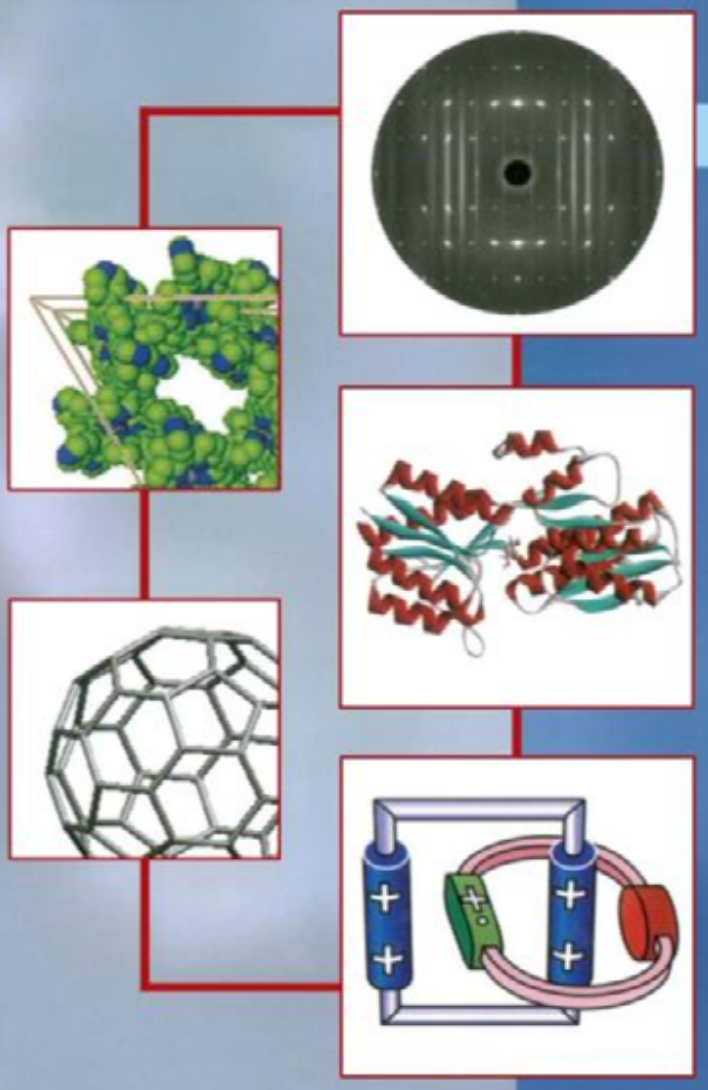

ENCYCLOPEDIA OF SUPRAMOLECULAR CHEMISTRY

EDITED BY
JERRY L. ATWOOD
JONATHAN W. STEED

Encyclopedia of Supramolecular Chemistry

Encyclopedia of Supramolecular Chemistry

Volume 1
A–Min
Pages 1–872

edited by

Jerry L. Atwood
University of Missouri, Columbia, Missouri, U.S.A.

Jonathan W. Steed
University of Durham, Durham, United Kingdom

Taylor & Francis
Taylor & Francis Group
Boca Raton London New York

CRC is an imprint of the Taylor & Francis Croup,
an informa business

Encyclopedia of Supramolecular Chemistry

Volume 2
Mod–Z
Pages 873–1648

edited by

Jerry L. Atwood
University of Missouri, Columbia, Missouri, U.S.A.

Jonathan W. Steed
University of Durham, Durham, United Kingdom

Taylor & Francis
Taylor & Francis Croup
Boca Raton London New York

CRC is an imprint of the Taylor & Francis Croup,
an informa business

Published in 2004 by
CRC Press
Taylor & Francis Group
6000 Broken Sound Parkway NW, Suite 300
Boca Raton, FL 33487-2742

Printed in the United States of America on acid-free paper
10 9 8 7 6 5 4 3 2

International Standard Book Number-10: 0-8247-5056-X (Hardcover)
International Standard Book Number-13: 978-0-8247-5056-5 (Hardcover)
ISBN Volume 1: 0-8247-4723-2
ISBN Volume 2: 0-8247-4724-0
ISBN Online: 0-8247-4725-9
ISBN Print/Online Combo: 0-8247-4720-8

Volume 1:
Front cover, top left and back cover detail: Courtesy of I. Goldberg, author of "Porphyrin-Based Clathrates."
Front cover, lower left: Courtesy of I. Goldberg, author of "Porphyrin-Based Clathrates."
Front cover, top right: Courtesy of T. Richard Welberry, author of "Disorder and Diffuse Scattering."
Front cover, middle right: Courtesy of Dr. Arne Lützen, author of "Carbohydrates, Recognition of."
Front cover, lower right and back cover detail: Courtesy of Dr. Alberto Credi, author of "Molecular-Level Machines."

Volume 2:
Front cover, top left and back cover detail: Courtesy of Dr. Alberto Credi, author of "Molecular-Level Machines."
Front cover, lower left and back cover detail: Courtesy of Irina S. Terekhova and the estate of Yuri A. Dyadin, authors of "Classical Descriptionsof Inclusion Compounds."
Front cover, top right: Courtesy of Martin Schröder and Neil Champness, authors of "Supramolecular Isomerism."
Front cover middle right: Courtesy of Dr. Alberto Credi, author of "Molecular-Level Machines."
Front cover lower right: Courtesy of Dr. Dmitry M. Rudkevich, author of "Self-Assembling Capsules."

Library of Congress Cataloging-in-Publication Data

Catalog record is available from the Library of Congress

informa
Taylor & Francis Group is the Academic Division of Informa plc.

Visit the Taylor & Francis Web site at
http://www.taylorandfrancis.com

and the CRC Press Web site at
http://www.crcpress.com

Jerry L. Atwood
University of Missouri, Columbia, Missouri, U.S.A.
Jonathan W. Steed
University of Durham, Durham, United Kingdom

Editorial Advisory Board

List of Contributors

Ghrister B. Aakeroy / *Kansas State University, Manhattan, Kansas, U.S.A.*
Rebecca J. Aarons *University of Manchester, Manchester, United Kingdom*
Alaa S. Abd-El-Aziz / *The University of Winnipeg, Winnipeg, Manitoba, Canada*
Saad A. M. Ali / *Smith & Nephew Group Research Centre, York, United Kingdom*
Frank H. Allen *Cambridge Crystallographic Data Centre (CCDC), Cambridge, United Kingdom*
Mark Allen *Montana State University, Bozeman, Montana, U.S.A.*
David B. Amabilino *Institut de Ciència de Materials de Barcelona (CSIC), Cerdanyola del Vallès, Spain*
Jörg Andrä *Research Center Borstel, Leibniz-Center for Medicine and Biosciences, Borstel, Germany*
Marius Andruh *University of Bucharest, Bucharest, Romania*
Eric V. Anslyn *University of Texas at Austin, Austin, Texas, U.S.A.*
Jun-ichi Anzai / *Tohoku University, Sendai, Japan*
Pavel Anzenbacher, Jr. / *Bowling Green State University, Bowling Green, Ohio, U.S.A.*
Vladimir A. Azov / *ETH Zurich, Zurich, Switzerland*
Alan L. Balch *University of California, Davis, California, U.S.A.*
Philip Ball *Nature, London, United Kingdom*
Vincenzo Balzani *Università di Bologna, Bologna, Italy*
Arindam Banerjee *Indian Association for the Cultivation of Science, Calcutta, West Bengal, India*
José Osío Barcina / *Universidad Complutense, Madrid, Spain*
Francesco Barigelletti *Istituto per la Sintesi Organica e la Fotoreattività CNR-ISOF, Bologna, Italy*
Craig E. Barnes *University of Tennessee, Knoxville, Tennessee, U.S.A.*
Stuart R. Batten / *Monash University, Clayton, Victoria, Australia*
Derek A. Beauchamp *University of Windsor, Windsor, Ontario, Canada*
Marc Bée / *Université J. Fourie Grenoble, France*
Paul D. Beer *University of Oxford, Oxford, United Kingdom*
Thomas W. Bell *University of Nevada, Retzo, Nevada, U.S.A.*
Andrew C. Benniston *University of Newcastle, Newcastle upon Tyne, United Kingdom*
Katja E. Berg *Stanford University, Stanford, California, U.S.A.*
Nicholas Blagden *Bradford University, Bradford, United Kingdom*
Kristin Bowman-James *University of Kansas, Lawrence, Kansas, U.S.A.*
Dario Braga *Università degli Studi di Bologna, Bologna, Italy*
Klaus Brandenburg / *Research Center Borstel, Leibniz-Center for Medicine and Biosciences, Borstel, Germany*
Perla Breccia / *Universidad Autónoma de Madrid, Madrid, Spain*
Gareth J. Brown *The Queen's University of Belfast, Belfast, Northern Ireland*
Andrew D. Burrows *University of Bath, Bath, United Kingdom*
Daryle H. Busch / *University of Kansas, Lawrence, Kansas, U.S.A.*
Mino R. Caira *University of Cape Town, Rondebosch, Western Cape Province, South Africa*

Salvatore **Camiolo** / *University of Southampton, Southampton, United Kingdom*
Jiří Čejka *Academy of Sciences of the Czech Republic, Prague, Czech Republic*
Neil R. Champness / *The University of Nottingham, Nottingham, United Kingdom*
Gervais **Chapuis** / *University of Lausanne, Lausanne, Switzerland*
Da-Wei Chen / *Achillian Pharmaceuticals Inc., New Haven, Connecticut, U.S.A.*
Kihang Choi *Yale University, New Haven, Connecticut, U.S.A.*
Alberto **Ciferri** / *University of Genoa, Genova, Ituly*
Anthony **W.** Coleman / *Institut de Biologie et Chimie des Protéines, Lyon, France*
James **P.** Collman / *Stanford University, Stanford, California, U.S.A.*
Ruud G. E. Coumans / *University of Nijmegen, Nijmegen, The Netherlands*
Robert **H. Crabtree** *Yule University, New Haven, Connecticut, U.S.A.*
Peter J. **Cragg** / *University of Brighton, Brighton, United Kingdom*
Alberto Credi / *Università di Bologna, Bologna, Italy*
Leroy **Cronin** / *The University of Glasgow, Glasgow, United Kingdom*
Sheng **Dai** *Oak Ridge National Laboratory, Oak Ridge, Tennessee, U.S.A.*
Ian Dance / *University of New South Wales, Sydney, New South Wales, Australia*
Eric Da Silva / *Institut de Biologie et Chimie des Protéines, Lyon, France*
Anthony **P.** Davis / *University of Bristol, Bristol, United Kingdom*
Steven De Feyter / *Katholieke Universiteit Leuven (K.U.Leuven), Leuven, Belgium*
Javier de **Mendoza** / *Universidad Autónoma de Madrid, Madrid, Spain*
Frans C. **De** Schryver / *Katholieke Universiteit Leuven (K.U.Leuven), Leuven, Belgium*
A. **Prasanna** de **Silva** / *The Queen's University of Belfast, Belfast, Northern Ireland*
Gautam **R.** Desiraju / *University of Hyderabad, Hyderabad, Andhra Pradesh, India*
Christian **Detellier** / *University of Ottawa, Ottawa, Ontario, Canada*
Bernard **Dietrich** / *ISIS –Université Louis Pasteur, Strasbourg, France*
Peter **H.** Dinolfo / *Northwestern University, Evanston, Ilinois, U.S.A.*
Stefano Di Stefano / *Università degli Studi di Roma La Sapienza, Roma, Italy*
Dennis A. **Dougherty** / *California Institute of Technology, Pasadena, California, U S.A.*
Trevor Douglas / *Montana State University, Bozeman, Montana, U.S.A.*
Yuri Alexseevich Dyadin (Deceased) / *The Siberian Branch of the Russian Academy of Sciences, Novosibirsk, Russia*
James **L.** Dye / *Michigan State University, East Lansing, Michigan, U.S.A.*
Claude Ecolivet / *Université de Rennes, Rennes, France*
Johannes **A. A. W. Elemans** / *University of Nijmegen, Nijmegen, The Netherlands*
Marco Evangelisti / *Leiden University, Leiden, The Netherlands*
John **S. O.** Evans / *University of Durham, Durham, United Kingdom*
Jean-Yves Exposito *Centre National de la Recherche Scientifique, Lyon, France*
Luigi Fabbrizzi / *Università di Pavia, Pavia, Italy*
Stephen **Faulkner** / *University of Manchester, Manchester, United Kingdom*
Riccardo Ferdani / *Washington University School of Medicine, St. Louis, Missouri, U.S.A.*
Ben **L. Feringa** / *University of Groningen, Groningen, The Netherlands*
Eduardo **J. Fernández** / *Universidad de La Rioja, UA –CSIC, Logroño, Spain*
Michelle **Flenniken** / *Montana State University, Bozeman, Montana, U.S.A.*
Thomas **M. Fyles** / *University of Victoria, Victoria, British Columbia, Canada*
Philip A. Gale / *University of Southampton, Southampton, United Kingdom*
Peter **Gans** *The University of Leeds, Leeds, United Kingdom*
Patrick **Garidel** / *Martin-Luther-Universität, Halle/Wittenberg, Halle/Saale, Germany*

Maria Gdaniec / *Adam Mickiewicz University, Poznań, Poland*

Bruce G. Gibb / *University of New Orleans, New Orleans, Louisiana, U.S.A.*

Hermann Gies / *Ruhr-Universität Bochum, Bochum, Germany*

Karsten Gloe / *Technische Universitat Dresden, Dresden, Germany*

George W. Gokel / *Washington University School of Medicine, St. Louis, Missouri, U.S.A.*

Israel Goldberg / *Tel Aviv University, Tel Aviv, Israel*

Carl Hensik Görbitz / *University of Oslo, Oslo, Norway*

Fabrizia Grepioni / *Università di Sassari, Sassari, Italy*

Manuela Grotjahn / *Technische Universitat Dresden, Dresden, Germany*

G. David Gutsche / *Texas Christian University, Fort Worth, Texas, U.S.A.*

Ionel Aaiduc / *Universitatea "Babeş-Bolyai," Cluj-Napoca, Romania*

Andrew D. Namilton / *Yule University, New Haven, Connecticut, U.S.A.*

Tamara D. Hamilton *University of Iowa, Iowa City, Iowa, U.S.A.*

Michaele J. Hardie / *University of Leeds, Leeds, United Kingdom*

Michael Harmata / *University of Missouri—Columbia, Columbia, Missouri, U.S.A.*

Kenneth D. M. Harris / *Cardiff University, Cardiff, Wales*

Jeffrey H. Harwell / *University of Oklahoma, Norman, Oklahoma, U.S.A.*

Takashi Hayashi / *Kyushu University, Fukuoka, Japan*

Elizabeth J. Hayes / *University of Oxford, Oxford, United Kingdom*

Tino Hertzsch *University of Berne, Berne, Switzerland*

Robert C. Hides / *King's College London, London, United Kingdom*

Andrew Hinton , *University of Edinburgh, Edinburgh, United Kingdom*

John D. Holbrey / *The University of Alabama, Tuscaloosa, Alabama, U.S.A.*

K. Travis Holman / *Georgetown University, Washington, District of Columbia, U.S.A.*

Antony M. Hooper / *Rothamsted Research, Harpenden, Hertfordshire, United Kingdom*

Junhua Huang / *Commonwealth Scientific and Industrial Research Organization (CSIRO), Melbourne, Victoria, Australia*

Jürg Hulliger *University of Bet-ne, Berne, Switzerland*

Joseph T. Hupp *Northwestern University, Evanston, Ilinois, U.S.A.*

Bakhtiyar T. Ibragimov / *Institute of Bioorganic Chemistry of Uzbekistan Academy of Sciences, Tashkent, Uzbekistan*

Yoshihisa Inoue / *Entropy Control Project, International Cooperative Research Project (ICORP), Toyonaka, Japan*

Yasuhiro Ishida / *The University of Tokyo, Tokyo, Japan*

Toschitake Iwamoto / *Iwaki Meisei University, Iwaki, Fukushima, Japan*

Stuart L. James / *Queen's University Belfast, Belfast, Northern Ireland*

Kim D. Janda / *The Scripps Research Institute and The Skaggs Institute for Chemical Biology, La Jolla, California, U.S.A.*

Sei-Hum Jang , *University of Washington, Seattle, Washington, U.S.A.*

Janarthanan Jayawiekramarajah / *University of Texas at Austin, Austin, Texas, U.S.A.*

Gunnar Jeschke / *Max Planck Institute for Polymer Research, Mainz, Germany*

Gyan P. Johari / *McMaster University, Hamilton, Ontario, Canada*

Bart Kahr *University of Washington, Seattle, Washington, U.S.A.*

Angel E. Kaifer / *University of Miami, Coral Gables, Florida, U.S.A.*

Gerd Kaupp / *University of Oldenburg, Oldenburg, Germany*

Jun-ichi Kikuchi / *Nara Institute of Science and Technology, Nara, Japan*

Hee-Joon Kim / *Pohang University of Science and Technology, Pohang, Republic of Korea*

Kimoon Kim / *Pohang University of Science and Technology, Pohang, Republic of Korea*

Eiichi Kimura / *Hiroshima University, Hiroshima, Japan*
Yoshiyaki Kobuke , *Nara Institute of Science and Technology, Nara, Japan; Crest, Japan Science and Technology, Nara, Japan*
Carolyn A. Koh *King's College London, London, United Kingdom*
Tohru Koike ' *Hiroshima University, Hiroshima, Japan*
Hiroki Kondo *Kyushu Institute of Technology, Fukuoka, Japan*
Shin-ichi Kugimiya ' *Nara Institute of Science and Technology, Tokyo, Japan*
Jayant Kumar ' *University of Massachusetts Lowell, Lowell, Massachusetts, U.S.A.*
Antonio Laguna , *Universidad de Zaragoza—CSIC, Zaragoza, Spain*
Chi-Keung Lam / *The Chinese University of Hong Kong, Hong Kong SAR, People's Republic of China*
Dario Landini , *Università degli Studi di Milano, Milano, Italy*
Adrian J. Lapthorn *University of Glasgow, Glasgow, United Kingdom*
Adina N. Lazar / *Institut de Biologie et Chimie des Protéines, Lyon, France*
Pavel Lhoták *Institute of Chemical Technology, Prague, Czech Republic*
Li Li *Nankai University, Tianjin, People's Republic of China*
Leonard F. Lindoy ' *The University of Sydney, Sydney, New South Wales, Australia*
Petra Linnartz *Kekulé-Institut für Organische Chemie und Biochemie der Universität, Bonn, Germany*
Karen J. Lipscomb , *Cambridge Crystallographic Data Centre (CCDC), Cambridge, United Kingdom*
Yu Liu *Nankai University, Tianjin, People's Republic of China*
Zu Dong Liu *King's College London, London, United Kingdom*
José M. Llinares *University of Kansas, Lawrence, Kansas, U.S.A.*
Stephen J. Loeb *University of Windsor, Windsor, Ontario, Canada*
José M. López-de-Luzuriaga , *Universidad de La Rioja, UA—CSIC, Logroño, Spain*
Ulrich Lüning , *Universitat Kiel, Kiel, Germany*
Arne Lützen / *University of Oldenburg, Oldenburg, Germany*
Donal H. Macartney *Queen's University, Kingston, Ontario, Canada*
Leonard R. MacGillivray ' *University of Iowa, Iowa City, Iowa, U.S.A.*
Joseph M. Mahoney *University of Notre Dame, Notre Dame, Indiana, U.S.A.*
Angelamaria Maia ' *Università degli Studi di Milano, Milano, Italy*
Thomas C. W. Mak , *The Chinese University of Hong Kong, Hong Kong SAR, People's Republic of China*
Luigi Mandolini *Università degli Studi di Roma La Sapienza, Roma, Italy*
Amedea Manfredi *CNR-Istituto di Scienze e Technologic, Molecolari, Milano, Italy*
Christian R. Marcilly ' *French Institute of Petroleum (IFP), Rueil Malmaison, France*
Bernd Marler *Ruhr-Universität Bochum, Bochum, Germany*
Michael J. Marsella / *University of California, Riverside, California, U.S.A.*
Antonio Garcia Martinez , *Universidad Complutense, Madrid Spain*
Takasuke Matsuo , *Osaka University, Osaka, Japan*
Karen R. Maxcy ' *IBM T.J. Watson Research Center, Yorktown Heights, New York, U.S.A.*
J. Andrew McCammon *University of California—San Diego, La Jolla, California, U.S.A.*
Gareth D. McClean *The Queen's University of Belfast, Belfast, Northern Ireland*
Judith R. Meakin *University of Aberdeen, Foresterhill, Aberdeen, United Kingdom*
Pierangelo Metrangolo *Polytechnic of Milan, Milan, Italy*
Robert M. Metzger *The University of Alabama, Tuscaloosa, Alabama, U.S.A.*
Amaresh Mishra *University of Akron, Akron, Ohio, U.S.A.*
Karycia D. D. Mitchell *University of Victoria, Victoria, British Columbia, Canada*
Mikiji Miyata *Osaka University, Osaka, Japan*

Sandra Monti / *Istituto per la Sintesi Organica e la Fotoreattività CNR-ISOF, Bologna, Italy*
Thomas S. Moody *The Queen's University of Belfast, Belfast, Northern Ireland*
Charles N. Moorefield / *University of Akron, Akron, Ohio, U.S.A.*
Arvin Moser *University of Ottawa, Ottawa, Ontario, Canada*
Ravi Mssurkal *University of Massachusetts Lowell, Lowell, Massachusetts, U.S.A.*
Ashwini Nangia / *University of Hyderabad, Hyderabad, India*
Luigi R. Nassimbeni / *University of Cape Town, Rondebosch, Western Cape Province, South Africa*
George R. Newkome *University of Akron, Akron, Ohio, U.S.A.*
Motorhiro Nishio / *The CHPI Institute, Tokyo, Japan*
Roeland J. M. Nolte / *University of Nijmegen, Nijmegen, The Netherlands*
Tomás C. O'Riordan *University College Cork, Cork, Ireland*
Sijbren Otto / *University of Cambridge, Cambridge, United Kingdom*
Giannis S. Papaefstathiou *University of Iowa, Iowa City, Iowa, U.S.A.*
Dmitri B. Papkovsky *University College Cork, Cork, Ireland*
Gerard Parkin *Columbia University, New York, New York, U.S.A.*
Alexandra L. Pickering / *The University of Glasgow, Glasgow, United Kingdom*
John A. Pickett / *Rothamsted Research, Harpenden, Hertfordshire, United Kingdom*
Lucidalva S. Pinheiro / *Instituto de Química da Universidade de São Paulo, São Paulo, Brazil*
Sebastian Polarz / *Ruhr-University Bochum, Bochum, Germany*
Gianluca Pozzi *CNR-Istituto di Scienze e Tecnologie Molecolari, Milano, Italy*
Nicholas C. Price *University of Glasgow, Glasgow, United Kingdom*
Sarah L. Price *University College London, London, United Kingdom*
Silvio Quici / *CNR-Istituto di Scienze e Tecnologie Molecolari, Milano, Italy*
Torsten Rambusch / *Technische Universitat Dresden, Dresden, Germany*
Alexander Rang *Kekulé-Institut für Organische Chemie und Biochemie der Universität, Bonn, Germany*
Colin L. Raston / *University of Western Australia, Crawley, Perth, Australia*
Christopher I. Ratcliffe / *National Research Council Canada, Ottawa, Ontario, Canada*
Mikhail Rekharsky *Entropy Control Project, International Cooperative Research Project (ICORP), Osaka, Japan*
Giuseppe Resnati *Polytechnic of Milan, Milan, Italy*
Marcos Caroli Rezende *Universidad de Santiago de Chile, Santiago, Chile*
John A. Ripmeester / *National Research Council Canada, Ottawa, Ontario, Canada*
Kari Rissanen / *University of Jyväskylä, Jyväskylä, Finland*
Michael A. J. Rodgers / *Bowling Green State University, Bowling Green, Ohio, U.S.A.*
Robin D. Rogers / *The University of Alabama, Tuscaloosa, Alabama, U.S.A.*
Alan E. Rowan / *University of Nijmegen, Nijmegen, The Netherlands; NSRIM, University of Nijmegen, Nijmegen The Netherlands*
Dmitry M. Rudkevich *The University of Texas at Arlington, Arlington, Texas, U.S.A.*
David A. Sabatini / *University of Oklahoma, Norman, Oklahoma, U.S.A.*
Kazuki Sada *Osaka University, Osaka, Japan*
J. Timothy Sage *Northeastern University, Boston, Massachusetts, U.S.A.*
Lynne A. Samuelson / *U.S. Army RDECOM, Natick, Massachusetts, U.S.A.*
Jeremy K. M. Sanders *University of Cambridge, Cambridge, United Kingdom*
Muhunthan Sathiosatham *Eastman Kodak Company, Rochester, New York, U.S.A.*
Abdelhamid Sayari *University of Ottawa, Ottawa, Ontario, Canada*
John F. Scamehorn *University of Oklahoma, Norman, Oklahoma, U.S.A.*
Franco Scandola *Università degli Studi di Ferrara, Ferrara, Italy*

Contents

Preface

Chemistry has witnessed a phenomenal change in the last decades of the twentieth century. Research in two areas in particular have driven the emergence and significance of supramolecular chemistry. Since the Nobel prize–winning work of Cram, Lehn, and Pedersen in the late 1960's and early 1970's, work in solution host guest compounds, and latterly self-assembling and self-organizing systems, has seen a veritable explosion. The older field of solid-state inclusion chemistry has, to a very great extent, paralleled these developments with a great deal of recent effort in crystal engineering being regarded as solid-state supramolecular synthesis. Boih subfields rely crucially on an understanding of the noncovalent bond—the quintessence of supramolecular chemistry. The evolution of these areas underscores the dynamic growth of supramolecular research and the explosion of interest in the field.

Clearly one of the most important goals of the *Encyclopedia* of *Supramolecular Chemistry* then is to provide a broad-based overview of the discipline and to capture the significance of research in this area, with special emphasis on a synthesis of the concepts and language of supramolecular chemistry across a wide range of related disciplines. Furthermore, this Encyclopedia is not written by, nor written exclusively for "supramolecular chemists"; it is for students and practitioners of the chemistry (indeed science) of the noncovalent bond wherever it occurs. We have made specific efforts to direct the reader to the defining literature in the field and specifically included cross-references to help the researcher locate other entries of interest.

We hope that this two-volume work will become a useful and well-thumbed source of information and ideas, as well as a helpful teaching aid as courses in intermolecular interactions continue to grow. If browsing through this work stimulates a new idea or a new collaboration from an unusual combination of topics, or if it clarifies a point of confusion for an undergraduate or senior researcher, then we will have succeeded.

As editors, we would very much like to thank the very many contributors and the members of the Editorial Advisory Board who have donated their time and insights to this work. It is very much a community effort and we have spent more time listening and nodding, than talking. Finally, we would like to express our heartfelt thanks to the editorial and production staff at Marcel Dekker, Inc. who have organized the monumental task of gathering together all of the elements of such a diverse production. We are especially grateful to Oona Schmid not just for her extremely hard work, but also for her insight into the needs of this work and the community as a whole.

Jerry L. Atwood
Columbia, Missouri, U.S.A.

Jonathan W. Steed
Durham, United Kingdom
July 2003

Foreword

Molecular chemistry has, over many years, developed a wide range of very powerful procedures for constructing ever more sophisticated molecules from atoms linked by covalent bonds. Beyond molecular chemistry lies supramolecular chemistry which aims at setting up highly complex chemical systems from components interacting via noncovalent intermolecular forces.

The concept and the term supramolecular chemistry were introduced in 1978, in the words: "Just as there is a field of molecular chemistry based on the covalent bond, there is a field of supramolccular chemistry, the chemistry of molecular assemblies and of the intermolecular bond," reformulated on various occasions, e.g., "Supramolecular chemistry may be defined as 'chemistry beyond the molecule,' bearing on the organized entities of higher complexity that result from the association of two or more chemical species held together by intermolecular forces."

The breadth and especially the unifying power of the concept became progressively more and more apparent, so that recent years have seen an explosive growth, as measured by the increasing number of laboratories that join the Geld and whose work has been reported in a vast range of publications, books, journals, meetings. and research networks.

By the appropriate manipulation of noncovalent interactions, supramolecular chemistry became the chemistry of molecular information, involving the storage of information at the molecular level, in the structural features, and its retrieval, transfer, processing at the supramolccular level, through molecular recognition processcs operating via specific interactional algorithms. A further step consisted of the design of systems undergoing self-organization, i.e., systems capable of spontaneously generating well-defined supramolecular architectures by self-assembly from their components under the control of the molecular information stored in the covalent framework of the components and read out at the supramolecular level through specific interactions. Self-organization processes thus represent the operation of programmed chemical systems leading to the spccific generation of well-defined entities.

The design of such molecular information-controlled. "programmed," and functional self-organizing systems provides an original approach to nanosciencc and nanotechnology, offering a powerful alternative/complement to nanofabrication and to nanomanipulation.

Supramolecular chemistry is also intrinsically a dynamic chemistry in view of the lability of the interactions connecting the molecular components of a supramolecular entity and the resulting ability of supramolccular species to exchange their constituents. Thus, in addition to self-organization by design, which strives to achieve full control over the output supramolecular entity by explicit programming, a new development resides in the implementation of self-organization by selection, operating on dynamic constitutional diversity in response to either internal or external factors to achieve adaptation.

From molecular recognition to self-organization, to prograinmed chemical systems, supramolecular chemistry progressively leads up the ladder of complexity and opens new horizons for chemistry toward a science of informed, organized, and adaptative matter.

Supramolecular chemistry is a highly interdisciplinary field of science. A major feature is the range of perspectives offered by the cross-fertilization of supramolecular chemical research

due to its location at the intersection of chemistry, biology, and physics. Drawing on the physics of organized condensed matter and extending *to the complex entities and processes of biology,* supramolecular *chemistry expands into a supramolecular science. It has penetrated such diverse areas as for instance: polyiner chemistry and materials science, solid-state chemistry and crystal engineering, species for nonlinear optics, biological interactions and drug design, sensor and diagnostic procedures, nanoscience and nanotechnology, etc.*

Supramolecular *chemistry has thus* become *a highly diverse but coherent and lively body of concepts and objects, generating and incorporating novel areas of investigation. Such wide horizons are a challenge and a stimulus to the creative imagination of the chemist.*

As a new field of science emerges, grows, and matures, it generates novel terminology to name the concepts that define it and to describe the *objects that constitute it. The language of supramolccular chemistry, its vocabulary, and syntax have been progressively developed, leading to the introduction of new terms or to the reappropriation of old ones.*

Such conceptualizing and naming play a very important role, not only for shaping the *field but also by the ground they offer to the creative imagination. Indeed, one may let one's imagination be carried by the magic of the word and pulled by the evocative and stimulating power* of the concept.

It *is clear that the time is* ripe *for an Encyclopedia of Supramolecular Chemistry, presenting its basic concepts, its various objects, and processes as* well *as its relations to other areas of basic and applied science. It will be of great value to the many practitioners in the field as well as to those, perhaps even more numerous newcomers, who wish to get acquainted with it and may wish to join the family and become part of the adventure!*

The editors and authors deserve our warmest thanks for their timely work to the benefit of the common good.

Jean-Marie Lehn
Strasbourg, France
September 2003

General references

- *Lehn, J.-M. Supramolecular chemistry: Concepts and perspectives. VCH Weinheim* 1995.
- *Lehn, J.-M. Supramolecular* Chemistry/Science—Some *Conjectures and Perspectives. In Supramolecular Chemistry: Where It Is and Where It Is Going; Ungaro, R., Dalcanale, E.. Eds.; Kluwer: Dordrecht, 1999;* 287–304.
- *Lehn,* J.-M. *Toward complex matter: Supramolecular chemistry and self-organization. Proc. Natl. Acad. Sci. USA, 2002, 99,* 4763.

Alkali Metal Cations in Biochemistry

A

Yoshiyaki Kobuke
Nara Institute of Science and Technology, Nara, Japan;
CREST, Japan Science and Technology, Nara, Japan

Shin-ichi Kugimiya
Nara Institute of Science and Technology, Tokyo, Japan

INTRODUCTION

Alkali metals easily lose one electron at the outer s-shell to form singly charged cations. Among these, the Na^+ and K^+ ions play the most important biological roles. Because of the weak and nonspecific nature of the interaction with other ligands, the biological significance is determined primarily by the magnitude of the concentrations. Similar chemical principles are applicable in a series of alkaline earth metal cations, except these are doubly positively charged. Moreover, the sizes become smaller, because the biologically important Mg^{2+} (0.60 Å) and Ca^{2+} (1 A) ions correspond to Li^+ (0.6 A) and Na^+ (0.95 Å) ions, respectively. These concentrations of the alkali and alkaline earth metal ions reflect those of seawater, and this coincidence evidences that the first life was born in archeological seawater. Therefore, the "physiological salt solution" employs concentrations in which $Na^+ > K^+ > Mg^{2+} > Ca^{2+}$. This order, however, shows a discrepancy from the one found in the earth's crust, where Ca, Na, K, and Mg occupy the fifth to the eighth elements in this order. The reason for this difference is that the Ca^{2+} ion is selectively eliminated from solution by the tendency to form insoluble precipitates such as $CaCO_3$ or Ca_4 (PO,),. According to this tendency, $CaCO_3$ is accumulated in rocks, and Ca_4 $(PO_4)_3$ is an important component of bone and tooth in the biological systems.

Dominant alkali metal ions, Na^+ and K^+, are highly soluble in aqueous solution and are the most important components in maintaining the salt concentrations inside and outside the cell, necessary to keep homeostasis of biological cells. At the same time, their single charge is associated with relatively small solvation energies, 98.5 and 80.5 kcal mol^{-1} for Na^+ and K^+ ions, respectively, reflecting the size difference on delocalizing the positive charges. These ions are most appropriately employed as messengers of biological signal transduction by mass (i.e., charge) transport across the membrane.[1] Compared to these ions, Mg^{2+} with two positive charges is constrained in a small atomic volume and must compensate by strong ion pairing with anionic counterparts of high charge densities. Phosphate anions are the most satisfactory as a pair component, and Mg—phosphates behave like molecules in many chemical events. The high solvation energy of the Mg^{2+} ion (454 kcal mol^{-1}) makes it difficult to use as the charge messenger of signal transduction.

The Ca^{2+} ion possesses properties that are intermediate, and it is associated with various biologically important roles. It does not favor any specific coordination structure but still interacts strongly with ligands, especially with an oxygen anion, to alter the charged state and geometrical structure of the ligands, just as transition metal ions do. At the same time, the Ca^{2+} ion can be transferred into the cell across the biological membrane, in spite of its high hydration energy (379 kcal mol^{-1}), and plays a role as a second messenger in the cell. For example, acetylcholine is ejected into a synaptic crevasse triggered by the entry of a Ca^{2+} ion. However, the presence of the Ca^{2+} ion in the cell is hazardous because of its wide spectrum of actions and is eliminated from the inside cell and stored in endocellular cavities immediately after the completion of the specific role. When the Ca^{2+} concentration is monitored by, e.g., Ca^{2+}-specific sensors, a Ca^{2+} wave can actually be observed. When this control system is destroyed, cells suffer fatal damage. For example, Alzheimer's and other related diseases are believed to induce such an uncontrolled entry of Ca^{2+} ion and to cause fatal damage to nerve cells. The entry of the Ca^{2+} ion was demonstrated by single channel measurements, and its close relationship with diseases was invoked.[2]

BIOLOGICAL ENERGY CONVERSION AND ION CHANNELS

A biological energy conversion system stores energy first in the form of a proton concentration gradient across the biological membrane via coupled electron and proton transport using the action of a photosynthetic or metabolic energy-producing pathway in many plants and animals.[3] This is a universal expression of energy storage, but it relies on the presence of the membrane as the separation barrier of the H^+-concentration gradient and must be

Encyclopedia of Supramolecular Chemistry
DOI: 10.1081/E-ESMC 120012671

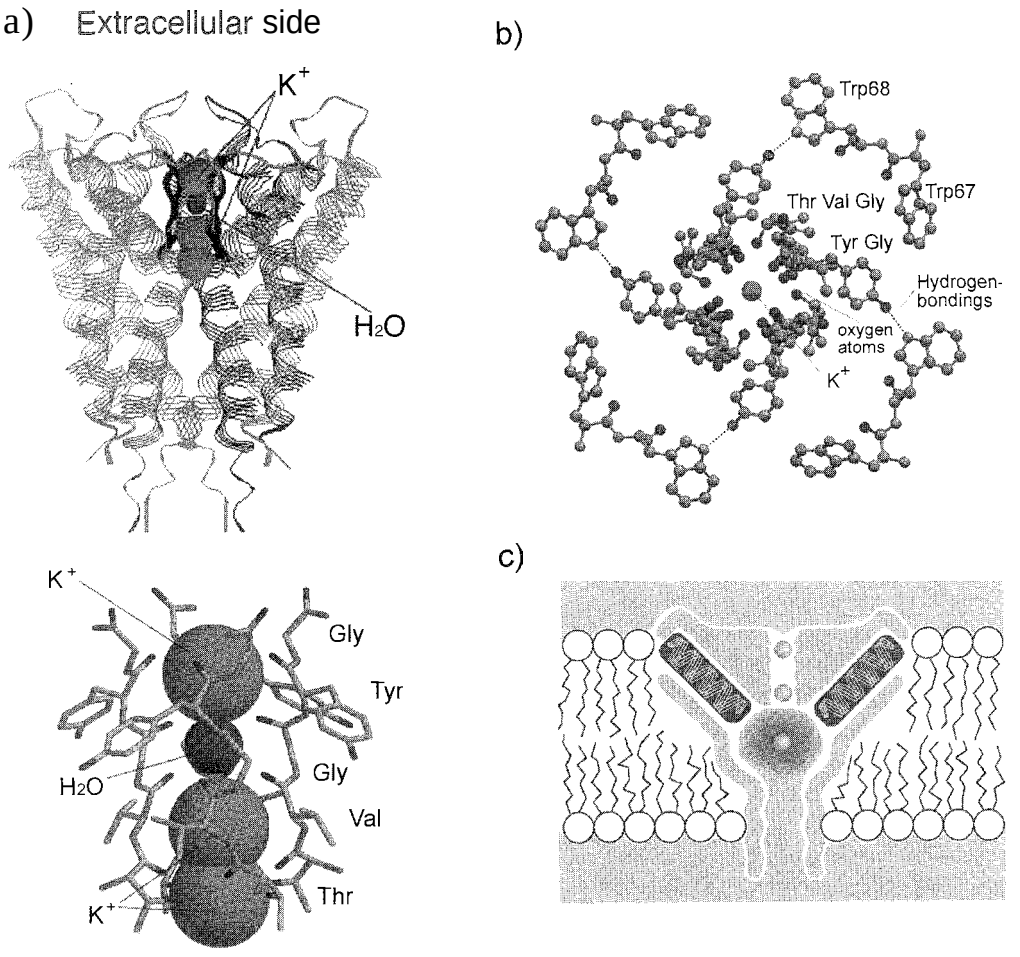

Fig. 1 Crystal structure of K^+ channel from *Streptomyces lividans*. a) Top: A ribbon representation of the KcsA tetramer viewed from the side. The four subunits are distinguished by color. Selectivity filter (black sticks) locates extracellular side in interface. K^+ ions are represented by green spheres. Bottom: Selectivity filter with four chains represented are comprised of the signature sequence amino acids Thr, Val. Gly, Tyr. Gly running from bottom to top. Two K^+ ions (green) are located at opposite ends of the selectivity filter, roughly 7.5 A apart. with a single water molecule (red) in between. The inner K^+ is in rapid equilibrium between adjacent coordination sites. b) K^+ channel selectivity filter viewed from the extracellular side. Carbonyl oxygens of the main chain Thr75-Gly79, and the side chain of the Thr are shown as red spheres. The Tyr side chains are directed away from the ion conduction pathway. Blue dotted line represents hydrogen-bondings. c) Overall representation of K^+ channel stabilizing a cation in the middle of the membrane. A large aqueous cavity stabilizes an ion (green) in the otherwise hydrophobic membrane interior. Oriented helices point their partial negative charge (carboxyl end. red) toward the cavity. Fig. 1a and b were produced with a PDB file (code: 1BL8.pdb from Ref. [5]) and Raswin Molecular Graphics (version 2.7.2. Glaxo Research and Development. U.K.).

converted to another form of stable energy in order to be transferred to the spot where energy is required This transformation is accomplished by H^+-ATPase. where the vectorial proton flux across the membrane can produce adenosine triphosphate as molecular energy or the so-called "energy coin `` This energy in the form of pyrophosphate bonds can be transported to numerous energy-demanding organs. Around one-third to one-fourth of this ATP is then consumed for the generation of Na^+/K^+ concentration gradient across the membrane of nerve cells through the action of Na^+/K^+-ATPase [4] Consumption of one molecule of ATP transports $3Na^+$ and 2K' ions outside or inside the cell. respectively. These concentration gradients are maintained across the impermeable membrane, but large ionic fluxes are generated once these ions becoine permeable through the membrane. This ion-permeating device, the ion channel, is a inolecular machine of signal transduction located in the brain and nervous systems.[1] Ion transport across the membrane, generally in a form of a large flux, induces a rapid change of membrane potentials. The opening and closing of the ion channels are controlled by

the gate systems equipped intrinsically in the channel. Ion channels can recognize cation and anion and K^+/Na^+ ions with high selectivities. Once a Na^+ channel is opened. Na^+ ions accumulated outside the membrane enter into the cell, shifting the membrane potential toward a positive value. This channel is then inactivated and followed by the opening of a K^+ channel to shift the potential toward a negative value by the outflux of K^+ ions. The temporary shift of the membrane potential is large enough to induce the opening of a second Na^+ channel. located close to the first channel, and a second cycle follows. In this way. the wave of membrane potential, termed an ''action potential.'' is transferred along the nerve axon. The ion channel is regarded, therefore; as a molecular device of signal transduction, relying on Na^+. K^+, Ca^{2+}. and C l ions as thepredominant messengers.

The chemistry of alkali and alkaline earth metal ions is understood most comprehensively through analyzing the function of ion channels, especially mechanisms of ion selectivity and gating. An ion channel with a typical conductance of 10 *pS* allows the passage of 5×10^6 ions per second through a single molecular pore. Even operating at such large ionic fluxes, ion channels generally discriminate between different ionic species. for example, cation and anion and K^+/Na^+, by passing them through the selectivity filter. Permeability ratios. P_{Na}/P_K, for several K^+ channels are less than $0.01 \sim 0.07$.[1] This remarkable selectivity of K^+ may be understood by examining how the structure of a selectivity filter manages different hydration energies and ionic radii. In this article, recent advances in this area will be described in light of mechanisms of high selectivity and gating based on x-ray crystallographies. Furthermore. approaches to the construction of artificial ion channels are focused on these specific functions.

STRUCTURE OF ION CHANNELS

X-Ray Analysis of Selectivity Filter and ion-Conducting Mechanism

The first x-ray crystal structure of an ion channel appeared in 1998 from MacKinnon's group (Fig. 1).[5] The structure of the selectivity filter forced scientists to abandon the previous hypothesis that K^+ ion should be stabilized by cation–n interactions in the aromatic cage when surrounded by four tyrosine residues. In the selectivity filter located near the extracellular surface. one Thr OH and four main-chain amide carbonyls from Val-Gly-Tyr-Gly are lined up in a 12Å length. Because the K^+ channel is composed of four identical subunits. this provides four consecutive spherical cavities for K^+ binding by wrapping each K^+ with eight neutral oxygen atoms. This mode of binding is reminiscent of valinomycin and sandwiched crown complexes. The Tyr unit does not contribute to the direct stabilization. but it is directed outwardly toward the pore and interacts with a Trp residue by a phenolic

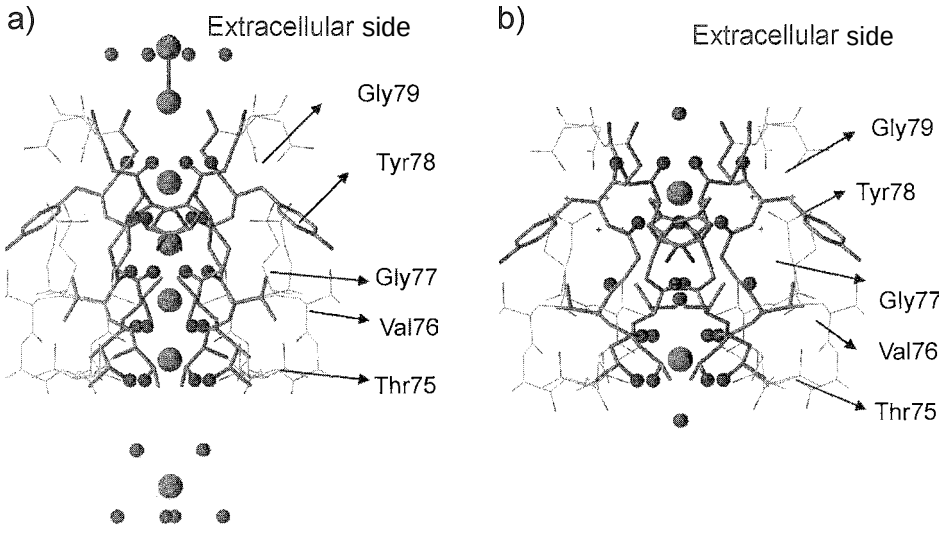

Fig. *2* Crystal structures of K^+ ion channel with different K^+ concentrations. a) K^+ channel selectivity filter with high concentration of K^+ ions (green spheres) along the ion pathway. and water molecules (pink spheres) in the vicinity. b) K^+ channel selectivity filter with low K^+ concentration of K^+ ion (green spheres). Main-chains of the selectivity filter are disordered. Fig. 2a and b were produced with PDB files (code: 1K4C and 1K4D from Ref. [8]) and ViewerLite (version 5.0 Accelrys. Inc.. U.K.).

OH···N (indolyl) hydrogen bond (Fig. 1b). This unit may keep the pore wide and contribute to the K^+/Na^+ selectivity through decreasing the stabilizing power for a smaller Na^+ ion. The selectivity filter is composed completely of neutral oxygen atoms in favor of stabilizing the K^+ rather than the Na^+ ion, which demands stronger electrostatic interactions. The selectivity filter of the Na^+ ion is believed to contain ionic pairs,[6] and its structural elucidation is highly desirable. Furthermore, the selectivity ratio P_K/P_{Na} of this K^+ channel KcsA shows only a moderate value of 11,[7] and it is interesting to imagine how highly selective K^+ channels introduce any additional recognition principle(s). Another characteristic point of this x-ray structure is that the transmeinbrane pore contains a Iarge water pool in the middle of the membrane. to which helical negative dipoles direct. Further, the inner half of the conduction pathway is lined with hydrophobic side chains and is wide enough to be filled completely with water molecules. These are thought to be features that allow a high throughput of K^+ ions (Fig. 1c).

The above selectivity filter constrained two K^+ ions about *7.5* Å apart. This configuration was thought to promote ion conduction by electrostatic repulsion. With an increased resolution, MacKinnon also determined two crystal structures at high and low K^+ concentration states.[8] At the high concentration, they found four K^+ ions in the selectivity filter instead of two, and two more hydrated K^+ ions at its extracellular entryway. Furthermore, the K^+ ion in the central cavity was fully surrounded by eight water molecules. All of these K^+ ions were embedded in a square antiprismatic geometry by water, carbonyl. and hydroxyl oxygen-donor ligand groups (Fig. 2). These ordered water molecules make dehydration and hydration interconversion processes of K^+ ion at both entryways easy. The similarity of the coordination structures, one at the central cavity, four in the selectivity filter, and two at the extracellular entryway, can promote the smooth structural interconversion and explain the rapid transport of K^+ ion through the K^+ channel.

The Cl^- channel is a physiological counterpart of cation channels, and the analysis of C l selectivity may contribute to the true understanding of the whole series of ion selectivities. In the x-ray crystal structure of the closed state of the Cl^- channel, two Cl^- ions detected inside the pore were stabilized by hydrogen bonding with main-chain amide NH and side-chain hydroxyl groups of Ser and Tyr (Fig. 3).[9,10]

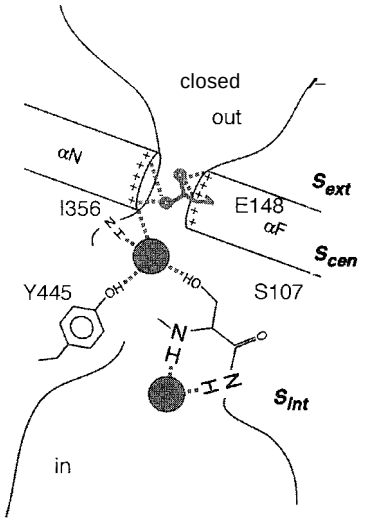

Fig. **3** Schematic illustration of the closed conformation of a ClC chloride channel. The ion-binding sites S_{int} and S_{cen} are occupied by chloride ions (red sphere) stabilized by $Cl^-\cdots H$ hydrogen bondings (dashed lines). The external ion-binding site S_{ext} constitutes the gate and is blocked by the side chain of Glul48 (red).

Gating Mechanisms of Ion Channels

Gating is one of the principal functions of ion channels. Ion permeation occurs only when the corresponding ion channels open on accepting their own stimuli. This gating information is classified into three types: voltage across the membrane (voltage-gated): binding of ligands such as neurotransmitters or second messengers (ligand-gated): and membrane deformation (inechanosensitive). In any event, in opening the gate, massive mechanical variations of channel structure must be performed when responding to the sensor unit. Recent developments in crystallographic structure determination enabled the identification of the open and closed states of several ion channels and discussion of the mechanisms based on these experimental structures.

In voltage-dependent K^+ channels, the number of gating charges amounts to 12–14 electron charges as a result of the assembly of four identical subunits having 3–3.5 charges. This large gating charge responds sharply to change of the membrane voltage. X-ray analysis elucidated the movement of this gating charge across the membrane, as shown in Fig. 4.[11,12] Here. the sensor units are composed of a highly conserved Arg-rich domain in the S4 helix. Its movement across almost the entire membrane can deform the channel geometry from trapezoidal to cylindrical forms and open the central pore (Fig. 4b). This new proposal differs from the conventional hypothesis of charge movement within the "gating pore."[13]

Voltage-dependent K^+ channels close by a process called "inactivation," rapidly after opening. In *drosophila* mutant K^+ channels, the cytoplasmic amino terminus in its own channel forms the inactivation gate. The central

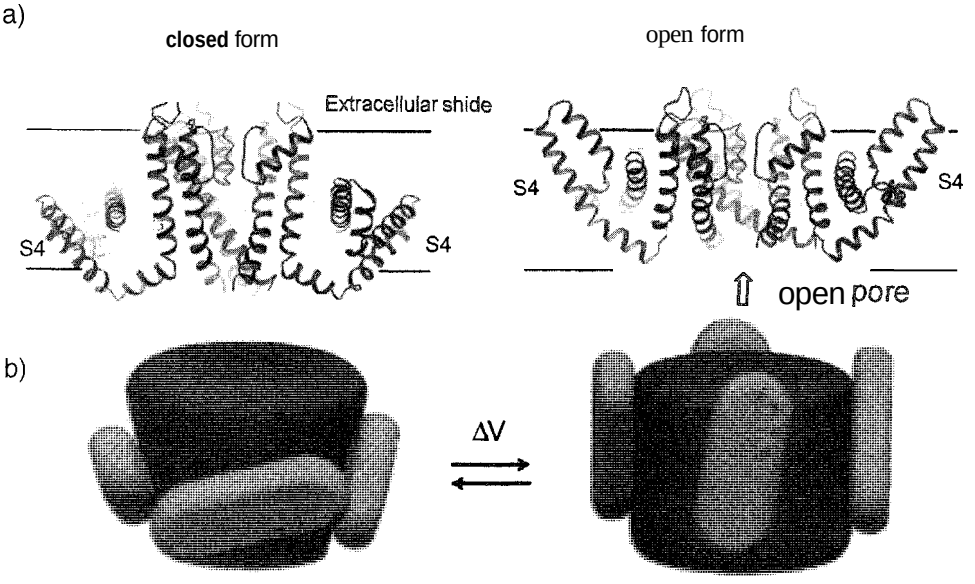

Fig. 4 Movement of voltage-sensor in voltage-gated K^+ channel. a) Positions within the membrane of the voltage-sensor paddles S4 (red) during closed and opened conformations. with coupling to pore opening. b) Gating charges (red plus signs) are carried through the membrane from inside (bottom) to outside (top) by *movements* of the voltage-sensor paddles against the lipid *membrane* and the open pore.

cavity and the inner pore of the K^+ channel provide the receptor site for the inactivation gate and inhibitors such as hydrophobic quaternary ammonium ions (Fig 5a).[14] The inactivation occurs by a sequential reaction. in which the gate peptide is bound initially to the cytoplasmic channel surface and then enters the pore (Fig. 5b).

The structural basis of ligand gating was reported for a Ca^{2+}-gated K^+ channel. Here, eight RCK (regulator of K^+

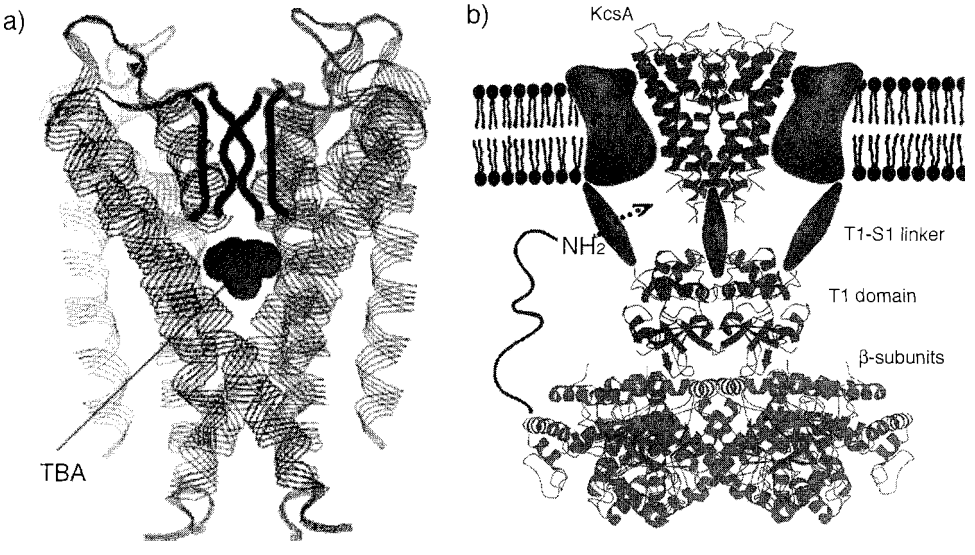

Fig. 5 Inactivation of K^+ channel. a) Crystal structure of KcsA K^+ channel with a hydrophobic cation, tetrabutylammonium TBA. b) Composite model of a voltage-dependent K^+ channel. The α-subunit is shown in blue and the β-subunit in red. The pore is represented by the KcsA K^+ channel *(5)* and the Tl-β complex (15). The structures of the linker (T1-S1) connecting the voltage sensors to the TI domain are unknown. An N-terminal inactivation gate is shown entering a lateral opening to gain access to the pore. Fig. 5a was produced with a PDB file (1J95.pdb from Ref. [14]) and Raswin Molecular Graphics (version 2.7.2. Glaxo Research and Development. U.K.).

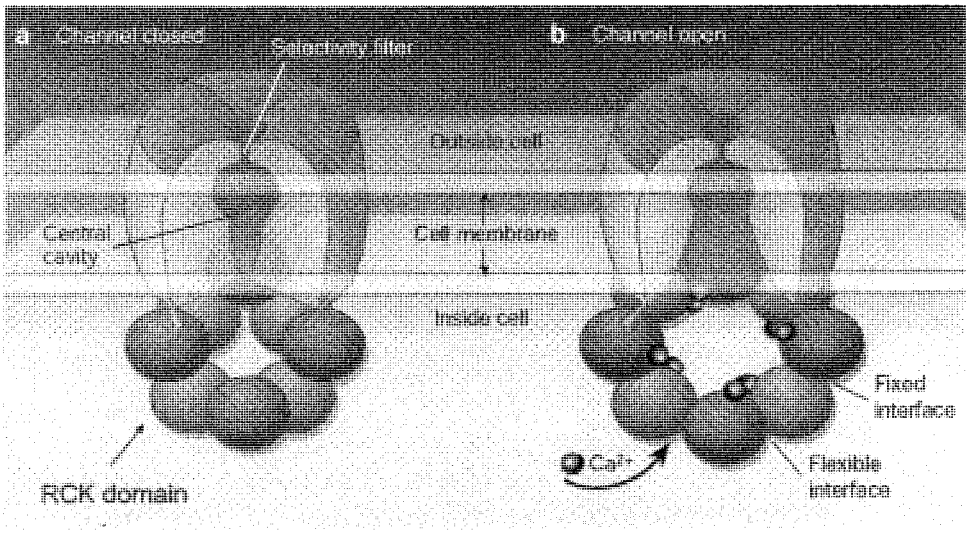

Fig. **6** Schematic model for the gating and opening of a bacterial Ca^{2+}-gated K^+ channel a) The closed and b) the open conformations Three of the four subunits of a K^+ channel are shown in brown The purple and red circles represent the eight RCK domains, a hich. after binding Ca^{2+}, are thought to deform with respect to each other, causing changes in the pore in the center of the channel

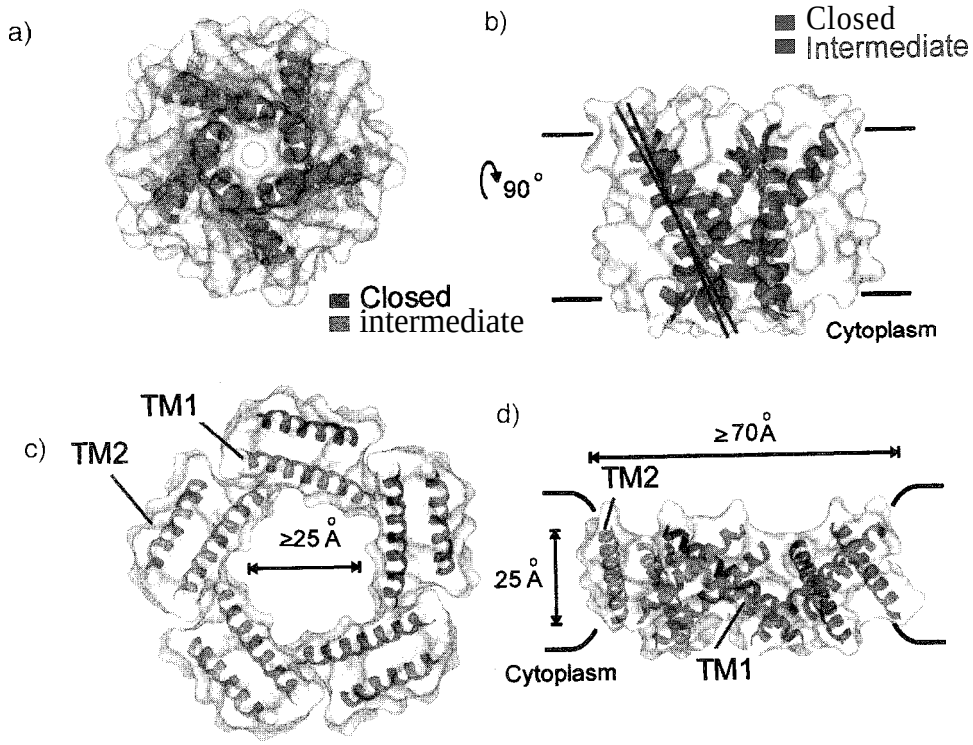

Fig. 7 Modeling structure of the MscL transmembrane segments. a) Top view (from extracellular) and bj side view in the intermediate closed state (orange ribbon) compared with closed structure (green ribbon). Not much difference betaeen closed and intermediate states. c) Top view of open from (from extracellular) with a wide open pore. d) Side view of the open form.

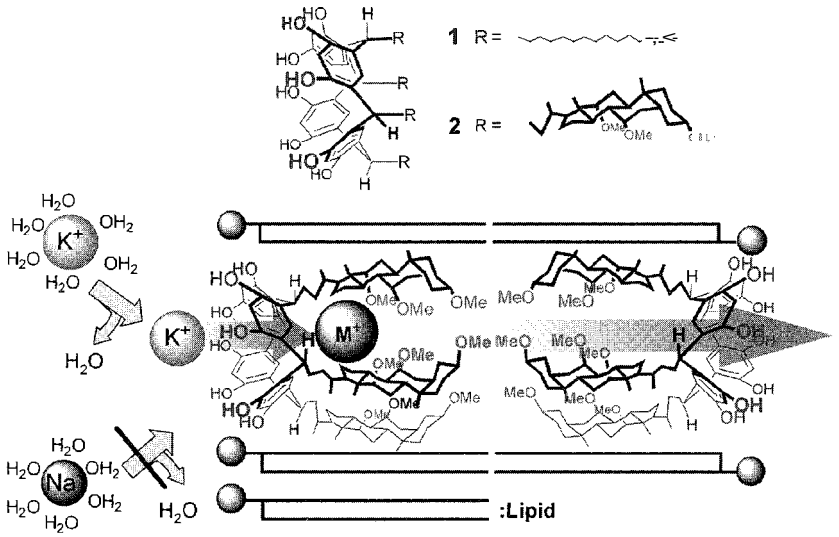

Fig. 8 Chemical structures of molecular ion channels with K^+ ion selectivity, **1,** 2. Schematical illustration of expected structures of a tail-to-tail dimer. The side chain opposite to the reader is eliminated for clarity.

conductance) domains assemble to form a large gating ring at the intracellular membrane surface. The cooperative binding of eight Ca^{2+} ions from the intracellular solution induces conformational change of the gating ring in such a way that it can open the inner helices of the pore to permit ion conduction. The gating behavior is shown schematically in Fig. 6, where the upper part forms an ion conduction pore in the membrane. The lower part from solution represents the RCK domain, where eight Ca^{2+} ions are bound allosterically.[16,17]

The open and closed conformations on binding ligands to the nicotinic acetylcholine receptor channel were already trapped and observed by electron microscopy. Here again. the cooperative binding of ligands induces large rotational movements of the pore-defining subunit~.~'~'

Mechanosensitive ion channels act as membrane-embedded mechanoelectrical switches that open a large pore in response to membrane deformations. It is a way of biological signal transformation of physical stresses such as touch and hearing to changes into electrochemical responses. The gating mechanism of a large-conductance mechanosensitive pentameric channel (MscL) was elucidated as shown in Fig. 7.[19,20] Transitions from the closed or intermediate state to the open states upon application of tension to the membrane are accompanied by massive rearrangements of the two transmembrane helices TM1 and TM2. The inner TM1, creating the bulk hydrophilic pore containing Thr, Lys, and Asp units, rotates along its principal axis and shifts away from the symmetrical axis to open the water-filled pore of 3040 Å, leading to conductance at nano-Siemens levels (Figs. 7c,d).

ARTIFICIAL ION CHANNELS

Construction of artificial ion channels according to simple principles[21,22] is interesting for obtaining molecular devices that mimic the biological signal transduction system. There are two ways to prepare ion-conducting artificial pores—molecular and supramolecular methodologies, along with modification of ionophoric antibiotics.

Molecular Ion Channels

A macrocyclic resorcin[4]arene with four hydrophobic substituents in the axial position provides an ion-conducting molecular pore by tail-to-tail dimerization.[23] Because the pore size and characteristics of the entryway are defined explicitly by the molecule, only one conductance level is observed. The relatively simple structure is amenable to systematic structural modifications and is, therefore, appropriate in establishing the structure–function relationships. When a methyl ether derivative of cholic acid was employed as the axial substituent,[24] the conductance was increased by 50% to 9.9 *pS*, compared with the value 6.1 *pS* observed for **1** with simple alkyl substituents.[23] The cation and anion selectivity ratio P_K/P_{Cl} was 20 for **2**. showing a significantly larger selectivity factor compared to 8 for **1**. A hydrophilic molecular plane of methoxy substituents certainly contributes to the increase of conductance and a higher cation and anion selectivity by the arrangement of a more hydrophilic environment at the central pore. Both ion channels exhibited moderate K^+ preferences compared to Na^+ by a facior of ca. 3. The aromatic moiety provides a weak electric field

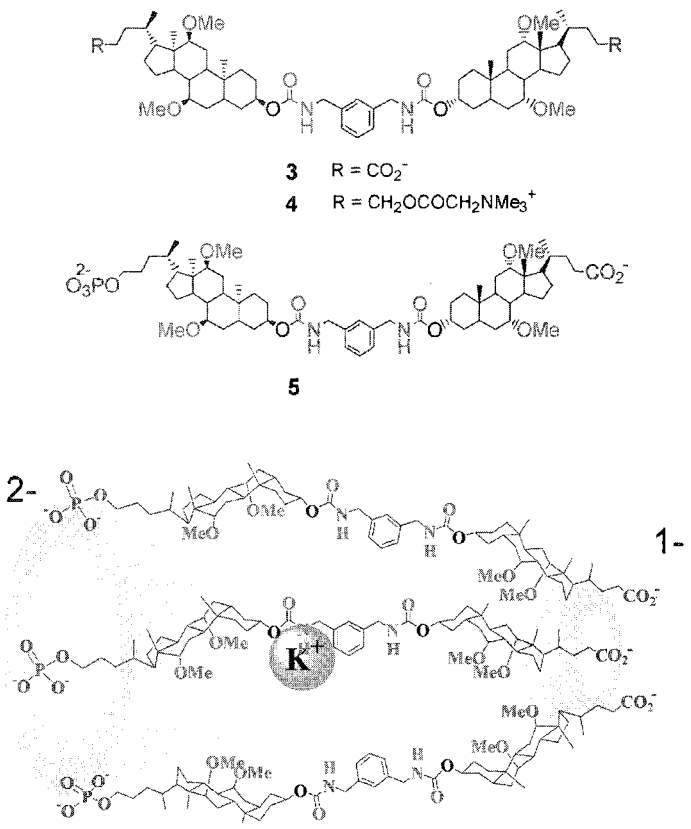

Fig. 9 Chemical structure of supramolecular ion channels with K^+ ion selectivity, 3, 4 and with voltage-dependent properties 5. Schematic illustration of supramolecular ion channels **5** with different mouth diameters in bilayer lipid membranes.

that can desolvate the K^+ ion with a lower dehydration energy to pass through the cavity but can only partly desolvate the more hydrophilic Na^+ ion (Fig. 8). The inverse selectivities. a preference for Na^+ and Cl^-, were not yet obtained. and their embodiment remains a challenging target in this field.

Supramolecular Ion Channels

r

Besides synthesizing a molecular pore of a definite diameter. supramolecular pore formation provides an attractive alternative. This methodology is also adopted in Nature for the formation of the K- and acetylcholine receptor channels as homotetrarner and heteropentamer. respectively.[1] The assembly numbe of artificial supramolecular channels is generally not controlled, and various levels of conductance are usually observed. Two cholic acid methyl ether derivatives were connected via bisurethane linkages to obtain a membrane-penetrating component in its extended conformation. The carboxylate 3 and ammonium 4 head groups provide supramolecular ion channels showing stable open durations.[25,26] Both channels are cation selective. irrespective of different charges of head groups. The cation and anion selectivity values P_K/P_{Cl} were 17 and 7.9 for **3** with negative head groups, and 4 with positive head groups, respectively. Therefore, the terminal charges reasonably perturbed the entry of the cation relative to the anion. The discrimination factor between K^+ and Na^+ ions was again moderate. P_K/P_{Na} being three for both channels. The metal ion selectivity is determined primarily at the critical domain of the pore environment and is separated substantially from the charged head groups.

Two head groups of carboxylic and phosphoric acids were introduced to displace different charges at the ends of the membrane-penetrating cholic acid dimer unit **5**.[27] The head group charges should be asymmetric under basic conditions ($-1/-2$ at pH *8.2)*. When 5 was introduced into a planar bilayer membrane under an application of the asymmetric voltage to facilitate the vectorial incorporation of the channel, the current values at a positive voltage range were larger than the corresponding values at the negative one. The current–voltage plots were fitted by curves passing through a zero point to show clear rectification properties. Without asymmetric voltage application. the current observed was symmetric. The rectification currents observed seem to be a result of the different radii of the channel mouths controlled by the displacement of different charge numbers at the molecular terminals. as shown in Fig. 9.

Ion channels can produce large ionic fluxes across the bilayer lipid membrane. Because living cells. including bacteria, rigorously maintain ionic concentrations and rely on the ion impermeability of the biological membrane. incosporation of foreign ion channels disrupts such osmotic balance. Recently, antibiotic activities of artificial ion channels were demonstrated independently by Ghadiri[28] and Gokel.[29] Supramolecular assembly of cyclic oligopeptides increased ion permeability in bacterial membranes. induced the collapse of the transinembrane ionic potentials, and finally caused rapid death of the cell. Similar activities were observed for crown-ether-based artificial ion channels against the bacterium *Escherichia coli.* These are thought to have considerable potential against the rapid emergence of drug-resistant bacterial infections.

Antibiotic-Based Ion Channels

Gramicidin antibiotics form a head-to-head dimer in a bilayer lipid membrane to afford a stable cation-selective ion channel. A half-gramicidin unit was introduced into an inner half-membrane with anchoring on gold surface and the other half counterpart was incorporated into the outer half membrane as a mobile unit.[30] The diffusion of the mobile half gramicidin unit carrying a guest molecule

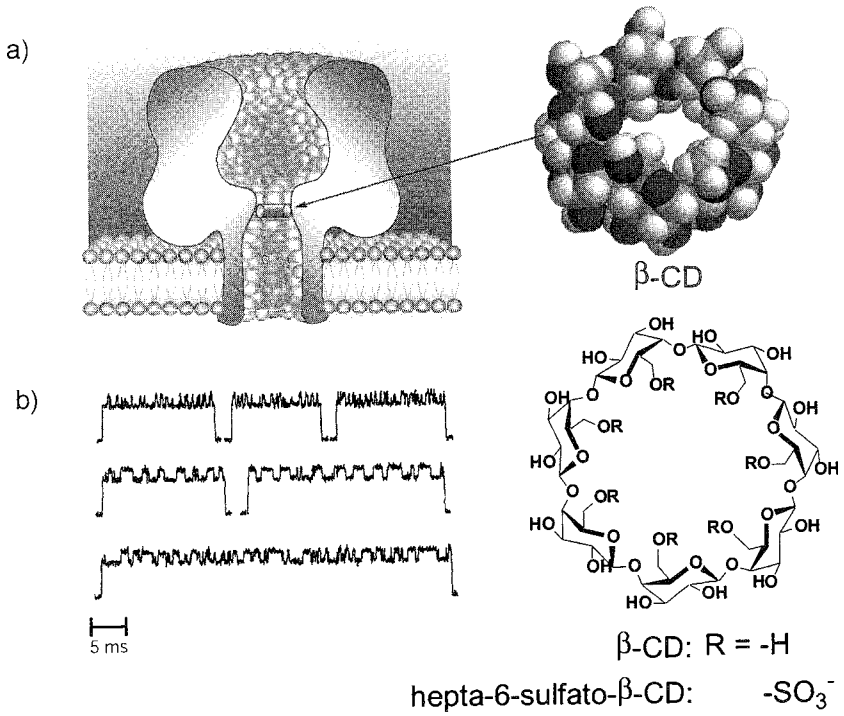

Fig. 10 Artificial ion channel with *staphylococcal α-hemolysin* (αHL) with a molecular adaptor. a) Schematic of the αHL pore showing βCD loged in the lumen of the channel with adapters. βCD and hepta-6-sulfato-β-cyclodextrin. b) Detection of organic molecules by stochastic sensing. The pore contains a noncovalent βCD adapter. which is capable of carrying out host–guest chemistry while lodged in the lumen. Upper trace, promethazine: middle trace, imipramine; loner trace, mixture of promethazine (100 μM), and imipramine (100 μM).

within the outer half of the membrane was switched off by an interaction with a receptor immobilized at the membrane surface. This prevented the grarnicidin dimer formation and decreased the ionic currents across the membrane. The addition of competitive guests recovered the conductance state. In this way, the population of molecular ion channels could be switched on and off by recognition events mimicking biological sensory functions.

α-Hemolysin (αHL) is a heptameric assembly of /?-sheet turns to make a mushroom-shaped large pore (near 30 Å diameter) surrounded by 14 *β*-sheets in a biological membrane. Through this cavity. a large ionic flux can be generated. and a-HL is a highly toxic material. This cavity interestingly can accommodate *β*-cyclodextrin (*β*-CD) to make an ion channel of a moderate pore size, therefore. affording inoderate conductivities.[31,32] Weakly anion-selective α-HL becomes more anion selective when *β*-CD is accommodated in the middle of the channel pore due to a favorable interaction of *β*-CD with anions. By contrast, hepta-6-sulfato-*β*-cyclodextrin carrying high negative charges produces reversed cation selectivities. It is noteworthy that this molecular adapter system can generate high permeability ratios (P_K/P_{Cl}) over a 200-fold range.'''']

As *β*-CD is an effective host for various substrates, the binding of guests in the cavity modifies the mode of ionic flux of the *β*-CD adapter channel. Depending on the binding characteristics of the guests. the conductance and time profiles of open–closed transitions can be modified. Because an ion channel is a molecular device used to amplify events at a single molecular level into a massive ionic flux. it affords a highly sensitive stochastic sensor for guest molecules (Fig. 10).

CONCLUSION

Alkali metal ions carry important messages and biological signals by their movements. By controlling the ionic species (Na^+, K^+, along with Ca^{2+} and Cl^- ions), magnitude of the flux (conductivity). triggering signals (voltage variation; ligand binding. and ineinbrane deformation), and dynamic behavior (duration of open–closed times), ion channels play critical roles in biological processes in the brain and nervous system. The mode of information transfer is totally different from the electronic systems we developed for computer systems. Although the achievements of dry electronic systems are magnificent.

the wet biological system is still far advanced in many respects. However, the use of wet systems in vitro is far less developed, and we need to gain an understanding of numerous principles of such biological systems. The construction of artificial ion channels may help scientists develop ways to comprehend these basic units and their systems. With further exploration to be undertaken in this area. the future picture can not easily be foreseen.

ARTICLES OF FURTHER INTEREST

The Allosteric Effect, p. 20
Biological Ligands, p. 88
Biological Models and Their Characteristics, p. *101*
Calixarenes and Their Analogues: Cation Complexation, p. 137
Calixarenes: Synthesis and Historical Perspectives, p. *153*
Cation–π Interactions, p. 214
Crown Ethers. p. *326*
Cryptands, p. 334
Cyclodextrins, p. 398
Induced Fit, p. *717*
Ion Channels and Their Models, p. 742
Ionophores, p. 760
Lariat Ethers, p. 782
Molecular Logic Gates. p. 893
Preorganization and Complementarity, p. 1158
Protein Supramolecular Chemistn. p. *1161*
Spherands, p. 1344
X-Ray Crystallography p. 1586

REFERENCES

1. Hill. B. *Ionic Channels of Excitable Membranes,* 3rd Ed.: Sinauer Associate: Sunderland, MA, 2001.
2. Lin. H.; Zhu. Y.J.; Lal. R. Amyloid protein (1–40) forms calcium-permeable, Zn^{2+}-sensitive channel in reconstituted lipid vesicles. Biochem. 1999. 38 (34), 11189–11196.
3. Alberts. B.: Johnson, A.; Lewis, J.: Raff, M.: Robert, K.: Walter, P. *Molecular Biology of The Cell,* 4th Ed.: Garland Science: New Uork. 2001.
4. Nicholls, D.G.; Freguson, S.J. *Bioenergetics* 3; Academic Press: San Diego, 2003.
5. Doyle. D.A.: Cabral, J.M.; Pfuetzner. R.A.; Kuo, A.: Gulbis, J.M.: Cohen. S.L.; Chait, B.T.: MacKinnon. R. The structure of the potassium channel: Molecular basis of K^+ conduction and selectivity. Science 1998. 260 (5360). 69–77.
6. Favre. I.: Moczydlowski, E.: Schild. L. On the structural basis for ionic selectivity among Na^+, K^+, and Ca^{2+} in the voltage-gated sodium channel. Biophys. J. 1996, 71 (6). 3110–3125.
7. Meuser, D.: Splitt, H.: Wagner. R.: Schrempf. H. Exploring the open pore of the potassium channel from *Streptomyces lividans.* FEBS Lett. 1999. 462 (3). 447–452.
8. Zhou. Y.; Morais-Cabral. J.H.; Kaufman. A.: MacKinnon, R. Chemistry of ion coordination and hydration revealed by a K^+ channel-Fab complex at 2.0 A resolution. Nature 2001. 414 (6859), 43–48.
9. Dutzler, R.; Campbell. E.B.; Cadene, M.; Chait, B.T.: MacKinnon, R. X-ray structure of a ClC chloride channel at 3.0 Å reveals the molecular basis of anion selectivity. Nature 2002, 415 (6869). 287–294.
10. Dutzler. R.: Campbell, E.B.; MacKinnon. R. Gating the selectivity filter in ClC chloride channels. Science 2003, *300* (5616). 108–112.
11. Jiang. U.: Lee. A.: Chen, J.: Ruta. V.: Cadene. M.: Chait. B.T.; MacKinnon. R. X-ray structure of a voltage-dependent K^+ channel. Nature 2003. 423 (6935). 33– 41.
12. Jiang, U.: Ruta. V.: Chen, J.: Lee, A.; MacKinnon. R. The principle of gating charge movement in a voltage-dependent K(+) channel. Nature 2003.423 (6935). 42–47.
13. Horn. R. Coupled movements in voltage-gated ion channels. J. Gen. Physiol. 2002. *120* (4). 449–453.
14. Zhou. M.; Cabralc. J.H.M.-: Mann, S.; Mackinnon. R. Potassium channel receptor site for the inactivation gate and quaternary amine inhibitors. Nature 2001. 411 (6838). 657–661.
15. Gulbis. J.M.; Zhou. M.; Mann. S.: MacKinnon. R. Structure of the cytoplasmic β subunit-T1 assembly of voltage-dependent K^+ channels. Science 2060. *289* (5476), 123–127.
16. Jiang. Y.; Lee, A.; Chen, J.; Cadene. M.; Chait. B.T.: Mackinnon. R. Crystal structure and mechanism of a calcium-gated potassium channel. Nature 2002. 417 (6888). 515–522.
17. Schumacher. M.: Adelman. J.P. An open and shut case. Nature 2002, 417 (6888), 501–502.
18. Unwin. N. Acetylcholine receptor channel imaged in the open state. Nature 1995. 373 (6509). 37–43.
19. Chang, *G.;* Spencer. R.H.: Lee, A.T.: Barclay, M.T.: Rees. D.C. Structure of the MscL homolog from *Mycobacterium tuberculosis*: A gated mechanosensitive ion channel. Science 1998, 282 (5397), 2220–2226.
20. Perozo. E.: Cortes. D.M.; Sompornpisut. P.; Kloda, A.; Martinac. B. Open channel structure of MscL and the gating mechanism of mechanosensitive channels. Nature 2002. 418 (6901), 942–948.
21. Kobuke. Y. Artificial Ion Channels. In *Advances in Supramolecular Chemistry*; Gokel. G.W., Ed.; JAI Press: New York, 1997; Vol. 4. 163–209.
22. Kobuke. Y.: Tanaka. Y.: Sokabe. M. Artificial Non-Peptide Single Ion Channels. In *Towards Biophysics of Ion Channels, Progress in Cell Research;* Sokabe. M.. Ed.: Elsevier: Amsterdam. 1997: Vol. 6. 167–188.
23. Tanaka. Y.; Kobuke, Y.: Sokabe. M. Non-peptidic ion channel with K^+ selectivity. Angew. Chem.. Int. Ed. Engl. 1995. 34 (6), 693–694.
24. Uoshino. N.; Satake, A.; Kobuke. Y. Artificial ion channel by rnacrocyclic resorcin[4]arene having amphiphilic cholic

acid ethers. Angew. Chem., Int. Ed. **2001,** *40* (2), 457–459.
25. Kobuke, Y.; Nagatani, T. A supramolecular ion channel based on amphiphilic cholic acid derivatives. Chcm. Lett. **2000,** *4*, 298–299.
26. Kobuke, Y.: Nagatani, T. Transmembrane ion channels constructed of cholic acid derivatives and characterizations by single channel current measuremcnts. J. Org. Chem. **2001,** 66 (15), 5094–5101.
27. Goto, C.; Yamamura, M.; Satake, A.; Kobuke, Y. Artificial ion channels showing rectified current behavior. J. Am. Chem. Soc. **2001,** *123* (49), 12152–12159.
28. Fernandez-Lopez, S.; Kim, H.S.; Choi, E.C.; Delgado, M.; Granja, J.R.; Khasanov, A.; Kraehenbuehl, K.; Long, G.; Weinhergcr, D.A.; Wilcoxen, K.M.; Ghadiri, M.R. Antibacterial agents based on the cyclic D,L-α-peptide architecture. Nature **2001,** *412* (6845), 452–455.
29. Leevy, W.M.; Donato, G.M.; Ferdani, R.; Goldman, W.E.; Schlesinger, P.E.; Gokel, G.W. Synthetic hydrophile channels of appropriate length kill *Escherichia coli*. J. Am. Chem. Soc. **2002.** *124* (31), 9022–9023.
30. Cornell, B.A.: Braach-Maksvytis, V.L.B.; King, L.G.; Osman, P.D.J.; Raguse, B.; Wicczorek, L.: Pace, K.J. A biosensor that uses ion-channel switches. Nature **1997.** *387* (6633), 580–583.
31. Gu, L.-Q.; Braha, O.; Conlan, S.; Cheley, S.; Baylcy. H. Stochastic sensing of organic analytes by a pore-forming protein containing a molecular adapter. Nature **1999,** 398 (6729), 686–690.
32. Gu, L.-Q.; Serra, M.D.; Vincent, J.B.; Vigh, G.; Cheley. S.; Braha, O.; Bayley, H. Reversal of charge selectivity in transmemhrane protein pores by using noncovalent molecular adapters. Proc. Natl. Acad. Sci. U. S. A. **2000.** 97 (8), 3959–3964.
33. Baylcy, H.: Cremer, P.S. Stochasic sensors inspired by biology. Nature **2001,** *413* (6852), 226–230.

Alkalides and Electrides

James L. Dye
Michigan State University, East Lansing, Michigan, U.S.A.

INTRODUCTION

Crystalline alkalides are salts with alkali metal anions (Na , K , Rb , or Cs) that have been known since 1974, when the first sodide was synthesized.[1] The first crystalline electride, in which trapped electrons serve as the anions, was first fully characterized in 1986.[2] The key to the formation of both classes of materials is complexation of the countercation (Li^+ through Cs^+) by organic macrocyclic or macrobicyclic molecules such as crown ethers and cryptands. Seven clcctrides and 37 alkalides have now been synthesized and their structures were determined by single crystal x-ray crystallography.[3] Their properties were studied by a number of methods, including optical, electron paramagnetic resonance (EPR), and nuclear magnetic resonance (NMR) spectroscopy, magnetic susceptibility, conductivity, and differential scanning calorimetry (DSC).

Both alkalidcs and electridcs are powerful reducing agents; so powerful, in fact, that most cannot survive, even in vacuo at temperatures above about $-30°C$. The organic complexant is irreversibly destroyed by cleavage of the O—C or N—C bonds of the complexant. This reducing ability of alkalides is, however, useful in organic synthesis when a powerful two-electron reducing agent is needed.[4] Alkalides and electridcs in solution are able to reduce nearly all metallic cations to form nanoscale metal particles.[5]

In this overview of alkalides and electrides, the methodologies and special techniques used will be briefly described, and the structural features and electronic, optical and magnetic properties will be summarized. The reference list is far from complete, but the information given can provide many additional references to the original literature in this field.

EXPERIMENTAL METHODS

The major concern in the preparation and study of alkalides and clcctrides is their extreme sensitivity to air, moisture, and especially elevated temperatures. Thus, ordinary glove box procedures do not suffice without provision to keep the samples cold (below about $-40°C$) at all times during and after synthesis. It should be noted, however, that the formation and use of alkalides such as $K^+(15\text{-crown-}5)_2\ Na^-$ in solution (in THF, for example) can bc carried out at room temperature in a glove box, Schlenk line, or by syringe techniques. Thus, organic synthetic methods that need a powerful two-electron reducing agent need not be as rigorous as those required to prepare crystalline alkalides and electrides.

Synthesis is simple and straightforward in principle. One merely needs to prepare a solution of the complexant and alkali metal in a pure aprotic solvent such as methylamine ($MeNH_2$) or dimethyl ether (Me_2O), filter the solution through a porous glass frit into a second compartment of a K-cell,[6] and add a less polar cosolvent such as diethyl ether (Et_2O) or trimethylaminc (Me_3N). Then the more polar primary solvent is removed by evaporation until the solution is saturated at about $-40°C$. Slow cooling over a I-or 2-day period (sometimes with temperature cycling back to the starting temperature to dissolve small crystals) results in crystal growth. The crystals can then be washed with the secondary solvent by pouring the liquid back through the frit and redistilling it for further washes. Finally. vacuum evaporation of all solvents leaves dry crystals for study. In some cases, solvent molecules are included in the crystal structure so that wet crystals must be harvested.

In practice, things arc not as simple as indicated above. Because the metal solutions are thermodynamically unstable, all glassware used must be rigorously cleaned, and solvents must be free of reducible impurities. Control of the stoichiometry can sometimes dctcrmine whether an clectride or an alkalide (or a mixture of the two) is formed. For example, the preparation of an electridc or a ceside can bc controlled by the relative amounts of 18-crown-6 (18C6) and ccsium metal according to

$$Cs + 2(18C6) \rightarrow Cs^+(18C6)_2e^- \quad (1)$$

or

$$2Cs + 2(18C6) \rightarrow Cs^+(18C6)_2Cs^- \quad (2)$$

By using a slight excess of 18C6, the electride is formed, while an excess of cesium gives the ceside. Because cesium mctal is insoluble in Me_2O, this solvent can bc used as a primary solvent. When preparing the clcctride, excess 18C6 is removed by washing with the secondary

Encyclopedia of Supramolecular Chemistry
DOI: 10.1081/E-ESMC 120012700

solvent. Again. complications often occur. It is easy to use cryptand[2.2.2], (C222) to prepare K^+(C222) Na by using a mixture of K and Na metals and to prepare Na^+ (C222)Na with just sodium. But, we have never been able to make crystalline Na^+(C222)e^-. Whenever sodium is present in solution, regardless of the complexant used, a sodide is formed. Another complication that can occur, especially with $MeNH_2$ and either Et_2O or Me_3N, is phase separation of the liquid solutions. One gets a concentrated $MeNH_2$-rich phase and a more dilute cosolvent-rich phase. Also, of course, the growth of high-quality crystals remains more an art than a science; we frequently obtain apparently well-formed crystals that do not diffract x-rays well enough to permit structure determination. In the descriptions of structures and properties that constitute the balance of this article, only alkalides and electrides of known structure will be considered. Many other polycrystalline alkalides and electrides were prepared and studied, but without a structure, one can never be confident that a pure compound was prepared. This is particularly true of electrides, which are frequently contaminated with alkali metal anions.

In this article. we will not describe in detail the experimental equipment used to determine the optical, electronic, and magnetic properties of these materials. Standard instruments were used for EPR, ENDOR. solid-state NMR. SQUID susceptibility, powder conductivity, optical reflectance and transmittance, and DSC. although some home-built instruments were involved. The specific equipment used is described in the references. The major consideration in designing and using equipment is the need to keep the samples cold and away from air and moisture at all times.

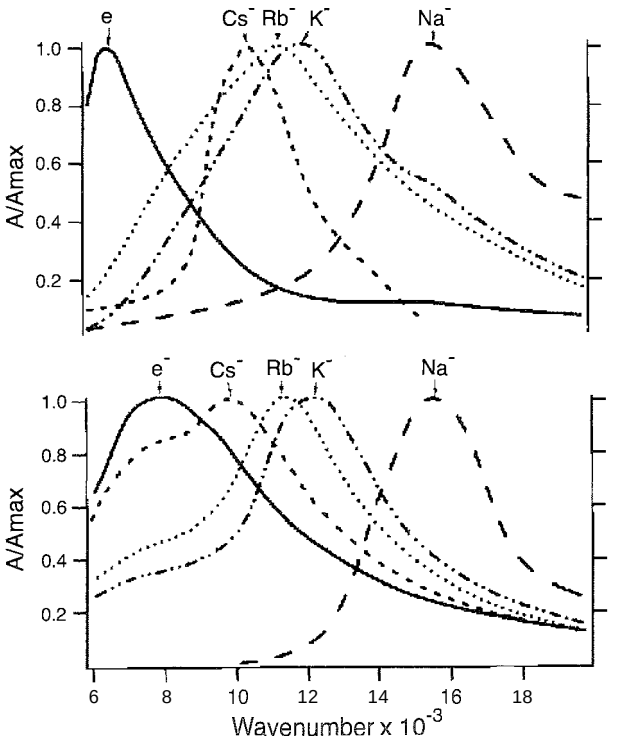

Fig. 1 Optical spectra of alkali metal solutions in ethylenediamine (8), corrected for sodide absorption (bottom) and from thin solvent-free films (top). The solution spectrum labeled e^- is that of lithium. Note also the shoulder due to e^-_{solv} in Cs. Rb. and K solutions.

ALKALIDES

Origin and Synthesis

The synthesis of crystalline alkalides had its origins in the study of alkali metal solutions in amines and ethers. Although genuine alkali metal anions apparently do not form in metal–ammonia solutions, they are ubiquitous in less-polar solvents. A great deal of confusion in early work was removed when Hurley. Tuttle, and Golden[7] showed that Na' in sodium borosilicate glass was readily exchanged by other alkali cations in solution. This exchange yielded the peak of Na^-, even when no sodium was added to the solution. The optical absorption spectra of alkali metal solutions in ethylenediamine at room temperature (shown in Fig. 1) (corrected for Na contamination when necessary) were obtained by Dewald and Dye in 1964.[8] Later work[9] clearly identified the peaks of e , Cs , Rb^-, K^-, and Na^-, as labeled in the figure. Note the absence of Li . a result of the high solvation energy of Li^+.

The study of more concentrated alkali metal solutions in a variety of solvents became possible in 1970, when crown ethers were used[10] to enhance the solubility of the metal. The use of crown ethers and cryptands permitted extensive studies of the optical spectra of solvated electrons and alkali metal anions in solution. After the isolation of the first sodide salt in 1974,[1] the optical spectra of polycrystalline films of various alkalides and electrides were determined by rapid evaporation of all solvent from a liquid film on the walls of the optical cell.[11] Displayed in Fig. 1 are the optical spectra obtained in this way. Clearly. there is a 1:1 correspondence between the spectra in solution and in the solid state. Although the peak positions shift somewhat with temperature and with the complexant used, the optical peaks can be used to verify the presence of particular alkali metal anions or trapped electrons. In addition to rapid solvent evaporation. solvent-free alkalide and electride films can be made by codeposition of the complexant and alkali metal in high vacuum (10^{-8} torr).[12] This permitted the study of optical

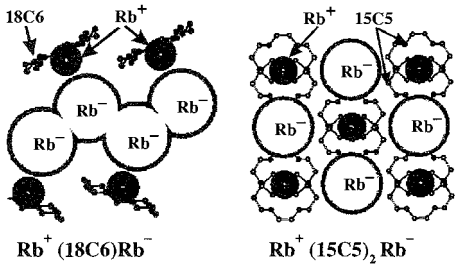

Fig. 2 Examples of M^- chain formation (left) and isolated M^- (right) in two rubidium rubidides. The Rb^+ and Rb^- ions are drawn to scale. while ball-and-stick models are used for 18C6 and 15C5.

transmission spectra, conductivity, and thermionic electron emission.[13]

Structural Features

Alkali metal anions are large and highly polarizable. With two electrons sharing the outer s-orbital, expansion occurs to yield radii of about 2.8, 3.1. 3.2, and 3.5Å for Na . K . Rb , and Cs , respectively.[14] Crystal structure determination permitted the identification of a variety of structural motifs. In addition to isolated anions. various structures include contact ion pairs between M^+ and M . dimers of the anions. $(M^-)_2$, and anionic chains. $(M^-)_n$.[14] Although one might think that coulomb repulsion would prevent dimerization of M . a theoretical study[15] showed that such dimers can be stabilized by adjacent cations. Dimers and chains presumably form by partial hybridization of the diffuse s-orbital with empty p-or *d*-orbitals.

Two extremes are shown in Fig. 2. Isolated anions, separated from the cations by the complexant. are present in $Rb^+(15C5)_2Rb^-$, while chains of Rb^- in close contact with Rb^+ form in $Rb^+(18C6)Rb^-$. The cesides, $Li^+(C211)Cs^-$ and $Cs^+(C222)Cs^-$ also form chains of anions. while anionic dimers are present in $K^+(C222)K^-$ and $Rb^+(C222)$ Wb . In most alkalides. the alkali metal anions are isolated from one another and from the cations. However. cation–anion contact pairs are present in M^+ (hexamethyl hexacyclen) Na . with M=K, Rb. Cs.[16]

Properties

Many properties of alkalide crystals. powders. and films were measured. The original alkalide, $Na^+(C222)Na^-$, has been most thoroughly studied, in part because of the high stability of pure samples. In contrast to most alkalides, single crystals and vapor-deposited films of this sodide are stable in vacuo for many hours, even at room temperature. In addition to the crystal structure, we measured the thermodynamics of formation by an EMF method, optical transmission spectra of polycrystalline films. reflectance spectra of single crystals, single-crystal fluorescence spectra, EPR of defect electrons, ^{23}Na-NMR spectra of powder and oriented single crystals. powder-and single-crystal conductivity, exciton formation and mobility, photoelectron emission spectra, and multiphoton photobleaching. Only limited sets of such measurements were made on other alkalides; Na·(C222)Na could be viewed as the best-understood model of an alkalide with isolated alkali metal anions.

Optical spectra

The optical transmission spectra of polycrystalline films are shown in Fig. 1. The spectrum clearly arises primarily from an $np \leftarrow ns$ transition. The peak positions correlate well with the corresponding dissociation transitions in the gas phase. The anisotropy in the solid leads to a small orientation dependence of the peak position in the single-crystal reflectance spectrum of $Na^+(C222)Na^-$.[12] Recent unpublished work in our laboratory showed that the effect is much larger in $Li^+(C211)Cs^-$, which forms extended chains of ceside anions.[17] This orientation dependence is a natural consequence of the removal of excited p-state degeneracy in the anisotropic solid.

Pure alkalides are diamagnetic insulators or semiconductors. It is practically impossible, however. to avoid the incorporation of defect electrons in the structure. They are easily detectable by EPR spectroscopy and contribute to defect conductivity and a "Curie tail" in the magnetic susceptibility. When defect electrons in $Na^+(C222)Na^-$ are photoexcited. they remain for many minutes in states near the vacuum level and can be photoejected with infrared (IR) photons.[18] The effect is completely absent in defect-free crystals of this sodide.

NMR spectra

Alkali metal NMR spectroscopy provides a good diagnostic tool for isolated alkali metal anions in solution and in solid alkalides. The chemical shifts are close to those calculated for the gaseous anions: much more diamagnetic (negative) than the reference state of $M^+(aq.)$. In solution, the chemical shifts of M are about -62, -100, -190. and -290 ppm for M=Na. K. Rb, and Cs. respectively, compared with calculated gas-phase values of -63, -103, -214. and -346 ppm.[19] The values in solid alkalides are somewhat dependent on the compound, but for salts with isolated anions, the values are about -61, -10.5. -190. and -220 ppm, in agreement with the solution values and. at least for Na and K, nearly the same as the gas-phase chemical shifts. The absence of significant shifts from those of gaseous M^- is a consequence of the large size of the anions and their nearly spherical shape. Shifts in the paramagnetic direction (Ramsey

shifts) are caused by mixing of the unoccupied orbitals of the alkali metals with those of surrounding molecules. The large size of the alkali metal anions tends to minimize such shifts.

When dimers or chains of alkali metal atoms are present, the anion chemical shift is considerably more paramagnetic, even to the extent of having the shift of Cs^- confused with that of Cs^+ in early work.[19] Recent studies indicate that dimer or chain formation can shift the peaks of K^-, Rb^-, and Cs^- by hundreds of ppm. The mixing of *p* or *d* orbitals to provide some bonding between adjacent anions would introduce considerable spin-orbit coupling that would result in a pronounced paramagnetic shift.

Because the alkali metal nuclei have quadrupole moments. the lines are considerably broader than those of nuclei with spin 1/2. The effect is small for ^{7}Li and ^{133}Cs and only moderate for ^{23}Na. With ^{39}K, ^{85}Rb, and ^{87}Rb, quadrupole broadening makes solid-state NMR studies difficult. but even in these cases, the static line shapes can provide considerable information about the quadrupole coupling constants. asymmetry paramete s, and chemical shifts.[20]

Stability

The tendency of alkalides to decompose above about −30°C made the study of iheir properties difficult. The decomposition mode with crown ethers and cryptands is the rupture of O—C bonds. For example. $M_a^+(C222)M_b^-$ (with M_a and M_b the same or different alkali metals) releases ethylene from the —O—CH_2—CH_2—O— moiety with formation of alkoxide units.[21] The N—C bonds in perazacryptands and cyclens is considerably more resistant to reduction. We recently prepared the sodide and potasside of fully methylated perazacryptand [2.2.2] and found them to be stable at room temperature for months.[22] The flip-side of this story is that aza coinplexants have generally much poorer complexing ability for alkali cations. When a complex forms, it frequently dissociates at elevated temperatures to yield the metal and free complexant. Thus, a synthetic challenge in this field is to find peraza complexants with just the right size and lone pair orientation to form strong complexes with alkali cations.

ELECTRIDES

Background and Definitions

In contrast to alkali metal anions. which were first positively identified as solution species in 1970. solvated and trapped electrons have been known for more than a century.[23] With the advent of pulse radiolysis, the solvated electron has become probably the most widely studied species in chemistry. Electrons trapped at defect sites in crystals (F-centers and clusters) have also been studied extensively for over a century.[24] Alkali metal incorporation in alumino-silicate zeolites to yield electrons trapped near clusters of cations has been the subject of many experimental and theoretical studies[25] since first observed in 1966.[26] Even simple alkali metals, with a "sea" of electrons filling the space between cations. have one electron per cation. What then distinguishes true electrides from all these other materials?

As the "-ide" ending suggests. the electrons in electrides take on the role of anions.[27] This implies that electrides are crystalline ionic compounds with one electron per cation. They could be viewed as salts that contain stoichiometric F-centers. with electrons as the only anions. But because one cannot suppress the quantum nature of electrons, these "anions" are special. The line between localized weakly interacting electrons and delocalized, or metallic electrons is blurred. and both extremes are encountered in electrides. Because most of the electron density in electrides is present in otherwise empty, well-defined pseudo-one-dimensional cavities and channels, they could also be viewed as forming low-dimensional correlated electron gasses.

General Structural Features

Except for zeolite-based electrides. to be considered later. the cations in all electrides synthesized to date are alkali cations, Li^+, K^+, Rb^+, or Cs^+, sequestered inside a cryptand cage or sandwiched between two crown ether molecules. Thus, the cations are well shielded from the electrons. The temperature dependence of the ^{133}Cs-NMR chemical shift (Knight shift) in two electrides shows that the unpaired electron density at the Cs^+ cation is less than 0.1% of the value for the isolated atom.[28] The structures of the complexed cations are practically identical to those of corresponding allialides and normal salts. Because the electron density of the trapped electrons is too low to detect by x-ray crystallography, the major structural difference between an electride and the corresponding alkalide is that the former has large voids at the anionic sites. To a first approximation, then. the electrons could be viewed as particles in adjacent, nearly spherical boxes. The common feature of an intense optical absorption band in the near IR at 1200–1500 nm. with a long tail into the visible, is the counterpart of the optical behavior of solvated electrons. The optical bands of solvated electrons were attributed, for many years. to electrons trapped in otherwise empty cavities.[23] The similarity to electrons in electride cavities is striking.

A complication that caused confusion in the study of electrides is structural polymorphism. Each of the electrides $Cs^+(18C6)_2e^-$, $Cs^+(15C5)_2e^-$, $Li^+(C211)e^-$, and $Rb^+(C222)e^-$ exists in at least two polymorphs.[3] Only

Fig. 3 Channel structures of four electrides. The general shapes of the cavities and channels are represented. (From Ref. [29].)

one form of each eiectride has a known structure, but the properties of the two forms are different. The factors that determine which form precipitates from solution are not known, and transitions between the types are slow. In the case of $Rb^+(C222)e^-$, mixtures of the two forms were usually produced, and it was necessary to use the magnetic properties to determine the amount of each present.[3]

Electron–Electron Interactions

The cavities and channels left by close-packing of the complexed cations tend to form uniform one-dimensional chains, like beads on a string, in five of the seven electrides of known structure.[29] The electrons are coupled antiferromagnetically, and the magnetic susceptibilities are well-fit by the Heisenberg linear-chain model, with a single negative coupling constant, J.[30] The mixed crown ether electride, $[Cs^+(15C5)(18C6)e^-]_6{\cdot}(18C6)$, has a complex structure.[''' while $K^+(C222)e^-$ has a two-dimensional channel-cavity structure with open channels in one direction and constricted channels in a second direction.[''' As with the corresponding potasside $K^+(C222)K^-$, this electride has open dumbbell-shaped cavities that contain two electrons.[32] The coupling is so strong in this case that the electride is nearly diamagnetic. The temperature dependence of the susceptibility is well-described by the alternating chain antiferromagnetic Heisenberg model.

The correlation between the magnetic coupling constant, J, and the geometry of the cavity-channel systems is remarkable. It provides strong experimental evidence for the theoretical finding that the excess electron density resides primarily in the cavities and channels.[33] The geometry of the channels in three electrides is shown in Fig. 3. Becaue the distance between cavity centers only slightly varies from one electride to another, the major effect on the interelectron coupling is the size of the connecting channel. Shown in Fig. 4 is the stron,σ correlation between the magnitude of the coupling constant and the cross-sectional area at the minimum diameter of the channel. Clearly, the overlap of the electronic wave functions is strongly influenced by the available void space between the electrons. This behavior of a well-defined; one-dimensional correlated electron gas of electrons should be a fruitful area for theoretical treatment.

Optical and Electrical Properties

The intense near-IR absorption of electride films (Fig. 1) is characteristic of localized electrons with little inter-

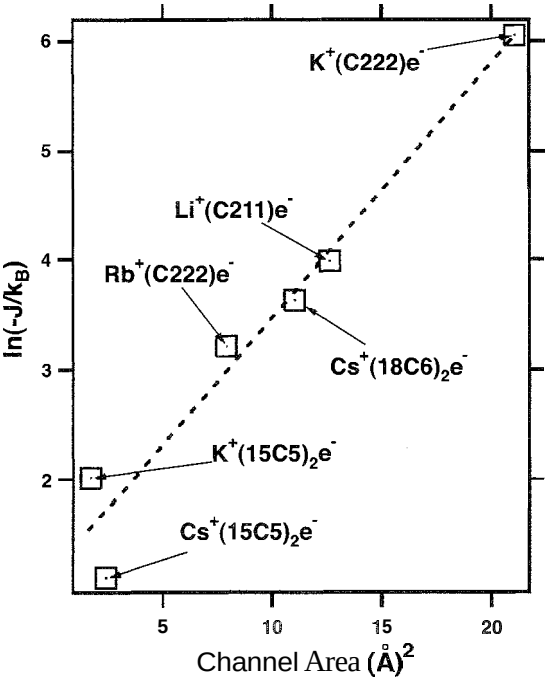

Fig. 4 Correlation of the antiferromagnetic coupling constants of electrides with the minimum cross-sectional area of the channels that connect the cavities. Reprinted with permission from Ref. [30]. Copyright 1997. American Chemical Society.

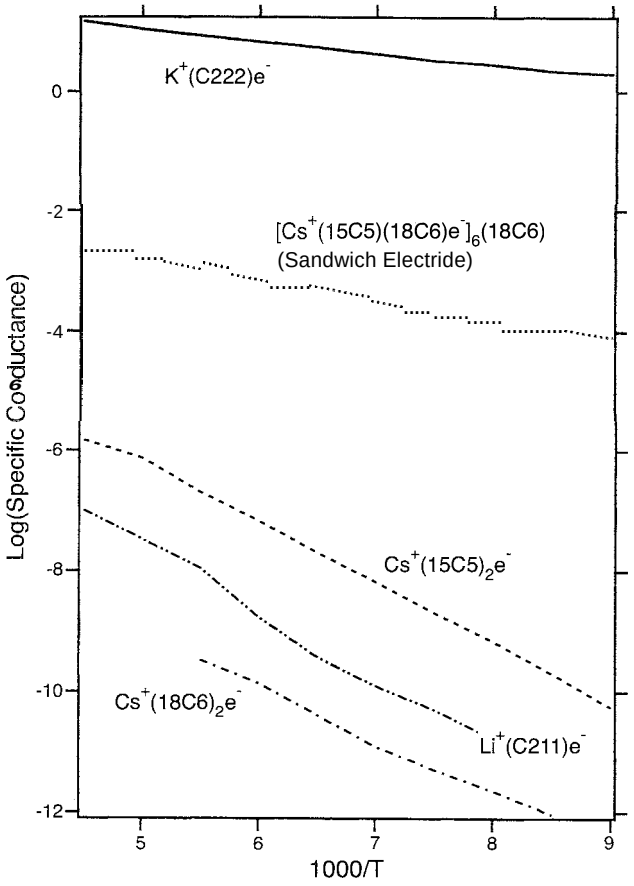

Fig. 5 Comparison of the conductivities of various electrides as functions of temperature. Reprinted with permission from Ref. [3]. Copyright 1997. American Chemical Society.

electron coupling. The electride $K^+(C222)e^-$ has a more open structure and far stronger coupling between electrons. This also has a profound effect on the optical spectrum and conductivity. Films of this electride. formed by high vacuum codeposition of K metal and cryptand [2.2.2] in 1:1 stoichiometry were extensively studied by optical transmission spectroscopy and four-probe conductivity.[34]

Freshly prepared films show the absorption peak of K . This tends to anneal with time to a combination of a localized electron peak at $\sim$1250 nm and an absorbance that rises steadily with increasing wavelength. The spectra are remarkably similar to those of concentrated metal–ammonia solutions as they move through the nonmetal to metal transition.[35] The rising absorbance is attributed to the plasma edge that is characteristic of metallic behavior. The electrical conductivity of powders and films of this electride is far greater than that of other electrides, as shown in Fig. 5. Whether these conductivities are intrinsic or defect-dominated is uncertain; but clearly. the open-channel nature of $K^+(C222)e^-$ has a profound effect, bringing this electride to the threshold of metallic behavior. Four-probe single crystal studies show that the conductivity is highly anisotropic.[36] It is nearly metallic along one direction in the plane of the channels and insulating perpendicular to this plane.

The Search for Stable Electrides

It is likely that the study of electrides would be more widespread if thermal stability at room temperature could be achieved. The recent success in synthesizing a sodide and potasside that are stable at room temperature[22] provided the incentive to find aza-based complexants that will permit the crystallization of stable electrides. The cation of choice would be Li^+, because there would be no competition from Li . an alkalide that has never been made. A number of candidates were tried. from methylated cyclens to fully methylated azacryptands to adamanzane-like complexants. Thus far: none produced a crystalline electride of known structure. When the cation is kinetically able to leave the complexant. dissociation without decomposition occurs. The aza complexants used to date apparently do not form strong enough complexes to yield thermodynamically stable electrides. although alkalides can be made in some cases. The search for the ideal aza complexant continues.

Inorganic Electrides

F-centers in alkali halides are stable. In 1966 Kasai and coworkers found that electrons could be trapped in a zeolite by incorporation of sodium from the vapor phase.[26] They identified the species Na_4^{3+}, an electron trapped by a cluster of four sodium cations. Since that time, a great deal of work was done on the inclusion of alkali metals in various aluminosilicates,[25] including the formation of a stoichiometric sodium sodalite that has Na_4^{3+} units inside every sodalite cage.[37] In common with electrides, these paramagnetic centers are coupled antiferromagnetically and undergo a Néel transition at 48 K. While these metal adducts to zealots could be (and have been) called ''electrides,''[25] they differ from the organic electrides by having several cations for each electron.

We recently added alkali metals from the vapor phase to two pure silica zealots to yield adducts that have a 1:1 stoichiometry of cations to electrons.[38] The properties strongly point to ionization to yield alkali cations that interact with the Si—O—Si units that line the zeolite channels. Apparently, the released electrons occupy the open spaces of the channels, which have diameters of -7 Å. The electrons are strongly coupled to form nearly diamagnetic materials. These inorganic electrides are stable to at least 100°C. Potentially, zeolite-based systems

might be made that would have an even closer relationship to organic electrides. If a pure silica zeolite could be made that contains open channels and separate cation-trapping sites, it should be possible to prepare a stoichiometric electride with trapped cations and electrons that are free to roam the channels. Such systems might have interesting properties. including, perhaps, metallic conductivity.

CONCLUSION

Although we studied alkalides and electrides for nearly 30 years. there is much that remains to be done to make them useful members of the chemistry–physics communities We hope that the existence of stable, easy-to-prepare alkalides and electrides will prompt a number of other researchers to entei this intriguing field

ARTICLES OF FURTHER INTEREST

Crown Ethers, p. 326
Cryptands, p. 333
Electron Paramagnetic Resonance Spectroscopy, p. 520
Energy and Electron Transfer in Supramolecular Systems, p. 535
Inclusion Compounds: Selectivity, Thermal Stability, arzd Kinetics, p. *696*
Macrocye Synthesis, p. 830
Molecular Modeling arzd Related Computational Techniques, p. 901
Nuclear Magnetic Resonance Spectroscopy, p. 981
Solid-State Nuclear Magnetic Resonance Spectroscopy, p. 1307
Space Groups and Crystal-Packing Modes, p. 1337
X-Ray Crystallography. p. 1586
X-Ray and Neutron Powder Diffraction, p. 1592

REFERENCES

1. Dye. J.L.: Ceraso. J.M.; Lok. M.T.: Bamett. B.L.; Tehan. F.J. A crystalline salt of the sodium anion (Na^-). J. Am. Chern. Soc. **1974**. *96*, 608–609.
2. Dawes, S.B.: Ward, D.L.; Huang, R.H.: Dye. J.L. First electride crystal structure. J. Am. Chem. Soc. 1984. *108*. 3534–3535.
3. Xie. Q.; Huang, R.H.: Ichimura. A.S.; Phillips, R.C.: Pratt. W.P., Jr.: Dye, J.L. Structure and properties of a new electride, Rb^+(cryptand[2.2.2]e^-. J. Am. Chem. Soc. 2000, *122*. 6971–6978.
4. Jedlinski. Z. Novel electron-transfer reactions mediated by alkali metals complexed by macrocyclic ligand. Acc. Chern. Res. 1998, *31*, 55–61.
5. Tsai. K.L.; Dye, J.L. Nanoscale metal particles by homogeneous reduction with alkalides or electrides. J. Am. Chem. Soc. **1991**. *113*. 1605–1652.
6. Wagner. M.J.; Dye, J.L. Alkalides and Electrides. In *Molecular Recognition: Receptors for Cationic Guests*, 1st Ed.: Gokel. G.W.. Ed.: Pergamon Press: Oxford. U.K.. 1996: 477–510.
7. Hurley, I.: Tuttle. T.R.J.: Golden, S. Origin of the 660-mu band in the spectra of alkali-metal-arnine solutions. J. Chem. Phys. 1968. *48*. 2818–2819.
8. Dewald, R.R.: Dye. J.L. Absorption spectra of the alkali metals in ethylenediamine. J. Phys. Chem. **1964**. *68*. 121–127.
9. Lok, M.T.; Tehan. F.J.: Dye. J.L. Spectra of N a . K and e^-_{solv} in amines and ethers. J. Phys. Chem. 1972. *76*. 2975–2981.
10. Dye. J.L.; DeBacker. M.G.; Nicely, V.A. Soluhilization of alkali metals in tetrahydrofuran and diethyl ether by use of a cyclic polyether. J. Am. Chem. Soc. **1970**. *92*. 5226–5228.
11. Dye. J.L.; Yemen. M.R.: DaGue. M.G.: Lehn. J.-M. Optical spectra of alkali metal anion and 'electride' films. J. Chem. Phys. 1978. *68*. 1665–1670.
12. Hendrickson. J.E.: Kuo. C.T.: Xie. Q.; Pratt. W.P., Jr.: Dye, J.L. Optical absorption and reflection spectra of Na^+(C222)Na . J. Phys. Chem. **1996**. *100*, 3395–3401.
13. Phillips. R.C.; Dye. J.L. Thermionic emission from cold electride films. Chem. Mater. **2000**, *12*. 3642--3647.
14. Huang, R.H.: Ward, D.L.; Dye. J.L. Alkali-metal-anion dimers and chains in alkalide structures. J. Am. Chem. Soc. **1989**. *111*. 5707–5708.
15. Tientega. F.: Dye. J.L.: Harrison. J.F. The electronic structure of K_2^{-2}. J. Am. Chem. Soc. 1991. *113*. 3206–3208.
16. Kuchenmeister. M.E.: Dye. J.L. Synthesis and structures of two thermally stable sodides with the macrocyclic complexant hexamethyl hexacyclen. J. Am. Chem. Soc. 1989. *111*, 935–938.
17. Ichimura. A.S. Unpublished results. this laboratory.
18. Kuo. C.-T.; Dye. J.L.: Pratt. W.P.,Jr. Effect of laser pulses on the photoelectron emission from Na^+(C222)Na^-. J. Phys. Chem. 1994. *98*. 13575–13582.
19. Dames. S.B.: Ellaboudy. A.S.; Dye, J.L. Cesium-133 solid state nuclear magnetic resonance spectroscopy of alkalides and electrides. J. Am. Chem. Soc. **1987**, 109. 3508–3513.
20. Kim. J.: Eglin. J.L.: Ellaboudy. A.S.: McMills. L.E.H.; Huang. S.: Dye. J.L. ^{87}Rb, ^{85}Rb. and ^{39}K NMR studies of alkalides. electrides and related compounds. J. Phys. Chem. 1996. *100*. 2885–2891.
21. Cauliez, P.M.: Jackson. J.E.; Dye. J.L. An unusual reduction of ethylene occurring during the thermal decomposition of alkalides and electrides. Tetrahedron Lett. **1991**. *32*. 5039–5042.
22. Kim. J.; Ichimura. A.S.: Huang, R.H.: Redko. M.: Phillips. R.C.: Jackson, J.E.: Dye. J.L. Crystalline salts of Na^- and K^- that are stable at room temperature. J. Am. Chem. Soc. 1999. *121*. 10666–10667.
23. Thompson. J.C. *Electrons in Liquid Ammonia*; Oxford Univ. Press: Oxford. 1976.

24. Markham. J.J. *F-Centers* in Alkali *Halides*; Academic Press: New York, 1966.
25. Edwards, P.P.; Anderson, P.A.; Thomas, J.M. Dissolved alkali metals in zeolites. Acc. Chem. Res. **1996.** 29, 23–29.
26. Rabo, J.A.; Angell, P.H.; Kasai, P.H.; Schomaker, V. Studies of cations in zeolites: Adsorption of carbon monoxide; formation of Ni ions and Na_4^{3+} centres. Discuss. Faraday Soc. **1966,** *41,* 328–349.
27. Dye, J.L. Elcctrides: Tonic salts with electrons as the anions. Science **1990,** 247, 663–668.
28. Dawes, S.B.; Eglin, J.L.; Mocggenborg, K.J.; Kim, J.; Dye, J.T. Cs^+(15-crown-5)2e , a crystalline antiferromagnetic electride. J. Am. Chcm. Soc. **1991,** *113,* 1605–1609.
29. Dye, J.L.; Wagner, M.J.: Overney, G.; Huang, R.H.; Nagy, T.F.; Tomanek, D. Cavities and channels in electrides. J. Am. Chem. Soc. **1996,** *118,* 7329–7336.
30. Dye, J.L. Electrides: From ID Heisenberg chains to 2D pseudo-metals. Inorg. Chem. **1997,** *36*, 3816 3826.
31. Wagner, M.J.; Huang, R.H.; Eglin, J.L.; Dye, J.L. An electride with a giant 6-electron ring. Nature **1994,** *368,* 726–729.
32. Huang, R.H.; Faber, M.K.; Moeggcnborg, K.J.; Ward, D.L.: Dye, J.L. Structure of K^+(cryptand[2.2.2]) electride and evidence for trapped electron pairs. Nature **1988,** *331,* 599 601.
33. Singh. D.J.; Krakauer, H.; Haas, C.; Pickett, W.E. Theoretical determination that electrons act as anions in the electride $Cs^+(15\text{-crown-}5)_2e^-$. Nature **1993.** *36.5.* 39 42.
34. Hendrickson, J.E.; Pratt, W.P., Jr.; Phillips, K.C.: Dye, J.L. Optical spectra and conductivities of thin films of the electride $K^+(C222)e^-$. J. Phys. Chem., B **1998,** *102,* 3917 3926.
35. Beckrnan, T.A.; Pitrer, K.S. The infrared spectra of marginally metallic systems: Sodium-ammonia solutions. J. Phys. Chem. **1961,** *65.* 1527 1532.
36. Ichimura, A.S.: Wagner, M.J.; Dye, J.L. Anistropic charge transport and spin–spin interactions in K^+(cryptand[2.2.2]) electride. J. Phys. Chem., B. 2002, *106*, 11196–11202.
37. Srdanov, V.T.; Stucky, G.D.; Lippma, E.; Engelhardt, G. Evidence for an antiferromagnetic transition in a zeolite-supported cubic lattice of F-centers. Phys. Rev. Lett. **1998,** *80,* 2449–2452.
38. Ichirnura, A.S.; Dye, J.L.; Camblor, M.A.; Villaescusa, L.A. Toward inorganic electrides. J. Am. Chcm. Soc. 2002; *124,* 1170 1171.

The Allosteric Effect

Anatoly K. Yatsimirsky
Universidad Nacional Autónoma de Mexico, Mexico City, Mexico

INTRODUCTION

The allosteric regulation of ligand binding to proteins is the principal regulatory mechanism in living systems on the molecular level.[1–3] The allosteric effect means the situation when the binding of one ligand at its binding site is influenced by the occupation of another binding site by another identical (homotropic effect) or different (heterotropic effect) ligand (effector). In biological systems. the allosteric effect is usually considered for oligomeric proteins, e.g., hemoglobin. and reflects interactions between subunits. In chemistry. it is studied with low-molecular-weight receptors possessing two or more binding sites, the interaction between which is mediated by conformational changes induced in the receptor upon occupation of one site. The positive allosteric effect, when the occupation of one site increases the affinity to the ligand on the other site, leads to positive cooperativity in ligand binding and may be used for amplification of the signal produced by the effector.[4,5] Allosteric regulation is a possible way to operate molecular switches. and it is important for the functioning of molecular machines.'''

BINDING ISOTHERMS FOR ALLOSTERIC SYSTEMS

In a general case of a receptor possessing N binding sites, the stepwise stoichiometric formation constants are defined as follows

$$K_i = [RL_i]/([RL_{i-1}][L])$$

where $1 \leq \iota \leq N$, and the overall formation constants are defined as

$$\beta_i = K_1 K_2 \; K_{i-1} K_i$$

In addition. one can define a single-site binding constant Q as

$$Q = [\text{occupied single site}]/([\text{free single site}][L])$$

The expression for the degree of complexation (or degree of saturation) Y is defined as follows:

$$Y = (\text{concentration of occupied sites})/(\text{total concentration of binding sites})$$

It has the following form:

$$Y = \frac{\sum_{i=1}^{N} i\beta_i[L]^i}{N\left(1 + \sum_{i=1}^{N} \beta_i[L]^i\right)} \quad (1)$$

Another useful function for the analysis of binding is the Bjerrum complex formation function $\bar{n}$, which gives an average number of ligand inolecules bound per receptor:

$$\bar{n} = YN$$

In the case when the receptor possesses N identical and independent sites:

$$K_i = Q(N - i + 1)/i$$

and the ratio of two successive stability constants is[6]

$$K_{i+1}/K_i = i(N - i)/((i + 1)(N - i + 1)) \quad (2)$$

Evidently each next stability constant is smaller than the preceding one due to only statistical factors. Any deviation from the statistical ratio K_{i+1}/K_i implies a nonequivalence of binding sites or some sort of interaction between sites, in particular due to the allosteric effect. In the latter case. deviations from statistical binding are commonly referred to as cooperativity, which can be positive or negative. depending on whether the ratio of successive stability constants is higher or lower than the statistically expected value.[6]

The binding isotherm for the statistical binding takes a form of Eq. 3:

$$Y = Q[L]/(1 + Q[L]) \quad (3)$$

A modified linear form[r6] of Eq. 3 is as below:

$$\bar{n}/[L] = NQ - \bar{n}Q \quad (4)$$

This is known as the Scatchard equation. Eq. 3 describes a simple hyperbolic binding isotherm, like in a case of a 1:1 complexation. The cooperative binding. however. modifies to a smaller or greater extent the shape of the isotherm, in particular. positive cooperativity leads to ''sigmoid'' binding isotherms. The oldest and still popular way to diagnose cooperativity by the analysis of the shape of the binding isotherm is to calculate the so-called Hill

Encyclopedia of Supramolecular Chemistry
DOI: 10.1081/E-ESMC 120012884

coefficient h. which is the slope of the plot of $\log(Y/(1-Y))$ versus $\log[L]$:[6]

$$h = d\log(Y/(1-Y))/d\log[L] \quad (5)$$

The Hill equation was derived originally for a complexation process, which involves only one equilibrium between R and h molecules of L affording the single complex RL_h. The degree of saturation is given in this case by the following equation:

$$Y = [RL_h]/[R]_t = \beta_h[L]^h/(1+\beta_h[L]^h) \quad (6)$$

which for $h>1$ describes a sigmoid-binding isotherm. Usually a linearized form given by Eq. 7 is used for the data fitting:

$$\log(Y/(1-Y)) = h\log[L] + \log\beta_h \quad (7)$$

Evidently this equation implies an infinite cooperativity when the binding constants for all complexation processes with $i<h=N$ equal to zero. In real cases. the value of h defined as in Eq. 5 is approximately constant only in a restricted range of concentrations of L, typically around 50% of saturation. It approaches N when the positive cooperativity is high, equals unity for statistical binding. and is smaller than unity for negative cooperativity.

Typical sigmoid isotherms are shown in Fig. I for cooperative binding of dicarboxylic acids 16 and **17** to a double-decker porphyrin with pyridine substituents **15a** (see below, Fig. 5*)*. The Hill coefficient for these systems $h=4$ equals the total number of bound guests as a result of a strong positive allosteric effect.[4]

Classical models for the cooperative binding to oligomeric proteins, which are formally applicable also for synthetic receptors, include the symmetry model of

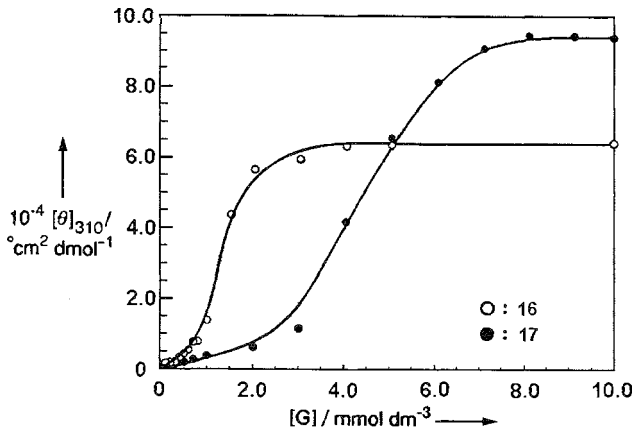

Fig. I Binding isotherms of Guests **16** and **17** to Receptor **15a** (see Fig. 5*)* followed by the complexation-induced circular dichroism.[4,25] Reprinted with permission from Ref. [4]. Copyright 2001 by American Chemical Society.

Monod–Wyman–Changeux (MWC model)[7] and the sequential or induced-fit model of Koshland–Nemethy–Filmer (MNF model).[8,9] In the MWC model. the positive cooperativity is due to a mechanism that does not involve any positive site interactions. It results from the complexation-induced shift of preequilibrium between two states of the receptor. in which all binding sites have different conformations possessing different affinities to the ligand [the tense (T) or relaxed (R) state in hemoglobin]. In the KNF model, ligand binding induces a conformational change in the receptor-binding site, which is transmitted to other binding sites. If the interaction between sites is strong, the conformational change may occur in a concerted manner involving all binding sites and, in this case, the model formally coincides with the MWC model.

A large number of allosteric systems discussed below involve a receptor R possessing two binding sites for two different ligands (heterotropic system). Analysis of such a system is straightforward: one can measure the single-site binding constant for any ligand in the absence of the other ligand and then compare it with the binding constant determined in the presence of the other ligand. Analysis of homotropic systems is more complicated. Eqs. 8–11 describe such a system:

$$R + L \rightleftharpoons RL^1 \quad (Q_1) \quad (8)$$

$$R + L \rightleftharpoons RL^2 \quad (Q_2) \quad (9)$$

$$RL^1 + L \rightleftharpoons RL_2 \quad (\alpha Q_2) \quad (10)$$

$$RL^2 + L \rightleftharpoons RL_2 \quad (\alpha Q_1) \quad (11)$$

Here. superscripts 1 and 2 refer to first and second binding sites: Q_1 and Q_2 are the respective single-site binding constants; and a is the interaction factor that shows how the binding constant for a given site changes upon occupation of the other site. Note that the interaction factor is the same for both binding sites. The stepwise stoichiometric formation constants equal:

$$K_1 = Q_1 + Q_2 \quad (12)$$

$$K_2 = \alpha Q_1 Q_2/(Q_1 + Q_2) \quad (13)$$

Obviously. in this case, the single-site binding constants and the site interaction factor cannot be calculated from the experimentally determined constants K_1 and K_2 without making additional assumptions concerning possible equivalence or mutual dependence of the binding sites. In the case of statistical binding. $Q_1=Q_2=Q$ and $a=1$: therefore $K_1=2Q$, $K_2=Q/2$, and the ratio $K_2/K_1=1/4$. If the binding sites are equivalent ($Q_1=Q_2=Q$) but not independent ($\alpha\neq1$), one observes positive ($K_2/K_1>114$) or negative ($K_2/K_1<114$) cooperativity when α is larger or smaller than unity, respectively. Alternatively. if the

binding sites are nonequivalent ($Q_1 \neq Q_2$) but independent ($\alpha = 1$), the ratio K_2/K_1 equals

$$K_2/K_1 = Q_1Q_2/(Q_1 + Q_2)^2$$
$$= (Q_2/Q_1)/(1 + Q_2/Q_1)^2 \quad (14)$$

Predicted with Eq. 14 is that K_2/K_1 has the maximum value of 1/4 at $Q_2/Q_1 = 1$, and, therefore. at all nonequal values of Q_1 and Q_2, the ratio K_2/K_1 is less than 114. In this case. a negative cooperativity without negative interaction between the binding sites is obcerved.

It should be noted that cooperativity does not necessarily result from site interaction. Often. the mutual attraction or repulsion of bound ligands leads to positive or negative cooperativity, respectively. For example. highly cooperative binding of four moleculec of n-octyl β-D-glucopyranozide to the resorcinol cyclic tetramer in $CHCl_3$, which is characterized by the Hill coefficient $h = 4$. results from intracomplex guest–guest hydrogen bonding involving the 5-CH_2OH and 2-OH groups of adjacent glucopyranozide molecules.[9]

ALLOSTERIC SYSTEMS BASED ON CROWN ETHERS AND PODANDS

The earliest examples of synthetic allosteric systems involved modification of binding properties of crown ethers by changing their conformations as a result of complexation with another metal cation at an adjacent binding site. For example, complexation of a bipyridine moiety of **1** (Fig. 2) with $W(CO)_4$ changes the selectivity of the crown ether from preferable binding of K^+ over Na^+ to preferable binding of Na^+ over K^+.[10] In a more recent study of the cooperative binding of K^+ or Ca^{2+} and monosaccharides to Receptor 2 (Fig. 2). reminiscent by its design of **1**, a negative allosteric effect was reported.[11] Cation-induced changes in the macrocycle conformation produced a disposition of boronic acids unfavorable for the saccharide complexation.

The bis-crown ether **3** (Fig. 2) showed a negative cooperativity in binding two K^+ or Na^+ cations. which resulted, however. from mutual repulsion of metal ions rather than from a negative allosteric effect.[12] Binding of two neutral Lewis acids. e.g., $Hg(CN)_2$ showed a positive cooperativity with the Hill coefficient $h = 1.5$.[12] This was interpreted as a result of positive allosteric effect due to the reduction of the conformational freedom of the second macrocycle favorable for complexation conformation upon binding of the first $Hg(CN)_2$ molecule.

A strong negative allosteric effect was found for the complexation of diquate dication by *bis*-crown receptor **4** (Fig. 2) in the presence of transition metal complexes like $Cr(CO)_4$ and $Ru(Bipy)_2^{2+}$.[13] Binding of these complexes to a bipyridine moiety of **4** induces rotation of the aromatic rings and formation of a planar structure, which does not bind diquat dication.

A large group of receptors showing a positive cooperativity in metal ion complexation is based on polyether (podand) compounds bearing terminal groups capable of chelation of transition metal ions.[14] As an example, in Fig. 2 (**5**), a complexation-induced cyclization of a podand bearing β-diketone terminal groups is shown.[15] The resulting complex is capable of complexation of alkali metal cations. Other examples of such pseudocrown ethers can be found in Ref. [14]. As pointed out in the preceding section, the interaction factor must be the same for two binding sites of a receptor. Therefore, one should expect that the complexation of a podand with an alkali metal cation in its turn must promote the interaction between the terminal groups. Such an effect was demonstrated for system **6** (Fig. 2).[16] A podand bearing two Zn(II) porphyrin complexes recognizes diamines by sandwiching them between two metal centers. The addition of sodium cations increases by a factor of 2 the affinity of the receptor to 1,2-diaminocyclohexane.

The allosteric regulation of the binding of an organic guest by complexation with alkali cations is illustrated by the molecular clip **7a**, Fig. 2.[17] It exists in three conformations *ss*. *sa*, and *aa*. interconverting slowly on the NMR time scale. The predominant conformer *sa* (as well as a minor conformer *sa)* converts upon uptake of a potassium ion in the crown ether bottom unit to *an* conformer, which then binds an aromatic guest. such as 1.3-dinitsobenzene. about four times better than without K^+ (Fig. 2. **7b**).

The allosteric effect also plays a role in the cooperative binding of anions and cations by some ditopic receptors, such as in the case of Receptor **8**, Fig. 2.[18] The positive cooperativity in the binding of Cl^- in the presence of K^+ partly results from the electrostatic attraction between oppositely charged ions. But, at the same time. binding of $H_2PO_4^-$ shows a negative cooperativity with K^+, and this specificity to the type of anion indicates a contribution of some nonelectrostatic. most probably, conformational effects.

ALLOSTERIC SYSTEMS BASED QN CYCLOPHANES

A cyclophane possesses a hydrophobic cavity suitable for complexation of nonpolar organic guests. Several heterotropic allosteric systems based on cavity formation induced by complexation with transition metal cations were reported. The idea is generally similar to metal-induced

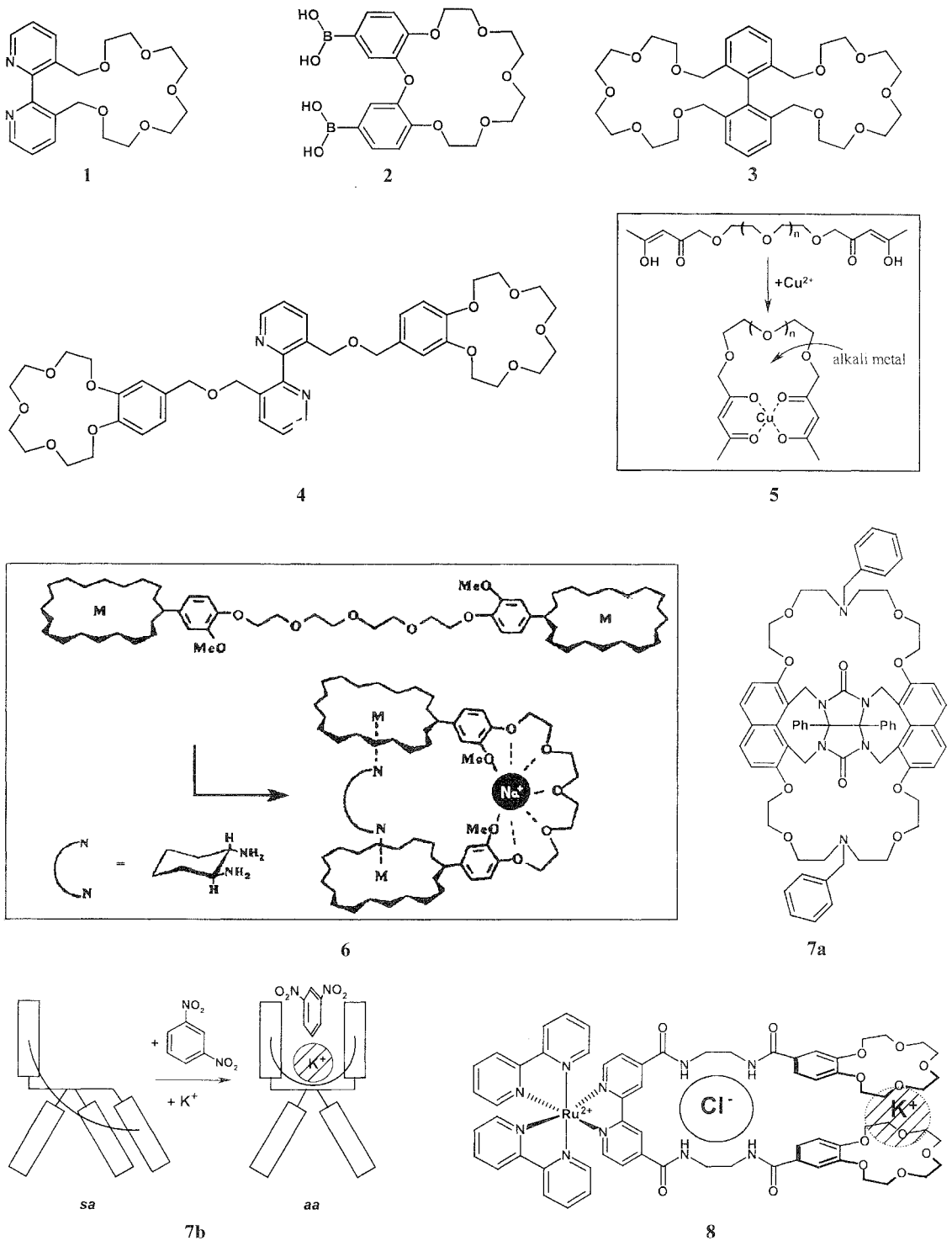

Fig. 2 Allosteric systems based on complexation with crown ethers and podands Fntry 6 From Ref [16] Reproduced by permission of The Royal Society of Chemistry (RSC) on behalf of the Centre National de la Recherche Scientifique (CNRS)

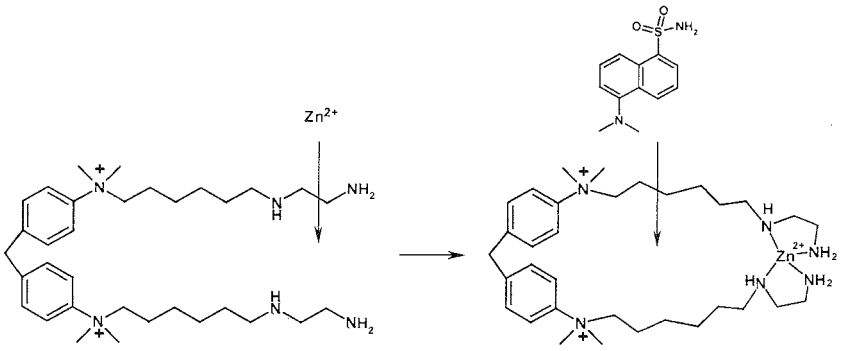

9

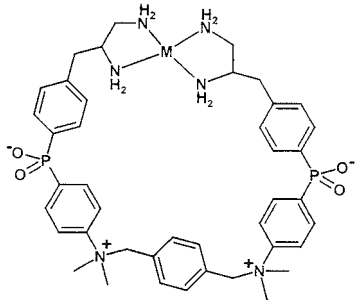

10

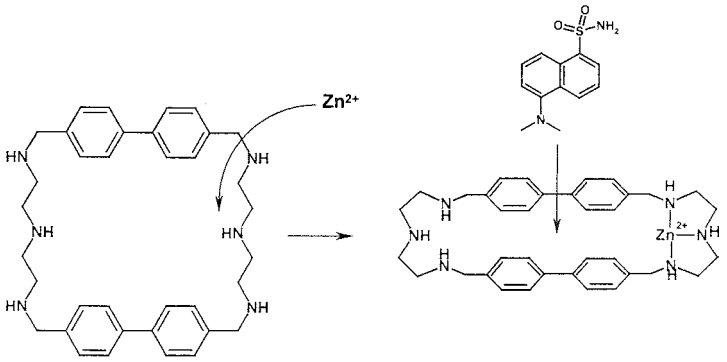

11

Fig. 3 Allosteric systems based on complexation with cyclophanes

cyclization of podands described in the preceding section [see Fig. 2 (5) as an example], but instead of leading to cooperativity between binding of two different metal ions. it leads to the cooperativity between binding of a metal ion and an organic molecule. Illustrated in Fig. 3 (9) is a coope ative complexation of Zn(II) or Cu(II) and a fluorescent indicator dansylamide to an open cyclophane precursor bearing ethylenediamine terminal groups.[19] Addition of the metal ion closes the cavity and allows the indicator to form an inclusion complex with the stability constant ca. 10 M^{-1} in water. This is ca. 100 times less than the stability constant for inclusion of the same guest in a normal azaniacyclophane of the same size. but the important thing is that in the absence of metal ions, the open host does not bind the indicator.

A similar principle was applied for the construction of metallocyclophanes 10, Fig. 3.[20] For this system. it was shown that the shape of the hydrophobic cavity depends

on the type of metal cation: when M=Zn, *the host* more strongly binds *a guest that is a naphthalene derivative than a guest that* is *a biphenyl derivative. but when* M=Cu, *the binding preference is inverted. Thus. the* distinct *coordination geometries of these metals differently affect the shape of the cavity.*

Another principle operates in System **11** *(Fig.* 3).[21] *Here. the metal binding leads to the ring contraction* and *better* accommodation *of* the *organic guest in the cavity, which is too large. The stability constant for guest inclusion increases by a factor of* 100.

ALLOSTERIC SYSTEMS BASED ON CALIXARENES

Calix[4]arenes *are* conformationally flexible *hosts particularly suitable* for *design of allosteric receptors due to a possible* communication *between binding sites situated at the upper and lower* rims.[5,22] *Positive and negative heterotropic* allosterism *was demonstrated* by *using* a calix[4]arene with *the metai-binding lower rim and the sugar-binding upper* rim *created by introducing two boronic acid* groups.[22] *Additions of hard cations* (Ca^{2+}, Mg^{2+}, *or* Na^{+}) *decreased,* but *additions of soft cations like* K^{+}, *Rb'. or* Cs^{+} *increased the sugar binding. This switch* from *a negative to a positive heterotropic allosteric effect, depending on the type of* metal *cation* within *a series of cations. which are similar by their chemical natures.* demonstrates *a possibility of a fine tuning of the binding site* conformation *of calixarene hosts.*

Receptor 12 (Fig. 4) binds urea derivatives *in* $CHCl_3$ *via hydrogen bonding to* two aryl carboxylate *groups with a positive allosteric effect based on the conformation change induced by complexation of* Na^{+} *with the* crown *ether* fragment *of the receptor.''''* In *the free receptor. carboxylic groups are at* a *short distance. favoring intramolecular hydrogen bonding. The addition of* Na^{+} *leads to a larger separation* between *the carboxylic groups. favoring the intermolecular hydrogen bonding* with *the guest.*

A similar effect of metal-induced conversion of a calixarene conformation with intramolecularly bound amide groups (closed form unable to bind guest molecules) into a conformation *with more separated unbound* amide *groups (open form) capable of complexation with* amide *guests operates in the allosteric* regulation *of the host* **13** *(Fig.* 4).[5]

Widening the opposite side of a calixarene upon complexation *of* small *cations to the oxygen* atoms *of a calixarene lower riin leads* to *the positive heterotropic allosteric effect in the inclusion of* [60]fullerene *in a cage molecule* **14** *(Fig. 4) derived* from *two* calix[3]aryl *esters by* complexation *of their pyridine groups* with Pd(II).[24]

Receptor 14 binds [60]fullerene *in* $CHCl_2CHCl_2$ *with the stability constant* $K=39\ M^{-1}$. *The addition of* Li^{+} cations *induces flattening of the cage and an increase in* K *up to 2100* M^{-1}. *Interestingly, the addition of* Na^{+} *cations produces a strong negative allosteric effect.*

DIMERIC PORPHYRINS

Face-to-face dimeric metalloporphyrins represent a new class of homotropic allosteric receptors that show strong positive cooperativity in binding different guests.[4,5,25] As *an example, in Fig. 5. the* cerium(IV) *bis*[tetrakis(4-pyridyl)-porphyrinate] *double* decker *is shown,* with **15a** *designed for* complexation *of* dicarboxylic *acids 16 and* **17**. *The addition of any of these guests to* **15a** *in* dichloromethane/ethyl *acetate (3011) leads to the appearance of circular dichroism spectra. The value of* $[\theta]_{max}$ *at* 310 *nm was found to be proportional to the amount of complexed receptor. Shown in Fig.* 1 *are the respective plots of* $[\theta]_{max}$ *versus guest concentration. which have typical sigmoid shape and give* $h=4$ *in the Hill coordinates. The binding mode of the guests* is illustrated in *Fig.* 5 *(18). It* is *proposed that successive binding of guest molecules reduces the degree of free* rotation *of porpliyrin rings in the double decker, which makes the binding of each next guest more energetically favorable. Binding of the same guests to* **15b**, *which can bind* only *one guest molecule, is too weak to be detectable in agreement with weak binding of the first guest to* **15a** *required for high cooperativity.*

Interestingly, a similarly designed double decker for the complexation *of saccharide guests.* **19** *(Fig.* 5), *shows negative cooperativity: only one guest can be bound to the receptor.* The *differencebetween these two systems is that in the case of* **15a**, *binding of the guests does not change the basic structure of the double decker. But* in *the case of 19, binding of the first guest induces deformation of the receptor structure. which makes more distant other boronic acid groups and thus precludes the binding of additional guests.*

ALLOSTERIC REGULATION OF REACTIVITY AND CATALYSIS

Enzyme regulation *is one of the most important biological applications of the allosteric effect. There is. however, little progress in reproducing regulation of reactivity and catalysis in chemical systems. Earlier works demonstrated a possibility of allosteric regulation of reactivity in several simple systems possessing a* 2,2′-bipyridyl *unit as a regulatory switch relevant to allosteric receptors of type* **1**.[26]

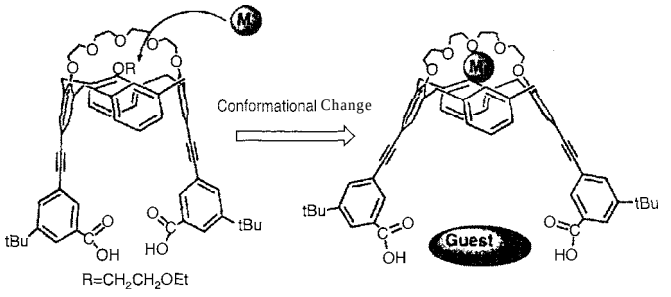

12

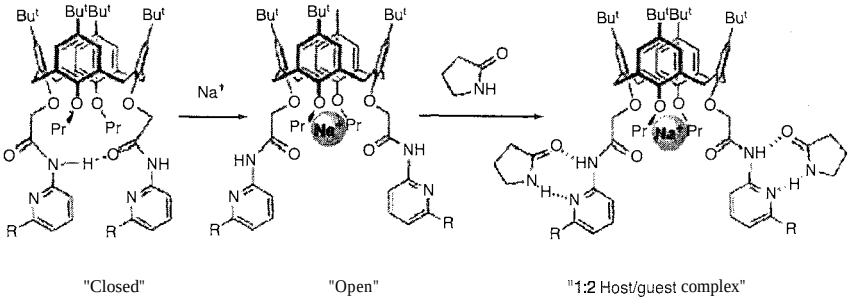

13

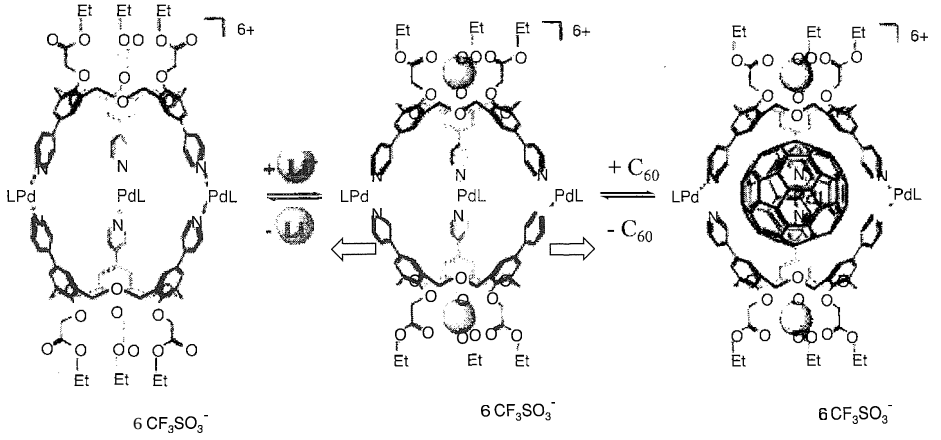

14 | 14 $(Li^+)_2$ complex with a flattened structure | 14 $(Li^+)_2$ [60]fullerene complex

Fig. 4 Positive heterotropic allosteric regulation of complexation with calixarene hosts. Entry 12: Reprinted from Ref. [23]. Copyright 1998. with permission from Elsevier; Entry 13: Reprinted with permission from Ref. [5]. Copyright 2001 by American Chemical Society; Entry 14: Reprinted from Ref. [24]. Copyright 2000, with permission from Elsevier.

For example, rate of cyclization of 20 strongly increases in the presence of Ni(II) cations. Rates of nucleophilic substitution in and elimination from **21** strongly increase in the presence of Pd(II) (Fig. 6). These systems, however. did not allow a clear separation of conformational and electronic, in particular, inductive effects.

The allosteric 30-fold acceleration of the reduction of a podand bearing a quinone group by 1-propyl-1,4-dihydronicotinamide in the presence of potassium cations[27] is illustrated in Fig. 6 (22). The system is based on the same principle as 6 (Fig. 2). A different approach was proposed for the allosteric regulation of a catalyst for the phosphodiester cleavage, 23 (Fig. 6).[28] The catalyst is a trinuclear metal complex with two functional metal ions (M_F), which activate the phosphodiester substrate. and one structural ion (M_S), which has the regulatory function. With M_F=Cu(II), variation in M_S=Cu(II), Ni(II), or Pd(II) leads to significant changes in the catalytic activity attributed to subtle differences in the ionic radius and coordination geometry of the allosteric metal ion.

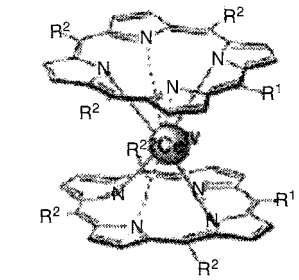

$R^1=R^2=$ 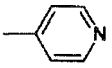 **15a**

$R^1=$  , $R^2=Ph$ **15b**

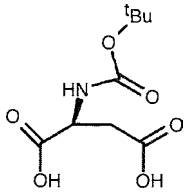

16

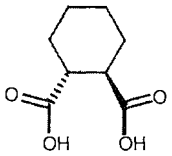

17

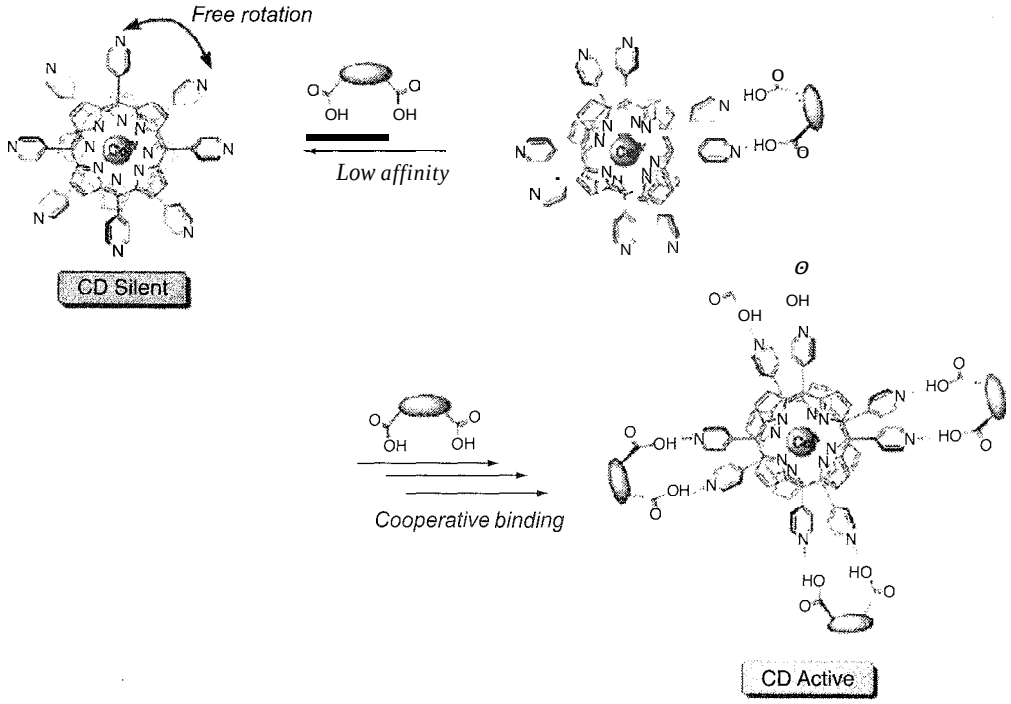

18

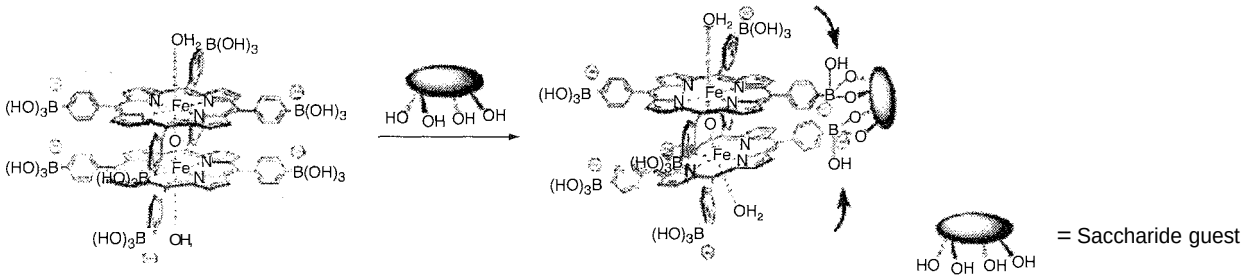

19

Fig. 5 Allosteric systems based on porphyrin face-to-face dimers. Entries **18** and 19: Reprinted with permission from Ref. [4]. Copyright 2001 by American Chemical Society.

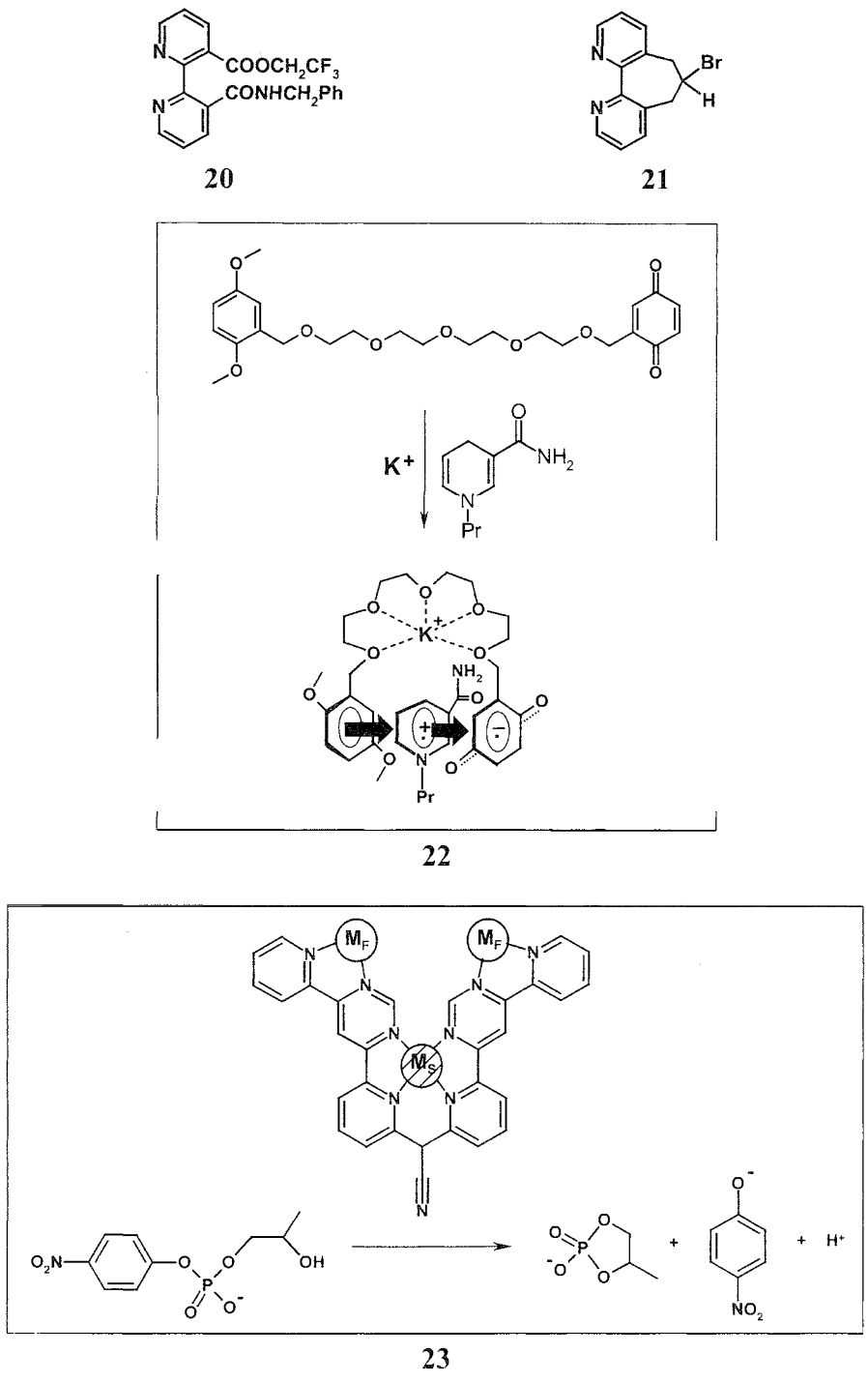

Fig. *4* Allosteric regulation of reactivity.

MISCELLANEOUS ALLOSTERIC SYSTEMS

Not unexpectedly. many attempts were made to imitate the cooperativity of oxygen binding by hemoglobin, e.g., by using his-metalioporphyrin complexes.[29] Allosteric preorganiration of oligobipyridine ligands by coordination with Cu(I) leads to self-assembly of interesting metal helicates with strand characteristics of DNA.[30] A similar effect was reported in complexation of Fe(III) with tripodal hydroxamate ligands: each next step in the consecutive

complexation of three metal ions has a larger stability constant.[31] Strong cooperativity between cation and anion binding to a cyclopeptide in $CHCl_3$ was attributed at least partially to the allosteric effect.[32]

CONCLUSION

Allosteric regulation requires a certain conformational flexibility of the receptor. The positive allosteric effect may be considered a preorganization of one binding site by a conformational change induced by the occupation of the other binding site. Many widely used types of synthetic hosts, such as crown ethers, cyclophanes, and calixarenes. have suitable conformational dynamic properties, but the recent discovery of other highly efficient allosteric systems based on. e.g., porphyrin double-decker structures points to the possibility of using receptors of different structural types. It should be noted that the actual mechanism of the allsoteric effect in many systems remains essentially hypothetical. With oligomeric proteins, binding sites are separated by large distances, excluding any mutual interaction between bound guests. In synthetic hosts. binding sites are close enough to expect some contribution of such interaction to the observed cooperativity. which is difficult to separate from the purely conformational effect. Practically. further development of allosteric systems promises considerable progress in the creation of new receptors and catalysts with tunable properties. as well as new analytical and other devices with improved sensitivity and selectivity.

ARTICLES OF FURTHER INTEREST

Hemoglobins: O_2 Uptake and Transport, p. 636
Induced Fit, p. *717*
The Lock and Key Principle, p. 809
Molecular Switches, p. *917*
Molecular-Level Machines, p. 931
O_2 Uptake and Transport, Models of, p. 1023
Preorganization and Complementarity, p. *1158*

REFERENCES

1. Fersht. A. *Enzyme Structure* and *Mechanism*, 2nd Ed.: W. H. Freeman: New York. 1985.
2. Levitzki. A. *Quantitative Aspects* of Allosteric *Mechanism*: Springer: New York. 1978.
3. Perutz. M.F. Mechanisms of cooperativity and allosteric regulation in proteins. Q. Rev. Biophys. 1989.22, 139–236.
4. Shinkai. S.: Ikeda, M.; Sugasaki. A.; Takeuchi, M. Positive allosteric systems designed on dynamic supramolecular scaffolds: Toward switching and amplification of guest affinity and selectivity. Acc. Chem. Res. 2001. *34* (6), 494–503.
5. Takeuchi. M.: Ikeda, M.; Sugasaki, A.; Shinkai, S. Molecular design of artificial molecular and ion recognition systems with allosteric geust responses. Acc. Chem. Res. 2001. *34* (11). 865–873.
6. Perlmutter-Hayman. B. Cooperative binding to macromolecules. A formal approach. Acc. Chem. Res. 1986. 19 (3), 90–96.
7. Monod. J.; Wyman, J.: Changeux. J. D. On the nature of allosteric transitions: A plausible model. J. Mol. Biol. 1965. 12 (1), 88–118.
8. Koshland. D.E.; Nemethy. G.: Filmer, D. Comparison of experimental binding data and theoretical models in proteins containing subunits. Biochemistry 1966, *5* (1), 365–385.
9. Kikuchi, Y.; Tanaka. Y.; Sutarto, S.: Kobayashi, K.: Toi. H.; Aoyama, Y. Highly cooperative binding of alkyl glucopyranosides to the resorcinol cyclic tetramer due to intracomplex guest–guest hydrogen-bonding: Solvophobicity/solvophilicity control by an alkyl group of the geometry, stoichiometry, stereoselectivity, and cooperativity. J. Am. Chem. Soc. 1992. *114* (26), 10302–10306.
10. Rebek, J.. Jr.: Wattley. R.V. Allosteric effects. Remote control of ion transport selectivity. J. Am. Chem. Soc. 1980. 102 (14). 4853–4854.
11. Deng. G.; James. T. D.; Shinkai. S. Allosteric interaction of metal ions with saccharides in a crowned diboronic acid. J. Am. Chem. Soc. 1994. *116* (11), 4567–4572.
12. Rebek. J.. Jr.: Cosltello. T.: Marshall. L.: Wattley. R.: Gadwood. R.C.: Onan. K. Allosteric effects in organic chemistry: Binding cooperativity in a model of subunit interactions. J. Am. Chem. Soc. 1985. *107* (25), 7481–7487.
13. Beer. P.D.; Rothin, A.B. A new allosteric bis crown ether ligand that displays negative binding cooperativity of the diquat dication by the complexation of a transition metal guest. J. Chem. Soc. Chem. Commun. 1988. (1). 52–54.
14. Nabeshima, T. Regulation of ion recognition by utilizing information at the molecular level. Coord. Chem. Rev. 1996. 148. 151–169.
15. Kobuke, Y.: Satoh. Y. Positive cooperativity in cation binding by novel polyether *bis*(β-diketone) hosts. J. Am. Chem. Soc. 1992. *114* (2). 789–790.
16. Monti, D.: La Monica. L.: Scipioni. A.; Mancini, G. Effect of the inclusion of sodium caitons on the binding properties of a switchable diporphyrin receptor. New. J. Chem. 2001. *25*. 780–782.
17. Sijbesma, R.P.: Notle. R.J.M. A molecular clip with allosteric binding properties. J. Am. Chem. Soc. 1991. *113* (17), 6695–6696.
18. Beer. P.D.: Dent. S.W. Potassium cation induced switch in anion selectivity exhibited by heteroditopic ruthenium(II) and rhenium(I) bipyridyl *bis*(benzo-15-crown-5) ion pair receptors. Chern. Commun. 1998. (7). 825–826.
19. Schneider. H.-J.; Ruf. D. A synthetic allosteric sytem with high cooperativity between polar and hydrophobic binding

sites. Angcw. Chcm. Int. Ed. Engl. **1990,** 29 (10), 1159–1160.
20. Wang, F.; Schwabachcr, A.W. Metal control of non-polar binding shape selectivity. Tetrahedron Lett. **1999.** 40 (43), 7641–7644.
21. Baldes, R.; Schneider, H.-J. Complcxcs from polyazacyclophanes, fluorescent indicators, and metal cations—An example of allosterism through ring contraction. Angew. Chem. Int. Ed. Engl. **1995,** *34* (3), 321–323.
22. Ohseto, F.; Yamamoto. H.; Matsumoto. H.; Shinkai, S. Allosteric communication between the metal-binding lower rim and the sugar-binding upper rim in a calix[4]crown platform. Tetrahedron Lett. **1995,** 36 (38). 6911–6914.
23. Haino, T.; Katsutani, Y.: Akii, H.; Fukazawa, Y. Allosteric receptor based on monodeoxycalix[4]arene crown ether. Tetrahedron Lett. **1998.** 39 (44), 8133–8136.
24. Ikeda, A.; Udzu, H.; Yoshimura, M.; Shinkai, S. Inclusion of [60]fullerene in a self-assembled homocalix[3]arene-based dimeric capsule constructed by a Pd(II)-pyridine interaction. The Li^+ binding to the lower rims can improve the inclusion ability. Tetrahedron 2000, *56* (13), 1825–1832.
25. Takeuchi, M.; Imada, T.; Shinkai, S. A strong positive allostcric effect in the molecular recognition of dicarboxylic acids by a cerium(IV) *bis*[tetrakis(4-pyridyl)-porphyrinate] double decker. Angew. Chem. Int. Ed. Engl. **1998,** 37 (15). 2096–2099.
26. Rebek, J., Jr. Binding forces, equilibria, and rates: New model for enzymic catalysis. Acc. Chcm. Res. **1984,** 17, 258–264.
27. Pierre, J.-L.; Gagnaire, G.; Chautemps, P. An artificial allosteric system: Regulation of a biomimetic reduction (NADH model) by potassium ions. Tetrahedron Lett. **1992,** *33* (2), 217–220.
28. Fritsky, I.O.; Ott, R.; Pritzkow, H.; Krämer, R. An allostcric synthetic catalyst: Metal ions tune the activity of an artificial phosphodiesterase. Chem. Eur. J. **2001,** 7 (6), 1221–1231.
29. Tabushi, I. Artificial allostcric systems. Pure Appl. Chem. **1988.** 60 (4), 581–586.
30. Pfeil, A.; Lehn, J.-M. Hclicate self-organization: Positive coopcrativity in the self-assembly of double-helical metal complexes. Chem. Commun. **1992.** 838–840.
31. Blanc, S.; Yakirevich, P.; Laize, E.; Mcycr, M.; Libman, J.; Dorsselaer, A.V.; Albrecht-Gary, A.-M.; Shanzer, A. Allosteric effects in polynuclear triple-strand ferric complexes. J. Am. Chem. Soc. **1997,** *119* (21), 4934–4944.
32. Kubik, S. Large increase in cation binding affinity of artificial cyclopcpide receptors by an allosteric effect. J. Am. Chcm. Soc. **1999,** *121* (25). 5846–5855.

Amide- and Urea-Based Anion Receptors

A

Philip A. Gale
University of Southampton, Southainpton, United Kingdom

INTRODUCTION

Among the armory of functional groups capable of binding anions,[1–4] the amides and the ureas are the most commonly employed anion binding sites in neutral organic anion receptor species (Fig. 1a. b). Oxyanion binding in proteins occurs through hydrogen bond donation from. most commonly. the peptide backbone NH groupr and from arginine.[5,6] One challenge that has been increasingly well met by the supramolecular chemistry community over the last 15 years, has been to design anion receptors with increasing selectivity for particular anionic guests. Of course. the supramolecular chemist does not (yet) have the precise control over the positioning of functional groups in three-dimensional space offered by the tertiary structure of a protein. In spite of this. great progress has been made in the design of neutral anion receptors, with systems now displaying exceptionally high association constants with anions. One of the major design criteria used in developing these systems is to prevent self-association (Fig. 1c) that competes with anion complexation and. hence. lowers association constants.

AMIDES

The first synthetic amide-based anion receptor **1** was reported in 1986 by Pascal Jr. and coworkers.[7] This neutral cyclophane-type receptor was synthesized by reaction of 1,3,5-*tris*-(bromomethyl)benzene with three equivalents of cystearnine to form a triamine which was then clipped with one equivalent of the tris-acid chloride of 1,3,5-benzenetriacetic acid. The receptor contains three amide NH groups chat may be directed into the center of the receptor to form a binding site for smaller anions. Preliminary ^{1}H- and ^{19}F-NMR studies in DMSO-d_6 suggested that there was an interaction with fluoride anions in solution.

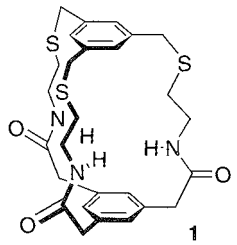

1

In early work. *tris*-amide-based anion receptors were also prepared by the groups of Reinhoudt and Beer. Reinhoudt and coworkers prepared a series of tr-is-amides and sulfonamides (2–7) that are selective for dihydrogenphosphate.[8] The receptors were synthesized from *tris*(aminoethyl)amine (tren) by reaction with an appropriate acid chloride in the presence of triethylamine and were purified by recrystallization from methanol with isolated yields ranging from 70–90%. Association constants were determined with tetrabutylammonium dihydrogen phosphate. hydrogen sulfate. and chloride in acetonitrile by conductometry. The receptors show the selectivity trend $H_2PO_4^- > Cl^- > HSO_4^-$. with receptor **7** having the highest affinity for dihydrogen phosphate (presumably due to the increased acidity of the sulfonamide NH group and π-stacking effects of the naphthalene groups.) Beer and coworkers also synthesized tren-based anion receptors in the early 1990s.[9] These systems

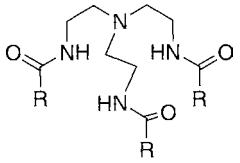

2 R = CH_2Cl
3 R = $(CH_2)_4CH_3$
4 R = C_6H_5
5 R = 4-$MeOC_6H_4$

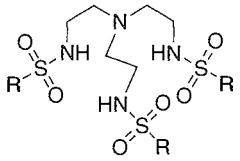

6 R = 4-MeC_6H_4

7 R = 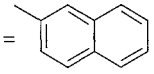

Encyclopedia of Supramolecular Chemistry
DOI: in 1081/E-ESMC 120012830

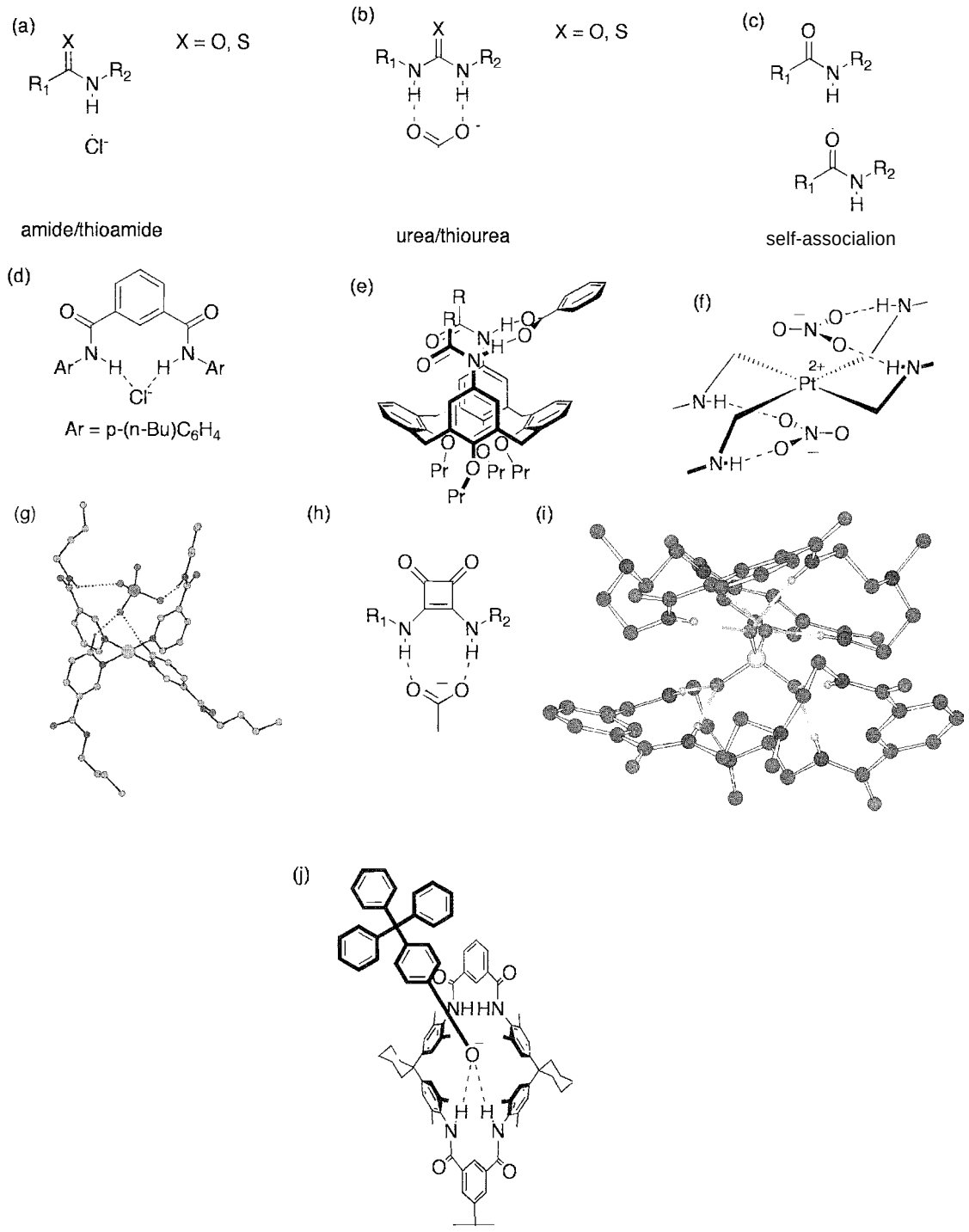

Fig. 1 (a) Amides and thioamides are excellent hydrogen bond donors to anions; (b) ureas and thioureas are complementary hydrogen bond donors for carboxylates: (c) amides can self-associate so lowering their affinity for anions: (d) Crabtree's isophthalamide 11–chloride complex: (e) Loeb's upper-rim amide functionalized calix[4]arene–benzoate complex: (f) a schematic diagram of Gale and Loeb's receptor 18 forming a 1:2 receptor:nitrate complex: (g) crystal structure of the perrhenate complex of receptor 18; (h) a squaramide-acetate complex; (i) crystal structure of the sulfate sandwich formed by receptor 20 and the anion; (j) a phenolate anion bound to a tetralactam macrocycle—a precursor to rotaxane formation. (*View* this *art* in *color at www.dekker.com.*)

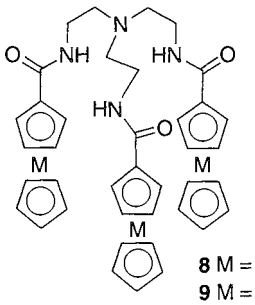

8 M = Fe
9 M = Co^+

contained ferrocene **8** or cobaltocenium **9** moieties that act as electrochemical reporter groups and. in the case of **9**, add an electrostatic component to the anion complexation.[9] These systems show similar anion selectivity trends as those shown by receptors **2**–**7**. in addition to being able to sense the presence of anions via cathodic shifts in the metallocenes' redox potentials. Receptor **8**, for example. is capable of detecting dihydrogen phosphate anions in the presence of 10-fold excesses of chloride and hydrogen sulfate.

More recently, some simple and yet highly effective amide-cleft-based anion receptors were synthesized by Crabtree and coworkers.[10] Receptors **10**–**14** are based upon benzene or pyridine rings that are substituted in the 1- and 3-positions, or in the case of pyridine 2- and 6-positions. with either amide or sulfonamide groups. Proton NMR titrations in dichloromethane-d_2 were used to determine the association constants of the receptors with halide anions and acetate. All the receptors displayed solely 1:1 receptor:anion complex stoichiometry in solution. except receptor **13** that showed behavior consistent with the formation of 1:1 and 1:2 receptor:anion complexes with fluoride and acetate. Among the halides, the receptors have association constants following the trend $Cl^- > Br^- > I^-$ with fluoride and acetate binding being either stronger or weaker than chloride binding depending upon the nature of the receptor. The highest association constant observed with this set of receptors was that of the chloride complex of **11** (K_a=61,000 M^{-1}; Fig. 1d). Interestingly. the presence of the pyridine nitrogen lone pair in receptor **14** serves to decrease the affinity of larger anions for this receptor and so increases the selectivity for smaller anions. For example, fluoride and chloride bind to **14** with association constants of 24,000 and 1500 M^{-1}, respectively, compared to 31,000 and 61,000 M^{-1} for fluoride and chloride binding to receptor **11**.

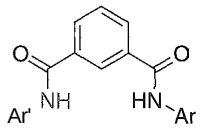

10 Ar = Ph
11 Ar = p-(n-Bu)C_6H_4
12 Ar = 2,4,6-$Me_3C_6H_2$

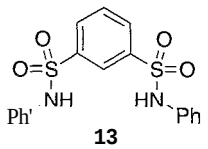

13

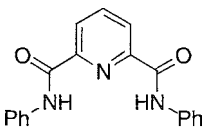

14

By arranging two amide groups in a parallel arrangement in space, Cameron and Loeb developed a set of receptors that are selective for Y-shaped carboxylate anions over tetrahedral or pseudotetrahedral 0x0-anions.[11] Calix[4]arenes **15**.**16**, and **17** were synthesized by reaction of the upper-rim calix[4]arene *bis*-amine with mono-, di-. or trichloroacetyl chloride. Receptor **16** proved to have the highest affinity for anionic guests. For example, receptor **15** binds benzoate in chloroform-d with a stability constant of 107 M^{-1}, whereas the receptor **16**– benzoate complex has an association constant of **5**160 M^{-1}. This increase in binding strength is attributed to the increased electron withdrawing effect of the dichloromethyl group in **16** compared to the monochloromethyl group in **15**. Compound **17** did not interact with anions. which model studies suggest is due to the steric bulk of the trichloromethyl groups that prevent the putative anionic guest approaching the upper-rim anion-binding site. These receptors proved to be selective for carboxylates over tetrahedral anions such as perrhenate. The stronger binding of Y-shaped anions is attributed to the calixarene adopting a so-called "pinched cone" conformation, with the calixarene rings attached to the two amide groups becoming parallel, so allowing the amide groups to align in a complementary manner to the carboxylate guest (Fig. 1e).

As we have seen. calix[4]arenes offer an organic scaffold upon which receptors may be constructed. Gale, Loeb, and coworkers also used a platinum tetrapyridine complex as an inorganic scaffold with which to arrange amide groups in space.[12] The square planar Pt(II)

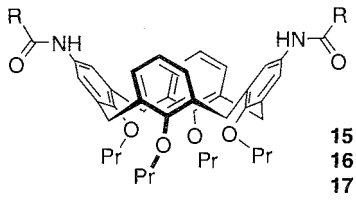

15 R = CH_2Cl
16 R = $CHCl_2$
17 R = CCl_3

complex was prepared by reaction of one equivalent of $PtCl_2(EtCN)_2$ with four equivalents of *n*-butylnicotinamide and two equivalents of $AgPF_6$ in acetonitrile. The anion coniplexation properties of **18**$[PF_6]_2$ were studied using ^{1}H-NMR titration techniques. Unfortunately, a variety of solvent conditions were required due to solubility problems during the titrations. and therefore. association constants are not directly comparable. It was found that tetrahedral or pseudotetrahedral anions such as ReO_4^-, $CF_3SO_3^-$, and HSO_4^- form exclusively 1:1 receptor:anion complexes with receptor 18. However flat anions such as acetate and nitrate form 1:2 receptor:anion complexes (shown schematically in Fig. 1f). Of particular note is the fact that acetate anions are relatively strongly bound even in the very polar 9:1 DMSO/acetonitrile solvent mixture. The fact that K_2 (491 M^{-1}) is greater than K_1 (230 M^{-1}) infers that binding of the first anion has a positive allosteric effect.which favors binding of the second. The 1:1 receptor:anion binding observed for the weakly coordinated ReO_4^-, $CF_3SO_3^-$, and HSOJ anions is supported by the x-ray structure of **18**$[ReO_4]_2$. In particular. it can be seen that in order to try and maximize hydrogen bonding. the relatively acidic nicotinamide CHs from the ligands on the opposite side of the square plane form hydrogen bonds to the perrhenate anion (Fig. 1g). To do this. the complex must significantly distort from centrosymmetry, a fact that presumably disfavors the interaction with a second anion. resulting in the observation of 1:1 binding in solution (Fig. 1g).

In a different approach to carboxylate coniplexation, squaramide (i.e., 3,4-diamino-cyclobutene-1,2-dione) derivatives have been used by Prohens et al. as selective receptors (Fig. 1h).[13] These receptors possess a parallel ditopic hydrogen bond donor array (c.f. urea) that show good to moderate association constants with acetate anions. A variety of mono-. di-. and tritopic receptors were synthesized, including the *tris*-squaramide receptor **19** that forms strong complexes with *tris*-carboxylates such as trimesoate and *cis*-cyclohexentricarboxylate (K_a=3.9 x 10^3 M^{-1} and 7.7 x 10^3 M^{-1}, respectively, in 10% D_2O/DMSO.)

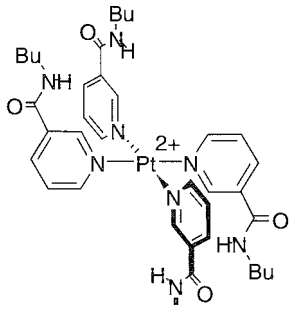

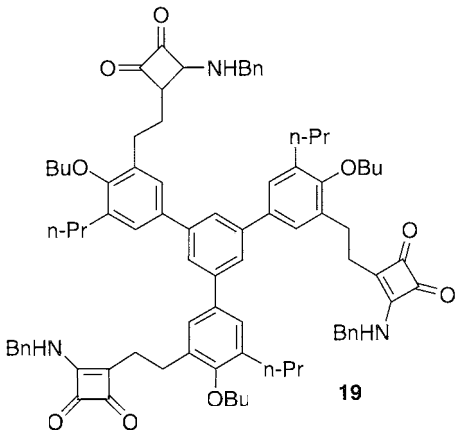

19

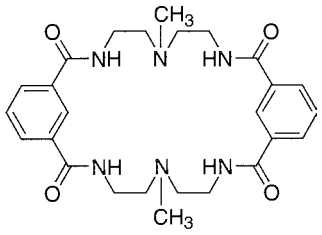

20

Bowman-James and coworkers showed that receptor **20**, a tetraamide-bisamine macrocycle. forms strong complexes with oxo-anions in chloroform solution.'''' Proton NMR titration experiments show that hydrogen sulfate binds with an association constant log K of 4.50, while dihydrogen phosphate has an association constant log K of 4.66. In these cases, a broadening of the NMW spectrum during the titration may be indicative of the anions protonating the amine moieties present in the macrocycle. Therefore. the simple 1:1 solution-binding model used to calculate the stability constants may no longer be valid. In contrast, aprotic anions such as nitrate. perchlorate. chloride, and iodide are bound more weakly (of these anions; chloride is most strongly bound log K_a=2.70.) Most notably, the receptor forms a sandwich complex with sulfate in the solid state. This complex was formed by slow diffusion of diethylether into a chloroform solution of 20 and tetrabutylammonium hydrogensulfate. The sulfate anion is bound by eight hydrogen bonds from the eight amide groups in the sandwich (Fig. 1i).

Receptors 21 and 22. reported by Choi and Hamilton. show a particularly high affinity for iodide and oxo-anions such as nitrate.'''' The receptor features a central hole of around 5 Å diameter lined with three amide NH groups and six aryl CH groups. The receptors are skewed in a way that allows the three NH groups to form a complementary hydrogen-bonding site suitable for pseudo-tetrahedral anions (e.g., p-tosylate.) Proton NMR spectroscopic titration studies were carried out in the

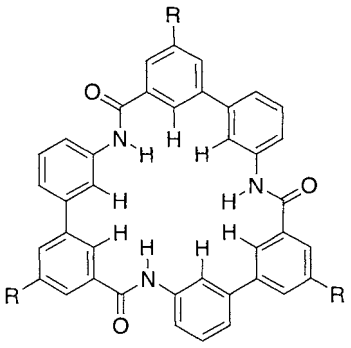

21 R = CO_2Et
22 R = NHBoc

case of both receptors using either 2% DMSO-d_6/$CDCl_3$ or pure DMSO-d_6 as the solvent. The results revealed that the best-bound anion substrates, namely I^-. NO_3^-, and TsO^-, are bound with affinity constants that are on the order of $10^5\ M^{-1}$. Both receptors were found to display similar affinities for anions, indicating that the functional groups on the periphery of the macrocycles do not serve to modulate anion binding selectivity or affinity. Proton WMR titration curves involving tosylate anion and subsequent Job plot analysis revealed the exclusive formation of a 1:1 receptor:tosylate complex in the case of both receptors. However, other anions displayed more complex binding behavior. For example, the shift of the amide NM resonance of 22 observed upon the addition of iodide anions reflected the formation of a 2:1 receptor:-iodide complex during the initial phases of the titration (i.e., an iodide sandwich complex in solution), with the equilibrium at higher iodide concentrations being pushed in favor of a 1:1 receptor:iodide complex.

Anslyn and coworkers used receptor 23. a trigonal box containing six convergently arranged amide NH groups designed to hydrogen bond to the n-clouds of included guests, to examine the role of hydrogen bonding in the stabilization of enolate intermediates.[16] In particular, the role of hydrogen bonding to the enolate n-cloud versus binding to the enolate oxygen atom lone pairs was examined by comparing the pK_a shifts of a variety of ketones in the presence of 23 and also in the presence of another receptor designed to form hydrogen bonds only to the enolates' oxygen atoms. It was found that NH-π hydrogen bonding has a greater effect on carbon acidity than hydrogen bonding to oxygen lone-pair electrons.

Vogtle and coworkers employed anion complexation in new strategies for high-yielding rotaxane syntheses.[17] These workers discovered that phenolate anions. when bound to tetralactam macrocycles (Fig. 1j) such as 24. are capable of reacting with acid chlorides and therefore may be used to form ester rotaxanes. A variety of different rotaxanes were synthesized via this method, including systems with carbonate and acetyl axles.

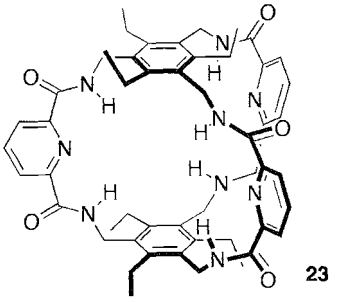

23

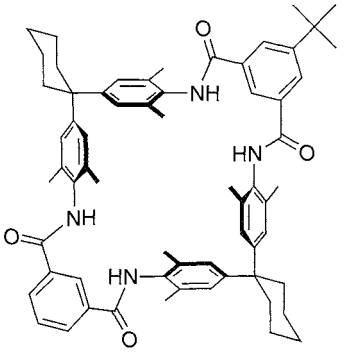

24

UREA

While an amide group can donate a single hydrogen bond, urea can donate two in a parallel fashion, and so it is complementary to oxyanions such as carboxylates (Fig. 1b). One of the earliest examples of anion complexation to urea-based receptors (e.g., 25 and 26) was reported in 1992 by Wilcox and coworkers.[18] Although receptor 26 (the thiourea) proved to have a higher affinity for carboxylates than the urea-based receptor 25, the binding properties of 25 were studied in detail, as thioureas are more susceptible to electrophilic and nucleophilic attacks. NMR experiments revealed large downfield shifts of the urea NM protons upon addition of oxyanions such as carboxylates, sulfonates. and phosphates (as their tetrabutylammonium salts in chloroform-d), however, the association constants were too high to be accurately determined by ^{1}H-NMR titration methods. Therefore, ultraviolet/visible (UV/Vis) titration experiments were employed. It was found that of the oxyanions used. receptor 25 binds benzoate most strongly (K_a=2.7 x $10^4\ M^{-1}$).

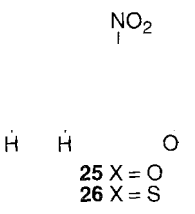

25 X = O
26 X = S

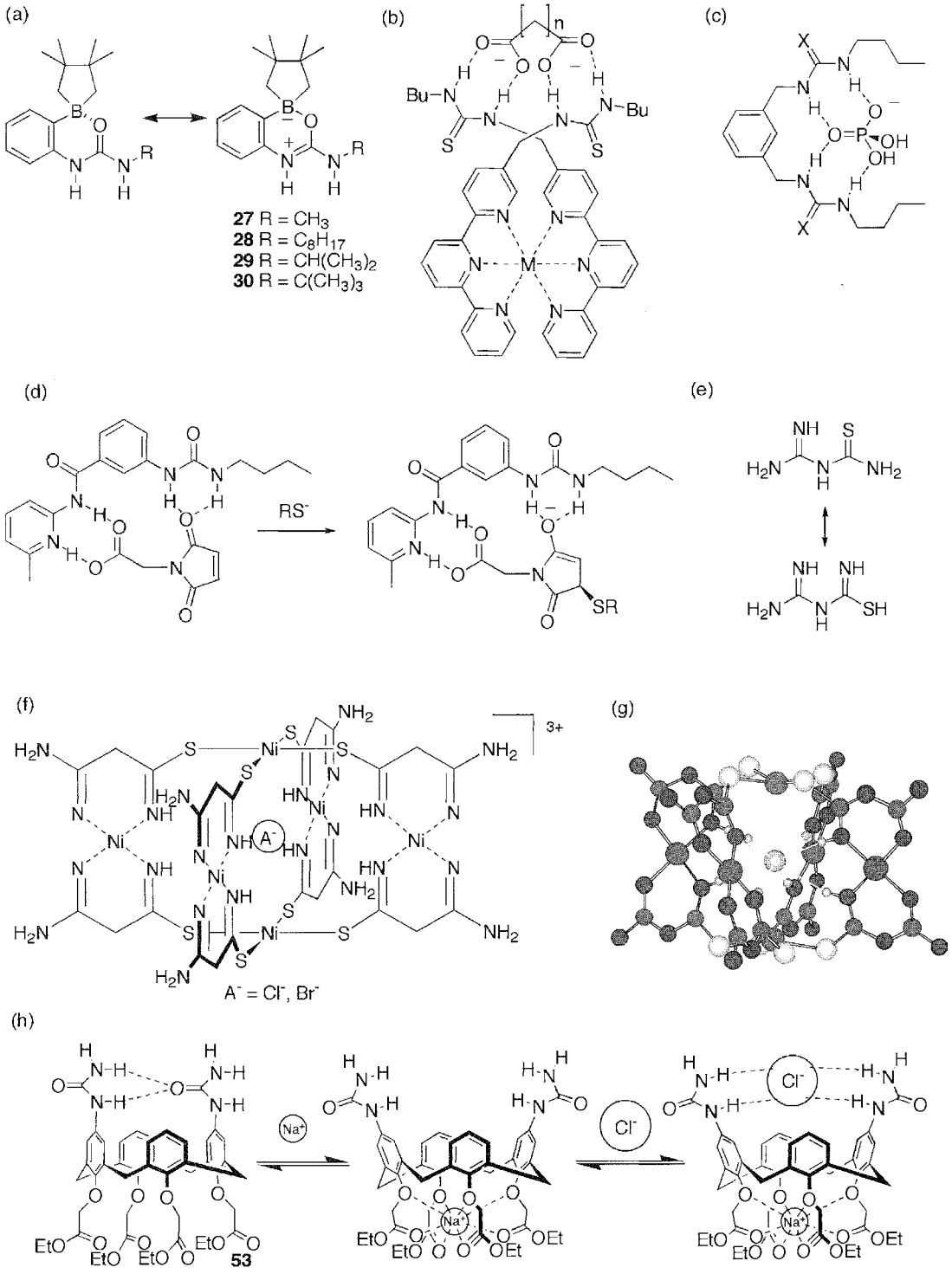

Fig. 2 (a) A boronate group enhances the acidity of the urea NH protons in Smith's receptors: (b) a dicarboxylate complex of Hamilton's combinatorial type ditopic terpy based receptor **34:** (c) the dihydrogen phosphate complex of receptors 36 and **37** (X = 0, S); (d) an example of catalysis by stabilization of an anionic intermediate by receptor 49: (e) amidinothiourea; (9 Mingo's anion templated nickel-amidinothiourea cage and (g) the crystal structure of this complex: (h) Reinhoudt's metal ion switched chloride receptor **53**. (*View this art in color at www.dekker.com.*)

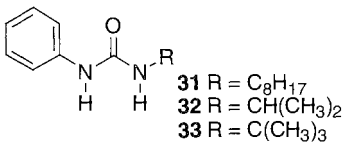

31 R = C_8H_{17}
32 R = $CH(CH_3)_2$
33 R = $C(CH_3)_3$

Smith and coworkers increased the affinity of both amides *and ureas for anions by polarizing the hydrogen* bond *donor site using an intramolecular interaction* from *a boronate* group.[19] *A variety of receptors were synthesized, including receptors 27–30 (Fig.* 2a). *Proton NMR* titrations *in* DMSO-d_6 *with acetate anions were conducted with receptors 28–30 and analogues* 31–33 *which do not contain a boronate group. The following association constants* (M^{-1}) *were determined: 28/31* K_a=7 *x* 10^3/ *3.7 x* 10^2, *29/32* K_a=6.9 *x* 10^3/3.1 *x* 10^2. *30133* K_a=7.1 *x* 10^3/2.6 *x* 10^2. *These results clearly show the enhanced carboxylate complexation properties of the boronate receptors as compared to the regular urea systems* 31–33. *Similar results were observed with* amide-based *receptors.*

A number *of research groups synthesized ditopic receptors containing two urea moieties for the* complexation *of dicarboxylates.* Hamilton *and coworkers used* metal-templated *receptors for this* purpose.[20] *A* thiourea-substituted terpyridine *was synthesized from inethylterpyridine by bromination with* *N*-bromosuccinimide *(WBS) followed by Gabriel amine synthesis and* finally *treatment with* butyl *isothiocyanate. The ruthenium complex 34 was obtained by heating the* ligand *with 0.5 equivalent of* $RuCl_2(DMSO)_4$ *in ethylene glycol and the iron complex 35 by mixing aqueous solutions of the receptor and* $Fe(NH_4)_2(SO_4)_2$. *Both* complexes *were isolaied as their* PF_6 *salts. Upon addition of dicarboxylates to receptor* 35, *displacement of the* terpyridine *ligands* occurred. *However. in the case of the inert ruthenium receptor 34. displacement did not occur, instead the dicarboxylate anions bound to the thiourea groups (Fig.* 2b). *Association* constants *were determined in* 5% D_2O/DMSO-d_6. Similar *association constants were obtained for a variety of* guests

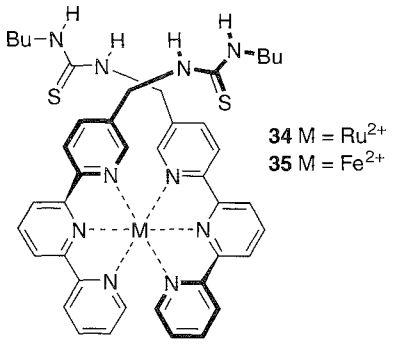

34 M = Ru^{2+}
35 M = Fe^{2+}

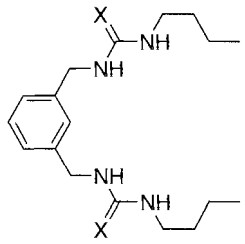

36 X = O
37 X = S

(glutarate K_a=8.3 *x* 10^3 M^{-1}, *adipate* K_a=2.9 × 10^3 M^{-1}, *and* pimelate=6.0 *x* 10^3 M^{-1}), *suggesting a degree of flexibility in the anion-binding site.*

By producing a ditopic receptor containing urea or thiourea groups in close proximity, Umezawa and coworkers produced dihydrogenphosphate *selective* receptors.[21] *Receptors* 36 *and* 37 *are selective for dihydrogenphosphate* over *a variety of other 0x0-anions. The* two *urea groups present in the receptor can* simultaneously *coordinate to the same dihydrogen phosphate anion (Fig.* 2c). *Thus,* NMR titration *studies in* DMSO-d_6 *revealed receptors 36 and 37* bind $H_2PO_4^-$ with *association constants of 110 and 820* M^{-1}. *respectively. while* non-*complementary anions such as acetate are* bound *with* association *constants of 43 and 470* M^{-1}. *respectively.*

Reinhoudt, *Ungaro, and coworkers synthesized* calix[6]arenes *38 and 39 that are substituted at the* lower *rim with three urea or thiourea groups* linked via alkyl *chains.''''' The threefold symmetry* of *the receptor imparts a selectivity for threefold symmetric tricarboxylates* such *as* 1,3,5-benzenetricarboxylate. *This anion was* bound *by receptor 39* with *an association constant of 290,000* M^{-1} *in* chloroform-d_3, *while benzoate was bound with an association constant of 1400* M^{-1}.

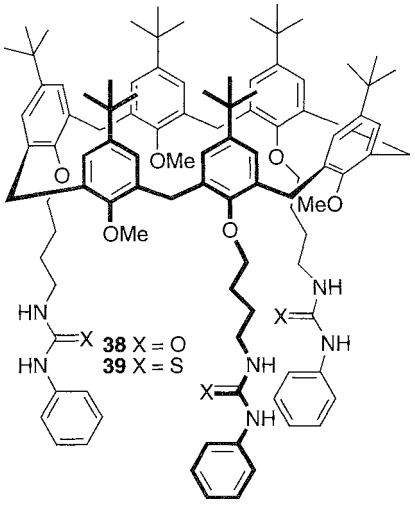

38 X = O
39 X = S

RECEPTORS THAT UTILIZE AMIDES AND UREAS

The complexation of biologically important amino acid derivatives has been the driving force behind Kilburn and coworkers' research in this area.[23] By combining thiourea and amide moieties in cryptand-like macrobicyclic structures. e.g., 40, Kilburn and coworkers synthesized receptors for amino acid derivatives that show selectivity for particular side-chain residues. Extraction methods were used to calculate association constants with a number of N-protected tetrabutylammonium amino acid salts in chloroform. Receptor 40 is selective for N^{α}-Ac-L-lysine (K_a=13 x 10^4 M^{-1}) over N-Ac-L-glycine (K_a=68,600 M^{-1}), N-Ac-L-alanine (K_a=16,900 M^{-1}), and several other protected amino-acid carboxylate salts. Kilburn showed that D-amino acid substrates bind predominantly on the outside of the macrocycle. whereas L-amino acid derivatives bind within the cavity of the receptor with the acetyl amide in a cis-configuration, the energetic penalty for forming the ***cis*** configuration being offset by the formation of hydrogen bonds between the ***cis*** amide and the rim of the macrocycle.

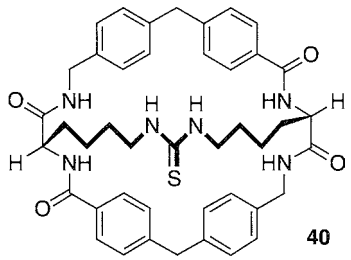

40

Over recent years, Davis and coworkers produced a variety of anion receptors based upon cholic acid. Recently, new urea derivatized receptors termed ''cholapods'' have been synthesized that form remarkably strong complexes with bromide and chloride anions in water-saturated chloroform solution.[24] Receptors 41–44 contain two urea or thiourea groups with electron withdrawing substituents linked to the chloic acid skeleton, while

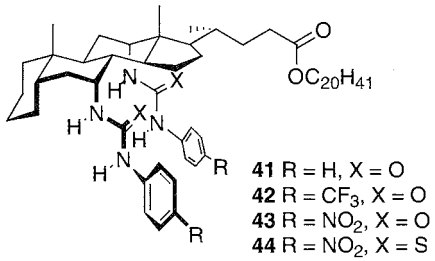

41 R = H, X = O
42 R = CF_3, X = O
43 R = NO_2, X = O
44 R = NO_2, X = S

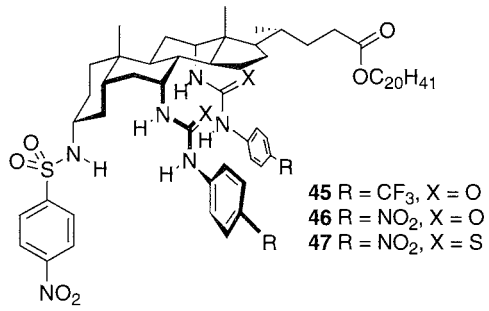

45 R = CF_3, X = O
46 R = NO_2, X = O
47 R = NO_2, X = S

45–49 contain an additional sulfonamide group. The attachment of the hydrogen bonding groups to the steroid skeleton largely prevents the formation of intramolecular hydrogen bonding. while the electron-withdrawing units serve to increase the acidity of the urea moieties and, hence, increase their affinity for anions. This is reflected in the very high association constants with chloride (K_a=1.03 x 10^{11} M^{-1} with receptor 49). These molecules may show excellent phase-transfer properties as well as display biological activity possibly as membrane transport agents for chloride.

Morán and coworkers also combined urea and amide moieties, in this case, in chiral receptors that are recognized chiral hydroxycarboxylates such as lactic or mandelic acid.[25] Receptor 48 combines a *bis*-chromenylurea with a spirobifluorenone linker in a macrocyclic structure and is capable of resolving a racemic mixture of the tetramethylainmonium salt of mandelic acid by thin-layer chromatography. Proton NMR titrations in DMSO-d_6 gave association constants for lactic acid [(*R*)-lactic acid K_a= 3.5 x 10^4 M^{-1}, (*S*)-lactic acid K_a=3.5 x 10^3 M^{-1}).

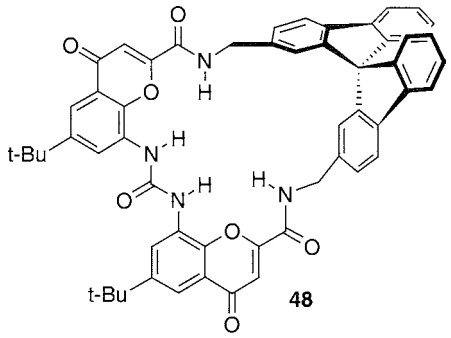

48

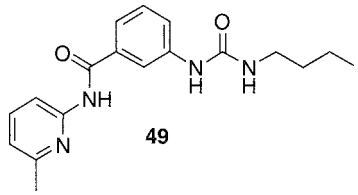

49

Hamilton used an anion-binding strategy with an amidourea receptor (49) to stabilize an oxyanion transition state and so catalyze the 1.4-addition reaction of a thiol to maleimide (Fig. 2d).[26] The enolate intermediate is stabilized via two hydrogen bonds to the urea group in 49, to a greater extent than the carbonyl oxygen present in the starting material. Therefore, the transition state of this reaction is stabilized relative to the starting material, and the reaction is accelerated.

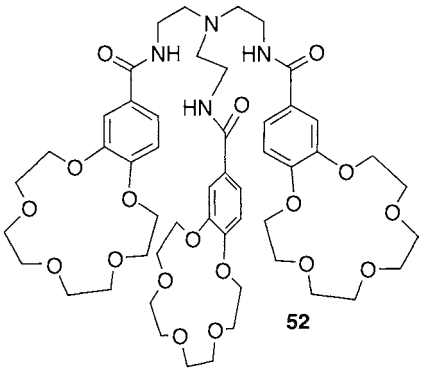

52

ION PAIR COMPLEXATION BY AMIDE- AND UREA-BASED RECEPTORS

Finally we will briefly examine receptors for ion pairs that contain amide or urea groups. An elegant self-assembly process of an amidinothiourea (50) (Fig. 2e) with $NiCl_2$ has been reported by Mingos and coworkers.[27] Complexation of $NiCl_2$ by amidinothiourea in methanol yields crystals of a cage complex (Fig. 2f). The cage $[Ni_6(atu)_8Cl]Cl_3$ consists of eight amidinothiourea units that coordinate six nickel ions through both nitrogen and sulfur donor atoms. A chloride anion is encapsulated within the cage by eight NH···Cl hydrogen bonds (as revealed by the crystal structure shown in Fig. 2g). An analogous complex can be formed between amidinothiourea and $NiBr_2$, however. when nickel salts containing noncage complementary anions such as nitrate, acetate. or perchlorate salts are used. the simple monomer $[Ni(atu)_2]^{2+}$ complexes are formed. Interestingly, if chloride anions are subsequently added to these complexes, the cage complex spontaneously assembles.

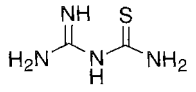

50

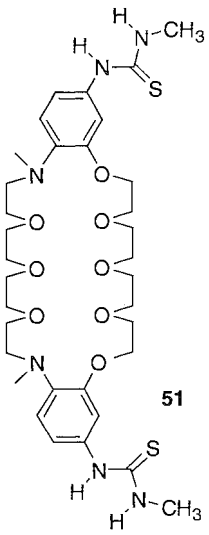

51

Kubo and coworkers synthesized a *bis*-thiourea functionalized dibenzo-diaza-30-crown-10 51 that wraps around potassium cations, so bringing the two thiourea groups into close proximity, forming an anion binding site.[28] NMR titration experiments with $(PhO)_2P(O)O^-$ anions (which form both 1:1 and 1:2 receptor:anion complexes with 51) in acetonitrile-d_3 solution in the absence and presence of potassium cations show an increase in K_1 from 490 to 9200 M^{-1} upon addition of three equivalents of potassium cations.

In the area of amidic receptors, the tris-crown-ether tren-based receptor **52**. synthesized by Beer and coworkers was recently shown to efficiently extract pertechnetate anions from simulated nuclear waste streams in the presence of sodium cations.[29]

Reinhoudt and coworkers produced a switchable anion receptor.[30] Receptor 53 (Fig. 2h) is a calix[4]arene substituted at the lower rim with cation-binding ester groups and at the upper rim with two distally arranged urea groups. In chloroform solution; intramolecular hydrogen bonds between the urea moieties block the potential anion-binding site. Upon addition of sodium cations, the lower rim of the calixarene contracts as the sodium ions are bound by the four ester groups. This conformational rearrangement separates the two urea groups at the upper rim, so disrupting the intramolecular hydrogen bonding and. therefore. allowing anions such as chloride to complex the receptor (Fig. 2h).

CONCLUSION

Amides and ureas have proven to be excellent anion receptor groups, widely employed by the supramolecular

chemistry community in receptors for anions and ion pairs. This is due in no small part to their ease of synthesis and stability. The roles amides play in binding to anions in protein structures is being revealed by protein crystallography, and these structures are inspiring new generations of synthetic receptors containing peptide groups capable of functioning as anion receptors in aqueous solution~.rThere is much yet to be explored in this fascinating a ea of supramolecular chemistry. For more information. the reader is directed to reviews[1-11] that provide entry to the extensive literature in this area.

ACKNOWLEDGMENT

The author would like to acknowledge the Royal Society for a University Research Fellowship.

ARTICLES OF FURTHER INTEREST

Anion-Directed Assembly, p. 51
Guanidinium-Based Anion Receptors, p. *615*
Hydrogen Bonding, p. *658*
Organometallic Anion Receptors. p. *1006*
Protonated Aza-Macrocycles for Anion Complexation, p. 1170
Pyrrole- and Polypyrrole-Based Anion Receptors, p. *1176*
Simultaneous Binding of Cations and Anions, p. *1291*

REFERENCES

1. Gale, P.A. Anion receptor chemistry: Highlights from 1999. Coord. Chem. Rev. 2001, *213*, 79–128.
2. Beer. P.D.: Gale. P.A. Anion recognition and sensing: The state of the art and future perspectives. Angew. Chem.. Int. Ed. 2001. *40* (3). 486–516.
3. Schmidtchen. F.P.: Berger. M. Artificial organic host molecules for anions. Chem. Rev. 1997. *97* (5). 1609–1646.
4. Antonisse. M.M.G.: Reinhoudt. D.N. Neutral anion receptors: Design and application. Chein. Cornmun. 1998, (4). 443–448.
5. Chakrabarti. P. Anion binding sites in protein structures. J. Mol. Biol. 1993. *234* (2). 463–482.
6. Mangani, S.: Ferraroni, M. Natural Anion Receptors: Anion Recognition by Proteins. In *Supramolecular Chemistry of Anions*. 1st Ed.: Bianchi, A., Bowman-James, K.. García-España, E., Eds.: WILEY-VCH: New York, 1997: 63–78.
7. Pascal. R.A.. Jr.: Spergel. J.: Van Engen, D. Synthesis and x-ray crystallographic characterisation of a (1,3,5) cyclophane with three amide NH groups surrounding a central cavity. A neutral host for anion complexation. Tetrahedron Lett. 1986, *27* (35). 4099–4102.
8. Valiyaveetil. S.: Engbersen. J.F.J.: Verboom. W.; Reinhoudt, D.N. Synthesis and complexation studies of neutral anion receptors. Angew. Chem.. Int. Ed. Engl. 1993. *32* (6). 900–901.
9. Beer. P.D. Transition-metal receptor systems for the selective recognition and sensing of anionic guest species. Acc. Chem. Rec. 1998. *31* (2). 71–80.
10. Kavallieratos. K.: Bertao, C.M.; Crabtree, R.H. Hydrogen bonding in anion recognition: A family of versatile nonpreorganised neutral and acyclic receptors. J. Org. Chem. 1999. *64* (5), 1675–1683.
11. Cameron, B.R.; Loeb, S.J. Bis(amido)calix[4]arenes in the pinched cone conformatioii as tuneable hydrogen-bonding anion receptors. Chem. Commun. 1997. (6), 573–574.
12. Bondy, C.R.; Gale. P.A.; Loeb. S.J. Platinum(II) nicotinamide complexes as receptors for 0x0-anions. Chein. Commun. 2001, (8). 729–730.
13. Prohens. R.; Tomàs. S.; Morey, J.: Deyà, P.M.: Ballester. P.; Costa. A. Squaramido-based receptors: Molecular recognition of carboxylate anions in highly competitive media. Tetrahedron Lett. 1998. *39* (9). 1063–1066.
14. Hossain, Md.A.; Llinares. J.M.; Powell, D.: Bowman-James, K. Multiple hydrogen bond stabilisation of a sandwich complex of sulfate between two macrocyclic tetraamides. Inorg. Chem. 2001. 40 (13). 2936–2937.
15. Choi, K.: Hamilton, A.D. Selective anion binding by a macrocycle with convergent hydrogen bonding functionality. J. Am. Chem. Soc. 2001. 123 (10), 2456–2457.
16. Snowden. T.S.; Bisson, A.P.; Anslyn. E.V. A comparison of NH-π versus lone pair hydrogen bonding effects on carbon acid pK_a shifts. J. Am. Chem. Soc. 1999. *121* (26). 6324–6325.
17. Reuter. C.; Wienand, W.; Hübner. G.M.; Scel, C.; Vögtle, F. High-yield synthesis of ester. carbonate. and acetal rotaxanes by anion template assistance and their hydrolytic dethreading. Chem. Eur. J. 1999. *5* (9). 2692–2697.
18. Smith. P.J.: Reddington. M.V.; Wilcox. C.S. Ion pair binding by a urea in chloroform solution. Tetrahedron Lett. 1992. *33* (41), 6085–6088.
19. Hughes. M.P.: Smith. B.D. Enhanced carboxylate binding using urea and amide-based receptors with internal Lewis acid coordination: A cooperative polarization effect. J. Org. Chem. 1997. *62* (13). 4492–4499.
20. Goodman. M.S.; Jubian. V.: Hamilton. A.D. Metal templated receptors for the effective complexation of dicarboxylates. Tetrahedron Lett. 1995, *36* (15), 2551–2554.
21. Nishizawa. S.: Bühlmann. P.; Iwao. M.: Umezawa. Y. Anion recognition by urea and thiourea groups: Remarkably simple neutral receptors for dihydrogenphosphate. Tetrahedron Lett. 1995. *36* (36). 6483–6486.
22. Scheerder. J.; Engbersen. J.F.J.: Casnati. A.; Ungaro, R.: Reinhoudt. D.N. Gomplexation of halide anions and tricarboxylate anions by neutral urea-derivitized *p-tert*-butylcalix[6]arenes. J. Org. Chem. 1995. *60* (20), 6448–6454.

23. Pcrnia, G.J.; Kilburn, J.D.; Essex, J.W.; Mortishire-Smith, R.J.; Rowley, M. Stabilization of a ***cis*** amide bond in a host–guest complex. J. Am. Chem. Soc. **1996;** *118* (42), 10220–10227.
24. Ayling, A.J.; Pérez-Payán, M.N.; Davis, A.P. New ''cholapod'' anionophores: High-affinity halide receptors derived lrom cholie acid. J. Am. Chem. Soc. **2001.** 123 (50), 12716–12717.
25. Tejeda, A.; Oliva. A.I.; Simón, L.; Grande. M.; Caballero, Ma.C.; Morán, J.R. A macrocyclic receptor for the chiral recognition of hydrocarboxylates. Tetrahedron Lett. **2000.** 41 (23), 4563–4566.
26. Fan, E.; Vicent, C.; Hamilton, A.D. Molecular recognition and catalysis: Incorporation of an "oxyanion hole" into a synthetic receptor. New J. Chem. **1997,** *21* (1), 81–85.
27. Vilár, R.; Mingos, D.M.P.; White, A.J.P.; Williams, D.J. Anion control in the sell-assembly of a cage coordination complex. Angew. Chem., Int. Ed. **1998,** 37 (9), 1258–1261.
28. Tozawa, T.; Misawa, Y.; Tokita, S.; Kubo, Y. A regioselectivelybis(thiourea)-substituted dibenzo-diaza-30-crown-10: A new strategy for the development of multi-site receptors. Tetrahedron Lett. **2000,** *41* (27), 5219–5223.
29. Beer, P.D.; Hopkins, P.K.; McKinney, J.D. Cooperative halide, perrhenate anion–sodium cation binding and pertechnetate extraction and transport by a novel tripodal tris-(amido benzo-15-crown-5) ligand. Chem. Commun. **1999,** (13), 1253–1254.
30. Scheerder, J.; van Duynhoven, J.P.M.; Engbersen, J.F.J.; Reinhoudt, D.N. Solubilization of NaX salts in chloroform by bifunctional receptors. Angew. Chem., Int. Ed. Engl. **1996**. *35* (10), 1090–1093.
31. Kubik, S.; Kirchner, R.; Nolting, D.; Seidel, J. A molecular oyster: A neutral anion receptor containing two cyclopeptide subunits with a remarkable sulfate affinity in aqueous solution. J. Am. Chem. Soc. **2002.** *124* (43), 12752–12760.

Amino Acids: Applications

Arindam Banerjee
Indian Association for the Cultivation of Science, Calcutta, West Bengal, India

INTRODUCTION

J.M. Lehn first introduced the term "supramolecular chemistry" in the literature in 1969 while he was studying the inclusion complexes of Eu^{3+} with its receptor-molecule cryptands. Eehn defined supramolecular chemistry as "the chemistry of intermolecular bonds"; in a supramolecular system. the same or different chemical compounds are held together by various noncovalent interactions. Amino acids. the building blocks of proteins and peptides, are useful in constructing various supramolecular architectures and forming inclusion complexes with different receptor molecules. including cyclodextrins and calixarenes. Amino acid derivatives also form host–guest inclusion complexes with structurally different receptor molecules. such as chiral crown ethers and cyclodextrines. α-Amino-acid-derived lipids become supramolecular receptors through self-assembly. and they host styryl dyes. Many α-amino acids form complexes with various types of transition metals, including Pt^{2+} and lanthanides. Leading to the formation of different supramolecular architectures.

Peptides composed of various coded and noncoded amino acid residues self-assemble to form various types of supramolecular architectures. including supramolecular helices and sheets, nanotubes, nanorods, nanovesicles, and nanofibers. The higher-order self-assembly of supramolecular β-sheets or supramolecular helices composed of short synthetic acyclic peptides leads to the formation of amyloid-like fibrils. Synthetic cyclic peptides were used in supramolecular chemistry as molecular scaffolding for artificial receptors. so as to host various chiral and achiral ions and other small neutral substrates. Cyclic peptides also self-assemble like their acyclic counterparts to form supramolecular structures, including hollow nanotubes. Self-assembling cyclic peptides can be served as artificial ion channels. and some of them exhibit potential antimicrobial activities against drug-resistant bacteria.

SYNTHETIC CYCLIC PEPTIDES AS RECEPTORS

Artificial receptor design is an Important aspect of supramolecular chemistry. Synthetic cyclic peptides were not used extensively so far. probably due to their usual relative flexibility compared to other macrocycles that contain a rigid framework or backbone (e.g., crown ethers, calixarenes. etc.). In spite of their cyclic structure, they are hardly able to bind guests in a well-defined cavity. However, cyclic peptides with conformationally constrained subunits like aromatic or alicyclic backbones or those containing rigid subunits were used for binding substrate molecules such as amino acid derivatives,[1] aromatic compounds,[2] or dicarboxylic acids.[3] Following this approach. Ishida and his colleagues demonstrated the complexation of phosphate ions with cyclic oligopeptides (with six to 14 residues) containing 3-aminobenzoic acid (AB) and protein amino acids in an alternating sequence.[4] Kubik established that a cyclic hexapeptide composed of alternating L-glutamic and 3-aminobenzoic acids binds to quaternary ammonium ions in $CHCl_3$ through cation–π interactions.[1] The cation-binding property of this cyclic peptide was enhanced by a factor of 10^3–10^4 in presence of certain anions (e.g., tosylate or phenyl phosphonate). This is due to the allosteric effects of these anions from binding to the cyclopeptide NH groups and stabilizing the receptor structure, which is essentially appropriate for interactions with positively charged ions.[5] The introduction of L-Pro in the cyclic peptide backbone was shown to rigidify the cyclic peptide structure and to increase the cation-and anion-binding affinities. Kubik and his coworkers established that cyclo[(L-Pro-AB)$_3$] has greater cation and anion affinity than the receptor molecule cyclo[(L-Glu-AB)$_3$].[6] This is because anion complexation is reduced to a great extent. As in the latter peptide, the amide NH groups in the L-Glu residues are involved in strong intramolecular hydrogen bonds, and are. therefore. not available for binding with host anions. Consequently. the stability of the cation complex also decreases. Using different amino acid subunits in the cyclic peptide backbone can regulate the solution conformation of these cyclic hexapeptides, which. in turn, can tune receptor properties. All these above-mentioned cyclic oligopeptides exhibit ditopic receptor properties for simultaneous complexation of cations and anions. Kubik and his coworkers improved the cation-binding affinity and incurred a significant loss of anion-binding ability by using intramolecular conformational control in a cyclic hexapeptide containing alternating L-proline and

Encyclopedia of Supramolecular Chemistry
DOI: 10.1081/E-ESMC 120019163

substituted 3-aminobenzoic acid residues.[7] The presence of methoxy carbonyl groups in the fourth-position of the aromatic ring of the 3-aminobenzoic acid subunits helps to form hydrogen bonds to adjacent amide NH protons. inducing the orientation of an amide group parallel to the aromatic rings. This causes the amide protons to point away from the central cavity and to be unavailable for binding with anions. The investigation of the optimum ring size required for good cation binding revealed that cyclotetrapeptides with alternating L-Pro and 3-aminobenzoic acid possess a lower affinity toward cations than the corresponding hexapeptides.[8] it was observed that the phenyl urea substituted at the benzene ring of cyclotetrapeptide can be used as the anion (iodide or acetate) receptor in DMSO-d_6 solution.[8] Artificial receptors that discriminate between two enantiomers of a given substrate are important in bioorganic and supramolecular chemistry. Recently. Kubik and his coworkers achieved the enantioselective recognition of a chiral quaternary ammonium ion (e.g., *N,N,N*-trimethyl,1-phenyl ethyl ammonium cation) using C_3 symmetric cyclic hexapeptides cornposed of L-proline and substituted 3-aminophenyl benzoic acid in 0.1% DMSO-d_6–$CDCl_3$ solution.[9]

INCLUSION COMPLEXES OF AMINO ACIDS AND THEIR DERIVATIVES WITH THEIR HOSTS

Host–guest complexation. by cyclodextrins for example. plays an important role in biomiinetic and supramolecular chemistry. Cyclodextrins (CDs) are barrel-shaped cyclic carbohydrate molecules composed of six, seven or eight glucose residues. which are termed α, β, or γ cyclodextrin. respectively. Due to the presence of an internal cavity. CDs can be used as versatile hosts. Amino acids form gas-phase inclusion complexes with CDs and they can be detected using ES-MS and a gas-phase guest exchange reaction.[10] Chiral discrimination of amino acid guests in CDs hosts was also achieved in the gas phase. The αCDs and βCDs form inclusion coinplexes with cumarin-6-sulfonyl amino acid derivatives in water. Theoretical modeling and fluorescence experimental results suggest the possibility of forming 1:2 guest–host coinplexes for βCD.[11] A recent report described the complexation of native L-α-amino acids with aliphatic or aromatic side chains by water-soluble substituted calix[4]arenes.[12] The host–guest cornplexation was studied using ^{1}H-NMR experiments. The upfield shift of some specific aromatic protons (H *meta* and H *para*) of the guest molecules compared to the free guest. due to the ring current effect of the aromatic nuclei of the host, confirms the formation of an inclusion complex. The inclusion of aliphatic or aromatic apolar amino acid residues within the calix[4]-arene cavity occurs either by CH–π interaction (for L-Val and L-Leu) or by π–π interaction (for L-Phe. L-His. L-Trp.). Another macrocyclic receptor, cyclotetrachromotropylene, forms 1:I host–guest complexes with various native Y-amino acids in water at pH 7 and 25°C. This phenomenon was studied using ^{1}H-NMR spectroscopy.[13] Sometimes host–guest complexation helps in useful chemical transformations like hydrolysis. A recent study indicated the formation of inclusion complexes of γ-CD and various amino acid methyl esters. This formation eventually leads to hydrolysis of host molecules. In the entire process. a high stereoselectivity was observed.[14]

METAL ION–AMINO ACID COMPLEXATION IN SUPRAMOLECULAR CHEMISTRY

A pentadecanuclear complex of Eu^{III} with tyrosine at high pH provides a novel supramolecular architecture, which involves 15 Eu^{III} ions and 10 tyrosine ligands plus hydroxo and aquo ligands associated with hydrolysis. In this structure. the europium(III) ions are assembled into three parallel layers. and each of the layers contains five Eu^{III} ions that occupy the vertical positions of a nearly perfect pentagon. The 10 tyrosine ligands can be grouped into two equivalent classes. each of which extends its 4-hydroxybenzyl side chains orthogonal to the crystallographically imposed C2 axis.[15] The side chains do not take part in coordination. while the amino and the carboxylate groups of each tyrosine residue participate in metal ion chelation. making each of the 10 tyrosinate groups become a tetradentate ligand. Near physiological pH (which is 6–7), multinuclear lanthanide complexes of various α-amino acids (e.g., Gly. Ala, Val. Giu) form a cubane-like cluster core that assembles to form 3D porous framework structures.[16]

SELF-ASSEMBLY OF α-AMINO-ACID-DERIVED LIPIDS

Study of the inclusion behaviors of the cavity of many commonly known macrocyclic receptors like calixarenes, cyclodextrins and cyclic oligopeptides draws considerable interest in supramolecular chemistry. However. the construction of inclusion compounds using self-assembly of α-amino-acid-derived lipids is relatively rare.[17–20] L-Glutamic-acid-derived anionic lipids act as supramolecular receptors and provide specific hydrophobic cavities for accommodating cationic dyes.[17,18] Cationic dyes are incorporated inside. due to their molecular planarity. Hachisako and his coworkers studied various types

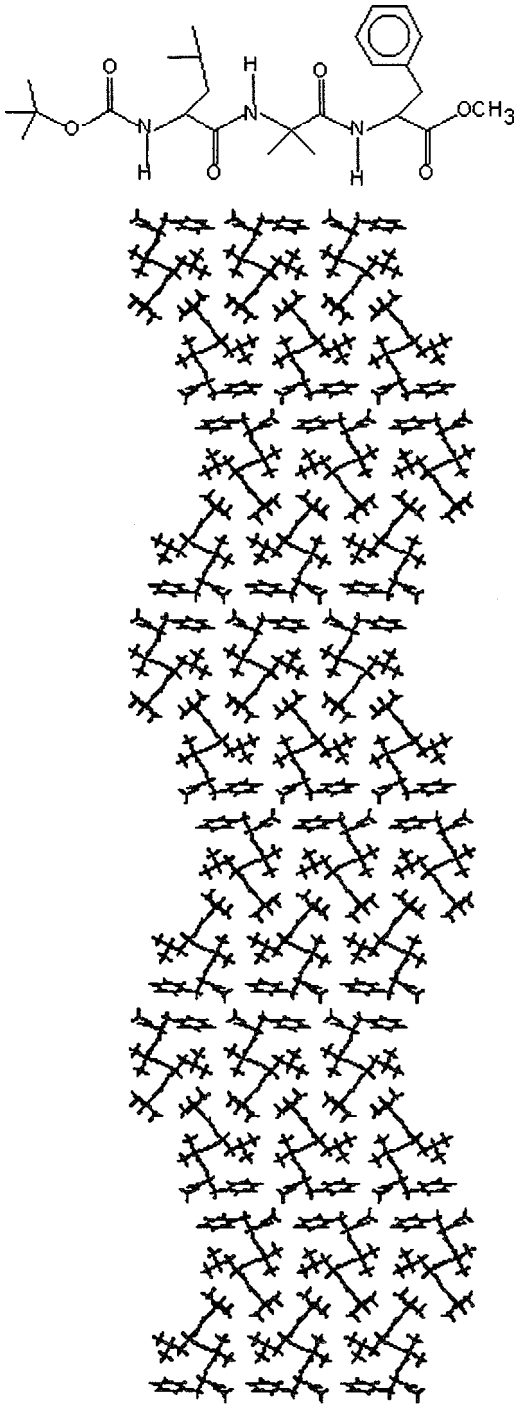

Fig. 1 Packing diagram of individual columns of the tripeptide Boc-Leu-Aib-Phe-OMe in the *c* projection, illustrating the formation of a highly ordered supramolecular helical assembly via van der Waals' interactions.

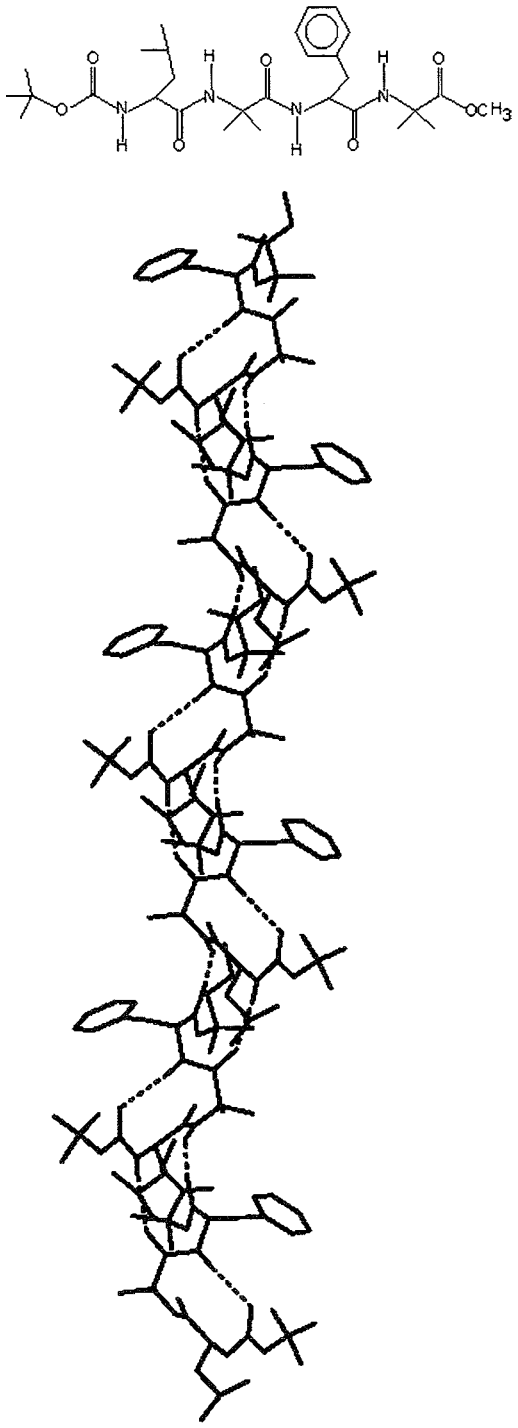

Fig. 2 The packing diagram of the tetrapeptide Boc-Leu-Aib-Phe-Aib-OMe showing a higher-ordered supramolecular helical assembly as determined by x-ray crystal structure analysis along the b axis. Hydrogen bonds are shown as dotted lines. Side chains of Lue. Phe, and nonhydrogen-bonded hydrogen atoms are omitted for clarity.

of α-amino-acid-derived cationic lipids containing multiple amide linkages per molecule. to probe the role of α-amino-acid residues and the chemical structural requirements needed to form specific hydrophobic cavities of supramolecular receptors in aqueous solution.[20] The role of amino acid residues on inclusion and molecular recognition were examined using structurally related cationic styryl dyes like 4[4-(dimethylamino)styryl]-*N*-methyl pyridinium iodide, 2-[4-(dimethylamino)styryl]-*N*-ethyl pyridinium iodide. and 2-[4-(dimethylamino)styryl]-*N*-methyl pyridiniuln iodide. These dyes not only act as host molecules but also serve as microenvironmental probes due to their sovatochromic nature.

SELF-ASSEMBLY OF CYCLIC AND ACYCLIC SYNTHETIC PEPTIDES

Supramolecular Peptide Helices

The design and construction of monomolecular peptide helical structures using appropriate, conformationally restricted amino acid residues were extensively studied. However. relatively less attention was paid to the construction of a supramolecular peptide helix. In biological systems. supramolecular helices with various levels of self-organization and self-assembly of the peptide backbone are common. My research group is involved in constructing various supramolecular helical structures from acyclic oligopeptides containing noncoded amino acids with appropriate conformations, which can act as subunits for self-assembly.[21–25]

The majority of the backbone torsion angles of the terminally blocked tripeptide Boc-Leu-Aib-Phe-QMe [Aib: α-aminoisobutyric acid] falls within the helical region. and it fails to form any intramolecularly hydrogen-bonded turn structures. However, this helps to form a supramolecular helical structure (Fig. 1) through noncovalent interactions in the solid state.[21] The scanning electron microscopic (SEM) picture of the tripeptide Boc-Leu-Aib-Phe-OMe shows the filamentous ribbon-like fibrillar morphology that is reminiscent of neurodegenerative disease-causing amyloid fibrils.

The terminally protected tetrapeptide Boc-Leu-Aib-Phe-Aib-OMe adopts a consecutive double-bend conformation with two successive β-turns. It self-assembles through various noncovalent interactions, including intermolecular hydrogen bonds, to form a supramolecular helical structure in crystals (Fig. 2).[22] Similarly, another double-bend-forming peptide Boc-Ala-Aib-Leu-Bib-OMe self-associates to form a supramolecular helix via intermolecular hydrogen bonding in the crystal structure.[22] However, the tetrapeptide Boc-β-Ala-Aib-Leu-Aib-OMe [β-Ala: β-alanine] adopts a new type of consecutive

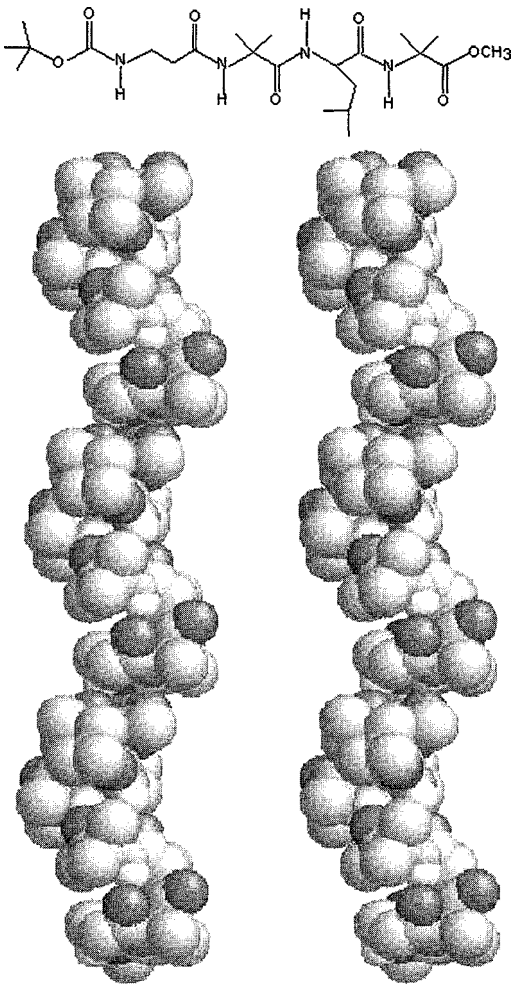

Fig. *3* A cross-eye stereo, space-filling representation of the tetrapeptide Boc-β-Ala-Aib-Leu-Aib-OMe showing a higher-ordered supramolecular helical assembly. as determined by single-crystal x-ray diffraction studies. Nitrogen atoms are blue. oxygen atoms are red. and carbon atoms are gray. Nonhydrogen-bonded hydrogen atoms and side chains of Lue are omitted for clarity. (*View* ***this*** *art in color at www.dekker.com.*)

double-turn structure, which self-associates to form a unique supramolecular helix (Fig. 3).[24] The terminally protected tetrapeptide Boc-Aib-Val-Aib-β-Ala-OMe adopts a double-turn molecular conformation that self-assembles to form an anisotropic intermolecularly hydrogen-bonded supramolecular helix with an average diameter of 1 nm in the crystal (Fig. 4). This suprainolecular helical structure further self-assembles to form polydisperse nanorods with diameters ranging from 10–40 nm.[25]

Supramolecular Acyclic Peptide β-Sheets

The design and construction of acyclic oligopeptide molecules. which form supramolecular (3-sheet structures,

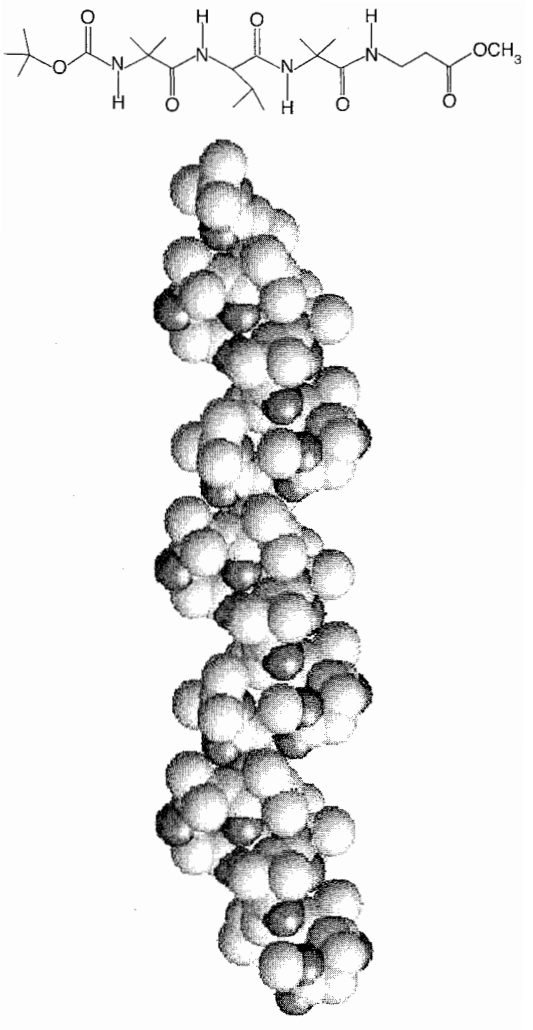

Fig. 4 Space-filling model of the supramolecular helical array of the tetrapeptide Boc-Aib-Val-Aib-β-Ala-OMe showing the staking of subunits maintaining proper registry, generating a helical structure as determined by x-ray crystallographic analysis. Nitrogen atoms are blue. oxygen atoms are red. and carbon atorns are gray. Hydrogen atoms are omitted for clarity. (*View this art in color at www.dekker.com.*)

comprise an emerging field. Formation of supramolecular β-sheet structures using various noncovalent interactions and their further self-association into highly ordered fibrillar structures are responsible for causing many fatal progressive neurodegenerative amyloid diseases, like Alzheimer's and Parkinson's. To understand the molecular bases of pathogenesis and therapeutics of these diseases. it is important to construct supramolecular peptide β-sheet assemblage. There are many reports of β-sheet stabilization involving unimolecular β-sheet formation and subsequent stabilization by only intramolecular interactions.[26,27] However, there are limited reports elucidating peptide β-sheet formation and stabilization in crystals and in solution by purely intermolecular interactions,[28–32] My research group is actively engaged in constructing amyloid-like fibril-forming supramolecular β-sheets.[28–32] The terminally blocked ti-ipeptide containing noncoded amino acids [viz., β-alanine (β-Ala) and α-aminoisobutyric acid (Aib)]. Boc-β-Ala-Aib-β-Ala-OMe, adopts a β-strand structure with an overall extended backbone conformation with a slight kink at the middle. It self-assembles to form a supramolecular parallel β-sheet structure in crystal (Fig. 5) and amyloid-like fibrils in the solid state.[28] The supramolecular β-sheet structure is formed by various noncovalent interactions, including intermolecular hydrogen bonding. This is the first crystallographic evidence of an amyloid-like fibril-forming parallel β-sheet assemblage of a synthetic tripeptide coinposed of only nonprotein amino acids. A recent report describes that components of a series of terminally protected dipeptides. composed of 3-aminophenyi acetic acid and Aib/Val/Pro, share a common structural feature—an extended backbone conformation—and they self-assemble to form an intermolecularly hydrogen-

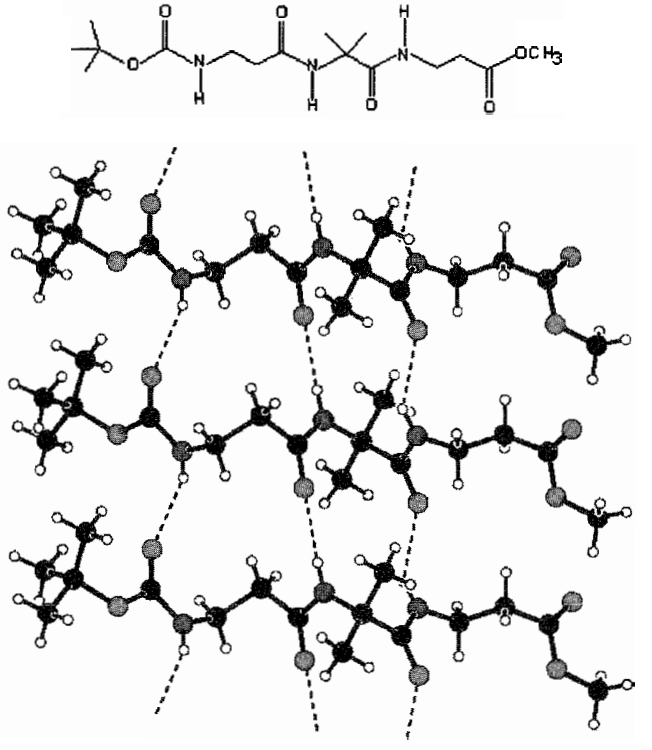

Fig. 5 Packing diagram of the terminally protected tripeptide Boc-β-Ala-Aib-β-Ala-OMe in the *b* projection, illustrating intermolecular hydrogen bonding in solid state and formation of the supramolecular β-sheet. Nitrogen atoms are blue. oxygen atorns are red. carbon atoms are black. and hydrogen atoms are white circles. Dashed lines indicate hydrogen bonds. (*View this art in* color- *at www.dekker.com.*)

bonded supramolecular β-sheet structure and show amyloid-like fibrillar morphology in the solid state.[29] Similarly. other terminally protected tripeptides Boc-Ala-Gly-β-Ala-OMe[30] and Boc-Leu-Aib-Leu-OMe[31] self-assemble through intermolecular hydrogen bonding to form supramolecular β-sheet structures in crystals. Both tripeptides form the antiparallel β-sheet structure. The tripeptide Boc-Leu-Aib-β-Ala-OMe adopts an intramolecularly hydrogen-bonded β-turn conformation in the crystals. There are two molecules in the asymeric unit to form a molecular dimer of two different conformers.[32] This peptide celf-assembles by intermolecular hydrogen bonds and other noncovalent interactions to form a supramolecular β-sheet structure in crystals (Fig. 6). This is the first example of a β-turn forming short acyclic peptide, which forms the supramolecular β-sheet structure in crystals instead of a supramolecular helix.

Self-Assembling Cyclic Peptides

Cyclic peptides with an even number of alternating D-and L-α-amino acids adopt flat ring-shaped structures in which the backbone amide groups are arranged perpendicular to the side chains and the plane of the ring conformation.

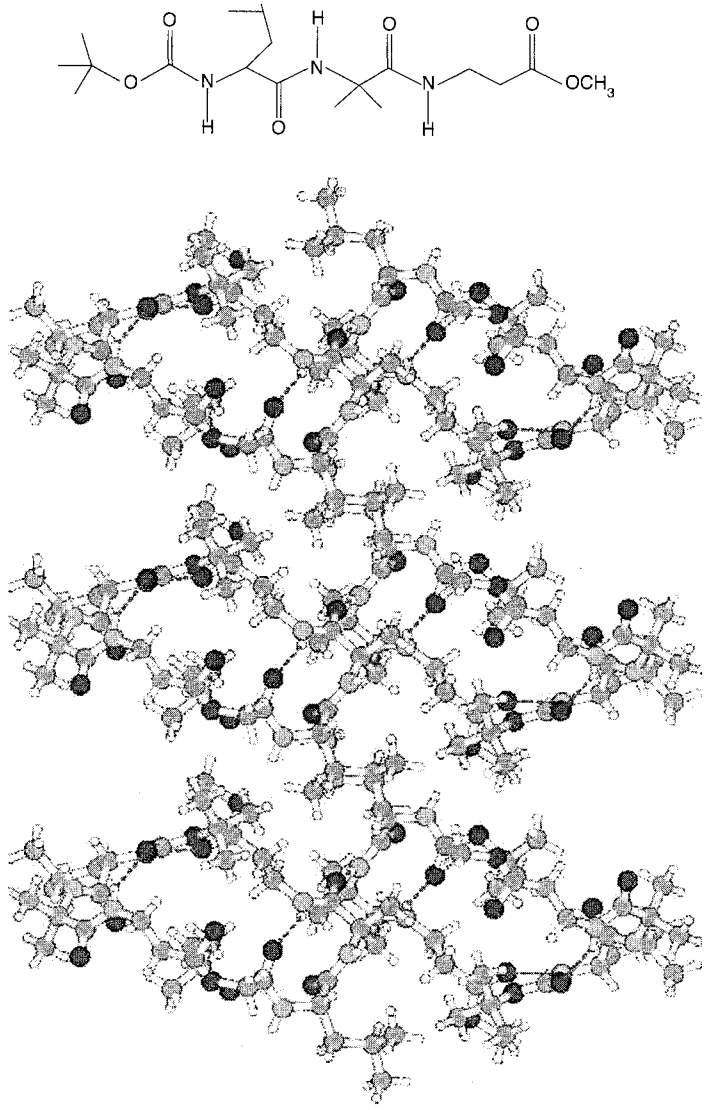

Fig. 6 The packing of the terminally protected tripeptide Boc-Leu-Aib-β-Ala-OMe, showing the formation of a continuous β-sheet column along the crystallographic *b* axis via intermolecular hydrogen bonds and van der Waals' interactions in the crystal. Dashed lines indicate hydrogen bonds. Nitrogen atoms are blue. oxygen atoms are red. carbon atoms are green, and hydrogen atoms are white. (*View this art in color. at www.dekker.com.*)

Under favorable conditions. these cyclic peptide rings self-assemble through intermolecular hydrogen bonding to form open-ended hollow β-sheet-like nanotubular structures. keeping the amino acid side chains outside the surface of the ensemble. In a pioneering work. Ghadiri and his coworkers demonstrated the formation of hollow tubular supramolecular structures with an appropriate internal diameter of 7 Å from a self-assembling cyclic octapeptide cyclo-[-(L-Glu-D-Ala-L-Glu-D-Ala-)$_2$].[33] The internal diameter of cyclic peptide nanotubes can be altered by varying the peptide ring size. The 12-residue peptide cyclo-[-(L-Glu-D-Ala-L-Glu-D-Ala-)$_3$][34] was shown to undergo proton-triggered self-assembly. which leads to the formation of a nanotubular structure of an enhanced van der Waals' diameter of 13 Å. A remarkable feature of these cyclic peptide nanotubes is that the surface properties of the tubular structures can be varied by appropriateiy selecting the amino acid side chains. Cyclic D, L-peptides with appropriate hydrophobic side chains can be partitioned in nonpolar lipid bilayers and undergo self-association to form transmembrane ion channels. In 1994, Ghadiri and his coworkers demonstrated the formation of a transmembrane ion channel based on a self-assembled. cyclic D,L-octapeptide.[35] Single-channel conductance measurements and fluorescence proton transfer assays were used to examine the channel-forming properties of cyclic D,L-peptides. These ion channels exhibit transport activity for Na^+ and K^+ greater than 10^7 ions s^{-1}. The cyclic clecapeptide cyclo[-(-L-Trp-D-Leu)$_4$-L-Gln-D-Leu] with an internal van der Waals diameter of 10 Å, was shown to transport glucose molecules across the lipid bilayer membrane.[36] A report from Seebach and his group noted that cyciic tetrapeptides containing only chiral β^3-amino acids can form hollow tubes similar to those exhibited by cyclic D,L-α-peptides.[37] Ghadiri et al. demonstrated the formation of ion channels by two self-assembling cyclic β^3-peptides.[38] Described in recent report from Ghadiri's group was that self-assembling cyclic D,L-α-peptides coinposed of six and eight residues can serve as potent antibacterial agents against drug-resistant bacteria[13''] by enhancing the membrane permeability, collapsing the transmembrane potential. and eventually causing rapid cell death. These antibacterial cyclic oligopeptides were found to be nontoxic in mice, and they hoid considerable promise in combating many drug-resistant bacterial infections in human beings.

CONCLUSION

The applications of amino acids in supramolecular chemistry are multipurpose. One purpose is to make inclusion complexes with common macrocyclic hosts. like CDs or calixarenes. Other applications include complexations of metal ions with amino acids, leading to various supramolecular architectures. In addition, various amino acids are used to synthesize cyclic and acyclic peptides that have wide applications in supramolecular chemistry. such as creating nonself-assembling cyclic oligopeptides with well-defined cavities that can be used as hosts for various cations (including the chiral one), anions, and electroneutral substrates. Finally, self-assembling cyclic and acyclic peptides not only form various supramolecular architectures, but also, cyclic oligopeptides can be used as artificial ion channels and antibacterial agents.

ACKNOWLEDGMENTS

I am thankful to Debashis Haldar, Arijit Banerjee, Apurba Kumar Das. Sudipta Rap, and Partha Pratim Bose for their help in the preparation of the entire manuscript. I am very grateful to my collaborator Prof. M.G.B. Drew, The University of Readings, Whiteknights, U.K.. for solving numerous cryrtal structures of my peptides that are cited within this article.

ARTICLES OF FURTHER INTEREST

Alkali Metal Cations in Biochemistry, p. 1
Artificial Enzymes, p. 76
Biological Ligands, p. 88
Biological Models and Their Characteristics, p. 101
Channel Inclusion Compounds, p. 223
Cyclodextrins, p. 398
Emergence of Life. p. 528
Enzyme Mimics, p. 546
Hydrogen Bonding, p. 658
Ion Channels and Their Models; p. 742
Peptide Nanotubes, p. 1035
Protein Supramolecular Chemistry, p. 1161

REFERENCES

1. Miyake. H.; Yamashita. T.: Kojima, Y.; Tsukube. H. Enantioselective transport of amino acid ester salts by macrocyclic pseudopeptides containing N,N′-ethylene-bridged-dipeptide units. Tetrahedron Lett. 1995, 36. 7669–7672.
2. Garcia, M.E.: Gavin. J.A.: Deng. N.; Andrievsky, A.A.; Mallouk, T.E. Combinatorial synthesis of modular chiral cyclophanes. Tetrahedron Lett. 1996, 37. 8313–8316.
3. Ranganathan. D.; Haridas, V.: Karle. I.L. Cystinophanse. a novel family of aromatic-bridged cystine cyclic peptides:

Synthesis, crystal structure, molecular recognition, and conformational studies. J. Am. Chem. Soc. 1998, *120.* 2695–2702.
4. Ishida. H.: Suga, M.: Donowaki. K.; Ohkubo. K. Highly effective binding of phosphornonoesters with neutral cyclic peptides which include a non-natural amino acid. J. Org. Chem. 1995, *60.* 5374–5375.
5. Kubik, S. Large increase in cation binding affinity of artificial cyclopeptide receptors by an allosteric effect. J. Am. Chem. Soc. 1999. *121.* 5846–5855.
6. Kubik, S.: Goddard. R. A new cyclic pseudopeptide composed of L-proline and 3-aminobenzoic acid subunits as a ditopic receptor for the simultaneous complexation of cations and anions. J. Org. Chem. 1999, *64,* 9475–9486.
7. Kubik, S.; Goddard. R. Interinolecular conformational control in a cyclic peptide composed of alternating L-proline and substituted 3-aminobenzoic acid subunits. Chem. Commun. 2000. 633–634.
8. Pohl, S.; Goddard. R.; Kubik. S. A new cyclic peptide composed of alternating L-proline and 3-aminobenzoic acid subunits. Tetrahedron Lett. 2001. *42.* 7555–7558.
9. Heinrichs, G.: Vial, L.: Lacour, L.; Kubik. S. Enantioselective recognition of a chiral quaternary ammonium ion by C_3 symmetric cyclic hexapeptides. Chem. Commun. 2003. 1252–1253.
10. Ramirez, J.; He, F.: Lebrilla. C.B. Gas-phase chiral differentiation of amino acid guests in cyclodextrin hosts. J. Am. Chem. Soc. 1998, *120.* 7387–7388.
11. Al-Mindy, S.M.Z.: Suliman, F.E.O.: Al-Hamadi. A.A. Fluoroscence enhancement of coumarin-6-sulfonyl chloride amino acid derivatives in cyclodextrin media. Anal. Sci. 2001. *17.* 539–543.
12. Arena. G.; Contino, A.: Gulino, F.G.; Margi. A.; Sansone, F.: Scitto, D.; Ungaro. R. Complexation of native L-α-aminoacids by water soluble calix[4]arenes. Tetrahedron Lett. 1999. *40,* 1597–1600.
13. Poh. B.L.: Tan. C.M. Complexation of amino acids by cyclotetrachromotropylene in aqueous solution — Importance of CH-π and π–π interactions. Tetrahedron 1994. *50.* 3453–3462.
14. Goto, K.: Wakamisha. K.: Tanone. O.; Nakushina, S.; Toudo, I.: Imamuro, C.: Ihara. Y.: Matsumoto. Y.: Ueoka. R. Cyclodextrin-mediated deacylation of amino acid esters with marked stereoselectivity. Chem. Pham. Bull. 2002, *50.* 1283–1285.
15. Wang, R.; Zheng. Z.: Jin. T.; Staples, R.J. Coordination chemistry of lanthanides at "high" pH: Synthesis and structure of the pentadecanuclear complex of europium (III) with tyrosine. Angew. Chem.. Int. Ed. 1999. *38.* 1813–1815.
16. Wang. R.; Liu. H.: Carducci, M.D.: Jin, T.; Zheng. C.: Zheng. Z. Lanthanide coordination with α-amino acids under near physiological pH conditions: Polymetallic complexes containing the cubane like $[Ln_4(\mu_3\text{-}OH)_4]^{8+}$ cluster core. Inorg. Chem. 2001. *40.* 2743–2750.
17. Nachisako, H.; Yamazaki. T.; Ihara, H.: Hirayama, C.: Yamada, K. Formation of specific hydrophobic sites for incorporation of methylene blue by laterally arranged L-glutainate residue in crystalline bilayer aggregates. J. Chem. Soc., Perkin Trans. 1994. (2). 1671–1680.
18. Hachisako. H.; Motozato, Y.: Murakani. R.: Yamada. K. Extraordinary monomer–dimer transition of methylene blue induced by the phase transition of telomer-bilayer membranes formed from dialkyl L-glutamate amphiphiles with oligo acrylic acid head group. Chem. Lett. 1992. 219–222.
19. Hachisako, H.: Yamazaki, T.: Ihara, H.; Hirayama. C.: Yamada, K. Recognition of molecular planarity of cationic dyes by anionic crystalline bilayer aggregates: Evidence using metachromatic and solvochromatic properties. J. Chem. Soc., Perkin Trans. 1994. (2), 1681–1690.
20. Hachisako, H.; Murata, Y.; Ihara, H. Supramolecular receptors from α-amino acid-derived lipids. J. Chem. Soc., Perkin Trans. 1999; (2), 2569–2577.
21. Haldar, D.: Maji, S.K.: Sheldrick, W.S.: Banerjee, A. First crystallographic signature of the highly ordered supramolecular helical assemblage from a tripeptide containing a non-coded amino acid. Tetrahedron Lett. 2002, *43.* 2653–2656.
22. Haldar. D.; Maji, S.K.: Drew. M.G.B.: Banerjee. A.; Banerjee, A. Self-assembly of a short peptide monomer into the continuous hydrogen bonded supramolecular helix: The crystallographic evidence. Tetrahedron Lett. 2002. *43.* 5465–5468.
23. Maji. S.K.: Banerjee. A.; Drew, M.G.B.; Haldar. D.; Banerjee. A. Self-assembly of a tetrapeptide in which a unique supramolecular helical structure is formed via intermolecular hydrogen bonding in the solid state. Tetrahedron Lett. 2802, *43,* 6759–6762.
24. Banerjee. A.: Maji. S.K.; Drew. M.G.B.: Haldar, D.; Banerjee, A. Suprainolecular peptide helix from a novel double turn forming peptide containing a β-amino acid. Tetrahedron Lett. 2003. *44.* 699–702.
25. Haldar. D.: Banerjee, A.; Drew. M.G.B.: Das. A.K.; Banerjee, A. First crystallographic signature of an acyclic peptide nanorod: Molecular mechanism of nanorod formation by a self-assembled tetrapeptide. Chem. Commun. 2003, 1406–1407.
26. Fisk. J.D.; Gellman. S.H. A parallel β-sheet model system that folds in water. J. Am. Chein. Soc. *2001.123.* 343–344.
27. Das, C.: Raghothama, S.: Balaram. P. A designed three stranded β-sheet peptide as a multiple β-hairpin model. J. Am. Chem. Soc. 1998, *120.* 5812–5813. and references cited therein.
28. Maji, S.K.: Drew, M.G.B.: Banerjee, A. First crystallographic signature of amyloid-like fibril forming 0-sheet assemblage from a tripeptide with non-coded amino acids. Chein. Commun. 2001. 1946–1947.
29. Maji. S.K.: Haldar, D.; Banerjee. A.; Banerjee, A. Fibril-forming model synthetic peptides containing 3-aminophenyl acetic acid. Tetrahedron 2002. 58. 8695–8702.
30. Maji. S.K.: Malik, S.; Drew, M.G.B.: Nandi, A.K.; Banerjee. A. A synthetic tripeptide as a novel organogelator: A structural investigation. Tetrahedron Lett. 2003. *44.* 4103–4107.
31. Banerjee, A.: Maji, S.K.: Drew. M.G.B.: Haldar. D.; Banerjee. A. Amyloid-like fibril forming antiparallel

supramolccular β-sheet from a synthetic tripeptide : A crystallographic signature. Tetrahedron Lett. **2003,** 44, 6741–6744.

32. Bancrjee. A.; Maji, S.K.: Drew, M.G.B.; Haldar, D.; Bancrjee, A. Amyloid-like fibril-forming supramolecular β-sheet from a β-turn forming tripcptide containing non-coded amino acids: Thc crystallographic signature. Tetrahedron Lett. **2003,** 44, 335–339.
33. Ghadiri, M.R.; Granja, J.R.; Milligan, R.A.; Mcree, D.E.; Khazanovich, N. Self-assembling organic nanotubes based on a cyclic peptide architecture. Nature **1993.** 366, 324–327.
34. Khazanovich, N.; Granja, J.R.; McRec, D.E.; Milligan, R.A.; Ghadiri, M.R. Nanoscale tubular ensembles with specified internal diameters. Design of a self-assembled nanotube with a 13 Å pore. J. Am. Chcm. Soc. **1994,** *116*, 6011–6012.
35. Ghadiri, M.R.; Granja, J.R.; Buehler, L.K. Artificial transmembrane ion channels from self-assembling peptide nanotubes. Nature **1994,** *369*. 301–304.
36. Granja, J.R.; Ghadiri, M.R. Channel-mediated transport of glucose across lipid bilayers. J. Am. Chem. Soc. **1994.** 116. 10785–10786.
37. Sccbach, D.; Mathews, J.L.; Meden, A.; Wessels, T.; Baerlocher, C.; McCusker, L.B. Cyclo-[β]-peptides: Structure and tubular stacking of cyclic tetramers of 3-aminobutanoic acid as determined from powder diffraction data. Helv. Chim. Acta **1997**, *80*. 173–182.
38. Clark, T.D.; Buehler, L.K.; Ghadiri, M.R. Self-assembling cyclic β^3-peptide nanotubes as artificial transmembrane ion channels. J. Am. Chcm. Soc. 1998, 120. 651–656.
39. Fernandez-Lopez, S.; Kim, H.S.; Chot. E.C.: Delgado, M.; Granja, J.R.; Khasnov, A.; Krachenbuehl, K.; Long, G.: Weinbeger, D.A.; Wilcoxen, K.M.; Ghadiri, M.R. Antibacterial agents based on the cyclic D, L-a-peplide architecture. Nature **2001,** *412*, 452–455.

Anion-Directed Assembly

Ramón Vilar
Imperial College of Science, Technology, and Medicine, London, United Kingdom

INTRODUCTION

There is great current interest in developing strategies for the synthesis of complex molecular architectures with novel properties and potential in a wide range of applications. During the past few years, supramolecular chemistry provided important advances in this direction. The increased control over the assembly of molecular components led to the rational synthesis of novel species such as molecular cages, helicates, rotaxanes, and catenanes, among several others. A common strategy used to prepare such assemblies involves the use of chemical templates. As defined by Busch, "A chemical template organizes an assembly of atoms. with respect to one or more geometric loci, in order to achieve a particular linking of atoms" (p. 389).[1] When there are several potential ways of linking a group of molecular components, the template provides the instructions for the formation of a single product. In the presence of another template. a different assembly is expected. and as a consequence, a different product should be formed. In generai, after the ternplate has directed the formation of the assembly. it can be removed to yield the template-free product. However. this is not possible if the templating agent is an integral part of the final product. In this entry. a template (or directing agent) will be considered to be any species that organizes an assembly of atoms or molecules for specific linking and is either removed from the final product or kept as an integral part of it.

ANIONS AS TEMPLATES

In contrast to the well-studied templating properties of cationic and neutral species,[2,3] anions have been largely neglected as templating agents until recently. Up to 1996 there were only a handful of examples of anion-directed assemblies, the first ones being reported in the early 1990s.[4,5] The relative lack of anion-templated assemblies bas been partially attributed to intrinsic properties of anions. such as their diffuse nature (i.e., small charge-to-radius ratio); pH sensitivity, and their relative high solvation-free energies.[9] However, as demonstrated over the past few years, these limitations can be overcome by appropriately modifying the experimental conditions, and several anion-directed assemblies have now been reported. The importance of anions as templates is also seen in biological processes where, for example. anions have been identified as directing agents in protein folding.[6]

This entry provides a compilation of anion-directed assemblies and analyzes some of the factors that have made these syntheses possible. This is the first time that the subject is specifically reviewed, even though Beer and Gale incorporated a section on this topic in their three reviews on supramolecular chemistry of anions.[7–9] The current entry will be divided into two main sections: anion-directed synthesis of metalla-assemblies. and anion-directed assembly in organic synthesis. While in the first type of assemblies the anions use mainly electrostatic and Lewis-acid–base interactions to direct the syntheses. in the second case hydrogen bonds play a very important role. The size and geometry of the ternplating anions are also essential in dictating the final structure to be formed (as it is in any other templated reaction). Due to space limitations, this entry will concentrate on anion-directed assemblies that yield well-defined molecular species. The anion-directed assembly of polymeric materials, although an important area within supramolecular chemistry. is out of the scope of this review.

ANION-DIRECTED SYNTHESIS OF METALLA-ASSEMBLIES

Metalla-Macrocycles and Circular Helicates

One of the first anion-directed assemblies is the [12]mercuracarborand-4 (1) reported by Hawthorne in 1991. which can be prepared in high yields by reacting 1,2-dilithio-carborane with mercuric chloride (see Fig. 1).[4] This compound consists of four bivalent 1.2-carborane cages linked by four mercury atoms forming a macrocycle with a chloride ion located at its center. The anion displays strong Lewis-acid–base interactions with the four mercury atoms of the macrocycle. Such interactions play an important role in directing the formation of the cyclic

Encyclopedia of Supramolecular Chemistry
DOI: 10.1081/E-ESMC 120012836

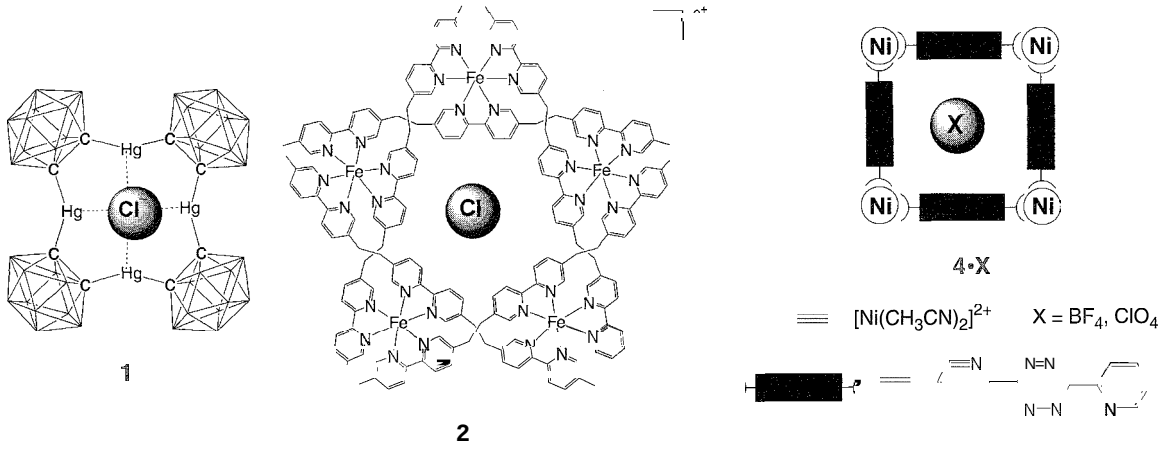

Fig. 1 The anion-templated assemblies reported by Hawthorne.[4,10] Lehn,[11,12] and Dunbar.[14,15] (*View this art in color ut www.dekker.com.*)

structures as opposed to the noncyclic ones. The same authors later showed that an analogous cyclic tetramer is obtained when mercuric iodide is used for the cyclization reaction but, *in contrast, an acyclic polymer is formed in the presence of mercuric acetate.'''''*

Elegant examples of anion-templated *synthesis are the* penta- *and hexanuclear circular helicates reported by Lehn (see Fig.* 1).[11,12] *In this work it was demonstrated that the self-assembly of* iron(II) *salts and a tris-*bipyridyl *ligand* (L) *is highly dependent on the presence of specific anions. With* $FeCl_2$, *the pentanuclear circular helicate* $[Fe_5L_5Cl]^{9+}$ *(2) is obtained. while the hexanuclear analogue* $[Fe_6L_6(SO_4)]^{10+}$ *(3)* is *formed in quantitative yields with* $FeSO_4$ *[hexanuclear systems are also formed with* $Fe(BF_4)_2$ *and* $FeSiF_6$]. *The structural characterization of* $[Fe_5L_5Cl]^{9+}$ *demonstrated it to be a circular double helix with an inner cavity radius of* 1.75 Å. *The chloride ion is contained within this cavity (which provides an excellent size match for this halide)* and *is tightly bound thanks to the* 10 *positive charges from the five* iron(II) *centers located in the periphery. By increasing the size of the* templating anion, it *is then possible to assemble structures with larger cavities such as* $[Fe_6L_6(SO_4)]^{10+}$. *In these examples, electrostatic interactions and good* ion-to-cavity *size match are the directing forces behind the* anion-templated *self-assembly process.* Using *a similar approach,* McCleverty *and Ward reported the synthesis of the cyclic supramolecular complex* $[Co_8L_{12}(ClO_4)]^{3+}$ *(where* L = *bis* {3-(2-pyridyl)pyrazol-1-yl}dihydroborate) *with a* perchlorate *anion encapsulated in the central cavity.'''' The anion is likely to play an important role in the selective formation of this structure.*

More recently, Dunbar *demonstrated that the structures resulting from the self-assembly of* metal *cations with the bis-*chelating *ligand* 3,6-*bis*(2-pyridyl)1,2,4,5-tetrazine *(bptz) are strongly dependant on the anions present in the reaction* mixture.[14,15] *In the presence of* BF_4^- *and* ClO_4^-, *the molecular squares* $[Ni_4(bptz)_4(CH_3CN)_8][X]_8$ (**4·X**) *(X =* BF_4^-, ClO_4^-*) are formed in approximately* 75% *yield (see Fig. 1). while in the presence of* SbF_6^-, *the molecular pentagon* $[Ni_5(bptz)_5(CH_3CN)_{10}][SbF_6]_{10}$ (5) *is obtained (in* 60–70% *yields). The structural characterization of the molecular square* **4·BF$_4$** *showed that it has a void space with an approximate diameter of* 4.6 Å, *which is of the ideal size match for the* BF_4^- *anion. In the case of the pentagon, the void space at its center is larger, providing a better size match for larger anions such as* SbF_6^-. *The structures observed in the solid state are retained in solution,* as *demonstrated by ESI mass spectrometry.*

Examples of metalla-macrocycles where hydrogen bonding (in addition to electrostatic and Lewis-acid–base *interactions) is used by the templating anion to direct the assembly are the* Ni/Pd *boxes reported by* Vilar *(see Fig.* 2).[16] *The* $Ni(atu)_2$ *fragment* (atu=deprotonated *arnidinothiourea) reacts with* $PdX_2(PPh_3)_2$ *to selectively form the metalla-macrocycles* $[Pd_2Ni_2(atu)_4(PPh_3)_4X]^{3+}$ (**6·X**) (X=Cl, Br, *and I) in* 55–74% *yields. In the presence of other anions such as triflate. nitrate, or acetate: the formation of the* macrocycle *is not observed, and instead* monometallic *species are obtained. Interestingly, if stoichiometric amounts of chloride, bromide, or iodide are added to these mixtures, the corresponding macrocycles are formed quantitatively.* confirming *the* templating *role of the halide anions. The structural characterization of these macrocycles demonstrates that, in the solid state, the halides located at their center form hydrogen bonds with four* NH *groups from the amidinothiourea ligands and with several* C–H groups from *the phenyl rings of the phosphines. The halides also interact with the palladium centers in a* Lewis-acid–base *fashion.* ^{31}P-NMR *studies revealed that the halides*

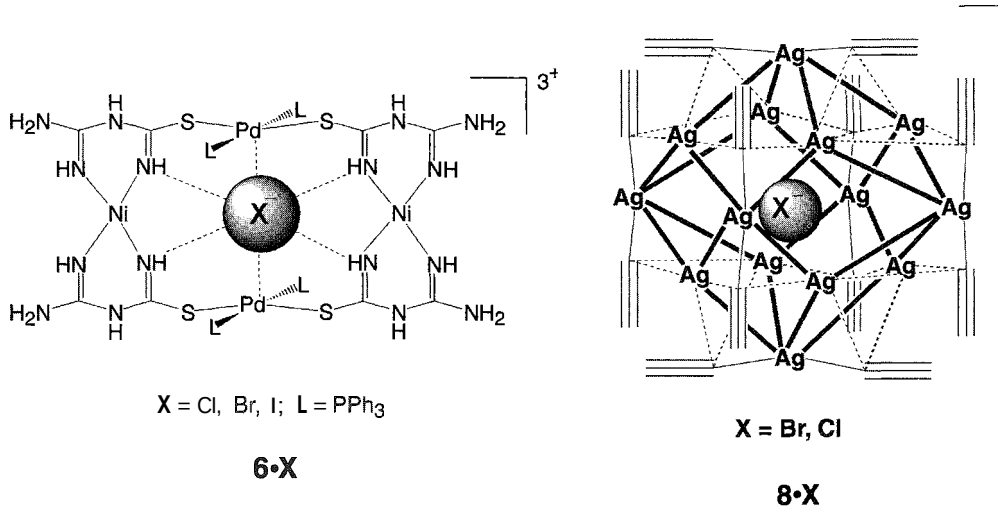

Fig. 2 Anion-templated metalla-macrocycles **6•X**[16] and silver-alkynyl cages **8•X**.[21] (*View this art in color ut www.dekker.com.*)

bound to the metalla-macrocycles can be exchanged in solution.

Metalla-Cages

The first examples of metalla-cages synthesized by anion-directed processes are a series of polyoxometallates reported by Müller.[5,17] In these species, anions control the aggregation of $V^{n+}O_x$ polyhedra into cage-type structures such as $[HV_{18}O_{44}(NO_3)]^{10+}$, $[HV_{22}O_{54}(SCN)]^{6+}$, and $[H_4V_{15}O_{40}(PO_4)]^{7+}$, in which the anions are situated inside the cavity of the cages. With other anions such as acetate. V–O aggregates are formed in which the anions are located on the outer surface of the shell. Similarly, Zubieta reported that the synthesis of a series of oxovanadium-organophosphates such as $[(VO)_6(t\text{-}BuPO_3)_8Cl]$ may be directed by the encapsulated chloride anion.[18]

An interesting example of anion-directed assembly is the "super-adamatoid" silver cage $[Ag_6(triphos)_4X_4]^{2+}$ (**7•X**) [X=O_3SCF_3, ClO_4, and NO_3; triphos=$(PPh_2CH_2)_3$-CMe] reported by James and Mingos.[19] The formation of these cages is anion-specific, because they are only obtained in the presence of the above-mentioned anions. When other species such as BF_4^- and SbF_6^- were used. the corresponding rigid cages were not formed but instead. more labile products in which the phosphines dissociate were obtained. These results indicate that, in order to form the silver cages, a nucleophilic anion with the appropriate geometry to bridge three silver atoms is essential. This process has been further exploited by James to prepare metallo-dendrimers by using benzylsulfate dendrons to direct the assembly of the silver cage.[20]

Another example of silver assemblies obtained by anion-directed synthesis[21] are the silver cages $[Ag_{14}(C{\equiv}C^tBu)_{12}X]^+$ (**8•X**) (X=F,Cl,Br). The reaction of *t*-butylalkyne and $AgBF_4$ in the presence of a base yields the organometallic polymer $[Ag(C{\equiv}C^tBu)]_n$, which is converted (in high yields) into the cages $[Ag_{14}(C{\equiv}C^tBu)_{12}X]^+$ (see Fig. 2) upon addition of fluoride. chloride, or bromide salts (but not when other anions such as triflate or tosylate are used). Their structural characterization demonstrated cages **8•X** to have a rhombohedra1 geometry with the corresponding halide encapsulated at their center. The cavity generated by this specific assembly is of the right geometry and dimensions to encapsulate spherical anions with a maximum radius of approximately 2.0 Å. Electrospray ionization mass spectometry (ESI-MS) and solution state infrared (IR) studies demonstrated that the cage-type structure is retained in solution. The silver atoms are held together by the bridging alkynyls and a combination of metallophilic attractions between the silver centers and Lewis-acid–base interactions between the silver atoms and the encapsulated halide.

Fujita reported a wide range of systems formed by the self-assembly of several nitrogen-donor ligands and palladium and platinum centers.[22] In the assembly of some of these systems, the ternplating properties of anions play an important role. When the square planar complex $[Pd(en)_2(NO_3)_2]$ is reacted with 1,3,5-*tris*(4-pyridylmethyl)benzene in the presence of anionic species having a hydrophobic moiety (such as 4-methoxyphenylacetate), the nearly quantitative formation of the cage structure **9** is observed (see Fig. 3).[23] In the absence of the anionic/hydrophobic species, this reaction gives rise to a considerable amount of polymeric material. Similarly, the

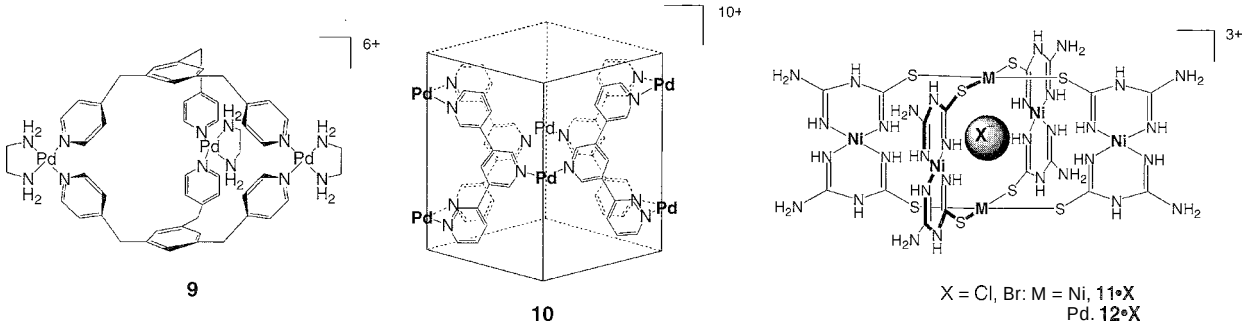

9 10

Fig. 3 Anion-directed cages 9. **11·X**, **12·X**,[23,25,26] and Fujita's nanochannels.[24] (*View this art in color at www.dekker.com.*)

quantitative formation of coordination channels such as **10** has been reported to occur when $[Pd(en)_2(NO_3)_2]$ is reacted with oligo(3,5-oligopyridine)s in the presence of rod-like anion species such as 4.4'-biphenylenedicarboxplate (see Fig. 3).[24] In these examples. the template directs the assembly not only through electrostatic interactions but also through π-π stacking and the use of hydrophobic effects.

A combination of metal. . .anion and hydrogen-bonding interactions has been used in the anion-directed synthesis of a series of hexametal cages.[25,26] The nickel complexes $[Ni_6(atu)_8X]^{3+}$ (**11·X**) can be prepared by mixing stoichiometric amounts of NiX_2 and Hatu (X = Cl,Br; Hatu = amidinothiourea) in methanol. The structural characterization of the resulting compounds demonstrated that the six nickel atoms are assembled in an octahedral geometry around a central anion and are linked by eight deprotonated Hatu ligands. The corresponding halide anion is encapsulated at the center of the cage and forms eight M-bonds with the ligands' NH groups. There is also an important attraction between the NiS_4 units located at the poles of the cage and the central anion. The analogous hexanuclear cages $[Ni_2Pd_2(atu)_8X]^{3+}$ (**12·X**) (X = Cl,Br) can be prepared by reacting four equivalents of the preformed $Ni(atu)_2$ complex and two equivalents of $Pd(PhCN)_2X_2$. In the presence of other anions (such as I^-, ClO_4^-, OAc^-. or NO_3^-), the hexanuclear cages do not form, indicating the important geometrical constrains (both regarding their volume and spherical shape) imposed by the templating halides for the formation of these specific structures.

ANION-DIRECTED ASSEMBLY IN ORGANIC SYNTHESIS

Macrocycles

Cation-directed synthesis of organic macrocycles such as crown ethers is a well-established procedure that has been widely utilized for many years. However: the use of anionic species for this purpose has only recently begun to be exploited. One of the first examples of anion-directed organic synthesis is the oligopyrrolic macrocycle **13** reported by Sessler (see Fig. 4).[27] This macrocycle was

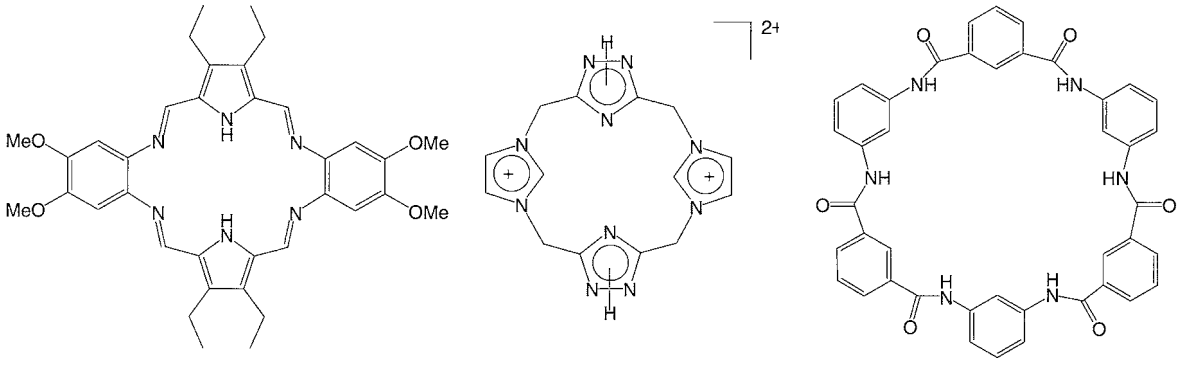

13 14 15

Fig. **4** Products of the anion-directed macrocyclization reactions reported by Sessler,[27] Alcalde,[28] and Kim [29]

prepared quantitatively using HNO_3 (rather than HCl) as acid catalyst for the cyclization. Under these conditions. the nitrate salt of the protonated macrocycle precipitated out of the reaction mixture. These results led the authors to suggest a possible ternplating effect exerted by the anionic species. Similarly, Alcalde recently reported[28] the chloride-directed synthesis of a series of [1_4]imidazoliophanes such as **14** (see Fig. 4). The macrocyclization reaction leading to these species was studied in the presence of a wide range of anions and demonstrated to give greatly increased yields when chloride (and in some cases, bromide) was used. In the presence of larger anions (such as BF_4^-, PF_6^-, and $H_2PO_4^-$), the yields were considerably lower, suggesting a good size-match between the cavity of the macrocycles and the two halides.

Another example in which anions seem to play an important directing role is in the synthesis of oligoamide macrocycles.[29] Following observations that certain salts (such as LiCl and $CaCl_2$) have an influence on the formation of polyamides. Kim engaged in studying the influence of such salts in model macrocyclic compounds. Specifically. the high dilution reaction between isophthalic acid chloride and *m*-phenylenediamine was studied and reported to yield a complex mixture of cyclic and oligomeric species. However, when this reaction was repeated in the presence of $CaCl_2$, the main product obtained was the cyclic hexamer **15** (see Fig. 4) in preference to the other cyclic and oligomeric species. Structural characterization of **15** demonstrated it to have a $CaCl_3^-$ anion (formed in situ from $CaCl_2$ and free chloride) positioned in the inner cavity of the macrocycle. These results suggested a directing effect of the anion. because in its absence. the main product of the reactions was not the hexamer **15** but oligomers and rings of different sizes.

Rotaxanes and Pseudorotaxanes

The interest in rotaxanes, pseudorotaxanes, and catenanes (i.e., molecules that contain non-covalently interlocked components) stems from their potential use as building blocks in molecular devices. Their syntheses usually rely on some sort of template assistance, such as the preorganization of the assembly's components around a metal center. While cationic templates have been widely used in this context, only a few examples of anion-directed synthesis of interlocked molecules have been reported. In fact, although rotaxanes and pseudorotaxanes have been prepared in this way (as discussed in this section), to date there is no reported example of anion-directed synthesis of catenanes.

Stoddart and Williams reported the first example of anion-assisted self-assembly of a pseudorotaxane.[30] By mixing four equivalents of $[NH_2(CH_2Ph)_2][PF_6]$ with one equivalent of a large macrocycle (tetrakis-*p*-phenylene [68]crown-20), the pseudorotaxane (16) shown in Fig. 5 was obtained. This superstructure was structurally characterized, revealing the presence of the PF_6^- anion at its center, which forms multiple C–H . . . F hydrogen bonds with the hydroquinone methine and the benzylic methylene hydrogen atoms. The presence of an encapsulated PF_6^- and its multiple interactions with the receptor suggest that it plays an important directing role in the self-assembly of this superstructure. Further studies in

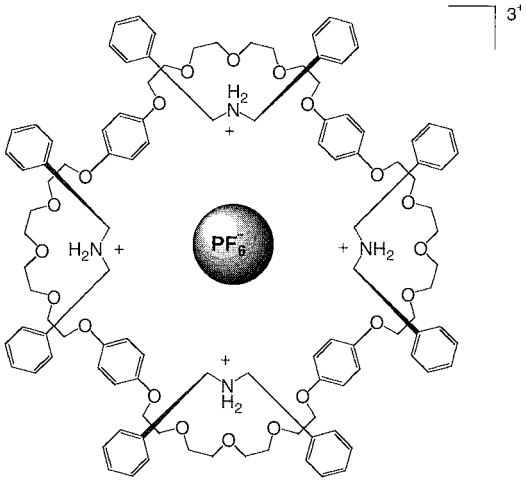

16

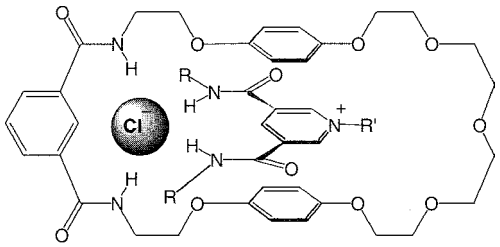

17

Fig. 5 Two examples of pseudorotaxanes reported by Stoddart and Williams[30] and by Beer.[31] (*View this art in color at www.dekker.com.*)

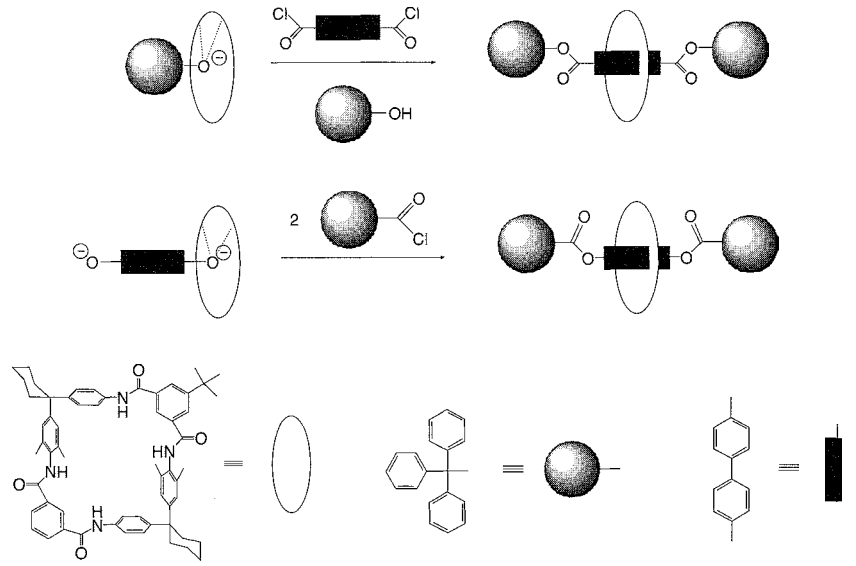

Fig. 6 Reaction scheme for the anion-directed synthesis of Vogtle's rotaxanes.[32] (*View* this art *in color at www.dekker.com.*)

the presence *of other anions would provide interesting insight into this reaction.*

Beer recently reported the anion-directed assembly of the [2]pseudorotaxane **17**.[31] *In this system (see Fig.* 5), *a chloride anion has been employed as the central core about* which *two ligands (the macrocycle and the liner species) are orthogonally disposed by means of* H-*bonding to the anion. The formation of 17 was studied in solution by* UV/Vis *spectroscopy and* ^{1}H-NMR *and confirmed in* the *solid state by an x-ray crystal structure. While chloride was demonstrated to be a good directing agent for the formation of* **17**, *other anions such as* Br^-, I^-, *and* PF_6^- *proved to be poor templates. This demonstrates the importance of the geometries and dimensions of the templating anion for the formation of a specific assembly.*

In 1999 Vögtle *reported the first example of* anion-*directed synthesis of* rotaxanes.[32] *The first step in this synthesis consisted of forming a strong host–guest complex between a* tetralactam macrocycle *and a phenolate anion (see Fig. 6). With this, the anion (also a good* nu-*cleophile)* is *properly positioned to further react with the adequate component to form a rotaxane. Using this* meth-*odology. different rotaxanes were prepared depending on whether the phenolic functionality was located at the stopper component or at the axle precursor.*

Helicates

In contrast to the well-documented assembly of helicates around metal *centers. there are only two examples of well-identified anion-assembled helicates. De Mendoza reported the first in* 1996,[33] *while Kruger and Martin only recently published the* second.[34] *The former reported that a tetraguanidinium strand self-assembled around a sulfate anion to produce a double helical structure. The formation of this* assembly *was proposed on the basis of NMR and* CD *spectroscopic studies. More recently,* Kruger *and Martin structurally* characterized *a double helicate formed by assembling a* diammonium-*bis-*pyridinium *salt around two chloride anions.* In *both of these examples, the directing forces to form the assemblies are based on H-bonding interactions between the anions and the N–H groups present in the ligands.*

CONCLUSION AND OUTLOOK

Important developments in the supramolecular chemistry of anions were seen in the last few years. As a consequence; anion-directed assemblies have started to emerge, providing synthetic chemists with a new approach for the synthesis of complex molecular architectures. The anion-directed assembly of macrocycles, *molecular cages,* nanotubes, *helicates, rotaxanes. and pseudorotaxanes is already a reality. These examples have established the foundations for a systematic and rational approach to the anion-directed synthesis of novel* supra-molecular (and *molecular) structures. Moreover, they suggest that even in well-known reactions. the participation of anions might have been ignored until now. In the years to come. we will certainly see an increasing number of assemblies prepared through anion-directed*

approaches, which will provide new methodologies for synthetic chemistry.

ACKNOWLEDGMENTS

Daniela Rais and Joachim Steinke are thanked for proofreading this manuscript and for providing valuable suggestions for improving it.

ARTICLES OF FURTHER INTEREST

Amide- and Urea-Based Anion Receptors, p. 31
Fluorescence Sensing of Anions, p. 566
Guanidium-Based Anion Receptors, p. 615
Halogen Bonding, p. 628
Macrocyclic Synthesis, p. 830
Molecular Squares, Boxes, and Cubes, p. 909
Naked Anion Effect, p. 939
Organometallic Anion Receptors, p. 1006
Rotaxanes and Pseudorotaxanes, p. 1194
Self-Assembly: Definition and Kinetic and Thermodynamic Considerations, p. 1248
The Template Effect, p. 1493

REFERENCES

1. Busch, D.H. Structural definition of chemical templates and the prediction of new and unusual materials. J. Inclusion Phenom. 1992. *12* (1–4), 389--395.
2. Anderson. S.: Anderson. H.L.: Sanders, J.K.M. Expanding roles for templates in synthesis. Acc. Chern. Res. 1993. 26 (9). 469–475.
3. Hoss, R.: Vogtle, F. Template synthesis. Angew. Chem.. Int. Ed. Engl. 1994. *33* (4). 375--384.
4. Yang, X.; Knobler, C.B.: Hawthorne. M.F. ''[12]Mercuracarborand-4''. the first representative of a new class of rigid macrocyclic electrophiles: The chloride ion complex of a charge-reversed analogue of [12]crown-4. Angew. Chem., Int. Ed. Engl. 1991. *30* (11). 1507–1508.
5. Miiller, A.: Penk, M.: Rohlfing. R.; Krickemeyer, E.: Döring, J. Topologically interesting cages for negative ions with extremely high "coordination number": An unusual property of V–O clusters. Angew. Chem.. Int. Ed. Engl. 1990, *29* (8). 926–927.
6. Henkels, C.H.: Kurz. J.C.; Fierke. C.A.; Oas. T.C. Linked folding and anion binding of the Bacillus *subtilis* ribonuclease P protein. Biochemistry 2001. *40* (9). 2777–2789.
7. Gale. P.A. Anion receptor chemistry: Highlights from 1999. Coord. Chem. Rev. 2001. *213*. 79–128.
8. Gale. P.A. Anion coordination and anion-directed assembly: Highlights from 1997 and 1998. Coord. Chern. Rev. *2000. 199*. 181–233.
9. Beer. P.D.: Gale, P.A. Anion recognition and sensing: The state of the art and future perspectives. Angew. Chem.. Int. Ed. 2001. *40* (3). 487–516.
10. Zheng, Z.: Knobler. C.B.: Hawthorne. M.F. Stereoselective anion template effects: Syntheses and molecular structures of tetraphenyl [12]mercuracarborand-4 complexes of halide ions. J. Am. Chem. Soc. 1995. *117* (18), 5105–5113.
11. Hasenknopf. B.: Lehn, J.-M.: Kneisel, B.O.: Baum. G.; Fenske, D. Self-assembly of a circular double helicate. Angew. Chem.. Int. Ed. Engl. 1996. *35* (16). 1838–1840.
12. Hasenknopf. B.; Lehn, J.-M.; Boumediene. N.; Dupont-Gervais, A.; Van Dorsselaer. A.; Kneisel. B.O.; Fenske, D. Self-assembly of tetra- and hexanuclear circular helicate. J. Am. Chem. Soc. 1994. 119 (45). 10956- 10962.
13. Jones, P.L.: Byrom. K.J.; Jeffery, J.C.; McCleverty, J.A.: Ward. M.D. A cyclic supramolecular complex containing eight metal ions, twelve bridging ligands, and an anion encapsulated in the central cavity. Chem. Commun. 1997. 1361–1362.
14. Campos-Fernández, C.S.: Clérac. R.: Dunbar, K.R. A one-pot, high yield synthesis of a paramagnetic nickel square from divergent precursors by anion template assembly. Angew. Chem.. Int. Ed. 1999. *38* (23). 3469–3477.
15. Campos-Fernández, C.S.: Clérac, R.: Koomen. J.M.: Rusell, D.H.: Dunbar, K.R. A fine-tuning the ring-size of metallacyclophanes: A rational approach to molecular pentagons. J. Am. Chem. Soc. 2001. *123* (4). 773–774.
16. Cheng, S.-T.; Doxiadi. E.: Vilar, R.: White. A.J.P.; Williams. D.J. Anion templated synthesis of Ni/Pd containing metalla-macrocycles. J. Chem. Soc. Dalton Trans. 2001. 2239–2244.
17. Müller, A.: Rohlfing. R.: Krickemeyer. E.: Bogge. H. Control of the linkage of inorganic fragments of V–O conipounds: From cluster shells as carcerands via cluster aggregates to solid-state structures. Angeu. Chem.. Int. Ed. Engl. 1993. *32* (6). 909–912.
18. Salta, J.: Chen. Q.: Chang, Y.-D.; Zubieta, J. The oxovanadium-organophosphonate system: Complex cluster structures $[(VO)_6(t\mathrm{BuPO_3})_8\mathrm{Cl}]$, $[(VO)_4\{\mathrm{PhP(O)_2\text{-}OP(O)_2Ph}\}_4\mathrm{Cl}]^-$, and $[V_{18}O_{25}(H_2))_2(\mathrm{PhPO_3})_{20}\mathrm{Cl_4}]^{4-}$ with encapsulated chloride anions prepared from simple precursors. Angew. Chern.. Int. Ed. Engl. 1994. *33* (7). 757–760.
19. James. S.L.: Mingos. D.M.P.: White. A.J.P.: Williams. D.J. Anion-templated formation of a unique inorganic 'superadamantoid' cage $[\mathrm{Ag_6(triphos)_4(O_3SCF_3)_4}]^{2+}$ [triphos=$(\mathrm{PPh_2CH_2})_3\mathrm{CMe}$]. Chem. Commun. 1998, (2323-2324.
20. Xu. X.: MacLean, E.J.: Teat, S.J.: Nieuwenhuyzen. M.; Chambers, M.: James. S.L. Labile co-ordination dendrimers. Chem. Commun. 2002, 78–79.
21. Rais, D.; Yau, J.: Mingos. D.M.P.; Vilar. R.: White. A.J.P.: Williams. D.J. Anion-templated syntheses of rhombohedra] silver-alkynyl cage compounds. Angew. Chern.. Int. Ed. 2001. *40* (18). 3464–3467.
22. Fujita, M. Metal-directed self-assembly of two- and three-dimensional synthetic receptors. Chem. Soc. Rev. 1998. *27* (6). 417–425.

23. Fujita, M.; Nagao, S.; Ogura, K. Guest-induced organization of a three-dimensional palladium(II) cagelike complex. A prototype for "induced-fit" molecular recognition. J. Am. Chem. Soc. **1995,** *117* (5), 1649 1650.
24. Aoyagi, M.; Biradha, K.; Fujita, M. Quantitative formation of coordination nanotubes templated by rodlike guests. J. Am. Chcm. Soc. **1999**, *121* (32). 7457 -7458.
25. Vilar, R.: Mingos, D.M.P.; White, A.J.P.; Williams, D.J. Anion control in the self-assembly of a cage coordination complex. Angcw. Chcm., Int. Ed. **1998,** 37 (9), 1258 1261.
26. Vilar, R.; Mingos, D.M.P.; White. A.J.P.; Williams, D.J. Aufbau synthesis of a mixed-metal anion receptor cage. Chem. Commun. **1999,** 229–230.
27. Sessler, J.L.; Mody, T.D.; Lynch, V. Synthesis and x-ray characterization of a unranyl(VI) Schiff base complex derived from 2:2 condensation product of 3,4-diethylpyrrole-2,5-dicarbaldehyde and 1,2-diamino-4,5-dimethoxybenzene. Inorg. Chem. **1992.** 31 (4), 529–531.
28. Alcalde, E.; Ramos, S.; Pérez-García. L. Anion template-directed synthesis of dicationic [1_4]imidazoliophanes. Org. Lett. **1999,** *1* (7), 1035–1038.
29. Kim, Y.H.; Calabrese, J.; McEwen. C. $CaCl_3$ or Ca_2Cl_4 complcxing cyclic aromatic amide. Tcmplatc effect on cyclization. J. Am. Chern. Soc. **1996**, 118 (6). 1545–1546.
30. Fyfe, M.C.T.: Glink, P.T.; Menzer, S.; Stoddart, J.F.; White, A.J.P.; Williams, D.J. Anion-assisted self-assembly. Angew. Chem.. Int. Ed. Engl. **1997**, 36 (19), 2068 2070.
31. Wisncr, J.A.; Beer, P.D.; Drew: M.G.R. A demonstration of anion tcmplation and selectivity in pseudorotaxane formation. Angew. Chem., Int. Ed. **2001**, *40* (19). 3606–3609.
32. Reuter, C.; Wienand, W.; Hiibner, G.M.; Seel, C.; Vogtlc, F. High-yield synthesis of ester, carbonate, and acetal rotaxanes by anion template assistance and their hydrolytic dethreading. Chem. Eur. J. **1999,** *5* (9), 2692 2697.
33. Sánchez-Quesada, J.; Seel, C.; Prados, P.; de Mendoza, J. Anion helicates: Double strand helical self-assembly of chiral bicyclic guanidinium dimers and tetramers around sulfate templates. J. Am. Chem. Soc. **1996,** *118* (1), 277–278.
34. Keegan, J.; Kruger, P.E.: Nieuwenhuyzen, M.; O'Brien, J.; Martin, N. Anion directed assembly of a dinuclear double helicate. Chem. Commun. 2001, 2192 -2193.

Annulenes

Michael J. Marsella
University of California, Riverside, California, U.S.A.

INTRODUCTION

The [nlannulenes may be defined as cyclic polyalkenes possessing a closed circuit of n π-conjugated p_z-orbitals. The first three small annulenes are shown in Fig. 1 and include [4]annulene (cyclobutadiene), [6]annulene (benzene), and [8]annulene (cyclooctatetraene). The bracketed number, n, can be classified as either a $4n+2$ (Hiickel aromatic/Möbous antiasomatic) or 4n (Huckel antiaromatic/Mobius aromatic) delocalized n-electron species. That said, it is not surprising that the concept of aromaticity[1] is closely associated with the annulenes. Indeed, the first three annulenes listed cover the concepts of Hiickel aromatic, antiaromatic, and nonaromatic properties (see Fig. 1).

Given that the annulene literature is vast and has already been covered within many excellent reviews,[2,3] this work is not intended to be comprehensive. Instead, this review will reflect a sampling of current annulene chemistry. focusing on representative aspects of [4]-, [6]-, [8]-, [12]-, [14]-, [16]-, and [18]annulenes.

DEFINITIONS AND ACRONYMS

For convenience, definitions of key terms and acronyms used in this review are provided below:

ACID (Anisotropy of the Current-Induced Density): A theoretical method for visualizing, as an isosurface, delocalization of electrons in molecules.

[*n*]Annulene: A cyclic polyalkene possessing a closed circuit of n n-conjugated p_z-orbitals.

Antiaromaticity: A property associated with [n]annulenes possessing either $4n$ electrons (Huckel) or $4n+2$ electrons (Mobius). such that the acyclic homologue is more stable than the cycle. A paratropic compound.

Aromaticity: A property associated with [nlannulenes possessing either a 4tz + 2 (Hiickel) or 4n (Mobius) number of delocalized n-electrons capable of sustaining a ring current.[1]

Hückel aromaticity: An aromatic annulene composed of a continuous circuit of p_z-orbitals oriented along the same axis (or plane) and possessing $4n+2$ electrons.

Möbius Aromaticity: An aromatic annulene composed of a continuous array of p_z-orbitals containing a $4n$ number of n-electrons, arranged such that an (ideal) 180° twist occurs within the orbital circuit.

BEE (Bond Localization Energy): The energy necessary to localize a common bond between two cyclic n-systems. See the work of Mitchell, sited herein.[4,5]

Diatropic ring current (**^{1}H-NMR**)**:** An induced ring current within the annulene n-circuit that opposes the applied magnetic field, resulting in a downfield shift of protons on the outside of an aromatic annulene.

Frost's circle: A simple, geometrical approach to approximating the HMO energy levels for planar annulenes. The lowest energy MO has an HMO energy of α+2β.

HMO theory (**Hückel** Molecular Orbital theory): A simple molecular orbital theory applied to planar π-conjugated systems. A key simplification involves treatment of the n-system independently from the σ-system. The HMO molecular orbital energies are in terms of α and β, where α is equated with the energy of an isolated p_z orbital, and β is the resonance integral, equated to the energy associated with having electrons shared by atoms. As reference, benzene is 4β more stable than an isolated p_z orbital.

Homoaromaticity: Cyclic conjugation of a n-system that bypasses one (or more) saturated atoms.

NICS (Nucleus-Independen&Chemical **Shifts**)**:** A theoretical method for determining the ring current at the center (or any position in space) of an annulene or other delocalized system.

Paratropic ring current (**^{1}H-NMR**)**:** An induced ring current within the annulene n-circuit that aligns with the applied magnetic field, resulting in an upfield shift of affected protons.

[4]ANNULENES

The instability of [4]annulene (a neutral $4n$ n-electron annulene) can be gleaned from either Frost's Circle[6] or HMO theory.[7] As shown in Fig. 2. the former predicts an open-shell triplet, implicating instability. The latter reports no gain in energy (0 β) relative to its acyclic analogue, butadiene. Experimental evidence shows that cyclobutadiene is. in fact, a closed shell species, with alternate single and double bonds. Regardless, as predicted. [4]annulene proved to be an unstable compound.

Encyclopedia of Supramolecular Chemistry
DOI: 10.1081/E-ESMC 120019198

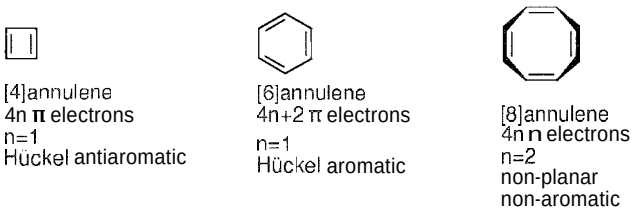

Fig. 1 Depicting the first three simple [n]annulenes along with their π-electron count and Hiickel aromatic/antiaromatic/nonaromatic classification.

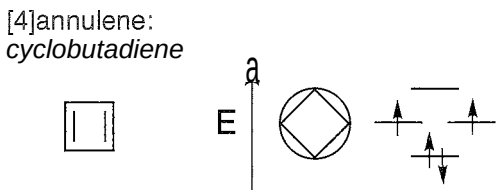

Fig. 2 Frost's circle applied to [4]annulene.

Harnessing the reactivity of [4]annulenes has allowed for their controlled use in [$4\pi_s+2\pi_s$] cycloaddition reactions, playing the role of diene, dieneophile, or both.[8–11] Transient tetraalkylcyclobutadienes can be readily prepared via DMF-promoted decomposition of the corresponding tetraalkylcyclobutadiene-aluminum trichloride complex. The complex is stable and can be readily prepared by reaction of aluminum trichloride with a dialkylacetylene. In the absence of a good dienophile. the reactive tetraalkylcyclobutadienes undergo dimerization to yield 1,2,3,4,5,6,7,8-octaalkyl-tricyclo[4.2.0.$0^{0,0}$]octa-3.7-dienes (Scheme 1). In the presence of a good dienophile, such as acetylenedicarboxylic acid or its corresponding esters, the Diels–Alder adduct can be isolated in high yield.[10,11] It is noteworthy to mention that the product of this [$4\pi+2\pi$] reaction is a substituted Dewar benzene, itself a high-energy isomer of [6]annulene. Thus, from a synthetic standpoint, a substituted [4]annulene can be converted to its isomeric [6]annulene via two pericyclic reactions: a thermal [$4\pi_s + 2\pi_s$] followed by a photochemical 4π electrocyclic ring opening (Scheme 1). Due to this fact, Dewar benzene was proposed as a supramolecular protecting group for aromatic rings, preventing aryl–aryl stacking interactions from biasing solid-state properties.[11]

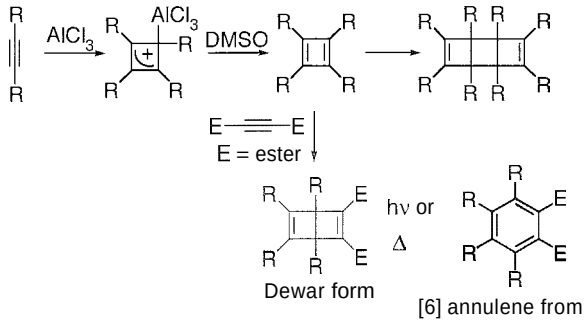

Scheme 1 Synthesis of a [6]annulene via its Dewar benzene isomer. The Dewar form is prepared via a [$4\pi+2\pi$] cycloaddition with [4]annulene and a substituted acetylene.

An elegant use of [4]annulene chemistry utilizes the stable tricarbonylcyclobutadiene iron complex as a protected cyclobutadiene.[8,9] One advantage over the aluminum cyclobutadiene complex is the ability of the tricarbonylcyclobutadiene iron complex to be amenable to synthetic modifications of the four-membered ring. Typically. ceric ammonium nitrate (CAN; or other oxidants) may be used to oxidize the iron and liberate free cyclobutadiene. An example of this methodology is shown in Scheme 2, as applied to the synthesis of (+)-asteriscanolide. Further examples of reactions utilizing this chemistry are shown in Table 1.

[6]ANNULENES

Benzene embodies arornaticity and is the standard by which the property of aromaticity is measured. Given that fact. it is worthwhile to provide an overview of recent techniques that attempt to quantify the property of aromaticity.

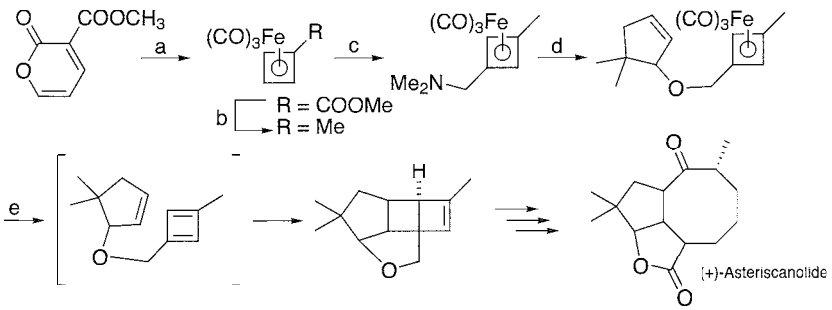

Scheme 2 (a) hν, C_6H_6; $Fe_2(CO)_9$, 50°C (64%); (b) LAH, BF_3 OEt_2 (93%); (c) $Me_2NCH_2NMe_2$, H_3PO_4, CH_3CO_2H, 100°C (67%). (d) MeI, THF; NaH, 5.5-dimethyl-cyclopent-2-enol. THF/DMF (50%). and (e) Me_3NO, acetone. 56°C (63%)

Table 1 Showing substrate and cycloadduct product from the intramolecular [4π+2π] cycloaddition involving the [4]annulene moiety

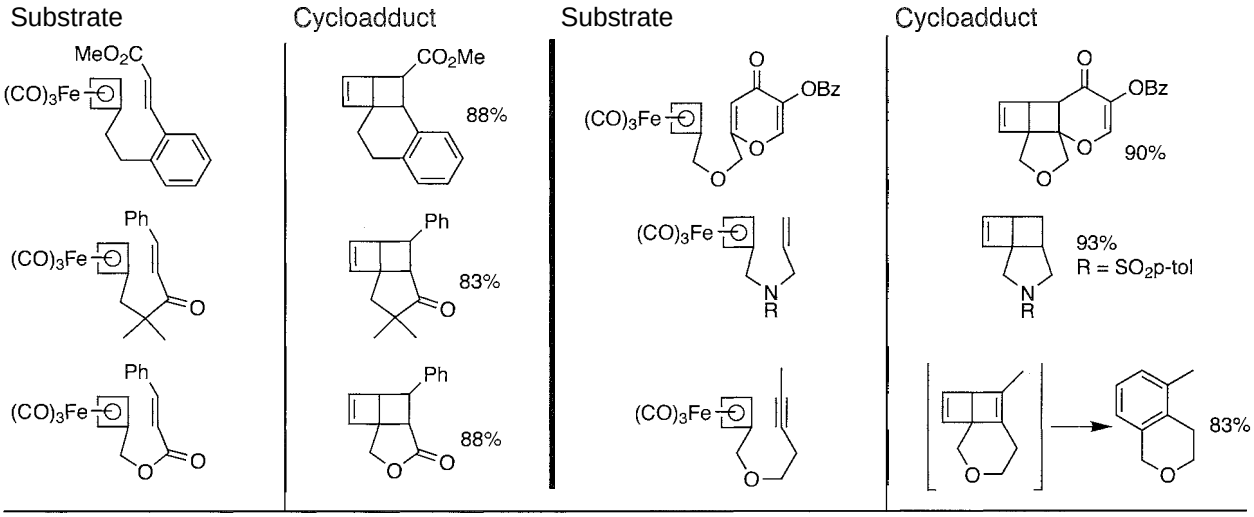

From a theoretical standpoint, simple analysis via Frost's circle yields a closed-shell system, implying stability (compare to cyclobutadiene) (Fig. 3). The HMO theory renders benzene ca. 1 β more stable than its acyclic analogue, hexatriene. Although these pen and paper methods cannot compare to modern computational methods presently available for a desktop computer. they are elegant in their simplicity and qualitative predictive power. However, given the interest in quantifying some measure of aromaticity (or antiaromaticity) among different annulenes,[a] much higher levels of theory are desired and have been developed. Recently, two new techniques were reported that integrate the power of ab initio calculations with simple protocols that are generally applicable to a wide variety of annulenes and related compounds. Both methods can take advantage of the popular Gaussian[12] suite of computational chemistry programs. Given their generality, availability. and ease of setup, they were highlighted in brief below.

NICS

Proton chemical shifts of annulenes have long been utilized as probes of ring currents.[13] For example. protons outside and inside of an aromatic annulene will shift downfield and upfield, respectively, as a function of the induced ring current. In general, those protons at (or above) the annulene center experience a greater magnitude of shift than those outside the annulene ring. One synthetic/experimental limitation of this "internal probe" technique is the ability to place an NMR active nucleus at a ring center. A theoretical technique designed to overcome this problem places a ghost atom at the ring center (or any position in space). Absolute magnetic shieldings can then be calculated using available computational chemistry programs. This facile technique, known as Nucleus-Independent Chemical Shifts (NICS), is establirhed as an effective aromaticity criterion. Some values are given in Table 2 (note that negative NICS values denote aromaticity, and positive NICS values denote antiaromaticity).

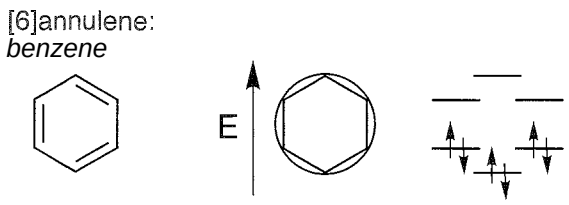

Fig. 3 Frost's circle applied to [6]annulene.

ACID

The ACID method (anisotropy of the current-induced density) provides a method to visualize, as an isosurface. delocalization of electrons in molecules.[14–16] One major advantage of this method is its invariance with respect to the relative orientation between molecule and magnetic

Table 2 Nics values for several aromatic and antiaromatic species

Annulene	Point group	NICS (6–31+G*)
Benzene	D_{6h}	−9.7
[8]Annulene dianion	D_{8h}	−13.9
[4]Annulene	D_{2h}	+27.6
Naphthalene	D_{2h}	−9.9

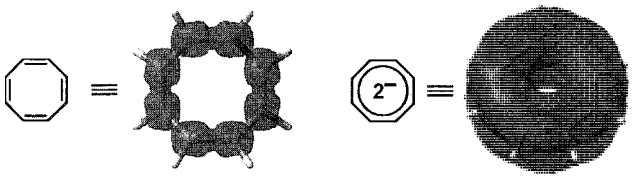

Fig. 4 ACID surface mapped onto the localized, tub conformer of [8]annulene (left), and the planar. delocalized [8]annulene dianion (right). Discontinuous surfaces imply no delocalization at those corresponding points in space (with respect to the selected isosurface value: here set at 0.05). (*View this art in color at www.dekker.com.*)

field. Furthermore. it is not a simple function of the electron density. and it utilizes the same symmetry as the wave function. In the proverbial sense that ''one picture is worth a thousand words.'' the ACID technique is best summarized by direct visualization of such an isosurface. As such, illustrated in Fig. 4 is an ACID isosurface mapped onto both the (localized) tub conformer and (delocalized) planar conformer of [8]annulene and its aromatic dianion. respectively.

In addition to the classical [6]annulene, benzene, neutral in-plane trishomoaromatic ''benzene'' frameworks (such as that depicted in Fig. 5*)* were also studied.[17] Although not yet synthesized, these compounds were collectively studied using a variety of computational techniques. Unique from benzene, the six overlapping p-orbitals lie in-plane (as opposed to orthogonal). Given that this arrangement constitutes a closed circuit of $4n+2$ π-electrons, the system. according to the definition provided herein. constitutes a (homo-) [6]annulene. Within the reported series. a maximum NICS value of -30.1 ppm was found at the ring center. Ultimately, it was determined that such in-plane annulenes may possess more than one third the aromatic stabilization energy of benzene, thus constituting the best candidates yet proposed for a neutral *tris*homoaroinatic compound.

[8]ANNULENES

[8]Annulene is a $4n$ π-electron system, and thus, the (neutral) planar form would be expected to exhibit antiaromatic behavior. Indeed, Frost's circle analysis predicts an open-shell species (as with [4]annulene; see Figs. 2 and 6). Extensive studies of cyclooctatetraene were performed,[18,19] and it was established that the neutral state avoids the problem of antiaromaticity by adopting a tub conformation. Both the anion and dianion are known to exist in a planar conformation, the latter being aromatic.[19] This fact is also predicted by simple analysis of the [8]annulene dianion by Frost's circle (see Fig. 6). It is predicted that the planar [8]annulene dianion is a closed-shell system.

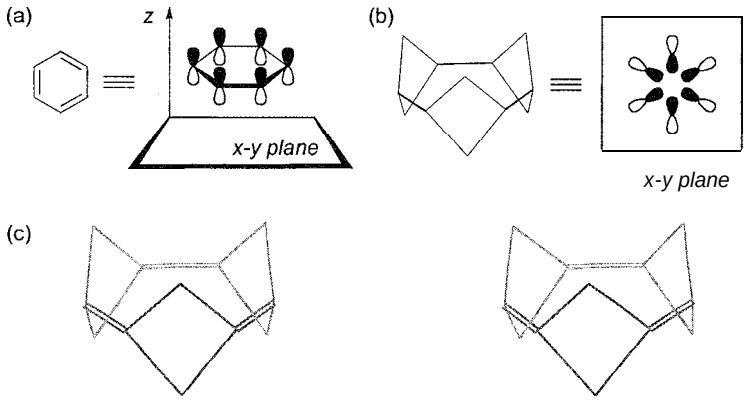

Fig. 5 (a) Benzene p-orbitals are orthogonal to the x–y plane. (h) In an in-plane benzene. six p-orbitals lie in-plane. (c) Stereoview (cross-eye) of an in-plane benzene skeleton.

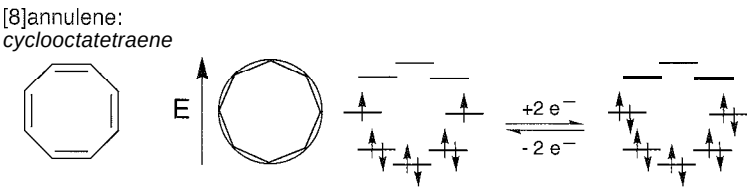

Fig. 6 Frost's circle applied to [8]annulene and its dianion.

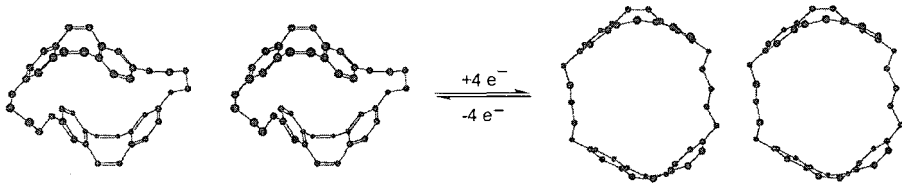

Fig. 7 Stereoviews (cross-eye) of a shape-changing cyclophane composed of two [8]annulene moieties. The stereoviews were modeled at ihe PM3 level of theory and optimized only for illustrative purposes (structures may not correspond to true global minima).

At the ab initio level of theory, a NICS calculation of the dianion yields an (aromatic) value of -13.9[13] (see Table 2). and ACID[14] clearly illustrates the corresponding shift from the localized neutral tub conformer to the delocalized planar dianion (see Fig. 4).

The redox-induced conformational change associated with [8]annulene was utilized as the key element in the design of shape-changing molecules. A shape-changing cyclophane was reported,[20] likely capable of functioning as a redox-triggered two-state host (Fig. 7). In an analogous manner. a polymer composed of tetra[2,3-thienylene] monomers (a thiophene-fused [8]annulene) was also reported,[21–23] a design intended to translate additive tub-to-planar conformational changes into an overall perturbation of polymer chain length (i.e., a polymeric electromechanical actuator or molecular muscle, see Fig. 8a,b and Table 3). In contrast to the aforementioned conformationally dynamic [8]annulenes, oxidation of the constrained tub conformer of octamethoxytetraphenylene (an *o*-dialkoxybenzene-fused [8]annulene), yields electrochromic switching via redox-triggered reversible carbon–carbon bond formation (Fig. 8c).[24]

Tetra[2,3-thienylene] was also utilized as a rigid unit, a double-helical scaffold.[25] Specifically, a racemic mixture of the corresponding octaaryl double helix. shown in Fig. 9, crystallizes to yield homochiral, supramolecular polymer chains extending in the direction of the long crystal axis. Edge-to-face stacking of neighboring (intermolecular) terminal phenyl groups dominated the homochiral supramolecular assembly (Fig. 9). Similarly, tetraphenylene was also used as a scaffold for the synthesis of octaaryl double-helical monomers (Fig. 10).[26]

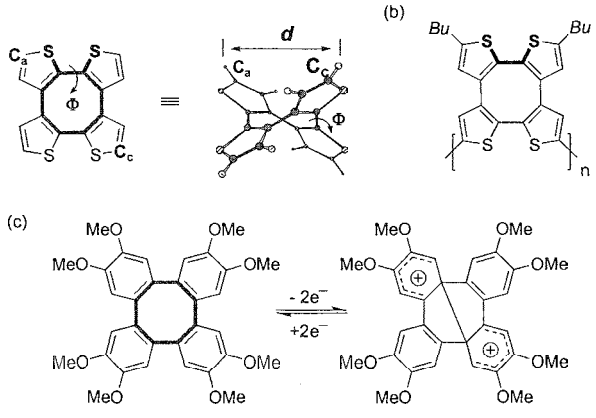

Fig. 8 (a) Depicting tetra(2,3-thienylene) and corresponding descriptors. @ and *d* (see Table 3). (b) Poly(tetra[2, 3-thienylene]). a putative molecular muscle. (c) Depicting redox-induced reversible carbon–carbon bond formation in octamethoxytetraphenylene.

MöBIUS [4*N*]ANNULENES: [12]-, [16]-, AND [20]ANNULENE

Although the concept of Mobius aromaticity was put forth in 1964,[27] no neutral [4*n*]annulene exhibiting a Mobius strip conformation (Fig. 1I) and Mobius aromatic character has yet been prepared. It was originally predicted that all [4*n*]anulenes $\geq$ [20]annulene should be capable of accommodating a Mobius strip conformation with minimal strain. Recent theoretical studies revealed that the [4*n*]annulenes, [12]-, [16]-, and [20]annulene, exhibit Mobius conformers (local minima) and corresponding aromatic character (NICS values of -14.6. -15.6, and -10.2 ppin at ring center, respectively), although the lowest-energy conformers (global minima). in all cases. are of Hückel topology.[28] Clearly, control of conformation via the targeted synthetic design of a [4*n*]annulene

Table 3 Reporting the redox-induced perturbation of S-C-C-S dihedral angle. Φ. and corresponding dimensional change, *d* (see Fig 8a)

Compound	Charge	Φ(deg)	*d* (Å)	Ad (%)
Monomer	0	49.5	6.87	—
Monomer	1+	34.8	7.27	5.69
Dimer	0	48.9	6.90	—
Dimer	1+	38.6	7.14	3.54
Dimer	2+	31.4	7.33	5.92

Charges were determined via electrochemical analysis of tetra(2. 3-thienylene) monomer and dimer. and conformer data was calculated at the B3LYP/6-31G(*d,p*) level of theory.

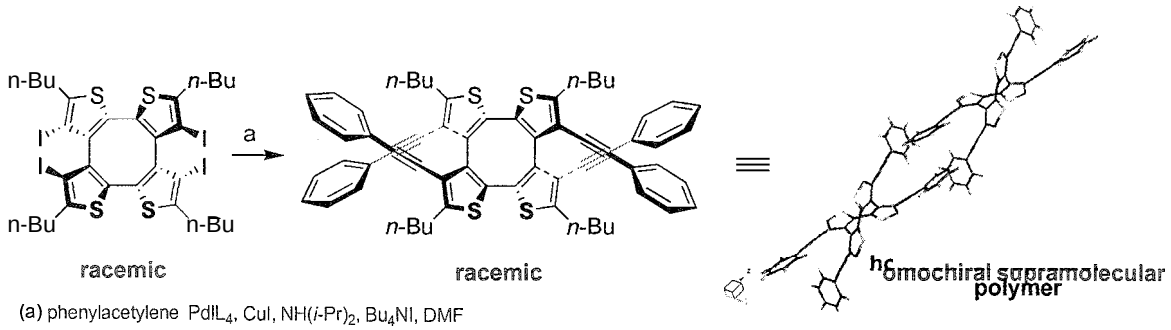

Fig. **9** Synthesis of a racemic octaaryl double helix utilizing tetra[2,3-thienylene] as a core. Supramolecular self-assembly of the racemic mixture yields homochiral supramolecular polymers (dimer repeat shown).

with true Mobius topology will be required to provide supporting experimental data to this study.

[14]ANNULENE: DIHYDROPYRENE VALENCE TAUTOMERISM AND APPLICATIONS DERIVED THEREFROM

The [14]annulene, diinethyldihydropyrene (DHP), exhibits rich cheinistry that was reviewed elsewhere in detail.[2,29] A key reaction of this annulene is the symmetry-allowed photochemical transformation between the closed [14]annulene form. and the open metacyclophanediene form (CPD; see Scheme 3a). The transition between colorless and colored forms, the perturbations in conjugation pathways, and the ^{1}H-NMR shift associated with the two methyl groups poised near the ring center (thus, reporting changes in ring currents) made DHP an excellent scaffold from which to design photochrornic switches and other n-functional molecules.

The current state-of-the-art DHP photochrornic switch is capable of accessing three unique states (CPD–CPD, CPD–DHP. and DHP–DHP; see Scheme I3b).[29,30] This multistate photochromic switch was prepared by fusion of two benzo[*e*]dimethyldihydropyrene moieties. The states can be optically read and written. although the DHP–DMP state rapidly converts back to the CPD–DHP state via a thermal (symmetry forbidden) process.

The DHP to CPD interconversion also perturbs conjugation pathways around the perimeter of the molecule. This fact was capitalized upon to yield an optoelectronic redox switch (Scheme 3c).[31] Specifically, the 16-π linear circuit extending from thiophene A through DHP to thiophene B is interrupted upon conversion to Th-CPD-Th. This process is reversible, and only the DHP form exhibits anodic activity within a window of 0.0–0.75 V. Thus, the state of the photochromic switch can be written photochemically and read electrochemically (the CPD form is redox silent, and the DHP form is redox active).

In addition to functioning as a switch. DHP also serves as a tool with which to probe aromatic character by NMR (via monitoring the "reporter" methyl groups).[4] It was shown that the BLE of any aromatic annulene benzannulated onto DHP (i.e., [*n*]annulene, shown in Fig. 3d) can be determined by the following equation:

$$\text{BLE} = [4.18 + \delta(\text{Ar})]/2.59$$

where δ(Ar) is the average chemical shift of ihe internal methyl groups.

This equation is true due to the sensitivity of the methyl groupr to the ring current of the DMP skeleton, as well as to the fact that annulated DHPs can be dissected into two π-circuits (i.e.. red and blue according to Scheme 3d). The

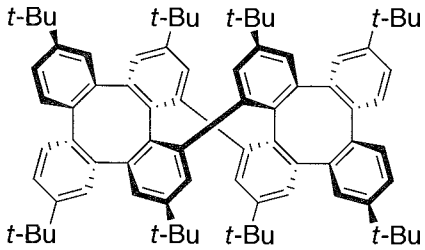

Fig. 10 An octaaryl double helix formed from the fusion of two tetraphenylene units.

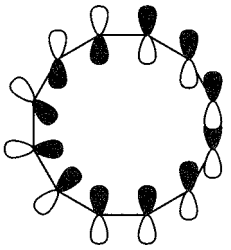

Fig. 11 A conceptual illustration of 12 p_z orbitals arranged in a Mobius strip conformation.

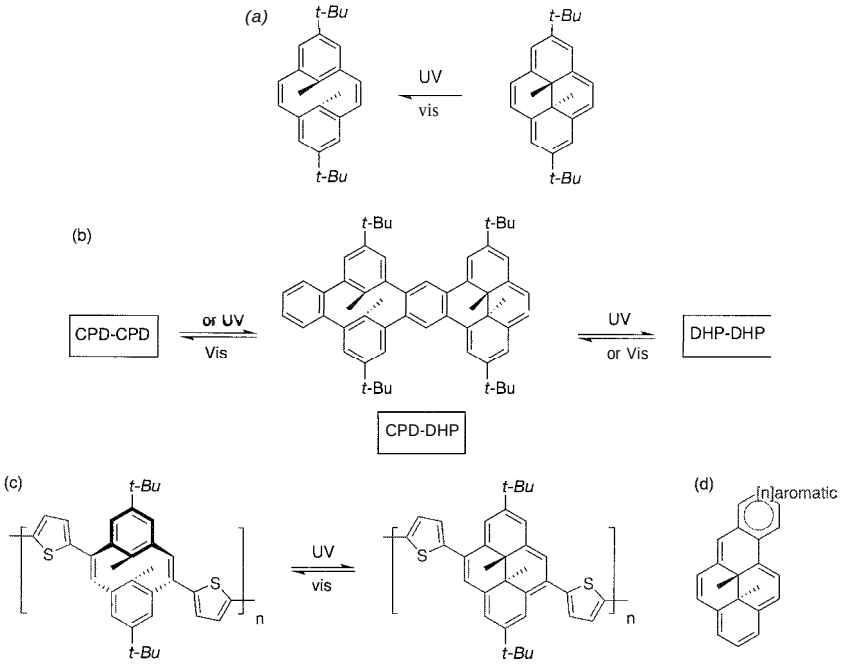

Scheme *3* (a) The DHP–CPD photochemical interconversion; (b) a DHP-based three-way switch: (c) a thiophene-DHP copolymer capable of attenuating effective conjugation length via the DHP–CPD photochemical interconversion; and (d) the two π-circuits in a benzannulated-DHP: blue corresponds to the DHP skeleton. and red corresponds to a benzannulated aromatic. (View *this* art *in* color *at www.dekker.com.*)

larger the resonance energy in the red fragment, the less delocalization in the blue circuit (i.e., DHP), hence, the smaller the diatropic shift of the methyl groups. Of course, one drawback of this method is that it requires covalent attachment between the DHP "probe" and the aromatic [*n*]annulene to be studied.

[16]- AND [18]ANNULENE

The [16]-annulene and [18]annulene are the smallest annulenes (antiaromatic and aromatic, respectively), possessing internal protons to be thermodynamically stable at room temperature (Fig. 12). Not surprisingly, steric interactions between internal protons affect the conformer distribution of these systems. Perdeuterated [16]- and [18]annulenes were synthesized in an effort to attenuate these internal sterics, given that C–D bonds are shorter than C–H bonds.[32] The results demonstrated increased ring currents in both of the perdeuterated annulenes, as determined by ^{1}H-NMR analysis (paratropic and diatropic, respectively). It is proposed that the shorter C–D versus C–H bond reduces internal sterics, allowing the σ-framework of the annulenes to achieve near ideal (120°) C–C=C bond angles, and thus increasing the enforcement of π-delocalization. It should be emphasized that achieving near ideal bond angles was determined to be more important than achieving complete planarity (i.e., all internal H/D atoms in the same plane).

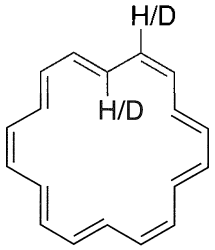

Fig. **12** [18]Annulene, emphasizing internal versus external HID environments.

CONCLUSION

Selected examples of recent properties and applications of [*n*]annulenes ($n = 4$, 6, 8. 12, 14. 16. and 18) were presented. Despite years of investigation. it is apparent that these cyclic systems possess many unique properties of

applications (for example. molecular devices). Furthermore, some interesting properties of as-yet unprepared

annulenes were predicted from accurate levels of ab initio theory. When coupling these facts and recognizing that the area of annulene chemistry extends far beyond this review, it is clear that interest in these systems will remain keen for many years to come.

ARTICLES OF FURTHER **INTEREST**

Calixarenes: Synthesis and Historical Perspectives, p. 153
Cation–π Inter-actions, p. *214*
Chemical Topology, p. *229*
Cyclophanes: Definition and Scope. p. 414
Molecular Switches, p. 917
Molecular Wires. p. 925
Nuclear Magnetic Resonance Spectroscopy, p. *981*
π–π Interactions: Theory and Scope, p. 1076
Spherands, p. 1344
Supramolecular Photochemistry, p. 1434

REFERENCES

1. Aromaticity, C. Aromaticity. Chem. Rev. 2001. *101*, 1115–1566.
2. Garratt. P.J. *Aromaticity*; John Wiley and Sons: New York. 1986.
3. Kennedy. R.D.: Lloyd, D.: McNab, H. Annulenes. 1980–2000. J. Chem. Soc., Perkin Trans. 1 2002, 1601–1621.
4. Mitchell. R.H.: Iyer, V.S.: Khalifa, N.: Mahadevan. R.; Venugopalan. S.: Weerawarna. S.A.; Zhou, P.Z. An experimental estimation of aromaticity relative to that of benzene: The synthesis and NMR properties of a series of highly annelated dimethyldihydropyrenes—Bridged benzannulenes. J. Am. Chem. Soc. 1995. *117*. 1514–1532.
5. Mitchell, R.H.: Iyer. V.S.; Khalifa. N.: Mahadevan. R.: Venugopalan, S.: Weerawarna. S.A.: Zhou, P.Z. An experimental estimation of aromaticity relative to that of benzene—The synthesis and NMR properties of a series of highly annelated dimethyldihydropyrenes—Bridged benzannulenes. J. Am. Chem. Soc. 1995. *117*. 1514.
6. Frost, A.A.; Musulin. B.J. Mnemonic device for molecular-orbital energies. Chem. Phys. 1953. *21*. 572.
7. Yates. K. *Hückel Molecular* Orbital *Theory*; Academic Press, Inc.: Orlando. 1978.
8. Limanto. J.; Tallarico. J.A.: Porter, J.R.: Khuong, K.S.; Houk, K.N.: Snapper. M.L. Intramolecular cycloadditions of cyclobutadiene with olefins. J. Am. Chem. Soc. 2002, *124*. 14748–14758.
9. Limanto. J.: Snapper. M.L. Sequential intramolecular cyclobutadiene cycloaddition. ring-opening metathesis. and cope rearrangement: Total syntheses of (+)- and (−)-asteriscanolide. J. Am. Chem. Soc. 2000. 122. 8071–8072.
10. Koster. J.B.; Timmermans. G.J.; van Bekkum. H. Reaction of the tetramethylcyclobutadiene-aluminum chloride complex with dienophilic esters. Synthesis 1971. *139*.
11. Marsella. M.J.; Meyer. M.M.; Tham. F.S. Dewar benzene as a protecting group? Demonstration of photolithographic crystallization. Org. Lett. 2001. *V3*. 3847–3849.
12. Gaussian: Frisch, M.J.: Trucks, G.W.: Schlegel. H.B.: Scuseria. G.E.; Robb, M.A.; Cheeseman. J.R.; Montgomery, J.A., Jr.: Vreven. T.: Kudin. K.N.; Burant. J.C.: Millam, J.M.: Iyengar, S.S.: Tomasi, J.: Barone. V.; Mennucci. B.; Cossi, M.: Scalmani, G.; Rega, N.; Petersson, G.A.: Nakatsuji. H.: Hada. M.: Ehara. M.; Toyota, K.; Fukuda. R.: Hasegawa, J.: Ishida. M.: Nakajima. T.: Honda, Y.: Kitao. O.: Nakai, H.: Klene, M.; Li, X.: Knox, J.E.: Hratchian, H.P.; Cross. J.B.: Adamo, C.: Jaramillo. J.; Gomperts, R.: Stratmann. R.E.: Yazyev, O.; Austin, A.J.; Cammi, R.: Pomelli, C.; Ochterski, J.W.: Ayala, P.Y.: Morokuma. K.: Voth. G.A.: Salvador. P.; Dannenberg. J.J.; Zakrzewski. V.G.; Dapprich. S.: Daniels, A.D.: Strain. M.C.: Farkas, O.; Malick, D.K.: Rabuck. A.D.: Raghavachari, K.: Foresman. J.B.; Ortiz, J.V.: Cui. Q.; Baboul, A.G.: Clifford, S.; Cioslowski. J.; Stefanov. B.B.; Liu, G.; Liashenko. A.; Piskorz. P.: Komaromi. I.: Martin. R.L.: Fox. D.J.; Keith. T.: Al-Laham. M.A.; Peng, C.Y.: Nanayakkara, A.: Challacombe. M.: Gill. P.M.W.: Johnson, B.: Chen, W.: Wong. M.W.; Gonzalez, C.: Pople, J.A. Gaussian. Inc.: Pittsburgh. PA, 2003.
13. Schleyer. P.V.; Maerker. C.: Dransfeld. A.; Jiao, H.J.; Hommes, N. Nucleus-independent chemical shifts—A simple and efficient aromaticity probe. J. Am. Chem. Soc. 1996. *V118*, 6317–6318.
14. Herges. R.; Geuenich, D. Delocalization of electrons in molecules. J. Phys. Chem. 2001. *105*, 3214–3220.
15. Herges. *R.:* Papafilippopoulos. A. Homoaroinaticity in *tris*(ethylene)nickel(0) and *tris*(ethyne)nickel(0). Angew. Chern.. Int. Ed. 2001. *40*. 4671.
16. Kimball. D.B.: Herges. R.: Haley. M.M. Two unusual. competitive mechanisms for (2-ethynylphenyl)triazene cyclization: Pseudocoarctate versus pericyclic reactivity. J. Am. Chem. Soc. 2002, *124*. 1572–1573.
17. Stahl. F.: Schleyer. P.V.: Jiao. H.J.; Schaefer, H.F.: Chen. K.H.: Allinger. N.L. Resurrection of neutral tris-homoaromaticity [Review]. J. Org. Chem. 2002. 67. 6599–6611.
18. Paquette. L.A. Cyclooctatetraenes: Conformational and π-electronic dynamics within polyolefinic [8]annulene frameworks. Adv. Theor. Interest. Mol. 1992. *2*. 1–77.
19. Strauss. H.L.: Katz. T.J.: Fraenkel, C.K. Electron spin resonance studies of the cyclooctatetraenyl anions. J. Am. Chem. Soc. 1963. *85*, 2360–2364.
20. Heinz. W.: Rader, H.-J.: Müllen. K. Changing the size of a cavity via an electron-transfer: Synthesis and reduction of 1. 5. 22, 26-tetraoxa-[5,5]-(2,8)-dibenzo[*a,e*]-cyclooctatetraeneophane. Tetrahedron Lett. 1989. *30*. 159–162.
21. Marsella. M.J.: Piao. C.Z.: Tham. F.S. Expanding

tetra[2,3-thicnylene]-based molecular muscles to larger [4*n*]annulenes. Synthesis **2002.** 1133–1135.
22. Marsclla, M.J.: Reid, R.J. Toward molecular muscles: Design and synthesis of an electrically conducting poly[cyclooctatetrathiophene]. Macromolcculcs **1999,** *32*, 5982–5984.
23. Marsclla, M.J.; Reid, R.J.; Estassi, S.; Wang, L.S. Tetra[2,3-thienylene]: A building block for single-molecule electromechanical actuators. J. Am. Chem. Soc. **2002,** *124*. 12507–12510.
24. Rathore, R.; Le Magueres, P.; Lindeman, S.V.; Kochi, J.K. A redox-controlled molecular switch based on the reversible C–C bond formation in octamethoxytetraphenylene. Angew. Chem., Int. Ed. **2000,** 39, 809–812. 663.
25. Marsella, M.J.; Kim, I.T.: Tham, F. Toward double helical ladder polymers: Cyclooctatetrathiophene as a highly versatile double helical scaffold. J. Am. Chem. Soc. **2000,** *122*, 974–975.
26. Rajca, A.; Safronov, A.; Rajca, S.; Shoemaker, R. Double helical octaphenylene. Angew. Chem., Int. Ed. Engl. **1997.** 36. 489–491.
27. Heilbronner, E. Hueckel molecular orbitals of Moebius-type conformations of annulenes. Tetrahedron Lett. **1964,** *1923*.
28. Castro, C.; Isborn, C.M.; Karney, W.L.; Mauksch, M.; Schleyer, P.V. Aromaticity with a twist: Mobius [4*n*]annulenes. Org. Lett. **2002,** *4*, 3431–3434.
29. Mitchell, R.H. The metacyclophanediene-dihydropyrene photochromic π switch. Eur. J. Org. Chem. **1999,** 2695–2703.
30. Mitchell, K.H.; Ward, T.R.; Wang, Y.X.; Dibble, P.W. π-Switches: Synthesis of three-way molecular switches based on the dimethyldihydropyrene-metacyclophanediene valence isomerization. J. Am. Chem. Soc. **1999,** *121*, 2601–2602.
31. Marsella, M.J.; Wang, Z.Q.; Mitchell, R.H. Backbone photochromic polymers containing the dimethyldihydropyrene moiety: Toward optoclcctronic switches. Org. Lett. **2000,** *2*, 2979.
32. Stevenson, C.D.; Kurth, T.L. Isotopic perturbations in aromatic character and new closely related conformers found in [16]- and [18]annulene. J. Am. Chem. Soc. **2000,** *122*. 722–723.

Anticrowns

Vladimir B. Shur
Irina A. Tikhonova
Russian Academy of Sciences, Moscow, Russia

INTRODUCTION

Anticrowns are peculiar antipodes of crown ethers and their thia and aza analogues. They contain several Lewis acidic centers in the macrocyclic chain and so are able to efficiently bind various anions and neutral Lewis bases with the formation of unusual complexes, wherein the Lewis basic species is simultaneously bonded to all Lewis acidic atoms of the macrocycle. This remarkable property of anticrowns, being reminiscent of the behavior of conventional crown compounds in metal cation binding, makes them prospective aids in the areas of molecular recognition. ion transport. as well as organic synthesis and catalysis.

The first reports on the anion-binding capacity of anticrowns emerged in the late 1980s–early 1990s. Subsequently, a considerable amount of information on different aspects of the chemistry of these novel reagents was accumulated. Nowadays. data on coinplexing properties of macrocycles containing two, three. four: and five Lewis acidic centers in the chain were published. Especially impressive results were obtained for polymer-curamacrocycles. which proved to be efficient hosts for binding various anionic and neutral Lewis basic species. Polytin- and polysilicon-containing macrocycles were also studied as anticrowns.

In the present article. host–guest chemistry of anticrowns as well as available data on their applications in catalysis and as ionophores will be briefly reviewed. Strictly speaking. only macrocycles with three and more Lewis acidic centers in the chain can be considered as genuine anticrowns. Nevertheless. the binding properties of some macrocycles containing only two Lewis acidic atoms in the ring will also be discussed.

HOST-GUEST CHEMISTRY OF ANTICROWNS

Polytin- and Polysilicon-Containing Macrocycles

In 1987, Newcomb et al.[1] reported the synthesis of the macrocycles $[Cl_2Sn(CH_2)_n]_2$ (n=8, 10. 12) containing two tin atoms in the macrocyclic chain. and they showed by ^{119}Sn-NMR method that these macrocycles form complexes with chloride anion in an acetonitrile solution. It was suggested that the anionic species in the resulting complexes is bonded to both tin atoms of the cycle. The most stable adduct was formed from the macrocycle with n=8.

The interaction of halide anions with a series of macrobicyclic compounds (**1**–**4**) containing two tin atoms in bridgehead positions was also studied by ^{119}Sn–NMR.[2] It turned out that bicyclic host **1** is able to bind fluoride anion. but it does not react with bulkier chloride. bromide, and iodide ions. By contrast, compounds 2–4 readily coordinate chloride ion but they are unable to bind fluoride anion. According to x-ray diffraction data, the fluoride ion in the complex with 1 is bonded to both tin centers of the Lewis acidic host. whereas the chloride ion in its adduct with 2 is coordinated only to a single tin atom.

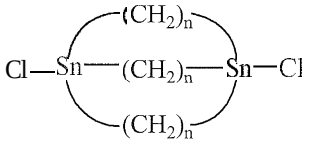

1 (n = 6), **2** (n = 8), **3** (n = 10), **4** (n = 12)

In 1989, Jurkschat et al.[3] described the synthesis of the 12-membered rnacrocycles $[R^1R^2Sn(CH_2)_3]_3$ [$R^1=R^2=Cl$ ***(5)***; $R^1=Me$, $R^2=Cl$ (**6**)] containing three tin atoms in the macrocyclic chain. According to ^{119}Sn-NMR spectra, both rnacrocycles are able to bind successively at first one and then the second chloride ions. The complex of 5 with one chloride ion was isolated from the reaction solution. An x-ray diffraction study of this complex revealed that the anionic species is coordinated here with two Lewis acidic centers of the cycle. For the analogous 1:1 complex of macrocycle 6. the structure including the simultaneous coordination of Cl^- with all three tin atoms of the cycle was proposed.

In a subsequent study. the ability of the 15-membered polytin-containing macrocycle $[Me_2Sn(CH_2)_4]_3$ to bind chloride and bromide anions as well as to transport them through liquid membrane was demonstrated.[4] Similar capacity to transport halide anions (Cl^-, Br^-) through

Encyclopedia of Supramolecular Chemistry
DOI: 10.1081/E-ESMC 120019199

liquid membranes was previously established for the macrocycle $[Me_2Si(CH_2)_3]_3$ containing three silicon atoms.[11] Recently, the synthesis of the eight-membered macrocycle [*cyclo*-$CH_2\{Sn(Cl_2)CH_2Si(Me_2)\}_2O$] with two tin and two silicon atoms in the ring was described.[6] This macrocycle reacts with chloride, fluoride. and hydroxide ions to form 1:1 complexes, wherein only tin atoms of the cycle are involved in the coordination with the anionic guest.

Perfluorinated Polymercuramacrocycles

The possibility of using polymercuramacrocycles as anion receptors was demonstrated for the first time in 1989. when it was reported that cyclic trimeric *o*-phenylenemercury (*o*-$C_6H_4Hg)_3$ (**7**)[7] containing three Hg atoms in a planar nine-membered cycle is capable of binding halide anions (Cl^-, Br^-, I^-) in halomethane solutions.[11] However, the resulting complexes could not be isolated here due to. apparently, their insufficient stability. Further progress in mercury anticrown chemistry was achieved when the perfluorinated analogue of **7**, viz. cyclic trimeric perfluoro-*o*-phenylenemercury (*o*-$C_6F_4Hg)_3$ (**8**)[9] was employed as a macrocyclic host.[10,11] The presence of fluorine atoms in the aromatic rings of 8 sharply increases the Lewis acidity of the Hg centers and. as a consequence. quite stable and isolable complexes of unusual structures are formed in the interaction of this macrocycle with anions and neutral Lewis bases. Subsequently, one other perfluorinated polymercuramacrocycle. $[(CF_3)_2CHg]_5$ (**9**),[12] with five Hg atoms in a planar 10-membered ring was also successfully used as an anticrown.

Macrocycle **8** exhibits a high affinity toward various anionic species (Cl^-, Br^-, I^-, SCN^-, BH_4^-, *closo*-$[B_{10}H_{10}]^{2-}$, *closo*-$[B_{12}H_{12}]^{2-}$, etc.), forming complexes with coinpositions and structures that are strongly dependent on the nature of the anion and the reagent ratio. In the case of bromide. iodide, and thiocyanate ions, the isolated compounds $[(o\text{-}C_6F_4Hg)_3X]^-$ (X=Br, I, SCN) contain one anionic guest per one molecule of the macrocycle.[10,11,13] The reaction of **8** with chloride ions gives the complex $\{[(o\text{-}C_6F_4Hg)_3]_3Cl_2\}^{2-}$, containing two anionic species per three macrocycle molecules.[11]

An x-ray diffraction study of the complexes of **8** with bromide and iodide anions showed[10,11] that they are polymeric in the solid state and have unprecedented structures of polydecker bent sandwiches $[(\cdots\mathbf{8}\cdot\cdot X\cdot\cdot)_n]^{n-}$ (X=Br, I), wherein every halide anion is simultaneously coordinated to six Hg atoms of two neighboring molecules of 8. A unique feature of the complexes is that the role of the coordinating centers in their molecules is played not by the metal atoms or cations. as in the case of normal sandwich complexes, but by the anions of the halogen. An analogous polydecker sandwich structure was established for a 1:1 complex of 8 with thiocyanate anion.[13] The anionic species in this complex is bonded to the Hg centers of **8** through the sulfur atom. However, the coordination of the anionic guest with Lewis acidic host is here less symmetrical: every S C N ion forms with each of the macrocycles two relatively short and one considerably longer Hg–S bonds. One may suggest that the above-mentioned complex of 8 with chloride anions. $\{[(o\text{-}C_6F_4Hg)_3]_3Cl_2\}^{2-}$, has a structure of triple-decker sandwich.[10] Quantum–chemical calculations also predict the possibility of the existence of double-decker sandwich complexes of macrocycle 8 with halide and sulfide anions.[14]

In the interaction of 8 with borohydride anions in THF. the complexes of three different compositions, viz. $\{[(o\text{-}C_6F_4Hg)_3]_2(BH_4)\}^-$, $\{[(o\text{-}C_6F_4Hg)_3](BH_4)\}^-$, and $\{[(o\text{-}C_6F_4Hg)_3](BH_4)_2\}^{2-}$ are formed depending on the reagent ratio.[11] According to IR spectra, the bonding of the BH_4^- ions to the Hg atoms is accomplished here through B–H–Hg bridges. Quantum–chemical calculations of the complexes suggest that they should have unusual double-decker sandwich, half-sandwich (pyramidal), and bipyramidal structures. respectively. The complexes are quite stable. For example, the stability constant of $\{[(o\text{-}C_6F_4Hg)_3]_2(BH_4)\}^-$ in THF at 20°C reaches a value of 10^7 l mol^{-2}.

The first structurally characterized double-decker sandwich complexes of perfluorinated polymercuramacrocycles with anions were obtained from the reactions of polyhedral *closo*-$[B_{10}H_{10}]^{2}$ and *closo*-$[B_{12}H_{12}]^{2}$ dianions with the excess of 8.[16] The anionic guest in these remarkable complexes $\{[(o\text{-}C_6F_4Hg)_3]_2(B_nH_n)\}^{2}$ (n=10, 12) is located between the planes of two macrocycles and is bonded to each through B–H–Hg bridges of two types. One type is the simultaneous coordination of the B–H group to all Hg centers of the neighboring molecule of the macrocycle. The other type is the coordination of the B–H

moiety only to a single Hg atom of the cycle. When the interaction of 8 with the above polyhedral dianions is conducted at an equimolar ratio of the reagents. the corresponding half-sandwiches $\{[(o\text{-}C_6F_4Hg)_3](B_nH_n)\}^{2-}$ are produced.[16]

For macrocycle 9. complexes with halide, acetate, trifluoroacetate, and sulfate anions were obtained. In the case of halide ions, the isolated compounds, $\{[(CF_3)_2CHg]_5X_2\}^{2-}$ (X=Cl, Br, I), contain two anionic species per one macrocycle molecule and have bipyramidal structures.[14,17,18] The halide anions in these adducts are arranged above and below the metallacycle plane, and each is symmetrically bonded to all Lewis acidic centers of the cycle, so that the coordination number of the halogen atoms here becomes equal to five. In the *bis*-acetate and *bis*-trifluoroacetate complexes of 9. the anionic guests are also disposed on different sides of the metallacycle plane and are bonded to 9 in the same manner.[19] In each of the carboxylate ligands. one of the oxygen atoms is coordinated with three metallic centers of the cycle, whereas the other is bonded to two remaining metal atoms. Different coordinated geometry is observed in the complex of 9 with sulfate anion.[19] In this 1:1 complex $\{[(CF_3)_2CHg]_5(SO_4)\}^{2-}$, the anionic guest behaves as a tetradentate ligand and forms three types of the Hg–O bonds with the macrocycle. One type is the cooperative binding of one of the oxygen atoms of the SO_4^{2-} ion by all Lewis acidic sites of the host. This oxygen atom is located nearly in the plane of a 10-membered mercuracarbon ring. Two other oxygen atoms are coordinated each to a single Hg atom of 9, while the fourth oxygen atom is bonded to two Hg centers.

Macrocycle 8 is able to bind effectively not only anions but also various neutral Lewis bases. such as nitriles,[20] carbonyl compounds,[21,22] aromatic hydrocarbons,[23] and some others.[21] As a result of the reactions. complexes containing one, two. or three Lewis basic species per one macrocycle molecule are produced. depending on the nature of a Lewis base. For example. the interaction of

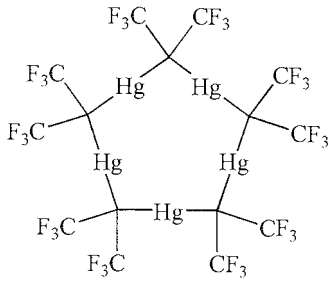

8 with acrylonitrile,[20] acetone,[22] acetaldehyde,[22] and benzophenone[22] gives 1:1 complexes having pyramidal structures in which the Lewis basic species is coordinated with all mercury centers of 8. The reactions of 8 with acetonitrile,[20] *N*,*N*-dimethylformamide,[21] and acetophenone[22] afford complexes containing two Lewis bases per molecule of 8. and these complexes have the corresponding bipyramidal structures, with the Lewis basic moieties being located on different sides of the metallacycle plane. And, at last, from the interaction of 8 with benzonitrile,[20] ethyl acetate,[21] and acetone,[22] complexes containing three molecules of a Lewis base were isolated. Interestingly, in the case of the benzonitrile complex $[(o\text{-}C_6F_4Hg)_3(PhCN)_3]$, all the nitrile ligands are disposed on one side of the metallacycle plane and, in addition, differ from each other in the geometry of coordination with the macrocycle. By contrast, in the 1:3 complexes of 8 with ethyl acetate and acetone, two of three molecules of a Lewis base are located above and below the metallacycle plane. It should be stressed that independent of their structure. all the 1:3 complexes contain at least one fragment wherein the Lewis basic guest is simultaneously bonded to all Lewis acidic sites of the macrocycle. Note also that according to IR spectra. the complexation of the above carbonyl compounds with 8 leads to a significant weakening of their C=O bonds, which is of interest for organic synthesis and catalysis.

The reactions of macrocycle 8 with benzene. biphenyl, naphthalene, and triphenylene result in the formation of 1:1 complexes with polydecker sandwich structures in the solid state.[7,8] The bonding of the aromatic molecules to 8 in these unusual complexes is due to secondary π-interactions between the C=C bonds of the arenes and the Lewis acidic Hg centers. Thus, even weak Lewis bases such as aromatic hydrocarbons are able to form host–guest complexes with 8.

o-Carboranylmercury Macrocycles (Mercuracarborands)

o-Carboranylmercury macrocycles or mercuracarborands[24,25] also exhibit a high efficiency in the binding of anions and neutral Lewis bases. which is due to the electron-withdrawing character of the carborane cages increasing the Lewis acidity of the mercury centers. This class of anticrowns was developed by Hawthorne et al.[24,25] At present. data on the synthesis and complexing properties of mercuracarborands $(o\text{-}C_2B_{10}H_{10}Hg)_4$ (10). $(o\text{-}C_2B_{10}H_{10}Hg)_3$ (11). and their substituted derivatives. containing four and three Hg atoms in 12- and 9-membered cycles, respectively, are available.

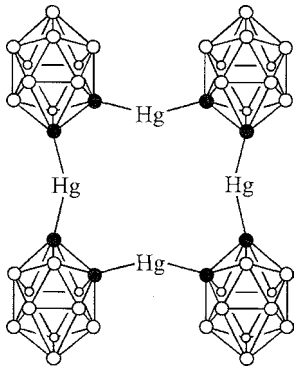

10

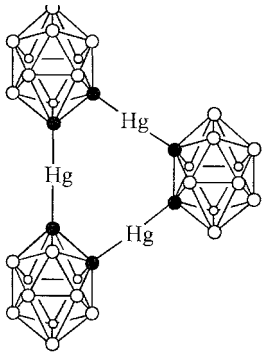

11

In 1991, Hawthorne et al. reported that the reaction of 1.2-dilithio-o-carborane *o*-$C_2B_{10}H_{10}Li_2$ *with* $HgCl_2$ *results in the formation of a* 1:1 *complex of* mercuracarborand *10 with chloride* ion.[24,25] *The anionic guest in this* unique *complex* $[(o\text{-}C_2B_{10}H_{10}Hg)_4Cl]^-$ *(12) resides nearly in the center of the mercuracarbon ring and is symmetrically coordinated to the four* Hg *atoms of the cycle. It was proposed that the chloride ion plays a role of a template in this macrocyclization reaction. Similarly. a treatment of* *o*-$C_2B_{10}H_{10}Li_2$ *with* HgI_2 *afforded the corresponding mono- or diiodide complexes,* $[(o\text{-}C_2B_{10}H_{10}Hg)_4I]^-$ *and* $[(o\text{-}C_2B_{10}H_{10}Hg)_4I_2]^{2-}$ *(13). depending on the reaction* conditions.[24,25] *As in the above-mentioned diiodide complex* $\{[(CF_3)_2CHg]_5I_2\}^2$ *, the anionic species in* **13** *are arranged above and below the* metallacycle *plane, but their coordination with the mercury atoms is less symmetrical here. which can be explained by the electrostatic repulsion of the iodide anions. The same indirect procedure was utilized successfully for the synthesis of halide complexes with a number of substituted derivatives of* **10**.[24,25] *In particular, a 1:1 complex of the tetraphenyl derivative of* **10** *with iodide ion,* $[(3\text{-Ph-}o\text{-}C_2B_{10}H_9Hg)_4I]^-$, *having a symmetrical pyramidal structure, was synthesized in this* way.[25]

The free macrocyclic host **10** *was prepared by the reaction of its diiodide* 13 *with silver* acetate.[24,25] *In a similar fashion. a series of substituted derivatives of 10 was obtained from the corresponding dihalide complexes and silver acetate. The structure of* **10** *in a form of the* $\mathbf{10}\cdot(THF)_4\cdot(H_2O)_2$ adduct *was established by an x-ray diffraction study. A treatment of* **10** *with I regenerates the initial* 13.

Macrocycle **10** *reacts with two equivalents of* KNO_3 *in acetone in the presence of 18-crown-6 to give the bis-nitrate complex* $[(o\text{-}C_2B_{10}H_{10}Hg)_4(NO_3)_2(H_2O)]^{2-}$ *(14) containing one coordinated water* molecule.[26] *Both nitrate ions in 14 behave as monodentate ligands but differ strongly from each other in the mode of coordination with the host.* One *of the* NO_3^- *ions in* 14 *is bonded through the oxygen atom to all four Hg centers of 10, while the second nitrate is bonded to only two Hg atoms. The remaining coordination site between two other* Hg *centers is occupied by a molecule* of *water. Interestingly, when the reaction of* **10** *with potassium nitrate is conducted at a* NO_3^-:**10** *molar ratio of 3:1 the bis-nitrate complex* $[(o\text{-}C_2B_{10}H_{10}Hg)_4(NO_3)_2]^{2-}$ *(15) containing no water is formed, and this complex has a different* structure.[26] *A remarkable feature of* 15 *is that each of the nitrate ions here is coordinated to* **10** *in an unprecedented tridentate, face-on fashion, and, in addition, all four* Hg *atoms of the* macrocycle *are involved in the bonding to the anionic guests.*

The interaction of 10 and its octaethyl derivative (9,12-Et_2-*o*-$C_2B_{10}H_8Hg)_4$ *(16) with closo-*$[B_{10}H_{10}]^{2-}$ *anions in acetone solution affords 1:1* adducts even *in the presence of an excess of the anionic guest, which is indicated by NMR spectra. However. the crystal product isolated from the reaction of* **16** *with closo-*$[B_{10}H_{10}]^{2-}$ *contained two polyhedral dianions per one macrocycle molecule. This unusual supramolecular aggregate has a bipyramidal structure wherein each of the* $[B_{10}H_{10}]^{2-}$ *species is bonded to all* Hg *atoms of the cycle through B–H–Hg* bridges.[24,25] *In the case of the bulkier closo-*$[B_{12}H_{12}]^{2-}$ *ion, no complexation with 10 and* **16** *occurs. The* bi*pyramidal complexes of 16 with neutral closo-*9,12-I_2-*o*-$C_2B_{10}H_{10}$ *and closo-*9-I-12-Et-*o*-$C_2B_{10}H_{10}$ *species were also* described.[25] *In these* 1:2 *complexes, an iodine atom of each of the boron-containing guests is bound to four Hg centers of the macrocyclic host.*

Mercuracarborand **11** *is structurally similar to the above-mentioned perfluorinated* polymercuramacrocycle *8.* It *was synthesized by the interaction of* 1.2-dilithio-*o*-*carborane with* $Hg(OAc)_2$.[24,25] *The same method was applied for the synthesis of hexamethyl derivative of* **11**, (9,12-Me_2-*o*-$C_2B_{10}H_8Hg)_3$ *(17). The formation of* **11**

rather than acetate complex of 10 or free PO in the above reaction can be explained by the greater strength of a mercuracarbon ring in **11** than in 10, as well as by the inability of noncoordinating acetate ion (in contrast to halide ions) to act as a template and thereby to direct the process of the cyclization toward PO.

Both mercuracarborands **11** and **17** are able to bind halide anions and acetonitrile molecules. In the case of **17**, the resulting complexes with halide anions (Cl^-, Br^-, I^-) contain two molecules of the macrocycle per one anionic guest and have unique structures of double-decker sandwiches.[27] The halide ion is situated here between two parallel rnercuracarbon rings and is syinmetrically bonded to six Hg centers. Thus. the coordination number of the halogen atom in these sandwiches as in the above-discussed polydecker bent sandwich complexes of 8 with bromide and iodide anions is equal to six. Structures of the halide adducts formed by macrocycle **11** are not yet determined.

From the interaction of **11** with acetonitrile. two cocrystallized complexes, $[(o\text{-}C_2B_{10}H_{10}Hg)_3(MeCN)_3]$ and $[(o\text{-}C_2B_{10}H_{10}Hg)_3(MeCN)_5]$, containing three and five nitrile molecules. were isolated.[24,25] In each of these complexes, two acetonitrile ligands are coordinated through the nitrogen atoms with all Hg atoms of the cycle. In contrast to **11**. macrocycle 17 gives with acetonitrile the sole complex $[(o\text{-}C_2B_{10}H_8Me_2Hg)_3\ (MeCN)_3]$, wherein only one MeCN ligand is simultaneously bonded to all Hg centers of the mercuracarbon ring.

The reaction of **17** with acetone/water (50:1) mixture yields the complex containing one water and three acetone species per one inacrocyclic host.[28] The water molecule in this complex is coordinated by its oxygen atom to three mercury atoms. while the carbonyl oxygen atom of each of the acetone ligands is bound only to a single Hg center. Interestingly, all four guest species in this adduct are arranged on one side of the metallacycle plane. An even more unusual host–guest complex $\{[(o\text{-}C_2B_{10}H_8Me_2Hg)_3(H_2O)]_2(C_6H_6)\}$ was obtained from the interaction of 17 with benzene and water in dichloromethane.[29] In this complex, every H_2O molecule is η^3–coordinated at the center of 17. and the benzene ligand is disposed between two $[(o\text{-}C_2B_{10}H_8Me_2Hg)_3(H_2O)]$ fragments, forming n-hydrogen bonds with both hydrogen atoms of each water molecule. The driving force for the formation of such multiple n-hydrogen bonds with benzene seems to be an increase in the acidity of the hydrogen atoms of water due to its η^3-coordination with the Lewis acidic centers of **17**.

Other Polymercuramacrocycles

In 1987. Wuest et al. published data on the synthesis of a 2:1 complex of THF with the 22-membered macrocycle $[o\text{-}C_6H_4HgOC(O)(CF_2)_3C(O)OHg]_2$ (18) containing four mercury atoms in the ring.[29,30] In this adduct, each of the THF ligands is coordinated with two Hg centers of the corresponding o-phenylenedimercury unit. Subsequently, a complex of the octamethyl derivative of **18**. $[o\text{-}C_6Me_4HgOC(O)(CF_2)_3C(O)OHg]_2$, with four 1,2-dimethoxyethane (DME) ligands was prepared and structurally characterized.[30,31] In this complex, one oxygen atom of each molecule of DME is bound with two Hg atoms of a o-phenylenedimercury moiety, while the other oxygen atom is bonded to a single mercury center. Evidently, the sizes of both macrocycles are too large, and the distance between o-phenylenedimercury fragments is too long for cooperative binding of a Lewis base by all Lewis acidic sites of these macrocyclic compounds. Wuest et al. also described a 2:1 complex of diethylformamide with dicationic macrocycle $[(o\text{-}C_6Me_4HgO(H)Hg)_2]^{2+}$ (**19**) containing four Hg atoms in a planar 10-membered ring.[30,32] The complex has a bipyramidal structure. The amide molecules in **19** are located above and below the metallacycle plane, and each is symmetrically coordinated through the oxygen atom with all four metal centers of the host. A high Lewis acidity of this macrocycle is due to its dicationic character.

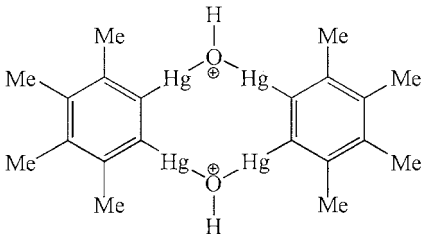

19

APPLICATIONS OF ANTICROWNS IN CATALYSIS AND AS IONOPHORES

There are at least two types of reactions wherein anticrowns could be successfully used as catalysts. The first type is reactions catalyzed or promoted by conventional monodentate Lewis acids. An application of anticrowns in such reactions could result in an additional increase in the reaction rate due to cooperative effects of several Lewis acidic centers. The ability of anticrowns to form lipophilic anionic species as a result of the complexation with anions suggests that these compounds will be capable of effectively transferring various organic and inorganic cations from an aqueous phase to an organic phase. Therefore, another field of synthetic o ganic chemistry in which anticrowns could be useful is phase-transfer catalysis of electrophilic reactions.

The first example of the successful application of anticrowns in phase-transfer catalysis was reported in 1989, when it was shown that nonfluorinated polymercuramacrocycle 3 is able to catalyze the azo-coupling reaction between benzenediazonium halides $PhN_2^+X^-$ (X=Cl, Br) and β-naphthol in the two-phase H_2O–CH_2Br_2 system.[''] Diphenylmercury proved to be totally inactive in this reaction.

Subsequently. it turned out that perfluorinated polymercuramacrocycle 8 displays high efficiency in the phase-transfer nitration of acenaphthene with 21% nitric acid in the presence of sodium nitrite as an initiator and NaCl as a promoter.[33] The process proceeds at room temperature and gives a quantitative yield of 5-nitro- and 3-nitroacenaphthenes (in a 90–93:10–7 ratio) after 40 min ($[acenaphthene]_o$=0.5 M. a 100:15 PhH–$PhNO_2$ mixture as an organic phase). In the absence of 8. the yield of the nitro compounds does not exceed 1%. even in 3 h. Noteworthy is that macrocycle 8 is stable under the nitration conditions for at least ! h and can be recovered from the reaction mixture in a 95% yield. Even greater activity in the nitration of acenaphthene with 21% HNO_3 is exhibited by macrocycle 9. in the presence of which a practically full conversion of the starting aromatic substrate into its nitro products is reached after 10 min.[34] According to the kinetic data. the introduction of 9 in the system increases the initial nitration rate by more than three orders of magnitude. Mercury dichloride and *bis*(perfluorophenyl)-mercury show no cataiytic activity.

Macrocycles 8 and **9** also catalyze the phase-transfer nitration of pyrene, acenaphthene and 1,3-dimethylnaphthalene with a mixture of sodium nitrite and 25.6% H_2SO_4 (i.e., with nitrous acid) in the presence of sodium chloride.[35] The reaction proceeds according to the following stoichiometric equation:

$$ArH + 3\ HNO_2 \rightarrow ArNO_2 + 2\ NO + 2\ H_2O$$

The highest nitration rates are observed for pyrene. which in the presence of 8 is quantitatively transformed into 1-nitropyrene within 9 min in a dinitrogen atmosphere ($[ArH]_o$=0.092 M. a $NaNO_2$:ArH molar ratio is 4:1). When the catalyst is absent. no nitration occurs for at least 4 h. The ability of 8 and **9** to transfer protons from an aqueous phase to benzene was also reported.[33,34] This result opens prospects for using macrocycles of such a type in the phase-transfer catalysis of acid-catalyzed reactions.

Mercuracarborand **17** and octamethyl derivative of 10. ($9.12\text{-}Me_2\text{-}o\text{-}C_2B_{10}H_8Hg)_4$ (20) were applied as catalysts for the Diels–Alder reactiori of a thionoester *trans*-MeCH=CHC(S)OMe with cyclopentadiene.[36] It was found that on carrying out the reaction in CH_2C1_2 at 0°C in the presence of 20 (diene:20=7.5:1, $[thioester]_o$=1 M) racemic mixtures of *endo* and *exo* adducts (in a 60 40 ratio) are formed with an 89% total ^{1}H-NMR yield (75% isolated yield) after 2 5 days When 17 is used as a catalyst almost exclusively, the *endo* isomer in a 94% 'H-NMR yield (83% recovered yield) is produced after 7.5 days under similar conditions. The replacement of *I f* or **20** by monodentate *bis*(*closo*-9,12-dimethyl-l,2-carboran-l-yl)mercury (21) leads to a further decrease in the rate of the process (65% isolated yield of the *endo* isomer after 11 days). in the absence of a catalyst or when HgI_2 or $Hg(OAc)_2$ were employed instead of **17** or 20, no reaction was observed. For an explanation of the greater activity level of macrocycle 28 as compared to **17** and **21** in this reaction. it was assumed that among the carboranylmercury compounds tested. only **20** is capable of cooperatively binding the C=S group of the thionoester by all Lewis acidic centers. Methyl crotonate does not form Diels–Alder adducts with cyclopentadiene in the presence of 17. 20. or **21**. which is due to its inability to coordinate with the mercury atoms, as indicated by ^{199}Hg-NMR spectra.

Anticrowns are also promising reagents for the development of a new type of anion-selective electrodes. The first success in this important area was achieved by Hawthorne et al.,[37] who described highly sensitive and selective chloride liquid/polymeric membrane electrodes based on mercuracarborand **11** as an ionophore and tridodecylmethylammonium chloride as a cationic additive. Optimized electrodes show a near-Nernstian behavior toward chloride anions over a wide concentration range and are characterized by a fast response time. short recovery time. long lifetime. insensitivity to pH changes over the pH range of 2.5–7.0 as well as by micromolar detection limits. Subsequently, highly selective optical sensors for chloride ions based on the same mercuracarborand **11** as an ionophore were developed.[38] In their selectivity coefficients toward chloride. both types of sensors meet the requirements for clinical applications.

CONCLUSION

Investigations of latter years led to the discovery of a novel class of highly efficient anion receptors–anticrowns that can be considered as charge-reversed analogues of crown ethers. The host–guest chemistry of anticrowns toward various anionic species was explored: the first promising results were also obtained on the use of anticrowns as catalysts and ionophores. The efficacy of the anion binding by anticrowns depends strongly on the Lewis acidity of metal centers incorporated in their macrocyclic chain. the number of these electron-deficient centers. and size of the macrocycle. The most effective anticrowns were found among perfluorinated polymercu-

ramacrocycles and mercuracarborands containing three. four. and five Lewis acidic Hg atoms in 9-. 10-, and 12-membered mercuracarbon rings. Various neutral Lewis bases such as nitriles. carbonyl compounds, aromatic hydrocarbons. and some others can also be bound by anticrowns. A unique feature of anticrowns is their capacity to bind Lewis basic species simultaneously by all Lewis acidic centers of the macrocycle. Such cooperative binding sharply increases the strength of the host–guest interaction and leads to the formation of complexes of unprecedented structures.

One of the serious problems of anticrown chemistry is a poor assortment of synthetic routes to these remarkable reagents. As a result, the range of the presently known anticrowns is narrow. being limited only by a number of polymercury-, polytin-, and polysilicon-containing macrocycles. One may expect that a successful solution of this important synthetic problem will lead to the wide application of anticrowns in various branches of chemistry.

ACKNOWLEDGMENTS

The authors wish to thank the Russian Foundation for Basic Research (Project code 02-03-33304) for financial support and Mr. Kirill I. Tugashov for his assistance in the preparation of the manuscript of this article.

ARTICLES OF FURTHER INTEREST

Anion-Directed Assembly. p. *51*
Cryptands, p. 334
Ionophores, p. 760
Organometallic Anion Receptors, p. 1056
Protonated Aza-Macrocycles for Anion Complexation, p. 1175
Secondary Bonding, p. *1215*

REFERENCES

1. Newcomb, M.; Madonik. A.M.: Blanda. M.T.: Judice. J.K. Macrocycles containing tin. ^{119}Sn NMR studies of chloride binding by Lewis acidic tin compounds. Organometallics 1987. 6. 145–150.
2. Newcomb, M.: Horner. J.H.: Blanda. M.T.; Squattrito. P.J. Macrocycles containing tin. Solid complexes of anions encrypted in macrobicyclic Lewis acidic hosts. J. Am. Chem. Soc. 1989. **111.** 6294–6301.
3. Jurkschat, K.; Kuivila. H.G.: Liu. S.: Zubieta, J.A. 1,5,9-Tristannacyclododecanes as Lewis acids. Novel structure of a chloride complex. Organoinetallics 1989. *8*. 2755–2759.
4. Jurkschat, K.; Rühlemann, A.: Tzschach, A. Synthese und transporteigenschaften von 1,1,6,6,11,11-hexamethyl-1.6.11-tristannacyclopentadecan. J. Organomet. Chem. 1990, *381*. C53–C56.
5. Jung, M.E.: Xia, H. Synthesis and transport properties of 12-silacrown-3, a new type of anion complexing agent. Tetrahedron Lett. 1988. *29*. 297–300.
6. Schulte, M.: Schiirmann, M.; Jurkschat, K. [*cyclo*-$CH_2\{Sn(Cl_2)CH_2Si(Me_2)\}_2O$]: Synthesis and complexation behavior of a novel, cyclic, bidentate Lewis acid and its conversion into a tin-containing fluorosilane with intermolecular Si-F···Sn bridges. Chern. Eur. J. 2001. 7. 347–355.
7. Brown, D.S.; Massey. A.G.; Wickens, D.A. A reinvestigation of o-phenylenemercurials (V) [I]: The crystal and molecular structure of inonoclinic tribenzo[b,e,h][1,4,7]trimercuronin. Inorg. Chim. Acta 1980. 44. L193–L194.
8. Shur. V.B.; Tikhonova. I.A.; Petrovskii, P.V.; Vol'pin, M.E. Complex formation between trimeric *o*-phenylenemercury and halide anions and the phase transfer catalysis of the azo-coupling reaction. Metalloorg. Khim. 1989. *2*, 1431–1432. [Organomet. Chem. USSR 1989, 2, 759–760 (Engl. Transl.)].
9. Ball. M.C.: Brown, D.S.: Massey. A.G.; Wickens, D.A. A reinvestigation of o-phenylenemercurials. IV. Adducts of perfluorotribenzo[*b,e,h*][1,4,7]trimercuronin and the crystal and molecular structure of its I:I 4-phenylpyridine solvate. J. Organomet. Chem. 1981. *206*, 265–277.
10. Sliur. V.B.; Tikhonova, I.A.: Uanovsky. A.I.: Struchkov, Yu.T.; Petrovskii. P.V.; Panov. S.Yu.; Furin. G.G.: Vol'pin. M.E. Crown compounds for anions. Unusual complex of trimeric perfluoro-o-phenylenemercury with the bromide anion having a polydecker sandwich structure. J. Organomet. Chem. 1991. *418*. C29–C32.
11. Shur. V.B.; Tikhonova. I.A.; Yanovsky, A.I.; Struchkov. Yu.T.: Petrovskii. P.V.; Panov. S.Yu.: Furin, G.G.; Vol'pin, M.E. Polydecker sandwich complex of trimeric perfluoro-*o*-phenylenemercury with iodide anion. Dokl. Akad. Nauk SSSR 1991. 321; 1002–1004. [Dokl. Chem. 1991, 321. 391-393 (Engl. Transl.)].
12. Antipin, M.Yu.; Struchkov. Yu.T.: Volkousky. A.Yu.; Rokhlin. E.M. X-ray study of 2,2,4,4,6,6,8,8,10,10-decakis(trifluoromethyl)-1,3,5,7,9-pentamercuracyclodecane $[(CF_3)_2CHg]_5 \cdot 2C_5H_5N \cdot 2H_2O$. Izv. Akad. Nauk SSSR. Ser. Khim. 1983. 452–455.
13. Tikhonova. I.A.; Dolgushin, F.M.; Yanovsky. A.I.: Struchkov. Yu.T.; Gavrilova, A.N.: Saitkulova. L.N.; Shubina, E.S.; Epstein. L.M.; Furin. G.G.; Shur. V.B. Crown compounds for anions. A polymeric complex of cyclic trimeric perfluoro-*o*-phenylenemercury with thiocyanate anion containing an infinite helical chain of alternating molecules of mercury-containing macrocycle and S C N ions. J. Organomet. Chem. 1996. 508, 271–273.
14. Chistyakov, A.L.: Stankevich. I.V.; Gambaryan, N.P.: Struchkov, Yu.T.; Yanovsky, A.I.; Tikhonova, I.A.; Shur, V.B. Crown compounds for anions. A new approach to the description of chemical bonds in the complexes of halide anions with polpmercury-containing macrocycles. J. Organomet. Cheni. 1997, *536–537*, 413–424.
15. Saitkulova, L.N.; Bakhmutova. E.V.: Shubina. E.S.;

Tikhonova, I.A.; Furin, G.G.; Bakhmutov, V.I.: Gambaryan. N.P.: Chistyakov, A.L.: Stankevich. I.V.: Shur. V.B.; Epstein, L.M. Crown compounds for anions. Spectroscopic and theoretical studies of complexation of borohydride anions with cyclic trimeric perfluoro-o-phenylenemercury. J. Organomet. Chem. 1999. *585*, 201–210.

16. Shubina. E.S.: Tilthonova, I.A.; Bakhmutova. E.V.: Dolgushin, F.M.: Antipin, M.Yu.; Bakhmutov, V.I.; Sivaev. I.B.; Teplitskaya. L.N.; Chirhevsky, I.T.; Pisareva, I.V.: Bregadze. V.I.; Epstein. L.M.; Shur. V.B. Crown compounds for anions: Sandwich and half-sandwich complexes of cyclic trimeric perfluoro-o-phenylenemercury with polyhedral *closo*-$[B_{10}H_{10}]^{2}$ and *closo*-$[B_{12}H_{12}]^{2-}$ anions. Chem. Eur. J. 2001. 7. 3783–3790.
17. Shur, V.B.: Tikhonova. I.A.; Dolgushin, F.M.; Yanovsky. A.I.: Struchkov, Yu.T.; Volkonsky, A.Yu.; Solodova. E.V.; Panov, S.Yu.: Petrovskii. P.V.: Vol'pin, M.E. Crown compounds for anions. A spinning top-shaped complex of cyclic pentameric perfluoroisopropylidenemercury with two chloride anions. J. Organornet. Chem. 1993, 443. C19–C20.
18. Shur. V.B.; Tikhonova, I.A.; Dolgushin. F.M.: Yanovsky, A.I.; Struchkov. Yu.T.; Volkonsky, A.Yu.; Petrovskii. P.V.: Solodova. E.V.; Panov, S.Yu.; Vol'pin, M.E. Crown compounds for anions. A spinning top-shaped complex of cyclic pentameric perfluoroisopropylidenemercury with two bromide anions. Dokl. Akad. Nauk 1993. 328. 339–341.
19. Tugashov, K.I.; Tikhonova. I.A.: Dolgushin. F.M.: Petrovskii, P.V.: Volkonsky, A.Yu.; Shur. V.B. Crown Coinpounds for Anions. Unusual Complexes of Cyclic Pentameric Perfluoroisopropylidenemercury with Sulphate, Acetate and Trifluoroacetate Anions. In Book *of Abstracts*, Mark Vol'pin (1923-1996) Memorial International Symposium "Modern Trends in Organometallic and Catalytic Chemistry", Moscow. Russia, May 18–23. 2003. 151.
20. Tikhonova. I.A.: Dolgushin. F.M.: Yanovsky, A.I.: Starikova, Z.A.: Petrol sltii. P.V.: Furin. G.G.: Shur. V.B. Complexation of cyclic trinieric perfluoro-*o*-phenylenemercury with nitriles. A remarkable sensitivity of the composition and structure of the resulting complexes to the nature of a nitrile. J. Organomet. Chem. **2000**. **613**. 60–67.
21. Tikhonova, I.A.; Dolgushin. F.M.; Tugashov. K.I.: Petrovskii, P.V.; Furin. G.G.; Shur, V.B. Coordination chemistry of polymercuramacrocycles. Complexation of cyclic trimeric perfluoro-*o*-phenylenemercury with neutral oxygeneous Lewis bases. J. Organomet. Chem. **2002**, *654*, 123–131.
22. King. J.B.: Tsunoda. M.: Gabbaï, F.P. Complexation of aldehydes and ketones by trimeric perfluoro-*ortho*-phenylene mercury. a tridentate Lewis acid. Organometallics 2002. 21. 4201–4205.
23. Haneline. M.R.: Tsunoda. M.: Gabbaï, F.P. π-Complexation of biphenyl. naphthalene. and triphenylene to trimeric perfluoro-*ortho*-phenylene mercury. Formation of extended binary stacks with unusual luminescent properties. J. Am. Chem. Soc. 2002. 124. 3737–3742.
24. Hawthorne, M.F.: Yang. X.: Zheng, Z. Host-guest chemistry of anion-complexation by macrocyclic multidentate Lewis acids. Pure Appl. Chem. 1994. 66, 245–254.
25. Hawthorne. M.F.; Zheng, Z. Recognition of electron-donating guests by carborane-supported multidentate macrocyclic Lewis acid hosts: Mercuracarborand chemistry. Acc. Chem. Res. **1997**. 30. 267–276.
26. Zinn, A.A.: Knobler, C.B.: Karwell. D.E.: Hawthorne, M.F. Molecular aggregates of nitrate ion with the tetravalent Lewis acid host 12-mercuracarborand-4: Novel trihapto coordination of NO_3^-. Inorg. Chem. **1999**, *38*. 2227–2230.
27. Lee, H.: Knobler, C.B.: Hawthorne. M.F. Octahedral coordination of halide ions (I^-, Br^-, Cl^-) sandwich bonded with tridentate mercuracarbovand-3 receptors. J. Am. Chem. Soc. 2001. 123. 8543–8549.
28. Lee, H.; Knobler, C.B.; Hawthorne. M.F. A hydrogen-bonded [(mercuracarborand–water)$_2$–benzene] π-sandwich complex. Angew. Chem. Int. Ed. **2001**. 40. 3058–3060.
29. Wuest. J.D.; Zacharie, B. Multidentate Lewis acids. Complex of macrocyclic tetradentate organomercuric perfluoroglutarate. J. Am. Chem. Soc. **1987**, 109, 4714–4715.
30. Wuest. J.D. Multiple coordination and activation of Lewis bases by multidentate Lewis acids. Acc. Chem. Res. 1999. 32, 81–89.
31. Nadeau, F.; Simard. M.; Wuest, J.D. Multidentate Lewis acids. Complex of a macrocyclic host with a bidentate guest. Organometallics 1990. 9. 1311–1314.
32. Vaugeois. J.: Simard, M.; Wuest, J.D. Quadruple coordination of the carbonyl oxygen atom of an amide by a cyclic tetradentate Lewis acid. Organometallics 1998, 17. 1215–1219.
33. Zaraisky. A.P.: Kachurin. O.I.; Velichko. L.H.: Tikhonova. I.A.; Furin, G.G.; Shur, V.B.: Vol'pin. M.E. Cyclic trimeric perfluoro-*o*-phenylenemercury as the phase transfer catalyst for nitration with dilute nitric acid. Izv. Akad. Nauk, Ser. Khirn. 1994. 547–548. [Russ. Chem. Bull. 1994. 43. 507–508. (Engl. Transl.)].
34. Zaraislty. A.P.; Kachurin. 0.1.; Velichko, L.I.; Tikhonova, I.A.: Volkonsky. A.Yu.: Shur. V.B. New highly efficient phase transfer catalyst for nitration with dilute nitric acid. Izv. Akad. Nauk. Ser. Khim. 1994, 2047–2048. [Russ. Chem. Bull. 1994, 43. 1936–1937. (Engl. Transl.)].
35. Zaraisky. A.P.: Kachurin. O.I.; Velichko, L.I.; Shur. V.B.: Tikhonova. I.A.: Furin, G.G. Phase transfer catalysis in reactions of electrophilic substitution. VIII. Phase transfer catalytic nitration of arenes with sodium nitrite in an acidic medium. Zh. Org. Khim. **1999**, *35*. 1063–1067.
36. Lee. H.; Diaz. M.: Hawthorne. M.F. Mercuracarborand-catalyzed Diels–Alder reactions of a thionoester with cyclopentadiene. Tetrahedron Lett. 1999, 40. 7651–7655.
37. Badr. I.H.A.: Diaz. M.: Hawthorne, M.F.; Bachas, L.G. Mercuracarborand "anti-crown ether"-based chloride-sensitive liquid/polymeric membrane electrodes. Anal. Chem. 1999. 71. 1371–1377.
38. Badr. I.K.A.: Johnson. R.D.: Diaz. M.: Hawthorne. M.F.; Bachas. L.G. A selective optical sensor based on [9]mercuracarborancl-3. a new type of ionophore with a chloride complexing cavity. Anal. Chem. **2000**. 72. 4249–4254.

Artificial Enzymes

Jun-ichi Kikuchi
Nara Institute of Science and Technology, Nara, Japan

Hiroki Kondo
Kyushu Institute of Technology, Fukuoka, Japan

INTRODUCTION

Study of artificial enzymes began as early as in the mid-twentieth century in pioneering work on enzyme model reactions.[1–3] On the basis of a vast amount of findings on structures and catalytic mechanisms of naturally occurring enzymes from the physical, chemical, and bioiogical viewpoints, we can now discuss the properties and reactions of enzymes in great detail at the molecular level. In general, enzymes are ingeniously designed biocatalysts. exhibiting marked rate enhancement. high substrate specificity. and distinct reaction selectivity under mild reaction conditions. Such characteristic features of enzymes are generated essentially through the formation of specific enzyme–substrate complexes as key intermediates. On these grounds. various artificial enzymes capable of performing substrate-binding behavior were developed up to the present time. In addition, while well-known hydrolases such as α-chymotrypsin, lysozyme, and ribonuclease do not require cofactors, many enzymes exhibit catalytic activity in collaboration with coenzymes and metal ions. For simulation of the latter class of enzymatic reactions, molecular design of artificial holoenzymes comprising an apoenzyme model and a cofactor is important.[5–8] Artificial enzymes can be classified mainly into the following three categories: macrocyclic compounds, molecular assemblies. and macromolecules.

MACROCYCLIC COMPOUNDS AS ARTIFICIAL ENZYMES

In general. the active site of an enzyme is regarded as a hydrophobic cavity or cleft created by folding of the polypeptide chain. Such a substrate-binding site is provided by macrocyclic compounds such as cyclodextrins[9] ((Fig. 1). crown ethers,[10–12] cyclophanes,[13–15] and calixarenes.[16–18] each having an inclusion cavity as a basic skeleton of potent artificial enzymes.

Cyclodextrins (1) are cyclic glucose oligomers of cylindrical shape having primary hydroxyl groups at the more restricted rim of the cylinder. The three most common cyclodextrins are α-, β-, y-species, which are composed of six. seven, and eight giucopyranose units. respectively. In early work in the 1950s and 1960s, it was shown that the oxyanion of cyclodextrin could react with pyrophosphates and carboxylate esters bound in the cyclodextrin cavity in aqueous media. and that acyl-group transfer from the esters could be accelerated with moderate substrate selectivity. Since then, many kinds of modified cyclodextrins were developed by introducing a catalytic group selectively into the primary or the secondary hydroxyl moieties. By employing the functional groups similar to those in the side chain of amino acids. such as imidazolyl and thiol groups. the resulting cyclodextrin derivatives were expected to serve as mimics of hydrolases. In fact. cyclodextrins bearing a metal-binding site worked as hydrolytic metalloenzyme models. Various functionalized cyciodextrins bearing a cofactor, such as vitamin B_1, B_2, B_6, B_{12}, nicotinamide. or porphyrin. were prepared as holoenzyme models. The introduction of multiple functional groups into cyclodextrins is essential to design more sophisticated artificial enzymes. For example. a β-cyclodextrin bearing two imidazolyl groups *(2)* acts as an excellent artificial ribonuclease. showing turnover behavior possibly through bifunctional catalytic assistance of the imidazolyl groups. A compound **(3)** carrying a pyridoxamine and an ethylenediamine unit attached to β-cyclodextrin on the neighboring primary methylene groups behaved as a potent artificial aminotransferase. Aromatic L-α-amino acids such as phenylalanine, tryptophan. and phenylglycine were generated with high (90–96% ee) enantiomeric excess by the catalysis of **3.** In addition, the prototropy rate observed with 3 was drastically enhanced relative to simple pyridoxamine. However. the true catalytic cycle, exhibiting amino group transfer from an α-amino acid to an α-keto acid. was not successful with this modified cyclodextrin.

While cyclodextrins are used as enzyme mimics in aqueous media, crown ethers can act as a key component of artificial enzymes in organic solutions (Fig. 2). Crown ether was discovered by Pedersen in 1967.[10] which

Encyclopedia of Supramolecular Chemistry
DOI: 10.1081/E-ESMC 120012839

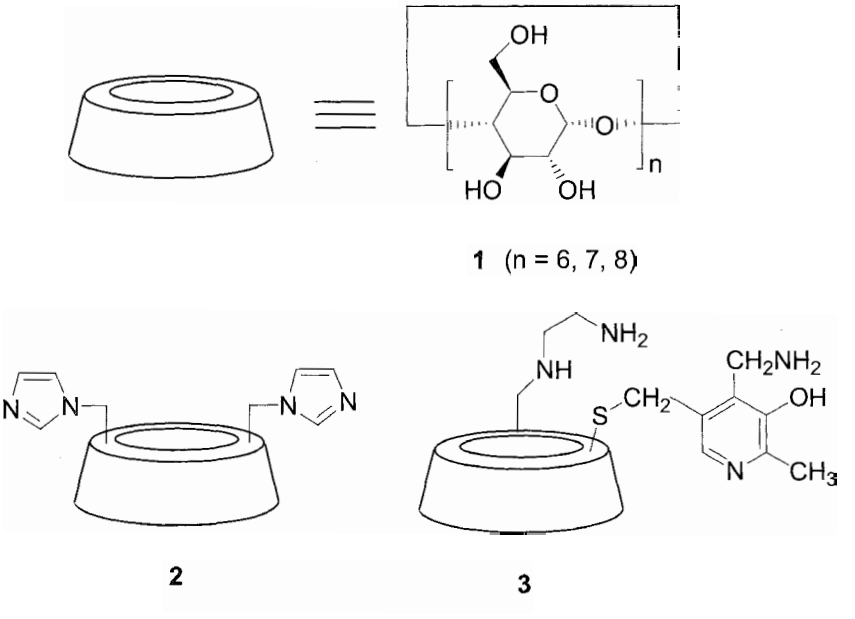

Fig. 1 Cyclodextrin (1) and its derivatives (2 and 3) as artificial enzymes.

eventually won him, together with Cram and Lehn. the Nobel prize in 1987. This discovery triggered the research on host–guest chemistry and artificial enzymes at large, including practical applications. For example. binding of a pyridinium substrate to a crown ether bearing dihydronicotinarnide moieties (4) led to enhancement of the hydrogen-transfer rate from the dihydropyridine moiety to the pyridinium within the intermediate complex in acetonitrile. In addition, the potentiality in enantioselective reductions was examined with a series of chirally bridged macrocyclic 1,4-dihydropyridines of crown ether type. In the reduction of ethyl benzoylformate by 5 having L-valine residues in the macrocyclic skeleton. (*S*)-mandelate was obtained with an enantiomeric excess of 90% in

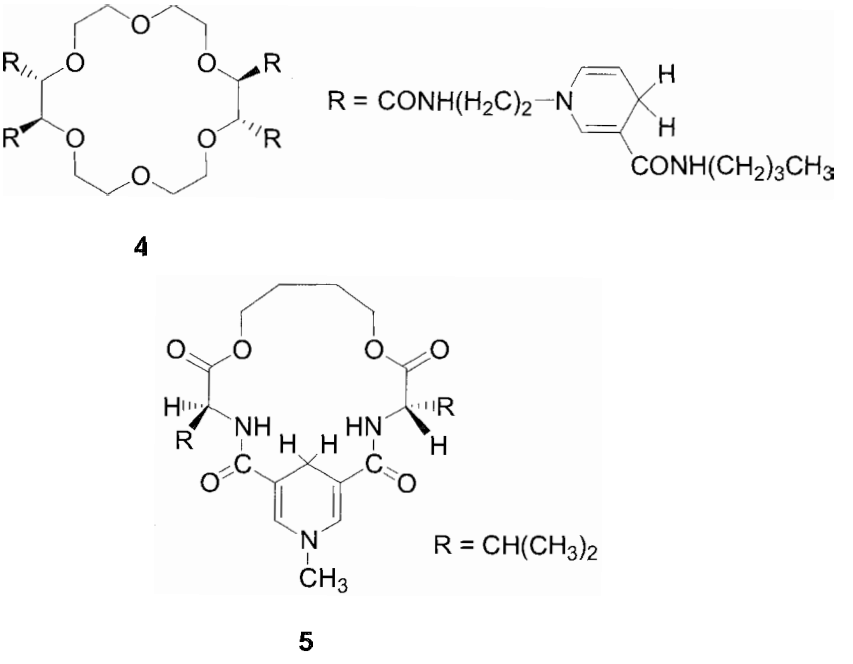

Fig. 2 Examples of crown ether derivatives (4 and 5) as artificial enzymes

acetonitrile-chloroform at room temperature in the presence of Mg(II) ions.

Cyclophanes with a sizable internal cavity also proved to be useful as supramolecular elements of artificial enzymes. While a relatively limited range of st uctural modifications is possible with cyclodextrins. a wide synthetic variation of cyclophanes can be achieved so that an appropriate recognition site with regard to size. shape, and microenvironment is provided for a target substrate molecule. In an early study in the 1970s. [20]paracyclophanes and [10.10]paracyclophanes were employed to demonstrate that cyclophanes are effective as macrocyclic enzyme models. Since then; various cyclophane derivatives were developed as artificial enzymes. While binding constants of simple cyclodextrins with typical substrates in aqueous media are ca. $10^4\ M^{-1}$ or less in general, the substrate-binding ability can be enhanced by various types of molecular design of the cyclophane skeleton, especially by creating three-dimensionally extended hydrophobic cavities. Enzyme mimetic reactions catalyzed by the artificial enzymes of cyclodextrin type would be duplicated and improvable by employing functionalized cyclophanes. For example, the octopus cyclophane (6) bearing eight hydrocarbon chains on a macrocyclic tetraazacyclophane ring provides a large and flexible hydrophobic cavity in which to incorporate as large as a hydrophobic vitamin B_{12} derivative (7) through the induced-fit mechanism (Fig. 3). The resulting host–guest complex acted as an efficient vitamin B_{12}-dependent artificial holoenzyme. showing turnover behavior for carbon-skeleton rearrangement reactions specifically catalyzed by methylmalonyl-CoA mutase and glutamate mutase. In addition, this artificial enzyme also catalyzed unique ring-expansion reactions for which naturally occurring vitamin B_{12}-dependent enzymes are not known.

Calixarenes developed by Gutsche[16] belong to a family of cyclophanes by definition. and much attention has focused on their catalytic functions as artificial enzymes based on their versatile molecular recognition

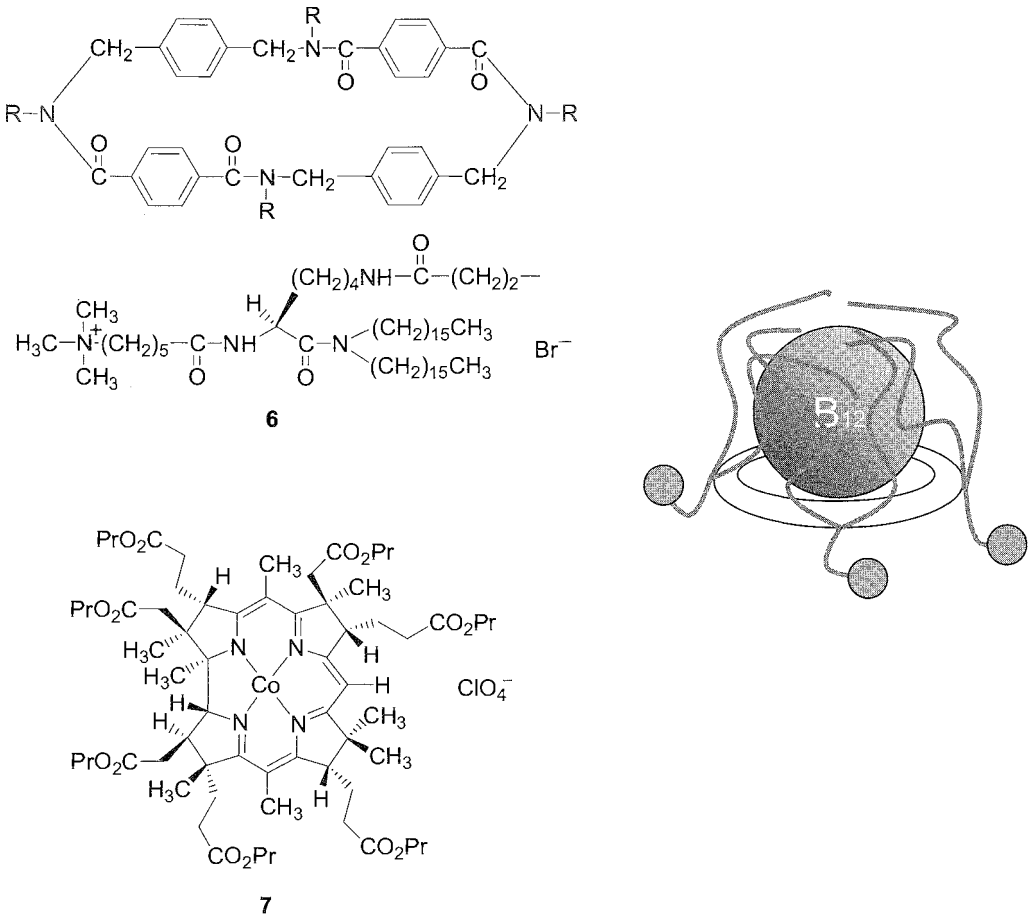

Fig. 3 An example of artificial holoenzyme formed with the octopus cyclophane (6) and the hydrophobic vitamin B_{12} derivative (7). (*View this art in color at www.dekker.com.*)

abilities. Other macrocyclic compounds such as cryptands, spherands. and cucurbiturils seem to be feasible as equally promising enzyme mimics.

MOLECULAR ASSEMBLIES AS ARTIFICIAL ENZYMES

There is another type of enzyme mimics that provide a substrate-binding site as a result of self-aggregation of functional elements through noncovalent intermolecular interactions in solution: reversed micelles in organic solutions. and micelles and lipid bilayer membranes in aqueous media.[4,18–21]

Reversed micelles formed with various surfactants in apolar solvents in the presence of small amounts of water were extensively studied on their characteristic features of cores in enzyme-mimetic reactions. In the spatially restricted microenvironment of reversed micelles, a unique catalytic behavior analogous to enzymatic reaciions was observed.

Aqueous micelles are typical and simple aggregates of surfactants, and numerous applications as enzyme models were accumulated up to 1980 (Fig. 4). In general, molecular structures characteristic of micelle-forming amphiphiles are composed of a polar head moiety, a long hydrophobic chain, and in some cases; an additional functional group for effective catalysis. Cationic amphiphiles having an imidazolyl (8)or a thiol moiety (9) in the polar head are typical examples. While micelles provide hydrophobic reaction sites effective for the acceleration of various enzyme-mimetic reactions, those aggregates are generally soft, and it is difficult to fix the disposition of substrates in space for regio- and siereospecificity of reactions to appear.

Another type of well-known molecular aggregate in an aqueous media is a bilayer membrane. In general. the bilayer membrane is superior to aqueous micelles with respect to aggregate rigidity and spacial orientation of component molecules, so that substrate specificity. catalytic activity. and reaction selectivity are more readily exhibited. In addition. phase states, gel and liquid crystalline, and phase-separation behavior among the component species can be utilized to control catalytic pathways.

Preparation and characterization of liposomes formed with natural phospholipids were well established. However, in using liposomes for simulation of enzymatic functions, especially in acid–base catalysis. difficulties would be encountered due to their chemicai and morphological instabilities. Thus, bilayer membranes composed of synthetic amphiphiles are more favorable candidates for enzyme mimics. For example, artificial vitamin B_6-dependent enzymes were constructed from catalytic bilayer membranes in combination with a bilayer-forming peptide lipid (**10**), a hydrophobic vitamin B_6 derivative (**11**), and metal ions (Fig. *5)*. The catalyst acts as an artificial aminotransferase. showing marked substrate specificity, high enantioselectivity, and turnover behavior for the transamination of α-amino acid with α-keto acids. In addition. the reaction fields provided by the catalytic bilayer membranes are suitable to establish multienzyme systems through functional alignments of artificial enzymes and natural ones in a sequential manner.

MACROMOLECULES AS ARTIFICIAL ENZYMES

On the basis of structural resemblance to enzymes, various kinds of macromolecules were developed as artificial enzymes. These macromolecules are classified mainly into two categories: modification of biopolymers and totally synthetic functional polymers.

The design of artificial enzymes through site-directed rnutagenesis is well established.[22] By single or muitiple replacement of an amino acid residue placed in the enzyme protein, enzymatic functions such as reactivity, substrate specificity. and reaction selectivity, can be altered. Although the site-directed rnutagenesis gives rise to only a small change in the amino acid sequence of a target protein, such modification can induce a drastic change in the catalytic behavior. Incorporation of unnatural amino acids and nonamino acids into proteins is also possible.

Development of catalytic antibodies or abzymes is another fascinating approach to artificial enzymes.[5] The concept of catalytic antibodies is that if a putative transition state analogue of a reaction for which a selective and efficient catalyst is desired is used to elicit antibodies,

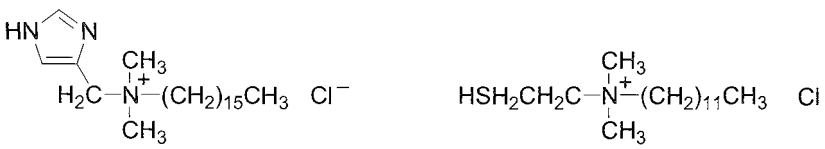

8 **9**

Fig. 4 Examples of micelle-forming amphiphiies (8 and 9) as a component of artificial enzyme

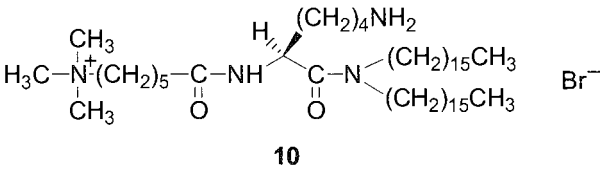

10

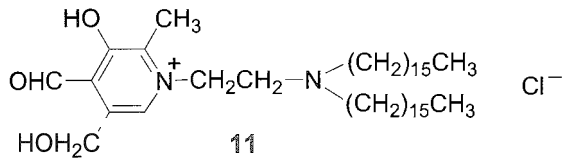

11

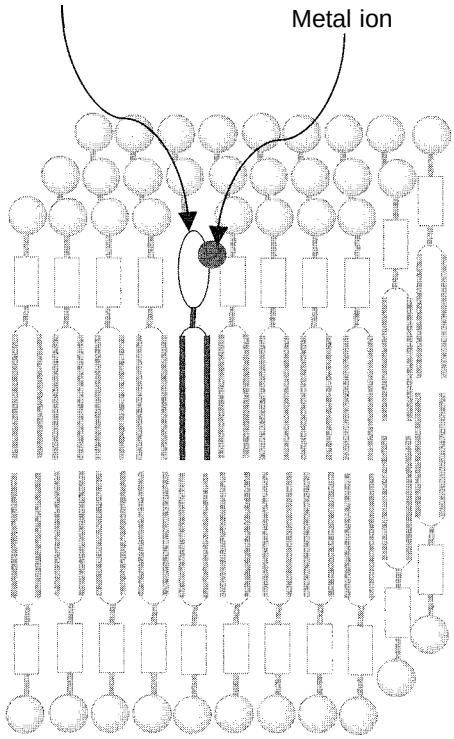

Fig. 5 An example of an artificial holoenzyme formed with the bilayer-forming peptide lipid (10). the hydrophobic vitamin B_6 derivative (11), and metal ions..(*View this art in color at www.dekker.com.*)

they are likely to catalyze the reaction of a parent compound. Because antibodies are specialized only for binding of ligands called antigens or haptens, semisynthetic strategies for introducing catalytic functionalities into the active site of an antibody is additionally necessary in some cases. Catalytic antibodies were elicited for reactions for which no enzyme exists. such as the Diels–Alder reaction, Claisen rearrangement. and oxy-Cope rearrangement.

Although the site-directed mutagenesis and catalytic antibody technique are useful genetic methods, chemical modification of enzymes remains a valuable tooi for protein engineering. The latter approaches are divided into direct modification of an enzyme protein and modification of a cofactor bound to the enzyme.[23–26] These chemical methods led to modification of existing enzyme activity or introduction of new enzyme functions into proteins and enzymes.

As regard to enzyme mimics formed with totally synthetic polymers, relatively simple water-soluble polymers with catalytic functionalities were employed in the early work before 1980.[4] Although simulation of enzymatic behavior was successful to a certain extent by employing such prototype models, recent interests focused on more intelligent synthetic polymers, such as imprinted polymers[5] and dendrimers.[27]

When a polymer is prepared in the presence of "print molecules" as the transition state or intermediate analogues, which are extracted after polymerization. the remaining polymer may contain catalytic cavities capable of recognizing the print molecules. By analogy to the catalytic antibodies. where a function complementary to that of the hapten can be induced in a specific place, polymers can be imprinted with print molecules containing suitable catalytic functionalities. Because dendrimers are structurally regulated polymers with an inner core like an enzyme active site, their characteristics as enzyme mimics also attract attention.

CONCLUSION

In recent years. the traditional definition of biocatalysts with enzymes that are proteins having catalytic functions in biological systems was expanded to a point where a series of ribonucleic acids, called ribozymes, also acts as a biocatalyst. Much effort was devoted to developing artificial ribozymes as well."'' In such approaches: a combination of strategies to mimic ribonucleases and to simulate complementary molecular recognition of nucleic acids is essential.

As mentioned above, studies on artificial enzymes were extensively developed to date. Although the catalytic performance of artificial enzymes rarely surpasses that of the corresponding naturally occurring enzymes from every point of view, some of them close in on catalytic performance of the natural counterparts. In addition, advantages of artificial enzymes relative to those of natural ones are flexibility in molecular design, structural stability, and possible applications to substrates and reactions for which natural enzymes are not available.

One of the targets in the study of artificial enzymes would be creation of integrated reaction systems on the nanometer scale inspired by the reaction network in cells. from the viewpoint of nanoscience and nanotechnology. For such a purpose, construction of artificial multienzyme systems. collaboration between enzymes and receptors,

and synchronization of individual supramolecules seem to be essential.[7 21,25,29]

ARTICLES OF FURTHER INTEREST

Biological Models and Their Characteristics, p. 101
Carbonic Anhydrase Models: p. *178*
Enzyme Mimics. p. 546
Enzymes: Characteristics and Mechanisms, p. 554
Ion Channels and Their Models, p. *742*
Molecular-Level Machines. p. *931*
O_2 Uptake and Transport, Models of. p. *1023*
Selectivity: Thermodynamic and Kinetic. p. 1225
Vitamin B_{12} and Heme Models, p. 1569
Zinc-Containing Enzymes and Their Models, p. 1631

REFERENCES

1. Bruice, T.C.: Benkovic. S.J. *Bioorganic Mechanisms*; W.A. Benjamin Inc.: New York, 1966.
2. Jencks, W.P. *Catalysis in Chemistry and Enzymology*; McGraw-Hill: New York, 1969.
3. Bender. M.L. *Mechanisms of Homogeneous Catalysis from Protons to Proteins:* Wiley Interscience: New York, 1971.
4. Fendler. J.H.: Fendler, E.J. *Catalysis in Micellar and Macromolecular Systems*; Academic Press: New York, 1975.
5. Feiters. M.C. Supramolecular Catalysis. In *Comprehensive Supramolecular Chemistry*; Atwood. J.L., Davies, J.E.D.. MacNicol. D.D.. Vigtle. F., Lehn. J.-M., Reinhoudt. D.N.. Eds.: Pergarnon: Oxford. 1996: Vol. 10. 268–360.
6. Ogoshi, H.: Mizutani, T. Biomimetic Reactions Catalyzed by Metalloporphyrins. In *Comprehensive Supramolecular Chemistry*; Atwood, J.L., Davies, J.E.D.. MacNicol, D.D.. Vigtle. F., Lehn, J.-M.. Murakami. Y., Eds.; Pergamon: Oxford. 1996; Vol. 4, 337–385.
7. Murakami. Y.: Kikuchi. J.; Hisaeda. Y.: Hayashida, O. Artificial enzymes. Chem. Rev. 1996. 96 (2). 721–758.
8. Ridder. A.M.; Kellogg, R.M. Models for Zinc-Containing Enzymes. In *Comprehensive Supramolecular Chemistry*; Atwood. J.L.. Davies. J.E.D.. MacNicol. D.D.. Vigtle. F.. Lehn. J.-M.. Murakami, Y., Eds.; Pergamon: Oxford, 1996: Vol. 4, 387–413.
9. Breslow, R.: Dong, S.D. Biomimetic reactions catalyzed by cyclodextrins and their derivatives. Chem. Rev. 1998. 98 (5), 1997–2011.
10. Pedersen. C.J. The discovery of crown ether. Angew. Chem., Int. Ed. Engl. 1988. 27 (8). 1021–1027.
11. Cram. D.J. The design of molecular hosts. guests. and their complexes. Angew. Chem.. Int. Ed. Engl. 1988. 27 (8). 1009–1020.
12. Lehn. J.-M. Supramolecular chemistry—Scope and perspectives. Molecules. supramolecules. and molecular devices. Angew. Chem.. Int. Ed. Engl. 1988. 27 (1). 89–112.
13. Murakami. Y. Functionalized cyclophanes as catalysts and enzyme models. Top. Curr. Chem. 1983, *115*, 107–155.
14. Murakami. Y.: Kikuchi. J.: Hisaeda. Y. Catalytic Applications of Cyclophanes. In *Inclusion Compounds*; Atwood, J.L.. Davies. J.E.D.. MacNicol. D.D., Eds.; Oxford Univ. Press: Oxford, 1991: Vol. 4. 448–478.
15. Seel, C.; Vigtle. F. Molecules with large cavities in supramolecular chemistry. Angew. Chem., Int. Ed. Engl. 1992. *31*, 528–549.
16. Gutsche. C.D. Calixarenes. In *Monographs in Supramolecular Chemistry*; Stoddart. J.F.. Ed.; The Royal Society of Chemistry: Cambridge, England. 1989: Vol. 1.
17. *Calixarenes: A Versatile Class of Macrocyclic Compounds:* Vecens, J.. Bíhmer. V., Eds.; Kluwer Academic Publishers: Dordrecht, 1991.
18. Fendler, J.H. *Membrane Mimetic Chemistry*; John Wiley & Sons: New York, 1982.
19. Kunitake. T. Synthetic bilayer membranes: Molecular design, self-organization. and application. Angew. Chem., Int. Ed. Engl. 1992. 31. 709–726.
20. Murakami. Y.: Kikuchi. J. Supramolecular Assemblies Formed with Synthetic Peptide Lipids. Functional Models of Biomembranes and Enzymes. In *Bioorganic Chemistry Frontiers*: Dugas, H., Ed.; Springer-Verlag: Berlin. 1991: Vol. 2. 73–113.
21. Murakami. Y.: Kikuchi. J.: Hisaeda, U.: Ohno. T. Artificial Enzymes with Vitamin B_6 and B_{12} Activity. In *Comprehensive Supramolecular Chemistry*; Atwood, J.L., Davies. J.E.D.. MacNicol, D.D.. Vígtle, F.. Lehn, J.-M., Murakami, Y., Eds.; Pergamon: Oxford. 1996; Vol. 4, 415–472.
22. Kondo. H. Towards Design of Artificial Enzymes and Receptors Through Site-Directed Mutagenesis of Proteins. In *Comprehensive Supramolecular Chemistry*; Atwood, J.L.. Davies, J.E.D.. MacNicol. D.D.. Vigtle, F., Lehn. J.-M.. Murakami. Y.. Eds.; Pergamon: Oxford. 1996: Vol. 4, 528–547.
23. Kaiser, E.T.: Lawrence. D.S. Chemical mutation of enzyme active sites. Science 1984. *226*, 505–511.
24. Qi, D.: Tann. C.-M.; Haring, D.: Distefano. M.D. Generation of new enzymes via covalent modification of existing proteins. Chem. Rev. 2001. *101* (10), 3081–3111.
25. Hayashi, T.: Hisaeda, Y. New functionalization of myoglobin by chemical modification of heme-propionates. Acc. Chem. Res. 2002. *35* (1). 35–43.
26. Hamachi. I.; Watanabe. J.; Eboshi. R.: Hiraoka. T.; Shinkai, S. Incorporation of artificial receptors into a protein/peptide surface: A strategy for on/off type of switching of semisynthetic enzymes. Biopolymers 2000, *55* (6). 459–468.
27. Astruc, D.: Chardac, F. Dendritic catalysts and dendrimers in catalysis. Chem. Rev. 2001, *101* (9). 2991–3023.
28. Trawick, B.N.; Daniher. A.T.: Bachkin. J.K. Inorganic mimics of ribonucleases and ribozymes: From random cleavage to sequence-specific chemistry to catalytic antisense drugs. Chem. Rev. 1998, 98 (3). 939–960.
29. Kikuchi, J.: Ariga, K.: Sasaki. Y. Molecular Recognition and Functional Connection in Lipid Membranes. In *Advances in Supramolecular Chemistry*; Gokel, G.W., Ed.: Cerberus Press: Miami. 2001: 131–173.

Aurophilic Interactions

Antonio Laguna
Universidad de Zaragoza—CSIC, Zaragoza, Spain

Eduardo J. Fernández
José M. López-de-Luzuriaga
Universidad de La Rioja, UA—CSIC, Logroño, Spain

INTRODUCTION

The word "aurophilic." derived from the Latin word ''Aurum'' (gold) and the Greek word ''Philos'' (with an affinity for). was coined in the late 1980s[1–3] to describe the tendency of gold(I) compounds to form dimers. oligomers, chains. or even layers via gold(I)–gold(I) interactions. In these interactions. the distances between the adjacent gold atoms range from *2.7–3.6* A. and are shorter than the sum of their van der Waals radii (3.6 A). These interactions have a strength between 20–50 kJ/mol, close to that found in hydrogen bonds. This result is surprising. as two gold(I) centers with an external d^{10} configuration would normally be expected to repel each other. In addition. gold attractions are already present in metallic gold; where the gold–gold distances are shorter than the corresponding silver–silver distances. This phenomenon, although it can be consider a general feature when comparing the metallic radii of the second- and third-row elements. cannot be considered as the result of a lanthanoid contraction, because the rest of the "anomalies" of gold. such as its high electroaffinity and electronegativity or the presence of highly stable Au_2 molecules in the gas phase. cannot be explained in these terms. Of course. with these properties. it is considered to be the "king of the metals."

THEORETICAL CONSIDERATIONS

The latest contributions of physicists and the theoretical chemists to the explanation of this phenomenon stem from the results of ab initio and density functional theory calculations.. which refute the previous *s-d* hybridization proposed by the extended Hückel theory. They suggest that the metallophilic attraction can be considered a correlation effect strengthened by the relativistic effect. which is important in the case of gold.[4,5]

Postlanthanide elements have a large number of protons in their atomic nuclei *(79* protons for gold). Moreover, the electrons move in a field with a high nuclear charge, and therefore. their speed is similar to that of light. Electrons moving at such a speed cannot be treated in terms of classical physics. rather they have to be treated on the basis of Einstein's Theory of Relativity: $m_r=m_o(1-v^2/c^2)^{-1/2}$. According to this equation. the relativistic mass (m_r) of these electrons is larger than the conventional nonrelativistic mass (m_o), resulting in a contraction of orbital radius. This effect. known as relativistic contraction. is particularly important for the orbitals with radial functions that have local maxima in the neighborhood of the nucleus, pa ticularly in the s-orbitals. Thus, the expected marked effect on the Is electrons of postlanthanide elements also has continuity in the 2s. 3*s*, 4*s*, 5s. and *6s* orbitals. as they are orthogonal to one another. The ratio of the relativistic radius of the valence electrons to their nonrelativistic radius as a function of the atomic number strongly deviates from unity and reaches a local minimum for gold. Therefore, gold occupies a unique position among all the elements.

The main consequences for gold are that the energy gap between the 5*d*. 6*s*, and 6*p* orbitals diminishes. the closed-shell configuration $5d^{10}$ is no longer chemically inert. and the interaction between two gold(I) centers can be explained. Furthermore. the formation of linear two-coordinate gold(%)complexes is also favored.

Let us analyze some examples where this interaction is present. These examples establish a great affinity between gold atoms, which are as close as possible to each other and. generally, at distances even shorter than the ones found in metallic gold (2.88 A). We excluded gold clusters with formal metal–metal bonds and oxidation states between 0 and +i from the description. We will refer only to the interactions among atoms with closed-shell configurations.

GOLD(I)–GOLD(I) INTERACTIONS

The term "aurophilic interactions" was first coined in connection with the chemistry of gold(I). Gold(I)

Encyclopedia of Supramolecular Chemistry
DOI: 10.1081/E-ESMC 120012925

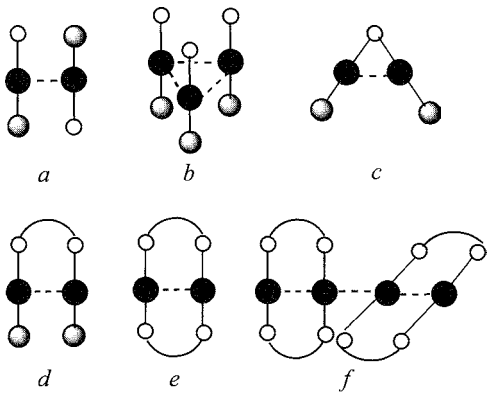

Scheme 1 Some attractive interactions in gold(I) complexes.

complexes are of general formula X-Au-L, where the ligands X and *L* may be neutral or anionic and have a linear geometry. After the advent of crystal structure analysis in the 1960s, it became apparent that virtually all such complexes are packed or arranged in such a way that the gold(I) atoms are as close as possible to each other. This attractive interaction gathers the gold atoms in pairs, rings, chains. or even layers (Scheme 1).

As can be seen in the scheme, the presence of ligands acting as bridges between the gold centers favors the appearance of such interactions *(c.d, e, f)* and, sometimes, ligands have even been considered responsible for their presence. In the e case, inter- and intramolecular interactions are present in the same molecule. Nevertheless, the existence of these interactions is undoubtedly evident in hundreds of examples of nonbridged complexes (types *a* and b), where the distances between the adjacent gold atoms depend on the electronic nature of the ligands and their steric requirements.[6–10] A particularly sophisticated structural arrangement appears in the complex $[Au(C_5H_5NS)_2]ClO_4$, where five of the six cations in the unit cell are linked to one another by short Au···Au contacts leading to a linear chain. The sixth cation is inonomeric and does not show interaction with other cations.[10] In the *c* case. dinuclear complexes with two gold centers bonded by a monoatomic bridge ligand are limited to elements of the 16 and 17 groups. Therefore, the structure proves the existence of metal–metal interactions in the cationic complex $[Au_2(\mu\text{-}Cl)(PPh_3)_2]ClO_4$[11] or the neutral derivatives $[Au_2(\mu\text{-}X)(PPh_3)_2]$ (X=S,[12] Se[13]). In these examples, the environment surrounding gold is almost linear and, interestingly. the Au-X-Au angle is shorter than expected from the involvement of p orbitals of the heteroatom.

An aryl group can also act as a bridging ligand, bonding the two metal atoms with a carbon center. This is the case of the complex $[Au_2(\mu\text{-}C_6F_3H_2)(PPh_3)_2]ClO_4$ obtained by substituting the chloro atom of the chloro-bridged complex by its reaction with $[Ag(2,4,6\text{-}C_6F_3H_2)]$ In this case, due to the narrow Au-C-Au angle (79 3°), a three-center two-electron bond was suggested [14]

Other amazing cases of a single atom bridging more than two gold(I) metal centers are the complexes with O,[15] S [16] Se [17] N [18,19] P [20] or C,[21 22] which include striking cases of hypervalence at these atoms, a situation unknown to typical p-block chemistry or postulated as an unstable intermediate. In these examples, the aurophilic interactions seem to be the driving force that stabilizes these complexes and determines their geometry. For example. the complex $[S(AuPPh_3)_4]^{2+}$ adopts a pyramidal structure instead of the expected tetrahedral one (Fig. 1).

On the other hand, some complexes that attracted considerable attention for the study of aurophilicity are the homo- or heterobridged diauracycles. In these complexes, the two metallic centers are bonded by two bidentate ligands such as diphosphines, *bis*(ylide) or dithiocarbamates, and intra- or intermolecular interactions appear. In most of the examples described, it is possible to observe a deviation from linearity around the gold centers caused by gold–gold interactions. Besides, the nature of the bridging ligands also has an impact on their strength. Thus. while $[Au_2(\mu\text{-}S_2CNEt_2)_2]$ has gold–gold distances of 2.782 (intramolecular) and 3.004 Å (intermolecular), the heterobridged complex $[Au_2(\mu\text{-}(CH_2)_2PPh_2)(\mu\text{-}S_2CNEt_2)]$ shows distances of 2.865 (intramolecular) and 2.9839 Å (intermolecular), and the complex $[Au_2(\mu\text{-}(CH_2)_2PPh_2)_2]$ only has an intramolecular distance of 2.977 Å.[23]

A hexanuclear complex with three pairs of gold atoms displaying short contacts can be obtained by using *bis*-(diphenylphosphino)methanediide as ligand. which can act as an eight-electron donor bonded to four gold atoms. The reaction of $[Au_2(\mu\text{-}(PPh_2)_2CH)_2]$ with $[Au(PPh_3)(tht)]ClO_4$ leads to a tetranuclear derivative that can be further deprotonated by reaction with [Au(acac)(PPh3)] to give the hexanuclear complex[24] (Scheme 2).

On the other hand, and as we already mentioned. gold(I) usually has a linear two-coordinate geometry. Nevertheless, three- and four-coordination. although much less abundant, is also well established.'''' Unlike linear coordination, where the gold(I) molecules are often

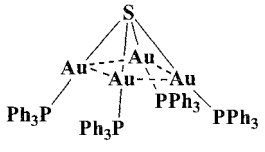

Fig. 1 Structural arrangement of the cation $[S(AuPPh_3)_4]^{2+}$.

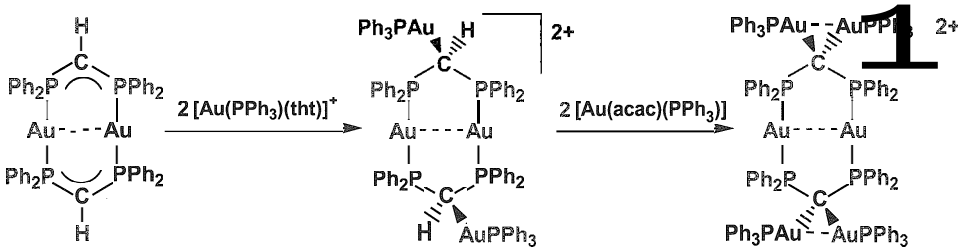

Scheme 2 Reactions from $[Au_2(\mu\text{-}(PPh_2)_2CH)_2]$

associated to form dimers, trimers. chains. or even layers through gold–gold interactions. in the rest of geometries, the presence of these interactions is almost an anecdote. Thus, there are a few cases reported. and most are examples of gold diauracycles, where solvent molecules or anions, with a coordinating capacity, interact with one or more gold centers. For instance, this is the case of the complex $[Au_2Cl_2(dppm)_2]$[26] with a gold–gold distance of 3.028 Å, visibly longer than that of the homologous $[Au_2(dppm)_2](BF_4)_2$ complex[27] with a distance of 2.931 Å, and with anions that do not interact with the gold atoms. In addition, the ligand coordination causes a small deviation from the original linearity in the L-Au-L angles.

An outstanding example of mixed coordination numbers and geometries of gold(I) is the complex $[Au_2(PPh_3)_3(SCH_2CH(OH)CH_2OH)](BF_4)$, where the coordination spheres of the two gold atoms are completely different. One of the atoms has a conventional linear two-coordination. whereas the other has a slightly distorted trigonal planar coordination with one sulfur and two phosphorus atoms. The gold centers exhibit a short gold–gold contact of 3.0162 Å, which is not forced by the presence of bidentate bridging ligands[28] ((Fig. 2).

Che's laboratory studied the strength of the three-coordinate gold–gold interaction by Raman spectroscopy in the coinplex $[Au_2(dmpm)_3](ClO_4)_2$ [*dmpm*=*bis*(dimemethylphosphine)methane], with atoms that exhibit an interaction of 3.050 Å. They obtained a wave number of 79 cm^{-1} for the gold–gold stretching mode. Significantly, the wave number increased to 165 cm^{-1}. and the gold–gold distances decreased when the sample was irradiated with 256 nm ultraviolet radiation, suggesting that the gold–gold interaction was strengthened in the excited state.[29] This result opens a new research field.

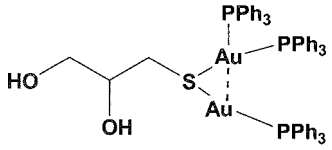

Fig. 2 Structural arrangement of the cation $[Au_2(PPh_3)_3(SCH_2CH(OH)CH_2OH)]^+$.

GOLD(I)–GOLD(III) INTERACTIONS

In addition to gold(I), gold(III) with a d^8 configuration and a square-planar geometry can be considered a closed-shell cation. Thus. interactions with other closed-shell centers such as gold(I) can be covered by the general term aurophilicity. Nevertheless, in spite of the huge number of examples of gold(I)–gold(I) contacts, interactions involving gold(III) centers are less represented, and many times. the oxidation states of the gold atoms are not completely clear. This is the case of the complexes obtained in the reaction of double-bridge ylide derivatives with gold(I) or gold(III) precursor complexes, such as $[Au_2(\mu\text{-}(CH_2)_2PPh_2)_2Au(C_6F_5)_3]$ obtained by reaction of the dimer $[Au_2(\mu\text{-}(CH_2)_2PPh_2)_2]$ with the gold(III) complex $[Au(C_6F_5)_3(OEt_2)]$. Nevertheless. the shorter distance between the two gold(I) centers of the dimer compared with the starting product, as well as the gold(I)–gold(III) distance of just 2.572 Å, are indicative of a more convincing Au(I)-Au(II)-Au(II) sequence than the expected Au(I)-Au(I)-Au(III) one.[30]

On the other hand, the reaction between the gold(II) dimer $[Au_2(\mu\text{-}(CH_2)_2PPh_2)_2(C_6F_5)(tht)]ClO_4$ and $NBu_4[Au(C_6F_5)_2]$ leads. after the displacement of the weakly coordinated *tht*. to a pentanuclear complex, where a formal gold(I) unit acts as a bridge between two adjacent gold(II) dimers. But. in this case, the theoretical calculations provide a sequence of Au(III)-Au(I)-Au(I)-Au(I)-Au(III) oxidation states based on the charges identified in the gold atoms.[31] Interactions in mixed-valence double-bridged ylide systems are often proposed due to the geometry of the ligands.[32–35]

Apart from these cases where the double-bridged ylide systems force the gold atoms to be in close proximity, there are some other examples where the gold(I)–gold(III)

interaction *seems not to be influenced by the* ligand architecture *This is. for instance, the case of the poly nuclear sulfur-centered* complex $[\{S(Au_2^{I}dppf)\}\{Au^{III}(C_6F_5)_3\}]OTf$ [*dppf*=1,1-*bis*(diphenylphosphino)ferrocene, *OTf*=trifluoromethylsulfonate],[36] *the* derivative $[Au^{I}Au^{III}Me_2(C_4F_6(PMe_3)_2)]$[37] *or the novel* $[Au^{III}(C_6F_5)_2\{PPh_2C_6H_4N(Au^{I}PPh_3)_2\}]ClO_4$,[38] which have Au(I)–Au(III) distances close to *3 3* Å

Finally, *the case of* interacting gold(III) centers with *a* d^8 configuration is *unknown* Even *with the most* appropriate structural *arrangement. i e.* a single *atom* bridging *two* gold(III) *metal centers.* this *type of* interaction *does* not *appeal Examples of this are.* among others. $[S(AuPPh_3)_2(Au(C_6F_5)_3)_2]$[39] *or* $[Se(AuPPh_3)_2(Au(C_6F_5)_3)_2]$ [40] *In all these cases. the* Au(III)–Au(III) *distances are* longer *than the sum of* their van *der* Waals radii

FUTURE PERSPECTIVES

The great development *of structural* analyses *in the last few years allowed us to realize that the interactions among metal centers at distances shorter than the sum of their* van *der* Waals *radii are not exclusive to* homometallic *gold systems. In fact, they also appear in molecules containing gold* and *other closed-shell metal centers. Therefore, words such as* aurophilicity *or* aurophilic *interactions are being replaced with* more *general* terms such *as* metallophilicity *or metallophilic interactions. Apart from the unquestionable interest of these* molecules from *a theoretical point of view, recent studies on their synthesis are being performed due to their fascinating and* unique physicochemical *properties, properties such as luminescence or conductivity. for instance. which might be exploited by industry in the near* future.[41]

There are many examples *of* heterometallic molecules *with gold-closed-shell interactions, including ions such as* Rh(I), Ir(I), Pd(II), *or* Pt(II) *with a* d^8-square planar *configuration, or* Cu(I), Ag(I), *or* Hg(II) *and* Tl(I) *and* Pb(II) with d^{10} *and* s^2 *configurations,* respectively.[4,5] *A recent ab* initio *study on bridged* dinuclear *Au–Ag and* Au–Cu *molecules concludes that the presence of* just *one gold atom is enough to induce metallophilic attractions in their group congeners and that this effect can be modulated depending on the gold* ligand[42] *involved.* In this *case,* the *relativistic effects of gold force a* numismophilicity. *On the other hand. theoretical studies on an* Au–Pd *interaction show* that *the dispersion* is *the key* contribution *to ihe* Pd(II)–Au(I) *attraction, whereas the* charge-transfer *type* contributions *are about half as important.* considering *that the* two *contributions Pd* → *Au and* Au → Pd *are energetically comparable.'''*

In short, it is *clear that gold makes an essential contribution to metallophilic interactions.* Thus, *the design of synthetic strategies to prepare systems* with *these bonds of unique versatility and flexibility must* include *gold as an essential building block.*

ACKNOWLEDGMENT

We thank the Dirección *General de* Investigación (M.C.T.)(BQU2001-2409) *for financial rupport.*

ARTICLES OF FURTHER INTEREST

Cation–π Interactions, p. *214*
Hydrogen Bonding, *p.* 658
Hydrogen Bonds to Metals and Metal Hydrides, *p.* 666
Second-Sphere Coordination, p. *1209*
Secondary Bonding, *p. 1215*
X-Ray Crystallography, *p* 1586

REFERENCES

1. Schmidbaur. H. The fascinating implications of new results in gold chemistry. Cold Bull. 1990, *23.* 11.
2. Schmidbaur, H. High-carat gold compounds. Cheni. Soc. Rev. 1995. 24. 391.
3. Schmidbaur. H. The aurophilicity phenomenon: A decade of experimental finding. theoretical concepts and emerging applications. Cold Bull. 2000. 33. 3.
4. Pyykko. P. Strong closecl-shell interactions in inorganic chemistry. Chem. Rev. 1997. 97. 597.
5. Kaltsoyannis, N. Relativistic effects in inorganic and organometallic chemistry. J. Chem. Soc. Dalton Trans. 1997. 1.
6. Pyykkö, P.: Runeberg. N. Pretlicted ligand dependence of the Au(I)···Au(I) attraction in $(XauPh_3)_2$. Chem. Phys. Lett. 1994, *218*. 133.
7. Assefa. Z.: McBurnett. B.G.; Staples. R.J.; Fackler, J.P., Jr. Structures and spectroscopic properties of gold(I) complexes of 1,3,5-Triaza-7-phosphaadamantane (TPA). 2. Multiple-itate emission from (TPA)AuX (X = Cl. Br, I) complexes. Inorg. Chem. 1995. *34.* 4965.
8. Assefa. Z.: McBurnett. B.G.: Staples. R.J.: Fackler. J.P., Jr.: Assmann, B.: Angermaier, K.; Schmidbaur. H. Synthesis, structures, and spectroscopic properties of gold(I) complexes of 1,3,5-Triaza-7-phosphaadamantane (TPA). Correlation of the supramolecular Au···Au interaction and photoluminescence for the species (TPA)AuCl and [(TPA-HCl)AuCl]. Inorg. Chem. 1995. 34. 3475.

9. Pyykko, P.; Runeberg, N.: Mendizábal, F. Theory of the d^{10}-d^{10} closed-shell attraction: 1. Dimers near equilibrium. Chem. Eur. J. 1997, 3, 1451.
10. Usón, R.; Laguna. A.: Laguna, M.: Jiménez, J.: Cbmez, M.P.; Jones. P.C. Gold complexes with heterocyclic thiones as ligands. X-ray structure determination of $[AuC_5H_5NS)_2]ClO_4$. J. Chem. Soc. Dalton Trans. 1990. 3457.
11. Jones, P.G.; Sheldrick, G.M.; Usón, R.: Laguna. A. μ-Cl-bis(triphenylphosphine)digold(I) perchlorate. dichloromethane solvate. Acta Crystallogr. 1980, B36. 1486.
12. Lensch. C.: Jones. P.G.: Sheldrick. G.M. Crystal structures of the selenide- and sulfide-bridged gold(I) complexes $[Se(AuPPh_3)_3]PF_6$ and $[S(AuPPh_3)_2{\cdot}CH_6Cl_2$. Z. Naturforch 1982. 37b. 944.
13. Li. J.; Pyykkö, P. Relativistic pseudo-potential analysis of the weak gold(+1)-gold(+1) attraction. Chem. Phys. Lett. 1992, *197*, 586.
14. Usón, R.: Laguna. A.; Fernhndez, E.J.: Mendia. A.: Jones, P.G. (Polyhalophenyl)silver(I) complexes as arylating agents: Crystal structure of $[(\mu\text{-}2,4,6\text{-}C_6F_3H_2(AuPPh_3)_2]$ ClO_4. J. Organomet. Chem. 1988.350. 129.
15. Schmidbaur. H.; Hofreiter. S.: Paul, M. Synthesis of the gold analog of the elusive doubly protonated water molecule. Nature 1995. 377. 503.
16. Canales. F.: Cimeno. M.C.; Jones. P.G.: Laguna, A. Aurophilicity at sulfur centers: Synthesis and structure of the tetragold species $[(PPh_3PAu)_4S](CF_3SO_3)_2{\cdot}2CH_2Cl_2$. Angew. Chem.. Int. Ed. Engl. 1994, 33. 769.
17. Canales. S.: Crespo, O.; Gimeno, M.C.; Jones. P.G.; Laguna, A. Synthesis of the first gold complex with a central μ^4-seleninido ligand. J. Chem. Commun. 1999. 679.
18. Crohmann. A.; Riede, J.: Schmidbaur, H. Electron-deficient bonding at pentacoordinate nitrogen. Nature 1990. 345. 140.
19. Schier. A.; Crohmann. A.; López-de-Luzuriaga, J.M.; Schmidbaur, H. The elusive structures of pentakis[triphenylphosphine)gold]ammonium(2+) bis[tetrafluoroborate(1-)]. Inorg. Chem. 2000. *39*, 547.
20. Bachman, R.E.; Schmidbaur, H. Isolation and structural characterization of $[P(AuPPh_3)_5](BF_4)_2$ via cleavage of a P-P bond by cationic gold fragments. Direct evidence of the structure of the elusive tetrakis[phosphineaurio(I)]phosphonium(+) cation. Inorg. Chem. 1996. 35. 1399.
21. Scherbaum, F.: Crohmann. A.; Huber. B.: Krüger, C.: Schmidbaur. H. "Aurophilicity" as a consequence of relativistic effects: The hexalus-(triphenylphosphinaneaurio)methane dication $[(Ph_3PAu\}_6C]^+$. Angew. Chem.. Int. Ed. Engl. 1988.27. 1544.
22. Scherbaum. F.: Crohmann. A.; Miiller, G.; Schmidbaur, H. Synthesis. structure and bonding of the cation $[\{(C_6F_5)_3PAu\}_5C]^+$. Angew. Chem., Int. Ed. Engl. 1989. *28*. 463.
23. Bardaji. M.: Connelly, N.C.; Cimeno. M.C.: Jiménez. J.: Jones. P.G.; Laguna, A.: Laguna. M. Synthesis of dinuclear gold(I) ring complexes containing two different bridging ligands. Crystal structure of $[Au_2\{\mu\text{-}(CH_2)_2PPh_2\}(\mu\text{-}S_2CNEt_2))]$. J. Chem. Soc. Dalton Trans. 1994. 1163.
24. Fernhndez. E.J.; Gimeno. M.C.: Jones. P.G.; Laguna. A.; Laguna. M.: Lbpez-de-Luzuriaga. J.M. A hexanuclear gold(I) complex: $[\{(Ph_3PAu)_2C(PPh_2AuPPh_2)\}_2](ClO_4)_2$. Angew. Chem., Int. Ed. Engl. 1994. 33. 87.
25. Girneno, M.C.: Laguna. A. Three- and four-coordinate gold(I) complexes. Chem. Rev. 1997, 97. 511.
26. Schmidbaur. H.: Wohlleben, A.: Schubert, U.; Frank, A.: Huttner. G. Synthese und Kistallstrukter achtgliedriger Ringverbindungen von gold(I) mit Au-Au-Wechselwirkung. Cheni. Ber. 1977, *110*. 2751.
27. Porter. L.C.; Khan. N.I., Md.: King. C.: Fackler. J.P.. Jr. Structure of the bis[bis(diphenylphosphino)methane]digold(I) cation in $[Au_2(dppm)_2](BF_4)_2$. Acta Crystallogr., C 1989; 45. 947.
28. López-de-Luzuriaga, J.M.; Sladek, A.: Schmidbaur, H. Mixed coordination numbers and geometries of gold(I) in a dinuclear complex of thioglycerol. J. Chem. Soc. Dalton Trans. 1996. 4511.
29. Leung. K.H.: Phillips. D.L.: Mao, Z.; Che. C.M.: Miskowski. V.M.; Chan. C.K. Electronic excited states of $[Au_2(dmpm)_3]_3](ClO_4)_2$ (dmpm = bis(dimethylphosphine)-methane. Inorg. Chem. 2002. 41. 2054.
30. Usón, R.: Laguna. A.; Laguna, M.: Tartbn. M.T.; Jones. P.G. The first example of a direct formal gold(I)-gold(III) bond. Synthesis and structure of $[\{Au(CH_2)_2PPh_2\}_2$ $Au(C_6F_5)_3]$. J. Chem. Soc., Chem. Commun. 1988.740.
31. Usbn. R.: Laguna, A.; Laguna, M.; Jiménez. J.: Jones, P.C. A mixed-valent pentanuclear gold complex containing a linear Au_5 chain. Angew. Chem., Int. Ed. Engl. 1991. 30. 198.
32. Mazany. A.M.: Fackler. J.P.. Jr. Isomeric species of $[AuCH_2P(S)(C_6H_5)_2I]_2$. Mixed-valent Au(I)/Au(III) and isovalent Au(II)/Au(II) complexes with the same methyl-eiiethiophosphinate ligand. J. Am. Chem. Soc. 1984, 106, 801.
33. Fackler, J.P., Jr.: Trzcinska-Bancroft. B. Isomerization of a symmetrical metal-metal bonded gold(II) ylide dimer to a mixed-valence gold(III)/gold(I) species. Organometallics 1985. *4*, 1891.
34. Raptis, R.G.; Porter, L.C.; Emrich, R.J.; Murray, H.H.; Fackler, J.P., Jr. Synthesis of a mixed-valence Au^I/Au^{III} complex, $\{Au(CH_2)_2PPh_2\}_2Br_2$, and its characterization by x-ray crystallography and x-ray photoelectron-spectroscopy. Inorg. Chem. 1990, 29. 4408.
35. Schmidbaur. H.: Hartmann, C.: Reber. G.; Müller, G. Isovalent and mixed-valent ylide complexes of gold: The synthesis of trinuclear coinpounds having double paddle-wheel structure. Angew. Chem.. Int. Ed. Engl. 1987. 26. 1146.
36. Calhorda, M.J.; Canales. F.; Cimeno. M.C.; Jiménez, J.; Jones. P.G.; Laguna. A.: Veirós, L.F. Gold(I)-gold(III) interactions in polynuclear sulfur-centered complexes. Synthesis and structural characterization of [S(Au2dppf){Au(C6F5)3}] and [{S(Au2dppf)}2{Au(C6F5)2}]OTf (dppf = 1,1′-bis(diphenylphosphino)ferrocene). Organometallics 1994. 16. 3837.

37. Jarvis, J.A.; Johnson, A.; Puddephatt, R.J. The mechanism of insertion of an acetylene into the methylgold bond: Structure of a reaction intermediate. J. Chem. Soc., Chcm. Cornmun. **1973**. 373.
38. Fernández, E.J.; Gil, M.; Olmos, M.E.; Crespo, O.; Laguna, A.; Jones, P.C. The ability of a Au_3-N unit to bond two aurophilically interacting gold(I) centers. Inorg. Chem. **2001,** *40*. 3018.
39. Canales. F.: Gimeno, M.C.; Laguna, A.; Jones, P.G. Synthesis and structural characterization of tetranuclear sulfur-centered complexes with mixed-valent gold atoms: $[S(Au_2dppf)\{Au(C_6F_5)_3\}_2]$ (dppf = 1,1′-bis(diphenylphosphino)ferrocene) and $[S(AuPPh_3)_2\{Au(C_6F_5)_3\}_2]$. Organometallics **1996**, *15*, 3412.
40. Canales, O.; Crcspo, O.; Girneno, M.C.; Jones, P.G.; Laguna. A.; Mendizábal, F. Mixed gold(I)-gold(III) complexes with bridging selenido ligands. Theoretical studies of the gold(I)-gold(III) Interactions. Organometallics **2001**, 20, 4985.
41. Fernández. E.J.; Laguna, A.: López-de-Luzuriaga, J.M. Luminescence in gold-heterometal complexes. Gold Bull. **2001.** *34*, 14.
42. Fernández, E.J.; López-de-Luzuriaga, J.M.; Monge, M.; Rodriguez. M.A.: Crespo, O.; Gimeno, M.C.; Laguna, A.; Jones, P.G. Heteropolynuclear complexes with the ligand PPh_2CH_2SPh. Theoretical evidence of relativistic Au-M interactions. Chern. Eur. J. **2000.** *6*, 636.
43. Crespo. O.; Laguna, A.; Fernández, E.J.; López-de-Luzuriaga. J.M.; Jones; P.G.; Teichert, M.; Monge, M.; Pyykkö, P.; Runeberg. N.; Schütz, M.; Werner, H. Experimental and theoretical studies of the d^8-d^{10} interactions between Pd(II) and Au(I): bis(chlorophenylthiomethyldiphenylphosphinegold(I))dichloropalladium (II) and related systems. J. Inorg. Chem. **2000,** 39. 4786.

Biological Ligands

Andrew Hinton
Paul Taylor
Malcolm D. Walkinshaw
University of Edinburgh, Edinburgh, United Kingdom

INTRODUCTION

The binding of a small-molecule ligand to a protein enzyme or receptor is governed by a host of weak nonbonding electrostatic effects like hydrogen bonds and van der Waals interactions. Entropic changes caused by displacement of water and by changes in ligand flexibility are also important in determining binding strength. An understanding of these processes is crucial for the design of novel enzyme inhibitors and other protein ligands. This is an area of great importance in the pharmaceutical industry, where more protein targets are becoming available. We now have high-resolution structures of over 1700 protein–ligand complexes as determined by protein x-ray crystallography.[1] This information coupled with the measured binding data of many protein–ligand systems is now providing insight into what factors are important for ligand binding. We provide a broad overview of the field, with examples of structures from a variety of ligand classes (Table 1). Current computational approaches for discovering new ligands and estimating the strength of ligand binding are also described.

ENERGETICS OF PROTEIN–LIGAND INTERACTIONS

The simple picture of protein–ligand binding is given by a bimolecular equilibrium (Eq. 1) in which a ligand in solution binds to the receptor protein to form a complex. In the context of this article, we define a ligand to be a mainly organic molecule with a molecular weight of up to 1500 Dalton, which may be reasonably expected to form a complex with a protein. We restrict our discussion to noncovalent complexes, though as in the case of enzymatic reactions or the binding of suicide inhibitors, covalent bonds can frequently be formed. The binding constant (or equilibrium constant) relates the concentrations of free and bound components.

$$\mathbf{P \cdot L} \rightleftarrows \mathbf{P} + \mathbf{L} \qquad (1)$$

where $K_d = [P][L]/[P{\cdot}L]$ or (the reverse reaction) $K_b = [P{\cdot}L]/[P][L]$, K_d = dissociation constant. K_b = binding constant, $[P{\cdot}L]$ = concentration of protein–ligand complex, $[P]$ = concentration of unbound protein, and $[L]$ = concentration of unbound ligand.

Drug–protein interactions tend to have dissociation constants (K_d) in the nanomolar to picomolar range. In the field of drug discovery, so-called lead ligands with potentials for being developed into drug candidates bind to their target proteins with K_d values in the micromolar range. The dissociation constants[i''] can be converted (Eq. 2) to binding energies from the following:

$$\begin{aligned} \Delta G^\circ &= -RT \ln Kd \\ &= -5.6 \log_{10} K \end{aligned}$$

x (at room temperature 20°C or 293°K) (2)

where K_d = dissociation constant (Mol), ΔG° = Gibbs free energy change of the reaction (kJ mol^{-1}), R = 8.31 (J/° mol), and T = temperature (°K).

Thus, a change in the binding constant by an order of magnitude only corresponds to a difference in binding energy of about 5.6 kJ/mol. A K_d of 10^{-9} M gives a calculated dissociation energy of +50.4 kJ/mol (which equals a free energy of binding of −50.4 kJ/mol), while a ligand that binds with a micromolar K_d has a dissociation energy of +33.6 kJ/mol (see also Table 5).

This overall binding energy can be regarded as consisting of a number of components including hydrogen bonding, van der Waals interactions, and other thermodynamic terms. Approximate energies for these components (Table 2) were calculated by correlating structural data with measured thermodynamic binding data.[3,4] A number of empirical energy terms were published, and one such example is shown in Eq. 3.[3,4]

$$\begin{aligned} \Delta G_{binding} &= \Delta G_0 + \Delta G_{polar} + \Delta G_{apolar} + \Delta G_{solv} \\ &\quad + \Delta G_{flexi} \end{aligned} \qquad (3)$$

As shown in Table 2. ΔG_0, ΔG_{hb}, ΔG_{ion}, ΔG_{rot}, ΔG_{aro}, and ΔG_{esrep} are enthalpic terms that describe contributions made by H-bond, ionic, rotational, aromatic, and nonspecific interaction energies. The ΔG_{lipo} includes lipophilic

Encyclopedia of Supramolecular Chemistry
DOI: 10.1081/E-ESMC 120012673

Table I Selected PDB entries of protein–ligand complexes indicating structural diversity and biological function

Biological class	Protein–ligand complex	Ligand structure	PDB ID
Saccharide	Porcine pancreatic amylase	Pseudo-octasaccharide V-1532 (trestatin A)	1PIG
	Human lysozyme	Hexa–*N*-acetyl-chitohexose	1LZS
	Strep. *Pneumonia* hyaluronate Lysase	Hyaluronic acid	1C82
	Concanavalin-A	**Alpha-methyl-D-mannopyanoside**[a]	**5CNA**
Lipid	Human serum albumin	Decanoic acid	1E7F
	Bovine β-lactoglobulin	**Palmitate**[a]	**1BO0**
	Mycobacterium tuberculosis enoyl-ACP reductase	Hexadecenoyl-thioester	1BVR
	RAt P-450:nadph-p450 reductase	Butenoic acid	1LFO
Signal molecule	Rat phosphatidylinositol transfer protein (Pitp)	Phosphatidylcholine	1FVZ
	Catalytic domain of human **c-H-ras p21.**	**Guanosine diphosphate**[a]	**4Q21**
	Growth factor receptor-bound protein 2	Phosphatyrosyl heptapeptide	1TZE
Retinol related	Rat cellular retinol binding Protein **c-RBP**	***Trans*-retinol**	**1CRB**
	Bovine plasma retinol-binding protein (bRBP)	Fenretinide	1FEL
Steroid	Rat α-hydroxysteroid dehydrogenases (3 α-HSDs)	Testosterone	1AFS
	Human sex hormone-binding globulin (SHBG)	Dihydrotestosterone. (androgen)	1D2S
	17-β-hydroxysteroid dehydrogenase	**17-β-estradiol (estradiol)**[a]	**1FDT**
Antibiotic	**β-Lactamase** mutant	Penicillin-6 (open)"	1GHP
		Cephaloridine	1GHM
Drug molecule	**HIV-1, protease**	**C33-cyclic urea inihibitor Aha001**[a]	**1AJX**
Drug molecule	Human rhinovirus. 16 coat protein	Vp63843 (Pleconaril)	1C8M
Drug molecule	Influenza virus. neuraminidase	Carboxamide inhibitor	2QWK
Thyroxin	Human transthyretin (TTR)	Thyroxin	2ROX

"Denotes structure shown.
Source: From Ref. [1].

Table *2* The relationship and approximate value of individual energy terms to the change in Gibbs free energy of binding (ΔG)

Energy component	Value (kJ/mol)	Interaction type	Example
ΔG_0	−2 8	ΔG_0	Nonspecific
ΔG_{hb}	−3 2	ΔG_{polar}	=O − − −H− − −O
ΔG_{ionic}	−5 7	ΔG_{polar}	NH_4^+ − − −COO^-
ΔG_{lipo}	−0 09	ΔG_{solv}	C_n− − −H_2O
ΔG_{rot}	+1 0	ΔG_{flexi}	C− − −CH_3 Rotation about single bond
ΔG_{aro}	−26	ΔG_{apolar}	C− − −C
$\Delta G_{lipo\ water}$	−1.3	ΔG_{solv}	C_n− − −H_2O
ΔG_{esrep}	+0 5	ΔG_{polar}	NH_4^+− − −COO

interaction energy as a function of all pair-wise atom−atom interaction energies. The $\Delta G_{lipo\ water}$ describes energy change through desolvation effects. These energy terms contribute to a simple representation of the components that make up $\Delta G_{binding}$, including polar (ΔG_{polar}), apolar (ΔG_{apolar}), solvation (ΔG_{solv}), and flexibility (ΔG_{flexi}) interactions as given in Eq. 3. Approximate energies for these terms were calculated by correlating structmal data with measured thermodynamic binding data.[3,4]

MEASUREMENT OF LIGAND BINDING STRENGTH

A number of spectroscopic and thermodynamic measurements can be used to measure the strength of protein–ligand interactions. including fluorescence spectroscopy, surface plasmon resonance, calorimetry, and enzyme inhibition. The change in property (for example, fluorescence signal,[5] heat of reaction,[6] crystallographic occupancy,[7] and NMR chemical shift[8,9]) is measured as a function of increasing concentration of added ligand until a maximum signal is obtained. For a simple protein–ligand binding experiment (with no substrate or other inhibitory ligand present); the K_d value can be simply determined by titrating a ligand solution into a protein solution of known concentration. The K_d is the slope of

Table *3* Techniques for measuring binding constants

Technique	Description	Example	Ref.
NMR (^{15}N-HSQC)	Observation of change in two-dimensional ^{1}H- or ^{15}N-heteronuclear single quantum correlation (HSQC) backbone chemical shift spectra upon ligand binding; described as $\Delta\delta(^1H,^{15}N) = [L]/([L] + K_d)$	FKBP	[9]
Fluorescence spectrophotometry	Measurement of fluorescence signal quenching of an active-site tryptophan as a function of ligand binding: described as $\Delta F = \Delta F_{max} - K_d(\Delta F/[L])$	FKBP	[5]
X-ray cry-stallography	Crystallographic refinement of ligand occupancy from a range of ligand soaking concentrations	Cyclophilin	[7]
Isothermal calorimetry (ITC)	Isothermal titration calorimetry (ITC) measures the enthalpy change caused by a binding event; the gradient of the generated ITC curve can be used to determine the binding constant K_b	OppA	[10]
Surface plasmon resonance (SPR)	SPR-biosensors measure the change in refractive index units (RU) of a solvent near the surface that occurs during complex formation with an immobilized protein target	HIV1-protease	[6]
Enzyme inhibition	The measurement of the rate (v) of products/reactants formation can be measured by spectrophotometry; the dissociation constant K_d corresponds to the concentration of inhibitor at which the observed constant (k_{obs}) is half its maximum value	Bovine cyclophilin	[9]

the straight-line plot of *[PL]* against $[PL]/[L]$ used to fit Eq. 4.

$$[PL] = P_o - K_d([PL]/[L]) \quad (4)$$

where $[PL]$ = concentration of the ligated protein, $[L]$ = concentration of the ligand. and $[P_o]$ = total protein concentration.

The IC_{50} value is the ligand concentration that produces *50%* reduction (or increase) in the measured effect (i.e., the coilcentration of unbound protein *[Pj* equals the concentration of ligand-bound protein *[PL])*For a simple binary protein–iigand mixture. the dissociation constant K_d is identical to the IC_{50} value.

In Table 3. a description of different techniques employed in the measurement of binding constants is presented, where $\Delta\delta(^1H,^{15}N)$ is the average weighted change in ^{15}N- or ^1H-amide chemical shift in two-dimensional ^1H- or ^{15}N-heteronuclear single quantum correlation (HSQC) spectra, where $[L]$ and K_d are ligand concentration and dissociation constants, respectively. The ΔF and ΔF_{max} is the change in fluorescence measured at 340 nm.

The relationship between IC_{50} and K_d (Eq. *5)* for competitive enzyme inhibition or competitive receptor ligand studies is complicated by the additional presence of substrate (S). Note that in such experiments, K_d the dissociation constant and K_i the inhibition constant can be used synonymously:

$$K_i = IC_{50}{*}K_m/([S] + K_m) \quad (5)$$

where K_i = equilibrium dissociation constant of the inhibitor ligand. IC_{50} = inhibitor concentration that produces 50% change in the measured effect. [S] = substrate concentration used in the assay. and K_m = substrate concentration (in the absence of inhibitor) at which the velocity of the reaction is half-maximal.

The K_i is an equilibrium dissociation constant corresponding to the concentration of the inhibitor ligand [I] that would bind to half of the binding sites at equilibrium (in the absence of other substrates). If [S] is small (usually in the nanomolar range) and the IC_{50} is in the micromolar range. then measured IC_{50} still closely approximates the K_i.

FINDING MEW LIGANDS

Over the last 10 years, the pharmaceutical industry invested in automating high-throughput screening (HTS) methods that enable libraries of ligands consisting of over 250.000 compounds to be screened in biological assays. A typical threshold for a hit is binding to or inhibiting a ligand with a K_i of less than about 10^{-6} M. It was estimated that it takes over 2 million trials to discover one lead compound (roughly defined as a ligand that proceeds to preclinical trials). A complementary approach to high-throughput screening is a structure-based computer-aided approach. A prerequisite is the availability of an accurate three-dimensional structure of the protein target. The protein data bank PDB[1] now contains nearly 20,000 entries mainly determined by protein x-ray crystallography. Of these, over 650 are different domain folds,[111] and 1700 are protein–ligand complexes.[1]

The structure of a protein's ligand-binding pocket provides a template into which novel (mainly inhibitory) ligands can be designed and visualized with the aid of computer graphics. The traditional method is to make use of a known inhibitor complex and make small changes to the ligand to modify the binding properties. This is exemplified in the development of influenza neuraminidase antivirals.[12] Prior to the elucidation of the crystal structure of influenza neuraminidase, N-acetylneuraminic (Neu5Ac) inhibitors had K_i values of above 1 μM. Knowledge of the enzyme structure allowed the addition of the bulky basic substituents at the 4-position to produce the 4-guanidino-Neu5Ac2en. Known as Zanamivir, this compound has a K_i of 0.1 nM. An ester prodrug of a cyclohexene–carboxylic derivative of Zanamivir called GS4071 was resolved to 1.8 Å (2QWK) complexed with wild-type neuraminidase. GS4071 has subnanomolar potency against Types A and 5 influenza neuraminidase.[12] An overlay of the crystal forms of wild-type neuraminidase complexed with GS4071 and a carboxyamide analogue (G2800) can be seen in Fig. 1.

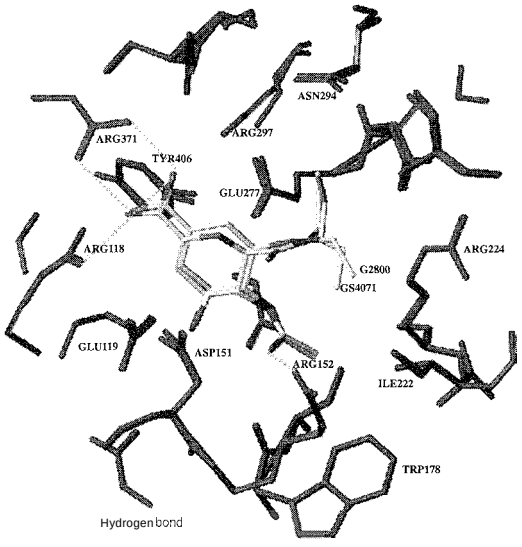

Fig. 1 A superimposition of two neurainidase–inhibitor complexes. (*View this art in color at www.dekker.com.*)

Shown in Fig. 1 is a superimposition of the inhibitor 634071 and a carboxyamide analogue crystallized with wild-type influenza neuraminidase. *The clinical inhibitor 634071* (2QWK) *and the carboxyamide analogue* G2800 (2QWG) *can be seen to be making a range of electrostatic and hydrophobic* interactions *with the residues of the sialic acid-binding pocket of wild-type influenza* neuraminidase (blue).[12]

COMPUTATIONAL TECHNIQUES IN LIGAND DISCOVERY

De novo Design, Database Mining, and Filtering

A more radical approach is to attempt *the design of completely novel entities in the binding pocket with the required* complementarity *of shape and charge properties. Computer programs such as* LUDI[13] *and* SMoG[14] use *libraries of small* chemical *building blocks to generate such theoretical inhibitors.*

Another related computational approach to ligand discovery is the method of database mining. Here. the HTS *approach* is *essentially carried out* in-silico. *Libraries of* small *molecules are converted to three-dimensional structures using molecular mechanics methods incorporated into programs such as* CONCORD[15] *and* CORINA.[16] *These three-dimensional libraries of small* molecules *can. in theory. contain almost infinite numbers of potential ligands.* In *practice, it is convenient to consider compounds that are already (commercially) available. The Available Chemicals Database* (ACD),[17] *for example. contains some* 260,000 *compounds and is frequently used as the basis for database mining trials.*

Further prescreening steps in the search for potential drug ligands can be made *by excluding molecules with properties that make them unlikely to be biologically accessible. These properties are summarized in Lipinski's* Rules,[18] *which are based on the fact that 2245 known small molecular drugs* (as *cataloged in the* USAN[19]) *show poor absorption or permeation when the following occur:*

1. *There are more than five H-bond* donors *(expressed as the sum of* OHs *and* NHs).
2. *The molecular weight is over 500.*
3. *The* LogP *is over 5.*
4. *There are more than 10* H-bond *acceptors (expressed as the sum of* Ns *and* Os).

LogP *is a partition coefficient defined as the ratio of concentrations of a compound in aqueous phase to the concentration in an* immiscible *solvent* (e.g., *octanol). According to Ghose et* al.,[20] 80% *of all drugs fall in the range of* 160–480 Da, *with an average of 357 Da, and have calculated log* P *values in the range of* −0.4–5.6, *with an average value of 2.3. Theoretically. there are at least* 10^{12} compounds *that would fit these* Lipinski *criteria. (The estimate is based* on *molecules derived from* consideration *of a tetrahedral lattice of 20 points. each of which can be occupied by four possible* substituents.) *Current FITS approaches. even using libraries of 1* million *compounds, are therefore sampling* less *than one* millionth *of potential ligands.*

Automated Docking

A number of computer programs are now available to carry out the automated docking of molecules selected from databases into the pi-otein-binding pocket.

Shown in *Fig. 2* is *a schematic representation of the stages of automated docking of ligands into a* protein-*binding pocket. The stapes include* the *generation of a description of a binding pocket using spheres or grid points (1). matching the ligand to the points or spheres (2). Finally, the fitted ligand is given an energy score (3).*

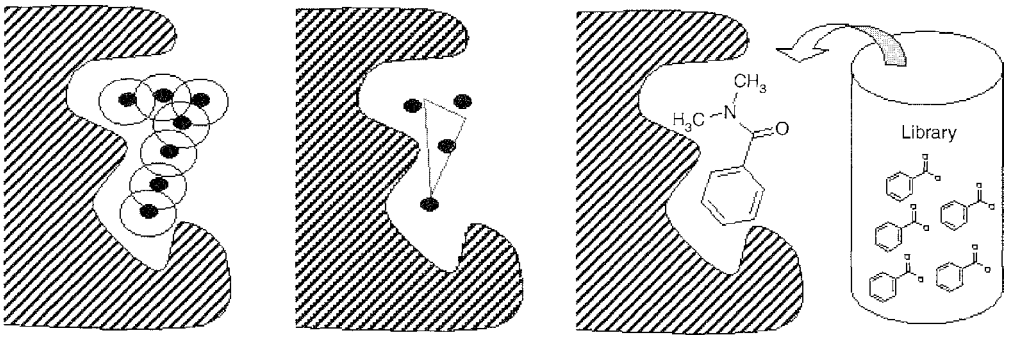

Fig. 2 Stages of automated docking

Table 4 Scoring functions employed in docking algorithms

Docking algorithm	Scoring functions	Attributes	Ref.
GLIDE	$\Delta G_{binding} = \Delta G_0 + \Delta G_{hbond} \sum_{il} g_1(\Delta r) g_2(\Delta\alpha) + \Delta G_{metal} \sum_{aM} f(r_{aM}) + \Delta G_{lipo} \sum_{IL} f(r_{IL}) + \Delta G_{rot} H_{rot}$ ΔG_0 is a nonspecific energy term. $\Delta G_{hbond} \sum_{il} g_1(\Delta r) g_2(\Delta\alpha)$ is an H-bond term between ligand and receptor atoms with an ideal bond length and angle deviation penalty. $\Delta G_{metal} \sum_{aM} f(r_{aM})$ is a term accounting for metal atoms. $\Delta G_{lipo} \sum_{IL} f(r_{IL})$ accounts for lipophilic atoms. $\Delta G_{rot} H_{rot}$ is a flexibility penalty for frozen bonds.	• Screens at 6 min per ligand • Includes entropic flexibility penalty • Lipophilic terms account for long-range terms • Incorporates metal ligand binding	[24]
GOLD	Score $= \sum(-E_{pair} - (E_{ij} + (E_{ijkl} + Eij)))$ $=$ −H-bond energy − (Internal energy + Complex energy) E_{pair} is a weighted H-bond interaction energy term between donor–acceptor aiom pairs, accounting for water displacement. E,, is a ligand steric energy using 6–12 Leonard–Jones factors accounting for dispersion of atom pairs caused by ionization and polarization. E_{ijkl} is a ligand torsion angle value calculated with a Tripos forcefield for four connected atoms. Eij is an energy distance constraint with a 4–8 Leonard–Jones potential, accounting for close contacts with a covalent bond energy term.	• Screens 12 min per ligand • The genetic algorithm (GA) explores full ligand and partial receptor flexibility • AG difficult to calculate, as only enthalpic consideration is considered • Surface-accessible area. term is not included	[25]
FlexX	$\Delta G = \Delta G_0 - \Delta G_{rot} \times N_{rot} - \Delta G_{hb} \sum_{\text{natural hbonds}} f(\Delta R, Ax) + \Delta G_{io} \sum_{\text{ionic int}} f(\Delta R, Ax) + \Delta G_{aro} \sum_{\text{aro int.}} f(\Delta R, An) + \Delta G_{lipo} \sum_{\text{lipo cont.}} f^*(\Delta R)$ ΔG_0, ΔG_{hb}, ΔG_{io}, ΔG_{rot}, ΔG_{aro} are entropic terms that describe contributions made by nonspecific, H-bond. ionic. rotational, and aromatic interaction energies offset by an idealized penalty function $f(\Delta R,\Delta\alpha)$. ΔG_{lipo} includees lipophilic interaction energy as a function of all pair-wise atom–atom interaction energies.	• Screens at 3 min per ligand • Large number of ligand conformations are generated • Lipophilic interactions are accounted for • Limited to ligands with less than 17–20 rotatable bonds	[23]
DOCKv4 GB/SA	$G_{binding} = \sigma_1 \Delta(SA_{hp}) + \beta .VDW - \sigma_2 \Delta(SA) + G_{pol}$ $\Delta(SA_{hp})$ and $\Delta(SA)$ are a measure of change in hydrophobic and total accessible surface areas. σ_1, σ_2 are solvation parameters for nonpolar atoms and a linear coefficient for the scaling of van der Waals interactions β.VDW. G_{pol} includes ligand-receptor electrostatic energy and partial desolvation energy terms for receptor and ligand atoms.	• Screens at 7 min per ligand • The desolvation states of ligand and receptor are included in term accounts for hydrophobic interactions • Effects of translational. rotational. and conformational entropy loss upon binding not included in function	[22]

Table 5 Structural and thermodynamic data for a selection of different classes of protein–ligand complexes

Protein–ligand		Number of H-bonds contacts	Number of non-H-bond contacts	Solvent accessible surface area (Å^2) of the ligand				K_i M^{-1}	$\Delta G°$ kJ mol^{-1}
				Uncomplexed Å^2	Complexed Å^2	Buried Å^2	%Buried		Calculated ($\Delta G° = -RT \ln K_i$)
OppA (1B1H.pdb)	K–Hph–K	12	103	201.151	5.687	195.464	97.17	9.3×10^{-8}	+40.1
Cyclophilin-A (1CWA.pdb)	CsA	5	15	342.429	193.203	149.226	43.57	5–200 10	45.6 to + 51.5
FKBP (1FKF.pdb)	FK506	3	110	261.332	126.936	134.396	51.42	4.0×10^{-10}	+52.6
FABP (2IFB.pdb)	Palmitate	1	109	154.195	9.744	144.451	93.68	$7 \times 10^{-}$	+46.4
ConA (1I3H.pdb)	Dimannose	8	58	121.752	51.562	70.19	57.64	4.2×10^{-3}	+13.5
HIV-1-protease (1HVR.pdb)	Cyclic urea inhibitor complex XK2 263	6	153	230.994	17.829	213.165	92.28	3.1 10^{-10}	+54.2
Estrogen receptor (1ERR.pdb)aps	Raloxifene	3	137	196.285	16.911	179.374	91.38	IC_{50} = 0.2 nm	+55.3

The process allows for whole libraries of ligands to be screened against a single binding pocket.

The steps in the process are as follows:

1. Generate a description of the binding pocket. This is usually in the form of a set of grid points or spheres.
2. Match the ligand to the grid points by fitting atoms of the ligand onto grid points that have appropriate electrostatic propesties.
3. Calculate an energy score showing how well the ligand fits into the binding pocket.
4. Rank and order the hits.

The well-established DOCK algorithm[21] generates a sphere-filled inverse representation of the binding pocket, subsequently matching thousands of ligand orientations to the spheres. DOCK version 5[22] includes a desolvation term in its scoring system to account for the shedding of water upon ligand binding. The incremental construction algorithm FlexX[23] considers ligands as totally flexible: fragment placing allows subsequent reconstruction of the ligand within the receptor. The scoring function (Table 4) is relatively computationally efficient and includes entropic terms covering lipophilic, aromatic, and ionic interactions. The GOLD (genetic optimization for the ligand docking) program[25] developed at the Cambridge Crystallographic Data Centre (CCDC) employs a genetic algorithm to fully explore ligand flexibility within a partially flexible receptor. The scoring system uses observations of nonbonded contacts from crystal structures to rank ligand orientations.

A BROAD SURVEY OF LIGAND CLASSES

For structural and thermodynamic data for a selection of differentclasses of protein–ligand complexes, see Table 5.

Peptides: OppA Complexed with 8-Peptides

The structures of eight OppA–peptide complexes were determined by protein x-ray crystallography[10] (Fig. 3a). OppA is a peptide transport receptor in gram-negative bacteria that binds a wide range of peptides between two to five amino acids in length. In a study by Davies et al.,[10] eight complexes of tripeptides K–X–K (X = abnormal side chain) were prepared. and the enthalpy, entropy, and binding affinity were measured when bound to OppA. The resultant K_d values ranged from 15 nm–29 ym. The complexes revealed a rigid binding pocket with well-ordered water molecules. The OppA system shows preferential binding for hydrophobic groups over positively charged groups. Small differences in ligand side chains cause a disproportionately large effect on ligand binding, resulting in an inability to rank or predict binding affinities within classes of ligands. Predictions of binding affinities are complicated due to favorable enthalpy changes being offset by a compensating cost in entropy change, making it difficultto correlate structure with binding affinity. The observed water displacement upon ligand binding associated with the Opp–A system and the resultant enthalpy–entropy compensation makes predicting binding affinities using scoring functions that do not account for unreliable solvent interactions.

Peptides: Cyclophilin A Complexed with Cyclosporin A

Cyclosporin A (CsA) is a cyclic undecapeptide that has seven of the 11 amides in the N-methylated form and is used as an immunosuppressent to prevent the rejection of organs after transplant sugery. CsA's immunosuppressive qualities arise from the formation of a tightly bound complex of CsA with Cyclophilin A (CypA); a ubiquitous 165 amino long cytosolic protein. The CsA/CypA composite surface binds and inhibits the serine/threonine phosphatase calcineurin. preventing further signal transduction. The CsA/CypA complex was solved to 1.8 Å resolution. Analysis of 11 CypA/CsA derivative crystal complexes by Kallen et al.[27] provides a useful database of protein–ligand interactions. revealing the effect of small chemical differences on hydrogen bond, van der Waals. and water interactions. Only six of the CsA residues form van der Waals or hydrogen-bonded contacts with the binding pocket of cyclophilin. There is an excellent complementarity of fit between the MeVal side chain and the hydrophobic active site pocket of cyclophilin, which is designed to accommodate proline. There are five direct hydrogen bonds between CsA and CypA and a solvent-excluded area of 150 $Å^2$. Despite only half the residues being involved in the interaction with the protein, there is a strong interaction with a K_d of 15 nM. The conformation of the ligand undergoes a dramatic conformational change from its uncomplexed state in organic solvents.

Macrolides: FKBP Complexed with FK506 and Rapamycin

FKBP is the soluble receptor for the immunosuppressant drug FK506 (see Fig. 3b). The native crystal structure of FKBP as well as with FK506 and rapamycin-bound forms were determined to a resolution of better than 2.0 Å.[5] A range of bound ligands describes the enthalpic and entropic contributions caused by differing electrostatic, chiral, and solvation properties of the ligand. X-ray

structures of a series of ligand molecules related to dimethylsulfoxide were complexed with FKBP. The structures allow for the correlation of physiochemical properties with experimentally observed binding affinities.[''] Analysis of rnacrolide and small-ligand FKBP complexes reveals an active site cavity able to flex in relation to the size of the bound ligand. Coinparison of FKBP complexed with DMSO and methyl sulfinylmethylsulfoxide (DSS) shows similar protein and solvent structures. The observed threefold increase in K_d in the FKBP/DSS complex compared to DMSO can be contributed to increase in enthalpic (van der Waals) interactions energy due to the presence of the methyl sulfide group. The correlation of three-dimensional structure with

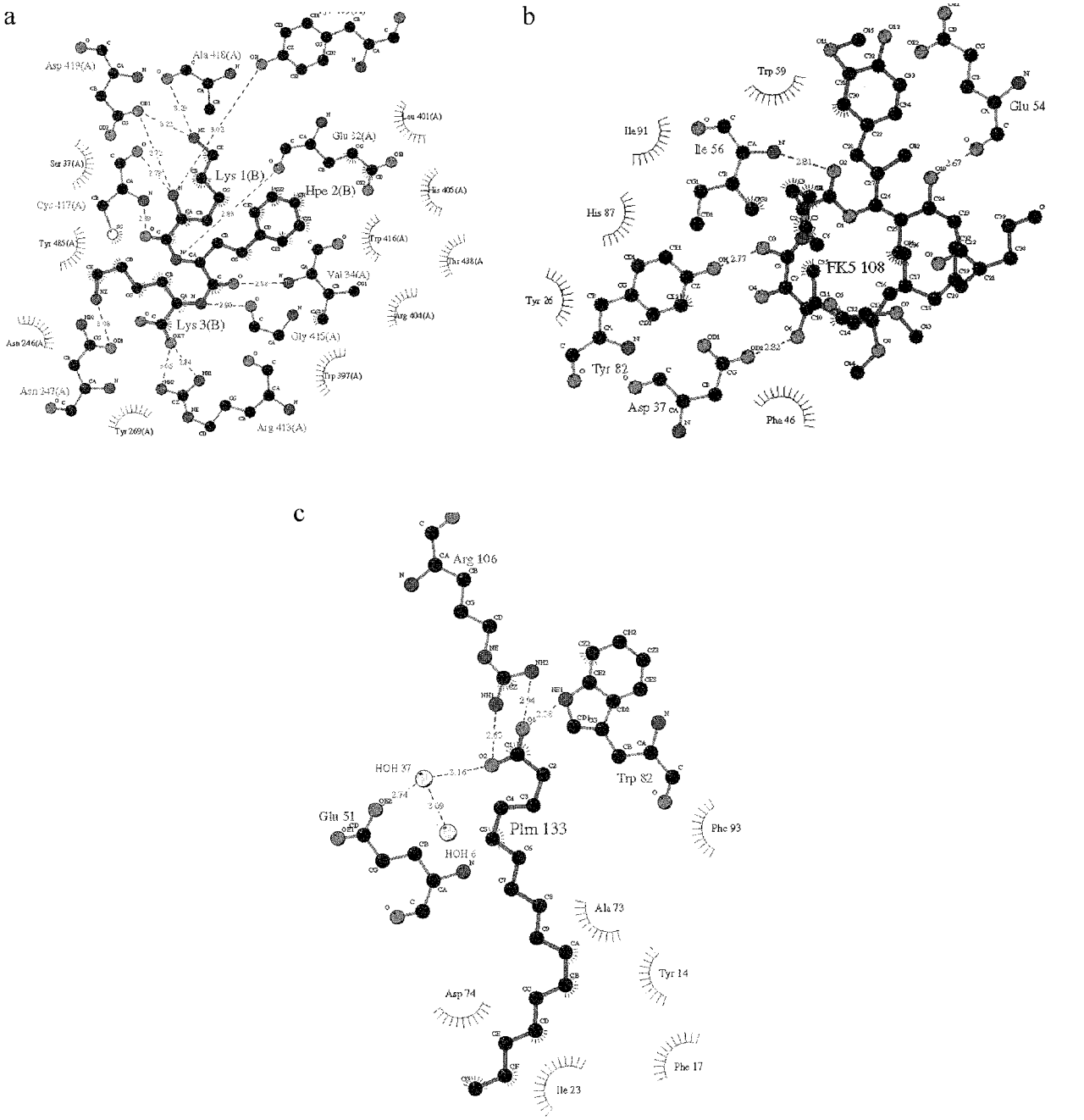

Fig. 3 (a) OppA K–HpH–K complex (1B1H.pdb); (b) FKBP–FK506 complex (1FKF.pdb); (c) FABP–palmitate complex (2IFB.pdb); id) ConA–dimannose complex (1I3H.pdb); (e) HIV-I protease–cyclic urea inhibitor (1HVR.pdb). Pictures generated using LigPlotv4.0. *Source*: From Ref. [26]. (*View this art in* color. *at www.dekker.com.*)

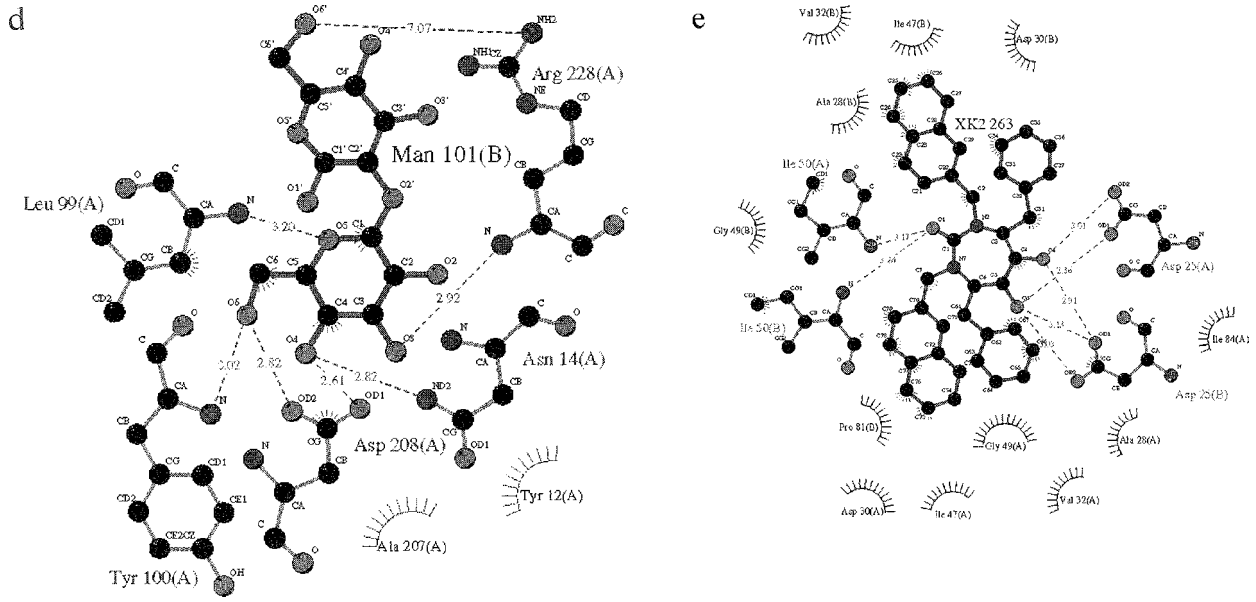

Fig. 3 (*Continued*).

ligand-binding data suggests that for each Å^2 contact between ligand and protein contributes between -0.1 kJ/mol[4] up to an estimated -0.5 kJ/mol binding energy.[5] FK506 binds to human FKBP with a K_d of 0.4 nM. With an estimated 134 Å^2 buried contact area. each Å^2 contact contributes -0.4 kJ/mol binding energy.

r

Lipids and Fatty Acids: FABP–Palmitate Complex

Fatty acid binding protein (FABP) is involved in fatty acid transport (Fig. 3c). High-resolution crystal- and NMR-derived structures of apo and holo forms of rat intestinal FABP complexed with palmitate allowed Bakowies et al.[28] to derive a 5 nsec molecular dynamics (MD) simulation.'''' The FABP family shares a common β-barrel motif with a large internal binding cavity, which when uncomplexed, contains 20 to 25 well-ordered wate molecules. Thermodynamic studies conclude that binding is enthalpically driven but cannot distinguish between entropic compensations between the ligand and water effects. Side-chain PI-bond interactions are consistent between MD simulations and crystal structures. however, crystal and NMR representations show poor agreement in the apo-FABP form. The holo-FABP complex MD simulation shows that palmitate ligand moves 3–4 Å back toward the cavity entrance. Crystal structures overestimated the electrostatic contribution, while the MD simulation shows that palmitate is able to sustain substantial flexibility and motion while bound in the protein cavity. The apo-FABP shows a high-density droplet of water in the cavity center. The holo-FABP complex reveals that water molecules are displaced from the cavity by palmitate, with one water molecule being replaced by three methylene fragments. The observed high mobility of water molecules within the interior and exterior of FABP when palmitate binds is due to a combination of water droplet dispersion and a more favorable exchange pathway via the portal region of FABP. Displacement of several β-strands around the exit channel observed in the NMR and MD representations but absent from ihe crystal form of apo-FABP show the importance of solvation on the overall protein structure.

Saccharides: Concanavalin-A Complexed with Dimannose

The interaction of plant lectin concanvalin-A (Con A) with different saccharides was studied in great depth and provides a unique insight into protein–oligosaccharide interactions. Sanders et al.[29] crystallized the structure of Jack Bean Con A in complex with dimannose (Man-(XI-2)Man) to a resolution of 1.2 Å.[29] Comparison with the complexed and uncomplexed forms shows that the water displacement that occurs upon ligand binding forms a network of well-defined H-bonds that helps to stabilize the Con A–dimannose complex. The H-bonding network provides an explanation for the observed preferences in

binding α1-2 linked disaccharides. The formation of eight direct hydrogen bonds (and seven indirect interactions. with well-observed waters) between dimannose and Con A combined with a buried contact area of 70.2 Å^2 gives a K_d of 4.2 mM. The high resolution of the structure revealed the protonation of an Asp208 OD1. a feature that was unaccounted for in previous modeling studies (Fig. 3d).

Steroids: Estrogen Receptor Complexed with 17β-Estradiol and Raloxifene

Estrogens play an important role in tissue growth, development, and homeostasis. These steroids mediate their effects ihrough direct interactions with a ligand-inducible nuclear transcription factor termed the estrogen receptor (ER), resulting in the activation or repression of target genes. How estrogens mediated their biological effects at the molecular level has been a source of continuous debate. The cocrystallization of the endogenous estrogen agonist 17β-estradiol (3.1 A) and the clinically used selective antagonist Raloxifene (2.6 A) with the α-estrogen receptor, respectively. by Brzozowski et al. provided insight into the molecular basis of agonism and antagonism of the ER.[30] Comparison between these structures reveals that the large side chain of Raloxifene protrudes from the cavity and causes a 10 A rigid body displacement of one of the receptor helices (Helix 12). The formation of three hydrogen-bond interactions and a 179 Å^2 buried contact area between Raloxifene and the ER results in Raloxifene having an IC_{50} of 0.2 nM. It is proposed char the failure of Helix 12 to fully cap the entrance of the binding cavity prevents the forination of a competent transcriptional activation function (AF-2) site that is able to effectively recruit coactivators. It is thought that this observed helical rearrangement of Helix 12 leads Raloxifene to behave as an antagonist in certain tissues.

Related in Table 5 are protein–ligand complexes described with the number of intermolecular contacts made and solvent-accessible surface area to thermodynamic binding data. The number of H-bonds, inhibition concentration (K_i), and change in Gibbs free energy (AG), respectively. were taken from original sources. The number of non-H-bonded contacts was generated using the Ligand–Protein Contact software.[31] The solvent-accessible surface was generated using the Connolly[32] accessible surface of the ligand in isolation and when bound in the protein (without water). The buried surface is taken as the difference between these values. A probe radius of 1.5 A was used with the implementation of the Connolly algorithm within the modeling program WIT-NOTP.[33]

Synthetic Drugs: HIV-1 Protease Inhibitors

In the fight against HIV. the National Cancer Institute developed a database of HIV protease–ligand complexes. The HIV-PR database[34] holds the coordinates for 142 different crystal structures of HIV protease–ligand complexes (Table 6). In conjunction with the Autodock3 docking package, a modified combined energy weighted grid system was used to predict the correct ligand-binding conformation for 21 of these complexes. The results showed ihat the energy grid could allow structural flexibility of the binding site and distinguish between ligands that required water for binding. The cyclic urea inhibitor that was tested, which does not require the presence of water for binding to HIV protease. was accommodated within the energy grid system. returning a predicted conformation close to that of the crystal structure.[35]

Table 6 Online ligand–protein databases

Database	Description	Web address
LIGAND	Contains compound. metabolic. and enzymatic information	http://www.genome.ad.jp/ligand/
RELIBASE	Easy searching of protein–ligand complexes	http://relibase.ccdc.cam.ac.uk/
PLD	Binding data for 150 protein–lipand complex's	http://www-mitchell.ch.cam.ac.uk/pld/pld2.html
BindingDB	Database of measured binding affinities	http:l/www.bindingdb.org
LPC	Automated analysis of interatomic contacts in protein–ligand complexes	http://bioinfo.weizmann.ac.il:8500/oca-bin/lpccsu/
HIV Protease Database	Structure database of HIV proteases complexed with their inhibitors	**http:l/srdata.nist.gov/hivdb/**

Described in Table 6 is a list of online databases that hold thermodynamic data on protein–ligand complexes.

CONCLUSION

The event of ligand binding is thermodynamically complex and is composed from a range of enthalpic and entropic factors. Recent technological developments allowed for improved experimental measurement of ligand binding. Linking binding data to the type of intermolecular forces observed within protein–ligand complexes (Table 5 and Fig. 3) provides a route to improving energy terms used in structure-based drug design. Listed in Table 6 are online databases that give thermodynamic and enzymatic information about relected protein–ligand complexes. However, current techniques can still only sample a small percentage of the total available ligands. Increasingly. computational techniques such as de novo design. database mining. and automated docking are being employed to predict new sources of protein–ligand interactions

The future prospects for this in-silco technology depends on incorporating improved parameters for describing the dynamic effects of water and protein flexibility in the system. The ability to achieve these coinputational advances will be helped by the increasing number of high-resolution crystal structures of protein–ligand complexes becoming available in publicly accessible databases. Such structures provide an opportunity for the detailed analysis of the poorly defined factors that influence the strength of protein–ligand interactions.

ACKNOWLEDGMENTS

We are grateful to Prof. J.W. Keillor at the Universite de Montreal. Department of Chimie, for his many useful discussions.

The authors would like to thank the BBSRC for their financial support.

ARTICLES OF FURTHER INTEREST

The Cambridge Structural Database, p. 161
Drug Delivery, p. *484*
Hydrogen Bonding, p. 658
The Hydrophobic Effect, *p.* 673
Kinetics of Complexation, *p.* 776
Molecular Modeling and Related Computational Techniques, p. 901
Nuclear Magnetic Resonance Spectroscopy, p. 981
van der Waals Forces, p. 1550
Weak Hydrogen Bonds, p. 1576
X-Ray Crystallography, p. 1586

B

REFERENCES

1. Berman, H.M.; Westbrook. J.: Feng, Z.: Gilliland. G.: Bhat. T.N.: Weissig, H.; Shindyalov, I.N.: Bourne. P.E. The protein data bank. Nucleic Acids Res. 2000. *28.* 235–242.
2. Knegtel, R.M.A.; Grootenhuis. P.D.J. Binding affinities and non-bonded interaction energies. Pers. Drug Dis. Des. 1998. *9–11.* 99–114.
3. Klebe. G.; Bohm. H.J. Energetic and entropic factors determining binding affinity in protein–ligand complexes. J. Recep. Signal Transduc. Res. 1997. *17.* 459- 473.
4. Bohm. H.J. Prediction of binding constants of protein ligands: A fast method for the prioritisation of hits obtained from de-novo design or 3D-database search programs. J. Comput. Aided Mol. Des. 1998. *12.* 309–323.
5. Burkhard. P.: Taylor. P.: Walkinshaw. M.D. X-ray structures of small ligand FKBP complexes provide an estimate for hydrophobic interaction energies. J. Mol. Biol. 2000. 295. 953–962.
6. Rich. R.L.: Myszka, D.G. Advances in surface plasmon resonance biosensor analysis. Curr. Opin. Biotechnol. 2000, *11.* 54–61.
7. Wu, S.Y.: Dornan, J.; Kontopidis, C.: Taylor. P.; Walkinshaw, M.D. The first direct determination of a ligand binding constant in protein crystals. Angewandte Chemie–International Edition 2001. *40.* 582–586.
8. Shuker, S.B.: Hajduk, P.J.: Meadows. R.P.: Fesik, S.W. Discovering high affinity ligands for proteins: SAR by NMR. Science 1996. *274.* 1531–1534.
9. Mofron. J.L.: Kuzmic, P.: Kishore, V.: Colonbonilla. E.: Rich. D.H. Determination of kinetic constants for peptidyl prolyl *cis trans* isomerases by an improved spectrophotometric assay. Biochemistry 1991. 30, 6127–6134.
10. Davies, T.C.; Hubbard, R.E.: Tame, J.R.H. Relating structure to thermodynamics: The crystal structures and binding affinity of eight OppA–peptide complexes. Protein Science 1999, *8.* 1432–1444.
11. Murzin. A.G.; Brenner, S.E.: Hubbard, T.; Chothia. C. SCOP—A structural classification of proteins database for the investigation of sequences and structures. J. Mol. Biol. 1995; *247.* 536–540.
12. Varghese, J.N.; Smith. P.W.: Sollis. S.L.; Blick. T.J.; Sahasrabudlie. A.: McKimm-Breschin. J.L.: Colman. P.M. Drug design against a shifting target: A structural basis for resistance to inhibitors in a variant of influenza virus neuraminidase. Structure 1998. 6. 735–746.
13. Bohm. H.J. The computer-program ludi—A new method for the de novo design of enzyme-inhibitors. J. Comput. Aided Mol. Des. 1992. 6. 61 78.
14. DeWitte. R.S.: Ishchenko. A.V.: Shakhnovich. E.I. SMoG. de Novo—Design method based on simple fast and accurate free energy estimates 2. Case studies in molecular design. J. Am. Chem. Soc. 1997. *119.* 4608–4617.

15. Ricketts, E.M.; Rradshaw, J.: Hann, M.; Hayes, F.; Tanna, N.; Ricketts. D.M. Comparison of conformations of small-molecule structures from the Protein Data-Bank with those generated by concord, cobra, chemdbs-3D, and converter and those extracted from the Cambridge Structural Database. J. Chem. Inf. Comput. Sci. **1993,** *33*. 905–925.
16. Sadowski, J.; Gasteiger, J.; Klede, G. Comparison of automatic 3-dimensional model builders using 639 x-ray structures. J. Chem. Inf. Comput. Sci. **1994**, 34, 1000–1008.
17. *ACD Available* Chemicals *Directory*; http://www.mdli.com (accessed July 2002).
18. Lipinski, C.A.; Lombardo, F.; Dominy, B.W.; Fecncy, P.J. Experimental and computational approaches to estimate solubility and permeability in drug discovery and development settings. Advances in Drug Delivery Review **1997.** *23,* 3–25.
19. *USP Dictionary of USAN and* International Drug *Names*; http://www.usp.org (accessed July 2002).
20. Ghose, A.K.; Viswanadhan, V.N.; Wendoloski, J.J. A knowledge-based approach in designing combinatorial or medicinal chemistry libraries for drug discovery. 1. A qualitative and quantitative characterisation of known drug databases. Journal of Combinatorial Chemistry **1999,** *1*, 55–68.
21. Ewing, T.J.A.: Makino, S.; Skillman. A.G.; Kuntz, I.D. DOCK 4.0: Search strategies for automated molecular docking of flexible molecule databases. J. Comput. Aided Mol. Des. **2001**, *15*. 411 428.
22. Zou, X.Q.; Sun. Y.X.; Kuntz, I.D. Inclusion of solvation in ligand binding free energy calculations using the generalized-Born model. Journal of the American Chemical Society **1999,** *121*, 8033–8043.
23. Rarey, M.; Kramer, B.; Lengauer, T.; Klebe, G. A fast flexible docking method using an incremental construction algorithm. J. Mol. Biol. **1996,** *261*. 470 489.
24. Eldridge, M.D.; Murray, C.W.; Auton, T.R.; Paolini. G.V.: Mee, R.P. Empirical scoring functions: I. The development of a fast empirical scoring function to estimate the binding affinity of ligands in receptor complexes. J. Comput. Aided Mol. Des. **1997.** *11*, 425–445.
25. Jones, G.; Willett. P.; Glen, R.C.: Leach, A.R.; Taylor, R. Development and validation of a genetic algorithm for flexible docking. J. Mol. Biol. **1997,** *267*, 727 748.
26. Wallace. A.C.; Laskowski, R.A.: Thornton. J.M. LIGPLOT: A program to generate schematic diagrams of protein–ligand interactions. Prot. Eng. **1995**. *8*, 127 134.
27. Kallen, J.; Mikol, V.: Taylor, P.; Walkinshaw, M.D. X-ray structures and analysis of 11 cyclosporin derivatives complexed with Cyclophilin A. J. Mol. Biol. **1998,** *283*. 435 449.
28. Bakowies, D.; Van Cunsteren, W.F. Simulations of apo and holo-fatty acid binding protein. Structure and dynamics of protein, ligand and internal water. J. Mol. Biol. **2002,** *315*, 713–736.
29. Sanders, D.A.R.; Moothoo, D.N.; Raftery, J.; Howard. A.J.; Helliwell. J.R.; Naismith, J.H. The 1.2 Å resolution structure of the Con A–dimannose complex. J. Mol. Biol. **2001.** *310*, 875–884.
30. Brzozowski, A.M.; Pike, A.C.W.; Dautcr, Z.; Hubbard, R.E.; Bonn, T.; Engstrorn, O.; Ohman, L.; Greene, G.L.; Gustafsson, J.A.; Carlquist, M. Molecular basis of agonism and antagonism in the oestrogen receptor. Nature **1997,** *389*. 753–758.
31. Sobolcv, V.; Sorokine, A.; Prilusky, J.; Abola, E.E.; Edelrnan, M. Automated analysis of interatomic contacts in proteins. Bioinformatics **1999.** *15*, 327 332.
32. Connolly, M.L. Solvent-accessible surfaces of proteins and nucleic-acids. Science **1983,** *221*. 709 713.
33. Widmer, A. *WITNOTP:* A *Computer Program for Molecular* Modelling; Novartis AG: Basel, 1997.
34. The HIV *Protease Databank*; http://mcll.ncifcrf.gov/hivdb (accessed July 2002).
35. Osterberg. F.; Morris. G.M.; Sanner. M.F.: Olson, A.J.: Goodscll, D.S. Automated docking to multiple target structures: Incorporation of protein [nobility and structural water heterogeneity. Proteins **2002,** 46, 34 -40.

Biological Models and Their Characteristics

Paolo Scrimin
University of Padova, Padova, Italy

Paolo Tecilla
University of Trieste, Trieste, Italy

INTRODUCTION

The ability to mimic and take advantage of the complexity of living matter as a way to store and transfer information, accelerate chemical reactions, selectively recognize chemical species, self-replicate, and so on is at the basis of supramolecular chemistry in the biological field. The concepts that spurred the growth of supramolecular chemistry came from the biological world, as scientists started to comprehend the extreme difficulty (if not the impossibility) of obtaining complex systems with specific function just by connecting building blocks via covalent synthesis. It is apparent that in the biological world, the most challenging and intriguing systems express their functions as collections of simpler elements held together not by covalent bonds but by reversible, singularly weak, interactions. Supramolecular chemistry was the response of scientists to this clear evidence: complex structures able to perform spectacular achievements can be obtained minirnizing chemical synthesis and relying on weak interactions, i.e., the way molecules reciprocally communicate without the formation of covalent bonds."] In order to do this; they had to master the way these weak interactions (like hydrogen bonds. hydrophobic forces, for instance) operate.

In order to address the characteristics of biological models, we have to first define the basic principles of biological systems that a supramolecular model may mimic. Among the most important are selective molecular recognition of a molecular entity: selective and highly accelerated modification of a substrate (typical role of enzymes): compartmentalization and selective translocation of chemical species across boundaries (typical role of biomembranes): harvesting and transformation of energy; and self-replication.

SELECTIVE MOLECULAR RECOGNITION

Molecular recognition relies on weak to moderate forces,[2] and the process depends critically on the structure of the molecular partners involved as well as on the nature of the surrounding solvent. Typical interactions involved in molecular recognition are ion–ion, ion–dipole, dipole–dipole, cation–π, π–π stacking, dispersion (London), and solvent effects. The classical recognition process requires two entities: the molecular receptor (host) and the recognized molecule (guest). However; self-recognition should not be overlooked, as it is one of the most important processes in the biological world. Self-recognition, for instance. is what dictates the folding of a protein into its secondary and tertiary structures. Those synthetic oligomers showing the property to fold into a specific conformation following the information encoded in their synthesis were dubbed Foldamers.[3] Interesting examples are those constituted by β-peptides[4,5] (unnatural oligomers composed of β-amino acids) that fold into a 3_{14} helix already at the level of a dodecamer. Even more striking are short oligomers (six to eight units) composed of Cα-tetrasubstituted unnatural amino acids[6] that fold into 3_{10} helices. Probably the system most studied as a model for molecular recognition is that constituted by cyclodextrins (CDs), cyclic oligomers (six to eight units) composed of glucose units with a doughnut shape and an hydrophobic interior.[7] This property led to the use of functional cyclodextrins as enzyme models (see below). However, as an example to illustrate molecular recognition, we will show a cage receptor for glucose able to extract the sugar from an aqueous solution into an organic one.[8,9] This is a challenging endeavor. because water is obviously an excellent solvent for a saccharide. The molecule (Fig. 1) comprises a rigid cavity (a tricycle), with amide groups pointing inward into the cavity and suitable for hydrogen bonding the sugar molecule. The design resembles key structural motifs present in carbohydrate-binding proteins that, as stated by the authors. "commonly place aromatic surfaces against patches of carbohydrate CH groups while accepting the hydroxyl groups into networks of hydrogen bonds." This receptor has an affinity for D-glucose, which is five times larger than that for D-galactose and >10 times that for D-mannose.

DOI: 10.1081/E-ESMC 120012671

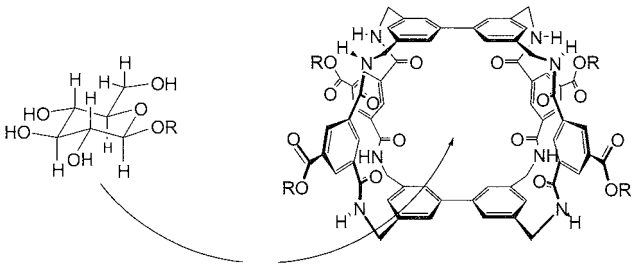

Fig. 1 Structure of the macrotricycle receptor for the selective extraction of glucose from aqueous solutions: the sugar binds inside the cavity, taking advantage of the forination of a hydrogen bonds network.

CATALYSIS

An essential prerequisite for enzymatic catalysis is the binding of the substrate to the protein before its transformation into products. The two processes (binding and modification) may occur on different sites of the protein. The binding site should not change during the catalytic process. while. in the reactive site, bonds are broken and new ones are formed, charge is developed or disappears.[10] Accordingly. the mimicry of a recognition site, compared with a catalytic site that is dynamic in nature: is much easier in a supramolecular system. Supramolecular (enzyme-like) catalysts typically provide the recognition site for a substrate, while they are much less effective as far as the catalytic site is concerned. Apart from the dynamic aspect mentioned above. a catalytic site requires the refinement of the pKa of acids or bases eventually involved in the process and accurate control of the solvation of all species. Nevertheless. effective supramolecular catalysts were reported, because just the proximity of reactant and catalyst achieved upon binding is enough to guarantee (sometimes) impressive rate accelerations. A typical example is that provided by cyclodextrins.[11] The hydrophobic cavity of these natural molecules was used to recognize substrates, while the hydroxyl rim was used as a source of a nucleophile for a transacylation process. By optimizing the substrate, Breslow and collaborators[12] were able to achieve 6-million-fold rate accelerations compared with the uncatalyzed hydrolysis reaction. The critical aspect stressed by these systems is that a substrate, rather rigid and complementary to the cavity, may be designed with the ester group sitting precisely over the CD secondary side

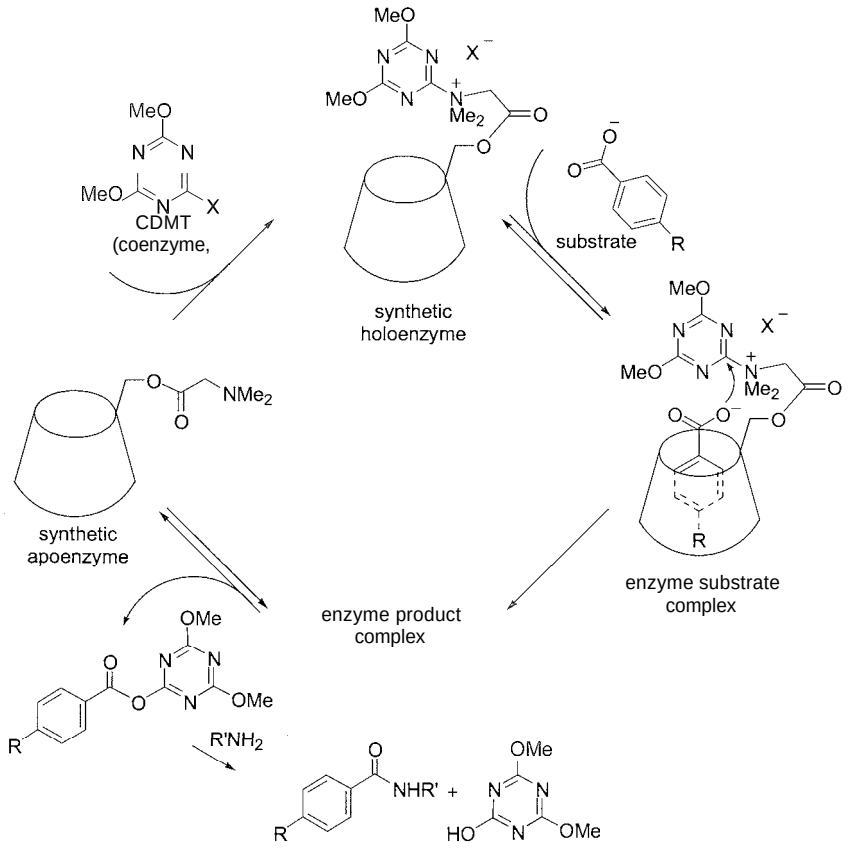

Fig. 2 Catalytic cycle for a CD-based artificial acyltransferase

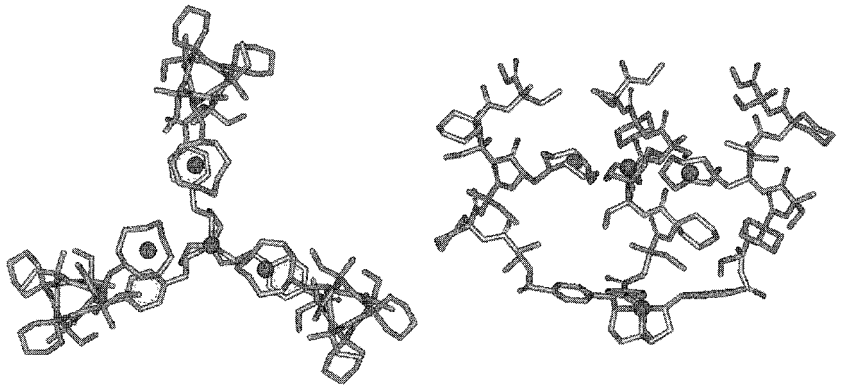

Fig. *3* Tripodal polypeptide used as a biomimetic supramolecular catalyst for the cleavage of phosphate esters. The tren platform is an allosteric control site. (*View this art* in *color at www.dekker.com.*)

hydroxyl group. Thus, the proximity is the source of the rate acceleration. More sophisticated systems require the modification of the cyclodextrin so that a catalytic site can be designed by placing suitable functional groups. An example[13] illustrating this point was recently reported by Kunishima et al. They simply esterified one of the primary hydroxyls of β-CD with *N,N*-dimethylglycine (see Fig. 2), transforming it into a catalyst (holoenzyme) for the amidation of carboxylic acids in aqueous solution. The process requires 2-chloro-4,6-dimethoxy-1,3,5-triazine (CDMT) as a coenzyme consumed during the reaction. The results indicate that, in the catalyst. the substrate-binding site (the CD cavity) and the catalytic site (the dimethylamino group at the rim) must be linked to each other in order to achieve substrate-specific amidation. Other molecuiar receptors can be used as supramolecular. biomimetic catalysts. For instance, Diederich[14] functionalized a cationic cyclophane with flavin and thiazolium groups and obtained a pyruvate oxidase mimic. Pyruvate oxidase is an enzyme that employs two cofactors: flavin and thiamine-diphosphate to catalyze the transformation of pyruvate to acetyl phosphate. The coexistence of the two cofactors on the same inolecular receptor makes this molecule one of the most active artificial enzymes known to date. In an attempt to mimic the catalytic site of a nuclease we synthesized[15] the molecule shown in Fig. 3 by attaching three copies of an helical heptapeptide to a derivative of tren (tris-aminoethylamine). The sequence of each single peptide is designed in such a way that by folding into an helical conformation, two ammonium groups are placed on one side of the helix. and a triazacyclononane ligand of synthetic amino acid ATANP is placed on the other. The tripodal derivative can bind up to four metal ions: one on the tren platform and three on the triazacyclononane moieties. The tren site is used to control the conformation of the molecule (like an allosteric site in proteins). while the remaining triazacyclononane coinplexes define a catalytic site for the metal-catalyzed hydrolysis of a phosphate. The metal complex is active in the cleavage of a phosphate model of RNA, with clear evidence of cooperativity between the metal centers. Surprisingly. however, it is active as the free amine in the cleavage of linear RNA. It appears that the allosteric site is responsible for this behavior of striking selectivity in the interaction with the substrate. By using natural sequences the group of Baltzer[16–19] recently described a series of fully synthetic polypeptides that are good catalysts of the cleavage of esters. The molecules contain 42 amino acids and were designed to fold into a helix-loop-helix conformation. The monomers dimerize into a four-helix bundle that provides a shallow reactive site for the substrate (Fig. 4). Here, the emphasis is on the careful control of the properties of the catalytic units placed on

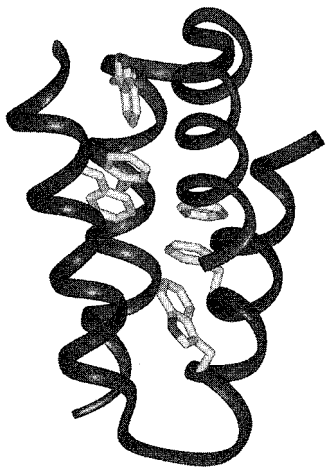

Fig. 4 Four-helix bundle formed by two helix-loop-helix peptides. The self-assembly of the two monomers provides a shallow reactive site for the substrate. (*View this art in color at www.dekker.com.*)

the reactive site. Thus. by introducing flanking amino acids with charged side chains. the authors were able to finely tune the pKa of the imidazole of the histidines so as to maximize their cooperative role at the optimum pH for the occuri-ence of the catalytic process. As stated above, this is a major challenge for everybody trying to prepare an artificial (supramolecular) catalyst. To conclude this section. we will mention two extremes in the design of supramoiecular enzyme models. The first takes advantage of putting together. in a polymer, several functional groups and hydrophobic units. These successful molecules were called synzimes.[20–22] The second is that represented by catalytic antibodies,[23] where the catalyst is a protein generated by the immune system against a model of the transition state of the reaction under investigation. The first is rude and devoid of any specific geometrical design of the catalytic site, while the second is highly sophisticated, although the recognition of the model of a transition state does not necessarily imply acceleration of the related reaction. Nevertheless, both provided promising results.

COMPARTMENTALIZATION AND TRANSLOCATION

Biological membranes play a fundamental role in compartmentalizing and insulating the living cell from the external medium. However. an organized trafficking of molecules and ions across the membrane is needed to sustain life. In nature. this traffic is regulated by a variety of systems able to form ion channels or to act as molecular carriers and to selectively affect the membrane permeability.[24] In particular, ion channels are formed following two general approaches: the first rely on molecules that, due to their peculiar structures. form a discrete pore in the membrane as exemplified by the β-helix of the gramicidin A dimer. The second is based on the hydrophobically driven self-assembling of amphipatic units in the membrane that form a cluster where the hydrophilic face of each unit points inward, defining a channel with a polar inner surface (barrel-stave model).[''' Examples of this include the ion channel proteins of the nervous system in which the channel is formed by four or five homologous α-helices containing several serine residues lining the pore.[26] Several other shorter peptides like peptaibols[27] or nonpeptidic systems like amphotericin B[28] are thought to affect rnembrane permeability with this mechanism. Supramolecular chemists undertook the ambitious challenge of preparing systems able to rival the natural ones. Example of models inspired to both types of ion channels described above are present in the literature. Recently. the group of Ghadiri[29–32] reported channel obtained from self-assembled cyclic peptides. The key feature of these cyclopeptides is the presence of alternating L, D amino acids; so that hydrogen bonding assembles them in a stack of rings. This strategy resembles that adopted by gramicidin A. When the assembling of the tubes (diameter > 7 Å, depending on the size of the cycle) occurs in a membrane, this leads to the alteration of its permeability (Fig. 5, left). The group of Voyer[33] synthesized a 21 amino acid peptide composed of 15 L-leucines and six 21-crown-7-L-phenylalanines: the sequence is such to allow the partial alignment of the macrocycles, one over the other, when the peptide adopts an α-helical conformation (Fig. 5, right). forming a pore in the membrane. A similar design was used by Matile in realizing a rigid oligo(*p*-phenylene) rod functionalized with several monoaza-18-crown-6 subunits.[34] Models based on the self-assembling of amphipatic subunits were also developed. They are based on peptides,[26] polyhydroxylated p-biphenyl oligomers,[35] cholic acid.'''' or polyhydroxylated steroid[37] derivatives. Often. the design of these systems is inspired by the naturally occurring ionophores. amphotericin B (AmB) and squalamine,[38] which are thought to form pores in lipid bilayers. The analysis of these two ionophores made by Regen is interesting in understanding how a biological model may be constructed.[39] AmB and squalamine have different structures but share some common elements: a long and rigid hydrophobic unit; a hydrophilic chain that is linked to the hydrophobic unit and can extend across its ''face''; and a polar head group. On these bases, the author designed the sterol derivative shown in Fig. 6. which mixes elements taken from squalamine. like the sterol-based hydrophobic unit and the polar head group, with the polyoxygenated chain, taken from AmB. This derivative is able to affect the membrane permeability of model liposomes with an activity and a mechanism of action comparable with that of AmB.[40] In particular, it is suggested that the ionophore assumes a folded conformation, like the one shown in Fig. 6, and is inserted in the rnembrane with the sulfate and the protonated amino group anchored to the surface of the liposome. Eventually, clusters are formed where the oxygenated chain points inward. toward a water-Filled pore. Furthermore. because the system is too short, the alignment of two of these clusters is needed to span the membrane across and alter its permeability.

HARVESTING AND TRANSFORMING ENERGY

Photoinduced electron and energy transfer are fundamental processes in nature[41] In photosynthetic organisms, photoinduced electron transfer that induces conversion of light into chemical energy begins when photonic excitation reaches the so-called reaction center (RC) Usually.

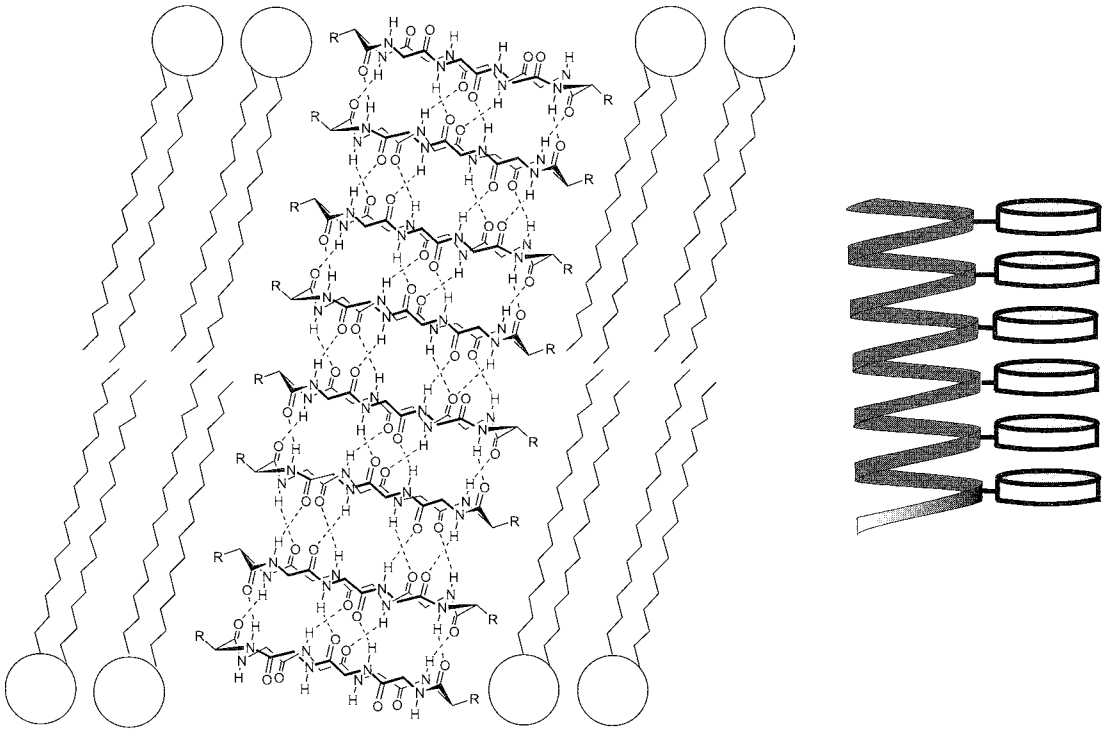

Fig. 5 Examples of systems able to form channels in membranes. Left: the Ghadiri's self-assembled nanotube formed by cyclopeptides. Right: The Voyer's 21 amino acid peptide containing six 21-crown-7 L-phenylalanines. In a membrane. the peptide adopts an α-helical conformation that allows the partial alignment of the macrocycles, one over the other.

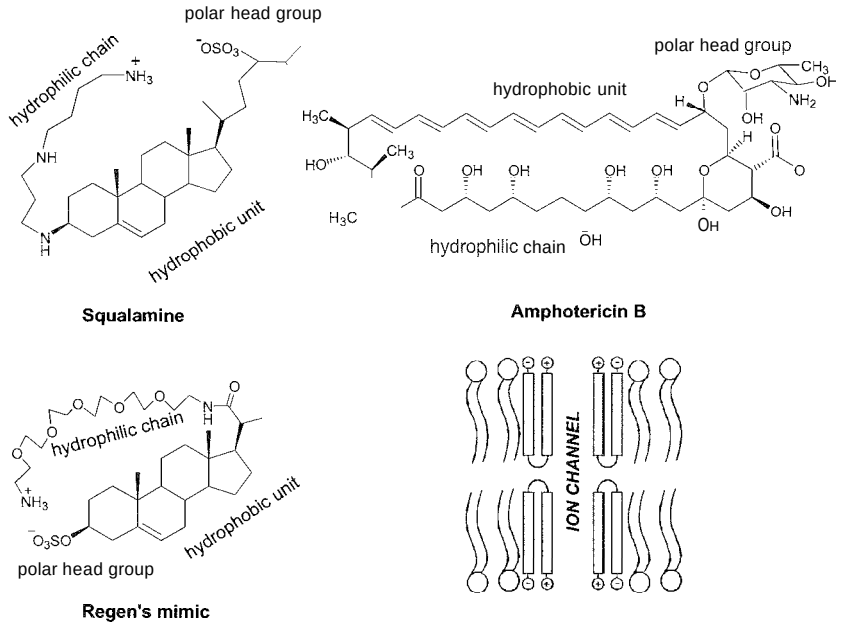

Fig. 6 Regen's mimic of amphotevicin B and squalamine. In the bottom left corner. the cartoon illustrates the proposed mode of action of this ionophore.

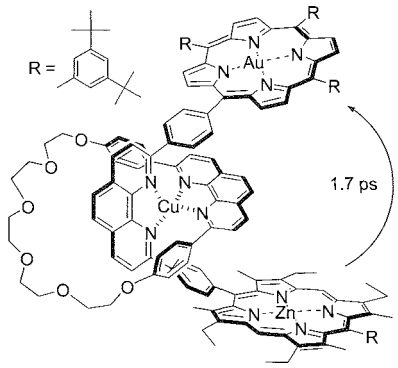

Fig. 7 A rotaxane that mimics the special pair/bacteriopheophytin (BPh) arrangement and electron-transfer properties of the bacterial photosynthetic reaction center.

light is trapped and transferred through a pool of well-organized chromophores included in the light-harvesting antenna protein. For example, in the bacteria *Rhodopseudomonas acidofila*, the light-harvesting system is formed by two rings of noncovalently linked bacteriochlorophyll chrornophores (BCh), one consisting of nine pigments and the other of 18 chromophores. This highly organized structure enhances the spectral width of the light trapped and the efficiency of energy transfer toward the RC. where electron transfer to a quinone group generates a long-lived charge separation state.[42]

Energy-transfer and electron-transfer processes inspired many research groups. and a variety of systems employing different chromophores were exploited.[43] Popular are tetrapyrrolic systems, the naturally occurring chromophores in the photosynthetic reaction center. In particular. supramolecular chemists are trying to reproduce the naturally occurring electron- and energy-transfer processes occurring through noncovalently linked proteins, using self-assembled systems. Sophisticated and efficient models of the photosynthetic RC and antenna systems were obtained.[44] For instance, Sauvage designed the rotaxane shown in Fig. 7 that mimics the special pair (SP, a closely associated dimer of BCh)/bacteriopheophytin (BPh) arrangement and electron-transfer properties of the bacterial photosynthetic RC.[45] In the natural system, the electron transfer from the excited state of SF to BPh occurs at a rate of 3 ps^{-1}. In the synthetic model, the electron donor is a zinc porphyrin in its excited state, and the electron acceptor is an Au(III) porphyrin. Light irradiation of the zinc porphyrin chromophore is followed by electron transfer to the gold porphyrin acceptor. which occurs at a rate similar to the natural system (1.7 ps^{-1}). The rotaxane structure is important, and in the absence of the Cu(I) ion that positions the second phenanthroline ligand in between the two porphyrin rings, the electron transfer process is substantially slower (36 ps^{-1}).

Self-assembling of multiporphyrin arrays was also exploited to model the properties of the antenna system. For instance, using a cooperative self-assembly process based on hydrogen bonding and metal–ligand interaction, Hunter was able to assemble five porphyrin rings in a well-defined structure in which a central free-base porphyrin is encapsulated in a spherical array of four zinc porphyrins.[46] Light excitation of these peripheral chromophores results in an efficient energy transfer to the central one, mimicking the funneling effect of the antenna system. A step forward is constituted by a self-assembled array of 16 zinc-porphyrins delivering energy to a central free-base porphyrin.[47]

SELF-REPLICATION

One of the peculiar characteristics of the living world is the ability to self-replicate. Undoubtedly, reproducing such a characteristic in the abiotic world is a demanding challenge. Supramolecular chemists have done it. Historically. the first example is that provided by von Kiedrowski,[48] who reported evidence of self-replication in a nonenzymatic nucleotide-based system. More exciting examples were subsequently reported.[49–51] These systems rely on the fact that the product of a reaction recognizes the reactants and catalyzes their transformations into the product. A typical problem of these systems is product inhibition. circumvented by von Kiedrowski by using solid-phase cycling. Examples of self-replicating peptides[52] were also reported by Ghadiri[53,54] and Chmielewski.[55–57] These systems take advantage of Kent's chemical ligation strategy for the formation of a peptide bond.[58] Recent advances comprise the mimicry of many fundamental properties of living systems, like sensitivity to the environment,[59] sensitivity to chirality,[60] and ability to correct errors.[61] A recent example from the work of Chmielewski[62] provides an illustration of the principle. Two halves of the peptide **I**. namely, **Ia** and **Ib** (Fig. 8), are subject to ligation under Kent's conditions in the presence and absence of **I**. Peptide **I** provides a remarkable rate acceleration to the process due

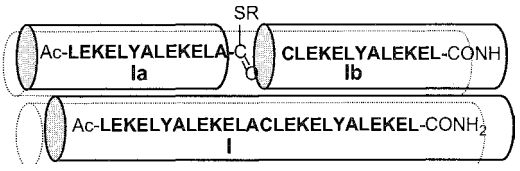

Fig. 8 A self-replicating system. Peptide **I** binds the two halves of **I** (actually a coiled-coil trimer. I_3), acting as a template, and placing **Ia** and **Ib** in the correct position for the occurrence of the ligation reaction.

to the binding of the two halves to I (actually a coiled-coil trimer. I_3) that acts as a template. thus placing Ia and Ib in the correct positions for the occurrence of the ligation reaction. The relative stability of the coiled-coil complexes appears to be the basis of the enhanced catalytic efficiency and low product inhibition of this system. A step forward into complexity in self-replication is provided by many of the systems described by Luisi and his group.[63–65] The basic idea behind this chemistry is that the lipid aggregates that are the constituents of a liposome (or vesicle) provide the elements for the minimal reaction vessel, a protocell. where reactions pertinent to living systems may occurr.[66] They were able to show that under appropriate conditions; these lipids can be continuously generated from a precursor. thus providing new constituents for new vesicle formation. If the vesicles catalyze the process of the generation of the constituent lipids from the precursor. the system becomes self-replicating. This proved to be the case. and self-replicating vesicles were reported. Now the system can be even more complex, in that self-replication may be controlled via a competing reaction that consumes the lipids. Depending on the conditions. the relative rates of lipid formation (v_f) and consumption (v,) may be such as to produce the growth of the vesicles ($v_f > v_c$), their death ($v_f < v_c$), or homeostasis ($v_c = v_f$). A chemical model for such a system was reported.[67] The basic component of this chemical model is a vesicular solution composed of an oleic acid/oleate lipid mixture charged with dihydroquinidine and OsO_4. These vesicles are continuously fed with oleic anhydride that is hydrolyzed in the oleic acid/oleate bilayer thus providing the source of new lipids (and, hence, new vesicles) and an oxidizing agent [$K_3Fe(CN)_6$]. This latter oxidizes the *cis* double bond of the lipid in a process that is OsO_4 catalyzed. If the hydrolysis reaction induces the growth of the vesicles, the oxidation one brings about their destruction, because the dihydroxystearic acid derivatives produced do not form vesicles. The careful control of the conditions leads to $v_f = v_c$ and to homeostasis of the system. As pointed out by the authors, the model is primitive, but it sets the basis for the obtainment of more complex and biologically relevant systems and, perhaps, to a metabolic model of a cell.

CONCLUSION

The mimicry of biological systems and, even more interesting, the synthesis of molecules working on the basis of the same principles that govern the natural ones but with unprecedented properties. are the challenges that supramolecular chemistry faces in this new century. The overview provided above gives readers an idea of some of the avenues chemists working in this field are undertaking. More exciting results are expected in the future.

ARTICLES OF **FURTHER** INTEREST

The Allosteric Effect, p. 20
Artificial Enzymes, p. 76
Catalytic Antibodies, p. 193
Crown Ethers, p. 326
Cyclodextrins, p. 398
DNA Nanotechnology, p. 475
Enzyme Mimics. p. 546
Enzymes: Characteristics and Mechanisms, p. 554
Hydrogen Bonding, p. 658
Hydrophobic Effects, p. 673
Ion Channels and Their Models, p. 742
Ionophores, p. 760
Molecular-Level Machines, p. 931
Rotawanes and Pseudorotaxanes, p. 1194
Self-Assembly in Biochemistry, p. 1257
The Template Effect, p. 1493
Vitamin B_{12} and Heme Models. p. 1569

REFERENCES

1. Lehn. J.-M. Toward complex matter: Sypramolecular chemistry and self-organization. Proc. Natl. Acad. Sci. U. S. A. 2002, *99*, 4763–4768.
2. Goshe, A.J.: Steele, I.M.: Ceccarelli. C.; Rheingold, A.: Bosnich, B. Supramolecular recognition: On the kinetic lability of thermodynamically stable host-guest association complexes. Proc. Natl. Acad. Sci. U. S. A. **2002**, *99*, 4823–4829.
3. Gellman, S.H. Foldamers: A manifesto. Acc. Chem. Res. 1998. 31, 173–180.
4. Etezady-Esfarjani, T.; Hilty. C.: Wiitrich. K.: Rueping, M.; Schreiber. J.; Seebach. D. NMR-structural investigations of a β^3-dodecapeptide with proteinogenic side chains in methanol and in aqueous solutions. Helv. Chim. Acta 2002.85, 1197–1209.
5. Raguse, T.L.: Porter, E.A.: Weisblum, B.: Gellman, S.H. J. Structure-activity studies of 14-helical antimicrobial β-peptides: Probing the relationship between conformational stability and antimicrobial potency. Am. Chem. Soc. **2002**, 124, 12774–12785.
6. Toniolo, C.; Crisma. M.; Formaggio, F.: Valle, G.; Cavicchioni. G.; Précigoux, G.; Aubry, A.; Kamphuis. J. Linear oligopeptide. 279. Structures of peptides from alpha-amino-acids methylated at the alpha-carbon. Biopolymers 1993, 33. 1061–1073.
7. Connors, K.A. The stability of cyclodextrin complexes in solution. Chem. Rev. **1997**. 97, 1325–1357.
8. Davis, A.P.; Wareham, R.S. A tricyclic polyamide receptor

for carbohydrates in organic media. Angew. Chem.. Int. Ed. 1998. *37*, 2270–2273.
9. Ryan. T.J.; Lecollinet. G.; Velasco, T.: Davis. A.P. Phase transfer of Monosaccharides through noncovalent interactions: Selective extraction of glucose by a lipophilic cage receptor. Proc. Natl. Acad. Sci. U. S. A. 2002, *99.* 4863–4866.
10. Kirby. A.J. Enzyme mechanisms. models, and mimics. Angew. Chem.. Int. Ed. 1996. *35*, 707–724.
11. Breslow, R.; Dong. S.D. Biornimetic reactions catalyzed by cyclodextrins and their derivatives. Chem. Rev. 1998, *98.* 1997–2011.
12. Breslow. R.: Trainor. G.: Ueno. J. Optimization of metallocene substrates for β-cyclodextrin in reactions. Am. Chem. Soc. 1983. *105*, 2739–2740.
13. Kunishima, M.: Yoshimura, K.: Morigaki. H.; Kawamata, R.: Terao, K.: Tani. S. Cyclodextrin-based artificial acyltransferase: Substrate-specific catalytic amidation of carboxylic acids in aqueous solvent. J. Am. Chem. Soc 2001, *123.* 10760–10761.
14. Mattei. P.: Diederich. F. Catalytic cyclophanes. 11. A flavo-thiazolio-cyclophane as a biomirnetic catalyst for the preparative-scale electro-oxidation of aromatic aldehydes to methyl esters. Helv. Chim. Acta 1997, *80*, 1555–1588.
15. Scarso, A.: Scheffer. U.; Göbel. M.; Broxterman. Q.B.; Kaptein. B.: Formaggio. F.; Toniolo. C.: Scrimin. P. A peptide template as an allosteric supramolecular catalyst for the cleavage of phosphate esters. Proc. Natl. Acad. Sci. U. S. A. 2002, *99.* 5144–5149.
16. Baltzer. L. Functionalization of designed folded polypeptides. Curr. Opin. Struc. Biol. 1998, *8.* 466–470.
17. Nilsson. J.: Baltzer, L. Reactive-site design in folded-polypeptide catalyst—The leaving group pK_a of reactive esters sets the stage for cooperativity in nucleophilic and general-acid catalysis. Chem. Eur. J. 2008. 6. 2214–2220.
18. Baltzer. L.: Nilsson, H.: Nilsson. J. De Novo design of proteins. What are the rules? Chem. Rev. 2001. *101*, 3153–3163.
19. Anderson, L.K.: Caspersson. M.; Baltzer. L. Control of lysine reactivity in four-helix bundle proteins by site-selective pK_a depression: Expanding the versatility of proteins by postsynthetic functionalisation. Chern. Eur. J. *2002, 8.* 3687–3697.
20. Klotz. I. *Enzyme Models-Synthetic Polymers*; Williams. A.. Page. M.. Eds.; The Royal Society of Chemistry: London. 1987: 14–34.
21. Hollfelder. F.: Kirby, A.J.; Tawfik, D.S. Efficient catalysis of proton transfer by synzymes. J. Am. Chem. Soc. 1997. *119.* 9578–9579.
22. Lie, L.: Breslow. R. A potent polymer/pyridoxamine enzyme mimic. J. Am. Chem. Soc. 2002. *124*, 4978–4979.
23. Wentworth. P. Antibody design by man and nature. Science 2002. *296.* 2247–2249.
24. Jain. M. *Introduction to* Biological *Membranes*. 2nd Ed.: Wiley: New York, 1992.
25. Urry, D.W. Chemical basis of ion transport specificity in biological membranes. Top. Curr. Chem. 1985. *128*, 175–191.
26. Åkerfeldt, K.S.: Lear. J.D.; Wasserman, Z.R.: Chung. L.A.: DeGrado. W.F. Synthetic pepticles as models for ion channel protein. Acc. Chem. Res. 1993. *26.* 191–197.
27. Benedetti, E.; Bavoso. A.: Di Blasio, B.: Pavone, V.; Pedone, C.; Toniolo. C.; Bonora, G.M. Peptaibol antibiotics: A study on the helical structure of the 2-9 sequence of emerimicins III and IV. Proc. Natl. Acad. Sci. U. S. A. 1982. *79.* 7951–7955.
28. Gennis. R.B. *Biomembranes: Molecular Structure and* Function: Springer-Verlag: New York. 1989.
29. Ghadiri, R.M.: Granja, J.R.; Buehler, L.K. Artificial transmembrane ion channels from self-assembling peptide nanotubes. Nature 1994, *369*, 301–305.
30. Khazanovich, N.: Granja, J.R.; McRee. D.E.; Milligan. R.A.; Ghadiri. M.R. Wanoscale tubular ensembles with specified internal diameters. Design of a self-assembled nanotube with a 13-Å pore. J. Am. Chern. Soc. 1994, *116*, 6011–6012.
31. Ghadiri, M.R.; Granja. J.R.; Milligan. R.A.: McRee. D.E.: Khazanovich. N. Self-assembling organic nanotubes based on a cyclic peptide architecture. Nature 1993, *366*, 324–328.
32. Kim, H.S.: Hartgerink, J.D.; Ghadiri. M.R. Oriented self-assembly of cyclic peptide nanotubes in lipid membranes. J. Am. Chem. Soc. 1998. *120*, 4417–4418.
33. Voyer. N.; Robitaille, M. Novel functional artificial ion channel. J. Am. Chem. Soc. 1995, *117*, 6599–6600.
34. Winum, J.-Y.; Matile, S. J. Rigid push-pull oligo(p-Phenylene) rods: Depolarization of bilayer membranes with negative membrane potential. Am. Chem. Soc. 8999. *121*, 7961–7962.
35. Sakai, N.: Brennan, K.C.: Weiss. L.A.: Matile. S. Toward biomimetic ion channels formed by rigid-rod molecules: Length-dependent ion-transport activity of substituted oligo(p-phenylene)s. J. Am. Chem. Soc. 1997, *119.* 8726–8727.
36. Goto. C.; Yamamura, M.; Satake. A.: Kobuke, Y. J. Artificial ion channels showing rectified current behavior. Am. Chem. Soc. 2001, *123*, 12152–12153.
37. De Riccardis, F.; Di Filippo, M.; Garrisi, D.: Izzo. I.: Mancin. F.; Pasquato, L.; Scrimin. P.; Tecilla, P. An artificial ionophore based on a polyhydroxylated steriod dimer. Chern. Commun. 2002. 3066–3067.
38. Moore. K.S.: Wehrli, S.; Roder, H.: Rogers, M.; Forrest, J.N.. Jr.; McCrimmon. D.: Zasloff, M. Squalamine: An aminosterol antibiotic from the shark. Proc. Natl. Acad. Sci. U. S. A. 1993. *90.* 1354–1357.
39. Sadownik. A.; Deng. G.; Janout, V.; Regen, S.L. Rapid construction of squalamine mimic. J. Am. Chem. Soc. 1995. *117.* 6138–6139.
40. Otto. S.; Osifchin. M.; Regen, S.L. Squeezing a synthetic ionophore and mechanistic insight out of a lipid bilayer. J. Am. Chem. Soc. 1999. *121.* 10440–10441.
41. Balzani. V.: Scandola, F. Photochemical and PhotoPhysical Devices. In *Comprehensive Supramolecular Chemistry*; Atwood, J.L., Davies, J.E.D., MacNicol. D.D.. Vogtle. F.. Lehn, J.-M., Reinhoudt, D.N.. Eds.: Pergamon: Oxford, 1996: Vol. 10.

42. Chambron, J.-C.; Heitz, V.; Sauvage, J.-P. Noncovalent Multiporphyrin Assemblies. In *The Porphyrin Handbook*; Kadish, K.M., Smith, K.M., Guilard, R., Eds.; Academic Press: New York, 2000; Vol. 6, 1–42.
43. *Supramolecular Photochemistry*; Balzani, V., Scandola, F., Eds.; Ellis Horwood Ltd.: New York, 1991.
44. Ward, M.D. Photo-induced electron and energy transfer in non-covalently bonded supramolecular assemblies. Chem. Soc. Rev. **1997**, *26*, 365–375.
45. Blanco, M.-J.; Jimenez, M.C.; Chambron, J.-C.; Heitz, V.; Linke, M.; Sauvage, J-P. Rotaxanes as new architectures for photoinduced electron transfer and molecular motions. Chem. Soc. Rev. **1999**, *28*, 293–305.
46. Haycock, R.A.; Yartsev, A.; Michelsen, U.; Sundstrom, V.; Hunter, C.A. Self-assembly of pentameric porphyrin light-harvesting antennae complexes. Angew. Chem., Int. Ed. **2000**, *39*, 3616–3619.
47. Sugou, K.; Sasaki, K.; Kitajima, K.; Iwaki, T.; Kuroda, Y. J. Light-harvesting heptadecameric porphyrin assemblies. Am. Chem. Soc. **2002**, *124*, 1182–1183.
48. von Kiedrowski, G. A self-replicating hexadeoxynucleotide. Angew. Chem., Int. Ed. Engl. **1986**, *25*, 932–934.
49. Li, T.; Nicolaou, K.C. Chemical self-replication of palindromic duplex DNA. Nature **1994**, *369*, 218–221.
50. Sievers, D.; von Kiedrowski, G. Self-replication of complementary nucleotide-based oligomers. Nature **1994**, *369*, 221–224.
51. Luther, A.; Brandsch, R.; von Kiedrowski, G. Surface-promoted replication and exponential amplification of DNA analogues. Nature **1998**, *396*, 245–248.
52. Issac, R.; Ham, Y.-W.; Chmielewski, J. The design of self-replicating helical peptides. Curr. Opin. Struct. Biol. **2001**, *11*, 458–463.
53. Lee, D.H.; Granja, J.R.; Martinez, J.A.; Severin, K.; Ghadiri, M.R. A self-replicating peptide. Nature **1996**, *382*, 525–529.
54. Severin, K.; Lee, D.B.; Martinez, J.A.; Ghadiri, M.R. Peptide self-replication via template-directed ligation. Chem. Eur. J. **1997**, *3*, 1017–1023.
55. Yao, S.; Ghosh, I.G.; Zutshi, R.; Chmielewski, J. A pH-modulated, self-replicating peptide. J. Am. Chem. Soc. **1997**, *119*, 10559–10560.
56. Yao, S.; Ghosh, I.G.; Zutshi, R.; Chmielewski, J. Selective amplification by auto- and cross-catalysis in a replicating peptide system. Nature **1998**, *396*, 447–450.
57. Yao, S.; Ghosh, I.G.; Zutshi, R.; Chmielewski, J. A self-replicating peptide under ionic control. Angew. Chem., Int. Ed. **1998**, *37*, 478–481.
58. Dawson, P.E.; Muir, T.W.; Clark-Lewis, L.; Kent, S.B.H. Synthesis of proteins by native chemical ligation. Science **1994**, *266*, 776–778.
59. Yao, S.; Chmielewski, J. A pH-tunable peptide ligase. Biopolymers **1999**, *51*, 370–375.
60. Saghtelian, A.; Yobobayeshi, Y.; Soltani, K.; Ghadiri, M.R. A chiroselective peptide replicator. Nature **2001**, *409*, 797–801.
61. Severin, K.; Lee, D.H.; Martinez, J.A.; Vieth, M.; Ghadiri, M.R. Dynamic error correction in autocatalytic peptide networks. Angew. Chem., Int. Ed. **1998**, *37*, 126–128.
62. Issac, R.; Chmielewski, J. Approaching exponential growth with a self-replicating peptide. J. Am. Chem. Soc. **2002**, *124*, 6808–6809.
63. Bachmann, P.A.; Luisi, P.L.; Lang, J. Autocatalytic self-replicating micelles as models for prebiotic structures. Nature **1992**, *357*, 57–59.
64. Walde, P.; Wick, R.; Fresta, M.; Mangone, A.; Luisi, P.L. Autopoietic self-reproduction of fatty acid vesicles. J. Am. Chem. Soc. **1994**, *116*, 11649–11654.
65. Morigaki, K.; Dallavalle, S.; Walde, P.; Colonna, S.; Luisi, P.L. Autopoietic self-reproduction of chiral fatty acid vesicles 301. J. Am. Chem. Soc. **1997**, *119*, 292–301.
66. Szostak, J.W.; Barteld, P.; Luisi, P.L. Synthesizing life. Nature **2001**, *409*, 387–390.
67. Zepik, H.H.; Blöchliger, E.; Luisi, P.L. A chemical model of homeostasis. Angew. Chem., Int. Ed. **2001**, *40*, 199–202.

Biomaterials

Judith R. Meakin
University of Aberdeen, Foresterhill, Aberdeen, United Kingdom

INTRODUCTION

A biomaterial is any natural or synthetic material that is employed as. or part of. a medical device. Typical materials include metals, ceramics, glasses. polymers, and tissue-engineered materials. The requirements of a biomaterial are that it should have the correct properties to allow it to achieve its intended function and be biocompatible. Over recent decades. there have been many developments in biomaterials research. Some of these developments have involved a movement from the use of inert materials to more sophisticated ones, which actively invoke a beneficial response from the body.

WHAT ARE BIOMATERIALS AND WHY DO WE NEED THEM?

Biomaterials are natural or synthetic materials that can be used as. or part of, a medical device to augment, repair, or replace a natural tissue within the body. They include tissue from the recipient's body (autograft), from another human being (allograft). from an animal of another species (xenograft). or a synthetic substitute. In this article. emphasis will be given to synthetic materials (metals, glasses. ceramics, polymers. and tissue-engineered materials) and some of the recent developments in this field.

The types of medical devices that require biornaterials arc wide ranging across most medical disciplines.[1] Artificial heart valves. contact lenses, drug delivery implants. urinary catheters. and replacement hip joints are just a few examples that demonstrate where biomaterials can be employed in the body.

Medical devices, and hence biomaterials, are becoining increasingly important in developed countries due to changes in society. With increasing life expectancy and better health care. people expect to remain active into their seventies and eighties. An increase in leisure time has led to an increase in injuries frotn sports. e.g., skiing. Furthermore. diseases such as heart disease and diabetes. which have become more prevalent in recent decades. require biornaterials to provide long-term solutions rather than the palliative treatments currently available.[2]

In the U.K.. there is a demand for medical devices that are quick and easy to implant, that minimize postsurgical complications, and that last the intended duration.[1] The importance given to this demand is demonstrated by the "Building up Biomaterials" program. which was recently launched by the Department of Trade and Industry. This program aims to promote the growth and competitiveness of the Bioinaterials industry in the U.K. by bringing together clinicians. researchers, and the medical device industry.

GENERAL REQUIREMENTS OF A BIOMATERIAL

The two principal requirements of any biomaterial used in a medical device are that it should have the correct physical properties in order for it to perform its intended function, and it should be biocompatible. Other requirements are that it can be easily manufactured and can be suitably sterilized. There are various sterilization methods; the use depends mainly on the material being sterilized. Gamma-ray or high-temperature sterilization methods, for example, are unsuitable for polyurethanes. as they produce toxic and carcinogenic compounds.[3]

The physical properties of a biomaterial include mechanical properties. such as stiffness. strength. and durability, together with other properties. such as oxygen permeability. The properties need to be suitable for the intended lifetime of the implant, which can range from the few weeks required for resorbable sutures to the lifetime of the patient receiving a hip replacement.

Biocompatibility essentially means that the material produces no adverse response from the body; this may be toxic, allergenic, carcinogenic, or mechanical. However. the body can tolerate even nonbiocompatible materials if the quantity of the material is small enough. Adverse responses can arise in response to chemical or particulate products that are released from a biomaterial. Metals, for example. are particularly susceptible to corrosion by body fluids. and the products of corrosion, such as metallic ions. salts. and oxides, can induce an immune response.[4] Particles. resulting from mechanical wear of an implant. may also invoke an immune response, even if this would

Encyclopedia of Supramolecular Chemistry
DOI: 10.1081/E-ESMC 120012816

not be induced by the bulk material.[5] Not only can loss of material from an implant lead to an adverse reaction, but it can also compromise the integrity. and hence function, of the device.

As well as physiological effects, implants can have adverse mechanical effects. Ideally. the mechanical properties of an implant should be compatible with those of the surrounding tissues. Large differences in stiffness though, can result in high interfacial shear stresses. The resulting micromovement may then lead to loosening and eventual failure of the implant. A difference in stiffness also changes the distribution of mechanical stress on the surrounding tissues. This can cause the tissue to degenerate or reinodel. In hip replacements. for example, the high stiffness of the implants compared to the bone of the femur can reduce the stress in the bone.[6] This "stress shielding" results in the bone being resorbed by the body. It is also hypothesized that modified stress distributions may result in continuing pain for the patient.[7]

TYPICAL BIOMATERIALS

Metals

The metals commonly used in medical devices are stainless steel (Types 316 and 316 L), cobalt-chromium-based alloys, titanium. and titanium-based alloys. Metals are used extensively in orthopedic surgery for load-bearing devices. such as artificial joints and fixation devices (wires. pins. screws; fracture plates. etc.). Other metals include tantalum, gold, and mercury alloys: the latter two are used predominantly in dentistry.

One of the main problems of metallic orthopedic implants is that they are much stiffer than the natural tissues they replace (see Table 1). As described above, a difference in stiffness between adjacent materials can lead to a number of problems. including loosening as a result of micromovement and bone resorption due to stress shielding. Adequate fixation of an orthopedic implant to the surrounding bone is therefore of paramount importance. It can be achieved using a number of methods. such as interference fitting. screws, poly(methyl methacrylate) bone cement. and coatings to achieve a chemical bond or porous ingrowth.[5]

Table I Typical material properties of metals and bone

Material	Elastic modulus (GPa)
Stainless steel	200
Co-Cr-Mb alloy	230
Titanium	110
Cortical bone	12–17
Cancellous bone	0 1

Cortical bone it a dense structure located at the surfaces of bones: cancellous bone is an open pore structure located internally. (From Ref. [5].)

Titanium may appear to be the ideal metal. as its stiffness is the closest to bone (Table 1). It has the lowest density (nearly half that of the other two metals). and it has the highest resistance to corrosion due to the formation of a nonreactive layer of titanium oxide on the surface of the metal. However. its shear strength is low, making it unsuitable for use in screws and bone plates. It also has a high coefficient of friction when in contact with itself or another metal. making it unsuitable as a load-bearing surface.

Stainless steel. which is typically used for bone plates, screws, and nails. is particularly susceptible to corrosion, although its chromium and molybdenum content (about 17% and 3%. respectively) helps to make it more resistant. Cobalt-chromium-molybdenum alloys exhibit excellent durability and strength. making them apposite for artificial joints, although their coefficients of friction make them unsuitable for load-bearing surfaces.

One interesting alloy of titanium and nickel, called Nitinol, exhibits shape-memory properties. Below a particular temperature (the transformation temperature), the crystal structure of the alloy is such that it can be plastically deformed (martensitic). As the alloy is heated, the crystal structure alters to one that is more ordered and rigid (austenitic). and the deformed metal reverts to its original shape.[8] This effect has been exploited in a number of devices. including a stent (a device used to hold open passageways such as arteries). The stent is placed inside a small-diameter catheter for insertion into the body, where it expands on being warmed to body temperature.[8]

Tantalum, which is used for a number of applications,[9] was recently made into a porous material that could be used for bone reconstruction. The porous structure is made by depositing the metal onto a vitreous carbon scaffold using chemical vapor deposition/infiltration techniques. Its low structural density means that its stiffness (2.5–4 GPa) is closer to that of natural bone than the solid metal. and the porosity means that bone can fully integrate into the structure. forming an excellent bond.[9]

Ceramics and Glasses

Ceramics, such as the coinmonly used Alumina ($A1_2O_3$) and Zirconia (ZrO_2), tend to have a very high elastic modulus (around 400 GPa), have a low coefficient of friction. and are resistant to wear. These properties make them useful as the load-bearing surfaces in orthopedic implants,

such as hip prostheses.[6] Another of their properties. which leads to them being popular for dental applications. is their inertness, which makes them very biocompatible. However, more interesting ceramics exist that, rather than being inert. provoke a beneficial response from the body.

Calcium phosphate is a mineral found in several different forms. including hydroxyapatite. β-whitlockite, and tricalcium phosphate. The crystal structure of hydroxyapatite [$Ca_{10}(PO_4)_6(OH)_2$], is similar to that of the calcium and phosphate apatites that are present in the mineral phase of bone. It was found that if a metallic implant is coated with a calcium-phosphate-based material, the formation of bone around the implant is accelerated, and surface contact in the early stages of healing is improved.[10,11] This is because, in addition to providing a porous surface with which the bone can integrate. the coatings are able to form a direct chemical bond with the bone.

Bioactive glasses are another type of material that actively promote a useful response from the tissue into which they are implanted. Bioactive glasses are a family of glass materials made from Na_2O–CaO–P_2O_5–SiO_2. Certain formulations of these glasses are able to form very strong bonds with bone. When the glass is exposed to fluids in the body. a 12-stage reaction occurs[1*] that involves formation of a hydroxyl carbonate apatite (HCA) layer on the outer surface of the glass. It is this outer layer that is thought to be crucial for bonding to bone to occur.

A smaller subset of the bioactive glasses can also form bonds with collagen.[12] In vitro tests showed that the collagen fibrils integrate into the outer HCA layer. This is similar to the way that collagen fibrils in natural tissues such as cartilage. ligament. etc.. bond to the underlying bone. Hence. bioactive glasses have the potential to provide a solution to the problem of how to attach replacement soft tissues such as ligaments or the menisci of the knee.

The main drawback of bioactive glasses is their brittle properties and insufficient strength, making them unsuitable for load-bearing applications. However, combining them with polymers was shown to improve the mechanical properties while retaining the bioactivity.[13]

Polymers

Many different polymers are used in a variety of medical devices.[1] These range from ultrahigh-density polyethylene, which is used as the load-bearing surface of artificial joints,[6] to much softer elastomers. such as silicones. which are employed. among other uses, as finger joint replacements and maxillofacial prostheses.

One particular class of polymers that absorb and retain significant amounts of water are called hydrogels. The water in a hydrogel is retained in the gel by hydrogen bonding to hydroxyl groups along the polymer backbone. Over the years, there has been considerable controversy on the exact state of the water.[14] However, some of the most recent research, using thermal analysis suggests that the water is present as three different phases in dynamic equilibrium.[15]

Bydrogels have many actual or potential uses—most notably as contact lenses, wound dressings. coatings, and drug delivery systems.[16] The hydrophilic nature of hydrogels, plus their high water content. makes them extremely biocornpatible. As a coating on a device such as a catheter, particularly in combination with antimicrobial agents. they can help prevent the buildup of bacteria that may otherwise lead to blockage and infection.

As a contact lens. their soft rubbery properties make them comfortable to wear. However. one of their limitations is the high water content and thin cross section required to achieve sufficient oxygen transport to the cornea. This is extremely important. as the cornea does not have its own vascular supply and relies on obtaining oxygen in this way.

The more recently developed silicone hydrogels have the potential to solve this problem because although they have relatively low water contents (about 30%). in comparison to the conventionally used hydrogels, their oxygen permeability is far higher.[1] This characteristic, combined with their good biocompatibility, has allowed them to be manufactured into lenses that can be worn continuously for up to a month.

Another exciting development for hydrogels is self-assembly.[18] Self-assembly means that the constituent molecules of a material organize themselves, under thermodynamic equilibrium, into a well-defined and stable configuration, held together by noncovalent bonds. The structural form of the molecules determines the way they fit together. and this can be influenced by environmental factors including temperature and pH value.[18]

Biodegradable polymers. as their name suggests. slowly degrade once they are implanted into the body. Several biodegradable polymers have been approved for implantation [poly(glycolide), poly(lactide), poly(ε-caprolactone), poly(dioxanone), and their copolymers] and have been manufactured into a number of medical devices, such as sutures, screws, and tissue repair barbs.[1] One advantage of using a biodegradable material is that additional surgery to remove a temporary device is unnecessary. Also, in applications such as fixation of a broken bone, the gradual degradation of the device means that load is transferred to the bone as it heals; this can help the bone regain its complete strength.

Degradation occurs due to hydrolysis of the polymer backbone or by enzymatic attack. which breaks the polymer into increasingly smaller units. The resulting

compounds may then dissolve into the surrounding body fluids or may be metabolized and excreted by the body [e.g., lactic acid removed as a product of poly(lactide)].

Tissue-Engineered Materials

Tissue engineering is perhaps most memorable to many people as an image of an ear growing on the back of a mouse.[20] Currently, the only commercially available product is skin grown from human fibroblasts on a biodegradable mesh. However, research continues toward achieving the ultimate aim of growing a fully functioning tissue or organ using cells from the patient's own body (e.g., Ref. [21]).

One of the potential benefits of tissue engineering is that it could eliminate the need for donor tissue and organs, which are in short supply. Additionally, there is less likely to be the problems of rejection or disease transfer that occur when using allografts or xenografts.

Essentially; the technique involves seeding cells onto a scaffold and providing them with the appropriate nutrients, growth factors. and environmental conditions.[22] When they sufficiently proliferated, the structure can be implanted into the patient, where it becomes integrated into its surroundings with the formation of blood vessels, etc. The scaffold not only determines the shape of the tissue but can also provide mechanical support as it develops. Once the tissue forms. the scaffold becomes redundant. Hence, materials for scaffolds are ideally made from synthetic biodegradable polymers, as described in the previous section. or from natural polymers such as collagen.

Fabrication of a three-dimensional scaffold can be achieved using a number of methods. One technique that was recently explored is fused deposition modeling (FDM). This is a rapid prototyping method, where the material [poly(ε-caprolactone)] is heated to just above its melting temperature and extruded as a thin thread that is laid down in layers.[23] Effectively. any three-dimensional structure can be made providing there is a computer file describing its geometry; this has useful applications for defining scaffolds from medical images.

The future success of tissue engineering is heavily dependent on understanding what external factors influence cell behavior (e.g., cell attachment, proliferation, migration, and expression of extracellular matrix). The laying down of extracellular matrix components such as collagen, for example, is important for growing tissues like ligaments, which require the collagen to be aligned in a specific direction.[24] So far, various external stimuli have been shown to influence cell behavior. These include surface topography in the form of grooves or surface texture and mechanical deformation.[22]

CONCLUSION

Since the first metal implants used in the early part of the twentieth century, biomaterials for use in medical devices have developed significantly. In the last few decades, materials technology has become more sophisticated, and there has been a move from the use of passive, inert materials toward ones that interact with the body to elicit a beneficial response or more closely mimic the natural tissues. However, there is still a need for further developments, and a recent report highlighted the desperate need for new biomaterials in all clinical disciplines.[2]

In the shorter term. improvements in existing materials are required. For example, 10% of hip replacement operations are revision surgeries. These are more technically difficult than the primary surgeries, are considerably more expensive, and tend to be less successful.[2] Hence, improvements can still be made in the materials used for hip prostheses and the methods used to fix them in place.

Over the longer term, a demand exists for materials that can provide permanent solutions. Tissue engineering may provide solutions to some of these needs in the future. However, despite recent success in this area, the development of functional tissue may still be a long way off. For example, it was estimated that it may take another 10–15 years to develop tissue-engineered kidneys.[2] Furthermore, for load-bearing tissues such as ligaments. the mere development of a material with suitable mechanical properties is only one concern. A major problem that requires resolution. is how to attach the ligament to the bones. However: as previously described, bioactive glasses may provide a solution.

In this article. the various biomaterials described have, in general, been considered separately. However, the use of biodegradable polymers in tissue engineering[23] and the fabrication of hydrogels by self-assembly[25] suggest that future developments in biomaterials research may benefit from an increasingly integrated approach.

ACKNOWLEDGMENTS

I would like to thank the Welcome Trust for funding my current research. I would also like to thank Dr. Simon Lee for his helpful comments concerning this manuscript.

ARTICLES OF FURTHER INTEREST

Crystal Growth *Mechanisms*, p. 364
Drug Delivery, p. 484
Gels. p. 586

Mesoporous Silicas and Silica-Organic Hybrids, p. *852*
Nanocasting Strategies and Porous Materials, p. 950
Self-Assembly: Definition and Kinetic and Thermodynamic Considerations, p. *1248*
Self-Assembly: Terminology, p. *1263*

REFERENCES

1. Bromhead. J. Biomaterials State *of* ***the*** Art Report 2002; 2002. LGC/GEN/2002/002, LGC (Teddington) Limited.
2. Bromhead, J. *Directory of Clinical Need*; 2002. LGC/GEN/2002/004, LGC (Teddington) Limited.
3. Yoda, R. Elastomers for biomedical applications. J. Biomatcr. Sci., Polym. Ed. **1998,** *9* (6), 561–626.
4. Hallab, N.; Merritt, K.; Jacobs, J.J. Metal sensitivity in patients with orthopaedic implants. J. Bonc Jt. Surg., Am. **2001,** *83A* (3). 428–436.
5. Park, J.B.; Lakes, R.S. *Biomaterials:* An Introduction, 2nd Ed.: Plenum Prcss: New York, 1992.
6. Huo, M.H. What's new in hip arthroplasty. J. Bone Jt. Surg., Am. **2002,** K4A (10), 1894–1905.
7. Mulholland, R.C.; Scngupta. D.K. Rationale, principles and experimental evaluation of the concept of soft stabilization. Eur. Spine J. Suppl. **2002,** 11. S198–S205.
8. Barras, C.D.J.; Myers, K.A. Nitinol—Its use in vascular surgery and other applications. Eur. J. Vasc. Endovasc. Surg. **2000.** 19, 564–569.
9. Bobyn, J.D.; Stackpool, G.J.; Hacking, S.A.; Tanzer, M.; Krygier, J.J. Characteristics of bone ingrowth and interface mechanics of a new porous tantalum hiomaterial. J. Bone Jt. Surg., Rr. **1999.** *81B* (5). 907–914.
10. Barrere, F.; van der Valk, C.M.; Dalmeijer, R.A.J.: van Blitterswijk, C.A.; de Groot. K.; Layrolle, P. In vitro and in vivo degradation of biomimctic octacalcium phosphate and carbonate apatite coatings on titanium implants. J. Biomed. Matcr. Res., A **2003,** 64A (2), 378–387.
11. Schliephake, H.; Scharnweher. D.; Dard, M.; Rossler, S.; Sewing, A.; Huttmann, C. Biological performance of biomimetic calcium phosphate coating of titanium implants in the dog mandible. J. Riomed. Matcr. Res., A **2003**, 64A (2). 225–234.
12. Hench, L.L. Rioceramics. J. Am. Chem. Soc. **1998**, 81 (7). 1705–1728.
13. Thompson, I.D.; Hcnch, L.L. Mechanical properties of bioaetivc glasses, glass-ceramics and composites. J. Eng. Med. **1998.** 212. 127–137.
14. McBrierty, V.J.; Martin, S.J.; Karasx. F.E. Understanding hydrated polymers: The perspective of NMR. J. Mol. Liq. **1999;** *80* (2 3). 179–205.
15. Meakin, J.R.; Imrie, C.T.; Hukins, D.W.L.; Aspden, R.M. Thermal analysis of poly(2-hydroxyethyl methacrylate) (pHEMA) hydrogels. J. Mater. Sci., Mater. Med. **2003,** 14 (1), 9–15.
16. Rosiak, J.M.; Yoshii, F. Hydrogels and their medical applications. Nucl. Instrum. Methods, B **1999,** *151*, 56–64.
17. Tighe, B. Silicone hydrogels—What are they and how should they be used in everyday practice'! Optician **1999.** *281* (5726). 31–32.
18. Zhang, S. Emerging biological materials through molecular self-assembly. Biotcchnol. Adv. **2002,** 20, 321–339.
19. Middleton, J.C.; Tipton, A.J. Synthetic hiodegradable polymers as orthopedic devices. Biomatcrials **2000**, 21, 2335–2346.
20. Cao, Y.L.; Vacanti, J.P.; Paige. K.T.; Upton, J.; Vacanti, C.A. Transplantation of chondrocytes utilizing a polymer-cell construct to produce tissue-engineered cartilage in the shape of a human ear. Plast. Reconstr. Surg. **1997**, 100 (2). 297–302.
21. Kim, T.H.; Vacanti, J.P. Tissue Engineering of thc Liver. In *The Biomedical Engineering Handbook,* Volume *II,* 2nd Ed.; Bronzino, J.D., Ed.; CRC Press LLC: Boca Raton, FL, 2000; 121,1–121,9.
22. Bcrthiaume, F.; Yarmush, M.L. Tissue Engineering. In *The* Biomedical Engineering *Handbook, Volume II,* 2nd Ed.; Bronzino. J.D., Ed.; CRC Prcss LLC: Boca Raton, FL, 2000; 109,1–109,12.
23. Hutmacher, D.W. Scaffolds in tissue engineering bonc and cartilage. Biomaterials **2000.** *21*, 2529–2543.
24. Hukins, D.W.L.; Aspden, R.M. Composition and properlies of connective tissues. Trends Biochem. Sci. **1985.** *10* (7), 260–264.
25. Otsuka. H.; Nagasaki, Y.; Kataoka, K. Self-assembly of poly(ethylene glycol)based block copolymers for biomedical applications. Curr. Opin. Colloid Interface **2001**. 6, 3–10.

Biosensors

Jun-ichi Anzai
Tohoku University, Sendai, Japan

INTRODUCTION

Enzyme–substrate, antibody–antigen, and other protein–ligand interactions are representative constituents of biological supramolecular systems. The structure and function of some of these biological supramolecular systems were mimicked by chemists in order to construct synthetic counterparts such as host-guest compounds, self-assembled monolayers and ordered multilayers, and related molecular assemblies. On the other hand, little was reported on the development of artificial supramolecular systems that use proteins as building blocks. Described in this article is the fabrication of biosensors using protein-based supramolecules based on avidin–biotin and lectin–sugar interactions.

BIOSENSORS

Biosensors comprise a class of analytical devices that are fabricated by combining transducers. such as electrodes and optodes, with biological materials. including enzyme. antibody, and other proteins, for medical. environmental. or industrial applications. The biological materials are usually immobilized on the surface of the sensing part of the transducers in order to fabricate biosensors. Therefore, the technique of protein immobilization is crucial for developing high-performance biosensors. Numerous procedures for protein immobilization. including physical adsorption. entrapment into a polymer matrix, covalent bonding to a reactive surface, self-assembling on the surface, and others were reported. Physical adsorption is a convenient and simple way to immobilize proteins on the surface of the transducer, because proteins tend to be adsorbed more or less to any type of solid surfaces. Thus. the surface of the transducer can be modified irreversibly by immersing the transducer in an aqueous solution of dissolved proteins, which are then adsorbed into the transducer. However. this protocol suffers from the drawback that proteins often lose their biological activity due to denaturing on the surface (i.e., surface-induced conformational changes). resulting in a short life of the sensor. This drawback can be overcome by entrapping proteins into a polymer matrix on the surface of transducer. because the proteins are entrapped in organic materials without direct contact with the surface of transducer. On the other hand: covalent bonding and self-assembly of proteins on the surface are sophisticated techniques that enable one to design structures and functions of sensors, although training to learn certain skills is often required. Recently, attention was devoted to the molecular-level modification of the surface of an electrode with proteins, in which the electrode surface is covered with a nanometer-sized thin film. One of the advantages of the molecular-level modification is that rapid-response sensors can be fabricated by removing the conventional type of thick membrane from the surface of the electrode. Another merit is that this method makes it possible to arbitrarily tune the performance of the sensors on the basis of the molecular-level design of the protein film.

AVIDIN–BIOTIN SYSTEMS

Avidin is a tetramer protein (molecular mass: 67.000) found in egg white, and each subunit of avidin contains a binding site to biotin and forms a highly stable complex noncovalently (the binding constant; $10^{15}\ M^{-1}$) (Fig. 1).[1] Therefore, a single avidin molecule can accommodate up to four biotin molecules simultaneously. This strong and specific binding led to its widespread use in diagnostic and biochemical assays in which the formation of practically irreversible complexes is required. This is because avidin binds not only biotin but also its derivatives, with a carboxyl side chain that is modified covalently with protein and other macromolecules. Many kinds of activated biotins for labeling and biotin- or avidin-labeled reagents were developed for this purpose and are now commer-. cially available.

A crystallographic study of avidin shows that the interactions include a hydrogen-bond network between the biotin ureide group and amino acid residues in the binding site, an interaction between the biotin sulfur atom and hydroxyl group of threonine in avidin, and a hydrogen bond between carboxylate in the biotin side chain and protein backbone.[2,3] Among these. the first interaction plays a dominant role in biotin binding. In the binding pocket, several polar residues are available, including asparagine, tyrosine, serine. and threonine, which participate in the network of hydrogen bonds with biotin

Encyclopedia of Supramolecular Chemistry
DOI: 10.1081/E-ESMC 120019155

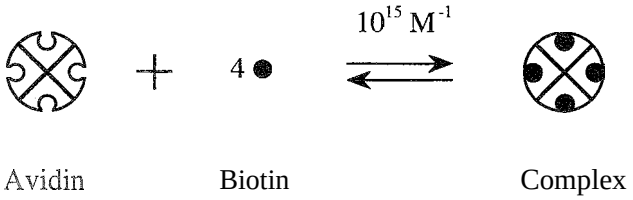

Fig. 1 Avidin–biotin complexation

ureide groups. In addition, the contributions of hydrophobic and van der Waals' interactions between biotin and aromatic residues in the binding pocket were also suggested. Avidin is a tetrameric protein with 222 molecular symmetry. and each subunit is organized in an eight-stranded antiparallel orthogonal β-barrel.[4] An avidin molecule (tetramer) is in a cubic-like shape (ca. 5.5 x 6 *x* 4 nm). The binding sites to biotin are arranged in two pairs on opposed faces of the molecule. The two binding sites on the same faces (6 x 5.5 nm) are separated 2–2.5 nm from each other.[5] The shape and size of avidin makes its use promising as a building block for constructing supramolecular protein architectures.

BIOSENSORS MODIFIED WITH AVIDIN–BIOTIN ARCHITECTURES

Electrochemical biosensors are usually fabricated by immobilizing enzymes or other functional proteins on the surface of electrodes. Illustrated in Fig. 2 is a typical structure and reactions involved in a glucose sensor fabricated by immobilizing glucose oxidase (GOx) on the surface of a inetal electrode. The chemical events on the electrode surface induced by GOx can be transferred into the output signals (i.e., electric current). Thus, the immobilization technique of enzyme is crucial to the development of high-performance biosensors. Therefore. many techniques were developed for immobilizing proteins. Early studies of enzyme biosensors often employed thick polymer membranes (thickness: 0.01–1 mm) in which enzymes are physically or chemically anchored. They sometimes suffer from such drawbacks as insufficient reusability and slow response due to the suppressed diffusion of analytes in the thick polymer membrane. To overcome these probiems. attention was recently devoted to the molecular-level modification of electrode surfaces (thickness: 10–100 nm) with enzymes or other proteins. An avidin–biotin system was employed for this purpose. For another example. in 1989, Walt and coworkers iinmobilized biotin-modified enzymes (urease. esterase. and penicillinase) on the surface of biotin-modified optical fibers using avidin as a binder.[6] They demonstrated the general use of this procedure in immobilizing any kind of enzyme. Gunaratna and Wilson also used an enzyme column in which enzymes were immobilized through avidin–biotin complexation.[7]

It may be possible to build up a two- or three-dimensional architecture composed of proteins. using avidin and biotin-labeled enzymes as building blocks. An enzyme multilayer (illustrated in Fig. 3) would be constructed using enzymes tagged with more than two biotin residues. because avidin contains four biotin-binding sites per molecule. The biotin-binding sites are fortunately located in two pairs on the opposing faces of an avidin molecule. In order to check the possibility of multilayer formation, we immobilized fluorescein-5-isothiocyanate (FITC)-conjugated avidin and biotin-labeled GOx alternately on a quartz slide and monitored the absorption spectra of the modified slide.[8] A silylated quartz slide was immersed in FITC-avidin and biotin-labeled GOx solutions alternately and repeatedly. which provided both sides of the slide with the protein multilayer. FITC-avidin is immobilized in each layer as a roughly monomolecular layer.

An electrochemical technique. cyclic voltammetry (CV), was employed for further characterization of the GOx multilayer film.[9] In the GOx-catalyzed oxidation reaction of glucose, a cofactor flavine adenine dinucleotide (FAD), which is contained at the active center of GOx, oxidizes glucose to gluconolactone. The resultant $FADH_2$ is converted back to the active FAD form by O_2. In the conventional type of enzyme sensor. the H_2O_2 generated from O_2 is oxidized at the electrode surface. It was reported that a GOx-catalyzed reaction can be mediated by synthetic redox compounds such as hydroquinone and ferrocene.[10–13] These redox compounds mediate electron relay from $FADH_2$ in GOx to electrode (i.e., electron mediator). In this situation, the magnitude of oxidation current in CV of the electron mediator would be a function of the loading of the enzyme on the electrode surface. Therefore. the CV measurements in the solution of a constant amount of dissolved mediator and glucose

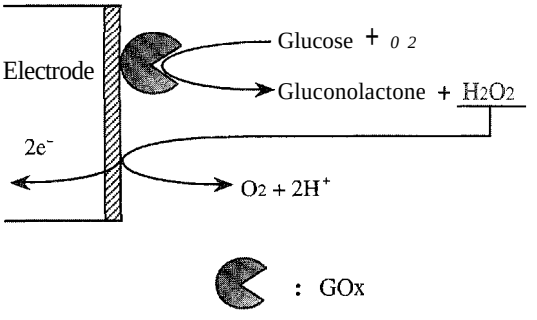

Fig. 2 Chemical reactions of a glucose sensor

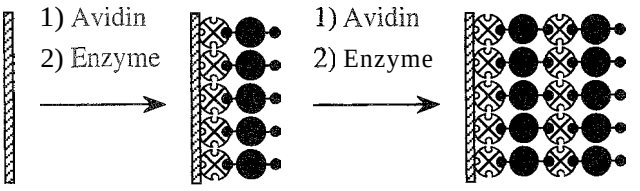

Fig. 3 Enzyme multilayer films composed of avidin and biotin-labeled enzymes

reveal the loading of GOx immobilized on the electrode. Thus, the oxidation current in CV was measured in the presence of ferrocenemethanol as mediator. The oxidation current depended linearly on the number of GOx layers. confirming that the present procedure can afford an enzyme multilayer composed of layers containing a constant amount of GOx.

A merit of enzyme multilayer films is that two or more different kinds of enzymes can be assembled simultaneously in the film, resulting in multienzyme biosensors. As an example, we prepared interference-free glucose sensors by assembling ascorbate oxidase (AOx) together with GOx on the Pt electrode.[14] Glucose sensors often suffer from interference arising from the direct oxidation of oxidizable substances such as ascorbic acid (vitamin C) and uric acid in biological fluids.[15] For the elimination of ascorbate interference, the enzyme multilayers composed of 10 GOx layers and an additional 10 AOx layers were assembled by depositing avidin and biotin-labeled GOx and AOx in a stepwise formation. In this glucose sensor, ascorbic acid is oxidized to an electrochemically inactive clehydroascorbic acid in the outer AOx layer, and the interference can be eliminated. Another example of the bienzyme multilayer-modified sensor includes acetylcholine sensors prepared using choline oxidase (ChOx) and choline esterase (ChE).[16]

It should be noted here that the avidin–biotin system can be applicable to the construction of many different types of protein architectures containing enzymes[17–19] and antibodies.[20,21] The biggest advantage of an avidin–biotin system is that the proteins can be strongly immobilized through biological affinity without cross-linking or chemical bonding. resulting in acceptable long-term stability.

LECTIN–SUGAR SYSTEMS

Eectins are made up of a group of sugar-binding proteins widely found in plants and animals. Concanavalin A (Con A) is isolated from jack bean (*Canavalia ensiformis*) and is studied extensively among lectins. Con A (molecular mass: 104.000) is known to contain four identical binding sites to α-D-mannose and α-D-glucose (binding constant: 10^5–10^6 M^{-1}).[22,23] Therefore, if an enzyme molecule is labeled with several residues of mannose or glucose units. one can expect that an alternate deposition of Con A and the sugar-labeled enzyme gives rnultilayer structures. as in the case of an avidin–biotin system. Glycoproteins can be used directly as materials for this purpose. because they inherently contain sugar chains on the surface. In case proteins do not contain a sugar chain. the surface of the protein may be labeled with sugar by using phenyliso-thiocyanate derivatives of sugar (Fig. 4). which react to an amino group in the protein. We used Con A and GOx and horseradish peroxidase (HRP), which contain sugar chains on the surface, for constructing supramolecular protein architectures, and they are employed as a sensitive layer of enzyme biosensors.

BIOSENSORS MODIFIED WITH CON A–SUGAR ARCHITECTURES

Con A–GOx inultilayer films were constructed using a native GOx, which inherently contains mannose residues on the surface of the polypeptide chains.[23,24] A layer-by-layer deposition of Con A and native GOx afforded a inultilayer thin film composed of Con A and GOx layers. The multilayer film was coated on the surface of a Pt electrode to prepare glucose biosensors. The output current of the Con A/GOx inultilayer film-modified electrode increased with an increasing number of layers; confirming that GOx is catalytically active in the film. Also, a constant amount of GOx was immobilized upon each deposition. The Con A–GOx multilayer-modified glucose sensors showed rapid responses to glucose. the response times being 10–15 sec for the sensors modified with 10 Con A–Gox layers. The rapid responses of the sensors can be ascribed to the thin nature of the rnultilayer films (the thickness of the unit layer: 10–15 nmj. The sensors exhibited a linear calibration over the concentration range of 1×10^{-5} to 2×10^{-2} M glucose, which covers the normal and diabetic blood levels of glucose.

We also used HRP. because this enzyme is reported to contain ca. 18% sugar chains on the surface.[25,26] A layer-by-layer deposition of Con A and HRP afforded a rnultilayer film as expected. and HRP exhibited catalytic

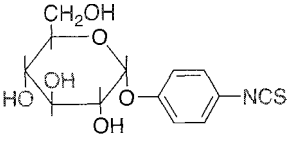

Fig. 4 Phenylisothiocyanate derivative of sugar

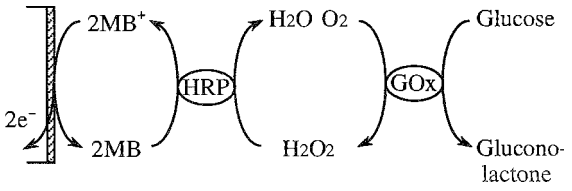

Fig. 5 Successive reactions of GOx and HRP.

activity to H_2O_2 *in the presence of methylene blue* (MB) *as the electron mediator. The* HRP–GOx *bienzyme* multilayer *films were prepared on the surface of a* Pt *electrode so as to develop glucose sensors. which detect glucose through successive reactions depicted in* Fig. 5. *In these bienzyme sensors. the response* current *depended on the geometry of the enzymes in the film. In practice, we prepared* four *different types of* multilayer *films:* $(HRP)_5$ + $(GOx)_5$, $(GOx)_5$ + $(HRP)_5$, $(HRP + GOx)_5$, *and* (GOx + HRP)$_5$. *These* films *contained an identical* number *of enzyme layers. but the sequence* of *enzyme layers differed. Among* the *films, the highest response was observed for the* $(HRP)_5$ + $(GOx)_5$ *film. which* is *composed of inner* $(HRP)_5$ *and outer* $(GOx)_5$ *layers. Thus. the present technique is useful for designing the* molecular geometry *of the* film.

We emphasize here that the Con A system can be used for immobilizing glycoproteins directly, without chemical modifications. which often induce deactivation of the biological activity of the protein.

CONCLUSION

Supramolecular protein assemblies prepared by a layer-*by-layer deposition technique are useful in the development of high-performance biosensors. Avidin–biotin and* lectin–sugar *systems are employed for this purpose. Many* kinds *of enzymes can be used as building blocks for the protein* assemblies *by modifying them with biotin and sugar residues.* Glycoenzymes *can be used to prepare* Con *A and enzyme* multilayer *assemblies without pretreatment. The advantages of this technique include rapid response of the biosensors due to the thinness of the* multilayer *film and versatile design of the geometries of bienzyme films.*

ARTICLES OF FURTHER INTEREST

Biological Ligands, p. 88
Electrochemical Sensors. p. 505
Protein Supramolecular Chemistry. p. 1161
Supramolecular Electrochemistry, p. 1412

REFERENCES

1. Wilchek, M.: Bayer, E.A. The avidin–biotin complex in bioanalytical applications. Anal. Biochern. 1988, *171.* 117.
2. Pugliese, L.; Coda, A.; Malcovati, M.: Bolognesi. M. Three-dimensional structure of the tetragonal crystal form of egg-white avidin in its functional complex with biotin at 2.7 A resolution. J. Mol. Biol. 1993. *231*, 698.
3. Weber, P.C.; Ohlendorf, D.H.; Wendoloski. J.J.; Salemme, F.R. Structural origin of high-affinity binding to streptavidin. Science 1989. *243.* 85.
4. Chilkoti. A.; Stayton, P.S. Molecular origin of the slow streptavidin-biotin dissociation kinetics. J. Am. Chem. Soc. 1995. *117.* 10622.
5. Green. N.M.; Konievzny, L.; Toms. E.J.: Valentine. R.C. The use of bifunctional biotinyl compounds to determine the arrangement of subunits in avidin. Biochem. J. 1971. *125.* 781.
6. Luo. S.; Walt, D.R. Avidin–biotin coupling as a general method for preparing enzyme-based fiber-optic sensors. Anal. Chern. 1989. *61.* 1069.
7. Gunaratna, P.C.; Wilson. G.S. Optimization of multienzyme flow reactors for determination of acetylcholine. Anal. Chem. 1990. *62*, 402.
8. Hoshi. T.; Anzai. J.; Osa, T. Controlled deposition of glucose oxidase on platinum electrode based on an avidin/biotin system for the regulation of output current of glucose sensors. Anal. Chem. 1995. 67, 770.
9. Anzai, J.; Kobayashi, Y.; Suzuki. Y.; Takeshita. M.; Chen, Q.; Osa. T.; Hoshi. T.; Du, X.-Y. Enzyme sensors prepared by layer-by-layer deposition of enzymes on a platinum electrode through avidin-biotin interaction. Sens. Actuators, B 1998. *52.* 3.
10. Cass. A.E.G.; Davis, G.; Francis. G.D.; Hill. H.A.O.; Aston. W.J.; Higgins, I.J.; Plotkin. E.V.; Scott. L.D.L.; Turner. A.P.F. Ferrocene-mediated enzyme electrode for amperometric determination of glucose. Anal. Chem. 1984. *56*, 667.
11. Frew. J.E.; Hill. H.A.O. Direct and indirect electron transfer between electrodes and redox proteins. Eur. J. Biochem. 1988. *172*, 261.
12. Heller. A. Electrical connection of enzyme redox centers to electrodes. J. Phys. Chem. 1992, *96*. 3579.
13. Yang, L.; Janle. E.; Huang, T.; Citzen. J.; Kissinger. P.; Vreeke. M.; Heller, A. Applications of "wired" peroxidase electrodes for peroxide determination in liquid chromatography coupled to oxidase immobilized enzyme reactions. Anal. Chem. 1995. 67. 1326.
14. Anzai. J.; Takeshita. H.; Kobayashi. Y.; Osa. T.; Hoshi. T. Layer-by-layer construction of enzyme multilayers on an electrode for the preparation of glucose and lactate sensors: Elimination of ascorbate interference by means of an ascorbate oxidase multilayer. Anal. Chem. 1998. *70*. 811.

15. Sasso, S.V.; Pierce, R.J.; Walla, R.; Yacynych, A.M. Electropolymerized 1,2-diaminobenzene as a means to prevent interferences and fouling and to stabilize immobilized enzyme in electrochemical biosensors. Anal. Chem. **1990.** *62*. 1111.
16. Chen, Q.; Kobayashi, Y.; Takeshita, H.; Hoshi, T.; Anzai, J. Avidin–biotin system-based enzyme multilayer membranes for biosensor applications: Optimization of loading of choline estcrase and choline oxidase in the bienzyme membrane for acetylcholine biosensors. Elcctroanalysis **1998,** 10, 94.
17. Anzai, J.; Takeshita, H.; Hoshi, T.; Osa, T. Regulation of output current of L-lactate sensors based on alternate deposition of avidin and biotinylated lactate oxidase on electrode surface through avidin–biotin complexation. Chem. Pharm. Bull. **1995,** 43. 520.
18. Du, X.-Y.; Anzai. J.; Osa, T.; Motohashi, R. Amperometric alcohol sensors based on protein multilaycrs composed of avidin and biotin-labeled alcohol oxidase. Electroanalysis **1996,** *8*, 813.
19. Hoshi, T.; Saiki, H.; Takeuchi, K.: Anzai, J. Enzyme coupled lactose sensors based on bicnzyme membrane prepared by an avidin/biotin method. Trans. IEE Jpn. **1999,** *119E*, 576.
20. Hoshi, T.; Saiki, H.; Anzai, J. Layer-by-layer deposition of avidin and biotin-labcled antibody on a solid surface to prepare a multilayer array of antibody. J. Chem. Soc., Perkin Trans. 2 **1999,** 1293.
21. Hoshi, T.; Saiki, H.; Anzai, J. Preparation of spatially ordered multilayer thin films of antibody and their binding properties. Biosens. Bioclcctron. **2000,** *15*. 623.
22. Beckcr, J.W.; Reeke, G.N., Jr.; Cunningham, B.A.: Edelman, G.M. New evidence on the location of the saccharide-binding site of concanavalin A. Nature **1976**, *259*, 406.
23. Anzai, J.; Kobayashi, Y. Construction of multilayer thin films of enzymes by means of sugar-lectin interactions. Langmuir **2000,** *16*, 2851.
24. Anzai, J.; Kobayashi, Y.; Nakamura, N. Alternate deposition of concanavalin A and mannose-labeled enzymes on a solid surface to prepare catalytically active enzyme thin films. J. Chem. Soc., Perkin Trans. 2 **1998,** 461.
25. Kobayashi, Y.; Hoshi, T.; Anzai, J. Glucose and lactate biosensors prepared by a layer-by-layer deposition of concanavalin A and mannose-labeled enzymes: electrochemical response in the presence of electron mediators. Chem. Pharm. Bull. **2001,** 49, 755.
26. Kobayashi, Y.; Anzai, J. Preparation and optimization of bienzyme multilayer films using lectin and glyco-enzymes for biosensor applications. J. Electroanal. Chem. **2001,** 507, 250.

Bond-Stretch Isomerism

Gerard Parkin
Columbia University, New York, New York, U.S.A.

INTRODUCTION

Bond-stretch isomerism may be defined as the phenomenon whereby molecules of the same spin state, on the same potential energy surface, differ only in the length of one or several bonds.[1–4] In contrast to exhibiting a single-minimum on the potential energy surface for the stretching of a bond. the existence of bond-stretch isomers requires the presence of a double-minimum, with a significant barrier between the two minima (Fig. 1). The theoretical concept of bond-stretch isomerism, with the existence of a double-minimum on a potential energy surface. was first discussed by Hoffmann in a 1972 study on a series of hypothetical organic molecules, of the types illustrated in Fig. 2.[5–7] Interestingly. experimental evidence in support of bond-stretch isomerism was actually reported shortly prior to Hoffmann's proposal. Specifically. Chatt reported in 1970 that the molybdenum oxo complex *mer*-$MoOCl_2(PMe_2Ph)_3$ could be isolated in blue and green isomeric forms.[6] Originally, these complexes were considered to be geometric isomers, namely *cis-mer*-$MoOCl_2(PMe_2Ph)_3$ and *trans-mer*-$MoOCl_2(PMe_2Ph)_3$, differing only in whether the two chloride ligands were cis or *trans*. X-ray diffraction studies on the blue isomer established a *cis* configuration. from which it was assumed that the green isomer possessed a *trans* configuration (Fig. 3).[6,8] However, X-ray diffraction studies on the green analogue *mer*-$MoOCl_2(PEt_2Ph)_3$ revealed that the chloride ligands were also cis and not *trans*.[8] Thus, the structures of blue *cis-mer*-$MoOCl_2(PMe_2Ph)_3$ and green *cis-mer*-$MoOCl_2(PEt_2Ph)_3$ were similar. with the exception that the Mo=O bond length in green *cis-mer*-$MoOCl_2(PEt_2Ph)_3$ [1.803(11) Å] was significantly longer than that observed in blue *cis-mer*-$MoOCl_2(PMe_2Ph)_3$ [1.676(7) Å]. As a result, Chatt suggested that the principal difference in the blue and green isomers of *cis-mer*-$MoOCl_2(PMe_2Ph)_3$ centered on their Mo=O bond lengths, and he termed these complexes "distortional isomers" (Fig. 3).[7a] In accord with his proposal. the actual green isomer of *cis-mer*-$MoOCl_2(PMe_2Ph)_3$ was structurally characterized and also found to possess a long Mo=O bond length of 1.80(2) Å.[10] Consistent with the different Mo=O bond lengths, the blue and green isomers exhibited slightly different $\nu_{Mo=O}$ stretching frequencies (blue. 954 cm^{-1}; green 943 cm^{-1}), and different stabilities, with solutions of the green isomer irreversibly converting to the blue isomer upon gentle heating.

Following Chatt's report, experimental evidence for bond-stretch (or distortional) isomerism was reported for a variety of systems, as illustrated in Fig. 4.[3] The blue and green tungsten oxo derivatives $[(Me_3tacn)W(O)Cl_2]^+$ represented particularly important examples. since these were reported to be the first set of bond-stretch isomers that were stable in solution for several days and also did not interconvert at temperatures up to ca. 180°C. The blue and green isomers also exhibited different $\nu_{W=O}$ stretching frequencies of 980 cm^{-1} and 960 cm^{-1}, respectively, with the higher energy vibration corresponding to the shorter W=O bond. With a series of transition metal complexes that exhibit bond-stretch isomerism now in existence. Jean, Lledos. Burdett, and Hoffmann extended the earlier calculations on hypothetical species to rationalize the presence of double-minima in the potential energy surfaces of the complexes actually reported to exhibit the phenomenon.[11]

A REINVESTIGATION OF BOND-STRETCH ISOMERISM IN *cis-mer*-$MoOCl_2(PMe_2Ph)_3$

In 1991, a series of detailed crystallographic studies resulted in the discovery that the original example of bond-stretch isomerism in transition metal complexes was an artifact due to crystallographic disorder."'".'" Specifically, the green "isomer" of *cis-mer*-$MoOCl_2(PMe_2Ph)_3$ was identified as a mixture of *blue cis-mer*-$MoOCl_2(PMe_2Ph)_3$ and yellow *mer*-$MoCl_3(PMe_2Ph)_3$. Evidence for the presence of *mer*-$MoCl_3(PMe_2Ph)_3$ was provided by ^{1}H-NMR spectroscopy. Thus, although the ^{1}H-NMR spectrum of *mer*-$MoCl_3(PMe_2Ph)_3$ is characterized by broad paramagnetically shifted signals, careful examination provided evidence that the green ''isomer'' of *cis-mer*-$MoOCl_2(PMe_2Ph)_3$ was contaminated by *mer*-$MoCl_3(PMe_2Ph)_3$. It is important to emphasize that the green "isomer" of *cis-mer*-$MoOCl_2(PMe_2Ph)_3$ was not a heterogenous mixture of crystals of *cis-mer*-$MoOCl_2(PMe_2Ph)_3$ and *mer*-$MoCl_3(PMe_2Ph)_3$ but was actually a homogenous mixture such that each single crystal was a solid solution of the two compounds. The formation of

Encyclopedia of Supramolecular Chemistry
DOI: 10.1081/E-ESMC 120012748

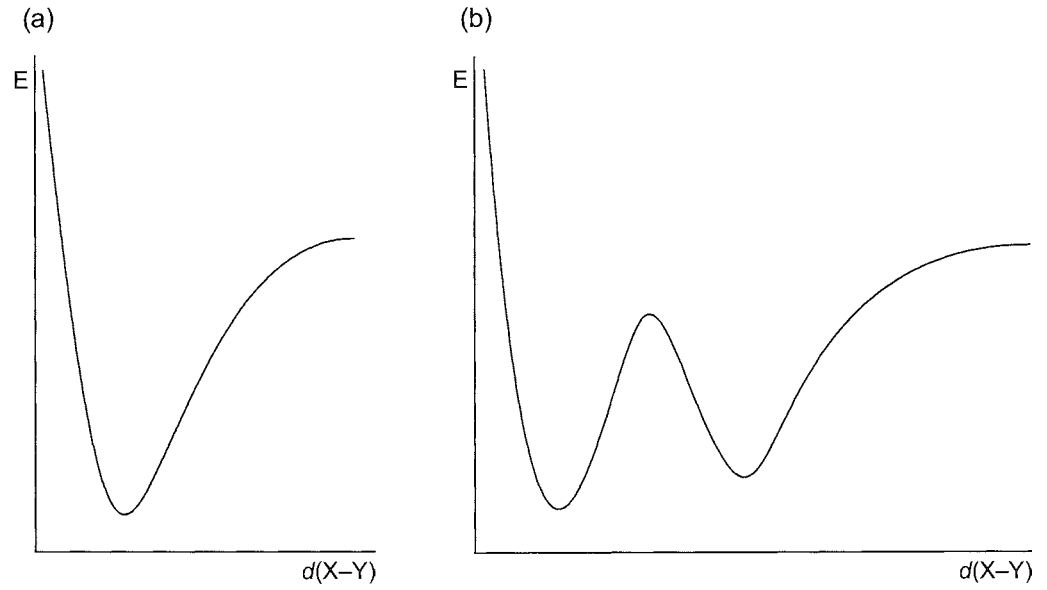

Fig. **I** Potential energy surfaces for (a) a normal X–Y bond and (b) a pair of X–Y bond-stretch isomers

such a solid solution is made possible by the fact that ***cis***-*mer*-$MoOCl_2(PMe_2Ph)_3$ and *mer*-$MoCl_3(PMe_2Ph)_3$ are isostructural and only differ by the exchange of oxygen for chlorine.

The impact of small amounts of the impurity *mer*-$MoCl_3(PMe_2Ph)_3$ on the structure determination is profound and strongly influences the *apparent* Mo=O bond length. The apparent lengthening is a result of the fact that the location of an ''atom'' at the disordered site is a weighted average of oxygen and chlorine positions (Fig. 5). Since the Mo–Cl bond is longer than the Mo=O bond. the presence of a chloride contaminant has the effect of apparently lengthening the Mo=O bond. Examination of Fig. 5 indicates that only very small amounts of the *mer*-$MoCl_3(PMe_2Ph)_3$ impurity are required to have a significant effect on the apparent Mo=O

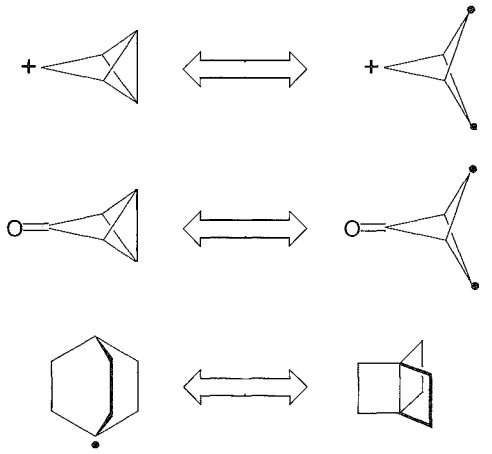

Fig. *2* Some hypothetical isomers that were studied theo retically.

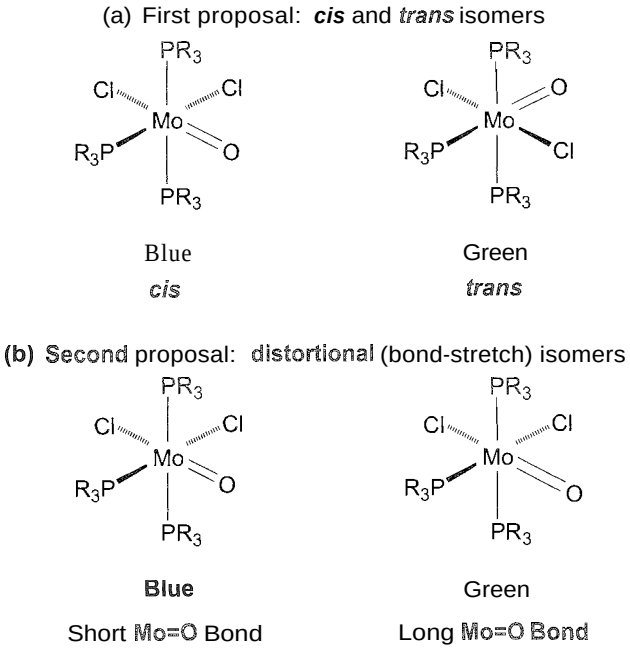

Fig. *3* Original. incorrect proposals for the structures of blue and green isomers of $MoOCl_2(PMe_2Ph)_3$. (a) ***cis*** and *trans* isomers: (b) distortional (bond-stretch) isomers with short and long Mo=O bonds.

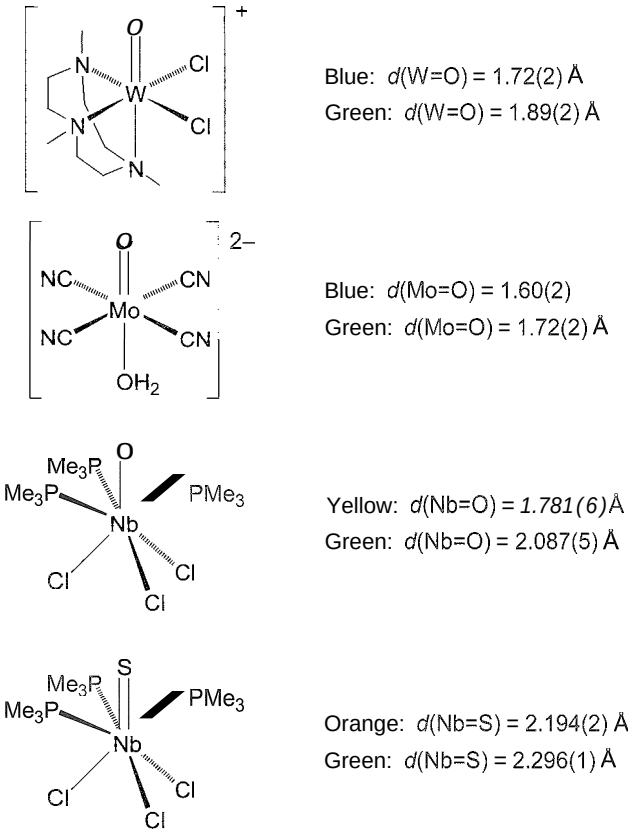

Fig. **4** Other examples of originally proposed bond-stretch isomers.

bond length. The reasons for this are twofold: (i) the Mo–Cl bond (ca. 2.45 Å) is considerably longer than the Mo=O bond (ca. 1.68 Å), and (ii) the scattering power (which is a function of the number of electrons) of chlorine is much greater than that of oxygen. Despite the contamination by chlorine being sufficient to apparently lengthen the Mo=O bond, the thermal parameter was not abnormal, and so the x-ray structure provided no evidence for contamination.

The reevaluation of the structures of *cis-mer*-$MoOCl_2(PMe_2Ph)_3$ demonstrated that there was no structural evidence for bond-stretch isomerism for the complexes that were originaily proposed to exhibit the phenomenon. Furthermore. the origin of the two different $\nu_{Mo=O}$ stretching frequencies for *cis-mer*-$MoOCl_2(PMe_2Ph)_3$ in the solid state was attributed to the existence of two different modifications, with only one value being observed in solution.[9,10] This reevaluation of bond-stretch isomerism in *cis-mer*-$MoOCl_2(PMe_2Ph)_3$ also cast doubt on the other proposed examples of bond-stretch isomerism. Indeed. subsequent studies on $[(Me_3tacn)W(O)Cl_2]^+$ demonstrated that the system was considerably more complex than that for *cis-mer*-$MoOCl_2(PMe_2Ph)_3$ and was composed of three components with different oxidation states: $[(Me_3tacn)W(O)Cl_2]^+$, $[(Me_3tacn)W(O)_2Cl]^+$, and $[(Me_3tacn)W(O)Cl(solv)]^+$.[15] Likewise, $NbCl_4(PMe_3)_3$ has been recognized as an impurity for influencing the apparent Nb=O and Nb=S bond lengths in $Nb(O)Cl_3(PMe_3)_3$ and $Nb(O)Cl_3(PMe_3)_3$, respectively.[16]

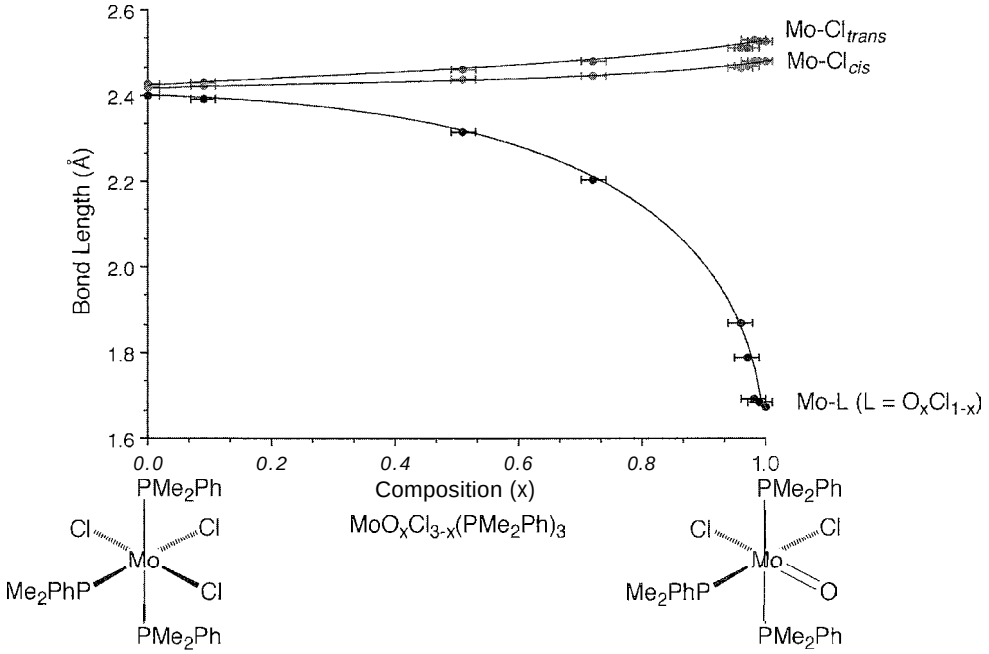

Fig. 5 Variation of apparent Mo=O bond length as a function of composition.

SPIN-STATE ISOMERISM AND RELATED PHENOMENA

Blue and green *cis-mer*-$Mo(O)Cl_2(PMe_2Ph)_3$ were originally classified as bond-stretch (distortional) isomers because there was no simple explanation for the existence of a pair of complexes in which the only significant difference resided in the length of one of the bonds. In this regard, it is important to note that there are several other examples of isomerism in which a bond between a pair of atoms differs in length. but the situation is fundamentally different than that proposed for *cis-mer*-$Mo(O)Cl_2(PMe_2Ph)_3$, because the change in bond length is accompanied by other significant geometric and/or spin-state changes.[17] For example. there are many transition–metal complexes that exhibit different spin states (high-spin/low-spin equilibria) for which significant structural changes are also observed.[18,19] Likewise, $[Cp^*RuCl_2]_2$ exists as singlet and triplet isomers that differ substantially in their Ru–Ru separations (2.93 A versus 3.75 Å), Ru–Cl–Ru bond angles (76.5° versus 100.2°), and Ru–Cl bond lengths (Fig. 6).[20] In addition. $[(MesP^*)_2CHCSiMe_3]$ exists in monocyclic and bicyclic structures (Fig. 6) with planar and puckered geometries. respectively, with the latter having a shorter C–C bond length (1.52 A versus 2.47 Å).[21] The trinuclear dipyridylamide cobalt complex $Co_3(dpa)_4Cl_2$ [dpaH = di(2-pyridyl)amine] exhibits a particularly interesting structural variability (Fig. 6).[22] Specifically. depending on the crystalline form. the Co_3 chain may be symmetrical (*s*-), with Co—Co distances of ca. 2.3 Å, or unsymmetrical (u-) with Co—Co distances of ca. 2.29 Å and 2.47 Å; however, only the symmetrical species exists in solution. It should also be noted that while the *s*-$Co_3(dpa)_4Cl_2$ and *u*-$Co_3(dpa)_4Cl_2$ species are isomeric, the compositions of the crystals are different by virtue of the solvents of crystallization, and thus the crystalline materials are not isomeric. Related chromium complexes $Cr_3(dpa)_4X_2$ are also known. and depending upon the nature of the axial ligands and the solvent of crystallization. the Cr_3 chain is likewise either symmetrical or unsymmetrical.[23] The complexes $(Cp^*RuCl_2)_2$, $[(MesP^*)_2CHCSiMe_3]$, and $Co_3(dpa)_4Cl_2$ represent extremely interesting examples of isomerism but are distinct from the bond-stretch isomerism proposed for *cis-mer*-$Mo(O)Cl_2(PMe_2Ph)_3$ by virtue of the fact that the lengthening of one bond is compensated for by other significant geometrical changes.

OTHER EXAMPLES OF CRYSTALLOGRAPHIC DISORDER RESULTING IN ANOMALOUS BOND LENGTHS AND THE INCORRECT FORMULATION OF COMPOUNDS

The interpretation of x-ray diffraction data in providing experimental evidence for bond-stretch isomerism in *cis-mer*-$Mo(O)Cl_2(PMe_2Ph)_3$ provides an extreme illustration

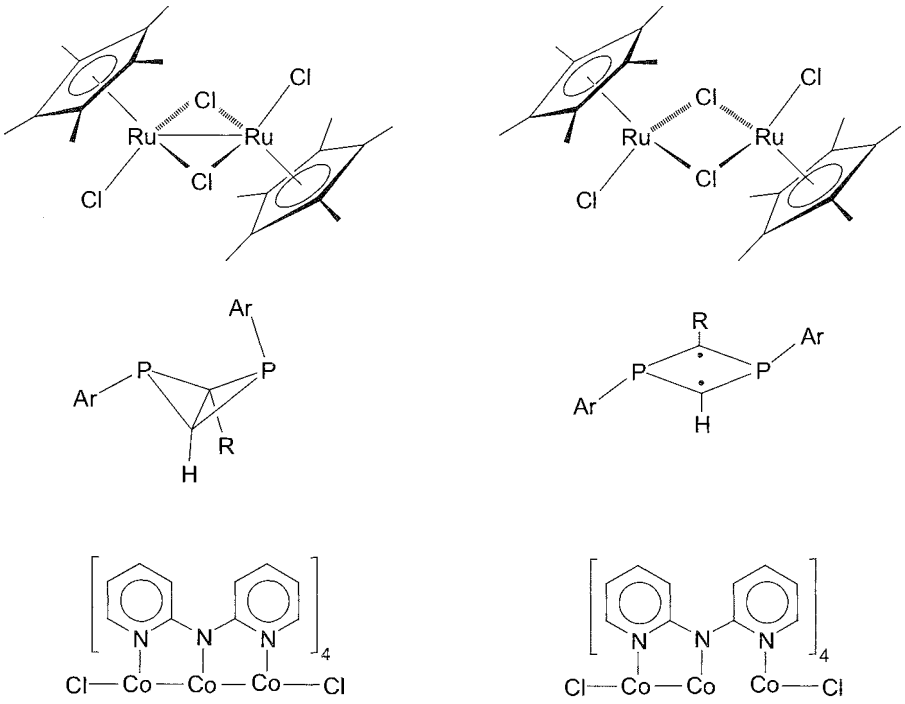

Fig. 6 Structurally characterized examples of isomers with different X–X bond lengths and other structural modifications

of how crystallographic disorder may be deceptive. In this regard. although crystallographic disorder is well known. the presence of a disorder is normally only discerned at the stage of refinement when an anomaly is detected. It is likely that there are many other circumstances where disorder has gone undetected but has, nevertheless, had an impact on the derived structure. Indeed. this notion was reinforced by a series of studies on *tris*(pyrazolyl)hydroborato zinc complexes $[Tp^{Bu^t}]ZnX$ to quantify the sensitivity of the apparent bond length to the composition of a disordered site.[24] Significantly, it was noted that for the series $[Tp^{Bu^t}]ZnCl_{1-n}I_n$, reasonable thermal parameters could still be obtained at irnpurity levels that were sufficient to result in a significant apparent change in the true bond length. Furthermore. the disordered site of the crystal of composition $[Tp^{Bu^t}]ZnCl_{0.5}I_{0.5}$ could be refined very well as bromine. with none of the unusual lengthening of the thermal ellipsoid along the bond vector that would have been anticipated given the true locations of Cl and I. Representative examples of how initially unrecognized disorder resulted in incorrect bond-length determinations include the following:

1. The complex *mer*-$WCl_3(PMe_2Ph)_3$ was reported to possess three different W–Cl bond lengths [2.295(2) Å, 2.437(1) Å, and 2.441(1) Å], with one exceptionally short W–Cl bond.[25] Further studies demonstrated that the origin of the short W–Cl bond was due to disorder with the isostructural oxo complex *cis-mer*-$WOCl_2(PMe_2Ph)_3$.[26]
2. The molecular structure of $Cp_2Hf(CH_3)_2$ was originally reported to exhibit two significantly distinct Hf–CH_3 bond lengths [2.318(8) A and 2.382(7) Å].[27] The origin of this inequivalence was subsequently reinterpreted as arising from cocrystallization with the chloride derivative $Cp_2Hf(CH_3)Cl$.[28]

Crystallographic disorder is not restricted to pairs of structurally similar groups, and controlled disorder between structurally inequivalent groups was investigated by determining the effect that partial occupancy of a halide ligand (X = Cl. Br. I) may exert upon the apparent structure of the cyanide derivative $[Tp^{Bu^t}]ZnCN$.[29] For chloride- and bromide-doped crystals of composition $[Tp^{Bu^t}]Zn(CN)_{0.8}Cl_{0.2}$ and $[Tp^{Bu^t}]Zn(CN)_{0.95}Br_{0.05}$, the disorder between the halide and the carbon of the cyanide ligand was not resolved. Although $[Tp^{Bu^t}]Zn(CN)_{0.8}Cl_{0.2}$ did not refine well in the absence of a disorder model. the bromide-doped crystal of composition $[Tp^{Bu^t}]Zn(CN)_{0.95}Br_{0.05}$ refined well; however, the bond lengths associated with the CN ligand were observed to be incorrect. with a iong Zn–C bond length and a short C≡N bond length. More extreme examples of disorder may also occur. For example, the complex $[Tp^{Ant}]Tl$ cocrystallizes with $[Tp^{Ant}]CoNCS$, so that in effect, a site that is disordered between a vacancy and a chain of *three* atoms results.[30] A representative example of how initially unrecognized disorder between pairs of structurally dissimilar groups resulted in incorrect bond length determinations is provided by the observation that the dinitrogen complex *trans*-$Cr(dmpe)_2(N_2)_2$ was reported to have an unusually short N–N bond length of 0.985(4) Å;[31] however, subsequent studies suggested that the origin of the exceptionally short N–N bond length in this molecule is compositionai disorder with the chloride impurity. *trans*-$Cr(dmpe)_2Cl_2$.[32]

It is important to note that crystallographic disorder is not restricted to the positions of ligands. and the metal centers may also be disordered. As an illustration, the entire $Zr(\eta^2\text{-}Te_2)(CO)$ moiety of the tetragonal modification of $Cp^*_2Zr(\eta^2\text{-}Te_2)(CO)$ is disordered.[33] The nature of the disorder is such that the $Cp^*_2Zr(\eta^2\text{-}Te_2)(CO)$ molecules pack so that the carbonyl ligands are statistically distributed about the crystallographic twofold axis, which bisects the two Zr–Te bond vectors. In the absence of modeling disorder of the zirconium atom, the derived Zr–CO bond was observed to be anomalously long. However. after deliberately displacing the Zr from the twofold axis and refining with half-occupancy, a more reasonable value for Zr–C bond length is obtained.

In addition to affecting observed bond lengths, crystallographic disorder may also result in the incorrect formulation of a compound. Furthermore. the incorrect determination of bond lengths, or misformulation of a compound. do not require a crystal to be impure. because disorder between inequivalent groups can also be achieved as a result of packing identical molecules in different orientations in the crystal. As an illustration. a molecule originally believed to be a dicarbonyl derivative of a ruthenium porphyrin complex, $Ru(TPP)(CO)_2$ (TPP = *meso*-tetraphenylporphyrin dianion) was reported to possess *bent* carbonyl ligands. with a Ru–C–O bond angle of 153.3(9)°.[34] The structure was reinvestigated and determined to be. in fact. a monocarbonyl–ethanol complex Ru(TPP)(CO)(EtOH).[35] However. the CO and EtOH ligands were statistically disordered so that a superposition was observed, resulting in the appearance of an apparently bent carbonyl ligand.

A related example of undetected disorder between the methyl (CH_3) and ethylidyne (CCH_3) ligands of $W(PMe_3)_4(CH_3)(CCH_3)$ resulted in the terminal carbon atom of the disordered ethylidyne ligand not being located. so that the molecule was originally formulated as the dimethyl derivative $W(PMe_3)_4(CH_3)_2$.[36] However. x-ray diffraction studies on a better-quality crystal successfully revealed the presence of the disordered methyl group of the ethylidyne ligand. thereby reformulating $W(PMe_3)_4(CH_3)_2$ as $W(PMe_3)_4(CH_3)(CCH_3)$.[37]

Other examples of disorder resulting in misformulation, include: (1) the structure of the unusual technetium

oxo polymer $[Cp^*Tc(\mu\text{-}O)_3Tc]_n$ has been reinterpreted as that of the monomeric rhenium complex, $Cp^*Re(O)_3$, with the original misassignment having been due to a combination of disorder and twinning;[38] and (2) dinitrogen molecules of crystallization have been reinterpreted as disordered dichloromethane solvent.[39]

ANOMALOUS BOND LENGTHS AND INCORRECT FORMULATION OF COMPOUNDS IN THE ABSENCE OF CRYSTALLOGRAPHIC DISORDER

Structural errors in interpretation of x-ray diffraction data are by no means limited to problems resulting from disorder. Thus. it is well known that errors in atom assignment. apace group assignment, and the refinement into a false minimum may each have a dramatic impact upon the accuracy of a structure determination.'" In terms of atom assignment; atoms of similar atomic number have similar x-ray scattering powers, and so it is often difficult to distinguish definitively between such pairs by using x-ray diffraction techniques. As such, the incorrect formulation of a compound can occur even when the crystal is pure and there is no crystallographic disorder. For example, the structures of the bridging chloride complexes $Nb_2(\mu\text{-}Cl)_2Cl_4(SMe_2)_4$, $Ta_2(\mu\text{-}Cl)_2Cl_4(SMe_2)_4$, and $Nb_2(\mu\text{-}Cl)_2Cl_4(EtSCH_2CH_2SEt)_2$ were reformulated as having two μ-S groups. rather than two μ-Cl groups;[40] the structures of the cobalt complex $Co(\eta^2\text{-}S_2CSEt)_3$ were reformulated as that of the chromium derivative $Cr(\eta^2\text{-}S_2CSEt)_3$;[41] the structure of the nickel(III) 1,4,7-triazacyclononane-*N*,*N*′,*N*″-triacetate was shown to be that of the cobalt(III) derivative;[42] the structure of the unusual compound $[ClF_6]^+[CuF_4]^-$ was proposed to be that of $[SiF_6]^-[Cu(OH_2)_4]^+$;[43] the structures of both the copper and silver complexes $[1,3,5\text{-}C_6Ph_3H_2]Cu$ and $[1,3,5\text{-}C_6Ph_3H_2]Ag$ were reforinulated as that of the bromine compound $[1,3,5\text{-}C_6Ph_3H_2]Br$[44] and the structure of $Mo(PMe_3)_2Cl_2$ was reformulated as $Zn(PMe_3)_2Cl_2$.[45] The latter is a particularly striking example. because the scattering powers of Zn ($Z = 30$) and Mo ($Z = 42$) are very different.[46]

Knowledge of the correct space group is essential for obtaining the correct structure of a molecule. Frequently, however. the space group is incorrectly assigned,[47] with the result that derived bond lengths are in error. In many such examples. the noncentrosymmetric space group is erroneously selected in preference to the true centrosymmetric space group. Noncentrosymmetric space groups present an additional problem in that it is important to establish that the correct absolute structure was determined. For a molecule that crystallizes in a polar space group. two minima exist in a least-squares refinement procedure, corresponding to chemically identical structures related by a reflection perpendicular to the polar axis. The structures corresponding to the two polar configurations typically differ slightly in bond lengths as a consequence of the ''polar dispersion error.''''' so that it is essential to establish that the correct polarity was determined by refining both configurations. As an illustration, the alternating C–C bond lengths in *s-cis*-1,3-butadiene transition metal complexes, and specifically $(\eta^4\text{-}C_4H_6)_2Mn(CO)$, is an artifact due to the incorrect absolute structure being refined.'''' The redetermined nonalternation of bond lengths is more in line with calculations. which predict that donation from the butadiene HOMO and back-donation into the butadiene LUMO should lengthen the terminal C–C bond.

A more extreme problem associated with polar space group results when the derived structure is a hybrid of the two possible polar configurations. Such a situation becomes feasible when the x-ray scattering is dominated by a heavy atom. As an illustration, the structures of $W(PMe_3)_4H_2Cl_2$[50] corresponding to false minima in the refinements are compared to its true structure in Fig. 7. A similar effect was observed for $[\eta^4\text{-}Me_8taa]Pb$.[51] Since the incorrect structures are related to the true structure by a reflection perpendicular to the polar axis of only a *selection* of the atoms. the effect is described as a ''partial polar ambiguity'' to distinguish it from the well-known ''polar dispersion error,'' an effect concerned with two structures related by a reflection perpendicular to the polar axis of *all* atoms. The severity of the pseudosymmetry problem is such that truly noncentrosymmetric structures were incorrectly refined as disordered centrosymmetric structures. For example. the *tris*(pyrazolyl)hydroborato indium complex $[Tp^{Bu^t}]In$ was originally reported to possess an unusual twofold disorder in such a manner that a nitrogen atom of one molecule was coincident with the boron atom of its disordered configuration, as illustrated in Fig. 8. Thus, the disordered configurations are related by a twofold rotation about the In···**B** axis, coupled with a canting of the molecules. Further studies. however. demonstrated that refinement of the correct model in the noncentrosymmetric space

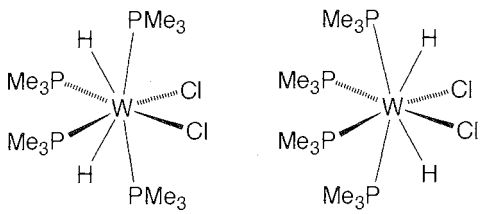

True Minimum False Minimum

Fig. 7 *True and false minima* for $W(PMe_3)_4H_2Cl_2$.

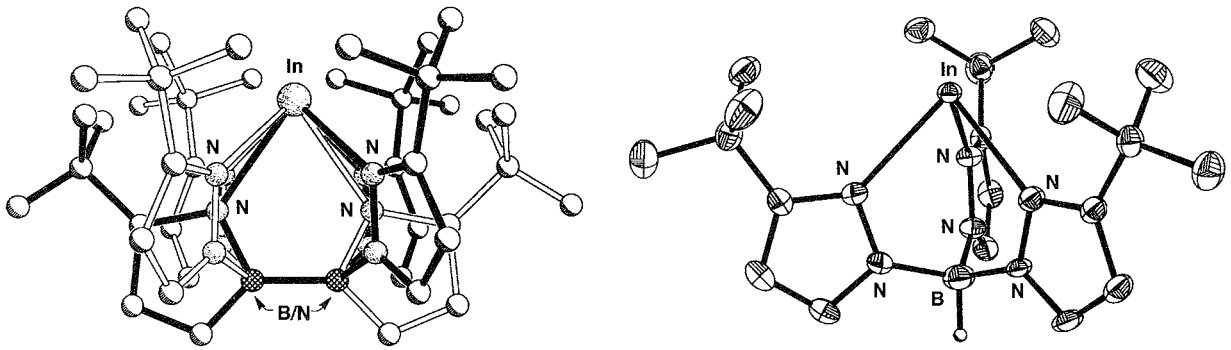

disordered structure in centrosymrnetric space group

ordered structure in non-centrosymrnetric space group

Fig. *8* Incorrect. disordered structure of [Tp^{Bu^t}]In refined in the centrosymmetric space group (left). The true structure refined in the noncentrosymmetric space group (right).

group resulted in a well-behaved. ordered structure.[7,9] Thus. [Tp^{Bu^t}]In provides an interesting counter example, where the structure is much better described as ordered in the noncentrosymmetric space group, rather than disordered in the centrosymmetric alternative.

CONCLUSION

Reinvestigation of *cis-mer*-$MoOCl_2(PMe_2Ph)_3$ demonstrated that the original proposai for bond-stretch isomerism is erroneous due to a crystallographic artifact resulting from disorder. The fact that the original x-ray diffraction study was not questioned at the time it was reported, and was considered sufficiently reliable to prove the existence of such isomers, is a consequence of two facts: first. the widespread notion that x-ray diffraction is the ultimate arbiter of a chemical structure; and second, the disorder was not detected, even though it had a significant effect on the apparent bond length. The apparent experimental verification of bond-stretch isomerism represents the tip of the iceberg and indicates that other unrecognized problems exist. as illustrated by the examples described above. These problems range from incorrect atom assignments to incorrect molecular geometries.

A variety of molecules, such as [$Cp^*RuCl_2]_2$, [$(MesP^*)_2CHCSiMe_3$], and $Co_3(dpa)_4Cl_2$, exhibit isomerism in which there is a variation in bond lengths. However, to date there has been no convincing evidence presented to support the existence of isomers analogous to the bond-stretch isomerism proposed for cis-met-$Mo(O)Cl_2(PMe_2Ph)_3$, in which the difference is principally associated with the mere lengthening of a bond between a single pair of atoms.

REFERENCES

Parkin. G.; Hoffmann, R. Bond-stretch isomers and spin-state isomers: A comment on the article 'Bond-Stretch Isomers: Fact not Fiction'. Angew. Chem., Int. Ed. Engl. 1994. 33, 1462.

2. Parkin. G. Do bond-stretch isomers really exist? Acc. Chem. Res. 1992. 25. 455–460.
3. Parkin. G. Bond-stretch isomerism in transition metal complexes: A reevaluation of crystallographic data. Chem. Rev. 1993, 93. 887–911.
4. Labinger. J.A. Bond-stretch isomerism: A case study of a quiet controversy. C. R. Chim. 2882. 5. 235–244.

5a. Stohrer, W.-D.: Hoffmann. R. Electronic-structure and reactivity of strained tricyclic hydrocarbons. J. Am. Chem. Soc. 1972. *94.* 779–786.

5b. Stolirer. W.-D.: Hoffmann. R. Bond-stretch isomerism and polytopal rearrangements in $(CH)_5^+$, $(CH)_5^-$, and $(CH)_4CO$. J. Am. Chem. Soc. 1972, *94.* 1661–1668.

6. Nagase, S. Polyhedral compounds of the heavier group-14 elements — Silicon. germanium. tin. and lead. Acc. Chern. Res. 1995. 28. 469–476.

Butcher. A.V.: Chatt. J. Complexes of tertiary phosphines and tertiary arsines with molybdenum(IV). J. Chem. Soc., A 1970. 2652–2656.

8a. Manojlovic-Muir, L. X-ray crystal structure of oxodichlorotris(dimethylphenylphosphine)molybdenum(IV) [$MoOCl_2(PMe_2Ph)_3$]. Chem. Commun. 1971. 147.

8b. Manojlovic-Muir, L. Molybdenum(IV) oxo-complexes. 1. Crystal and molecular structure of the blue isomer of oxodichlorotris(dimethylphenylphosphine)molybdenum(IV), *cis-mer*-[$MoOCl_2(PMe_2Ph)_3$]. J. Chem. Soc., A 1971. 2796–2800.

9a. Chatt. J.; Manojlovic-Muir, L.; Muir, K.W. X-ray determination of molecular structures of molybdenum(IV) 0x0-complexes — Possibility of a new type of isomerism. Chem. Commun. 1971. 655–656.

9b. Manojlovic-Muir. L.: Muir. M.W. Molybdenum(IV) oxo-complexes. 2. Crystal and molecular structure of dichlo-

rotris(diethylphenylphosphine)oxomolybdenum(IV), *cis-mer*-[$MoOCl_2(PEt_2Ph)_3$]. J. Chem. Soc., Dalton Trans. 1972. 686–690.

10. Hayniore. B.L.: Goddarcl. W.A.. III; Allison, J.N. Proc. Int. Conf. Coord. Cheni.. 23rd 1984. 535.

11a. Jean, Y.; Lledos. A.; Burdett, J.K.; Hoffmann. R. Bond-stretch isomerism in transition–metal complexes. J. Am. Chern. Soc. 1988, *110.* 4506–4516.

11b. Jean. Y.; Lledos, A.; Burdett. J.K.; Hoffmann, R. Electronic mechanisms associated with bond-stretch isomerism in transition–metal complexes. J. Chem. Soc., Cheni. Commun. 1988. 140–142.

12a. Uoon, K.; Parkin, G.; Rheingold. A.L. A re-investigation of the molecular structures of *cis-mer*-$MoOCl_2(PR_3)_3$: Do bond-stretch isomers really exist? J. Am. Chem. Soc. 1991. *113*, 1437–1438.

12b. Uoon. K.; Parkin. G.; Rheingold. A.L. Bond-stretch isomerism in the complexes *cis-mer*-$MoOCl_2(PR_3)_3$: A re-investigation. J. Am. Chem. Soc. 1992, *114*, 2210–2218.

13. Desrochers, P.J.: Nebesny, K.W.: LaBarre. M.J.: Lincoln. S.E.; Loehr. T.M.; Enemark. J.H. Studies of distortional isomers—Spectroscopic evidence that green *cis,mer*-dichlorotris(dimethylphenylphosphine)-oxomolybdenum-(IV) is a mixture. J. Am. Chern. Soc. 1991. *113.* 9193–9200.

14. Bashall, A.P.: Bligh, S.W.A.: Edwards, A.J.; Gibson. V.C.: McPartlin. M.: Robinson. O.B. Distortional isomerism in oxomolybdenum systems—The evidence reevaluated. Angew. Chem.. Int. Ed. Engl. 1992, *31.* 1607–1609.

15. Desrochers, P.J.: Nebesny, K.W.: Labarre. M.J.: Bruck, M.A.: Neilson. G.F.: Sperline, R.P.; Enemark, J.H.: Backes. G.; Wieghardt, K. Studies of distortional isomers. 2. Evidence that green $[LWOCl_2]PF_6$ is a ternary mixture. Inorg. Chern. 1994. *33.* 15–24.

16. Gibson. V.C.: McPartlin. M. Bond stretch isomerism—Fact or artifact. J. Chem. Soc., Dalton Trans. 1992. 947–956.

17. Rohmer. M.-M.; Bénard. M. Bond-stretch isomerism in strained inorganic molecules and in transition metal complexes: A revival? Chem. Soc. Rev. 2001, *30.* 340–354.

18. König, E. Structural-changes accompanying continuous and discontinuous spin-state transitions. Prog. Inorg. Chem. 1987. *35*, 527–622.

19. Gütlich, P.: Goodwin. H.A.; Hendrickson. D.N. Bond-stretch isomers—Fact not fiction. Angew. Chem., Int. Ed. Engl. 1994. *33*, 425–427.

20. Kölle. U.; Kossakowski. J.; Klaff, W.: Wesemann. L.: Englert. U.; Heberich. C.E. Dichloro(pentamethylcyclopentadienyl)ruthenium—Novel dichotomy in a molecular-structure. Angew. Cheni.. Int. Ed. Engl. 1991. *30.* 690–691.

21. Niecke. E.; Fuchs. A.; Nieger. M.; Schmidt. O.; Schoeller. W.W. Valence Isomerization of a 1.3-diphosphacyclobutane-2,4-diyl: Photochemical ring closure to 2.4-diphosphabicyclo[1.1.0]butane and its thermal ring opening to gauche-1.4-diphosphabutadiene. Angew. Chem., Int. Ed. Engl. 1999. *38.* 3028–3031.

22a. Clérac, R.; Cotton. F.A.: Daniels. L.M.; Dunbar. K.R.: Murillo. C.A.; Wang, X. Tuning the metal–metal bonds in the linear tricobalt compound $Co_3(dpa)_4Cl_2$: Bond-stretch and spin-state isomers. Inorg. Chem. *2001. 40.* 1256–1264.

22b. Clérac. R.: Cotton. F.A.: Daniels. L.M.: Dunbar. K.R.: Kirschbaum, K.: Murillo, C.A.; Pinkerton, A.A.: Schultz. A.J.; Wang. X. Linear tricobalt compounds with di(2-pyridyl)amide (dpa) ligands: Temperature dependence of the structural and magnetic properties of symmetrical and unsymmetrical forms of $Co_3(dpa)_4Cl_2$ in the solid state. J. Am. Chem. Soc. *2000. 122.* 6226–6236.

23. Clérac. *R.:* Cotton, F.A.; Daniels. L.M.; Dunbar. K.R.: Murillo. C.A.: Pascual. I. Linear trichromium complexes with direct Cr to Cr contacts. 1. Compounds with Cr_3 (dipyridylamide)$_4^{2+}$ cores. Inorg. Chem. 2000, *39*, 748–751.

24. Yoon, K.; Parkin, G. Artificial manipulation of apparent bond lengths as determined by single crystal x-ray diffraction. J. Am. Cheni. Soc. 1991. *113,* 8414–8418.

25. Hills. A.; Hughes. D.L.; Leigh, G.J.: Prieto-Alcùn. R. Preparation and structure of trichlorotris(dimethylphenylphosphine)tungsten(III), the 1st structurally characterized neutral mononuclear complex of tungsten(III). J. Cheni. Soc., Dalton Trans. 1991. 1515–1517.

26. Yoon. K.: Parkin. G.; Hughes. D.L.: Leigh. G.J. Origin of the two significantly different W–Cl bond lengths for chemically equivalent bonds in *mer*-$WCl_3(PMe_2Ph)_3$. J. Chem. Soc., Dalton Trans. 1992. 769–773.

27. Fronczek, F.R.: Baker, E.C.; Sharp. P.R.; Raymond. K.N.: Alt. H.G.; Rausch. M.D. Structures of dimethylhafnocene and its hydrolysis product. μ-oxo-bis(methylhafnocene). Inorg. Chern. 1976. *15.* 2284–2289.

28. Hunter. W.E.: Hrncir. D.C.: Bynum, R.V.; Penttila, R.A.: Atwood. J.L. The search for dimethylzirconocene—Crystal-structures of dimethylzirconocene, dimethylhafnocene. chloromethylzirconocene, and (μ-oxo)bis(methylzirconocene). Organometallics 1983. *2.* 750–755.

29. Yoon, K.: Parkin. G. Resolved and unresolved crystallographic disorder between {η^3-HB(3-Bu^{t}pz)$_3$}ZnCN and {η^3-HB(3-Bu^{t}pz)$_3$}ZnX (X = Cl. Br. I). Inorg. Chem. 1992. 31. 1656–1662.

30. Han. R.; Parkin, G.: Trofimenko. S. The *tris*[3-(9-anthryl)pyrazol-1-yl]hydroborato Ligand, [Tp^{Ant}]: Compositional disorder between a vacancy and a chain of three atoms. Polyhedron 1995. *14.* 387–391.

31. Girolami. G.S.: Salt. J.E.; Wilkinson. G.; Thornton-Pett. M.: Hursthouse. M.B. Alkyl. hydride. and dinitrogen 1,2-bis(dimethylphosphino)ethane complexes of chromium—Crystal-structures of $Cr(CH_3)_2(dmpe)_2$, $CrH_4(dmpe)_2$, and $Cr(N_2)_2(dmpe)_2$. J. Am. Chem. Soc. 1983. *105.* 5954–5956.

32. Salt. J.E.: Girolami. G.S.: Wilkinson. G.; Motevalli. M.: Thornton-Pett. M.; Hursthouse, M.B. Synthesis and characterixation of 1,2-bis(dimethylphosphino)ethane (dmpe) complexes of chromium(0) and chromium(IV)—X-ray crystal-structures of *trans*-$Cr(N_2)_2(dmpe)_2$, *cis*-$Cr(CO)_2(dmpe)_2$, $Cr(C_2Ph_2)_2(dmpe)$, and $CrH_4(dmpe)_2$. J. Chem. Soc., Dalton Trans. 1985. 685–692.

33. Howard. W.A.: Parkin, G.: Rheingold. A.L. Non-classical carbonyl complexes of zirconium: The syntheses.

characterization. and reactivities of (η^5-$C_5Me_5)_2Zr(\eta^2$-E_2)(CO) (E = S. Se, Te). Polyhedron 8995. 14.25–44.

34. Cullen. D.: Meyer, E., Jr.: Srivastava. T.S.: Tsutsui. M. Unusual metalloporphyrins — Structure of product frorn reaction of dodecacarbonylruthenium with meso-tetraphenylporphine—Dicarbonyltetraphenylporphinatoruthenium (IT). J. Chem. Soc., Chem. Commun. 1972. 584–585.
35. Bonnet, J.J.: Eaton, S.S.; Eaton. C.R.; Holm, R.H.; Ibers. J.A. Spectroscopic and structural characterization of ruthenium(II) carbonyl-porphine complexes. J. Am. Chem. Soc. 1973. 95, 2141–2149.
36. Jones, R.A.; Wilkinson. G.; Gaias. A.M.R.: Hursthouse. M.B. Interaction of hexamethyltungsten(VI) with trimethylphosphine — X-ray crystal-structure of dimethyltetrakistrimethylphosphinetungsten(II). J. Chern. Soc., Chem. Commun. 1979, 926–927.
37. Chiu, K.W.; Jones, R.A.; Wilkinson, G.; Galas, A.M.R.: Hursthouse. M.B.: Malik. K.M.A. Reactions of hexamethyltungsten(VI) in the presence of trimethylphosphine—Synthesis of methyl, ethylidyne. hydrido-tungsten. alkoxo-tungsten, and other tungsten compounds — X-ray crystal-structures of *trans*-ethylidyne-(methyl)tetrakis(trimethylphosphine)tungsten(IV) and trihydrido-(phenoxo)-tetrakis(trimethylphosphine)tungsten(IV). J. Chem. Soc., Dalton Trans. 1981. 1204–1211.
38. Burrell, A.K.; Cotton. F.A.; Daniels, L.M.: Petricek. V. Structure of crystalline (C_5Me_5)ReO_3 and implied nonexistence of (C_5Me_5)Tc_2O_3. Inorg. Chem. 1995. 34. 4253–4255.
39. Marsh. R.E.: Olmstead, M.M.; Schaefer, W.P.: Schomaker. V. Dinitrogen or dichloromethane? Inorg. Chem. 1993.32. 4658–4659.
40. Babaian-Kibala, E.: Cotton. F.A.: Kibala, P.A. A new bis(μ-sulfido)ditantalum(IV) edge-sharing bioctahedral molecule and a reassessment of some earlier bis(μ-chloro) molecules. Inorg. Chem. 1990. 29, 4002–4005.
41. Li. T.-I.: Lippard, S.J. Crystal and molecular-structure of tris(ethylthioxanthato)cobalt(III)—Reinvestigation. Inorg. Chern. 1974. 13. 1791–1792.
42. Boeyens. J.C.A.: van der Merwe. M.J. The nonexistent crystals of macrocyclic nickel(III). Structure of the cobalt(III) complex of 1,4,7-triazacyclononane-N,N′,N″-triacetate. Inorg. Chem. 1997. 36, 3779–3780.
43. von Schnering, H.G.: Vu. D. Are the previously described [ClF_6][CuF_4] and [$Cu(H_2O)_4$][SiF_6] identical? Angew. Chem.. Int. Ed. Engl. 1983, 22. 408.
44. Haaland. A.; Rypdal, K.; Verne. H.P.; Scherer. W.; Thiel. W.R. The crystal-structures of base-free. monomeric arylcopper(I) and arylsilver(I) compounds—2 cases of mistaken identity. Angew. Chem.. Int. Ed. Engl. 1995. 33. 2443–2445.
45. Cotton. F.A.: Schmid. G. Proposed reformulation of recently reported "tetrahedral molybdenum(II)'' complexes: Trimethylphosphine complexes of zinc chloride. Polyhedron 1996. *15*. 4053–4059.
46a. Marsh, R.E. Is there any Zr in $Na_2NiZr(P_2O_7)_2$ or $Na_2CoZr(P_2O_7)_2$? Acta Crystallogr. 1990. *C46*, 2497–2499.
46b. Marsh, R.E. On the structure of $Zn(C_4H_8N_2O_6)$. Acta Crystallogr. 1986, *C42*. 1327–1328.
47. Marsh. R.E. Some thoughts on choosing the correct space group. Acta Crystallogr. 1995. *B51*. 897–907.
48. Templeton, L.K.; Templeton, D.H.; Zalkin. A.: Ruben. H.W. Anomalous scattering by praseodymium, samarium and gadolinium and structures of their ethylenediaminetetraacetate (edta) salts. Acta Crystallogr. 1982. *B38*. 2155–2159.
49. Reiβ, G.J.; Konietzny. S. How realistic are alternating C–C-bond lengths in *s-cis*-1,3-butadiene transition metal complexes? J. Chem. Soc., Dalton Trans. 2002. 862–864.
50a. Murphy, V.J.; Rabinovich. D.; Parkin. G. False minima and the perils of a polar axis in x-ray structure solutions: The molecular structures of $W(PMe_3)_4H_2X_2$ (X = F, Cl, Br) and $W(PMe_3)_4H_2F_2(H_2O)$. J. Am. Chem. Soc. 1995. *117*, 9762–9763.
50b. Murphy. V.J.: Rabinovich, D.: Hascall. T.: Klooster. W.T.; Koetzle. T.F.; Parkin. G. False minima in x-ray structure solutions associated with a 'partial polar ambiguity': Single crystal x-ray and neutron diffraction studies on the eight-coordinate tungsten hydride complexes, $W(PMe_3)_4H_2X_2$ (X = F. CI. Br, I) and $W(PMe_3)_4$-$H_2F(FHF)$. J. Am. Chem. Soc. 1998. 120. 4372–4387.
51. Kuchta. M.C.; Parkin. G. Incorrect atom connectivity in x-ray structures associated with a 'partial polar ambiguity': A nou-macrocyclic structure for the macrocyclic lead complex. [η^4-Me_8taa]Pb. New J. Chem. 1998. *22*, 523–530.
52. Kuchta. M.C.: Dias, H.V.R.: Bott, S.G.; Parkin. G. The synthesis and structure of [$Tp^{Bu^t_2}$] In, a highly twisted *tris*(3,5-di-t-butylpyrazolyl)hydroborato indium(I) complex: Comparison with the re-evaluated ordered structure of [Tp^{Bu^t}]In. Inorg. Chem. 1996. 35, 943–948.

Brillouin Scattering

Claude Ecolivet
Université de Rennes, Rennes, France

INTRODUCTION

Brillouin scattering is a technique in which, through an inelastic scattering process of photons by acoustic waves (also called acoustic phonons),[1,2] the investigation of the elastic properties of materials can take place. Although transparent materials make experiments easier and more fruitful, some measurements can be successfully performed on opaque semiconductors and even metals.[3,4] One of the interests of this noncontact technique is that it does not require large samples. Some experimental setups even use microscopes to collect the scattered light, allowing measurements on microscopic or heterogeneous samples.[5] This is an advantage on ultrasonics or inelastic neutron scattering that can also measure sound velocities but usually necessitate larger samples. The essential microscopic physical information provided by Brillouin scattering is the magnitude of the interatomic or intermolecular elastic interactions revealing what actually occurs inside the material. In supramolecuiar crystals consisting in host and guest molecules, it can then be possible to identify and evaluate the interactions between the different constituents.

Moreover, the technical progress in Brillouin scattering spectroscopy, mainly due to the use of tandems of Fabry Perot interferometers,[6] allows us to investigate. in the same experiment, the acoustic phonons and the low-lying Raman lines and the Rayleigh wings often generated by instabilities and relaxations.[7] Often, these modes are coupled to ihe acoustic waves. and their scattering geometries and polarizations facilitate their assignment and give a deeper insight to their dynamics. Brillouin spectra. like the Raman spectra, appear as doublets. where their intensity. frequency. and line width are the main characteristics that can be used to produce quantitative data about elastic, photoelastic,[8] and anharmonic properties of the materials.

In this article. we briefly recall the principles of the technique and the state of the art of the technique as it is currently used in laboratories. Then we present some results obtained on supramolecular compounds: charge–transfer crystals and inclusion compounds (clathrates and channel-like composites). These results were chosen to give a broad scope of what the interest of Brillouin scattering is for supramolecular scientists. More details on the technique or its application to other materials can be found in other review papers.[9,10]

PRINCIPLE

It is well known since the beginning of the last century that acoustic waves (longitudinal and transverse) are generated by thermal agitation even at very low temperatures. The Debye T^3 law of specific heat is but one of the numerous consequences. These waves of frequency v and wave vector $q = 2\pi/\lambda$ have a linear dispersion:

$$2\pi v = Vq$$

where V is the phase velocity (longitudinal or transverse). They carry a (pseudo) momentum $\hbar\mathbf{q}$ that can combine with the one of an incident photon $\hbar\mathbf{k_i}$ to satisfy a conservation law defining the wave vector of scattered photons $\mathbf{k_s}$:

$$\hbar\mathbf{k_s} = \hbar(\mathbf{k_i} \pm \mathbf{q})$$

This process can also be considered a Bragg diffraction of incident photons by an index grating resulting from the refractive index modulation by the density variations of the longitudinal acoustic mode or the shearing strains for the transverse modes. Because the energy of the incident photon ($\approx$2 eV) is much larger than that of the acoustic phonon ($\approx$0.1 meV), the magnitude of $\mathbf{k_s}$ is similar to the one of $\mathbf{k_i}$, yielding:

$$\|\mathbf{k_s} - \mathbf{k_i}\| \approx 2\|\mathbf{k_i}\| \sin(\theta/2)$$

like in a Bragg reflection, where θ is the scattering angle; which will define the magnitude of the phonon wavevector. Because the scattering grating moves at the sound of velocity in opposite directions $\pm\mathbf{q}$, the scattered intensity is Doppler shifted and appears as a double? centered on the incident photon frequency:

$$v_s = v_i \pm v_{phonon} = v_i \pm 2(nV/\lambda)\sin(\theta/2)$$

This relation is obtained through the linear dispersion relation of acoustic phonons and photons in the simple case

DOI: 10.1081/E-ESMC 120012848

of an optically isotropic material of index n. The last term of the righi-hand side (rhs) of the above equation is called the Brillouin shift. which is equal to the frequency of the detected phonon. In the case of an optically anisotropic material. the scattered and incident wave vectors can be very different, and the $2n\sin(\theta/2)$ term in the above formula is replaced by: $(n_i^2+n_s^2-2n_in_s\cos\theta)^{1/2}$, where n_i and n_s are the refractive indices for the incident and scattered beams.

Thus, the choice of an incident radiation λ_i defines $\mathbf{k}_i$, whereas the choice of a scattering angle (usually 90° or 180") unambiguously determines $\mathbf{k}_s$ and, henceforth. the Brillouin shifi related to each of the three acoustic modes with their own velocities. Typically. for an incident visible radiation. and a material characterized by an index of refraction about 1.5 and sound velocities of a few km/s, the Brillouin shift lies in the range of 10–30 GHz (0.33–1 cm^{-1}) in backscattering geometry. Obviously, the study of Brillouin lines requires a more consequent resoiution than the one of a conventional Raman spectrometer.

In the absence of any perturbation by other modes. the Brillouin lines can be described by a damped oscillator profile derived from the imaginary part $\chi''(\omega)$ of the oscillator susceptibility:

$$I(\omega) = I_0[n(\omega,T) + 1/2 \pm 1/2]\chi''(\omega)$$
$$\approx I_0kT\gamma/\{[\omega^2 - (\omega_i \mp Vq)^2]^2 + \gamma^2\omega^2\}$$

where $n(\omega,T)$ is the Bose factor defining the phonon population at a given temperature T; γ is the half-width at half height; and ω_i is the pulsation of the incident light. The upper sign is related to what is called the Stokes process. where an acoustic phonon is created by a photon inside the sample. and the associated frequency is then:

$$\nu_s(\text{Stokes}) = \nu_i - \nu_{\text{phonon}}$$

whereas the lower sign is related to the opposite case, called Antistokes, where an acoustic photon is destroyed in the scattering process corresponding to a line located at a frequency higher than the incident one:

$$\nu_s(\text{antiStokes}) = \nu_i + \nu_{\text{phonon}}$$

The probability of this process being strictly proportional to the phonon population by the Bose factor decreases at low temperatures. Except at very low temperatures. there is no detectable intensity difference between the Stokes and anti-Stokes contributions at variance to Raman scattering.

The intensity I_0 depends on geometric factors characteristic of the setup and also on the photoelastic constants. which relate the refractive index variations to the elastic strains and soine internal rotations. Brillouin scattering. by comparison with a substance where the photoelastic constants are well known (usually benzene. quartz,...). is a method for determining these coefficients.[8] In some scattering geometries, the calculated intensity of some well-polarized modes can be zero. but at variance to Raman scattering where optic modes are not always active. acoustic modes can always be seen. at least theoretically. in some other scattering geometry. usually labeled in the Porto notation $\mathbf{k}_i(\mathbf{E}_i, \mathbf{E}_s)\mathbf{k}_s$, where $\mathbf{E}$ is the radiation electric field (Fig. 1).

The line width γ is related to the damping of elastic waves. which results from anharmonic interactions of the acoustic phonons with other phonons, relaxation

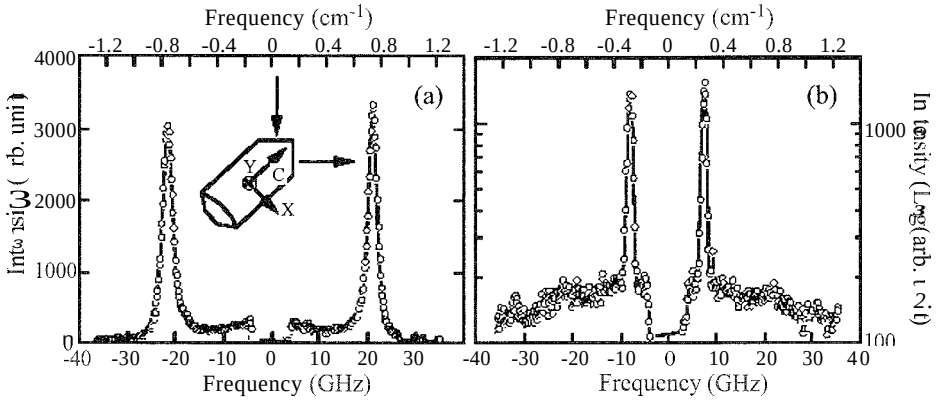

Fig. 1 Example of Brillouin scattering spectra taken in right-angle geometry in an hexagonal crystal showing the effect of beams polarization. The hexagonal axis is C. The orthogonal directions in the basal plane are X and Y. (a) $C-X(Y,Y)$ C+X scattering geometry showing a broad longitudinal doublet sitting on a quasielastic component. (b) $C-X(Y,C-X)$ C+X scattering geometry revealing the only narrow transverse doublet expected. Notice through the logarithmic intensity scale the practical absence of the longitudinal component in that spectrum. (From Ref. [30].)

processes, or structural disorder. Due to the high frequency of the investigated phonons, inherent to the technique. the influence of linear defects like dislocations is usually negligible. In solids. typical line widths are within tens to hundreds of MHz, and because it is the same order of magnitude as the experimental broadening due to the apparatus function and the finite aperture contribution, a deconvolution is needed in order to obtain a better estimation of the true line width.

The phonon frequency $\nu_{phonon}=Vq/2\pi$ is determined by the Christoffel equation,[11] which relates the phase velocity of acoustic waves to the elastic constants of the material. The number of elastic constants of a material depends on its symmetry. varying from one for liquids to three for cubic crystals and up to 21 in triclinic crystals. By measuring a number of independent sound velocities at least equal to the number of elastic constants in nonequivalent directions, it is theoretically possible to determine all the elastic constants of the material. Often, structural phase transitions generate acoustic anomalies. which can then be studied by Brillouin scattering by following the evolution versus temperature or pressure of the Brillouin shift and the line width of selected phonons.[9] High-frequency noncritical relaxations, in the ps range. also create some anomalies that are more gradual.

EXPERIMENTAL

Due to the small value of the Brillouin shifts and their line widths. experimental techniques involve interferometric devices. However. resolution is not all. perhaps the more important quality is the contrast, i.e., the ability to distinguish a small Brillouin line in the wing of a huge elastic Rayleigh line. In the case of a low contrast like in nonscanning interferometers,[12] studies are limited to high optical quality materials in right-angle scattering geometry. where the stray light is minimum. Obviously, usual samples are most of the time not of high optical quality, and they do not always present right-angle faces oriented along the more interesting directions. Nowadays. the best trade-off for Brillouin spectrometers is the tandem of plane Fabry-Perot (FP) interferoineters (Sandercock mounting) that may offer a resolution about 0.1 GHz and a contrast larger than 10^{11} with an acceptable transmission.[6] An FP interferometer consists in two partially reflecting parallel mirrors between which light undergoes multiple reflections. ensuring a higher contrast than with a two-wave interferometer like a Michelson device. A drawback of FP interferometers is the periodicity of their transmission characterized by the free spectral range $\Delta=c/2ne$ obtained by scanning the distance e (or the refractive index n) between the mirrors by more than a half-wavelength. An interesting feature of the tandem is the "vernier" ratio between the periodicities of the FPs defined by the ratio between their distances e_1 and e_2 chosen to be close to an incommensurate value. In such a case. the free spectral range of the tandem may be 20 times the one of an individual FP. The apparatus function of an FP interferometer characterized by its maximum transmission T_M is an Airy function:

$$T_i(\nu) = T_M/[1 + (2F_E/\pi)^2 \cos^2(\pi\nu/\Delta_i)]$$

where F_E is the effective finesse defined as the ratio of the free spectral range Δ over the width at half height of the

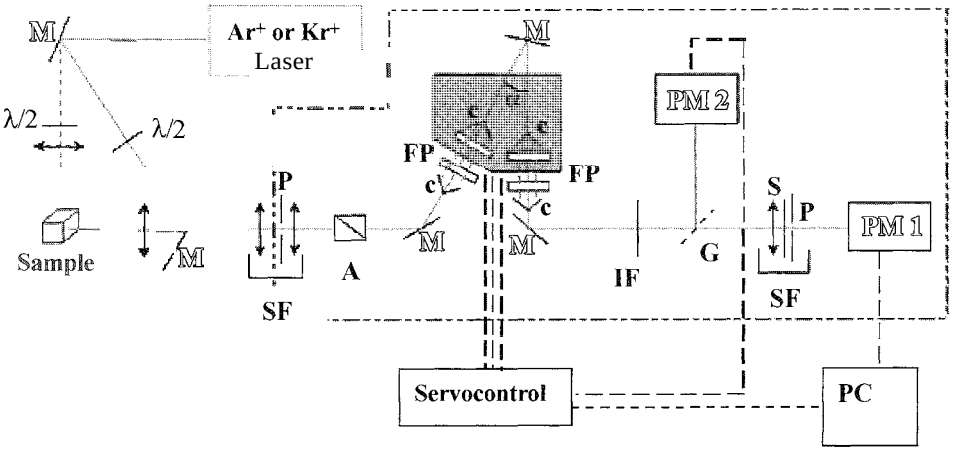

Fig. 2 Typical Brillouin scattering setup using a tandem of triple-passed Fabry-Perot interferometers. M: mirrors, SF: spatial filters. FP: Fabry Perot interferometers. c: corner cubes. IF: interferential filter, 1-12: half-wave plate. PM: photomultipliers, P: pinholes. A: Glan analyzer. S: fast shutter. G: glass plate, and PC: personal computer for data acquisition. (From Ref. [13].) (*View this art in color at www.dekker.com.*)

maximum of the Airy function. The apparatus function of the tandem being the product of the individual Airy functions, the interest of the loss of periodicity in the total apparatus function is that it allows for easier measurement of the Brillouin shifts, and more specifically. it allows in the same experiment the observation of sharp Brillouin lines and broad quasielastic components with a good rejection of the contribution of higher-order interferences.

The high contrast of the spectrometer is achieved either by triple passing each FP or the whole tandem setup. It results theoretically in an elevation of the apparatus function of each interferometer to the cube, which strongly enhances the contrast defined as the ratio of the maximum transmission over its minimum value. In order to achieve this high contrast, the tandem sits in a highly collimated beam between spatial filters, which also allows the stray light at the entrance to be diminished and the bandwidth at the exit pinhole in front of a photoinultiplier or an avalanche diode to be selected (Fig. 2).

Spectra are acquired by a linear scan of the piezoelectrically driven tandem, and data acquisition lasts between a few seconds and several hours, according to experimental conditions and sample characteristics. The long-term stability usually required to collect spectra is realized via a maximum transmission servo-controi keeping the best alignment of the tandem checlted by an auxiliary photodetector (PM2).

RESULTS

Results obtained by Brillouin scattering range from the determination of the elastic and photoelastic constants of materials to the analysis of material transformations: phase transitions. polymerization. glass transitions, photoinduced transformations. etc. (It is out of the scope of this presentation to present all.) We will limit our discussion to some examples selected in the field of supramolecular products defined as complexes consisting of two or more chemical entities associated through van der Waals interactions, hydrogen bonds, or charge-transfer mechanisms.[14]

Weak Charge-Transfer (CT) Complex Crystals

Tetracyanobenzene (TCWB) is an electron acceptor that forms charge-transfer complexes with aromatic donor molecules: anthracene (A), naphthalene (N), phenantrene (Ph), etc. These weak CT complexes crystallize in alternated stacks, leading to insulating properties with CT bands of rather high energy, yielding to colored but transparent crystals. Like many organic crystals, they crystallize in a monoclinic group and are known to present

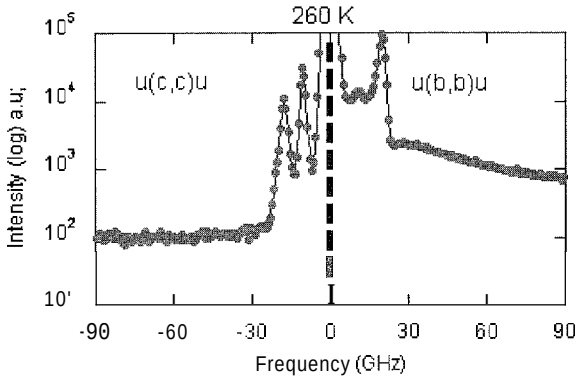

Fig. 3 Brillouin spectra of naphthalene-tetracyanobenzene taken in a backscattering geometry showing (on the right) the interference scattering between acoustic modes and a quasi-elastic component generated by an overdamped reorientational optic mode. (*View this* art *in* color at *www.dekker.com.*)

an orientational disorder, because the cyanide arms of the acceptor define a volume larger than that of donors.[15]

In N-TCNB, the disorder is well characterized by molecular jumps of the donor molecule between orientations separated by 36°.[16] At room temperature, the relaxation time of these jumps in the few ps range lead to a coupling with acoustic phonons. Then the quasielastic component generated by this relaxational behavior with a width in the 10 GHz range is distorted by coupling with the acoustic modes, which also undergo a severe asymmetry of their profile with a dip on the high-frequency wing (Fig. 3). These profiles can be described by a coupled susceptibilities equation[17] relating the oscillator susceptibility of the acoustic phonon with a relaxational susceptibility (Debye type). Another common result from coupling the acoustic modes to other modes is the increase of their line-width. Shown in Fig. 3. on a semi-log scale, are two spectra demonstrating this coupling. On the left side. one observes a usual uncoupled Brillouin spectrum with two peaks: a QL mode around 20 GHz and a QT mode around 10 GHz. In this experiment, the incident and scattered electric fields are perpendicular to the molecular plane (c,c) and, consequently, are not influenced by the electric polarization generated by the rotation of an asymmetric molecule. On the contrary, the right side was recorded along the same direction but with incident and scattered electric fields in the molecular plane (b,b). One also sees two Brillouin lines at about the same frequencies as with fie other polarization (except for the birefringence shift). but they are accompanied by a quasielastic component of about 22 GHz half-height half-line-width interfering severely with the QL mode. A signature of this interference scattering is the difference of intensity between the low- and high-frequency wings of a Brillouin line. The dots on the spectra are the

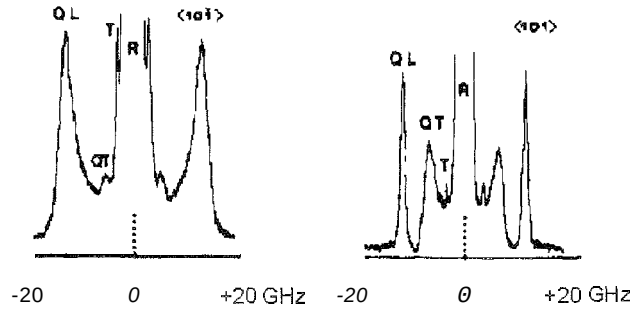

Fig. 4 Brillouin spectra recorded at atmospheric pressure at T_c 5 K in right-angle geometry along the direction $(10\bar{1})$, nearly parallel to the anthracene long axis (left), and the (101) direction almost perpendicular to this long axis (right). The R. *T*, *QT*, and *QL* indicate. respectively. the Rayleigh elastic line. the transverse mode polarized along the b monoclinic axis. and the quasitransverse and quasilongitudinal modes polarized in the (a,c) plane. The free spectral range is 39.15 GHz. (From Ref. [18].)

experimental data. whereas the continuous line is the fit by the coupled susceptibilities.

By cooling the sample. one observes a narrowing of the quasielastic component and the apparition in the Raman spectrum of a low-frequency mode (40 cm^{-1}) at about 200 K. This mode shifts toward higher frequencies due to the decrease of its damping and presents only a small frequency anomaly at the phase transition (T_C=73 K).

The disorder is so fast in A-TCNB at atinospheric pressure, that no physical method is able to distinguish well-defined orientations of the donor, which librates in an anharmonic double well. but above the internal energy barrier. It then results in a displacive structural transition characterized by an optical soft mode coupled to acoustic phonons and leading to large elastic anomalies of the relaxational type.[18] However, under pressure. this disorder slows. probably under the effect of an increase of the internal barrier, and the structural transition becomes an order–disorder one with an overdamped optic mode that no longer softens."'' This structural phase transition was extensively studied by different techniques, including Brillouin scattering. In particular. it was shown that all elastic anomalies occurring in that compound derive from the coupling between the (A) librations and the longitudinal acoustic mode propagating along the molecular long axis. The relaxation time of the order parameter presents a critical slowing $\tau(T)=\tau_0/(T_C-T)$, with T_C=212 K and τ_0=50 ps. Shown in Fig. 4. at T_c-5 K. is the effect of the coupling with the soft optic mode on the Brillouin spectra related to acoustic phonons propagating nearly along the (A) Long molecular axis $(10\bar{1})$, where the quasilongitudinal acoustic mode (QL) is strongly coupled to the soft mode and is, consequently. broadened. In a perpendicular direction (101), this occurs for the quasitransverse mode (QT). also polarized along the (A) long axis. The true transverse mode polarized along the monoclinic axis is always narrow. because it is not good symmetry to be coupled to the soft mode. Further studies of the fluctuation dynamics also revealed the contribution of disorder to this typical displacive transition.

Clathrates

Clathrates are typical supramolecular objects with molecules playing the role of host. whereas others are guests. A large variety of structures were imagined and realized (for a recent review see Ref. [20]), but they can be sorted by the dimensionality of the guest asse bly. At the lowest level. we get cages inside with zero, one, or two rnolecules included. With a dimension one, we have tubular or cylindrical pores inside which guests molecules will have a longitudinal interaction. At two dimensions, we will have intercalated molecules between host planes.

A general problem of clathrates is the interaction of guests and host molecules and eventually between guests. In the simplest approach, these interactions are neglected, and it is expected that the elastic properties of the clathrate are only sensitive to the degree of filling of the cages and to the mass of the guest molecules.[21] Brillouin scattering is a well-suited technique for such investigations, which should look into the sound velocities of the empty clathrand and differently filled clathrates. First Brillouin scattering experiments on such materials were performed in the early 1990s on methane and xenon clathrate hydrates.[22] In these compounds. water rnolecules build a cubic lattice through hydrogen bonds and define two types of cages inside the lattice—large and small ones—inside which atoms or small molecules are present. Further studies on a larger variety of guests show a decrease in proportion to the square root of the guest mass but not as large as expected in the absence of guest–host interactions. which are found to be repulsive.[23]

For these clathrate hydrates. a problem is the comparison to the empty clathrand properties. because the stability of the empty clathrate is often a problem. Dianin's compound and its clathrates are an opposite case. because the stability of the pure compound is good. Consequently, they were more extensively investigated. The structure of this compound is based on a hexamer linked by a network of hydrogen bonds involving the phenolic hydroxyl groups of 4-(*p*-hydroxyphenyl)-2,2,4-tritrimethylchroman, which is represented in Fig. 5b. A projection of the cell perpendicular to the threefold axis of the space group (R3i) is represented in Fig. 5a,[24] showing the six arms of the hexamer. which are

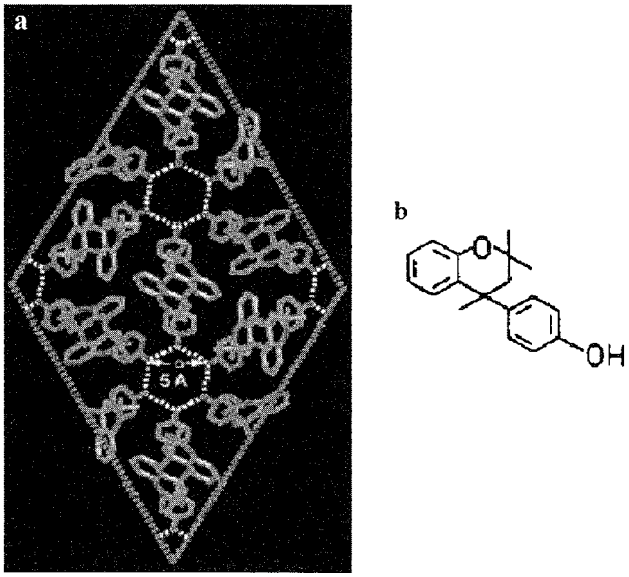

Fig. 5 (a) Projection of the structure of the Dianin clathrand in the basal plane.[24] Carbon atoms are represented in green; oxygen in red: and H bonding by yellow dashed lines. (b) Its building molecule. (From Ref. [24].) (*View this art in color at www.dekker.com.*)

alternately up and down. building around each H-bonded ring an hourglass-like architecture. In the next above layer, three downward arms with the three upwards arms of the represented layer build a cage that is locked by van der Waals interactions. It was shown that the dimensions of the unit cell increase when the cages are occupied, but the more affected distance is the c axis, which is mainly dependent from the van der Waals interactions between hexamers.

Recently, by comparing sound velocities and elastic constants between Dianin clathrand and the ethanol and heptanol clathrates. quantitative data related to the interactions were reported.[25] The main difference between both clathrates lies in the number of molecules per cage: two for ethanol with a noticeable disorder. but only one for heptanol which adopts a folded "gauche" conformation for a better fit inside the cage. Brillouin scattering results show that for the clathrand and the ethanol clathrate, similar sound velocities are observed for the longitudinal modes in the basal plane, whereas the longitudinal mode along the threefold axis presents a 15% decrease of its velocity for the ethanol clathrate. This fact could be explained by the 0.5% elongation strain along the c axis produced by the two guest molecules. If one compares the heptanol clathrate to the clathrand, more isotropic longitudinal sound velocity decreases are observed in the basal plane (12%) and along the c axis (18%). This seems in agreement with the more isotropic elongations of the a and c parameters of these compounds, 0.67% and 0.7310, respectively. These strain values lead to the concept of internal pressure that guest molecules would apply to the host ones. It reaches 1 kbar for the heptanol clathrate and two to three times less for the ethanol one. This pressure is produced by an energetically less-favorable state of the guest molecules. estimated at 18 kJ/mol for heptanol. Such studies exemplify the interest of what can be learned from Brillouin scattering experiments coupled with other data sources.

Urea Inclusion Compounds

Channel-like compounds can also be considered clathrates, because guest molecules are confined inside these channels. Here also, the nature and magnitude of the interactions between the different kinds of molecules are major problems. In addition to the cage situation, the channel geometry may allow longitudinal end-to-end interactions between the guests. Depending on the thickness of the channel walls. a weaker lateral guest–guest interaction is also possible. Elastic properties are again a good probe for all of these interactions. Such compounds are commonly obtained with molecules such as urea or thiourea. but in the case of thiourea, the channel diameter is strongly modulated and firmly localizes guest molecules in pockets along the channels, in a similar fashion as in cages rejoining the previous cage-like compounds. Consequently. we will be more interested in smoother channels like those of urea. Depending on the nature of interactions developed between the host and the guest molecules, it will be possible to obtain a regular crystal by periodic packing of the guests along the channels or to obtain an aperiodic structure.[26] The first case is, for example, obtained when firm hydrogen bonds are developed with the host, like in 2–10 undecanedione.[27] whereas the second case is typical of alkane molecules that only interact by van der Waals forces. All of these structures are derived from infinite honeycomb-like channels made up of three urea helices interwoven by hydrogen bonds. inside which guest molecules are densely packed to ensure the stability of the composite. The symmetry is often hexagonal. but distortions resulting from the shape of the guest molecules usually lead to orthorhombic symmetries at low temperatures. When such a ferroelastic transition occurs, Brillouin scattering gives valuable data on the order and the regime of transition by recording sound velocity anomalies.[13,28]

In aperiodic composites, another degree of freedom occurs due to the infinite degeneracy of the ground state. i.e., all relative positions of the host and guest molecules exist in the structure due to its incommensurability, so that the whole composite has the same energy for any relative

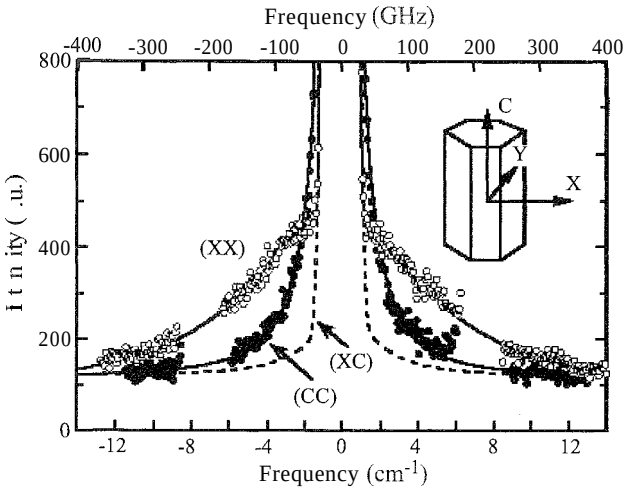

Fig. 6 Quasielastic components observed in nonadecanelurea at room temperature in tandem with Fabry-Perot interferometers. The central intensity is due to the longitudinal Brillouin doublets. The (XX) component is assigned to the reorientation of alkane molecules, whereas the (ZZ) component is compatible with an overdamped "sliding" motion. (From Ref. [30].)

position of a given host–guest pair. Such a degeneracy leads to a possible sliding motion of the whole urea sublattice with respect to the guest sublattice without any energy cost. This feature is also the one of acoustic phonons. which have zero energy *for infinite wavelengths. The main difference is located in the energy dissipation of these vibration modes: sound waves are* hydrodynamic *modes. and their damping goes* to *zero like* q^2, *because the atomic relative* motion *also goes* to *zero for infinite wavelengths. On the contrary.* the *relative sliding motion is. by essence.* optic-like *with large relative motions of the hosts and guests so* that *rhis* motion *will dissipate energy or* can *also be* quenched *by* Nabarro *barriers that in crystals.* impede *the* dislocation *motion. giving birth to a gap in its dispersion branch at low wave-vectors. The search of an experimental observation of sliding modes is* still *active and relies on inelastic techniques like neutron and light scattering. Many experiments were performed* in alkane/urea *compounds* without *any direct observation of an inelastic* peak *unambiguously assignable to rhis sliding mode. The apparition of an extraneous fourth Brillouin peak in the spectrum of* heptadecane/urea[29] *was not confirmed by* the following experiments,[30] *which evidenced the existence of quasielastic components (Fig. 4): one related to the reorientational–librational motion of alkane molecules around their long axis and another one polarized along the channel. which could be compatible with an* overdamped *sliding mode. Elastic properties* of *several urea inclusion* compounds *were investigated, and they showed the weak influence* of *the nature of the guest molecules on the sound velocities inside the* composites. *This is striking, because, along the channel axis. one can expect that the addition of the* sublattice *stiffness and the one of the guest sublattice should vary with the length and the end-to-end interactions between these molecules. Recently, by applying a hydrostatic pressure to the guest* molecules *by He atoms directly inside the channels. it was possible to determine the force constant between alkane* ($C_{19}D_{40}$) molecules.[31] *Its weak value* 1 N/m *compared to the average* 10–15 N/m *for H-bonded molecules allows us to understand the very small influence of the alkane length on* the *composite sound velocity. Another characteristic of the* dynamics *of such* a *system is the broadening of the longitudinal Brillouin line along the channels, as shown in Fig. 1a, which was taken on nonadecanelurea. High-pressure experiments showed that about* 25% of *this anomalous broadening (1.7* GHz) *is due to the* conformational *defects of alkane chain* ends.[13] *but the* major *part is still nonidentified and could be due to a coupling between the overdamped sliding* motion *and the longitudinal phonon. It should be noticed that the transverse acoustic mode seen in Fig. 1b has a very small* damping *that is barely measurable on this spectrum. Recent experiments on periodic and aperiodic ketones included in urea also showed relaxations coupled differentlyto the acoustic phonons than those in* alkane/urea *inclusion compounds. and this will be reported elsewhere.*

CONCLUSION

All of these results and many *others not reported here due to a lack of space prove* the *interest of Brillouin scattering as a technique of investigation of the elastic and* dynamical *properties of materials.* in *particular. for* supramolecular *compounds. The conclusions derived give better insight to the materials when they are carefully crossed with structural or other* dynamical *results provided for by complementary techniques.* In *photoexcitable materials. Brillouin scattering offers the unique opportunity of measuring the elastic properties of the excited volume. because at the* same *time, the light* beams *modify the sample and* measure *its properties. Despite the high technical* level *reached now. there is* still room *for further* experimental *improvements allowing faster and more precise measurements to be made.*

ARTICLES OF FURTHER INTEREST

Channel Inclusion Compounds, p. 223
Clathrate Inclusion Compounds, Phase Transitions irz. p. 289

Disorder and Diffuse Scattering, p. 457
Energy- and Electron-Transfer in Supramolecular Systerns, p. 535
Inclusion Compounds: Selectivity, Thermal Stability, and Kinetics, p. 696
Incommensurate and Commensurate Structures. p. 712
Inelastic Neutron Scatter-ing, p. 727
Modulated Structures, p. 873
Polymorphism, p. 1129
Soft and Smart Materials, p. 1302
Solid-State Reactivity and Topochemistry, p. *1316*

REFERENCES

1. Mandel'shtam. L.I. (in *Russian*) Zh. Russ. Fiz. Khim. Obshchestva 1926. *58*, 381.
2. Brillouin. L. (*in French*) Ann. Phys. (Paris) 1922. *17*. 88.
3. Dil. J.C.: Brody, E.M. Brillouin scattering from isotropic metals. Phys. Rev. B 1976, *14*. 5218.
4. Sandercock, J.R. Light scattering from surface acoustic phonons in metals and semiconductors. Solid State Comm. 1978, *26*. 547.
5. Jiang, F.M.: Kojima. S. Microheterogeneity and relaxation in $0.65Pb(Mn_{1/3}Nb_{2/3})O_3$-$0.35PbTiO_3$ relaxor single crystals. Appl. Phys. Lett. 2000. *77*. 1271.
6. Sandercock, J.R. U.S. Patent 4,014.614, 1977.
7. Ecolivet. C.; Sougotti, M.: Delugeard, D.: Beaufils. S. High resolution Raman study of the soft mode in tlie incommensurate bis(4-chlorophenyl sulfone) J. Phys. I (France) 1994. *4*. 1451.
8. Vacher. R.; Boyer, L. Brillouin scattering: A tool for the measurement of elastic and photoelastic constants. Phys. Rev. B 1972, *6*, 639.
9. Cummins, H.Z. *Light Scattering* Near *Phase Transitions*: Cummins. H.Z., Levanyuk, A.P.. Eds.; North-Holland: Amsterdam. 1983; 359.
10. Sandercock. J.R. Topics *in Applied Physics:* Light *Scattering in* Solids III: Springer Verlag: Berlin. 1982: 173.
11. Musgrave, M.J.P. Crystal Acoustics; Holden Day: San Francisco, 1970.
12. Ko, J.-Y.; Kojima, S. Non scanning Brillouin spectroscopy applied to solid materials. Rev. Sci. Instr. 2002. *73*. 4390.
13. Bourgeois. L. Ph.D. Thesis: 2002. Rennes (unpublished).
14. Lehn. J.M. Cryptates: Inclusion complexes of macropolycyclic receptor molecules. Pure Appl. Chem. 1978. *50*. 871.
15. Lcfebvre, J.; Odou. G.: Muller. M.; Mierzejewski, A.: Luty, T. Characterisation of an orientational disorder in two charge-transfer complexes: anthracene-tetracyanobenzene (A-TCNB) and naphthalene-tetracyanobenzene (N-TCNB). Acta Cryst. B 1989. *45*. 323.
16. Kumakura, S.: Iwasaki, F.: Saito. Y. Bull. Chem. Soc. Jpn. 1967, *40*. 1826.
17. Katiyar, R.S.; Ryan. J.F.: Scott. J.F. Proton-phonon coupling in CsH_2AsO_4 and KH_2AsO_4. Phys. Rev. B 1971. 4, 2635.
18. Ecolivet. C.; Mierzejewski, A. Brillouin scattering study of the elastic anomalies at the structural phase transition in anthracene-tetracyanobenzene. Phys. Rev. B 1990.42 (13). 8471.
19. Bourges. P.: Ecolivet. C.; Mierzejewski, A.: Delugeard, Y.; Girard, A. *Phonons* 89: Hunklinger, S., Ludwig, W.. Weiss. G., Eds.: World Scientific: Singapore. 1990; 1147.
20. Langley, P.J.: Hulliger, J. Nanoporous and mesoporous organic structures: New openings for materials research. Chem. Soc. Rev. 1999. *28*. 279.
21. Whalley, E. J. Geopliys. Kes. 1980. *85*, 2539.
22. Whiffen, B.L.: Kiefte. H.: Clouter. M.J. Determination of acoustic velocities in xenon and methane hydrates by Brillouin spectroscopy. Geophys. Res. Lett. 1982. 9. 645.
23. Kiefte. H.; Clouter, M.J.; Gagnon, R.E. Determination of acoustic velocities of clathrate hydrates by Brillouin spectroscopy. J. Phys. Chem. 1985. 89. 3103.
24. Kiang. Y.-H.; Lee. S.: Xu, Z.: Choe, W.: Cardner. G.B. Persistent honeycomb structures in porous and other two-component solids. Adv. Mat. 2000, *12* (10). 767.
25. Sandstedt. C.A.: Michalski, D.; Eckhardt. C.J. Quantitative measurement of guest-host interactions in supramolecular systems: A comparative Brillouin scattering study of the Dianin's compound clathrand and two of its isostructural clathrates. J. Chem. Phys. 2000. 112 (7). 7606.
26. Hollingsworth, M.D.; Harris. K.D.M. *Comprehensive Supramolecular Chemistry*; Pergamon: New York, 1996; Vol. 6. 177.
27. Brown. M.E.; Hollingsworth, M.D. Strees-induced domain reorientation in urea inclusion compounds. Nature 1995, *376*, 323.
28. Ollivier. J. Ph.D. Thesis: 1997. Rennes (unpublished).
29. Smicker. D.; Van Smaalen. S.V.: de Boers. J.L.: Haas. C.: Harris. K.D.M. Observation of the sliding mode in incommensurate intergrowth compounds: Brillouin scattering from the inclusion compound of urea and heptadecane. Phys. Rev. Lett. 1995, *74*. 734.
30. Ollivier. J.: Ecolivet. C.; Beaufils. S.: Guillaunie. F.: Breczewski, T. Light scattering by lo\\-frequency excitations in quasi-periodic n-alkane/urea adducts. Europhys. Lett. 1998. 43. 546.
31. Bourgeois, L.: Ecolivet. C.; Toudic. B.: Bourges. P.: Breczewski, T. First one-dimensional stress-strain experiments inside an aperiodic inclusion compound: Evidence of depinning effects. Phys. Rev. Lett. 2003. 91 (2). 25503.

Calixarenes and Their Analogues: Cation Complexation

Anthony W. Coleman
Adina N. Lazar
Eric Da Silva
Institut de Biologie et Chimie des Protéines, Lyon, France

INTRODUCTION

The calixarenes. calixresorcinarenes. and analogues are macrocyclic molecules containing phenolic rings bridged by methylene functions and are among the most ubiquitous of organic molecular host molecules in supramolecular chemistry.[1] The basic molecular scaffolds are, in general. simple to prepare in high yields from inexpensive starting compounds. In the case of the calixarenes; the size of the macrocycle synthesized is dependent on the nature of the cation used in the base-catalyzed cyclization, demonstrating that from the start, these molecules are excellent choices for cation complexation.

They possess sterically divergent reactive centers, either phenolic or aromatic in chemical nature. that may be modified fully or selectively to introduce functionalities capable of complexing a wide variety of cations. The chemical and physical robustness of the macrocycles allows their use for the complexation of a wide range of metal cations, including radioactive isotopes.

The introduction of ligand groups, such as ethers or crown ethers. amides. esters, or caroboxylic acids, or sulfonates and phosphonates allows for the fine tuning of capacity for coinplexation with regard to mono-, di-. tri-. and tetravalent metal cations: cationic metal complexes; and organic cations. including mono-, di-. and trivalent ammonium systems, amino acids. peptides. and even certain proteins.

Further fine-tuning of the physicochemical and chemical properties of the derivatives allows for their use for extraction of cations, sensing at surfaces and interfaces, conducting of polymers. and specific-site targeting in biological macromolecules.

CATION COMPLEXATION: GENERALITIES

The structures of the calixarenes and analogues are given in Figs. 1A.B. While calix[4]arene possesses four conformers—cone, partial cone. 1,2-alternate cone, and 1,3-alternate cone—that are sufficiently stable to be separated or to be blocked in place under certain conditions, the higher analogues have a much higher degree of conformational mobility. These conformational properties were used to prepare preformed receptors for cation binding or to allow the ligands to wrap around the cation to form the binding site.

The basic molecular skeletons do not possess useful ligand sites for the binding of cations and a large body of research was devoted to the selective introduction of ligand groups for cations Fig. 1c. In general. these groups are of two types: soft or hard electron donor groups for coordination (sulfur. nitrogen, and oxygen donor atoms). or negatively charged groups for electrostatic (ion-pairing) interactions with cations (phosphonates, phosphates. sulfonaies, and carboxylates).

INORGANIC CATION COMPLEXATION

Direct Complexation

Direct complexation of cations to unmodified calixarenes or their analogues occurs generally by formation of ion pairs arising from deprotonation of one or more phenolic groups under basic conditions. A comprehensive study of alkali metal–calixarene ion-pair complexes in soluton and the solid state was undertaken by Gutsche.[1] Extraction of alkali metals from basic aqueous solutions shows strong selectivity for Cs^+ by calix[4]arene and calix[6]arene and selectivity for both Rb^+ and Cs^+ for calix[8]arene.[2]

Interfacial complexation of various alkali cations by the amphiphilic acyl-calix[4]arenes is achieved without deprotonation and shows strong selective binding for Rb''. The binding of cations by these molecules is also strongly dependent on the counteranion.[3]

Ester, Amide, and Ketone Derivatives

The main classes of calixarene derivatives for the complexation and extraction of alkali and alkali earth cations are based on the total subsitution at the lower rim by alkoxyester. alkoxyamide. or alkoxyketone functions. Fig. 2. In this way. suitable donor ligand functions for cation complexation are introduced. Such derivatives were used for the complexation and solvent-to-solvent

DOI: 10.1081/E-ESMC 120012850

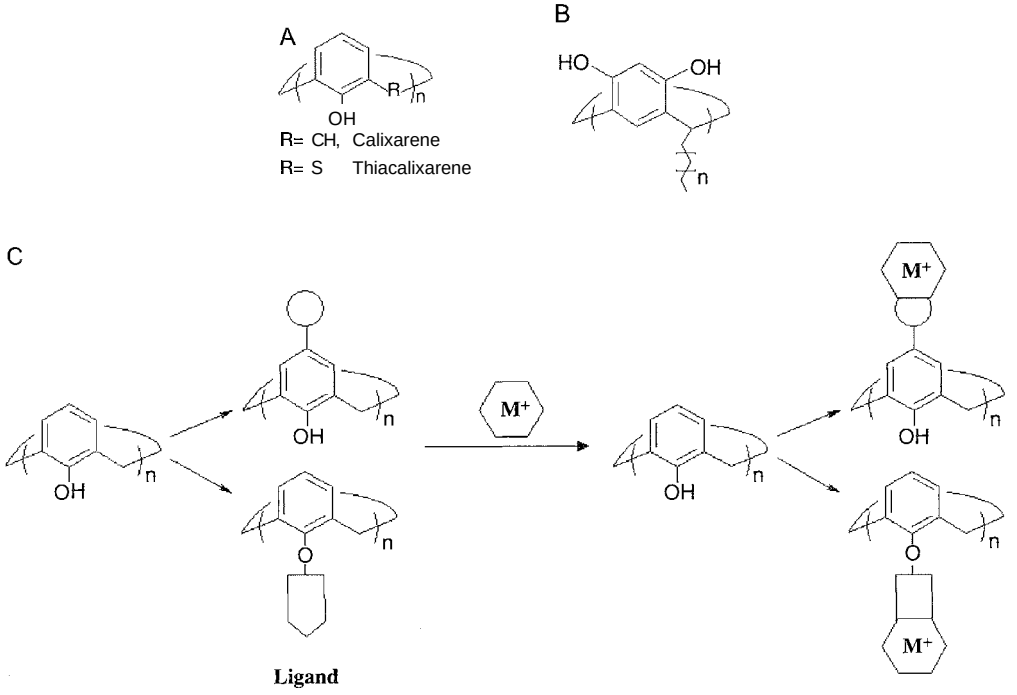

Fig. 1 Molecular structures of the calixarenes, where, commonly, $n = 4$. 6. and 8 and the calixresorcinarene (A). The strategy for cation complexation by the introduction of ligand groups at either the lower or upper rims of calixarene derivatives (B). Metal complex with upper and lower rim functionalized calix-[n]-arenes (C).

extraction of a wide range of metal ions. including alkali metals Li^+, Na^+, K^+, Rb^+, Cs^+, Ag^+; alkali earth metals Mn^{2+}, Mg^{2+}, Ca^{2+}, Cu^{2+}, Sr^{2+}, Ba^{2+} and lanthanides La^{3+}.

The size of the calixarene macrocycle can govern the selectivity with regard to the different cations. For example. the ester derivative of calix[4]arene presents a high selectivity for the smaller cations Na^+ and Li^+.[4] However, the analogous ester derivative of calix[5]arene and calix[6]arene interact strongly with $Cs^+ = Rb^+ > K^+$. No selectivity with regard to cations is observed for the calix[7]arene and calix[8]arene ester derivatives.

The conformation of the calixarene derivative also plays a role, and thus. the 1,3-alternate conformation of calix[4]arene can interact with other metals such as silver.[9]

The selectivity of the complexation and extraction is also determined by the chemical nature of the ligand group, where inversion of the selectivity between Na^+ and Cs^+ is achieved by changing the ligand function from ester to ketone or amide for the calix[4]arene derivatives. Amide substituents play a role in the extraction of alkali metals or alkali earth metals.[6] The calixarene amide derivatives interact with $Na^+ > K^+ = Li^+ >> Rb^+ = Cs^+$. With regard to the divalent cations, Ca^{2+} and Sr^{2+}, high selectivity in complexation is seen for derivatives carrying amide functions, and similar selectivity is seen for the mixed diacid, diamide derivative.[7,8]

Ether and Crown Ether Derivatives

Given the structural analogy with the crown ethers, the calixarenes were alkylated to produce ether ligands at the phenolic face. These molecules complex various cations including alkali metals ions. Coinplexation may take place

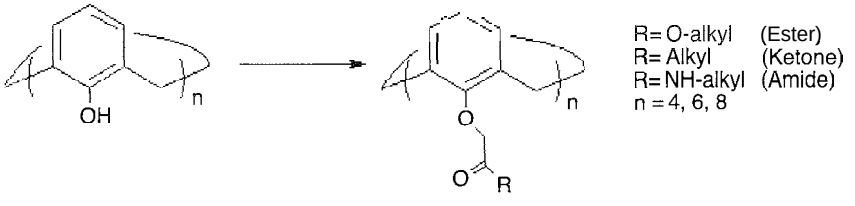

Fig. 2 Molecular structure of calixarene derivatives substituted at the lower rim

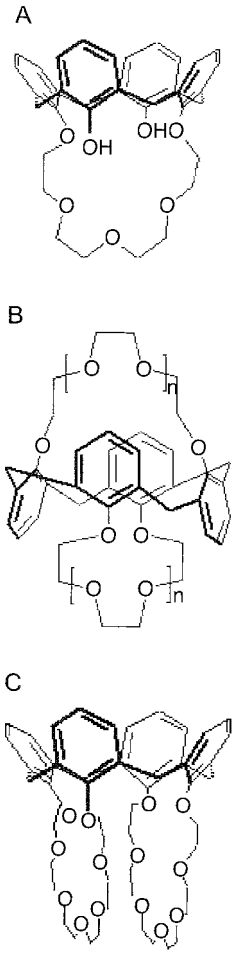

Fig. **3** Molecular structure of 1.2-his-calix crown ether (A): 1–3 alternate calix crown ether (B); and 1.3-his-calix crown ether (C).

at the phenolic groups for Na^+ and by cation–aromatic interaction in the case of Ag^+ and K^+.[9,10]

The construction of calix-crown molecules is achieved by grafting ethylene glycol chains in a loop at two of the phenolic functions (Fig. 3A).

The 1.3-bis crown-ether calix[4]arene (Fig. 3B) was shown to be highly effective in the extraction of the radioactive isotope cation Cs^+.[11] As compared to other possible extractants, the stability of the calix[*n*]arene skeleton is an important factor in their potential use. The 1.2-*bis*-crown ether calix[4]arene (Fig. 3C) interacts more strongly with the Rb^+ cation than with the K^+ and Na^+ cations. In this case. the binding of the Cs^+ is relatively weak.[12]

Amino Derivatives

In order to complex transition metal cations. including chromium (VI), molybdenum (VI), rhenium (VII) and selenium (VI), suitable hard ligands based on nitrogen donor groups were introduced onto the basic calix[*n*]arene skeleton, for example, alkyl amino chains.[''] Recently, Regnouf de Vains synthesized calixarene derivatives having heterocyclic pendant ligands. including bipyridyl, and observed strong bonding of transition metal cations, including Co^{2+}. Cu^+, and Cu^{2+}.[14,15]

Sulfonate Derivatives

The sulfonate derivatives (Fig. 4A), in which introduction of suitable ligand functions takes place at the *para*-position of the aromatic ring, are the most widely studied of the water-soluble calixarenes. Their solid-state binding to a wide range of metallic cations and complexes was reviewed by Raston and Atwood.[16] The ability of these molecules to intercalate cations in expandable layers between bilayers of *para*-sulfonato-calix[4]arene led Atwood and Coleman in 1988 to name these systems ''Organic Clays.'' (Fig. 4C).[17] Since then. Atwood extended the structural types observed to include liposomal analogues. tubes. and various Archimedian and Platonic solids.''[8]

Phosphonate Derivatives

The calix[4]arene molecule was modified at both the upper (para) and lower (phenolic) rims by the introduction of phosphate and phosphonate groups, mainly by the group of Kalchenko (Fig. 4B).[19] Such derivatives complex and allow the extraction of lanthanide and actinide tri- and tetravalent cations. Detoxification of radioactive waters may be possible in this way, as the chemical and physical robustness of the calix[*n*]arenes makes them particularly suitable for this task.

Double complexation of the Zn^{2+} and Histidine amin oacid cations to 1.3-diphosphate cation occurs selectively with regard to the cation and the amino acid. as demonstrated by electrospray mass spectrometry.[20]

Miscellaneous

Cations bind to nanoscopic colloidal assemblies, supramolecular solid lipid nanoparticles of amphiphilic calix[4]arene derivatives, leading, in certain cases. to the clustering of such assemblies in the presence of divalent cations Mg^{2+} and Ca^{2+}. Such clustering was imaged by atomic force microscopy.[21] Such effects have particular relevance to the use of such transport systems in physiological media.

Others

The interaction of thiacalixarene ester derivatives (Fig. 1A) alkali metal cations. is strongly conformation of calixarene

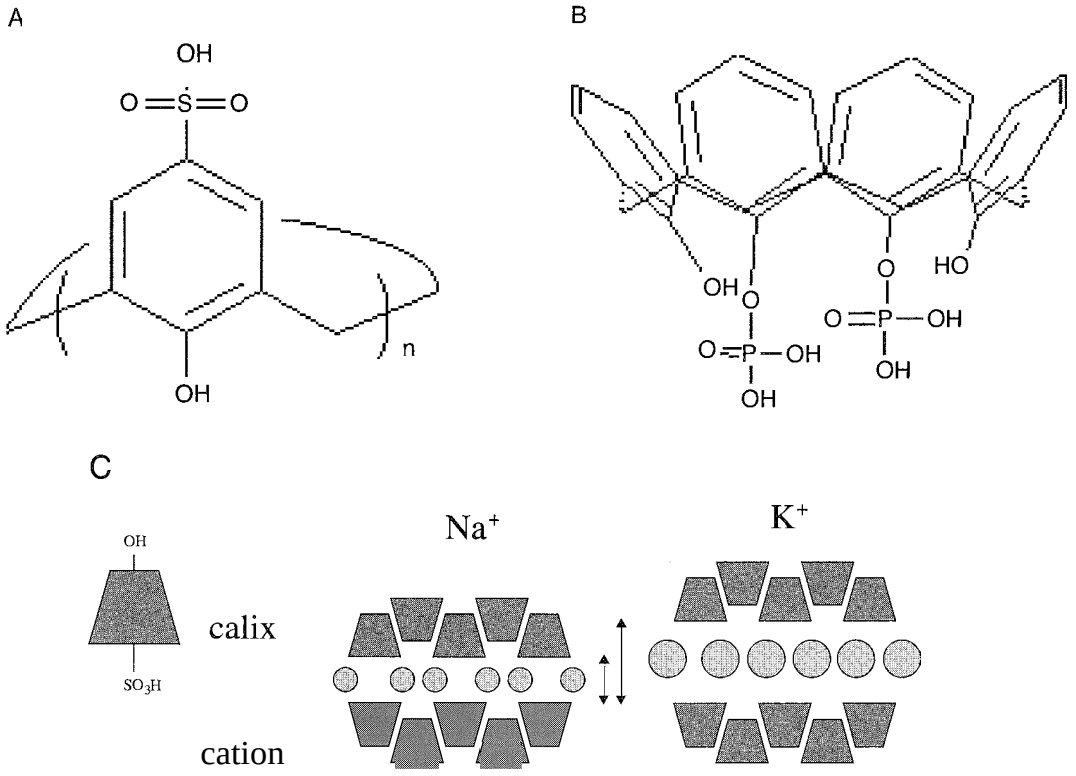

Fig. 4 Molecular structure of water-soluble calixarene: (A) *p*-sulfonato-calix[*n*]arene, where $n = 4$, 6, 8; (B) crystal packing of *p*-sulfonato-calix[4]arene in the presence of salts b calix[4]arene diphosphonic acid: and (C) schematic of the bilayer packing of para-sulfonato-calix[4]arene showing how, as with clays, an increase in the cation size leads to an increase in the height of the hydrophilic interbilayer space. (*View this art in color at www.dekker.com.*)

The cone conformation presents a high selectivity for the sodium cation, while the partial cone and 1,3-alternate conformations show selectivity for potassium and cesium cations.[22]

In the presence of cations, such as bipyridinium, included as guests. *c*-methylcalix[4]resorcinarene is induced to adopt a boat conformation.[23]

ORGANIC CATION COMPLEXATION

In 2002. Abraham published an extensive review of organic cation complexation by calixarenes.[24]

Direct Complexation

The receptor cavity of calix[*n*]arenes favors the formation of complexes with amines by proton transfer. NMR spectrometry and calorimetry techniques allowed for the evaluation of the role of the cavity and the phenolic oxygens in the case of calix[4]arene complexes with aliphatic amines. Hydrophobicity and bas strength are important, and thus, the order of binding is *tert*-butylamine>iso-propylamine (>*n*-hexylamine>piperazine>-diethylamine>piperidine)>triethylamine.[25]

For *p-tert*-butylcalix[6]arene, the tetramethylammonium cation is one of the cations included in the cavity. the other one forms an exterior ion pair.[26]

The use of electrospray mass spectrometry allowed for observation of complexes of calix[4]arenes with alkylammonium ions. either directly from solution[27] or by gas-phase ion–molecule reactions.[28]

Ether and Grown Ether Derivatives

The crown ether derivatives of calixarenes, having a more rigid structure. prove to be more selective in their complexation of organic ammonium cations and are only large enough to accommodate the mono-methylammonium ion and not the larger di-, tri-. and tetramethylammonium ions.[29]

A significant improvement in the ammonium-ion-binding properties can be achieved by covalent bridging of two cone conformation crown-ether derivatives. By adjusting the ethylene bridge length and rigidity. the

association constants can be increased by several orders of magnitude.[30]

Esters, Amides, and Carboxylic Acid Derivatives

Selective recognition of butylamines by *p-tert*-butylcalix[6]arene ester derivatives shows the influence of steric effects on the binding strength, with *n*-butyl>iso-butyl-*sec*-butyl>*tert*-butyl.[31]

NMR studies proved that the calix[4]arene tetracarboxylaie is able to form complexes with tetramethylammonium and trimethylanilinium cations, but with a lower stability than in the case where the calixarene is sulfonated at the upper rim.[32]

Sulfonate Derivatives

The presence of a hydophobic cavity and multiple anionic ligand groups in the *para*-sulfonato-calix[*n*]arenes coupled with their high aqueous solubility, made these molecules the derivatives of choice for the study of binding of organic cations, usually containing ammonium functions.

The stoichiometries of binding organic ammonium cations, such as trimethylanilinium and adamantrimethylammonium, to the para-sulfonato-calix[*n*]arenes is controlled by the macrocycle size formed. Thus, for the calix[4]arene and calix[6]arene derivatives, complexes of stoichiometry I:1 are observed, while for the larger calix[8]arene derivatives a 1:2 stoichiometry occurs.[33]

As with the inorganic cations, solid-state organic clay bilayer structures are favored by *p*-sulfonatocalix[4]arene and were observed with organic cations such as, $[H_4TMTAA^{2+}]_2$ [*trans*-{$Na^+\subset$(18-crown-6)$(H_2O)_2$ and $[H_4TMTAA^{2+}]_2$ $[(C_7N_2OH_7^+)_2$.[34]

Phosphonate Derivatives

1,3-Diphosphatecalix[4]arene is present in the solid state as a self-included dimer with two sets of anionic ligands capable of complexing a wide range of organic ammonium cations, with the propane diammonium cation a complex structure containing a selective water channel (Fig. 5a).[35]

The calix[4]arene α-aminophosphonates are highly selective receptors for amino acids. They exhibit excellent selectivity as carriers of the zwitterionic form of aromatic amino acids through supported liquid membranes.

BIOMOLECULAR COMPLEXATION

The study of the interaction between calix[*n*]arene derivatives and biomolecular cationic functions is mainly limited to two groups of anionic water-soluble calix[*n*]arene derivatives. the *para*-sulfonato- and 1,3-diphosphate systems. These anionic molecules complex strongly to the cationic lateral chains of the amino acids, lysine (Lys, K). arginine (Arg, R). and histidine (His. M). Association constants. as determined by NMR and microcalorimetry, for these three amino acids vary as follows: His <Lys <Arg for the three *para*-sulfonato-calix[*n*]arenes, where *n*=4, 6. or 8; the stoichiometries of the observed complexes are 1:1 with *para*-sulfonato-calix[4]arene, and are

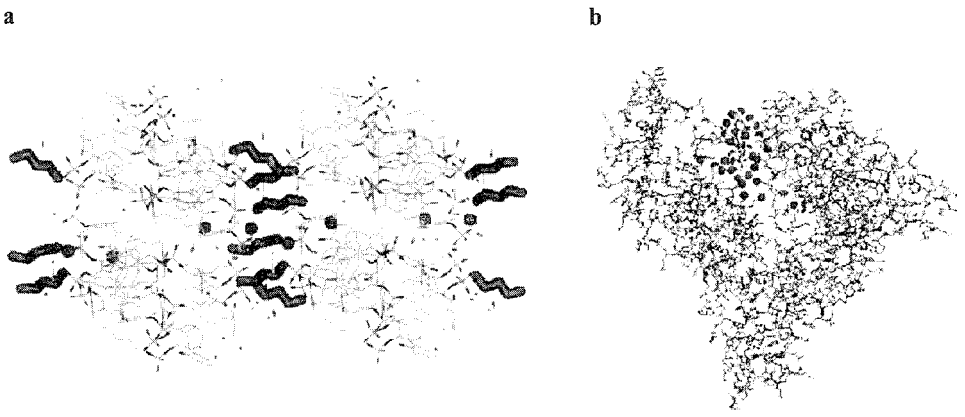

Fig. 5 View of the large self-asembled structure generated by the complexation of the propane diammoniuin cation by calix[4]arene diposphonic acid showing a selective water channel in the crystal packing. The propane diammonium groups act as linkers along the channel (a). Molecular model of bovine serum albumin showing one of the binding sites for *para*-sulphonato-calixarenes. The cationic residues lysine and arginine within the binding pocket are shown in blue: the calixarene molecule is shown as colored spheres (b). (View *this art in color at www.dekker.com.*)

1:2 *for para*-sulfonato-calix[6]arene *and para*-sulfonato-calix[8]arene. *Di-and* tri-peptides *based on* Lys *and Arg binding increase with the number of basic amino acids*

Recognition *of this binding to* cationic *amino acids present* at *the surface of* many *proteins and often clustered either by the amino acid sequence or by the tertiary protein structure explains the biological activity of the para*-sulfonato-calix[*n*]arenes, *for example. their enzyme inhibition properties with regard to* lysyl oxidase.[38]

The binding of the para-sulfonato-calix[*n*]arenes *to bovine serum albumin* (BSA), *as demonstrated by* electrospray mass *spectrometry,* involves *complexation to* lysine *and arginine* present *in anion-binding pockets* on *the protein surface (Fig.* 5b).[39]

APPLICATIONS

The capacity of *the calixarenes to exhibit cation selection or to recognize the chirality of* amines *and amino acids, as well as their ability to form complexes with quaternary ammonium. led to a number of potential and actual applications.*

The use of the *ethoxycarbonylmethyl derivative of p-tert*-butylcalix[6]arene *as a selective carrier for the separation of amino acids through a chloroform liquid* membrane *was demonstrated by Chang et* al.[40] Ion*ophoric calixarene esters and ethers were applied to* ion *transport through phospholipid bilayer membranes.*

The most *widely studied and developed application of* the *calixarenes* is in *sensing devices for cation* recogniton. *Devices based on* Langmuir Blodgett *films. thermally deposited thin films. or where the calixarene derivatives are immobilized into polymer films have been used in such applications. Sensing may occur through* potentio*metric. fluorometric, or* photometric measurements.[41]

Their application in the biomedical field is clearly demonstrated by the preponderance of patents as compared to publications in the field. Calixarenes functionalized at the wide rim with sulfonic *acid and* sulfonamide *groups showed anticoagulant and antithrombotic properties. approaching the activity of heparin and* coumarin, *currently used as* anticoagulants *in antithrombotic therapy.* Calixarene *derivatives are also active as antiviral, antimicrobial. and antifunga! agents.*

CONCLUSION

Since the recognition *of the cyclic nature of the calixarenes by* Zinke in *1942. their use in* supramolecular *chemistry and for the* complexation *of cations has seen* almost *exponential growth. Given the diversity of the nature of the* chemical modification *is* seemingly *only limited by* the *imagination of the chemist. we can expect this growth to continue. The design and construction of calixarenes carrying highly specific ligand functions are leading to their application* in *the areas of environmental control for detoxification of poisonous metal ions. The field of biological application of calixarenes by their cornplexation to* cationic *groups present in* biomacromolecules *is* just *starting. but it can be expected that this field* will *prove to be of great impact in the* future.

ARTICLES OF FURTHER INTEREST

Amino Acids: Applications, p. *42*
Biologic01 Ligands, *p. 88*
Calixarenes and Their Analogues: Molecular Complexation, *p.* 145
Calixarenes: Synthesis and Historical Perspectives, *p. 153*
Cation–π Interactions, p. *214*
Crown Ethers. p. 326
Fluorescent Sensors, p. *572*
Ionophores, *p. 760*
Organic Zeolites. p. 996
Platonic and Archimedean Solids. p. 1100
Protein Supramolecular Chemistry, *p. 1161*
Simultaneous Binding of Cations and Neutral Molecules. p. 1295
Stability Constants: Definition and Determination. p. 1360
Supermicroscopy: AFM, SNOM, and SXM, p. *1394*
Supramolecular Chemistry: Definition, *p. 1401*
X-Ray Crystallography, p. *1586*
Zwitterion Receptors, *p. 1639*

REFERENCES

1. Gutsche. C.D. *Monographs in Supramolecular Chemistry, Calixarenes Revisited*; Stoddart. J.F.. Ed.: The Royal Society of Chemistry: Cambridge, U.K.. 1998.
2. Roundhill. M.D. Metal Complexes of Calixarenes. In *Progress in Inorganic Chemistry*; Kenneth. *D.M.*. Ed.: John Wiley & Sons, Inc., 1995: 533 pp.
3. Shahgaldian, P.: Coleman. A.W. Anion and cation interactions with *p*-dodecanoylcalix[4]arene monolayers at the air–water interface. Langmuir 2001. *17*, 6851–6854.
4. Arnaud-Neu, F.: Collins, E.M.: Deasy, M.: Ferguson. G.; Harris. S.J.: Kaitner. B.: Lough, A.J.: McKervey, M.A.: Marques. E.: Ruhl. B.L.; Schwing-Weill, M.J.: Seward. E.M. Synthesis, x-ray crystal structures, and cation-binding properties of alkyl calixaryl esters and ketones. a new

family of macrocyclic molecular receptors. J. Am. Chem. Soc. 1989. *111*, 8681–8691.
5. Akdas. H.; Graf. E.: Hosseini. M.W.: De Cian. A.; Harrowfield, J.McB. Design, synthesis and structural investigation of a 2-D-coordination network based on the self-assembly of the tetracarboxylate derivative of tetrathiacalix[4]arene and silver cation. Chem. Commun. 2000, *22*. 2219–2220.
6. Arnaud-Neu, *F.*: Barrett. G.; Fanni. S.: Marrs. D.; McGregor, W.: McKervey, M.A.: Schwing-Weill, M.-J.; Vetrogon. V.: Wechsler, S. Extraction and solution thermodynamics of coinplexation of alkali and alkaline-earth cations by calix[4]arene amides. J. Chem. Soc., Perkin Trans., 2 Phys. Org. Chem. 1995, 3. 453–461.
7. Ogata. M.: Fujimoto, K.: Shinkai. S. Molecular design of calix[4]arene-based extractants which show high Ca^{2+} selectivity. J. Am. Chem. Soc. 1994, *116*. 4505–4506.
8. Aime. S.: Barge, A.; Botta. M.: Casnati. A.; Fragai. M.; Luchinat. C.: Ungaro, R. A calix[4]arene GdIII complex endowed with high stability, relaxivity, and binding affinity to serum albumin. Angew. Chem.. Int. Ed. 2001. *40*. 4737–4739.
9. Bott. S.G.: Coleman, A.W.: Atwood. J.L. Inclusion of both cation and neutral molecule by a calixarene—Structure of the [para-tert-butylmethoxycalix[4]arene sodium toluene]+ cation. J. Am. Chem. Soc. 1986, *108*. 1709.
10. Ikeda, A.; Shinkai. S. On the origin of high ionophoricity of 1.3-alternate calix[4]arenes: p-donor participation in complexation of cations and evidence for metal-tunneling through the calix[4]arene cavity. J. Am. Chem. Soc. 1994. *116*. 3102–3110.
11. Thuery. P.: Nierlich, M.; Arnaud-Neu, F.: Souley, B.; Asfari, Z.: Vicens, J. Silver ion complexation by a calix[4]arene bis(crown ether). Ambivalence towards ether and polyhapto coordinations. Supramol. Chem. 1999, *11*. 143–150.
12. Arduini. A.; Casnati, A.: Dodi, L.; Pochini. A.: Ungaro. R. Selective 1.2-functionalization of calix[4]arenes at the lower rim. Synthesis of a new type of bis-calixcrown ether. Chem. Commun. 1990. *22*, 1597–1598.
13. Georgiev, E.M.: Wolf, N.: Roundhill. D.N. Lower riin alkylammonium-substituted calix[4]arenes as "proton-switchable" extractants for chromate and dichromate anions. Polyhedron 1997, *16*. 1581–1584.
14. Molard, Y.: Bureau, C.; Parrot-Lopez. H.: Lamartine. R.; Regnouf-de-Vains. J.-B. Synthesis of calix[4]arene podands bearing two and four histidine or glycine groups at the lower rim. Complexation properties towards cobalt (II) chloride. Tetrahedron Lett. 1999. *40*. 6383–6387.
15. Pellet-Rostaing. S.; Lamartine. R.; Regnouf-de-Vains. J.-B.; Fennet. B. A bithiazole-containing calix[4]arene podand as versatile ligand for copper(I) and copper(II). Inorg. Chem. Commun. 1999. *2*. 44–47.
16. Atwood. J.L.; Barbour. L.J.: Hardie, M.J.: Raston. C.L. Metal sulfonatocalix[4,5]arene complexes: Bi-layers, capsules. spheres. tubular arrays and beyond. Coord. Chem. Rev. 2001. *222*. 3–32.
17. Coleman. A.W.: Bott. S.G.; Morley, S.D.; Means. C.M.; Robinson. M.D.: Zhang, H.; Atwood. J.L. Sodium calix[4]arenesulfonate with a layered structure. An organic clay'? Angew. Chem., Int. Ed. 1988. *100*. 1412–1413.
18. Atwood. J.L.; Barbour. L.J. Molecular graphics: From science to art. Cryst. Growth Des. 2003. 3. 3–8.
19. Lipkowski. J.; Simonov. Y.; Kalchenko. V.I.; Vysotsky. M.A.; Markovsky, L.N. Molecular and crystal structure of water-soluble 25,57-bis(dihydroxyphosphoryloxy)calix[4]-arene. An. Quim. Int. Ed. 1998. *94*. 328–331.
20. Perret. F.: Morel-Desrosiers. N.; Coleman. A.W. An ESI/MS study of the formation of ternary 25,27-bis(dihydroxyphosphoryloxy) calix[4]arene-metal ion-aminoacid complexes. J. Suprainol. Chem. 2003. *in* press.
21. Dubes. A.; Parrot-Lopez, H.: Shahgaldian. P.: Coleman. A.W. Interfacial interactions between amphiphilic cyclodextrins and physiologically relevant cations. J. Colloid Int. Sci. 2003. *259*. 103–111.
22. Stoikov. I.I.; Omran. O.A.; Solovieva. S.E.: Latypov. S.K.; Enikeev, K.M.; Gubaidullin, A.T.: Antipin, I.S.; Konovalov, A.I. The synthesis of tetracarbonyl derivatives of thiacalix4arene in different conformations and their complexation properties towards alkali metal ions. Tetrahedron 2003; *59*. 1469–1476.
23. Brown, P.O.; Enright, G.D.: Ripmeester, J.A. Cationic guests in extended anionic c-methylcalix[4]resorcinarene-inorganic frameworks: Exercising conformational control over c-methylcalix[4]resorcinarene. J. Supramol. Chem. 2002. *2* (4–5), 497–500.
24. Abraham. W. Inclusion of organic cations by calix[n]arenes. J. Incl. Phenom. Macrocycl. Chem. 2002, *43*, 159–174.
25. Nachtigall, F.F.; Lazzarotto. M.: Noine, F. Interaction of Calix[4]arene and amines: A combined NMR. spectrometric and conductimetric investigation. J. Braz. Chem. Soc. 2002, *13*. 295–299.
26. Harrowfield, J.M.; Richmond. W.R.: Sobolev. A. Inclusion of quaternary ammonium compounds by calixarenes. J. Incl. Phenoin. Mol. Recognit. Chem. 1994. *19*. 257.
27. Lippmann, T.; Wilde. H.; Pink. M.: Schaefer. A.; Hesse. M.; Mann. G. Host–guest complexes between resorcinol-derived calix[4]arenas and alkylammonium ions. Angew. Chem. 1993, *105*, 1258–1260.
28. Wong, P.S.H.; Yu. X.; Dearden. D.V. Complexes of p-tert-butylcalix[4]arene with mono- and dipositive cations in the gas phase. Inorg. Chim. Acta 1996. *246*. 259–265.
29. Arduini. A.; McGregor, W.: Paganuzri. D.; Pochini. A.; Secchi, A.: Ugozzoli, F.: Ungaro. R. Rigid cone calix[4]-arenes as π-donor systems: Complexation of organic molecules and ammonium ions in organic media. J. Cheni. Soc., Perkin Trans.. 2 Phys. Org. 1996. 5. 839–846.
30. Arduini. A.; Pochini. A.; Secchi, A. Rigid calix[4]arene as a building block for the synthesis of new quaternary ammonium cation receptors. Eur. J. Org. Chem. 2000, 2325.
31. Chang, S.K.: Jang, M.J.; Han. S.Y.; Lee. J.K.: Hang, Y.S.: No. M.T. Molecular recognition of butylamines by calixarene-based ester ligands. Chem. Lett. 1992. 1937.
32. Arena, G.; Casnati, A.: Contino, A.; Lombardo, G.G.: Sciotto. D.; Ungaro. R. Water-soluble calixarene hosts that specifically recognize the trimethylammonium group or the benzene ring of aromatic ammonium cations: A combined ^{1}H NMR, calorimetric, and molecular mechanics

investigation. J. Chem. Soc., Perkin Trans. **2000,** *2*, 419–423.

33. Shinkai, S.; Araki, K.; Matsuda, T.; Manabe, O. NMR determination of association constants for aqueous calixarene complexes and guest template effects on the conformational freedom. Bull. Chcm. Soc. Jpn. **1989.** *62*, 3856.
34. Ness, T.; Nichols, P.J.; Raston, C.L. Bi-Layer complexes incorporating large organic cations and anionic tetra-p-sulfonated calix[4]arene capsules. Eur. J. Inorg. Chcm. **2001,** *8*. 1993–1997.
35. Coleman, A.W.: Da Silva, E.; Nouar, F.; Nierlich, M.; Navaza, A. The structure of self-assembled calixarene aqua-channel system. Chem. Commun. **2003.** 7, 826–827.
36. Kalchenko, **O.1.;**Da Silva, E.; Coleman, A.W. Determination of the stability constants of inclusion complexes of p-H-37-(2-carboxy-methyloxy)-calix-[6]-arene and p-sulphonato-37-(2-carboxy-methyloxy)-calix-[6]-arene with 15 amino acids by KP-HPLC. J. Incl. Phenom. Macrocycl. Chem. **2002,** 43. 305–310.
37. Guevel-Douteau, N.; Pcrrct, F.: Morel-Desrosiers, N.; Morel, J.-P.; Coleman, A.W. Molecular organisation of positively charged di- and tri-peptides by anioinic calix-[n]-arene-sulfonates. J. Chem. Soc., Perkin Trans. **2002,** *2*, 524–532.
38. Hulmes, D.; Coleman, A.W.; Aubert-Foucher, E. Use of calix(n)arenes for treating fibrotic diseases. PCT Int. Appl. **2000.**
39. Memmi, L.; Lazar, A.; Rrioude, A.; Ball, V.; Coleman. A.W. Protein–calixarene interactions: Complexation of bovine serum albumin by sulfonatocalix[n]arenes. Chem. Commun. **2001,** *23*, 2474–2475.
40. Chang, S.K.; Hwang, H.S.; Son, H.; Youk, J.; Kang, Y.S. Sclcctivc transport of amino acid esters through a chloroform liquid membrane by a calix[6]arene-based ester carrier. J. Chcm. Soc., Chem. Commun. **1991,** 217.
41. Diamond, D.; Nolan, K. Calixarenes: Designer ligands for chemical sensors. Anal. Chem. **2001,** 73 (1). 22A–29A.

Calixarenes and Their Analogues: Molecular Complexation

C

Ivan Stibor
Pavel Lhoták
Institute of Chemical Technology, Prague, Czech Republic

INTRODUCTION

The ability of calixarenes to act as baskets is said to be one of their most intriguing properties, accounting for much of the interest they received.''' Generally speaking, molecules having convergent concave surfaces are frequently potent receptors; and their cavity can form a binding site where recognition events take place. It is well known that calix[4]arenes and calix[5]arenes, particularly when in their cone conformations, possess an intramolecular cavity that can host neutral molecules or their neutral parts of complementary size. Other conformations of calix[n]arenes (n=4,5) as well as larger calix[n]arenes are also known to form numerous molecular complexes, but factors controlling their complexation selectivity are not well understood, mainly due to their greater conformational flexibilities.[2–4]

This entry deals with various facets of molecular complexation by calixarenes. Most studies published on this subject are connected with cone conformation of calixarene skeleton.

The subject is traditionally divided into two parts, considering solid-state systems, first and then proceeding to solution-state systems, having in mind aqueous and nonaqueous solvents. Finally; gas-phase recognition will be mentioned briefly.

SOLID-STATE COMPLEXES

Many calixarenes form complexes in the solid state, this property having been observed even before the structure of compounds was established. Among the simple calix[n]arenes, for example, *p-tert*-butylcalix[4]arene forms complexes with chloroform, benzene. toluene. xylene, nitrobenzene, nitromethane, acetonitrile, and many others, while *p-tert*-butylcalix[5]arene complexes were studied with lower alcohols, ethyl acetate, toluene. and tetraline. More flexible *p-tert*-butylcalix[6]arene was found to form complexes with acetonitrile and *p-tert*-butylcalix[8]arene with chloroform. The tenacity with which the guest molecule is held by the calixarene hosts varies widely with the size of macrocycle. Whereas tetramers to hexamers usually hold their guests tightly. retaining a residual amount of the crystallization solvent even after prolonged heating at high temperature under vacuum (which makes traditional elemental analysis completely useless at times), *p-tert*-butylcalix[8]arene crystallizes from chloroform in beautiful glistening needles that change to white powder within a few minutes at atmospheric pressure.

The structures of complexes of calixarenes are most effectively revealed by x-ray crystallography. The first solid-state complex published was that of *p-tert*-butylcalix[4]arene with toluene[5] (Fig. 1).

It was quickly found that there are many difficulties connected with the structural studies of even the simplest calixarene complexes.[6] In general: the compounds are disordered, often with involvement of guest and host sublattices. and there is evidence for dynamic coupling between them. That is why the use of a synoptic approach has been advanced, where the use of complementary techniques resulted in improved structural models. Without doubt, the combination of crystallography and solid-state nuclear magnetic resonance (NMR) spectroscopy has proven to be remarkably effective in solving a number of complex problems. We can illustrate the complexity of these studies by looking at an almost 10-year-long structural study of the first crystalline calixarene complex mentioned above. The parent *p-tert*-butylcalix[4]arene has a flexible upper rim defined by *tert*-butyl groups. In contrast, the lower rim is fixed by in-plane hydrogen bonding. It was found that at room temperature, the toluene guest rapidly reorients between equivalent guest sites, but that below 248 K, the transition to a lower symmetry host lattice takes place. There are two crystallographically distinct molecules. each with a toluene guest that is disordered over two equivalent sites. More detailed study using ^{2}H, ^{13}C, variable temperature NMR, calorimetry. and 150 K crystallography show that toluene is static at 129 K. and that it undergoes rapid 180° flip about the molecular C_2 symmetry axis at 180 K and above (E_a=34±3 kJ mol^{-1}). These results are consistent with the final structural analysis in which each of two crystallographically different complexes has only a twofold axis of symmetry. Apparently, the structure of solid-state

DOI: 10.1081/E-ESMC *120012851*

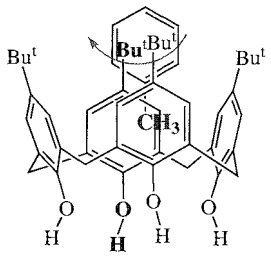

Fig. **I** The structure of *p-tert*-butylcalix[4]arene with toluene. (*View this art in* color *at www.dekker.com.*)

calixarene molecular coinplexes is far from being trivial because of the dynamic structural complexity. Similarly, the dynamic structures of other calixarene complexes were recently examined,[6] namely. complexes of *p-tert*-butylcalix[4]arene with benzene, pyridine, 4-nitrobenzene, cyclohexane, hexane. dodecane, heptane-1-ol, octane-1-ol, and. 1,4-dichlorobenzene. The following extremely important conclusions can be drawn from this pioneering work:

> "Most. if not all, molecules of appropriate size form reasonably stable inclusion compounds with *p-tert*-butylcalix[4]arene, and this observation suggest that considerable caution should be exercised in interpreting compound stability in terms of specific interactions. By examining series of structurally-related guest compounds it can be seen that the deep cavity is chlorophobic, but the space filling seems to be more important than the avoidance of unfavorable interactions in determining whether compound formation will take place. A similar conclusion can be drawn from the fact that a long molecule will curl up in order to fill space effectively in an inclusion compound rather than exist in a favored all-trans conformation without inclusion compound formation."[6]

In an alternative approach. all data available in the Cambridge Structural Database (CDS) for inclusion complexes formed by calix[4]arenes, calix[4]resorcinols, and thiacalix[4]arenes in the cone conformation with neutral organic molecules having acidic CH groups were retrieved. The data for 39 guests and two types of organic molecules with CH acidic groups. namely, CH_3X and CH_2XY (X,*Y*=EWG groups) were critically evaluated.[7] First; suitable geometrical descriptors were introduced for precise definition of host geometry as well as position and orientation of the guest inside the cavity. Nitromethane and acetonitrile were chosen as typical guests of CH_3X type. No obvious correlation between simple geometrical characteristics of the host or guest and the strength of inclusion was found. Nonetheless, what is important is the specific position of the guest methyl group inside the cavity, a position that must facilitate the strongest possible intermolecular interaction with all aromatic wails of the host. Accordingly. dichloromethane, chloroacetonitrile. and malononitrile were chosen as typical guests of the CH_2XY type. The data obtained showed that the intermolecular interactions between the aromatic cavity of the calix[4]arene hosts and the molecule having acidic CH groups are different for CH_3X and CH_2XY guests. There is no evidence for hydrogen-bond-like characteristics of CH_3X interactions. These results are in agreement with more sophisticated studies (e.g., inelastic neutron scattering) that show that the guest methyl group behaves as an almost free quantum rotor. Conversely, rotation of CH_2XY guests is somewhat inhibited by complex formation. This entropic cost is partially compensated for by a higher value of the enthalpic contribution to the bonding, as reflected by the cotrelation of CH-aromatic distance and acidity of the guest.

There have been several attempts to apply quantum chemistry to the evaluation of structure and properties of solid-state complexes of calix[4]arene receptors. Usually, only inolecular mechanics and dynamics can be used to do this job, and information obtained has usually been regarded as supporting evidence of the structure of the complex formed. Recently. an advanced approach was applied to structure elucidation of solid-state inclusion complexes formed by *p-tert*-butylcalix[4]arene with different solvents. The method reported[8] is based on the following procedure. Various possible geometries of host–guest complexes are modeled using fast force-field optimization. Based on minima structures obtained by this approach, quantum chemical (GIAO)-DFT NMR calculations were performed. Then comparison of theoretical and experimental chemical shifts for free ligand and complex with solvent furnish the spatial arrangements of host and guest. Thus, it is possible for calix[4]arene complexes. using a combination of force-field geometry optimization and CIAO-GFT NMR shift calculations. to screen various starting geometries against experimental data, yielding good structural models for these complexes in the solid state.

COMPLEX FORMATION IN LIQUID PHASE

Apolar Media

Calixarenes in general are known to form weak complexes with neutral organic guests in apolar media. This behavior is different from that of cavitands based on calix[4]resorcinols. Molecules of solvent compete with the guest with respect to interaction with the host molecule. That is why the crucial problem to be solved is the proper choice of solvent that is able to dissolve both components and that is not able to interact with the host molecule. For

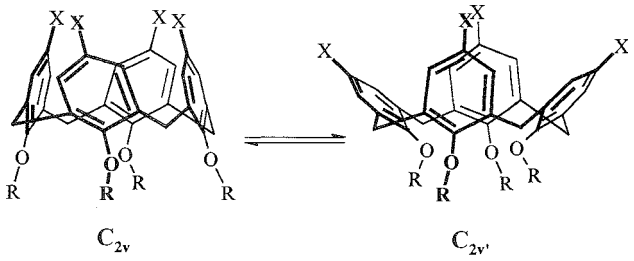

Fig. 2 Dynamic stereochemistry of tetraalkoxycalix[4]arenes in the cone conformation.

calix[4]arenes in the cone conformation, tetrachloromethane is a good example. as it is too big to fit within the cavity and at the same time it has acceptable properties as a solvent. This is perfectly true for calixarenes with rigid cavities, as for example. parent *p-tert*-butylcalix[4]arene. with a circular array of four hydrogen bonds. It is. however. not true for tetraalkylated *p-tert*-butylcalix[4]arenes. where large alkyl substituents are believed to lock the cone conformation. The reason is that most of these compounds retain a limited degree of conformational flexibility, as their cone conformation in which apparent C_{4v} symmetry is in fact the result of fast interchange between two C_{2v} flattened cone structures. These are sometimes referred to as pinched cone conformations. This behavior was directly established by variable temperature NMR measurement of tetrakis-*n*-octyloxy-*p-tert*-butylcalix[4]arene (Fig. 2).[9]

The role of the lower-rim substitution pattern of *p-tert*-butylcalix[4]arene was studied for a series of complexes formed by 12 *p-tert*-butylcalix[4]arene hosts with 13 guests (eight nitriles and five nitroalkanes).[10] It was proven that the complexation ability of these hosts follows the order: monosubstituted > disubstituted > unsubstituted > tetrasubstituted. The suggested explanation of this order is based on the shape of the host cavity and the time-averaged proportion of the host molecule adopting transition shapes during flipping through the annulus. The structure of complex acetonitrile **C 1** was proven by ^{1}H-NMR spectroscopy, in which NOEs were found between metaprotons of ail the phenolic units of hosts. with the methyl protons of acetonitrile as guests (Fig. 3).

Doing the same study with propionitrile, it was found that methyl and methylene groups are found inside the cavity of the host. with the methylene group positioned somewhat deeper.

These findings are in perfect agreement with other approaches to binding enhancement by "covalent shaping" of the *p-tert*-butylcalix[4]arene cavity. The first involves selective 1,2 (proximal) lower-rim functionalization of parent *p-tert*-butylcalix[4]arene, yielding the series of *p-tert*-butylcalix[4]arene *bis*crowns 2–6 (Fig. 4), where the conformational flexibility can be tuned by varying the length of the bridging unit.[11]

In fact, *p-tert*-butylcalix[4]arene *bis*crown-5 6 is flexible and adopts a flattened-cone conformation in solid state, while *p-tert*-butylcalix[4]arene *bis*crown-3 derivatives 2–4 possess a rigid cone structure. The recognition properties of **3** in solution were evaluated in organic solvents ($CDCl_3$ and CCl_4) using nitromethane as guest.[12] By adding variable amounts of guest to a solution of **3,** a significant upfield shift of the CH protons of the guest and fast exchange conditions were observed. These shifts clearly show an interaction of the acidic protons of the guest with the n-electrons of the calixarene cavity, while excluding a possible interaction of these protons with the crown-ether region. which should result in a downfield shift. The analysis of the data showed the formation of 1:1 complexes and provided quantitative information on host–guest interactions (Table 1).

To gain further insight into the role of rigidity on the molecular recognition properties of hosts. comparison was made with the more mobile hosts 6 and **7**. Interestingly, in **6** and **7**. with nitromethane and malononitrile, nu variation of the chemical shift of the guest was observed, while with 5, coinplexation occured but only in CCl_4 and with a lower association constant than with the more rigid 3. These results deinonstrate the importance of rigidity in determining the complexation properties of the n-donor cavity of calix[4]arenes. The group present at the upper rim strongly affects the stability of complexes formed as witnessed by data for compounds **2–4**. In fact. increasing the extension of the cavity increases the complexation efficiency toward nitromethane (Table 1). In contrast, malonodinitrile is bound with comparable efficiency by all three hosts. probably for steric reasons. Another interesting observation. which confirms the importance of rigidity and, consequently. the preorganization of the calix[4]arene in the cone conformation, was observed by comparison between hosts 8 and 9. Here. the well-known

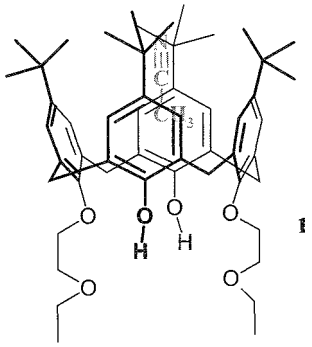

Fig. *3* Complex **1**⊂ acetonitrile in CCl_4 proven by ^{1}H-NMR (*View this art in* color *at www.dekker.com.*)

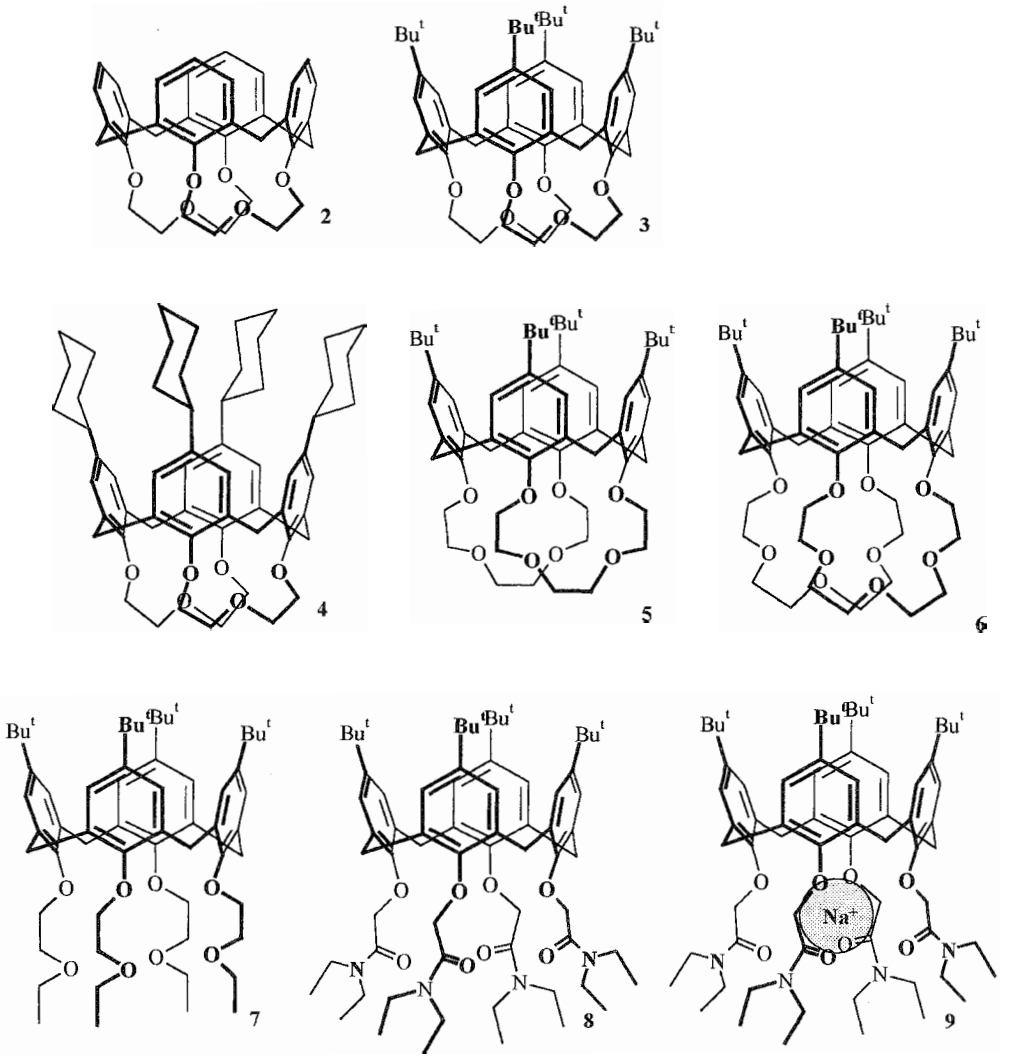

Fig. 4 *p-tert*-Butylcalix[4]arenes with different flexibilities of cone conformation

free ligand and its codium picrate complex were compared in the complexation of nitromethane in $CDCl_3$. While the conformationally mobile 8 does not show significant complexation, its rigid sodium complex 9. through a positive allosteric effect, binds nitromethane (Table 1). Similar results were obtained with a corresponding tetraester–acetonitrile system.[10] There is also a recent report involving the correlation between the guest acidity and the association constants in the recognition of neutral CH_3X and CH_2XZ species by rigidified calix[4]arene.[13] Comparison of K_{ass} of acetonitrile (pK_a – DMSO = 31.3) and nitromethane (pK_a – DMSO = 17.2), measured in CCl_4, shows that these two guests are bound with similar efficiency. This indicates. in agreement with the results obtained in solid state,[7] that the complexation of the CH_3X guests is not determined by their acidity. Conversely. as verified in the solid state, the similar. data on guests CH_2XZ strongly suggest their dependence on the acidity of the CH_2 group. This finding is also in agreement with the solid-state study.[7] The energetics of the inclusion of guests by rigidified cone conformer of calix[4]-arenes in CCl_4 was also recently reported.[14]

Table 1 Association constants (K_{ass}, M^{-1}) of 1:1 complexes of nitromethane and malononitrile with rigidified calix[4]arenes 2–9 at 300 K

	CH_3NO_2		$CH_2(CN)_2$
Calix[4]arene	$CDCl_3$	CCl_4	$CDCl_3$
2	5±2	28±7	17±2
3	27±4	230±60	6±2
4	36±8	123±25	23±5
5	[a]	50±10	[a]
9	34±7	[a]	[a]

[a] Not determined.

The influence of upper-rim substitution was also studied in the series of calix[4]arenes with identical substitution patterns on the lower rim but differing in their upper-rim substitution pattern. Namely, hydrogen, *tert*-butyl, and adamantyl were used as upper-rim substituents.[15] The association constants obtained for *p*-adamantylcalix[4]arene complexes are close in their values to those of the corresponding *p-tert*-butylcalix[4]arene complexes. The ^{1}H-NMR spectra of these compounds undergo similar changes caused by complexation as the spectra of their *p-tert*-butyl analogues. Thus. complexation-induced shifts of OH and aryl protons of the ligands of both types have similar values, and a significant upfield shift of the protons of the substrate (up to 6 ppm) is observed. It seems apparent that both hosts behave in a similar way, at least in tetrachloromethane solution. In contrast. upper-rim unsubstituted calix[4]arene derivatives form weak complexes with all guests studied. This result can be explained by the fact that the calixerene apolar cavities are not shielded by any substituent and are easily accessible for solvent molecules of any shapes and sizes. The results from all the above studies can be rationalized in the following way. First. the ability of calix[4]arene hosts to form complexes with neutral molecules is controlled by the solvation of its cavity. Second. C–H···π interactions play an important role in the complexation process—the strength of complexes formed by the guests with similar geometries and nature strongly depends on their C–H acidity. Third, the association constants of observed complexes do not exceed 300 M^{-1} in CCl_4 and 30 M^{-1} in $CDCl_3$.[15]

In order to improve the recognition efficiency of neutral organic species. suitable binding sites were attached at one or two rims of calix[4]arene or calix[5]arene platform. usually with the ability to act as hydrogen bond donor or acceptor groups. Using this approach, selective binding of several primary amines by a carefully designed dicarboxy- calix[5]arene receptor was studied. As usual with calix[5]arenes, the synthesis of the receptor is complicated and results from a low-yielding synthetic sequence.[16] Also, a molecule of water was found to be complexed selectively by adamantylated calix[4]arene diamide.[17] Clear evidence that the hydrogen-bonding groups linked at the upper rim and the cavity are able to cooperate in binding was obtained when rigidified calix[4]arene **10** bearing a methylenephenylureido additional binding site at the upper rim was exploited to recognize low-molecular-weight amides.[18] The structure of host and the cooperative binding is shown in (Fig. 5).

The complexation properties of host **10** were evaluated in $CDCl_3$, and it was found that it is able to efficiently recognize amides with NH_2 or NHR groups, whereas the substantial decrease of this ability was observed with the guests bearing *N,N*-dialkylamino groups.

Aqueous Media

One of the main reasons for studying the interactions of calixarenes in water is to exploit hydrophobic effects in order to enhance complexation of apolar guests in their cavities. In order to study this phenomenon, the water-soluble calixarenes are needed in analogy of cyclodextrins and water-soluble cyclophanes. To engender water solubility generally, calixarenes need to be functionalized with groups containing positive or negative charges or with neutral but highly hydrophilic moieties. A predominant part of the work concerning the complexation of neutral molecules by water-soluble calixarenes was carried out in the 1980s and was critically reviewed.[19] Classical work was devoted to the inclusion of small neutral organic guests (alcohols. ketones, and nitriles) by water-soluble calix[4]arene hosts (solubility was introduced by sulfonyl groups at the upper rim or carboxy groups at the lower rim, sometimes in combination, and with an ethoxyethoxy group at the lower rim). The guests are included in the host hydrophobic cavity by their apolar aliphatic residues.

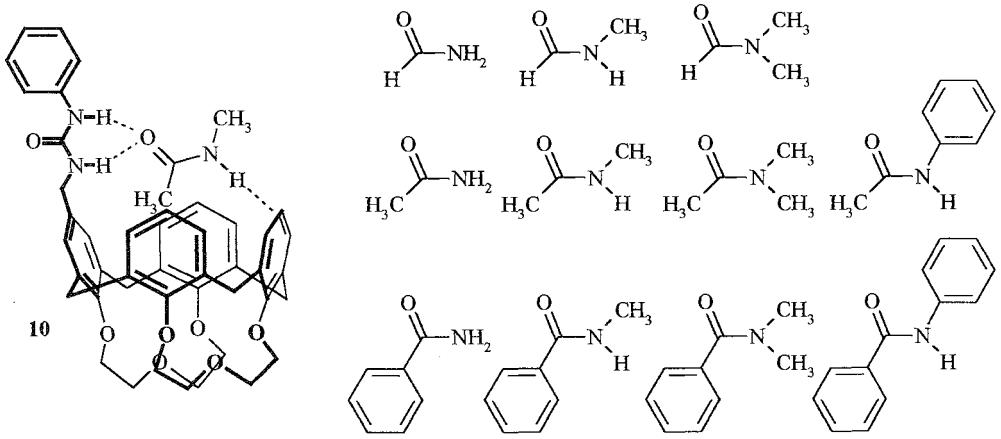

Fig. 5 Structure of complex formed by **10** and several amides

The binding constants at neutral pH confirm the importance of charge assistance in the apolar binding of guests inside calixarene cavities, and they highlight the role played by the conformational properties of host in the recognition process."'' Recently, the rennaissance of interest in all aspects of molecular recognition in water were easily observed in chemical literature. A number of papers appeared on the application of water-soluble calix[*n*]arenes as catalysts or cocatalysts. Thus, Wacker oxidation of alkenes,[20] aldol-type condensation and Michael addition,[21] and Suzuki coupling,[22] were recently reported to be catalyzed by water-soluble calix[*n*]-arenes. These results are apparently connected with ''green chemistry'' procedures with the potential for industrial application, a fact that should boost the research in this area profoundly. The second subject of recent interest is centered around medicinal chemistry application in a broad sense. Water-soluble *p*-sulfonatocalixarenes were recently reported to bind dipeptides and tripeptides containing lysine and arginine. This process, taken as a model for interaction of glycosylaminoglycans with polypeptides, was thoroughly studied by NMR and microcalorimetry.[23] There are, however, many examples of water-soluble neutral calixarenes, and most of them belong to the neoglycoconjugates family.[24] Such compounds can be used as models of important biological processes like interactions taking place on the surface of the cell. Among them, embryogenesis, cancer metastasis, inflammation. and bacterial and viral infections are examples of biological events that involve the selective recognition of carbohydrates by proteins. However, isolated carbohydrate–protein interactions are typically weak. Nature compensates for the weakness of these isolated interactions by tending to cluster together multiple copies of carbohydrate receptors in order to allow for stronger cooperative binding to take place—the so-called multivalent effect. The role of calixarenes as cyclic oligomers of phenolic nuclei is immediately apparent. No wonder that many water-soluble carbohydrate-appended calixarenes were reported and their properties studied. A recent report on this subject illustrates the state-of-art in this direction.[25]

Gas-Phase and Gas–Solid Interface

The study of host–guest interactions recently expanded from solution chemistry to the gas phase. where solvent effects are not present. allowing better understanding of the intrinsic phenomena responsible for molecular recognition. Many calixarenes were used as hosts in this respect[26,27] using CI MS. The less-demanding approach (at least as far as the instrument costs are concerned) involves the application of GC headspace analysis applied for gas-phase complexation of parent calixarene[28,29] and thiacalixarene.[29]

CONCLUSION

No conclusion can adequately summarize the developments in the topic of this article. Host–guest chemistry is still in its infancy as a typical multidisciplinary subject. The progress in all basic disciplines will immediately provoke progress in the level of our knowledge on molecular complex formation by calixarenes. The synthesis of many new ligands and their thorough study will definitely be required to better understand the multifaceted problem of molecular recognition and complex formation.

NOTE ADDED IN PROOF

Parent *p-tert*-butylcalix[4]arene has been found to undergo unprecedented single-crystal-to-single crystal phase transition upon guest uptake and release. Despite the lack of porosity of the material, guest transport through the solid occurs readily until a thermodynamically stable structure is achieved. In order to actively facilitate this dynamic process, the host molecule undergo significant positional and/or orientational rearrangement. This transformation is triggered by weak van der Waals interaction between host (*p-tert*-butylcalix[4]arene) and guest (vinyl bromide) molecules.

Atwood, J.L.; Barbour, L.J.; Merta, A.: Schottel, A. Guest transport in nonporous solid via dynamic van der Waals cooperativity. Science 2002, 298, 1000–1002.

ARTICLES OF FURTHER INTEREST

The Allosteric Effect, p. 20
Biological Ligands, p. 88
Calixarenes and Their Analogues: Cation Complexation, p. 137
Calixarenes: Synthesis and Historical Perspectives, p. 153
Carbohydrates, Recognition of, p. 169
Cavitands, p. 219
Chiral Guest Recognition, p. 236
Classical Description of Inclusion Compounds, p. 253
Complexation of Fullerenes, p. 302
Concave Reagents, p. 311
Concepts in Crystal Engineering, p. 319
Dendrimers, p. 432
Disorder and Diffuse Scattering, p. 457
Drug Delivery, p. 484
Guanidinium-Based Anion Receptors, p. 615

Homocalixarenes, p. 649
Hydrogen Bonding, p. 658
Hydrophobic Effects, p. 673
Inclusion Compounds: Selectivity, Thermal Stability, and Kinetics. p. 696
Inelastic Neutron Scattering, p. 727
Isostructurality of Inclusion Compounds. p. 767
The Lock and Key Principle. p. 809
Macrocycle Synthesis, p. 830
Molecular Wires. p. 925
Self-Assembling Capsules, p. 1231
Simultaneous Binding of Cations and Anions, p. 1291
Simultaneous Binding of Cations and Neutral Molecules, p. 1295
Solvation Effects in Guest Binding. p. 1322
Strong Hydrogen Bonds. p. 1379
The Template Effect, p. 1493
van der Waals Forces, p. 1550
Weak Hydrogen Bonds, p. 1576
X-Ray Crystallography, p. 1586
Zeolites: Structure and Inclusion Properties: p. 1623

REFERENCES

1. Gutsche, C.D. Filling the Baskets: Complex Formation with Calixarenes. In *Calixarenes*; Monograph in Supramolecular Chemistry: Royal Society of Chemistry: Cambridge, 1989; Vol. 1. 149–185.
2. Gutsche. C.D. Filling the Baskets: Complex Fonnation With Calixarenes. In Calixarenes Revisited: Monograph in Supramolecular Chemistry; Royal Society of Chemistry: Cambridge. 1998: Vol. 6, 169–177.
3. Arduini. A.; Pochini, A.; Secchi, A.: Ugozzoli, F. Recognition of Neutral Molecules. In *Calixarenes* 2001; Asfari, Z.. Bohmer, V., Harrowfield, J., Vicens. J.. Eds.: Kluwer Academic Publisher: Dordrecht, 2001: 457–475.
4. Casnati, A.; Sciotto, D.; Arena. G. Water-Soluble Calixarenes. Ill *Calixarenes* 2001; Asfari, Z., Bohmer. V.. Harrowfield, J., Vicens, J., Eds.; Kluwer Academic Publisher: Dordrecht. 2001: 440–456.
5. Andreetti. G.D.: Ungaro. R.; Pochini. A. Crystal and molecular structure of cyclo{quarter[(5-*t*-butyl-2-hydroxy-1,3-phenylene)methylene]} toluene (1:1) clathrate. J. Chern. Soc., Chem. Commun. 1979. 1005–1006.
6. Brouwer. E.B.; Enright, G.D.; Ratcliffe. C.I.; Ripmeester, J.A.: Udachin. K.A. Dynamic Structures of Host–Guest Systems. In *Calixarenes* 2001: Asfari. Z.. Bohmer, V., Harrowfield. J., Vicens. J., Eds.: Kluwer Academic Publisher: Dordrecht. 2001: 296–311.
7. Arduini, A.; Nachtigall, F.F.; Secchi. A.; Pochini, A.; Ugozzoli. F. Calix[4]arene cavitands: A solid state study on the interactions of their aromatic cavity with neutral organic guests characterised by acid CH_3 or CH_2 groups. Supramol. Chem. 2001. 12, 273–291.
8. Backes, A.C.: Schatz. J.: Siehl. H.-U. GIAO-DFT calculated and experimentally derived complexation-induced chemical shifts of calix[4]arene-solvent inclusion complexes. J. Chem. Soc., Perkin Trans. 2 2002. 484–488.
9. Arduini, A.; Fabbi. M.: Mantovani, M.; Mirone. L.; Pochini, A.; Secchi, A.; Ungaro. R. Calix[4]arenes blocked in a rigid cone conformation by selective functionalization at the lower rim. J. Org. Chern. 1995. *60.* 1454–1457.
10. Smirnov. S.; Sidorov, V.; Pinkhassik, Z.; Havlicek, J.: Stibor. I. Complexes of *p-tert*-butylcalix[4]arene derivatives with neutral molecules: Structure and stabilities. Supramol. Chem. 1997. *8*. 187–196.
11. Arduini, A.: Domiano, L.: Pochini. A.; Secchi. A.: Ungaro. R.: Ugozzoli. F.; Struck. O.; Verboom. W.; Reinhoudt, D.N. Synthesis of 1,2-bridged calix[4]arene-biscrowns in the 1,2-alternate conformation. Tetrahedron 1997. *53*, 3767–3776.
12. Arduini. A.; McGregor, W.M.; Paganuzzi, A.; Pochini, A.; Secchi, A.; Ugozzoli. F.; Ungaro, R. Rigid cone calix[4]-arenes as π-donor systems: Complexation of organic molecules and ammonium ions in organic media. J. Chem. Soc., Perkin Trans 1996. 2. 839–846.
13. Arduini. A.; Giorgi. G.; Pochini. A.; Secchi. A.; Ugozzoli, F. Interaction of the aromatic cavity of rigid calix[4]arene cone conformers with acid CH_3 and CH_2 containing guests in apolar solvents. Tetrahedron 2001. *57.* 2411–2417.
14. Arena, G.: Contino. A.; Magri, A.; Sciotto, D.; Arduini, A.; Pochini, A.: Secchi. A. Energetics of the inclusion of organic molecules by rigidified cone calix[4]arenes in carbon tetrachloride. Supramol. Chem. 2001.13. 379–386.
15. Sidorov. V.: Smirnov. S.: Pinkhassik, E.; Koča, J.; Kovalev, V.V.: Khomich, A.N.; Shokova. E.A.: Lhoták, P.: Stibor. I. Binding of *Neutral* Molecules *by Calix[4]arene Ligands* in *Solution—A Systematic* Approach: unpublished.
16. Haino. T.; Natsumura. K.: Harano, T.; Uamada. K.; Saijyo. Y.; Fukazawa, Y. Synthesis and binding behavior of an artificial receptor based on "Upper Rim" functionalired calix[5]arene. Tetrahedron 1998. 54. 12185–12196.
17. Pinkhassik, E.; Sidorov. V.: Stibor. I. Calix[4]arene-based receptors with hydrogen-bonding groups immersed into large cavity. J. Org. Chem. 1998. *63.* 9644–9651.
18. Arduini. A.; Pochini. A.; Secchi, A. Recognition of amides by new rigid calix[4]arene-based cavitands. J. Org. Chern. 2000. 65, 9085–9091.
19. Arena. G.; Contino, A.: Gulino. F.G.: Magri, A.; Sciotto. D.; Ungaro. R. Complexation of small neutral organic molecules by water soluble calix[4]arenes. Tetrahedron Lett. 2000. 41. 9327–9330.
20. Karakhanov. E.: Buchneva. T.: Maximov, A.; Zavertyaeva, M. Substrate selectivity on byphasic Wacker-oxidation of alkenes in the presence of water-soluble calixarenes. J. Mol. Catal. A 2001. *3416.* 1–7.
21. Shimizu. *S.:* Shirakawa. S.: Suzuki, T.: Sasaki, Y. Water-soluble calixarenes as new inverse phase-transfer catalysts. Their application to aldol-type condensation and Michael addition reaction in water. Tetrahedron 2001. *57,* 6169–6173.
22. Baur. M.: Frank. M.; Schatz, J.: Schildbach. F. Water-soluble calix[*n*]arenes as receptor molecules for non-polar

substrates and inverse phase transfer catalysts. Tetrahedron **2001.** *57,* 6985–6991.

23. Douteau-Guével, N.: Perret, F.; Coleman, A.W.; Morel, J.-P.: Morel-Desrosiers, N. Binding of dipeptides and tripeptides containing lysine or arginine by *p*-sulfonato-calixarenes in water: NMR and microcalorimetric studies. J. Chem. Soc., Perkin Trans. 2 **2002,** 524–532.
24. Fulton, D.A.; Stoddart, J.F. Neoglycoconjugates based on cyclodextrins and calixarenes. Bioconjug. Chem. **2001,** 12, 655–672.
25. Dondoni, A.; Kleban, M.; Hu, X.; Marra, A.; Banks, H.D. Glycoside-clustering round calixarenes towards the development of' multivalent carbohydrate ligands. Synthesis and conformational analysis of' calix[4]arene **O-** and C-glycoconjugates. J. Org. Chem. **2002.** *67,* 4722 4733.
26. Vincenti, M.; Minero, C.; Pelizzetti, E.; Secchi. A.; Dalcanale, E. Host-guest chemistry in the gas phase and at the gas-solid interface: Fundamental aspects and practical applications. Pure Appl. Chem. 1995, 67, 1075–1084.
27. Arduini. A.; Cantoni, M.; Graviani, E.; Poehini, A.; Scchi. A.; Sicuri, A.R.; Ungaro. R.; Vincenti, M. Gas-phase complexation of neutral molecules by upper rim bridged calix[4]arenes. Tetrahedron **1995,** *51,* 599- 600.
28. Gorbatchuk, V.V.; Tsifarkin, A.G.; Antipin, I.S.; Solomonov. B.N.: Konovalov, A.I.; Seidel, J.; Baitalov, F. Thermodynamic comparison of molecular recognition of vaporous guests by solid calixarene and diol hosts. J. Chem. Soc., Pcrkin Trans. 2 **2000.** 2287 22'94.
29. Gorbatchuk, V.V.; Tsifarkin, A.G.: Antipin, I.S.: Solomonov. B.N.; Konovalov, A.I.; Lhoták, P.; Stibor, I. Nonlinear structure-affinity relationships for vapour guest inclusion by solid calixarenes. J. Phys. Chem., B **2002,** 106, 5845–5851.

Calixarenes: Synthesis and Historical Perspectives

C. David Gutsche
Texas Christian University, Fort Worth, Texas, U.S.A.

INTRODUCTION

The modern era of calixarene chemistry had its inception in the early 1970s in the laboratories of Washington University in Saint Louis." Motivated by an interest in designing enzyme mimics but faced with a paucity of easily synthesized basket-like molecules. Gutsche and his research group became intrigued with the compounds involved in an industrial process at the Petrolite Corporation in nearby Webster Groves. In response to a problem of sludge formation in one of the crude oil-demulsifying surfactants marketed by this company. the Petrolite chemists isolated a high melting material that seemed to be similar to compounds described by the Austrian chemist Alois Zinke in the 1940s. Zinke treated various phenols with formaldehyde along with a strong base in boiling linseed oil and obtained materials assumed to be pure entities to which he assigned cyclic tetrameric structures.[b] This conclusion appeared to be substantiated by a rational. stepwise synthesis of a cyclic tetramer by the English chemists Hayes and Hunter[7,8] in the 1950s, although a direct coinparison with the Zinke compound was not made. The first hint of a problem with the Zinke inaterials emerged at about the same time from the work of another English chemist, Sir John Cornforth. who isolated pairs of compounds fi-om *p-tert*-butylphenol and *p*-(1,1,3,3-tetramethylbutyl)-phenol and who noted the extraordinarily capricious nature of the reaction.''' The work of the Gutsche group in the 1970s confirmed the fact of mixtures'''' and showed that by careful control of the reaction conditions, pure samples of the cyclic tetramer, cyclic hexamer, and cyclic octamer can be easily and reproducibly obtained from *p-tert*-butylphenol.[11] The structures of these,[12 14] and now many other calixarenes that have been made, have been firmly established by x-ray crystailographic analyses. Work in many laboratories shows that a number of other phenols also yield cyclic oligomers. although none allow as precise product control as does *p-tert*-butylphenol. Perceiving a visual resemblance between the CPK space-filling model of the cyclic tetramer and a type of Greek vase known as a Calix Crater. the name ''calixarene'' was chosen to define this particular class of [1_n]metacyclophanes, using a bracketed number [*n*] to designate the size of the calixarene, i.e.. calix[4]arene for the cyclic tetramer, calix[6]arene for the cyclic hexamer, etc. The special ease of synthesis of the major calixarenes 1, 3, and 5 (R = *tert*-Bu) followed by the relative ease of synthesis of the minor calixarenes 2 and 4 (R = *tert*-Bu) played a key role in the rapid expansion of the field. bringing dozens of laboratories and hundreds of chemists into the fold of calixarene chemistry. As the early experiments of Hayes and Hunter demonstrated. however. the one-step synthesis is not the only route to calixarenes, and stepwise syntheses, now called fragment condensations, have aiso played a significant role.

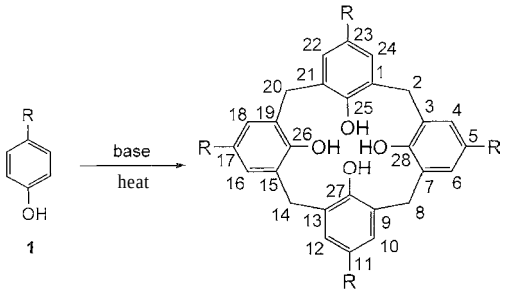

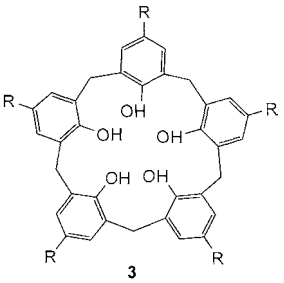

[a]For treatises on calixarenes see Refs. [1–5].
[b]Detailed accounts of the history of the calixarenes arc found in Refs. [5,6].

Encyclopedia of Supramolecular Chemistry
DOI: 10.1081/E-ESMC 120011849

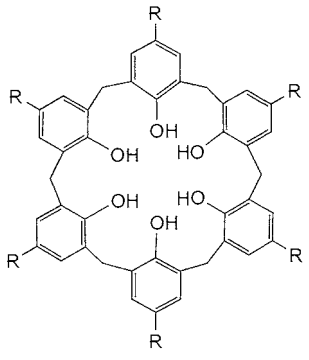

4

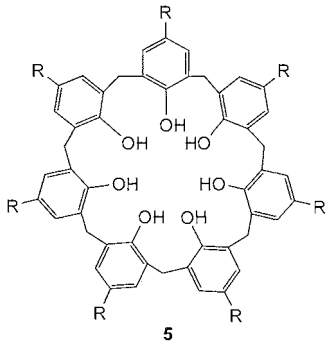

5

SINGLE-STEP CONDENSATION OF PHENOLS AND FORMALDEHYDE

The original Zinke *synthesis employed* NaOH *as the base to induce the condensation of* *p*-alkylphenols *and formaldehyde, and base induction* remains *the method of choice noi only for the three major calixarenes* 2, *4, and* 6 (R = *tert*-Bu) but *also for the* two *minor calixarenes 3 and* 5 (R = *tert*-Bu). *With* NaOH *(in* small *amounts) as the base and* refluxing *diphenyl ether as the solvent, a* 50% *yield of pure* *p-tert*-butylcalix[4]arene *2 is produced.*[16] *With* KOH *(in larger amounts) as the base and* refluxing xylene *as the solvent. ca.* 85% yields *of p-tert*-butylcalix[6]arene *4 are* produced.[16] *With* NaOH *(in small amounts) as the base and* refluxing *xylene as the solvent, ca.* 65% yields *of p-tert*-butylcalix[8]arene 6 *are* produced.[17] *The* *p-tert*-butylcalix[5]arene **3**[18,19] *and* *p-tert*-butylcalix[7]arene **5**[20] *require more effort to synthesize, entailing separation* from *the various other calixarenes* in *the product* mixture, *but are isolable in pure form in yieids of ca.* 15–20%. *Phenols that do* not *yield calixarenes* when *treated with formaldehyde and base include* *p*-nitro, *p-cyano,* *p*-phenoxyphenyl, *p*-carboxy, *p*-acetyl, *p*-hydroxymethyl, *and* *p*-hydroxy (hydroquinone) *Success* is generally limited *to phenols carrying* nondeactivating *p*-substituents *For example, p-*cresol gives *4* (R = *Me) in* 74% yield[21] *or* 5 *(R = Me) in* 22% yield[22] *p*-phenylphenol gives *a* mixture *of 4* (R = *Ph),* 5 (R = Ph), *and* **6** *(R =* Ph),[23] *p*-benzyloxy-*phenol* gives *6* (R = Bn) in 48% yield,[24] *but* p-methoxyphenol *yields a* complex mixture *ol* oligomeric *compounds Phenol, carrying long-cham* *p*-alkyl substit-*uents often* give poor *results.* but *those* carrying alkyl groups highly *branched near the point of attachment at the* *p*-position sometimes react *more* like *p-tert*-butylphe-nol *For example.* *p*-(1,1,3,3-tetramethylbutyl)phenol *gives 2 and 6* (R = 1,1,3,3-tetramethylbutyl) in *modest* yields,[25,26] *and* *p*-adamantylphenol gives *6* (R = ada-mantyl) in 72% *yield* [27]

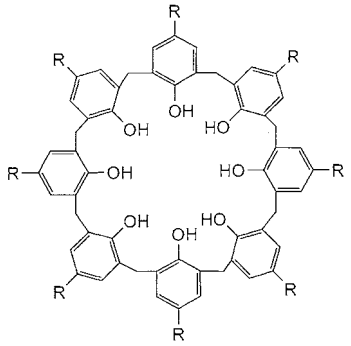

6

For many years, it was thought that no calixarenes larger than $n = 8$ *are formed in the one-step process. However, it* is *now known that calixarenes* with *sires well beyond this can be formed, extending to at least* 20 *aryl* residues.[28] *Although several of the "large" calixarenes* ($n > 8$) *can be obtained via base-induced condensation. an acid-catalyzed reaction provides a better source: treatment of* *p-tert*-butylphenol *with s-trioxane and* *p*-toluenesulfonic *acid in* $CHCl_3$ *solution produces an almost quantitative yield of a calixarene mixture that is richer in the large calixarenes than the product from base* induction.[28]

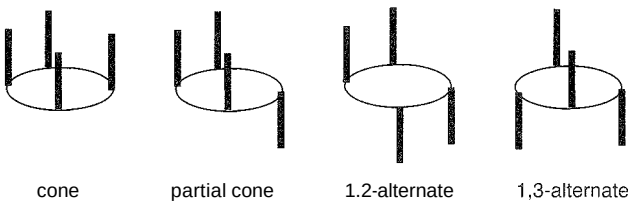

Fig. 1 Conformations *of* calix[4]arenes

One of the interesting characteristics of calixarenes is their ability to assume a variety of conformations in which the aryl groups are oriented *syn* or *anti* with respect to one another. Calix[4]arenes, for example. can assume a cone, partial cone, 1.2-alternate, or 1,3-alternate conformation, and the energy barrier to interconversion among the conformers can be determined by dynamic ^{1}H-NMR spectral measurements (Fig. 1). A study of the entire family of *p-tert*-butylcalix[n]arenes shows that conformational stabilities (i.e., higher barriers to interconversion) reach maxima when n = 4,8,12,16, and 20, probably the result of the interplay of intramolecular hydrogen bonding and molecular packing.[28]

SINGLE-STEP CONDENSATION OF NAPHTHOLS AND BISPHENOLS WITH FORMALDEHYDE

r-Naphthol reacts with formaldehyde in a comparable fashion to p-alkylphenols to furnish calix[4]naphthol **7** along with two positional isomers in which, in contrast to the phenol-derived calixarenes. all of the OH groups are *exo* rather than *endo* to the annulus.[29–32] Analogously. 1,8-naphthalene-sultone 8 yields the sulfonated calix[4]naphthalene 9. Bisphenols of the general structure **10** (m = 0, 2, and 3) produce calixarenes **11** (a = 2 and 3) upon reaction with paraformaldehyde in the presence of bases including NaOH. KOH. and CsOH.[33–38]

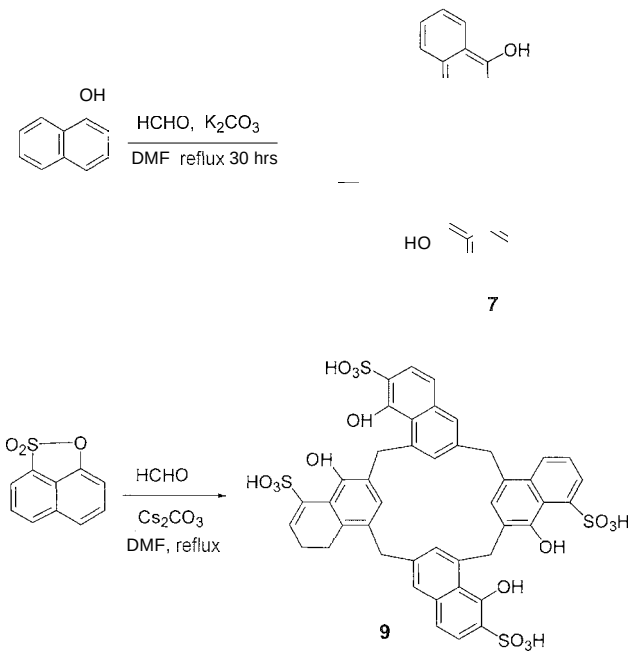

MECHANISM OF BASE-INDUCED CALIXARENE FORMATION

Although the mechanism of the base-induced formation of calixarenes has been studied in some detail, the reaction pathways remain uncertain. The most intuitively reasonable proposal is that the immediate precursor of any particular calixarene, regardless of size, is the linear oligomer carrying the requisite number of aryl residues. Another proposal, however, postulates that calix[8]arenes, for example, arise from intermolecularly hydrogen-bonded dimers (hemicalixarenes) formed from a pair of crescent-shaped, intramolecularly hydrogen-bonded linear tetramers.[3] Calix[4]arenes, formed under considerably more strenuous conditions. have been postulated to be the result not of direct cyclization of the linear tetramer but of reversion of the calix[8]arene.[39] The cyclic octamer is viewed as the product of kinetic control, and the cyclic tetramer is viewed as the product of thermodynamic control. The particular efficacy of KOH and RbOH for the formation of calix[6]arenes suggests that the hexamer is the product of template control.

SINGLE-STEP CONDENSATION OF RESORCINOLS AND ALDEHYDES

Concurrent with Zinke's work with phenols and base in the 1940s was Niederl's[40,41] reinterpretation of the structures of the products formed by the acid-catalyzed reaction of resorcinol and aldehydes, which he postulated to be cyclic tetramers 12. The cyclic tetrameric structure was conclusively established in 1968 by Erdtman[42] through x-ray crystallographic analysis, and the synthesis of the Niederl tetramers was greatly improved through the work of Högberg[43,44] in the 1980s. A wide variety of aldehydes were condensed with resorcinol and substituted resorcinols, including aliphatic aldehydes (saturated, unsaturated, functionalized). aromatic aldehydes [with R. OH. NO_2, halogen; CN, NH_2, RCO, and $B(OR)_2$ substituents]. heterocyclic aldehydes, and ferrocenylaldehyde. Failing to yield cyclic tetramers are HCHO (which forms a polymeric glue), highly hindered aldehydes such as 2,4,6-trimethylbenzaldehyde, and aldehydes containing functionality proximate to the CHO, such as $ClCH_2CHO$. Employing the Wiederl coinpounds as starting materials. Cram elaborated them into enforced baskets called cavitands, and these, in turn, into hollow spheres called

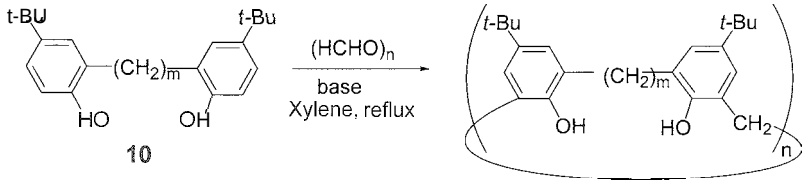

10 11

carcerands, capable of incarcerating molecules with no way of escape.[45]

NOMENCLATURE

The name "calixarene" (the prefix ***calix*** because of the vase-like shape of the cyclic tetramer; the suffix *arene* because of the aryl groups in the cyclic array) most accurately describes the shape of the cone conformers, of the cyclic tetramers and cyclic pentamers. However, the descriptor is less apt for the other three conformers. of these two calixarenes as well as for the larger members of the series that can assume a wide variety of conformations. Nevertheless, calixarene provides a convenient name for the entire extended family of cyclooligomers in which aryl (or heterocyclic) moieties are connected at the 1 and 3 positions by bridging moieties. Thus, the phenol-derived. naphthol-derived, and resorcinol-derived cyclooiigomers belong to the calixarene family and are appropriately named calix[*n*]phenarenes, calix[*n*]-naphtharenes, and calix[*n*]resorcarenes, respectively. The first of this group. however, are more generally designated simply as calix[*n*]arenes, the second as calix[*n*]naphthalenes, and the last as resorc[*n*]arenes which. lamentably lacking the prefix calix. belies their membership in the family. Substituents attached to calixarenes are specified as being on the upper (or wide) rim or on the lower (or narrow) rim. The OH groups of p-*tert*-butylcalix[4]arene, for example, are on the lower rim, and the tert-butyl groups are on the upper rim. When applying systematic nomenclature to a calixarene compound; the calixarene descriptor is taken to designate only the basic carbon framework, and all substituents (OH, tert-butyl, etc.) are specified by name and position. Thus, *p-tert*-butylcalix[4]arene becomes 5.11,17,23-tetra-*tert*-butylcalix[4]-25,26,27,28-tetrol; the calix[4]resorcarene derived from acetaldehyde becomes 2,8,14,20-tetramethylcalix[4]arene-4,6,10,12, 16.18,22,24-octol.

STEPWISE SYNTHESIS OF CALIXARENES

The multistep synthesis of calixarenes. introduced by Hayes and Hunter[7,8] and perfected by Kämmerer,[46] has been largely supplanted by the more convergent approaches for which the terms "fragment condensation" and "directed synthesis" have been applied by Böhmer.[47] In a ''3 + 1'' fragment condensation[48–50] for synthesizing **15** a linear trimer **13** is condensed with a monomer 14, one or the other of these units carrying a pair of appropriately placed hydroxymethyl or halomethyl groups. In similar fashion. a ''2 + 2'' fragment condensation[51] involves the reaction of the two linear dimers **16** and **17**. Other variations on the fragment condensation include ''2 + 1 + 1'' and ''1 + 1 + 1 + 1'' processes for the synthesis of calix[4]arenes (15), "3 + 2'' and "4 + 1'' processes for calix[5]arenes, "3 + 3'' processes for calix[6]arenes, etc. The major advantage of the fragment condensation over the one-step process resides in the control that it affords over the identity of the *p*-substituents. The major disadvantage is that it is generally more time consuming and provides lower yields, often in the 15–30% range, sometimes lower than 15% and rarely higher than 40%.

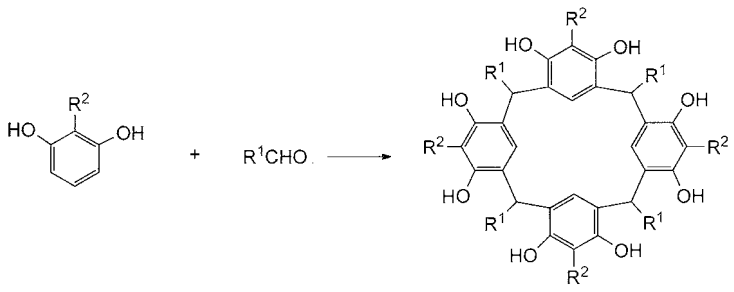

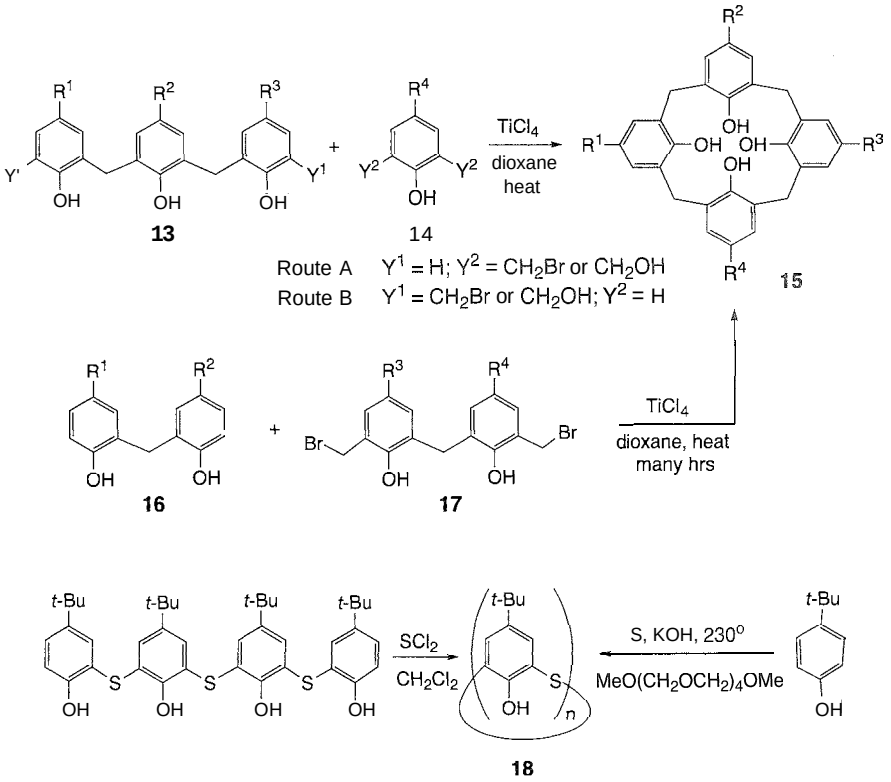

THIACALIXARENES

When p-tert-butylphenol. elemental sulfur, and NaOH are heated at 230°C in tetraethylene glycol dimethyl ether, the thiacalixarene 18 is produced in better than 50% yield [52 53] The same material was rynthesized in stepwise fashion but in far lower overall yield [54]

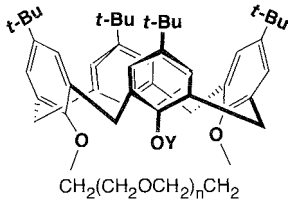

19

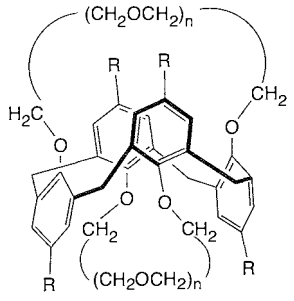
20

FUNCTIONALIZATION OF CALIXARENES

The *p-tert*-butylphenol, in addition to making the major and minor calixarenes readiiy available. provides these compounds in an easily functionalized form. The OH groups on the lower rim can be directly converted to a wide variety of esters and ethers. The tert-butyl groups on the upper rim can be readily removed by treatment with $AlCl_3$ and then replaced by a wide variety of functional groups. In this fashion. hundreds of calixarenes have been prepared carrying all manners of groups on the two riins. Saryl groups themselves have been achieved, as exemplified by the calixspirodienones.[55] Among the many interesting examples of functionalized calixarenes are the calix crowns, in which crown-ether moieties are introduced onto pairs of OH groups, as illustrated by 19 and 20.

CALIXARENE-RELATED COMPOUNDS

The calixarene family has become increasingly extended with the passage of time. and a variety of compounds now claim membership. Among the present family members.

inter alia. are homocalixarenes **21**,[56] homooxacalixarenes **22**.[57] homoazacalixarenes **23**,[58] calixfurans **24**,[59] calixpyrroles **25**,[60] calixthiophenes **26**,[61] and silacalixarenes 27 [62]

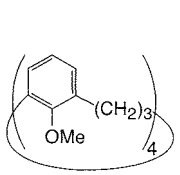

21

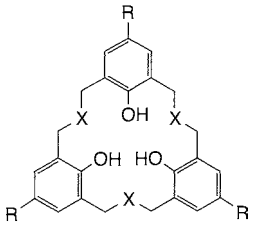

22 X = O

23 X = NR

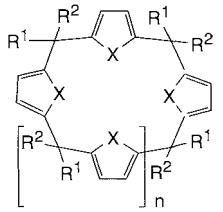

24 X = O

25 X = NH

26 X = S

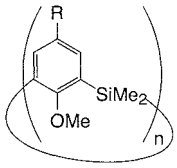

27

APPLICATIONS OF CALIXARENES

Among the early commercial applications of calixarenes are their use by the Petrolite Corp as demulsifiers and the Loctite Corp as adhesive moderators. Among the more recent commercial applications is the sequestration of cesium ions from nuclear wastes, using calix crowns such as 19. Much of the intense research activity in calixarene chemistry during the last decade focused on the ability of appropriately functionalized calixarenes to form complexes. In addition to complexation with cesium cation, the complexation of many other cations of the elements in the periodic table has been studied; with the promise of useful applications.[63] Complexation of anions as well as molecules has also been demonstrated. the latter providing the basis for investigations of enzyme mimics. Particularly interesting applications are illustrated by the wide variety of sensors that take advantage of the complexation properties of calixarenes.[2] Calix[4]arenes fixed in a cone conformation by large OR groups on the lower rim provide rigid platforms from which metal-based catalysts can be elaborated.[64] Two hundred or more patents have been issued in which calixarenes play the central role and deal. inter alia. with adhesion promoters. electrophotographic photoreceptors, photographic toners. hair dyes. diesel fuel additives. curing agents. antistatic agents. antioxidants. stabilizers. temperature-sensing devices. pressure-sensitive recording materials. flame-proofing compounds. safety glass composition, optical recording materials. and antibacterial agents.

CONCLUSION

Calixarenes. now easily synthesized on any scale in a variety of ring sizes by the one-step process and also accessible by the more flexible fragment condensation process. have taken their place alongside the cyclodextrins and crown ethers as the dominant ring structures in host–guest chemistry. Research in the field of calixarene chemistry continues at a rapid pace throughout the world, and new. interesting: and useful applications of these molecules are certain to be revealed in the years ahead.

ARTICLES OF FURTHER INTEREST

Calixarenes and Their Analogues: Cation Complexation, p. 137
Carcerands and Hemicarcerands, p. *189*
Concave Reagents, p. 311
Crown Ethers. p. *326*
Cryptophanes, p. 340
Cyclodextrins, p. 398
Cyclodextrins, Applications. p. 405
Cyclophanes: Definition and Scope, p. 414
Enzyme Mimics. p. 546
Macrocycle Synthesis, p. 830
Organometallic Anion Receptors, p. 1006
Soft and Smart Materials, p. *1302*
X-Ray Crystallography, p. *1586*

REFERENCES

1. *Calixarenes* 2001; Asfari, Z.. Böhmer. V.. Harrowfield, J.. Vicens. J.. Eds.: Kluwer Academic Publishers: Dordrecht. 2001.
2. *Calixarenes* in *Action*: Ungaro, R., Mandolini. M., Eds.; Imperial College Press: London. 2000: 37–143.
3. Gutsche. C.D. Calixarenes Revisited. In *Monographs in Supramolecular Chemistry*; The Royal Society of Chemistry: Cambridge. 1998: 50–58.
4. *Calixarenes: A Versatile Class of Macrocyclic Compounds*: Vicens. J., Bohmer. V., Eds.: Kluwer Academic Publishers: Dordrectht. 1991.
5. Gutsche, C.D. Calixarenes. In *Monographs in Supramolecular Chemistry*; The Royal Society of Chemistry: Cambridge, 1989; 1–26.

6. Kappe, T. The early history of calixarene chemistry. J. Inclusion Phenom. Mol. Recognit. Chem. 1994. *19*. 3–15.
7. Hayes. B.T.: Hunter. R.F. Rational synthesis of cyclic tetranuclear *p*-cresol novolak. Chem. Ind. 1956. 193.
8. Hayes. B.T.; Hunter. R.F. Phenol-formaldehyde and allied resins VI: Rational synthesis of a 'cyclic' tetranuclear *p*-cresol novolak. J. Applied Chern. 1958. *8*. 743.
9. Cornforth, J.W.: D'Arcy Hart. P.D.; Nicholls, G.A.: Rees. R.J.W.: Stock. J.A. Antituberculosis effects of certain surface-actixe polyoxyethhylene ethers. Br. J. Pharmacol. 1955. *10*. 73.
10. Gutsche. C.D.: Muthukrishnan. R. Calixarenes. I. Analysis of the product mixtures produced by the base-catalyzed condensation of formaldehyde with para-substituted phenols. J. Org. Chem 1978. 43. 4905.
11. Gutsche. C.D.: Dhawan. B.; No. M.H.; Muthukrishnan. R. The synthesis. characterization. and properties of the calixarenes from *p-tert*-Butylphenol. J. Am. Chem. Soc. 1981. *103*. 3782.
12. Andreetti. G.D.: Ungaro. R.: Pochini. A. Crystal and molecular structure of cyclo {quater[5-*t*-butyl-2-hydroxyo-1.3-phenylene)methylene]] toluene {1:1} clathrate. J. Chem. Soc. Chem. Commun. 1979. 1005.
13. Andreetti. G.D.: Pochini. A.: Ungaro. R. Molecular inclusion in functionalized macrocycles. Part 6. The crystal and molecular structures of the calix[4]arene from p-(1,1,3,3-tetramethylbutyl)phenol and its 1:1 complex with toluene. J. Chem. Soc., Perkin Trans. 1983. 2. 1773.
14. Gutsche. C.D.: Cutsche, A.E.: Karaulov, A.I. Calixarenes. 11. Crystal and molecular structure of *p-tert*-Butylcalix[8]-arene. J. Inclusion Phenom. 1985. 3. 447.
15. Gutsche. C.D.; Iqbal. M. *p-tert*-Butylcalix[4]arene. Org. Synth. 1990. *68*. 234.
16. Cutsche. C.D.: Dhawan. B.: Leonis. M.; Stewart. D. *p-tert*-Butylcalix[6]arene. Org. Synth. 1990. 68. 238.
17. Munch, J.H.: Cutsche, C.D. *p-tert*-Butylcalix[8]arene. Org. Synth. 1990. 68. 243.
18. Stewart. D.R.: Gutsche. C.D. The one-step synthesis f *p-tert*-Butylcalix[5]arene. Org. Prep. Proced. Intl. 1993. *25*, 137.
19. Iwamoto, M.; Araki, M.: Shinkai, S. Improved synthesis of 5.11,17,23,29-penta-*t*-butylcalix[5]arene-31,32,33,34,35-pentol and immobilization of the conformation by O-alkylation. Bull. Chern. Soc. Jpn. 1994. *67*. 1499.
20. Vocanson, F.: Lamartine, R.: Lanteri. R.; Longeray. R.: Gauvrit, J.Y. Synthese du *p-tert*-Butylcalix[7]arene. Optimisation du rendement par la methode des plans d'experiences. Neu J. Chem 1995. *19*. 825.
21. Seki. Y.; Morishige. Y.: Wamme. N.; Ohnishi. Y.: Kishida. S. Nonpolymer new organic film for local insulation in laser-directed circuit restructuring for large-scale circuits. Appl. Phys. Lett 1993. *62*. 3375.
22. Asfari. Z.; Vicens. J. isolation and characterization of bis-homooxacalix[4]arene from condensation product of 4-octadecylphenol with formaldehyde. Makromol. Chem. Rapid Commun. 1989. *10*. 181.
23. Stewart. D.R.; Gutsche. C.D.. unpublished observations.
24. Casnati. A.; Ferdani. R.: Pochiiii. A.; Ungaro. R. *p*-(Benzyloxy)calix[8]arenes: One-pot synthesis and functionalization. J. Org. Chem 1997. *62*. 6236.
25. Foina. *D.:* Pochini. A.: Ungaro. R.: Andreetti. G.D. Isolation and characterization of calix[4]arene from the condensation product of 4-(1,1,3,3-tetramethylbutyl)phenol and formaldehyde. Makromol. Chem. Rapid Commun. 1983. *4*. 71.
26. Bocchi. V.: Foina. D.: Pochini. A.: Ungaro. R.; Andreetti, G.D. Synthesis. ^{1}H NMR, ^{13}C NMR spectra and conformation preferences of open chain ligands on lipophilic macrocycles. Tetrahedron 1982, *38*. 373.
27. Lubitov, I.E.: Shokova. E.A.: Kovalev, V.V. New class of host molecules, *p*-1-adamantylcalix[8]arenes. Synlett. 1993. 647.
28. Stewart. D.R.: Gutsche. C.D. Isolation. characterization, and conformational characteristics of *p-tert*-Butylcalixp[9-20]arenes. J. Am. Chem. Soc 1999. *121*. 4136.
29. Georghiou. P.E.: Li, Z. Calix[4]naphthalenes: Cyclic tetramers of 1-naphthol and formaldehyde. Tetrahedron Lett. 1993. *34*. 2887.
30. Georghiou. P.E.; Li. Z. Conforinational properties of the calix[4]naphthalenes. J. Inclusion Phenorn. Molec. Recognit. Chem. 1994, 19. 55.
31. Georghiou. P.E.: Ashram. M.: Li. Z.: Chaulk. S.G. Synthesis of calix[4]naphthalenes derived from 1-naphthol. J. Org. Chem. 1995. *60*. 7284.
32. Georghiou. P.E.: Li. Z.: Ashram. M.: Miller. D.O. Synthesis of dihomacalix[4]naphthalenes: First members of a new class of [1.2.1.2](1,3)naphthalenophanes. J. Org. Cliem. 1996. *61*. 3865.
33. Yamato. *T.:* Saruwatari. Y.: Nagayama, S.: Maeda. M.: Tashiro, M. Preparation and conformational properties of tetrahydroxy[3.1.3.10]-metacyclophanes. J. Chem. Soc. Chem. Commun. 1992. 861.
34. Yamato. T.: Saruwatari, Y.; Doemekpor, L.K.; Hasegawa, K.-I.: Koike. M. Preparation and conformational studies of ethylene-bridge calixarene-analogous macrocyclic metacyclophanes. Chem. Ber. 1993. *126*. 2501.
35. Yamato, T.: Hasegawa, K.-I.: Saruwatari. Y.: Doamekpor, L.K. Novel spherancl-type calixarenes—Synthesis, conformational studies. and isomer separation. Chem. Ber. 1993. *126*. 1435.
36. Yamato. T.: Yasumatsu. M.: Saruwatari. Y.; Doamekpor, L.K. Synthesis and ion selectivity of macrocyclic metacyclophanes analogous to spherand-type calixarenes. J. Inclusion Phenorn. Molec. Recognit. Chem. 1994. *19*, 315.
37. Yamato. T.: Zhang, F.; Yasumatsu. M. Isolation of a cyclic octainer in the caesium hydroxide catalysed calixarene condensation of a dihydroxybiphenyl. J. Chem. Res. Synop. 1997. 466.
38. O'Sullivan. P.: Bohmer. V.: Vogt. W.; Paulus, E.F.; Jakobi. R.A. Diasteoselective functionalization of a spherand-type calixarene. Chem. Ber. 1994. *127*. 427.
39. Gutsche. C.D.; Johnston. D.E., Jr.: Stewart. D.R. Pathways for the reversion of *p-tert*-Butylcalix[8]arene to *p-tert*-Butylcalix[4]arene. J. Org. Chem. 1999. 64, 3717.
40. Niederl. J.B.: Vogel, H.J. Aldehyde-resorcinal condensations. J. Am. Chem. Soc. 1940. *62*. 2512.

41. Niederl, J.B.: McCoy, J.S. Indirect phenol-aldehyde condensations. J. Am. Chem. Soc. 1943, *65*. 629.
42. Erdtman. *H.:* Högberg, S.: Abramson. S.: Nilsson. B. Cyclooligomeric phenol-aldehyde condensation products. Tetrahedron Lett. 1968. 1679.
43. Högberg, A.G.S. Two stereoisomeric macrocyclic resorcinol-acetaldehyde condensation products. J. Org. Chem. 1980. *45*. 4498.
44. Högberg, A.G.S. Stereoselective synthesis and DNMR study of two 1,3,15,22-tetraphenyl[14]metacyclophan-3,5,10, 12,17,19,24,26-octols. J. Am. Chem. Soc. 1980, *102*. 6046.
45. Cram, D.J.: Cram. J.M. Container Molecules and Their Guests. In *Monographs in Supramolecular Chemistry*; Stoddart, J.F., Ed.: Royal Society of Chemistry: Cambridge, 1994.
46. Kammerer. H.; Happel, G. *Weyerhaeuser* Science *Symposium* on Phenolic Resins, 2; Weyerhaeuser Publishing Co.: Tacoma. 1981: 143.
47. Böhmer, V. Special calixarenes by directed synthesis. Liebigs Ann./Recueil 1997. 2019.
48. Bohmer. V.: Chhim, P.: Kämmerer, H. A new synthesis access to cyclic oligonuclear phenolic compounds. Makromol. Chern. 1979, 180. 2503.
49. Bohmer. V.; Marschollek, F.: Zetta. L. Calix[4]arenes with four differently substituted phenolic units. J. Org. Chem 1987, *52*. 3200.
50. Zetta. L.: Wolff. A.; Vogt. W.: Platt, K.-L.: Bohmer. V. Asymmetrically substituted calix[4]arenes: A two-dimensional proton NMR study of a tetraester derivative in the cone conformation. Tetrahedron 1991, *47*. 1911.
51. Böhmer, V.; Merkel, L.; Kunz, U. Asymmetrically substituted calix[4]arenes. J. Chem. Soc. Chem. Commun. 1987. 896.
52. Kumagai, H.: Hasegawa. M.; Miyanari. S.: Sugawa. Y.: Sato. Y.; Hori, T.; Ueda, S.; Kamiyama, H.; Miyano, S. Facile synthesis of *p-tert*-Butylthiacalix[4]arene by the reaction of *p-tert*-Butylphenol with elemental sulfur in the presence of a base. Tetrahedron Lett. 1997, *38*. 3971.
53. Iki, H.: Kabuto. C.: Fukushima. T.; Kuniagai. H.; Takeya. M.; Miyanari. S.: Miyashi. T.; Miyano. S. Synthesis of *p-tert*-Butylthiacalix[4]arene and its inclusion property. Tetrahedron 2000. *56*. 1437.
54. Sone. T.: Ohba, Y.; Moriya, K.; Kumada. H.; Ito. K. Synthesis and properties of sulfur-bridge analogs of *p-tert*-Butylcalix[4]arene. Tetrahedron 1997. *53*. 10689.
55. Aleksiuk. O.: Grynszpan. F.: Litwak. A.M.: Biali, S.E. Spirodienone calixarene derivative. New J. Chem. 1996. *20*. 473.
56. Ibach, S.; Prautzsch. V.: Vögtle, F.: Chartroux. C.: Gloe. K. Homocalixarenes. Acc.Chem. Res. 1999, 32. 729.
57. Tsubaki. K.; Otsubo, T.; Tanaka. K.; Fuji, K. Stepwise construction of some hemahomooxacalix[3]arenes and their conformations in solid state. J. Org. Chern. 1998. *63*. 3260.
58. Hampton. P.D.: Tong, W.: Wu. S.: Duesler. E.N. Synthesis, x-ray structure. and alkali-metal binding properties of a new hexahomotriazacalix[3]arene. J. Chem. Soc. Perkin Trans. 1996. *2*. 1127.
59. Chastrette. *M.;* Chastrette, F.; Sabadie. J. 2.2.7.7.12.12. 17,17-Octamethyl-21,22,23,24-tetraoxaperhydroquaterene. Org. Syn. 1977. *57*. 74.
60. Anzenbacher, P.: Jursíková, K.; Lynch. V.M.: Gale. P.A.: Sessler. J.L. Calix[4]pyrroles containing deep cavities and fixed walls. Synthesis structural studies, and anion binding properties of the isomeric products derived from the condensation of p-hydroxyacetophenone and pyrrole. J. Am. Chern. Soc. 1999, *121*. 11020.
61. Ahmed, *M.;* Meth-Cohn. O. The preparation and properties of thiophene analogues of porphyrins and related systems. Part III. J. Chem. Soc. (C) 1971. 2104.
62. Yoshida. M.; Goto, M.; Nakanishi, F. Silicon-bridge metacyclophanes as parent compounds of silacalix[*n*]-arenes. Synthesis, structures, and confrmational analysis by semiempirical MO calculations. Organometallics 1999. *18*, 1465.
63. *Calixarenes fur Separations*; Lumetta. G.J., Rogers, R.D.. Gopalan, A.S., Eds.: ACS Symposium Series 757. American Chemical Society: Washington. DC, 2000.
64. Guillemot. G.: Solari, E.: Scopelliti, R.; Floriani. C. Molybdenum(IV)-d^2 reactivity in a quasiplanar oxo-environment modeled by calix[4]arene: The reductive cleavage of N=N double bond and the formation of 1-metallocyclopropene from the corresponding alkyne complexes. Organometallics 2001. *20*. 2446.

The Cambridge Structural Database

Frank H. Allen
Karen J. Lipscomb
Cambridge Crystallographic Data Centre (CCDC), Cambridge, United Kingdom

INTRODUCTION

The Cambridge Structural Database (CSD) is the world's repository of crystal structure data for organic and metal–organic compounds. In addition to the primary results of each diffraction experiment. the CSD also contains bibliographic and chemical text, two-dimensional (2D) chemical structural diagrams, and any crystal properties that are available in the formal publication. The CSD will exceed 300,000 structural entries during 2003. The CSD System comprises the database together with software for the search and retrieval of information, structure visualization and data analysis. and is distributed to scientists in 56 countries worldwide. The CCDC is also developing structural knowledge bases derived from the CSD: IsoStar is a knowledge base of intermolecular interactions, and Mogul is a knowledge base of intramolecular geometry (bond lengths, valence angles, and torsion angles). The CSD is widely used as a basis for fundamental research, and nearly 1000 papers in the open literature are collated in a subsidiary database that is freely available via the CCDC web site.

BACKGROUND

The value of crystal structure data to the understanding of supramolecular processes is inestimable, because a crystal structure is the archetypal supermolecule. X-ray and neutron diffraction are the only experimental techniques that routinely generate precise and detailed information about nonbonded interactions at atomic resolution. This information forms the basis for the recognition, description and understanding of the key interactions through which molecules associate in the condensed phase, an understanding that is vital in supramolecular synthesis: crystal engineering, and the study and prediction of protein–protein and protein–ligand interactions.

In October 2001. the CCDC archived its 250,000th small-molecule crystal structure to the Cambridge Structural Database (CSD),[1,2] and this total will exceed 300,000 structures during 2003. The ongoing creation and maintenance of the CSD has been the CCDC's core activity since its inception in 1965. The CSD System, the database together with associated access software,[1,3] is now widely used in industry and in academic institutions in 56 countries.

The CCDC began life in the Department of Chemistry, University of Cambridge, U.K., with the aim of compiling a database of small-molecule crystal structures, i.e., organics and metallo-organics, determined using x-ray and neutron diffraction. A specific aim was to store the key numerical results of each analysis (cell parameters, atomic coordinates, etc.), which are embellished with chemical and bibliographic information, together with any physical and biological property data that can be gleaned from published crystal structure reports. In the late 1960s, just a few hundred structures were published each year, but fueled by scientific and technological advances, annual totals increased to more than 20,000 structures since 2001.

Early software development centered on systems for validating and storing crystal structure data. but systems for search, retrieval, analysis, and visualization began to be developed in the late 1970s and were significantly upgraded over recent years.[3] During the 1990s, the CCDC began to develop structural knowledge bases derived from the CSD and other data. The first of these. IsoStar—a knowledge base of information about intermolecular interactions,[4]—has been available since 1997, and Mogul, a knowledge base of intramolecular geometry, will be available during 2004. Since the late 1970s, the CSD has been increasingly used as a basis for fundamental research in structural chemistry,[5,6] crystal chemistry,[5] and the life sciences,[7] and nearly 1000 papers use CSD data as the basis for detailed research investigations. References to these applications are gathered in a database, DBUse,[5] which is available via the CCDC web site at http://www.ccdc.cain.ac.uk/dbuse.

INFORMATION CONTENT OF THE CSD

Each crystal structure forms an entry in the CSD and is identified by a CSD reference code (refcode). e.g., BAGFIT02. Six letters identify the chemical compound.

DOI: 10.1081/E-ESMC 120012882

and two suppleinentary digits identify additional determinations of the same structure. e.g., an improved refinement. studies by different scientists, studies under different experimental conditions, etc. The information content of each entry is summarized in Table 1.

The most important information item added by CCDC staff is the 2D chemical structure representation, which forms the basis for 2D and three-dimensional (3D) substructure searching[3] at the molecular and supramolecular levels. To increase the speed of these searches, each connection table is analyzed in order to assign cyclic/acyclic flags to bonds and to generate a bitmap or "screen" record. This contains codified yes/no information indicating the presence or absence of specific substructural features in each chemical diagram. e.g., atoms with specific connectivity patterns, coinmon functional groups, rings of specific sizes and constitutions, etc. The screens then act as search heuristics: screens generated from a search substructure must all be present in a candidate CSD entry before that entry is further analyzed using cpu-intensive atom-by-atom and bond-by-bond substructure matching. Bit screens are also generated from other CSD information fields, including text fields, for similar reasons.

Table I Information content of the Cambridge Structural Database.

Bibliographic and chemical text
Compound name(s): systematic and trivial
Amino-acid sequence for peptides
Chemical formula
Author name
Journal name and literature citation
Text indicating special experimental conditions or results (e.g., neutron study, powder study, polymorph, nonambient temperature or pressure, absolute configuration determined. etc.)
Chemical class (e.g., alkaloid. steroid. etc.)
Text comment concerning disorder and errors located during validation
Crystal data
Cell dimensions and standard uncertainties
Space group and symmetry operators
Reduced-cell parameters
Z' (number of chemical entities per asymmetric unit)
Calculated density
Chemical connection table
Formal two-dimensional chemical structure diagram in terms of atom and bond properties. Bond types used in the CSD are single, double, triple, quadruple (metal–metal), aromatic. delocalized double, and π-bonds
Bit-encoded screen records (see text)
Crystal structure data
Atomic coordinates and standard uncertainties

DATA ACQUISITION

Until the mid-1990s much of the information entering the CSD was laboriously retyped from coordinate listings in published papers or associated deposition documents. All that has now changed since the universal acceptance of the Crystallographic Information File (CIF) format,[8] adopted as an international standard for the electronic interchange of crystal structure data by the International Union of Crystallography in 1991. Most major journals now require electronic data deposition using the CIF, and 90% of new structures now enter the CSD processing system via this route. The CCDC currently acts as the official depository for over 70 journals, receiving data at the same time as the associated manuscript is submitted for publication. Full details of CSD data deposition facilities can be found at http://www.ccdc.cam.ac.uk/conts/depositing.html. The vast majority (>99%) of CSD entries arise from published work abstracted from the 1011 cited journals. However, the CCDC also encourages Personal Communications of data that would otherwise be lost to the scientific community. Only 262 such entries were archived in the period up to 1995. but since the general acceptance of the CIF. a further 1286 structures were deposited via this route.

DATA PROCESSING AND VALIDATION

The addition of chemical information forms a vital part of CSD data-processing activities. This involves the encoding of chemical connectivity data via the generation of a formal 2D chemical diagram and the checking or adding of chemical compound names and any common synonyms. Scientific Editors also add bibliographic data. together with any other CSD information that may be in the printed paper but not recorded in the CIF.

Complete information, crystallographic and chemical. is then validated using the CCDC program PreQuest. The principal checks carried out are self-consistency of crystal data (i.e., cell parameters, Z-value and density) and chemical constitution; a cross-check that the atomic connectivity derived from the coordinate data and standard covalent radii matches that in the encoded 2D chemical diagram; self-consistency of the geometry calculated from the atomic coordinates with the published geometry; and a check that there are no unreasonably short intermolecular contacts or any large unexplained voids in the extended crystal structure, perhaps indicative

Table 2 CSD entry statistics (June 1, 2003)

	Structures	%
Total number of structures	291,965	100.0
Number of different compounds	264,576	—
Number of literature sources	1011	—
Organic structures	128,367	44.0
Transition metal present	141,449	48.4
Li–Fr or Be–Ra present	16,080	5.5
Main group metal present	19,058	6.5
3D coordinates present	261,622	89.6
Error-free coordinates	255,795	97.8[a]
Neutron studies	1155	0.4
Low/high temperature studies	75,124	25.7
Absolute configuration determined	5376	1.8
Disorder present in structure	55,415	19.0
Polymorphic structures	9384	3.2
R-factor <0.100	264,903	90.7
R-factor <0.070	225,763	77.3
R-factor <0.050	144,027	49.3
R-factor <0.030	24,422	8.4
Average *N*(atoms)/structure in 2002[b]	75	—
Data added in 2002 (Mb)[c]	95	—

[a]Taken as a percentage of structures for which coordinates are present in the CSD.
[b]Data for 1970. 1980. 1990. 2000 were 27. 44. 53. 73 atoms. respectively.
[c]Data for 1970, 1980. 1990. 2000 were 2. 14. 29, 84 Mb, respectively.

of an incorrect space group or missing solvent molecule(s). Any unresolved errors are referred back to the original author(s) for clarification. Editors also resolve issues connected with crystallographic disorder and add text remarks concerning special aspects of the crystallographic experiment or its results.

STATISTICS

Some summary statistics for the CSD as of October 30, 2001 are given in Table 2, and more detailed information is presented elsewhere.[2] Shown in Fig. 1 is the cumulative rate of growth of the CSD for the period 1970–2000. These data can be analyzed to reveal two related facts: the time taken for the CSD to double its number of entries increased from 3.6 years in the 1980s to 8.0 years in 2001; and continuation of current trends indicates that the CSD will archive its 500,000th structure during the year 2010. However, these projections cannot take account of increased publication rates due to improved technology or any changes that may occur in methodologies for placing crystal structure data into the public domain.

CSD SYSTEM SOFTWARE

The distributed CSD System comprises the database, together with software for search. retrieval. visualization, and analysis of CSD content.

Searching The CSD: The ConQuest Program

ConQuest provides search, retrieval. and display facilities for the CSD.[3] Individual queries can be set up to interrogate the bibliographic, chemical text, and crystal data fields listed in Table 2, and, in particular, the program provides extensive graphical facilities for the definition of 2D and 3D substructure searches. The 2D searches interrogate the chemical connection tables alone, while

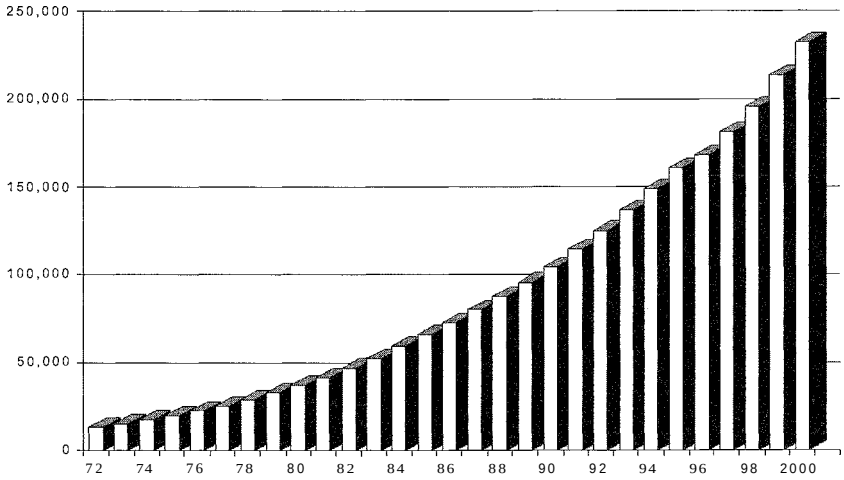

Fig. 1 Growth of the CSD over the period 1970–2000.

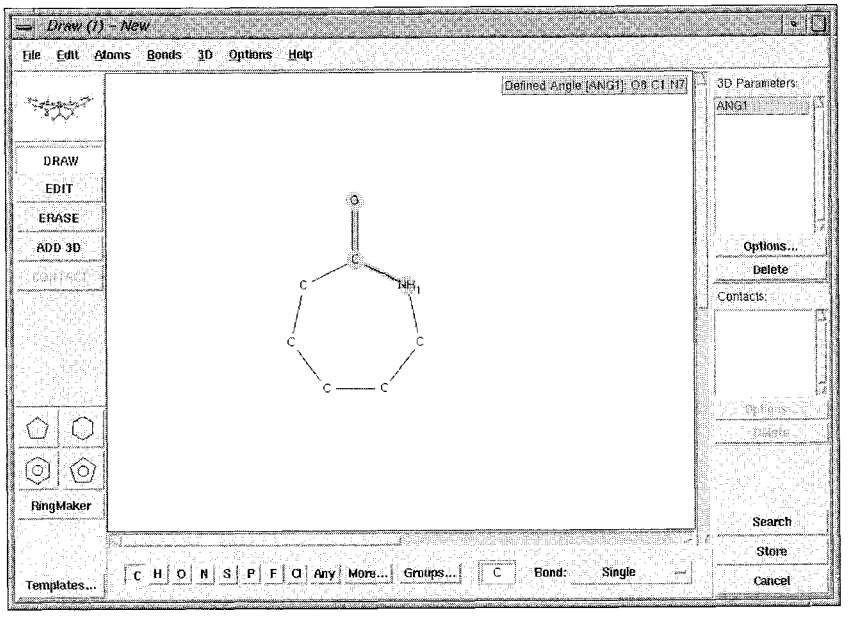

Fig. *2* Substructure search defined in the drawing window of ConQuest; output of a specific valence angle for each hit fragement is requested. (*View* this *art in* color at *www.dekker.com.*)

the atomic coordinates and connection tables. used together, form the basis for the following:

The retrieval of calculated 3D geometrical parameters for a substructure, as shown in Fig. 2, which can be used in further analyses. e.g., using the Vista program described below.

- 3D substructure searching, either in molecules (e.g., to locate substructures with specific conformations, 3D pharinacophoric patterns. etc.), or in extended crystal structures (e.g., to locate hydrogen bonds or other nonbonded interactions), using specific chemical and geometrical constraints in both cases.

ConQuest has facilities for combining individual queries, including 2D and 3D substructure queries. using Boolean logic. The program also displays the information content of CSD entries. selected from the main database (browse function) or from a subset of entries resulting from a search. Display panes show bibliographic and chemical text. crystal data, 2D chemical diagrams, and 3D structures. ConQuest can call up Mercury

Table *3* Principal facilities of the Mercury visualizer

- Browse the entire CSD. load hit lists from ConQuest searches. or read in crystal structure data in other common formats (*mol2*, *pdb*, *cif*, *mol*), supporting drag-and-drop on suitable platforms.
- Rotate. translate. and scale the 3D crystal-structure display and view cell axes, reciprocal cell axes. and normals to planes.
- Range of visualization options. e.g., different display styles. coloring, and labeling options. ability to hide and then redisplay atoms, molecules. etc
- Measure distances. angles. and torsion angles.
- Create and display centroids. least-squares mean planes. and Miller planes
- Display unit cell axes and the contents of any number of unit cells in any direction (including fractions of unit cells).
- Locate. display. and build networks of hydrogen bonds or other nonbouded contacts.
- Display a slice through the crystal in any direction.
- Undo and redo actions.
- Save the display as a file of molecules or as a graphics image, and copy images onto a PC clipboard.
- Save and read displays using its own binary format, retaining all program settings (except view direction and scale).

(see below, and Table 3) to provide more extensive 3D structure visualization facilities. Finally, ConQuest can output information for search hits in a variety of formats (e.g., cif, mol2, etc.), and transfer data to other programs.

Visualizing Crystal Structures: The Mercury Program

Mercury provides general and advanced Sunctionality for viewing crystal structures in 3D, as summarized in Table 3.[3,9] A unique feature of Mercury applied to CSD entries is its ability to import chemical bond types from the 2D connection tables and display them on the 3D image, as shown in Fig. 3. However, the most important functionality in Mercury, and one that is vital in supramolecular studies, is the ability to locate, build, and display networks of intermolecular and intramolecular hydrogen bonds, short nonbonded contacts, and user-specified contact types. Mercury will use distance criteria relative to van der Waals radii sums, or direct (Å) values. An example H-bonded network, constructed and viewed in Mercury, is shown in Fig. 4a. The facilities for displaying a slice through a crystal in any direction are illustrated in Fig. 4b, and such displays can be valuable in rationalizing crystal morphology and predicting how to control it.

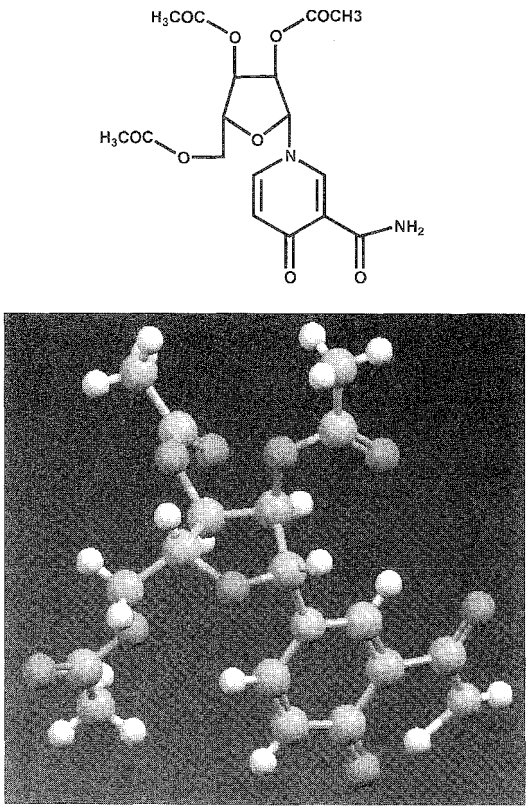

Fig. 3 Chemical diagram from the CSD and a Mercury representation of the 3D structure with imposed chemical bond types. (*View this art in color at www.dekker.com.*)

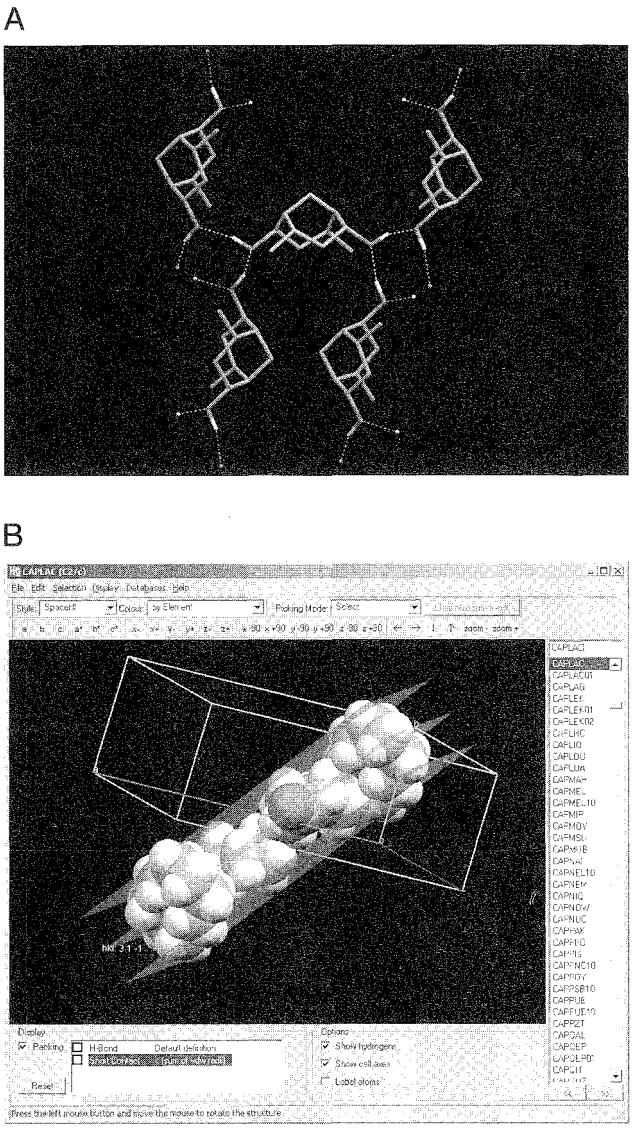

Fig. 4 Mercury plots of (a) an extended H-bonded network in CSD refcode KAPNAQ,[10] and (b) a slice through the crystal structure of caprolactam,[11] showing molecules with centroids that lie within 2.5 A of the (3 1-1) Miller plane. (*View this art in color at www.dekker.com.*)

Display and Analysis of Geometrical Parameters: The Vista Program

Vista displays molecular geometry and other parameters relating to a molecular or supramolecular substructure in a

spreadsheet format.[12] Such data are retrieved from the CSD by ConQuest according to user-supplied specifications. Vista performs a variety of analytical and display functions, including generation of the following

- Simple descriptive statistics for parameter distributions.
- Histograms and scattergrams referred to Cartesian or polar axes.
- Statistical analyses, including linear regression and principal component analysis.
- Hyperlinks from geometrical data back to the original CSD entry.
- Preparation of plots for reports and publications.

Exploring Intermolecular interactions: The IsoStar Knowledge Base

IsoStar gathers a vast amount of information on intermolecular interactions in a readily accessible form.[4] For a given contact between a central group (A) and a contact group (B), the CSD search results for an interaction A...B are transformed into an easily visualized form by overlaying the A moieties. This results in a 3D scatterplot showing the experimental distribution of the B-moieties around the (static) central group A (see Fig. 5a), which can also be presented in contoured form (Fig. 5b). IsoStar contains data retrieved from the CSD and from protein–ligand complexes stored in the Protein Data Bank (PDB),[13] and also contains nearly 1000 potential energy minima calculated using distributed multipole analysis and intermolecular perturbation theory calculations.[4]

Version 1.5 of IsoStar, released in October 2002, covers 300 central groups, 45 contact groups, and contains over 25.000 scatterplots. The user may interact with the basic scatterplots to generate contoured surfaces, to change the A...B distance limit for data presentation, to control the display style, etc. Importantly, the scatterplot data are hyperlinked to the master CSD and PDB files, so that the structural environments of specific interactions can be examined in detail. IsoStar, therefore, contains a vast amount of information of use in supramolecular chemistry, crystal engineering, and organic crystal chemistry,[5,6] and also provides ready access to information that is invaluable in rational drug design.[7]

RESEARCH APPLICATIONS OF THE CSD: THE DBUSE DATABASE

Research applications of the accumulated data in the CSD began to be published in the mid-1970s, as software for searching, manipulating, and analyzing the data began to be widely distributed. Indeed, software developments and research methodologies were always closely intertwined. Since the mid-1970s, nearly 1000 publications made use of CSD data as the essential basis for research projects that address topics such as the following:

- Mean molecular dimensions.[14,15]
- Structure correlation and reaction pathways.[16]
- Conformational analysis.[17,18]
- Hydrogen-bond geometry and directionality.[19,20]
- Weak hydrogen bonds.[21]
- Nonbonded interactions not mediated by H.[22,23]
- Crystal engineering.[24]
- Crystal structure prediction.[5]

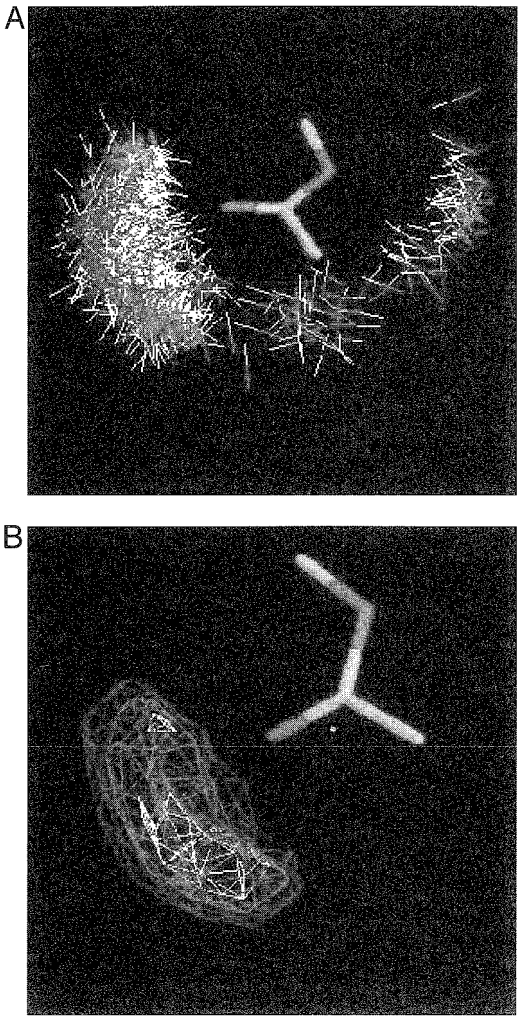

Fig. 5 IsoStar plots of N—H and O—H contact groups around a carboxylic ester central group (a) basic IsoStar plot and (b) contoured plot. (*View this art* in color *at www.dekker.com.*)

Protein–ligand interactions and protein–ligand docking.[25,26]
Applications in metallo-organic chemistry.[6]

All of these topics. and more, are covered in three recent reviews[5–7] published in a special issue of *Acta Crystallographica* devoted to the status and research applications of all of the crystallographic databases.

While these articles[5–7] and the other papers and monographs noted above cite many relevant CSD studies, the CCDC compiled a more complete and classified collection of references to CSD research applications in its DBUse database. This database not only provides full bibliographic data but also contains short synopses of each published project, prepared by CCDC staff. The DBUse is freely available and searchable via the CCDC web site at http://www.ccdc.cam.ac.uk/dbuse.

CONCLUSION

The CSD system. comprising the complete database. together with ConQuest, Mercury. Vista. IsoStar, and PreQuest (software for database creation) is available on CD for Unix, Linux, and Windows platforms. and full subscription details can be found at http://www.ccdc.cam.ac.uk/ or by e-mailing admin@ccdc.cam.ac.uk. The web site also contains full details of other CSD-related products. Data for individual crystal structures are freely available on request for bona fide research use, by citing CCDC Deposition Numbers (printed in many journals) and bibliographic information. Full details of this service are given at http:/lwww.ccdc.carn.ac.uW.

ARTICLES OF FURTHER **INTEREST**

Aurophilic Interactions, p. 82
Biological Ligands, p. 88
Crystal Engineering with Hydrogen Bonds. p. 357
Crystal Growth Mechanisms, p. 364
Crystal Structure Prediction, p. 371
Drug Design. p. 490
Halogen Bonding, p. 628
Hydrogen Bonding, p. 658
Hydrogen Bonds to Metals and Metal Hydrides, p. 666
The Lock and Key Principle, p. 809
Neutron Diffractiorz. p. 959
π–π Stacking as a Crystal Engineering Tool, p. 1093
Polymorphism, p. 1129
Secondary Bonding, p. 1215
Space Groups and Crystal Packing Modes. p. 1337
Strong Hydrogen Bonds, *p.* 1379
Weak Hydrogen Bonds, p. 1576
X-Ray Crystallography. p. 1586
X-Ray and Neutron Powder Diffraction, p. 1592

C

REFERENCES

1. Allen. F.H.: Davies, J.E.; Galloy, J.J.; Johnson. **O.:** Kennard, 0.; Macrae, C.F.; Mitchell, E.M.; Mitchell, G.F.; Smith, J.M.; Watson, D.G. Development of versions 3 and 4 of the Cambridge Structural Database system. J. Chem. Inf. Comput. Sci. 1991, *31*. 187–204.
2. Allen, F.H. The Cambridge Structural Database: A quarter of a million structures and rising. Acta Crystallogr. 2002. *B58*. 380–388.
3. Bruno, I.J.: Cole, J.C.; Edgington, P.R.: Kessler, M.: Macrae, C.F.; McCabe, P.; Pearson, J.: Taylor, R. New software for searching the Cambridge Structural Database and visualising crystal structures. Acta Crystallogr. 2002. *B58*. 389–397.
4. Bruno, I.J.; Cole, J.C.; Lommerse, J.P.M.; Rowland. R.S.; Taylor, R.; Verdonk, M.L. IsoStar: A library of information about nonbonded interactions. J. Comput.-Aided Mol. Des. 1997. *11*. 525–537.
5. Allen. F.H.; Motherwell. W.D.S. Applications of the Cambridge Structural Database in organic chemistry and organic crystal chemistry. Acta Crystallogr. 2002, *B58*. 407–422.
6. Orpen, A.G. Applications of the Cambridge Structural Database in molecular inorganic chemistry. Acta Crystallogr. 2002, *B58*, 398–406.
7. Taylor. R. Life-science applications of the Cambridge Structural Database. Acta Crystallogr. 2002. *D58*, 879–888.
8. Hall. S.R.; Allen. F.H.: Brown. I.D. The crystallographic information file (CIF). Acta Crystallogr. 1991. *A47*. 655–685.
9. Taylor. R.: Macrae, C.F. Rules governing the crystal packing of mono- and dialcohols. Acta Crystallogr. 2001, *B57*, 815–827.
10. Nguyen, V.T.; Bishop. R.: Craig, D.C.; Scudder, M.L. A versatile but unexpected new clathrate inclusion host. CrystEngComm 2000, 2. 46–48.
11. Winkler. F.K.: Dunitz, J.D. Crystal and molecular structure of caprolactam. Acta Crystallogr. 1975, *B31*, 268–269.
12. *Vista* 2.0 *Users* Guide: Cambridge Crystallographic Data Centre: 12 Union Road. Cambridge, CB2 1EZ. UK. 1995.
13. Berman. H.M.; Battistuz, T.: Bhat, T.N.; Bluhm. W.F.: Bourne. P.E.; Burkhardt, K.: Feng. Z.; Gilliland, G.L.; Iype, L.; Jain, S.: Fagan, P.: Marvin. J.; Ravichanran. V.; Schneider, B.; Thanki, N.; Padilla, D.: Weissig, H.: Westbrook, J.D.: Zardecki, C. The protein data bank. Acta Crystallogr. 2002, *D58*, 899–907.
14. Allen, F.H.: Kennard. 0.; Watson. D.G.; Brammer. L.: Orpen, A.G.: Taylor. R. Tables of bond lengths determined by x-ray and neutron diffraction. Part I: Bond lengths in organic compounds. J. Chem. Soc., Perkin Trans. 2 1987, S1–S19.

15. Orpen, A.G.; Brammer, L.; Allen, F.H.; Kennard, O.; Watson: D.G.: Taylor, R. Tables of bond lengths determined by x-ray and neutron diffraction. Part 2: Organometallic compounds and coordination complexes of the d- and *f*-block metals. J. Chem. Soc., Dalton Trans. 1989. S1–S83.
16. Bürgi, H.-B.; Dunitz, J.D. *Structure* Correlation; VCH Publishers: Weinheim, Germany, 1994.
17. Allen. F.H.; Doyle, M.J.: Auf der Heyde, T.P.E. Automated conformational analysis from crystallographic data. 6. Principal component analysis for *n*-membered carbocyclic rings (n=4,5,6). Symmetry considerations and correlations with ring-puckering parameters. Acta Crystallogr. **1991**, B47. 412–428.
18. Allen, F.H.: Harris, S.E.; Taylor, R. Comparison of conformer distributions in the crystalline state with conformational energies calculated by ab initio techniques. J. Cornput.-Aided Mol. Des. 1996, *10*, 247–254.
19. Taylor, K.; Kennard. O. Hydrogen-bond geometry in organic crystals. Acc. Chem. Res. 1984. *17*, 320–326.
20. Jeffrey, G.A.; Saenger, W. Hydrogen Bonding in Biological Structures; Springer Verlag: Berlin, Germany, 1991.
21. Desiraju, G.R.; Steiner, T. The Weak *Hydrogen* Bond in *Structural Chemistry* and Biology; Oxford University Press: Oxford, UK, 1999.
22. Lommerse, J.P.M.; Stone, A.J.; Taylor, R.; Allen, F.H. The nature and geometry of intermolecular interactions between halogens and oxygen or nitrogen. J. Am. Chem. Soc. 1996, 118, 3108–3116.
23. Allen, F.H.; Baalham, C.A.; Lommerse, J.P.M.; Raithby, P.R. Carbonyl–carbonyl interactions can be competitive with hydrogen bonds. Acta Crystallogr. **1998**, *B54*, 320–329.
24. Nangia, A. Database research in crystal engineering. Cryst. Eng. Comm. 2002, 4, 93–101.
25. Verdonk, M.L.; Cole, J.C.; Taylor, R. Superstar: A knowledge-based approach for identifying interaction sites in proteins. J. Mol. Biol. 1999, 289, 1093–1108.
26. Jones. G.; Willett, P.; Glen, R.C.; Leach, A.R.; Taylor, R. Development and validation of a genetic algorithm for flexible docking. J. Mol. Biol. 1997, 267. 727–748.

Carbohydrates, Recognition of

Arne Lützen
University of Oldenburg, Oldenburg, Germany

INTRODUCTION

Carbohydrates are now recognized to be among the most important compounds involved in intercellular recognition events. Viral or bacterial infections. certain immune responses. fertilization, or the regulation of enzyme and other protein functions and even protein folding, are all processes that are—at least to some extent—ruled by carbohydrate recognition through specific proteins. This binding is achieved by complex arrays of weak noncovalent interactions involving hydrogen bonding, hydrophobic interactions. as well as metal ion coordination.

Given the importance of the above-mentioned processes, it is not surprising that a lot of effort was made in supramolecular chemistry over the last 15 years to develop artificial receptors for these classes of compounds. which is. however. a challenging problem. because saccharides provide a complex three-dimensional array of functional groups that makes the design of a suitable receptor a difficult task. Up to now. mainly two binding motifs were employed to approach this problem: boronic acids that bind to the saccharides through the formation of covalent boronic ester linkages, which provides strong binding even in highly polar solvents: and the more supramolecular and biomimetic approach to use a mixture of hydrogen bonds and hydrophobic effects. which is. however, still in its infancy with regard to effective binding in polar solvents. especially water.

CARBOHYDRATE RECOGNITION IN BIOLOGICAL SYSTEMS

Saccharides have an enormous information-storing potential that is substantially higher than that of peptides and nucleotides of comparable molecular weights.'" Thus. it is not surprising that carbohydrates. beside their structural, property-modulatory. and energy-storing functions. can act as recognition markers in numerous physiological and pathological processes.[2–4] Many of these processes occur on cell surfaces, where oligosaccharides are found in the glycocalix as components of giycoproreins and glycolipids. The encoded information is deciphered by carbohydrate-binding proteins that can be subdivided into antibodies, enzymes involved in sugar utilization and glycoconjugate turnover, and other carbohydrate-binding proteins—also called lectins. which are neither enzymes nor immunoglobulins.[5] Especially. carbohydrate–lectin interactions play a crucial role in many intra- and intercellular recognition and communication processes, including protein folding, clearance of glycoproteins from the circulatory system. control of intracellular traffic of glycoproteins, cell adhesion, bacterial and viral infections, tumor metastasis, certain immune reactions, like. e.g., the recruitment of leukocytes to inflammatory sites. and fertilization, just to name a few.

But how do these proteins actually recognize carbohydrate structures on a molecular level?

The structural basis for selective recognition was mainly investigated by x-ray crystallography and. more recently, by advanced NMR spectroscopic techniques.[2,5–12] According to the broad variety of events involving carbohydrate recognition processes, a multitude of diverse protein frameworks evolved. providing binding sites for carbohydrates either deeply buried in the protein structure as found in most enzymes and bacterial periplasmic carbohydrate-binding proteins or in rather shallow indentations in the protein surface, as is typically the case for lectins (Fig. 1).

However, despite this enormous diversity, they share some common key features.

Hydrogen Bonding

Carbohydrates display a high density of hydroxyl groups, and therefore. it is not surprising that hydrogen bonding plays an important role in their recognition. Although the energetic contributions of hydrogen bonds to protein–carbohydrate binding are still uncertain, it is clear that the directionality of hydrogen bonds is critical to the specificity of the recognition process.

As shown in Fig. 2, the protein usually exploits cooperative hydrogen bonding in which a sugar hydroxyl group acts simultaneously as a hydrogen bond donor and acceptor in order to distinguish between different carbohydrate epitopes. Generally. one acidic amino acid side chain is used as a hydrogen-bond acceptor for one or two sugar OH groups. The primary hydrogen bond donors

Encyclopedia of Supramolecular Chemistry
DOI: 10.1081/E-ESMC *120019891*

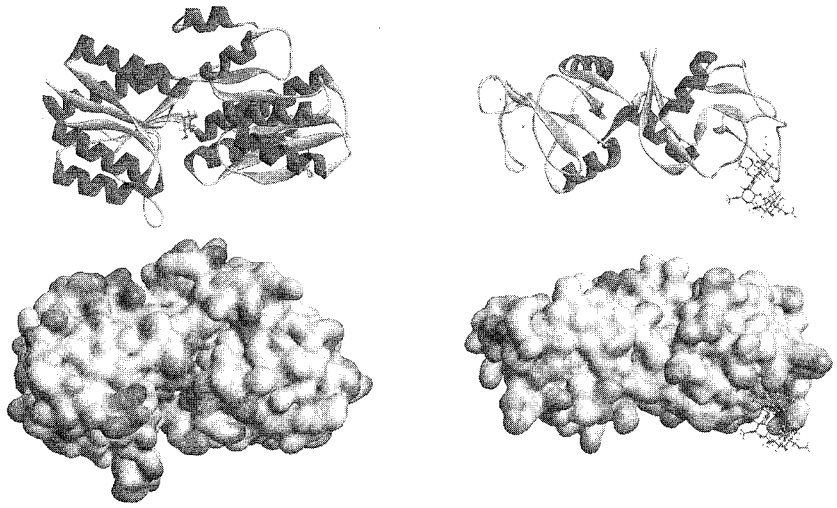

Fig. 1 Crystal structures of the periplasmic L-arabinose-binding protein (ABP) of *Escherichia coli* cornplexed to α-L-arabinose (left. PDB entry IABE) and of galectin-1 complexed to *N*-acetyllactosamine (right, PDB entry 1SLT). (Frorn Refs. [13–15]). *(View this art* in color *at www.dekker.com.*)

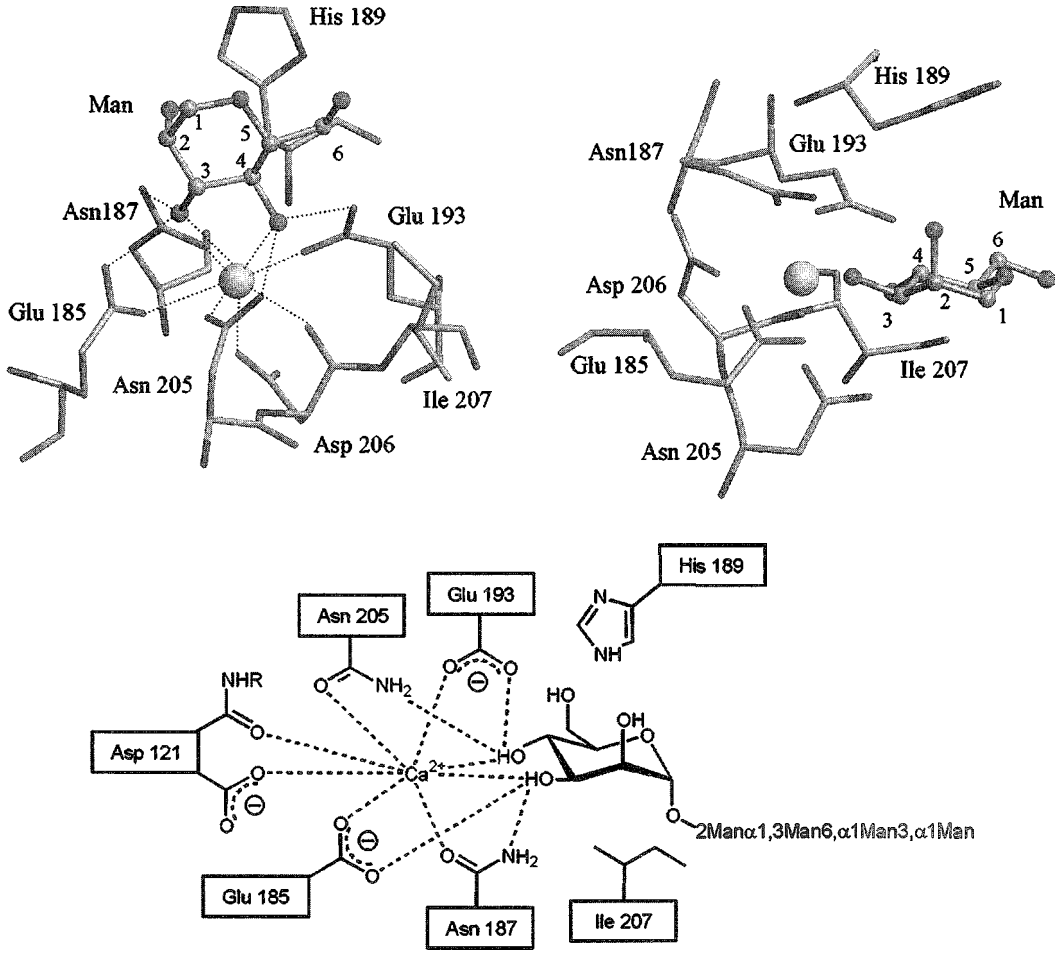

Fig. 2 Crystal structure of an α-D-mannose unit bound to the C-type lectin rat mannose-binding protein A (MBP-A, PDB entry 2MSB). Dashed lines indicate hydrogen and coordinative bonds. (From Ref. [16].) (View *this art* in color at *www.dekker.com.*)

are main-chain amide groups and side-chain amide groups. Charged side-chain donors also occur with some frequency. However, protein hpdroxyls are much less common. Thus. the most common hydrogen-bonding scheme is as follows:

protein $(NH)_n \rightarrow$ sugar OH $\rightarrow$ protein C=O

Water-mediated hydrogen bonds

In addition to direct interactions between the protein and the sugar hydroxyl groups, water was also observed to mediate (indirect) hydrogen bonds between amino acid residues and the saccharide OH groups. In these cases. the water molecules act as fixed structural elements, equivalent to hydrogen-bonding groups of the protein, and can. therefore, be considered as part of the binding site architecture.

The particular sugar functionalities that form hydrogen bonds with the protein are those required for specific recognition and discrimination. whereas those positions not used as recognition elements tend to stay solvent exposed and form no direct contact with the protein (Fig. 2). However. in these cases, higher selectivity is often achieved by extending binding sites through additional contacts between oligosaccharide structures and the protein surface (''subsite multivalency''[11]).

In this context, it is also interesting to note that charged groups on sugars like carboxylate moieties usually interact with main-chain amides. polar side chains (especially serine), or ordered water molecules by means of charged hydrogen bonds rather than through salt-bridge formation with fully charged side chains. In many cases, it is even energetically favorable to maintain these highly polar groups exposed to solvent.

Nonpolar interactions

Although carbohydrates have many polar functional groups. most biologicaliy relevant saccharides still present nonpolar patches on their surfaces that can interact with complementary hydrophobic amino acid residues. This is particularly true for β-D-galactose, which is almost always observed to pack against aromatic amino acid side chains. Also. the binding of other sugars. like mannose, was observed to involve hydrophobic interactions of nonpolar areas of the saccharide unit. with aromatic and aliphatic amino acid side chains (Fig. 2). Hydrophobic interactions are believed to provide a significant contribution to the overall binding energy, because apolar patches on the sugar as well as the compleinentary side chains of the protein are removed from bulk solvent. thereby expelling unfavorably bound water molecules.

Divalent Cations

Direct interactions with the sugar

C-Type lectins are unique among the structurally characterized lectins, because most of them require a calcium(II) ion to form direct coordinative bonds with the sugar ligand. Shown in Fig. 2 is such a case, where the full noncovalent binding potential of two vicinal OH groups is used: One lone pair of electrons from each OW group forms a coordinative bond with Ca^{2+}, and the other lone pair accepts a hydrogen bond from a side-chain amino group, and the proton is donated to an acidic oxygen in a hydrogen bond.

Indirect roles

However. calcium as well as other ions like manganese(II) ions are required for the activity of many families of carbohydrate-binding proteins, even when they do not directly interact with the ligands. In these cases. the most common function of these ions is structural. in that the metal ion coordination shell orients important protein functional groups for optimal ligand binding.

Multivalency

Despite the manifold interactions between proteins and carbohydrates described above that result in a lot of cases in specific binding of single monosaccharide epitopes, the binding affinity of Iectins is still surprisingly low—usually in the order of millimolar dissociation constants. However. multivalency, i.e., the simultaneous association of several ligands of one biological unit (macromolecule, cell surface, etc.) with several receptors of another biological unit, is applied by nature to accomplish high-affinity interactions.[12,17,18] Thus, high-affinity carbohydrate–protein interactions in the nanomolar range can be achieved through oligomerization of several lectin polypeptides. each containing similar or identical simple binding sites (''subunit multivalency''[11]) or through clustering of several lectins on cell surfaces and interaction of these architectures with multiple carbohydrate epitopes presented in an appropriate manner on lipid or protein carriers.[19]

The strategy of employing structurally defined multivalen: interactions is also efficient to get maximum recognition of certain carbohydrate-coated surfaces, like cell surfaces. while minimizing competitive binding to smaller or soluble saccharides at the same time. Structural studies revealed that many Iectins that bind surfaces achieve the required planar array of sugar-binding sites by arrangement of polypeptide subunits in oligomers that

have cyclic symmetry, with all binding sites located on one end of the oligomer.

CARBOHYDRATE RECOGNITION BY ARTIFICIAL RECEPTORS

Given the importance of the various processes involving carbohydrate recognition events in nature. it is not surprising that a lot of efforts were made in supramolecu-Iar chemistry to develop efficient artificial receptors for these substrates over the last 15 years.[20–23] However, the recognition of carbohydrates is one of the biggest challenges for structurally as well as for preparatively orientated chemists. because they dispiay a complex three-dimensional array of functional groups. This presents an interesting problem for the design of suitable receptors. and supramolecular "bottom up" approaches could help to further elucidate natural processes. although one has to admit that effective. truly biomimetic carbohydrate recognition is still far away at the moment. Nonetheless. nonbiomimetic systems also promise some interesting (future) applications in medicinal chemistry in that they could possibly be employed in the prevention of bacterial and viral infections: in the monitoring of the health condition of cells, and in the identification of malignant cells. for instance. cancer cells: as transport vehicles for saccharides or 'elated pharmaceuticals; or as sensors for saccharides in biological fluids.

Like lectins that undergo few if any changes in their global conformations upon binding to sugars, most of the receptors reported so far have rigid structures that provide more or less well-preorganized binding sites for the substrates. According to the high density of hydroxy groups displayed by carbohydrates, it is not surprising that most receptors are designed to target these functions to obtain binding. So far, there are mainly two classes of receptors:

First. there are a number of effective receptors that use boronic acid functions to form five- or six-membered cyclic boronate esters with two appropriately orientated hydroxy groups (at least in organic and basic aqueous media). This approach was used intensively with regard to sensing applications. However, this approach is neither biomimetic nor strictly supramolecular. because. although

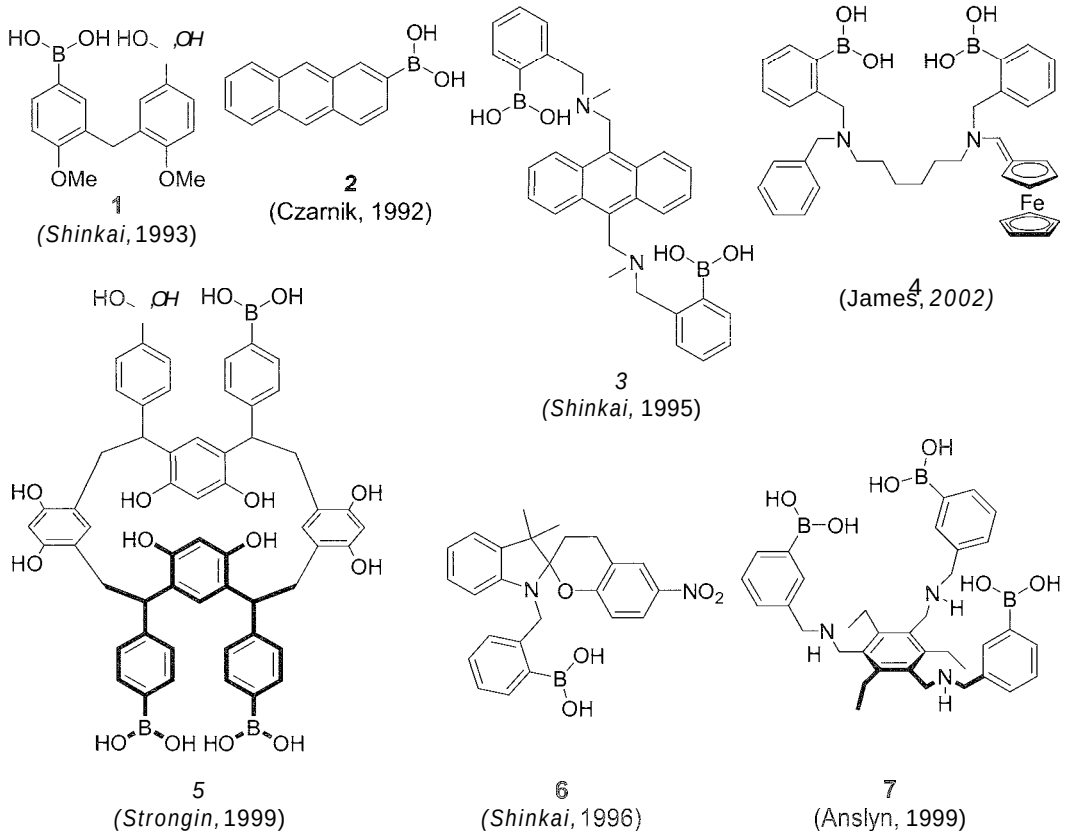

Fig. 3 Boronic-acid-based receptors for carbohydrate sensing. (From Refs. [21–25].)

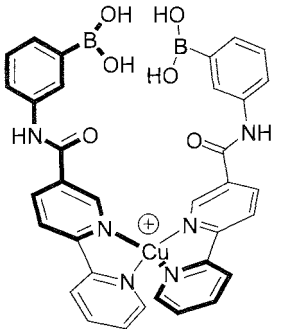

8
(Shinkai, 1998)

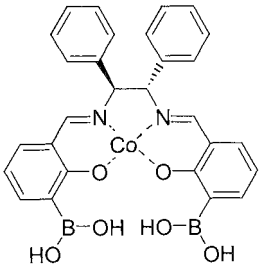

9
(Shinkai, 1999)

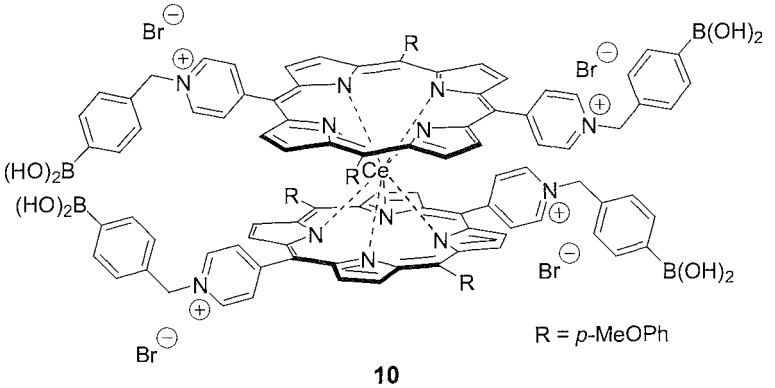

10
(Shinkai, 2000)

Fig. 4 Boronic-acid-based receptors for carbohydrates with metal coordination elements as structure-determining elements. (From Ref. [36–39].)

only moderately strong and reversible, covalent bonds are formed during binding.[21–28]

Second, noncovalent intermolecular binding can be achieved by means of hydrogen bonding through (an)ionic or neutral hydrogen bond donor and acceptor groups. as in their natural examples." However. other than their natural models. most of the receptors reported so far are designed to be effective in organic solutions in order to profit not only from the directionality of hydrogen bonds but also to get a maximum energetic contribution to overall binding.

Molecular Receptors Based on Boronic Acids

Boronic acids are extensively used in carbohydrate chemistry. for example, in chromatographic separations, for a long time. However, Wulff and coworkers were the first to employ boronic esters in imprinted polymer carbohydrate receptors.[35] About a decade later. the first aryl-boronic-acid-based receptors and sensors other than the long-known phenyl boronic acid mere reported and the area has seen tremendous development since.[20–27] The most noticeable advantages of this binding motif are that strong binding can even be obtained in water. and that boronic acids can easiiy be incorporated in molecular architectures useful for different sensing techniques. Shown in Fig. 3 are some examples for boronic-acid-based saccharide sensors.

Sensing methods reported include circular dichroism (**1**),[21–23] fluorescence (**2–3**),[21–23] mainly based on photoinduced electron transfer but also on intramolecular energy transfer. electrochemistry (**4**),[24] and visible color changes (**5–7**).[21–23,26] However, boronic-acid-based receptors were also used for the transport of monosaccharides.[27,28]

In addition, boronic-acid–carbohydrate interactions can be used to transfer stereochemical information. e.g., to a newly formed stereogenic center (usually the metal ion) in

[a]Selected recent examples not covered by Ref. [20]: Refs, [29–34]

metal coordination compounds (8) built from ligands that carry one boronic acid group each. These can only bind to a saccharide in a cooperative fashion when the complex has the proper configuration (Fig. 4).[36,37]

Furthermore, boronic-acid-substituted metal coordination compounds were used as heterotropic allosteric receptors (9), where the coordination to a metal ion changes the conformation of a covalently assembled ditopic ligand in a way that the boronic acids can cooperatively bind to a single saccharide substrate.[38] This strategy was further extended when cerium *bis*(porphyrin) double-decker systems (10) were demonstrated to show positive homotropic allosteric effects in the binding of two saccharide guest molecules.[39]

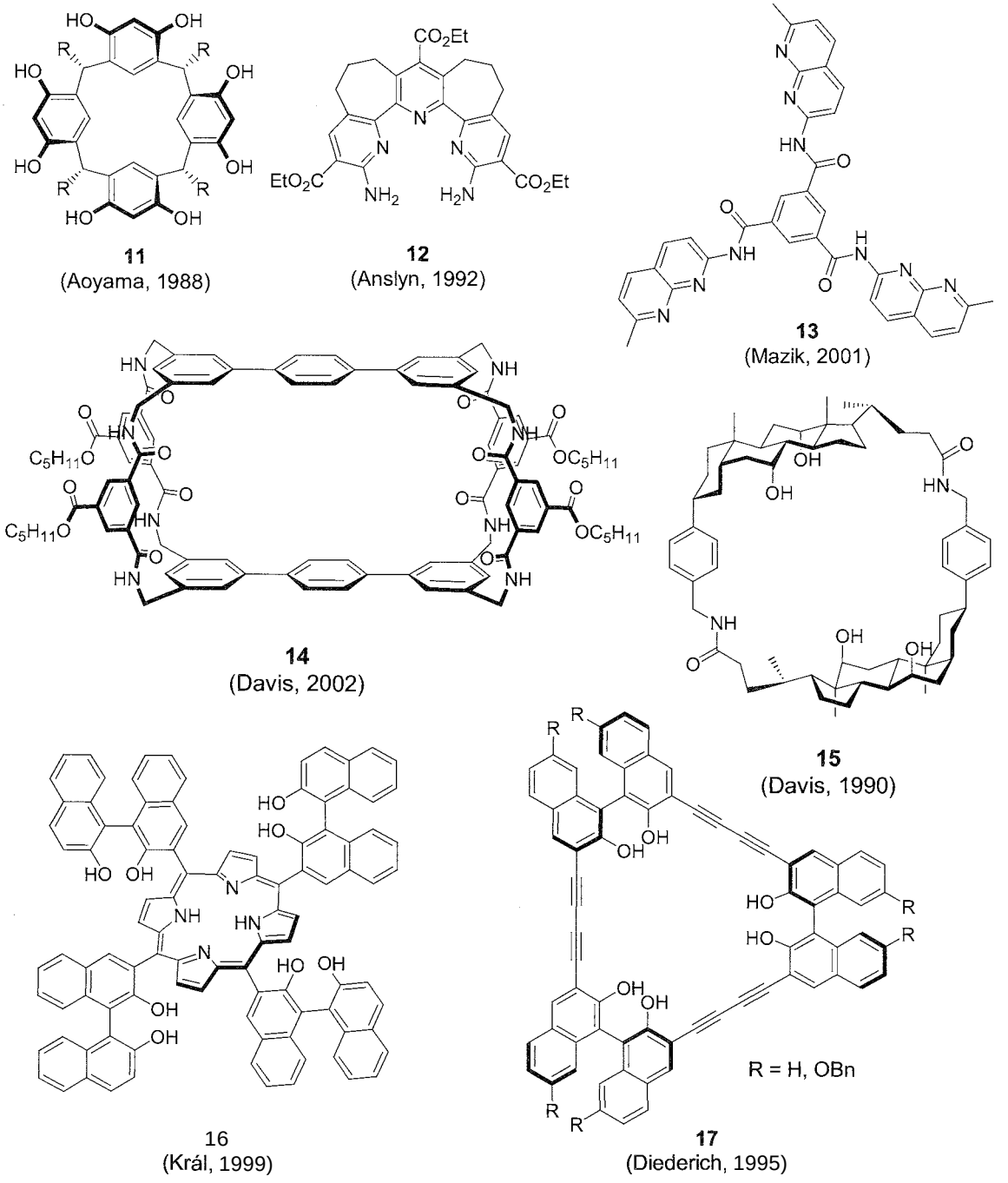

Fig. 5 Achiral and chiral artificial receptors for the recognition of carbohydrates via neutral hydrogen bonds. (From Refs. [20,29–34].)

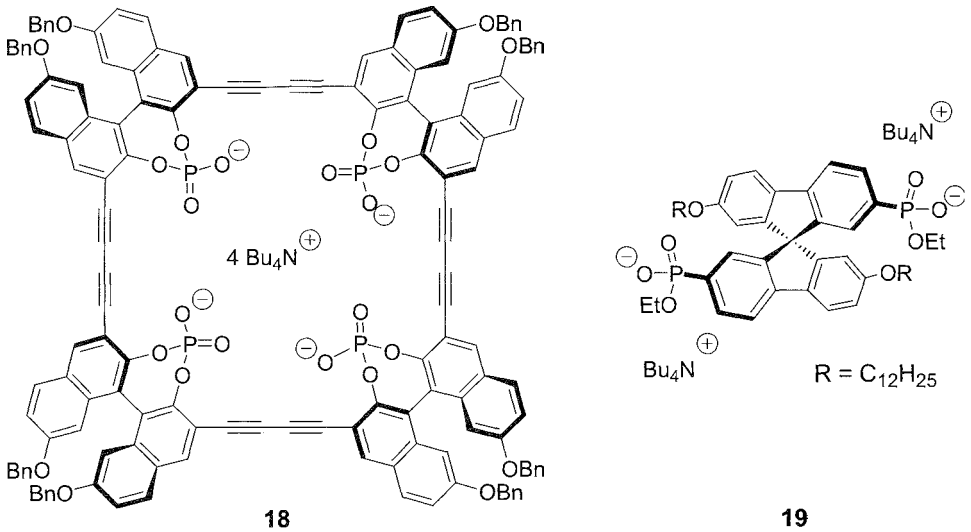

18
(Diederich, 1995)

19
(Hamilton, 1997)

Fig. 6 Chiral artificial receptors for the recognition of carbohydrates via charged hydrogen bonds. (From Ref. [20].)

Molecular Receptors with Hydrogen-Banding Functionalities

Like their natural examples, almost all artificial receptors of this type offer an array of functional groups (pyridines. amide NH and CO groups. amino, or phenolic hydroxyl groups) in order to exploit cooperative hydrogen bonding. in which the sugar hydroxyl groups can act simultaneously as a hydrogen-bond donor and acceptor (**11–17**,[20,29-34] Fig. 5). Only in the cases where phosphonates or phosphate groups (**18** and **19**,[20] Fig. 6) are used to bind carbohydrates via strong ionic hydrogen bonds. can the sugar OHs act as hydrogen-bond donors.

In addition. most of the receptors bear hydrophobic patches in their binding sites in order to bind complementary areas of carbohydrates. Although the energetic contributions of this interaction to overall binding are obviously neglectable in organic solutions. these contacts might play a more prominent role in terms of specificity and in recognition events in more polar solvents. like DMSO, acetonitrile/methanol, or even mixtures containing water, as observed for instance for **14**,[34] **16**[30–31] **18**,[20] and **19**.[20]

The results obtained with these receptors show that diastereoselective binding of single sugar epitopes is. to some degree, possible even with nonchirai structures although the order of preferred binding often reflects the monosaccharides' tendency to self-aggregate in the order α-galactosides≤α-glucosides<β-glucosides<α-mannosides. Improved diastereoselectivity and. of course. enantioselectivity can be observed with chiral receptors; where **19** was found to show the highest enantioselectivity of approximately 5:1 for the binding of *n*-octyl β-glucopyranosides.

Association constants for the binding of mono- or disaccharides are usually in the range of $1 \times 10^2\ M^{-1}$ (12 and **17**) to $3 \times 10^4\ M^{-1}$ (13 and 15) in organic solvents, like chloroform or dichloromethane. but can also reach up to $1 \times 10^4\ M^{-1}$ (14, 16. 18, and 19) when measured in more competitive solvents. like acetonitrile. acetonitrile/methanol, DMSO. or dichloromethane/water.

CONCLUSION

Nature developed a diversity of independent protein architectures for the recognition of carbohydrates. However. these structures share some common key features. as the molecular basis of carbohydrate binding involves a complex array of noncovalent interactions. like hydrogen bonds; hydrophobic interactions. and in some cases, an essential contribution of divalent cations to protein structure fixing and direct coordination to the substrate. In the end. it is a question of the number of attractive contacts and the degree of shielding from aqueous solution that cause the differences in binding affinity to a single saccharide epitope.

However. on a higher level of molecular organization. the affinity and specificity of carbohydrate-mediated cell–cell recognition events depend not only on the inherent specificity of one binding site for a specific saccharide epitope but also on factors that are not operative in monovalent interactions. These multivalent factors include. for example. the location of a protein.

the oligomerization state of the protein, its display of saccharide binding sites. and the display of saccharide recognition epitopes. Given this range of variables, the factors that contribute to favorable multivalent protein–carbohydrate interactions are difficult to dissect. Much work remains to be done to fully elucidate these important and fascinating processes.

For biomimetic and for other reasons. a lot of efforts in supramolecular chemistry are directed to the development of artificial receptors for carbohydrates over the last 15 years. Like their natural examples — the lectins — most receptors have rigid structures and try to address the saccharide's hydroxyl functions through the formation of covalently linked aryl boronic acid esters or hydrogen bonding to obtain binding. Although the first approach is not biomirnetic or truly supramolecular, it provides strong binding in polar solvents and even in water. Because these functionalities can easily be incorporated in aggregates with signaling abilities, boronic-acid-based receptors are currently mainly used as chemosensors for carbohydrates.

Although a number of examples of receptors capable of binding saccharides through hydrogen bonding were reported, nearly all were designed to bind carbohydrates in nonpolar solvents. Thus, much work needs to be done to develop artificial receptors that combine sufficient orientation through an array of hydrogen-bond contacts with favorable hydrophobic effects, in order to provide sufficient binding energy and reach the ultimate goal — the effective and biomirnetic recognition of carbohydrates in water.

ARTICLES OF FURTHER INTEREST

Biological Ligands, p. 88
***Biological Models** and Their Characteristics.* p. *101*
Fluorescent ***Sensors,*** p. 572
Hydrogen ***Bonding.*** p. 658
Hydrophobic ***Effects,*** p. 673
Preorganization and Complementarity, p. 1158

REFERENCES

1. Laine. R.A. *Glycosciences:* Stutus *and Perspectives*; Cabius. H.-J., Gabius. S.. Eds.; Chapman & Hall: Weinheim, 1997: 1 – 14.
2. Lee. Y.C.: Lee, R.T. Carbohydrate–protein interactions: Basis of glycobiology. Acc. Chem. Res. 1995. 28 (8). 321 – 327.
3. Dwek, R.A. Glycobiology: Toward understanding the function of sugars. Chem. Rev. 1996. *96* (2). 683 – 720.
4. Essentials of *Glycobiology*; Varki, A.. Cummings, R.. Esko. J., Freeze. H.. Hart. G., Marth, J.. Eds.; Cold Spring Harbor Laboratory Press: Cold Spring Harbor. 1999.
5. Lis. H.; Sharon. N. Lectins: Carbohydrate-specific proteins that mediate cellular recognition. Chem. Rev. 1998. *98* (2). 637 – 674.
6. Quiocho, F.A. Carbohydrate-binding proteins: Tertiary structures and protein–sugar interactions. Ann. Rev. Biochein. 1986. *55.* 287 – 315.
7. Weis. W.I.: Drickamer. K. Structural basis of lectin–carbohydrate recognition. Ann. Rev. Biochein. 1996, *65.* 441 – 473.
8. Bezouška, K. *Glycoscience:* Chemistry *and Chemical* Biology: Fraser-Reid. B., Tatsuta, K.. Thiem. J.. Eds.: Springer-Verlag: Heidelberg, 2001: Vol. II, 1325 – 1331.
9. Evers. D.L.: Rice. K.G. *Glycoscience: Chemistry and* Chenzicnl *Biology*; Fraser-Reid. B.. Tatsuta, K., Thiem, J., Eds.; Springer-Verlag: Heidelberg. 2001; Vol. II, 1779 – 1816.
10. *Nuclear* Magnetic *Resonance* of Biologicnl *Macromolecules, Part* A *and* B; James. T.L., Dotsch. V., Schmitz, U., Eds.: Methods Enzymol.. Academic Press: San Diego, 2001; Vols. 338 and 339.
11. Rini. J.M. Lectin structure. Annu. Rev. Biophys. Biomol. Struct. 1995. 24. 551 – 577.
12. Kiessling, L.L.; Young. T.; Mortell. K.H. *Glycoscience: Chemistry and Chemical* Biology; Fraser-Reid. B., Tatsuta, K., Thiern, J., Eds.: Springer-Verlag: Heidelberg, 2001: Vol. II, 1817 – 1861.
13. The Research Collaboratory for Structural Bioinformatics — Protein Data Bank (RCSB—PDB) is available online at http: www.pdb.org . (accessed April 2003).
14. Quiocho, F.A.; Vyas, N.K. Novel stereospecificity of the L-arabinose-binding protein. Nature 1984. *310* (5976). 381 – 386.
15. Liao. D.I.: Kapadia. G.: Ahmed, H.: Vasta, G.R.: Herzberg. O. Structure of S-Lectin, a developmentally regulated vertebrate β-galactoside-binding protein. Proc. Natl. Acad. Sci. U. S. A. 1994. 91 (4). 1428–1432.
16. Weis, W.I.: Drickamer. K.; Hendrickson. W.A. Structure of a C-type mannose-binding protein complexed with an oligosaccharide. Nature 1992, *360.* 127 – 134.
17. Mammen. M.; Choi. S.-K.; Whitesides. G.M. Polyvalent interactions in biological systems: Implications for design and use of multivalent ligands and inhibitors. Angew. Cliern. Int. Ed. 1998. 37 (20). 2755 – 2794.
18. Brewer. C.F.; Miceli. M.C.: Baum. L.G. Clusters. bundles. arrays and lattices: Novel mechanisms for lectin–saccharide-mediated cellular interactions. Curr. Opin. Struct. Biol. 2002. *12* (5). 616 – 623.
19. Crocker, P.R.: Feizi, T. Carbohydrate recognition systems: Functional triads in cell–cell interactions. Curr. Opin. Struct. Biol. 1996, *6 (5).* 679 – 691.
20. Davis. A.P.: Wareham. R.S. Carbohydrate recognition through noncovalent interactions: A challenge for biomimetic and supramolecular chemistry. Angew. Chem. Int. Ed. 8999. 38 (20). 2978 – 2996.
21. James, T.D.: Linnane. P.; Shinkai. S. Fluorescent saccharide receptors: A sweet solution to the design. assembly

and evaluation of boronic acid derived PET sensors. Chem. Commun. **1996**, (3), 281–288.

22. James, T.D.; Sandanayake, K.R.A.S.; Shinkai. S. Saccharide sensing with molecular receptors based on boronic acid. Angew. Chem. fnt. Ed. **1996**. *35* (17), 1910–1922.
23. James. T.D.; Shinkai, S. Artificial receptors as chemosensors for carbohydrates. Top Curr. Chem. 2002, *218*, 159–200.
24. Arimori, S.; Ushiroda, S.; Peter, L.M.; Jenkins, A.T.A.; James, T.D. A modular electrochemical sensor for saccharides. Chcm. Commun. 2002. (20). 2368–2369.
25. Arimori, S.; Bell, M.L.; Oh. C.S.; James, T.D. A modular fluorescence intramolecular energy transfer saccharide sensor. Org. Lett. 2002, *4* (24), 4249–4251.
26. He, M.; Johnson, R.J.; Escobedo, J.O.; Beck, P.A.; Kim, K.K.; St. Luce, N.N.: Davis, C.J.; Lewis, P.T.; Fronczek, F.R.; Melancon, B.J.: Mrse, A.A.; Treleaven, W.D.; Strongin, R.M. Chromophore formation in resorcinarene solutions and the visual detection of mono- and oligosaccharides. J. Am. Chem. Soc. 2002. *124* (18), 5000–5009.
27. Draffin, S.P.; Duggan, P.J.: Duggan, S.A.M. Highly fructose selective transport promoted by boronic acids based on a pentaerythritiol core. Org. Lett. 2001. 3 (6). 917–920.
28. Altamore, T.M.: Barrett, E.S.; Duggan, P.J.; Sherburn, M.S.; Szydzik, M.L. Cavitand boronic acids mediate highly selective fructose transport. Org. Lett. 2002, *4* (20). 3489–3491.
29. Droz, A.S.; Neidlein. U.; Anderson, S.; Seiler, P.; Diederich, F. Optically active cyclophanc receptors for mono- and disaccharides: The role of bidentate ionic hydrogen bonding in carbohydrate recognition. Helv. Chim. Acta 2001, *84* (8), 2243–2289.
30. Rusin. O.: Král, V. Novel macrocycles with 1,1′-binaphthyl substituents for the recognition of saccharides. Chem. Commun. **1999**. (23). 2367–2368.
31. Rusin, O.: Lang, K.; Král, V. 1,1′-Binaphthyl-substituted macrocycles as receptors for saccharide recognition. Chem. Eur. J. 2002. *8* (3), 655–663.
32. Mazik, M.; Bandmann, H.; Sicking, W. Molecular recognition of carbohydrates by artificial polypyridine and polypyrimidine receptors. Angcw. Chem. Int. Ed. 2000. *39* (3), 551–554.
33. Mazik, M.: Sicking, W. Molecular recognition of carbohydratcs by artificial receptors: Systematic studies towards recognition motifs for carbohydrates. Chem. Eur. J. **2001**, 7 (3). 664–670.
34. Lecollinet, G.; Dominey, A.P.; Velasco, T.; Davis. A.P. Highly selective disaccharide recognition by a tricyclic octaamide cage. Angew. Chem. Int. Ed. 2002, *41* (21), 4093–4096.
35. Wulff, G. Selective binding to polymers via covalent bonds. The construction of chiral cavities as specific receptor sites. Pure Appl. Chem. 1982. *54* (11), 2093–2102.
36. Yamamoto, M.; Takeuchi. M.: Shinkai. S.; Tani, F.: Naruta, Y. Chirality control of a Cu(I)·(phenanthroline)$_2$ complex by a sugar–boronic acid interaction. A preliminary step toward the total chain helicity control by a chain-end sugar-binding. J. Chcm. Soc., Perkin Trans. 2 2000; (1), 9–16.
37. Yamamoto, M.; Takcuchi. M.; Shinaki, S. Oligosaccharide binding to a boroiiic-acid-appended phenanthroline.Cu(I) complex which creates superstructural helicates and catenates Tetrahedron 2002. 58 (36), 7251–7258, and cited references therein.
38. Mizuno, T.: Takeuchi, M.; Shinkai, S. Sugar sensing using chiral salen-Co(II) complex. Tetrahedron 1999. *55* (31), 9455–9468.
39. Sugasaki. A.: Ikeda, M.; Takeuchi, M.; Shinkai, S. Novel oligosaccharide binding to the cerium(IV) *bis*(porphyrinate) double decker: Effective amplification of binding signal through positive homotropic allosterism Angew Chem Int Ed **2000** 39 (21), 3839–3842

Carbonic Anhydrase Models

Tohru Koike
Eiichi Kimura
Hiroshima University, Hiroshima, Japan

INTRODUCTION

The zinc(II) ion is a biologically essential element. Recognition of its importance is ever increasing. as more enzymes are discovered containing zinc(II) at the active centers. Model studies of zinc enzymes (e.g., carbonic anhydrase and alkaline phosphatase) by us and a number of other groups are establishing a deeper and wider scope of knowledge about the zinc(II) ion in relation to its biological functions. In this article, we present the latest results obtained with recently designed carbonic anhydrase models. Although these models are simple zinc(II) complexes. they have helped to disclose the hitherto unsettled intrinsic properties of zinc(II)-dependent enzyme functions. The discussion emphasizes how H_2O is activated by zinc(II) for nucleophilic attack toward electrophilic substrates (i.e., CO_2) and also how the HCO_3^- ion is dehydrated by zinc(II) ion in carbonic anhydrase.

CARBONIC ANHYDRASE MODELS WITH MACROCYCLIC TRIAMINES

There are several kinds of mononuclear zinc(II) complexes· **1**,[1–6] **2**,[1–4,7–10] **3**,[11] **4**,[12–15] and **5**.[16] designed to mimic the zinc(II)-coordination structure or the function of zinc(II) ions at the active center of carbonic anhydrase (CA), the enzyme that catalyzes CO_2 hydration ($CO_2+H_2O \rightarrow HCO_3^-+H^+$) and its reverse reaction HCO_3^- dehydration ($HCO_3^- \rightarrow CO_2+OH^-$).[17]

However. the 12-membered macrocyclic triamine ([12]aneN$_3$) zinc(II) coinplex **1** has. for the first time, provided a chemical mechanism that shows the role of zinc(II) ion in the reversible CO_2 hydration and HCO_3^- dehydration catalyzed by CA.[6] The fast kinetics of the CO_2 hydration catalyzed by **1** was followed by H^+ production at 25°C. which was detected by using a pH-indicator in buffer solution (pH 6–10). The kinetics demonstrated the catalytic nature of the zinc(II) complex **1** at various pHs. A plot of the initial rates against total zinc(II) complex concentrations (=$[\mathbf{1}]_{total}$) indicated that the CO_2 hydration rate varied linearly with $[\mathbf{1}]_{total}$ and $[CO_2]$ to give an observed second-order rate constant $(k_{cat}^h)_{obs}$. Shown in Fig. 1a is a plot of $(k_{cat}^h)_{obs}$ data as a function of pH. The sigmoidal curve is characteristic of a kinetic process controlled by an acid–base equilibrium and exhibits an inflection point (pK_{kin}) at about pH 7.4. which is almost the same as the potentiometrically determined pK_a value of 7.3 for zinc(II)-bound water of **1a**.[3] Thus. **1b** must be the genuine active species in the catalytic hydration of CO_2. The sigmoidal pH dependence for the CO_2 hydration with CA (although its pK_a is 6.9)[17] can thus be accounted for by a hydroxo complex zinc(II)–O H at the active center of CA reacting with CO_2. A proposed CO_2 hydration mechanism by CA is shown in Fig. 2. The rate law for the suggested CO_2 hydration mechanism by **1** is more precisely given by $(k_{cat}^h)_{obs} = k_{cat}^h \cdot K_a/([H^+]+K_a)$, and from this were calculated the kinetically obtained pK_a value of 7.4 and the k_{cat}^h value of 6×10^2 M^{-1} sec^{-1} at 25°C. The much faster reaction of CA [e.g., k_{cat}=ca. 10^8 M^{-1} sec^{-1} for human CA II at 25°C].[18] in comparison to **I** may partially be explained by an effective preassociation of CO_2 within the hydrophobic pocket in CA.[19,20] If this preassociation of CO_2 is characterized by a large binding constant of 10^5 M^{-1}. it can account for the large difference observed in the catalytic activity during the hydration of CO_2.

The kinetic study of the reverse HCO_3^- dehydration catalyzed by a model complex was successfully conducted for the first time with the zinc(II) complex **1** at 25°C.[6] The rate was followed by measuring the evolution of O H for the reaction ($HCO_3^- \rightarrow CO_2+OH^-$) in a similar fashion to the CO_2 hydration in buffer solution (pH 6–9). The rates increased with iowering pH (see Fig. lb). The kinetic data showed that the kinetically reactive species was **1a**, and the second-order rate was followed with [Pa] and $[HCO_3^-]$, each first-order dependent. The dehydration constant k_{cat}^d with **1a** was found to be 5 M^{-1} sec^{-1}, and the kinetically obtained pK_a value of 1a was 7.3 at 25°C. Important conclusions for HCO_3^- dehydration with the catalyst **1** are that the reactive species is the zinc(II)–OH_2 form: substitution of the zinc(II)-bound H_2O with HCO_3^- is rate determining; and decarboxylation of the zinc(II)-bound HCO_3^- is much faster (see a similar proposed mechanism for CA-catalyzed reaction in Fig. 2).

Although the magnitude for the k_{cat}^h and k_{cat}^d significantly differs, the two curves (Fig. 1a and b) have an inflection point at the same pH (ca. 7.4) and are symmetrical (a·ith scales adjusted). Thus, the model complex **I** is the first example to mimic the pH-dependent

Encyclopedia of Supramolecular Chemistry
DOI: 10.1081/E-ESMC 120017675

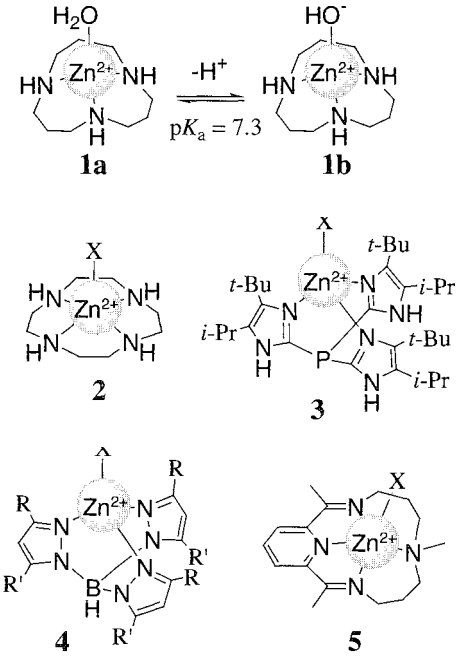

behavior of reversible CO_2 hydration catalyzed by CA. This fact implies that in CA, too, the CO_2 hydration1 HCO_3^- dehydration is determined by the zinc(II)–OH^-/ zinc(II)–OH_2 equilibrium at the active center. A similar CA model study with macrocyclic tetraamine zinc(II) complex 2 gave an analogous reaction mechanism.[10]

The zinc(II) complex **1b** is significantly more reactive (k_{cat}^h=6 x 10^2 M^{-1} sec^{-1}) than Woolley's model complex (X=OH) (k_{cat}^h=2 x 10^2 M^{-1} sec^{-1}).[16] In another model involving *tris*(imidazole) zinc(II) complexes (analogues of **3**), higher rate constants of HCO_3^- dehydration (k_{cat}^d=900–2800 M^{-1} sec^{-1}) were reported in 80% EtOH/H_2O at pH ca. 6.5. However, the system failed to mimic the characteristic pH profile for the hydration

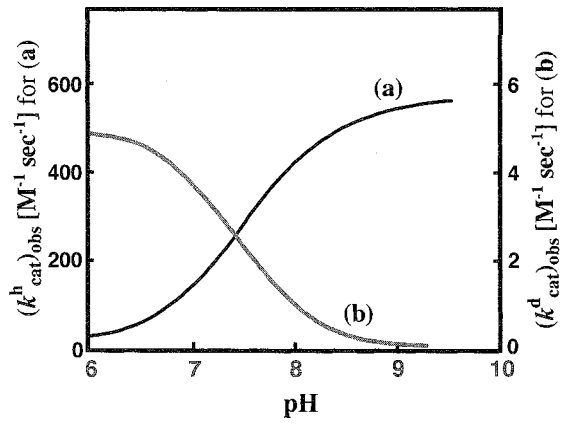

Fig. 1 The rate-pH profile for (a) CO_2 hydration and (b) HCO_3^- dehydration catalyzed by 1.

reaction and dehydration reaction of CA. The model complex 1 demonstrated the unique properties of a labile water molecule that is susceptible to substitution reactions with substrate HCO_3^-, anion inhibitors. and a nonlabile OH– ligand that acts as a nucieophile to attack CO_2. By changing the pH (around physiological pH). zinc(II) can choose either reactant. The zinc(II)-bound HCO_3^- has the choice to be substituted by O H for the reverse aqueous reaction at alkaline pH, or to lose CO_2 for the decasboxylation at acidic pH. In this context. it is of great significance that the bicarbonate anion (HCO_3^-) has the highest 1:1 affinity constant (K=[ZnL–$^-OCO_2H$]/ [ZnL][HCO_3^-]=$10^{4.0}$ M^{-1}) to 1a, only next to hydroxide anion (K=$10^{6.4}$ M^{-1}): e.g., K=$10^{1.3}$ M^{-1} for Cl^-, $10^{2.6}$ M^{-1} for CH_3COO^-.[5] Taken together. it is concluded that zinc(II) with a pK_a value of ca. 7 for the zinc(II)-bound H_2O is probably the most appropriate metal ion to perform the functions of CA at physiological pH. Also. the very high affinity of zinc(II) to HCO_3^- that binds as a monodentate ligand is a critical property of zinc(II) ion. If the metal were more acidic or had higher coordination numbers [e.g., cobalt(III) ion], HCO_3^- may be deprotonated to CO_3^{2-} and act as a bidentate ligand that would no longer be susceptible to decarboxylation.

OTHER CARBONIC ANHYDRASE MODELS

A *tris*(imidazolyl)phosphine zinc(II) complex 3. where X is a monodentate ligand (=OH . I^-, and NO_3^-), was synthesized and examined by x-ray crystal analysis.[11] The zinc@)-bound OH^- complex is claimed to be the first structurally characterized monomeric zinc(II) hydroxide complex sequestered by three imidazole groups and. therefore, may become an excellent structural model for the active site of carbonic anhydrase.

A *tris*(pyrazolyl)borate zinc(II) complex 4 (*R*=*p*-isopropylphenyl. *R'*=Me. *X*=OH^-) was prepared by mixing zinc(II) ion. ligand. and KOH in MeOH/ CH_2Cl_2.[15] Due to insolubility or instability of the zinc(II) complex in aqueous solution. the pK_a value for the zinc(II)-bound H_2O was not reported. The zinc(II)–OH in 4 showed sufficient nucleophilicity toward hydrolyzable substrates. carboxylesters, activated amides (β-lactam or CF_3CONH_2), and phosphonates in organic solvent. where the reactions are not catalytic but are stoichiometric. The seemingly high nucleophilicity of the *tris*(pyrazolyl)borate zinc(II) complex was attributed to steric hindrance and hydrophobic environment around the zinc(II)-bound OH . It is of interest to see whether 4 acts as a catalyst in H_2O-containing solvents. The earlier zinc(II)–OH^- species 1b and 2 (*X*=OH^-) catalytically hydrolyze esters,[3] β-lactams,[8] and *bis*(4-nitrophenyl) phosphodiester in aqueous solution.[4]

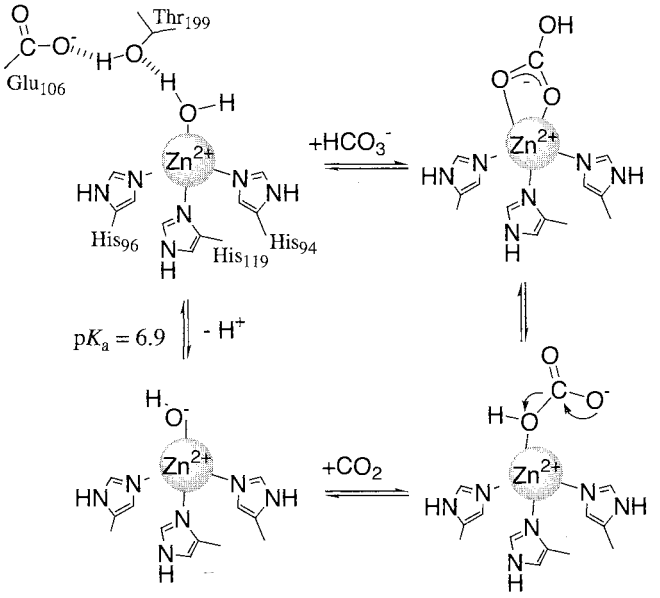

Fig. 2 A proposed mechanism of CO_2 hydration at the HCA II active center

As a structural model of the zinc(II)–OH^- species of carbonic anhydrase. the first mononuclear OH -bound zinc(II) complex 6 was prepared by mixing zinc(II) ion. the ligand. and KOH. and was characterized by x-ray crystal analysis.[12] The zinc(II)–OH^- complex **1b** is a cyclic trimer linked by three hydrogen bonds between each zinc(II)-bound hydroxide group, as shown by x-ray crystal study.[3] However, in aqueous solution. this trimer dissociates into monomeric zinc(II)–OH^- species **1b**. The zinc(II) complex **6** in $CHCl_3$ reacted immediately with CO_2, possibly to form a HCO_3^- complex 7 that ultimately and irreversibly gave a bridging carbonato complex 8. However. quantitative determination of the pK_a value for the zinc(II)-bound H_2O or of the nucleophilicity of 6 was not reported. The HCO_3^- complex **7** was characterized by IR spectroscopy [1675 and 1302 cm^{-1} for zinc(II)-bound bicarbonate].[11] The formation of the bicarbonate complex **7** is reversible, and removal of the CO_2 atmosphere results in regeneration of *6*. In view of the labile equilibrium between 6 and **7**. attempts to crystallize **7** were made under CO_2. However. a syminetrically bridging carbonato complex 8 was isolated instead. The hydroxide complex 6 effectively promoted the exchange of oxygen atoms (^{17}O) between CO_2 and H_2O, which somewhat served as a good functional model for CA. The authors suggested that the facile equilibrium between zinc (11)–OH– and zinc(II)–$^-OCO_2H$ may be a critical function for CA activity. An increased tendency toward bidentate coordination (due to stronger acidity) across the metal series (Zn^{2+}<Co^{2+}<Ni^{2+} and Cu^{2+}) was observed that resulted from stronger binding of the bicarbonate ligand. The authors concluded that in this context, too. zinc(II) ion is probably the best-suited metal for CA.

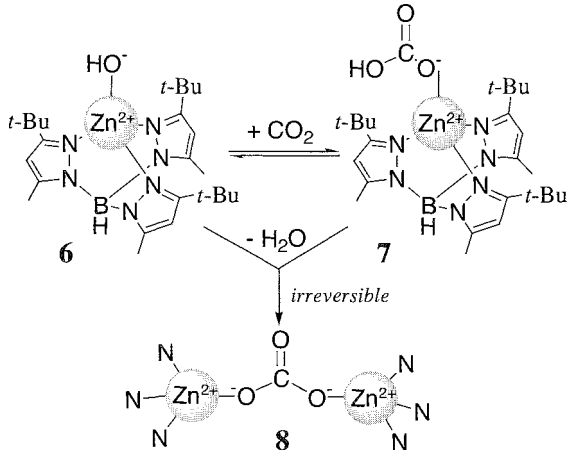

BASICITY OF ZINC(II)–BOUND HYDROXIDE IN CARBONIC ANHYDRASE

Aromatic sulfonamides are strong inhibitors of carbonic anhydrase. among which acetazolamide [K_D=6.0 nM for

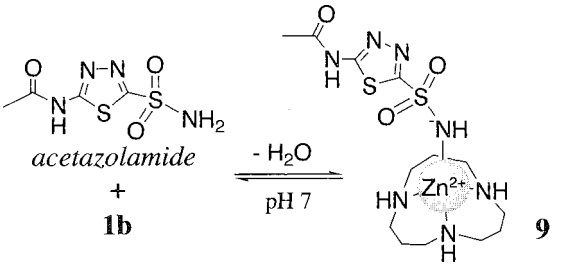

human carbonic anhydrase II (HCA *II)] at pH 7.4 is therapeutically prescribed as a diuretic* drug.[17] *A question as to how acetazolamide is bound to the active center appears to have been settled by x-ray crystal studies.''' although the precise inner-sphere binding* mode *of the sulfonamide to* zinc(II) *ion is not completely solved. The focal point is whether or not the sulfonamides are deprotonated. The resolution of* the *x-ray study was insufficient to afford a clear-cut answer. Chemically, it is puzzling that undeprotonated sulfonarnides* (pK_a=7–10) *can be good* donors, *forming strong coordination bonds with the* zinc(II) *ion.* One *of the pieces of indirect evidence for the deprotonation is that the lower the* pK_a *values of the* sulfonamides (e.g., pK_a *value of 7.4 for acetazolarnide). the* higher *the* 1:1 *affinity constants. On the basis of strong fluorescent complex formation of* CA *with dansylamide* (pK_a=9.9 *for the sulfonamide.* K_D = 0.25 μM *with HCA* II *at pH* 7.4[122]), *it was concluded that the deprotonated form of dansylamide binds to* zinc(II) *ion* at *the CA-active center. In any case, an interaction of the aromatic group of* dansylamide *with the protein must* make *a large contribution to the observed stability* of *the complex.* A *question concerning the intrinsic* zinc(II) *properties was whether it is acidic enough to displace the proton of sulfonamides, or* whether *the* zinc(II)-bound *O H (generated at physiological pH) is basic enough to neutralize the weak acid* sulfonamide *group. However, this fundamental* study *remained unaddressed. To date, only* model *studies give insight* into *the interaction of aromatic* sulfonamides *with* zinc(II) *ion.*

Treatment of a typical CA inhibitor. acetazolamidc with la. yields the product as a precipitate, which was identified as a 1:1 *complex 9. wherein the sulfonamide is deprotonated to coordinate with* zinc(II) *ions.''' It is of interest to point out that with other transition metal ions* (e.g., Ni^{2+}), *acetazolamide binds to the thiazole* N *but not to the deprotonated sulfonamide nitrogen. This different behavior of* zinc(II) *best illustrates its outstanding (hard) acid nature that favors the anionic* N^- *donor over the neutral (soft)* N *donor. The* pK_a value *of 7.4 for deprotonation of acetazolarnide is close to that for the* zinc(II)-bound H_2O *in 1. which would be extremely favorable for* simultaneous *coordination and* deprotonation *to yield the* 1:1 *complex* 9. *Aromatic sulfonamides*

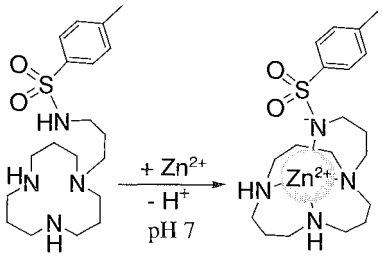

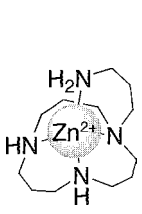

12

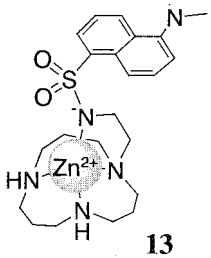

13

with higher pK_a *values are* more *difficultto deprotonate at neutral pH, and hence. the apparent* 1:1 *affinity with* zinc(II) *is weaker. More convincing evidence of the basicity of* zinc(II)-bound *O H was obtained at the interaction of* tosylamidopropyl-[12]aneN$_3$**10** *(HL) with* zinc(II) *ion.''' A* stable *amide-deprotonated complex* **11** (ZnL) *was formed at physiological pH, despite the* pK_a *of the* tosylamide *being 11.2. The structure of* **11** *was determined by an x-ray crystal analysis. The comparison of the complex stability for* **11** *(log* K=log([ZnL]/[Zn][L])=*14.7) with those of* ***la*** *(log* K=8.4) *and 12 (log* K=*11.7) indicates that* zinc(II) *ion in the* triamine *complex prefers the fourth ligand in the order of anionic nitrogen>neutral nitrogen>water. The complex 9 does not catalyze ester hydrolysis. Thus,* 9 *may represent chemically the* sulfonamide *inhibition of CA.* On the *basis of this model study, we consider that the* zinc(II) *coordinated by three* histidyl *imidazoles at the active center of* CA *(see Fig. 2)* is *sufficiently acidic to deprotonate the aromatic sulfonamides. Other neutral organic compounds, such as phenols and carboxylic acids. are also inhibitors of* CA.[17] *Similar acid–base properties should operate in their interactions.*

Recently. dansylamidoethyl-[12]aneN$_3$ *(the ligand of 13) as a model for the CA–dansylamide* complex *has been* synthesized.[23] *The* 1:1 zinc(II) *coinplex 13 was shown* again *to contain* zinc(II)-bound *sulfonamide*N^- *anion as a monodentate ligand by x-ray crystal analysis. The dan-*sylamidoethyl-[12]aneN$_3$ *is a novel type of* zinc(II)-fluo*rophore, which forms stable complexes with* zinc(II) *and* copper(II) *ions under physiological conditions. The* 1:1 zinc(II) complex *13 shows a* fluorescent *maximum at 538 (quantum* yield=0.19, 320-nm *excitation) in aqueous solution, while the free ligand shows a weaker fluorescence (quantum* yield=0.05). *The* copper(II) *complex. on the contrary.* completely *quenches the fluorescence. The* zinc(II)-dependent *fluorescence is quantitatively responsive at* μM *concentrations of* zinc(II) *ion and is not affected by the presence of* mM concentration *of biologically important metal ions. such as* Na^+, K^+, Mg^{2+}, *and* Ca^{2+}. *Because* Cu^{2+} *is strongly bound to amino acids, peptides, or proteins in ordinary biological* systems, *dan-*sylamidoethyl-[12]aneN$_3$ may *be useful for the* dynamic *analysis of the biologically important* zinc(II) *ion.*

From the kinetic study of **1b**-catalyzed *hydrolysis of 4-nitrophenyl acetate inhibited by various aromatic sulfonamides, the apparent* 1:1 *affinity constants* were *determined at pH* 8.4.[5] *A* comparison *of* intramolecular [$K_{intra}=10^{6.3}=K$(for **11**)/K(for *1a*)] *and intermolecular* ($K=10^{2.4}$ M^{-1} *for* **1a** *with p*-toluenesulfonamide) *contribution of p-toluenesulfonamide anion coordination to the* zinc(II)-[12]aneN$_3$ complex *gives an effective* molarity *of* $K_{intra}/K=10^{3.9}$ M *by the intramolecular location. These* 1:1 *anion complexation constants for the* zinc(II) *macrocyclic triamine complexes with various aromatic sulfonamides exhibit a trend paralleling that reported for* CA,[24] suggesting *a similar inhibition mechanism* [i.e., *the deprotonated sulfonamide anions can coordinate to the* zinc(II) *in a CA-active center].The effectivemolarity of the pendant sulfonamide in the model complex may be viewed as the noncoordinating contributions to bring the inhibitors to* the zinc(II) *center of CA.*

When going back to the question of the basicity of zinc(II)-bound OH^-, *we can conclude that despite* **1b** ($pK_a=7.3$ *for its conjugate acid* 1a) *being a weaker base than* aromatic sulfonamides *of higher* pK_a (e.g., $pK_a=10.5$ *for p*-toluenesulfonamide), zinc(II)–OH^- *can still* deprotonate *the aromatic sulfonamides. because the resulting sulfonamide anions* ($ArSO_2NH^-$) *have extremely strong interactions with* zinc(II), *compensating for the unfavorable* interaction *between the weak base and the weak acid. It may be inferred that while* NaOH *releases* OH^- *anion without any favorable contribution from* Na^+, ZnL–OH^- *releases OH-, with* ZnL^{2+} *waiting to accept the conjugate base.*

CONCLUSION

All of these recent CA *models qualitatively or quantitatively illustrate the importance of nucleophilicity of* zinc(II)-bound OH^- *species in aqueous or nonaqueous solutions. This aspect is important in almost all of the zinc enzymes and will be presented again* for *models of other hydrolytic enzymes. However, in* CA *and many other zinc enzymes. the basicity of the* zinc(II)-bound *hydroxide is similarly important. Although I offers an excellent* CA *model, its catalytic activity is moderate in* comparison *to* CA. *Model* 1 simply *shows the essence of the intrinsic properties of* zinc(II) *at the active center of CA. Other important features such as the hydrophobic pocket for* CO_2, *proton relay (network), and other structures in* CA[25,26] *are missing. More sophisticated next-generation models should be equipped with these functions.*

ARTICLES OF FURTHER INTEREST

Artificial *Enzymes*, p. 76
Enzyme Mimics. *p.* 546
Fluorescent *Sensors*, *p.* 572
Kinetics o j *Complexation*, *p.* 776
Zinc-Containing Enzymes and Their- Models, *p.* 1631

REFERENCES

1. Kimura. E.: Koike. T. Metalloenzyme Models that Answer Mysteries Surrounding the Intrinsic Properties of Zinc(II). In *Comprehensive Supramolecular Chemistry*; Reinhoudt. D.N.. Ed.; Elsevier Science Ltd.: Oxford, 1996: Vol. 10, 429–444.
2. Kimura. E.: Koike. T. Comments Inorg. Chem. 1991. 11. 285–301.
3. Kimura, E.: Shiota. T.: Koike. T.: Shiro, M.: Kodama, M. J. Am. Chem. Soc. 1990. 112. 5805–5811.
4. Koike. T.: Kimura. E. J. Am. Chem. Soc. 1991. 113. 8935–8941.
5. Koike, T.: Kimura. E.; Nakamura. I.: Hashimoto, Y.; Shiro. M. J. Am. Chem. Soc. 1992. 114. 7338–7345.
6. Zhang, X.: von Eldic, R.; Koike. T.: Kimura. E. Inorg. Chem. 1993, 32. 5749–5755.
7. Kimura. E.: Nakamura. I.; Koike. T.; Shionoya. M.: Kodama. Y.: Ikeda. T.: Shiro. M. J. Am. Chem. Soc. 1994. 116. 4764–4771.
8. Koike. T.; Takamura, M.: Kimura. E. J. Am. Chem. Soc. 1994. 116. 8443–8449.
9. Koike, T.: Kajitani, S.; Nakamura, I.: Kirnura, E.: Shiro. M. J. Am. Chem. Soc. 1995. 117. 1210–1219.
10. Zhang, X.: von Eldik, R. Inorg. Chem. 1995. 34. 5606–5614.
11. Kimblin. C.: Allen. W.E.: Parkin, G. J. Chem. Soc. Chem. Commun. 1995. 1813–1815.
12. Alsfasser. R.; Trofimenko. S.; Looney, A.: Parkin, G.: Vahrenkamp, H. Inorg. Chern. 1991. 30. 4098–4100.
13. Looney. A.: Han. R.; McNeill. K.: Parkin, G. J. Am. Chem. Soc. 1993. 115. 4690–4697.
14. Looney. A.; Parkin, G. Inorg. Chern. 1994.33. 1234–1237.
15. Ruf. M.: Weis. K.; Vahrenkamp. H. J. Chern. Soc. Chem. Commun. 1994. 135–136.
16. Woolley, P. Nature 1975, *258*, 677–682.
17. Botrè, F.; Cros. G.: Storey. B.T. *Carbonic Anhydrase*; VCH: Weinheim. 1991.
18. Khalifah. R.G. J. Biol. Chem. 1971. 246, 2561–2573.
19. Nair, S.K.: Calderone. T.L.: Christianson. D.W.: Fierker. C.A. J. Biol. Chem. 1991, 266. 17320–17325.
20. Eriksson. A.E.; Jones, T.A.; Lilijas, A. Proteins 1988. 4. 274–282.
21. Eriksson. A.E.: Kylsten. P.: Jones. T.A.: Lilijas, A. Proteins 1988. 4. 283–293.
22. Chen. R.C.: Kernohan. J.C. J. Biol. Chem. 1967. 242. 5813–5823.
23. Koike. T.: Abe, T.: Takahashi. M.: Ohtani, K.: Kimura. E.: Shiro, M. J. Chem. Soc., Dalton Trans. 2002. 1764–1768.
24. Taylor. P.W.: King. R.W.: Burgen, A.S.V. Biochemistry 1970. 9, 2638–2645.
25. Silverman. D.K. Acc. Chem. Kes. 1988. 21. 30–36.
26. Christianson. D.W.: Fierke. C.A. Acc. Chem. Res. 1996, 29. 331–339.

Carboxypeptidase A

Shinji Sueda
Hiroki Kondo
Kyushu Institute of Technology, Fukuoka, Japan

INTRODUCTION

Hydrolysis of proteins is found in all scenes of life, from fertilization. growth, and aging. to disease. Thus, it is not surprising to see a *large* number *of proteases that mediate these* proteolyses *to occur within or outside the cell. But when viewed from a* mechanistic *standpoint, they are classified into one of only several groups. They are serine proteases, cysteine proteases. acid* proteases, *and* metalloproteases. *Carboxypeptidase A (CPA. peptidyi-L-amino acid* hydrolase, EC *3.4.17.1) belongs to the last group and requires zinc ion for activity.* Another *way of dividing proteases is by using endopeptidase and exopeptidase. which cleave inner and terminal* peptide *bonds, respectively. As its* name *indicates. CPA cleaves* peptide *bonds* from *the carboxyl terminus sequentially. Herein.* the *structure and catalytic mechanism of* CPA *are described. but because a number of* excellent *reviews are already* available,[1–3] *emphasis is placed* mainly on *recent topics concerning this thoroughly studied enzyme.*

HISTORY AND OVERVIEW

The occurrence of CPA was first noted by Walschmidt-*Eeitz and Purr in* 1929.[4] *The physiological* function *of CPA is* to *digest foodstuffsin the intestine. Proteinaceous foodstuffspartially digested by pepsin in the stomach are further processed into smaller* peptide fragments *or even into amino acids for reabsorption in the large intestine. CPA* is *synthesized in the pancreas and secreted to the intestine as inactive* zymogen (preproenzyme) *together with other proteases (see below). During this process,* multiple proteolytic *events occur on* CPA; *the signal* peptide is *cleaved from the* amino *terminus to form a proenzyme, and then an activation* peptide is *lost to* form *a fully active mature* enzyme *(see below).*

It is interesting to note that there is another carboxy-*peptidase. carboxypeptidase* B (CPB), *in the* same *tissue that has an* amino *acid sequence homologous to that of* CPA *but differs in substrate specificity. Whereas CPA prefers aromatic (phenylalanine. tyrosine, and tryptophan) or hydrophobic amino acid residues* (valine, leucine. *and isoleucine) at the C terminus; CPB prefers basic arginine and lysine residues there. This situation is reminiscent of the fact that the* same *tissue secrets other proteases, such as chymotrypsin and trypsin, both serine endopeptidases. which differ* in *their substrate specificity: the former prefers aromatic or hydrophobic amino acid residues. whereas the latter prefers basic residues.*

CPA seems to *occur only in mammals. but it should be noted that there is a related* Zn *endopeptidase,* thermolysin *(EC* 3.4.24.4), *in* thermophilic *bacterium Bacillus thermoproteolyticus. Although its amino acid sequence and three-dimensional structure are unrelated to CPA. the active site structure is similar. and the mechanism of action also seems to be* similar.[5] *This is an example of convergent evolution; just like the case of serine proteases mammalian chymotrypsin and microbial subtilisin.*

ASSAY

CPA is available commercially *in pure form.* Benzyloxycarbonylglycylphenylalanine (Z-Gly-Phe) *is one of the* commonly *used* substrates.[1] *The progress of reaction is conveniently tnonitored spectrophotometrically at* 220–*225 nm.* In *addition to* peptides, *esters such as* O-(*N*-benzoylglycyl)-L-β-phenyllactate (Bz-Gly-(O)Phe) *and* -L-mandelate *are hydrolyzed easily by* CPA. *Typical* Km *values for these artificial substrates are* 0.5–5 mM *with a turnover* number *of* 20 s^{-1} *for* amides *and* 100 s^{-1} *for esters under standard assay* conditions.[1]

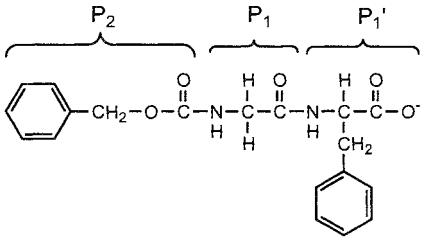

Z-Gly-Phe

Encyclopedia of Supramolecular Chemistry
DOI: 10.1081/E-ESMC 120012676

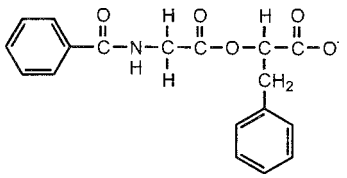

Bz-Gly-(O)Phe

PRIMARY STRUCTURE

The primary structure of CPA was determined first in 1969 for bovine enzyme.[1] Because of heterogeneity in the *N*-terminal sequence. three forms of CPA are generated: Form a is the largest with 307 residues, and Forms b and g lack 2 and 7 of the N-terminal residues, respectively. of Form a. In addition. allelic polymorphism was observed at three sites: Ile/Val, Ala/Glu, and Val/Leu at residues 179. 228. and 305. respectively.

It later turned out that there are isozymes of CPA, CPA1,[7] and CPA2[8] in some organisms. According to the cDNA sequence for rat CPA! gene,[7] the prepro-enzyme is coinposed of 419 amino acids (Fig. 1). The N-terminal 16 residues are cleaved upon secretion. and the following 94 residues are cleaved for activation of the enzyme, making the 111th residue (Ala) constitute the *N*-terminus of mature CPA. The gene for CPA1 is composed of 10 exons of 80–200 base pairs each, while that for CPB of 11 exons.[9] The N-terminus is encoded on Exon 2 in both cases. All of these carboxypeptidases seem to have evolved from a common ancestral protein, and their estimated evolutional relationship is illustrated in Fig. 2.[8]

```
atg aag aga cta ctg att ctg agt ctg ctg ctg gaa gca gtc tgt ggc aat gag aac ttt gtg gga cac cag gtt
MET LYS ARG LEU LEU ILE LEU SER LEU LEU LEU GLU ALA VAL CYS GLY ASM GLU ASN PHE VAL GLY HIS GLN VAL  -86

ctc cga atc tct gca gcc gat gaa gcc cag gtg cag aaa gtg aag gag ttg gag gac ctg gag cac ttg cag ttg
LEU ARG ILE SER ALA ALA ASP GLU ALA GLM VAL GLM LYS VAL LYS GLU LEU GLU ASP LEU GLU HIS LEU GLN LEU  -61

gac ttc tgg cgg gac gct gcc cgg gcc ggt stc ccc att gat gtc aga gtg ccc ttc ccc agc atc caa tct gtg
ASP PHE TRP ARG ASP WLA ALA ARG ALA GLY ILE PRO ILE ASP VAL ARG VAL PRO PHE PRO SER ILE GLN SER VAL  -36

aaa gca ttc ttg gaa tat cat ggt att agc tat gag atc atg att gas gat gtg cag tta ctg ctc gat gag gag
LYS ALA PHE LEU GLU TYR HIS GLY ILE SER TYR GLU ILE MET ILE GLU ASP VAL GLN LEU LEU LEU ASP GLU GLU  -11

                                  1
aaa cag cag atg tct gcc ttc cag gcc agg gcc ttg tcc act gac tct ttc aat tat gcc acc tat cat acg ctg
LYS GLN GLN MET SEW ALA PHE GLN ALA ARG ALA LEU SER THR ASP SER PKE ASN TYR ALA THR TYR HIS THR LEU   15

gat gag atc tac gaa ttc atg gac ctg ctg gtg gct gag cac cca cag ctt gtg agc aag atc cag atc ggc aac
ASP GLU ILE TYR GLU PHE MET ASP LEU LEU VAL ALA GLU HIS PRO GLN LEU VAL SER LYS ILE GLN ILE GLY ASN   40

acc ttt gaa ggt cgc ccc atc cat gtg ctg aag ttc agc act gga ggg acc aat cgc cca gca atc tgg atc gac
THR PHE GLU GLY ARG PRO ILE HIS VAL LEU LYS PHE SER THR GLY GLY THR ASM ARG PRO ALA ILE TRP ILE ASP   65

act ggc atc cat tct agg gag tgg gtc acc cag gct agt gag gtc tgg ttt gca aag aag gtc acc aaa gac tat
THR GLY ILE HIS SER ARG GLU TRP VAL THR GLN ALA SER GLY VAL TRP PHE ALA LYS LYS VAL THR LYS ASP TYR   90

ggc cag gac ccc acc ttc aca gcc gtt ctt gac aac atg gac atc ttc ttg gag att gtc acc aac cct gat ggt
GLY GLN ASP PRO THR PHE THR ALA VAL LEU ASP ASN MET ASP ILE PHE LEU GLU ILE VAL THR ASN PRO ASP GLY  145

ttt gcc tac acc cac aaa acg aat cgc atg tgg cgc aag act cga tca cac acc cag ggc tcc ctc tgt gtt ggt
PHE ALA TYR THR HIS LYS THR ASN ARG MET TRP ARG LYS THR ARG SER HIS THR GLN GLY SER LEU CYS VAL GLY  140

gtg gac ccc aac agg aac tgg gac gct ggc tta ggg aag gcc gga gca agt agc aac ccc tgc tcg gaa act tac
VAL ASP PRO ASN ARG ASW TRP ASP ALA GLY LEU GLY LYS ALA GLY ALA SER SER ASN PRO CYS SER GLU THR TYR  165

cga ggc aaa ttt ccc aac tct gag gtg gag gtc aag tcc atc gtg gac ttt gtg acg agc cat ggg aac atc aag
ARG GLY LYS PHE PRO ASN SER GLU VAL GLU VAL LYS SER ILE VAL ASP PHE VAL THR SEX HIS GLY ASN ILE LYS  190

gcc ttc atc tcc atc cac agc tat tcc cag ctc ctg ctc tac ccc tac ggc tac acg tcg gaa cca gcc cct gac
ALA PHE ILE SER ILE HIS SER TYR SER GLN LEU LEU LEU TYR PRO TYR GLY TYR THR SER GLU PRO ALA PRO ASP  215

cag gca gag ctg gat cag cta gct aag tct gct gtg aca gcc ttg acg tct cta cac ggg acc gag ttc aag tat
GLN ALA GLU LEU ASP GLN LEU ALA LYS SER ALA VAL THR ALA LEU THR SER LEU HIS GLY THR GLU PHE LYS TYR  240

ggc agc atc atc gat aca atc tat caa gcc agt ggg agc act atc gat tgg acc tac agc cag ggc atc aag tac
GLY SER ILE ILE ASP THR ILE TYR GLM ALA SER GLY SER THR ILE ASP TRP THR TYR SER GLN GLY ILE LYS TYR  265

tct ttc act ttt gaa ctg agg gac act ggg ctt aga gga ttc ctg ctg cct gcc tcc cag atc atc cct acg gcg
SER PHE THR PHE GLU LEU ARG ASP TWR GLY LEU ARG GLY PHE LEU LEU PRO ALA SER GLM ILE ILE PRO THR ALA  290

gag gag aca tgg ctg gcc ctt ttg acc atc atg gac cac aca gtc aaa cac ccc tac tga
GLU GLU THR TRP LEU ALA LEU LEU THR ILE MET ASP HIS THR VAL LYS HIS PRO TYR *                      309
```

Fig. 1 Amino acid sequence of the prepro form of rat CPA1 deducecl from its cDNA sequence. taken from Ref. [6] with GenBank accession number 500713. The peptide bonds cleaved during secretion and activation are indicated by arrows, and some of the key residues that appear in the text are boxed.

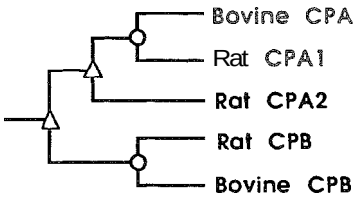

Fig. 2 Phylogenetic tree for carboxypeptidases CPA1. CPA2. and CPB from rat and cow, taken from Ref. [7]. The three enzymes seem to have evolved from a common ancestor. and the individual proteins were generated by gene duplication (triangles) and upon speciation (circles).

THREE-DIMENSIONAL STRUCTURE

The three-dimensional structures of bovine CPA alone and complexed with a poor substrate were solved by x-ray diffraction to high sesolution in 1970.[10] CPA is a globular protein of roughly ellipsoidal shape, with a dimension of 50 Å x 42 Å x 38 Å (Fig. 3a). The structure is composed of eight-stranded twisted β-sheets and nine x-helices which seemingly constitute two "bowls" facing each other. Between their boundary is the active site cleft, where His-49, Glu-72, and His-196 bind to Zn to form a nearly tetrahedral metal complex with the fourth ligand being water (Fig. 3b). Arg-145 forms a salt bridge with the C-terminal carboxylate of substrate, and Tyr-198, Ile-247. Tyr-265, and Phe-279 constitute a hydrophobic pocket to accommodate the side chain of the residue at P1′ (designating the residue nearest to the scissile peptide bond in the leaving group) of substrate. Some other residues that seem to play an important role in catalysis are Glu-270. Arg-127. and Tyr-248. The former is supposed to participate directly in catalysis, either as a base to abstract a proton from the zinc-bound water or as a nucleophile to undergo attack on the substrate carbonyl, as described below. The latter two residues seem to assist in the formation and collapse of a tetrahedral intermediate that forms during hydrolysis of amides and esters by donating a proton.

CHEMICAL MODIFICATION AND SITE-DIRECTED MUTAGENESIS

CPA is inactivated by alkylation of Glu-270 with *N*-bromoacetyl-*N*-methyl-L-phenylalanine,[11] suggesting that it plays an essential role during catalysis (see above). In addition to Glu-270. Tyr-248 is located in proximity to the reaction center, undergoes a large conformational change upon substrate binding. and is regarded to be one of the key residues for catalysis. For one thing, chemical modification of this and probably other tyrosine residues by acetylation or nitration affected the catalytic activity of CPA drastically.[12] Peculiarly. however. these types of modification enhanced the esterase activity up to sixfold, whereas the peptidase activity decreased to Lower than 10%. suggesting that the catalytic mechanism may be different between peptides and esters. Alternatively. however. it is also possible that the rate-determining step may be different between the two types of substrates. though the mechanism is basically the same. It is easily

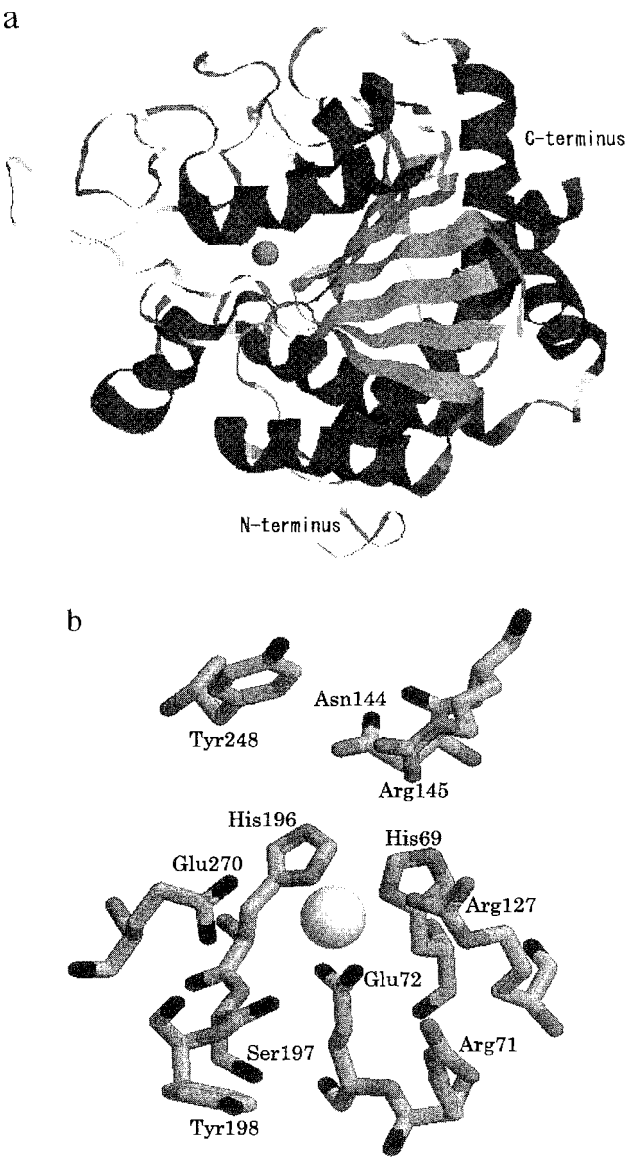

Fig. 3 (a) Three-dimensional structure of bovine CPA. taken from Ref. [10], with Protein Data Bank accession number 5CPA. For clarity. only the peptide backbone is depicted. (b) Nearly in the center of the ellipsoidal protein is the active site cleft where zinc (central sphere) is coordinated by His-69, Glu-72. His-196, and water (not shown).

imagined that in amides with a poor leaving group, the formation of a tetrahedral intermediate can be rate determining, whereas in esters having a good leaving group. the collapse of the intermediate could be the rate-limiting step. At any rate. the role assigned to Tyr-248 was a proton donor; it may donate a proton during the formation and collapse of a tetrahedral intermediate. If this is the case. replacement of Tyr-248 with any other amino acid will abolish all or most of its catalytic activity. Contrary to this expectation, an engineered enzyme with this Tyr replaced by Phe lost little activity, though the Km for substrates increased severalfold.[13] These data may be best interpreted to suggest that Tyr-248 does not serve as a key proton donor but instead is involved somehow in substrate binding. Instead of Tyr-248, which had long been regarded to be a plausible candidate, this electrophilic function seems to be played by Arg-127, as described below.

CATALYTIC MECHANISM

Upon binding to the enzyme, the carbonyl oxygen of a substrate seems to interact with the guanidium group of Arg-127. thereby enhancing polarization of the carbonyl to facilitate nucleophilic attack on the carbonyl carbon by Zn-bound water or Glu-270. The negative charge developing on the carbonyl oxygen and subsequent departure of the amino anion should be stabilized by proton donation from some group of the enzyme. Arg-127, rather than Tyr-248. seems to do this job.

There is dispute over the role of the active site Glu-270: one theory advocates a general base mechanism, while the other advocates a nucleophilic mechanism. If a nucleophilic attack on the substrate carbonyl by Glu-270 occurs, an acyl anhydride intermediate covalently bound to the enzyme is generated. If the general base is the real mechanism. no such intermediate intervenes. The putative acyl intermediate may be detected by some means, such as spectroscopic ones under cryo conditions or those trapped by suitable chemical agents such as hydroxylamine. There are claims for successful detection of a covalent intermediate.[14] but this assertion does not seem to be widely approved. In fact, the alternative general base mechanism appears to be more consistent with various data. Hence, the hydrolytic mechanism of CPA depicted in Fig. 4 is based on this notion.

SPECIFIC INHIBITORS

There are a number of natural and synthetic inhibitors known for CPA. Thus, a potent proteinaceous inhibitor was isolated from potato tuber that can inhibit not only CPA but also CPB with a Ki of 5 and 50 nM, respectively, but is inactive toward other common proteases, such as chymotrypsin and trypsin.[15] The mode of its inhibition was found to be a classical competitive one with respect to substrate, i.e., it binds to the same active site of the enzyme as do substrates; as later proven by x-ray crystallography.[16] The inhibitor is a mixture of two sequences of 38 or 39 amino acid residues with a single difference of whether a glutamine residue is present or not in Position 2 from the amino terminus. These proteins possess three disulfide bonds within the molecule. which may be responsible for the high thermostability for their size. This inhibitor binds to CPA at its C-terminus, but it is interesting to note that the C-terminal peptide bond between valine and glycine was already cleaved in the complex. In other words, the enzyme-inhibitor complex represents a complex of CPA and products. It is not known why further proteolysis of the truncated inhibitor does not proceed.

There are other CPA inhibitors reported from a parasitic roundworm *Ascaris lumbricoides*.[17] They have a molecular weight of 7.5 kDa. with about 65 residues that seem to be charge isomers. The apparent Ki values for

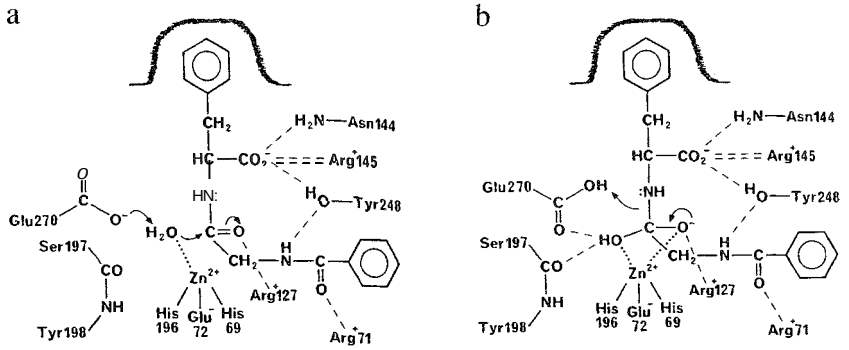

Fig. 4 The catalytic mechanism of CPA in the hydrolysis of peptides. taken from Ref. [3]. (a) Upon anchorage of a substrate to the active site, the carboxylate of Glu-270 triggers the reaction by abstracting a proton from zinc-bound water. which in turn. undergoes nucleophilic attack on the scissile carbonyl. (b) A tetrahedral intermediate is generated: its formation and collapse may be assisted by proton donation from Arg-127 or other residues.

bovine CPA lie in the nM range, but the stoichioinetry of binding is anomalous in that two moles of inhibitor bind per enzyme. The exact mode of binding to enzyme remains to be clarified. There is another CPA inhibitor known from the medicinal leech *Hirudo medicinalis*.[18] This inhibitor is composed of 66 amino acids. contains four disulfide bonds within the protein. and binds not only to CPA but also to CPB with a subnanomolar Ki (0.2–0.4 nM). Although amino acid sequence homology is rarely found between the inhibitors from potatoes and medicinal leech except for their C-termini, the mode of binding is siinilar in that their C-terminal carboxylate coordinates to the active-site zinc.[19]

Phosphoramidon [*N*-((*a*-L-rhamnopyranosyloxy)hydroxy-phosphinyl)-L-leucyl-L-tryptophan], a metabolite produced by *Streptomyces tanashiensis*. is a potent inhibitor of zinc metalloproteases, especially of thermolysin.[20] Synthetic phosphonate and phosphonamidate analogues of substrates are also potent inhibitors of CPA. The inhibitors containing (O)Phe at the PI' position of tri- or tetrapeptides are the most potent inhibitors; for example, the Ki of Z-Phe-Val^{P}-(O)Phe for CPA is as low as 11 fM.[21] a potency not far from that (1 fM) for the well-known. tightest binding of biotin with avidin. The phosphonate replacing the scissile peptide bond of substrates confers much higher affinity for CPA because of the resemblance of its structure to that of a putative tetrahedral intermediate of amide or ester hydrolysis (transition-state analogy). In fact, both of the phosphonate oxygen atoms are bound to zinc in the crystal of a complex of CPA and inhibitor.[22]

Much less potent as they are. aldehyde. ketone, and haloketone analogues of substrates are also reversible inhibitors of CPA. For example, (RS)-2-benzyl-4-oxobutanoic acid is a competitive inhibitor of CPA with a Ki of 480 nM.[23] These classes of compounds are more or less hydrated in water to form a gem-diol(ate), with a structure that mimics that of a putative intermediate of hydrolysis of substrates (see above). In other words. these compounds seem to serve as a transition-state analogue. just like the phosphonates described above. and hence. they bind more tightly than substrates. It may be noted that the structure of these transition-state analogues more closely resembles that of a putative intermediate of hydrolysis generated by

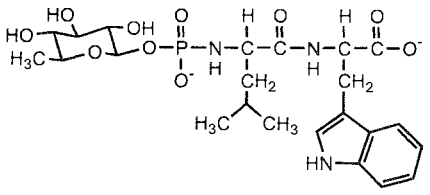

Phosphoramidon

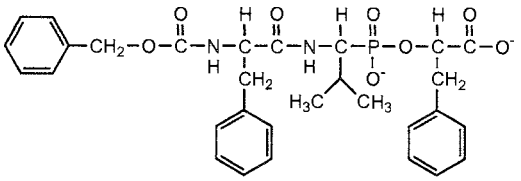

Z-Phe-Val^{P}-(O)Phe

the general base pathway than that generated by a nucleophilic attack by Glu-270.

TISSUE DISTRIBUTION AND ENZYMES RELATED TO CPA

CPA is basically localized in the digestive tract. but a transcript of its gene or the messenger RNA is detected in nonpancreatic tissues. such as in brain tissues, though CPA activity is not observable there.''] A plausible explanation for this observation is the occurrence of an inhibitor. In fact: such an inhibitor was reported. with a molecular weight of 26 kDa and a Ki for CPA of 3 nM.[25] The physiological significance of CPA activity and its inhibitor(s) in nonpancrealic tissues remain to be clarified.

CPA does not seem to have been a target of medication. but there are a number of related zinc metalloproteases in the human body, such as angiotensin-converting enzyme (ACE. EC 3.4.15.1), collagenase (EC 3.4.24.7), and enkephalinase (EC 3.4.24.11). Because these enzymes play a role in various physiological processes. they are good targets for the rational design of therapeutic agents.[26] In this respect. because CPA may be regarded as the prototype of all the zinc metalloproteases, its structure. free and complexed with substrate or inhibitor, and the mechanism of its action should give clues to the development of lead compounds capable of specifically regulating one of the zinc metalloproteases.

CONCLUSION

CPA is often used for sequencing protein samples. Whereas there is an effective way to sequence from the amino terminus, such as with Edman degradation with phenyl isothiocyanate, there are few such methods for sequencing from the carboxyl terminus (hyclrazinolysis is one such chemical method). Hence, digestion with CPA is a choice whe e one needs to know the amino acid sequence from the C-terminus. The time course of amino acid release is monitored on the amino acid analyzer. This way to use CPA seems to be made even more effective by immobilizing it on a solid support. Bovine enzyine was

immobilized covalently to polyacrylamide beads to 125 U/g solid.[27] The immobilized CPA exhibited characteristics nearly equivalent to chose of intact enzyme.

ARTICLES OF FURTHER INTEREST

Enzymes: Characteristics and Mechanisms, p. 554
Hydrogen Bonding, p. 658
Zinc-Containing Enzymes and Their Models, p. 1631

REFERENCES

1. Petra, P.W. Bovine procarboxypeptidase and carboxypeptidase A. Methods Enzymol. 1970, *31*. 460–503.
2. Kaiser. E.T.: Kaiser, B.L. Carboxypeptidase A: A mechanistic analysis. Acc. Chem. Res. 1972. *5*. 219–224.
3. Christianson. D.W.: Lipscomb. W.N. Carboxypeptidase A. Acc. Chem. Res. 1989. *22*, 62–69.
4. Walschmidt-Leitz. *E.;* Purr. A. Uber proteinase und carboxy-polypeptidase aus pankreas. Chem. Ber. 1929. *62B*, 2217–2226.
5. Matthews, B.W. Structural basis of the action of thermolysin and related zinc peptidases. Acc. Chem. Res. 1988, *21*. 333–340.
6. Bradshaw, R.A.; Ericsson. L.H.: Walsh. K.A.: Neurath. H. The amino acid sequence of bovine carboxypeptidase A. Proc. Natl. Acad. Sci. U. S. A. 1969. *78*, 1389–1394.
7. Quinto. C.: Quiroga. M.: Swain, W.F.: Nikovits. W.C.. Jr.; Standring. D.N.: Pictet, R.L.; Valenzurela, P.: Rutter, W.J. Rat preprocarboxypeptidase A: cDNA sequence and preliminary characterization of the gene. Proc. Natl. Acad. Sci. U. S. A. 1969; *79*. 31–35.
8. Gardell, S.J.; Craik. C.S.: Clauser, E.: Goldsmith. E.J.: Stewart. C.-B.; Graf, M.: Rutter, W.J. A novel rat carboxypeptidase. CPA2: Characterization. molecular cloning. and evolutionary implications on substrate specificity in the carboxypeptidase gene family. J. Biol. Chem. 1988. *263*, 17828–17836.
9. Clauser. E.; Gardell, S.J.: Craik. C.S.: MacDonald. R.J.: Rutter, W.J. Structural characterization of the rat carboxypeptidase A1 and B genes. Comparative analysis of the rat carboxypeptidase gene family. J. Biol. Chem. 1988. *263*, 17837–17845.
10. Lipscomb, W.N.: Reeke. G.N., Jr.; Hartsuck, J.A.: Quiocho. F.A.: Tethge. P.H. The structure of carboxypeptidase A. VIII. Atomic interpretation at 0.2 nm resolution. a new study of the complex of glycyl-L-tyrosine with CPA. and mechanistic deductions. Philos. Trans. R. Soc. Lond., B 1970. *257*. 177–214.
11. Hass, *C.M.:* Neurath. H. Affinity labeling of bovine carboxypeptidase AgLeu by *N*-bromoacetyl-*N*-methyl-L-phenylalanine. II. Biochemistry 1971, *10*, 3541–3546.
12. Riordan, J.F.: Sokolovsky. M.: Vallee. B.L. The functional tyrosyl residues of carboxypeptidase A. nitration u-ith tetranitromethane. Biochemistry 1967, 6. 3609–3617.
13. Gardell, S.J.: Craik. C.S.: Hilvert. D.; Urdea. M.S.: Rutter. W.J. Site-directed mutagenesis shows that tyrosine 248 of carboxypeptidase A does not play a crucial role in catalysis. Nature 1985, *317*. 551–555.
14. Makinen. M.W.; Kuo, L.C.: Dymowski. J.J.; Jaffer. S. Catalytic role of the metal ion of carboxypeptidase A in ester hydrolysis. J. Biol. Chem. 1979. *254*. 356–366.
15. Ryan. C.A.: Hass. G.M.: Kuhn. R.W. Purification and properties of a carboxypeptidase inhibitor from potatoes. J. Biol. Chem. 1974. *249*, 5495–5499.
16. Rees. D.C.; Lipscomb. W.N. Refined crystal structure of the potato inhibitor complex of carboxypeptidase A at 2.5 A resolution. J. Mol. Biol. 1982, *160*. 475–498.
17. Homandberg, G.A.: Peanasky. R.J. Characterization of proteins from *Ascaris lumbricoides* which bind specifically to carboxypeptidase. J. Biol. Chem. 1976. *251*. 2226–2233.
18. Reverter, D.: Vendrell. J.; Canals. F.: Horstmann, J.; Aviles. F.X.: Fritz. H.: Sommerhoff. C.P. A carboxypeptidase inhibitor from the medical leech *Hirudo medicinalis*. J. Biol. Chem. 1998. *273*. 32927–32933.
19. Reverter. D.; Fernandez-Catalan, C.; Baumgartner. R.: Pfandler. R.: Huber, R.; Bode, W.; Vendrell. J.; Holak. T.A.: Aviles. F.X. Structure of a novel leech carboxypeptidase inhibitor determined free in solution and in complex with human carboxypeptidase A2. Nat. Struct. Biol. 1999, 7. 322–328.
20. Komiyama, T.; Suda. H.; Aoyagi, T.; Takeuchi, T.; Umezawa. H.; Fujimoto, K.; Umezawa. S. Studies on inhibitory effect of phosphoramidon and its analogs on thermolysin. Arch. Biochem. Biophys. 1975, *171*. 727–731.
21. Hanson. J.E.: Kaplan. A.P.: Bartlett. P.A. Phosphonate analogues of carboxypeptidase A substrates are potent transition-state analogue inhibitors. Biochemistry 1989. *28*, 6294–6305.
22. Kim. H.: Lipscomb. W.N. Comparison of the structures of three carboxypeptidase A-phosphonate complexes determined by X-ray crystallography. Biochemistry 1991. *30*. 8171–8180.
23. Galardy, R.E.: Kortylewicz, Z.P. Inhibition of carboxypeptidase A by aldehyde and ketone substrate analogues. Biochemistry 1984. *23*, 2083–2087.
24. Normant. E.; Gros. C.; Schwartz, J.-C. Carboxypeptidase A isofornis produced by distinct genes or alternative splicing in brain and other extrapancreatic tissues. J. Biol. Chem. 1995. *270*. 20543–20549.
25. Normant. *E.:* Martres, M.: Schwartz. J.: Gros, C. Purification. cDNA cloning. functional expression, and characterization of 26-kDa endogenous mammalian carboxypeptidase inhibitor. Proc. Natl. Acad. Sci. U. S. A. 1995. *92*. 12225–12229.
26. Patchett. A.A.: Harris, E.: Tristram. E.W.: Wyvratt, M.J.: Wu. M.T.; Taub. D.: Peterson. E.R.: Ikeler. T.J.: ten Broeke. J.: Payne. L.G.: Ondeyka, D.L.: Thorsett. E.D.: Greenlee, W.J.; Lohr. N.S.: Hoffsommer, R.D.: Joshua, H.; Ruyle, W.V.: Rothrock. J.W.: Aster. S.D.: Maycock, A.L.: Robinson. F.M.: Hirschmann. R.; Sweet. C.S.: Ulm, E.H.: Gross. D.M.: Vassil, T.C.: Stone. C.A. A new class of angiotensin-converting enzyme inhibitors. Nature 1980, *288*. 280–283.
27. Vertesi. A.A.: Simon. L.M.: Kiss, I.; Szajani, B. Preparation, characterization and application of immobilized carboxypeptidase. Enzyme Microb. Technol. 1999, *25*. 73–79.

Carcerands and Hemicarcerands

Bruce C. Gibb
University of New Orleans, New Orleans, Louisiana, U.S.A

INTRODUCTION

In the words of Cram,[1] ''Carcerands are closed-surface, globe-shaped molecules with enforced hollow interiors large enough to incarcerate simple organic compounds, inorganic ions. or both.'' Although this term can be applied to a number of different chemical systems including cryptophanes[2,3] and even C_{60},[4] the term has become synonymous with shell-like molecules based on cavitands. More often than not, the hollow interior of a carcerand is occupied by a guest molecule. In these cases, the term. ''carceplex'' is used to describe the carcerand–guest complex.

By definition,'' it is not possible for the guest molecule or ion in a carceplex to escape without rupturing covalent bonds in the shell of the host or the guest. For those cavitand-based hosts that possess holes large enough for guest entry or egression to occur, the term ''hemicarcerands'' has been coined. The term for the corresponding host–guest complex is a ''hemicarceplex.'' In the archetypical hemicarceplex (vide infra), guest exchange is usually slow at room temperature.

Since their conception.'' carcerands and hemicarcerands have been used for a number of applications including trapping reactive intermediates and studying templation processes.[6] Examples of these applications,

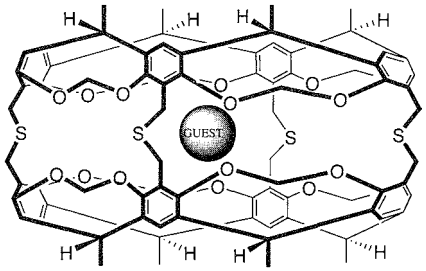

1

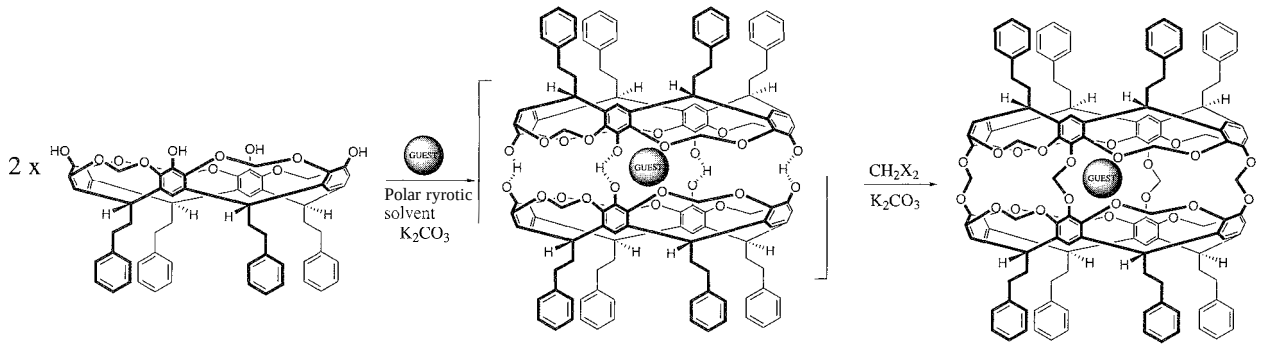

2 3

Scheme 1 The formation of carceplex 2.

as well as examples that demonstrate the structural variations to these types of molecules. are given belou.

CARCERANDS AND CARCEPLEXES

The first carcepiexes that were formed. 1, possessed very poor solubility.''' As a result. it was only possible to partially characterize mixtures of carcerands containing, among other species. dimethyl formamide and cesium chloride. The next generation of carcerands possessed larger. phenethyl ''feet'' and a different mode of linking together the two cavitand hemispheres.[8] Thus. two molecules of tetrol 2 were Iinked by acetal groups to form the more soluble 3 (Scheme 1). In the first examples of these types of carceplex reactions. the entrapped guests were the solvents of each reaction: dimethyl sulfoxide (DMSO). dimethyl acetamide (DMA), or dimethyl formamide (DMF). Yields of the isolated complexes were reinarkable: 61% for the DMSO complex. 54% for the DMA species. and 49% for the carcerand containing DMF. Addressing the question as to why these processes are so efficient has led to a greater understanding of templation by neutral molecules.[9,10] Thus, Sherman et al. identified the importance of the charged hydrogen bond ternary complex shown in Scheme 1. and determined that the differing topology of guests leads to a one-million-fold template effect.'''[11-14] The best template for the shell closure is pyrazine. which gave a yield of 87% of the corresponding carceplex when the poorly templating solvent, *N*-methyl-2-pyrrolidinone (NMP) was used. This

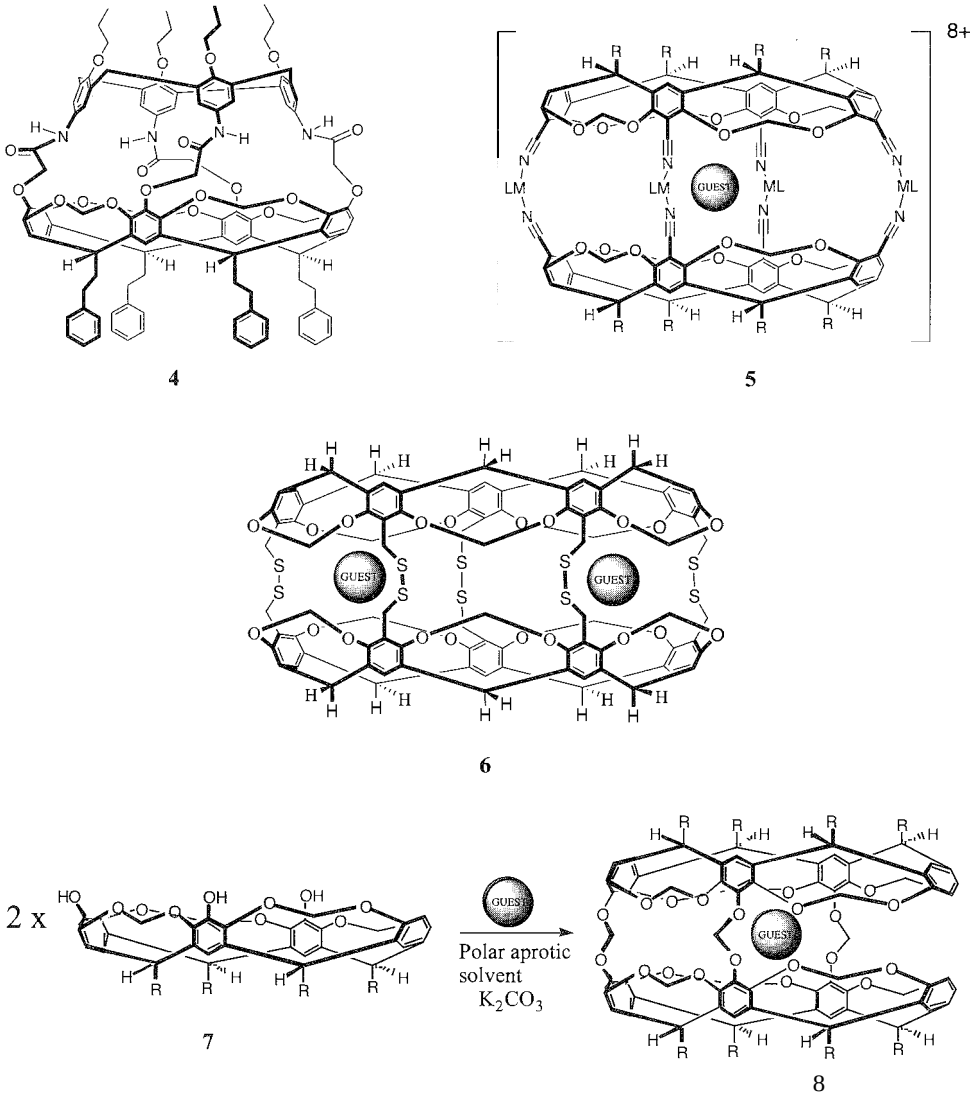

Scheme 4 Synthesis of the first hemicarceplex 8.

yield corresponds to a greater than 98% efficiency for each of the eight bonds formed.

A number of important variations to carceplexes such as **3** have been reported. For example, the Reinhoudt group synthesized carceplex **4**, which is one half cavitand and one half calixarene.[15] The lower symmetry of this derivative provided the opportunity to study how the guest can adopt different orientations within the confines of the shell. Another fascinating class of carceplex includes those that utilize metal links to join the two cavitand hemispheres. For example, Dalcanale's group in Parma synthesized carceplex **5** (M = Pd or Pt, R = $C_{11}H_{23}$), where the guest within the shell is one of the eight, triflate counterions.[16] The good thermal stability of the complex confirms its status as a carceplex, however, the shell-forming process was confirmed to be fully reversible by the addition of competing ligands such as triethylamine. Finally, a recent report from Sherman's group detailed the synthesis of complex **6** (Guest = DMF or DMA), the first carceplex derived from a [5]cavitand.[17] Details of how templation affects the synthesis of carceplex **6** were not given; however, the ideal guest is likely to be somewhat larger than the guests in complex **3**.

HEMICARCERANDS AND HEMICARCEPLEXES

There are two general types of hemicarcerand (and likewise two types of hemicarceplex).[6] Either one or two of the linking groups that join the hemispheres of molecules such as **3** can be removed to form lower symmetry analogues, or the linking groups can be elongated to engender D_{4h} hosts with much larger portals in their sides. It was the former that were synthesized first. As Sherman pointed out,[6] the isolation of significant quantities of triol **7** as a by-product in the synthesis of tetrol **2** inevitably led to the synthesis of the prototypical hemicarceplex **8** (Scheme 2). As expected, the formation of **8** is templated by the same types molecules as those most efficient in promoting the formation of **3**.[6]

The shell of **8** can be considered to be a molecular-sized reaction chamber capable of isolating reactive species from the external environment.[18] The first example arising from this line of reasoning was the photolysis of encapsulated α-pyrone and the resulting generation of cyclobutadiene.[19] Protected by the hemicarcerand shell, the normally highly reactive diene is stable at room temperature and was shown to exist in a singlet ground state.

As a rule, the longer the linking group inserted between the cavitand hemispheres, the weaker the templation and the lower the overall yield of the reaction. Be that as it may, the second approach to hemicarcerand formation, whereby four large linking units are inserted between the cavitand hemispheres, has led to a broad range of different hosts and host–guest complexes. A series of illustrative examples follow. Methylene-linked hemicarceplexes with up to six methylene units have been synthesized. The tetramethylene-linked derivative **9**[20] (Fig. 1) is perhaps the most studied of these, with a number of guest molecules as large as 1,2,3-trisubstituted benzene derivatives successfully encapsulated.[21–23] One of the more interesting guests reported inside **9** is *o*-benzyne.[21] Following on from using the shell of **8** as an inert reaction vessel, benzyne·**9** was synthesized by the photolysis of benzocyclobutenedione·**9**. As always, no reaction vessel is impervious to attack. Thus, over time, the highly reactive guest reacted with the relatively inert walls of **9** in an unusual intermolecular Diels–Alder reaction.[24]

By linking together cavitands with moieties that possess elements of chirality, a number of chiral hemicarceplexes including **10**[25] and **11**[26] were synthesized. These chiral hosts demonstrated chiral recognition in the presence of racemate guests. Linking groups can also be used to bestow sought after solubility properties to these hosts. The water-soluble hemicarceplex **12**, which was capable of binding a number of organic molecules, is one such example.[27]

All these hemicarcerands demonstrate hosting properties, the thermodynamic and kinetic aspects of which are intrinsically tied to the sizes and shapes of the cavity, portal, and guest. There is, however, a limitation to the

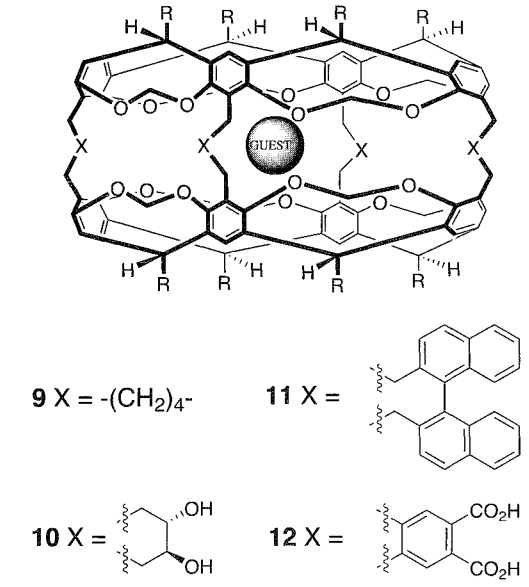

Fig. 1 Examples of hemicarceplexes based on tetrol **2**.

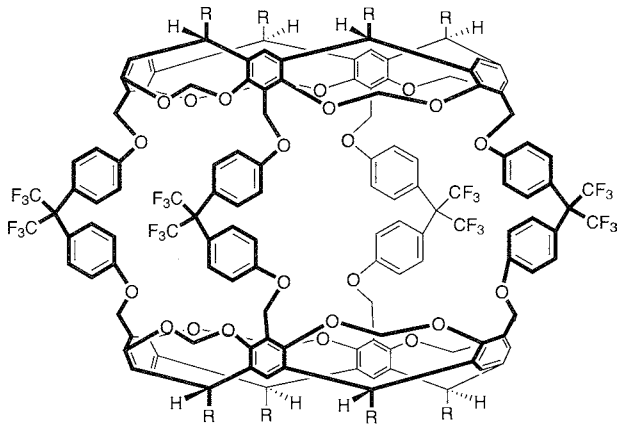

13

Scheme **3**

size of the host. Thus, as the linker groups and hence the portals increase in size, the cavity tends to become less defined. and guest complexation becomes more transient. Correspondingly, no complexation properties of large hemicarcerand **13**[28] have been reported.

CONCLUSION

d

We have defined the terms carcerand, carceplex, hemicarcerand. and hemicarceplex The formation of carcerands an carceplexes has led to some important information regarding templation by neutral molecules Similarly, the properties of hemicarcerands and hemicarceplexes has led to some interesting host–guest properties, including the storage of highly reactive species such as cyclobutadiene or benzyne

ACKNOWLEDGMENTS

This work was supported by the National Science Foundation (CHE-0111033) and the Donors of the Petroleum Research Fund. administered by the American Chemical Society.

ARTICLES OF FURTHER INTEREST

Cavitands, p. 219
The Template Effect, p. *1493*

REFERENCES

1. Cram. D.J.: Cram. J.M. *Container* Molecules *and Their Guests*; Royal Society of Chemistry: Cambridge. 1994.
2. Collet. A. Tetrahedron 1987. *43.* 5725–5759.
3. *Comprehensive Supramolecular Chemistry*; Lehn. J.-M., Atwood. J.L., Davis. J.E.D., MacNicol, D.D., Vögtle, F.. Eds.: Collet, A. Pergamon: New York. 1996: Vol. 2. Chapter 11.
4. Kobayashi. K.: Nagase, S. J. Am. Chem. Soc. 1997, *119*, 12639–12694.
5. Cram. D.J. Science 1983, *219.* 1177–1183.
6. Jasat, A.; Sherman. J.C. Chem. Rev. 1999. *99,* 932–967.
7. Cram. D.J.: Stewart, K.D.: Goldberg, I.; Trueblood, K.N. J. Am. Chern. Soc. 1985. *107.* 2575–2576.
8. Sherman, J.C.; Knobler. C.B.; Cram, D.J. J. Am. Chem. Soc. 1991, *113,* 2194–2204.
9. *Templated Organic Synthesis*; Diederich, F., Stang, P.J., Eds.: Wiley-VCH: Weinheim, 2000.
10. Chapman, R.G.: Sherman. J.C. Tetrahedron 1997, *53.* 15911–15945.
11. Chapman, R.G.: Chopra, N.; Cochien, E.D.; Sherman. J.C. J. Am. Chem. Soc. 1994. *116.* 369–370.
12. Chapman. R.G.: Sherman. J.C. J. Am. Chem. Soc. 1995. *117.* 9081–9082.
13. Nakamura, K.: Sheu, C.: Keating. A.E.: Houk. K.N.: Sherman. J.C.: Chapman, R.G.: Jorgensen, W.L. J. Am. Chem. Soc. 1997. *119.* 4321–4322.
14. Chapman. R.G.: Sherman. J.C. J. Org. Chem. 1998. *63.* 4103–4110.
15. Timmerman. P.: Verboom. W.: van Veggel. F.C.J.M.: van Duynhoven, J.P.M.: Reinhoudt. D.N. Angew. Chem., Int. Ed. Engl. 1994. *33.* 2345–2348.
16. Jacopozzi. P.; Dalcanale, E. Angew. Chem., Int. Ed. Engl. 1997, *36.* 613–615.
17. Naumann, C.: Place. S.; Sherman. J.C. J. Am. Chem. Soc. 2002. *124.* 16--17.
18. Warmuth. R. Eur. J. Org. Chem. 2001. 423–437.
19. Cram. D.J.; Tanner, M.E.; Thomas. R. Angew. Chem., Int. Ed. Engl. 1991. *30.* 1024–1027.
20. Robbins. T.A.; Knobler. C.B.; Bellew, D.R.: Cram. D.J. J. Am. Chem. Soc. 1994, *116.* 111–122.
21. Warmuth. R. Angew. Chern., Int. Ed. Engl. 1998. *36.* 1347–1350.
22. Kurdistani, S.K.: Helgeson, R.C.: Cram, D.J. J. Am. Chem. Soc. 1995, *117.* 1659–1660.
23. Robbins. *T.A.;* Cram. D.J. J. Am. Chem. Soc. 1993. *115.* 12199.
24. Warmuth. *R.* Chem. Commun. 1998. 59–60.
25. Park, B.S.; Knobler, C.B.: Eid. C.N.; Warmuth. R.; Cram. D.J. Chem. Commun. 1998. 55 - 56.
26. Judice, J.K.; Cram. D.J. J. Am. Chem. Soc. 1991, *113.* 2790–2791.
27. Yoon. J.: Cram, D.J. Chem. Commun. 1997. 497–498.
28. von dem Bussche-Hünnefeld. C.; Bühring, D.; Knobier. C.B.: Cram. D.J. Chem. Commun. 1995. 1085–1087.

Catalytic Antibodies

Kim D. Janda
The Scripps Research Institute and The Skaggs Institute for Chemical Biology, La Jolla, California, U.S.A.

Da-Wei Chen
Achillian Pharmaceuticals Inc., New Haven, Connecticut, U.S.A.

INTRODUCTION

Catalytic antibody research was derived from the demand for new biocatalysts and the existing knowledge of enzyme catalysis mechanisms. By challenging the immune system with haptens mimicking the structure of the transition state of a given reaction; antibodies can be elicited to bind congruent substrates, to stabilize the transition state of the reaction, and ultimately. to catalyze the targeted reaction."' Following this concept, antibodies succeeded in the catalysis of more than 50 chemical transformations.[2–4] Summarized in this article are important technologies used in generating catalytic antibodies and interesting applications derived from these biocatalyses.

BACKGROUND

An antibody, also termed an immunoglobulin, is a component of the immune system produced by B cells. Typically, an antibody (G-type) molecule is around 150 kDa in mass and has a Y-shaped configuration consisting of two longer identical polypeptide chains (heavy chains) and two shorter identical polypeptide chains (light chains). They are intimately held together by disulfide bonds. Each of these chains folds into domains of approximately 110 amino acids. At the *N*-terminal end of each chain are three regions of greatest sequence variability (nine to 12 amino acids long for each), referred to as complementarity-determining regions (CDRs). These hypervariable regions in total form the antigen-binding site. This combining region can be deep cleft for a small molecule or extended surface for a binding protein. Up to 20 kcal mol^{-1} of binding energy is estimated to be deliverable by an antibody. Within the human body, approximately 10^{10} different antibodies reside. Each has a unique specificity that can be made to recognize nonself substances. This diversity and specificity of an antibody results from the integration of a series of complicated but elegant DNA processes in a B cell known as gene rearrangements, which entail imprecise joining. and somatic hypermutations. during its maturation and differentiation. Because of the limitless number of antibodies that are available and the potential to tap into their binding energies makes antibodies attractive vehicles for catalysis.

Standard protocols with the key component known as hybridoma technology were established to produce monoclonal antibodies with predetermined specificity for small organic molecules.[5] The technique is based on three steps: 1) preparation and immunization of mice with a hapten-carrier protein conjugate; 2) immortalization of the antibody-producing B cells and the production of antibodies; and 3) selection and screening for catalysis.

Because antigen–antibody interactions occur in a defined region, the antigen-binding fragment of an antibody termed Fab usually provides the same binding affinity as a whole antibody molecule. Proteolytic cleavage of an antibody by papain leads to a Fab fragment, which also can be constructed by recombinant engineering. A single-chain variable fragment (ScFv) is a highly simplified version of an antibody containing the two essential V_H and V_L domains that form the binding site and a peptide linker (10–14 amino acids long) that prevents two domains from dissociating. Combinatorial libraries of ScFv can be created and are usually displayed on the surface of filamentous phage for high throughput selection.

ANTIBODIES AND CATALYSIS

Similar in many ways to the binding of enzymes to their substrates. antibodies bind to their antigens. with noncovalent interactions exhibiting high specificities and high affinities (association constants range from 10^4–10^{14} M^{-1}). Several mechanisms employed by enzymes to accelerate reactions can be adopted as rules to follow for creating catalysis in antibodies. These include transition-state stabilization, proximity effects. general acid–base, and cofactor catalysis. Hapten design is typically based on the mechanism for the reaction of interest and usually combines several external mechanistic factors in order to obtain highly efficient catalytic antibodies.

Encyclopedia of Supramolecular Chemistry
DOI 10.1081/E-ESMC 120012677

Transition-State Stabilization

The transition-state analogue (TSA) strategy is one of the major methods used to elicit catalytic antibodies. A tremendous number of studies were directed at producing antibodies with hydrolytic activity toward activated esters. carbonates, and amides because of the potential biological importance of these reactions. The mechanistic features of these reactions are well known to involve the attack of a water or hydroxide ion at a carbonyl center. forming an oxyanion. which is a transient tetrahedral intermediate. This is followed by decomposition of the tetrahedral intermediate to the corresponding acid and alcohol or amine. More than 80 cataiytic antibodies were generated against a variety of transition-state analogues, including phosphonates. phosphates, phosphonamidates. sulfones, sulfonamides, boronic acids. and hemiketals. Among this group. the tetrahedral phosphorus compounds have been the most successful in the generation of catalytic antibodies. This success was rationalized by the ability of these structures to resemble the oxyanion intermediate of a hydrolytic reaction in terms of configuration, negative charge distribution. and bond lengths. Catalytic antibodies elicited with phosphorus-based haptens usually have a key basic residue in their combining site that forms an oxyanion hole. This residue stabilizes the transient intermediate electrostatically and provides hydrogen bonds necessary for the catalytic process.

Antibody 48G7,[6] generated against a *p*-nitrophenyl phosphonate hapten, catalyzes the hydrolysis of an activated ester (Fig. 1A). From the crystal structure of the 48G7 Fab–hapten complex,[7] it is hypothesized that the source of catalysis is the stabilization of an oxyanion transition state formed in the reaction. Binding energy for catalysis is mainly derived from ArgL96, which forms an electrostatic interaction with the anionic phosphonate moiety embedded in the hapten, as well as the TyrH33 and HisH35 residues that form hydrogen bonds with the phosphonyl oxygen atoms in the hapten.

Analysis of the binding and catalysis data of 48G7 and its precursor germline antibody (which differs by nine amino acid residues) reveals that the dissociation constant K_d of the hapten–antibody complex decreased by $>10^4$ during affinity maturation, while the k_{cat}/K_m (catalytic efficiency) increased by 100-fold.[8] This study indicates that improvements in transition-state binding are positively correlated with improvements in catalysis, although only a small fraction of the additionally gained binding energy is converted to transition-state stabilization. Interestingly, none of the nine residues in which somatic mutations were fixed directly contact the hapten. This further indicates that the catalytic motifs were determined by a TSA at an early stage of antibody evolution. Affinity maturation in the case of 48G7 merely plays a conformational role. wherein there is reorganization of active-site residues to an optimal geometry for hapten binding rather than provision of new functional residues in the active site for catalysis.

Sequence comparison between 4867 and other hydrolytic antibodies generated with similar phosphonate TSAs reveals a high degree of conservation in the binding-site residues.'" Similar observations are obtained for three catalytic antibodies D2.3. D2.4, and D2.5. also elicited against a phosphonate TSA and identified by screening for catalytic activity through the entire hybridoma repertoire.[10] X-ray structural data indicate that the three antibodies use identical binding-site residues to stabilize the oxyanion intermediate, thus they all achieve catalysis in essentially the same mode. This strongly supports the notion that the immune system tends to quickly reduce the broad diversity initially existent in the antibody repertoire to a small number of "best solutions." However, structural convergence is not always the only solution adopted by the immune system to create catalytic antibodies using the TSA method.

Antibodies 6D9 and 7C8,[11] generated against a phosphonate transition-state analogue. hydrolyze a prodrug of chloramphenicol monoester to yield the parent drug chloramphenicol (Fig. 1B). Amino acid sequence analysis demonstrates that these antibodies share only 55% and 44% homology in V_L and V_H, respectively. Evidence from catalytic and binding assays. substrate specificity investigations, pH profiles, and chemical modifications indicates that different motifs and mechanisms are employed to achieve catalysis by these two antibodies. Judging by comparisons of differential binding energies K_S/K_{TSA} (dissociation constants for substrate *S* and TSA with antibody) and rate enhancements k_{cat}/k_{nucat}, the antibody 6D9 catalyzes hydrolysis solely by transition-state stabilization ($K_S/K_{TSA}=900$; $k_{cat}/k_{nucat}=895$). but 7C8 does not ($K_S/K_{TSA}=12$: $k_{cat}/k_{nucat}=707$).

Different binding modes are clearly shown in the structure complexes of the TSA (a compound without glutaroyl linker in the hapten) with 6D9 Fab and 7C8 Fab.[12] TSA binds to 6D9 in a folded form. with its two aromatic rings stacked and the trifluoroacetyl group buried deeply in the combining site. In contrast, the TSA is extended in a shallow groove in 7C8. The key side-chain residue is HisL27d, in 5D9 forming a hydrogen bond to the phosphoryl oxygen. In 7C8, TyrH95 is the critical residue that also determines a completely distinct catalytic mechanism from the former antibody. This diversity of catalytic antibodies generated against a single TSA hapten demonstrates that several catalytic solutions are available throughout the complete immune repertoire for a same reaction. Each provides a distinct starting point for reaching higher optimized efficiency.

More interestingly; functional residue arrays that provide a well-fashioned binding mode with a transition-state

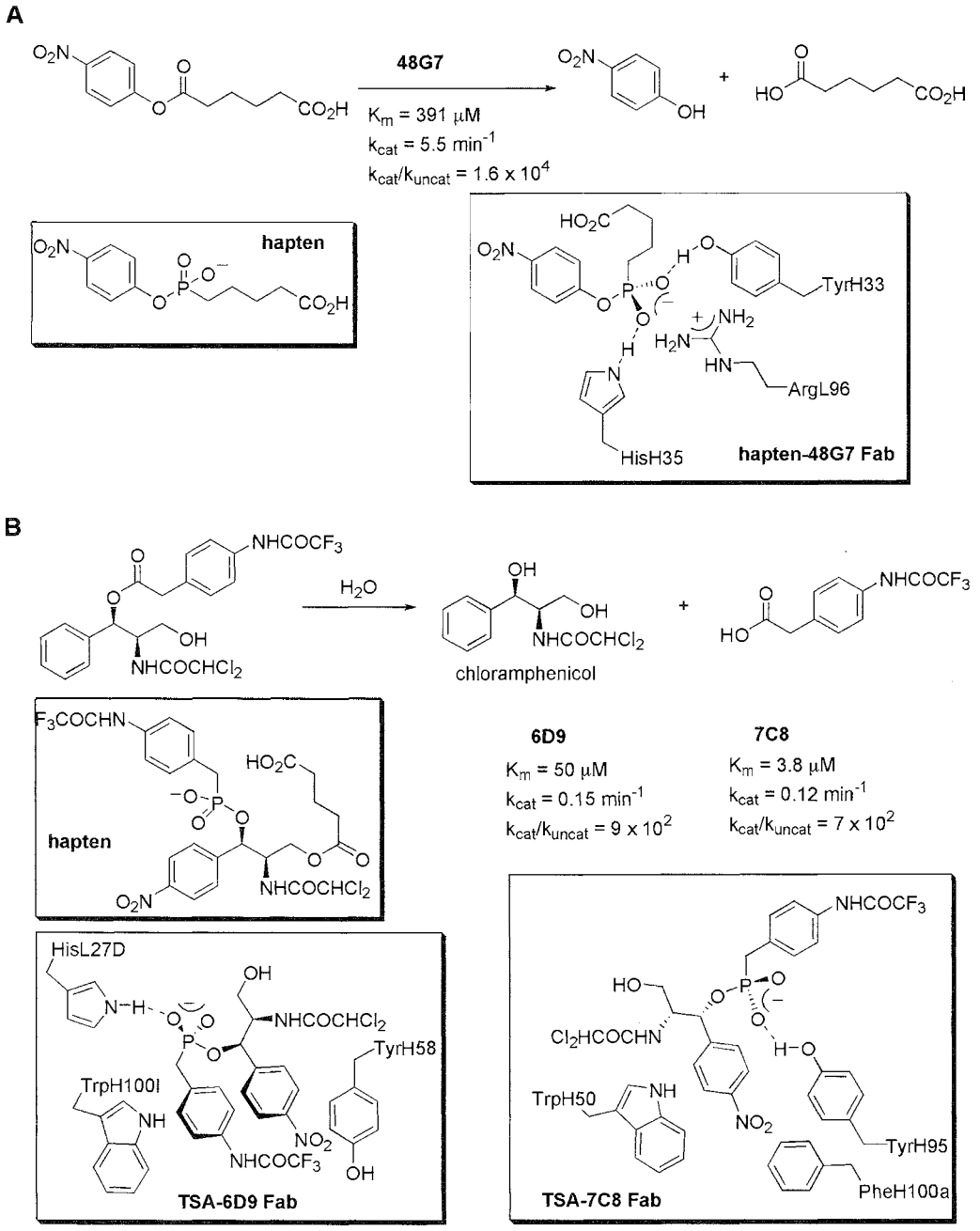

Fig. 1 (A) Antibody 48G7, elicited against a phosphonate hapten, catalyzes the hydrolysis of an activated ester. The hapten-48G7 Fab coinplex shows the key residues that comprise the oxyanion hole. (B) Two antibodies. 6D9 and 7C8, elicited against a phosphonate hapten, catalyze the release of chloramphenicol from its prodrug ester. The Fabs of 6D9 and 7C8, cocrystallized with a TSA (with the glutaroyl linker removed from the hapten), reveal completely different binding modes for the TSA.

analogue in the combining site can transform the antibody into a new catalytic factor in the reaction process. Antibody 43C9.[13] which was generated against a phosphonamidate, significantly accelerates the hydrolysis of an activated amide by a factor of 10^5 (Fig. 2A). Although there is a good match between the differential binding energy and rate enhancement (K_m/K_d=2.3 x 10^5; k_{cat}/k_{uncat}=2.5 x 10^5), solid evidence reveals that 43C9 employs covalent catalysis forming an acyl-antibody intermediate as its chemical mechanism to hydrolyze the p-nitroanilide substrate.[14]

Crystal structural data combined with a computational model of 43C9 scFv explained how active residues arrayed to bind a hapten turned to play an unexpected role of

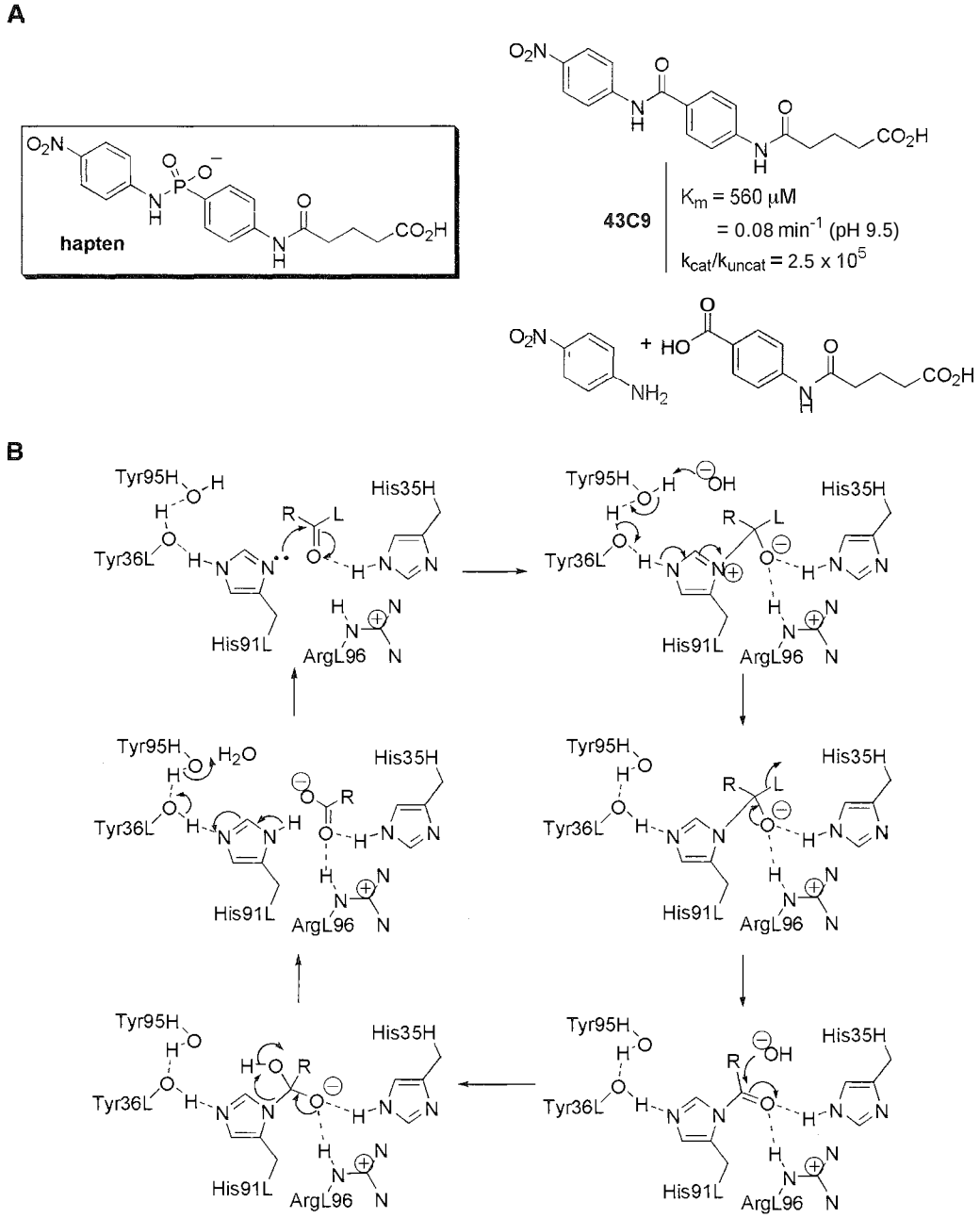

Fig. 2 (A) Antibody 43C9. elicited against a phosphonamidate hapten, catalyzes the hydrolysis of an activated amide. (B) Evidence reveals that antibody 43C9 employs a covalent catalytic mechanism. HisL91 is the nucleophile that attacks the substrate's amide carbonyl. Residue HisH35 assists in transition-state stabilization. while TryL36 and TryH95 are probably involved in proton transfer.

nucleophilic catalysis in the reaction.[15] In the combining site. HisL91 is arranged in a perfect orientation (N to carbonyl $C-4$ Å) for nucleophilic attack on the substrate. while TyrL36 and TyrL95 are involved in proton transfer. Residues ArgL96 and HisH35 assist in transition-state stabilization of the reaction by forming hydrogen bonds (Fig. 2B). This covalent mechanism demonstrates that the immune system has the ability to evolve unprogammed catalysis in antibodies with a simple TSA hapten to achieve higher catalytic efficiency.

Proximity Effects and Entropy Trap

In many cases. enzymes catalyze bi- or unimolecular reactions by providing organized active sites that collect substrates in sufficient proximity to react with one

another. or by freezing the substrates into reactive conformations. These processes lead to a decrease in the enthalpy of activation or an increase in the entropy of activation, or both, compared to the uncatalyzed reaction. Hence. they reduce the Gibbs' activation energy of reaction and accelerate the process.[16] An antibody combining site can be sculpted for shape complementarity to the reaction's transition state. Thus, changes in activation enthalpy and entropy from uncatalyzed to catalyzed reactions could be compensated with binding energy provided by the preorganized combining site.

Antibody 11F1-2E11[17] catalyzes a [3,3] sigmatropic rearrangement of chorismate to prephenate with a rate acceleration of 10^4 over the uncatalyzed reaction (Fig. 3A). This is only two orders of magnitude lower than the enzyme isolated from B. *subtilis*. In this scenario, the hapten is a shape mimic of a cyclic transition state having a pseudodiaxial conformation. It was programmed to induce a complementary combining site in the antibody that restricts the rotational degrees of freedom of chorismate and constrains it into a chair-like conformation; thereby inducing the reaction to occur. Kinetic analysis showed that the antibody-catalyzed reaction has 18.3 kcal mol^{-1} and -1.2 e.u. of activation enthalpy and entropy.[18] Compared to the 20.5 kcal mol^{-1} and -12.9 e.u. of activation enthalpy and entropy for uncatalyzed reaction. it is clear that antibody 11F1-2E11 successfully acts as an entropy trap to -accelerate the reaction.

Antibody 1E9,[19] the first catalytic antibody for the Diels–Alder reaction. catalyzes the cycloaddition between terachlorothiophene dioxide and *N*-ethylmaleimide. This reaction occurs via a bridged sulfone intermediate forming tetrachlorophthalimide through sulfone elimination and spontaneously oxidative aromatization (Fig. 3B). This catalyst displays an effective molarity ($EM = k_{cat}/k_{uncat}$) of 1000 M, which is extremely efficient for a bimolecular reaction catalyzed by an antibody. The hapten used to elicit this antibody is a derivative of endo hexachloronorbornene. which is a shape mimic of the transition state. Because it has less structural similarity to the aromatic product, product inhibition in the 1E9-catalyzed reaction is avoided.

Interestingly, experimentally determined entropy and enthalpy of activation for the catalyzed reaction indicate that 1E9 does not function as a classical entropy trap. as the activation entropy is even more negative than that of the uncatalyzed reaction in solution (-22.1 e.u. and -21.5 e.u for catalyzed and uncatalyzed reactions, respectively).[20] Instead. the enthalpy-controlled process by which the substrates are arranged to a reactive conformation in the combining site dominates the reaction. Thus, the rate enhancement of 1E9 is derived entirely from a reduction of the activation enthalpy of the reaction (11.3 kcal mol^{-1} and 15.5 kcal mol^{-1} for the catalyzed and uncatalyzed reactions. respectively). In fact, as crystallographic structural data and quantitative calculations indicated. the binding site of 1E9 provides over 120 van der Waal interactions to facilitate the correct organization of the substrate and an increased electrostatic complementarity compared to water to yield the catalysis observed.[21]

A particularly efficient mechanism for manipulating the entropic issue to attain rate acceleration is through covalent catalysis. Antibody 21H3 is a remarkably efficient catalyst for the transesterification reaction between sec-phenethyl alcohol and an enolic ester in water to form the corresponding chiral ester (Fig. 3C).[22]

The antibody is found to be highly efficient, with an effective molarity of approximately 10^6–10^8 M, corresponding to a gain of about 35 e.u. in entropy of activation. Steady-state kinetics show classic ping-pong behavior in double-reciprocal plots: indicating that the reaction proceeds through two half-reactions in which the initial step consists of formation of a covalent antibody complex. The maximum entropy loss is achieved with a tight fixation of one of the reacting partners to the antibody combining site. Moreover. the second step of the reaction shows an induced fit mechanism that involves transferring the acyl group from the covalent intermediate to the alcohol acceptor to form the product ester. The observed covalent intermediate and the induced fit mechanism of catalysis are the most notable features of this catalytic antibody, as it possesses catalytic machinery previously thought to be the purview of only highly evolved enzymes.

General Acid/Base Catalysis

For the reactions where the appropriate transition state analogues are not accessible or that require the involvement of a specific catalytic group in the reaction process, the strategic use of haptenic charges could generate antibody active residues acting as general acid/base catalysis. This strategy, also known as "bait and switch,"[23] relies on the fact that point charges in hapten can induce complementary but opposite point charges in the combining site of an antibody.

Antibody 43D4-3D3,[24] which catalyzes the β-elimination of a β-fluoro ketone with a rate acceleration of approximately 10^5 over that of the corresponding background reaction, is generated against an ammonium hapten (Fig. 4A). The positively charged alkyl ammonium ion is expected to induce a complementary negatively charged carboxylate residue in the antibody combining site. positioned to function as a general base in the reaction. Because hapten structure has less resemblance to the transition state of reaction, achieved catalysis is largely due to the presence of a catalytic base. Chemical modification and affinity-labeling experiments confirm

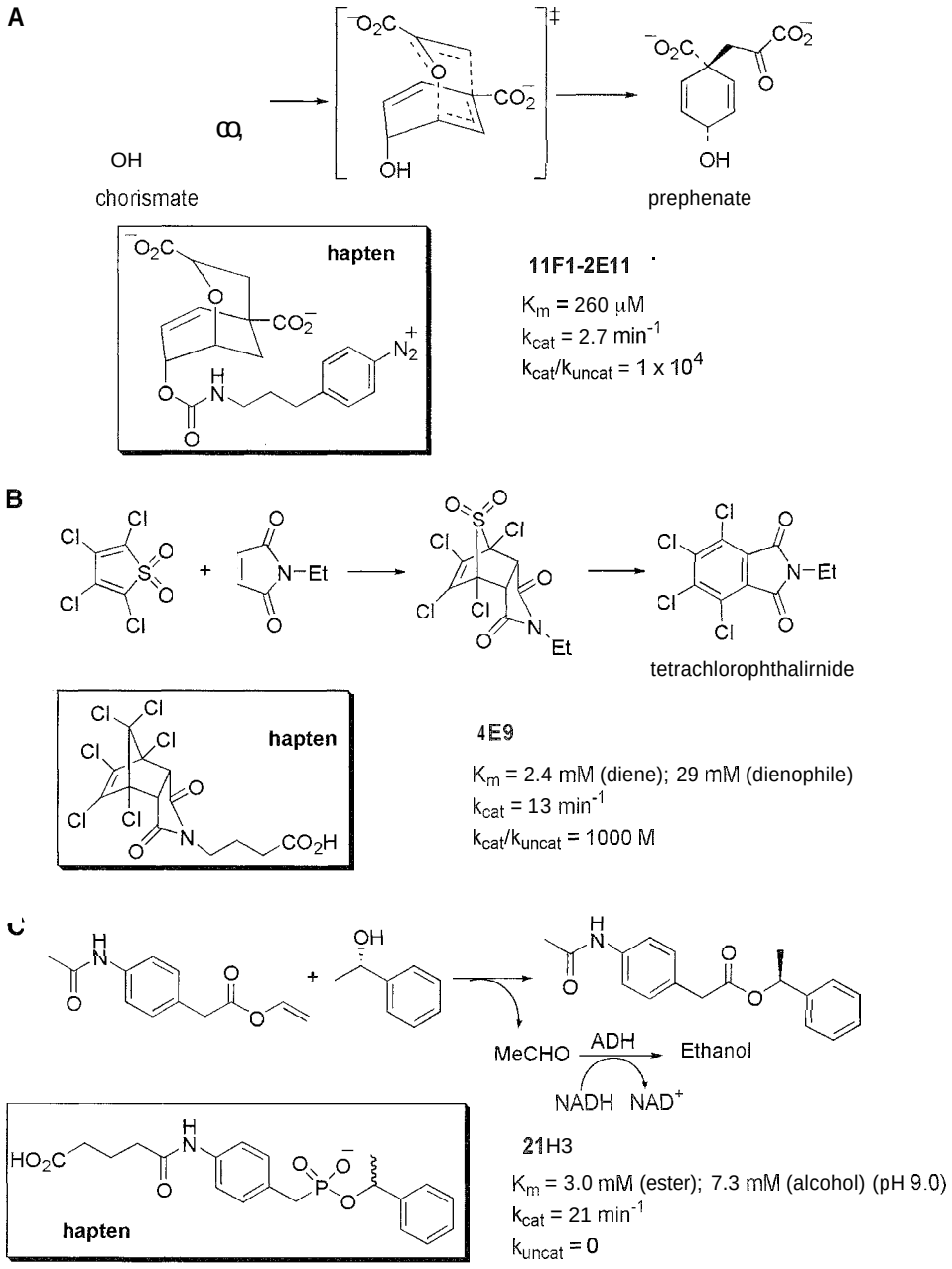

Fig. 3 (A) [3,3] Sigrnatropic rearrangement of chorismate to prephenate catalyzed by antibody 11F1-2E11. The hapten is a shape mimic of the cyclic transition state. (B) Antibody 1E9 catalyzes a Diels–Alder reaction of tetrachlorothiophene dioxide and *N*-ethylmaleimide. The hapten is comprised of the endo hexachloronorbornene unit. (C) Antibody 21H3A catalyzes the transesterification reaction between *sec*-phenethyl alcohol and an enolic ester to form a chiral ester. The hapten here is racernic phosphonate.

that the carboxylate side chain of GluH46 on 43D4-3D3 is responsible for removal of the proton in the elimination reaction.

General acid/base catalysis was also exploited to generate highly efficient catalytic antibodies for hydrolytic reactions.[25] A hapten with an *N*-methyl-pyridinium group was designed with a positive charge in order to elicit a negatively charged carboxylate, with an appropriate distance in space, acting as a general base or nucleophile for the acyl moiety to be hydrolyzed (Fig. 4B). Antibody 30C6, generated against this hapten, is found to accelerate the hydrolysis over a million-fold with its ester substrate. A pH rate profile of it reveals a basic form of a dissociable group with pKa of 6.25 evolved in the catalytic process. As a clear comparison for the success of the bait and switch strategy, no antibodies against a

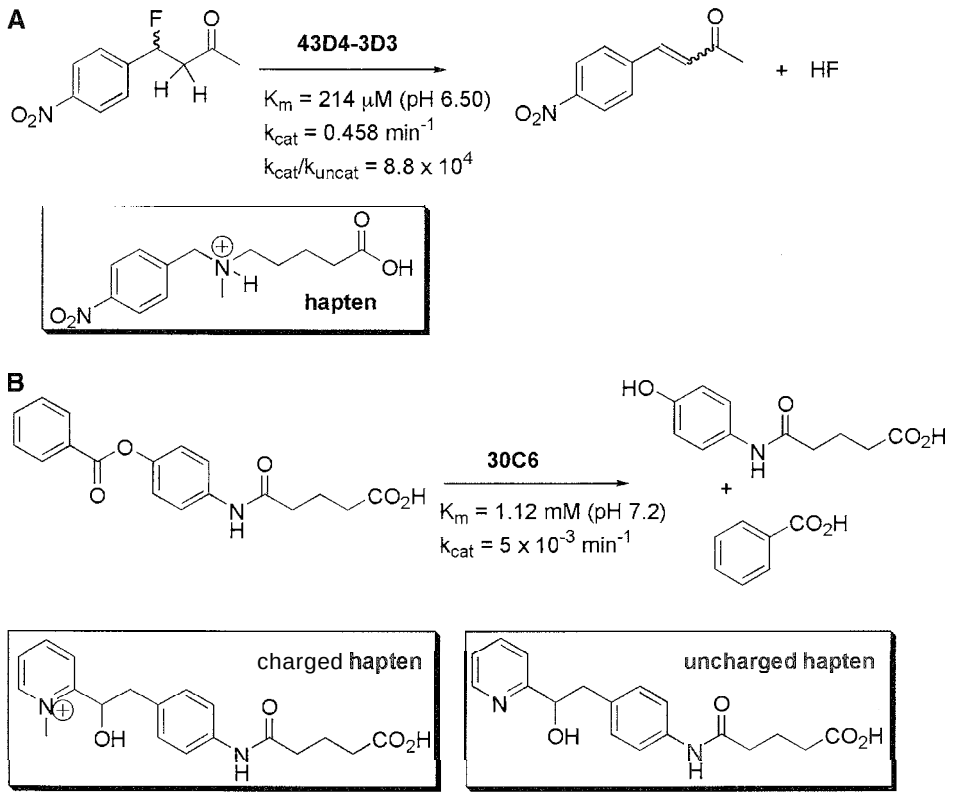

Fig. **4** (A) Antibody 43D4-3D3, elicited against an ammonium hapten, catalyzes an elimination reaction. (B) The hydrolytic reaction of an ester catalyzed by antibody 30C6. The pyridinium compound is the hapten used to elicit catalytic antibody 30C6. The uncharged hapten did not elicit catalysis for this reaction.

hapten that differs from the charged hapten by simply lacking a positive charge at physicological conditions are found to be catalytic.

It has further been demonstrated that by appropriate presentation of point charges on haptens, general acid/base catalysis could be achieved in a variety of catalytic antibody reactions, including condensation, isomerization, elimination, and hydrolytic reactions.

Cofactor Catalysis

Enzymes use nonpeptidyl catalytic auxiliaries termed cofactors to gain additional chemical functionality. These include metal ions, hemes, thiamine, flavins, and pyridoxal. To expand the scope of antibody catalysis, the introduction of cofactors into an antibody-combining site could be a powerful tool to improve catalysis. The diversity of the immune response should allow one to use not only the natural cofactors but also a host of unnatural cofactors unavailable to enzymes.

Antibody 28F11 achieves sequence-specific cleavage of the Gly-Phe bond at neutral pH with metal complex cofactor (Fig. 5A).[126] The hapten is designed to ensure correct approximation of the functional portions of the cofactor and substrate. Thus, a stable cobalt(III)-trien is linked to a peptide substrate for immunization, so that the antibody binding site could accommodate the substrate and trien simultaneously. The trien can form complexes with Co(III) as well as many other metal ions in the antibody binding site. Particularly effective metal ions include Zn(II), Fe(III), Ga(III), Cu(III), and Ni(II). The trien-Zn(II) as a cofactor is determined to have a k_{cat} of 6×10^{-4} s^{-1} and 400 turnovers per antibody binding site.

This principle of using a ligand analog or metal–ligand complex as a hapten to produce antibodies with cofactor catalysis was also applied to a number of redox-active cofactors.[27,28] Basically. antibodies generated by this method do not bind metal ions directly but bind them through ligand binding induce a metal ion into its combining site.

Antibody 3862 is a metalloantibody that incorporates mercury(II) as a Lewis acid cofactor.[29] It is generated against a coordinatively unsaturated mercury complex with the phosphorodithioate shown in Fig. 5B. In this case, the antibody-combining site is developed to coordinate directly to the metal and stabilize the

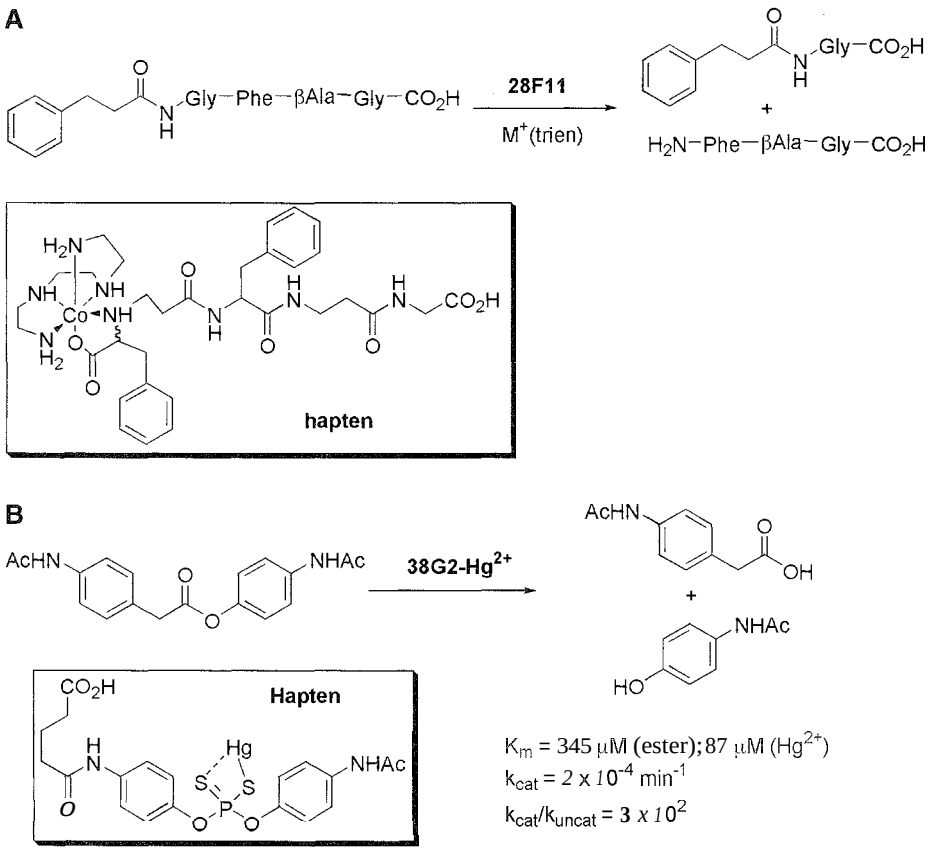

Fig. 5 (A) Antibody 28F11 catalyzes Gly-Phe bond cleavage. The hapten is a stable cobalt(III)-trien complex. (B) Antibody 38G2 specifically uses Hg(II) as a cofactor to catalyze the hydrolysis of an ester. The hapten in this case is a phosphorodithioate-Hg(II) complex.

transition state of the hydrolysis reaction simultaneously. Antibody 3802 is highly specific for Hg(II) *catalysis of the ester hydrolysis with a race enhancement of over 300-fold with multiple turnovers. Significantly, this approach opens new avenues for the exploitation of* metal cofactors *thought previously beyond the* realm *of even enzymes.*

IMPROVEMENTS IN THE GENERATION OF CATALYTIC ANTIBODIES

Toward the end of finding antibodies with new catalytic properties or greater efficiency,methodological and technical improvements have been continuously explored through the aspects of novel hapten design/immunization, enlargement *of pooi size of hapten-specific antibodies, and new screening and selection methods.*

One *of the* methods *has been termed "reactive* immunization."[30] *This strategy requires a reactive compound for immunization so that a chemical reaction takes place in the combining site of antibody during the process of induction. This chemical reaction is "ingrained" in the hybridoma and used later as part of the catalytic mechanism. Phosphonate diesters and* β-diketones *are two types of compounds explored as* haptens *to generate hydrolytic antibodies[31] and aldolase antibodies.[32]Reactive residues such as cysteine, serine, and lysine are elicited to form a covalent bond with the* haptens *in combining site.*

Combining transition state theory and reactive immunization *design into a single* hapten *can result in an increase in the output of catalysts* from *the immune* system *as well as their efficiency.[33]The synergistic application of these two approaches has been* employed *in the design of aidolase antibody 8463 (Fig.* 6A). In *the structure of* hapten *for this antibody. a* 1,3-diketone *moiety is* strategically *placed to induce lysine in the binding site,* mimicking *the mechanism of a Type I aldolas. In addition, a sulfone* is embedded *in the molecule, acting as transition state analogue of* C–C *bond formation between the enaminone intermediate and the acceptor aldehyde. Antibody 8463 catalyzes a retro-aldo reaction*

with rate enhancement of 10^8, and its catalytic proficiency is found to be 1000-fold higher than that of any other catalytic antibody.

A successful immune response to a given hapten will generate a large diversity of antibody-producing B cells. However. current procedures generally termed ''hybrid.ma technology'' are limited to the production of only a few hundred hybridoma clones. This inevitably results in a significant loss of initial diversity. Alternatively, antibodies can be produced using combinatorial cDNA libraries from immunized mouse spleen cells to generate antibody (or functional antibody fragments like Fab and scFv) libraries for screening and selection.[34] This technique provides libraries on the order of 10^8–10^9.

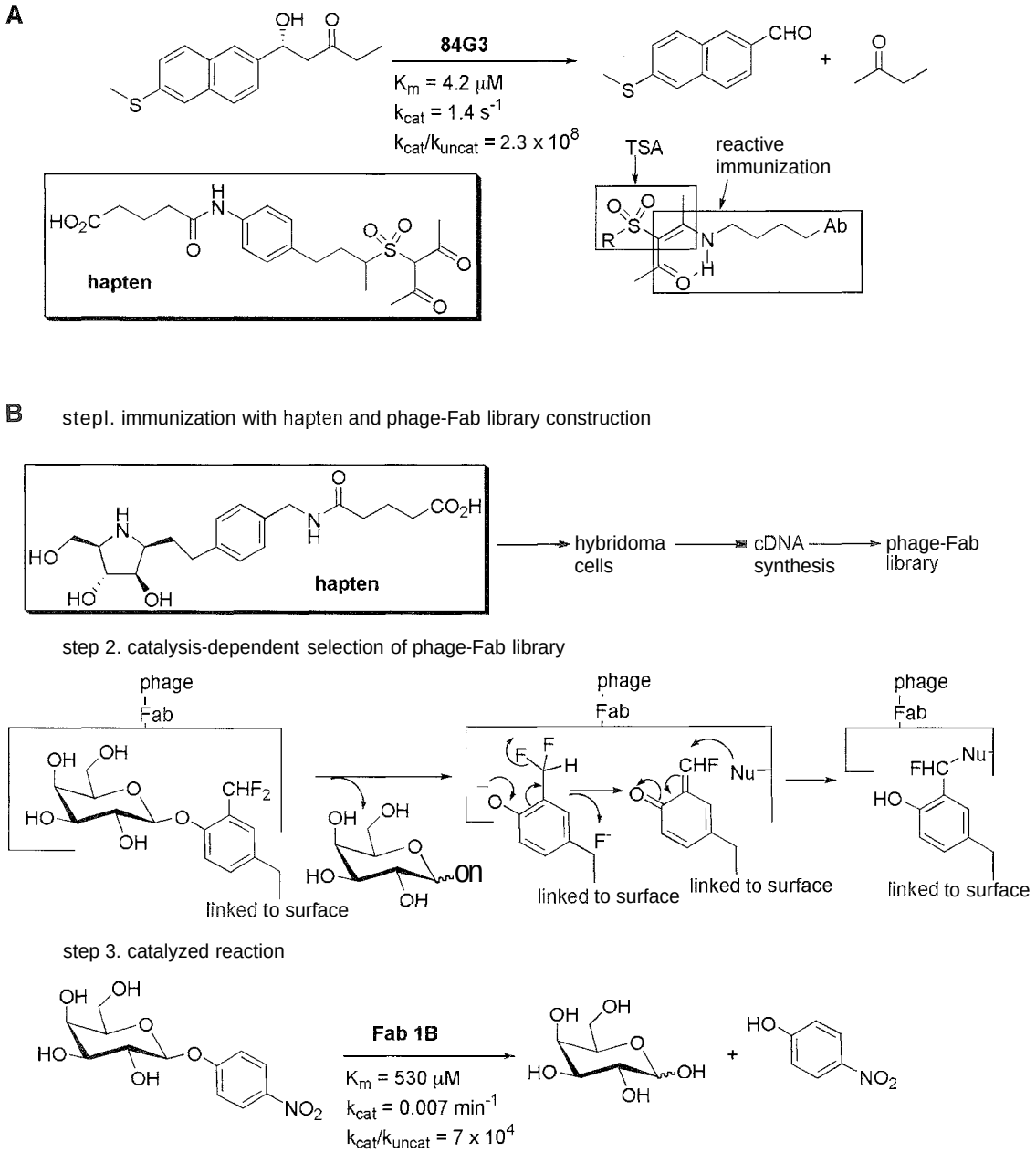

Fig. 6 (A) A retro-aldol reaction catalyzed by the antibody 8403. The hapten's structure combines reactive immunization and transition state analogue theory. (B) A phage-Fab library combined with direct selection of catalytic activity was used to discover the antibody catalyst Fab 1B for glycocidic bond cleavage.

Phage display technology facilitates the creation of such large libraries so tha-t the odds of finding a desired catalytic antibody are greatly increased.

Whether one uses hybridomas or phage libraries, screening and selection methods are crucial.[35] In essence, the screen or selection determines what products will be obtained from a library. and a poorly organized screen or selection can severely hamper catalytic searches. CatELISA,[36] which was developed from the conventional enzyme-linked immunosorbent assay (ELISA) for antibody affinity, uses substrate instead of hapten in the screening process. This then provides a more direct link to effectively screen for catalysis.

Fab 1B,[37] a catalyst for glycocidic bond cleavage, is selected from a phage-Fab library using a mechanism-based "trap" to uncover catalysts (Fig. 6B). Compared to the best antibody obtained from a simple hybridoma screen for binding, catalytic activity of Fab 1B is 700 times greater. This provides an excellent example, showing that if one can couple a clever design and selection strategy with a large diverse library, improved catalysts can be identified.

APPLICATIONS OF CATALYTIC ANTIBODIES

In Organic Synthesis

As antibody catalysis has progressed; one catalytic antibody, 38C2,[33] became commercially available, with much attention being drawn to its practical application in organic synthesis. In fact, there are many publications reviewing applications of antibody catalysis in asymmetric reactions,[38,39] pericyclic reactions,[40] cationic reactions:[41] and general organic synthesis.[42,43]

One of the most exciting developments in the catalytic antibody field is the demonstration of a disfavored

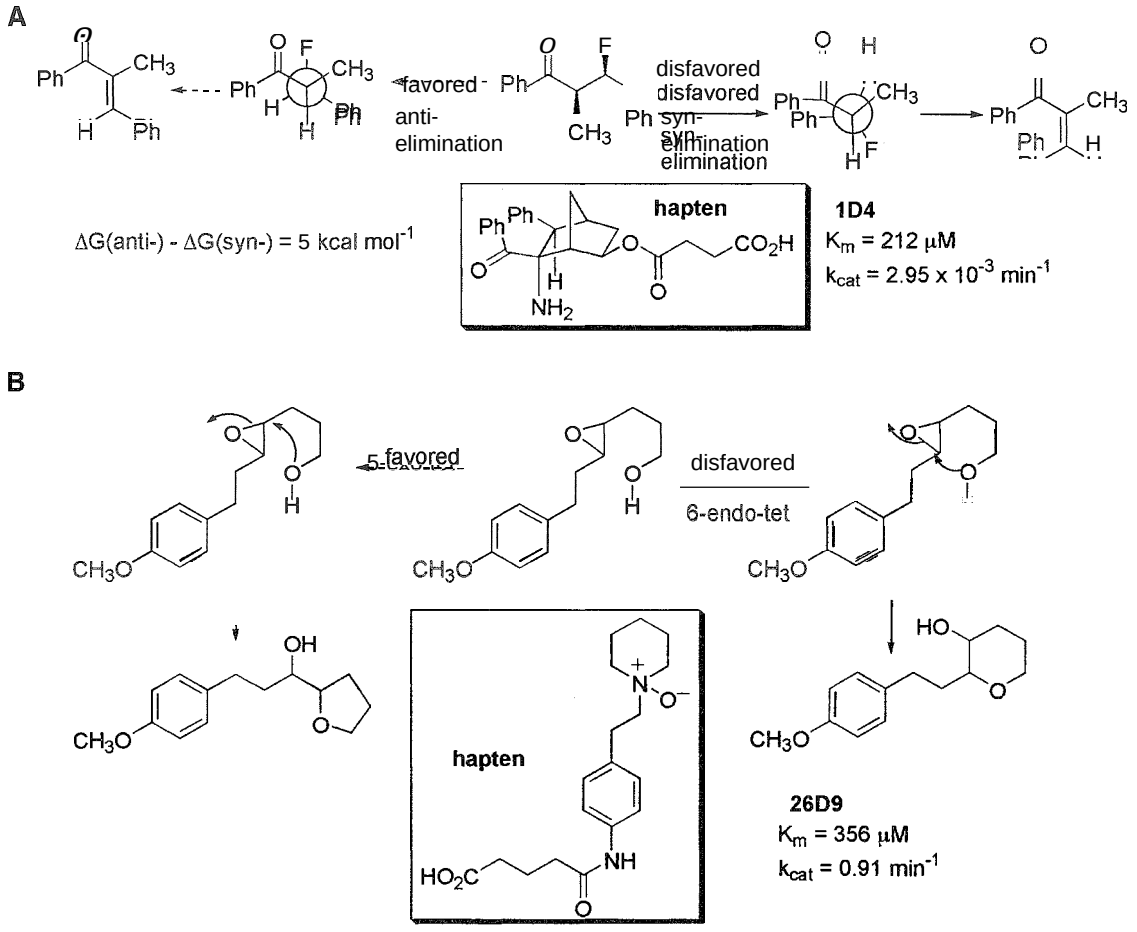

Fig. 7 (A) Antibody 1D4 catalyzes a disfavored *syn*-elimination reaction. (B) Antibody 26D9 catalyzes a difavored 6-endo-tet reaction.

chemical reaction providing products and stereochemical results that cannot be obtained under uncatalyzed conditions. Syn elimination[44,45] and an anti-Baldwin rules' cyclization[46,47] are examples of processes having unfavorable energy barriers that were surinounted through the use of antibody catalysis (Fig. 7A, B). Antibodies elicited against the appropriate hapten can provide sufficient binding energy to allow the disfavored process to become the only viable direction of a reaction in the antibody-combining site.

Other Developments

As a logical outgrowth of their utility in organic synthesis. catalytic antibodies are finding new applications in a wide variety of areas. Therapeutic use of catalytic antibodies is one of these emerging applications.[48] Acting as a local activation reagent, a catalytic antibody was found that demonstrates promising treatment for cancer.[49] Antibody catalysis to cure drug addiction[50] received broad interest from scientific and public communities. In addition, the generation of catalytic antibodies for polymer degradation[51] is another new avenue with industrial and environmental potential.

CONCLUSION

Catalytic antibodies have proven to be an outstanding platform on which to provide biocatalysts for many types of chemical transformations on a practical time scale. Antibodies can be programmed to achieve catalysis using the same mechanistic features employed by enzymes. Significantly, the short evolution time of a catalytic antibody is a highly desirable feature that allows for the discovery of catalysts in a matter of months versus enzyme evolution that takes years. As concepts and methods are no longer restricted to the TSA approach only, we are now seeing upper rate limits for catalytic antibodies on the order of 10^8, with some antibodies displaying catalytic efficiencies superior to the comparable natural enzymes. For many antibodies, however. improvement of catalytic efficiency is still necessary for their widespread utility. The increasing understanding in the structure–function relationship between haptens, combining sites, and catalysis should be helpful for designing and preparing better catalytic antibodies.[52] Clearly. biotechnological methods such as in vitro evolution could provide a powerful solution for the production of future generations of catalytic antibodies with greater efficiency.[53] The chemical versatility of catalytic antibodies in rerouting chemical transformations and the catalysis of nonenzymatic reactions. as well as the broad substrate tolerance, were demonstrated in organic synthesis. However. the most exciting feature for this new type of biocatalyst likely lies in the catalysis of reactions for which there are no natural enzyme counterparts.

ACKNOWLEDGMENT

We thank Mr. Jason Moss for reviewing the manuscript.

ARTICLES OF FURTHER INTEREST

Biological Ligands, p. *88*
Biosensors, p. *115*
Imaging und Targeting, p. 687

REFERENCES

1. Jencks. W.P. Strain, Distortion and Conformational Change. In *Catalysis* in Chemstn and *Enzymology*; McCraw-Hill: New York, 1969; 288–289.
2. Schultz. P.G.; Lerner, R.A. From molecular diversity to catalysis: Lessons from the immune system. Science 1995. 269. 1835–1842.
3. Thomas, N.R. Catalytic antibodies—Reaching adolescence. Nat. Prod. Rep. 1996. *13,* 479–511.
4. Blackburn. G.M.: Datta, A.; Denham, H.; Wentworth, P., Jr. Catalytic antibodies. Adv. Phys. Org. Chem. 1998. *31*, 249–392.
5. Harlow, E.; Lane. D. *Using Antibody:* A *Laboratory Manual*; Cold Spring Harbor Lab: Plainview, NY, 1999.
6. Lesley, S.A.; Patten, P.A.; Schultz, P.Z. A genetic approach to the generation of antibodies with enhanced catalytic activities. Proc. Natl. Acad. Sci. U. S. A. 1993. *90*, 1160–1165.
7. Wedemayer, G.J.; Patten, P.A.: Wang, L.H.: Schultz, P.Z.; Stevens, R.C. Structural insights into the evolution of an antibody combining site. Science 1997. 276, 1665–1669.
8. Patten. P.A.; Gray. N.S.: Yang, P.L.: Marks. C.B.: Wedemayer, G.J.; Boniface. J.J.: Stevens. R.C.: Schultz, P.Z. The immunological evolution of catalysis. Science 1996. 271. 1086–1091.
9. MacBeath, G.; Hilvert. D. Hydrolytic antibodies: Variations on a theme. Chem. Biol. 1996. *3*. 433–445.
10. Charbonnier, J.-B.: Golinelli-pimpaneau. B.; Gigant, B.; Tawfik, D.S.; Chap. R.: Schindler, D.G.: Kim, S.-H.; Green, B.S.: Eshhar. Z.: Knossow. M. Structural conver-

gence in the active sites of a family of catalytic antibodies. Science 1997, 275, 1140–1142.
11. Fujii, I.: Tanaka. F.: Miyashita. H.; Tanimura. R.; Kinoshita, K. Correlation between antigen-combining-site structures and functions within a panel of catalytic. antibodies generated against a single transition state analog. J. Am. Chem. Soc. 1995. *117*. 6199–6209.
12. Gigant, B.: Tsumuraya, T.; Fujii, I.; Knossow, M. Diverse structural solutions to catalysis in a family of antibodies. Structure 1999. 7. 1385–1393.
13. Janda. K.D.: Schloeder. D.; Benkovic. S.J.; Lerner. R.A. Induction of an antibody that catalyzes the hydrolysis of an amide bond. Science 1988. 241. 1188–1191.
14. Stewart, J.D.: Krebs. J.F.: Siuzdak, G.; Berdis, A.J.; Smithrud, D.B.: Benkovic, S.J. Dissection of an antibody-catalyzed reaction. Proc. Natl. Acad. Sci. U. S. A. 1994. 91, 7404–7409.
15. Thayer, M.M.: Olender, E.H.: Arvai, A.S.; Koike, C.K.; Canestrelli, I.L.; Stewart, J.D.: Benkovic. S.J.; Getzoof. E.D.: Roberts, V.A. Structural basis for amide hydrolysis catalyzed by the 43C9 antibody. J. Mol. Biol. 1999. 291, 329–345.
16. Bruice, T.C.: Lightstone, F.C. Ground state and transition state contributions to the rates of intramolecular and enzymatic reactions. Acc. Cheni. Res. 1999, 32, 127–136.
17. Jackson, D.Y.: Jacobs, J.W.; Sugasawara, R.; Reich, S.H.: Bartlett, P.A.: Schultz, P.G. An antibody-catalyzed Claisen rearrangement. J. Am. Chem. Soc. 1988. 110, 4841–4842.
18. Jackson, D.Y.; Liang. M.N.: Bartlett, P.A.: Schultz, P.G. Activation parameters and stereochemistry of an antibody-catalyzed Claisen rearrangement. Angew. Chem., Int. Ed. Engl. 1992, 31, 182–183.
19. Hilvert. D.: Hill. K.W.: Nared, K.D.: Auditor, M.-T.M. Antibody catalysis of a Diels–Alder reaction. J. Am. Chem. Soc. 1989. *111*. 9261–9262.
20. Xu, J.: Deng. Q.: Chen. J.: Houk, K.N.; Bartek. J.; Hilvert. D.; Wilson. I.A. Evolution of shape complementarity and catalytic efficiency from a primordial antibody template. Science 1999. *286*. 2345–2348.
21. Chen, J.: Deng, Q.; Wang, R.; Houk. K.N.; Bartek. J.: Hilvert, D. Shape, complementarity, binding-site dynamics, and transition state stabilization: A theoretical study of Diels–Alder catalysis by antibody 1E9. ChemBioChem 2000. *1*, 255–261.
22. Wirsching, P.; Ashley. J.A.; Benkovic, S.J.: Janda. K.D.: Lerner, R.A. An unexpectedly efficient catalytic antibody operating by ping-pong and induced fit mechanisms. Science 1991, 252. 680–685.
23. Lerner. R.A.: Benkovic, S.J. Principles of antibody catalysis. Bioassays 1988. 9. 107–112.
24. Shokat. K.M.: Leumann. C.J.; Sugasawara, R.: Schultz, P.G. A new strategy for the generation of catalytic antibodies. Nature 1989, *338*. 269–271.
25. Janda. K.D.; Weinhouse. M.I.; Schloeder, D.M.; Lerner, R.A. Bait and switch strategy for obtaining catalytic antibodies with acyl-transfer capabilities. J. Am. Chem. Soc. 1990, 112, 1274–1275.
26. Iverson, B.L.: Lerner. R.A. Sequence-specific peptide cleavage catalyzed by an antibody. Science 1989. 243, 1184–1188.
27. Cochran, A.C.: Schultz, P.G. Peroxidase activity of an antibody-heme complex. J. Am. Chem. Soc. 1990. 112. 9414–9415.
28. Nimri, S.: Keinan, E. Antibody-metalloporphyrin catalytic assembly mimic natural oxidation enzymes. J. Am. Chem. Soc. 1999, 121, 8978–8982.
29. Brummer. O.: Hoffman. T.Z.: Janda. K.D. Metalloantibody: Mercury(II)-dependent acyl transferases. Bioorg. Med. Chern. Lett. 2001. 9. 2253–2257.
30. Wirsching, P.; Ashley. J.A.; Lo. C.-H.L.; Janda. K.D.: Lerner. R.A. Reactive immunization. Science 1995. 270, 1775–1782.
31. Datta, A.; Wentworth. P., Jr.: Show, J.P.: Simeonov, A.; Janda, K.D. Catalytically distinct antibodies prepared by the reactive immunization versus transition state analogue hapten manifolds. J. Am. Chem. Soc. 1999, 121. 10461–10467.
32. Wagner, J.; Lerner, R.A.; Barbas, C.F., III. Efficient aldolase catalytic antibodies that use the enamine mechanism of natural enzymes. Science 1995. 270. 1797–1800.
33. Zhong. G.; Lerner. R.A.; Barbas. C.F., III. Broadening the aldolase catalytic antibody repertoire by combining reactive immunization and transition state theory: New enatio- and diastereoselectivities. Angew. Chem.. Int. Ed. 1999. 38, 3738–3741.
34. Burton, D. Monoclonal antibodies from combinatorial libraries. Acc. Chern. Res. 1993. *26*. 405–411.
35. Griffiths, A.D.: Tawfik, D.S. Man-made enzymes—From design to in vitro compartmentalization. Curr. Opin. Biotechnol. 2000. 11. 338–353.
36. Tawfik, D.S.; Green. B.S.: Chap, R.: Sela, M.; Eshhar. Z. catELISA: A facile general route to catalytic antibodies. Proc. Natl. Acad. Sci. U. S. A. 1993, 90. 373–377.
37. Janda, K.D.; Lo. L.-C.; Lo, C.-H.L.: Sim, M.-M.: Wang, R.; Wong, C.-H.; Lerner. R.A. Chemical selection for catalysis in combinatorial antibody libraries. Science 1997. 275, 945–948.
38. Hilvert. D. Stereoselective reactions with catalytic antibodies. Top. Stereochem. 8999. 22, 83–135.
39. Wentworth, P.. Jr.; Janda. K.D. Catalytic Antibodies. In *Comprehensive Asymmetric Catalysis*; Jacobsen, E.N.. Pfaltz, A.. Yamamoto. H.. Eds.; Springer-Verlag: New York, 1999: 1403–1426.
40. Tremblay. M.R.: Dickerson. T.J.; Janda, K.D. Advances in antibody catalysis of cycloaddition reactions. Adv. Synth. Catal. 2001. 343. 577–585.
41. Li. T.; Lerner, R.A.: Janda, K.D. Antibody-catalyzed cationic reactions: Rerouting of chemical transformations via antibody catalysis. Acc. Chem. Res. 1997. *30*, 115–121.
42. Rasserodt. J. Organic synthesis supported by antibody catalysis. Synlett 8999. 12. 2007–2022.
43. Reymond, J.-L. Catalytic antibodies for organic synthesis. Top. Curr. Chem. 1999. 200, 59–93.
44. Cravatt. B.F.: Ashley, J.A.: Janda. K.D.: Boger, D.L.;

Lerner, R.A. Crossing extreme mechanistic barriers by antibody catalysis: Syn elimination to a cis olefin. J. Am. Chem. Soc. 1994, *116*, 6013–6014.
45. Larsen, N.A.; Heine, C.L.; Cravatt, B.F.; Lerner, R.A.; Wilson, I.A. Structural basis for a disfavored elimination reaction in catalytic antibody 1D4. J. Mol. Biol. **2001,** 314, 93–102.
46. Janda, K.D.; Shevlin, C.G.; Lerner, R.A. Antibody catalysis of a disfavored chemical transformation. Science 1993. 259, 490–493.
47. Gruber, K.; Zhou, B.; Houk, K.N.; Lerner, R.A.; Shevlin, C.G.; Wilson, I.A. Structural basis for antibodycatalysis of a disfavored ring closure reaction. Biochemistry 1999, *38*, 7062–7074.
48. Jones, L.H.; Wentworth, P., Jr. The therapeutic potential for catalytic antibodies: From a concept to a promise. Mini-rev. Med. Chem. **2001,** 1, 125–132.
49. Shabat, D.; Lode, H.N.; Pertl, U.; Reisfeld, R.A.; Radcr, C.; Lerner. R.A.; Barbas, C.F., III. In vivo activity in a catalytic antibody-prodrug system: Antibody catalyzed etoposidc prodrug activation for selectivc chcmothcrapy. Proc. Natl. Acad. Soc. U. S. A. **2001.** 98, 7528–7533.
50. Carrera, M.R.A.; Ashley. J.A.; Parsons, L.H.; Wirsching, P.; Koob, G.F.; Janda, K.D. Suppression of psychoactive effects of cocaine by active immunization. Nature 1995. *378*, 727–730.
51. Chen, D.-W.; Kubiak, R.J.; Ashley, J.A.; Janda, K.D. Reactive immunization elicits catalytic antibodies for polyester hydrolysis. J. Chem. Soc., Perkin Trans., **12001,** 2796–2803.
52. Wentworth, P., Jr.; Janda, K.D. Catalytic antibodies: Structure and function. Cell Biochem. Biophys. **2001**, *35*, 63–87.
53. Takahashi, N.; Kaninuma. H.; Liu, L.; Nishi, Y.; Fujii, I. In vitro abzymes evolution to optimize antibody recognition for catalysis. Nat. Biotechnol. **2001,** *19*, 563–567.

Catenanes and Other Interlocked Molecules

Alexander Rang
Christoph A. Schalley
Kekulé-Institut für Organische Chemie und Biochemie der Universitdt, Bonn, Germany

INTRODUCTION

Since the concepts of "asymmetry" were developed by Jacobus Henricus van't Hoff, a scholar of Friedrich August Kekulé, and Joseph Achille Le Bel, in 1874. dealing with asymmetric carbon atoms. chemistry has developed rapidly: meso-compounds were found, and chiral allenes and biaryl systems with high rotational barriers were discovered. synthesized, and separated into their enantiorners. The same is true for molecules with planar and helical chirality. A newer form of chirality is topological chirality. which is, nevertheless. as fascinating as the long-known types. Catenanes (from the latin word "catena" for "chain") are two entangled macrocycles mechanically linked with each other. They cannot be separated without breaking a covalent bond, although they are not bound to each other by such a bond. These and other interlocked molecules are perfect examples with which to outline this topic in greater detail. These complex molecules cannot be obtained in adequate yields without templated synthesis. Therefore. we would like to address this topic in this article. New supramolecular complexes were found by the participating research groups as precursors for interlocked species and will be discussed. Also, catenanes feature some challenging properties as polymers. switches, or potentially as molecular machines. in that they are able to circumrotate. But how exactly do they rotate? The article will terminate with a brief discussion of their dynamic properties, which are due to the high flexibility of the mechanical bond.

MOLECULAR TOPOLOGY OF CATENANES AND KNOTS

Catenanes are not only mechanically bound molecules with enormous aesthetic appeal but also feature interesting topologies. The topology of a molecule is described by reducing the structure to its simplest form. the molecular graph, which neglects substituents and just follows the backbone of the molecule. Consequently, a inacrocycle is reduced to a simple circle that can be represented in a flat graph (Scheme 1). In topology. which as a certain type of geometry is a mathematical discipline. all transformations of an object are allowed that can be done and reversed by a continuous transition. Consequently, if two macrocycles are intertwined and connected by a mechanical bond, the result equals the molecular graph of a catenane. The graph is nonplanar. because both circles cross each other two times.[1] In other words. a simple catenane is characterized by the fact that any projection of the molecular graph on a plane will have two crossing points."' It is important to realize that the two rings cannot be separated without opening one of them. This would be a noncontinuous transition and is. therefore, forbidden in topology. The number of crossing points of a trefoil knot's graph is three, and once again, the graph is nonplanar (Scheme 1). Naturally. an infinite number of knots with more than three crossings exists and is waiting to be synthesized as chemical molecules.

TOPOLOGICAL CHIRALITY OF CATENANES AND KNOTS

Molecules possessing a nonplanar graph can. but do not necessarily. exhibit topological chirality. While molecular trefoil knots are inherently chiral. i.e., they do not require a particular arrangement of atoms to be chiral;[3,4] catenanes are achiral. because they require a particular arrangement of atoms or otherwise can easily be mirrored. As discussed by Schill,[5] an achiral catenane can be dissyinmetrized by suitable substitution. In fact, this approach is equivalent to one making use of macrocycles that bear a defined directionality due to a nonsyminetrical sequence of atoms. In 1995. Vogtle and his group reported the first synthesis of a chiral amide-based catenane containing one sulfonamide group in each of the two macrocycles[6,7] (Scheme 2). Due to the directionality defined from *S* to *N* in these sulfonamides, this catenane is topologically chiral. The enantioseparation of the catenane via HPEC on a chiral column was successful. and the CD spectra shown in Scheme 2 could be obtained.

It should be noted that in contrast to the mentioned trefoil knot. the square knot (Scheme 1) is achiral. Like the classical mesoform of tartaric acid. the square knot bears a mirror plane and. consequently, shows that symmetry considerations are important. For more complex

Encyclopedia of Supramolecular Chemistry
DOI: 10.1081/E-ESMC 120012769

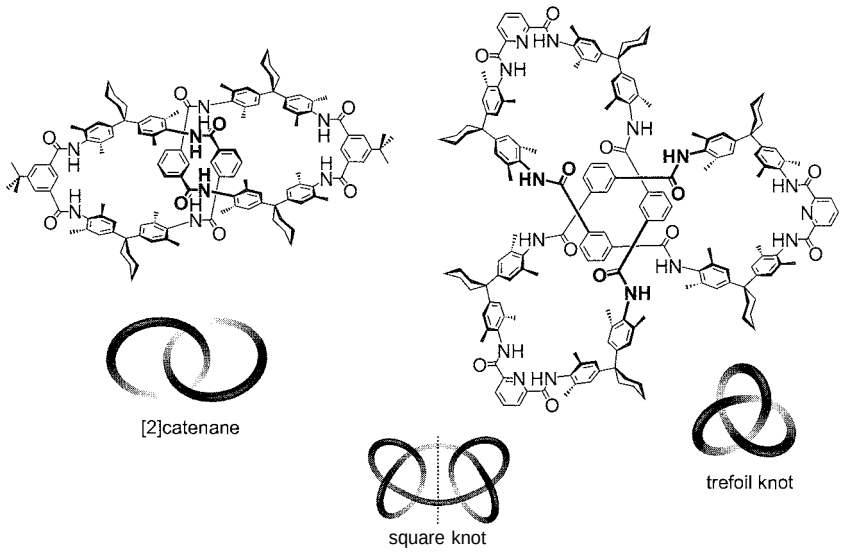

Scheme I Molecular formulae and molecular graphs of a [2]catenane and a trefoil knot. Bottom: Graph of a square knot.

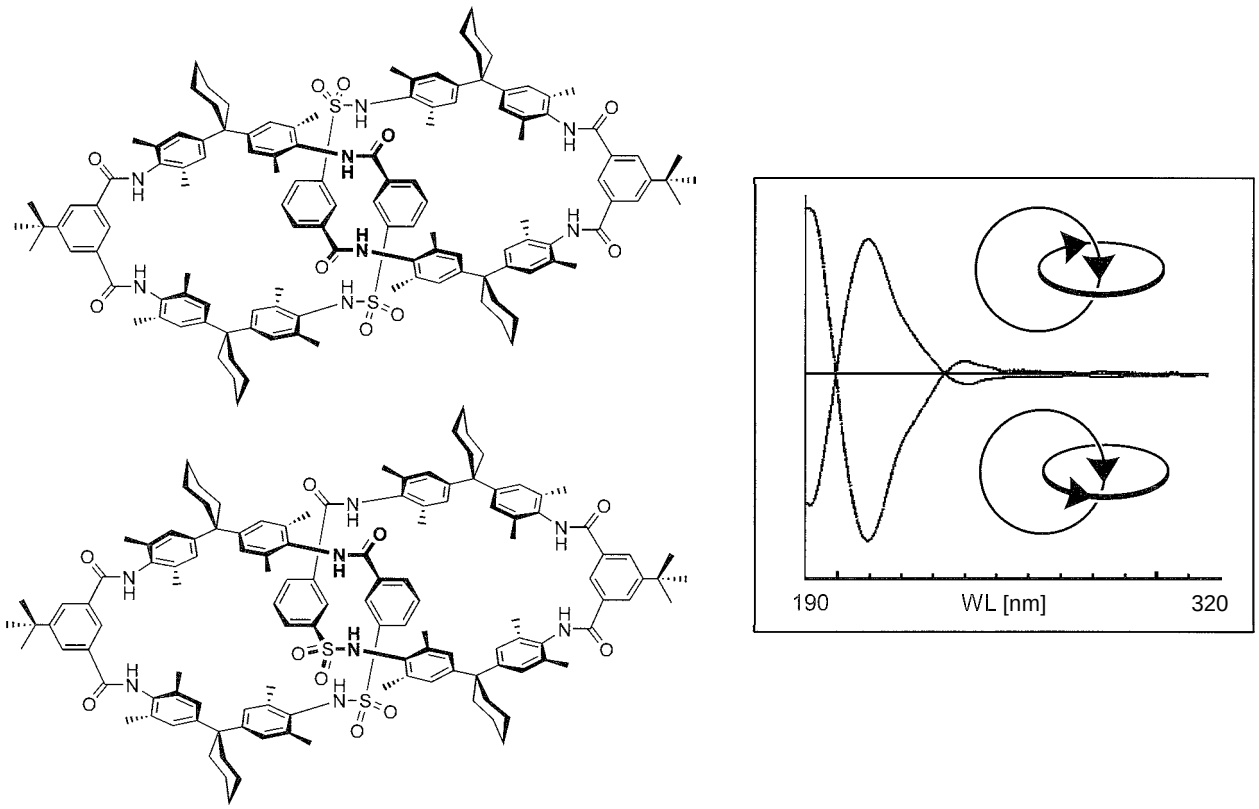

Scheme 2 Two enantiomers of a topologically chiral sulfonamide [2]catenane and their CD spectra

knots. it may even be impossible to determine with complete certainty whether or not a knot is topologically chiral. To find such invariants remains an unsolved problem to this day.[4]

TEMPLATED CATENANE SYNTHESIS

Three different synthetic strategies toward catenanes can be distinguished:

1. A preformed macrocycle binds the open precursor of a second one inside its cavity to form what could be called a pseudorotaxane. The threading step is then followed by connecting the two ends of the pseudorotaxane with each other in a inacrocyclization reaction.
2. Two open precursors are brought together into a suitably preorganized supramolecular complex and are then cyclized in a one-pot-two-step sequence.
3. The third possibility requires a reversible bond formation. Then, preexisting rings could be opened, threaded into each other, and cyclized again when intertwined.

All of these strategies require ihe operation of suitable template effects for an efficient threading.

The first templated synthesis of a catenane was published 20 years ago.[8,9] Since then, synthetic strategies based on various template effects were proposed by several groups. Therefore. modern template strategies[10] give satisfying yields and make these molecules accessible from a preparative viewpoint. How important template strategies are becomes clear when considering the synthetic efforts needed for the first statistical catenane syntheses in the early 1960s.[11] Since the modern template effects used for catenane synthesis resemble those employed for the preparation of rotaxanes, the reader is referred to the article on "'Rotaxanes and Pseudorotaxanes" of this Encyclopedia, where they are discussed in greater detail. Here. we would like to focus on several other aspects in order to avoid unnecessary repetition.

SELF-ASSEMBLY AS A SYNTHETIC STRATEGY

In the following examples, self-assembly may be regarded as another form of templated synthesis. but because of the topicality of this synthetic strategy and the achieved results, this approach should be discussed in greater detail. Metal-directed self-assembly is particularly attractive, as the metal-to-ligand bonds are reversibly formed, and the catenanes can often be obtained almost quantitatively as the thermodynamically most stable products. In 2001. Fujita, Sauvage. and their groups presented a [2]catenane consisting of 41-membered interlocking rings, which is formed quantitatively: following strategy based on two different metal coordination steps.[12] Two building blocks of the [2]catenane, i.e., the unclosed rings, are held together by attractive interactions between a copper(I) ion and two [1,10]-phenanthroline moieties to form a precursor of the desired [2]catenane. Furthermore. the organic building blocks of the [2]catenane are equipped with two pyridine ends. which can be "closed" with palladium(II) ethylene diamine [enPd(II)] corners (Scheme 3).

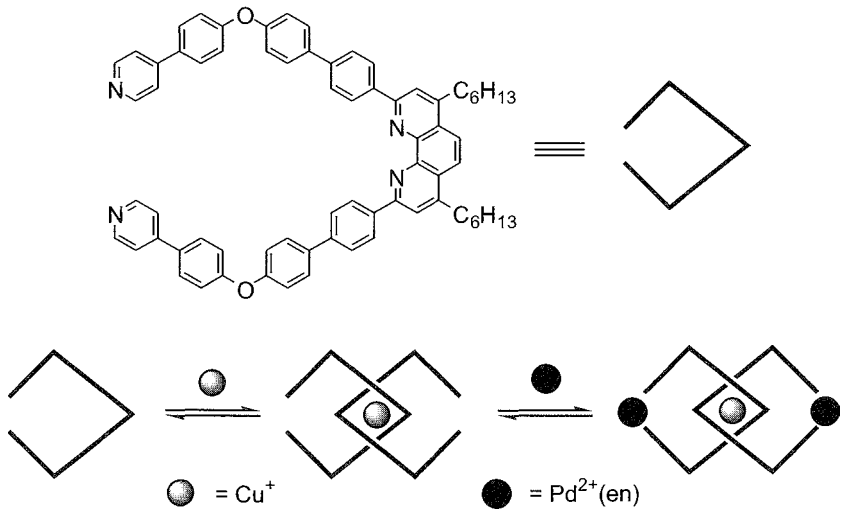

Scheme 3 *Self-assembly* of *a* [2]catenane using *a metal–ion template effect*.

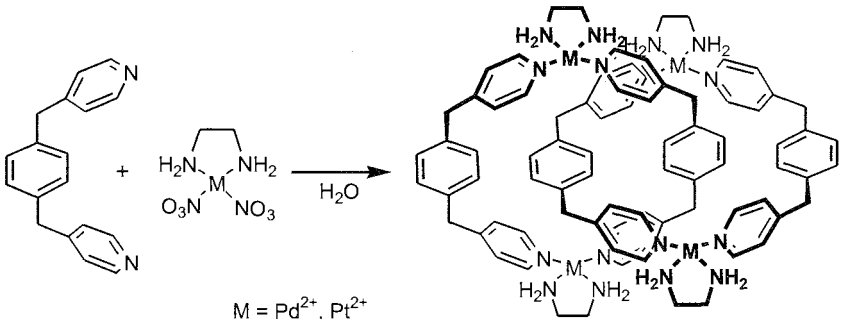

Scheme 4 Self-assembly of a [2]catenane using a solvophobic template effect.

A different type of catenane is formed through the action of hydrophobic forces through self-assembly of building blocks bearing inetal ions (M=Pd, Pt) and ditopic pyridine ligands (Scheme 4).[113] When the two components are mixed in water, the catenane forms spontaneously, minimizing the hydrophobic surfaces by including unpolar ligands of one macrocycle in the cavity of the other and vice versa. An interesting feature of these compounds is the reversibility of catenane formation. if the metai is Pd(II). Even at room temperature, the Pd complexes equilibrate, while the analogous Pt(II) complexes require higher temperatures or high salt concentrations in order to make the coordinative bonds sufficiently labile for an exchange of the ligands.

MORE COMPLEX CATENANES

A catenane may bear more than two intertwined macrocycles. In this section, we wish to introduce several more complex topologies. The increasing complexity not only caused synthetic problems but also prompted Vogtle et al. to introduce a systematic nomenclature for mechanically linked molecules.''''

The synthesis of larger [n]catenanes with $n>3$ is a fascinating challenge for preparative organic chemistry. A prerequisite for the formation of oligocatenanes is to find appropriate ditopic host macrocycles that can bind two guests from the other catenane wheels in a subsequent macrocyclization step. So far, catenanev with up to seven

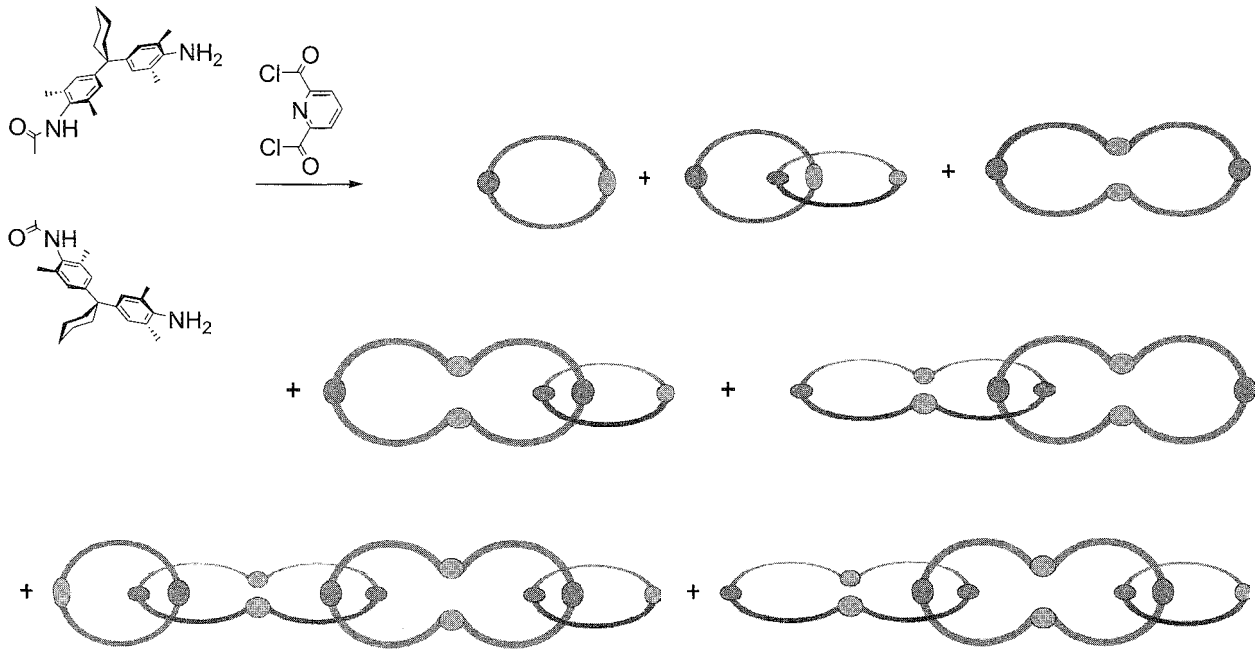

Scheme 5 Vogtle's [n]catenanes

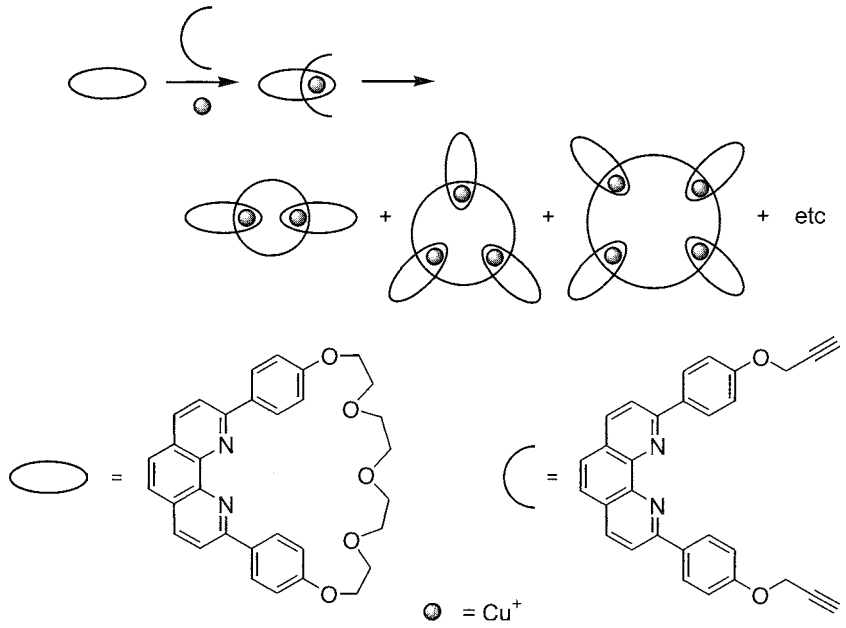

Scheme 6 Multiring Interlocked [*n*]catenanes synthesized by Glaser's oxidative coupling

intertwined rings have been published. Stoddart et al. developed an approach to larger self-assembling catenanes in 1995.[15] The methodology relies on the stereoelectronic complementarity between n-electron-deficient bipyridinium-based components and n-electron-rich hydroquinone- or 1.5-dioxynaphthalene-based components. The driving forces responsible for the self-assembly are π–π stacking and C—H···O hydrogen-bonding interactions. By employing this approach. they were able to self-assemble a large number of [2]catenanes, [3]catenanes, [4]catenanes, and two [5]catenanes (including the so-called olympiadane). A related approach by Stoddart and Balzani led to the construction of catenanes, comprised of up to seven interlocked rings.[16] Two *tris*-1,5-naphtho-57-crown-15 macrocycles template the formation of cyclo*bis*(paraquat-4,4′-biphenylene) to yield a [3]catenane, acting as a template for the construction of one and then another cyclo*bis*(paraquat-*p*-phenylene) to give a [4]- and a [5]catenane. When high pressure was used in these templated syntheses, the corresponding [6]- and [7]catenanes were obtained.

In 2000. Vogtle et al. found another route toward [*n*]catenanes[17] —new tetralactarn and octalactam macrocycles were used to obtain [*n*]catenanes (Scheme 5) with up to five rings. The largest of these is the first amide-type olympiadane, which, however, could not be isolated. The octalactam macrocycle served as a ditopic host permitting the threading of two other macrocycles.

Topological isomers of linear [*n*]catenanes are the so-called multiring interlocked systems that bear a number of smaller rings all threaded on the saine larger macrocycle.[18] The ends of the axles of n pseudo-rotaxanes are covalently connected by Glaser's coupling of triple bonds to form a large macrocycle that carries all the smaller rings (Scheme 6). Higher catenanes with up to seven rings are found that display similar ^{1}H-NMR properties and have identical elemental analyses. They can, however, easily be distinguished from one another by electrospray ionization mass spectrometry (ESI-MS).

While simple [2]catenanes that have two crossings in their molecular graphs were among the first interlocked species synthesized, the development of a doubly interlocking [2]catenane with four crossings in the molecular graph has taken a few decades and was not realized before the 1990s. Two similar self-assembly routes toward the same chiral catenane were developed by the groups of Fujita and Sauvage[19] (Scheme 7), which differ by the sequence of metal addition. Both lead to the desired four-crossing-[2]catenane in quantitative yields.

REGIO- AND STEREOSELECTIVITY IN CATENANE SYNTHESIS

Wegio- and stereoselectivity in chemical reactions are long known to chemists, whereas their supramolecular analogues are just starting to be discovered and are yet to be understood. In the beginning of the current millennium, Vögtle and his group described a regioselective templated synthesis of a topological chiral sulfonamide [2]catenane.[20] The large cyclohexylidene residues hinder circumrotation of both wheels by steric bulk. Due to these

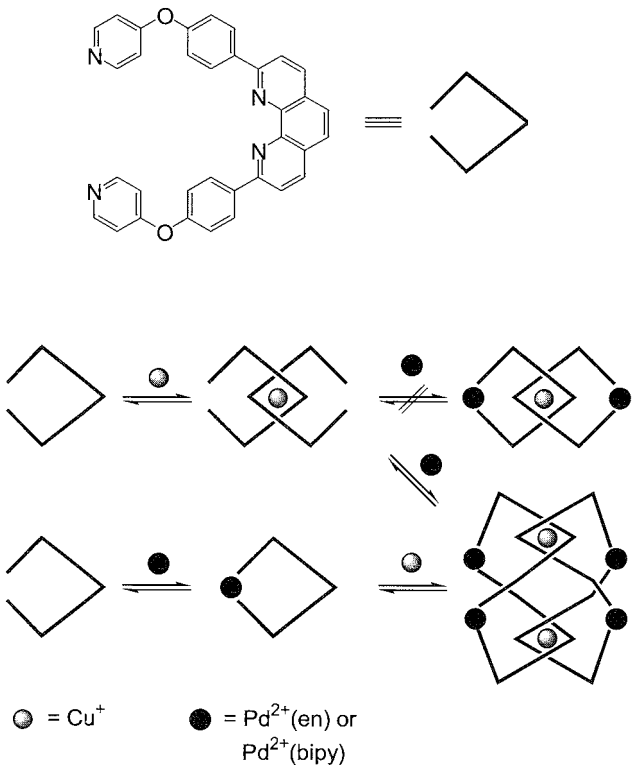

Scheme 7 Four-crossing-[2]catenane

effects, the structure of the catenane reveals an interesting control of selectivity during formation of the intertwined ring system. Only two out of four possible isomers are formed. This allows more distinct conclusions regarding the reaction mechanism leading to amide-based catenanes. The already-formed macrocycle is able to interact with the yet to be closed diamine through hydrogen bonds, forming a precursor of the desired catenane, once again a pseudorotaxane. Differences in hydrogen bonding between the intermediates finally gives rise to the products. and those that would lead to the products not observed are likely the reason for this "supramolecular regioselectivity effect." The x-ray single crystal structure analysis, at the same time, is the first crystal structure of an amide-based topologically chiral catenane.

One year before, Stoddart et al. described the diastereoselective self-assembly of [2]catenanes[21] (Scheme 8). Catenanes incorporating complementary π-electron-rich and π-electron-deficient macrocyclic components with binaphthol building blocks self-assemble from appropriate precursors. If one of the components is present as a racemate and the other as an enantiopure compound, the formation of two diastereoisomers is possible. The diastereoselective self-assembly into [2]catenanes occurs through the formation of intermediate diastereoisomeric complexes. In a subsequent step, the open ring is again cyclized and the catenane formed with a diastereomeric excess of 33%.

DYNAMIC PROCESSES IN **CATENANES: HOW DO** CATENANES CIRCUMROTATE?

Most catenanes can undergo rotation of one ring through the cavity of the other. Benzylic amide catenanes show unambiguous evidence for the spinning of the interlocked macrocycles about one another in solution.[22] Leigh, Zerbetto, and colleagues showed for benzylic amide [2]catenanes how this circumrotation happens.[23,24] They investigated the structure and dynamics of these catenanes using molecular mechanics calculations and employed unimolecular reaction rate theory. Lowest-energy pathways for the circumrotation of the macrocycles were identified. The process is a sequence of several large-amplitude motions. involving several rearrangements to minimize steric and electrostatic interactions via the interplay of weak interactions. The rate constants and barriers

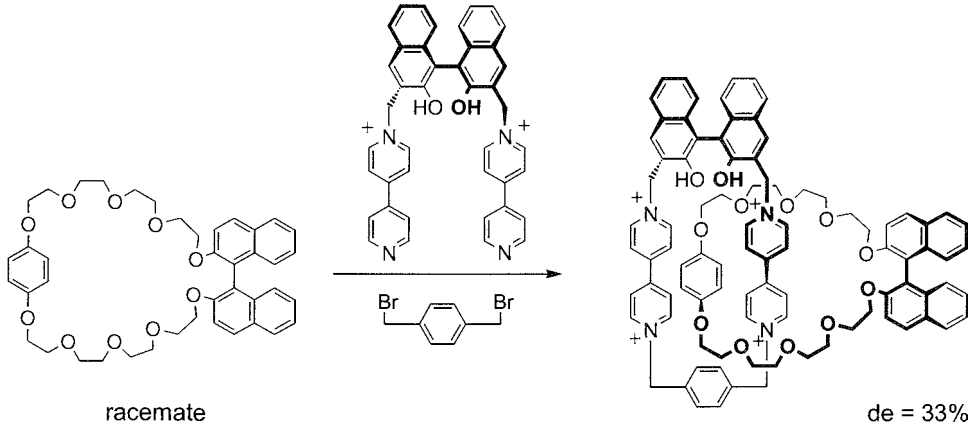

Scheme 8 *Diastereoselective formation of a* [2]catenane.

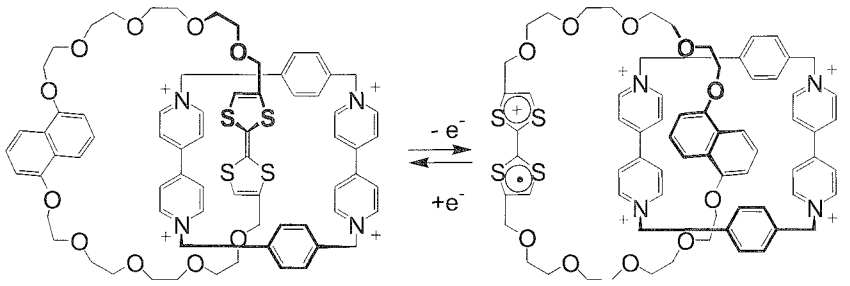

Scheme 9 A molecular switch, based on redox reactions at tetrathiafulvalen subunits

are in agreement with temperature-dependent NMR experiments. The rate-determining steps do not necessarily correspond to the passage of the bulkiest groups. Rather. the transition structures suggest that circumrotation of one macrocyclic ring induces — or synergistically eases — rotation of the other in a coupled motion.

A detailed experimental investigation of circumrotation in catenanes is limited by the complexity of the network of hydrogen bonds and other weak interactions as well as the steric constraints that exist in most catenanes, leading to a large number of degrees of freedom. Complete circumrotation must involve some breaking of attractive inter-ring interactions. If hydrogen bonds are involved, variation of the solvent can control the rate constants of the circumrotational motions of catenanes. Therefore, the circumrotation in benzylic amide catenanes can, to a fair approximation, be described in a classical manner.

PROPERTIES AND POSSIBLE APPLICATIONS

Catenanes are experiencing a spectacular revival in relation to topology as well as to their possible applications as polymers, switches, machines, and motors at the molecular level. Several poly([2]catenane)s together with poly(*bis*[2]catenane)s poly([2]catenand)s, and poly([2]catenate)s were described over the last decade by different groups;[25] the synthesis of cyclic oligo[2]catenands is also possible.[26] The characterization of these compounds includes NMR spectroscopy and mass spectrometry as well as gel permeation chromatography for the determination of the molecular weight distribution and viscometry. These molecules are rare examples of mechanically interlocked polymers, a class of intriguing supramolecular polymers with potentially unusual properties.

Another topic of current chemistry should be addressed here briefly, again with reference to the article on "Rotaxanes and Pseudorotaxanes," where further aspects of molecular machinery are discussed in greater detail. A solid state, electronically addressable, bistable [2]catenane-based molecular switching device was fabricated from a single monolayer of the [2]catenane.[27] The catenane can be switched at +2 V and switched back at −2 V, thus allowing us to write information into it that is stored in the catenane structure through circumrotations. It is possible to read out that information between 0.1 and 0.3 V, and the switch survives at least a few hundred cycles of switching back and forth over a period of 2 months without substantial changes in its properties. Upon further engineering and optimization, this system may be useful as a memory device at the molecular level (Scheme 9).

CONCLUSION

Catenanes and other interlocked molecules remain fascinating, even if their first successful synthesis was accomplished 45 years ago. Since the early days of the first catenane synthesis, more and more functionality has been introduced into molecules, either in relation to electron and energy transfer processes or with regard to controlled molecular motions. While Vögtle et al. claim that "with the natural ATP synthase as a prototype in mind, it is comforting to know that the generation of such a motor is at least in principle possible, and we trust that the goal to build an artificial analogue will be reached within a decade or so",[28] Sauvage argues that "it would of course be unwise to predict that nanoscopic motors and related machines will have any practical application in the future as molecular storage devices or as nanoscale components in electronics".[2] The future will show who will be right in this controversy. But the search for further, more complex, interlocked molecules should not be terminated, because in Sauvage's words, "the search for such molecules or molecular assemblies is important in itself."

ACKNOWLEDGMENTS

We would like to thank Prof. F. Vogtle and Patrick Dragut for helpful discussions and Gregor Pawlitzki for the CD spectra. AR is thankful to the German National Merit Foundation for a scholarship.

ARTICLES OF FURTHER INTEREST

Chemical Topology, p *229*
Molecular Logic Gates, p. 893
Molecular Switches, p *917*
Molecular-Level Machines, p. *931*
π–π Interactions. Theory and Scope, p *1076*
Rotaxanes and Pseudorotaxanes, p. 1194
Self-Assembling Catenanes, p. 1240
The Template Effect, p. 1493

REFERENCES

1. Sauvage, J.-P.; Dietrich-Buchecker, C.O. *Molecular Catenanes, Rotaxanes and Knots*: Wiley-VCH: Weinheim, Germany, 1999.
2. Sauvage. J.-P. Transition metal-containing rotaxanes and catenanes in motion: Toward molecular machines and motors. Acc. Chern. Res. 1998, *31*. 611–619.
3. Chanibron. J.-C.: Dietrich-Buchecker. C.O.: Sauvage, J.-P. From classical chirality to topological chiral catenands and knots. Top. Curr. Chem. 1993. *165*. 131–162.
4. Mislow. K. Molecular Chirality. In Topics in *Stereochemistry*; Denmark. S.E.. Ed.: John Wiley & Sons, Inc.: New York. 1999: Vol. 22.
5. Schill. G. *Catenanes, Rotaxanes and Knots*; Academic Press: New York, USA. 1971.
6. Ottens-Hildebrand. S.: Schmidt, T.; Harren. J.: Vögtle, F. Sulfonamide-based catenanes—Regioselective template synthesis. Liebigs Ann. 1995. 1855–1860.
7. Vögtle, F.; Dünnwald. T.: Schmidt. T. Catenanes and rotaxanes of the amide type. Acc. Chem. Res. 1996. *29*, 45.
8. Dietrich-Buchecker. C.O.; Sauvage, J.-P.: Kintzinger, J.-P. Une nouvelle faniille de molécules: les métallo-caténanes. Tetrahedron Lett. 1983. *24*. 5098.
9. Dietrich-Buchecker. C.O.: Sauvage. J.-P.; Kern, J.M. Synthesis and electrochemical studies of catenates: Stabilization of low oxidation states by interlocked macrocyclic ligands. 3. Am. Chern. Soc. 1989. *111*. 7791–7800.
10. Amabilino, D.B.; Stoddart. J.F. Interlocked and intertwined structures and superstructures. Chem. Rev. 1995, *95*, 2725–2828.
11. Wassermann, E. The preparation of interlocking rings: A catenane. J. Am. Chem. Soc. 1960. *82*. 4433–4434.
12. Dietrich-Buchecker. C.O.: Geum, N.; Hori. A.; Fujita. M.: Sakamoto. S.: Yamaguchi. K.: Sauvage. J.-P. A [2]catenane quantitatively assembled via copper(I) and pallaadium(II) coordination. Chem. Commun. 2001. 1182–1183.
13. Fujita, M.: Oguro, D.: Miyazawa, M.: Oka. H.: Yamaguchi. K.: Ogura, K. Self assembly of 10 molecules into nanometer-sized organic host frameworks. Nature 1995, *378*, 469–471.
14. Safarowsky, O.: Windisch. B.; Mohry. A.; Vogtle, F. Nomenclature for catenanes. rotaxanes, molecular knots. and assemblies derived from these structural elements. J. Prakt. Chem. 2000. *342* (5). 437–444.
15. Pasini. D.: Raymo. F.M.;Stoddart. J.F. Self-assembling catenanes and rotaxanes. Cazz. Chim. Ital. 1995.125.431 –443.
16. Amabilino, D.B.; Ashton, P.R.: Balzani. V.: Boyd. S.E.; Credi. A.; Lee. J.Y.; Menzer, S.: Stoddart. J.F.; Venturi. M.; Williams. D.J. Oligocatenanes made to order. J. Am. Chem. Soc. 1998. *120*. 4295–4307.
17. Schwanke, F.; Safarowsky. O.; Heim. C.: Silva, G.: Vogtle. F. Amide-based oligocatenanes by an iterative template strategy. Helv. Chim. Acta 2000. *83*. 3279–3290.
18. Bitsch, F.: Dietrich-Buchecker, C.O.; Khemiss. A.-K.: Sauvage. J.-P.; Van Dorsselaer, A. Multiring interlocked systems: Structure elucidation by electrospray mass spectrometry. J. Am. Chem. Soc. 1991. *113*. 4023–4025.
19. Ibukuro. F.; Fujita, M.: Yamaguchi, K.: Sauvage, J.-P. Quantitative and spontaneous formation of a doubly interlocking [2]catenane using copper(I) arid palladium(II) as templating and assembling centers. J. Am. Chem. Soc. 1999, 121. 11014–11015.
20. Mohry, A.: Vogtle. F.; Nieger. M.; Hupfer. H. Regioselective template synthesis. x-ray structure. and chiroptical properties of a topologically chiral sulfonamide catenane. Chirality 2000. *12*. 76–83.
21. Ashton, P.R.; Heiss, A.M.; Pasini. D.; Raymo. F.M.: Shipway, A.N.; Stoddart. J.F.: Spencer. N. Molecular meccano. 51—Diastereoselective self-assembly of [2]catenanes. Eur. J. Org. Chem. 1999. 995–1004.
22. Johnston, A.G.: Leigh. D.A.: Nezhat. L.: Smart. J.P.; Deegan. M.D. Structurally diverse and dynamically versatile benzylic amide [2]catenanes assembled directly from commercially available precursors. Angew. Chem., Int. Ed. Engl. 1995. *34*. 1212–1216.
23. Deleuze. M.S.; Leigh. D.A.: Zerbetto. F. How do benzylic amide [2]catenane rings rotate? J. Am. Chem. Soc. 1999, *121*. 2364–2379.
24. Leigh. D.A.: Troisi. A.; Zesbetto. F. A quantum-mechanical description of macrocyclic ring rotation in benzylic amide [2]catenanes. Chern. Eur. J. 2002. 7. 1450–1454.
25. Hamers, C.: Raymo, F.M.: Stoddart. J.F. Molecular meccano. 42—Maill-chain and pendant poly([2]catenane)s incorporating complementary π-electron-rich and -deficient components. Eur. J. Org. Chem. 1998, *10*. 2109–2117.
26. Weidmann. J.L.; Kern. J.M.: Sauvage. J.P.: Muscat. D.; Mullins. S.; Kohler, W.: Rosenauer. C.; Rader, H.J.: Martin. K.; Geerts, Y. Poly[2]catenanes and cyclic oligo[2]catenanes containing alternating topological and covalent bonds: Synthesis and characterization. Chem. Eur. J. 1999, *5*. 1841–1851.
27. Collier. C.P.: Mattersteig. G.: Wong, E.W.: Luo, Y.: Beverly. K.: Sampaio, J.: Raymo. F.M.: Stoddart. J.F.; Heath. J.R. A [2]catenane-based solid state electronically reconfigurable snitch. Science 2000. *289*. 1172–1175.
28. Schalley. C.A.: Beizai, K.: Vogtle, F. On the way to rotaxaae-based molecular motors: Studies in molecular mobility and topological chirality. Acc. Chem. Res. 2001. *34*. 465–476.

Cation–π Interactions

Dennis A. Dougherty
California Institute of Technology, Pasadena, California, U.S.A.

INTRODUCTION

The cation–n interaction is a noncovalent binding force of broad importance in biological systems and in supramolecular chemistry." It is defined as the attraction between a cation and the face of a simple π system. such as in benzene or ethylene (Fig. 1). The physical origin of the cation–n interaction is primarily electrostatic. involving an attraction of the cation to a locus of negative electrostatic potential associated with the face of the n system. It is a common and pervasive contributor to protein secondary structure and to a wide range of small molecule–macromolecule binding interactions in biology. The cation–π interaction was also used as a key design component in a number of synthetic supramolecular systems.

Intensive studies in recent years led to the conclusion that the cation–n interaction should be considered along with the hydrophobic effect, hydrogen bonding. and ion pairing (salt bridges) as a major structural force in biology. It was also extensively characterized using gas-phase ion methodologies and was used to design artificial receptors and supramolecular systems. Although usually associated with aromatic systems, it should be emphasized from the start that the effect has nothing to do with aromaticity. Ethylenes and acetylenes can also participate in cation–n interactions.

THE ESSENTIAL INTERACTION

Many studies of simple cations binding to prototype π systems were carried out in the gas phase, and these provided crucial insights into the fundamental nature of the interaction. Some of these studies are summarized in Table 1. High-level theory accurately reproduces the experimental data. For simple cations, such as alkali metals. lower-level ab initio quantum mechanical methods provide acceptable descriptions of cation–π interactions, allowing more extensive studies of trends (Table 1).

As early as 1981. Kebarle showed that K^+ binds well to benzene.[8] Importantly, these studies also established that the binding of K^+ to benzene was enthalpically stronger than the binding of K^+ to water. a remarkable result that presaged the importance of cation–π interactions in biological recognition. These early studies were confirmed and extensively expanded by Lisy using more advanced techniques.[13] Studies of the full series of alkali ions reveal a classical electrostatic trend (Table 1). Smaller ions bind more tightly, with correlation between ionic radius and binding energy. Because all the ions have the same total charge, the smaller ions must have a more intensely focused charge, enhancing an electrostatic interaction. Comparable trends are seen for binding to ethylene and acetylene.

In this light, Meot-Ner's early results on the binding of NH_4^+ and $N(CH_3)_4^+$ to benzene[9,10] are easily understood (Table 1). It is generally accepted that NH_4^+ and K^+ have comparable ionic radii, and their cation–n binding energies are similar. The reason $N(CH_3)_4^+$ has a much smaller binding energy is simply explained by noting the much larger effective ionic radius of this quaternary ammonium ion. There is no need to invoke special effects like "hydrogen bonds to benzene" or "C—H hydrogen bonds" to explain the data for ammonium ions. These "organic" ions follow the same patterns as the alkali metal ions.

Substituent effects on the π system follow an intriguing and telling pattern (Table 1).[12] Not surprisingly. fluorine is deactivating. consistent with the expected electron-withdrawing effect. However, OH (and OCH_3) substituents have no significant effect on the cation–n interaction, although they are often considered to be "electron donating." This theoretical prediction was confirmed experimentally. An amino substituent is strongly activating, and in fact. only nitrogen-based substituents enhance the cation–π interaction. This novel sequence (NH_2 > OR ~ H > F) is nicely rationalized by electrostatic arguments. Qualitative inspection of electrostatic potential surfaces (Fig. 2) and quantitative analysis of the electrostatic component of binding lead to the conclusion that the variation in cation–n binding ability is due to a substituent's modulation of the electrostatic component. That is not to say that other factors—induced dipoles, polarizability, dispersion forces, and so on—make no

"Several comprehensive reviews of the cation–π interaction were published,[1–4] and the reader should consult these for further details and original references. Especially significant and more recent articles are explicitly cited here.

Encyclopedia of Supramolecular Chemistry
DOI: 10.1081/E-ESMC 120012650

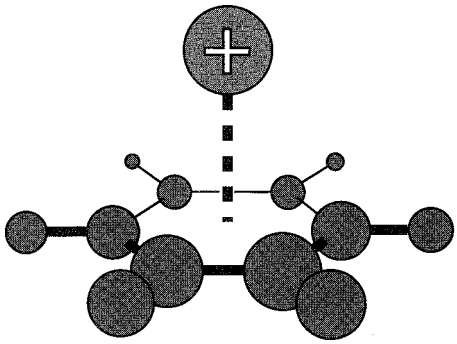

Fig. 1 The cation–n interaction. Shown is the interaction of a generic cation with the face of a benzene ring. (*View this art* in color *at www.dekker.com.*)

contribution to the cation–rt interaction. However, none of these other forces provide the defining characteristic of the interaction. For example. cyclohexane is more polarizable than benzene, but it is a decidedly weaker cation binder.

What is the origin of this electrostatic effect? Simply, all the major observations concerning the cation–n interaction can be understood by recognizing that sp^2 carbon is more electronegative than hydrogen. This introduces $C^{\delta-}$—$H^{\delta+}$ bond dipoles into the system. In the geometries of prototype structures such as benzene and ethylene, these bond dipoles combine to create a focused buildup of negative charge over the center of the π system. Cations bind to this region. Of course, the edges of these structures, the location of the hydrogens. are positively charged. The net effect is the now-familiar electrostatic map for benzene (Fig. 2). with a focus of negative (red) electrostatic potential over each face of the ring and a belt of positive (blue) electrostatic potential around the edge.

In benzene and ethylene: the sum of the individual bond dipoles produces an overall molecular quadrupole moment, and this is an alternative way to describe the electrostatics of these molecules. More extensive discussions of the quadrupole moments of benzene and ethylene were presented elsewhere.[1,3,14,15] We simply note here that it is well established that just as the dipole moment of a molecule like water can bind ions strongly, so can the quadrupole moment of a molecule like benzene or ethylene.

While the gas-phase studies provide insights into the fundamental nature of the cation–n interaction, a key question is the viability of the interaction in solution. A recent computational study[16] indicated that, unlike an ion pair (salt bridge) interaction, the cation–n interaction is not dramatically attenuated when it moves from the gas phase to an aqueous medium. In fact. in water, a simple cation–rt interaction is predicted to be stronger than a comparable salt bridge. The many examples of biological recognition cited below support the view that the cation–π interaction is viable in aqueous media.

LIGAND RECOGNITION USING CATION–π INTERACTIONS

Beginning in the 1980s, a number of studies of cyclophanes, calixarenes, and related structures established that the cation–rt interaction can be a potent force for molecular recognition in aqueous media.[3] Quaternary ammonium ions, including acetylcholine [ACh; $CH_3C(O)OCH_2CH_2N(CH_3)_3^+$], and alklylated pyridine/quinoline derivatives, such as *N*-methylquinolinium, proved to be especially effective substrates. These studies clearly established that a hydrophobic binding site could pull a cation out of the highly favorable environment associated with aqueous solvation and into the binding site, as long as the binding site is comprised of aromatic groups.

An important result to emerge from such studies was a better appreciation of where the positive charge is actually

Table 1 Gas-phase, cation-π binding energies"

$C_6H_6\cdots Li^+$	38.5[b] (38.3)[c]
$C_6H_6\cdots Na^+$	22.1[b] (28.0)[d]
$C_6H_6\cdots K^+$	17.5[b] (19.2)[e]
$C_6H_6\cdots Rb^+$	16.4[b]
$C_6H_6\cdots Cs^+$	15.4[b]
$C_6H_6\cdots NH_4^+$	19.3[f]
$C_6H_6\cdots N(CH_3)_4^+$	9.4[g]
$C_2H_4\cdots Li^+$	20[h]
$C_2H_4\cdots Na^+$	13[h]
$C_2H_2\cdots Li^+$	20[h]
$C_2H_2\cdots Na^+$	14[h]
Calculated substituent effects",'	
$C_6H_6\cdots Na^+$	27.1
$C_6H_5F\cdots Na^+$	22.0
$C_6H_5OH\cdots Na^+$	26.9
$C_6H_5NH_2\cdots Na^+$	31.8
$C_6H_5Cl\cdots Na^+$	21.5
$C_6H_5CN\cdots Na^+$	15.7
Pyridine$\cdots Na^+$	20.0
Indole$\cdots Na^+$	32.6

Note: These are not the highest-level calculations. However, all systems were done at the same level of theory. allowing for direct comparisons.
[a]kcal/mol.
[b]Ref. [5].
'Ref. [6].
[d]Ref. [7].
"Ref. [8].
'Ref. [9].
▾▾ef. [10].
"Ref. [11].
'Ref. [12].

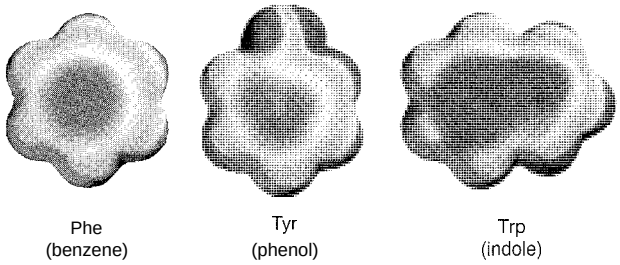

Fig. 2 Electrostatic potential maps for benzene, phenol, and indole, models for the side cnains of phenylalanine. tyrosine. and tryptophan. (*View this art in color at www.dekker.com.*)

located in cations such as ACh and other "onium" compounds. Although we draw a positive charge (+) associated with the nitrogen, high-level theory consistently reveals that the CH_3 and CH_2 groups attached to the nitrogen carry the charge. Most models of tetramethylammonium $[(CH_3)_4N^+]$ place a charge of $\sim+0.25$ on each methyl and roughly a charge of zero on the nitrogen. Thus, when an alkylated ammonium or similar-type structure makes contact with the face of a π system, it is delivering a region of positive charge to the buildup of negative potential on the π system.

Systems that combine a crown ether-like structure with an appropriately positioned π system have proven to form effective binding sites for alkali metal cations.[17] Cation–π interactions were also used to incorporate n facial selectivity into catalysts for asymmetric synthesis.[18]

Cation–n interactions were also established as important contributors to a large number of binding events between small organic molecules and protein-binding sites.[1–4] In proteins. the side chains of phenylalanine (Phe). tyrosine (Tyr), and tryptophan (Trp) can contribute to ligand recognition through a cation–n interaction. Given the substituent effects mentioned above (Table 1). it can be anticipated that Trp should provide the best cation–π binding site. and this result is supported by electrostatic potential maps (Fig. 2) and by several experimental studies (see below). To first order. Phe and Tyr are predicted to be similar, and electrostatic maps (Fig. 1) support this view. Note, however, that hydrogen bonding to the OH of Tyr can make it a more effective cation–n binding site."'' and certainly. this is expected to be operative in some protein structures. Interestingly. theory predicts that for Trp. the optimal cation–n binding site is over the 6-ring of the indole, not the 5-ring. This prediction is supported by statistical studies of preferred binding modes to Trp in proteins.

It has been known for some time that Phe, Tpr, and Trp are overrepresented at protein-binding sites, and part of the reason for this is, no doubt. the potential to use cation–π interactions in binding. Antibody binding sites. including those in catalytic antibodies, are well documented in using cation–n interactions in binding cationic ligands or transition states. Other "generic" binding sites have binding regions that are rich in aromatics, including the multidrug resistance protein (*P*-glycoprotein), which pumps a wide range of compounds out of cells.

A considerable array of small molecules of biological importance make use of cation–n interactions when binding to their protein targets. A well-documented example is the neurotransmitter acetylcholine (ACh). At two different binding sites — acetylcholine esterase (AChE), the enzyme that terminates synaptic transmission by hydrolyzing ACh; and the nicotinic acetylcholine receptor (nAChR), a prototype membrane-spanning neuroreceptor involved in synaptic transmission — the quaternary ammonium ion of ACh makes close contact with a Trp side chain. Note that this was anticipated by earlier cyclophane studies.

Most neurotransmitters have a cationic group, and cation–π interactions are likely involved generally in their binding sites. A similar cation–n interaction to that seen in the nAChR is involved in binding serotonin (5-HT) to the $5\text{-}HT_3$ receptor,[20] and it may be present in the $GABA_A$ receptor. Glutamate. the most common excitatory neurotransmitter of the CNS. is recognized in part by a cation–n interaction in both the metabotropic glutamate receptor (mGluR), a G-protein-coupled receptor, and in the ionotropic glutamate receptors, such as the NMDA receptor.

Another prominent ligand-binding site that exploits cation–π interactions is the SH2 domain, a ubiquitous regulatory unit that binds phosphotyrosine. The cationic side chain of an arginine from the protein makes contact with the π face of the phosphotyrosine.

A well-documented example is the binding of the N7-methylated guanosine (m^7G) present at the 5' end of eukaryotic mRNA. This "5′ cap" is essential for proper processing of mRNA. Crystal structures of VP39, a viral mRNA methyltransferase, and eIF4E, a eukaryotic translation initiation factor with no structural homology to VP39, show the cationic m^7G sandwiched between two aromatic amino acid side chains. exactly as was anticipated by cyclophane studies of N-methylquinolinium. It was also proposed that the "inverse" of such an interaction — a cationic amino acid (Arg) stacking on a DNA base — is important in DNA repair enzymes and perhaps in other proteins that recognize DNA.

Cation–π interactions are also prominent at the active sites of enzymes involving cationic substrates. Key examples include the blood coagulation serine proteases Factor Xa and thrombin. and a number of enzymes that use S-adenosylmethionine. a sulfonium ion that serves as nature's ubiquitous methyl transfer agent. A spectacular series of examples is the array of enzymes that catalyze the cationic cyclizations of polyenes in a key step of terpene and steroid biosynthesis. It is now clear that

precisely positioned aromatic side chains guide the migrating positive charge and influence the structure and stereochemistry of the final product.

An interesting question is the energetic contribution to an overall binding event that can be made by a cation–n interaction. As with all noncovalent binding interactions. determining the magnitude of a cation–π interaction is challenging and expected to be significantly context-dependent. Still, several studies using unnatural amino acid mutagenesis led to estimates of 2–4 kcal/mol for binding of a cation to an aromatic side chain.[20,21] That Trp is the optimal side chain for ligand binding and is supported by mutagenesis studies on the VP39 protein mentioned above. When the Phe and Tyr that bind m^{7}6 are replaced by Trp, either individually or simultaneously, the single and double mutants bind more tightly by 10-fold and 50-fold, respectively.[''] These data show the enhanced binding ability of Trp relative to Phe/Tyr, and they are also in line with the overall magnitude expected for a cation–n interaction.

CATION–π INTERACTIONS IN STRUCTURAL BIOLOGY

Another prominent role for cation–n interactions is in stabilizing the secondary structures of proteins. The cationic amino acids Arg and Lys can interact with Phe, Tyr, and Trp in favorable ways. His, if protonated, can serve as the cation of a cation–n interaction. and several studies showed that the pK_a of a His side chain can be inodulated by a cation–π interaction. Neutral His is not a favorable n system for a cation–π interaction. A pioneering analysis by Burley and Petsko considered the ''amino-aromatic interaction,'' in which NH groups from Arg. Lys, Asn, or Gln contact Phe, Tyr. or Trp.[23] It is now appreciated that Arg and Lys are involved in cation–n interactions. while interactions involving Asn or Gln must be "polar-n" interactions. which are inherently much weaker than cation–n interactions. While this coupling of two different interactions clouded the statistics,[24] the importance of pointing out the potential for such interactions was substantial.

Several more modern analyses established how prominent cation–n interactions are in structural biology. Considering only (Arg/Lys)···(Phe/Tyr/Trp) interactions, Gallivan and Dougherty showed that, throughout the protein data bank. there is one cation–n interaction for every 77 amino acids.[''] Thus. a typical protein will have several cation–π interactions. As expected. Trp is overrepresented in the data set. In fact. a remarkable 25% of all trypiophans are involved in cation–n interactions. A recent study suggests that proteins from thermophilic organisms are enriched in cation–π interactions.[''] further supporting the notion that cation–π interactions are a significant stabilizing force.

Note that when considering such interactions. it is again important to appreciate where the positive charge is on an amino acid side chain. For Lys, the ε CH_2 group, i.e., the CH_2 next to the NH_3^+, carries a substantial positive charge. Just like positioning a CH_3 group of ACh over an aromatic ring is a cation–n interaction, so too is placing the ε CH_2 of Lys over an aromatic. A large fraction of cation–n interactions involving Lys are of this type. which frees the NH_3^+ for other types of interactions, such as hydrogen bonds and salt bridges.

All possible combinations of amino acids and interacting geometries were documented to occur in protein structures. The key feature; of course, is that the cation must be oriented toward the face of the Phe/Tyr/Trp side chain, not the edge. An especially iinpressive cation–n interaction was first noted by Wilson in the erythropoietin receptor extracellular domain.[27] An interdigitated stack of side chains follows the sequence Lys-Tyr-Arg-Phe-Arg-Trp-Lys, a remarkable string of cation–π interactions. Similar motifs are seen in growth hormone receptors and related structures.

CONCLUSION

It is now clear that the cation–π interaction is a significant noncovalent binding force in the gas phase, in solution. and in biological systems. It should be considered on par with the hydrophobic effect. hydrogen bonding. and ion pairs (salt bridges), when considering molecular recognition and supramolecular chemistry in aqueous media.

ARTICLES OF FURTHER INTEREST

Alkali Metal Cations in Biochemistry, p. 1
Calixarenes and Their Analogues: Cation Complexation, p. 137
Cyclophanes: Endoacidic, Endobasic, and Endolipophilic Cavities, p. *424*
Hydrogen Bonding, p. 658
Ion Channels and Their Models, p. 742
n–n *Interactions: Theory and Scope*, p. *1076*
van der Waals Forces, p. 1550

REFERENCES

1. Dougherty, D.A. Cation–π interactions in chemistry and biology A new view of benzene. Phe. Tyr, and Trp Science **1996**. 271. 163–168

2. Scrutton. N.S.: Raine, A.R.C. Cation–π bonding and amino-aromatic interactions in the biomolecular recognition of substituted ammonium ligands. Biochem. J. 1996, *319*. 1–8.
3. Ma, J.C.: Dougherty, D.A. The cation–π interaction. Chein. Rev. 1997. *97*. 1303–1324.
4. Zacharias. N.: Dougherty. D.A. Cation–x interactions in ligand recognition catalysis. Trends Pharmacol. Sci. 2002. *23* (6). 281–287.
5. Amicangelo, J.C.; Armentrout, P.B. Absolute binding energies of alkali-metal cation complexes with benzene determined by threshold collision-induced dissociation experiments and ab initio theory. J. Phys. Chem., A 2000. *104*. 11420–11432.
6. Taft, R.W.: Anvia, F.: Gal. J.-F.: Walsh, S.: Capon. M.: Holmes. M.C.; Hosn. K.: Oloumi, G.: Vasanwala. R.: Yazdani. S. Free energies of cation-molecule complex formation and of cation-solvent transfers. Pure Appl. Chem. 1990, *62*, 17–23.
7. Guo. B.C.; Purnell, J.W.: Castleman. A.W.. Jr. The clustering reactions of benzene with sodium and lead ions. Chem. Phys. Lett. *1990. 168*, 155–160.
8. Sunner. J.: Nishizawa, K.: Kebarle. P. Ion-solvent molecule interactions in the gas phase. The potassium ion and benzene. J. Phys. Chem. 1981. *85*. 1814–1820.
9. Deakyne. C.A.; Meot-Ner (Mautner). M. Unconventional ionic hydrogen bonds. 2. $NH^{+}\cdots\pi$. Complexes of onium ions with olefins and benzene derivatives. J. Am. Chem. Soc. 1985. *107*. 474–479.
10. Meot-Ner (Mautner), M.; Deakyne. C.A. Unconventional ionic hydrogen bonds. 1. $CH^{\delta+}\cdots X$. Complexes of quaternary ions with n- and π-donors. J. Am. Chem. Soc. 1985. *107*. 469–474.
11. Kar. T.: Ponec, R.; Sannigrahi. A.B. Electronic structure. stability and nature of bonding of the complexes of C_2H_2, and C_2H_4 with H^+, Li^+, and Na^+ ions. Extensive ab initio and density functional study. J. Phys. Chem.. A 2001. *105*. 7737–7744.
12. Mecozzi, S.: West, A.P.. Jr.: Dougherty. D.A. Cation–π interactions in simple aromatics. Electrostatics provide a predictive tool. J. Am. Chem. Soc. *1996. 118*. 2307–2308.
13. Cabarcos, O.M.; Weinheimer. C.J.: Lisy, J.M. Size selectivity by cation–π interactions: Solvation of K^+ and Na^+ by benzene and water. J. Chem. Phys. *1999.110* (17). 8234–8429.
14. Luhmer. M.; Bartik. K.; Dejaegere. A.; Bovy, P.; Reisse. J. The importance of quadrupolar interactions in molecular recognition processes involving a phenyl group. Bull. Soc. Chim. Fr. *1994. 131,* 603–606.
15. Williams. J.H. The molecular electric quadrupole moment and solid-state architecture. Acc. Chem. Res. *1993. 26*, 593–598.
16. Gallivan, J.P.; Dougherty. D.A. A computational study of cation–ITinteractions vs. salt bridges in aqueous media: Implications for protein engineering. J. Am. Chem. Soc. 2000. *122*. 870–874.
17. Gokel. C.W.; Barbour, L.J.: Ferdani, R.: Hu. J. Lariat ether receptor systems show experimental evidence for alkali metal cation–π interactions. Acc. Chem. Res. 2002, *35*. 878–886.
18. Yamada. S.; Morita. C. Face-selective addition to a cation–π complex of a pyridinium salt: Synthesis of chiral 1.4-dihydrophridines. J. Am. Chem. Soc. 2002, *124*. 8184–8185.
19. Mecozzi. S.: West. A.P.. Jr.; Dougherty. D.A. Cation–π interactions in aromatics of biological and medicinal interest: Electrostatic potential surfaces as a useful qualitative guide. Proc. Natl. Acad. Sci. U. S. A. *1996*, 93. 10566–10571.
20. Beene. D.L.; Brandt. G.S.; Zhong, W.; Zacharias, N.M.; Lester. H.A.: Dougherty, D.A. Cation–π interactions in ligand recognition at serotonergic (5-HT_{3A}) and nicotinic acetylcholie receptors. The anomalous binding properties of nicotine. Biochemistry 2002. *41*. 10262–10269.
21. Ting. A.Y.: Shin. I.: Lucero. C.; Schultz. P.G. Energetic analysis of an engineered cation–π interaction in staphylococcal nuclease. J. Am. Chem. Soc. 1998. *120*. 7135–7136.
22. Hu. **G.:** Oguro. A.; Li. C.: Gershon, P.D.; Quiocho. F.A. The 'cap-binding slot' of an mRNA cap-binding protein: Quantitative effects of aromatic side chain choice in the double-stacking sandwich with cap. Biochemistry 2002. *41*, 7677–7687.
23. Burley. S.K.: Petsko, G.A. Amino-aromatic interactions in proteins. FEBS Lett. 1986. *203*, 139–143.
24. Singh, J.; Thornton. J.M.; Sirius. An automated method for the analysis of the preferred packing arrangements between protein groups. J. Mol. Biol. *1990, 211*. 595–615.
25. Cailivan. J.P.: Dougherty. D.A. Cation–π interactions in structural biology. Proc. Natl. Acad. Sci. U. S. A. 1999. 96. 9459–9464.
26. Chakravarty. S.: Varadarajan. R. Elucidation of factors responsible for enhanced thermal stability of proteins: A structural genomics based study. Biochemistry 2002. *41,* 8152–8161.
27. Livnah. O.; Stura. E.A.: Johnson. D.L.; Middleton, S.A.: Mulcahy. L.S.; Wrighton, N.C.: Dower. W.J.: Jolliffe. L.K.: Wilson. I.A. Functional mimicry of a protein horinone by a peptide agonist: The EPO receptor complex at 2.8 Å. Science *1996. 273*. 464–471.

Cavitands

Bruce C. Gibb
University of New Orleans, New Orleans, Louisiana, U.S.A

C

INTRODUCTION

As originally defined by Cram. cavitands are "synthetic organic compounds *with enforced cavities large* enough *to complex* complementary *organic compounds or* ions.''[1,2] *The two key words in this definition are "enforced" and "cavity." The former implies highly preorganized, rigid molecules.* i.e., *those types of molecules constructed in such a way that few (if* any) *conformational or rotational options are available to them. Cavitands are then generally* macrocyclic *compounds. comprised of multiple aromatic rings covalently linked in a highly constrictive manner. Implicit in the word "cavity"* is *a range of topologies ranging* from *a concave, or bowl-shaped feature, to a fully* encapsulating *molecular surface. When Cram originally* invoked *the* term, *he did not differentiate between these two different degrees of* curvature.[1] *However with the development* of *bowl-shaped molecules, along with Cram's introduction of the* term *"carcerand" to define hosts that can* fully *encapsulate guest molecules. the term cavitand has become synonymous with open.* concave-*shaped hosts. The two most* prominent *examples of* bowl-*shaped hosts are those based on* resorcin[4]arenes[3–5] *and* cyclotriveratrylenes[6,7] *(Fig. 1). It is the former. having shown a broader repertoire of chemical and structural variabilities.* that *have come to epitomize the definition of* .'cavitand.''

STRUCTURES OF CAVITANDS

Resorcinarene cavitands can be broken down into roughly three types. examples of which are shown in Fig. 2. "Normal" cavitands are simple *derivatives of resorcin* [4]arenes. *The second type, formed by adding a second layer of aromatic rings to the resorcinarene* framework, is termed *"deep-cavity* cavitands.'' *Recently. a third group of molecules emerged. We will use the term* ''wide-*bodied" cavitands to relate to these molecules derived from resorcinarenes* comprised *of more than four* resor-cinol *rings. The structure of all these cavitands lends* them *to a* number *of uses and potential applications that require their hosting properties or the spatial arrangement of their functionality. As such, it* is *their structural features rhat define* them. Correspondingly, we *focus here on structure and avoid expressly highlighting the uses and applications of cavitands to specific problems. Readers interested in these examples should consult some of the more recent* reviews.[2,5,8.9]

Apart from the overall concave topology, there are three structurally important *features of cavitands to which we frequently refer. The "feet" of a cavitand are the R-groups situated at the base of the molecule (Fig.* 1). *These often significantly influence the solubility of a cavitand. Frequent reference is also* made *to the "rim" of a cavitand. This corresponds to the upper-most portions of the cavity of the host, where functional groups can he readily attached. Finally. the "bridging groups" of a* cavitand *are the moieties rhat bridge between the pairs of phenol OH groups of the original resorcinarene. These groups control the splay of the aromatic rings,* i.e., *the steepness of the walls of the cavity.* and *the width of the rim of the cavity. They can also serve as introduction points for the extra row of* aromatic *rings in deep-cavity cavitands. We will highlight some examples* from *each of the three categories to emphasize the wide variety of structures that have been synthesized.*

CAVITANDS

The earliest cavitands[2,5,9] *(Fig. 3) were designed and synthesized in the Cram* group.[1,2] *The first reported was a series of methyl-footed,* methylene-bridged *cavitands* **1** (X=H, *Br,* CO_2CH_3). Variations *to this first series concentrated on changes to the rim of the cavitand and the bridging groups. In terms of the functionalization of the rim, we will note here in passing that it is relatively straightforward to introduce* functionality *into* the *rim of a cavitand. The primary reason for this is that even if the desired functionality is not compatible* with *the resorcin-arene-forming process, the highly activated aromatic rings of resorcinarenes or cavitands inake electrophilic substitution at the 2-position readily accomplishable. A more difficult task is to selectively functionalize some of the positions on the rim. However. the* Sherburn *group* is making *advances into this* area.[10]

In terms of different bridging groups. the first variations to methylene *bridging* were *ethylene. propylene. or* dialkylsilyl *bridges. These resulted in cavitands with*

DOI: 10.1081/E-ESMC 120012742

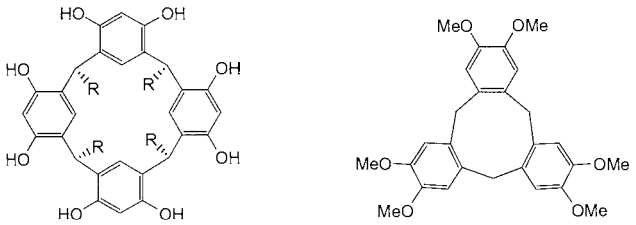

Fig. 1 A resorcin[4]arenes and cyclotriveratrylene. (From Refs. [3–7])

slightly deeper- or wider-rimmed cavities.[11,12] Compounds 2 and 3 are examples. By controlling the bridging conditions, it is aiso possible to introduce less than the maximal four bridges (see references in Ref. [5]). Methylene bridging is typical. Usually, the first three bridges are ı-elatively easy to insert. whereas the fourth bridge is more difficult. Hence, isolation of a ti-is-bridged derivative is easier than the corresponding *mono-* and A/B or A/C his-bridged derivatives. Finally. it should be noted that bridging groups are not limited to the Group 14 elements. For example, phosphorous-bridged cavitands have also been synthesized.[13,14]

Investigations into varying the feet of cavitands were conducted subsequent to the studies into rim functionalization or bridging reactions: presumably because the feet do not directly affect the size and shape of the most

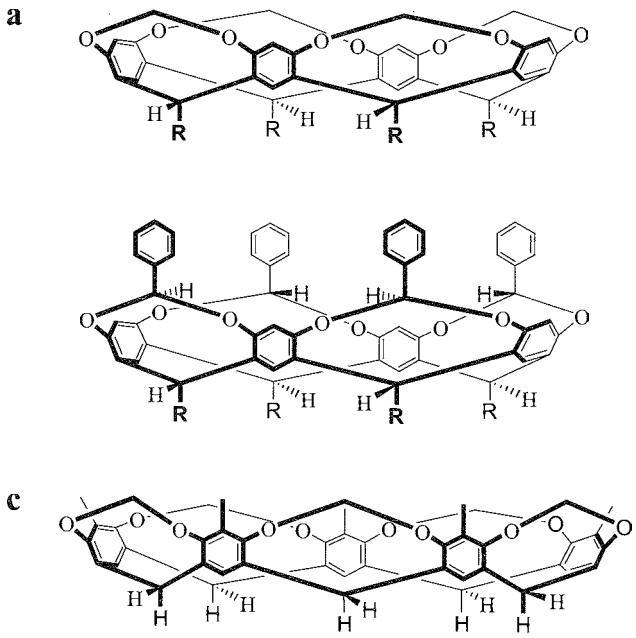

Fig. 2 Typical frameworks of (a) normal cavitands. (b) deep-cavity cavitands. and (c) wide-bodied cavitands.

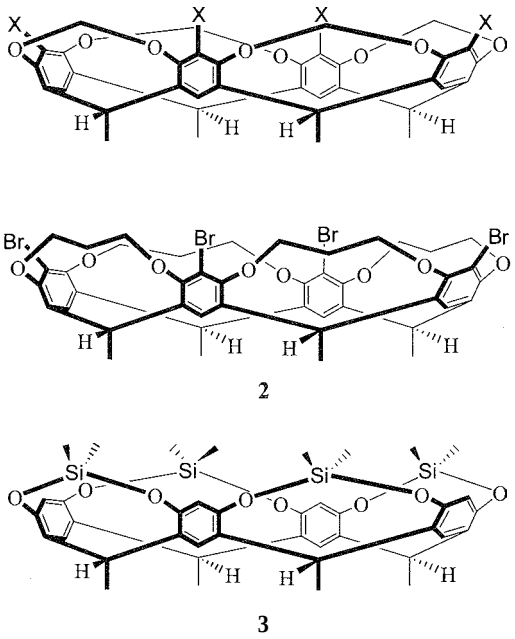

Fig. *3* Three example5 of normal cavitands.

interesting part of the molecules (the cavity), and because the corresponding resorcinarenes had to be synthesized.[4] Once investigated. however. it became apparent that the feet have considerable influence on properties such as solubility. For example. it is possible to bestow water solubility on the cavitand framework by suitable functionalization of the feet.'''' Partially as a result of their importance to solubility, there are now literally dozens of

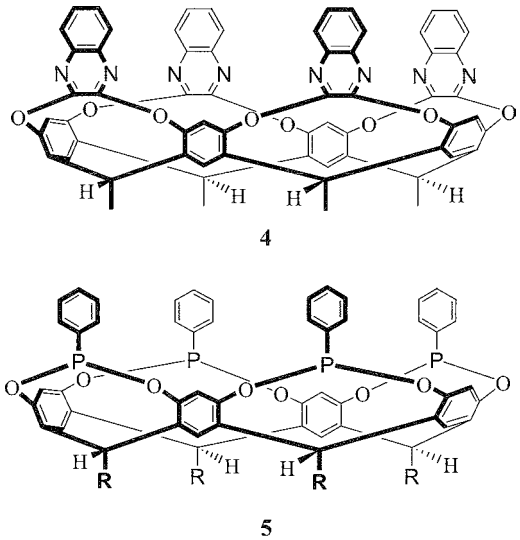

Fig. 4 Representative example5 of deep-cavity cavitands

different feet to chose from when considering a cavitand target.[5]

DEEP-CAVITY CAVITANDS

The first deep-cavity cavitand[8] to be synthesized was the 2.3-quinoxaline derivative 4 (Fig. 4).[1] This second row of aromatic rings in this cavitand. and related cavitands formed by the condensation of resorcinarenes with 2,3-dichloropyrazines. is conformationally flexible. Thus. they exist in a range of conformers between the vase-like C_{4v} form (shown) and a flat C_{2v} form.[16] These families of compounds were termed velcrands, because in the flat. "kite-like" form, they have a propensity to dimerize.[2] When not binding themselves, these types of cal-itands also bind mono-[17] or di-substituted[18] benzene derivatives.

An alternative to deepening the cavity in the manner of cavitand 4 comes in the form of the stereoselective bridging of resorcinarenes. The first successes in this regard were carried out with a number of phosphorus derivatives, e.g., **5**.[13,14,19] Stereoselective bridging with carbon (benzal bridging), for example. see Fig. 2b. followed shortly thereafter.[20,21] In these derivatives, there is a degree of flexibility to the structure, but instead of a conformational flipping being available to the second row of aroinatic rings. each ring is free to rotate.

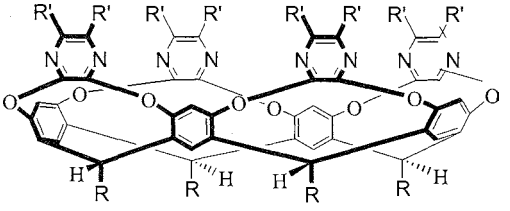

6

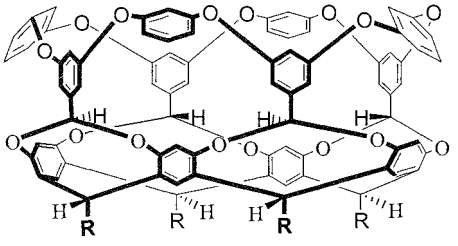

7

Fig. **5** Rigidified deep-cavity cavitands.

It is also possible to increase the depth of the cavity of a cavitand by adding a second row of aromatic rings to the 2-position of each resorcinol moiety.[22] However, in the resulting biaryl derivative, the second row rings must adopt an orientation perpendicular to the cavity wall defined by the first row. Consequently. the cavities of such derivatives, although deeper, are narrower.

With the idea of improved or more selective guest binding, recent efforts were made to instill in deep-cavity cavitands some of the structural integrity seen in normal cavitands. Two general approaches have been demonstrated (Fig. 5). In the first. hydrogen-bonding groups were introduced into the rims of deep-cavity cavitands to engender a more defined but still highly dynamic cavity.[8,23–25] Cavitand 6 is one such example. Alternatively, just like the first row of aromatic rings. the second row can be covalently bridged to prevent their moveinent. Molecular basket **7** is one such example.[26,27] In both of these examples, the cavity of the cavitand is large enough to bind disubstituted adamantanes.

WIDE-BODBED CAVITANDS

Following on from the work of Monishi and cowork-e r ~ , ' ~ the Maier and Sherman groups recently reported the synthesis of the first cavitands coinprised of more than four resorcinol rings.'"' These [*n*]cavitands, where $n = 5$, 6. or 7. were isolated in low yield by direct bridging of the crude kinetic products of the reaction beiween 2-methylresorcinol and formaldehyde. The NMR evidence and x-ray crystallography detnonstrated that the [5]cavitand (see Fig. 2c) adopts the familiar bowl-shaped structure seen in [4]cavitands. However, by similar means. it was shown that the structures of the [6]- and [7]cavitands are more complex. For example. because of steric crowding, the former adopts a conformation that results in a rectangular C_{2v} cavity.

CONCLUSION

We have outlined the range of cavitands derived from resorcinol. There are currently three general families of these cavitands. Two are prominent in the general trend toward synthesizing large cavities for the selective binding of sizable guest molecules. Hence. deep-cavity and wide-bodied cavitands show promise in a number of developing areas of supramolecular chemistry.

ACKNOWLEDGMENTS

This work was supported by the National Science Foundation (CHE-0111033) and the Donors of the

Petroleum Research Fund, administered by the American Chemical Society.

ARTICLES OF FURTHER INTEREST

Carcerands and Hemicarcerands, p. 189
Concave Reagents. p. 311

REFERENCES

1. Moran. J.R.: Karbach. S.: Cram. D.J. Cavitands: Synthetic molecular vessels. J. Am. Chem. Soc. 1982. *104,* 5826–5828.
2. Cram. D.J.; Cram. J.M. *Container Molecules and Their Guests*: Royal Society of Chemistry: Cambridge, 1994.
3. Högberg, A.G.S. Two stereoisomeric macrocyclic resorcinol-acetaldehyde condensation products. J. Org. Chem. 1980. *45,* 4498–4500.
4. Tunstad. L.M.; Tucker. J.A.; Dalcanale, E.: Weiser. J.: Bryant, J.A.: Sherman. J.C.: Helgeson, R.C.: Knobler, C.B.: Cram. D.J. Octol building blocks for cavitands and carcerands. J. Org. Cliein. 1989. *54,* 1305–1312.
5. Timmerman. P.: Verbooin. W.; Reinhoudt. D.N. Resorcinarenes. Tetrahedron 1996, *52,* 2663–2704.
6. Lindsey, A.S. The structure of cyclotriveratrylene (10,15-Dihydro-2,3,7,8,12,13-hexamethoxy-5H-tribenzo[a,d,g]cyclononene) and related compounds. J. Cheni. Soc. 1965. 1685–1692.
7. Collet, A. Cyclotriveratrylenes and cryptophanes. Tetrahedron 1987, *43.* 5725–5759.
8. Rudkevich. D.M.: Rebek. J.. Jr. Deepening cavitands. Eur. J. Org. Chem. 1999. 1991–2005.
9. Bohmer, V. Calixarenes, Macrocycles with (almost) unlimited possibilities. Angew. Chern., Int. Ed. Engl. 1995. *34,* 713–745.
10. Barrett, E.S.: Irwin, J.L.: Turner. P.; Sherburn, M.S. Efficient distal-difunctionalization of cavitand bowls. J. Org. Chem. 2001. *66,* 8227–8229.
11. Cram. D.J.; Karbach, S.; Kim. H.-E.: Knobler. C.B.; Maverick, E.F.: Ericson, J.L.: Helgeson. R.C. Host-guest complexation. 46. Cavitands as open molecular vessels form solvates. J. Am. Chem. Soc. 1988. *110,* 2229–2237.
12. Cram. D.J.: Stewart. K.D.: Goldberg. I.: Trueblood, K.N. Complementary solutes enter nonpolar preorganized cavities in lipophilic noncoinplementary media. J. Am. Cheni. Soc. 1985. *107,* 2574–2575.
13. Lippmann, T.: Wilde, H.; Dalcanale. E.: Mavilla. L.: Mann. G.: Heyer, U.; Spera. S. Synthesis and configurational analyis of a novel class of cavitands containing four dioxaphosphocin moieties. J. Org. Chem. 1995. *60,* 235–242.
14. Delangle, P.: Dutasta, J.-P. Tetraphosphate-calix[4]octol. A powerful host for alkali metal and ammonium cations encapsulation. Tetrahedron Lett. 1995, *36,* 9325–9328.
15. Mezo. A.R.: Sherman. J.C. Water-soluble cavitands: Synthesis of methylene-bridged resorcin[4]arenes containing hydroxyls and phosphates at their feet and bromomethyls and thiomethyls at their rims. J. Org. Chem. 1998, *63.* 6824–6829.
16. Cram. D.J.: Heung-Jin, C.: Bryant. J.A.: Knobler. C.B. Solvophobic and entropic driving forces for forming velcraplexes. which are four-fold, lock-key dimers in organic media. J. Am. Chem. Soc. 1992. *114.* 7748–7765.
17. Dalcanale. E.: Soncini. P.; Bacchilega. G.: Ugozzoli. F. Selective complexation of neutral molecules in organic solvents. Host-guest complexes and cavitates between cavitands and aromatic compounds. Chem. Commun. 1989. 500–503.
18. Soncini. P.: Bonsignore. S.: Dalcanale, E.: Ugozzoli. F. Cavitands as versatile molecular receptors. J. Org. Chem. 1992. *57.* 4608–4612.
19. Xu. W.: Vittal, J.J.: Puddephatt. R.J. Inorganic inclusion chemistry: A novel anion inclusion system. J. Am. Chem. Soc. 1995. *117.* 8362–8371.
20. Xi, H.; Gibb, C.L.D.; Stevens. E.D.: Gibb. B.C. Deep-cavity cavitands: The synthesis and solid state structure of host molecules possessing large, bowl-shaped cavities. Chem. Commun. 8998. 1743–1744.
21. Xi. H.: Gibb. C.L.D.: Gibb. B.C. Functionalized deep-cavity cavitands. J. Org. Chem. 1999. *64.* 9286–9288.
22. von dem Bussche-Hiinnefeld. C.: Helgeson, R.C.; Bühring, D.: Knobler, C.B.: Cram, D.J. Bowl shaped cavitands dimerize and complex certain organic guests in organic solvents which themselves are poor guests. Croat. Chem. Acta 1996. *69,* 447–458.
23. Lücking, U.: Chen. J.: Rudkevich, D.M.; Rebek. J. Jr. A self-folding metallocavitand. J. Am. Chem. Soc. 2001, 123. 9929–9934.
24. Starnes. S.D.; Rudkevich, D.M.: Rebek. J.. Jr. Cavitand-porphyrins. J. Am. Chem. Soc. 2001, *123.* 4659–4669.
25. Rudkevich, D.M.: Hilmersson. G.: Rebek, J., Jr. Self-folding cavitands. J. Am. Chem. Soc. 1998. *120.* 12216–12217.
26. Gibb, C.L.D.: Stevens. E.D.: Cibb. B.C. C-H···X-R hydrogen bonds drive the complexation properties of a nano-scale molecular basket. J. Am. Chem. Soc. 2001. *123.* 5849–5850.
27. Gibb. C.L.D.; Xi. H.: Politzer, P.A.; Concha, M.: Gibb, B.C. The synthesis and binding properties of nano-scale hydrophobic pockets. Tetrahedron 2002. *58,* 673–681.
28. Konishi. H.; Ohata. K.: Morikawa. O.: Kobayashi. K. Calix[6]resorcinarenes: The first examples of[1_6]metacyclophanes derived from resorcinols. Chern. Commun. 1995. 309–310.
29. Konishi, H.: Nakamura. T.: Ohata. K.; Kobayashi, K.: Morikawa. O. The acid-catalyzed condensation of 2-propylresorcinol with formaldehyde diethyl acetal. The formation and isomerization of calix[4]octol, calix[5]octol, and calix[6]octol. Tetrahedron Lett. 1996, *37.* 7383–7386.
30. Naumann, C.: Roman. E.: Peinador, C.; Ren. T.: Patrick. B.O.: Kaifer. A.E.: Sherman, J.C. Expanding cavitand chemistry: The preparation and characterization of [n]cavitands with $N \geq 4$. Chem. Eur. J. 2001. 7. 1637–1645.

Channel Inclusion Compounds

Maria Gdaniec
Adam Mickiewicz University, Poznań, Poland

INTRODUCTION

The occurrence of channels is a relatively common structural feature of inclusion compounds encountered across a range of different host structures. Among well-known solid organic inclusion compounds belonging to the channel-type family are those formed by urea, thiourea, perhydrotriphenylene (PHTP), tri-o-thymotide (TOT). 2,2,6,6-tetramethyl-4-oxopiperidine N-oxide (TANO). bile acids. alicyclic diols. cyclodextrins. and others. The wide-ranging interest in these compounds has a theoretical and a practical background. Confining the functionalized guest molecules in one-dimensional. parallel channels is one of the routes toward the design of new materials with attractive structural, electronic, optical, and magnetic properties.

Different terms like "channel," "tunnel." "canal," and ''tube'' were used to describe host cavities extended in one dimension without introducing any restrictions on the cross-sectional contours of these cavities. Channels can be of cylindrical shape with only small fluctuations in channel diameter on moving along the channel (e.g., urea inclusion compounds). Thread-like guest molecules pack closely in these channels. end to end: and form stable inclusion compounds when some critical value of the molecular length is exceeded. Significant bulges and constrictions at different positions along the channel (e.g., thiourea inclusion compounds) are sometimes observed. These constricted regions give channels partially cage-like properties. and the guest molecules occupy preferred sites along the channel. In general. the distinction between channels and cages is poorly defined.

Crystalline inclusion coinpounds are usually composed of two chemically discernible species. the host and the guest. The guest molecules act as templating agents on which the porous host substructure is constructed. In a prevailing number of cases. the guest inolecules are needed to maintain the stability of the host structure. which collapses on removal of the guest component. Many efforts are currently being made to design organic and coordination channel-type host networks, analogues of channel-type inorganic zeolites. which would reinain stable when the guest component is removed (see *Organic Zeolites*).

EXAMPLES OF CHANNEL-TYPE HOST STRUCTURES

The host architecture has some gross structural characteristics, which are repeated in a series of its inclusion compounds. Among the most extensively studied channel-type inclusion coinpounds are the conventional urea inclusion compounds (see *Urea)*, in which the urea molecules form an extensive hydrogen-bonded honeycomb network containing parallel helical tunnels (Fig. 1a) with diameter between 5.5–5.8 A and the tunnel centers separated by ca. 8.2 Å.[1,2] The walls of the tunnels are covered with the smooth faces of the urea molecules joined together via hydrogen bonds into two helical ribbons running in opposite directions. A variety of guest molecules, among which are not only *n*-alkanes. *n*-alkenes. and their derivatives but also linear polymers. pack in the tunnel. The minimum chain length required for inclusion of a given class of guest molecules depends strongly on the size, polarity, and position of the substituent. Guest molecules interact only weakly with the channel walls and undergo substantial translational and vibrational motions about the tunnel axis. Urea inclusion compounds are frequently nonstoichiometric.

Honeycomb-type network-containing tunnels (Fig. 1b) are also typical of the conventional thiourea inclusion compounds[1,2] (see *Thiourea and Selenourea*). However, in contrast with the urea inclusion compounds the tunnels are not helical, and there are large fluctuations in tunnel diameters (5.8–7.1 A). The distance between centers of adjacent channels is ca. 1 Å longer than in the urea inclusion compounds. Guest molecules enclosed in the thiourea channels are larger and differently shaped than those accommodated in the urea channels, e.g., linear 12-paraffins do not form inclusion compounds with thiourea. while branched hydrocarbons are easily included. Thiourea uses all of its hydrogen-bonding potential for construction of the host network. Guest molecules, which occupy specific sites along the channel. interact only weakly with the host and are generally disordered. Thiourea inclusion compounds are typically stoichiometric.

The inclusion compounds formed by triangularly shaped hydrocarbon host molecule perhydrotriphenylene

Encyclopedia of Supramolecular Chemistry
DOI: 10.1081/E-ESMC *120012855*

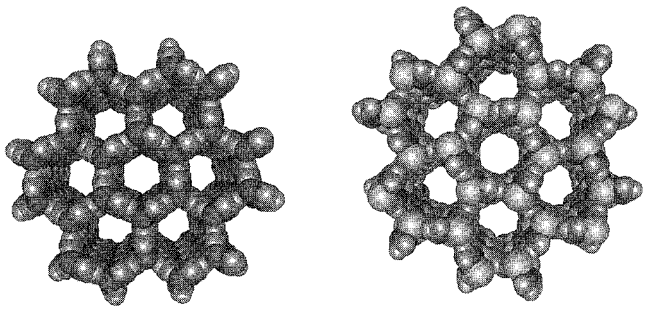

Fig. 1 Perspectir e view along the channel axis of the honeycomb host network in (a) an urea inclusion compound and (b) a thiourea inclusion compound (*View this* art *in color at www dekker corn*)

(PHTP) also exhibit the honeycomb arrangement of narrow tunnels (Fig. 2). The hose lattice is built from the stacks of PMTP molecules; which are placed in corners of the honeycomb motif.[3] The channels are formed between six closely packed host stacks and have their walls covered with equatorial hydrogen atoms of PHTP. Their diameters are ca. 5 Å, and channel centers are 15 Å apart. The PHTP forms channel inclusion compounds of similar construction in the racemic and in the optically active forms. In the racemic PHTP, host molecules are statistically disordered: however, there is strong evidence that individual stacks of PHTP are homochiral.[4] The spectrum of guest molecules accommodated in the flexible PHTP channels is much wider than that for urea inclusion compounds. Moreover, a special class of guest molecules consists of macromolecular substances. which easily cocrystallize with PHTP.[3]

The free radical nitroxide 2,2,6,6-tetramethyl-4-oxopiperidine *N*-oxide (TANO) forms stable channel inclusion compounds with linear or slightly branched molecules.[5] The arrangement of the host inolecules is close to a 3_1 helix, and two such helices define a channel lined with methyl groups of TANO. Again, nearly cylindrical parallel channels, which are 18 Å apart and have effective diameter ca. 5 Å, show a honeycomb arrangement. The TANO and guest molecules are dynamically disordered in the crystal. The most studied of the compounds of TANO are its inclusion compounds with n-alkanes.

Tri-o-thymotide (TOT) is able to include an enormous variety of guest molecules. and depending on the guest component, it forms cage-type or channel-type structure~.'-With unbranched long-chain guests (longer than ca. 9.5 Å), a TOT host network comprises linear, parallel tunnels of effective diameter 5.5–6 Å, with their centers separated by ca. 14.2 Å. During crystallization. TOT spontaneously resolves into (−)-*M* and (+)-*P* conformers, forming chiral crystals with space group symmetries $P6_1$, $P6_2$, or $P3_1$, with the screw axis directed along the tunnel.

Porous host substructures with parallel channels are typical of many inclusion compounds formed by bile acids and their derivatives[7] (see *Deoxycholic, Cholic,* and *Apocholic Acids). In* this class of compounds. host molecules are always optically active. and the resulting host networks are chiral. The best known among them are inclusion compounds of deoxycholic acid (DCA) (also known as choleic acidsj. With most guests. DCA molecules assemble via hydrogen bonds into a corrugated

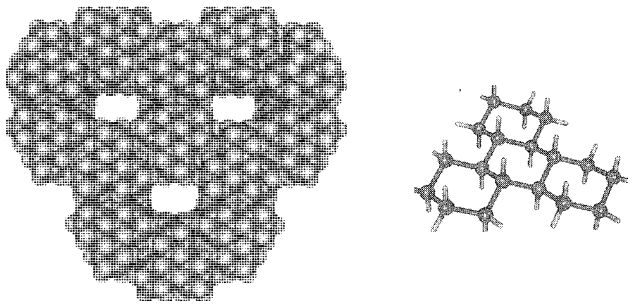

Fig. 2 The PHTP molecule and slightly deformed honejcomb-type netnork of PHTP with channels formed between six PHTP stacks

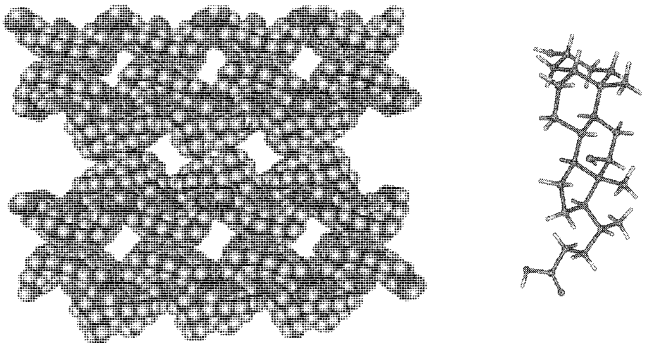

Fig. 3 A DCA molecule and CPK model of the DCA host substructure Channels are formed between corrugated host bilayers constructed from hydrogen-bonded DCA molecules *(View this art in color at www dekker com)*

bilayer structure with a hydrophilic interior and hydrophobic outer surface. Parallel hydrophobic channels running in one direction are formed between adjacent host bilayers (Fig. 3). The shape of the channel can be adjusted to the template guest molecule, mainly via translations in the directions parallel to the layer. In the presence of thread-like molecules, the channels have nearly uniform rectangular cross-sections. For more spherical guests. they exhibit considerable constrictions and bulges. as in thiourea inclusion compounds.

Channel structures can also be produced when monomolecular species with intramolecular tubular cavities arrange into an one-dimensional stack. For example, cyclodextrins (see *Cyclodextrins*), with their truncated funnel shapes, can form channels that have an effective diameter dependent on the number of monosaccharide units of the cyclodextrin.[8] This type of packing enables cyclodextrin accommodation not only of small molecules but also of longer guests,[8] which can be extended over several host cavities (e.g., the α-cyclodextrin–methyl orange complex). Cyclodextrin molecules can be threaded onto a polymeric chain (e.g., the α-cyclodextrin–polyethylene glycol complex) producing a molecular "necklace" that. after the cross-linking of adjacent cyclodextrin units. transforrns into a molecular nanotube able to reversibly bind small molecules.[9]

DESIGN OF CHANNEL INCLUSION COMPOUNDS

Discovery of the inclusion properties of many channel-type compounds was mainly made by chance. The creation of crystal lattices with tailor-made properties or even the fine tuning of properties of known crystal architectures represent significant challenges for materials chemists. Worth mentioning here is a large family of alicyclic diols, called helical tubulands.[10] These compounds have structures closely related to urea and thiourea inclusion compounds. The diol molecules form a three-dimensional hydrogen-bonded network with helical parallel channels (Fig. 4). The common hydrogen-bonding motif of the host lattices is a spiral chain of hydrogen-bonded O—H groups arranged about a 3_1 axis. In contrast with the urea and thiourea hosts. which cannot be modified without destroying their host networks, helical tubulands can be designed and engineered by preparing modified alicyclic diol molecules with structures conforming to certain rules. These modifications do not alter the hydrogen-bond motif, host packing, or crystal symmetry, but by changing dimensions of the channel, they significantly influence inclusion properties of the alicyclic diol host.

STRUCTURAL ASPECTS OF CHANNEL INCLUSION COMPOUNDS

An important property of the channel inclusion compound, which has significant implications with regard to its structural and dynamic properties. is the degree of structural registry between the host and guest substructures (see *Commensurate and Incommensurate Structures*). When the guest molecules are arranged inside a one-dimensional extended cavity in a periodic manner, the relationship between the periodicities of the host and guest components along the channel axis can be of two types.[2] A channel inclusion compound is considered to be commensurate if the ratio of the guest repeat distance c_g and the host repeat distance c_h along the channel axis is rational, i.e.. the relationship $pc_h = qc_g$ holds true when p and q are sufficiently small integers. An incommensurate relationship between the host and guest substructures occurs if the ratio c_g/c_h is not a reasonably small integer. Incommensurate phases are mainly observed ainong channel inclusion cornpounds of urea,

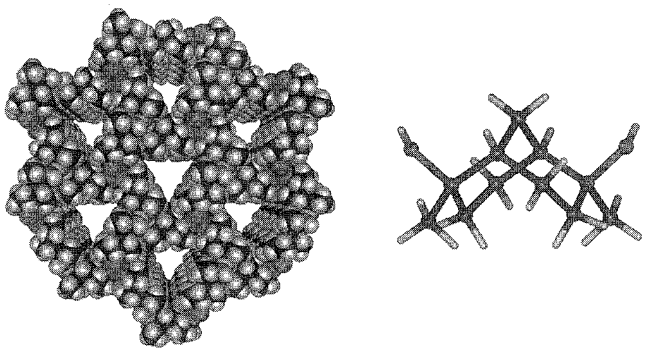

Fig. 4 Representative alicyclic diol molecule and CPK model of its helical channel-type host structure. (*View* this *art in color at www.dekker.com.*)

PHTP. TOT. TANO, and DCA. In many cases, it is difficult to distinguish commensurate from incommensurate inclusion compounds. In an incommensurate relationship between the host and guest structures, the guest molecules are found in a wide range of environments with respect to the host. The fluctuation in interaction energy associated with translating the guest substructure relative to the host substructure along channel direction should be relatively small for true incommensurate behavior. This property is related to the appearance of an additional acoustic mode in the incommensurate crystal. so-called ''sliding mode.'' Observation of the sliding mode can prove the incommensurate nature of the system.'']

Some information about periodic properties of channel inclusion compound can be obtained from x-ray diffraction oscillation photographs. For incommensurate crystals rotating about the channel axis. this photograph will contain layer lines of reflections arising mainly from the guest substructure and layer lines arising mainly from the host substructure and the ''0'' line. which can be attributed to guest and host substructures.[2] The positions of the guest layer lines depend on the periodicity of the guest molecules along the channel. while their patterns, which usually contain discrete Wragg scattering or diffuse scattering. depend on degree of disorder within the guest substructure. The discrete Bragg scattering in the guest diffraction pattern is observed when some interchannel ordering of the guest molecules takes place in the inclusion crystal.

The structure periodicity of composite incommensurate inclusion compounds generally requires four basis reciprocal lattice vectors for lattice description and a four-dimensional superspace group to characterize its symmetry.[2] The use of the superspace approach in structure determination of channel inclusion compounds is scarce but was applied recently in the study of urea inclusion compounds.[11] For a commensurate inclusion compound, its periodicity can be described by a three-dimensional lattice and symmetry represented by a three-dimensional space group. In the diffraction pattern; there is no need to assign separate contributions from the host and guest subsystems.

In addition to periodic properties. incommensurate channel inclusion compounds provide an opportunity to study local structural properties like. for example, the pairwise interaction of functional groups of guest molecule~.'Narrow channels allow the functional groups of the guests to interact only with one nearest guest molecule on each end. Incorporation into inclusion compounds of an asymmetsic guest molecule with two different functional groups as the end groups permits us to study the recognition properties of functional groups by solid-state NMR techniques.

APPLICATIONS OF CHANNEL INCLUSION COMPOUNDS

Channel inclusion compounds are of great importance from theoretical and practical points of view. Many of their properties are related to the alignment of closely packed guest molecules in parallel channels.''' However. the most widespread practical application of channel inclusion compounds is their use for separation of mixtures of different molecules based on discrimination of molecular size and shape. For example, urea is employed by industrial and research chemists to separate linear from branched molecules. The narrow urea channel selectively includes straighi-chain alkanes over their small, branched analogues.[2] It is important that the requirement of size and shape compatibility of the host and guest offers a means of separating compounds that differ only slightly in chemical functionality and that cannot be separated by other methods. Chiral channel-type host networks were successfully used in enantioselective separations. Not only are inherently chiral hosts like, e.g., DCA or cholic acid,

able to discriminate between the enatiomers of the guest,[13] but also achiral urea and configurationally labile TOT, which crystallize in chiral space groups and exist in the forms of enantiomorphous crystals, exhibit some degree of chiral recognition.[2,6]

Many interesting chemical reactions can be carried out in channels, however. the most specific for channel inclusion compounds are polymerization reactions (see *Inclusion Polymerization*). Soon after the channel-type structure was proposed for urea and thiourea inclusion compounds. Classen carried out for the first time the polymerization reaction of 2.3-dimethylbutadiene in channels of thiourea.'''' Further extensive studies of Brown and White on urea and thiourea and some 30 monomers showed that inclusion polymerization can be initiated by high-energy radiation leading to highly stereoregular polymers. Later. PHTP was shown to be an excellent host for inclusion polymerization, and a series of highly stereoregular polymers was synthesized from 1,3-butadiene and its derivatives. The most spectacular was the synthesis of an optically active polymer from achiral monomers, *trans*-1.3-pentadiene. using optically active PHTP as a host.[15]

Polymer inclusion compounds. which can be prepared not only by inclusion polymerization but also by direct cocrystallization of polymers with small molecule hosts, are interesting composite materials awaiting practical applications, e.g., incorporation of conjugated polymers into channels should lead to new composite materials with potential use as molecular wires.[12] New polymer–polymer molecular composites with interesting properties can be produced by embedding polymer inclusion compound into a carrier polymer.[16]

In recent years, considerable effort has been devoted to the design of organic solid materials exhibiting nonlinear optical effects (NLO), such as second harmonic generation (SHG; doubling frequency of light) or electrooptical (EO; modulation of the refractive indices of materials by application of an electrostatic field). In order for a crystalline solid to exhibit SHG or EO, the crystal structure must be noncentrosymmetric. In the case of organic or metalloorganic substances, the constituent molecules should have high molecular hyperpolarizabilities. Typically, such molecules have rod-like shapes with an electron-withdrawing group and an electron-donating group attached to the ends of a π-conjugated core. However, to minimize electrostatic repulsions. such molecules tend to pack antiparallel in their crystals, giving rise to centrosymmetric structures. One of the ways to produce noncentrosymmetric NLO materials is to confine these molecules to channels formed in a substructure of the organic host. With hosts such as TOT. PHTP. DCA, and thiourea. a variety of channel inclusion compounds with organic and metalloorganic guest molecules exhibiting high molecular hyperpolarizabilities were prepared. Many exhibited pronounced SHC and EO effects.[17,18] Interestingly. macroscopically. polar inclusion compounds are surprisingly often formed when dipolar guest molecules are incorporated into the host substructures that are typically centrosymmetric (e.g., thiourea or raceinic PHTP). The fact that dipolar guest molecules in neighboring channels of PHTP point in the same direction was explained in terms of a Markov model of a crystal growth.[4,19]

CONCLUSION

As shown above, channel inclusion compounds exhibit a wide range of interesting properties and fundamental physicochemical phenomena. An enormous amount of progress was made in recent years in understanding the physical and chemical properties of these compounds.'' [2] and there is no doubt that new applications of channel-type composite materials are to be expected in the future.

ARTICLES OF FURTHER INTEREST

Concepts in Crystal Engineering, p. 319
Crystal Engineering with Hydrogen Bonds, p. 357
Inclusion Compounds: Selectivity, Thermal Stability, and Kinetics, p. 696
Inclusion Reactions and Polymerization, p. 705
Incommensurate and Commensurate Structures, p. 712
Isostructurality of Inclusion Compounds, p. 767
Mineralomimetic Structures. p. 868
Nomenclature in Crystal Engineering, p. 967
Soft and Smart Materials, p. 1302
Space Groups and Crystal Packing Modes. p. 1337
Supramolecular Isomerism. p. 1420
van der Waals Forces. p. 1550
Zeolites: Structures and Inclusion Properties, p. 1623

REFERENCES

1. Harris. K.D.M. Meldola lecture: Understanding the properties of urea and thiourea inclusion compounds. Chem. Soc. Rev. **1997**. *26*. 279–289.
2. Hollingsworth, M.D.; Harris. K.D.M. Urea. Tiourea, and Selenourea. In *Comprehensive Supramolecular Chemistry*; MacNicol, D.D., Toda, F.. Bishop. R.. Eds.; Pergamon Press: Oxford. 1996: Vol. 6. 177–237.
3. Farina. M. Inclusion Compounds of Perhydrotriphenylene. In *Inclusion Compounds*; Atwood, J.L., Davies, J.E.D.,

MacNicol, D.D., Eds.; Academic Press: London, 1984; Vol. 2, 69–122.

König, O.; Bürgi, H.-B.; Armbruster, T.; Hulliger, T.; Wcbcr, T. A study in crystal engineering: Structure, crystal growth. and physical properties of a polar perhydrotriphenylene inclusion compound. J. Am. Chem. Soc. **1997,** *119*, 10632 10640.

Le Bars-Combe, M.: Lajzerowicz, J. Ordering in channel inclusion compounds of TANO with linear-chain compounds. 1. High- and low-temperature structures of TANO-a-heplane. Acta Crystallogr. **1987.** *B37*. 386–393.

Gerdil, R. Tri-o-Thymotide Clathrates. In Topics in *Current Chemistry*; Weber, E.. Ed.; Springer: Berlin, 1986: Vol. 140, 71–105.

Miyata, M.; Sada, K. Deoxycholic Acid and Related Hosts. In *Comprehensive Supramolecular Chemistry*; MacNicol, D.D., Toda. F., Bishop, R., Eds.; Pergamon Press: Oxford. 1996; Vol. 6, 147–176.

8. Harata. K. Crystallographic Studies. In Comprehensive *Supramolecular* Chenzistry; Szejtli, J., Osa, T., Eds.; Pcrgamon Press: Oxford, 1996; Vol. 3. 279–304.
9. Harada, A.; Li, J.; Kamachi. M. Synthesis of a tubular polymer from threaded cyclodcxtrins. Nature (Lond.) **1993**, *364*. 516–518.
10. Yue, W.; Bishop, R.; Craig, D.C.; Scudder, M.L. Fine-control of helical tubuland inclusion properties through the pendant group approach. Tetrahedron 2000, 56, 6667–6673.

Petral. I.; Madriaga, G.; Petricek, V.; Rrcczcwski, T. Average structure of the composite crystal urea/octanedioic acid at room temperature within the superspace formalism Acta Crystallogr. **2001**, *B57*, 386 393

12. Langley. P.J.; Hulliger, J. Nanoporous and mesoporous organic structures: New openings for materials research. Chcm. Soc. Rev. **1999,** 28, 279 291.
13. Gdaniec, M.; Milewska, M.J.; Poloński, T. Enantioselectivc complexation of N-nitrosopiperidines by the crystal lattices of steroidal bile acids. Angew. Chem., Int. Ed. Engl. **1999,** *38*, 392–395.
14. Farina, M. Inclusion Polymerization. In Inclusion Compounds: Atwood, J.L., Davies, J.E.D., MacNicol, D.D., Eds.; Academic Press: London, 1984; Vol. 3, 297–329.
15. Farina, M.; Audisio, G.: Natta, G. A new kind of asymmetric synthesis. The radiation polymerization of *trans*-1,3-pentadiene included in optically active perhydrotriphenylcne. J. Am. Chem. Soc. **1967,** *89*, 5071.
16. Tonelli, A.E. Polymer inclusion compounds: Model systems for ordered hulk polymer phases and starting materials for fabricating polymer-polymer molecular composites. Polym. Int. **1997,** *43*, 295–309.
17. Tarn. *W.;* Eaton, D.F.; Calabrese, J.C.; Williams, I.D.; Wang, Y., Anderson, A.G. Channel inclusion complexation of organometallics: Dipolar alignment for second harmonic generation. Chem. Mater. **1989,** *1*. 128–140.
18. Hulliger, J.; Konig, 0.: Hoss. R. Polar inclusion compounds of perhydrotriphenylene (PHTP) and efficient nonlinear optical molecules. Adv. Mater. **1995,** *7*, 719 721.
19. Hulliger, J.; Langley, P.J.; Roth, S.W. A new design strategy lor efficient electro optic single-component organic crystals Cryst Fng. **1998,** 1 177

Chemical Topology

David B. Amabilino
Institut de Ciència de Materials de Barcelona (CSIC), Cerdanyola del Vallès, Spain

INTRODUCTION

The importance of topology of molecules on their supramolecular chemistries and, consequently, on the properties of their aggregates, is absolute. Chemical topology. in general; is the connectivity and linkage of atoms and molecules in space."' This connectivity and linkage play vital roles in determining the chemical and physical characteristics of the molecules (such as the boiling points of differently branched alkanes) and assemblies of them (such as the inclusion properties of crystals).

In terms of connectivity, chemists normally consider principally the covalent bonds between atoms, where the latter are regarded as points. In terms of linkage. we infer crossing points between chains of molecules, as in catenanes—from the Latin *catena* meaning chain, comprised of two or more interlocked macrocycles (with catenands and catenates being ligands and complexes, respectively)—and knots—self-crossing macrocycles. (Refs. [2,3] see also articles on ''Catenanes and Interlinked Structures.'') Supramolecular chemistry played a pivotal role in the preparation of different topological stereoisomers such as catenanes, that have topological diasatereomers that are the component macrocycles. and knots.[4] Just as the topology of molecules can be described. so can the topology of assemblies of them, in which the noncovalent bonds are regarded as a connection. in addition to the covalent bonds. Perhaps the most striking example of this idea is in the study of nets in the solid state.[5,6] All of these aspects are discussed in this short overview, which should act as a springboard to further reading; of the wide implications of chemical topology.

MOLECULAR GRAPHS AND TOPOLOGICAL ISOMERS AND DIASTEREOMERS

It is perhaps easiest to envision the concepts of topological isomerism and diastereoisomerism for the case of molecules, although all the concepts can be extended in dimensionality to interpenetrating supramolecular networks. For understanding the chemical topology of any system. it is important to define the molecular and supramolecular graphs. Any graph is a collection of points and lines. which in the chemical world are generally defined as atoms or ions and bonds; respectively. Changes in connectivities of atoms give rise to constitutional isomers. with different molecular graphs that are planar, that is to say they can be represented in a plane with no crossing points.[1,2] This case pertains to the isomers of linear or branched alkanes or the isomers pyrazine and pyrimidine (Fig. 1). The latter example is particularly relevant because it demonstrates the importance of constitution in determining topology. The coordination compounds of these two heterocycles show different conneciivities in the solid state. It should also be pointed out that enantiomers that are chiral by virtue of stereogenic centers or planar chirality are identical from the topologicai point of view. Topology only distinguishes geometrical properties that remain unchanged upon continuous deformation. Increasing the connectivity leads to the Platonic and Archimedean polyhedra, each with distinct planar molecular graphs.

Topological isomers cannot be converted into one another by continual deformation of the bonds between the atoms that comprise them. They have nonplanar graphs in three-dimensional space—a [2]catenane cannot be represented without having at least two crossing points or nodes (to avoid confusion with point nodes, here we will call these crossing points topological nodes) and is, therefore. a topological isomer of its component rings. Rotaxanes are not topological isomers of their component macrocycle and dumbbell. because by (hypothetically) expanding the ring until it can slip over the stoppers. they may be interconverted.

Increasing the number of crossing points in the molecular graph increases the topological complexity of the compound. A macrocycle presenting three crossing points is better known as the trefoil knot. A simple [2]catenane is not chiral: however. a trefoil knot is topologically chiral because the two enantiomers cannot be interconverted without breaking the link. They are topological diastereomers of the macrocycle that has no crossing points. Note that the synthetic template for the formation of a trefoil knot is a double helix. which is not topologically chiral. although in principle. its helical chirality. if presented in the synthesis, could be converted into topological chirality. When a [2]catenane presents four crossing points. the doubly interlocked [2]catenane,

DOI: 10.1081/E-ESMC 120012651

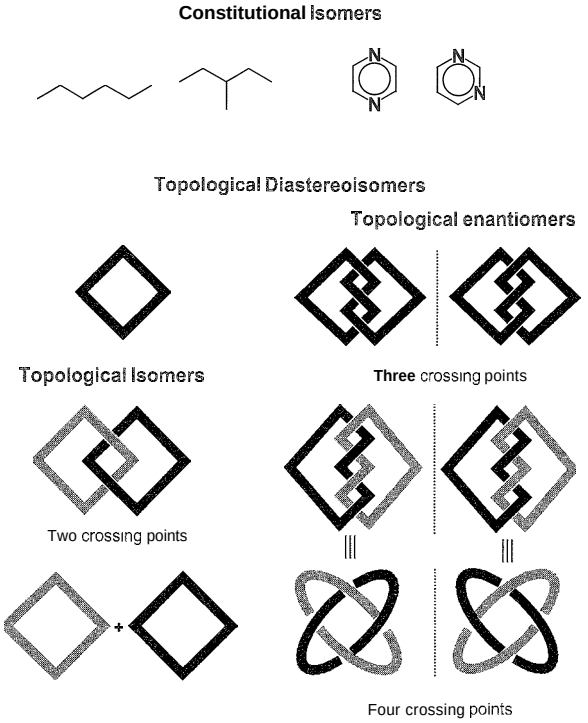

Fig. 1 Constitutional isomers, topological isomers. topological diastereomers, and topological enantiomers. (*View* this *art* in color *at www.dekker.com.*)

two enantiomers exist that are diastereomeric with the singly linked molecule and topologically isomeric with the component macrocycles.

SUPRAMOLECULAR POLYGONS AND POLYHEDRA

Dramatic advances, in resent years, were made in preparing supramolecular polyhedra (the tetrahedron. cube, dodecahedron, etc) from molecular and supramolecular polygons (triangles, squares. pentagons, and so on), especially because of potential interest in them as supramolecular hosts This statement holds true for the more developed coordination compounds[7] as well as for hydrogen-bonded ''containers ''[8] For example, a capsule with the topology of a tetrahedron can be constructed fiom four triaminoguanidine-based ligands and 12 cadmium ions. in which the planar triangular blocks are hinged through Cd–O interactions between chelated metal ions and oxygen atoms from the adjoining faces [9] Also, a truncated trigonal bipyramid can be prepared from a palladium(II) diamine complex and the hexadentate ligand 1,3,5-*tris*(3,5pyrimidinyl)benzene [10] Here, 24 components self-assemble to give the unique polyhedron structure in solution

The formation of polyhedra can also be achieved using hydrogen bonds as the directing force [8] An example is the formation of a chiral spherical supramolecular capsule with the topology of a snub cube (Fig 2A) by six calix[4]resorcinarene moleculer (Fig 2B) in combination with eight water molecules [11] A partial view of the hydrogen-bonding network around the sphere is shown in Fig. 2C. The vertices of the square faces of the snub cube correlate with the corners of the calixarenes. while the centroids of the eight triangles thai link the three squares are represented by the eight water molecules.

SUPRAMOLECULAR CHEMISTRY AIDING THE FORMATION OF TOPOLOGICALLY COMPLEX MOLECULES

It is clear from the drawings in Fig. I that pure chance is an inefficient way to make topologically complex molecules. While covalent-bonding strategies are valid, supramolecular chemistry has all but come into its own in the

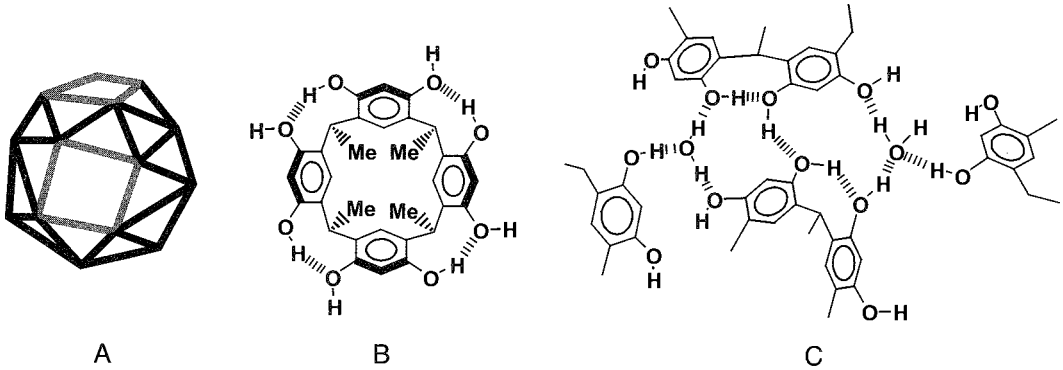

Fig. 2 (A) A representation of the snub cube. (B) The calix[4]resorcinarene that forms the polyhedron. six in combination with eight water molecules. (C) A partial view of the hydrogen-bonding network around the sphere. (From Ref. [1I].) (*View* this *art in* color *at www.dekker.com.*)

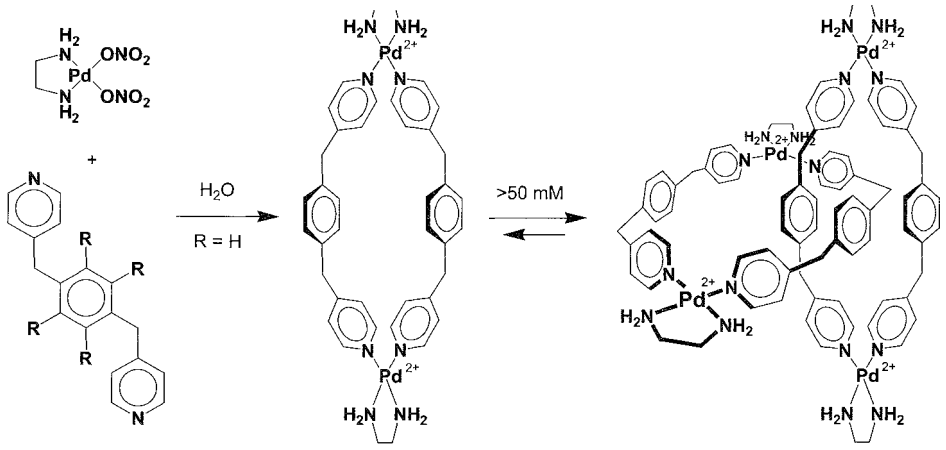

Fig. 3 The equilibrium-controlled self-assembly of a metallo-organic [2]catenane. (From Ref. [12].)

preparation of molecular catenanes and knots. Metal ion. π–π stacking (aided by edge-to-face and [C–H···O] hydrogen bonding), ammonium to crown hydrogen bonding, and amide hydrogen-bond-assisted templating afford isolable. stable molecules with an element of entanglement.[3] Because these methods were amply reviewed elsewhere, emblematic examples follow. All show that orthogonally oriented fragments are a prerequisite for interlocking.

The use of reversible metal ion coordination to pyridinic ligands can be used to form [2]catenanes in a quantitative way.[12] Thus: the mixing of 1,4-*bis*[4-pyridyl)methyl]benzene (Fig. 3, *R*=H) with ethylenediamine palladium(II) nitrate in aqueous sodium nitrate leads to practically total conversion to the [2]catenane. It is believed, on the basis of the x-ray crystal structure of the platinum analogue and the fact that the ligand with R = F is not so efficient in catenane formation, that edge-to-face aromatic interactions play a key role in the formation of this catenane. The *para*-xylyl unit acting as a spacer unit is particularly efficient for the formation of nets of difunctional ligands with metal ions (vide infra).

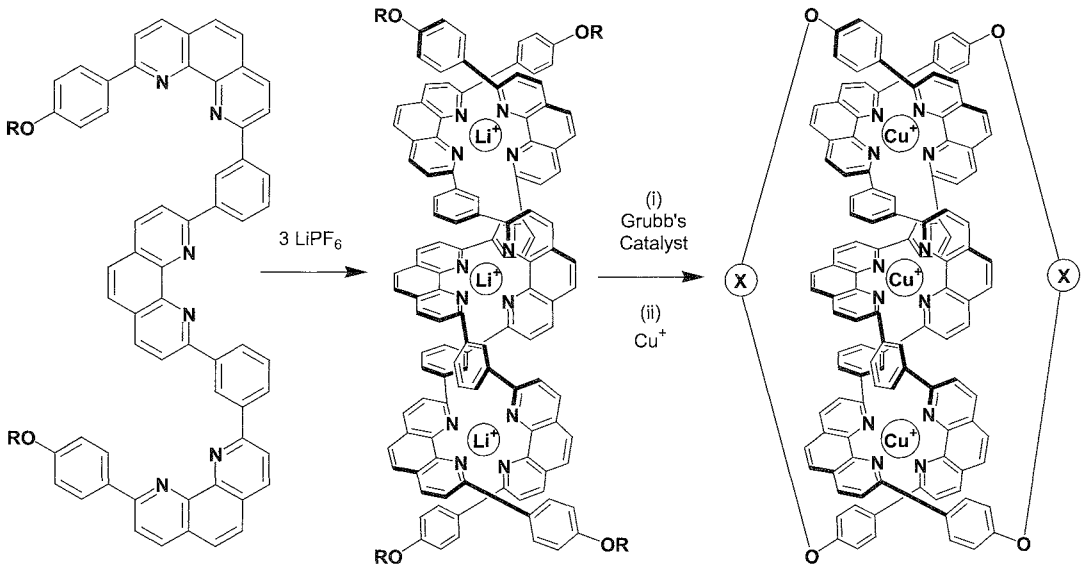

R = $CH_2(CH_2OCH_2)_3CH{=}CH_2$ X = $CH_2(CH_2OCH_2)_3CH{=}CH(CH_2OCH_2)CH_2$

Fig. 4 Lithium-ion-templated formation of a doubly interlocked [2]catenane. (From Ref. [13].)

The preparation of the challenging doubly interlocked [2]catenane, with four crossing points, was achieved on several occasions. One example involves the intertwining of molecular strands incorporating three 1,10-phenanthroline units linked by *meta*-phenylene spacers around three lithium ions (Fig. 4).[13] The mild ring-closing metathesis of the resulting trinuclear double helicate followed by exchange of the lithium ion for copper(I) afforded the catenate (in a remarkable 30% yield) that was liberated of its metal ions using KCN to give the doubly interlocked catenand. This metal-free compound shows the kind of slow dynamics in NMR spectroscopy characteristic of the hindered intramolecular motions in the self-entangled compounds.

The double-helical topography is not the only one to be able to produce the doubly interlocked topology of a [2]catenane. For example, a precatenate based on coordination of phenanthroline units to copper(I) ions can be linked through the coordination of pendant pyridine groups to palladium(II), as described previously.[14] The interaction of the gold(I) ion with alkynes [both end-on with the anions and side-on (η^1 and η^2 modes)] led to the formation of simple [2]catenanes as well as to the creation of a doubly interlocked [2]catenane.[15] In the latter example, the compound is formed under thermodynamic control, because the gold(I)-acetylide link is relatively labile, which leads to formation of the compounds in high yields when the ligand design is good."''

Higher catenanes showing topological stereoisomerism were prepared. For example, a [5]catenane that is the topological equivalent of the Olympic rings is formed along with a branched isomer through a two-step procedure based on self-assembly of π-electron-rich and deficient components.[16] Although noncovalent interactions were used to great effect for the preparation of these and other topologically nontrivial compounds, the control in their syntheses makes the formation of molecules with more crossing points challenging. The use of DNA as a construction unit, on the other hand, makes possible the synthesis of extremely complex molecules,[17] as will be discussed in a subsequent section.

TOPOLOGY OF NETS IN CRYSTALS AND POLYMERS

Two levels of topology can be defined in nets in crystals: first, the connectivity in sheets or frameworks: and second, the way in which the nets interpenetrate, or not. In coordination chemistry, the degree of connectivity is determined largely by the nature of the metal ion and the number of coordinating groups in the ligands, which are usually rigid or at least semirigid.[6,18] The topology of noncovalent interactions in compounds containing organic coinponents can also be rationalized using graph set analysis.[19] A good example with which to show the different levels of topology is that of the organic compound 1,3,5-benzenetricarboxylic (trimesic) acid.[20] The dimerizations of carboxylic acid groups are defined by various topologies, in this case, the $R_2^2(8)$ (a ring, *R*, with eight members maintained by two hydrogen bond donors, the subscript 2, and two hydrogen bond acceptors, the superscript 2) holds any pair of molecules together (Fig. 5). The planar topography and trigonal symmetry of these molecuies makes them ideal for the formation of an infinite two-dimensional hexagonal net. This net is designated (6,3), because the complete circuit involves six sides, and each point (which is at the center of each benzene ring in the structure) is connected to three others.[6] Because the presence of void space in crystals is usually disfavored, the compound relieves this effect through interpenetration. Each net is interpenetrated by three others, as indicated schematically in Fig. 5. For many, interpenetration is not desired, for example, if the aim is to prepare an "organic zeolite." The interpenetration can be avoided through complexation with guest molecules in the net.[20] Changing the functionality, topology, and topography of the molecule to adamantine-1,3,5,7-tetracarboxylic acid leads to three-dimensional fivefold interpenetration.[21] The size of the connectors in the hexagonal nets of 1.3.5-benzenetricarboxylic acid can be increased in a supramolecular way by crystallization with 4.4'-bipyridine, giving rise to a triply interpenetrated undulating hexagonal sheet.[22]

In these organic structures, the connecting points are the centers of the molecuies, while in coordination compounds, the metal ions are usually considered as the points; and the organic ligands form the sides of the nets.[5,6,18] The connectivity of the nets (which is determined by the point metals), usually between two and six for the early transition metals, can be pushed as far as seven and eight in the case of lanthanide ions complexed to 4,4-bipyridine-*N,N'*-dioxide.[23] The interpenetration of nets is observed frequently, although the rules determining whether or not it will take place are not established in a general sense. These nets were reviewed extensively,[6] and it is beyond the scope of this short overview to give more detail. It is interesting to note that the *para*-xylyl unit is often present in interpenetrating networks of various topologies,[6] presumably because of its penchant for edge-to-face hydrogen bonds.[24] A recent article by Carlucci et al. illustrated that the interpenetration is often anion dependent, and as many as 10 diamondoid nets car! be interwoven by the use of 1,12-dodecanedinitrile and silver(I) salts.[25] This example has additional interest in the sense that the ligand is flexible and can "breathe in'' to its fully extended

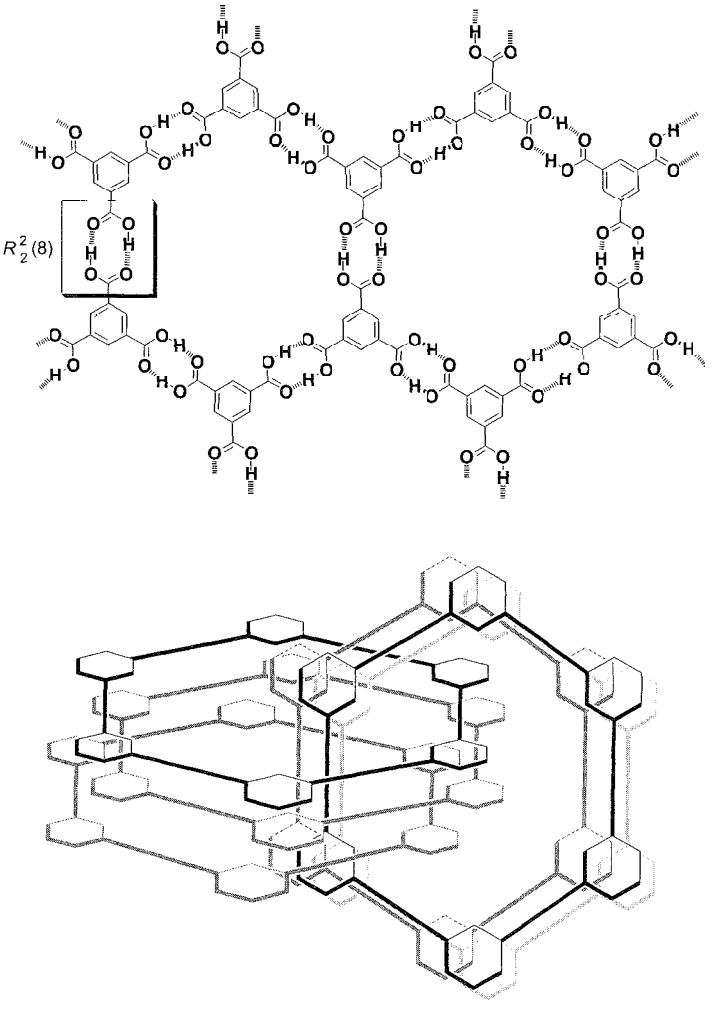

Fig. 5 The (6,3) net formed by 1,3,5-benzenetricarboxylic acid and its triple interpenetration. (From Refs. [6,20].) (*View this art in color at www.dekker.com.*)

all-trans form to give the 10-fold net when nitrate acts as counterion to the silver(I). In the hexafluorophosphate salt, the ligand adopts gauche conformations at the termini of the spacing chain in half of the molecules, resulting in an eightfold network with an unusual [4 + 4] interpenetration, while in the perchlorate salt, all molecules present gauche conformations at their termini; and a fourfold net results.

Interpenetration is not limited to ordered crystalline materials. The polymeric interpenetrating networks are frequently believed to contain mechanically trapped polymer chains.[4,26] Interpenetration has effects on the properties of the polymers when compared to their noninterpenetrating counterparts and is important in their applications. It is extremely difficult to define the exact topology of many of these systems. due to their polymeric nature, and the interested reader is recommended to read around the subject to explore the importance of chemical topology in these interesting materials.[26,27]

EFFECTS OF MOLECULAR TOPOLOGY ON SUPRAMOLECULAR CHEMISTRY

The topology of molecules can drastically influence their supramolecular chemistries and properties in general. For example. dendrimers or hyperbranched polymers show dramatically different properties when compared with their linear counterparts. To take a recent example. hyperbranched polyglycerols with a core-shell amphiphile structure encapsulate guests and thereby act as phase-transfer agents. while their strictly linear counterparts do not.[28]

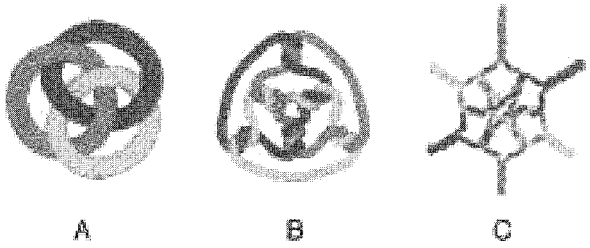

Fig. 6 (A) The classic Borromean rings. (B) The Borromean rings as in A, but with each single topological node (crossing point) replaced with three. (C) The DNA molecule that was synthesized. (From Ref. [17].) (Many thanks to Ned Seeman for providing the images.) (*View this art in color at www.dekker.com.*)

The effect of interlocking on the properties of molecules is dramatic. For example, the basicity of the 2,9-diphenyl-1.10-phenanthroline unit is enhanced by several orders of magnitude when it is present in a [2]catenand.[29] The proton catenate displays a similar molecular structure to that of the corresponding copper(I) catenate. whereas that of the catenand is completely different. The special topology of the catenands and knots makes them unique ligands, with strong complexes being formed with a variety of metal ions.[30]

TOPOLOGICALLY INTRICATE DNA-BASED MOLECULES

The topological complexity of the synthetic compounds described above pales in insignificance when compared with that observed in naturally occurring DNA[31] and with that created using the nucleic acids as building blocks for the construction of molecular objects, including polyhedra and all kinds of knots.[17]

in naturally occurring DNA, catenanes and knots are observed that are crucial for the replication cycle of the genetic data with the help of the various families of topoisomerase proteins.[31] However, to quote Ned Seeman. "there is far more to DNA than a repository for genetic information!"[17] The use of "sticky-ended" DNA duplex strands. in combination with control of branch junctions. design of B-DNA and Z-DNA segments. and restriction and ligation sequences led to the creation of molecules beyond the dreams of non-DNA chemists. The synthetic DNA chemistry even provided the challenging Borrornean rings—three macrocycles linked together. but no two of which are entwined, and the breaking of any one of the macrocycles results in the disconnection of the other two (Fig. 6). The Borromean rings remain a daunting confrontation for those involved in the synthesis of topologically complex molecules through supramolecular assistance.

CONCLUSION

Topology in all of its forms has important consequences in molecular and supramolecular chemistry, and in the properties of the materials that result. Great control was demonstrated over the creation of polyhedra using coordination chemistry based on appropriate design of the topology and topography of ligands and the coordination numbers of the metal ions employed, strategies that also apply to the formation of coordination nets. Purely organic systems of analogous nature. in which the branch points are located at the center of the component molecules, are in their early days, although significant progress has been made. The preparation of topologically complex molecules and assemblies through the employ of noncovalent bonds has made remarkable progress, but it is fair to say that the doubly interlocked [2]catenane and the [5]catenanes are at the limit of present capabilities. it is likely that new supramolecular motifs with orthogonal topography will be needed to progress in this area. These motifs would also be applicable to the preparation of interpenetrating nets. Precise control over polymeric structures and detailed proof of their topologies are still challenging. and a lot can be learned from the topological heights that were reached in DNA structures.

ACKNOWLEDGMENTS

The author is indebted to Professors J. Fraser Stoddart and Jean-Pierre Sauvage for their teachings in matters topological. Ned Seeman (New York University) is warmly thanked for supplying the Borromean images in Fig. 6.

ARTICLES OF FURTHER INTEREST

Catenanes and Other Interlocked Molecules, p. 206
DNA Nanotechnology, p. 475
Nomenclature in Crystal Engineering, p. 967
Plutonic and Archimedean Solids, p. 1100
Self-Assembling Catenanes, p. 1240
Strict Self-Assembly and Self-Assembly with Covalent Modifications, p. 1372
Supramolecular Isomerism, p. *1420*
The Template Effect, p. 1493

REFERENCES

1. *Topology in Chemistry—Discrete Mathematics* of Molecules: Rouvray, D.H., King. R.B., Eds.: Horwood Publishing: Chichester. 2002.
2. Walba, D.M. Topological stereochemistry. Tetrahedron 1985, *41* (16). 3161–3212.
3. *Molecular Catenanes, Rotaxanes and Knots:* A *Journey Through* the *World of Molecular Topology*; Sauvage, J.-P., Dietrich-Buchecker. C.O., Eds.: Wiley-VCH: Weinheim. 1999.
4. Amabilino. D.B.: Stocldart, J.F. Interlocked and intertwined structures and superstructures. Chem. Rev. 1995. 95 (8). 2725–2828. and references cited therein.
5. Wells. A.F. *Three-Dimensional Nets and Polyhedra*; Wiley Interscience: New York, 1977.
6. Batten. S.R.: Robson. R. Interpenetrating nets: Ordered. periodic entanglement. Angew. Cheni.. Int. Ed. 1998. 37 (11). 1460–1494. and references cited therein.
7. Leininger, S.: Olenyuk, B.: Stang. P.J. Self-assembly of discrete cyclic nanostructures mediated by transition metals. Chern. Rev. 2000. *100* (3). 853–908, and references cited therein.
8. MacGillivray, L.R.; Atwood, J.L. Structural classification and general principles for the design of spherical molecular hosts. Angew. Chem., Int. Ed. 1999. *38* (8). 1018–1033, and references cited therein.
9. Müller, I.M.: Robson. R.: Separovic. F. A metallosupramolecular capsule with the topology of the tetrahedron, 3. assembled from four guanidine-based ligands and twelve cadmium centers. Angew. Chem.. Int. Ed. 2001. *40* (23). 4385–4386.
10. Takeda. N.: Umemoto. K.: Yamaguchi, K.: Fujita, M. A nanometre-sized hexahedral coordination capsule assembled from 24 components. Nature 1999. *398*. 794–796.
11. MacGillivray, L.R.: Atwood, J.L. A chiral spherical molecular assembly held together by 60 hydrogen bonds. Nature 1997, *389*. 469–472.
12. Fujita. M. Self-assesnbly of [2]catenanes containing metals in their backbones. Acc. Chem. Res. 1999. 32 (1), 53–61.
13. Dietrich-Buchecker. C.: Sauvage, J.-P. Lithium templated synthesis of catenanes: Efficient synthesis of doubly interlocked [2]-catenanes. Chem. Commun. 1999. 615–616.
14. Ibukuro. F.: Fujita, M.: Yamaguchi, K.: Sauvage, J.-P. Quantitative and spontaneous formation of a doubly interlocking [2]catenane using copper(I) and paladium(II) as templating and assembling centres. J. Am. Chem. Soc. 1999, *121* (47). 11014–11015.
15. McArdle. C.P.: Jennings, M.C.: Vittal. J.J.: Pudclephatt. R.J. Self-assembly of rings. catenanes, and a doubly braided catenane containing gold(I): The hinge-group effect in diacetylide ligands. Chem. Eur. J. 2001. 7 (16). 3572–3822.
16. Amabilino. D.B.: Ashton. P.R.: Balzani. V.; Boyd. S.E.: Credi. A.; Lee. J.Y.: Menzer. S.; Stoddart. J.F.: Venturi, M.: Williams. D.J. Oligocatenanes made to order. J. Am. Chern. Soc. 1998. 120 (18). 4295–4307.
17. Seeman. N.C. Nucleic acid nanostructures and topology. Angew. Chem.. Int. Ed. 1998. 37 (23). 3220–3238.
18. Moulton. B.: Zawarotko. M.J. From molecules to crystal engineering: Supramolecular isomerism and polymorphism in network solids. Chem Rev 2001. *101* (6). 1629–1658.
19. Etter. M.C.; MacDonald, J.C.: Bernstein. 3. Graph set analysis of hydrogen-bond patterns in organic crystals. Acta Crystallogr. 1990. *B46* (2). 256–262.
20. Kolotuchin, S.V.: Thiessen. P.A.; Fenlom. E.E.: Wilson. S.R.: Loweth, C.J.: Zimnierman, S.C. Self-assembly of 1.3.5-benzenetricarbovylic (trimesic) acid and its analogues. Chem. Eur. J. 1999. *5* (9). 2537–2547, and references cited therein.
21. Ermer. O. Fivefold-diamond structure of adamantine-1.3.5.7-tetracarboxylic acid. J. Am. Cheni. Soc. 1988. *110* (12). 3747–3754.
22. Sharma. C.V.K.: Zawarotko. M.J. X-ray crystal structure of $C_6H_3(CO_2H)_3$-1.3.5·1.5(4,4′-bipy): A 'super trimesic acid' chicken-\?ire grid. Chem. Cornmun. 1996, (23), 2655–2656.
23. Long, D.-L.: Blake. A.J.: Champness. N.R.: Wilson. C.: Schröder. M. Unprecedented seven- and eight-connected lanthanide coordination networks. Angew. Chein., Int. Ed. 2001. *40* (13), 2444–2447.
24. Goodgame, D.M.L.; Menzer. S.: Smith, A.M.; Williams. D.J. $[Mn(C_{18}H_{16}N_2O_2)_3](ClO_4)_2$: A polymeric 34- and 68-mambered metallacyclic network forming a novel woven polycatenanted framework. Angew. Chern., Int. Ed. Engl. 1995, *34 (5)*. 574–575.
25. Carlucci. L.: Ciani. G.; Proserpio, D.M.: Rizzato. S. Three novel interpenetratirig diamondoid networks from self-assembly of 1.12-dodecanedinitrile with silver(I) salts. Chem. Eur. J. 2002, *8* (7). 1520–1526.
26. *Interpenetrating Polymer Networks*; Klempner, D., Sperling, H., Utracki, L.A., Eds.; Advances in Chemistry Series, American Chemical Society: Washington. DC. 1994; Vol. 239.
27. Lipatov, Y.S. Polymer blends and interpenetrating polymer networks at the interface witli solids. Prog. Polym. Sci. 2002. *27* (9). 1721–1801.
28. Stiriba. S.-E.; Kautr. H.: Frey. H. Hyperbranched molecular nanocapsules: Comparison of the hyperbranched architecture with the perfectly linear analogue. J. Am. Chem. Soc. 2002, *124* (33). 9698–9699.
29. Cesario, M.: Dietrich. C.O.: Edel, A.: Guilheni, J.: Mintzinger. J.-P.; Pascard, C.: Sauvage. J.-P. Topological enhancement of basicity: Molecular structure and solution study of a monoprotonated catenand. J. Am. Chem. Soc. 1986. *108* (20). 6250–6254.
30. Meyer, M.: Albrecht-Gary, A.-M.; Dietrich-Buchecker. C.O.; Sauvage. J.-P. Dicopper(I) trefoil knots: Topological and structural effects on the demetalation rates and mechanism. J. Am. Cheni. Soc. 1997, *119* (20). 4599–4607. and references cited therein.
31. Postow. L.: Peter. B.J.: Cozzarelli. N.R. Knot what we thought before: The twisted story of replication. BioEssays 1999. *21* (10). 805–808.

Chiral Guest Recognition

Anthony P. Davis
University of Bristol, Bristol, United Kingdom

INTRODUCTION

Enantioselective recognition is a long-standing preoccupation of supramolecular chemistry. On the one hand. the phenomenon is of great theoretical interest, being critical to the functioning of biology. On the other, it has practical importance deriving from the need for enantiomerically pure compounds in the chemical industry. To quote from a recent monograph. "The separation of enantiomers may well represent the economically most important application of supramolecular chemistry."[1] It is a substantial topic, and coverage herein must be selective. This entry will focus on recognition in solution and selectivity in the sense of differential binding free energies. Solid-state host–guest chemistry and spectroscopic differentiation (as for chiral NMR shift reagents) will not receive general consideration. Chromatographic chiral stationary phases (CSPs) will be mentioned only briefly; for more detailed discussions, see reviews by Pirkle and Pochapsky[2] and Okamoto and Yashima.[3] After a short section on general principles, the account will be organized according to substrate type. following the sequence amines/ammonium ions. carboxylic acids/carboxylates, underivatized amino acids, peptides and peptide models, carbohydrates, and nonpolar guest molecules.

GENERAL PRINCIPLES

General discussions of enantioselective recognition are given in a number of reviews.[2,4,5] A prevalent concept is the "three-point rule."[6] formulated by Pirkle. as "Chiral recognition requires a minimum of three simultaneous interactions between the CSP(/receptor) and at least one of the enantiomers, with one of these interactions being stereochemically dependent."[2] Schematically; receptor 1 is a match for 2 but not for ***3***. However, while undoubtedly true, this principle encourages a design concept that may not be optimal. When 1 and **3** interact. they should be capable of two interactions as in 4, and it is the third interaction C···C′ that determines the degree of enantioselectivity. This third interaction will be the weakest of three noncovalent bonds and, in most cases, is not likely to represent a large energy difference. In practice, the most successful enantioselective receptors seem to present a complex array of functional groups and steric barriers. such that one enantiomer can make good binding contacts but the other has minimal opportunities for interaction. Beyond this, it may be difficult to generalize, but there is a case for saying that rigidity and bulky substituents are often helpful for achieving good selectivity,[4] and it is true that strong interactions are necessary (the larger of the binding energies sets an upper limit for the useful difference in binding energies).

ENANTIOSELECTIVE RECOGNITION OF AMINES AND AMMONIUM IONS

Primary ammonium ions can bind to crown ethers, especially 18-crown-A derivatives. via formation of three H-bonds as shown in ***5***. In seminal work by Cram and coworkers, this interaction was exploited in a series of chiral receptors based on the twisted 1,1′-binaphthyl and 1,1′-ditetralyl units. A key example is receptor 6, containing two binaphthyl units. of which one carries methyl substituents. This cornpound was capable of extracting protonated methyl D- and L-phenylglycinates (**7**.H^+ and **8**.H^+, respectively) from racemic aqueous solutions into chloroform in the ratio 31:1,[7] setting a standard that has proved difficult to match with newer systems. The system was used to demonstrate a "resolving machine" based on the transport of the cations through a chloroform barrier.[8] The machine consisted effectively of two U-tubes filled with chloroform and placed in contact with a central reservoir of aqueous racemate. One chloroform soiution contained 6 and selectively removed **7** from the central reservoir into a receiving phase. while the second contained ent-6 and transported 8. The two receiving phases accumulated phenylglycinates in up to 90% e.e.

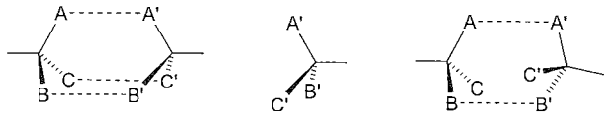

1 2 3 4

Encyclopedia of Supramolecular Chemistry
DOI: 10.1081/E-ESMC 120012857

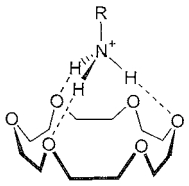

5

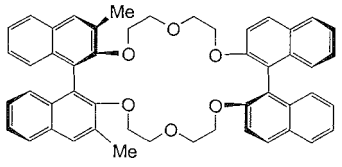

6

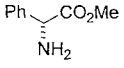

7 (D)

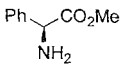

8 (L)

A variety of other chiral crown ethers were studied. although selectivities usually peaked at 10:1 or less.[4] Pyridine-based systems. typified by **9**,[9] were subject to especially detailed investigations. The incorporation of phenolic units allows the crowns to bind amines, as opposed to ammonium ions, and may also be used to introduce a spectroscopic response to binding.[10,11] For example. the calixarene-crown **10** acts as a colorimetric chiral sensor for amino alcohols, changing from red to blue on exposure to *R*-phenylglycinol **11** in ethanol (K_a=66 M^{-1}) but unresponsive to the enantiomeric substrate.[11]

An alternative strategy for binding amines is to use a Lewis acidic metal atom. Zn-porphyrin complexes prove especially useful in this context. For example, the doubly bridged α,α,β,β-system **12** bound the methyl esters of α-amino acids with moderate but fairly general enantioselectivities (7.5:1 for valinate, 4:1 for alaninate) in dichloromethane.[12] The "Troger's-base-linked" *bis*-porphyrin **13** was designed to make two Zn–*N* interactions and was shown to bind histidine methyl ester **14** with an enantioselectivity of 13:1 in $CDCl_3$.[13] Recently, the relatively accessible α,β,α,β-complex **15** was found to give 22:1 selectivity in binding the enantiomers of methyl phenylglycinate (**7**+**8**) in dichloromethane.[14]

ENANTIOSELECTIVE RECOGNITION OF CARBOXYLIC ACIDS AND CARBOXYLATES

Carboxylic acids/carboxylates are popular substrates in supramolecular chemistry. offering various opportunities for hydrogen bonding and electrostatic and donor–acceptor interactions.[15] Especially prevalent are duplex H-bonded motifs. as shown in **16**–**18**. A number of groups incorporated these motifs in enantioselective receptors. A simple but effective example is **19**, due to Morán.[16] This receptor was targeted at *O*-carbamoyl lactic and mandelic acids **20** and is thought to bind them via an array of H-bonds, as shown. The chiral centers in host and guest are held close in space. allowing the receptor to differentiate between guest enantiomers. The best results were obtained with lactic derivatives **20** (R = Me), for which the *R* receptor (shown) preferentially bound the *S* substrate with exceptional enantioselectivity of 90:1 in $CDCl_3$.

Motif **16** was also employed in receptors **21** and **23**. designed respectively to bind dicarboxylic acids and C-terminus dipeptides. Receptor **21** is part of a series in which different linkers were used to connect the binaphthol oxygens and thus control the dihedral angle between the naphthyl groups.[17] The $MeN(CH_2CH_2)_2$ unit in **21** gave optimum results, including an affinity ratio of 16:1 in $CDCl_3$ for L-aspartic derivative **22** versus the D-enantiomer. Tweezer **23** was aimed especially at the D-Ala-D-Ala unit in **24**, the target in nature of the Valinomycin family of antibiotics. In $CDCl_3$, **24** was bound 23 times more strongly than its enantiomer.[18] The guanidinium-based motif **17** was exploited in the steroid-based receptors **25**.

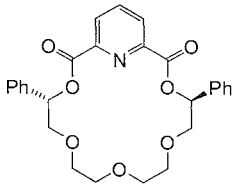

9

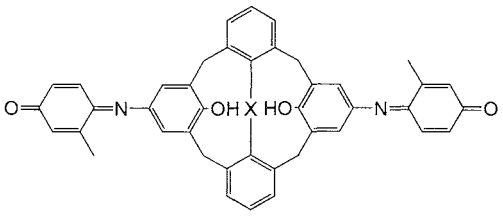

10

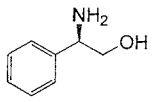

11

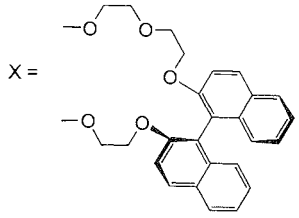

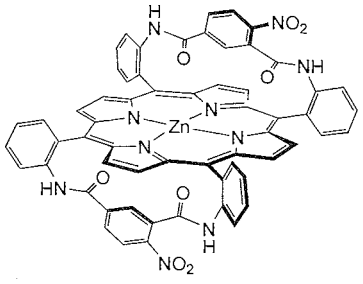

12

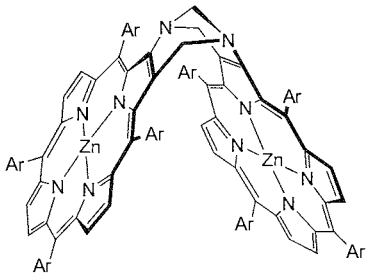

13 Ar =

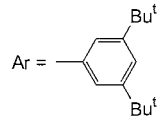

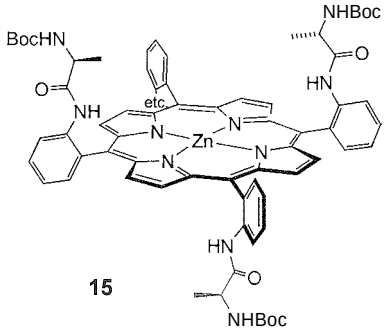

15

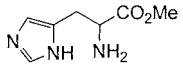

14

The methyl *ester* **25a** *was found to extract* *N*-acetyl alanine/phenylalanine *carboxylates from aqueous solution into* chloroform *with* L:D *selectivities of* 10:1, *while the lipophilic* analogue **25b** *transported* *N*-acetyl phenylalanine *through* apolar *solvent barriers in up to 70%* e.e.[19]

In special cases, n-donor–n-acceptor interactions *can supplement* H-bonding *to achieve good chiral* recognition. *The group of Pirkle applied this approach to* carboxylic *acids as well* as *other classes of compounds (vide* infra). *For example. derivatization of* leucine *with the n-acidic 3.5-dinitrobenzopl group,* to *give 26,* provides *a "handle" that allows* enantiodiscrimination *by selector* 23. *A combination* of *23 and* tetrahexylammonium *chloride in hexane can transport 26 between aqueous phases with up to* 95% e.e., *in favor of the S* enantiomer.[20] *The Pirkle group also addressed the* enantioselective *recognition of Naproxen 28, seen as a difficulttarget due to the relative dearth of polar functional groups* and *the small difference in bulk between methyl and hydrogen at the* asymmetric *center.* In *this case, the* 3,5-dinitrobenzoyl *group can be incorporated in the receptor. complementing the electron-rich* aromatic system *in the substrate.* CSPs *incorporating selector 29 gave* α-values *(equivalent to a ratio of binding constants) of up to 2.6 for 28. retaining the S enantiomer more* strongly.[21]

Carboxylates (like amino groups) can also bind to Lewis acidic metal *complexes, such as Zn-porphyrinates. In* receptor *30. derived from an* *N*-methyl porphyrin, *the methyl group* blocks *an approach from the* lower *face. A carboxylate* counterion *must, therefore. coordinate to the top face. in the chiral* environment *created by the strap. When 30 (X* = OAc) *was dissolved in* $CHCl_3$ *and* shaken *with aqueous* *N*-acyl *amino acids. many of the* carboxylates *were extracted with* >80% e.e.[22]

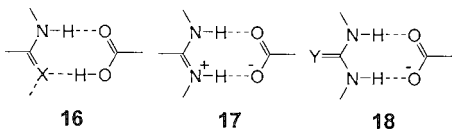

16 17 18

UNDERIVATIZED AMINO ACIDS

From the previous two *sections. it is clear that* α-amino *acid derivatives are popular* substrates *for studies of*

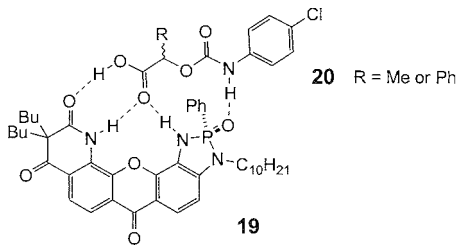

20 R = Me or Ph

19

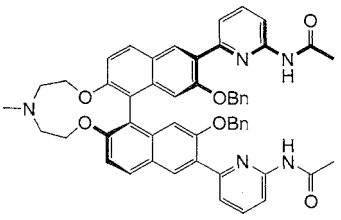

21

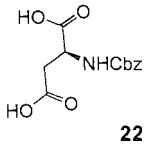

22

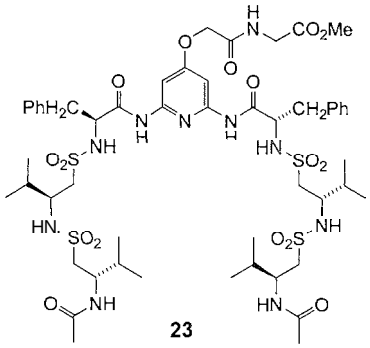

23

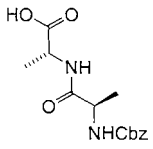

24

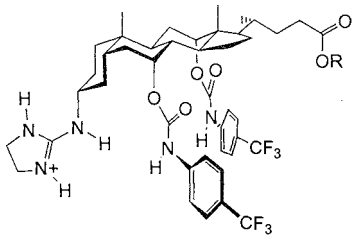

25a R = Me
25b R = $C_{20}H_{41}$

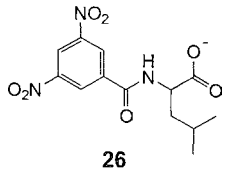

26

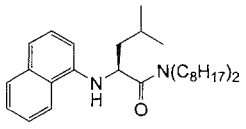

27

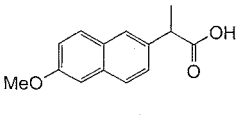

28

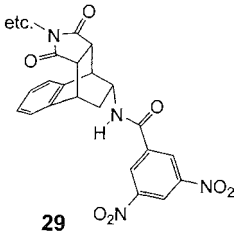

29

enantioselective recognition. The amino acids themselves are of particular interest, considering their direct participation in biocheinistry. A natural approach to the enantioselective recognition of amino acids is the incorporation of well-established ammonium- and carboxylate-binding motifs in a chiral framework. The bicyclic guanidinium receptor 31 conforms to this strategy. It also features a naphthoyl unit that should bind to the side chains of aromatic amino acids. providing an especially clear example of three-point contact. Indeed, 31 binds L-tryptophan 32 and L-phenylalanine with good enantioselectivity, extracting them from racemic aqueous solutions into chloroform in ca. 80% e.e.[23,24]

Metal ions can bind amino and carboxylate groups (vide supra), so are well-adapted to amino acid recognition. The cobalt(II) coinplex 33 (racemic) reacts with DL-alanine to give diastereomeric products **34** and 35 in ~2:1 ratio. A controlling influence is the tendency of the carboxylates to locate *trans* to each other. Interestingly, ***35*** is converted almost exclusively to 34 upon treatment with

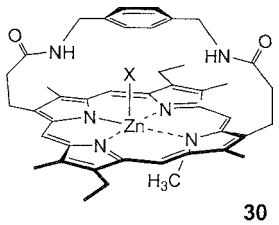

30

X = OAc or substrate carboxyiate

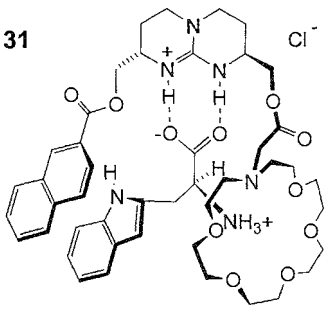

31

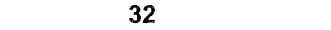

32

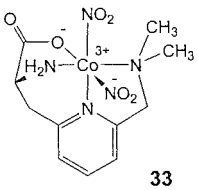

33

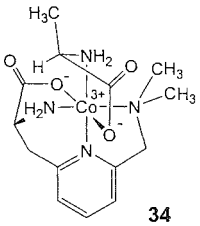

34

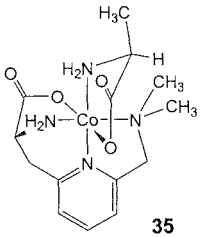

35

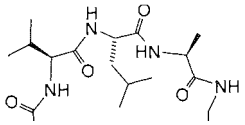

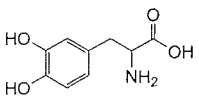

37

38

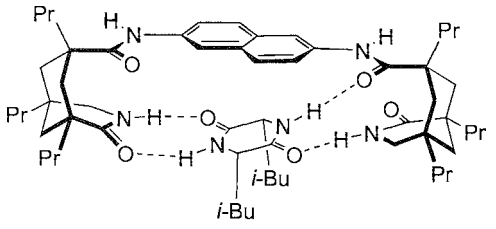

39

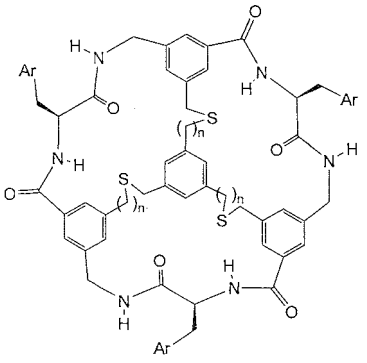

43

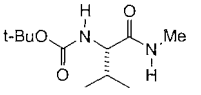

44

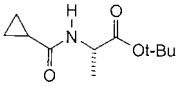

40 n = 0, Ar = Ph

41 n = 1, Ar = Ph

42 n = 0, Ar =

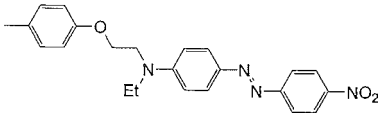

aqueous base. implying *a substantial energy difference between the two* complexes.[25]

Amino acids may be bound in *water by* molecules *with hydrophobic cavities. Cyclodextrin derivatives were studied extensively. Enantioselectivities are usually modest, with some exceptions. For example, a* diphenoxyphosphoryl-substituted β-cyclodextrin *bound serine with* 3.6:1 enantioselectivity[26] *and an* α-cyclodextrin *with a* pyridinium substituent *showed* 10:1 enantioselectivity *toward the same* substrate.[27] *Synthetic cyclophanes were also used. The* bipyridinium-based *macrocycle 36 bound DOPA 37 with 13:1 R:S selectivity in acidic aqueous* solution.[28]

PEPTIDES AND PEPTIDE MODELS

Peptides *and* peptide *models* (i.e., amides *derived from* α-*amino acids) are also important targets for* enantioselective *receptors:* many *of the* most extreme *selectivities were obtained* with *these substrates. An example is Rebek's tetra-amide 38. derived from two* molecules *of*

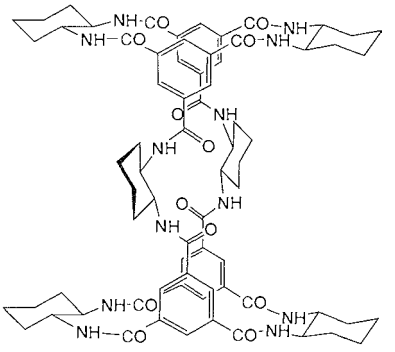

45

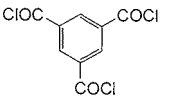

46

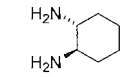

47

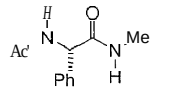

48

"Kemp's *triacid." One enantiomer of the* diketopiperazine *(cyclodipeptide) substrate 39 can bind through four hydrogen bonds. as shown. The other enantiomer cannot form a similar complex without a steric clash between the* isobutyl *groups and the naphthyl system. Accordingly, the receptor gives* ~*100:1* enantioselectivity *with this substrate in* $CDCl_3$.[29]

Still *and coworkers also described some remarkably selective* peptide *receptors. Tricyclic systems 40–42 represent an interesting sequence. These* molecules *adopt bowl-shaped* conformations *in which the central aromatic ring serves as the "base." and the outer rings of* amide *groups define the* "rim." *The first example 40 was found to bind a range of N-Boc* α-amino *acid* amides *with excellent enantioselectivities, peaking at* 130:1 *for valine derivative 43* in $CDCl_3$.[30] *Receptor 41 was then used to demonstrate, with unusual clarity. the importance of a well-defined preorganized architecture. This slightly* more *flexible molecule* was still *a good receptor but showed just 9:1* enantioselectivity *for 43.*[31] *The colored system 42 was used to explore the application of combinatorial chemistry to molecular recognition. When exposed to a library of bead-bound peptidic substrates, it bound preferentially to certain members.* turning *the*

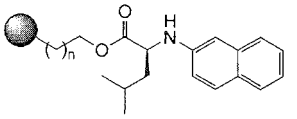

49

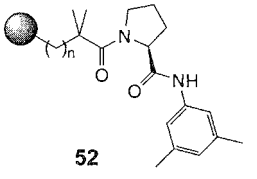

52

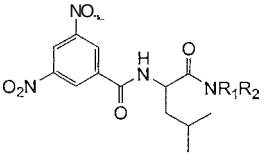

50 R_1 = H, R_2 = Bu

51 R_1 = R_2 = Me

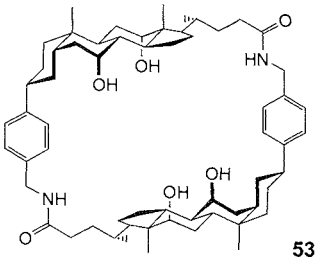

53

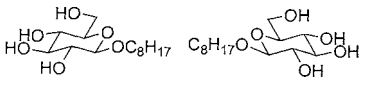

55 (β-D) 56 (β-L)

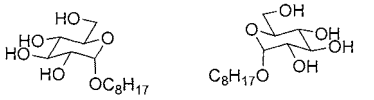

57 (α-D) 58 (α-L)

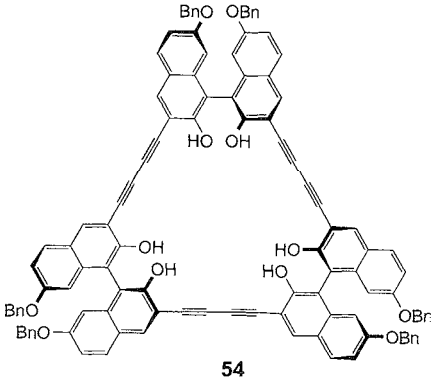

54

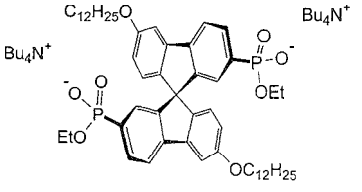

59

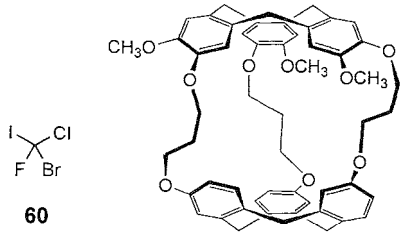

61

60

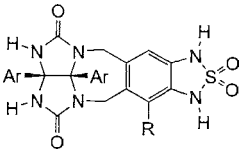

Ar = 4-dodecylphenyl

62 R = H
63 R = OH

64

corresponding beads a deep red. High affinities were indicated for peptides with terminal cyclopropanoyl groups, and when amide 44 was tested in solution, it was bound exceptionally strongly. Strong binding will often imply an exact fit and, therefore, high selectivity. in this case. 44 was bound with ~300:1 enantioselectivity, probably the highest recorded value for a synthetic receptor.[31,32]

Still and coworkers reported a second tricyclic system 45. This host was accessible in a single step from 46 and 47 (13% yield) and also showed exceptional enantiodiscrimination. For example, L-phenylglycine derivative 48 and its enantionier were bound in the ratio ~160:1, with $CDCl_3$ as solvent.[33]

Finally, Pirkle's pioneering work on enantioselective separations was especially successful with *N*-3,5-dinitrobenzoyl peptide models. For example, a CSP of form 49 was able to separate the enantiomers of 50 with $\alpha=18$,[34] while the later-generation phase **52** gave $\alpha=30$ for **51**.[35] These simple but effective systems are amenable to detailed structural analysis and, thus, can be especially informative. For example, NMR[35] and x-ray crystallography[36] were used to show that the more stable 51.52 complex possesses a compact structure held together by a π–π interaction and two intermolecular NH···O=C hydrogen bonds.

CARBOHYDRATES

Carbohydrates are challenging targets for molecular recognition. being complex yet only subtly different from

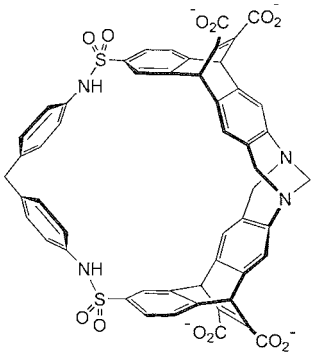

65

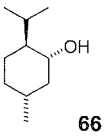

66

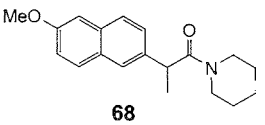

68

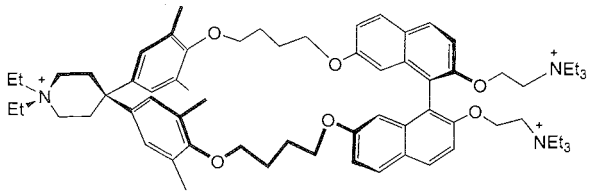

67

each other.[37] *Enantioselectivity is usually achieved through host structures that can* surround *the carbohydrate nucleus. accessing all the recognition features of the substrate.* Examples *are* **40**. ***53.*** *and* **54**, *which were tested against organic-soluble octyl glucosides* ***55–58*** *in* $CDCl_3$. *The steroid-based system 53 showed moderate* selectivities in α- *and* β-series, *preferring* **58** (α-L) *over* **57** (α-D) *by a factor of 2. and* 55 (β-D) *over 56* (β-L) *by a factor of* 3.[38] *Chiral "bow!" 40 gave values of 2 and 4 in the* α- *and* β-series, *respectively, favoring the* D-*substrate in each case."'"* Receptor **54** *(the S,S,R-*member *of* a *family of* stereoisomers) *showed better selectivity in the* α-series, *binding* **58** *and* **57** *in the ratio* 4:1.[40] *Unfortunately. a figure could not be obtained for the* β *anomers, because* **56** *bound* with *slow kinetics.*

Bis-phosphonate 59 *is exceptional in that it cannot* encapsulate *the substrate, providing instead a chiral cleft to act as binding site. The receptor was not resolved, but* NMR *studies with* **55** *and* **57** *in* CD_3CN *could be analyzed to give binding constants for both diastereo*meric *complexes. The selectivity was only* 1.4:1 *for the* α-series. *but the ratio for* β-anomer *55 was 5:1.*[41] *This* figure, though *moderate, is still the record for enantioselective carbohydrate recognition through non-covalent interactions."*

"An alternative approach to carbohydrate recognition involves covalent B-O bond formation. For a review of this area see Ref. [42].

ENANTIOSELECTIVE RECOGNITION OF LESS-FUNCTIONALIZED SUBSTRATES

Selective molecular recognition usually relies on strong and specific attractions involving *polar functional groups.* Enantioselective *recognition is favored by several such interactions. Substrates with* just *one functional group. or none at all, are therefore especially challenging targets. An extreme* example is *the chiral* haloform CHFClBr *(60). Merely binding this* molecule *is nontrivial. especially* in organic *solvents. The solution was found in* "cryptophane" *61, a host molecule with an enclosed chiral cavity that is closely matched in size to* **60**. *The cavity appears to be too small for* $CDCl_3$, *so this solvent does not* compete *with the substrate. At low temperature (215 K), receptor* **61** formed *a* 2:1 *ratio of diastereoineric complexes with excess of* racemic **60**.[43] *A related chiral* hemicarcerand, *constructed from two calixarenes linked face to face via a binaphthyl unit. was employed for soinewhat larger substrates. In this case. the substrates were used neat or dissolved in* noncompeting *diphenyl ether. The* hemicarcerand *showed an enantioselectivity of* 2.7:1 *with* $BrCH_2CH_2CHBrMe$ *as guest, and it appeared to be* completely *selective for one* enantiomer *of p-*tolyl *methyl* sulfoxide.[44] An *interesting recent development is the formation of capsular hosts by self-assembly. The sulfa*mido-glycoluril *unit* **62** forms *an enclosed, symmetrical* tetrameric *structure capable of accepting sizeable guests. Desymmetrization as in 63 distorts this structure so that it can show* enantioselectivity. *With ketone 64 as guest. the results are remarkable: the self-assembled capsule* shows *4:1 selectivity in favor of the S-*substrate.[45]

With water as solvent. hydrophobic interactions can be used to drive complex *formation. Cyclodextrins were widely used to study hydrophobic binding. and* they *often show enantioselectivity.* However, *strong enantiodiscrim*ination *is* rare, *especially* for less-functionalized *substrates."'" synthetic water-soluble receptors gave* similar *results. For example,* cyclophane *65 bound the enantiomers of menthol* **66** *in the ratio* 5:4,[47] *while macrocycle* **67** *bound Naproxen derivatives 68 in* D_2O/MeOH (60:40) *with 1.9:1* enantioselectivity.[48]

CONCLUSION

*Chiral guest recognition is a success story in supramo*lecular *chemistry. with* many *examples of good selectivity and some that are impressive. However. there is plenty of room for improvement. By their nature, the most effective receptors are complementary to specific substrates and, therefore.tend to be limited in scope. Also, some substrate classes have proved far* more *resistant than others. The goal of binding a wide range of substrates with. say.* >95% e.e., is *still unrealized. Success* will *probably require an*

equally wide range of receptors, and one may foresee an increased role for combinatorial chemistry in future work.[49] It is unlikely that interest will lapse—chirality continues to fascinate chemists. and the supramolecular community is unlikely to drop this challenge for many years to come.

ACKNOWLEDGMENT

The author thanks his coworkers for their efforts toward chiral. and achiral, molecular recognition over the past two decades. Funding for our programs has been provided by the EPSRC, the European Commission, the University of Bristol, and Enterprise Ireland.

ARTICLES OF FURTHER INTEREST

Amide- and Urea-Based Anion Receptors, p. 31
Amino Acids, Applications, p. 42
Calixarenes and Their Analogues: Molecular Complexation, p. 145
Carbohydrates, Recognition of, p. 169
Chiral Induction, p. 245
Crown Ethers. p. 326
Cryptophanes, p. 340
Cyclodextrins, p. 398
Cyclodextrins, Applications, p. 405
Cyclophanes: Eizdoacidic, Endobasic, and Endolipophilic Cavities, p. 424
Guanidium-Based Anion Receptors, p. 615
Hydrogen Bonding, p. 658
Hydrophobic Effects, p. 673
Molecular Clefts and Tweezers, p. 887
Porphyrin Derivatives, Functional, p. 1139
Steroid-Based Anion Complexation Agents, p. 1365
*Tröeger's Base Derivatives, p. 15*16
Zwitterion Receptors, p. 1639

REFERENCES

1. Schneider. H.-J.; Uatsimirsky, A. *Principles and Methods in Supramolecular Chemistry*; Wiley: Chichester. 2000: 287.
2. Pirkle. W.H.; Pochapsky, T.C. Considerations of chiral recognition relevant to the liquid-chromatographic separation of enantiomers. Chem. Rev. 1989. 89 (2). 347–362.
3. Okamoto. Y.; Yashima. E. Polysaccharide derivatives for chromatographic separation of enantiomers. Angew. Chem.. Int. Ed. Engl. 1998. *37* (8). 1021–1043.
4. Zhang, X.X.; Bradshaw. J.S.; Izatt. R.M. Enantiomeric recognition of amine compounds by chiral tnacrocyclic receptors. Chern. Rev. 1997. *97* (8). 3313–3361.
5. Webb. T.H.; Wilcox. C.S. Enantioselective and diastereoselective molecular recognition of neutral molecules. Chem. Soc. Rev. 1993. 22. 383–395.
6. Dalgliesh. C. The optical resolution of aromatic amino acids on paper chromatograms. J. Chem. Soc. 1952. 3940–3942.
7. Peacock. S.C.: Domeier. L.A.; Gaeta. F.C.A.: Hegelson. R.C.; Timko, J.M.: Cram, D.J. Host-guest complexation. 13. High chiral recognition of amino esters by dilocular hosts containing extended steric barriers. J. Am. Chern. Soc. 1978. *100*. 8190–8202.
8. Newcomb, M.; Toner. J.L.: Hegelson. R.C.: Cram, D.J. Host-guest complexation. 20. Chiral recognition in transport as a molecular basis for a catalytic resolving machine. J. Am. Chem. Soc. 1979. *101*. 4941–4947.
9. Huszthy, P.; Bradshaw. J.S.: Zhu. C.Y.; Izatt. R.M.; Lifson, S. Recognition by new symmetrically substituted chiral diphenyl- butylpyridino-18-crown-6 and di-tert-butylpyridino- IS-crown-6 and asymmetrically substituted chiral dimethylpyridino-18-crow-6 ligands of the enantiomers of various organic ammonium perchlorates. J. Org. Chem. 1991. *56* (10). 3330–3336.
10. Naemura, K.: Ogasahara. K.; Hirose, K.: Tobe. Y. Preparation of homochiral azophenolic crown ethers containing I-phenylethane-1.2-diol and 2,4-dimethyl-3-oxapentane-1,5-diol as a chiral subunit: Enantiomer recognition behaviour towards chiral 2-aminoetlianol derivatives. Tetrahedron: Asymmetry 1997. *8* (1). 19–22.
11. Kubo. Y.; Maeda. S.; Tokita. S.: Kubo. M. Colorimetric chiral recognition by a molecular sensor. Nature 1996. 382 (6591). 522–524.
12. Kuroda, Y.: Kato, Y.; Wigashioji, T.; Hasegawa. J.: Kawanami. S.: Takahashi. M.; Shiraishi. N.: Tanabe, K.; Ogoshi. H. Chiral amino acid recognition by a porphyrin-based artificial receptor. J. Am. Chem. Soc. 1995. *117* (44). 10950–10958.
13. Crossley. M.J.; Mackay, L.G.: Try, A.C. Enantioselective recognition of histidine and lysine esters by porphyrin chiral clefts and detection of amino acid conformations in the bound state. J. Chem. Soc., Ser. Chern. Commun. 1995. *18*. 1925–1927.
14. Wang, C.Z.: Zhu. Z.A.: Li. Y.: Chen. Y.T.; Wen, X.: Miao, F.M.: Chan. W.L.: Chan. A.S.C. Chiral recognition of amino acid esters by zinc porphyrin derivatives. New J. Chem. 2001. *25* (6). 801–806.
15. Fitzmaurice. R.J.; Kyne. G.M.; Douheret. D.; Kilburn. J.D. Synthetic receptors for carboxylic acids and carboxylates. J. Chem. Soc., Perkin Trans. 1 2002: (7). 841–864.
16. Martin, M.: Raposo, C.; Almaraz. M.: Crego. M.: Caballero. C.: Grande. M.; Morán, J.R. Efficient recognition of chiral carbamoyl-α-hydroxyacids with a cleft-type receptor. Angew. Chem., Int. Ed. Engl. 1996. *35* (20). 2386–2388.
17. Lustenberger. P.: Martinborough, E.: Denti, T.M.: Diederich. F. Geometrical optimisation of 1,1'-binaphthalene receptors for enantioselective molecular recognition of excitatory amino acid derivatives. J. Chem. Soc., Perkin Trans. 2 1998; (4). 747–761.
18. Botana, E.; Ongeri. S.: Arienzo, R.: Demarcus, M.: Frey, J.C.: Piarulli. U.; Potenza, D.; Gennari. C.: Kilburn. J.D. Enantioselective binding of dipeptides using acyclic receptors. Chem. Commun. 2001; (15), 1358–1359.
19. Baragaña, B.: Blackburn. A.G.: Breccia. P.: Davis. A.P.: de

Mendoza, J.; Padrón-Carrillo, J.M.; Prados. P.: Riedner. J.: de Vries. J.G. Enantioselective transport by a steroidal guanidinium receptor. Chem. Eur. J. 2002. *8*. 2931–2936.
20. Pirkle. W.H.; Bowen, W.E. Preparative separation of enantiomers using hollow-fiber membrane technology. Tetrahedron: Asymmetry 1994. *5* (5). 773–776.
21. Pirkle, W.H.: Liu, Y. Design. synthesis, resolution. determination of absolute configuration, and evaluation of a chiral naproxen selector. J. Org. Chem. 1994. *59*. 6911–6916.
22. Konishi. K.: Yahara. K.: Toshishige, H.; Aida, T.: Inoue. S. A novel anion-binding chiral receptor based on a metalloporphyrin with molecular asymmetry. Highly enantioselective recognition of amino acid derivatives. J. Am. Chem. Soc. 1994. 116. 1337–1344.
23. Galan. A.; Andreu. D.; Echavarren. A.M.; Prados, P.; de Mendoza, J. A receptor for the enantioselective recognition of phenylalanine and tryptophan under neutral conditions. J. Am. Chem. Soc. 1992. *114*. 1511–1512.
24. de Mendoza. J.; Gago, F. Molecular Recognition of Dinucleotides and Amino-Acids by Artifical Receptors Containing a Bicyclic Guanidinium Unit. In *Computational Approaches in Supramolecular Chemistry*; Wipff. G., Ed.: Kluwer Academic Publishers. 1994: 79–99.
25. Chin, J.: Lee. S.S.; Lee. K.J.: Park, S.: Kim, D.H. A metal complex that binds α-amino acids with high and predictable stereospecificity. Nature 1999. 401 (6750). 254–257.
26. Liu. Y.: Bin. L.: Han. B.H.; Li. Y.M.; Chen, R.T. Enantioselective recognition of amino acids by β-cyclodextrin 6-*O*-monophosphates. J. Chem. Soc., Perkin Trans. 2 1997. (7). 1275–1278.
27. Liu. Y.: Han, B.H.; Qi, A.D.: Chen. R.T. Molecular recognition study of a suprarnolecular system. 11. Chiial recognition of aliphatic amino acids by natural and modified α-cyclodextrins in acidic aqueous solution. Bioorg. Chem. 1997. 25 (3), 155–162.
28. Gavin, J.A.: Gal-cia. M.E.; Benesi, A.J.: Mallouk. T.E. Chiral molecular recognition in a tripeptide benzylviologen cyclophane host. J. Org. Chem. 1998. 63 (22). 7663–7669.
29. Jeong, K.S.; Muehldorf. A.V.; Rebek, J. Molecular recognition—asymmetric complexation of diketopiperazines. J. Am. Chem. Soc. 1990. 112 (16), 6144–6145.
30. Hong, J.-I.: Namgoong, S.K.: Bernardi, A.; Still. W.C. Highly selective binding of simple peptides by a C_3 macrotricyclic receptor. J. Am. Chem. Soc. 1991. 113. 5111.
31. Yoon. S.S.; Georgiadis. T.M.; Still. W.C. Conformational flexibility and binding selectivity in a synthetic receptor for peptides. Tetrahedron Lett. 1993. 34, 6697.
32. Borchardt, A.; Still. W.C. Synthetic receptor binding elucidated with an encoded combinatorial library. J. Am. Chem. Soc. 1994. 116. 373–374.
33. Yoon. S.S.: Still. W.C. An exceptional synthetic receptor for peptides. J. Am. Chem. Soc. 1993. 115. 823.
34. Pirkle, W.H.: Pochapsky. T.C.; Mahler, G.S.; Corey. D.E.: Reno. D.S.; Alessi. D.M. Useful and easily prepared chiral stationary phases for the direct chromatographic separation of the enantiomers of a variety of derivatised amines. ammo acids, alcohols. and related compounds. J. Org. Chem. 1986. 51.4991–5000.
35. Pirkle. W.H.; Murray, P.G.: Rausch. D.J.: McKenna, S.T. Intermolecular H-1-H-I two dimensional nuclear overhauser enhancements in the characterization of a rationally designed chiral recognition system. J. Org. Chem. 1996. 61 (14). 4769–4774.
36. Pirkle, W.H.: Murray, P.G.; Wilson. S.R. X-ray crystallographic evidence in support of a proposed chiral recognition mechanism. J. Org. Chem. 1996. 61 (14). 4775–4777.
37. Davis. A.P.: Wareham, R.S. Carbohydrate recognition through noncovalent interactions: A challenge for biomimetic and supramolecular chemistry. Angeu-. Chem., Int. Ed. 1999. 38 (20). 2978–2996.
38. Bhattarai. K.M.: Bonar-Law, R.P.: Davis, A.P.: Murray. B.A. Diastereo- and enantio-selective binding of octyl glucosides by a tetrahydroxycholaphane. J. Chem. Soc., Chem. Commun. 1992, 752.
39. Liu. R.; Still. W.C. Highly selective binding of diverse neutral donor/acceptor substrates by a C_3 macrotricyclic receptor. Tetrahedron Lett. 1993. 34. 2573.
40. Bahr. A.; Droz, A.S.; Püntener, M.: Neidlein. U.: Anderson. S.; Seiler. P.; Diederich, F. Molecular recognition of pyranosides by a family of trimeric. 1,1′-binaphthalene-derived cyclophane receptors. Helv. Chim. Acta 1998, *81* (11). 1931–1963.
41. Das, G.: Hamilton. A.D. Carbohydrate recognition: Enantioselective spirobiiluorene diphosplionate receptors. Tetrahedron Lett. 1997. 38 (21). 3675–3678.
42. James. T.D.: Sandanayake. K.R.A.S.;Shinkai, S. Saccharide sensing with molecular receptors based on boronic acid. Angew. Chem.. Int. Ed. Engl. 1996, 35 (17). 1911–1922.
43. Canceill. J.; Lacombe, L.: Collet. A. Analytical optical resolution of bromochlorofluoromethane by enantioselective inclusion into a tailor-made cryptophane and determination of its maximum rotation. J. Am. Chem. Soc. 1985. *107* (24). 6993–6996.
44. Yoon. J.Y.; Cram. D.J. Chiral recognition properties in complexation of two asymmetric hemicarcerands. J. Am. Chem. Soc. 1997. 119 (49). 11796–11806.
45. Nuckolls, C.; Hof, F.: Martin. T.: Rebek, J. Chiral microenvironments in self-assembled capsules. J. Am. Chem. Soc. 1999. *121* (44), 10281–10285.
46. Rekharsky, M.V.; Inoue. Y. Complexation thermodynamics of cyclodextrins. Chem. Rev. 1998.98 *(5)*. 1875–1917.
47. Webb. T.H.; Suh, H.; Wilcox. C.S. Enantioselective and diastereoselective molecular recognition of alicyclic substrates in aqueous media by a chiral. resolved synthetic receptor. J. Am. Chern. Soc. 1991. 113. 8554–8555.
48. Castro. P.P.: Georgiadis. T.M.; Diederich, F. Chiral recognition in clefts and cyclophane cavities shaped by the 1.1'-binaphthyl major groove. J. Org. Chem. 1989. 54. 5835–5838.
49. Gennari, C.: Nestler, H.P.; Piarulli. U.; Salom. B. Combinatorial libraries: Studies in molecular recognition and the quest for new catalysts. Liebigs Ann. 1997. (4). 637–647.

Chiral Induction

David B. Amabilino
Jaume Veciana
Institut de Ciència de Materials de Barcelona (CSIC), Cerdanyola del Vallès, Spain

INTRODUCTION

Chiral induction is the generation of a chiral molecular structure or superstructure in an otherwise achiral or racemic system by use of some stimulus (Fig. 1).[1] It is important, because it guarantees creation of chiral organizations of a determined handedness. which is not available through spontaneous resolution.[2] The chirality of the organization is determined from the molecular level in the conformations that the molecules adopt: the way the molecules come together through covalent or noncovalent means, and the way in which these aggregates self-assemble.

The most obvious stimulus to chiral induction is the use of stereogenic centers, but external perturbation, such as physical fields; can also be used to induce chirality.[3] The term is applied to traditional asymmetric synthesis through covalent bonds as well as to supramolecular synthesis. which is our interest here. Mention the word "chirality" to any chemist. and thoughts will be conjured of the right-handed B-DNA double helix. the right-handed α-helices formed by peptides of the natural L-amino acids, of thalidomide, and other emblematic and dramatic examples of the importance of stereochemistry. It is clear that the chirality of the components of biological systems play a key role in their function. in which induction of chirality through noncovalent bonds is inherent. But beyond natural systems and related phenomena, there is a wealth of unnatural chemical systems that display remarkable and important properties.

The scope of the area is so wide that all we can attempt to do here is discuss key examples and encourage the interested reader to investigate the other interesting results cited therein. We concentrate strictly on supramolecular effects in chiral induction. There is a separate article in this Encyclopedia that deals with the related field of chiral guest recognition.

OBSERVING CHIRAL INDUCTION

Induction of chiral structure is precisely observed in the crystal structures of compounds. In this sense. x-ray crystallography is a precise and informative tool in the study of chiral induction. Ideas can be given of how chirality is transmitted through the systems via the conformations and intermolecular interactions from the packing of molecules in the crystal. The obvious limitation is that high-quality single crystals are essential. Electron microscopy is useful when it comes to the induction of chirality in fibrous self-assembled systems. especially transmission electron microscopy (TEM), where direct observation of the twisted threads can be realized, as we will discuss. The use of scanning tunneling microscopy (STM) and atomic force microscopy (AFM) are also emerging rapidly as alternatives in this regard,[4] as well as in the study of chiral induction in monolayers.[5]

However. perhaps the most widely used techniques for observing chiral induction are the optical ones. polarimetry and, especially. circular dichroism (CD) spectroscopy, both in solution and in the solid state.[6] While induction of chirality implies the formation of a chiral structure, care must be exercised when drawing parallels between optical activity (as witnessed by these methods) and "real" structural chirality. For example, binding of a rigid achiral molecule to another chiral molecule may give rise to a Cotton effect in the absorption of the chromphores of the former. Optical activity was induced, but was chirality induced? The electronic structure is clearly chiral, there is a Cotton effect, but the conformation of the molecule is not. If the achiral molecule is flexible, and a Cotton effect is observed upon complexation with a chiral molecule, we cannot be sure that this is the result of a chiral conformation or merely the influence of the chiral complexing molecule on the electronic transitions. The problem becomes more complex in the case of complexation of a chiral agent to a racemic molecule, as highlighted by Krois and Lehner for the case of bilirubins.[7] These problems do not apply when the chirality is amplified to larger assemblies, where the increase in the magnitude of the Cotton effects cannot possibly be caused by proximity effects.

CHIRALITY IN CRYSTALS

The induction of chirality in crystals is usually achieved through the incorporation of stereogenic centers in one

Encyclopedia of Supramolecular Chemistry
DOI: 10.1081/E-ESMC 120012719

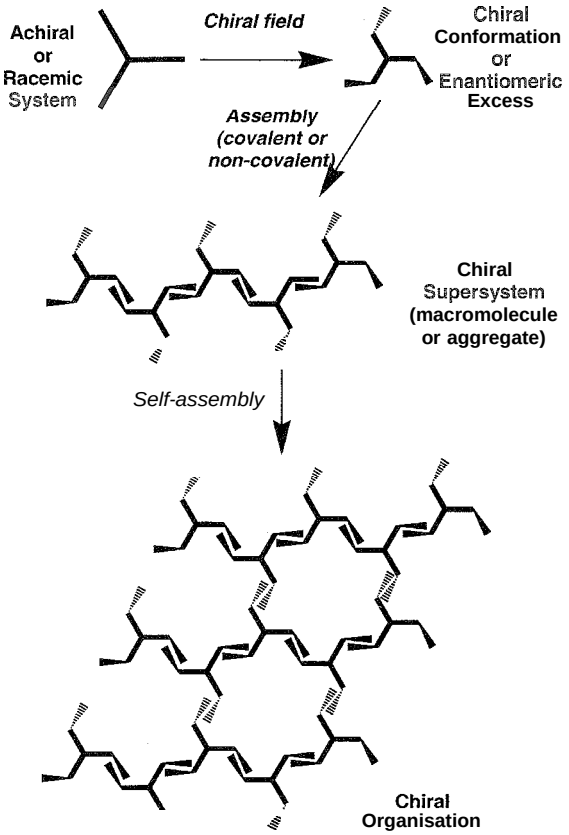

Fig. 1 A representation of the hierarchy of chiral induction, leading in this case to a principally two-dimensional chiral assembly.

molecule. which is complementary with an achiral or racemic compound. The resolution of racemates is a model example. but chiral compounds can also be used to confer chiral structures on otherwise achiral systems. The inclusion compounds formed by the chiral cholic acid host and achiral N-aryl-N-nitrosamine guests result in the adoption of a chiral conformation of the latter.[9] Here, the conformation observed by x-ray crystallography was correlated with the Cotton effects observed in the solid-state CD spectra. This type of trapping of chiral conformations in the solid state can be used to perform covalent-bond-forming photochemistry.[9] Thus, the inclusion compound formed between the chiral host 1 and the achiral anilide 2 contains the latter in a chiral conformation (Fig. 2). Irradiation of the crystals with UV light results in photocyclization of the anilide to form compound 3 in 98% ee and in a yield of 46%, and the reaction could be followed by x-ray crystallography. Even more efficient reactions. in which chiral host crystals act to induce chiral conformations in reagents prone to photocyclization, were observed.[9]

The use of anions or organic ligands as inducers of chirality to metal ion centers is well documented. if not entirely predictable because of high coordination numbers and a throng of possible metals.[10] As an example of induction by organic ligands, we take our own work on the formation of metal complexes by α-nitronyl nitroxide radicals, such as 3MLNN, in which a basic phenyl α-nitronyl nitroxide is substituted with a methyl lactate moiety.[11] When (*R*)-3MLNN is crystallized with manganese(II) hexafluoroacetylacetonate, a coordination polymer is formed through coordination of the radical's oxygen atoms to the metal ion (Fig. 3), and in which the chirality in the ligand induces a chiral A configuration in the manganese coordination sphere. Interestingly. the chiral conformation adopted by the ligand—regarding the helicity between the phenyl ring and the imidazolyl ring and that of the imidazolyl ring—is of the same type as that seen in the isolated ligand's crystal structure. In addition to being chiral, this metal-radical-based material is interesting, because it is a magnet at low temperatures.

CHEMICALLY INDUCED CHIRALITY IN SUPRAMOLECULAR SYSTEMS IN EQUILIBRIUM

The induction of chiral structure in supramolecular systems at equilibrium was widely studied, partially because of surging interest in the hierarchical nature of the self-assembly of chiral aggregates. It is also of utmost relevance in the study of chiral information in unnatural systems displaying new properties.

The transmission of chirality in membranes and other types of aggregates formed by surfactants was widely studied. The superstructures of bilayers formed by gemini dicationic surfactants based on quaternary ammonium centers can be modulated through the employ of enantiomeric tartrate salts.[12] The twisted ribbons (Fig. 4) are formed when an enantiomeric excess of one of the tartrates is present, with the period (helical pitch) shorten-

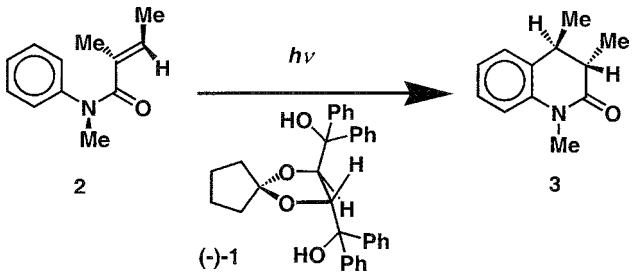

Fig. 2 Chiral induction in the photochemical reaction of *2* included in **1.** (From Ref. [9].)

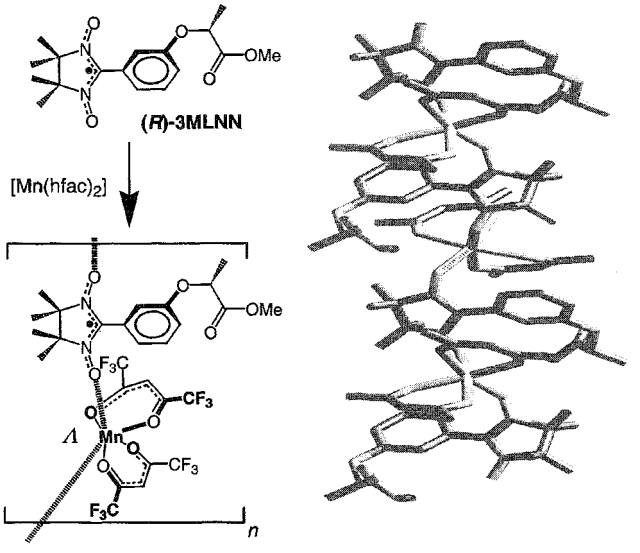

Fig. 3 Formation of the coordination polymer (*R*)-**3MLNN**·$Mn(hfac)_2$ and a view of the crystal structure of the molecular material showing part of the 2_1 chain. (From Ref. [11].)

ing as the enantiomeric excess of the anion increases. When there is no enantiomeric excess of tartarate or in the presence of achiral anions, flat ribbons are observed. The gemini nature of the surfactant is crucial in observing the effects. This effect is probably due the possible chiral conformers that the surfactant head group can adopt.[13]

Perhaps one of the most important applications of chiral induction is in the area of liquid crystals. Upon addition of a wide range of appropriate chiral compounds, the achiral nematic, smectic C, and discotic phases are converted into the chiral cholesteric (or twisted nematic). the ferroelectric smectic C*, and the chiral discotic phases. As a first example, we take the induction of chirality in the columns of aromatic chromophores present in some liquid-crystalline polymers.[14] The polymers. achiral polyesters incorporating triphenylene moieties, display discotic mesophases, which upon doping with chiral electron acceptors based on tetranitro-9-fluorene, form chiral discotic phases in which the chirality is determined by the dopant. These conclusions were reached on the basis of CD spectra in which strong Cotton effects were observed. Interestingly, the chiral dopants were unable to dramatically influence the chiral winding of triphenylene polymers that already incorporated stereogenic centers.

The induction in smectic C phases of chirai order in the form of smectic C* phases is interesting and important in view of the applications of this phase in displays.[15] The calamitic (rod-like) molecules in this phase are organized in layers, with the long axes of the molecules forming an angle with the normal to the layer plane. Upon addition of a suitable chiral dopant, this angle is forced into a helical arrangement about the normal to the layer plane, with a pitch of a few microns. The induction mechanism is believed to operate by incorporation of the dopant into the layers of achiral molecules, which interact in a host–guest type of way such that an orientational bias is inferred on the host. These chiral superstructures may be induced by molecules with stereogenic centers in the alkyl chains attached to rigid cores, with relatively high flexibility of the stereogenic center in general, which induce chirality in host phases with a wide variety of structural features.[16] Meanwhile. when rigid atropoisomeric cores are used in the dopant molecules. specific interactions take place between host and guest, and a more pronounced dependence on the structure of the two is observed.[17] Dopant molecules of Type 4 in Fig. 5 interact with host smectic C liquid crystals with a phenyl pyrimidine core (**PhP1**) in such a way that a preferred axially chiral conformation of the host is induced by the dopant guest, and this conformation is propagated through the layers.

Just as chiral induction can be realized in discotic liquid crystals, so it can in assemblies of disc-like molecules or disc-like aggregates. As far as molecules are concerned, C_3-symmetrical *tris*-amides (Fig. 6), which exhibit discotic liquid-crystalline phases, also form chiral columnar stacks through π–π interactions when dissolved in apolar solvents,[17] which are depicted schematically in

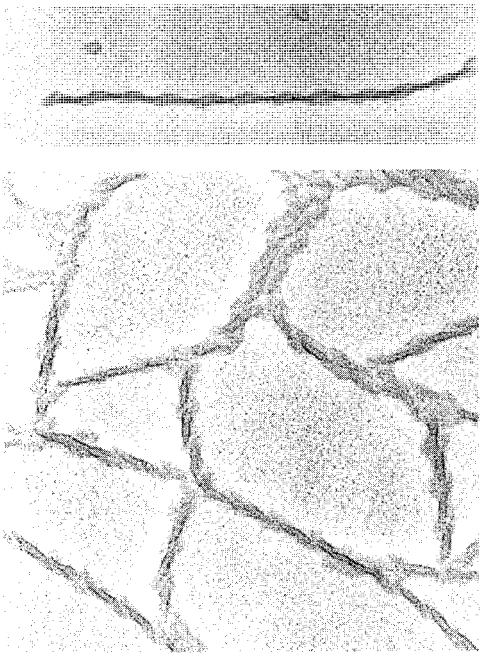

Fig. 4 The twisted ribbons formed by the addition of tartrate ions to aggregates formed by gemini ammonium surfactants. (From Ref. [12].) The authors thank Dr. Reiko Oda for supplying these TEM images.

Fig. 4. An achiral compound of this type exhibits no optical activity in dodecane, but when the compound is dissolved in the chiral (*R*)-(−)-2,6-dimethyloctane, significant Cotton effects (only slightly less intense than those observed in a chiral derivative) are detected. A chiral disc-like *tris*-amide compound can also be used as a dopant at concentrations as low as 2.5% to induce supramolecular chirality in the stacks of achiral compound. The presence of the additional hydrogen bonds in the form of the self-complementary urea unit is detrimental to chiral induction in this case.

Disc-like aggregates are also capable of forming chiral aggregates, in which chiral induction can be realized. The rosette-type aggregates formed by melamine derivatives and cyanurates or barbiturates form the basis of chiral aggregates formed from a calix[4]arene dimelamine **Mel1** and a complementary cyanurate or barbiturate.[18] Because there is a twist between the layered rosettes in the 3:6 aggregate, a helical twist exists between upper and lower decks, as seen in Fig. 7 by the orientation of the calixes. In the absence of any chiral influence. the *M* and *P* enantiomers are formed in equal amounts (Fig. 7), but when a stereogenic center is included in the barbiturate component (for example, **Bar1**), the point chirality is transmitted to the twist between the two decks of the assembly. Furthermore. the chiral component can be replaced through equilibration with an achiral cyanurate derivative (**CY1**), and the assembly retains the induced chirality. This kind of memory effect can also be achieved using an achiral calix[4]arene dimelamine with pendant pyridine moieties combined with achiral cyanurate to form the double-decker rosette and inducing a chiral secondary structure by adding tartaric acid derivatives that hydrogen bond to the pyridine moieties.[17] Efficient chiral induction requires the presence of two sterogenic centers in the his-acid. Subsequent precipitation of the acids through slat formation leaves the enantiomerically enriched supramolecules.

The chiral induction seen in the double-decker supramolecule we just discussed can also be seen in stacked systems that form nanotubes. A self-complementary heterobicyclic base CC—which incorporates the hydrogen bond donor–donor–acceptor sequence of guanine and the acceptor–acceptor donor sequence of cytoseine—suitably substituted with crown ether rings, undergoes formation of a cyclic hexamer which in methanol subsequently piles up on itself to give a nanotube-type structure, as observed by TEM. dynamic light scattering, and small-angle x-ray scattering.[17] When chiral amino acids are added to this preassernbled nonchiral system in concentrated methanol solution, the ammonium moieties bind the crown ether ring and induce a CD spectrum indicative of a helical superstructure. At lower concentrations, where the aggregation number is lower, the addition of amino acids leads

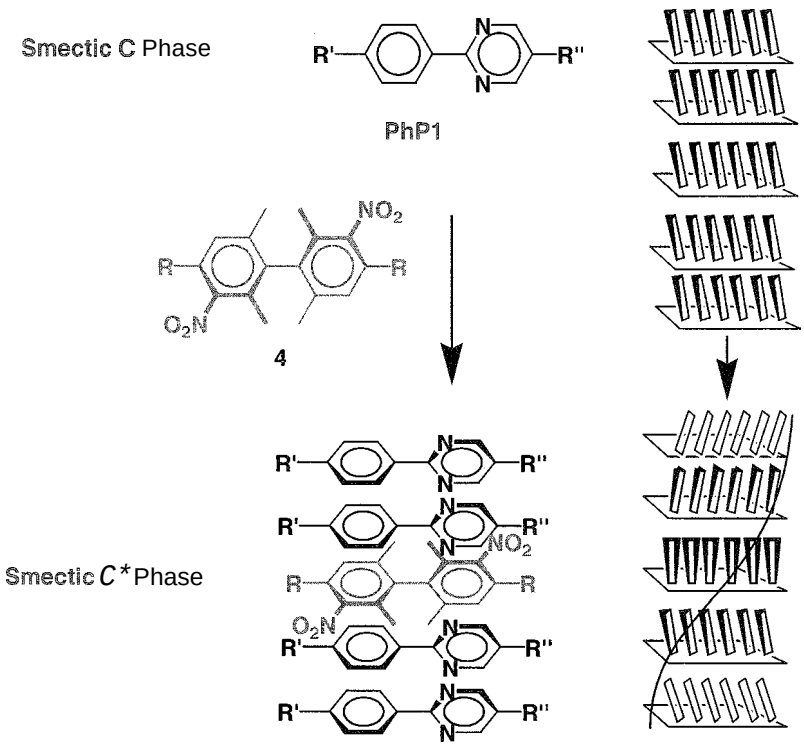

Fig. 5 The chiral induction of the srnectic C* phase in the smectic C phase of **PhP1** by atropoisomeric compound 4. (From Ref. [15].)

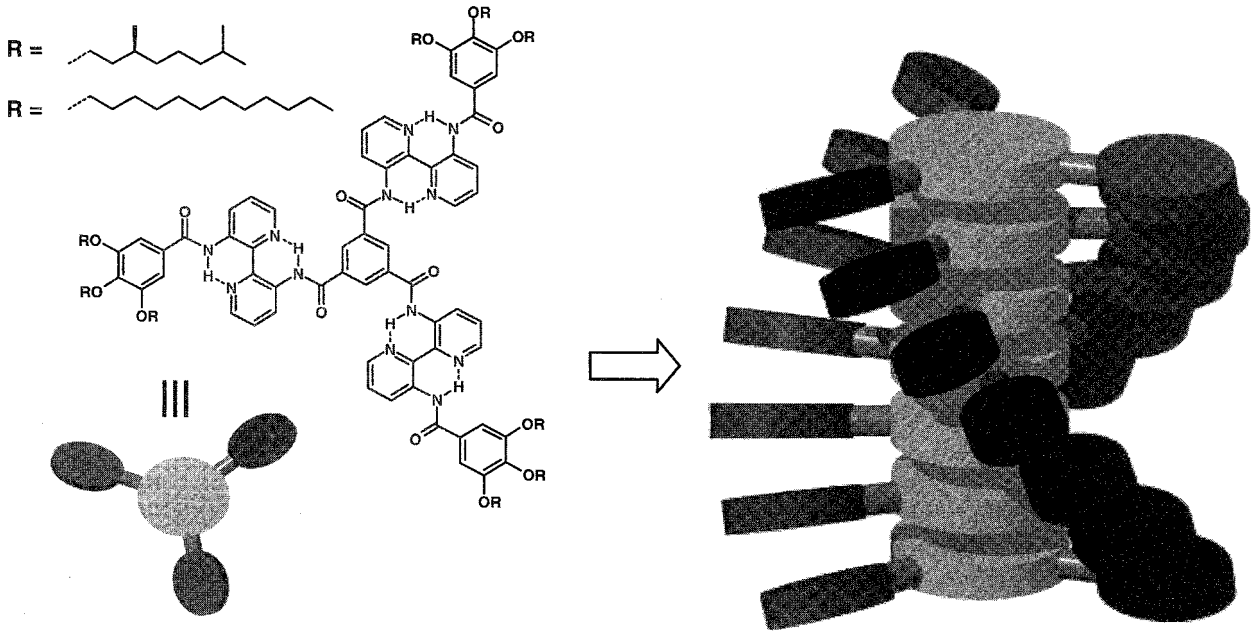

Fig. 6 Chiral and achiral *tris*-amides that display chiral induction phenomena and a representation of the n-stacked aggregates that they form. (From Ref. [17].) The authors thank Dr. "Bert" Meijer for supplying these images.

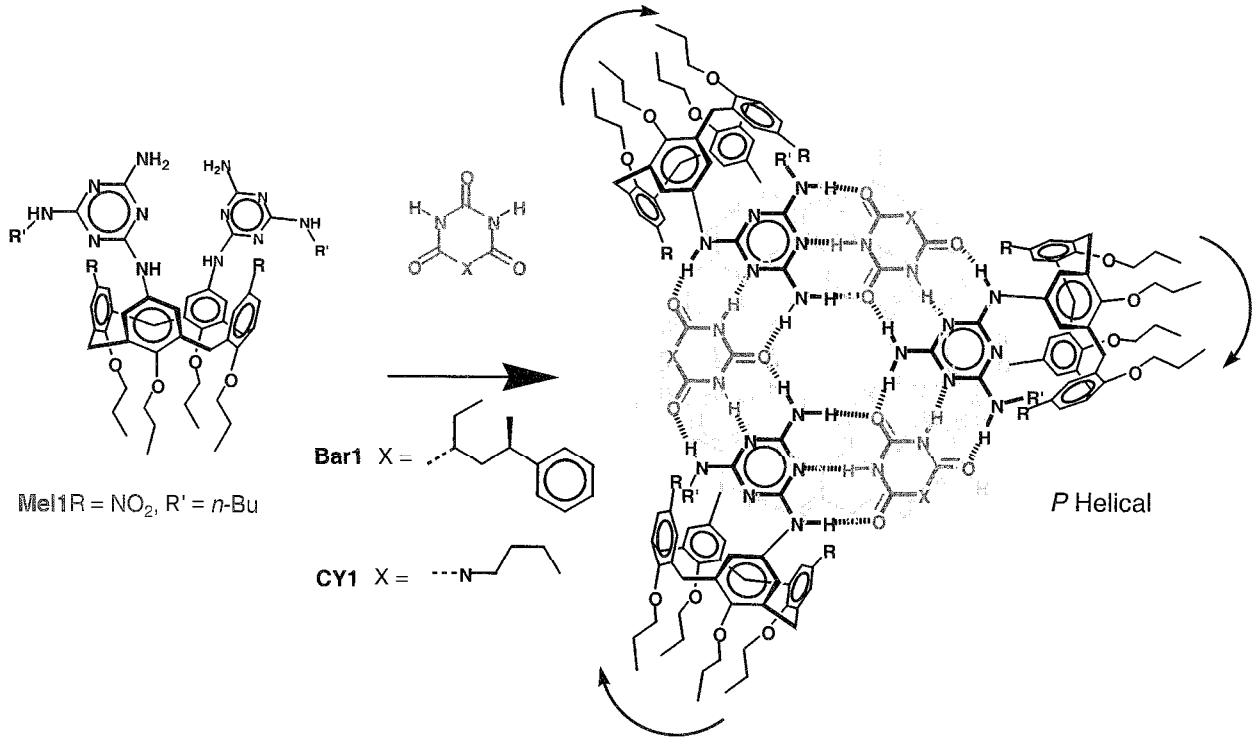

Fig. 7 Chiral double-decker rosettes formed by dimelamine calix-[4]-arenes and barbiturates and cyanurates. (From Ref. [18].) One of the helical forms, the P. is shown.

to a slow hierarchichal assembly of the rosette nanotubes with chirality that is determined by the nature of the amino acid used as the inducer. The optical activity of the helical nanotubes formed from the stacked rosettes depends critically on the nature of the amino acid inducer. L-Met being the best. Furthermore, the assembly process seems to be all or nothing. the maximum optical activity is obtained in a small range of concentrations and the aggregate can be disassembled upon heating and reassembled on cooling.

Treatment of a number of covalent polymers substituted with molecular recognition capability with suitable guests leads to chiral induction. The same crown ether–amino acid complementary pair described for the rosettes above was employed in the form of crown-ether pendant cis-transoidai poly(phenylacetylene).[20] When the achiral polymer is treated with amino acids (in the form of their hydroperchlorate salts in acetonitdle) a large induced CD signal is observed in the backbone of the polymer. The polymer is sensitive to small enantiomeric excesses in the amino acid, as little as 0.005% enantiomeric excess of alanine can be detected. In a similar vein, *cis*-transoidal poly(carboxyphenylacetylene) shows induced circular dichroism when treated with nonracemic chiral amines.[21] In addition, the system displays chiral memory, in that treatment of the complex with achiral amino alcohols results in retention of the chiral polymer backbone.

Supramolecular polymers are also partial to induction of chiral structures.[22] Biureidotriazines form polymeric chains maintained by the extremely strong complex formed by the self-complementary unit through four hydrogen bonds. When chiral "arms" are attached well away from the ureidotriazine units, chiral induction is seen in the polymers of the difunctional monomers, thanks to stacking of the neighboring hydrogen-bonded pairs.[23] Also, startlingly. when a chiral monofunctional ureidotriazine was used to cap a polymer formed in dodecane from an achiral biureidotriazine, significant chiral induction was observed from the end of the polymer chain through the secondary structure. Heterocomplementary monomers, just one of which contained a stereogenic centers, were also used for the formation of chiral suprarnolecular polymers.[24] In this case, the transfer of chirality was observed in the helical fibers witnessed in electron microscope images.

SUPRAMOLECULAR ASSISTANCE IN REACTIONS DISPLAYING CHIRAL INDUCTION

The diastereoselectivity of covalent bond-forming reactions can also be influenced by supramolecular effects. The polymerization of isocyanides shows this effect. When isocyanopeptides are polymerized under certain conditions. a dramatic dependence of reactivity on the stereochemical nature of the amino acid residues present in the monomer.[25] The origin of this difference appears to lie in the orientation of the hydrogen bonds acting between the monomers, which line the isocyanides up into chains in the solid state as well are present in the polymer chains.

Supramolecular effects were also observed during the formation of poly(isocyanide)s derived from chiral promesogenic phenyl benzoate-containing monomers.[26] These effects were seen through the degree of chiral induction from the stereogenic centers in the side chains to the polymer backbone during the kinetically controlled polymerization in different solvents and at different concentrations. Importantly, the sense of chiral induction seen during the polymerizations in certain cases was identical with the helicity induced in nematic and smectic C phases by the monomers.

PHYSICAL FIELD-INDUCED CHIRALITY IN SUPRAMOLECULAR SYSTEMS IN EQUILIBRIUM

Simple stirring is known to induce chirality through different mechanisms. Stirring during crystallization, for example, can lead to enantiomerically enriched samples. The origin of this chiral induction lies in the breaking of the first formed crystals into many pieces, which in turn, act as nucleation sites. Stirring solutions of protonated porphysins — which form aggregates as concentration is increased or as the ionic strength is changed — results in the formation of vortices that are able to influence the chirality of the growing supramolecular system,[27] as observed in the CD spectra of the aggregates. It was suggested that this kind of vortex effect, observed under rotary evaporation and stirring, may be general for supramolecular systems that are formed under kinetic control.[28]

Irradiation of switchable systems by circularly polarized light is another way of inducing chirality in racemic compounds. Racemic sterically hindered alkenes can be switched in solution using circularly polarized light to give enantiomeric excesses of only about 0.1%.[29] In order to amplify this small effect, the racemate was used as a dopant in a nematic liquid-crystal phase. and the resulting achiral mesophase was irradiated with circularly polarized light. A cholesteric phase resulted because of the small enantiomeric excess of the sterically hindered alkene. This system is a three-way switch. Irradiation with left or right circularly polarized light generates differently handed cholesteric phases. while irradiation with linearly polarized light affords the nematic phase.

Irradiation of racemizing species in solution with unpolarized light in a strong magnetic field can also give rise to small enantiomeric excesses. thanks to magneto-chiral anisotropy.[30] The effect was observed for the potassium salt of chromium *tris*(oxalate)—an ideal system for magnetochiral anisotropy in that it has high natural CD and magnetic CD asymmetry factors—in water. In a field of 10 Tesla, an enantiomeric excess of about 1×10^{-4} was observed. which equilibrated back to zero with time. But it was proved beyond doubt that photochemistry with unpolarized light in a magnetic field are enantioselective, and it was suggested that it be considered when addressing the origins of the homochirality of biological systems.

CONCLUSION

The ability of chemists to induce chirality through noncovalent bonds in systems in which it is absent was achieved in certain systems with efficiency on a number of occasions. some of which were highlighted in this review. The phenomenon is dramatic and potentially useful. However, the exact pathways of chiral transfer from the molecular through supramolecuiar to the macroscopic level are poorly understood in general. The use of physical fields in the induction of chirality has a long history but is still poorly understood. It is surely the conformations of molecules and their relative dispositions in aggregates that are key in the propagation of chirality. and the battery of analytical and theoretical techniques available today are sure to help in determining these factors and will aid in the rationalization and prediction of chiral induction.

ACKNOWLEDGMENTS

We warmly thank Dr. Reiko Oda (Institut Européen de Chimie et Biologie, Pessac, France) for supplying the TEM images in Fig. 3. and Dr. "Bert" Meijer (Eindhoven University of Technology, Holland) for supplying the graphics for Fig. 6. Our research in this area is supported by the DGI (Spain. Projects BQU2000-1157 and BQU2003-00760) and DGR (Catalonia. Project 2001SGR00362).

ARTICLES OF FURTHER INTEREST

Calixarenes and Their Analogues: Molecular Complexation, p. *145*
Chiral Guest Recognition. p. 236
Molecular Switches, p. *917*
Scanning Tunneling Microscopy. p. 1202
Self-Assembly: Definition and Kinetic and Thermodynamic Considerations, p. *1248*
Strict Self-Assembly and Self-Assembly with Covalent Modifications, p *1372*
Supramolecular Isomerism, p. 1420
Supramolecular Polymers, p. 1443

REFERENCES

1. Feringa, B.L.; van Delden. R.A. Absolute asymmetric synthesis: The origin, control, and amplification of chirality. Angew. Chem. Int. Ed. **1999**, *38* (23). 3418–3438.
2. Pérez-García, L.: Amabilino, D.B. Spontaneous resolution under supramolecular control. Chem. Soc. Rev. *2002. 31* (6). 342–356.
3. Avalos, M.: Babiano, R.; Cintas. P.; Jiménez. J.L.: Palacios, J.C.: Barron, L.D. Absolute asymmetric synthesis under physical fields: Facts and fictions. Chem. Rev. 1998.98 (7), 2391–2404.
4. Shinohara. K.-i.; Yasuda. S.: Kato, G.: Fujita, M.; Shigekawa. H. Direct measurement of the chiral quaternary structure in a π-conjugated polymer at room temperature. J. Am. Chem. Soc. **2001**. *123* (15). 3619–3620.
5. De Feyter. S.; Gesquiere, A.; Abdel-Mottaleb, M.M.; Grim, P.C.M.; De Schryver. F.C.; Meiners, C.; Sieffert. M.; Valiyaveettil, S.: Müllen, K. Scanning tunnelling microscopy: A unique tool in the study of chirality. dynamics. and reactivity in physisorbed monolayers. Acc. Chem. Res. 2800. *33* (8), 520–531.
6. Minguet. M.; Amabilino, D.B.; Wurst, K.: Veciana, J. Circular dichroism studies of crystalline chiral and achiral α-nitronyl nitroxide radicals in KBr matrix. J. Chem. Soc., Perkin Trans. 2 *2001,* (5), 670–676.
7. Krois. D.: Lehner, H. Induced circular dichroism and chiral discrimination of racemates revisited: Bilirubins as illustrative examples. J. Chem. Soc., Perkin Trans. 2 1995. (3), 489–494.
8. Szyrszyng. M.: Nowak. E.; Gdaniec, M.: Milewska, M.J.; Herman, A.; Połoński, T. Circular dichroism spectra of the achiral guest *N*-aryl-*N*-nitrosamines included in the crystal host matrices of cholic acid. J. Org. Chem. **2001**, 66 (22); 7380–7384.
9. Toda. F. Crystal engineering for molecular dynamics. CrystEngComm 2002, *4* (40). 215–222, and references cited therein.
10. Knof. U.: von Zelewsky, A. Predetermined chirality at metal centres. Angew. Chem. Int. Ed. 1999. 38 (3). 302–322.
11. Minguet. M.; Luneau, D.: L'hotel. E.: Villar. V.: Paulsen, C.; Amabilino. D.B.; Veciana, J. An enantiopure molecular fenornagnet. Angew. Chem. Int. Ed. *2002.41* (4), 586–589.
12. Oda. R.: Huc. I.: Scmutz. M.; Candau. S.J.: MacKintosh. F.C. Tuning bilayer twist using chiral counterions. Nature **1999**. *399*. 566–569.
13. Berthier, D.; Buffeteau, T.; Léger, J.-M.; Oda, R.; Huc, I. From chiral counterions to twisted membranes. J. Am. Chem. Soc. *2002,124* (45). 13486–13494.

Green, M.M.; Ringsdorf, H.; Wagner, J.; Wiistefeld, R. Induction and variation of chirality in discotic liquid crystalline polymers. Angcw. Chcm.. Int. Ed. Engl. 1990, 29 (12). 1478–1481.

15. Lemieux, R.P. Chirality transfer in ferroelectric liquid crystals. Acc. Chem. Res. 2001, 34 (11), 845–853, and references cited therein.
16. Walba, D.M.: Slates, S.C.: Thurmes, W.N.; Clark, N.A.; Handschy, M.A.; Supon, F. Design and synthesis of a new ferroelectric liquid crystal family. Liquid crystals containing non-racemic 2-alkoxy-1-propoxy unit. J. Am. Chem. Soc. 1986, 108 (17). 5210–5221.

van Gorp, J.J.; Vekemans, J.A.J.M.; Meijer, E.W. C_3-Symmetrical supramolecular architectures: Fibers and organic gels from discotic trisamides and trisureas. J. Am. Chem. Soc. 2002, 124 (49), 14759–14769. and references cited therein.

Ishi-i, T.; Crego-Calama, M.: Timmerman, P.; Reinhoudt, D.N.; Shinkai, S. Bnantioselective formation of a dynamic hydrogen-bonded assembly based on chiral memory concept. J. Am. Chem. Soc. 2002, 124 (49), 14631–14641, and rcfcrences cited thcrcin.

19. Fenniri, H.; Deng, B.L.; Ribbe, A.E. Helical rosette nanotubcs with tunablc chiroptical properties. J. Am. Chem. Soc. 2002, 124 (37), 11064–11072.
20. Nonokawa. R.; Yashirna, E. Detection and amplification of a small enantiorneric imbalance in α-amino acids by a helical poly(phenylacetylene) with crown ether pendants. J. Am. Chem. Soc. 2003, *125* (5), 1278–1283.
21. Yashima, E.; Maeda, K.; Okamoto, Y. Memory of macromolecular helicity assisted by interaction with achiral small molecules. Nature **1999**, *399*, 449–451.
22. Rrunsvcld. L.; Folmer. B.J.B.; Meijer, E.W.; Sijbesma, R.P. Supramolecular polymers. Chem. Rev. 2001. 101 (12), 4071–4097, and references cited therein.
23. Hirschberg, J.H.K.K.;Brunsveld, L.; Ramzi, A.; Vekemans, J.A.J.M.; Sijbesma, R.P.; Meijer, E.W. Helical self-assembled polymers from cooperative stacking of hydrogen-bonded pairs. Nature 2000, 407, 167–170.
24. Berl, V.; Schmutz, M.; Krische, M.J.; Khoury, R.G.: Lehn, J.-M. Supramolecular polymers generated from heterocomplementary monomers linked through multiple hydrogen-bonding arrays — Formation, characterization and properties. Chem. Eur. J. 2002, *8* (5), 1227–1244.
25. Cornelissen, J.J.L.M.; Donners, J.J.J.M.; de Gelder, R.; Graswincliel, W.S.; Metselaar, G.A.; Rowan, A.E.; Sommerdijk, N.A.J.M.; Nolte, R.J.M. β-Helical polymers from isocyanopeptides. Science 2001.293, 676–680.
26. Amabilino,D.B.;Ramos,E.;Serrano,J.-L.;Sierra,T.;Veciana, J. Long-range chiral induction in chemical systems with helical organization — Promesogenic monomers in the formation of poly(isocyanides) and in the organization of liquidcrystals.J.Am.Chem.Soc.1998;*120*(36),9126–9134.
27. Ribó, J.M.; Crusats, J.; Sagués, F.; Claret: J.; Rubires, R. Chiral sign induction by vortices during the formation of mesophases in stirred solutions. Scicnce 2001, 292, 2063–2066.
28. Rubires, R.: Farrcra. J.-A.; Ribó, J.M. Stirring effects on the spontaneous formation of chirality in the homoassociation of diprotonated *meso*-tetraphenylsulfonato porphyrins. Chem. Eur. J. 2001, 7 (2). 436–446.
29. Huck, N.P.M.; .lager, W.F.; de Lange, R.; Feringa, B. Dynamic control and amplification of molecular chirality by circular polarised light. Science 1996. 273, 1686–1688.
30. Rikken, G.L.J.A.; Raupach, E. Enantioselective magneto-chiral photochemistry. Nature 2000, 405, 932–935.

Classical Descriptions of Inclusion Compounds

Yuri Alexseevich Dyadin (Deceased)
Irina Sergeevna Terekhova
The Siberian Branch of the Russian Academy of Sciences, Novosibirsk, Russia

INTRODUCTION

Clathrates. or inclusion compounds, are the typical representatives of supennolecular species. We may define them as the compounds formed by inclusion of one kind of molecules, called guest molecules. into the cavities of a crystalline framework composed of the molecules of another kind (or into a cavity of one large molecule), called host molecules, without forming any specific chemical bond between guest and host. Unlike the case of traditional chemical compounds, favorable spatial complementarity of the guest and host subsystems. not chemical reactivity. plays the important role in formation of these compounds from the components. This principle of formation allows molecules that are coordination saturated and do not interact chemically with each other to be brought together, so that they form supermolecules or supermolecular crystalline phases that are thermodynamically more stable than a mixture of initial components.

BRIEF HISTORY

J. Priestley (1778) seems to be the first to have observed the formation of a compound that today we call clathrate. He described "anomalous" ice formed at positive temperature. which sank in the aqueous solution of sulfur dioxide (also discovered by him). Since then, for nearly 170 years, outstanding chemists of the world H. Davy, M. Faraday, F. Wohler, and B. Rooseboom[1] often encountered these compounds. In some cases, they approached the understanding of their nature, however, for a long time these coinpounds were mainly considered as laboratory curiosity. The crucial role of van der Waals forces in the formation of these compounds was highlighted for the first time by Russian chemist B. A. Nikitin in 1936–1938 during the investigation of molecular compounds of noble gases.[2] However, the nature of the compounds under question was discovered in the most complete manner by H. M. Powell in 1947–1948 in x-ray crystallographic studies on the compound of β-hydroquinone with SO_2 (and also with other volatile components: HCl. HBr. Ar, Xe), which showed that the guest molecules were enclosed into the cavities of the framework formed by hydroquinone molecules and were not bound to the framework by any other forces than weak van der Waals interactions.[1] Independently, but somewhat later (in 1949); the same conclusion was made by M. von Stackelberg on the basis of x-ray analysis of the hydrate of sulfur dioxide,"' and by W. Schlenk who investigated channel adducts of urea and thiourea.[4] In 1956 to 1959, van der Waals and Platteeuw[5] constructed a statistical–thermodynamical ideal model of clathrate formation. Later, the compounds were discovered in which weak chemical interactions occur between guest and host molecules; these compounds are coordinatoclathrates, an example being trimethylamine hydrate $(CH_3)_3N{\cdot}10{,}25H_2O$, in which the amine molecule occupies the cavity of the water framework and is bonded to it through a hydrogen bond."' In the 1960s, C. J. Pedersen[7] and J. -M. Lehn[8] introduced new species into the class of inclusion compounds: complexes of the alkali metal salts with crown ethers and cryptands (clathratocornplexes): in this case. the interaction between guest and host subsystems is rather strong, but spatial complementarity has a pronounced effect on the properties of the resulting compounds.

MAJOR IDEAS, TERMS, CLASSIFICATIONS

The term "clathrate" (originating from Latin word ''clathratus,'' which means closed, surrounded from all sides (in turn, originating from the Greek words κλειθρον, κλεις=lock, key) was introduced by H. M. Powell in 1948, as we mentioned above, for the inclusion compounds of β-hydroquinone that have a crystalline framework with cavities shaped as isometric cages in which the guest molecules are located. In 1949, W. Schlenk introduced the term "inclusion compounds" (Einschluβ-verbindungen) for channel compounds of urea and thiourea. At first, the term clathrate was used to denote only cage inclusion compounds. At present: along with the term inclusion compounds, it is used independently of the shape of cavity; this points to the fact that there are no specific chemical interactions between the guest and host.

Clathrates may be classified according to the shape of the cavity into the following types: cryptatoclathrates— the compounds of this type have cage structures (κρυπτον is secrecy in Creek); tubulatoclathrates — one-dimensional channel inclusion compounds (tubus is the Latin tube):

DOI: 10.1081/E-ESMC 120006062

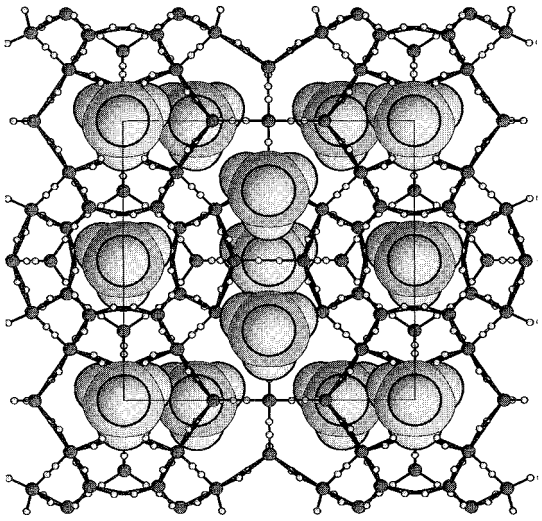

Fig. 1 The cubic structure I (CS-I) hydrate with methane molecules accommodated in the dodecahedra] (D) and in the tetradecahedral (T) cavities. (*View this art in color at www.dekker.com.*)

iiltercalatoclathrates — layered inclusion compounds. Another classification is based on the type of bonding of the host molecules in the framework. The host framework in lattice clathrates is composed of molecules bonded with each other with relatively weak specific bonds (most often hydrogen bonds). The guest molecule located within a cavity of such a frainework is surrounded by several host molecules (for example, by six molecules in hydroquinone clathrates or 20–38 molecules in aqueous clathrates). When dissolved or melted. the clathrate compound of this type decomposes. Thermal stability of a clathrate may be higher than that of a host component by several tens of degrees but not more: for lattice clathrates, the upper limit of stability is about 200–250°C. The host framework in macromolecular clathrates is completely constructed using covalent bonds: it is impossible to distinguish an individual host molecule. and the framework is a macromolecule as a whole. Clathrasils[9] may serve as an example of this type of clathrates. SiO_2 being the formula unit in the framework. The structure of melanophlogite is identical to that of methane or xenon hydrate (Fig. 1). with silicon atoms occupying the positions of oxygen atoms of water molecules, and Si–0–Si bonds presenting instead of H-bonds. Guest molecules in clathrasils can be the same as those in the hydrates. because the cavities are close in size; however, it is clear that tremendous differences are observed in thermal properties. The host molecules in monomolecular clathrates are large: each has one (or more) cavities in which guest molecules can be located. A feature of monomolecular clathrates is that they can also exist in the liquid phase. The typical examples of monomolecular clathrates are inclusion compounds of cyclodextrins.[10] Some examples of inclusion compounds classified in accordance with the type of cavities are given below.

Cage-Type Inclusion Compounds

The major structural motif determining the structure of host framework in β-hydroquinone clathrates is a hexagonal ring $(OH)_6$ composed of hydrogen-bonded terminal OH groups of six hydroquinone molecules (Fig. 2). Because a hydroquinone molecule has two hydroxyl groups occupying *p*-positions, a three-dimensional hydrogen-bonded single β-hydroquinone structure (δ-framework) can be constructed; however. it is absolutely

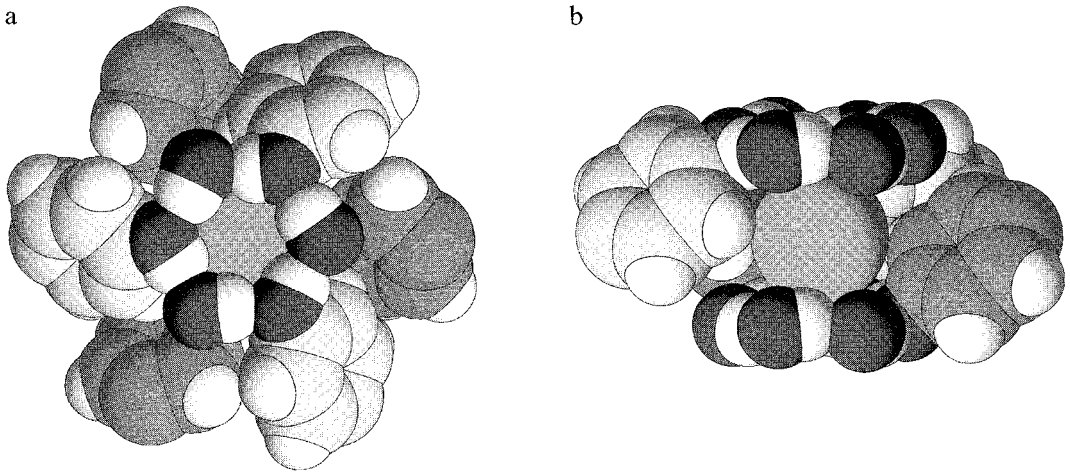

Fig. 2 The cavity in the β-hydroquinone structure with included Xe molecule. (a) the top view. (b) the side view. (*View this art in color at www.dekker.com.*)

unstable in the absence of a guest. The host framework in β-hydroquinone clathrates consists of these two mutually interpenetrating translation-equivalent unconnected networks. Cavities in this structure can accommodate small guest species HCl, HBr, CH_4, and CH_3OH, inert gases, each sandwiched between two $(OH)_6$ rings positioned at distance 5.5–5.6 A. The structural stoichiometry (ratio of the number of cavities to the number of host molecules) is 1:3, however, the real degree of cage occupancy can change depending on clathrate formation conditions.[11] The molecules of phenol and Dianin's compound (which can be considered as a phenol derivative with a large substituent) do not have a second functional OH group and, hence, cannot create the three-dimensional network, so the structural fragment described; composed of 12 host molecules (Fig. 2) is a supermolecule with a cavity inside of it. These supermolecules are packed in a structure tightly (in this case, cavities are only inside a supermolecuie, as in the structure of Dianin's compound), or there is a free space of a molecular size between them, in which the guest molecules can also be accommodated (phenol clathrates). Small cavities in the phenol clathrate framework of a size of 4–4.5 Å may enclose the same guests as the cavities in the β-hydroquinone framework: HCl, HBr, inert gases. SO_2. Each large cavity can enclose several molecules: 4HCl. 4HBr, $3SO_2$; thus, the stoichiometry of clathrates with small guests like HCl is 5:12, and for SO_2 and similar molecules it is 4:12.[12] In the cavities of Dianin's cornpound clathrate framework, the distance between hexagonal $(OH)_6$ rings is ~11 A, and different numbers of guest molecules (CCI_4, CH_3OH, CH_3NO_2, C_6H_5Br), depending on their size, can be located within the cavity. At present, several 10s of analogues of Dianin's compound capable of clathrate forination were synthesized.[12] Replacement of the structure-defining motif in the host frameworks of phenol clathrates and similar compounds, i.e., a six-membered $(OH)_6$ ring, by a benzene molecule with voluminous substituents led to the synthesis of a new type of host, the "hexahost.'' Hexahosts based on polynuclear aromatic hydrocarbons (naphthalene, anthracene, coronene) were also synthesized.[13]

Water can build a number of frameworks close in energy content. Because of this, clathrate hydrates of different structures can be formed, depending on the sizes and shapes of the guest molecules and on the conditions of clathrate formation. More than a dozen water clathrate frameworks are known.[6] The most common structures found in the gas hydrates are Cubic Structure I (CS-I), Cubic Structure II (CS-II), Hexagonal Structure III (HS-III), and Tetragonal Structure I (TS-I). The first two occur most frequently. Such guest molecules as argon, krypton, xenon; methane, acetylene, and hydrogen sulfide, chlorine stabilize CS-I (Fig. 1). The unit cell contains 46 water molecules and eight cavities. The eight cavities contain two so-called ''small'' dodecahedral *D*-cavities and six ''large'' tetradecahedral *T*-cavities, thus giving the stoichiometry 8:46=1:5.75; however, because a small fraction of cavities remains empty, the hydrate number often increases to six or more. If a guest molecule is larger [for example: $CHCl_3$, CCl_4, tetrahydrofuran (THF), etc.], CS-II hydrates are formed, their stoichiometry being 1:17. In this case, guest molecules occupy only large cavities (hexadecahedral H-cavities that are somewhat larger than T-cavities in CS-I). Small D-cavities, the number of which in the structure is two times more than the number of large ones (unit cell formula is $8H{\cdot}16D{\cdot}136H_2O$), remain unoccupied. More complicated molecules can aiso stabilize the water clathrate frameworks. For example, tetrabutylammonium and tetra-i-amylammonium salts with water form clathrate polyhydrates under definite conditions. Water molecules with simple anions (like halide, hydroxy, nitrate, formiate, etc.) build a crystalline water–anion framework, forming hydrogen bonds between them (hydrophilic inclusion), while each substituent of the cation occupies one of the large cavities arranged in the structure tetrahedrally. The vertex shared by all four cavities is occupied by the central atom of a cation (nitrogen in the case under consideration) that displaces a water molecule and does not form any H-bonds with adjacent molecules (hydrophobic inclusion). Hydrophobic–hydrophilic inclusion of an anion is also possible. For example, a carboxylate anion displacing two water molecules with its oxygen atoms builds one of the framework edges, while the hydrocarbon part of the anion (starting frorn acetate) occupies vacant dodecahedral (small) cavities, the number of which in these structures is not less than the number of anions.

Because in the structures of different hydrates the ratio of the small cavities to the large ones varies within the broad range $(2 > Rt > 0)$ (if the small D-cavities are vacant), the packing coefficients (k) vary considerably $(0.47 < k < 0.60)$. Therefore, the behavior of hydrates under pressure varies, too: from destabilization (dt/dp = −2.5 K/kbar for $THF{\cdot}17H_2O$; k = 0.485) in the case of CS-II, to a considerable stabilizaion in the case of CS-I hydrates (dt/dp=7.0 Wkbar for $C_2H_4O{\cdot}6.7H_2O$; k = 0.537), and of hydrates with completely occupied cavities (dt/dp=10 K/kbar for $THF{\cdot}0.5(C_3H_7)_4NF{\cdot}16H_2O$; k = 0.591).[14,15] In the latter example, the large *H*-cavities are occupied by the TMF guest molecules, and the small dodecahedra1 ones are occupied by tetrapropylammonium-cation guests. The CS-II hydrates can also be stabilized with the help of small molecules of inert gases (for example, Xe) or CH_4. In the case of THF hydrate, the double hydrates of the composition $THF{\cdot}2Xe{\cdot}17H_2O$ (k = 0.619), $THF{\cdot}2CH_4{\cdot}17H_2O$ (k = 0.568) are formed that are stabilized by pressure (Fig. 3). In the classic CS-II hydrates with 1:17 stoichiometry, *R*t is the largest (for the hydrates that can exist with absolutely vacant small

cavities). their packing coefficients are the smallest (k = 0.47–0.52, after the ice *Ih*. k = 0.43). and, therefore, they are destabilized by pressure. With a pressure increase, they become thermodynamically unstable, and a? relatively low pressure (P < 3 kbar), they are replaced by hydrates with a stoichiometry about 1:7 (CS-I hydrates), which are stabilized by pressure (Fig. 3).

Clathrates sf Metal Complexes

In Hofmann's compounds. the clathrate nature discovered by H. M. Powell in 1952,[1] the host coordination molecule. composing the framework: has a chemical formula $[Ni(CN)_4Ni(NH_3)_2]$. These units are bound with covalent bonds via bridging CN ligands, forming layers of the host framework positioned one above another at a distance of 8.28 Å and touching each other with ammine ligands, protruding above and below the layer at the octahedral Ni atom (Fig. 4). Cavities between layers are efficiently filled with guest molecules. for example, benzene, forming the compound $[Ni(CN)_4Ni(NH_3)_2]\cdot 2C_6H_6$. Replacement of one of the two nickel atoms in the structure, i.e., octahedral nickel, by the metal ions with the same coordination geometry (divalent Mn. Fe, Cu. Cd) does not result in any substantial change in clathrate formation ability. Replacement of the square planar $Ni(CN)_4$ by tetrahedral $Cd(CN)_4$ or $Hg(CN)_4$ groups leads to a substantial change in the structure and the cavity shape, but the ability to form clathrates is not lost.[16] Similar clathrates form so-called Schaeffer complexes. The host complex has a formula $[M(MePy)_4(A)_2]$, (here, *MePy*=4-methylpyridine, *M*=divalent octahedrally coordinated metal atom, *A*=monovalent acido ligands like halides, nitrate, and, most frequently, NCS).[17] Unlike the Hoffmann clathrates, the host molecules in the Schaeffer clathrates are not bound by covalent bonds; they are packed in a crystal together with guest molecules by van der Waals forces. Some host complexes are stable in their own crystalline phase. for example, $[NiPy_4(NCS)_2]$; clathrate formation causes their additional stabilization. Others can exist in a crystal only when cocrystallized with guest molecules, which stabilizes the structure. For example. the complexes $[Zn(MePy)_4(NCS)_2]$ and $[Cu(MePy)_4(NCS)_2]$ are completely unstable, although clathrates $[Zn(MePy)_4\text{-}(NCS)_2]\cdot G$, $[Zn(MePy)_4(NCS)_2]\cdot 2/3G$, or $[Cu(MePy)_4\text{-}(NCS)_2]\cdot 2G$ are stable—they were isolated, and their structures were determined. However. when a guest molecule is removed, two methyl pyridine ligands split off immediately, and the complex $[M(MePy)_2\text{-}(NCS)_2]$ is formed. These examples demonstrate contact stabilization of molecules, in this case. of the host molecules.[18] Contact stabilization is responsible for the stability of polyiodide guest molecules in the channels of starch amylose or polyvinyl alcohol. The polymeric guest molecule composed of iodine atoms is unstable without noncovalent support of the host.

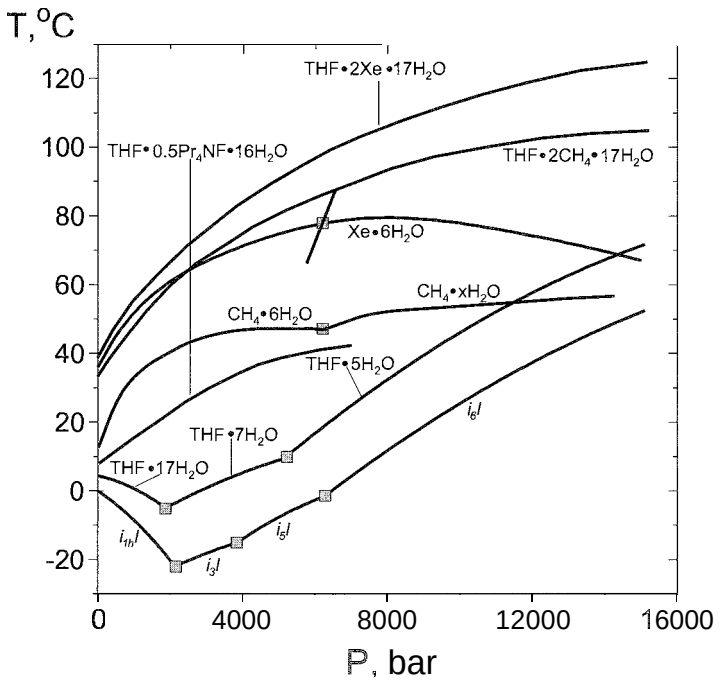

Fig. 3 The P.T decomposition curves of the simple and double hydrates. The melting curves of different ices are given.

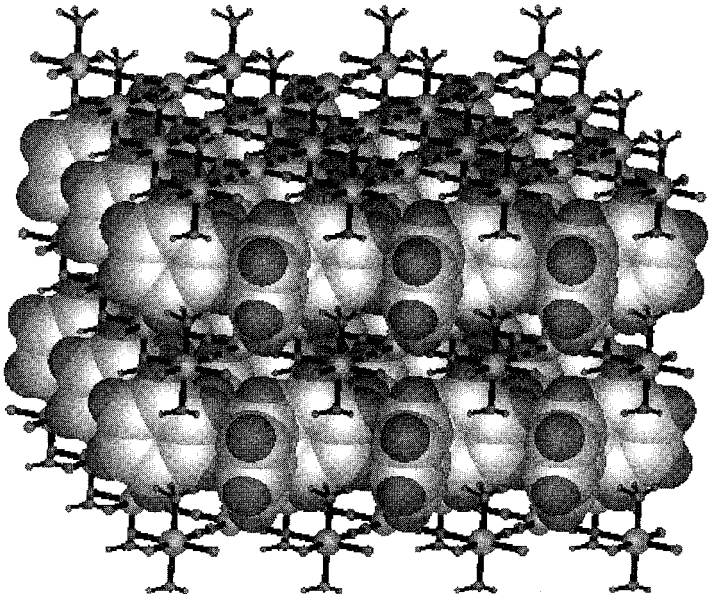

Fig. 4 The structure of Hofmann compound $[Ni(CN)_4Ni(NH_3)_2]\cdot 2C_6H_6$.

Channel-Type Inclusion Compounds

In urea clathrates,[1-4] the hydrogen-bonded host framework (β-urea) consists of an array of parallel hexagonal channels, the diameter of which (5.5 Å) is practically the same along their length (Fig. 5). There are six urea molecules in the unit cell of β-urea, and the corresponding channel length is 11.00 Å. So. the composition of a clathrate (the ratio of a number of urea molecules to a number of guest molecules) is $m=6\cdot l:11.00$, where l is the length of the guest molecule in Å. The most suitable guests are *n*-alkanes and others with minimal branching (alcohols. amines). With an increase of the length of a guest molecule, the thermal stability of urea clathrates increases; for example, the compound of urea with *n*-hexane decomposes at 38°C, with *n*-hexadecane at 106°C and with polyethylene at 148°C (which is 15° above the melting point of pure urea). In the absence of a guest. the clathrate β-framework is absolutely unstable. Channel compounds of thiourea are similar to those of urea. but the channels have broadened (≈7 Å) and narrowed (≈6.2 Å) regions. Clathrates are formed with CCl_4, cyclo-C_6H_{12} and isoparaffins. Perhydrotriphenylene forms a hexagonal β-framework with channels about 5.5 Å in diameter when cocrystaliized with nonbranched guest molecules (*n*-paraffins). Because the host molecules, constituting the channel walls, are bound by van der Waals forces, the structure is flexible; clathrates can be formed with larger guest molecules (cyclohexane, bromoform, butadiene).[20] Triorthothymotide (TOT) is a universal host molecule able to form inclusion compounds of channel and cage types. As in the case of perhydrotriphenylene, host–host interactions in the host framework are only of the van der Waals-type, resulting in flexibility of the structure. Surprising is the ability of TOT to form inclusion compounds with guest molecules of various sizes, from alcohols to polynuclear aromatics and organometallic complexes of Cr, Mn, W.[21] Cholic acids belong to channel inclusion compounds in which desoxycholic acid is the host, while the guests are such molecules as stearic, palmitic, and oleic acids.[22]

Layered-Type Inclusion Compounds

A characteristic feature of layered compounds is that the interaction within a layer is much stronger than the interaction between the layers. In the majority of layered compounds (graphite: sulfides of transition metals, clays, phosphates and phosphonates of Croup IV metals). molecules of a layer are bonded by covalent bonds, thus forming a giant macromolecule, while the interaction between the layers is mainly via van der Waals forces. As a consequence. layered solids usually exhibit a high degree of anisotropy in physical properties. There are several classifications of layered solids.[23] Based on layer charge, they can be divided into two groups: layers characterized by the presence of charge and uncharged layers. The first group includes some cationic and anionic clays: montmorillonite. muscovite, hydrotalcite-type anionic clays, and Group IV metal phosphates α-$M(HPO_4)_2\cdot H_2O$ (M=Ti, Zr, Ge, Pb, Sn). The compounds

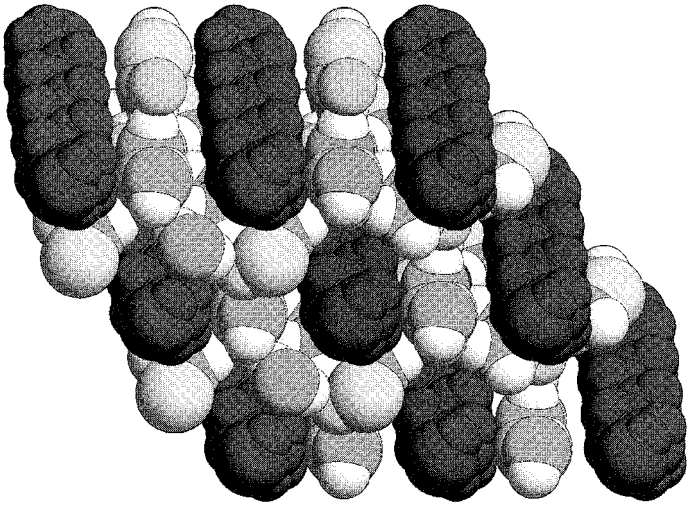

Fig. 5 The molecules of n-alkane in the urea channels. (*View this art in color at www.dekker.com.*)

of the second group. in turn. can be subdivided into insulators and electronic conducting layers.

The typical examples of insulators are nickel cyanide, nickel hydroxide. and alkyl- and arylphosphonates of Group IV metals. Among this group. α-Zr diphosphonates of general formulae $Zr(O_3P-R-PO_3)$ (pillared compounds) are of interest due to their application potential as ion and molecular sieves. In these compounds, adjacent inorganic layers consisting of tetravalent Zr atoms bound to oxygen atoms belonging to $R(PO_3)_2$ groups are covalently joined by divalent organic groups R (aryl, alkyl). Changing the length of organic pillar R and the distance between adjacent voluminous pillars, materials of desired interlayer distance and porosity can be obtained.[7,8]

The electronic conducting layers include graphite and transition metal dichalcogenides exhibiting intercalation and redox properties. Graphite layers can act as acceptors of electrons in the interaction with strong reducing agents (alkali metals) and as donors of electrons in the interaction with oxidizers (halogens. metal halides PtF_6, IrF_6, OsF_6, AsF_6). Intercalation of metal atoms (M) makes carbon layers (A) move apart and shift, so that they stand exactly one above another (an *AMAMA*. . .stacking sequence, unlike pristine graphite, in which layers are shifted with respect to each other and form an *ABABABA*. . .stacking sequence). If the interlayer space is completely occupied by metal atoms. Stage 1 intercalation compounds are formed. The stoichiometry for this arrangement of atoms is MC_8 for heavy alkali metals (starting from potassium) (Fig. 6). If metal layers are separated from each other by two, three, or more graphite layers. Stage 2, Stage 3, and so on compounds are formed. Stage 1 compounds with alkali earth metals (Ca, Sr. Ba) and lanthanides (Sm, Eu, Yb) were synthesized and under definite conditions, compounds with iron were obtained. Graphite acts as a donor of electrons when it interacts with halogens. and intercalation compounds with Br_2, ICl, IBr molecules are easily formed, while the compound with Cl_2 is extremely unstable. At low temperatures (15–100°C), graphite interacts with fluorine with the help of catalysts (HF, AgF). This fluorination results in the formation of graphite

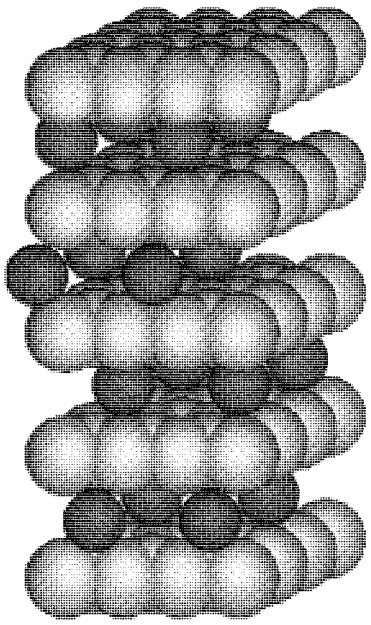

Fig. 6 The Stage 1 graphite intercalation compound of potassium KC_8. (*View this art in color at www.dekker.com.*)

fluorides with different compositions. Among them, C_6F[25] is the intercalation compound of fluoride ions into graphite. In layered compounds of Ti, Zr. Hf, Nb and Ta dichalcogenides, the slabs comprising the structure are not monolayers. as in the case of graphite or boron nitride, but are coinposed of two anionic monolayers framing a cationic layer. Dichalcogenides of transition metals form inclusion compounds with alkali metals. some alkali earths, as well as with Eu and Yb. Similar to the case of graphite, compounds of different staging can be formed with alkali metals.[26]

STOICHIOMETRY

The stoichiometry of clathrates may be easily determined from structural data—it is numerically equal to the ratio of the number of cavities to the number of host molecules in the unit cell. The real stoichioinetry can differ from the structural if the cavities are only partially filled with guest molecules. It is reasonable to consider three cases:

1. The composition of the clathrate compound is constant. as is possible in the case of host frameworks that are extremely unstable in the absence of a guest. As examples, the compound of urea with n-decane $C_{10}H_{22}\cdot(8.06 \pm 0.06)(NH_2)_2CO$, or the hydrate $(i\text{-}C_5H_{11})_4NF\cdot(26.8 \pm 0.03)H_2O$ may be cited. In both cases, the clathrate composition corresponds to the structural within the experimental error and remains constant in the whole stability region.
2. The host framework is thermodynamically stable in the absence of the guest molecules. In this case. solid clathrate solutions are formed on the basis of the α-modification of the host. which means that no new phase is formed. The inclusion of the guests results in additional stabilization of the α-structure. For example. α-hydroquinone with included krypton melts at a temperature 1°C higher than that of the pure α-phase.
3. The host component has a metastable modification with cavities of molecular size, which becomes stable above a certain value of the degree of filling the cavities. In this case. the clathrate is a new phase of variable composition due to changing the degree of cavity filling upon changing equilibriuin conditions. Examples include the classic hydroyuinone clathrates based on the β-hydroquinone framework, with such guests as Ar. Kr, Xe, H_2S, SO_2, HCl, HBr, etc.[11]

CONCLUSION

Similarity in the chemical behavior of atoms. molecules, or their fragments (functional groups) is determined predominantly by the similarity of their electronic structures. It suffices to look at the elements in the groups of the Periodic Table or to compare chemical reactions, for examples, those of amines, ketones, or alcohols. The decisive role in supramolecular chemistry is played by the sizes and shapes of molecules rather than their chemical natures. For example, from the viewpoint of clathrate chemistry, xenon. hydrogen sulfide. chlorine, methane, sulfur dioxide, and phosphine are all analogous. In spite of different chemical natures, these molecules have a common feature, which is the correspondence in size and shape to the geometry of the cavities in the CS-I hydrate framework. And. all of these form hydrates of this structure. These guest molecules can also stabilize the β-hydroquinone framework (besides chlorine, which oxidizes hydroquinone). On the other hand, the behavior of chemical analogs, for example, normal and branched secondary alkylamines, differs significantly on reaction with urea: the first ones form tubulatoclathrates, while the latter do not. This difference provides the possibility of efficient separation of isomers. As the cavity shape becomes more complicated. the selectivity of clathrate formation reactions increases substantially. In 1894, the Canadian scientist Emil Fisher introduced the lock and key principle (see "The Lock and Key Principle") to explain highly specific enzyme reactions. In other words, if the substrate is complementary to enzyme (or guest–host in our terms). like a key to a lock, the reaction proceeds. However, as a rule, a host (and a guest if its molecule is complicated) does not exist beforehand in the clathrate form. The necessary modification of the host framework and proper conformation of the guest is induced during their interaction. Cascade inclusion processes are possible. For example, hernoglobin is composed of a protein part (globin). including a nonprotein heme molecule (iron porphyrin complex) without any valent bonding. This heme molecule attains a conformation with a basket-shaped cavity which. in turn, includes an oxygen or carbon dioxide molecule. known to exchange for each other easily.

As a discipline, clathrate cheinistry is the most advanced part of supramolecular chemistry. because its subjects. despite relative complexity, are amenable to strict quantitative experiment and interpretation. which allows for the forming of concepts that would simplify the understanding of more complicated supermolecular species (as in the example mentioned above).

ARTICLES OF FURTHER INTEREST

Channel Inclusion Compounds, p. 223
Clathrate Hydrates, p. *274*
Deoxycholic, Cholic, and Apocholic Acids, p. 441
Gossypol, p. *606*

REFERENCES

1. Powell. H.M. Clathrate Compounds. In *Non-Stoichiometric Compounds*; Mandelcorn. L.. Ed.: Academic Press: New Uork. 1964; 398–450.
2. Nikitin. B.A. Issledvanija po khimii blagorodnykh garov. In *Izbrannye trudy (Russian)*; Izd-vo AN SSSR. 1956; 104–240.
3. Stackelberg. M. Feste Gashydrate. Naturwissenschaften 1949. **36** (11). 327–333.
4. Schlenk. W. Die Harnstoff-Addition der aliphatischen Verbindungen. Ann. Chem. **1949**. *565*. 204–240.
5. Van der Waals. J.H.: Platteeuw. J.C. Clathrate solutions. Adv. Chem. Phys. **1959**. *2*, 1–57.
6. Jeffrey. G.A. Hydrate Inclusion Compounds. In *Comprehensive Supramolecular Chemistry*; Atwood. J.L.. Davies. J.E.D.. MacNicol. D.D.. Vogtle. F.. Eds.: Pergamon: Oxford. 1996; Vol. 6, 757–788.
7. Pedersen. C.J. The discovery of crown ethers. J. Incl. Phenorn. 1988. 6. 337–350.
8. Lehn. J.-M. Supramolecular chemistry—Scope and perspectives: Molecules–supermolecules–molecular devices. J. Incl. Phenom. 1988. *6*, 351–396.
9. Gies. H. Clathrasils and Zeosils: Inclusion Cornpounds with Silica Host Frameworks. In *Inclusion Compounds*; Atwood. J.L.. Davies. J.E.D.. MacNicol, D.D., Eds.: Oxford University Press: Oxford. 1991; Vol. 5. 1–36.
10. Szejtli, J. Chemistry, Physical and Biological Properties of Cyclodextrines. In *Comprehensive Supramolecular Chemistry*; Atwood. J.L.. Davies. J.E.D.. MacNicol, D.D.. Vogtle, F.. Eds.: Pergamon: Oxford. 1996; Vol. 3. 5–40.
11. Dyadin, Yu.A. On the stoichiometry of clathrates. Supramol. Chem. 1995. 6. 59–70.
12. MacNicol. D.D. Structure and Design of Inclusion Compounds: The Clathrates of Hydroquinone. Phenol. Dianin's Compound and Related Systems. In *Inclusion Compounds*; Atwoocl. J.L.. Davies. J.E.D.. MacNicol. D.D., Eds.: Academic Press: London, 1984; Vol. 2, 1–45.
13. MacNicol, D.D.; Downing. G.A. Symmetry in the Evolution of Host Design. In *Comprehensive Supramolecular Chemistry*; Atu-ood. J.L.. Davies. J.E.D.. MacNicol. D.D., Vogtle. F.. Eds.; Pergamon: Oxford. 1996: Vol. 6. 421–464.
14. Dyadin, Yu.A.: Bondaryuk, I.V.; Zhurko, F.V. Clathrate Hydrates at High Pressures. In *Inclusion Compounds*; Atwood, J.L., Davies. J.E.D.. MacNicol. D.D.. Eds.: Oxford University Press: Oxford. 1991: Vol. 5. 213–275.
15. Dyadin, Yu.A. Constitution and Stability of Clathrate Hydrates. In *Crystallography* of *Supramolecular Compounds,* Proceedings of the NATO Advanced Study Institute on Crystallography of Supramolecular Compounds. Erice, Italy. June 1–11. 1995: Tsoucaris. G., Atwood, J.L.. Lipkowski. J.. Eds.; Kluu-er Academic Publishers: Dordrecht. 1996.
16. Iwamoto, T. Supramolecular chemistry in cyanometallate systems. In *Comprehensive Supramolecular Chemistry*; Atwood, J.L.. Davies. J.E.D.. MacNicol, D.D.. Vogtle, F.. Eds.; Pergamon Press: Oxford. 1996; Vol. 6. 643–690.
17. Lipkowski, J. Werner Clathrates. In *Comprehensive Supramolecular Chemistry*; Atu-ood, J.L.. Davies. J.E.D., MacNicol. D.D., Vogtle. F.. Eds.: Pergamon: Oxford. 1996; Vol. 6. 691–714.
18. Dyadin, Yu.A.; Kislykh, N.V. Contact stabilization of host molecules during clathrate formation. Mendeleev Commun. **1991**. 4. 134–135.
19. Hollingsworth. M.D.; Harris. K.D.M. Urea. Thiourea. and Selenourea. In *Comprehensive Supramolecular Chemistry*; Atwood, J.L.. Davies. J.E.D.. MacNicol, D.D., Vogtle. F., Eds.: Pergamon: Oxford. 1996: Vol. 6. 177–237.
20. Farina. M.: Silvestro. *G.*: Sozzani. P. Perhydrotriphenylene: AD_3 Symmetric Host. In *Comprehensive Supramolecular Chemistry*; Atwood. J.L.. Davies. J.E.D., MacNicol. D.D.. Vogtle, F.. Eds.: Pergamon: Oxford. 1996: Vol. 6. 371–398.
21. Gerdil. R. Tri-o-thymotide and Related Hosts. In *Comprehensive Supramolecular Chemistry*; Atwood. J.L.. Davies, J.E.D.. MacNicol. D.D.. Vogtle. F.. Eds.: Pergamon: Oxford. 1996: Vol. 6. 239–280.
22. Miyata. M.: Sada. K. Deoxycholic Acid and Related Hosts. In *Comprehensive Supramolecular Chemistry*; Atwood. J.L.. Davies. J.E.D.. MacNicol. D.D.. Vogtle. F.. Eds.: Pergamon: Oxford. 1996: Vol. 6. 147–176.
23. Alberti. G.: Costantino, U. Layered Solids and Their Intercalation Chemistry. Ill *Comprehensive Supramolecular Chemistry*; Atwood, J.L.. Davies. J.E.D.. MacNicol. D.D., Vogtle. F.. Eds.: Pergamon: Oxford, 1996: Vol. 7. 1–23.
24. Alberti. G.: Costantino, U. Intercalates of Zirconium Phosphates and Phosphonates. In *Inclusion Compounds*; Atwood, J.L.. Davies. J.E.D.. MacNicol, D.D.. Eds.; Oxford University Press: Oxford. 1991: Vol. 5. 137–176.
25. Okino, F.: Touhara. H. Graphite and Fullerene Intercalation Compounds. In *Comprehensive Supramolecular Chemistry*; Atwood. J.L.. Davies. J.E.D.. MacNicol. D.D.. Vogtle. F., Eds.: Pergamon: Oxford, 1996: Vol. 7. 25–76.
26. Rouxel. J. Layered Metal Chalcogenides and Their Intercalation Chemistry. In *Comprehensive Supramolecular Chemistry*; Atwood. J.L.. Davies. J.E.D.. MacNicol. D.D.. Vogtle. F., Eds.: Pergamon: Oxford. 1996: Vol. 7. 77–105.

Classification and Nomenclature of Supramolecular Compounds

Edwin Weber
Technische Universität Bergakademie Freiberg, Freiberg, *Germany*

INTRODUCTION

Although suprainolecular compounds are general and were recognized more than 100 years ago, beginning with Emil Fisher's "lock-and-key principle" of enzyme-substrate recognition."' the real rise of this field started in the late 1960s or early 1970s. after the discovery of the crown compounds and cryptands by the pioneers of the field, C. J. Pedersen and J.-M. Lehn, and also including the pioneering work on host–guest chemistry by D. J. Cram. In 1987. these leading proponents of what is now called supramolecular chemistry[1,2] were awarded the Nobel prize in chemistry.[3–11] With this. the era of supramolecular coinpounds rapidly expanded into different disciplines and fields, from supramolecular organic to the rising new field of nanotechnology, including special subjects such as molecular recognition. self-assembly. and crystal engineering.'".'" All that produced new classes of compounds, with new names, scientific terms, acronyms, and notations being illustrated and specified briefly in the following. However. as the so-called host–guest chemistry[14] sponsored to the great majority and most remarkable structural variations in the field, having as a consequence a variety of detailed nomenclature, the host–guest (or receptor–substrate) compounds take precedence over other supramolecular compounds. which are discussed more briefly or referred to under specific keywords (see cross-references at the end of the article).

DEFINITION AND BASIC CLASSIFICATION

Supramolecular chemistry may be defined as ''chemistry beyond the molecule." bearing on the organized entities of higher complexity that result from the association of two or more chemical species held together by intermolecular noncovalent forces, such as metal ion coordination, electrostatic forces. hydrogen bonding. van der Waals interactions, and others.[6–15] These supramolecular entities derived from supramolecular association are generally called supermolecules or supramolecular compounds. Thus. one may say that ''supramolecules are to molecules and the intermolecular bond what molecules are to atoms and the covalent bond." This kind of definition is highlighted in Fig. 1a.

Supramolecular Compounds Designed for Host–Guest/Receptor–Substrate interactions

Within the above context. host–guest chemistry and host–guest compounds[1,"] might be seen as particular cases of suprainolecular chemistry and supramolecules, respectively (Fig. 1a). In a more specific determination. hosts are defined as (organic) molecules containin,g convergent binding sites. and guests are defined as molecules or ions containing convergent binding sites.'"[11] The terms receptor and substrate, originating from biological systems and inodels, are now largely synonymous with host and guest. respectively. in artificial supramolecular systems. However, while the hosts are usually convergent in the construction of the binding sites, receptors can be convergent or divergent, i.e., forming endo- or exoreceptor-type supramolecular associations (Fig. 1b). In particular, when the host or the receptor provides a hollow space. or any not precisely defined cavity. an inclusion compound results."' Moreover, it has become useful to divide inclusion compounds into two major classes (Fig. Ic). Those where the host substance is a single molecule possessing intramolecular cavities, and the guest molecule or molecules reside completely within the host. are designated ''cavitates'' (used here in a broad sense). In this case. the supermolecule is limited to the particular host–guest entity, accounting also for the descriptions of intramolecular. endomolecular. or monomolecular inclusion compound. Concerning the second class of inclusion compounds. there is more than one host molecule with which to construct the cavity for accommodation of the guest. In the terminology of supramolecular compounds, this species is called an extramolecular. exomolecular, or multimolecular inclusion compound. The vast majority of inclusion compounds where predominantly formed in the solid state belong to this latter category. These inclusion compounds of relevance only in the solid state are

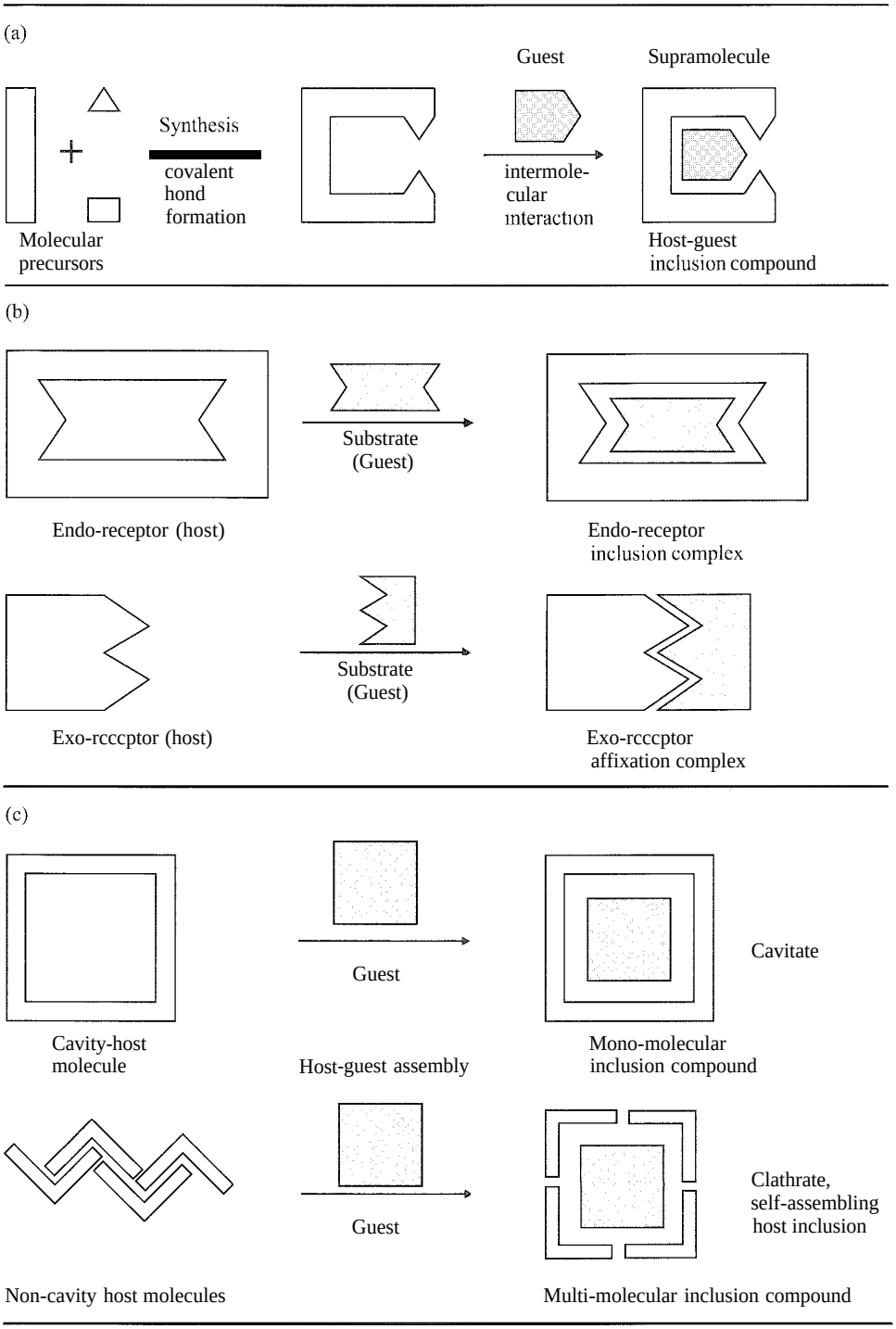

Fig. 1 Definitions and overall scheme of supramolecular events: (a) chemical host synthesis and formation of a supramolecule (host–guest inclusion compound); (b) endo- and exosupramolecular receptor–substrate (host–guest) chemistry; and (c) formation of mono- and multimolecular inclusion compounds.

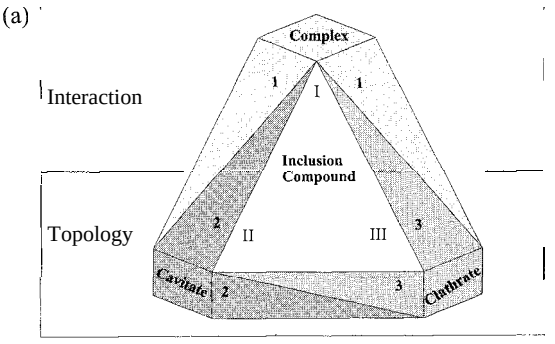

I Coordination-typ/polar interaction host-guest inclusion compound

II Intrainolecular host cavity inclusion compound

III Extramolecular lattice cavity inclusion compound

(1) Coordinative/electrostatic force interaction; (2) monomolecular shielding interaction; (3j lattice barrier interaction

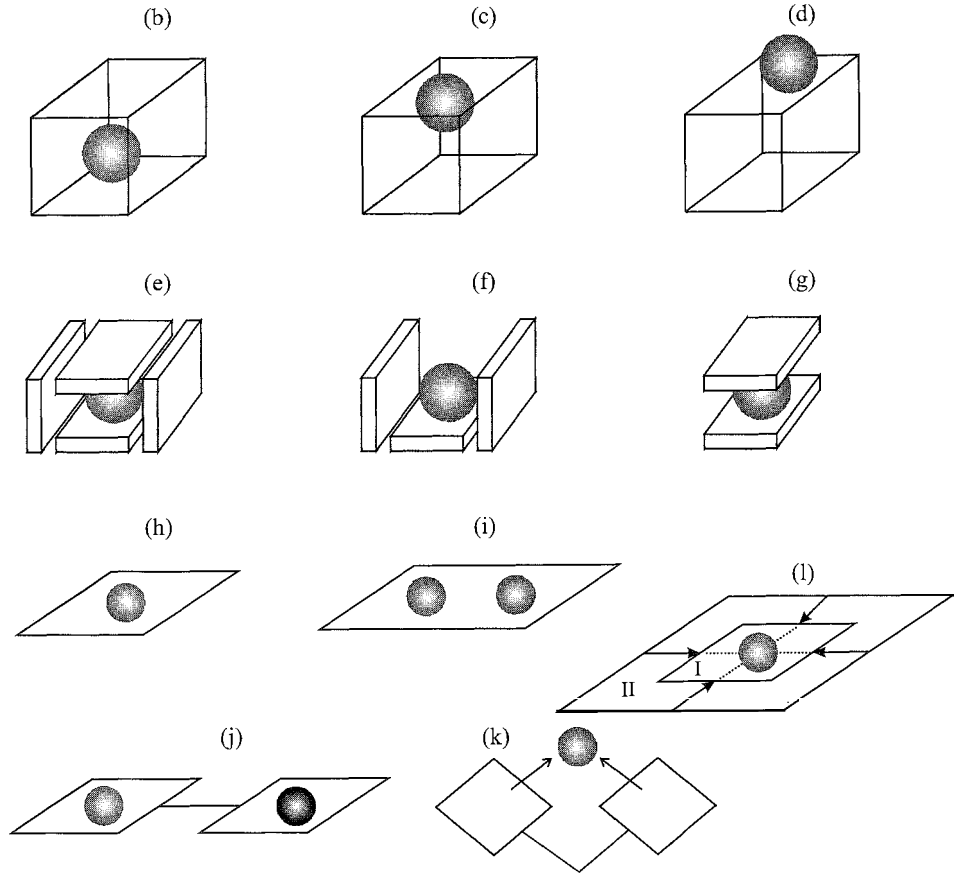

(b) capsular; (c) nesting: (d) perching; (e) tubular; (f) wrapping; (g) sandwich; (h) monomolecular; (i) dinuclear, homonuclear; (j) dinuclear, heteronuclear, ditopic; (k) monomolecular, dihapto: (l) second-sphere

Fig. 2 General classification/nomenclature and descriptive terminology of host–guest supramolecular inclusion compounds

commonly termed ''clathrates'' or "lattice-type inclusion compounds.''[17]

A further fundamental subdivision of supramolecular host–guest compounds may be made on the basis of the forces between host and guest (Fig. 2a). If the host–guest aggregate holds together by primarily electrostatic forces. including ion–dipole, dipole–dipole. hydrogen bonding, etc., the term "complex" is used. On the other hand, if species are held together by less specific and often weaker, nondirectional interactions, such as hydrophobic, van der Waals, or crystal close-packing effects, then the terms ''cavitate'' and ''clathrate'' are more appropriate.[17] Thus;

another potential way of distinguishing between complexes. cavitates. and clathrates is to make use of the fact that complexes mostly retain their identity in solution, which is largely observed also for cavitates. whereas clathrates decompose on dissolution. However, it should be noted here that there is a significant trend in the current literature to use the word "complex" to cover all of these phenomena. Nevertheless. because a great number of intermediate types of host–guest compounds exist; these borderline cases are sometimes treated as hybrids between the most applicable terms, such as "clathratocomplex" or "coordinatoclathrate." In the first case, the host–guest interaction is largely of the complex type. but there is also a distinct crystal close-packing participation. while it is the reverse in the latter case. The hybride terms ''cavitatocomplex'' and "cavitatoclathrate" are also topologically descriptive designations describing that the guest resides partly in a host cavity of a complex- or clathrate-type inclusion compound.[18]

Other subsidiary descriptive terms used to illustrate the spatial relationships between host and guest refer to the designations "layer-type" (two-dimensionally open), "channel-type" (one-dimensionally open). and ''cage-type" (totally enclosed) inclusion compound, also termed "intercalates." "tubulates.'' and "cryptates," respectively, which makes further coinbinations of descriptive hybrid terms possible, e.g., tubulatoclathrate indicating a channel-type clathrate: and so on.[15] Even more precise descriptions are possible when using terms such as ''capsular..' ''nesting,'' "perching," "sandwich." or ''wrapping" to visualize spatial relationships between host and guest (Fig. 2b–g). In addition. with respect to the number and nature of the bound guests (substrates), the resulting supermolecule (host–guest compound/receptor–substrate complex) may be mono- or polynuclear and homo- or heteronuclear, if the guests (substrates) are identical or different. The respective hosts (receptors) are monotopic or polytopic. i.e., containing one or more discrete binding subunits. Moreover, the mode of guest (substrate) binding may be monohapto or polyhapto, depending whether fixation occurs via a single or via multiple association(s)[15] (Fig. 2h–k). Another specific phenomenon involving an onion-skin- or cascade-type structure of the supermolecule is defined as a "second-sphere''[19,20] or "doll in the doll" complex (Fig. 21).

Finally. it is advantageous to distinguish in the naming between the free host (receptor) capable of forming the host–guest aggregate and the complete host–guest compound. This is achieved by using the suffix-"and.' to mean free host or uncomplexed ligand, and the ending "-ate" for the host–guest compound.[17] Thus. the cavitate-forming host cornpound is termed a cavitand. tubulands correspond to tubulates. and so on (Table 1). However, it was pointed out that this naming is misleading.

Table 1 Specification/nomenclature of hosts (ligands) and suplamolecular compounds they form (decriptive terms or names of supramolecular compounds, if existing. are given in parentheses)

a) Hosts/ligands typical of supramolecular complex formation:
Catenand (catenate)
Corand (coraplex)
Coronand (coronate)
Crown ether
Cryptand (cryptate)
Cryptaspherand (cryptaspheraplex)
Cyclam
Glyme
Helicand (helicate)
Hemispherand (hemispheraplex)
Hexacylen
Lariat ether (lariate)
Metallacoronand (metallacoronate)
Metallacryptand (metallacryptate)
Molecular cleft host
Octopus host
Pincer host
Podand (podate, podaplex)
Sargophagine
Sepulchrand (sepulchrate)
Siderophore, siderand (sideraplex)
Soccer ball cryptand
Spherand (spheraplex)

b) Hosts typical of cavitate inclusion formation
Calixarene
Capsule host
Carcerand (carceplex)
Cavitand (cavitate. caviplex)
Cyclodextrin
Cyclointercaland (cyclointercalate)
Cyclophane
Cryptophane
Hemicarcerand (hemicarceplex)
Kohnkene
Metal array host
Molecular box
Molecular square
Resorcarene
Speleand (speleate)
Softball host
Tennis ball host
Torand (toraplex)
Tubuland (tubulate)

c) Hosts typical of clathrate (crystal inclusion) formation
Clathrand (clathrate. clathraplex)
Coordinatoclathrand (coordinatoclathrate)
Hexahost
Piedfort host
Roof host
Scissors host
Spider host
Wheel-and-axle host

Specific cases: Cyclotriphosphazene. cyclotriveratrylene, Dianin's compound, hydroquinone, perhydrotriphenylene. tetraphenylene. trimesic acid. tri-o-thymotide.

because the suffix ''-ate'' is usefully used for anions, whereas a great many of the host–guest compounds referred to are cations or uncharged species. This is why it was proposed to replace it with the suffix ''-plex,'' to give caviplex, clathraplex, and so on[1**] (Table 1). Unfortunately. this suggestion for improvement has not yet been generally accepted.

Supramolecular Compounds Involving Objects Other Than Host–Guest/Receptor–Substrate Association

Because by definition supramolecular coinpounds include any chemical species resulting from association of molecules, the number and variety of compounds or materials that fall under the category are immense,[2] and the host–guest compounds. although important, make up only a relatively small segment of the whole range. Nevertheless. this majority of supramolecular compounds is far from producing descriptive terms and names compared to the host–guest compounds. Generally. they are classified into different bur broad fields, where engineered supramolecular structures and pattern motifs, mostly of nanoscale or communicating functional systems, are the center of interest. They include the so-called interlocked and interwoven systems, the crystal engineering supramolecular materials and liquid crystals. the surfactant-type aggregates and mono-/multilayers, the catalytic systems and biological mimics. the self-replicating systems, and the supramolecular devices. to mention only relevant fields of classification.[12,13,23] The structures belonging to these supramolecular compounds or materials are usually complex. yet in many cases they contain a host–guest component as part of the framework.

STRUCTURAL VARIATIONS AND TRIVIAL NAMES

Apart from the basic classification scheme given above. extremely varied structural types of supermolecules were developed. supplying a more detailed specification of supramolecular compounds by using trivial names. In the cases of the host–guest compounds. they normally refer to a particular feature of the host molecule.

Crown-Type and Cryptand Hosts

Typical examples of this category of compounds[24,25] are illustrated in Fig. 3. The essential property common to this family of host molecules is a flexible framework of multidentate donor atoms, such as oxygen. nitrogen. or sulfur. to mention but the most important. Depending on the topology with which these donor atoms are arranged. one basically distinguishes between the acyclic podands (from Greek. meaning ''foot''j. the macrocyclic ''coronands'' (from Latin. meaning "wreath or ring"). and the macropolycyclic cryptands (from Greek, meaning ''hidden'').[26] Another term occasionally used for the multidentate monocyclic coronands is ''corand,''[21,22] while the term ''crown ether" is reserved for cyclic oligoethers containing oxygen donor atoms only (Fig. 3a). Historically, these appealing structures of crown ethers are the basic units of the nowadays varieties of supramolecular hosts. That is why the term "crown compound" is also loosely used for any macrocyclic ligand having a crown-like shape. and even the acyclic podands are sometimes called ''open-chain crown compounds" in this connection. Moreover. structure types of higher category involving each compound family and hybrids between the three basic compound families are known. Thus. extending the podand concept to three dimensions gives a tripodal molecule specified as "tripodand" (see Fig. 3d). Important examples of this compound type are the naturally occurring siderophores and synthetic siderands (from Greek, meaning "iron bearer'').[12] Multiarmed representatives of the podands are the "octopus molecules",[27,28] and in the final analysis, also the ''dendrimers''[2] when containing donor sites. A molecular combination of two separate coronand rings leads to a dicoronand. and so on. The podandocoronands, e.g., are hybride compounds featuring a coronand ring with a podand side arm. Because of their graphic resemblance to a lasso they are usually called "lariat compounds'' (lariat ethers, from the Spanish ''la reata." meaning "the rope'').[29] The analogs with two side arms are named "bibracchial ethers" (BIBLEs).[29]

Other descriptive names for particular cornpounds are common in the literature. The term ''glyme'' (mono-. di-. triglyme. etc.), is actually short for ethyleneglycol dimethylethers, which are perhaps the simplest representatives of podands[27,28] (see Fig. 3b). Furthermore. azacoronands (azaanalogues of crown ethers, cf. Fig. 3g) often have unusual names. such as ''cyclam'' or ''hexacyclen'' for the respective 14- or 18-membered tetra- or haxaaza-coronands.[30] Similarly; there are trivial names such as sarcophagine (from the Greek meaning ''luxory coffin made from stone") and sepulchrates (from the Latin meaning "grave") named by analogy with the bicyclic cryptands with nitrogen (cf. Fig. 3h) and carbon bridgehead atoms, respectively. but having all-aza donor sites.[2] Another special case of an amphiphilic cryptand combining the macrocycle cyclotriveratrylene and a coronand fragment as hydrophobic and polar binding sites, respectively. is called speleand (from the Greek meaning ''cave'').[15]

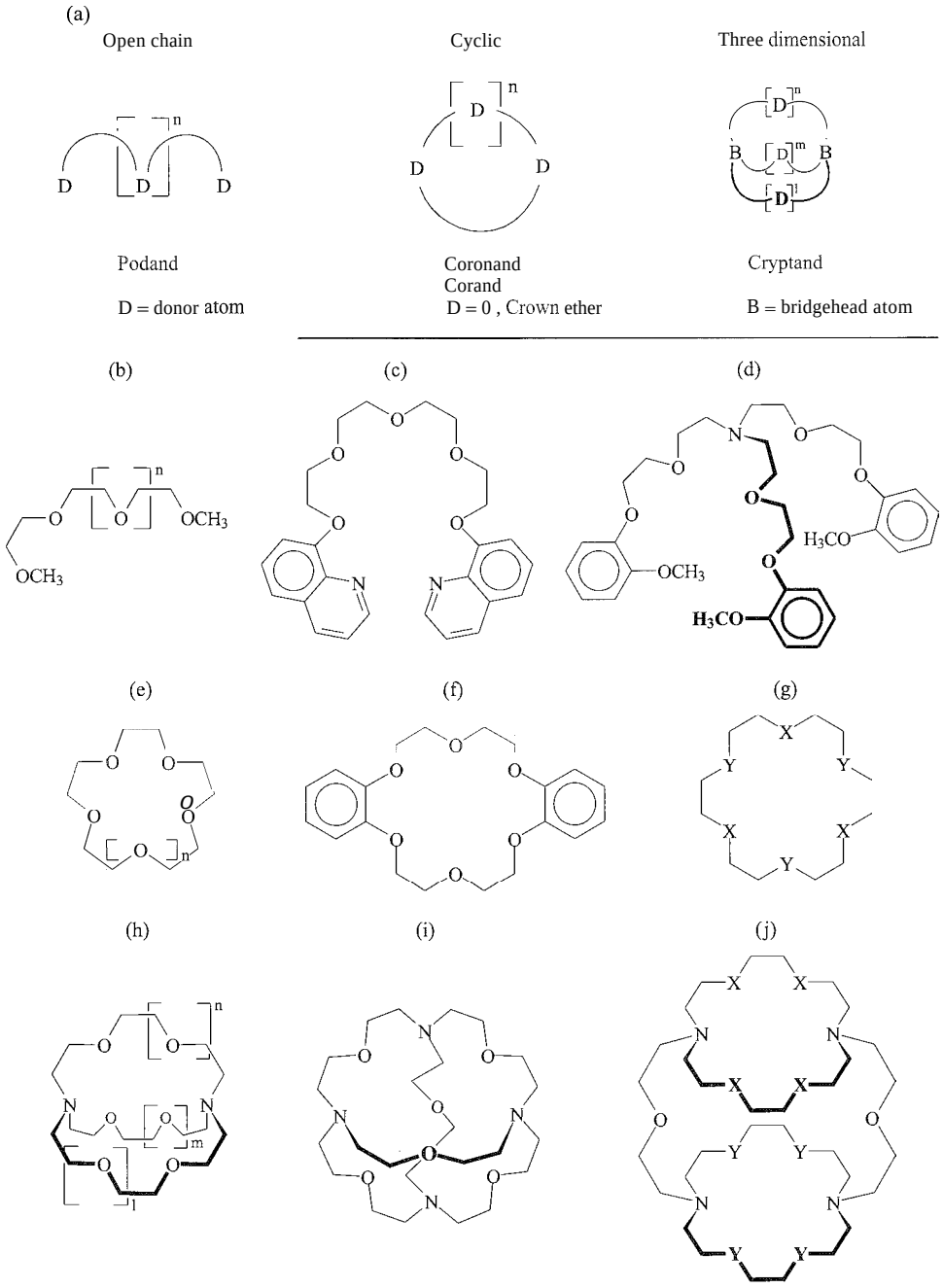

Fig. *3* Crown-type and cryptand hosts: (a) Class specification: (b)–(j) representative cases of compounds: (b,c) linear (n = 0, 1. 2. etc.) and (d) tripodal podands: (e,f) crown ethers (n = 0. 1. 2. etc.). and (g) coronand/corand (X = NH. S): (h) bicyclic (l, m, n = 0. 1. 2). (i) tricyclic spherical. and (j) tricyclic cylindrical cryptands (x = O, S).

All of these host molecules (ligands) were synthesized with the inclusion or complexation of guest species in mind, mostly of metal ions. Thus. transformation from the free host molecule to the host–guest complex changes the ending of the host name from "-and" to "-ate" or "-plex" (podate or podaplex, coronate or coraplex, etc.: see Table 1).[17,21,22]

Enforced Cavity Hosts

The features shared by all of the host molecules of this category are a high degree of structural rigidity coupled with multipoint binding, thus leading to rigid preorganization of the host for accommodation and binding of the guest[21,22] (Fig. 4). While the usual flexible podands have

a low degree of preorganization, the rigid molecular clefts (Fig. 4a) and tweezers (Fig. 4b) are much more organized in this respect.[31–33] In a sense, they may therefore be understood as highly preorganized podands. Similarly, the hemispherands, spherands (Fig. 4c), and cryptaspherands, showing enforced spherical arrangement of donor atoms, with increasing preorganization in this order, are the preorganized analogues of crown compounds and cryptands, respectively.[9,10,21] Typical of their rigid backbone are the ortho-connected anisyl units replacing the flexible ethyleneoxy fragments in the conventional crown compounds and cryptands. The stable inclusion complexes formed of the spherands are mostly called "spheraplexes."

Actually, these aromatic groups containing spherands fall under the extensive range of cyclophane hosts."] By definition, a cyclophane host must contain at least one macrocyclic ring comprising a bridged aromatic unit. This has been realized in numerous structural types (cf. Fig. 4d–g) that can be grouped to different compound classes, including the above cavitands (in a more specific sense) and carcerands, mostly having a rigid cyclophane-type framework and being generally termed container molecules.[35] The difference between the two species lies in the fact that the molecular cavity of the cavitands is usually open at one end (cf. Fig. 4f), while the carcerand (Fig. 4g) is defined as a closed molecular container or capsule without portals of significant size through which guests can enter or leave. Guest species within a carcerand to yield a carceplex are, therefore, permanently trapped or intercarcerated within the internal volume, unless covalent bond breaking within the host occurs.[36] Other individual cyclophane-type hosts making use of a characteristic kind of building block are the "calixarenes"[37,38] They are macrocycles formed from the condensation of a *p*-substituted phenol (e.g., *p*-tert-butylphenol) with formaldehyde. The most common calixarene is the cyclic tetramer derived from these components (Fig. 4h). The descriptive name "calixarene" for the whole family of compounds is indicative of the bowl-shaped conformatioil of the smaller calixarenes resembling a Greek vase called a "calix crater". Hybrid calixarenes such as calix-crowns, -cryptands, or -spherands are also known.[37,38] Closely related to the calixarenes are the resorcarenes or calixresorcarenes, which are derived in similar fashion by condensation of resorcinol with aldehydes[37,38] (Fig. 4i). Calixarenes and resorcarenes form cavitates. The torands and the kohnkene (named after his creator) are toroidal-shaped, rigid host cornpounds featming a macrocycle of condensed six-membered rings, while the characteristic curved molecular building block for the formation of cryptophanes (Fig. 4j) is cyclotriveratrylene (CTV).[2,33] These capsular hosts were given the name cryptophanes by analogy with the cryptands, while the ending "–phane" comes from membership in the class of cyclophanes. From another view, the cryptophanes fail under the class of "hemicarcerands" (closed molecular containers allowing guests enter to and exit), thus yielding hemicarceplexes on inclusion of a guest species.[36]

However, using linked aromatic rings of cyclophane type is not the only way to introduce rigidity into a host design. The most common, most studied and cheapest commercially available hosts, the cyclodextrins (CDs), are fully saturated cyclic oligosaccharides comprising usually six to eight D-glucopyranoside units, linked by a 1,4-glycosidic bond[39] (Fig. 4k). The name comes from dextrose, an early synonym for glucose. The shape of a cyclodextrin is often represented as a tapering torus or truncated funnel, making available a hydrophobic cavity into which guests can be included."[40] Another well-known host compound based on the fully saturated rigid glycoluril building block is cucurbituril[41] (Fig. 41). This barrel-shaped compound is named because of the resemblance to a gourd or pumpkin of the Cucurbitaceae family. The inclusion compounds formed of cucurbituril are of cavitate type with a likeness to a hemicarceplex.

Self-Assembling Inclusion Hosts

While the above host compounds were obtained by conventional covalent synthesis, formation of the present type of host compounds is based on a so-called self-assembling process: as a synthetic ltey step, i.e., programmed molecular components or tectons (from the Greek meaning "builder") come together spontaneously, in a well-defined way, to give noncovalent assemblies that are stable in solution.[42–44] Thus, the host assembly as such is already a supermolecule constituting the first level of hierarchy in the construction completed by formation of the inclusion compound, which is the second level of supramolecular construction. Characteristic examples of this class of host compounds are the self-assembling tennis ball and softball capsules formed of two self-complementary building blocks (see Fig. 5a) or the so-called giant capsules, being larger self-assembling cavity systems."[45] A different approach than assembling closed capsules via hydrogen bonding, as above, is to form self-assembling coordination compounds, where transition metals as structural components are used in the construction of containers. This was realized by a range of supramolecular triangles, squares, spheres, and boxes composed of different coordinatively effective building units and metal centers or partly protected metal fragments[46] (see Fig. 5b). In analogy to the conventional coronands and cryptands, the terms "metallacoronands," "metallacryptands," etc. (metallacoronates, rnetallacryptates for the inclusions) are in use for this type of supramolecular compound.[44]

(a)

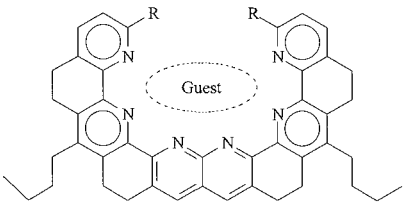

R = OH NHR

(b)

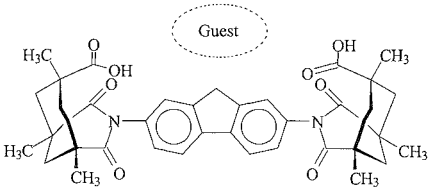

(c)

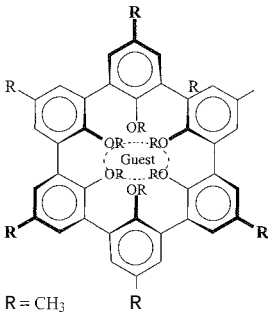

R = CH_3

(d)

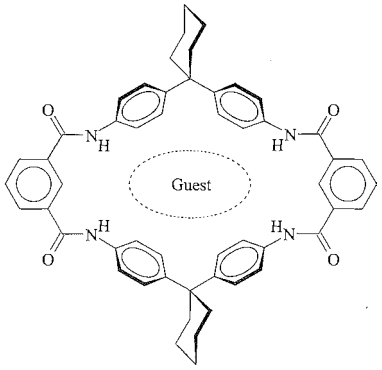

(e)

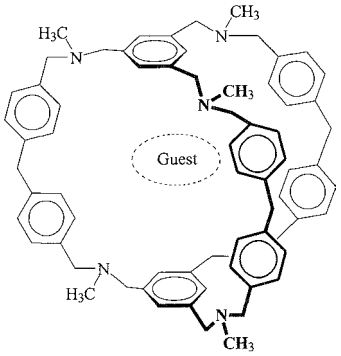

(f)

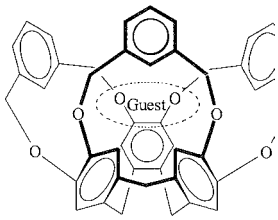

(g)

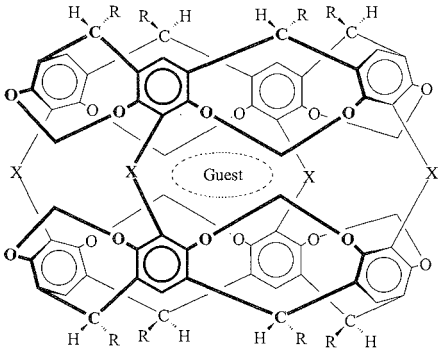

X = CH_2SCH_2
R = CH_3

(h)

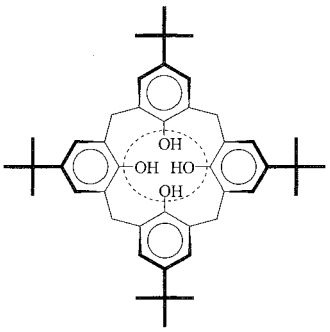

(i)

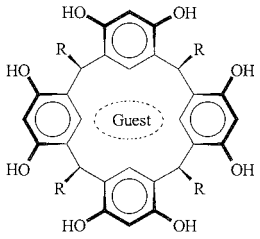

R = Alkyl, Aryl

(j)

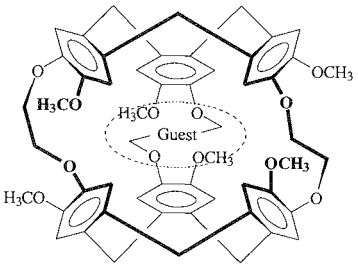

(k)

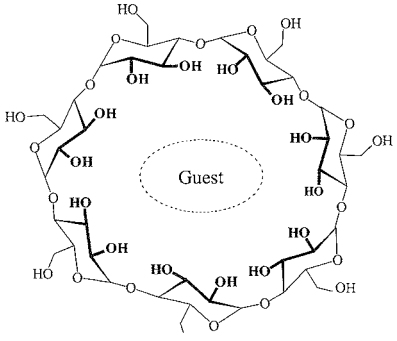

(l)

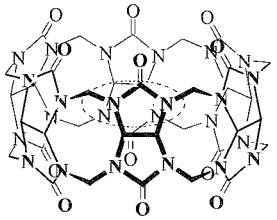

Moving away from closed capsules. a number of rack, ladder. and grid structures were produced via metal-directed self-assembly using multidentate bridging ligands of different geometries to yield two- and three-dimensional synthetic receptors'"' (see Fig. 5c). From a more general point of view. this type of self-assembling metal arrays, also specified as open structures or porous systems. fa11 under the class of "coordination polymer~," an active field. Early types of coordination polyiners to be mentioned here are the Hofmann compounds and Werner clathrates, that are also classified into the below family of solid-state inclusion hosts.'"'

Interlocked and Interwoven Systems

Typical exainples of this category of supramolecular structures are the catenanes,[48] consisting of two or more rings that are interlocked mechanically without any chemical interaction between the two except nonbonding interaction (see Fig. 5d). Generally. the rings cannot be separated without breaking a chemical bond. A particular case of catenane being composed of five interlocked rings. such as in the international Olympic Games symbol. is dubbed ''olympiadane.''[49] In circumstances where the interlocked ring system is capable of acting as a ligand, the terms "catenate.' for the complex apply.[2] Compounds related to the catenanes are the rotaxanes.[48] They consist of a long. fairly linear molecule threaded through a macrocyclic ring with the linear part of the molecule terminated by bulky groups preventing slip out (see Fig. 5e). Rotaxanes without such physical barriers that can take apart are called pseudorotaxanes. They are frequently necessary precursors to rotaxanes and catenanes. The self-assembling double-helical structure of DNA provided the inspiration for a further area of supramolecular compounds called helicates.[50] Usually. they consist of extended. multidentate bridging ligands (helicands. a particular type of podands) capable of chelating different metal centers that gives rise to helical coordination complexes (see Fig. 5f). but hydrogen bonding analogues of such helical assemblies and much higher complex interwoven systems are also known.[42,43,47]

Solid-State Inclusion Hosts

The previous hosts produced host–guest compounds that usually exist in solution and in the solid state. By way of contrast; inclusion compounds of a so-called solid-state host are only in existence in the solid state. As stated above. host–guest compounds of this type are generally termed clathrates.[17,18] Although, here, a distinction between host and guest is sometimes subjective, because there are prototypes of organic and inorganic structures of host compounds following particular lines of molecular construction and concepts taken up in the trivial names.[2,47,51,52] In the first place. a distinction can be made between host molecules that feature strong mutual interactions (mostly via hydrogen bonding: see Fig. 5g,h), and those that have remarkable frames (specifically curved or propeller-type backbone, or a kind of awkward shape: see Fig. 5i,j). They result in an inefficient filling of space when host molecules are packed together in the crystalline form. thus providing voids.

The mutually interacting hosts can be simple molecules, such as water, on the inorganic and urea or thiourea on the organic side of compounds. The inclusions of ice are usually called clathrate hydrates or gas hydrates.[16] Trimesic acid (Fig. 5g) and derivatives, Dianin's compound (named after the creator), and other phenols. including hydroquinone, are further exainples of this particular compound type. Derivatives of cyclotriphosphazene. tri-o-thymotide, cyclotriveratrylene (CTV; Fig. 5i), perhydrotriphenylene (PMTP) and tetraphenylene are exempiary cases for the second category of host compounds characteristic of a curved or propeller-like framework structure. The host molecules typical of an awkward shape include all kinds of triarylmethanols and their derivatives. as well as molecular frameworks resembling a pair of scissors (Fig. 5h), a roof. or a wheel-and-axle shape[47,51,52] (Fig. 5j). Other design strategies leading to hexahosts (six-armed derivatives of benzene) or piedfort analogues (two trisubstituted aromatic rings juxtaposed: the term comes from a special coin stuck) were also successfully developed.[16,18,47] The most general approach to designing a solid structure (diamondiod network. rosette, tape motif. etc.) including host–guest systems. however. is to make use of the supramolecular synthon and crystal engineering concepts,[53–55]

Finally. the layered solids and intercalates of inorganic clay minerals and graphite as well as the zeolites as porous aluminosilicates have to be quoted here.[47]

SPECIFIED NOMENCLATURE

Due to their complex structure, systematic names of supramolecular compounds are cumbersome in use. This has given rise to many trivial names and descriptive

Fig. 4 Exemplary cases of enforced cavity hosts and their supramolecular compounds (guests symbolized in broken rings): (a) Cleft-type: (b) tweezer-type: (c) spherand; (d) cyclophane (monocyclic): (e) cyclophane ibicyclic): (f) cavitand; (g) carcerand; (h) calixarene (calix[4]arene); (i) resorcarene; (j) cryptophane; (k) cyclodextrin (β-cyclodextrin); and (l) cucurbituril.

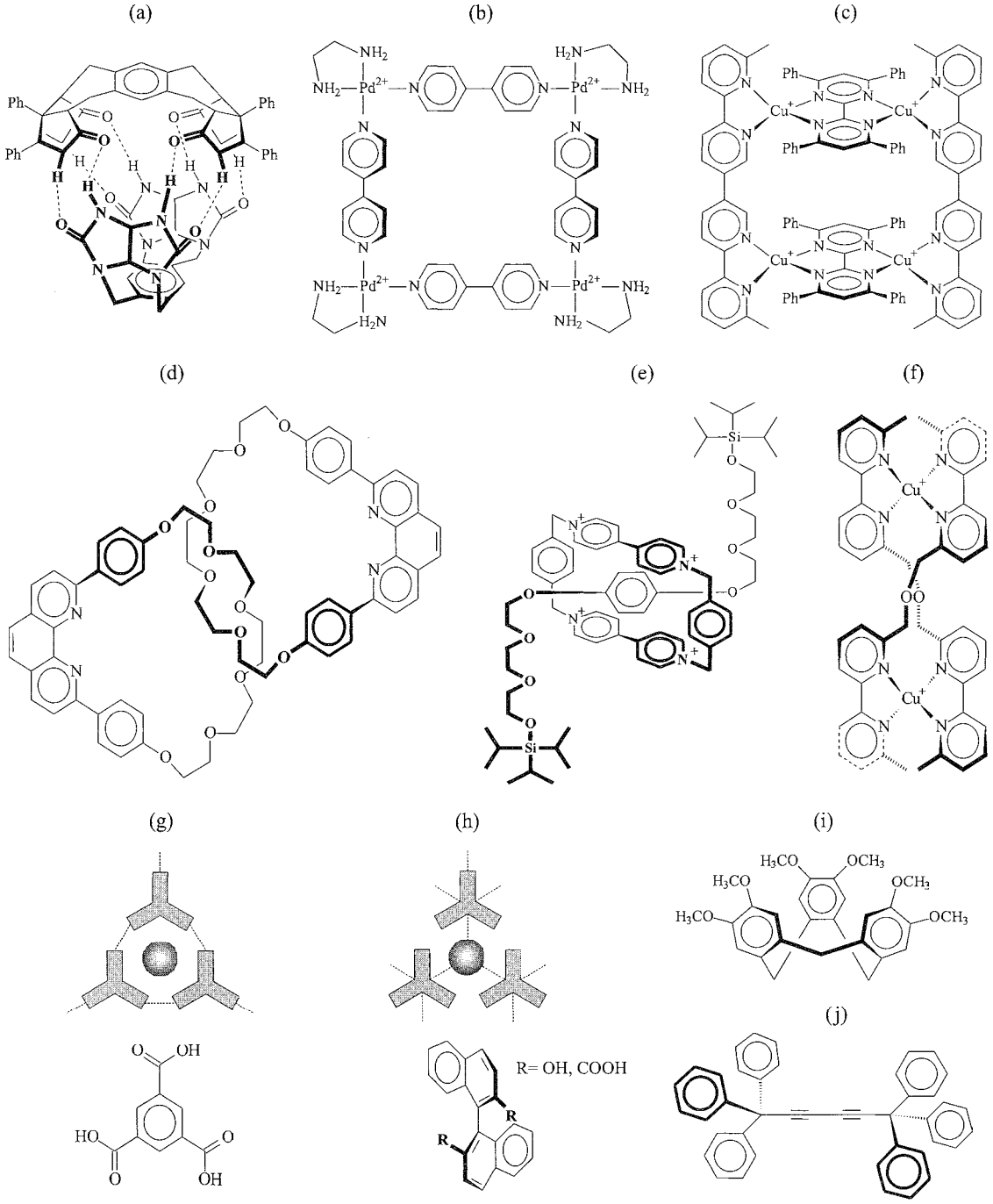

Fig. 5 Typical examples of (a–c) self-assembling inclusion hosts; (d–f) interlocked and interwoven systems: and (g–j) solid state inclusion hosts: (a) tennis ball dimer; (b) metallamacrocycle; (c) ladder-structured metal array: (d) catenane: (e) rotaxane: (f) helicate: (g) network lattice host (exemplary host molecule): (h) coorclinatoclathrate host (exemplary hosts): (i) curved framework host molecule: and (j) aukward-shape host molecule.

terms. as shown above. On the other nand. systems of more detailed terminology were established for particular classes of compounds in order to make smooth yet sufficiently precise expert conversation possible.

Seen from this point of view, the naming of crown ether compounds is relatively simple.[3–5,24] The first number in the crown name designates the number of atoms in the ring and is usually given in square brackets. The second number

following the class specification crown gives the number of oxygen atoms involved. Substituents or condensations are denoted with a prefix such as benzo-. dicyclohexano-, and so on. For example, [18]crown-6 (Fig. 3e, n = 2) is a crown ether with an 18-membered macrocyclic ring containing six oxygen atoms, and dibenzo[18]crown-6 is an analogue with two benzo condensations (Fig. 3f). These are sometimes modified to 18-crown-6 and dibenz(en)o-18-crown-6 (abbreviations: 18C6 and DB18C6). Although this kind of notation is cotnmonly accepted. it gives only a rough characterization of the structure and is not clearly defined (positions of *O* atoms and substituents). In an improved notation system,[26] the name [18]crown-6 (cf. Fig. 3f) becomes 18⟨$O_6$2$_6$-coronand-6⟩, meaning an 18-membered monocyclic compound containing six oxygen atoms linked by six spacers containing two carbon atorns each to give a total of six donor atoms. Similarly, a corresponding azacoronand (azacorand) compound containing alternate oxygen and nitrogen atoms (Fig. 3g; X = O,Y = NH) is callen triaza[18]crown-6, 18⟨O_3N_3-2$_6$-coronand-6) or 18⟨$(ON)_3$-2$_6$-coronand-6⟩ showing upward precision in naming. Especially for coronands containing multiple nitrogen or sulphur donors. a notation based on the suffix ''-ane,'' along with numbers denoting the ring size and donor atorns. is in use.[30] Thus. the hexaaza analogue of 18C6, 18⟨$N_6$2$_6$-coronand-6⟩ (Fig. 3g: X.Y = NK). is denoted [18]ane-N_6, and its sulfur analogue (Fig. 3g; X,Y = S) [18]ane-S_6.

The spherical cryptands have a somewhat different nomenclature.[6–8,24] Each host is denoted by a series of numbers, given in square brackets, followed by the class name "cryptand". The numbers in square brackets and separated by dots indicate the number of donor atoms in each of the bridges between the bridgehead atoms. Thus. the most common cryptand (Fig. 3h) is termed [2.2.2] cryptand. sometimes abbreviated [2.2.2]. in accordance, the analogous compound with sulfur atorns in the bridges is designated [2$_S$.2$_S$.2$_S$]. A more specific nomenclature as for the coronands was also been developed for the cryptands but is only scarcely in use.[26] Commercially, the cryptands are sold under the trade name Kryptofix®.

By way of contrast, the podands cannot refer to a simple notation system for naming,[26] except for the glymes (e.g., gyme-6: Fig. 3b, n = 3) where the number following the class name denotes the number of oxygen atoms connected to the ethylene glycol linkages.[27,28]

Regarding the big family of enforced cavity hosts. a more specific nomenclature than class names is more or less in use only for the calixarenes and cyciodextrins. In case of the calixarenes, the number of phenolic residues is denoted by a number in square brackets.[37,38] Thus. the most common cyclic tetramer with *p-t*-butyl substituents (Fig. 4h) is termed *p-t*-butyl-calix[4]arene. When using the cyclophane nomenclature,[56] the calix[4]arene would go by the name of [1.1.1] metacyclophane. The other cyclophane-type hosts, if not too complex in structure, are named correspondingly. The three most important members of the cyclodextrin family are α-, β-, and γ-cyclodextrin (sometimes abbreviated to *r*-. β-, and ;/-CD), which possess, respectively, six. seven. and eight glucopyranoside units. Thus. the Greek letters serve to distinguish the different ring sizes of the homologous series and are essentially historical in nature.'''' Numbers in square brackets of a nomenclature rnay still have another meaning than mentioned above. In catenanes[2,48] these denote numbers of interlocked rings, e.g., a [2]catenane consists of two interlocked rings (Fig. 5d), and in the case of the helicates,[2,50] they denote the binding sites of the helicand used for coordination of a metal ion. e.g., [4 + 4]helicate for the structure shown in Fig. 5f.

While a distinction between the free host (ligand) and the host–guest compound (inclusion complex) is easy to make for all hosts ending their name with "-and." simply by changing the ending to ''-ate'' or ''-plex'' for the host–guest compound[17,21,22] (Table 1), the other hosts cannot be treated in a similar way. e.g., the calixarenes or cyclodextrins. Here, paraphrastic wording may be used for specification of the host–guest compound. However. there is also the possibility of using formula terms denoted by the mathematical symbol ⊂, meaning "part of the set of.''[15] Thus. the coronand 18-crown-6, when including a metal ion M^+, forms the corollate [M^+⊂18C6], or β-cyclodextrin including benzene gives the cavitate [benzene ⊂ β-cyclodextrin].

CONCLUSION

Due to the fast growth in the number of supramolecular compounds, assemblies, or materials. it becomes difficult to distinguish between the different chemical species. It is true that. in principle, naming by using the systematic nomenclature could help in telling the species apart, but most of the compounds under discussion are so complex in structure that systematic names are cumbersome and thus impracticable in common use. This is the reason for the many trivial names, mostly of high pictorial nature, that have been coined. However, this is anything but a solution to the problem. because new trivial names constantly have to be found. On ihe other hand, efforts have been undertaken to find a generalized system of nomenclature for all supramolecular compounds. or at least for the host–guest compounds.[17,26] As shown, this is possible up to a point. but naming also tends become intricate and thus relatively troublesome. The main problem, however. is more complicated. owing to the noncovalent binding type a supramolecular compound rests upon. Interactions of this kind are not contained in the conventional nomenclature

systems that are designed only for covalent-bonded molecules or ions. Another insurmountable problem met with the naming of solid supramolecular compounds is connected with the phenomenon of polymorphism,[53] i.e., the ability of a compound to crystallize in different crystal arrangements. Thus, at present. it is more or less impossible to unambiguously name a moderately complex supramolecular compound using the existing nomenclature. In a way, the circuinstances are similar to the single compound nomenclature used somewhere near the end of the nineteenth century. A glimmer of hope might come from the so-called "supramolecular synthons"[54,55] to lay the foundation for a new system of nomenclature. They are related to the functional groups on the molecular level that. as known, are the bases of conventional nomenclature. Apart from this potential approach, a long-dated solution of the problem is not in the offering, although this would be profitable for the development of the whole field.

To summarize, it can be said that basic classification of supramolecular compounds has been developed using several criteria, of which the type of interaction and topological considerations are most important. On the other hand, a strict systematic nomenclature for any type of supramolecular compounds is lacking. Instead, a number of trivial names, notations. and semi-systematic names are presently in use.

ARTICLES OF FURTHER INTEREST

Carcerands and Hemicarcerands, p. 189
Catenanes and Other Interlocked Molecules. p. 206
Cavitands, p. 219
Classical Descriptions of Inclusion Compounds, p. 253
Concepts in Crystal Engineer-ing with Hydrogen Bonds, p. 319
Crown Ethers, p. 324
Cryptands, p. 334
Cryptophanes, p. 340
Cucurbituril, Its Homologues, and Derivatives, p. 390
Cyclodextrins, p. 398
Cyclophanes: Definition and Scope. p. 414
Dendrimers, p. 432
Glycoluril-Based Hosts, p. 597
Lariat Ethers. p. 782
Liquid Clathrates, p. 804
Micelles and Vesicles, p. 841
Molecular Clefts and Tweezers, p. *887*
Molecular Squares, Boxes, and Cubes. p. 909
Nomenclature in Crystal Engineering, p. 967
Organic Zeolites, p. 996
Podands, p. 1106
Polymorphism, p. 1129
Rotaxnnes and Pseudorotaxanes. p. 1194
Second-Sphere Coordination, p. 1209
Self-Assembly: Definition and Kinetic and Thermodynamic Considerations. p. 1248
Self-Assembly: Terminology, p. 1263
Siderophores, p.1278
Spherands, p. 1344
Supramolecular Chemistry: Definition, p. 1401
Supramolecular Polymers, p. 1443
Surfactants, Part I: Fundamentals. p. 1458
Surfactants, Part II: Applications, p. 1470
Zeolites: Structures and Inclusion Properties, p. 1623

REFERENCES

1. *The Lock and Key Principle*; Behr. J.-P., Ed.; Perspectives in Supramolecular Chemistry, Wiley: Chichester. UK. 1994: Vol. 1.
2. Steed. J.W.: Atwood. J.L. *Supramolecular Chemistry*; Wiley: Chichester. UK, 2000.
3. Pedersen, C.J. The discovery of crown ethers (Nobel Lecture). Angew. Chern. 1988. 100. 1053–1059.
4. Pedersen. C.J. The discovery of crown ethers (Nobel Lecture). Angew. Chem. Int. Ed. Engl. 1998. 27. 1021–1027.
5. Pedersen. C.J. The discovery of crown ethers (Nobel Lecture). J. Incl. Phenom. 1998. 6. 337–350.
6. Lehn, J.-M. Supramolecular chemistry—Scope and perspectives—Molecules. supermolecules and molecular devices (Nobel Lecture). Angew. Chem. 1988, *100.* 91–116.
7. Lehn. J.-M. Supramolecular chemistry—Scope and perspectives—Molecules, supermolecules and molecular devices (Nobel Lecture). Angew. Chem. Int. Ed. Engl. 1988. 27, 89–112.
8. Lehn. J.-M. Supramolecular chemistry—Scope and perspectives—Molecules. supermolecules and molecular devices (Nobel Lecture). J. Incl. Phenom. 1988. 6. 351–396.
9. Cram. D.J. The design of molecular hosts, guests. and their complexes (Nobel Lecture). Angew. Chem. Int. Ed. Engl. 1988. *100.* 1041–1052.
10. Cram. D.J. The design of molecular hosts, guests, and their complexes (Nobel Lecture). Angew. Chem. Int. Ed. Engl. 1988. 27. 1009–1020.
11. Cram. D.J. The design of molecular hosts, guests. and their complexes (Nobel Lecture). J. Incl. Phenom. 1988. 6. 397–413.
12. *Comprehensive Supramolecular Chemistry*; Atwood, J.L., Davies, J.E.D., MacNicol, D.D., Vogtle, F., Eds.: Elsevier Science: Oxford. UK, 1996: Vols. 1–10.
13. Schneider. H.-J.: Yatsirnirsky. A. *Principles and Methods in Supramolecular Chemistry*; Wiley: Chichester. UK, 2000.
14. *Host–Guest Complex Chemistry*; Vogtle, *F.,* Weber. E., Eds.; Springer Verlag: Berlin. Germany. 1985.
15. Lehn. J.-M. *Supramolecular Chemistry*; VCH Verlagsgesellschaft: Weinheim. Germany. 1995.

16. Weber, E. Inclusion Compounds. In *Kirk-Othmer Encyclopedia of Chemical* Technology, 4th Ed.; Ksoschwitz. J.I., Ed.: Wiley: New York, 1995: Vol. 14: 122–154.
17. Weber, E.; Josel, H.-P. A proposal for classification and nomenclature of host–guest-type compounds. J. Incl. Phenom. 1983. I. 79–85.
18. Weber. E. Clathrate chemistry today—Some problems and reflections. In Molecular *Inclusion and Molecular* Recognition-*Clathrates* I: Weber. E., Ed.; Topics in Current Chemistry. Springer-Verlag: Berlin. Germany. 1987: Vol. 140.
19. Colquhoun, H.M.; Stoddart. J.F.; Williams, D.J. Second-sphere coordination—A new role for molecular receptors. Angew. Chem. 1986. 98. 483–503.
20. Colquhoun, H.M.Stoddart. J.F.; Williams, D.J. Second-sphere coordination—A new role for molecular receptors. Angew. Chem. Int. Ed. Engl. 1986, 25. 487–507.
21. Cram, D.J. Preorganization—From solvents to spherands. Angew. Chem. 1986. 98. 1041–1060.
22. Cram. D.J. Preorganization—from solvents to spherands. Angew. Chem. Int. Ed. Engl. 1986. *25.* 1039–1057.
23. Vogtle. F. *Supramolecular Chemistry*; Wiley: Chichester. UK, 1991.
24. Cokel. G.W. *Crown* Ethers *and Cryptands*; Monographs in Supramolecular Chemistry. The Royal Society of Chemistry: Cambridge, UK. 1991; Vol. 3.
25. *Crown Ethers and Analogs*; Patai, S.. Raort. Z.. Eds.: Wiley: Chichester. UK, 1989.
26. Weber. E.; Vogtle. F. Classification and nomenclature of coronands, cryptands, podands, and their complexes. Inorg. Chim. Acta 1980, *45*, L65–L67.
27. Vogtle, F.: Weber. E. Multidendate acyclic neutral ligands and their complexation. Angew. Chem. 1979, 91. 813–837.
28. Vogtle. F.: Weber. E. Multidendate acyclic neutral ligands and their complexation. Angew. Chem. Int. Ed. Engl. 1979, 18. 753–776.
29. Gokel. G.W.; Schall, O.F. Lariat Ethers. In *Comprehensive Supramolecular Chemistry*; Atwood, J.L., Davies. J.E.D., MacNicol, D.D.. Vogtle, F., Eds.; Elsevier Science: Oxford. UK, 1996: Vol. 1: 97–152.
30. Lindoy, L.F. The *Chemistry* of Macrocyclic *Ligand* Complexes: Cambridge University Press: Cambridge. UK, 1989.
31. Rebek. J. Molecular recognition with model systems. Angew. Chem. 1990. 102. 261–272.
32. Rebek. J. Molecular recognition with model systems. Angeu. Chem. Int. Ed. Engl. 1990. *29*, 245–255.
33. *Supramolecular Chemistry* I—Directed *Synthesis and Molecular Recognition.* Weber. E.. Ed.: Topics in Current Chemistry. Springer-Verlag: Berlin. Germany. 1993; Vol. 165.
34. Diederich, F. *Cyclophanes*; Monographs in Supramolecular Chemistry, The Royal Society of Chemistry: Cambridge. UK, 1991: Vol. 2.
35. Cram. D.J.: Cram, J.M. Container *Molecules* and *Their Guests*; Monographs in Supramolecular Chemistry. The Royal Society of Chemistry: Cambridge. UK, 1994: Vol. 4.
36. Jasat, A.: Sherman. J.C. Carceplexes and hemicarceplexes. Chem. Rev. 1999. 99. 931–967.
37. Gutsche, C.D. *Calixarenes*: Monographs in Supramolecular Chemistry, The Royal Society of Chemistry: Cambridge. UK, 1989: Vol. 1.
38. Gutsche, C.D. *Calixarenes Revisited*: Monographs in Supramolecular Chemistry. The Royal Society of Chemistry: Cambridge. UK. 1998: Vol. 6.
39. Szejtli. J. Introduction and overview of cyclodextrin chemistry. Chem. Rev. 1998. 98. 1743–1753.
40. *Comprehensive Supramolecular Chemistry*; Atwood, J.L., Davies. J.E.D.. MacNicol, D.D.. Vogtle. F.. Eds.: Elsevier Science: Oxford. UK. 1996: Vol. 3.
41. *Supramolecular Chemistry* II—Host *Design and* Molecular *Recognition*; Weber. E.. Ed.: Topics in Current Chemistry. Springer-Verlag: Berlin, Germany. 1995: Vol. 175.
42. Philip, D.: Stoddart. J.F. Self-assembly in natural and unnatural systems. Angew. Chern. 1996, 108. 1242–1286.
43. Philip. D.: Stoddart. J.F. Self-assembly in natural and unnatural systems. Angew. Chem. Int. Ed. Engl. 1996. *35.* 1154–1196.
44. Molecular *Self-Assembly—Organic Versus Inorganic Approaches*; Fujita, M.. Ed.: Structure and Bonding, Springer-Verlag: Berlin, Germany. 2000: Vol. 96.
45. Conn. M.M.: Rebek. J., Jr. Self-assembling capsules. Chem. Rev. 1997.97. 1647–1668.
46. Suiegers, C.F.: Malefetse, T.J. New self-assembled structural motifs in coordination chemistry. Chem. Rev. 2000, 100. 3483–3537.
47. *Comprehensive Supramolecular Chemistry*; Atwood, J.L., Davies. J.E.D., MacNicol. D.D.. Vogtle, F., Eds.; Elsevier Science: Oxford, UK, 1996: Vol. 6.
48. *Molecular Catenanes, Rotaxanes and Knots*; Sauvage, J.-P.. Dietrich-Buchecker. C., Eds.: Wiley-VCH: Weinheim, Germany, 1999.
49. Raymo, F.M.: Stoddart. J.F. Interlocked macromolecules. Chem. Rev. 1999. *99*, 1643–1666.
50. Piguet, C.: Bernardinelli, G.; Hopfgartner. G. Helicates as versatile supramolecular complexes. Chem. Rev. 1997, 97. 2005–2062.
51. *Molecular Inclusion and Molecular Recognition—Clathrates* I: Weber, E., Ed.: Topics in Current Chemistry, Springer-Verlag: Berlin. Geriiiany. 1987: Vol. 140.
52. *Molecular Inclusion and Molecular Recognition—Clath*rates *II*; Weber. E.. Ed.: Topics in Current Chemistry. Springer-Verlag: Berlin, Germany. 1988: Vol. 149.
53. *Design* of *Organic* Solids: Weber. E.. Ed.: Topics in Current Chemistry. Springer-Verlag: Berlin-Heidelberg. 1998; Vol. 198.
54. Desiraju, G.R. Supramolecular synthons in crystal engineering—A new organic synthesis. Angew. Cheni. 1995, 107. 2541–2558.
55. Desiraju, G.R. Supramolecular synthons in crystal engineering—A new organic synthesis. Angew. Chem. Int. Ed. Engl. 1995. *34.* 2311–2327.
56. Vogtle, F. *Cyclophane Chemistry*; Wile) : Chichester. UK, 1993.

Clathrate Hydrates

John A. Ripmeester
Christopher I. Ratcliffe
Konstantin A. Udachin
National Research Council Canada, Ottawa, Ontario, Canada

INTRODUCTION

A clathrate hydrate is a crystalline inclusion compound in which small guest molecules. usually hydrophobic. are trapped in polyhedral cages formed by hydrogen-bonded water molecules.[1] True clathrates are formed by guests that interact with the hydrate lattice only by weak, nondirectional forces. In such cases. the water molecules form a completely hydrogen-bonded network, and the inaterials effectively are ices. A number of structures are known for true clathrate hydrates. including the three major families of clathrate hydrate structures[2] that will be discussed later.

Clathrate hydrates are of interest today for a number of reasons. It probably is fair to say that they were the first-recognized suprarnolecular coinpounds. with a history going back 200 years. Scientifically. they are of interest as perhaps the best-understood class of inclusion compounds, and they serve as the archetypal model for hydrophobic hydration. Technically, hydrates proved to be a hazard in the exploration and transport of hydrocarbon resources because of solid plug formation in pipelines.[3] Last. the existence of naturally occurring hydrates sparked an interest in their roles in the geosphere, especially pertaining to their possible roles as agents of climate change. as sources of clean-burning methane gas, and as geohazards.[4] The last features are related to the fact that a hydrate is an extremely efficient storage medium for gases. as each volume of Structure I hydrate, for example, is known to hold $\sim$160 volumes of gas at standard temperature and pressure (STP).

Several classes of materials closely related to clathrates are known as well, generally classified as semiclathrates, and ionic or salt hydrates.[3] Semiclathrates are crystalline hydrates formed mainly by amine guests, where there is some interaction between guest and host. This often takes the form of hydrogen bonding between the guest molecule and host lattices. which leaves some water molecules incompletely incorporated in the hydrogen-bonded clathrate framework. There is a large variety of structures. some of which are related to the true clathrates.

The ionic clathrates are formed by onium salts MR^+_4 and SR^+_3 (M = N, P. and R = C_1-isoC_5), where the anions can be inorganic or organic ions.[2] For these structures, it is also possible to substitute NH_4F for some of the water molecules. As well, acids such as perchloric, tetrafluoroboric, and HXF_6 (X = P, As. Sb). form clathrate structures with the anion in a hydrate cage and the proton incorporated into the hydrate lattice. Again, some substitution of lattice water molecules is possible for these compounds with HF. Oxides with formula R_3NO, R_3PO, and R_3AsO, where $R = C_4H_9$, isoC_5H_{11}, also form clathrate hydrates.

HISTORICAL PERSPECTIVE

Although some researchers claim that the initial observation of a clathrate hydrate took place in the eighteenth century. it is generally accepted that the first official report was made by Davy to the Royal Society and published in 1811.[5] He reported that a compound of muriatic oxide (chlorine) and water had a melting point higher than that of ice, and Faraday measured its composition to be $Cl_2.10H_2O$ in 1823.[6] Thus, clathrate science is. in fact, older than the concepts of modern chemistry. It can also be said that the clathrate hydrates often did not obey the general rules that were being discovered for chemical compounds. and until the first structure was determined in the early 1950s, remained somewhat of a mystery. Many eminent scientists contributed to clathrate science. developing a number of general concepts.[7] For instance. clathrates formed definite compounds. but their components could be recovered unchanged on decomposition: they were generally nonstoichiometric with fractional hydration numbers; and mixtures of guests often gave coinpounds as readily as pure guests.

The observation that solid hydrates of hydrocarbons might more easily form blockages in gas pipelines than ice[8] was the impetus for a vigorous research program with the aim of predicting hydrate formation conditions and preventing blockages, an effort that continues today. The early work led to a comprehensive package of practical knowledge on phase equilibria of gases and gas mixtures. either in the presence or absence of hydrate inhibitors. such as methanol and salt.[9]

Encyclopedia of Supramolecular Chemistry
DOI: 10.1081/E-ESMC 120012723

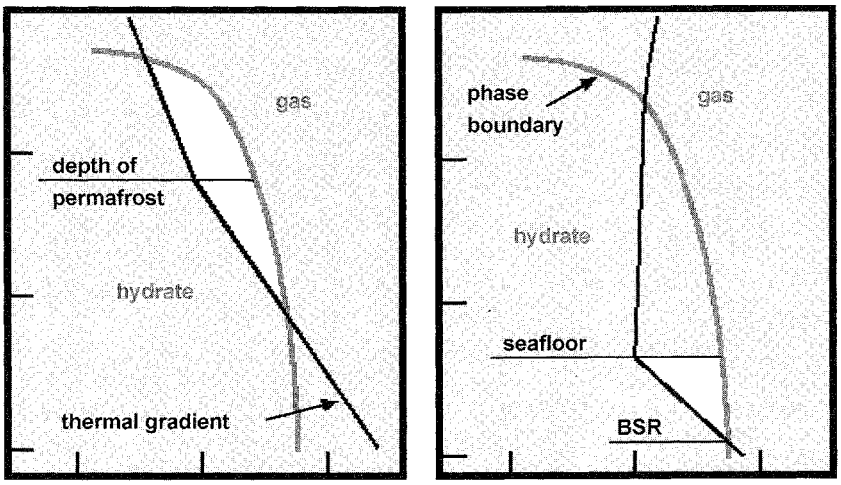

Fig. 1 Methane hydrate. which is stable belou· and to the left of the phase boundary line. Also shown is the geothermal gradient in permafrost as well as marine environments. Where the curves intersect, natural methane hydrate is stable. Natural methane hydrates are found in the lightly shaded region. BSR labels the "bottorn-simulating reflector." an unexpected interface found by sonic exploration techniques and usually associated with the interface between sediments with and without hydrate. (*View this art in color at www.dekker.com.*)

The first crystal structures for the clathrate hydrates now known as Structures I and II were published in the early 1950s, giving answers to many of the questions raised during the previous 150 years of hydrate work.[10–14] They were seen to fit the class of materials known as "clathrates." a term coined a few years earlier by Powell[15] to describe inclusion compounds of quinol and trapped guests. The knowledge of structural information and compositional data on clathrates. including the hydrates. led van der Waals and Platteeuw to propose their elegant "solid-solution" theory for clathrates,[16] still the basis for much of the predictive modeling of clathrate stability conditions today.

Interest in clathrate hydrates was sparked again when it was realized that hydrates might exist naturally in the geosphere. and when this hypothesis was subsequently confirmed. This includes "air" hydrates deep inside glaciers[17] and natural gas hydrates, both under the permafrost[18,19] and offshore on the continental margins (see Fig. 1).[20] On a more speculative note. it was also conjectured that gas hydrates exist on the outer planets and in comets.[21,22]

In the last 30 years or so. clathrate science has blossomed. with the reports of many new guests, a new hydrate structural family, a complete revision of the structure–size relationships. new approaches for hydrate characterization. refined models for hydrate stability prediction, high-level calculations and computational work on hydrate physical properties, experimental work and models for kinetic processes, etc.

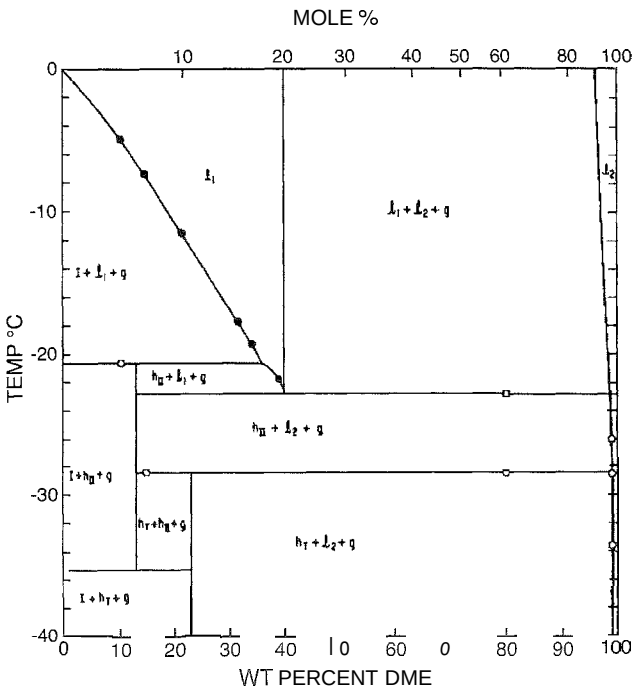

Fig. 2 Temperature–composition diagram for the water–dimethyl ether system. The two hydrates that form at −12 and 22 Wt% DME are Structure II ($DME.17H_2O$) and Structure T (DME.8 2/3 H_2O hydrates. respectively), Both decompose incongruently. (S.L. Miller, S.R. Gough, D.W. Davidson. J. Phys. Chem. 1977. *81,* 2154: K.A. Udachin. C.I. Ratcliffe. and J.A. Ripmeester, Angew. Chem. Int. Ed. 2001. *113.* 1343.)

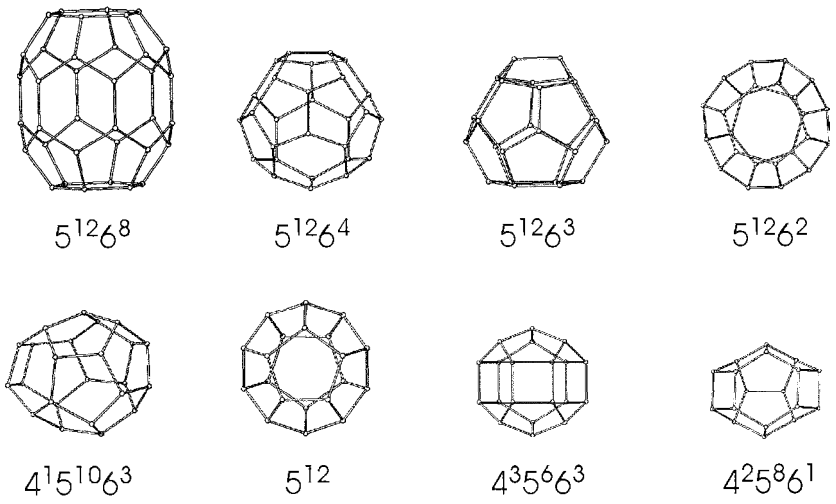

Fig. 3 Polyhedra present in the true clathrate hydrates

STRUCTURES

The true clathrates can be classified as belonging to three major families. commonly known as Structures I, II[1,2] and H,[23,24] and several unique structures formed by bromine,[25] dimethyl ether (see Fig. 2),[26] and *tert*-butylamine.[27] The polyhedra that make up these various structures are shown in Fig. 3. In contrast to Ice Ih, in which hexagonal rings of hydrogen-bonded water molecules occur exclusively. Fig. 3 and Table 1 show that pentagonal rings predominate in the clathrate hydrates. although hexagonal and, sometimes, square rings are necessary in order to give space-filling frameworks. The polyhedra, which must comply with Euler's relationship, F + V = E + 2 (where *F*, V. and *E* are the number of faces. vertices, and edges. respectively), stack together by sharing faces to fill three-dimensional space. They are usually described by the descriptor n^m, where *m* is the number of faces with *n* edges. Of the hydrate cages, the pentagonal dodecahedron (5^{12}), also referred to as "nature's second favorite structure",[26] is the only polyhedron that can have equal edges and interedge angles while maintaining planar faces. The cages of various types stack together to fill three-dimensional space. as shown in Fig. 4.

Table 1 Hydrate structure types. unit cell contents. and cage types

Structure type	Unit cell content *Space group*	Cage	Symmetry of cages
Structure I	$2D \cdot 6T \cdot 46H_2O$	5^{12}(D)	m3
	Pm3n	$5^{12}6^2$(T)	$\bar{4}$2m
Structure II	$16D \cdot 8H \cdot 136H_20$	5^{12}(D)	3m
	Fd3m	$5^{12}6^4$(H)	$\bar{4}$3m
Structure H	$E \cdot 3D \cdot 2D' \cdot 34H_2O$	5^{12}(D)	mmm
	P6/mmm	$4^35^66^3$(D)	$\bar{6}$m2
		$5^{12}6^8$(E)	6/mmm
Structure II/H polytype (ideal form)	$3E\ 12H \cdot 6D' \cdot 33D \cdot 306H_2O$	5^{12}(D)	3. 3m
	R-3m	$4^35^66^3$(D′)	3m
		$5^{12}6^4$(H)	3m, 3ln
		$5^{12}6^8$(E)	3m
Structure T	$12U \cdot 12T\ 24T'\ 12P\ 348H_2O$	$4^25^86^1$(U)	2. 2. 1
	P321	$5^{12}6^2$(T)	2, 2, 1
		$5^{12}6^3$(P)	32, 3, 2
		$4^15^{10}6^3$(T)	1, 1, 1, 1
Bromine hydrate	$2D_A \cdot 8D_B \cdot 8T_A \cdot 8T_B \cdot 4P \cdot 172H_2O$	5^{12} (D)	1
	$P4_2/mmm$	$5^{12}6^2$ (T)	m, m
		$5^{12}6^3$ (P)	m

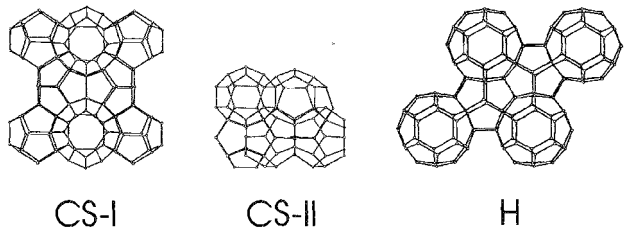

Fig. 4 Clathrate hydrate structures. Hydrates of cubic Structures I, II. and hexagonal Structure H are illustrated to indicate the stacking of the polyhedra.

As well. a summary of the structural details and the cages in each structure is given in Table 1.

Suitable guest materials for true clathrate hydrates vary widely in size and chemical nature and number well over a hundred. The main criterion is that the guest molecule should not interact too strongly with water, as in the solid hydrates, the guest and host must interaci hydrophobically. Thus. the classes of hydrate formers include monatomic (Ar. Kr, Xe), diatomics (N_2, O_2, CO, Br_2, Cl_2), other inorganics [H_2S, H_2Se, CO_2, COS, PH_3, NF_3, ClO_3F, SO_2F_2, MF_6 (M=S, Se, Te)], organic hydrocarbons (aliphatic. alicyclic. olefinic, acetylenic, aromatic). and substituted organics (halides. including CFCs HCFCs, sulfides. mercaptans, ethers, ketones, some alcohols. aldehydes, and acids). Size limits (van der Waals' diameter) on the guests vary from 4–8 A (Ar to ~dimethylcyclohexane). On the basis of high-pressure experiments. it was suggested that Ne, He, and H_2 are also able to form classical hydrate structures.[28]

The actual hydrate structure that forms is usually determined by the size of the guest. In two-phase systems, the relationship between guest size and structure is reasonably straightforward. When there is more than one guest type, the relationship is far more complex. as shown in Fig. 5.

PREPARATION AND PHYSICAL PROPERTIES

Pure hydrates are crystalline ice-like solids usually prepared from water or ice and an appropriate guest species. Hydrates of water-soluble guests have well-defined phase diagrams characteristic of two-phase systems with compound formation.".'' If the hydrate melts congruently, it is simply a matter of freezing a solution of the correct composition to obtain the hydrate. For systems that melt incongruently, the aqueous solution must be quenched below the peritectic temperature and conditioned so that the crystalline hydrate can form on annealing the frozen mixture. In cases where the guest species is a poorly water-soluble liquid or gas, hydrates can be made by contacting powdered ice with the guest in a sealed tube or in a pressure vessel and leaving the sample for periods of several days to weeks. Often it helps to cycle the temperature through 0°C in order to promote

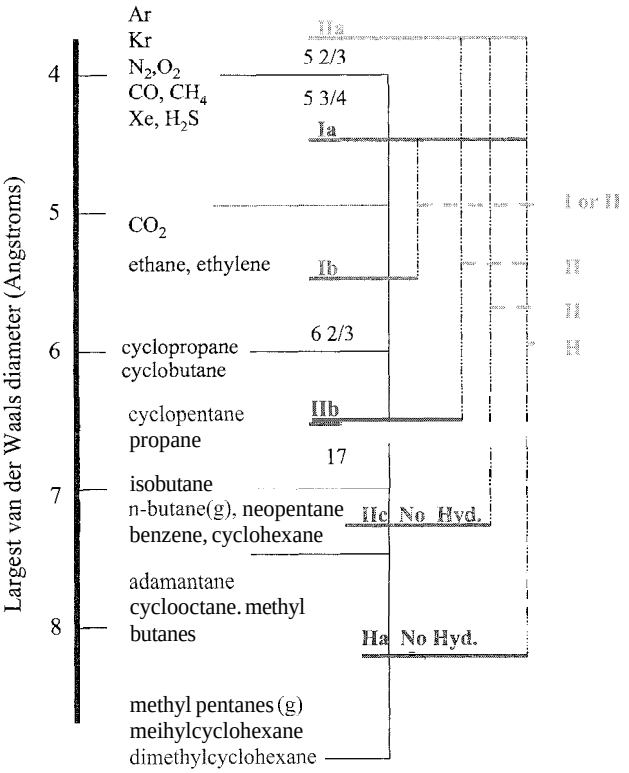

Fig. 5 Structure–sire relationships. A number of representative guests are shown at their largest van der Waals' diameters. Guests are classified as I and II. those being the structures formed if a single guest of that type were present. The **a.** b, c letters classify different subgroups, with the guest size of a smaller than that of b. which, in turn. is smaller than that classified as c. Also indicated are the ideal hydration numbers: 5 213 for guests of IIa. 5 3/4 for Ia if all cages are full. For guests ot Ia and Ib, some of the small cages are empty. so that hydration numbers tend toward 6 2/3 as the guest size increases. For guests of IIb, the small cages are empty. so that the hydration number is 17 Some guests at the Ib–IIb boundary can gıve either Structure I or IT Guests ın Groups IIc and Ha are not known to form hydrates by themselves but need small help gas molecules (trorn Groups Ia. IIa, some hom IIb) If guest types from Ia or IIa are present together with guests from Group Pb. Structures I or II maq occur depending on P.T conditions and relative concentrations. Guests of Type IIa. Ia. or Ib together with IIb or IIc give double hydrates of Structure II, and guests of Type Ia. IIa, or Ib with Ha give structure H. (J.A. Ripmeester. Ann. N. Y. Acad. Sciences 2000. *912*. 1.) (*View this art in color at www.*

hydrate formation, and continuous grinding of the reaction mixture has also been used effectively.

On the other hand, it is also possible to react water with liquid or gaseous guest in bulk. However, the hydrate usually forms at the interface, and agitation is needed in order to produce significant amounts of hydrate. The pressure of a gaseous guest must be maintained within the P–T range of stability for the hydrate, and usually a significant overpressure is needed in order to nucleate hydrate initially. For the clathrates with gaseous guests, it is difficult to form a "pure" hydrate in which there is neither ice nor hydrate former in excess. This is especially difficult if the hydrate is to be homogeneous in terms of composition. as it needs to be made under fom-phase equilibrium (usually water–liquid guest–hydrate–gas or water–ice–hydrate–gas) conditions.

Because hydrates are nonstoichiometric, the determination of the composition, especially for gaseous guests. has been a challenge.[1,3] This determination can be done by direct measurement of water and guests for samples known to be pure hydrate, or more generally by a variety of wet chemistry techniques. One of these is the application of the Clausius–Clapeyron equation to P–T data for the hydrate–liquid–gas and hydrate–ice–gas equilibria in systems of water plus one guest component, which yields the heats of forination for these two reactions, H_l and H_s. The difference divided by the molar heat of fusion of ice then gives an estimate of the number of moles of water in the hydrate. Because natural hydrates often occur in the presence of sediment and excess water. there is a strong interest in developing instrumental techniques that will allow the determination of composition in situ or in the presence of impurities.

THERMODYNAMIC DESCRIPTION

The best simple description of clathrate hydrates is the solid solution model of van der Waals and Platteeuw.[16] It assumes that there is an hypothetical empty hydrate lattice that is metastable with respect to ice, and that the lattice is stabilized by the presence of the guest molecules. Further assumption5 are that there is single occupancy of hydrate cages, and that guest–guest interactions can be neglected. Then, for a single-guest component at the quadruple point (hydrate, ice, water. gas), the hydrate will have the minimum cage occupancy for lattice stability. and the chemical potential difference $\Delta\mu$ between the hypothetical empty lattice and ice can be expressed in terms of the fractional cage occupancies θ_i as:

$$\Delta\mu = RT\Sigma_i[n_i \ln(1 - \theta_i)]/N \quad (1)$$

where n_i is the number of cages of type i, and N is the number of water molecules per unit cell, respectively. For Structure I hydrate, the best estimate of $\Delta\mu$ is 1297 J/m, which means that for guests such as methane and xenon. the large cages are essentially full and the small cages are $\sim$75% occupied, giving hydration numbers of 6–6.2. The thermodynamics of clathrates were recently reviewed.[29]

CHARACTERIZATION OF HYDRATES

A complete description of a hydrate requires knowing the detailed structure; including the distribution of the guest molecules over the cages. which then fixes the composition. and its phase diagram (P–T-composition, or a two-dimensional cross section thereof).[1–3,29] Other important parameters. especially for engineering and geophysical applications, include the thermal parameters, such as the various hears of reaction. the heat capacity, and physical properties. such as the dielectric permittivity, the thermal conductivity, the speed of sound. and the refractive index.

As for other crystalline solids, the primary method for determining hydrate structure is by diffraction techniques. High-quality single-crystal x-ray data obtained on a modern diffractometer can be good enough to determine the framework structure and the highly disordered guest positions. Refinement of the data with the cage occupancy as a variable can then be used to determine the composition of the hydrate.[30] Powder data (x-ray or neutron) can be refined by Rietveldt analysis, although the coupling of parameters tends to preclude a completely independent determination of structure and composition.[31]

Other techniques for the characterization of hydrates[32,33] include calorimetry, dielectric measurements. and spectroscopic techniques such as NMR,[34] Raman,[35,36] and IR spectroscopy.[37] These techniques depend on providing a structure-dependent spectral signature. In NMR spectroscopy. isotropic chemical shifts of the guests are affected by the size of the cages. As well. the anisotropic chemical shifts or quadrupolar coupling constants observed for the guests reflect the guest dynamics and the symmetry of the cages. Quantitative information can yield relative cage occupancies, which through expression I can be related to the hydration number. In vibrational spectroscopy. the size of the cage affects some of the vibrational modes of the guests. again allowing for identification of guests in different cages. However. there is evidence of guest–guest coupling. suggesting that intensity information needs to be treated with caution. especially in Raman spectroscopy, where the intensities depend on the polarizability tensor at the guest site.[35,36]

CONCLUSION

Gas hydrates continue to challenge researchers in scientific and technical areas. There is much current interest in understanding and controlling nucleation and kinetic processes; in discovering new hydrate phases, especially at high pressures; in viewing the nature of the hydrate in natural settings; in determining the location and extent of natural hydrate deposits and their roles in the geosphere: and in determining the feasibility of producing gas from natural deposits.

Over time, various applications were demonstrated on laboratory or pilot plant scale, including the fractionation of gases, the concentration of aqueous solutions. the desalination of water, cool energy storage, and the storage and transport of natural gas. All of these await future developments of commercially viable technologies.

ARTICLES OF FURTHER INTEREST

Cavitands, p. *219*
Clathrate Hydrates, p. *274*
Disorder and Diffuse Scattering, p. *457*
Hydrogen Bonding, p. *658*
Hydrophobic Effects, p. 673
Isostructurality of Inclusion Compounds, p. *767*
Neutron Diffraction, p. *959*
Soft and Smart Materials, p. *1302*
Solid-State Nuclear Magnetic Resonance Spectroscopy, p. 1307
Vibrational Spectroscopy, p. *1557*
X-Ray Crystallography, p. 1586
Zeolites: Structures and Inclusion Properties, p. *1623*

REFERENCES

1. Davidson. D.W. *Clathrate Hydrates* in *Water. A Comprehensive Treatise*; Frank. F.. Ed.; Plenum: NY. 1973; Vol. 2. 115–234.
2. Jeffrey, C.A. *Comprehensive Supramolecular Chemistry*; MacNicol. D.D., Toda. F.. Bishop. R., Eds.; Pergamon. 1996; Vol. 6, 757–788.
3. Sloan, E.D.. Jr. *Clathrate Hydrates of Natural* Gas; Marcel Dekker: New York. 1998.
4. *Proceedings of the Third International Conference* on *Gas Hydrates*; New York Academy of Sciences. 2000: Vol. 912.
5. Davy, H. The Bakerian lecture. On some of the combinations of oxymuriatic gas and oxygen. and on the chemical relations of these principles to inflammable bodies. Philos. Trans. R. Soc. 1811. *101*. 1–35.
6. Earaday. M. Q. J. Sci. 1823. *15*. 71.
7. Schroeder. W. Die geschichte der gashydrate. Samml. Chem. Chem.-Tech. Vortr. 1926. 1. 29.
8. Hanimerschmidt. E.C. Formation of gas hydrates in natural gas transmission lines. Ind. Eng. Chem. 1934.26, 851–855.
9. Katz. D.L.; Cornell. D.; Kobayashi. R.: Poettmann. F.H.; Vary, J.A.: Elenbaas. J.R.: Weinaug. C.F. *Handbook of Natural* Gas *Engineering*; McGraw-Hill: New York, 1959.
10. Clausen. W.F. Suggested structures for water in inert gas hydrates. J. Chem. Phys. 1951. *19*. 259–260. erratum 662.
11. von Stackelberg. M.: Muller, H.R. On the structure of gas hydrates. J. Chem. Phys. 4951. 19. 1319–1320.
12. Clausen. W.F. A second structure for inert gas hydrates. J. Chem. Phys. 1951. *19*, 1425–1426.
13. Muller. H.R.: von Stackelberg. M. Zur struktur der gashydrate. Naturwiss. 1952. 39. 20–21.
14. Paulinp, L.: Marsh. R.E. The structure of chlorine hydrate. Proc. Natl. Acad. Sci. U.S.A. 1952. *38*. 112–1 18.
15. Powell. H.M. The structure of molecular compounds. Part IV. Clathrate compounds. J. Chem. Soc. 1948, 61–73.
16. Van der Waals. J.H.; Platteeuw. J.C. Clathrate solutions. Adv. Chem. Phys. 1959. 2. 1–57.
17. Miller, S.L. Clathrate hydrates of air in Antarctica. Science 1969. *165*, 489–490.
18. Makogon, Y.F.: Trebin. F.A.: Trofimuk, A.A.: Tsarev. V.P.: Cherskiy, N.V. Detection of a pool of natural gas in a solid (hydrated gas) state. Dokl. Acad. Sci. USSR, Earth Sci. Sect. 1972. *196*. 197–200.
19. Bily, *C.:* Dick, J.W.L. Naturally occurring gas hydrates in the Mackenzie Delta. Bull. Can. Pet. Ceol. 1974. 32. 340–352.
20. Stoll. R.D.; Ewing, J.I.: Bryan. G.M. Anomalous wave velocities in sediments containing gas hydrates. J. Geophys. Res. 1971, *76*, 2090–2094.
21. Miller. S.L. The occurrence of gas hydrates in the solar system. Proc. Natl. Acad. Sci. U.S.A. 1961. 47. 1798–1808.
22. Delsernme. A.H.: Miller. D.C. Physico-chemical phenomena in comets TI. Gas adsorption in the snows of the nucleus. Planet. Space Sci. 1970. 18. 717–730.
23. Ripmeester, J.A.; Tse. J.S.: Ratcliffe. C.I.: Powell, B.M. A new clathrate hydrate structure. Nature 1987. 325, 135–136.
24. Udachin. K.A.: Ratcliffe. C.I.: Enright, G.D.; Ripmeester. J.A. Structure H hydrate: A single crystal diffraction study of 2,2-dimethylpentane.5(Xe,H_2S).34H_2O. Supramol. Chem. 1997. *8*, 173–176.
25. Udachin. K.A.; Enright, G.D.: Ratcliffe, C.I.: Ripmeester, J.A. Structure. stoichiometry and morphology of bromine hydrate. J. Am. Chem. Soc. 1997, *119*. 11481–11356.
26. Udachin. K.A.; Ratcliffe. C.I.; Ripmeester. J.A. A dense and efficient clathrate hydrate structure with unusual cages. Angew. Chem., Int. Ed. 2001. *40*. 1303–1305.
27. McMullan, R.K.; Jeffrey. G.A.; Jordan, T.H. Polyhedral clathrate hydrates XIV. The structure of $(CH_3)_3CNH_2.9\frac{3}{4}H_2O$. J. Chem. Phys. 1967. 47. 1229–1234.
28. Dyadin. Y.A.: Larionov. E.; Manakov, A.Y.: Zhurko, F.V.; Aladko, E.Y.: Mikina, T.V.: Komarov, V.Y. Clathrate

hydrates of hydrogen and neon. Mendeleev Commun. 1999, *9*, 209–210.
29. Dyadin, Y.A.; Belosludov, V.R. Stoichiometry and Thermodynamics of Clathrate Hydrates. In *Comprehensive Supramolecular Chemistry*; MacNicol, *D.D.*, Toda, F., Bishop, R.. Eds.; Pergamon: New York, 1996; Vol. 6. 789–824.
30. Udachin, K.A.; Ratcliffe, C.I.; Ripmeester. J.A. Structure, composition and thermal expansion of CO_2 hydrate from single crystal X-ray diffraction measurements. J. Phys. Chem. 2001, *105*. 4200–4204.
31. Henning, R.W.; Schultz, A.J.; Thieu, V.; Halpern, Y. Neutron diffraction studies of CO_2 clathrate hydrate: Formation from deuterated ice. J. Phys. Chcm. A 2000, *104*, 5066–5071.
32. Davidson, D.W.; Garg, S.K.; Gough, S.R.; Handa. Y.P.; Ratcliffe, C.I.; Ripmeester, J.A.; Tse, J.S.; Lawson, W.F. Laboratory analysis of a naturally occurring gas hydrate from sediment of the Gulf of Mexico. Geochim. Cosmochim. Acta 1986. *50*. 619–623.
33. Tulk, C.A.; Ratcliffe, C.I.; Ripmeester, J.A. Chemical and physical analysis of natural gas hydrate from the JAPEX/JNOC/GSC Mallik 21,-38 gas hydrate research well. Bull. Geol. Surv. Can. 1999. *544*, 251–262.
34. (a) Ripmeester, J.A.; Ratcliffe, C.I. Solid-State NMR Spectroscopy: Applications to Supramolecular Chemistry. In *Comprehensive Supramolecular Chemistry*, 8th Ed.; Atwood, J.L., Davies, J.E.D., MacNikol, D.D.. Vogtle, F., Lehn, J.-M., Eds; Pergamon: New York, 1996; Vol. 8, 323–380. (b) Ripmeester, J.A., Ratcliffe, C.I., Brouwer, E.B. Inclusion Compounds. In *Encyclopedia of Nuclear Magnetic Resonance;* Grant, D.M.. Harris, R.K.. Eds: John Wiley and Sons: Chichester, 2002; Vol. 9. 558–570.
35. Sum, A.K.; Burruss, R.C.; Sloan, E.D. Measurement of clathrate hydrates via Raman spectroscopy. J. Phys. Chem., B 1994, *101*, 7371–7377.
36. Tulk, C.A.; Klug, D.D.; Kipmeester, J.A. The application of Raman spectroscopy to the study of gas hydrates. Ann. N. Y. Acad. Sci. 2000; *912*. 859–872.
37. Richardson, H.H.; Wooldridge, P.J.; Devlin, J.P. FT-TR spectroscopy of vacuum deposited clathrate hydrates of oxirane H_2S, THF, and ethane. J. Chem. Phys. 1985, *83*, 4387–4394.

Clathrate Hydrates: Occurrence, Uses, and Problems

Christopher I. Ratcliffe
John A. Ripmeester
National Research Council Canada, Ottawa, Ontario, Canada

INTRODUCTION

Clathrate hydrates are supramolecular framework materials in which guest molecules are physically trapped inside cages made of hydrogen-bonded water molecules. Naturally occurring hydrocarbon gas hydrates constitute a vast untapped energy resource, generally little known by the layman, though receiving increasing attention in the media. Ice-like in appearance, methane hydrate can generate about 160 times its own volume of gas at standard temperature and pressure (STP). Gas hydrates already have a huge impact on industry, as the cause of numerous problems for the oil and gas industry, but they also have a few specialized beneficial applications. and they have potential for use in a number of other areas. This review will be rather eclectic. because the study of hydrates cuts across many sciences, from the basic physics and chemistry of hydrates to their involvement in biological systerns, in geological processes, in astronomy. and in climatology. They even have a place as a source of entertainment. The sources for much of the current information, especially regarding natural gas hydrates, are a number of books. reviews, and conference proceedings, to which the interested reader may refer.[1–15]

First, we will present a little history and basic science. Although gas hydrates have been known to scientists since the early nineteenth century, with the work of Davy (in 1811) and Faraday (in 1823) on chlorine hydrate, their true nature as clathrates was not demonstrated until the advent of x-ray crystallographic studies in the 1950s. Gas hydrates began to gain more attention when their potential for causing blockages in natural gas pipelines was first noted in 1933. Their existence as natural deposits in permafrost regions of the Earth was recognized in Siberia in 1965 and in Canada in 1974. Off-shore deposits were found with the advent of the Deep Sea Drilling Project, with the first indications of hydrate recorded around 1972 and the first samples recovered around 1983.

The detailed physical science of hydrates can be found in a number of reviews.[2,4–9] Three principal crystal structures are known: Structures I and II, which are cubic, and Structure H. which is hexagonal. All have small cages together with cages of increasing size (in the order I, II, H) that can accommodate larger guest molecules. They are nonstoichiometric, and their stabilities depend on the particular guest molecules and the pressure (P) and temperature (T) conditions. Stability models are based on the statistical thermodynamic description formulated by van der Waals and Platteeuw.[16] Many hydrates can exist above the melting point of ice, some up to 28°C under pressure. Because the guest does not have any chemical bonds to the host. it has considerable translational and rotational freedom within its cage. Resonant coupling between these guest motions and the low-frequency lattice vibrational modes results in a thermal conductivity for hydrates that is considerably lower than that in ice. Many different techniques have been applied to study hydrate compositions and physical properties. The most reliable methods for determining structure type are x-ray diffraction, solid-state nuclear magnetic resonance (NMR), and (to a lesser extent) Raman spectroscopy.

OCCURRENCE

Hydrates can and will occur wherever the components exist in sufficient concentrations and the conditions of temperature and pressure are right for stability of the hydrate relative to ice (or water) and the particular encaged gas molecules.

Natural Gas Hydrates on Earth

Naturally occurring hydrocarbon hydrates occur in permafrost regions, i.e., in the north of Canada. Alaska, and Russia (Siberia), in marine deposits on the continental margins (probably everywhere around the globe), and in the beds of smaller seas and large deep lakes (Black Sea, Caspian Sea. Sea of Okhotsk, Lake Baikal. Gulf of Mexico) (Fig. 1). The most widespread gas hydrates (permafrost and continental margins) appear to be largely of Structure I type. with methane as the principal component, though other gases that form clathrate hydrates are usually present in much smaller amounts, e.g., H_2S, CO_2, and some hydrocarbons. However, hydrates associated with major marine oil and gas deposits and seeps. as in the Gulf of Mexico. are more often of

Encyclopedia of Supramolecular Chemistry
DOI: 10.1081/E-ESMC 120012832

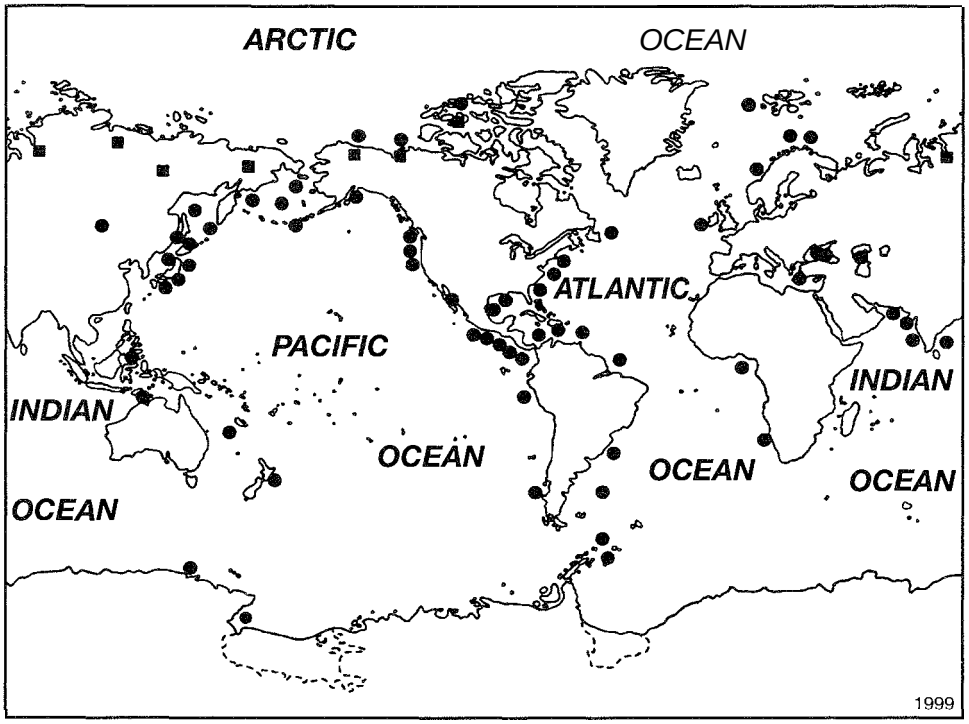

Fig. 1 Gas hydrate locations around the world. (Courtesy of K. Kvenvolden, U.S. Geological Survey. from Ref. [13], p. 18.)

Structure II *type because of the high content of the higher hydrocarbons' propane and butane. which are too large to form Structure* I. *There is even a suggestion that Structure* H *(first* discovered *in laboratory preparations in* 1987[17]) *may also occur naturally in the Gulf of Mexico* deposits:[18,19] Isopentane *is* found *to be excluded from the Structure* II *hydrate beds (this molecule is too large for Structure* II), *but it remains in quantity in the surrounding sediments. Thus. the coexistence of Structure* II *and Structure* H *at petroleum seep sites is postulated. and the* Structure HH *hybrid recently discovered in the lab* may *also be* relevant in *this* context.[20] *Structures* II *and* H *can contain the smaller gas molecules, including* CH_4, *in their small cages, and, in fact, Structure* H is *only known to exist* when *such* small *help gases are present. Double hydrates involving methane are quite likely to occur.*

"Massive" hydrate deposits outcropping on the sea floor have been found in the Gulf of Mexico and off the West coast of Canada. In *the latter* case, *geolo,gists were alerted to their existence when large frothing chunks were pulled* up *in a fishing net.*

On the continental *slopes, gas hydrates typically occur below* 500 *m water depth and within the upper* 700 *m of sediment. though they can go significantly deeper.* In *the permafrost regions. the zones can range between 100* m *(in places in Siberia) and as deep as* 2000 *m. The exact conditions of stability depend on the composition of the hydrate. The zones where they are found depend on the heat* flux *from* below *and the temperatures above.* Thus, *the bottom of* the *hydrate zone occurs where the temperature is just too high for stability at the local pressure (Fig. 2).* Large *quantities of gas can accumulate beneath the hydrate zone. There are also relict deposits, reflecting all earlier enlarged zone of hydrate stability, presumably still present because of self-preservation (a state in which hydrate particles develop a coat of ice that prevents further decomposition).*

Much effort is expended in making assessments of these geological occurrences; exploratory drilling often produces fizzing cores. and numerous other down-well sensor logging techniques are used. Besides these direct probe techniques, much use has been inade of seismic exploration. Bottom-simulating reflectors (BSRs) *are sound reflectors (they depend* on *a discontinuity in sediment density) that follow the contours of the sea floor, usually cutting through the bedding planes of the sediments* in *which they occur. The* BSR's *images are generally taken to indicate the presence of gas hydrates. and thus have been* very useful *in mapping potential hydrate areas. Follow-up drilling has confirmed the presence of hydrates in many instances, though* BSRs *are not an* 100% *reliable indicator.*

The origin of the gases that form the hydrates can be biogenic. involving the natural breakdown of organic detritus and bacterial action. or thermogenic, involving thermal fractionation of oil sediments. The latter usually generates the higher hydrocarbons and. thus, is *usually the*

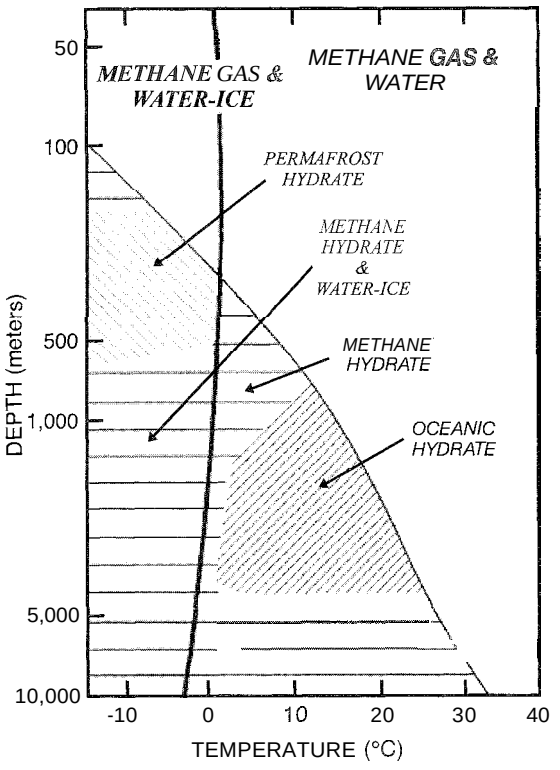

Fig. 2 Pressure (depth) versus ternperature stability diagram for methane hydrate. (From "Oceanic Gas Hydrate Research and Activities Review." U.S. Department of the Interior. Minerals Management Service. Gulf of Mexico OCS Region. OCS Report MMS 2000-017.)

source for Structure II *(or* H*) hydrate deposits. Carbon isotope analysis is* used *to distinguish between hydrocarbons of these different origins.*

Natural hydrates of air have been found in *ice cores obtained from the deep ice caps of Greenland and the Antarctic. Because the main guests are nitrogen and oxygen molecules. the* material *is of* Structure II *type, and considerable pressures and. hence. depths are required for their stability.* In *these environments. the temperatures are* low. -20 *to* $-28°C$, *for which* minimum *depths for air hydrates are* 800–700 m. respectively.[21] *These have been studied principally by microscopy,* Raman *spectroscopy, and powder x-ray diffraction.*

Artificial Hydrates

Laboratory production

There are a number of laboratories *around the world where hydrates are produced artificially for* study. *The* bulk *of our knowledge of the structures and properties of gas hydrates emerged from such synthetic materials.* Additionally, many *hydrates with* unusual *guest species that are unlikely to be* found *in nature have been* studied *in this* way. *Structural types. usually specific to one or two particular guest molecules, beyond the* major *Structures* I. *11. and H. have also been found. Recently.* a *Structure IT* H_2 *hydrate with multiple cage* occupancy[22] *and new hydrate forms of methane*[1] *''' were discovered by work* at *very high pressures. These high-pressure forms have relevance to* extraterrestrial *hydrates.*

In *laboratory prepared samples. if air* is *not excluded during the formation of the hydrate, then* O_2 *and* N_2 *can end up in the cages not occupied by* the *main guest. This shows up as extra electron density in x-ray diffraction single-crystal structural studies, and paramagnetic* O_2 *molecules cause relaxation effects and line-shape distortions in* NMR *spectra.*

Incidental production

Of *course, there are situations in which hydrates* can *form where they are not wanted, for instance, in gas and oil pipelines and in* tank *cars used for transporting liquid hydrocarbons. These will be discussed in more detail as* problem *areas.*

Extraterrestrial Gas Hydrates

It is thought to be highly *probable that gas hydrates exist elsewhere in the solar system and beyond, wherever the right conditions prevail,* e.g., *in the gaseous giant planets and on many of their* moons. *The crust of the Jovian satellite Europa* probably *contains clathrate hydrates in* abundance,[24] *and* it *was postulated that* CO_2 *hydrate exists* on *Mars.*

Much attention has recently been given *to the possibility of vast amounts of methane hydrate and high-pressure structural forms of methane hydrate existing on Titan, the largest* moon *of Saturn. Previously. it was thought that methane hydrate would phase separate into* methane *and ice at very high pressures, and that. consequently. Titan would have lost most of its methane.* However. *the discovery of the new high-pressure structures*[23] initiated *major revisions of* models *of the geology and* atmosphere *of Titan.*

Hydrates may also be involved in the outgassing from cornets. which are often described as dirty snowballs, as they warm during their *close approach to the sun.*

USES

Hydrocarbon and Energy Source

The natural *gas hydrates constitute a vast hydrocarbon and energy resource. Though the* numbers *are constantly* revised as exploration *and* measurements *of hydrate*

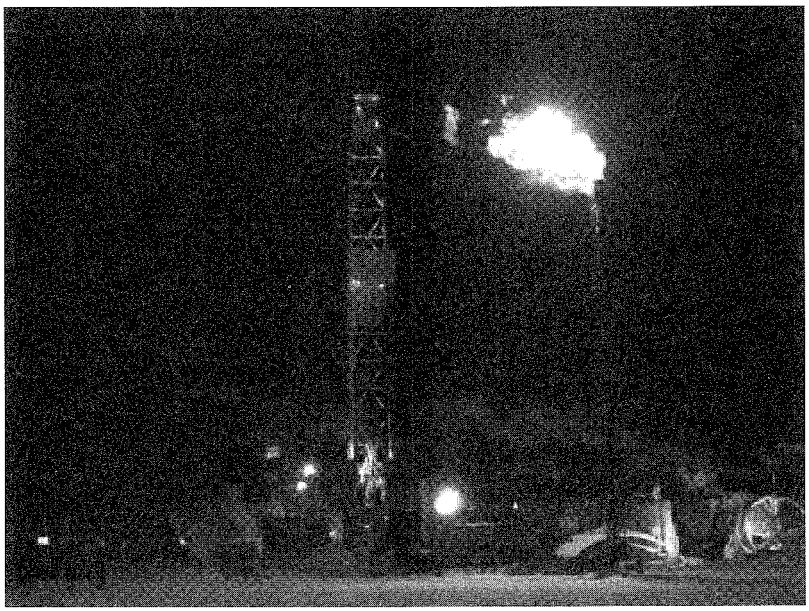

Fig. 3 Flaring of natural gas produced by thermal stimulation of gas hydrates at the Mallik 5L-38 production research well located in the Mackenzie Delta of Canada's Northwest Territories. (Photo provided courtesy of the Geological Survey of Canada from the Mallik 2002 field program.) *(View this art in color at www.dekker.com.)*

content in different deposits are made, there have been estimates suggesting that the world has 5.6×10^{18} m^3 of methane stored as hydrate, though more conservative current estimates suggest somewhere on the order of $1–50 \times 10^{15}$ m^3. On land, gas was obtained for years from hydrate beds in Messoyakha in Siberia, and gas was successfully generated and flared from hydrate buried under the permafrost at the exprimental well at Mallik in Canada in 2002 (Fig. 3). There was drilling into marine hydrate deposits in the Nankai trough off Japan in 1999–2000, and further drilling is planned to recover usable methane.

Gas Storage and Transport

Because a hydrate can contain, volume for volume, a large amount of gas, this is potentially a useful solid storage and transport medium, though it has to compete economically with liquefied gas. There is active research to find storage systems that will work at pressures less than 1 MP, involving "additives" to give double hydrates that are more stable.

CO_2 Sequestration

There has been considerable interest in the possibility of disposing of industrial CO_2 waste as hydrate in the deep ocean trenches. There have even been experiments conducted with liquid CO_2 on the ocean floor using submersibles to demonstrate the formation of hydrate from seawater. While this would remove a greenhouse gas, its disposal in this form raises other environmental concerns.

Gas Separation

Some gas mixtures can be separated by exploiting the different stability conditions for their hydrates, e.g., have been hydrofluorocarbons (HFCs) have been separated from nitrogen by forming the HFC hydrate that requires much less pressure than N_2 hydrate.

Desalination

This involves producing a hydrate from cold seawater (deeper ocean temperatures are close to 2–4°C around the world) and a guest that does not require much pressure for stability and then recovering and draining the saltwater. The hydrate can then be decomposed to obtain fresh water, and the hydrate former can be recycled.

Sludge Remediation

This can be effected by producing hydrates that remove excess water and thus concentrate the sludge.

Cold Energy Storage

Storage systems have been produced that make use of cheap off-peak electricity to produce hydrates. Then. at peak demand periods, the hydrate is used for air-conditioning.

Hydrogen Storage

The new high-pressure hydrogen hydrate[22] has been touted as a potential hydrogen storage medium, with implications for fuel cell applications and the "Hydrogen Economy," because it appears that it can be recovered at atmospheric pressures at liquid nitrogen temperature. With $4H_2$ in tne large cages and $2H_2$ in the small cages. a filled hydrate would have a substantial 4.97 wt% of hydrogen.

A Role in Anesthesia?

Hydrates enjoyed a period in the spotlight many years ago. when Pauling suggested chat they might have a mechanistic role in anesthesia. because many gases that cause anesthesia will also form clathrate hydrates. However, with our current knowledge of the stability conditions of these gases, it is not likely that such hydrates can exist in the body at normal body temperature and pressure. Nevertheless, this theory may have an element of truth, because clathrate hydrate-like structures involving other materials. such as amines, are stable at higher temperatures and normal pressures, or perhaps hybrid hydrate–organic structures could develop.

Hydrates and Biological Systems

It has been found over the last few years that there are marine ecosystems that depend on the existence of methane hydrates. There are certain methane-consuming archaea and bacteria associated with methane hydrate deposits in temperature and pressure regions where the hydrate is close to its decomposition threshold.[25–27] In one system studied, the archaea interact symbiotically with sulfate-reducing bacteria. with the net result that methane is oxidized and sulfate is reduced:

$$CH_4 + SO_4^{2-} \rightarrow HCO_3^- + HS^- + H_2O$$

The sulfide produced is then processed by communities of sulfide-based organisms also found around the hydrate deposits. All of these organisms, in turn. provide a food source for the aptly named "ice worms." a new species recently discovered apparently feeding on the surfaces of exposed massive gas hydrate outcrops on the sea floor[28] (Fig. 4).

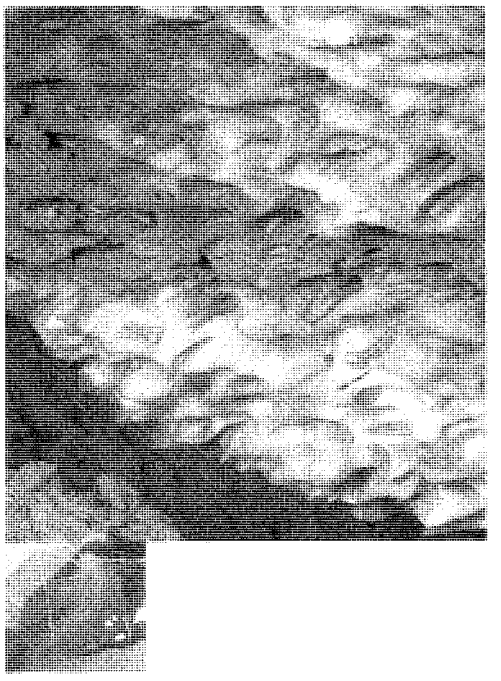

Fig. 4 "Ice worms'' in their natural habitat. The white ice-like material is gas hydrate. (From Ref. [28] and Fisher, C., Penn. State Eberly College of Science. Web site: www.science.psu.edu/iceworms/iceworms.html.) (Inset) Detailed view of an ice worm. (From MacDonald, I.R.; Joye. S.. Quarterdeck 1997. 5(3), TAMU. Department of Oceanography. Web site: www-ocean.tamu.edu/Quarterdeck/QD5.3/macdonald.html.) (*View this art in color at www.dekker.com.*)

It has been inferred that the waters of Lake Vostok and numerous other subglacial Antarctic lakes contain oxygen sufficient to support life in an unique ecosystem. at 350 atm and −3°C. in permanent darkness. Though the lake water has not been sampled for fear of introducing bacteria from above. oxygen is found in the refrozen lake water just above the lake. The oxygen comes from the decomposition of air hydrates present in the ice overburden.[29]

As a Source of Entertainment

There has been recurring media interest in gas hydrates ever since it was postulated by McIvor that they might be the cause of mysterious events in the Bermuda Triangle.[30] The notion is that ships might sink from loss of buoyancy, and aircraft could stall from lack of oxygen, due to large-volume gas release when a hydrate cap cracks or slides and the gas reservoir below bursts to the surface. While it is probably safe to say that this suggestion regarding the folklore of the Triangle now has little

credence in the scientific community, especially since the discovery of deposits all around the globe. the science regarding disturbances of hydrate deposits has relevance in the context of hydrate "problems.' discussed later.

Gas hydrates were used inadvertently as a plot theme in the movie "Total Recall," (starring O_2 hydrate). Set on Mars at a mining colony, it transpires that the whole interior of Mars is "ice." and that 0.5 M years ago, an alien race constructed machinery in huge underground caverns, which when set in motion sends huge heaters plunging into the "ice," which melts, generating vast amounts of water vapor and oxygen and creating a breathable atmosphere on Mars. From a scientific viewpoint, the implication is that the atmosphere was stored or trapped as air hydrate, and hence, it must have been of Structure II type.

Submarine hydrates feature prominently in the recent novel "Fire Ice'' (by Clive Cussler with Paul Kemprecos). in which a scheme is developed by a megalomaniac Russian tycoon to explode methane hydrate deposits off the East coast of the United States, creating destructive tidal waves.

The "burning snowball" is an often-repeated pyrotechnic demonstration (Fig. 5). Methane hydrate is allowed to warm to the point where the surface begins to decompose. and the evolved methane can be ignited (methane hydrate requires 26 atmospheres pressure of methane at 273 K to keep it stable). The burning snowball is self-sustaining until all the hydrate decomposes and the methane is consumed.

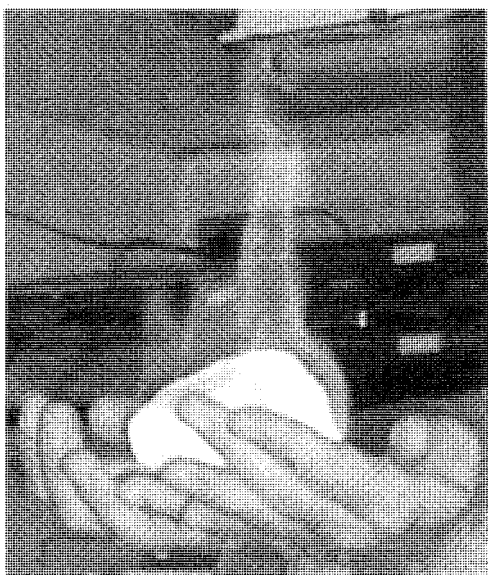

Fig. 5 The "burning snowball." Methane hydrate decomposing to gas, which is burning, and water. (Photo courtesy of the GEOMAR Research Center, Kiel. Germany.) *(View* this *art in* color *at www.dekker.com.)*

PROBLEMS

Pipeline Blockages

In the oil and gas industry. the occurrence and deterrence of gas hydrate plugs in pipelines has a tremendous cost. for example, on one occasion, the gas supply to all major users in Melbourne was shut down for 3 days because of a hydrate plug in a 30-inch pipeline. It is estimated that roughly $1 billion USD is spent annually to prevent and remove hydrate plugs. Consequently, there is great interest in both the formation and inhibition of gas hydrates. Water can be removed where possible, but from subaquatic sources especially, this is not feasible. Instead, large quantities of chemical additives are used, such as methanol or ethylene glycol, which act as thermodynamic inhibitors, shifting the stability conditions. Kinetic inhibitors, such as poly(*N*-vinylpyrrolidone), delay nucleation and slow the growth of hydrates. Quaternary ion salts can act as emulsifiers and antiagglornerants; any hydrates that form remain as small particles that are carried away in the flow. When plugs occur, attempts to unblock by releasing pressure on one side of the plug can be hazardous, because the plug tends to decompose from the outside in. Then, when it releases from the sides of the pipe. the high pressure on the other side turns the hydrate slug into a high-velocity projectile, until it meets a restriction or turn in the pipeline, with predictably disastrous consequences; i.e.. failure and rupture of the pipeline at the point of impact. Consequently, it is recommended that the pressure be released on both sides of the plug.

Methane Hydrate and the Global Environment

As a greenhouse gas. CH_4 is more than 10 times worse than CO_2, and as such. may be an important factor in climate change.[31] Concerns have been raised that its rapid release from hydrates due to increased global temperatures may exacerbate the greenhouse problem. causing runaway warming. It has been suggested that CH_4 released from gas fields and hydrate deposits caused two sudden strong warming pulses at the end of the last glaciation episode. Hydrates have also been associated with other prehistoric sudden warming episodes in the Jurassic (183 million years ago) and the Late Palaeocene (55.5 million years ago) periods.[32,33] But, at the same time, hydrate plays a role in the global carbon cycle, acting like a great carbon–methane capacitor (a source or a sink).

Marine Geohazard

There is a great deal of geological evidence linking hydrate destabilization with massive submarine slides and slumps. Such slides can run large distances. and the huge masses displaced create destructive tsunamis.[10,13,30,34]

Drilling and Construction Hazards

Drilling and production through hydrate formations above oil and gas reservoirs can cause dissociation and well blowouts. Similarly, the possible instability of the sea floor sediments over hydrate deposits where oil and gas is extracted raises concerns over the collapse and loss of engineering structures.

Tanker Car Explosions in Cold Climates

Though there do not seem to be any generally available technical reports. there are genuine stories of explosions and burn accidents caused by the inadvertent formation and subsequent decomposition of hydrates of hydrocarbons in railway tank cars in the cold climate of Canada. Incidents occurred due to the practice of washing ''empty'' tank carr following their use for transporting liquid hydrocarbons. In a cold winter climate, it is possible to form hydrates with small amounts of hydrocarbon residues. which later decompose when the tank car warms up, e.g., when exposed to sunshine. For example, the clathrate hydrate of isobutene (2-methyl-propene, b.p. $-6.9^{\circ}C$) needs only 1.12 bar at 273 K to be stable. Precautions were not taken around such nominally "clean and empty" tankers, and exposure to sparks or naked flames led to flash fires and explosions. While the main content of the tankers was butane, other hydrocarbons were present. In another kind of industrial accident, a worker was killed by H_2S gas liberated from H_2S hydrate residue in a heavy water production plant. during a shutdown for maintenance.

Problems in the Sense of Insufficient Knowledge

Prediction

The phase stability diagrams for natural source hydrates can become very complicated. especially when there are several guest components. This poses a major problem when assessing the quantity of gas, stability zones, structural types, etc. Also, the delicate physical balances determining structural types means that very small changes in the relative amount of a third component may trigger a structural transformation.

Exploitation

The exploitation of gas from natural hydrates poses many problems in terms of the technology needed to mine or extract them, environmental impact. and economics. One noble idea is to replace CH_4 with CO_2, and although lab experiments show that the physical exchange is possible, whether it can be done in situ in natural hydrate beds is another question.

Hydrate formation

The mechanisms of hydrate formation are still somewhat of a mystery. as neither component is soluble enough in the other to convert bulk material completely.

CONCLUSION

Clathrate hydrates are seen to be widespread in Nature wherever the stability conditions are met, occurring in vast. hidden quantities. It is surprising that these materials with such far-reaching potential and consequences for mankind have received so little attention beyond the oil and gas industries and the scientific community. But that must surely change in the coming decade and as conventional hydrocarbon sources decline. In closing. let us not forget that the amazing universe of clathrate hydrates and associated systems ultimately depends on one of the pillars of supramolecular chemistry. namely. the hydrogen bond, which in this case provides the glue for the assembly of clathrate hydrate frameworks.

ARTICLES OF FURTHER INTEREST

Classical Descriptions of Inclusion Compounds, p. 253
Clathrate Hydrates, p. *274*
Crystal Growth Mechanisms, p. 364
Hydrogen Bonding, p. 658
Hydrophobic Effects, p. 673
Inclusion Compounds: Selectivity, Thermal Stability, and Kinetics, p. *696*
Isostructurality of Inclusion Compounds, p. 767
Neutron Diffraction, p. *959*
Solid-State Nuclear Magnetic Resonance Spectroscopy, p. 1307
Space Groups and Crystal Packing Modes, p. 1337
van der Waals Forces, p. *1550*
X-Ray Crystallography, p. 1586
X-Ray and Neutron Powder Diffraction, p. *1592*

REFERENCES

1. *Natural Gas Hydrates:* Proper-ties, *Occurrence and* Recovery: Cox. J.L.. Ed.: Butterworth Pubs.: Boston. 1983.
2. Sloan, E.D.. Jr. *Clathrate Hydrates* of *Natural Gases,* 2nd Ed.: Marcel Dekker: New York. 1998.
3. Makogan, Y.F. *Hydrates of Hydrocarbons;* PennWell Publishing Co.: Tulsa. OK. 1997.
4. Davidson, D.W. Clathrate Hydrates. In *Water.* A *Comprehensive Treatise;* Frank. F.. Ed.: Plenum: New York. 1973; Vol. 2. 115–234. Chp. 3.
5. Davidson. D.W.: Ripmeester. J.A. NMR. NQR and Dielectric Properties of Clathrates. In *Inclusion Compounds, Vol.* 3; Atwood, J.L.. Davies. J.E.D., MacNicol. D.D.. Eds.: Academic Press: London. 1984: Vol. 3. 69–128.
6. Ripmeester, J.A.: Ratcliffe. C.I. Solid State NMR Studies of Inclusion Compounds. In *Inclusion Compounds, Vol.* 5; Atwood, J.L., Davies. J.E.D.. MacNicol. D.D.. Eds.: Oxford Univ. Press: Oxford. 1991; Vol. 5. 37–89.
7. Ripmeester, J.A.: Ratcliffe. C.I. Solid-State NMR Spectroscopy: Applications to Supramolecular Chemistry. In *Comprehensive Supramolecular Chemistry, Vol.* 8: Atwood, J.L.. Davies. J.E.D.. MacNicol. D.D.. Vogtle, F., Lehn, J.-M., Eds.: Pergamon: New York. 1996: Vol. 8. 323–380.
8. Jeffrey. G.A. Hydrate Inclusion Compounds. In *Comprehensive Supramolecular* Chemistry, *Vol.* 6; MacNicol. D.D.. Toda. F., Bishop. R., Eds.: Pergamon. 1966: Vol. 6. 757–788.
9. Dyadin, Y.A.: Belosludov. V.R. Stoichiometry and Thermodynamics of Clathrate Hydrates. In *Comprehensive Supramolecular Chemistry,* Vol. *6;* MacNicol. D.D.. Toda, F., Bishop, R.. Eds.: Pergamon. 1966; Vol. 6. 789–824.
10. *International Conference on Natural* Gas *Hydrates;* Sloan, E.D.. Jr.. Happel, J.. Hnatow. M.A., Eds.: Ann. N. Y. Acad. Sci.. 1994; Vol. 715.
11. Proc. 2nd International conference on Natural Gas Hydrates. Toulouse, 1996.
12. Proc. Int. Symp. on Methane Hydrates: Resources in the Near Future'? National Oil Corporation: Chiba, Japan. 1998.
13. Gas Hydrates: Challenges for the Future. In Proc. *Third Int. Conf. on Gas Hydrates;* Holder, G.D.. Bishnoi, P.R.. Eds.: Ann. N. Y. Acad. Sci.. 2000: Vol. 912.
14. Proc. Fourth International Conference on Gas Hydrates. Yokohama. 2002: Vol. 1 and 2.
15. Scientific *Results from JAPEX/JNOC/GSC Mallik 2L-38* Gns *Hydrate Research Well:* Dallimore. S.R., Uchida. T., Collett, T.S.. Eds.; Bulletin. Geological Survey of Canada. 1999: Vol. 544.
16. Van der Waals, J.H.: Platteeuw. J.C. Clathrate solutions. Adv. Chem. Phys. **1959**. *2.* 1–57.
17. Ripmeester. J.A.: Tse. J.S.; Ratcliffe. C.I.; Powell, B.M. A new clatlirate hydrate structure. Nature **1987**. *325.* 135–136.
18. Sassen, R.: MacDonald. I.R. Evidence of Structure H hydrate, Gulf of Mexico continental slope. Org. Geochem. **1994**. *22.* 1029–1032.
19. Sassen, R.: Sweet, S.T.: DeFreitas. D.A.: Milkov. A.V. Exclusion of 2-methylbutane (isopentane) during crystallization of Structure II gas hydrate in sea-floor sediment. Gulf of Mexico. Org. Geochem. 2000. *31.* 1257–1262.
20. Udachin. *K.A.:* Ripmeester, J.A. A complex clathrate hydrate structure showing bimodal guest hydration. Nature **1999**, *397.* 420–423.
21. Nakahara, J.: Shigesato. Y.: Higashi, A.; Hondoh. T.; Langway. C.C.. Jr. Raman spectra of natural clathrates in deep ice cores. Philos. Magn., B 1988. *3.* 421–430.
22. Mao, W.L.; Mao. H.-K.; Goncharov. A.F.; Struahkin. V.V.: Guo, Q.; Hu, J.: Shu, J.: Hemley, R.J.: Somayazulu. M.: Zhao. Y. Hydrogen clusters in clathrate hydrate. Science **2002**, *297.* 2247–2249.
23. Loveday, J.S.: Nelmes. R.J.: Guthrie. M.; Belmonte. S.A.: Allan, D.R.; Klug, D.D.: Tse. J.S.: Handa, U.P. Stable methane hydrate above 2 GPa and the source of Titan's atmospheric methane. Nature **2001**. *410.* 661–663.
24. Kargel, J.S.; Kaye, J.Z.; Head, J.W.. III; Marion. G.M.: Sassen. R.: Crowley. J.K.; Ballesteros. O.P.: Grant, S.A.: Hogenboom, D.L. Europa's crust and ocean: Origin, composition. and the prospects for life. Icarus 2000. 148. 226–265.
25. Hinrichs. K.-U.; Hayes. J.M.; Sylva, S.P.; Brewer. P.G.: DeLong, E.F. Methane-consuming archaebacteria in marine sediments. Nature 1999. *398.* 802–805.
26. Boetius, A.: Ravenschlag. K.; Schubert, C.J.; Ricltert, D.; Widdel, F.: Gieseke. A.; Amann. R.; Jorgensen, B.B.: Witte, U.; Pfannkuche. O. A marine consortium apparently mediating anaerobic oxidation of methane. Nature 2000. *407.* 623–626.
27. Lanoil, B.D.; Sassen, R.: La Duc. M.T.: Sweet. S.T.; Nealson, K.H. Bacteria and archaea physically associated with Gulf of Mexico gas hydrates. Appl. Environ. Microbiol. **2001**. *67.* 5143–5153.
28. Fisher; C.R.: MacDonald. I.R.: Sassen. R.; Young, C.M.; Macko. S.A.: Hourdez. S.: Carney. R.S.: Joye. S.; McMullin, E. Methane ice worms: *Hesiocaeca methanicola* colonizing fossil fuel reserves. Naturwissenschaften 2000. *87,* 184–187.
29. Siegert. M.J.; Ellis-Evans. J.C.: Tranter, M.; Mayer. C.; Petit. J.-R.: Salamatin. A.: Priscu. J.C. Physical. chemical and biological processes in Lake Vostok and other antarctic subglacial lakes. Nature 2001. *414.* 603–609.
30. McIvor, R.D. Role of naturally occun-ing gas hydrates in sediment transport. Am. Assoc. Petrol. Geol. Bull. **1982**. 66. 789.
31. Nisbet. E. Climate change and methane. Nature 1990, *347.* 23.
32. Katz. M.E.: Pak. D.K.: Dickens, G.R.: Miller. M.G. The source and fate of massive carbon input during the latest paleocene thermal maximum. Science 1999. 286. 1531–1533.
33. Hesselbo. S.P.; Grocke. D.R.: Jenkyns, H.C.; Bjerru, C.J.; Farrimond. P.: Morgans Bell, H.S.; Green, O.R. Massive dissociation of gas hydrate during a jurassic oceanic anoxic event. Nature **2000**. 406. 392–395.
34. Nisbet. E.G.: Piper. D.J.W. Giant submarine landslides: Slumps, megaturbidities and their impact. Nature 1998. *392.* 329–330.

Clathrate Inclusion Compounds, Phase Transitions in

C

Takasuke Matsuo
Osaka University, Osaka, Japan

INTRODUCTION

Interaction between guest molecules is a weak secondary energy compared with the primary host–guest interaction, and it contributes a small additional stabilization to the formation of the supramolecular system. However, in some inclusion compounds. the anisotropic part of the guest–guest interation plays a decisive role in determining their structures and properties, especially the temperature dependence of these characteristics. This occurs in disordered clathrate crystals for which the entropy is the important thermodynamic parameter underlying the occurrence of phase transitions. In this article. we discuss phase transitions arising from the guest–guest interactions in inclusion coinpounds based on urea, thiourea. and hydroquinone hosts and in clathrate hydrates and several other supramolecular systems from the structural and thermodynamic point of view.

PHASE TRANSITIONS

Phase transition is a general term meaning change of the physical state of matter. It includes melting. vaporization, sublimation, and the changes opposite these. In solid state and condensed matter. appearance and disappearance of ferromagnetistn. ferroelectricity, superconductivity. superfluidity, and liquid crystalline phases are among the important phase transitions. Phase transitions in clathrate inclusion compounds are structural phase transitions. The term "structural" means that the crystal structure (rather than the electronic states or spin states) changes in the transition.

The symmetry of the crystal changes as it undergoes a phase transition. Here, the symmetry is that of the distribution of atoms and molecules in the crystals. For an ordered crystal, it is simply the symmetry of the periodic structure; whereas. for a disordered crystal. it is the symmetry of the positions of the atoms and molecules averaged over space and time. Thus, the symmetry is that of the distribution functions of the atoms and molecules in the crystal. It is generally believed that two phases separated by a phase boundary in a phase diagram have different symmetries[1] (such as characterized by the presence or lack of an inversion symmetry). even if their actual space group symmetries are not known or have not been studied. A notable exception of this general statement is the vaporization: the liquid and the vapor of a substance have the same uniform distribution of molecules in the two phases. Also, there are several exceptional phase transitions. known as isomorphous transitions, where the symmetries of the distribution of the molecules in the two phases involved are the same, but the degree of the order of the atomic positions changes discontinuously.

The discussion based on symmetry becomes less clear when we consider modulated and incommensurate phases. In some crystals (notably thiourea), the crystal structure does not repeat Itself precisely with the periodicity of an ordinary crystal lattice but is modulated with a longer periodicity of several unit cells. The periodicity is, in general, not an integral multiple of the original lattice. Hence, the modulated structure is incommensurate with the basic structure. The symmetry of such a crystal cannot be described by one of the 230 space groups. although the space group representation theory copes with modulated structures and phase transitions involving them. Incommensurate phases can be identified by single-crystal diffraction experiments and are relevant to phase transitions in clathrate crystals.

Another important characteristic of a phase transition is the occurrence of discontinuities or singularities in the thermodynainic properties as functions of temperature, pressure. and other parameters. In the Ehrenfest classification,['.''] a phase transition is of the nth order if the free energy of the substance changes in such a manner that its nth derivative with respect to an independent variable (e.g., the temperature) is discontinuous at the transition point. Thus, a phase transition is of the first order if it is accompanied by a latent heat, because the entropy, one of the first derivatives of the free energy. is discontinuous at the transition point. This classification forms the basis of the Ehrenfest relations connecting the slope of the phase boundaries with the magnitude of the discontinuities in thermodynamic quantities.[2,3] However, the Ehrenfest classification is not general enough to cover all types of phase transitions. Important classes of phase transitions in which various the modynamic derivatives, such as the heat capacity. diverge to infinity are not included. The singularites in such cases are dealt with by the Pippard

Encyclopedia of Supramolecular Chemistry
DOI: 10.1081/E-ESMC 120012841

relation in thermodynamics and by critical exponent formulations in statistical mechanics.[2,3]

There are two major types of structural phase transitions: order–disorder and displacive.[2,3] An order–disorder phase transition is characterized by disorder of the atoms or molecules in the structure of one of the phases. Sometimes both phases are disordered in different degrees. The disordered (or more disordered) phase is more symmetric. because disorder makes the average distribution of atoms more even. Most of the phase transitions in clathrate crystals are of this type.

In a displacive phase transition. the positions of atoms are ordered in both phases. but the position changes from a less symmetric site to a more symmetric one as the crystal undergoes the phase transition. Order–disorder transitions are distinguished from displacive transitions by, among other properties, a large entropy of phase transition. dielectric dispersion at low frequencies. and directly, by crystal structure revealing two or more sites fractionally occupied by the same atom.

Phase transitions are often accompanied by changes in the mobility of molecules. Nuclear magnetic resonance (NMR) is a sensitive technique used to detect the occurrence of phase transitions and to determine the type, magnitude, and timescale of the molecular motion involved in the phase transition. Neutron scattering also gives quantitative knowledge about the molecular motion involved in phase transitions. On account of the large scattering power of protons to a neutron beam. this is especially useful if the substance being studied contains hydrogen. a condition readily met in organic clathrate compounds.

Phase transitions in clathrate inclusion compounds are of interest in the general viewpoint of phase transition study because of the structural peculiarity of inclusion compounds that distinguishes them from ordinary molecular crystals. Phase transitions occur in clathrate inclusion compounds as a result of interactions between the guest molecules. (Clathrate hydrates are exceptional in that the host lattice is also disordered.) Host–guest interaction is not sufficient for the occurrence of a phase transition. however strong it may be. Thus. occurrence of a phase transition shows that there are strong enough interactions between the second nearest pair of molecules in the crystal. The first neighbor interaction is, of course, the host–guest interaction. The guest–guest interaction thus deduced from the phase transition also contributes to the stability of the clathrate crystal to some extent.

UREA AND THIOUREA INCLUSION COMPOUNDS

Long-chain hydrocarbons such as decane. dodecane, hexadecane, and eicosane form channel-type inclusion coinpounds with urea. Low-temperature calorimetry on these compounds reported in 1965[4] appears to be the first work that introduced inclusion compounds into the study of phase transitions. The hexagonal space group $P6_122$ requires that the guest molecules in the all-*trans* conformation be disordered, with their molecular planes lying in one of the three equivalent orientations. The phase transitions occur at temperatures between 100–200 K. depending on the chain length of the guest molecules. For the urea–hexadecane inclusion compound. the low-temperature phase stable below 150 K is orthorhombic, belonging to the space group $P2_12_12_1$. The transition entropies are consistent with the threefold disorder of the molecular plane in the hexagonal phase and its ordering in the orthorhombic structure at low temperature.[4] Because the length of the hydrocarbon chain is not always an integral multiple of the repeating unit of the host lattice; the structure may be incommensurate.[5,6] This complicates the structure analysis. For smaller guest molecules such as trioxane, the stoichiometry $(urea)_3G$ suggests a commensurate structure.[7] These stoichiometric inclusion compounds also undergo phase transitions. Deuteron magnetic resonance gives detailed knowledge about the reorientation of the guest molecules in the high-temperature phase. Undecane-1,11-dicarboxylic acid and dodecane-1,12-dicarboxylic acid form similar inclusion compounds with urea. They also undergo phase transitions at low temperatures arising from the order–disorder mechanism.[8]

Thiourea forms channel-type inclusion compounds with globular molecules.[9] This is partly because the space group $R\bar{3}c$ lacks a screw axis that the space group of the urea inclusion compounds $P6_122$ possesses. The larger diameter of the channel than in the urea compounds accommodates cyclohexane and monosubstituted cyclohexane as well as carbon tetrachloride and hexachloroethane in the channel. With these more or less spherical molecules as the guest species. thiourea inclusion compounds are rich in their polymorphism. most undergoing two or more phase transitions below room temperature.

The thiourea–cyclohexane inclusion compound undergoes phase transition at 127 K and 148 K.[10] The reorientational motion of the guest molecule approaches the spherical rotation at a higher temperature. with discontinuous increase of its rate at these temperatures. as detected by deuteron magnetic resonance.[10] Neutron scattering was used to study the molecular motion in space and time, simultaneously giving detailed knowledge of geometry and time rate of the reorientation.[11]

The thiourea–CCl_4 compound shows that a rigid molecule can also form an inclusion compound with thiourea.[9,12] It undergoes phase transitions of an order–disorder type. as the entropy change and the crystal structure suggest.[13,14] The $CBrCl_3$ forms a similar

compound with thiourea. The heat capacity reproduced in Fig. 1 shows the two thermal anomalies due to first-order (84 K) and second-order (92 K) phase transitions. The former is characterized by a Δ-function peak, whereas the latter is characterized by a discontinuous decrease of the heat capacity, exemplifying the first two cases of the Ehrenfest classification of phase transitions.[2,3] Interestingly, the orientational disorder corresponding to the exchange of Br and Cl atoms persists in the low-temperature phase and ultimately becomes frozen in a glass transition at 20 K (see the reference given in the caption of Fig. 1). Persistence of the residual disorder down to 4 K was also deduced from nuclear quadrupole resonance of the Cl nuclei. The high sensitivity of this technique contributed to detection and quantification of the critical properties of the phase transition in the CCl_4–clathrate compound.[15,16] This was achieved by studying the temperature dependence of the electric field gradient at the nitrogen nucleus in the host molecule, arising from disordering of the guest species.

A recent development in this area is the finding of an incommensurate structure in the thiourea–C_2C_6 compound,[17] a contribution from clathrate research to the general solid-state physics of incommensurate crystals. The stoichiometry of this compound is 2.95:1. The slight deviation from the ideal ratio 3:1 arises from discommensuration over several unit cells, where the location of the guest molecules does not mesh with the host structure, alternating with nearly commensurate regions persisting over several tens of the unit cells. The compound is disordered above 96 K, where a phase transition occurs, accompanied by an entropy change of 6.57 $JK^{-1}mol^{-1}$.[18] The soliton, another name of discommensuration, becomes less mobile at low temperature and finally freezes into a glassy state at 59 K.[18,19]

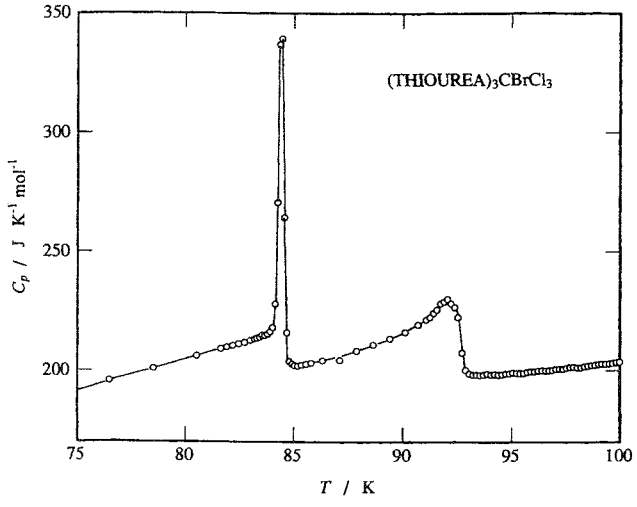

Fig. 1 The heat capacity of $(thiourea)_3CBrCl_3$ in the temperature range of the phase transitions. [From T. Matsuo and O. Yamamuro, *Supramolec. Chem.*, **6** (1995) 103.]

In the thiourea 1,1,2,2-tetrachloroethane compound, phase transitions occur at 224 K and 248 K with much larger transition entropies (28.1 and 11.3 $J K^{-1} mol^{-1}$[20]). This is related to the lower symmetry of the guest molecule than C_2Cl_6, giving a larger number of equivalent and distinguishable orientations of the guest molecule in the high-temperature phase. The ordered structure was not studied.

HYDROQUINONE–CLATHRATE COMPOUNDS

In hydroquinone–clathrate compounds, the host molecules form nearly spherical cavities in which small guest molecules reside. This structure, determined by x-ray diffraction in 1947 and the first recognized as such, was the starting point of clathrate research.[21] The phase transition in $(hydroquinone)_3MeOH$ was found in 1967 by heat capacity measurement at low temperature.[22] The entropy of transition (comparable with the molar gas constant for a mole of the guest molecule) suggested an order–disorder mechanism. The Debye-type dielectric loss (occurring above the transition temperature 67 K) is an important characteristic of an order–disorder mechanism involving motion of a polar molecule. Other hydroquinone clathrate compounds formed by small polar molecules also undergo phase transitions. Polarity of the guest molecule is necessary for a phase transition to take place in hydroquinone–clathrate compounds, because the mutually orienting interactions essential for an ordering phase transition are possible only with long-range electrostatic forces. In fact, the temperatures of the phase transitions of hydroquinone clathrate compounds correlate well with the square of the dipole moment of the guest molecule, as shown in Fig. 2. The figure includes recent data (on HCl and CH_3CN) added to the original plot on H_2S, CH_3OH, and HCN. The slope of this correlation line T_{trs} versus μ^2, related to the dipole lattice sum and electrostatic shielding factor of the host lattice, is also of the correct magnitude. However, actual ordering patterns are complicated, as shown by x-ray diffraction[23] and NMR[24] for the methanol clathrate. Macroscopic measurements (dielectric constant and spontaneous polarization) and vibrational spectroscopy are also useful for this purpose. Energy calculation, molecular dynamics, and comprehensive statistical mechanical calculations were performed with an important result about the stabilization of nonstoichiometric clathrates.[25]

The transition temperatures 7–15 K of hydroquinone–clathrate compounds containing very small polar molecules (HCl and H_2S) are comparable with the separation

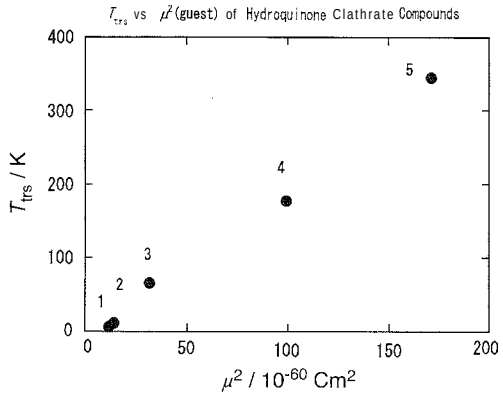

Fig. 2 Transition temperatures of hydroquinone clathrate compounds plotted against the electric dipole moment of the guest molecule: 1: H_2S, 2: HCl, 3: MeOH, 4: HCN, and 5: CH_3CN. [The original plot from T. Matsuo and H. Suga, **J.** *Inclus. Phenom.*, *2* (1984) 49, was extended with recent experimental data from Refs. [26] and [29].]

between the rotational energy levels of the guest species in the gaseous state. Far infrared absorption and neutron scattering showed the unusually high rotational mobility of these guest molecules at very low temperatures.[26] Quantum mechanical effects may be important in these compounds. as discussed in a quantum version of the mean field theory.[27]

The nonstoichiometric property of this compound presents a new type of cooperative behavior of the guest molecules. At lower concentrations of the guest MeOH, the transition temperature is lower. because the effective ordering energy is smaller. However, the reorientation rate of the guest molecule in the cavity decreases faster than the ordering temperature. This results in strong short-range correlation of the guest orientation. while the crystal remains in the high-temperature phase. Eventually. this leads to the freezing of the guest orientation in a spin-glass-like state.[28]

CLATHRATE–HYDRATE CRYSTALS

The guest molecules in clathrate hydrates are confined in nearly spherical cavities. The symmetry of the cavities is high, most having fourfold. threefold, inversion, or other symmetry elements and their combinations.[29] Therefore, the guest molecules of low symmetry (e.g., polar molecules) have several equivalent orientations in the cavity and, hence, are disordered. The disorder persists to 4.2 K, as dielectric and NMR measurements show for, e.g., dimethyl ether in a Structure II hydrate.[29] A phase transition to ail ordered phase may be expected to occur. as we saw in hydroquinone compounds discussed above. In fact, in trimethylene oxide hydrate; the ordering of orientation of the guest occurs in a phase transition at 105 K.[30] In other clathrate hydrates, it appears that the guest molecules remain disordered, even at low enough temperatures where the ordering is expected to take place from the thermodynamic point of view. Interestingly, the guest molecules reorient themselves fast. even at the lowest temperature (4 K) examined. Slow kinetics is thus excluded as the reason for the absence of ordering.

It was pointed out that the ordering is inhibited by the random electric field due to the disorder in the host lattice. The host lattice formed by tetrahedraily hydrogen-bonded water molecules has the same local structure as in ice *Ih* and has the same disorder as to the position of hydrogen atoms. Ice *Ih* becomes ordered below 72 K when doped with KOH (see the reference cited in the caption of Fig. 3). The dopant is effective even at concentrations less than 0.1 mole %. Clathrate hydrates undergo similar ordering transitions under the action of doped KOH. In Fig. 3, the heat capacities of tetrahydrofuran (THF) hydrate samples (pure and KOH-doped) are shown. Pure THF hydrate undergoes a glass transition at 85 K, and doped THF hydrate undergoes a phase transition at 61.9 K. The transition entropy includes contributions from the host lattice

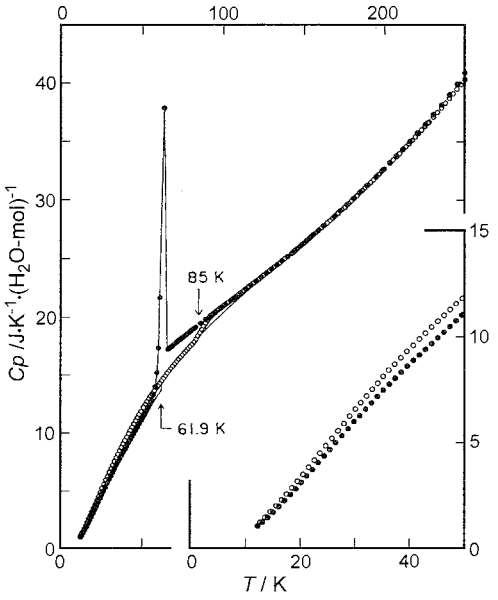

Fig. **3** The heat capacity curves of tetrahydrofuran clathrate hydrate (open circles) and tetrahydrofuran clathrate hydrate doped with KOH (mole fraction 1.8×10^{-4}, filled circles). showing the glass transition at 85 K for the former and phase transition at 61.9 K for the latter. [From O. Yamamuro, M. Oguni. T. Matsuo and H. Suga, **J.** *Phys. Chem. Solids.* 49 (1988) 425. See also O. Yamamuro and H. Suga, **J.** *Thermal Analysis, 35* (1989) *2025.1*

and guest molecules. The dielectric permittivity showed that the guest inolecules are disordered above 61.9 K and are ordered below. Other clathrate hydrates behave in a similar way. undergoing phase transitions when doped with KOH. For these, see the references given in Fig. 3.

OTHER CLATHRATE INCLUSION COMPOUNDS UNDERGOING PHASE TRANSITIONS

Phase transitions were reported in other clathrate systems. Although these were not studied systematically, they are important as indications of generality of phase transitions in supramolecular systems. Some are of interest because of the transition mechanism. others are of interest for molecular recognition involving cooperative effects, and still others are for potential use in practical applications.

In the toluene clathrate of *t*-butylcalix[4]arene, disorder of the molecules is suspected from the crystal structure. The NMR nieasurements showed that the spectrum changes at 248 K.[30,31] The more complicated spectrum recorded at a lower temperature is evidence for ordering of the host and guest molecules. Disorder of the guest molecule appears to also be involved in the phase transitions of the Werner clathrate compound containing p-xylene, studied by low-temperature calorimetry. Removal of xylene from the crystal does not destroy the crystal, but the peaks (at 45 K and 75 K) in the heat capacity curve disappear.[32] They are most likely ordering transitions arising from the guest molecules: though there were no structural studies of this compound at low temperatures.

β-Cyclodextrin undecahydrate undergoes a first-order transition at 226 K. accompanied by an entropy change of 45 $JK^{-1}mol^{-1}$.[33] The large transition entropy is related to disorder of the water molecules in the channel of cyclodextrin. Disorder of the water molecules is also involved in a clathrate-like hydrate crystal $[H_{31}O_{14}][CdCu_2(CN)_7]$ studied by calorimetry and dielectric measurement.[34]

CONCLUSION

The most interesting aspect of phase transitions in clathrate compounds is probably the cooperativity among the guest molecules that underlies their ordering. This arises from guest–guest interactions that are weak secondary interactions. usually disregarded in comparison with host–guest interactions. Despite the weak energy involved, guest–guest interactions can generate long-range cooperative effects that determine even macroscopic properties and the symmetry of the compound. Various clathrate systems undergoing phase transitions have so far been studied mostly for the purely theoretical purpose of understanding the basic mechanism of cooperativity. Clathrate systems will continue to provide actual cheinical compounds in which we will be given new aspects of cooperativity. They will include equilibrium as well as time-dependent cooperative phenomena. Nonstoichiometry, an original defining property of a clathrate compound[21] (but not stressed in recent years), offers the possibility of uniformly random cooperative systems.

Molecular recognition. as understood now, is a local concept meaning preferential stabilization of a pair of molecules in a specific mutual configuration. It appears that molecular recognition may be generalized to include cooperativity extending over a large distance. There is actually cooperative molecular recognition in the simplest clathrate crystal. When a hydroquinone acetonitrile clathrate crystal grows in acetonitrile solution, acetonitrile molecules enter the crystal lattice exactly in the orientation dictated by the guest molecules already in the crystal lattice. In the crystal thus formed. all the guest molecules recognize their own orientation relative to the orientations of their neighbors. Hence, cooperative molecular recognition. Although the hydroquinone clathrate is too rigid to be of use in actual application, the cooperative molecular recognition enunciated by this case may be a useful concept arising from phase transitions in clathrate compounds.

ARTICLES OF FURTHER INTEREST

Hydroquinone, p. 679
Incommensurate and Commensurate Structures, p. 712
Inelastic Neutron Scattering. p. 727
Nuclear Magnetic Resonance Spectroscopy. p. 981
Nuclear Quadrupole Resonance Spectroscopy. p. 989
Thiourea Inclusion Compounds. p. 1501
Urea Inclusion Compounds, p. 1538

REFERENCES

1. *Landau. L.D.: Lifshitz. E.M.:* Pitaevskii, *L.P. Statistical Physics;* Pergamon *Press,* 1971: *Vol. 1.*
2. *Parsonage. N.G.:* Staveley, *L.A.K. Disorder in Crystals*; Clarendon *Press: Oxford*. 1977.
3. *Huang. K. Statistical Mechanics, 2nd* Ed.; *John Wiley and Sons,* 1987: *35.*
4. *Pemberton.* R.C.; *Parsonage,* N.G. *Thermodynamic properties of urea + hydrocarbon adducts. Part 1. Heat capacities of* adducts *of* n-$C_{10}H_{22}$, n-$C_{12}H_{26}$, n-$C_{16}H_{34}$, *and* n-$C_{20}H_{42}$. *Trans.* Faraday Soc. 1965, *61. 2112.*
5. *Yeo. L.; Kariuki.* B.M.; Serrano-Gonzalez, *H.: Harris.*

K.D.M. Structural properties of the low temperature phase of the hexadecane/urea inclusion compounds, investigated by synchrotron x-ray powder diffraction. J. Phys. Chem. **1997**, *101*, 9926.
6. Le Lann, H.; Odin, C.; Toudic, B.; Ameline, J.C.; Gallier, J. Single-crystal deuterium NMR study of the symmetry breaking in an incommensurate organic inclusion compound. Phys. Rev. **2000**, *B62*, 5442.
7. Gelerinter, E.; Luz, Z.; Poupko, R.; Zimmermann, H. Structure and dynamics of the urea-trixane inclusion compound phases, studied by ^{2}H NMR spectroscopy. J. Phys. Chem. **1990**, *94*, 5391.
8. Brustolon, M.; Maniero, A.L.; Segre, U. Guest-guest interactions in urea inclusion compounds. J. Chem. Soc., Perkin trans., II **1997**, 2521.
9. Chekhova, G.N.; Dyadin, Yu.A.; Rodionova, T.U. Clathrates of urea and thiourea. Part IV. Stoichiometry of thiourea clathrates with small molecules and the nature of their packing in the matrix channels. Izv. Sibirskogo Otd. Akad. Nauk SSSR, Ser. Khim. Nauk **1979**, *N5* (78).
10. Desmedt, A.; Kitchin, S.J.; Guillaume, S.; Couzi, M.; Harris, K.D.M.; Bocanegra, E.H. Phase transitions and molecular dynamics in the cyclohexane/thiourea inclusion compound. Phys. Rev. **2001**, *B64*, 054106.
11. Desmedt, A.; Guillaume, F.; Combet, J.; Dianoux, A.J. A high resolution quasielastic neutron scattering study of the guest molecules dynamics in the cyclohexane/thiourea inclusion compound. Physica **2001**, *B301*, 59.
12. Fait, J.F.; Fitsgerald, A.; Caughlin, C.N.; McCandless, F.P. Carbon tetrachloride-thiourea(1/3) adduct at 170 K. Acta Crystallogr. **1991**, *C47*, 332.
13. Sekii, M.; Matsuo, T.; Suga, H. Calorimetric study of phase transitions in the thiourea carbon tetrachloride inclusion compound. J. Incl. Phenom. Mol. Recognit. **1990**, *9*, 243.
14. Yagi, K.; Shima, S.; Terauchi, H.; Matsuo, T. Phase transitions of (thiourea)$_3$-CCl_4 clathrate compound. J. Phys. Soc. Jpn. **1997**, *66*, 2737.
15. El Ghallali, J.; Gourdji; Guibe, L.; Peneau, A. Investigation of the phase transition at 67.17 K in the thiourea-CCl_4 inclusion compound as studied by ^{14}NQR. Z. Naturforsch **1993**, *49a*, 433.
16. Adolphi, N.L.; Conradi, M.S.; Matsuo, T. ^{35}Cl NQR study of thiourea-CCl_4 and thiourea-CCl_3Br inclusion compounds. J. Phys. Chem. **1994**, *98*, 1968.
17. Panich, A.M.; Krieger, J.H.; Semenov, A.R.; Goren, S.D.; Chekhova, G.N. Chlorine-35 NQR and $^{1}HNMR$ study of guest structure and dynamics in the thiourea-hexachloroethane inclusion compound. J. Phys., Condens. Matter. **2000**, *12*, 5765.
18. Mizutani, Y.; Tamura, H.; Matsuo, T.; Suga abd, H.; Matsubayashi, G. Single crystal x-ray diffraction and low temperature calorimetric studies of the thiourea-hexachlororethane adducts. Netsu Sokutei **2000**, *27*, 118.
19. Krieger, J.H.; Panich, A.M.; Semenov, A.R. Utraslow motion of domain wall in channel inclusion compound studied by means of NMR cross-relaxation. Solid State Commun. **2001**, *120*, 69.
20. Sekii, M.; Matsuo, T.; Suga, H. Calorimetric study of phase transitions in the thiourea 1,1,2,2,-tetrachloroethane clathrate compound. J. Thermal Anal. **1992**, *38*, 1861.
21. Palin, D.E.; Powell, H.M. The structure of molecular compounds. Part III. Crystal structure of addition complexes of quinol with certain volatile compounds. J. Chem. Soc. **1947**, 208.
22. Matsuo, T.; Suga, H.; Seki, S. A phase transition and dielectric absorption in the quinol methanol clathrate compound. J. Phys. Soc. Jpn. **1967**, *22*, 677.
23. Mak, T.C.W. Orientation of methanol enclathrated in the β–hydroquinone lattice: An x-ray crystallographic study. J. Chem. Soc Perkin Trans. II **1982**, 1435.
24. Matsui, S.; Terao, T.; Saika, A. Study of static and dynamic structure of β–quinol clathrate by ^{13}C high-resolution solid-state NMR and proton T_1 measurement. J. Chem. Phys. **1982**, *77*, 1788.
25. Zubkus, V.E.; Tornau, E.E.; Belosludov, V.R. Theoretic physico-chemical problems of clathrate compounds. Adv. Chem. Phys. **1992**, *81*, 296.
26. Ukegawa, H.; Matsuo, T.; Suga, H.; Leadbtter, A.J.; Ward, R.; Clark, J.W. Static and dynamic properties of hydrogen sulfide in hydroquinone clathrates. Can. J. Chem. **1988**, *66*, 443.
27. Hirokawa, S.; Imasaka, I.; Matsuo, T. Quantum effects on the orientational ordering of H_2S and D_2S molecules enclosed in β–quinol clathrate. J. Phys. Soc. Jpn. **1994**, *63*, 593. Errata **1994**, *63*, 634.
28. Woll, H.; Rhainstadter, M.C.; Kruchten, F.; Kiefer, K.; Enderle, M.; Klopperpieper, A.; Albers, J.; Knorr, K. Dipolar ordering and glassy freezing in methanol-β-hydroquinone-clathrate. Phys. Rev. **2001**, *B63*, 224202.
29. *Inclusion Compounds*; Atwood, J.L., Davies, J.E.D., McNicol, D.D., Eds.; Academic Press, 1984; Vol. 1–3.
30. Facey, G.A.; Dubois, R.H.; Zakrzewski, M.; Radcliffe, C.I.; Atwood, J.L.; Ripmeester, J.A. Phase transition and dynamic structure in the toluene clathrate of t-butylcalix[4]arene. Supramolec. Chem. **1993**, *1*, 199.
31. Ripmeester, J.A.; Ratcliffe, C.I.; Enright, G.; Brouwer, E. Thermodynamic and resonance studies of structural changes in crystals. Acta Crystallogr. **1995**, *B51*, 513.
32. Ishida, K.; Matsuo, T.; Suga, H.; Zielenkiewicz, W.; Lipkowski, J. Low temperature properties of the Werner clathrate inclusion compounds. Isotopic p-xylenes in tetrakis (4-methylpyridine) nickel(II) thiocyanate. J. Chem. Thermodyn. **1998**, *30*, 1289.
33. Hanabata, H.; Matsuo, T.; Suga, H. Calorimetric study of β–cyclodextrin undecahydrate. J. Incl. Phenom. **1987**, *5*, 325.
34. Okishiro, K.; Yamamuro, O.; Tsukushi, I.; Matsuo, T.; Nishikiori, S.; Iwamoto, T. Calorimetric and dielectric studies on the water reorientation in the two-dimensional hydrogen-bond system of $Cd(H_2O)_2Ni(CN)_4{\cdot}4H_2O$. J. Phys. Chem. **1997**, *101*, 5804.

Collagens

Jean-Yves Exposito
Centre National de la Recherche Scientifique, Lyon, France

INTRODUCTION

Collagens are a family of extracellular matrix proteins that represents up to one-third of protein mass in higher animals. They are often associated with the emergence and evolution of metazoa. By definition, collagens are proteins that contain at least one triple-helical domain and that form supramolecular aggregates in the extracellular matrix. The triple-helical domain results from the conformational association of three polypeptides consisting of Gly–X–Y triplets and has to be considered as one of the multiple modules used to build multimodular proteins. Collagens were first known as the key elements of the extracellular matrix, providing the structural integrity of tissues, and ultimately, of animals. Involvement of many collagens in human diseases and their numerous interactions with neighboring extracellular components and cellular receptors clearly support their functional importance in developmental processes and tissue remodeling. Their roles in these functions are closely related to their ability to oligomerize and to create multivalent supramolecular networks.

COLLAGEN DEFINITION

In mammals. collagen is the most abundant protein (about 30%) and was first known as gelatin, which corresponds to heat-denatured collagen. A useful history of collagens was presented by van der Rest and Garrone.[1] The word collagen came from the properties of some connective tissues to give glue or gelatin after boiling (from the Greek; κολλα, glue, and γενοξ, birth). During the last century. biochemical and molecular investigations led to a clearer definition of this family of proteins. Collagens are extracellular matrix proteins that contain at least one collagenous domain or triple helix and that form supramolecular networks. More recently. biological activities other than their involvement in the structural integrity of organisms were demonstrated for collagens. Consequently. their fundamental role in developmental and biological processes such as cell behavior should be included in a current definition of collagens. In this article, we will describe collagens in terms of structure. metazoan evolution, and function.

THE COLLAGEN TRIPLE HELIX

The triple helix is a hallmark of collagens. which are trimeric molecules. This structural motif corresponds to a right-handed super helix and represents the conformation resulting from the association of three left-handed polyproline-11-like polypeptide a chains (Fig. 1). The sequence involved in this left-handed conformation consists of the repetition of Gly–X–Y triplets. where X and *Y* are often proline and 4-hydroxyproline, respectively. The imino acids stabilize the triple helix. while the sterically small glycine residue is the only amino acid that can fit into the central position of the three intertwining helices that are closely packed (1.5 nm in diameter). Within the triple helix, the neighboring α chains are staggered by one amino acid. During the last decades. diffraction and x-ray crystal structure analyses of collagen and synthetic peptides improved the knowledge of this supercoiled protein motif. The main conclusion is that the triple-helical structure is dependent on the collagen sequence[i3] Hence, the triple-helical twist is smaller in imino-acid-rich regions, but there are generally 3.33 residues per helical turn, with a rise of 2.86 Å per residue (see Fig. 1).

COLLAGEN AND COLLAGEN-LIKE FAMILIES

Collagen-hike Proteins

A collagenous domain is not peculiar to collagens and is present in proteins that are not implicated in extracellular matrix structure.[''''] Some of the collagen-like proteins are involved in host defense, and for this reason, they were called defense collagens.[6] In this group of proteins are the collectins that possess a short collagenous domain. connected to a C-type (calcium-dependent) lectin via an α-helical coiled neck region; the ficolins. which are structurally similar to collectins but with the lectin region replaced with a fibrinogen-like module: the complement C1q and adiponectin. which both consist of a carboxyl-terminal C1q domain connected to a collagenous region: and membrane-associated Type-II proteins, including three isoforms of the macrophage scavenger receptor and the so-called macrophage receptor MARCO. Other

Encyclopedia of Supramolecular Chemistry
DOI: 10.1081/E-ESMC 120019201

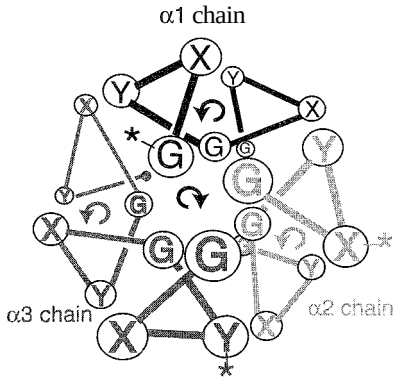

Fig. 1 The triple helix motif. Shown is a cross-section of a right-handed triple helix made of three left-handed α chains (adapted from Ref. [2]). The symbol (*) shows one example of amino acid residues present at the same axial level and the one residue stagger between two adjacent α chains. Note the location of every third glycine residue at the center of this structural motif and the availability of the side chains of the X and Y residues at the surface. (*View this art* in *color at www.dekker.com.*)

noncollagenous proteins possessing a triple helix are emilins, the collagen tail of acetyl cholinesterase, and the Type II transmembrane protein, ectodysplasin.

Human Collagens

Collagens are present in organisms from the sponge to a human.[5,7] In humans, 27 types were characterized, and their sequences are available online (Ref. [4]). Collagens are made by the association of three identical α-chains for homotrimeric molecules or by the association of two or three genetically distinct α-chains for heterotrimeric molecules. The collagen nomenclature results mostly from the order of characterization of the collagen types (I, II, III...). More precisely, an α*n*(*Y*) collagen polypeptide corresponds to the α chain *n* of type *Y*, where *n* and Yare Arabic and Roman numerals, respectively. Collagens can be divided into several subfamilies according to their primary structures and their resulting supramolecular structures. The first and best known are the so-called fibrillar collagens (Types I–III, V, and XI) that generate cross-striated fibrils. The procollagen procursors of all fibrillar α-chains present the same overall structure, i.e., a central uninterrupted triple helix of approximately 338 Gly–X–Y triplets flanked by two noncollagenous doinains, the amino- and carboxyl-propeptides (Fig. 2A). Other subfamilies are known as nonfibrillar collagens, because they present short interruptions in their collagenous domains. Among them, Type IV collagen is specific to basement membranes and is a network-forming collagen. Other nonfibrillar collagen subfamilies include the fibril-associated collagens with interrupted triple helices or FACITs (Types IX, XII, XIV, XX, XXI); the FACIT-related collagens (Types XVI and XIX); collagens that form beaded filaments and hexagonal networks (Type VI); Type VII, which is the major component of anchoring

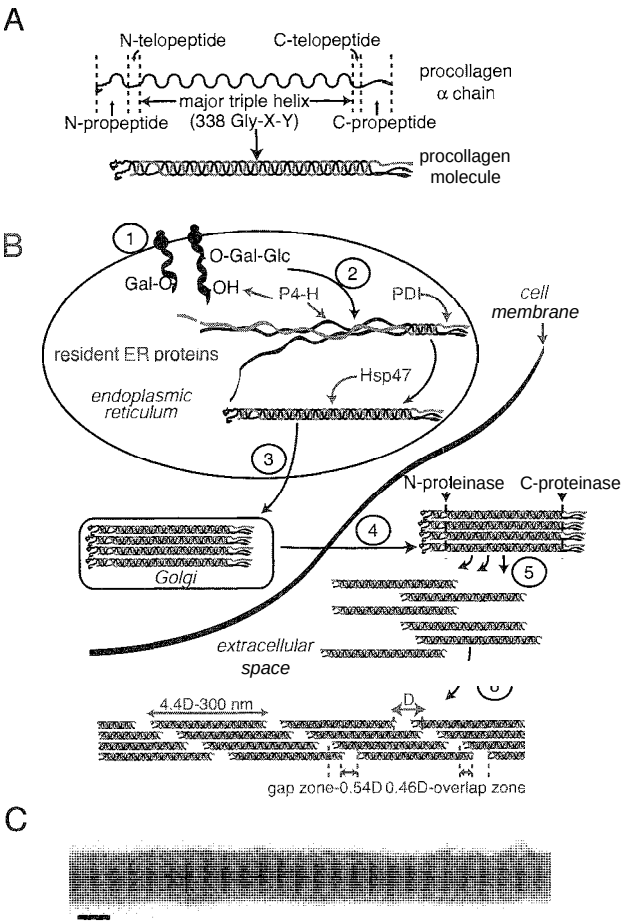

Fig. 2 Biosynthesis of collagens. a view based on the fibrillar collagens. (A) The domains of a fibrillar α-chain arid of a procollagen molecule. (B) From procollagen mRNAs to fibril formation: 1) Procollagen mRNAs are translated into procollagen 2-chains on polysomes of the rough endoplasmic reticulum. and cotranslational events take place on nascent α chains. i.e., hydroxylation and glycosylation reactions: 2) after translocation into the endoplasmic reticulurn lumen, the C-propeptides of three appropriate 9-chains trimerize. and the triple helix elongates from its carboxyl-terminus to the amino-terminus: 3) translocation of procollagen molecules into the Golgi and lateral association of the procollagen molecules: 4) secretion of procollagen molecules; 5) cleavage of the *N*- and C-propeptides by specific proteinases; and 6) formation of the fibril. (C) Sea urchin fibril visualized after negative staining (courtesy of Claire Lethias). Bar: 100 nm. Resident endoplasmic reticulurn proteins are indicated: P4-H, prolyl-4 hydroxylase: PDI, protein disulfide isomerase: and Hsp47, heat shock protein 47. (*View this art* in color *at www.dekker.com.*)

Table 1 Fibrillar collagens

Type	Molecule	Tissue distribution	Disease
I			
α1(I) α2(I)	$(\alpha1)_2$, α2	Ubiquitous skin. tendon bone etc	Osteogenesis imperfecta, Ehlers–Danlos syndrome (arthrochalasia), osteoporosis
	$(\alpha1)_3$ (minor form)	Dentin. tumors, skin	
II			
α1(II)	$(\alpha1)_3$	Hyaline cartilage, vitreous body	Chondrodysplasia (severe to mild disease) osteodrthrosis
III			
α1(III)	$(\alpha1)_3$	Skin, blocd vessels intestine	Ehlers–Danlos syndrome (vascular)
V			
α1(V), α2(V), α3(V)	$(\alpha1)_2$ α2 (major form)	Same as Type I	Ehlers–Danlos syndrome (classical)
	$(\alpha1)_3$	Hamster lung cell culture	
	α1 α2. α3	Placenta. Synovial membranes	
		V/XI heterotypic molecules	
XI			
α1(XI), α2(XI), α3(XI)	α1. 22. α3	Hyaline cartilage	Chondrodyslasia (mild disease). osteoarthrosis no-syndromic hearing loss

The α3(XI) chain appears to be a posttranslationally modified form of the α1(II) collagen chain.

fibrils that participate in the attachment of basement membranes to the underlying extracellular matrix; and short-chain collagens forming hexagonal networks (Types VIII and X). Finally, the latest families include Type II transmembrane collagens (Types XIII. XVII. XXIII, and XXV); multiplexins (collagens including multiple collagenous domains and interruptions. Types XV and XVIII); and the newly characterized Type XXVI.

COLLAGEN BIOSYNTHESIS

In the extracellular matrix, collagens form supramolecular organizations. To follow the different steps leading to these structures. we will focus our attention on fibrillar collagens for which most of the work was done. Illustrated in Fig. 2B are the fates of fibrillar collagen chains from their syntheses to their incorporations into fibrils. The first step is the translation of collagen mRNA in the rough endoplasmic reticulum on membrane-bound polysomes. Concornitant with the translocation of the nascent procollagen chain into the lumen of the endoplasmic reticulum, cotranslational events occur. These include the hydroxylation of some proline and lysine residues by prolyl and lysyl hydroxylases. respectively. Modified prolines are 3-hydroxyproline and 4-hydroxyproline in the X and *Y* positions. respectively. Other cotranslational modifications are the glycosylation of certain hydroxylysines by galactosyltransferase or glucosyltransferase, the addition of mannose-rich oligosaccharides to the W-linked oligosaccharide attachment site in one or both propeptides, and the formation of disulfide bonds in the *C*-propeptide. mediated by the protein disulfide isomerase (PDI). After complete translocation of the procollagen chain and removal of the signal peptide, the formation of procollagen molecules begins. As indicated in Table I. not all of the possible molecular compositions are produced indeed—one cell can synthesize different types of fibrillar collagen. It was demonstrated that a short sequence located in the C-propeptide is involved in the recognition of relevant pro-α chains.[8] Interestingly, this sequence is absent in all the invertebrate fibrillar α-chains characterized to date.[7] The formation of the procollagen molecules begins by the recognition and association of the C-propeptides, this structure being stabilized by intra- and interdisulfide bridges. At this point, the formation of the triple helix is propagated from the C-terminus toward the amino-terminus. Even though a triple-helical conformation can be formed in the absence of the C-propeptide, proper α-chain recruitment and correct register of the collagenous regions requires this domain. The next step is the transfer of the procollagen molecules into the Golgi without leaving the lumen of the cisternae.[9] During cisternal maturation, procollagen is laterally aggregated. The final step is the secretion of these aggregates from vesicles. During ail of these processes, several chaperone

proteins are involved in the proper folding. the retention of unfolded molecules. and the vesicular trafficking of collagen molecules.[10] In addition to being involved in the hydroxylation of proline residues in position *Y*. prolyl-4 hydroxylase (P4-H) also acts as a chaperone by interacting with the correctly folded monomeric triple helix. The PDI is the enzyme used in the formation of disulfide bridges in the C-propeptides, but it is also involved in quality control of collagens in the endoplasmic reticulum. Hence, PDH mediates retention in the endoplasmic reticulum of unassembled procollagen C-propeptides. The Hsp47 is an endoplasmic reticulum collagen chaperone that seems to prevent the lateral aggregation of collagen molecules before their transfer to the golgi. An in vitro study indicated that Type I collagen is thermally unstable at body temperature.''' As indicated by Persikov and Brodsky,[12] the collagen triple helix is more stable in cells, and an increase in collagen stability might be correlated with the interaction between chaperones and the triple helix.

After secretion, the soluble aggregated procollagen molecules are generally processed by amino and carboxyl proteinases, leading to the formation of insoluble collagen molecules ready to be incorporated into fibrils. The mature collagen molecule consists of a central triple helix flanked by two shori noncollagenous extensions, the N- and the *C*-telopeptides. In fibrils, collagen molecules, approximately 300 nm or 4.4 D in length. are aligned in parallel. with a *D*-stagger, including a gap zone and an overlap region (see Fig. 2B). This molecular staggering explains the striated appearance of negatively stained fibrils as revealed by transmission microscopy (Fig. 2C). How are the fibrils organized and how can we explain the shape heterogeneity of fibrils? Although numerous studies and models were made from structural analyses, these questions were not completely answered. In this article, we will present data concerning heterotypic fibrils in cornea composed of Types I and V collagens. Corneal stroma fibrils are uniformly thin and are arranged into a highly ordered lattice-like structure. This orthogonal structure was postulated to be of importance in the transparency of cornea. Holmes et al.[13] used automated eiectron tomography to analyze the structures of corneal fibrils. The authors indicated that these fibrils are composed of microfibril units (five collagen molecules). which are tilted by 15° with respect to the long axis of the fibrils in a right-handed helix. Moreover. the microfibrils exhibit an ordered lateral arrangement at the boundaries of the overlap regions (*N*- and *C*-telopeptides) and in a region of the gap zone. Disordered arrangements were observed in other regions of the *D*-period. The *N*- and *C*-telopeptide regions are involved in intermolecular cross-linking in fibrils. Moreover, their presence improves fibril formation: as revealed by in vitro fibrillogenesis experiments. Analyses of these heterofibrils reveal that macromolecules are located at their surfaces in regions exhibiting a relatively ordered arrangement. These macromolecules might be the *N*-propeptide of Type V collagen that is not fully processed in mature fibrils. Linsenmayer et al.[14] suggested that the retention of Type V *N*-propeptide at the surface of the fibrils prevents, by sterical hindrance, the addition of new collagen molecules and permits the formation of thin fibrils of regular diameters. Other macromolecules are the small leucine-rich repeat proteoglycans such as lumican. Lumican-null mice present an opacification of the cornea and a disorganization of the fibril network.'''' The presence of lumican in normal mice seems to prevent the lateral fusion of collagen fibrils. Hence. different parameters might explain variations in fibril shape, including the collagen types involved and their ratios, retention of the *N*-propeptide, interaction with neighboring components such as the small leucine-rich repeat proteoglycans or the FACIT collagens, and the intrinsic sequence of the triple

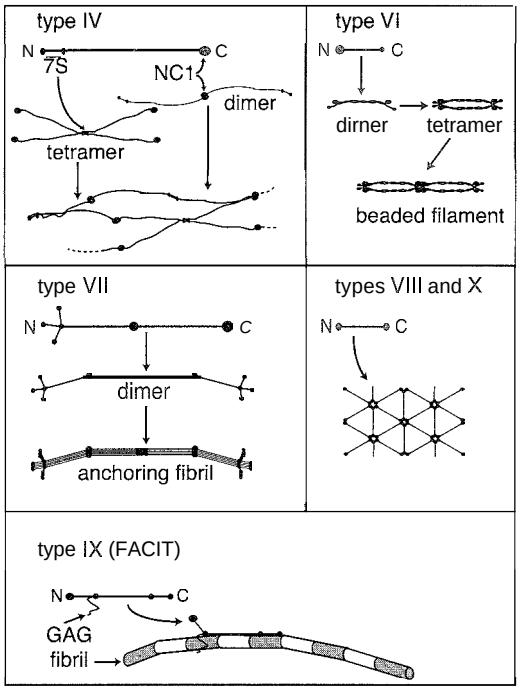

Fig. *3* Supramolecular organizations of some nonfibrillar collagens. The steps leading to the formation of supramolecular structures from monomeric molecules. N and C: *N*-terminus and *C*-terminus of the molecules: closed circles and thick black lines indicate noncollagenous and triple-helical domains. respectively: GAG: glycosaminoglycan: 7S is the triple-helical region of the Type IV collagen molecules involved in the formation of tetramers; NC1 is the carboxyl-terminal noncollagenous domain of Type IV collagen molecules involved in the formation of dimers.

helix. To complete this section. the supramolecular organizations of some nonfibrillar collagens are illustrated in Fig. 3.

EVOLUTION OF COLLAGENS

From the first multicellular animals, sponge and hydra. to humans, only two classes of collagens seem to be maintained to date: the fibrillar and the basement-membrane Type IV collagens. For fibrillar collagens, their absence was demonstrated in a few species such as *Drosophila melanogaster* and *Caenorhabditis elegans*. It was suggested that flies and nematodes do not need the mechanical resistance produced by fibrillar collagens, because they have a chitinous or a cuticular exoskeleton, respectively.[5,16] The complete genome sequences of these two protostome animals are available, and subsequent analyses indicated that in addition to Type IV collagen. only a vertebrate collagen ortholog, Type XVIII, is present in these animals. Collagens that appear to be unique to some invertebrate phyla were characterized. We can cite the cuticular collagens of nematodes. These short-chain collagens are encoded by a large family of genes and are involved in part in the physical properties of the cuticle.[17] Another family of short-chain exocollagens (collagens outside the animal) was described in sponges.[18] These collagens are termed spongin and play two major roles. One is to attach the animal to its substratum, while it can also act as cement between the spicules forming the sponge skeleton. Hence. in the well-known bath sponge, spongin collagen replaces the inorganic skeleton. Other invertebrate collagens described to date are the collagen from mussel bysus, hydra minicollagens, and the cuticle collagen of annelid.[''''] From the diversity of collagen and collagen-like proteins and the presence of this structural motif in prokaryotes. several questions come to mind. How old is collagen? How should the triple helix be perceived? From sequence and fossil analyses. its metazoan origin was dated to approximately 600 to 1000 million years ago.[20] Environmental changes. such as the increases in oxygen in the late proteozomic, were postulated to be involved in the burst of metazoan radiation during the Vendian–Cambrian period. Oxygen is important for animal respiration and for the evolution of metabolic processes in animals.[21] Moreover. through its involvement in the posttranslational hydroxylation of proline and lysine residues. the increase of oxygen can also be considered a key step favoring the synthesis of coilagen. which can be considered an hallmark of metazoans. En fact. collagen and collagen-like molecules were also described in plants and prokaryotes. In metazoans, extracellular matrix proteins and the extracellular region of transmembrane proteins are composed of modules. By definition, a module should be present in multiple copies in one protein or in otherwise unrelated proteins,[22] it should be able to fold independently, and it is generally encoded by one exon. Several authors indicated that the triple helix might be considered a module.[5,23] From its short repeating primary motif (Gly–X–Y), the size of this module can easily be changed. Hence. in fibrillar collagen genes, most of the exons encoding the triple helix are 54 bp or 45 bp long. In Type VI gene, there is a prevalence of 63 bp exons. Another important function of the triple helix is its involvement in oligomerization. a structural function permitting the formation of inultivalent supramolecular networks.

FUNCTIONS OF COLLAGENS

The structural and biological importance of collagens is clearly demonstrated by the study of human genetic diseases resulting from mutations in genes encoding collagens or enzymes involved in their posttranslational modification. The catalog of human diseases is available in a recent review[''] and is indicated in Table 1 for the fibrillar collagens. Natural disease and knock-out experiments in mice confirmed the human data and also permitted the identification of other potential genetic diseases. In this article; we will focus on the Ehlers–Danlos syndrome. This syndrome is divided into several subtypes, but it is generally associated with joint hypermobility and skin fragility. The genes involved in this syndrome encode Type I and III collagens, and the α1 and α2 chains of Type V collagen. lysyl hydroxylase and, more recently identified, tenascin-X.[24] Tenascin-X is also an extracellular matrix protein detected at the surface of fibrils in the skin that interacts with decorin, a small leucine-rich repeat proteoglycan.[25] Decorin interacts with Type I collagen and tenascin via its core protein and its dermatan sulfate chains. respectively. Moreover, decorin-null mice present a phenotype related to the Ehlers–Danlos syndrome.[26] Altogether, these data clearly show that maintainance of the supramolecular fibrillar network is important for the structural integrity of skin.

The functional importance of collagens in biological activities can be considered on two levels. The first results from the triple-helical sequence. Hence, as previously indicated[i1]] and shown in Fig. 1. residues X and Y are exposed at the surface of the triple helix and are available for lateral interactions. Ligands of the triple helix were characterized. such as several integrins and proteoglycans. The second level concerns the noncollagenous domains of collagen. One of the best known is endostatin, which represents the C-terminal region of collagen XVIII, a component of endothelial and epithelial basement membranes. Endostatin is the major molecular form in

several tissues. Functions associated with this protein are the inhibition of endothelial cell proliferation, migration, and angiogenesis.[27] Another function is the reduction of tumor growth in animal models. Actually, different modules form the noncollagenous domains of collagens, and some of their putative functions might be suggested from their obvious biological importance in other extracellular matrix proteins. Hence, chordin, which possesses several cysteine-rich modules (Tsp-2), is involved in dorsal-ventral patterning. Chordin interacts with different bone morphogenetic proteins (BMPs).[28] Type IIA collagen includes a Tsp-2 module in its N-propeptide. The dorsalizing activity of Type IIA collagen was shown by injecting Type IIA mRNA in *Xenopus* embryos.[29] The Tsp-2 module of Type IIA collagen, which is required for this activity, binds to TGF-β1 and BMP-2.[30] Hence; the retention and the concentration of growth factors or cytokines might be some of the nonstructural functions of collagen fibrils. The availability of these sequestering molecules during remodeling or tissue differentiation might be realized by the action of different metalloproteinases.

CONCLUSION

The metazoan extracellular matrix is composed of large supramolecular networks that involve modular glycoproteins and proteoglycans. Structural elements (coiled-coil motif, triple helix) permitting oligomerization are of importance in generating these networks. The triple-helical structure. the common structural element of collagens. allows the formation of trimeric molecules. This first structural order is often associated with higher oligomerization levels involving the self-association of the triple helix or multimerization from the noncollagenous domains of these molecules. Networks including collagens are implicated in the structural properties of tissues. The best known are the collagen fibril networks that provide protection against mechanical constraints in skin and tendon. However, collagens are also important in numerous physiological events. Future directions in the collagen Geld will include dissecting their functions during development, tissue remodeling, and tumor invasion. Their use in biomedical applications will also be explored. Hence. from their biological properties, collagens are of use in several biomedical applications (hemostatic sponges. surgical sutures, sponges for burns and wounds, etc.). Private companies and academic institutes used different systems (plant, yeast. mammalian cells) to produce recombinant collagens. Improvements in production in terms of quality, quantity, and cost will be considered in the future. This approach will be further improved with a better understanding of the biological functions of the noncollagenous domains. Actually. future progress will come in the understanding of collagens, not as an individual component of an extracellular matrix but as one of the elements of the extracellular macroaggregates. Mow do these macromolecular networks influence cell signaling events and what are the roles of the extracellular matrix on the control of distinct morphogenetic processes. are some of the questions that will mobilize laboratories working in the collagen field during the next few years.

ACKNOWLEDGMENTS

I apologize to all the scientists whose works I could not cite due to space restrictions. The author thanks Claire Lethias for the electron micrograph in Fig. 2.

ARTICLES OF FURTHER INTEREST

Amino Acids: Applications, p. 42
Gels, p. 586
Hydrogen Bonding, p. *658*
Macrocycle Synthesis, p. 830
Micelles and Vesicles, p. 861
Protein Supramolecular Chemistry, p. *1161*
Self-Assembly in Biochemistry, p. *1257*
Self-Assembly: Terminology, p. 1263

REFERENCES

1. Van der Rest, M.: Garrone, R. Collagen family of proteins. FASEB J. 1991, *5*, 2814–2823.
2. Beck, K.: Brodsky. B. Supercoiled protein motifs: The collagen triple-helix and the α-helical coiled coil. J. Struct. Biol. 1998. *122.* 17–29.
3. Kramer, R.Z.: Bella. J.: Mayville. P.; Brodsky, B.; Berman, H.M. Sequence dependent conformational variations of collagen triple-helical structure. Nat. Struct. Biol. 1999. 6 (5). 454–457.
4. Myllyharju, J.; Kivirikko. K.I. Collagens and collagen-related diseases. Ann. Med. 2001. *33,* 7–21.
5. Exposito, J.Y.: Cluzel. C.; Garrone. R.: Lethias. C. Evolution of collagens. Anat. Rec. 2002, 268 (3), 302–316.
6. Acton. S.; Resnick. D.: Freeman. M.: Ekkel. Y.; Ashkenas, J.; Krieger, M. The collagenous domains of macrophage scavenger receptors and complement C1q mediate their similar. but not identical. binding specificities for polyanionic ligands. J. Biol. Chem. 1993. *268* (5), 3530–3537.
7. Boot-Handford, R.P.: Tuckwell. D.S. Fibrillar collagen: The key to vertebrate evolution? A tale of molecular incest. BioEssays 2003. *25.* 142–151.

8. Tasab, M.; Jenkinson, L.; Bulleid, N.J. Sequence-specific recognition of collagen triple helices by the collagen-specific molecular chaperone HSP47. J. Biol. Chem. 2002. *277* (38). 35007–35012.
9. Bonfanti. L.: Mironov. A.A., Jr.; Martinez-Menarguer, J.A.; Martella, O.; Fusella, A.; Baldassarre. M.; Buccione, R.; Geuze, H.J.; Mironov, A.A.; Luini, A. Procollagen traverses the golgi stack without leaving the lumen of cisternae: Evidence for cisternal maturation. Ccll **1998.** *95* (7), 883–889.
10. Hendershot, L.M.; Bulleid. N.J. Protein-specific chaperones: The role of hsp47 begins to gel. Curr. Biol. 2000. *10* (24), R912–R915.
11. Leikina, E.; Mertts, M.V.; Kuznetsova, N.; Leikin, S. Type I collagen is thermally unstable at body temperature. Proc. Natl. Acad. Sci. U. S. A. 2002, *99* (3), 1314–1318.
12. Persikov. A.V.; Brodsky, B. Unstable molecules form stable tissues. Proc. Natl. Acad. Sci. U. S. A. 2002, *99* (3), 1101–1103.
13. Holmes, D.F.; Gilpin, C.J.; Baldock, C.; Ziese, U.; Koster, A.J.; Kadler, K.E. Corneal collagen fibril structure in three dimensions: Structural insights into fibril assembly, mechanical properties, and tissue organization. Proc. Natl. Acad. Sci. U. S. A. 2001, *08* (13), 7307–7312.
14. Linsenmayer, T.F.; Gibney, E.; Igoe, F.; Gordon. M.K.; Fitch, J.M.; Fessler, L.I.; Birk, D.E. Type V collagen: Molecular structure and fibrillar organization of the chicken α1(V) NH2-terminal domain, a putative regulator of corneal fibrillogenesis. J. Ccll Biol. **1993,** *121* (5), 1181–1189.
15. Chakravarti, S.; Petroll, W.M.; Hassell, J.R.; Jester, J.V.; Lass. J.H.; Paul, J.; Birk, D.E. Corneal opacity in lumican-null mice: Defects in collagen fibril structure and packing in the posterior stroma. Invest. Ophthalmol. Vis. Sci. 2000, *41* (11), 3365–3373.
16. Hynes, R.O.; Zhao, Q. The evolution of cell adhesion. J. Cell Biol. 2000. *150* (2), F89–F96.
17. Johnstone, I.L. Cuticle collagen genes. Expression in *Caenorhabditis elegans*. Trends Genet. 2000, *16* (1), 21–27.
18. Exposito, J.Y.; Le Guellec, D.; Lu, Q.; Garrone, R. Short chain collagens in sponges are cncodcd by a family of closely related genes. J. Biol. Chem. **1991,** *266* (32). 21923–21928.
19. Gaill, F.; Wiedernann, H.; Mann, K.; Kuhn, K.; Timpl, R.; Engel, J. Molecular characterization of cuticle and interstitial collagens from worms collected at deep sea hydrothermal vents. J. Mol. Biol. **1991;** *221* (1), 209–223.
20. Knoll. A.H.; Carroll, S.B. Early animal evolution: Emerging views from comparative biology and geology. Science **1999,** *284* (5423), 2129–2137.
21. Canfield, D.E.; Tcske, A. Late Proterozoic rise in atmospheric oxygen concentration inferred from phylogenetic and sulphur-isotope studies. Nature **1996.** *382* (6587). 127–132.
22. Patthy, L. Genome evolution and the evolution of exon-shuffling—A review. Gene **1999,** *238* (1), 103–114.
23. Bork, P. The modular architecture of vertebrate collagens. FEBS Lett. **1992,** *307* (1), 49–54.
24. Burch, G.H.; Gong, Y.; Liu, W.; Dettman, R.W.; Curry, C.J.; Smith, L.; Miller. W.L.; Bristow, J. Tenascin-X deficiency is associated with Ehlers–Danlos syndrome. Nat. Genet. **1997;** *17* (1). 104–108.
25. Elefteriou, F.; Exposito, J.Y.; Garrone, R.; Lethias, C. Binding of tenascin-X to decorin. FEBS Lett. 2001. *495* (1–2). 44–47.
26. Danielson, K.G.; Baribault, H.; Holmes, D.F.; Graham, H.; Kadler, K.E.; Iozzo, R.V. Targeted disruption of decorin leads to abnormal collagen fibril morphology and skin fragility. J. Ccll Biol. **199'7.** *136* (3), 729–743.
27. Zatterstrom, U.K.; Felhor, IJ.; Fukai, N.; Olsen, B.R. Collagen XVIII/endostatin structure and functional role in angiogencsis. Ccll Struct. Funct. 2000. *25* (2), 97–101.
28. Piccolo, S.; Sasai. Y.; Lu, B.; De Kobertis, E.M. Dorsoventral patterning in Xenopus: Inhibition of ventral signals by direct binding of chordin to BMP-4. Ccll. **1996.** *86* (4). 589–598.
29. Larrain, J.; Bachiller, D.; Lu. B.; Agius, E.; Piccolo, S.: De Kobertis, E.M. BMP-binding modules in chordin: A model for signalling regulation in the extracellular space. Development 2000, *127* (4). 821–830.
30. Zhu, Y.; Ogancsian, A.; Keene, D.R.; Sandell, L.J. Type IIA procollagen containing the cystcine-rich amino propeptide is deposited in the extracellular matrix of prechondrogenic tissue and bincls to TGF-betal and BMP-2. J. Ccll. Biol. **1999.** *144* (5), 1069–1080.

Complexation of Fullerenes

Colin L. Raston
University of Western Australia, Crawley, Perth, Australia

INTRODUCTION

Complexation of fullerenes covers a diverse range of interactions and structural types. ranging from simple host–guest complexes through to oligomeric structures and continuous arrays, and structures with covalent metal-fullerene interplay.[1–5] The later organometallic chemistry is extensive and beyond the scope of this article,[6] except where the complexes show supramolecular interactions, such as in the complexation with silver nitrate, where the fullerene effectively templates a curved silver nitrate network.'" Accordingly, the focus of this article is on the host–guest chernistry of fullerenes and higher complexity supramolecular chemistry based on organization of fullerenes with one or more other synthons.

GENERAL CONSIDERATIONS

Fullerenes are electron-deficient molecules comprised exclusively of carbon, collectively representing a new allotropic form of carbon. for which C_{60} is the most abundant, smallest. and most widely studied. having a truncated icosahedral structure 10.0 A in diameter at the van der Waals limit. They can undergo addition organic reactions that have been extensively mapped out for C_{60}; the addition is across the 6,6′-position ring junction of two six-membered rings. which is consistent with the double bonds *in* the fullerene avoiding the five-membered rings of the polyhedran, an area reviewed by Diederich and Gomez-Lopez.[4] Recent advances *in* the supramolecular chemistry of such modified fullerenes include the organization of the potassium salt of a penta-substituted fullerene into −17 nm spherical bilayer vesicles,[8] assembling fullerenes on surfaces,[9] and binding porphyrins.[10] In general. surface assembly of fullerenes on continuous flat surfaces and on the surface of nanoparticles is possible and includes the use of aza-crown ether to complex C_{60} at air–water interfaces. and the assembly of 64 C_{60}^- anions on the surface of a dendimer with terminal ferricinium moieties.[11] Dendrimers can also bind fullerenes within their internal cavities,[12,13] and this includes porphyrin-containing systems.[14,15] In addition, self-assembly processes can stabilize nanoparticles of fullerenes, such as a diblock polymer shrouding 10^{10} fullerene molecules.[16]

In embracing the principles of supramolecular chemistry, the goal is to encourage the interplay of fullerene molecules, or reduced fullerenes, noting that they can be readily reduced, in the case of C_{60} this is reversible to C_{60}^{n-}, $n = 1$ to 6. with other synthons in an organized way. This chemistry is inherently complicated by the tendency of fullerenes to aggregate at the van der Waals limit in the presence of other synthons, but this offers potential for building new arrays and materials based on both types of interactions. i.e., host–guest and interfullerene. Optimizing complementarity of curvature of fullerenes with host molecules, such as bowl-shaped cavitands and saddle-shaped molecules was a successful but not essential strategy for host–guest chemistry, as was the choice of solvent. which can tip the balance from complexation to coinplexation with aggregation of the fullerenes, through to little or no complexation. Summarized in Fig. 1 are the main types of host molecules, including cavitands 1–4. 7,[17] and 9:[18] saddle-shaped molecules, 5: porphyrins, 6: siloxanes, 8: curved-face tryptophanes. 10;[19] and β,γ-cyclodextrins, 11. Where complexation is not prevalent. the addition of other synthons can be effective. Group 1 ions. for example. bind to modified calixarenes (R' =ester) and now results in complexation of C_{60}.[20] Seemingly most molecules with aromatic ring systems and electroll-rich moieties can form complexes with fullerenes. including benzene and extended aromatic systems and tetrathiafulvalenes,[4,21] but the conditions to effect complexation are varied. Essentially planar porphydns. 6. form a myriad of complexes. despite the lack of complementarity of curvature with fullerenes. The synthesis of fullerene complexes is often simple. for example, the mixing of equimolar amounts of the two components usually in toluene, or with an excess of the "host," with the complex crystallizing over several hours or sometimes days. Only where special conditions are required, is this discussed below for specific synthons.

Fullerenes can also be taken up in the pores of mesoporous silica, with aggregation of the fullerenes in the presence of cavitand molecules such as 1–4. This is a qualitative test for host–guest chemistry between the

Encyclopedia of Supramolecular Chemistry
DOI: 10.1081/E-ESMC 120012741

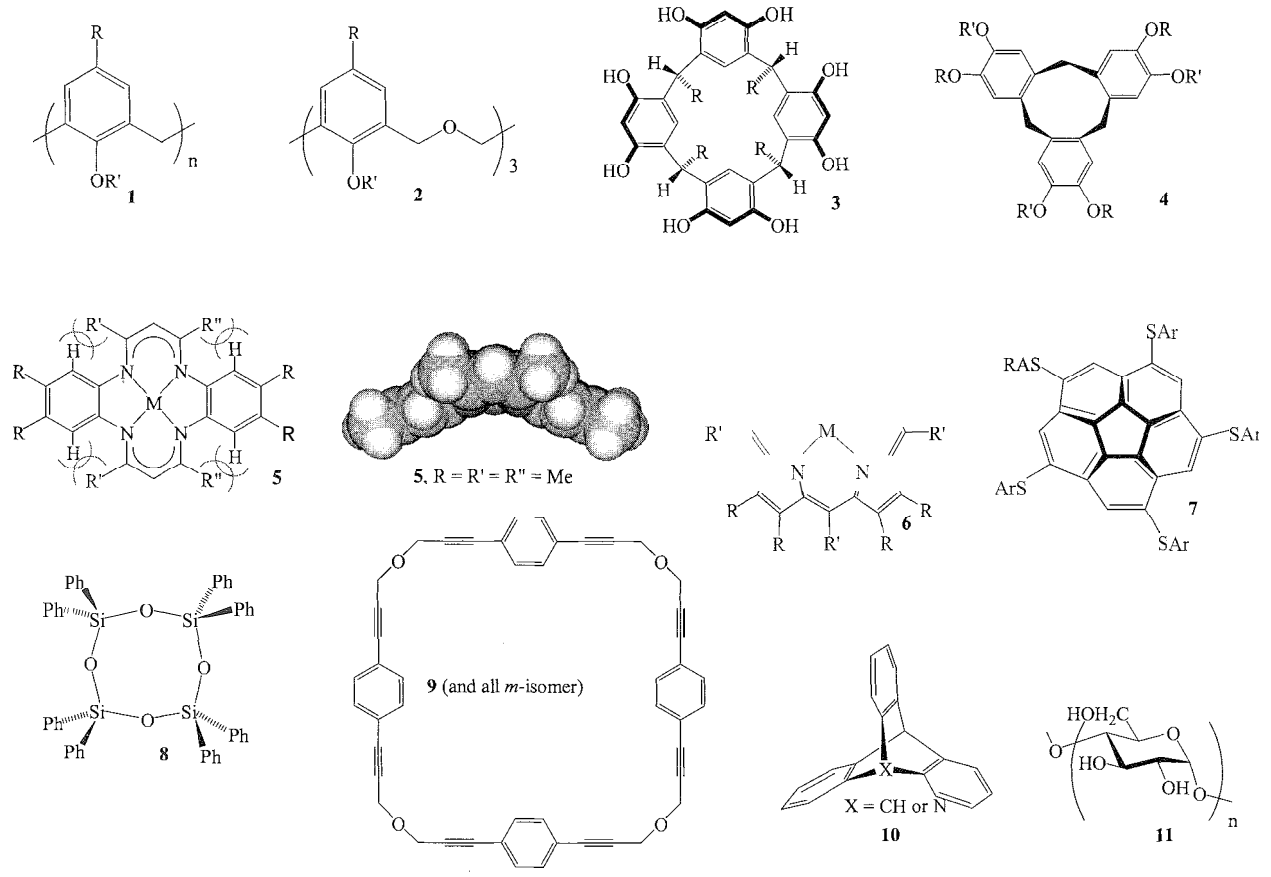

Fig. 1 Types of molecules that form complexes with fullerenes with a specific example for **5** shown as space filling. (*View this art in color at www.dekker.com.*)

fullerene and the cavitand,[2] *and confinement of the fullerene can be used to form hydrated* C_{60} *at* 350°C, i.e., controlled *synthesis in confined* space.[22] *Fullerenes. including* metallofullerenes *such as* $Sm@C_{82}$,[23] *can also be drawn into carbon nanotubes. Salient aspects of supramolecular chemistry of* fullerenes *are now elaborated below. making reference to leading papers in the field and review articles."-"* The *class* of *complexes formed are dealt* with *according to the nature of the host molecules. Simple donor–acceptor* complexes *were reviewed*[5] *and dealt with in the article Fullerene Intercalates. Each class of host* molecules *often afford different structural types. which are also elaborated below.*

Supramolecular chemistry *of fullerenes can be used to controi the interplay of fullerenes in the solid state, for then covalently linking the* fullerenes *under high pressure and temperature. The pioneering work for the synthesis of dumbbell-shaped* C_{120} *was done by Iwasa et al. This was followed by Sun and Reed preparing a linear* polymer *of covalently linked* C_{60} molecules.[24]

HOST–GUEST COMPLEXES

Calixarenes and Related Molecules

Calix[8]arenes, **1**, $n = 8$

Historically, complexation *of* fullerenes with *p*-Bu^t-calix[8]arene, **1**, $R = Bu^t$, $R' = H$, *was an important development in the field, independently reported in 1994 by* Atwood *et al. and Shinkai et al.. although there was an earlier report on the* binding *of a water-soluble calixarene bearing sulfonate groups on* the *lower* rim.[1,21] *p*-Bu^t-calix[8]arene *is effective in retrieving high-purity* C_{60} *from toluene solutions of* fullerite, *which is a mixture of* all *the* toluene-soluble *fullerenes in carbon soot. This involves recrystallization of the precipitate from toluene followed by* decomposition *of the* 1:1 *complex when added to chlorinated hydrocarbons* in *which the fullerene* is *only sparingly soluble (Scheme* 1). *Significant advances were made in understanding the nature of the host–guest*

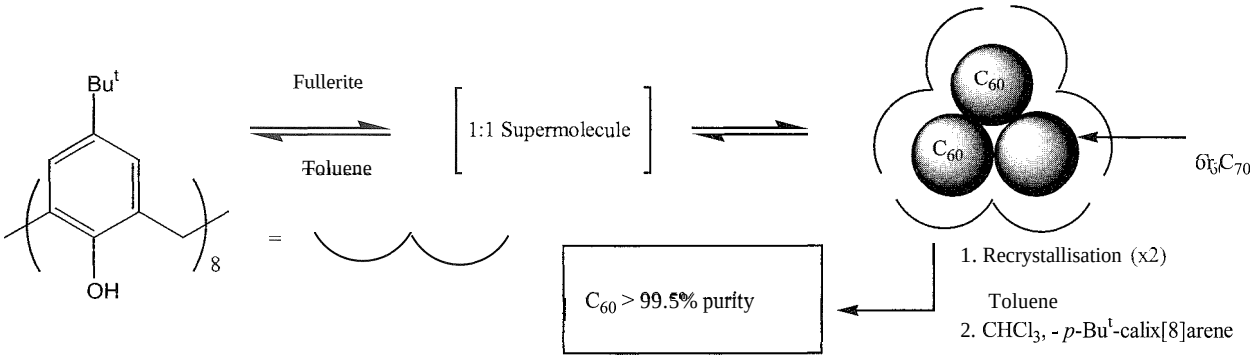

Scheme 1 Purification of C_{60} by complexation

complex,[2] albeit with some conflicting reports. The *p*-Bu^t-calix[8]arene/C_{60} complex has a resonant inter-fullerene molecular transition at 470 nm, similar to that observed in thin films of C_{60}.[2] Formation of the cornplex is thought to involve a monomeric 1:1 transient intermediate that may be a genera! phenomenon for complexation of the fullerene with other host molecules. The proposed structure of the final complex is a triangular arrangement of three fullerenes surrounded by a sheath of three calixarenes in the double-cone conformation. [$(C_{60})_3$(*p*-Bu^t-calix[8]arene)$_3$] (Scheme 1). In contrast. the vibrational spectrum of the complex was probed, using Raman. IR. and neutron scattering,'" with the results consistent with the C_{60} molecules being almost isolated. suggesting that any fullerene–fullerene interactions are weak.

The electrochemistry of the *p*-Bu^t-calix[8]arene/C_{60} complex was extensively studied with the complex breaking apart on reduction (at 400 mV more negative potential).'" Other calix[8]arene complexes were reported, **1**, $n=8$. R = Pr^i and Et, R′ = H,[25] but they also were not structurally authenticated.

Fullerene C_{70} does not form a complex with the same calixarene in toluene. but it does so in benzene. crystallizing as the 2:1 complex, $(C_{70})_2$(*p*-Bu^t-calix[8]arene) (structme unknown).[25] The same fullerene also forms a 2:1 complex with *p*-Bu^t-calix[6]arene, and its precipitation from toluene solutions can be used to retrieve 87% purity C_{70} from C_{60}-depleted fullerite.[26]

Calix[6]arenes, **1**, $n=6$

The fullerene-rich calix[6]arene complexes. (C_{60} or $C_{70})_2$calix[6]arene, were structurally authenticated as isomorphous complexes,[2] showing the calixarene in the double-cone conformation with a fullerene perched in each of the shallow cavities. resembling the jaws of a pincer acting on two adjacent cage molecules; the extended structures have continuous three-dimensional interplay of the fullerenes close to the van der Waals limit (Fig. 2j). In the case of the C_{70} complex, the principle axis of the fullerene is aligned such that the end of the fullerene close to this axis, where the curvature of the cage is similar to that of C_{60}, resides in the cavity. Calix[6]-arenes bearing *N*,*N*-dialkylaniline or m-phenylenediamine units also form complexes of C_{60} in toluene solution (ill defined).

Calix[5]arenes, **1**, $n=5$

These can be grouped with oxacalix[3]arenes (see below), because they have single-cone conformations. at least for R' = H, which have a cyclic hydrogen bond array, and they have good complementarity of curvature with fullerene C_{60}.[2] In addition, there is the potential for "symmetry matching," whereby the fullerene lines up with the C_5 or C_3 symmetry axis of the cavitand, thereby optimizing π...π overlap between the synthons. For both calixarenes, there is little or no preorganizational requirement prior to forming host–guest interactions; unlike for the more flexible. larger-ring systems for calix[6,8]arenes.

Calix[5]arene, **1.** $n=5$, R = R′ = H, forms a complicated 4:5 complex with C_{60},[27] where the fullerenes assemble into five closed packed columns in a Z-arrangement. surrounded by a sheath of calixarenes (Fig. 2g). Initially. the complex was thought to be a 1:1 complex, and in this context, care needs to be exercised in establishing the stoichiometry of fullerene host–guest complexes. Moreover, the presence of otiher fullerenes and other globular molecules in solution dramatically changes the nature of the crystalline complex. In the presence of C_{70}, which is the other major fullerene in fullerite, a 1:1 calixarene:C_{60} complex forms with NO C_{70} incorporated in the structure, which is now comprised of a single zigzag array of fullerenes surrounded by a sheath of calixarenes

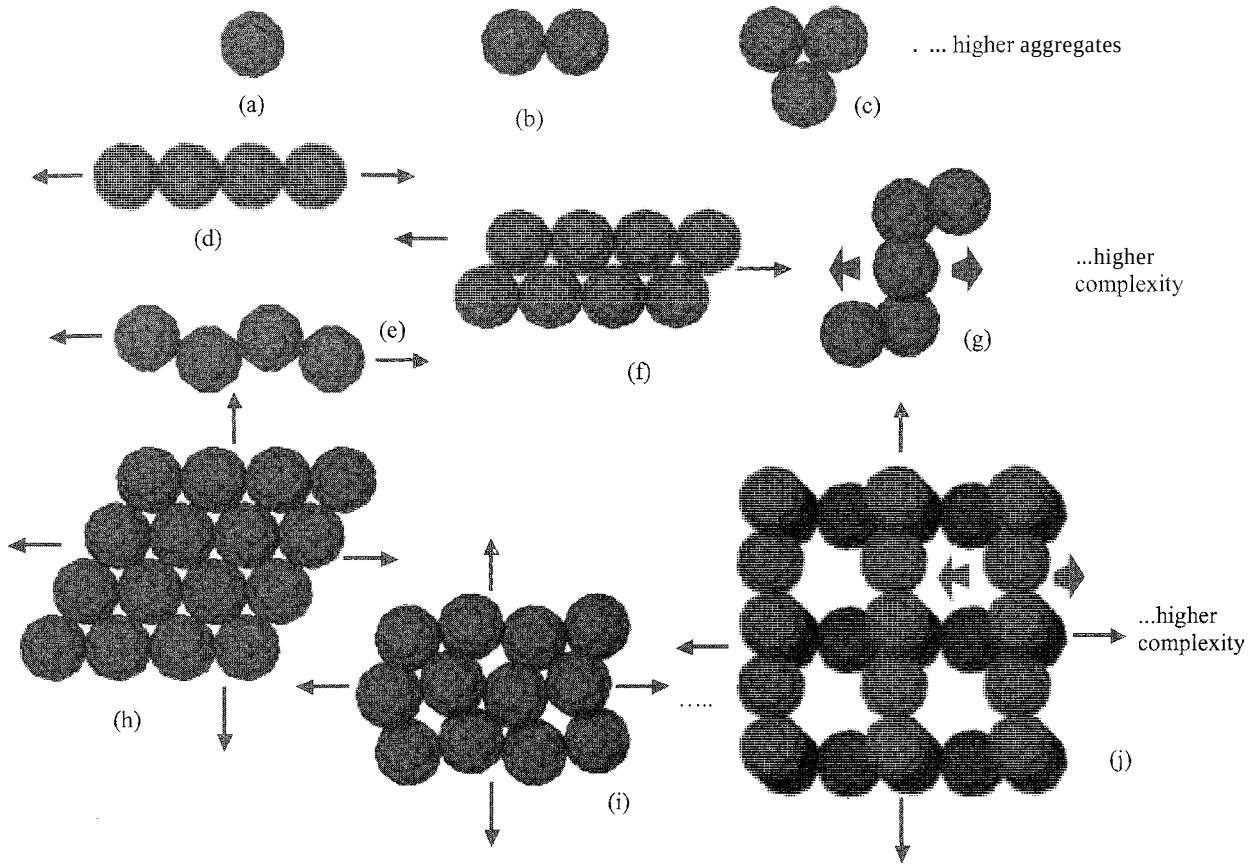

Fig. 2 The types of arrangements of fullerenes (van der Waals contacts) in their host–guest complexes (host molecules not shown). These cover finite structures. (a) monomeric (encapsulated). (b) dimeric. and (c) the proposed trimeric complex involving *p*-Bu^t-calixa[8]arene,[2] and higher aggregates. and continuous structures, all of which were established in parts (d–j),[2,27] with scope for structures of higher complexity. (*View* this *art in* color at *www.dekker.com.*)

(Fig. 2e). This is despite solution-binding constants favoring C_{70} complexation of C_{60}, and thus crystal-packing forces are important. The same 1:1 complex also forms in the presence of C_{84} and 1.2-dicarborane (1,2-$C_2B_{10}H_{12}$), an icosahedral molecule that is independently drawn into the cavity of the calixarene.[2]

p-Benzylcalix[5]arene forms 2:1 complexes with C_{60}. The fullerene is shrouded by two staggered *trans*-host molecules that are in the cone conformations with dangling benzyl groups (Figs. 2a and 3).[2,28] There is alignment of the symmetry axis of the calixarene with a C_5 symmetry element of C_{60}. However, in the case of *p*-phenylcalix[5]arene,[29] the rigid extended arms interdigitate on one hemisphere of the 2:1 supermolecule such that symmetry matching for both calixarenes is not possible. and interestingly. the fullerene here is now completely disordered.[''''] Other authenticated structures with C_{60} encapsulated by two calix[5]arenes, hence precluding

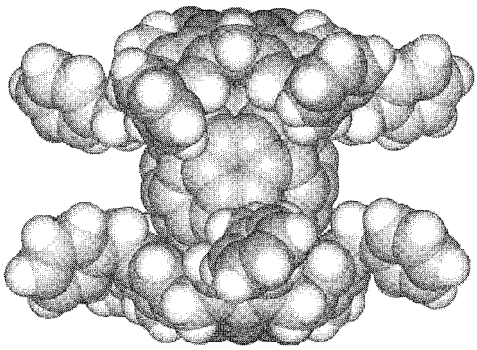

Fig. 3 Space-filling arrangement of the 2:1 supermolecules in [C_{60}⊂(*p*-benzylcalix[5]arene)2].8(toluene). (From Ref. [2].) (*View* ***this*** art *in* color *at www.dekker.com.*)

interfullerene contacts, is a calix[5]arene complex with three methyl and two iodo groups (1,3 disposition) in the p-positions of the upper rim.[2]

Solutions studies on complexation of **1**, R = benzyl, R' = H, with C_{60} in toluene gives a high K_1 association constant (2800 ± 200 dm^{3}mol^{-1}) and a relatively low K_2 (230 ± 50 dm^{3}mol^{-1}). This is consistent with the initial formation of a 1:1 complex [$C_{60} \subset$ (**1**)] (*cf* calix[8]arene intermediate. Scheme 1), followed by the formation of a 2:1 supermolecule, [$C_{60} \subset (\mathbf{1})_2$], and is in agreement with densitometry studies.[2] Similar UV/Vis studies involving 2, R = benzyl. R' = H, suggest the presence of more than one species in solution. In contrast, Fuji et al. obtained a 1:1 association constant of 35.6 dm'mol' for a related oxacalixarene (*R*= Bu^t, *2)* (or 64 ± 5 dm^{3}mol^{-1} for an independent study); and obtained 1:1 complexes rather than a 2:1 complex in the solid state, showing interfullerene interactions.[2] Other solution studies on calix[5]arenes were also reported.[27] including the electrochemical behavior of C_{60} with *p*-Bu^t-calix[5]arene[2] and *p*-benzylcalix[5]arene (solution and solid state).[28] Two calixarenes covalently linked show exceptional affinity for binding fullerenes (Fig. 4). One such system has a space between the calixarenes capable of binding metal ions (Fig. 4), and metal complexation triggers complexation of the fullerene, selectively for C_{70}.[30] Hydrogen bonding through urea moieties of single substituted calix[5]arene is another approach to entrap C_{60}, which can be retrieved under acidic conditions. The coinplexation proceeds via a 1:1 supermolecule that then takes up a second functionalized calixarene (association constants 450 and 110 dm'mol', respectively). The findings have major implications in the separation of fullerenes.[31] Elaborate monofunctionalized metal-complexed calix[5]arenes and bis-calixarenes (Fig. 4) can act as highly selective sensors for the detection of C_{60} and C_{70}.[32]

Calix[4]arenes and calix[4]resorcinarenes

The cavity of these calixarenes is usually too small to accommodate fullerenes, and is confirmed by solution, unless they have extended cavity walls as in calix[4]-naphthalenes.[27] Nevertheless, some calix[4]arenes were shown to form stable crystalline complexes with C_{60} with the fullerene eno- to the calixarene cavity. and they include *p*-Ph-calix[4]arene, which has a toluene molecule in the cavity, the overall structure dominated by fullerene–fullerene and eso-calixarene fullerene interactions;[2] *p*-Br-calix[4]arene propyl ether, the structure showing very close interfullerene contacts in a columnar structure (Fig. 2d), which most likely results in opposing induced dipoles from the unidirectionally aligned calixarenes;[34] and *p*-I-calix[4]arene benzyl ether. where the fullerenes are ordered without appreciable interfullerene interactions.[27] There is also a calix[4]resorcinarene, $R = CH_2CH_2Ph$, **3**, which has a molecular capsule derived from head-to-head hydrogen bonding of two resorcinarenes and propan-2-01 molecules, with the fullerenes also

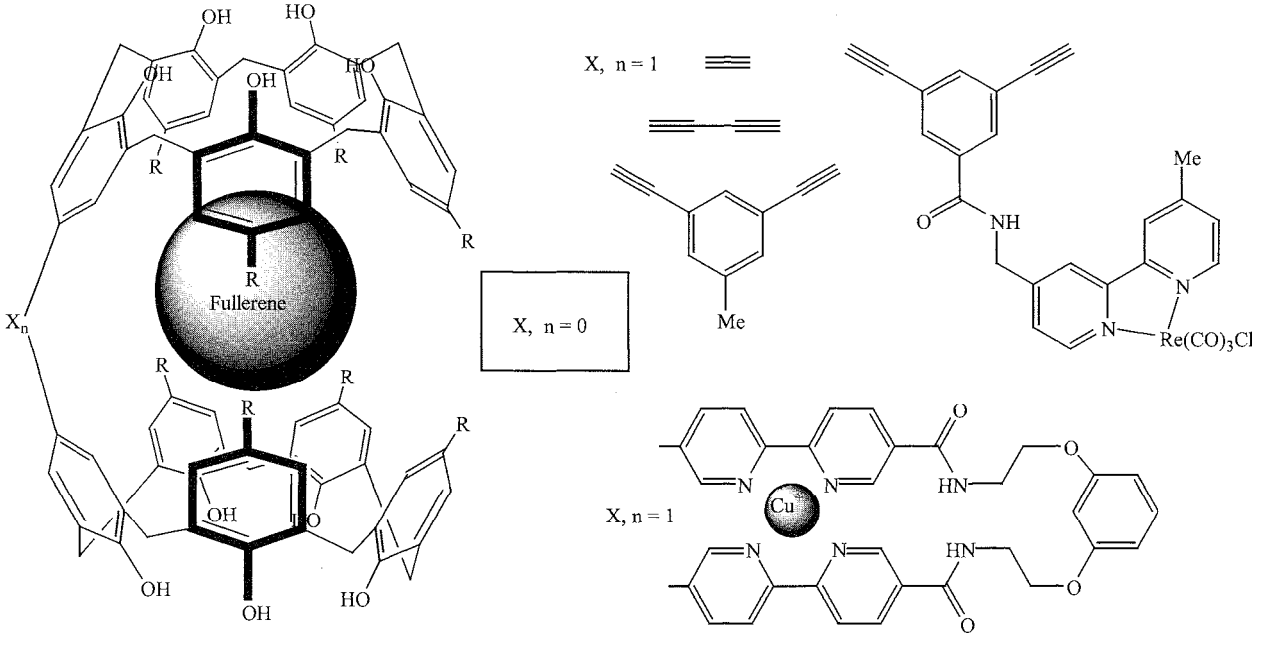

Fig. 4 Encapsulation of fullerenes by bridged calix[5]arenes. (From Refs. [30,32].)

arranged in columns.[2] A *bis*-calix[4]resorcinarene is effective in binding C_{60} (cf. his-calixarenes; Fig. 4),[35] and calix[4]resorcinarenes bearing dithiocarbamate groups between the oxo group, R = alkyl chains, and with methylene groups between adjacent 0x0-groups, 3, form torus-shaped complexes comprised of three calixarenes with divalent cadmium and zinc ions, which effectively bind C_{60}.[36]

The four-fold symmetry of calixarenes and resorcinarenes relates to complexation of the siloxane. 8, with C_{60} in toluene.[2] Here the fullerenes are arranged in double columnar arrays shrouded by edge on siloxanes (Fig. 2f), the siloxanes interlocking by one of the phenyl groups of one molecule residing in the cavity of another.

Oxacalix[3]arenes 2

These calixarenes form 2:1 complexes with C_{60} and include R = benzyl. R' = H, for which the complex was structurally authenticated (see above);''' R = 4-pyridyl, R' = $CH_2C(O)OEt$, which can be assembled with Pd^{2+} via pyridyl complexation into hexacationic capsules confining C_{60} (NMR studies);'''' and R = Bu^t, R' = water-solubilizing $CH_2C(O)N(H)(CH_2)_3NMe_3^+$.[38] Here the hexacationic capsules assemble as a monolayer on anion-coated gold surfaces and indium tin oxide surfaces. For the structure including R = benzyl. the benzyl groups are edge-on to the fullerene with C-H...fullerene interactions rather than face-on for n...π interactions.

Cyclotriveratrylene, 4

Complexation of C_{60} in toluene solutions of CTV. 4, R = R' = Me, results in poiymeric structures in the solid. either a fullerene-rich phase $(C_{60})_{1.5}$(CTV) or a 1:1 phase (C_{60})(CTV),[2,39] both complexes being studied electrocheinically (solution and solid state). The structures are dominated by fullerene–fullerene interactions, and each CTV has a C_{60} associated within the cavity of the CTV as a ''ball and socket'' nanostructure. For $(C_{60})_{1.5}$(CTV), the fullerenes collectively comprise a two-dimensional close-packed array with half of the fullerenes devoid of CTV (Fig. 2h).[2] Solvated host–guest species, [(CTV)(C_{60})], are formed first in solution. This results in polarization of the fullerene promoting aggregation, which is evident by a resonant interfullerene transition band as 475 nm. The substituted analogue 4. R = Me, R = allyl, with C_{60} shows only solvated host–guest species. C_{70} does not form an isolable complex with CTV. yet remarkably in the presence of 1.2-dicarborane, a ternary complex results with each fullerene in the cavity of a CTV. and each of these supermolecules is linked by bifurcated H-bonding to two carborane molecules. forming a helical arrangement. Thus. additional synthons can encourage host–guest chemistry.[2]

The incorporation of aromatic pendant arms on CTV leads to strong binding of C_{60}, that of *N*-methylpyrrole showing the highest association constant, 48×10^3 dm^3mol^{-1} in benzene. With six benzoyl arms. a 1:1 complex forms in the solid state. with two host molecules surrounding one fullerene, with a second ''bare'' C_{60} in the lattice.[2] The host molecule, R = benzoyl, 4. can be used to retrieve C_{60} from fullerite A planar analogue of CTV with a central six-membered ring (without the bridging methylene units of CTV) forms a 1 2 complex in the solid state. with isolated fullerenes surrounded by four planar molecules.[40]

Metal Macrocycles

Nonaromatic macrocycles 5

These have two divergent concave surfaces in a saddle-shape arrangement that arises from the otherwise unfavorable interactions between the methyl groups and the adjacent H-atoms on the aromatic rings. It can act as a divergent heterotopic receptor toward C_{60}. In the structure of (C_{60})Ni(TMTAA) (5, R = H, R' = R'' = Me), two host molecules shroud the fullerene such that a fullerene is in the saddle of one Ni(TMTAA) molecule with the methyl groups directed toward it and in the opposite saddle of another Ni(TMTAA) molecule, the overall host–guest contacts form a continuous zigzag array. with the fullerenes forming a corrugated two-dimensional sheet (Fig. 2i).[2] Cu(II) and Zn(II) TMTAA molecules similarly bind C_{60} and are isostructural with the Ni(II) analogue. For R = Me, **5**, (=OMTAA), a 1:1 complex is formed with C_{60} with the extended supramolecular array based on linear chains of close contact C_{60} molecules, and linear chains of n-stacked alternating molecules of C_{60} and Ni(OMTAA), with adjacent chains running in opposite directions and thus cancelling out dipole moments. The same macrocycle forms a 1:1 complex with C_{70}, which is isostructural with the C_{60} complex of Ni(TMTAA). In all of these Ni(II) macrocycle structures, there are no significant contacts between the metal centers and the fullerenes. As in other systems, there is evidence for the formation of 1:1 solvated supermolecules in solution. which then go on to form micelle-like species.''' The unsymmetrical macrocycle, **5**. R = H. R' = Me, R'' = Ph, also forms a 1:1 complex with C_{60}.[41]

Porphyrins, 6

Strong complexes form between n-curved surfaces of fullerenes. including C_{60}, C_{70}, Kr@C_{60}, NSc_3@C_{80}, and Er_2@C_{82}, and the airnost-planar π-surface of porphyrins,

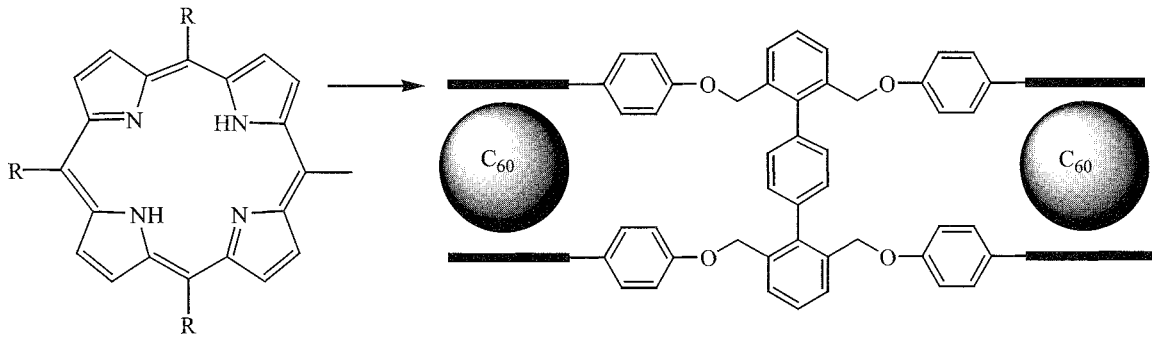

Fig. 5 A tertaporphyrin host designed for cooperative binding of C_{60} molecules (From Ref [47])

6. The most widely studied porphyrins are 6, $R = Et$, $R' = H$ (OEP), for M = Zn, Ru(CO), Pd, Cu, Ag, Ni, VO, Co, and Fe, with much of the work covered in a recent review article.[3] The complexes fall into two types: The first type includes ethyl groups in the *syn*-form, with the alkyl groups directed toward the fullerene, either one or two porphyrins associated with each fullerene (includes endohedral fullerenes).'''' and in the latter case, they almost shroud the fullerene. The second type includes four adjacent ethyl groups in either side of the porphyrin plane (*anti*-form), allowing slipped porphyrin–porphyrin contacts (includes endohedral fullerenes),[43] in structures where fullerene–fullerene contacts prevail.

Bulky groups incorporated into the porphyrin. 6, $R = H$. $R' = C_6H_3$-3,5-$(Bu^t)_2$, result in a 1:1 complex with C_{60}, but there is a fullerene on either side of the porphyrin, such that the continuous structure has the fullerene encapsulated. In the case of C_{70} complexes, the fullerene lies side-on to the principle axis, which maximizes $\pi\ldots\pi$ interactions with the flat porphyrin.[44] Amino-substituted porphyrins. 6, $R = NMe_2$, $R' = H$, M = Ni or Cu, or where the porphyrin is metal free, show a variety of structural types.[45] More elaborate porphyrin ligands were developed, including covalently linking two units to shroud a fullerene,[46] and attaching four units around a terphenyl axis (Fig. 5),[47] and assembling two porphyrins via metal complexation to form a "jaws porphyrin" host.[48] In this context, dendritic porphyrins strongly bind fullerenes.[14,15] A silica-supported zinc(II) tetraphenylporphyrin is effective in separating metallofullerenes from C_{60} and higher fullerenes (HPLC).[2]

CONCLUSION

The original work focused mainly on the larger -!-cyclodextrin, **11.** $n = 8$,[49] associated with solubilizing fullerenes in aqueous media, which was achieved for more hydrophobic cavitands, namely, lower-rim sulfonated calix[8]arenes[2] and amine-substituted oxacalix[3]arenes.[40] which are of interest in the separation of fullerenes as well as in biomedical applications. Earlier work used heterogeneous reaction to effect complexation, and here there is no binding with α- or β-cyclodextrins, **11,** $n = 6$ and 7, respectively. This was thought to be a consequence of the smaller cavity size of these cyclodextrins.[50] However, by using a mixed DMF/toluene solvent system, now as a homogeneous reaction, a 2:1 complex results, and the isolated complex is water soluble, 4 gL^{-1}. Covalently attaching fullerenes to cyclodextrins also results in binding in the cavity of two β-cyclodextrins, also as a water-soluble complex.[51]

ARTICLES OF FURTHER INTEREST

Calixarenes and Their Analogues: Molecular Complexation, p. *145*
Concave Reagents, p. *311*
Concepts in Crystal Engineering, p. 319
Fullerenes as Encapsulating Hosts: Preparation, Detection, and Structures of Endohedral Fullerenes, p. 579
Self-Assembling Capsules, p. *1231*

REFERENCES

1. Raston, C.L. Complexation of Fullerenes. In *Comprehensive Supramolecular Chemistry*; Atwood, J.L., Davies, J.E.D., Macnicol, D.D., Eds.; Vogtle, Pergamon: Oxford, 1996; Vol. 1, 777–787.
2. Hardie, M.J.; Raston, C.L. Confinement and recognition of icosahedral main group cage molecules: Fullerene C_{60} and o-, *m*-, *p*-dicarbadodecaborane(12). Chem. Commun. 1999. 1153–1163.
3. Ishii, T.; Aizawa, N.; Kanehama, R.; Yamashita, M.; Sugiura, K.; Miyasaka, H. Cocrystallites consisting of

metal macrocycles with fullerenes. Coord. Chem. Rev. 2002. *226.* 113–124.
4. Diedrich, F.: Comez-Lopez. M. Supramolecular fullerene chemistry. Chem. Soc. Rev. 1999. 28. 263–277.
5. Konarev, D.V.; Lyubovskaya, R.N.; Drichko, N.V. Donor–acceptor complexes of fullerene C_{60} with organic and organometallic donors. J. Mater. Chem. 2000. *10.* 803.
6. Balch, A.L.: Olmstead. M.M. Reactions of transition metal complexes with fullerenes (C_{60}, C_{70}, etc.) and related materials. Chem. Rev. 1998. *98.* 2123.
7. Olmstead. M.M.: Maitra. K.: Blach. A.L. Formation of a cur\ed silver nitrate network that conforms to the shape of C_{60} and encapsulates the fullerene. Angew. Chem.. Int. Ed. Engl. 1999. *38.* 231–233.
8. Zhou. S.: Burger. C.; Chu. B.: Sawamura, M.: Nagahama, N.; Toganoh, M.; Hackler, U.E.; Isobe, H.: Nakamura. E. Sperical bilayer vesicles of fullerene-based surfactants in water: A laser light scattering study. Science 2001, *291.* 1944–1946.
9. Guldi, D.M.; Martin. N. Fullerene architectures made to order. Biomimetic motifs—Design and features. J. Mater. Chern. 2002. *12.* 1978–1992.
10. Konarev. D.V.: Khasanov, S.S.: Otsuka. A.; Yoshida, Y.; Saito. G. Synthesis and crystal structure of ionic multi-component complex. J. Am. Chem. Soc. 2002. *124.* 7648–7649.
11. Ruiz. J.: Pradet. C.; Varret. F.; Astruc. D. Molecular batteries: Synthesis and characterisation of a dendritic 19-electron Fe^{I} complex that reduces C_{60} to its mono-anion. Chem. Commun. 2002. 1108–1109.
12. Majoral. J.-P.: Caminade, A.-M. Dendrimers containing heteroatoms (Si, P. B. Ge. Bi). Chem. Rev. 1999. *99.* 845–880.
13. Nierengarten, J.-F.: Oswald, L.: Eckert, J.-F.: Nicoud. J.-F.; Armaroli. N. Complexation of fullerenes with dendritic cyclotriveratrylene derivatives. Tetrahedron Lett. 1999. *40.* 5681–5684.
14. Ayabe. M.: Ikeda, A.; Kubo, Y.: Takeuchi. M.: Shinkai, S. A dendritic porphyrin receptor for C_{60} which features a profound positive allosteric effect. Angew. Chem.. Int. Ed. Engl. 2002. *41,* 2790–2792.
15. Kimura. M.: Saito. Y.: Hanabusa. K.: Shiral. H.; Kobayashi, N. Self-organization of supramolecular complex composed of rigid dendritic porphyrin and fullerene. J. Am. Chem. Soc. 2002. *124,* 5274–5275.
16. Jenekhe, S.A.: Chen. X.L. Self-assernbled aggregates of rod-coil block copolymers and their solubilisation and encapsulation of fullerenes. Science 1998, *279.* 1903–1906.
17. Mizyed. S.; Geroghiou, P.E.: Bancu, M.: Cuadra, B.: Rai. A.K.: Cheng. P.: Scott. L.T. Embracing C_{60} with multiarmed geodesic partners. J. Am. Chem. Soc. 2001. *123.* 12770–12774.
18. Yamaguchi, U.: Kobayashi, S.: Amita. N.: Wakamiya, T. Creation of nano-scale oxaarenecyclynes and their C_{60} complexes. Tetrahedron Lett. 2002. 43. 3277–3280.
19. Veen, E.M.: Postma, P.M.: Jonkman, H.T.; Spek. A.L.: Feringa. B.L. Solid state organization of C_{60} by inclusion crystallisation with triptycenes. Chem. Commun. 1999. 1709–1710.
20. Ikeda, A.; Suzuki. Y.: Yoshimura. M.: Shinkai. S. On the prerequisites for the formation of solution complexes from [60]fullerene and calix[n]arenes: A novel allosteric effect between [6]fullerene and metal cations in calix[-n]aryl ether complexes. Tetrahedron 1998. *54.* 2497–2508.
21. Konarev, D.V.: Kovalevsky, A.Y.: Coppens, P.; Lyubovskaya, Synthesis and crystal structure of a C_{60} complex with a bis(ethylenedithio)tetrathisfulvalene radical salt: [BEDT-TTF.I_3)C_{60}. Chem. Commun. 2000. 2358–2359.
22. Moller. K.; Bein. T. Inclusion chemistry in periodic niesoporous hosts. Chem. Mater. 1998. *10.* 2950–2963.
23. Okazaki, T.; Suenaga. K.; Hirahara. K.: Banow. S. Iijima, S.: Shinohara. H. Real time reaction dynamics in carbon nano-tubes. J. Am. Chem. Soc. 2001. *123.* 9673–9674.
24. Sun, D.: Reed. C.A. Crystal engineering a linear polymer of C_{60} fullerene via supramolecular pre-organisation. Chem. Commun. 2000, 2391–2392.
25. Haino, T.: Yanase, M.: Fukazawa, Y. New supramolecular complex of C_{60} based on calix[5]arene—Its structure in the crystal and in solution. Angew. Chem., Int. Ed.. Engl. 1997. *36.* 259–260.
26. Atwood, J.L.; Koutsantonis, G.A.: Raston. C.L. Purification of C_{60} and C_{70} by selective complexation with calixarenes. Nature 1994. *368.* 229–312.
27. Atwood. 3.L.: Barbour. L.J.: Raston. C.L. Supramolecular organization of C_{60} into linear columns of five-fold. Z-shaped strands. Cryst. Growth Des. 2002, *2,* 3–6.
28. Bond, A.M.; Miao. W.: Raston, C.L.: Sandoval, C.A. Electrochemical, EPR. and magnetic studies on micro-crystals of the [C_{60}⊂(*p*-benzylcalix[5]arene)$_2$].8toluene and its one-electron-reduced encapsulation complex. J. Phys. Chem.. B 2000. *104.* 8129–8137.
29. Majaka, *M.:* Hardie. M.J.; Raston. C.L. Inter-digitation approach to encapsulation of C_{60}:[C_{60}⊂(*p*-phenylcalix[5]-arene)$_2$]. Chem. Commun. 2002. 1446–1447.
30. Haino. T.; Yamanaka, Y.: Araki, H.: Fukazawa. Y. Metal-induced regulation of fullerene complexation with double-calix[5]arene. Chem. Commun. 2002. 402–403.
31. Yansase. M.: Haino, Y.; Fukazawa. Y. A self assembling molecular container for fullerenes. Tetrahedron Lett. 1999. *49.* 2781–2784.
32. Haino. T.: Araki. H.: Fujiwara, Y.: Tanimoto. Y.: Fukazawa. Y. Fullerene sensors based on calix[5]arene. Chern. Commun. 2002. 2148–2149.
33. Mizyed. S.; Tremaine. P.R.: Ceorghiou. P.E. Partial molar volume study of the complexes of calix[4]naphthalenes with [60]fullerene in different solvents. J. Chem. Soc.. Perkin Trans. 2001: (2). 3–6.
34. Barbour. L.J.; Orr, G.W.; Atwood. J.L. Supramolecular assembly of well-separated. linear columns of closely-spaced C_{60} molecules facilitated by dipole interactions. Cheni. Commun. 1998. 1901–1902.
35. Wan, Y.; Mitkin. O.: Barnhurst, L.: Kurchan. A.; Kutateladre. A. Molecular assembly and disassembly: Novel photolabile molecular hosts. Org. Lett. 2000. *2.* 3817–3819.
36. Fox. G.D.: Drew, M.G.B.; Wilkinson. E.J.S.; Beer, P.D. Cadmium- and zinc-directed assembly of a llano-sized.

resorcinarene-based host architecture which strongly bind C_{60}. Chern. Commun. **2000,** 391–392.

37. Ikcda, A.; Yoshimura, M.; Udzu, H.; Fukuhara. C.; Shinkai, S. Inclusion of [60]fullerene in a homooxacalix[3]arene-based dimeric capsule cross-linked by a Pd^{II}-pyridine intercalation. J. Am. Chem. Soc. 1999. *121,* 4296–4297.
38. Ikeda. A.; Hatana, T.; Shinkai, S.; Akiyama, T.; Yamada, S. Efficient photocurrent generation in novel self assembled multilayers comprised of [60]fullerene-cationic homooxacalix[3]arene inclusion complex and anionic porphyrin polymers. J. Am. Chem. Soc. **2001,** *123*, 4855–4856.
39. Bond, A.M.; Miao, W.; Raston, C.L.; Ness, T.J.; Barnes, M.J.; Atwood, J.L. Electrochemical and structural studies on microcrystals of the $(C_{60})_x$(CTV) complexes (x = 1, 1.5: CTV = cyclotriveratrylcnc). J. Phys. Chern., B **2001,** *105*, 1687–1695.
40. Chiang, L.Y.; Swirczewski, J.W.; Liang, K.; Millar Synthesis and complex crystal structure of C_{60} with symmetrical donor of 2,3,6,7,10,11-hexamethyltriphenylcne (HMT). J. Chern. Lett. 1994. 981.
41. Soldatov, D.V.; Diamente. P.R.; Ratcliffe, C.L.; Ripmeester, J.A. (6,17-Dimethyl-8,15-diphenyldibenzo[*b,i*][1.4.8.11]-tetra-aza[14]annulenato)nickel(II) in solids: Two guest-free polymorphs and inclusion compounds with methylene chloride. Inorg. Chcm. **2001**, *40,* 5660–5667.
42. Olmstead, M.M.; Bettencourt-Dias, A. de: Stevenson, S.; Dorn, H.C.; Balch, A.L. Crystallographic charactcrisation of the structure of the endohedral fullerene $\{Er_2@C_{82}$ isomer I). J. Am. Chcm. Soc. **2002,** *124,* 4172–4173.
43. Lee, M.H.; Olmstead, M.M.; Suctsuna, T.; Shimotani, H.; Dragoe, W.; Cross, R.J.; Kitazawa, K.; Balch, A.L. Crystallographic characterisation of $K@C_{60}$ in $(0.09Kr@C_{60}/0.91C_{60}).\{Ni^{II}(OEP)\}.2C_6H_6$. Chcm. Commun. **2002**, 1352–1353.
44. Konarev, D.V.; Nerctin, I.S.; Slovokhotov, Y.L.: Yudanova, E.I.; Drichko, N.V.; Shul'ga, Y.M.; Tarasov, B.P.; Gumanov, L.L.; Hatsanov, A.S.; Howard. J.A.K.; Lyubovskaya, R.N. New molecular complexes of fullerene C_{60} and C_{70} with tetraphcnylporphyrins [M(tpp)], in which M = H_2, Mn, Co, Cu, Zn, FeCl. Chem. Eur. J. **2001.** 7. 2605–2616.
45. Hochmuth, D.H.; Michel, S.L.J.; White. A.P.J.; Williams, D.J.; Barret. A.G.M.; Hoffman: H.M. C_i Symmetric and non-centrosymmctric crystalline complcxcs of [60]fullerene with octakis(dimethylamino)porphyrazinato-copper(II) and -nickel(II). Eur. J. Inorg. Chem. **2000**, 593–596.
46. Zheng, J.-Y.; Tashiro, K.; Hirabayashi, Y.; Kinbara. K.: Saigo, K.; Aida, T.; Sakamaoto, S.; Yamaguchi, K. Cyclic dimers of metalloporphyrins as tunable hosts for fullerenes: A remarkable effect of Rhodium(III). Angew. Chem., Int. Ed. Engl. **2001,** *40,* 1858–1861.
47. Kubo. Y.; Sugasaki, A.; Ikcda, M.; Sugiyasu, K.; Sonoda. K.; Ikeda, A.; Takeuchi, M.; Shinkai. S. Coperative C_{60} binding to a porphyrin tetramer arranged around a p-terphenyl axis in 1:2 host–guest stoichiometry. Org. Lett. **2002,** *4*. 925–928.
48. Sun; *D.;* Tham, F.S.; Reed, C.A.; Chaker. L.; Boyd, P.D.W. Supramolecular fullerene–porphyrin chemistry. Fullerene complexation by metalled "jaws porphyrin" hosts. J. Am. Chem. Soc. **2002,** *124*, 6604–6612.
49. Cyclodextrins. In *Comprehensive Supramolecular Chemistry*; Atwood, J.L., Davies, J.E.D., MacNicol, D.D., Vogtle, F., Eds.; Elsevier: New York, 1996: Vol. 3.
50. Murthy, C.N.; Geckeler. K.E. The water-soluble β-cyclodextrin-[60]fullerene complex. Chem. Commun. **2001,** 1194–1195.
51. Filipponc, S.; Heimann, F.: Rassat, A. A highly water-soluble 2:1 β-cyclodextrin-fullerene conjugate. Chem. Commun. **2002,** 1508–1509.

Concave Reagents

Ulrich Lüning
Universitat Kiel, Kiel, Germany

INTRODUCTION

The selectivity of enzymatic reactions is mainly caused by the concave shielding of the active site. However. enzymes do not exist for all purposes. For some substrates and reactions, no enzymes have yet been found. Furthermore, most enzymes do not survive extreme reaction conditions (high temperatures, concentrated salt solutions, extreme pH, nonaqueous solvents). Therefore, the concave geometry of enzymes has been combined with artificial reagents. Standard organic reagents and catalysts have been placed in a concave environment in order to amplify or alter selectivities. Such concave molecules need not be made from amino acids. Almost any building block of organic chemistry may be used. Therefore, the structural components can be varied broadly. In addition, if compared to enzymes. the molecular weights of concave reagents will be reduced, because no large amino acid backbone is necessary to build up the concave structure.

The key feature of these new synthetic tools is the concave shielding of the functional group. In order to guarantee a concave geometry, the concave reagents or concave catalysts" have to be very rigid (see cleft molecules) or the potential rotational freedom has to be limited to avoid the functional group from turning to the convex outside. This can be achieved by incorporating the functional group into a polymacrocycle (cavity molecules). In the latter case. the overall geometry of such a concave reagent can be compared to a lightbulb in a lamp shade: the lamp shade is the concave shielding. and the lightbulb is the reactive functionality. Several classes of such concave reagents have been realized. and the most prominent classes will be discussed below.

In principle, all functional groups of organic chemistry can be incorporated into a concave structure. Especially acids, bases. and transition metal ions have been investigated in detail. Shown in Fig. 1 are important examples of concave reagents.

[a]In the context of this article. the term concave reagent will not differentiate between reagents and catalysts.

SYNTHESES

Before any concave reagent can be employed in a reaction. it has to be synthesized in acceptable quantities. For the translation of the structure "lightbulb in a lamp shade" into molecular dimensions, one conceivable geometrical form is a bimacrocycle. In a concave reagent. the rim must be large enough to let a molecule or a part of a molecule pass for a contact with the lightbulb. Therefore. it must be macrocyclic. This macrocycle must then be spanned by a bridge that carries the functional group, the lightbulb. Therefore, at least bimacrocycles must be synthesized. Such a synthesis is not necessarily trivial. Nevertheless, for bimacrocyclic concave pyridines **1** and concave 1.10-phenanthrolines 2, cyclization methods have been established with more than 50% overall yield for the cyclization steps. For other classes. the yields are not yet optimized.

Kinetically and thermodynamically controlled macrocyclizations have been used. A kinetically controlled reaction has the advantage in that once a macrocycle is formed; it remains a macrocycle. In contrast. the products of a thermodynamically controlled equilibrium may be interconverted into one another. If the desired macrocycle is the most stable molecule. potential side products will be transformed into the desired bimacrocycle.

Among the "library" of potential macrocycles, oligo- and polymers, the concave 1,10-phenanthrolines **2b** are the thermodynamically most stable products and can be formed by ring-closing metathesis of the tetra-alkenylated precursors 4 (see Fig. 2) in excellent yields (>70–92% for a double macrocyclization).[7] In contrast, the first macrocyclization in the synthesis of the concave pyridines **1**. the formation of the macrocyclic diimines **7**, can only be realized using a thermodynamical approach if a stabilizing template ion is added. When mixing a dialdehyde **5** and one or more diamines 6, a huge variety of possible products is or can be formed. and only the addition of a suitable template ion. an earth alkaline ion in this case, will shift the equilibrium to one macrocycle **7.** The final stable macrocyclic dianiines **8** can be isolated after reduction. If the iibrary is large and contains several diamines 6, then the addition of more than one template ion can give more than one inacrocyclic diamine 8 in good yields (>70%) in parallel.[8]

Encyclopedia of Supramolecular Chemistry
DOI: 10.1081/E-ESMC 120012859

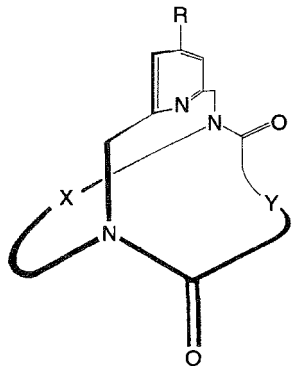

1

a R = OMe, X = $CH_2(CH_2OCH_2)_3CH_2$, Y = $(CH_2)_{10}$

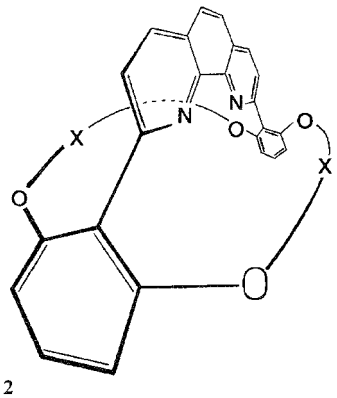

2

a X = $(CH_2)_n$ or $CH_2(CH_2OCH_2)_nCH_2$

b X = $(CH_2)_{n-1}(CH{=}CH)(CH_2)_n$,

c X = no chain, but two methyl groups

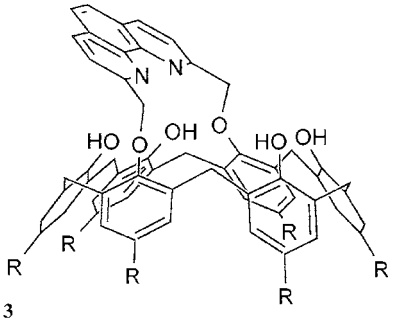

3

a: R = *t*Bu

Fig. 1 Important classes of concave reagents: concave pyridines **1**[1–3] and concave 1,10-phenanthrolines **2**[4,5] and **3**.[6] which may complex transition metal ions.

But in most macrocyclizations, thermodynamic control is not yet possible. These macrocyclizations have therefore been carried out under kinetic control, often using high dilution conditions. Typical reactions are the formation of lactams, for instance. in the second macrocyclization during the synthesis of concave pyridines **1** by reaction of the macrocyclic diamines **8** with diacid dichlorides,[1–3] or the reaction of calix[6]arene with dibromides to give A,D-bridged calix[6]arenes like **3** by a double substitution reaction.[11,12]

Not only cavity-containing molecules can be employed as concave reagents, but also, cleft molecules have been realized. The necessary stiffness usually is realized by an aryl-aryl backbone (Fig. 3). In particular, two classes of concave reagents have been successfully employed to enhance selectivities: concave reagents based on 2′-substituted *m*-terphenyls **10**[13–18] and 2,9-diaryl-1,10-phenanthroline-derived transition metal ion complexes **2c**·M^{n+}.[4,5,7,19,20] The key synthetic steps are the formation of the aryl–aryl bonds. The synthesis of *m*-terphenyls **10** uses the addition of Grignard compounds to dichloroiodoarenes like **9**.[13–18] The resulting 2′-magnesium function in the m-terphenyl **10** can then be transformed into a broad variety of other functional groups like Hal. Li, COOH (and its esters), CHO (and its acetals), CH=NOH, CH_2OH, $CH{=}CH_2$, SO_2Cl, SO_3H, SO_2H, SH, SAc, and H.[13–18] The stiff *m*-terphenyl moiety has been used successfully for these cleft molecules and also in bimacrocyclic concave reagents.[13–15] Due to its special geometry. the stabilization of less stable fiinctional groups like selenic and sulfenic acids is allowed.[21] 2,9-Disubstituted 1,10-phenanthrolines like **2c** or 4 can be obtained either by adding aryl lithium compounds to 1,10-phenanthroline and following with rearomatization[4,5] or by Suzuki coupling of areneboronic acids with 2,9-dihalogeno-1,10-phenanthrolines.[22]

REACTIONS

Three different classes of reactions have been investigated using concave reagents:

1. Stoichiometric use of concave reagents in protonations.
2. Base catalyses.
3. Catalyses by transition metal ions.

Protonations

All concave reagents carrying a proton within the cavity can be used as concave acids. This includes protonated concave bases. If a proton is delivered directly from the proton source to the substrate (general protonation[b]) and the protonation is irreversible, the concave shielding will

[b]The term general and specific protonation is used in the same sense as the terms general and specific acid catalyses are used: specific means that a specific protonated solvent molecule is the reacting species. while general means that in general, all acids in solution contribute to the reaction.

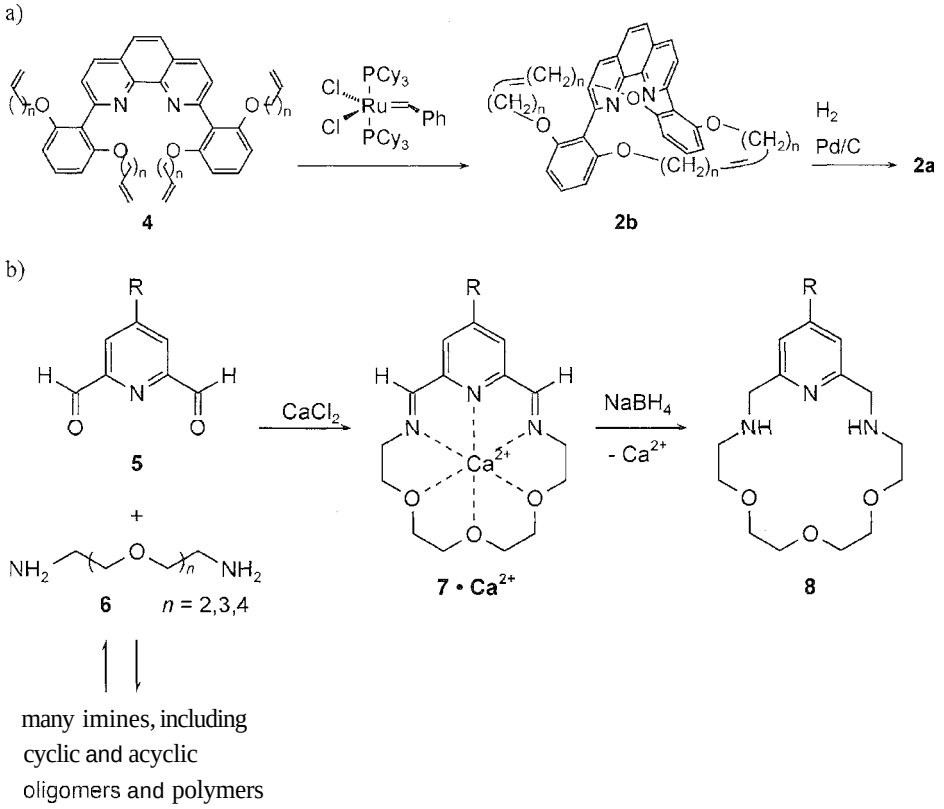

Fig. *2* Efficient syntheses of macrocycles for concave reagents using thermodynamic control for macrocyclizations: (a) Formation of concave 1,10-phenanthrolines 2 by ring-closing metathesis; (b) selection of niacrocyclic diimines **7** from a dynamic combinatorial library with the help of transition metal ions as templates and subsequent reduction to 8. here: formation of an 18-membered macrocycle by using Ca^{2+}.

influence the selectivity of the protonation (see Fig. 4a). Such a selective protonation would be extremely useful. especially if carried out stereoselectively, because most asymmetrically substituted carbon atoms carry a hydrogen atom as one of the four different substituents. But if

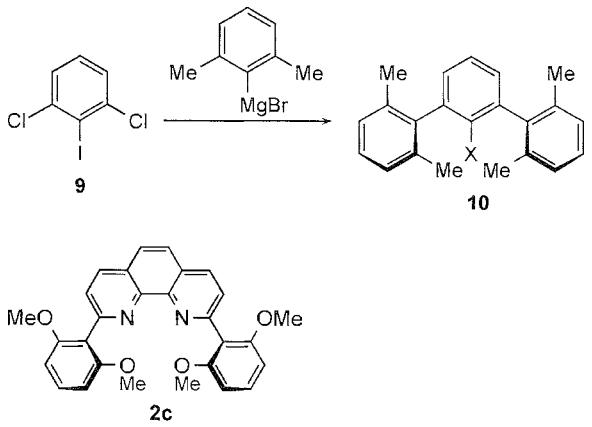

Fig. *3* Cleft molecules based on 2′-substituted *m*-terphenyls **10** (for X see text) and 2.9-diaryl-1,10-phenanthrolines like **2c**.

the acid protonates a solvent molecule first (k_{solv}), and this then transports the proton to the substrate (specific protonation[b]), then all proton sources will exhibit the same selectivity. Also. if the protonation is reversible (k_{deprot}), no influence of the proton source will be detectable, because the thermodynamical stability of the products would determine the selectivity. In order to avoid the equilibrium, the conjugate base of the acid should not be too basic, and the acid should not be too strong to avoid the protonation of the solvent. These limitations only allow a small window of acidities and basicities. and therefore, not too many examples for a selective kinetically controlled general protonation exist to date. However, some concave acids have been successfully employed in selective protonations.[23–25]

These selective protonations include the "soft Nef reaction" (Nef reaction in buffers at high pH), in which a nitronate ion is selectively protonated (proper buffer) to form the aci-nitro compound *aci*-**11** that ultimatively gives the corresponding carbonyl compound **12**.[26,27] Due to the steric shielding of the protons in the concave reagents. the competing C-protonation to give the nitro compound **11** is much slower (Fig. 4b).

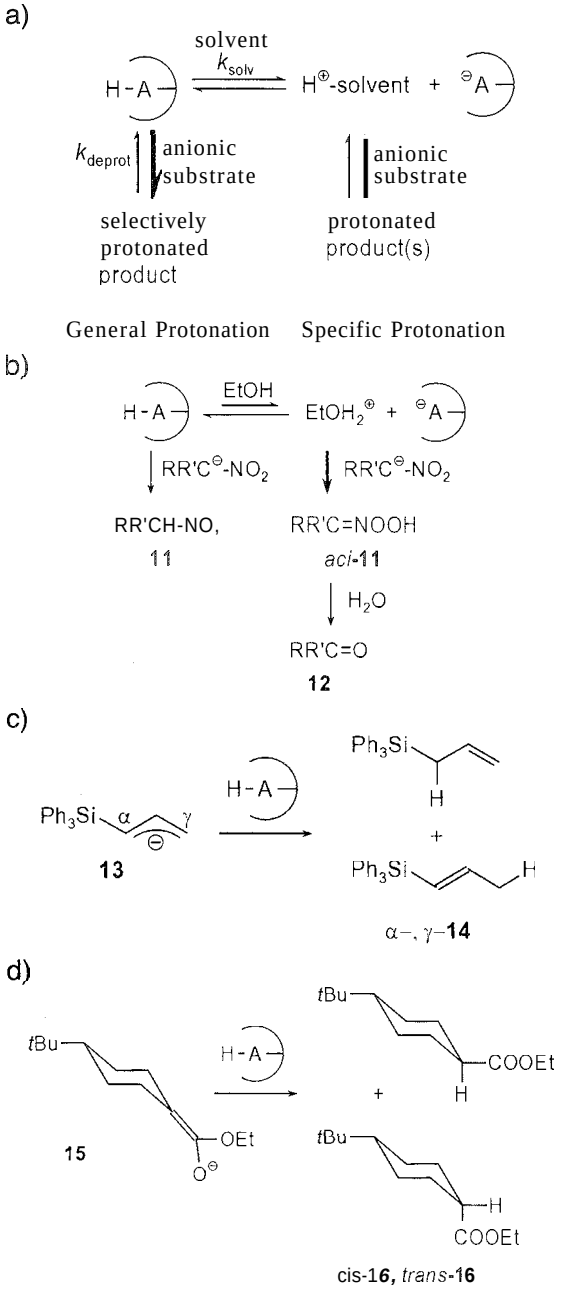

Fig. 4 (a) The change of the structure of an acid can enhance the selectivity of a protonation only in a kinetically controlled general protonation. (b) in the "soft Nef reaction,"[26,27] (c) in regioselective protonations of allyl anions.[25] and (d) in stereoselective protonations.[25]

A regioselective protonation (of allyl anions 13[25]) is also possible (Fig. 4c), as is the stereorelective protonation of esterenolates like 15 (Fig. 4d)[25] In the latter case, a contrathermodynamical diastereoselectivity (*cis/trans* for **15** or *threo/erythro* for noncyclic substrates) was observed, which was explained by a concave wrapping of the protons in the concave reagent. In the transition state, the wrapped proton is very large, while in the product. the transferred proton is the smallest substituent.

Base Catalyses

Pyridine is well known as a catalyst in organic reactions. However, in a large number of reactions, only pyridine is reactive. α-substitution diminishes the reaction rates considerably, because it hinders the reaction of pyridine as a nucleophile. The formation of hydrogen bonds to the nitrogen atom of a pyridine is also hindered by α-substitution but only if these substituents are huge (for example tert-butyl). Therefore, concave pyridines 1 also form hydrogen bonds, and they thus can be used, for instance, to enhance the nucleophilicity of hydroxyl groups. This has been exploited for the addition of alcohols to ketenes. and rate enhancements with several concave pyridines have been measured[28–30] (see Fig. 5).

In competition experiments, the relative rates for the addition of various hydroxyl groups to diphenylketene have been determined, and selectivity improvements have been found for inter- and intramolecular competitions.[28–30] Steric factors are dominant. and primary alcohols are added much faster than secondary ones. But by variation of the concave base. some concave pyridines could be identified that were able to differentiate even between similar secondary hydroxyl groups within one molecule. The glucose derivative 19 possesses two secondary. equatorial alcohol functions. Nevertheless. the 2-OH group can be acylated exclusively by using the concave pyridine 1a and diphenylketene.[31] With 2% of the catalyst and 85% conversion, only the 2-acylated carbohydrate 20 (not 3-acylated or doubly functionalized sugar) could be found. Also. a chinovose derivative could be acylated to give one out of seven conceivable products with 60% selectivity.[32]

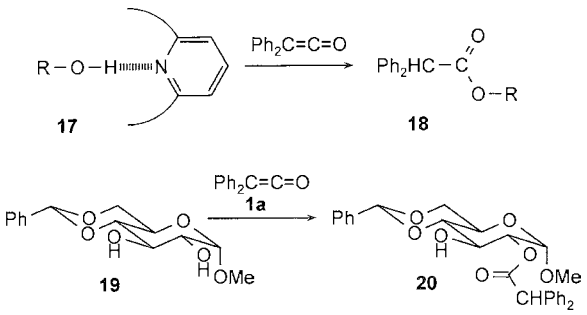

Fig. 5 Base-catalyzed addition of alcohols to diphenylketene. Formation of a complex 17 between a concave pyridine and an alcohol activates the OH group and facilitates the formation of the ester 18. When the concave pyridine Pa is used, the carbohydrate 19 can be acylated exclusively in 2-position to give 20.

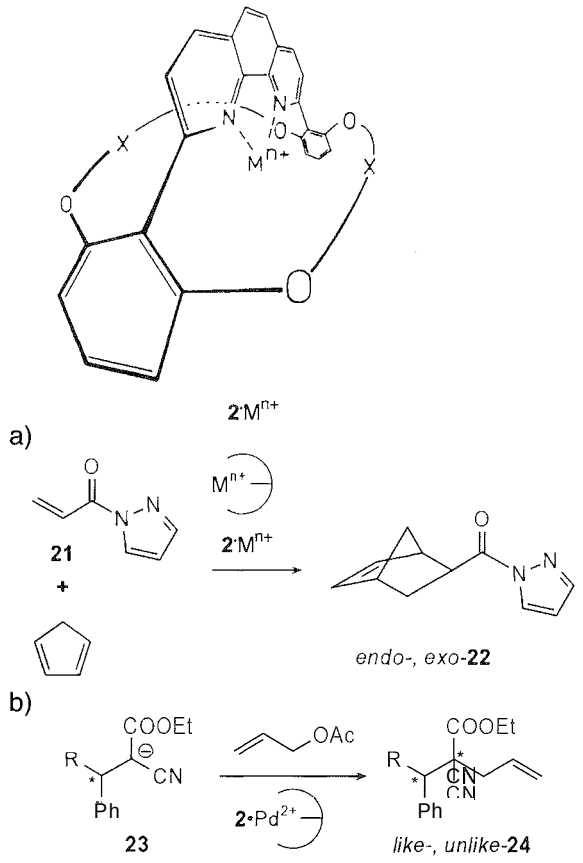

Fig. 6 (a) Transition metal ion complexes of concave 1,10-phenanthrolines $2{\cdot}M^{n+}$ can enhance the *exo*-selectivity of Lewis-acid-catalyzed Diels–Alder reactions. (b) The use of concave 1,10-phenanthrolines 2 as ligands can enhance the diastereoselectivity of palladium-catalyzed allylations.

Complexes of Concave 1,10-Phenanthrolines 2 and 3 with Transition Metal Ions

In *organic chemistry (and in enzymes),* many *reactions and especially catalyses take place at a transition metal ion. Concave* 1,10-phenanthrolines *2* and *3 offer two nitrogen atoms that can bind a metal ion in a bidentate fashion. In complexes such as* $2{\cdot}M^{n+}$, the *concave shielding ensures a* 1:1 *sioichiometry. leaving coordination* sites *open* for *the binding of substrates. Numerous* complexes *have* been investigated,[19,20] *and in many cases; these complexes are catalytically active. Then* the *selectivity of the catalyses can be determined by the shape of the concave shielding.*

For instance. the exo/endo-selectivity *of Lewis-acid-catalyzed Diels–Alder reactions can be shifted toward exo-products by incorporating* the metal *ion into a concave* 1,10*-phenanthroline 2* (Fig. 6a).[20]

Palladium-catalyzed allylations *can be carried out in the presence of a concave ligand* **2**[33] *(Fig.* 6b). *Due to the square-planar orientation of all ligands at the palladium center. non-macrocyclic and bimacrocyclic* 1,10-phenanthrolines **2a**, **2b**, *and* **2c** *do not differ much in their selectivity. The* 2,9-*bis*-aryl-substitution *is the* important *feature for this catalysis.*

In copper(I)-catalyzed *cyclopropanations of cyclic or noncyclic alkenes 25 with diazoacetates, two classes of* bimacrocyclic 1,10-phenanthrolines *2 and 3 have been checked (see* Fig. 7).[34–36] *Surprisingly. bath ligands are reactive and selective but give complementary anti/syn-selectivities* (*exo/endo or trans/cis for cyclic or* noncyclic alkenes *25, respectively). While the bimacrocyciic* diaryl-phenanthrolines *2 showed a strong arzti-selectivity* (e.g., up *to 140:*1 *with indene),* 1,10-phenanthroline-*bridged* calix[6]arenes *3 led to the syn*-cyclopropanes *26* (e.g., *up to* 14:86 *with indene). With 2, the selectivity was better when large residues* R′ *at the diazoacetate were used, while in the latter case. using 3, the smallest* substituent R′, *the* methyl substituent, *gave the* best *syn-selectivity.* Responsible *for this striking difference is the*

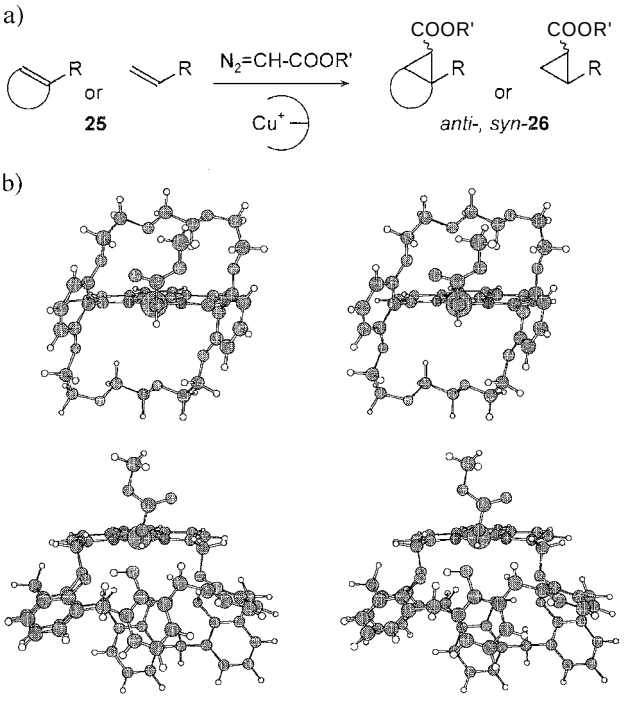

Fig. 7 (a) Copper(I)-catalyzed cyclopropanation of alltenes 25 with diazoacetates. (b) Explanation of the different *anti/syn*-selectivities of the cyclopropanation of alltenes 25 by diazoacetates in the presence of either concave diaryl-1, 10-phenanthrolines 2 or of A,D-1,10-phenanthroline-bridged calix[6]arenes **3:** stereopictures of the copper(I)-bound carbenoide iiitermediates. For details see text. (*View this art in* color *at www.dekker.com.*)

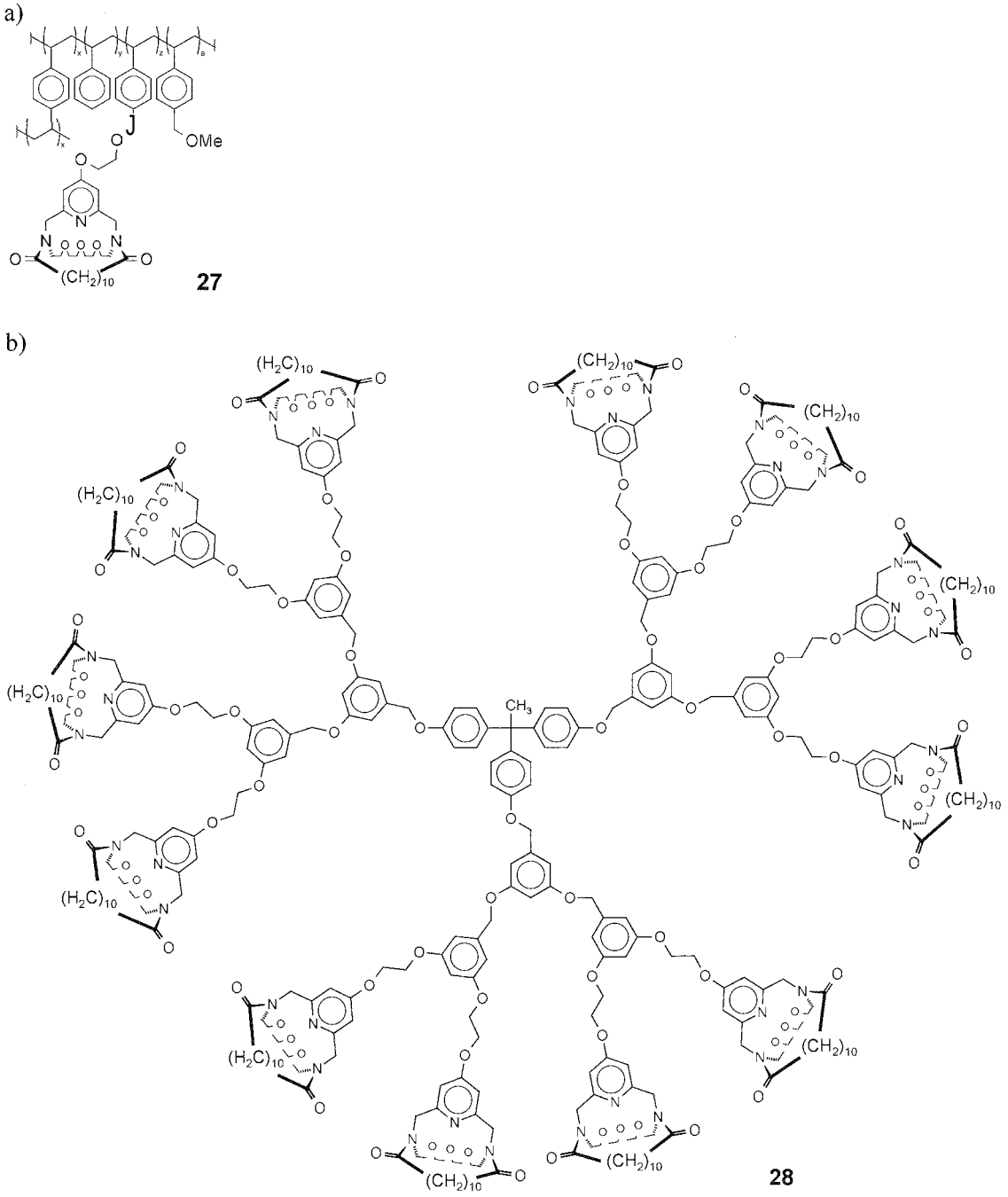

Fig. 8 (a) Polymer and (b) dendrimer fixed concave pyridines **27** and 28.

flexibility of the two ligands. In the case of the diaryl-1,10-phenanthrolines **2**. only a slight twist along the aryl-1.10-phenanthroline bonds is possible. Therefore, the overall geometry cannot be much different from the concave structure found in x-ray analyses. In the selectivity determining step. the carbene moiety transfered to the alkene 25 is attached to the copper ion that is bound to the concave ligand 2. In the resulting intermediate, the concave reaction site is partly covered by the ester substituent of the carbene moieiy. allowing the approach of an alkene only *anti* to this group. The validity of these intermediates has been investigated by calculations, and Fig. 7b shows a stereopicture of the minimized structure based on the x-ray geometry of a ligand **2a**.

In contrast to the diaryl-1,10-phenanthrolines **2**. the calix[6]arene derivatives **3** contain an oxygen atom and a methylene group between the aryl bridgehead and the 1,10-phenanthroline. This allows twists within the

bimacrocycle and leads to a structure in which the 1,10-*phenanthroline bridge is tilted against the vertical on the calixarene plane. This was proven by x-ray* analyses[37] and *by !ow-temperature NMR experiments.* A *complexed metal ion is still strongly shielded but is accessible from another direction if compared to the stiff* complexes *of 2. When a carbene moiety is bound to the* copper(I) *ion in the calixarene ligand 3, the ester group receives a strong sterical repulsion by the calixarene macrocycle that also forces the copper atom to leave the plane of the* 1,10-*phenanthroline a little bit (see Fig. 7b). An incoming* alkene can *now have two possible orientations: syn to the ester substituent of the former diazoacetate and thus anti to the calixarene, or* vice *versa. This difference is largest in* the *case of the small methyl group. which explains the finding* of *the highest syn-*selectivity for *methyl diazoacetate.*

Thus. with two classes of concave ligands. 2 and 3, respectively. which *only differ a little in* their *flexibility, opposing* selectivities *are accessible. Modification of each class of ligands with* chiral *substituents shall now allow these reactions to be carried out enantioselectively.*

RECYCLING

To justify the synthetic efforts for the synthesis of concave reagents, the gain in selectivity must be combined with an easy recovery. Usually. polymer fixation allows easy recycling, and therefore. the concave pyridine 1a has been attached to a Merrifield resin (27, see Fig. 8a).[38,39] *Indeed, the polymeric material 27 was able to catalyze the alcohol addition to diphenylketene comparably to the soluble concave pyridine* **1a**, *but complications may exist due to swelling of the resin and substrate depletion deep within the polymer. Therefore. soluble polymers loaded* with *the concave pyridine 1a have also been synthesized. However, this material behaved unreproducibly, especially because side reactions led to cross-polymerized insoluble material. Furthermore. due to reptation (leakage through membrane), an easy separation of product and catalyst would* not *be possible by ultrafiltration.*

Dendritic *compounds avoid such a reptation due to their branched structure. Thus, the concave pyridine 1a was incorporated into* Fréchet-type *dendrimers by a convergent synthesis (see Fig.* 8b).[40,41] *The resulting products like 28 can be retained by nanofiltration.*

CONCLUSION

A variety *of concave reagents and catalysts is now accessible In* protonations, *base catalyses and metal- on-assisted catalyses. they* have *been successfully* employed *enabling chemo-. regio-, and stereoselectivity. By introducing chirality into the* concave *structures. the* problem *of enantioselectivity shall be tackled next. The class of concave 1.10-phenanthrolines (and related molecules)* seems *to be especially promising for other* selective *reactions. which have not been investigated yet. because different concave catalysts can be provided by binding different metal ions to one given concave* 1,10-phenanthroline.

ARTICLES OF FURTHER INTEREST

Artificial Enzymes, *p. 76*
Calixarenes: Synthesis and Historical Perspectives, p. 153
Calixarenes and Their Analogues: Cation Complexation, *p.* 137
Calixarenes and Their Analogues: Molecular Complexation, *p.* 145
Chemical Topology, p. 229
Dendrimers, *p.* 432
Macrocyclic Synthesis, *p.* 830
Molecular Clefts and Tweezers, *p. 887*
Selectivity: Thermodynamic and Kinetic, *p.* 1225
The Template Effect, *p.* 1493

REFERENCES

1. Luning. U. Concave reagents: Syntheses of macrobicyclic pyridines. Liebigs Ann. Chem. 1987. 949–955.
2. Liining. U.; Baumstark. R.; Peters. K.: von Schnering, H.G. Concave reagents, 3: Synthesis. basicity and conformation of new concave pyridines. Liebigs Ann. Chem. 1990. 129–143.
3. Liining. U.; Baumstark. R.: Müller. M. Concave reagents. 8: Concave pyridines and 1.10-phenanthrolines with sulfonarnide bridgeheads. Increased basicity by 4-diethylamino substitution of the pyridine unit. Liebigs Ann. Chern. **1991**, 987–998.
4. Luning. U.; Müller, M. Concave reagents, 5: Bimacrocyclic 1.10-phenanthroline cyclophanes. Chern. Ber. **1990**, 123. 643–645.
5. Luning. U.: Miiller. M.: Gelbert. M.: Peters. K.; von Schnering, H.G.: Keller. M. Concave reagents. 15: New concave 1.10-phenanthrolines: Catalysts for the alcohol addition to ketenes. and ligands in transition metal complexes. Chem. Ber. 1994. 127. 2297–2306.
6. Ross. H.; Luning. U. Concave reagents. 23: Synthesis of a calix[6]arene bridged by a 1.10-phenanthroline. Tetrahedron Lett. 1997. *38.* 4539–4542.
7. Liining, U.; Fahrenkrug. F.; Hagen, M. Concave reagents. 35: Concave 1.10-phenanthrolines via ring-closing metathesis. Eur. J. Org. Chem. 2001. 2161–2163.
8. Storm, O.; Liining. U. How to synthesize macrocycles efficiently using virtual combinatorial libraries. Chem. Eur. J. **2002**. *8.* 793–798.
9. Ross. H.; Lüning, U. Concave reagents. 16: Concave

reagents based on calixarenes. Angew. Chem. 1995. *107*. 2723–2725.
10. Ross, H.; Liining. U. Concave reagentr. 16: Concave reagents based on calixarenes. Int. Ed. Engl. 1995. 34. 2555–2557.
11. Ross. H.; Liining, U. Concave reagents. 18: Synthesis, conformational behaviour. and basicity of new pyridine-bridged calix[6]arenes Liebigs Ann 1996. 1367–1373
12. Ross. H.: Liining. U. Concave reagents, 19: Synthesis. structure and basicity of a calix[6]arene bridged by an aniline. Tetrahedron 1996; 52. 10879–10882.
13. Liining. U.: Wangnick, C.: Peters. K.; von Schnering, H.G. Concave reagents. 7: Concave benzoic acids. Chem. Ber. 1991. 124. 397–402.
14. Liining. U.: Wangnick, C. Concave reagents, 11: Concave benzoates. sterically extremely shielded esters. Liebigs Ann. Chem. 1992. 481–484.
15. Lüning, U.: Baumgartner. H.: Wangnick, C. Concave reagents. 17: Steric effects on the acidity of concave sulfinic acids and concave benzoic acids. Tetrahedron 1996. 52. 599–604.
16. Liining. U.: Baumgartner. H. Concave reagents. 13: 2′-Substituted *m*-terphenyls as building blocks. Synthesis of a concave thiol acetate. Synlett 1993. 571–572.
17. Baumgartner, H. 2'-Substituierte *m*-Terphenyle. Von sterisch gehinderten Verbindungen zu Konltaven Reagenzien. Ph.D. Thesis: 1996; Freiburg.
18. Manthey, C. *m*-Terphenyl-verbindungen als Basis fur selektive Reagentien Ph.D. Thesis: 1998. Kiel.
19. Celbert. M.: Korber. C.: Friedrich. O.: Fahrenkrug, F.: Keller, M.: Liining. U. Concave reagents. 36: Transition metal complexes with concave 1,10-phenanthrolines. Supramolecular Chem. 2002. 14. 199–210.
20. Gelbert, M.: Liining, U. Concave reagents. 25: Transition metal complexes of concave 1.10-phenanthroiines as catalysts for [4+2]-cycloadditions. Ligand effects on the *exo/endo*-selectivity. Supramolecular Chem. 2001. *12*, 435–444.
21. Goto, K.: Okazaki, R. Molecular bowls and capsules with an endohedral functionality: The stabilization of highly reactive species in their inner phase. Liebigs Ann./Recueil 1997, 2393–2407.
22. Luning. U.; Abbass. M.; Fahrenkrug. F. Concave reagents, 37: A facile route to aryl-substituted 1.10-phenanthrolines by means of Suzuki coupling reactions between substituted areneboronic acids and halogeno-1.10-phenanthrolines. Eur. J. Org. Chem. 2002. 3294–3303.
23. Liining. U.: Müller. M. Konkave Reagenzien. 10: Konkav verpackte Protonen: Reagenzien für kontra-thermodynarnische Protonierungen. Angew. Chem. 1992. *104*, 99–102.
24. Liining. U.: Müller. M. Konkave Reagenzien. 10: Konkav verpackte Protonen: Reagenzien für kontra-thermodynamische Protonierungen. Int. Ed. Engl. 1992. 31. 80–82.
25. Liining. U.: Baumgartner, H.; Manthey, C.; Meynhardt. B. Concave reagents. 20: Sterically shielded *m*-terphenyls as selective agents in general protonations. J. Org. Cheni. 1996. *61*. 7922–7926.
26. Lüning, U.: Baumstark, R.: Müller, M.; Wangnick, C.: Schillinger, F. Concave reagents. 4: Protonation of nitronate anions via concave pyridines. Stereoselective C-protonation versus Nef reaction. Chern. Ber. 1990. 123. 221–223.
27. Lüning, U.; Schillinger. F. Concave reagents, 6: Can the structure of concave reagents determine selectivities? Chern. Ber. 1990. 123. 2073–2075.
28. Luning. U.: Baumstark. R.: Schyja, W. Concave reagents. 9: Alcoholysis of diphenylketene catalyzed by concave pyridines and open-chain analogs. Liebigs Ann. Chem. 1991. 999–1002.
29. Schyja. W.; Petersen. S.: Liining. U. Concave reagents, 21: Selective acylations of primary and secondary alcohols by ketenes. Liebigs Ann. 1996. 2099–2105.
30. Liining, U.: Petersen. S.: Schyja. W.: Hacker. W.: Marquardt. T.: Wagner, K.: Bolte. M. Concave reagents. 26: Concave pyridines for selective acylations of polyols. Eur. J. Org. Chem. 1998. 1077–1084.
31. Petersea. S.: Liining. U. Concave reagents, 28: Comparison of bimacrocyclic, monomacrocyclic and non-macrocyclic bis(amidomethyl)pyridines as catalysts in the base catalyzed addition of alcohols to ketenes. Eur. J. Org. Chem. 1999. 847–854.
32. Liining. U.: Schyja. W. Selectivity Enhancement by Concave Reagents. In NATO *ASI* Series, *Series C: Mathematical and* Physical *Sciences*; Siegel. J.S.. Ed.: Supramolecular Stereochemistry, Kluwer Academic Publishers. 1995: Vol. 473. 223–226.
33. Meynhardt, B.; Liining. U.; Wolff, C.; Nather. C. Concave reagents. 30: Diastereoselective generation of quarternary stereocenters by ligand controlled palladium catalyzed allylations. Eur. J. Org. Chem. 1999. 2327–2335.
34. Hagen, M.; Liining. U. Concave reagents, 22: Cyclopropanation of alkenes with ethyl diazoacetate: Copper (I) complexes of concave 1.10-phenanthrolines as diastereoselective catalysts. Chem. Ber./Recueil 1997. 130. 231–234.
35. Löffler, F.: Hagen, M.; Liining. U. Concave reagents. 32: Syn- and anti-selective cyclopropanation of alkenes with diazoacetates catalyzed by copper(I) complexes of concave 1,10-phenanthrolines. Synlett 1999. 1826–1828.
36. Biihl, M.: Terstegen. F.: Loffler. F.; Meynhardt, B.: Kierse. S.; Müller, M.; Nather. C.: Liining, U. Concave reagents. 34: On the mechanism and stereoselectivity of the copper(I) catalyzed cyclopropanation of oiefins. A combined experimental and density-functional study. Eur. J. Org. Chem. 2001. 2151-2160.
37. Eggert. J.: Harrowfield, J.: Liining. U.: Skelton. B.W.: White. A.H.; Löffler. F.. to be submitted.
38. Lüning, U.: Gerst. M. Concave reagents. 12: Polymer fixation of concave pyridines. J. Prakt. Chem./Chem.-Ztg. 1992. 334. 656–660.
39. Lüning, U.: Hacker, W. Concave reagents. 31: A Merrifield bound concave pyridine for the selective acylation of polyols. J. Prakt. Chem. 1999. *341*, 662–667.
40. Marquardt, T.: Liining. U. Ton-ards golf ball shaped reagents. Dendrimer fixed concave pyridines (concave reagents 24). Chem. Commun. 1997, 1681–1682.
41. Liining. U.: Marquardt, T. Concave reagents. 29: Dendrimer fixed concave pyridines. J. Prakt. Cheni. 1999.341. 222–227.

Concepts in Crystal Engineering

Andrew D. Burrows
University of Bath, Bath, United Kingdom

INTRODUCTION

Crystal engineering involves the design and synthesis of solid-state structures with desired properties, based on an understanding and exploitation of intermolecular interactions. The two main strategies currently in use for crystal engineering. based on hydrogen bonds and coordination bonds respectively, are discussed together with key concepts such as those of the supramolecular synthon and the secondary building unit.

CRYSTAL ENGINEERING

Crystal engineering is a rapidly expanding discipline, as witnessed by the steady increase of publications in the area over the past 6 years (Fig. 1) and the recent inauguration of several international journals in which the topic plays a major role, including *Crystal Engineering*, *CrystEngComm*, and *Crystal Growth and Design*.

The term "crystal engineering'. was first used in 1971 by Schmidt'" in connection with photodimerization reactions in crystalline cinnamic acids. Since this initial use, the meaning of the term has broadened considerably to include many aspects of solid-state supramolecular chemistry. A useful modern definition is that provided by Desiraju. who defined crystal engineering as ''*the understanding of intermolecular interactions in the context of crystal packing and the utilisation of such understanding in the design of new solids with desired physical and chemical properties*''.[2] Since many of the bulk properties of molecular materials are dictated by the manner in which the molecules are ordered in the solid state, it is clear that an ability to control this ordering would afford control over these properties.

MOLECULAR RECOGNITION AND SUPRAMOLECULAR SYNTHONS

Crystal engineering relies on noncovalent forces to achieve the organization of molecules and ions in the solid state. Much of the initial work on purely organic systems focused on the use of hydrogen bonds. though with the more recent extension to inorganic systems, the coordination bond has also emerged as a powerful tool. Other intermolecular forces such as π···π. halogen···halo-halogen, and Au···Au interactions have all been exploited in crystal engineering studies. and ionic interactions can also be important. However, the two most commonly used strategies in crystal engineering exploit hydrogen bonds'"."] and coordination bonds.[5]

Molecular recognition lies at the heart of crystal engineering, with the molecular recognition event typically involving an interaction between complementary hydi-ogen-bonding faces or a metal and a ligand. By analogy with the retrosynthetic approach to organic synthesis, Desiraju coined the term "supramolecular synthon" to describe building blocks that are common to many structures and hence can be used to order specific groups in the solid state.'" The carboxylic acid dimer (Fig. 2a) represents a simple supramolecular synthon, though in practice this is only observed in approximately 30% of crystal structures in which it is possible.[7] The alternative catemer (Fig. 2b) avoids the unfavorable secondary interactions present in the dimer (vide infra). The Cambridge Structural Database (CSD)[8] provides an excellent tool for assessing the efficiency of particular synthons. The supramolecular synthon approach has been successfully applied in the synthesis of one-dimensional tapes. two-dimensional sheets. and three-dimensional structures.

CRYSTAL ENGINEERING USING HYDROGEN BONDS

Examples of supramolecular synthons based on hydrogen bonds that have been used in crystal engineering studies are shown in Fig. 2. In an X—H···Y hydrogen bond. the X—H group is referred to as a hydrogen bond donor and the Y group a hydrogen bond acceptor. It might be expected that the greater the number of hydrogen bond donors and acceptors on each face. the greater would be both the degree and the specificity of the inte actions between the faces. This is true to some extent. though in systems containing multiple hydrogen bonds, secondary interactions are also important.[9] Hydrogen bonds are mainly electrostatic in origin. and secondary interactions

DOI: 10.1081/E-ESMC 120012750

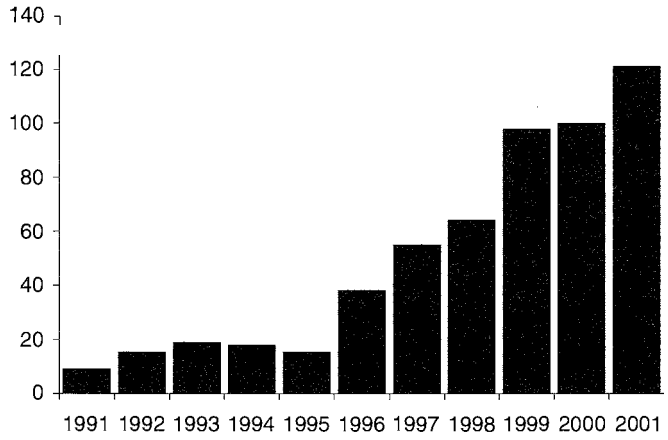

Fig. 1 The number of publications per year including the term "crystal engineering" in the title. keywords, or abstract from 1991 to 2001. Source: ISI Web of Science.

arise from the electrostatic interactions between those hydrogen-bonding groups on the two faces that are not hydrogen bonded together. Thus, in a synthon that contains two hydrogen bond donors on one face and two hydrogen bond acceptors on the other. denoted DD:AA (Fig. 2d), the secondary interactions are attractive, whereas in a synthon in which each face contains one donor and one acceptor, denoted DA:AD (Fig. 2a), the secondary interactions are repulsive. Since each secondary interaction has been calculated at approximately one-third the energy of a hydrogen bond. synthons based on DD:AA interactions would be expected to be more robust than those based on DA:AD interactions, a prediction borne out by theoretical studies, NMR experiments, and an analysis of the CSD.

One of the most highly studied hydrogen bond systems is that based on the triple hydrogen bond interaction between melamine and cyanuric acid. Melamine possesses three DAD faces, whereas cyanuric acid possesses three complementary ADA faces (Fig. 3a). The two molecules cocrystallize to form hexagonal two-dimensional sheets in which all hydrogen bond donors and acceptors are satisfied. a fact that despite earlier predictions was only

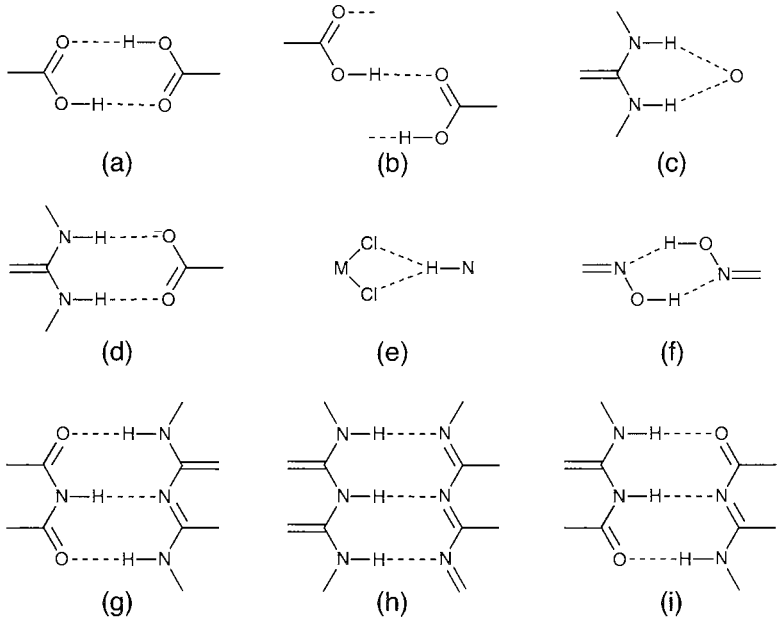

Fig. 2 Supramolecular synthons based on hydrogen bonds that have been used in crystal engineering studies. (From Refs. [3,4].)

confirmed crystallographically in 1999 (Fig. 3a).[10] Whitesides[11] and Lehn[12] and their respective coworkers showed that by introducing substituents onto the two components, they could reduce the number of hydrogen-bonding faces on each molecule, which reduces the dimensionality of the resultant aggregate forming either one-dimensional tapes (Fig. 3b) or discrete rosettes, depending on the steric demands of the substituents.

Guanidinium sulfonates form similar hexagonal two-dimensional sheet structures. though because each guanidinium cation contains three hydrogen-bonding faces bearing two hydrogen bond donors and each sulfonate anion contains three hydrogen-bonding faces bearing two hydrogen bond acceptors, in this case, charge-augmented DD:AA interactions serve to link the ions into the sheets. Ward and coworkers studied the influence of the sulfonate alkyl or aryl substituent on the structure[13] and demonstrated that use of a disulfonate enables the guanidinium sulfonate sheets to be linked together to form pillared structures capable of including guest molecules.[14]

Bifunctional ligands containing metal-binding and hydrogen-bonding faces are used in crystal engineering studies.[15] A metal center can serve to orientate the hydrogen-bonding faces in a predetermined direction, such as in the square-planar cation *trans*-[Ni{SC(NH_2)($NHNH_2$)-κ^2*S,N*}$_2$]$^{2+}$, which contains two DD hydrogen-bonding faces directed at 180° from each other and forms tapes with dicarboxyiate anions.[16] Unlike organochlorine compounds, metal-bound chloride can act as a hydrogen bond acceptor (Fig. 2e). This has been exploited in the formation of tapes based on protonated amine cations and polychiorometallate anions. typified by [4,4′-H_2bipy][$PtCl_4$].[17]

Hydrogen bonding in the solid state can also serve to bring reagents together. Hydrogen bonds between pyridyl-substituted alkenes and a resorcinol template have been used to orient the alkene double bonds into appropriate positions for solid-state photoreaction to occur, giving much higher yields of the [2 + 2] cycloaddition product than is observed in solution.[18]

Although most of the synthetic strategies employing hydrogen bonds use relatively strong interactions, weaker hydrogen bonds such as C—H···O and C—H···π interactions are also important. The recognition of the frequent occurrence of multiple phenyl embraces involving combinations of C—H···π and π···π interactions is particularly noteworthy, as the total energy of interactions between two triphenyl moieties can be as high as 80 kJ mol^{-1}.[19]

CRYSTAL ENGINEERING USING COORDINATION BONDS

The use of bridging di-or polyeopic ligands in conjunction with metal centers to construct predictable one-, two-, or three-dimensional coordination networks has received

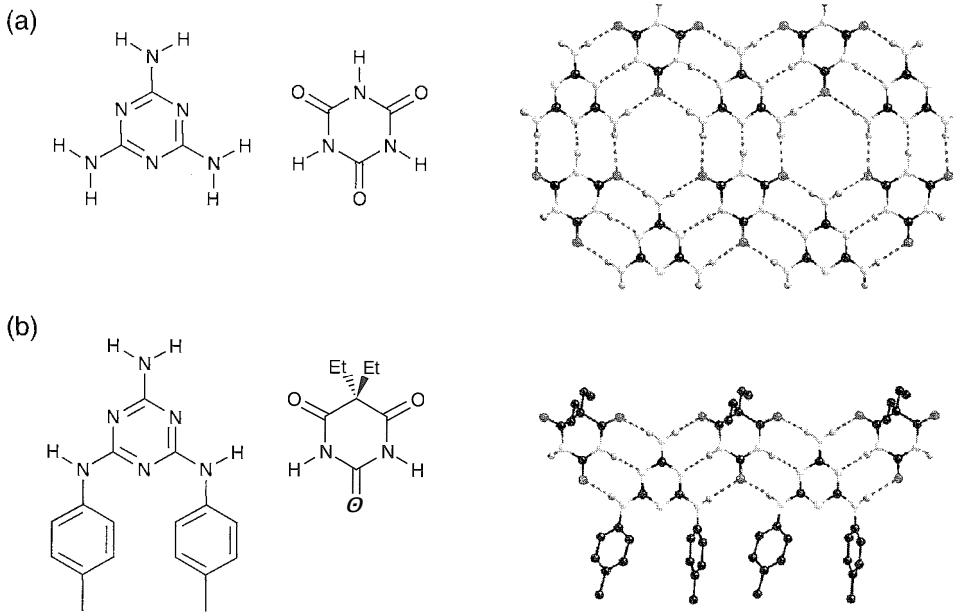

Fig. 3 (a) The structures of melamine and cyanuric acid and the hydrogen-bonded sheet formed by a 1:1 combination of them. (b) The structures of *N,N′-bis*(*p*-tolyl)melamine and 5.5-diethylbarbituric acid. and the hydrogen-bonded tape formed by a 1:1 combination of them. (From Ref. [11].) (*View this art* in *color at www.dekker.com.*)

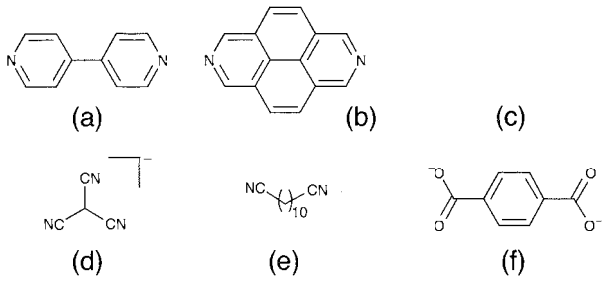

Fig. 4 Ditopic bridging ligands that have been used in crystal engineering studies involving coordination bonds. (From Refs. [5,20].)

considerable atiention recently.[20] The predictability arises from knowledge of the relative orientation of the ligand donor sites and the preferred metal ion coordination geometries, though variations in counterion and solvent can sometimes have unexpected effects. Examples of bridging ligands used in crystal engineering studies are shown in Fig. 4.

A 1:1 mixture of $AgBF_4$ and the linear spacer ligand 4,4′-bipyridine (4,4′-bipy, Fig. 4a) gives the one-dimensional coordination polymer $\{[Ag(4,4'\text{-bipy})]BF_4\}_n$ containing linear two-coordinate silver(I) centers.[20] Square-grid coordination polymers represent a common class of two-dimensional network. These structures are based upon a 1:2 ratio of metal centers containing square-planar coordination sites and linear spacer ligands such as 4,4′-bipy.[21]

Robson pioneered a net-based approach to the generation of three-dimensional coordination networks.[22] A net is a collection of nodes with clearly defined connectivity or topology.[23] The strategy involves identifying molecular building blocks with the functionality and stereochemistry appropriate to a particular target net. For example. the rutile net consists of octahedral and trigonal nodes in 1:2 ratio, and in rutile the titanium centers are octahedral and the oxides trigonal. The tricyanomethanide ion $[C(CN)_3]^-$ (Fig. 4d) contains trigonally arranged nitrogen donors, and the structures of $M[C(CN)_3]$ (M=Cr, Mn,Fe,Co,Ni,Cu,Zn,Cd, or Hg) all contain two interpenetrating rutile networks (Fig. 5).[24]

Interpenetration is a common phenomenon when networks contain large channels. It occurs when the channeis created by one framework are filled with one or more independent networks that may or may not be identical to the first. By using 1,12-dodecanedinitrile (Fig. 4e), interpenetration of as many as 10 independent networks has been observed.[25] Intel-penetration may be problematic when using coordination networks to prepare porous materials. though there is evidence it can lead to the strengthening of network structures.[26]

In some Instances, more than one structuie may be possible for a given set of molecular components. and such structures can be described as supramolecular isomers For example, three forms of $[Co_2(NO_3)_4\{1,2\text{-}bis(4\text{-pyridyl})ethane\}_3]_n$ have been structurally characterized with different network structures This results from the conformational freedom of 1,2-*bis*(4-pyridyl)ethane (Fig 4c), which unlike 4,4-bipy can adopt *gauche* or *anti* conformations [27]

SYNTHETIC STRATEGIES FOR CRYSTAL ENGINEERING

Crystal engineering requires information on intermolecular interactions in the solid state, which necessitates crystal structure determinations. Despite the increasing importance of structure solution using powder diffraction data, this generally implies a need for single crystals. Recent developments in diffractometer technology and access to synchrotron radiation have afforded the opportunity to obtain information using crystals of smaller size and poorer quality than previously possible. and on a vastly greater scale. However, the need for single crystals remains. Many elaborate experiments have been devised in order to ensure slow mixing of reagents and enhance the likelihood of growing single crystals. This is particularly important in coordination-based systems in which the product is usually insoluble. The reversibility of hydrogen bond and coordination bond formation is likely to be crucial in the formation of single crystals.

Two-component systems typically use cocrystallization or metathesis techniques. and in these experiments. the solvent needs to be chosen carefully to prevent the components from crystallizing separately. Grinding the components together can also be used sometimes to prepare cocrystalline compounds.[28]

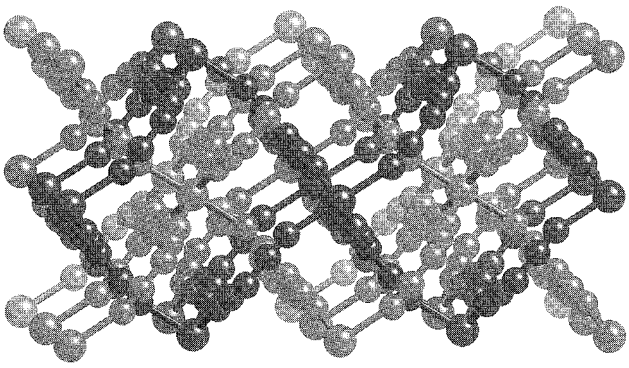

Fig. 5 The structure of $Cr[C(CN)_3]_2$, which is based on two interpenetrating nets with the rutile topology. (From Refs. [22,24].) (*View this art in color at www.dekker.com.*)

STRUCTURE–PROPERTY RELATIONSHIPS

Much of the crystal engineering literature is concerned with attempts to dictate organization in the solid state through control of intermolecular interactions. A criticism occasionally leveled at crystal engineering is that this can easily become a simple data gathering exercise. Although it can be argued with some validity that the discipline is at a stage where its tools are still being evaluated, it is clear that future progress will focus predominantly on function.[29] Many properties of materials are related to the manner in which the component molecules or ions pack. Thus. for example, for second-order nonlinear optical activity, the components need to be arranged in a noncentrosymmetric manner, whereas for magnetism. the components need to be organized so that communication between spins is possible. For porous materials that can be used for separations or gas storage, close-packing and interpenetration need to be prevented. Yaghi and coworkers have prepared a range of highly porous materials using the concept of the secondary building unit (SBU).[30]

The secondary building units utilized by Yaghi and others are metal carboxylate clusters such as copper acetate [$Cu_2(\mu\text{-}OAc)_4$], and basic zinc acetate [$Zn_4(\mu_4\text{-}O)(\mu\text{-}OAc)_6$], shown in Fig. 4. The bridging coordination mode of the carboxylates in these compounds imparts rigidity, and these SBUs can be linked together into two- or three-dimensional structures (Fig. 6) by use of dicarboxylates such as terephthalate (Fig. 4f) instead of acetate. Unlike many coordination networks. the resulting structures are maintained when the solvent is removed. The compound in which $Zn_4(\mu_4\text{-}O)$ units are linked by triphenyldicarboxylate dianions is, following removal of the solvent, the least dense crystalline material currently known, with a calculated crystal density of 0.21 gcm^{-3} and a free volume of 91.1%. The series of compounds prepared by linking $Zn_4(\mu_4\text{-}O)$ units by linear dicarboxylates shows reversible isotherm behavior characteristic of microporous materials.[31]

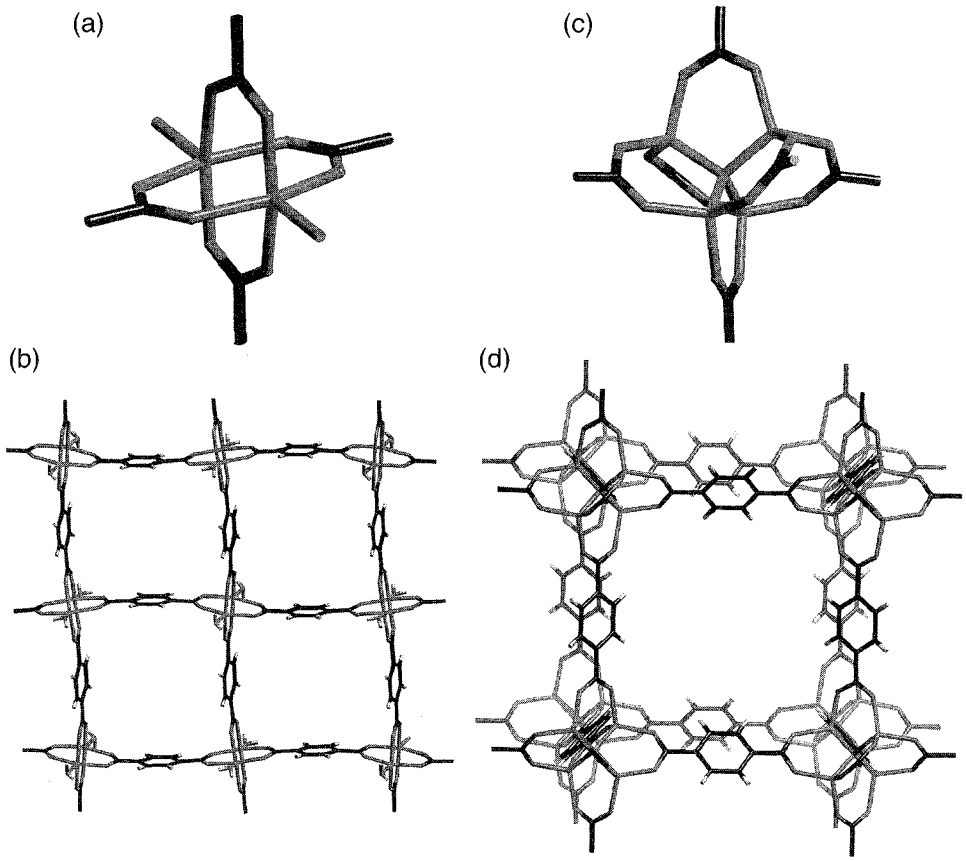

Fig. 6 (a) The $M_2(\mu\text{-}O_2R)_4$ SBU containing a square-planar arrangement of carboxylate groups. (b) The structure of $[Zn_2(\mu\text{-terephthalate})_2(OH_2)_2]_n$ formed from linking $M_2(\mu\text{-}O_2R)_4$ SBUs. (c) The $M_4(\mu_4\text{-}O)(\mu\text{-}O_2R)_6$ SBU containing an octahedral arrangement of carboxylate groups: (d) The structure of $[Zn_4(\mu_4\text{-}O)(\mu\text{-terephthalate})_3]_n$ formed from linking $M_4(\mu_4\text{-}O)(\mu\text{-}O_2R)_6$ SBUs. (From Refs. [30 and 31].) (*View this art in* color *at www.dekker.com.*)

CONCLUSION

Although concerned with the design and synthesis of one-, two-. and three-dimensional structures, crystal engineering is not synonymous with crystal structure prediction. which is a far more precise and complex task. Crystal engineering at the current time also cannot seek to control. in anything but a very imprecise way. the factors involved in crystal nucleation and growth, though these obviously impact heavily upon the results obtained.

Crystal engineering is. however. a truly interdisciplinary area, coinbining organic and inorganic synthesis with material science. Much progress has been made over the past few years in the design and synthesis of new materials and, although much more work is needed before crystal engineering can be considered a mature area, it is clear that the discipline has a very promising future.

ARTICLES OF FURTHER INTEREST

The Cambridge Crystallographic Structural Database, p. 161
Crystal Engineering with Hydrogen Bonds, p. 357
Interpenetration, p. 735
Nomenclature in Crystal Engineering, p. 967
$\pi-\pi$ *Stacking as a Crystal Engineering Tool,* p. 1093
Polymorphism, p. 1129

REFERENCES

1. Schmidt. G.M.J. Photodimerization in the solid state. Pure Appl. Chem. 19711. 27. 647.
2. Desiraju. G.M. *Crystal Engineering, the Design of Organic Solids:* Elsevier: Amsterdam, 1989.
3. Aakeroy. C.B.; Beatty. A.M. Crystal engineering of hydrogen-bonded assemblies—A progress report. Aust. J. Chem. 2001. *54* (7), 409–421.
4. Meléndez. R.E.: Hamilton. A.D. Hydrogen-bonded ribbons, tapes and sheets as motifs for crystal engineering. Top. Curr. Chem. 1998. 198. 97–129.
5. Zaworotko. M.J. Superstructural diversity in two dimensions: Crystal engineering of laminated solids. Chem. Commun. 2001. (1). 1–9.
6. Desiraju. G.R. Supramolecular synthons in crystal engineering—A new organic-synthesis. Angew. Chem., Int. Ed. Engl. 1995. 34 (21). 2311–2327.
7. Allen. F.H.: Motherwell. W.D.S.: Raithby. P.R.: Shields. G.P.; Taylor, R. Systematic analysis of the probabilities of formation of bimolecular hydrogen-bonded ring motifs in organic crystal structures. New J. Chem. 1999. *23* (1). 25–34.
8. Allen. F.H.; Kennard, O. 3D search and research using the Cambridge Structural Database. Chem. Des. Automat. News 1993, *8*, 31–37.
9. Pranata. J.: Wierschke. S.G.; Jorgensen. W.L. OPES potential functions for nucleotide bases—Relative association constants of hydrogen-bonded base-pairs in chlorofonn. J. Am. Chem. Soc. 1991. *113* (8). 2810–2819.
10. Ranganathan, A.: Pedireddi, V.R.: Rao. C.N.R. Hydrothermal synthesis of organic channel structures: 1 : 1 hydrogen-bonded adducts of melamine with cyanuric and trithiocyanuric acids. J. Am. Chem. Soc. 1999. *121* (8), 1752–1753.
11. Zerkowski. J.A.: Macdonald, J.C.; Seto. C.T.: Wierda. D.A.: Whitesides. G.M. Design of organic structures in the solid-state — molecular tapes based on the network of hydrogen-bonds present in the cyanuric acid melamine complex. J. Am. Chem. Soc. 1994. *116* (6). 2382–2391.
12. Lehn, J.-M.; Mascal, M.: DeCian. A.; Fischer. J. Molecular ribbons from molecular recognition directed self-assembly of self-complementary molecular-components. J. Chem. Soc. Perkin Trans. 2 1992. (4). 461–467.
13. Russell. V.A.; Etter, M.C.: Ward. M.D. Layered materials by molecular design—Structural enforcement by hydrogen-bonding in guanidinium alkanesulfonate and arenesulfonate. J. Am. Chem. Soc. 1994. *116* (5). 1941–1952.
14. Russell. V.A.: Evans. C.C.: Li. W.J.: Ward. M.D. Nanoporous molecular sandaiches: Pillared two-dimensional hydrogen-bonded networks with adjustable porosity. Science 1997. 276 (5312). 575--579.
15. Burrows. A.D.; Chan. C.-W.: Chowdhry. M.M.: McGrady, J.E.: Mingos. D.M.P. Multidimensional crystal engineering of bifunctional metal complexes containing complementary triple hydrogen bonds. Chern. Soc. Rev. 1995, 24 (5). 329–339.
16. Burrows. A.D.: Mingos. D.M.P.: White. A.J.P.; Williams. D.J. Crystal engineering of metal complexes based on charge-augmented double hydrogen-bond interactions between thiosemicarbazides and carboxylates. Chem. Commun. 1996, (1), 97–99.
17. Gillon. A.L.: Lewis. G.R.: Orpen, A.G.: Rotter. S.: Starbuck, J.: Wang. X.M.: Rodriguez-Martin. Y.: Ruiz-Perez. C. Organic-inorganic hybrid solids: Control of perhalometallate solid state structures. J. Chem. Soc. Dalton Trans. 2000. (21). 3897–3905.
18. MacGillivray, L.R.: Reid. J.L.: Ripmeester. J.A. Supramolecular control of reactivity in the solid state using linear molecular templates. J. Am. Chem. Soc. 2000. *122* (32). 7817–7818.
19. Dance. I.: Scudder, M. Supramolecular motifs: Concerted multiple phenyl embraces between Ph_4P^+ cations are attractive and ubiquitous. Chem. Eur. J. 1996. 2 (5), 481–486.
20. Blake. A.J.; Champness, N.R.: Hubberstey, P.; Li. W.S.; Withersby. M.A.; Schroder. M. Inorganic crystal engineering using self-assembly of tailored building-blocks. Coord. Chem. Rev. 1999. *183,* 117--138.
21. Fujita, M.: Kwon, Y.J.; Washizu. S.: Ogura, K. Preparation. clathration ability, and catalysis of a 2-dimensional square network material composed of cadmium(II) and 4.4'-bipyridine. J. Am. Chem. Soc. 1994. *116* (3). 1151–1152.

22. Robson, R. A net-based approach to coordination polymess. J. Chem. Soc. Dalton Trans. **2000.** (21), 3735–3744.
23. Wells, A.F. *Three-Dimensional Nets and Polyhedra*; Wiley-Interscience: New York, 1977.
24. Batten, S.R.; Hoskins, B.F.; Moubaraki, B.: Murray, K.S.; Rohson, R. Crystal structures and magnetic properties of the interpenetrating rutilc-related compounds $M(tcm)_2$ [M=octahedral, divalent metal; tcm =tricyanomethanide, ide, $C(CN)_3^-$] and the sheet structures of $[M(tcm)_2(EtOH)_2]$ (M=Co or Ni). J. Chem. Soc. Dalton Trans. **1999**, (17), 2977 -2986.
25. Carlucci, I,.; Ciani, G.; Proserpio, D.M.; Rizzato, S. Three novel interpenetrating diamondoid networks from self-assembly of 1,12-dodecanedinitrile with silver(I) salts. Chem. Eur. J. **2002.** *8* (7), 1520–1526.
26. Chen. B.L.: Eddaoudi, M.; Hyde, S.T.; O'Keeffe, M.; Yaghi, O.M. Interwoven metal-organic framework on a periodic minimal surface with extra-large pores. Science **2001**, *291* (5506), 1021 1023.
27. Hennigar, T.L.; MacQuarrie, D.C.; Losier, P.; Rogers, R.D.; Zaworotko, M.J. Supramolecular isomerism in coordination polymers: Conformational freedom o1 ligands in $[Co(NO_3)_2(1,2\text{-}bis(4\text{-pyridyl})ethane)_{1.5}]_n$. Angcw. Chem., Int. Ed. Engl. 1997, *36* (9), 972–973.
28. Toda, F. Crystal engineering for molecular dynamics. CrystEngComm. **2002,** *4*, 215–222.
29. Braga, D. Inorganic crystal engineering: A personal perspective. J. Chem. Soc. Dalton Trans. **2000.** (21). 3705–3713.
30. Eddaoudi, M.; Moler, D.B.; Li, H.L.; Chen, B.L.; Reineke, T.M.; O'Keeffe, M.; Yaghi, O.M. Modular chemistry: Secondary building units as a basis for the design of highly porous and robust metal-organic carboxylate frameworks. Acc. Chem. Res. **2001.** *34* (4). 319–330.
31. Eddaoudi, M.: Kim, J.; Rosi, N.; Vodak, D.; Wachter, J.: O'Keeffe, M.; Yaghi, O.M. Systematic design of pore size and functionality in isorcticular MOFs and their application in rncthane storage. Science **2002.** *295* (5554), 469 472.

Crown Ethers

George W. Gokel
Washington University School of Medicine,
St. Louis, Missouri, U.S.A.

INTRODUCTION

Crown ethers are organic ring compounds, typically larger than 12 atoms in the cycle, that contain oxygen. nitrogen, sulfur: or other heteroatoms. These heteroatoms alternate with carbon bridges that may be ethylene (CH_2CH_2) units, or they may be part of more complex structures. One example of such an element is catechol (1,2-dihydroxybenzene), which may be thought of as an O-C-C-O unit fused to a benzene ring. The key property of crown ethers on which interest has centered for decades is their ability to complex various ions. Initially; studies were focused on such alkali metal ions as sodium and potassium, but ammonium ion, diazonium ion, transition metals, and even neutral species were complexed by these versatile macrocycles. Their applications in modern supramolecular chemistry now extend to their uses as functional elements or structural scaffolds in even more complex structures.

THE DISCOVERY OF CROWN ETHERS

Crown ethers were known as structural types as early as the 1950s, when 12-crown-4 was prepared and patented. As a class, however, the discovery is credited to Charles Pedersen, who obtained dibenzo-18-crown-6 serendipitously, while attempting to prepare open-chained complexing agents for vanadium cations that he planned to use as polymerization catalysts.[1,2] The target structures had phenolic hydroxyl groups that could readily be deprotonated and interact with a metal ion. The cyclic compound that was isolated had no detectable hydroxyl group. but an interaction with a metal ion was still apparent. Pedersen deduced that the cyclic. rather than open-chained, compound was formed. He then undertook an extensive and systematic study of macrocycles in which ring size, heteroatoms. and substructural elements were all varied. For this discovery, Pedersen shared the 1987 Nobel Prize in Chemistry.

DEFINING FEATURES OF CROWNS

Structural Features of **Crown** Ethers

Thousands of different macrocycles that fall under the general description "crown ether" are now known. It is, therefore, impossible to define the structural features beyond the presence of a macrocyclic ring (generally, but not always: considered to be $\geq$12 members), in which heteroatoms (generally $\geq$4) are separated by a carbon-containing unit of two or more atoms. Oxygen is probably the predominant heteroatom in macrocycles intended to bind alkali metals. Nitrogen is often incorporated into these structures and may predominate when binding to transition metals is the object. Likewise, crowns containing sulfur atoms in the donor array favor transition over alkali metal ions.

The two-carbon unit that separates heteroatoms may be part of an aromatic system (e.g., benzene, naphthalene, pyridine). In the case of a heteroaromatic component such as furan or pyridine. the subcyclic unit may contribute a heteroatom to the donor array. In aliphatic crown ethers, the preference for ethyleneoxy units (OCH_2CH_2) results from chemical and practical considerations. Repeating ethyleneoxy units are readily available by polymerization of ethylene oxide (oxirane). Construction of a crown from such a simple and readily available starting material is economical. Use of the ethyleneoxy unit also means that every third atom is a donor, so the macrocycle's interior void is electron rich. A higher concentration of donors would be possible if methyleneoxy (OCH_2) chains were used, but the acetal (OCH_2O) linkage is hydrolytically unstable. Fewer donors would be available in the same size of macroring if propyleneoxy ($OCH_2CH_2CH_2$) units were used for construction of the macrocycle. A problem in the latter case is that unfavorable conformational interactions would occur. Rotation about the ethylene linkage is facile when oxygens occupy the 1,2-positions (i.e., O-CH_2CH_2-O). The corresponding O-CH_2CH_2-CH_2 interaction is energetically less favorable. The conformation

Encyclopedia of Supramolecular Chemistry
DOI: 10.1081/E-ESMC 120012703

problem increases with the number of carbons between the heteroatoms.

Grown Ether Nomenclature

A macrocycle comprised of six ethyleneoxy units $[(CH_2CH_2O)_6]$ is named 1,4,7,10,13,16-hexaoxacyclooctadecane Alternate heteroatoms and other structural elements consrderably complicate this already cumbersome nomenclature Because of the appearance of their molecular models and the fact that these macrocycles "crowned" cations. Pedersen suggested the family name "crown ether ' He called $(CH_2CH_2O)_6$ 18-crown-6 The analogs $(CH_2CH_2O)_4$ and $(CH_2CH_2O)_5$ are named 12-crown-4 and 15-crown-5. respectively When the ethyleneoxy unit is part of the arene catechol, the compound is named as a benzo-3*n*-crown-*n* in which "3*n*" is the total number of atoms in the macroring, and "*n*" is the number of heteroatoms In Fig 1. 14 clown ethers are illustrated along with their semi-systematic names

Problems with the nomenclature will be immediately apparent The naming system assumes the presence of two-carbon spacers. This is clearly impossible for 20-crown-6. but the relative positions of the 3-carbon bridges are not revealed by the name. This lack of clarity is also a problem wlienever more than one substituent is present. The two cyclohexane rings of dicyclohexano-18-crown-6 may be adjacent, separated by one ethyleneoxy unit, or as illustrated. This ambiguity applies as well to the dibenzo and dipyrido crowns. Because the systematic names are so cumbersome, structures are typically expressed by a combination of an illustration and a short name.

Crown Ether Toxicity

Early studies conducted at Dow Chemical Company showed that 12-crown-4 caused testicular atrophy in test animals.[3] Pedersen also found in early studies that at least one of his macrocycles was an irritant in the eyes of a dog.[4] These observations and a variety of anecdotal evidence gave crown ethers a reputation for toxicity. Later studies showed that for some macrocycles. toxicity was low.[5] In particular. the lethal dose for rats of 18-crown-6 and aspirin is similar. Of course, crown ethers should be

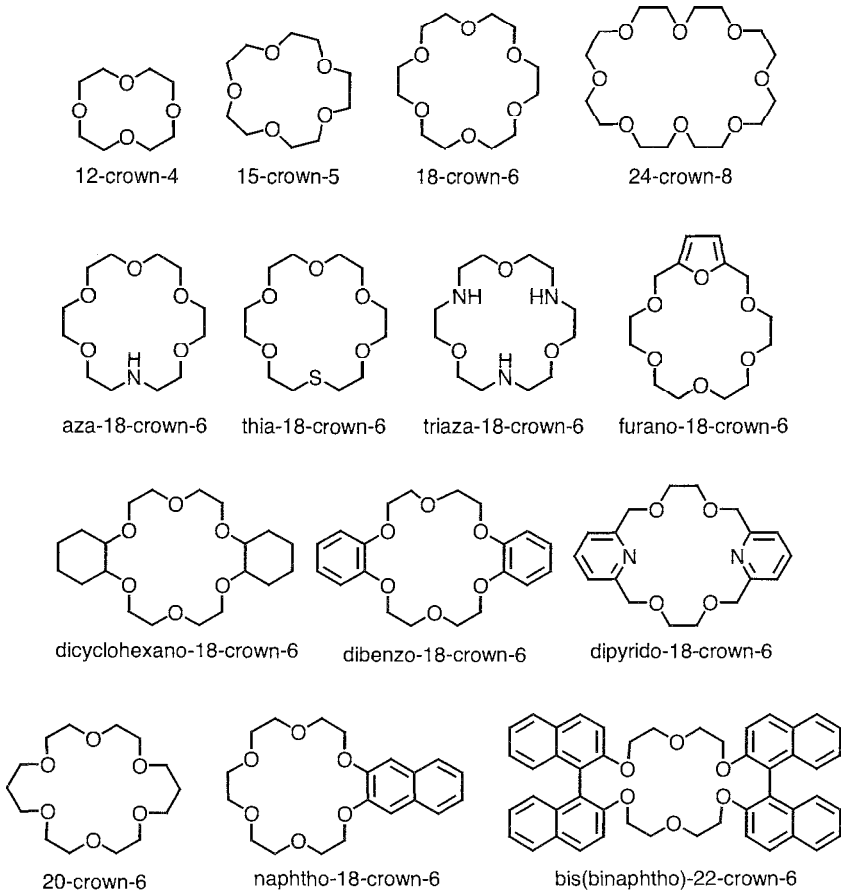

Fig. 1 Representative crown ethers and their semi-systematic names.

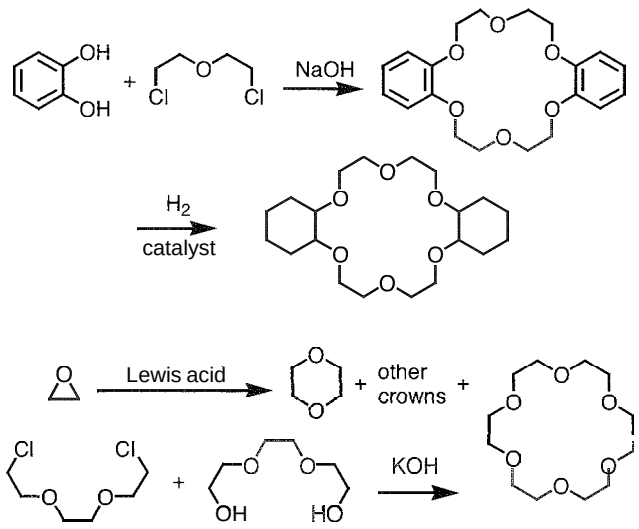

Pig. 2 Schemes depicting synthetic access to dibenzo-18-crown-6 dicyclohexano-18-crown-6, and 18-crown-6

handled with care. and all chemicals for which biological data are not available should be treated as potentially toxic.

STRUCTURAL TYPES AND SYNTHETIC ACCESS

Synthetic Methods

Unsubstituted crowns such as 15-crown-5 or 21-crown-7 may be prepared by cyclooligomerization of ethylene oxide (oxirane) under Lewis acidic conditions.[6] The products form in a mixture and must be separated by distillation. The predominant product of the reaction is dioxane, but the distribution of crowns may be influenced by the addition of alkali metal cations of different diameters. Unsubstituted crowns may also be formed by reaction of a diol fragment with a complementary fragment activated for substitution by dihalide or ditosylate. Reaction of $Cl(CH_2CH_2O)_2CH_2CH_2Cl$ with $H(OCH_2CH_2)_3OH$ in the presence of KOH can result in 18-crown-6 being obtained.[7,8] The crown is obtained by distillation and is further purified by forming a crystalline acetonitrile solvate (Fig. 2). Preparation of 15-crown-5 can be done similarly, by reaction of $Cl(CH_2CH_2O)_2CH_2CH_2Cl$ with $H(OCH_2CH_2)_2OH$ or $ClCH_2CH_2OCH_2CH_2Cl$ with $H(OCH_2CH_2)_3OH$. A difficulty with the approach in this case is that the leaving groups may exchange; leading to mixtures of 9- and 18-membered rings contaminating the desired 15-crown-5.

Pedersen's original preparation of dibenzo-18-crown-6 involved the reaction of $ClCH_2CH_2OCH_2CH_2Cl$ and catechol (1.2-dihydroxybenzene) with NaOH in *n*-butanol solution. The macrocycle was isolated as a white solid. Hydrogenation produced dicyclohexano-18-crown-6 as a mixture of stereoisomers.[4] Compounds such as dipyrido-18-crown-6 (see Fig. 1) may be produced by a similar 2+2 strategy. In this case, either 2,6-*bis*(chloromethyl)pyridine and ethylene glycol or 2,6-*bis*(hydroxymethyl)pyridine and ethylene glycol ditosylate must be used. When a compound that includes a single subcyclic unit is desired, it may be produced from the diol and an appropriately sized dihalide or ditosylate. For example, the reaction of 2,5-*bis*(hydroxymethyl)furan and pentaethylene glycol ditosylate will give furano-18-crown-6, shown in Fig. 1.

Macrocycles. especially azacrowns, were prepared by reaction at high dilution between diamines and diacid chlorides. The cyclic *bis*(amide) is then reduced (e.g., $LiAlH_4$) to afford the cyclic diamine. Other general and compound-specific inethods were developed (Fig. 3).[9,10]

The Template Effect

Crown ethers complex cations. as discussed later in this article. Conversely, cations can organize the reactive partners to form the macrocyclic products. In the absence of some organizing principle. the formation of large rings is an improbable process. The reaction of triethylene glycol with triethylene glycol dichloride in the presence of KOH. for example, begins with ether formation:

$$H(OCH_2CH_2)_3OK + ClCH_2CH_2(OCH_2CH_2)_2Cl$$
$$\rightarrow H(OCH_2CH_2)_3OCH_2CH_2(OCH_2CH_2)_2Cl$$
$$\equiv H(OCH_2CH_2)_6Cl$$

The next step in this process is likely to be a further extension of this intermediate to form the next longer

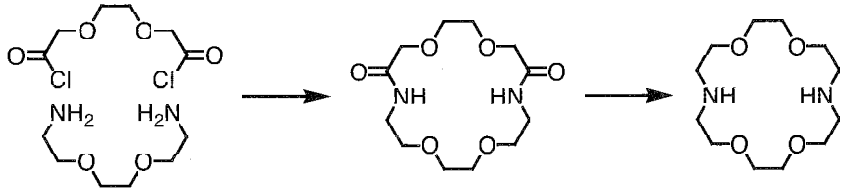

Fig. 3 A cyclization-reduction synthesis of 4,13-diaza-18-crown-6.

analog, $H(OCH_2CH_2)_9OH$. In addition, two inolecules of $H(OCH_2CH_2)_6Cl$ may combine to give $H(OCH_2CH_2)_{12}Cl$. This is a polymerization process. and many chain lengths will be formed. The process is favored because it is more likely that one molecule will find a second one with which to react than to find its other end. The latter can be made more probable by working at high dilution (i.e., low concentration). In that case. the odds of finding the other end are not increased, but finding another molecule is made more difficult.

There are two notions implicit in the idea of a "template effect." as discussed by Greene in reactions to form 18-crown-6.[11] The first is that the two reactive ends of the crown precursor are brought together by what is tantamount to a complexation phenomenon. This is illustrated in Fig. 4. Mandolini and Masci studied the template effect in a cyclization that formed benzo-18-crown-6.[12] The presence and absence of cations demonstrated that the presence of an organizing cation was beneficial. These reactions are illustrated in Fig. 4.

The second concept inherent in the template effect is that cations of different sizes favor the formation of different ring sizes. In the cyclooligomerization of ethylene oxide reported by Dale et al.[6] relatively more 15-crown-5 was formed in the presence of Na^+ and more 18-crown-6 was formed when K^+ was added to the reaction mixture. When the reacting components are triethylene glycol and triethylene glycol dichloride, the possibilities are the formation of rings having sizes of 9.

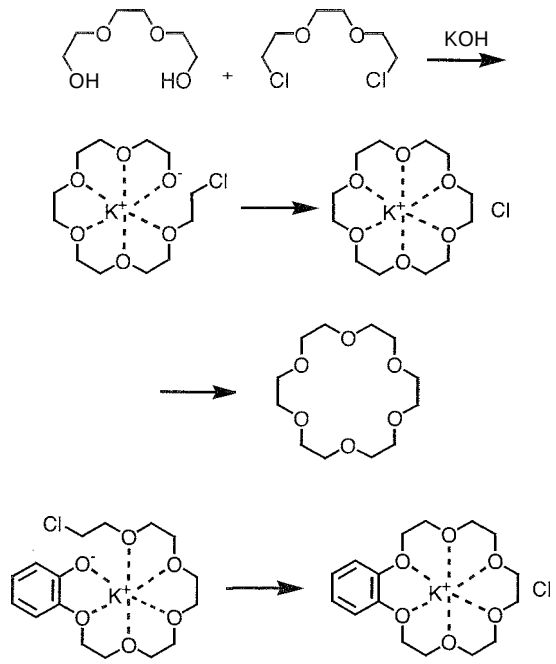

Fig. **4** Cyclization to form crown ethers assisted by cation complexation.

18. 27. etc. Cram showed that a 27-membered ring was favored by the large cationic template—guanidinium ion.[13] Often, though, the differences in the reaction products are subtle. and the demonstration of a clear template effect is problematic.

COMPLEXATION

The earliest and most studied properties of crown ethers concern their ability to cornplex cations.[14–16] A crown ether is, in a sense, a unirnolecular solvation gradient. The exterior of the macrocycle (alkyl) is lipophilic (hydrophobic), and the interior (heteroatoms) is hydrophilic (lipophobic). An 18-crown-6 may be likened structurally to a doughnut. An appropriately sized cation may fit in the "hole" to give a complex. The question of appropriate size is complicated. When the macroring hole and the cation diameter are identical, the cation is typically ernbedded within the ring. When the ring is larger than the cation, the ring may pucker so that donor-group-to-ion contacts are of appropriate length and geometry. When the cation is larger than the ring. the cation may "perch" on the ring or be "sandwiched" between two rings. Other geometric arrangements are also possible.

Organic cations may also bind to crown ethers. In particular. the macroring oxygen atoms may function as PI-bond acceptors. Alternate oxygen atoms in 18-crown-6 are positioned to form three $N—H\cdots O$ bonds with an ammonium ion. Hydronium ion. H_3O^+, has nearly the same geometry as $R—NH_3^+$ and forms a similar complex.

Shown in Fig. 5 are several complex structures. The top row illustrates typical alkali metal complexation. A sphere and the macrocycle structure represent the complex between 15-crown-5 and Na^+. This type of illustration is also used for the K^+ structure of 18-crown-6, shown in structural form in the center. The middle row illustrates H-bond complexes of an ammonium ion, a hydronium ion,[17–19] and a water complex of a protonated aza-crown.[20] The left-hand structure shown in the third row is a so-called "second-sphere" complex. The Pt—N bond renders the nitrogen atom partially positive, so the $Pt—NH_3$ structure is like $R—N^+H_3$. At the right is shown an arenediazonium cation complex.

Complexation sf Anions

The "bole" of a crown ether is lined with electronegative atoms. This nicely complements cations but repels anions. Complexation of anions proved to be possible. however. for azacrowns, protonated azacrowns, and related species. In these cases. the complex is stabilized by multiple hydrogen bonds. Although the anion complexation field is

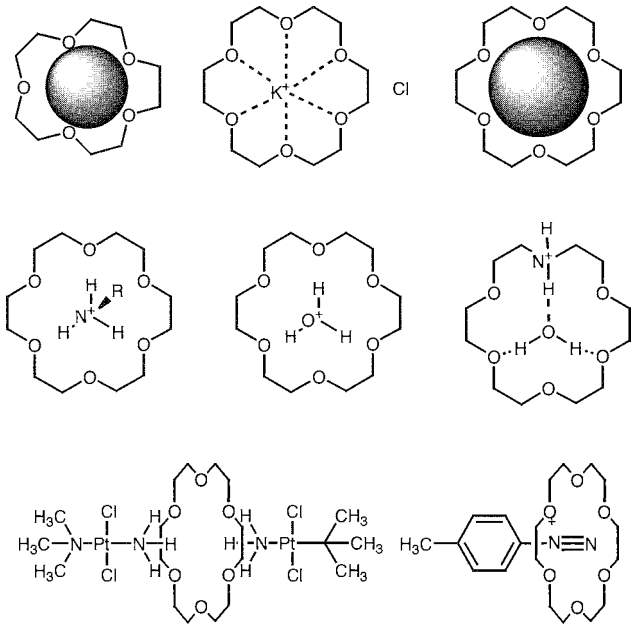

Fig. *5* Crown ether coinplexation of a range of cationic guests (see text for details).

growing rapidly,[21] the number of examples is dwarfed by the literature on cation complexation.

Methods to Detect and Measure Cation Complexation

The complexation of ions by crown ethers can be detected in solution, but evidence was also obtained by studies in gas and solid phases. Most complexation chemistry is conducted in solution. Complexation reactions can be expressed generally by the equilibrium:

$$\text{host} + \text{guest} = \text{complex}$$

The critical requirement is. therefore, to detect the complex quantitatively. From the amount of complex formed; the position of the equilibrium and, therefore, the equilibrium constant will be known. at least under the conditions of the measurement.

At an early stage. Frensdorff, a colleague of Pedersen's at Dupont, developed a useful method for determining the equilibrium complexation constant in solution.[22,23] The method required the use of ion-selective electrodes and an appropriate voltmeter. Calorimetric methods were applied early in the development of crown ethers by Arnett and by Izatt and Christensen and their coworkers.[24,25] The latter group reported extensive solution calorimetric studies of complexation involving metal and organic guest molecules with a variety of hosts. Considerable data on cation binding by macrocycles may be found in the literature.[14–16]

Cram and coworkers developed a convenient extraction method that they used to assess the structural factors that influence cornplexation of metal ions and protonated amino acids.[26–28] (For a review of chiral complexation see Ref. [29].) The method was used extensively enough to merit a description here. An aqueous solution of, for example, sodium picrate, is prepared. The solution is yellow owing to the trinitrophenoxide anion. A potential host molecule is dissolved in $CHCl_3$, and the two phases are shaken together. If successful, the host molecule will extract the cation picrate salt into the organic phase. The extent of the extraction can be quantitated by UV spectroscopy, based on the assumption that the amount of picrate anion observed corresponds to the amount of cation extracted. For obvious reasons, this method is called the ''picrate extraction technique.'' For comparisons to be made between data sets obtained by this method, solvents, volumes. concentrations. temperatures, etc., must be controlled. The influence of the anion on complexation was also studied.[30]

Enantioselective complexation between chiral host molecules and racemic guests was also achieved.[29] One enantiomer of phenylethylammonium cation can be selectively complexed by optically pure *bis*(binaphtho)-22-crown-6.[26–29] The racemic ammonium salt, dissolved in water. and the chiral crown, dissolved in an immiscible solvent such as $CHCl_3$, are shaken together. If one of the two diastereomeric complexes is favored, it can be detected (e.g., by NMR) or separated. When the chiral macrocycle is bound to a resin. a multi-plate, chiral organic separation is possible.

Solid-state complexes

Modern chemistry is aided profoundly by the advancement of x-ray techniques. and crown ether chemistry is no exception. Our understanding of solution coinplexaiion has been augmented by numerous solid-state structures. Among the earliest crown ether complexes to appear were those reported by Truter and Bush.[31] Numerous other contributions to this area were reviewed by Dobler.[32] In brief, many crown ethers are solid and form regular crystals. Because they possess an empty central space, one or more methylene residues typically turns inward to fill the molecular void. When complexation of a cation occurs, the methylene rotates outward so that the bound cation will be accessible to all of the macroring donors.

Shown clearly by solid-state structures is that crowns are versatile binders. Although the fit between K^+ and 18-crown-6 is nearly perfect. this host can complex numerous other cations. In addition, other crowns can complex K^+, even if the host is larger or smaller than the guest. For

example, 15-crown-5 forms a 2:1 "sandwich" complex with K^+. Likewise. 14-crown-4 forms a 2:1 sandwich complex with Na^+. The structure of $Na^+ \cdot$18-crown-6 shows that the macroring contracts so that the $O—Na^+$ distances are optimized for five donors. essentially in a plane. The sixth oxygen puckers upward but also coordinates the cation. A complex was also reported in which two Na^+ ions are complexed within a 24-crown-8 macroring. Literally hundreds of solid-state structures are known for crown ethers with cations and molecular species. and these may be found in the Cambridge Structural Database.

Six structures are shown in Fig. 6. Unbound 12-crown-4 is shown in panel (a). It is shown complexed in panel (b), along with 18-crown-6, in an unsymmetrical sandwich. Two additional molecules of 18-crown-6 are present in the unit cell but do not bind the cation. Note that because 10 oxygen donors are present. K^+ is not in the 18-crown-6 macroring's plane. Potassium cation is in the plane in (c), (d). and (e). The ClO_4^- ion is shown in contact with the cation in (d). The counterions are not shown for (c) and (e) (*N*-heptylaza-15-crown-5). The molecular complex between 18-crown-6 and acetonitrile is shown in panel (f).

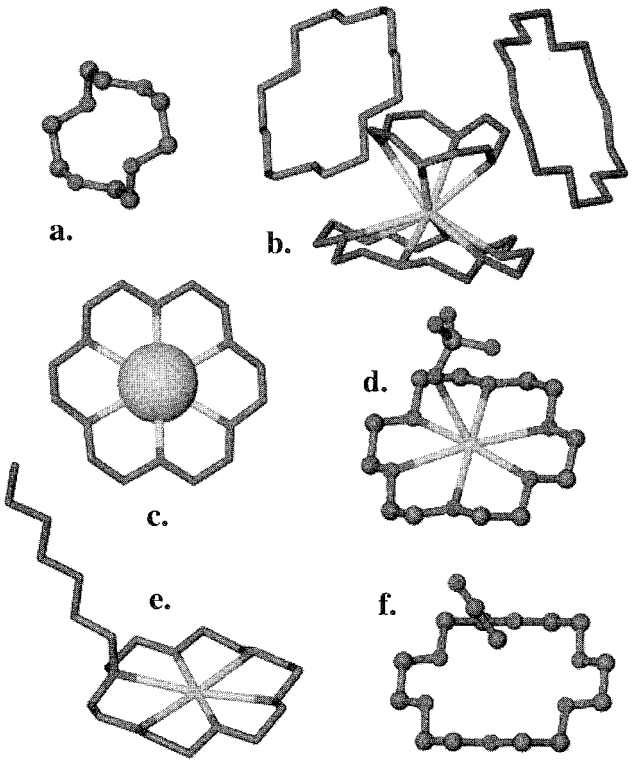

Fig. 6 Solid-state structures of crown ethers and several potassium complexes. (*View this art in color at www.dekker.com.*)

Complex detection by mass spectrometry

The advent of such low-fragmentation techniques as fast-atom bombardinent (FAB) and electrospray ionization (ESI) permitted the direct observation of crown ether complexes in the gas phase. Complexation of a species such as $(18\text{-crown-6} \cdot Na)^+$ is readily detectable as a species having mlz (264 + 23) = 287. The corresponding K^+ complex would have a mass of 303. Selectivities were inferred by comparing peak intensities. The mass spectrometric method is of great value, but comparisons between gas, solution. and solid phases should be made with appropriate circumspection.[33]

APPLICATIONS

The applications of crown ethers in modern chemistry could fill many volumes. Initially, they were used to complex metal ions. This was expanded to organic ions and molecular species. Eventually, crowns became scaffolds upon which other. more ambitious structures were built. This section presents a limited number of these interesting and important applications and in only the briefest outline.

Dye and coworkers formed complexes of the type $M^+ \cdot \text{crown} \cdot M^-$. A cryptand complex of Na^+ permitted the first observation of Na^-. This work was extended from alkalides to cation complexes having an electron ("electride") as counterion.[34,35]

Chromophoric groups can be appended to or integrated with crown ethers. If absorption of light induces a conformational change in the macrocycle, complexation selectivity may be controlled and switched. This was recognized almost simultaneously by Misumi,[36] Vögtle,[37] Takagi,[38] and Shinkai,[39] who all reported "crown ether dyes" or photoresponsive crown ethers. Another means of altering the conformation is to use a redox reaction. Shinkai used oxidative formation of a disulfide linkage to achieve this end.[40] Another means of "switching" is to vary the electron density rather than the conformation. If this can be accomplished electrochemically. it is a convenient and reversible process. Enhancement of electron density by reduction of appended nitroaromatic residues in crown ethers was reported by Maifer. Echegoyen, and Gokel.[41–43] During the past decade, numerous and diverse applications were made for crown ethers. These include the formation of rotaxanes. catenanes, and knots,[44,45] membrane[46–49] and monolayer[50] formation, and ion channels.[51–53] They were used as fluorescent probes[54–56] and to demonstrate cation–π interactions.[57]

CONCLUSION

The original concept and report of crown ethers is now more than three decades old. Even so, the field remains vital. and many applications in modern science are found for crowns. They are used as complexing agents and as substructural elements in complex chemical architectures. The number of literature reports involving crown ethers continues to increase, and undiscovered applications are still ahead.

ARTICLES OF FURTHER INTEREST

Cryptands, p. *334*
Ionophores, p. *760*
Lariat Ethers, p. *782*

REFERENCES

1. Pedersen, C.J. Cyclic polyethers and their complexes with metal salts. J. Am. Chem. Soc. 1967. 89, 2495–2496. 7017–7036.
2. Pedersen. C.J. The discovery of crown ethers. Science 1988, 241. 536–540.
3. Leong. B.K.J.: Ts'o. T.O.T. Testicular atrophy from inhalation of ethylene oxide cyclic tetramer. Toxicol. Appl. Pharmacol. 1974. 27. 342–354.
4. Pedersen, C.J. Macrocyclic polyethers. Dibenzo-18-crown-6 polyether and dicyclohexyl-18-crown-6 polyether. Org. Synth. 1972, 52. 66–74.
5. Hendrixson. R.R.: Mack. M.P.; Palmer, R.A.; Ottolenghi, A.; Ghirardelli. R.G. Oral toxicity of the cyclic polyethers 12-crown-4. 15-crown-5, and 18-crown-6 in mice. Toxicol. Appl. Pharmacol. 1978. 44. 263.
6. Dale, J.: Borgen, G.; Daasvatn, K. Oligomerization of ethylene oxide to macrocyclic ethers, including 1,4,7-trioxacyclononane. Acta Chem. Scand., Ser. B 1974, *28*, 378–379.
7. Cokel, G.W.; Cram. D.J.; Liotta. C.L.: Harris. H.P.: Cook. F.L. Preparation and purification of 18-crown-6. J. Org. Chem. 1974. 39. 2445–2446.
8. Gokel. G.W.: Cram. D.J.; Liotta. C.L.; Harris. H.P.: Cook. F.L. 18-crown-6. Org. Synth. 1977. 57, 30.
9. Gokel. G.W.: Korzeniowski. S.H. *Macrocyclic* Polyether *Syntheses*; Springer Verlag: Berlin, 1982: 415 pp.
10. Parker, D. *Macrocycle* Synthesis: A Practical *Approach*; Oxford University Press: Oxford, 1996; 252 pp.
11. Creene. R.N. 18-crown-6. A strong complexing agent for alkali metal cations. Tetrahedron Lett. 1972. 1793–1796.
12. Mandolini, L.: Masci. B. Kinetic evidence for the template effect of added cations on the rate of formation of benzo-18-crown-6 in water solution. J. Am. Chem. Soc. 1977, 99. 7709–7710.
13. Madan, K.; Cram. D.J. Guanidinium ion as a guest during and after formation of 27-crown-9 polyether hosts. J. Chem. Soc., Chem. Commun. 1975, 427–428.
14. *Cation Binding* by *Macrocycles*; Inoue. Y.. Gokel, G.W., Eds.; Marcel Dekker: New York. 1990: 762 pp.
15. Gokel, G.W. *Crown* Ethers *and Cryptands*; The Royal Society of Chemistry: London, England. 1991: 190 pp.
16. *Comprehensive Supramolecular* Chemistry: Gokel, G.W.. Ed.; Pergamon Press: Oxford. 1996: 787 pp.
17. Izatt. R.M.; Hayinore, B.L.: Christensen. J.J. Stable oxonium-cyclic polyether complex characterized by infrared spectroscopy. J. Chem. Soc., Chem. Commun. 1972, 1308–1309.
18. Chenevert. R.; Rodrigue, A.: Beauchesne. P.; Savoie. R. New complexes of the hydronium ion with crown ethers: Synthesis and vibrational spectra. Can. J. Chem. 1984. 62. 2293–2298.
19. Junk. P.C.: Atwood, J.L. Synthesis and x-ray crystal structure of [H5O2+.21-crown-7][WOCl5-], a complex in which the 21-crown-7 molecule adopts a rigid, bowl-like conformation. J. Chem. Soc., Chern. Commun. 1995. 1551–1552.
20. Gokel. G.W.: Garcia. B.J. Crown-cation complex effects. III. Chemistry and complexes of monoaza-18-crown-6. Tetrahedron Lett. 1977. 317–320.
21. Bianchi. A.; Bowman-James. K.: Garcia-Espaiia. E. *Supramolecular* Chemistry of Anions: Wiley-VCH: New York, 1997: 461 pp.
22. Frensdorff, H.K. Salt complexes of cyclic polyethers. Distribution equilibriums. J. Am. Chem. Soc. 1971, 93. 4684–4688.
23. Pedersen. C.J.: Frensdorff. H.K. Macrocyclic polyethers and their complexes. Angew. Chem., Int. Ed. Engl. 1972. 11. 16–25.
24. Christensen. J.J.; Hill. J.O.: Izatt. R.M. Ion binding by synthetic macrocyclic compounds. Science 1971, 174. 459–467.
25. Izatt, R.M.; Terry. R.E.: Haymore, B.L.: Hansen. L.D.; Dalley, N.K.: Avondet, A.G.: Christensen, J.J. Calorimetric titration study of the interaction of several uni- and bivalent cations with 15-crown-5. 18-crown-6, and two isomers of dicyclohexo-18-crown-6 in aqueous solution at 25°C and m=0.1. J. Am. Chem. Soc. 1976, 98. 7620–7626.
26. Kyba. E.B.; Koga. K.; Sousa. L.R.; Siegel. M.G.; Cram, D.J. Chiral recognition in molecular complexing. J. Am. Chem. Soc. 1973, 95, 2692–2693.
27. Kyba, E.P.: Siegel, M.G.; Sousa, L.R.: Sogah. G.D.Y.; Cram. D.J. Chiral, hinged, and functionalized multiheteromacrocycles. J. Am. Chem. Soc. 1973. 95. 2691–2692.
28. Helgeson. R.C.: Timko, J.M.: Cram, D.J. Structural requirements for cyclic ethers to complex and lipophilize metal cations or α-amino acids. J. Am. Chem. Soc. 1973. 95. 3023–3025.
29. Zhang. X.X.; Bradshaw. J.S.; Izatt, R.M. Enantiomeric recognition of amine compounds by chiral macrocyclic receptors. Chein. Rev. 1997. *97*, 3313–3361.
30. Olsher, U.; Hankins, M.G.; Kim. Y.D.: Bartsch. R.A. Anion effect on selectivity in crown ether extraction of alkali metal cations. J. Am. Chem. Soc 1993. *115*, 3370–3371.
31. Truter, M.R.; Bush. M.A. Crystal structures of three

alkali-metal complexes with cyclic polyethers. J. Chem. Soc., D 1970. 1439–1440.
32. Dobler. M. *Ionophores and Their Structures*; J. Wiley & Sons: New York. 1981: 379 pp.
33. Fyles, T.M.; Zeng. B. On the assessment of complex cation-crown ether equilibria by electrospray mass spectrometry. Supramol. Chem. 1998. 10. 143–153.
34. Lok. M.T.: Tehan, F.J.: Dye. J.L. Spectra of Na-, K-. and e-solv in amines and ethers. J. Phys. Chern. 1972. 76. 2975–2981.
35. Dye. J.L. Anions of the alkali metals. Sci. Am. 1977, *237*. 92–96. 98. 100. 102. 104–105.
36. Yamashita, I.; Fujii. M.: Kaneda, T.: Misumi. S.: Otsubo. T. Synthetic macrocyclic ligands. II. Synthesis of a photochromic crown ether. Tetrahedron Lett. 1980.21.541–544.
37. Dix, J.P.: Voegtle. F. Ligand structure and complexation. L. Ion-selective crown ether dyes. Chern. Ber. 1980, *113*. 457–470.
38. Yamashita. T.: Nakamura, H.: Takagi, M.; Ueno, K. Synthesis of crown ether dyes. Bull. Chern. Soc. Jpn. 1980, *53*. 1550–1554.
39. Shinkai, S.: Shigematsu. K.: Kusano, Y.; Manabe. O. Photoresponsive crown ethers. Part 3. Photocontrol of ion extraction and ion transport by several photofunctional bis(crown ethers). J. Chem. Soc., Perkin Trans. 1 1981. 3279–3283.
40. Minami. T.; Shinkai. S.: Manabe, O. Redox-switched crown ethers. Monocrown-biscrown interconversion coupled with redox of a thiol-disulfide couple. Tetrahedron Lett. 1982. *23*. 5167–5170.
41. Gustowski. D.A.; Echegoyen, L.: Goli. D.M.; Kaifer. A.; Schultz, R.A.: Gokel. G.W. Electrochemically switched cation binding in nitrobenzene-substituted. nitrogen-pivot lariat ethers. J. Am. Chem. Soc. 1984, 106. 1633–1635.
42. Kaifer. A.; Echegoyen, L.: Gustowski. D.: Goli, D.M.; Gokel. G.W. Enhanced sodium cation binding by electrochemically-reduced, nitrobenzene-substituted lariat ethers. J. Am. Chem. Soc. 1983. 105. 7168–7169.
43. Kaifer, A.E.; Comez-Kaifer, M. *Supramolecular Electrochemistry*; Wiley-VCH: Weinheini, 1999.
44. Dietrich-Buchecker. C.: Frommberger. B.: Luer. I.: Sauvage, J.P.; Vögtle, F. Catenanes with a macrobicyclic central unit. Angew. Chem. 1993, *105*, 1526–1529.
45. Ashton. P.R.; Baldoni, V.; Balzani. V.: Claessens. C.G.; Credi. A.; Hoffmann. H.D.A.: Raymo. F.M.: Stoddart. J.F.; Venturi. M.; White, A.J.P.; Williams. D.J. Template-directed syntheses. spectroscopic properties. and electrochemical behavior of [*n*]catenanes. Eur. J. Org. Chem. 2000. 1121–1130.
46. Furusawa. K.: Obata. C.: Matsumura, H.: Takeuchi, M.; Kuwamura. T. Bilayer membranes of amphiphilic crown ethers with amino acid residue. Chem. Lett. 1990. 1047–1050.
47. Diederich. F.: Effing. J.: Jonas, U.: Jullien, L.: Plesnivy, T.; Ringsdorf, H.; Thilgen, C.: Weinstein, D. C60 and C70 in cages? Mono- and multilayers of azacrown compounds and fullerenes. Angew. Chem.. Int. Ed. Engl. 1992. *31*. 1599–1602.
48. Tai. Z.: Qian. X.: Wu, L.: Zhu, C. Self assembly of bilayer membranes from single-chain aza crown ether. J. Chem. Soc., Chem. Commun. 1994. 1965–1966.
49. De Wall, S.L.: Wang, K.: Berger, D.R.; Watanabe, S.: Hernandez. J.C.; Gokel. G.W. Azacrown ethers as amphiphile headgroups: Formation of stable aggregates from two- and three-armed lariat ethers. J. Org. Chem. 1997, *62*. 6784–6791.
50. Flink. S.: van Veggel. F.C.J.M.: Reinhoudt, D.N. Recognition of cations by self-assernbled monolayers of crown ethers. J. Phys. Chem.. B 1999. 103, 6515–6520.
51. Fyles, T.M.: James. T.D.: Pryhitka, A.; Zojaji. M. Assembly of ion channel mimics from a modular construction set. J. Org. Chem. 1993. *58*. 7456–7468.
52. Pregel. M.J.; Jullien. L.: Canceill, 3.: Lacombe, L.: Lehn, J.-M. Channel-type molecular structures. Part 4. Transmembrane transport of alkali-metal ions by 'bouquet' molecules. J. Chem. Soc., Perkin Trans. 2 1995. 417–426.
53. Gokel. G.W.; Murillo, O. Synthetic organic chemical models for transmembrane channels. Acc. Chem. Res. 1996. *29*. 425–432.
54. Fages. F.: Desvergne, J.-P.; Bouas-Laurent. H.: Lehn, J.-M.; Barrans. Y.: Marsau, P.; Meyer. M.; Albrecht-Gary, A.-M. Synthesis, structural. spectroscopic, and alkali-metal cations complexation studies of a bis-anthracenediyl macrotricyclic ditopic receptor. J. Org. Chem. 1994. *59*. 5264–5271.
55. De Silva, A.P.; Gunaratne, H.Q.N.: Rice, T.E.: Stewart. S. Switching "on" the luminescence of one metal ion with another: Selectivity characteristics with respect to the emitting and triggering metal. Chern. Commun. 1997. 1891–1892.
56. De Silva. A.P.: McClenaghan, N.D. Proof-of-principle of molecular-scale arithmetic. J. Am. Chem. Soc. 2000. *122*. 3965–3966.
57. De Wall. S.L.: Meadows. E.S.: Barbour, L.J.: Gokel. G.W. Synthetic receptors as models for alkali metal cation-pi binding sites in proteins. Proc. Natl. Acad. Sci. U. S. A. 2000, *97* (12), 6271–6276.

Cryptands

Bernard Dietrich
ISIS—Université Louis Pasteur, Strasbourg, France

INTRODUCTION

Shortly after the discovery of crown ethers by Pedersen in 1967. Lehn designed the first cryptand. and the synthesis of this compound was achieved in the fall of 1968.[1,2] Thus, at the end of the 1960s, one of the largest fields of research was opened by these two classes of compounds, and the origin of supramolecular chemistry goes back to that time. Not often mentioned in the foundation of this large field are the cyclodextrins. Nevertheless, credit should be given to the pioneer workers in this area, since as early as 1952, "Einschlussverbindungen" (inclusion compounds) were studied by F. Cramer.[3] Some of the numerous achievements of cryptand chemistry will be presented after a brief historical introduction.

HISTORY

In the mid-1960s. Jean-Marie Lehn developed interest in the process occurring in the nervous system, in particular, in the fact that the electrical events in nerve cells rest on changes in the distribution of sodium and potassium ions across the membrane. Around the same period, several research groups established that some natural macrocyclic antibiotics (nonactin, valinomycin) have a complexing ability toward alkali cations, and the first x-ray investigation on the K'-nonactin complex revealed the efficient surrounding of the cation by eight oxygen atoms of the macrocyclic ligand. Thus, when Charles Pedersen reported the cation binding properties of crown ether. Lehn rapidly realized that the recognition of a spherical species (an alkali cation) would be much more efficient if the ligand has a sphericai three-diinensional (3D) cavity instead of the circular two-dimensional (2D) surrounding of the cation observed with the crown ether.[4] This idea led to the synthesis of the first cryptand **1** (Fig. 1) that forms a stable potassium complex 2 (Fig. 2), named "cryptate." In addition to the high stability. the ligand also has a large selectivity for the potassium cation versus the smaller (Na^+) and the larger (Rb^+) cations. The crystal structure determination confirmed the inclusion of the cation in the 3D cavity and the perfect matching between size of cation and size of cavity.

CRYPTATES OF METAL CATIONS

This first synthesis was followed by the modification of the cavity size by altering the length of the bridging chains. This led to a series of cryptands exhibiting high selectivity of complexation toward almost all cations of Groups I and II. For example, the smaller cryptands **3** and 4 (Figs. 3 and 4) are selective for Li^+ and Na^+, respectively. Cryptands incorporating other donor atoms (nitrogen, sulfur) or heterocyclic rings were also synthesized (Figs. 5–7). These ligands present attractive coordination chemistry features: depending on their specific structures. they can bind transition metal ions, heavy metals, or lanthanides cations. Thus, most of the cations of the periodic table can be complexed with variable stabilities and selectivities. In addition, by virtue of molecular design. a tuned ligand exhibiting specific properties may be obtained by making appropriate modifications of an existing ligand.

A further step in complexity was accomplished by designing ligands able to complex more than one cation: cryptand **8** (Fig. 8), for example. forms a homodinuclear complex with silver or copper.[5] The crystal structure of the dinuclear Cu(I) complex formed with the hexaimine macrobicycle **8** shows the inclusion of the two copper ions, which are tetracoordinated at each end of the cavity. the Cu...Cu distance being very large (11.07 A). The small hexaimine macrobicycle **9** (Fig. 9) forms a Cu(I) dinuclear complex in which the Cu(I)...Cu(I) distance is short (2.45 A). In the reduced ligand **10** (Fig. 10), the Cu(I) is not stable, and only the $[Cu_2(\mathbf{10})]^{3+}$ cryptate was obtained. The Cu...Cu distance in this complex is 2.42 Å, and on the basis of ESW measurements, an average redox state (di $Cu^{1.5}$) was postulated rather than a Cu(I)...Cu(II) dinuclear complex.[6]

Mention has to be given to the synthetic aspects of cryptands. It is obvious that after the intellectual process of ligand design and despite the various new (efficient) modelization tools found for the computer. the necessity still exists to obtain the actual compound. Numerous methods were developed over the years.[7] Many symmetrical cryptands can be obtained in a few steps and with high yields. For the more elaborate cryptands, synthesis is usually more cumbersome. and the number of steps is high.

Encyclopedia of Supramolecular Chemistry
DOI: 10.1081/E-ESMC 120012704

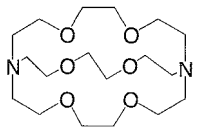

Fig. 1 1: Diazahexaoxa macrobicycle cryptand [2.2.2]

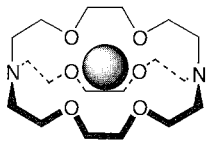

Fig. 2 2: Potassium coinplex of cryptand **1**. An example of cryptate.

The nomenclature used to describe the simplest cryptands is simple, it is formed by three numbers, each designing the numbers of oxygen atoms in each chain For example 1 is called [2 2 2]

PROTON CRYPTATES

The small cryptand 11 (Fig. 11) was obtained with difficulty. because the major compound obtained was a macrotricyclic tetraarnide resulting from a dimerization reaction. It was observed that stable proton cryptates of 11 can be obtained. The [1.1.1] bicycle binds one or two protons inside its intramolecular cavity. The diprotonated cryptate 11, $2H^+$, has a high resistance to deprotonation. The monoprotonated cryptate may be obtained with difficulty; but this latter species cannot be fully deprotonated by base to afford the free cryptand.[8] Smaller analogues of **11** containing only carbon atoms in the three chains were also described. They present similar behavior toward the proton.'" Another class of cryptands able to strongly bind the proton was developed more recently.

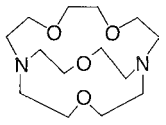

Fig. **3** **3:** Cryptand [2.1.1].

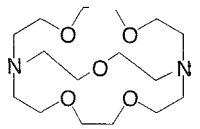

Fig. 4 4: Cryptand [2.2.1]

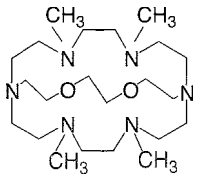

Fig. **5** **5:** Wexaazadioxa macrobicycle

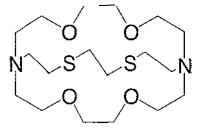

Fig. 6 6: Diazatetraoxa-dithia macrobicycle

The tetraazamacrotricycle 12 (Fig. 12) is an example of this type of cryptand. The name adamanzane was proposed for these compounds. As for the cryptands described above, in this new type of "proton sponge," one can observe the same inertness of the inside coordinated proton toward strong bases.[10] The simplicity of the synthesis of this class of compounds will allow for the preparation of many new representatives.

CRYPTATES OF AMMONIUM AND ORGANIC CATIONS

The binding by cryptand 1 of the nonspherical ammonium cation was observed. but not surprisingly, the receptor–substrate binding complementarity is poor. and therefore.

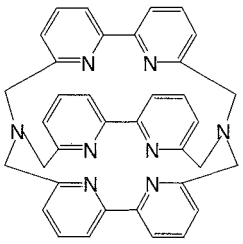

Fig. 7 7: Ti-is-bipyridine cryptand.

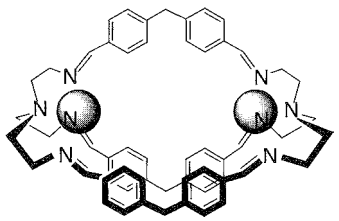

Fig. 8 Homodinuclear complex of the hexaimine cryptand 8 containing a diphenylmethane spacer

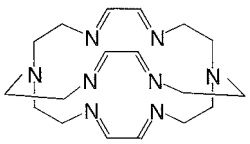

Fig. 9 9: Hexaimine cryptand

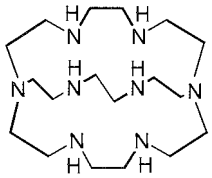

Fig. 10 10: Octaazacryptand

the stability constant of the coinplex [$NH_4^+ \subset$ 2.2.2] is in the medium range. By contrast, the macrotricyclic cryptand **13** (Fig. 13) forms a stable ammonium cryptate. The cation is held inside the cavity by a tetrahedral array of N–H^+...N hydrogen bonds with the four bridgehead nitrogen atoms. The binding is completed by electrostatic interaction between the partial charges on the NH_4^+ hydrogens and the remaining heteroatoms of the ligand.[4]

A new approach for efficient binding of the ammonium cation was postulated. It relies on the use of cation–π interactions in addition to hydrogen bonding. The ligand 14 (Fig. 14) was synthesized, and the binding of NH_4^+ was studied. The x-ray investigations revealed that the benzene rings are positioned at an appropriate distance from the cation so as to allow efficient cation–π interactions.[11]

The above-described spherical macrotricyclic cryptand 13 was designed for the ammonium cation, whereas the series of cylindrical macrotricycles **15** (Fig. 15) was

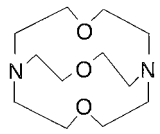

Fig. 11 11: Cryptand [1.1.1].

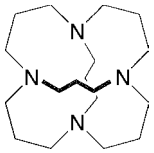

Fig. 12 12: Tetraazatricyclo cryptand

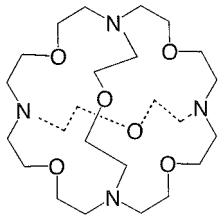

Fig. 13 13: Tetraaza-hexaoxamacrotricyclic cryptand.

synthesized for the linear recognition of diammonium salts $^+H_3N(CH_2)_n–NH_3^+$. The various bridges (R) allow specific binding of the substrate of complementarity length (n=2–12). Definitive proof that these molecular complexes display cryptate-like behavior was obtained by x-ray structure analysis of the complex [$^+H_3N(CH_2)_5–NH_3^+ \subset$**15b**].[12]

ANION CRYPTATES

Compared to cations. the field of anion coordination was developed more recently. but due to the efforts realized over the years in several laboratories, the area of anion complexation is by now a full member of the supramolecular chemistry family. The delayed exploration of the field can be mainly ascribed to the limited choices of appropriate binding sites for anions. The most studied are the ammonium binding sites that present. unfortunately, an intrinsic drawback: their positively charged status is pH dependent (except for the tetraalkylammonium derivatives). Nevertheless. many polyammonium macrocycles were synthesized and studied. These ligands exhibit good binding properties toward large poiyatomic anions (phosphates, sulfates, adenosine phosphates. tartrates, etc.). For the smaller spherical halide anions. efficient binding requires macrobicyclic structures. Thus, the octaaza analogue of the [2.2.2] cryptand, compound **10**. binds in its hexaprotonated form the F^- halide, with a high stability constant and a sharp F^-/Cl^- selectivity (>10^8).[13] The slightly larger macrobicycle **16** (Fig. 16) binds well the

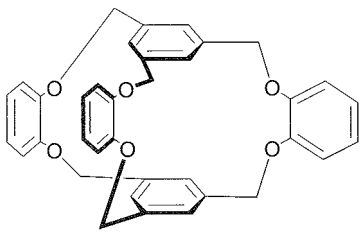

Fig. 14 14: Cage-type receptor for NH_4^+. In the top and bottom benzene rings, the 2.4.6 ethyl substituents are omitted for clarity.

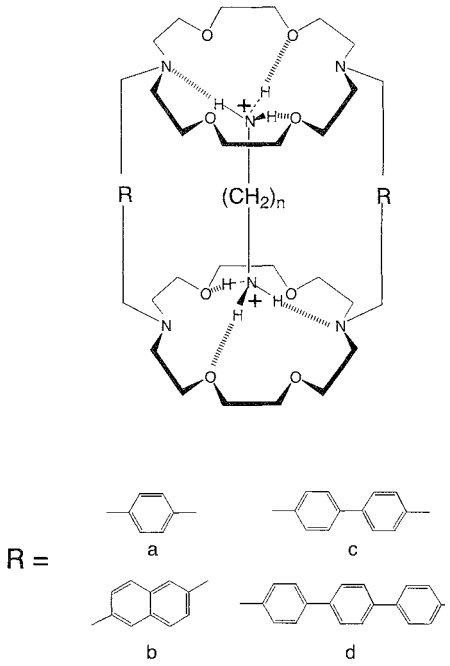

Fig. 15 15: Cylindrical macrotricyclic ligands.

Cl^- *anion. X-ray investigations confirm the inclusion of the anion in the macrobicyclic cavity.* Ligand *13 described above for the ammonium cation* complexation *is able to complex, in its tetraprotonated form. the* Cl^- *anion, a high* Cl^-/Br^- *selectivity being observed for this compound. An x-ray structure of the complex* [Cl^- *C* 13–$4H^+$] *confirmed the anion* inclusion *in the cavity and also the binding* of the *anion by a tetrahedral array of* four *ionic hydrogen bonds.*

Successful anion complexation *was also achieved with larger* macrobicyclic *ligands. Thus, the macrobicycle* 17 *(Fig. 17).6H' binds halide anions and the linear triatomic azide anion with a* very *high stability constant. The x-ray structure revealed an efficient shape and size complementarity between* N_3^- *and the* cavity.[14] *A whole series of* polyazacryptands *was obtained in high yields by a simple* Schiff *base* [2 + 3] *condensation between the* triaminotriethylamine *(tren) and various* dicarboxaldehydes. *The hexaimine macrobicycles prepared by this* way *lead, after reduction, to the polyaza cryptands, which* in

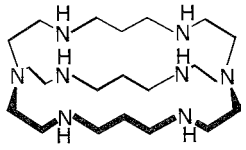

Fig. 16 16: Octaazacryptand containing a propyl spacer.

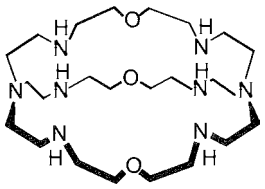

Fig. 17 17: Octaaza-trioxa cryptand.

their hexaprotonated form were shown to complex numerous polyatomic *anions. The examples presented here were characterized by x-ray structures: terephtalate anion by* cryptand 18 (Fig. 18), $6H^+$,[15] *perchlorate and nitrate by* 19 *(Fig.* 19), $6H^+$, *and 20 (Fig.* 20), $6H^+$.[16] *Encapsulation of two nitrates by the latter compound was also observed. and the x-ray structure revealed that the two planar nitrate anions were maintained inside the cavity by hydrogen-bonding interactions between the protonated amine* functions *and the* anions.[17]

The large cavity of cryptand 17 *allows another approach to anion coordination, the "cascade anion binding." In a first step, the ligand binds by* its *tren subunits two* Cu(II) *cations. In a second step.* the *axial vacant hollow between the two already bound* Cu(II) *cations* will *allow the binding of an anion. An early example was based on* computer *analysis of potentiometric titrations data, and the efficientbinding of* the *chloride anion by the dicopper complex of* 17 *was* postulated.[18] *Many other bis-tren-type figands were studied, and the cascade binding of anions such as Br , OH , N_3^-, WCO . etc. was demonstrated. Many x-ray structures confirm the location of the anions between the various metal* cations.[6,19]

An interesting novel approach to anion binding is the use of NH–π *hydrogen bonds. It has to be emphasized that this type of receptor rests on neutral hydrogen bonding, a seldom-encountered situation in the field of anion coordination. In Compound* 21 *(Fig.* 21). *it can be seen that the amide hydrogens are orientated toward the inside of the cavity and are* able *to* interact with *the* π *electron system of an anion. Crystal structure of the acetate coniplex reveals that the anion* is *bound within the* cavity.[20]

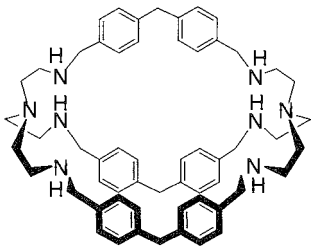

Fig. 18 18: Octaazacryptand containing a diphenyl-methane spacer.

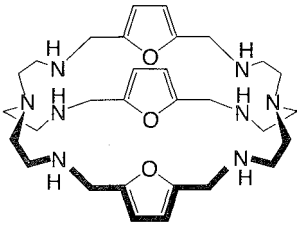

Fig. 19 19: Octaazacryptand containing a furan spacer.

APPLICATIONS OF CRYPTANDS

The development of the cryptand field has been rapid for two major reasons. First. a few years after the first publication on cryptands syntheses. several representatives became commercially available, allowing subsequent wide inquiries into numerous areas. A second explanation for rapid multifield developments rests on the large number of researchers in various fields who immediately realized the potentialities of cryptands in their ow11 spheres of expertise.

Few examples will illustrate the revolution introduced in some domains by the cryptands. In 1974. J. L. Dye published the first x-ray structure of an alkalide. a new species containing a sodium anion (Na^-) (a rather offensive discovery for a traditional trained chemist in the 1970s) as counterion of the sodium cryptate of cryptand [2.2.2]. The cryptate has a stabilizing effect on the fairly unstable anion. and by using this procedure, a large number of alkalides were isolated. A further step was the isolation of electrides species in which the counterion of the cryptate is an electron.[21,22] The field of polyanionic clusters was largely studied by J. D. Corbett, and many of these systems could be isolated owing to the stabilization of the polyanion by the associated alkali cation cryptand.[23,24] Other interesting new species were generated by L. Echegoyen using the electroreductive crystallization of the sodium cryptate of ligand 7. This process leads to a neutral entity formed by the positively charged cation cryptate and one electron located on one of the bipy units of the cryptand. The name cryptatium was proposed

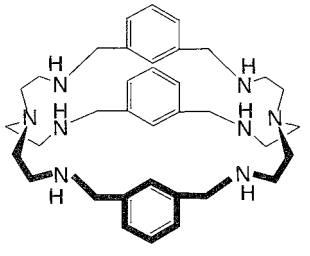

Fig. 20 20: Octaazacryptand containing anxylyl spacer

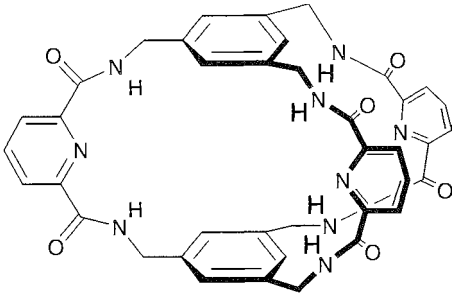

Fig. 21 21: Cage-type receptor for anion. In the top and bottom benzene rings. the 2.4.6 ethyl substituents are omitted for clarity.

for this new class of compounds.[25] The Eu^{3+} cryptate formed with cryptand **7** showed attractive luminescent properties,[26] and practical applications in fluoroimmunoassays were realized.

Other areas of interest include stabilization of noncommon oxidation states, solvent extraction of cations. transfer of cations through membranes, isotopic separation, detoxification of harmful and radioactive metals, metal recovery, metal trace analysis. ion chromatography on polymer-supported cryptands, and chromo- and fluoroionophores. More organic-chemistry-orientated applications can be mentioned, including enhancement of metal salt solubility in organic solvents, anion activation, phase-transfer catalysis. and anionic polymerization. Many of these applications are covered in other articles in this encyclopedia as well as in the literature.[27]

CONCLUSION

In this short presentation, the author tried to give a short survey of this enormous field. There was not enough room to mention many other types of cryptands, like the metallocene-containing cryptands. the sepulchrate and sarcophagine cage complexes, the photocleavable cryptands, the borocryptands, the phosphorus cryptands, and the macrobicyclic polyethers with carbon atoms bridgehead. to cite just a few. Concerning the future. there is no doubt that the design of new cryptands displaying specific properiies will remain a major challenge for the people active in this area. Improvements of already existing compounds[12''] and new trials[29] will lead to new achievements and progress.

ARTICLES OF FURTHER INTEREST

Alkalides and Electrides, p. 12
Cation–π Interactions, p. 214

Crown Ether,, p *326*
Hydrogen Bonding, p. *658*
Ionophores, *p. 760*
Protonated Aza-Macrocycles for Anion Complexation, p. 1170
Simultaneous Binding of Cations arid Anions. p. *1291*

REFERENCES

1. Dietrich. B.: Lehn, J.-M.; Sauvage. J.-P. Diaza-polyoxa-macrocycles et macrobicycles. Tetrahedron Lett. 1969. *34*. 2885–2888.
2. Dietrich. B.: Lehn. J.-M.; Sauvage. J.-P. Les Cryptates. Tetrahedron Lett. 1969, *34*. 2889–2892.
3. Cramer. *F*. Einschlussverbindungen. Angew. Chem. 1952. *64*. 437–447.
4. Lehn, J.-M. Supramolecular chemistry—Scope and perspectives molecules. supermolecules. and molecular devices (Nobel Lecture). Angew. Chem.. Int. Ed. Engl. 1988. *27*. 90–112.
5. Jazwinski, J.: Lehn. J.-M.: Lilienbaum. D.: Ziessel. R.: Guilheni. J.; Pascard, C. Polyaza macrobicyclic cryptands: Synthesis, crystal structure of a cyclophane type macrobicyclic cryptand and of its dinuclear copper(I) cryptate, and anion binding features. J. Chem. Soc., Chem. Commun. 1987. *22*. 1491–1694.
6. Nelson, J.; McKee. V.; Morgan. G. Coordination chemistry of azacryptands. Prog. Inorg. Chem. 1998. *47*. 167–316.
7. Dietrich, B. Cryptands. In *Comprehensive Supramolecular Chemistry*; Cokel, G.W., Ed.: Elsevier Science: New York, 1996; Vol. 1, 153–211. Chapter 4.
8. Dietrich, B.: Viout, P.: Lehn. J.-M. *Macrocyclic Chemistry—Aspects of Organic and Inorganic Supramolecular Chemistry*; VCH Publishers: Weinheim. 1993.
9. Alder. R.W.: East. S.P. In/out isomerism. Chem. Rev. 1996. 96. 2097–2111.
10. Springborg, J.: Pretzmann. U.; Olsen, C.E. An inert proton coordinated inside tetrahedral cage [3^6] adamanzane. Synthesis of the inside monoprotonated amine 1.5.9.13-tetraazatricyclo [7.7.3.$3^{5,13}$] docosane. Acta Chem. Scand. 1996. *50*. 294–298.
11. Jon. S.Y.; Kim. J.: Kim. M.; Park. S.-H.: Jeon. W.S.; Heo. J.; Kim. K. A rationally designed NH_4^+ receptor based on cation–π interaction and hydrogen bonding. Angew. Chem. Int. Ed. 2001. *40*. 2116–2119.
12. Pascard, C.: Riche, C.: Cesario. M.: Kotzyba-Hibert. F.: Lehn. J.-M. Coreceptor–substrate binding. Crystal structures of a macrotricyclic ligand and of its molecular cryptate with cadaverine dication. J. Chem. Soc., Chem. Commun. 1982. *10*. 557–560.
13. Dietrich, B.: Dilworth. B.; Lehn. J.-M.; Souchez. J.-P.; Cesario. M.; Guilhem. J.: Pascard, C. Anion cryptates: Synthesis, crystal structures. and cornplexation constants of fluoride and chloride inclusion complexes of polyammonium macrobicyclic ligands. Helv. Chim. Acta 1996. 79, 569–587.
14. Dietrich. B.: Guilhem. J.: Lehn. J.-M.: Pascard. C.; Sonveaux. E. Molecular recognition in anion coordination chemistry. Structure, binding constants and receptor–substrate complementarity of a series of anion cryptater of a macrobicyclic receptor molecule. Helv. Chim. Acta 1984. *67*. 91–104.
15. Lehn. J.-M.; Méric. R.; Vigneron, J.-P.; Bkouche-Waksman. I.: Pascard. C. Molecular recognition of anionic substrates. Binding of carboxylates by a macrobicyclic coreceptor and crystal structure of its supramolecular cryptate with the terephtalate dianion. J. Chem. Soc., Chem. Commun. 1991. *2*, 62–64.
16. Hynes. M.J.: Maubert. B.; McKee. V.: Town. R.M.: Nelson. J. Protonated aracryptates hosts for nitrate and perchlorate. J. Chem. Soc., Dalton Trans. 2000. *16*. 2853–2859.
17. Mason, S.: Clifford, T.: Seib. L.: Kuczera. K.: Bowman-James. K. Unusual encapsulation of two nitrates in a single bicyclic cage. J. Am. Chem. Soc. 1998. *120*. 8899–8900.
18. Motekaitis. R.J.: Martell. A.E.: Dietrich. B.: Lehn. J.-M. Anion binding in macrobicyclic metal cryptate complexes: Copper(II)-bistren. Inorg. Chem. 1984. *23*. 1588–1591.
19. Amendola. V.: Bastianello. E.: Fabbrizzi. L.: Mangano. C.: Pallavicini. P.; Perroti. A.: Lanfredi, A.M.: Ugozzoli. F. Halide–ion encapsulation by a flexible dicopper(II) *bistren* cryptate. Angew. Chem. Int. Ed. 2000. *39*, 2917–2920.
20. Bisson. A.P.; Lynch, V.M.: Monahan. M.-K.C.: Anslyn, E.V. Recognition of anion through NH–π hydrogen bonds in a bicyclic cyclophane—Selectivity for nitrate. Angew. Chem. Int. Ed. 1997. *36*. 2340–2342.
21. Dye. J.L. Alkali metals plus complexants: From alkalides and electrides to aromatic anions. Macromol. Symp. 1998. *134*. 29–39.
22. Dye. J.L. Electrides: From 1D Heisenberg chains to 2D pseudo-metals. Inorg. Chem. 1997, *36*. 3816–3826.
23. Corbett. J.D. Exploratory synthesis in the solid state. Endless wonders. Inorg. Chein. 2000. *39*. 5178–5191.
24. Corbett, J.D. Diverse naked clusters of the heavy main-group elements. Electronic regularities and analogies. Struct. Bond. 1997, *87*. 157–193.
25. Boulas. P.L.: Gomez-Kaifer. M.; Echegoyen, L. Electrochemistry of supramolecular systems. Angew. Chern. Int. Ed. 1998. 37. 216–247.
26. Sabbatini. N.: Cuardigli. M.: Lehn. J.-M. Luminescent lanthanide complexes as photochemical supramolecular devices. Coord. Chem. Rev. 1993. *123*. 201–228.
27. Atwood, J.L.; Davies. J.E.D.: MacNicol. D.D.: Vogtle. F. *Comprehensive Supramolecular Chemistry*; Elsevier Science: New York. 1996; (11 volumes).
28. Zhang, X.X.: Izatt. R.M.: Bradshaw. J.S.; Krakowiak, K.E. Approaches to improvement of metal ion selectivity by cryptands. Coord. Chem. Rev. 1998. *174*, 179–189.
29. MacGillivray, *L.R.:* Atwood. J.L. Structural classification and general principle? for the design of spherical molecular hosts. Angew. Chem. Int. Ed. 1999. *38*. 1018–1033.

Cryptophanes: Molecular Containers

K. Travis Holman
Georgetown University, Washington, District of Columbia, U.S.A

INTRODUCTION

In the past few decades, we have witnessed the profusion in synthetic chemical systems that highlight an elegance of design in the field of supramolecuiar chemistry, with many examples arising as models that help to deconvolute the supramolecular operations of biological systems. To this end. a large variety of molecules appeared possessing concave hydrophobic surfaces that can serve as binding sites for convex substrates. Cryptophanes hold a special place in this historical context. First reported by Collet and coworliers in 1981,[1] they are among the first examples of synthetic "container molecules"—that is, closed-surface macrocycles that possess the defining ability to completely encapsulate molecule-sized substrates.[2–5] Molecules of this unusual form, including such members as the (hemi)carcerands and self-assembled capsules. immediately bring to mind poiential applications as microreaction vessels, sensors. molecular delivery devices, and separations agents. to name but a few possibilities. Research is ongoing in these areas, and technological applications based upon the remarkable recognition cheinistry that is characteristic of these container-like species appear to be forthcoming.

The defining features of the cryptophanes are structural. They are composed of two cup-shaped. C_3-symmetric, [1.1.1]orthocyclophane units, connected by three bridges (Y, Fig. 1). This construction effectively ensures that. with appropriate bridges. cryptophanes possess enclosed (or nearly so) elliptical cavities with interior volumes on the size-scale of individual small molecules. The closed-surface nature of the cryptophanes is exemplified by a space-fill rendition of the so-called cryptophane-E, a well-studied member of the cryptophane family (Fig. 1). Enforced cavities make these molecules exceptionally well suited for molecular recognition studies—particularly. the sort that shed light on the nature of substrate binding within a generally hydrophobic pocket. The existence of two diastereomeric forms of these compounds (*syn* and *anti*, Fig. 1). together with chemical variety in the bridging (Y) and peripheral substituents (R), makes available a large number of cryptophanes with readily adjustable cavity volumes. aperture sizes, solubilities, and, ultimately, recognition properties.

The remarkable recognition properties displayed by the cryptophanes have attracted a great deal of attention. In this article, an attempt will be made to provide general insights into the supramolecular chemistry of these remarkable hosts by highlighting selected studies in the context of the field. Collet, the late father of cryptophane chemistry. provided more in-depth reviews elsewhere.[6]

CRYPTOPHANE STRUCTURE AND SYNTHESIS

As the details of cryptophane structure greatly affect the molecular recognition properties of these hosts. some discussion of structure and synthesis is pertinent. The construction of a cryptophane skeleton can be accomplished via any of three basic methods: (i)the "template" method. (ii)the "two-step" method, or (iii)a "capping" method. These approaches are generalized in Fig. 2. Each relies. at some stage. on a cyclization reaction that leads to the formation of the trimeric [1.1.1]-orthocyclophane moiety that provides the critical element of curvature to the cryptophane structure. This electrophilic aromatic substitution reaction is made regioselective, promoting C_3-symmetric trimeric products, by employing an appropriately 3,4-disubstituted benzyl alcohol as a starting material. For obvious reasons, the choice of substituents is limited. To achieve reasonable yields. the R substituent is almost exclusively limited to the strongly activating methoxy group. The identity of the X substituent is less important; typically. X needs only to be activating (e.g., -OR. -SR, NHCOR), but some limitations exist. These synthetic limitations dictate that functionalization of the peripheral substituents (R), which ultimately define the apertures of the cryptophane cavity. usually occurs after the critical cup-forming steps.

The C_3 symmetry of the cup-lilie trimers indicates that they are chiral. typically being formed as a racemate. In some cases, the cups are resolvable via suitable diastereomers. as the enantiomers are somewhat stable to racemization via conformational inversion of the nine-membered cyclophane ring ($\Delta G^{\ddagger}_{298}$ = 110–115 kJ/mol). Chirality in the cup-shaped units implies that two types of cryptophanes exist. Joining two cups of opposite

Encyclopedia of Supramolecular Chemistry
DOI: 10.1081/E-ESMC 120012710

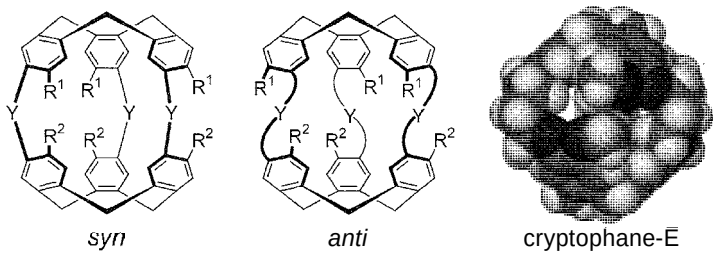

Fig. 1 Cryptophane structure.

handedness; as defined by the arrangement of the bridging *Y* substituents, results in a cryptophane, where the R substituents display a *syn* relationship. Alternatively, joining two cups of the same handedness results in a chiral *anti* cryptophane (only one enantiomer is depicted in Fig. 1). If $R^1 = R^2$, the *syn* diastereomer will be the achiral *meso* form, with C_{3h} symmetry, whereas the anti diastereomer will be chiral, possessing D_3 symmetry. Fortunately, most cryptophane *syn* and *anti* diastereomers can be readily separated, but unambiguous assignment of their identity can be more difficult. Additionally, if the top and bottom cups differ with respect to their peripheral substituents ($R^1 \neq R^2$), the *syn* and *anti* forms will both be chiral (C_3). It is relatively straightforward to impart top/bottom asymmetry in the cryptophanes, but only recently have lower-symmetry C_2 varieties, bearing different Y bridges. been achieved."]

Method (i), the "template method," was the first employed by Collet for the synthesis of cryptophanes.[1] A suitably substituted benzyl alcohol is first cyclized to form a trimeric cup. Additional benzyl alcohol substituents are then appended via a bridging Y group, and these groups are then subjected to an intramolecular cyclization to yield the corresponding cryptophanes. The initially fonned C_3-cup thus serves as a template for the second cup-forming reaction, with the reaction typically proceeding in good yields (often > 60%) and with appreciable diastereoselectivity. Though this method normally requires high dilution conditions (10^{-4} M in formic acid), it provides distinct advantages in some respects. This approach. for instance, allows the synthesis of cryptophanes that are asymmetric with respect to the peripheral substituents attached to the top and the bottom cups ($R^1 \neq R^2$). Second, provided that the initially formed trirner can be resolved, this route can be employed to provide optically active *anti* cryptophanes of known absolute configuration.

Method (ii), known as Collet's ''two step'' synthesis, yields suitable cryptophanes in only two synthetic steps from readily available vanillyl alcohol (R = OCH_3, X = OH).[8] In this approach. a monomer possessing two vanillyl alcohol residues is synthesized and then cyclized directly, under acidic conditions, to the con-esponding

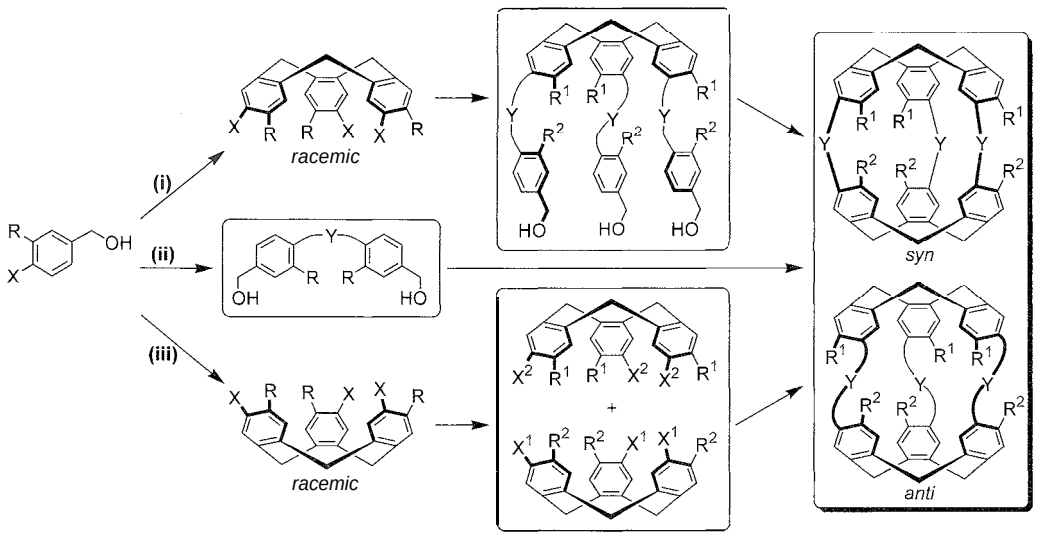

Fig. 2 Synthesis of cryptophanes.

cryptophanes. The reaction entails the formation of both orthocyclophane cups in a single pot and. although the yields are generally low (< 20%), gram quantities of cryptophanes can be readily prepared by this convenient approach. Notably, this reaction tends to display diastereoselectivity in favor of the chiral anti cryptophanes: making available some chiral *anti* cryptophanes that give low yields by the "template" method.

Cram and coworkers demonstrated that Method (iii). the "capping" of one preformed C_3-trimer with another. is also viable.[9] Though Cram's synthesis involved the oxidative coupling of two identical cups possessing terminal acetylenic groups (R = CH_3; X = $OCH_2C{\equiv}CH$), "capping" one C_3-trimer with a dissimilar trimer can also be envisaged ($R^1 \neq R^2$ or $X^1 \neq X^2$). Though the yields of cryptophanes synthesized by the "capping" method were low (< 15%), lessons learned from similar approaches toward the syntheses of (hemi)carcerand molecular containers suggest that it may be possible to improve yields by employing suitable guest templates.[10]

To date, several dozen cryptophanes have been synthesized. A detailed list of these is beyond the scope of this short review; but most cryptophanes are of the form where the bridging Y substituents are simple oxyhydrocarbons {e.g., Y = –OZO-: Z = $(CH_2)_n$ [n = 2–10], CH_2ArCH_2, $CH_2CH{=}CHCH_2$, $CH_2C{\equiv}CCH_2$, $OCH_2C{\equiv}CC{\equiv}CCH_2O$, $(OCH_2CH_2)_2O$}.[6] Moreover, the peripheral R substituents of as-synthesized cryptophanes are often methoxy groups, but these may be selectively cleaved to the phenol, providing a synthetic entry point to cryptophanes with varying peripheral R substituents. Interestingly, there are two examples of cryptophanes that were synthesized in effectively quantitative yields via supramolecular self-assembly. These examples highlight the growing importance of self-assembly as a synthetic approach toward increasingly complex macrocycles.[11,12]

CRYPTOPHANE COMPLEXES

Of the 70 or so cryptophanes that have been reported, relatively few were characterized with respect to their supramolecular chemistry. Listed in Table 1 are those examples that were shown to display some kind of complex-forming behavior. As the IUPAC names for cryptophanes are exceedingly complex, an alphabetical system based simply on the chronology of synthesis was used and, as much as possible. will be adopted here.

Discovery

The cryptophane story begins in 1981 with Collet's template-directed synthesis of the first and smallest known cryptophane, the so-called cryptophane-A (*anti*; $Y = O(CH_2)_2O$; $R^1 = R^2 = OCH_3$).[1] At the time. the field of supramolecular or host–guest chemistry was entering

Table I Cryptophanes *possessing demonstrated complex-forming* abilities

Structure			Name		
Bridges, -Y-	R^1	R^2	*anti*	*syn*	Ref.
3 × $O(CX_2)_2O$, X = H/D	OCX_3	OCX_3	**A**		[13,14]
	OCH_2CO_2H	OCH_2CO_2H	**A3**		[15]
	OCH_3	*H*	**C**	**D**	[16,17]
3 × $O(CH_2)_3O$	OCH_3	OCH_3	**E**	**F**	[18,19]
	OCH_2CO_2H	OCH_2CO_2H	**E3**		[20]
3 × $O(CH_2)_5O$	OCH_3	OCH_3	**O**	**P**	
	OCH_2CO_2H	OCH_2CO_2H	**O3**		[21]
3 × $OCH_2C{\equiv}CC{\equiv}CH_2O$	CH_3	CH_3	γ	δ	[9]
3 × $O(CH_2CH_2O)_2$	OCH_3	*OCH;*		†	[22]
3 × 1,2-$(OCH_2C_6H_4CH_2O)$	OCH_3	OCH_3	†	†	[23]
3 × 1,2-$(OCH_2C_6H_4(3,4\text{-}(CO_2Me)_2)CH_2O)$	OCH_3	OCH_3	†	†	[23]
3 × 1,4-$(OCH_2C_6H_4CH_2O)$	OCH_3	OCH_3		†	[23]
3 × 1,3-$(OCH_2(2\text{-}CO_2H\text{-}5\text{-}Bu^t)C_6H_4CH_2O)$	OCH_3	OCH_3		†	[24]
2 × $O(CH_2)_2O$, 1 × $O(CH_2)_3O$	OCH_3	OCH_3	**223**		[7]
2 × $O(CH_2)_3O$, 1 × $O(CH_2)_2O$	OCH_3	OCH_3	**233**		[7]
2 × $O(CH_2)_2O$, 1 × $O(CH_2)_4O$	OCH_3	OCH_3	**224**		[7]
3 × $OCH_2COO^-\cdots{}^+H_3N(CH_3)HCOCO$	OCH_3	OCH_3	†,‡	†,‡	[12]

A common name was not assigned

[+]*Syn/anti* form not specified.

its developing stages. and, though many examples of synthetic molecules capable of the selective binding of cations (or even anions) were known. nonnatural systems. wherein complexes persist in solution between uncharged apolar host, and similar, uncharged apolar guests, were essentially unknown. Though naturally occurring cyclodextrins had long been observed to complex uncharged molecules in aqueous solution via their hydrophobic cavities. the question remained whether the design of synthetic molecules for such purposes could be achieved. It was generally recognized, however, that synthetic hosts capable of discriminatory binding according to size. shape; and especially chirality. could prove useful for a variety of technologies.

Examination of space-filling models of cryptophane-A indicated it to be an effectively closed surface container. suggesting that it would be exceedingly difficult for certain solvent molecules. such as $CHCl_3$, to enter the cavity through the methoxy-guarded apertures. Accordingly. $CDCl_3$ was originally chosen as a noncompetitive solvent to initiate complexation studies. but the evidence showed that substrates like CH_2Cl_2 were only weakly bound under these conditions. It was thought. therefore. that the cryptophane-A cavity may be too well guarded, and that the cavity apertures needed to be enlarged in order to allow potential substrates access to the cavity. Collet and coworkers thus synthesized cryptophanes-**C** and -**D**, the anti and *syn* cousins of cryptophane-A, wherein one of the two cups was absent the methoxy substituents.[16,17] Despite similar cavity sizes, the ^{1}H-NMR spectrum in $CDCl_3$ showed cryptophane-C to complex CH_2Cl_2 more effectively than cryptophane-A, though the association was modest ($K_a = 1.8\ M^{-1}$). Further studies showed that CH_2ClBr ($K_a \approx 0.9\ M^{-1}$) and CH_2Br_2 ($K_a \approx 0.15\ M^{-1}$) were also weakly bound by cryptophane-**C** under these conditions, and effective size discrimination was clearly operative. Remarkably, the *syn* diastereomer, cryptophane-D, forms complexes with the same guests. but the association constants are an order of magnitude smaller.

In 1985, Collet and coworkers demonstrated the first example of enantioselective recognition by a cryptophane. Optically pure cryptophane-**C** was used as an ^{1}H-NMR shift reagent for the analytical resolution and first experimental determination of the maximum rotation of bromochlorofluoromethane (CHFClBr), one of the simplest chiral molecules.'''' At *332* K, the difference in association constants (in $CDCl_3$) between the diastereomeric conipiexes ($K_a = 0.22\ M^{-1}$ and $0.30\ M^{-1}$) were sufficient to effect the separation of the fast exchange resonances of the guest, and the enantiomeric excess of a weakly resolved sample could be determined; thus yielding the maximum rotation as $[\alpha]^{25}_D = 1.7 \pm 0.5°$—data that were sought for nearly a century. The (*R*)-(−) absolute configuration of the haloform was later assigned with the aid of corroborating molecular dynamics simulations and Raman optical activity spectra of the cryptophane-**C**⊙CHFClBr complexes.[26 27]

Lessons in Molecular Recognition

Given the modest association constants. it originaliy appeared that thermodynamic driving forces for the formation of cryptophane complexes were destined to be extremely small. Binding of CH_2Cl_2 by cryptophane-A, for instance, was immeasurably weak in chloroforin solution. As experiments progressed, however, it became clear that, contrary to earlier beliefs, the chloroform solvent was, in fact. a significant competitor for the cryptophane cavity. In $(CDCl_2)_2$, a much larger solvent, the binding of CH_2Cl_2 by cryptophane-A is strong ($K_a = 475\ M^{-1}$ at 300 K). Moreover, under these conditions. the strong affinity of cryptophane-A for chloroform also became apparent ($K_a = 230\ M^{-1}$).[14] Binding of CH_2Cl_2 by cryptophane-**C** was observable in chloroform, not because the apertures of the cryptophane cavity are larger, but because chloroform does not compete as effectively for the cavity of cryptophane-C [$K_a = 10\ M^{-1}$ at 300 **K** in $(CDCl_2)_2$].

These results highlight a general caveat in supramolecular chemistry: the significance of complexation behavior must always be interpreted in the context of the solvent. In special cases where the solvent is bound by the host in competition with the intended guest. the observed association constant is only an apparent association constant (K_{app}). Thus, K_{app} will be comparable to the "true" association constant, K_a, only when the binding of the solvent, K_s, is extremely weak ($K_s < 10^{-2}$–10^{-3}). This considered, molecular recognition studies involving container compounds are typically performed in less conventional solvent systems, where the solvent is usually too large to be accommodated by the cavity (e.g., mesitylene. phenyl ether, hexachloroacetone, 1,1,2,2-tetrachloroethane) or has a poor affinity for the, typically hydrophobic, cavity (e.g., water).

The subtleties of the molecular recognition properties exhibited by cryptophanes are best appreciated by comparing a series of structurally similar cryptophanes in a common solvent system. In this respect, the binding of neutral guests by cryptophanes-**A**, -**C**, and -**E** (*anti*, $Y = O(CH_2)_3O$, $R^1 = R^2 = OCH_3$) are directly comparable in $(CDCl_2)_2$, as this solvent is sufficiently large that it cannot compete with the guests. Depicted in Fig. *3* are the free energies of association, at *300* K, as a function of guest volume for a series of neutral molecules that are bound by these three cryptophanes.[6,14,18] The identities of selected guests are indicated. The most notable feature of this plot is the sharp size discrimination displayed by all

of all of the cryptophanes and particularly for cryptophanes-C and -E. The intrinsic thermodynainic driving forces for complexation of optimal guests ($-\Delta G_i^0$) range from 15–21 kJmol^{-1}, meaning that these hosts will effectively. scavenge complementary guests. even in the absence of solvophobic effects. The optimal guest volume increases smoothly with increasing cryptophane cavity size: Xe, CH_2Cl_2, and $CHCl_3$ for -**A**. -**C**. and -E. respectively. Guests smaller or larger than the experimental optimal volume are bound less effectively; and those that, according to molecular models. are too large to occupy a particular cryptophane cavity are simply not complexed. Notably, the cryptophanes can effectively differentiate guests on the basis of subtle volume differences (< 5%). Cryptophane-C, for instance, discriminates between CH_2Cl_2 and CH_2ClBr by 1.5 kJmol^{-1}. Similarly, cryptophane-E discriminates between $CHCl_3$ and $CHCl_2Br$ by 1.2 kJmol^{-1}. In terms of shape recognition. guests of roughly tetrahedral or elliptical shape tend to be bound more effectively than planar or linear guests. Isobutane, for example, is bound more strongly by cryptophane-E than is *n*-butane ($\Delta\Delta G^0 = 6.0$ kJmol^{-1}). Additionally. the cryptophanes tend to have a low affinity for fluorinated guests. Cryptophane-A, for example. has almost no affinity for CHF_2Cl, though the size and shape of this guest would suggest that it should be bound strongly.

Cryptophanes also readily bind and recognize suitable cations in organic solvents.[20] The free energies of association, at 300 K in $(CD_2Cl_2)_2$, between cryptophane-E and alkyl ammonium cations ranging in size from Me_3NH^+ to Me_3PrN^+ are plotted in Fig. 3. along with the corresponding data for the binding of neutral molecules by the same host. A similarly sharp size selectivity profile is observed for the binding of these cations. with Me_4N^+ being the most strongly bound. The K_a of cryptophane-E binding to Me_4N^+ (2.25×10^5 M^{-1}), however, is three orders of magnitude greater than that of the most favored neutral molecule complex (cryptophane-E⊙$CHCl_3$), reflecting the strong preference of the cation for the electron-rich. aryl-lined cryptophane cavity as compared to the halogenated solvent. Moreover. Me_4N^+ is 33% larger than $CHCl_3$. Remarkably, neutral molecules of this size are essentially unbound under the same experimental conditions. and these results raise some serious questions concerning the criteria by which one defines inolecular "size."

Collet and coworkers also synthesized cryptophanes of a water-soluble variety. Cryptophanes-A3, E3. and **O3** are water-soluble derivatives of cryptophanes-A, **C**. and **O**. possessing six pendant ionizable –OCH_2COOH groups in place of the methoxy groups.[15,20,21] As expected, the stability of the neutral molecule cryptophane complexes is increased on moving to aqueous solvent due to the hydrophobic effect. and the stabilizing effect is more pronounced as the size of the guest increases. Notably. the larger cryptophane-03 displays an affinity for comparatively larger guests (Me_4Sn, Et_4Ge, Me_4Pb), an observation in accord with expectations. The water-soluble cryptophanes are far less effective at binding small alkyl ammonium cations in aqueous solution than their parent cryptophanes in organic solvents, though

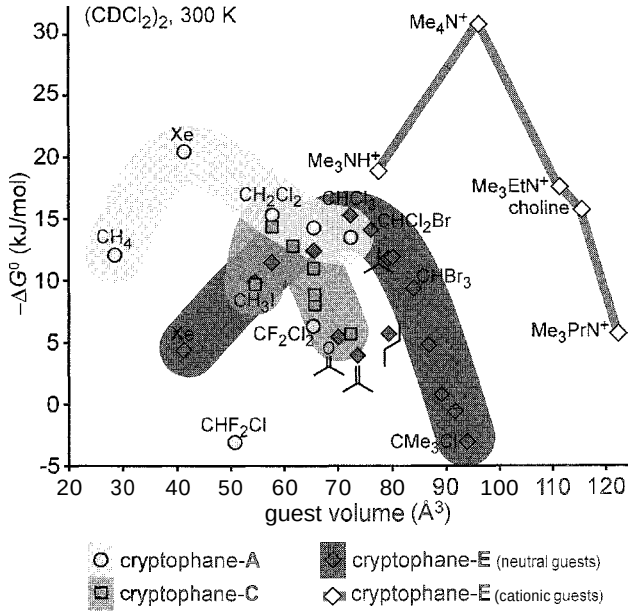

Fig. 3 Gibb's molar free energies of complexation for various cryptophane⊙guest complexes in $(CDCl_2)_2$ at 300 K.

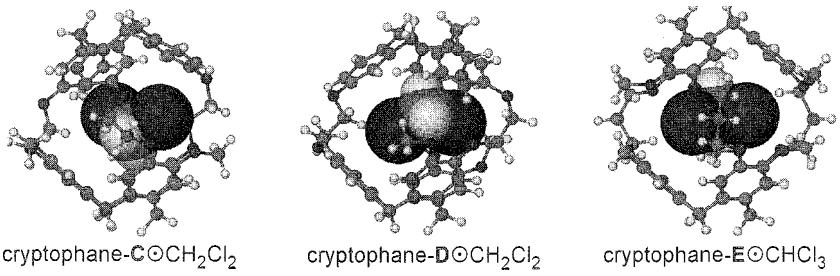

Fig. 4 Crystal structures of well-resolved cryptophane⊙guest complexes.

similar trends are observed with respect to size selectivity. The K_a for the binding of Me_4N^+ by cryptophane-E3, for example. is only 320 M^{-1}, as compared to the aforementioned K_a of 2.25 x 10^5 M^{-1} for the cryptophane-E⊙Me_4N^+ complex in $(CD_2Cl_2)_2$. Lower association constants are attributable to the hydrophilic nature of the small alkyl ammonium cations. As the size of an alkyl ammonium ion is increased, however. it tends to become more hydrophobic. Thus, the larger cryptophane-03 forms a complex with acetylcholine that is of comparable stability to that of acetylcholine esterase.

Variable temperature studies allow deconstruction of the free energy of association into the enthalpic and entropic contributions.[6] Though complex formation is typically favored from an enthalpy standpoint, these studies show that complex formation may also be entropically favored. The binding of CH_2Cl_2 by cryptophane-E. for instance, is driven strictly by entropy, with values for ΔH^0 and ΔS^0 equal to 4.2 kJmol^{-1} and 25 Jmol^{-1}K^{-1}, respectively. Similarly. the binding of methane by cryptophane-A is both enthalpically (AN" = – 6.7 kJmol^{-1}) and entropically (ΔS^0 = 17 Jmol^{-1}K^{-1}) favored. Moreover, Cram and Rebek observed similar results for hemicarceplexes and self-assembled capsules. respectiv e~~.These extraordinary observations are counterintuitive for an association of two molecules, in an apolar solvent, wherein the motions of the molecules would be anticipated to be relatively restricted. Collet and coworkers rationalized these observations by pointing out that the guest molecules of such entropy-favored complexes often do not efficiently fill the volume of the host cavities, suggesting that in such cases, the cryptophane interiors may best be described as a supercritical fluid and the guests may readily disorder within the host. The methane molecule of the cryptophane-A⊙CH_4 complex, for example, occupies a mere 35% of the cavity volume. Cram used related arguments to make the case for a ''new phase of matter'' within carcerand interiors and pointed out the entropic benefits of diluting empty space on complex formation.[4] Additionally, it should be considered that complexation may release somewhat organized solvent molecules from the solvation sphere of the guest, a factor that is known to assist complex formation in aqueous solutions.

The crystal structures of only a few well-defined cryptophane complexes were reported. The complexes cryptophane-C⊙CH_2Cl_2,[16] cryptophane-D⊙CH_2Cl_2,[17] and cryptophane-E⊙$CHCl_3$[19] are depicted in Fig. 4. Each depicts an arrangement wherein the guest is completely encapsulated by the pseudo-C_3 symmetric cryptophane.

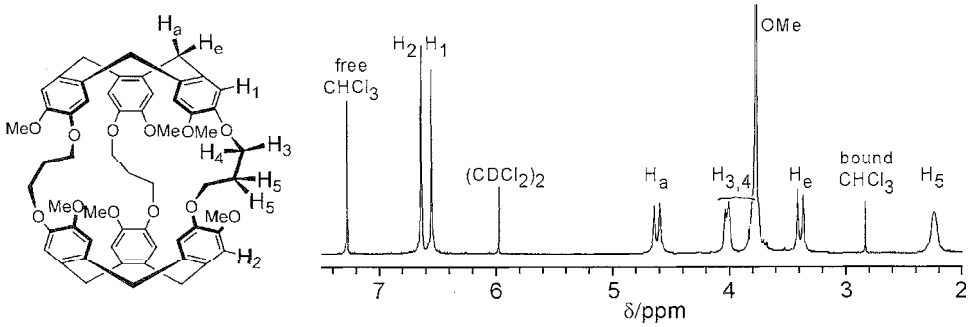

Fig. 5 Slow exchange binding of $CHCl_3$ by cryptophane-E in $(CDCl_2)_2$ as revealed by ^{1}H-NMR.

The two CH_2Cl_2 complexes possess ordered guest molecules This ıs ın accord with a negative entropy of complexation for the cryptophane-C complex (ΔS° = -4 $Jmol^{-1}K^{-1}$) and the fact that the guest can occupy roughly 70% of the available cavıty volume, a value sımılar to the packing fraction of close-packed crystals

Constrictive binding: the "container effect"

In an appropriate solvent. guests encapsulated by cryptophanes typically exchange slowly, with many complexes exhibiting half-lives on the order of milliseconds-seconds at room temperature. Thus, in a typical NMR experiment, separate signals for free and complexed guest species can often be observed simultaneously. Fig. 5 depicts the room temperature 300 MHz ^{1}H-NMR spectrum of cryptophane-E in $(CDCl_2)_2$ in the presence of four equivalents of $CHCl_3$. The peaks at δ 7.28 and δ 2.84 correspond to free and cryptophane-bound $CHCl_3$, respectively. The dramatic upfield shifts ($\Delta\delta \approx 4$ ppm) for encapsulated species are consistent with the close proximity to the shielding regions of the aryl rings of the host. Similar spectroscopic signatures were noted for guests encapsulated within other container molecules.

Observation of slow exchange in these systems is remarkable. considering that the negative free energies for complexation of neutral molecules rarely exceed 15 $kJmol^{-1}$. The activation barriers for dissociation. $\Delta G_d^{\ddagger}$, were measured by line shape analysis for some cryptophane complexes of uncharged substrates.[6] The $\Delta G_d^{\ddagger}$ for complexes of cryptophane-E are found to be nearly independent of the guest identity, ranging only from 66-71 $kJmol^{-1}$ for a relatively wide range of guests. Cram and coworkers recognized similar behavior for hemicarceplexes and put forth the notion of a container effect. termed constrictive binding, as an explanation.'" Constrictive binding ($\Delta G_c^{\ddagger}$) is a manifestation of the physical consequences of encapsulation and is defined as the activation free energy for host–guest association or. alternatively, the activation free energy of dissociation ($\Delta G_d^{\ddagger}$) less the intrinsic thermodynamic driving force for complexation, $-\Delta G_i^0$ (Fig. 4). As for some hemicarceplexes. the constrictive binding energy for cryptophane-E [$\Delta G_c^{\ddagger} = \Delta G_d^{\ddagger} - (-\Delta G_i^0) \approx 56$ $kJmol^{-1}$] remains relatively constant for a series of guests, implying that exchange of guests is governed by a (somewhat costly) conformational gating by the host. As a result. complexes of relatively Iow intrinsic thermodynamic stability (e.g., $\Delta G_i^0 \approx 15$ $kJmol^{-1}$) can display impressive kinetic stabilities (upwards of $\Delta G_d^{\ddagger} > 70$ $kJmol^{-1}$), a feature that should be regarded as a defining trait for true molecular containers. This concept is illustrated schematically in Fig. 6 by cornparing the binding behavior of container molecules with that of related cup-shaped cavitands. which display similar values for $-\Delta G_i^0$ but differ greatly with respect to their ability to constrictively bind guests via encapsulation. McCammon and coworkers performed molecular dynamics simulations on some cryptophane complexes and found that the conformational sampling of the host can depend on the identity of the encapsulated guest.[28,29] In related work. Houk and coworkers performed gas-phase calculations on several members from the hemicarcerand family and identified two operative mechanisms. termed "French door*' and "sliding door,.' responsible for the gating of encapsulated guests.[30] Taken together, the experimental and computational findings suggest opportunities to finely tune the kinetics of complexation by modifying the cavity-guarding periphery, without appreciably affecting the thermodynamics. It is clear that more insight can be gained from continued complementary computational and experimental work.

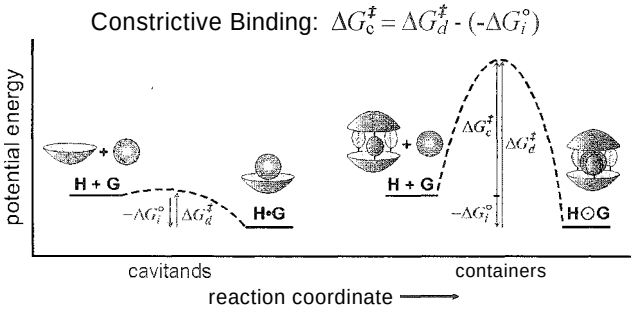

Fig. 6 Constrictive binding via encapsulation results in complexes with relatively high kinetic stabilities.

CONCLUSION

The study of cryptophanes has led to a greater understanding of molecular recognition phenomena. and particularly that which occurs within a hydrophobic binding site. Moreover, the ability of these and other molecular containers to discriminate between small molecule substrates on the basis of size. shape, chirality. and electronic characteristics is extraordinary. and the feasibility of practical applications derived from these characteristics is clear, though much work remains to be done. The development of higher-yield synthetic procedures or efficient optical resolutions, for instance. would increase availability and promote the use of cryptophanes for practical, recognition-based technologies. Additionally. much remains to be learned about the relationship between the kinetics and thermodynamics of complexation, the mechanisms by which these hosts select their guests,

and the properties of materials that might be derived from these remarkable compounds. Moreover, larger cryptophane-like molecular containers should be able to encapsulate larger or even greater numbers of substrates, opening the door for use as delivery devices or miniature reaction chambers. To be sure, much remains to be written in the story of container molecule chemistry.

ARTICLES OF FURTHER INTEREST

Calixarenes and Their Analogues: Molecular Complexation, p. 145
Calixarenes: Synthesis and Historical Perspectives. p. 153
Carcerands and Hemicarcerands, p. 189
Cavitands, p. 219
Chiral Guest Recognition, p. 236
Classification and Nomenclature of Supramolecular Compounds, p. 261
Concave Reagents. p. 311
Cryptands, p. 334
Cyclophanes: Definition and Scope, p. 414
Cyclophanes: Endoacidic, Endobasic, and Endolipophilic Cavities, p. 424
The Diphenylmethane Moiety, p. 452
Fullerenes as Encapsulating Hosts: Preparation, Detection, and Structures of Endohedral Fullerenes. p. 579
Hydrophobic Effects, p. 673
Inclusion Compounds: Selectivity, Thermal Stability, and Kinetics, p. 696
Induced Fit. p. 717
Kinetics of Complexation, p. 774
Macrocycle Synthesis, p. 830
The Template Effect, p. 1493

REFERENCES

1. Gabard. J.; Collet, A. Synthesis of D_3-bis(cyclotriveratrylenyl) macrocage by stereospecific replication of a C_3-subunit. J. Chem. Soc., Chem. Commun. 1981. 1137–1139.
2. Macgillivray, L.R.: Atwood, J.L. Structural classification and general principles for the design of spherical molecular hosts. Angew. Chem.. Int. Ed. 1999. *38*, 1019–1034.
3. Jasat. A.; Sherman. J.C. Carceplexes and hemicarceplexes. Chem. Rev. 1999. 99. 931–967.
4. Cram. D.J.: Cram. J.M. *Container Molecules and Their Guests*; Royal Society of Chemistry: Cambridge, 1994.
5. Conn. M.M.: Rebek, J. Self-assembling capsules. Chem. Rev. 1997. 97. 1647–1668.
6. Collet, A. Cryptophanes. In *Comprehensive Supramolecular Chemistry*; Atwood. J.A.. Atwood. J.L., Davies, J.E.D.. MacNicol. D.D.. Vögtle, F.. Suslick. K.S., Eds.; Pergamon Press: Oxford. 1996: Vol. 2. 325–365.
7. Brotin. T.: Dutasta. J.P. Xe@cryptophane complexes with C_2 symmetry. Eur. J. Org. Chern. 2003. 973–984.
8. Canceill. J.; Collet, A. Two-step synthesis of D_3 and C_{3h} cryptophanes. J. Chern. Soc., Chem. Commun. 1988. 582–584.
9. Cram. D.J.: Tanner. M.E.: Keipert, S.J.; Knobler, C.B. Two chiral [1.1.1]orthocyclophane units bridged by three biacetylene units as a host which binds medium-sized organic guests. J. Am. Chem. Soc. 1991. 113. 8909–8916.
10. Fraser, J.R.: Borecka. B.; Trotter, J.; Sherman, J.C. An asymmetric carceplex and new crystal-structure yield information regarding a one-million-fold template effect. J. Org. Chem. 1995. 60. 1207–1213.
11. Zhong, Z.L.; Ikeda, A.; Shinkai, S.: Sakamoto. S.; Yamaguchi, K. Creation of novel chiral cryptophanes by a self-assembling method utilizing a pyridyl-Pd(II) interaction. Org. Lett. 2001, 3. 1085–1087.
12. Lee. S.B.: Hong. J.I. Encapsulation of small organic molecules by a self-assembled molecular capsule through charged hydrogen bonding interaction. Tetrahedron Lett. 1996. 37. 8501–8504.
13. Brotin, T.; Devic. T.: Lesage. A.; Emsley, L.; Collet, A. Synthesis of deuterium-labeled Cryptophane-A and investigation of Xe@cryptophane complexation dynamics by 1D-EXSY NMR experiments. Chem. Eur. J. 2001. 7. 1561–1573.
14. Garel, L.: Dutasta, J.P.: Collet. A. Complexation of methane and chlorofluorocarbons by Cryptophane-A in organic solution. Angew. Chem., Int. Ed. Engl. 1993. 32. 1169–1171.
15. Canceill, J.; Lacombe, L.; Collet. A. Water-soluble cryptophane binding lipophilic guests in aqueous solution. J. Chem. Soc.. Chem. Commun. 1987, 219–221.
16. Canceill, J.; Cesario. M.; Collet. A.; Guilhem. J.; Pascard. C. A new bis-cyclotribenzyl cavitand capable of selective inclusion of neutral molecules in solution. Crystal structure of its CH_2Cl_2 cavitate. J. Chem. Soc., Chem. Commun. 1985. 361–363.
17. Canceill, J.: Cesario. M.: Collet; A.; Guilhem, J.: Riche, C.; Pascard. C. Selective recognition of neutral molecules: ^1H NMR study of the complexation of CH_2Cl_2 and CH_2Br_2 by Cryptophane-D in solution and crystal-structure of its CH_2Cl_2 cavitate. J. Chem. Soc., Chem. Commun. 1986. 339–341.
18. Canceill, J.; Lacombe. L.; Collet. A. New cryptophane forming unusually stable inclusion complexes with neutral guests in a lipophilic solvent. J. Am. Chem. Soc. 1986, *108*. 4230–4232.
19. Canceill. J.: Cesario, M.: Collet, A.; Guilhem. J.: Lacombe, L.; Lozach, B.; Pascard, C. Structure and properties of the Cryptophane-E $CHCl_3$ complex. a stable van der Waals molecule. Angew. Chem.. Int. Ed. Engl. 1989. 28. 1246–1248.
20. Garel. L.: Lozach, B.: Dutasta, J.P.; Collet. A. Remarkable effect of receptor size in the binding of acetylcholine and related ammonium-ions to water-soluble cryptophanes. J. Am. Chem. Soc. 1993. *115*. 11652–11653.
21. Garel, L.: Dutasta, J.P.; Collet, A. Complexation of

tetraalkylated derivatives of silicium. germanium, tin and lead by a water soluble cryptophane. New J. Chem. **1996.** *20*, 1265–1271.

22. Akabori, S.; Takeda, M.; Miura, M. The complexing abilities of diethylcneoxy- and xylene-bridged cryptophanes with alkanes. Supramol. Chem. **1999,** *10*, 253–262.
23. Miura, M.; Yuzawa, S.; Takeda. M.; Takeda, M.; Habata, Y.; Tanase, T.; Akabori, S. Syntheses of aromatic bridged cryptophanes and their complexing abilities with alkyl ammonium cations. Supramol. Chem. **1996,** *8*, 53–66.
24. Roesky, C.E.O.: Weber, E.; Rambusch, T.; Stephan, H.; Gloe, K.; Czugler, M. A new cryptophane receptor featuring three cndo-carboxylic acid groups: Synthesis, host behavior and structural study. Chcm. Eur. J. **2003,** 9, 1104–1112.
25. Canceill, J.: Lacombc, L.; Collet, A. Analytical optical resolution of bromochlorofluoromethanc by enantioselectivc inclusion into a tailor-made cryptophane and determination of its maximum rotation. J. Am. Chem. Soc. **1985.** 107, 6993–6996.
26. Costante, J.; Hecht, L.; Polavarapu, P.L.; Collet, A.; Barron, L.D. Absolute configuration of bromochlorofluoromethanc from experimental and ab initio theoretical vibrational Raman optical activity. Angew. Chem., Int. Ed. Engl. **1997,** 36. 885–887.
27. Costantecrassous, J.; Marronc, T.J.; Briggs, J.M.; Mccammon, J.A.; Collet, A. Absolute configuration of bromochlorofluoromethane from molecular dynamics simulation of its enantioselective complexation by Cryptophane-C. J. Am. Chem. Soc. **1997**, *119*, 3818–3823.
28. Kirchhoff, P.D.: Bass, M.B.; Hanks, B.A.; Briggs, J.M.; Collet, A.; McCammon, J.A. Structural fluctuations of a cryptophane host: A molecular dynamics simulation. J. Am. Chcm. Soc. **1996,** *118*, 3237–3246.
29. Kirchhoff, P.D.; Dutasta, J.P.; Collet, A.; Mccammon, J.A. Structural fluctuations of a cryptophane-tetramethylammonium host–guest system: A molecular dynamics simulation. J. Am. Chem. Soc. **1997,** 119, 8015–8022.
30. Houk, K.N.; Nakamura, K.; Sheu, C.M.; Keating, A.E. Gating as a control element in constrictive binding and guest release by hemicarcerands. Science **1996,** *273*. 627–629.

Crystal Deconstruction

Fabrizia Grepioni
Università di Sassari, Sassari, Italy

Dario Braga
Università degli Studi di Bologna, Bologna, Italy

INTRODUCTION

Crystal deconstruction is the process that leads backwards. in a reverse ''aufbau'' process. from the structure of a molecular crystal to the component molecules or ions. Crystal deconstruction allows one to focus on the interactions that are more relevant for crystal structure cohesion. The objective of the deconstruction process is also that of learning about the factors responsible for molecular/ionic recognition and self-assembly in the solid state. Insights into crystal polymorphism can be gained by comparing the different distributions of intermolecular interactions associated with the existence of different crystal forms of the same molecular species.

FROM BONDS BETWEEN ATOMS TO BONDS BETWEEN MOLECULES

Understanding the interactions that control molecular or ion recognition and self-assembly is one of the most relevant chemical problems of our time. with implications in all areas of chemistry, from biochemistry to organic, organometallic, and physical chemistry, to encompass inaterials chemistry. The interest in the bonds between molecules is paradigmatic of supramolecular chemistry.[1,2] This perception is shared with molecular crystal engineering[3,4] if the concept of bonds between molecules is convoluted with the translational symmetry of a molecular crystal (see Fig. I).

Molecular crystals can. in fact, be viewed as periodical supermolecules, in which a large number of molecules or ions interact via noncovalent interactions, generating collective physical and chemical properties.[5] According to the same reasoning. polymorphic modifications of a molecular crystal. i.e., different crystals of the same constituent molecule/ions,[6–9] can be regarded as periodical supramolecular isomers, differing in distribution of the noncovalent bonds.

In the context of this article, we will use the term ''*intermolecular*'' as a synonym of noncovalent. with this encompassing all types of secondary interionic or intermolecular interactions, e.g., electrostatic, hydrogen bonds, and van der Waals interactions. which do not imply two-electron σ-bonds. Accordingly, it is useful to identify neutral molecules and molecular ions (e.g., those formed by an ensemble of covalently bonded atoms) as molecular systems.

INTERNAL VERSUS EXTERNAL INTERACTIONS

The assembling of molecules to form stable three-dimensional aggregates is the quintessence of the self-recognition and self-aggregation processes that are behind the construction of any supramolecular system. The understanding of these processes requires a profound knowledge of the interactions among molecules and ions in the solid state.[10]

Crystal deconstruction is a logical process that allows one to "decode" the crystal structure organization of a given molecular or ionic crystal by sifting out those interactions. that are relevant to supramolecular recognition and to crystal cohesion.[11]

Supramolecular recognition is a process that applies when two different or identical entities (two molecules. two ions) approach each other in the vacuum or in a solvent medium to form a stable aggregate. In the absence of directing interactions, such as those resulting, for example, from the presence of strong dipoles or hydrogen-bonding donor–acceptor groups, the recognition process will be controlled by the outer shape of the molecule and by the nature of the peripheral atoms. The formation of a stable dimolecular aggregate. whether formed by the same molecule, i.e., *AA*, or by two different molecules/ions, i.e., AB, or $A^{+/-}B^{-/+}$, will depend primarily on the complementarity of shape. This concept was put forward by Linus Pauling long ago:[12]

> ...in order to achieve the maximum stability, the two molecules must have complementary surfaces. like die and coin. and also a complementary distribution of active

Encyclopedia of Supramolecular Chemistry
DOJ: 10.1081/E-ESMC 120012751

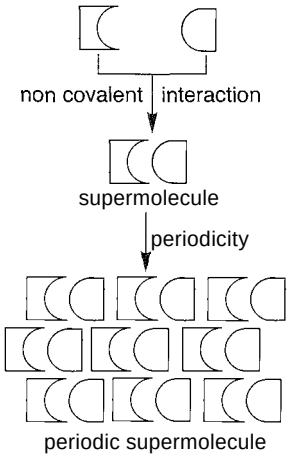

Fig. I The relationship between an aggregate at the molecular level—a supermolecule—and an aggregate at the crystal level—a periodic supermolecule.

groups. The case might occur in which the two complementary structure5 happened to be identical: however. in this case also the stability of the complex of two molecules would be due to their complementariness rather than their identity.

The pairwise approach of two molecules is the most elementary aggregation step in the nucleation of a crystal. This first nucleus will respond to the need to optimize the pairwise interaction; possibly in competition with the solvation/desolvation process. However, as the first nucleus begins to grow. with molecules/ions clinging to it one after the other, the cohesion of the overall aggregate becomes more important, to the extent that an optimum pairwise interaction may be sacrificed in favor of a more stable multicomponent aggregation. In other words. the construction of the crystal responds to a process of global energy minimization. which has to compromise between various factors in order to optimize the following:

I. Pairwise atoni–atom interactions between first neighbors (strong "local" repulsions are not tolerated).
2. Cohesive energy of the crystal aggregate (with its trillions of molecules).
3. Conformational energy for the isolated molecules. (This term is relevant in the case of flexible. structurally nonrigid molecules/ions.)

In addition. the temperature of the system must be taken into account, because molecules in thermal motion or undergoing low-energy reorientational/fluxional processes have temperature-dependent shapes and geometries. It should not be surprising, therefore. that there is no unique answer to the optimization process. and that different compromises between internal and external energy terms (both of enthalpic and entropic natures) may be reached for a given species. This inay well be the fundamental reason for the existence of polymorphic modifications of the same substance or for the occurrence of solid-state processes, such as solid-to-solid phase transitions between enantiotropic forms, order–disorder transitions, temperature-dependent isomerization in the solid state, etc. Crystal deconstruction is also useful for exploring the different distributions of intermolecular interactions that are consequences of crystal polymorphism.

ANALOGIC CRYSTAL DECODING

The crystal structure formed by neutral molecules or by molecular ions can be efficiently decoded by focusing on the number and distribution of the nearest neighbors around the reference molecule or ion in the crystal, the so-called molecular "enclosure shell" (ES) approach.[13] The ES approach avoids the strictness of translational and point symmetry and affords a direct appreciation of the most relevant interinolecular interactions involving the molecule of interest. One commences from the known molecular structure to study how the observed crystal can be reconstructed. This logical process recalls Kitaigorodsky's molecular ''aufbau'' process.'[14] In general, if possible, it is useful to first prepare a "one-dimensional" crystal by linking molecules to form a inolecular row. then a "two-dimensional" system by coupling molecular rows. and finally. a three-dimensional crystal by stacking molecular layers as depicted in Fig. 2. The decoding process can be carried out by using computer-aided graphic programs exploiting atomic coordinates determined by x-ray diffraction.

A practical application of the decoding process is afforded by the investigation of the crystal structure of two chemically different molecular systems. namely. benzene and *bis*benzenechromium,[13] compared in Fig. 3. The analogy between the two crystals is remarkable. even though the two molecules greatly differ in terms of chemistry. This is because the periphery of most organometallic molecules and coordination complexes is "organic" in nature.'''' while the metal centers are mostly situated in the molecular cores and are shielded from neighboring molecules. Because the surface atoms. besides determining the outer shape of the molecules/ions, are crucial in determining the nature and extent of intermolecular interactions, the packing problem of most molecular organometallic compounds reduces to the organic case. Under this viewpoint. it should be no surprise that the structures of benzene and *bis*benzenechromium are topologically similar. The peripheral.

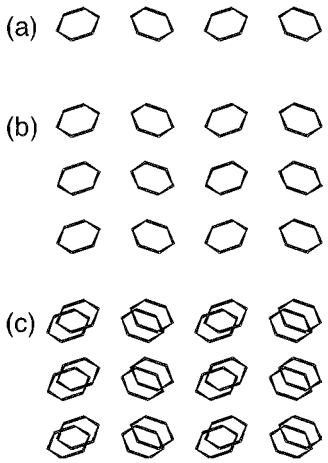

Fig. 2 The "crystal construction" process. Formation of (a) a one-dimensional crystal by linking molecules to form a molecular row: (b) a two-dimensional system by coupling molecular rows: and finally. (c) a three-dimensional crystal by stacking molecular layers.

crystal-structure-determining features of the two molecules are the same. with discoid. aromatic C_6H_6 moieties. which are able to form C–H· · ·π interactions.[15,16]

A more complex application of the deconstruction algorithm is provided by a prototypical transition metal carbonyl cluster molecule. $Ru_3(CO)_{12}$.[17] In this crystal. a row of molecules forming the crystal backbone is obtained by inserting of one axial CO-ligand into a tetragona! cavity — formed by two axial and two radial COs—on a next neighboring. equally oriented molecule (see Fig. 4). This intermolecular interaction is responsible for deviation of the molecular symmetry from the

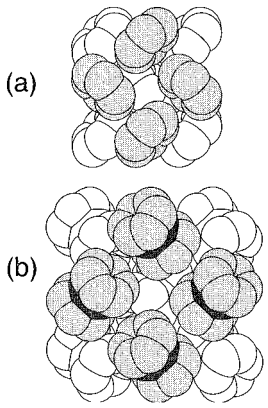

Fig. **3** Space-filling representation of the crystal structures of benzene (a) and *bis*benzenechromium (b). showing the similarity between the two packing arrangements.[12] The H atoms were omitted for clarity.

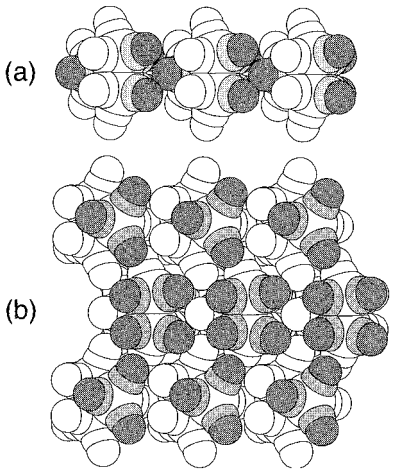

Fig. **4** Deconstruction of crystalline $Ru_3(CO)_{12}$: (a) a row of molecules constituting the crystal backbone is obtained by inserting one axial CO-ligand into a tetragonal cavity. formed by two axial and two radial COs on a next neighboring. equally oriented molecule: (b) a molecular layer is obtained by placing other rows on both sides of the central one. uith the $(CO)_3$ and $(CO)_4$ units protruding from the surface affording a "Velcro"-type interaction for the incoming molecular layers. (From Ref. [17].)

idealized D_{3h} symmetry. Once a row of $Ru_3(CO)_{12}$ molecules is formed. a molecular layer is obtained by placing other rows on both sides of the central one. The layer presents $(CO)_3$ and $(CO)_4$ units protruding from the surface. These units afford a ''Velcro''-type interaction between molecular layers, which can then pile up. generating a three-dimensional stacking. viz. the observed crystal structure.[18]

An example of crystal deconstruction is provided by Dance's study[19] of the packing of molecules containing PPh_3 peripheral groups. Dance showed that molecules with multiple PPh_3 ligands recurrently form one-. two-, and three-dimensional supramolecular networks. based on

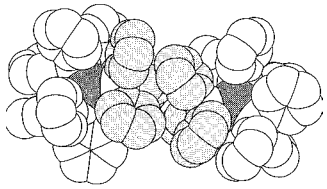

Fig. **5** A sixfold phenyl embrace involving two PPh_3 ligands on adjacent $Ni(PPH_3)_3$ molecules. The remaining PPh_3 ligands are participating in analogous interactions in the crystal. thus originating an extended network.[18,19] The H atoms were omitted for clarity.

a precise supramolecular packing motif, called multiple phenyl embrace. This packing motif is transferable from crystal to crystal and possesses clear directionality (topological) features. An example, reported in Dance's paper. of a sixfold phenyl embrace is shown in Fig. 5. It can be seen that three phenyl rings on each of two PPh_3 ligands belonging to adjacent $Ni(PPH_3)_3$[20] molecules form a dimer. which is part of an extended network of similar interactions.

ATOM–ATOM POTENTIAL ENERGY CALCULATIONS: A VALUABLE TOOL FOR PACKING DECODING

The examples discussed above show the importance of analogic crystal deconstruction. Clearly, this is not the only means by which to investigate crystal packings. Computational methods can also be used. For example, the atom–atom potential energy method, in use for more than 50 years in the organic solid-state chemistry field[14,21,22] has proven to be a valuable tool with which to estimate noncovalent interactions of the van der Waals type incrystals. The most commonly used expression for the empirical estimate of the packing potential energy (PPE) of a molecul ar crystal is the 6-exp-l potential, with $PPE = \Sigma_i\Sigma_j Ae^{-Brij} - Cr_{ij}^{-6} + q_i q_j r_{ij}^{-1}$.[21,22] In this expression. index *i* runs over all atoms of a molecule taken as reference in the lattice: index *j* runs over the atoms of the surrounding molecules distributed according to crystallographic symmetry; r_{ij} is an atom–atom intermolecular distance; and q_i and q_j are the formal atomic charges if a coulombic term is included in the calculations. The basic assumption underlying the use of most atom–atom potential calculations is that only central forces operate between pairs of atoms. and chat the total interaction energy is the sum of the interactions between all atomic pairs. Repulsions arising from short contacts between atoms belonging to different molecules are taken into account by the exponential function. A number of independent tabulations for the coefficients to be used in each type of atom–atom contact for organic substances, including hydrogen-bonded ones, are available in the literature.[23,24] They are obtained by fitting observed crystal properties (heat of sublimation and known crystal structures) or via ab initio calculations of the intermolecular potential energy.[25]

The atom–atom method is extraordinarily flexible and transferable and can be applied to a great variety of molecular crysialiine systems. including metal-containing materials.[''''] Rather than use the atom–atom potential energy method to obtain (more or less reliable) estimates of the enthalpy of the crystal. the method can be used as a computational tool to explore the ES. i.e., the surroundings of a molecule within an observed crystal structure. For the pu pose of crystal deconstruction. the lack of suitable parameters for the metal atoms does not seriously affect the calculations; the metal atoms, in fact. are usually deeply embedded in a sheath of ligands and screened from the surroundings, to the extent that their contribution to crystal cohesion is often minor, if not negligible. The molecules forming the first-neighbor shell of the one chosen for reference can be selected and ranked on a relative scale of pairwise van der Waals energy.[27,28]

COMPARISON OF PACKINGS CAN BE USEFUL TO UNDERSTAND PHASE TRANSITIONS AND CRYSTAL TRANSFORMATIONS

It was amply demonstrated in studies of organic solids that little differences in free energy are sufficient to yield alternative packing modes, and that, in the absence of highly directional forces; there is no unique way to organize the complex web of intermolecular interactions responsible for the choice of packing arrangement. This is at the basis of the phenomenon of crystal polymorphism.[6–9] One way to tackle this problem is to computationally generate theoretical crystal structures, which often goes under the epithet of crystal structure prediction.[29–32] This is an important area of research, but it falls outside the scope of this article and will not be discussed.

A crystal deconstruction application of the atom–atom potential energy method to tackle a problem of conformational polymorphism is provided by ferrocene.[33] for which a disordered monoclinic phase is stable at room temperature and to 163.9 K. below which it forms an ordered triclinic phase. An orthorhombic phase can also be grown by seeding at low temperature with crystals of orthorhombic ruthenocene. At the crystal level, the three phases differ in the relative orientation of the molecules (see Fig. 6). which. in turn, possess different relative conformations of the cyclopentadienyl ligands. In terms of van der Waals energy, it was shown that the difference between the various phases is small (of the order of 1 kcal . mol^{-1}), and that the phase transition behavior can be understood as a need to alleviate interatomic repulsions as the temperature is decreased and the hydrogen atoms at the periphery are brought in to closer contact.[34] Crystal deconstruction also allows for the modeling of the transition between the orthorhombic and the monoclinic phases as the temperature is increased;[34] as it can be appreciated on comparing Figs. 6b and 6c, a relatively simple geared motion in the plane of the drawings can lead from one phase to the other.

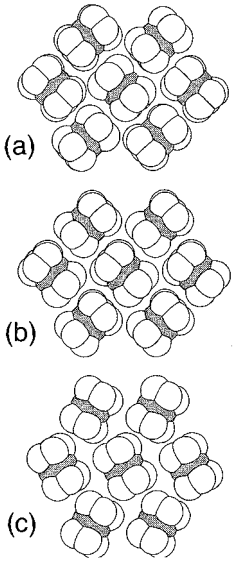

Fig. 6 Space-filling representation of the molecular organization in the triclinic (a). monoclinic (b). and orthorhombic (c) forms of ferrocene [32,33] The H atoms were omitted for clarity

CRYSTAL CONSTRUCTION WITH VAN DER WAALS INTERACTIONS

In van der Waals solids. the attractive forces acting between molecules. regarded as ensembles of atoms, are not particularly sensitive to molecular shape. rather they depend on the distance and fall off rapidly ($E \propto r^{-6}$). Repulsions are effective at very short distances and are dependent on the nature of the peripheral atoms. In this way, the bulk of the molecule provides attraction, while surface atoms determine recognition. optimum relative orientation, and interlocking of molecules in the solid state. In general, a given supramolecular arrangement in the solid state can be seen as the result of the minimization of short-range repulsions rather than the optimization of attractions. Therefore. it is important, when considering a van der Waals solid. to focus on the relationship between molecular shape and nature of the peripheral atoms.

An example is provided by the work of Hosseini and collaborators, who designed one-dimensional van der Waals networks by joining calix[4]arene derivatives, bearing two receptor cavities arranged in a divergent fashion. by means of neutral molecules employed as linear connectors.[35,36] The example in Fig. 7 shows the result of utilizing symmetrical calix[4]arenes obtained from the double fusion of two different calix[4]arenes by silicon atoms. The koilands so formed are joined together with hexadyine. which acts as a symmetrical connector.[''''] The resulting one-dimensional network, or koilate, is obtained by translating the assembling core defined by the inclusion connector into the cavity of the receptor. Recognition. self-assembly, and cohesion of the solid-state networks are based on van der Waals interactions.

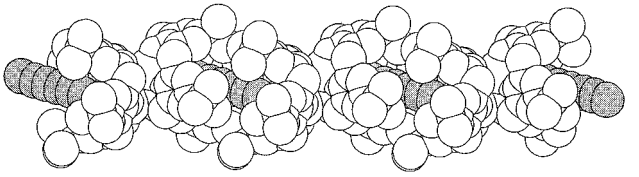

Fig. 7 Space-filling representation of the koilate (one-dimensional molecular array) formed between a symmetrical calix[4]-arene derivative and hexadyine as a connector.[''''] The H atoms were omitted for clarity.

CRYSTAL DECONSTRUCTION IN CRYSTALLINE SALTS

When dealing with molecular ions, the nature of the interactions changes considerably. The energies involved when ions are present are greater by at least an order of magnitude with respect to molecular neutral crystals. The dispersion energies are always attractive at long distances. while coulombic terms depend on the sign of the interaction. The evaluation of the crystal energetics. even on an empirical basis, becomes more difficult when large polyatomic anions or cations are involved. The packing of molecular ions has to fulfill the same requirements for optimization of next-neighbors interlocking and of pairwise interactions with the additional, not trivial, constraint of minimizing the sum of repulsive interactions

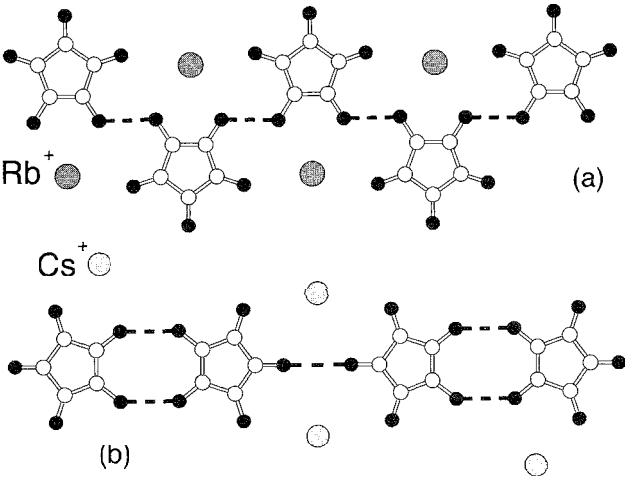

Fig. 8 Hydrogen croconate anions joined in chains (a) and ring dimers (b) in crystalline $RbHC_5O_5$ and $CsHC_5O_5$, respectively. (From Ref. [36].)

between like charges and maximizing the attraction between ions of opposite signs.

The crystals of $RbHC_5O_5$ and $CsHC_5O_5$ are good examples of the relationship between directional hydrogen-bonding interactions and ionic charges[37] (see Fig. 8). The structure of the rubidium salt contains chains of hydrogen croconate anions, while the cesium salt is characterized by the presence of ring dimers (Fig. 8b). An ab initio computational analysis provides the notion that the $^{(-)}O—H\cdots O^{(-)}$ hydrogen-bonding interactions between like ions are not sufficient to bind the ions together, as the stability is provided by attractive next-neighbor anion. . ·cation interactions, which largely overcompensate for the combined effect of next-neighbor anion . ·anion and cation. . ·cation repulsions. These observations lead to the recognition that $^{(-)}O—H\ldots O^{(-)}$ interactions are not energetically determinant in the cohesion of these salts, while they are responsible for the spatial organization of the anions. The $^{(-)}O—H\cdots O^{(-)}$ interactions contribute to cohesion by reducing interanion repulsions.

Another example is afforded by potassium croconate $K_2C_5O_5$, which was isolated and characterized as $K_2C_5O_5 \cdot 2H_2O$ by Dunitz[38] and subsequently by us.[39] The coordination around the potassium cation is depicted in Fig. 9a. The croconate dianions form columns. extending parallel to the c-axis. completely surrounded by cations and water molecules, with these latter acting as "pinchers" on the dianions (see Fig. 9b.c). The short interplanar separation (3.30 Å) is thus a result of the external interactions that "compress" the anions together.

The deconstruction of the potassium croconate crystal allows us to recognize the analogies with another member of the family of oxocarbon anions, rubidium rodizhonate $Rb_2C_6O_6$.[40] The crystals possess some remarkable

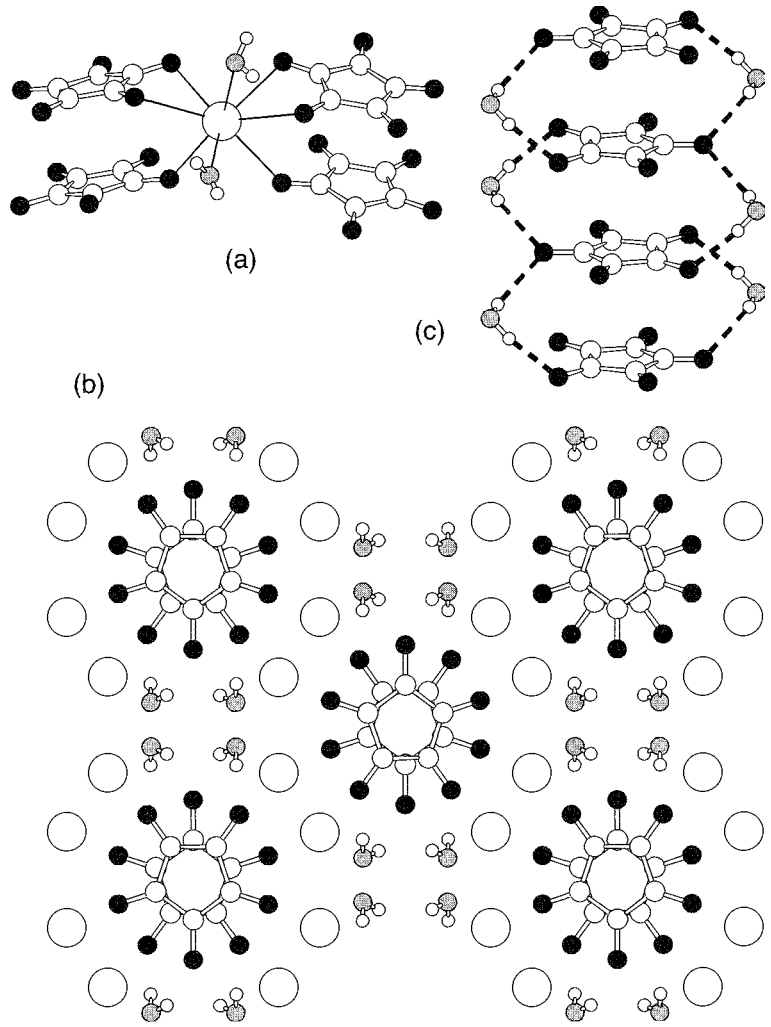

Fig. 9 Crystal deconstruction in $K_2C_5O_5 \cdot 2H_2O$: (a) the coordination of two water molecules and four croconate dianions around the K^+ cation in crystalline; (b) the dianions are stacked in columns surrounded by the cations and the water molecules (b); the latter act as ''pinchers'' along the columns (c). (From Refs. [37,38].)

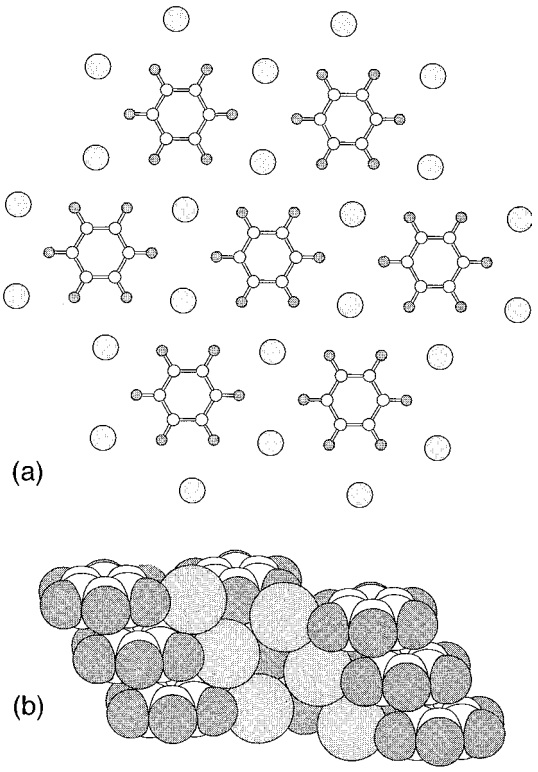

Fig. 10 (a) The pseudosixfold symmetry of $C_6O_6^{2-}$ dianions and Rb^+ cations in a layer of crystalline $Rb_2C_6O_6$; and (b) the stacking of layers. showing how the dianions are shifted and the Rb^+ ions are in close contact. forming cationic piles. (From Ref. [39].)

features: I) there are layers of rhodizonate dianions $C_6O_6^{2-}$ organized with pseudosixfold symmetry within the layer (see Fig. 10a), and the $C_6O_6^{2-}$ units lie flat on each other at an interplanar distance of 3.30 Å; and 2) the Rb^+ ions form cationic rows in between the rhodizonate units (see Fig. 10b).

CONCLUSION

The design of solids starting from molecular and ionic building blocks with predefined shapes and functions has become the forefront of molecular assembly and recognition studies. as well as of materials chemistry research. This is witnessed by the rapidly increasing number of publications that deal specifically with intermolecular interactions in molecular solids. A great contribution to these studies came from the development of structural databases, in particular, the CSD (Cambridge Structu e Database), and, to a smaller extent, the ICSD (Inorganic Crystallographic Structural Database),[41,42] which permitted statistical evaluation of the topology of noncovalent interactions on a large basis. The "quest for intermolecular interactions" afforded remarkable insight into ihe factors responsible for recognition and cohesion. Some cautionary words are. however. in order. It is argued that it is dangerous to focus exclusively on pairwise interactions. as one may forget that it is the overall balance of interactions. some acting at short range only, some acting at very long range, that accounts for cohesion in molecular crystals. At the same time, very weak interactions. falling in the fluctuations of the crystal structure energetics (due, for instance: to motion of atoms or atomic groups), may be useless in design strategies, because they are too feeble to control crystal construction. Only strong pairwise interactions (e.g., an O—H···O bond) may stand out of the noise and act as true packing directors. Because interactions of this type are often already present in solution; nucleation and crystal growth occur around preformed long-living aggregates. On the other hand. crystallization of structurally nonrigid molecules often requires complicated compromises between intra-and intermolecular interactions. The dynamic behavior of molecules or ions in the solid state (from libration, to large amplitude and reorientational motions, and fluxionality) will also be controlled by intermolecular interactions and by the way these will convolute with the internal energy barriers to structural rearrangement.[7,9] Insights into the relationship between size. shape, and charge of the component molecules and the molecular organization in the crystal can be obtained by decoding observed crystal packings by means of empirical packing potential energy calculations and computer graphics.

ACKNOWLEDGMENTS

We acknowledge useful discussions with a number of scientists through the years: including A. Gavezzotti, H.-B. Bürgi, and J. Dunitz. This research work was possible thanks to financial support through the years from MIUR and CNR and from the universities of Bologna and Sassari.

REFERENCES

1. Lehn. J.M. *Supramolecular Chemistry: Concepts and Perspectives*; *VCH:* Weinheim. Germany, 1995.
2. Steed. J.W.; Atwood. J.L. *Supramolecular Chemistry*; J. Wiley: Chichester, UK. 2000.
3. Braga. D.; Grepioni, F. Intermolecular interactions in nonorganic crystal engineering. Acc. Chem. Res. 2000. 33. 601--608.
4. Braga. D.: Crepioni, F.: Desiraju. C.R. Crystal engineering and organometallic architecture. Chem. Rev. 1998. 98, 1375–1405.
5. Braga, D.; Crepioni. F.; Orpen, A.G. *Crystal Engineering:*

from Molecules and Crystals to *Materials*: Kluwer Academic Publishers: Dordrecht. Germany. 1999.
6. Bernstein. J. *Polymorphism in Molecular Crystals*; Oxford University Press: Oxford, UK, 2002.
7. Dunitz, J.; Bernstein. J. Disappearing polymorphs. Acc. Chern. Res. 1995. *28*. 193–200.
8. Braga. *D.*; Grepioni. F. Organometallic polymorphism and phase transitions. Chem. Soc. Rev. 2000. 4. 229–238.
9. Braga. D.: Grepioni. F. Static and Dynamic Structures of Organometallic Molecules and Crystals. In *Organometallic Bonding and Reactivity—Fundamental Studies*; Brown, J.M.. Hofmann, P., Eds.: Springer Verlag: Berlin, 1999: Vol. 4. 47–68.
10. Dunitz. J.D.: Gavezzotti. A. Attraction and repulsions in molecular crystals: What can be learned from the crystal structures of condensed ring aromatic hydrocarbons? Acc. Chern. Res. 1999. *32*. 677–684.
11. Braga, D.: Grepioni. F. From molecule to molecular aggregation: Clusters and crystals of clusters. Acc. Chem. Res. 1994. *27*. 51–56.
12. Pauling. L.; Delbrück. M. Science 1940. 77.
13. Braga. D.: Grepioni. F. Effect of molecular shapes on crystal building and dynamic behavior in the solid state: From crystalline arenes to crystalline metal-arene complexes. Organometallics 1991. 10. 2563–2569.
14. Kitaigorodsky, A.I. *Molecular Crystal and Molecules*: Academic Press: New Uork. 1973.
15. Desiraju, G.R.; Gavezzotti. A. Crystal structures of polynuclear aromatic hydrocarbons. Classification. rationalization and prediction from molecular structure. Acta Crystallogr. 1989. *B45*. 473–482.
16. Takahashi. O.; Kohno, Y.; Iwasaki, S.: Saito. K.: Iwaoka, M.: Tomoda. S.: Umezawa, Y.: Tsuboyama. S.: Nishio. M. Hydrogen-bond-like nature of the CH···π interaction as evidenced by crystallographic database analyses and ab initio molecular orbital calculations. Bull. Chem. Soc. Jpn. 2001. 74. 2421–2430.
17. Churchill. M.R.: Hollander, F.J.; Hutchinson. J.P. An accurate redetermination of the structure of triruthenium dodecacarbonyl. $Ru_3(CO)_{12}$. Inorg. Chem. **1977.** 16. 2655–2659.
18. Braga. D.: Grepioni. F. Molecular self-recognition and crystal building in transition-metal carbonyl clusters: The cases of $Ru_3(CO)_{12}$ and $Fe_3(CO)_{12}$. Organometallics 1991, 10. 1254–1259.
19. Dance. I.: Scudder. M. Crystal supramolecularity: Sixfold phenyl embraces between PPh_3 ligands. forming extended nets in one-. two-. and three-dimensions. J. Chem. Soc., Dalton Trans. 2000. 1587 1594.
20. Dick. D.J.: Stephan, D.W.; Campana, C.F. The crystal and molecular structure of the coordinatively unsaturated Ni(0) species $Ni(PPh_3)_3$. Can. J. Chem. 1990. 68. 628 -632.
21. Pertsin, A.J.; Kitaigorodsky, A.I. *The Atom-Atom Potential Method*: Springer-Verlag: Berlin. Germany. 1987.
22. Gaverzotti. A.; Simonetta. M. Crystal chemistry in organic solids. Chern. Rev. 1981, 82. 1–11.
23. Gavezzotti. A.: Filippini. G. Empirical intermolecular potentials for organic crystals: The '6-exp' approximation revisited. Acta Crystallogr. 1993. *B49*, 868–880.
24. Gavezzotti. A.; Filippini. G. Geometry of the intermolecular X-H—Y (X. Y=N. O) hydrogen bond and the calibration of empirical hydrogen-bond potentials. J. Phys. Chem. 1994. *98*. 4831–4837.
25. Gavezzotti. A. The crystal packing of organic molecules: Challenge and fascination below 1000 Da. Crystallogr. Rev. 1998. *7*, 5–121.
26. Braga. D.: Grepioni. F.: Orpen, A.G. $Ni(CO)_4$ and $Fe(CO)_5$. A study of molecular recognition and crystal construction. Organornetallics 1994, 13. 3544 3556.
27. Gavezzotti, A. Molecular packing and other structural properties of crystalline oxohydrocarbons. J. Phys. Chem. 1991, *95*. 8948–8955.
28. Gavezzotti. A. Statistical analysis of some structural properties of solid hydrocarbons. J. Am. Chem. Soc. 1989. 111. 1835–1843.
29. Gavezrotti, A. Are crystal structures predictable? Acc. Chem. Res. 1994. *27*. 309–314.
30. Lommerse. J.P.M.: Motherwell, W.D.S.: Ammon, H.L.: Dunitz. J.D.; Gavezrotti, A.: Hofmann. D.W.M.: Leusen. F.J.J.; Mooij, W.T.M.: Price. S.L.; Schweizer. B.: Schmidt. M.U.; van Eijck. B.P.: Verwer. P.: Williams. D.E. 4 test of crystal prediction of small organic molecules. Acta Crystallogr. 2000. *B56*. 697–714.
31. Beyer. T.: Lewis. T.: Price. S.L. Which organic crystal structures are predictable by lattice energy minimisation'? CrystEngComm. 2001. *3*. 178–212.
32. Gavezzotti, A. A molecular dynamics test of the different stability of crystal polymorphs under thermal strain. J. Am. Chem. Soc. 2000. *122*. 10724–10725.
33. Dunitz, J.D. Phase changes and chemical reactions in molecular crystals. Acta Crystallogr. 1995. *B51*. 619–631.
34. Braga. D.: Grepioni, F. Crystal construction and molecular interplay in solid ferrocene. nickelocene and ruthenocene. Organometallics 1992. 11. 711–718.
35. Hosseini. M.W.; De Cian. A. Molecular tectonics: An approach to organic networks. Chem. Commun. 1998. 727.
36. Martr. J.: Graf. E.: Hosseini. M.W.; De Cian. A.: Fischer. J. Directional 1-D inclusion networks: Self-assembly of unsymmetrical koilands into directional koilates in the crystalline phase. 3. Chem. Soc. Dalton Trans. 2000. 3791.
37. Braga. D.: Maini. L.: Grepioni. F.; Mota. F.: Rovira. C.: Novoa. J.J. Inter-anionic $^{(-)}$O-H···O$^{(-)}$ interactions: A solid state and computational study of the ring and chain motifs. Chem. Eur. J. 2000. 6. 4536–4551.
38. Dunitz. J.D.; Seiler. P.; Czechtizky. W. Crystal structure of potassium croconate dihydrate. after 175 years. Angew. Chem.. Int. Ed. 2001. 40. 1779–1780.
39. Braga. D.: Maini. L.; Grepioni, F. Croconic acid and alkali metal croconate salts: Some new insights into an old story. Chem. Eur. 3. 2002. *8*. 1804–1812.
40. Braga. D.: Cojazri. 6.: Maini, L.: Grepioni. F. Reversible solid-state interconversion of rhodironic acid $H_2C_6O_6$ into $H_6C_6O_8$ and the solid-state structure of the rhodizonate dianion $C_6O_6^{2-}$ (aromatic or non-aromatic?). New J. Chern. 2001. *25*. 1221–1223.
41. Allen, F.H.: Kennard. O. Chem. Des. Autom. News 1993, *8*, 31.
42. *Inorganic Crystal Structure Database (ICSD)*; Fachinformationszentrum (FIZ) Karlsruhe and Gmelin Institut. Release 2002.
43. Braga. D. Dynamical processes in solid organometallic compounds. Chem. Rev. 1992. *92*. 369–685.

Crystal Engineering with Hydrogen Bonds

Dario Braga
Università degli Studi di Bologna, Bologna, Italy

Fabrizia Grepioni
Università di Sassari, Sassari, Italy

INTRODUCTION

Molecular crystal engineering is the bottom-up construction of functional *materials, starting from molecular or ionic building blocks assembled by means of noncovalent interactions. The hydrogen bond (MB)is the interaction of choice, because it* combines *strength and directionality. These properties guarantee* materials *cohesion and stability as* well *as reproducibility of crystal-directed syntheses.*

THE INTERACTION OF CHOICE IN MOLECULAR CRYSTAL ENGINEERING—THE HYDROGEN BOND

Molecular *crystal engineering can be viewed as the area of supramolecular* chemistry[1,2] *devoted to the controlled design of* crystalline materials.[3] *As noncovalent interactions are responsible for the existence and functioning of* supermolecules, *intermolecular and interionic interactions are responsible for crystal cohesion and solid-state properties. The* HB *is the interaction of choice in molecular crystal engineering, because it combines strength and* directionality.[4,5] *Strength* is *a synonym of cohesion and stability. while directionality implies topological control and selectivity, which guarantee reproducibility to the* supramolecular *assembly process. These properties are quintessential for an interaction to be useful in crystal engineering. A* nondirectional, i.e., *nonselective, intermolecular interaction wili not possess specific topological properties, and its performance within different structural environments will not always be predictable.*

Strength *deserves a more subtle comment, because it brings about the definition of the hydrogen bond. What is a* hydrogen *bond? The answer to this question is controversial and depends on the objective of the investigator. For* the *purpose of crystal engineering, however, Etter's elaboration*[6] *of the* Linus Pauling *definition of a* bond[7] is *probably the* most *appropriate:*

> A hydrogen bond is an interaction that directs the association of a covalently bound hydrogen atom with one or more other atoms, groups of atoms. or molecules into an aggregate structure that is sufficiently stable to make it convenient for the chemist to consider it as an independent chemical species.

The focus is on *the concept of "directed"* association *and of stability. The existence of an* intermolecular *bond is* conceptually *associated with the energetic stability of the aggregate.*

For most purposes, *however. the HB can be described as a stable interaction of essentially electrostatic nature between an X-H donor and an* Y *acceptor, being X- and* Y-electronegative *atoms or electron-rich* groups.[8] *The HB interaction is* generally *stronger than the strongest van der Waals* interaction. *The* H···Y *and* X···Y *separations are shorter than van der Waals contact distances, and* X—H···Y *angles that tend to linearity are* considered *diagnostic of the presence of strong* HBs.[9] The *same topological rules are followed by hydrogen-bonding interactions between ions,* even *though the energetic scale is* different.[10] In *the case of* HB *interactions between neutral molecules. the* length/strength *analogy is believed to hold.* i.e., *the shorter the acceptor–donor distance.* the *stronger the bond. This relationship. however, fails to apply satisfactorily in the case of weak and very weak HB interactions,"" where the electrostatic* component *is active at a distance larger than van der Waals contacts: and in the case of HB interactions between ions. where the* dominant *energetic terms come from* coulombic *attractions and* repulsions.[12] *This latter aspect. in particular, is often overlooked.*

In terms of energy, HB interactions span a large interval. ranging from tiny energies (ca. *10* kJ/mol *in the case of* C—H···O, *vide infra) to large values* when *the acceptor is an anion (ca. 120–130* kJ/mol *in the case of* O—H···$O^{(-)}$). *Negatively charge-assisted."" positively charge-assisted."" as well as* resonance-assisted[15] HBs *were identified. Metal atoms* can *also be directly involved in* HB formation.[16]

A *discussion of the energetics of the HB is beyond the scope of this article. What* is *relevant for crystal engineering is the* notion *that the strongest of weak hydrogen bonds are comparable to the weakest of strong hydrogen*

DOI: 10.1081/E-ESMC 120012752

bonds (−20 kJ/mol) and. in terms of crystal structure directing effects. there seems to be little difference between these two categories. As in conventional covalent bonding, there is a continuum of energy, and the distinction between strong and weak HBs is, often, only conventional. It is essential. however, to know the exact nature of the interactions one is trying to control. If discrimination needs to be made. this is between noncovalent interactions in ionic and neutral crystalline materials because of the differencesin physical properties (solubility, melting point, behavior under mechanical stress. etc.) arising from the presence of ions or neutral molecules.

In general. strong donor/acceptor groups such as -COOH and -OH systems. as well as primary -$CONH_2$ and secondary -CONHR amido groups, form essentially the same type of HB interactions, whether as part of organic molecules or of metal coordinated ligands. This is not surprising. as HBs formed by such strong donor and acceptor groups are at least one order of magnitude stronger than most noncovalent interactions and are most often already present in solution. For the purposes of crystal construction, the utilization of a single very strong interaction; as the O—H···$O^{(-)}$ mentioned above, is not necessarily the best or only way to provide cohesion. The "Gulliver effect" can also be exploited: the collective strength of weaker bonds may be equivalent. in terms of cohesion. to the strength of a single bond, although the directionality component may be lost or greatly diminished with respect to that of single strong bonds, e.g., O—H···O or N—H···O. etc.

HYDROGEN BONDING AND CRYSTAL ENGINEERING INVOLVING NEUTRAL MOLECULES

Some examples of utilization of HB in crystal engineering strategies are presented in the following. The reader is referred to the entries on crystal engineering and to those on the hydrogen bond for more details. The selection of examples is clearly arbitrary and cannot do justice to the number of scientific groups involved in this booming field of research."""

An early entry into the crystal engineering of organic crystals using strong O—H···O bonds is provided by the work of Etter.[18] The molecuie 1,3-cyclohexanedione, [$C_6H_8O_2$], capable of forming O—H···O HB interactions, can be crystallized from THF in linear chains (Fig. 1a) or in hexarneric units (Fig. 1b) when the solvent is benzene. which acts as a templating unit through the self-assembly of the dione molecules. We were later able to mimic such behavior by replacing benzene with his-benzene chromium (vide infra).[19]

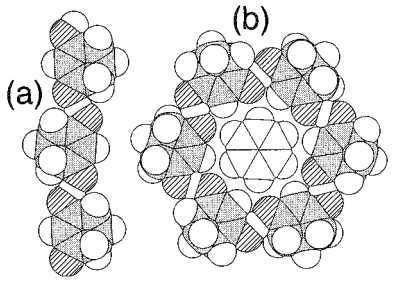

Fig. 1 Etter's example of crystal engineering with O—H···O hydrogen bonds: (a) a space-filling representation of the chain of O—H···O bonded 1.3-cyclohexanedione molecules, crystallized from THF; and (b) the cyclamer formed by 1.3-cyclohexanedione with benzene—note how the benzene molecule is surrounded by six neutral molecules linked by O—H···O interactions.

Hanessian utilized N—H···O interactions between *trans*-1,2-diaminocyclohexane and 1,2-diols to construct supramolecular helicate structures that, depending on the chirality of the diols. can be left-handed or right-handed.[20] An example is given in Fig. 2. which shows the left-handed helical structure formed by the self-assembly of (R,R)-1,2-diaminocyclohexane with (R,R)-2,3-butanediol via N—H···O hydrogen bonds.

Crystal engineering endeavors based on weak HBs are less frequent for the reasons given above. One may wonder if weak HBs are "good enough" to direct molecular recognition and crystal packing. While there is consensus on the relevance of C—H···O bonds in crystals, C—H···N bonds have not been investigated to the same extent. Boese showed that C—H···N bonds can be used likewise for producing predictable patterns. For instance. C—H···N bonds can be used between sp^2 CH groups and nitrogen atoms in pyrazines and methyl-substituted pyrazines[21] to form layered structures (see Fig. 3): the methyl groups are involved in sp^3 C—H···π interactions and govern the interlayer packing.

Combining coordination bonds with hydrogen bonds is another attractive crystal engineering perspective. Brammer and collaborators elaborated the idea of incorporating transition metals into the design of hydrogen-bonded crystalline solids.[22–24] The metal centers can be used to provide a directing influence upon the hydrogen-bonded links between neighboring building blocks (Fig. 4a)[22] or are appended as a potentially functional group to the parent hydrogen-bonded organic network, as in π-bonded organometallic systems (Fig. 4b).[23] Coordination of halide ligands to transition metals leads to good HB-acceptor capability. New supramolecular hydrogen-bonding motifs, such as N—H···X_3M and N—H···X_2M, that have no precedents in organic crystal engineering were used to construct hydrogen-bonded assemblies using ammonium salts of perhalometallate ions.[24]

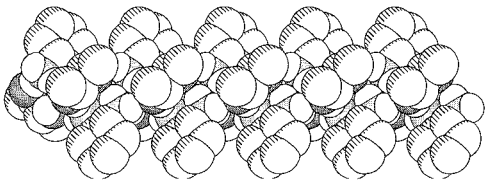

Fig. 2 Space-filling representation of the left-handed helical structure formed by self-assembly of (R,R)-1,2-diaminocyclohexane with (R,R)-2,3-butanediol via N—H···O hydrogen bonds.[20] For clarity. H_{CH} atoms are not shown.

Aakeröy and collaborators[25,26] elaborated a strategy based on the assembly of inorganiclorganic architectures through a combination of copper(I) coordination polymers and self-complementary hydrogen bonds. The design strategy yields lamellar inorganiclorganic hybrid materials (see Fig. 5). Infinite copper(I) halide coordination polymers provide robust one-dimensional building blocks, and these are subsequently linked into two-dimensional layers by attaching one pyridine ligand to each metal ion. The ligand, which carries a self-complementary hydrogen-bond moiety (e.g., carboxylic acid. carboxamide, oxime). provides a noncovalent directional tool for connecting neighboring coordination polymers into an extended two-dimensional network.

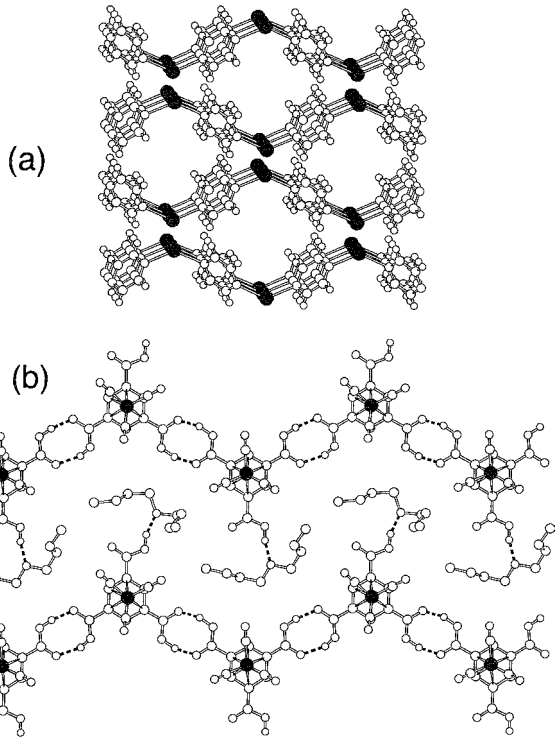

Fig. 4 Examples of hydrogen bonds combined with coordination chemistry: (a) stacking of adjacent layers (anions omitted) in crystalline $Ag(O_2CCF_3)L$ (*L*=pyrazine); and (b) zigzag tapes of $[Cr(CO)_3(\eta^6\text{-TMA})]$ with Bu_2O hydrogen bonded in channels.

HYDROGEN-BONDING INTERACTIONS BETWEEN IONS

A practical instrument in devising new solids is afforded by the possibility of combining ionic charges and HB interactions. Because the HB has a fundamentally electrostatic nature, the presence of ionic charges on the building blocks can be exploited to strengthen the interaction. Charge assistance to HB is the enhancement of the polarity of donor and acceptor systems by utilizing cationic

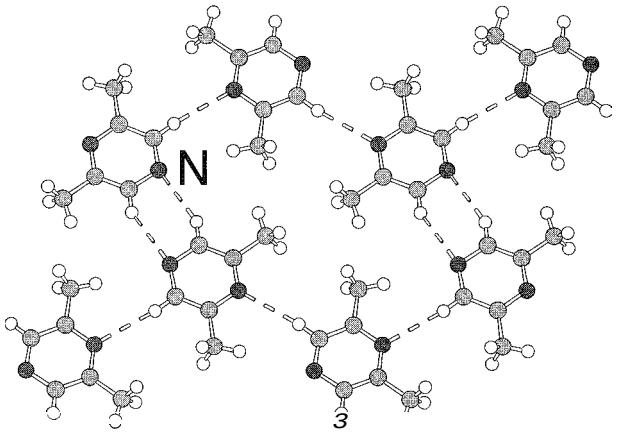

Fig. 3 The use of C—H N hydrogen bonds allows for formation of a layered structure in 2,6-dimethylpyrazine The methyl groups are involved ın sp^3 C—H π ınteractıons (not shonn) and govern the interlayer packing

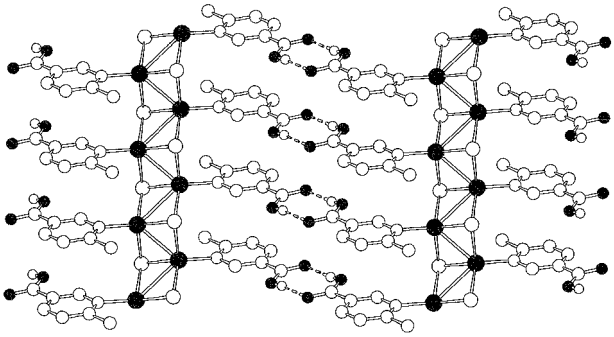

Fig. 5 Pyridine ligands carrying a self-complementary hydrogen-bond moiety (carboxylic acid. in this example) provide a noncovalent directional tool for connecting infinite copper(I) chloride coordination polymers into an extended two-dimensional network.

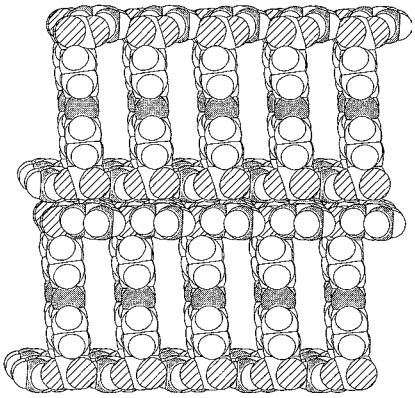

Fig. 6 An example of guanidinium–sulfonate superstructures. The fundamental interaction responsible for robustness and flexibility is the charge-assisted $^{(+)}N—H\cdots O^{(-)}$ hydrogen bonding between the guanidinium cations and the sulfonate anions, which can be varied in shape and length.

donors and anionic acceptors instead of neutral systems, i.e., $X—H^{(+)}\cdots Y^{(-)}$ rather than $X—H\cdots Y$. The favorable location of ionic charges enhances proton acidity and acceptor basicity in the solid state. Hydrogen-bonding interactions between ions need to occupy a special place in the library of noncovalent interactions of interest to supramolecular chemists and crystal engineers. because they optimally convolute the strength of the coulombic field generated by the ions with the high level of directionality afforded by the $X—H\cdots Y$ interaction.

Interionic hydrogen-bonding interactions are easily accessed via homogeneous or heterogeneous acid–base reactions. By choosing the number of potential donor/acceptor groups on the building block and the acid–base stoichiometric ratio, one can control the formation of homo- or heteroionic interactions. For example. partially deprotonated polyprotic acids possess "loaded" and "unloaded" hydrogen-bonding donor groups. i.e., COOH and $COO^{(-)}$, that can take part in the formation of heteroionic bridges with competing donors. This fairly comrnon situation arises when the base participates in the HB interactions. This is the case, for instance, of nitrogen-containing bases (ainines. amidines, etc.) that are protonated upon reaction with acid molecules. e.g., $RCOOH+NR_3\rightarrow RCOO^{(-)}\cdots{}^{(+)}HNR_3$, leading to anion–cation pairing in the solid state. and hence, to formation of $^{(+)}N—H\cdots O^{(-)}$ charge-assisted interactions.[27]

With an analogous approach, "soft" molecular host networks were developed by Ward et al. They combine two relatively simple structural units: layers of guanidinium cations spaced by pillars of sulfonate anions (see Fig. 6).[28] The $^{(+)}N—H\cdots O^{(-)}$ interactions between guanidinium cations and sulfonate anions render the superstructures robust and adaptable to the guest requirements, while the porosity can be tuned by changing the length of the pillars. These properties were exploited in several applications, such as shape-selective separation of molecular isomers.

A less common situation is observed when the counterion cannot form HB interactions with the acid moiety. as in the case of the reaction with inorganic or organometallic hydroxides.[29]

Partially deprotonated polyprotic acids. possessing COOH and $COO^{(-)}$ HB donor groups. can thus take part in the formation of homoionic bridges with themselves.

This strategy was applied, rather unawarely, when 1,3-cyclohexanedione, $[C_6H_8O_2]$ was reacted with bis-benzene chromium.[19] The reaction afforded the pseudocyclamer formed by two $[Cr^I(C_6H_6)_2][(C_6H_8O_2)_3(C_6H_7O_2)]$ units held together by $O—H\cdots O$ and $C—H\cdots O$ interactions (Fig. 7). The product differs substantially from Etter's compound mentioned above: the reaction between the acidic molecule and $[Cr(C_6H_6)_2]$ leads to the oxidation product $[Cr^I(\eta^6\text{-}C_6H_6)_2]^+$ and to partial deprotonation of the dione.

A recent example of engineering a supramolecular arrangement with target magnetic properties is provided by crystalline $[Cr^I(\eta^6\text{-}C_6H_6)_2][HC_4O_4]$, obtained by reacting squaric acid (3,4-dihydroxy-3-cyclobutene-1,2-dione, $H_2C_4O_4$) with $[Cr(\eta^6\text{-}C_6H_6)_2]$.[30] The intercalation of the hydrogen squarate chains between the sandwich cations leads to the formation of one-dimensional $D^+A^-D^+A^-$ structures comprised of alternating cation donors (D) and anion acceptors (A). The presence of a charge-transfer transition was detected in the reflectance spectrum, while magnetic measurements showed that the weak, but appreciable, antifersomagnetic interaction between the S=1/2 of the $[Cr^I(\eta^6\text{-}C_6H_6)_2]^+$ cations could be attributed to the anion–cation π-stacking interaction.

Orpen and collaborators developed the use of salts of perhalometallate complexes $[MX_n]^{m-}$(X=Cl, Br, etc.:

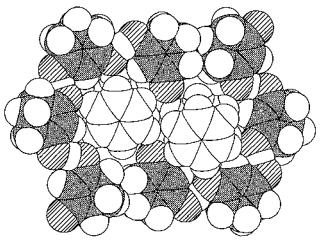

Fig. 7 An organometallic mimic of Etter's cyclamer (see Fig. 1b): space-filling representation of the pseudocyclamer formed by two $[Cr^I(C_6H_6)_2][(C_6H_8O_2)_3(C_6H_7O_2)]$.

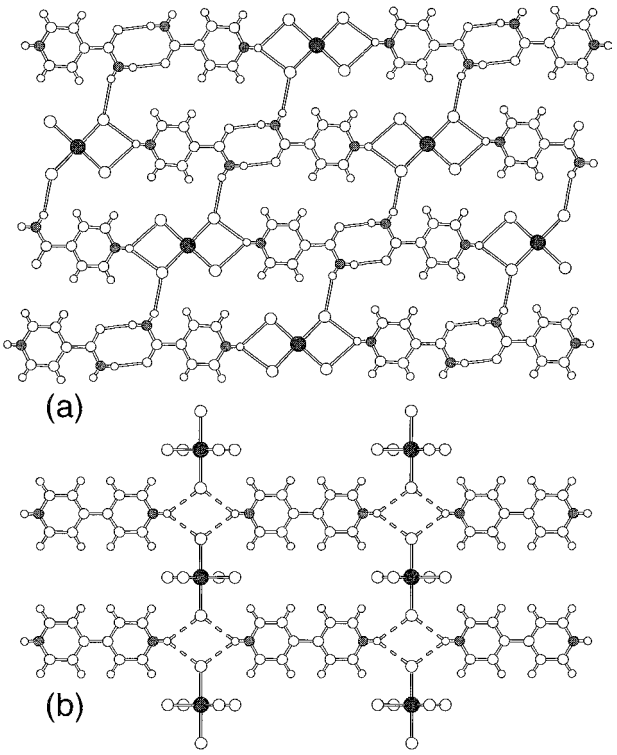

Fig. 8 Hydrogen-bonding networks in salts of perhalometallate complexes $[MX_n]^{m-}$ (X=Cl, Br. etc.; M=Pt, Zn, Mn. Pb. etc.) with organic cations possessing N—H hydrogen-bond donor functionality.

M=Pt, Zn, Mn, Pb, etc.) with organic cations possessing N—H HB-donor functionality (Fig. 8).[31,32] These systems are modular and robust and offer the opportunity to exploit the shape, charge, and functional groups of the ions in order to control the crystal structures they form and. in particular. the HB networks they contain.

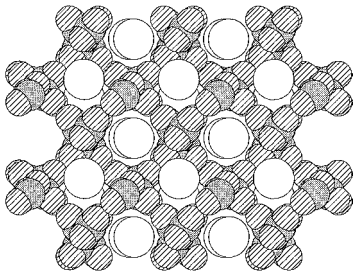

Fig. 9 Space-filling representation of the L-tartaric acid framework in crystalline $[Co^{III}(\eta^5\text{-}C_5H_5)_2]$[L-hydrogentartrate], with the $[Co^{III}(\eta^5\text{-}C_5H_5)_2]^+$ cations (represented as large spheres) occupying the channels.

Chiral crystals based on hydrogen L-malate anions were assembled via $^{(-)}O—H\cdots O^{(-)}$ bridges in anionic layers.[33] Because the two-dimensional network is highly reproducible, it can be transferred from crystal to crystal, inducing noncentrosymmetry, a target on the route to materials for a second-harmonic generation. We used analogous strategy to self-assemble chiral frameworks around organometallic cations (Fig. 9).[29]

Lehn et al. used interionic hydrogen bridges to direct the recognition and self-aggregation of metal complexes carrying terpyridine-derived ligands joined by intercation $^{(+)}N—H\cdots N^{(+)}$ bridges.'''' The solid-state arrangement of the $Co(terpy)_2^{2+}$ complex is highly dependent on the choice of counterion: in the $[PF_6]^-$ salt, a two-dimensional infinite network is formed via pairs of N—H···N interactions. while in the $[BF_4]^-$ salt. a broken network is observed (Fig. 10). This provides an example of competition between formation of N—H···N interactions and optimization of the coulombic interactions that. in turn. depend on the size of the ions.

The possibility of switching between neutral hydrogen-bonded systems and charged systems is at the basis of the reversible gas-trap system obtained on reacting the cobalticinium zwitterion $[Co^{III}(\eta^5\text{-}C_5H_4COOH)(\eta^5\text{-}C_5H_4COO)]$ with acid and base vapors (HCl, CF_3COOH, HBF_4, and NH_3, NH_2Me, NMe_3).[35,36] The salts resulting from the heterogeneous reaction contain the organometallic moiety in its fully protonated form $[Co^{III}(\eta^5\text{-}C_5H_4COOH)_2]^+$ (in the reaction with acids) or in its fully deprotonated form $[Co^{III}(\eta^5\text{-}C_5H_4COO)_2]^-$ (in the reaction with bases), as shown in Fig. 11. The two types

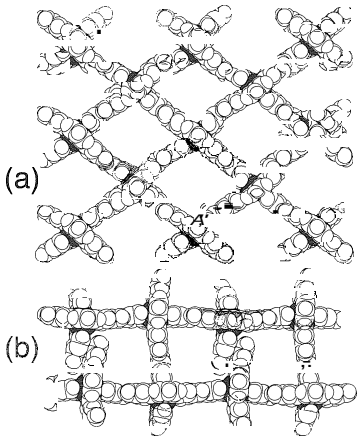

Fig. 10 A two-dimensional infinite netuork is formed via pairs of $^{(+)}N—H\cdots N^{(+)}$ interactions in the $[PF_6]^-$ salt of the cobalt complex $Co(terpy)_2^{2+}$ (a), while a quarter of the potential hydrogen-bond interactions are not formed. leading to a broken network in the case of the $[BF_4]^-$ salt (b).

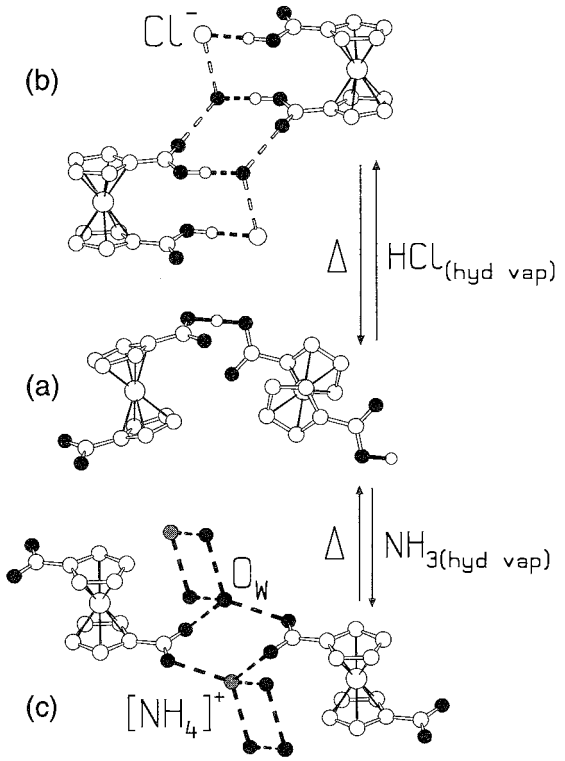

Fig. 11 The zwitterion $[Co^{III}(\eta^5\text{-}C_5H_4COOH)(\eta^5\text{-}C_5H_4COO)]$ (a) reacts reversibly with HCl (b) and NH_3 (c) hydrated vapors to give the corresponding salts.

of reactions imply the interconversion between neutral O—H . ·O hydrogen-bonding interactions and $^{(+)}$O—H- . . .X and $^{(-)}$O· . ·H—N$^{(+)}$ interactions. respectively.

CONCLUSION

Molecular crystal engineering is supramolecular solid-state chemistry. Crystal engineers concentrate their efforts on developing synthetic strategies aimed at the preparation of periodic supermolecules. Engineering implies function-oriented design of the superstructure. selection of the building blocks (on the basis of their chemical and physical stabilities and of their extramolecular bonding capacity), their assembly and characterization. to end with evaluation of the properties of the resulting supramolecular aggregate. In order to be satisfactory, a supramolecular/crystal engineering synthetic strategy should be reproducible. Hence. the utilization of interactions that are strong and, at the same time. highly directional, such as hydrogen bonding; are favored for the assembly of molecular components. These interactions are transferable from crystal to crystal and retain the same assembly-directing capacity, even on changing the nature of the forces holding the building blocks together in the crystal. For these reasons, the hydrogen bond is the interaction of choice in the engineering of molecular and ionic crystals constructed from neutral molecules or molecular ions.

ACKNOWLEDGMENTS

We acknowledge useful discussions with a number of scientists. C.R. Desiraju, A.G. Orpen, and J. Bernstein. Crystal engineering research work has been possible thanks to financial support from MIUR and CNR and from the universities of Bologna and Sassari.

ARTICLES OF FURTHER INTEREST

Concepts in Crystal Engineering, p. *319*
Crystal Engineering with Hydrogen Bonds, p. *357*
Hydrogen Bonding, p. *658*
Strong Hydrogen Bonds, p. *1379*
Weak Hydrogen Bonds, p. *1576*

REFERENCES

1. Lehn, J.M. *Supramolecular Chemistry: Concepts and Perspectives*; VCH: Weinheini, Germany. 1995.
2. Steed. J.W.: Atwood, J.L. *Supramolecular Chemistry*; J. Wiley: Chichester. UK, 2000.
3. Braga. D.; Grepioni, F.; Orpen, A.G. *Crystal Engineering: from Molecules and Crystals to Materials;* Kluwer Academic Publishers: Dordrecht, Germany. 1999.
4. Prins, L.J.: Reinhoudt. D.N.; Timmerman. P. Noncovalent synthesis using hydrogen bonding. Angew. Chem.. Int. Ed. Engl. 2001. 40, 2382–2426.
5. Braga. D.: Grepioni. F. Intermolecular interactions in non-organic crystal engineering. Acc. Chem. Res. 2000. 33, 601–608.
6. Etter. M.C. Encoding and decoding hydrogen-bond patterns of organic compounds. Acc. Chem. Res. 1990. 23, 120–126.
7. Pauling. U.L. *The Nature* of *the Chemical Bond,* 3rd Ed.: Cornell University Press: Ithaca. NY. 1960: 6.
8. Gordon, M.S.; Jensen, J.H. Understanding the hydrogen bond using quantum chemistry. Acc. Chem. Res. 8996. 29. 536–543.
9. Jeffrey. G.A.: Saenger, W. *Hydrogen Bonding in Biological Structures*: Springer-Verlag: Berlin, 1991.
10. Braga, D.; Maini. L.: Grepioni, F.; Mota, F.: Rovira. C.: Novoa. J.J. Inter-anionic $^{(-)}$O—H· ·O$^{(-)}$ interactions: A solid state and computational study of the ring and chain motifs. Chem. Eur. J. 2000, *6*. 4536–4551.
11. Desiraju, G.R.; Steiner. T. *The Weak Hydrogen Bond in Structural Chemistry and Biology* Oxford University Press: Oxford, 1999.

12. Novoa, J.J.; Nobeli, I.; Grepioni, F.; Braga, D. Are all short O—H···O contacts hydrogen bonds? A quantitative look at the nature of the O—H···O intermolecular hydrogen bonds. New J. Chem. 2000, 24, 5–7.
13. Meot-Ner (Mautner), M.; Sieck, L.W. The ionic hydrogen bond and ion solvation. 5. $OH\cdots O^-$ bonds. Gas-phase solvation and clustering of alkoxide and carboxylate anions. J. Am. Chem. Soc. 1986, *108*, 7525–7529.
14. Meot-Ner (Mautner), M. The ionic hydrogen bond and ion solvation. 1. $NH^+\cdots O$, $NH^+\cdots N$, $OH^+\cdots O$ bonds. Correlation with proton affinity. Deviations due to structural effects. J. Am. Chem. Soc. 1984, *106*, 1257–1264.
15. Gilli, G.; Bellucci, F.; Ferretti, V.; Bertolasi, V. Evidence for resonance-assisted hydrogen bonding from crystal-structure correlation on the enol form of the β-diketone fragment. J. Am. Chem. Soc. 1989, *111*, 1023–1028.
16. Braga, D.; Grepioni, F.; Desiraju, G.R. Crystal engineering and organometallic architecture. Chem. Rev. 1998, 98, 1375–1405.
17. Beatty, A.M. Hydrogen bonded networks of coordination complexes. CrystEngComm. 2001, 243–355.
18. Etter, M.C.; Urbonczyck-Lipkowska, Z.; Jahn, D.A.; Frye, J.S. Solid-state structural characterization of 1.3-cyclohexanedione and of a 6:1 cyclohexanedione: Benzene cyclamer, a novel host-guest species. J. Am. Chem. Soc. 1986, *108*, 5871–5876.
19. Braga, D.; Grepioni, F.; Byrne, J.J.; Wolf, A. Hosting paramagnetic $[(C_6H_6)_2Cr]^+$ in an organic anion framework *via* CH···O hydrogen bonds. J. Chem. Soc., Chem. Cornmun. 1995, 1023–1024.
20. Hanessian, S.; Siniard, M.; Roelens, S. Molecular recognition and self-assembly by non-amidic hydrogen-bonding—An exceptional assembler of neutral and charged supramolecular structures. J. Am. Chem. Soc. 1995, *117*, 7630–7645.
21. Thalladi, V.R.; Gehrke, A.; Boese, R. C—H group acidity and the nature of C—H···N interactions: Crystal structural analysis of pyrazine and methyl substituted pyrazines. New J. Chem. 2000, 24, 463–470.
22. Branimer, L.; Burgard, M.D.; Rodger, C.S.; Swearingen, J.K.; Rath, N.P. Silver(I) carboxylates: Versatile inorganic analogs of carboxylic acids for supramolecular network formation. Chem. Commun. 2001, 2468–2469.
23. Brammer, L.; Mareque Rivas, J.C.; Atencio, R.; Fang, S.; Pigge, F.C. Combining hydrogen bonds with coordination chemistry or organometallic π-arene chemistry: Strategies for inorganic crystal engineering. J. Chem. Soc., Dalton Trans. 2000, 3855–3867.
24. Brammer, L.; Mareque Rivas, J.C. Self-assembly of I-D chains of different topologies using the hydrogen-bonded inorganic supramolecular synthons N—H···Cl_2M or N—H···Cl_3M. Inorg. Chem. 1998, 37, 4756–4757.
25. Aakeroy, C.B.; Beatty, A.M.; Lorimer, K.R. Assembly of 2-D inorganiclorganic lamellar structures through a combination of copper(I) coordination polymers and self-complementary hydrogen bonds. J. Chem. Soc., Dalton Trans. 2000, 3869–3872.
26. Aakeroy, C.B.; Beatty, A.M.; Leinen, D.S.; Lorimer, K.R. Deliberate combination of coordination polymers and hydrogen bonds in a supramolecular design strategy for inorganiclorganic hybrid networks. Chem. Commun. 2000, 935–936.
27. Braga, D.; Maini, L.; Grepioni, F.; DeCian, A.; Felix, O.; Fisher, J.; Hosseini, M.W. Charge-assisted $N—H^{(+)}\cdots O^{(-)}$ and O—H···$O^{(-)}$ hydrogen bonds control the supramolecular aggregation of ferrocenedicarboxylic acid and *bis*-amidines. New J. Chem. 2000, 24, 547–553.
28. Holman, K.T.; Pivovar, A.M.; Swift, J.A.; Ward, M.D. Metric engineering of soft molecular host frameworks. Acc. Chem. Res. 34, 107–118.
29. Braga, D.; Grepioni, F. Complementary hydrogen bonds and ionic interactions give access to the engineering of organometallic crystals. 3. Chem. Soc., Dalton Trans. 1999, 1–8.
30. Braga, D.; Maini, L.; Prodi, L.; Caneschi, A.; Sessoli, R.; Grepioni, F. Anions derived from squaric acid form interionic π-stack and layered hydrogen bonded superstructures with organometallic sandwich cations. The magnetic behaviour of crystalline $[(\eta^6C_6H_6)_2Cr]^+[HC_4O_4]^-$. Chem. Eur. J. 2000, 6, 1310–1318.
31. Angeloni, A.; Orpen, A.G. Control of hydrogen bond network dimensionality in tetrachloroplatinate salts. Chem. Commun. 2001, 343–344.
32. Dolling, A.; Gillon, A.L.; Orpen, A.G.; Starbuck, J.; Wang, X.-M. Homologous families of chloride-rich 4,4-bipyridinium salt structures. Chem. Commun. 2001, 567–568.
33. Aakeroy, C.B.; Nieuwenbuyzen, M. Hydrogen bonded layers of hydrogen malate anions: A framework for crystal engineering. J. Am. Chem. Soc. 1994, *116*, 10983–10991.
34. Ziener, U.; Breuning, E.; Lehn, J.-M.; Wegelius, E.; Rissanen, K.; Bauni, G.; Fenske, D.; Vaughan, G. Recognition directed supramolecular assemblies of metal complexes of terpyridine derived ligands with self complementary hydrogen bonding sites. Chem. Eur. J. 2000, 6, 4132–4139.
35. Braga, D.; Cojazzi, G.; Emiliani, D.; Maini, L.; Grepioni, F. Reversible trapping of acid and base vapours into an amphoteric crystalline material. Chem. Comniun. 2081, 2272–2273.
36. Braga, D.; Cojazzi, G.; Emiliani, D.; Maini, L.; Grepioni, F. Reversible gas-solid reactions between the organometallic rwitterion $[(\eta^5\text{-}C_5H_4COOH)(\eta^5\text{-}C_5H_4COO)Co^{III}]$ and vapors of trifluoroacetic and tetrafluoroboric acids. Organometallics 2002, 21, 1315–1318.

Crystal Growth Mechanisms

Nicholas Blagden
Bradford University, Bradford, United Kingdom

INTRODUCTION

Crystal growth in a synthetic or suprarnolecular chemistry context is usually from solution and is undertaken to purify a material or is used as a synthesis step in a crystal engineering strategy. The process of crystal growth may have a great effect on the final form and cornposition of the targeted crystalline material. An objective of this contribution is to contrast the classical descriptions and the molecular recognition description of how molecules self-assemble into crystals from solution in order to describe the core mechanism and processes of crystal growth. In the classical interpretation. the vehicle for this process is the growth unit: for suprarnolecular chemists. the comparable vehicle is the synthon. Both perspectives rely on a hierarchical description of overall assembly directed by the Sunctionality inherent to the crystallizing species. This process naturally forms the basis for understanding how the growth units assemble (crystal graph. for crystal growth or motif, for crystal engineer). Such an understanding of the molecular assembly at the crystallographic level is widely used to describe the functionality and stereochemistry inherent in the bulk and surface of the crystal, and this information can be utilized to direct crystal growth.

GROWTH THEORIES

Two aspects of crystal growth".'' will be covered: One aspect pertains to surface processes and the second to transport processes at the growing crystal face. However. it is first necessary to describe the nature and mechanism of a crystal face capturing growth units from solution. According to Hartman and Perdock,[3] for a three-dimensional crystal face. the capture of growth units can be classified according to how many contacts form between the adsorbed growth unit and the crystal surface. If three orientations of surface contacts are involved, then incorporation is at a kinked face: if two orientations of surface contacts are involved. then incorporation is at a stepped face: and if one surface contact is involved. then incorporation is at a flat face (Fig. 1). According to Temkin.[4] (for any of the above incorporation steps). the energy change occurring when a solvated flat surface is roughened by the transfer of a solvated growth block from one layer of the surface to form a new layer can be expressed as the overall calculated energy of dissolution. then adsorption, and is given by Eq. 1:

$$\Delta E = 4\Phi_{sf} - 2\Phi_{ss} - 2\Phi_{ff} \quad (1)$$

where Φ is a binding energy of a growth unit, and the subscripts indicate the type of binding interaction: *ss* for solid-to-solid binding. *ff* for fluid-to-fluid binding, and sf for solid-to-fluid binding.

According to Jackson.[5] which growth mechanism a crystallographic unique face obeys depends on the magnitude of the surface roughing factor, α. which is a function of $\Delta E/kT$. Human et al.[6] modified the Jackson α-factor function to include paramaters that account for the supersaturation contribution and the contribution arising from the binding energy of the crystallographic plane and crystal lattice under consideration. E_{ss}^{face} and $E_{ss}^{crystal}$. respectively, see Eq. 2:

$$\alpha = E_{ss}^{face}/E_{ss}^{crystal}[\Delta E/kT - \ln\Omega] \quad (2)$$

where Ω=solubility relative to the density of the crystallizing solute.

In this scheme (the respective growth processes are illustrated in Fig. 2), as supersaturation decreases, a region occurs where $\alpha<2$–3. This range is where the growth process is without a layer mechanism and grows without any crystallographically defined orientation. If $3>\alpha>5$, then the system moves to growth dominated by nucleation with subsequent layer growth. When $\alpha>6$. then sequential layer growth occurs. and this is when the supersaturation reaches the metastable zone on the solubility curve.[7]

In general. at low supersaturation, the growth is via flat faces according to the solubility modified α-factor. In addition. the general analysis of α indicates that if ΔE is a kinked, stepped. or flat face, the energy change decreases according to the following inequality:

$$kinked < stepped < flat$$

and thus indicates that a flat face is the energetically most unfavorable. So. growth via a flat face requires an energetically cheap mechanism for the growth process.

Crystal growth theories aim to describe how an energetically unfavorable flat faces grows and how a set

Encyclopedia of Supramolecular Chemistry
DOI: 10.1081/E-ESMC 120012753

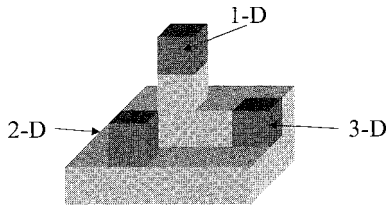

Fig. I The classification of surface contacts according to Hartman and Perdock: 1-D—flat. one contact: 2-D—step, two contacts: 3-D—kink. three contacts. (View *this* art *in* color *at www.dekker.com.*)

of possible flat faces may grow relative to each other. It was Cabrerra, Burton, and Frank[8] who first proposed that the energetically cheap process that enables a flat surface to grow is mediated by the presence of the screw dislocation lattice defect. In this model of how a lattice surface grows. the growth rate for a flat surface is described by a complex product of the flux of growth units entering kink sites: the step velocity (v_{step}); the density of kink sites (ρ_{step}); and the height of the step (h_{step}). The theoretical expression for the rate of a crystal surface growing (G_{sdl}) is described by an involved set of paraineters for a flat surface. using screw dislocation lattice defects. but can be simply put according to Eq. 3.

$$G_{sdl} = v_{step}^{x} h_{step}^{y} \rho_{step}^{z} \tag{3}$$

The complexity of each variable arises as the flux of growth units entering a kink site is determined by a function describing the diffusion of growth units to the kink sites. The density of steps is related to the spiral curvature. which is a function of supersaturation: the height of the step depends on the initial number of defects in the nucleating crystal. The exact form of Eq. 3 can be found in the literature.[7–9]

For moderate supersaturation, the mechanism of growth is described by a site nucleation process. followed by growth from this nucleation center.[10,12] In this process. the growth rate is determined by a complex product of nucleation rate N_s, step height H_s, and step velocity V_s. Again. the theoretical expression for the rate of a crystal surface growth (G_{ns}) is described by an involved set of parameters for nucleation and spread mechanism but can be simply put according to Eq. 4.

$$G_{ns} = N_s H_s V_s \tag{4}$$

The nucleation rate N_s is determined by a function that relates the surface energetics of the nucleation process and the supersaturation. The step height H_s describes the number of growth sites available from the nucleation center. and it is determined by the type of growth site, which is also a function of supersaturation. Step velocity V_s is determined by a function that describes the rate of the diffusion of growth units over the surface from the nucleation center.

At high supersaturation, a surface is deemed to contain a large number of kinks and steps. The surface diffusion step that describes how a growth unit finds a growth site depends on supersaturation only. In this situation. it is assumed that all growth units find a growth site. and under this mechanism, the growth rate takes on a simple form.[1,2] as shown in Eq. 5.

$$G_c = K\sigma \tag{5}$$

To describe the bulk growth of crystals in solution where the solvent is in excess, the growth rate G is described by two contributions. These are the mass transport to the particle surface and the reaction or integration step, the process whereby incoming growth units incorporate into the crystal surface. Again. the quantities involved are complex, and the details are to be found elsewhere.'''' Shown in Eq. 6 is the bulk growth rate expression. G, derived using first-order kinetics:

$$G = \frac{k_I k_d}{k_I + k_d}\sigma \tag{6}$$

where σ is the supersaturation and represents the difference between the concentration in solution: k, and k_d represent the rates of incorporation and diffusion. respectively. at the incorporating interface. See Fig. 3 for an overall schematic representation of the mass transport

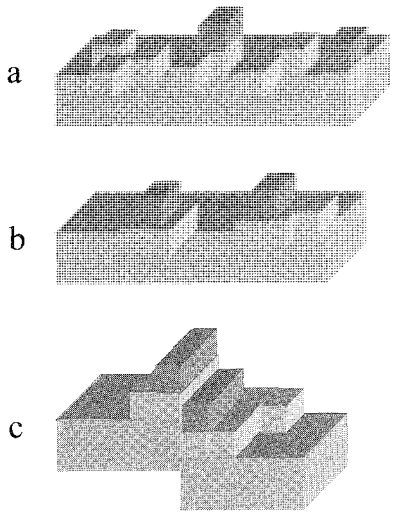

Fig. *2* The classification of the crystal growth process according to Jackson α-factor: (a) rough growth; (b) island growth (nucleation and spread): and (c) spiral growth. (*View this* nrt in color *at www.dekker.com.*)

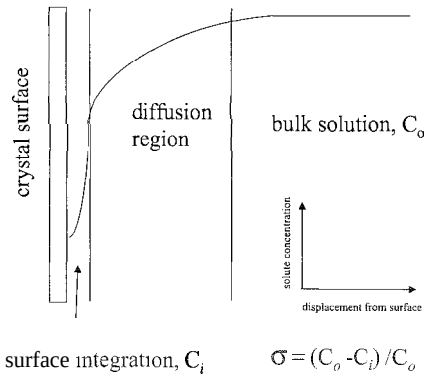

Fig. 3 The diffusion model of crystal growth. (*View this art in color at www.dekker.com.*)

process. Over the range of supersaturation and *differing* k_I and k_d, *three regimes of growth are usually observed. When* $k_I < k_d$, *then the integration step dominates growth: if* $k_d < k_I$, *then the diffusion step* dominates *the growth; and* when $k_d = k_I$, *then the growth process is a cornbination of both processes.*

In summary. whichever *mechanism appropriately describes the mechanism of crystal growth from solution. crystal growth is the balance between adsorption and desorption processes* at *the solid–liquid interface.* Conse*quentiy. temperature,* supersaturation, *surface process, diffusion process. and the energy transfer associated with incorporation* contribute *to the description of the overall crystal growth process.*

CRYSTAL GROWTH AND CRYSTAL HABIT

It is the overall relative growth rates of crystal faces described by the internai structure of the crystalline inaterial under consideration that *determine the observed* equilibrium *morphology of crystal.* referred *to as* habit.[12,13] Gibbs *and* Wulf[14] *described the attainment of an equilibrium* form *acco ding to surface free-energy sums being* minimized, *later relating* the *dominance of a face to the distance a face* was *from* a *growth center. according to the relative surface-energy* contribution *of each possible face. An* implication is *that the relative growth rate of faces defines the final shape of* the *crystal. As flat faces are the slowest growing faces. then the habit is defined by the relative gron-th rate of these flat faces (see* Fig. *4). In addition. if spiral growth conditions hold. the enerpetics of the process can be written* in terms *of a sequential lattice layer concept of face formation. With these two criteria, the habit of a crystal* is *defined by a set of expressed faces based upon relating face growth to* the *individual surface energy of each plane in* the *set of crystallographic planes defining the crystal. In order to do this, two* assumptions *are made, which are reviewed in the* literature:[15,16]

1. *Crystals* grow *by the addition of complete* layers *of* thickness d_{hkl} *that* have *the same crystal structure* as *the bulk, as* given *by the crystal structure. taking* into *account* systematic *absences.*
2. *The energy* released *per* mole *of layer—the so-called attachment energy.* E_{att}, is *directly proportional to the growth rate of the face.*

The introduction *and* use *of these* assumptions *are often attributed to the pioneering* work *of* Hartman *and Perdok in the* 1950s.[9] *In* making *these assumptions,* they *extended* the *treatment of crystal* morphology *described by* Gibbs *and* Wulf. *In this system of analysis of expressed faces. the faces* that *bound a crystal will be those with the* more *positive* E_{att} *consistent with the point group* symmetry. *Additional assumptions are made* that *relate to fluid–fluid contributions and fluid–solid contributions. These are assumed to be isotropic interactions. in that they are nonface specific,* and *that the anisotropic contribution* from *the solid–solid interaction* is *the critical* quantity *describing* E_{att}. *For this to be* valid, *the assumption* is *made that there is no differentiation between bulk and interface interactions.* In *conclusion, of the factors that affectcrystal habit, the morphology is dominated by the slowest growing faces, with the exact habit described by the relative growth rates of all flat faces. As we will see. modern theories* attempt *to account for the process* at *a molecular level.*

HABIT MODELING THEORY

Various approaches exist for predicting crystal habit. The basic concepts of those commonly *used will be described.*

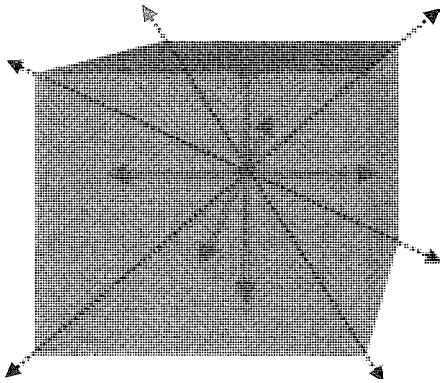

Fig. 4 The relationship between habit and the relative growth rates of faces: the faces are defined by the weakest interactions and slowest growth: and the edge defined by the strongest interactions and the fastest growth. (*View this urt in color at www.dekker.com.*)

The methods. as described. are not able to accommodate modifications to deal with solvent or impurity effects. How these effects might be included in the model will be discussed later. The following are three commonly used approaches:

1. The Donnay Harker[17] approach — The attachment energy is assumed to be inversely proportional to the interplanar spacing. Thus, the relative growth rates of faces in a series can be assessed purely on the basis of their structures.
2. The Hartman and Perdok[9] approach — An examination of the crystal structure is undertaken. in order to identify molecular chains within the crystal structure (referred to as the crystal graph). For each molecular chain identified, the intermolecular interactions within the molecular chains are classified. The weakest intermolecular contacts within these chains are identified and are taken to be the molecular contacts that determine the growth rate of that particular chain. These points are then used to identify sets in the crystallographic plane that describe the crystal (the crystal net) and are taken as the flat growth face that defines the habit. It is from this work chat the importance of attachment energy in describing rate of growth of a specific crystal face in low supersaturation was made.
3. The attachment energy approach—Bennema[18] and coworkers initially, and more recently Docherty and Roberts (HABIT code)[19] and Berkovitch-Yellin,[20] utilized the attachment energy as derived from differences between the lattice energy (the potential energy summation derived from a central inolecule to all other molecules in the lattice) and the slice energy. The slice energy is defined as the potential energy summation from the central molecule along the direction of a Miller plane that characterizes a set of lattice planes that describe a specific face. Parameterized Leonard-Jones-type potentials are commonly used, and a pairwise summation of all the nonbond interactions and an Ewald summation for either point charges or multipole contributions to the electrostatic interactions are used in the calculations. As with all calculations of this type. the calculated morphology obtained is sensitive to the combination of charge treatment and potential set used.

SOLVENT AND IMPURITY EFFECT ON CRYSTAL GROWTH

As stated earlier. the internal structure controls the energetics of a molecule or ion attachment to the cryrtal surface. For different crystal surfaces, the energetics vary. and it is this variation that differentiates between the growth rates of respective faces.[21] External factors, such as the levels of supersaturation, solvent. and impurities, may contribute additional influences on the attachment energy for a set of growing faces, with the result that a modification to the overall habit is observed as the growth conditions are varied. In particular, because crystal growth is a surface-specific process, with the distinct feature that if a recognition process between a crystal face and impurity or solvent occurs, then a dramatic influence on crystal habit is achievable.

A problematic area is how to ratify the effect of solvent or impurities. When analyzing the effect of solvent or impurities on crystal habit. two factors are essential to understanding the process.

The first is the process of solvent or impurity inclusion at the growth site. Here, attachment energy calculations are used to assess the effect. Two parameters are used to evaluate the impact of inclusion. One parameter is the binding affinity of the solvent or impurity to a specific lattice plane. this is used to characterize the affinity of the solvent or impurity for a specific face. The second key parameter is the inclusion effect on the attachment energy. What must be envisaged in this process is that the habit is altered as a result of an impurity or solvent molecule blocking a growth site. such as a kink, and so reducing the growth rate of one face relative to the others. i.e., increasing the attachment energy. As the binding affinity increases, the probability of incorporation increases. This approach to the mechanism of impurities and solvent is effective, because the concentration of active growth sites on the surface is low, and an impurity or solvent may be specific to one particular face.

The second factor in quantifying the influence of solvents or impurities is the effect of solvent or additive on the growth mechanism. particularly when solubility is affected. Because solubility defines supersaturation, any change in supersaturation can cause the growth mechanism to move from screw dislocation to surface nucleation and eventually to continuous growth. This is the change in growth behavior as previously discussed. Predicting the transition of the growth process from one of continuous growth to one of spiral growth requires detailed calculations that include surface diffusion, collision, and exchange processes at the growth interface. The transition of the growth process that includes the above phenomena is usually modeled using an Ising Net and Monte Carlo simulation techniques.

It is important to note that the comparison of experimental morphologies to calculations is also problematic. due to the effect of solvent. It is usual to compare the habit of a crystal grown by sublimation with those generated by varying the solvent. For example, when the

calculated sublimation and solvent-grown crystal morphologies of succinic are compared, the role of the solvent becomes clear. As morphology and binding modeling indicate, the presence of water results in the rhomb morphology elongating. as the water molecule has a preference for the (100) faces and, with the presence of 2-propanol. has a preference for the (010) faces, resulting in needle morphology.

CRYSTAL GROWTH: ADDITIVES AND HABIT MODIFICATION

If solvents or impurities are added to produce a specific effect on morphology, they are referred to as "tailor-made additives." In recent years, the principle of selecting a molecule to selectively disrupt or block the growth of specific faces and, consequently, to modify the habit or inhibit growth has been widely applied. Which process occurs depends on the additive loading and to what degree the additive blocks the subsequent growth layer. This work was guided by the habit calculations using attachment energies. In many cases, the choice of additive is made purely on considerations of surface geometry.

In all cases. the objective is to identify additives that will either cap a growing face and thus act as a blocker to growth from the target face or that will maintain the ability to support the next face layer but distort the attachment of the next layer, thus acting as a disrupter to growth from the target face (see Fig. 5). The reason for modifying crystal morphology relates to the effect of particle geometry on the physical properties, such as particle flow, filtration characteristics, or optical properties.

Some examples of the attachment energy calculation approach to additive effects can be found in the Clydesdale, Roberts. and Docherty article on HABIT 95[23,27] and Davey, Polywka, and Magin.[22] For instance; the effect of benzoic acid on the growth of benzamide and the impact of biphenyl on the growth of naphthalene were modeled and analyzed in these articles. An example in which laboratory experiments and calculations were used is the work on the disruptive additive benzoic acid on benzamide.[23] Pure benzamide grows in needle-plate geometry. but in the presence of benzoic acid. the morphology changes to a rhombohedra1 plate. In this system. the aim was to block the formation of the hydrogen-bond ribbon characteristic of the structure along the [010] axis.[26] This was achieved using benzoic acid, as the incorporation of this molecule into the hydrogen-bond ribbon disrupts the attachment of the next incoming layer, as no -H–O- contact is available for benzamide attaching to benzoic acid incorporated in the chain. Consequently, the (010) faces dominate the habit. and the crystal elongates along the [100] axis.

Calculations are not always carried out; often, a geometric approach is used. Again. there are many examples to be found in the literature: one example is the selective inhibition of prochiral faces (viz. when a pair of faces are described by lattice planes that are mirror images of each other). for glycine[24] by chiral additives, such as *L*- or R- serine. Here, the solution was doped with either the L- or *R*- form of the amino acid serine. Both forms of the amino acid cause the glycine crystal to grow as a pyramid. instead of growing as the usual bipyrainid. This occurs as glycine posseses a prochiral axis along [010]. This prochiral axis arises as the glycine molecules form two antipolar sets (the relative mirror orientation of the molecule within prochiral lattices gives rise to alternating pairs of lattices within the structure) within the structure and lie perpendicular to the orientation of prochiral lattice planes. The habit modification was rationalized in terms of the R-serine being specific for the (010) face only and the L-serine being specific for the (0-10) face only. The overall habit arises as the antipolar set typifies the plane intersecting the bipyramid, and each component of the antipolar set characterizes one of the respective top faces of the bipyramid.

A variation of the principles of habit modification is the inhibition or retardation of crystal growth. In this strategy, the additive is selected to mimic and block the fastest-growing face of the crystalline material under study. This has led to additives, which control encrustation, fouling the surfaces in many industrial situations, i.e. barium sulfate precipitation in oil wells.[25]

A common theme for all of these examples is the application of an impurity that partially mimics the stereochemistry of the next incoming growth layer of a specific lattice plane, and in doing so, manipulates the significance of the targeted faces in the overall morphology. Not only is the crystal engineered to express a specific morphology. but influences on size are also observed.

To conclude the discussion of habit modification by additives, additive choice is based either on a geometrical

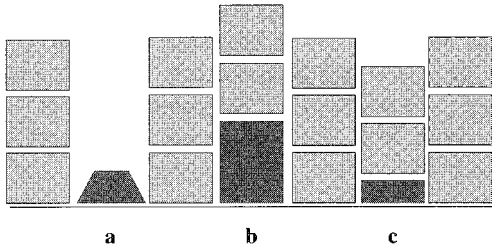

Fig. 5 Additive strategies for habit modification: (a) capping of a growth layer site; (b) disruption of contacts due to an additive larger than the site: (c) disruption of contacts due to an additive smaller than the site. (*View this art in color at www.dekker.coin.)*

match between the additive geometry and the host site or on calculations. Calculations are used to determine the affinity of the additive for the surface, and the influence of the additives on the energetics of the growth process. In certain cases, the choice is based on a guess using derivatives of the molecule under study.

CRYSTAL GROWTH AND POLYMORPH SELECTION

A variation on the application of impurities, which affect the crystal growth process, has been the selection of polymorphs[26,27] grown from solutions using solvents and additives. In this area, the route to polymorph selection and stabilization is to employ additives or solvents (impurities) that have the ability to inhibit or to interfere with the fastest growth directions of a stable polymorph over that of the metastable form exhibited by the system. Such studies highlight the subtle role growth conditions play in crystallization and have direct ramifications for the supramolecular chemist engaged in crystal engineering. as such work highlights the effects kinetics and growth conditions may have on the durability of a synthon to generate a particular architecture. This arises. as such systems are subject to the issue of the growth of one form over another, which is described by Ostwald's rule of stages,[28] which states:

> "...when a change in phase occurs. the transformation proceeds not directly to the most stable phase but to the next stable...."

Consequently. for solution crystallization, polymorphism adds a kinetic dimension to crystal growth, whereby the kinetics requires that the transformation of one phase (G_I) to another (G_{II}) in solution is dependeat on the dissolution (k_d)of the metastable phase (as stated in Eq 7). driving the supersaturation of the growth of the stable phase (k_g) (as stated in Eq 8)

$$G_I = -k_d(\sigma - \sigma_{(i-ii)}) \tag{7}$$

$$G_{II} = k_g(\sigma_{(i-ii)}) \tag{8}$$

Experimentally. this process can be verified using time-lapse micrographs of a polymorphic system crystallizing. and this is illustrated for dimorphic system L-glutainic in Fig. 6. In this figure. a series of time-sequence micrographs clearly show the dissolution of the metastable rhomb phase (I) and the growth of the stable needle phase

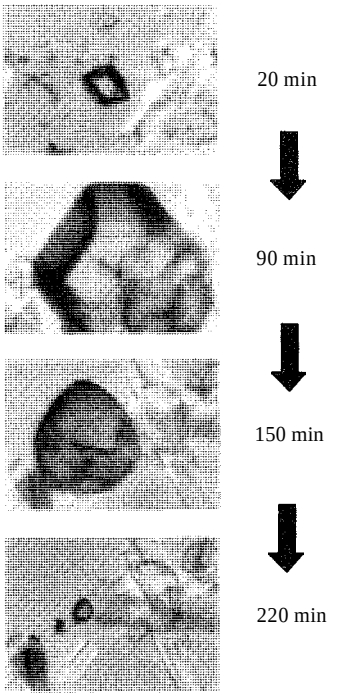

Fig. 6 Dissolution and growth process of polymorphic transformations in solution of L-glutamic acid from Form I to Form II. (*View this art in color at www.dekker.com.*)

(II). Such a description of the transforination kinetics suggests that the stabilization of the metastable form using an impurity would require the impurity to affect the growth kinetics of the stable phase. In the case of glutamic acid, the impurity used was trimesic acid, as this impurity is a conformational mimic of glutamic acid in the stable form. Consequently, an impurity of this type will disrupt the growth of the stable form of glutamic acid via disruption of the fastest growth direction, and this arises as the trimesic acid possesses a larger volume than the host site within the fastest growth direction, thus disrupting the next incoming layer.

CONCLUSION

Selectivity of crystal growth processes based on a firm understanding of the mechanism of crystal growth should enable the practitioner to manipulate the habit: isomer, or polymorph of a molecular solid grown from solution. Also. the suprainolecular chemist. as a crystal engineer. will be able to make better use of the underlying crystallographic principles that govern crystal growth to better understand the appearance of habit or polymorph variation.

ARTICLES OF FURTHER INTEREST

Biomaterials, p. 110
Crystal Deconstruction, p. *349*
Hydrogen Bonding, p. 658
The Lock *and Key Principle*, p. *809*
Polymorphism, p. 1*129*

REFERENCES

1. Bennema, P.: Gilmer, G.H. Kinetic of Crystal Growth. In *Crystal Growth*: Hartman, P.. Ed.; North-Holland: Amsterdam. 1973: Vol 1, 263–327.
2. Pfeiffer, H.; Klupsch, T.: Haubenreiber. W. *Micrscopic Theory* of *Crystal Growth*: Akadeinie-Verlag: Berlin. 1989.
3. Hartman, P.: Perdok. W.G. On the relationship between structure and morphology. Acta Crystallogr. 1955, *8*. 49–52.
4. Temkin, D.E. *Crystallisation Processes*: Consultants Bureau: New York. 1966: 15. Chp 1.
5. Jackson, K.A. *Liquid Metals and Solidification*; Craichvitch, A.. Ed.: American Society of Metals: Cleveland, 1958: 174–186.
6. Human, H.J.: van der Eerden. J.P.: Jetten, L.A.M.J.; Oderkerken, J.G.M. On the surface roughening transition of faceted to non faceted growth of diphenyl for different organic solvents and the melt. J. Cryst. Growth 1981. *51*. 598–600.
7. Davey, R.J.: Mullin, J.W.: Whiting. M.J.L. Habit modification of succinic acid crystals grown from different solvents. J. Cryst. Growth 198%*58*, 304–312.
8. Burton. W.K.; Cabrera. N.: Frank. F.C. The growth of crystals. Philos. Trans. R. Soc. 1951, *243*. 299–358.
9. Ohara, M.: Reid. R.C. *Modelling* Crystal *Growth* Rates *From Solution*; Prentice Hall: New York, 1973.
10. Aquilano, D. Basic Mechanism of Crystal Growth. In NATO *ASI*. Series *B* 210: Arend. H.. Hulliger, J.. Eds.: Plenum: London, 1989; 49–67.
11. Carberry. J.J. *Chemical and Cataytic Reaction* Engineering: McGraw Hill: New York. 1976.
12. Toschev, S. Equlibrium Forms. In Crystal *Growth*; Hartman, P.. Ed.; North-Holland: Amsterdam. 1973; Vol 1, 328–341.
13. Bennema, P. Generalized Treatment of the Equlibrium Form. In Crystal *Growth*; Hartman, P., Ed.: North-Holland: Amsterdam. 1973: Vol 1. 342–401.
14. Cibbs. J.W. Collected *Works: Thermodynamics*; Yale University Press. 1948: Vol. I.
15. Docherty. R. The Application of Computational Chemistry to the Study of Molecular Materials. In *Crystal Growth of Organic Materials*: Conference Series. USA. 1996; 2–14.
16. Bennerna, P. On the Crystallographic and Statistical Mechanical Foundation of the Hartman Perdok Theory. In *Crystal Growth of Organic Materials*: Conference Series, USA. 1996: 15–21.
17. Donay, G.D.H.; Harker, D.Am. Mineral. 1937, *22*. 446–451.
18. Bennema, P.; van des Eerden, J.P. *Morpholgy* of Crystals: Sunagagwa, I.. Ed.: Terra Pub.: Tokyo. 1987: 1–75.
19. Clydesdale. G.: Roberts. K.J.; Docherty. R. HABIT 95. In Crystal *Growth* of Organic Materials: ACS Conference Series. USA, 1996; 43–52.
20. Berkovitch-Yellin, Z. Towards an ABINITIO derivation of crystal morphology. J. Am. Chem. Soc. **1985**, 107. 8239–8253.
21. Buckly H.E. *Crystal Growth*: John Wiley: New York. 1951: 339–460.
22. Davey. R.J.: Polywka. L.A.; Magin, S. The Control of Morphology by Additives: Molecular Recognition. Kinetics and Technology. In *Advances* in *Industrial Crystallisation*; Butterworth. 1991: 150–179.
23. Berkovitch-Yellin. Z.; Addadi. L.: IdelsonM.; Lahav. M.: Leiserwitz, L. Controlled modification of crystal habit by tailor made impurities: Application to benzamide. Angew. Chem. Suppl. 1982. 1336–1345.
24. Addadi. L.; Berkovitch-Yellin, Z.: Weissbuch, I.: Lahav, M.; Leiserwitz. L. A link between macroscopic phenomena and molecular chirality crystals as probes for the direct assignment of absolute configuration of chiral molecules. Top. Stereochem. 1986, 16, 2–83.
25. Black. S.N.; Bromley, L.A.; Coltier. D.: Davey. R.J.: Dobbs. B.; Rout. J.E. Molecular design based upon recognition at inorganic surfaces. Nature 1991. *353*. 549–550.
26. Davey. R.J.: Blagden, N.; Potts. G.D.: Docherty. R. Polymorphism in molecular crystals: Stabilization of a metastable form by conformational mimicry. J. Am. Chern. Soc. 1997. 119 (7). 1767–1772.
27. Blagden, N. Powder technology. Cryst. Eng. Polymorph Appearance 2001, *121*. 46–52.
28. Ostwald, W. Rule of stage,. Z. Phys. Chem. 1897. 22. 306.

Crystal Structure Prediction

Sarah L. Price
University College London, London, United Kingdom

INTRODUCTION

Programs are available for the computational prediction of organic crystal structures. usually based on searching for the most thermodynamically stable unit cell. Such programs will generally predict any dominant supramolecular motif and are often successful at predicting the complete crystal structure for simple organic molecules in common space groups. Although there have been successful predictions, even under blind test conditions, no method is yet reliable for any type of organic molecule. The methods will become more widely useful as accurate quantitative models for the intermolecular and intramolecular forces are developed and the range of possible crystal structures covered in the searches is extended. Nevertheless, there is a fundamental limitation when: as is often found. the search generates more energetically feasible crystal structures than experimentally known polyinorphs. In such cases, the kinetics of nucleation and crystal growth will determine which of these crystal structures are observed. Work on incorporating kinetic factors into crystal structure prediction is only just beginning.

WHAT IS CRYSTAL STRUCTURE PREDICTION?

Crystal structure prediction can simply mean using a computer to predict the crystal structure of an organic molecule from its chemical diagram. The aim is to predict the space group, cell dimensions, and atomic fractional coordinates that will be observed should the molecule be successfully synthesized and crystals obtained that allow the structure to be solved by diffraction methods. Such a computational method would be practically valuable in the development of molecular materials, where the crystal structure as well as the molecule affect the property of industrial or scientific interest. For example, a molecule with a high nonlinear optical coefficient will only produce an active material if it crystallizes in a noncentrosymmetric space group. Crystal structure predictions could also reduce synthetic effort in the development of energetic materials and pigments.

Crystal structure prediction is considerably complicated by polymorphism. When a inolecule can adopt more than one crystal structure. we want to be able to predict all the crystal structures that are likely to be found and the conditions to control the form produced. This would benefit the pharmaceutical industry, where the unexpected appearance of a new polyinorphic form is a disaster. However, until there is an experimental screening method that reliably establishes all the polymorphs that could exist for a given molecule. it is impossible to conclude with certainty that a crystal structure prediction study was completely successful. A predicted polymorph may yet be found. A known crystal structure could be thermodynamically metastable, but there may be no kinetically feasible route to forming the more stable form. Hence, the development of crystal structure prediction is intrinsically linked with progress in demystifying polymorphism.

Thus. crystal structure prediction is a forinidable problem and a major test of our quantitative ability to model the details of supramolecular recognition. The answer to the question as to whether crystal structures are predictable has only recently advanced from an emphatic "no" to a ''maybe''.[1] Experience in this field is still relatively limited.[2] Although there have been cases where the crystal structure of a molecule was genuinely predicted just from the chemical diagram, it is certainly not yet possible to predict ab initio the crystal structures of any organic molecule. Indeed. it is not yet possible to define the molecules for which current methods are likely to be adequate.

The distinction that crystal structure prediction should completely predict an unknown crystal structure makes it intrinsically more precise and difficult than crystal engineering, which seeks to predict broad structural patterns and motifs. For example. crystal structure prediction may indicate that a molecule has a strong preference for a certain hydrogen-bonding motif. for example, forming a sheet. If this sheet was observed in all polymorphs. then the prediction would be a success for crystal engineering. However. it would only be deemed a successful crystal structure prediction if the stacking of the sheets was accurately predicted to give the correct space group and cell dimensions.

The emphasis on no prior experimental knowledge is important in distinguishing crystal structure prediction from methods of solving crystal structures using known unit cell parameters. For most fairly rigid organic molecules. the problem is much simpler when the unit cell parameters are known, as seen by recent progress in solving crystal structures from x-ray ponder diffraction.

Encyclopedia of Supramolecular Chemistry
DOI: 10.1081/E-ESMC 120012751

However. a set of computed feasible crystal structures can be useful in solving structures from x-ray powder data when the pattern cannot be indexed to give the cell dimensions. This only requires that a set of feasible crystal structures. containing one with a simulated powder pattern close enough that it can act as a starting point for refinement: be generated by the prediction.

Thus, there will be many practical uses for a reliable computational method of predicting the crystal structures of organic molecules. It is a fundamental challenge that underpins crystal engineering. We cannot claim to understand crystallization until we can at least predict the crystal structures that will be observed. It is probable that a reliable method of crystal structure prediction will have to represent in a quantitative way the factors that control crystallization.

THE BASIC ASSUMPTION OF CRYSTAL STRUCTURE PREDICTION

Most crystal structure prediction methods are based on the assumption that the observed crystal structure will correspond to the global minimum of the Iattice energy. This is essentially assuming thermodynamic control of crystallization. It also simplifies the calculation of the thermodynamics by neglecting all temperature. pressure, and quantum effects and by replacing the appropriate free energy by the lattice energy. the classical energy at 0 K. According to this zero-order assumption, any local minima in the lattice energy that are sufficiently close to the global minimum may be potential polymorphs.

Implementing this crude assumption requires a method of evaluating the lattice energy and of searching through the wide range of possible crystal structures. Quantifying inter - and intramolecular forces and global optimization are all major research fields, and so many alternative schemes were developed. Many of the programs[3–16] developed for crystal structure prediction based on lattice energy minimization are listed in Table 1. The main features of the search methods were reviewed[''' and compared.[17,18] Their limitations in terms of the techniques used in molecular crystal modeling,[''' particularly in the types of intermolecular and intramolecular potentials that can be used. usually reflect the type of organic molecules that were the main focus of the developmental work.

SEARCH METHOD

Even for a simple rigid organic molecule, the number of variables required to define the crystal structure presents a major search problem. and the search is limited to the most probable space groups. Some programs[8,14] use information on most likely packing modes within each space group. Most methods are. in practice; confined to considering just one molecule in the asymmetric unit ($Z'=1$) of the most common space groups for organic molecules. So, consideration of $P2_1/c$, $P\bar{1}$, and $P2_12_12_1$ is routine, and most programs can consider many others, such as $P1$ (as trivial), $P2_1$, $Pna2_1$, $Pca2_1$, $Pbca$, $C2/c$, Cc, $C2$, etc., though the computing time increases with the number of molecules in the unit celi (Z). During a search in a given space group. minimization could place molecular symmetry elements so as to generate a higher symmetry space group. Similarly; a stationary point found by minimizing within a space group symmetry could be a transition state between lower-symmetry structures. and reducing the symmetry in these cases can generate a minimized structure with more than one crystallographically independent molecule in the unit cell ($Z'>1$). Searches in $P1$ with varying numbers of independent molecules in the unit cell may become more effective in the future. However, to date, only in one published study. of hydrates of pyranoses and alcohols,[''' was the search explicitly for structures with more than one independent molecular unit in the cell. though this extension is urgently required for considering salts and solvates.

Crystal structure prediction only really started in the 1990s, when the increases in computer power made it possible to consider even this limited range of possible types of crystal structures. Some methods sample the potential energy landscape systematically. relying on efficiently eliminating impossible structures where ihe molecules overlap significantly. or use other criteria, such as the density of pseudo-hard sphere packing or the interaction energy of symmetry-constrained nuclei, to select a more limited number of structures for starting points for lattice energy minimization. Other methods use Monte Carlo simulated annealing or molecular dynamics to search for minima. repeating the runs to overcome the random element. However, all methods are extremely computer intensive. involving some sort of consideration of millions of hypothetical structures to span the potential energy surfaces and resulting in at least thousands of lattice energy minimizations. The problem is difficult because of the complex shape of the potential energy hypersurface: the energy barriers for converting between different approximately close-packed structures are high, and so only a small range of the surface will minimize to the global minimum. A key practical issue is in how to cluster similar hypothetical crystal structures, in the process of being relaxed or as minima. The clustering must remove structures that would correspond to the same

Table 1 Overview of programs developed for organic crystal structure prediction by searching for minima in the lattice energy. The types of molecules for which the program was originally developed are given. though all programs with emboldened names were used in the blind tests and so have been used for a wider range of systems (Fig. 4).

Program	Type of molecules used in development (Ref.)	Search type
Chin	Crystal engineering—diketopiperazines[3]	Monte Carlo simulated annealing with hydrogen-bonding bias
CRYSTALG	Rigid organics — amides, bases[4]	Self-consistent basin-to-deformed-basin mapping global optimization
CRYSCA	Pigments. organometallics[5]	Random search with steepest descent
ICE9	Rigid hydrocarbons[6]	Systematic grid search to generate close-packed structures
MDCP	Small rigid[7]	Constant pressure molecular dynamics to find crude structures
MOLPAK	Energetic materials. rigid[8]	Systematic search for high-density
(and DMAREL)	Rigid polar and hydrogen bonded[9]	structures in common coordination types
MPA, extended to Mpg	Small rigid[10]	Lattman systematic, or random generation of expanded trial unit cell
Perlstein	Moderate sized. semiflexible organics[11]	Aufbau search for low-energy one-dimensional and two-dimensional aggregates. primarily for monolayer predictions
PMC	Hydrocarbons[12]	Symmetry-adapted grid systematic
Polymorph Predictor	Flexible organics, including	Monte Carlo simulated annealing with intemediate clustering
PROMET	Rigid hydrocarbons[14]	Selecting cohesive dimer, ribbons and layer substructures of partial space-group
SySe and PP	Pigments[15]	Grid-based systematic
UPACK	Sugars and alcohols[16]	Systematic grid or random search. with intermediate clustering

observed crystal structure, while ensuring that minima that correspond to two closely related polymorphs are not eliminated.

Thus, a crystal structure prediction search will generate many hundreds to thousands of different lattice energy minima. The example in Fig. 1 shows the distinct minima obtained from about 1500 MOLPAK-generated starting points for a rigid nonplanar molecule with a CH-CO-NH-CO-CH functional group. The low-energy structures include hydrogen-bonded dimers and catemers and cover a range of distinct structures with relatively little difference in densities. Such crystal structure prediction results, where the energy gap separating the global from other minima is very small. and there are many distinct minima within the energy range of possible polymorphism. currently appear to be common. Examples where the known structure is found at the global minimum. with a sufficient energy separation from hypothetical structures to rule out polymorphism, are rare. The number of energetically feasible minima will obviously depend on the search method and force field. However. the main determinant is the molecule, as there is considerable similarity[18] between the low-energy hypothetical structures found by different methods with different force fields.

TREATMENT OF MOLECULAR FLEXIBILITY

The number of variables that need optimizing severely limits the degree of conformational flexibility in the types of molecules that can be studied. Many workers restrict their studies to molecules that can be reasonably assumed to be rigid. The gas-phase molecular structure is estimated by ab initio optimization, or sometimes molecular mechanics methods, and this molecular structure is kept fixed during the lattice energy minimizations. The molecular model can be taken from x-ray diffraction results, with suitable adjustment for the errors in locating the hydrogen atoms. for developing crystal structure prediction methodologies. However, the distortions in the molecular structure caused by the crystal environment will bias the calculated lattice energies toward the crystal structure used. It is clear[19]

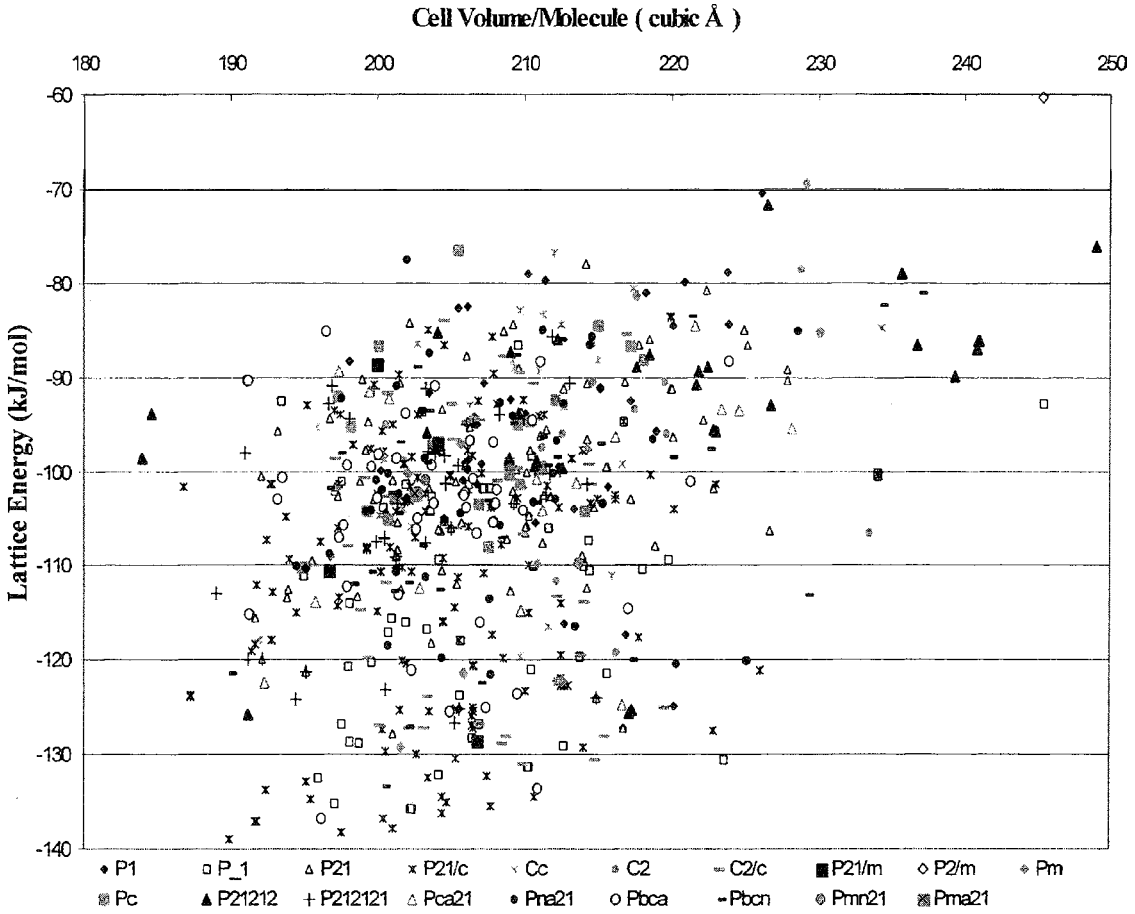

Fig. 1 A plot of the lattice energy minima found in the crystal structure prediction search for the rigid CHNO molecule in the 2001 blind test[18] (Fig. 4). in the search by Price. This diagram illustrates the plurality of distinct minima in different space groups found in a relatively sparse search. which did not locate the experimental structure.

that even minor distortions of the molecular structure, arising from crystal packing or experimental uncertainties, can change the calculated lattice energies significantly, compared with the lattice energy differences associated with polymorphism.

The other alternative is to use an intramolecular force field that allows the molecular structure to change torsion and bond angles and bond lengths in the course of the minimization. This is essential for considering flexible molecules like sugars. In this case, the lattice energy being optimized has to accurately represent the balance between the energetic cost for distorting the molecule and the intermolecular energy gain from, for example, improving the hydrogen bond geometry. In order to treat systems where conformational polymorphism is possible (i.e., there are low-energy molecular conformations with distinctly different molecular shapes), it is often prudent to start a search with each conformer, as the search/minimization procedure may not cross the intramolecular energy barrier effectively. Thus. crystal structure predictions for molecules with only one or two degrees of conformational freedom are currently considered challenging, but this will change with increasing computer power.

THE INTERMOLECULAR POTENTIAL

For all molecules, the reliability of the relative lattice energies for different hypothetical crystal structures depends on the accuracy of the intermolecular potential, and this is the key factor in the generation of the energetically feasible crystal structures. The range of molecules with crystal structures that can be predicted by lattice energy minimization is therefore limited to the ones for which a sufficient:~reliable potential is available. This is dependent

on the functional groups within the molecule. The lattice energies of different hypothetical crystal structures may be balancing van der Waals forces in different orientations with the energy differences between different types and orientations of hydrogen bonds and π – n stacking. A crystal structure can only be predicted as accurately as the lattice energy minimum closest to the experimental structure, which even with the best potentials. is likely to be only within a few percent in the cell dimensions because of the neglect of thermal effects. Because in most crystal structure prediction studies there are many structures within the energy range of possible polymorphism (c.f. Fig. 1), the desired accuracy in the relative lattice energies is often only a fraction of a kJ/mol. This provides a major challenge to the development of intermolecular potentials.[21,22] Empirically fitted model atom–atom potentials are often used, and the confidence in their accuracy increases with the number of crystal structures used in the fitting and testing. Because the accuracy of such empirical potentials is limited by the transferability of the parameters between different molecules, the parameters should be specific to the functional groups. For polar and hydrogen-bonding molecules. where the electrostatic contribution dominates the lattice energy and its orientation dependence, then the most accurate representations of the molecular charge distribution. such as distributed multipoles[21] or models with explicit lone pair or π electron point charges. are theoretically more reliable. The requirements of crystal structure prediction for accurate intermolecular and intermolecular potential are driving the development of increasingly accurate. elaborate, and computationally intensive methods of evaluating the inter-and intramolecular forces.[22] Improvements are envisaged even on the most elaborate force fields combined with ab initio intramolecular energies developed for sugars.''''

WHAT AWE THE RESULTS LIKE?

A survey[2] of ail the published crystal structure prediction papers in approximately the first decade of significant activity in this area reveals a considerable degree of success for lattice energy minimization methods over a range of types of molecules (Fig. 2). In approximately 250 searches for a particular polymorphic form, there was only a 10% reported failure rate to locate the structure: with the experimental structure being located as the global minimum in approximately half the cases (Fig. 3). However. these published studies were generally aimed at developing the methodology for specific types of molecules. and so the reported failures were generally within a

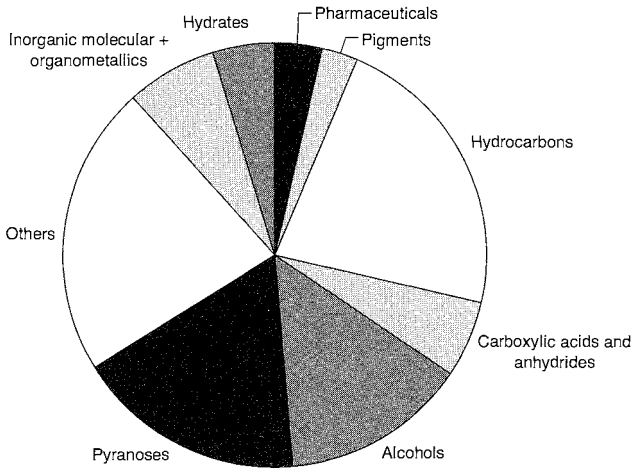

Fig. 2 The types of molecules studied in the first decade of crystal structure prediction. as derived from a survey of published lattice energy minimisation based studies.[2] Within each category, the molecules are generally the smaller and more rigid molecules whose published crystal structures are in common space groups with Z'=1.

sample of chemically similar molecules or in locating a particular polymorph. This literature will also not reflect the use of crystal structure prediction methods in industry. where predictions of feasible crystal structures for more complex molecules may be required to help solve particular problems in conjunction with experimental data. Suggested by Fig. 3 is that the ''global minimum'' assumption is useful but far from reliable, but this may reflect the makeup of the small sample as well as force field inadequacies. The molecules studied contained a large proportion of hydrocarbons and sugars, with nearly 30 known polymorphic systems, and hence, a low proportion of molecules that would be considered easy to predict or suitable for use in crystal engineering. It may be that more complex molecules, with irregular shapes and a well-defined hierarchy of functional group interactions may be more readily predicted as having a unique thermodynamically favored structure. For example, Pigment Yellow 74 (Hansa-Brillantgelb 5GX), which has two phenyl rings and a variety of nitrogen and oxygen functional groups producing four intramolecular hydrogen bonds, had its known experimental structure correctly predicted[1''''] as the global minimum. over 12 kJ/mol more stable than any hypothetical structures. Various syntheses and recrystallizations confirmed this prediction that no other polymorphic form is energetically feasible.

A more meaningful test of whether an arbitrary molecule can be genuinely predicted from its chemical diagram

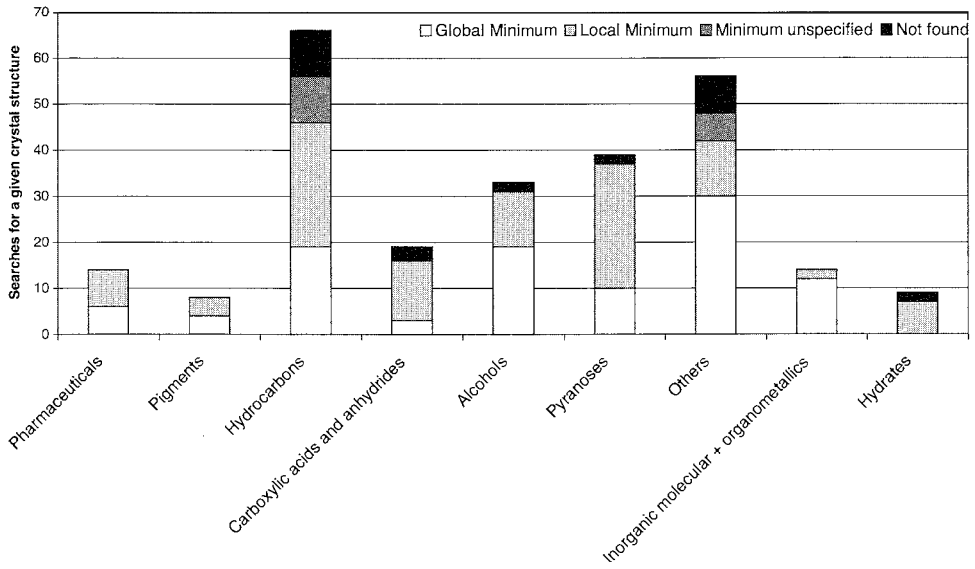

Fig. **3** The success rate of searches for a given crystal structure by lattice energy minimization, as derived from a survey of published studies.[2] The results are distinguished as to whether the known structure was found as the global or local minimum or not found. The number of searches significantly exceeds the 189 molecules categorized in Fig. 2. because of searches for polymorphic systems (where one structure is necessarily a local minimum) and where different groups have published a search for the same molecule.

is provided by the blind tests in 1999[17] and 2001,[18] organized by the Cambridge Crystallographic Data Centre. The participants were sent the chemical diagrams of the molecules. as in Fig. 4, which although arbitrarily chosen by an independent referee. fell into three categories within the capabilities of at least some of the programs. and thus illustrate the current limitations. One molecule was to be rigid with only C, H, N. or O atoms. another also rigid but allowing a wider range of atomic types as a test of force field development, and the third had a limited degree of conformational flexibility. The participants were allowed to submit up to three predictions per molecule of the crystal structure for comparison with the unpublished crystal structures. The success rate shown in Fig. 4 indicates that genuine crystal structure prediction is possible. However; the overall success rate was low. and might have seemed discouraging had a metastable polymorph not been characterized in 1999. It must be stressed that most of the participants correctly indicated a low level of confidence in their predictions, particularly when the search gave results such as in Fig. 1, where the energetic discrimination between different structures was very small compared with the expected accuracy of the force field.

It is. of course; possible to analyze the reasons for failure of a crystal structure prediction study using the experimental structure. The search is inadequate if it does not find the minimum obtained starting from the experimental structure, using the same force field. If this

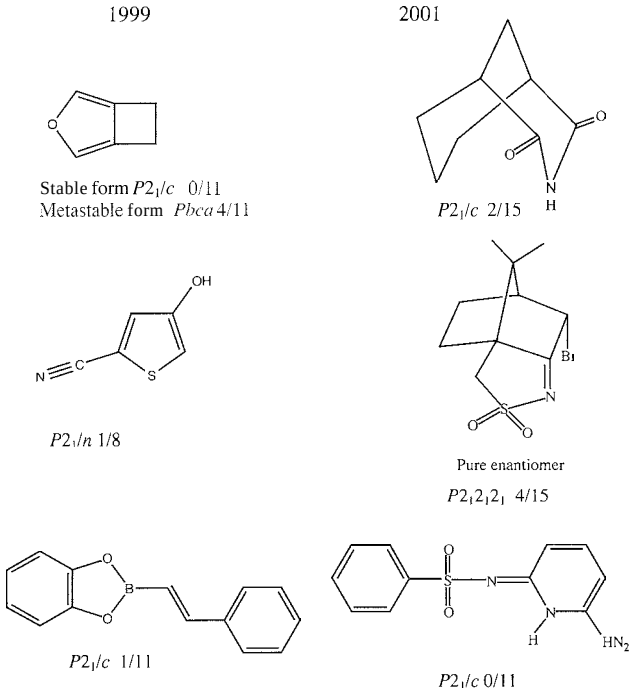

Fig. 4 The molecules used in the blind tests of crystal structure prediction, organized by the Cambridge Crystallographic Data Centre in 1999[17] and 2001.[18] For each molecule. the success rate is given as *x*/*y*, where *x* is the number of successful predictions, and *y* is the number of groups that submitted (usually) three guesses for the crystal structure.

minimum is not a good approximation to the experimental structure or is found to be considerably less stable than the global minimum, then the force field is inadequate. However. when this minimum is found among a plurality of minima within a few kcal/mol of the global minimum, then the observed polymorph could be metastable. In this case, it is probably a fundamental problem that there are more energetically feasible polymorphs than known structures. Improvements in the calculation of the relative thermodynamic stabilities of hypothetical crystal structures, and expansions of the search procedures, are definitely required. Some progress has been made in estimating entropic and zero-point energy contributions to the relative free energies of the crystal, using calculations of the lattice dynamical frequencies. Although the differences in these entropic terms are small, they may re-order structures that are approximately equi-energetic on lattice energy.[25] Further advances are anticipated in the future. However, the more fundamental problem is the limitations of the basic assumption that the observed crystal structure will correspond to the global minimum in the lattice energy.

BEYOND LATTICE ENERGY MIMIMIBIZATION—KINETIC EFFECTS

The phenomenon of polymorphism demonstrates that metastable crystal structures are observed, and it is not always obvious that such crystal structures are metastable. The energy differences between different polymorphs crystallized out of different solvent are small, and those between concomitant polymorphs presumably are very small. Kinetics must play a major role in determining which of the approximately equi-energetic hypothetical crystal structures are actually observed. How do the kinetics of nucleation and growth, and the variations with crystallization conditions. affect which thermodynamically feasible crystal structures are actually seen? How can this be incorporated in the crystal structure prediction model to produce a polymorph prediction model?

One approach is to assume that these kinetic factors are in some way represented in experimental crystal structures. Thus, analyses using the information in the Cambridge Structural Database were developed.[26,27] Although there have yet to be successful independent predictions by this method in the blind tests. this approach holds promise for discriminating among the hypothetical crystal structures within the energy range of potential polymorphism and force field uncertainty.

An alternative approach is to develop methods of calculating relative nucleation and growth rates, and their solvent dependence, for the hypothetical structures that are energetically feasible lattice energy minima. Thus, crystal structure prediction is pushing for further development of computational models. Preliminary attempts include estimating the mechanical properties of the hypothetical structures. Crystal structures that have an unphysically low resistance to shear can be eliminated as unlikely to be able to grow in competition with more mechanically stable crystallites.[9] The relative growth rates of the faces of the different hypothetical structures, as used to predict the morphologies of the crystals when the growing from the vapor by a birth and spread crystal growth mechanism, can be used to eliminate particularly slow-growing structures from being plausible polymorphs.[9] When there is a distinction in predicted growth rate among the low-energy structures, as observed for paracetamol[9] and pyridine,[25] the observed structures are favored. However. calculations on the kinetics of the crystal structure can only distinguish between the structures that readily nucleate. Thus, a method of predicting which crystal structures correspond to readily formed nuclei in different solvents would be a major step forward in polymorph prediction.

CONCLUSION

Crystal structure prediction is a technique that is in the relatively early stages of development. It is unlikely to become a reliabie method of predicting crystal structures, and particularly polymorphism, until our fundamental understanding of crystallization considerably improves. However, the methodology for generating energetically feasible hypothetical crystal structures for a molecule is well-developed, and foreseeable improvements in force fields and computational resources will allow such studies to be applied to an increasing range of molecules. When this extends to more of the molecules of interest in supramolecular chemistry. it may be found that when the molecular recognition is sufficiently strong, there will be one well-defined global minimum in the lattice energy. and the crystal structure will therefore be readily predictable.

Crystal structure prediction is already sufficiently mature to show the more subtle interplay between the nature and disposition of functional groups that determines which recognition motifs are feasible. For example, it demonstrates that the smaller carboxylic acids have low-energy minima corresponding to catemer and dimer structures, whereas benzoic acid has a significant energy preference for dimes-based structures. 5-Azauracil has a marked energy preference for forming a layer structure. which produces a more stable crystal[30] than is possible for 6-azauracil. where a variety of a three-dimensional

hydrogen-bonded networks are almost equi-energetic. The ability to generate a set of energetically feasible crystal structures will often be useful in understanding a given system. Although the ambitious goals of crystal structure prediction are only sometimes achieved. the calculations have the potential to be a valuable tool in developing supramolecular chemistry.

ACKNOWLEDGMENTS

The Cambridge Crystallographic Data Centre is thanked for arranging the blind tests. which advanced the area of crystal structure prediction and provided an objective test of the progress. My postgraduate students. Graeme Day and Theresa Beyer. are thanked for providing data for this article.

ARTICLES OF FURTHER INTEREST

The Cambridge Structural Database, p. *I41*
Crystal Growth Mechanisms, p. *364*
Hydrogen Bonding, p. *658*
π–π Interactions: Theory and Scope, p. 1076
Polymorphism, p. 1129
Space Groups and Crystal Packing Modes, p. 1337
van der Waals Forces, p. *1550*
X-Ray and Neutron Powder Diffraction, p. *1592*

REFERENCES

1. Gavezzotti. A. Are crystal-structures predictable? Acc. Chem. Res. 1994. 27 (10). 309–314.
2. Beyer. T.: Lewis. T.; Price, S.L. Which organic crystal structures are predictable by lattice energy minimisation? CrystEngComm 2001. *3* (44), 178–212. http://www.rsc.org/is/journals/current/crystengcomm/cecpub.htm.
3. Chin, D.N.: Palmore. G.T.R.; Whitesides. G.M. Predicting crystalline packing arrangements of molecules that form hydrogen-bonded tapes. J. Am. Chem. Soc. 1999.121 (10). 2115 -2122.
4. Pillardy, J.: Wawak, R.J.: Arnautova, U.A.: Czaplewski, C.: Scheraga. M.A. Crystal structure prediction by global optimization as a tool for evaluating potentials: Role of the dipole moment corsection term in successful predictions. J. Am. Chem. Soc. 2000. 122 (5). 907–921.
5. Schmidt. M.U.; Englert. U. Prediction of crystal structures. J. Chern. Soc. Dalton Trans. 1996. (10). 2077–2082.
6. Chaka, A.M.; Zaniewski. R.; Youngs, W.; Tessier, C.: Klopman, G. Predicting the crystal-structure of organic molecular materials. Acta Crystallogr., B 1996. 52 (1), 165–183.
7. Tajima, N.; Tanaka. T.; Arikawa. T.: Sakurai. T.: Teramae. S.: Hirano. T. A heuristic molecular-dynamics approach for the prediction of a molecular-crystal structure. Bull. Chem. Soc. Jpn. 1995. *68* (2). 519–527.
8. Holden. J.R.: Du. Z.Y.; Ammon. H.L. Prediction of possible crystal-structures for C-. H-. N-. O -and F-Containing Organic-Compounds. J. Comput. Chern. **1993**, 14 (4). 422–437.
9. Beyer. T.: Day. G.M.: Price, S.L. The prediction, morphology. and mechanical properties of the polymorphs of paracetamol. J. Am. Chem. Soc. 2001. 123. 5086–5094.
10. Williams. D.E. Ab initio molecular packing analysis. Acta Crystallogr.. A 1996. *52* (2), 326–328.
11. Perlstein, J. Introduction to Packing Patterns and Packing Energetics of Crystalline Self-Assembled Structures—Predicting Crystal Structures Using Kitaigorodskii's Aufbau Principle. In *Crystal Engineering: From Molecules and Crystals* to *Materials*: Braga. D.. Grepioni. F.. Orpen, A.G., Eds.; Kluwer: Dordrecht. 1999; Vol. 538. 23–42.
12. Dryabchenko. A.V.; Agafonov, V.: Davydov, V.A. A theoretical study of the pressure-induced dimerization of C-60 fullerene. J. Phys. Chem.. A 1999. *103* (15). 2812–2820.
13. Verwer. P.: Leusen. F.J.J. Computer Simulation to Predict Possible Crystal Polymorphs. In *Reviews in Computational Chemistry*; Lipkowitz, K.B., Boyd. D.B.. Eds.: Wiley-VCH: New Uork. 1998: Vol. 12, 327–365.
14. Gavezzotti. A. Generation of possible crystal-structures from the molecular-structure for lo\\-polarity organic-compounds. J. Am. Chem. Soc. 1991. *113* (12). 4622–4629.
15. Erk, P. Crystal Design: From Molecular to Application Properties. In *Crystal Engineering: From Molecules and Crystals* to *Materials*; Braga, D.. Crepioni, F.. Orpen, A.G., Eds.: Kluwer: Dordrechr. 1999; Vol. 538, 143–161.
16. van Eijck. B.P.; Kroon. J. Structure predictions allowing more than one molecule in the asymmetric unit. Acta Crystallogr., B 2000. *56,* 535–542.
17. Lommerse. J.P.M.: Motherwell, W.D.S.; Ammon, H.L.: Dunitz. J.D.; Gavezzotti. A.: Hofmann. D.W.M.; Leusen, F.J.J.; Mooij, W.T.M.: Price. S.L.: Schweizer. B.: Schmidt, M.U.; van Eijcli. B.P.: Verwer. P.: Williams. D.E. A test of crystal structure prediction of small organic molecules. Acta Cryst. B 2000. *56*, 697–714.
18. Motherwell, W.D.S.; Ammon, H.L.: Dunitz, J.D.; Dzyabchenko. A.; Erk, P.: Gavezzotti, A.: Hofmann. D.W.M.: Leusen, F.J.J.; Lommerse. J.P.M.; Mooij. W.T.M.: Price. S.L.: Scheraga, H.; Schweizer. B.: Schmidt. M.U.; van Eijck. B.P.: Verwer. P.: Williams. D.E. Crystal structure prediction of small organic molecules: A second blind test. Acta Cryst. B 2002, *B58*. 647–661.
19. Gavezzotti. A. Theoretical *Aspects* and *Computer Modeling of the Molecular Solid State*; John Wiley: Chichester. 1997.
20. Beyer. T.: Price. S.L. The errors in lattice energy minimisation studies: Sensitivity to experimental variations in the molecular structure of paracetamol. CrystEngComm

2000. 2 (34); 183–190. http://www.rsc.org/is/journals/current/crystengcomm/cecpub.htm.

21. Stone, A.J. The Theory *of Intermolecular* Forces; Clarendon Press: Oxford. 1996.
22. Price, S.L. Toward More Accurate Model Intermolecular Potentials for Organic Molecules. In *Reviews* in *Computational* Chemistry; Lipkopwitz, K.B., Royd, D.B., Eds.; John Wiley & Sons: New York, 2000: Vol. 14, 225–289.
23. van Eijck, B.P.; Mooij, W.T.M.; Kroon, J. Ab initio crystal structure predictions for flexible hydrogen-bonded molecules. Part II. Accurate energy minimization. J. Comput. Chem. 2001, 22 (X), 805–815.
24. Schmidt, M.U. Energy Minimisation as a Tool for Crystal Structure Determination of Industrial Pigments. In *Crystal Engineering: From Molecules* and *Crystals to Materials*; Braga, D.. Grepioni. F., Orpen, A., Eds.; Kluwer: Dordrecht, 1999; Vol. 538, 331–348.
25. Anghel. A.T.: Day, G.M.; Price, S.L. A study of the known and hypothetical crystal structures of pyridine. Why are there four molecules in the asymmetric unit cell? CrystEngComm 2002, 4, 348- 355.
26. Motherwell, W.D.S. Crystal structure prediction and the Cambridge Structural Database. Mol. Crystals Liq. Crystals 2001. *356*, 559 567.
27. Apostolakis, J.; Hofmann, D.W.M.; Lengauer, T. Derivation of a scoring function for crystal structure prediction. Acta Crystallogr., A 2001. *57*, 442–450.
28. Sarma, J.; Desiraju, G.R. The supramolecular synthon approach to crystal structure prediction. Cryst. Growth Des. 2002, 2 (2), 93–100.
29. Beyer, T.; Price, S.L. Dimer or catemer? Low-energy crystal packings for small carboxylic acids. J. Phys. Chem., B 2000, 104 (12), 2647–2655.
30. Potter, B.S.; Palmer, R.A.; Withnall, R.; Chowdhry, B.Z.; Price, S.L. Aza analogues of nucleic acid bases: Experimental determination and computational prediction of the crystal structure of anhydrous 5-azauracil. J. Mol. Struct. 1999, 485 486, 349–361.

Crystalline Microporous Silicas

Hermann Gies
Bernd Marler
Ruhr-Universität Bochum, Bochum, Germany

INTRODUCTION

Crystalline microporous silicas, the porosils, are a family of materials based on [TO_4] units with tetrahedral densities below 21 T-atoms per 1000 $Å^3$, which are synthesized in the presence of teinplating guest molecules. Their silica host frameworks are three-dimensionally four-connected, and in their calcined form, they belong to the large family of silica polymorphs. Porosils with pore openings too small to let the occluded guest molecules out are called clathrasils; porosils in which the guests can be removed are called zeosils.

In the course of synthesis, the template molecules act as structure-directing agents. Size and shape of the ternplate determines the geometry of the pore. During crystallization. the amphiphilic nature of the template (mainly organic amines) allows for molecular interaction between the aqueous silicate solution and the growing hydrophobic silica framework. Thermodynamic analyses suggest that the kinetics of nucleation are the most important factors in the crystallization process.

Experiments employing model systems show that nanoblocks of ~10 Å organize to macroscopic crystals in a second stage. However, there is still no deep understanding of the synthesis of crystalline microporous silicas.

The impact of computer modeling on development in the field is increasing. Databases store all possible tetrahedral frameworks. More detailed analyses allow for the optimization of the host–guest interaction for the synthesis of new materials. Finally, molecular dynamic calculations potentially show the molecular details of the nucleation and crystallization of micropoi-ous crystals. This article lists the most important geometric and crystallographic properties, points out possible applications of microporous silicas, summarizes the recent developments; and presents ideas for future progress in the field.

MICROPOROSITY IN FRAMEWORK SILICAS

The highly covalent nature of the Si—O bond in silicas, SiO_2, with tetrahedral silicon coordinated by oxygen, [SiO_4], leads to open, three-dimensional bonding networks. Silica polymorphs with high densities have Si in octahedral coordination and are natural or synthetic high-pressure phases with oxygen in close-packed arrangements. As an example, the crystal structure of stishovite. one of the densest naturally occurring silica minerals, can be seen as distorted hexagonally close-packed array of O atoms with Si in octahedral interstices. Its density is $\rho=4.28$. The naturally occurring silica minerals quartz. cristobalite, etc.. are crystalline solids with tetrahedrally coordinated Si, and they have densities of less than 60% compared to high-pressure phases. There are also the microcrystalline silicas, like opals, chalcedon. etc., and the amorphous silicas. such as lechatelierite, hyalite, and opal AG (gemstone opal), the latter two containing water. which possess three-dimensional bonding networks with densities even below that of tridymite. the least dense natural crystalline polymorph of silica ($\rho=2.27$). Their density is $p-2.1$, which corresponds to approximately 21 tetrahedral units [SiO_4] per 1000 $Å^3$. The composition independent value was introduced as framework density. FD. However, none of these silicas is porous in the sense of having accessible pore space. By definition, porous structures have framework densities below 21 T-atoms (T=tetrahedral) per 1000 Å', which leads to open space within the silica framework wide enough for the incorporation of guest molecules. If the size of the pore opening in these materials is less than 20 A, they are microporous; in the range between 20 and 1000 Å. they are mesoporous; and finally. above 1000 Å, the macropore regime begins. The crystalline porous silicas, the topic of this article, typically are microporous and contain guest molecules as templates for their pores in the as-made form. which can be exchanged or removed by thermal treatment to render all-silica porous framework structures, the porosils. A compilation of all crystalline and noncrystalline silicas is given in Table 1.[1,2]

The crystalline microporous silicas. [SiO_2]·(template), (Tables 2a and 2b) are considered solid solution end members of aluminosilicate zeolites, $(cation)^{x+}[Al_xSi_{1-x}O_2]^{x-}$ (nonframework constitutents). The topology of the host framework is the same. however, the composition and, with it. the properties, are distinct for every material. A

Encyclopedia of Supramolecular Chemistn
DOI: 10.1081/E-ESMC 120012795

Table 1 List of silica materials arranged according to their density

Silica material!	Density [g/cm^3]	Structural characteristics	CN* of Si
Baddeleyite-type	4.30	Dense. crystalline	6
α-PbO_2-type	4.30		
$CaCl_2$-type	Not determined		
3 x 2 zigzag chain form	1.29		
Stishovite	4.28		
Fe_2N-type	4.27		
Coesite	2.92	Dense, crystalline	4
Quartz	2.65		
Keatite	2.50		
Cristobalite	2.32		
Tridymite	2.26–2.28		
Silica-W	ca. 1.97		
Moganite	2.55	Dense, microcrystalline (1–8 wt% lion-essential water)'	4
Opal-C	2.1–2.2		
Opal-CT	1.9–2.1		
Opal-A_N (Hyalite)	2.1–2.2	Dense. noncrystalline (3–8 wt% noo-essential water)'	4
Opal-AG	1.9–2.5		
Silica glass	2.20	Dense, noncrystalline	4
Porosils	**1.5–2.1**	**Microporous, crystalline**	**4**
MCM-48 (3D-Channels)	ca. 1.0	Mesoporous, ordered pore structure	4
MCM-41 (1D-Channels)	ca. 1.0	Silanol group water (ca 10 wt%)	
SBA-1 (cage-like)	ca. 1.0		
SBA-2 (cage-like)	ca. 1.0		

*CN = coordination number.
#Molecular water and silanol group water located at interstices of the microstructure and as structural defects.

complete survey of all known *zeolite host frameworks, including the* crystalline *rnicroporous silicas, is given in the Atlas of* Zeolite *Framework* Types[3] *or on the Internet in the zeolite database.'" Every framework* type *has a three-letter code (approved by* IUPAC) *to which* it will *be referred.* In this *article. only the* family *of crystalline rnicroporous silicas is* dealt *with.*

The Porosils

The porosils comprise *all crystalline microporous silicas with framework densities of* less *than 21.* In all *three-dimensional silica frameworks, the* [SiO_4] *tetrahedral building units are four-connected. Ieading to* electroneutral *three-dimensional* host *framework structures. The calcined crystals are colorless and hydrophobic. The hardnesses* of *the microporous silicas are similar to that of quartz. The refractive indices of* the *different crystalline phases are directly* correlated *with the frainework* density, *as expected from the general refractivity* equation.[5] *The framework density varies between 20.9 and* 15.0 *T*-atoms/1000 Å^3, *which is equivalent to density values between* $\rho = 2.1$ *and* $\rho = 1.5$. *The family of porosils is further subdivided in claihrasiis* and *zeosils, depending on their pore openings. The microporous silicas with maximum pore openings confined by six tetrahedral* [SiO_4] *units, six membered rings* (6 *MR). corresponding to pore diameters of less than 2.5* Å, *are called clathrasiis. They cannot exchange the templating guest molecules without the guest's* decomposition. Also, *sorption is restricted to the smallest molecules, such as* H_2 *or Ar. The zeosils, in contrast,* have *pore openings greater than 2.5 A, confined by 7–14 MR. Here, the whole. undamaged guest species* might *be removed by exchange or thermal processes, making the* pore volume *available for sorbates for various purposes.*

With the exception of the mineral *melanophlogite, all porosils are synthetic products. All porosils were directly* synthesized *with structure-directing agents (SDA) as templates, in general, organic* molecules. *There are a few* more *cases where postsynthesis treatment of* aluminosilicate *zeolites leads to the complete* dealumination *of silicate* framework *structures, yielding all-silica*

Table 2a Structural properties of clathrasils

Clathrasil	Zeolite framework type	Framework density*	Composition per unit cell	Type of cage	Max. possible symmetry of the cage	Approx. volume of the cage
MCM-35	MTF	20.9	$44[SiO_2]\cdot 8M^8 2M^{16}$§	$[5^8]$	mm2	25 Å^3
				$[4^2 5^8 6^2 8^4]$#	2/m	300 Å^3
Silica-RUB-10	RUT	18.1	$36[SiO_2]\cdot 2M^{10} 4M^{16}$	$[4^4 5^4 6^2]$	2111	35 Å^3
				$[4^4 5^6 6^5 8^1]$	m	250 Å^3
Melanophlogite	MEP	17.9	$46[SiO_2]\cdot 2M^{12} 6M^{14}$	$[5^{12}]$	m3	80 Å^3
				$[5^{12} 6^2]$	4m2	160 Å^3
Decadodecasil 3R	DDR	17.8	$120[SiO_2]\cdot 6M^{10} 9M^{12} 3M^{19}$	$[4^3 5^6 6^1]$	3m	35 Å^3
				$[5^{12}]$	m3	80 Å^3
				$[4^3 5^{12} 6^1 8^3]$	3m	350 Å^3
Decadodecasil 3H		17.8	$120[SiO_2]\cdot$- $6M^{10} 9M^{12} 1M^{15} 4M^{19} 1M^{23}$	$[4^3 5^6 6^1]$	3m	35 Å^3
				$[5^{12}]$	m3	80 Å^3
				$[4^6 5^6 8^3]$	62m	230 Å^3
				$[4^3 5^{12} 6^1 8^3]$	3m	350 Å^3
				$[5^{18} 6^2 8^3]$	6/mmm	540 Å^3
Nonasil	NON	17.6	$88[SiO_2]\cdot 8M^8 8M^9 4M^{20}$	$[5^4 6^4]$	222	25 Å^3
				$[4^1 5^8]$	mm2	30 Å^3
				$[5^8 6^{12}]$	mmm	290 Å^3
Sigma-2	SCT	17.5	$64[SiO_2]\cdot 8M^9 4M^{20}$	$[4^3 5^6]$	mm2	25 Å^3
				$[5^{12} 6^8]$(SGT)	4m2	390 Å^3
Dodecasil 3C	MTN	17.3	$132[SiO_2]\cdot 16M^{12} 8M^{16}$	$[5^{12}]$	m3	80 Å^3
				$[5^{12} 6^4]$	m3	240 Å^3
RUB-3	RTE	17.2	$24[SiO_2]\cdot 2M^8 2M^{18}$	$[4^4 5^4 6^2]$	mmm	35Å^3
				$[4^6 5^4 6^6 8^2]$	2/m	300 Å^3
Dodecasil 1H	DOH	16.9	$34[SiO_2]\cdot 3M^{12} 2M^{12'} 1M^{20}$	$[5^{12}]$	m3	80 Å^3
				$[4^3 5^6 6^3]$	62m	70 Å^3
				$[5^{12} 6^8]$(DOH)	6/mmm	430 Å^3
Silica-sodalite	SOD	16.5	$12[SiO_2]\cdot 2M^{14}$	$[4^6 6^8]$	m3m	130 Å^3
Silica-RUB-13	RTH	16.0	$24[SiO_2]\cdot 2M^8 2M^{22}$	$[4^4 5^4]$	mm2	20 Å^3
				$[4^6 5^8 6^4 8^4]$	mm2	500 Å^3
Octadecasil	AST	15.9	$20[SiO_2]\cdot 2M^6 2M^{18}$	$[4^6]$	4/mmm	5 Å^3
				$[4^6 6^{12}]$	4/mmm	280 Å^3
NU-3	LEV	15.8	$54[SiO_2]\cdot 3M^8 6M^{14}$	$[4^6 6^2]$	6/mmm	10 Å^3
				$[4^9 6^5 8^3]$	3m	300 Å^3
ITQ-3	ITE	15.7	$64[SiO_2]\cdot 2M^8 2M^{22}$	$[4^4 5^4]$	mm2	20 Å^3
				$[4^6 5^8 6^4 8^4]$	mm2	500 Å^3
Silica-chabazite	CHA	15.0	$36[SiO_2]\cdot 2M^8 2M^{20}$	$[4^6 6^2]$	6/mmm	10 Å^3
				$[4^{12} 6^2 8^6]$	3m	260 Å^3

*Number of Si atoms per 1000Å^3 based on idealized cell constants.
§M^n = cage like void (polyhedron) confined by n faces.
#$[4^2 5^8 6^2 8^4]$ is a 16-hedron built by two 4-membered rings. eight 5-mernhered rings. two 6-membered rings and four 8-membered rings.
(From Refs. [3,4].)

composition materials that are otherwise not accessible. For reasons of systematics, those are not included in this compilation.

Recently, a mathematical, rigorous enumeration of all possible tetrahedral networks (three-dimensional four-connected nets) in three-dimensional space was presented.[6] This included all existing and hypothetical porosil framework structure types. Geometrically feasible models are potential candidates for new framework structure types, provided a suitable SDA can be made.

Clathrasils

The silica frameworks of the clathrasil family are built from cage-like polyhedral structural subunits containing the guest molecules (Fig. 1). The cages are bound by

Table 2b Structural properties of zeosils

Zeosil	Zeolite framework type	Framework density*	Composition per unit cell	Type of channel	Approx. cross section of the limiting pore [Å]	Dimensionality of the pore system
MCM-35	MTF	20.9	44[SiO_2]·P8MR[§]	8-MR	3.9 × 3.6	1-D
VPI-8	VET	20.5	17[SiO_2]·P12MR	12-MR	5.9 × 5.9	1-D
Silica-ZSM-48	—	Ca. 19.9	48[SiO_2]·P10MR	10-MR	5.6 × 5.3	1-D
Silica-ZSM-5	MFI	18.5	96[SiO_2]·P10MR·P10′MR	10-MR	5.6 × 5.3	3-D
				10-MR	5.5 × 5.1	
Silica-ZSM-12	MTW	18.1	56[SiO_2]·P12MR	12-MR	6.0 × 5.6	1-D
Silica-ZSM-23	MTT	18.1	24[SiO_2]·P10MR	10-MR	5.2 × 4.5	1-D
Silica-theta-1	TON	18.0	24[SiO_2]·P10MR	10-MR	5.5 × 4.4	1-D
Decadodecasil 3R	DDR	17.8	120[SiO_2]·P8MR	8-MR	4.4 × 3.6	2-D
Decadodecasil 3H	—	Ca. 17.8	120[SiO_2]·P8MR	8-MR	4.4 × 3.8	2-D
Silica-SSZ-44	SFF	17.8	32[SiO_2]·P10MR	10-MR	5.4 × 5.7	1-D
Silica-ferrierite	FER	17.7	36[SiO_2]·P8MR·P10MR	8-MR	4.8 × 3.5	2-D
				10-MR	5.4 × 4.2	
SSZ-48	SFE	17.6	14[SiO_2]·P12MR	12-MR	5.4 × 7.6	1-D
Silica-ZSM-11	MEL	17.3	96[SiO_2]·P10MR	10-MR	5.4 × 5.3	2-D
ITQ-4	IFR	17.3	32[SiO_2]·P12MR	12-MR	7.2 × 6.2	1-D
RUB-3	RTE	17.2	24[SiO_2]·P8MR	8-MR	4.4 × 3.7	1-D
Silica-mordenite	MOR	17.1	64[SiO_2]·P8MR·P8′MR·P12′MR	8-MR	3.4 × 4.8	2-D
				8-MR	5.7 × 2.6	
				12-MR	7.0 × 6.5	
UTD-1F	DON	17.0	64[SiO_2]·P14MR	14-MR	8.2 × 8.1	1-D
Silica-SSZ-24	AFI	16.9	24[SiO_2]·P12MR	12-MR	7.3 × 7.3	1-D
SSZ-23	STT	16.8	64[SiO_2]·P7MR·P9MR	7-MR	3.5 × 2.4	2-D
				9-MR	5.3 × 3.7	
Silica-SSZ-35	STF	16.8	16[SiO_2]·P10MR	10-MR	5.4 × 5.7	1-D
CIT-5	CFI	16.6	32[SiO_2]·P14MR	14-MR	7.5 × 7.2	1-D
SSZ-55	ATS	16.1	24[SiO_2]·P12MR	12-MR	6.5 × 7.5	1-D
Silica-RUB-13	RTH	16.0	32[SiO_2]·P8MR·P8′MR	8-MR	3.8 × 4.1	2-D
				8-MR	5.6 × 2.5	
Silica-GUS-1	CON	15.9	32[SiO_2]·P12MR	12-MR	6.8 × 5.4	1-D
Silica-MCM-22	MWW	15.9	72[SiO_2]·P10MR·P10′MR	10-MR	5.5 × 4.0	2-D
				10-MR	5.1 × 4.1	
NU-3	LEV	15.8	54[SiO_2]·P8MR	8-MR	4.8 × 3.6	2-D
ITQ-3	ITE	15.7	64[SiO_2]·P8MR·P8′MR	8-MR	3.8 × 4.3	2-D
				8-MR	5.8 × 2.7	
Silica-beta	BEA	15.4	64[SiO_2]·P12MR·P12′MR	12-MR	5.6 × 5.6	3-D
				12-MR	7.6 × 6.6	
ITQ-14	BEC	15.1	64[SiO_2]·P12MR·P12′MR	12-MR	6.9 × 6.0	3-D
				12-MR	7.5 × 6.3	
ITQ-7	ISV	15.0	64[SiO_2]·P12MR·P12′MR	12-MR	6.1 × 6.5	3-D
				12-MR	5.9 × 6.6	
Silica-chabasite	CHA	15.0	36[SiO_2]·P8MR	8-MR	3.8 × 3.8	3-D

*Number of Si atoms per 1000 Å^3 based on idealized cell constants.
[§]PxMR = channel like void with a cross section which is defined by an x-membered ring of $[TO]_4$ units.
(From Refs. [3,4].)

polygons with 4-, 5-. or 6-tetrahedral $[SiO]_4$ units. i.e., 4, 5, or 6 MR. With the exception of silica sodalite (SOD), all clathrasils known so far are composed of more than one type of cage (Table 2a). In general, the biggest cage contains as template the SDA, whereas the smaller cages are occupied by help guest species (e.g., N_2, Ar) or are empty. The size and shape of the cage reflect the size and shape of the SDA. Because of the electroneutral nature of the silica framework, the interaction with the SDA is weak, at least in the completed structure. Among the clathrasil structures, the smallest cage containing a SDA is the $[5^{12}]$ cage, the pentagonal dodecahedron. with 90 Å^3:

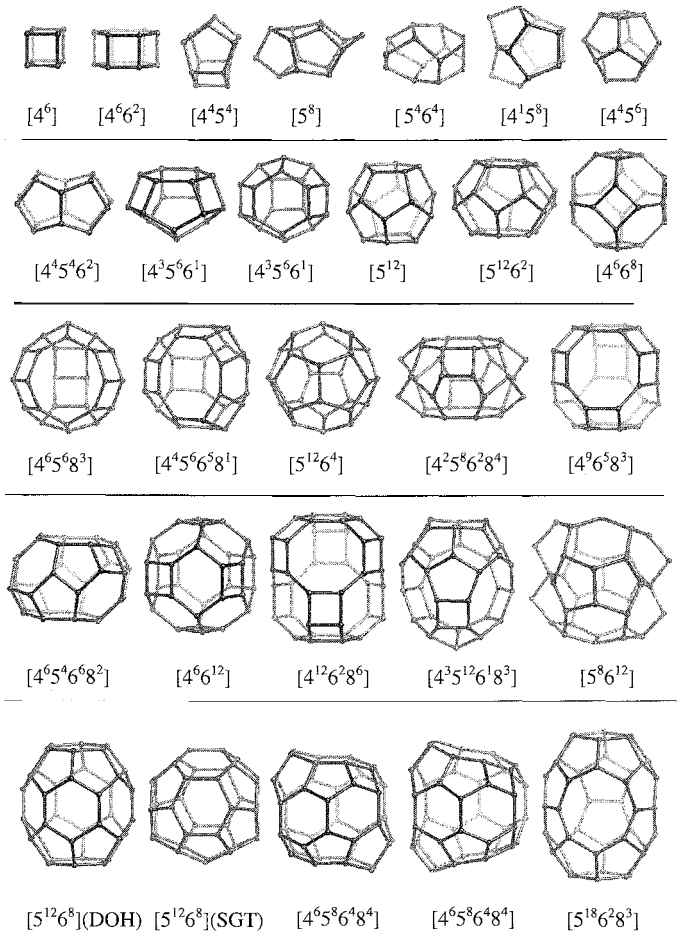

Fig. 1 Compilation of cage-like voids observed in clathrasils. For more information on the cage properties and the symbols used see Table 2a. (*View this art in color at www.dekker.com.*)

the biggest found so *far is the* $[5^{18}6^2 8^3]$, *with 560* Å^3 *as free cage volume in the framework of* DD3H. *The silica* framework *of* the *clathrasils* is *thermally stable,* e.g., *dodecasil 3C (MTN) was held for more than 3 months at* 950°C. *In* DTA *analyses. the framework breakdown was observed above 1000°C for melanophlogite, dodecasil 3C. dodecasil* 1H, *and decadodecasil 3R when heating with a* 5°/min *heating rate. Because of* the *high thermal resistance. all clathrasils* were *calcined successfully and obtained as* pure porous *silicas. This leads* to *a reduction of* the symmetry *caused by distortion of the silica framework through cooperatively tilting the rigid* $[SiO_4]$ *unit for* melanophlogite, *sodalite, and dodecasil* 3C, *whereas no lowering of the space group symmetry was observed for the other clathrasils. At higher* tempertures, *the distorted silica frameworks undergo a* displacive *phase transition to the highest possible space group symmetry for* the given *framework topology. Surprisingly. the silica frameworks of all clathrasiis in their highest symmetry forms contract when raising the temperature above the phase-transition temperature. The thermal* contraction *is* in the *order of* $\alpha \sim -1*10^{-6}$ *over a wide* temperature *range. in the case of dodecasil 3C. between 100°C* and 1000°C, *before an expansion of the* unit *cell sets in* again.[7]

The study of the morphology of the clathrasils shows that ail materials *synthesized so far crystallize with a typical crystal morphology. Because the crystal growth faces developed grow slowest;* they *are indicative for the rate-determining step* in *crystal growth. All* morphologies *studied so far show* dominant *faces, ivhere the cage containing the SDA* is *involved in high concentration. This indicates that the trapping of the SDA on the respective growth face is the rate-limiting* step *for the progress of crystal* growth.[8]

Zeosils

The typical structural feature of a zeosil is *channel-like voids in the silica framework that extend in one* dimension *or intersect to* two- *or* three-dimensional *channel*

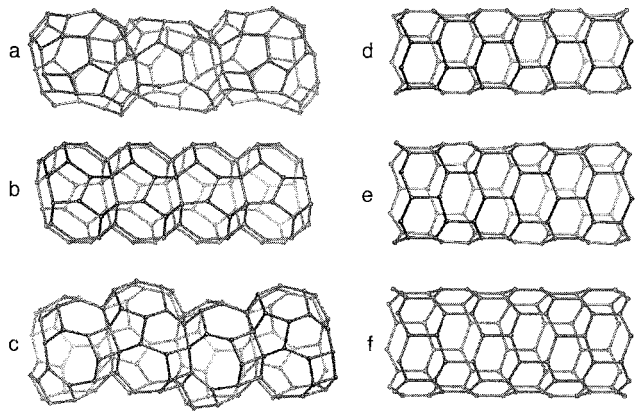

Fig. 2 Typical channel-like voids observed in zeosils of different framework structure type. The channel-like voids possess pore openings limited by n-membered rings (nMR) a) 7MR of the STT type, b) 8MR of the RTE type, c) 9MR of the STT type. d) 10MR of the Silica ZSM-48, e) 12MR of the AFI type. f) 14MR of the DON type. (*View this art in color at www.dekker.com.*)

systems Fig. 2). The channel opening is confined by 7 MR (2.4 * 3.5 A. SSZ-23) at least. The widest channel has 14 tetrahedral units. with a free diameter of ~8.2 Å for UTD-1. The typical SDAs for zeosils are molecules that extend in one or two dimensions. As for the clathrasils, the pore geometry reflects the molecular shape of the SDA. After calcination at moderate temperatures, the channel pores are accessible for suitable sorbate molecules. In general, the physical and chemical properties of porosils are comparable to those of clathrasils—they are transparent. colorless, hard, thermally resistant, have negative thermal expansion coefficients in a wide temperature regime, and show typical crystal morphologies. As an example, zeosils with a one-dimensional channel system always crystallize in a needle morphology. with the needle axis parallel to the channel pore. As already discussed for clathrasils. the growth-limiting step is the formation of a new channel by trapping the SDA along the needle axis.[8]

In contrast to zeolites. which are porous aluminosilicates. water does not enter the zeosil pore; however. hydrophobic molecules of appropriate size are readily taken up. The hydrophobicity index characterizes this property. The materials are useful for the separation of hydrophobic, nonpolar, or aprotic molecules in the presence of water in the liquid and gaseous states. As an example. the zeosil DD3R was a candidate for the separation of CO_2 in the presence of moisture for air-conditioning in spacecrafts.

The accessibility of the pore space of zeosils was also used for the encapsulation of functional molecules inside the silica matrix. Because the channels are anisotropic and provide a mold for molecules with polar properties, they are ideally suited as supports. Dipolar molecules will line up inside the channel, create polar symmetry, and might imprint interesting properties on the composite material, e.g., nonlinear optical properties. Dye molecules can be arranged within the silica matrix in favorable distances. so that their dipolar interactions can be used for light harvesting, and magnetic nanocrystals might be deposited inside zeosil matrix in well-defined sites.[9]

Silica is a material with a low dielectric constant of k—4.0. In order to increase the packing density between multilevel interconnects, new. ultralow-k inaterials are needed. Because k decreases with decreasing density, crystalline and noncrystalline porous silicas with DK as low as $k<2.0$ were introduced to replace the current wire insulators in microelectronics for multilayer devices. Because of their low density, ordered mesoporous materials are used for practical purposes.[10]

SYNTHESIS OF POROSILS

Mechanism of Porosil Synthesis

Porosils are synthesized using hydrothermal techniques in the typical temperature range of 140–200°C in the presence of SDA. Here. the SDA act as templates for the formation of the pores in the silica framework.'"] Therefore. the as-synthesized porosil is not porous but is a composite material that contains molecular or ionic species inside a crystalline silica framework. The bonding interaction between host and guest is of van der Waals type and is weak. Although research on crystalline porous materials, including porosils, is more than 50 years old. and there are several hundreds of examples of host–guest pairs for porosils only, the principles of the early stages of formation are poorly understood. From the thermodynamic standpoint, the porous silica frameworks are between 4–14 kJ/mol SiO_2 metastable with respect to quartz and similar to amorphous silica and silica glasses.[12] The thermal energy at 150°C, a typical synthesis temperature. is 3.5 kJ/mol, so the formation of crystalline porous silicas from amorphous silica sources is not generally hindered. However. in order to understand the details of the nucleation process. the interaction of solvent. silica, and organic template must be taken into account. The analysis shows that the seif-assembly process depends upon a delicate interplay between a large number of weak interactions. The thermodynamic analysis suggests that the kinetic factors are of major importance, and the kinetics of nucleation are likely to be the critical factors in determining the material obtained from a particular preparation."[3,14]

It is difficult to experimentally identify the molecular structure of the critical species from which crystal growth continues to bulk dimensions. One approach is to use the crystal structure analysis of the as-made material. including the guest species, as a protocol of the synthesis process. Using fragments of the structure as building blocks from which the porosil framework can be made, a rational model can be developed and tested against experimental evidence from syntheses experience. This concept was used to enumerate so-called secondary building units (SBU),[3] from which a particular structure can be built entirely. However, the building blocks are not framework-specific, and one SBU-type can be used to construct different porosil structures. Recently. a number of studies on the nucleation, seed formation. and crystal growth of silicalite were presented.[15–17] Over several orders of magnitude, starting from the species in solutions until the coherently scattering crystals, the formation of the silicate framework was monitored. Under the conditions of a clear. homogeneous starting solution. the formation of nanoblocks of $\sim$10 Å under synthesis conditions was postulated. These nanoblocks then assemble to three-dimensional periodic crystals.[17] The model as the general mechanism of nucleation is discussed controversially. However, for the specific synthesis conditions of the model system, nanoblocks containing the templating species play a crucial role in the development of the extended silicate framework.

On the other hand. silicate oligomers in aqueous solution were analyzed for their potentials as structure precursors.[18] The multitude of silicate species in solution and the complicated equilibrium between different oligomers, however, make it impossible to unambiguously identify those species involved in seed formation. In an attempt to identify silicate species attached to SDA molecules in solution. it was shown that there is no distinct structural entity as an SDA/silicate complex, but silicate oligomers segregate close to the organic guest species. matching the charge, size, and shape of the template.[19]

Computer modeling also offers the opportunity to investigate the nucleation process. A new approach was described.[20] Instead of starting with structural subunits typical for porous silicas. a random arrangement of silicate monomers and solvent describing the synthesis solution was observed over time, however, without the template present. For temperature and pressure conditions typical for silicate synthesis and using Monte Carlo techniques. the silicate cluster forination was studied. The analysis showed that condensation reaction in the computational procedure was sensitive to pH and silica concentration. which is in agreement with the experiment. Critical clusters were calculated to have 25–50 Si atoms. In addition. the geometrical analysis of the cluster showed a close relationship to structural units of dense silicas. In the future, it is hoped that the calculations. run in the presence of templates. will yield clusters that resemble subunits of zeolite framework structures.

Synthesis Rules for Porosil Synthesis

Based on wide experimental experience, a set of rules for porosil synthesis was established that characterizes the fundamental relation of host and guest in a descriptive and intuitive way. There are general physical and chemical properties an SDA must possess. It must be stable under the conditions of synthesis. physically and chemically. Because the solvent for synthesis is water, the SDA should be soluble. however, it must not hydrolyze. Most guest molecules are rigid or have a limited nuinber of conformer states. The basic organic amines and ammonium coinpounds comprise the group of molecules most successfully used as SDA. They are soluble in water, stable under the conditions of synthesis. and because of their basicity. dissolve silicates. If used as ammonium fluorides. the anion. in addition, acts as a help species in a multifunctional way. Fluoride is a common mineralizer and enhances the solubility of silicates. In the presence of fluoride, porosils were synthesized even in acidic conditions. In addition, the anion has properties of an SDA or help species, because it is often incorporated in the small cavities of porosils (Fig. 3a). leading to the stabilization of materials otherwise not accessible. The characteristic property of organic amines as SDA is their amphiphilic nature. They are hydrophilic at the N-carrying head group and hydrophobic at the hydrocarbon tail. This specific property. the positive ionic charge in the protonated form. and the basicity of the SDA lead to pairwise interaction with the anionic silicate species in solution responsible for the nucleation process. Once the critical size of the nucleus is reached, growth determines the progress of crystallization. The amphiphilic property of the SDA matches the dominant growth faces of the porosils. because they consist of hydrophobic parts, e.g., half-complete cavities and channels where the internal silica surface is already complete, and of hydrophilic parts where silanol groups terminate the growing host framework. The role of the SDA now is to fill the developing pore with the hydrophobic tail and to interact with the solvent. the silicate species in solution, and the silanol groups of the silicate framework. At the interface between framework and solution. the N-carrying head group of the amine that can easily be protonated and deprotonated, probably acts as a catalyst for the condensation of the silicate species in solution and the

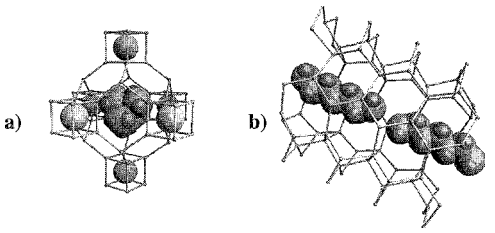

Fig. 3 a) Section of the structure of octadecasil (zeolite framework type: AST) showing the isometric tetramethylammonium cation as the guest species occluded in the $[4^6 6^{12}]$-cage and the fluoride anion occupying the small $[4^6]$-cage. b) The channel-like void of Silica-theta-I (zeolite framework type: TON) possessing a LO-membered ring pore opening and being occupied by a chain-like amine. (*View this art in color- at www.dekker.com.*)

silanol groups of the framework. The continuing condensation process of the silicate species finally traps the SDA inside the pore. In a series of AFM studies of zeolite crystal growth, this picture is convincingly supported. On growth surfaces, terrace steps are observed that are higher than one atomic layer but are of the same height as the characteristic, SDA-containing structural subunits.[''']

SDA for Clathrasils

As explained above. most clathrasils are built from several types of cages with different volumes. The SDA occupies the cage characteristic for a framework structure type: the framework-specific cage. The cage-like voids of the clathrasils require isometric SDA of appropriate size and shape (Fig. 3a).[11] Size and shape are the dominant attributes of tlte SDA. In general, the SDA interacts as a template only weakly with the host framework through van der Waals forces. Therefore. different SDA function as templates for one framework structure type. e.g., there are 26 SDA known for the synthesis of dodecasil 3C (Fig. 4a). On the other hand. a number of SDA stabilize different framework structure types (Fig. 4b) under different conditions of synthesis; occupying cages of different volumes. At lower synthesis temperature and higher pressures. the cage volume of the framework-specific cage is smaller for the SDA than at a higher synthesis temperature and lower pressure, respectively. Although there are a large number of hypothetical framework structure types. with bonding geometries comparable with the known clathrasil phases, only a limited selection was synthesized. Despite all efforts with computer modeling, combinatorial synthesis. and high-throughput experimentation, none of the framework structure types was "tailor made" but was discovered by systematically varying SDA and synthesis conditions. This shows that the process of nucleation is not well understood and that energy differences between various nuclei are small, which makes predictions from modeling difficult.

Another important factor influencing the product in clathrasil synthesis is the active concentration of the SDA. For some SDA, high concentrations lead to frameworks with higher densities of framework-specific cages. Pyrrolidine, for example, gives silica sodalite (2.9 cages per 1000 A') at high concentrations of SDA. whereas RUB-10 (2.0 per 1000 $Å^3$) and dodecasil 3C (1.1 per 1000 $Å^3$) form at lower concentrations.

SDA for Zeosils

The characteristic feature of a zeosil is channel-like pores wide enough for the exchange of SDA with sorbate molecules. The ring size must be larger than six and is typically eight and more. Some zeosils have spacious. cage-like voids, however. the interconnecting pore windows are much smaller (Fig. 2a–c). As an example. decadodecasil 3R (DDR) contains 1-aminoadamantane

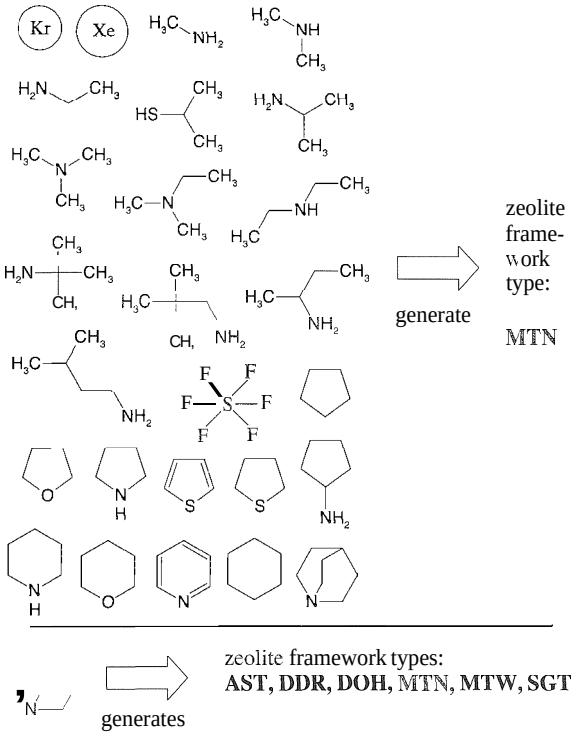

Fig. 4 top) Compilation of structure directing agents (SDA) which all lead to the formation of MTN-type materials. bottom) Zeolite framework types obtained with quinuclidine as SDA under different synthesis conditions.

as SDA in the as-synthesized form and is a typical clathrasil. After calcination and the removal of the decomposition fragments, a two-dimensional channels system becomes accessible through the 8 MR.

The typical zeosils have channel-like voids that extend in one dimension or are interconnected to two- and three-dimensional channel systems, respectively. The channels are bound by 10, 12. or 14 MR housing the SDA (Fig. 2d–f). As for clathrasils. the sizes and shapes of the SDA are imprinted on the host framework. Chain-like amines, polyazacompounds, and di- and trialkylamines are typical SDA for zeosils with 10 MR (Fig. 3b).[11] Here. the di- and trialkylamines create intersecting channel systems. In order to obtain the larger 12 MR pore. bulkier SDA. such as phenyl groups containing templates. are needed. For the even larger 14 MR zeosils. the diameter of the SDA is further increased. However. the SDA for the large-pore zeosils show only limited conformationa! freedom. The geometries of tricyclic molecules or metal–organic compounds are almost rigid. Because the channel cross section is the only characteristic feature of zeosil host framework structures that reflect SDA geometry, a number of different SDA can be used for the synthesis of every zeosi? framework structure type. As already mentioned for the clathrasils. there are many hypothetical framework structure types derived from existing models and through rigorous mathematical enumerations. However. modeling calculations with the aim of identifying specific SDA for new host framework structure types has not been successful so far.

Help guest species

In recent years, the fluoride route[i]**.*'' was successfully used for the synthesis of a series of new framework structure types. Often. SDA are ion pairs with a quarternary ammonium cation and fluoride anions as constituents. The structure-directing influence of the fluoride anion is such that the framework structure type forms only in its presence. The ammonium cation yields a different framework structure type. This finding led to a new direction in the research of the synthesis of porosils, the use of combinations of SDA for different structural subunits. Whereas the ammonium cation occupies the major void in the host framework. the fluoride anion resides in small cages that are rigid. Typical cages are the cube, [4^6] cage (Fig. 3a), and the [5^8] cage. Therefore. the fluoride-containing cages are the backbones for the otherwise open host framework. Careful calcination also removes the fluoride anion and leads to porous silicas. The influence of help species on the structure-directing effect of guest species was also reported for atmospheric gases in combination with pyrroiidine as SDA.[24]

CONCLUSION

Developing new directions in the synthesis of porosils includes all of the possibilities outlined above. The design of new and the modification of existing SDA was successful until now. Attempts to use nonaqueous solvents and dry gels were intensively researched for some time. however. without a major breakthrough. The use of mixtures of SDA, in particular, the combination of small and spacious molecules. was promising in the recent past. High-throughput experimentation will increase the efficiency of experiments and help to explore the vast parameter space in porosil synthesis. The fact that we know all possible porosil framework structure types and that computational chemistry has the power to calculate the SDA–host framework interaction should provide powerful tools for the synthetic chemist.[25] This combination of database knowledge. computer modeling, and experimental synthesis has not yet been exploited, or. at least, there is no successful example of the beneficial collaboration of the different disciplines in a joint effort. However. modern and successful synthesis research on porosils must include these disciplines in order to achieve the long-awaited goal of tailored synthesis of porous silicas.

ARTICLES OF FURTHER INTEREST

Channel Inclusion Compounds, p. 223
Mesoporous Materials, p. 845
Mesoporous Silica and Silica-Organic Hybrids, p. *852*
Organic Zeolites, p. 996
Solid-Stcite Nuclear Magnetic Resonance Spectroscopy, p. 1307
The Template Effect. p. 1493
Vibrational Spectroscopy. p. 1557
X-Ray and Neutron Power Diffraction, p. *1592*
Zeolites: Catalysis. p. 1610
Zeolites: Separation Science, p. 1617
Zeolites: Structures and Inclusion Properties, p. 1623

REFERENCES

1. Flörke. O.W.; Graetsch, H.; Brunk, F.: Benda. L.; Paschen, S.: Bergna, H.E.: Roberts, W.O.: Welsh, W.A.; Chapman, D.M.: Ettlinger, M.; Kerner. D.; Maier, M.; Meon. W.; Schmoll. R.; Gies. H.: Schiffmann. D.

SILICA. In *Ullmann's Encyclopedia of Industrial Chemist~:* 6th Ed.: Wiley-VCH Verlag GmbH: Weinheim. 2001.
2. Liebau, F. Structural Similarities and Dissimilarities Between SiO_2 and H_2O. In *The Physics* and *Technology of Amorphous* SiO_2; Devine. R.A.B., Ed.: Plenum Press: New York, 1988: 15–35.
3. Baerlocher, Ch.: Meier. W.M.;Olson. D.H. *Atlas of Zeolite Framework Types.* 5th Ed.: Elsevier: Amsterdam. 2001.
4. http://www.iza-structure.org/databases/ (accessed January 2003).
5. Marler. B. On the relationship between refractive index and density for SiO_2-polymorphs. Phys. Chem. Miner. 1988. *16,* 286–290.
6. Friedrichs, O.D.; Dress. A.W.M.: Huson. D.H.: Klinowski, J.; Mackay. A.L. Systematic enumeration of crystalline networks. Nature 1999, **400.** 644–647.
7. Park. S.H.; Große Kunstleve. R.-W.; Graetsch, H.: Gies. H. The Thermal Expansion of the Zeolites MFI. AFI, DOH. DDR. and MTN in Their Calcined and as Synthesized Form. In *Proceedings of the 11th IZA Conference, Progress in Zeolite and Microporous Materials;* Chon. H.. Ihm, S.-K.. Uh. Y.S.. Eds.: Studies in Surface Science, Elsevier: Amsterdam. 1996; Vol. 105. 1989–1994.
8. Gies. H. Clathrasils and Zeosils: Inclusion Compounds with Silica Host Frameworks. In *Inclusion Compounds*; Atwood. J.L., Davies. J.E.D.. MacNicol, D.D.. Eds.; Oxford Science Publications: Oxford. 1991; Vol. 5. 1–36.
9. Maas. H.; Calzaferri, G. Trapping energy from and injecting energy into dye-zeolite nanoantennae. Angew. Chem. Int. Ed. 2002. *41* (13). 2284–2288.
10. Yang. S.; Mirau, P.A.: Pai, C.S.: Nalsmasu, O.; Pai. J.C.; Obeng, Y.S.: Seputro, J.: Lin. E.K.: Lee. H.J.: Sun, J.N.; Gidley, D.W. Nanoporous ultralow dielectric constant organosilicates ternplated by triblock copolymers. Chem. Mater. 2002. *14,* 369–374.
11. Gies. H.: Marler. B. The structure controlling role of organic templates for the synthesis of porosils in the system SiO_2/template/H_2O. Zeolites 1992. **12,** 42–49.
12. Piccione. P.M.: Laberty, C.: Yang. S.; Camblor, M.A.: Navrotsky. A.; Davis, M.E. Thermodynamics of pure-silica zeolites. J. Phys. Chem., B 2000, **104.** 10001–10011.
13. Helmkamp, M.M.; Davis. M.E. Synthesis of porous silicates. Annu. Rev. Mater. Sci. 1995. *25,* 1–13.
14. Yang. S.; Navrotsky, A. In situ calorimetric study of the growth of silica TPA-MFI crystals from an initially clear solution. Chem. Mater. 2002. **14.** 2803–2811.
15. Schoeman, B.J.: Regev. O. A study of the initial stage in the crystallization of TPA-silicalite-1. Zeolites 1996. **17,** 447–456.
16. deMoor. P.P.E.A.: Beelen. T.P.M.; Komanschek, B.U.: Beck. L.W.; Wagner, P.: Davis. M.E.; van Santen, R.A. Imaging the assembly process of the organic-mediated synthesis of a zeolite. Chem. Eur. J. 1999. *5,* 2083–2088.
17. Kirschhock. C.E.A.: Buschmann, V.: Kremer. S.; Ravishankar, R.: Houssin, C.J.Y.;Mojet, B.L.: van Santen, R.A.; Grobet, P.J.; Jacobs. P.A.: Martens, J.A. Angew. Chern. Int. Ed. 2001, **40** (14), 2637–2640.
18. Knight; C.T.G.:Kinrade. S.D. Comment on "Identification of precursor species in the formation of MFI zeolite in the TPAOH-TEOS-H_2O system". J. Phys. Chem. 2002. **B106** (12). 3329–3332.
19. Burkett, S.L.: Davis, M.E. Mechanism of structure direction in the synthesis of ZSM-5: An investigation by intermolecular ^1H-^{29}Si-CP MAS NMR. J. Phys. Chem. 1994. *98.* 4647–4653.
20. Wu, M.G.: Deem, M.W. Monte Carlo study of the nucleation process during zeolite synthesis. J. Chern. Phys. 2002. **116.** 2125–2137.
21. Anderson. M.W.: Agger. J.R.: Hanif, N.: Terasaki, O. Growth models in microporous materials. Microporous Mesoporous Mater. 2001, **48,** 1–9.
22. Guth. J.L.: Kessler. H.: Wey, R. New route to pentasil-type zeolites using a non-alkaline medium in the presence of fluoride ions. Stud. Surf. Sci. Catal. 1986, *28.* 121–128.
23. Camblor. M.A.: Villaescusa. L.A.; Dias-Canañas, M.N. Synthesis of all-silica and high-silica molecular sieves in high fluoride medium. Top. Catal. 1999. 9, 59–76.
24. Gunawardane, R.P.: Gies, H.; Liebau. F. The effect of help gases on the formation and stability of clathrasils. Z. Anorg. Allg. Chem. 1983. *546,* 189–198.
25. Lewis. D.W.: Catlow, C.R.A.: Thomas, J.M. Application of computer modeling to the mechanisms of synthesis of microporous catalytic materials. Faraday Discuss. 1997, **106.** 451–471.

Cucurbituril, Its Homologues, and Derivatives

Kimoon Kim
Hee-Joon Kim
Pohang University of Science and Technology, Pohang, Republic of Korea

INTRODUCTION

Cucurbituril (cucurbit[6]uril, or CB[6]) is a hexameric macrocyclic compound self-assembled from an acid-catalyzed condensation reaction of glycoluril and formaldehyde (Scheme 1). Although its synthesis was first reported by Behrend and coworkers in 1905,[1] its chemical nature and structure were unknown until they were revealed by Mock and coworkers in 1981.[2] CB[6] has a cavity of ~ 5.5 Å diameter, accessible from the exterior by two carbonyl-laced portals of ~ 4 Å diameter. Although the size of the cavity is similar to that of a-cyclodextrin (!-CD), the highly symmetrical structure with two identical openings distinguishes CB[6] from α-CD. In a similar way to CDs, the hydrophobic interior of CB[6] provides a potential site for inclusion of hydrocarbon molecules. Unlike CDs, however, the polar carbonyl groups at the portals allow CB[6] to bind ions and molecules through charge-dipole and hydrogen-bonding interactions. The rigid structure and capability of forming complexes with molecules make CB[6] attractive as a synthetic receptor[3,4] and as a building block for the construction of supramolecular architectures.[5] Recent syntheses of cucurbituril homologues (cucurbit[*n*]uril) and derivatives opened up new opportunities in supramolecular chemistry of cucurbituril. In this entry, we briefly survey recent developments of supramolecular chemistry based on cucurbituril, its homologues and derivatives.

CUCURBITURIL (CUCURBIT[6]URIL)

Host–Guest Chemistry with Organic Molecules

Host–guest chemistry using CB[6] as a host has been studied mostly in strongly acidic aqueous solution, typically a 1:1 mixture of formic acid and water, because CB[6] is sparingly soluble in virtually any solvent except strongly acidic aqueous solution. Thus, early studies on the host–guest chemistry of CB[6] were mainly focused on the complexation with alkyl amines or diamines, which exist as ammonium ions in acidic solution.[6] The thermodynamics and kinetics of the binding were investigated.[7] The binding affinities of selected amines are summarized in Table 1 and a more extensive collection of such data is available.[4] Charge–dipole interaction as well as hydrogen bonding between the protonated amine group of the guest and the carbonyl groups at the entrance of CB[6] is responsible for the high affinity of these substrates. In addition, hydrophobic interactions between the alkyl group and the inside wall of the cavity contribute to the stability of these host–guest complexes. Shape-selectivity associated with the inclusion phenomenon is demonstrated by the fact that par-a-substituted benzene rings are able to access the cavity, whereas *ortho-* and ineta-substituted counterparts are not included (Table 1). Complex formation between CB[6] and other organic substrates, including alcohols. acids. nitriles. nonionic surfactants. and polyethylene glycols was recently studied by calorimetric titration in aqueous formic acid (50 vol%) solution.[7]

The kinetics of the host–guest complexation between cyclohexylmethylamine and CB[6] was recently investigated in a wide range of pH.[8] Interestingly. the rate of inclusion is related not to the thermodynamics of complexation but to the degree of protonation of the guest. The ingress of the protonated guest is retarded by the formation of an association complex. while the unprotonated guest can enter the cavity directly with a 20-fold larger rate.

Despite the poor solubility of CB[6] in pure, neutral water, it dissolves appreciably in neutral aqueous solutions containing alkali metal ions in high concentration. For example, $\sim 6.6 \times 10^{-2}$ mol of CB[6] dissolves in 1/L of 0.2 M Na_2SO_4 solution.[9] The markedly increased solubility has been ascribed to binding of alkali metal ions to the carbonyl groups at the portal. The X-ray structure of CB[6] crystallized from Na_2SO_4 solution reveals that two sodium ions are coordinated to each portal, and these ions along with water molecules cover each portal of CB[6] like "a lid on a barrel." Encapsulation of simple organic molecules such as tetrahydrofuran (THF), cyclopentanone, furan. and benzene in the cavity of CB[6] in alkali metal ion solutions was studied.[9] The inclusion of xenon into CB[6] dissolved in aqueous Na_2SO_4 solution was also investigated by ^{129}Xe- and 'H-NMR spectroscopy.[10] Xenon is reversibly trapped into

Encyclopedia of Supramolecular Chemistry
DOI: 10.1081/E-ESMC 120012364

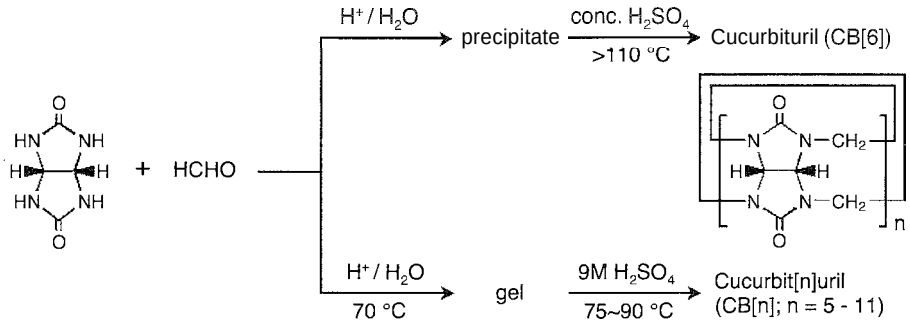

Scheme I. Synthesis of cucurbit[6]uril and its homologues.

the cavity to form a 1:1 host–guest complex. The exchange between the free and the complexed xenon is slow on the ^{129}Xe-NMR time scale but fast on the ^{1}H-NMR time scale.

Fluorescence enhancement of 2-anilinonaphthalene-6-sulfonate (2,6-ANS) in aqueous Na_2SO_4 solution caused by the complexation with CB[6] was reported.[11] In addition. a solid precipitate formed from aqueous Na_2SO_4 solution containing 1-anilino-8-naphthalenesulfonate (1,8-ANS) and CB[6] is highly fluorescent.[12] The X-ray crystal structure of the fluorescent solid revealed that 1,8-ANS molecules are clathrated in the lattice of CB[6] molecules with an overall 1,8-ANS/CB[6] stoichiometry of 2:1.[12]

Sorption of Organic Dyes for Water Treatment

Potential applications of CB[6] for the treatment of waste water containing organic dyes from the textile industry were investigated. In general. the solubility of CB[6] decreases significantly when dyes are present. Buschmann and coworkers measured stability constants for the complexation of some organic dyes by CB[6] in formic acid/water solution.[13] Karcher et al. also investigated the sorption of reactive dyes by CB[6] and effects of metal salt concentration. pH, and temperature on the dye sorption.[14]

Quantitative Studies of Metal Ion Binding

The two carbonyl-fringed portals of CB[6] are potential binding sites for metal ions. Buschmann and coworkers investigated the binding of alkali metal ions and other cations ($<5 \times 10^{-4}$ M) to CB[6] in aqueous solution by UV/Vis spectroscopy.[15] Assuming that CB[6] binds metal ions in a 1:2 stoichiometry and K_1 and K_2 are equal, they reported stability constants of Na^+ and K^+ complexes with log K of 3.69 and 3.96. respectively. Later. the metal ion binding was studied by calorimetry in a 50% formic acid/water solution where 1:1 complexes were observed.[16] The complexation of CB[6] with some transition metal ions was also reported.[17]

Reactions Inside CB[6]

Mock et al. reported that 1.3-dipolar cycloaddition of alkynes with alkyl azides, both substituted with a terminal amine group, yielding triazoles. is catalyzed by CB[6] in aqueous acid solutions.[18] The reaction proceeds with

Table 1 Affinity data for ligand–receptor complexes of cucurbituril.[a]

Ammonium ion	K_f (rel)[b]	Ammonium ion	K_f (rel)[b]
$Me(CH_2)_2NH_2$	37 6	$NH_2(CH_2)_3NH_2$	2 8
$Me(CH_2)_3NH_2$	307	$NH_2(CH_2)_4NH_2$	480
$Me(CH_2)_4NH_2$	74	$NH_2(CH_2)_5NH_2$	7600
$Me(CH_2)_5NH_2$	7.0	$NH_2(CH_2)_6NH_2$	8600
cyclo-$(CH_2)_3CHCH_2NH_2$	1130	$C_6H_5NH_2$	16.6
cyclo-$(CH_2)_4CHCH_2NH_2$	1040	$C_6H_5CH_2NH_2$	0 8
o- or *m*-$MeC_6H_4CH_2NH_2$	Not bound	*p*-$MeC_6H_4CH_2NH_2$	1 0
$NH_2(CH_2)_3NH(CH_2)_4NH(CH_2)_3NH_2$	40.000		

[a]From Ref. [6].
[b]Formation constant relative to *p*-Me-$C_6H_4CH_2NH_2$, for which the absolute value of K_1 = 320 M^{-1} in 1:1 formic acid/water solution at 40°C.

large rate acceleration by a factor of 10^5 and high regiospecificity, yielding only 1,4-disubstituted triazoles, via formation of a ternary host–guest complex with CB[6] in solution.

Mechanically Interlocked Molecules and Their Supramolecular Assemblies

CB[6] has been used as a molecular bead to synthesize mechanically interlocked molecules such as rotaxanes and catenanes.[5] The first rotaxane containing CB[6] was synthesized by Kim and coworkers.[19] The highly efficient, one-pot synthesis involves the threading of CB[6] with sperminc followed by attaching a dinitrophenyl group to each end of the spcrmine unit to prevent dethreading. They also developed a novel strategy to polyrotaxane using metal-ion-directed self-assembly. It involves threading a CB[6] "bead" with a short "string" to form a stable pseudorotaxane, followed by joining the pseudorotaxanes with transition or lanthanide metal ions such as Cu^{2+},[20] Ag^{+} (Fig. 1a),[21] or Tb^{3+}[22] as "linkers" to organize into a polyrotaxane. A wide variety of one-dimensional (1D), 2D, and 3D polyrotaxanes were synthesized, and their structures wcre characterized by single-crystal X-ray crystallography.[23] This strategy was extended to the synthesis of molecular necklaces, in which a number of small rings arc threaded onto a large ring. In the synthesis of molecular necklaces, however, a metal complex with *cis* "vacant" coordination sites such as $Pt(en)(NO_3)_2$ (en = ethylenediamine), instead of simple metal salt, is used as a "90 degree angle connector." Molecular necklaces [4]MN (Fig. Ib) and [5]MN having three and four CB[6] beads threaded on trianglar and square frameworks, respectively, were synthesized.[24] Reaction between a prcorganized L-shaped pscudorotaxane, in which two molecular beads arc already in place, and metal ions or metal complexes, produced a molecular necklace [5]MN containing four molecular beads.[25]

(Pseudo)polyrotaxanes containing CB[6] thrcaded on organic: polymers wcrc also reported. Such (pseudo)polyrotaxanes were synthesized by interfacial polymerization of CB[6]/polyamine pseudorotaxane with diacid chlorides such as 1,6-hexanedioyl chloride (adipoyl chloride).[26] Steinke and coworkers recently reported a novel way to produce polyrotaxanes utilizing 1,3-dipolar cycloaddition between azide and alkyne inside the cavity of CB[6].[27] They also synthesized pseudopolyrotaxanes by threading CB[6] onto poly(iminohexamcthylene chloride).[28]

Dendrimcrs with terminal groups that are modified with pseudorotaxanes were reported.[29] Kim et al. attached diaminobutane units at the terminals of polypropylimine (PPT) dendrimers (G1–G5), and then threaded CB[6] onto the diaminobutane terminals to produce pseudorotaxane-terminated dendrimers. The structures and properties of the dendrimers can be reversibly changed by threading and dethreading CB[6].

Interaction of (pseudo)rotaxanes containing CB[6]/polyamine with DNA was investigated by Nakamura and Kim.[30] Pscudorotaxancs containing a CB[6] bead threaded on polyamines with an acridinc terminal bind to DNA strongly. Furthermore, the activities of polyamines, such as spermine and spermidine, which are known to accelerate transcription and nuclcasc activities, are greatly affected by their formation of pseudorotaxanes with CB[6].

Molecular Switches and Machines

One of the potential applications of mechanically interlocked molecules is construction of molecular-scale devices such as molecular machines and switches. [2](Pseudo)rotaxanes containing CB[6] were studied along

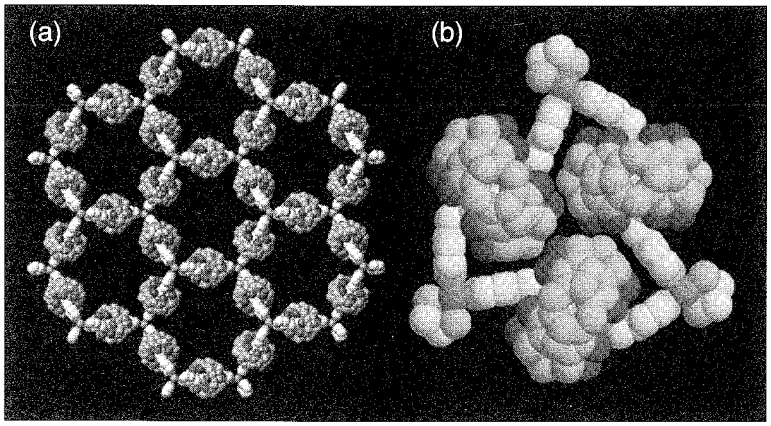

Fig. 1 X-ray crystal structures of a two-dimensional polyrotaxane (a) and a molecular necklace [4]MN (b). (*View this art in color at www.dekker.com.*)

this line. In 1990. Mock reported a pseudorotaxane-based molecular switch consisting of a CB[6] "bead" and a triamine "string" $PhNH(CH_2)_6NH(CH_2)_4NH_2$.[31] At low pH, the "bead" resides at the protonated diaminohexane site. because CB[6] forms a more stable complex with diprotonated diaminohexane than with diprotonated diaminobutane. Upon deprotonation of the aniline nitrogen (pK_a = 6.7). however, the "bead" migrates to the diprotonated diaminobutane site, because binding with the monoprotonated diaminohexane is weaker. Recently, Kim et al. extended this work to design a fluorescent molecular switch that can signal the change in the "bead" position by color and fluorescence changes.[32] They also reported another bistable [2]rotaxane containing CB[6] that behaves as a kinetically controlled switch.[33]

Other Supramolecular Assemblies Formed with CB[6] end Metal Ions or Metal Complexes

CB[6] and K^+ or Rb^+ ion form a columnar one-dimensional coordination polymer in the solid state, in which CB[6] molecules stack atop one another through coordination of their carbonyl groups to K^+ or Rb^+ ions in between. In the case of Rb^+, the coordination polymer chains are arranged in such a way as to produce a honeycomb-like structure with large. linear hexagonal channels parallel to the polymer chains.[34] Supramolecular assemblies of CB[6] and transition metal ion clusters were investigated. For example, an infinite one-dimensional chain structure was reported, in which a double cube cluster cation $\{[M_3E_4(H_2O)_7Cl_2]_2Hg\}^{4+}$ (M = Mo, W; E = S. Se) is sandwiched between two CB[6] units via hydrogen bonds.[35]

CUCURBITURIL HOMOLOGUES

Syntheses, Structures, and General Properties

Cucurbituril homologues having glycoluril units fewer or greater than six were recently reported by Kim and coworkers.[36] The cyclization at lower temperatures (75–90°C) compared to that (> 110°C) employed in the conventional synthesis of CB[6] allows formation of significant amounts of other CB homologues besides CB[6] (Scheme 1). The homologues (cucurbit[*n*]uril or CB[*n*], *n* = 5–8) can be isolated by a series of fractional crystallizations. The higher homologues (CB[*n*], *n* = 9–11) were also detected by mass spectrometry, although they have not yet been isolated due to the very low level of production. Recently. Day and coworkers examined a wide range of reaction conditions. including acid type. acid concentration, reactant concentrations. and temperature to probe the mechanism as well as to optimize the yield of individual CB homologues.[37]

The CB homologues CB[5], CB[7], and CB[8] were fully characterized by various spectroscopic methods. including x-ray crystallography (Fig. 2).[36] Compared in Table 2 are some structural parameters of the CB homologues. As we go from CB[5] to CB[8], the mean diameter of the internal cavity increases progressively from ~ 4.4 to ~ 8.8 Å. Likewise, the oxygen-bounded portal increases its mean diameter from ~ 2.4 to ~ 6.9 Å. In terms of cavity size, CB[6], CB[7], and CB[8] are close to α, β, and γ-CDs, respectively. The different cavity size of the CB homologues is manifested in their host–guest chemistry. Protonated 2,6-*bis*(4,5-dihydro-1*H*-imidazol-2-yl)naphthalene is too large to be included in CB[6] but forms a 1:1 host–guest complex with CB[7] and a 1:2 complex with CB[8].[36]

Similar to CB[6], solubility of CB homologues. except CB[7], is extremely low in common solvents. including water. However, CB[7] has a moderate solubility in water (3×10^{-2} M),[38] which is comparable to that of β-CD. All CB homologues (n = 5–8) have high thermal stability in the solid state. No decomposition is observed up to 420°C for CB[n] (n = 5, 6, and 8), although CB[7] starts decomposing at a somewhat lower temperature (370°C).[38,39] Prolonged heating of CB[8] in concentrated HCl at 100°C produces the smaller hornologues. while smaller CB homologues do not show interconversion or detectable decomposition.[37]

Cucurbit[5]uril

Although cucurbit[5]uril (CB[5]) became available only recently, along with other CB homologues. its derivative decamethylcucurbit[5]uril (Me-CB[5])[40] was known since 1992, and its chemistry was studied (see *Cucurbituril Derivatives*). Because CB[5] and Me-CB[5] have essentially identical cavity structures, their chemistry is also expected to be the same.

Cucurbit[7]uril

Nau and Marquez examined the photophysicai properties of 2,3-diazabicyclo-[2,2,2]oct-2-ene (DBO) inside CB[7] to characterize the chemical environment of the CB[7] cavity.[41] The encapsulation of DBO by CB[7] strongly affects the photophysical properties of DBO. Interestingly, the polarizability inside CB[7] cavity is even lower than that in perfluorohexane, and thus, the environment of the cavity inside CB[7] is closer to the gas phase than the solution phase.

Kim et al. discovered that CB[7] forms a stable 1:1 inclusion complex with methylviologen dication (MV^{2+};

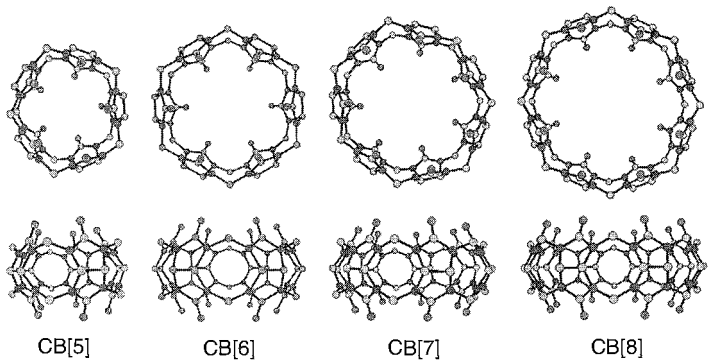

Fig. 2 X-ray crystal structures of cucurbit[*n*]uril (*n* = 5–8)

log K = 5.30).[42] It is in sharp contrast to the fact that β-cyclodextrin, which has a similar cavity size, does not bind MV^{2+} appreciably. Unusual electrochemical behavior of the inclusion complex was also observed. Inclusion of o-carborane in CB[7] was recently reported.[43]

Cucurbit[8]uril

The selective inclusion of a hetero-guest pair in CB[8] driven by charge–transfer interaction between the electron-rich and electron-deficient guests. such as methylviologen and 2,6-dihydroxynaphthalene or 1.4-dihydroxybenzene was reported (Fig. 3a).[44] The 1:1:1 ternary complexes exhibit largely red-shifted charge–transfer absorptions with a concomitant high increase in intensity and the strong fluorescence quenching of 2.6-dihydroxynaphthalene compared to those of a 1:1 mixture of the guest molecules in the absence of CB[8].

Macrocycles within macrocycles were synthesized; where tetraazamacrocycles and their metal complexes are encapsulated within CB[8].[45] The 1:1 inclusion complexes cyclen·4HCl-CB[8], cyclam·4HCl-CB[8], and [Cu(cyclen)(H_2O)](NO_3)$_2$-CB[8] (Fig. 3b) were characterized by X-ray crystallography. An electrochemical study shows that the encapsulation of Cu(cyclen) in CB[8] increases the stability of the Cu(I) state but considerably slows the electron transfer between the electrode and the redox center.

The synthetic utility of CB[8] as a reaction vessel was also demonstrated. The [2 + 2] photoreaction of *trans*-diarninostilbene dihydrochloride proceeds with large rate acceleration and high stereoselectivity via formation of a stable 1:2 host–guest complex with CB[8] in solution.[46]

Table 2 Structural parameters for cucurbit[*n*]uril (*n* = 5–8).[a]

	CB[5]	CB[6][b]	CB[7]	CB[8]
Portal diameter (Å)	2.4	3.9	5.4	6.9
Cavity diameter (A)'	4.4	*5.8*	7.3	*8.8*
Cavity volume (Å^3)	*82*	164	279	479
Outer diameter (Å)[c]	13.1	14.4	16.0	17.5
Height (Å)	9.1	9.1	9.1	9.1

"From Ref. [36].
[b]From Ref. [2].
'Values measured at the equator of the receptors

CUCURBITURIL DERIVATIVES

Decamethylcucurbit[5]uril

The first cucurbituril derivative decamethylcucurbit[5]uril (Me-CB[5]) (Chart I) was synthesized from dimethylglycoluril and formaldehyde in 1992.[40] The X-ray structural analysis shows a cavity of 4 Å in diameter and two identical portals of ~ 2.5 A in diameter. Bradshaw and coworkers studied complexation of Me-CB[5] with metal ions in 50% formic acid/water solution by calorimetric and potentiometric methods.[47] Me-CB[5] binds most metal ions in a 1:1 stoichiometry in the acidic solution. Interestingly, Me-CB[5] shows exceptionally high affinity for Pb^{2+} ion (log K > 9). which is mainly due to the size match between Pb^{2+} and Me-CB[5] portals. The pK_a value (9.56) for protonation of Me-CB[5] indicates that Me-CB[5] behaves as a base in an aqueous solution.

The encapsulation of small molecules, such as N_2, O_2, methanol, or acetonitrile in ammonium ion complexed Me-CB[5] in the gas phase. was observed using electrospray ionization Fourier transform mass spectrometry.[48] The guest is released in the gas phase upon removing an ammonium ion "lid" using 18-crown-6. The rate of guest release depends on the size of the guest molecules.

Cyclohexanocucurbit[*n*]uril (*n* = 5 and 6)

Cyclohexanocucurbit[*n*]uril (n = 5 and 6: CB*[5] and CB*[6]) (Chart 1) were recently synthesized from

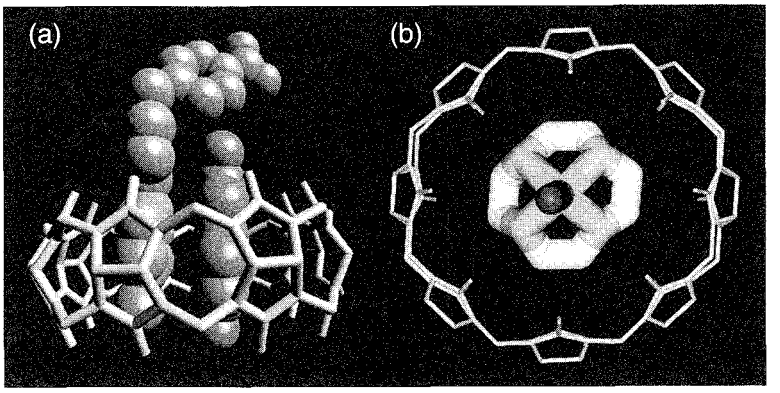

Fig. 3 X-ray crystal structures of inclusion complexes of a hetero-guest pair (a) and Cu(cyclen) (b) in CB[8]. (View this art *in* color *at www.dekker.com.*)

cyclohexanoglycoluril and formaldehyde.[49] Their X-ray crystal structures reveal 5 and 6 fused cyclohexane rings, respectively, decorating outside the "equators" of CB[n] (n = 5 and 6). The portal and cavity sizes of CB*[5] and CB*[6] are essentially the same as those of CB[5] and CB[6], respectively.

Remarkably, the new CB derivatives CB*[5] and CB*[6] are soluble in common solvents, such as water, methanol, and DMSO, and moderately soluble in ethanol, DMF, and acetonitrile. They are both more soluble in water ($\sim 2 \times 10^{-1}$ mol L^{-1}) than in organic solvents ($\sim 3 \times 10^{-2}$ mol L^{-1} or less) despite the presence of the equator-decorating fused cyclohexane units. The solubility of CB*[6] in water is comparable to that of x-CD.

A study of the complex formation of CB*[5] with K^+ ion in neutral water using titration calorimetry showed that CB*[5] binds K^+ ion in a 1:2 stoichiometry. The utility of water-soluble CB*[6] was also illustrated by formation of a stable 1:1 host–guest complex with acetylcholine in neutral water. The good solubilities of CB*[5] and CB*[6] in organic solvents make their applications in ion-selective electrodes (ISEs) possible. Membrane electrodes prepared with CB*[5] and CB*[6] behave as ISEs for sensing Pb^{2+} ion and acetylcholine, respectively, with good sensitivity and selectivity.

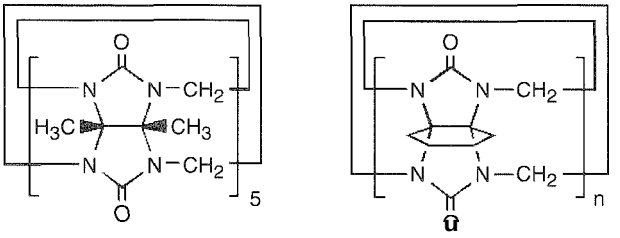

Decamethylcucurbit[5]uril (Me-CB[5])

Cyclohexanocucurbit[n]uril (CB*[n]; n = 5 and 6)

Chart 1.

CONCLUSION

Cucurbit[6]uril is attractive not only as a synthetic receptor but also as a building block for supramolecular assemblies. Recent syntheses of its homologues and derivatives further broadened the scope of cucurbituril chemistry.[50] Many challenges remain, including direct functioualization of CB[n] and synthesis of CB analogues, particularly chiral ones. Considering what has been done with cyclodextrins, nevertheless, we believe that the CB homologues and derivatives provide new opportunities in many areas of supramolecular chemistry, including recognition, catalysis, separation, transport, and many others.

ARTICLES OF FURTHER INTEREST

Catenanes and Other Interlocked Molecules, p. 206
Cavitands, p. 219
Cyclodextrins, p. 398
Dendrimers, p. 432
Drug Delivery, p. 484
Dye Inclusion Crystals, p. 497
Enzyme Mimics, p. 546
Glycoluvil-Based Hosts, p. 597
Hydrogen Bonding, p. 658
Hydrophobic Effects, p. 673
Inclusion Compounds: Selectivity, Thermal Stability, und Kinetics, p. 696
Ion Channels and Their Models, p. 742
Ion-Selective Electrodes, p. 747
The Lock and Key Principle, p. 809
Molecular Squares, Boxes, and Cubes, p. 909

Molecular Switches, p. *917*
Molecular-Level Machines, p. 931
Nuclear Magnetic Resonance Spectroscopy, p. 981
Rotaxanes and Pseudorotaxanes, p. 1194
Self-Assembly: Definition and Kinetic and Thermodynamic Considerations, p. *1248*
Stability Constants: Definition and Determination, p. *1360*
The Template Effect, p. 1493
X-Ray Crystallography, p. *1586*

REFERENCES

1. Behrend. R.: Meyer. E.: Rusche, F. Condensation products from glycoluril and formaldehyde. Liebigs Ann. Chem. 1905. *339*. 1–37.
2. Freeman, W.A.: Mock. W.L.; Shih. N.-Y. Cucurbituril. J. Am. Chem. Soc. 1981. *103* (24). 7367–7368.
3. Cintas. P. Cucurbituril: Supramolecular perspectives for an old ligand. J. Incl. Phenom. Mol. Recognit. Chem. 1994. *17* (3). 205–220.
4. Mock, W.L. Cucurbituril. In *Comprehensive Supramolecular Chemistry*; Vogtle. F., Ed.: Pergamon: Oxford, 1996; Vol. 2, 477–493.
5. Kim. K. Mechanically interlocked structures incorporating cucurbituril. Chem. Soc. Rev. 2002. *31* (2). 96–107.
6. Mock. W.L.: Shih, N.-Y. Structure and selectivity in host–guest coinplexes of cucurbituril. J. Org. Chem. 1986. *51* (23). 4440–4446.
7. Buschmann. H.-J.; Jansen. K.: Schollmeyer. E. Cucurbituril as host molecule for the complexation of aliphatic alcohols. acids and nitriles in aqueous solution. Thermochim. Acta 2000, *346* (1–2). 33–36.
8. Marquez. C.: Kau. W.M. Two mechanisms of slow host–guest complexation between cucurbit[6]uril and cyclohexylmethylamine: pH-responsive supramolecular kinetics. Angew. Chem., Int. Ed. 2001. *40* (17). 3155–3160.
9. Jeon. Y.-M.: Kim, J.: Whang. D.: Kim. K. Molecular container assembly capable of controlling binding and release of its guest molecules: Reversible encapsulation of organic molecules in sodium ion complexed cucurbituril. J. Am. Chem. Soc. 1996. *118* (40). 9790–9791.
10. Haouaj, M.E.; Luhmer. M.: Ko, Y.H.; Kim. K.; Bartik. K. NMR study of the reversible complexation of xenon by cucurbituril. J. Cheni. Soc., Perkin Trans. 2 2001, (5), 804–807.
11. Wagner. B.D.; Fitzpatrick, S.J.; Gill. M.A.: MacRae, A.I.; Stojanovic, N. A fluorescent host–guest complex of cucurbituril in solution: A molecular Jack O'Lantern. Can. J. Chern. 2001, 79 (7). 1101–1104.
12. Wagner, B.D.: MacRae. A.I. The lattice inclusion compound of 1.8-4NS and cucurbituril: A unique fluorescent solid. J. Phys. Chern., B 1999. *103* 146). 10114–10119.
13. Buschmann, H.-J.: Schollmeyer. E. Cucurbituril and β-cyclodextrin as hosts for the complexation of organic dyes. J. Incl. Phenom. Mol. Recognit. Chem. 1997. *29* (2). 167–174.
14. Karcher, S.: Kornmüller. A.: Jekel. M. Cucurbituril for water treatment. Part I: Solubility of cucurbituril and sorption of reactive dyes. Water Res. 2001. *35* (14), 3309–3316.
15. Buschmann. H.-J.; Cleve. E.; Schollmeyer, E. Cucurbituril as a ligand for the complexation of cations in aqueous solutions. Inorg. Chim. Acta 1992, *193* (1), 93–97.
16. Buschmann, H.-J.: Jansen, K.: Meschke. C.: Schollmeyer. E. Thermodynamic data for complex formation between cucurbituril and alkali and alkaline earth cations in aqueous formic acid solution. J. Solution Chem. 1998, 27 (2). 135–140.
17. Buschmann, H.-J.; Cleve. E.: Jansen. K.: Schollmeyer, E. Determination of complex stabilities with nearly insoluble host molecules: Cucurbit[5]uril, decamethylcucurbit[5]uril and cucurbit[6]uril as ligands for the complexation of some multicharged cations in aqueous solution. Anal. Chim. Acta 2001. *437* (1). 157–163.
18. Mock, W.L.; Irra. T.A.: Wepsiec. J.P.; Adhya, M. Catalysis by cucurbituril. The significance of bound-substrate destabilization for induced triazole formation. J. Org. Chem. 1989. *54* (22), 5302–5308.
19. Jeon. Y.-M.: Whang. D.: Kim, J.: Kim. K. A simple construction of a rotaxane and pseudorotaxane: Syntheses and X-ray crystal structures of cucurbituril threaded on substituted spermine. Chem. Lett. 1996. (7), 503–504.
20. Whang. D.; Jeon. Y.-M.: Heo, J.; Kim. K. Self-assembly of a polyrotaxane contaning a cyclic "bead" in every structural unit in the solid state: Cucurbituril molecules threaded on a one-dimensional coordination polymer. J. Am. Chem. Soc. 1996, *118* (45). 11333–11334.
21. Whang, D.: Kim. K. Polycatenated two-dimensional polyrotaxane net. J. Am. Chem. Soc. 1997, *119* (2). 451–452.
22. Lee. E.: Heo. J.; Kim. K. A three-dimensional polyrotaxane network. Angew. Chem.. Int. Ed. 2000. *39* (15). 2699–2701.
23. Park, K.-M.: Whang. D.: Lee. E.: Heo. J.: Kim. K. Transion metal ion directed supramolecular assembly of one- and two-dimensional polyrotaxanes incorporating cucurbituril. Chern. Eur. J. 2002. 8 (2). 498–508.
24. Whang, D.; Park, K.-M.; Heo. J.: Ashton. P.; Kim. K. Molecular necklace: Quantitative self-assembly of a cyclic oligorotaxane from nine molecules. J. Am. Chem. Soc. 1998. *120* 119). 4899–4900.
25. Roh. S.-G.; Park. K.-M.; Park, G.-J.: Sakamoto, S.; Yamaguchi. K.: Kim, K. Synthesis of a five-membered molecular necklace: A 2 + 2 approach. Angew. Chem.. Int. Ed. 8999. *38 (5)*. 638–640.
26. Meschke. C.: Buschmann. H.-J.: Schollmeyer, E. Polyrotaxanes and pseudorotaxanes of polyamides and cucurbituril. Polymer 1999. *40* (4). 945–949.
27. Tuncel. D.; Steinke. J.H.C. Catalytically self-threading polyrotaxanes. Chem. Commun. 1999, (16). 1509–1510.
28. Tuncel. D.; Steinke, J.H.G. Mainchain pseudorotaxanes via post-threading with cucurbituril. Chern. Commun. 2001, (3). 253–254.
29. Lee. J.W.: Ko. Y.H.: Park. S.-H.: Yamaguchi. K.: Kim. K. Novel pseudorotaxane-terminated dendrimers: Supramo-

lecular modification of dendrimer periphery. Angew. Chem., Int. Ed. 2001, *40* (4). 746–749.
30. Isobe, H.; Tomita, N.: Lee. J.W.: Kim. H.-J.; Kim, K.; Nakamura, E. Ternary complexes between DNA. polyamine. and cucurbituril: A modular approach to DNA-binding molecules. Angew. Chem.. Int. Ed. 2000. 39 (23). 4257–4260.
31. Mock, W.L.: Pierpoiit. J. A cucurbituril-based molecular switch. Chem. Commun. 1990, (21), 1509–1511.
32. Jun. S.I.; Lee. J.W.: Sakamoto. S.; Yamaguchi, K.; Kim, K. Rotaxane-based molecular switch with fluorescence signaling. Tetrahedron Lett. 2000, *41* (4), 471–475.
33. Lee. J.W.: Kirn. K.P.; Kim. K. A kinetically controlled molecular switch based on bistable [2]rotaxane. Chem. Commun. 2001. (11), 1042–1043.
34. Heo, J.; Kirn. S.-Y.; Whang, D.; Kim, K. Shape-induced. hexagonal, open frameworks: Rubidium ion complexed cucurbituril. Angew. Chem.. Int. Ed. 1999.38 (5). 641–643.
35. Sokolov. M.N.: Virovets, A.V.: Dybtsev, D.N.; Gerasko. O.A.; Fedin. V.P.; Nernandez-Molina, R.: Clegg. W.; Sykes, A.G. Metal incorporation into and dilnerization of M_3E_4 clusters (M = Mo. W: E = S. Se) in supramolecular assemblies with cucurbituril: A molecular model of intercalation. Angew. Chem.. Int. Ed. 2000. *39* (9), 1659–1661.
36. Kim. J.: Jung, I.-S.: Kim. S.-Y.: Lee, E.; Kang, J.-K.: Sakamoto. S.: Yamaguchi, K.: Kim. K. New cucurbituril homologues: Syntheses. isolation, characterization, and X-ray crystal structures of cucurbit[*n*]uril (*n* = 5, 7. and 8). J. Am. Chem. Soc. 2000. 122 (3), 540–541.
37. Day, A.: Arnold. A.P.: Blanch. R.J.: Snushal!. B. Controlling factors in the synthesis of cucurbituril and its homologues. J. Org. Chem. 2001. 66 (24), 8094–8100.
38. Kim. K. unpublished results.
39. Germain. P.; Létoffé. J.M.: Merlin. M.P.: Buschmann. H.-J. Thermal behaviour of hydrated and anhydrous cucurbituril: A DSC. T.G. and calorimetric study in temperature range from 100 to 800 K. Thermochim. Acta 1998. 315 (2). 87–92.
40. Flinn, A.: Hough, C.C.: Stoddart. J.F.; Williams. D.J. Decamethylcucurbit[5]uril. Angew. Chem., Int. Ed. Engl. 1992. *31* (11). 1475–1477.
41. Marquez, C.; Nau. W.M. Polariaabilities inside molecular containers. Angew. Chem.. Int. Ed. 2001. *40* (23), 4387–4390.
42. Kim. H.-J.; Jeon. W.S.; Ko, Y.W.: Kim, K. Inclusion of methylviologen in cucurbit[7]uril. Proc. Natl. Acad. Sci. U.S.A. 2002. 99 (8). 5007–5011.
43. Blanch. R.J.: Sleeman. A.J.: White, T.J.; Arnold, A.P.: Day. A.I. Cucurbit[7]uril and *o*-carborane self-assemble to form a molecular ball bearing. Nano Lett. 2002. 2 (1), 147–149.
44. Kim. H.-J.: Heo. J.: Jeon. W.S.; Lee. E.: Kim. J.; Sakamoto, S.; Yamaguchi, K.: Kim. K. Selective inclusion of a hetero-guest pair in a molecular host: Formation of stable charge-transfer complexes in cucurbit[8]uril. Angew. Chem.. Pnt. Ed. 2001. *40* (8). 1526–1529.
45. Kim. S.-Y.: Jung. I.-S.; Lee, E.: Kim, J.: Sakamoto, S.: Yamaguchi. K.; Kim, K. Macrocycles within macrocycles: Cyclen, cyclam, and their transition metal complexes encapsulated in cucurbit[8]uril. Angew. Chem.. Int. Ed. 2001. *40* (11), 2119–2121.
46. Jon. S.Y.; Ko, Y.H.; Park, S.H.; Kim. H.-J.; Kim, K. A facile, stereoselective [2 + 2] photoreaction mediated by cucurbit[8]uril. Chem. Commun. 2001, (19). 1938–1939.
47. Zhang, X.X.: Krakowiak. K.E.: Xue. G.: Bradshaw. J.S.; Izatt. R.M. A highly selective compound for lead: Complexation studies of decamethylcucurbit[5]uril with metal ions. Ind. Eng. Chem. Res. 2000. 39 (10). 3516–3520.
48. Kellersberger. K.A.: Anderson. J.D.: Ward. S.M.; Krakowiak. K.E.: Dearden, D.V. Encapsulation of N_2, O_2, methanol. or acetonitrile by decamethylcucurbit[5]uril$(NH_4^+)_2$ complexes in the gas phase: Influence of the guest on "lid" tightness. J. Am. Chem. Soc. 2001. *123* (45). 11316–11317.
49. Zhao. J.; Kini, H.-J.: Oh. J.; Kim, S.-Y.; Lee. J.W.: Sakamoto. S.: Yamaguchi. K.; Kim. K. Cucurbit[n]uril derivatives soluble in water and organic solvents. Angew. Chem.. Int. Ed. 2001. *40* (22). 4233–4235.
50. Lee. J.W.: Samal. S.: Selvapalam, N.: Kim, H.-J.: Kim. K. Cucurbituril hornologues and derivatives: New opportunities in supramolecular chemistry. Acc. Chem. Res. 2003. in press (DOI: 10.1021/ar020254k).

Cyclodextrins

József Szejtli
CYCLOLAB, Cyclodextrin Research and Development Laboratory Ltd., Budapest, Hungary

INTRODUCTION

Cyclodextrins (CD) are the most widely used molecules that form host–guest-type inclusion complexes. Although as recently as the 1970s these long-known molecules were merely scientific curiosities. available only as expensive fine chemicals. by the end of the twentieth century, they we e produced and used industrially in thousand-tons amounts.

The spectacular development of CD technology relies on a series of reasons:

- They are seminatural products. produced from a renewable natural material (starch) by employing a relatively simple enzymic conversion.
- They are produced in thousand ton/year amounts by environment-friendly technologies.
- Their initially high prices have dropped to levels where they become acceptable for most industrial purposes. Through their inclusion complex-forming ability. important properties of the complexed substances can be modified significantly. This unprecedented "molecular encapsulation'' is widely utilized in many industrial products. technologies, and analytical methods. Their toxic effects are of secondary character and can be eliminated by selecting the appropriate CD type or derivative or mode of application.
- They can be consumed by humans as ingredients of drugs. foods, or cosmetics.

STRUCTURAL FEATURES OF CYCLODEXTRINS

Cyclodextrins comprise a family of three well-known industrially produced major. and several rare. minor cyclic oligosaccharides. The three major cyclodextrins are crystalline, homogeneous. nonhygroscopic substances. which are torus-like macro-rings built up from glucopyranose units. The α-cyclodextrin (Schardinger's α-dextrin, cyclomaltohexaose. cyclohexaglucan, cyclohexaamylose, αCD, ACD, C6A) comprises six glucopyranose units, βCD (Schardinger's β-dextrin, cyclornaltoheptaose, cycloheptaglucan, cycloheptaamylose, βCD, BCD. C7A) comprises seven such units, and γCD (Schardinger's y-dextrin. cyclomaltooctaose, cyclooctaglucan, cyclooctaamylose. γCD, GCD, CXA) comprises eight such units (Fig. 1). The most important characteristics of the CDs are summarized in Table 1.

The nomenclature of CDs is not exact. Maltose is a disaccharide. i.e., a cyclomaltopentaose could be interpreted as a 10-glucopyranose-containing cyclic oligosaccharide. Otherwise. this is the five-membered pre-αCD. How would a four-membered CD be named?

Fortunately, the practically important. industrially produced CDs are the E-, p-, and γCDs. Their names are unambiguous and need not be changed. A complete and unanimous nomenclature was suggested by Lichtenthaler and Immel,[1] e.g., the pre-αCD is named cyclo-α(1 → 4)-glucopentaoside. This nomeilclature is recommended for the so-called minor CDs as well as for any other cyclic oligosaccharides.

As a consequence of the $^4C_1$ conformation of the glucopyranose units. all seconclary hydroxyl groups are situated on one of the two edges of the ring, whereas all the primary ones are placed on the other edge. The ring, in reality. is a cylinder, or better said. a conical cylinder. which is frequently characterized as a doughnut or wreath-shaped truncated cone. The cavity is lined by the hydrogen atoms and the glycosidic oxygen bridges. respectively. The nonbonding electron pairs of the glycosidic–oxygen bridges are directed toward the inside of the cavity. producing a high electron density there and lending to it some Lewis-base characteristics.

The C–2–OH group of one glucopyranoside unit can form a hydrogen bond with the C–3–OH group of the adjacent glucopyranose unit. In the βCD molecule, a complete secondary belt is formed by these H-bonds. and therefore, the βCD is a rigid structure. This intramolecular hydrogen-bond formation is probably the explanation for the observation that βCD has the lowest water solubility of all CDs.

The hydrogen-bond belt is incomplete in the αCD molecule. because one glucopyranose unit is in a distorted position. Consequently. instead of the six possible H-bonds. only four can be established simultaneosly. The γCD is a noncoplanar, more flexible structure. and therefore. it is the more soluble of the three CDs.[2–8]

Shown in Fig. 2 is a sketch of the characteristic structural features of CDs. On the side where the secondary

Encyclopedia of Supramolecular Chemistry
DOI: 10.1081/E-ESMC 120012731

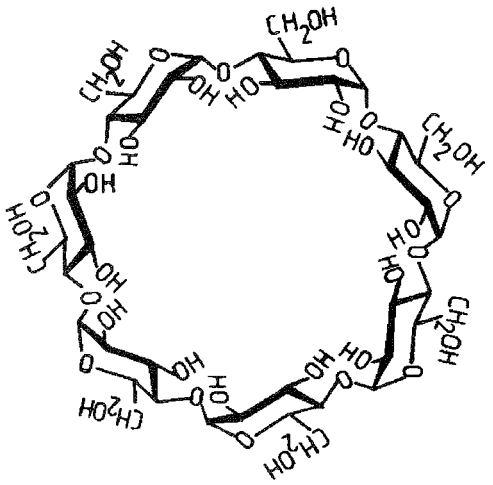

βCD

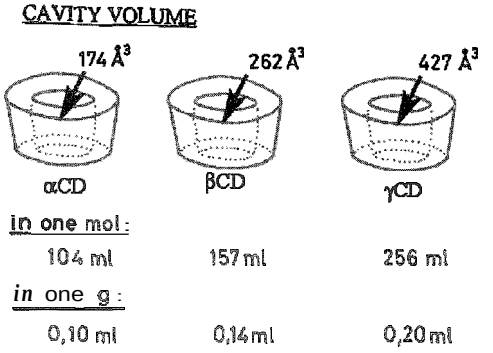

Fig. 1 Structure of βCD and approximate geometric dimensions of α-, β-, and γCD molecules. (*View this art in color at www.dekker.com.*)

hydroxy! groups are situated, the cavity is wider than on the other side, where free rotation of the primary *hydroxyls reduces the effective diameter of the cavity.*

For a *long time.* only *the three parent (or major)* CDs (α-, β-, *and* γCD) *were known and well characterized.*

In *the* 1990s, *a series of larger* CDs *was* isolated *and studied. For example. the nine-membered* δCD *was isolated from the* commercially *available CD-conversion mixture by chromatography. The 6CD has greater aqueous solubility than the* βCD *but less than that of* α- *and* γCD. *It was the least stable* among *the* CDs *known at that time; their acidic hydrolysis* rate *increases in the order of* αCD<βCD<γCD<δCD. *The* δCD *did not show significant solubilization effect on slightly soluble drugs* in *water. except in the cases of some large guest molecules, like spironolactone and digitoxin.*

The larger CDs *are not regular cylinder-shaped structures. They are collapsed. and their real cavity is* even smaller *than that in* the γCD. *The proposed principal driving force of the complex formation, the substitution of the high-enthalpy water molecules in the CD-cavity, is weaker in the case of larger* CDs, *and therefore. their utilization as inclusion-complexing agents will probably* remain *restricted.*

PRODUCTION OF CDS

The cyclodextrin glucosyl *transferase enzyme (CGT-ase)* is *produced by a large number of microorganisms, like Bacillus macerans, Klebsiella oxytoca, Bacillus circulans. Alkalophylic bacillus No. 38-2. etc. Genetic engineering provided more active enzymes, and probably, in the future. these enzymes will be used for industrial* CD *production.*[7]

The first step in CD *production is the liquefaction of starch at an elevated temperature. To reduce the viscosity of the concentrated (around 30% dry weight) starch solution, it has to be hydrolyzed to an optimum degree. The prehydrolyzed starch* must *not contain glucose, or low-molecular oligosaccharides, because they strongly reduce the yield of the* CDs *formed. After cooling to the optimum temperature, the* CGT-ase enzyme *is added to the starch solution. In the so-called nonsolvent technology, the* α-, β-, *and* γCDs *formed have to be separated from the complicated partially hydrolyzed mixture.* In *the case of solvent technology. an appropriate* complex-*forming agent is added to the* conversion *mixture. If toluene is added to this system. the* toluene–βCD-formed *complex is separated immediately. and the conversion is shifted toward the formation of* βCD. *If n-*decanol *is added to the conversion mixture. mainly* αCD *will be produced. while in the case of cyclohexadecenol. the main product is* γCD. *Various other complex-forming agents can be used. The selection depends on price, toxicity. and explosivity,* and most *importantly, on the efficiency of the removal of the solvents* from *the crystalline end product. The insoluble complexes are separated from the conversion mixture by filtration. The removal of the solvents from the filtered and washed complex is generally* made *after suspending it in water by distillation or extraction. The aqueous solution obtained after removal of the* complexing *solvent is treated with activated carbon and then filtered. The cyclodextrins are then separated* from *this solution by crystallization and filtration. The* homogeneity *of the industrially produced cyclodextrins* is *generally better than 99%.*

CYCLODEXTRIN DERIVATIVES

For many reasons *(price. availability. approval status, cavity dimensions, etc.).* βCD *is the* most *widely used and*

Table 1 Characteristics of α-, β-, and γCD

	a	β	γ
No. of glucose	6	7	8
Mol. wt.	972	1135	1297
Solubility in water g 100 ml $^{-1}$ at room temperature	14.5	1.85	23.2
$[\alpha]_D$ 25"	150±0.5	162.5±0.5	177.4±0.5
Cavity diameter Å	4.7–5.3	6.0–6.5	7.5–8.3
Height of torus Å	7.9±0.1	7.9±0.1	7.9±0.1
Diameter of outer periphery Å	14.6t0.4	15.4±0.4	17.5±0.4
Approximate volume of cavity Å^3	174	262	427
Approximate cavity volume in 1 mol CD (ml)	104	157	256
Approximate cavity volume in 1 g CD (ml)	0.10	0.14	0.20
Crystal forms (from water)	Hexagonal plates	Monoclinic parallelograms	Quadratic prisms
Crystal water wt%	10.2	13.2–14.5	8.13–17.7
Diffusion constants at 40°C	3.443	3.224	3.000
Hydrolysis by A. *oryzae* α-amylase	Negligible	Slow	Rapid
pK (by potentiometry) at 25°C	12.332	12.202	12.081
Partial molar volumes in solution ml.mol^{-1}	611.4	703.8	801.2
Adiabatic compressibility in aqueous solutions ml.mol^{-1} bar^{-1}.10^4	7.2	0.4	−5.0

represents at least 95% of all CDs produced and consumed. It is used for many purposes; however. its anomalous low aqueous solubility (and the low solubility of most of its complexes) is a serious barrier in its wider utilization. Fortunately by chemical or enzymatic modifications. the solubility of all CDs can be strongly improved, and instead of the 18 g/L aqueous βCD solutions 500 g (or more)/L aqueous βCD derivative solutions can easily be prepared.

In the cyclodextrins. every glucopyranose unit has three free hydroxyl groups that differ in their functions and reactivity. The relative reactivities of C(2) and C(3) secondary, and the C(6) primary hydroxyls, depend on the reaction conditions (pH. temperature, reagents). In βCD, 21 hydroxyl groups can be modified by substituting the hydrogen atom or the hydroxyl group with a large variety of substituting groups (like alkyl-, hydroxyalkyl-. carboxyalkyl-, amino-. thio-. tosyl-, glucosyl-, maltosyl-, etc., groups). And. thousands of ethers. esters. anhydro- deoxy-, acidic, basic. etc.. derivatives can be prepared by chemical or enzymatic reactions.[110] The aim of such derivatizations may be as follows:

To improve the solubility of the CD derivative (and its complexes).
- To improve the fitting. or the association between the CD and its guest, with concomitant stabilization of the guest, reducing its reactivity and mobility.
- To attach specific (catalytic) groups to the binding site (e.g., in enzyme modeling).

To form insoluble, immobilized CD-containing structures, polymers. e.g., for chromatographic purposes.

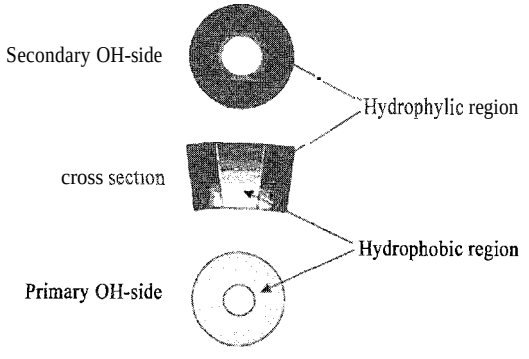

Fig. 2 Schematic representation of the hydrophilic/hydrophobic regions of a CD molecule. (*View this* art *in color at www. dekker.com.*)

From the thousands of CD derivatives described in hundreds of scientific papers and patents, only a few can be taken into consideration for industrial-scale synthesis and utilization. Complicated muitistep reactions, using expensive. toxic. environment-polluting reagents, and purification of the products by chromatography are feasible for preparing derivatives only on laboratory scale. To produce tons, at an acceptable price. only about a dozen of the known CD derivatives can be taken into consideration.

Among industrially produced. standardized, and available (even in ton amounts) βCD derivatives. the most important are the heterogeneous, amorphous. highly water-soluble methylated βCD and 2-hydroxypropylated βCDs. Due to their heterogeneity, these products cannot be crystallized, which is an important advantage (e.g., at

producing liquid drug formulations). More important. however. is that these derivatives cannot form crystalline cholesterol complexes; because the nonmodified βCD has a particularly high affinity to cholesterol. If administered parenterally, it is not metabolized in the organism but forms insoluble cholesterol complex crystals in the kidneys, resulting in nephrotoxicity.

The first hydroxypropyl-βCD and hydropropyl-γCD to contain drug formulations are already approved and marketed in several countries.

A methylated βCD is more hydrophobic than the βCD, therefore, it forms a more stable (but soluble) complex with cholesterol. Its affinity to cholesterol is so strong that it extracts cholesterol from the blood cell membranes: resulting in hemolysis in around 1 mg/mL concentration.

A particular inethylated βCD, the heptakis (2,6-di-*O*-methyl-βCD, called DIMEB) is a crystalline product. It is extremely soluble in cold water but insoluble in hot water, therefore, its purification, and also the isolation, of its complexes is technically simple. Up to now, no better solubilizer was found among the CDs. It is available in better than 95% isomeric purity for injectable drug formulation. but for widespread industrial application, the cheaper randomly methylated βCD (called RAMEB) is produced and marketed.

Reacting βCD with starch in the presence of pullulanase enzyme results in the attachment of one or two maltosyl or glycosyl groups to the primary side of the CD ring with α-1,6 glycosidic linkage. The product is the so-called "branched" CD (mono- or dimaltosyl or mono- or diglucosyl CD). which is very soluble in water, being a heterogeneous, noncrystallizable substance. It is produced and used in the food industry, mainly in Japan. for example, for production of stable flavor-powders.

There is also increasing interest in the per-acyl-CDs. All acetylated CDs from per-acetyl to per-octanoyl esters were studied partly as retard drug carriers (to retard the drug release for absorption from its pharmaceutical formulation). partly as bioadhesive, film-forming substances to be used in transdermal drug delivery systems.

The heptakis-(sulfobutyl)-βCD is very soluble in water. noncrystallizable. and even at extremely high doses seems to be free from any toxic side effects. It can be used as a chiral separating agent in capillary zone electrophoresis. But, the aim of intensive research is to develop it as a parenteral drug carrier, for preparation of aqueous injectable solutions of poorly soluble drugs.

The GD sulfates possesses many similar properties as heparin. without its anticoagulating effect. Apparently, they can reduce the blood supply of tumor tissues through inhibiting the formation of new arteries.

The monochloro-triazinyl βCD is produced on industrial scale from CDs and cyanuric chloride. It is reactive with cellulose fibers in alkaline medium (see the entry *Cyclodextrins: Applications).*

To elongate the actual CD cavity, substituents are attached to the primary or secondary side. This elongation may be hydrophylic, in which case: hydroxyalkyl groups are attached to the ring, or it might be hydrophobic, for example, by substituting the primary hydroxyl groups with long fatty-acid chains: "medusa"-like molecules can be prepared. These molecules behave as detergents while retaining their complex-forming ability. In the coming years. it will be decided how these derivatives may be utilized.

The chair conformation of the CD ring can be modified by inverting the position of some hydroxyl groups. For example, eliminating the tosyl group in alkaline medium from a CD-tosyl derivative, 2,3-anhydro derivatives can be prepared. When opening the anhydro ring, one hydroxyl group will take up an inverted position, and in this way, cycloaltrins are formed. By eliminating an appropriate leaving group from the primary side, 3,6-anhydro-CDs are formed. Because of the twisted conformation of the anhydro-glucopyranose unit, the properties of CDs (for example, their solubility) are strongly changed.

It is possible to close one side of the CD cavity, for example, by overbridging the primary or secondary side with an appropriate bifunctional substituent. It is expected that these overbridged CDs will form more stable complexes with certain guests.

The essence of photodynamic tumor therapy is that particular compounds have to be delivered to the tumor tissues. which upon the effects of strong light, become toxic through isomerization or splitting, etc. In this case, upon strong light irradiation, the photosensitive molecules will become toxic just for the tumor cells. For such targeting of the drug, very stable (10^5–10^7 M^{-1}) complexes are needed. The duplex homo- or heterodimers of CDs (constructed only from one or two different CDs) form complexes that are more stable by orders of magnitude than those of the single CDs. By interconnecting two CDs with appropriate bridges, such duplex CD derivatives were prepared that can form stable complexes with photosensitive posphyrinoid structures and transport them to the target organs.

In "antennae"-bearing CDs, receptor-specific oligosaccharide units are attached to the CDs, which will bond only to specific receptors in the living organisms. The aim of these efforts is to synthesize a receptor-targeting carrier, that is, the drug complexed with an antenna-bearing duplex CD would transport the specific drug solely to the target organ.

The most complicated CD derivatives are synthesized for enzyme-modeling experiments. By dimerizing amino acid CD derivatives. hydrolase enzyme models were prepared. that approximate the activity of natural enzymes.

A dozen CD derivatives of various types are used in gas chromatography. liquid chromatography: and capillary zone electrophoresis.

For other industrial purposes where toxicological demands do not play a decisive role, epichlorohydrin crosslinked. hydroxyethylated, or sometimes apparently fancy (but justified by their usefulness) mixed ethers–esters, like heptakis (2,6-di-*O*-methyl)-3-*O*-trifluoracetyl-βCD and similar derivatives are produced and utilized.

It seems to be probable that for drug carrier purposes, four or five different CDs will be developed and produced in the future, because no one of them alone is able to fulfill all of the strict requirements, which are usual in case of a parenteral drug carrier.

For other industrial purposes. the production of hundreds of tons of alkylated, hydroxyalkylated, and acylated CDs is forecast by the end of the first decade of the twentieth century.

CYCLODEXTRIN COMPLEXES

In an aqueous solution, the slightly apolar cyclodextrin cavity is occupied by water molecules that are energetically unfavored (polar–apolar interaction) and, therefore, can be readily substituted by appropriate "guest molecules" that are less polar than water (Fig. 3). The dissolved cyclodextrin is the ''host'' molecule. and part of the "driving force" of the complex formation is the substitution of the high-enthalpy water molecules by an appropriate "guest" molecule. One, two. or three cyclodextrin molecules contain one or more entrapped "guest" molecules. Frequently, the host:guest ratio is 1:1. This is the essence of "molecular encapsulation."

This is the simplest and most frequent case. However 2:1, 1:2, 2:2, or even more complicated associations, and higher-order equilibria exist, almost always simultaneously.

The inclusion complexes formed can be isolated as stable crystalline substances. Upon dissolving these complexes, an equilibrium is established between dissociated and associated species. and this is expressed by the complex stability constant K_a. The association of the CD and guest (D) molecules, and the dissociation of the CD/guest complex formed is governed by a thermodynamic equilibrium:

$$\mathrm{CD} + \mathrm{D} \rightleftharpoons \mathrm{CD.D} \tag{1}$$

$$K_{1:1} = \frac{[CD.D]}{[CD][D]} \tag{2}$$

The most important primary consequences of the interaction between a poorly soluble guest and a CD in aqueous solution are as follows:

1. The concentration of the guest in the dissolved phase increases significantly, while the concentration of the dissolved free CD decreases. In case of ionized guests or hydrogen-bond-establishing (e.g., phenolic) guest molecules. the solubility of the CD increases. After reaching the solubility limit of the complex, its precipitation begins.
2. The spectral properties of the guest are modified. For example, the chemical shifts of the anisotropically shielded atoms are modified in the NMR spectra. Also. when achiral guests are inserted into the chiral CD cavity. they become optically active and show strong induced Cotton effects on the circular dichroism spectra. Sometimes the maxima of the UV spectra are shifted by several nm, and fluorescence is strongly improved, because the fluorescing molecule is transferred from the aqueous milieu into an apolar surrounding.
3. The reactivity of the included molecule is modified. In most cases. the reactivity decreases. i.e., the guest is stabilized. but in many cases, the CD behaves as an

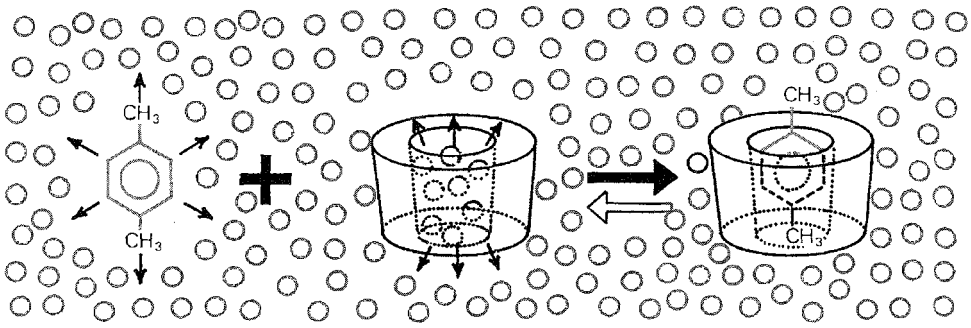

Fig. **3** CD inclusion complex formation. p-Xylene is the guest molecule. and the small circles represent the water molecules. (*View this art in color at www.dekker.com.*)

artificial enzyme. accelerating various reactions and modifying the reaction pathway.
4. The diffusion and volatility (in case of volatile substances) of the included guest decrease strongly.
5. The formerly hydrophobic guest, upon complexation. becomes hydrophilic, and therefore. its chromatographic mobility is modified.
6. In the solid state. the complexed substance is molecularly dispersed in a carbohydrate matrix forming a microcrystalline or amorphous powder, even with gaseous guest molecules.
7. The complexed substance in the solid state is effectively protected against any type of reaction, except that with the CD hydroxyls or reactions catalyzed by them.
8. Sublimation and volatility in the solid state are reduced to a low level.
9. The complex in the solid state is hydrophilic, easily wettable, and rapidly soluble.

When, in an aqueous system, the formation of the CD-inclusion coinplex can be detected, e.g., by NMR or circular dichroism or through a catalytic effect, this does not necessarily mean that a well-defined crystalline inclusion complex can be isolated. The two main components of the driving force of the inclusion process are the repulsive forces between the included water molecules and the apolar CD cavity on the one hand, and between the bulk water and the apolar guest, on the other hand. This second factor does not exist in the crystalline (dry) state. Therefore. it is common to find that the complex formation is convincingly proven in solution, but the isolated product is only a very fine dispersion of the CD and the guest.

The absolute majority of all practical applications of CDs (see *Cyclodextrins:* Applications) is based on their inclusion complex-forming capacity.

THE CD LITERATURE [REF. 9]*

By the end of 2003, the number of CD-related publications will be more than 26,000, representing more than 160,000 printed pages.

The only way to exploit the enormous potential hidden in the vast amount of literature is to summarize it in specific, well-limited critical reviews. More than 450 reviews were published on cyclodextrins. Less than 10% can be considered "critical evaluations." The majority comprise an uncritical compilation of that literature that the author was able to find and read (frequently only as an abstract), mixing significant, industrially important observations and products with unfounded speculations and nonfeasible ideas. While 30 years ago about four to five CD papers were published monthly, in 2002 just that many are published daily.

About 16% of all CD-relevant publications are dedicated to the fundamentals of cyclodextrin chemistry and technology, i.e., the physical and chemical properties of cyclodextrins, their enzymology, toxicology, production. and derivatives. This section also includes the numerous review articles on CDs.

Nearly 22% of the publications are dedicated to studies of the CD-inclusion phenomena. These works are generally not directly practice-oriented, dealing with energetics and kinetics of inclusion, x-ray, FT-IR, liquid- and solid-phase NMR, EPR, circular dichroism, Raman spectroscopy, enhancement of luminescence and phosphorescence. thermal analysis, interaction of CDs, with specific guest types, enzyme modeling with CDs and CD derivatives, preparation, analysis of cyclodextrin complexes, etc. These methods, as well as the correlation between the complexation and various structural and external parameters. form the basis for all practical applications of CDs.

The largest group of CD papers, nearly 25%, is dedicated to the pharmaceutical applications of CDs. The large number (nearly 5000) of drug/CD-related papers and patents is misleading, because many authors publish the same results in different journals under different titles but with virtually identical content. Rediscoveries are published frequently, simply because the authors did not read the earlier literature: in essence, they discovered something that was published earlier. Because of the many repetitions and the nonfeasible ideas. only about 30% of the published papers disclose new and significant results. Actually. only 7% of the CD-related papers are dedicated directly to the food, cosmetic, and toiletry applications of CDs, but at the same time, about 70% of all cyclodextrins produced are used in this field. The approval process for CD-containing products in this field is much simpler and faster than in the case of the drug/CD formulations. The amount of CD used in a cosmetic or toiletry product might be larger, by orders of magnitude, than the amount used in a drug.

Presently, about 11% of the CD literature is dedicated to the application of CDs in the chemical and biotechnological industries.

Approximately 25% of the CD literature involves the applications of cyclodextrins in analytical chemistry and diagnostic preparations. The analytical applications of CDs refer mainly to the application of cyclodextrins in gas chromatography. in high-performance liquid

*The most comprehensive source of CD literature is the *Cyclodextrin-News*, published monthly, since 1986.

chromatography. and in capillary zone electrophoresis. but some research was dedicated to thin-layer chromatography. to enhancement of UV-Vis absorption. luminescence/phosphorescence by CDs, and to increasing the sensitivity of the related analytical methods. Apparently. it is difficult to find a separation problem on an analytical scale that could not be solved by using the appropriate CD.

CONCLUSION

Cyclodextrins are, by far. the most important organic host molecules. The raw material for their production is starch: available, cheap. and its conversion to cyclodextrin is a relatively simple enzymatic process. A continuous, steady increase in production is expected in the following decade. both for CDs and their derivatives.

ARTICLES OF **FURTHER** INTEREST

Artificial Enzymes, p. *76*
Calixarenes and Their Analogues: Cation Complexation, p. 137
Calixarenes: Synthesis and Historical Perspectives, p. 153
Cucurbituril, Its Homologues, and Derivatives. p. 390
Cyclodextrins: Applications; p. 405
Drug Delivery, p. 484
Enzyme Mimics, p. 546
Nanocasting Strategies and Porous Materials. p. *950*

REFERENCES

1. Lichtenthaler. F.V.: Immel. S. Molecular modeling of saccharides. Tetrahedron: Asymmetry 1994. *5, 2045.*
2. French. D. The Schardinger Dextrins. In *Adv. Carbohydrate Chem.*: Academic Press: New York. *1957:* Vol. *12, 189.*
3. Srejtli. J. *Cyclodextrins and Their Inclusion Complexes*; Akadémiai Kiadó: Budapest. *1982: 296.*
4. *Cyclodextrins and Their Industrial Uses;* Duchene. *D.*. Ed.: Editions de Santé: Paris. *1987; 448.*
5. Szejtli. J. *Cyclodextrin Technology*; Kluwer Academic Publisher: Dordrecht, *1988: 450.*
6. *New Trends in Cyclodextrins and Derivatives*; Duchene. D., Ed.: Editions de Sante: Paris, *1991: 635.*
7. *Comprehensive Supramolecular Chemistry*; Szejtli, J.. Osa. T.. Eds.: Cyclodextrins, Pergamon: Oxford. *1996;* Vol. *3,* 693.
8. Chem. Rev. 1998. 98 *(5).* 1741–*2076.* (Special issue on Cyclodextrins).
9. Cyclodextrin News. Cyclolab Ltd.: Budapest. Vol. 1–17. 1986–2003.
10. Easton. N.J.: Lincoln, S.F. *Modified Cyclodextrins, Scaffolds and Templates for Supramolecular Chemistry*; Imperial College Press. London and World Scientific Publishing Co.: Singapore. *1999:* 393.

Cyclodextrins: Applications

József Szejtli
CYCLOLAB, Cyclodextrin Research and Development Laboratory Ltd., Budapest, Hungary

INTRODUCTION

The vast majority of cyclodextrin (CD) applications involve the formation of inclusion complexes between CDs and appropriate guest molecules. The complex formed (Fig. 1) may be used as follows:

Might be isolated as a solid inicrocrystalline or amorphous powder.

- Might be utilized in (mostly) aqueous solutions to modify solubility. spectral properties, reactivity, etc., of the guest.
- Complex formation might be utilized only as a transient, discriminating operation, as in catalysis or in chromatographic separation processes.

The actual arid potential uses of CDs in products and technologies seem to be inexhaustible.

The amount of relevant literature keeps steadily growing. An incoinplete list of relevant papers and patents would consist of at least 15 thousand references. which grows, at least in the next few years, by at least 1000 new entries per year. Therefore, the following few pages can give only a superficial impression of the enormous versatility of CD applications.

CYCLODEXTRINS IN DRUGS

The complexation of a drug molecule with a CD (Fig. 2) is generally considered in the following cases:

The drug is poorly soluble, and therefore, its bioavailability (upon oral, dermal. pulmonar, mucosal, etc.. applications) is incomplete or irregular.
The time to reach the effective blood level of the orally administered drug is too long because of the low dissolution rate. even in case of a complete absorption.

- There is no aqueous eye drop or injectable solution or other liquid formulation that can be prepared because of the low solubility.
The drug is chemically unstable. Because of its autodecomposition, polymerization, or degradation by atmospheric oxygen, absorbed humidity. light, etc., no marketable formulation with satisfactory shelf-life can be produced.
- The drug is physically unstable. Volatilization or sublimation results in losses. By migration. the originally homogeneous product becomes heterogeneous. or on account of its hygroscopicity, it liquifies by atmospheric humidity.
The acceptability of the drug is bad. because of bad smell, bitter, astringent, or irritating taste.
- The drug is a liquid, but its preferred pharmaceutical form would be a stable tablet. powder, aqueous spray, etc.
- The dose of the lipid(-like) poorly homogenizable drug is extremely low, and therefore. content uniformity of the product is problematic.
The drug is incompatible with other components of the formulation.
The relief of serious side effects (throat, eye, skin, or stomach ill-itation) is required.
- The extremely high biological activity (in case of drugs, requires extremely low doses) makes working with such powder dangerous.

The advantageous results of CD complexation of (CD-complexable) drugs are as follows:

Improved bioavailability from solid or semisolid formulations.
Enhanced stability and prolonged shelf life.
Reduced side-effects.
Uniform, easy-to-handle powders. even from liquids.
Aqueous. injectable solutions from poorly soluble drugs can be prepared (Fig. 3).

Speaking only of the numerous advantages of drug/CD complexation can be misleading, because there are just as many limiting factors that restrict the applicability of CDs to certain types of drugs. In addition. not all drugs are suitable for CD complexation. Many compounds cannot be complexed. or complexation results in no essential advantages. Inorganic compounds generally are not suitable for CD complexation. The exceptions include nondissociated acids (HCl, HI. H_3PO_4, etc.) halogens. and gases (CO_2, C_2H_4, Kr, Xe, etc.). Inorganic salts such as KCl, Fe-salts. etc., cannot be complexed.

General preconditions (which are not without exceptions) to form a medicinally useful CD complex of a drug molecule include characteristics such as a need for more

DOI: 10.1081/E-ESMC 120012796

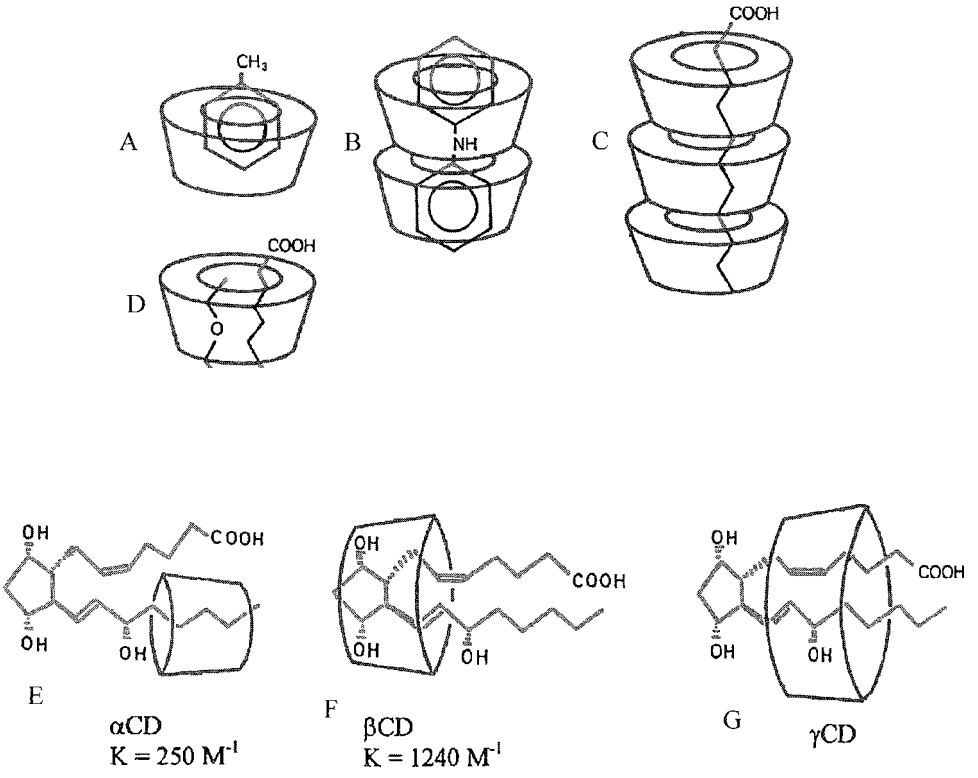

Fig. 1 Structures of various CD complexes. Toluene fits well into a βCD cavity. for diphenylamine, two βCDs form a "capsule." A long-chain fatty acid can take up three or more αCDs. A short-chain fatty acid and diethylether form a stable ternary complex. In the case of prostaglandin E_1 the αCD accomodates only the aliphatic chain of the unsaturated cyclic hydroxy-fatty acid. but it is enough to convert it into a water-soluble complex. The βCD can accomodate the cyclopentane moiety. but γCD is too wide for this guest. (*View this art in color. at www.dekker.com.*)

than five atoms (C, P, S, N) to form the skeleton of the drug molecule:a solubility in water of less than 10 mg/ml; a melting point temperature below 250°C (otherwise the cohesive forces between the molecules are too strong); a inolecule that consists of less than five condensed rings; and a molecular weight between 100 and 400 (with smaller molecules, the drug content of the complex is too low, and large molecules do not fit the CD cavity).

Strongly hydrophilic and moiecules that are too small or too large, such as peptides, proteins, enzymes, sugars. polysaccharides. etc., generally cannot be complexed. Nevertheless, when large water-soluble molecules contain appropriate complex-forming side chains, e.g., an aromatic amino acid in a polypeptide. they will react with CDs in aqueous solutions, resulting in modified solubility and stability. (For example, the stability of an aqueous solution of insulin, or many other peptides, proteins, hormones. and enzymes, is significantly improved in the presence of an appropriate CD.)

An unavoidable limiting factor in selecting the drug for complexation is the dose of the complex that has to be administered. A fundamental requirement is that the mass of a tablet should not exceed 500 mg. Because the drugs to be complexed have molecular weights between 100400, and the CDs have large molecular weights (972. 1132, and 1297 for α-, β-, and γCDs, respectively), a 100 mg complex contains only about 5–25 mg of active ingredient. If the single dose of a drug is not more than 25 mg. then even a complex of 5% active substance content can carry the necessary dose in a single tablet of 500 mg weight, otherwise the possibility of a powder sachet or sparkling-tablet formulation has to be taken into consideration. Thus, in the case of complex-forming drugs. the relationship of the required dose and the molecular weight determines the feasibility of oral administration in CD-complexed form.

Similarly, the volume of an injection should be less than 5 inl, or even better, not more than 2–3 ml, i.e., sufficient to dissolve the necessary amount of drug in 2–3 ml of 40% HPBCD (=2-hydroxypropyl-β-cyclodextrin) solution—800–1200 mg HPBCD can be used. In liquid formulations: the use of CD derivatives in excess is possible. In the case of Prostavasin injection, the molar ratio of prostaglandin E_1 to αCD is 1:11 (20 μg

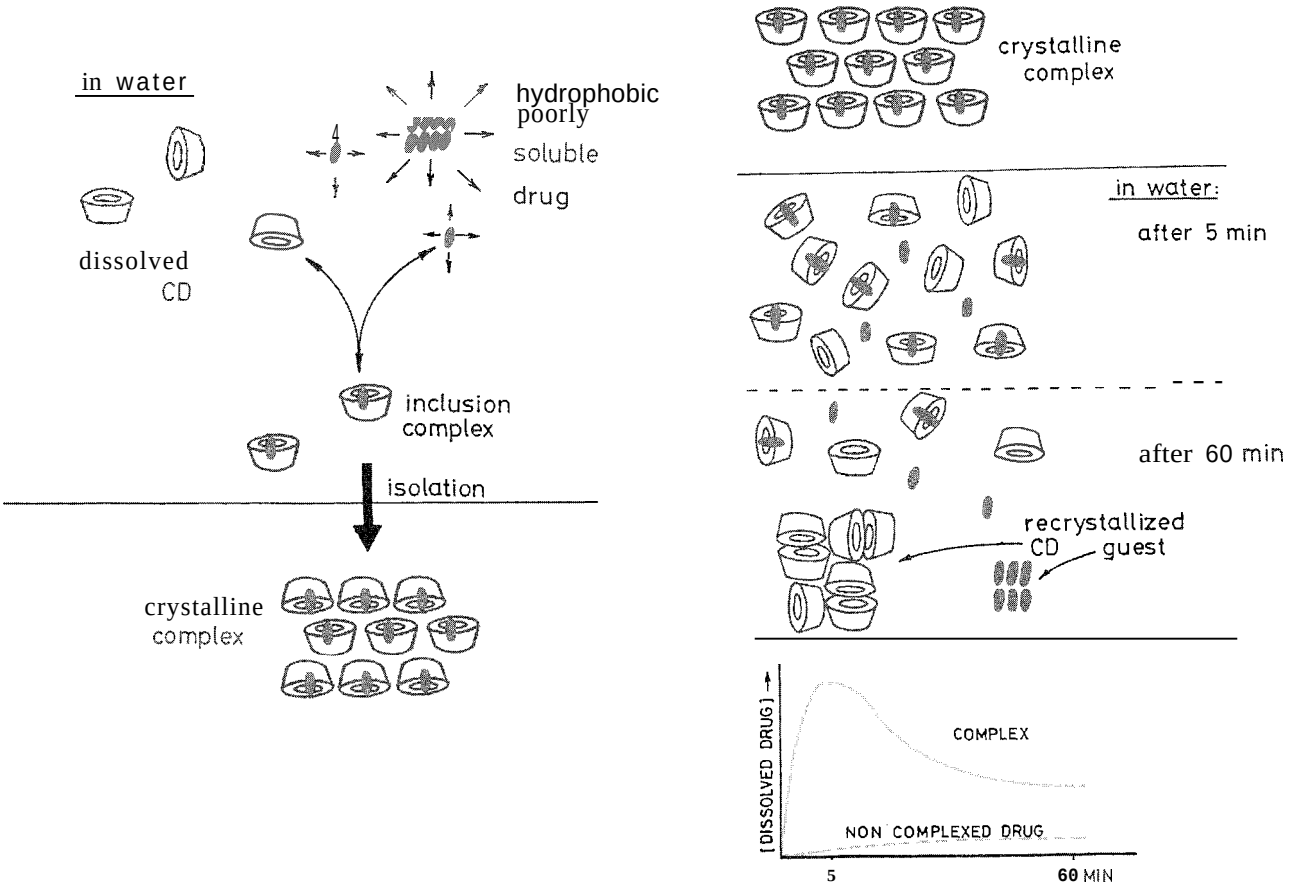

Fig. *2* Preparation and redissolution of a drug/CD complex. (Left) The poorly soluble drug is dissolved in an aqueous CD solution. The formed complex is isolated by cooling or removing the water by freeze-drying. spray-drying, or evaporating to dryness as a microcrystalline or amorphous powder. (Right) The drug/CD complex (e.g., compressed to tablet) in water. In gastric juice, the complex is dissolved within seconds. resulting in an oversaturated solution. Both recrystallization (separation) of the host (CD) and the guest (drug) and absorption of the drug begin immediately. Dissolving the complex results in a much higher dissolved level of the drug than in case of the plain drug. (*View this art* in color *at www.dekker.com.*)

PGE_1 + 646 μg αCD/dose). In slow infusion. the parenteral administration of several grams of a noncrystallizable CD derivative is possible. for example, in a liquid itraconazole formulation; the weight ratio of the drug to hydroxypropyl βCD is 1:40.

A 3000 I.U. D_3-vitamin tablet contains only 0.075 mg cholecalciferol; a Prostarmon-E tablet contains only 0.5 mg PGE_2; the active ingredient content of a nitroglycerin tablet is 0.5–4 mg—these and similar drugs are ideal for CD complexation, but even the 20 mg piroxicam containing BREXIN tablet is a widely marketed successful product.

If the K_a stability constant of a complex is low (less than 10^2 mol^{-1}), the existence of the complex can be demonstrated in solution. but on removing the water, the product obtained is often only a mixture (e.g., a coprecipitate) that contains the host and guest in a fine dispersion. Also, on removing the water, an important component of the driving force for complexation is eliminated: the repulsive forces between water and the hydrophobic drug. Upon contact with water, the complex formation is an instantaneous process, i.e., in solution, the guest is included in the CD cavity, and the dissociation–association equilibrium is reached within seconds.

In such cases. the guest is not protected against external destructive factors, like oxygen or humidity. but if the guest is stable enough. and only its low solubility is problematic, such intimate mixtures can be utilized for preparation. e.g., solid formulations of improved bioavailability. If. however. the guest is unstable, then only full complexation. even in the anhydrous state, can be of use.

In cases of extremely high complex stability constants (over about 10^4 M^{-1}), the bioavailability of a drug can be reduced. The complex is practically not absorbed and actively arises only from the free, molecularly dispersed (dissolved) drug molecules. In such cases, the

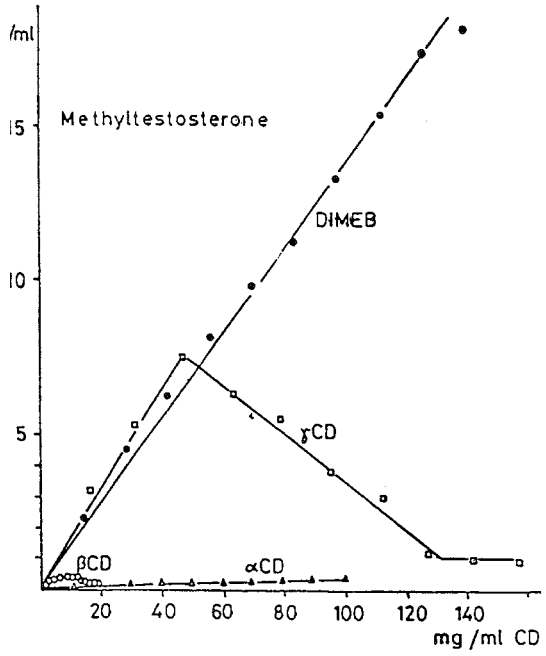

Fig. *3* In aqueous solutions of crystallizable CDs. depending on their concentrations. the solubility of poorly soluble compounds is increased. When reaching the solubility limit of the formed inclusion complex, the concentration dissolved drug reaches a plateau or even drops back. In the case of non-crystallizable CD derivatives, no such limit is attained, therefore. to form practically water-insoluble steroid. 10 or 20 or even more mg substances can be dissolved in the 1 ml solution of an appropriate CD derivative.

coadministration of a better complex-forming competitor molecule (e.g., phenylalanine) can help.

Hundreds of published examples illustrate the stabilizing, solubilizing and bioavailability enhancing, side-effect reducing, and advantageous technological effects of CD complexation of unstable. poorly soluble, locally irritating drugs. Illustrated in Table 1 is a selection of CD-containing drugs that are approved and marketed in various countries.

CYCLODEXTRINS IN **COSMETICS** AND TOILETRIES

Many active principles of interest in cosmetics were complexed with cyclodextrins. achieving positive and interesting results. For instance, the inclusion of retinol in hydroxypropyl-β-cyclodextrin leads to a water-soluble product, sufficiently stable, of higher bioavailability and lower toxicity compared to free retinol. Similarly, it is possible to include almost all vitamins in cyclodextrins. with unquestionable advantages with regard to their stability and bioavailability (Table 2). The main advantages of using CD complexes in functional dermocosmetics are similar to those in pharmaceutical formulations:

- Increase in the bioavailability of incosporated active components(vitamins, hormones. glycolic acid, depigmenting agents, etc.).
- Protection from oxidation (vitamin A. retinol, hydroquinone, arbutin, DHA, etc.).
- Reduction of toxicity and aggressivity (glycolic acid, hydroquinone. essential oils, fragrances, etc.).
- Formation of hydrosoluble complexes, even if the incorporated molecule is liposoluble.
- Increased stability of emulsion and gel products.
- Easy formulation: the complex is added to the final formulation, dispersing it in the aqueous phase at 35–40°C.
  No preservatives added.

Some special advantages were observed for sunscreen agent/CD complexes:

- Increased stability (photostability) of cream formulations.
- Decreared cytotoxicity.
  Increased/improved functional activity.
- Reduced smell.
  Reduced fabric staining.

Thus, the markedly increased photostability is associated with decreased phototoxicity and photosensitization risk coming from the production of free radicals primed by solar photochemical attack on the filter molecule.

Cyclodextrins are suitable for skin treatment products and for the formulation of makeup cosmetics. which are to stay on the face and skin for a number of hours (up to one day).

CD complexation can be used to stabilize emulsion and color, perfume, or aroma. For instance, most perfume concentrates. such as rose oil, citral, and citronella1 can form complexes and can be used in any solid preparation. such as powdered detergents: the collateral irritant effect caused by a scent in a shampoo can be reduced through the use of CD complexes: a solution of iodine-βCD can be used as deodorant for the body. for baths, or as a refresher for the oral cavity; a CD complex with detergent molecules can act as antifoam agents: etc.

CYCLODEXTRINS IN FOODS

Flavor substances are generally volatile and easily deteriorate. Most (e.g., tespenoids and phenylpropan derivatives) form stable complexes with CDs, and in dry

Table 1 Some approved and marketed CD-containing pharmaceutical products

Drug	*Trade name*	*Indication*	Formulation	Company/country
PGE_2/βCD	Prostarmon E	Induction of labor	Sublingual tablet	Ono, Japan
PGE_1/αCD 20 μg/amp	Prostavasin	Chronic arterial occlusive disease	Intraarterial	Ono, Japan: Schwarz. Germany
PGE_1/αCD 500 μg/amp	Prostadin 500	Controlled hypotension during surgery	Infusion	Ono. Japan
OP-1206/γCD	Opalmon	Buerger's disease	Tablet	Ono. Japan
Piroxicam/βCD	Cicladol. Brexin	Antiinflammatory, analgesic	Tablet, sachet, and suppositorq	Masterpharma, Chiesi, Italy
Garlic oil/βCD	Xund, Tegra, Allidex, Garlessence	Antiatherosclerotic	Dragees	Bipharm, Hermes, Germany: Pharmafontana. HU CTD, U.S.A.
Benexate/βCD	Ulgut, Lonmiel	Antiulcerant	Capsules	Teikoku, Japan: Shionogi, Japan
Iodine/βCD	Mena-Gargle	Throat disinfectant	Garling	Kyushin. Japan
Dexamethanose.Glyteer/βCD	Glymesason	Analgesic, antiinfammatory	Ointment	Fujinaga, Japan
Niroglycerin/βCD	Nitropen	Coronary dilator	Sublingual tablet	Nippon Kayaku, Japan
Cefotiam-hexetil/αCD	Pansporin T	Antibiotics	Tablet	Takeda. Japan
New oral cephalosporin (ME 107)/βCD	Meiact	Antibiotics	Tablet	Meiji Seika, Japan
Thiaprofenic acid/βCD	Surgamyl	Analgesic	Tablet	Roussel-Maestrelli, Italy
Diphenylhydramine.HCI chlortheophylline+βCD	Stada-Travel	Travel sickness	Chewing tablet	Stada. Germany
Chlordiazepoxide-βCD	Transillium	Tranquilizer	Tablet	Gador. Argentina
Piroxicam/βCD	Flogene	Antiinflammatory. analgesic for pediatric use	Liquid	Aché, Brazil
Hydrocortisone/HPβCD	Dexacort	Mouth wash against aphta, gingivitis, etc.	Liquid	Icelandic Pharm, Iceland
Itraconazole/HPβCD	Sporanox	Esophageal candidiosis	Liquid	Janssen, Belgium
Cloramphenicol/methyl βCD	Clorocil	Eye drop, antibiotic agent	Liquid	Oftalder. Portugal
Cisapride/βCD	Coordinax	Gastrointestinal mobility stimulant	Rectal supository	Janssen. Belgium
Nimesulide/βCD	Mesulid Fast	Nonsteroid antiinflammatory	Oral sachet	Boehringer, Italy
Ziprasidone mesylate/Captisol®	Zeldox. Ceodon	Antischizophrenic	Infusion	Pfizer. USA
Nicotine/βCD	Nicogum		Chewing gum	Pierre Fabre, France
Nicotine/βCD	Nicorette		Chewing gum	Pharmacia Upjohn, Sweden
Cetrizine/βCD	Cetrizin	Antiallergic		Losan Pharma. Germany
Voriconazole/sulfobutyl-βCD	VFEND®	Antimycotic	Tablet	Pfizer. USA
Mitomycin/HPβCD	MitoExtra	Antiinflammatory	Infusion	Novartis. Switzerland
Diclofenac Na/HPγCD	Voltaren ophtha	Nonsteroid antiinflammatory	Eye drop	Novartis. Switzerland
Omeprazole/βCD	Omebeta	Proton pump inhibitor	Tablet	Betapharm. Germany

complexed form remain stable for a long time, without further protection, at room temperature. Such powder-flavors are approved, produced. and used in several countries. like France. Japan, and Hungary. For example, lemon-peel oil/βCD complex mixed with powdered sugar is used in pastries: spice–flavor mixtures are complexed with CDs in the preparation of canned meat, and sausages: peppermint oil/βCD complex is used in chewing gum. etc. In Germany, the garlic-oil/βCD complex is marketed as odorless dragées (to substitute garlic. and a number of unstable garlic preparations. consumed to reduce blood cholesterol levels). The βCD cannot be considered tasteless. and its sweetness cannot be ignored. Its taste threshold value is lower than that of sucrose (detection: 0.039% c.f. 0.27%: recognition: 0.11% c.f. 0.25%). An aqueous solution of a 0.5% βCD proved to be as sweet

Table 2 Examples of CD-containing cosmetic products

Product name	Type	Produces
KLORANE	Dry shampoo	Klorane Laboratories
L EAU D ISSEY	Deodorant	Issei Miyake
EXCEPTIONAL	Lipstick	Elisabeth Arden
SELF ACTION TANNING CREME	Creme	Estée Lauder
ADVANCED SUN CARE	Sun protection	Estee Lauder
AKTIV COMPLEX PLUS	Sun protecting	AOK
CELLUTEX	Creme	Regena nex
LUMINIS	Tinted cieam	Roan SpA
VIVACE	Powder cologne	Shiseido
NOVOFLEX	Vitamin shampoo	Revlon
COLORAMA	Silicona-shampoo	Revlon
EUCERIN Q10 ACTIVE	Q10 vitamin creme	Beierisdorf
EUCERIN VITAL RETINOL	Vitamin A creme	Beiersdorf

as a 0.5% aqueous solution of sucrose, and a 2.5% solution was proven as sweet as a 1.71% sucrose solution. When βCD is used in food processing. its sweetness cannot be ignored. Sucrose sweetness and βCD sweetness are additive.

Emulsion stability, water retention, and storability can be improved in many cases by adding cyclodextrins to the food component or food. A solid composition containing sugars and amino acids for food or pharmaceutical purposes is known to undergo browning and caking. This can be prevented by incorporating in such a composition at least 40% of an oligo- or polysaccharide. such as dextrin, starch. or CD, with a water content of not more than 3%. For example, adding 20% βCD to a powdered juice consisting of anhydrous glucose: sodium L-aspartate. DL-alanine, citric acid. and inorganic salts, resulted in a product of excellent stability. After 30 days at 40°C, there was no apparent discoloration or caking. The control, without βCD, began to cake on the second day and to turn brown on the fourth day.

The CD can be utilized for preparing stable water-in-oil emulsions, such as mayonnaise and salad dressing. Natural food-coloring components in tomato ketchup can be stabilized by adding 0.2% βCD. The ketchup thus prepared did not discolor on heating at 100°C for 2 h, whereas the control did. The addition of CDs to emulsified foods or cheese can increase the water retention and the shelf life. In processed meat products. CD improves water retention and texture.

In Belgium. low-cholesterol butter is produced. The molten butter is mixed with βCD, which does not react with triglicerides but forms complexes with cholesterol. The βCD complex is easily removable from the butter. More than 90% of the choleste ol can be removed in one step. The butter does not retain any CD. Other low-cholesterol milk products, like cheese, cream. and even low-cholesterol eggs. are produced by this technology.

CYCLODEXTRINS IN CHEMICAL PRODUCTS AND TECHNOLOGIES

It is impossible to list all products that contain CDs. In the following, only a few examples will be given to illustrate the possibilities of CD utilization.

Binding CD to textile fibers chemically or by adsorption opens new ways for the preparation of perfumed textiles, with slow release of the perfume. The immobilized (wash-fast) cyclodextrin can be loaded with perfumes, or insect repellents, which will be released only slowly as a result of th reaction of body heat and released humidity (perspiration). Simultaneously. these hosts can bind distasteful smelling components of perspiration (deodorizing effect).

By mixing CD or CD-polymer fragrance complexes to a melt mixture of synthetic fiber polymers (e.g., polyester) and weaving fabric from such fibers. wash-fast fragrant fabrics can be produced.

The CDs represent a new class of auxiliary substances for the textile industry. It is important that their chemical oxygen demand (in wastewater) is lower than that of the usual textile auxiliary substances. While the chemical oxygen demand (in mg/g) for the widely used tensides NP10 is 2020, Uniperol O is 1930, and Gisapon 1555 is 2290. for βCD this value is only 1060.

For coloration of polyester fibers, so-called dispersion dyes are used, which are poorly soluble in water (0.1–10 mg/l). Without using solubility-enhancing agents, such as tensides. uniform dyeing is not possible. However; CDs can substitute tensides. e.g., 0.3 g/l conversion mixture (which contains three cyclic and noncyclic dextrins) proved to be about equivalent to 1 g/l Eevegal HTN (a nonionic tenside).

Fragrant paper or paper containing protective substances can be prepared using CD complexes of perfumes, insecticides, rust inhibitors, mold- and mildew-proofing

agents. fungicides. and bactericides. For example. the fenitrothion βCD complex sprayed on a wet paper web, passed between drying rollers heated to 100°C, and wound to give insecticide-containing paper, was shown to be effective for more than 6 months.

Silane resins are made using a 1,5-cyclooctadieneplatinum catalyst. Once the catalyst is added, the reaction proceeds. On complexing the catalyst with βCD, it became possible to produce a single-component heat-curable silicone with a shelf life exceeding 7 months. because complexation prevented immediate catalysis and reaction. No gelation occurred at ambient temperature. Gelation began only when the mixture was heated to 150°C.

The conservation of wooden products, which are prone to attack by microorganisms. like the frames of windows, doors. and buildings constructed from wood; was usually done by impregnating, the wood with fungicides, which are generally water insoluble and therefore had to be dissolved in organic solvents. After impregnation, the solvents escape into the atmosphere. A new process dissolves the fungicides in aqueous CD solutions, and thus, the impregnation and conservation of the wood can be carried out without using organic solvents.

Emulsion-type coatings (paints) contain emulsion polymer binders to give. after drying, a resistant. continuous protecting film on the coated surface. To ensure the formation of a good film, the applied layer has to contain various coinpatible components, like solvent, pigment, thickener, and binder. The rheological properties of the paint are determined by the thickener. which is usually a hydrophobically modified polymer. like polyurethanes. polyacrylamides, cellulose ethers, etc. To avoid a concomittant excessive viscosity (which makes the formation of uniform coating on the surface to be covered difficult). viscosity suppressors have to be added to the emulsion. On adding CDs to this emulsion. the CD molecules will associate with the hydrophobic sites of the polymer and, being strongly hydrated. inhibit the association of the macromolecules, resulting in a strong reduction of the viscosity.

The CD complexes are compatible with thermoplastic resins. Mixing a dry pulverized CD complex of a perfume, for example, a geraniol αCD complex. with a thermoplastic resin (polyethylene), and molding it, yielded plastic products with a long-lasting (at least 6 months) fragrance. Rapid loss of the perfume by volatility and thermal decomposition can be avoided in this way.

Mixing CD complexes of thymol, eugeneol, isobutylquinoline, etc., to inolten PVC. a natural leather odor-emitting (leather-like) material. was prepared. e.g., for automobile door internal coverings.

Important properties, such as the relative sensitivity and fog of silver halide containing photographic materials can be improved by adding CDs to the light-sensitive photographic gelatin layers.

Additives, dyes, stabilizers, and fog inhibitors used in the photographic industry should be fixed to a certain layer of the film or photo paper. This can be achieved by using derivatives with "heavy" side chains. It seems to be more convenient to prepare water-soluble polymer complexes of these substances. In complexed form, their mobility is markedly reduced, and they become fixed to the layer required. A diminished diffusion can be observed either on preparing, processing, or storing the film. Another advantage of the soluble polymer complex is that poorly soluble or even water-insoluble stabilizers can be applied to the film in aqueous solutions. The CD–gelatin composition as in the photographic layer shows lower water absorption and accelerated diffusion of the developing agents.

The biological remediation of carcinogenic polyaromatic hydrocarbon polluted soils is a slow process. because the dangerous polluting hydrocarbons are adhered strongly to the soil particles, and hence, they are not available for the soil microorganisms. Adding CDs (for example. randomly methlyated βCD) to such soils results in mobilization of the hydrocarbons by the CD, which makes them available for the microorganisms. resulting in an accelerated remediation of the soil.

Explosive substances, like nitroglycerine, or isosorbide-dinitrate. when complexed, can be handled without any danger. The pernitro-γCD complex of the extremely explosive nitramine can be used as a controlled missile propellant.

Incorporated into food packaging plastic films, CDs effectively reduce the loss of aroma substances. Incorporating fungicide CD complexes into films, for example, packaging of hard cheeses, significantly elongates the shelf life of the product by inhibiting the rapid development of mold colonies on the surface of the packaged cheese.

CYCLODEXTRINS IN BIOTECHNOLOGY

The application of cyclodextrins in biotechnology began only in the 1980s. but rapid development is expected in this field.

The majority of biotechnology processes constitute an enzyme-catalyzed transformation of a substrate in aqueour media. The main difficulties that used to arise include the following:

- The substrate is hydrophobic and sparingly (or hardly) soluble in water.
  The enzyme or the enzyme-producing microbial cells are sensitive to the toxic effects of the substrate or to inhibitors that can be the product of the transformation.

- The substrate or the product is unstable under the conditions of the enzymatic transformation.
- Isolation of the product from the heterogeneous system is difficult.

Cyclodextrins and their derivatives enhance the solubility of complexed substrates in aqueous media and reduce their toxicity. but they do not damage the microbial cells or the enzymes. As a result, the enzymatic conversion of lipophilic substrates can be intensified (accelerated. or performed at higher substrate concentrations) in industrial processes and in diagnostic reagents, the yield of product-inhibited fermentation can be improved, organic toxic compounds can be tolerated and metabolized by microbial cells at higher concentrations, and compounds in small amounts can be isolated simply and economically from complicated mixtures.

Examples illustrate the rapidly-growing and promising uses of cyclodextrins in various operations: the intensification of the conversion of hydrocortisone to prednisolone, the improvement in the yield of fermentation of lankacidine and podophyllotoxin, the stereoselective reduction of benzaldehyde to L-phenylacetyl carbinol, and the reduction in toxicity of vanillin to yeast, or organic toxic substances to detoxificating microorganisms. In the presence of an appropriate cyclodextrin derivative (e.g., 2,6-dimethyl-β-cyclodextrin), lipid-like inhibitor substances are complexed. The propagation of *Bordatella pertussis* and the production of pertussis toxin therefore increases up to hundred-fold. Cyclodextrins and their fatty acid complexes can substitute for mammalian serum in tissue cultures.

Until recent years, the *Leprae bacillus* (Mycobacterium leprae) was considered not to be cultivable under in vitro conditions. The most important energy source for the bacillus is palmitic (or stearic) acid, which, however, cannot penetrate the thick. strongly hydrophobic shell of the mycobacterium. On solubilizing, the fatty acids (or fatty alcohols) with dimethyl-β-cyclodextrin, however, the Mycobacterium can be cultivated in vitro, on synthetic media. This discovery will facilitate the screening of drugs against similar difficultly-to-cultivate microorganisms.

MISCELLANEOUS USES

The active ingredients of pesticides (insecticides. fungicides. herbicides, etc.) can be complexed with the same technologies and same consequences as drug molecules.

The selectivity of an insecticide can be improved. For example, by complexing. the insecticide that kills the herbivorous insect will not be toxic for the honeybee. The stability against sunlight-accelerated decomposition of pyrethroids can be improved, ensuring a longer-lasting insecticidal effect. Wettability or solubility of poorly-soluble benzimidazole-type antifungicides can be improved. allowing reduction of the dose and reducing the pollution of the environment. The possibilities of utilization of CD in pesticide formulations were elucidated in numerous scientific papers; however, until the last years, the price of βCD did not allow for its application in such fields, because the pesticide industry is cost sensitive. By end of the twentieth century, the price of βCD dropped to such a low level that the price was no longer a restricting factor.

In medicinal diagnostic kits, a frequent problem is the limited, uncertain solubility of some essential component and the stability and storability of the kit. On complexing. the typical components with such problems can be

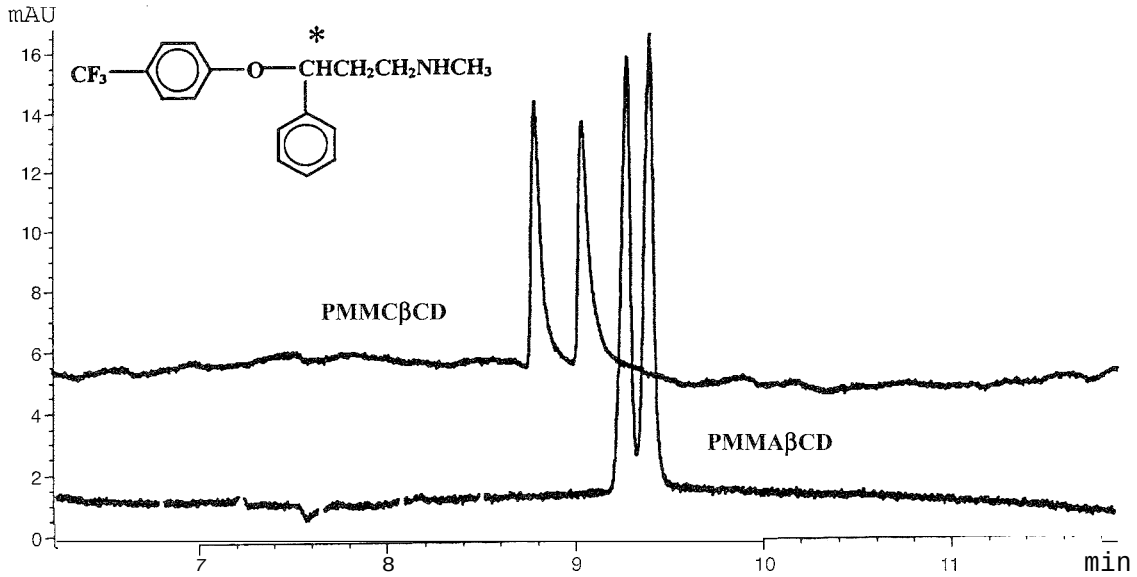

Fig. 4 Enantioseparation of Fluoxetine by capillary zone electrophoresis using permethyl-monodeoxy-monocarboxy-βCD or permethyl-monodeoxy-monoamino-βCD as chiral selector (10 mmol CD derivate pH 3.0 or 3.9).

eliminated. Also, frequently, the intensity of color reactions or of fluorescence can be significantly enhanced by the presence of CDs, resulting in higher sensitivity of the method.

There are some cases when the human taste and smell sensors cannot be substituted, even by the most sophisticated analytical instruments. In an organoleptic evaluation (comparison of identical food products of different origins, for example, beers), the dosing of extremely small but exactly known amounts of flavor components (for example, ppm amounts of mercaptanes. butyric acid, hydrogen sulfide, etc.) is necessary. To store and dose these volatile. unstable substances becomes simple when they are complexed with CDs, diluted with inert excipient to the appropriate grade, and filled in known amounts into hard gelatin capsules. By adding the content of one or more capsules of different flavors to the sample during sensoric "titration," the differences between the products can be expressed unambiguously and numerically.

In chromatographic separations, CDs and mainly specific derivatives are used widely. In the years 1990–2000, about 25 papers monthly were published on successful application of some CD in gas or liquid chromatography. In gas chromatography, CDs are used only in the stationary phase, while in HPLC, the CD is used either dissolved in the mobile phase. or bound to a surface in the stationary phase. In capillary zone electrophoresis. the most used chiral selectors are CDs. as their anionic: cationic. or alkylated derivatives (Fig. 4).

CONCLUSION

It is difficult to find an industry in which CDs are not or cannot be applied. In steadily increasing amounts, in the drug. food. cosmetic, textile. plastic, paper. pesticide, wood. toiletry; etc., industries, and in analytical chemistry. diagnostic. environment protection, packaging material production, etc.. CDs and CD derivatives are being used. Extrapolating the trends of the applications of CDs observed during the last two decades, no leveling-off is expected in the upcoming decades.

ARTICLES OF FURTHER INTEREST

Artificial Enzymes, p. *76*
Calixarenes and Their Analogues: Cation Complexation, p. 137
Calixarenes and Their Analogues: Molecular Complexation, p. 145
Cucurbituril, Its Homologues, and Derivatives, p. 390
Drug Deliver?, p. 484
Enzyme Mimics, p. 546
Stability Constants: Definition and Determination, p. 1360

REFERENCES

1. Proc. First Int. Symp. on Cyclodextrins. Budapest. 1981: Szejtli. J., Ed.; D. Reidel Publ.: Dordrecht, 1982: 544.
2. Atwood. J.L.; Davies. J.E.D.: Osa. T. Ill *Clathrate Compounds, Molecular Inclusion Phenomena and Cyclodextrins*. Proc. of Third Int. Symp. on Clathrate Compounds and Molecular Inclusion and the Second Int. Symp. on Cyclodextrins. Tokyo. 1981: D. Reidel Publ., Co.: Dordrecht, 1985; 426.
3. In *Inclusion Phenomena in Inorganic, Organic and Organometallic Hosts*. Proc. Fourth Int. Symp. on Inclusion Phenomena and the Third Int. Sympt. on Cyclodextrins. Lancaster. 1986: Atwood. J.L., Davies. E.D.. Eds.: D. Reidel Publ.: Dordrecht, 1987: 455.
4. Proc. Fourth Int. Symp. on Cyclodextrins. Munich. 1988: Huber. O., Szejtli, J.. Eds.: Kluwer Academic Publ.: Dordrecht. 1988: 576.
5. Minutes of the Fifth Int. Symp. on Cyclodextrins. Paris, 1990; Duchene. D.. Ed.: Editions de Santé: Paris. 1990: 722.
6. Minutes of the Sixth Int. Symp. on Cyclodextrins, Chicago. 1992: Hedges. A.R.. Ed.: Editions de Santé: Paris, 1992; 693.
7. Proceedings of the Seventh International Cyclodestrin Symposium, Tokyo. 1994: Osa. T., Ed.: Publ. Office of Business Center for Academic Societies: Tokyo, Japan. p. 554.
8. Proceedings of the Eighth International Cyclodextrin Symposium, Budapest. 1996: Szejtli, J., Szente, L.. Eds.: Kluwer Acad. Publ.: Dordrecht. 1996; 685.
9. *Proc. Ninth Int. Symp. on Cyclodextrins Santiago de Compostela*; Torres-Labandeira. J.J., Vila-Jato, J.L.. Eds.: Kluwer Acad. Publ.: Dordrecht. 1999: 707.
10. *Inclusion Compounds*; Atwood. J.L.. Davies, J.E.D.. MacNicol, D.D.. Eds.; Academic Press: London. 1984: Vol. 1–3.
11. *Comprehensive Supramolecular Chemistry*; Lehn. J.M., Atwood. J.L., Davies. J.E.D.. MacNicol. D.D.. Vogtle. F.. Eds.: Pergamon: Oxford. 1996: Vol. 1–11.
12. Fromming. K.H.: Szejtli. J. *Cyclodextrins in Pharmacy*; Kluwer Acad. Publ.: Dordrecht. 1993.

Cyclophanes: Definition and Scope

Carlo Thilgen
Vladimir A. Azov
ETH Zürich, Zürich, Switzerland

INTRODUCTION

The beginning of the more than centenarian history of cyclophane chemistry[1–4] can be related to the preparation of [2.2]metacyclophane (**1**, Fig. 1) by Pellegrin in 1899.[5] The ''modern age'' of cyclophanes started in 1951 when Cram and Steinberg reported a rational synthesis for the isomer **2**.[6,7] In the following decades, such ''small'' or strained cyclophanes were extensively used to study intramolecular interactions between braced arenes held in close proximity with defined relative orientation. The gained insights provided a strong basis for the understanding of weak intermolecular interactions involving aromatic rings.[8] Together with the exploitation of the restricted conformational flexibility of arene-based building blocks, this knowledge spurred the creation of highly preorganized macrocyclic cyclophane receptors and self-assembled superstructures, thus contributing significantly to the exuberant development of supramolecular chemistry during the last 30 years.

DEFINITION

Cram and Steinberg proposed the class name *paracyclophane*s for compounds in which two benzene rings are rigidly held in a face-to-face orientation by methylene bridges in the *para* positions,[6,7] the term *cyclophane* constituting a contraction of ''*cyclophe*nylene alk*ane*.'' The concept was subsequently systematized by Smith[1] and extended to a broader range of structural elements by Vögtle and Neumann, who designated as ''*phane*'' every molecule containing at least one aromatic nucleus and at least one n-membered bridge with $n \geq 0$.[3] A recent recommendation of the IUPAC defines *cyclophanes* as compounds having (i) mancude (*ma*ximum number of *n*on*cu*mulative *d*ouble bonds)-ring systems, or assemblies of mancude-ring systems, and (ii) atoms and/or saturated or unsaturated chains as alternate components of a large ring.[9]

NOMENCLATURE

According to the commonly used nomenclature of Vögtle and Neumann, two sets of numbers precede the components of the name that carries the suffix *-phane*: numbers in brackets indicate the length(s) of the bridge(s), starting with the longest one, and numbers in parentheses define the substitution pattern of the aromatic moieties (**1–5**, Fig. 1).[3] For multibridged arenes, the number of equal bridges can be indicated as a subscript to the number of *C*-atoms they contain (**1–3**).

The IUPAC recently published recommendations on phane nomenclature, representing a new approach for building names of complex organic structures.[10,11] In principle, each arene is collapsed to a ''superatom'' that, together with the remaining backbone, is named and numbered as an alicyclic system, the typical *-ne* ending being replaced by *-phane* (**5a,b**). Superatoms are cited as prefixes derived from the names of the corresponding arenes by changing their terminal *-e* to *-a*, e.g., *benzena*. These prefixes are incorporated in the name in analogy to heteroatoms in replacement (''a'') nomenclature. Arene positions that are connected to the remainder of the cyclophane backbone are indicated within parentheses, following the locants for superatoms. As an example, the simplified skeleton for cyclophane **5a** corresponds to ''cycloheptaphane'' **5b** with two superatoms in positions 1 and 4; the amplified full name is 1(2,7)-naphthalena-4(1,3)-benzenacycloheptaphane.

SYNTHESIS

In line with the immense structural diversity of cyclophanes, the synthetic approaches are extremely heterogeneous[1–3,12] and cannot be reviewed in a short synopsis. Progress in the preparation of cyclophanes is closely associated with the development of synthetic methodology for ring closure and ring contraction. Three principles of general importance in cyclophane synthesis should be mentioned.

Molecular Building Block Principle

A common aspect of many cyclophane syntheses is the modular assembly of simple structural subunits.[12] Macrocyclization can involve one or several components. The

Encyclopedia of Supramolecular Chemistry
DOI: 10.1081/E-ESMC 120012737

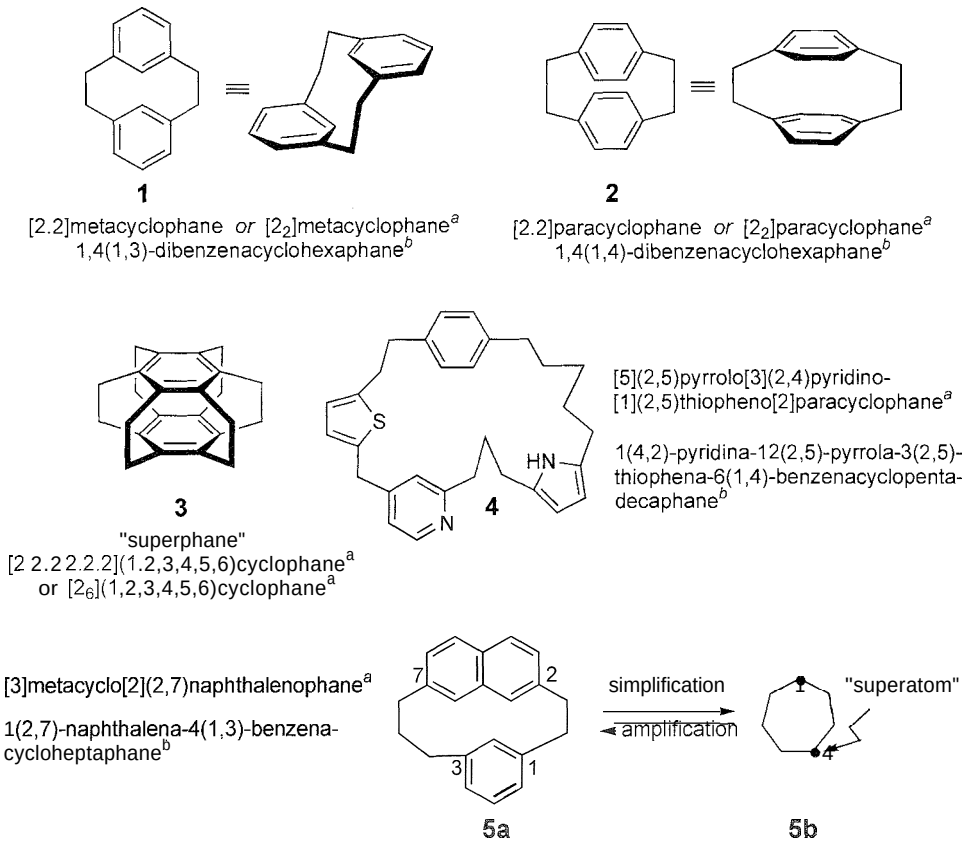

Fig. 1 Selected cyclophane structures and their nomenclature according to *Vögtle/Neumann*[a] and to IUPAC[b]

fewer bond formations it comprises, the higher the yields, in general. On the other hand, the synthesis of more elaborate precursors requires a higher number of steps. In practice, a compromise is made between synthetic effort and cyclization yield. The most important approaches to promote cyclization versus polymerization make use of the dilution principle and the template effect.

Dilution Principle

Cyclizations typically start from cornpounds with two or more reactive centers. Whereas the ring-closure is an intramolecular first-order reaction. intermolecular second-order reactions lead to undesired oligo- or polymerization. To favor cyclization over polymerization, reactions should be run at low concentration, a principle referred to as Ruggli's dilution principle.[13] However, in multicomponent syntheses including bimolecular steps prior to cyclization. the total reaction rate becomes too low at extreme dilution, and component concentrations between 5 and 50 mM are generally recommended. These can be achieved by slow addition of the starting materials to the reaction flask, for example, using syringe pumps.

Template Effect

Molecular templates are control elements leading to predominant or exclusive formation of a specific product from reactant5 that can, in principle, assemble in different wayc [''' They are often used to favor the formation of cycles over oligomers or of cycles of a certain size through specific interactions with the components during the assembly process.

'"SMALL" CYCLOPHANES

Small and, therefore, often strained cyclophanes encompass an enormous structural diversity (**1–13**, Figs. 1 and 2) that was reviewed in detail.[1–3] Their preparation initiated studies of weak noncovalent interactions between chromophores fixed in a rigid. geometrically defined arrangement. and thus, contributed substantially to paving the way for the development of supramolecular chemistry.

The "bent and battered''[6,7] arene rings of many cyclophanes with short bridges, e.g., **1** and **2**, or the *ansa* (lat.: handle) compounds [6]paracyclophane (6) (Jones)

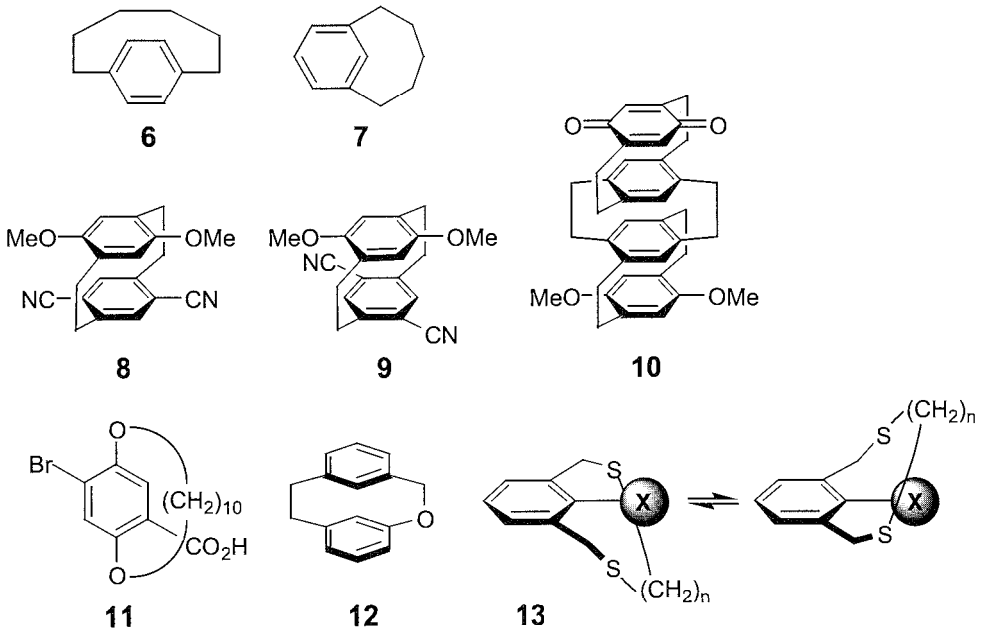

Fig. 2 "Small" cyclophanes with interesting structural, optical, and stereochemical properties.

and [5]metacyclophane (7) (Bickelhaupt),[3] deviate strongly from planarity. Together with transannular effects, the corresponding π-system distortions significantly affect chemical reactivity and spectroscopic properties.

Small cyclophanes generally exhibit an enhanced reactivity compared to the constituent arenes.[6,7,15] In [2_n]cyclophanes, for example, electrophilic aromatic substitution is facilitated by transannular interactions with the n-basic second deck; furthermore, Lewis-basic substituents direct a substitution in the second ring predominantly to the pseudogeminal position. Strain relief plays an important role in reactions like catalytic hydrogenation, cycloadditions, and cleavage or rearrangement of bridges.

Transannular interactions between arenes held in defined proximity and orientation within a cyclophane are easily detected in their electronic absorption or emission spectra, as shown by the groups of Staab, Haenel, and Misumi.[4] In combination with the deviation from planarity, these interactions result in a loss of fine structure and the appearance of a new long-wavelength transition centered around 300 nm in the UV/Vis spectrum of [2.2]paracyclophane, when compared to an open-chain reference.[6,7] Likewise, cyclophanes served as models for intermolecular excimers and exciplexes: most show a red-shifted, poorly structured fluorescence, reflecting the typical binding energy of an excimer or exciplex as well as the repulsion energy of the corresponding ground state. In an elegant study with donor–acceptor cyclophanes such as 8 and 9, Staab and coworkers investigated the orientation and distance dependence of charge–transfer interactions.[3] Typically. the pseudogeminal derivative (8) gave a red-shifted and more intense charge–transfer band compared to the pseudoortho isomer (9). Such interactions are effective even over several stacked chromophores, for example, in 10.

The incorporation of arenes in small cyclophanes hinders rotation around certain bonds and can afford isolable enantiomers with appropriately substituted backbones, e.g., planar-chiral 11 (Liittringhaus) or helical-chiral 12 (Vögtle).[1,16] Studies of the dynamic properties of small cyclophanes with intraannular substituents X (13) provided insight into the space occupancy of atoms or functional groups.[3]

CYCLOPHANE RECEPTORS

During the rapid development of supramolecular chemistry over the last two to three decades, a great variety of synthetic hosts was designed, many of them with a cyclophane backbone.[4,17–21] Aromatic building blocks confer a certain rigidity to cyclophanes and, if connected appropriately, span a preorganized cavity that can act as a binding site for guests.

The aromatic "walls" or spacers delimiting the cavity can participate in nondirectional binding through disperrion (van der Waals) interactions that are inherently weak but can add up to considerable values for large surfaces. Depending on the nature of the substrate and the

functionalization of the receptor, other possible interactions include aromatic π–π stacking and edge-to-face interactions, cation–π interactions: ion pairing (Coulomb interactions), ion–dipole and dipole–dipole interactions, and hydrogen bonding.[4,8,21] Binding selectivity: on the other hand, relies on size and shape of the cavity. and, most importantly, on directional interactions such as hydrogen bonding between appropriate functional groups of host and guest.

Extracavity functionalization is often required to make the inherently apolar cyciophanes soluble in polar solvents. Water solubility, in particular, may be desirable to take advantage of the hydrophobic effect as a strong driving force in the complexation of apolar guests.'''."]

Cyclophanes for Apolar Binding

Apolar binding plays a key role in the complexation by cyclophanes and will be discussed in some detail before specific classes of receptors are reviewed. Apolar complexation is mostly studied in water or polar organic solvents, because binding energies. largely determined by dispersion interactions and the desolvation of hydrophobic surfaces, are highest in these solvents. Polar functional groups that may be present are favorably solvated in the unbound receptor or substrate. To avoid a strong reduction in binding free enthalpy, full solvation must be maintained upon complexation or replaced by energetically equivalent host–guest interactions.[4,21]

In 1980, Koga and coworkers reported the inclusion complexation of benzene and naphthalene derivatives by 14 (Fig. 3) in aqueous HCl.[2] To inspect the driving forces for inclusion complexation by completely lipophilic cavities in detail. Diederich and coworkers investigated a series of cyclophanes (**15a–c**) displaying the following features:[4]

- The diphenylmethane moieties open and preorganize a cavity lined by benzene rings that are nearly orthogonal to the mean molecular plane.

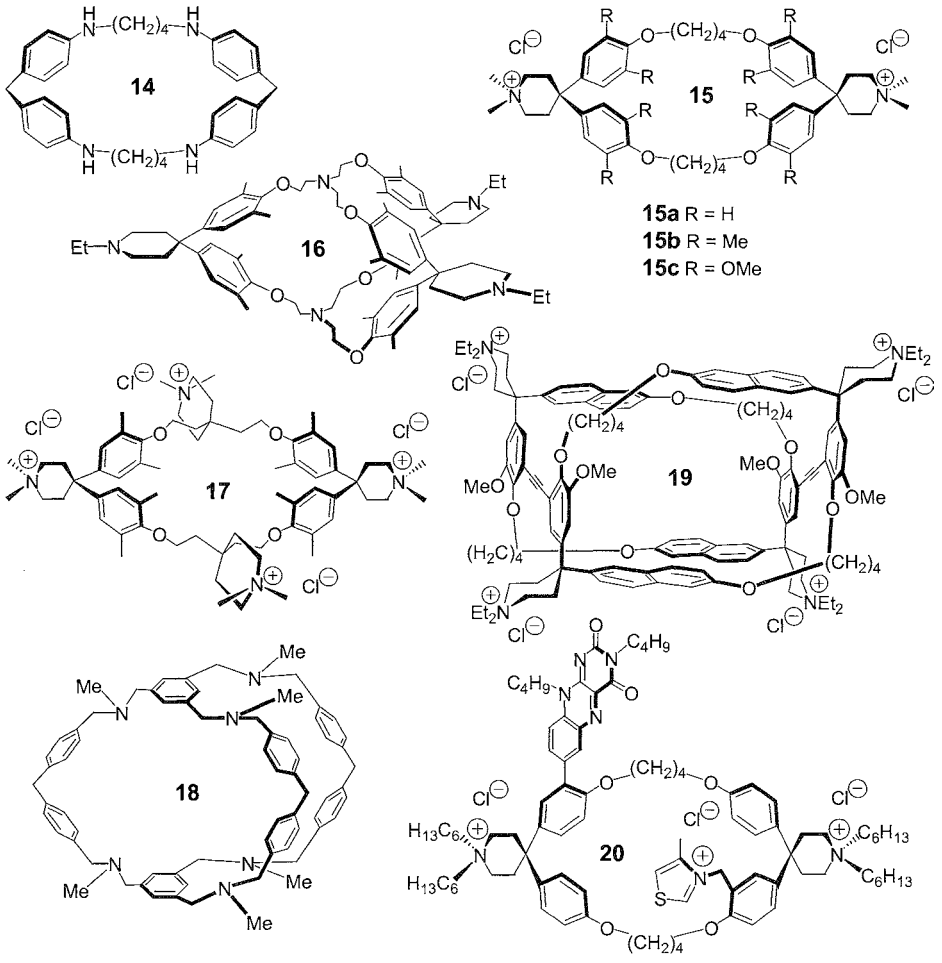

Fig. *3 Cyclophanes for apolar* complexation.

The length of the chains between the diphenylinethane substructures determines the size of the cavity. Careful conformational analysis of flexible units is crucial for succesful host design.

- The depth of the cavity is influenced by substituents on the benzene rings.

  The quaternary ammonium ions provide water solubility. Being remote from the binding site, they do not influence its polarity or solvation.
- In the absence of guests, the cavity is filled with solvent.

A coinplexation study (CD_3OD) of **15b** with 2,6-disubstituted naphthalenes carrying donor or acceptor substituents revealed that relative binding strength is controlled by polar effects that can also be considered donor–acceptor interactions:[4,21] increasing acceptor strength of the guest substituents enhances π–π-stacking interactions with the electron-rich benzene rings of the host and $C–H_{guest} \cdots \pi_{host}$ edge-to-face interactions.[8]

The thermodynamics of tight complexation of *para*-disubstituted benzene derivatives by **15c** in water are in conflict with the classical hydrophobic effect. i.e., large favorable entropy change. small enthalpy change. and large negative change in heat capacity. Deeper insight into the enthalpic driving force for apolar complexation and the role of the solvent was provided by calorimetric investigation of the coinplexation between **16** and pyrene in a series of solvents ranging from H_2O to CS_2.[4,21] Tight apolar colnplexation is mostly enthalpy driven and increases from apolar over dipolar aprotic to protic solvents with water at one end of the scale but in accord with the entire series. The main enthalpic contributions appear to be favorable changes in solvent cohesive interactions and gain in dispersion interactions (nonclassical hydrophobic effect).

Cyclophane **17** undergoes strong colnplexation with polycylic aromatic hydrocarbons (PAHs) of complementary size and shape in water.[4,21] Peryiene. with its large surface providing significant dispersion interactions and releasing many H_2O molecules into the bulk solvent, shows the strongest binding that may benefit also from ammonium ion–π interactions. For naphthalene derivatives with ionic substituents, ion-pairing interactions lead to extraordinary substrate selectivity. Cyclophane **17** can act as a carrier for the passive transport of PAHs between two hexane phases across an aqueous interphase. Another strong size-and shape-selective receptor for PAHs in acidic aqueous medium is hexaamine 18. reported by Vögtle and coworkers.[3,17]

Thanks to their modular design. cyclophanes are easily adjusted to bind target substrates. Thus, when the cavity of 15c was enlarged by replacing two benzene by naphthalene units and deepened by .'stacking" two macrocycles on top of each other. the resulting D_2-symmetrical double-decker cyclophane 19 was suitably shaped and preorganized for inclusion of steroids such as cholesterol.[21]

Water-soluble cyclophanes are also studied as possible catalysts or artificial enzymes: the hydrophobic cavitiy serves as substrate binding site while appended functional groups act as cofactors. The pyruvate oxidase mimic 20 performed remarkably in the oxidation of aromatic aldehydes to the cossesponding esters (MeOH/H_2O), and it displayed Michaelis–Menten kinetics comparable to those of natural enzymes.''' The encapsulation of cyclophanes in dendrimers creates binding sites within microenvironments. resembling those existing in protein superstructures.

Calixarenes, Resorcinarenes, and Cavitands

Calixarenes (**21**) and resorcinarenes (22) (Fig. 4)[22] are condensation products of phenol or resorcinol (benzene-1.3-diol) and aldehydes. Depending on the reaction conditions and the substitution of the starting benzenols. size and shape (conforination) of the cyclooligomers and, therefore. of their basket-shaped cavities can be varied. They can be further modified by functionalization of the hydroxy groups or the benzene rings. This modular concept makes them versatile receptors with regard to structure and function.

The bridging of vicinal arene units of resorcinarenes via their hydroxy functions leads to deeper and more rigid cavities in cavitands (23 and **24**).[23] Quinoxaline-2.3-diyl-bridged cavitands (24) can be switched between the so-called *vase* and *kite* conformers as a function of temperature or pH. Whereas the *vase*, predominant at higher temperature or lower pH, possesses a deeper cavity, the *kite* displays an extended, relatively flat surface.

Carcerands and Hemicarcerands

Carcerands are large, closed molecular containers that are assembled by fourfold interconnection of two cavitands (**25**).[23] They irreversibly incarcerate substrates, for example, solvent molecules, that are required as necessary templates for the assembly and cannot escape the cage for steric reasons unless it is destroyed. Hemicarcerands (26), on the other hand. include fewer or longer linkers. thus containing portals large enough for guests to get in and out at elevated temperatures. This allowed highly reactive species, such as cyclobutadiene and benzyne. to be generated from appropriate entrapped precursors and to be characterized in the ''inner phase'' at ambient temperature.

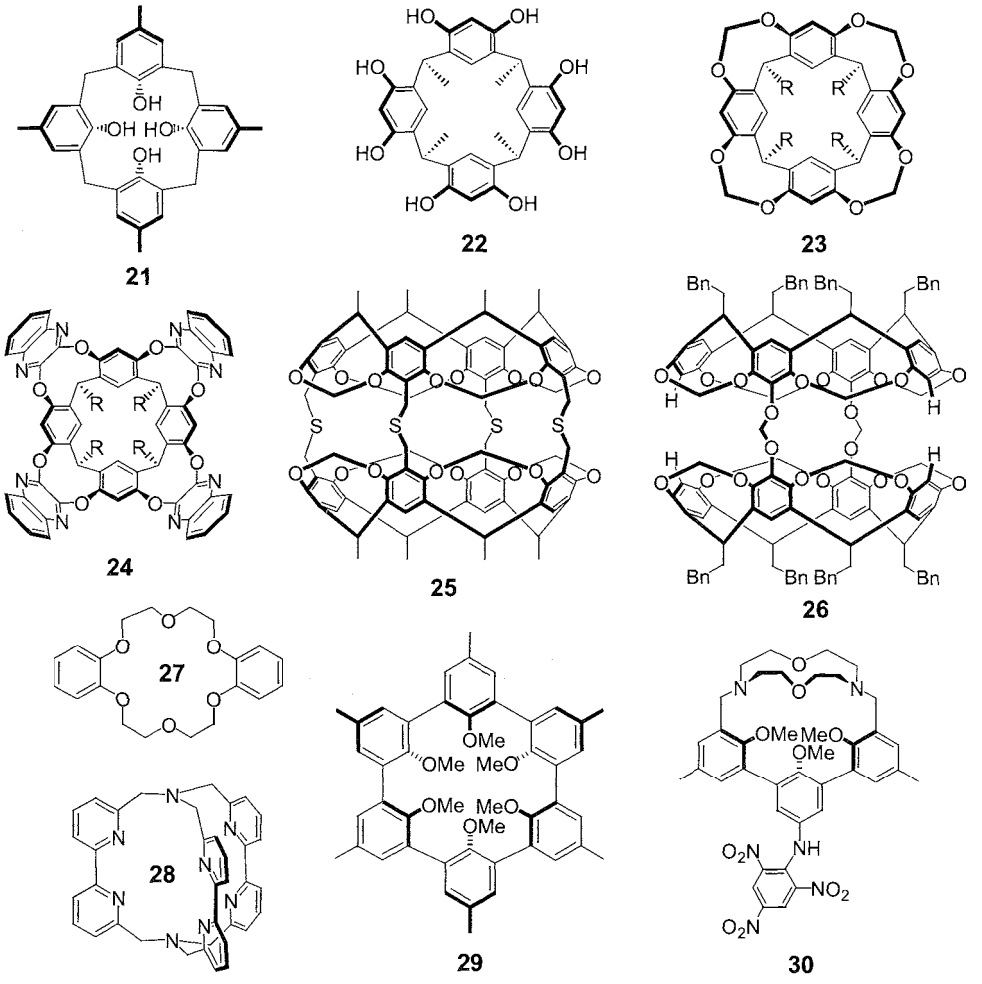

Fig. 4 Representatives of typical cyclophane host families calixarene (21), resorcinarene (22), cavitands **(23,** 24), cdrcerand (25). hemicarcerand (26), crown ether (27), cryptand (28), spherand **(29).** and hemispherand (30)

Fullerenes also represent container molecules that are able to Incarcerate metals, noble gases, or extremely reactive species such as *N*-atoms

Cyclophane-Type Ionophores

Compared to chemically similar individual ligands. macrocyclic cyclophanes with several donor centers may be potent complexing agents for metal ions. Next to the chelate effect, this is often related to a productive preorganization of convergent donor functionality providing favorable coordination sites.

Although many crown ethers are entirely alicyclic, the first representative. obtained by Pedersen in 1967, was a cyclophane (**27**).[24] Generally, the fusion of arenes to crown ethers and cryptands[25] makes the ionophores more lipophilic and confers a handle for functionalization. Also, the cyclophane backbone may include heterocycles that simultaneously provide the donor atoms for complexation. as illustrated by cryptand 28 (Lehn).[3,17]

Spherands[23] are typically derived from a hexa-*m*-phenylene backbone with donor substituents converging toward the center of the macrocycle (29). The close proximity forces the donor atoms to line a small and extremely preorganized cavity appropriate for very strong and specific binding of metal ions. As a consequence of the exceptional preorganization, decomplexation kinetics are exceedingly slow. Hemispherands (30) have a more flexible structure that reduces binding strength to some extent, but selectivities can still be very high. This has led to their incorporation into chromoionophores used for the determination of Na^+ (30) or K' in blood serum.[23]

Macrobicyclic cyclophanes with three highly preorganized catechol units were prepared by the groups of Vogtle and Raymond.[3,17] As an example. 31 (Fig. 5)

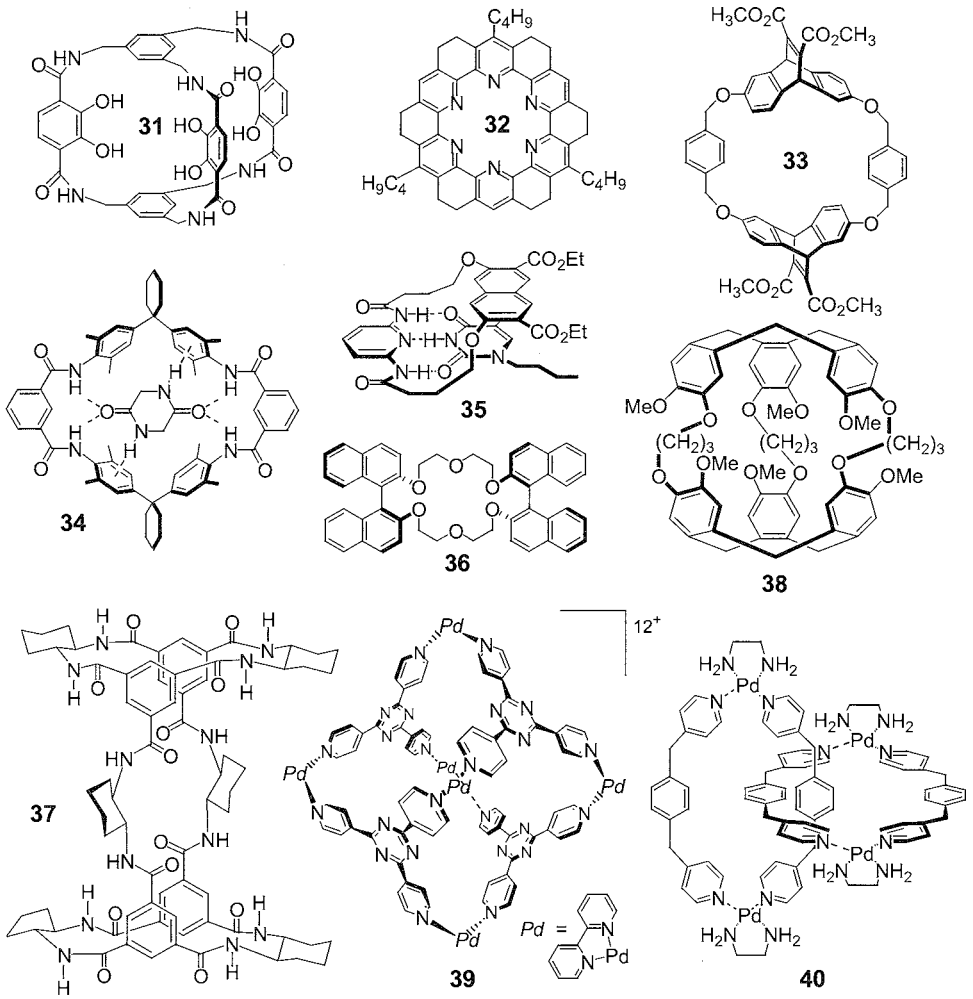

Fig. 5 Typical cyclophane receptors for metal ion complexation (siderophore 31. torand 32, crown ether 36), onium ion-π interactions (33, crpptophane 38). hydrogen bonding interactions (34–37), and chiral recognition (36–38). Self-assembled cyclophanes 39 and 40.

displays extremely strong complexation of Fe(III) upon deprotonation. exceeding that of the related natural siderophore enterobactin. Other well preorganized cyclophane-type ionophores include torands (Bell), e.g., 32 and a multitude of bridged and unbridged porphyrins.[3]

Cation–π interactions

While studying the coinplexation of ammonium ions by cyclophanes, Dougherty and coworkers recognized the interaction between cations and the electron-rich, polarizable π-systems of arenes.[26] Receptor 33 thus encapsulates *N*-methylquinolinium ions ($CDCl_3$) but not quinoline. Furthermore. complexation-induced changes in ^{1}H-NMR chemical shifts of the bound adamantyltrimethylammonium ion demonstrated that the ionic rather than the hydrocarbon moiety is included in the cavity. Cation–π interactions[18] play an important role in many natural systems such as proteins.

Hydrogen Bonding and Binding Selectivity

The directionality of hydrogen bonding makes cyclophanes with hydrogen-bond donor or acceptor sites very selective hosts for guests with a complementary hydrogen-bonding pattern. and high association constants are usually observed in noncompetitive solvents. Receptor 34, prepared by Hunter and coworkers,[27] strongly binds cyclo-diglycine ($CDCl_3$): in addition to the H-bonding between N–H groups of the cyclophane and the C=O groups of the guest, $N–H_{guest}\cdots\pi_{host}$ interactions[18] became evident by x-ray crystallography. In the complex of 35 with *n*-butylthymine, hydrogen-bonding interactions are complemented by π–π stacking which, as shown by

Hamilton and coworkers, is controlled by partial charge complementarity between the stacked naphthalene and heterocycle moieties.[28]

A number of cyclophanes with acidic NW groups, often belonging to pyrroles or amide functions, are suitable for anion binding.

Cyclophane Receptors for Chiral Recognition

Enantioselective recognition between chiral hosts and guests is of great interest. The required difference in stability between diastereoisomeric complexes often relies on three-point interactions between a well-preorganized receptor and the substrate. Hydrogen bonding as a directional interaction is of particular importance in this context, often in combination with steric host–guest complementarity.

Early reports from the groups of Cram[23] and Prelog[29] describe the use of chiral crown ethers derived from binaphthalene *(36)*and spirobifluorene. respectively, for the recognition, among others, of ammonium salts of D- or L-amino-acid esters. A model was proposed for the observed chiral recognition by *36*, and it was tested as a carrier in a machine for the preparative resolution of guest enantiomers by differential passive transport through a liquid membrane. However, developing back transport limited separations to "initial transport rate" conditions, thus hampering large-scale applications.

Still and coworkers prepared the highly selective, D_2-symmetric receptor 37 for amino acids and small peptides by simple condensation of (*R*,*R*)-cyclohexane-1,2-diamine and trimesic acid.[30] Complexes are held together by four intermolecular hydrogen bonds and resemble a peptidic three-strand β-sheet. A further, enantiomer-discriminating interaction is based on steric complementarity between the amino acid side chain and the cleft-type cavity of the receptor.

The aesthetically pleasing cryptophanes reported by Collet et al. include two cyclotriveratrylene (CTV) units

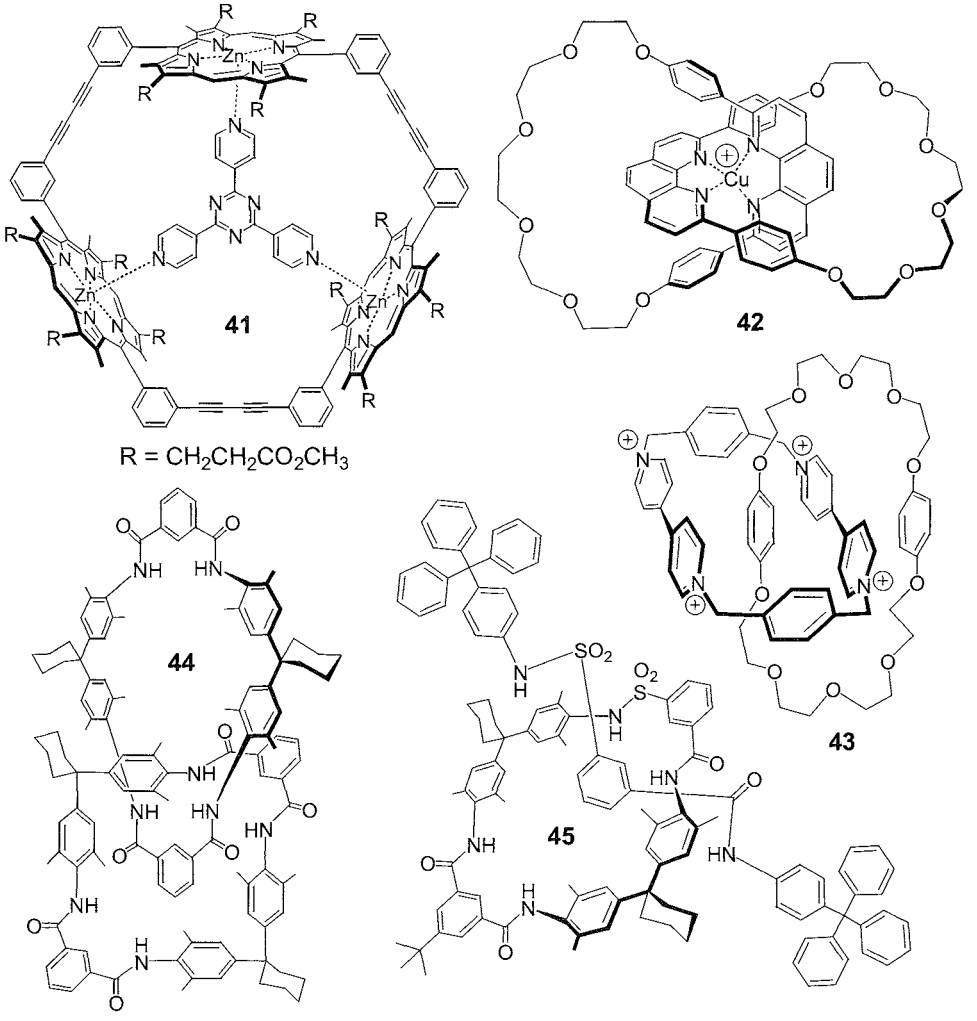

Fig. *6* Cyclophanes obtained by templated synthesis or self-assembly.

with a chiral substitution pattern, interlinked by three aliphatic chains.[31] Depending on the configuration of the CTV moieties, either an achiral (*meso* form) or a chiral cryptophane. e.g., **38**, results. The latter forms inclusion complexes with small apolar methane derivatives and onium ions [$CHCl_3$, $(H_3C)_4N^+$, etc.] in $CD_2Cl–CD_2Cl$. Nonracemic cryptophanes allowed the first chiral recognition, defined enantiomeric enrichment and configurational assignment of CHBrClF.

TEMPLATED SYNTHESIS AND SELF-ASSEMBLY OF CYCLOPHANES [REF. 203]

Based on coordinational preferences and the resulting spatial arrangement of ligands. certain transition-metal ions were used. sometimes in combination with covalent bond formation: as structural building blocks for rational self-assembly of molecular components into well-defined cyclophanes. The groups of Stang and Fujita thus exploited the coordination of ligands containing pyridine units to Pd and Pt to obtain some remarkable square cyclophanes. cage-type receptors (**39**), or catenanes (**40**).[32–34]

The metal-ion-mediated template effect was widely used in crown ether synthesis. Templated syntheses of cyclophanes such as **41** (Fig. 6) (Sanders)'''' are generally impressive by their efficacy and selectivity. Besides, they made structures such as rotaxanes, catenanes. and knots easily accessible for the first time. Sauvage and coworkers. taking advantage of a Cu(I)-mediated preorganization of phenanthroline building blocks. reported the first efficient rotaxane and catenane (**42**) syntheses and the first preparation of a molecular knot.[33,34] A strategy developed by Stoddart and coworkers for the synthesis of rotaxanes and catenanes, e.g., **43**, uses interactions between electron-deficient *N*-alkylated 4.4'-bipyridine units and electron-rich dialkoxyarene-based crown ethers.[33,34] The modular architectures were investigated in great detail and extended to interlocked multicomponent structures and functional systems on the way to molecular machines and motors. An efficient synthesis of macrotetralactam-based catenanes such as **44**, relying on templated self-assembly mediated through hydrogen bonding and, to a lesser extent, aromatic π–π-stacking, was reported by the groups of Hunter and Vögtle.[33,34] By subtly varying the structure and the combination of building blocks. the latter group was able to prepare unusual interlocked structures, including topologically chiral knots. catenanes, and rotaxanes (**45**). The cycloenantiomerism associated with the latter two compound families is a consequence of the directionality originating from asymmetric atom sequences within the macrocycles and the dumbbell component.

CONCLUSION

The building block principle applied successfully to the synthesis of cyclophane receptors allows for an enormous structural diversity with regard to shape and function. In combination with template-directed synthesis. self-ascembly, and other recent advances in macrocyclization methodology. it is hard to imagine limits as to the potential of cyclophane hosts in the foreseeable future. Similarly and despite the ''old age'' of small and nonhost-type cyclophanes, aesthetically pleasing, stereochemically remarkable, and extremely strained new structures are still being created.

ACKNOWLEDGMENT

We thank Prof. Dr. F. Diederich for providing a number of structural drawings.

ARTICLES OF FURTHER INTEREST

Amide- and Urea-Based Anion Receptors, p. 31
Artificial Enzymes, p. 76
Calixarenes and Their Analogues: Cation Complexation, p. 137
Calixarenes and Their Analogues: Molecular Complexation, p. 145
Calixarenes: Synthesis and Historical Perspectives. p. 153
Carcerands and Hemicarcerands, p. 189
Catenanes and Other Interlocked Molecules. p. 206
Cation–n Interactions, p. 214
Cavitands, p. 219
Chemical Topology, p. 229
Chiral Guest Recognition, p. 236
Classification and Nomenclature of Supramolecular Compounds, p. 261
Crown Ethers. p. 326
Cryptands, p. 334
Cryptophanes, p. 340
Cyclophanes: Endoacidic, Endobasic, and Endolipophilic Cavities. p. 424
Dendrimers. p. 432
The Diphenylmethane Moiety, p. 452
Enzyme Mimics, p. 546
Fullerenes as Encapsulating Hosts: Preparation, Detection, and Structures of Endohedral Fullerenes, p. 579
Hydrogen Bonding, p. 658
Hydrophobic Effects, p. 673
Ionophores, p. 760
Macrocycle Synthesis, p. 830

REFERENCES

1. Smith, B.H. Bridged *Aromatic Compounds*; Academic Press: New York, 1964.
2. Keehn. P.M.: Rosenfeld. S.M. *Cyclophanes*; Academic Press: New York. 1983: Vol. I and TI.
3. Vögtle, F. *Cyclophane Chemistry*; Wiley & Sons: Chichester, 1993.
4. Diederich, F. *Cyclophanes*; Stoddart, J.F., Ed.; The Royal Society of Chemistry: Cambridge, 1991.
5. Pellegrin. M.M. Contribution à l'étude de la reaction de Fittig. Recl. Trav. Chim. Pays-Bas 1899. *18.* 457–465.
6. Cram, D.J.: Steinberg. H. Macro rings 1. Preparation and spectra of the paracyclophanes. J. Am. Chem. Soc. **1951**, *73* (12). 5691–5704.
7. Cram. D.J.: Cram, J.M. Cyclophane chemistry—Bent and battered benzene rings. Acc. Chem. Res. 1971.4 (6). 204–213.
8. Meyer, E.A.: Castellano. R.K.: Diederich. F. Interactions with aromatic rings in chemical and biological recognition. Angew. Chem.. Int. Ed. **2003**, 42 (11), 1210–1250.
9. Moss, G.P.: Smith. P.A.S.: Tavernier. D. Glossary of class names of organic compounds and reactive intermediates based on structure. Pure Appl. Chem. 1995. 67 (8–9). 1307–1375.
10. Powell, W.H. Phane noinenclature—Part I: Phane parent names. Pure Appl. Chem. 1998. 70 (8). 1513–1545. See also: http://www.chem.qmul.ac.uk/iupac/phane (accessed July 2003).
11. Favre. H.A.; Hellwinkel. D.: Powell. W.H.: Smith, H.A.. Jr.: Tsay, S.S.-C. Phane nomenclature. Part II. Modification of the degree of hydrogenation and substitution derivatives of phane parent hydrides. Pure Appl. Chem. 2002. 74 *(5)*. 809–834. See also: http://www.chem.qmul.ac.uk/iupac/phane2 (accessed July 2003).
12. Seel, C.; Vogtle. F. Molecules with large cavities in supramolecular chemistry. Angew. Chem., Int. Ed. 1992, *31* (5). 528–549.
13. Knops. P.: Sendhoff, N.; Mekelburger, H.-B.: Vogtle. F. High dilution reactions—New synthetic applications. Top. Curr. Chem. 1991. 161. 3–36.
14. Diederich. F.; Stang, P. *Templated* Organic Synthesis; Wiley-VCH: Weinheim, 2000.
15. Boekelheide. V. Syntheses and properties of the [2_n]cyclophanes. Top. Curr. Chem. **1983**, *113*. 87–143.
16. Grimme. S.: Harren, J.; Sobanski. A.; Vogtle, F. Structure1 chiroptics relationships of planar chiral and helical molecules. Eur. J. Org. Chem. **1998**, (8). 1491–1509.
17. Vögtle, F. *Supramolecular Chemistry*; Wiley & Sons: Chichester. 1991.
18. *Molecular* Recognition: *Receptors for Cationic* Guests; Gokel. G.W.. Ed.: Comprehensive Supramolecular Chemistry, Elsevier Science Ltd.: Oxford, 1996; Vol. 1.
19. *Molecular Recognition: Receptors for* Molecular *Guests*; Vögtle, F.. Ed.: Comprehensive Supramolecular Chemistry, Elsevier Science Ltd.: Oxford. 1996: Vol. 2.
20. *Templating, Self-Assembly, and Self-Organization*; Sauvage, J.-P., Hosseini. M.W.. Eds.: Comprehensive Supramolecular Chemistry. Elsevier Science Ltd.: Oxford. 1996; Vol. 9.
21. Diederich. F. Molecular Recognition with Cyclophane Receptors in Aqueous Solution. In *Modern Cyclophane Chemistry*; Hopf. H.. Gleiter. R., Eds.: *in* press.
22. Gutsche. D. *Calixarenes*: Stoddart. J.F., Ed.: The Royal Society of Chemistry: Cambridge. 1989.
23. Cram, D.J.: Cram, J.M. Container *Molecules* and Their *Guests*; The Royal Society of Chemistry: Cambridge, 1994.
24. Pedersen. C.J. The discovery of crown ethers. Angew. Chem., Int. Ed. 1988. 27 (8). 1021–1027.
25. Gokel, G. Crown *Ethers* and *Cryptands*; The Royal Society of Chemistry: Cambridge, 1991.
26. Ma. J.C.; Dougherty. D.A. The cation–n interaction. Chem. Rev. 1997. 97 (5), 1303–1324.
27. Allott, C.: Adams. H.: Bernad. P.L.; Hunter, C.A.: Rotger, C.: Thomas. J.A. Hydrogen-bond recognition of cyclic dipeptides in water. Chem. Commun. 1998. (22). 2449–2450.
28. Hamilton, A.D.; Van Engen, D. Induced fit in synthetic receptors—Nucleotide base recognition by a molecular hinge. J. Am. Chem. Soc. **1987**, *109* (16). 5035–5036.
29. Prelog. V. Chiral ionophores. Pure Appl. Chem. 1978, *50* (9–10), 893–904.
30. Yoon. S.S.; Still. W.C. An exceptional synthetic receptor for peptides. J. Am. Chem. Soc. 1993. *115* (2). 823–824.
31. Collet. A.; Dutasta. J.-P.; Lozach, B. Cryptophanes: Receptors for Tetrahedral Molecules. In *Advances* in *Supramolecular Chemistry*; Gokel. G.W., Ed.: JAI Press Inc.: Greenwich, USA. 1993: Vol. 3, 1–35.
32. Holliday, B.J.: Mirkin, C.A. Strategies for the construction of supramolecular compounds through coordination chemistry. Angew. Chem.. Int. Ed. 2004. 40 (11), 2022–2043.
33. *Molecular Catenanes, Rotaxanes and Knots*; Sauvage, J.-P., Dietrich-Buchecker. C.. Eds.: Wiley-VCH: Weinheim, 1999.
34. Lindoy, L.F.: Atltinson. I.M. *Self-Assembly* in *Supramolecular* Systems: Stoddart, J.F., Ed.: The Royal Society of Chemistry: Cambridge, 2000.

Cyclophanes: Endoacidic, Endobasic, and Endolipophilic Cavities

Andrew C. Benniston
University of Newcastle, Newcastle upon Tyne, United Kingdom

INTRODUCTION

The name "cyclophane" is specific and literally means organic compound containing bridge aromatic ring."' However. as time has gone by, the generic term "cyclophane" has come into play, and scientists now use the name to encompass a multitude of molecular assemblies that have various cavities capable of binding guests. Indeed. some of the intricate and sophisticated molecules created today are a far cry from the first cyclophane chemistry started in 1899, when Pellegrin succeeded in preparing [2,2]-metacyclophane.[2] In this article. we will tie down a few specific examples and categorize the cavities of the cyclophanes according to the type of molecules they bind and the driving force for complexation. Why this is important will become clear later on, but it should not be forgotten that binding studies are carried out in solvents, and all entities in solution will be solvated to some extent. Hence. upon complexation. degrees of desolvation of the molecular species must occur so that binding is allowed to take place. Even this simplified picture does not explain the binding of certain cyclophane structures. because, for example, ion-pairing effects and solvotophobic effects play an important role in molecular association.

Over the last 10 years or so, numerous books (Diederich[3] and Vögtle[4] are particularly recommended) and chapters in books were published, covering many aspects of cyclophane chemistry.[5] Readers are pointed to a recent review on "Synthetic Receptors'' that also embraces many aspects of cyclophane chemistry.[6] It is the intention of this article in the *Encyclopedia* to focus on more recent developments toward the end of the last century and the turn of the new millennium. The examples chosen are in no way exhaustive but rather serve as pertinent examples to emphasize the types of cavities the cyclophane receptors possess and interactions that drive complexation. Where possible, the bioinimetic nature of the receptors will be discussed; because the ultimate goal in much of cyclophane work is to mimic nature's processes. It is hoped that the reader will see the cross-fertilization of cyclophane chemistry and how examples discussed in other articles on. for example, cyclodextrins, cryptophanes. cavitands, crown ethers, etc.. are just as relevant to this article.

ENDOACIDIC CYCLOPHANES

Endoacidic cyclophanes contain cavities with functional groups thai are acidic; and hence. they have the potential to bind cation guests such as metal ions. quaternary ammonium salts, positively charged species, and H-bonding solvents. Obvious acidic groups that could be part of the cyclophane skeleton structure include carboxylic acids, phenols, etc. In the general definition. we can also include cyclophane structures that are π-acidic (electron accepting) and use intimate donor–acceptor interactions to drive binding.

Cryptophanes comprise a class of compounds made up of two cone-shaped cyclotriveratrylene units attached to one another by three bridges. This feature leads to a highly preorganized three-dimensional enforced cavity suitable for accommodating organic substrates. In general. these classes of compounds contain, on the periphery, substituted methoxy groups, and examples are rare where substitution with ionizable groups was carried out. This situation was recently rectified by the group of Weber,[7] who successfully prepared the new cyclophane receptor **1** featuring three *endo*-carboxylic acid groups (Fig. 1). Complexation studies were performed using **1** in $CDCl_3$ and a range of alcohols (methanol, ethanol, and isopropanol). because proton donor–acceptor interactions were considered to operate. No binding to isopropanol was observed to take place, which is attributed to its inability to pass through the narrow openings of the cyclophane wall. The smaller alcohols were. however, found to navigate the passages. and binding constants for 1:1 complexation of methanol and ethanol were determined to be 7500 and 41 dm' mol ^{1}. respectively. Interestingly, small dipolar solvents with proton acceptor capabilities. such as acetonitrile, nitromethane, acetaldehyde, and acetone. also tested as guests. failed to form detectable complexes. Solvent extraction studies of metal ions were fortunately more rewarding and highlighted the capability of **1** to act as an ion carrier. Cyclophane **1** acts as an efficient transporter of highly charged. hard metal ions of matching size. including divalent alkaline earth metals (e.g., Ca^{2+}, Sr^{2+}) and trivalent lanthanide metal ions (e.g., Yb^{3+}).

it is worth noting that **1** represents the spherical analogue of the proposed *endo*-cyclophanes **2a** and **2b**

Encyclopedia of Supramolecular Chemistry
DOI: 10.1081/E-ESMC 120012738

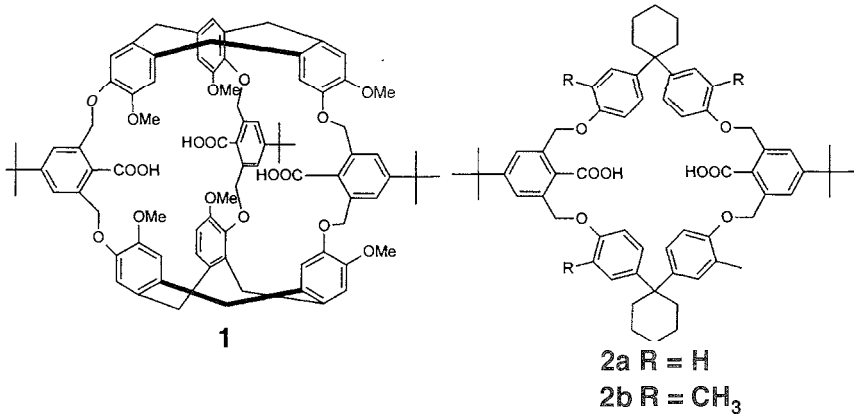

Fig. 1 Examples of endoacidic cyclophane hosts containing carboxylate binding sites.

prepared by the same group. which once again contain carboxylate moieties capable of convergent binding.[8] The cyclophane **2b** was found to be an excellent host for numerous solvents, where host:guest ratios vary from 1:1 (benzoquinone, benzene, cyclohexane, toluene: and DABCO) to 1:2 (DMSO, propionic acid, and methanol) to 1:4 (acetic acid. acetone). For these host–guest complexes, the structures of the adducts are not unique along the series. The single-crystal x-ray structure of **2b**.4 (acetic acid) $2H_2O$ (Fig. 2A) clearly demonstrates that the cavity is filled by methyl groups, thus forcing both the carboxylate units to an exo orientation. On the other hand, the carboxylate groups do not take an exo or *endo* orientation in the host–guest complex 2b.2 (propionic acid), as illustrated in Fig. 2B.

Without doubt, the most widely known *endo* π-acidic cyclophane is Stoddart's "blue-box" **3** that incorporates in the cyclic framework two electron-deficient (electron acceptor) *N,N'*-bipyridinium units.[9] The cavity size is consummate for binding a wide range of electron-rich (electron donor) aromatics in organic and aqueous solvents. The intimate interaction between donor and acceptor groups is evident, because a broad charge-transfer absorption band is observed in the visible spectral region. Because of the rigidity and highly beneficial photophysical properties of cyclophane **3**, and its host–guest complexes, many applications have emerged, including testing electron-transfer theory,[10] mimicking photosynthesis,[11] and light-activated devices,[12] to name a few. Since this pioneering work. new n-acceptor cyclophanes based on. and similar to, **3** emerged. by Stoddart and other groups as well.[13] The work of the group of Mallouk[14] is highlighted here, because they took the basic design of 3, incorporated extra recognition sites, and exchanged the cation electron-affinic groups with neutral electron acceptor units (Fig. 3). It could be argued that these cyclophanes cannot be considered as endoacidic cyclophanes, which to an extent is true, because other functional groups are added. Hopefully. the reader will see that there is a great deal of crossover when categorizing cyclophane structures; and many could be included in other sections.

The cyclophane 4 incorporating the tripeptide backbone was the first attempt at creating a chiral host for shape-selective molecular recognition. This group is mainly interested in intercalating host molecules into α-zirconium phosphate (α-ZrP) for applications in such areas as preparative-scale chiral separation. Although 4 displayed considerable promise in chiral recognition of racemic DOPA [3-(3,4-dihydroxyphenyl)-DL-alanine) in a water–acetone mixture, the same molecule embedded in (α-ZrP) was not an effective chiral separation agent. It was hypothesized that this lack of recognition was caused by reduction in the n-acidic nature of the cyclophane, caused by close association of the negative α-ZrP with the *N,N*-bipyridinium group. Cyclophanes **5**–**7** represent the next stage of development by Mallouk et al. to overcome this problem. An association constant (K) of 13 ± 1 dm^3 mol^{-1} was determined for **5** and indole in chloroform. Unfortunately, the low solubility of **6** and **7** in chloroform (the curse for all binding studies) meant that similar binding constants could not be obtained with indole. Even more disappointing was that no obvious binding of **6** and **7** with indole could be detected when the solvent was changed to DMSO. Why should this be the case, because indole is a good electron donor, and the aromatics used are recognized to be adequate electron acceptors? The strength of the cyciophane–guest interaction depends on several factors. The first is the stereoelectronic complementarity between host and guest. which leads to favorable donor–acceptor, hydrogen bonding, and other interactions. The second is the preorganization of the host, i.e.. the existence of a rigid binding pocket that does not require loss of entropy to accommodate the guest. The third. and often neglected, is the donor ability of the solvent. which determines how heavily solvated the separated molecular

species really are, i.e., association will only take place if it is favorable for the host and guest to bind rather than be solvated in solution. In this case. DMSO is a strong donor solvent and would solvate strongly the indole and cyclophanes. Other steric factors could also play a role. especially in cyclophane **7**, where molecular modeling shows that nitro groups sterically inhibit π-complexation.

ENDOBASIC CYCLOPHANES

The internal cavity of a cyclophane is endobasic if functional groups are present that are basic or electron donating: the most obvious groups include the ethers, pyridines, amines. and phosphorus-based donors. Cyclophanes in this category would be expected to bind metal ions and also promote H-bonding interactions within the cavity. Hence, in this section, crown ethers and azamacrocycles could easily be included. Under this heading, we can also

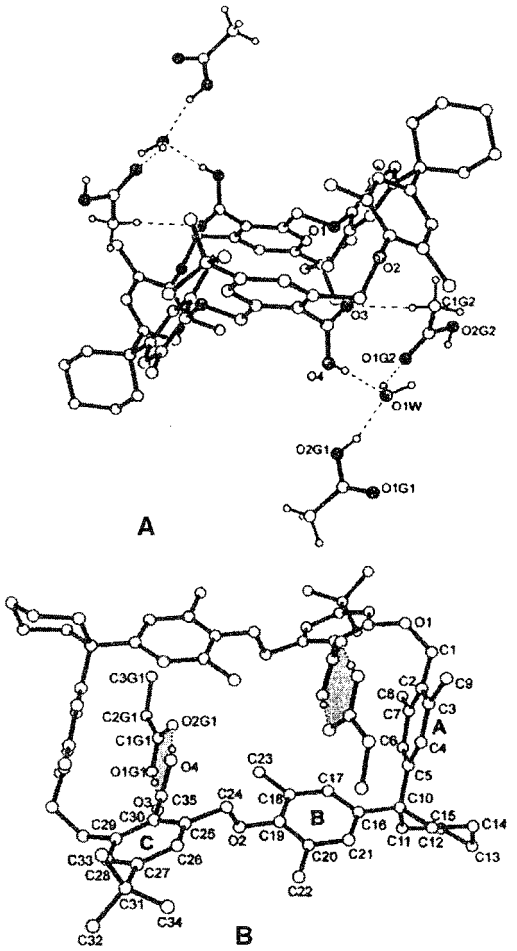

Fig. 2 Crystal structures of cyclophane complexes 2b.4 (acetic acid) $2H_2O$ (A) and **2b**.2 (propionic acid) (B).

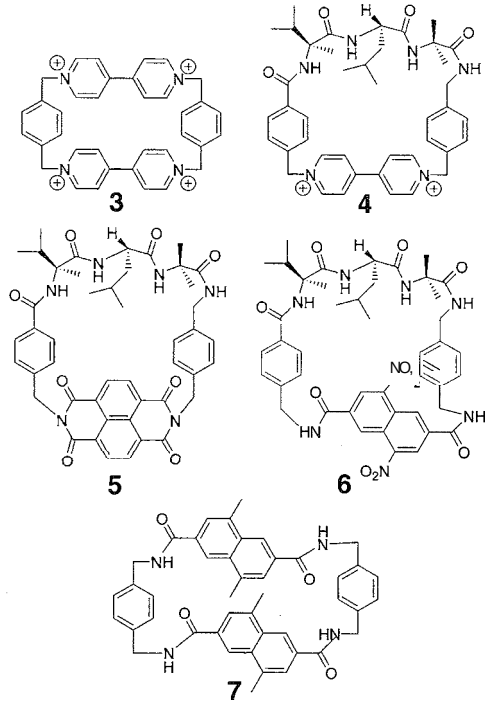

Fig. **3** The *endo* π-acidic cyclophanes incorporating cationic and neutral electron acceptors.

incorporate electron-rich aromatics, because n-donation to an electron acceptor will result in host–guest binding.

Collected in Fig. 4 are examples of cyclophanes containing the correct functional groups for inclusion in this section. The three-dimensional Structure *8* prepared by Takemura and coworkers[''''] incorporates four pyridine donor sites. as well as potential N and O donors as part of the connecting straps. The x-ray structure of the potassium adduct of **8** clearly established the *endo* binding nature of the pyridine. nitrogen. and oxygen atoms. The cyclophane cavity is consummate for host–guest complexation of other cations. Inclusion properties of the cyclophane were also carried out with varying anions (Cl^-, F , Br , I , BF_4^-) in 10% D_2SO_4; the protonated form of the cyclophane enhances binding because of favorable cation–anion interactions. A binding constant of 24 ± 2 dm^3 mol^{-1} for Cl^- complexation was determined, and thermodynamic data obtained by a van't Hoff plot afforded ΔH° (-2.9 kcal mol ') and AS" (-3.9 cal K^{-1} mol '). Larger anions Br^-, I , and BF_4^- were not complexed by the cyclophane.

Twistophanes **10** and **11** represent a new class of cyclophanes that recently emerged as the follow-up compounds to the endobasic host **9** first prepared by Baxter.[16] The cyclic structures comprise substituted 2,2′-bipyridyl groups linked via acetylinic linkers, and they are primarily developed as sensors for metal ions. For both

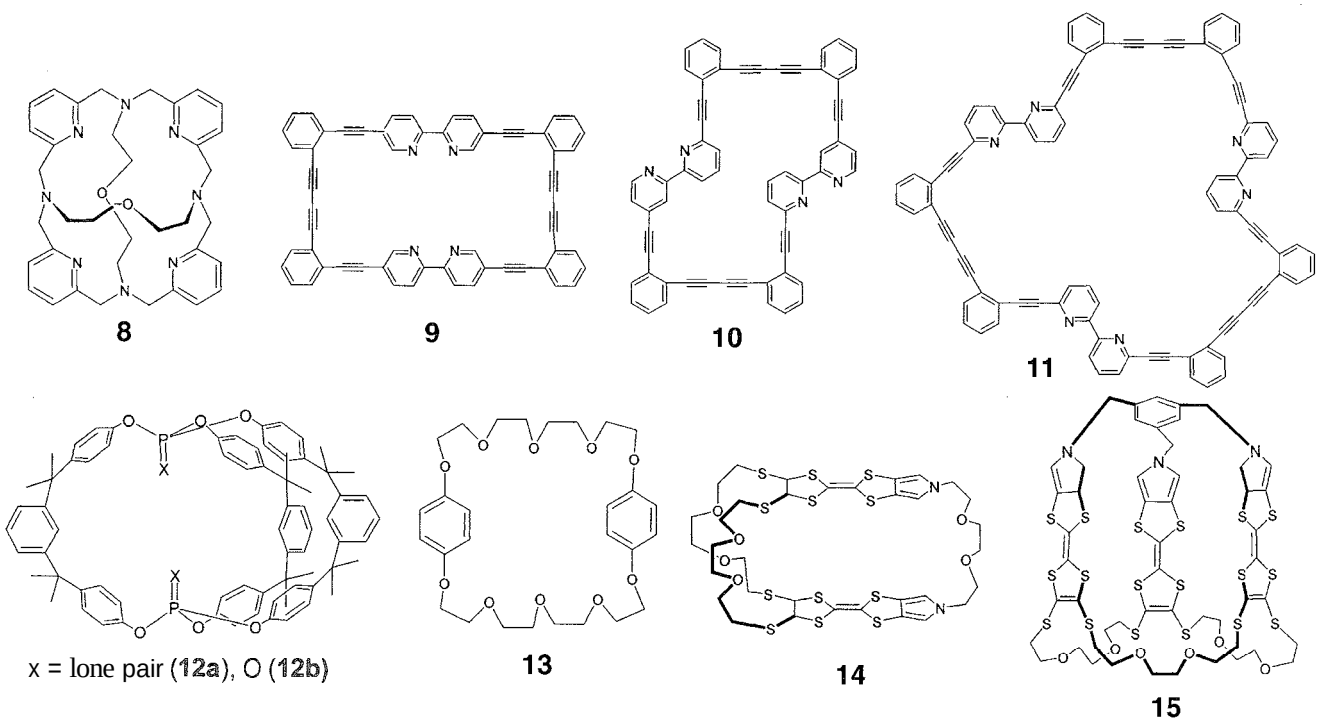

Fig. 4 Examples of multidimensional structures containing donor sites for molecular recognition.

bipyridine subunits of **9** to bind a single metal ion, the twisted carbon backbone must slightly unwind, thus permitting the bipyridine rings to rotate about the long axis and orient the four nitrogen lone pairs in an *endo* orientation. In this case, only a minimal change in conformation is required. So, a spectroscopic response from metal-ion binding originates only from electron distribution perturbations communicated through the bipyridine nitrogen lone pairs. The new cyclophanes 10 and **11**, however, must undergo larger structural alterations and, hence, more significant electronic perturbations upon metal ion binding. Ultraviolet-Visible spectroscopic studies revealed that **10** and **11** bind with dissimilar selectivities to the following metal ions: Cu(II), Ag(I), Hg(II), Th(I), and Pd(II). Fluorescence quenching observed for **10** and **11** (1: 2 $CHCl_3$/MeOH) in the presence of Cu(II) ions also support that these new twistophanes could be used as sensors. It is also worth noting that the cyclophanes function also as chromogenic fluorescence sensors for protons.

Endo-functionalized cyclophanes incorporating trivalent phosphorus are potentially interesting, because the soft donor site is perfect for binding soft transition metals that have applications in many catalysis reactions. Trivalent phosphorus atoms easily undergo oxidation to afford pentavalent species such as phosphoryl moieties. Thus, the phosphoryl oxygen can act as a hard donor site. which once again, can be used for metal ion binding, but also molecular recognition of H-bonding substrates such as biologically interesting amino acids. Cyclophane systems incorporating P-bridgehead atoms are not common, and reported assemblies show the expected *endo*/*exo* isomerism. A recent example of the synthesis of *endo*–*endo* P-based cyclophanes (**12a**/**12b**) was reported by Bauer and Habicher.[17] The x-ray structure of endo–endo **12a** shows two flat cyclic conformers with P–P distances of 4.5 Å and 5.3 Å, respectively.

In the previous article, the n-acidic "blue box" of Stoddart was introduced as a cyclophane capable of binding electron donor groups. Here. we introduce the reverse analogue of this cyclophane. 13, in which the donor groups form part of the cyclic structure, and hence, bind electron-deficient molecules.[18] Cyclophane 13 and its analogues now have a central role in the creation of more exotic structures such as rotaxanes[19] and catenanes.[20] More recently. a move toward tetrathiafulvalene-based cyclophanes was made because of their unique π-electron donor properties. Structures **14** and **15** represent two such examples prepared by the group of Becher.[21] The central cavity of cyclophane 14 is a little too small to accommodate electron-deficient guests such as 7,7,8,8-tetracycano-π-quinodimethane. Preliminary complexation studies with **15** and 1,3,5-trinitrobenzene have been more encouraging. The addition of one equivalent of 1,3,5-trinitrobenzene to a solution of 15 in chloroform resulted in a color change from orange to light green and the

appearance of a CT absorption band at 646 nm. The 'H-NMR evidence was also consistent with the formation of a 1:1 host–guest complex, presumably with the 1,3,5-trinitrobenzene moiety residing in the donor cage.

ENDOLIPOPHILIC CYCLOPHANES

The final category in this series is the endolipophilic cyclophanes that possess internal cavities that bind organic entities through $\pi-\pi$ stacking or other dispersive forces. This class of cyclophanes is probably the most extensive, and examples are numerous. Illustrated in Fig. 5 are just a handful of recent diverse examples from the literature. A common thread running in these examples is their biomimetic nature, in which host–guest chemistry involves the binding of biologically relevant molecules.

Cyclophane 16 represents a lipophilic host specifically prepared by Roelens and Bartoli,[22] as part of their continuing research effort. to ascertain the influence of cation–n interaction on the binding of numerous acetylcholine (Ac) derivatives and tetramethylammonium (TMA) salts.[23] Association constants were measured for 17 salts of commonly used anions; binding energies ($-\Delta G^{\circ}$) ranged from over 8 kJ mol^{-1} down to the limit of detection. Thermodynamic parameters ascertained for the association of 16 with TMA.picrate demonstrate that binding is enthalpic in origin, with a substantial enthalpy gain ($\Delta H^{\circ} = -16.7$ kJ mol^{-1}) and an unfavorable entropic contribution ($AS^{\circ} = -27.9$ J mol^{-1} K^{-1}). Interestingly. there is a good correlation between the ''goodness'' of anions as guest partners and the solubility of their salts. When the salts were converted to more charge-dispersed species such as dialkyltrichlorostannate salts. cation binding substantially improved, which indicates that charge dispersion is a main factor determining the influence of the anion on the cation–n interaction. Detailed high-level computational studies were also performed to ascertain the influence of the counterion on the binding free energy of TMA with Cyclophane 16. It was found that binding energies correlated with the electrostatic potential of the ion pair. In other words, the guest binding behavior is determined by the cation's

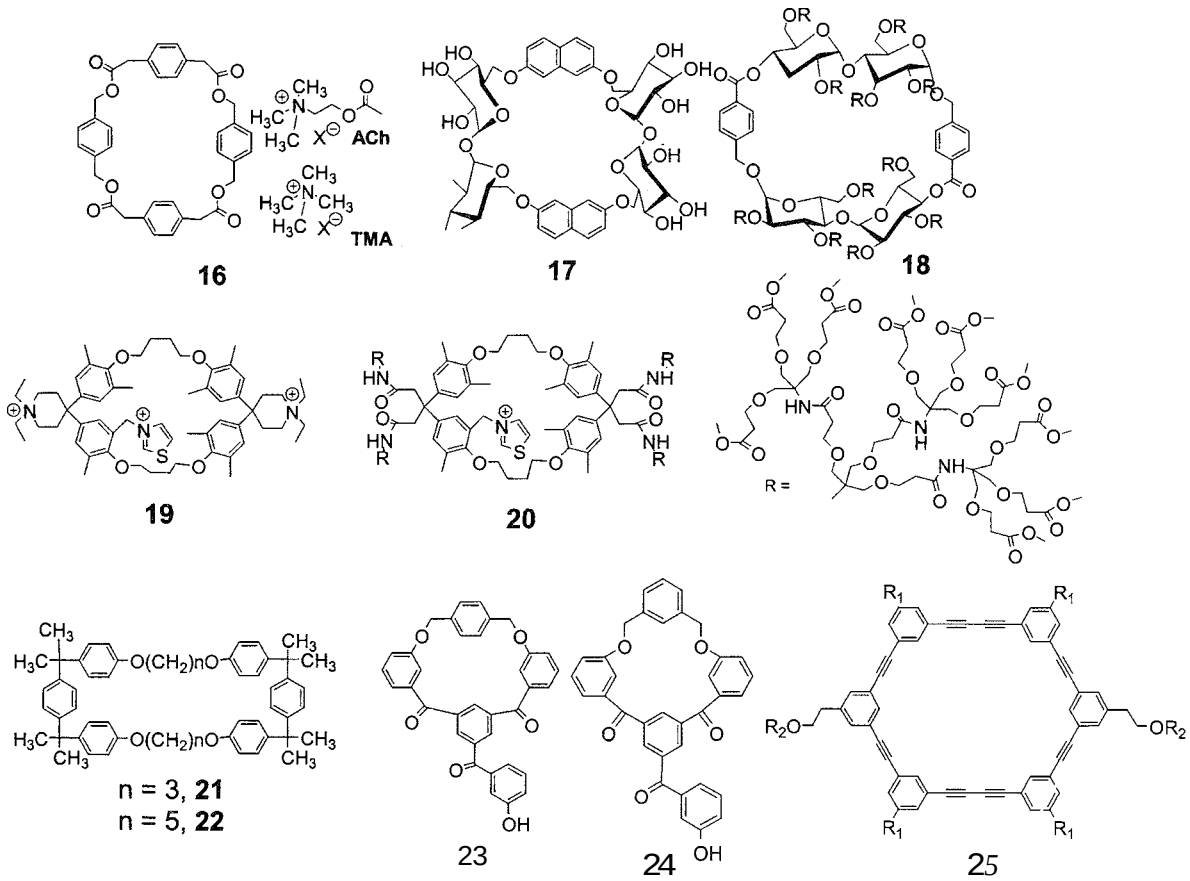

Fig. 5 A selection of endolipophilic cyclophanes for binding a range of guest molecules

charge density exposed to the receptor, which is determined by the anion's charge density by way of a polarization mechanism.

The cyclic sugar compounds cyclodextrins have long been recognized as water-soluble hosts for aromatics. The internal cavity is hydrophobic (or lipophilic), and complexation of aromatics is driven by solvotophobic response. Glycophanes represent a class of compounds incorporating sugar residues associated with cyclodextrins and aromatics more in fitting with cyclophanes; hence, the name glycophane. meaning cyclodextrin+cyclophane. The compounds **17** and **18** are two such examples reported by the group of Penadés.[24] Carbohydrate–carbohydrate interactions are recognized as important interactions that manipulate processes within cells. Hence. the two cyclophanes were developed to establish the strength of carbohydrate–carbohydrate interactions in water. Binding of **17** and **18** in water toward a series of 4-nitrophenyl glycosides with axial α-D-gluco(α-Glc), α-D-galacto (α-Gal), α-D-manno (αMan), β-L-arabino (βLAra), and α-L-fucopyranoside (αLFuc), plus equatorial β-D-gluco (βGlc), β-D-galacto (βGal), β-D-manno (βMan), z-L-arabino (αLAra), and β-L-fucopyranoside (βLFuc) configurations at the anomeric center were measured by ^{1}H-NMR spectroscopy. The overall findings of the work suggest that within glycophanes, carbohydrate–carbohydrate interactions in water contribute to the affinity of binding. Thus. the systems seem to reproduce the nonpolar interactions between lipophilic surfaces found in sugars binding to proteins.

Enzymes are nature's work horses. specifically designed for carrying out many essential transformations in biological systems. Small molecule mimics of enzymes based on cyclophanes are highly sought-after commodities in the supramolecular chemistry field. Compounds 19 and 20 are a class of thiazolio-based cyclophanes developed by Diederich et al.[25] for mimicking the action of thiamine diphosphate-dependent enzymes. Cyclophane 19 is a mimic of pyruvate oxidase and was shown to catalytically oxidize napthalene-2-carbaldehyde to methyl naphthalene-2-carboxylate, as illustrated in the cycle of Fig. 6. In basic MeOH. solution 19 is in equilibrium with the thiazolium ylide that reacts with bound aromatic aldehyde to afford an activated aldehyde. In the presence of an oxidant, the intermediate is transforined to the 2-acylthiazolium ion. The methyi ester is generated in a rapid reaction of the intermediate with the solvent. One outcome of this work was the understanding of how the microenvironment at the active site is critical for rate enhancement. That is, the large contribution to the catalytic behavior is the reduced polarity at the active site. Hence. the dendritic cyclophane *20* was designed and synthesized so as to alter the microenvironrnent at the active site. Unfortunately. **20** exhibited only a weak catalytic activity hypothesized to be due to steric hindrance of reaction transition states by the dendritic branches.

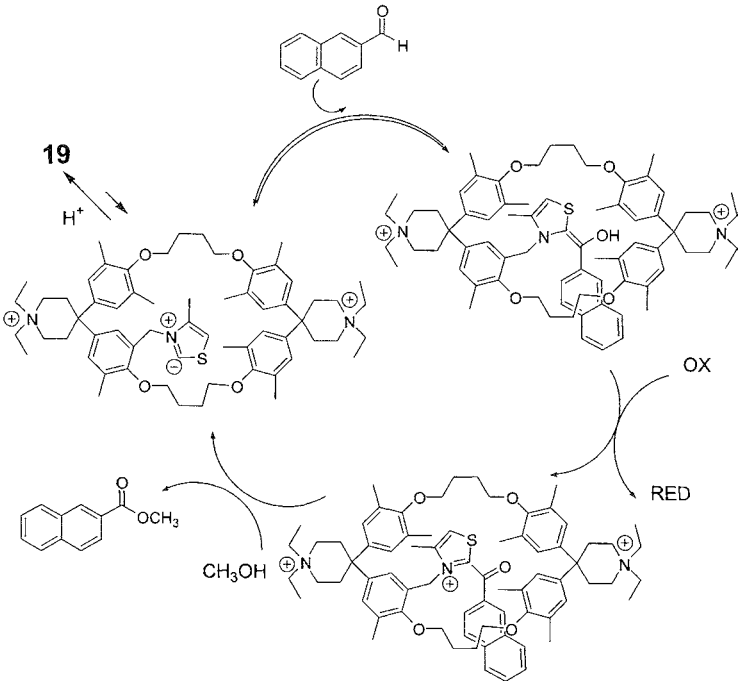

Fig. 6 Proposed catalytic oxidation cycle for conversion of napthalene-2-carbaldehyde to methyl naphthalene-2-carboxylate using a functionalized cyclophane

To conclude this final section. the cyclophanes 21–25 are illustrated as recent new additions to the host–guest arena. Bartsch and coworkers[26] recently reported the synthesis of the π-electron-rich hydrophobic cyclophanes 21–22 that are termed "corrals" because of the walled enclosure. The binding ability of 2%is limited, but the crystal structure of the anthracene adduct confirms that the cavity is consummate for binding, with edge-to-face π-interactions locking the guest in place. The linked aromatic motif is a popular approach in cyclophane construction. and 23–24 are two examples of Pigge et al.[27] constructed via an enaminone-directed benzannulation macrocyclization reaction. Although no binding studies were reported so far. x-ray crystal structures confirm that the cyclophanes adopt conformations suited for molecular association. The shape-persistent cyclophanes (SPCs) 25 (R_1=$OC_{12}H_{25}$, R_2=TBS; R_1=$COOC_{12}H_{25}$, R_2=TBS; R_1=$OC_{12}H_{25}$, R_2=H; R_1=$COOC_{12}H_{25}$, R_2=H) comprise an interesting class of compounds recently reported by Tour and Lin.[27] In a sense, the cavities in these compounds are not as important as their intermolecular π-stacking ability. The cyclophanes were shown to dimerize in solution using n-stacking and hydrogen-bonding interactions. Clearly. further oligomerization is eventually the goal so that well-defined suprainolecular assemblies (nanostructures) are generated containing internal cavities for aromatic encapsulation.

CONCLUSION

Cyclophane chemistry is flourishing and important field in the general area of supramolecular science. The hosts bind a multitude of species to varying degrees using a wide range of intermolecular noncovalent forces. In specific cases, they can help us understand the role these weak forces play in biological receptors. or offer the possibility of mimicking the enzyme reactions that nature uses so well. In an attempt to keep up with the most up-to-date advances in the field of cyclophanes, references to works were, where possible, taken from recent papers. However. the field is expanding so rapidly that new examples will be in the literature as this article is published.

ACKNOWLEDGMENTS

This work was supported by the Molecular Photonics Laboratory and the University of Newcastle.

ARTICLES OF FURTHER INTEREST

Artificial Enzymes, p. 76
Biological Models and Their Characteristics, p. 101
Calixarenes: Synthesis and Historical Perspectives, p. 153
Carcerands and Hemicarcerands, p. *189*
Cavitands, p. *219*
Crown Ethers. p. *326*
Cyclodextrins, p. 398
Cyclodextrins: Applications, p. 405
Cyclophanes: Definition and Scope, p. 414
Macrocycle Synthesis, p. *830*
π–π Interactions: Theory and Scope. p. 1076
π–π Stacking as a Crystal Engineering Tool, p. 1093

REFERENCES

1. Steed. J.W.: Atwood, J.L. *Supramolecular Chemistry*; John Wiley & Sons. 2000; 337.
2. Pellegrin. M.M. Contribution a l'étude de la réaction de Fittig. Rec. Trav. Chim. Pays-Bas 1899, *18*, 457–465.
3. Diederich. F. *Cyclophanes: Monographs* in *Supramolecular Chemistry*; The Royal Society of Chemistry, 1991.
4. Vögtle, F. *Cyclophane Chemistry:* Synthesis *Structures and Reactions*; John Wiley & Sons. 1993.
5. Lehn, J.-M. *Supramolecular Chemistry: Concepts and Perspectives*; VCH. 1995.
6. Hartley, J.H.: James. T.D.; Ward. C.J. Synthetic receptors. J. Chem. Soc., Perkin Trans. 1 2000. 3155–3184.
7. Roesky, C.E.O.; Weber, E.; Rambusch, T.: Stephan. H.: Gloe, K.: Czugler. M. Anew cryptophanereceptorfeaturing three endo-carboxylic acid groups: Synthesis, host behavior and structural study. Chem. Eur. J. 2003. 9. 1104–1112.
8. Weber. E.: Helbig, C.: Seichter, W.; Czugler, M. A new functional cyclophane host. Synthesis. complex formation and crystal structures of three inclusion compounds. J. Incl. Phenom. Macro Chem. 2002, 43. 239–246.
9. Odell, B.: Reddington, M.V.: Slawin. A.M.Z.: Stoddart. J.F.: Williams. D.J. Cyclobis(paraquat-para-phenylene)-a tetracationic multipurpose receptor. Angew. Chem.. Int. Ed. 1988, *27*, 1547–1550.
10. Benniston. A.C.; Harriman. A.: Philp. D.; Stoddart, J.F. Charge recombination in cyclophane-derived intimate radical ion pairs. J. Am. Chem. Soc. 1993. 115. 5298–5299.
11. Benniston. A.C.: Harriman. A.: Mackie. P.R. Artificial photosynthesis: Mimicking redos asymmetry. Angew. Chem.. Int. Ed. 1998. 37. 354–356.
12. Ballardini. R.; Balzani. V.: Gandolfi. M.T.: Prodi. L.; Venturi, M.: Philp. D.; Ricketts, H.G.: Stoddart. J.F. A photochemically driven molecular machine. Angew. Chem., Int. Ed. 1993. 32, 1301–1303.
13. Benniston. A.C.: Mackie. P.R. Functional Nanostructures Incorporating Responsive Modules. In *Handbook* of *Nanostructured* Materials *and Nanotechnology—Concise Edition*; Nalwa. H.S., Ed.; Academic Press, 2002; 693–747.
14. Chen. G.; Lean. J.T.: Alcalá. M.; Mallouk. T.E. Modular synthesis of π-acceptor cyclophanes derived from 1.4.5.8-naphthalenetetracarboxylic diimide and 1.5-dinitronaphthalene. J. Org. Chem. 2001. 66. 3027–3034.

15. Takemura. H.: Otsuka, K.; Kon. N.: Yasutake. M.: Shinmyozu. T.: Inazu. T. A pyridine cage as a bireceptor: Inclusion of cations and anions. Tetrahedron Lett. 1999. *40.* 5561–5564.
16. Baxter. P.N.W. Twistophane macrocycles with integrated 6,6′-connected-2,2′-bipyridine units: A new lead class of fluorescent sensors for metal ions. Chem. Eur. J. 2002. 8. 5250–5264.
17. Bauer. I.; Frohlich. R.; Yu. Zigganshina, A.: Prosvirkin. A.V.; Gruner, M.; Kh. Kazakova, E.; Habicher. W.D. Synthesis and structural peculiarities of homomorphic phosphorus bridgehead macrobicyclic compounds and novel dioxaphospa[3.1.1]*p,m,p*-cyclophanes. Chem. Eur. J. 2002. 8. 5622–5629.
18. Allwood. B.L.: Spencer. N.: Shahriarizavareth, H.: Stoddart. J.F.: Williams. D.J. Complexation of diquat by a bisparaphenylene-34-crown-10 derivative. Chem. Commun. 1987, 1061–1064.
19. Ashton, P.R.; Philp. D.; Spencer, N.: Stoddart, J.F. A new strategy for the self-assembly of molecular shuttles. Chern. Commun. 1992, 1124–1128.
20. Philp, D.: Stoddart, J.F. Self-assembly in organic synthesis. Synlett 1991. 445–457.
21. Nielson. K.A.; Jeppesen, J.O.: Levillain. E.: Thorup. N.; Becher, J. A pyrrolo-tetrathiafulvalene cage: Synthesis and X-ray crystal structure. Org. Lett. 2802. *4.* 4189–4192.
22. Bartoli, S.: Roelens. S. Binding acetylcholine and tetramethylammonium to a cyclophane receptor: Anion's contribution to the cation-π interaction. J. Am. Chem. Soc. 2002. *124.* 8307–8315.
23. Roelens, S.: Torriti. R. Binding of acetylcholine and quaternary ammonium cations to macrocyclic and acyclic "phane" esters. Evaluation of the cation π-primary interaction through adaptive aromatic hosts. J. Am. Chem. Soc. 1998. *120.* 12443–12452.
24. Morales. J.C.; Zurita. D.: Penadés. S. Carbohydrate–carbohydrate interactions in water with glycophanes as model systems. J. Org. Chern. 1998. *63.* 9212–9222.
25. Habicher. T.: Diederich, F. Catalytic dendrophanes as enzyme mimics: Synthesis. binding properties. micropolarity effect, and catalytic activity of dendritic thiazolio-cyclophanes. Helv. Chim. Acta 1999. *82,* 1066–1094.
26. Bartsch, R.A.: Kus, P.; Dalley, N.K.: Kou. X. A novel cyclophane-anthracene complex. Tetrahedron Lett. 2002. *43.* 5017–5019.
27. Lin, C.-H.; Tour. J. Hydrogen-bond assisted x-stacking of shape persistent cyclophanes. J. Org. Chem. 2002. 67. 7761–7768.

Dendrimers

Charles N. Moorefield
George R. Newkome
Amaresh Mishra
University of Akron, Akron, Ohio, U.S.A.

INTRODUCTION

From the time that chemists could characterize and manipulate molecular architecture, methods have been sought to enhance and modify molecular properties with an eye toward, among other attributes. intra- and intermolecular interactions based on covalent and noncovalent means. Evolution of the study of these properties and interactions has led to the supramolecular regime, whereby noncovalent molecular interplay produces effects and properties not ordinarily exhibited by the individual components.

This supramolecular tenant, defined by J.M. Lehn, is classically exhibited by the action of a micelle, whereby surfactant molecules aggregate into a globular motif that is capable of enhancing molecular guests' solubilities or acting as nanoscale reactors and transport vehicles, to mention but a few utilities. The micelle architecture, as well as the lipophilic-hydrophilic character, leads logically to the consideration of dendrimers as supramolecular components; this potential is herein chronicled.

Dendrimers are first examined with respect to their ability to soiubilize molecular guests in environments that, without added dendrirner. would exhibit unfavorable solubility properties. such as dissolution of water-insoluble molecules. Numerous dendritic architectures are highlighted with respect to this phenomenon.

The potential of dendrimers to encapsulate molecular species is further examined from the perspective of catalysis and the ability to improve reaction rates and yields. As well. their use as components facilitating chroinatographic separations is discussed. Finally, the use of dendrimers to effect noncovalent molecular ordering is examined.

MICELLAR ASPECTS

Consideration of the generally globular. or pseudo-spherical. 3-dimensional architecture of dendritic molecules".'' naturally leads to a comparison with the idealized concept of micellar organization and properties (Fig. I). From the perspective of classical, charged amphiphilic aggregation (1) above the critical micelle concentration (cmc). dendrimers (2) are structurally similar in that charged, or polar, surfaces connected to more lipophilic interior frameworks are readily attainable. Of course, reversible micellar characteristics (i.e., lipophilic exteriors and hydrophilic interiors) are also conceivable and have been demonstrated. Thus, to date, a structurally diverse array of nanoscopic-sized dendrirners has been shown to possess structural parameters comparable to that of supramolecular aggregates known as micelles.[3] Notably, even though in most cases monomer connectivity is covalent, the iterative nature of dendritic construction imparts an ordering to the building blocks that creates molecular characteristics inaccessible by a collection of simple unordered monomers.

However. it is not only from an architectural viewpoint that dendrirners can be contrasted to organized assemblies. but micellar stabilization and organization of species in uncharacteristic environments are also suggested. Thus. structural attributes of branched frameworks can be employed for such applications as aqueous solubilization of inherently water-insoluble species as well as molecular ordering based on noncovalent interactions, such as *H*-bonding and ionic associations. The advent and current status of several dendritic micelles are herein chronicled.

Internal Inclusion

With the beginning[4,5] of dendrirner chemistry in 1985, and the successful construction of branched, multifunctional architectures such as polyols **3** and 4 (Fig. 2), the logical application of supramolecular chemistry to this field was obvious, as noted by the original introduction[4] of the ierm ''unimolecular micelle.'' It would, however, be several years before the actual proof-of-concept for covalently connected surfactant moieties was unequivocally demonstrated[6,7] in the all-hydrocarbon micellane series;[8] this was the first example of a unimolecular micelle that incorporated the lipophilic/hydrophilic features of a classical micelle into a single molecule. Pivotal to its construction was access to monomers possessing

Encyclopedia of Supramolecular Chemistry
DOI: 10.1081/E-ESMC 120012783

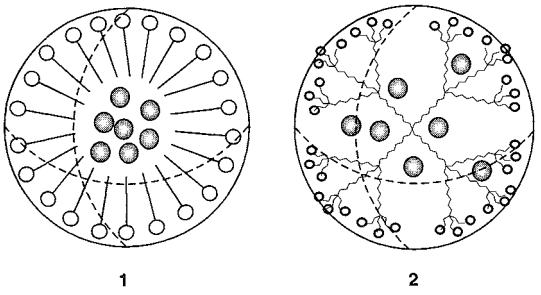

Fig. 1 Idealized representations of guest (●) encapsulation via a classical micelle aggregate 1 and a dendritic unimolecular micelle 2

tetraalkyl-substituted quaternary carbon branching centers via the free radical-promoted replacement of a tertiary nitro *group with an electron-deficient alkene* (i.e., *acrylonitrile or an* alkyl *acrylate).*

Thus reaction of the tetrabromide core 5 *with four equivalents of the requisite terminal alkyne building block* 6 *via generation of the alkynide anion afforded the first generation polyalkyne; concomitant reduction and* deprotection *yielded the polyol. which was transformed to the corresponding polybromide for iteration. Following reduction and conversion of the periphery to carboxylic acid moieties, aqueous solubility was imparted by treatment with* $Me_4N^{[+]}OH^{[-]}$ to *form the* poly(ammonium *carboxylate)* 7.

Molecular inclusion was demonstrated by the aqueous solubilization and UV *and fluorescence analysis of the guest dyes phenol blue* (8), *pinacyanol chloride (9). chlortetracycline (10).and naphthalene (11).Fluorescence lifetime decay experiments using* 1,*6-diphenylhexatriene* (12) *as the probe further supported the host–guest relationship: while electron microscopy (EM)* corroborated *the single molecule. non-aggregated state. Calculated molecular modeling diameters of* 48 Å in *a fully extended conformation were also substantiated via EM.*

Prior to micellane construction, ca. 1989, *Tomalia and* coworkers[9] *examined the* $^{[13]}$C-NMR T_1 (spin-*lattice) relaxation times of* 2,4-dichlorophenoxyacetic

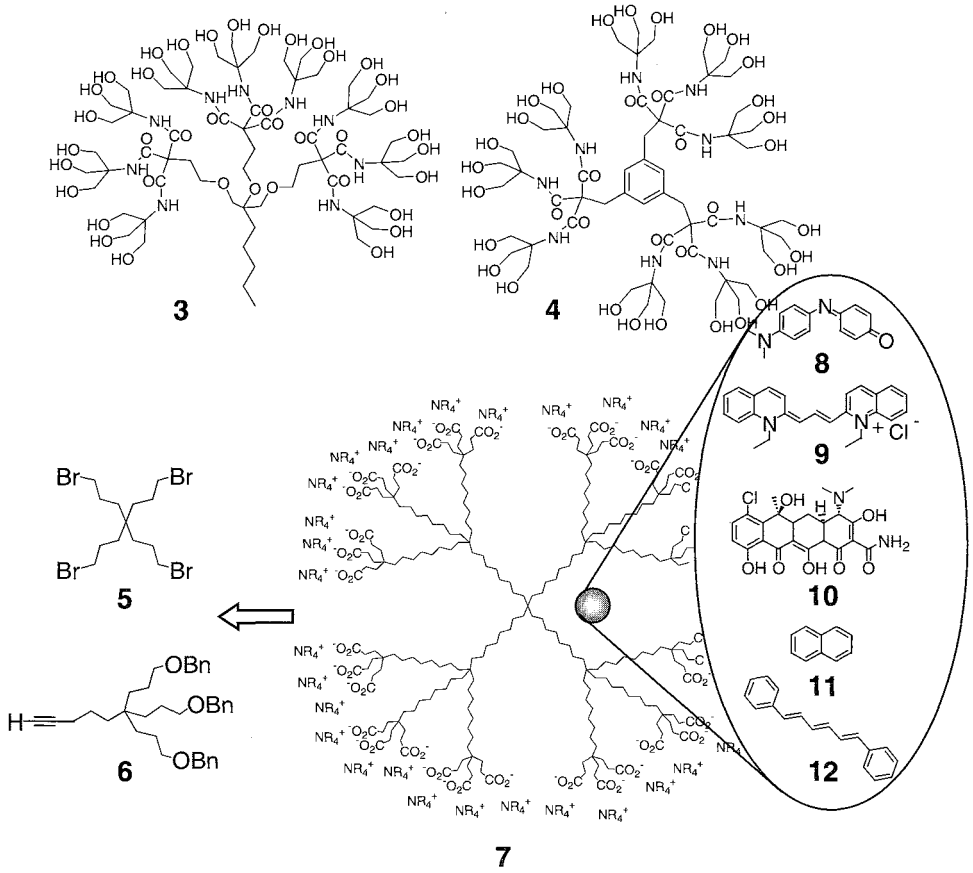

Fig. 2 Early *tris*-terminated, branched architectures (i.e., 3 and 4) were described as possessing micellar architecture and character: and study of the properties of nuinerous encapsulated molecular guests proved the micellar character of the first, all-alkyl hydrocarbon dendrimer 7.

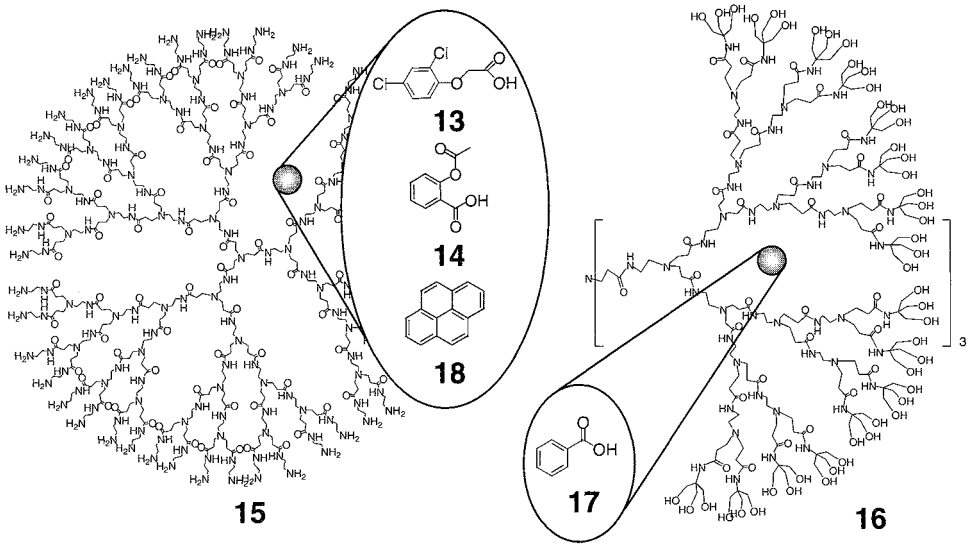

Fig. 3 [13]C-NMR spin-lattice (T_1) relaxation studies of guests, such as acetylsalisylic acid (14), encapsulated in polyamidoamine dendrimers (15) and the enhanced *aqueous* solubility of guests (i.e., 17) reveal the micellar nature of dendrimers.

acid (13) and acetylsalicylic acid (14) in the presence of PAMAM (polyamidoamine) *dendrimers* (15; *Fig. 3, prepared via repetition of two steps. exhaustive amine alkylation with methyl acrylate followed by amidation of the resulting ester* moieties with *1.2-diaminoethane to regenerate the* amine *surface) and in bulk solution alone. Relaxation* times *were found to be significantly* lower *with added host. suggesting molecular inclusion within the dendrimer. or a dendrimer aggregate, as noted by the authors.*

Other notable PAMAM-based host–guest studies have appeared. Tris(hydroxymethyl)aminomethane-(TRIS) *terminated* PAMAMs (16) *have been* created[10] *by reaction of* TRIS *with the ester groups on the surface. Inclusion complexes with, for example, benzoic acid* (17), *significantly increased guest aqueous solubility 300-fold at neutral pH; while the above* PAMAM *examples denote an acid–base interaction,* Turro *and* coworkers[11,12] *used pyrene* (18) *in* photoluminescent *experiments to evaluate internal hydophobicity and thereby corroborate a predicted morphology change* for *this family* [i.e., *changing* to *a* more *globular shape with a more closed and congested surface'" beyond generation* 3.5].

PAMAMs *constructed starting with lipophilic* C_{12} *cores have been exploited as hosts for studies using the dye Nile* red.[13] *Notably. aqueous fluorescence emission was significantly enhanced by the formation of a* dendrimer-surfactant *assembly upon amphiphile addition. Modification of* PAMAM *surfaces by* treatment *with* epoxyalkanes,[14] such *as* 1,2-epoxyhexane *and* 1,2-*epoxyoctane. produced* nanoscopic *container molecules that facilitated the solubilization of* $CuSO_4$ *in toluene when placed in contact with a 0.1 M aqueous solution.*

Meijer *and* coworkers[15] *provided a striking example of dendrimer-based. host–guest interaction (Fig. 4) by successfully sterically trapping 3-carboxyproxyl radicals (19).* 7,7,8,8-tetracyanoquinodimethane *(20:TCNQ), and the dye Rose Bengal* (21) *within the interior of fifth-generation* poly(propyleneimine) (PPIs; *accessed by repetitive terrninal* amine *alkylation* with *acrylonitrile and subsequent* nitrile reduction *to regenerate a set of new amines for further elaboration) dendrimers described as a dendritic box (22). A filled dendritic box was prepared by reacting the* amine *surface with an activated ester of a t-*BOC-protected *amino acid. such as phenylalanine, in the presence of encapsulated guests; notably, complete impermeability of the shell by trapped molecules was observed.*

The PPI *series has also been used to craft inverted* micelles[16] *via termini modification with long-chain* ($C_{5,9-15}$) *acid chlorides. Ethanol solutions of these dendrimers and Rose Bengal afforded second- and fifth-generation* unimolecular *micelles entrapping an average of one and seven (or eight) guests. respectively.* Dynamic *light scattering experiments supported single particle behavior. Also. coating the surface with palmitoyl chloride and subjecting to low pH gave rise to efficient anionic dye* extractors;[17] *however. higher* pH *environments* (i.e., >6), *afforded less-effective extractors. Similar materials have been* employed *for* oxyanion-*based extraction of pertechnetate, perrhenate, AMP. ADP, and* ATP.[18] *As well. host–guest binding constants using*

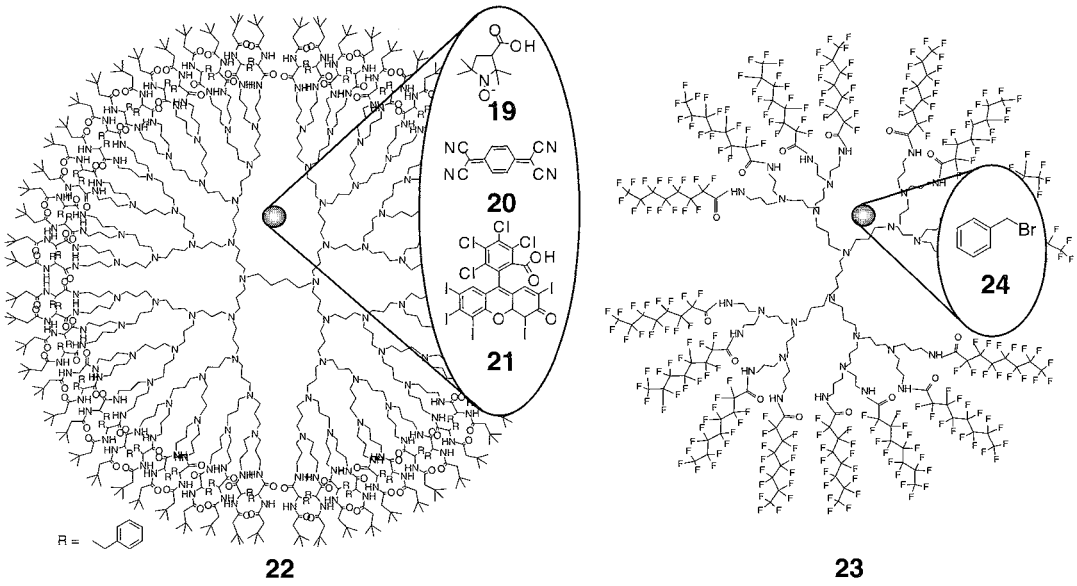

Fig. **4** A dendritic box has been shown to trap molecular guests (i.e., **22**), while fluorinated constructs (23) show promise as phase-transfer catalysts.

pyrene as the probe,[19] PPIs quaternized with glycidyltrimethylammonium chloride as pH-sensitive. controlled drug release systems,[20] and unimolecular micelles crafted by the preparation of oligo(ethyleneoxy)-terminated PPIs[21] have also been reported.

Researchers van der Broeke and coworkers[''' created perfluoro-functionalized poly(propyleneimine) dendrimers (23; Fig. 4) and demonstrated their potential as phase-transfer catalysts in supercritical carbon-dioxide–water mixtures and as anionic species extractants. The dendrimers were accessed via reaction of perfluorinated, linear alkyl acid chlorides with the terminal amines. Extraction of perinanganate or dichromate from aqueous to CO_2 solution was described as rather low, whereas their use as phase-transfer catalysts in a halogen exchange reaction [benzyl chloride to benzyi bromide (24)] resulted in high rates of conversion.

Dykes et al.[23] reported that peptide-coupled L-lysine amino-acid-based dendrimers solubilized proflavin hydrochloride and aurin tricarboxylic acid in CH_2Cl_2. The degree of dye solubilization increased as the degree of branching increased (i.e., at higher generations), with generation 4 incorporating up to 97% of suspended proflavin •HCl in the best case. Dye incorporation was enhanced by focal carboxylic acid or amine coordination with a proflavin-free amine or an aurin acid moiety, respectively. Control experiments with unbranched hosts. such as acetic acid, showed very little dye uptake, as expected, further suggesting that ''ddedritic branching does indeed play a key role in the dye solubilization process.''[23]

Soon after the introduction of convergent dendrimer synthesis,[24] hemispherical. aryl-ester-coated, benzyl ether-based dendrons were reported.[25] Attachment to a divalent core and conversion to the polycarboxylate 25 (Fig. 5) yielded dendriiners that facilitated a 200-fold increase in pyrene (26) solubility in water compared with that of pure water without the dendrirner. Notably, use of sodium dodecyl sulfate (SDS; above cmc: $9 \times 10^{[-3]}$ M) for pyrene encapsulation resulted in only an 100-fold enhancement.

Piotti et al.[26] reported the construction of Fréchet-type reverse unimolecular micelles possessing polar internal aryl methyl esters at each generation and linear C_{14} alkyl chains at the periphery. Construction began with reaction of 3,5-*bis*(tetradecylaryl ether)benzyl bromide (27) with the 3,5-dihydroxybenzene (28). Repetition of the standard benzyl alcohol to bromide conversion[24] followed by phenolic substitution of the benzylic halide produced fourth-generation wedges that were subsequently attached to a *tris*(phenolic) core to afford the desired architecture 29. The internal methyl aryl ester groups were also converted to alcohols via $LiAlH_4$ reduction. Micellar potential was demonstrated by use of these dendrimers as catalysts in elimination reactions of tertiary iodoalkanes. The greatest effect was observed for the transformation of 2-iodo-2-methylheptane (30), with a recorded 99% conversion to alkene (dendrimer to substrate ratio. 1:17,600), while the lowest observed conversion was 83%.

Acid-terminated, amide-based dendrimers (i.e., 31) have been shown to be effective surfactant substitutes in

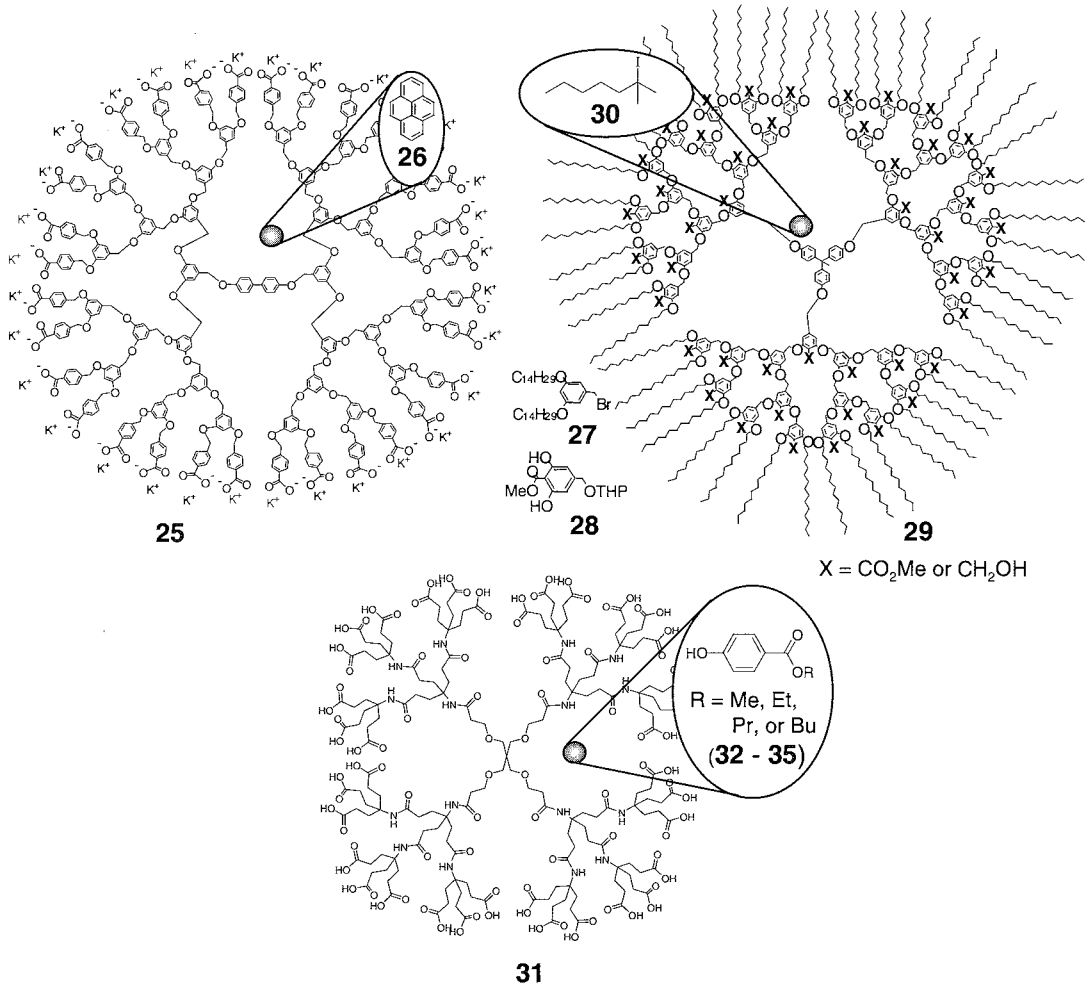

Fig. 5 A variety of architectures have been demonstrated to be useful aqueous solubility enhancements (**25**), catalysts for elimination reactions (**29**), and vehicles for chromatographic separations **(31).**

the analytical separation technique of micellar electrokinetic capillary chromatography (MECC).[27] The dendrimers were prepared by iterative peptide-type coupling followed by carboxylic acid deprotection using an amino*tris*(*tert*-butyl ester) building block: divergent synthesis began with a *tetrakis*(carboxylic acid) core. A series of alkyl parabens (methyl, ethyl, *n*-propyl, and *n*-butyl 4-hydroxybenzoate; **32–35)** were separated, employing first-, second-, and third-generation polyacids, with the higher construct affording the best results. Essentially, the greater the analyte:micellar (i.e., dendrimer) interaction, the longer the analyte retention time in the capillary. Thus, the observed order of elution started with the least lipophilic benzoate and progressed sucessively to the most lipophilic. Separations were shown to be strongly pH dependent, with acidic buffers yielding no results due to dendrimer interaction with the fused-silica capillary surface effectively stopping mobility. MECC has also been examined using PAMAM dendrimers as surfactant substitutes.[28]

Ordered Positioning

Whereas the majority of dendrimer-based lipophilic-hydrophilic inclusion phenomena discussed thus far results in random guest positioning on a branched framework. ordered interactions in supramolecular assemblies are also of interest. For example, González et al.[29] reported the surface modification of poly(propyleneimine)s with cobaltocenium groups that are easily reduced to Co(0). Reaction of the amine termini with 1-chlorocarbonylcobaltocenium afforded the metal-terminated dendrimers. The lipophilic, charge-neutral polycobaltocenes were rendered H_2O soluble via addition of β-cyclodextrin (36, β-CD) based on its cylindrical

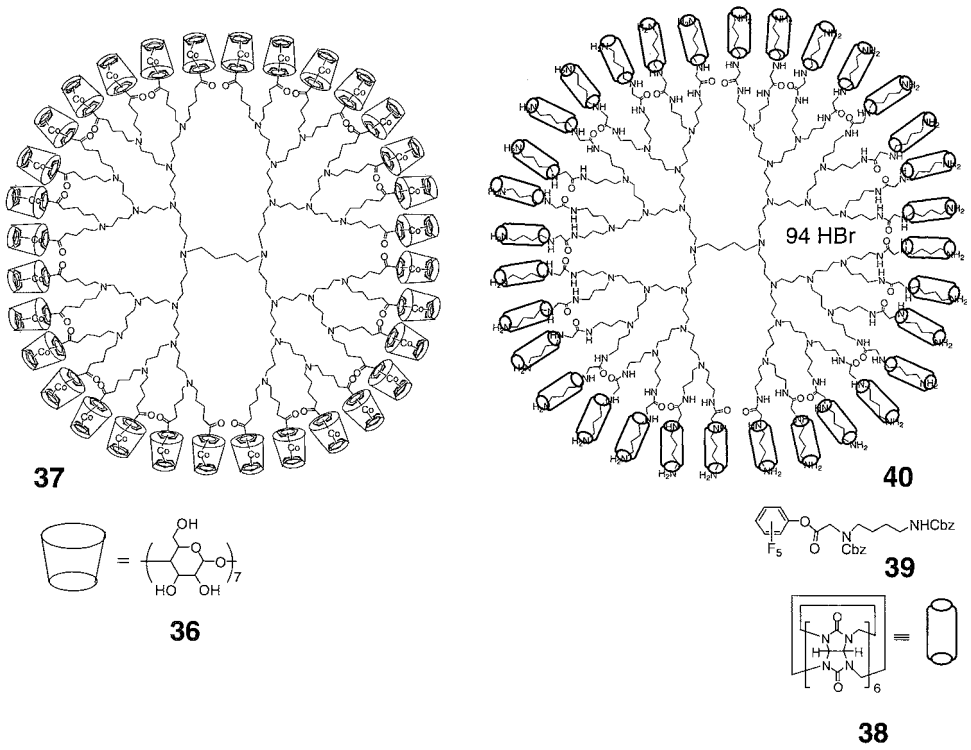

Fig. 6 Branched architectures have also demonstrated their utilitarian nature by facilitating supramolecular ordering on modified surfaces (i.e., 37 and 40).

encapsulation of the metallocene moieties (37; Fig. 6). Reversible electrochemical oxidation to the charged state afforded the uncomplexed dendrimer form. Similar ferrocenyl-terminated PPIs are also known.[30]

Kim and coworkers[31] adapted the periphery of PPIs for a similar, albeit more ionic, coordination with cylindrical cucurbituril (CB; 38) units to give a stable, poly(pseudorotaxane) architecture. The required *bis*(ammonium)-coated scaffolding was accessed via treatment of the dendriiner amine surface with the perfluorophenyl-activated ester of a *bis*(protected) diamine-modified acetate 39 followed by deprotection (HBr) of the diamine chains. Dissolution of the polyprotonated framework in H_2O followed by the addition of CB afforded the self-assembled product 40. Preliminary studies aimed at decomplexation via treatment with base yielded partial separation. T_1 (spin-lattice) relaxation experiments with the CB-dendrimer complex showed a sharp increase with higher generations, suggesting that the outer shell possessed attributes of a solid phase; such behavior has also been noted by Jansen et al.[15]

Newkome and coworkers[32] employed site-specific, *H*-bonding-based, molecular recognition on the interior of a branched framework for guest positioning. Incorporation of the binding sites was facilitated by a single-pot, three-component reaction, whereby 1,5-glutaryl dichloride was reacted with one equivalent of an amino-*tris*(*tert*-butyl ester) followed by treatment of an excess of 2,6-diaminopyridine to form an extended aminotriester useful in iteration. NMR titration experiments using glutarimide and 3'-azido-3'-deoxythimidine (AZT) revealed downfield shifts of the pyridyl diamide protons substantiating the dendrimer–guests complexes (e.g., 41).

Baars et al.[33] reported the peripheral amine modification of PPI frameworks with adamantane isocyanate to afforded terminal urea moieties. Supramolecular surface ordering of carboxylic acid-modified urea guests was achieved based on ionic-acid–base association at the outermost dendritic tertiary amine moieties and urea promoted H-bonding. T_1 relaxations were found to significantly increase at the complex surface verifying enhanced rigidity. Other assemblies of interest include PAMAM–fatty acid[12''] and PAMAM–surfactant''' mixtures.

CONCLUSION

Progress in supramolecular chemistry and nanotechnology is inherently linked to the building blocks that are available. Attributes of desirable building blocks include the potential to effect noncovalent molecular interactions

on their environment. Due to the modular and iterative features of branched. macromolecular architecture syntheses that facilitate the fine-tuning of physicochemical parameters. and from the perspective of multifunctional and multilevel interactions, dendrimers are uniquely and logically suited as supramolecular monomers.[36–58]

ACKNOWLEDGMENTS

We gratefully acknowledge the Office of Naval Research (N00014-99-0082) and the National Science Foundation (DMR-9901393).

ARTICLES OF FURTHER INTEREST

Amide- and Urea-Based Anion Receptors, p. *31*
Amino Acids, Applications in Supramolecular Chemistry, p. 42
Anion-Directed Assembly, p. 51
Calixarenes and Their Analogues: Cation Complexation, p. 137
Calixarenes and Their Analogues: Molecular Complexation, p. 145
Catenanes and Interlinked Structures, p. 206
Cation–π Interactions, p. 214
Chemical Topology, p. 229
Chiral Guest Recognition, p. 236
Concepts in Crystal Engineering, p. 319
Cucurbituril, Its Homologues, and Derivatives, p. 390
DNA as a Supramolecular Scaffold, p. 467
DNA Nanotechnology, p. 475
Fullerenes as Encapsulating Hosts, p. 579
Guanidium-Based Anion Receptors, p. 615
Hydrogen Bonding. p. 658
Hydrophobic Effects, p. 673
Induced Fit, p. 717
Micelles and Vesicles, p. *861*
Self-Assembling Capsules, p. 1231
Supramolecular Chemistry: Definition, p. 1401
Supramolecular Polymers, p. 1443
Surfactants, Part I: Fundamentals, p. 1458
Surfactants, Part II: Applicatiorzs, p. 1470

REFERENCES

1. Newkome, G.R.; Moorefield, C.N.; Vogtle. F. *Dendrimers and Dendrons: Concepts, Syntheses, Applications*; Wiley-VCH: Weinheirn, Germany, 2001.
2. *Dendrimers and Other Dendritic Polymers;* Frechet, J.M.J.. Tomalia, D.A.. Eds.: John Wiley & Sons: West Sussex, UK, 2001.
3. Menger, F.M. On the structure of micelles. Acc. Chem. Res. **1979,** *12.* 110–117.
4. Newkome, G.R.; Yao, Z.; Baker. G.R.: Gupta. V.K. Cascade molecules: A new approach to rnicelles. A [27]-arborol. J. Org. Chem. **1985.** *50.* 2003–2004.
5. Tomalia. D.A.; Baker, H.; Dewald, J.: Hall. M.; Kallos, G.: Martin. S.: Roeck, J.; Ryder, J.: Smith. P. A new class of polymers: Starburst-dendritic macromolecules. Polym. J. (Tokyo) **1985.** *17.* 117–132.
6. Newkome. G.R.; Baker. G.R.; Saunders. M.J.: Russo. P.S.; Gupta, V.K.; Yao. Z.: Miller. J.E.; Bouillion, K. Two-directional cascade molecules: Synthesis and characterization of [9]-*n*-[9] arborols. J. Chem. Soc., Chem. Commun. **1986,** 752–753.
7. Newkome. G.R.: Moorefield, C.N.: Baker. G.R.: Saunders, M.J.; Grossman, S.H. Unimolecular micelles. Angew. Chem., Int. Ed. Engl. **1991,** *30.* 1178–1180.
8. Newkorne, G.R.; Moorefield, C.N.; Baker. G.R.: Johnson, A.L.: Behera, R.K. Alkane cascade polymers with a micellar topology: Micellanoic acid derivatives. Angew. Chern., Int. Ed. Engl. **1991,** *30,* 1176–1178.
9. Naylor, A.M.: Goddard. W.A., III: Kiefer. G.E.; Tomalia, D.A. Starburst dendrimers. 5. Molecular shape control. J. Am. Chern. Soc. **1989,** *111.* 2339–2341.
10. Twyman. L.J.; Beezer. A.E.; Esfand, R.; Hardy. M.J.; Mitchell. J.C. The synthesis of water soluble dendrimers, and their application as possible drug delivery systems. Tetrahedron Lett. **1999.** *40.* 1743–1746.
11. Gopidas, K.R.: Leheny. A.R.: Caminati. G.; Turro, N.J.: Tomalia, D.A. Photophysical investigation of similarities between starburst dendrimers and anionic micelles. J. Am. Chem. Soc. **1991,** *113.* 7335–7342.
12. Carninati. G.; Ottaviani, M.F.; Gopidas, K.: Jockusch. S.; Turro. N.J.: Tomalia, D.A. Photochemical and spectroscopic probes of starburst dendrimers: restricted spaces for photoinduced electron transfer and surfaces for the construction of supramolecular aggregates. Polym. Mater. Sci. Eng. **1995.** *73.* 80–81.
13. Watkins. D.M.: Sayed-Sweet. Y.; Klimash, J.W.; Turro. N.J.: Tomalia, D.A. Dendrimers with hydrophobic cores and the formation of supramolecular dendrimer-surfactant assemblies. Langmuir **1997,** *13.* 3136–3141.
14. Sayed-Sweet. Y.: Hedstrand, D.M.: Spindles, R.; Tornalia, D.A. Hydrophobically modified poly(amidoamine) (PAMAM) dendrimers: Their properties at the air–water interface and use as nanoscopic container molecules. J. Mater. Chem. **1997.** 7, 1199–1205.
15. Jansen, J.F.G.A.; de Brabander-van den Berg. E.M.M.; Meijer, E.W. Encapsulation of guest molecules into a dendritic box. Science 1994, 266. 1226–1229.
16. Stevelmans, S.: van Hest, J.C.M.; Jansen. J.F.G.A.; van Boxtel. D.A.F.J.: de Brabander-van den Berg, E.M.M.; Meijer. E.W. Synthesis, characterization. and guest–host properties of inverted unirnolecular dendritic micelles. J. Am. Chem. Soc. **1996.** *118,* 7398–7399.

17. Baars, M.W.P.L.: Froehling, P.E.; Meijer, E.W. Liquid–liquid extractions using poly(propylene imine) dendrimers with an apolar periphery. Chem. Commun. 199'7, 1959–1960.
18. Stephan. H.: Spies. H.; Johannsen, B.; Klein. L.: Vogtle. F. Lipophilic urea-functiorialized dendrimers as efficient carriers for oxyanions. Chem. Cornmun. 1999. 1875–1876.
19. Pistolis, G.: Malliaris. A.; Tsiourvas. D.; Paleos. C.M. Poly(propyleneimine) deiidrimers as pH-sensitive controllecl-release systems. Chem. Eur. J. 1999, 5. 1440–1444.
20. Sideratou. Z.: Tsiourvas, D.; Paleos, C.M. Quaternized poly(propylene imine) dendrimers as novel pH-sensitive controlled-release systems. Langmuir 2000, 16. 1766–1769.
21. Baars. M.W.P.L.; Kleppinger. R.; Koch, M.H.J.; Yeu. S.-L.; Meijer. E.W. The localization of guests in water-soluble oligoethyleneoxy-modified poly(propyleneimine) dendrimers. Angew. Chem.. Int. Ed. **2000**, *39*, 1285–1288.
22. Goetheer. E.L.V.: Baars, M.W.P.L.; van den Broeke, L.J.P.: Meijer, E.W.: Keurentjes, J.T.F. Functionalized poly(propylene imine) dendrirners as novel phase transfer catalysts in supercritical carbon dioxide. Ind. Eng. Chem. Res. 2000. *39*, 4634–4640.
23. Dykes. G.M.: Brierley. L.J.: Smith. D.K.; McGrail. P.T.; Seeley, G.J. Supramolecular solubilisation of hydrophilic dyes by using individual dendritic branches. Chem. Eur. J. 2001, 7. 4730–4739.
24. Hawker, C.; Fréchet, J.M.J. A new convergent approach to monodisperse dendritic macroinolecules. J. Chem. Soc., Chem. Cominun. 1990. 1010–1013.
25. Hawker, C.J.: Wooley. K.L.; Fréchet. J.M.J. Unimolecular micelles and globular amphiphiles: Dendritic macromolecules as novel recyclable solubilization agents. J. Cliem. Soc., Perkin Trans. 1 1993, 1287–1297.
26. Piotti. M.E.: Rivera. F., Jr.; Bond, R.; Hawker. C.J.: Fréchet. J.M.J. Synthesis and catalytic activity of unimolecular dendritic reverse micelles with "internal" functional groups. J. Am. Chem. Soc. **1999**, *121*, 9471–9472.
27. Kuzdzal, S.A.; Monnig, C.A.: Newkome. G.R.: Moorefield, C.N. Dendrimer electrolcinetic capillary chromatography: Unimolecular micellar behavior of carboxylic acid terminated cascade macromolecules. J. Chem. Soc., Chem. Commun. 1994. 2139–2140.
28. Tanaka, N.: Tanigawa, T.: Hosoya, K.: Kimata. K.: Araki. K.; Terabe. S. Starburst dendrimers as carriers in electrokinetic chromatography. Chem. Lett. 1992. 959–962.
29. González, B.; Casado. C.M.; Alonso, B.: Cuadrado. I.: Morán. M.; Wang, Y.: Kaifer. A.E. Synthesis. electrochemistry and cyclodextrin binding of novel cobaltocenium-functionalized dendrimers. Chem. Commun. 1998, 2569–2570.
30. Cuadrado. I.: Moran, M.: Casado. C.M.; Alonso. B.; Lobete. F.: Garcia. B.: Ibisate. M.; Losada, J. Ferrocenyl-functionalized poly(propylenimine) dendrimers. Organometallics **1996**. *15*. 5278–5280.
31. Lee, J.W.: Ko, Y.H.; Park, S.-H.; Yarnaguchi. K.: Kim. K. Novel pseudorotaxane-terminated dendrimers: Supramolecular modification of the dendrimer periphery. Angew. Chem., Int. Ed. 2001. 40. 746–749.
32. Newkome, G.R.; Woosley, B.D.; He, E.; Moorefield, C.N.; Güther, R.: Baker, G.R.: Escaniilla, G.H.; Merrill, J.: Luftmann. H. Supramolecular chemistry of flexible. dendritic–based structures employing molecular recognition. Chem. Commun. 1996, 2737–2738.
33. Baars. M.W.P.L.; Karlsson. A.J.; Sorokin, V.: de Waal. B.F.W.; Meijer. E.W. Supramolecular modification of the periphery of dendrimers resulting in rigidity and functionality. Angew. Chern., Int. Ed. **2000**. 39, 4262–4265.
34. Chechik, V.; Zhao. M.; Crooks, R.M. Self-assembled inverted micelles prepared from a dendrimer template: Phase transfer of encapsulated guests. J. Am. Chem. Soc. 1999. 121, 4910–491 1.
35. Uppuluri, S.; Swanson. D.R.: Piehler, L.T.; Li. J.; Hagnauer, G.L.; Tomalia, D.A. Core-shell tecto(dendrimers): I. Synthesis and characterization of saturated shell models. Adv. Mater. **2000**. 12. 796–800.
36. Piotti. M.E.: Rivera. F., Jr.; Bond. R.: Hawker. C.J.; Fréchet, J.M.J. Synthesis and catalytic activity of unimolecular dendritic reverse micelles with "internal" functional groups. J. Am. Chem. Soc. 1999. 121.9471–9472.
37. Vas. C.R. *"Amphiphilic Dendrimers"* Dissertation; Eindhoven University of Technology. 1999.
38. Huang. H.; Remsen. E.E.; Kowalewski, T.: Wooley. K.L. Nanocages derived from shell cross-linked micelle templates. J. Am. Chem. Soc. 1999. 121. 3805–3806.
39. Chechik, V.: Zhao, M.: Crooks, R.M. Self-assembled inverted micelles prepared from a dendrirner template: Phase transfer of encapsulated guests. J. Am. Chem. Soc. 1999. 121. 4910–4911.
40. Liu, H.: Jiang, A.; Guo, J.: Uhrich, K.E. Unimolecular micelles: Synthesis and characterization of amphiphilic polymer systems. J. Polym. Sci., A. Polym. Chem. **1999**. 37. 703–711.
41. Guo. J.: Farrell. S.; Liu. H.; Uhrich, K.E. Interactions between hyperbranched unimolecular micelles and liposomes as cell membrane-mimics. Polym. Prepr. 1999, 40, 209–210.
42. Heise. A.; Hedrick. J.L.; Franlc, C.W.; Miller. R.D. Starlike block copolymers with amphiphilic arms as models for unimolecular micelles. J. Am. Chem. Soc. **1999**. 121. 8647–8648.
43. Palmer, C.P. Micelle polymers, polymer surfactants and dendrimers as xpseudostationary phases in micellar electrokinetic chromatography. J. Cliromatogr., A **1997**, *780*, 75–92.
44. Templeton. A.C.: Wuelfing, W.P.: Murray. R.W. Monolayer-protected cluster molecules. Acc. Chem. Res. **2000**. 33. 27–36.
45. Liu, M.; Kono, K.: Fréchet. J.M.J. Water-soluble dendritic unimolecular micelles: Their potential as drug delivery agents. J. Control. Release 2000, *65*, 121–131.
46. Gitsov. I.: Lambrych. K.R.; Remnant. V.A.: Pracitto. R. Micelles with highly branched nanoporous interior: Solution properties and binding capabilities of amphiphilic copolymers with linear dendritic architecture. J. Polym. Sci., A, Polym. Chem. **2000**. 38, 2711–2727.

47. Stapart, H.R.: Nishiyania. N.; Jiang. D.-L.: Aida. T.: Kataoka. K. Polyion complex micelles encapsulating light-harvesting ionic dendrimer zinc porphyrins. Langmuir 2000. **16** (21), 8182–8188.
48. Wade. D.A.: Torres. P.A.: Tucker, S.A. Spectrochemical investigations in dendritic media: Evaluation of nitromethane as a selective fluorescence quenching agent in aqueous carboxylate-terminated polyamido amine (PAMAM) dendrimers. Anal. Chim. Acta 1999. 397, 17–31.
49. Hanabusa. K.; Hirata. T.: Inoue. D.; Kimura, M.: Shirai, H. Formation of physical hydrogels with terpyridine-containing carboxylic acids. Colloids Surf., A Physicochem. Eng. Asp. 2000. *169*, 307–315.
50. Gröhn, F.; Bauer, B.J.; Amis, E.J. Hydrophobically modified dendrimers as inverse micelles: Formation of cylindrical multidendrimer nanostructures. Macromolecules 2001. 34 (19). 6701–6707.
51. Topchieva. I.N.; Kalashnikov, Ph.A.: Mel'nikov, A.B.; Polushina, G.E.: Lezov. A.V. Self-assembly of dendritic micellar structures based on triton X-100 and branched poly(ethylene oxide)-containing cyclodextrins. Colloid J. 2002. 64 (1). 106–111.
52. Schmalenberg, K.E.; Frauchiger, L.: Nikkhouy-Albers, L.; Uhrich. K.E. Cytotoxicity of a unimolecular polymeric micelle and its degradation products. Biomacromolecules 2001, 2 (3). 851–855.
53. Gohy, J.-F.; Lohmeijer. B.G.G.: Schubert. U.S. Metallo-supramolecular block copolymer micelles. Macromolecules 2002, *35* (12), 4560–4563.
54. Yusa, S.; Sakakibara. A.; Yarnamoto. T.: Morishima. Y. Reversible pH-induced formation and disruption of unimolecular rnicelles of an amphiphilic polyelectrolyte. Macromolecules 2002, *35* (13). 5243–5249.
55. Gohy. J.-F.; Lohmeijer. B.G.G.; Varshney, S.K.; Schubert, U.S. Covalent vs metallo-supramolecular block copolymer micelles. Macromolecules 2002. *35* (19). 7427–7435.
56. Slagt. M.Q.: Stiriba, S.E.; Klein Gebbink, R.J.M.; Kautz. H.: Frey, H.; van Koten, G. Encapsulation of hydrophilic pincer–platinum(II) complexes iii amphiphilic hyperbranched polyglycerol nanocapsules. Macromolecules 2002. *35* (15), 5734–5737.
57. Xu. Z.; Ford. W.T. Polystyrene latexes containing poly(polypropyleneimine) dendrimers. Macromolecules 2002, *35* (20). 7662–7668.
58. Menger. F.M.: Azov, V.A. Synthesis and properties of water-soluble asterisk molecules. J. Am. Chem. Soc. 2002, 124 (37), 11159–11166.

Deoxycholic, Cholic, and Apocholic Acids

D

Mikiji Miyata
Kazuki Sada
Nungruethai Yoswathananont
Osaka University, Osaka, Japan

INTRODUCTION

Deoxycholic, cholic, and apocholic acids were established to have abilities for including various organic compounds. They exhibit characteristic inclusion behaviors with different arrangements and hydrogen-bonding schemes. Their structures are equally the same but different in hydrogen-bonding groups. This prompts us to verify the other derivatives by simple modified the numbers of hydroxy groups with different locations and directions on the skeletons. as well as different side-chain length and functional groups on the side chains. This article will describe their inclusion compounds from the viewpoint of molecular assemblies and hydrogen-bond motifs.

ORIGIN OF BILE ACIDS

Bile acids are natural compounds that are produced in livers of vertebrate animals for digestion and absorption of fats and fat-soluble vitamins. Shown in Fig. 1 is the synthetic process of bile acids through cholesterol from isoprene. Cholesterol is converted to primary bile acids. such as cholic acid (CA). deoxycholic acid (DCA), chenodeoxychoiic acid (CDCA), and lithocholic acid (LCA).

FACIALLY AMPHIPHILIC AND ASYMMETRIC STRUCTURES OF BILE ACIDS

Bile acids are aliphatic compounds with unique structures. Shown in Fig. 2a is the molecular structure of **CA**. as compared to the turtle for simplicity. CA consists of large, rigid, facial skeletons as well as small, flexible, axial side chains. The skeletons accompany three hydroxyl groups and two methyl groups, which brings about facial amphiphilicity. The former groups point below the steroidal plane to form a hydrophilic face. while the latter groups point above the plane to form a lipophilic face. The facially asymmetric structure enables us to distinguish three axes of the skeletons. First, we call the hydrophilic and lipophilic sides "belly" and .'back." respectively. Second, we separate the small side chain as the "tail" and the reverse part of the skeleton as "head." Third, we discriminate the hydroxyl groups at carbon 7 and 12 positions as left and right. respectively.

HISTORICAL RESEARCH OF INCLUSION COMPOUNDS OF BILE ACIDS

Deoxycholic acid (DCA) is the first bile acid with inclusion ability that was established in a crystalline state."' So far, many research groups reported the inclusion compounds of DCA with various guest molecules, such as aliphatics. aromatics. alcohols, fatty acids, esters, ketones, and ethers. In mid-1980.~"Giglio overviewed the compounds and gave significant insight for flexible bilayer structures by means of energy calculation. Although DCA is a well-known host, there were no detailed reports on inclusion abilities of the related compounds. Only a little description is seen for apocholic acid (ACA). which has the same structure as DCA except for a double bond in the skeleton."' In 1986, Miyata and Miki et al. discovered lots of inclusion coinpounds of CA with channel structures."' This is the starting point at which to investigate inclusion phenomena of the other bile acids and their derivatives. Since then. several research groups dealt with their crystal structures and inclusion abilities. leading to the interpretation of comprehensive molecular recognition in size, shape. polarity. and chirality.

MODIFICATION OF BILE ACIDS AS HOST COMPOUNDS

The primary bile acids can be modified in many derivattves, as shown in Table 1 As for the side chains, we can change the carboxylic group to amide, hydroxyl, ester. and so on And we can decrease or increace the methylene number of the side chains Moreover, we can regulate the

Encyclopedia of Supramolecular Chemistry
DGI: 10.1081/E-ESMC 120012746

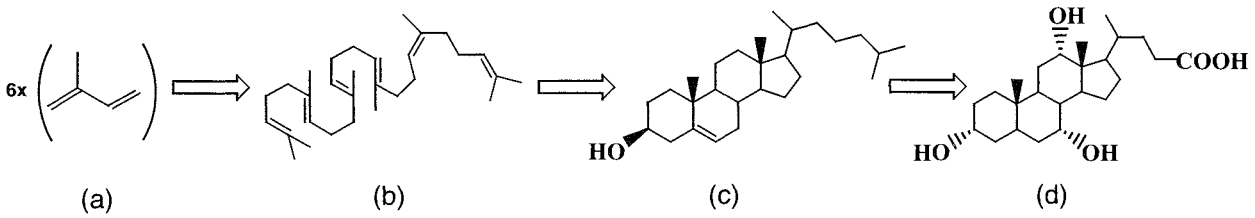

Fig. I Synthetic process of bile acids from (a) isoprene, through (b) squalene and. (c) cholesterol, to (d) CA.

direction of hydroxpl groups of the skeletons at axial or equatorial positions.

We usually search their inclusion abilities by using more than 100 organic compounds as guest candidates. The inclusion phenomena vary from one case to another. meaning that we do not always obtain their crystalline molecular assemblies. X-ray diffraction studies display that the steroidal hosts form various molecular assemblies such as monolayers. bilayers, helical tubes, and so on. In addition, we see diverse relationships among multiple host molecules and guest compounds. Such diversities originate from subtle differences on the hydrogen-bonding groups with respect to their positions and numbers. enabling us to compare hydrogen-bonding networks. molecular arrangements, inclusion behaviors, and so on, from a viewpoint of various donor–acceptor relationships between the hydrogen-bonding groups.

INCLUSION COMPOUNDS OF BILE ACIDS AND THEIR DERIVATIVES

Bile Acid Hosts

Deoxycholic acid (DCA)

DCA, one of the classical hosts, is known to form crystalline inclusion compounds with a wide range of organic substances. Craven and De Titta[5] reported the first crystal structure of DCA with acetic acid in 1972. Most of the crystals of DCA inclusion compounds belong to orchorhombic. and have cumulated bilayer structure5 with channels (Fig. 3a). The host molecules are arranged in a parallel fashion on the hydrophilic faces and in an antiparallel fashion on the lipophilic faces. as depicted in Fig. 2b. Also refer to the constant helical motif among hydrogen-bonding groups (see Fig. 6a).

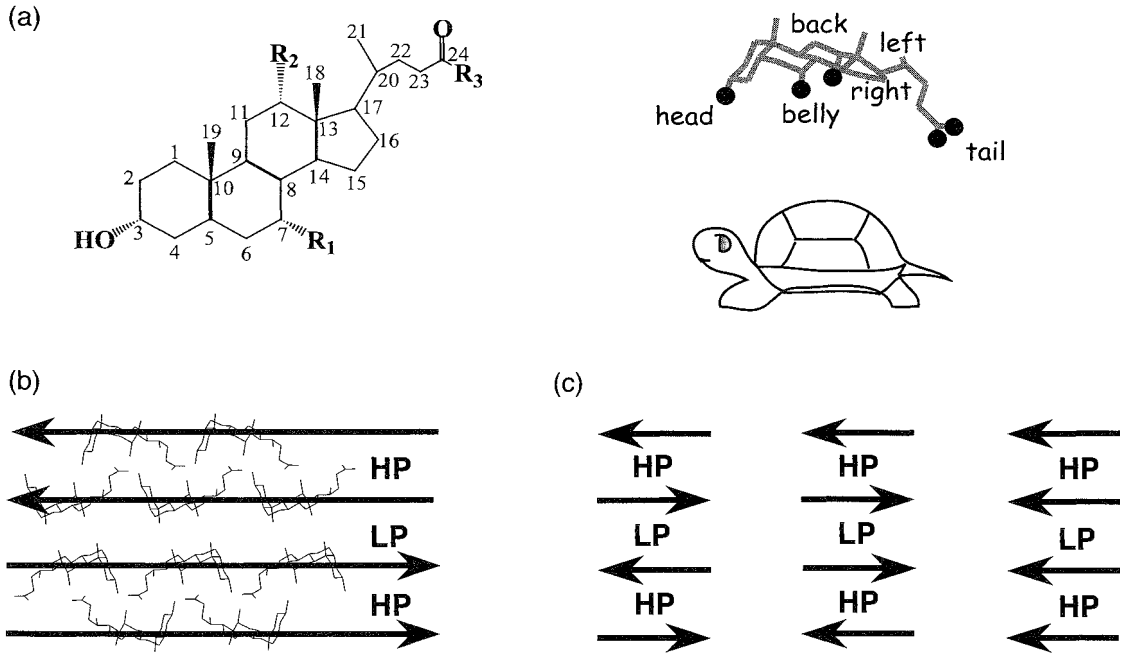

Fig. *2* (a) A facial amphiphilic and asymmetric structure of CA compared to turtle: (b) arrangements of the host molecules—parallel on the hydrophilic side (HP) and antiparallel on the lipophilic side (LP); and (c) three different arrangements in the bilayers.

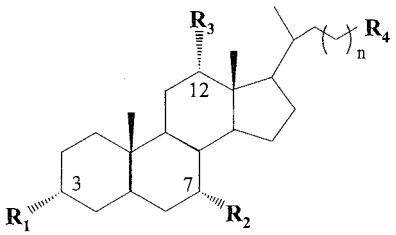

Table 1 Bile acid derivatives and their abbreviations used in this article

R_1	R_4	n	R_2 = α-H, R_3 = α-OH	R_2 = α-OH, R_3 = α-OH
N-OH	COOH	1	Deoxycholic acid (DCA)	Cholic acid (CA)
a-OH	$CONH_2$	1	Deoxycholamide (DCAM)	Cholamide (CAM)
x-OH	$CONHCH_3$	1	N-Methyldeoxycholamide (MDCAM)	N-Methylcholamide (MCAM)
α-OH	$CONHCH_2CH_3$	1	N-Ethyldeoxycholamide (EDCAM)	N-Ethylcholainide (ECAM)
α-OH	CH_2OH	1	3a.12a,24-Trihydroxy-5b-cholane (DCAtriol)	3a,7a,12a.24-Tetrahydroxy-5b-cholane (CAtetraol)
α-OH	$COOCH_3$	1	Methyl deoxycholate (MDC)	Methyl cholate (MC)
α-OH	COOH	0	Nordeoxycholic acid (NDCA)	Norcholic acid (NCA)
α-OH	COOH	2	Hoinodeoxycholic acid (WDCA)	Homocholic acid (HCA)
α-OH	COOH	3	Bishomodeoxycholic acid (BHDCA)	Bishomocholic acid (BHCA)
β-OH	COOH	1	3-Epideoxychol~cacid (3EDCA)	3-Epicholic acid (SECA)
	R_4	n	R_2 = α-OH, R_3 = α-H	R_2 = α-H, R_3 = α-H
α-OH	COOH	1	Chenodeoxycholic acid (CDCA)	Lithocholic acid (ECA)
α-OH	$CONH_2$	1	Chenodeoxycholamide (CDCAM)	Lithocholamide (ECAM)
α-OH	$CONHCH_3$	1	N-Methylchenodeoxycholamide (MCDCAM)	N-Methyllithocholamide (MLCAM)
α-OH	$CONHCH_2CH_3$	1	*N*-Ethylchenodeoxycholamide (ECDCAM)	N-Ethyllithocholamide (ELCAM)
α-OH	CH_2OH	1	3a,7a,24-Trihydroxy-5b-cholane (CDCAtriol)	3a,24-dihydroxy-5b-cholane (LCAdiol)
α-OH	$COOCH_3$	1	Methyl chenodeoxycholate (MCDC)	Methyl lithocholate (LMC)
α-OH	COOH	0	Norchenodeoxycholic acid (NCDCA)	Norlithocholic acid (NLCA)
α-OH	COOH	2	Homochenodeoxycholic acid (HCDCA)	Homolithocholic acid (HECA)
α-OH	COOH	3	Bishomochenodeoxycholic acid (BHCDCA)	Bishomolithocholic acid (BHLCA)
β-OH	COOH	1	3-Epichenodeoxycholic acid (3ECDCA)	3-Epilithocholic acid (3ELCA)

Apocholic acid (APA)

APA[3] has long been known to form the inclusion compounds similar to DCA. The crystal structures and inclusion abilities are nearly the same as shown in Fig. 4. They are served as hosts for inclusion polymerization. The former has larger channels than the latter.

Cholic acid (CA)

Inclusion compounds of CA with some alcohols were first reported by Mylius in 1887.[6] One hundred years later. Johnson and Schaefer[7] determined a crossing type of crystal structure for the inclusion compound of CA with ethanol. On the other hand, Miki et al. found a bilayer structure for the one with acetophenone.[8] Further studies made clear that CA forms various host frameworks to include different kinds of organic guest compounds. such as carboxylic acids, alcohols, nitriles. esters, aldehydes, ketones, and aromatic compounds. It is noteworthy that CA includes small alcohols such as methanol, ethanol, and propanol, in contrast to DCA. Shown in Fig. 5 are the guest-dependent crystal structures of CA. Small alcohols, carboxylic acids. as well as nitriles are incorporated in the crossing structure. On the other hand, aromatic compounds are done in the bilayer structure, where the host molecules are arranged in an antiparallel fashion on hydrophilic and lipophilic sides. CA has a cyclic hydrogen-bond network among four hydrogen-bonding groups of four different host molecules, which is different from the helical one of DCA. The versatile enclathration of CA comes from isomerization of the host frameworks on the basis of layer sliding on the lipophilic sides and conformational changes of the side chains.

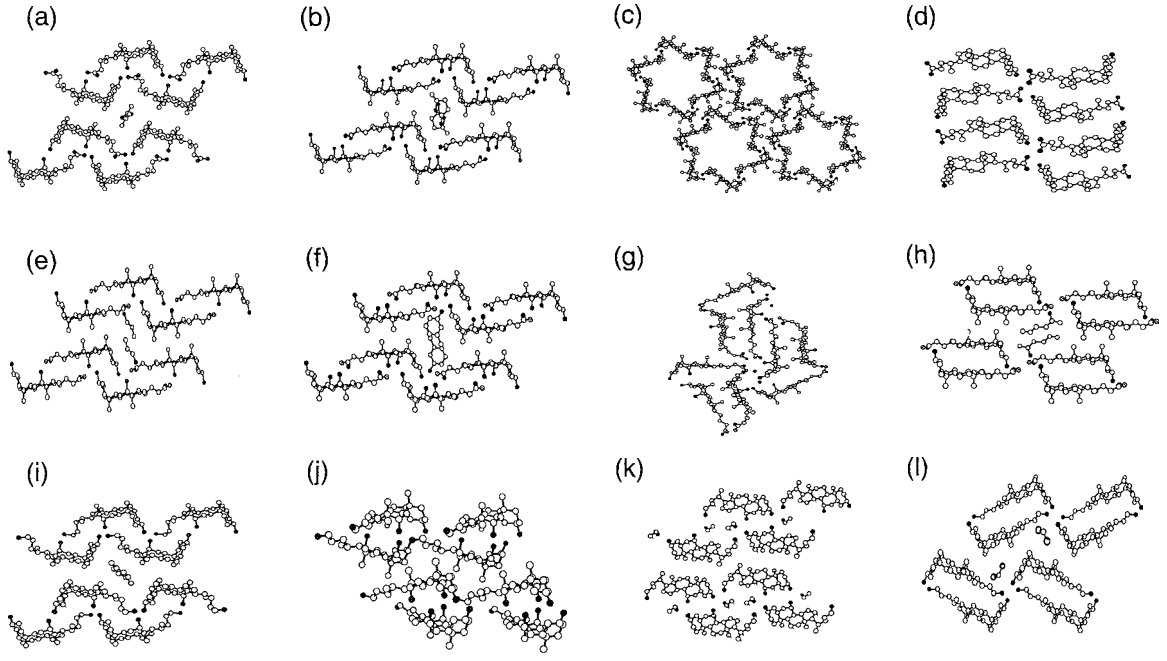

Fig. **3** Crystal structures of (a) DCA with acetone: (b) CA with γ-valerolactone; (c) guest-free crystal of CDCA: (d) guest-free crystal of LCA; (e) DCAM with 1-propanol; (f) CAM with *m*-cresol; (g) CDCAM with water; (h) LCAM with 2-hexanol; (i) DCAtriol with p-xylene: (j) guest free of CAtetraol; (k) CDCAtriol with ethanol: and (1) LCAdiol with dichloromethane.

Chenodeoxycholic acid (CDCA)

There are several reports[9–12] on the inclusion compounds of CDCA, despite many articles on those of DCA and CA. It is known that CDCA forms guest-free crystals (monoclinic $P2_1$)[9] as well as inclusion crystals with helical assemblies (hexagonal $P6_5$),[10] as depicted in Fig. 3c. The hexagonal type provides a large channel, where various guest compounds are included. Recently, Sada et al. succeeded in producing large crystals from the gel state, leading to the study on the intercalation and polymerization in the CDCA channels with retention of the crystalline state.[13]

Lithocholic acid (LCA)

It seems that LCA will not include any organic guests. as can be seen from the fact that only structures of guest-free and hydrate crystals are known[11] (Fig. 3d). In fact, we attempted to recrystallize LCA with over 100 organic compounds but inclusion compound still remains unknown.

MODIFICATION OF SIDE-CHAIN FUNCTIONAL GROUPS

Bile Amide Hosts

Replacement of the carboxyl group at the side chain to an amide group led to a great change of the inclusion abilities. One additional hydrogen-bond donor acts as a "hook" for catching a guest molecule with an hydrogen-bond acceptor. As a result, bile amide hosts can include many aliphatic alcohols in contrast to the original bile acids.

DCAM includes various types of organic compounds, regardless of their functional groups, and do not give

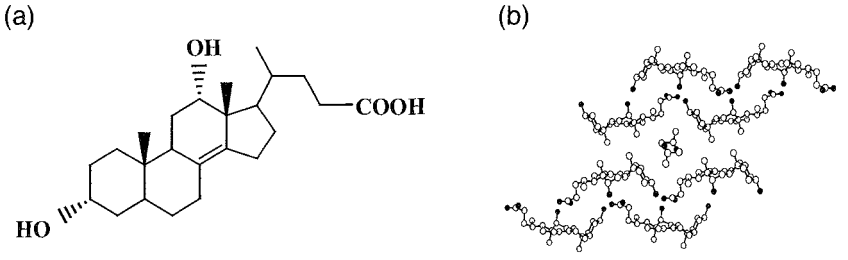

Fig. 4 (a) Molecular structure of APA and (b) crystal structure of APA with acetone.

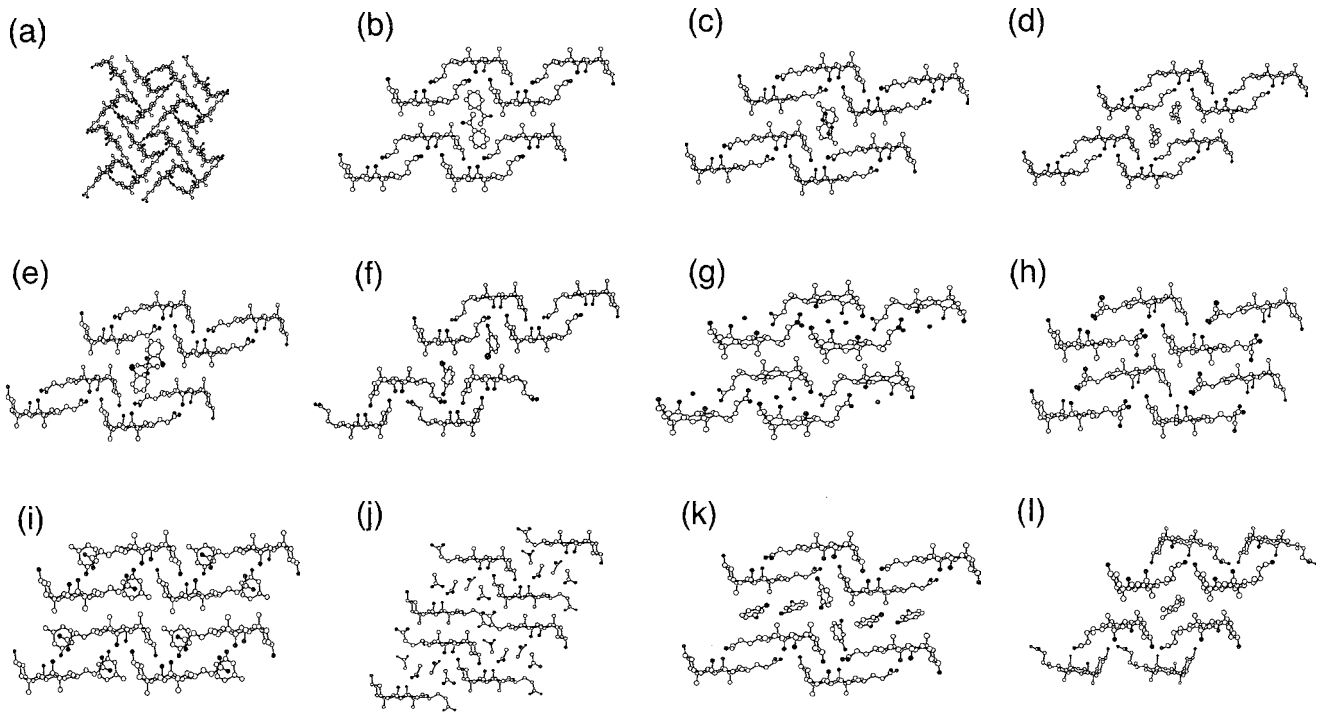

Fig. 5 Various host frameworks of CA with (a) methanol: (b) acetophenone: (c) γ-valerolactone; (d) ethylnylbenzene; (e) 2-fluoropropiophenone; (f) *m*-chloroaniline; (g) water: (h) acetonitrile; (i) 3-methylcyclohexanone; (j) acetic acid: (k) *m*-fluoroaniline; and (l) 1,2,3-trimethylbenzene.

guest-free crystals at all. It forms several host frameworks that depend on guests. In the case of small alcohols, the crystals have bilayer structures, where the host molecules are arranged in an antiparallel fashion on the hydrophilic and lipophilic sides as depicted in Fig. 3e. This arrangement is the same as that of CA. The hydroxyl groups of the guest molecules are inserted into the cyclic hydrogen-bond networks (Fig. 6e). On the other hand, in the case of large alcohols or aromatic compounds, DCAM employs the bilayer structure similar to DCA, where the host molecules are arranged in a parallel fashion on the hydrophilic sides and in an antiparallel fashion on the lipophilic sides. The guest molecules do not join the helical hydrogen-bond networks like DCA (Fig. 6f).

CAM forms the same bilayer structure as CA. Although the steric dimensions of the host cavities are identical. CAM has hydrogen-bond hooks on the wall of the channels for catching guest inolecules with hydrogen-bond acceptors. Therefore. CAM prefers to form inclusion compounds with guest molecules involving hydrogen-bonding groups.[15] Most of nonpolar guests do not give stable inclusion crystals, but CA has the opposite preference. For example. CAM forms the stable inclusion crystals with a wide range of alcohols, from methanol to decanol. The hydroxyl groups of the guest molecules are linked between two cyclic hydrogen-bond networks among the host molecules, as depicted in Fig. 6g.

CDCAM do not yield inclusion crystals with organic guest molecules but hydrate crystals, as shown in Fig. 3g. In contrast, LCAM constructs a bilayer structure with channels for including various organic molecules. LCAM tends to include aliphatic alcohols involving over five carbon atoms, while it does not include small alcohols, such as methanol, ethanol. and propanol.[16,17] LCAM forms flexible molecular assemblies due to the sliding of the bilayer as well as to the conformational change of the side chain. In the case of LCAM. replacement of the carboxyl group to amide leads to a change of the hydrogen-bond network from helical to ladder type,[16] as shown in Fig. 6h.

Bile Alcohol Hosts

DCAtriol prefers to form inclusion compounds with nonpolar guests. such as aromatic compounds. but not with polar guests, such as alcohols. The helical hydrogen-bond network of DCAtriol is similar to that of DCA. DCAtriol has a parallel arrangement on the hydrophilic side and an antiparallel one on the lipophilic side, as shown in Fig. 3i. However. in the benzene clathrate,[18] host molecules are arranged in the parallel fashion on hydrophilic and Iipophilic sides. Although DCAtriol includes various aromatic compounds: CAtetraol does not include organic guests and gives only guest-free

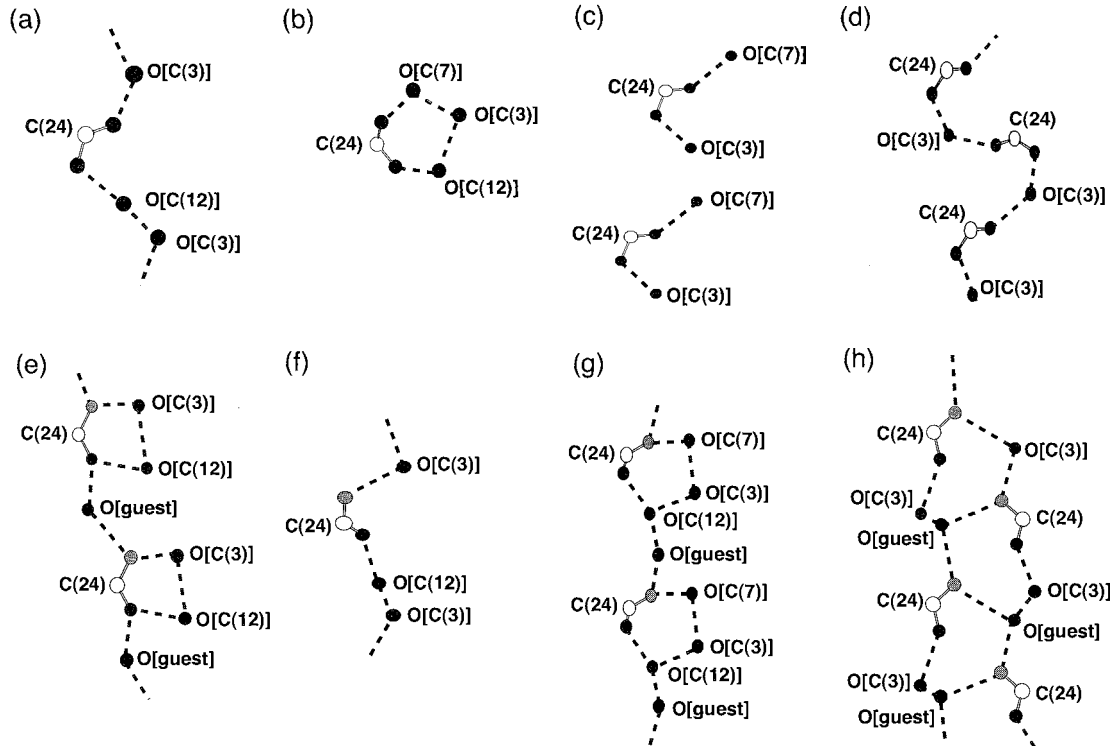

Fig. 6 Hydrogen-bonding networks of (a) DCA; (b) CA; (c) CDCA: (d) LCA; (e) DCAM with hydrogen-bond guest: (f) DCAM with nonhydrogen bond guest; (g) CAM; and (h) LCAM. Carbon. nitrogen. and oxygen atoms are represented by open, shadowed, and filled circles. respectively.

crystals,[19] as depicted in Fig. 3j. **CDCAtriol** constructs a bilayer structure. which is different from a tubular structure of CDCA. Small alcohols are included in the hydrophilic layers through hydrogen bonds between host and guest molecules. LCAdiol forms inclusion crystals with only small guests (Fig. 31).

Bile Ester Hosts

Esterification of the carboxylic acid decreases the number of hydrogen-bond donor group at the steroidal side chain, leading to a reduction of their inclusion abilities. MDC includes only methanol[20] and do not form the bilayer structure (Fig. 7a). MC includes only small polar guests, as shown in Fig. 7b, c. The inclusion compounds of MC with small nitriles have the same crystal structures as that of CA with acetonitrile.[21,22] Although there are no channels on the lipophilic sides, the guest molecules are held in the cavities between the pleated bilayers. No hydrogen bonds between the host and guest molecules are found. However. when the alcoholic guests are included, the side chains of the host molecules are leaned toward to the lipophilic face and do not form hydrogen bond.[23] The hydroxyl groups of alcoholic guests are inserted into the helical hydrogen-bond

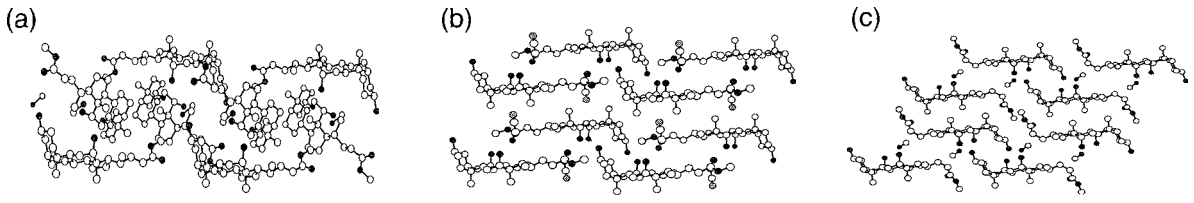

Fig. 7 Crystal structures of bile ester derivatives: (a) MDCA with methanol: (b) MCA with acetonitrile: and (c) MCA with methanol.

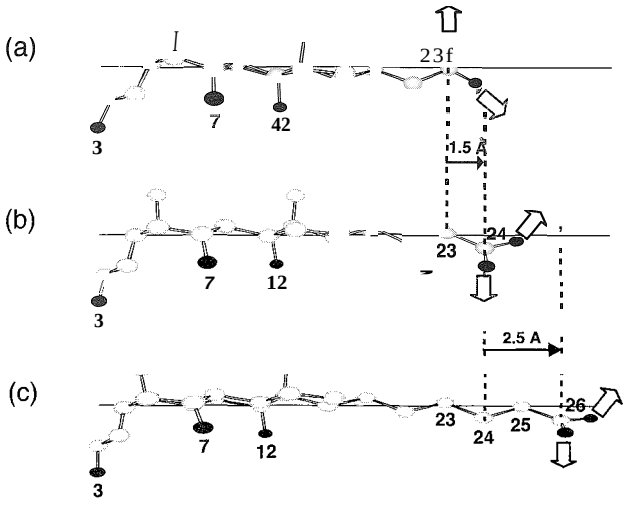

Fig. 8 Different distances and directions of carboxylic acid groups of (a) NCA; (b) **CA**; and (c) BHCA

networks. On the other hand, MCDC and **MLC** do not seem to include any organic compounds.

MODIFICATION OF THE SIDE-CHAIN LENGTH

Norbile Acids

Norbile acids have shorter side-chain lengths by one methylene unit than original bile acids. They form inclusion crystals with various organic substances.[24,25] Shortening the side-chain length brings about a change in the orientation of the carboxyl group and deforms the hydrogen-bonding motif, as shown in Fig. 8. The cyclic hydrogen-bond network is formed among two hydroxyl groups at the 3-position and two carboxyl groups at the side chains from four different host molecules. In Fig. 9, the crystal structures of four norbile acid, with acetone. They are all the same bilayer structures with cage-like cavities. Compare to the lack of inclusion abilities of LCA and **CDCA**, NLCA and NCDCA include a wide range of organic substances, as shown in Table 2.

Bishomobile Acids

The elongation of the side chain of CA gives rise to the expansion of the host cavity. BHCA. which have longer side-chain length by two methylene units than CA. was reported to form inclusion compounds with various guests[26] in a 1:1 host-to-guest ratio. X-ray crystallographic studies reveal that BHCA have two kinds of host frameworks: a bilayer structure and crossing structure, like CG. Larger aromatic compounds. such as 1-methylnaphthalene, are included in the former host framework with a cyclic hydrogen-bond motif among host molecules, while smaller aromatic compounds. nitriles. and alcohols. are included in the latter, with helical hydrogen-bond motif (as shown in Fig. 10a, b). In contrast, the other bishomobile acids do not tend to include any guest molecules and yield only guest-free crystals.

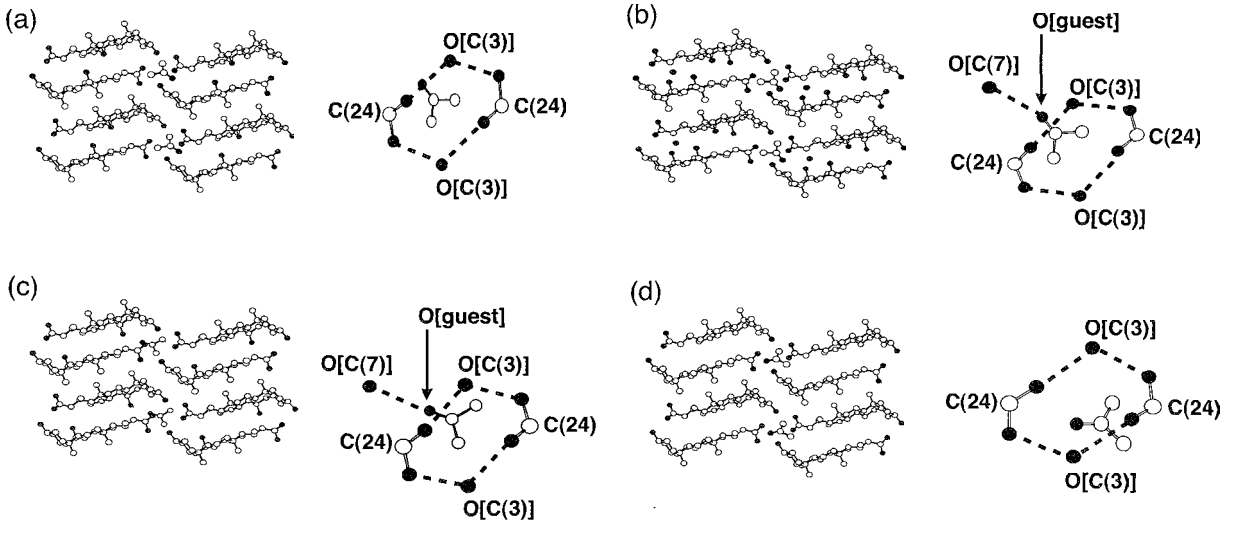

Fig. 9 Crystal structures of norbile acids with acetone together with hydrogen-bonding networks of (a) NDCA: (b) NCA: (c) NCDCA: and (d) NLCA.

Table 2 Formation of the inclusion compounds of bile acids and their derivatives with their host–guest ratios

	DCA	CA	CDCA	LCA	NDCA	NCA	NCDCA	NLCA	DCAM	CAM
Guest (G_1)	**H:G_1:G_2**[a]	**H:G_1:G_2**	**H:G_1:G_2**	**H:G_1:G_2**	**H:G_1:G_2**	**H:G_1:G_2**	**H:G_1:G_2**	**H:G_1:G_2**	**H:G_1:G_2**	**H:G_1:G_2**
Methanol	NC[b]	1:1	NC	NC	W[c]	1:1	1:1	1:1	1:1	1:1
Ethanol	NC	1:1	NC	NC	1:1	1:1	1:1	1:1	1:1	1:1
1-Propanol	NC	1:1	NC	NC	1:1	2:1	1:1	2:1	1:1	1:1
2-Propanol	1:1	1:1	NC	NC	1:1	2:1:1	2:1	2:1	1:1	1:1
1-Butanol	NC	GF[d]	NC	NC	2:1:1	2:1	2:1	W	1:1	1:1
2-Butanol	NC	GF	NC	NC	1:1	NC	2:1	2:1	1:1	1:1
Acetone	1:1	GF	NC	NC	2:1	2:1:1	2:1	2:1	1:1:	NC
Ethylene glycol	NC	1:1	NC	NC	W	1:1	1:1	2:1	NC	1:1:1
Acetophenone	1:1	1:1	NC	NC	2:1	2:3	GF	2:1	NC	1:1

[a] G_2 = water.
[b] NC = not crystallized.
[c] W = water-included crystal.
[d] GF = guest-free crystal.

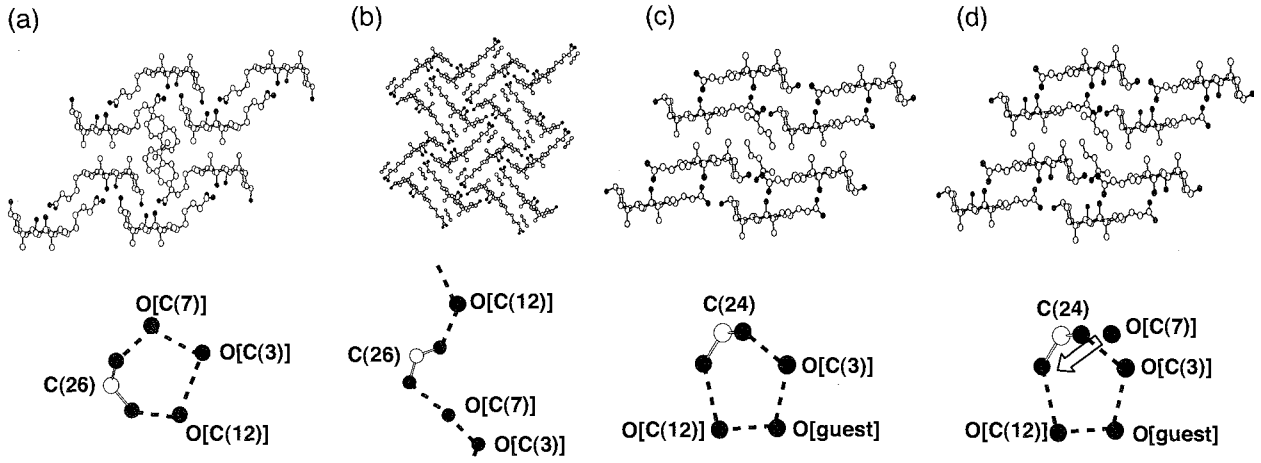

Fig. 10 Crystal structures and hydrogen-bonding networks of BNCA: (a) bilayer structure: (b) crossing structure: and epibile acids with 2-pentanol (c) 3EDCA: (d) 3ECA.

CHANGE OF DIRECTIONS OF HYDROXYL GROUPS OF THE SKELETONS

3-Epibile Acids

Change of direction of the hydroxyl groups at 3-position of the bile acids from α to β give 3-epibile acids. 3EDCA tends to include hydrophilic guests, such as alcohols and lactones, whereas DCA forms inclusion crystals with a wide range of organic compounds. except for alcohols. In Fig. 10c, the crystal structure of 3EDCA with 2-pentanol is shown. The host molecules arrange in an antiparallel fashion on hydrophilic and lipophilic sides. The hydroxyl groups of the guest molecules join the cyclic hydrogen-bond networks.

3ECA also gives the inclusion crystals with various aliphatic alcohols. Shown in Fig. 10d is a crystal structure of 3ECA with 2-pentanol, indicating the same bilayer structure in the case of CA. 3ECA forms a cyclic hydrogen-bond network, which is the same as that of 3EDCA. The extra hydroxyl group at 7-position is branched to the carboxylic group. because the direction change forces the hydroxy group at carbon 3-position to combine with carboxylic groups of the side chains. The alcoholic guest is inserted between the 3- and 12-positioned hpdroxy groups. as shown in Fig. 10c,d.

PACKING COEFFICIENT OF HOST CAVITY (*PCcavity*)

Key and lock mechanism has been established as a principle for molecular recognition. Steric and electronic complementary between guest molecules and host cavities play an important role for formation of the host–guest compounds. Only the guest molecules with steric size fitness to the host cavities are included as a result of size-selective binding. Guests that are too large or too small do not form stable inclusion complexes due to misfitting between guest and host cavities. Comparison of the volumes between the guest molecules and the host cavities may explain the size-selective guest recognition. In order to understand the steric fitness between guests and host cavities, we introduced the term; "packing coefficient of the host cavity" or *PCcavity* in the inclusion compounds of CA with monosubstituted benzenes.[27] *PCcavity* is the ratio between molecular volume of the guest molecules and free volume of the host cavities in a unit cell. This ratio is indicated by the equation shown below (see Eq. below):

The optimal *PCcavity* values are in the range of 55–70% (Table 3) for the complexes in which the guest molecules are included via steric complementation and no interaction between host and guest molecules. Complexes

$$PCcavity(\%) = \frac{\text{(Molecular volume of guest)} \times \text{(Number of guests in the unit cell)}}{\text{Volume of the host cavity}} \times 100$$

Table 3 Molecular volume of guests, host cavity, and *PCcavity* in the inclusion compounds of CA with monosubstituted benzenes

Guest	Molecular volume [Å^3]	*V*cavity [Å^3][a]	*PCcavity* (%)[b]
Benzene	83.4	298.1	56.0
Fluorobenzene	88.4	319.2	55.4
Aniline	95.8	336.0	57.0
Chlorobenzene	97.5	327.6	58.0
Toluene	100.8	334.5	60.3
Bromobenzene	101.8	318.9	63.8
Benzaldehyde	104.0	331.0	62.8
Iodobenzene	107.9	351.6	61.4
Nitrobenzene	109.6	326.4	67.2
Anisole	110.4	332.0	66.5
Styrene	111.2	345.7	64.3
Benzyl chloride	114.5	370.1	61.9
Ethylbenrene	117.7	386.1	61.0
Benzyl bromide	119.1	400.4	59.5
Acetophenone	120.9	344.9	70.1
Allylbenzene	127.9	393.9	64.9
Phenetol	128.1	389.2	65.8
Phenyl acetate	131.0	399.4	65.6

[a] *V*cavity is the volume of the cavity in the unit cell calculated with a 0.7 Å radius probe.
[b] *PCcavity* is the packing coefficient of the guest components in the host cavity: *PCcavity* = (molecular volume of guest molecule) x 2/*V*cavity x 100.

with *PCcavity* out of this range give rise to the isomerization of the host frameworks or change of the host-to-guest ratios due to steric misfit. However, the interaction between host and guest molecules, such as hydrogen bonds, could be expanding the range of the *PCcavity*. Calculations of the *PCcavity* should be helpful in estimating the boundary in changing the host framework as well as the host:guest ratio., and also in designing the included guests.

CONCLUSION

Designing the robust host molecules is one of the fascinating researches for future chemistry. In this article. we demonstrated that the bile acids and their derivatives serve as host molecules for various guest compounds. Each derivative exhibits individual characteristic that vary from one case to another. Finally, bile acids tell us their information and expression through their molecular assemblies. that we should listen from them.

ACKNOWLEDGMENTS

This work was supported by a Grant-in-Aid for Scientific Research from the Ministry of Education. Science, Sports and Culture, Japan.

ARTICLES OF FURTHER INTEREST

Classical Descriptions of Inclusion Compounds, p. *253*
Concepts in Crystal Engineering, p. *319*
Deoxycholic, Cholic, and Apocholic Acids, p. *441*
Hydrogen Bonds, p. *658*
Inclusion Compounds, p. 696
The Lock and Key Principle. p. 809
X-Ray Crystallography, p. 1586
X-Ray and Neutron Powder Diffraction, p. 1592

REFERENCES

1. Herndon. W.C. The structure of choleic acids. J. Chem. Educ. 1967. 44. 724.
2. Giglio. E. Inclusion Coinpounds of Deoxycholeic Acid. In *Inclusion Compounds*; Atwood. J.L.. Davies, J.E.D.. MacNicol, D.D.. Eds.; Academic Press: London. 1984: Vol. 2. 207.
3. Miyata, M.; Sada. K. Deoxycholic Acid and Related Hosts. In *Comprehensive Supramolecular Chemistry*; MacNicol, D.D., Toda. F.. Bishop, R.. Eds.; Pergamon: Oxford, 1996; Vol. 6, 147. Chapter 6.
4. Rheinboldt. H.; Flume, E.: Konig. O. Uber das Molekulbindungsvermogen von Gallensauren und Sterinen. Z. Phpsiol. Chem. 1929. *180*, 180.
5. Craven. B.M.; DeTitta, G.T. Crystal structure determination of the 1:1 complex of deoxycholic acid and acetic acid. J. Chem. Soc., Chem. Commun. 1972. 530.
6. Mylius. F. Uber die cholsaure. Chem. Ber. 1887. *20*, 1968.
7. Johnson, *P.L.:* Schaefer, J.P. The crystal and molecular structure of an addition compound of cholic acid and ethanol. Acta Crystallogr.. B 1972. *28*. 3083.
8. Miki. *K.;* Masui, A.: Kasai. N.: Miyata, M.; Shibakami. M.; Takemoto. K. New channel-type inclusion compound of steroidal bile acid. Structure of a 1:1 complex between cholic acid and acetophenone. J. Am. Chem. Soc. 1988. *110*. 6594.
9. Lindley, P.F.; Mahmound. M.M.: Watson, F.E.: Jones, W.A. The structure of chenodeoxycholic acid, $C_{24}H_{40}O_4$. Acta Crystallogr., B **1980**, 36. 1893.
10. Rizkallah. P.J.: Harding. M.M.; Lindley. P.F.: Aigner, A.; Bauer. A. Structure of a low-temperature polymorph of chenodeoxycholic acid, $C_{24}H_{40}O_4$, determined with synchrotron radiation. Acta Crystallogr.. B 1990. 46, 262.
11. Sluis, P.: Schouten. A.: Kanters. J.A. Structure of chenodeoxycholic acid in chenodeoxycholic acid ethyl acetate solvate. Acta Crystallogr.. C 1990. 46, 2165.
12. Giuseppetti, G.; Paciotti. M. Polymorphism of chenodeoxycholic acid. Farmaco. Ed. Sci. 1978.33. 64.
13. Chikada. M.: Sada, K.: Miyata. M. Intercalation and polymerization in chenodeoxycholic acid channels with retention of a crystalline state. Polymer 1999, 31. 1061.
14. Arora. S.K.; Germain. G.; Declercq. J.P. The crystal and molecular structure of lithocholic acid. Acta Crystallogr.. B 1976. 32. 415.
15. Sada. K.: Kondo. T.; Ushioda. M.: Matsuura. Y.; Nakano, K.; Miyata, M.: Miki. K. Functionalization of inclusion

cavities of bile acid hosts. Channel-type inclusion compounds of cholamide. Bull. Chem. Soc. Jpn. 1998.71. 1931.
16. Hishikawa, Y.; Aoki. Y.: Sada. K.; Miyata. M. Selective inclusion phenomena in lithocholaminde crystal lattices: design of bilayered assemblies through ladder-type hydrogen bonding network. Chem. Lett. 1998, 1289.
17. Aoki. Y.; Hishikawa. Y.: Sada, K.: Miyata. M. Enantioresolution of aliphatic alcohols by lithocholamide. Enantiomer 2000. *5*. 95.
18. Sada, K.; Matsuo, A.; Miyata. M. Novel molecular arrangement in asymmetric bilayered crystals of the inclusion compounds of 3α, 12α, 24-trihydroxy-5β-cholane. Chem. Lett. 1995. 877.
19. Sada. K.: Kondo, T.; Yasuda. Y.; Miyata. M.; Miki, K. Interpretation of variable inclusion abilities of cholic acid and its derivatives on the basis of the crystal structure of 5β-petromyzonol. Cheni. Lett. 1994. 727.
20. Miki, K.; Masui, A.: Kasai, N.; Miyata. M.; Goonewardena, W.; Shibakami, M.: Takemoto, K. Structure of a 2:1 addition compound of methyl deoxycholate with methanol. Acta Crystallogr., C 1989. *45*, 79.
21. Scott, J.L. Solid-vapour reactions of cholic acid and methyl cholate with acetonitrile: Structures and reaction kinetics. J. Chem. Soc.. Perkin Trans. 2 1995. 495.
22. Goonewardena, W.; Miyata, M.; Takemoto, K. One-dimensional inclusion polymerization of diene and vinyl monomers by using methyl cholate as a host. Polym. J. 1993. *25*. 731.
23. Miki, K.: Masui, A.; Kasai, N.: Shibakami. M.; Takemoto, K.: Miyata, M. Structures of 1:1 addition cornpounds of methyl cholate with methanol and with 2-propanol. Acta Crystallogr., C. 1992. *48*. 503.
24. Sada, K.; Sugahara, M.; Nakahata. Y.: Yasuda. Y.: Nishio. A.: Miyata, M. First columnar monolayer structure of bile acids inclusion crystal. Inclusion compounds of 23-nordeoxycholic acid. Chem. Lett. 1998. 31.
25. Sugahara, M.; Sada, K.: Miyata, M. A robust structural motif in inclusion crystals of norbile acids. Chem. Commun. 1999. 293.
26. Sada, K.; Sugahara, M.: Kato. K.; Miyata. M. Controlled expansion of a molecular cavity in a steroid host compound. J. Am. Chem. Soc. 2001. 123. 4386.
27. Nakano, K.: Sada. K.; Kurozumi. Y.: Miyata, M. Importance of packing coefficients of host cavities in the isomerizatioii of open host frameworks: Guest-size-dependent isomerization in cholic acid and inclusion crystals with monosubstituted benzenes. Chem. Eur. J. 2001. 7, 1.

The Diphenylmethane Moiety

Antonio García Martinez
José Osío Barcina
Universidad Complutense, Madrid, Spain

INTRODUCTION

Diphenylmethane (DPM) and some of its derivatives are often used as subunits in the design of supramolecular structures. One of the factors controlling the stability of the resulting complexes is the conforrnational flexibility of the host. Therefore. an entropic cost is paid upon complexation with DPM derivatives, because they must organize into a binding conformation. An efficient way to reduce this entropic cost is by stabilizing the gable conformation. This can be done by employing 7,7-diphenylnorbornane (DPN) as a building block.

THE DIPHENYLMETHANE MOIETY

The DPM moiety is easily recognized as a basic constituent of the most important cyclophanes (diphenylmethanophanes).[1] The supramolecular properties of these compounds cannot be understood without knowledge of the structure, energy. and molecular dynamics of DPM.

The complete potential energy surfaces (PES) of DPM were calculated with semiempirical, ab initio. and density functional theory (DFT) methods.[2,3] The stationary points correspond to the conforinations given in Scheme 1. Frequency calculations reveal that conformations **1–3** are transition states (one imaginary frequency was found). and 4 is the only minimum energy conformation.

For comparison, the relative total energy (BE) values computed for DPM with the semieinpirical (AM1), ab initio. and DFT methods are listed in Table 1, as well as geometrical data (torsional angles ϕ_A and ϕ_B and angle 0, Scheme 1 j.

All computed PES show a large flat minimum between 30" and 95° (ϕ_A or ϕ_B) with a C_2 minimum structure 4. The geometry of this structure is similar to the experimental C_1 conformation of DPM in the solid state (x-ray)[4] with ϕ_A=63.9°, ϕ_B=71.1°, and θ=112.5°. The results of the ab initio and DFT methods agree with the semiempirical AM1 method. with the exception of the relative energy of the gable conformation **2**.[3] There is also agreement with the PES computed with other semiempirical and molecular mechanics methods."' although some of them (e.g., PM3 and MM2) indicate a gable (2) ground state for the isolated molecule, but only 0.1–0.5 kcal/mol lower in energy than the helical conformation 4. Therefore, inexpensive semiempirical and molecular mechanics methods, especially AM1, seem to be useful for all problems related to the phenyl rotation.[3]

The bending angle θ depends on the dihedral angles ϕ_A and ϕ_B.[2] Typical examples are the conformers 2 and 3 (Table 1), where 8 varies from 113.6° to 116.4'. As expected, the angle 0 increases when the dihedral angles approach zero. Thus, the T-shaped conformation **3** is destabilized due to the repulsive short-range C—H···π interaction (vide infra). On the other hand, angle 8 of DPM determined by x-ray analysis (112.5") is significantly smaller than any other similar angle reported for ring-substituted DPM with electron-donor substituents.[2,4] Conformation 1 is expected to be unstable due to the short H.H distance of the o-hydrogen atoms. The steric repulsion between the filled π orbitals at the C_{ipso} atoms of conformation 2 causes its relative instability; which shows two aryl rings in an apical cofacial disposition (vide infra).[5] Conformation 4 seems to correspond to the equilibrium point between the π,π and C—H,π repulsions.

The relative population of each rotamer can be expressed quantitatively using the Boltzmann distribution:

$$N_A/N_B = e^{-\Delta G/RT} \quad (1)$$

where N_i represents the population of each conformation and AG the free energy difference associated to the rotation from A to *B* conformations. On the other hand. AG is given by the following equation:

$$\Delta G = \Delta H - T(\Delta S_R + \Delta S_V + \Delta S_T + \Delta S_L) - RT \ln \Delta\sigma \quad (2)$$

where AH is the difference in enthalpy [AE corrected by the work term (−RT)]. ΔS_i the differences in entropy (R = rotational. *V* = vibrational, *T* = translational, and *L* = librational), and $\Delta\sigma$ the difference in the symmetry numbers (degeneracy).[6–8]

The thermocheinical properties (H and *S*) arise from the energetics of vibrational frequencies obtained by frequency analysis of the wave functions of each conformation. The so-obtained ΔG values must be corrected by the entropy term $RT\ln\sigma$.

Encyclopedia of Supramolecular Chemistry
DOI: 10.1081/E-ESMC 120012881

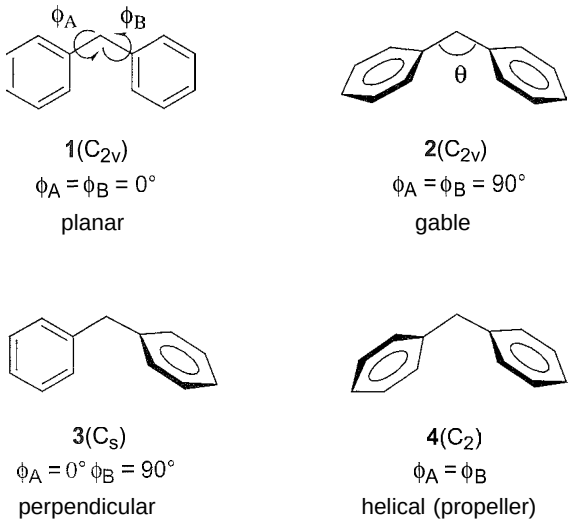

Scheme 1 Torsional angles (ϕ), point symmetry group. and name[***] of the conformations of DPM.

In supramolecular chemistry, separation of librational (configurational) entropy from the rest of the entropic contributions is often useful. The contribution of librational (torsional angle vibrations) modes to the configurational entropy can be calculated in a good approximation using Eq. 3:[9,10]

$$TS_L = RT\Sigma_i[(\theta_i/e^{\theta_i} - 1) + \ln(1/1 - e^{-\theta_i})] \quad (3)$$

where frequency θ_i is given by

$$\theta_i = h\omega_i c/RT \quad (4)$$

where h is Planck's constant. c the speed of light. and ω_i the wave number (in cm^{-1}) of the vibrations (ranging from 0–650 cm^{-1}).

Table 1 Computed AE values (in kcal/mol) for the conformations of DPM using several methods

	AM1*	HF/6-31G*	B3LYP/ 3-28G	B3LYP/ 6-31G*
1	8.89	—	10.48	—
2	0.01	0.61 θ=113.6°	0.66	0.61 θ=116.4°
3	0.33	0.76 θ=116.4°	0.34	0.65 θ=116.4°
4	0.0 $\phi_A=\phi_B$ =54.5°	0.0 $\phi_A=\phi_B$ =58.5° θ=114.6°	0.0 $\phi_A=\phi_B$ =57.0°	0.0 $\phi_A=\phi_B$ =57.0° θ=114.6°

[*]Difference in heat of formation (ΔH_f).

MOLECULAR DYNAMICS

In order to obtain information on the fluctuations in the DPM moiety, we performed molecular dynamics (MD) computations on DPM and 1,1-diphenylcyclohexane (5, DPC). often used as spacers in supramolecular chemistry, as well as on DPN 6 (Scheme 2).[11] The aryl rings of DPN are disposed in a gable conformation forced by the steric effect of the four exo-norbornylic C–H bonds.[***] In contrast to DPN, DPC adopts a helical conformation like DPM.[5]

The MD studies of DPM, DPC. and DPN were carried out with the MM2 force-field method implemented in CHEM3D.[13] Dynamic trajectories were generated for 20.0 ns at 300 K (target temperature), with 2.0 fs step interval, 10 fs frame interval, and a heating (cooling) rate of 1.0 kcal/atom/ps. The mean values of torsional angles (ϕ_m) and the corresponding standard deviations were calculated from the φ values of 60 frames (configurations) statistically sampled. During the whole equilibration time. the phenyl rings of DPM underwent five rotations. On the contrary, the aryl rings of DPC and DPN did not rotate but carried out librations, with amplitudes given in Table 2 as standard deviations of the mean torsional angle (ϕ_m). The ϕ_m values were similar (or identical) to the equilibrium values coinputed with the MM2 method. Noteworthy, the librational mobility of the equatorial (e) ring is higher than that of the axial *(a)* ring. As expected. the lowest librational amplitude corresponds to DPN.

The computed rotational barriers ($\Delta E^{\neq}$) using the AM1 method are given in Table 2. The C_{2v} symmetrical structure 2 of DPM is the lowest energy transition state between the C_2 symmetrical minimum 4 and its mirror image.[3] Hence. the racemization takes place according to the conrotatory two-ring-flip mechanism.[14,15] Conrotatory and disrotatory librations are allowed in the ground state of DPM[2] and its derivatives DPC and DPN. In the case of DPC, the perpendicular conformation is slightly more stable (by 0.24 kcal/mol) than the gable

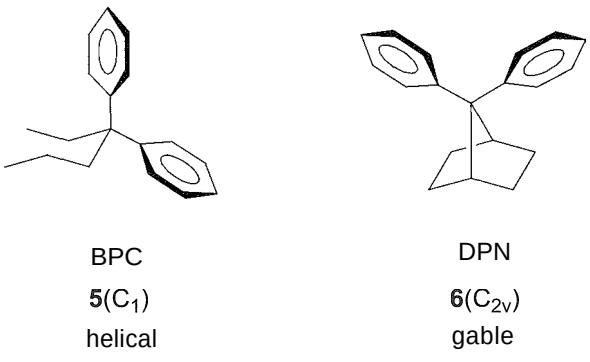

Scheme 2 More stable conformations of DPC and DPN.

Table 2 AM1 rotational barriers ($\Delta E^{\neq}$, in kcallmol) and molecular dynamics of DPM. *DPC*. and *DPN* (MM2)

	DPM	DPC	DPN
$\Delta E^{\neq}$	0 01	0.43	12.5
φ_m	Rotor	$\phi_e=69\pm20°$	$\phi_A=93\pm15°$
		$\phi_a=67\pm30°$	
○	—	$\phi_e=69°$	$\phi_A=93°$
		$\phi_a=65°$	$\varphi_B=83°$

conformation, and the racemization takes place mainly according to a disrotatory one-ring-flip mechanism[14,15] through a C_s symmetrical structure similar to **3.** The amplitude of the librations in DPN is much higher than the deviations from the planarity ($\sim3°$). Therefore, DPN can be considered as a librating C_{2v} structure. On the contrary, according to the MD results, at 300 K, DPM and DPC can be described as a free rotator (propeller) and a high-amplitude librator. respectively. This has important consequences on the properties of both compounds. In the case of DPN, the gable conformation shows both phenyl rings in a disposition favorable for a π,π interaction, a kind that we named apical homoconjugated.[5] This repulsive interaction between filled orbitals gives place to new binding and antibinding MOs and, therefore, to new electronic transitions. Thus, the UV spectrum of DPN (in MeOH) shows a strong absorption at 228 nm ($\varepsilon=12.300$) that is not observed in the UV spectra of 2,2-diphenylpropane (DPP), that has phenyl rings arranged in a helical conformation. Besides this homoconjugation band (AHK band),[5] DPN shows the ^1L_b and the fine-structured ^1L_a bands (β and α bands, respectively). which are common to all DPM and alkylbenzenes,[16] due to intraannular transitions. However, methylene-bridged donor–acceptor systems exhibit weak intramolecular charge-transfer absorptions.[16] Intramolecular through-space donor–acceptor interactions are feasible even in the case of orthogonality of the donor and acceptor chromophores.[17] On the other hand. the orthogonality of donor and acceptor orbitals exclude an intramolecular through-bond ground-state interaction.[16]

Moreover, the second-order nonlinear susceptibility (β_z) of DPN derivatives is higher than the value of related DPM derivatives, due to the π–π interaction in the gable conformation.[18] Both transannular electronic transitions and hyperpoiarizability are Franck–Condon processes, which are favored in DPN, because the probability of a photon impacting the gable conformation in a free rotor is negligible.

The conformational instability of DPM is partially transmitted to derivatives that are important in supramolecular chemistry, such as cavitands.[19,20] Resorcarenes are conformationally mobile, with a $\Delta G^{\neq}$ for the rotation of one ring of 4.5 kcallmol for *p-n*-hexyl[4]resorcarene,[19] whereas the $\Delta G^{\neq}$ range for calixarenes is higher (15–16 kcallmol). The reason for this is the strong cyclic lower-rim intramolecular hydrogen bonding of the calixarenes in comparison to the analogous upper-rim interaction in resorcarenes. As a consequence, the cavities of calixarenes are relatively small and too conformationally mobile to offer significant solvophobic protection.

A inacrobicyclic cyclophane host containing three *N*-ethyl-4.4-diarylpiperidine units was the subject of MD simulations. At 300 K, no conformations with a collapsed or significant distorted cavity were observed.[20] However, a relatively high degree of flexibility is maintained in complexes of macrocyclic hosts containing two diarylmethane moieties bonded by isophthaloyl and phosphonate subunits, with one adrenaline molecule. despite the high binding enthalpies resulting from the combination of electrostatic interactions, hydrogen bonds, and van der Waals interactions.[21]

FORMATION **OF INCLUSION COMPLEXES**

The chemical equation for the reaction of formation of an inclusion complex between the gable conformation of DPM and a symmetrical guest G, is

$$\mathbf{2}(C_{2v}) + \mathrm{G} \leftrightarrows \mathbf{2}\ (C_{2v})\cdot\mathrm{G}$$

The thermochemistry is given by Eq. 2, where ΔH now represents the binding enthalpy and AS, the differences in entropy between the complex and the gable conformation $2\,(C_{2v})$. Only the stable conformations in equilibrium with the host conformation contribute to the term $\Delta\sigma$. Thus, in the case of DPM and DPC,[22] $\Delta\sigma=2$, and a loss of mixing entropy by $RT\ln2=0.41$ kcallmol (at 300 K) must be taken into account.

The computational packages usually calculate the ΔS_T using the Sackur–Tetrode equation. This equation predicts the entropy of monoatomic gases successfully. The ΔS_T values predicted with this equation in the liquid or solution phase are. however, significantly lower than the experimental ones.[23] These discrepancies can be corrected; considering the idea of free volume in condensed phases.[24]

The uncertainty regarding the value of AS_{m} in solution is low, because the value of rotational entropy in solution is, in most cases. the same as that in the gas phase. Thus, AS_{m} is predicted with reasonable accuracy using an existing model based on statistical mechanics.[24]

The changes in high-frequency harmonic vibration ΔS_V upon assembly are negligible. By contrast, the contribution of low-frequency vibrations associated with torsions about single bonds (librations), expressed by ΔS_L, is high.

Unlike high-frequency vibrations, low-frequency vibrations cannot be modeled as accurately as harmonic oscillations.[24,25]

A simple model for the determination of conformational entropy (ΔS_L) is based on the assumption that accessible conformational space has the same potential energy. From the classical (nonquantum mechanical) definition of the partition function, the conformational entropy is given by the following equation:

$$S_L = R \ln(V_{conf}/V_{mol}) \quad (5)$$

where V_{conf} is the available volume to a rigid molecule of volume V_{mol}.[24]

An interesting approach to the estimation of ΔS_L is offered by Eq. 3. The amplitude of the host librations decreases upon binding and implies a reduction of conformational entropy, because the frequency θ_i in Eq. 4 increases. Therefore, the complexation takes place with an additional entropy cost, which increases with the binding enthalpy. It is higher in the case of strongly bonded complexes and, for the same host, depending on the nature of the guest. Hence, it is to be expected that the loss in conformational entropy is accompanied by a compensatory enthalpy change. The decrease in librational amplitude leads to a better preorganized host structure. The configurational (conformational) entropy term, ΔS_L, can be considered as the entropic cost of the assembly of the conformations (microstates) that disappear upon binding, placed between the stable conformations.

The tightly bonded inclusion complexes in aqueous solution, between aromatic and aliphatic guests (steroids, among others) and cyclophane receptors with tetraoxa[*n*.1.n.1]paracyclophanes and quaternary ammonium cyclophanes is entropically unfavorable and strongly enthalpically driven.[26,27] The thermodynamic characteristics of tight inclusion complexes differ from those measured for weak apolar association processes, which are characterized by small enthalpic changes and favorable entropic terms. This is the usual interpretation of the so-called hydrophobic effect.[28]

The enthalpic contribution to ΔG of formation of a complex depends on the geometry. Sometimes. the DPM moiety in the cyclophane complex adopts a helical conformation, as observed in synthetic adrenaline receptor~,[~in' which the guest is placed outside the DPM cavity and undergoes double π-staking interactions with two DPM moieties. But, most of the cyclophane–arene complexes prefer a gable conformation of the DPM moiety,'''' because this geometry allows for a deeper docking of the arene guest in the cavity than does the helical conformation. Hence, DPM hosts are enthalpically favored in comparison to 2,2-diphenyl propane (DPP) or DPC hosts. because the ΔE between the gable and the helical conformation is lower. When the complex formation is enthalpically controlled. DPM hosts should be better receptors than DPP hosts. This was observed in the case of cyclophanes incorporating Troger's base and DPM or DPP moieties.[30,31] Thus, substituents at the methylene group of DPM influence the complex stability. However, the DPM derivatives used as building blocks in the design of hosts are often selected in order to increase only the solubility.

TOWARD THE REDUCTION OF CONFIGURATIONAL ENTROPY

The high configurational entropy of DPM is a serious disadvantage in its use as a building block in the construction of macrocyclic hosts,[10,21,24] although some flexibility is needed for a fast guest complexation.[32]

In order to decrease the configurational entropy, several strategies are possible. Thus, the introduction of *ortho* substituents causes an increase of the rotational barriers. A $\Delta G^{\neq}$ value of 16.4 kcallmol (323 K) for the conrotatory racemization of the helical conformation of *bis*(2-ethyl-6-methylphenyl)methane was determined by dynamic nuclear magnetic resonance (DNMR).[33] This result is in agreement with that calculated with the MM2 program (16.4 kcallmol for a zero-ring-flip mechanism).[34] However, according to our MD calculations, this compound shows the C_2 conformation ($\phi_B = 52 \pm 14°$) as the more stable and, therefore, is not preorganized for the formation of inclusion complexes.

Another improvement of the DPM rigidity and preorganization without alteration of the substitution pattern is the back-stabilization of the gable conformation. The 1.1-diphenylcyclopropane derivatives invariably show preference for the gable conformation. as revealed from x-ray data.[35] Also, in diarylmethane-bridged fullerenes, the gable disposition was described as the most stable conformation.[36] However, no experimental rotational barriers were reported until now.

The best approach reported to date to solve this problem is DPN,[5,12,18,22,37] with a gable conformation that is the most stable described until now (vide supra). From Eq. 2, using the RHF/STO-3G method for the computation of ΔE and AS, and taking into account the mixing entropy, the formation of inclusion complexes of DPN in the gable conformation should be disfavored by 2.27 kcallmol in comparison to complexes of DPN and the same guest.[22]

Interestingly, hosts containing the DPN moiety form complexes with isophthaloyl derivatives, which are only slightly more stable (by 0.29 kcal/mol) than analogous complexes with DPC hosts.[22] These results clearly show that DPC is in the helical conformation, with a small loss

of configurational (librational) entropy caused by the interaction with the guest. The entropic contribution to the energy of complexation with DPC hosts can be as high as 1 kcal/mol, a value that can be important in the determination of weak noncovalent interactions.[38,39] The entropy loss due to the configurational term becomes higher in the case of macrocyclic hosts.[10]

CONCLUSION

The DPM moiety is a convenient building block for the design of cyclophanes able to form inclusion complexes with neutral molecules. However, an entropic cost must be assumed due to the conformational flexibility of DPM and derivatives. The best way to reduce the conformational entropy is to stabilize the gable conforination by back substitution, just as carried out in the case of DPN.

ARTICLES OF FURTHER INTEREST

Calixarenes: Synthesis and Historical Perspectives, p. 153
Cation–π Interactions, p. 214
Cavitands, p. 219
Cyclophanes: Endoacidic, Endobasic, and Endolipophilic Cavities, p. 424

REFERENCES

1. *Comprehensive Supramolecular Chemistry*; Atwood, J.L.. Davies, J.E.D.. MacNicol, D.D.. Vogtle, F., Lehn. J.M.. Eds.; Pergamon. 1996.
2. Feigel. M. Theochem 1966. *366.* 83–88.
3. Strassner, T. Can. J. Chem. 1997, *75.* 1011–1022.
4. Barnes. J.C.: Paton, J.D.: Damewood, J.R.; Mislow, K. J. Org. Chem. 1981. *46.* 4975–4979.
5. Garcia Martinez. A.: Osio Barcina, J.: Fresno Cerezo, A.; Gutierrez Rios. R. J. Am. Chem. Soc. 1998. *120.* 673–679.
6. Williams. D.H.: Westwell. M.S. Chem. Soc. Rev. 1998. *27,* 57–63.
7. Searle, M.S.: Williams, D.H. J. Am. Chem. Soc. 1992, *114,* 10690–10697.
8. Searle. M.S.: Williams, D.H.; Gerhard, U. J. Am. Chem. Soc. 1992. *114.* 10697–10704.
9. Brooks, B.R.: Janezic. D.; Karplus, M.J. J. Comput. Chem. 1995. *16,* 1522–1542.
10. Jusuf. S.: Loll, P.J.; Axelsen, P.H. J. Am. Chern. Soc. 2002. *124.* 3490–3491.
11. Garcia Martinez. A.; Osio Barcina. J. Unpublished work.
12. Garcia Martinez, A.: Osio Barcina, J.: Albert, A.; Cano. F.H. Tetrahedron Lett. 1993. *34,* 6736–6753.
13. *CHEM3D*, version 7.0 (2002): CambridgeSoft Corporation: Cambridge. MA. USA. Licensed to A.G.M.
14. Mislow, K.: Gust, D. J. Am. Chem. Soc. 1973, *95,* 1535–1547.
15. Mislow, K. Acc. Chem. Res. 1976. 9, 26–33.
16. van Walree, C.A.; Roest, M.R.: Schuddeboom. W.; Jenneskens, L.W.: Verhoeven. J.W.: Warman, J.M.: Kooijman, H.: Spek, A.L. J. Am. Chem. Soc. 1996. *118.* 8395–8407.
17. Pérez. S.; Scaringe. R.P. Macromolecules 1987, *20.* 68–77.
18. Garcia Martinez, A.; Osio Barcina. J.: Fresno Cerezo, A.; Rojo. G.; Agulló-López, F. J. Phys. Chem., B 2000. *104.* 43–47.
19. Bohmer. V. Angew. Chem.. Int. Ed. Engl. 1995. *34.* 713–745.
20. Mordasini-Denti. T.: van Gunsteren, W.: Diederich, F. Computational *Approaches in Supramolecular Chemistry*; Wipff. G.. Ed.: Kluwer Academic Publishers: The Netherlands, 1994: 117–136.
21. Herm, M.: Molt, O.; Schrader. T. Chem. Eur. J. 2002. *8.* 1485–1499. and references therein.
22. Garcia Martinez. A.: Osio Barcina, J.: Fresno Cerezo, A. Chern. Eur. J. 2001. 7. 1171–1175.
23. Fujiwara, H.: Ohtaku. I.: Takagi, T.; Murata, S.; Sasaki. Y. Bull. Chem. Soc. Jpn. 1988. *61.* 1853–1856.
24. Mammen, M.: Shakhonovich, I.; Deutch. J.M.; Whitesides. G.M. J. Org. Chem. 1998, *63.* 3821–3830.
25. Go, N.: Scheraga. H.A. Macromolecules 1976. 9. 535–542.
26. Peterson. B.R.; Walliman, P.: Carcanague, D.R.: Diederich, F. Tetrahedron 1995. *51,* 401–421. and references therein.
27. Odashima. K.: Kawakami, H.: Miwa, A.: Sasaki, I.; Koga. K. Chem. Pharm. Bull. 1989. *37,* 257–259.
28. Diederich, F. Angew. Chem.. Int. Ed. 1988, *27.* 362–386.
29. Wilcox, C.S.; Cowart, M.D.; Sucholeiki, I.: Bukownik. R.R.: Lynch. V. *Inclusion Phenomena and Molecular Recognition*; Atwood, J.L.. Ed.: Plenum: New York, 1990.
30. Cowart, M.D.; Sucholeiki, I.: Bukownik, R.R.: Wilcox. C.S. J. Am. Chem. Soc. 1988. *110.* 6204–6210.
31. Hunter. C.A.: Packer. M.J. Chem. Eur. J. 1999; *5.* 1891–1895. and references therein.
32. Rudkevich. D.M.; Hilmersson, G.; Rebek. J.. Jr. J. Am. Chem. Soc. 1997. *119.* 9911–9912.
33. Weissensteimer, W. Monatsch. Chern. 1992, *123.* 1135–1147.
34. Weissensteimer, W.; Scharf. J.; Schlögl, K. J. Org. Chem. 1987. *52.* 1210–1215.
35. Gawronski. J.: Gawronska. K.: Radocki. D. Tetrahedron: Assymmetry 1993. *4.* 383–392.
36. Djojo. *F.:* Herzog. A.: Lamparth. I.: Hampel, F.; Hirsch, A. Chem. Eur. J. 1996, 2, 1537–1547.
37. Garcia Martinez. A.: Osio Barcina. J.: Fresno Cerezo. A.: Schlüter. A.-D.; Frahn, J. Adv. Mater. 1999, *11,* 27–31.
38. Schneider, H.-J. Angew. Chem., Int. Ed. 1997, *36.* 1072–1073.
39. Hunter. C.A. Angew. Chern.. Int. Ed. 1997. *36.* 1073.

Disorder and Diffuse Scattering

T. Richard Welberry
Australian National University, Canberra, Australia

INTRODUCTION

The strong sharp Bragg reflections that occur in diffraction patterns of all real crystals are used by conventional x-ray crystallography to deduce the average repetitive arrangements of atoms or molecules. Diffuse scattering. on the other hand, contains information about the deviations from the average (i.e., different types of disorder) and gives structural information on a scale that goes beyond that of the average unit cell and extends over a range of ~1 A–1000 A. In many important materials, it is this extended range of structural information that is crucial in determining the unique or novel properties of the material. rather than the average unit cell structure.

METHODS OF ANALYSIS

Despite potentially providing a rich source of information about local and nanoscale structural detail in materials and about hour atoms and molecules interact with each other to produce this structure, the development of methods to analyze diffuse scattering lagged well behind conventional average structure determination. There are two main reasons. First, diffuse scattering intensities are weak in comparison to Bragg peaks, making the experimental observation vastly more demanding and time consuming. Second, the sheer diversity of different types of disorder makes it difficult to formulate a solution strategy that will work for all problems.

The recent advent of intense synchrotron sources and various kinds of multidetectors has meant that even weak diffuse scattering can now be readily observed.[1,2] but the second problem remains. However. the ever-increasing power and decreasing cost of computers facilitated the development of model-building techniques that are beginning to bear fruit in terms of their use as aids in the interpretation and analysis of the scatte ing for an increasingly diverse range of materials.[3–5] In these methods. the basic aim is to construct a computer model of the disordered structure using suitably parameterized basic interatomic or intermolecular interactions and a prescription for the particular type of disorder. A diffraction pattern computed from this model can then be cornpared with the observed pattern. Following this comparison, the model parameters can be adjusted and the process repeated until satisfactory agreement is obtained. Although agreement between an observed pattern and a calculated pattern does not guarantee the correctness of a model, the fact that sound chemical and physical principles were built into it at the outset lends considerable confidence to its validity. A model giving poor agreement can certainly be rejected. This methodology can be applied to a wide range of disorder problems with equal facility.

In order to be able to construct such a computer model, it is necessary to be able to identify particular types of disorder and understand the basic diffraction theory that describes how these affect the diffraction pattern. Our aim in this article is to give a brief overview of the theory of diffraction from disordered crystals and then present a number of real example patterns that illustrate some of the important principles. These examples were chosen to illustrate the diversity of the patterns that can be encountered and the types of disorders that cause them. We do not attempt to present details of the modeling of these examples. which is beyond the scope of the present article. For this. the reader is referred to the original literature on these systems.

DISORDER INVOLVING OCCUPANCIES AND DISPLACEMENTS

General

A description of diffuse scattering that allows for short-range substitutional disorder and local atomic displacements that accompany the SRO can be obtained by expanding the exponential in the general diffraction equation in terms of powers of displacement [6,7]

$$\begin{aligned} I(\mathbf{k}) &= \sum_m \sum_{m'} f_m f_{m'} \exp(i\mathbf{k}\cdot(\mathbf{r}_m + \mathbf{u}_m - \mathbf{r}_{m'} - \mathbf{u}_{m'})) \\ &\approx \sum_m \sum_{m'} f_m f_{m'} \exp(i\mathbf{k}\cdot(\mathbf{r}_m - \mathbf{r}_{m'})) \\ &\quad \times \left\{ 1 + i\mathbf{k}\cdot(\mathbf{u}_m - \mathbf{u}_{m'}) - \frac{1}{2}[\mathbf{k}\cdot(\mathbf{u}_m - \mathbf{u}_{m'})]^2 \right. \\ &\quad \left. - i\frac{1}{6}[\mathbf{k}\cdot(\mathbf{u}_m - \mathbf{u}_{m'})]^3 + \ldots \right\} \end{aligned} \quad (1)$$

Encyclopedia of Supramolecular Chemistry
DOI: 10.1081/E-ESMC 120012736

In this equation. f_m is the scattering factor of the atom m associated with the lattice site at the locator $\mathbf{r}_m$ and which is displaced from its mean position by a small amount $\mathbf{u}_m$. Expressed in Eq. 1 is the fact that the scattered intensity may be written as the sum of component intensities. The zero'th-order term is independent of the displacements. The first-order term is dependent on the first moment of displacements, the second-order term on the second moments, etc. If we carry out a reduction of Eq. 1 by separating terms into those corresponding to the average lattice and those corresponding to the deviations from the average, this separation into scattering components is preserved. We can then express the total intensity as follows:

$$I_{\text{Total}} = I_{\text{Bragg}} + I_0 + I_1 + I_2 + I_3 + \ldots \text{etc.} \tag{2}$$

I_{Bragg}, The Bragg Scattering Term

The term I_{Bragg} is the intensity due to the average lattice. This has a form that includes the Debye–Waller factor. $\exp(-2M)$, where $M = 8\pi^2\langle \mathbf{u}^2\rangle\lambda^2/\sin^2\theta$ (see Ref. [8]):

$$I_{\text{Bragg}}(\mathbf{k}) = (m_A f_A + m_B f_B)^2 \exp(-2M) \sum \exp(i\mathbf{k} \cdot \mathbf{r}_N) \tag{3}$$

The Debye–Waller factor takes account of the mean-square amplitude of displacements. (u^2). The equation describes how the Bragg peaks are still sharp, but their intensities are depressed at high angles.

I_0, The Short-Range Order Component

The term I_0 is known as the SRO component and may be expressed in the following general form:

$$I_0(h_1,h_2,h_3) = -N \sum_{i,j} \sum_{l,m,n} c_i\ c_j\ f_i\ f_j^* \times C_{lmn}^{ij} \cos(2\pi(h_1 l + h_2 m + h_3 n)) \tag{4}$$

The summation over i,j is over all atomic species and sublattices, and the summation over l,m,n represents all interatomic vectors. The N is the number of unit cells; c and f are the concentration and scattering factors for the species, respectively. The C_{lmn} are short-range order (SRO) parameters that may alternatively be called correlation coefficients.

The SRO parameters or correlation coefficients measure the degree of mutual dependence of the type of atom (or molecule) occupying a particular site in the crystal with that occupying another site. For $C_{lmn}=0$, there is no dependence, and the chance of finding an A-atom, say. in one site. is the same whether the second site contains either an A-atom or a B-atom. For $0 < C_{lmn} < 1$. the pair are more likely to be (A...A or B...B), and this is called positive correlation. For $0 > C_{lmn} > -1$, the pair is more likely to be (A...B or B...A), and this is called negative correlation. In a later section. we consider how a particular set of C_{lmn} might have arisen in a crystal or how in we might construct a model to contain such a set of values.

Note that presented in Eq. 4 is a summation over cosine functions so that the form of the diffuse scattering due to this component is symmetric about the Bragg peak positions.

I_1, The Size–Effect Component

The I_1 is the Warren size–effect term that takes account of the fact that interatomic vectors. $\mathbf{r}_N$, nominally all of equal length in the average lattice. have different lengths depending on whether the vector joins sites occupied by A–A, A–B, B–A, or B–B. This component includes all terms that are linear in the displacements $\mathbf{u}_m$. In contrast to I_0, therefore, the intensity for each term varies in reciprocal space relative to the displacement direction. If $\mathbf{k} = h_1\mathrm{a} + h_2\mathrm{b} + h_3\mathrm{c}$ and $\mathbf{r}_N = l\mathrm{a} + m\mathrm{b} + n\mathrm{c}$, then the size–effect intensity can be written in the following form:

$$I_1(h_1,h_2,h_3) = -2\pi N \sum_{ij} \sum_{lmn} c_i\ c_j\ f_i\ f_j^* (1 - C_{lmn}^{ij}) \times \sin(2\pi(h_1 l + h_2 m + h_3 n)) \times (h_1\langle X_{lmn}^{ij}\rangle + h_2\langle Y_{lmn}^{ij}\rangle + h_3\langle Z_{lmn}^{ij}\rangle) \tag{5}$$

The quantities in angle brackets are averages of various kinds of displacement. For example.

$$X_{lmn}^{ij} = u_{lmn}^{xj} - u_0^{xi}, \text{etc.} \tag{6}$$

Here u_{lmn}^{xj} is the displacement in the x direction of an atom with label j situated at the end of the vector $\mathbf{r}_{lmn}$ from the origin, where an atom with label i is displaced u_0^{xi}, also in the x direction. Note that Eq. 5 is a summation over sine functions so that the form of the diffuse scattering due to this component is antisymmetric about the Bragg peak positions. That is to say. it has the effect of transferring intensity from one side of the Bragg position to the other.

I_2, The Huang Scattering and First-Order TDS Component

The I_2 is the Huang scattering and first-order thermal diffuse scattering (TDS) component. It can be written in the following form:

$$\begin{aligned} I_2(h_1,h_2,h_3) = & -2\pi^2 N \sum_{ij} \sum_{lmn} c_i\ c_j\ f_i\ f_j^* (1 - C_{lmn}^{ij}) \\ & \times \cos(2\pi(h_1 l + h_2 m + h_3 n))[(h_1^2\langle (X_{lmn}^{ij})^2\rangle \\ & - (1 - C_{lmn}^{ij})^{-1}\langle (X_{\infty}^{ij})^2\rangle) + (h_2^2\langle (Y_{lmn}^{ij})^2\rangle \\ & - (1 - C_{lmn}^{ij})^{-1}\langle (Y_{\infty}^{ij})^2\rangle) + (h_3^2\langle (Z_{lmn}^{ij})^2\rangle \\ & - (1 - C_{lmn}^{ij})^{-1}\langle (Z_{\infty}^{ij})^2\rangle) \\ & + 2h_1 h_2\langle X_{lmn}^{ij} Y_{lmn}^{ij}\rangle + 2h_2 h_3\langle Y_{lmn}^{ij} Z_{lmn}^{ij}\rangle \\ & + 2h_1 h_3\langle X_{lmn}^{ij} Z_{lmn}^{ij}\rangle] \end{aligned} \tag{7}$$

Note that Eq. 7 is a summation over cosine functions so that the form of the diffuse scattering due to this component is again symmetric about the Bragg peak positions.

I_3, The Third-Order Sine–Effect Component

The expression for I_3 is even more complex than that for I_2. It involves averages of displacements, such as

$$\langle (X_{lmn}^{ij})^3 \rangle, \langle (X_{lmn}^{ij})^2 Y_{lmn}^{ij} \rangle, \langle X_{lmn}^{ij} Y_{lmn}^{ij} Z_{lmn}^{ij} \rangle, \text{etc.} \tag{8}$$

and the different terms are dependent on factors such as h_1^3, $h_1^2 h_2$, $h_1 h_2 h_3$, etc. This third component, in common with all odd components. is again the sum of sines. Consequently, scattering due to this component is antisymmetric about the Bragg peak positions. and it has the effect of transferring intensity from one side of the Bragg position to the other. The effect of this component is thus similar to that of the I_1 term. but it should be noted that it is of opposite sign. This and other higher-order component terins are usually negligible at low scattering angles but become increasingly important at large angles.

SOME PARTICULAR DISORDER MODELS

The theory outlined in the previous section shows how diffuse scattering can be described in terins of various kinds of lattice averages.''' These include simple occupancy correlations, averages involving atomic displacements; and cross terms where dispiacements are coupled with occupancy. In their most general form. the equations are not useful. because they contain many unknowns for each type of interatomic vector. However, the general form of the equations and the fact that the intensity can be broken into different components is of prime importance, because it allows different diffraction features to be identified. In any particular disorder problem. not all of the possible types of lattice average will be important, and correct identification of what is causing a particular pattern of diffuse scattering is the initial key question.

The Eqs. 4, 5. and 7 are general, and detailed elaboration of how these apply in particular systems is beyond the scope of the present article. In this section, we instead illustrate some aspects of the general problem by elaborating the form of particular terms in more detail for some important simple models.

One-Dimensional Occupancy Disorder

Nearest-neighbor Markov chain

The general problem in Eq. 4 is to consider how a particular set of C_{lmn} might have arisen in a crystal or how we might construct a model to contain such a set of values. In one dimension (1D), a simple way of constructing a disordered crystal is to use a simple Markov chain. We first choose an atom (or molecule) to be A or *B* at random and then add subsequent atoins one at a time using a probability that depends only on the previous one. If x_i is a (0.1) random variable, such that $x_i=1$ corresponds to an A-atom and a value $x_i=0$ corresponds to a B-atom, then a disordered sequence can be generated using the following simple expression:

$$P(x_i = 1/x_{i-1}) = \alpha + \beta x_{i-1} \tag{9}$$

Here. the expression $P(x_i=1/x_{i-1})$ means "the probability that x_i takes the value 1 given the value of x_{i-1}.'' This model can be shown to have the property that the fraction of atoms that are A, m_A, and the set of correlations, C_n, are simply related to the parameters α and β.

$$m_A = \alpha/(1-\beta) \text{ and } C_n = \beta^n \tag{10}$$

(note $C_1 = \beta$ and $C_0 = 1$)

It can then be shown that the diffuse intensity is entirely defined by these two parameters:

$$I(\mathbf{k})_{\text{diffuse}} = m_A m_B (f_A - f_B)^2 \times \left[1 + 2 \sum_{n=1}^{N-1} \beta^n \cos(\mathbf{k} \cdot n\mathbf{a}) \right] \tag{11}$$

As the number of atoms (or molecules), N. tends to infinity, the summation can be carried out to give

$$I(\mathbf{k})_{\text{diffuse}} = K \frac{1-\beta^2}{1+\beta^2-2\beta\cos(\mathbf{k}\cdot\mathbf{a})} \tag{12}$$

Here. K replaces the constant terms involving m_A and f_A, etc. In Fig. 1a, we show plots of this function for different values of the nearest-neighbor correlation coefficient $C_1=\beta$. Note that m_A only appears in the constant term and therefore affects only the overall intensity of the diffuse peaks and not their shapes. The shape is entirely dependent on β. Positive correlations produce a diffuse peak centered on the Bragg peak positions ($\mathbf{k}=0, 2\pi, 4\pi$, etc., if $a=1$), while negative correlations produce a peak midway between them ($\mathbf{k}=\pi, 3\pi$. etc.). The higher the absolute value of β, the sharper the diffuse peak. The geometrically decaying correlations seen in Eq. 11 and the corresponding diffuse peak shapes seen in Fig. 1a are characteristic of ID disorder.

Second-nearest-neighbor Markov chain

Eq. 9 can be readily extended to include second-nearest-neighbor (or higher) effects:

$$P(x_i = 1/x_{i-1}, x_{i-2}) = \alpha + \beta x_{i-1} + \gamma x_{i-2} \tag{13}$$

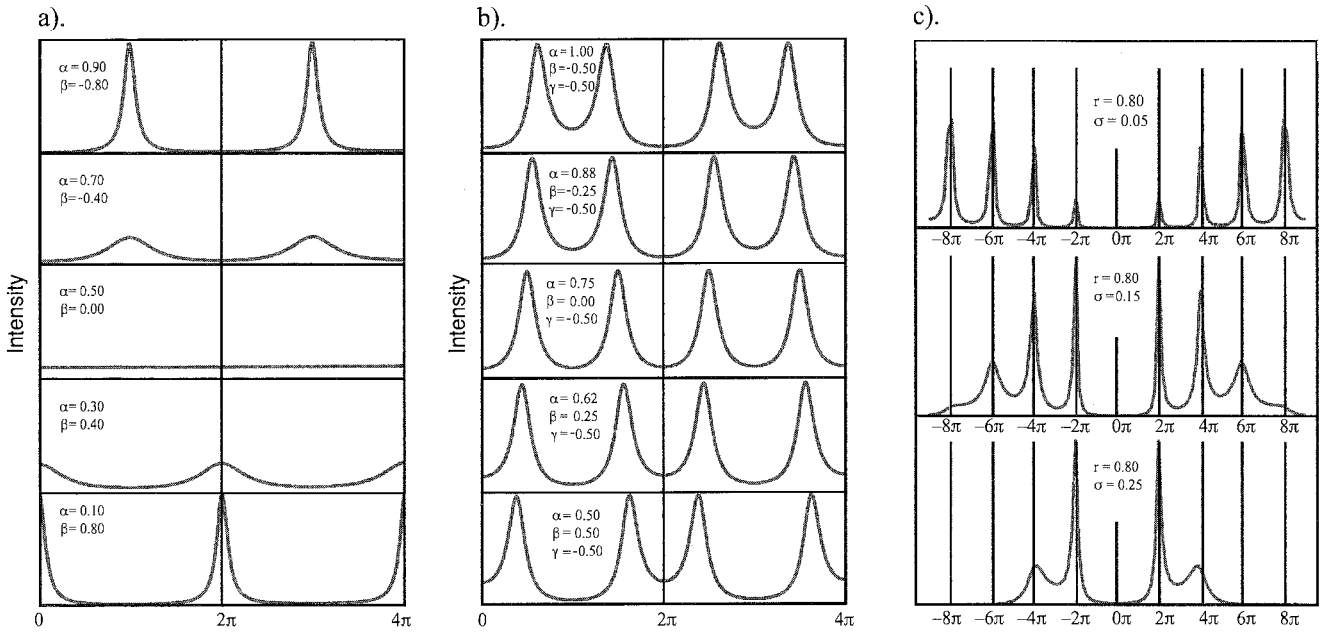

Fig. 1 Diffuse intensity plots for various 1D models discussed in the text. (a) The nearest-neighbor Markov chain. (b) The second-nearest-neighbor Markov chain. (c) The perturbed regular lattice. (See the text for details.) (*View this art in color at www.dekker.com.*)

This model can again be readily solved, and the diffuse intensity is now of the following form:

$$I(\mathbf{k})_{\text{diffuse}} = K\left(c_1\frac{1-\beta_1^2}{1+\beta_1^2-2\beta_1\cos(\mathbf{k}\cdot\mathbf{a})} + c_2\frac{1-\beta_2^2}{1+\beta_2^2-2\beta_2\cos(\mathbf{k}\cdot\mathbf{a})}\right) \tag{14}$$

Here, β_1, β_2 and c_1, c_2 depend on the parameters α, β, γ, and they may be complex. but $I(\mathbf{k})_{\text{diffuse}}$ is real. Example plots of this function are shown in Fig. 1b. It is seen that diffuse peaks may occur at positions other than k=O or $\mathbf{k}=\pi$. For the plots that have diffuse peaks at positions close to $\mathbf{k}=2\pi/3$ and $\mathbf{k}=4\pi/3$, the atom sequence tends to be *AABAABAAB*... or BBABBABBA..., while for ones with peaks close to $\mathbf{k}=2\pi/4$ and $\mathbf{k}=6\pi/4$, the sequences tend to be *AABBAABB*....

The second-neighbor Markov chain is the simplest system that gives rise to diffuse peaks at incommensurate positions. Incommensurate peaks occurring in real materials invariably arise from a competition between nearest-neighbor forces and some more distant force.

Ising models in 1D

Although at first sight they appear different, 1D Markov chain models are formally equivalent to Ising models. In the Ising formulation, it is more convenient to change from the x_i (0,1) variables to σ_i (−1, +1) variables, where $\sigma_i=2x_i-1$. In the simplest 1D Ising model, the random variables interact only with nearest-neighbor variables on either side. A given configuration of the lattice (a disordered sequence of As and Bs) is assumed to occur with a probability given by a Boltzmann partition:

$$P_{\text{config}} = \frac{\exp(-E_c/kT)}{\sum_c \exp(-E_c/kT)}$$

where the summation is over all configurations, c, and the interaction energy is given by

$$E_c = \sum J\sigma_i\sigma_{i-1} \tag{16}$$

This simple pair-interaction Ising model is equivalent to the Markov chain model of Eq. 9 for $m_A=0.5$. The interaction parameter J is related to the correlation β by the following:

$$\beta = \tanh(-J/kT) \tag{17}$$

1D Displacement Disorder

Perturbed regular lattice

We consider for simplicity the displacement equivalent of the simple 1D Markov chain model given in Eq. 9. We suppose that x_i is now a zero-mean normally distributed random variable that represents the longitudinal displacement of the site i from its regular position on a 1D lattice

of spacing **a.** The spacing d_i between the $(i-1)^{th}$ and ith points is $x_i - x_{i-1} + a$. We construct the distribution by choosing the position of the first point and then adding subsequent points using a conditional probability relation:

$$P(x_i/x_{i-1}) = K\exp\left(-\frac{1}{2\sigma_L^2}\frac{(d_i-\mathbf{a})^2}{2(1-r)}\right) \tag{18}$$

This produces a distribution that has the property that the probability distribution of the variables x, is a simple Gaussian function:

$$P(x_i) = K\exp\left(-\frac{x_i^2}{2\sigma_L^2}\right) \tag{19}$$

and the joint probability distribution of two neighboring points is also Gaussian:

$$P(x_i, x_{i-1}) = K\exp\left(-\frac{1}{2\sigma_L^2}\frac{(x_{i-1}^2 + x_i^2 - 2rx_{i-1}x_i)}{(1 \quad r^2)}\right) \tag{20}$$

Here r is a correlation coefficient with properties similar to the occupancy correlations discussed above. Positive values of r correspond to neighboring points tending to be displaced in the same direction and negative r to neighboring points tending to be displaced in opposite directions. The diffracted intensity for this model again consists of two parts: a Bragg intensity that comes from the average lattice and a diffuse component that comes from the differences from the average. It can be shown[9] that

$$I(\mathbf{k})_{\text{Bragg}} = \exp(-\mathbf{k}^2\sigma^2)\sum_n \exp(i\mathbf{k}\cdot n\mathbf{a}) \tag{21}$$

$$I(\mathbf{k})_{\text{Diffuse}} = \exp(-\mathbf{k}^2\sigma^2)\sum_{P=1}^{\infty}\frac{\exp(\mathbf{k}^2\sigma^2)^P}{P!} \times \frac{(1 - r^{2P})}{(1 + r^{2P} - 2r^P\cos(\mathbf{k}\,.\,\mathbf{a}))} \tag{22}$$

Some plots of this diffuse intensity function are shown in Fig. 1c. All plots use the same value of the correlation coefficient r. When the value of σ is a small fraction of the lattice spacing (n.b. typical values for thermal displacements may be $\sim$0.05), only the P=1 term in the summation is appreciable. In this case: the form of the diffuse scattering is practically the same as for substitution disorder (Eq. 12). However, here the overall intensity is zero at the origin and rises with k. As the value of a is increased. higher-angle diffuse peaks become broader as a result of the increasing contribution of the $P=2, P=3$, etc., terms in the summation. At the same time. the exponential before the summation (the Debye–Waller factor) reduces the overall intensity at high angles.

It should be noted that when σ reaches about 0.3 (of the repeat distance), the intensity of even the first Bragg peak is so small that it is virtually undetectable, and all the scattering can then be considered to be diffuse scattering. In this case, increasing the value of r to values > 0.95 will result in a scattering pattern consisting of moderately sharp diffuse peaks but no actual Bragg peaks.

Disorder in 3D

Although 1D models provide useful insight into the various concepts of correlation and disorder. and there are real systems for which 1D models are appropriate. for most purposes, it is necessary to consider the possibility of disorder in higher dimensions. Unfortunately, the change from 1D to higher dimensions is decidedly nontrivial. At the conclusion of his work on the 1D Ising model, Ising considered that the extension to higher dimensions would be a simple matter. It was not until 1944[10] that the 2D nearest-neighbor Ising model was solved. and there is still no analytical solution for the 3D model. The correlation coefficients, C_{lmn}, are now present on a fully 3D array. and the constraints and interdependencies of these are much more complex.

In general terms. it is easy to see why the extra complexity occurs. In ID, a given lattice site can be influenced by its neighbor only via a direct interaction. In 2D or 3D systems, there is a multitude of other indirect pathways that can transmit the interaction. This has a marked effect on the way in which correlations spread through a lattice. For the 1D models discussed earlier, it was seen that there was a geometric progression of the correlations with distance. For the corresponding 2D or 3D nearest-neighbor Ising model with the same value of the nearest-neighbor correlation coefficient β, the decay is much less rapid. The corresponding diffraction peaks have a profile that is correspondingly sharper than those seen for the 1D model in Fig, 1a.

Despite the difficulty in obtaining analytical solutions for higher-dimension Ising models, they are still simple to formulate, and realizations of them can readily be obtained via Monte Carlo simulation (although care must be taken. because there may be phase transitions present). Such models are routinely used in a wide range of different systems (see, e.g., Refs. [3–5,7,12,14]).

EXAMPLES

Example 1: The Molecular Crystal 1,3-dibromo-2,5-diethyl-4,6-dimethylbenzene

Shown in Fig. 2a is the $(0kl)$ section of the diffraction pattern from the pure molecular crystal 1.3-dibromo-2.

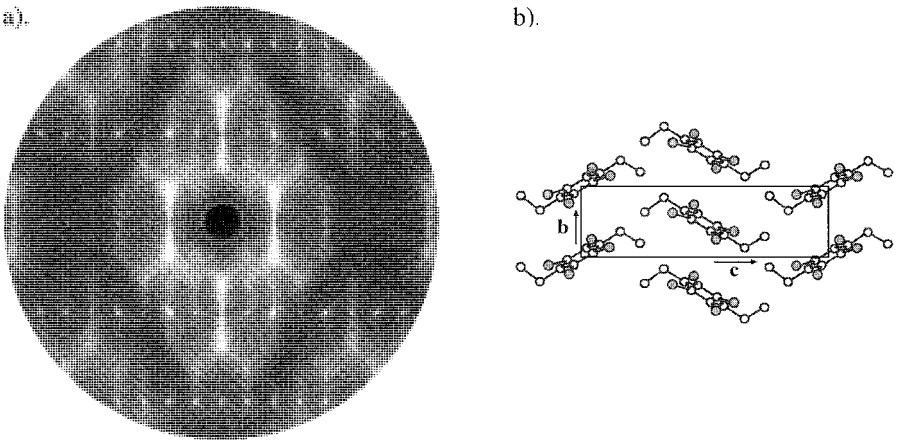

Fig. 2 (a) The (*0kl*) section of the diffraction pattern of 1,3-dibromo-2,5-diethyl-4,6-dimethylbenzene. (b) A corresponding projection of the average crystal structure. (*View this art in color. at www.dekker.com.*)

5-diethyl-4,6-dimethylbenzene recorded at low temperatures (100 K).[7] Shown in Fig. 2b is the corresponding projection of the average crystal structure. This material is disordered because of the similarity in size of the methyl- and bromo-substituents, and in the drawing. the atomic sites shaded in gray are revealed by conventional crystal structure determination to be occupied by 50% Br and 50% methyl.

Although the intensity distribution in Fig. 2a looks complex, it can be described purely in terms of substitutional disorder. in which there are two different possible molecular orientations A and *B* in each site and can be understood in terms of a small set of C_{lmn} intermolecular occupancy correlations. In addition. and most importantly. the overall form of the scattering is modulated by the difference of the molecular scattering factors, $|F_A - F_B|^2$. Because there are two different molecular sites (cell corners and cell centers), with different average orientations, some terms arise from pairs of molecules on a single sublattice (e.g., the cell corners). while others arise from pairs comprising a molecule on one sublattice (cell corner), with a molecule on the other sublattice (cell center).

Example 2: The Zeolite Material, Mordenite

Shown in Fig. 3a is part of the (*hk5*) section of the diffraction pattern of the zeolite mordenite." The origin of the reciprocal section is near the center at the top of the figure. Two different diffuse scattering features can be seen: narrow diffuse streaks emanating from the Bragg reflection positions and broad uniform diffuse regions each extending over several reciprocal lattice cells.

A schematic drawing of the structure is shown in Fig. 3b. This is made up of corner-connected SiO_4 tetrahedra that appear as triangles in this figure. The basic building blocks for the structure are the clusters of tetrahedra (eight triangles) shown in two different shades of gray. These form columns along the **c** (projection) direction. The origins of the light and dark columns differ by 0.5**c**. The perfect structure consists of alternating light and dark columns, as seen in the lower-right portion of the figure.

Two types of defects can occur. First. a single isolated column is able to slip by 0.5**c**. Such a slip of origin corresponds to a change of shading from dark to light or vice versa. Second, stacking faults can occur where one whole region of the structure slips 0.5**c** relative to the adjacent region. The dark line running diagonally across the figure indicates such a fault line. Note that the shading of columns on opposite sides of the fault is in antiphase.

For this example, the two different diffuse features can also be described purely in terms of substitutional disorder and understood in terms of sets of correlation parameters. For both types of defects, F_A and F_B represent the structural factors for the two different types of columns (one shifted 0.5**c** relative to the other). The difference between these $|F_A - F_B|^2$ gives a function with the broad areas of scattering that are seen. For isolated random defects, only the origin term C_0 is present: all other C_{lmn} are zero. This produces uniform (unmodulated) scattering in the noted broad areas.

The sharp streaks caused by the stacking faults involve strong correlations that modulate the scattering in the same broad regions. Parallel to the fault line, there is strong positive correlation, i.e., neighboring columns fol-

"Data supplied by kind permission of Dr. Branton Campbell. Advanced Photon Source. Argonne, USA.

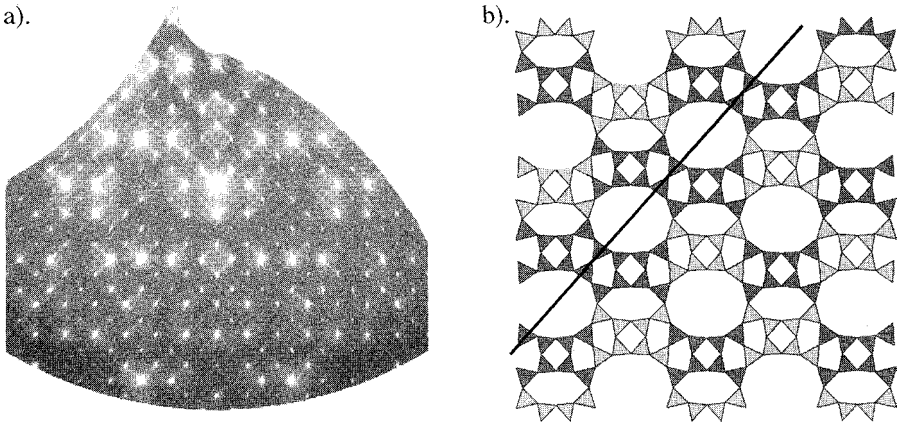

Fig. **3** (a) Part of the (*hk5*) section of the diffraction pattern of the zeolite mordenite. together with (b) a schematic plot of the structure illustrating the formation of a stacking fault. (See the text for details.) (*View this art in color at www.dekker.com.*)

low the perfect structure sequence. This gives the streaks their narrow widths. Normal to the fault line, there is also positive correlation, as neighboring sheets of structure still tend to conform to the perfect structure sequence, but depending on the faulting probability. the range of order is only moderate. This results in the streak being most intense at the Bragg position and diminishing away from it.

Example 3: Dibromodecane/Urea Inclusion Compound (BBD–Urea)

Shown in Fig 4a is the (*0kl*) section of the diffraction pattern from the DBD–Urea inclusion compound In urea inclusion compounds, the urea molecules form a hydrogen-bonded network containing hexagonal channels that run along the c-direction The channels can accommodate various kinds of long-chain molecules. of which DBD is an interesting example.[11,12] The DBD molecules pack end-to-end in an individual channel to form a pseudo-ID crystal, the repeat distance of which is not commensurate with the crystallographic repeat of the urea framework. At room temperature, the molecules are able to rotate about their long axes and are also able to slide along the channels. To a first approximation, the molecules in one channel are independent of those in neighboring channels. This is shown schematically in Fig. 4b. The average crystal structure obtained from the Bragg peaks reveals details of the urea framework, but little information is obtainable about the guest molecules' positions or orientations.

The vertical diffuse bands in Fig. 4a arise from the chains of molecules that form a pseudo-1D crystal along each urea channel. Each band is virtually uniform in intensity, because there are no correlations linking one

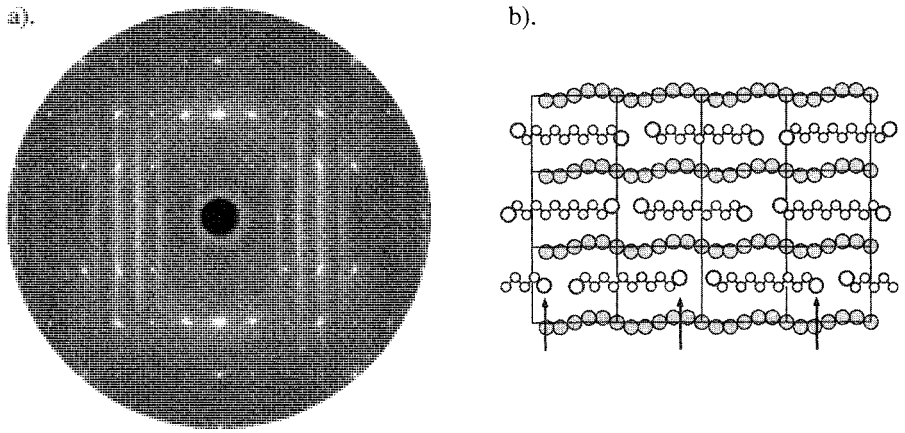

Fig. 4 (a) The (*0kl*) section of the diffraction pattern of the dibromodecane/urea inclusion compound, together with (b) a schematic diagram of the structure showing that the dibromodecane molecules form a pseudo-1D crystal within each channel of the urea host. (*View* this *art in color ut www.dekker.com.*)

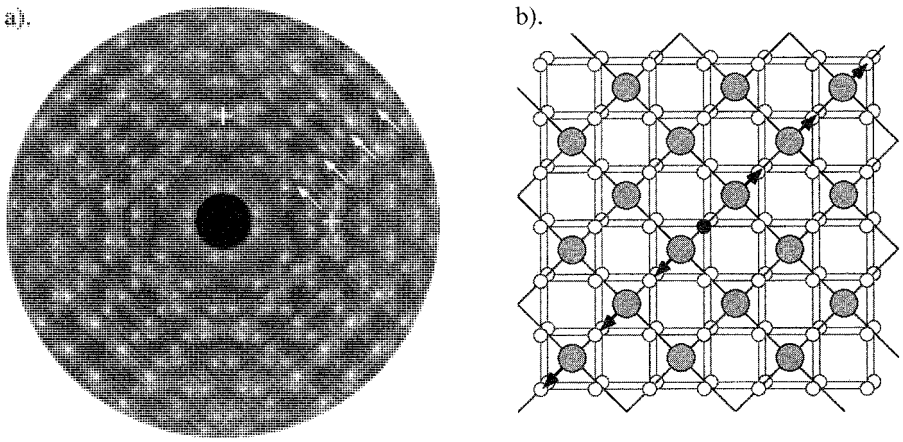

Fig. 5 (a) The (*hk0.5*) section of the diffraction pattern of a calcia-stabilized cubic zirconia, together with (b) a schematic drawing of part of the structure showing how the cations move away from a vacancy in the oxygen lattice. The ''+'' signs in (a) mark the reciprocal points (4 0 0.5) and (0 4 0.5). The arrows are drawn to indicate pairs of diffuse spots refel-red to in the text. (*View this art* in *color at www.dekker.com.*)

channel with the next. It is seen that the firct diffuse band is narrow. but higher-order ones get progressively broader. This behavior is in accord with the 1D displacement model described by Eq. 22. Note also that the spacing of the bands is incommensurate with the Bragg peak spacing. [It should be noted that the second band is absent due to the particular form of the molecular structure factor (omitted from Eq. 22).]

Example 4: Calcia-Stabilized Cubic Zirconia (Ca-CSZ)

Shown in Fig. 5a is the *(hk0.5)* section of the diffraction pattern of a Ca-CSZ of composition. $Ca_{0.125}Zr_{0.875}O_{1.875}$.[13] CSZs have the fcc fluorite average structure, with all atoms in special positions. A drawing of part of the fluorite structure viewed down **c** is shown in Fig. 5b. Only two layers of anion sites are shown, together with the cations they contain. In CSZs, the cation sites are all occupied but are disordered; the anion sites have partial occupancy. Between two cations, there are two bridging oxygen sites, as shown in Fig. 5b, and the black circle near the center of the figure is drawn to represent a vacancy in one of these sites. The figure illustrates the proposed mechanism by which the cations are displaced away from a vacancy. This distortion mechanism accounts for the dark lines (indicated in Fig. 5a by the direction of the arrows) (see Ref. [7]).

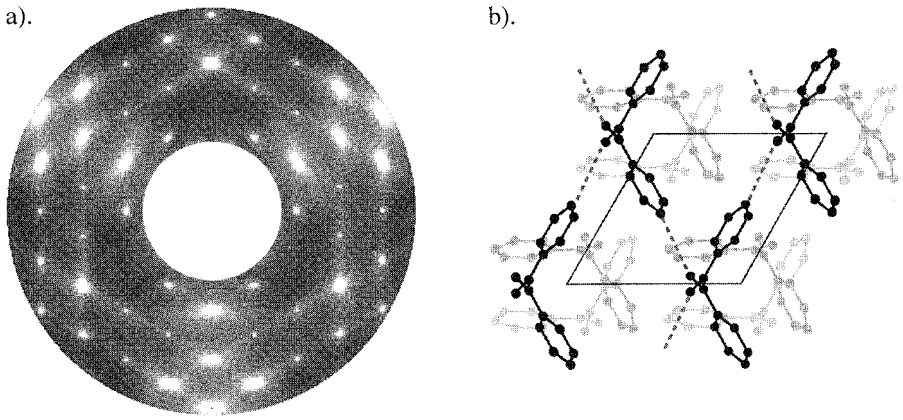

Fig. **6** (a) The (*hk2*) section of the diffraction pattern of benzil. $C_{14}H_{10}O_2$, together with (b) a plot of the corresponding projection of the structure (H atoms omitted). The structure consists of three symmetry-related molecular planes, two of which are drawn in light shading for clarity. The dashed line indicates the important vectors along which the internal motion of one molecule is coupled to its neighbors. (View *this art* in *color at www.dekker.com.*)

The second-neighbor Markov chain, described earlier, is the simplest system that gives rise to diffuse peaks at incommensurate positions. Incommensurate peaks occurring in real materials invariably arise in a similar way from a competition between nearest-neighbor forces and some more distant force. The CSZ example of Fig. 5 is one such system. It was recently shown[4] that the diffuse peaks in this system can be understood in terms of a competition between nearest-neighbor forces and a longer-range strain that builds up as the locally prefen-ed structure tries to fit into the average lattice.

The CSZ diffraction pattern shown in Fig. 5a also demonstrates the importance of the higher-order diffuse scattering components that involve interaction between occupancy and displacements. The diffuse spots mentioned above are due to the presence of occupancy correlations (i.e., the I_0 component), but their intensities are modified by the various other components. Each pair of spots spans a particular dark line, four of which are indicated by the directions of the arrows in Fig. 5a. The point of each arrow indicates a particular pair of spots. Of particular interest is the relative intensity of the two spots comprising each pair. At low diffraction angles, the lower-angle spot is stronger. but as the diffraction angle increases, the higher-angle spot progressively becomes stronger. The asymmetry of the spot intensity arises from the size-effect term; I_1, and the other odd higher-order components. such as I_3. At low angles, I_1 dominates. but at higher angles, the I_3 term becomes progressively more important. Because I_1 and I_3 are of opposite signs. the asymmetry switches the signs.

Example 5: The Molecular Crystal, Benzil

The $(hk2)$ section of the diffraction pattern of benzil is shown in Fig. 6a.[5] This is an example of a system where the scattering is purely TDS and does not involve any occupancy disorder. The molecule has internal degrees of flexibility, and the diffuse scattering results from motions in which the internal degrees of flexibility are coupled from molecule to molecule via intermolecular interactions. The corresponding c-axis projection of the structure and the most important intermolecular vectors are shown in Fig. 6b. These vectors run between the O atoms in the flexible bridge of one molecule to the C–H terminus of a neighboring molecule. This hydrogen-bond network enables the internal motions of molecules to be coupled over relatively large distances.

Because there is no occupational disorder, the diffuse scattering in Fig. 4a is essentially made up of terms from the second-order diffuse component I_2 (Eq. 7). Because this is a sum of cosine terms. the intensity is symmetric about Bragg peak positions. This is true for the strong anisotropic peaks that surround some strong Bragg peaks and for the narrow diffuse bands that run between them. The diffuse peaks that surround the Bragg peaks indicate that there are strong positive correlations between the displacements of atoms and molecules. The anisotropy of the peaks (relatively narrow on a radial vector and broader in directions normal to this) is indicative of the fact that correlations are stronger in directions parallel to the displacement direction and weaker in directions normal to the displacement direction. This information is present in the relative magnitudes of the different displacement averages that appear in Eq. 7.

CONCLUSION

In this article, we attempted to show, using a selection of real diffraction examples, the range and diversity of different types of disorder that occur in many materials. We also gave a brief survey of some important aspects of diffraction theory. an understanding of which enables the different disorder effects to be identified. Correct identification of the origins of a particular diffuse scattering pattern is a prerequisite to being able to correctly analyze it. This is particularly important, because the diffraction experiment can only give information concerning pair correlations and so there is always the possibility of ambiguity.

Perhaps of most importance to chemists is the last example of the molecular crystal benzil.[5] In this, the diffuse scattering arises entirely from thermal disorder and so is essentially similar to a whole range of molecular crystal systems that are nominally considered to be perfect. Whereas conventional crystal structure determination will provide such quantities as mean-square atomic displacement ellipsoids. the diffuse scattering analysis reveals details of how the molecules are interacting and moving. The analysis of benzil is indicative of the level of detail that can be obtained using current modeling techniques. The agreement between model calculations and the observed diffuse scattering is approaching the level that is routinely obtained for Bragg reflections. At this level of quantitative agreement, for example, it was possible to measure the torsional force constant for the internal degrees of flexibility in the benzil molecule. As the modeling methods develop and computers become ever more powerful, the future looks bright for this kind of detailed information to become routinely available.

ARTICLES OF FURTHER INTEREST

Channel Inclusion Compounds, p. 223
Classical Descriptions of Inclusion Compounds, p. 253
Hydrogen Bonding, p. 658

Molecular Modeling and Related Computational Techniques, p *901*
Organic Zeolites, p *996*
Polymorphism, p *1129*
X-Ray Crystallography, p. *1586*
Zeolites Structures and Inclusion Properties, p. *1623*

REFERENCES

1. Weber, T.: Estermann, M.A.; Bürgi, H.-B. The structural complexity of a polar perhydrotriphenylene inclusion compound brought to light by synchrotron radiation. Acta Crystallogr. 2001. B57. 579–590.
2. Estermann, M.A.; Steurer, W. Diffuse scattering data acquisition techniques. Phase Transit. 1998. *B67*, 165–195.
3. Welberry, T.R.; Proffen. Th.; Bown. M. Analysis of single-crystal diffuse x-ray scattering via automatic refinement of a Monte Carlo model. Acta Crystallogr. 1998. A54.661–674.
4. Welberry. T.R. Diffuse x-ray scattering and disorder in *p*-methyl-*N*-(*p*-chlorobenzylidene)aniline, $C_{14}H_{12}ClN$ (ClMe): Analysis via automatic refinement of a Monte Carlo model. Acta Crystallogr. 2000. *A56*, 348–358.
5. Welberry, T.R.; Coossens, D.J.: Edwards. A.J.: David. W.I.F. Diffuse x-ray scattering from benzil, $C_{14}H_{10}O_2$: Analysis via automatic refinement of a Monte Carlo model. Acta Crystallogr. 2001. *A57*, 101–109.
6. Hayakawa. M.: Cohen, J.B. Equations for diffuse scattering from materials with multiple sublattices. Acta Crystallogr. 1975; *A31*, 635–645.
7. Welberry, T.R.: Butler, B.D. Interpretation of diffuse x-ray scattering via models of disorder. J. Appl. Crystallogr. 1994. 27, 205–231.
8. Warren. B.E. *X-ray Diffraction*; Dover: New York. 1990: 35–38.
9. Welberry, T.R. Diffuse x-ray scattering and models of disorder. Rep. Prog. Phys. 1985, *48*, 1481–1541.
10. Onsager, L. Phys. Rev. 1944. 44. 117–149.
11. George. A.R.; Harris, K.D.M. Properties of the guest molecules in the 1.10-dibromodecane/urea inclusion compound. J. Mater. Chem. 1994. 4. 1731–1735.
12. Welberry. T.R.; Mayo, S.C. Diffuse x-ray scattering and Monte Carlo study of guest–host interactions in urea inclusion compounds. J. Appl. Crystallogr. 1996. 29. 353–364.
13. Welberry. T.R.: Withers. R.L.; Mayo, S.C. A modulation wave approach to understanding the disordered structure of cubic stabilized zirconias (CSZs). J. Solid State Chem. 1995. *115*, 43–54.
14. Welberry, T.R. Diffuse x-ray scattering and strain effects in disordered crystals. Acta Crystallogr. 2001. *A57*, 244–255.

DNA as a Supramolecular Scaffold

Alexandra L. Pickering
Leroy Cronin
The University of Glasgow, Glasgow, United Kingdom

INTRODUCTION

Since the elucidation of the structure of DNA in 1953, a revolution has occurred in molecular biology that recently culminated in the sequencing of the entire human genome. However, the properties that define DNA as a macromolecule with the most essential role in biology are also of tremendous importance in the design and understanding of DNA as a stnictural component in nanotechnology. After all. it could be argued that DNA is the ultimate supramolecular architecture. In this article, we describe the structural features of DNA that allow application as what promises to be one of the most fundamental supramolecular scaffolds. In describing this, we discuss the importance of molecular recognition and DNA binding in the design of synthetic DNA architectures. diagnostic agents, and the growth of new DNA-hybrid materials. The understanding of how DNA acts as a template, both to allow its own replication and to assemble cations; is also vital, as is an appreciation of topological concepts in the design of new materials. Finally, we describe how these ideas were applied to the design of DNA-based architectures for nanolithography, DNA machines. molecular wires, and as chiral memory devices.

DNA STRUCTURE

Considering its integral importance to life, the structural components of deoxyribose nucleic acid (DNA) are reinarkably simple. Each strand of DNA is a linear polymer comprising a constant backbone of alternating deoxyribose sugars and negatively charged phosphodiesters, and a selection of four heterocyclic bases (Fig. 1). The uniqueness of the DNA strand is defined purely in terms of the sequence of the bases.

Two polymeric nucleic acid strands are held together by Watson–Crick hydrogen bonds (2.8–3.0 Å) between two bases to form a double helix. Adenine and thymine base pairs hydrogen bond together via two interactions, and guanine and cytosine through three. The conformation of the base pairing defines the mutual positions of the two sugar–phosphate strands in DNA. Hydrophobic and van der Waals interactions as well as π stacking between sets of base pairs also contribute to the stability of the overall structure.

Although the individual bases are planar heterocycles. considerable flexibility is conferred upon the entire structure from a number of contributing factors. Base pairing, for example, can deviate from planarity by up to 35° to minimize steric interactions without appreciable loss of hydrogen-bonding energy.[1] Furthermore, there are 12 different torsion angles associated with the sugar–phosphate backbone that can adopt a range of values. and hence, can have significant effects on the overall structure of the oligonucleotide. Linking the bases to the deoxyribose sugars is a glycosidic bond. which can have a torsion angle (χ) dependent on the orientation of the base in relation to the sugar. The sugar has a nonplanar "puckered" conformation dependent on its five internal torsion angles (τ_0–τ_4). The relative populations of the conformations arise from the type of base attached, and in solution, it is possible for these to interconvert, which alters the orientation of the substituents and, hence, the backbone of the entire structure. The final six variable torsion angles (α–ζ) define the conformation of the phosphodiester backbone. Steric restrictions prevent large angular variations between 0–360°; however, many possible low-energy conformations of the oligonucleotide exist.[2]

As a function of both flexibility and restraint, the overall structure of DNA can adopt several polyrnorphs, including left- and right-handed helices. Four major secondary structures of DNA are known; A-DNA. B-DNA, and triple helices are right-handed. and Z-DNA structures are left-handed[i]" ((Fig. 2). The A-conformer is the most compact, being wider and having a helical rise of 1I bases (25.6 Å). Z-DNA is composed of alternating purine-pyrimidine nucleotides, giving the structure a zigzag appearance and has a rise of 12 bases (37 A). A triple helix, comprising one purine and two pyrimidine strands, results from a "base triplet" hydrogen-bonding system. Its dimensions are similar to those of A-DNA. with the second pyrimidine strand lying in the grooves formed by a pyrimidine and a purine strand.

B-DNA is the most common polymorph due to its chirality and geometry along the sugar–phosphate backbone. The overall width of the helix is approximately 20 Å and completes one turn every 10 bases (34 Å).[4] As with

DOI: 10.1081/E-ESMC 120019196

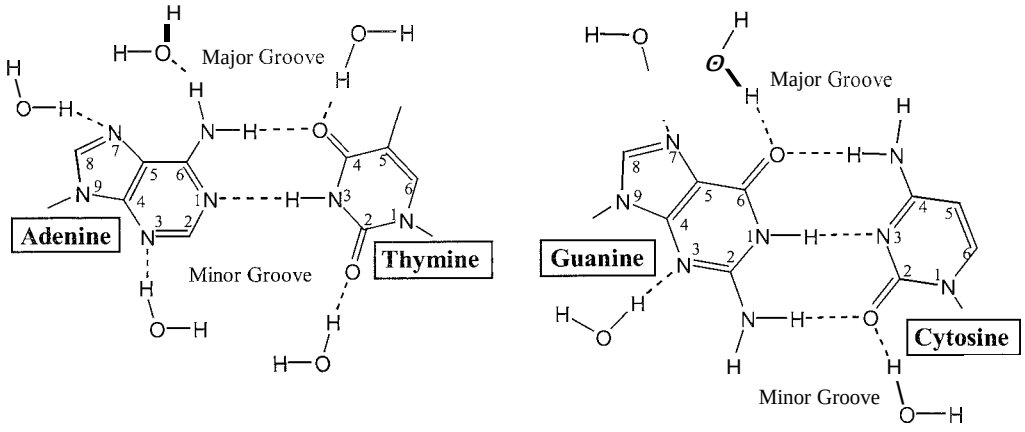

Fig. 1 *Base-pairing of DNA* nucleotides

each double helix. the asymmetry of the base pairs results in major *and minor grooves along the helical axis. with dimensions that are related to the distance and orientation of the base pairs in relation to the axis. The major groove is approximately 13* Å *wide and 8* Å *deep. whereas the minor groove is 4.5 A and 6* Å, *respectively. The minor groove has hydrophobic hydrogen* atoms *of the sugar groups forming its walls. The major groove is richer in base* substituents, *having the* O_6, N_6 *atoms of the purine moieties and the* N_6, O_4 *atoms of pyrimidines available.*

DNA BINDING

The two major ways in which DNA *interacts with other eniities can be classed as nonspecific covalent bonding via either the phosphodiesicr or sugar moieties or electrostatic dominated noncovalent bonding. Nonreversible covalent interactions are important when considering the cellular processing of many drugs, but it is the ability to form* noncovalent *interactions that defines* DNA *as the ultimate supramolecular building block.*

Fig. 2 *The common* polymorphs *of DNA. (View this art in color at www.dekker.com.)*

Noncovalent interactions *with* DNA *occur via two binding modes: groove binding and intercalation. Much research has been carried out* to *exploit the properties of DNA* in *the design of targeted intercalating and* groove-*binding drugs in such areas as anticancer. antibacterial. and antiviral agents. and in the postgenomic era, the* need *for a deeper understanding of how* DNA *interacts with other* molecules *is* becoming more *apparent. However. analyses of the integral features of the structure of* DNA *allow a much* more *comprehensive view of its noncellular potential.*

Conventionally. the structures of the molecules designed for each binding mode followed certain distinctive criteria."' Boundaries are now *being extended and* becoming *less clear. and an ever-increasing number of physical and chemical techniques are emerging to aid in the determination of the structures, sequence specificity. energies. and binding stoichiometries of these* noncova-*lent* interactions.[6] *The specific binding mode of interaction can now be determined by a combination of such techniques as x-ray crystallography, NMR. gel* footprint-*ing, circular* dichroism. and *fluorescence.* UV. IR, *and mass spectroscopy.*

In the biological environment, it is *important to understand the processing of the genetic code stored in the* DNA. *The ability to stimulate or prevent this processing is of great importance in terms of molecular biology and drug design. and also in* terms *of* supramo-*lecular chemistry. as the noncovalent interactions* in-volved *in such "switching"* mechanisms *are of great interest. These mechanisms involve a variety of molecular tools in order to recognize the genetic code in a* sequence-*specific manner. Biology achieves this through the surface motifs of proteins. which are too large to fit into the minor*

groove and instead interact in or around the major groove.[7] This acts as a particularly attractive macroreceptor site for DNA recognition agents, as the dimensions of the major groove are dependent to a large extent on the base sequence and so can be seen as a molecular "lock" that is activated by a highly specific recognition "key." For example, distortion of the DNA backbone is activated by transcription regulators that incorporate cylindrical binding units such as α helices or zinc fingers that insert into the major groove.

It is possible to mimic the biological mechanisms used to bind DNA. For example, oligonucleotides of natural and synthetic origins are capable of forming triplexes by sequence-specific binding to the major groove, and the area of metallosupramolecular assembly can provide cationic charge around the metallocenters, which confer a substantial electrostatic contribution by interactions with the anionic sugar–phosphate backbone.

Such large arrays of macromolecular recognition contrast sharply with the mode of *DNA* binding of small molecule recognition agents. Typically, cationic at physiological pH and much smaller than proteins. these agents are able to bind preferentially to the minor groove. where the electrostatic potential is negative, displacing the hydrogen-bonded water molecules. Strong electronic interactions along with the formation of significant van der Waals contacts make the complex stable, with dissociation constants in the order of 10^{-5} M^{-1}. The natural antibiotic distamycin *A* (Fig. 3) and its derivatives are well-established reversible minor-groove binding agents. It incorporates an oligopeptidic pyrrolic framework with a terminal amidino moiety and is highly selective for A·T-rich regions containing more than four A·T base pairs. Typical minor-groove binders include an extended ring syctem with unfused rings, although recent developments in sequence-dependent DNA binding included ligands with polyaromatic nuclei. These conjugated systems form strong hydrophobic contacts with the sugar-containing walls of the minor groove. Increased interactions can be introduced through hydrogen-bonding moieties to improve the affinity of the groove binders for G·C-rich regions. Derivatives of such groove binders as distamycin A can be used for alkylating and nonalkylating agents in anticancer therapeutics.[8] It is believed that the ability of small molecule recognition agents to alkylate DNA in a sequence-specific manner and modify the function of nucleic acids irreversibly will increase the specificity for target cells.

In general, groove binding effects only subtle changes in the overall structure by bending or kinking the DNA. Intercalation, on the other hand: has a much more dramatic structural effect in terms of helical twist and compression. Intercalators are typically polycyclic aromatic compounds that bind reversibly to the DNA double-helical structure by inserting into the central hydrophobic region of the helix between the stacked base pairs. These chromophores are conventionally two or three six-membered rings, for example, doxorubicin (Fig. 3), of approximately the same size as a base pair. This means that, in addition to π-stacking interactions between the intercalator and the adjacent base pairs, strong van der Waals contacts further contribute to the stability of the complex. There are also a number of intercalating agents containing side chains that play vital roles in both the stablization and sequence specificity of interactions with *DNA* by binding in the minor groove.[9]

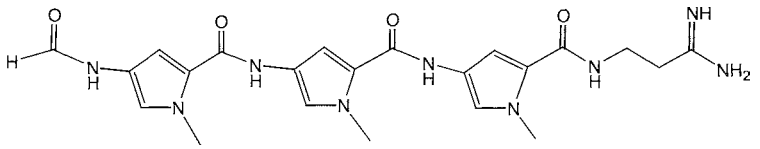

Distamycin A

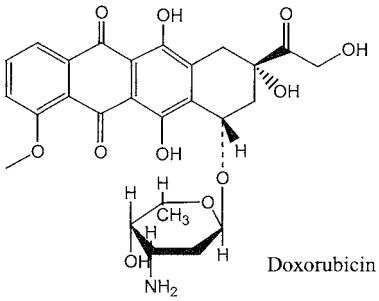

Doxorubicin

Fig. 3 Minor groove binder distamycin A and intercalator doxorubicin

The process of intercalation demands an alteration of the $\alpha-\zeta$ torsion angles along the sugar–phosphate backbone in order to accommodate the aromatic ring system. Rotation around these torsion angles results in a separation of the base pairs and a subsequent extension of the helical axis (approximately 3.4 Å per bound intercalator) and "unwinding" of the two DNA strands. The extent of the unwinding is dependent on the individual intercalator. Polyintercalators are well known,[10] containing two or more aromatic ring systems bridged by appropriate linker chains that facilitate simultaneous intercalation along the DNA strands and the potential for increased sequence specificity.

DNA AS A TEMPLATE

DNA as a helical anion can be viewed as a macromolecular template. The fact that DNA is comprised of two self-complementary strands of base pairs is responsible for its ability to replicate upon dissociation of these strands. In fact, the replication of DNA via a templating effect to form a coinpleinentary strand aided by Watson–Crick base pairing is linked to the central dogma of molecular biology.[11] By utilizing a self-complementary and "self-templating" molecule such as DNA, the emergence of life and the possibility for evolution was realized. This is because the use of a double helix of DNA, containing two identical copies of genetic information, allowed the development of an exquisite DNA repair mechanism. Furthermore, the supramolecular coiling of DNA in the chromosomes of a cell is the key to cellular development via protein expression; this is thought to occur through a kind of unwrapping process in which DNA is the key molecule.

The anionic nature of DNA also has important implications in the construction of virus capsids. in which the protective capsid is either assembled around the DNA from a large number of repeating protein building blocks or preformed for DNA insertion. This self-assembly process is partly responsible for the fast spread of viral infection, as many viruses can spontaneously assemble from a soup of DNA and protein-based building blocks.[12] The ability to manipulate the structure of the DNA duplex by altering the code should therefore affect the ability of DNA to coil in chromatin formation as well as gene therapy vector design and in the manipulation of virus structure. It was shown that DNA can also direct the assembly of small molecular units that can undergo a template-driven polymerization process.[13] The covalent casting of noncovalent architectures serves to determine large molecular constructs that express well-defined modes of aggregation. In the case of one-dimensional hydrogen-bonding motifs, covalent casting yields molecular strands that adopt a duplex mode of aggregation.

It is well known that nucleic acids are capable of promoting chemical reactions, and catalytic nucleic acids were found in nature or evolved through in vitro selection processes. Interestingly, it appears that the DNA acts in a similar manner to enzymes and promotes chemical reactions through spatial alignment of the reaction partners; i.e., via a template effect.[14] Recent reports reveal new facets of nucleic acid promoted chemistry and indicate that DNA strands are able to promote chemical reactions by bringing reaction partners into close proximity of each other rather than by precisely aligning the reactive groups. Therefore. it appears that DNA-templated synthesis is a phenomenon that applies to a remarkable variety of chemical reactions (Fig. 4). The ease of automated DNA synthesis. predictable binding, and established methods for nucleic acid amplification and sequence analysis render DNA a promising template for future developments.[15]

DNA TOPOLOGY

Research into the application of noncovalent metal–ligand interactions to direct self-assembly resulted in a number of interesting topological structures.[16] It is well established that DNA topology is a crucial factor in many biological processes. such as topoisomerism and DNA supercoiling. Highly ordered DNA topology is also of considerable interest with respect to the

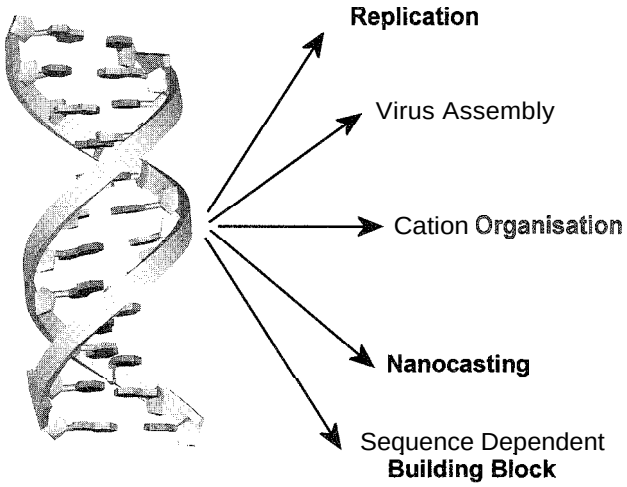

Fig. 4 Examples of DNA chemical reactions. (*View this art in color at www.dekker.com.*)

design of sequence-specific DNA binding agents, allowing targeted recognition and precise regioselectivity along the polymeric strands. The crystallographic motivation for such developments lies in the desire to organize DNA in a periodic array in order to provide a scaffold on which other macromolecules, which are difficult to crystallize by conventional methods, may be arranged.

The first-known topological polymorph of DNA, discovered in 1967,[17] was the DNA catenane consisting of two interlocked rings of circular DNA. It was recognized that these structures had important implications in the cellular functioning of DNA. If, during the replication of circular DNA. a catenane structure is formed upon the interlocking of parent and daughter molecules, continuation of the replication process is impeded. Topoisomerases are a class of enzymes capable of changing the topology of DNA by an incision and repair mechanism. Once the DNA strand is broken, another strand may pass through the rupture; and then repair mechanisms reseal the original strand. Type I topoisomerases effect topological transformations during the disruption of one DNA strand, and Type II topoisornerases are capable of breaking two strands.[18] The design of

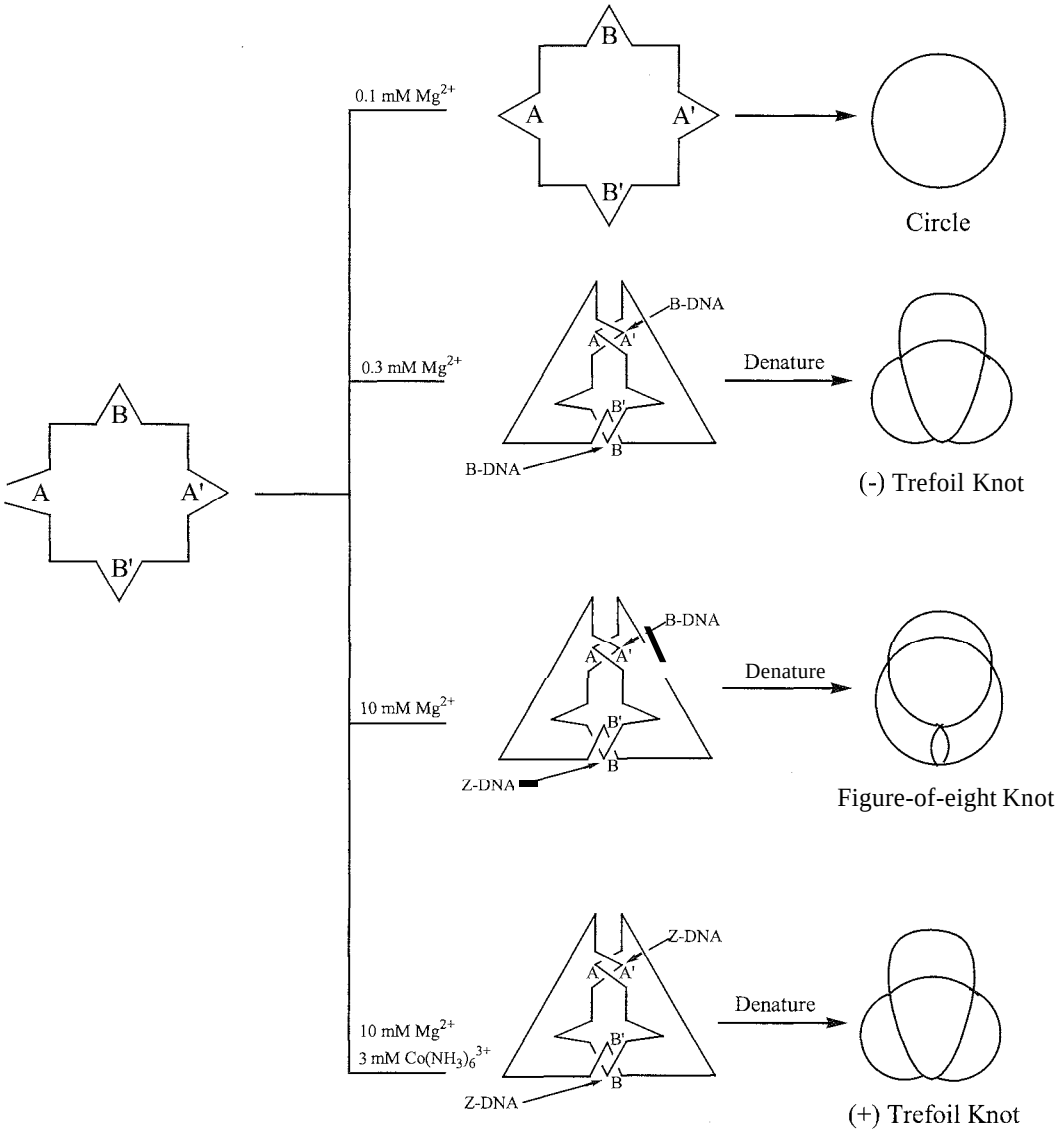

Fig. **5** Seeman's synthesis of DNA knots. (From Du. S.M.: Stollar, B.D.: Seeman, N.C. A synthetic DNA molecule in three knotted topologies. J. Am. Chem. Soc. 1995, *117*, 1194–1200.)

topoisomerase-inspired synthetic agents could provide a much desired control of highly ordered topology in the area of nanotechnology.

The replication of DNA is controlled by its topology in another vital process known as supercoiling. Topological isomers of circular double-stranded DNA can be made by incision of the duplex and twisting of the strands through 360° before repairing the incision. The overall three-dimensional structure of the DNA undergoes a significant change in the number of helical twists, and a compression along the helical axis in coinparison to the uncomplexed B-DNA is observed.

In addition to naturally occurring complex helical DNA topologies, it is also possible to design topologically interesting structures with linear DNA. The differences in chirality between right-handed B-DNA and left-handed Z-DNA duplex formation as well as engineered effects of specific base-pair complimentarity facilitate the formation of a number of molecular knots from a single-stranded DNA oligomer as a function of salt concentration (Fig. 5).[19,20]

Other remarkable complex structures were assembled from both single strands, for example, the DNA ''padlock,''[16] and multiple strands. such as the DNA cube[21] and a truncated octahedron.[22] The formation of a linear double-helical structure from two strands of oligodeoxyribonucleotides is the most energetically favorable, and as such, it would appear that other configurations are unlikely. However, the principles of genetic recombination. a biological process forming new genetic inaterial from the interaction of two pieces of DNA. can be applied to generate novel, topologically interesting architectures. A key structural intermediate in the recombination mechanism is the Holliday junction,[23] which joins four double helices in a branched molecule. The sequence of nucleotides that converge at the junction is generically twofold symmetric, which allows isomerization of the branch point to the region of symmetry. This is not, however. crucial to the forination of DNA branched molecules, and so it is possible to develop junction structures with fixed branch points.

DNA, MOLECULAR ARCHITECTURE, AND NANOTECHNOLOGY

A significant challenge faced in the use of nanoscale building blocks lies in developing parallel methods for interconnecting and patterning assemblies of the individual components. Molecular scaffolds based on the structure of DNA have the potential of preparing closely spaced, specifically arranged nanoscale assemblies. The ease in which DNA can be synthesized and manipulated means that it is an ideal building block for nanostructured materials.[24] Furthermore, the fact that DNA can interact with other molecular assemblies in a sequence-specific manner means that DNA is a perfect functional scaffold for application in nanotechnology as a molecular device.

The ability to cause DNA to branch is being used in the design of new molecular devices and materials. Such DNA branch junctions are often found in biology; they occur as ephemeral structures in cellular DNA metabolism, including the processes of replication and repair. A particularly significant structure in such systems is the four arm branched Holliday intermediate crucial to the process of genetic recombination.[23] It is fairly simple to design sequences of DNA molecules that lead to stable synthetic variants of Holliday junctions, branched molecules with varied numbers of arms. as well as more complex motifs; it is also elementary to synthesize their constituent strands and engineer subsequent self-assembly of target systems. The use of branched intermediates allows us to make N-connected objects from DNA as well as periodic and aperiodic arrays. Similarly, branched DNA motifs were the basis for several nanomechanical devices.[25]

Further applications of the DNA scaffold are as molecular wires in nanoelectronic circuits, facilitated by

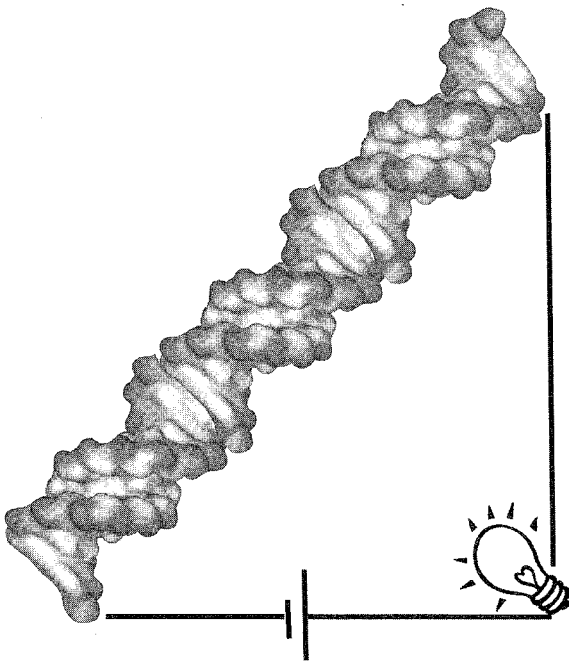

Fig. 6 DNA as a conducting molecular wire. *(View this art in color at www.dekker.com.)*

the fact that electron-transfer processes appear to be mediated by DNA via the π–π-stacked arrangements of the base pairs.[26] This idea, although still the subject of controversy, appears to be limited by recent observations that such events can only occur over small distances.[27] However, DNA has now been used as a template to provide a surface that can be coated with metal atoms to form a conducting or semiconducting sheath.[28] Therefore, should the conducting properties of the polymeric DNA be proven to be insignificant, it appears possible to use the linear framework as a scaffold to assemble or grow a conducting sheath (Fig. 6).

DNA can also be used as a template for the assembly of extended. close-packed nanoparticle structures. Electrostatic binding of ligand-stabilized nanoparticles to the DNA backbone results in extended linear polymers of ribbon-like structures composed of parallel nanoparticle chains and branched structures. Furthermore, the functionalization of DNA with gold nanoparticles led to the design of a DNA array detection method.[29] As such, DNA shows tremendous potential for a variation of biomolecular nanolithography. and the arrangement of nanoscale building blocks on biomolecular scaffolds is a viable approach to interconnecting individual devices into extended, close-packed assemblies.[30]

CONCLUSION

Perfected by nature, the cellular functioning of DNA is an important model for the design of binding agents and therapeutics. However. the potential of such a splendid example of supramolecular architecture as a prototype for the future development of advanced and functional supramolecular scaffolds is now being realized.

ARTICLES OF FURTHER INTEREST

Catenanes and Interlinked Structures, p. 206
Chemical Topology, p. 229
DNA *Nanotechnology*, p. 475
Emergence of Life, p. 528
Molecular Wires: p. 925
Molecular-Level Machines. p. 931
π–π Stacking as a Crystal Engineering Tool, p. 1093
Self-Assembly in *Biochemistry*, p. 1257
Soft and Smart Materials, p. 1302
Strict Self-Assembly and Self-Assembly with Covalent Modification, p. 1372
Supramolecular Polymers, p. 1443
The Template Effect. p. 1493
Zinc-Containing Enzymes and Their Models, p. 1631

REFERENCES

1. Navarro. J.A.; Lippert, B. Molecular architecture with metal ions, nucleobases and other heterocycles. Coord. Chem. Rev. 1999. *186.* 653–667.
2. Dervan, P.B. Design of sequence specific DNA-binding molecules. Science 1986. *232.* 464–471.
3. Mitchell, A. The A to Z of DNA. Nature 1998. *396.* 524.
4. Watson. J.D.: Crick. F.H.C. Molecular structure of nucleic acids. Nature 1953, *171,* 737–738.
5. Tanious, F.A.; Wilson, W.D.; Patrick. D.A.: Tidwell, R.R.; Colson, P.: Houssier, C.: Tardy. C.; Bailly, C. Sequence dependent binding of bis-amidine carbazole dications to DNA. Eur. J. Biochem. 2001. 268, 3455–3464.
6. Suh, D.; Oh. Y.-K.; Chaires, J.B. Determining the binding modes of DNA sequence specific compounds. Process Biochem. 2001, 37. 521–525.
7. Hannon, M.J.; Moreno, V.: Prieto, M.J.; Moldrheim, E.: Sletton. E.: Meistermann, I.: Isaac, C.J.; Sanders, K.J.; Rodger, A. Intramolecular DNA coiling mediated by a metallo-supramolecular cylinder. Angew. Chem., Int. Ed. Engl. 2001. *40* (5). 880–884.
8. Baraldi. P.C.: Balboni, G.; Pavani. M.G.: Bando. T.: Sugiyama, H.; Romagnoli. R. Design. synthesis. DNA binding and biological evaluation of water-soluble hybrid molecules containing two pyrazole analogues of the alkylating cyclopropylpyrroloindone (CPI) subunit of the antitumor agents CC-1065 and polypyrrole minor groove binders. J. Med. Chem. 2001, 4, 2536–2543.
9. Medhi, C.: Mitchell, J.B.O.; Price. S.L.: Tabor, A.B. Electrostatic factors in DNA intercalation. Biopoly 1999. *52.* 84–93.
10. Lockey, R.S.; Kwok. Y.; Guelev. V.: Pursell. C.J.: Hurley. L.H.; Iverson. B.L. A new class of polyintercalating molecules. J. Am. Chem. Soc. 1997. *119,* 7202–7210.
11. Alberts, B. DNA replication and recombination. Nature 2003. 421, 431–435.
12. Bustamante. C.: Bryant. Z.: Smith. S.B. Ten years of tension: Single-molecule DNA mechanics. Nature 2003, *421.* 423–427.
13. Trubetskoy. V.S.: Budker. V.G.: Hanson. L.J.: Slattum. P.M.; Wolff, J.A.: Hagstrom, J.E. Self-assembly of DNA-polymer complexes using template polymerization. Nuc. Acid Res. 1998. *26* (18). 4178–4185.
14. Summerer. D.: Marx. A. DNA-templated synthesis: More versatile than expected. Angew. Chem., Int. Ed. Engl. 2002, *41.* 89–90.
15. Yurke. B.: Turberfield, A.J.: Mills. A.P.: Simmel. F.C.; Neumann. J.L. A DNA-fuelled molecular machine made of DNA. Nature 2000. *406.* 605–608.
16. Kuhn, H.: Demidov. V.V.: Frank-Kamenetskii. M.D.

Topological links between duplex DNA and a circular DNA single strand. Angew. Chem.. Int. Ed. Engl. 1999. *38* (10). 1446–1439.
17. Hudson, B.; Vinograd. J. Catenated circular DNA molecules in HeLa cell mitochondria. Nature 1967. *216*. 647–652.
18. Breault, G.A.; Hunter. C.A.; Mayers. P.C. Supramolecular topology. Tetrahedron 1995, *55*, 5265–5293.
19. Seeman. N.C. Nucleic acids, nanostructures and topology. Angew. Chem.. Int. Ed. Engl. 1998. *37*. 3220–3288.
20. Du. S.M.; Stollar. B.D.; Seeman. N.C. A synthetic DNA molecule in three knotted topologies. J. Am. Chem. Soc. 1995. *117*. 1193–1200.
21. Chen. J.; Seemaa, N.C. The synthesis from DNA of a molecule with the connectivity of a cube. Nature 1991. *350*. 631–633.
22. Zhang. Y.; Seeman, N.C. Construction of a DNA-truncated octahedron. 3. Am. Chem. Soc. 1994. *116*. 1661–1669.
23. Holliday, R. A mechanism for gene conversion in fungi. Gen. Res. 1964. *5*. 282–304.
24. Seeman. N.C. DNA in a material world. Nature **2003,** *421*, 427–431.
25. Yan. H.; Zhang. X.P.; Shen. Z.Y.; Seernan. N.C. A robust DNA mechanical device controlled by hybridization topology. Nature **2002.** *415*. 62–65.
26. Kelley, S.O.: Barton. J.K. Electron transfer between bases in double helical DNA. Science 1999. *283*. 375–381.
27. Wan, C.Z.: Fiebig, T.: Schiemann. O.; Barton, J.K.; Zewail. A.H. Femtosecond direct observation of charge transfer between bases in DNA. Proc. Natl. Acad. Sci. U. S. A. **2000,** *97* (26), 14052–14055.
28. Braun. E.: Eichen. Y.: Sivan. U.; Yoseph, C.B. DNA-templated assembly and electrode attachment of a conducting silver wire. Nature 1998. *391*. 775–778.
29. Park. S.J.: Taton. T.A.: Mirkin. C.A. Array-based electrical detection of DNA with nanoparticle probes. Science 2002, *295*. 1503–1504.
30. Demers. L.M.: Ginger, D.S.; Park. S.J.: Li. Z.; Chung. S.W.: Mirkin. *C.A.* Direct patterning of modified oligonucleotides on metals and insulators by dip-pen nanolithography. Science **2002.** *296*, 1836–1838.

DNA Nanotechnology

Nadrian C. Seeman
New York University, New York, New York, U.S.A

r

INTRODUCTION

DNA nanotechnology is a new area of research. It has many goals, but few of its practical aims have been achieved. Nevertheless. the results obtained to date are encouraging and suggest that the application targets of the endeavor are within reach. Before going into the specific aims that the field seems well-poised to accomplish, it might be useful to explain just what DNA nanotechnology is, and where its niche is likely to lie. We all know that DNA is the genetic material of living organisms. DNA nanotechnology utilizes the features of DNA that enable it to function in this role, but the field is not exclusively a biologically oriented enterprise. It seeks to control the a chitecture of matter on the nanometer scale. with the aims of creating well-defined two-dimensional (2D) and three-dimensional (3D) molecular arrangements.

The key to DNA's biological role lies in the specificity of the base pairing that holds the two strands of the double helix together: adenine (A) pairs with thymine (T). and guanine (G) pairs with cytosine (C). The familiar double helix that results from these complementary interactions is a linear molecule. in the topological sense that its axis is not branched. However, by designing appropriate sequences for synthetic molecules, it is possible to produce more complex molecular topologies from synthetic strands,[1,2] for example. the branched DNA molecule, termed a "junction." shown in Fig. 1. The sequence of this molecule has been optimized so that the likelihood of the four strands associating as shown is very high. In addition. twofold symmetry is forbidden about the branch point to prevent its relocation via an isomerizaiion known as branch migration.

DNA NANOTECHNOLOGY COMBINES BRANCHED DNA WITH INTERMOLECULAR COHESION THAT USES BASE PAIRING

Genetic engineers frequently produce their constructs by using DNA molecules that contain short overhangs on one end or the other of their double helices. These overhangs, known as sticky ends. will bind with their complements in solution to produce concatenated species that cohere by hydrogen bonding; if desired, DNA ligase can seal the nicks in these complexes to convert them to covalent molecules.[3] Thus, specific intermolecular associations between DNA components can be designed by the simple method of designing complementary sticky ends. It is important to recognize that sticky-ended cohesion is not merely a means of generating programmed affinity. Sticky ends form the classical B-DNA structure when they cohere; thus, the 3D structure near the point of cohesion is known, without need for further characterization.[" In this article, attention will be confined to those instances in which tight structural control of this sort is inherent to the molecular design.

DNA nanotechnology combines the two concepts of programmable intermolecular assembly using sticky ends with DNA topologies based on branched molecules. The addition of sticky ends to branched molecules produces components that can lead to association and ligation products more complex than could be obtained from linear DNA. These products include stick polyhedra, knots and catenanes, and devices and networks. A simple example is shown in Fig. 2, where four identical branched molecules containing sticky ends are assembled into a quadrilateral. The edges are double helical DNA, and the vertices correspond to the branch points. The quadrilateral has open valences on the outside, so the construct could be extended, in principle. to produce an infinite array. The arsay could be two-dimensional. as suggested by the drawing. or three-dimensional. The scale of DNA is important to keep in mind. The B-DNA double helix is about 20 Å wide. and its helical repeat is 10–10.6 nucleotide pairs for a pitch of 34–36 Å. Thus. constructions made from DNA will have features on the nanoscale.

DNA NANOTECHNOLOGY SEEKS TO BUILD USEFUL ARCHITECTURES ON THE NANOSCALE

What is the value of producing DNA objects, devices, and arrays'? Several applications have been suggested. The original motivation for the program was based on the

Encyclopedia of Supramolecular Chemistry
DOI: 10.1081/E-ESMC 120012867

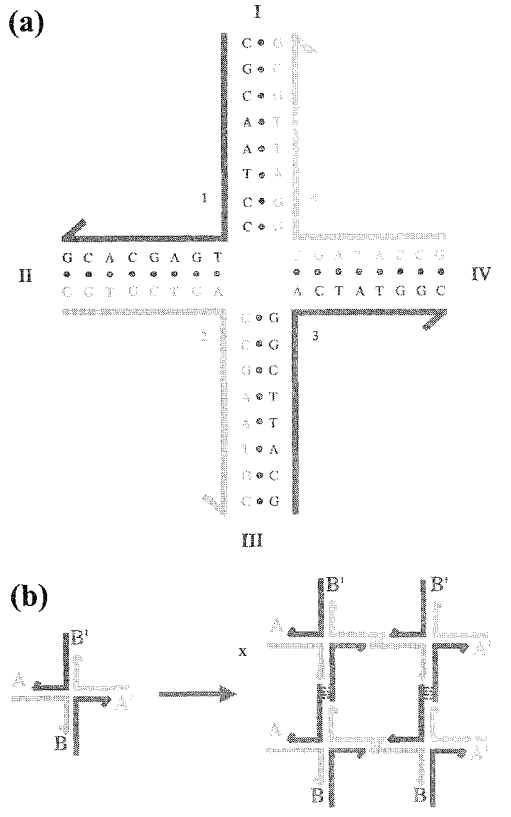

Fig. 1 (a) A branched molecule with four arms. The four strands labeled with Arabic numerals combine to produce four arms, labeled with Roman numerals. The branch point of this molecule is fixed by lack of twofold sequence symmetry. (b) Formation of a two-dimensional lattice from a four-arm junction with sticky ends. A is a sticky end, and A' is its complement. The same relationship exists between B and B'. Four of the monomeric junctions on the left are complexed in parallel orientation to yield the structure on the right. DNA ligase could close the gaps in the complex, Note that the complex could be extended by the addition of more monomers. (*View this art* in color *at www.dekker.com.*)

notion that spatially periodic networks are crystals.[1] The ability to build stick-figure crystalline cages on the nanometer scale could be used to orient other molecules as guests inside those cages, thereby rendering their structures tractable to diffraction analysis. as shown in Fig. 2a. Using the same logic, one could use the architectural properties of branched DNA to position and orient components of molecular electronic devices with nanometer-scale precision,[5] as shown in Fig. 2b. DNA nanomechanical devices will eventually lead to robotics on the nanometer scale. with applications in molecular fabrication and assembly. In addition. the motifs produced by DNA nanotechnology appear to be useful for DNA-based computation and the algorithmic assembly of materials.[9,10] Finally, DNA objects offer the possibility for self-replication, although the only route yet suggested to self-replicating branched DNA systems is somewhat oblique."[11]

THE REASONS TO USE DNA AS A MEDIUM FOR NANOARCHITECTURE

The key reason for using DNA to make nanoscale constructs is that DNA sticky ends provide the most predictable. diverse, reliable, and programmable set of intermolecular interactions available. In contrast to other molecules their scale. e.g., proteins, it is simple to program associations between specific molecules through

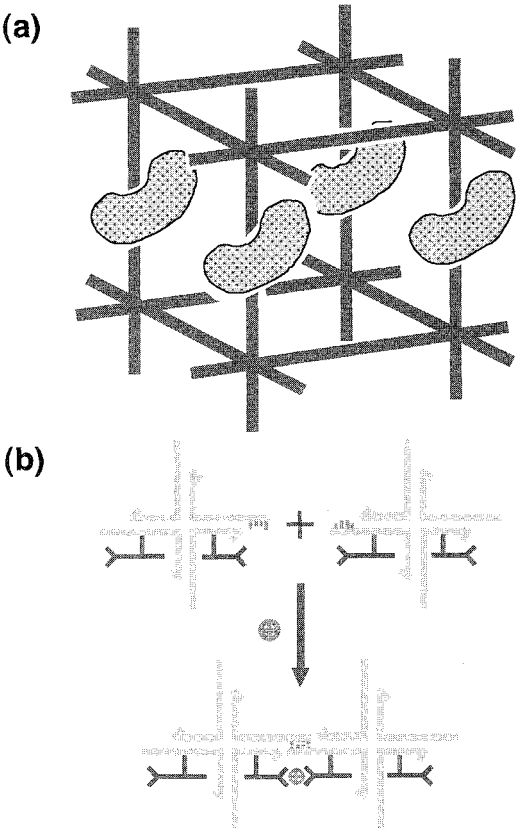

Fig. 2 Future applications of DNA nanotechnology. (a) A guest in a simple cubic lattice. The DNA lattice is drawn as a portion of simple cubic lattice made from 6-arm junctions. The guests are represented by the kidney-bean-shaped features in every unit cell. (b) DNA as scaffolding. Two branched junctions are shown. and a molecular wire is attached to them. When the two junctions cohere with each other. so does the molecular wire, which forms a synapse. (*View* this *art in* color *at www. dekker.com.*)

complementarity. In addition. convenient automated phosphoramidite chemistry[12] permits the assembly of arbitrary sequences containing 100 or more conventional or modified nucleotides. Likewise. it is key that DNA molecules can be manipulated by commercially available modifying enzymes. such as ligases. restriction endonucleases, exonucleases, or topoisomerases. The long persistence length of DNA (--500 A, or ~15 turns) ensures a stiff segment[13] when one uses lengths consisting of two to three double helical turns. DNA also contains an externally readable code''] that ultimately may be used to position and orient scaffolded molecules within arrays. Although most effort today is devoted to conventional DNA molecules. there are many variants that may be used ultimately in specific applications.[15] It is also worth noting that DNA has a very high density of functional groups: consequently, any given molecular motif may be decorated richly with derivatives.

MOTIF GENERATION

The key operation in generating motifs used in DNA nanotechnology is reciprocal exchange between two different strands.[2] This operation can be performed between strands of the same or different polarities, leading to parallel or antiparallel helices. These terms are derived from the biological recombination literature. but they really refer to the relative phasing between two adjacent helices. Illustrated in Fig. 3 is this operation at the top. and shown on the bottom are useful molecules derived from this operation. two double crossover (DX) molecules. a double crossover molecule with an extra junction (DX + J), and a triple crossover (TX) molecule.

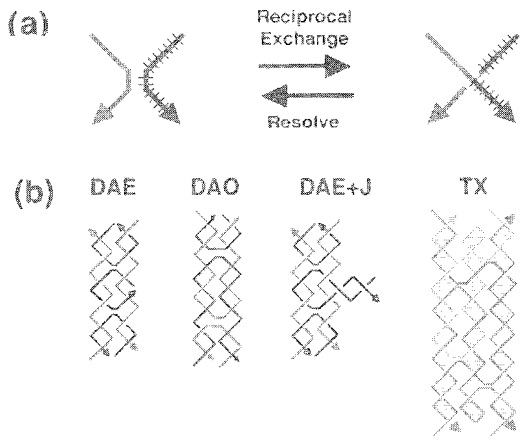

Fig. **3** Complex DNA Motifs. (a) Reciprocal exchange. Two strands are juxtaposed on the left. Arrowheads indicate their 3' ends. After reciprocal exchange, each resulting strand consists of a mixture of the two initial strands. (b) Rigid DNA motifs. The DAE and DAO motifs are generated by double reciprocal exchange between two helices. The separation of the crossover sites is an even number of half-turns in DAE and an odd number of half-turns in DAO. DAE + J contains an extra DNA domain: when this domain is oriented perpendicular to the plane of the other helix axes. it can be detected by the AFM. The base pairs are indicated in the triple crossover motif. (*View* this art in color *at www.dekker.com.*)

SEQUENCE SELECTION

We noted above the designing stable branch points requires avoiding twofold symmetry. In addition, the design of junction sequences entails the elimination of sequence symmetry among contiguous nucleotide groups. Sequences are divided into a series of overlapping 4–6 nucleotide elements, and repeated elements are forbidden during the sequence selection process; likewise. the complements to all elements flanking branch points are also avoided.''.''' This approach aims to eliminate all possible alternative structures that the system could assume: branched target molecules correspond to an excited state, and care must be taken to ensure that the excited product obtained is the one that is sought. The algorithm is a simplification of a more formal thermodynamic protocol,[17] and. with the motifs investigated so far, has proved remarkably successful in the design of DNA molecules containing branch points.

BRANCH FLEXIBILITY

The assembly of the quadrilateral product shown in Fig. 1b assumes not only that the sticky ends associate in a specific fashion. but also that the junctions maintain fixed angles between their double helical arms. Unfortunately, this assumption is not correct. Individual junctions have flexible angles around their branch points,[18,19] so rigid variants on simple branches must be used. The DX, DX + J, and TX molecules shown in Fig. 3 are systems in which this problem has been solved. They contain multiple branch points, with undistorted or minimally distorted helical domains. By contrast. control over the ligation products of single junctions is restricted to the topological level, and likewise, proof of synthesis is only topological and not geometrical. A group of single junctions with unique sticky ends can be joined to form discrete low-symmetry closed products, but rigid subunits

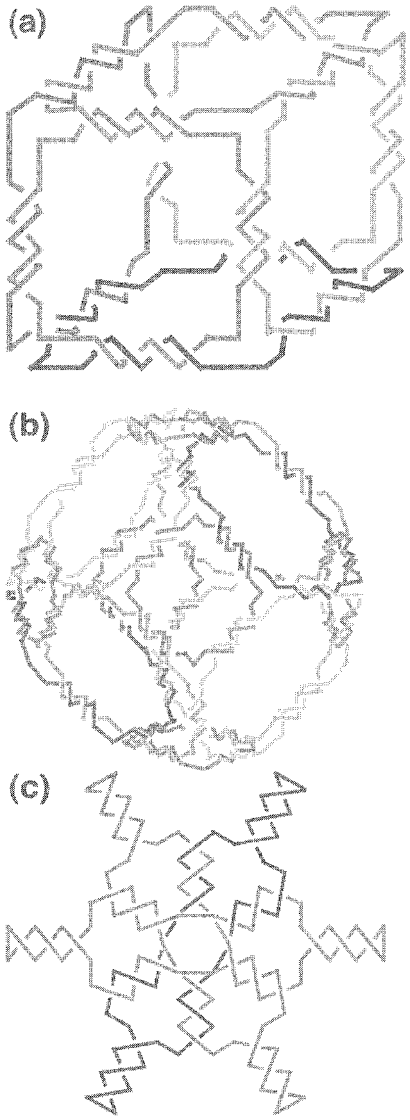

Fig. 4 Ligated linked products from flexible DNA components. (a) A stick cube and (b) a stick truncated octahedron. Each edge of the cube and the truncated octahedron contains two turns of double-helical DNA. The twisting is confined to the central portion of each edge for clarity. but it actually extends from vertex to vertex. (c) Borromean rings. Scission of any of the three rings shown results in the unlinking of the other two rings. (*View* ***this*** art *in color at www.dekker.com.*)

are necessary to form high-symmetry targets, such as periodic arrays.

POLYHEDRAL CATENANES AND KNOTS BUILT FROM SINGLE-BRANCH JUNCTIONS

Flexible single-branch junction building blocks have been used to construct a variety of topological targets. The first of these (Fig. 4a) is a DNA molecule with heiix axes connected like the edges of a cube or a rhombohedron.[20] Each edge contains two turns of double-helical DNA; as a consequence of this design, each face corresponds to a cyclic single strand. Each of these strands is linked twice to each of its neighbors, resulting in a complex hexacatenane. The topology has been demonstrated by designing a unique restriction site in each edge and then digesting the product at those sites to yield predicted subcatenanes. Illustrated in Fig. 4b is a more complex DNA molecule, a molecule with the connectivity of a truncated octahedron[21] that was built using a solid-support-based methodology.[22] This figure contains 14 faces, six squares, and eight hexagons. Each edge contains two turns of DNA. so this molecule is a complex 14-catenane; its topology has been demonstrated by techniques similar to those used to prove synthesis of the cube.

The half-turn of DNA corresponds to the fundamental unit of braiding topology. the node or a crossing seen when a topological figure is projected in two dimensions.[23] This feature makes branched DNA a particularly useful component with which to build complex topological figures. The half-turn of right-handed B-DNA produces negative nodes, and a half-turn of left-handed Z-DNA[24] produces positive nodes. Borromean rings consist of a set of linked circles that completely unlink upon the scission of any one of them. Combining a three-arm branched junction built from B-DNA and a three-arm branched junction built from Z-DNA produces the three-ring Borromean rings shown in Fig. 4c.[25]

The convenience of DNA as a topological synthon has been taken advantage of in constructing a variety of DNA

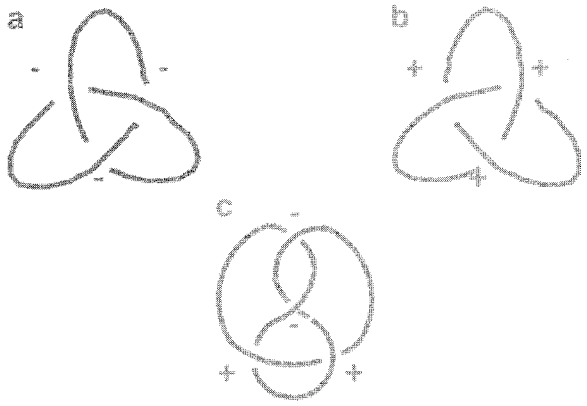

Fig. 5 Knots constructed from DNA. The signs of the nodes are indicated. A trefoil knot with negative nodes is shown in panel (a), a trefoil knot with positive nodes is shown on panel (b), and a figure-eight knot with two positive and two negative nodes is shown in panel (c). (*View this art in color at www.dekker.com.*)

knots. A trefoil knot with negative nodes is shown in Fig. 5a, and a trefoil knot with positive nodes is shown in Fig. 5b. An amphichiral figure-eight knot, with two positive and two negative nodes, has also been constructed: using B-DNA to produce the negative nodes and Z-DNA to produce the positive nodes (Fig. 5c). All of these knots can be produced from the same strand by varying conditions.[26] An RNA knot built similarly has been used to demonstrate that E. coli DNA topoisomerase III has an RNA topoisomerase activity.[27]

PERIODIC **ARRAYS** FROM **DNA MOTIFS**

The key goal of this system is to produce periodic (or aperiodic) assays from DNA motifs that can act as tiling elements in two or three dimensions. These tiles must be rigid components, because flexibility can lead to undesired structures. As noted above. the antiparallel DNA DX molecules. DAO and DAE and DAE + J (shown in Fig. 3b), have this property, as does the TX molecule shown there. Rigidity has been demonstrated experimentally for the DAF and DAE + J molecules[28] and inferred for the rest because of their successful use as tiling components. The two topological isomers of antiparallel DX molecules, DAO and DAE. differ by whether there are an odd (DAO) or even (DAE) number of double helical half-turns between crossover points. The DAE + J motif. consists of one or more bulged junctions positioned between the crossovers; the bulge consists of two nucleotides, with a presence that enables the stacking of the helix that is interrupted. The extra helix can act as a topographic marker in the atomic force microscope (AFM), when positioned so that it protrudes from the plane of the two DX helices.

Illustrated in Fig. 6 is a variety of two-dimensional arrays that have been formed from DNA tiles. Illustrated

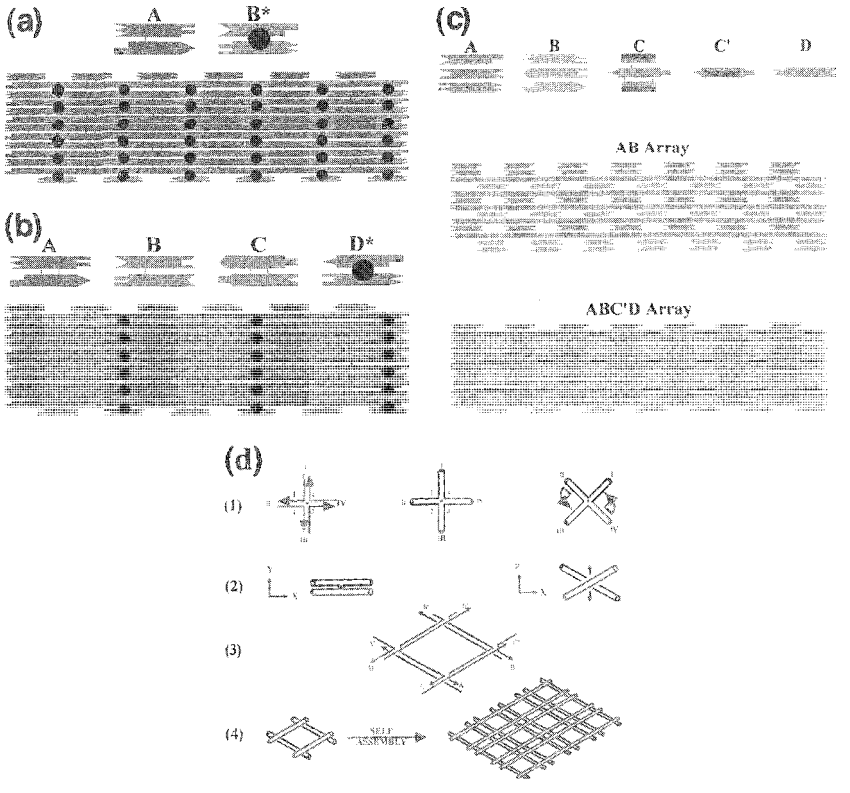

Fig. 6 Two-dimensional arrays assembled from DNA components. (a) A two-component array made from a DAE and a DAE + J motif. both 4 x 16 nm in this projection. where the extra domain is indicated by a filled black circle. Sticky ends are represented geometrically. (b) A four-component array. where the stripes occur every 64 nm. (c) An array made of two TX molecules (A and B), a rotated TX molecule (C'). and a double helix (D). (d) A four-arm junction can also be used to produce an array. (d.1) and (d.2) show that the four-arm junction assumes a two-domain structure, where the two domains are at an angle 60° to each other. Although flexible in its own right. four of them can produce a well-structured parallelogram (d.3) that can self-assemble into a 2D array (d.4). (*View this art in color at www.dekker.com.*)

in Figs. 6a and 6b are 2D arrays composed of DX and DX + J molecules. represented by A and **B***, respectively, in Fig. 6a; likewise, A. **B**, and **C** are DX molecules in Fig. 6b, whereas **D*** is a DX + **J** molecule. The dimensions of these tiles are about 4 nm x 16 nm, so the protruding stripe-like features on the DX + J tiles are separated by 32 nm in Fig. 6a and by 64 nm in Fig. 6b. Indeed. these features are readily apparent in AFM examination of these arrays.[29] These patterns may be modified by restriction. ligation, and hydrogen-bonded annealing.[30]

In Fig. 6c. patterns obtained from TX molecules are illustrated. At the top of the panel, one can see four molecules. A. B. **C**, and **D**. A and **B** are TX molecules that are connected 1–3 in the AB array illustrated below the individual molecules. This type of connection leads to gaps in the array. **D** is a simple double helix that can be fit into one of the gaps. **C** is another TX molecule, but it can be shifted by three nucleotide pairs from the phasing of A and B. This shift results in rotating it about 102°, nearly perpendicular to the array. This rotated molecule. called **C′**, can be fit into the gaps in the lattice that **D** does not fill. This arrangement provides a robust way of extending helices out of the A–B plane.[31]

In Fig. 6d, a different kind of array is illustrated—one made of DNA parallelograms. The single branch does not assume the conformation shown in Fig. 1 but rather folds, as illustrated in Figs. 6d.1 and 6d.2, to produce two stacking domains with an angle of about 60° between them. This angle is flexible, but when four of these junctions are assembled into a parallelogram. the angle focuses to its most favored value. These parallelograms yield an array containing cavities with sizes that can be tuned by design.[32]

ALGORITHMIC ARRAYS

The arrays described in the last section are all periodic arrays. Winfree suggested[9] that DNA molecules can be assembled in arrays based on algorithms more complex than simple periodicity. Thus, in principle, the self-assembly of DNA tiles can be used to generate complex arrangements, without using a unique tile for every component of the asyininetric unit. A preliminary test of this notion has been executed,[10] in which a one-dimensional cumulative exclusive OR (XOR) calculation was performed over four steps with high accuracy.

DNA NANOMECHANICAL DEVICES

DNA is not a static molecule. During its life cycle in the cell. it undergoes pairing, unpairing, cleavage. ligation. topoisomerization, branch migration, and changes of double helical structure. Hence. it seems reasonable to try to use DNA as the basis for nanomechanical systems. as well as fixed structural systems. The minimal mechanical device is a inolecule with a structure that switches between two alternatives in response to an external signal. Four such devices have been described to date. In the first, somewhat unwieldly system, the dimensions of a DNA cruciform were altered via branch migration, caused by the addition of ethidium to the solution.[33] Fhe first two-state device with a well defined structure is predicted on the B-Z transition of DNA.[34] Conventional DNA, known as B-DNA, is a right-handed molecule. However. there is another structure of DNA that is radically different from DNA, known as Z-DNA.[24] Z-DNA is a left-handed double helix. but it is not the mirror image of B-DNA. because it is also composed of sugars in the D-configuration. Two conditions must be met to obtain the Z-DNA structure: first is a sequence (called a proto-Z sequence) that can be converted from B-DNA to Z-DNA: the second is a solution environment that will promote the B → Z transition. The best-known of the proto-Z sequences contains alternating C and G [$(dCdG)_n$]. High ionic strength. and effectors such as $Co(NH_3)_6Cl_3$, can promote the B-Z transition.[24] The sequence requirement can be used to delimit the B-Z transition in space, and the environmental requirement can be used to delimit it in time. The device consists of two DAO molecules joined by a double-helical shaft that contains 20 nucleotide pairs capable of undergoing the B-Z transition. The operation of the B-Z device is illustrated in Fig. 7a.

Despite their appeal. the problem with both of the devices described above is that they are activated by small molecules. To approach nanorobotics succesfully. one needs many different devices incorporated into a larger matrix, such as the 2D arrays described above. However, both the cruciform and the B-Z devices are activated by small molecules. so that the action of these effectors could not be targeted easily to a specific device within the assay. Given the informational nature of DNA, it seems that sequence-dependent devices should be developed to fulfill this purpose. Two such devices have been developed, both based on the same principle of activation by strand addition and strand removal. This approach was pioneered by Yurke et al.[35] who developed molecular tweezers that were closed by adding a strand of DNA. The strand contained an unpaired segment and could be removed from the tweezers by the addition of its full complement; removal of the strand resulted in the tweezers relaxing to their open state.

A robust rotary device based on this principle has been developed using a new DNA motif, PX DNA, and one of its variants. JX_2 DNA. PX DNA consists of two parallel double helices, wherein crossovers occur at all possible sites:[36] two crossovers are absent in the JX_2 molecule.

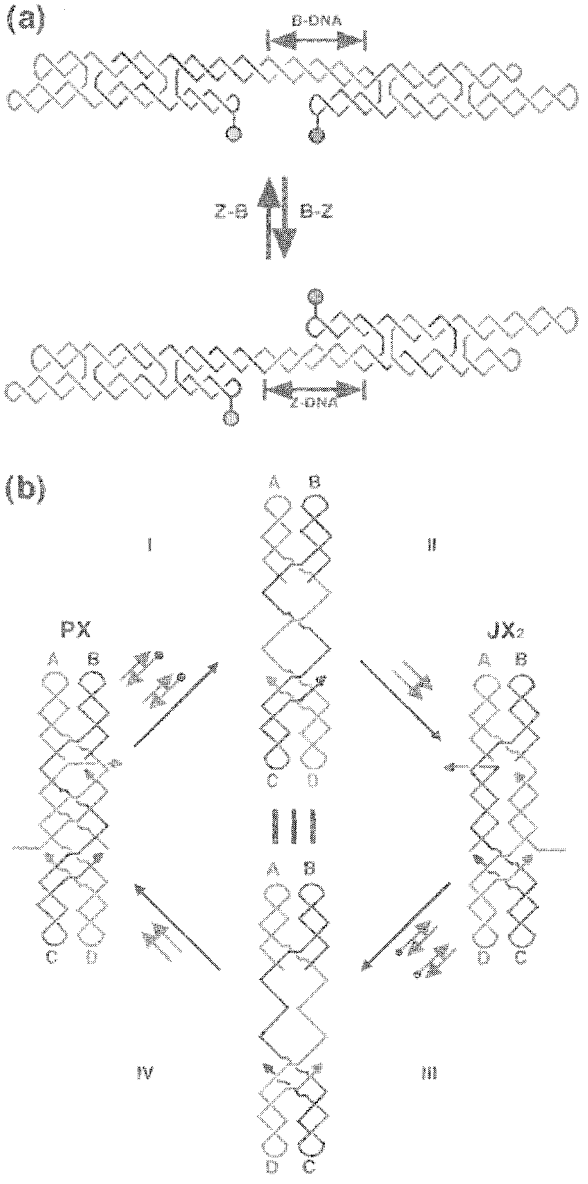

Fig. 7 DNA nanomechanical devices. (a) A device based on the B-Z transition. The device consists of two DNA DX molecules (DAO motif) connected by 4.5 turns of DNA between the nearest crossover points. The upper portion of the drawing illustrates the molecule constructed entirely from right-handed B-DNA. Fluorescent dyes are drawn schematically as filled (fluorescein) and unfilled (Cy3) circles attached to the free hairpins near the middle of the molecule. When this transition occurs. the two double crossover molecules change their relative positions. increasing the separation of the dyes. (b) A sequence-dependent device. This device uses two motifs. PX and JX_2. The labels A. B, C. and D on both show that there is a 180° difference between their total wrapping. There are two thick strands at the center of the PX motif. and two thin strands at the center of the JX_2 motif; in addition to the parts pairing to the larger motifs, each has an unpaired segment. These strands can be removed and inserted by the addition of their total cornplements (including the segments unpaired in the larger motifs) to the solution: these complements are shown in the processes I and III as strands with black dots (representing biotins) on their ends. Starting with the PX. one can add the complements strands (process I). to produce an unstructured intermediate. Adding the set strands in process II leads to the JX_2 structure. Removing them (III) and adding the PX set strands (IV) completes the machine cycle.

leading to a 180° rotation. These two motifs and the machine cycle are shown in Fig. 7b. The short strands at the centers of the PX and JX_2 molecules are set strands that set the state of the device. Starting from the PX device on the left, the addition of the complements to the set strands extracts them from the molecule, leading to an ill-defined intermediate at the top. The addition of the other set of strands puts the device in the JX_2 state, and return to PX is also available through the intermediate shown on the bottom. Many different groups of sequences can be used in the set strand regions. leading to many devices, all of which can be addressed individually.[36]

CONCLUSION

The experimental results described above augur well for the use of DNA self-assembly to produce structural targets on the nanometer scale. The resolution of control in this system is about an order of magnitude above the atomic scale; however, this is the scale on which the cell builds its structural components, and it is likely to be appropriate for biological goals, Among the challenges for DNA nanotechnology are to extend 2D periodic arrays to 3D. to extend algorithmic assembly to 2D and 3D systems, and to incorporate sequence-dependent DNA devices into those arrays. Although difficult. none of these goals seems to require chemistry beyond that already known for these systems. At some point. DNA must incorporate heterologous materials into the arrays, either biological macromolecular structures or nanoelectronic components. This incorporation will require further advances in the chemistry of these systems. DNA constructs appear potentially capable of self-replication, although the difficulties of combining branched systems with DNA polymerase are not likely to be simple.[37] Ultimately, DNA nanotechnology must advance from the biokleptic to the biomimetic, and from there to the abiological. This progression is likely to take some time, but the field appears to be gathering momentum, so the prospects are promising.

ACKNOWLEDGMENTS

The science described dbove represent, the efforts of many individuals. largely the coauthors of this writer I wish to thank all of them for their contributions to the founding of DNA Nanotechnology This work has been supported by grants GM-29554 from the National Institute of General Medical Sciences. N00014-98-1-0093 from the Office of Naval Research, NSF-CCR-97-25021 from DARPA/National Sctence Foundation, grants CTS-9986512, EIA-0086015, DMR-01138790, and CTS-0103002 from the National Science Foundation, and F30602-01-2-0561 from DARPA/AFSOR.

ARTICLES OF FURTHER INTEREST

Biomaterials. p. 110
Chemical Topology, p. 229
Concepts in Crystal Engineering: p. 319
Crystal Engineering with Hydrogen Bonds, p. 357
DNA as a Supramolecular Scaffold, p. 467
DNA Nanotechnology, p. 475
Hydrogen Bonding, p. 658
The Lock and Key Principle, p. 809
Molecular Logic Gates, p. 893
Molecular Squares, Boxes, and Cubes, p. 909
Molecular Switches, p. 917
Molecular-Level Machines, p. 931
Platonic and Archimedean Solids, p. 1100
Self-Assembling Catenanes, p. 1240
Self-Assembly in *Biochemistry*, p. 1257
Soft and Smart Material, p. 1302

REFERENCES

1. Seeman, N.C. DNA junctions and lattices. J. Theor. Biol. 1982, 99. 237–247.
2. Seeman, N.C. DNA nicks and nodes and nanotechnology. NanoLett. 2001, *1*. 22–26.
3. Cohen, S.N.: Chang. A.C.Y.: Boyer, H.W.; Helling, R.B. Construction of biologically functional bacterial plasmids in vitro. Proc. Natl. Acad. Sci. U. S. A. 1973, 70, 3240–3244.
4. Qui. H.; Dewan, J.C.; Seeman, N.C. A DNA decamer with a sticky end: The crystal structure of d-CGACGATCGT. J. Mol. Biol. 1997, 267, 881–898.
5. Robinson, B.H.; Seeman, N.C. The design of a biochip: A self-assembling molecular-scale memory device. Prot. Eng. 1987, *1*. 295–300.
6. Mao, C.; Sun, W.; Seeman, N.C. A DNA nanomechanical device based on the B-Z transition. Nature 1997, *386*, 137–138.
7. Yurke, B.: Turberfield. A.J.: Mills. A.P., Jr.; Simmel. F.C.; Neumann, J.L. A DNA-fueled molecular machine made of DIVA. Nature 2000. 406, 605–608.
8. Yan, X.; Zhang. X.; Shen, Z.; Seeman, N.C. A robust DNA mechanical device controlled by hybridization topology. Nature 2002. *415*, 62–65.
9. Winfree, E. On the Computational Power of DNA Annealing and Ligation. In DNA Based *Computer-s;* Lipton, R., Baum, E.. Eds.; American Mathematical Society: Providence, 1995: 199–215.
10. Mao, C.; LaBean, T.; Reif, J.H.: Seeman, N.C. Logical computation using algorithmic self-assembly of DNA

triple crossover molecules. Nature 2000. *407,* 493–496. *Erratum*: *Nature* 408, 750–750 (2000).
11. Seeman, N.C. The construction of 3-D stick figures from branched DNA. DNA Cell Biol. 1991, *10,* 475–486.
12. Caruthers, M.H. Gene synthesis machines: DNA chemistry and its uses. Science 1985. *230,* 281–285.
13. Hagerman, P.J. Flexibility of DNA. Ann. Rev. Biophys. Biophys. Chem. 1988. *17,* 265–286.
14. Seernan, N.C.: Rosenberg, J.M.: Rich. A. Sequence specific recognition of double helical nucleic acids by proteins. Proc. Natl. Acad. Sci. U. S. A. 1976, 73. 804–808.
15. Freier. S.M.: Altmann, K.-H. The ups and downs of nucleic acid stability: Structure-stability studies on chemically-modified DNA:RNA complexes. Nucl. Acids Res. 1997. *25.* 4429–4443.
16. Seeman, N.C. De novo design of sequences for nucleic acid structure engineering. J. Biomol. Struct. Dyns. 1990. *8,* 573–581.
17. Seernan, N.C.; Kallenbach, N.R. Design of immobile nucleic acid junctions. Biophys. J. 1983. *44,* 201–209.
18. Ma. R.-I.; Kallenbach. N.R.; Sheardy. R.D.; Petrillo, M.L.; Seeman, N.C. 3-Arm nucleic acid junctions are flexible. Nucl. Acids Res. 1986. *14.* 9745–9753.
19. Petrillo, M.L.: Newton, C.J.: Cunningham, R.P.: Ma, R.-I.; Kallenbach. N.R.: Seeman. N.C. The ligation and flexibility of 4-arm DNA junctions. Biopolymers 1988.27. 1337–1352.
20. Chen, J.; Seeman, N.C. The synthesis from DNA of a molecule with the connectivity of a cube. Nature (London) 1991. *350.* 631–633.
21. Zhang, Y.: Seeman. N.C. The construction of a DNA truncated octahedron. J. Am. Chem. Soc. 1994. *116.* 1661–1669.
22. Zhang, Y.; Seeman, N.C. A solid-support methodology for the construction of geometrical objects from DNA. J. Am. Chern. Soc. 1992, *114.* 2656–2663.
23. Seernan, N.C. The design of single-stranded nucleic acid knots. Mol. Eng. 1992. *2,* 297–307.
24. Rich, A.: Nordheim. A.: Wang. A.H.-J. The chemistry and biology of left-handed Z-DNA Ann Rev Biochem 1984. *53,* 791–846
25. Mao. C , Sun. W . Seeman, N C Assembly of Borromean rings from DNA Nature 1997. *386,* 137–138
26. Du. S.M.: Stollar, B.D.: Seeman, N.C. A synthetic DNA molecule in three knotted topologies. J. Am. Chern. Soc. 1995. *117.* 1194–1200.
27. Wang, H.; Di Gate. R.J.: Seeman, N.C. An RNA topoisomerase. Proc. Natl. Acad. Sci. U. S. A. 1996. *93,* 9477–9482.
28. Li. X.; Yang, X.; Qi, J.: Seeman, N.C. Antiparallel DNA double crossover molecules as components for nanoconstruction. J. Am. Chem. Soc. 1996. *118.* 6131–6140.
29. Winfree. E.; Liu, F.: Wenzler, L.A.: Seeman. N.C. Design and self-assembly of two-dimensional DNA crystals. Nature 1998, *394.* 539–544.
30. Liu, *F.;* Sha. R.: Seeman, N.C. Modifying the surface features of two-dimensioiial DNA crystals. J. Am. Chem. Soc. 1999, *121.* 917–922.
31. LaBean, T.; Yan, H.: Kopatsch. J.: Liu, F.: Winfree. E.; Reif. J.H.; Seeman, N.C. The construction. analysis. ligation and self-assembly of DNA triple crossover complexes. J. Am. Chem. Soc. 2000. *122.* 1848–1860.
32. Mao. C.: Sun, W.; Seeman, N.C. Designed two-dimensional DNA Holliday junction arrays visualized by atomic force microscopy. J. Am. Chem. Soc. 1999. *121,* 5437–5443.
33. Yang, X.: Vologodskii. A.V.; Liu. B.; Kemper. B.: Seeman, N.C. Torsional control of double stranded DNA branch migration. Biopolymers 1998, *45.* 69–83.
34. Mao. C.: Sun. W.: Shen. Z.: Seernan, N.C. A DNA nanomechanical device based on the B-Z transition. Nature 1999. *397.* 144–146.
35. Yurke, B.: Turberfield, A.J.: Mills. A.P.. Jr.: Simmel, F.C.: Neumann, J.L. A DNA-fueled molecular machine made of DNA. Nature 2000. *406.* 605–608.
36. Yan. H.; Zhang. X.; Shen. Z.; Seeman, N.C. A robust DNA mechanical device controlled by hybridization topology. Nature 2002. *415,* 62–65.

Drug Delivery

Saad A. M. Ali
Smith & Nephew Group Research Centre, York, United Kingdom

INTRODUCTION

The modes in which chemicals or drugs are administered have gained increasing attention in the past two decades. Normally, a *chemical is administered in a high dose at a given tiine only to have to repeat that dose several hours or days later. This is not economical and sometimes* results *in damaging side effects. As a consequence, increasing attention has been focused on* methods *of giving drugs continually for prolonged time periods and in a controlled manner. The primary method of accomplishing this controlled release has been through incorporating the chemicals within polymers. This technology now extends across many fields and includes pharmaceutical, food and* agricultural *applications, pesticides, cosmetics, and household products. In the pharmaceutical field; in addition to the importance of polymers, an understanding of the physiological barriers in the human body is also critical to developing appropriate* controlled-*release systems. The skin. the gastrointestinal tract, the lung, the nose, and the eye are of particular importance. Recent advances in genetic engineering produced numerous new polypeptide agents. Novel approaches for delivering and stabilizing these therapeutic molecules are being developed.*

BACKGROUND

Drug research has evolved and matured through several phases, beginning with the botanical phase of early human *civilization. through to the synthetic chemistry age in the middle of* the *20th century, and finally the biotechnology era* at *the dawn of the* 21st *century. Rapid developments in* molecular *biology, immunology, genetics. biochemistry, and information technology have converged and culminated* in *the deciphering of the human genome. Functional genomics and proteomics are likely to expand the therapeutic agents to incredible levels. once the gene–protein and protein–protein relationships are firmly established for the 5000–10.000 drug targets expected from the human genome map. In tandem. drug delivery has also progressed from conventional pills* to sustained/controlled *release and sophisticated* programmable *delivery systems. Meanwhile,* drug *delivery has also become more specific from* systemic *to organ and cellular targeting.*

Drug *discovery and development has* undergone *a paradigm shift from serendipity to a more rational approach. However, drug discovery remains a costly (US $400–650 million), time-consuming (10–15 years). and risky* process.[1] *As a consequence. new drug delivery systems have been developed at 20% of the cost and in half the time, which allows pharmaceutical companies to maximize the return on their investment, giving second life to old drugs, with better efficacy and patient* compliance.[2]

Since the formation of the pioneering companies in this area, Alza Corporation (U.S.A.) and Elan Corporation (Ireland), in the 1960s. more than 350 drug delivery and 1000 medical *device companies have come into existence, with worldwide drug delivery sales of US $22 billion.''' At the present rate of growth, the drug delivery market is expected to* comprise *20% of the total pharmaceutical market by* 2005.[2]

Novel drug delivery systems evolved over a period of time *to* improve *patient compliance and optimize the dosage regimen without* compromising *the therapeutic efficacy. The foundations were laid in 1952, with the introduction of the first sustained-release capsule of* Dexedrine.[4] Subsequently, *several concepts originated. including prolonged, timed, and extended release: and finally matured to controlled-release systems.*

MODES OF DELIVERY

Drug delivery covers a wide range of techniques used to deliver therapeutic agents into the human body. Many limitations have been recognized for the most widely used drug delivery techniques, those of the ingested tablet and *of the* intravenous/subcutaneous/intramuscular *injections. The ingested tablet delivers the drug into the blood only through the hepatic system. and hence; the amount in the bloodstream* may *be* much *lower than the amount formulated into the tablet, which results* in *low* bioavail-*ability;* furthermore, *liver damage is a side effect of many soluble tableted drugs. The injection mode of delivery can be used to deliver any size of drug molecules and* is *versatile in this regard, but it suffers from the disadvantages*

Encyclopedia of Supramolecular Chemistry
DOI: 10.1081/E-ESMC 120012797

of being invasive and painful and the shortness of duration of residence for drugs with short half-lives.

To address some of these limitations. other modes of delivery of drugs into the body were investigated in the early 1970s. Transdermal (through the intact skin), transmucosal (through the intact mucosa of the mouth, intestine, rectum. vagina, or nose), transocular (through the eye), transalveolar (inhalation, through lung tissue). implantable (subcutaneous and deeper implants, delivery into surrounding tissue). and injectable (intramuscular or subcutaneous) modes of delivery have been investigated extensively over the last 30 years, with varying degrees of commercial and therapeutic success.

Two other modes of injectable drug delivery are receiving increased attention. One focuses on the use of nanoparticles for delivering DNA or genes to cells for transfection. These particles have the unique ability to be taken up by targeted cells via various transcellular entry mechanisms. Another mode is needleless (and hence, painless) injectables. which are being explored.

The common features underlying these delivery modes are increased therapeutic efficiency and increased patient compliance.

FORMULATION REQUIREMENTS

The polymeric component of the delivery device is required to perform a set of functions in order to address some of the shortcomings of the most widely used forms of drug delivery. i.e., oral tablets and intravenous injections. The most important shortcomings are the duration of action and its relationship to the controlled release needed to achieve the desired plasma profile for the drug. In addition, the alternative delivery system must be acceptable to the patient (noninvasive) and must increase the level of patient compliance. Thus, the polymeric component is required, in these alternative drug delivery approaches. to extend and control the release of the drug into the bloodstream via various portals of entry (skin, oral mucosa, etc.). The primary role of the polymer is diffusional control of active agents, and the secondary role is disintegration or dissolution control of the dosage form employed.

ORAL DELIVERY

Among all routes of administration, the oral route has been most widely used and successful. This is. in part, because of the inherent simplicity of the oral route and oral delivery systems. On the other hand. the oral route is constrained by short and variable gastrointestinal tract and the size of the system.

Dissolution-Controlled Release

Dissolution-controlled release can be achieved by slowing the dissolution rate of a drug in the gastrointestinal medium, incorporating the drug in an insoluble polymer, and coating drug particles or granules with polymeric materials of varying thicknesses. The rate-limiting step for dissolution of a drug is the diffusion across an aqueous boundary layer. The solubility of the drug provides the source of energy for drug release, which is countered by the stagnant-fluid diffusional boundary layer.

Drug delivery using rate of dissolution as a controlled release mechanism can be achieved by encapsulation of a drug-polymer matrix with a relatively insoluble polymeric membrane. The coated beads can be compressed into tablets or capsulated, as was done with the Spansule® products.[5] Because the time required for the membrane coat to dissolve is a function of membrane thickness, granules with varying thicknesses can be employed to achieve sustained release of the drug. Examples of drugs delivered in this manner include antispasmodic-sedative combinations,[6] phenothiazines,[7,8] and anticholinesterase agents.[9]

One of the most common approaches used to achieve sustained release is to incorporate a drug in a hydrophobic matrix, such as wax, polyethylene, polypropylene. and ethylcellulose. or in a hydrophilic matrix, such as hydroxypropylcellulose. hydroxypropylmethylcellulose, methylcellulose. and sodium carboxymethylcellulose. The rate of drug release is controlled by the rate of penetration of the dissolution fluid into the matrix.

Diffusion-Controlled Release

Diffusion of a drug molecule through a polymeric membrane forms the basis of these controlled drug delivery systems. Similar to the dissolution-controlled systems, the diffusion-controlled devices are manufactured by encapsulating the drug particle in a polymeric membrane or by dispersing the drug in a polymeric matrix. Unlike the dissolution-controlled systems, the drug is made available as a result of partitioning through the polymer.

Another configuration of diffusion-controlled systems includes matrix devices, which are common because of ease of fabrication. Diffusion control involves dispersion of drug in either a water-insoluble or a hydrophilic polymer.[10–13] For instance, bupropion hydrochloride (Zyban®, GlaxoSmithKline) is formulated using carnuba wax and hydroxypropylmethylcellulose.[13]

Osmotically-Controlled Release

Theeuwes et al.[14] developed an elementary osmotic pump to achieve controlled drug delivery. The delivery of

the drug from the system is controlled by solvent influx across a semipermeable membrane. which in turn carries the drug outside through a laser-drilled orifice. The osmotic and hydrostatic pressure differences on either side of the semipermeable membrane govern fluid transport into the system.

Oral controlled-release forms generally involve either dispersing the drug into a polymeric matrix or encapsulating the drug containing core or granules with a rate-controlling membrane. Several techniques, such as wet granulation. spray drying, or spray congealing, are being used in the manufacture of oral controlled-release products.[15]

Despite great strides in the development of successful commercial oral novel drug delivery systems for small molecules, delivery of macromolecules is still a remote goal. Nevertheless, there are a number of emerging approaches[16] to deliver macromolecules, which include stabilizing the macromolecules in the harsh environment of the gastrointestinal tract (GIT) and increasing the membrane permeability, either by using of sorption promoters or exploiting natural carrier systems in the GIT.[17,18] A promising strategy from Emisphere Technologies Inc. uses small synthetic molecules, consisting of both α and non-α amino acids capable of interacting reversibly with macromolecules and facilitating their membrane permeability.[19] Various prodrugs of peptides and proteins have been explored to improve the proteolytic stability as well as membrane permeability.[18] Efforts are also focused on oral gene delivery for both systemic and local action; however, there are several critical issues that need to be addressed to improve their bioavailabilities.[20]

NASAL DELIVERY

Of all the mucosal, nasal mucosa is considered to be the most permeable, offering tremendous scope for peptide delivery, particularly for vaccines (90% of pathogens invade via mucosa).[21,22] Already, several peptide formulations are on the market. and further developments will depend on clarifying the immunogenicity of bioactive agents on the nasal mucosa and the long-term effect of enhancers on the nasal mucociliary activity.

PULMONARY DELIVERY

The lung also offers an exciting opportunity for systemic delivery because of the enormous surface area and rich blood supply.[23] However, the major limitations are high-dose requirements and low efficiency of deposition on alveolar surfaces. Although it is possible to design aerosol particles of desired characteristics using supercritical fluid technology,[24] improved aerosol design awaits further progress. Unlike the pressurized metered dose inhalers. new dry powder inhalers are breath-activated, deriving the energy from the patient's inhalation.[25] However, the real commercial feasibility of the pulmonary route for macromolecules will only be realized when inhaled insulin reaches the market.

TRANSDERMAL DELIVERY

Because of significant obstacles posed by the oral route. focus has shifted to alternative routes of administration, of which the transdermal route has generated much interest, beginning with the introduction of the scopolamine patch in 1983. Since then, only eight drugs have been commercialized, with a market share of US $2 billion, indicating that drug delivery through the skin is also far from easy.[26] Chemical and physical enhancement techniques (iontophoresis. electroporation, sonophoresis, and high-speed powdered delivery) are under active investigation to expand the scope of drugs (in terms of size, lipophilicity, and charge) that can be delivered through the skin.[27] Iontophoresis, which uses a small electric current, offers promise for delivery of small peptides, but there are several developmental and skin-safety considerations that need to be resolved before reaching a stage of commercialization.[28] Newer approaches involving a synergistic combination of the above-mentioned enhancement techniques are evolving to deliver very large proteins, while at the same time overcoming the skin-toxicity issues.[29]

There are two designs in transdermal systems: membrane-controlled systems and matrix systems.[30] A brief discussion of the features of each is given below.

Membrane-Controlled Systems

This design consists of three major components: the drug reservoir. the rate-controlling membrane, and the adhesive. The drug permeates the membrane and the adhesive to reach the skin. The drug reservoir contains a solution of the drug and liquid excipients. One excipient used is an enhancer that permeates the layers to the skin, where it exerts its enhancing effects by modulating the skin permeability.

Matrix Systems

In this design, the adhesive performs the role of the drug reservoir. The drug and excipients are formulated into the adhesive, typically into adhesive solution, and the solvent is evaporated to yield the matrix film. The matrix-adhesive film is then laminated to a backing film.

The main factors limiting the progress of transdermal technology are the ability to push small molecules through the skin faster and the problems associated with sensitization from certain drug classes. Advancement will occur through the development of new enhancers. Co-administration of immune suppressants or modification of drug structure to an immunologically inert form may be required to address the issue of sensitization.

IMPLANTABLE DELIVERY SYSTEMS

Implantable drug delivery systems are defined as long-term (>30 days) implantable products that are resorbable or removable. The resorbable implants are injectables incorporating lyophilized microspheres. The removable version is typically a subcutaneous implant, requiring minor outpatient procedures for insertion and removal. The main commercialized product in this category is Norplant®, a contraceptive implant. Medtronic Corporation has two products in the implantable area that allow drug delivery into the intrathecal space (where the spinal fluid circulates). One of these products delivers baclofen for spasticity, and the other delivers anaesthetics for pain control. Both products utilize Medtronic's SynchroMed® infusion pump, which can be electronically programmed to deliver any type of preset dose.

MICROPARTICLE AND NANOPARTICLE DELIVERY SYSTEMS

Microparticles and nanoparticles incorporate drug in matrix or encapsulated form, delivered to the body via injection (intramuscular; intravenous. or subcutaneous), via the oral cavity or via the nose. For nasal or oral delivery. the particles are typically in the 20–100 μm size range, because smaller particles can be inhaled and may make their way to the lung for alveolar delivery. For injectable delivery, to achieve prolonged duration of effect, the particles tend to be in the 50–100 μm range. Nanoparticles are classified as having diameters below I μm and tend to be used specifically for targeted delivery, usually via the injectable route.

SYSTEMIC AND LOCAL DELIVERY

Parenteral administration (injection). which is the immediate option for orally undeliverable drugs. has advanced greatly in recent years for systemic and local drug delivery.[31] The novel drug delivery system has metamorphosed from simple polymer and antibody conjugates to sterically stabilized colloidal systems. Liposomes and nanoparticles can improve pharmacokinetic-pharmacodynamic profiles of antibiotics (e.g., aminoglycosides and fluoroquinolones) and antifungal agents with enhanced intracellular accumulation and activity against dormant forms.[32]

Now, it is possible to deliver antineoplastic agents, toxins, proteins and peptides, and antisense oligonucleotides by conjugating to polymers such as polyethylene glycol or hydroxypropyl methacrylate, or by entrapping them in colloidal carriers leading to a decrease in the clearance of drugs and offering protection against hostile plasma constituents. This passive targeting of antineoplastic agents to tumors is based on the leaky vasculature hydrodynamics and enhanced permeation and retention effect. On the basis of this principle, styrene maleic acid neocarzinostatin, a polymer conjugate, has been approved for the treatment of primary hepatoma.[33] Further. to augment targeted therapy of tumors, cytotoxic agents and radioisotopes can be conjugated to antibodies.[34]

Local delivery for cancer therapy is accomplished using biodegradable polymeric systems or infusion pumps, where the drug is distributed throughout the tumor by passive diffusion, leading to increased drug levels at the tumor site and thereby minimizing systemic burden.[35] FeRx Corporation is developing magnetic-targeted systems, which make use of elemental iron magnets with drug adsorbed to the surface of carriers. These carriers that localize within tumors because of the applied magnetic field are being developed for the treatment of metastatic liver cancer.[36] Delivery of drugs for treatment of central nervous system (CNS) disorders is challenging because of the significant barriers posed by the blood-brain barrier (BBB) and the blood cerebrospinal fluid barrier.[37] Drug delivery to the brain has been attempted by targeting drug-and growth-factor-conjugates/liposomal formulations to specific transporters in the BBB. The discovery of cell-penetrating peptides (penetratin, transportan) has opened the scope for cellular delivery of drugs and macromolecules across the BBB and other biological membranes.[38] Chemical approaches using retro-metabolic design (soft drug-and chemical-delivery systems) offer the promise of targeting drugs to the brain.[39] Gene therapy using viral (retrovirus and adenoviruses) and nonviral (cationic liposomes and DNA-ligand complexes) vectors is gaining momentum for the transfer of genetic information to target cells; enabling them to synthesize the protein encoded by the gene.[40]

SUPRAMOLECULAR STRUCTURES

Micelles self-assembled from amphiphilic block copolymers have attracted interest because of their ability to solubilize hydrophobic molecules in water.[41,42] Interest is particularly keen in the context of drug solubilization,

where many existing drugs and many new ones coming out of drug discovery lack water solubility. Efforts focused on the synthesis of micelle-forming block copolymers that can be safely administered to humans and that can adequately solubilize drugs.[43]

Nanocapsules for controlled drug delivery are being developed using supramolecular structures. These capsules are made from polyelectrolyte multilayers and are produced using a patented process called layer-by-layer deposition.[44] The building blocks are naturaily occurring charged polymers. such as pectins. gelatins, polyglutamic acid. chitosan, and hyaluronic acid. These are adsorbed around the drug particle in alternating layers of oppositely charged material. The supramolecular structure is held together electrostatically through the formation of complexes between the polycations and polyanions. The resulting capsules have a wall thickness of 10–40 nm and range from 20 nm–20 mm in diameter, with the exact size controlled via the production process. Their physical, chemical, and pharmacokinetic properties can be manipulated as required by varying the polymers used and incorporating other materials into the layer structure, including lipids, nanoparticles. and biological molecules. such as ligands or receptors. Drug particles can be carried in the lumen of the capsule or incorporated into the wall layers.

FUTURE PROSPECTS

One of the most recent developments is the use of microchips as controlled drug delivery devices.[''' This novel technology is based on tiny silicon or polymeric chips containing hundreds or thousands of microreservoirs, each of which can be filled with any combination of bioactive agents. In this way. complex release patterns can be achieved with programmed microprocessors.

CONCLUSION

Novel delivery strategies have begun to diversify outside the realm of mere drug delivery to tissue engineering and diagnostics. In tissue engineering, controlled-release concepts are being applied for the delivery of growth factors to nurture the cells encapsulated in biocompatible polymers so as to expedite tissue regeneration.[46] Diagnostic application can be exeinplified by the recent premarket approval granted by the U.S. Food and Drug Administration (US FDA) for a blood-glucose-monitoring device (Glucowatch™) that can extract glucose through skin using reverse iontophoresis coupled to an enzyme-based detection system.

ARTICLES OF FURTHER INTEREST

Biomaterials, p. 1*10*
Collagens, p. *295*
Dsug Delivery, p. *484*
Gels, p. *586*
Micelles and Vesicles, p. *861*
Supramolecular Polymers, p. *1443*

REFERENCES

1. Chess. R. Economic aspects of drug delivery. Pharm. Res. **1998**. *15.* 172–174.
2. Speers, M. Economic Aspects of Controlled Drug Delivery. In *Encyclopaedia* of Controlled Drug *Delivery*; Mathowitz. E.. Ed.: John Wiley and Sons: New York. 1999: Vol. 1, 341–347.
3. Verma, R.K.; Garg. S. Current status of drug delivery technologies and future directions. Pharm. Technol. 2001, *25.* 1–14.
4. Stan, C. Innovations in drug delivery. Patient Care 2000, *15.* 107–137.
5. Benita, S.; Donbrow, M. Release kinetics of sparingly soluble drugs from ethylcellulose walled microcapsules. Theophylline microcapsules. J. Pharm. Pharmacol. **1982**, 34, 547–551.
6. Steigmann. F.; Kaminski. L.; Nasatir. S. Clinical-experimental evaluation of a prolonged acting antispasmodic-sedative. Am. J. Dig. **1959**. 4. 534–544.
7. Mellinger, T.J. Serum concentration of thioridazine after different oral medication forms. Am. J. Psychiatry **1965**, *121,* 1119–1139.
8. Wollister, L.E. Studies of prolonged action medication. 11. Two phenothiazine tranquilizers (thoradizine and chlorpromazine) administered as coated tablets and prolonged action preparation. Curr. Pharm. Ther. 1965. *6,* 486–496.
9. Magee, K.R.: Westerberg, M.R. Treatment of myasthenia gravis with prolonged-action mestinon. Neurology 1959, 9. 348–368.
10. Viega, F.; Salsa. T.; Pina. M.E. Oral controlled release dosage forms. Part 2. Glassy polymers in hydrophilic matrices. Drug Dev. Ind. Pharm. 1998. 24 (1), 1–10.
11. Viega, F.; Salsa, T.; Pina. M.E. Oral controlled release dosage forms. I. Cellulose ether polymers in hydrophilic matrices. Drug Dev. Ind. Pharm. 1997. *23* (9), 929–938.
12. Khan. M.A.: Reddy, I.K. Controlled drug delivery development of solid oral dosage forms with acrylate polymers. STP Pharm. Sci. 1997. 7 (6), 483–493.
13. *Physician's* Desk *Reference*, 53rd Ed.; Medical Economics: Oradell, NJ, 1999: 1277.
14. Theeuwes. F.: Higuchi. T. Osmotic Dispensing Device with Maximum and Minimum Sizes for the Passageway. US Patent 3,916,899, November 4. 1975.
15. Venkatraman. S.; Davar. N.: Chester. A.; Kleiner, L. An Overview of Controlled Release Systems. In *Handbook* of *Pharmaceutical Controlled* Release *Technology*; Wise, D.L., Ed.: Marcel Dekker: New York. 2000: 431–463.

16. Sood. A.; Panchagnula, R. Peroral route: An opportunity for protein and peptide delivery. Chem. Rev. 2001. 101 (11), 3275–3303.
17. Sharnia. P.; Chawla. H.P.S.: Panchagnula. R. The role of sorption promoters in increasing the bioavailability of drugs in oral preparations. Drugs Future 1999. *24.* 1221–1240.
18. Orellana, I.G.; Paton, D.R. Advances in oral delivery of proteins. Exp. Opin. Ther. Pat. 1998. 8, 223–234.
19. Bay. A.L.: Paton, D.R.; Eeidner. J.J. The development of delivery agents that facilitate the oral absorption of macrornolecular drugs. Med. Res. Rev. **2000**, 20, 169–186.
20. Page. D.T.; Cudmore. S. Innovations in oral gene delivery. Drug Discov. Today 2001. 6. 92–101.
21. Patridos. C.D. Intranasal vaccines: Forthcoming challenges. Pharm. Sci. Technol. Today **2000**, *3*, 273–281.
22. Brayden, D.J. Vaccinology—The challenges for non-injected approaches. Pharm. Sci. Technol. Today 2000, 3, 115–117.
23. Gonda, I. The ascent of pulmonary drug delivery. J. Pharm. Sci. 2000, 89, 940–945.
24. York. P. Strategies for particle design using supercritical fluid technologies. Pharm. Sci. Technol. Today 1999. 2, 430–440.
25. Ashrst, I.; Malton, A.; Prime. D.; Sumy. B. Latest advances in the development of dry powder inhalers. Pharm. Sci. Technol. Today 2000. 3. 246–256.
26. Naik, A.; Kalia, Y.N.: Guy, R.H. Transdermal drug delivery: Overcoming the skin's barrier function. Pharm. Sci. Technol. Today 2000. 3. 318–326.
27. Pillai. O.; Nair. V.; Jain. A.K.: Thomas, N.S.: Panchangnula. R. Non-invasive delivery of peptides and proteins through skin. Drugs Future 2001. *26* (8), 779–791.
28. Panchagnula, R.: Pillai. O.; Nair. V.B.; Ramarao, P. Transdermal iontophoresis revisited. Curr. Opin. Chem. Biol. 2009, 4, 468–473.
29. Mitragotri. S. Synergistic effect of enhancers for transdermal drug delivery. Pharm. Res. **2000**, 17, 1354–1359.
30. Venkatraman. S.: Gale, R.M. Skin adhesives and skin adhesion 1. Transdermal drug delivery systems: A review. Biomaterials 1998, *19*, 1119–1136.
31. Cleland. J.L.: Daughtery. A.; Mrsny, R. Emerging protein delivery methods. Curr. Opin. Biotechnol. 2001. 12. 212–219.
32. Pinto-Alphandry, H.; Andermont, A.; Couvreur, P. Targeted delivery of antibiotics using liposoines and nanoparticles: Research and applications. Int. J. Antimicrob. Agents **2000**, *13*, 155–168.
33. Duncan. R. Polymer conjugates for tumour targeting and intracytoplasmic delivery. The EPR effect as a common gateway? Pharm. Sci. Technol. Today 1999. 2, 341–449.
34. Trail, P.A.; Bianchi, A.B. Monoclonal antibody conjugates in the treatment of cancer. Curr. Opin. Immunol. 1999, 11. 584–588.
35. Dhanikula, A.B.; Panchagnula, R. Localised paclitaxel delivery. Int. J. Pharm. 1999. *183*, 85–100.
36. Fricker, J.: Writer, F. Drugs with a magnetic attraction to tumours. Drug Discov. Today **2001**. 6, 387–389.
37. Bruke, M.; Langer, R.; Brem. H. Central Nervous System—Drug Delivery to Treat. In *Encyclopaedia* of *Controlled* Drug *Delivery*; Mathowitz E.. Ed.; John Wiley and Sons: New York. 1999; Vol. 1, 184–212.
38. Lindgren. M.; Hallbrink. M.; Prochiantz, A.; Langel, U. Cell-penetrating peptides. Trends Pharmacol. Sci. 2000. 21, 99–103.
39. Bodor, N. Chemical Approaches to Drug Delivery. In *Encyclopaedia of* Controlled *Drug Delivery*; Mathowitz, E., Ed.; John Wiley and Sons: New York, 1999; Vol. 1, 285–298.
40. Mountain. A. Gene therapy: The first decade. Trends Biotechnol. 2000. 18, 119–128.
41. Kwon, G.S.: Okano, T. Soluble self-assembled block copolymers for drug delivery. Pharm. Res. 1999. *16*. 597–600.
42. Kwon. G.S. Doblock copolymer nanoparticles for drug delivery. Crit. Rev. Ther. Drug Carr. Syst. **1998**. *15*, 481–512.
43. Lavasanifar, A.; Samuel. J.: Kwon, G.S. Micelles of poly(ethylene oxide)-*block*-poly(*N*-alkyl stearate L-aspartamide: Synthetic analogues of lipoproteins for drug delivery. J. Biomed. Mater. Res. **2000**, *52*. 831–835.
44. Donath. E. Novel hollow polymer shells by colloid-templated assembly of polyelectrolytes. Angew. Cheni., Int. Ed. Engl. 2998. 37. 2202–2205.
45. Santini. J.T.. Jr.; Richards, A.C.: Scheidt. R.: Cima, M.J.; Langer. R. Microchips as controlled drug delivery devices. Angew. Chem., Int. Ed. Engl. 2000. *39*. 2396–2407.
46. Tabaia, *Y*. The importance of drug delivery in tissue engineering. Pharm. Sci. Technol. Today 2000. 3, 80–89.

D

Drug Design

Chung F. Wong
J. Andrew McCammon
University of California—San Diego, La Jolla, California, U.S.A.

INTRODUCTION

Computer-aided drug design is playing an increasing role in the development of pharmaceuticals. *Computers can now be used in* many *ways to aid the design of therapeutic drugs. Molecular graphics software running on powerful workstations can draw useful qualitative insights from the experimental structure of a receptor and its complex with ligands. Rapid advances in computer technology and computational chemistry facilitated the generation of quantitative data to help sort promising drug leads from real and virtual chemical libraries and to aid in rational drug design. These methods range from rigid structural models* employing simple *but easy-to-compute scoring functions to flexible structural models with sophisticated descriptions of intra- and intermolecular interactions. Structural predictions* programs *were developed to provide structural models of receptors when experimental structure is not yet available. Alternatively, useful insights into drug design can be obtained by conducting comparative analyses of a* number *of inhibitors that are known to bind to* a *receptor. This ligand-based approach can be used without knowledge of the three-dimensional structure of the receptor. Each approach has its pros and cons. and effective computer-aided drug design usually utilizes a* number *of methods. Mere, we give a* glimpse *of some of these approaches* with *a short selected list of references that aids interested readers in* further *exploring the subject.*

MOLECULAR MODELING

For a long time, *chemists learned and predicted the properties of molecules based on their structures. This has now gone beyond two* dimensions *to three and more, as the physical and* chemical *properties of a molecule obviously depend on how different* functional *groups of the molecule are presented in three-dimensional* (3D) *space at different* conformations. *These properties will; in turn, determine* whether *a* small *molecule binds favorably* to *a receptor and whether* the *molecule possesses drug-like characteristics. Molecular graphics help a drug designer visualize the three-dimensional structure of a receptor so that useful insight can be gained into what* molecules *may fit into a suitable pocket of the receptor so as to modulate its activity and achieve therapeutic effects. The receptor can be rendered in a variety of ways to aid in drug design. For example, molecular surfaces can be displayed to provide ideas of the shapes and sizes of different pockets. In addition, the surface can be colored according to the electrostatic potential to suggest where positively charged, negatively charged, and nonpolar groups of an inhibitor may fit into the receptor. Fast computers made it feasible to quickly obtain the electrostatic potentials surrounding a receptor by solving the Poisson–Boltzmann equation, taking into account the detailed shape of the* receptor,[1,2] *and to display the resulting potentials in high resolution. In Fig.* 1, *an* example *of the electrostatic potential calculated on the van der Waal surface of protein kinase* A *using the APBS program is given.''* Small *molecules can be displayed simultaneously and manually* docked *to different sites of a receptor, interactively. Molecular graphics also allows one to overlay structures of* similar *proteins on a graphics screen to facilitate comparison. Such visualization can provide useful insight into designing inhibitors that are selective toward the intended targets. A molecular editor embedded within a graphics* program *can be used to edit the inhibitor in a* receptor–*inhibitor complex to examine what modifications may be profitable in order to enhance interactions with the receptor. Based on the structural features of a binding pocket, one can also design three-dimensional* pharmaco*phore models*[i4,] *to help mine drug candidates from chemical libraries.*

Pharmacophore Model

A 3D *pharmacophore model contains features. arranged in 3D space, with which a* molecule *can act on a drug* target.[4] *These features include hydrogen-bond donors. hydrogen-bond acceptors, hydrophobic groups, and charged moieties. Knowing the structure of a suitable binding pocket of a receptor can generate such a pharmacophore* model *by putting suitable features near complementary groups on the receptor. One can then search a chemical database, which can be a virtual database containing cornpounds that have not yet been made, to find real or virtual molecules that match the*

Encyclopedia of *Supramolecular Chemistry*
DOI: 10.1081/E-ESMC 120012696

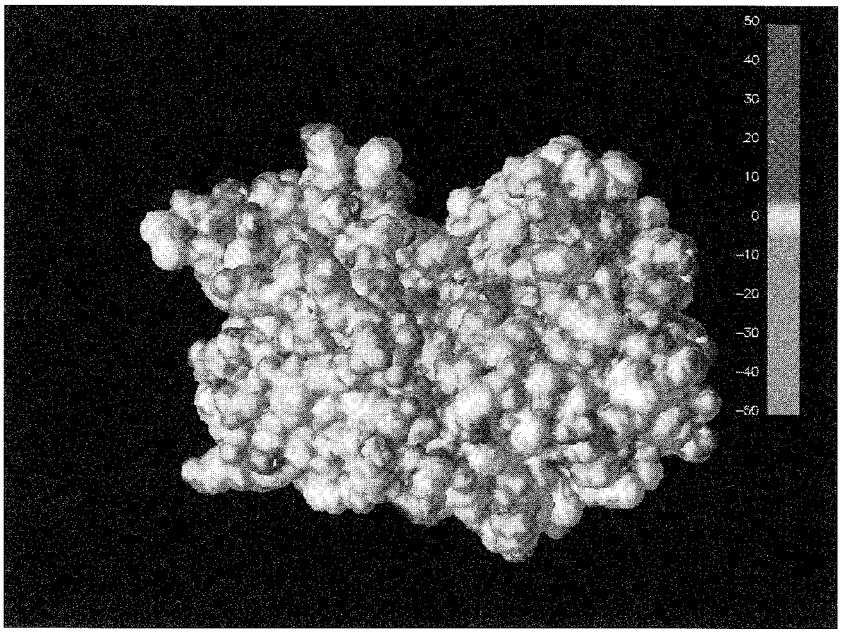

Fig. 1 Electrostatic potentials calculated on the van der Waals surface of protein kinase A

pharmacophore model and therefore may be active toward the desired receptor. Usually, many conformations of each compound in a library need to be generated and examined for fit to a pharmacophore model. Modern computing power can now permit thousands of compounds to be screened within hours. Higher-quality pharmacophore models can be constructed when the crystal structure of the complex of a receptor with one of its ligands was determined, as the coordinates of the ligand can provide a precise definition of the features of a pharmacophore. However, the interplay among many factors can sometimes complicate the development of pharmacophore models relying on visual inspection of crystal structures. For example, the mere presence of a functional group in the ligand in the vicinity of an apparently complementary group does not necessarily imply that these groups interact to enhance binding. This is partly because the binding of a ligand to a receptor is accompanied by the desolvation of ligand functional groups and receptor residues. For example, it is not obvious whether the formation of an intermolecular hydrogen bond upon complex formation can overcome the penalty associated with the desolvation of the hydrogen-bond donor and acceptor before the complex is formed. Quantitative calculations can remove these ambiguities. For example, one can calculate the binding free energy using a suitable computational model (some are discussed below) and knock out parameters of different functional groups of the ligand to examine whether they affect binding.[4,5] The truly significant functional groups can then be selected to construct a pharmacophore model. Quantitative calculations also allow one to quantify the relative significance of different pharmacophoric features and assign them different weights in mining chemical databases. Methods that dock simple molecules to a receptor can also aid the placement of different features of a pharmacophore. For example, Monte Carlo docking of methanol molecules to HIV integrase revealed possible sites for placing hydrogen-bond donors.[7]

Structure and Ligand-Based Models

When the structure of a receptor has not yet been determined experimentally, structural modeling of receptors and ligand-based approaches can be used. If a protein has a similar amino acid sequence as one previously determined, homology modeling can be carried out to construct a structural model for the target protein from the known structures. Here, one usually starts with a sequence alignment of the target protein with the proteins with structures that were determined. This will direct how the sequence of the target protein will be threaded into a template structure. The backbone coordinates are usually built first by simply taking the corresponding coordinates from a known structure. When more than one template is available, a structural alignment of the known structures can first be done to get an idea of which parts of the proteins are structurally conserved. These parts do not vary significantly from one template structure to another and the target protein is likely to have similar structure in

these regions. These portions of the structural model can be constructed most reliably. The other parts of the backbone, loosely called the loops, can then be built. If the sequence of a loop of the target is similar to one or more of the templates, one may use the template coordinates to build the structure of the loops. If the sequence of the loop is different from the ones in the templates, two approaches are commonly used. One is a database approach in which one searches from a structural database of proteins for loops with N and C termini that have similar local structures as the anchoring points in the corresponding structural conserved regions. Those loops that also have high sequence similarity to the loop of the target can then be used to build models for the loop if they do not overlap with the backbone coordinates that were already built. Another approach is to carry out conformational samplings that give low-energy structures. The energy is calculated based on models similar to those described below. A side chain can be built by taking coordinates from the templates, if they contain similar amino acids. If the side chain contains groups that cannot be built from the templates. a structure from a rotamer library can be tried. Energy refinement can then be carried out to further improve the model. Different algorithms may work somewhat differently. But the above descriptions summarize some key features of homology modeling. Swiss-Model[8] is an example of a Web-accessible resource that helps researchers build homology models.

Homology modeling only works when the target sequence is more than about 30% homologous to proteins in a structural database. When it is difficult to find proteins with significant sequence identity with the target, one can use methods such as threading. In a threading experiment, one threads the sequence of the target into template structures in a structural database, and a scoring function is used to help determine which threaded structures are more likely. A scoring function can be derived from a database approach in which residue–pair interaction potentials. for example, are determined by their probability of being observed in the database. Empirical force fields (described below) commonly used in molecular simulations can also be used. Once a structural model of the receptor is determined, pharmacophore models can be constructed using methods such as those described above. A recent article[9] gives an overview of several structural prediction methods.

Another way to construct pharmacophore models when the structure of a receptor is not known is to use a ligand-based approach. Here, one does not try to predict the structure of the receptor but focuses on analyzing similar and dissimilar features among a number of ligands that are known to act on a receptor. A long-used qualitative method is to simply draw the structure of a number of inhibitors along with their measured activity levels. Common features shared among them are likely important for their activities. Such a qualitative study of the structure–activity relationship (SAR) can be quantified with mathematical models. For example, one can express the activity of a number of bioactive compounds in terms of a set of descriptors:

$$activity = A[\log(P_{o/w})] + B[\log(P_{o/w})]^2 + C\sigma + DS + \ldots \quad (1)$$

where example descriptors include the partition coefficient of a compound between a nonpolar solvent and water $P_{o/w}$, the electron-withdrawing or -donating ability of a functional group a, and the size of a functional group S. Many such models with different descriptors can be constructed and evaluated for their abilities to explain a set of experimental data. The mathematical relationship provided by the best models can then be used to estimate the activity of compounds not yet synthesized. The best models also give useful insight into which features may be important for biological activity, by examining which descriptors remain in the model. Such studies on quantitative structure–activity relationship (QSAR). pioneered by Hansch,[10] went further into 3D QSAR,[11] in which the 3D conformations of compounds are taken into account. Here, one needs to spend extra effort on determining optimal structure–property alignment of a number of active compounds, and descriptors such as the 3D electrostatic field surrounding these compounds can be used.

Methods based on quantitative modeling of molecular interactions

There are also methods that rely on quantitative descriptions of the interactions between drug candidates and receptors. For example, molecular docking programs attempt to determine where a compound may bind to a receptor using sampling techniques that explore an interaction potential energy surface. A potential energy surface is often represented by a simple analytical function, such as the following:

$$V = \sum_{bond} \frac{1}{2} k_b (b - b_o)^2 + \sum_{angle} \frac{1}{2} k_\theta (\theta - \theta_o)^2 + \sum_{dihedral} k_\phi [1 + \cos(n\phi - \delta)] + \sum_{improper} \frac{1}{2} k_\omega \times (\omega - \omega_o)^2 + \sum_{pairwise} \left[\frac{C_{12}}{r^{12}} - \frac{C_6}{r^6} \right] + \sum_{pairwise} \left[\frac{q_i q_j}{r} \right]$$

The term "summing over bonds" describes the energy costs in compressing or stretching bonds. A Hook's-law-type relationship is commonly used to model these costs, in which b is a bond length; b_o is its corresponding equilibrium value: and k_b is the force constant. A similar term "summing over angles" is used to describe angle bending, with θ a bond angle, θ_o its equilibrium value, and k_θ its force constant. A periodic function is used to describe rotational energy profiles about bonds. The sum over dihedral angles involves a periodic cosine function with $n\phi - 6$ its argument. Here. ϕ is a dihedral angle, n is an integer determining how many maxima and minima there are in a span of 360°, and 6 is a phase factor. A harmonic improper dihedral term, with the parameters k„, and ω_o, is also used to keep aromatic rings approximately planer. tetrahedral groups nearly tetrahedral. etc.[6–12] Lennard–Jones potentials, with the parameters C_6 and C_{12}, depend on the distance between two atoms r and are often used to describe the attractive forces between them due to electronic dispersion effects and to keep the two atoms from crashing into each other. Finally, Coulomb terms, which depend on the charges of two interacting atoms, q_i and q_j, are used to describe the electrostatic interactions between the atoms. When solvent molecules are not included explicitly to save coinputational time, their effects on electrostatics are modeled by introducing additional screening functions to the Coulomb terms. More sophisticated ways of modeling solvation effects such as those based on solving the Poisson–Boltzmann equation[1,2] and on generalizing the Born models[12] were also developed.

Once a model for the potential energy function is adopted, a conformational search algorithm can be used to move a ligand around in the receptor to find its most favorable binding site. The potential energy surface has a complicated landscape and requires an efficient algorithm to go over energy barriers during a conformational search. Simulated annealing Monte Carlo or molecular dynamics is one method with which to do it. This involves heating and cooling a system, while the system is evolving according to a Monte Carlo or molecular dynamics simulation algorithm. Genetic algorithms were also used. In such algorithms, one represents a ligand state—involving position. orientation, and conformation—with "genes," such as a series of bits that encode a particular conformation. One first starts with a random population containing a ligand in different states. The population is then allowed to evolve by selection, mutation. and gene crossing. A fitness function, which can depend on the potential energy function described earlier. can be used to determine which states fit better and survive after many generations. Autodock[13,14] is an example of a docking program that can utilize a simulated annealing Monte Carlo method or a genetic algorithm.

Quantitative calculations based on rigorous principles of quantum mechanics and statistical mechanics were also performed to discriminate strong inhibitors from weak ones.[6] Rigorous theories for calculating binding free energy were worked out.[15] A general approach not only accounts for ligand but also receptor flexibility. However; such approaches are expensive to use and are harder to apply to a large number of systems in a short time. Nevertheless, they provide more rigorous theoretical frameworks for evaluating approximations used in simpler models and can be applied in the later stage of a drug development process, when only a small number of potential drug candidates need to be investigated in further detail.

One approach is the thermodynamic cycle-perturbation method that allows one to compare the relative binding affinity of a number of similar ligands.[16] This approach recognizes the difficulty in simulating the absolute binding affinity ΔG between a ligand and its receptor:

$$\Delta G = G_{complex} - G_{receptor} - G_{ligand} \tag{2}$$

In principle. one can calculate the free energy of the receptor $G_{receptor}$, the ligand G_{lig^2} & and their complex $G_{complex}$ to obtain AG. However, it is usually difficult to carry out simulations long enough to obtain sufficiently good statistics for the free energies, which have large magnitude and statistical errors. and add them according to Eq. 2 to obtain ΔG with a much smaller magnitude. The thermodynamics cycle-perturbation method avoids this problem by focusing on comparing the free energy of binding among similar ligands. It makes use of a thermodynamic cycle to facilitate the comparison between two inhibitors:

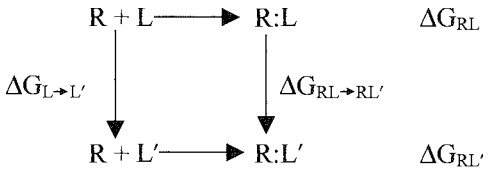

Because free energy is a state function:

$$\Delta\Delta G = \Delta G_{RL'} - \Delta G_{RL} \tag{3}$$

which coinpares the binding affinity of two ligands, L and L', to a receptor R. it can also be obtained from

$$\Delta\Delta G = \Delta G_{RL\rightarrow RL'} - \Delta G_{L\rightarrow L'} \tag{4}$$

$\Delta G_{RL\rightarrow RL}$ and $\Delta G_{L\rightarrow L}$ are usually much easier to calculate, because each corresponds to the free energy difference between two similar systems. Moreover, methods such as Zwanzig's perturbation theory[17] can

be used to facilitate the calculations of $\Delta G_{\mathrm{RL}\rightarrow\mathrm{RL}}$ and $\Delta G_{\mathrm{L}\rightarrow\mathrm{L}'}$. For the Helmholtz free energy, Zwanzig's perturbation theory reads

$$\Delta A = -RT\ln\langle\exp(-\Delta H/RT)\rangle_r \quad (5)$$

where $\Delta H = H_p - H_r$, in which H_p and H_r are the classical Hamiltonians of the perturbed and reference systems, respectively; and $\langle\ldots\rangle_r$ represents an ensemble average over the reference state. By choosing the reference and perturbed systems to be those containing two similar ligands. the free energy difference between the two systems can be calculated directly rather than by first calculating the free energy of each and then taking their difference. Extensive efforts were also spent by a number of research groups to improve the range of applications of the thermodynainic cycle-perturbation method. These methods facilitate the calculation of a free energy difference when the direct application of Zwanzig's formula[17] gives poor statistics, such as when the two ligands are not sufficiently similar. Instead of changing a ligand into another in one step. the windowing technique introduces a number of intermediate steps, calculates the free energy difference between two adjacent intermediates, and sums the results to obtain the overall ΔA. Kirkwood's integration formula[18] utilizes a coupling parameter λ to change the classical Hamiltonian $H(\lambda)$ of one system into another. when λ goes from 0 to 1, and to obtain a free energy difference ΔG according to

$$\Delta G = \int_0^1 \left\langle \frac{\partial H(\lambda)}{\partial \lambda} \right\rangle_\lambda d\lambda \quad (6)$$

A recent derivation[19] showed that the free energy difference between two states can also be obtained by averaging the irreversible work in taking one state into the otl-ier, as follows:

$$\overline{\exp(-\beta W)} \equiv \int dW \rho(W,t)\exp(-\beta W) = \exp(-\beta\Delta G) \quad (7)$$

where W is the work associated with switching one system into another in a finite time t, β is the inverse of the product between the gas constant R and the absolute temperature T, and $\rho(W,t)dW$ is the probability of work found within the range W and $W+dW$. This formula was also evaluated experimentally by the mechanical unfolding of single RNA molecules.[21]

FASTER APPROXIMATE MODELS

Although the methods just described have firm theoretical bases. they are expensive to use. Faster approximate methods were developed to permit quick early evaluation of a larger number of potential drug candidates. One trick is to expand a binding free energy ΔA in terms of a Taylor's series of the model parameters λ_i, such as atomic partial charge and size of a lead compound:[15,16,22]

$$\Delta A = \sum_i \frac{\partial A}{\partial \lambda_i}\Delta\lambda_i + \frac{1}{2}\sum_{i,j}\frac{\partial^2 A}{\partial\lambda_i\partial\lambda_j}\Delta\lambda_i\Delta\lambda_j + \ldots \quad (8)$$

The key here is that analytical mathematical formulas can be worked out to calculate the derivatives: $\frac{\partial A}{\partial\lambda_i}, \frac{\partial^2 A}{\partial\lambda_i\partial\lambda_j}, \ldots$, and only simulation results involving the lead compound are required in calculating them. Once the expensive derivatives are calculated, they can be used in the Taylor's series expansion to predict the effects of making many different combinations of parameter change ($\Delta\lambda_i$) on the binding affinity. Because one usually only includes the first few order terms in the expansion, the parameter change cannot be made too large. However, thoroughly exploring a chemical space near the lead compound can point out useful compounds to synthesize. If some of the synthesized compounds are more active, similar calculations can be performed by using one or more of the new compounds as novel leads to gradually expand the chemical space. Sometimes, one can also obtain useful insights into inhibitor design simply by analyzing the derivatives, because they provide useful information about what parameter changes may improve activity. This approach was applied to study protein kinases, for example.[5] Other approaches that focus on examining a small chemical space near a lead compound to save computational time include the use of single-step perturbation methods. the Gaussian perturbation formula, and free energy perturbation calculations utilizing soft-core potentials.[6]

Another way to speed simulations is to use implicit rather than explicit solvent models. Solvent can play an important role in influencing binding, as both the ligand and the binding site of the receptor need to be desolvated before a receptor–ligand complex can be formed. Favorable binding can only occur when the gain in interaction energy upon binding can override the loss in solvation energy. Computational models need to account for solvation effects sufficiently well to be useful. Including a large number of solvent molecules surrounding a solute in a simulation provides a detailed molecular description of solvation effects. but this is very expensive. Recently. implicit solvent models became popular. Two major contributions of solvation effects are usually taken into account: electrostatic and hydrophobic. Different electrostatic models were introduced. Numerical solutions of the Poisson–Boltzmann equation,[1,2] taking into account the detailed shape of the solutes, are now used extensively.

Cheaper electrostatic models include various generalized Born models[12] and approaches that utilize screened Coulomb potentials.[23] The hydrophobic effects are most commonly modeled by using terms proportional to the surface area of a solute, as experimental results for simple alkanes suggest such a relationship.[24]

Another approximation commonly used to speed calculations is to assume the ligand and receptor to be rigid. This approximation may be crude, but calculations can be done on more hypothetical structures to identify promising ones for further computational and experimental explorations. This approximation can be partially relaxed by allowing only the smaller ligand to be flexible, with the receptor held fixed. Many molecular docking experiments were done with this approximation. Various approximate methods accounting for receptor flexibility are also being developed.[25] Some methods only allow side chains near the docking site to move. Others may take the receptor portions of crystal structures of different receptor–ligand complexes for docking, as these structures reflect the plasticity of the receptor when different ligands are bound. Snapshots of a receptor obtained from a molecular dynamics simulation can also be used. A traditional molecular dynamics simulation performed at a constant temperature may not be able to sample conformational space well enough in a short simulation, methods for improving conformational samplings can be put to use here. One inethod that became popular is the replica-exchange method.[26] In addition to simulating a system at the desired temperature, this method also simulates the system at higher temperatures and allows snapshots at different temperatures to exchange at regular intervals according to the Metropolis criteria. The runs at higher temperatures facilitate barrier crossing. and larger conformational switching can be realized at the lower desired temperature due to the replica exchange.

CONCLUSION

Computational chemistry can be used together with genomics information to aid in the design of selective drugs. Besides pointing out new targets for drug development. genomics information can also help in the design of more selective therapeutics. Computational chemists are beginning to be able to take many related targets into account so as to maximize the impact of a drug candidate on its intended target but not on the unintended ones.''' In addition. it should eventually be feasible to develop drugs that are tailored to the genetic traits of specific patients.

Computer-aided drug design is becoming more useful due to rapid improvement in computer speed, development of new algorithms, and rapid growth of experimental data that can be utilized in modeling studies. Here, we are able to introduce only some of the approaches being used and developed in the field. Other useful tools include diversity and similarity analysis methods that help in selecting a more manageable set of compounds for synthesizing, screening, and testing, methods that help to predict ADME (absorption, distribution, metabolism, and elimination) properties to aid in the design of molecules with good pharmacokinetic properties. and Web servers that provide useful databases and tools for modeling studies. Together with new developments in various experimental techniques, computer-aided drug design is playing its part in speeding the development of new pharmaceuticals. The rapid development of computer-aided drug design is fueled by the diligent work of many research groups. Due to limits in the number of citations that can be included here, we selected a short list of references that hopefully can lead readers to explore the works of a larger community.

ACKNOWLEDGMENTS

The authors acknowledge support from the Howard Hughes Medical Institute, the National Institutes of Health. the National Science Foundation. the Keck Foundation. the National Biomedical Computing Resource, the San Diego Supercomputer Center, and Accelrys Inc.

ARTICLES OF FURTHER INTEREST

Biological Ligands, p. *88*
The Cambridge Structural Database, p. *161*
Drug Delivery, p. 484
Enzymes: Characteristics and Mechanisms, p. 554
Molecular Modeling and Related Computational Techniques, p. *901*
Stability Constants: Definition and Determination, p. *1360*
Viruses as Host Assemblies, p. *1563*

REFERENCES

1. Honig, B.; Nicholls. A. Classical electrostatics in biology and chemistry. Science 1995, 268 (5214). 1144–1139.
2. Warshel. A.; Papazyan, A. Electrostatic effects in macromolecules: Fundamental concepts and practical modeling. Curr. Opin. Struct. Biol. 1998. 8 (2). 211–217.
3. Baker, N.A.: Sept. D.: Joseph, S.; Holst, M.J.; McCammon.

J.A. Electrostatics of nanosystems: Application to microtubules and the ribosome. Proc. Natl. Acad. Sci. U. S. A. 2001. *98* (18). 10037–10041.
4. Güner, O.F. *Pharmacophore: Perception, Development, and Use in Drug Design*; International University Line: La Jolla, CA. 2000.
5. Sims. P.: Wong. C.F.; McCammon. J.A. A computational model of binding thermodynamics: The design of CDK2 inhibitors. J. Med. Chem. 2003. 46 (15) 3314–3325.
6. Wong, C.F.: McCammon, J.A. Protein simulation and drug design. Adv. Protein Cliem. 2003, *in press.*
7. Carlson. H.A.: Masukawa. K.M.; Rubins, K.: Bushman. F.D.: Jorgensen, W.L.: Lins. R.D.: Briggs. J.M.; McCammon. J.A. Developing a dynamic pharmacophore model for HIV-1 integrase. J. Med. Chem. 2000.43 (11), 2100–2114.
8. Guex. N.; Peitsch, M.C. SWISS-MODEL and the Swiss-PdbViewer: An environment for comparative protein modeling. Electrophoresis 1997, *18* (15). 2714–2723.
9. Fetrow. J.S.: Giammona. A.: Kolinski. A.; Skolnick, J. The protein folding problem: A biophysical enigma. Curr. Pharm. Biotechnol. 2002. 3 (4). 329–347.
10. Hansch, C.; Leo. A. *Exploring QSAR: Fundamentals and Applications in Chemistry and Biology*; American Chemical Society: Washington. D.C.. 1995.
11. 30 *QSAR in Drug Design*; Kubinyi. H.. Folkers. G.. Martin. Y.C.. Eds.; KLUWER/ESCOM: Dordrecht, 1998; Vol. 3.
12. Bashford, D.; Case. D.A. Generalized Born models of macromolecular solvation effects. Annu. Rev. Phys. Chem. 2000. *51*. 129–152.
13. Goodsell, D.S.; Morris, G.M.; Olson. A.J. Automated docking of flexible ligands: Applications of AutoDock. J. Mol. Recognit. 1996. *9* (1). 1–5.
14. Morris, G.M.: Goodsell. D.S.; Halliday, R.S.; Huey. R.: Hart. W.E.: Belew. R.K.; Olson, A.J. Automated docking using a Eamarckian genetic algorithm and an empirical binding free energy function. J. Comput. Chem. 1998. *19* (14). 1639–1662.
15. Gilson. M.K.: Given, J.A.: Bush. B.L.; McCammon. J.A. The statistical–thennodynamic basis for computation of binding affinities: A critical review. Biophys. J. 1997. 72 (3). 1047–1069.
16. Tembe. B.L.; McCammon. J.A. Ligand-receptor interactions. Comput. Chem. 1984, *8* (4). 281–283.
17. Zwanzig, R.W. High-temperature equation of state by perturbation method. I. Nonpolar gases. J. Chem. Phys. 1954, *22*, 1420.
18. Kirkwood. J.G. Statistical mechanics of fluid mixtures. J. Chem. Phys. 1935. 3, 300–313.
19. Jarzynski, C. Equilibrium free-energy differences from nonequilibrium measurements: A master-equation approach. Phys. Rev.. E 1997, *56* (5). 5018–5035.
20. Crooks. G.E. Nonequilibrium measurements of free energy differences for microscopically reversible Markovian systems. J. Stat. Phys. 1998, *90* (5–6). 1481–1487.
21. Liphardt, J.; Dumont. S.; Smith. S.B.; Tinoco, I.; Bustamante. C. Equilibrium information from nonequilibrium measurements in an experimental test of Jarzynski's equality. Science 2002, *296* (5574). 1832–1835.
22. Wong. C.F.: Thacher, T.; Rabitz, H. Sensitivity Analysis in Biomolecular Simulation. In *Reviews in Computational Chemistry*; Lipkowitz, K.B., Boyd. D.B., Eds.; Wiley-VCH: New York, 1998: Vol. 12. 281–326.
23. Hassan. S.A.; Mehler. E.L. A critical analysis of continuum electrostatics: The screened Coulomb potential-implicit solvent model and the study of the alanine dipeptide and discrimination of misfolded structures of proteins. Prot. Struct. Funct. Genet. 2002. 47 (1), 45–61.
24. Wolfenden. R.: Andersson. L.; Cullis. P.M.; Southgate. C.C.B. Affinities of amino acid side chains for solvent water. Biochemistry 1981. *20*. 849–855.
25. Carlson. H.A. Protein flexibility and drug design: How to hit a moving target. Curr. Opin. Chem. Biol. 2002, *6* (4). 447–452.
26. Mitsutake, A.; Sugita, Y.; Okamoto. Y. Generalized-ensemble algorithms for molecular simulations of biopolymers. Biopolymers 2001. *60* (2). 96–123.

Dye Inclusion Crystals

Bart Kahr
Sei-Hum Jang
University of Washington, Seattle, Washington, U.S.A.

INTRODUCTION

"Supramolecular chemistry" is of recent coinage. Therefore, it is no surprise that contemporary chemists rarely think of textile dyeing, a human occupation for thousands of years, as supramolecular chemistry. However, unlike pigments that color by the mechanical trapping of particles. genuine dyeing involves the tuning of equilibria of dye sorption on fibers in order to achieve a desired fastness. Dyeing, one of the oldest and most transforming of chemical technologies, is also a quintessential example of deliberate self-assembly. Dyeing, indeed, is supramolecular chemistry. broadly defined. Crystal growth from solution is another area of inquiry that is governed by the specificity of noncovalent interactions. Long shrouded in mystery, recent studies are beginning to specify relevant interactions between molecules or ions and growing crystal surfaces.[1] This article broaches the intersection of these two areas of supramolecular chemistry: dyeing and crystal growth from solution. Mere. we describe the process of dyeing crystals, whereby simple crystalline substances orient and overgrow chromophores during crystal growth from solution.

Compared with supramolecular chemistry, crystal dyeing is a comparatively old subject."' The crystallographic literature of the past 150 years contains examples of crystals stained by dyes that we call dye inclusion crystals (DICs). When dyes express different affinities for faces of growing crystals not related by symmetry, they produce strikingly colored,[3] dichroic polyhedra that captured the attention of generations of crystallographers, not only for their appearance but also for what they teach about crystal structure and crystal growth. How do dye molecules adopt oriented positions in otherwise close-packed lattices made from molecules or ions that bear no size. shape, or constitutional similarity to the dye molecules'! These mixed crystals were troublesome in the past. because they seemed to violate Mitscherlich's principle of isomorphism,"' the idea that host and guest molecules must "fit." Dyed crystals were studied in order to address a variety of other questions. including the nature of pleochroism, mechanisms of crystal growth, silver halide photosensitization, ceramics crystallization. colloid stabilization, habit modification. epitaxy, explosives preparation, and kidney stone inhibition.[2]

HISTORY

In 1854, Henri de Sénarmont (Fig. 1) contemplated whether pleochroism might analogously be imparted to an otherwise transparent crystal if a colored material present in solution should stain the crystal during growth. Sénarmont was satisfied by red, pleochroic crystals of $Sr(NO_3)_2 \cdot 4H_2O$ that he grew from a solution containing a natural red quinone called heinatein.

Retgers, motivated by the apparent violation of the principle of isomorphism in Sénarmont's salt, and appreciating the limitations of Sénarmont's singular study. attempted to produce a family of DICs by systematically adding dyes to solutions of three dozen simple salt crystals.[5] From some 1000 crystallizations, he observed only four mixed crystals that he thought were worthy of continued study. The paucity of successes suggests that the probability of staining an ionic crystal during growth with a randomly chosen dye is small.

Like Retgers, Lehmann was motivated to understand the limitations of the principle of isomorphism but focused his research on organic hosts, especially carboxylic acid derivatives.[6,7] Unlike Retgers, he obtained many dichroic crystals. illustrating a surprisingly general capacity of some crystalline substances to orient and overgrow organic dyes. Gaubert repeated many of Lehmann's studies. He was the first to describe the process of dyeing crystals with respect to specific crystallographic directions. For example. he clarified that methylene blue recognized the (021} growth sectors of phthalic acid[8,9] and the {101} growth sectors of poppy acid.[10]

Neuhaus[11–13] and France[14,15] were the first to use x-rays to study DICs. However. by and large. x-ray scattering[16] experiments were not informative, as minor components in single crystals (typically DICs contain 1 mole of dye to $10^3 - 10^5$ moles of host) are rarely manifest in the Bragg scattering. France determined that the lattice constants for pure and dyed alum crystals were the same within experimental error.

Fig. **I** Henri de Sénarmont.

Most scientists familiar with the process of dyeing crystals were first introduced to the subject by Buckley. who showed photographs of a number of DICs in his popular book. *Crystal Growth.*[17] In large measure. his work constitutes a reinvestigation of the previous studies of Gaubert. But, despite an extra generation of sophistication. he too was unable to interpret his results given the still-limited understanding of crystal structure and the conformations of complex dye molecules in the 1930s. Thereafter. contributions to the literature on DICs were incidental or highly restricted in scope and most often divorced from their antecedents, until recent investigations in the 1990s.[2]

Stained alums are suitable illustrations of DICs. They are appropriate in this context because of the important role that alum has long played in the dye industry. Dyes are often chemically fixed to textile fibers following adsorption; mordanting with alum is common. What if we chose alum crystals as the ground? In other words, can alum mordant a dye to itself, that is to an alum crystal? In this century, alum crystals were first dyed by France in 1928,[18,19] Milligan in 1929,[20] and Buckley in 1930,[21] using a variety of azo and triarylmethyl cation dyes. In Fig. 2, an alum crystal grown in the presence of the dye diamine sky blue that stained the {100} growth sectors only is shown. As small {111} faces were expressed, they eschewed the dye, thereby leaving behind the unstained "darts."

Potassium alum is structurally similar to NaCl; both crystals have two distinct planes, one checkerboard like [$(111)_{alum}$ and $(100)_{NaCl}$], and one with alternating layers of cations and anions [$(100)_{alum}$ and $(111)_{NaCl}$]. France believed that charged dye molecules would be more strongly attracted to faces comprised of like ions.[22,23] Buckley, nevertheless, found dyes that recognized both types of faces in K_2SO_4.[17] Moreover, Frondel found that the checkerboard {100} faces of NaF adsorbed a great number of ionic dyes.[24] Obviously. the process of dyeing crystals cannot be reduced to a few simple "rules." In fact; the entire range of noncovalent interactions determines the segregation of the dyes and their orientations and conforinations.

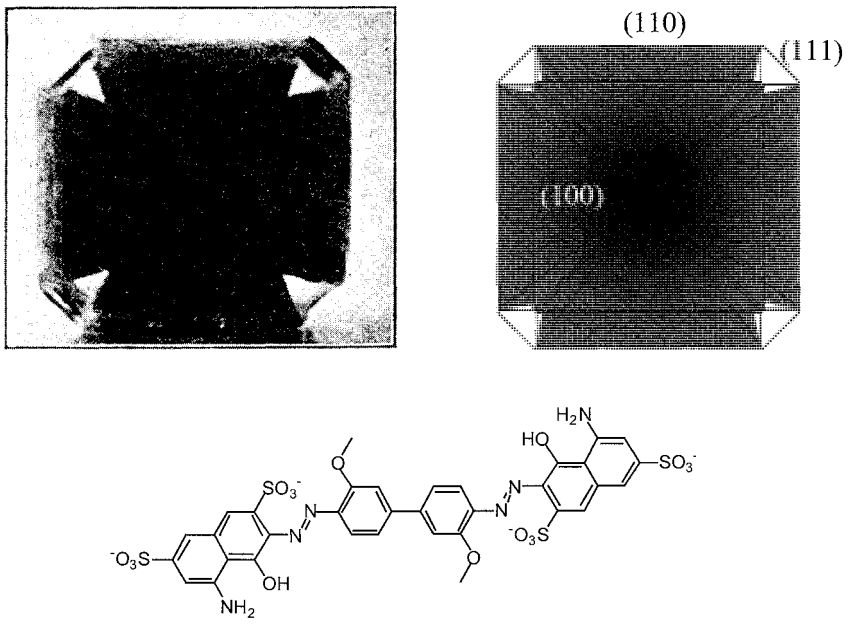

Fig. 2 France's photograph of a $NH_4AlSO_4 \cdot 12H_2O$ crystal stained by diamine sky blue in the {100} growth sectors. An idealized representation is shown on the right. (*View this art in color at www.dekker.com.*)

CHEMICAL ZONING

Additives interacting with growing crystals must discriminate between faces that are not symmetry related. Consequently: mixed crystals exhibiting more than one form will invariably display chemical zoning—the partitioning of impurities from one growth sector to another. While countless examples of such phenomena exist in mineralogy, as well as in the literature on dyeing crystals, a molecular-level understanding was first provided in a sweeping revision of the structure of solid solutions.[25,26] We explicitly designate this phenomenon intersectoral zoning. For example, many organic dyes. when included in saturated solutions of potassium hydrogen phthalate, give crystals in which the luminescence is confined to particular growth sectors (Fig. 3).[27] The orientations of the dye molecules can be ascertained by measuring the absorption spectrum in polarized light, so long as the electronic ctructures of the dyes are sufficiently well understood.

Organic impurities inhomogeneously deposit not only between growth sectors but also within single growth sectors depending on the crystal's surface topography. Surfaces of crystals grown in the lower supersaturation regime often propagate through dislocations that produce growth spirals or hillocks, shallow-stepped pyramids with single or multiple dislocations at the apexes. Polygonization of hillocks partitions faces into vicinal regions, each having slightly different inclinations. Impurity partitioning among vicinal slopes, intrasectoral zoning, results from the selective interactions of impurities with particular stepped hillock slopes. Tntrasectoral zoning, therefore, provides more detail about recognition mechanisms than intersectoral zoning, because the active growth surfaces at the time of incorporation can be more highly specified.

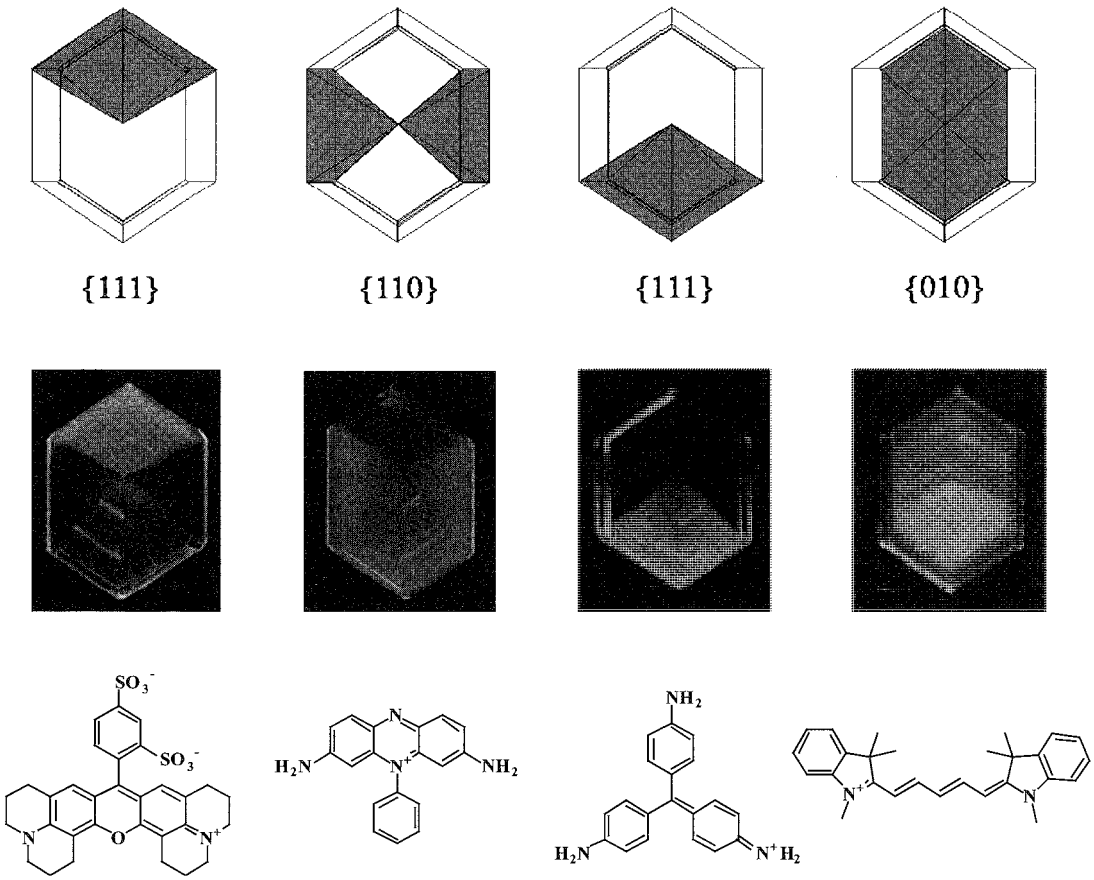

Fig. 3 Idealized representations of potassium hydrogen phthalate crystal habits viewed down [010] with growth sectors delineated. Red luminophores are included in each of principal growth sectors, as shown by the patterns of luminescence. (*View this art in color at www.dekker.com.*)

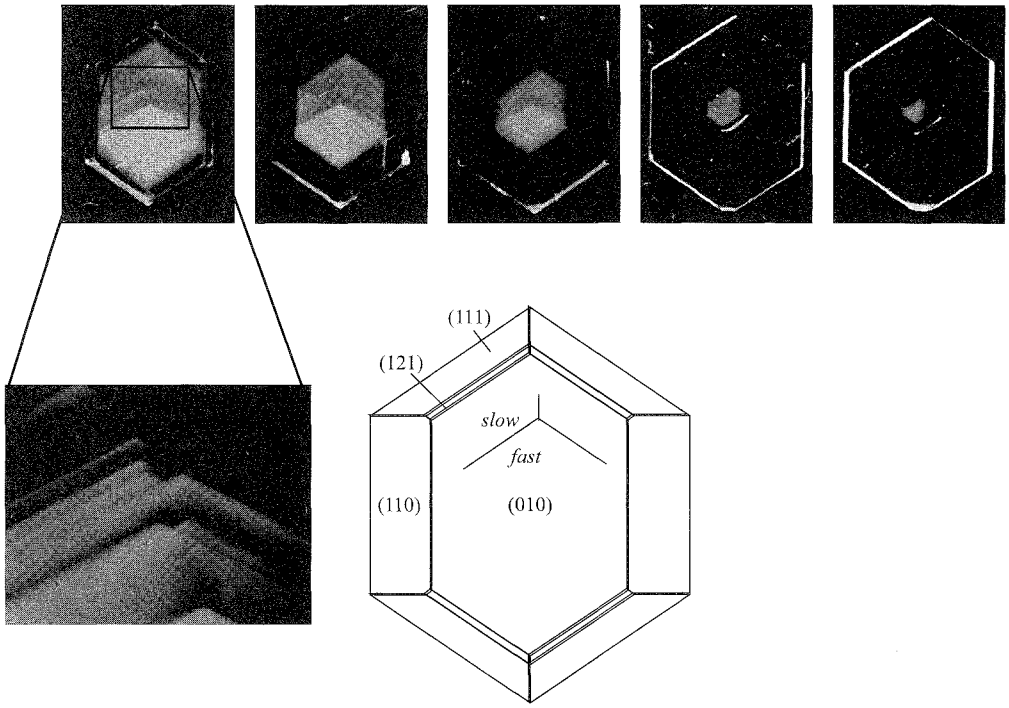

Fig. 4 Top row: Successive (010) slices (200 μ) of dyed potassium hydrogen phthalate crystals reveal the growth histories in their patterns of luminescence. Bottom row: The orientation of the fast- and slow-moving steps of a growth hillock are shown on the (010) face in a comparison of images made by differential interferencc contrast microscopy and fluorescence microscopy. (View this art *in color* at *www.dekker.com.*)

For example, the substructure in the luminescence from the crystal in Fig 4 results not only from intersectoral chemical zoning but also from intrasectoral zoning[28] on hillocks that arc manifest on these surfaces The dye recognizes the fast-growing steps in prcferencc to the slow-growing steps Other examples of the intrasectoral zoning of dyes were given by Zaitseva et al tor KH_2PO_4,[29] Gurney et al foi K_2SO_4,[28] and Kurtmoto et al for a-lactose monohydrate [30]

SUPRAMOLECULAR INTERACTIONS

We determined that the great range of host–guest interactions, including ionic forces, cation–π interactions, charge-transfer interactions, hydrogen bonding, and hydrophobic forccs are manifest in DICs. Of course, these categories are fuzzy at best. Cation–π interactions and hydrogen bonding could be considered charge-transfer interactions of a sort. Here, wc will not parse Coulomb's

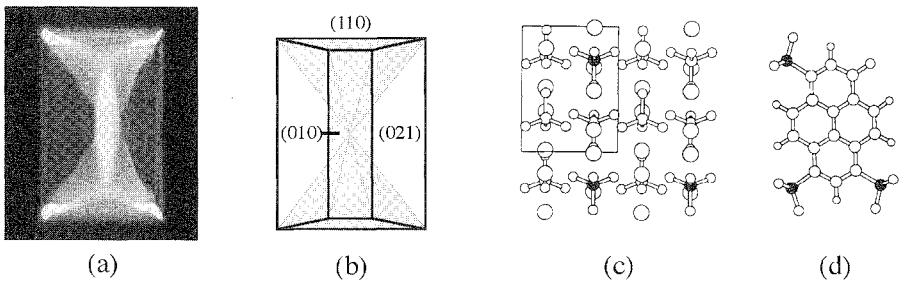

Fig. 5 Ionic forccs. (a) Fluorescence from K_2SO_4/pyranine. (b) Idealized representation of K_2SO_4/pyranine. K_2SO_4 (c) and pyranine (d) drawn to the same scale. Filled sulfur atoms define substituting sulfate (SO_4^{2-}) and sulfonate ($-SO_3^-$) groups. (*View this* art in color *at www.dekker.com.*)

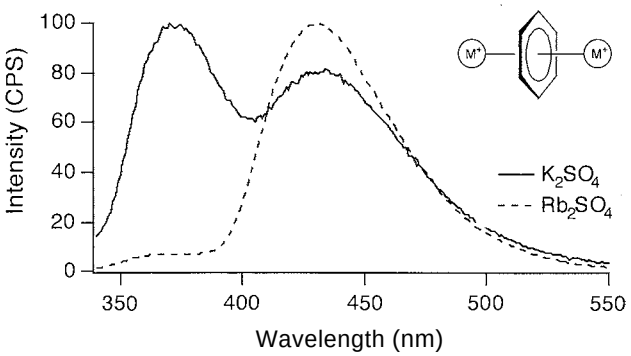

Fig. 6 Cation–n interactions. Comparison of fluorescence and phosphorescence yields from crystals of K_2SO_4 and Rb_2SO_4 containing aniline-2-sulfonate in the {001} growth sectors. (*View this art in color at www.dekker.com.*)

law into separate sublaws and statutes. We will adhere to the meanings of the aforementioned terms as they are commonly given in the literature.

Ionic Forces

Potassium sulfate can be straightforward in the mechanisms by which it incorporates chromophores. Ionic forces drive the mixed crystal formation in most cases. Buckley long ago suggested that the stereoregular substitution of sulfate ions in the lattice by sulfonate substituents on the dyes were responsible for the formation of some DICs.[17] We prepared more than 100 intersectorally zoned K_2SO_4 DICs containing sulfonated synthetic dyes.[17] A typical example. shown in Fig. 5. is K_2SO_4 containing pyranine in the (110) and (010) growth sectors. The disposition of sulfate ions in the lattice closely matches the rigidly disposed sulfonate substituents and drives the mixed crystal forination. This mixed crystal model can be confirmed by measurements of absorbance with polarized light.[38]

Cation–π Interactions

Gurney et al. studied the excited state lifetimes and zero-field splittings of rooin-temperature phosphorescent *ortho*-arninosulfonated benzenes and naphthalenes, through which they found evidence of cation–π interactions.[28] A number of these DICs are highly subject to heavy atom effects. The triplet lifetime of *ortho*-aminobenzenesulfonate was shorter in Rb_2SO_4 as compared with K_2SO_4 (Fig. 6). Similarly, phosphorescent lifetimes of *para*-aminobenzoate were considerably shorter in barium acetate crystals as compared to sodium acetate trihydrate crystals.[28] it was demonstrated by optical detection of magnetic resonance that intersystem crossing rates for aromatic compounds are only affected by heavy atoms if they are interacting with the face of the π-system.[32,33] Thus, there is reason to assume that cation–π interactions are important in determining the properties of aromatic guests in ionic salt crystals.[34]

Charge-Transfer Interactions

As first demonstrated by Gaubert and Lehmann, phthalic acid orients a great variety of cationic dyes, especially in its {021} growth sectors.[35] Red shifts in the absorption spectra of the crystals indicated the possibility of hydrogen phthalateldye charge-transfer complexes. Such associations were confirmed in crystal structures of stoichiometric hydrogen phthalatelmalachite green cocrystals (Fig. 7). This crystal structure was used in the interpretation of the linear dichroism of the corresponding DIC.

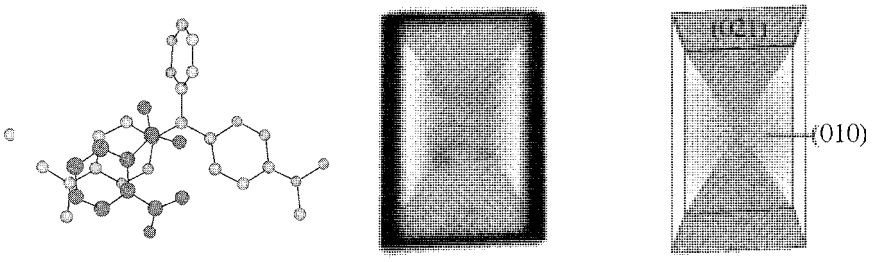

Fig. 7 Charge-transfer interactions. (a) Crystal structure of stoichiometric hydrogen phthalatelrnalachite green complex. Photograph (b) and ideal representation (c) of phthalic acid/malachite green mixed crystal. (*View this art in* color. *at www.dekker.com.*)

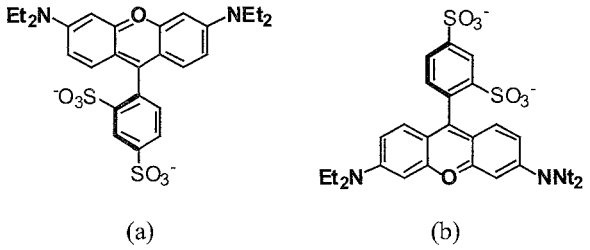

(a) (b)

Fig. 8 Hydrophobic effects. (a) Dimerization of sulforhodamines in K_2SO_4. (b) K_2SO_4 dyed in {110} growth sectors viewed along [010].

Hydrophobic Effects

Hydrophobic effects are manifest in the aggregation of dyes in some crystalline hosts. For example, sulforhodamine B absorbs light of 537 nm in the (110) growth sectors of K_2SO_4. This absorbance has been blue shifted with respect to that in solution and has been attributed to dimers, as shown in Fig. 8.[36]

Hydrogen Bonding

It is self-evident that hydrogen bonding plays an important role in the dyeing of many crystals, such as KH_2PO_4, phthalic acid, and α-lactose monohydrate. However, specifying the active hydrogen bonds is difficult. One example that lends itself to interpretation is the dyeing of benzamide in the $\{10\bar{2}\}$ sectors with Nile red (Fig. 9). The horizontal polarization of the excitation is consistent with the preorganized hydrogen bonding of Nile red to three benzamide molecules in a crystal chain. The luminescence is consistent with H-bonding found in polar protic solvents, where the $-NEt_2$ groups are turned out of plane.[37]

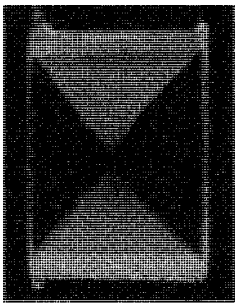

(a)

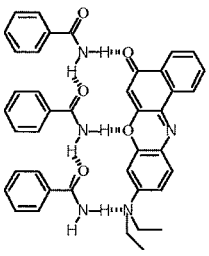

(b)

Fig. 9 Hydrogen bonding. (a) Benzamide crystal containing Nile red in the $\{10\bar{2}\}$ growth sectors. [100] is vertical. View along [010]. (b) Proposed structure of Nile red on the (102) face of benramide consistent with the linear dichroism and energy of the solvatochromic dye. (*View this art* in color *at www.dekker.com.*)

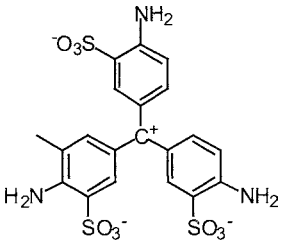

(a)

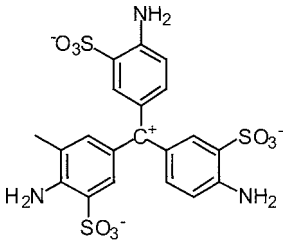

(b)

Fig. 10 Diastereoselectivity. Crystal spectra were interpreted as resulting from the incorporation of the asymmetric acid fuchsin diastereomer (a) in K_2SO_4 isomers. (b) The symmetric diastereomer.

STEREOSELECTIVITY

In principle, distinct facets of a single crystal might express different affinities for guests that can exist in more than one conformation. Such is the case with acid fuchsin in the {110) growth sectors of K_2SO_4.[38] The breaking of symmetry evident in the shape of the absorption spectrum suggested that of the two predominant conformations of acid fuchsin, one with all three sulfonates pointing to the same side of the mean molecular plane and one with two above and one below, only the latter was evident in the process of dyeing. Conformational selectivity was also observed in K_2SO_4 crystals containing naphthylamines.[28]

The process of crystal dyeing can be enantioselective as well as diastereoselective (Fig. 10). Blattner et al.

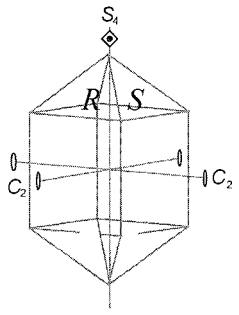

(a)

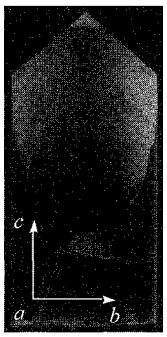

(b)

Fig. 11 Enantioselectivity. (a) Idealized habit of KH_2PO_4 crystal: R and S indicate mirror image faces. (b) Fluorescence photograph of KH_2PO_4/adenosine phosphate crystal viewed normal to the (100) face. (*View* this *art in* color *at www. dekker.com.*)

reported that solutions of hematein stained the {100} growth sectors of KH_2PO_4.[39] Recent reinvestigation of their work revealed that hematein stains every other prism face.[40] Hematein is chiral: adjacent prism faces of KH_2PO_4 are mirror symmetric. The adsorption, therefore, must be enantioselective.

Recently, Kurimoto et al. observed a visible blue luminescence localized in the pyramidal {101} growth sectors of KH_2PO_4 grown from a solution containing adenosine triphosphate).[30] This is a common pattern of zoning of anionic dyes in KH_2PO_4.[41,42] Comparisons of the luminescence viewed through the *a* and b faces revealed that the (011) sector was considerably brighter than the (101) sector (Fig. 1I). As these sectors are mirror images of one another, the chiral nucleotides must also have recognized these faces enantioselectively.

CONCLUSION

Crystal dyeing is an easy,[43] colorful, and often dramatic way of obtaining definitive evidence for specific noncovalent interactions controlling crystal growth. Moreover. the applications of DICs are numerous. DICs can be used as unique hosts in single-crystal matrix isolation experiments with metastable excited states[...] and biopolymers,[44,45] for conforrnational analysis. for separations, to interrogate mechanisms in biomineralization[...] and in matrix-assisted optical[47] and mass spectrometric chemical analyses,[48] to identify growth-active surface structures on crystalline faces, and as optical reporters of phase transitions.[49] During the past decade, we barely scratched the surface of a subject that was barely scratched by crystallographers of past generations. It is likely that we will learn much more about the process of dyeing crystals. as varied methods of contemporary analysis—particularly high spatially and temporally resolved electronic spectroscopies—are brought to bear upon the subject in the future.

ARTICLES OF FURTHER INTEREST

Cation–π Interactions, p. 214
Channel Inclusion Compounds, p. 223
Chiral Guest Recognition, p. 236
Crystal Growth Mechanisms, p. 364
Fluorescent Sensors, p. 572
Hydrogen Bonding, p. 658
Hydrophobic Effect, p. 673
Luminescent Materials, p. 816
Nonlinear Optical Materials, p. 973
Solvatochromism, p. 1330
Space Groups and Crystal Packing Modes, p. 1337

REFERENCES

1. Weissbuch, I.: Popovitz-Biro, R.: Leiserowitz, L.; Lahav, M. Lock-and-Key Processes at Crystalline Interfaces: Relevance to the Spontaneous Generation of Chirality. In *The* Lock *and Key Principle: The State of the Art—10 Years On*; Behr. J.-P., Ed.: Wiley: New York, *1994.*
2. Kahr. B.; Gurney, R.W. Dyeing crystals. Chem. Rev. **2001**, *101.* 893–951.
3. Kahr. B.: Vasquez. L. Painting crystals. CrystEngComm 2002, 514–516.
4. Kitaigorodsky, A.I. *Mixed Crystals*; Springer-Verlag: Berlin. *1994.*
5. Retgers. J.W. Beiträge zur kenntnis des isomorphismus. VII. Zeit. Phys. Chem. 1893. *12.* 583–622.
6. Lehmann. 0 . Uber kiinstliche färbung von krystallen. Zeit. Phys. Chem. 1891. *8. 543–553.*
7. Lehmann. O. Ueber kiinstliche färbung von krystallen und amorphen körpern. Ann. Phys. Chem. **1894**, *51. 47–76.*
8. Gaubert, P. Sur la coloration artificielle des cristaux d'acide phthalique. Bull. Soc. Mineral. Fr. 1905. *28.* 286–304.
9. Gaubert. P. Diffusion sous l'influence de la chaleur de la inatibre colorante dans les cristaux d'acide phthalique colorés artificiellement. Comptes Rendus **1937**, *204.* 599–*601.*
10. Caubert. P. Influence des metikres etrangkres dissoutes dans l'eau mère sur la facies des méconique et sur leur pseudopolychroi'sme. Cornptes Rendus 1910. *151.* 1134–*1136.*
11. Neuhaus, A. Anomale mischkristalle und orientierte abscheidung. Angew. Chem. 1941. *54*, 527–536.
12. Neuhaus. A. Das anomale mischsystem K_2SO_4-ponceaurot. (Anomale mischkritalle V.). Z. Krystallogr. 1942. *104. 197–224.*
13. Neuhaus. A. Partiell-isomorphe systeme. Zeitschrift für Kristallographie. 1943. *105.* 161–219.
14. Foote. F.G.: Blake. F.C.: France. W.G. Adsorption at crystal-solution interfaces. V. The effect of adsorbed dye on the lattice size of potassium alum crystals. J. Phys. Chem. **1930**. *34.* 2236–2240.
15. Paine. P.A.: France. W.G. Adorption at crystal-solution interfaces. IX. The concentration of adsorption at crystal solution interfaces. J. Phys. Chem. 1935. 39, 425–429.
16. Vetter. W.; Dudley. M.; Totsuka, H.: Kahr. B. The perfection and defect structure of organic hourglass inclusion K_2SO_4 crystals. J. Cryst. Growth 2002. *241. 498–506.*
17. Buckley, H.E. *Crystal Growth*; John Wiley: New York, *1951.*
18. Bennett, G.W.; France. W.G. Adsorption at crystal-solution interfaces. III. Individual macroscopic ammonium alum crystals grown in the presence of gelatin and dyes. J. Am. Ceram. Soc. 1928. *11*, 571–581.

19. France. W.G.; Davis. P.P. Adsorption at crystal-solution interfaces. IX. The concentration of foreign substances in solution relative to the quantity adsorbed by the host crystal. J. Phys. Chem. 1936. *40.* 177–185.
20. Milligan, A.G. The regional adsorption of dyes by growing crystals. J. Phys. Chem. 1929. 33, 1363–1373.
21. Buckley, W.E. The crystallization of potash alum and the effect of certain added impurities on its habit. Z. Kristallogr. 1930, *73.* 443–464.
22. Keenan, F.G.; France, W.G. Adsorption at crystal-solution interfaces. II. Individual macroscopic potassium alum crystals grown in the presence of gelatin and dyes. J. Am. Ceram. Soc. 1927. *10,* 821–827.
23. Lash. M.E.: France. W.G. Adsorption at crystal–solution interfaces. IV. Macroscopic ammonium. cesium and potassium alum crystals grown in the presence of dyes and other foreign materials. J. Phys. Chem. 1930, *34.* 724–736.
24. Frondel, C. Effect of dyes on the crystal habit and optics of NaF. LiF. NaCl. KCl. KBr. and KI. Am. Mineral. 1940. *25.* 91–110.
25. Vaida. M.: Shimon. L.J.W.: Weisinger-Lewin. Y.; Frolow. F.; Lahav. M.; Leiserowitz, L.: McMullan. R.K. The structure and symmetry of crystalline solid solutions: A general revision. Science 1988. *241.* 1475–1479.
26. Weissbuch. I.: Popovitz-Biro. R.: Lahav. M.; Leiserowitz. L. Understanding and control of nucleation. growth. habit. dissolution and structure of two- and three-dimensional crystals using 'tailor-made' auxiliaries. Acta Crystallogr. 1995. *B51.* 115–148.
27. Benedict. J.B.; Wallace. P.: Reid. P.; Jang, S.-H.: Kahr. B. Up-conversion luminescence in dye doped crystals of potassium hydrogen phthalate. Adv. Mater. 2003. *15.* 1068–1070.
28. Gurney, R.W.: Mitchell, C.A.; Ham. S.: Bastin. L.D.: Kahr, B. Salting benzenes. J. Phys. Chem.. B 2000, *104,* 878.
29. Zaitseva. N.: Carman. L.: Smolsky, I.; Torres, R.: Yan, M. The effect of impurities and supersatmation on the rapid growth of KDP crystals. J. Cryst. Growth 1999. *204.* 512–524.
30. Kurimoto. M.: Bastin, L.D.; Fredrickson. D.; Gustafson. P.N.: Jang. S.-H.: Kaminsky, W.; Lovell, S.; Mitchell. C.A.; Chmielewski. J.: Kahr. B. Intrasectoral Zoning of Proteins and Nucleotides in Simple Crystalline Hosts. In *Morphology and Dynamics of Crystal Surfaces in Complex Molecular Systems*; DeYoreo, J., Casey, W.. Malkin, A., Vleig, E., Ward. M.. Eds.; Mater. Res. Soc. Symp. Proc.. 2001: Vol. 620, M9.8.1.
31. Bastin, L.: Kahr, B. Engineering oriented gases: Dyeing K_2SO_4. Tetrahedron 2000. *56.* 8250–8260.
32. Ghosh. S.; Petrin, M.: Maki. A.H.: Sousa, L.R. Dependence of the triplet state properties on the orientation of metal ion perturbers in naphthalene-crown ether metal ion complexes. I. External heavy atom effect. J. Chem. Phys. 1987. *87.* 4315–4323.
33. Maki. A.H. Optically detected magnetic resonance of photoexcited triplet states. Methods Enzymol. 1995; *246,* 610–638.
34. Ma. J.C.; Dougherty. D.A. The cation–n interaction. Chem. Rev. 1997. *97.* 1303–1324.
35. Mitchell, C.A.; Lovell, S.; Thomas. K.: Savickas. P.; Kahr, B. Charge transfer interactions in dyed aromatic acid crystals and their relevance to MALDI mass spectrometry. Angew. Chem. Int., Ed. Engl. 1996. *35,* 1021–1023.
36. Chambers, R.W.: Kajiwara, T.; Kearns, D.R. Effect of dimer formation on the electronic absorption and emission spectra of ionic dyes. Rhodamines and other common dyes. J. Phys. Chem. 1974, *78,* 380–387.
37. Sarkar. N.; Das. K.: Nath. D.N.; Bhattacharvya, K. Twisted charge transfer processes of nile red in homogeneous solutions and in faujasite zeolite. Langmuir 1994. *10,* 326–329.
38. Kelley. *M.P.;* Janssens. B.; Kahr, B.: Vetter. M. Recognition of dyes by K_2SO_4 surfaces: Choosing organic guests for simple salts. J. Am. Chem. Soc. 1994. *116,* 5519–5520.
39. Blattner. H.: Matthias, B.: Merz. W. Charakeristicsche farbstoffeinlagerungen in seignetteelektrischen kristallen. Helv. Phys. Acta 1946, *19.* 415–417.
40. Kahr, *B.:* Lovell. S.: Subramony, J.A. The progress of logwood extract. Chirality 1998, *10.* 66–77.
41. Subramony. J.A.; Jang. S.-H.; Kahr, B. Dyeing KDP. Ferroelectrics 1997. *191.* 292–300.
42. Kahr. B.; Jang. S.H.; Subramony. J.A.: Kelley. M.P.; Bastin. L. Dyeing salt crystals for optical applications. Adv. Mater. 1996, *8.* 941–944.
43. Kahr, B.; Chow, J.K.: Peterson, M.L. Organic hourglass inclusions. J. Chem. Educ. 1994. *71.* 584–586.
44. Kurimoto, M.: Subramony, P.; Gurney, R.W.: Lovell. S.: Chmielewski. J.: Kahr. B. Stabilization of proteins in single crystal hosts: Green fluorescent protein and α-lactose monohydrate. J. Am. Chem. Soc. 1999, *121,* 6952–6953.
45. Wang, H.C.; Kudmoto. M.; Kahr, B.; Chmielewski, J. α-Lactose monohydrate single crystals as hosts for matrix isolation of guest biopolymers. Bio. Med. Chem. Lett. 2001. *9.* 2279–2283.
46. Touryan. L.: Clark, R.; Gurney. R.W.: Kahr, B.; Vogel, V. Growth of calcium oxalate monohydrate with fluorophores and fluorophore-labeled proteins. J. Cryst. Growth 2001, *233,* 380–388.
47. Mitchell. C.A.: Gurney. R.W.: Kahr. B. On the mechanism of matrix assisted room temperature phosphorescence. J. Am. Chem. Soc. 1998, *120.* 9726–9727.
48. Chmielewski. J.; Lewis, J.L.; Lovell. S.: Zutshi, R.; Savickas, P.: Mitchell. C.A.; Subramony. J.A.: Kahr, B. Single crystal matrix isolation of biopolymers. J. Am. Chem. Soc. 1997. *119.* 10565–10566.
49. Sedarous. S.; Subramony, J.A.; Kahr. B. Structure and optical characterization of Rochelle salt dye inclusion crystals and the fluorescence detection of their phase transitions. Ferroelectrics 1997, *191.* 302–306.

Electrochemical Sensors

James H. R. Tucker
University of Exeter, Exeter, United Kingdom

INTRODUCTION

There is considerable interest in electrochemical sensing within the field of supramolecular chemistry, and the topic has been identified as an important applicable area of host–guest chemistry.[1–3] This review covers developments in the area of supramolecular voltammetric/amperometric sensors. where current is measured as a function of applied potential. The area of supramolecular potentiometric sensors (e.g., ion-selective electrodes) is not covered here. and the reader is referred to a general review on electrochemical sensors that covers this topic.[1,2]

A number of methods for sensing or analyzing charged or neutral species in solution using voltammetric techniques have been identified.[1,2,4,5] So far. it is fair to say that many of the more successful approaches, in terms of applications and technological advances, have involved methods that fall outside the realm of supramolecular chemistry. particularly in the detection of electroactive (redox-active) species (e.g., the glucose biosensor).[4,5] This is not to say, however. that supramolecular receptors cannot be used to detect or respond to redox-active guests using electrochemical techniques.[6,7] However. it is no surprise that the electrochemical detection of non-redox-active species is less straightforward and requires an indirect method of detection. As far as voltammetric sensors are concerned. supramolecular chemistry can play an important role in this area with the use of redox-active receptors that can respond electrochemically to the cornplexation of a non-redox-active guest. This process is shown schematically in Scheme 1.

The complexation by a redox-active host. H. of a charged or neutral guest, **G**, imparts a change in its electrode potential that enables the binding process to be read out by an electrochemical technique. usually cyclic voltammetry. In the design of such a supramolecular sensor. the objectives are twofold; namely. guest selectivity and a significantly large redox response to complexation. This second aspect can be conveniently illustrated by the following square scheme (Scheme 2) and Eq. 1. Essentially. the change in the electrode potential (i.e., the redox response) of **H** upon complexation with **G** is related to the change in the host–guest binding constant upon its oxidation or reduction. In Eq. 1, $E_{\mathbf{H}}$ and $E_{[\mathbf{H-G}]}$ are the formal electrode potentials of **H** and the complex. **[H–G]**, respectively (each is usually approximated from the average of the anodic and cathodic peak potentials from cyclic voltammetry); K^+ and K are the binding constants in the oxidized and reduced form of the receptor, respectively: F is the Faraday constant; R is the universal gas constant, T is the temperature; and n is the number of electrons transferred (in Scheme 2, $n = 1$).

$$K^+/K = \exp[-nF(E_{[\mathbf{H-G}]} - E_{\mathbf{H}})/RT] \quad (1)$$

Therefore, a successful sensor will be selective for a particular target and bind it considerably more strongly in either its oxidized or its reduced form. The suitability of Eq. 1 for estimating the magnitude of the redox-switched binding enhancement from potential shifts has been examined in detail.[2,8] One finding is that the strength of the host–guest binding interaction appears to dictate whether cyclic voltammograms exhibit one-wave or two-wave behavior when adding aliquots of guest to the redox-active host.

The area of supramolecular electrochemistry and its relevance to sensing and redox-switched binding has been the subject of a book[1,2] and a number of reviews.[9–15] In

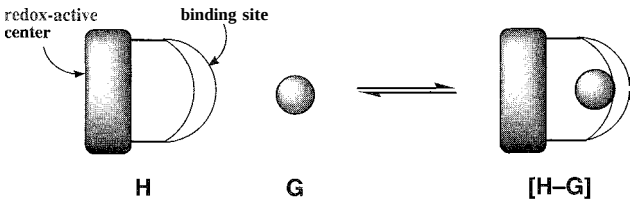

Scheme 1 The complexation of a guest. G. by a redox-active receptor. H.

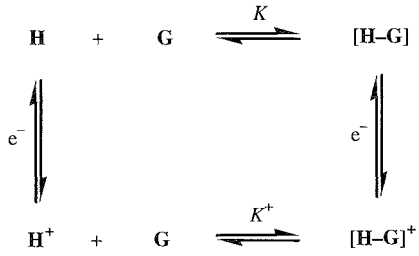

Scheme 2 Square scheme for a redox-switchable system

Encyclopedia of Supramolecular Chemistry
DOI: 10.1081/E-ESMC 120012784

a review by Gale, Beer, and Chen,[10] the different mechanisms by which complexation can impart a redox response. for example, via through-bond or through-space interactions, were discussed. In general, the proximity of the receptor site to the redox center and the charge density of the guest are important factors in determining the magnitude of the redox response and the effectiveness of the electrochemical read out. Here. an overview of the range of receptors designed for the binding and sensing of charged and neutral guest species will be given and will include examples of freely diffusing redox-active receptor species in solution and those immobilized at a surface.

RECEPTORS IN SOLUTION

In this section, freely diffusing receptors in solution will be discussed, in which the redox-active center or reporter group is, or is an integral part of. an inorganic or an organic group.

Inorganic Reporter Groups

Metallocenes

Ferrocene has been by far the most used redox-active group in a supramolecular sensor due its stability, its ease of functionalization and its well-understood and reversible redox chemistry. A host of ferrocene-containing compounds are now known that bind cations; anions, and neutral molecules. It can be argued that the first examples of redox-active receptors, for which the complexation of other species was demonstrated. were ferrocenyl crown ether compounds, as reported in the late 1970s and in 1980.[16–18] However, it was not until later that the structural. binding, and redox properties of these and related crown ether compounds were investigated in more detail.[19–28] Compounds such as **1**,[19] **2**.[20] **3**,[21] **4**,[22] and **5**[23] (Fig. 1), and related receptors containing two or more ferrocene centers, were found to bind and electrochemically respond to a range of hard (mainly Groups 1 and 2) metal cations in organic solvents, as well as. in some cases. ammonium ions[25] and ion pairs.[26] Almost without exception,[27] complexation imparts positive (anodic) shifts in the ferrocene-centered redox couples (Fc^+/Fc), as a result of the close proximity of the bound cation making ferrocene oxidation more difficult. Progress in this area has been reviewed extensively.[10,12] In addition to cyclic receptors, simple acyclic receptors have also been reported[29,30] (e.g., 6) that give a significant electrochemical response to the presence in solution of relatively charge-dense, hard cations.

Ferrocenyl receptors that bind and sense lanthanides.[31] as well as those that respond to a range of transition and soft metal cations, are now known. In the case of transition metal and soft metal cations; nitrogen-containing,[30,32–39] and to a lesser extent, sulfur-containing[40,41] ligands were used as receptor groups (e.g., Compounds 7–12. Fig. 2). A number of the aza-compounds can also bind anions, for example, Compound **9**.[35] As found with the crown ether derivatives, cation complexation generally imparts anodic shifts in the Fc^+/Fc redox couples of each receptor.

It is important that the factors responsible for generating a significant electrochemical response to complexation be fully understood if effective sensors are to be designed. In this respect, a detailed study by Plenio et al.[32] of transition metal complexation by a ferrocenyl molecule containing a cyclam ligand. 7, provided further

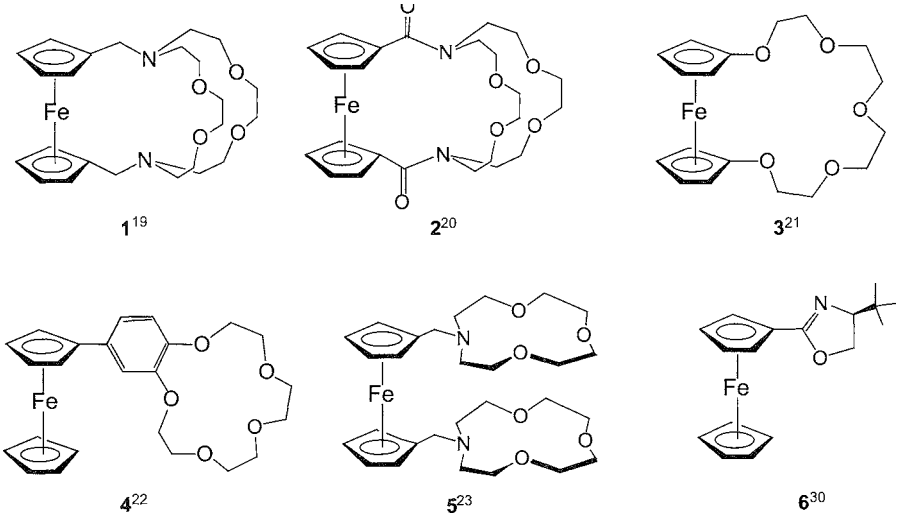

Fig. 1 Ferrocene receptors for hard metal cations

information on the iinportance of the Fe-metal distance and the solvent in governing the redox response to complexation. In particular. a linear dependence of the shift in the Fc^+/Fc couple upon complexation, AE, versus the intermetallic distance, 1/r, was found for the complexes $[M(FcCyclam)](CF_3SO_3)_2$ (M = Co. Ni. Cu, and Zn), which was clear evidence for a primarily coulombic, through space $Fe-M^{2+}$ interaction. Similar results were obtained previously. when the effect of protonation on the Fc^+/Fc redox couple of a series of tertiary amine derivatives was investigated.[''''] Found in other studies of the binding of hard metal cations by crown ether derivatives 1 and 2 were linear relationships between the shift in potential and either the charge/(radius)^2[19] or the charge/radius[20] of the bound cation. respectively. It was also shown by Plenio and Martínez-Mánez how the solvent can have a dramatic effect on the shift in potential, in that the complexation of $Zn(CF_3SO_3)_2$ by 7 imparted shifts ranging from + 280 mV in THF/CH_3CN (30:2 v/v) to + 409 mV in CH_3CN alone.[32] The expected trend toward larger shifts for solvents with lower dielectric constants was only observed for solvent mixtures of relatively high polarity. For solvent mixtures of relatively low polarity. the shifts were lower than expected due to ion-pairing effects.

There are now numerous reports of metallocene derivatives that bind and sense anions. Early work in this area was carried out by Beer, who first reported a redox-active anion receptor in 1989.[43] Beer published a number of cobaltocenium and fen-ocene anion receptors[10,11,43–48] some of which are shown in Fig. 3 (Compounds 13–16). In contrast to what is found with cations, the Fc^+/Fc redox couples undergo appreciable negative (cathodic) shifts upon complexation with inorganic anions in organic solvents. These negative shifts are consistent with a stabilization of the oxidized forms of each receptor by the negative charge of each guest. Beer found that amide receptors of this type (e.g., 13–15) bound anions through hydrogen-bonding interactions: with the cobaltocenium receptors binding anions more strongly due to the additional through-space electrostatic attraction between host and guest. Beer also developed sensors for organic anions,[45,46] for example; the cobaltocenium receptor 15 containing a calix[4]arene group that binds carboxylate ions selectively over halide ions. due to two rigidly held amide units on the upper rim of the calixarene that create an ideal site for bidentate coordination.

Beer and Martínez-Mánez also reported a number of fen-ocene-containing receptors that selectively bind and

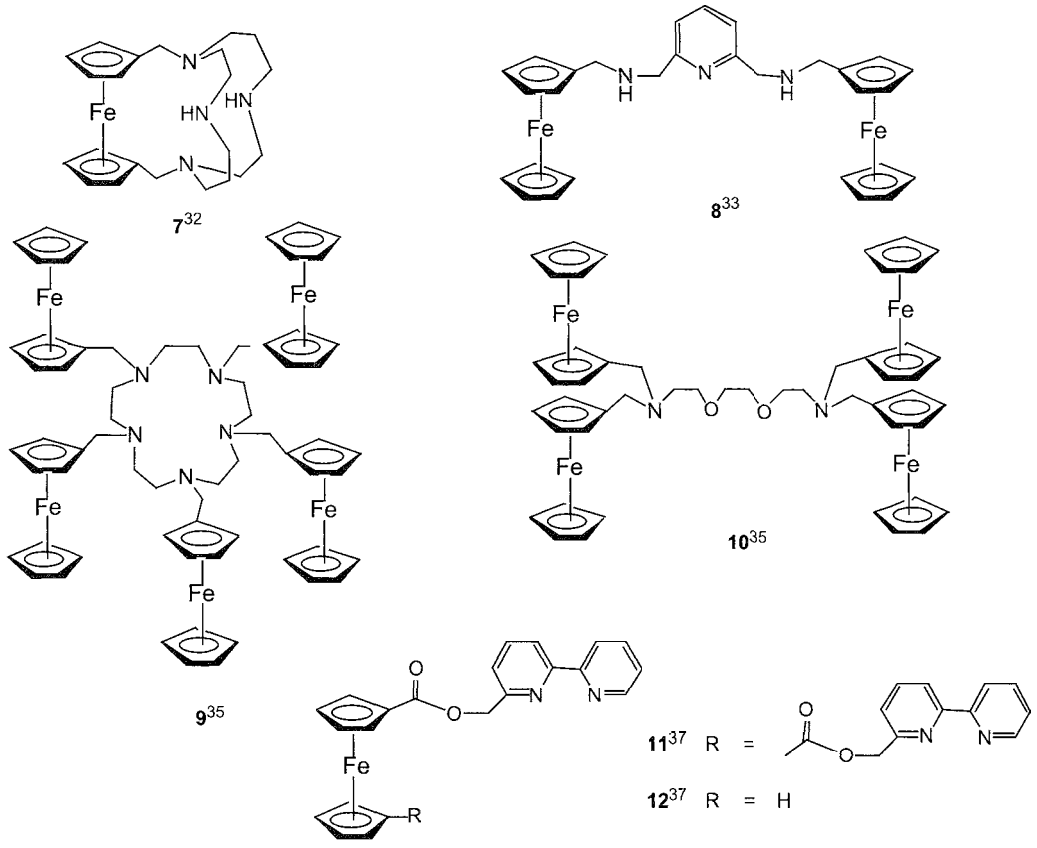

Fig. 2 Ferrocene receptors for transition metal and soft metal cations.

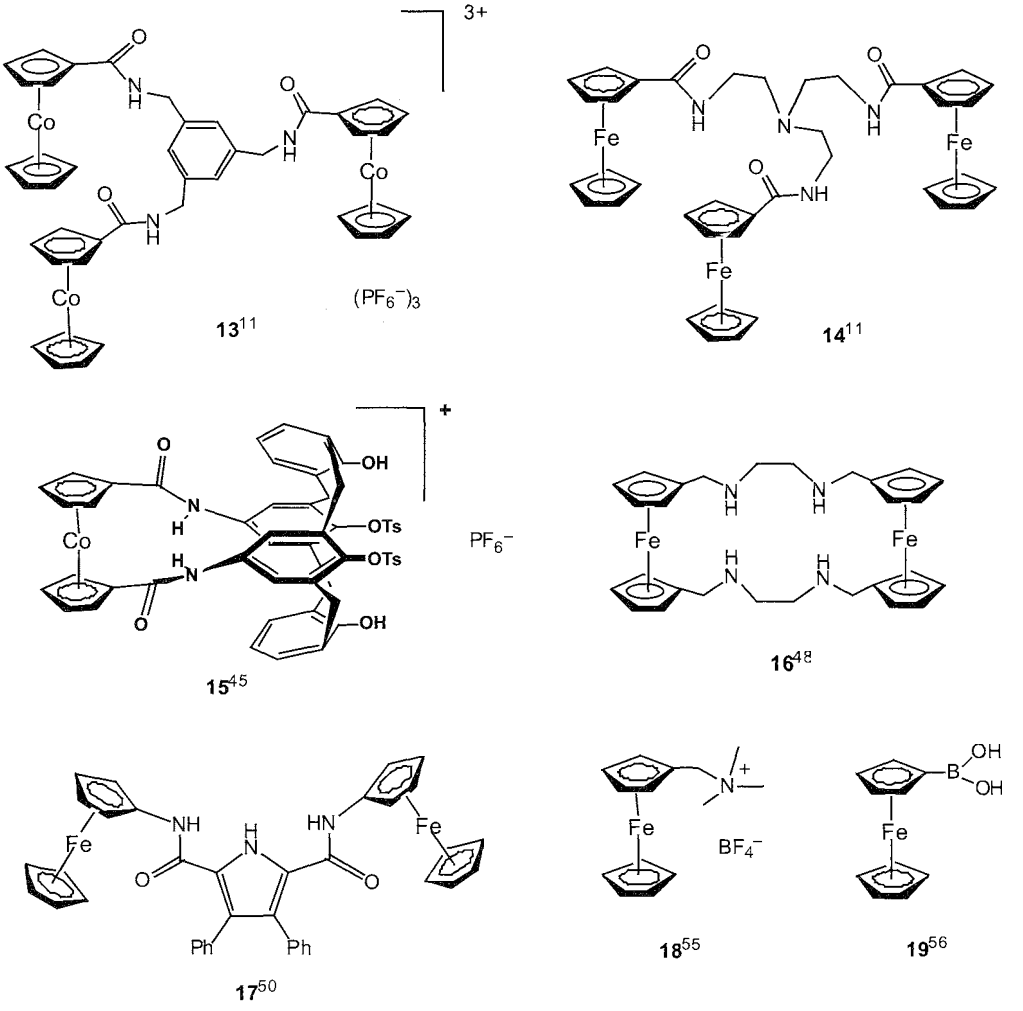

Fig. *3* Metallocene receptors for anions

sense oxoanions at a particular pH value. For example, at pH 4 in THF/water (70:30 v/v), ligand 16 selectively forms a 1:1 complex with sulfate in the presence of phosphate. with the Fc^+/Fc redox couple undergoing a shift of -54 mV upon complexation.[48] Under these conditions. all four secondary amines of the receptor are protonated. with the anion existing as HSO_4^-. The biological anion ATP can also shift the redox couple of **16** cathodically by up to -100 mV. depending on the pH of the medium.

Other groups reported a variety of ferrocene receptors for anions,[49–57] representative examples of which are shown in Fig. 3 (Compounds 17–19). Some of these are simple. for example, commercially available **18**, which can sense dihydrogen phosphate and ATP anions in organic media.[55] The large negative shifts of the Fc^+/Fc redox couple upon compiexation (e.g., $\Delta E = -470$ mV in CH_2Cl_2 upon addition of $H_2PO_4^-$) result from strong ion-pairing interactions between the anion and the double positive charge of the quaternary ammonium group and the oxidized ferrocenium ion. Another commercially available compound is ferrocene boronic acid. **19**,[56] one of a number of redox-active boronic acid and boronate receptors.[57–59] that recognizes fluoride selectively over a range of other halide ions and oxoanions in water. Cathodic shifts in the Fc^+/Fc redox couple of ca. -200 mV were observed upon the addition of excess amounts of fluoride. which forms an adduct with the Lewis acidic boron center. A study with a ferrocenyl *bis*(boronate) derivative demonstrated similar selectivity toward fluoride.[57]

In contrast to the recognition of cations or anions. the eiectrochemical sensing of neutral molecules by redox-active receptors is less common. A number of supramolecular ferrocene receptors for such species are now known,[59–67] but only a few are reported as undergoing significant electrochemical responses to complexation. As found with the anion receptors. complexation brings about a negative shift in the Fc^+/Fc redox couple. which is consistent with host–guest binding strength being stronger in the ferrocenium form. Beer utilized a neutral ferrocene-appended calix[5]arene to encapsulate and

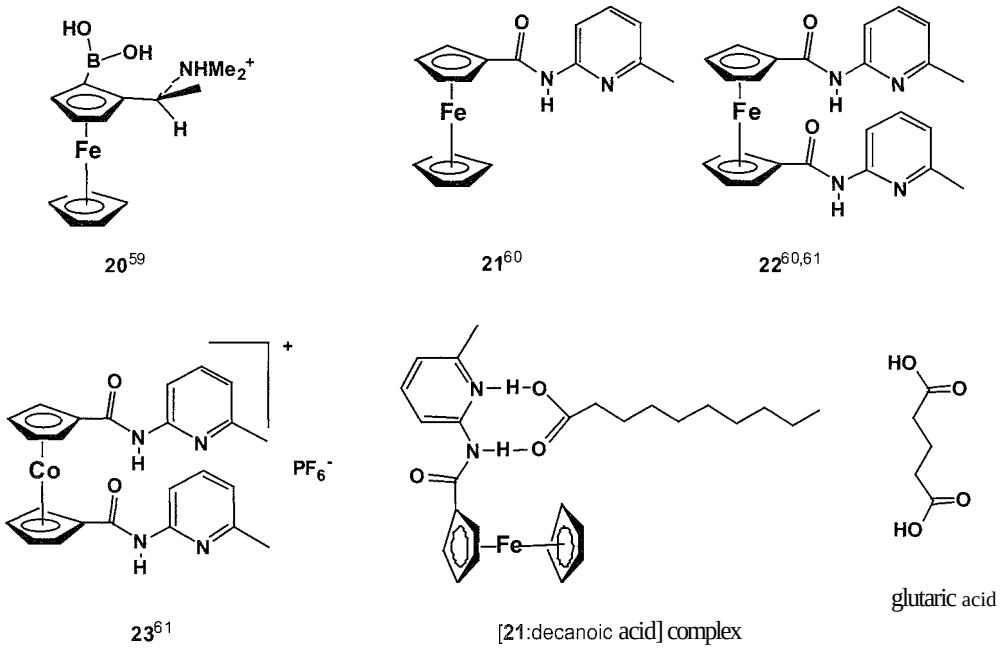

Fig. 4 Metallocene receptors for neutral molecules

sense the binding of polar organic molecules such as EtOH and DMF.[64] Electrocheinical studies revealed that inclusion of these molecules into the calixarene cavity induced small changes in the ferrocene-centered redox waves. Some other ferrocene compounds that electrochemically respond to neutral organic molecules are shown in Fig. 4.

The boronic acid 20 reported by Shinkai[59] is a rare example of an enantiopme chiral redox-active receptor." It was found to bind linear and cyclic sugars in aqueous solution at neutral pH due to the reversible reaction between the boronic acid moiety of the protonated ferrocene receptor and the sugar to form a boronate ester. Electrochemical studies revealed that complexation imparted cathodic (ca. -50 mV) shifts in the Fc^+/Fc redox couple. Interestingly, moderate enantioselectivity was observed in that (+) -1 bound the linear saccharide D-sorbitol more strongly than L-sorbitol (K_D/K_L = 1.4). However. differences in the electrochemical response to the binding of these enantiomers by 20 were not apparent.

Metallocenes 21–23 were found to bind mono- and dicarboxylic acids in organic solvents through complementary hydrogen bonds with their amide (N–H...O) and pyridine (O–H...N) groups.[60,61] Cyclic voltammetry studies in CH_2Cl_2 revealed cathodic shifts in the Fc^+/Fc redox couples, with the redox response to complexation of the monoacid decanoic acid by 21 and 22 (-25 mV and -55 mV, respectively) being approximately proportional to the number of hydrogen bonds in each complex (two and four. respectively).[60] Similar cathodic shifts were found in the complexation through hydrogen bonds of 3-aminopyrazole derivatives by ferrocene dipeptide receptors.[63] The binding of the dicarboxylic acid glutaric acid by metallocenes 22 and 23 in $CDCl_3$-0.5% DMSO. to give complexes of 1:1 stoichiometry. iinparted larger but identical cathodic shifts of -90 mV in the redox couples of each receptor. due to the guest being bridged between the Cp rings.[61]

Other inorganic reporter groups

A number of other metal-based redox-active centers have been incorporated into supramolecular receptors. representative examples of which are displayed in Fig. 5 (Compounds 24–28). Many of these receptors electrochemically respond to cations.[70–78] but species that respond to anions[58,79] and neutral molecules[80] are also known. A number of the cation binders are organometallic crown ether and metallocrown or metallothiacrown derivatives,[71–78] for example. Compound 24.[77] However, in many cases, the redox processes are not particularly reversible, and relatively small anodic shifts in the metal-centered redox couples are observed. A series of self-assembled [12]metallocrown-3 complexes. two of which are 25 and 26, were found by Severin to bind halide salts of small Group 1 metals strongly in organic solvents. with affinities similar to those of the cryptands.[71,72] X-ray crystal structures revealed that the metal cation was

"For two recent examples of electrochemical sensing by homochiral redox-active receptors. see Refs. [68,69].

bound in the center of the cavity, coordinated by three oxygen atoms of the metallocrown and the halide counterion. No detectable complexation of KCl was observed due to the small size of each cavity. These receptors were found to respond electrochemically to complexation, with shifts in oxidation peak potential of more than + 300 mV observed upon addition of LiCl and NaCl to 25. The $LiBF_4$ complex of 26 was also found to electrochemically sense fluoride anions in organic solvents.[72] A cathodic shift of −203 mV was observed upon the addition of excess NBu_4F, as a result of the fluoride anion forming an unusual molecular Li–F bond.

Transition metal bipyridine[79] and terpyridine[58] complexes were used as redox reporter groups for anions. The bimetallic receptor **27** was found to respond to chloride anions in CH_3CN, as evidenced by a cathodic shift of −110mV in the ligand-centered reduction couple of the two *bis*-substituted bipyridine groups.[79]

Organic Reporter Groups

There are numerous examples of organic redox-active reporter groups that have been incorporated into supramolecular receptors over the past 20 years. Many of these date to the 1980s and early 1990s. when Gokel and coworkers reported a number of crown ether and cryptand derivatives containing redox-active centeres. Much of this work has been reviewed.[2,13] A number of macrocylic receptors containing reducible redox-active groups are now known,[81–92] representative examples of which are shown in Fig. 6 (Compounds 29–33). Crown ethers and cryptands containing quinone/anthraquinone,[81–86] azobenzene,[87,88] and nitrobenzene[8,89] units sense Groups 1 and 2 metal cations through anodic shifts in reduction potential, as a result of the reduced forms binding these positively charged guests more strongly. The zinc(II) cyclen complex 30 was found to electroche~nicallydetect the DNA base thymidine in aqueous solution at physiological pH. This was possible through cathodic shifts in the anthraquinone reduction potential, as a result of π–π stacking interactions between host and guest decreasing upon anthraquinone reduction.[85]

A number of other reducible organic redox-active groups were used in receptors that can bind species through the formation of hydrogen bonds. However, most of these were used for i-edox-switched binding purposes rather than for electrochemical sensing.[9,93]

Some examples of receptors containing oxidizable organic groups that respond electrochemically to cat-i$_{ons}$[**–102] are depicted in Fig. 7 (Compounds 34–38). The tetrathiafulvalene (TTF) unit. which can undergo two reversible oxidations. is one of the most common redox-active groups to be incorporated into a supramolecular sensor over the past few years. The groups of Becher, Sallé. and Bryce are prominent in this field, publishing

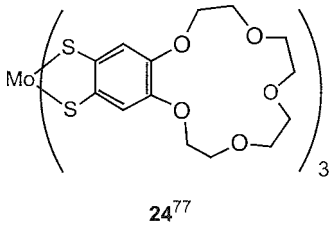

24[77]

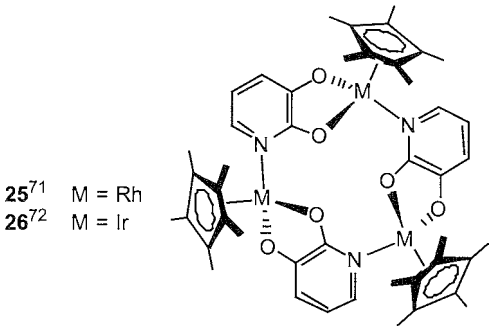

25[71] M = Rh
26[72] M = Ir

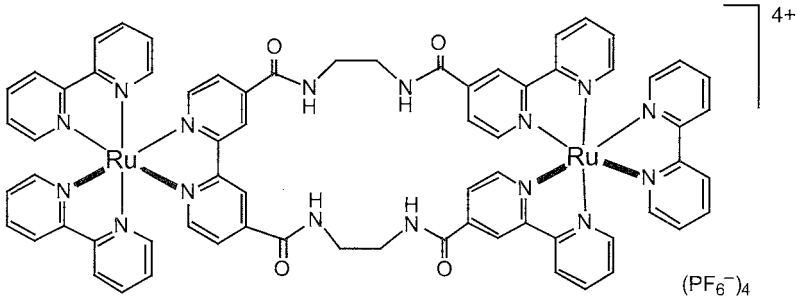

27[79]

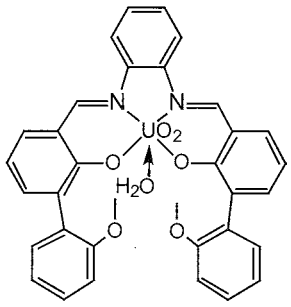

28[80]

Fig. 5 Redox-active receptors with non-metallocene-based inorganic reporter groups.

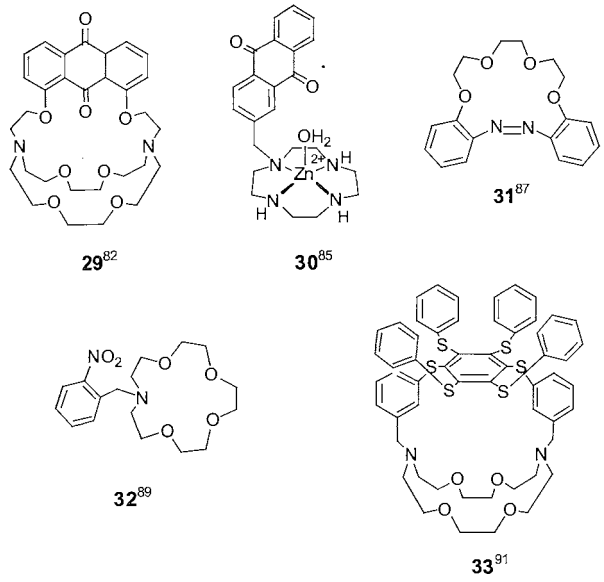

Fig. 6 Redox-active receptors containing reducible organic reporter groups.

receptors with cation binding sites located at the end of (e.g., **34**), or across (e.g., **35**), the TTF unit.[94–99]

TTF receptors are known for binding hard or soft metal cations, depending upon the type of donor atom used in the receptor unit, although hydrogen-bonding TTF receptors for neutral molecules[97] are also known. In general, cation binding produces a positive shift in the first TTF oxidation potential, with the second being largely unchanged, which is attributable to the expulsion of the bound cation from the positively charged cavity. Recent progress involved the preparation of a TTF receptor **36**[98] containing two pyrrole units that makes it devoid of the *cis*/*trans* isomerization found in 35. This compound can electrochemically sense Pb^{2+} and Ba^{2+} ions in organic solvents; with unprecedented large shifts observed in the first TTF oxidation potential.

RECEPTORS IMMOBILIZED AT A SURFACE

In order to assess the commercial viability of the supramolecular approach to voltammetric sensing. it is important for freely diffusing receptor species to be attached to a surface to assess whether changes in redox properties observed upon complexation in a homogenous system can still be observed once the receptor is immobilized. Accordingly, examples of thin filins of redox-active receptors on surfaces (e.g., chemically modified electodes. CMEs) are becoming increasingly common, as exemplified by a recent review.[6] The most common methods of iinmobilizing a receptor onto a surface involve the formation of either a polymer film or a self-assembled monolayer (SAM). An overview of both approaches, with appropriate examples, is given below.

Polymer-Based Electrochemical Sensors

Polymer-based materials are of immense interest to supramolecular chemists working in a number of fields. The area of polymer-based sensing is vast and was reviewed by Swager in 2000.[103] As far as electrochemical sensors are concerned, a number of approaches have been identified,[6] but they generally fall into two main categories. The first involves using a system in which the receptor site is simply attached to the electrode-immobilized polymer (e.g., polypyrrole or polythiophene) through covalent bonds, with the redox-active polymer film acting as the redox probe (e.g., Fig. 8, Compounds 39–41).

This approach was fairly popular in the past,[6,103] especially for the sensing of metal cations using crown ethers (e.g., Compound **39**[104]) or nitrogen-containing ligands.[105] More recently, calixarene-based polymers were shown to be effective voltammetric sensors for such species.[103,106] However, other charged or neutral species can also be sensed if an appropriate receptor group is used. For example. Fabre reported that a conjugated polymer film formed from the anodic oxidation of boronate-substituted pyrrole. 40, can selectively sense millimolar concentrations of flouride in an H_2O–CH_3CN solvent mixture.[107] Likewise, redox-active thiophene polymers covalently linked to hydrogen-bonding units were found to recognize complementary DNA base derivatives (e.g., Complex **41**).[108,109]

The second approach involves using a separate redox-active group as the reporter group, with the polymer merely providing a convenient means for immobilizing the receptor onto an electrode surface (e.g., Compounds 42–44, Fig. 9). Thus, a more defined and controlled redox response to complexation can be envisaged, and a direct comparison with the performance of freely diffusing receptors is possible.

The group of Moutet and coworkers published a number of reports on the sensing of Group 1 and Group 2 metal ions using ferrocenyl crown ethers in polypyrrole films."[10] In a recent study, a polypyrrole film was grown on a Pt electrode from the corresponding pyrrole-substituted monomer 42. A sole redox process corresponding to the Fc^+/Fc redox couple was observed in CH_3CN solution. The transfer of this film to a solution containing Ba^{2+} ions resulted in the immediate appearance of a new redox wave. anodically shifted by 0.12 V. The free receptor could be regenerated by holding the film at a positive potential in Ba^{2+}-free electrolyte or by soaking in an aqueous EDTA solution. Interestingly, the magnitude of the redox response and the selectivity pattern toward different cations were comparable to that of an analogous freely diffusing receptor.

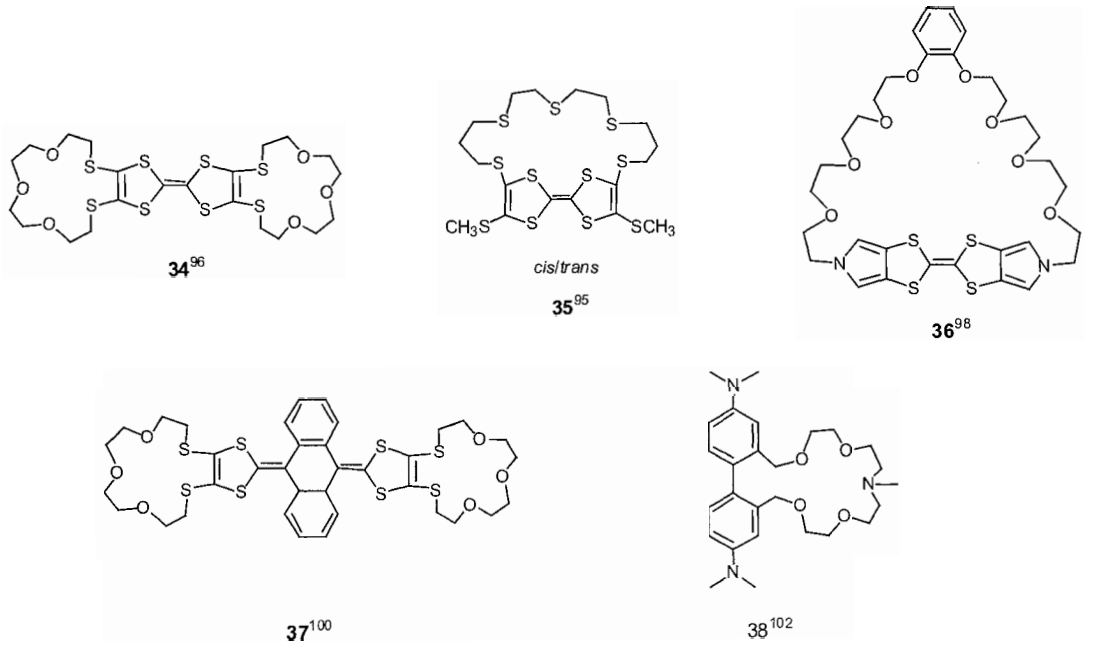

Fig. 7 Redox-active receptors containing oxidizable organic reporter groups.

Similar approaches were used by others to detect of anions and neutral molecules. For example, the cobaltocenium compound 43 was immobilized onto an electrode surface by electropolymerization.[111] The presence of submillimolar amounts of $H_2PO_4^-$ in CH_3CN caused a cathodic shift in the cobaltocenium$^+$/cobaltocene redox couple as well as the appearance of a new redox wave at more negative potentials. The film was selective toward this anion over HSO_4^- and halide ions. as was the monomer in homogenous solution. Smith built on previously described studies of hydrogen-bonding interactions in solution[93] with the synthesis of a phenanthrenequinone (PQ) pyrrole 44, which was electropolymerized at a glassy carbon disk electrode.[112] Electrodes derivatized with this polymer were found to be reasonably stable in organic solvents. The electrode was placed in CH_3CN solutions of various urea compounds. such as 1-phenyl-3-propylurea. As observed previously in solution phase studies, urea complexation through two compleinentary hydrogen bonds resulted in anodic shifts in the $PQ^{0/-1}$ redox couple, indicating a strong interaction between the surface-confined quinone radical anion and the urea. Interestingly. the surface-confined receptor was found to be more selective than the analogous compound in solution. with only aromatic ureas causing a significant shift in reduction potential.

SAM-Based Electrochemical Sensors

The use of self-assembled monolayers (SAMs) for Investigating the binding properties of redox-active groups at a surface has been explored over the pact few years by a number of research groups [13 14.113–117 119–123] Some examples of redox-active receptors that form monolayers and respond electrochemically to complexation are shown in Figs 10 and 11 (Compounds 45–49) An early example

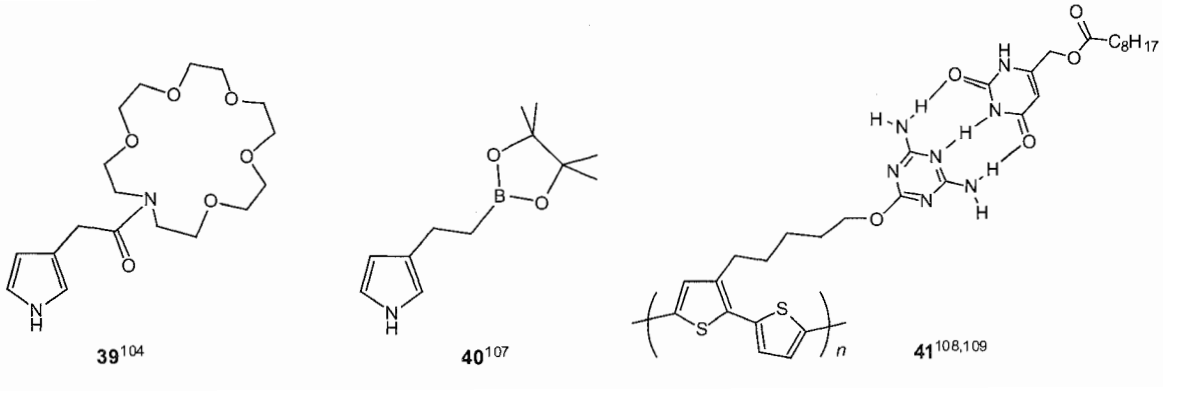

Fig. 8 Pyrrole and thiophene-based redox-active receptors.

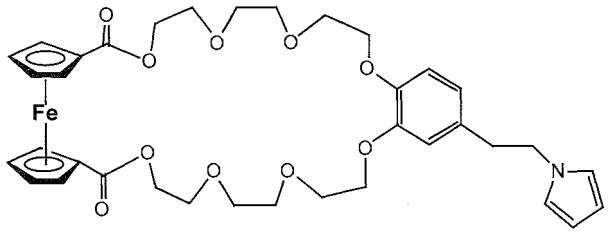

42[110]

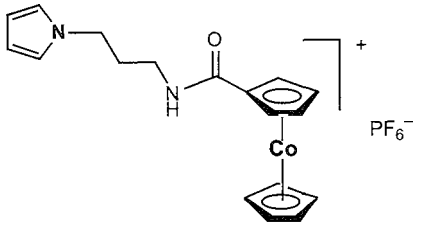

43[111]

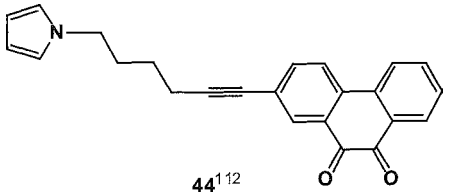

44[112]

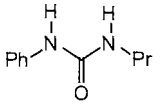

1-phenyl-3-propylurea

Fig. 9 Pyrrole and thiophene-based receptors containing separate redox-active reporter groups.

involved the disulfide 46, which formed a inixed monolayer with decanethiol on a gold electrode.[113] Micromolar concentrations of catechol and indole could be detected by shifts in the reduction potential of the viologen groups. More recently. a related viologen-based receptor[114] was found to bind and sense a series of ferrocene derivatives.

Ferrocene-containing SAMS have been used in a number of examples of molecular recognition processes at a surface. Kaifer and Gokel successfully used such species to probe the binding of β-cyclodextrin derivatives through shifts in ferrocene-centered oxidation potentials.[115] More recently, ferrocene-containing SAMS on spherical surfaces (gold colloids)[116] and planar surfaces

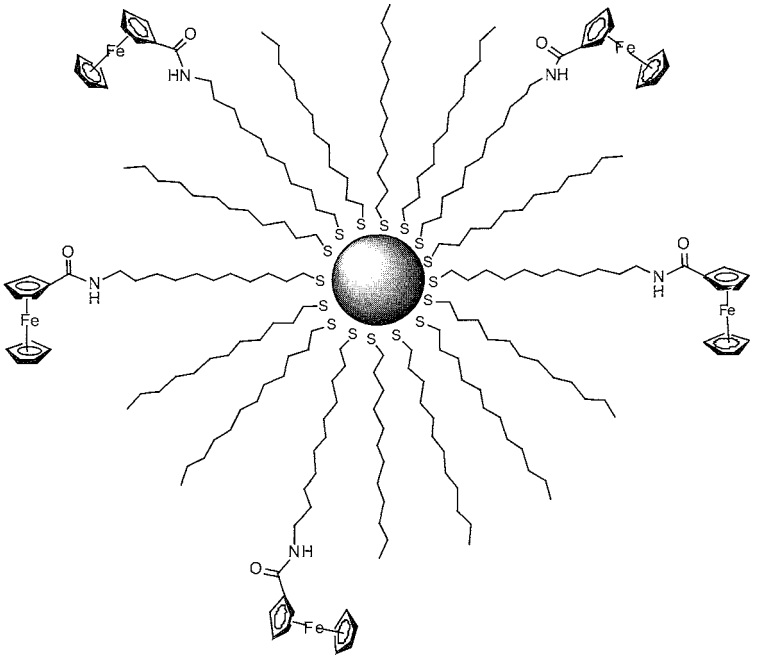

45[116]

Fig. 10 A gold colloid containing mixed dodecanethiol and amido(ferrocenyl) undecane thiol ligands

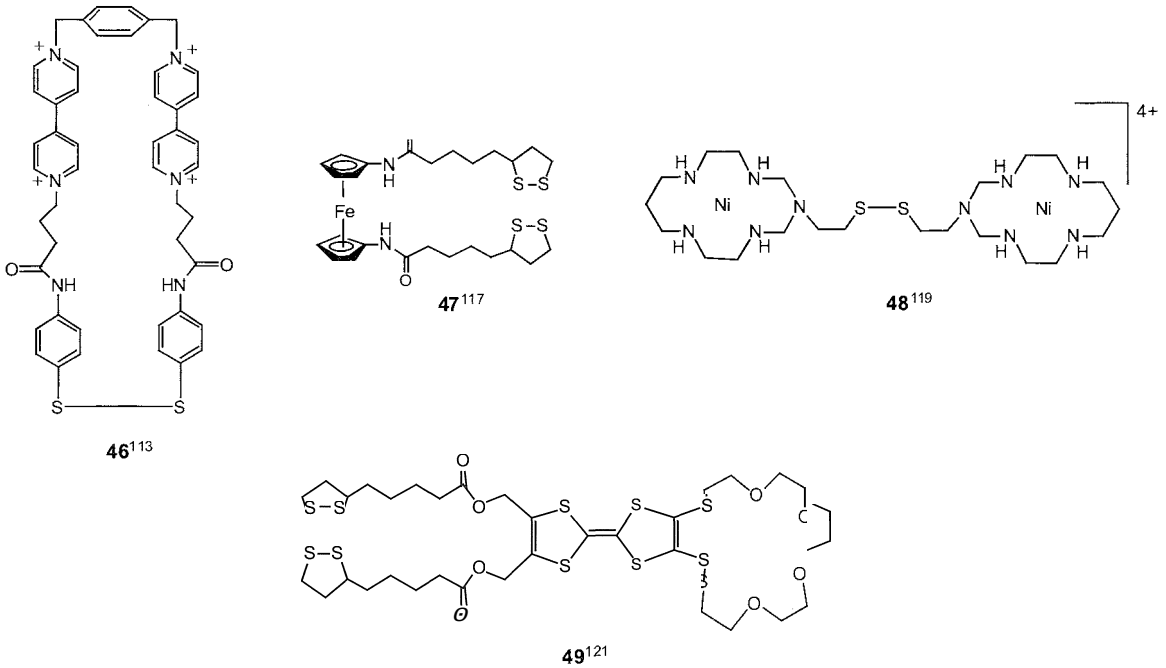

Fig. 11 *Redox-active receptors* that *form self-assembled monolayers* (SAMs) *on electrode* surfaces

(gold electrodes)[117] were *used to sense anions. Functional assemblies on gold colloids have been identified by Willner as potential nanostructured sensing* devices.[118] Astruc *synthesized a series of* mixed *monolayer gold colloids such as 45 (containing 39 ferrocene branches) that responded to anions* in CH_2Cl_2.[116] *Cyclic* voltammetry *studies revealed that the addition of* $H_2PO_4^-$ *to a solution of 45 induced the* formation *of a new ferrocene-centered* redox *wave that was cathodically shifted by* −220 mV *from the original couple that corresponded to the oxidation of the* unbound redox *sites.* An *electrochemical titration revealed that each ferrocene branch formed a 1:1 complex with the anion. Interestingly, the shifts in the* redox *couple were much less with* HSO_4^- *(−30* mV), *with no significant changes observed with nitrate or with the halide anions* Cl^- *or* Br^-.

Beer and Davis *reported* Compound **47**, *which formed a* 1:1 *complex* with $H_2PO_4^-$ *in organic* solvents.[117] *The addition of an excess amount of this anion to a monolayer of* **47** *on a gold electrode in* CH_2Cl_2–CH_3CN *brought about a large cathodic shift in the* Fc^+/Fc redox *couple of* −300 mV. *This shift was significantly larger than the response for the same compound as a freely diffusing species* (−210 mV), *which was indicative of a surface sensing* amplification *effect. As for other anion sensors, a SAM of a* dinickel(II) *complex 48 was found* to *electrochemically respond to a range of anions in aqueous solution. including ATP, as evidenced by cathodic shifts in the* Ni(III)/Ni(II) couple.[119] The *results were consistent with axial coordination of the nickel center by either one or two anions, but* only *in the* +3 *oxidation state.*

Cations can also be sensed by SAMs *containing* redox-active TTF[120,121] *or* calix[4]quinone[122] *moieties. The first example of a TTF-containing SAM that responded to cations was reported by Moore and* coworkers.[96,120] *Anodic shifts in the TTF-centered* redox *couple the surface-bound receptor were observed* in *the presence of Croup 1 and Group 2 cations and also* Ag^+. *Echegoyen reported a related dithia-crown ether, 49, containing two* disulfide *arms, that forms particularly stable monolayers and responds to Croup 1 cations* in *a similar* fashion.[121]

CONCLUSION

The objective of this review has been to show how supramolecular *chemistry has made, and is continuing to make. an important contribution to the area of electrochemical sensing. From an applications point of view, future developments will continue to be directed toward recognition and read out at a surface. so that robust voltammetric sensors that are viable alternatives* to *other sensors* (e.g., *biosensors) can be produced. However, fundamental studies are required to further our understanding of how to maximize substrate selectivity. while maintaining an effective electrochemical response to* complexation. *Switchable* ''on/off'' *binding processes,*[9,124,125] *where* complexation *strength can be closely controlled by* redox *processes. are likely to become increasingly important. Recent developments in molecular recognition and sensing using redox-active* dendrimers[126–129] and nanoparticles[116,118,123,130] *are*

likely to widen interest in this area even further, as will the continuing development of novel electrochemical methods[131–134] for the detection of a range of species.

ARTICLES OF FURTHER INTEREST

Crown Ethers, p. 326
Energy and Electron Transfer in Supramolecular Systems, p. 535
Fluorescent Sensors, p. 572
Ion-Selective Electrodes. p. 747
Organometallic Anion Receptors. p. *1006*

REFERENCES

1. Lehn. J.-M. *Supramolecular Chemistry,* Concepts and *Perspectives*; VCH: Weinheim, 1995.
2. Kaifer, A.E.: Gbmez-Kaifer. M. *Supramolecular* Electro-*chemistry*; Wiley–VCH, 1999.
3. Steed, J.W.; Atwood, J.L. *Supramolecular Chemistry*; Wiley, 2000.
4. Bakker, E.; Telting-Diaz, M. Electrochemical sensors. Anal. Chem. 2002; 74. 2781–2800.
5. Lawrence. N.S.: Beckett. E.L.; Davis. J.: Compton. R.C. Advances in the voltammetric analysis of small biologically relevant compounds. Anal. Biochem. 2002.303. 1–16.
6. Coldenberg, L.M.: Bryce. M.R.; Petty. M.C. Chemsensor devices: Voltammetric molecular recognition at solid interfaces. J. Mater. Chem. 1999. 9. 1957–1974.
7. Ashton. P.R.: Balzani. V.: Cleniente-Leon. M.; Colonna. B.; Credi, A.: Jayaraman. N.; Raymo. F.M.; Stoddart, J.F.: Venturi. M. Ferrocene-containing carbohydrate dendrimers. Chern. Eur. J. 2002. 8. 673–684 and references therein.
8. Miller, S.R.: Gutowski. D.A.: Chen, Z.-H.: Gokel, G.W.: Echegoyen. L.: Kaifer, A.E. Rationalization of the unusual electrocheniical-behavior observed in lariat ethers and other reducible macrocyclic systems. Anal. Chern. 1988. 60. 2021–2024.
9. Tucker. J.H.R.; Collinson, S.R. Recent developments in the redox-switched binding of organic compounds. Chem. Soc. Rev. 2002, *31*. 147–156.
10. Beer. P.D.; Gale. P.A.: Chen. G.Z. Electrochemical molecular recognition: Pathways between complexation and signalling. J. Chem. Soc., Dalton Trans. 1999. 1897–1909.
11. Beer, P.D. Transition metal receptor systems for the selective recognition and sensing of anionic guest species. Acc. Chem. Res. 1998. 31. 71–80.
12. Beer, P.D. Redox responsive macrocyclic receptor molecules containing transition-metal redox centers. Chem. Soc. Rev. 1989. *18*. 409–450.
13. Boulas. P.L.: Gómez-Kaifer. M.; Echegoyen, L. Electrochemistry of supramolecular systems. Angew. Chem. Int. Ed. 1998. 37, 216–247.
14. Kaifer. A.E. Interplay between molecular recogntion and redox chemistry. Acc. Chem. Res. 1999. 32. 62–71.
15. Niemz, 4.; Rotello. V.M. From enzyme to molecular device. Exploring the interdependence of redox and molecular recognition. Acc. Chem. Res. **1999**. *32*. 44–52.
16. Oepen, G.; Vogtle. F. Ligandstruktur und Komplexierung. XLVI. Ferrocen-Kronether. Liebigs Ann. Chem. **1979**. 1094–1101.
17. Biernat. J.F.; Wilczewski. T. Macrocyclic polyfunctional Lewis bases—VI. Polyoxaferrocenophanes. Tetrahedron **1980**. 36. 2521 and references therein.
18. Bell. A.P.; Hall. C.D. Synthesis of macrocyclic compounds containing the ferrocene unit. J. Chem. Soc., Chern. Commun. 1980, 163.
19. Medina. J.C.: Goodnow. T.T.: Rojas. M.T.: Atwood. J.L.: Lynn, B.C.: Kaifer, A.E.; Gokel, G.W. Ferrocenyl iron as a donor group for complexed silver in ferrocenyldimethyl[2.2]cryptand—A redox-switched receptor effective in water. J. Am. Chem. Soc. 1992.114. 10583–10595.
20. Hall. C.D.: Sharpe, N.W.: Danks, I.P.; Sang. Y.P.J. Cyclic voltammetry studies on the complexation of metal-cations by cryptands containing the ferrocene unit. Chem. Soc., Chem. Commun. 1989. 419–421.
21. Saji. T.; Kinoshita, Electrochemical ion-transport with ferrocene functionalized crown-ether I. J. Chem. Soc., Chem. Commun. 1986. 716–717.
22. Beer. P.D.; Sikanyika, H.: Blackburn, C.: McAleer, J.F.: Drew. M.G.B. Redox-responsive crown ethers containing a direct link between the ferrocene redox-active center and a benzo-crown ether—Crystal-structures of a ferrocene benzo-15-crown-5 ligand and of its sodium complex. J. Chem. Soc., Dalton Trans. 1990. 3295–3300.
23. Plenio. H.; Diodone, R. Complexation of Na^+ in redox-active ferrocene crown-ethers. a structural investigation. and an unexpected case of Li^+ selectivity. Inorg. Chem. 1995. 34. 3964–3972.
24. Grossel. M.C.: Goldspink. M.R.: Hriljac. J.A.: Weston. S.C. Metallocene-bridged cryptands. 2. Solid-state studies of some ferrocene amides and their cryptand analogs. Organometallics 1991. 10. 851–860.
25. Beer. P.D.: Crowe. D.B.; Ogden, M.I.; Drew, M.G.B.; Main. B. Ammonium redox-responsive receptors containing multiple ferrocene and quinone redox-active centers attached to di-aza and tri-aza crown-ether macrocycles. J. Chern. Soc., Dalton Trans. 1993. 2107–2116.
26. Beer, P.D.: Chen. Z.: Ogden, M.I. Voltammetric and NMR-studies of a *bis*(ferrocenecarboxamide)-substituted diara 18-crown-6 receptor that simultaneously complexes and electrochemically recognizes both cations and anions. J. Chem. Soc., Faraday Trans. 1995. 295–302.
27. Beer. P.D.; Danks. J.P.: Hesek. D.: McAleer. J.F. A potassium-selective sulfide-linked redox-active ferrocene ionophore that exhibits extraordinary electrochemical recognition behavior. J. Chem Soc., Chern. Commun. 8993. 1735–1737.
28. Dol. G.C.; Kamer. P.C.J.; Hartl. F.: van Leeuwen. P.W.N.M.: Nolte. R.J.M. Electrochemical and binding properties of a novel ferrocene-containing redox-active basket-shaped host molecule. J. Chem. Soc., Dalton Trans. 1998. 2083–2090.

29. Beer. P.D.: Sikanyika. H.: Blackburn, C.; McAleer, J.F. Lithium redox-responsive ferrocene bis-tertiary amide derivatives. J. Organomet. Chem. 1988. 350. C15–C19.
Sutcliffe. O.B.; Chesney. A.: Bryce. M.R. Voltammetric cation sensors based on ferrocene derivatives with oxaline and imine substituents. J. Organomet. Chem. 2001, *637–639*, 134–138.
Brindley, G.D.: Fox. O.D.; Beer, P.D. Ferrocene-appended and bridged calixarene ligands for the electrochemical sensing of trivalent lanthanide ions. J. Chern. Soc., Dalton Trans. 2000, 4354–4359.
Plenio. H.; Aberle, C.: Al Shihadeh. Y.: Lloris, J.M.: Martinez-Miner, R.: Pardo. T.; Soto. J. Ferrocene-cyclam: A redox-active macrocycle for the complexation of transition metal ions and a study on the influence of the relative permittivity on the coulombic interaction between metal cations. Chem. Eur. J. 2001. *7*, 2848–2861 and references therein.

33. Beer. P.D.: Smith, D.K. Tunable *bis*(ferrocenyl) receptors for the solution-phase electrochemical sensing of transition metal cations. J. Chern. Soc., Dalton Trans. 1998. 417–423 and references therein.

34. Costa. J.: Delgado, R.: Drew. M.G.B.: Félix, V.: Saint-Maurice, A. A new redox-responsive 14-membered tetraazamacrocycle with ferrocenylmethyl arms as receptor for sensing transition-metal ions. J. Chem. Soc., Dalton Trans. 2000. 1907–1916 and references therein.
Lloris. J.M.; Martinez-Miner. R.: Soto, J.: Pardo, T.J. An electrochemical study in acetonitrile of macrocyclic or open-chain ferrocene-containing oxa-aza or polyaza receptors in the presence of protons. metal cations and anions. J. Organornet. Chem. 2001. *637–639*. 151–158 and references therein.

36. Beer. P.D.: Bernhardt, P.V. A ferrocene-functionalised macrocyclic receptor for cations and anions. J. Chem. Soc., Dalton Trans. 2001. 1428–1431.

37. Ion. A.: Buda. M.; Moutet. J.-C.; Saint-Aman. E.; Royal. G.; Gautier-Luneau. I.: Bonin, M.; Ziessel. R. Coordination of ferrocenyl ligands bearing bipy subunits: Electrochemical. structural and spectroscopic studies. Eur. J. Inorg. Chern. 2002. 1357–1366.
Carr. J.D.: Coles. S.J.: Hursthouse, M.B.: Tucker, J.H.R. The effect of d-block metal cornplexation on the spectroscopic and redox properties of ferrocene derivatives containing pyridine ligands. J. Organomet. Chem. 2001. 637–639. 304–310.
Delavaux-Nicot, B.: Bigeard, A.: Bousseksou, A.: Comnienges. G. Reactivity of the acyclic diazadioxa redox active ligand $[(C_5H_5)Fe(C_5H_4CH_2N(CH_3)(CH_2)_2OCH_2-)]_2$: NMR. electrochemical. and Mössbauer studies. Crystal structure of its copper complex. Inorg. Chem. 1997, 36. 4789–4797.
Sato. M.; Anano. H. The transition-metal cornplexes of the thiamacrocycle containing two ferrocene nuclei in the main chain. Synthesis. properties, and molecular structure of Ag(I), Cu(I), Pd(II), and Pt(II) complexes of 1.5.16.21-tetrathia[5.5]ferrocenophane. J. Organomet. Chem. 1998. *555*. 167–175 and references therein.
Bushell, K.; Gialou. C.: Goh. C.H.: Long, W.J.: Martin, J.; White. A.J.P.: Williams, C.K.: Williams. D.J.; Fontani. M.; Zanello. P. Synthesis and characterisation of novel multidentate ferrocene ligands and their Re(I) and Pt(II) complexes. J. Organomet. Chem. 2001. 637–639. 418–425 and references therein.

42. Plenio, H.: Yang, J.J.; Diodone. R.; Heinze. J. Redox-switched bonding of protons to ferrocenophanes, ferrocene cryptands. and simple ferrocene amines—Correlation of x-ray structural data and cyclic voltammetry derived redox potentials. Inorg. Chem. 1994. 33. 4098–4104.

43. Beer, P.D.; Keefe. A.D. A new approach to the coordination of anions. novel polycobalticinium macrocyclic receptor molecules. J. Organomet. Chem. 1989. 375. C40.

44. Kingston. J.E.: Ashford. L.; Beer. P.D.; Drew. M.G.B. Anion recognition and sensing by neutral and charged transition metal co-ordinated ferrocene phosphine amide receptors. J. Chem. Soc., Dalton Trans. 1999. 251–257.

45. Beer. P.D.; Hesek. D.: Nam. K.C.: Drew. M.G.B. Anion recognition properties of new upper-rim cobaltocenium calix[4]arene receptors. Organometallics 1999. IS. 3933–3943.

46. Beer. P.D.: Drew, M.G.B.: Smith. D.K. Selective electrochemical recognition of bidentate anionic guests in competitive solvents using novel ferrocenyl thiourea and guanidinium receptors. J. Organomet. Chern. 1997. *543*, 259–261.

47. Beer, P.D.; Cadman, J.; Lloris. J.M.: Martinez-Miner. R.: Soto, J.; Pardo, T.; Marcos. M.D. Anion interaction with ferrocene-functionalised cyclic and open-chain polyaza and aza–oxa cycloalkanes. J. Chem. Soc., Dalton Trans. 2000. 1805 1812 and references therein.

48. Beer, P.D.: Cadman. J.: Lloris. J.M.: Martínez-Mánez, R.; Padilla. M.E.; Pardo. T.: Smith. D.K.: Soto. J. Selective electrochemical recognition of sulfate over phosphate and phosphate over sulfate using plyaza ferrocene macrocyclic receptors in aqueous solution. J. Chern. Soc., Dalton Trans. 1999, 127–133 and references therein.

49. Gale. P.A.: Hursthouse. M.B.: Light, M.E.; Sessler, J.L.; Warriner. C.N.: Zimmerman. R.S. Ferrocene-substituted calix[4]pyrole: A new electrochemical sensor for anions involving CH. . .anion hydrogen bonds. Tetrahedron Lett. 2001. 42. 6759–6762.

50. Denault, G.: Gale. P.A.: Hursthouse, M.B.: Light, M.E.; Warriner. C.N. Anion complexation and electrochemical behaviour of ferrocene-appended amido-pyrole clefts. New J. Chem. 2002. 26. 811–813.

51. Kavallieratos, K.; Hwang. S.: Crabtree. R.H. Amino-ferrocene derivatives in chloride recognition and electrochemical sensing. Inorg. Chem. 1999. 38. 5184–5186.

52. Abouderbala. L.O.: Belches, W.J.; Boutelle, M.G.: Cragg, P.J.; Steed. J.W.: Turner. D.R.: Wallace. K.J. Cooperative anion binding and electrochemical sensing by molecular podands. Proc. Nat. Acad. Sci. 2002. 99, 5001–5006.

53. Reynes, O.; Maillard, F.: Moutet. J.-C.; Royal, G.: Saint-Aman. E.: Stanciu. G.; Dutasta, J.-P.: Gosse. I.; Mulatier. J.-C. Complexation and electrochemical sensing of anions by amide-substituted ferrocenyl ligands. J. Organomet. Chem. 2001. 637–639. 356–363.
Sessler, J.P.: Zimmerman. R.S.: Kirkovits, G.J.; Gebauer.

A.; Scherer, M.J. Synthesis and dihydrogen phosphate binding properties of pyrrole containing ansa-ferrocenes. J. Organomet. Chem. **2001**, *637–639*, 343–348.
55. Reynes, O.; Moutet, J.-C.; Pecaut, J.; Royal, G.; Saint-Aman, E. (Ferrocenylmethyl)trimethylammonium cation: A very simple probe for the electrochemical sensing of dihydrogen phosphate and ATP anions. New. J. Chem. **2002**, *26*, 9–12.
56. Dusemund, C.; Sandanayake, K.R.A.S.; Shinkai, S. Chem. Commun. **1995**, 333–334.
57. Aldridge, S.; Bresner, C.; Fallis, I.A.; Coles, S.J.; Hursthouse, M.B. Multidentate Lewis acids: Synthesis, structure and mode of action of a redox-based fluoride ion sensor. Chem. Commun. **2002**, 740–741.
58. Fabre, B.; Lehmann, U.; Schlüter, A.D. Boronic ester-substituted terpyridine metal complex as a novel fluoride-sensitive redox receptor. Electrochim. Acta **2001**, *46*, 2855–2861 and references therein.
59. Ori, A.; Shinkai, S. Electrochemical detection of saccharides by the redox cycle of a chiral ferrocenylboronic acid-derivative—A novel method for sugar sensing J. Chem. Soc., Chem. Commun. **1995**, 1771–1772.
60. Carr, J.D.; Lambert, L.; Hibbs, D.E.; Hursthouse, M.B.; Malik, K.M.A.; Tucker, J.H.R. Novel electrochemical sensors for neutral molecules. Chem. Commun. **1997**, 1649–1651.
61. Carr, J.D.; Coles, S.J.; Hursthouse, M.B.; Light, M.E.; Tucker, J.H.R.; Westwood, J. Redox-switched control of binding strength in hydrogen-bonded metallocene complexes. Angew. Chem. Int. Ed. **2000**, *39*, 3296.
62. Collinson, S.R.; Gelbrich, T.; Hursthouse, M.B.; Tucker, J.H.R. Novel ferrocene receptors for barbiturates and ureas. Chem. Commun. **2001**, 555–556.
63. Saweczko, P.; Enright, G.D.; Kraatz, H.B. Interaction of ferrocenoyl-dipeptides with 3-aminopyrazole derivatives: β-sheet models? A synthetic, spectroscopic, structural, and electrochemical study. Inorg. Chem. **2001**, *40*, 4409–4419.
64. Beer, P.D.; Chen, Z.; Drew, M.G.B.; Gale, P.A. Synthesis and x-ray crystal structure of a new redox-active calix[5]arene containing a totally included ethanol molecule. J. Chem. Soc., Chem. Commun. **1995**, 1851–1852.
65. Inouye, M.; Itoh, M.S.; Nakazumi, H. Ferrocene-modified bis(sipropyridopyran)s as synthetic signaling receptors for guanine-guanine dinucleoside derivatives. Chem. Commun. **2001**, 2432–2433.
66. Li, C.S.; Medina, J.C.; Maguire, G.E.M.; Abel, E.; Atwood, J.L.; Gokel, G.W. Neutral molecule receptor systems using ferrocene's "atomic ball bearing" character as the flexible element. J. Am. Chem. Soc. **1997**, *119*, 1609–1618.
67. Arimori, A.; Ushiroda, S.; Peter, L.M.; Jenkins, A.T.A.; James, T.D. A modular electrochemical sensor for saccharides. Chem. Commun. **2002**, 2368–2369.
68. Laurent, P.; Miyaji, H.; Collinson, S.R.; Prokes, I.; Moody, C.J.; Tucker, J.H.R.; Slawin, A.M.Z. Asymmetric synthesis of chiral α-ferrocenylalkylamines and their use in the preparation of chiral redox-active receptors. Org. Lett. **2002**, *4*, 4037–4040.
69. Abbott, A.P.; Barker, G.W.; Davies, D.L.; Griffiths, G.A.; Walter, A.J.; Kocovsky, P. Electrochemical recognition of chiral species using quaternary ammonium binaphthyl salts. Anal. Chem. **2002**, *74*, 4002–4006.
70. Moutet, J.-C.; Saint-Aman, E.; Ungureanu, E.-M.; Arion, V.; Gerbeleu, N.; Revenco, M. Heterodinucleating macrocyclic compounds designed for electrochemical recognition. Electrochim. Acta **2001**, *46*, 2733–2740 and references therein.
71. Piotrowski, H.; Hilt, G.; Schulz, A.; Mayer, P.; Polborn, K.; Severin, K. Self-assembled organometallic [12]metallocrown-3 complexes. Chem. Eur. J. **2001**, *7*, 3197–3208.
72. Lehaire, M.-L.; Scopelliti, R.; Piotrowski, H.; Severin, K. Selective recognition of fluoride anion using a Li^+-metallacrown complex. Angew. Chem. Int. Ed. **2002**, *41*, 1419–1422.
73. Song, L.-C.; Guo, D.-S.; Su, Q.-M.; Hu, F.-H.; Sun, J.; Huang, X.-Y. Synthesis and electrochemical properties of organometallic macrocyclic crown ethers containing redox-active tetrahedral $Mo_2Fe(\mu_3\text{-}S)$ cluster cores. J. Organomet. Chem. **2001**, *622*, 210–220.
74. Shephard, D.S.; Johnson, B.F.G.; Matters, J.; Parsons, S. Novel redox-active ruthenium cluster crown compounds capable of host–guest chemistry. J. Chem. Soc., Dalton Trans. **1998**, 2289–2291.
75. Plenio, H.; Burth, D. Indenyl crown ethers: Heterotopic ligands with π- and s-faces and the synthesis of cymantrene and coboltocene crown ethers and their alkaline metal ion complexes. Organometallics **1996**, *15*, 1151–1156.
76. Yam, V.W.-W.; Lo, K.K.-W.; Cheung, K.-K. Synthesis and crystal structure of a novel copper(I) crown complex: A spectrochemical metal ion probe for alkali metal and alkaline earth metal cations. Inorg. Chem. **1995**, *34*, 4013–4014.
77. Lowe, N.D.; Garner, C.D. Transition-metal complexes of crown ether benzodithiolenes. Part 2. The effects of alkali-metal cation binding. J. Chem. Soc., Dalton Trans. **1993**, 3333–3340 and references therein.
78. Nadasdi, T.T.; Stephan, D.W. Redox-active macrocycles as metalloligands—Synthesis, electrochemistry, and structure of silver(I) and copper(I) complexes of $Cp_2Ti(eta\text{-}S(CH_2)_nS)_2TiCp_2$ (n = 2, 3). Organometallics **1992**, *11*, 116–122.
79. Beer, P.D.; Szemes, F.; Balzani, V.; Sala, C.M.; Drew, M.G.B.; Dent, S.W.; Maestri, M. Anion selective recognition and sensing by novel macrocyclic transition metal receptor systems. ^1H NMR, electrochemical and photophysical investigations. J. Am. Chem. Soc. **1997**, *119*, 11864–11875.
80. van Doorn, A.R.; Bos, M.; Harkema, S.; van Eerden, J.; Verboom, W.; Reinhoudt, D.N. Molecular recognition of neutral molecules by metalloclefts: Synthesis, X-ray structure, ^1H NMR spectroscopy, electrochemistry, and molecular recognition. J. Org. Chem. **1991**, *56*, 2371–2380.
81. Delgado, M.; Gutowski, D.A.; Yoo, H.K.; Gatto, V.J.; Gokel, G.W. Contrasting one-cation and 2-cation binding behavior in syn-anthraquinone and anti-anthraquinone

bibracchial podand (bip) mono-anions and dianions assessed by cyclic voltammetry and electron-paramagnetic resonance spectroscopy. J. Am. Chem. Soc. 1988. *110*, 119–124 and references therein.

82. Chen, Z.; Schall, O.F.; Alcalá, Y.; Li, Y.: Gokel. G.W.; Echegoyen. L. Unusual 1-2 ligand-metal complex-formation between an anthraquinone cryptand and Li^+. J. Am. Chem. Soc. **1992**, *114*. 444–451 and references therein.
83. Delgado, M.: Wolf. J.R.E.: Hartman, J.R.; McCafferty, G.; Yagbasan, R.; Rawle. S.C.; Watkin. D.J.: Cooper. S.R. Redox-active crown ethers—Electrochemical and electron-paramagnetic resonance studies on alkali-metal complexes of quinone crown ethers. J. Am. Chem. Soc. 1992, *114*, 8983–8991 and references therein.
84. Echegoyen. L.E.: Yoo. H.K.; Gatto, V.J.: Gokel, G.W. Cation-transport using anthraquinone-derived lariat ethers and podands—The 1st example of electrochemically switched on off activation deactivation. J. Am. Chem. Soc. 1989. *111*, 2440–2443.
85. Tucker. J.H.R.: Shionoya. M.; Koike. T.; Kimura. E. A zinc(II)-cyclen complex attached to an anthraquinone moiety that acts as a redox-active nucleobase receptor in aqueous solution. Bull. Chem. Soc. Jpn. **1995**, *68*. 2465–2469.
86. Webber. P.R.A.: Chen. G.Z.; Drew, M.G.B.: Beer. P.D. Cesium and rubidium-selective redox-active *bis*(calix[4]-diquinone) ionophores. Angew. Chem. Int. Ed. 2001. *40*, 2265–2268.
87. Goldenberg, L.M.; Denisov, N.N.; Biernat, J.F.: Petty, M.C. Electrochemical recognition properties of 13- and 16-membered azo- and azoxycrowns in solution. J. Electroanal. Chem. **2001**, *509*. 42–47 and references therein.
88. Gutowski, D.A.; Gatto, V.J.; Kaifer. A.: Echegoyen, L.; Godt. R.E.: Gokel. G.W. Cation effects on the cyclic voltammograms of azotoluene and the potassium cation selectivity of the electrochemically reduced azo-cryptand 7,16-azobis(1,3-phenylenemethylene)-1.4.10.13-tetraoxa-7,16-diazaoctadecane J. Chem. Soc., Chem. Commun. 1984. 923–925.
89. Gutowski. D.A.: Echegoyen. L.; Goli, D.M.: Kaifer, A.E.: Schultz. R.A.: Gokel. G.W. Electrochemically switched cation binding in nitrobenzene-substituted. nitrogen-pivot lariat ethers. J. Am. Chem. Soc. 1984. *106*. 1633–1635.
90. Bourgeois, J.-P.: Echegoyen. L.: Fibbioli, M.: Pretsch, E.: Diederich. F. Regioselective synthesis of *trans*-1 fullerene *bis*-adducts directed by a crown ether tether: Alkali metal cation modulated redox properties of fullerene-crown ether conjugates. Angew. Chem. Int. Ed. 1998. *37*. 2118–2121.
91. Mayor. M.; Lehn. J.-M. Potassium crpptate of a macrobicyclic ligand featuring a reducible hexakis(phenylthio)benzene electron-acceptor site. Helv. Chim. Acta **1997**, *80*, 2277–2284.
92. Beer, P.D.; Chen. Z.; Grieve. A.; Haggitt. J. A new bipyridinium bis benzo crown-ether ligand whose redox properties are dependent upon complexed cation-induced conformational switching effects. J. Chem. Soc., Chern. Commun. 1994, 2413–2414.
93. Ge, Y.: Miller. L.: Ouimet. T. Smith D.K. Electrochemically controlled hydrogen bonding. o-Quinones as simple redox-dependent receptors for arylureas. J. Org. Chem. **2000**. *65*. 8831–8838.
94. Le Derf, F.; Mazari. M.; Mercier. N.: Levillain, E.: Trippé, G.; Riou, A.; Richomme, P.: Becher. J.: Garín, J.; Orduna. J.: Gallego-Planas, N.; Gorgues, A.; Sallé. M. Tetrathiafulvalene crowns: Redox-switchable ligands. Chem Eur. J. **2001**. *7*. 447–455. and references therein.
95. Le Derf, F.: Mazari. M.; Mercier, N.: Levillain. E.; Richomme. P.: Becher, J.: Garin, J.; Orduna. J.; Gorgues. A.; Salle. M. Thiacrown ether tetrathiafulvalene derivatives as redox responsive ligands. Chem. Commun. 1999. 1417–1418.
96. Nielsen, M.B.; Lomholt, C.; Becher, J. Tetrathiafulvalenes as building blocks in supramolecular chemistry II. Chem. Soc. Rev. 2000. 29. 153–164.
97. Goldenberg. L.M.; Neilands, O. Hydrogen bond complexation of dimethyl-[1-butyl-2,4-dioxo-(1H,3H)pyrimido]tetrathiafulvalene with aminopyridine derivatives probed by cyclic voltammetry. J. Electroanal. Chem. 1999. *463*. 212–217.
98. Trippé, G.: Levillain, E.: Le Derf. F.: Trippé, 6.; Gorgues, A.: Becher. J.: Sallé, M.: Jeppesen. J.O.: Nielsen. K.; Becher, J. Electrochemical recognition of cations by *bis*(pyrrolo)tetrathiafulvalene macrocycles. Org. Lett. 2002. *4*, 2461–2464.
99. Johnston, *B.:* Goldenberg. L.M.: Bryce. M.R.; Kataky, R. A tetrathiafulvalene derivative with an acyclic S-4 domain as a voltammetric silver sensor. J. Chem. Soc. Perkin Trans. 2 2000. 189–190.
100. Bryce. M.R.: Batsanov, A.S.: Finn. T.: Hansen, T.K.: Howard. J.A.K.; Kamenjicki. M.; Lednev. I.K.; Asher, S.A. Crown-annelated 9,10-*bis*(1,3-dithiol-2-ylidene)-9,10-dihydroanthracene derivatives: A new efficient transducer in the electrochemical and spectroscopic monitoring of metal complexation. Chem. Commun. 2000. 295–296.
101. Pearson. A.J.: Hwang. J.-J. Crown-annelated *p*-phenylenediamine derivatives as electrochemical and fluorescence-responsive chemosensors: Cyclic voltammetry studies. Tetrahedron Lett. **2001**. 3541–3543.
102. Costero. A.M.: Monrabal. E.; Andreu, C.: Martínez-Mánez, R.: Soto, J.; Padilla-Tosta, M.: Pardo, T.; Ochando. L.E.: Amigó, J.M. Synthesis, solution and electrochemical behaviour of new aza-crown ethers derived from biphenyl. J. Chem. Soc., Dalton Trans. **2000**. 361–367.
103. McQuade, D.T.: Pullen, A.E.: Swager, T.M. Conjugated polymer-based chemical sensors. Chem. Rev. 2000. *100*. 2537–2574.
104. Korri Youssoufi. H.: Hmyene. M.; Garnier, F.: Delabouglise. D. Cation recognition properties of polypyrrole 3-substituted by azacrown ethers. J. Chem. Soc., Chem. Commun. 1993. 1550–1552.
105. Goldenberg, L.M.; Skabara, P.J.: Roberts. D.M.: Berridge. R.: Ortí, E.; Viruela, P.M.: Pou-Amérigo, R. Electrochemical molecular recognition of silver cation by electropolymerised thieno[3′,4′:5,6][1,4]dithiiono[2,3-b]quinoxaline: A joint experimental and theoretical study. J. Mater. Chem. **2000**. *10*. 2458–2465.
106. Giannetto, M.; Mori. G.; Notti. A.: Pappalardo, S.: Parisi,

M.F. Calixarene-poly(dithiophene)-based chemically modified electrodes. Chem Eur. J. 2001. 7. 3354–3362 and references therein.
107. Nicolas. M.; Fabre. B.: Simonet, J. Boronate-functionalized polypynole as a new fluoride sensing material. Chem. Cornmun. 1999. 881–882 and references therein.
108. Bauerle. P.; Emge, A. Specific recognition of nucleobase-functionalized polythiophenes. Adv. Mater. 1998, 10, 324–330.
109. Emge. A.; Bauerle. P. Molecular recognition properties of nucleobase-functionalized polythiophenes. Synth. Met. 1999, 102. 1370–1373.
110. Ion. A.; Ion. I.: Moutet. J.-C.; Pailleret. A.: Popescu. A.: Saint-Aman. E.: Ungureanu, E.; Siebert. E.: Ziessel. R. Electrochemical recognition of metal cations by redox-active receptors in homogenous solution and in polymer films: Some relevant examples. Sensors and Actuators B 1999. 59. 118–122 and references therein.
111. del Peso. I.; Alonso. B.: Lobete. F.: Casado, C.M.: Cuadrado. I.; del Barrio, J.L. A polymerizable pyrrole-cobaltocenium receptor for the electrochemical recognition of anions in solution and immobilized onto electrode surfaces. Inorg. Chem. Commun. 2002.5. 288–291.
112. Ge. Y.; Smith, D.K. Development of chemical sensors based on redox-dependent receptors. Preparation and characterization of phenanthrenequiiione-modified electrodes. Anal. Chern. 2000. 72. 1860–1865.
113. Rojas, M.T.: Kaifer, A.E. Molecular recognition at the electrode-solution interface. Design, self-assembly, and interfacial binding properties of a molecular sensor. J. Am. Chern. Soc. 1995, *117*, 5883.
114. Yamaguchi, T.: Takahashi, K.: Komura. T. Electrochemical characteristics of viologen carboxylic acid derivatives assembled onto Au electrode as a synthetic receptor for electron-rich compounds. Electrochim. Acta 2001, *46*, 2527–2535.
115. Zhang, L.; Codi'nez, L.A.: Lu, T.: Gokel. G.W.: Kaifer. A.E. Molecular recognition at an interface: Binding of monolayer-anchored ferrocenyl groups by an amphiphilic calixarene host. Angew. Chem. Int. Ed. Engl. 1995, 34. 235.
116. Labande, A.: Ruiz, J.; Astruc. D. Supramolecular gold nanoparticles for the redox recognition of oxoanious: Synthesis. titrations, stereoelectronic effects. and selectivity. J. Am. Chem. Soc. 2002. 124. 1782–1789.
117. Beer, P.D.: Davis. J.J.; Drillsma-Milgrom. D.A.: Szemes, F. Anion recognition and redox sensing amplification by self-assembled monolayers of 1,1′-*bis*(alkyl-*N*-amido)ferrocene. Chem. Commun. 2002, 1716–1717.
118. Shipway, A.N.: Katz. E.: Willner, I. Nanoparticle arrays on surfaces for electronic. optical and sensor applications. ChemPhysChem. 2000. **1.** 18–52.
119. Gobi, K.V.; Ohsaka, T. Anion recognition and electrochemical characteristics of the self-assembled monolayer of nickel(II) azamacrocyclic complex. J. Electroanal. Chem. 2000. *485*, 61–70.
120. Moore. A.J.; Coldenberg. L.; Bryce. M.R.; Petty. M.C.: Monkman. A.P.: Marenco, C.: Yarwood. J.: Joyce. M.J.: Port. S.N. Cation recognition by self-assembled layers of novel crown-annelated tetrathiafulvalenes. Adv. Mater. 1998. 10. 395--398.
121. Liu, S.-G.: Liu. H.: Bandyopadhyay. K.; Gao. Z.; Echegoyen. L. Dithia-crown-annelated tetrathiafulvalene disulfides: Synthesis, electrochemistry, self-assembled films. and metal ion recognition. J. Org. Chem. 2000, 65. 3292–3298.
122. Chung. T.D.; Park. J.: Kim. J.; Lim. H.; Choi. M.-J.; Kim, J.R.: Chang, S.-K.; Kim. H. Self-assembled monolayer of a redox-active calix[4]arene: Voltammetric recognition of the Ba^{2+} ion in aqueous media. Anal. Chem. 2001. 73. 3975–3980.
123. Boal, A.K.; Rotello. V.M. Redox-modulated recognition of flavin by functionalized gold nanoparticles. J. Am. Chem. Soc. 1999, *121*, 4914–4915.
124. Goldston. H.M.. Jr.; Scribner. A.N.; Trammell, S.A.: Tender. L.M. A model recognition switch. Electrochemical control and transduction of imidazole binding by electrode-immobilized microperoxidase-11. Chem. Commun. 2002. 416–417.
125. Balzani, V.; Credi. A.: Raymo. F.M.: Stoddart. F.S. Artificial molecular machines. Angew. Chem. Int. Ed. 2000. 39. 3348–3391.
126. Valério, C.; Fillaut. J.-L.: Ruiz. J.: Guittard, J.; Blais, J.-C.; Astruc, D. The dendritic effect in molecular recognition: Ferrocene dendriiners and their use as supramolecular redox sensors for the recognition of small inorganic anions. J. Am. Chem. Soc. 1997, 119. 2588–2589.
127. Le Derf. F.: Levillain, E.: Trippé, G.; Gorgues, A.; Sallé. M.; Sebastian. R.-M.; Caminade, A.-M.; Majoral, J.-P. Immobilization of redox-active ligands on an electrode: The dendrimer route. Angew. Chem. Int. Ed. 2001. *40*, 224--227.
128. Alonso. B.: Casado, C.M.; Cuadro. I.; Moran. M.; Kaifer. A.E. Effective recognition of $H_2PO_4^-$ by a new series of dendrimers functionalized with ferrocenpl-urea termini. Chem. Commun. 2002, 1778–1779.
129. Casado. C.M.; Cuadrado. I.: Alonso, B.; Moran. M.; Losada, J. Silicon-based fenocenyl dendrimers as anion receptors in solution and immobilized onto electrode surfaces. J. Electroanal. Chem. 1999. 463. 87–92.
130. Daniel. M.-C.; Ruiz. J.: Nlate. S.: Palumbo, J.: Blais, J.C.: Astruc, D. Gold nanoparticles containing redox-active supramolecular dendrons that recognize $H_2PO_4^-$. Chem. Cornmun. 2001. 2000–2001.
131. Choi. S.-J.: Choi, B.-G.; Park, S.-M. Electrochemical sensor for the electrochemically inactive β-D(+)-Glucose using α-cyclodextrin template molecules. Anal. Chem. 2002. 74. 1998–2002.
132. Shioya. T.: Swager, T.M. A reversible resistivity-based nitric oxide sensor. Chem. Commun. 2002. 1364–1365.
133. Takenaka. S. Highly sensitive probe for gene analysis by electrochemical approach. Bull. Chem. Soc. Jpn. 2001, 74. 217–224.
134. Flink. S.: Boukamp, B.A.: van den Berg. A.; van Veggel. F.C.J.M.: Reinhoudt. D.N. Electrochemical detection of electrochemically inactive cations by self-assembled monolayers of crown ethers. J. Am. Chern. Soc. 1998, 120. 4652–4657.

E

Electron Paramagnetic Resonance Spectroscopy

Gunnar Jeschke
Max Planck Institute for Polymer Research, Mainz, Gerrnany

INTRODUCTION

Structures on length scales between 0.3 and 10 nm and dynamics on time scales between approximately 10 ps and 1 ys can be characterized by electron paramagnetic resonance (EQR) spectroscopy if a suprainolecular system contains native paramagnetic centers. such as free radicals or transition metal ions, or if stable free radicals can be introduced as spin probes or labels. Probe concentrations as low as 10 $\mu mol \cdot L^{-1}$ and sample volumes down to *5* µl may be sufficient for recording continuous-wave (CW) EPR spectra at conventional frequencies of 9–35 GHz. Such experiments provide details on the reorientation dynamics of small molecules or paramagnetic side groups that are. in turn, related to weak interactions between molecules. For high-field EPR at frequencies of *95* GHz, sample volumes of 100 nL may suffice. while more sophisticated pulse techniques. such as pulse electron electron double resonance (ELDOR) and electron nuclear double resonance (ENDOR) at *9–35* GHz, require concentrations and sample amounts that may be *5–10* times larger than for CW EPR. The latter techniques can yield pair correlation functions corresponding to specific sites in a supramolecular system and can directly prove contact between different molecules or between molecules and inorganic surfaces. The highly selective addressing of sites of interest by probes or labels combined with the vast amount of information accessible by a broad arsenal of techniques makes EPR spectroscopy an attractive tool for studying complex suprarnolecular systems that lack long-range order.

SCOPE OF EPR SPECTROSCOPY

Native Paramagnetic Species

Paramagnetism is related to single occupation of molecular orbitals. Systems with an odd number of electrons are, thus, necessarily paramagnetic, while the more abundant systems with an even number of electrons have a diamagnetic low-spin state and paramagnetic high-spin states. For most stable molecules. the ground state is diamagnetic. and short-lived excited paramagnetic stales are accessible only by absorption of UV or visible light. In the absence of strong light irradiation, such species do not give rise to EPR signals. For this reason, EPR spectroscopy is not a generally applicable method for structure determination. On the other hand, the rareness of paramagnetic centers greatly enhances the resolution in the spectra and simplifies the assignment of the lines in applications to complex materials such as supramolecular assemblies.

A few stable molecules, notably NO and NO_2, have an odd number of electrons and are accessible to EPR spectroscopy. The most important class of such molecules is comprised of the nitroxide stable free radicals.[1,2] In the solid state. where diffusion is slow, dilute radicals may be metastable for long times, in particular, when the unpaired electron is strongly delocalized over a system of conjugated bonds. Further molecules and macromolecules have a high-spin ground state.[3] Some can be detected directly by EPR. while others, such as O_2 with an extremely fast-relaxing ground-state triplet enhance relaxation and thus broaden lines of other paramagnetic species.[4] Solid inorganic networks have structural discontinuity at their surface that often gives rise to so-called dangling bonds. For particle sizes in the nanometer to micrometer range, the specific surface and thus the concentration of such dangling bonds may be sufficient for detection by EPR spectroscopy.

Among transition metal and rare earth metal ions, there is a sizeable number of stable species with an odd number of electrons, prominent examples being Ti^{3+}, VO^{2+}, Cr^{3+}, Mn^{2+}, Fe^{3+}, Co^{2+}, Cu^{2+}, Ce^{3+}, Nd^{3+}, Dy^{3+}, and Er^{3+}. Most of these species are catalytically active, and a number of them were studied in zeolite-type materials.[4] For these ions. a low-spin ground state with total electron spin $S=1/2$ is attained due to electron pairing in strong ligand fields. Complexes with weak ligand fields may have high-spin ground states; for instance, $S=3/2$ for Co^{2+} ($3d^7$), and $S=5/2$ for Fe^{3+} ($3d^5$). This is significant. as high-spin species tend to have more complicated spectra and shorter relaxation times and are thus more difficult to study. However, transition metal ions with an even number of electrons can only be studied in their high-spin states. the low-spin states being diamagnetic. These species have integer spin and transitions that are observable only at high fields and frequencies,[6]

Encyclopedia of Supramolecular Chemistry
DOI: 10.1081/E-ESMC 120019194

unless symmetry is high enough to cause degeneracy of two states at zero field (cubic symmetry or at least one rotation axis C_n with $n \geq 3$).

Stable Free Radicals Suitable as Probes or Labels

The structures and dynamics of supramolecular assemblies are usually complex and cannot be completely characterized by a single technique. This is particularly true for functional systems, which require a minimum size of a few nanometers and a certain balance between flexibility and rigidity to allow for reproducible changes of their states. The difficulties in characterizing such systems are readily apparent for a natural class of supramolecular systems, namely, membrane proteins that are functional when embedded in a lipid bilayer and tend to be extremely difficult to crystallize. To understand structure-dynamics-function relationships of such systems, many pieces of information on length scales between 1 Å and several nanometers and time scales between picoseconds and milliseconds have to be assembled and interpreted. The samples are often macroscopically disordered systems, and the conformation of the molecules is distributed to some extent. Techniques for local characterization of structures and dynamics at selected sites are required to reduce the complexity of the problem.

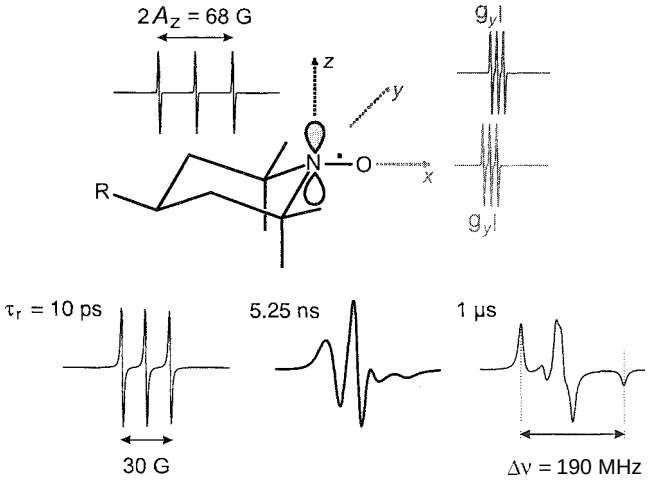

Fig. 1 Orientation dependence of nitroxide spin-probe EPR spectra and dynamical effects on line shapes (simulations). Maximum hyperfine splitting A, is observed along the lobes of the singly occupied molecular orbital (z direction). Within the xy plane, spectra at X band frequencies differ only slightly due to g anisotropy. Dynamic spectra are shown for rotational correlation times τ_r corresponding to the fast limit (10 ps), slow tumbling ($\tau_1 = 1/\Delta\nu = 5.25$ ns), and the rigid limit (1 ys). (*View* this *art* in *color* at *www.dekker.com.*)

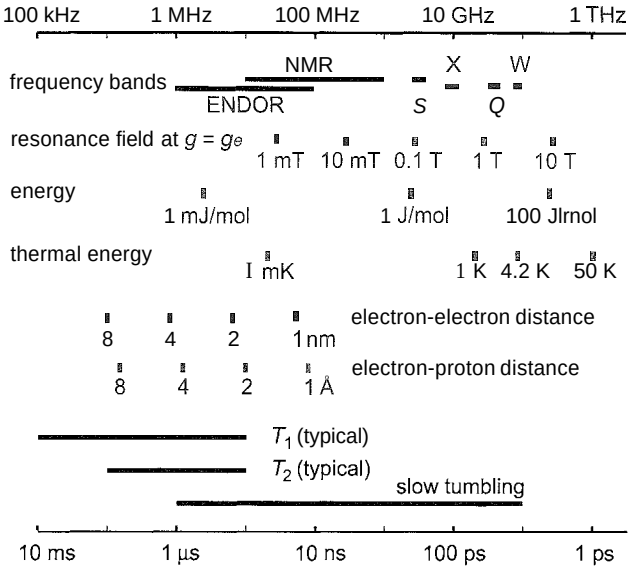

Fig. 2 Frequencies, magnetic fields, energies, length scales. and time scales relevant in EPR spectroscopy (logarithmic scale).

These factors represent the rationale for using probes, which mimic certain constituent parts of the system, or site-selective labels. In a spin probe (in the following, this term includes labels). the electron should be well localized to allow for measurements with high spatial resolution. Furthermore, a moderate anisotropy of the spin interactions is favorable, as this introduces information on reorientation dynamics of the probe into the spectra. Finally. probes should be as small as possible to avoid undue interference with the observed system. Nitroxide-free radicals (Fig. 1) nicely fulfill all the requirements and are available with a broad range of additional functional groups.[1,2,7] The spin is almost equally distributed between two p orbitals on the N and O atoms of the nitroxide group, with little spin density on adjacent carbon atoms. The anisotropies of the hyperfine coupling to the nitrogen nucleus and the g tensor correspond to widths of the powder pattern of a few 10 mT at typical EPR frequencies between 9.5 and 95 GHz (see Fig. 2 for designations of EPR frequency bands). The N–O group and the neighboring groups, which prevent dimerization by sterical hindrance, roughly fit into a rotational ellipsoid with an extension of 0.7 nm x 0.5 nm. Probes such as TEMPO (2,2,6,6-tetramethyl-piperidine-1-oxyl) are soluble with the required concentrations of approximately 1 mM in a broad range of solvents. including for instance toluene and water. as the molecule as a whole is largely unpolar, while the slightly polar N–O group can take part in hydrogen bonds.

Transition metal ions are less widely applicable as spin probes but may be convenient for addressing ionic clusters or ligand moieties[8] or for substituting diamagnetic ions.

For substitution of diamagnetic Mg^{2+} ions by paramagnetic Mn^{2+} ions. the perturbation of the system is almost not perceptible, as evidenced by some metalloproteins that function with both of these ions.

Sensitivity

In general. sensitivity of spectroscopies increases with frequencies of the photons that excite the transitions. EPR spectroscopy ($\sim 10^{10}$–10^{11} Hz) is thus significantly less sensitive than optical spectroscopy ($\sim 10^{15}$ Hz) and vibrational spectroscopy ($\sim 10^{13}$ Hz) and significantly more sensitive than NMR spectroscopy ($\sim 10^{7}$–10^{9} Hz). Typical concentrations of paramagnetic centers in EPR spectroscopy are between 50 μM and 2 mM. In this range, the whole arsenal of CW[9,10] and modern pulsed EPR methods[11] can be applied. Usually. CW EPR spectra of good quality can be acquired for concentrations as low as 10 μM, and free radicals can be detected at least down to concentrations of 1 μM. Typical sample volumes with standard equipment are 150 μl at X-band frequencies, which can be decreased to 5 μl using loop-gap resonators. A sample amount corresponding to 2.5 nmol paramagnetic centers is thus sufficient for a broad range of techniques at X band, while CW EPR can be performed down to sample amounts of approximately 0.1 nmol. As spectra of transition metal ions are broader, 5–10 times higher concentrations may be needed for those species.

The required sample volume in EPR spectroscopy roughly scales with the cube of the wavelength. A sample volume of 100 nL is sufficient for all experiments at W-band frequencies. Despite a moderate decrease in concentration sensitivity when going to frequencies higher than 35 GHz. high-frequency EPR can thus deal with minute amounts of paramagnetic centers.

RELATION OF SPIN INTERACTIONS TO STRUCTURE AND DYNAMICS

Spins are magnetic dipoles that interact with magnetic fields imposed externally or locally by other spins.[9–11] As the dipole–dipole interaction scales with the inverse cube of the distance between the two dipoles (Fig. 3), information on the spatial distribution of the spins in solids can be inferred. For electron spins, the apparent local magnetic field is influenced by the spatial distribution of the unpaired electron and modified by spin-orbit coupling, so that there is also information on the singly occupied molecular orbital (SOMO).

For spin quantum numbers larger than $^1/_2$, spins have an electric quadrupole moment that interacts with electric field gradients. For electron spins, this interaction is again related to the spatial distribution of the unpaired electron and modified by spin-orbit coupling. For spins of nuclei involved in covalent bonds, the quadrupole interaction is related to the type and specifics of bonding. For nuclear spins in ionic materials, it is related to the distribution of point charges in the vicinity of the nucleus.

The separation and analysis of all interactions can thus provide a detailed picture of the geometric and electronic

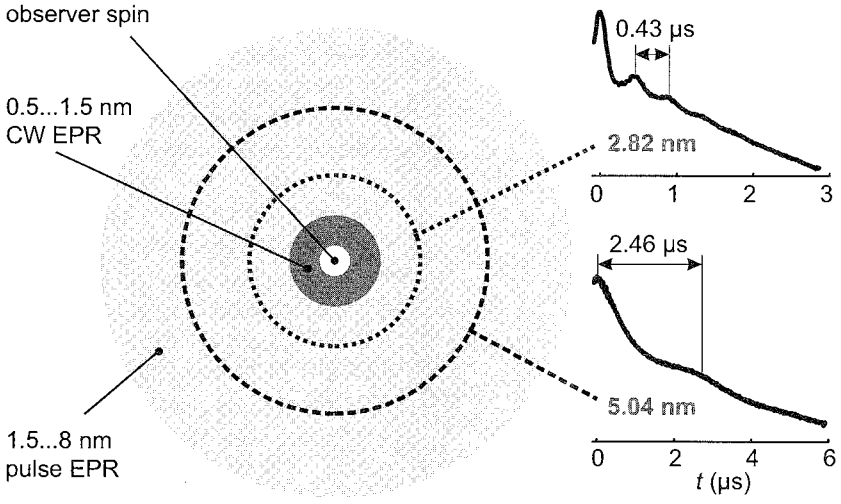

Fig. 3 Distance measurements between paramagnetic centers by EPR spectroscopy. Below 0.5 nm. distance estimates are unreliable: for $0.5<r<1.5$ nm. CW EPR is the method of choice; for $1.5<r<8$ nm, pair correlation functions can be obtained from pulse EPR data: and spins at larger distances (up to 40 nm) contribute only to background. Well-defined distances in shape-persistent molecules can be directly computed from the dipolar oscillation frequency (right). (View *this art in color at www.dekker.com.*)

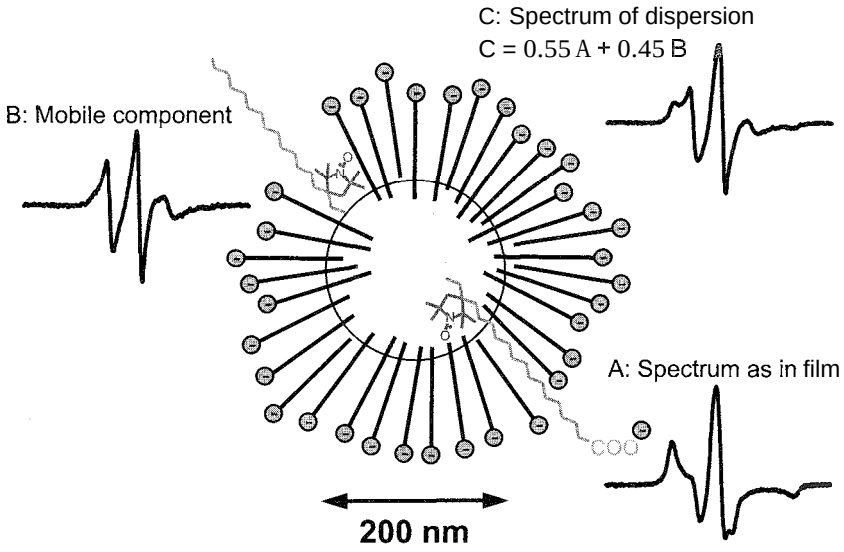

Fig. **4** Dynamical contrast between two surfactant sites in a colloidal polymer dispersion [poly(butylmethacrylate)]. Surfactant spin labels anchored with their tail end in the polymer particle exhibit a rigid limit line shape (A), while surfactants not anchored are more mobile (B). The total spectrum C of the dispersion is a superposition. with the fraction of the mobile component decreasing with decreasing water content (data taken from S. Cramer. Ph.D. thesis. University of Mainz, 2000). (*View this art in color at www.dekker.com.*)

structures of the system under investigation. Such a complete analysis can rarely be performed on the basis of only the CW EPR spectrum. The ENDOR, ELDOR, and electron spin-echo envelope modulation (ESEEM) techniques may be required to separate interactions.[11,12] Even with such a broad method arsenal, a full analysis is not usually undertaken. After the interactions of interest in a given context are identified. one tries to separate and measure them with the required precision and collects supporting information necessary for their unambiguous interpretations. The intricacies involved in this approach are discussed below. An overview of the interactions and their typical energies is given in Fig. 2.

The EPR, ENDOR, and ELDOR spectra are sensitive to dynamic processes that change electronic or geometric structures (chemical reactions, phase transitions. diffusional encounter of paramagnetic centers among each other or with macromolecules or surfaces), lead to a change in resonance frequency for a given structure (reorientation of centers with anisotropic interactions), or influence spin relaxation (fluctuation of interactions due lo reorientation, vibrational dynamics, Heisenberg spin exchange). The most reliable results on dynamics are usually obtained for spin probes with electronic and geometric structures that are well known. Dynamical contrast. i.e., differences in rotational dynamics, between probes located at different sites or in different domains of a complex material can be used to infer the distribution of the probes between the sites or domains (Fig. 4).

Geometric Structure—interactions Through Space

Dipole–dipole interaction between electron spins—The nanometer range

The dipole–dipole interaction between two electron spins $S=^1/_2$ with $g=g_e$ has a magnitude of 52 MHz or 1.9 mT at a distance $r=1$ nm. It scales with distance as r^{-3} and is proportional to the product of the two g factors (Fig. 3). Line splitting or broadening due to this interaction is significant in CW EPR spectra up to a distance of approximately 2 nm. For larger distances, broadening due to proton hyperfine couplings usually dominates. For distances below 0.5 nm, anisotropic contributions of exchange coupling may become significant, and distance estimates based on electron–electron coupling may become unreliable. Line-shape analysis of CW EPR spectra or related techniques can thus provide distance estimates in the range between 0.5 and 2 nm.[7,13]

Pulse EPR methods can measure dipole–dipole couplings with precision to 0.5 MHz for most paramagnetic centers. which corresponds to a distance range up to 5 nm.[13–15] If transverse electron spin relaxation caused by proton spin diffusion is slow, a precision of 0.1 MHz corresponding to a distance of 8 nm can be achieved. This is possible for materials that do not contain methyl groups or water or when the bulk of the material is perdeuterated. If part of a supramolecular system exhibits

a distribution of conformations, distances between sites may not be well defined but instead broadly distributed. Such situations can be addressed by direct conversion of pulse EPR data to a spin-to-spin pair correlation function.[14]

Anisotropic hyperfine interaction—The Angstrom range

The dipole–dipole interaction between an electron spin $S=1/2$ with $g=g_e$ and a proton has a magnitude of 79 MHz at a distance of 1 Å. It scales with distance as r^{-3} and is proportional to the product of the electron and nuclear g factors. Only in exceptional cases are splittings due to this interaction resolved in EPR spectra. Usually. ENDOR or ESEEM techniques are applied that measure nuclear transition frequencies with a sensitivity roughly comparable to an EPR experiment.[11] The resolution of the measurements is determined by the static NMR line width, which is typically up to 100 kHz for protons in solids and less for other nuclei. This indicates that distances up to 8 Å between an electron spin and a proton can be measured. The precision of the distance measurement is not usually limited by the precision of the frequency measurement but rather by the spatial distribution of the unpaired electron. For a paramagnetic center with known structure, the latter contribution can be estimated by quantum-chemical computations of the hyperfine coupling and can thus be corrected.

The direct relation between the anisotropic part of the hyperfine coupling and the electron-nuclear distance is spoiled when there is spin density in orbitals other than *s* orbitals on this nucleus. Except for protons, alkali. and earth alkali ions, this is usually expected. In this situation. a quantum-chemical computation is mandatory before any attempt can be made to relate the hyperfine splitting to a distance.

Electronic Structure—Singly Occupied Molecular Orbital and Interactions Through Bonds

The *g* tensor

Orbital angular momentum of the electron spin is usually quenched in the ground state, but due to relativistic effects. there is an admixture of excited states that manifests itself as spin-orbit coupling and. in turn. as a deviation of the g value from g_e. Often the deviation is anisotropic and has to be described as a g tensor. This tensor reflects point symmetry at the site of the paramagnetic center and can be considered a characteristic for the global distribution of the unpaired electron. In other words. the principal values of the g tensor can often be used as the fingerprint of a certain type of paramagnetic center.

For characterizing supramolecular interactions, it is of interest that g tensor principal values are sensitive to the polarity of the environment and are influenced by hydrogen bonding to an atom with significant spin density in a p orbital.[16] For nitroxide spin probes. it was demonstrated that the two effects can be separated by correlating g_{xx} to A_{zz}.[17]

Exchange interaction

Two electron spins interact through Heisenberg spin exchange when their wave functions overlap. Such an exchange can proceeed along a network of bonds (overlap of two molecular orbitals of the same molecule) or through space or through a matrix. Exchange through space or through an isolating matrix is isotropic and is negligible compared to the dipole–dipole interaction at distances longer than 1.5 nm.[7] Exchange through a network of conjugated bonds or in a conducting material can be significant at distances up to at least 5 nm. In solutions, exchange broadening of spectral lines occurs through short-time overlap of the wave functions of colliding paramagnetic species. It is thus related to the local concentration of these species (Fig. 5).

Exchange coupling is related to ferromagnetism (antibonding overlap) and antiferromagnetism (bonding overlap) and to the rate of electron transfer between the two centers. The EPR measurements are useful in studies of molecular magnets. in order to probe their inner structures and to separate intramolecular and intermolecular contributions to the exchange interaction.[18]

Isotropic hyperfine interaction

Spin density in *s* orbitals of an atom with a magnetic nucleus results in an isotropic hyperfine coupling (Fermi contact interaction of electron and nuclear spin). Proton *s* orbital spin densities are usually caused by spin polarization and are proportional to the spin density on the directly bound neighbor atom.[9] Isotropic hyperfine couplings are thus related to the delocalization of the SOMO.

Hyperfine couplings to nuclei of strongly electronegative elements are sizeable. even for the extremely low-spin densities transferred from a paramagnetic center to neighbor molecules. For instance, in the case of ^{19}F, a hyperfine splitting of 0.5 MHz corresponds to a spin density as low as 10^{-5}. Detection of such couplings can thus prove spatial proximity between different molecules.

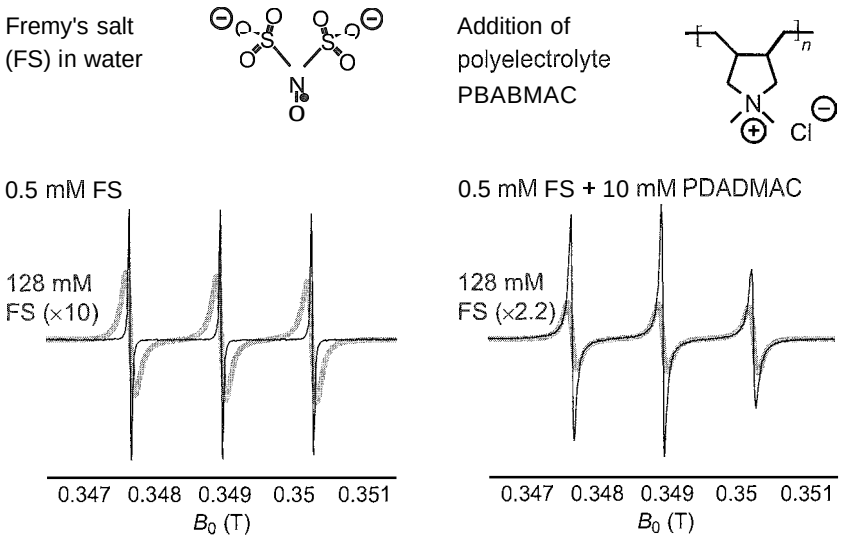

Fig. 5 Exchange broadening and slow down of rotational diffusion by dynamic electrostatic attachment of counterion spin probes to a polyelectrolyte. Left panel: Effect of exchange broadening on the spin probe EPR spectrum. Right panel: The broad wings of the center line indicate strong enrichment of counterions close to the polyelectrolyte. Broadening of the low-field and high-field lines cornpared to the center line stems from a slow down of the reorientation of the probe and is caused by formation of contact ion pairs with a subnanosecond lifetime (data provided by D. Hinderberger).

Dynamics—Anisotropy and Fluctuation of Interactions

Rotational dynamics and small-angle libration

Due to the anisotropy of g and of the hyperfine interaction, resonance frequencies of EPR transitions depend on the orientation of the paramagnetic center with respect to the magnetic field (Fig. 1). Hence. if rotational diffusion of the molecule or dynamics of a spin-carrying side group change this orientation on the time scale of the EPR experiment, spectral changes are observed. Such dynamics is observable up to rotational correlation times τ_r that are comparable to the transverse relaxation time T_2 of the electron spins (typical range 100 ns–10 μs). For $\tau_r \gg T_2$, the rigid limit is attained in which the spectrum of a macroscopically disordered sample is the superposition of the spectra of all orientations. The lower limit of τ_r for dynamics to be observable depends on the total anisotropy $\Delta\nu$ of the spectrum. Strictly speaking, $\Delta\nu$ is the largest possible frequency change of a single EPR transition during reorientation. however, the total width of the EPR spectrum in the rigid limit is usually a good approximation. For nitroxide spin probes at X-band frequencies, $\Delta\nu$ is well approximated by $2A_z \approx 200$ MHz, where A_z is the ^{14}N hyperfine coupling along the z direction (Fig. 1). For $\tau_r \ll 1/\Delta\nu$, the East limit is attained in which the anisotropy is averaged and the spectrum is characterized by narrow lines with frequencies that are determined by the isotropic averages of g and of the hyperfine splittings. For nitroxides, this requires rotational correlation times shorter than 10 ps.

For correlation times in between the rigid and fast limits (slow tumbling regime). spectral line shapes depend on τ_r and on specifics of the motion.[1,19] It is usually possible to decide whether rotational diffusion is isotropic (nearly spherical molecules) or has to be characterized by a rotational diffusion tensor (molecules with prolate or oblate shape). Spectral line shapes are also sensitive to reorienting potentials as they occur in microscopically ordered phases such a liquid crystals or lipid membranes. It is thus possible to recognize microscopic order in EPR spectra of macroscopically disordered samples.[19] Furthermore, restricted side-group motion is manifest in line shapes that are different from the line shapes for unhindered rotational diffusion. Sensitivity of the EPR spectra to all these details of reorientation dynamics is optimum at $\tau_r \approx 1/\Delta\nu$. In many supramolecular systems. this optimum can be attained by temperature variation. Restricted motion, such as small-angle libration. can be recognized by line-shape changes at the edges of the rigid limit that are induced by partial averaging of the anisotropy. Such motion can be characterized by pulse EPR experiments.[11]

Chemical exchange and Heisenberg spin exchange

The spin Hamiltonian changes suddenly when a paramagnetic molecule changes its conformation, undergoes chemical reaction. or exchanges spin with another para-

magnetic tnolecule. All of these processes cause changes in transition frequencies and are thus observable in EPR spectra. Detailed information can be obtained by time-domain experiments at time scales between approximately 10 ns and 1 ms.[11] Slow processes with characteristic times in the range of seconds to hours can be conveniently characterized by CW EPR spectroscopy.

Heisenberg spin exchange occurs upon collision of paramagnetic molecules in solution due to temporary overlap of the wave functions of the two unpaired electrons.[20] This process causes line broadening in the spectra. It can be noticed, even for collisions of like molecules, if hyperfine splittings are resolved in the EPR spectrum, because in that case, the two molecules may differ in their nuclear magnetic spin quantum numbers and thus in the local fields at the electron spins. Furthermore, even if one of the species is unobservable due to electron-spin relaxation that is too fast. collisions still cause line broadening in the spectrum of the other species. Generally, EPR spectra broadened by Heisenberg exchange contain information on the rate of collisions and their effectiveness in spin exchange. The rate of collisions, in turn, depends on the diffusion coefficients of the molecules and on their local concentrations, while their effectiveness can be described by a steric factor. A quantitative analysis of collisions between nitroxide radicals and transition metal ions ligated by crown ethers provides a good introduction to this topic.[21]

SPIN LABELS AND SPIN PROBES—ACCESS TO DIAMAGNETIC MATERIALS

Site-Directed Spin Labeling

Paramagnetic centers can be directly attached to the site of interest via covalent bonds. Such methodology is particularly well developed for proteins. where the amino acid residue of interest can be converted to a cysteine residue by site-directed mutagenesis, and a thiol-reactive spin label can be attached under mild conditions.[22] If a peptide or protein is synthesized, the nonnative spin-labeled amino acid TOAC can be incorporated directly into the chain.[23] In other synthetic systems. nitroxides can be conveniently attached via ether. ester, or amide bonds,[24] an approach that is also viable for labeling ceramic and metal oxide surfaces.[25] The complexity of supramolecular systems that can be investigated by this approach is exemplified by a study on the interaction between spin-labeled starburst dendrimers and DNA.[26]

Probing Weak Supramolecular interactions

The high sensitivity of the spectra to subtle changes in probereorientation dynamics combined with a concentration sensitivity in the 10 $\mu mol \cdot L^{-1}$ range and the large variety of commercially available nitroxide spin probes[1,2,7] makes CW EPR a valuable tool for studying weak interactions between molecules. Instructive application examples include the adsorption of inorganic[27] and organic molecules on zeolites,[28] hydrogen bonding between small additive molecules and epoxy polymers,[29] formation of surfactant layers on clay particles in a poly(acrylamide)/bentonite composite,[30] detection of dynamic electrostatic attachment of counterions to polyelectrolytes in solution.[31] and study of lipid–protein interactions.[32]

CONCLUSION

As a local method for characterization of dynamics at faster time scales and structures at longer distances than are accessible by NMR spectroscopy, EPR spectroscopy is a valuable technique for studying supramolecular systems. The absence of any background signals in most cases and the possibility to address sites of interest by a variety of relatively small spin probes allows for applications to complex materials. Weak interactions between molecules, such as electrostatic interaction, physisorption, and hydrogen bonding, can be detected in solutions, soft matter, and on large internal surfaces by simple, fast, and sensitive CW EPR measurements. While the principles of applying EPR spectroscopy to suprarnolecular systems were proved and impressive results were achieved on biological systems, the broad arsenal of existing techniques still appears to be underutilized in studies on synthetic materials.

ACKNOWLEDGMENTS

Helpful discussions with H.W. Spiess and H.-J. Steinhoff are gratefully acknowledged. The author thanks S. Cramer for providing the data for Fig. 4 and D. Hinderberger for providing the data for Fig. 5. This work was supported by BMBF "Zentrum für Multifunktionelle Werkstoffe und Miniaturisierte Funktionseinheiten" (03N 6500) and by a Dozentenstipendium of Fond der Chemischen Industrie.

ARTICLES OF FURTHER INTEREST

Amino Acids: Applications, p. *42*
Dendrimers, p. 432
DNA as a Supramolecular Scaffold. p *467*
Ionic, Dipolar, and Interfacial Processes. p. 753
Nuclear Magnetic Resonance Spectroscopy, p *981*

Protein Supramolecular Chemistry, p. 1161
Solid-State *Nuclear* Magnetic Resonance Spectroscopy, p. 1307
Zeolites: Catalysis, p. 1610

REFERENCES

1. *Spin Labeling: Theory* and Applications; Berliner, L.J.. Ed.: Academic Press: New York. 1976.
2. *Biological* Magnetic *Resonance*; Berliner. L.J.. Ed.: Plenum: New York, 1998: Vol. 14.
3. Bag, D.S.: Maiti, S. Magnetic polymers. J. Polym. Mater. 1999. *I6* (3), 187–208.
4. Crucker, D. Oxymetry by magnetic resonance: Applications to animal biology and medicine. Prog. Nucl. Magn. Reson. Spectrosc. 2000, *36* (3). 241–270.
5. Hartmann, M.; Kevan, L. Transition-metal ions in aluminophosphate and silicoaluminophosphate molecular sieves: Location, interaction with adsorbates and catalytic properties. Chem. Rev. 1999. 99 (3), 635–663.
6. Hassan. A.K.; Pardi, L.A.; Krzystek, J.: Sienkiewicz, A.: Coy, P.: Rohrer, M.; Brunel, L.C. Ultrawide band multifrequency high-field EMR technique: A methodology for increasing spectroscopic information. J. Magn. Reson. 2000. *142* (2), 300–312.
7. Jeschke, G. Determination of the nanostructure of polymer materials by electron paramagnetic resonance spectroscopy. Macromol. Rapid Commun. 2002. *23* (4), 227–246.
8. Ristori, S.; Martini. G.; Schlick. S. Paramagnetic probes for the investigation of ordered and disordered perfluorosurfactants, perfluoropolyethers and perfluorinated ionomers. Adv. Colloid Interface Sci. 1995, 57. 65–122.
9. Weil. J.A.: Bolton, J.R.: Wertz, J.E. Electron *Paramagnetic Resonance*: Wiley: New York, 1994.
10. Atherton, N.M. Principles of *Electron Spin Resonance*: Ellis Horwood: New York, 1993.
11. Schweiger, A.: Jeschke, G. Principles of Pulse Electron *Paramagnetic Resonance*; Oxford University Press: Oxford. 2001.
12. *Multiple Electron Resonance Spectroscopy*; Dorio. M., Freed. J.H.. Eds.; Plenum: New York. 1979.
13. Biological *Magnetic Resonance*; Berliner, L.J.. Eaton, S.S., Eaton, G.R.. Eds.; Kluwer: Amsterdam. 2001; Vol. 19.
14. Jeschke. G. Distance measurements in the nanometer range by pulse EPR. ChemPhysChem 2002, *3* (11). 927–932.
15. Milov, A.D.: Maryasov, A.G.: Tsvetkov, Y.D. Pulsed electron double resonance (PELDOR) and its applications in free-radicals research. Appl. Magn. Reson. 1998, 15 (1). 107–143.
16. Kawamura, T.; Matsunami, S.; Yonezawa, T. Solvent effects on the g-value of di-t-butyl nitric oxide. Bull. Chem. Soc. Jpn. 1967. *40* (5), 1111–1115.
17. Steinhoff. H.J.: Savitsky, A.; Wegener, C.; Pfeiffer, M.; Plato. M.; Mobius, K. High-field EPR studies of the structure and conformational changes of site-directed spin labeled bacteriorhodopsin. Biochim. Biophys. Acta 2000. *1457* (3). 253–262.
18. Gatteschi. D.: Sessoli. R. Quantum tunneling of magnetization and related phenomena in molecular materials. Angew. Chem.. Int. Ed. 2003. *42* (3). 268–297.
19. Schneider. D.J.; Freed, J.H. Calculating Slow Motional Magnetic Resonance Spectra: A User's Guide. In Biological *Magnetic* Resonance; Berliner, L.J., Reuben. J., Eds.: Plenum: New York. 1989; Vol. 8. 1–75.
20. Molin. Y.N.; Salikov, K.M.: Zamaraev, K.I. *Spin Exchange*; Springer-Verlag: New York, 1980.
21. Livshits, V.A.: Meshkov, B.B.: Mikhailov. A.L.; Alfimov. M.V. Spin exchange between transition metal complexes and nitroxyl radicals in nonaqeous media. Russ. Chem. Bull. Int. Ed. 2002, *51* (12). 2207–2215.
22. Columbus. L.; Hubbell, W.L. A new spin on protein dynamics. Trends Biochem. Sci. 2002. *27* (6). 288–295.
23. Smythe, M.L.: Nakaie. C.R.; Marshall, C.R. Alpha-helical versus 3(10)-helical conformation of alanine-based peptides in aqueous solution—An electron-spin-resonance investigation. J. Am. Chem. Soc. 1995. *117* (42). 10555–10562.
24. Miller. W.G. Spin-Labeled Synthetic Polymers. In Spin *Labeling II: Theory and* Applications; Berliner. L.J.. Ed.: Academic Press: New York. 1979: 173–221.
25. Auteri, F.P.; Belford, R.L.: Robinson. B.H.; Clarkson, R.B. Electron-paramagnetic-resonance nitroxide spin-labeling of ceramic and metal-oxide surface hydroxyls. and use in studying surface molecular-dynamics vs. temperature, solvent. and polymer additive. Colloids Surf., A 1993, 81, 25–42.
26. Ottaviani. M.F.; Furini, F.: Casini. A.; Turro. N.J.: Jockusch, S.; Tomalia. D.A.; Messori, L. Formation of supramolecular structures between DNA and starburst dendrimers studied by EPR, CD. UV, and melting profiles. Macroinolecules 2000. *33* (21). 7842–7851.
27. Rudolf. T.: Bohlmann, W.; Pöppl, A. Adsorption and desorption behavior of NO on H-ZSM-5, Na-ZSM-5, and Na-A as studied by EPR. J. Magn. Reson. 2002, *155* (1). 45–56.
28. Ottaviani. M.F.; Lei, X.G.; Liu. Z.Q.: Turro. N.J. Supramolecular structure and dynamics of organic molecules adsorbed on the external surface of MFI zeolites. A direct and indirect computational EPR analysis. J. Phys. Chern., B 2001. *105* (33), 7954–7962.
29. Pace. M.D.: Snow. A.W. Nitroxide spin-probe label of hydrogen-bonding and probe size effects in a linear epoxy polymer. Macromolecules 1995. *28* (15), 5300–5305.
30. Starodoubtsev. S.G.; Ryabova. A.A.; Dembo, A.T.: Dernbo. K.A.: Aliev, I.I.; Wasserman, A.M.; Khokhlov, A.R. Composite gels of poly(acrylamide) with incorporated bentonite. Interaction with cationic surfactants. ESR and SAXS study. Macromolecules 2002, *35* (16). 6362–6369.
31. Hinderberger. D.; Jeschke. G.: Spiess. H.W. Counterion condensation and conformational transitions of polyelectrolytes characterized by EPR spectroscopy. Macromolecules 2002. *35* (26). 9698–9706.
32. Marsh, D.: Horvath, L.I. Structure. dynamics and composition of the lipid-protein interface. Perspectives from spin-labelling. Biochim. Biophys. Acta 1998, *I376* (3). 267–296.

Emergence of Life

Pall Thordarson
The University of Sydney, Sydney, New South Wales, Australia

INTRODUCTION

How life emerged has occupied the thoughts of mankind for millennia. Life, of course, can be defined in a number of ways.[1] but here the NASA definition is the most appropriate. stating that: "Life is a self-sustained chemical system capable of undergoing Darwinian evolution."[2] Chemistry. together with biology and other disciplines of science. have now come a long way in explaining how life could have emerged from the once sterile primordial earth (or for that matter, elsewhere in the universe) to reach the complexity we now see around us. Evolutionary science and biology can trace the roots of modern lifeforms back to the "last common ancestor,"[1,3] while prebiotic chemistry"' gave us insight into how the building blocks of life (nucleotides, amino acids, etc.) could have been formed under the conditions that prevailed before life emerged. It is, however. what happened in the gap from the time the building blocks of life were formed until we had the first primitive lifeforms (the last common ancestor), that remains a challenge for modern science. Supramolecular chemistry is likely to play a major role here, as the key questions are how simple molecules can interact noncovalently in such a fashion to give rise to more complicated superstructures. in a hierarchical fashion. that eventually lead to living identities. The topics that (supramolecular) chemists have so far tried to cover in their quests to answer these questions range from self-replication, chiral amplification and templated synthesis. to temporal thermodynamics, self-reproduction. and *emergence*.

TIMELINE FOR THE EMERGENCE OF LIFE

Our solar system and the Earth are thought to be about 4.6 Ga (4.6 billion or 4.6×10^9 years) old (Fig. 1). Meteorite bombardment made the surface of our planet a rather inhospitable place during the first few hundred years after its formation, however. isotopic patterns in sediments from Greenland indicate that life already existed as early as 3.8 Ga ago.[5] The upper limit for the emergence of life is set by the intense bombardment of the Earth between 3.9–4.1 Ga ago, which without doubt sterilized it, e.g., by boiling off the oceans.[1] destroying the prebiotic matter (the prebiotic soup) that is necessary for life to emerge. Only when this heavy meteorite bombardinent ceased, about 3.8–3.9 Ga ago."' could life have started to evolve. Thus; it appears that life evolved from the prebiotic soup within the span of 100–200 million years.[1] A window as narrow as 10 million years was suggested for life to emerge.[6] There are, broadly speaking, two strategies that can be used to try to understand what happened during this period. They are the "top-down" biological strategy and the .'bottom-up" biogeochemical strategy."' Prebiotic bioorganic chemistry, and in particular, prebiotic supramolecular chemistry. clearly belong to the latter (Fig. I).

PREBIOTIC CHEMISTRY

As the famous Miller–Urey experiment showed,[7] many of the building blocks of life can be obtained under experimental conditions that resemble (as far as we know) conditions on primordial Earth. There is controversy about whether the early atmosphere of Earth was reducing or not,[1] but assuming it was so (i.e., a mixture CH_4, NH_3, H_2, and H_2O), one can obtain important prebiotic feedstock molecules like $HC{\equiv}N$, $CH_3C{\equiv}N$, $HC{\equiv}C{-}CN$, and HCHO. From these initial feedstock molecules, a range of amino acids, purines, pyrimidines, and sugars were obtained under prebiotic conditions. which upon further reaction can afford nucleosides. nucleotides, and activated amino acids. eventually leading to oligomers of these building blocks.[4,8] The prebiotic synthesis of other important building bloclcs such as lipids[9] and riboflavins[4] was demonstrated. however. under a cloud of considerable controversy.[1]

Calculations also showed that about 4 Ga ago, more carbon was delivered to Earth in less than a few million years by interplanetary dust particles than the current amount of organic carbon in the biosphere, or about 6×10^{14} kg.[10] Analyses of interstellar dust clouds and heavenly bodies found on Earth, such as the Murchison meteorite, showed the presence of a variety of important prebiotic compounds. such as amino acids. ureas. alcohols. aldehydes, purines. polycyclic aromatic hydrocarbons (PAH), and organic acids,"'' highlighting the significance of extraterrestrial carbon delivery to Earth.

Encyclopedia of Supramolecular Chemistry
DOI: 10.1081/E-ESMC 120019880

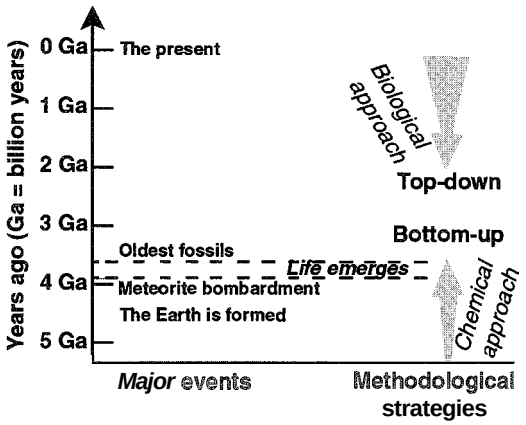

Fig. 1 A hypothetical timescale for the emergence of life. The dotted lines indicated the window within which life is thought to have emerged. On the right. the two main methodological approaches according to Lahav[11] are shown in relation to the timescale. (*View this art in color. at www. dekker.com.*)

Thus, it appears that most of the compounds necessary to form life were available. even abundant. in the "prebiotic soup" some 3.8–3.9 Ga ago, whether they were formed on Earth or were of extraterrestrial origin. How these then assembled to eventually beget life is less clear, but before going into the details, it is worthwhile to consider the thermodynamic aspects of forming complex systems such as those that make life possible.

THERMODYNAMIC CONSIDERATIONS FOR THE EMERGENCE OF LIFE

The first (conservation of energy) and the second (entropy of the universe is increasing) laws of thermodynamics are universal and, thus, will apply to the processes that led to life. Because energy can easily change from one form to another (e.g., light to electrical to chemical as in the photosynthetic reaction center). it is possible to explain how prebiotic (spontaneous) chemistry could have taken place without violating the first law. One might find it harder to see how life and living identities (and therefore the origin of life) can possibly obey the second law, as life seems to be characterized by a decrease in entropy. The answer is that the second law applies to a closed system (e.g., the universe). while life is an open system in which exchanges of energy and matter with its surroundings cause a net increase in the total entropy of life and its environment as a whole. But as every chemist understands, these two laws are related, and what really matters for the study of chemical processes is the free-energy (Gibbs) or more precisely the free-energy change ΔG within a given system, where $\Delta G = \mathrm{AH} - \mathrm{TAS}$ (AH= enthalpy change and AS = entropy change). Thus, processes that are unfavorable for the system in terms of entropy can be driven forward by enthalpy (energy input).

When it comes to considering these factors in a possible scenario for the emergence of life. it is useful to consider the level of organization at different stages in relation to energy flow.[12] On the first level is energy (such as electrical discharge and UV light) necessary to drive the synthesis of prebiotic molecules, like cyanides, nitriles, and formaldehyde. On the next level are concentration mechanisms necessary to gather dilute solution of potential building blocks. Here. the energy might come from adsorption to mineral surfaces, simple drying, or molecular self-assembly in the forms of films and vesicles. On the third level, energy input is required to drive polymerization reactions in "nonliving" assemblies. On the fourth level. these assemblies would grow using internal energy sources based on photosynthesis or metabolism, eventually leading to cellular life.[12] On the latter two levels, a variety of possible scenarios were postulated: from the energy of simple dehydration and heating, to redox properties of minerals, through to geothermal energy, light energy capture by primitive pigments, and ion gradients across lipid bilayers.

When the thermodynamics of self-assembly and the emergence of life are discussed, one critical factor is often overlooked—namely. time. Life is. after all, dynamic; and it is difficult to overlook the importance of energy flux in all living processes. Most of our understanding of self-assembly comes from examining static systems. Fortunately, this is now changing, and studies'into dynamic self-assembly are gaining increased popularity.[13] Within thermodynamics there is even a theory of "temporal hierarchies?" which, broadly speaking, states that supramolecular structures on one particular hierarchical level (j) that arise because of self-assembly of lower-hierarchy structures ($j-1$). have a lifetime inversely related to the level of hierarchy. i.e., $\tau_j \gg \tau_{j-1}$ (τ = lifetime of structure).[14]

TEMPLATED SYNTHESIS

Templaied synthesis plays a central role in any discussion about the emergence of life. This is because it was certainly involved in two stages of the evolution of life—self-replication and translation (protein synthesis)—and possibly in the third, polymerization of monomers or shorter oligomers of amino acids and nucleotides into peptides and (longer) oligonucleotides. The role of templated synthesis in supramolecular chemistry is ubiquitous and well documented.[7,9] Before going further, it is

useful to define it in the words of Busch: "A chemical template organizes an assembly of atoms with respect to one or more geometric loci; in order to achieve a particular linking of atoms."[16] The template is. therefore, distinguished from a reagent by its ability to interfere with the macroscopic geometry of the reaction rather than the intrinsic chemistry.[15] In the complicated case of protein synthesis. *messenger*-RNA (m-RNA) acts as a template for the assembly of amino acids linked to the *transfer*-RNA (t-RNA), leading to one combination of these amino acids only, instead of the many other possible combinations of amino acids that could form a peptide in the absence of the m-RNA template. Likewise, self-replication is nothing but a subclass of templated synthesis restricted to the template used being the same as the product.

Although it was demonstrated that montmorillonite clay particles can catalyze the condensation of nucleotides,[17] it is unclear if the surface shape of these clays can template a specific sequence or shape of the oligomers formed. Many other theories of how clays and minerals could have played a templating role or been used as compartmentation agents[1,8] were proposed, but all remain to be confirmed by experiments.

SELF-REPLICATION, CHIRALITY, AND MUTATION

The transition point in the evolution of life was the emergence of a molecule that was capable of replication." It should be noted that the DNA molecule does self-replicate. however, at present, only with the aid of several enzymes. What researchers are looking for is a molecule that can self-replicate without the aid of any (or many) complex cofactors, like enzymes. The "chicken–egg" paradox[11] that comes from DNA being synthesized by enzymes while enzymes are synthesized by instructions stored in DNA but mediated and cocatalyzed by RNA. led many researchers to suggest that RNA or a WNA-like molecule was the first self-replicating molecule. the so-called "RNA world" theory.[1] This is because RNA can function as a catalyst (ribozymes) and as a carrier for genetic information (retroviruses), offering a possible solution to the "chicken–egg" paradox. According to the "RNA world" theories, the formation of self-replicating RNA (RNA replicase) predates the formation of a primitive ribozyme RNA capable of protein synthesis.

It is not surprising that many researchers spent their time designing and synthesizing self-replicating systems." These efforts show that self-replication is possible, however, it is a complicated issue to study. One has to be careful here to define self-replication, as it is merely a subset of autocatalytic reactions (such as acid-catalyzed hydrolysis of esters, which in turn, makes more acid). Self-replicating molecules are selfish catalysts, i.e., they will only catalyze their own formation.[18] This also means that information is transferred during the reaction; in other words, molecular recognition between the product(s) and reagent(s) plays a major role in templating the reaction.

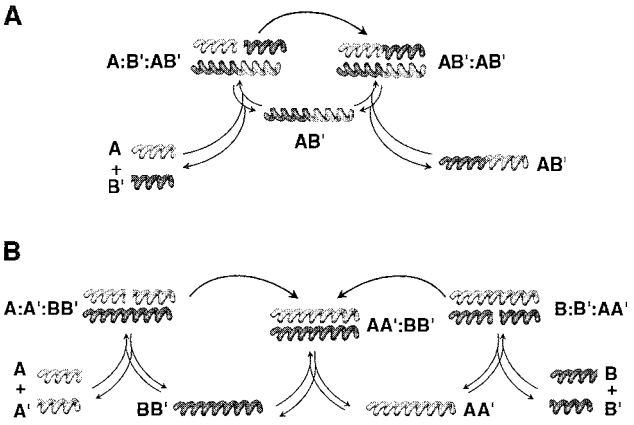

Fig. 2 *(A)Self-replication versus (B)cross-catalysis. according to* von *Kiedrowski et al. (Ref.* [19]). *A. A'. B. B' stands for oligomeric fragments that can combine to form the templates (AA',AB'. BB').* (*View this art* in *color at www.dekker.com.*)

Self-replication can occur through autocatalysis with a self-complementary template (Fig. 2A) or by cross-catalysis with a complementary template (Fig. 2B). In the latter case, two complementary units catalyze each other's formation. This is significant: as modern DNA is made up of two complementary strands that replicate in a cross-catalytic manner. Studies on a simple nonenzyinatic DNA system capable of competing auto- and cross-catalysis. show that in the absence of an initial template, both pathways are equally as likely, but that in the presence of a seeding template, the cross-catalytic route is more efficient.[19]

The self-replication of peptides was also demonstrated in the laboratory,[20] raising the question of whether peptides were the first molecules to self-replicate in the evolution of life. Whether this was the case or not. various interesting phenomena were demonstrated using self-replicating peptides. including dynamic error correction[21] and chiroselective amplification.[22] Both are significant in discussing the emergence of life. The dynamic error correction experiment is based on introducing two mutants to the system. The system as a whole was shown to be robust enough to suppress the formation of these mutants and capable of using the mutants to produce more of the nonmutated template.[21] Thus, small "errors" in

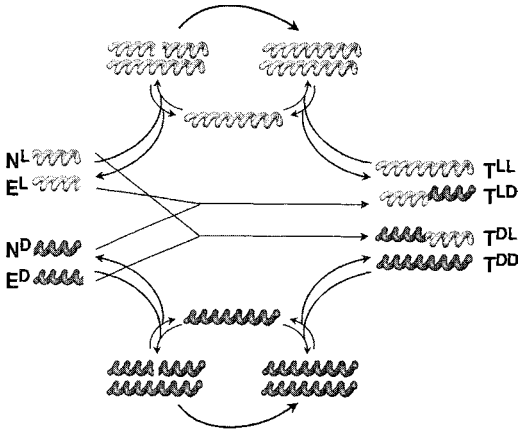

Fig. 3 Chiroselective amplification according to Saghatellan et al. (Ref. [22]). The potential ternplates T are formed by reacting nucleophilic *N* and electrophilic E peptide fragments together. The superscripts (L and D) indicate the different chiralities of the amino acids that rnake up the peptide fragments. *(View this urt in color at \vww.dekker.com.)*

the replicating system can be corrected again toward the native template. In the case of chiroselective amplification (Fig. 3), a similar correction mechanism was observed. More importantly, it was also observed that a chiral peptide template is capable of amplifying homochiral products from a racemic mixture of shorter fragments.[22] For instance. starting from a racemic mixture of the shorter peptide fragments, more than 70% diastereomeric (de) excess of the homochiral (template) versus heterochiral peptide was obtained under the conditions used. The origin of homochirality in biopolymers is still one of the great mysteries in the quest to understand the origin of life,[1] but these experiments help us understand how chirality can be amplified once an initial enantiomeric imbalance is established and indicate that self-replication of biopolymers might have played an important role.

TRANSLATION AND PROGRAMMED TEMPLATED SYNTHESIS

At least as important as the self-replication of information (DNA) is the ability of a living organism to carry out programmed templated synthesis of proteins using RNA. At the center of this system is the codon–anticodon recognition between m-RNA and t-RNA. This is the genetic code, as m-RNA is synthesized by complementary templated synthesis from a DNA (the genetic material) single-strand sequence. The t-RNA molecules carry a specific amino acid and. according to the anticodon they possess, form a compleinentary complex with a codon on m-RNA inside the ribosome, where the amino acid is added to the growing polypeptide chain. In modern organisms, this system is complex, but it is obvious that it must have been a lot simpler closer to the origin of life. How it evolved is one of the most contested topics in the whole discipline; some favor a graduai change from RNA-replication to RNA-coded protein synthesis (RNA-world), while others suggest a ''coevolution'' of RNA and catalytic peptides and proteins that eventually merged into one system.[1] The simulation or mimicking of this remarkable programmed templated synthesis system has. to date, not been attempted by wholly synthetic analogues, which is not surprising considering its complexity.

It should also be noted that the genetic code is twofold, with the second being the recognition between individual t-RNA anticodons and the specific ainino acids they stand for. This adds some weight to the theory that peptides were the first carriers of genetic information. or the coevolution theory.[1] This kind of template switching, or a transition between two different (albeit related) genetic systems, has been demonstrated, between RNA and PNA (peptide nucleic acid) oligomers.[23]

LIPIDS, MEMBRANES AND SELF-REPRODUCTION

Important but often overlooked players in the origin of life scenario are lipids. Lipids, and amphiphiles in general, can self-assemble into structures such as micelles, vesicles, and importantly. membranes. Their most important role in living organisms today is compartmentalization, but they also play a vital role in metabolism, respiration, and photosynthesis, to name a few examples. Normally, it is assumed that they play a passive role in these processes. However, the recent ''lipid world'' theory suggests that lipid-like molecules played a much more active role in metabolism[12,24,25] arid in the early stages of evolution, and even acted as information carriers.[24,25] The latter suggestion conies from the observation that cell membranes are always created by growth and division and not de novo and, thus. are direct ancestors of the first living cells.[24]

Another important observation in this context is that micelles are capable of self-reproduction. that is, the amphiphiles (fatty acids) within the micelles are capable of catalyzing the hydrolysis of fatty acid esters. causing the micelle to grow and eventually split into two new ones.[26] The term reproduction is used to distinguish it from self-replication as discussed above, as it is not limited to discrete (linear) molecular structures but rather is confined in geometry. Because each new micelle

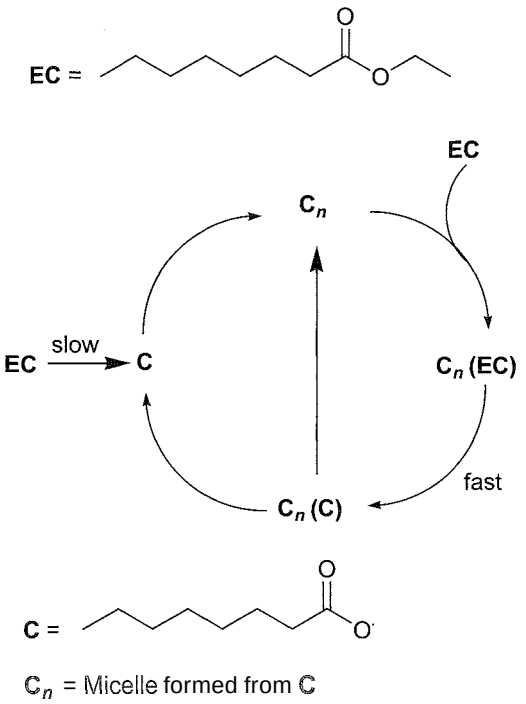

Fig. 4 Self-reproduction of a micelle according to Bachmann et al. (Ref. [26]). The ester *EC* is hydrolyzed slowly to C outside the micelles (indicated with C_n) but much quicker inside, and as the micelles grow. they generate new ones.

formed is capable of binding and then hydrolyzing about five ester molecules, the micellar growth is explosive once the first is formed from the very slow noncatalytic hydrolysis of fatty acid esters (Fig. 4). Although micelles are obviously too small and unstable to have played a significant role in the evolution of life, they are closely related to vesicles. which could more easily have served as envelopes for protocells.[26,27]

HIERARCHY, *EMERGENCE*, AND SYNTHETIC LIFE

Until now. the discussion was limited to how individual components of life might have developed. But living organisms, even as simple as the "last common ancestor",[1,3] are multilevel complex assemblies. A closer look reveals that biological self-assembly of complex structures can be explained based on a few simple principles.[28] One of the most important of these is that self-assembly occurs in an hierarchical fashion, i.e., it is a modular process by which stable subassemblies are formed before they assemble into a more elaborate structure. Hierarchical assembly was put into practice by supramolecular chemists: an early example concerns the formation of an helical stack from a chiral phthalocyanine where. in turn, two of these stacks form a superhelix.[29] This, and other examples of hierarchical assemblies, show that information within one molecule (e.g., chirality) can be transferred through several levels of hierarchy, forming very large structures that still contain that piece of information (a superhelix is chiral). As pointed out above, the lifetime of a particular superstructure seems to be linked to the level of hierarchy for that structure.[14] Therefore, as the complexity of prebiotic assemblies increased in a hierarchical fashion, the longer their lifetimes became. This could have ensured a smooth transition toward cellular life, once all the basic components were in place.

Another tool that could turn out to be helpful in comprehending how life reached its complexity is the concept of "*emergence*" (it should be stressed that this is a much broader term than used in the phrase "emergence of life"). *Emergence* as a concept can be defined in a number of ways, but often the statement "the whole is more than the sum of the parts" is used. Another definition would be that it describes how novel properties arise (emerge) on one particular level of hierarchy *(j)*,

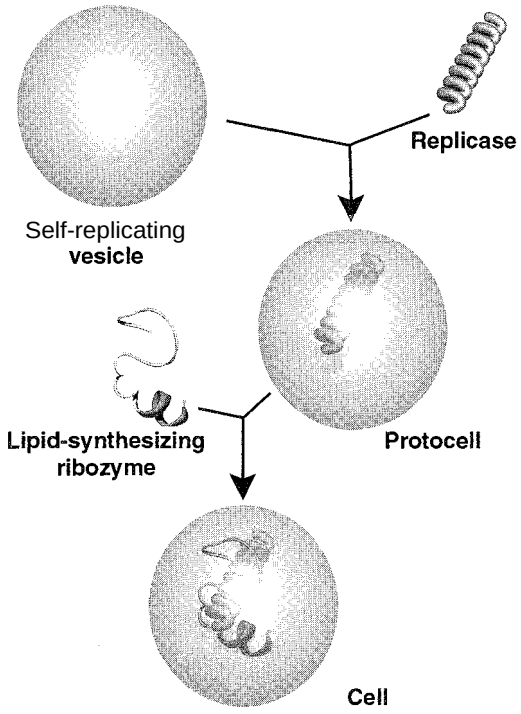

Fig. 5 A hypothetical pathway to a synthetic cell. according to Szostak et al. (Ref. [27]). ***(View** this art in color at www.dekker.corn.)*

when that was formed from the next hierarchical level $(j-1)$ below it. This concept clearly plays a major role in chemistry, despite having gone almost unnoticed until recently.[30] In the emergence of life, novel properties (self-replication, metabolism, etc.) arose as more complex assemblies formed. *Emergence* will undoubtedly help us to better understand the origin of life. An illustration comes from ambitious plans to make a minimal synthetic cell.[27] The plan is based on combining an RNA replicase and a self-replicating vesicle, forming a protocell. Incorporation of a lipid-synthesizing ribozyme would complete this minimal cell (Fig. 5). It is anticipated that novel properties will arise as complexity increases, providing major insights into the origin of life.

CONCLUSION

The problem of understanding how life emerged is as complex as it is fascinating. It is. however, impossible to travel back in time to actually observe how it happened. Therefore, we can only speculate how it could have happened and then test those theories in the laboratory. Supramolecular chemistry has already, and will certainly continue: to play a major role in this quest. Studies into self-replication, templated synthesis, and micellar replication, to name a few topics covered here, already gave valuable insight into how life might have emerged. Hierarchical assembly, *emergence*, and other more novel areas within supramolecular chemistry are also set to do the same. Practical applications, such as programmed templated synthesis of polymers. could also result from these studies. Synthesis of "living" cells was targeted, and other ambitious plans are likely to follow. Prebiotic supramolecular chemistry is therefore set to be a thriving field in the twenty-first century.

ACKNOWLEDGMENTS

I thank my mentors Prof. M.J. Crossley (Sydney, Australia), Prof. R.J.M. Nolte. and Dr. A.E. Rowan (Nijmegen, The Netherlands) for their inspiration and support.

ARTICLES OF FURTHER INTEREST

Chiral Induction, p. 245
***DNA** as a Supramolecular Scaffold*, p. 467
Energy and Electron Transfer in Supramolecular Systems, p. 535
Micelles and Vesicles, p. *861*
Preorganization and Complementarity, p. *1158*
Self-Assembly in *Biochemistry*, p. 1257
The Template Effect, p. 1493

REFERENCES

1. Lahav. N. *Biogenesis: Theories* of Life's Origin; Oxford University Press: Oxford, U. K.. 1999.
2. Joyce, G.F. Foreword. In *Origins* of Life: The *Central* Concept: Deamer. D.W.. Fleischaker, G.R.. Eds.; Jones and Bartlet Publishers: Boston. 1994: xi–xii.
3. Orgel, L.E. The origin of life on the earth. Sci. Am. 1994. *271*. 76–83.
4. Sutherland. J.D.; Whitfield, J.N. Prebiotic chemistry: A bioorganic perspective. Tetrahedron **1997**, *53*. 11493–11527.
5. Schidlowski, M.A. 3,800-million year isotopic record of life from carbon in sedimentary rocks. Nature 1998, 333. 313–318.
6. Lazcano, A.; Miller, S.L. The origin and early evolution of life: Prebiotic chemistry, the pre-RNA world, and time. Cell **1996**, *85*, 793–798.
7. Miller, S.L. A production of amino acids under possible primitive Earth conditions. Science **1953**, *117*. 528–529.
8. Kuhn, H.: Waser. J. Molecular self-organization and the origin of life. Angew. Chem., Int. Ed. Engl. **1981**, *20*, 500–520.
9. McCollom, T.M.; Ritter. G.; Simoneit, B.R.T. Lipid synthesis under hydrothermal conditions by Fischer-Tropsch-type reactions. Orig. Life Evol. Biosph. 1999, *29*, 153–166.
10. Chyba, C.; Sagan, C. Endogenous production. exogenous delivery. and impact-shock synthesis of organic molecules: An inventory for the origins of life. Nature 1992. *355*. 125–132.
11. Cronin, J.R. Origin of organic compounds in carbonaceous chondrites. Adv. Space Res. 1989, 9, 59–64.
12. Deamer. D.W. The first living systems: A bioenergetic perspective. Microbiol. Mol. Biol. Rev. 1997. 61, 239–261.
13. Whitesides. G.M.: Grzybowski. B. Self-assembly at all scales. Science **2002**, *295*. 2418–2421.
14. Gladyshew. G.P. On thermodynamics. entropy and evolution of biological systems: What is life from a physical chemist's viewpoint. Entropy 1999. *1*, 9–20.
15. Anderson. S.; Anderson, H.L.; Sanders. J.K.M. Expanding role for templates in synthesis. Acc. Chem. Res. 1993, *26*, 469–475.
16. Busch, D.H. Structural definition of chemical templates and the prediction of new and unusual materials. J. Incl. Phenom. 1992. 12. 389–395.
17. Ferris, J.P.; Hill, A.E.. Jr.: Liu, R.: Orgel, L.E. Synthesis

of long prebiotic oligomers on mineral surfaces. Nature **1996.** *381*. 59–61.
18. Robertson. A.; Sinclair. A.J.; Philp. D. Minimal self-replicating systems. Chem. Soc. Rev. **2000.** *29*. 141–152.
19. von Kiedrowski. G.; Sievers, D. Self-replication of hexodeoxynucleotide analogues: Autocatalysis versus cross-catalysis. Chem. Eur. J. **1998.** *4*, 629–641.
20. Lee, D.H.; Granja, J.R.: Martinez, J.A.; Severin, K.: Ghadiri. M.R. A self-replicating peptide. Nature **1996,** *382*. 525–528.
21. Severin. K.: Lee, D.H.; Martinez, J.A.: Vieth, M.; Ghadiri, M.R. Dynamic error correction in autocatalytic peptide networks. Angew. Chem.. Int. Ed. **1998.** *37*. 126–128.
22. Saghatellan. A.; Yokobayashi. Y.; Soltani. K.; Ghadiri, M.R. A chiroselective peptide replicator. Nature **2001,** *409*. 797–801.
23. Bohler. C.; Nielsen. P.E.; Orgel, L.E. Template switching between PNA and RNA oligonucleotides. Nature **1995,** 376, 578–581.
24. Cavalier-Smith, T. Obcells as proto-organisms: Membrane heredity, lithophosphorylation, and the origin of the genetic code, the first cells. and photosynthesis. J. Mol. Evol. **2001.** *53*, 555–595.
25. Sergé, D.; Ben-Eli. D.; Deamer, D.W.; Lancet, D. The lipid world. Orig. Life Evol. Biosph. **2001.** *31*, 119–145.
26. Bachmann. P.A.; Luisi, P.L.; Lang, J. Autocatalytic self-replicating micelles as models for prebiotic structures. Nature **1992.** *357*. 57–59.
27. Szostak, J.W.; Bartel. D.P.; Luisi, P.L. Synthesizing life. Nature **2001,** *409*. 387–390.
28. Whitesides, G.M.; Mathias, J.P.; Seto, C.T. Molecular self-assembly and nanochemistry: A chemical strategy for the synthesis of nanostructures. Science **1991,** *254*. 1312–1319.
29. Engelkamp. H.; Middelbeek, S.; Nolte, R.J.M. Self-assembly of disk-shaped molecules to coiled-coil aggregates with tunable helicity. Science **1999.** *284*, 785–788.
30. Luisi. P.L. Emergence in chemistry: Chemistry as the embodiment of emergence. Found. Chern. **2002.** *4*. 182–200.

Energy and Electron Transfer in Supramolecular Systems

Jonathan L. Sessler
Janarthanan Jayawickramarajah
University of Texas at Austin, Austin, Texas, U.S.A.

Muhunthan Sathiosatham
Eastman Kodak Company, Rochester, New York, U.S.A.

INTRODUCTION

In recent years; considerable effort has been devoted to elucidating the pathway of energy transfer in supramolecular assemblies. The impetus for this work stems from the fact that electron transfer reactions are endemic in biosynthesis. Such critical and well-known cellular activities as respiratory oxidative phosphorylation[1] and photosynthesis[2] rely on electron transfer processes. Most of these are mediated via protein–protein interactions. Currently, it remains uncertain whether a specific pathway is required for a given biological electron transfer event.[1,3–5] The study of synthetic donor–acceptor systems held together by noncovalent interactions resembling those found in proteins, nucleic acids, and other biological inacromolecules is thus being pursued with the goal of better understanding the full range of natural electron transfer processes. The aim of this chapter is to summarize recent advances in the area of electron and energy transfer model studies. with the focus being specifically on synthetic supramolecular model systems that are held together via hydrogen bonds. reported after 1998. This choice of emphasis, designed to be illustrative of how supramolecular approaches can help shed light on current problems of interest, is, of course, arbitrary. Indeed, it is important to appreciate that supramolecular assemblies based on hydrophobic interactions. salt bridges, aromatic π-stacking, van der Waals forces, etc., have been produced, and that they also have an important role to play in the area of electron and energy transfer modeling. The reader is directed to many excellent reviews for examples of these kinds of model systems as well as of early hydrogen-bond-derived ensembles.[6–9]

THEORY

Traditional transition state theory does not hold for long-distance electron transfer reactions. Due to weak electronic coupling between donor and acceptor moieties, formation of a transition state does not necessarily lead to an electron transfer event. Thus, electron transfer rates (k_{ET}) must be described by Fermi's golden rule. which has its basis in nonadiabatic quantum mechanical perturbation theory (Eq. 1). Here. T_{DA} is an electronic coupling factor that reflects the electronic structure of the donor. acceptor, and bridging groups." The second term is the Franck–Condon factor (FC), the weighted density of states that can be calculated using classical Marcus theory[10] or. more precisely, using its many quantum mechanical corrections.[11,12] Detailed in Eq. 2 is the FC factor in the high-temperature regime predicted by Marcus. In this equation, λ=reorganization energy, and ΔG^0=standard free energy for the reaction. When $-\Delta G^0 \approx \lambda$. the electron transfer rate reaches its maximum value and is dependent solely on T_{DA} (Eq. 3), where $|T_{DA}|_0$=electronic tunneling matrix element when the donor and acceptor are at van der Waals contact distance, r_0, and β=decay constant.

$$k_{ET} = \frac{2\pi}{\hbar}|T_{DA}|^2(FC) \quad (1)$$

$$(FG) = \frac{1}{\sqrt{4\pi\lambda kT}}\exp[-(\Delta G^0 + \lambda)^2/4\lambda\kappa T] \quad (2)$$

$$k_{ET} = \frac{2\pi}{\hbar}|T_{DA}|_0^2\exp[-\beta(r - r_0)] \quad (3)$$

Marcus theory deals with the first-order electron transfer rate constant for a donor-acceptor system presuming fixed separation. However, there are often systems that do not undergo Marcus behavior and have to be treated using the Rehm–Weller formalism.[13] Here. the second-order diffusion-mediated electron transfer rates are calculated using Eq. 4, where ΔG^*=free energy of activation for

"Some authors use H_{AB} instead of T_{DA}. Strictly speaking. these terms differ in that H_{AB} is the electronic coupling matrix element. and T_{DA} is defined as the electronic tunneling matrix element. However. this subtle difference in meaning is unimportant as far as the mostly qualitative conclusions of this review are concerned. Thus, T_{DA} is used throughout.

the electron transfer and is defined by Eq. 5, where ΔG^*_0=free energy of activation when there is no standard free energy for the reaction (i.e., $\Delta G^0=0$). The greater complexity associated with the study of systems that must be treated in accord with Eq. 4 has provided an impetus to make and study systems where the distance between the donor(s) and acceptor(s) are well defined. To date, this has largely been accomplished via the synthesis of covalently linked systems. Often these systems have proved hard to prepare. By contrast, a prime attraction of synthetic hydrogen-bond-mediated assemblies is that they allow donor and acceptor complexes to be placed at various preselected distances and orientations while providing systems that would allow the importance of noncovalent interactions to be assessed by experiment. Not surprisingly. therefore; such systems have attracted considerable attention of late.

$$k_{ET} = \frac{20 \times 10^9}{1 + 0.25[\exp(\Delta G^*/RT) + \exp(\Delta G^0/RT)]} \quad (4)$$

$$\Delta G^* = \frac{\Delta G^0}{2} + \left[\left(\frac{\Delta G^0}{2}\right)^2 + (\Delta G_0^*)^2\right]^{1/2} \quad (5)$$

Ensemble 1

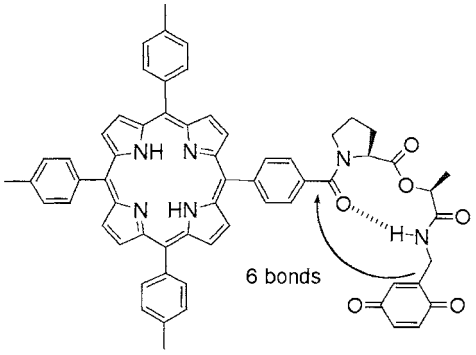

Ensemble *2*

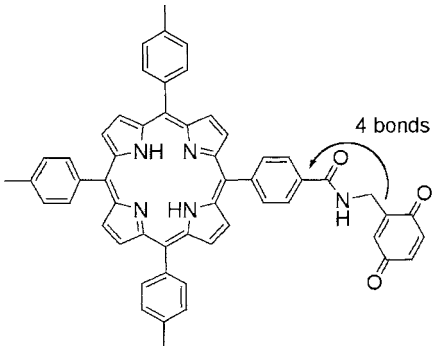

MODULES WITH A SINGLE TETHERING HYDROGEN BOND

Appropriate combinations of well-known functional groups such as amines. phenols. and carboxylates are known to assemble through one-point hydrogen-bonding motifs. Such combinations are thus attractive in the context of energy and electron transfer model construction. Unfortunately. supramolecular assemblies preorganized solely via a single H-bond have low association constants. While increasing the number of hydrogen bonds in a cooperative manner dramatically enhances the stability of supramolecular assemblies and abets their formation, analyses of photoinduced electron transfer events in ensembles tethered via a single H-bond are of considerable interest, because interprotein electron transfers are often mediated via a single H-bond. With these considerations in mind. Williamson and Bowler designed and synthesized a linked porphyrin-*p*-benzoquinone donor–acceptor dyad (Ensemble 1), in which the shortest bond electron transfer pathway requires electronic coupling through a hydrogen bond.[14] The authors chose a depsipeptide bridge that forms a β-turn due to an intramolecular hydrogen-bonding interaction. Temperature-dependent ^{1}H-NMR, ROESY ^{1}H-NMR. and FTIR spectroscopic measurements confirmed the presence of the β-turn in the predominant conformation. Time-resolved fluorescence studies of Ensemble 1 showed a biexponential fluorescence decay in dichloromethane [τ_1=0.85 ns; τ_2=8.76 ns]. The shorter lifetime was assigned to the conformation containing the β-turn, wherein electron transfer is found to be competitive with intrinsic fluorescence decay. In contrast, the longer lifetime is attributed to various non-β-turn conformations. From these lifetime values. the electron transfer rate in the hydrogen-bond-containing conformer was determined to be $k_{ET}=(1.1 \pm 0.1) \times 10^9$ s^{-1} in dichloromethane. This rate compares well with that of a covalent analog reported by Bolton and Archer (Ensemble 2)[15] for which $k_{ET}=(8.0 \pm 0.4) \times 10^8$ s^{-1}, thus illustrating the efficiency of electron transfer *via* the single hydrogen bond present in Ensemble 1. As part of their studies, Williamson and Bowler found that the coupling decay factor, ε_{hb},[b] was 0.8 ± 0.4, a value that correlates well with the theoretically predicted value of 0.36.[16]

[b] ε_{hb} is a decay factor representing the electronic coupling through a hydrogen bond. This factor is somewhat analogous to β; however. β refers to a decay through a homogeneous electronic coupling medium. while ε_{hb} is defined specifically for through-hydrogen-bond orbital interactions.

MODULES CONTAINING TWO HYDROGEN BONDS

Despite the relatively low enthalpy gain associated with using two hydrogen bonds to generate a supramolecular ensemble. numerous examples of photoinduced electron transfer in models linked via two-point hydrogen bonds have been reported. Part of the reason for this is that many polar groups containing H-bond donor and acceptor sites tend to self-associate. For instance, Gopidas and colleagues have taken advantage of the dimerization ability of carboxylic acid groups to generate systems wherein the rate of electron transfer between various donor and acceptor units could be studied.[17] In these models, the edge-to-edge distance between the donor–acceptor pairs was kept constant at 9.40 Å (Chart 1b, where $n=m=1$ and both m and n are the number of methylene units). The dependence of the electron transfer rate on driving force was then determined by systematically varying the redox potentials of the quenches molecules (Chart la). Fluorescence quenching experiments yielded k_{ET} values between [(1.9 + 0.19) x 10^7 s^{-1} and (144.0 + 14) x 10^7 s^{-1}]. The authors proposed two types of electron transfer mechanisms: intraensemble electron transfer, which obeys the Marcus equation; and bimolecular electron transfer. where an inverted region is not observed. The latter mechanism can be treated by the Rehm–Weller formalism (Eqs. 4 and 5) and is associated with diffusion in a regime where the driving force is moderately large ($\Delta G^0 \geq -1.5$ eV). Furthermore. Gopidas and coworkers realized that dyads PA/1 and **PA/2** (where PA dimerizes with **1** and **2**, respectively) fall into the Marcus normal and inverted regions, respectively. Subsequent experiments involving studies of distance on the electron transfer rates within dyads **PA/1** and PA/2 were made by varying the number of connecting methylene units (Chart 1b, where $m+n \leq 6$).[18] These studies confirmed the expected exponential decrease with increasing distance in the normal region. However, in the inverted region, the predicted increase in rate at larger distances was not seen. Novel experiments incorporating rigid linkers may be needed to further elucidate the role that distance plays in the inverted region of these two-point H-bond-mediated systems.

Taking advantage of a different kind of hydrogen bond interaction, Tanaka and colleagues assembled several cofacial p-benzoquinone-posphyrin systems that are tethered via two amide-quinone hydrogen bonds (Ensemble 3).[19] The authors ascribe the stability of the system to these interactions. However, x-stacking interactions could also be serving to stabilize Ensemble 3. Such interactions also serve to complicate interpretations of intraensemble electron transfer events, making these elegant systems less useful than they otherwise would be.

Arimura and coworkers were able to overcome the problem of x-stacking by using a calix[4]arene linker between the porphyrin unit and the quinone (Ensemble 4).[20] In this system, it is proposed that two-point hydrogen bonds between the two phenolic hydroxyl groups on the calix[4]arene and the oxygen atom on the p-benzoquinone

Chart 1 (a)

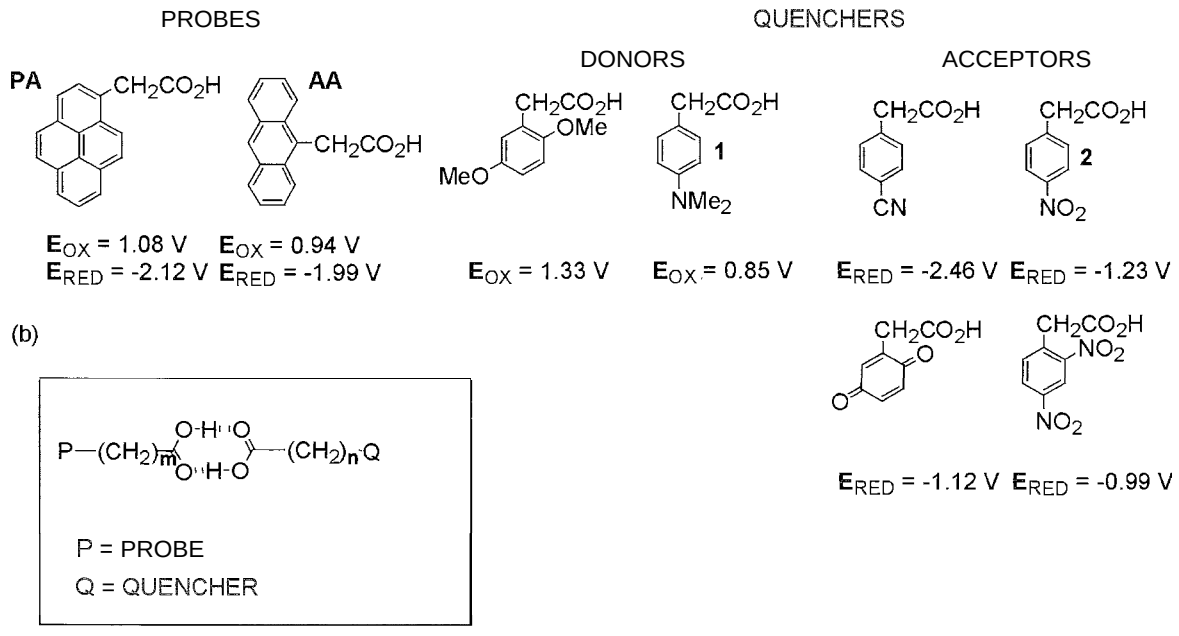

Ensemble 3

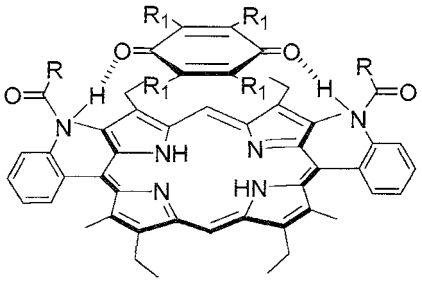

R = C_7F_{15}, C_7H_{15}, CF_3, CH_3 ,C_6F_5, or C_6H_5
R_1 = H, CH_3 or F

Ensemble 4

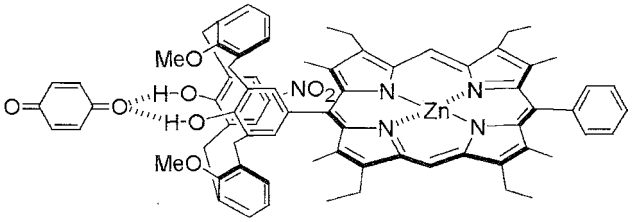

link the system. Further, the directionality of the H-bonds and the exo-cyclic nature of the OH groups are thought to preclude π-π porphyrin-quinone interactions. In point of fact, neither ^{1}H-NMR nor UV-Vis spectral shifts corresponding to n-stacking were observed. Proton-NMR binding studies in $CDCl_3$ gave a weak association constant [(70 a 10) M^{-1}] for the interaction between the quinone and the rest of the ensemble. Time-resolved fluorescence measurements indicated two lifetimes, τ_1=30 ps and τ_2=1.3 ns that are ascribed to intraensemble quenching and to diffusional quenching, respectively.

ENSEMBLES BASED ON THREE HYDROGEN BONDS: CYTOSINE-GUANINE MOTIFS

Watson–Crick hydrogen bonds between nucleic bases are ubiquitous in living systems. Their directionality and cooperativity renders them essential in the transfer of biological information. Similar considerations have made the cytosine-guanine (CC) base pair attractive for energy and electron transfer model studies. It possesses three hydrogen bonds and two attractive and two repulsive secondary interactions (referred to as DDA•AAD couples in the language of supramolecular chemistry, where D=donor and A=acceptor). Sessler and coworkers were the first to use CG base pairing to generate a redox-active supramolecular scaffold. In a first series of studies. a zinc porphyrin and a free-base porphyrin, tethered via flexible linkers were linked in a supramolecular sense via CG base pairing. Second-generation guanine-cytosine assemblies. designed to study electron-, as opposed to energy-, transfer processes, were then synthesized incorporating a porphyrin donor and a quinone acceptor into a GC-linked motif (Ensemble 5).[21] Proton NMR binding studies in CD_2Cl_2 gave an association constant (K) for the formation of Ensemble 5 of 3100 a 470 M^{-1}. Time-resolved fluorescence experiments involving subunit 3 alone gave a single exponential decay, which became biexponential upon the addition of 4. The associated lifetimes were found to be τ_1=(1.5 a 0.2) ns and τ_2=(0.94 a 0.07) ns, respectively. Here, τ_1 is the lifetime attributed to the uncomplexed porphyrin 3, while τ_2 (the shorter-lived decay) is ascribed to electron-transfer-derived quenching of the excited state of 3 by quinone 4. The derived rate constant was (4.2 ± 0.7) x 10^8 s^{-1}. The authors concluded that electron transfer was taking place as the result of the three-point hydrogen bond bridge, because no quenching was seen when a small quantity of ethanol (2% v/v), sufficient to break up the CG hydrogen bonds, was added.

Ensemble 5

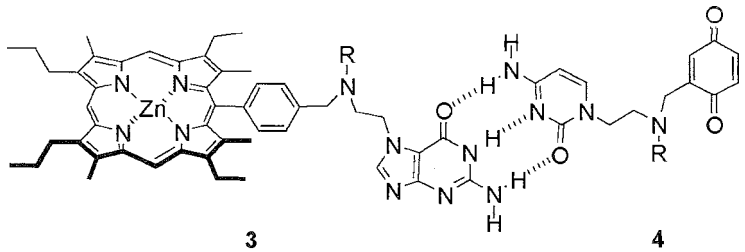

3 4

R = 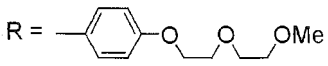

Ensemble 6

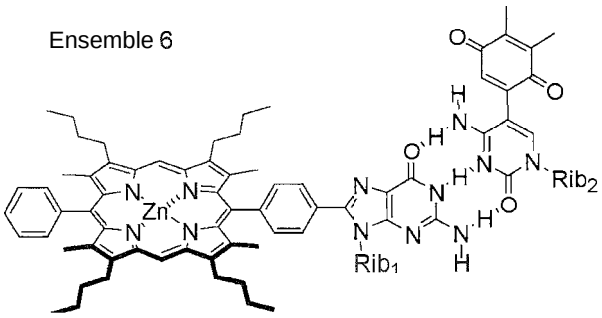

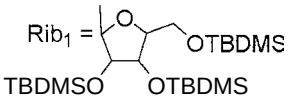

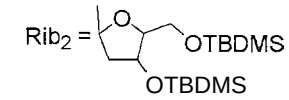

TBDMS = -SiMe$_2$^{t}Bu

Ensemble 5 is tethered via flexible linkers. This means that many conformations are possible even after formation of the sought-after hydrogen-bonded assembly. This leads to problems in defining the exact electron transfer pathway. To circumvent this problem, Sessler and coworkers synthesized systems containing rigid linkers (Ensemble 6).[22] The use of these latter models allowed the authors to calculate electron transfer rates and to conclude that the most probable electron transfer mechanism occurs through the hydrogen bond network. Ensemble 6 also has a larger association constant (8990 ± 600) M^{-1} as compared to Ensemble 5. Time-resolved fluorescence studies indicated two lifetimes: τ_1=(1.8 ± 0.2) ns and τ_2=(740 ± 90) ps, where the latter lifetime is ascribed. as in the case of Ensemble 5, to electron-transfer-mediated fluorescence quenching within the Watson–Crick defined complex. The rate of electron transfer was calculated to be $-8 \times 10^8\ s^{-1}$.

To gain further insight into the electron transfer properties of Watson–Crick linked donor–acceptor assemblies, the authors of the present chapter synthesized several dimethylaniline-anthracene electron transfer dyads (Ensembles 7 and 8).[23] The association constant for Ensemble 7 was found to be 38,500 ± 1300 M^{-1}. The large binding constant seen for this system is attributed to its increased rigidity relative to earlier CG ensembles. In this ensemble, the driving force for the initial photoinduced charge separation and the subsequent charge recombination processes were estimated as $\Delta G^0_{CS} = -0.41$ eV and $\Delta G^0_{RC} = -2.5$ eV, respectively. Fluorescence quenching experiments revealed substantial quenching of the anthracene chromophore 6 upon the addition of the dimethylaniline-guanosine donor ***5***. Further control experiments, using a masked donor: wherein the exocyclic amino group on 5 was protected, revealed little quenching, thus providing support for the idea that three-point hydrogen bonding is necessary for the observed photophysical process. Transient absorption spectroscopic studies were also carried out. Following irradiation with a 150 fs 417 nm laser pulse, two strong

Ensemble 7

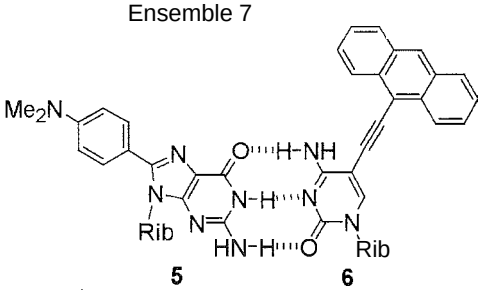

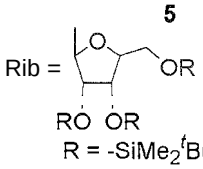

R = -SiMe$_2$^{t}Bu

Ensemble 8

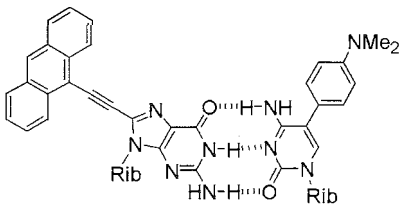

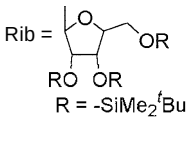

R = -SiMe$_2$^{t}Bu

Ensemble 9

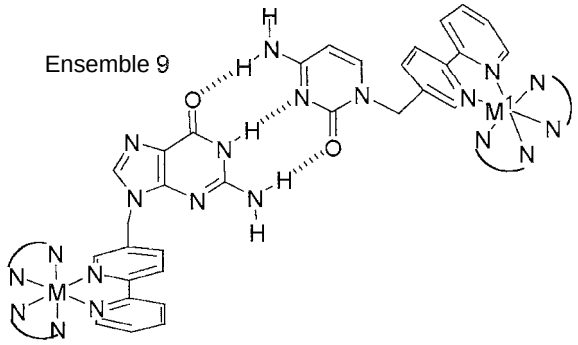

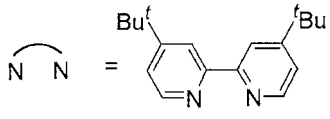

M = Os

M^1 = Ru

Ensemble 10

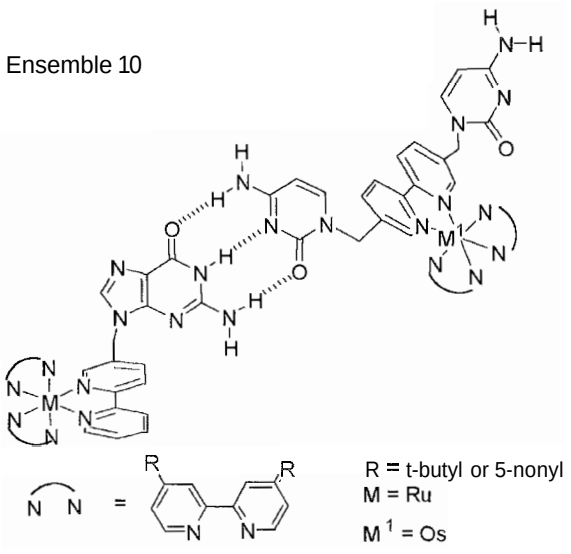

R = t-butyl or 5-nonyl
M = Ru
M^1 = Os

Ensemble 11

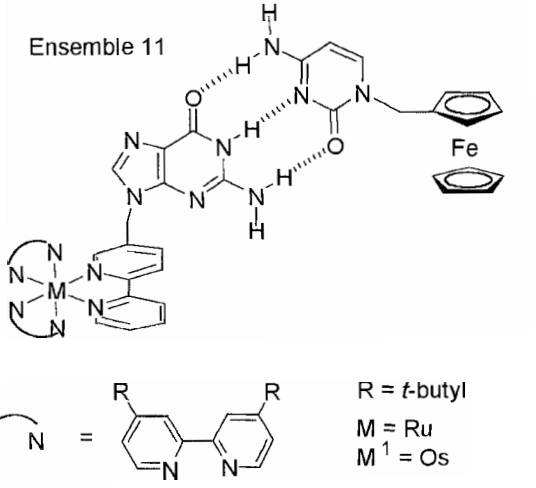

R = *t*-butyl
M = Ru
M^1 = Os

absorption bands, at 590 and 480 nm, were seen. The higher wavelength band is dominant 15 ps after photoexcitation and is ascribed to the $S_n \leftarrow S_1$ transition of the anthracene acceptor 6. From an analysis of the absorption band at 590 nm, A_{590}, as a function of time, a rate constant of $(2 \pm 0.5) \times 10^{10}\ s^{-1}$ was calculated for this forward electron transfer process. In contrast to what is seen at 590 nm, the absorption band at 480 nm is seen to rise and then decay in a monoexponential fashion after photoexcitation. Such a finding is consistent with the formation and disappearance of the presumed dimethylaniline cation. This latter absorption band was thus used to determine the charge separation and charge recombination rates, with values of $k_{CS} = (3.5 \pm 0.03) \times 10^{10}\ s^{-1}$ and $k_{CR} = (1.42 \pm 0.03) \times 10^{9}\ s^{-1}$ being calculated, respectively. These transient absorptions experiments are considered important, because they provided the first direct evidence for charge separation in a Watson–Crick-type model system under simple solution-phase photoexcitation conditions.

In spite of the apparent structural similarity, photophysical studies on the reverse Ensemble 8 revealed behavior that was different from that observed for Ensemble 7. In fact, fluorescence analyses of Ensemble 8 revealed the formation of an exciplex in dichloromethane. Subsequent experiments in toluene using time-resolved emission and transient absorption methods provided no evidence of quenching. These results illustrate the sensitivity of electron transfer processes toward the orientation of donor–acceptor moieties in a given intraensemble system.

Ward and coworlters extensively studied energy transfer between metal polypyridyl complexes preorganized via complementary Watson–Crick base pairing.[124] Ensemble 9 has an association constant of $5 \times 10^{7}\ M^{-1}$ in CD_2Cl_2, and the k_{EN} for the Ru → Os energy transfer

Ensemble 12

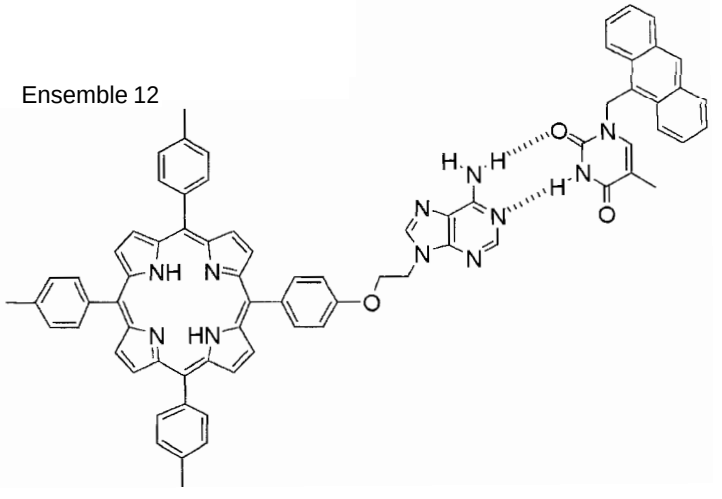

Ensemble 13

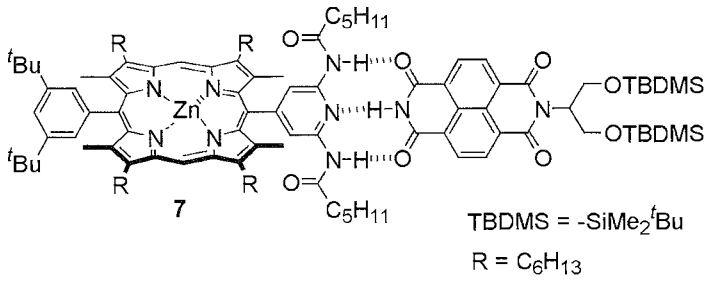

within the resulting dyad was calculated to be k_{EN} = 29.3 x 10^7 s^{-1} on the basis of time-resolved luminescence measurements. Ensuing studies by the authors[25] led them to conclude that the Ru → Os energy transfer process within the constrained Ru-G/C-Os-C Ensemble 10 is of the Forster type, implying that the role of the guanine–cytosine couple is merely structural. However. replacing the C-Os-C couple with a fen-ocene (Fc-C) moiety (Ensemble 11) gave experimental results consistent with a Dexter mechanism, a finding that implicates an electronic mediation role for the H-bonds.

Interestingly. Ward and his coworkers were unable to study the energy transfer properties of the analogous adenine–thymine linked systems. In this case, the less favorable two-point hydrogen bond interactions give rise to low association constants (i.e., K ~ 10^2 M^{-1} in CD_2Cl_2). Maiya and Sirish also reported an adenine–thymine linked system (Ensemble 12). where the donor is an anthracene and the acceptor is a porphyrin.[26] Here the authors attempted time-resolved fluorescence measurements but only observed a monoexponential decay. They suggest that there exists a short-lived component due to the foldover conformers. However; the lifetime of this component is too short to be measured. Another explanation for the lack of a biexponential decay may be due to the possibility that the lifetimes of the complexed (Ensemble 12) and uncomplexed forms (free anthracene–thymine unit) are similar. Be this as it may, it is clear from these studies that the use of adenine–thymine bridges provides electron transfer model systems that are harder to study than their guanine–cytosine counterparts.

ABIOTIC MOTIFS LINKED BY THREE HYDROGEN BONDS

Synthetic systems with three primary hydrogen bonds and four repulsive secondary interactions, ADA•DAD motifs in the supramolecular vernacular. are among the best known of all noncovalent host–guest systems. Although not generally as stable as the previously mentioned DDA•AAD system (because they have four repulsive secondary interactions, while the DDA•AAD models possess two attractive and two repulsive interactions), they have been widely used for electron transfer model construction. The naphthalene diisnide interface is one ADA system that is especially attractive, due to its distinct transient absorption properties when reduced. Furthermore, it serves as an efficient electron sink for excited zinc posphyrins. Hence, Mataga and Osaka recently reported a 2,6-diacylaminopyridylporphyrin-napthalene diimide complex (Ensemble 13).[27] The presence of the complex was confirmed by ^{1}H-NMR spectroscopic binding studies in C_6D_6 (K=2.8 x 10^2 M^{-1}). The rate of forward electron transfer (k_{CS}=4.1 x 10^{10} s^{-1}) was obtained from an analysis of the time profile of the transient absorption spectrum (λ_{ex}=532 nm) at 458 nm, where the main absorbing species was the S_1 state of the zinc porphyrin 7. Unambiguous evidence for the proposed electron transfer across the hydrogen-bonding interface within the supramolecular Ensemble 13 came from transient absorption spectroscopic measurements. The transient absorption spectrum of Ensemble 13 recorded 20 ps after laser excitation at 532 nm revealed absorption bands at 474 and 655 nm that correspond to a diimide radical anion and zinc porphyrin radical cation, respectively. The rate of back electron transfer (k_{CR}=3.7 x 10^9 s^{-1}) was calculated from the lifetime (τ=270 ps) of the transient species. Comparison of Ensemble 13 with a related covalent system[27] indicated similar forward and

Ensemble 14

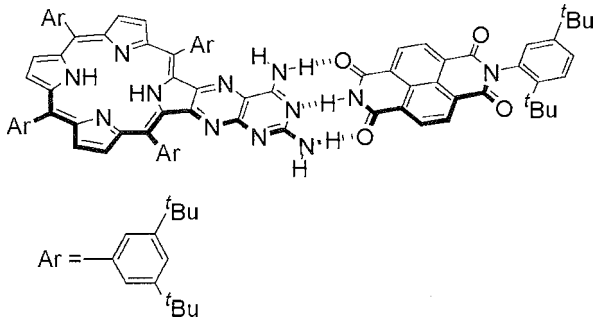

Ensemble 15

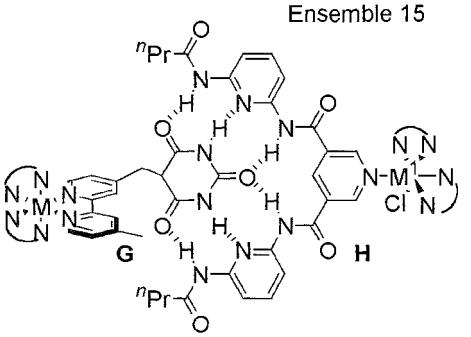

M = Ru^{II} or Os^{II}
M^1 = $Ru^{III/II}$ } R = *t*-butyl

M^1 = $Os^{III/II}$ R = methyl

G = guest

H = host

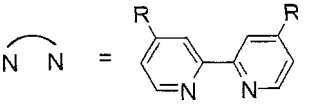

backward electron transfer rates. a finding that underscores the efficiency of hydrogen-bond-mediated electron transfer within (at least) ensembles such as this.

Sessler and Brown also studied a system wherein a naphthalene diimide moiety is linked via a three-point hydrogen bond to a rigid chlorin (see Ensemble 14).[28] The edge-to-edge distance was calculated to be 7 A. Proton NMR binding titrations in $CDCl_3$ gave an association constant. $K = 364 + 47\ M^{-1}$. Subsequent photoirradiation studies, carried out with excitation effected at 573 nm. allowed for various spectroscopic analyses. For instance. from single-photon counting studies, the electron transfer rate was determined to be $7.6 \times 10^8\ s^{-1}$. These studies, also revealed a biexponential decay, indicating two lifetimes ($\tau_1 = 13$ ns and $\tau_2 = 1.25$ ns), with the latter lifetime being characteristic of intracomplex photoinduced eiectron transfer. Unfortunately, in this system, no evidence for a diimide-derived radical anion was obtained, presumably as a consequence of rapid back electron transfer.

MODULES WITH MULTIPLE H-BONDS

In recent years. research has focused on the exploration of motifs with multiple hydrogen-bonding sites. Like the ensembles described earlier in this chapter. these systems can serve as models for photoinduced electron transfer. However, by virtue of possessing a greater number of hydrogen bonds, these newer systems offer the promise of increased preorganization and enhanced stability. As one example of a system with a high degree of self-complementarity, Isied and coworkers recently reported a new barbiturate-*bis*(2,6-diacylaminopyridine) template-mediated $*Ru^{II}$ or $*Os^{II}G \rightarrow Ru^{III}$ or $Os^{III}H$ (where *G* and *H* are defined as the guest and host. respectively) electron transfer model system (Ensemble 15).[29] Here. the barbiturate moiety allows for a six-point H-bonding array that contains the diacylaminopyridine unit. As a consequence, the donor ($M^{II}G$) and acceptor (HM^{III}) units assemble in CD_2Cl_2 with high affinity ($K = 2-5 \times 10^{n}\ M^{-1}$) as judged by steady-state fluorescence and 'H-NMR spectroscopic titrations. Upon laser excitation. in all cases, the excited singlet state is observed to decay in a biphasic manner. with the shorter lifetime corresponding to the intramolecular electron transfer across the 18 ± 1 A H-bond-linked donor–acceptor gap. The forward electron transfer rates from $*M^{II}G$ to $M^{III}H$ in dichlorornethane were calculated from the difference in fluorescence lifetimes of the complexed and uncomplexed components. Furthermore, the rate of thermal back electron transfer (charge recombination) was determined by transient absorption spectroscopic techniques. The results generated from the studies are suinmarized in Table 1. The authors were also able to fit the experimental electron transfer rates using classical Marcus theory (Eqs. 1 and 2), thereby obtaining both the electronic coupling matrix element T_{DA} ($1.2\ cm^{-1}$)[a] and the reorganization energy λ (1.2 eV).

The use of multiple hydrogen bonding also allows for the assembly of higher-order supramolecular structures that begin to mimic the complexity of biological arrays. In the bacterial photosynthetic system. many antenna

Table 1 Measured Electron-Transfer Rates and Estimated Driving Force Values for Ensemble 15[a]

Complex	k_{ET}/s^{-1}	$\Delta G°/eV$
$*Ru^{II}G\text{-}HRu^{III} \rightarrow Ru^{III}G\text{-}HRu^{II}$	1.5×10^8	1.68
$*Ru^{II}G\text{-}HOs^{III} \rightarrow Ru^{III}G\text{-}HOs^{II}$	2.5×10^8	−1.29
$*Os^{II}G\text{-}HOs^{III} \rightarrow Os^{III}G\text{-}HOs^{II}$	2.6×10^8	−1.37
$(Ru^{III}G\text{-}HRu^{II}) \rightarrow Ru^{II}G\text{-}HRu^{III}$	3.3×10^6	−0.44
$(Os^{III}G\text{-}HOs^{II}) \rightarrow Os^{II}G\text{-}HOs^{III}$	2.0×10^6	−0.39

[a]Data from Ref. [29].

Ensemble 16 (a)

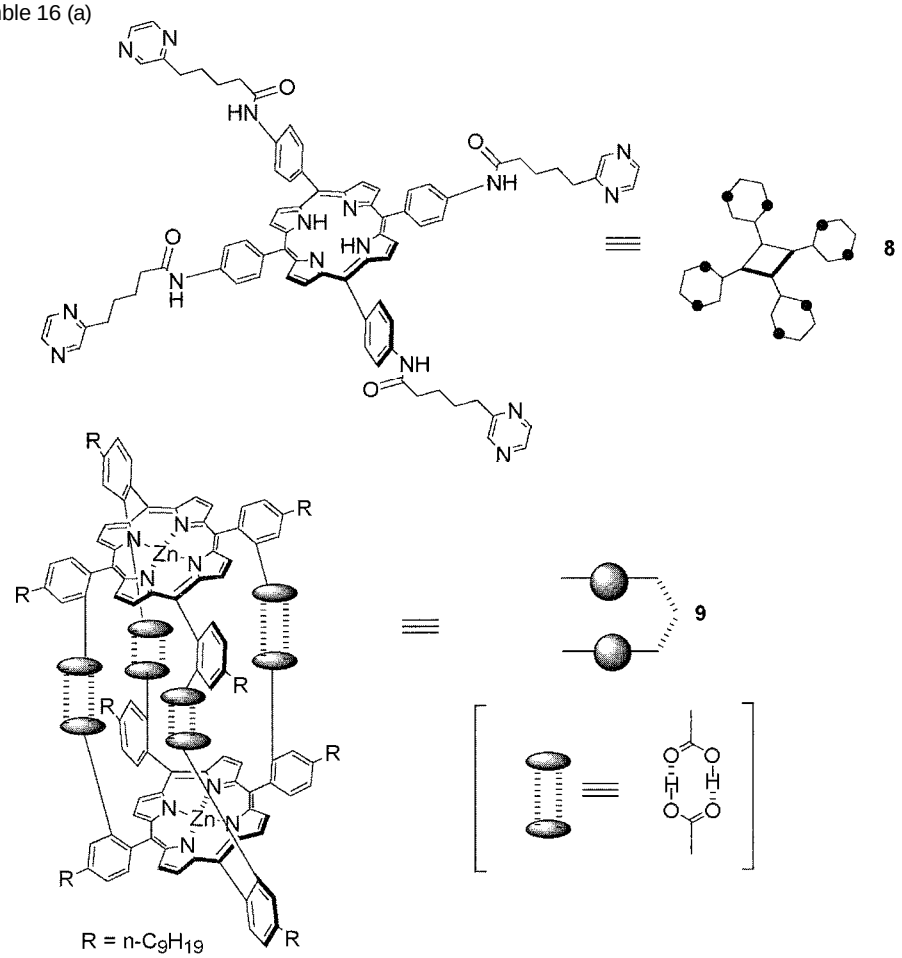

Ensemble 16 (b)

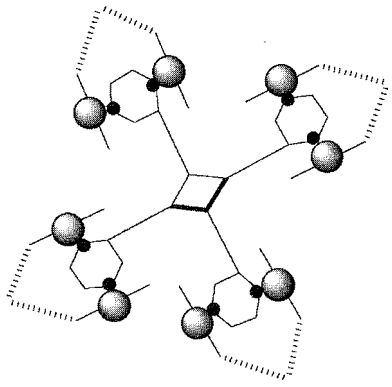

(*View this art in color at www.dekker.com.*)

pigments are located around the reaction center; these pigments serve to absorb and transmit light into the reaction center. Generating noncovalent analogues of these antennae has stood as an important challenge to the supramolecular chemist. Kuroda and colleagues made important progress toward this goal. They reported a novel synthetic porphyrin suprarnolecular assembly that illustrates the principle of the antenna effect. Their system

Ensemble 17

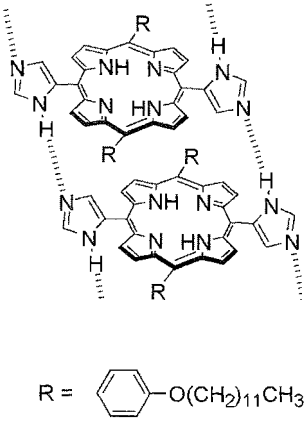

contains one energy acceptor porphyrin and four pairs of antenna porphyrins. Each dimeric antenna porphyrin pair is self-assembled via eight hydrogen bonds between carboxylic acid moieties (Ensemble 16a).[30] Absorption and fluorescence titrations indicate binding between 8 and 9 in a 1:4 ratio. The four individual binding processes are independent. and the association constants are identical ($K = 4$ a 1 x 10^7 M^{-1}). The free-base porphyrin 8 in the absence of 9 exhibits a weak emission. By contrast, Ensemble 16b shows a strong fluorescence emission. Using a best-fit analysis for the absorption spectrum, the authors calculated the efficiency of energy transfer from the zinc porphyrin 9 to the free-base porphyrin 8 at 82% for a process that takes place over a range of 16–21 Å. These results are consistent with the conclusion that the fluorescence of 8 is enhanced 18-fold. thereby achieving the proposed antenna effect.

Kobuke and coworkers also built a supramolecular system that mimics light harvesting arrays via an antenna effect (Ensemble 17).[31] Were, a polymeric complex is assembled through cooperative hydrogen-bonding interactions involving imidazole subunits and via slipped cofacial π-stacking interactions. In studying their systems, the authors used chloranil and tetraphenylporphyrinato-Mn(III) chloride (MnTPP·Cl) as external energy acceptors. It was found that chloranil and MnTPP·Cl quenched the fluorescence of the complex (Ensemble 17) 2.9 times faster than they did that of the monomer (porphyrin lacking the imidazole hydrogen-bonding sites). An explanation for these findings put forward by the authors is that the excitation energy is delocalized through the polymeric complex and can be quenched by an acceptor from any one of the monoineric components.

CONCLUSION

Investigations of electron and energy transfer processes in supramolecular model systems preorganized through hydrogen-bonding interactions have advanced our understanding of noncovalent assembly construction and electron- and energy-transfer theories. Among the most important take-home lessons are that the rate of electron transfer in ensembles tethered via hydrogen bonds is often comparable to what is seen in comparable covalent analogs. and the orientation and rigidity of the donor–acceptor pairs within a given intramolecular system can profoundly affect the nature of the electron transfer process. Yet another important finding is that working antenna systems can be generated by tethering multiple photoacceptors to an appropriate acceptor through multiple hydrogen-bonding interactions. Still. in these and all other cases, the models remain but oversimplified reflections of the natural systems they are designed to imitate. Thus, there remains a need to prepare yet more elaborate model systems that can provide further insights into why certain biological electron transfer pathways are favored over others.

ACKNOWLEDGMENT

This work was supported by the R.A. Welch Foundation (grant F-1018 to J. L. S.).

ARTICLES OF FURTHER INTEREST

Hydrogen Bonding, p. 658
Preorganization and Complementarity, p. 1158
Strong Hydrogen Bonds, p. 1379
Supramolecular Photochemistry, p. 1434
Weak Hydrogen Bonds. p. 1576

REFERENCES

1. Pelletier, H.; Kraut, J. Crystal structure of a complex between electron transfer partners, cytochrome c peroxidase and cytochroine c. Science 1992. *258* (5089). 1738–1755.
2. Deisenhofer. J.: Epp. O.; Miki. K.: Huber, R.; Michel, H. Structure of the protein subunits in the photosynthetic reaction centre of *Rhodopseudomonas viridis* at 3 A resolution. Nature 1985. *318* (19). *61*8–624.
3. Moser. C.C.: Keske. J.M.; Warncke. K.: Farid, R.S.; Dutton. P.L. Nature of biological electron transfer. Nature *1992. 355 (6363)*. 796–802.
4. Beratan. D.N.; Onuchic. J.N.: Winkler. J.: Gray. H.B. Electron-tunneling pathways in proteins. Science 1992. *258* (5089), 1740–1741.
5. Murphy, C.J.; Arkin, M.R.; Jenkins. Y.; Ghatlia. N.D.; Bossmann. S.H.; Turro, N.J.: Barton, J.M. Long-range photoinduced electron transfer through a DNA helix. Science 1993. *262* (5136), 1025–1029.

6. Sessler, J.L.; Wang, B.; Springs, S.L.; Brown. C.T. Electron- and energy-transfer reactions in noncovalently linked supramolecular model systems. Compr. Supramol. Chem. 1996, *4*. 311–336.
7. Ward. M.D. Photo-induced electron and energy transfer in non-covalently bonded supramolecular assemblies. Chem. Soc. Rev. 1997. 26 (5). 365–375.
8. Hayashi, T.; Ogoshi, H. Molecular modelling of electron transfer systems by noncovalently linked porphyrin-acceptor pairing. Chem. Soc. Rev. **1997**, 26 (5), 355–364.
9. Chang, C.J.; Brown. J.D.K.: Chang. M.C.Y.: Baker, E.A.: Nocera, D.G. Electron Transfer in Hydrogen-Bonded Donor–Acceptor Supramolecules. In *Electron Transfer in Chemistry*, 1st Ed.; Balzani, V., Ed.: Wiley-vch: Weinheim, 2001: Vol. 3. 409–461.
10. Marcus, R.A.: Sutin. N. Electron transfers in chemistry and biology. Biochim. Biophys. Acta. 1985. **811** (3). 265–322.
11. Levich. V.G. Present state of the theory of oxidation-reduction in solution (bulk and electrode reactions). Adv. Electrochem. Electrochem. Eng. 1966, 4. 249–371.
12. Jortner. J. Temperature dependent activation energy for electron transfer between biological molecules. J. Chem. Phys. 1976. 64 (12), 4860–4867.
13. Rehm. D.; Weller, A. Kinetics of fluorescence quenching by electron and H-atom transfer. Israel J. Chem 1970, *8*. 259–271.
14. Williamson, D.A.: Bowler. B.E. Electron transfer through the hydrogen-bonded interface of a β-turn-forming depsipeptide. J. Am. Chem. Soc. 1998, 120 (142). 10902–10911.
15. Bolton, J.R.; Schmidt, J.A.; Ho. T.-F.; Liu, J.-Y.; Roach, K.J.: Weedon, A.C.; Archer. M.D.; Wilford, J.H.: Gadzekpo, V.P.Y. Solvent. Temperature, and Bridge Dependence of Photoinduced Intramolecular Electron Transfer. In *Electron Transfer in Inorganic, Organic, and Biological Systems;* Bolton, J.R.. Mataga. N., McLendon. G., Eds.: American Chemical Society: Washington; 1991; Vol. 2. 117–131.
16. Onuchic. J.N.: Beratan, D.N.; Winkler, J.R.; Gray, H.B. Pathway analysis of protein electron-transfer reactions. Annu. Rev. Biophys. Biomol. Struct. 1992, 21, 349–377.
17. Prasad, E.; Gopidas, K.R. Photoinduced electron transfer in hydrogen bonded donor-acceptor systems. Study of the dependence of rate on free energy and simultaneous observation of the Marcus and Rehm–Weller behaviours. J. Am. Chem. Soc. 2000, 122 (13). 3191–3196.
18. Smitha. M.A.: Prasad, E.; Gopidas. K.R. Photoinduced electron transfer in hydrogen bonded donor-acceptor systems. Free energy and distance dependence studies and an analysis of the role of diffusion. J. Am. Chem. Soc. 2001, 123 (6), 1159–1165.
19. Tanaka, K.: Yamamoto. Y.: Machida. I.: Iwata. S. Quinone recognition by amide hydrogen bonding in porphyrin systems. J. Chem. Soc. Perkin Trans. 1999. 2, 285–288.
20. Arimura, T.; Ide. S.; Sugihara, H.; Murata, S.; Sessler, J.L. A non-covalent assembly for electron transfer based on a calixarene-porphyrin conjugate: Tweezers for a quinone. New J. Chem. **1999**, 23 (10), 977–979.
21. Harriman. A.: Kubo, Y.: Sessler, J.L. Molecular recognition via base pairing: Photoinduced electron transfer in hydrogen-bonded zinc porphyrin-benzoquinone conjugates. J. Am. Chem. Soc. 1992, 114 (1), 388–390.
22. Sessler, J.L.: Wang, B.; Harriman, A. Long-range photoinduced electron transfer in an associated but noncovalently linked photosynthetic model system. J. Am. Chem. Soc. 1993, *115* (22). 10418–10419.
23. Sessler. J.L.: Sathiosatham, M.; Brown, C.T.; Rhodes, T.A.; Wiederrecht, G. Hydrogen-bond-mediated photoinduced electron-transfer: Novel dimethylaniline-anthracene ensembles formed via Watson–Crick base-pairing. J. Am. Chem. Soc. **2001**, 123 (16), 3655–3660.
24. Armaroli. N.: Barigelletti. F.: Calogero, G.; Flamigni, L.; White, C.M.; Ward, M.D. Electronic energy transfer between ruthenium(II) and osmium(II) polypyridyl luminophores in a hydrogen-bonded supramolecular assembly. Chem. Commun. 1997, (22), 2181–2182.
25. Encinas. S.: Simpson, N.R.M.: Andrews, P.: Ward. M.D.; White, C.M.; Armaroli, N.; Barigelletti, F.; Houlton. A. Photoinduced energy transfer within hydrogen-bonded multi-component assemblies based on a ruthenium-polypyridyl donor and an osmium-polypyridyl or ferrocenyl acceptor. New J. Chern. 2000, 24 (12). 987–991.
26. Sirish, M.; Maipa, B.G. A porphyrin-anthracene supramolecular system assembled via complementary nucleic acid base pairing. J. Porphyrins Phthalocyanines. **1998**, *2* (4–5), 327–335.
27. Osuka, A.; Yoneshima, R.: Shiratori. H.; Okada, T.; Taniguchi, S.: Mataga. N. Electron transfer in a hydrogen-bonded assembly consisting of porphyrin-diimide. Chem. Commun. 1998.15, 1567–1568.
28. Sessler. J.L.: Brown, C.T.: O'Connor, D.; Springs. S.L.: Wang. R.; Sathiosatham, M.: Hirose, T. A rigid chlorin-naphthalene diimide conjugate. A possible new noncovalent electron transfer model system. J. Org. Chem. 1998. 63 (21). 7370–7374.
29. Ghaddar. T.H.: Castner, E.W.: Isied, S.S. Molecular recognition and electron transfer across a hydrogen bonding interface. J. Am. Chem. Soc. **2000**, 122 (6), 1233–1234.
30. Kuroda, Y.: Sugou, K.: Sasaki, K. Nonameric porphyrin assembly: Antenna effect on energy transfer. J. Am. Chem. Soc. 2000, 122 (32). 7833–7834.
31. Nagata, N.; Kugimiya. S.: Kobuke. Y. Antenna functions of 5,15-*bis*(imidazol-4-yl)-10,20-*bis*(4-dodecyloxyphenyl)-porphyrin supramolecular assembly through imidazole-imidazole hydrogen bonding. Chem. Commun. **2000**, (15), 1389–1390.

Enzyme **Mimics**

Anatoly K. Yatsimirsky
Universidad Nacional Autónoma de México, Mexico City, Mexico

INTRODUCTION

Biomimetic chemistry attempts to improve the performance of chemical reactants and catalysts by imitating enzymatic processes.[1] One may consider as enzyme mimics catalysts of a different nature, which use principles of enzyme action, such as an initial binding interaction between the substrate and catalyst, polyfunctional activation of the bound substrate by properly positioned organic catalytic groups or metal ions, transition-state stabilization and others.[2] Enzyme mimics are designed mainly for practical applications as artificial enzymes and less for understanding enzyme mechanisms, which is one of the goals of enzyme modeling. Although in some instances even simple organic molecules[3] or metal complexes[4] work as enzyme mimics, only more sophisticated supramolecular systems discussed in this article show an enzyme-like performance. A general feature is the presence of a host that recognizes the substrate and the reaction transition state, providing increased reactivity and selectivity. Several books[5,6] and reviews[2,7,8] may be recommended for general reading on this subject.

SURFACTANT AGGREGATES AND SYNTHETIC POLYMERS

Surfactants aggregate above so-called critical micelle concentration, forming spherical or cylindrical micelles, bilayers. vesicles, and other aggregates; depending on surfactant structure and conditions. Synthetic polymers. e.g., polyethyleneimine or polyvinylpyridine, modified (usually by quaternizaiton) by long-chain aliphatic groups behave similarly, forming intramolecular micelles already at low concentrations. All of these aggregates possess a hydrophobic interior or core made from surfactant hydrocarbon tails covered by a hydrophilic, usually ionic, surface layer made from surfactant head groups, reminiscent of the structural organizations of globular proteins and biological membranes. For this reason, reactivity in such aggregates was studied for a long time and represents. perhaps, the oldest suprainolecular imitation of enzyme catalysis.[9]

Surfactant aggregates serve as primitive hosts, due to their ability to incorporate apolar organic molecules into the hydrophobic core and to attract counterions to the surface layer. The origin of catalysis in micelles and other aggregates is principally the concentration effect: the partitioning of reactants between aqueous and micellar pseudophases leads to increased concentrations of reacting species in the micelles and, consequently. to an increased rate.[10] Remarkably, this simple effect explains large rate enhancements of up to 10^6 times.[11] Simple inert surfactants typically catalyze bimolecular reactions between a neutral organic molecule bound to micelles by hydrophobic interactions and an ionic species charged opposite to the micellar surface charge and bound electrostatically. For example, cleavage of 4-nitrophenyl carboxylates by deprotonated aryl oximes is accelerated 10^3–10^4 times in the presence of micelles of cationic surfactants. The acid hydrolysis of acetals is accelerated ca. 10^2 times by micelles of anionic surfactants.[10,11]

More successful enzyme mimics are aggregates with functionalized surfactants. In this approach, a functional group (a nucleophile, a metal complex, or an enzyme cofactor, e.g., nicotinamide or cobalamine) is attached to a long-chain molecule that has surfactant properties or can be incorporated into aggregates of an inert surfactant.[7,9] As an example of such a system, shown in Fig. 1 is a mechanism proposed for cleavage of a chiral ester of C-phenylglycine by a lipophilic chiral alkoxide Cu(II) complex incorporated into *n*-hexadecyltrimethylammonium bromide micelles.[12] The metal cation facilitates deprotonation of the ligand alcohol group and binds the substrate via coordination of the α-amino group. In comparison with a nonmicellar complex of similar structure, but with an N-methyl instead of an N-dodecyl group, the micellar catalyst is 140 times more active and shows much higher enantioselectivity (the ratio of the rate constants for cleavage of S and R enantiomers increases from 1.2 to 11.6). The nonmicellar catalyst uses coordinated hydroxide anion as a nucleophile, but the micellar environment favors formation of a stronger alkoxide nucleophile, which in addition, reacts more stereospecifically. Positive micellar charge and hydrophobic binding of the ester to micelles also contribute to catalysis and enantioselectivity. Incorporation of the

Encyclopedia of Supramolecular Chemistry
DOI: 10.1081/E-ESMC 120012678

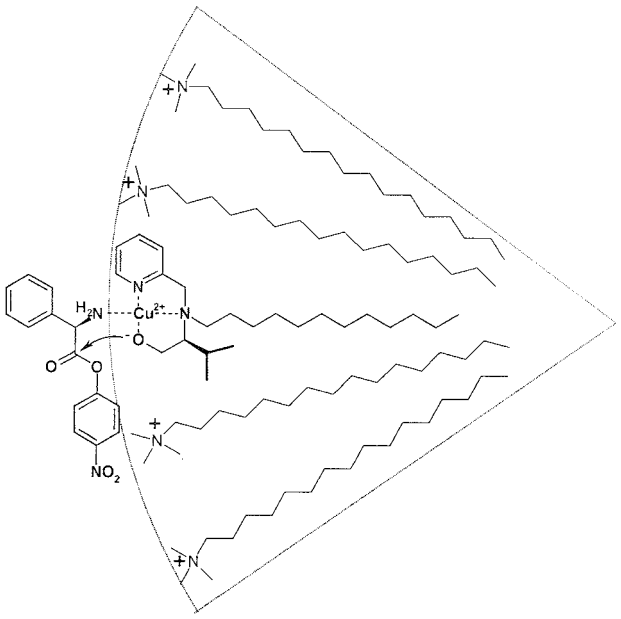

Fig. I Cleavage of an α-amino acid ester by a lipophilic Cu(II) complex incorporated into micelles of a cationic surfactant. A sector of a spherical micelle with incorporated ligancl is shown schematically. (From Ref. [12].)

same lipophilic complex into cationic bilayers leads to a further increase in enantioselectivity, probably due to the more rigid structure of bilayers as compared to spherical micelles.

Functionalized polymers behave similar to surfactant aggregates[9] but have some advantages for practical applications. Surfactant aggregates have low stability and exist only in solution at sufficiently high concentrations. Surfactant polymers have an advantage of being stable at any concentration. and they can easily be incorporated into, e.g., filters or other devices for analytical or biomedical applications. For example; polymeric surfactants. which are glutathione transferase mimics. were designed for such applications.[13]

CYCLODEXTRINS

Cyclodextrins (CDs) are useful components for biomimetic systems. They form well-characterized inclusion complexes with many organic compounds via hydrophobic interactions and possess a large number of alcohol groups that can serve as cataiytic groups or can be used to attach other functional groups. A large number of biomirnetic catalytic reactions using native or modified CDs were described.[14]

An important area of application of CDs as enzyme mimics involves hydrolysis of activated esters and amides via nucleophilic attack of a deprotonated secondary hydroxyl group of CD on the carboxyl group of the bound substrate. The enzyme-like Michaelis–Menten kinetics, turnover, and a mechanistic similarity of CD-catalyzed reactions to serine hydrolases were demonstrated in earlier studies with simple acetate and benzoate esters as substrates.[''' Further investigations guided by molecular modeling of CD-substrate and CD-transition-state complexes revealed the importance of the specially designed acyl part of the substrate for the efficiency of CD catalysis.[14] Thus. the rate enhancement by β-CD in the hydrolysis of 4-nitrophenyl acetate is only six times, but the hydrolysis of ferroceneacrylate esters is accelerated by ca. 6×10^6 times in the presence of β-CD. Binding constants for both substrates are similar. Therefore. the stronger catalysis for ferroceneacrylate esters is due to better complementarity of CD cavity to the reaction transition state.

For a long time, the hydrolase activity of CDs was restricted to activated substrates. such as aromatic esters, because CD hydroxyl groups are not basic enough to force out a poor leaving group. such as aliphatic alcohol. from the tetrahedral addition intermediate. Recently, successful catalytic hydrolysis of an unactivated aliphatic ester was achieved by using a *bis*-CD derivative with a Cu(II) bipyridine complex as the active site (Fig. 2).[15] The rate enhancement for this system is 1000-fold, and the attacking nucleophile is the coordinated hydroxide ion rather than a CD hydroxyl group.

Numerous biomimetic reactions catalyzed by CDs carrying catalytic or reactive functional groups, such as nucleophiles (imidazole. oxime, and amine). enzyme cofactors (pyridoxamine, thiazolium. nicotinamide, cobalainine, flavin), metal complexes. etc.. were reported.[14] Typically, enzyme-like kinetics and improved performance of a catalytic group, as compared to a simple analog lacking CD. are observed.

Besides enhanced reactivity, a higher selectivity may be achieved by using CDs. For example. chlorination of

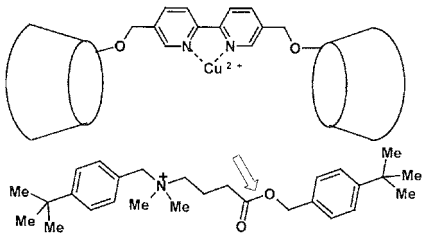

Fig. *2* Catalytic hydrolysis of an unactivated aliphatic ester by a Cu(II) bipyridine complex with two attached CDs. (From Ref. [15].)

anisole by hypochiorous acid in the presence of α-CD proceeds faster and exclusively in the *pal-a* position of the substrate.''' Also, the regioselectivity of the Diels–Alder reaction may be improved by CDs.[14]

Supramolecular catalysts that involve two or more CD units are especially promising. The presence of several CD units strongly increases binding constants for substrates. which can bind to two CD cavities. Binding constants exceeding 10^{10} M^{-1} were reported for CD dimers and guests, like 4-$(CH_3)_3C$–$C_6H_4COO(CH_2)_3$-$OOCC_6H_4$–$C(CH_3)_3$-4, while binding constants of typical organic guests to CDs are in the range of 10^2–10^4 M^{-1} only.[14] High activities and high selectivities were reported for catalysts of this type. Illustrated in Fig. 3 is the application of a cytochrome P-450 mimic based on a Mn(III)–porphyrin active site with three attached CD units for selective hydroxyiation of steroids.[16] The catalyst contains fluorinated phenyl groups that protect the porphyrin from oxidative destruction, three CDs for substrate complexation, and a pyridine group required for catalytic activity as an axial ligand stabilizing the active Mn=O species. In the first step, androstan-3,17-diol was modified by esterification with two fragments carrying bulky hydrophobic groups for binding into CDs cavities and sulfonate groups for solubility in water. Then, the modified steroid was hydroxylated by iodosobenzene in the presence of the enzyme mimic, and the ester groups were removed by hydrolysis. The only product was the 6α-hydroxy derivative. and the catalyst did the oxidation with 2000 turnovers. In a control experiment, a similar substrate, but lacking terminal *tert*-butylphenyl groups. was not oxidized. This remarkable selectivity is in line with results of molecular modeling that predict that bound to two CDs, the steroid diester is positioned above the posphyrin plane. and only the α-hydrogen at C-6 can be reached by reactive Mn=O species. A similar approach was successfully applied to mimic carotene dioxygenases: selective 15,15′ double-bond scission of β,β-carotene was achieved with a Ru(II) porphyrin with two CDs attached to opposite sides of the

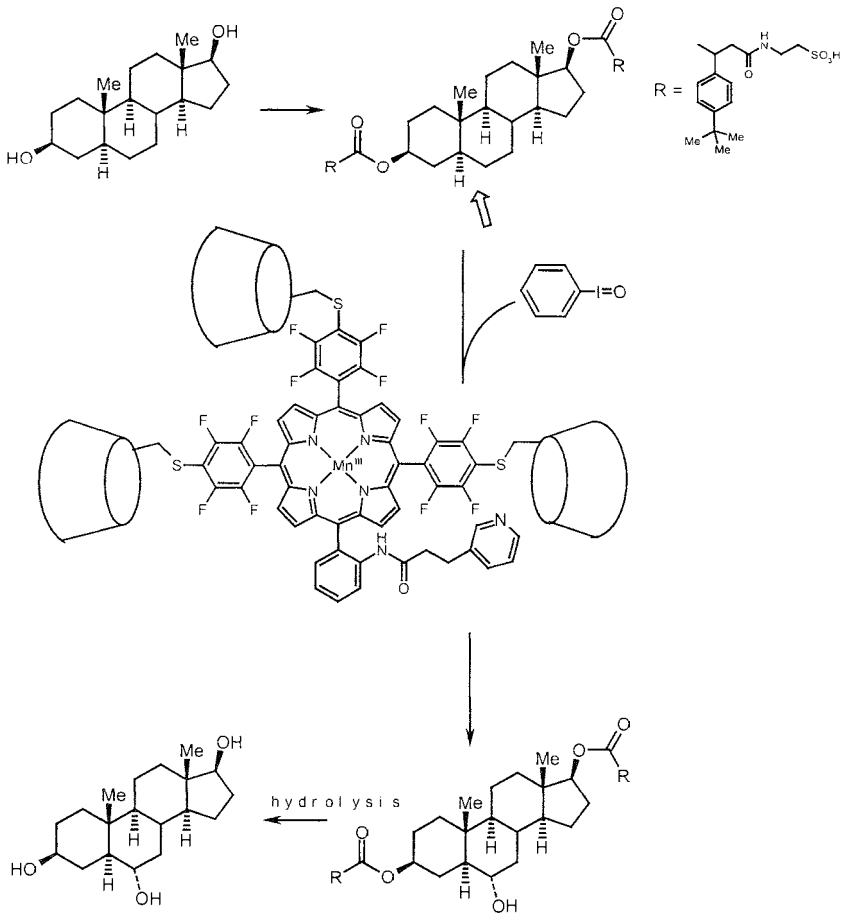

Fig. *3* A cytochrome P-450 mimic for selective hydroxylation of steroids. (From Ref. [16].)

porphyrin ring.[17] Other examples can be found in the literature.[7,8 14]

SYNTHETIC MACROCYCLES

Crown Ethers and Macrocyclic Polyamines

The ability of crown ethers to bind primary ammonium groups was used to achieve an enzyme-like cleavage of activated amino acid esters by attachment to the macrocycle nucleophilic group. Inclusion of the protonated amino group of the substrate into the crown ether approximates the ester group and the nucleophile, inducing significant rate enhancements.[2] Such systems were proposed to accelerate peptide synthesis by using dithiole crown ether derivatives like 1 (Fig. 4).[18] Both thiole groups of 1 are acylated by activated esters of amino acids, and then intramolecular aminolysis leads to formation of the dipeptide as the thioester at one thiole group and liberation of another thiole group. that again may be acylated.

Partially protonated macrocyclic polyamines possess a high positive charge that may attract and activate negatively charged substrates. This type of catalysis is illustrated by catalysis of H–D exchange in the malonate dianion in the presence of a tetraprotonated macrocyle (2; Fig. 4) that imitates enolase enzymes.[19] In addition, amino groups of the macrocycle, which remain unprotonated, may act as nucelophiles toward an anionic substrate bound to the protonated cationic part of the macrocycle. This type of catalysis operates in the ATP hydrolysis by the same macrocycle (3: Fig. 4).[20]

Cyclophanes

Guest-binding properties of cyclophanes resemble those of CDs. Nonfunctionalized cyclophanes with large cavity sizes may catalyze bimolecular reactions by bringing together two reactants.[2] Many cyclophanes carrying functional groups (nucleophiles and some enzyme cofactors) were prepared as enzyme mimics.[2,7,8] In Fig. 4 (Structure 4), one of the most successful cyclophane enzyme mimics, a flavo-thiazolio-cyclophane imitating the action of pyruvate oxidase,[21] is shown. The host 4 catalyzes oxidation of 2-naphthaldehyde to methyl 2-naphthoate in methanol. The reaction kinetics is of the Michaelis–Menten type. A similar, but not macrocyclic, compound reacts much slower and does not show any saturation upon variation of substrate concentration. The results show the importance of the macrocyclic binding site. The recycling of the flavin is possible by electro-

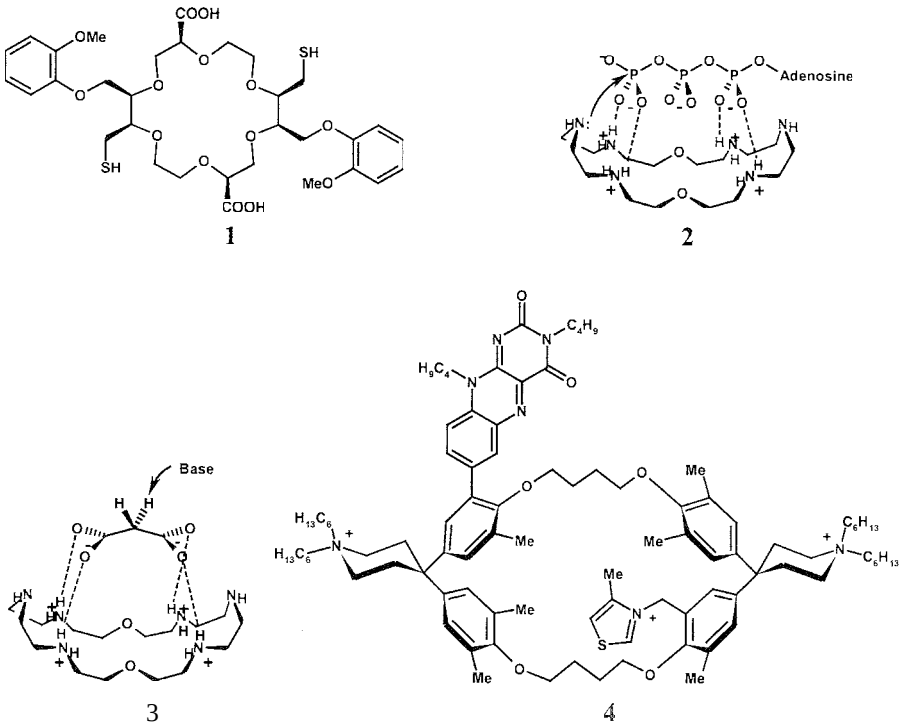

Fig. 4 Some synthetic macrocycles used as enzyme mimics

chemical reoxidation of the cofactor. and up to 100 cycles can be performed on a preparative scale.

MOLECULARLY IMPRINTED POLYMERS

Transition-state stabilization by complementary noncovalent binding to the active-site functional groups is the central idea in interpretating the remarkable activity and selectivity of enzymes.[2] From this point of view, a synthetic receptor designed as an enzyme mimic should recognize reactants in the transition rather than in the ground state. The most successful approach to such receptors is the development of catalytic antibodies (abzymes), discussed in a separate article. The general idea of this approach is to use a stable analogue of the transition state for a given reaction as a hapten (a small molecule that can stimulate antibody formation when combined with a protein) to induce production of antibodies. which will have combining sites capable of specifically interacting with the transition state. In chemical systems. this idea was realized (with much lower efficiency. however) by using molecularly imprinted polymers.[22]

Schematically shown in Fig. 5 is the preparation of an enzyme mimic for the hydrolysis of ester 6 by molecular imprinting.[22] Phosphonate 5 is an analog of the transition state for the alkaline hydrolysis of Ester 4. It was used as a template for polymerization with two equivalents of the binding-site monomer *N,N'*-diethyl-4-vinylbenzamidine. Amidinium groups were chosen, because they can interact electrostatically with the side carboxylate group as well as with the anionic transition state of the alkaline hydrolysis, thus achieving substrate recognition and transition-state stabilization. Polymerization of the preassembled binding-site monomer with the template (Fig. 5A) followed by template removal (Fig. 5B) leaves a cavity that acts as transition-state receptor for the ester substrate (Fig. 5C). The imprinted polymer accelerates the hydrolysis of 6 more than 100-fold compared to the reaction at the same pH in buffer solution without the polymer. The reaction kinetics is of the Michaelis–Menten type. A polymer obtained with amidinium benzoate as a control, with a statistical distribution of amidinium groups. is ca. one order of magnitude less active in the hydrolysis of 6.

Another often applied approach to enzyme mimics is imprinting a polymer containing catalytically active groups with a substrate analogue. For example, a polymer containing Co(II)–imidazole complexes imitating the active site of the phosphotriesterase enzyme was designed

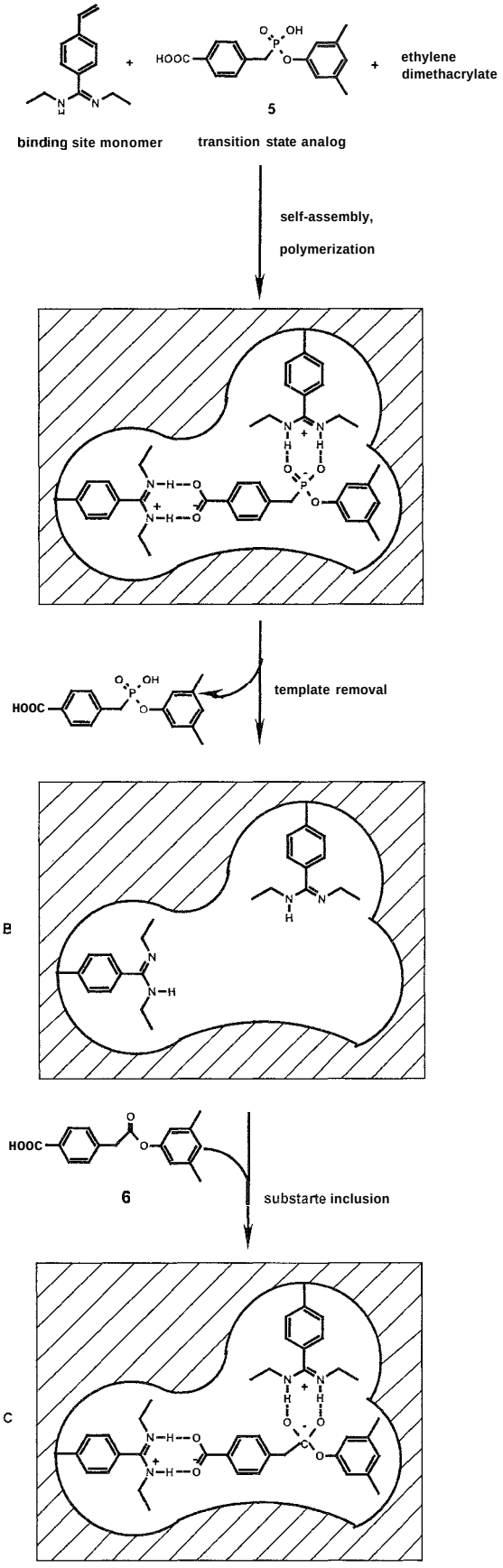

Fig. 5 Preparation of an enzyme mimic for the ester hydrolysis by molecular imprinting. (From Ref. [22].)

for the hydrolysis of paraoxon [$(EtO)_2P(=O)OC_6H_4$–NO_2-4)].[23] Imprinting this polymer with a substrate analogue stable toward hydrolysis [$(EtO)_2P(=O)CH_2$-C_6H_4–NO_2-4)] noticeably improved the catalyst activity. Catalytically active imprinted polymers were prepared, using both approaches discussed above, for many other reactions. such as elimination, carbon–carbon bond formation, oxidation. and hydrogen transfer.[22]

Bioimprinting is a more recent approach that employs a biological polymer for the imprinting.[18,22] Thus. a glutathione peroxidase mimic was prepared by imprinting egg albumin with *N*,*S*-*bis*(2,4-dinitrophenyl)glutathione and by having subsequent chemical modification.[24] The protein was denaturated and allowed to interact with the glutathione derivative. Then the new protein conformation was fixed by cross-linking with glutaraldehyde, the template was removed by dialysis, and protein serine residues were converted to selenocisteines. The resulting enzyme mimic was only seven times less active than the native glutathione peroxidase.

SOLID-STATE **ENZYME MIMICS**

The microporous structure of some solid materials makes possible incorporation of active species, e.g., metal complexes inside them, and these systems may show the shape-selective catalysis and an enzyme-like kinetics that allows one to consider them as enzyme mimics.[25]

The most important class of solid-state enzyme mimics is based on zeolites. Zeolites are solid materials composed of SiO_4 or AlO_4 tetrahedra linked at their corners, affording a three-dimensional network with small pores of molecular dimensions. They possess a unique feature of a strictly uniform pore diameter. In particular, zeolites with encapsulated metal complexes are used as inimics of cytochrome P-450.[26] An efficient enzyme mimic was obtained by encapsulating an iron phthalocyanine complex into crystals of zeolite Y, which were, in turn, embedded into a polydimethylsiloxane membrane acting as a mimic of the phospholipid membrane.[26] With t-butylhydroperoxide as the oxidant, the system hydroxylates alkanes at room temperature: with rates comparable to those for the enzyme. It shows similar selectivity (preference oxidation of tertiary C–H bonds) and a large kinetic isotope effect of nine.

Enzyme-like behavior was observed for electrocatalytic oxidation on Nafion/lead-ruthenium oxide pyrochlore chemically modified electrodes.[27] Nafion is loaded with lead(II) and ruthenium(III) cations by ion exchange, and then their oxides are prepared by in situ precipitation in such a way that the catalytically active sites remain

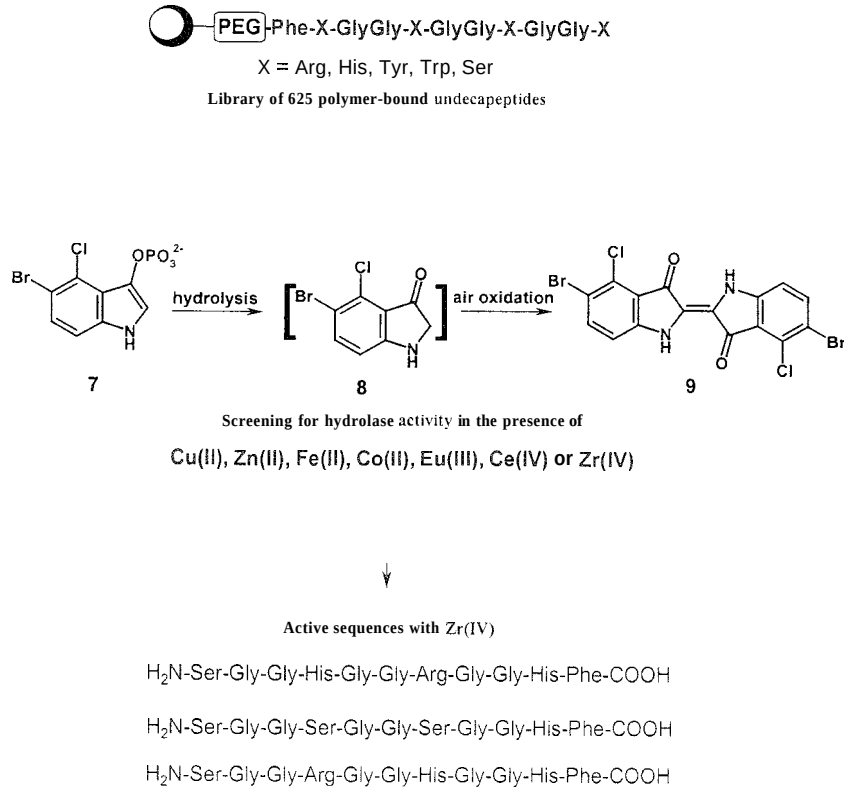

Fig. *4* Combinatorial development of phosphatase mimics on the basis of a peptide library. (From Ref. [30].)

covered with a hydrophobic core of the polymer. The electrooxidation of many biological compounds follows the Michaelis–Menten mechanism. Electrodes of this type were used as chemical sensors.

OTHERAPPROACHES

Using peptides in the design of enzyme mimics received increased attention. For example, nuclease mimics were prepared by incorporating lanthanide(III) cations into chimeric peptides composed of helices from the DNA-binding protein Engrailed and the binding turn from the Ca protein Calmodulin.[28] These 33- and 34-residue peptides were expected to possess metal-binding and DNA-recognition properties. They showed high affinity for Eu(III) [dissociation constant of the Eu(III)–peptide complex is 3 μM] and higher activity than free Eu(III) cation in the hydrolysis of supercoiled plasmid DNA. In another instance, attachment of a 14-residue peptide to a Mn(III) porphyrin complex allowed size-selective oxidation of alkenes.[29]

Impressive progress in combinatorial chemistry led to a new approach to the development of catalysts by the activity selection principle. A discussion of this aspect related to combinatorially developed enzyme mimics can be found in Ref. [8]. In Fig. 6. this approach is illustrated with an example of combinatorial development of phosphatase mimics on the basis of a peptide library.[30] In the first step. a library of 625 polymer-bound undecapeptides with five variable amino acids and three constant GlyGly spacer fragments was prepared. Variable amino acids were chosen on the basis of their possible ability to recognize anionic substrates (Arg). coordinate metal ions (His, Tyr). participate in π–π stacking interactions with aromatic groups of the substrate (Trp), and serve as a nucleophile (Ser). Screening for hydrolase activity was performed by using a specially designed phosphate monoester Substrate **7**, which affords, after hydrolysis, a deeply colored insoluble Product **9** via the air oxidation of the Intermediate 8. In the screening experiments, I mM solutions of different metal cations were added to approximately 2500 polymer beads, and in the case of Zr(IV), about 20 of these beads showed a typical turquoise color of 9. Peptide sequences shown at the bottom of Fig. 6 were determined for three intensively colored beads. Resynthesized peptides with these sequences mixed with Zr(IV) show catalytic activity in 4-nitrophenyl phosphate (a typical phosphatase substrate) hydrolysis in solution. Another original combinatorial approach to the development of phosphatase mimics is based on random functionalization of polyallylamine by potential metal coordinating and nucleophilic groups.[31]

CONCLUSION

Introducing the ideas and methodologies of supramolecular chemistry to the development of enzyme mimics allowed new catalysts to be obtained. which usually follow enzyme-like kinetics and show relatively high efficiency. Artificial enzymes are still inferior to natural enzymes in catalytic activity and selectivity.[2] Nevertheless, enzyme mimics already have practical applications, e.g., in the development of electrochemical sensors with solid enzyme mimics[27] or in organic synthesis with metal complexes of modified cyclodextrins.[32] Future progress in this area may be expected from more efficient designs of transition-state receptors,[2] improvement of the catalytic activity–selection approach based on combinatorial methodology,[8] and general progress in development of specific receptor molecules.

ARTICLES OF FURTHER INTEREST

Artificial Enzymes, p. 76
Carbonic Anhydrase Models, p. 178
Catalytic Antibodies. p. 193
Cyclodextrins, p. 398
Cyclophanes: Endoacidic, Endobasic, and Endolipophilic Cavities, p. 424
Enzymes: Characteristics and Mechanisms. p. 554
Micelles and Vesicles. p. 861
Surfactants, Part I: *Fundamentals*. p. 1458
Vitamin B_{12} and Heme Models, p. 1569
Zeolites: Catalysis, p. 1610
Zinc-Containing Enzymes and Their Models. p. 1631

REFERENCES

1. Breslow. R. Biomirnetic chemistry. Chem. Soc. Rev. 197%. *1* (6), 553–580.
2. Kirby. A.J. Enzyme mechanisms. models. and mimics. Angew. Chem.. Int. Ed. Engl. 1996. *35* (7). 707–724.
3. Groger. H.; Wilken, J. The application of L-proline as an enzyme mimic and further new asymmetric syntheses using small organic molecules as chiral catalysts. Angew. Chem.. Int. Ed. Engl. 2001, 40 (3). 529–532.
4. *Biominzetic Oxidations Catalyzed by Ti-ailsition Metal Complexes:* Meunier. *B.*. Ed.: Imperial College Press: London, 2000.
5. Dugas, H. *Bioorganic Chemistry: A Chemical Approach to Enzyme Action,* 3rd Ed.: Springer: New York. 1996.
6. *Molecular Design and Bioorganic Catalysis*; Wilcox, C.S.. Hamilton, A.D., Eds.; Kluwer Academic Publishers: Boston, 1996.
7. Murakami. Y.; Kikuchi. J.; Hisaeda. Y.; Hayashida. O. Artificial enzymes. Chem. Rev. 1996. *96* (2). 721–758.

8. Motherwell, W.B.; Bingham, M.J.; Six, Y. Recent progress in the design and synthesis of artificial enzymes. Tetrahedron **2001**, *57* (22), 4663–4686.
9. Kunitake, T.; Shinkai, S. Catalysis by micelles, membranes and other aqueous aggregates as models of enzyme action. Adv. Phys. Org. Chem. **1980**, *17*, 435–488.
10. Berezin, I.V.; Martinek, K.; Yatsimirsky, A.K. Physicochemical grounds of the micellar catalysis. Russ. Chem. Rev. Engl. Transl. **1973**, *42* (10), 787–802.
11. Bunton, C.A.; Nome, F.; Quina, F.H.; Romsted, L.S. Ion binding and reactivity at charged aqueous interfaces. Acc. Chem. Res. **1991**, *24* (12), 357–364.
12. Cleij, M.C.; Scrimin, P.; Tecilla, P.; Tonellato, U. Chiral Lipophilic ligands. 3. Control of enantioselectivity in copper(II)-catalyzed cleavage of α-amino acid esters by aggregate morphology. Langmuir **1996**, *12* (12), 2956–2960.
13. Svenson, R.; Pamedytyte, V.; Juodaityte, J.; Makuska, R.; Morgenstern, R. Characterization of polymeric surfactants that are glutathione transferase mimics. Toxicology **2001**, *168* (3), 251–258.
14. Breslow, R.; Dong, S.D. Biomimetic reactions catalyzed by cyclodextrins and their derivatives. Chem. Rev. **1998**, *98* (5), 1997–2011.
15. Yan, J.; Breslow, R. An enzyme mimic that hydrolyzes an unactivated ester with catalytic turnover. Tetrahedron Lett. **2000**, *41* (13), 2059–2062.
16. Breslow, R.; Yang, J.; Yan, J. Biomimetic hydroxylation of saturated carbons with artificial cytochrome P-450 enzymes—Liberating chemistry from the tyranny of functional groups. Tetrahedron **2002**, *58* (4), 653–659.
17. French, R.R.; Holzer, P.; Leuenberger, M.G.; Woggon, W.-D. A supramolecular enzyme mimic that catalyzes the 15,15′ double bond scission of β,β-carotene. Angew. Chem., Int. Ed. Engl. **2000**, *39* (7), 1267–1269.
18. Sasaki, S.; Takase, Y.; Koga, K. An attempt on acceleration of peptide synthesis using the enzyme model having preorganized catalytic groups. Tetrahedron Lett. **1990**, *31* (42), 6051–6054.
19. Fenniri, H.; Lehn, J.-M.; Marquis-Rigault, A. Supramolecular catalysis of H/D exchange in malonate ions by macrocyclic polyamines: A model enzyme with enolase activity. Angew. Chem., Int. Ed. Engl. **1996**, *35* (3), 337–339.
20. Hosseini, M.W.; Lehn, J.-M.; Jones, K.C.; Plute, K.E.; Mertes, K.B.; Mertes, M.P. Supramolecular catalysis: Polyammonium macrocycles as enzyme mimics for phosphoryl transfer in ATP hydrolysis. J. Am. Chem. Soc. **1989**, *111* (16), 6330–6335.
21. Mattei, P.; Diederich, F. A flavo-thiazolio-cyclophane as a functional model for pyruvate oxidase. Angew. Chem., Int. Ed. Engl. **1996**, *35* (12), 1341–1344.
22. Wulff, G. Enzyme-like catalysis by molecularly imprinted polymers. Chem. Rev. **2002**, *102* (1), 1–27.
23. Yamazaki, T.; Yilmaz, E.; Mosbach, K.; Sode, K. Towards the use of molecularly imprinted polymers containing imidazoles and bivalent metal complexes for the detection and degradation of organophosphotriester pesticides. Anal. Chim. Acta **2001**, *435* (1), 209–214.
24. Liu, J.; Luo, G.; Gao, S.; Zhang, K.; Chen, X.; Shen, J. Generation of a glutathione peroxidase-like mimic using bioimprinting and chemical mutation. Chem. Commun. **1999**; (2), 199–200.
25. De Vos, D.E.; Sels, B.F.; Jacobs, P.A. Heterogeneous enzyme mimics based on zeolites and layered hydroxides. CaTTech **2002**, *6* (1), 14–29.
26. Parton, R.F.; Vankelecom, I.F.J.; Casselman, M.J.A.; Bezoukhanova, C.P.; Uytterhoeven, J.B.; Jacobs, P.A. An efficient mimic of cytochrome P-450 from a zeolite-encaged iron complex in a polymer membrane. Nature **1994**, *370* (6490), 541–544, and references therein.
27. Zen, I.-M.; Kumar, A.S. A mimicking enzyme analogue for chemical sensors. Acc. Chem. Res. **2001**, *34* (10), 772–780.
28. Welch, J.T.; Sirish, M.; Lindstrom, K.M.; Franklin, S.J. De novo nucleases based on HTH and EF-hand chimeras. Inorg. Chem. **2001**, *40* (9), 1982–1984.
29. Geier, G.R., III; Sasaki, T. Catalytic oxidation of alkenes with a surface-bound metalloporphyrin-peptide conjugate. Tetrahedron **1999**, *55* (7), 1859–1870.
30. Berkessel, A.; Hérault, D.A. Discovery of peptide–zirconium complexes that mediate phosphate hydrolysis by batch screening of a combinatorial undecapeptide library. Angew. Chem., Int. Ed. Engl. **1999**, *38* (1/2), 102–105.
31. Menger, F.M.; Eliseev, A.V.; Migulin, V.A. Phosphatase catalysis developed via combinatorial organic chemistry. J. Org. Chem. **1995**, *60* (21), 6666–6667.
32. Reetz, M.T.; Frombgen, C. Chemoselective reduction of halo-nitro aromatic compounds by β-cyclodextrin-modified transition metal catalysts in a biphasic system. Synthesis **1999**, (9), 1555–1557.

Enzymes: Characteristics and Mechanisms

Nicholas C. Price
Adrian J. Lapthorn
University of Glasgow, Glasgow, United Kingdom

INTRODUCTION

Enzymes are remarkable catalysts. With a high degree of specificity, they can bring about rate enhancements greater than 10^{12}-fold for simple reactions, such as the hydrolysis of amide bonds or phosphate esters. The vast majority of the enzyme-catalyzed reactions in living systems do not occur on any reasonable time scale in their absence. In addition to the specificity and catalytic power, the third remarkable property of enzymes is that their activities can be regulated by a variety of mechanisms. thereby allowing the complex metabolic network of chemical reactions in organisms to be controlled. In short. enzymes provide the essential underpinning to life in organized systems.[1–4] Because of these remarkable properties, the application of enzymes to industrial processes attracted increasing attention, and a number of ways in which the obvious disadvantages of enzymes. such as high cost and ability to work over a limited range of experimental conditions, are being successfully overcome.[5] Over the last 20 years or so, it was recognized that certain RNA molecules can act as catalysts; these molecules were termed ribozymes.[6]

The purpose of this article is to explain the principal characteristics of enzyme catalysis and to focus on the approaches used by enzymologists to answer current questions. Over the last decade. developments in recombinant DNA technology that have led to high levels of expression of enzymes and provided the ability to mutate amino acid residues, coupled with those in structural characterization and bioinformatics over the same period. have led to a renaissance in enzymology. In the next decade. we will see the harvesting of the fruits of the genome sequencing projects.[7]

THE CLASSES OF ENZYME-CATALYZED REACTIONS

As of 2002, over 4000 different chemical reactions were characterized as being enzyme-catalyzed. The Enzyme Commission, established by the International Union of Biochemistry (now known as the International Union of Biochemistry and Molecular Biology), in consultation with the International Union of Pure and Applied Chemistry in the 1950s. proposed the basis for enzyme classification and nomenclature that is still in use.[8]

Reactions are divided into six classes:

Class	*Type of reaction*	*Category of enzyme*
1	Redox	Oxidoreductase
2	Group transfer	Transferase
3	Hydrolysis	Hydrolase
4	Elimination (to form a double bond)	Lyase
5	Isomerization	Isomerase
6	Ligation (joining molecules at the expense of any energy source. e.g., ATP)	Ligase (synthetase)

Enzymes are classified on the basis of the reaction catalyzed, not on the source from which they were isolated or on the precise details of the mechanism of the reaction. Each enzyme is then given an Enzyme Commission (EC) number consisting of four parts (A.B.C.D); this number serves as an identifier for interrogating databases. A is the Class number. i.e., it can take values from 1 to 6: B and C denote more precise descriptions of the type of reaction and substrate(s) acted on: and D is a serial number within the sub-subclass. Each enzyme is given a systematic name (usually too cumbersome for everyday use) and a common name. For example. lactate dehydrogenase is EC 1.1.1.27, and chymotrypsin is EC 3.4.21.1. Further details can be found in Ref. [8].

HOW MANY DISTINCT ENZYMES ARE REQUIRED BY AN ORGANISM?

Although well over 4000 different types of chemical reactions are now known to be catalyzed by enzymes, these do not all occur in every organism. In the well-studied enteric bacterium *Escherichia coli* K-12, the results of genome sequencing[9] indicate that 4288 different proteins can be coded for. and of these. 2656 (62%) are

Encyclopedia of Supramolecular Chemistry
DOI: 10.1081/E-ESMC 120012683

characterized. (The others are regarded as hypothetical, unclassified, or unknown.) Of the characterized proteins. 1701 (64%) are enzymes. This is likely to represent a reasonable estimate of the number of reactions required to sustain a simple free-living organism. In higher eukaryotic organisms such as mammals. this figure is likely to be five- to 10-fold higher. Of course, not all enzymes are equally abundant in the cell, and it is estimated that the 20 or so enzymes that catalyze the steps in the major energy-yielding pathways of glycolysis and the tricarboxylic acid cycle make up nearly 60% of the total number of actual enzyme molecules in the E. coli cell.[10]

WOW CAN ENZYMES BRING ABOUT CATALYSIS?

In order to achieve catalysis of so many different types of chemical reactions, enzymes have, at their disposal. an enormous variety of chemical weapons. Enzymes are proteins. i.e.. chains of amino acids Iinked by peptide (amide) bonds. There are 20 different amino acids, providing side chains with a variety of characteristics:

- Nonpolar (Ala, Val, Leu, Ile, Phe, Cys, and Met).
  Charged (Lys. Arg, Glu. Asp. and His).
- Nucleophiles (Cys, Lys. Tyr, and Ser).
  Proton donors/acceptors (His, Asp. and Glu).
  Hydrogen-bond donors/acceptors (Asn. Gln. Ser. and Thr. in addition to charged residues).
- Metal ion coordination (His, Asp, Glu, and Cys).

A number of amino acids display composite properties. For example. Lys is a charged amino acid due to a prinary amine group in the side chain; however. this group is at the end of an aliphatic chain $-(CH_2)_4-$, which can allow the residue to be significantly buried in a nonpolar environment.

Other side chains play important structural roles, e.g., Pro (an imino acid) disrupts regular secondary structural elements. stabilizes the conformation of exposed loops, and, although hydrophobic in nature. is often found surface-exposed at turns. Similarly, Gly is found performing a number of functions because of its small size, which allows it to adopt conformations that are sterically inaccessible to other amino acids. Gly is therefore critical to the correct folding of many proteins. can form hinge regions between domains (folded units), and can be necessary for the correct positioning of functional groups. which are all crucial roles for catalysis. Cys is the only amino acid residue that can form covalent cross-linking of the peptide chain by forming a disulfide linkage to another suitably positioned Cys under oxidizing conditions. This cross-linking provides significant stability to folded proteins but is not usually considered necessary for acquisition of the correct folded structure.

In addition to the repertoire of amino acids, a significant proportion (of the order of 30%) of enzymes exploits the properties of metal ions to assist catalysis; these metals include Zn to act as a Lewis acid and polarize bonds, Mg to neutralize charges on anions, and Cu and Fe to act as redox centers. The last role is especially important, because only one of the naturally occurring amino acids (Cys) has any significant redox chemistry: although it should be noted that certain redox cofactors such as TPQ (2,4,5-trihydroxyphenylalanine quinone) in E. coli amine oxidase can be formed by posttranslational modification of Tyr side chains.[11] Several other metals (Na, K, Ca, V, Mn, Ni. Co, Mo) also assist catalysis in specific cases. Biological systems generate a number of organic compounds with specific chemical functions, which are essential components (cofactors) of many enzymes. These cofactors include pyridixal-5'-phosphate (involved in elimination and replacement reactions of amino acids), biotin (involved in CO_2 fixation and carboxylation reactions), lipoic acid (involved in acyl transfer reactions), and heme (which is critical in monooxygenase reactions).[1–3]

The range of chemical functionalities available to enzymes means that an almost limitless range of environments for the correct binding: mutual orientation, and activation of reacting molecules can be created. The mechanisms by which catalysis can be achieved are discussed in a later section.

For a number of enzyme-catalyzed reactions, it is clear that nature evolved a number of distinct answers to the same chemical problem. Thus; for example, in the cases of 3-dehydroquinase[12] and phosphoglycerate mutase,[13] two distinct types of enzyme are known in each case. In the case of proteases, there are four main types of enzymes, each of which displays a distinct solution to the problem of breaking the (relatively stable) amide bond.[1,2] To illustrate the range of possibilities involved, the nucleophile attacking the electrophilic carbon of the carbonyl bond can be a Ser or Cys side chain or a water molecule activated by an Asp side chain. The polarization of the carbonyl bond is enhanced by a Zn ion or by hydrogen bonding. and the proton donor to the leaving (amino) group can be His or a dyad of carboxyl (Asp) side chains. These different types of enzymes presumably represent the outcomes of independent, parallel, evolutionary processes.

In comparison with proteins, the smaller variety of chemical functionalities available in nucleic acids (only four bases compared with 20 amino acids) restricts the range of structures they can adopt. It is therefore not surprising that ribozymes appear to catalyze a more

limited range of reactions (mainly those of phosphodiester transfer). While it is clear that the active site of the peptidyl transferase activity in ribosomes contains only RNA, some precise details of the catalytic process remain to be elucidated.[14]

THE THREE-DIMENSIONAL CONTEXT OF ENZYME CATALYSIS

The three-dimensional structures of enzymes provide the context within which the chemical functionalities are depioyed to bring about catalysis. The three-dimensional structure not only brings the individual functions into the correct spatial relationship. but also allows modulation of these functions. Thus. the effect of the microenvironment can be to alter the pK_a of a given side chain in an enzyme by several units from its value in model compounds: examples include the side chain of Glu 35 in lysozyme (pK_a raised to 6.2[2]) and Asp 32 in pepsin (pK_a lowered to <3[2]). In the case of the ''serine'' proteases. such as chymotrypsin. trypsin. and thrombin, a precise geometrical arrangement of three side chains (Ser...His...Asp) known as the "charge relay system'' serves to increase the nucleophilicity of the catalytic Ser by several orders of magnitude.[1,2] It is now appropriate to give a short overview of enzyme structure.

The Structures of Enzymes

Enzymes consist of polypeptide chains from about 100 to over 2000 amino acid residues in length. The three-dimensional structures of several thousand enzymes were determined, predominantly using the technique of X-ray crystallography, while NMR continues to be an important technique for determining the structure of smaller. often flexible; enzymes (<30 kDa). Advances such as the routine freezing of crystals to 100 K to prolong their lifetime, brighter synchrotron X-ray sources with tunable wavelengths to permit structure solution from a single crystal. and charged couple devices (CCD) detectors to speed up data collection times by an order of magnitude have revolutionized X-ray crystallography. These developments alongside those in the overexpression and purification of proteins resulted in faster structural characterization. From the large number of enzyme structures determined. we have a better understanding of enzymes than ever before. Databases such as SCOP[15] and CATH[16] attempt to catalog protein structures into a hierarchy of folds, superfamilies, and families of proteins (Fig. 1). These proteins can be further divided into motifs of secondary structural elements; for example, the ferredoxin-like fold is composed of two repeats of the common β-α-β motif. Although both databases highlight the potential diversity of enzyme folds. it must be stressed that many proteins share common folding architectures e.g., $(\alpha/\beta)_8$ or TIM barrel, which is estimated to represent 10% of all enzyme folds.

There are 58 classes of small proteins identified so far, which are dominated by disulfide bridges. metal ligands. or hemes; however, few can be considered enzymes. The small proteins consist of enzyme inhibitors, toxins, hormones, and discrete folded units or domains of larger proteins. The smallest enzymes (approximately 100 amino acid residues in length) include the bacterial ribonucleases and thioredoxins. At around 400–500 residues. enzymes such as cyiochrome P450s and the aminodeoxyisochorismate (ADC) synthase subunit are unusual in forming a single large globular protein. It is more common for proteins of this size and larger to be composed of a series of smaller folded domains joined by short and often flexible linker regions. This is clearly advantageous in terms of simplifying the folding of the protein as well as generating hinges between protein domains that permit the large conformational changes necessary for catalysis. For example, lactate dehydrogenase is a 330 amino acid polypeptide chain separated into two domains of approximately 160 amino acid residues in length (see "Lactate Dehydrogenase" later in this article). One domain is involved in binding NAD^+ and has a characteristic (Rossmann) fold, the other binds lactate. The two domains close together on binding both substrates to form the catalytically competent conformation of the enzyme. This pattern is found in other members of the dehydrogenase family.

Flexibility in the protein is often key to the functioning of the macromolecule as a catalyst. Regions of flexibility are often identified from crystallography by high thermal parameters and from information such as NMR relaxation times. rates of hydrogen exchange, and fluorescence polarization.[2,17] In some enzymes. such as adenylate kinase, multiple X-ray structures of the enzyme in the presence and absence of ligands precisely defined the hinge regions of the protein and the extent of conformational changes that occur during the catalytic cycle.[18]

Large enzymes are rarely cornposed of a single polypeptide chain but form larger syminetricai arrangements via self-assembly processes. This quaternary structure of the enzyme is often necessary for the formation of active protein, as the catalytic active site is often formed at the interface between subunits. Given that proteins are chiral molecules. almost all possible symmetrical arrangements of subunits were observed, from the simple 222 symmetry of the tetramer of various dehydrogenases such as lactate dehydrogenase to the cubic 23 symmetry of the Type II dehydroquinase dodecamer. The role of

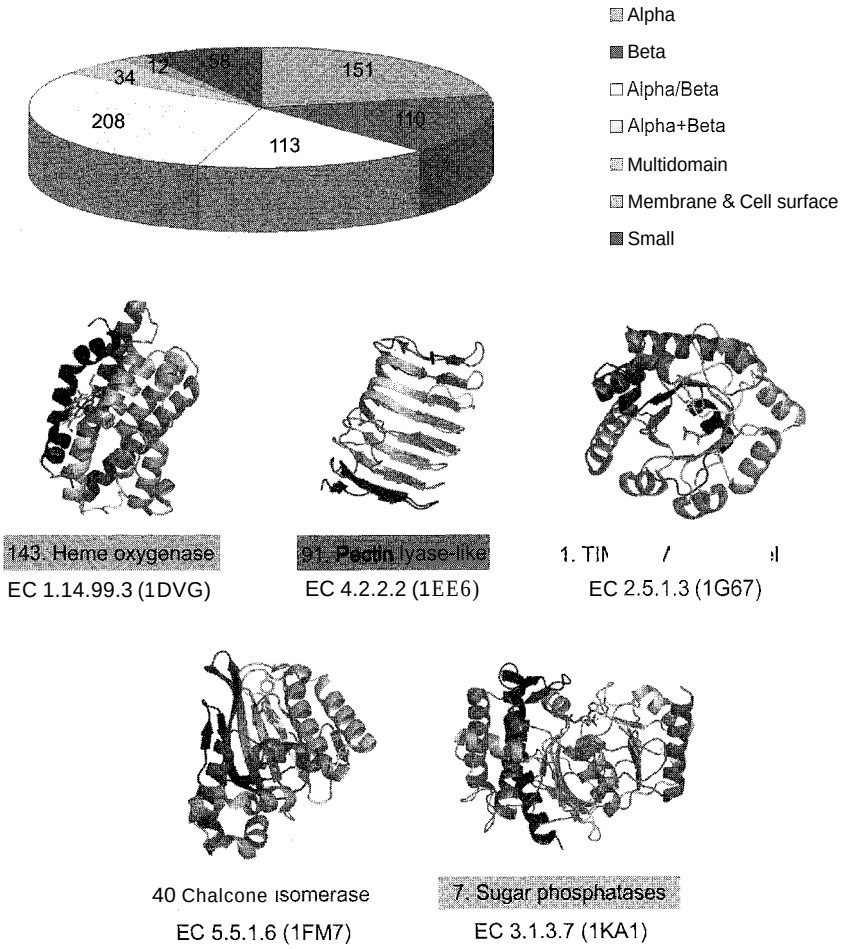

Fig. 1 The number of fold families identified from structural studies of proteins based on data obtained from SCOP.[15] Representative structures are shown from each of the classes of protein fold, e.g., alpha or beta, that include enzymes. The proteins are represented as ribbons. colored from blue at the N-terminus through to red at the C-terminus. Cofactors and inhibitors are colored according to atom type and are represented in stick. For example. the alpha fold of Heme oxygenase is fold 143 out of 151 in the classification. a multihelical bundle containing two structural repeats of three-helical motif. The enzyme is an oxidoreductase EC 1.14.99.3 and is represented by the crystal structure of rat heme oxygenase-1 (HO-1) protein data bank acession code IDVG. (*View this art in color at www.dekker.com.*)

oligomerization is not completely understood, but it is believed to contribute to increased stability of the protein,[19] as well as to offer possibilities of regulation of activity.[20] Oligomerization of multiple enzymes allows for the coordination of sequential steps in a metabolic pathway and the containment of potentially toxic intermediates.[21,22]

DETERMINATION OF ENZYME MECHANISMS

Understanding the mechanism of an enzyme requires the structural characterization of the various enzyme-containing complexes involved in the transformation of substrates to products. as well as the rates at which these complexes are interconverted. It follows that information from a variety of experimental approaches must be integrated.

Kinetic Aspects

Kinetic data (steady-state and rapid reaction) can be used to identify the sequence of enzyme-containing complexes as substrates are converted to products, and to identify the rates of some or all of the elementary steps in the overall reaction. For instance, in a two-substrate reaction such as that catalyzed by lactate dehydrogenase (lactate+ $NAD^+ \longleftrightarrow$ pyruvate+NADH), it can be shown that the

reaction proceeds via a ternary complex (E-NAD^+-lactate), which is formed in an ordered fashion. with binding of NAD^+ preceding that of lactate. Other two-substrate reactions, such as that catalyzed by creatine kinase (creatine + ATP $\longleftrightarrow$ phosphocreatine + ADP). proceed via a random ternary complex mechanism in which either substrate can bind first. A third group of two-substrate enzyme reactions proceed via enzyme substitution (or "ping-pong") mechanisms in which the first substrate combines with the enzyme to produce the first product and a modified enzyme (E*). In the second step, E* reacts with the second substrate to give the second product and regenerate enzyme. An example of an enzyme substitution mechanism is provided by nucleoside diphosphate kinase, where the first substrate (NTP, N=any nucleoside) transfers a phosphate group to an His side chain in the enzyme. The techniques involved in assigning a given enzyme to a particular mechanistic category have been described in detail.[1,23,24]

In addition to determining the sequence of complexes. kinetic studies provide fundamental parameters of the enzyme. For most enzymes, the dependence of rate (velocity. v) on substrate concentration ([S]) follows a hyperbolic saturation curve known as the Michaelis–Menten equation. i.e., $v = V_{max}[S]/(K_m + [S])$. The dependence is characterized by the parameters V_{max} (the maximum or limiting velocity at infinite substrate concentration) and K_m (Michaelis constant, corresponding to the concentration of substrate required for the velocity to reach half V_{max}). For reactions involving two or more substrates. the same general principles apply, although the equations are more complex. For some enzymes. particularly those with multiple polypeptide chains that play key roles in metabolic regulation. the dependence of rate on substrate concentration does not follow the Michaelis–Menten equation. and more complex mathematical descriptions are required to account for the kinetics. These involve interactions between the multiple active sites in the molecule.[1,2]

The parameter V_{max} can be converted to a turnover number or k_{cat} by taking account of the molar concentration of enzyme present in the assay mixture. The values of k_{cat} of enzymes are generally in the range of 10^2–10^6 s^{-1}.[2] This means that the catalytic events on the enzyme occur in the time range of milliseconds or less. In order to characterize such steps. it is necessary to employ rapid reaction techniques such as stopped-flow, which has a dead time of approximately 1 ms. Continuous-flow mixing techniques can have shorter dead times but make much greater demands in terms of quantities of sample required. The value of k_{cat}/K_m provides not only a quantitative measure of the specificity of an enzyme for a given substrate.[2] but it can also be used as a measure of cataiytic efficiency.[2]

Structural Aspects

The detailed three-dimensional picture of an enzyme obtained by techniques such as X-ray crystallography is effectively a time- and space-averaged view of a single conformation of a protein stabilized by the crystallization conditions. Protein crystals typically contain 50% (w/w) solvent. and. as a result. have large solvent channels running through them. In many cases. the enzymes are still capable of catalyzing reactions within the crystal. albeit at a somewhat reduced rate. The ideal approach with which to examine events at the active site would appear to exploit X-ray crystallography by diffusing substrates into enzyme crystals and thereby defining the side chains involved in substrate binding and the structural changes that occur during catalysis. Freezing techniques and complete data collection in microsecond or shorter time scales in the late 1980s seemed to hold great promise of time-resolved structural studies on enzymes.[25] However. technical difficulties associated with loss of order in the crystals during catalysis as a result of the spatial averaging necessary for the diffraction experiment, among other reasons, made this approach technically challenging. Success stories include the use of lasers to initiate a light-sensitive reaction, followed in real time by the use of Eaue diffraction in photoactive yellow protein,[26,27] and the use of conventional X-ray methods with a single-crystal spectrophotometer to identify stable highly populated intermediate states in amine oxidase[11] and cytochrorne cd_1 nitrite reductase.[28] These methods. together with traditional X-ray data collection using cocrystallization (often in preference to soaking of crystals) with poor substrates, transition state analogues. competitive inhibitors. catalytically compromised enzymes (by site-directed mutagenesis), or individual components of multisubstrate reactions, provided structural perspectives on many enzyme mechanisms.[29] In addition, conformational changes essential for catalysis were also characterized in much greater detail than was previously possible.

WOW CAN WE UNDERSTAND THE SPECIFICITY OF ENZYME-CATALYZED REACTIONS?

The term specificity is widely used in connection with enzymes but has a number of aspects.[1,2] Most enzymes are highly specific in the nature of the substrates they utilize and the reaction catalyzed. There are enzymes with relatively low specificities (bond specificityj. e.g., peptidases and phosphatases, which will act on a wide range of substrates provided they contain the requisite chemical band (peptide or phosphate ester. respectively). Low

specificity is commonly observed with degradative enzymes but rarely with biosynthetic enzymes. Hexokinase is an enzyme showing group specificity: it acts on a variety of sugars provided they are aldohexoses. A number of enzymes show absolute or near-absolute specificity and will work effectively on only one substrate or substrate combination; urease is an example of this type of enzyme. These classifications of specificity become more difficult when macromolecular substrates are considered. For example, restriction endonucleases catalyze the breaking of DNA chains at a recognition sequence of four to six base pairs in DNA. Any DNA molecule containing this sequence will be acted on: in this case, the specificity is for that portion of the substrate in immediate contact with the active site of the enzyme. A further aspect of specificity is the stereospecificity exhibited by enzymes: thus, a given dehydrogenase using the NAD(P)H/NAD(P)$^+$ redox pair will abstract only one of the two hydrogens (A-side or B-side) at the C4 of nicotinamide ring of NAD(P)H.[11] The precise mode of binding of the NAD(P)H substrate to the enzyme will dictate which hydrogen is available for transfer to the other substrate in the reaction.

A further aspect of specificity has become recognized in recent years. namely, proofreading.''' The accurate replication of DNA during cell division is an event of crucial importance to an organism. DNA polymerases catalyze this process with an error rate of as little as 1 in 10^{10}. This is achieved by a combination of Watson–Crick base pairing (error rate of the order of 1 in 10') in combination with a proofreading step in which checks are made after the addition of each base to the 3' end of the growing DNA chain that the correct pair was formed. Any incorrectly added bases are removed by a 3'–5' exonuclease activity that occurs at an active site distinct from the polymerase site.

Specificity can be understood in terms of the complementarity of interactions between enzyme and substrate. In addition, the binding of the substrate will generally bring about a conformational change in the enzyme, so as to bring the amino acid side chains necessary for catalysis into the correct spatial relationship. The adjustment of the structure accompanying complex formation has proven to be a complicating factor in the application of computer programs that ''dock'' the enzyme and substrates or other ligands.

HOW CAN WE UNDERSTAND THE CATALYTIC POWER OF ENZYMES?

From studies of the rates of organic reactions. several factors were identified that could be relevant to understanding the mechanism of enzyme-catalyzed reactions. More complete discussions of the importance of these have been given.[1,2,30]

The factors include the following:

- *Proximity and orientation effects*
  The binding of substrates at adjacent sites on an enzyme in the correct orientation for reaction leads to a reduction in the entropy of activation. It was estimated that for a bimolecular reaction, each factor could contribute approximately 10'-fold to rate enhancement.
  Acid–base catalysis
  The addition or removal of a proton can promote electron flow. i.e., bond formation and breakage. during the reaction. As far as enzymes are concerned. only general acid or base catalysis can occur. because enzymes have no means of concentrating H^+ or OH^- ions. A number of amino acid side chains can act as proton donors or acceptors, and in many Zn-dependent enzymes, such as carboxypeptidase. the metal ion acts as an effective Lewis acid to enhance polarization of the carbonyl moiety of the amide bond. Among the amino acids; His (which has a pK_a generally close to 7) plays an especially important role in enzyme catalysis. because at neutral pH, there is a good balance between its protonated and deprotonated forms. In most cases, enzymes have suitably positioned pairs of side chains to provide push and pull of electrons.
- *Covalent catalysis*
  Reactions can be accelerated by the formation of intermediates, provided that such intermediates are rapidly formed and broken down. This then provides a new reaction pathway of lower activation energy. Many enzyme-catalyzed reactions proceed via covalent catalysis. involving side chains such as Cys, Ser, Eys. or His acting as nucleophiles in the formation of intermediates such as acyl-enzymes or Schiff bases.
  Changes in environment
  The rates of many reactions involving polar species are low in water because of the energetic cost of desolvating the reactants. Such reactions can be accelerated drainatically by switching to dipolar aprotic solvents such as dimethylsulfoxide. Enzymes are capable of providing nonpolar environments for reactions in which water is essentially removed. In addition. charges that develop during the reaction can be effectively stabilized in a medium of low dielectric constant by appropriately positioned charged side chains.
- *Distortion of substrate/transition state stabilization*
  In model reactions, it was demonstrated that distortion of a reactant so as to make it more closely resemble the postulated transition state of the reaction can lead to dramatic acceleration. In a number of enzyme-catalyzed reactions. there is evidence for such strain or

distortion, but the quantitative effect of this on the rate of reaction was not always clear. In order to act as a catalyst. an enzyme must make more favorable interactions with the transition state than with the substrates or products. From this. it follows that a compound that resembles this state in terms of geometry and electronic structure should bind to the enzyme. Such tight binding transition state analogues were developed for many different types of enzymes. Apart from helping to confirm ideas about the nature of the proposed catalytic mechanism of a reaction, they offer scope as potential selective inhibitors for therapeutic intervention.

It is clear that in a qualitative sense, the factors outlined in this section help us to understand the origin of enzyme catalytic power. However. it is not clear that for any given enzyme we can yet account quantitatively for the magnitude of its rate enhancement.

Given recent developments in computer modeling of chemical reactions. there is considerable interest in attempting to develop a mathematical understanding of enzyme catalysis. The sheer complexity of enzymes means that at present, it is possible to apply a strict quantum mechanical approach to only a limited region, such as the active site, and classical molecular mechanics are used to describe the remainder of the molecule. This combined approach had some success in modeling some aspects of enzyme-catalyzed reactions. such as the importance of particular side chains in the catalytic process.[31] However, a complete mathematical description of enzyme catalysis remains a considerable way off.

Constraints on the Rates of Enzyme-Catalyzed Reactions

For a number of enzymes. such as triosephosphate isomerase. fumarase, and catalase. the value of the k_{cat}/K_m ratio approaches a value of 10^8 M^{-1} s^{-1}.[2] This is close to the diffusion limit. i.e., the enzyme cannot work any faster because the rate is limited by the rate at which substrate diffuses to the active site. Enzymes of this type were described as having achieved catalytic perfection in evolutionary terms.[32] However, it should be noted that "evolutionary perfection" may not always imply a high value of k_{cat}. In the case of aldose reductase. for example. the enzyme was considered perfectly evolved for its role as a detoxification catalyst with a broad specificity by developing high affinities for the redox substrates NADPH/$NADP^+$ in such a way that the equiiibrium is shifted in the direction of product formation. These properties thus achieve saturation of the enzyme at all times under cellular conditions and effective rapid removal of toxic aldehydes.[33]

In some enzymes. it appears that the upper limit of k_{cat} is set by the rate of structural changes that accompany the catalytic events. For example, in the cases of lactate dehydrogenase[34] and triosephosphate isomerase,[35] it was shown that the catalytic rate matches the movement of flexible loops that close over the active site to allow catalysis to occur. Because of the scarcity of data concerning the rates of catalytically relevant structural changes in enzyme, it is difficult to know how widespread this effect might be; however: the structural data indicate that substrate-induced conformational changes occur in many enzymes. In kinases (enzymes that catalyze ATP-dependent phosphorylation reactions), formation of the catalytically active complex requires closure of the two domains. preventing access of water to the active site. In large assemblies such as the motor systems of ATP synthase and the actin–myosin system, the linkages between the structural changes and the reaction catalyzed underpin their function in coupling H^+ movement to ATP synthesis and ATP hydrolysis to muscle contraction. respectively.[2]

EXAMPLES OF ENZYME MECHANISMS

In this section, the mechanisms of two enzymes will be outlined in order to illustrate the way in which the various experimental approaches were integrated to provide an understanding of enzyme mechanisms. For further examples. see Refs. [1–3].

Lactate Dehydrogenase

Lactate dehydrogenase (EC 1.1.1.27) catalyzes the reaction lactate+NAD^+⟷pyruvate+NADH, which in the reverse direction represents the last reaction of anaerobic glycolysis. The enzyme consists of four identical polypeptide chains (subunits), each of molecular mass about 35 kDa. For a summary of this work, see Ref. [1].

X-ray crystallographic studies of the enzymes from dogfish and pig muscle and from *Bacillus stearothermophilus*[36,37] show that the enzyme belongs to the α/β class of proteins, with about 40% of the amino acids in α helix and 23% in β structure (Fig. 2a). In the N-terminal domain. there is a six-stranded parallel β-sheet with interconnecting helices. This motif is found in all $NAD(P)^+$-dependent dehydrogenases and is referred to as the Rossmann fold. Binding of NAD^+ to lactate dehydrogenase involves a large number of interactions with different side chains, including hydrogen bonds. electrostatic bonds, and hydrophobic interactions. The mode of binding explains why $NADP^+$ is not a substrate and also why lactate dehydrogenase is an A-side dehydrogenase.

a)

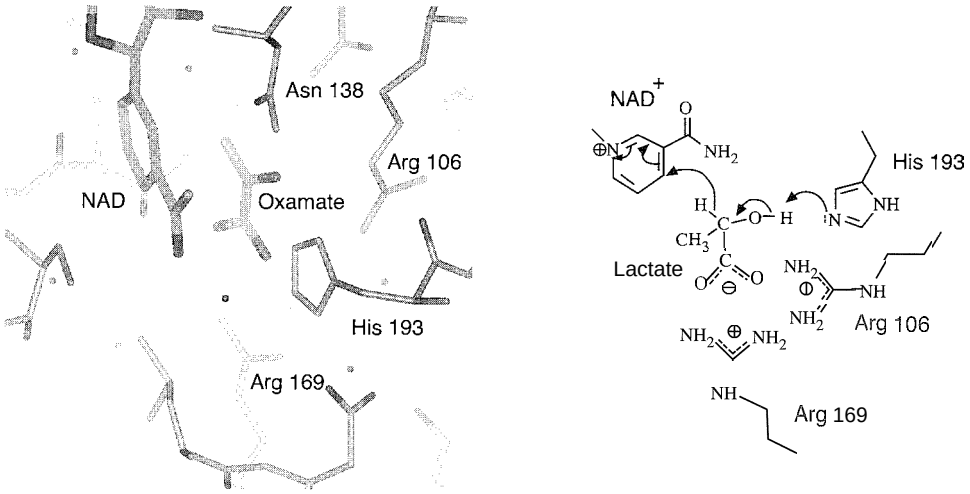

b)

Fig. 2 Lactate dehydrogenase: a) a ribbon representation of the tetramer of the B. *stearothermophilus* enzyme with each peptide chain depicted in a different color. The cofactor and oxamate inhibitor are colored according to atom type. as is fructose bisphosphate. which is an allosteric regulator of the enzyme. b) On the left is a detailed view of the enzyme active site as seen in the crystal structure. The ligand is highlighted in green and key amino acid residues are labeled. This is compared with the traditional two-dimensional representation of the enzyme mechanism on the right. Note that the residue numbers differ slightly from those of the muscle enzyme discussed in the test. (*View this art in color at www.dekker.com.*)

The structure of the catalytically active complex was deduced by the use of competitive inhibitors in abortive complexes (e.g., E.NADH.oxamate and $E.NAD^+$.oxalate). On this basis, the lactate is predicted to bind between the nicotimamide group of NAD^+ and the side chain of His 195 (which is close enough to form a hydrogen bond to the hydroxyl group of the lactate). The side chains of Arg 109 and Arg 171 are thought to anchor the carboxylate group

of lactate. (Note that these numbers are for the muscle enzyme and differ slightly from the corresponding residues in the *B. stearothermophilus* enzyme shown in Fig. 2).

Of key importance are the structural changes that accompany formation of the active, ternary complex. A flexible loop, consisting of Residues 98 to 120, which in the absence of substrates extends into solution, moves down in the ternary complex so as to exclude water from the active site. The side chain of Arg 109 moves some 1.4 nm: a smaller movement (0.15 nm) of the side chain of His 195 occurs to bring this into the correct position with respect to lactate.

As stated previously. kinetic studies showed that the enzyme-catalyzed reaction follows an ordered ternary complex mechanism in which the binding of NAD^+ occurs prior to that of lactate. and release of pyruvate precedes that of NADH. The use of rapid mixing methods allowed rates of many of the individual steps in the reaction sequence to be elucidated. including the hydride ion-transfer step in the catalytically active ternary complex.

The overall chemistry of the reaction involves the side chain of His 195 acting as a general base, abstracting the proton from the hydroxyl group of lactate and promoting electron flow in the direction of the positive charge on the nicotinamide ring of NAD^+ (Fig. 2b). The crucial features of the catalytic process are the correct positioning of the substrates. the conformational changes that aligned the appropriate side chains for reaction and binding. and the role of the side chain of His 195 as a general base.

Lactate dehydrogenase was subjected to extensive enzyme engineering studies using site-directed mutagenesis to explore the roles of a number of side chains in catalysis. to examine the nature of the rate-limiting step in the catalytic cycle. and to alter the specificity of the enzyme.[1,38,39] To examine the nature of the rate-limiting step, Gly 106 in the flexible loop was replaced by Trp. and the other Trp residues (80. 150. and 203) were replaced by Tyr, which has a much lower fluorescence. The mutant enzyme had similar catalytic activity to the wild-type. but essentially, only a single fluorescent group located within the flexible loop (Residues 98–120). Changes in the fluorescence of Trp 106 could be used to monitor the rate of structural changes associated with formation of the catalytically active complex. From this work. it was possible to conclude that the rate-limiting step in the catalytic cycle corresponded to the rate at which the flexible loop closed over the active site.

The active site of lactate dehydrogenase could be redesigned to convert it to a malate dehydrogenase. (It was already known that the tertiary structures of the two enzymes were similar.) To take account of the increased size and additional negative charge of malate, the volume of the active site was increased (Thr 246 replaced by Gly), and the basic character of the active site was enhanced (Asp 197 replaced by Asn, and Gln 102 replaced by Arg). The effect of these mutations was to change the ratio of the lactate/malate rates from 50011 to 1/1000. i.e., over 10^5-fold change in specificity. In further experiments. the active site of lactate dehydrogenase was altered to allow a broad range of bulky hydrophobic ketoacids to act as substrates, though at the expense of a significant reduction in the value of k_{cat}.[37]

Type II 3-Dehydroquinase

The dehydration of 3-dehydroquinate to 3-dehydroshikimate catalyzed by 3-dehydroquinase (EC 4.2.1.10) is common to two metabolic pathways, the inicrobial biosynthetic shikimate pathway and the catabolic quinate pathway. This reaction is catalyzed by two completely different enzymes: either a Type I enzyme that catalyzes a *syn* elimination: or a Type II enzyme that catalyzes an *anti* elimination.

The Type II 3-dehydroquinase is made up of 12 identical 16.5 kDa subunits of approximately 150 amino acid residues, which are arranged as a tetramer of trimers. The protein adopts a flavodoxin-like fold (i.e., belongs to the α/β class of proteins), with a parallel five-stranded β-sheet flanked on both sides by α-helices (Fig. 3a). The active site is located at the carboxyl end of the β-strands as in other α/β proteins, in the crevice produced by the specific topology of the β-sheet.[40] The loops from the P-strands 1 and 2 connect to helices in one direction. while those of β-strands 3, 4. and 5 connect to helices on the opposite face of the β-sheet. Between Strands 1 and 3, a crevice is formed, and this is where the active site is located (at least partially) in all α/β proteins. It should be noted that locating the active site of an enzyme is not as straightforward in the other classes of protein folds shown in Fig. 1.

Before the structure of the enzyme was determined, chemical modification experiments (using proteolysis and mass spectrometry to identify the modified residue) and site-directed mutagenesis were used to identify Arg 21, Tyr 28, and a His as catalytically important side chains.[41,42] Substrate and solvent ^2H isotope effects. proton inventory studies. and the pH-dependence of the kinetic parameters V_{max} and K_m were used to identify the enzyme mechanism[43] as an E_1CB elimination reaction proceeding via an enolate intermediate, with the initial proton abstraction as the rate-limiting step. The unusual sharp increase in k_{cat} and K_m above pH 9 was interpreted as the effect of an active-site Arg side chain on the basicity of a His.[43]

In the first crystal structure obtained for a Type II 3-dehydroquinase,[12] Arg 21 and Tyr 28 were disordered

a)

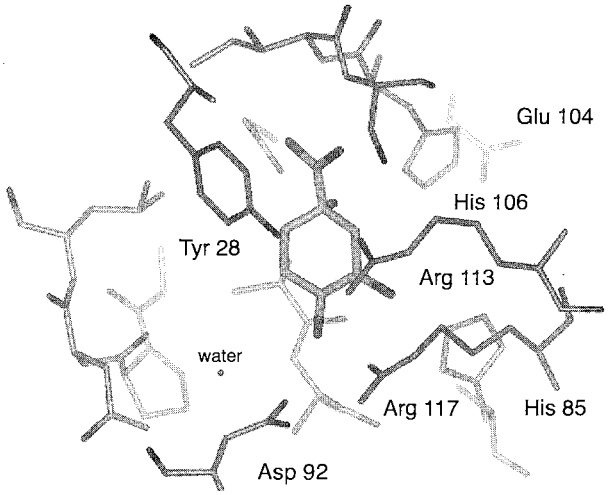

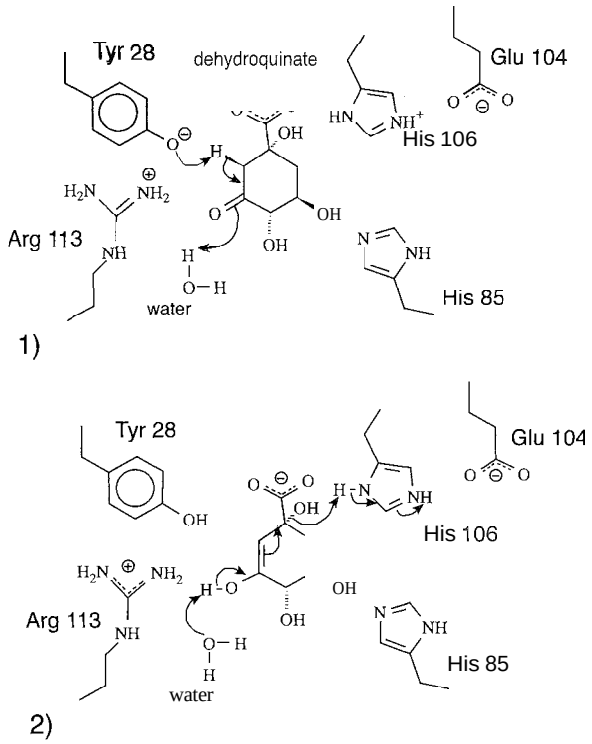

b)

Fig. **3** Type II dehydroquinase: a) a ribbon representation of the quaternary structure of the enzyme, with each peptide chain depicted in a different color. The inhibitor 2,3-anhydro-quinic acid is shown in space-filling representation. with atoms colored according to atom type. b) On the left is a detailed view of the enzyme active site as seen in the crystal structure. with the ligand highlighted in green and key amino acid residues labeled. This is compared with the traditional two-dimensional representation of the two steps of the enzyme mechanism on the right. *(View* this *art in color at www.dekker.com.*)

in a loop region of the structure. However, based on the conserved amino acid residues within the active site, His 106 was suggested as the residue involved in proton abstraction, with its basicity elevated by the neighboring side chain of Glu 104. Further structural characterization was made possible by the synthesis of a series of transition-state analogue inhibitors.[47] Four crystal structures including the catalytically compromised mutant enzyme in which Arg 21 was replaced by Ala in complex with the product dehydroshikimate and the wild-type enzyme with 2,3-anhydro-quinic acid bound (Fig. 3b) defined unambiguously the active site of the enzyme and the role of key amino acid residues and provided snapshots of the catalytic cycle.[45] Surprisingly, Tyr 28 is involved in the initial proton abstraction step rather than a His, its pK_a being lowered by the proximity of Arg 113. The absence of a residue to stabilize the negative charge of an enolate and the presence of a conserved water molecule strongly suggests that the reaction proceeds via an enol intermediate. The His 106–Glu 104 pair instead is involved in the elimination of water, with His 106 acting as an acid, not a base. Despite having identified the various catalytically important amino acid residues and the probable enzyme mechanism, several questions still need to be addressed. including the following: 1) is Tyr 28 present as a phenolate ion and. if so, how is this maintained in a flexible loop; and 2) what is the role of Glu 104, if any, in the enzyme mechanism? Different combinations of techniques will undoubtedly be needed to answer these and further questions.

CONCLUSION

In this article, we showed how the application of structural and kinetic methods allowed enzyme action to be understood at the atomic level. Higher-resolution definition of reaction intermediates together with computational methods will give increasing insights into the processes of bond breakage and formation as substrates are converted to products. Using exquisitely sensitive spectroscopic and mechanical methods, it is now possible to study the action of single-enzyme molecules.[46] It is expected that the application of these methods to enzyme systems catalyzing complex biosynthetic reactions will lead to the successful exploitation of enzymes for the manufacture of compounds of commercial and medical importance. The range of applications of enzymes is already wide[17] and is being extended by developments such as the generation of catalytic antibodies[14] and the directed evolution of enzymes.[49] Progress in the attempts to redesign enzymes has been reviewed.[50] The coming decade will be a rewarding one for enzymologists.

ARTICLES OF FURTHER INTEREST

The Allosteric Effect, p. 20
Artificial Enzymes, p. 76
Biological Models and Their Characteristics, p. 101
DNA Nanotechnology, p. 475
Enzyme Mimics, p. 546
Induced Fit, p. 717
The Lock and Key Principle, p. 809
Molecular-Level Machines, p. 931
O_2 Uptake und Transport, Models of, p. 1023
Peptide Nanotubes, p. 1035
Self-Assembly in Biochemistry, p. *1257*
X-Ray Crystallography, p. 1586
Zinc-Containing Enzymes und Their Models, p. 1631

REFERENCES

1. Price, *N.C.;* Stevens. L. *Fundamentals* of *Enzymology*, 3rd Ed.; Oxford University Press: Oxford, 1999: 5–7; 139–144; 154–161; 177–186; 200–206: 217–272.
2. Fersht, A. R *Structure and Mechanism in Protein Science; W.H.* Freeman: New York, 1999; 44–51; 54–102; 110–111: 164–168: 289–323; 377–400: 472–491; 497–500.
3. Berg, J.M.; Tymoczko, J.L.; Stryer. L. *Biochemistry*, 5th Ed.: *W.H.* Freeman: New York, 2002: 189–260.
4. BRENDA is a comprehensive enzyme information database. see www.brenda.uni-koeln.de/.
5. Walsh, *C.T.* Enabling the chemistry of life. Nature 2001. *409*. 226–240.
6. Doudna, J.A.; Cech, T.R. The chemical repertoire of natural ribozymes. Nature 2002. *418*, 222–228.
7. Updated information about genome sequencing projects can be found at web sites such as www.ensembl.org.
8. *Enzyme Nomenclature. Recommendations of the Nomenclature Committee of the International Union of Biochemistry and Molecular Biology*; Academic Press: San Diego, 1992. The enzyme nomenclature database is maintained at www.chem.qmul.ac.uk/iubmb/enzyme/.
9. Blattner, F.R.; Plunkett. G.; Bloch, C.A., et al. The coinplete genome sequence of *Escherichia coli* K-12. Science **1997**, *277*. 1453–1474.
10. Goodsell, D.S. Inside a living cell. Trends Biochem. Sci. **1991**. *16*, 203–206.
11. Wilmot, C.M.; Hajdu, J.; McPherson. M.J., et al. Visualization of dioxygen bound to copper during enzyme catalysis. Scicncc **1999**, *286*. 1724–1728.
12. Gourley, D.G.; Shrive, A.K.; Polikarpov, I., et al. The two types of 3-dehydroquinase have distinct structures but catalyse the same overall reaction. Nat. Struct. Biol. **1999,** *6*. 521–525.
13. Fraser. H.I.; Kvaratskliclia, M.; White. M.F. The two analogous phosphoglycerate mutases of *Escherichia coli*. FEBS Lett. **1999**. *455*, 344–348.
14. Moore, P.B.; Steitr, T.A. The involvement of RNA in ribosome function. Nature 2002. *418*, 229–235.

15. Lo Conte. L.: Ailey. B.: Hubbard. T.J.P., et al. SCOP: A structural classification of proteins database. Nucleic Acids Res. **2000**. *28*. 257–259.
16. Orengo, C.A.: Michie. A.D.; Jones, S.. et al. CATH—A hierarchic classification of protein domain structures. Structure 1997, *5*. 1093–1108.
17. Creighton. T.E. *Proteins: Structures and Molecular Properties*, 2nd Ed.: W.M. Freeman: New York, 1993: 243: 281–287.
18. Vonrhein. C.; Schlauderer, G.J.: Schulz, C.E. Movie of the structural changes during a catalytic cycle of nucleoside monophosphate kinases. Structure 1995. 3. 483–490.
19. Mandelman, D.: Schwarz. F.P.; Li. P.. et al. The role of quaternary interactions on the stability and activity of ascorbate peroxidase. Protein Sci. 1998. *7*, 2089–2098.
20. Nelmstaedt. *K.*: Krappmann, S.: Braus, G.H. Allosteric regulation of catalytic activity: *Escherichia coli* aspartate transcarbamoylase versus yeast chorismate mutase. Microbiol. Mol. Biol. Rev. 2001. *65*. 404–421.
21. Cane, D.E.; Walsh, C.T. The parallel and convergent universes of polyketide synthases and nonribosomal peptide synthetases. Chem. Biol. 1999. 6, R319–R325.
22. Huang, X.Y.: Holden, H.M.; Raushel, F.M. Channeling of substrates and intermediates in enzyme-catalyzed reactions. Ann. Rev. Biochem. 2001. *70*. 149–180.
23. Engel, P.C. *Enzyme Kinetics: The Steady State Approach*, 2nd Ed.: Chapman and Hall: London. 1981; 45–73.
24. Cornish-Bowden. A. *Fundamentals of Enzyme Kinetics*; Portland Press: London, 1995: 129–158.
25. Hajdu. J.: Machin, P.A.: Campbell, J.W., et al. Millisecond X-ray-diffraction and the 1st electron-density map from Laue photographs of a protein crystal. Nature 1987. *329*. 178–181.
26. Genick. U.K.; Borgstahl, G.E.O.: Ng, K.. et al. Structure of a protein photocycle intermediate by millisecond time-resolved Laue crystallography. Science 1997. *275*. 1471–1475.
27. Ren, Z.; Perman, B.; Srajer, V., et al. A molecular movie at 1.8 Å resolution displays the photocycle of photoactive yellow protein. a eubacterial blue-light receptor, from nanoseconds to seconds. Biochemistry 2001. *40*. 13788–13801.
28. Williams, P.A.: Fülöp, V.: Garman, E.F.. et al. Haem-ligand switching during catalysis in crystals of a nitrogen-cycle enzyme. Nature **1997**. *389*, 406–412.
29. Hajdu. J.; Neutre. R.; Sjogren, T.. et al. Analyzing protein functions in four dimensions. Nat. Struct. Biol. 2000. 7. 1006–1012.
30. Jencks. W.P. *Catalysis in Chemistry and Enzymology*; McGraw-Hill: New York, 1969.
31. Mulholland, A.J.; Lyne, P.D.: Karplus, M. Ab initio QM/MM study of the citrate synthase mechanism. A low-barrier hydrogen bond is not involved. J. Am. Chem. Soc. **2000**, *122*. 534–535.
32. Albery. W.J.; Knowles. J.R. Evolution of enzyme function and the development of catalytic efficiency. Biochemistry 1976. *15*. 5631–5640.
33. Grimshaw, C.E. Aldose reductase: Model of a new paradigm of enzymic perfection in detoxification catalysts. Biochemistry 1992, *31*. 10139–10145.
34. Waldman. A.D.: Hart, K.W.; Clarke, A.R., et al. The use of genetically engineered tryptophan to identify the movement of a domain of B. *stearothermophilus* lactate dehydrogenase with the process which limits the steady-state turnover of the enzyme. Biocheni. Biophys. Res. Commun. **1988**, *150*. 752–759.
35. Williams, J.C.; McDermott, A.E. Dynamics of the flexible loop of triose-phosphate isomerase—The loop motion is not ligand-gated. Biochemistry **1995**, *34*. 8309–8319.
36. Holbrook, J.J.: Liljas, A.: Steindel, S.J.. et al. Lactate dehpdrogenase. Enzymes 1975, *11*, 191–292. 3rd ed.
37. Wilks, H.M.; Halsall. D.J.; Atkinson, T., et al. Designs for a broad substrate-specificity keto acid dehydrogenase. Biochemistry **1990**. 29. 8587–8591.
38. Clarke. A.R.: Atkinson. T.: Holbrook, J.J. From analysis to synthesis: New ligand binding sites on the lactate dehydrogenase framework. Part I. Trends Biochem. Sci. 1989; *14*. 101–105.
39. Clarke. A.R.: Atkinson. T.; Holbrook, J.J. From analysis to synthesis: New ligand binding sites on the lactate dehydrogenase framework. Part II. Trends Biochem. Sci. 1989. *14*. 145–148.
40. Branden. C.: Tooze, J. Enzymes that Bind Nucleotides. In *Introduction to Protein Structure*: Garland Publishing. Inc.: New York. 1991; 43–57.
41. Krell. T.; Horsburgh, M.J.; Cooper. A., et al. Localization of the active site of type II dehydroquinases. Identification of a common arginine-containing motif in the two classes of dehydroquinases. J. Biol. Chem. 1996. *271*. 24492–24497.
42. Bottomley. J.R.; Hawkins, A.R.; Kleanthous. C. Conformational changes and the role of metals in the mechanism of type II dehydroquinase from *Aspergillus nidulans*. Biochem. J. 1996, *319*. 269–278.
43. Harris. J.M.: Gonzalez-Bello. C.; Kleanthous. C., et al. Evidence from kinetic isotope studies for an enolate intermediate in the mechanism of type II dehydroquinases. Biochem. J. 1996. *319*. 333–336.
44. Frederickson. M.; Parker. E.J.: Hawkins. A.R., et al. Selective inhibition of type II dehydroquinases. J. Org. Chem. **1999**. *64*. 2612–2613.
45. Roszak. *A.W.;* Robinson. D.A.; Krell, T., et al. The structure and mechanism of the type II dehydroquinase from *Streptomyces coelicolor*. Structure 2002. *10*. 493–503.
46. Xie, X.S.; Lu. H.P. Single molecule enzymology. J. Biol. Chem. 1999. *274*. 15967–15970.
47. Schmid. A.; Dordick. A.S.: Hauer. B.. et al. Industrial biocatalysis today and tomorrow. Nature 2001. *409*. 258–268.
48. Wagner, J.: Lerner. R.A.; Barbas. C.F.. III. Efficient aldolase catalytic antibodies that use the enamine mechanism of natural enzyme. Science 1995. *270*. 1797–1800.
49. Arnold. F.H. Combinatorial and computational challenges for biocatalyst design. Nature **2001**, *409*. 253–257.
50. Penning, T.M.; Jez, J.M. Enzyme redesign. Chem. Rev. 2001. *101*. 3027–3046.

Fluorescence Sensing of Anions

Kihang Choi
Andrew D. Hamilton
Yale University, New Haven, Connecticut, U.S.A

INTRODUCTION

Fluorescence is one of the most sensitive methods for converting molecular events to photophysical phenomena that can be easily detected using relatively simple devices and techniques. The powerful technique of fluorescence spectroscopy has been used for the analysis of many chemical and biological samples, especially when the quantity of the analyte is limited. Another key advantage of fluorescence sensing is that it is nondestructive; the analyte does not need to be isolated from its original environment as long as there is no background fluorescence blocking the detection of the signal.

Fluorescence sensors are usually constructed by conjugating a receptor (synthetic or biological) to a fluorophore.[1] The fluorescence properties of a fluorophore, such as emission intensity and wavelength. can be affected by the binding of an analyte to the receptor recognition domain. These changes can be monitored to determine the presence or. in a more quantitative way, the concentration of a given analyte. Effective connection of an analyte-binding domain to a fluorophore is important to produce a sensitive sensor with a significant fluorescence change. Many fluorophores with a wide range of excitation and emission wavelengths are available, and their fluorescence properties, such as excitation/emission mechanisms, decay processes; and excited state reactions are well characterized. Sensors using the chemical and physical properties of certain analytes to alter one of these fluorophore properties could give highly specific responses.

In this article. we will describe different approaches to the design of fluorescence sensors for anions that exploit distinctive mechanism-based concepts. In most case, synthetic receptors are used for anion binding and induce specific responses from the appended fluorophores, leading to selective and sensitive sensing.

LANTHANIDE COMPLEXES

An obvious approach to anion sensing would be to use cationic species as the anion-binding sites. In addition, some metal ions have well-characterized luminescent properties that can be utilized for sensing purposes. For example, the lanthanide f–f transition is forbidden. which makes direct excitation of the lanthanide ion difficult but also leads to slow radiative decay from the excited state.[2] The long-lived emission lifetime ranges from micro- to milliseconds. and by using time-gating detection methods, this can be distinguished from background short-lived emissions; which are common in biological systems. As a result: sensitive luminescence fluorophores can be obtained using this property.

Parker and coworkers showed that lanthanide complexes can be used as selective anion sensors.[3] Because lanthanide emission is quenched effectively by metal-bound water molecules through vibrational energy transfer to OH oscillators. displacement of water molecules by an anion changes the extent of vibrational quenching and can be signaled by increases in the intensity and lifetime of emission (Fig. 1). Macrocyclic heptadentate ligands containing aromatic chromophores were used to make coordinately unsaturated complexes of Eu and Tb ions. These in-built chromophores act as antennas to transfer energy from the chromophore excited state to the metal excited state. This indirect excitation solves the problem of direct excitation, and the excitation wavelength can be changed by using different chromophores. In aqueous solution; empty coordination sites are filled with one or two water molecules that can be replaced by certain anions with emission changes. When a chiral macrocyclic ligand was used, as in **1.** anion binding also induced changes in emission polarization.[4] HPO_4^{2-}, F^-, and SO_4^{2-} displaced one water molecule. while HCO_3^-, citrate, and lactate displaced two water molecules and formed chelated adducts. In particular. HCO_3^- binding was studied in a competitive anion background simulating an extracellular environment.

Another lanthanide-based anion sensor 2 exploits a bipyridine phosphine oxide derivative as a pentadentate ligand to coordinate Eu cation.[5] As anions bind to this complex, emission intensity was increased. presumably again due to the displacement of ligated water molecules.

RU(II) POLYPYRIDINE COMPLEXES

Another class of transition metal-based anion fluorescence sensors is based on ruthenium(II) *tris*(bipyridyl)

DOI: 10.1081/E-ESMC 120012885

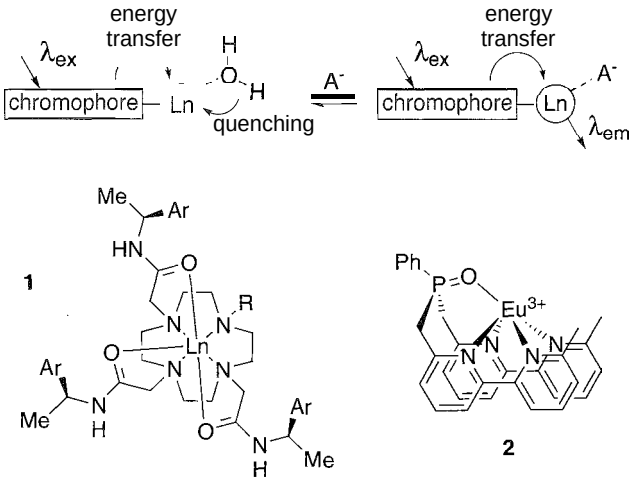

Fig. 1 Lanthanide complex sensors,

complexes. The electrochemical and photophysical properties of $Ru(bpy)_3^{2+}$ are well characterized[6] and are applied in the design of many sensors. The lowest excited state of the complex derives from a metal-to-ligand charge transfer (MLCT), so its nature can be controlled by the choice of ligands. The easy synthetic accessibility of the heteroleptic complex $Ru(L_2L')^{2+}$ is another advantage of this sensor system, as it allows ready incorporation of the anion recognition domain into one of the ligands.

Most sensors in this class, reported mainly by Beer and coworkers. have 4,4′-dicarboxamide-2,2′-bipyridine derivative as the anion-binding ligands (Fig. 2).[7,8] The two amides and additional binding groups on side-chain R constitute the anion-binding site. Negative charge develops on the ligand after photoinduced MLCT. and the charge interaction with a bound anion leads to a relative destabilization of this excited state. As a result, the emission shows a blue shift, which is usually accompanied by an increase in intensity. The anion is postulated to restrict the conformational flexibility of the receptor and. consequently, inhibit nonradiative decay processes.

When a metal complex like osmium(II) *tris*(bipyridyl) or a metallocene, as in compound **3,** is appended to the ligand, the MLCT excited state is quenched by energy transfer to the adjacent metal center. The rate of this quenching decreases as an anionic substrate binds between the two metal complexes. A similar switching mechanism is seen in the calix[4]diquinone-appended complex, 4. In this case. the fluorescence emission is quenched via an intramolecular electron transfer to the quinone. Anion binding between the Ru complex and the quinone blocks the quenching process, and the emission intensity is significantly recovered.

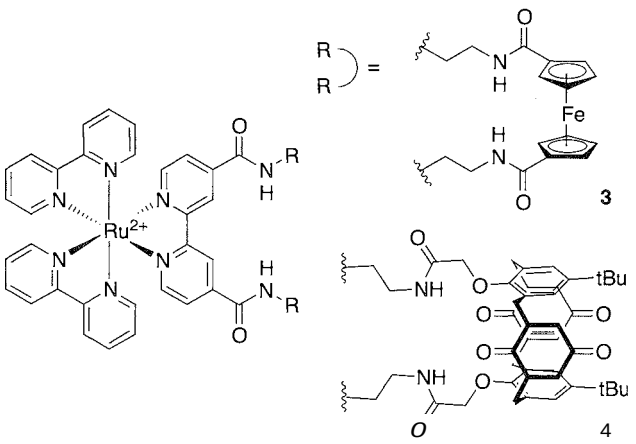

Fig. 2 Ru(II) polypyridine complex sensors.

PHOTOINDUCED ELECTRON TRANSFER

The fluorescence properties of aromatic alkylamines are critically dependent on the energy level of the amine functionality. After local excitation of the aromatic ring. electron transfer can occur from the amine nitrogen to the aromatic ring, preventing radiative decay of the excited state. This photoinduced electron transfer (PET) is suppressed by analyte binding to the amine functional group that lowers the energy of the nonbonding orbital, and as a

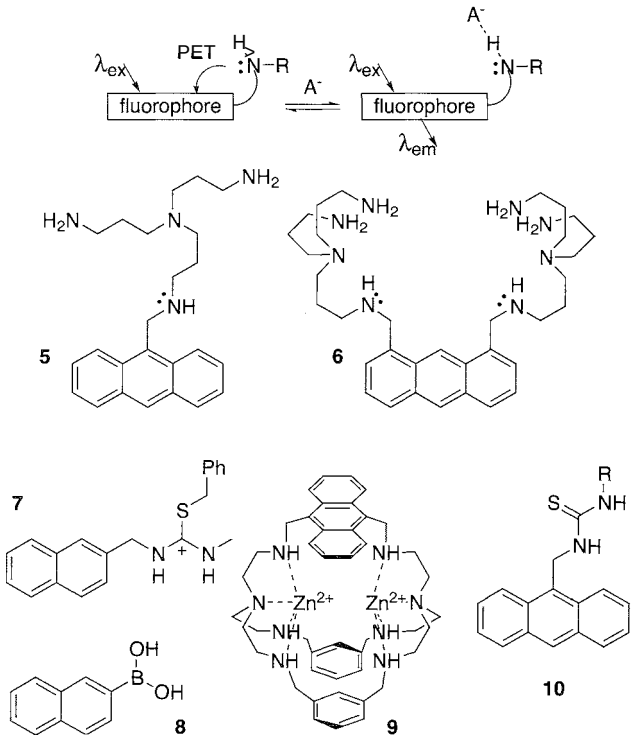

Fig. 3 PET sensors

result, enhanced emission intensity is observed (Fig. 3). This simple on–off switching mechanism and the undemanding chemistry of polyaromatic fluorophores led to extensive development of PET-based sensors for the detection of diverse analytes.

Czarnik and coworkers developed the first fluorescence anion sensor based on the PET mechanism using a polyamine as the anion-binding domain.[9] The polyamine-appended anthracene **5** showed enhanced emission upon HPO_4^{2-} binding in neutral aqueous condition. The anion interacts with the benzylic amine group, rendering the nitrogen electron pair unavailable for PET, probably by a proton transfer. and fluorescence of the anthracene is switched on. A closely related system was devised for pyrophosphate sensing.[10] Compound 6 has two polyamine chains attached to the I- and 8-positions of anthracene. These two arms effectively discriminate between pyrophosphate and phosphate at neutral pH. Thiouronium **7**. synthesized from the corresponding thiourea, also showed an increase in the maximum emission intensity after anion binding, with good selectivity for AcO^- over dialkylphosphate.[11]

There are several examples of the reversal of the PET mechanism being used for anion sensing. In these cases, anion binding enhances PET, leading to a reduction in the maximum emission intensity. Arylboronic acids. widely used for carbohydrate recognition, can also act as Lewis acids and bind to F^- to form the tetrahedral boronate. For example. F^- binding to Compound **8** quenches the fluorescence of the attached naphthalene ring due to increased PET from the boronate anion.[12] No fluorescence change was observed on addition of Cl^- or Br^-. Bis-zinc(II) Complex **9** selectively coordinates linear N_3^- over other anions, and the emission of the anthracene fluorophore is quenched through intracomplex electron transfer from the bound N_3^-.[13] Recently, neutral PET anion sensor **10** with a thiourea group linked to anthracene was shown to undergo significant fluorescence quenching on addition of F^-, AcO^-, and $H_2PO_4^-$.[14] The authors proposed that electron transfer from the anion–thiourea complex to the anthracene excited state is increased. because the reduction potential of the thiourea group is enhanced by anion binding.

EXCITED STATE COMPLEXES

Pyrene is an example of a ciass of fluorophores that form complexes with themselves. A concentration-dependent fluorescence behavior occurs due to intermolecular interaction between the flat hydrophobic surfaces in the dimer. A highly structured emission from the monomer is dominant at low concentration. but as the concentration increases; a long-wavelength emission from the excited state dimer, called an excimer. begins to appear. Shifting the monomer-to-excimer equilibrium can be exploited to develop ratiomeric fluorescence sensors. By measuring the intensity ratio of monomer-to-excimer emissions. analyte concentrations can be determined independently of sensor concentration or other artifacts that might affect emission intensity.

A guanidinium-functionalized pyrene was shown to assemble into a dimer, directed by pyrophosphate anion complexation (**11** in Fig. 4).[15] Characteristic emission of the pyrene excimer was observed from this anion-templated, self-assembled complex, and the concentration of pyrophosphate was measured by ratiomeric titration. The addition of phosphate did not cause any significant emission change. A closely related Compound 12 was also an effective ratiomeric anion sensor.[16] The emission of this thiourea-functionalized pyrene monomer was quenched by anion binding due to the increased PET from the thiourea group to the pyrene ring. The long-wavelength emission. however, was not significantly affected, and the ratio of two emission intensities showed ideal behavior as a function of changing anion concentration. The authors assigned the long-wavelength emission to an intramolecular exciplex formed between the pyrene ring and the thiourea group.

Cornpound 13 bearing four pyrene rings was recently reported as a selective phosphate sensor.[17] The pyrene rings. connected through amide bonds, undergo hydrophobic collapse and form an intramolecular pyrene exciplex. In the presence of phosphate anion; the intensity of the long-wavelength emission was reduced with simultaneous increase of pyrene monomer emission. Presumably. pyrene exciplex formation is inhibited by anion binding to the amide groups between fluorophores. The selectivity for phosphate was explained by the pseudo-tetrahedral arrangement of the hydrogen bond donating amide NH groups.

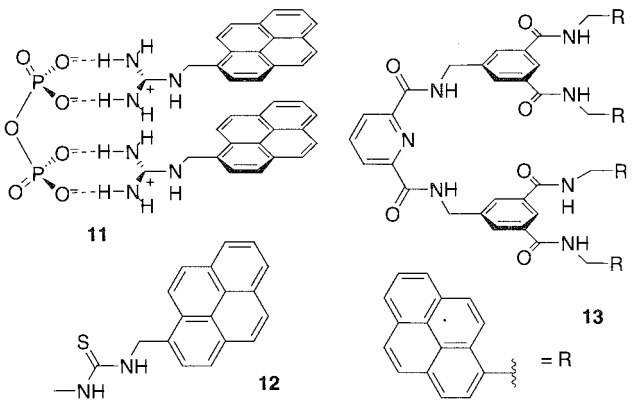

Fig. 4 Excimer/exciplex sensors.

SENSING ENSEMBLE

Competitive titration is another powerful method for anion fluorescence sensing. In this technique, the fluorophore and anion recognition domain are not linked together. Instead. changes in the fluorescence properties of the fluorophore are induced by its displacement from a noncovalent association with the recognition domain (the sensing ensemble) by the target anion. Sensing selectivity comes partially from the structural similarity between the fluorophore and the analyte, because these two molecules act as competitive guests for the receptor. A calibration curve, obtained by monitoring emission changes over a range of analyte concentrations. is used for quantification of the analyte. Several biologically important anions, including citrate, carbonate, and inositol triphosphate. were detected in a range of solvent mixtures using this method.

Many chemosensor ensembles were reported by Anslyn and coworkers.[18] Compound 14, with three guanidinium groups displayed in the same direction (Fig. 5). binds to the citrate tricarboxylate anion. Anionic fluorophore 5-carboxy-fluorescein **15** binds with modest affinity to this receptor and shows increased fluorescence intensity due to the decreased pKa of its phenol group. As citrate is added, the fluorophore is displaced from the receptor, and the emission intensity diminishes. The same fluorophore was used in another sensing ensemble for inositol-1,4,5-triphosphate (IP_3), an important second messenger involved in many cell regulatory functions. The fluorophore bound to positively charged hexa-guanidinium receptor **16** is displaced by added IP_3, and the fluorescence intensity decreases.

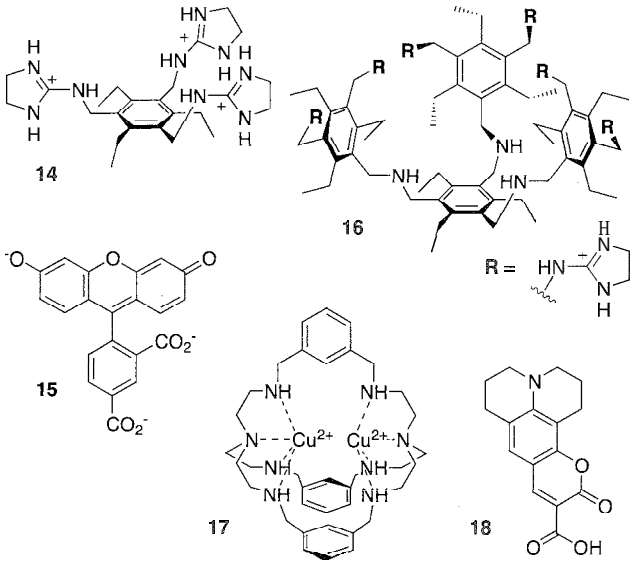

Fig. 5 Sensing ensembles.

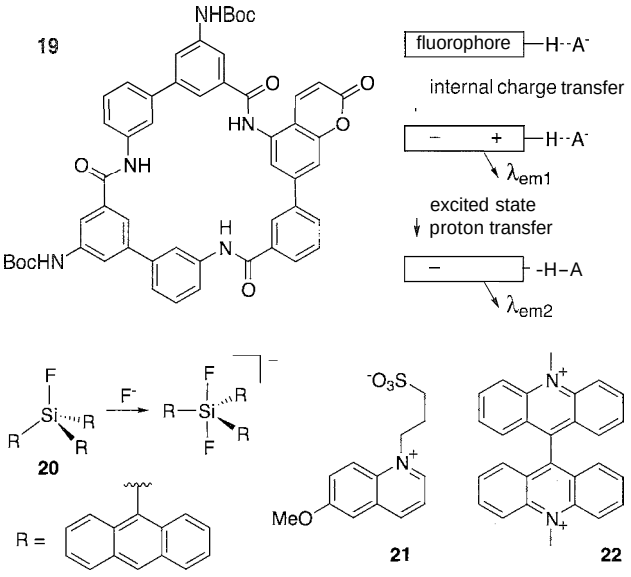

Fig. 6 Other anion chemosensors.

A coinpetitive method for carbonate sensing is based on dicopper complex **17** and coumarin 343 as anion receptor and external fluorophore, respectively.[19] The fluorophore 18 coordinates to the copper atoins through its carboxylic group. and energy transfer between coumarin ring and copper atoms quenches the fluorescence emission. Carbonate showed strong binding to the metal complex and coupled the displacement of the bound fluorophore with concomitant recovery of the coumarin emission. This ensemble showed selective response to carbonate over phosphate or carboxylate.

OTHER CHEMOSENSORS

We explored the strategy of linking an anion receptor to a fluorophore that exhibits emission from an internal charge transfer (ICT) excited state. This allowed us to obtain a high dynainic range of emission response, and in one case, the resulting design functions as a dual channel
In sensor **19** (Fig. 6), an aminocoumarin tluorophore is integrated into the binding domain of a macrocyclic receptor such that it is directly involved in hydrogen bonding to the anion. Anion binding caused an increase in intensity and red shift of the fluorescence emission of the coumarin. The red shift is due to stabilization of the ICT excited state relative to the ground state by electrostatic interaction with the bound anion. The intensity enhancement likely results from conformational restriction of the fluorophore that would otherwise lead to nonradiative decay through rotatory inotion of the amide group of the fluorophore. The most remarkable change was the

appearance of a second emission band at longer wavelength upon addition of anions like $H_2PO_4^-$. The increased acidity of the fluorophore after excitation facilitated proton transfer to the bound anion. and the second fluorescence emission channel was opened through intermolecular excited state proton transfer (ESPT).

Tri(9-anthryl)fluorosilane **20** was used for fluorescence sensing of fluoride anion.[21] The organosilane derivative binds with F^- to form a penta-coordinated organosilicate, and this hypercoordination changes the structure from tetrahedral to trigonal bipyramidal. Through-space interaction between the anthryl groups is reduced, and the emission intensity of the anthracene fluorophore increased significantly.

N-Alkyl-6-methoxyquinolinium and N-alkylacridinium derivatives like **21** and **22** were used to detect chloride anion in biological samples.[22,23] These simple derivatives are commercially available and, unlike the other sensors discussed so far, they detect Cl^- via collisional quenching of the fluorophore excited states. No molecular recognition event is involved in the sensing mechanism. Other halides. such as Br^- and I^-, and SCN^- are also efficient quenchers, but physiological concentrations of these anions do not significantly affect the fluorescence.

BIOSENSORS

Biosensors represent additional useful tools for fluorescence anion sensing. In this approach, an anion-binding protein is used as the recognition domain. and a fluorophorc is covalently linked to the region where conformational changes are expected after analyte binding. Variation of the microenvironment around the fluorophore is detected through changes in its spectroscopic properties.

E. coli phosphate-binding protein (PBP) is a monomeric protein that associates strongly and selectively with inorganic phosphate. The anion binds into a cleft between two domains of PBP and induces a large conformational change in the protein. One alanine residue at the edge of the binding cleft was replaced with cysteine. and the mutant protein was reacted with a thiol-reactive diethylaminocoumarin derivative.[24] On binding phosphate, the fluorophore-labeled protein exhibited a Slue shift and intensity increase in its fluorescence emission. The aminocoumarin is postulated to be constrained in a highly fluorescent conformation due to the reduced local flexibility of the phosphate-bound form of PBP.

A similar strategy was employed for an IP_3 biosensor.[25] Pleckstrin homology (PH) domain of phospholipase C (PEG) δ_1, which binds IP_3 with a submicromolar affinity. was mutated to incorporate a cysteine residue next to the anion-binding site. Labeling with thiol-reactive fluorescein or aminonaphthalene derivatives gave anion sensors that showed large fluorescence changes in response to IP_3, with good selectivity over other phosphates.

Mutants of yellow fluorescent protein (YFP), an engineered variant of green fluorescent protein (GFP). were developed as biosensors for Cl^-. YFP autocatalytically generates its own fluorophore. and its mutant YFP-H148Q showed decreased fluorescence in response to many anions. Crystallographic analysis confirmed that the anion is bound close to the protein fluorophore and increases its pKa, inducing fluorescence suppression.[27] To improve the halide anion selectivity. random mutants of YFP-H148Q were generated. and some variants with increased affinity and selectivity for C l and I were identified.[28]

CONCLUSION

Design of a receptor molecule that can bind to a target anion with high affinity and selectivity remains a challenging task. The properties of the target anion and the nature of its possible interactions with a receptor in different environments must be considered in the design. The key additional element in the design of a fluorescence sensor is the fluorophore. The interactions of a fluorophore with a receptor or an analyte before and after their binding determine the fluorescence behavior of the sensor. It is not enough to simply connect a receptor with a fluorophore to achieve sensitive and selective sensing. The anion fluorescence sensors described in this article provide good examples of how tluorophores can be coupled with selective anion-binding receptors to convert a molecular recognition event to fluorescence changes. Fluorophore properties such as the energy of the excited state. the extent of nonradiative decay. and the opening and closing of transfer processes can be modulated by direct interaction with an anion or by indirect changes in the receptor after binding an anion. Designs based on fluorescence mechanisms led to many sensors. The growing number of synthetic anion receptors suggests that in the future. more selective and sensitive anion sensors will be developed for diverse applications.

ACKNOWLEDGMENT

The portion of this work carried out at Yale was supported by the National Institutes of Health (GM35208).

ARTICLES OF FURTHER INTEREST

Amide- and Urea-Based Anion Receptors, p. 31
Energy and Electron Transfer in Supramolecular Systems, p. 535

Luminescent Materials, p. 816
Luminescent Probes, p. 821
Semiochemistry, p. 1270
Supramolecular Photochemistry, p. 1434

REFERENCES

1. de Silva. A.P.: Gunaratne, H.Q.N.: Gunnlaugsson. T.; Huxley, A.J.M.: McCoy. C.P.; Rademacher, J.T.; Rice. T.E. Signaling recognition events with fluorescent sensors and switches. Chem. Rev. 1997. 97 (5), 1515–1566.
2. Sabbatini, N.; Guardigli, M.; Lehn, J.M. Luminescent lanthanide complexes as photochemical supramolecular devices. Coord. Chem. Rev. 1993. 123 (1–2), 201–228.
3. Parker. D. Luminescent lanthanide sensors for pH, pO_2 and selected anions. Coord. Chem. Rev. 2000,205(1), 109–130.
4. Bruce, J.I.: Dickins, R.S.: Govenlock, L.J.: Gunnlaugsson. T.; Lopinski. S.; Lowe. M.P.: Parker. D.; Peacock. R.D.; Perry. J.J.B.: Aime, S.: Botta. M. The selectivity of reversible oxy-anion binding in aqueous solution at a chiral europium and terbium center: Signaling of carbonate chelation by changes in the form and circular polarization of luminescence emission. J. Am. Chem. Soc. 2000, 122 (40), 9674–9684.
5. Montalti. M.; Prodi. L.: Zaccheroni, N.: Charbonniere. L.; Douce, L.: Ziessel, R. A luminescent anion sensor based on a europium hybrid complex. J. Am. Chem. Soc. 2801. 123 (50), 12694–12695.
6. Juris. A.: Balzani, V.; Barigelletti. F.; Campagna. S.: Belser, P.; von Zelewsky. A. Ru(II) polypyridine complexes: Photophysics, photochemistry. electrochemistry. and chemiluminescence. Coord. Chem. Rev. 1988, 84. 85–277.
7. Beer, P.D.; Cadman, J. Electrochemical and optical sensing of anions by transition metal based receptors. Coord. Chem. Rev. 2000. 205 (1), 131–155.
8. Beer. P.D.: Gale. P.A. Anion recognition and sensing: The state of the art and future perspectives. Angew. Chem., Int. Ed. 2001, 40 (3), 487–516.
9. Huston. M.E.: Akkaya, E.U.; Czarnik. A.W. Chelation enhanced fluorescence detection of non-metal ions. J. Am. Chem. Soc. 1989. 111 (23), 8735–8737.
10. Vance, D.H.; Czarnik. A.W. Real-time assay of inorganic pyrophosphatase using a high-affinity chelation-enhanced fluorescence chemosensor. J. Am. Chem. Soc. 1994, 116 (20). 9397–9398.
11. Kubo. Y.; Tsukahara. M.: Ishihara. S.; Tokita. S. A simple anion chemosensor based on a naphthalene-thiouroniuin dyad. Chern. Cornmun. 2000, (8), 653–654.
12. Cooper, C.R.: Spencer, N.: James, T.D. Selective fluorescence detection of fluoride using boronic acids. Chem. Cornmun. 1998. (13), 1365–1366.
13. Fabbrizzi. L.: Faravelli, I.: Francese. G.; Licchelli, M.; Perotti, A.: Taglietti. A. A fluorescent cage for anion sensing in aqueous solution. Chem. Commun. 1998, (9). 971–972.
14. Gunnlaugsson, T.: Davis, A.P.; Glynn. M. Fluorescent photoinduced electron transfer (PET) sensing of anions using charge neutral chemosensors. Chem. Commun. 2001. (24). 2556–2557.
15. Nishizawa, S.; Kato. Y.; Teramae. N. Fluorescence sensing of anions via intramolecular excimer formation in a pyrophosphate-induced self-assembly of a pyrene-functionalized guanidinium receptor. J. Am. Chem. Soc. 1999. 121 (40). 9463–9464.
16. Nishizawa. S.; Kaneda, H.: Uchida. T.; Teramae. N. Anion sensing by a donor-spacer-acceptor system: An intramolecular exciplex emission enhanced by hydrogen bond-mediated complexation. J. Chem. Soc., Perkin Trans. 2 1998. (11), 2325–2327.
17. Liao, J.-H.; Chen, C.-T.; Fang, J.-M. A novel phosphate chemosensor utilizing anion-induced fluorescence change. Org. Lett. 2002. 4 (4). 561–564.
18. Wiskur. S.L.: Ait-Haddou. H.; Lavigne. J.J.: Anslyn. E.V. Teaching old indicators new tricks. Acc. Chem. Res. 2001, 34 (12), 963–972.
19. Fabbrizzi, L.: Leone. A.; Taglietti, A. A chemosensing ensemble for selective carbonate detection in water based on metal-ligand interactions. Angew. Chem.. Int. Ed. 2001. 40 (16), 3066–3069.
20. Choi. K.; Hamilton, A.D. A dual channel fluorescence chemosensor for anions involving intermolecular excited state proton transfer. Angew. Chem.. Int. Ed. 2001. 40 (20), 3912–3915.
21. Yamaguchi, S.: Akiyama, S.; Tamao. K. Photophysical properties changes caused by hypercoordination of organosilicon compounds: From trianthrylfluorosilane to trianthryldifluorosilicate. J. Am. Chem. Soc. 2000. 122 (28). 6793–6794.
22. Illsley, N.P.; Verkman, A.S. Membrane chloride transport measured using a chloride-sensitive fluorescent probe. Biochemistry 1987, 26 (5). 1215–1219.
23. Biwersi. J.: Tulk, B.: Verkman. A.S. Long-wavelength chloride-sensitive fluorescent indicators. Anal. Biochem. 1994, 219 (1). 139–143.
24. Brune. M.: Hunter. J.L.: Corrie. J.E.T.; Webb, M.R. Direct. real-time measurement of rapid inorganic-phosphate release using a novel fluorescent-probe and its application to actomyosin subfragment-1 ATPase. Biochemistry 1994.33 (27). 8262–8271.
25. Morii, T.; Sugimoto, K.: Makino, K.: Otsuka, M.: Imoto, K.: Mori. Y. A new fluorescent biosensor for inositol trisphosphate. J. Am. Chem. Soc. 2002. 124 (7). 1138–1139.
26. Jayaraman, S.: Haggie. P.; Wachter. R.M.: Remington, S.J.; Verkman, A.S. Mechanism and cellular applications of a green fluorescent protein-based halide sensor. J. Biol. Chem. 2000. 275 (9). 6047–6050.
27. Wachter. R.M.; Varbrough. D.: Kallio, K.: Remington. S.J. Crystallographic and energetic analysis of binding of selected anions to the yellow variants of green fluorescent protein. J. Mol. Biol. 2000. 301 (I), 157–171.
28. Galietta. L.J.V.; Haggie. P.M.: Verkman. A.S. Green fluorescent protein-based halide indicators with improved chloride and iodide affinities. FEBS Lett. 2001, 499 (3). 220–224.

Fluorescent Sensors

A. Prasanna de Silva
Gareth D. McClean
Thomas S. Moody
The Queen's University of Belfast, Belfast, Northern Ireland

INTRODUCTION

Following a brief introduction and justification, the design of fluorescent sensors is summarized. Three popular photochemical designs are highlighted. Then, with some examples, we will show how suitably selective receptors can give rise to excellent sensor systems. Cases showing considerable success in cellular physiology and in medical diagnostics are included among these examples. To conclude. a glance at the future will be taken.

WHY DO WE NEED FLUORESCENT SENSORS?

It is a truism that our environment exerts as much control over us as our genes. It is no wonder that most societies lay considerable emphasis on monitoring human environments. In practice, this means that such surveillance must extend to many chemical constituents of our external environment as well as those that exist within ourselves. The ideal spies for such operations must be small enough to enter the various spaces of interest and cause minimum disruption to the sensitively poised steady states existing therein.[1,2] In addition. such spies must be able to communicate their findings to human observers. Such tough criteria for the ideal spy are most satisfactorily met by fluorescent molecular sensors.[3–9]

HOW ARE FLUORESCENT SENSORS DESIGNED?

The bare essentials[10] of a fluorescent sensor molecule are as follows: 1) a means of temporarily capturing chemicai targets, i.e., a receptor: 2) a means of long-range communication with the observer/controller, i.e., a light absorber/emitter or a fluorophore; and 3) a means of shorter-range communication between the receptor and the fluorophore so that capture of a chemical target causes a light signal.

Several elaborations of Point 3 exist. The oldest of these[1,11] ensures receptor–fluorophore communication by simply overlapping the two units so that their x-electron systems merge (Fig. 1). Such x-systems are particularly useful if they show electronic push–pull character. These give rise to internal charge transfer (ICT) excited states that are significantly perturbed when the receptor captures its target species.[2] A color change in excitation or emission is the usual experimental outcome that can be of considerable value in physiological investigations.[12]

Another approach to implementing Point 3 has become particularly popular. In this method. the fluorophore and the receptor are forced to cominunicate through a short σ-bond spacer. Photoinduced electron transfer (PET) is a single-electron process that can cross this bridge with ease if the thermodynamics are right.[13,14] Naturally. the PET thermodynamics are substantially altered upon target capture by the receptor.[1] The experimental outcome can be a switching on or off of fluorescence (Fig. 2). Such a result creates considerable drama when compared to most laboratory experiments. and it may account for the rapid uptake of this design. However, PET is not the only process that can be profitably arranged within fluorophore–spacer–receptor systems. Electronic energy transfer (EET)[15] can also be useful in cases where the target possesses a rather low-energy excited state. The emission from the fluorophore is then switched off upon target capture.

A third way to tackle Point 3 is to arrange for the fluorophore and the receptor to be associated by means of one supramolecular interaction or another.[1,16] Such an association can mimic the situation discussed in the previous paragraph. Or else the proximity of the receptor to the fluorophore can disturb the emission properties of the latter.[17] Target capture by the receptor liberates the fluorophore so it can emit normally again.

ILLUSTRATIVE EXAMPLES OF FLUORESCENT SENSORS

There are literally hundreds of fluorescent sensors[2] that would merit discussion in a general introductory review of this kind. Many of these were already featured in the review literature.[1–10] For the present purpose. we allowed

Encyclopedia of Supramolecular Chemistry
DOI 10.1081/E-ESMC 120012870

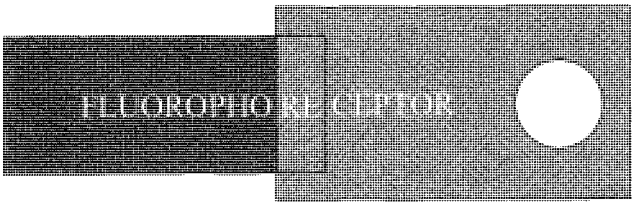

Fig. 1 Integrated fluorophore–receptor format, where ICT excited states can arise. (*View this* art *in* ***color*** *at www.dekker.* ***corn.)***

our choice to be dictated by the selectivity of cheinical target recognition as well as by the diversity of photochemical mechanisms.

A Fluorescent Sensor for Ma'

Tusa, keiner, and their colleagues at Roche Diagnostics Corporation produced a commercially successful diagnostic system for blood electrolytes and gases in critical care and point-of-care situations.[18] Its design platform is PET, with fluorescent sensors for each blood constituent being equipped with an adequately selective receptor. The case for Na^+**1**[19] is highlighted here. The *N*-(2-methoxyphenyl)monoaza-15-crown-5 ether picks out extracellular Na^+ (normally 1.5×10^{-1} M) from K^+ (normally 5×10^{-3} M) and a myriad of other species. Monoaza-15-crown-5 ether has similar preferences for binding Na^+ and K^+. besides sufficient attraction toward H^+, to be heavily protonated at the pH value found in the extracellular matrix (normally 7).[20] The fusion of the phenyl unit with an azacrown nitrogen essentially destroys the attraction toward H^+ under these conditions. The 2-methoxy substituent on the phenyl ring presents a ligating oxygen to supplement the NO_4 donor set as they confront Na^+. The three-dimensional pseudocryptand environment now shows higher selectivity[21,22] toward the size-complementary Na^+ than the larger K^+. All these selectivity aspects were considered and tackled previously by Tsien[12,23] during his groundbreaking program for imaging intracellular constituents. We subsequently constructed fluorescent PET sensors with Tsien's Na^+ receptor.['' importantly, receptors like that within **1** display clear conformational changes upon binding Na^+ which decouple the electron systems of the 2-methoxyphenyl unit and of the nitrogen atom.[24] This has important ramifications in a PET sensing context. because the oxidation potential of the receptor jumps from 0.8 V (versus SCE) to >1.2 V upon Na^+ binding.

Rational discussion of PET thermodynamics now cues the entry of the fluorophore. The 4-amino-1,8-naphthalimide was introduced by us into the field of PET sensors some time ago.[25] Its particular attractions for the present application are its complementarity with visible light-emitting diodes as excitation sources and its robust thermal stability. The oxidation potential of this fluorophore is 1.1 V. A molecular orbital diagram (Fig. 3) collects these oxidation potentials and their relationship to the sensory behavior of **1**. Excitation of the fluorophore leaves a hole in the highest occupied molecular orbital (HOMO) that can be filled by an electron from HOMO' but not by an electron from HOMO". where the Na^+ exerts its influence. So de-excitation of the excited fluorophore via fluorescence is only possible when Na' is present (Fig. 3b), i.e., "off–on" signaling of Na^+.

The dimethylene spacer between the fluorophore and the receptor is short enough to permit PET at a sufficient rate (when thermodynamically feasible. i.e.,

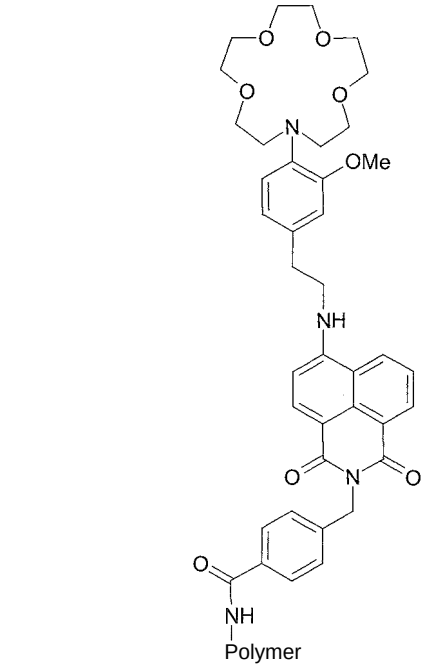

1

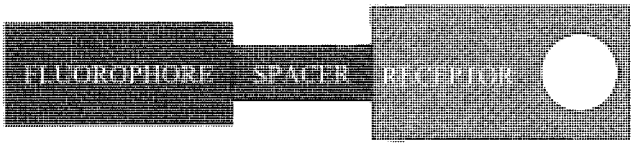

Fig. 2 Modular fluorophore–spacer–receptor format. where PET or EET processes can deactivate the excited state (either before or after capture of the target). (*View this art* ***in color*** *at www.dekker.com.*)

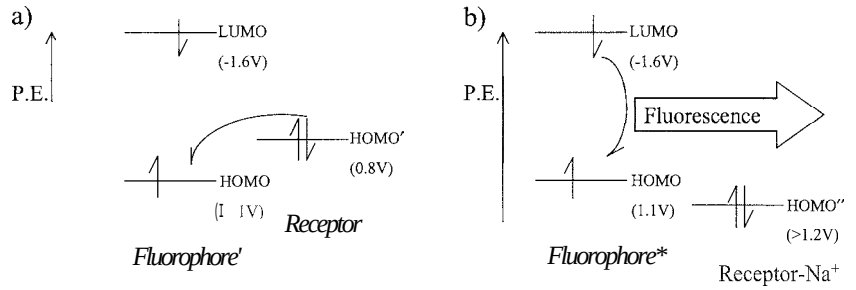

Fig. 3 *Molecular orbital potential energy* (P.E.) diagram *for* 1 *before (a) and after (b)* Na^+ *capture. The* redox *potentials are given* as *measures* of *orbital* energies.

in the absence of sufficient Na^+) *to overwhelm the competing process* of *fluorescence. Nevertheless,* it *is long enough to preserve the* modularity *of the fluorophore and the receptors. Besides these three photochemically essential components,* 1 *also contains an anchor to iink with a water-insoluble polymer. to* complete *the medical device.*

Fluorescent Sensors for Fe^{3+} and MoO_4

Siderophores are naturally honed to pick up Fe^{3+} with *excellent selectivity. without which many microorganisms would fail to achieve their essential iron* intake.[26] Some *of these siderophores are also* excellent *at recognizing* MoO_4^- *(see Fluorescent Sensing of Anions).*[27] *So it* is *natural that* such *receptors were incorporated into* fluo*rophore–spacer–recepcor* systems *without* compromising *their coordination properties.* It *is equally natural to design such systems* to *be intrinsically fluorescent, because targets such as* Fe^{3+} *and* MoO_4^- *will be* redox*active and, therefore. switch off the fluorescence via PET upon binding. As* mentioned *previously, the fluorescence quenching can also arise via EET for these colored targets, though this pathway appears to* be *experimentally ruled* out *in the cases to be* examined *here.*

Shanzer's team *uses a tris-*hydroxamate *motif within 2 to target* Fe^{3+}, *as the latter is transported into Pseudomonas putida* bacteria.[28] *On the other hand, a catecholcarboxamide serves as the receptor for* Fe^{3+} *and* MoO_4^- *within* 3 *designed by* Duhme-Klair, *Perutz, and* coworkers.[29] The Fe^{3+} *recognition by* **3** *can be* suppressed *by artificially adjusting the* pH *to 5.7, even though such action disqualifies it from* many in vivo *studies. Nevertheless, this leaves us with 3 as a brilliant assay* for MoO_4^-. *Both 2* and **3** *employ* fluoro*phores with solid track records: 4-amino-7-nitrobenzo-*2-oxa-1,3-diazole *(widely used as a biochemical label) and tris*bipyridylRu(II) *(the* most *famous metal* complex *in* photochemistry/physics).

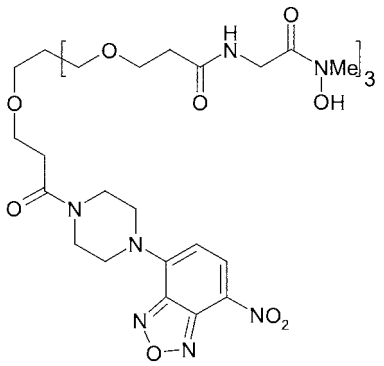

2

The relatively long spacers in 2 and **3** *again assist in maintaining modularity. Nevertheless, the spacers are short enough to* permit *rapid PET and switch fluorescence off* when *required. There is no significant (rate of) PET* in *the target-free 2 and 3. Poor* redox *activity of the hydroxamic acid receptor* in *2 is to be expected;* but *the* same *cannot be said of the catecholcarboxarnide receptor in 3 without more careful consideration. In fact, this receptor will undergo PET to the fluorophore if deprotonated. However, the* redox *activity of the receptor remains insufficient if the pH was pegged at acidic enough* values *(5.7) to prevent deprotonation. The arrival of targets* Fe^{3+} *and* MoO_4^- *into 2 and 3. respectively. causes clear fluorescence quenching. Proof of the PET nature of the quenching is seen in the case of 3: freezing of* **3**.MoO_4^- *solutions resurrects fluorescence. This is because PET changes the charge states of the receptor and the fluorophore. Such charge* changes require *reorientation of solvent dipoles, which. of course, cannot occur in a* frozen *glass.*

Fluorescent Sensors for Cu^{2+}

A feature common to a number of receptors showing *good* Cu^{2+} *selectivity is the presence of one or* more *primary*

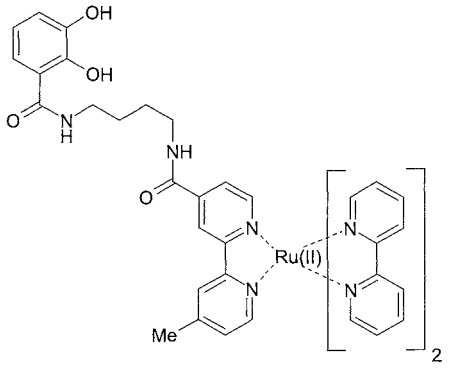

3

amide moieties that appear to lose the amide proton during the complexation process. Naturally, the complex is bolstered by the availability of other ligating units in chelating configurations. Sensor 4, due to Bhattacharya and Thomas, contains a receptor unit that illustrates these generalities.[30] It picks up micromolar concentrations of Cu^{2+} at neutral pH values. The fluorophore employed within 4 is 5-dimethylaminonaphthalene-1-sulfonamide (dansylamide), the common biochemical label. It seems that the fluorophore stands clear of the receptor-Cu^{2+} complex, even though the spacer component is flexible. The experimental upshot of all this is a clear switching off of the fluorescence of 4, though the off state is still emissive: upon encountering Cu^{2+}. Such a limited degree of switching off is probably caused by the relatively large separation between the fluorophore and the complexed Cu^{2+} center. Cu^{2+} shares several key properties, like redox activity and color, with Fe^{3+}, so the mechanistic arguments considered in the previous section are equally relevant here. Nevertheless, several studies, including a one by Prodi and coworkers,[31] find that Cu^{2+}-induced fluorescence quenching is not prevented by freezing. In other words, EET rather than PET is the likely channel of fluorescence switching.

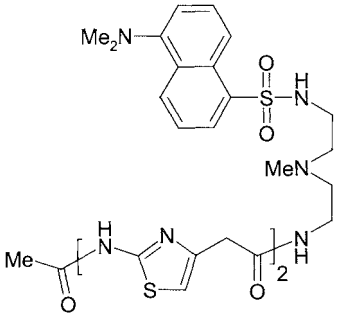

4

As indicated in the design section. supramolecular assembly of a fluorophore and a receptor creates a pseudointramolecular situation in which effective quenching via PET or EET becomes possible. Tecilla and Tonellato's team apply fluorophore 5 and receptor 6 in this way to selectively target Cu^{2+}.[16] Receptor 6 fits the generalizations opening the previous paragraph. However. 6 contains something else—a long hydrocarbon chain. This is the clue to the supramolecular assembly process of 5 and 6. In fact, there is a third species with a similar chain — cetyltrimethylammonium bromide (CTAB)—that supramolecularly assembles with many copies of itself in aqueous solution to form micelles. Receptor 6 naturally incorporates into CTAB micelles while locating its peptide/acid units in the micellar head-group region. Fluorophore 5 also locates in this region, owing to its dianionic nature being attracted to the cationic micellar surface, beside a modicum of hydrophobic association. Addition of Cu^{2+} causes fluorescence switching off, as seen with 4, even though the cationic micelle surface would somewhat hinder the approach of the target.

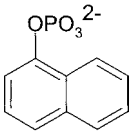

5

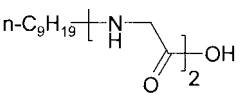

6

The study with 5, 6, and CTAB expose two advantages of general significance. Assembling rather than synthesizing a fluorescent sensor can be a big convenience, especially if the components can be obtained "off-the-shelf." Furthermore, 5, 6, and CTAB can be replaced by other pretenders and evaluated for their degrees of success as judged by the efficiency of fluorescence switching off in the presence of Cu^{2+}. However, self-assembled fluorescent sensors of this type have an Achilles' heel: they are not robust enough to be used within multi-compartmental environments. because each component may localize in a different environment.

A Fluorescent Sensor for Ca^{2+}

It is rare to have an opportunity to report on the birth of a revolution, but this is one such time. Tsien's 7,[32] though

not the first.''' supplied the molecular spy to enlighten physiologists about the Ca^{2+} *traffic within* living *cells.''' Prior to this, spying for ions within living cells was regarded as a hazardous occupation.* ''How *does the spy observe its target* amidst *a jungle of chemical species?''* was *the frequently asked question. In the case of* Ca^{2+}, *the spy* must look *for* 10^{-7} M concentrations *of its target,* while H^+ *lurks at* 10^{-7} *M.* Mg^{2+} *at* 10^{-3} M, Na^+ *at* 10^{-3} *M.* K^+ *at* 10^{-1} M, *and a myriad of others. Excellent selectivity of* Ca^{2+} *reception* is *called for. The receptor part of 7 discriminates against the monovalent cations as well as anions by* flaunting its *tetra-anionic cavity. It discriminates against* Mg^{2+} *by exploiting the spacious cavity.*

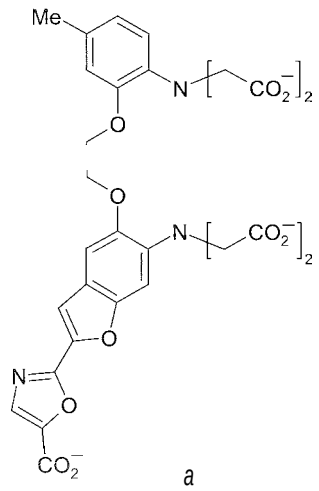

a

Being nonmodular, 7 *does not* employ *a popular* fluorophore. Rather, *the n-electron system of one of the* 1-amino-2-alkoxy *benzene moieties was extended by fusion with a* furan *ring and by further addition of an oxazole ring. This* extended *n-electron* system *is adequate for the* purpose at *hand, though the excitation wavelengths are short.* An example *is* 7, *showing an* ICT *excited state. Upon optical excitation. the* electron *density shifts away* from the *tertiary amino group toward the* furan *and oxazole heterocycles. The resulting* δ^+ *charge on the tertiary amino region will naturally suffer destabilization* upon *entry of* Ca^{2+} *into the cavity. So. a blue shift of the* emission *and excitation spectra of 7 would be the simple prediction.* In *practice;* the Ca^{2+}-induced *emission shift is nullified in 7 and* many *(but* not *all) of its relatives because of* Ca^{2+} *decoordination. The latter is a natural* consequence *of the* Ca^{2+} *being placed near the* δ^+ *charged tertiary amino group.* However, the *excitation shift is clearly observed. and the revolutionary is born.*

Suddenly. the life processes of the cell as reflected by the Ca^{2+} *traffic are visualized in every square micrometer and at every millisecond. Not surprisingly. bioresearchers have* taken *to the general approach in their thousands. As evidence, we offer a statistic:* Ref. [32] *was cited in over* 13.000 *publications at the time of writing.*

CONCLUSION

The previous discussion indicated how adequately *selective receptors for a given target species can be developed into typically* useful *fluorescent sensors. PET, EET, and* ICT *are the photochemical mechanisms underlying the sensing behavior. The road* immediately *ahead is likely to yield a broadening of the target set that* can *be practically sensed.* Sensor *families where each member goes after a given range of target concentrations are also set to emerge. Mechanistic consolidation of PET, EET,* and ICT *types can also be expected, though other designs''' will gather momentum.* Sensory *data transmission* from *specific* microenvironments *even below the* limit *of visual resolution will be encountered.* In *fact, the forerunners of this class are already with us. Small spaces adjoining detergent* micelle *surfaces and resin beads are the focus of* H^+-selective *fluorescent* PET *sensors 8 and 9, respectively. Our 8 is just one member of* a family *that maps the* H^+ *distribution* in *the Gouy–Chapman region bounded by the membrane with electric* and *dielectric* influences.[34] Copeland *and Miller's 9, when covalently linked to the* polymer *substrate, serves to signal local* H^+ *generation if a coresident on the bead serves as a catalyst for an* acid-*forming reaction.''''* It *seems that fluorescent sensors are heading for many problem areas looking for molecular or* supramolecular *solutions—and to a rosy future.*

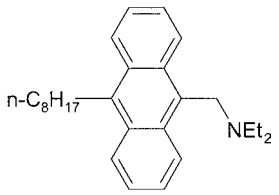

8

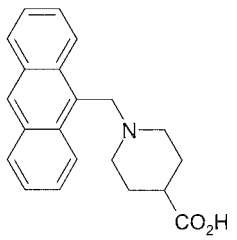

9

ACKNOWLEDGMENTS

We thank the Department of Employment and Learning, Northern Ireland. for support of our efforts in this area.

ARTICLES OF FURTHER INTEREST

Crown Ethers, p. 326
Electrochemical Sensors, p. 505
Energy and Electron Transfer in Supramolecular Systems, p. 535
Fluorescence Sensing of Anions. p. 566
Imaging and Targeting, p. 687
Ion-Selective Electrodes, p. 747
Ionophores, p. 760
Lariat Ethers, p. 782
Luminescent Materials. p. 816
Luminescent Probes, p. 821
Molecular-Level Machines, p. 931
Photophysical and Photochemical Methods, p. 1060
Semiochemistry, p. 1270
Supramolecular Photochemistry, p. 1434

REFERENCES

1. Bryan. A.J.; de Silva, A.P.: de Silva. S.A.; Rupasiiighe. R.A.D.D.: Sandanayake. K.R.A.S. Photoinduced electron transfer as a general design logic for fluorescent molecular sensors for cations. Biosensors 1989. 4, 169–179.
2. de Silva, A.P.: Gunaratne, H.Q.N.: Cunnlaugsson, T.: Huxley, A.J.M.; McCoy. C.P.: Rademacher, J.T.: Rice, T.E. Signaling recognition events with fluorescent sensors and switches. Chem. Rev. 1997. 97. 1515–1566.
3. *Fluorescent Chemosensors of* Ion *and Molecule Recognition*; Czarnik. A.W.. Ed.: ACS Symp. Ser., American Chemical Society: Washington. DC, 1993: Vol. 538.
4. *Chemosensors of Ion and* Molecule Recognition: Czarnik, A.W., Desvergne, J.-P., Eds.: Kluwer: Dordrecht. 1997.
5. Valeur. B. *Molecular* Fluorescence: Wiley-VCH: Weinheim. 2001.
6. *Luminescent Sensors*: Fabbrizzi. L.. Ed.: Coord. Chein. Rev.. 2000: Vol. 205, 1–228.
7. Bargossi, C.: Fiorini. M.C.: Montalti. M.: Prodi. L.: Zaccheroni, N. Recent developments in transition metal ion detection by luminescent chemosensors. Coord. Chem. Rev. 2000. 208. 17–32.
8. James. T.D.: Sandanayake. K.R.A.S.; Shinkai. S. Saccharide sensing with molecular receptors based on boronic acid. Angew. Chem., Int. Ed. Engl. 1996. *35*. 1911–1922.
9. Rurack, K. Flipping the light switch 'ON'—The design of sensor molecules that show cation-induced fluorescence enhancement with heavy and transition metal ions. Spectrochim. Acta, Part A: Mol. Biomol. Spectrosc. 2001. *57*. 2161–2195.
10. Bissell, R.A.; de Silva. A.P.; Cunaratne. H.Q.N.; Lynch, P.L.N.; Maguire, G.E.M.: Sandanayake. K.R.A.S. Molecular fluorescent signalling with ''fluor-spacer-receptor'' systeins—Approaches to sensing and switches devices via supramolecular photophysics. Chem. Soc. Rev. 1992. *21*, 187–195.
11. Kirkbright. G. Fluorescent Indicators. In *Indicators*; Bishop. E.. Ed.: Pergainon Press. 1972: 685–708.
12. Tsien. R.Y. Intracellular signal transduction in 4 dimensions—From molecular design to physiology. Am. J. Physiol. 1992. *263*. C723–C728.
13. Kavarnos. G.J. *Fundamentals* of Photoinduced *Electron Transfer*; VCH: Weinheim. 1993.
14. *Electron Transfer in Chemistry*; Balzani, V.. Ed.; Wiley-VCH: Weinheim, 2000.
15. Speiser. S. Photophysics and mechanisms of intramolecular electronic energy transfer in bichromophoric molecular systems: Solution and supersonic jet studies. Chem. Rev. 1996. 96. 1953–1976.
16. Grandini, P.: Mancin. F.: Tecilla, P.: Scriniin. P.: Tonellato, U. Exploiting the self-assembly strategy for the design of selective Cu-II ion chemosensors. Angew. Chem., Int. Ed. 1999, *38*. 3061–3064.
17. Wiskur, S.L.; Ait-Haddou. H.; Lavigne, J.J.; Anslyn. E.V. Teaching old indicators new tricks. Acc. Chem. Res. 2001. 34. 963–972.
18. See OPTI-CCA® and OPTI-R® under http://www.roche.com/diagnostics/products/prodlist.html (accessed February 2002).
19. Leiner. M.J.P.: He, H.: Boila-Gockel. A. Method of Determining an Alkali Ion. 2000, USP 5,952,491.
20. Izatt, R.M.; Pawlak. K.: Bradshaw. J.S.; Bruening, R.L. Thermodynamic and kinetic data for macrocycle interaction with cations, anions and neutral molecules. Chem. Rev. 1995. 95. 2529–2586.
21. Lehn. J.-M. *Supramolecular Chemistry*; VCH: Weinheim. 1995.
22. Balzani. V.: Scandola. F. *Supramolecular Photochemistry*; Ellis-Horwood: Chichester. 1991.
23. Minta, A.: Tsien. R.Y. Fluorescent indicators for cytosolic sodium. J. Biol. Chem. 1989, 264, 19449–19457.
24. de Silva, A.P.: Gunaratne, H.Q.N.; Gunnlaugsson, T.; Nieuwenhuizen, M. Fluorescent switches with high selectivity towards sodium ions: Correlation of ion-induced conformation switching with fluorescence function. Chem. Commun. 1996. 1967–1968.
25. de Silva. A.P.: Gunaratne, H.Q.N.: Habibjiwan. J.L.: McCoy, C.P.: Rice, T.E.; Soumillion. J.P. New fluorescent model compounds for the study of photoinduced electron transfer—The influence of a molecular electric field in the excited state. Angew. Chem., Int. Ed. Engl. 1995. 34. 1728–1731.
26. Neilands. J.B. Microbial iron compounds. Ann. Rev. Biochem. 1981. *50*. 715–731.

27. Hamilton. A.D. Fluorescent Sensing of Anions. In *Encyclopedia* of *Supramolecular Chemistry*; Atwood, J.L., Steed. J.W., Eds.: Dekker, 2002.
28. Nudelman. R.; Ardon, O.; Hadar, Y.; Chen. Y.N.: Libman, J.: Shanzer, A. Modular fluorescent-labeled siderophore analogues. J. Med. Chem. **1998,** *41,* 1671–1678.
29. Jedner, S.B.: James. R.: Perutz, R.N.; Duhme-Klair, A.K. Selective signalling of molybdate by a siderophore derivative. J. Chem. Soc., Dalton Trans. **2001**, 2327–2329.
30. Bhattacharya, S.; Thomas, M. Synthesis of a novel thiazole based dipeptide chemosensor for Cu(II) in water. Tetrahedron Lett. 2000, *41*. 10313–10317.
31. Prodi, L.: Montalti, M.; Zaccheroni, N.; Dallavalle, F.; Folesani, G.; Lanfranchi, M.; Corradini, R.; Pagliari, S.; Marchelli. R. Dansylated polyamines as fluorescent sensors for metal ions. Photophysical properties and stability of copper(II) complexes in solution. Helv. Chim. Acta **2001**, *84*. 690–706.
32. Grynkiewicz, G.; Poenie, M.: Tsien, R.Y. A new generation of Ca^{2+} indicators with greatly improved fluorescence properties. J. Biol. Chem. **1985.** *260*, 3440–3450.
33. Tsien, R.Y. New calcium indicators and buffers with high selectivity against magnesium and protons: Design, synthesis. and properties of prototype structures. Biochemistry **1980.** 19, 2396–2404.
34. Bissell. R.A.; Bryan. A.J.: de Silva, A.P.; McCoy, C.P. Fluorescent PET (photoinduced electron-transfer) sensors with targeting/anchoring modules as molecular versions of submarine periscopes for mapping membrane-bounded protons. J. Chem. Soc., Chem. Commun. **1994,** 405–407.
35. Copeland, G.T.; Miller. S.J. A chemosensor-based approach to catalyst discovery in solution and on solid support. J. Am. Chem. Soc. **1999,** *121*. 4306–4307.

Fullerenes as Encapsulating Hosts: Preparation, Detection, and Structures of Endohedral Fullerenes

Alan L. Balch
University of California, Davis, California, U.S.A.

INTRODUCTION

The prototypical fullerene, C_{60} consists of a closed icosahedral cage of 60 carbon atoms that enclose a small void space. and it is natural to expect that atoms may be trapped within this space. Indeed, shortly after C_{60} was discovered, Kroto, Smalley. and coworkers reported the detection of La@C_{60} by mass spectrometry and proposed a structure in which the lanthanum atom resided inside the fullerene cage.[1] Fullerene cages with varying numbers of carbon atoms are known, with the empty cages C_{60}, C_{70}, C_{76}, C_{78}, and C_{84} particularly abundant in normal fullerene preparations. Consequently, it is expected that there will be a variety of cage sizes available as intriguing hosts for the encapsulation of a variety of individual atoms or collections of atoms. Moreover. if the atom entrapment occurs during fullerene formation, the trapping procedure can produce new fullerene cages that are not generally found in conventional empty-cage fullerene preparations. Throughout this article, we will use the symbol A@C_n to indicate that an atom of element A is encapsulated within a cage of n carbon atoms to form a particular endohedral fullerene. In the alternative, but less widely adopted IUPAC nomenclature, one would use the symbol iAC_n for the same species.

What atoms are found within fullerene cages? Shown in Fig. 1 is a periodic table that highlights the atoms found in some type of fullerene cage. Moreover, endohedrals with two, three, and four atoms (not necessarily all of one kind) were detected. As seen in Fig. I, a wide range of atoms. including unreactive noble gas atoms, highly reactive and rarely encountered atomic nitrogen. electropositive metal atoms including alkali metals, alkaline earth metals, and lanthanide atoms, were found encapsulated in carbon cages. Representative examples include He@C_{60},[2] N@C_{60},[3] La@C_{82},[4] Sc_3N@C_{80},[5] and Sc_2C_2@C_{84}.[6] It is notable that there are few reports of transition metal atoms beyond Sc, Ti, Y. and Lu bound within fullerene cages, and those generally involve single studies that were not replicated in other laboratories.

In the following sections. we will consider in more detail some of the types of atoms and molecules that are found confined within the curved walls of carbon cages of various sizes. In many cases. these species were detected by a combination of spectroscopic methods as minor components in mixtures of fullerenes. Further work on separation and purification produced small quantities of isolated endohedrals.

NOBLE GAS ATOMS AS GUESTS

Noble gas atoms can be physically trapped within fullerene cages of various sizes.[1] An example is shown in Fig. 2. In these species. the interaction between the fullerene and the noble gas atoms largely involves van der Waals forces. How are they made? The conventional arc synthesis of empty cage fullerenes uses an electric arc between two graphite rods to vaporize graphite. This procedure is usually conducted under 0.2 atm of helium. Under these conditions, helium atoms may be trapped inside the fullerene as it is assembled from smaller carbon fragments starting with C_2 units. As a consequence, one atom of ^{3}He is present in every 880,000 molecules of C_{60}, and one atom of the less abundant ^{4}He is found in every 10^{12} C_{60} molecules formed in the conventional arc process. Sensitive mass spectrometric methods were utilized to detect the release of helium from these filled cages.

Enrichment of these endohedral species can be obtained by heating the intact solid fullerene under 3000 atm of a noble gas at 650°C.[2] Under these conditions, helium. neon, argon, krypton, and even xenon can be forced into the cavity within C_{60}. This process is believed to occur via a window mechanism in which a C—C bond of the fullerene breaks to provide a window through which the noble gas atom enters the fullerene. Subsequent reformation of the C—C bond can trap the noble gas atom inside the cage.[1] Recent work on creating orifices in C_{60} through chemical modification produced an interesting model system in which entry and exit of both He and H_2 can be monitored, as shown in Fig. 3.[7]

Because ^{3}He has a spin of 1/2 and a high gyromagnetic ratio, ^{3}He-NMR spectroscopy of fullerenes and chemically modified fullerenes containing helium atoms produces useful information in regard to the electronic and

Encyclopedia of Supramolecular Chemistry
DOI: 10.1081/E-ESMC 120012745

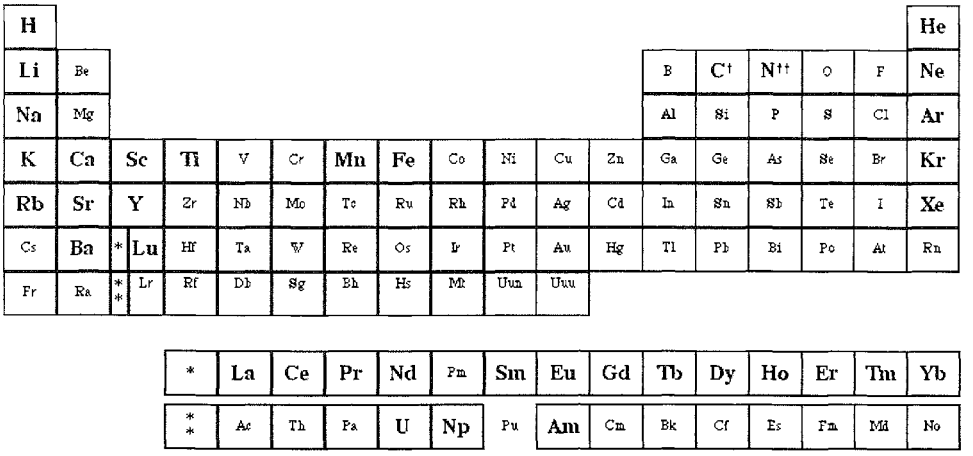

† only with metals, *i.e.* $Sc_2C_2@C_{84}$.
†† alone and with metals.

Fig. 1 The periodic table, with those atoms that were reported to be trapped within fullerene shown in boldface.

geometric structures of these molecules.[8] For example. the spectrum of $^3He@C_{60}$ consists of a single line with a chemical shift of −4.4 ppm (relative to dissolved ^3He at 0 ppm), while the spectrum of $^3He@C_{70}$ shows a single resonance at −28.8 ppm. The chemical shift of the ^3He nucleus monitors the magnetic field experienced by the ^3He atom within the fullerene and is a sensitive indicator of that environment. The large difference in chemical shift between $^3He@C_{60}$ and $^3He@C_{70}$ was ascribed to differences in the aromatic ring currents within these different cages. Thus, C_{70} shows a much larger diamagnetic ring current and has a greater aromatic character. Demonstrated in Fig. 4 is how useful ^3He-NMR spectroscopy can be in detecting individual species in a mixture of higher fullerenes.[9] Resonances of different isomers with varying cage geometries for C_{76}, C_{78}, and C_{84} are clearly differentiated.

However. the purification of endohedrals containing noble gases is challenging. Generally, only minute quantities of purified endohedrals like $Kr@C_{60}$ were separated. and this separation was accomplished only after using tedious sequential high-pressure liquid-chromatographic steps. Nevertheless, a sample containing 9% $Kr@C_{60}$ and 91% C_{60} is sufficiently enriched to allow the structure of this endohedral to be obtained by single-crystal x-ray diffraction.[10] The structure is shown in Fig. 2. In $Kr@C_{60}$, the krypton atom is found at the center of the fullerene cage. and the average Kr to C separation is 3.540 Å.[3] For comparison, the sum of the van der Waals radii for carbon (1.70 Å) and ksypton (2.02 Å) is 3.72 Å, so the krypton atom is tightly confined within the C_{60} cage. However, at the level of crystallographic refinement. the dimensions of the C_{60} cage are not significantly altered by the presence of the entrapped ksypton atom.

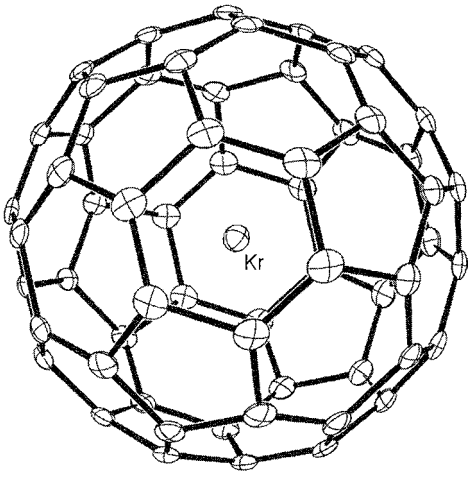

Fig. 2 The structure of $Kr@C_{60}$ as determined from a single-crystal x-ray diffraction study of $(0.09\ Kr@C_{60}/0.91\ C_{60})\cdot Ni^{II}$(octaethylporphyrin)·2 (benzene) from data in Ref. [10].

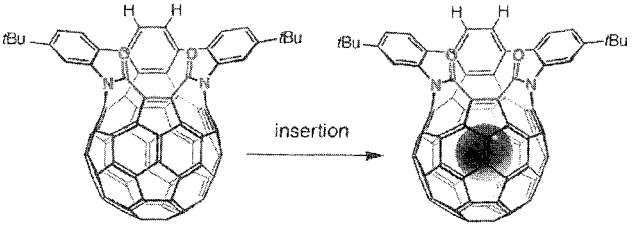

Fig. 3 Insertion of atomic helium into a chemically modified C_{60} molecule in which an orifice was engineered (see Ref. [7]).

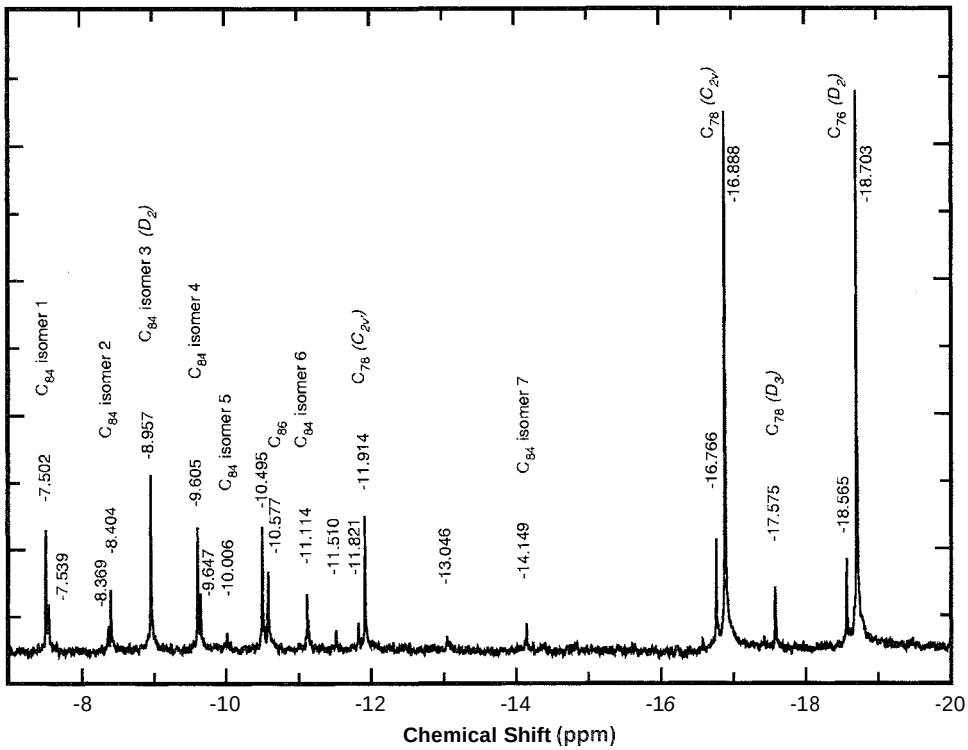

Fig. 4 The ^{3}He-NMR spectrum of a mixture of isomers of the higher fullerenes C_{78} and C_{84}, which shows the ability to resolve resonances of individual molecules. From Ref. [9], with permission.

ATOMIC NITROGEN AND MOLECULAR N_2 WITHIN C_{60}

Bombardment of C_{60} with nitrogen ions from a plasma discharge source or sublimation of C_{60} in a nitrogen glow discharge produces a mixture of neutral $N@C_{60}$ and empty C_{60}.[3,11] The presence of $N@C_{60}$ can be readily detected by electron spin resonance (ESR) spectroscopy, which shows an isotropic three-line spectrum for ^{14}N (with a weaker doublet due to lower abundant ^{15}N) that is characteristic of a paramagnetic nitrogen atom with three unpaired electrons (i.e., $S=3/2$). The ESR spectrum of $N@C_{60}$ strongly resembles that of the free nitrogen atom. However, unlike atomic nitrogen, $N@C_{60}$ is stable in the atmosphere. Samples containing $N@C_{60}$ can be dissolved in toluene and handled as any other stable endohedral species. In $N@C_{60}$, the three nitrogen p orbitals are degenerate, but chemical modification of the icosahedral C_{60} cage should destroy the degeneracy of these nitrogen p orbitals. Consequently, the series of adducts $N@C_{60}\{C(COOEt)_2\}_n$, with varying numbers (n) of cycloprophyl groups on the exterior of the fullerene cage. show additional features in their ESR spectra that reflect the different symmetries of each abduct.[9,11] These studies clearly demonstrate that the inside of the fullerene cage is chemically unreactive, unlike the outside of the cage, which readily undergoes a variety of addition reactions.

Not only can individual nitrogen atoms be trapped within C_{60}, but also N_2 (as well as CO) molecules were inserted into C_{60} cages.[13] The methodology for this follows the techniques for inserting the noble gases—heating the fullerene to 650°C under 3500 atm of N_2. Again, the ratio of empty to filled cages (200011) in the product is high, but the presence of $N_2@C_{60}$ can clearly be detected by mass spectrometry.

ELECTROPOSITIVE METAL IONS IN FULLERENES

Macroscopic amounts of a metallofullerene, $La@C_{82}$, were first obtained by the Rice group in 1991 through laser vaporization of a composite of La_2O_3 and graphite.[4] Although $La@C_{60}$, $La@C_{70}$, and $La@C_{82}$ were detected in the sublimed product of the reaction. only $La@C_{82}$ could be extracted into toluene and purified. The presence of $La@C_{82}$ is readily detected by ESR spectroscopy, and the observed hyperfine splittings were interpreted to indicated that the encapsulate metal is present as La^{3+}.[14] Consequently, the fullerene cage must bear a 3− charge, which is consistent with the observations that fullerenes

can readily accept electrons through a series of stepwise one-electron reductions. Many other metal-containing fullerenes were prepared through the laser vaporization of graphite in the presence of a metal salt or the conventional arc synthesis, in which graphite rods doped with metal oxides are vaporized in a low-pressure helium atmosphere. The resulting endohedrals can be detected by mass spectrometry in the soot that is generated, sublimed for an initial stage of purification, extracted into organic solvents, and purified by chromatographic techniques. In the process. fullerenes of various sizes can be produced. The components present can control the types of fullerene cages formed. For example, laser vaporization of a graphite-UO_2 composite rod produces the small cluster $U@C_{28}$, in which a uranium atom stabilizes a C_{28} cage with tetrahedral symmetry.[15] The mechanism of formation of these endohedral fullerenes received relatively little attention, but polycyclic polyene rings with metal atoms appended were detected during the gas-phase self-assembly of endohedrals.[16] Several reviews cover the progress made in the isolation and in the rudimentary characterization of these endohedrals.[17–19]

In order to illustrate the progress in separation and structural identification of endohedral metallofullerenes, we will focus our discussion on one such molecule, Isomer 1 of $Er_2@C_{82}$.[20,21] Three isomers of $Er_2@C_{82}$ were separated through high-pressure liquid chromatography and characterized by their chromatographic retention time, mass spectrometry, and UV/Vis spectroscopy. Isomer I has the shortest retention time. In characterizing the structure of such an endohedral, there are two main issues: the specific geometry of the fullerene cage and the locations of the metal atoms within that specific cage. Generally, empty-cage fullerenes obey the isolated pentagon rule (IPR), which requires that each pentagon be surrounded by five hexagons.[1,22] For the C_{82} cage, there are nine isomeric forms (three different C_2 isomers, three C_S isomers, two C_{3v} isomers, and one C_{2v} isomer) that obey the IPR. Small amounts of the empty-cage C_{82} were isolated and purified. Analysis of the ^{13}C-NMR spectrum of a mixture of these isomers reveals that the dominant isomer present has C_2 symmetry, while two other fullerenes are present in minor amounts.[23] Theoretical calculations indicate that the stability of the C_{82} cage isomers depends markedly upon the negative charge that resides on the cage,[24] and that there is no requirement for the endohedral coinplexes involving C_{82} cages to have the same symmetry as those of the empty cages.

The structure of Isomer 1 of $Er_2@C_{82}$ was identified through a low-temperature (113 K), single-crystal x-ray diffraction study of a crystalline complex [$Er_2@C_{82}$ Isomer $1 \cdot Co^{II}(OEP) \cdot 1.5$ (benzene). 0.3 (chloroform)], in which the endohedral was cocrystallized with cobalt-(II)octaethylporphyrin.[25] The structure of the endohedral is shown in Fig. 5. In Fig. 5A, a drawing of the C_{82} cage is shown, which is one of the three C_s isomers (82:6) that obey the isolated pentagon rule. In Parts B and C of Fig. 5, the entire endohedral from two different perspectives is shown. The two erbium atoms are disordered and distributed over 23 different sites, with fractional site occupancies ranging from 0.35–0.01. These erbium sites reside near the walls of the fullerene. with the closest Er–C distances in the 3.3–3.4 A range. Moreover, the erbium sites cluster near a band of 10 contiguous hexagons that encircle the carbon cage. This band is highlighted in Parts A and B of Fig. 5 by the use of solid lines to connect the carbon atoms within that band. Each of the two other isomers of C_{82} [C_{3v}(82:8) and C_{2v}(82:9)] has a similar band of 10 contiguous hexagons, and it was speculated that the other two known isomers of $Er_2@C_{82}$ involve these C_{82} isomers with their analogous bands of 10 hexagons.

HETERONUCLEAR ASSEMBLIES WITHIN FULLERENES, $Sc_3N@C_{80}$ AND RELATED MOLECULES

Conducting the normal Kratschmer–Muffman arc fullerene preparation, with graphite rods doped with Sc_2O_3 in a dynamic atmosphere that contains dinitrogen in addition

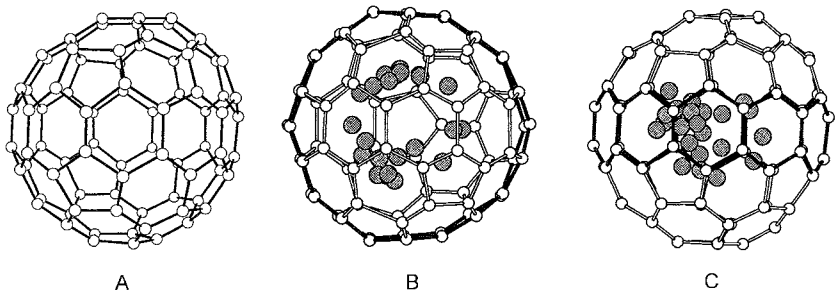

Fig. 5 The structure of Isomer 1 of $Er_2@C_{82}$ as determined from a single-crystal x-ray diffraction study of $Er_2@C_{82}$ Isomer $1 \cdot Co^{II}(OEP) \cdot 1.5$ $(C_6H_6) \cdot 0.3$ $(CHCl_3)$ from data in Ref. [25]. (A) The C_{82} cage alone. (B,C) The endohedral from two different perspectives showing the *23* fractionally occupied Ersil.

to helium, results in enhanced production of a new family of endohedral fullerenes: $Sc_3N@C_{80}$, $Sc_3N@C_{78}$,[26] and the novel $Sc_3N@C_{68}$[27] (with relative yields of 8:1:1). The fullerene cages in $Sc_3N@C_{68}$ [and in Sc_3C_{66}[28]] must violate the isolated pentagon rule, because there are no cages that can obey the IPR for C_{62}, C_{64}, C_{66}, or C_{68}. Significantly, $Sc_3N@C_{80}$ is more abundant than C_{84} (the third most abundant of the empty cage fullerenes after C_{60} and C_{70}). These endohedrals, which contain the planar tetraatomic Sc_3N unit within variously sized carbon cages, were isolated via three stages of high-pressure liquid chromatography. The structures of $Sc_3N@C_{80}$ and $Sc_3N@C_{78}$ as determined by low-temperature x-ray diffraction are shown in Fig. 6. The $Sc_3N@C_{80}$ consists of a C_{80} cage with icosahedral symmetry that encloses the planar Sc_3N unit.[5,27] Because the ^{13}C-NMR spectrum of $Sc_3N@C_{80}$ at 25°C consists of only two lines (as required by the I_h symmetry of the cage only, the Sc_3N unit must be freely moving inside the carbon cage.[5] The $Sc_3N@C_{78}$ consists of a C_{78} cage with D_{3h} symmetry, with the planar Sc_3N unit located in the horizontal mirror plane.[26]

The isolation of milligram quantities of pure $Sc_3N@C_{80}$ allowed its chemical reactivity to be explored. The icosahedral C_{80} cage of $Sc_3N@C_{80}$ lacks the usual sites (6:6 ring junctions between two pentagons) for addition reactions that are found to occur in all other fullerenes investigated so far, and hence, its reactivity will follow new patterns. Thus, it is significant that the first addition product involves a Diels–Alder reaction at a 5:6 ring junction.[30] The structure of the product $Sc_3N@C_{80}$-$C_{10}H_{12}O_2$ shown in Fig. 5 reveals that the scandium atoms are not near the site of addition, and that the Sc_3N portion retains its planar structure.[31]

The recent identification of $(Sc_2C_2)@C_{84}$, which was originally thought to be $Sc_2@C_{86}$, presents another example of a fullerene that encapsulates a combination of metal and main group atoms.[6] In this case: an acetylenic C_2 unit is believed to have two scandium

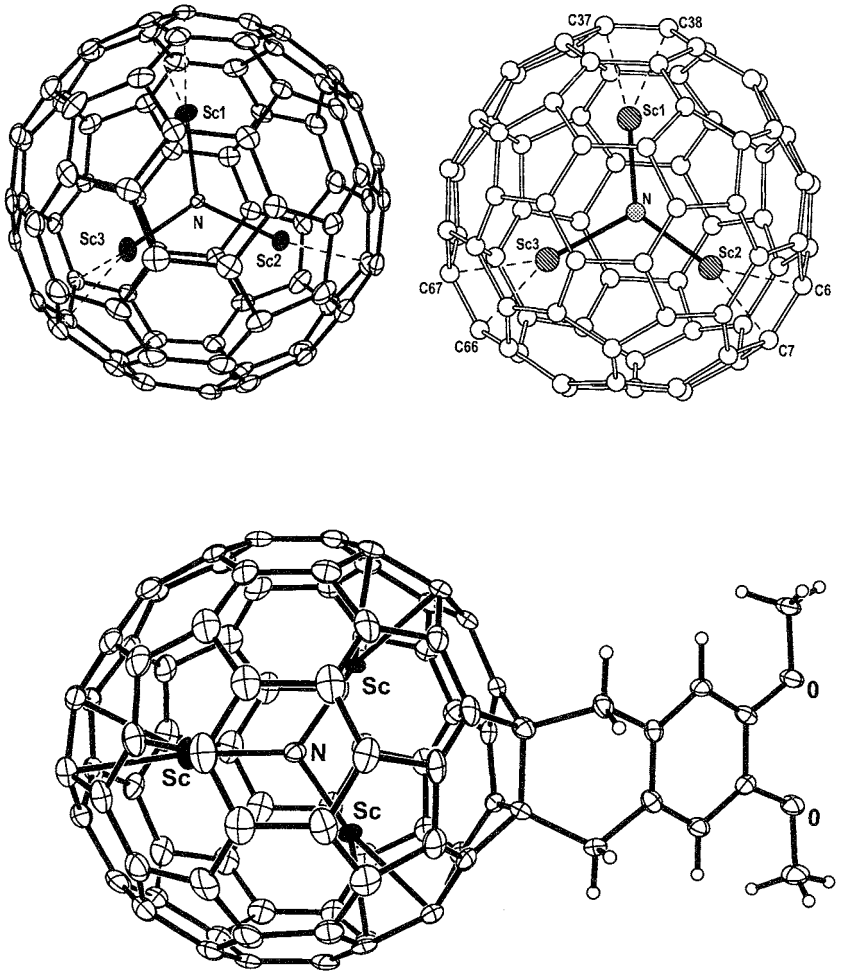

Fig. 6 The structures of $Sc_3N@C_{80}$ [in crystalline $Sc_3N@C_{80}\cdot 5(o\text{-xylene})$, Ref. [29]], $Sc_3N@C_{78}$ [in crystalline $Sc_3N@C_{78}\cdot Co(OEP)\cdot 1.5\ (C_6H_6)\cdot 0.3\ (CHCl_3)$, Ref. [26]], and the Diels–Alder cycloadduct $Sc_3N@C_{80}$-$C_{10}H_{12}O_2$ (Ref. [30]), as determined from single-crystal x-ray diffraction studies.

atoms located perpendicular to the C—C portion, which is then surrounded by a C_{84} cage. Further examples of fullerene cages containing complex combinations of electropositive metals and main group elements are likely to be created.

CONCLUSION

As seen in Fig. 1, fullerenes can encapsulate a variety of atoms from different parts of the periodic table. One to four atoms can be accommodated in cages of varying sizes. The interior face of the fullerene cage is remarkably inert toward the very reactive nitrogen atom, but the carbon cage can accept electrons when an electropositive metal atom is encapsulated. To date, most research focused on the preparation, identification, and characterization of these unusual molecules. However, applications for these novel molecular containers (which have low toxicity due to the inert carbon cages) are anticipated, including radioisotope delivery for imaging and diagnostic and therapeutic radiochemistry.[32] For example, recent work showed that polyhydroxylation of $Gd@C_{82}$ produces Gd-fullerenol that has an exceptionally high relaxivity and acts as an effective MRI (magnetic resonance imagining) contrast agent.[33]

ACKNOWLEDGMENTS

Research on endohedrals at the University of California, Davis, has been supported by the National Science Foundation (Grant CHE 0070291 to ALB). I thank Dr. Hon Man Lee for help in preparing Figs. 2, 5. and 6, Professor Y. Rubin for Fig. 3, and Professor R. J. Cross, Jr. for Fig. 4.

ARTICLES OF FURTHER INTEREST

Complexation of Fullerenes, p. 302
Molecular Squares, Boxes, *and Cubes,* p. 909
Platonic and Archimedean Solids, p. 1100
X-Ray Crystallography, p. *1586*

REFERENCES

1. Heath, J.R.; O'Brien, S.C.; Zhang, Q.; Liu. Y.; Curl. R.F.: Kroto. H.W.: Tittel. F.K.; Smalley. R.E. Lanthanum complexes of spheroidal carbon shells. J. Am. Chem. Soc. 1985. *107* (25). 7779–7780.
2. Saunders, M.; Cross, R.J.; Jiménez-Vázquez, A.: Shimshi, R.; Khong, A. Noble gas atoms inside fullerenes. Science 1996, 271 (5256). 1693–1697.
3. Murphy, T.A.; Pawlik. T.; Weidinger; A.; Hohne, M.; Alcala. R.: Spaeth, J.-M. Observation of atomlike nitrogen-implanted solid C_{60}. Phys, Rev. Lett. 1996, *77* (6), 1075–1078.
4. Chai. Y.; Guo, T.: Jin, C.: Haufler. R.E.: Felipe Chibante, L.P.: Fure. J.: Wang, L.; Alford, J.M.: Smalley, R.E. Fullerenes with metals inside. J. Phys. Chem. 1991, *95* (20), 7564–7568.
5. Stevenson. S.: Rice, G.; Glass, T.; Harich, K.: Cromer, F.; Jordan, M.R.: Craft, J.: Hadju, E.; Bible. R.; Olmstead, M.M.; Maitra, K.; Fisher. A.J.; Balch. A.L.; Dom. H.C. Small-bandgap endohedral metallofullerenes in high yield and purity. Nature 1999. 401 (6748), 55–57.
6. Wang, C.-R.; Kai. T.; Tomiyama, T.; Yoshida, T.: Kobayashi, Y.; Nishibori. E.; Takata, M.; Sakata, M.; Shinohara. H. A scandium carbide endohedral metallofullerene. $(Sc_2C_2)@C_{84}$. Angew. Chem. Int. Ed. 2001.40 (2), 397–399.
7. Rubin. Y.; Jarosson. T.: Wang. G.-W.; Bartberger. M.D.; Houk, K.N.: Schick. G.: Saunders. M.; Cross, R.J. Insertion of helium and molecular hydrogen through the orifice of an open fullerene. Angew. Chem. Int. Ed. **2001**, 40 (8). 1543–1546.
8. Saunders, M.; Jiménez-Vázquez, H.A.: Cross, R.J.; Mroczkowski, S.; Freedberg, D.I.; Anet. F.A.L. Probing the interior of fullerenes by ^{3}HE NMR spectroscopy of endohedral $^3He@C_{60}$ and $^3He@C_{70}$. Nature 1994, *367* (6460), 256–258.
9. Wang. G.-W.; Saunders, M.: Jiménez-Vázquez, H.A.; Khong, A.; Cross, R.J. A new method for separating the isomeric C_{84} fullerenes. J. Am. Chem. Soc. 2000. 122 (13). 3216–3217.
10. Lee, H.M.; Olmstead, M.M.: Suetsuna, T.: Shimotani. H.; Dragoe, N.: Cross. R.J.: Kitazawa, K.; Balch, A.L. Crystallographic characterization of $Kr@C_{60}$ in $(0.09Kr@C_{60}/0.91C_{60})\cdot Ni^{II}(OEP)\cdot 2C_6H_6$. Chem. Commun. **2002**, 1352–1353.
11. Pietzak. B.; Waiblinger M.: Murphy, T.A.: Weidinger. A.; Hohne. M.; Dietel, E.; Hirsch. A. Buckminsterfullerene C_{60}: A chemical Faraday cage for atomic nitrogen. Chem. Phys. Lett. 1997. *279* (5–6). 259–263.
12. Mauser, H.; van Eikema Hommes. N.J.R.: Clark, T.; Hirsch. A.; Pietzak. B.; Weidinger, A.: Dunsch, L. Stabilization of atomic nitrogen inside C_{60}. Angew. Chem., Int. Ed. Engl. **1997**. *36* (24). 2835–2838.
13. Peres. T.; Cao. B.: Cui. W.: Khong. A.: Cross. R.J., Jr.; Saunders, M.; Liffshitz. C. Some new diatomic molecule containing endohedral fullerenes. Int. J. Mass Spectrom. 2001. *210/211*, 241–247.
14. Johnson, R.D.: de Vries. M.S.: Salem. J.: Bethune. D.S.: Uannoni. C.S. Atoms in carbon cages—The structure and properties of endohedral fullerenes. Nature 1993. *366* (6451), 123–128.
15. Guo. T.; Diener, M.D.; Chai, Y.; Alford. M.J.: Haufler. R.E.: McClure, S.M.; Ohno, T.; Weaver. J.H.: Scuseria, G.E.: Smalley, R.E. Uranium stabilization of C_{28}: A

tetravalent fullerene. Science 1992. *257* (5077), 1661–1664.

16. Clemmer. D.E.: Shellmov, K.B.: Jarrold, M.F. Gas-phase self-assembly of endohedral metallofullerenes. Nature 1994, 367 (6465). 718–720.
17. Shinohara. H. Endohedral Metallofullerenes: Production, Separation, and Structural Properties. In *Fullerenes: Chemistry, Physics, and Technology*; Kadish. K.M., Ruoff. R.S.. Eds.; John Wiley & Sons, Inc. 2000; 357–393.
    Nagase, S.; Kobayashi, K.: Akasaka, T.: Wakahara. T. Endohedral Metallofullerenes: Theory. Electrochemistry. and Chemical Reactions. In Fullerenes: *Chemistry, Physics, and Technology*; Kadish. K.M.. Ruoff. R.S., Eds.: John Wiley & Sons, Inc. 2000: 395–436.
19. Shinohara. H. Endohedral metallofullerenes. Rep. Prog. Phys. 2000, *63* (6), 843–892.
20. Dorn. H.C.: Stevenson. S.: Burbank, P.: Sun. Z.: Glass, T.: Harach. K.: van Loosdrecht, P.M.H.; Johnson, R.D.: Beyers. R.: Salem. J.R.; de Vries, M.S.; Yannoni. C.S.; Kiang, C.H.; Bethune. D.S. Endohedral metallofullerenes: Isolation and characterization. Mater. Res. Soc. Symp. Proc. 1995. *359*, 123–135.
    Tagmatarchis, T.: Aslanis. E.: Shinohara, W.: Prassides. K. Isolation and spectroscopic study of a series of mono- and dierbium endohedral C_{82} and C_{84} metallofullerenes. J. Phys. Chem. 2000, *104* (47), 11010–11012.
22. Fowler, P.W.: Manoloupoulos, D.E. *An Atlas* of *Fullerenes*: Oxford Univ. Press: Oxford, 1995: 254.
23. Achiba. Y.: Kikuclii. K.; Aihara. Y.: Wakabayashi. T.; Miyake. Y.: Kainosho, M. Higher fullerenes: Structure and properties. Mater. Res. Soc. Symp. Proc. 1995, *359*, 3–9.
    Kobayashi, K.; Nagase. S. Structures and electronic states of $M@C_{82}$ (M=Sc, Y. La and lanthanides). Chern. Phys. Lett. 1998. *282* (3/4), 325–329.
    Olmstead, M.M.; de Bettencourt-Dias, A.: Stevenson. S.; Dorn, H.C.; Balch. A.L. Crystallographic characterization of the structure of the endohedral fullerene Er@C82 Isomer I with Cs cage symmetry and multiple sites for erbium along a band of ten contiguous hexagons. J. Am. Chem. Soc. 2802. *124* (16). 4172–4173.
26. Olmstead, M.M.; de Bettencourt-Dias. A.; Duchamp. J.C.; Stevenson. S.; Marciu, D.; Dorn. H.C.: Balch. A.L. Isolation and structural characterization of the endohedral fullerene $Sc_3N@C_{78}$. Angew. Chem.. Int. Ed. Engl. 2001. *40* (7), 1223–1225.
27. Stevenson. S.: Fowler. P.W.; Heine, T.: Duchamp, J.C.; Rice, G.: Glass. T.: Harich. K.: Hajdu, E.; Bible. R.: Dorn. H.C. A stable non-classical metallofullerene family. Nature 2000, *408* (6811), 427–428.
28. Wang. C.-R.: Kai, T.: Tomiyania. T.: Yoshida. T.: Kobayashi. Y.: Nishibori, E.: Takata. M.; Sakata. M.: Shinohara. H. C_{66} fullerene encasing a scandium dimer. Nature 2800. *408* (6811), 426–427.
29. Stevenson, S.: Lee. H.M.; Olmstead. M.M.; Balch. A.L. Characterization of $Lu_3N@C_{80}$-5*o*-xylene and comparison with $Sc_3N@C_{80}\cdot 5o$-xylene. Chem. Eur. J. 2002, *8*, 4528–4535.
30. Iezzi, E.B.: Duchamp. J.C.: Harich. K.; Glass. T.; Lee. H.M.: Olmstead, M.M.: Balch. A.L.; Dorn. H.C. A symmetric derivative of the trimetallic nitride endohedral metallofullerene. $Sc_3N@C_{80}$. J. Am. Chem. Soc. 2001, *124* (4), 524–525.
31. Lee, H.M.; Olmstead, M.M.; Iezzi. E.: Duchamp, J.C.; Dorn. H.C.; Balch. A.L. Crystallographic characterization and structural analysis of the first organic fuctionalization product of the endohedral fullerene $Sc_3N@C_{80}$. J. Am. Chem. Soc. 2002, *124* (14). 3494–3495.
32. Wilson. L.J.; Cagle. D.W.: Tharsh, T.P.; Kennel. S.J.: Mirzadeh. S.: Alford. J.M.; Ehrhardt, G.J. Metallofullerene drug design. Coord. Chem. Rev. 1999. *190–192*, 199–207.
33. Mikawa. M.: Kato. H.; Okumura. M.: Narazaki. M.: Kanazawa. Y.: Miwa, N.; Shinohara, H. Paramagnetic water-soluble metallofullerenes having the highest relaxivity for MRI contrast agents. Bioconjug. Chem. 2001, *12* (4), 510–514.

Gels

Jan H. van Esch
Ben L. Feringa
University of Groningen, Groningen, The Netherlands

INTRODUCTION

Everyone knows what a gel is. but from a scientific point of view, the term "gel" encompasses chemically diverse systems. Already in 1926, Jordon Lloyd wrote that ''A gel is easier to recognize then to define,''[1] however, an exact definition of a gel is still a problem. Perhaps the most general definition is given by Flory, who described gels as dilute mixtures of at least two components, in which both components form a separate continuous phase throughout the system.[2] This definition includes not only gels composed of a solid phase and a gas phase (so-called aerogels, in which the solid phase often consists of silicates)[3] but also gels consisting of a solid-like phase and a fluid phase. In most gels, the solid-like phase is the minor component that forms a network structure in the fluid phase. Because of the coexistence of a network structure with a liquid phase, a gel behaves like an elastic solid at low stress values. but above a finite yield stress, they turn into a viscous liquid. This was described by Tanaka as follows: "the solid network structure prevents the fluid from flowing, whereas the fluid prevents the solid from collapsing.''[4]

Gels can be divided into two groups depending on the types of interactions that hold the network structure together. Chemical gels are formed through covalent cross-linking of dilute solutions of polymers or inorganic oxides, and because of the covalent nature of the network, their formation is thermally irreversible.[3] Chemical gels can. nevertheless, have many interesting properties and applications. Smart gels. for example. are hydrogels from cross-linked polymers that can reversibly swell and shrink in response to a physical or chemical stimulus (Fig. 1A), and are of great interest for novel drug delivery systems or artificial muscles.[4] Opposite to the chemical gels are the physical gels.'" In physical gels, the network structure is built up from smaller subunits, which are held together by noncovalent interactions. Many gels formed by polymers, proteins, surfactants. small organic molecules, and even mineral clays, belong to this class. Despite the different natures of their constituents. they all exhibit a characteristic thermally reversible gel–sol phase transition at moderate temperatures. because the strengths of the noncovalent interactions are comparable to the thermal energy (Fig. 1B).

Also, certain low-molecular-weight organic molecules ($M_w \sim 300$–1000 Da) are capable of forming physical gels. Gelation of a solvent by low-molecular-weight organic molecules is the result of self-assembly of the compound into elongated fibers. which then form an entangled network within the solvent (Fig. 1B). In these networks, the fibers consist of infinite arrays of small molecules that are solely held together by noncovalent interactions. The focus of this article will be on gelation phenomena by low-molecular-weight organic molecules, because this is a striking macroscopic manifestation of self-assembly and supramolecular structure formation.

SMALL-MOLECULE GELLING AGENTS

Survey of the Literature

The gelation of liquids by small organic molecules is a phenomena known for a long time, and in 1921. Bradford considered gelation by small organic molecules as a kind of incomplete crystallization.[6] However, until 60 years ago, gel formation was not consistently reported as such, either because the gel state was not recognized or because the gelling agents were named after their main applications, for instance, as lubricants or thickeners. A fine introduction into the older literature was given by Beginn.[7] From 1940 onward. many cases of gel formation by small organic molecules were reported, and these gelaror systems were summarized in reviews by Terech and Weiss and van Esch and Feringa.[8,9]

Unfortunately, even nowadays, searching for literatme on low-molecular-weight gelators among the enormous number of papers on gels, is like searching for "a needle in a haystack." The main reason is that up to now, there were no generally accepted keywords with which to discriminate between the various types of gels or gel-forming substances. Because low-molecular-weight gelators were most frequently used for the gelation of organic solvents, the term "organogel" (as opposed to ''hydrogel") became more popular, but it is not clear whether it denotes the gelling agent or the liquid phase. and it becomes even more confusing when the small-molecule gelling agent is used to turn water into a ''hydrogel.'' Therefore, we propose to use the more accurate term

Encyclopedia of Supramolecular Chemistry
DOT: 10.1081/E-ESMC 120013879

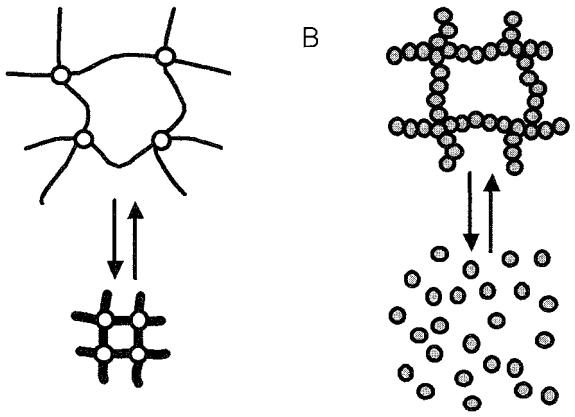

Fig. 1 A change of the environment can cause the reversible shrinking or swelling of a chemical gel, but the network structure remains intact (A). whereas a physical gel can undergo a reversible gel–sol phase transition (B).

"low-molecular-weight gelators" (LMWGs) for future reference.[8,10]

Structural Features of LMWGs

The LMWGs have in common the property that they self-assemble into fibrous aggregates; a process that can be driven by different noncovalent interactions like coulomb interactions, hydrogen bonding, π–π interactions, van der Waals forces, and solvophobic effects. For most of the early examples of LMWGs, the gelation properties were, however, discovered by accident, e.g., during attempts to crystallize the compound, and the diverse structures of the gelator molecules makes it difficult to identify the common structural features responsible for the gelation ability.

In some cases, the gelator structure bears a clear resemblance to surfactants. and one can distinguish a solvophobic part and a solvophilic part. The solvophobic part is prone to aggregate in a particular solvent, but this favorable contribution is opposed by the solvophilic part. Probably the best example is the gelation of aliphatic hydrocarbons or perfluorinated solvents by the perfluoralkane-perhydroalkane block compounds **1** (Fig. 2), which is believed to be caused by the immiscibility of either the perfluorocarbon or perhydrocarbon chains with the solvent.[9,11] In most other cases, specific interactions between (part of) the gelator molecules favor aggregation into fibers. The gelation of aliphatic solvents by the *bis*(alkyloxy)anthracene 2 is, for instance, driven by favorable π–π interactions between the aromatic moieties.[12] The gelation of apolar solvents by surfactant **3** is caused by electrostatic interactions between the ion pairs in the aggregates.[13] Many salts of fatty acids or phosphates were reported as potent gelators for organic solvents, an example being 12-hydroxystearic acid (12-HSA. 4) and especially its lithium salt.[14] For this compound, the clear distinction between the solvophilic and solvophobic part faded, and detailed investigations revealed that hydrogen bonding between the hydroxyl groups and electrostatic interactions between the head groups contribute to the stability of the fibrous aggregates.

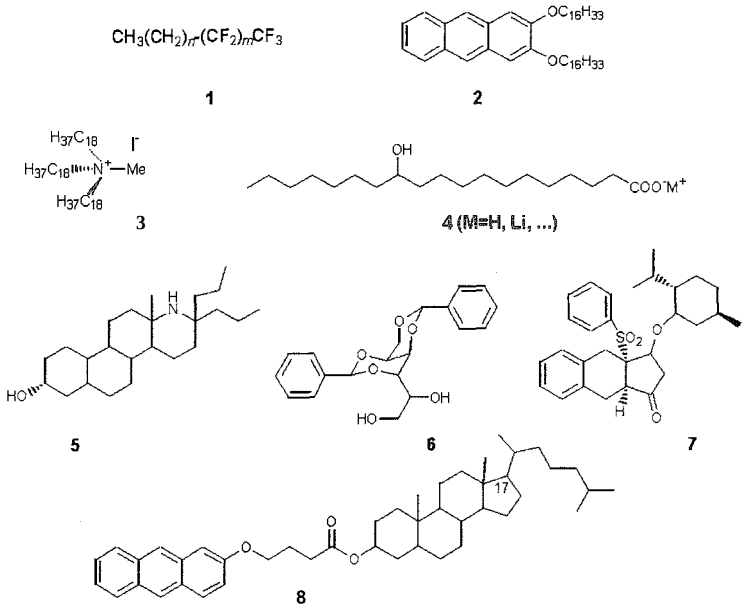

Fig. **2** Examples of well-known gelling agents for organic solvents.

Compounds 5–7 are also potent gelators for organic solvents. but for these compounds, it is less obvious which structural features contribute to their gelation ability. Gelator 5 is an example of a steroid-like compound that is able to gel saturated hydrocarbons.[15] Other steroids were also reported as efficient gelators,[8] and it was suggested that this gelation ability is related to the anisotropic aggregation properties of the rigid steroid skeleton, which is usually associated with their ability to form liquid crystalline mesophases.[16] Other gelators are also built around a rigid skeleton, like dibenzylidene-D-sorbitol (DBS. 6), which was known since 1942 as an efficient gelator,[17] and menthoxyfuranone derivative 7.[18] The broad scope of solvents, ranging from cyclohexane to ethylene glycol, that are gelated by enantiomerically pure DBS suggests that different intermolecular interactions like hydrogen bonding or π–π interactions contribute to its gelation ability, depending on the nature of the solvent.[19] However, racemic 6 does not show gelation ability, and the gelation ability of menthoxyfuranone 7 is susceptible to minor structural changes and stereochemical modifications. This sensitivity of the gelation ability to structural modification. solvent, number, and nature of intermolecular interactions. and stereochemical aspects is a common phenomenon among LMWGs.

In one approach to identify some of the molecular features that favor gelation. Weiss and coworkers systematically varied the structure of anthracene-steroid 8. which is an effective gelator for a large variety of organic solvents (Fig. 2).[20] It was found that some structural modifications are allowed, as long as the rod-like shape of the molecule is preserved, which emphasizes the importance of the inolecular shape. The dibenzoyl cysteine gelators **9a** and related compounds. which are potent gelators for water, represent another interesting case (Fig. 3). Guided by the crystal structure of ditoluoyl cysteine 9b, Menger and coworkers studied the relationship between gelation ability and molecular structure in detail and found that in addition to the capability to form an infinite hydrogen-bonded network, the kinetics of gel fonnation and the solubility are also crucial for gelation ability and stability of the gels.[21]

However, for most other gelators. the supramolecular arrangement in the gel fibers is still not known in detail; and in many cases, the explanation for the presence or absence of gelation ability remains speculative. It should be noted that the above-mentioned examples are only a selection of the many known gelling agents. and for an extensive overview, the reader is referred to the review by Terech and Weiss.[8]

Design of Small-Molecule Gelling Agents

The scientific challenges associated with the gelation phenomena by LMWGs together with the quest for robust gelators with tunable properties or additional functionality considerably stimulated research on organogelators and, in recent years, led to remarkable progress in the design of new LMWGs.

One approach to develop new gelling agents is to make use of one or more structural moieties that are known for their self-assembly or gelation properties, as building blocks (''tectons'')[23] for the construction of new gelators. Inspired by the anthranyl-cholesterol gelators 8, Shinkai and coworkers exploited the cholesterol moiety as a covalently attached tecton to turn peptides, carbohydrates, and even functional units like azobenzenes, crown ethers, and porphyrins into efficient gelators for organic solvents.[24] It was proposed that the cooperative effect of the anisotropic association properties of the cholesterol and the intermolecular interactions provided by the attached functional moiety leads to the gelation ability. because the separate units as single molecules do not display gelation behaviors. The structure of the powerful

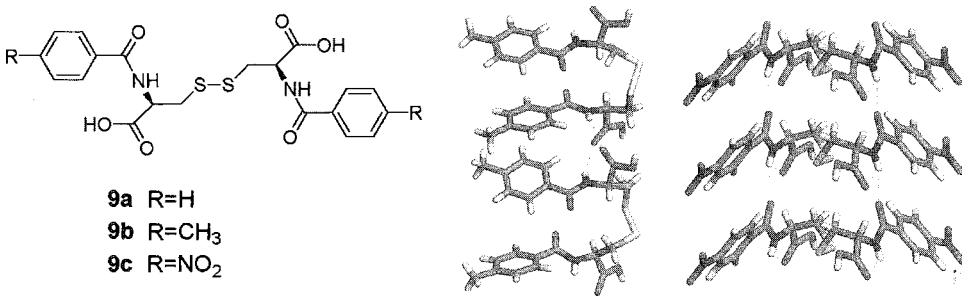

Fig. *3* Dibenzoyl cysteine family of gelators (9) and crystal structures of 9b (middle) and 9c (right). Compound **9a** is an excellent gelator for water, whereas the closely related compounds 9b and 9c form two-dimensional (0-network) and one-dimensional (α-network) arrays of hydrogen bonds, respectively, in the crystalline state. (From Refs. [21,22].) *(View this art in color at www. dekker.com.)*

gelator *dibenzylidene sorbitol clearly inspired Shinkai and coworkers to investigate the gelating properties of a* family *of saccharide gelators,* which *consists of a rigid molecular skeleton, with one or more hydrogen-bonding hydroxyl groups connected to* it.[10] *The well-defined molecular architecture with little conformational freedom and the large library of carbohydrates allowed for the evaluation of* gelation *properties in relation to* molecular *conformation and supramolecular arrangement in the crystal and gel states. The outcome of these studies confirms the presence of strongly anisotropic intermolecular interactions as a prerequisite for* gelation *(vide infra).*

In a different approach, new gelator *molecules were designed, starting from criteria derived from the events and intermolecular interactions that occurred during the* gelation process.[25] *Important guidelines for the design of new gelators that* emerged *from these studies are the presence of strong self-complementary and unidirectional interactions to enforce one-dimensional (1D) self-assembly; the control of fiber-solvent interfacial energy to tune solubility* and *prevent crystallization; and the presence of some factor to induce cross-linking of the fibers and* form *a network.*

Hydrogen-bonding groups appear to offera particularly useful self-assernbly motive *for the rational design of new gelators because of their strength and directionality. One of the earliest* examples *is the two-component system consisting of triaminopyrimidine- and barbituric acid derivatives. which self-assembles into linear tapes, whereas crystallization is prevented by the presence of the aliphatic side chains (Fig.* 4).[26] *The apparent preference for ID tape formation is sensitive to interactions between the substituents at the triaminopyrimidine and barbituric acid molecules. and slight changes in the nature of the substituents can shift the preference from* 1D *tapes to the formation of cyclic hexameric* assemblies.[27] *The problem of polymorphic self-assembled structures is not directly apparent with cyclic dipeptides and his-urea-based gelators, because in both types of compounds. all of the hydrogen-bonding groups are directed along a single molecular axis (Fig.* 4).[28,29] *These compounds are accessible and can* gelate *a wide range of solvents. and moreover. the hydrogen-bonding core can be used as a "gelating scaffold" to which other* functional *moieties can be attached without losing* gelation *ability.*

It *should be noted that these designs are not yet perfect, because they are mainly based on the concept of* 1D *self-assembly and do not include factors that would limit the diameter of the fibers.* In *most gels, the fibers are composed of* multiple *strands of molecules, and the fiber diameters show a broad distribution. It was proposed that fiber formation takes place via nucleation–growth*

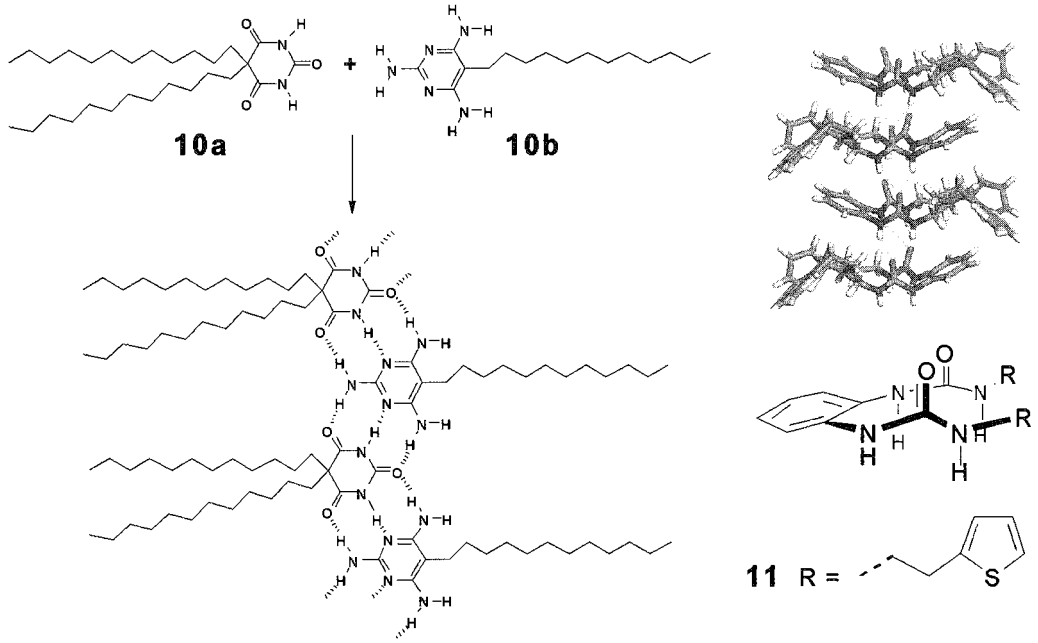

Fig. 4 Two-component (left) and single-component (right) 1D self-assernbly. Barbituric acid (10a) and triaminopyrimidine (10b) derivatives self-assemble through complementary hydrogen bonds into linear tapes (left).'''' At the right. the crystal packing of his-urea cornpound PI is shown. in which the urea groups form a ID (a-network) hydrogen-bonded array. (From Ref. [29].) (*View* this *art* in *color* at *www.dekker.com.*)

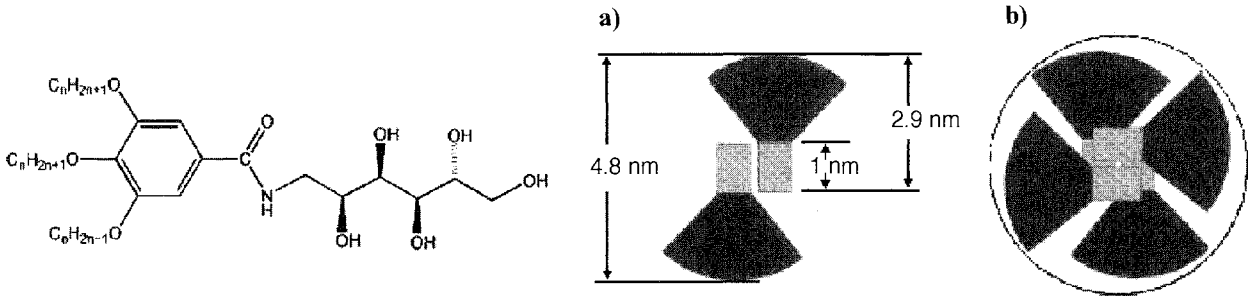

Fig. 5 Tentative head-to-head arrangement of 12 (a), and the cross section of a single strand of 12 (b). (Reproduced from Ref. [31].)

processes, similar to that of crystal formation, and kinetic factors play an important role in restricting the fiber diameter.[30,32] Furthermore, many gel systems suffer from instability due to the growth of small crystals (vide infra) with much lower aspect ratios than the original fibers. Gelators designed to form fibers with a finite diameter are the wedge-shaped amphiphilic carbohydrates 12 (Fig. 5).[31] A consequence of the wedge shape of the molecules is that an optimal packing can only be realized in columnar aggregates; and the observed structures show the presence of thin fibers with a discrete diameter. However, many thicker fibers can also be observed, indicating that there is still a significant driving force for the formation of multicolumnar fibers.

These studies clearly showed that the rational design of LMWGs became reality. and in recent years, these insights were exploited in the development of functional gelators for specific applications (see the section entitled "Applications." below). The design approach established that unidirectional intermolecular interactions are a prerequisite for gelation by LMWGs, but it remains a challenge to control, at the supramolecular level, other aspects of gel formation. like the fiber length and diameter, cross-linking of the fibers, and prevention of crystallization.

CHARACTERIZATION AND PROPERTIES OF THE GELS

Gels from LMWGs usually display a gel–sol phase transition at a characteristic temperature that depends on the nature of the solvent and the structure of the gelator as well as its concentration. Gels can, therefore, easily be prepared by crossing the gel–sol phase boundary by cooling or by adding a poor solvent. Significant supercooling is. however, often necessary, because gel formation is, in most cases, a kinetically controlled process that resembles in many aspects the nucleation and growth stages of crystallization.[30,32] On the other hand, the gel–sol equilibrium is maintained during melting of the gels if the heating rate is sufficient low. The gel–sol phase-transition temperatures (T_{GS}) can be determined by a number of different methods in which one monitors. for instance. the viscoelastic properties or a specific spectroscopic or optical feature as a function of the temperature.["] Particularly convenient are the "dropping ball" and "tilted tube" methods, which allow visual observation of the gel–sol transition (Fig. 6).

Gels from low-molecular-weight organic compounds can have remarkably high melting temperatures. even up to 150°C, despite the fact that the gels are solely held together by noncovalent interactions.[34,35] The gel–sol phase transition occurs through dissolution of the fibrous network. Analogous to the dissolution of crystals in ideal solutions, the variation of T_{GS} with the concentration usually obeys the van't Hoff or Schrader relation. from which one can calculate the gel–sol phase-transition enthalpy (ΔH_{GS}).[16,33] The melting enthalpy of a gel can also be measured by calorimetric methods, like differential scanning calorimetry, although the sensitivity is often a problem. More importantly, the ΔH_{GS} obtained from T_{GS} measurements and calorimetric methods can

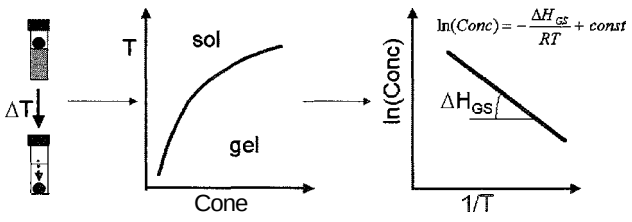

Fig. 6 In the dropping ball method, one records the temperature (T_{GS}) at which the gel can no longer bear the weight of the ball (left). The experiment is repeated at different concentrations. and from the variation of the T_{GS} with the concentration, one can construct the phase diagram (middle) and calculate ΔH_{GS} (left) using the van't Hoff equation.

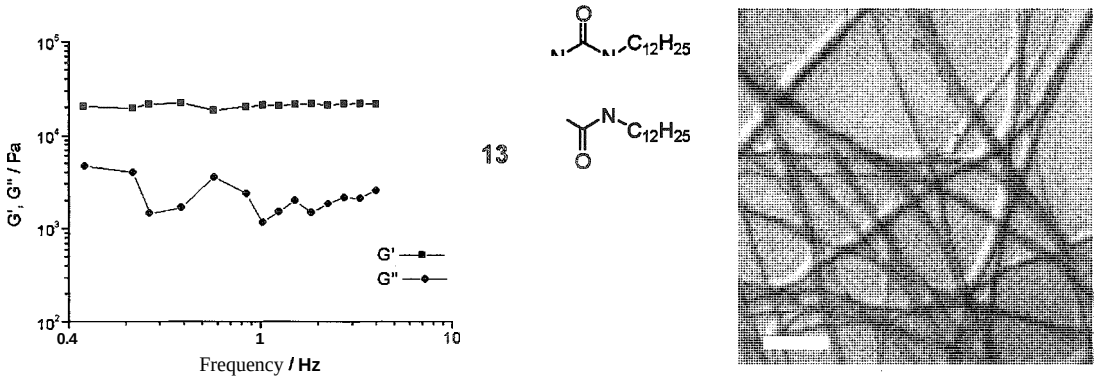

Fig. 7 Typical viscoelastic behavior of a strong gel. in this case, of his-urea gelator **13** in 1-hexanol (left). The TEM micrograph of this gel is shown at the right and reveals that the minimum width of the fibers amounts to 15–20 nm. which is still an order of magnitude larger than the molecular dimensions of **13**. (Scale bar is 500 nm. reproduced from Ref. [37].)

differ significantly, which is most likely due to the assumptions made and nonideal behaviors of the gels. It should be noted that in the long-term, many organogels tend to transform to crystals, most likely through Ostwald ripening, and this instability toward crystallization clearly indicates that the gel state is metastable.[30]

One of the most prominent features of a gel is its specific viscoelastic properties. The solid character of organogels at low stress values. for instance, provides a convenient test for gelation. because gels resist gravitational flow. This and other viscoelastic properties of organogels are direct consequences of the presence of a network structure. Therefore, rheological studies of the viscoelastic properties are. in the ideal case, complemented by characterization of the fiber and network morphology. Pioneering work in this area by Terech showed that most orpanogels can be classified as "strong" gels, but there are also few documented examples of ''weak'' organogels.[36]

Strong organogels are usually composed of a network of cross-linked fibers. The diameters of the fibers are at least an order of magnitude larger than the size of a single gelator molecule, and cross-linking of the fibers into the network structure occurs through entanglement or the formation of microcrystalline junction zones. The network appears as a static structure at timescales of minutes and shorter. because the fibers and junction zones are stabilized by multiple noncovalent interactions. and hence, the scission energy is much larger than kT. As a consequence, strong organogels behave as elastic solids up to a characteristic stress value (yield stress), with only little dependence on the timescale of the experiment. In an oscillatory rheology experiment, this behavior is reflected in the storage modulus G' being larger than the loss

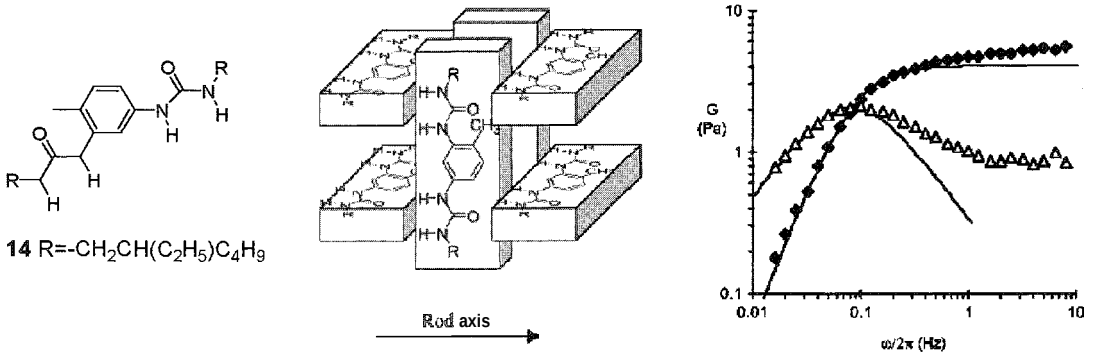

Fig. 8 A slight modification of the structure can lead to completely different properties, as is illustrated by methyl-substituted his-urea coinpound 14 that, in contrast to gelator 13. forms a typically weak gel. The oscillatory rheology experiment shows the weak gels characteristic frequency dependency of G' and G'' (right), and small-angle neutron scattering studies revealed that the molecular wires are only two molecules thick, as depicted in the tentative model in the middle. (Reproduced from Ref. [38].)

modulus G'' over a wide frequency range (Fig. 7), and if the applied stress (amplitude of the oscillation) exceeds the yield stress, the gel network breaks down to yield a viscous fluid. For most systems, the gel state can only be restored by a heating–cooling cycle through the gel–sol phase transition. but a few strong gels were reported to display thixotropy, i.e., a spontaneous restoration of the gel state occurs if the stress is taken away.[37]

Weak gels from LMWGs, on the other hand, are formed by the bis-urea compound 14 depicted in Fig. 8. which self-assembles into molecular wires in hydrocarbon solvents. and above a critical concentration, the wires entangle to form a network structure.[38] Because the molecular wires are only two molecules thick, there are only a few noncovalent interactions. resulting in small scission energies and short lifetimes of the wires. In such weak gels. the relaxation of stress is possible through mechanisms like reptation or scission and recombination of the chains. and their viscoelastic properties are governed by the relative timescales of these relaxation processes. This leads to a pronounced frequency dependency of G' and G'' in an oscillatory rheology experiment, and the lifetime of the wires is given by the frequency at which G' and G'' intersect (Fig. 8).

The strong correlation between viscoelastic properties of the gels and the fiber and network morphology stresses the importance of complementing the rheologicai studies with morphological studies. A first impression of the morphology of organogels can be obtained by microscopy techniques. Especially transmission electron inicroscopy (TEM) and more recently also atomic force microscopy (AFM),[39] are convenient methods to use to study fiber morphology. and high-resolution images can even reveal the fine structure of a fiber down to nanometer resolution. The 319 structure of the network can be studied by scanning electron microscopy on gel samples of which the liquid phase is removed by supercritical extraction. However-, with electron microscopy. one always has to deal with samples that are rather diverged from the native gel state with all risks of looking at artifacts. This limitation does not hold for x-ray or neutron scattering methods. which allow the characterization of the network morphology in the native state. but the downside is that analysis and interpretation of the data are more complicated, because the structural data are obtained in reciprocal space.[36] Especially high-flux x-ray sources as provided by synchrotrons are useful, because highly diluted gel systems (to circumvent multiple scattering) with low scattering intensities can be studied in real time, which allows one to follow the formation of a gel upon quenching from the solution state, or to study the deformation of the network upon application of stress. Moreover, the high-beam intensities makes it possible to collect data at very small angles, thereby probing structural features from one to several hundreds of nanometers, which allows characterization of the fiber shape and diameter. as well as mesh size of the network.

Together, microscopy, scattering methods, rheology, and thermotropic methods provide a detailed view of the gel network and its behavior. however, they do not provide information on the nature of the intermolecular interactions stabilizing the gel network and the supramolecular arrangement of the gelator molecules within the fibers. In supramolecular chemistry, such information is usually obtained from single x-ray crystal structures or 2D NMR spectroscopic studies: but unfortunately, these techniques are of limited value for organogels. The application of high-resolution solution-phase NMR techniques is limited to the pre-gel stage, because of the solid nature of the fibrous network.[40] and only in a few instances have LMWGs successfully been crystallized despite their tendency to gelate. Powder XRD is a powerful technique for native or dried gels, because it provides structural information on randomly oriented samples. Simple phases like lamellar or hexagonal phases can easily be recognized from the diffi-action patterns, and recent advances in this area made it possible to deduce even a crystal structure from high-resolution powder patterns. Such high-quality powder patterns were not yet reported for organogels, probably because the arrangement in the fibers is not as well defined as in crystals. Powder x-ray diffraction (XRD) patterns of gels were used to identify the gel-forming morph of hexatriacontane gels, by comparison with powder diffraction patterns of several crystalline forms of hexatriacontane,[41] but other examples showed that the arrangements in the gel and crystal states are not necessarily the same.[22,29] For insight into the supramolecular arrangement of the gelator molecules in these and most other gel systems, one has to rely on the nonconclusive information that emerges from changes in the electronic and vibrational spectra that occur by going from the solution to the gel state.

APPLICATIONS

The LMWGs are of great interest, because numerous applications for them are found in different areas, like cosmetics. drug delivery. separation technology, lubrication: and display technology. In particular. gels formed by salts of long-chain carboxylic acids or other organic acids. but also amide oligomers, have been known for a long time, and were used as lubricants or thickeners in commercial applications, but regrettably also as a

hardener of kerosene in Napalm. Dibenzylidene sorbitol is used on a large scale as a nucleating or clearing agent for polypropylene, and other LMWGs are used as rheology modifiers in personal care products like lipstick or antiperspirant sticks. It is foreseen that recent advances in the design and understanding of organogelators will lead to many more applications as rheology modifiers because of better possibilities for tuning the processing conditions or the molecular properties. And, the use of polymers to alter network morphology is a very promising development.[32]

The development of new LMWGs for water and nonclassical solvents is also of great interest. Low-molecular-weight hydrogelators based on carbohydrates or amino acids for water are potentially of interest for biomedical applications:[42–44] and recently, vancomycin was modified with pyrene, which turns it into a hydrogelator and enhances its antibacterial activity.[45] It was shown that the organogels can be used for the selective binding of guest molecules, which might be of interest for separation technology and drug delivery.[46] The gelation of supercritical CO_2 offers a new route to organic xerogels as new insulating material,[47] and gelled ionic liquids might find application as electrolytes in batteries or solar cells.[48] Functionalized organogels with, for instance, oligothiophene moieties: show enhanced electronic or ionic conductivity and are of potential interest in molecular electronics,[49] and the recent structuring of liquid-crystalline materials by organogelators led to liquid-crystalline materials with new electrooptical properties.[50]

Organogels were also used as templates for the construction of membranes and new hybrid materials. Polymeric membranes were prepared by the gel-template leaching method, in which membranes with defined channels were prepared by polymerization of a methacrylate ester liquid phase of an organogel, followed by extraction of the organogel gel matrix.[51–53] It is also possible to polymerize the gel phase of modified gelators containing a polymerizable group, resulting in a low-density xerogel.[54] The transcription of the organogel fibril structure into inorganic materials was pioneered by Shinkai et al. Toward this goal, the gelator molecules were extended with functional groups that strongly interact with the inorganic precursors, and as a consequence, the inorganic sol-gel process proceeds preferentially at the interface of the organogel network, to give an inorganic object of which the shape is reminiscent of the organic template (Fig. 9).[55]

The development of responsive organogels is a relatively unexplored area, but it might be of interest for, e.g., novel drug delivery systems or microfluidics. In contrast to chemical gels, the application of chemical or

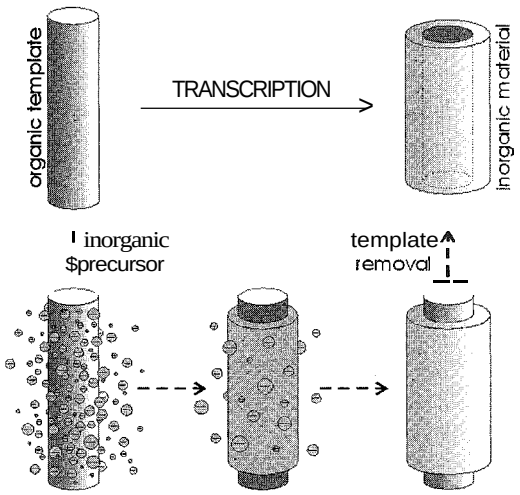

Fig. 9 Transcription of organic templates into an inorganic material. (Reproduced from Ref. [55].)

physical stimuli to organogels with encapsulated guest compounds can result in a reversible gel–sol phase transition (see also Fig. 1), thereby releasing its content. Shinkai and coworkers developed, for instance, an azobenzene-steroid gelator, of which only the trans azobenzene isomer and not the cis-isomer forms gels, and they found that the photochemically induced trans-cis isomerization is accompanied by a reversible gel–sol phase transition.[16] Unfortunately. the cis-isomer of employed azobenzenes is thermally unstable, resulting in a spontaneous (thermally induced) restoration of the gel state. The photo-bistable dithienylcyclopentenes do not suffer from this disadvantage, and recently it has been shown that also for these compounds the degree of aggregation can be controlled by light.[56] Other stimuli, like protonation in combination with light,[57] or ion-complexation[58] were also used to control the gel–sol phase transition. However, the response of organogels to stimuli is not limited to the gel–sol phase transition. Zinic and coworkers showed that a morphological transition from microspheres to a fibrous network can be induced by light,[59] and remarkably, a glycosylated amino-acid-based gelator for water displays a thermotropic volume-phase transition.[44]

CONCLUSION

The gelation of organic solvents by LMWGs is a phenomenon that has been known for a long time but, nevertheless, has been poorly understood. at least at the

molecular level. Only with the advance of supramolecular chemistry has it been realized that the formation of a fibrous network by small organic molecules is an example of self-assembly par excellence. From this perspective, the elucidation of several factors governing gelation and establishment of some of the design rules for new LMWGs were realized, and in recent years, this led to remarkable progress in the development of functional gelators with programmed properties. Applications of organogels in highly diverse areas ranging from cosmetics and drug delivery to material science and molecular electronics already are or will become reality within the near future.

It also became clear that the gelation of liquids by low-molecular-weight organic molecules is a complex process, of which the 1D assembly of gelator molecules is only a first step in a series of events that ultimately leads to the formation of a network structure. Understanding and controlling the different stages of the gelation process remain a huge scientific challenge, not only because the structural analysis of gels is still problematic. but also because of the prominent role of kinetics in the gelation process. Progress toward these goals, however, will be relevant not only for the possible applications of gels but also for related areas like crystallization and hierarchic structure assembly.

ARTICLES OF FURTHER INTEREST

Crystal Engineering with Hydrogen Bonds. p. 357
DNA Nanotechnology, p. 475
Hydrogen Bonding, p. 658
Liquid Clathrates, p. 804
Micelles and Vesicles, p. 861
Nanocasting: Strategies and Porous Materials. p. 950
Self-Assembly: Definition and Kinetic and Thermodynamic Considerations, p. 1248
Supramolecular Polymers, p. 1443
Surfactants, Part I: Fundamentals, p. 1458
Surfactants, Part II: Applications, p. 1470

REFERENCES

1. Jordon Lloyd. D. Colloid *Chemistry*; Alexander. J.. Ed.; The Chemical Catalog Co.: New York, 1926.
2. Flory. J.P. Gels and gelling processes. Faraday Discuss. Chem. Soc. 1974. *57.* 7–18.
3. Cesser. H.D.; Goswami. P.C. Aerogels and related porous materials. Chem. Rev. 1989. *89.* 765–788.
4. Tanaka. T. Gels. Sci. Am. 1981. *244.* 110–123.
5. Guenet, J.P. *Thermoreversible Gelation* of *Polymers and Biopolymers*; Acad. Press Ltd.: London. 1992.
6. Bradford, S.C. On the theory of gels. Biochem. J. 1921, *15.* 553.
7. Beginn, U. Rational Design of Supramolecular Organogelators and Their Application for the Preparation of Functional Membranes. Habil. Thesis: 2000. Ulm.
8. Terech, P.; Weiss. R.G. Low molecular mass gelators of organic liquids and the properties of their gels. Chem. Rev. 1997. 97. 3133–3159.
9. Van Esch. J.; Schoonbeek, F.; De Loos. M.: Veen, E.M.; Kellogg. R.M.: Feringa. B.L. Low Molecular Weight Gelators for Organic Solvents. From Serendipity Towards Design. In *Supramolecular* Science, *Where It* Is *and* Where **I**t Is *Going*; Ungaro, R., Dalcanale, E., Eds.; Kluwer Acad. Pub., 1999; 233–259.
10. Gronwald, O.: Snip. E.: Shinkai. S. Gelators for organic liquids based on self-assembly: A neu facet of supramolecular and combinatorial chemistry. Curr. Opin. Colloid Interface Sci. 2002, 7. 148–156.
11. Twieg, R.J.: Russell. T.P.; Siemens, R.; Rabolt. J.F. Observations of a gel phase in binary mixtures of semifluorinated n-alkanes with hydrocarbon liquids. Macromolecules 1985, *18*, 1361–1362.
12. Brotin. T.; Utermohlen. R.; Fages. F.; Bouas-Laurent. H.: Desvergne. J.P. A novel small molecular luminescent gelling agent for alcohols. J. Chem. Soc., Chem. Commun. 1991, 416–418.
13. Lu, L.D.; Weiss, R.G. Cholestanyl substituted quaternary ammonium-salts as gelators of organic liquids. Langmuir 1995. *11.* 3630–3632.
14. Terech. P.; Rodriguez. V.; Barnes. J.D.; McKenna. G.B. Organogels and aerogels of racemic and chiral 12-hydroxyoctadecanoic acid. Langmuir 1994. *10.* 3406–3418.
15. Terech. P.; Berthet, C. Magnetic orientational effects during the aggregation kinetics of a steroid cyclohexane gelling system. J. Phys. Chem. 1988. *92.* 4269–4272.
16. Murata, K.: Aoki, M.: Suzuki, T.: Harada, T.: Kawabata. H.; Komori, T.; Ohseto. F.: Ueda, K.: Shinkai. S. Thermal and light control of the sol–gel phase-transition in cholesterol-based organic gels—Novel helical aggregation modes as detected by circular-dichroism and electron-microscopic observation. J. Am. Chem. Soc. 1994, *116*, 6664–6676.
17. Wolfe. J.K.; Hann. R.M.; Hudson. C.S. 1. 2. 3, 4-Dibenzylidene-D-sorbitol. J. Am. Chem. Soc. 1942. 64. 1493–1496.
18. Snijder. C.S.: de Jong. J.C.; Meetsma. A.; van Bolhuis. F.: Feringa, B.L. A novel low molecular weight chiral gelator for apolar organic solvents. Chem. Eur. J. 1995, *1*, 594–597.
19. Uamasaki. S.: Tsutsumi. H. The dependence of the polarity of solvents on 1,3/2,4-di-*o*-benzylidene-D-sorbitol gel. Bull. Chein. Soc. Jpn. 1995, *68*, 123–127.
20. Lin. Y.; Kachar. B.: Weiss, R.G. Novel family of gelators of organic fluids and the structure of their gels. J. Am. Chem. Soc. 1989. **111,** 5542–5551.

21. Menger, F.M.: Caran. K.L. Anatomy of a gel. Amino acid derivatives that rigidify water at submillimolar concentrations. J. Am. Chem. Soc. 2000. *122*. 11679–11691.
22. Menger. F.M.; Yamasaki. Y.: Catlin, K.K.; Nishimi. T. X-ray structure of a self-assembled gelating fiber. Angew. Chem.. Int. Ed. 8995. *34*. 585–586.
23. Su. D.: Wang, X.; Simard, M.: Wuest, J.D. Molecular tectonics. Supramol. Chem. 1995. *6*, 171–178.
24. Shinkai. S.; Murata. K. Cholesterol-based functional tectons as versatile building-blocks for liquid crystals, organic gels and monolayers. J. Mater. Chern. 1998. *8*, 485–495.
25. Van Esch. J.H.: Feringa, B.L. New functional materials based on self-assembling organogels, from serendipity towards design. Angew. Chem.. Int. Ed. 2000. *39*. 2263–2266.
26. Hanabusa, K.; Miki, T.: Taguchi, Y.; Koyama, T.: Shirai, H. 2-Component, small-molecule gelling agents. J. Chem. Soc.. Chern. Commun. 1993. 1382–1384.
27. Bielejewska, A.G.; Marjo. C.E.; Prins. L.J.: Timmerman, P.: De Jong, F.: Reinhoudt, D.N. Thermodynainic stabilities of linear and crinkled tapes and cyclic rosettes in melamine-cyanurate assemblies. a model description. J. Am. Chem. Soc. 2001. 123. 7518–7533.
28. Hanabusa. K.: Matsumoto, Y.: Miki. T.: Koyama, T.: Shirai. H. Cyclo(dipeptide)s as low-molecular-mass gelling agents to harden organic fluids. J. Chem. Soc., Chem. Commun. 1994, 1401–1402.
29. Van Esch, J.: Schoonbeek. F.; De Loos. M.: Kooijman, H.: Spek. A.L.: Kellogg. R.M.; Feringa, B.L. Cyclic bis-urea compounds as gelators for organic solvents. Chem. J. Eur. 1999. *5*. 937–950.
30. Lescanne. M.: Colin. A.; Mondain-Monval. O.; Fages. F.; Pozzo, J.L. Structural aspects of the gelation process observed with low molecular mass organogelators. Langmuir 2003. *19*. 2013–2020.
31. Beginn, U.; Keinath, S.: Moller, M. New carbohydrate amphiphiles. 2. Gel formation and gel morphologies. Macromol. Chem. Phys. 1998, *199*. 2379–2384.
32. Liu. X.Y.: Sawant, P.D. Mechanism of the formation of self-organized microstructures in soft functional materials. Adv. Mater. 2002. *14*. 421.
33. Terech. P.: Rossat. C.: Volino. F. On the measurement of phase transition temperatures in physical molecular organogels. J. Colloid Interface Sci. 2000. *227*. 363–370.
34. Van Esch. J.: DeFeyter, S.: Kellogg, R.M.; DeSchryver, F.; Feringa. B.L. Self-assembly of bisurea compounds in organic solvents and on solid substrates. Chem. Eur. J. 1997, *3*. 1238–1243.
35. Makarevic, J.: Jokic. M.; Frkanec, L.; Katalenic. D.: Zinic, M. Gels with exceptional thermal stability formed by bis(amino acid) oxalamide gelators and solvents of low polarity. Chem. Commun. 2002. 2238–2239.
36. Terech. P. Fibers and wires in organogels from low-mass compounds. typical structural and rheological properties. Ber. Bunsen Ges. Phys. Chem. Chern. Phys. 1998. *102*. 1630–1643.
37. Brinksma, J.; Feringa, B.L.; Kellogg. R.M.: Vreeker. R.; Van Esch. J. Rheology and thermotropic properties of bis-urea-based organogels in various primary alcohols. Langmuir 2000. *16*. 9249–9255.
38. Lortie, *F.:* Boileau, S.: Bouteiller, L.; Chassenieux, C.: Deme, B.; Ducouret. G.: Jalabert, M.: Laupretre. F.: Terech. P. Structural and rheological study of a bis-urea based reversible polymer in an apolar solvent. Langmuir 2002. *18*. 7218–7222.
39. Wang. R.; Geiger, C.: Chen. L.H.: Swanson, B.; Whitten, D.G. Direct observation of sol–gel conversion: The role of the solvent in organogel formation. J. Am. Chem. Soc. 2000. *122*. 2399–2400.
40. Duncan, D.C.; Whitten, D.G. H-l NMR investigation of the composition. structure, and dynamics of cholesterol-stilbene tethered dyad organogels. Langmuir 2000, *16*, 6445–6452.
41. Abdallah, D.J.; Sirchio. S.A.: Weiss. R.G. Hexatriacontane organogels: The first determination of the conformation and molecular packing of a low-molecular-mass organogelator in its gelled state. Langmuir 2000. *16*. 7558–7561.
42. Makarevic. J.: Jokic, M.: Peric, B.: Tomisic, V.; Kojic-Prodic. B.; Zinic, M. Bis(amino acid) oxalyl amides as ambidextrous gelators of water and organic solvents. supramolecular gels with temperature dependent assembly/dissolution equilibrium. Chem. Eur. J. 2001, 7, 3328–3341.
43. Estroff. L.A.; Hamilton. A.D. Effective gelation of water using a series of bis-urea dicarboxylic acids. Angew. Chem., Int. Ed. 2000, *39*. 3447.
44. Kiyonaka. S.; Sugiyasu. K.; Shinkai, S.: Hamachi. I. First thermally responsive supramolecular polymer based on glycosylated amino acid. J. Am. Chern. Soc. 2002. *124*, 10954–10955.
45. Xing. B.G.: Yu, C.W.: Chow. K.H.; Ho, P.L.: Fu. D.G.; Xu. B. Hydrophobic interaction and hydrogen bonding cooperatively confer a Vanconiycin hydrogel. a potential candidate for biomaterials. J. Am. Chem. Soc. 2002; *124*. 14846–14847.
46. Maitra, U.: Mukhopadhyay. S.: Sarkar. A.; Rao, P.; Indi, S.S. Hydrophobic pockets in a nonpolymeric aqueous gel, observation of such a gelation process by color change. Angew. Chem.. Int. Ed. 2001. *40*. 2281.
47. Shi. *C.:* Huang. Z.: Kilic. S.: Xu, J.; Enick, R.M.; Beckman, E.J.: Carr. A.J.; Melendez. R.E.: Hamilton. A.D. The gelation of CO_2, a sustainable route to the creation of microcellular materials. Science 1999. *286*. 1540–1543.
48. Hanabusa, K.; Hiratsuka. K.: Kimura. M.: Shirai. H. Easy preparation and useful character of organogel electrolytes based on low molecular weight gelator. Chem. Mater. 8999, **11,** 649–655.
49. Schoonbeek. F.S.: Van Esch. J.H.: Wegewijs, B.: Rep, D.B.A.: De Haas, M.P.; Klapwijk. T.M.: Kellogg. R.M.: Feringa. B.L. Efficient intermolecular charge transport in self-assembled fibers of mono- and bithiophene bisurea compounds. Angew. Chem., Int. Ed. 1999. *38*, 1393–1397.

50. Kato. T. Self-assembly of phase-segregated liquid crystal structures. Science 2002, *295*. 2414–2418.
51. Beginn, U. Supramolecular templates as porogenes. Adv. Mater. 1998. *10*, 1391.
52. Gu. W.Q.: Lu. L.D.: Chapman, G.B.; Weiss, R.G. Polymerized gels and 'reverse aerogels' from methyl methacrylate or styrene and tetraoctadecylammonium bromide as gelator. Chem. Cornmun. 1997, 543–544.
53. Hafkamp, R.J.H.; Kokke. B.P.A.: Danke, I.M.: Geurts. H.P.M.: Rowan. A.E.: Feiters, M.C.: Nolte. R.J.M. Organogel formation and molecular imprinting by functionalized gluconamides and their metal complexes. Chem. Comniun. 1997. 545–546.
54. De Loos, M.: Van Esch. J.: Stokroos. I.; Kellogg, R.M.: Feringa. B.L. Remarkable stabilization of self-assembled organogels by polymerization. J. Am. Chern. Soc. 1997. *119*. 12675–12676.
55. Shinkai. S.: Van Bornmel, K.: Friggeri, A. Organic templates for the fabrication of inorganic materials. Angew. Chern.. Int. Ed. 2003, 42. 980–999.
56. Lucas. L.N.; Van Esch, J.: Kellogg. R.M.; Feringa, B.L. Photocontrolled self-assembly of molecular switches. Chem. Cornmun. 2001. 759–760.
57. Ahmed, S.A.; Sallenave, X.; Fages. F.; Mieden-Gundert, G.; Muller, W.M.: Muller. U.; Vogtle. F.; Pozzo. J.L. Multiaddressable self-assembling organogelators based on 2H-chroniene and *N*-acyl-1,omega-amino acid units. Langrnuir 2002. *18*. 7096–7101.
58. Sohna, J.E.S.; Fages, F. A trisbipyridine tripodal ligand as toluene gelator. Phase transition-triggered binding of iron(II). Chem. Comniun. 1997. 327–328.
59. Frkanec, L.: Jokic, M.; Makarevic, J.: Wolsperger, K.: Zinic. M. Bis(pheOH) maleic acid amide-fumaric acid arnide photoizomerization induces microsphere-to-gel fiber morphological transition: The photoinduced gelation system. J. Am. Chem. Soc. 2002. *124*, 9716–9717.

Glycoluril-Based Hosts

Johannes A. A. W. Elemans
Alan E. Rowan
Roeland J. M. Nolte
University of Nijmegen, Nijmegen, The Netherlands

INTRODUCTION

In the early 1980s our group began a study on the possibilities of using the cyclic glycoluril hexamer cucurbituril **1** (Fig. 1a) as a host for small organic guests. Until recently."] however, modification of cucurbituril was inhibited due to the extreme insolubility of this macrocycle in most common solvents. In attempts to overcome this problem of solubility by attaching lipophilic phenyl groups to the glycoluril units: it was discovered that the reaction of diphenylglycolmil (DPG) 2 with formaldehyde in benzene gave a clip-shaped molecule, **3a**. This molecule appeared to have a rigid, U-shaped cavity, and it turned out to be an ideal host for dihydroxybenzene derivatives such as resorcinol and catechol.[2] Since then. an enormous variety of glycoluril-based hosts possessing numerous functionalities has been synthesized. Nowadays, these hosts find their applications in many different research areas. e.g., as mimics of biological systems. as amphiphiles, and as liquid crystals.[3] In this overview, only the most recent developments in glycoluril-based host chemistry will be discussed.

BINDING FEATURES

The crystal structure of host **3b** (Fig. 1b) clearly shows that this molecule possesses a well-defined and preorganized cleft. ^{1}H-NMR studies revealed that glycoluril-based hosts are excellent receptors for neutral guests, e.g., (di-)hydroxybenzene molecules.[4] The binding strength toward these types of guests can reach values of $K_a > 10^5 M^{-1}$, depending on the binding functions in the host molecule and the substitution pattern in the guest. The binding is a result of three cooperative effects. viz. hydrogen bonding. $\pi-\pi$ stacking. and a so-called "cavity effect," which can be simply described as the entropically favorable filling of an empty cavity by the guest. Recent work within our group enabled the separation and quantification of each of these effects."] Upon binding of a 1,3-dihydroxybenzene in a host of type 3 in chloroform, two hydrogen bonds are formed simultaneously between the hydroxy groups of the guest and the urea carbonyl groups of the receptor (Fig. 1c). The strength of these hydrogen bonds is directly correlated to the 5-substituent of the guest. which determines the acidity of the phenolic OH groups. It was found that for a series of 5-substituted 1,3-dihydroxybenzenes. the ΔG of binding to **3b** increases linearly as a function of the Hammett substituent constant σ_m(R).

The $\pi-\pi$ interactions between host and guest are readily influenced by subtle variations in the host side walls. Altering the 1,4-substituents on the side walls from methoxy to methyl to hydrogen significantly weakens the $\pi-\pi$ interactions and reduces the contribution of the cavity effect. Host 4 with two p-benzoquinone n-acceptor side walls somewhat surprisingly turned out to be a poor receptor for n-donor 1,3-dihydroxybenzene guests. Although favorable interactions were expected between the host and the guest, their orientation, imposed by the hydrogen bonds, is energetically less favorable than that found in the related complex with host 3b. Enlargement of the aromatic surface of the side walls to 1.4-dimethoxynaphtalene (Host ***5***) completely inhibited guest binding. due to a combination of unfavorable $\pi-\pi$ interactions and blocking of the cavity by the methoxy side wall substituents. Connection of the naphthalene walls at their 1.8-positions (Host 6) removes these constraints. Host 6, however, exists in three slowly exchanging conformers. of which only the *anti–anti* one possesses a cleft in which substrates can be bound (Fig. Id). The large aromatic n-surfaces of the side walls in 6 interact favorably with electron-deficient guests and silver ions. Binding occurs by an induced-fit mechanism: upon binding of the guest, the relative amount of *anti–anti* conformer was found to increase.[6,7]

All the binding processes described above were carried out using hosts based on the DPG skeleton. Recently. this central core was modified. and new host molecules were synthesized based on the propane-diurea skeleton.[8] The x-ray structure of **7** revealed that its cavity resembles the cavities of DPG-based hosts, the only difference being

Encyclopedia of Supramolecular Chemistry
DOI: 10.1081/E-ESMC *120012733*

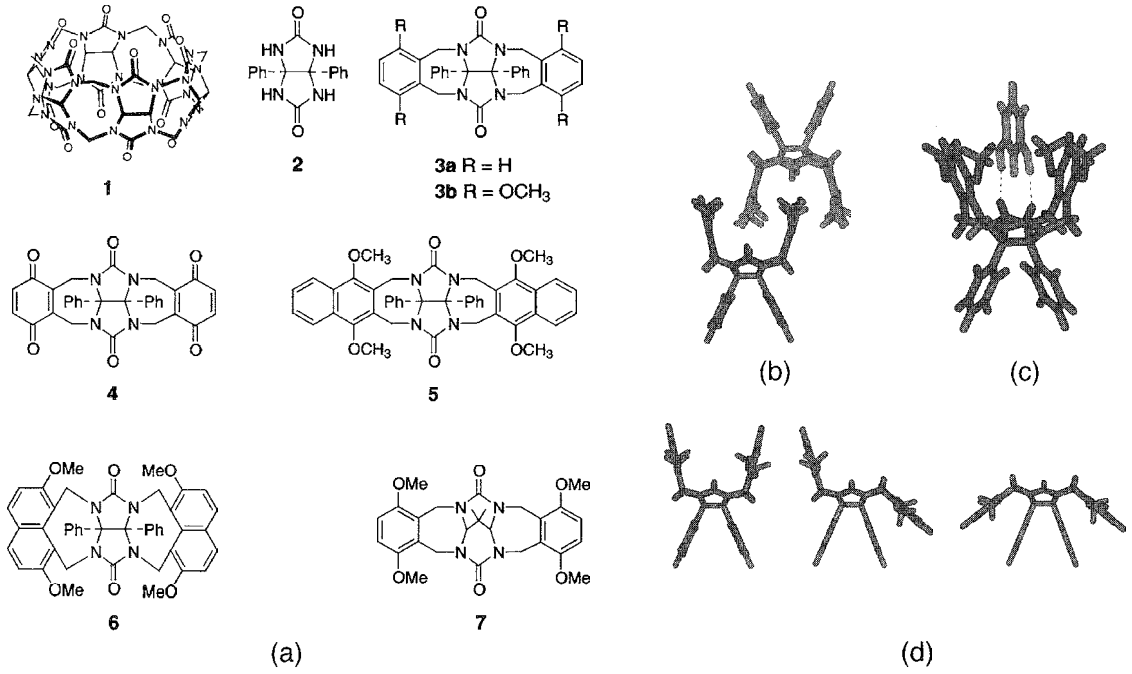

Fig. **I** (a) Glycoluril-based host molecules. (b) Dimeric arrangement of molecules in the crystal structure of 3b. (c) Computer-modeled representation of the binding of resorcinol in Host **3b.** (d) The three conformations of Host 6: (from left to right) anti-anti, *anti-syn*, and *syn-syn*. (*View* ***this*** *art in color at www.dekker.com.*)

that in the new host. the distance between the urea carbonyl groups is slightly shorter (5.2 A compared to 5.5 Å in the case of 3b). As a result of this closer distance. 1.3-dihydroxybenzene guests are bound by 7. approximately 10 times stronger. The exceptionally high binding constants measured for these guests (up to K_a = 2.4 *x* 10^6 M^{-1} for the complex between 7 and 5-cyanoresorcinol), highlight the fact that even a sub-Å

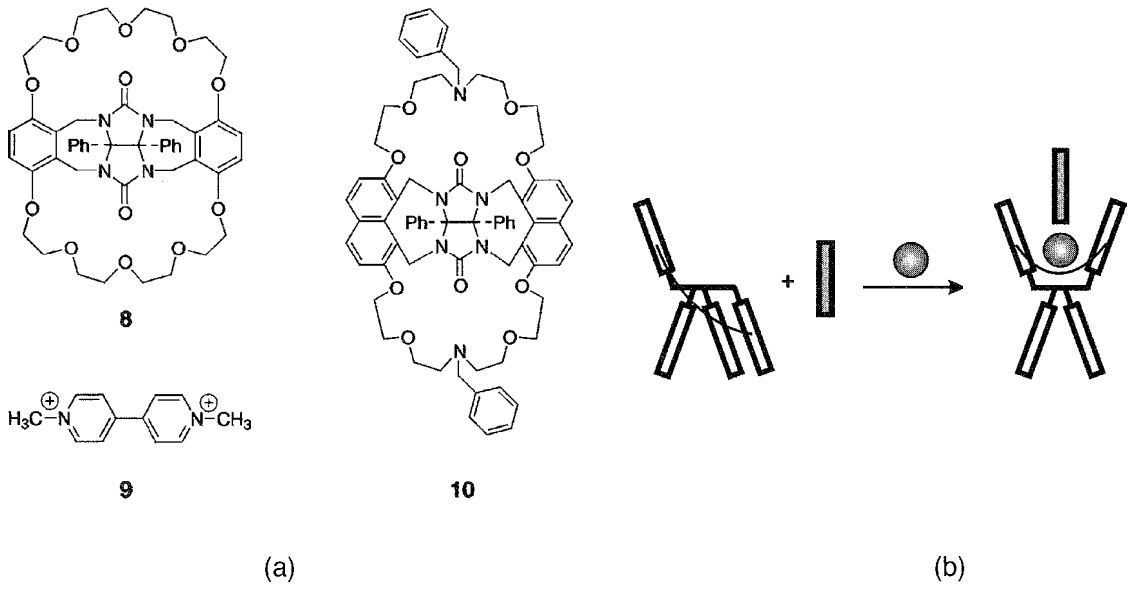

Fig. *2* (a) Basket-shaped host 8 and 10 dnd viologen guest 9 (b) The allosteric binding of a guest in Host 10. In the presence of Na^+ or K^+ (circle), electron-deficient aromatic substrates (rectangle) are bound more strongly

change in the host structure can have a dramatic effect on its binding properties.

Glycoluril-based hosts derivatized with crown ether moieties. such as 8, are known as molecular baskets because of their basket- or bowl-like shape (Fig. 2a). In addition to alkali metal ions and diammonium salts, these molecules are excellent receptors for charged aromatic compounds such as viologens (*N,N'*-disubstituted 4,4'-dipyridinium compounds) and polymeric derivatives thereof.[109] Host 8 binds 9 with a K_a of 5.7 x 10^4 M^{-1}, which is much stronger than the binding of 9 in the *bis*(paraphenylene)-[34]-crown-10 macrocycle studied by Stoddart and coworkers.[110] Upon complexation with **8,** the redox properties of 9 were modified, i.e., bound 9 is 100 mV more difficult to reduce than uncomplexed 9. Once reduced to its 1+ form, however, 9 is expelled from the cavity. In the case of polymeric derivatives of 9, the electrochemical properties of the polymer are altered by the addition of Host 8.

Another family of basket-shaped hosts was synthesized containing azacrown ethers that can act as linking points for functional groups. Naphthalene-walled basket 10 exists in three conformations and displays allosteric binding behavior.[111] Upon addition of alkali metal ions, the ***anti-anti*** conformation is induced, resulting in a host that is an ideal receptor for aromatic guests (Fig. 2b). As a result of this induced change, the binding of 1,3-dinitrobenzene is increased by a factor of 2 to 6, upon the addition of K^+ ions to a solution of 10, with two K^+ ions complexed between the crown ether rings in a cooperative manner. The second K^+ ion binds approximately 100 times stronger than the first.

MIMICS OF BIOLOGICAL SYSTEMS

Glycoluril-based host molecules were used as components of substrate-selective catalysts. Using nature as a guide, catalytically active metal centers were linked to the receptor cavities. These supramolecular systems were synthesized to mimic well-known processes in natural

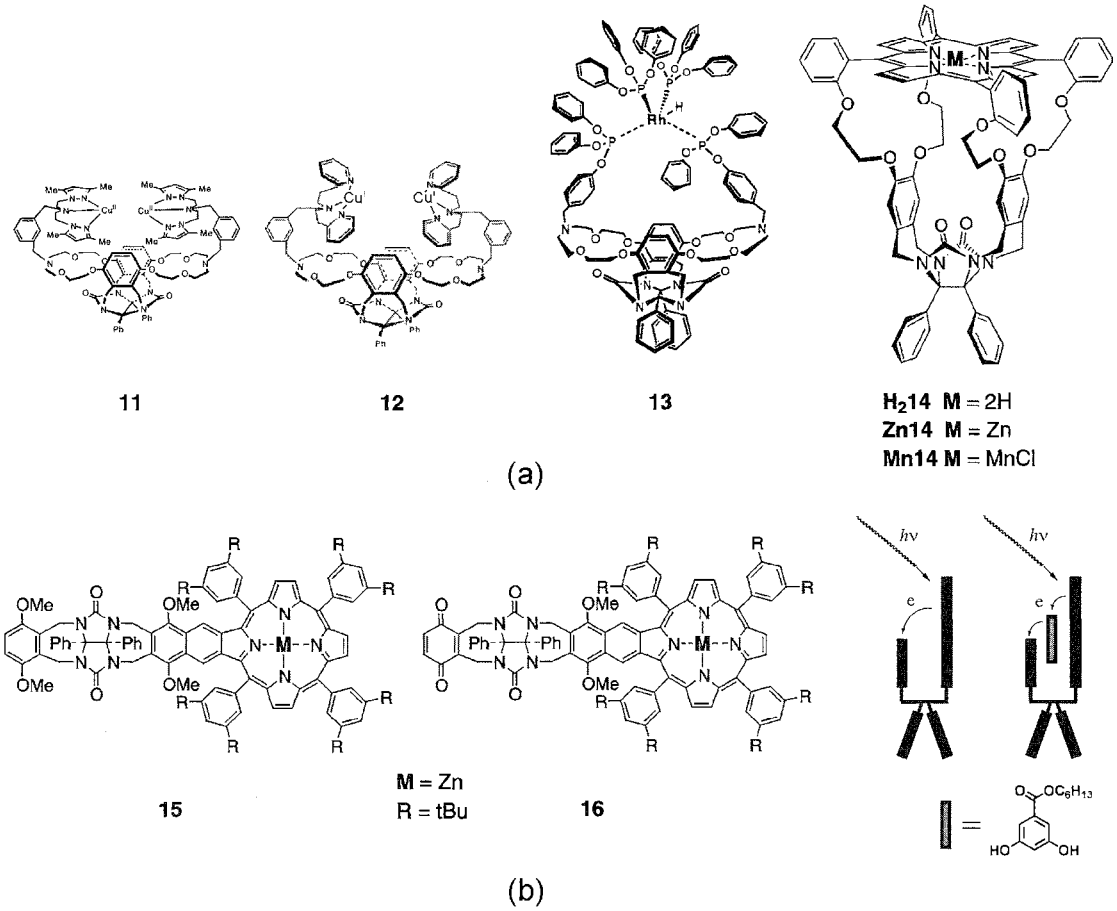

Fig. 3 (a) Examples of glycoluril-based supramolecular catalyst. (b) Porphyrin hosts **15** and **16** and the guest-mediated electron transfer occurring in these hosts.

enzymes, such as selective binding of a substrate, its catalytic conversion, and release of the product.

The first models were designed to carry out oxidation catalysis (Fig. 3a). Inspired by naturally occurring copper enzymes, pyrazole ligands were connected to a basket-shaped receptor. which, upon complexation of two Cu(II) metal centers, catalyzed the oxidation of alcohols to aldehydes (**11**).[12] The rate of oxidation of alcohols that were complexed in the receptor cavity, such as 3,5-dihydroxybenzyl alcohol: was accelerated more than 50,000 times compared to substrates that were not bound. The reaction, however, involved the irreversible reduction of Cu(II) to Cu(I) and, consequently. a stoichiometric amount of catalyst was required. The ideal oxidation catalyst would use molecular oxygen as the oxidant, e.g., as in the case of the tyrosinase enzyme. In order to mimic this property, the pyrazole ligands in **11** were replaced by pyridine ligands to give host molecule 12. This molecule, when complexed to two Cu(I) centers, was found to form metastable O_2 adducts in dichloromethane at $-85°C$, thus mimicking the naturally occurring hemocyanine oxygen carrier.[''''] Although 12 was still capable of complexing guests in its cavity. the host–guest geometry was not ideal. and oxidative splitting of the pyridine ligands of the host occurred in preference to oxidation of the guest. Molecular modeling confirmed that in the geometry formed upon O_2 complexation. the benzylic protons linking the pyridine functions to the basket are in direct proximity to the bound oxygen. Due to this close proximity. the host is oxidized in preference to the guest.

In addition to oxidative catalytic systems. glycoluril-based hydrogenation catalysts were developed. Following a synthetic methodology similar to that used for the preparation of **11** and 12. a tetrakis(triphenyl)phosphite Rh(I) hydride complex was linked to a molecular basket (13). The resulting supramolecular catalyst was capable of selectively catalyzing the hydrogenation of guests such as 5-allylresorcinol with a significant rate enhanceinent compared to nonbinding guests. e.g., 5-allyl-1,3-dimethoxybenzene.[14] The catalyst also exhibited many of the features encountered in enzymes. such as Michaelis–Menten kinetics. product inhibition, and rate enhanceinent by cooperative binding of a second substrate.

As a synthetic model of the enzyme cytochrome P450, a glycoluril-based host was equipped with a posphyrin roof.[15,16] Molecule H_2**14** possesses a rigid cavity in which a variety of guests. e.g., dihydroxybenzenes and viologen derivatives, can be bound. Because of cavity effects, **Zn14** displayed a high affinity for pyridine molecules ($K_a = 10^5\ M^{-1}$). As a result of a similar strong binding of pyridine in its cavity. host **Mn14** displayed an enhanced activity in the catalytic oxidation of alkenes.[17] Using **Mn14**, α-pinene was epoxidized at a 10 times higher rate than when manganese-tetrakis(*meso*-phenyl)porphyrin was used as the catalyst. When instead of pyridine the bulky ligand 4-t-butylpyridine was used, which does not fit in the cavity of **Mn14** and binds on the outside, no rate enhancement was observed. An advantage of this catalytic system was, however, that oxidative decomposition of the catalyst was inhibited, because the formation of μ-oxobridged manganese posphprin dimers no longer occurred.

Glycoluril-based hosts were also applied as mimics of the photosynthetic reaction center. One of the unresolved questions in the study of electron transfer processes in such a center is the role of intervening aromatic amino acid residues.[18] To study this role, a host was designed with one zinc-porphyrin side wall and one 1.4-dimethoxybenzene donor (15) or p-benzoquinone acceptor (16) side wall (Fig. 3b).[19,20] In a nonpolar solvent, such as cyclohexane or CCl_4, the fluorescence quantum yields of 15 and **16** were coinparable to that of zinc-tetrakis(*meso*-phenyl)porphyrin. In a more polar solvent, the quantum yield of **16** became much smaller due to solvent-mediated electron transfer from the porphyrin donor to the quinone side wall acceptor. A similar effect was observed when an excess of the guest hexyl 3.5-dihydroxybenzoate was added. Upon binding to Host 16 in CCl_4, this guest mediated the electron transfer, suggesting that in the natural system. the aromatic amino acid residues may play a similar role.

SELF-ASSEMBLY IN WATER

At the same time that Rebek's group began investigation of the hydrogen-bond self-assembly of glycoluril-based molecules into tennis-ball-like architectures,[21,22] we introduced water-soluble functionalities into glycoluril-based receptors with the objective to study the self-assembling behavior of the resulting molecules in water. The first approach was to attach long hydrocarbon tails to the nitrogen atoms of azacrown ether functionalized baskets. to give Compounds **17** and 18 (Fig. 4a). Upon dispersion of 17 in water, well-defined vesicles were formed with diameters between 500 and 4000 Å.[23,24] It was proposed that in these vesicles, the charged receptor cavities are directed toward the water layer, forming aggregates that possess a dimpled exterior. These supramolecular golf balls, as they became known. were still able to complex guests. such as magneson [4-(4-nitrophenylazo)resorcinol] in water. UV titrations indicated that below the critical aggregation constant (c.a.c.) of the compound, a 1:1 host–guest complex was formed ($K_a = 10^6\ M^{-1}$). Above the c.a.c., the titration data could only be fitted assuming a 2:1 host–guest complex ratio. This phenomenon was attributed to the fact that above the c.a.c., only the receptors on the outside of the

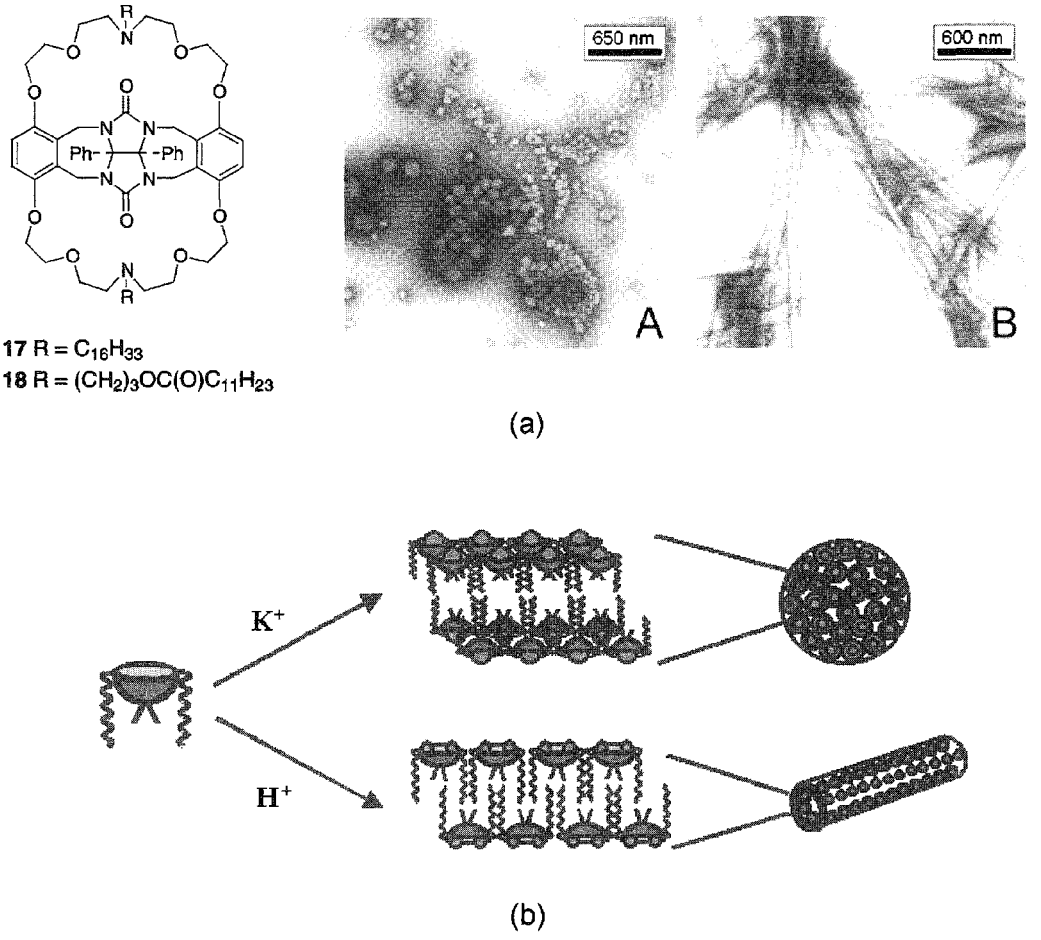

Fig. 4 (a) Transmission electron microscope images of aggregates formed by **17** in aqueous KCl solution (A) and in acidic water (B). (b) Proposed structures of the aggregates of 18 formed in the presence of K^+ and H^+ ions. (View *this art in color at www.dekker.com.*)

vesicle are able to bind magneson. and that the receptors on the inside of the vesicle are not accessible for the guests. Basket **18** was found to give tube-like assemblies with a diameter of 100 nm in aqueous HCl but vesicles in aqueous KCl or NaCl solution.[24,25] The morphologies of these superstructures could be manipulated by the addition of different alkali metal ions, such as Rb^+, which resulted in the formation of a mixture of tubes and vesicles. or Cs^+, which gave only nanotubes (Fig. 4a,b).

In the absence of guest molecules, Host 3b forms dimers in chloroforin as a result of cavity filling and favorable intermolecular π–π interactions (Fig. 1b). In chloroform. this dimerization was relatively weak (K_{dimer} = 16M^{-1}). It was reasoned, however. that this dimeriaation would be enhanced in water because of the hydrophobic effect. which acts as a driving force for self-assembly. Hosts **19**[26] and **20**[27,28] were designed and synthesized. both having a large hydrophobic cavity and on their convex side a water-soluble moiety, i.e., pyridinium in the case of **19** and a ruthenium–bipyridine coinplex in the case of 20 (Fig. 5a). Hosts **19** and 20 showed strong self-association in water (for both molecules K_{dimer} > 5000 M^{-1}). At concentrations above 1–2 mM, the solutions of **19** and **20** became turbid. and pearly dispersions were obtained. Samples of these dispersions were studied with the help of transmission electron microscopy (TEM) (Fig. 5b). A sample of **19** revealed the presence of well-defined razor-blade-like aggregates. which all had approximately the same shape and dimensions (1.2 x 8 μm) (Fig. 5b, A–C). Closer inspection of the aggregates showed that they were built up from a limited number of thin layers (approximately 50). Electron diffraction experiments revealed that the structures were not crystals but contained highly ordered arrays of molecules, displaying a repeating distance of 16.8 Å, which corresponds to approximately the length of one host molecule. Study of a sample of 20 showed the presence of rectangular aggregates that. similar to **19**, had well-defined

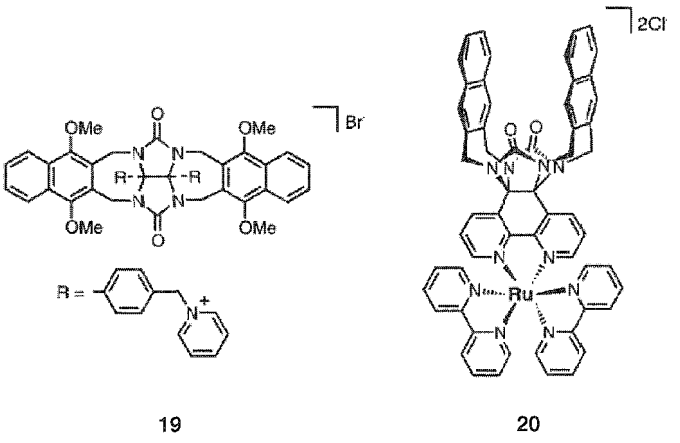

19 20

(a)

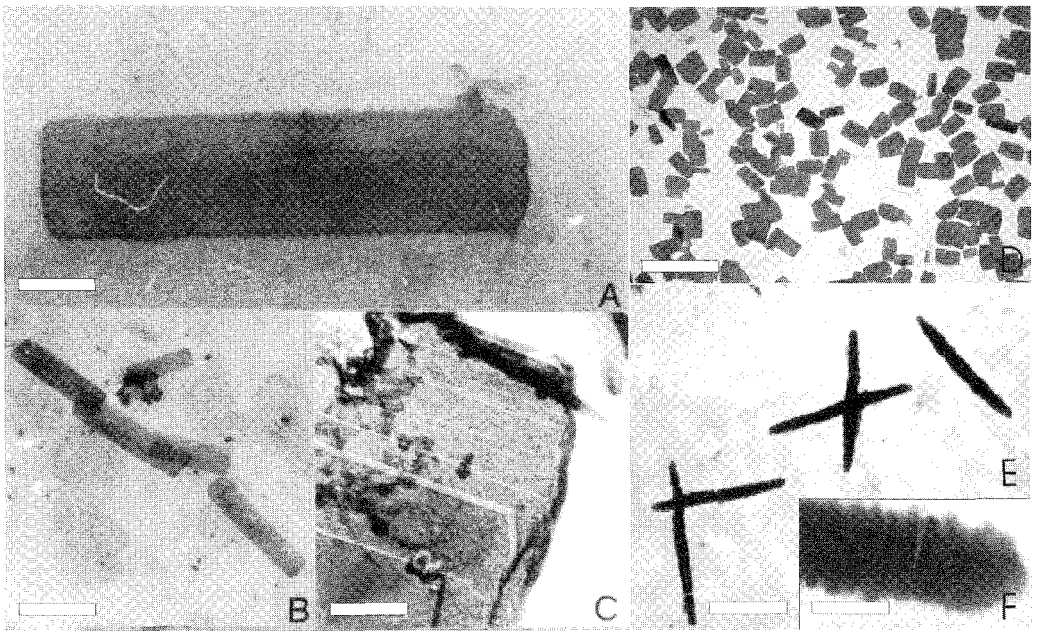

(b)

Fig. 5 (a) Water-soluble glycoluril hosts **19** and 20. (b) Transmission electron micrographs of dispersions of Hosts **19** and 20 in water: A,B—razor-blade structures formed by 19 (A: bar = 900 nm, B: bar = 3500 nm); C—layered structure of a razor blade formed by **19,** bar = 120 nm; D—rectangular aggregates formed by 20. bar = 800 nm; E—cigar-like superstructure of the rectangular aggregates formed by 20, bar = 1500 nm; F—close-up of a "cigar" formed by 20, showing its constituting components. bar = 350 nm. (c) Proposed mechanism of hierarchical growth of the aggregates derived from **20**.

shapes and sizes (350 x 150 nm) (Fig. 5b, D). Interestingly, in some cases no rectangular aggregates were formed by 20, but larger "cigar-like" aggregates were formed (Fig. 5b, E). Close inspection of these "cigars" revealed that they were built up from smaller subunits that had the same dimensions as the rectangular aggregates. It was concluded, therefore, that the cigars are a higher-order aggregate of the rectangles.

Based on NMR, fluorescence; and powder diffraction experiments, for both **19** and **20**, a similar aggregate growth process was proposed. In Fig. 5c, a schematic representation of this growth process is depicted for compound 20. It starts with the formation of a head-to-head dimer, in which two molecules of **20** dimerize as a result of hydrophobic cavity filling. In a next step, dimers of 20 form an array, to which in a competing process molecules of 20 are attached in a head-to-tail binding geometry. Eventually. lamellar sheets of host molecules are formed that stack on top of each other, forming a rectangular structure.

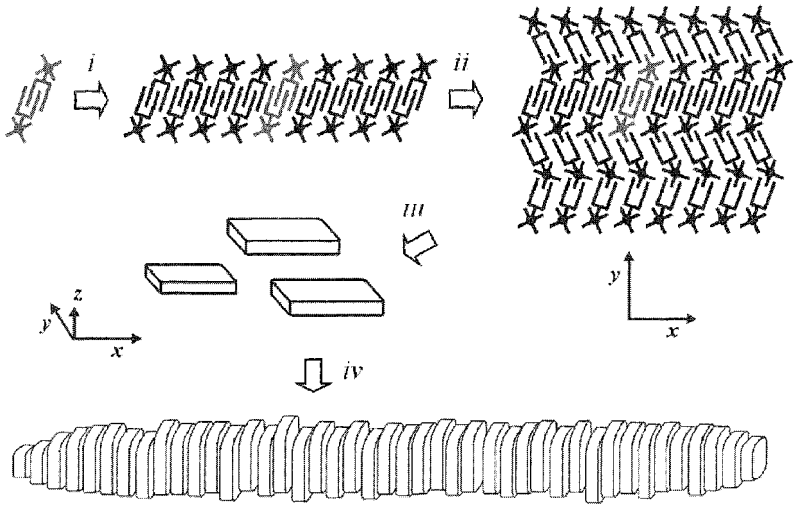

(c)

Fig. 5 (*Continued*)

A unique aspect of the aggregates formed by 19 and 20 is that they are so well-defined in shape and size. The final shape of the aggregates apparently is encoded within the glycoluril building block. The fact that the aggregates have a finite shape is attributed to a fine balance between the enthalpy, i.e., the strength of the interactions between the molecules. and the entropy of the growth processes. At a certain moment. it is not favorable to attach new monomeric units to the relatively hydrophilic exte ior of the aggregates. It appeared that when the dispersion of 28 was prepared at higher temperatures (e.g., 70°C), the rectangular aggregates became smaller and more well-defined in size. At elevated temperatures, as a result of the increased contribution of kinetics. only the inost favorable modes of aggregation occur, and hence, a more defined aggregate structure is obtained. This unique phenomenon resembles self-repair processes that are ubiquitous in self-assembling systems occurring in nature.

SOLID-STATE MATERIALS

In order to introduce the aspect of liquid crystallinity in glycoluril-based hosts. Compound **21**, which has 12 hydrocarbon chains connected to its side walls. was designed and synthesized (Fig. 6a).[25,29] Molecules of 21 predominantly exist in the *syn–anti* conformation. but upon binding of a guest. the *anti–anti* conformation is induced. and the resulting complex exhibits liquid-crystalline (LC) properties. By changing the host–guest ratio, the nature and temperature range of the various LC phases could be tuned. The versatility of this concept of supramolecular induction of liquid crystallinity was demonstrated when multifunctional guests were used. The 4:1 host–guest complex of **21** with porphyrin 22 also displayed LC behavior. If a porphyrin that cannot bind was used, no mesophases were formed, which confirmed that the host–guest complex is the mesogenic species. Not only were the material properties of the porphyrin changed but also were its redox properties. Electrochemical studies revealed that the porphyrin core is encapsulated in the 48 hydrocarbon tails of the four hosts (Fig. 6b), causing the reduction potentials of the porphyrin to alter in a similar way to certain porphyrin-containing enzymes. such as cytochrome C. Through an identical process, liquid crystallinity could also be induced in polymers. The host–guest complex of **21**, with a copolymer of styrene and 3,5-dihydroxystyrene, gave a stable, discotic-like mesophase.

In another approach to introduce liquid crystallinity, aliphatic tails were connected to the convex side of a glycoluril-based host (23. Fig. 6a).[30,31] It was reasoned that in the solid state. this host would form dimers. in a similar way as the parent compound **3b**. As can be seen in Fig. 6c. such a dimer resembles the structure of a typical rod-like mesogen. Although the material formed by 23 exhibited the typical features of a liquid crystal, i.e., birefringent optical textures and a high degree of malleability, calorimetric and powder diffraction measurements showed that it was a plastic crystal composed of lamellae of dimers (Fig. 6c). Strong π–π interactions between the aromatic surfaces of adjacent molecules are the reason the material is not liquid crystalline. The

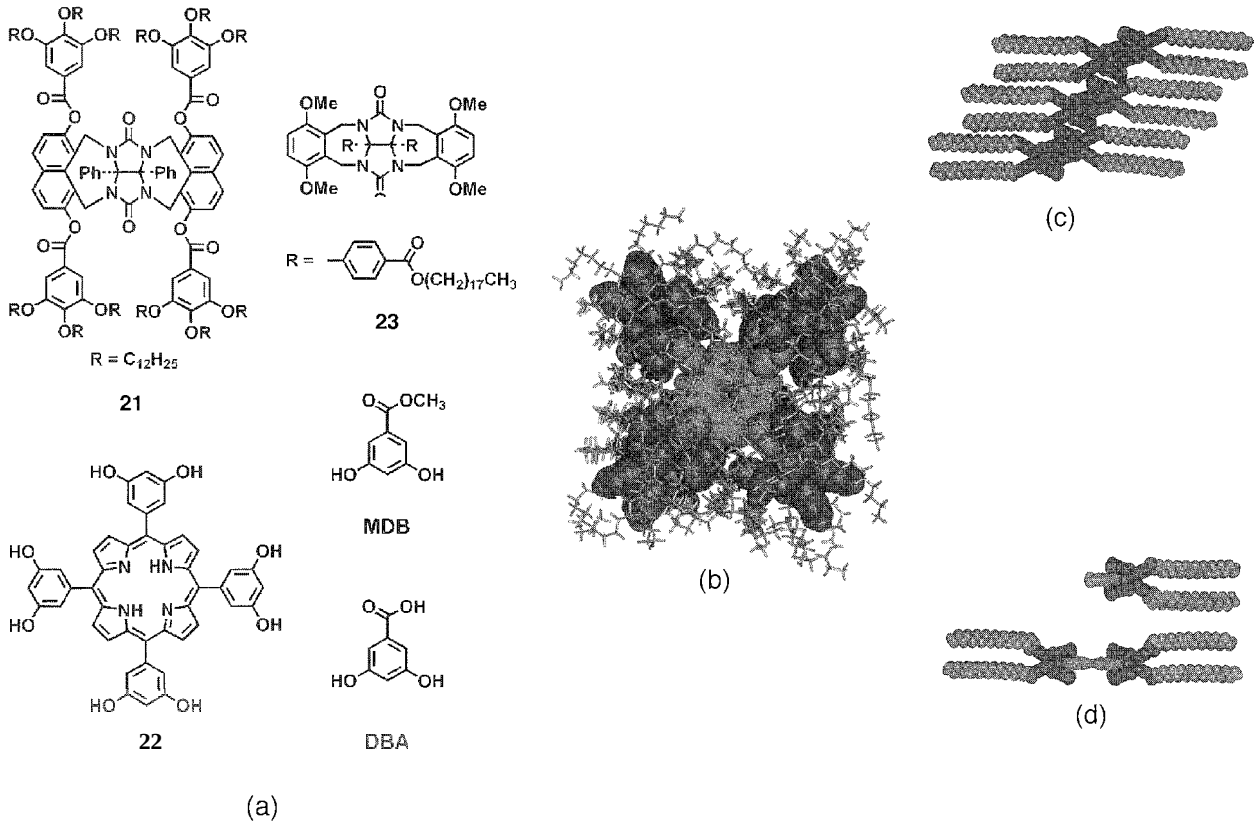

Fig. *6* (a) Host and guest molecules used in the glycoluril-based materials. (b) Computer–modeled representation of the liquid-crystalline host–guest complex between porphyrin %% and four molecules of Host 21. (c) Modeled structure of the arrangement of dimers in the lamellar plastic crystal formed by **23**. (d) Modeled structures of the 1:1 host–guest complexes between 23 and MDB (top) and between 23 and DBA (bottom). *(View this art in color at www.dekker.com.)*

materials properties of 23 could be tuned by the incorporation of guest molecules in the solid state (Fig. 6d). An equimolar complex of 23 and methyl 3,5-dihydroxybenzoate (**MDB**) lost its lamellar crystalline properties. due to the fact that the dimeric structure of the host was broken. A 1:1 complex of *23* and 3,5-dihydroxybenzoic acid (DBA). however, gave a material that showed a similar solid state behavior as free 23. Powder diffraction measurements revealed that the host–guest coinplex adopted a similar lamellar arrangement as the uncomplexed host, however, with an extended lamellar distance.

CONCLUSION

The preceding overview demonstrates that simple glycoluril building blocks can be used to create a wealth of host molecules capable of binding a variety of guests with very high binding constants. The host–guest systems proved their applications in functional mimics of biological systems. such as receptors, enzymes. and the photosynthetic reaction center. In recent years, the hosts were shown to be versatile building blocks in the self-assembly of well-defined nanosized materials, both in solution and in the solid state. It can be foreseen that in the near future, both features of glycoluril-based hosts, i.e., function and self-assembly, will be combined to generate highly ordered and functional supramolecular materials of which the properties can be precisely controlled.

ARTICLES OF FURTHER INTEREST

Artificial Enzymes, p. *76*
Concave Reagents, p. 311
Cucurbituril, Its Homologues, and Derivatives, p. 390
Enzyme Mimics, p. 546
Self-Assembling Capsules, p. *1231*
Supramolecular Polymers, p. 1443

REFERENCES

1. Zhao, J.: Kim. H.-J.; Oh. J.; Kim. S.-Y.; Lee, J.W.; Sakamoto. S.: Yamaguchi, K.; Kim. K. Cucurbit[n]uril derivatives soluble in water and organic solvents. Angew. Chem., Int. Ed. 2081. *40* (22). 4233.
2. Sijbesma. R.P.: Kentgens. A.P.M.: Nolte, R.J.M. Binding of dihydroxybenzenes in synthetic molecular clips. Effect of hydrogen bonding and n-stacking. J. Org. Chem. 1991. *56* (10). 3199.
3. Rowan. A.E.; Elemans. J.A.A.W.; Nolte. R.J.M. Molecular and supramolecular objects from glycoluril. Acc. Chem. Res. 1999. *32* (12), 995.
4. Sijbesma. R.P.; Kentgens, A.P.M.: Lutz. E.T.G.: Van der Maas. J.H.; Nolte, R.J.M. Binding features of molecular clips derived from diphenylglycoluril. J. Am. Chem. Soc. 1993, *115* (20). 8999.
5. Reek. J.N.H.; Priem, A.H.; Engelkamp, H.: Rowan, A.E.; Elemans, J.A.A.W.; Nolte, R.J.M. Binding features of molecular clips. Separation of the effects of hydrogen bonding and $\pi-\pi$ interactions. J. Am. Chem. Soc. **1997**, *119* (42), 9956.
6. Sijbesma. R.P.: Wijmenga, S.S.: Nolte. R.J.M. A molecular clip that binds aromatic guest by an induced fit mechanism. J. Am. Chem. Soc. **1992**, *114* (25). 9807.
7. Reek, J.N.H.; Engelkamp. H.; Rowan. A.E.; Elemans. J.A.A.W.: Nolte, R.J.M. Conformational behaviour and binding properties of naphthalene-walled clips. Chem. Eur. J. **1998**, *4* (4). 716.
8. Jansen. R.J.: de Gelder. R.: Rowan. A.E.: Scheeren. H.W.: Nolte, R.J.M. Molecular clips based on propanediurea. Exceptionally high binding affinities for resorcinol guests. J. Org. Chem. **2001**, *66* (8). 2643.
9. Schenning, A.P.H.J.; de Bruin. B.; Rowan, A.E.: Kooijman. H.; Spek. A.L.: Nolte. R.J.M. Strong binding of paraquat and polymeric paraquat derivatives by basket shaped hosts. Angew. Chem., Int. Ed. Engl. 1995. *34* (19). 2132.
10. Ashton, P.R.: Philp, D.; Reddington, M.V.: Slawin, A.M.Z.: Spencer. N.: Stoddart. J.F.: Williams, D.J. The self-assembly of complexes with [2]rotaxane superstructures. J. Chem. Soc., Chem. Commun. 1991, (23); 1680.
11. Sijbesma, R.P.; Nolte, R.J.M. A molecular clip with allosteric binding properties. J. Am. Chem. Soc. 1991. *113* (17), 6695.
12. Martens. C.F.: Klein Gebbink, R.J.M.: Feiters. M.C.: Nolte, R.J.M. Shape selective oxidation of benzylic alcohols by a receptor functionalized with a dicopper (TI) pyrazole complex. J. Am. Chem. Soc. 1994, *116* (13). 5667.
13. Klein Gebbink, R.J.M.: Martens. C.F.; Feiters, M.C.: Nolte, R.J.M. Novel molecular receptors capable of forming Cu_2-O_2 complexes. Effect of pre-organisation on O_2 binding. Chem. Cornmun. **1997**, (4), 389.
14. Coolen. H.K.A.C.: van Leeuwen. P.W.N.M.; Nolte. R.J.M. Substrate selective catalysis by rhodium metallohosts. J. Am. Chem. Soc. 1995. *117* (48). 11906.
15. Rowan, A.E.: Aarts. P.P.M.: Koutstaal. K.W.M. Novel porphyrin-viologen rotaxanes. Chem. Commun. 1998. (5). 611.
16. Elemans, J.A.A.W.: Claase, M.B.: Aarts, P.P.M.; Rowan, A.E.; Schenning, A.P.H.J.: Nolte, R.J.M. Porphyrin clip derivatives derived from diphenylglycoluril. Synthesis, conformational analysis and binding properties. J. Org. Chem. 1999, *64* (19). 7009.
17. Elemans. J.A.A.W.: Bijsterveld, E.J.A.: Rowan. A.E.; Nolte, R.J.M. A host–guest epoxidation catalyst with enhanced activity and stability. Chem. Commun. **2000**, (24), 2443.
18. Several authors. *Renction Centers of Photosynthetic Bncterin;* Michel-Beyerle. M.-E.. Ed.; Springer-Verlag: Berlin, 1992.
19. Reek. J.N.H.;Rowan. A.E.; de Gelder, R.: Beurskens, P.T.: Crossley. M.J.: de Feyter, S.: de Schryver, F.; Nolte, R.J.M. Novel cleft-containing porphyrins as models for studying electron transfer processes. Angew. Chem.. Int. Ed. Engl. **1997**, 36 (4), 361.
20. Reek. J.N.H.; Rowan, A.E.; Crossley. M.J.: Nolte. R.J.M. Synthesis and photophysical properties of porphyrin-functionalized molecular clips. J. Org. Chem. 1999. *64* (18), 6653.
21. Conn. M.M.: Rebek, J., Jr. Self-assembling capsules. Chem. Rev. 1997. 97 *(5)*. 1647.
22. Rebek. J., Jr. Reversible encapsulation and its consequences in solution. Acc. Chem. Res. 1999. *32* (4). 278.
23. Schenning, A.P.H.J.: de Bruin. B.; Feiters, C.M.; Nolte. R.J.M. Molecular golfballs: Vesicles from bowl-shaped host molecules. Angew. Chem., Int. Ed. Engl. 1994. *33* (15–16), 1662.
24. Schenning. A.P.H.J.: Escuder, B.; van Nunen. J.L.M.: de Bruin, B.: Lowik. D.W.P.M.: Rowan, A.E.; van der Gaast. S.: Feiters. M.C.: Nolte. R.J.M. Synthesis, aggregation. and binding properties of synthetic amphiphilic receptors. J. Org. Chem. **2001**, 66 (5). 1538.
25. Van Nunen, J.L.M.: Stevens. R.S.A.; Picken. S.J.; Nolte. R.J.M. Tunable supramolecular structures from clips and baskets derived from glycoluril. J. Am. Chem. Soc. 1994. *116* (19), 8825.
26. Reek. J.N.H.; Kros. A.; Nolte. R.J.M. Novel water soluble molecular clips. Toward nanostructures with controlled shape. Chem. Commun. 1996. (2). 245.
27. Elemans. J.A.A.W.: de Gelder. R.: Rowan. A.E.; Nolte. R.J.M. Bipyridine functionalized molecular clips. Self-assembly of their ruthenium complexes in water. Chein. Commun, 1998. (15). 1553.
28. Elemans. J.A.A.W.: Rowan. A.E.: Nolte. R.J.M. Hierarchical self-assembly of amphiphilic metallo-hosts to give discrete nanostructures. J. Am. Chem. Soc. 2002. *124* (7). 1532.
29. Van Nunen. J.L.M.: Folmer, B.F.B.; Nolte, R.J.M. Induction of liquid crystallinity by host–guest interactions. J. Am. Chem. Soc. **1997**, *119* (2). 283.
30. Holder. S.J.; Elemans. J.A.A.W.: Barberá. J.: Rowan, A.E.; Nolte. R.J.M. Host–guest complexes with tunable solid-state structures. Chem. Commun. 2000. (5). 355.
31. Holder, S.J.; Elemans. J.A.A.W.; Donners, J.J.J.M.: Boerakker. M.J.: de Gelder, R.: Barberá. J.; Rowan. A.E.: Nolte, R.J.M. Lamellar organic thin films through self-assembly and molecular recognition. J. Org. Chem. **2001**. 66 (2), 391.

Gossypol

Bakhtiyar T. Ibragimov
Samat A. Talipov
Institute of Bioorganic Chemistry of Uzbekistan Academy of Sciences, Tashkent, Uzbekistan

INTRODUCTION

Gossypol (Gp) is a natural polyphenolic compound[1] found in different organs of the cotton plant. This yellow pigment exists in plants as a protective agent against insects and diseases and is therefore sufficiently toxic even for human and animal organisms.[2] It is called Gossypol in order to indicate its plant origin (Gossypium) and chemical nature (phenol). Gp has been known from the end of the 19th century. Nevertheless, its unusual ability to demonstrate different types of biological activity and to form numerous supramolecular complexes has been discovered comparatively recently. In this entry. Gp's biological action. specific features of its chemical structure. stereochemistry. tautomerism. and optical activity will be briefly described. Special attention will be paid to its unique host properties, pseudopolymorphism (existing of the given host–guest complex in different crystal modifications) phenomenon. organic zeolite formation ability, and the reasons that make Gp a versatile host.

BIOLOGICAL ACTION AND STRUCTURE

Gp is not just harmful for humans and animals product. it may have a lot of useful applications. As it is one of the strongest antioxidants found in nature, investigators have tried to use it in the textile. rubber, and petroleum industries. but practical application of this natural compound is related mainly to its biological activity. Early investigations of Gp biological action revealed its antiviral and anticancer activities. Gp became the object of intensive biomedical studies after the discovery of its oral male contraceptive properties a quarter of century ago in China.[3] Later research showed that it has antifertility effects in males and females. A lot of other types of biological activity are characteristic for Gp, among which it is worth indicating its antimicrobial, antimalarial, antiparasitic, anti-HIV. immunosupressive, and interferon-inducing actions.'" To date, interest in the biological properties of Gp is still high, and dozens of papers devoted to it appear monthly.

The chemical structure of Gp was established by Adams[5] in the 1940s as a highly substituted symmetric binaphthalene (Scheme 1). The main factors defining stereochemistry of the molecule are the mutual arrangement of the naphthyl moieties (the dihedral angle) and disposition of the isopropyl groups relative to the appropriate halves. The dihedral angle between naphthyl moieties ranges from 70–106° in Gp crystals studied.[6] All polar substitutents are grouped on the one side of the naphthyl fragments, while hydrophobic parts are located on the opposite side. Such concentration of the polar groups makes possible the formation of an extensive system of intramolecular hydrogen bonds. The adjacent hydroxyl groups O3–H (O7–H) and O4–H (O8–H) are involved in H-bonding. giving rise to a five-membered conjugated ring system. whereas the H-bonded hydroxy O3–H (O7–H) and oxygen atom of the aldehyde group are part of a six-membered conjugated system. A coplanar arrangement of the naphthyl ring and aldehyde group forces the H-atom of the aldehyde group and hydroxy oxygen O1 (O5) to be displaced a short distance. This contact also can be considered as an intramolecular C–H...O hydrogen bond. The orientation of the hydroxy group O1–H (O5–H) enables an interaction of its H-atom with the π-electrons of the aromatic system in the other half of the molecule. In order to explain some features of Gp chemical behavior. Adams postulated the existence of the three tautomeric forms for Gp: aldehyde, quinoid. and hemiacetal.[5] The aldehyde form is the only tautomer found in numerous crystal modifications of Gp. The other two tautomers are fixed in Gp derivatives. The quinoid form is typical for solid-state Shiff's-base-type derivatives, while the hemiacetal tautomer is characteristic of crystalline Gp ethers.

Relatively bulky methyl and hydroxyl substitutents located in ortho-positions to the ordinary bond make a free rotation of the naphthyl moieties around the aryl–aryl bond impossible and give rise to the two distinguishable molecular conformations (atropoisomers) or two optically active forms (enantiomers). The racemization of chiral Gp takes place in raising the temperature up to 190°C. Only some kinds of cotton plants may synthesize enantiomeric Gp with a small excess (15–20%)—one of

Encyclopedia of Supramolecular Chemistry
DOI: 10.1081/E-ESMC 120012747

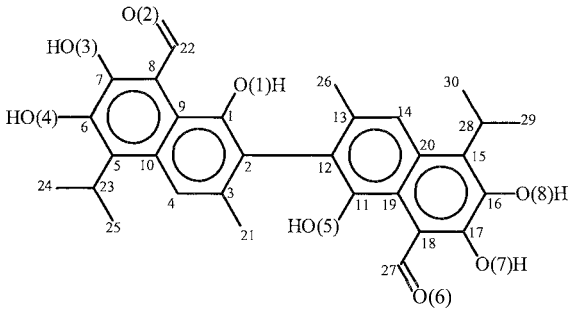

Scheme 1 Gossypol molecule.

the antipodes. Therefore, optically active Gp for biomedical research has been obtained by chroinatographic separation of diastereoisomeric derivatives.[7] Results demonstrated that for main types of Gp bioactivity, a (−)-isomer is responsible (the absolute configuration of this antipode is determined as R by circular dichroism experiments).[8] This situation stimulated a search for relatively cheap and quick resolution methods for large-scale preparation of the R-form. The classic technique for resolution of racemates by preparation of diastereisomeric salts or enamine-type derivatives with subsequent fractional crystallization failed because of the surprisingly strong resistance of Gp to separation. The resolution of racemic Gp, however, by direct crystallization. has been achieved recently using polymorphism phenomena of the given host–guest complex.[9] It has been known for some time that crystallization of Gp from solutions in acetone results in formation of the stable 1:1 host–guest complex of racemic Gp with solvent molecules.[10] The lowering of crystallization temperature to −20°C leads to formation of the unstable 1:3 solvate of enantiomeric Gp with acetone.[11] i.e., unique host properties of Gp have been used for resolution of the racemic product.

GOSSYPOL—A UNIQUELY VERSATILE HOST COMPOUND

Investigations carried out by Adams and coworkers identified Gp complexes with pyridine and the first four members of the homologous *n*-monocarboxylic acids. Three crystal forms of Gp recrystallized from chloroform, ligroin, and a mixture of diethyl ether with petroleum ether have different melting points and have been considered as polymorphs.[12] These compounds. however. have not been characterized structurally. and therefore. their natures remain unknown. The recently established fin the 1980s) bioactivity of Gp required its large-scale production. Therefore, an Experimental Plant of the Institute of Bioorganic Chemistry of the Uzbekistan Academy of Sciences initiated production of this compound from by-products of the cottonseed industry. The production encountered instability problems of the physicochemical parameters of the final product precipitated from solutions in the binary solvent diethyl ether–hexane. In order to explain such behavior. we studied crystallization of Gp from that solution. Results showed that Gp could be crystallized from this binary solvent in four different crystal forms (two solvates and two polymorphs). This situation prompted us to conduct systematic investigations of Gp crystallization from a large number of organic solvents (polar, nonpolar, protic, aprotic, acids, alcohols, ketones, aldehydes, etc.) and led to the discovery of its unusual host property: Gp can form inclusion (host–guest) complexes (clathrates) with every solvent (120 examples). Therefore, the preparation of host–guest complexes with solid-state guests using common solvent for both components is a problem in the case of Gp, because the solid-state product is forced out from the complex formation by competing solvent molecules. Despite this problem, clathrates of Gp with solid-state species such as tropolone and naphthalene have been obtained.

To date, single crystals of over 80 Gp inclusion compounds have been prepared and characterized. The x-my structure determination was carried out for 45 clathrates. Results attested that depending on chemical nature (polarity), guest molecules may interact with the host component by using specific forces such as hydrogen bonds (coordinatoclathrates), or they may have no such interactions (true clathrates). Guest inolecules may be located in channels (tubulates), layers between host molecules (intercalates or layer-type clathrates), or totally enclosed cages (cryptates).[6] Gp can easily adjust its packing mode to form voids with shape. size. and chemical natures complementary to the guest molecules to be accommodated. This is achieved by producing a large variety of hydrogen-bonded assembles. Geometrical parameters of the intermolecular H-bonds formed by any of six potential proton-donor or eight proton-acceptor groups of Gp indicate that they are not very strong. This means that association of the host molecules is not driven by a single type of interaction. instead, Gp molecules form numerous, weak. even bent and multicenter intermolecular H-bonds. Therefore, alteration of the host molecules' association modes does not have to be related to large energetic changes in the system. which may explain the diversity of Gp crystal forms (see below).

Gp inolecules may be incorporated into finite bimolecular associates by centrosymmetric H-bonds (O5–H...O3, 05–H...O2, and O1–H...O2) and axially symmetric bonds (O1–H...O8 and O1–H...O6). These

Table 1 Crystal data of the typical representatives of the isostructural groups of gossypol clathrates* (classification of gossypol clathrates)

Structural type	Isostructural group	Guest	Space group	H:G	Clathrate type	a, (Å)	b, (Å)	c, (Å)	α, (°)	β, (°)	γ, (°)	V, (Å^3)	d, g . cm^{-3}
I	A	Acetone	P-1	1:1	HT	10.665(2)	11.135(2)	14.379(3)	76.47(2)	108.67(1)	77.72(1)	1494	1.28
	B	Butanal	P-1	1:1	HT	10.190(2)	11.355(1)	15.618(2)	69.40(1)	108.48(1)	81.07(1)	1530	1.28
II	A	Acetic acid	P-1	1:1	HT	14.278(7)	6.924(5)	14.706(6)	91.90(5)	92.34(3)	98.71(5)	1435	1.34
	B	DMSO	P-1	1:1	HT	15.132(2)	7.207(1)	14.726(3)	90.90(1)	66.94(1)	96.15(1)	1468	1.35
	C	*n*-Valeric acid	P-1	1:2	HT	19.387(4)	6.912(2)	14.506(3)	93.22(3)	78.85(2)	96.08(3)	1895	1.27
III	A	Benzaldehyde	P-1	2:3	HC	10.959(2)	14.116(2)	11.418(2)	73.62(1)	92.27(1)	91.71(1)	1693	1.33
	B	Salicylaldehyde	$P2_1/n$	1:2	HC	11.130(2)	29.542(5)	11.744(2)		98.45(1)		3820	1.33
IV	A	Tetrachlormethane	P-1	1:1	VC	8.847(2)	14.304(6)	13.395(5)	102.54(3)	69.53(3)	91.12(3)	1547	1.44
	B	Diethyl ether	$P2_1/c$	1:1	VT	8.557(2)	14.474(5)	25.651(5)		107.22(2)		3035	1.30
	C	Diethyl ether	$P2_1$	2:1	VT	8.497(4)	14.546(5)	23.031(6)		99.53(2)		2807	1.32
V	A	Chloroform	C2/c	1:1	VI	28.464(4)	8.948(1)	26.480(4)		108.93(1)		6380	1.33
	B	Toluene	$P2_1/c$	4:3	VC	20.615(4)	16.134(3)	19.344(4)		109.14(2)		6078	1.28
	C	Benzene	P-1	2:1	VC	11.241(3)	14.986(4)	17.380(4)	98.89(2)	99.86(2)	98.91(2)	2800	1.32
VI	A	Amyl acrylate	P-1	2:1	HC	14.425(2)	15.519(1)	16.409(2)	97.89(1)	117.80(1)	67.01(1)	2987	1.31
VII	A	1,3-Dioxane	P-1	1:1	HT	12.149(4)	14.310(3)	18.687(3)	91.08(2)	94.16(2)	94.94(2)	3227	1.25
	B	Salicylaldehyde	P-1	1:1	HT	13.834(3)	14.874(3)	18.403(2)	66.60(1)	109.12(1)	109.63(2)	3190	1.33
VIII	A	Dichloromethane	C2/c	1:1	VT	21.320(4)	19.129(6)	15.765(2)		113.05(2)		5916	1.36
IX	A	Ethyl-(S) (−) lactate	C2	5:4	HC	21.562(3)	28.499(3)	25.783(6)		94.38(2)		15797	1.27
X	A	Ethyl acetate	C2/c	2:1	HC	11.143(2)	30.769(5)	16.507(3)		90.25(2)		5659	1.32
	B	Isobuthyl acetate	$P2_1/n$	2:1	HC	11.445(2)	30.724(5)	16.552(2)		91.83(2)		5817	1.32
XI	A	Pyridine	P21/c	1:3	HT	10.276(3)	20.380(4)	19.159(6)		93.95(2)		4003	1.25
XII	A	1,4-Dioxane	Pbcn	1:3	HT	25.459(9)	11.923(3)	13.608(2)				4131	1.26
XIII	A	Tropolone	C2/c	1:2	HT	35.589(3)	12.889(1)	18.591(2)		118.54(1)		7492	1.35
XIV	A	Acetone	$P2_12_12_1$	1:3	HT	9.0208(7)	17.488(1)	24.358(2)				3843	1.21

*H:G = host:guest ratio.

associates or single Gp molecules are further incorporated by O8–H...O4 bonds (there are three kinds of this bond with different symmetrical relationships between proton-donor and proton-acceptor groups) or by O8–H...O2 and O1–H...O6 M-bonds to infinite higher-order networks. The networks found are one-dimensional (chain or column-like) or two-dimensional (layer-like) associates. A three-dimensional network has not been revealed among gossypol crystals.[113] The similarities of hydrogen bond patterns of the host (0, 1-, and 2-dimensional sets) or host–guest interactions (true clathrates or coordinato-clathrates) give a basis for classifying gossypol inclusion complexes into 14 structural types (Table 1). The same host associate of the definite structural type may be packed by different modes, leading to various crystal systems with different host:guest ratios (e.g., types III–V, X; Table 1) or affected by slight changes from the disappearance or formation of certain H-bonds (e.g., types I. II, and VII). Such situations subdivide some structural types into up to three subtypes or isostructural groups, leading to 24 groups in total. Some of these groups are represented by one clathrate only (e.g., groups II C, XI A. or XII A), but there are many groups having more than five representatives (e.g., group X A has 14 members). For the designation of isostructural clathrate groups (clathrate types). two-lettered symbols have been used

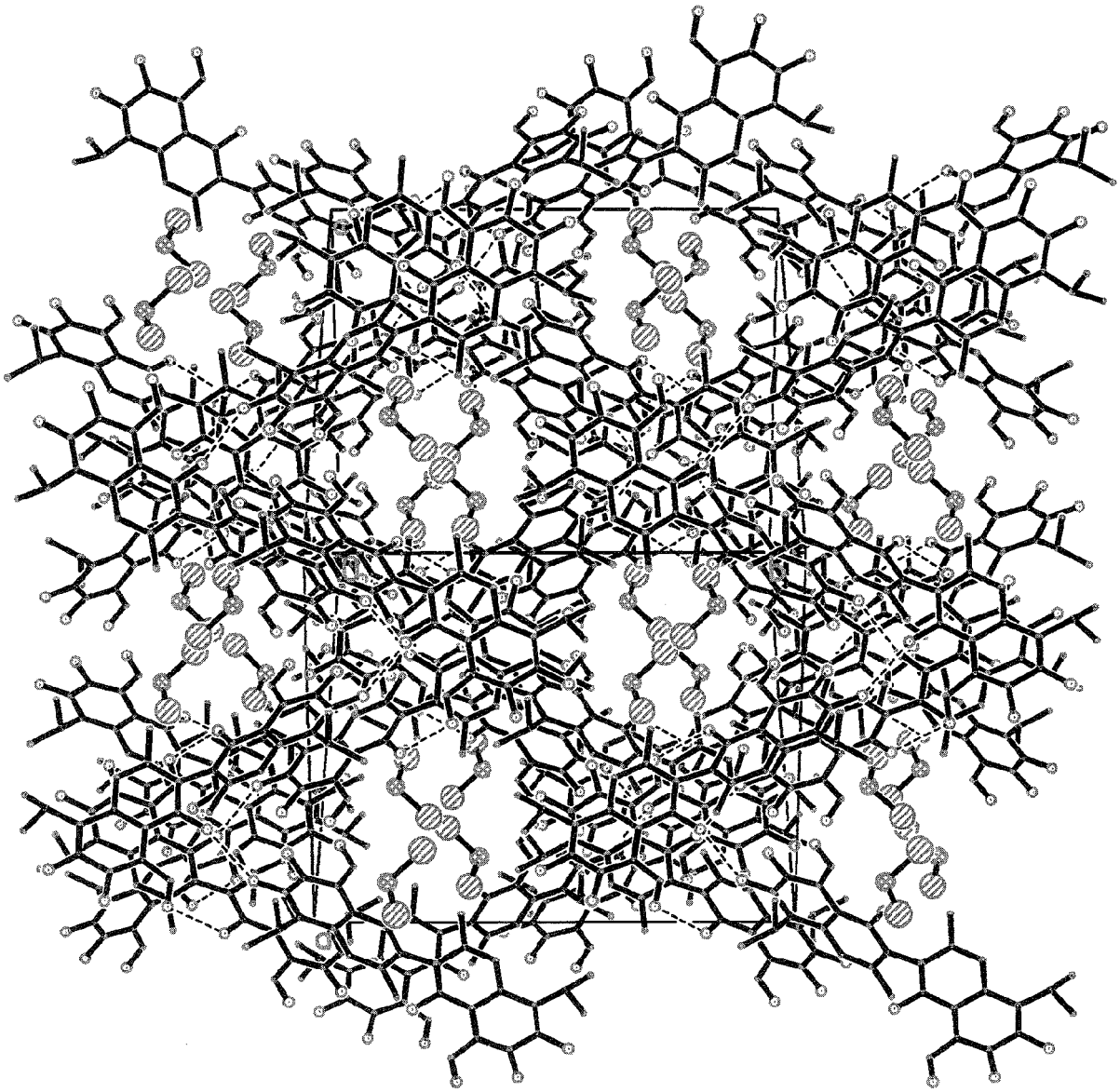

Fig. 1 *Clathrate* of gossypol with *dichloromethane.* (*View this art in color at www.dekker.com.*)

(Table 1). The first symbol indicates the host–guest interaction (M-coordinatoclathrates, V-true clathrates, or interaction with van-der-Waals forces), and the second specifies a topology of space occupied by guest molecules (T-tubulates, I-intercalates, and G-cryptates).

An inclusion compound of Gp may be sensitive to the shape and form of the guest molecule, e.g., each addition of a subsequent Cl atom to the CH_2Cl_2 molecule leads to formation of the new type of clathrate (rnorphotrophic transition): the host–guest complex of CH_2Cl_2 with Gp is an unstable tubulate (group VIII A; Fig. 1), the clathrate of $CHCl_3$ is a relatively stable intercalate (group V A; Fig. 2) and the solvate of CCl_4 is a very stable cryptate (group IV A; Fig. 3).[6] On the other hand, in some cases, inclusion complex formation by Gp may be not so sensitive to the geometry of the guest molecule, e.g., species relating to ketones, alcohols. acids, esters. dimethylformamide, acetonitrile, nitromethane. and tetrahydrofuran (16 entities) form isostructural inclusion compounds of group I A (Fig. 4).[14] In this example, different kinds of guest molecules form the same types of inclusion compound. The opposite situation is of great interest — formation of different types of Gp clathrates by the given guest molecule.

CAN GOSSYPOL FORM DIFFERENT INCLUSION COMPLEXES WITH THE SAME GUEST?

There were already two examples of such a possibility when we decided to investigate it in detail — diethyl ether and salisylaldehyde each form two different clathrates with Gp (Table I). The semisolvate of Gp with diethyl ether is obtained by desolvation of the monosolvate,[15] whereas clathrates of salisylaldehyde are formed from

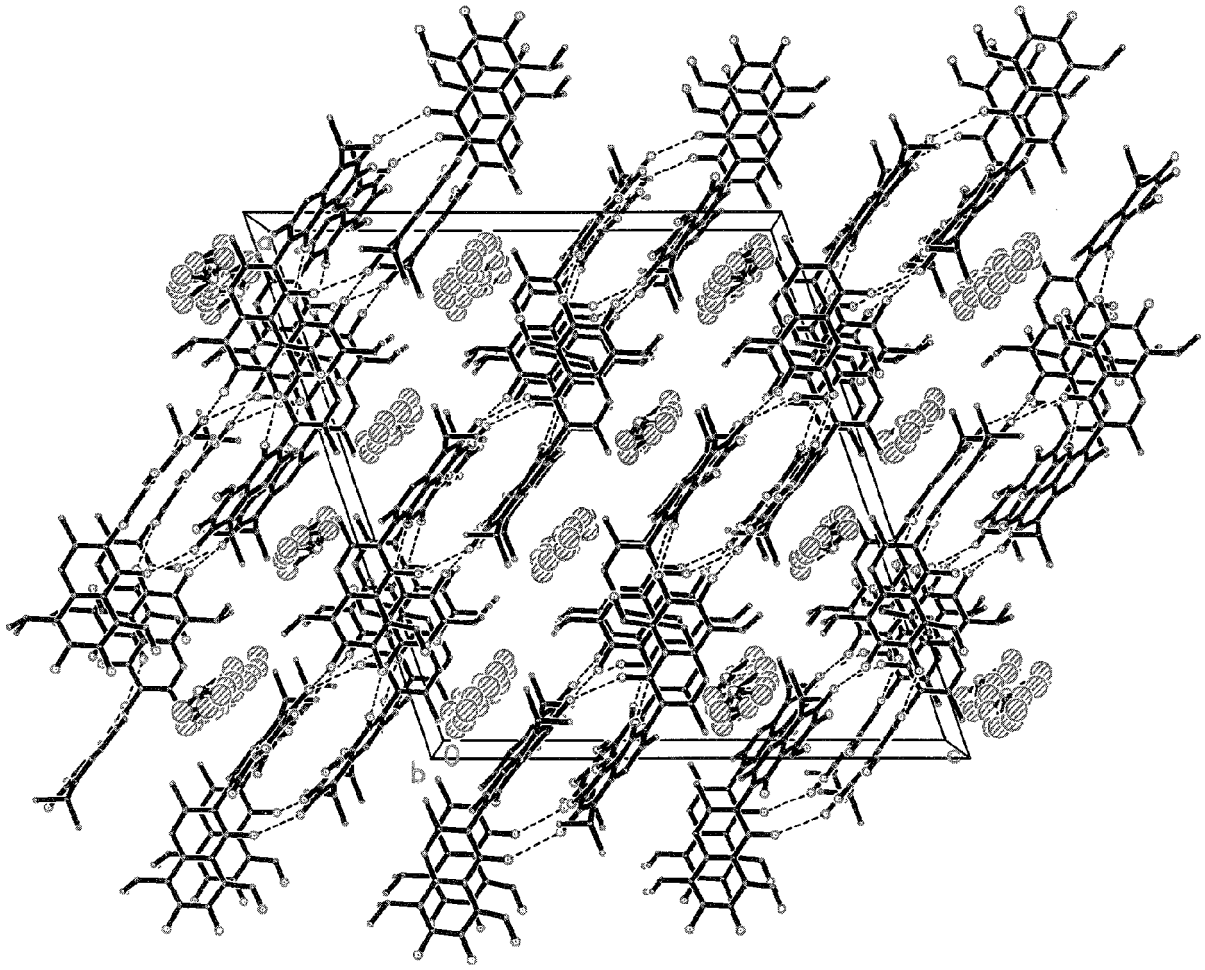

Fig. 2 Clathrate of gossypol with chloroform. Guest molecules are disordered in four positions. (*View this art in color at www.dekker.com.*)

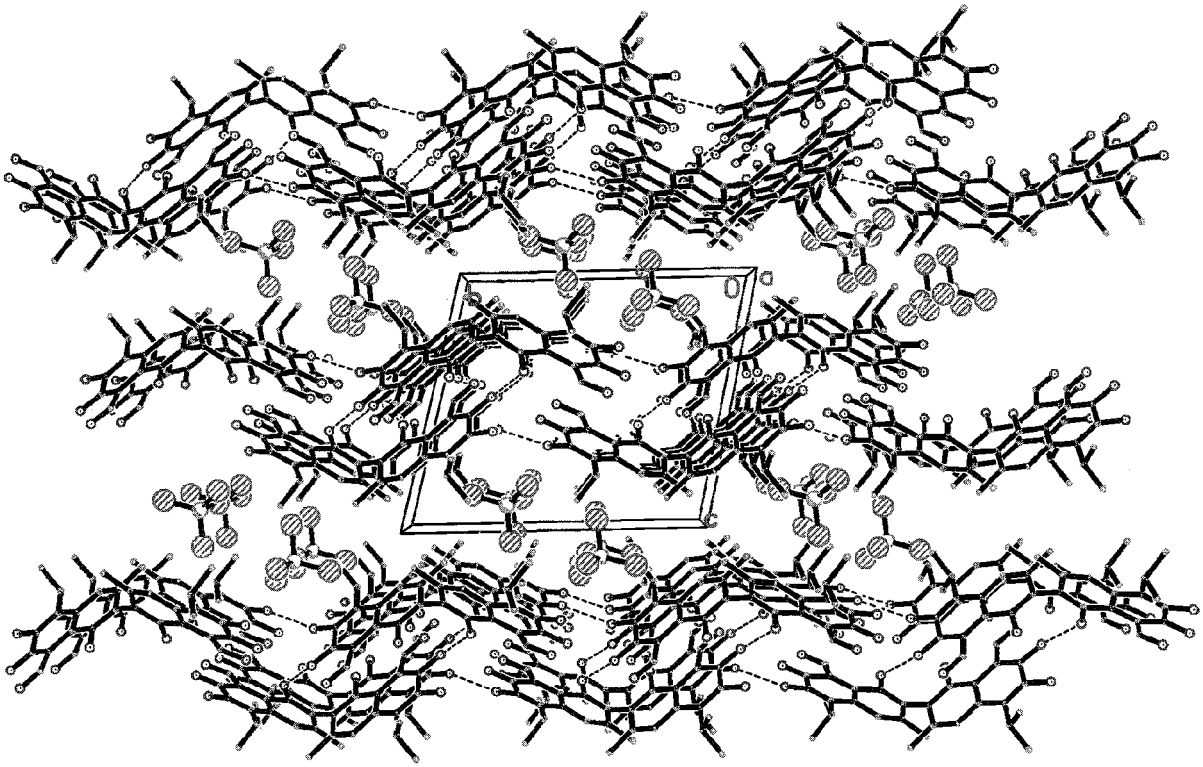

Fig. *3* Clathrate of gossypol with tetrachloromethane. (*View this art in color at www.dekker.com.*)

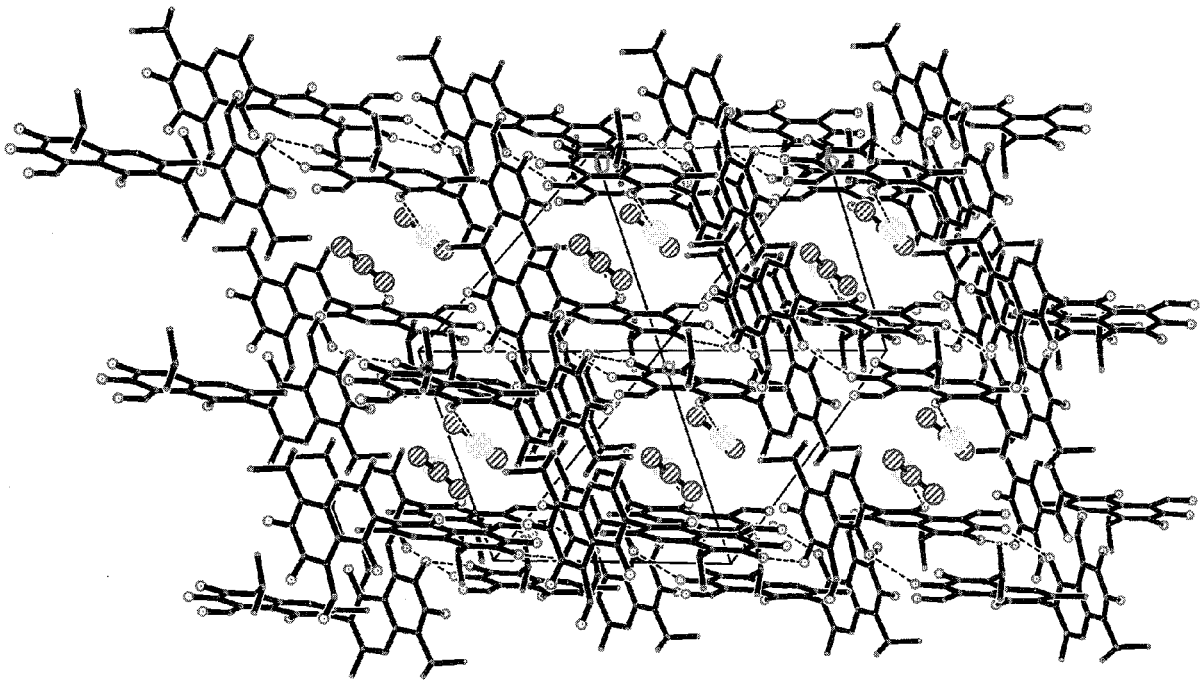

Fig. 4 Coordinatoclathrate of gossypol with acetone. (*View this art in color at rr.+i.+c,.dekker..com.)*

solutions with different supersaturations.[6] As these findings were accidental. in order to establish the versatility of this phenomenon, systematic studies have been carried out.

Under ambient conditions, crystallization of Gp from solutions in dichloroinethane forms, as mentioned above, an unstable 1:I clathrate or a-phase complex (group VIII A; Fig. 1). Increasing the crystallization temperature to 30°C gives rise to the 1:1 host–guest complex (β-phase) relating to the group IV A (Fig. 3). Further increasing of the formation temperature to 36°C results in crystallization of a third, very stable 2:1 y-phase isostructural with clathrates of group V C.[16] The observed phenomenon has been called pseudopolymorphism of the given host–guest complex. It also took place in case of 1.4-dioxane. pyridine. and acetone. Raising the crystallization temperature to 40°C gives 1:1 modifications relating to the I A group instead of the conventional 1:3 clathrates of 1.4-dioxane (type XII) and pyridine (type XI).[17] Pseudodimorphism is also characteristic for clathrates of Gp with acetone. but here a new 1:3 modification has been obtained by lowering the crystallization temperature to −20°C (type XPV). The remarkable feature of the latter phenomena is in resolution of the racemic Gp in such a manner that each separate crystal of the solvate contains only one Gp enantiomer.[11]

INCLUSION COMPLEXES OF GOSSYPOL BASED ON ITS ORGANIC ZEOLITE

The clathrate of Gp with dichloromethane or dibromomethane obtained under ordinary conditions is very unstable. and removing the crystal from the mother liquid leads to spontaneous desolvation. Channels occupied by guest molecules do not collapse after desolvation, giving rise to a porous structure with relatively wide (diameter about 6 Å), empty channels. In case of the complex in the form of a single crystal. the latter is retained without destruction. It is surprising that the structure of this organic zeolite is supported by weak Van-der-Waals forces. Guest-free porous Gp obtained from its unstable clathrate may serve as an initial solid-state product for preparation of Gp's nonstoichiometric supramolecular complexes with some linear molecules. Indeed. it may easily absorb from the environment molecules of ammonia. alkylamines, alcohols, etc.[18] High selectivity of this zeolite analogue toward inclusion of linear amines such as methyl- and ethylamine may serve for creation of sensors for detecting these compounds in the environment. Moreover, the channel walls of the Gp zeolite have a specific structure with only one aldehyde group on it. while another group is hidden inside the crystal. This situation makes a solid-state reaction with linear amines possible in the organic zeolite matrix, producing unsymmetric Shiff's-base-type derivatives of Gp. The solid-state reaction takes place spontaneously under ordinary conditions.[18] The Gp zeolite analogue may be used for the separation and storage of linear molecules that do not react with Gp.

Thus, Gp is a unique host molecule including any solvent molecule via the liquid phase and certain linear molecules in the solid state. To establish the driving forces behind this unique host versatility is of great interest for supramolecular chemistry and of importance for the design of new versatile host molecules.

WHY CAN GOSSYPOL INCLUDE ANY SOLVENT MOLECULE?

This ability of Gp is related to its unique molecular structure. The factors responsible are the following (in order of decreasing importance):

1. Conformational mobility of the molecule—rotation around a single aryl–aryl bond.
2. Plurality of polar functional groups and their mutual arrangement.
3. Racemic nature of the compound.
4. Hydrophobic–hydrophilic separation in the molecule.

The conformational mobility of the molecule is of crucial importance in the host versatility of Gp. By appropriate rotation around an ordinary bond. Gp adjusts its form and size for optimal packing in crystals of inclusion complexes. Plurality of proton-donor and proton-acceptor groups and their mutual arrangement make possible an inclusion of guest molecules with different types of polar groups and construction of the numerous H-bonded host aggregates. A racemic mixture is important for crystallization of inclusion complexes in many different lattices, because enantiomeric Gp complexes would be crystallized only in chirai space groups. Indeed, the inclusion ability of pure (−)-Gp is limited. Hydrophobic–hydrophilic separation in the molecule (see above) leads to such separation in Gp clathrates: hydrophobic voids are prepared for inclusion of hydrophobic guests, while polar guests are included to hydrophilic space, meaning that clathrates of polar and unpolar guests are never isostructural. However. a possible way of violating the hydrophobic–hydrophilic separation is to introduce the hydrophobic substitutents into the hydrophilic part of the molecule. This transformation may be achieved easily by preparation of the Shiff's-base-type derivatives.

HOST PROPERTIES OF GOSSYPOL DERIVATIVES

The host properties of Gp derivatives with violated hydrophobic–hydrophilic separation have been studied in the example of dianilinegossypol (DaGp). The condensation reaction of Gp with aniline proceeds spontaneously and produces a product that is chemically more stable and less soluble in organic solvents. Therefore, the synthesis of the derivative and its consequent crystallization in the clathrate form can be performed in the same vial. DaGp forms inclusion complexes with a variety of small organic molecules. However, in contrast to Gp. the derivative does not include protic solvent molecules. Moreover, deterioration of the hydrophobic–hydrophilic separation compared to the Gp molecule dramatically influences the derivative's aggregation mode. The centrosymmetric dimer O5–H...O3 or single host molecules are combined by centrosymrnetric H-bond O8–H...O7 into two types of higher-order one-dimensional networks.[6] In both cases, the networks are built from *R* and *S* host molecules. i.e., chains are heterochiral."'' The heterochiral chains are also characteristic for diastereomeric condensation products of Gp with optically active amines such as 1-phenyl-ethylamine[20] or 1-methylphenylethylamine prepared for resolution of racernic Gp by subsequent fractional crystallization. Undoubtedly, the heterochirality of the host networks is at the root of the failure of diastereomeric separation by fractional crystallization. So the most optimal combination of all factors favorable for the host versatility is found in the Gp molecule, and elimination of any of them leads to a compound with worse inclusion ability.

CONCLUSION

Gp is the only known host giving 25 types of the different isostructural supramolecular complexes (clathrates). This natural compound demonstrates dozens of kinds of biological activity. Such behavior is explained by its special molecular structure — diversity of the polar functional (six proton-donor and two proton-acceptor) groups, conformational mobility. and racemicity. This finding may be used in the future in order to design or look for the new versatile host compounds.

ACKNOWLEDGMENTS

The authors thank CRDF (grant ZC1-2451-TA-02) and SCOPES (grant 7UZPJ065576) for financial support.

ARTICLES OF FURTHER INTEREST

Channel Inclusion Compounds, p. 223
Hydrogen Bonding, p. 658
Inclusion Reactions and Polymerization, p. 705
Isostructurality of Inclusion Compounds, p. 767
Organic Zeolites, p. 996
Polymorphism, p. 1129
Space Groups and Crystal Packing Modes. p. 1337
van der Waals Forces, p. 1550
X-Ray Crystallography, p. *1586*

REFERENCES

1. Markman, A.L.: Rzhekhin, V.P. *Gossypol and Its Derivatives*; Pishevaya Promishlennost: Moscow, 1965; 1–242.
2. Berardi. L.C.; Goldblatt, L.A. Gossypol. In *Toxic Constituents of Plant Foodstuffs*, 2nd Ed.; Academic Press: New York. 1980; 183–237.
3. National Coordinating Group on Male Fertility. A new male contraceptive drug—Cotton phenol (gossypol). Chin. Med. J. 1978. *4*, 417–428.
4. Baram, N.I.; Ismailov, A.I. Biological activity of gossypol and its derivatives. Chimiya Prirodnih Soedinenie 1993, 334–351.
5. Adams, R.: Ceismann, T.A.: Edwards. J.D. Gossypol, a pigment of cottonseed. Chem. Rev. 1960. *60*. 555–574.
6. Gdaniec, M.; Ibragimov, B.T.: Talipov. S.A. Gossypol. In *Comprehensive Supramolecular Chemistry*; MacNicol. *D.D.*. Toda. F.. Bishop. R., Eds.; Elsevier Sciences: London. 1996: Vol. 6, 117–146.
7. Huang, L.: Zheng, D.K.: Si. Y.K. Resolution of racemic gossypol. J. Ethnopharmacol. 1987. *20*. 13–20.
8. Culan. M.Z.: Wang. N.G. Effect of (+)-, (–)- and (+ –)-gossypol on early pregnancy in rats. Acta Pharm. Sinica 1996. *31*. 10–12.
9. Ibragimov. B.T. A simple correlation between the structures of different crystal modifications of the given host–guest complex and their crystallization temperature. J. Incl. Phenom. Mol. Recognit. Chem. 1999; *34*. 345 - 353.
10. Talipov, S.A.: Ibragimov. B.T.; Tishenko, G.N.; Aripov. T.F. The crystal structure of gossypol solvate with acetone. Kristallografiya 1989. *34* (2), 327–332.
11. Dowd, M.K.; Thomas. L.M.: Calhoun, M.C. Crystal and molecular structure of an enantiomeric gossypol—Acetic acid clathrate. J. Am. Oil Chem. Soc. 1999. 76 (11), 1343–1350.
12. Campbell, K.N.; Morris. R.S.: Adams. R. The structure of gossypol. J. Am. Chem. Soc. 1937. *59*, 1723–1728.
13. Ibragimov, B.T.: Talipov. S.A. The modes of gossypol supramolecular association in the crystalline state. J. Structurnoe Khimii 1999. *40* (5), 849–871.

14. Ibragimov, B.T.; Gdaniec, M.; Dadabaev. B.N. Inclusion complexes of the natural product gossypol. Strong influence of the guest on the host structure in channel-type isostructural complexes of gossypol. J. Incl. Phenom. Mol. Recognit. Chem. **1990**, *8*, 333–348.
15. Talipov. S.A.; Ibragimov. B.T.: Tishenko. G.N.; Aripov. T.F.; Nazarov, G.B.: Strokopytov, B.V.: Polyakov. K.M. Crystal structures of gossypol mono- and semisolvate with diethyl ether. Kristallografiya **1988.** 33. 384–389.
16. Ibragimov. B.T.; Tiljakov, Z.G.; Beketov, K.M.: Talipov, S.A. Polymorphism of inclusion complexes and unsolvated hosts. I. Trimorphism of the host–guest complex of gossypol with dichloromethane. The structure of the β-phase. J. Incl. Phenom. Mol. Recognit. Chem. **1997**, 27. 99–104.
17. Talipov. S.A.: Tiljakov, Z.G.; Beketov, K.M.; Ibragimov. B.T. Polymorphism of crystalline inclusion complexes and unsolvated hosts. VII. Pseudodimorphism of the inclusion complex between gossypol and 1.4-dioxane and structure of the β-phase complex. Four different H-bonds possible in the gossypol molecule. J. Incl. Phenom. Mol. Recognit. Chem. **1998.** 32, 429–437.
18. Talipov, S.A.: Manakov. A.; Ibragimov, B.T.: Lipkowski. J.: Tiljakov, Z.G. Sorption of ammonia, methylamine and methanol by the P3 polymorph of gossypol. Synthesis of unsymmetric monoamine derivatives of gossypol by a solid-state reaction. J. Incl. Phenom. Mol. Recognit. Chem. **1997**. 29. 33–39.
19. Ibragimov, B.T.; Nazarov, G.B.: Talipov, S.A. X-ray structure investigation of gossypol and its derivatives. VIII. The new class inclusion compounds on the base of dianilinegossypol. Chimiya Prirodnih Soedinenie **1988.** 666–669.
20. Gdaniec, M. Crystal structure of the product of a condensation reaction of (+ –)-gossypol with R-(+)-1-phenylethylamine. Why do diastereoisorneric diaminogos-sypol cocrystallize? J. Incl. Phenom. Mol. Recognit. Chem. **1994**, 17, 365–376.

Guanidinium-Based Anion Receptors

Eric V. Anslyn
Suzanne L. Tobey
University of Texas at Austin, Austin, Texas, U.S.A

INTRODUCTION

The guanidinium functional group is characterized by three amines joined to a central carbon atom (Fig. 1A). In nature, the guanidinium group is found as a side chain of the amino acid arginine and as part of the ring structure of guanine. In enzymes, arginine residues often function in catalytic reactions through charge pairing or hydrogen bonding to the activated complex, thereby imparting stabilization.[1–3,6]

In the development of effective anion receptors. many researchers in the field of molecular recognition incorporate the guanidinium group into receptor designs. The presence of one or more guanidinium groups markedly enhances the assembly of host and guest in bulk solution through electrostatic and hydrogen-bonding interactions. The guanidinium group is protonated and hence positively charged in aqueous media, with a pH up to approximately 13,[4,5] a range over which several important targets exist as anions in water. The high degree of stability of the guanidinium moiety is in part due to the delocalization of the positive charge across the three nitrogen atoms. Additionally, this delocalization renders all of the three nitrogen centers effective hydrogen-bond donors, permitting the formation of multiple hydogen bonds with multiple hydrogen bond acceptors. Another key feature of the guanidinium group is its geometry. which allows directional hydrogen bonds to be formed with an intended anionic target. Three different bonding motifs have been identified[6] (Fig. 1B), which exemplify the utility of the guanidinium group as a bidentate moiety as opposed to that of an ammonium group, for example. The delocalization. geometry, and pK_a range of the guanidinium functional group makes it very useful in anion recognition.

Anions vary in shapes and sizes, and exist in multiply charged states. They can be spherical as in the case of chloride, linear as in the case of azide. trigonal planar as in the case of nitrate. tetrahedral as in the case of phosphate, octahedral as in the case of hexacyanoferrate. and complex as in the case of dioctanol-L-α-phosphatidylcholine. Some targets for anion recognition have multiple pK_a values and can therefore have multiple charges. which depend on the pH of the solution. These features have to be taken into consideration when designing a synthetic receptor. It is the goal of this entry to exemplify the use of guanidinium groups in synthetic receptors that are designed to recognize and bind a variety of anionic targetr.

RECEPTORS DERIVED FROM A MELAMINE CORE

Yano et al. exploited the hydrogen-bonding capabilities of the guanidinium group through incorporation into a melamine derivative.[7] The synthesis of the receptor commenced with substitutions on cyanuric chloride. Various substitutions permitted the isolation of three receptors. ^{1}H NMR, UV-Vis, and fluorescence studies in chloroform yielded association constants for the binding of 6-azaflavin and 3-methyl-6-azaflavin to each of the receptors. A $K_a = 1.4 \times 10^5\ M^{-1}$ was reported for complex formation between receptor 1 and 6-azaflavin in chloroform, the magnitude of which is attributed to a complex formed via quintuple hydrogen bonds.

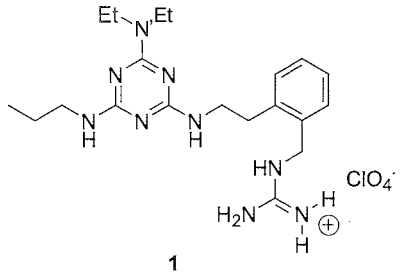

1

An extension of this receptor type led to complexation studies of 2 with the anionic semiquinone radical of 6-azaflavin.[8] The absorption spectrum of 6-azaflavin observed in the presence of 2 in chloroform indicated formation of the radical species. which was stabilized for a 48 h period. The anion radical was also observed by EPR spectroscopy. A binding constant of $7.7 \times 10^5\ M^{-1}$ was determined for the complexation of the anion radical, two orders of magnitude higher than complexation of 6-azaflavin with 2.

Encyclopedia of Supramolecular Chemistry
DOI: 10.1081/E-ESMC 120012718

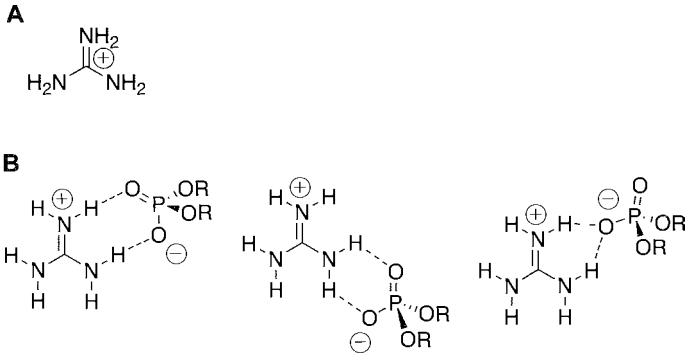

Fig. 1 A) A guanidinium group. B) The three types of bonding motifs to a guanidinium moiety.

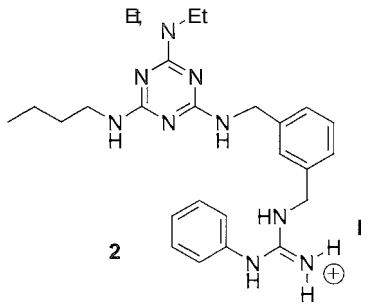

In later studies, several receptors were synthesized to incorporate the basic melamine core with different substitutions on the guanidiniurn moiety. These were used to explore the effectiveness of the hydrogen bonding of the guanidinium groups to various acceptor groups on the flavin rings.[9] Absorption studies were employed to determine pseudo first-order kinetics of the oxidation of N-benzyl-1.4-dihydronicotinamide and thiopheno! in the presence of 6-azaflavin and the receptors under anaerobic conditions. Complex formation of the flavin with the guanidiniurn moieties, through hydrogen bonding at N1 of the flavin, showed the largest rate accelerations for oxidation.

Making Use of the Steroid Scaffold

A scaffold that has been used for the design of abiotic receptors derives from steroids.[10] In research directed toward the use of abiotic receptors as mimics for RNase active sites, Malesse et al. developed a series of *bis*-(guanidinium) structures, including some derived from a steroid scaffold.[11] The compounds contain guanidiniurn and imidazole groups linked with spacers of different lengths. Hydrolysis experiments using 2-hydroxypropyl *p*-nitrophenylphosphate (HPPWP) as the substrate were monitored in acetonitrile and in water using UV-Vis spectroscopy. The observed rates were slower in acetonitrile (10^{-4} s^{-1}) when compared to water (10^{-7} s^{-1}), which the authors attributed to deactivation of the guanidinium moiety through intramolecular hydrogen bonding in acetonitrile. This was determined through ^{1}H-NMR studies on the steroid-based system. Steroid **3** had the largest rate constant for HPNPP cleavage in water (k = 14.3 x 10^{-7} s^{-1}), an increase by a factor of 10 over other (his)-guanidinium compounds studied. Receptor **3** also catalyzed transesterification behavior of the nucleotide Up(3′–5′)U with a pseudo first-order rate constant of 2.4 x 10^{-4} h^{-1}.

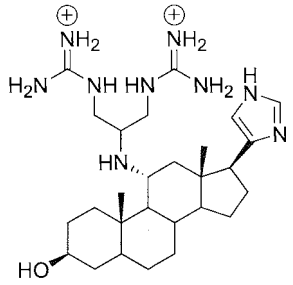

The steroid-based scaffold was also used by Davis and coworkers to effect the enantioselective extraction of *N*-acyl a-amino acids from aqueous media.[12,13] Synthetic manipulation of cholic acid delivers a family of steroid-type derivatives (4) with different binding units at C3, C7. and C12, which are predisposed to facilitate binding. A guanidinium group embedded in a six-membered ring was incorporated at C3 to enhance lipophilicity of the receptor. Variations in the asymmetry of the receptors using a variety of phenyl substituents permitted the researchers to tune the receptor for extraction of different amino acids.

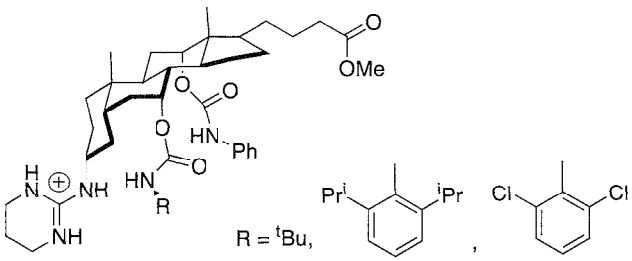

4

Metalloreceptors

A class of receptors that has gained increasing popularity is that of the metalloreceptors. The presence of a metallic center in a functionalized receptor ensemble can provide a binding site as well as an internal means of signaling the complexation of analytes. Beer et al. developed a ferrocenyl guanidinium binding unit for the recognition of inorganic and organic anions.[''' Receptor 5 was derived from ferrocenemethylamine and phenylmethylthiourea. Receptor ***5*** did not exhibit any binding affinities for phosphate, acetate, or benzoate based on ^{1}H-NMR studies in DMSO-d_6. However, pyrophosphate bound to **5** through hydrogen bonding with the guanidinium groupr in a 2:1 stoichiometry with K_a = 4.6 x 10^3 M^{-2}. The electrochemical behavior of the receptor in the presence of dihydrogenphosphate was monitored, and a reversible ferrocene redox wave was observed upon addition of pyrophosphate in H_2O/MeOH.

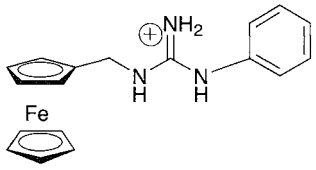

5

The work of Watanabe et al. provides another example of a receptor design inclusive of a metal center.[15] Receptor 6 makes use of an acylaminoimidazoline functionalized bipyridyl unit that simultaneously ligates a ruthenium center. The pK_a values of the acylaminoimidazoline groups were spectrophotometrically determined to be 2.0 and 3.9, significantly lower than alkyl or aryl analogues. This was thought to be a result of repulsive interactions between the metal center and the acylaminoimidazoline groups. Association of dibenzylhydrogenphosphate to 6 was monitored by ^{1}H-NMR in acetone to determine a binding stoichiometry of 1:1 and a K_a = 4.6 x 10^3 M^{-1}. Additionally, the changes in the absorption and luminescence spectra of 6, induced upon analyte addition. permitted the determination of binding constants for tetraethylammonium dipheny! phosphate and dibenzylhydrogen phosphate (3.3 x 10' M^{-1} and 4.8 x 10^3 M^{-1}, respectively) in acetone.

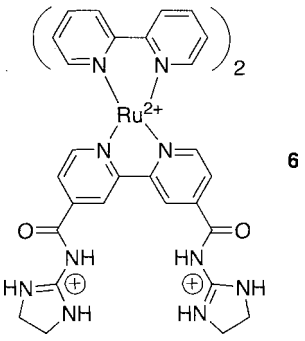

6

Anslyn and coworkers used a phenanthroline-bound copper moiety within a receptor design containing two aminoimidazoline functional groups.[16] The binding of citrate to 7 was monitored by fluorescence inodulation of the metallated phenanthroline unit. The complexation of 7 with citrate is thought to occur through charge pairing of two carboxylates with the guanidinium functional groups and coordination of one carboxylate to the copper center. Investigations on the photophysical properties of the system verify that the phenanthroline-bound copper and the pendant guanidinium groups work cooperatively in the binding of citrate. Application of this receptor to the analysis of commercially available beverages led to a successful quantification of citrate.

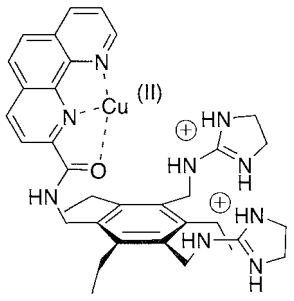

7

The Bicyclic Guanidinium Motif

A significant amount of work with guanidinium receptors revolves around a bicyclic motif exploited by Schmidtchen, de Mendoza. and Rebek. The design lends itself to a

preorganized compound. while maintaining the binding abilities of the guanidinium functionality.[17] The synthetic methodologies involving guanidiniums are not typically applicable to bicyclic compounds. The syntheses of such bicyclic compounds from L-asparagine and D- asparagine were reported by de Mendoza.[18] Alternate synthetic access to the bicyclic core was reported by Schmidtchen.[19–21]

Derivitization of the bicyclic core with napthoyl groups afforded compound 8, which quantitatively extracted p-nitrobenzoate from an aqueous solution.[22] ^{1}H-NMR studies in $CDCl_3$ confirmed a 1:1 complex of 8 with triethylammonium p-nitrobenzoate and gave an association constant of 1609 M^{-1}. Binding resulted from charge pairing of the carboxylate with the guanidinium group and π-stacking of the napthoyl groups of 8 with the phenyl group of the analyte. Three additional compounds were designed with various *R* groups to access a family of lipophilic receptors.'''' The receptors were used in extraction experiments of monophosphate adenine nucleotides from water with varying selectivities. ^{1}H-NMR analysis was used to characterize the 1:1 complexes in $CDCl_3$, DMSO-d_6, and MeOD/D_2O. The complexes observed in DMSO-d_6 and MeOD/D_2O were weaker than those in $CDCl_3$, indicating the role of hydrogen-bonding in host–guest association.

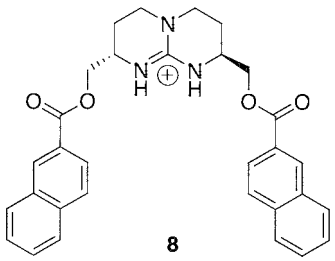

8

Incorporation of the bicyclic core into a larger macrocycle using a carbazole spacer and substituted Kemp's triacid yielded 9.[24,25] Based on extraction experiments from aqueous solutions, receptor 9 displayed a high affinity for 2'-deoxyadenyl(3'-5')-2'-deoxyadenosine. Additionally. NMR data of the complex suggested pairing the adenosine to the amide links of 9 and hydrogen bonding the phosphodiester link to the guanidinium moiety. Compound 10 was designed to incorporate the bicyclic guanidinium in a carbazole-based scaffold.[26,27] ^{1}H-NMR titrations in water were used to determine binding constants and the accompanying free energies of complexes formed between 10 and cyclic adenosine monophosphates. These data. when compared to those of a control host lacking the bicyclic guanidinium substituent. indicated that on average the guanidinium–phosphate interaction contributes 0.6 kcal/mol (ionic strength = 51 mM) and 0.3 kcal/mol (ionic strength = 501 mM) to the binding event (average ΔG of -3 kcal/mol).

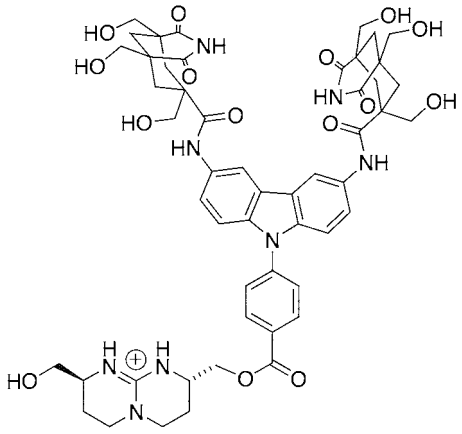

10

The design of 11 was aimed at the enantioselective recognition of zwitterionic aromatic amino acids[28] under neutral conditions.[29] The features of the receptor include a chiral structure. an aromatic substituent for n-stacking. and binding sites for a carboxylate group and an ammonium

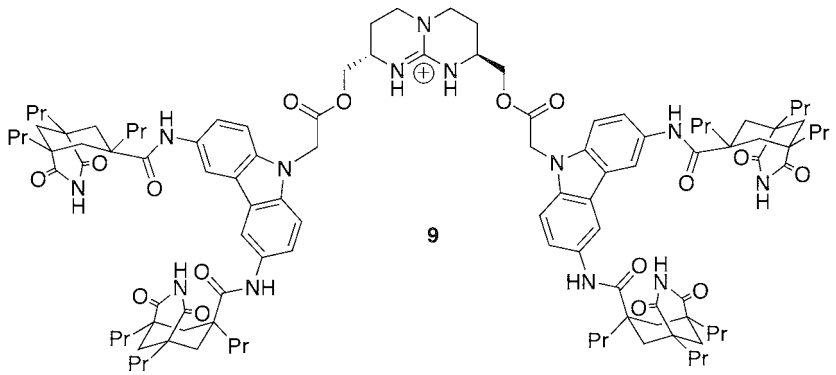

9

group. Liquid–liquid extractions were used to determine affinities of 19 seven amino acids. The largest response was found for L-tryptophan and L-phenylalanine, with extraction efficiencies of 40% as determined by ^{1}H-NMR integrations of the organic phase components. The D-enantiomers were not extracted when subjected to similar conditions. However, the (R,R)-11 receptor successfully extracted D-tryptophan and D-phenylalanine.

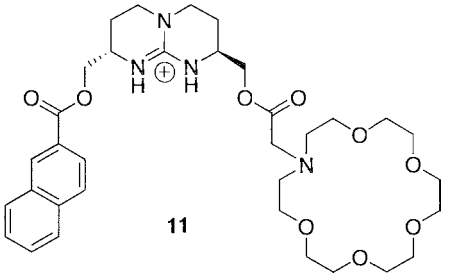

11

The introduction of silyl groups to the bicyclic core yielded **12**, which was shown to catalyze the Michael addition of pyrrolidine to unsaturated lactones.[30] Three receptor analogues were investigated. and the half-lives of the addition reactions were determined by ^{1}H-NMR. Compound **12** facilitated the largest decrease in half-life of 8.4-fold over the uncatalyzed reaction. The receptor is thought to stabilize the transition state through two-point hydrogen bonding to the guanidinium group. The catalysts did not show improvements in stereoselectivity over the uncatalyzed reaction.

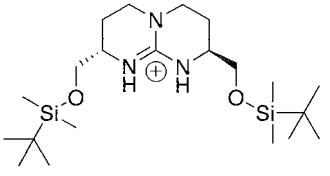

12

Modified deoxycholic side arms were placed on the bicyclic core (13) to provide a binding cavity for uronic acid salts.[31] The binding of the receptor to tetrabutylammonium D-gluconate and tetraethylammonium D-galacturonate was evaluated using ^{1}H-NMR studies in acetonitrile (K_a range = 7.0 x 10^3 M^{-1} to 3.2 x 10^3 M^{-1}). The binding constants were on the same order of magnitude when compared to a control compound, indicating that the steroid arms had little influence on the binding due to intramolecular hydrogen bonding.

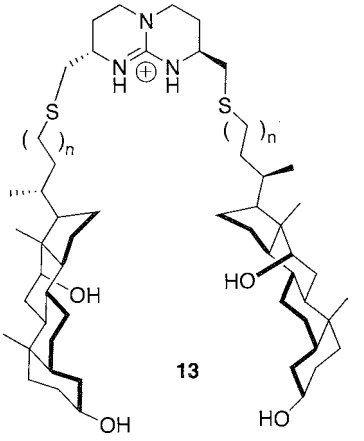

13

The bicyclic unit was incorporated into a macrocycle containing additional binding sites under the guise of urea groups.[32] The strength of the binding of diphenylphosphate to 14 was found to be greater than 10^5 M^{-1} in chloroform. The NMR data suggest that the analyte resides on the outside of the cavity.

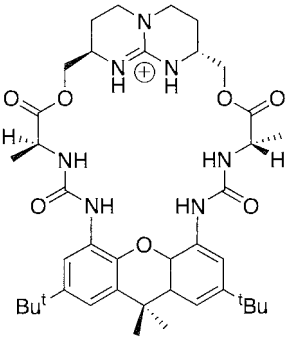

14

The combination of a calixarene subunit and the bicyclic guanidinium in macrocycle 15 demonstrates affinities for dicatonal-L-x-phosphatidylcholine (K_a = 7.3 × 10^4 M^{-1}) and acetylcholine (K_a = 7.3 x 10^2 M^{-1}) in chloroform.[33] These affinities are reduced in $CDCl_3$/CD_3OD (99:1). Kinetic studies were performed on the hydrolysis of p-nitrophenylcholine carbonate in the presence of 15, which showed a 149-fold rate enhancement over methanolysis. The guanidinium is thought to piay a role in the stabilization of the $B_{Ac}2$-type transition state. This provides an example of an artificial acetylcholinesterase.

Work by Schmidtchen involved the construction of a flexible receptor with two bicyclic guanidinium subunits appended to a 2,7,-dihydroxynapthalene core.[34] The complexation of this ditopic receptor (16) with a series of alkyl and aromatic dicarboxylates in methanol was

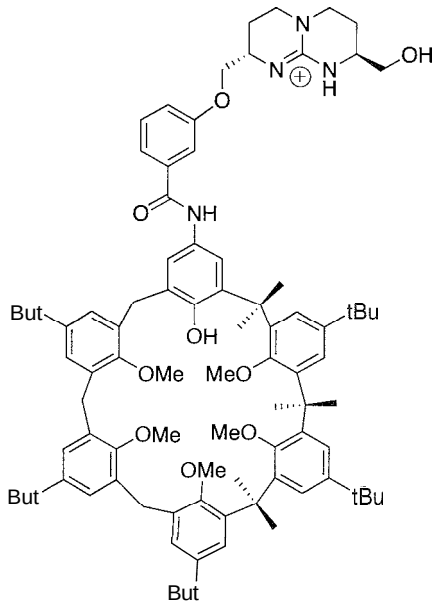

15

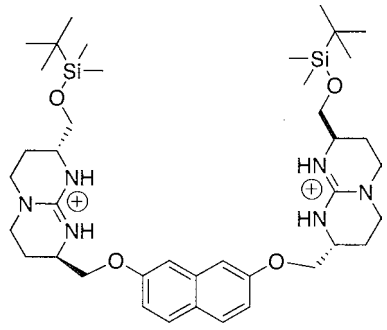

16

followed by ^{1}H-NMR techniques, resulting in binding constants ranging from 854–14,500 M^{-1}. Compound **16** also formed 1:1 complexes with phosphates in methanol and water when monitored by ^{1}H-NMR.[35] Alternate designs involved an alkyl spacer,[36] a peptide spacer,[37] a phenyl spacer,[38] and a phenyl spacer with an appended *closo*-borane cluster (**17**) to maintain the overall hydrophobicity of the receptor.[39] Association constants (on the order of 10^4 M^{-1}) were determined for **17** and different 0x0-anions in DMSO using ^{1}H-NMR techniques. Synthetic modifications of the receptor afforded a series of hosts that could bind sulfate in DMSO as determined by isothermal calorimetry.[40] The thermodynamic parameters indicate that complexation to 0x0-anions is entropically driven due to solvation effects.[41]

Phenyl-Based Receptors

bis(Acylguanidinium) receptors (**18**,**19**) were reported by Hamilton for the recognition of phosphodiesters.[42] The binding cavity of 19 is trigonal and complementary to dibenzyphosphate, resulting in a 1:1 complex with K_a = 4.6 x 10^4 M^{-1} in CD_3CN. Furthermore, this receptor exhibited rate enhancements of 700-fold in the hydrolysis of 2-hydroxypropyl p-nitrophenylphosphate in acetonitrile.[43] An analogue of the *bis*-guanidinium receptor was reported (20) and shown to have an affinity for glutarate of 4.8 x 10^2 M^{-1} in 12% D_2O/DMSO.[44] An extension of this receptor motif resulted in 21, with a bicyclooctane spacer that places the two guanidinium groups in proximity to interact with two carboxylates separated by 4–5 Å.[45] A 1:1 complex of **21** with aspartate pairs of peptide substrates was confirmed by NMR Job plots, and affinities ranged from 390–2200 M^{-1} in H_2O/MeOH. Binding studies of 24 with a series of peptides, using UV/Vis and CD techniques, supported the NMR studies.[46] The development of a tetraguanidinium receptor derived from the bicyclic guanidinium was reported by Hamilton and de Mendoza.[47] This receptor was used in the surface recognition of a tetraaspartate peptide based on shape and charge complimentarity in water and H_2O/MeOH mixtures. Reported are NMR, UV/Vis, and CD experiments and pH studies that confirm binding of **21** to the peptide surfaces.

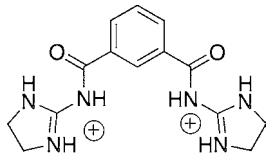

18

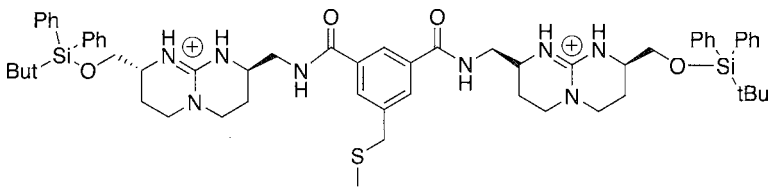

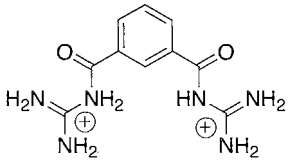

19

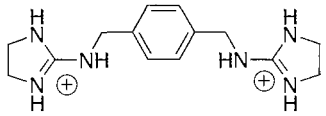

20

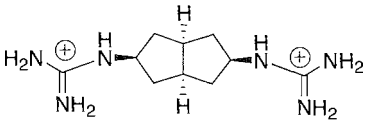

21

A variety of monoguanidinium scaffolds were used in isothermal calorimetry studies to determine the thermodynamic parameters involved in complexes with carboxylates.[48,49] The authors concluded that the guanidinium compounds form bidentate hydrogen bonds with acetate in DMSO with favorable enthalpy and entropy contributions (range K_a = 110–8700 M^{-1}). In one case. two acetates bind to one guanidinium group, which is characterized by endothermic heat patterns and positive entropy. This is suggestive of solvent reorganization.

Isothermal calorimetry and NMR titrations were used to characterize and quantify the binding of guanidinium receptors with nitronate anions in DMSO. The parameters of interest were the Gibb's free energy, enthalpy. and entropy.[50,51] The reported binding affinities indicate that nitronate anion complexation with a thiourea moiety is weaker than with a guanidinium moiety. The nitronate complex of 22 was used in investigations of nitronate alliylation reactions. A kinetic analysis of the reaction of nitronate with *p*-nitrophenylbromide in the presence of the receptor indicated that complex formation is responsible for the observed increase in the *C*-alkylation product over the *O*-alkylation product.

Göbel and coworkers reported the synthesis of *bis*(guanidinium) alcohols as mimics for the active site of staphylococcal nuclease.[52] The phosphorylation of these mimics with a cyclic phosphate was studied using ^{31}P-NMR methods.[53] The pseudo first-order rate constant for the phosphorylation of 23 was k_{obs} = 8.0 x 10^{-3} min ^{1} in DMF. Potentiometric titrations indicated that the acidities of the guanidinium groups are responsible for the differences observed in the k_{obs} values for various hosts.

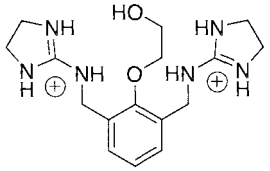

23

The HexaSubstituted Benzene Scaffold

Receptors are also derived from a 1,3,5-substituted-2,4,6-triethylbenzene compound. which provides a preorganized recognition scaffold with the binding moieties directed to one face of the ring. Substitutions at the 1,3,5 positions with aminoimidazoline groups resulted in **24**.[54] The complimentarity of the guanidiniums to carboxylates allowed for the determination of binding constants for several carboxylate-containing analytes. Compound 24 was found to be selective for citrate (K_a = 6.9 *x* 10^3 M^{-1} in D_2O). A crystal structure of 24 with tsicasballate bound to the cavity was reported, and it verified the orientation of the guanidinium groups to one face of the plane. Development of a competition assay in which a cavity-bound dye, 5-carboxyfluorescein, was displaced upon addition of citrate, was used to quantify the binding of citrate to the host. The assay was used to quantify the citrate content of eight commercial beverages containing competing analytes.

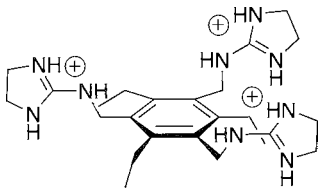

24

Another design involved receptor 25, in which one of the guanidinium-containing groups of 24 was replaced with a boronic acid.[55] The use of guanidinium groups for ion-pairing interactions and the boronic acid for complexing diols was intended to target the recognition of polyfunctionai analytes. The cavity of 25 was found to be effective in the recognition of tartrate (K_a = 5.5 x 10^4 M^{-1} in H_2O/MeOH 25:75) and malate (K_a = 4.8 *x*

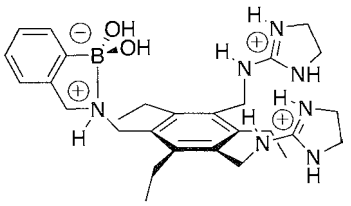

25

10^4 M^{-1}) based on a dye-displacement assay using alizarin complexone. The magnitude of the binding constants obtained suggests that the boronic acid and the guanidinium recognition units work cooperatively to effect binding of the analyte. Several wines were tested using this assay, and the tartaric and malate concentrations were accurately determined, as found by comparison to a control method in which ^{1}H-NMR studies were used.

Introduction of a second boronic acid functional group to the scaffold yielded compound 26, which was effective in binding phenolic acids.[56] A competition assay with pyrocatechol violet was used to determine the binding affinity for *26* for gallate (K_a = 1.0 x 10^4 M^{-1}). This sensing ensemble was used in the analysis of scotch whisky. The collective response of the host to the phenolic acid components of the whisky was correlated to the ages of the scotches.

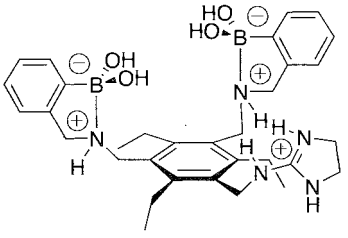

26

An alternate approach yielded a bowl-shaped cavity with six recognition elements on the periphery (**27**).[57] The triethylbenzene scaffold aids in the orientation of the recognition units toward the interior of the cavity. Fluorescent

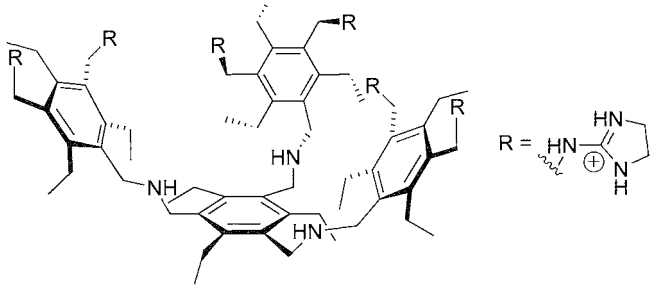

27

and UV/Vis methods were used to monitor the displacement of 5-carboxyflourescein from **27** upon addition of inositol-1,4,5-trisphosphate. This secondary messenger bound within the cavity with K_a = 4.7 $\times$ 10^5 M^{-1} in water.

Polyaza Clefts

Crescent-shaped polyaza clefts are commonly used in recognition ensembles.[58–62] Anslyn et al. reported the synthesis of several polyazaclefts characterized by a tricyclic core with appendant guanidiunium groups (28 and 29). ^{31}P-NMR titrations in DMSO/H_2O mixtures indicated that 29 bound dibenzyl phosphate with both 1:1 and 2:1 stoichiometries, with affinity constants on the order of 10^2 M^{-1}.[63] Receptor 29 bound dibenzylphosphate more strongly than a control host containing only one guanidinium group. An investigation on the extension of these binding motifs to phosphodiesters and phosphomonoesters yielded affinity constants on the order of 10^3 M^{-1} and 10' M^{-1} for 28 in DMSO.[64]

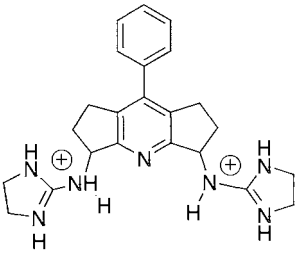

28

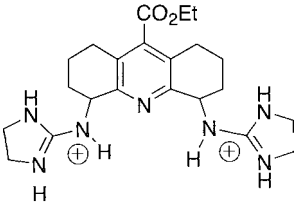

29

Modifications to the ring size of the spacer units and relative stereochemistry at C1 through synthetic means led to an array of clefts that were more or less rigid and more or less closed in architecture. These modifications resulted in manipulation of the guanidinium recognition units such that four-point hydrogen bonding with dibenzylphosphate as a surrogate was optimized. The complexes with dibenzylphosphate in DMSO/H_2O mixtures were enhanced by the presence of chloride and reduced by tetraphenylborate counterions.[65] The trends observed in the affinity constants were attributed to solvation effects of the complexes in the presence of these counterions. These observations were confirmed with a crystal structure analysis of meso-28-bound dibenzylphosphate. A participating chloride was found in the cocrystal

of *meso*-28 with bound dibenzyl phosphate. The physical studies indicated that 28 would be the most promising candidate for RNA hydrolysis studies. A kinetic assay was used to determine that 29 gave a 20.7-fold rate enhancement in the hydrolysis of mRNA when compared to imidazole alone.[66,67]

Recent work involves the use of a 2,2′:6,2″ terpyridine scaffold with a metal center and pendant guanidinium groups.[68] A dye displacement assay was employed in the determination of binding affinities for amino acids to the cavity of 30. The receptor was selective for aspartate with an affinity $1.5 \times 10^5\ M^{-1}$ in 1:1 water/methanol. Studies with the control host in which the guanidinium groups are absent indicate that the selectivity for aspartate is due to the interactions with the Zn(II) center and the guanidinium moieties.

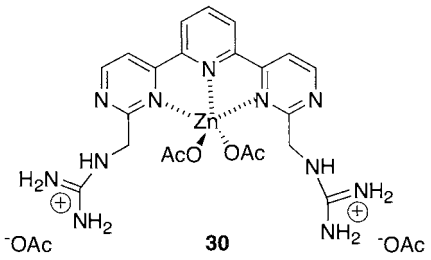

30

Miscellaneous Designs

The synthesis of three polymacrocyclic compounds (31) reminiscent of crown ether designs with imbedded guanidinium groups has been reported.[69] The stability constants for binding of the phosphate anion are reported as determined from pH titrations in $MeOH/H_2O$ (9:1).

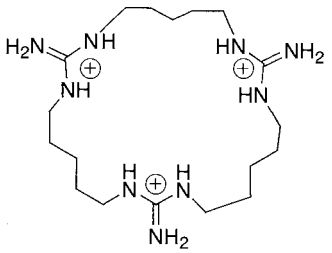

31

A xanthone-based receptor functionalized with a guanidinium group has been reported.[70] Complex formation with carboxylic acids is thought to occur through hydrogen bonding with the guanidinium. The association constants of several carboxylic acids with 32 in $CDCl_3$ were determined by ^{1}H-NMR studies. The reported values range from 10^9–$10^4\ M^{-1}$.

A tweezer-like receptor with arms derived from amino acids adjoined through a guanidinium group is

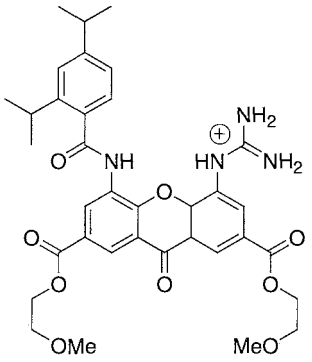

32

described.[71] Two such receptors were fluorescently labeled and used to screen a library of resin-bound peptides.[72] The receptor (33) is selective for peptides containing a carboxylic acid terminus in aqueous media. The mode of binding has not been verified but is deemed to be a result of carboxylate–guanidinium interactions.

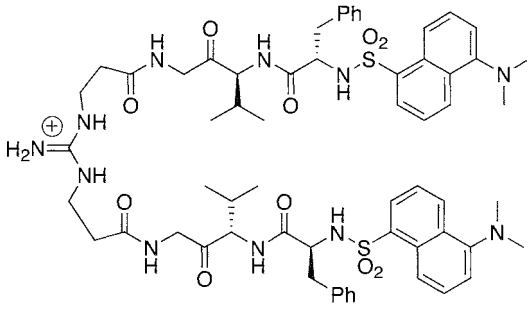

33

The development of a series of neutral anion receptors that undergo flourescent modulations upon complexation to anions has been reported.[73] The guanidine group in compound 34 is embedded in an iminolythiourea group. The emission intensity of the host was observed upon addition of various inorganic anions. Association of the guest to host is slow (72 h), but the increased rigidity of the host molecule upon anion complexation is thought to be responsible for the observed fluorescent enhancements. particularly in the presence of carbonate.

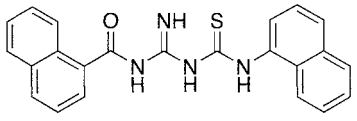

34

A pyrrole derivatized with a guanidinium moiety (**35a**) has been reported by Schmuck as an effective host for *N*-acetyl-α-amino acid carboxylates.[74] The binding constants as determined by ^{1}H-NMR titrations for a series of

analytes range from 10^6–10^2 in H_2O/DMSO mixtures. Further studies using a series of varied guanidiniocarbonyl pyrrole-type receptor molecules revealed that the guanidinium group and the amide NH on the pyrrole are necessary for the high K_a values reported.[75] A variation of this receptor in which a carboxylate group is appended at the 4 position (**35b**) has the propensity to oligomerize in DMSO.[76] ^{1}H-NMR titrations were used to determine dimerization constants at various temperatures for a van't Hoff plot. the results of which indicate that the oligomerization is entropy driven.

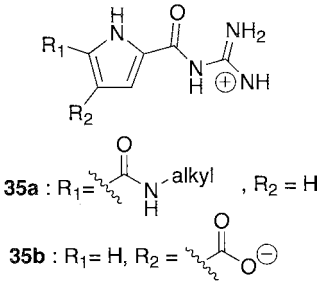

A recognition assembly (**36**) consisting of a cationic receptor (crown ether). fluorophore (anthracene), and an anion receptor (guanidinium) is used in the complexation of zwitterionic amino acids.[77] Complexation of amino acids to **36** at pH 9.5 led to an increase of the fluorescence intensity of the anthacene subunit in H_2O/MeOH. The binding constant for γ-aminobutyric acid was reported as 84 dm' mol^{-1}. while all other amino acids had lower affinities.

In tethering a designed core structure to solid phase with subsequent derivitization using peptide chemistry, a library of receptors as depicted in compound **37** was obtained.[78] The guanidinium group was incorporated for charge-pairing interactions, the peptide arms were intended to interact with the adenine moiety of ATP, and the fluorophore was necessary for detection protocols. Screening of the library with solutions of ATP permitted identification of derivatized beads selective for ATP. Further investigations indicated that an ATP-selective resin-bound receptor did not respond to AMP or GTP.

The incorporation of guanidinium groups in functionalized monolayers has been reported by Kunitake.[79–81] These functionalized monolayers were studied at an air–water interface and found to bind nucleotides. The reported binding affinities are on the order of 10^6 M^{-1} and were determined using XPS analyses. This was further manipulated to include mixed monolayers with guanidinium functional groups, as well as other recognition units.[82] The guanidinium and peptide amphiphiles bound peptides at the water–air surface with affinities of 10^3 M^{-1}.

Teramae and coworkers reported an example of self-assembly for anion recognition.[83] A pyrene with an appended guanidinium group (**38**) forms complexes in 2:1 and 1:1 stoichiometries with pyrophosphate. The self-assembled complex was monitored by fluorescence and ^{1}H-NMR spectroscopy in MeOH. The binding affinity for the 2:1 complex is 9.8 x 10^7 M^{-2}, and that of the 1:1 complex is 1.3 x 10^4 M^{-1}.

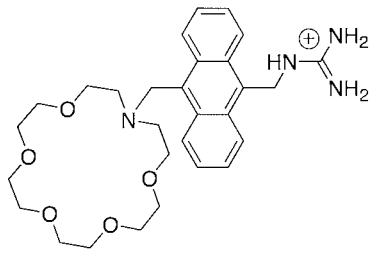

36

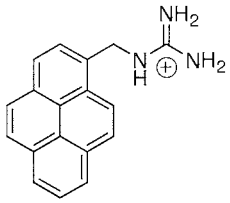

38

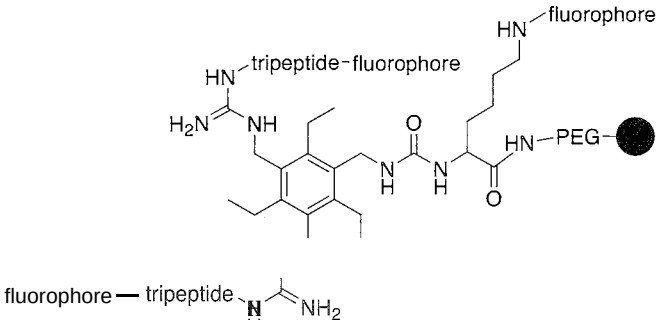

CONCLUSION

The research reviewed above is representative of the utility of the guanidinium functional group in receptor designs. This functional group has gained popularity due to its inherent ability to effectively bind anions through ion pairing and hydrogen bonding. There still remains a great deal to be gleaned from using the guanidiniurn group as a binding site in receptors that are potentially more intricate in design.

ARTICLES **OF** FURTHER INTEREST

Amide- and Urea-Based Anion Receptors, p. 31
Crown Ethers, p. 326
Fluorescent Sensors, p. 572
Organometallic Anion Receptors, p. 1006
Podands, p. 1106
Pyrrole- and Polypyrrole-Based Anion Receptors. p. 1176
Simultaneous Binding of Cations and Anions, p. 1291

REFERENCES

1. Hannon, C.L.: Anslyn. E.V. The Guanidinium Group. Its Biological Role and Synthetic Analogs. In *Bioorganic Chemistry* Frontiers: Dugas, H., Schmidtchen. F.P., Eds.; Springer-Verlag Berlin Heidelberg: Germany, 1993: 194–251.
2. Kim. E.E.; Wyckoff, H.W. Reaction Mechanism of alkaline phosphate based on crystal structures. Two-metal ion catalysis. J. Mol. Biol. 1991. *218* (2). 449–464.
3. Christianson. D.W.; Lipscomb. W.N. Carboxypeptidase A. Acc. Chern. Res. 1989. 22 (2). 62–69.
4. Dean. J.A. *Lange's Handbook* of Chemistry. 13th Ed.: McGraw Hill Book Co.: New York, 1985.
5. Angyal, S.J.: Warburton. W.K. The basic strengths of methylated guanidines. J. Chem. Soc. 1951. 2492–2494.
6. Cotton. F.A.: Hazen, E.E.; Legg. M.J. The role of arginine residues at enzyme active sites. The interaction between guanidinium ions and p-nitrophenyl phosphate and its effect on the rate of hydrolysis of the ester. Proc. Natl. Acad. Sci. U. S. A. 1979. 76 (6), 2551–2555.
7. Tamura. N.; Kajiki, T.: Nabeshima. T.: Yano, Y. A flavin receptor. Strong binding ability of a melamine derivative bearing a guanidinium ion of 4-azaflavin: Five hydrogen bonds formed in chloroforni. J. Chem. Soc., Chem. Commun. 1994, 2583–2584.
8. Kajiki, T.: Moriya. H.: Kondo. S.: Mabeshima. T.: Yano. Y. Remarkable stabilization of the anionic semiquinone radical of 6-azaflavin by hydrogen bonding with a receptor in chloroform. Chem. Commun. 1998. 2727–2728.
9. Kajiki, T.; Moriya, H.; Hoshino, K.: Kuroi. T.; Kondo. S.: Nabshima, T.: Yano. Y. Functionalized flavin receptors. Regulation of redox properties of 6-azaflavin via hydrogen bondings with melamine derivatives bearing guanidinium ion(s) in organic solvents. J. Org. Chern. 1999. 64 (26). 9679 - 9689.
10. Davis, A.P. Cholaphanes; Steroids as structural components in molecular engineering. Chem. Soc. Rev. 1993. *22* (4). 243–253.
11. Oost, T.; Filippazzi. A.: Kalesse. M. *Bis*(guanidinium) receptors as ribonuclease active-site model systems: Structural changes and solvent effects. Liebigs Ann. 1997, 1005–1011.
12. Lawless, L.J.; Davis. A.P. Steroidal guanidinium receptors for the enantioselective recognition of N-acyl e-amino acids. Chem. Commun. 1999. 9–10.
13. Lawless. L.J.; Blackburn, A.G.: Ayling, A.J.: Perez-Payan. M.; Davis, A.P. Steroidal guanidines as enantioselective receptors for N-acyl α-amino acids. Part 1. 3α-Guanylated carbanates derived from cholic acid. J. Chem. Soc., Perkin Trans. 1 2001. 1329–1341.
14. Beer, P.D.; Drew, M.G.B.: Smith. D.K. Selective electrochemical recognition of bidentate anionic guests in competative solvents using novel ferrocenyl thiourea and guanidinium receptors. J. Organomet. Chem. 1997. *543* (1–2). 259–261.
15. Watanabe. S.: Onogawa, O.: Komatsu. Y.: Yoshida. K. Luminescent metalloreceptor with a neutral *bis*(acylaminoimidazoline) binding site: Optical sensing of anionic and neutral phosphodiesters. J. Am. Chem. Soc. 1998. *120.* 229–230.
16. Cabell, L.A.: Best, M.D.: Lavigne, J.J.: Schneider. S.E.; Perreault, D.M.: Monohan, M.; Anslyn, E.V. Metal triggered fluorescence sensing of citrate using a synthetic receptor. J. Chem. Soc., Perkin Trans. 2 2001, 315–323.
17. Müller, C.: Riede, J.: Schmidtchen. F.P. Host–guest bonding of oxoanions to guanidinium anchor groups. Angew. Chem., Int. Ed. Engl. 1988. *27* (11), 1516–1518.
18. Echavarren, A.; Galan, A.: Mendoza, J.: Salmeron. A.; Lehn, J.-M. Anion receptor molecules: Synthesis of a chiral and functionalized binding subunit. a bicyclic guanidinium group derived from L- or D-asparagine. Helv. Chim. Acta 1988. *71* (4). 685–693.
19. Gleich. A.: Schmidtchen, F.P. Künstliche molekulare anion-wirte. Die synthese eins chiralen bicyclischen guanidinium-salzes als funktionlisierte ankergruppe für oxo-anionen. Chem. Ber. 1990. *123* (4). 907–915.
20. Kurzmeier. H.; Schmidtchen. F.P. Abiotic anion receptor functions. A facile and dependable access to chiral guanidinium anchor groups. J. Org. Chem. 1990. *55* (12). 3749–3755.
21. Metzger, A.; Peschke. W.; Schmidtchen. F.P. A convenient access to chiral monofunctionalized bicyclic guanidinium receptor groups. Synthesis 1994. 566–570.
22. Echavarren. A.: Galán. A.: Lehn. J.-M.; de Mendoza. J. Chiral recognition of aromatic carboxylate anions by an optically active abiotic receptor containing a rigid guanidinium binding subunit. J. Am. Chem. Soc. 1989. *111* (13). 4994–4995.
23. Galán. A.; Pueyo, E.: Salmeron. A.: de Mendoza. J. Selective complexation of adenosine monophosphate nucleotides by rigid bicyclic guanidinium abiotic receptors. Tetrahedron Lett. 1991, *32* (15). 1827–1830.

24. Galán, A.; Mendoza. J.; Bruix, C.M.: Deslongchamps. G.; Rebek, J., Jr. A synthetic receptor for dinucleotides. J. Am. Chem. Soc. 1991, *113* (24). 9424–9425.
25. Andreu. C.: Galán. A.: Kobiro. K.; de Mendoza, J.: Park, T.K.: Rebek, J.; Salmerón, A.; Usman, N. Transport of adenine mono- and dinucleoside monophosphates across liquid membranes and extraction of oligonucleotides with synthetic carriers. J. Am. Chern. Soc. 1994, *116* (12), 5501–5502.
26. Delongchamps, G.; Galán, A.; de Mendoza. J.: Rebek, J. A synthetic receptor for cyclic adenosine monophosphate. Angew. Chem.. Int. Ed. Engl. 1992. *31* (1). 61–63.
27. Kato, Y.: Conn. M.; Rebek. J.. Jr. Water-soluble receptors for cyclic-AMP and their use for evaluating phosphate–guanidinium interactions. J. Am. Chem. Soc. 1994. *116* (4). 3279–3284.
28. Galán. A.; Andreu. D.: Echavarren, A.; Prados, P.; de Mendoza. J. A receptor for enantioselective recognition of phenylanaline and tryptophan under neutral conditions. J. Am. Chern. Soc. 1992. *114* (4). 1511–1512.
29. Metzger, A.; Gloe. K.: Stephan, H.; Schmidtchen, F.P. Molecular recognition and phase transfer of underivatized amino acids by a foldable artificial host. J. Org. Chem. 1996. *61* (6). 2051–2055.
30. Alcazar, V.; Moran, J.R.; de Mendoza. J. Guanidinium catalyzed conjugate addition of pyrrolidine to unsaturated lactones. Tetrahedron Lett. 1995, *36* (22). 3941–3944.
31. Segura. M.: Alcazar. V.; Prados. P.; de Mendoza. J. Synthetic receptors for uronic acid salts based on bicyclic guanidinium and deoxycholic acid subunits. Tetrahedron 1997, *53* (38). 13119--13128.
32. Alcazar. V.: Segura. M.; Prados, P.; de Mendoza, J. A preorganized macrocycle based on a bicyclic guanidinium subunit with six convergent hydrogen bonds for anion recognition. Tetrahedron Lett. 1998, *39* (9). 1033–1036.
33. Cuevas, F.: Stefano, S.D.; Magrans, J.O.: Prados. P.; Maadolini. L.: de Mendoza, J. Toward an artificial acetylcholinesterase. Chem. Eur. J. 2000, *6* (17). 3228--3234.
34. Schießl, P.: Schmidtchen, F.P. Abiotic molecular recognition of dicarboxylic anions in methanol. Tetrahedron Lett. 1993, *34* (15). 2449–2452.
35. Schiessl. P.; Schmidtchen, F.P. Binding of phosphates to abiotic hosts. J. Org. Chein. 1994, *59* (3). 509- 511.
36. Peschke, W.: Schmidtchen, F.P. Incremental rigidification of a foldable anion host: Does it help in guest binding'? Tetrahedron Lett. 1995, *36* (29), 5155–5158.
37. Peczuh, M.W.; Hamilton, A.D.; Sànchez-Queseda, J.; de Mendoza. J.: Haack, T.; Giralt, E. Recognition and stabalization of an α-helical peptide by a synthetic receptor. J. Am. Chem. Soc. 1997, *119* (39), 9327–9328.
38. Schmidtchen. F.P. A non-macrocyclic host for binding organic phosphates in protic solvents. Tetrahedron Lett. 1989. *30* (34). 4493–4496.
39. Berger. M.; Schmidtchen. F.P. Electroneutral artificial hosts for oxoanions active in strong donor solvents. J. Am. Chem. Soc. 1996, *118* (37). 8947–8948.
40. Berger. M.; Schmidtchen, F.P. The binding of sulfate anions by guanidinium receptors is entropy-driven. Angew. Chem., Int. Ed. Engl. 1998, *37* (19), 2694–2696.
41. Berger. M.; Schrnidtchen. F.P. Zwiterionic guanidinium compounds serve as electroneutral anion hosts. J. Am. Chem. Soc. 1999. *121* (43). 9986–9993.
42. Dixon, R.P.; Geib, S.J.: Hamilton, A.D. Molecular recognition: *Bis*-acylguanidiniums provide a simple family of receptors for phosphodiesters. J. Am. Chem. Soc. 1992, 114, 365–366.
43. Jubian. V.: Dixou. R.P.: Hamilton, A.D. Molecular recognition and catalysis. Acceleration of phosphodiester cleavage by a simple hydrogen-bonding receptor. J. Am. Chem. Soc. 1992, *114* (3). 1120–1121.
44. Fan, E.; Arman, S.A.: Kincaid. S.: Hamilton, A. Molecular recognition: Hydrogen-bonding receptors that function in highly competitive solvents. J. Am. Chem. Soc. 1993. *115* (1). 369–370.
45. Albert. J.S.; Goodman, S.; Hamilton, A.D. Molecular recognition of proteins: Sequence-selective binding of aspartate pairs in helical peptides. J. Am. Chem. Soc. 1995. *117* (3). 1143–1144.
46. Albert. J.S.: Peczuh, M.W.; Hamilton, A.D. Design, synthesis and evaluation of synthetic receptors for the recognition of aspartate pairs in an α-helical conformation. Bioorg. Med. Chem. 1997. *5* (8). 1455–1467.
47. Haack, T.; Peczuh. M.W.; Salvatella. X.: Sanchez-Quesada, J.; de Mendoza, J.; Hamilton, E.; Giralt, E. Surface recognition and helix stabilization of a tetraaspartate peptide by shape and electrostatic complimentarity of an artificial receptor. J. Am. Chein. Soc. 1999, *121* (50), 11813–11820.
48. Linton. B.; Hamilton. A.D. Calorimetric investigation of guanidinium–carboxylate interactions. Tetrahedron 1999. *55* (19), 6027–6038.
49. Linton. B.R.; Goodman. M.S.: Fan, E.; Van Arman. S.A.; Hamilton, A.D. Thermodynamic aspects of dicarboxylate recognition by simple artificial receptors. J. Org. Chern. 2001. *66* (22). 7313–7319.
50. Davis, A.P.; Dempsey, K.J. Synthesis and investigation of a hindered. chiral, bicyclic guanidine. Tetrahedron: Asymmetry 1995. *6* (11). 2829–2840.
51. Linton. B.R.; Goodman, M.S.; Hamilton, A.D. Nitronate anion recognition and modualtion of ambient reactivity by hydrogen-bonding receptors. Chern. Eur. J. 2800, *6* (13), 2449–2455.
52. Gross, R.: Bats, J.W.: Göbel, M.W. Das trans-decalingerüst als Abstanshalter für axial konfigurierte diamine: Herstellung eines phosphatbindenden bis(guanidins). Liebigs Ann. Chem. 1994. 205–210.
53. Muche. M.-S.: Göbel, M.W. *Bis*(guanidinium) alcohols as models of staphylococcal nuclease: Substrate binding through ion pair complexes and fast phosphoryl transfer reactions. Angew. Cheni.. Int. Ed. Engl. 1996, *35* (IS). 2126–2129.
54. Metzger, A.: Lynch. V.M.: Anslyn, E.V. A synthetic receptor selective for citrate. Angew. Chem., Int. Ed. Engl. 1997, *36* (8), 862–864.

55. Lavigne, J.J.: Anslyn. E.V. Teaching old indicators new tricks: A colorimetric chemosensing ensemble for tartrate1 malate in beverages. Angew. Chern.. Int. Ed. Engl. **1999**. 38 (24), 3666–3669.
56. Wiskur. S.L.: Anslyn, E.V. Using a synthetic receptor to create an optical sensing ensemble for a class of analytes: A colorimetric assay for the aging of scotch. J. Am. Chern. Soc. **2001**, 123 (41). 10109–10110.
57. Niikura. K.: Metzger, A.; Anslyn, E.V. Chemoseiisor ensemble with selectivity for inositol-triphosphate. J. Am. Chem. Soc. 1998, 120 (33). 8533–8534.
58. Hedge, V.: Madhukar. P.: Madura. J.D.: Thummel, R.P. Fischer route to pyrido[3,2-g]indoles A novel receptor for urea derivatives. J. Am. Chem. Soc. **1990**, 112 (11), 4549–4550.
59. Hedge, V.: Hung, C.Y.; Cummingham. R.: Hopfiner. T.: Thunimel, R.P. Design of receptors for urea derivatives based on the pyrido[3,2-g]indole subunit. J. Am. Chem. Soc. 1993. 115 (3). 872–878.
60. Bell. T.W.; Hou, Z.; Zirnmerman, S.C.: Thiessen. P.A. Highly effective hydrogen-bonding receptors for guanine derivatives. Angew. Chem., Int. Ed. Engl. 1995. 34 (19). 2163–2165.
61. Bell. T.W.: Hext, N.M.: Khasanov, A.B. Binding biomolecules with designed, hydrogen-bonding receptors. Pure Appl. Chem. 1998. 70 (12). 2317–2377.
62. Cuntze. J.; Owens, L.: Alcazar. V.; Seiler. P.: Diederich. F. Molecular clefts derived from 9,9′-spirobi-9H-fluorene for enantioselective complexation of pyranosides and dicarboxylic acids. Helv. Chim. Acta 1995. 78 (2), 367–390.
63. Ariga. K.: Anslyn. E.V. Manipulating the stoichiometry and strength of phosphocliester binding to a Bis-guanidine cleft in DMSO/water solutions. J. Org. Cheni. 1992.57 (2). 417–419.
64. Perreault, D.M.; Chen. X.: Anslyn, E.V. The advantages of using rigid polyaza-clefts for hydrogen-bonding molecular recognition. Tetrahedron 1995, 51 (2). 353–362.
65. Kneeland, D.M.: Ariga. K.; Lynch. V.M.: Huang, C.: Anslyn. E.V. *Bis*(alkylguanidinium) receptors for phosphodiesters: Effects of counterions, solvent mixtures, and cavity flexibility on complexation. J. Am. Chern. Soc. **1993**, *115* (22). 10042–10055.
66. Anslyn. E.V.: Smith. J.: Kneeland, D.M.; Ariga. K.; Chu, F. Strategies for phosphodiester complexation and cleavage. Supramol. Chem. **1993**, *1*, 201–208.
67. Perreault. D.M.: Cabell. L.A.: Anslyn, E.V. Using guanidinium groups for the recognition of RNA and as catalysts for the hydrolysis of RNA. Bioorg. Med. Chem. 1997. *5* (6). 1209–1220.
68. Ait-Haddou. H.; Wiskur, S.L.; Lynch. V.M.; Anslyn. E.V. Achieving large color changes in response to the presence of amino acids: A molecular sensing ensemble with selectivity for aspartate. J. Am. Chem. Soc. **2001**, 123 (45). 11296–11297.
69. Dieterich. B.; Fyles, T.M.: Lehn. J.-M.; Pease. L.G.; Fyles. D.L. Anion receptor molecules. Synthesis and some anion binding properties of macrocyclic guanidinium salts. J. Chem. Soc., Chem. Commun. **1978**, 934–936.
70. Martin, M.: Almaraz. M.; Hernández. J.V.; Tejeda, A.: Caballero. M.C.; Morán. J.R. Xanthone receptors for carboxylic acids and carboxylates. Heterocycles 1999. *5* (1). 47–51.
71. Bonnat. M.: Bradley. M.; Kilburn. J.D. The solid phase synthesis of a guanidinium based 'tweezer' receptor. Tetrahedron Lett. 1996. 37 (30). 5409–5412.
72. Davies. M.: Bonnat. M.: Guillier, F.; Kilburn, J.D.: Bradley. M. Screening an inverted peptide library in water with a guanidinium-based tweezer receptor. J. Org. Chern. 1998, 63 (24). 8696–8703.
73. Hennrich, G.; Sonnenschein. H.; Resch-Genger. U. Fluorescent anion receptors with iminoyltliiourea binding sites-selective hydrogen bind mediated recognition of CO_3^{2-}. HCO_3^- and HPO_4^{2-}. Tetrahedron Lett. 2001. 42 (15). 2805–2808.
74. Schmuck: C. Side chain selective binding of *N*-acetyl-α-amino acid carboxylates by a 2-(guanidiniocarbonyl)pyrrole receptor in aqueous solvents. Chem. Commun. 1999. 9. 843–844.
75. Schmuck, C. Carboxylate binding by 2-(guanidiniocarbonyl)pyrrole receptors in aqueous solvents: Improving the binding properties of guanidinium cations through additional hydrogen bonds. Chem. Eur. J. **2000**, 6 (4), 709–718.
76. Schmuck. C. Self-assembly of 2-(guanidiniocarbony1)-4-carboxylate in dimethyl sulfoxide: An entropy driven oligermerization. Tetrahedron 2001. 57 (15). 3063–3067.
77. Silva. A.P.: Gunaratne. H.Q.N.; McVeigh, C.; Maguire, G.E.M.: Maxwell. P.R.S.; O'Hanlon. E. Fluorescent signalling of the brain neurotransmitter γ-aminobutyric acid and related amino acid zwitterions. Chem. Commun. 1996. 18. 2191–2192.
78. Schneider, S.E.; O'Neil. S.N.: Anslyn. E.V. Coupling rational design with libraries leads to the production of an ATP selective chemosensor. J. Am. Chern. Soc. 2000. 122 (8). 542–543.
79. Sasaki. D.Y.; Kurihara. K.: Kunitake. T. Specific. multiple-point binding of ATP and AMP to a guanidinium-functionalized monolayer. J. Am. Chem. Soc. 1991. 113 (25). 9685–9686.
80. Sasaki, D.Y.: Kuihara. K.; Kunitake. T. Self-assembled multifunctional receptors for nucleotides at the air–water interface. J. Am. Chem. Soc. 1992; 114 (27). 10994–10995.
81. Kamino, A.; Koyano, H.; Agria, K.: Kunitake. T. Control of the molecular packing in guanidinium rnonolayers through binding with aqueous polycarboxylates. Bull. Chem. Soc. Jpn. **1996**. 69. 3619–3631.
82. Ariga, K.: Kamino, A.; Cha, X.; Kunitake. T. Multisite recognition of aqueous dipeptides by oligoglycine arrays mixed with guanidinium and other receptor units at the air–water interface. Langmuir 1999, 15 (11). 3875–3585.
83. Nishizawa, S.: Kato, Y.: Teramae, N. Fluorescence sensing of anions via intramolecular excimer formation in a pyrophosphate-induced self-assembly of a pyrene-functionalized guanidinium receptor J Am Chem Soc 1999. 121 (40), 9463–9464

Halogen Bonding

Pierangelo Metrangolo
Giuseppe Resnati
Polytechnic of Milan, Milan, Italy

INTRODUCTION

"Halogen bonding" is the term *introduced by Dumas et* al.[1] *for describing the attractive donor–acceptor interactions that involve halogen atoms functioning as* Lewis *acids. Within the framework of* Mulliken's theory,[2] *the* Lewis *bases owe their donor properties to the presence of atoms possessing one or more "lone pairs" of electrons* (i.e., N, O, S, *Se, I* , Br^-,...). *The stronger the* electron-withdrawing *environment around the halogen* atoms, *the higher their ability to be engaged in such noncovalent interactions. The resulting complexes were* considered *by* Prout and *Kamenar as belonging to the* $n \rightarrow \sigma^*$ type.[3]

The halogen bonding was first reported in 1863,[4] *and pale yellow crystals with the composition* $(CH_3)_3N \cdot Br_2$ *were obtained by directly adding trimethylamine to bromine* more *than* 100 *years* ago.[5] *While its implications impact all the fields where design and manipulation of* aggregation *phenomena play a key role, halogen bonding only recently has become an object of serious study as a well-defined, strong. specific. and directional interaction for* assembling complex *supramolecular architectures.*

Hassel *first deinonstrated that* halogen *bonding* is *a powerful tool in* driving the *self-assembly of endless chains of alternating donor and acceptor* modules.[6] *His solid-phase studies (using x-ray crystallography)* unequivocally *established the existence of a* D···X (*D=electron-pair donor, X=electron-pair halogen acceptor) interaction with a defined linear* geometry.[7] *These studies* suggested *an analogy with the hydrogen bonding. Theoretical and* experimental *data show that the two interactions have* comparable strengths.[8] *loth are also highly directional.* Similar *to the binding geometry in hydrogen bonding, halogens are directly linked to donor* atoms *with a bonding direction that roughly coincides* with *the axes of the lone-pair orbitals in the* non-complexed donor *molecule. Moreover, as expected for an* $n \rightarrow \sigma^*$ *interaction, the* N···X–C *angle in intermolecular halogen bonding spans over the range of* 160–180°, even *for weak interactions* (>3 Å *when iodine or bromine are* involved). Interaction *strength and* directionality *support* the *idea that the halogen bonding is of a "specific" type.*

HALOGEN BONDING

Halogen atoms that are involved in halogen-bonding formation can be bound to other halogens (elemental halogens and interhalogens) or to carbon or nitrogen atoms. The electron-pair donors can be neutral (N, O, S, *Se,...) or anionic* (*I* , *Br* , Cl^-, *F* ...) species.[9] *Interaction of these motifs results in a wide diversity of* supramolecular synthons *(Fig.* 1).

Calculations and experimental *data (in solid, liquid. and gas phases) show that the tendency of different halogens to give strong halogen bondings is* I>Br>Cl>F, *namely, opposite to the sequence of their* electronegativies. *Due to this, reports* on *short contacts having fluorine as the acceptor site are* rare,[10] *and they were never encountered in the solid state.*

The interaction energy spans the range 10–200 kJ mol^{-1}. *The lower value* is *calculated for the weak* N···Cl *halogen bonding, while the higher one is reported for the very strong* $I^- \cdots I_2$ *halogen bonding in the* I_3^- anion.[11]

Statistical studies carried out on the Cambridge Structural Database (CSD) confirmed *the existence of the halogen bonding. An accurate study by Lommerse et* al.[12] *on the* D···X–C (*D*=O,N *and X*=F, Cl, *Br. I) interactions demonstrates that the more electron withdrawing the carbon framework of the halocarbon is, the stronger* the *halogen bonding. Usually, the order of acceptor strength is* X–X>X–C(sp)>X–C(sp^2)>X–C(sp^3). *According to these studies, the attractive nature of the interaction is mainly due to electrostatic effects.However, polarization.* charge-*transfer, and dispersion contributions play important roles in the interpenetration of van der Waals* volumes *of halogen and donor atoms. Whether or not electrostatic or charge-transfer effects are the* main *cause of the complex formation still* remains *an open question. This also holds for hydrogen bonding. another entry thus being added to the analogies listed between the two interactions.*

The relative donor ability of different heteroatoms depends on the halogen partner, the analytical *technique used for the measurements. and the aggregation state of the complex. Toward iodo- and bromoperfluorocarbons and in solution. the* ^{19}F-NMR *technique gives the donor strength scale* N>S≥O, *when that all the donor atoms are in the same* sp^3 *hybridization state."" In the solid*

Encyclopedia of Supramolecular Chemistry
DOI: 10.1081/E-ESMC 120019872

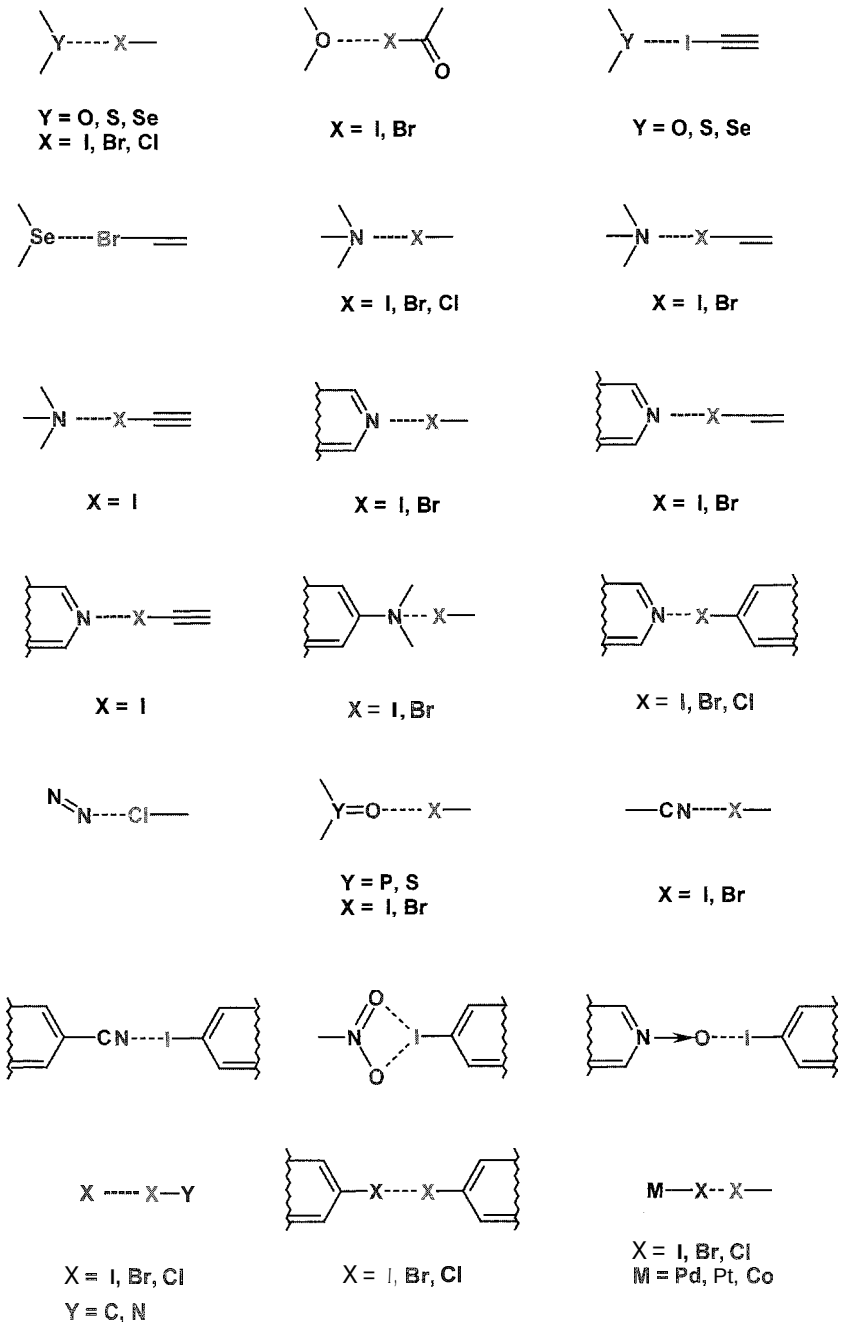

Fig. 1 Most frequently used halogen-bonding-based supramolecular synthons. Electron-pair donor sites were reported in black, while the acceptor sites are in grey. (*View this art in color at www.dekker.com.*)

state. the scale O>S was suggested, and recent theoretical calculations gave the scale P≥N>S [14] The donor strength scales N(sp^3)>N(sp^2)>N(sp) and O(sp^3)>O(sp^2) are fairly general, and increased electronegativity of substituents on the electron-donor atom decreases the strength of the halogen bond they form. Conversely, increased electron density on the electron donor results in stronger Interactions and it is thus not surprising that aromatic N-oxides or anions are good donors toward halocarbons.[15]

Some of the characteristics of halogen bonding depend on the nature of the interacting partners. for instance. the relative role of the specific forces acting between the atoms involved (e.g., electrostatic effects. polarization, charge-transfer, dispersion contributions). Some other characteristics remain constant in a wide variety of cases,

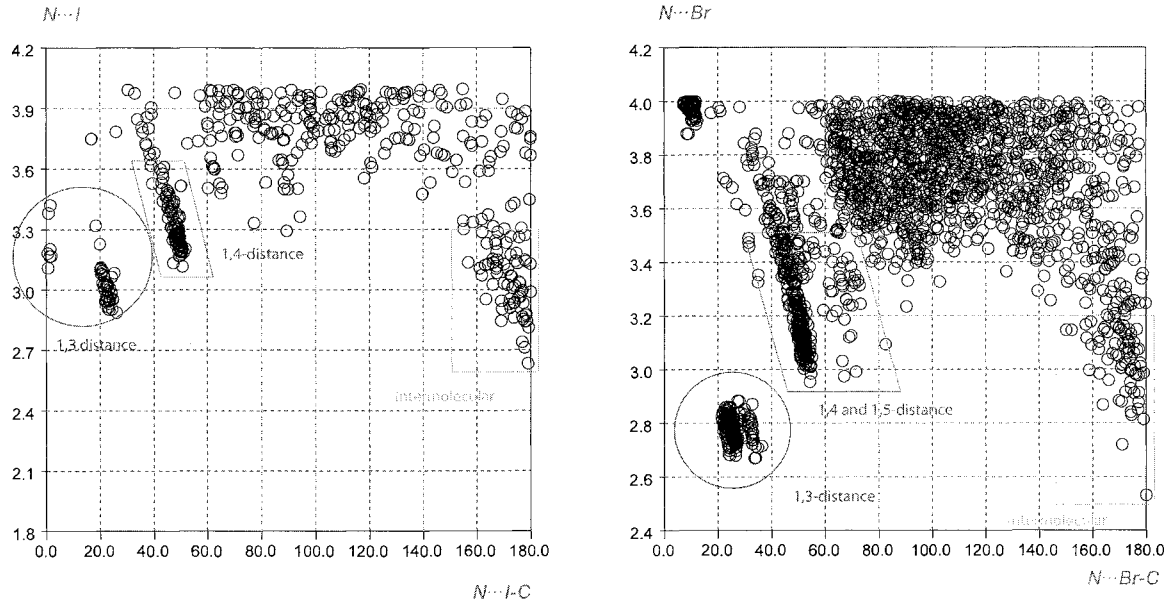

Fig. 2 The CSD scatterplots of N···X halogen-bonding distance versus N···X-C angle for X=I (left) and Br (right). Intra- (1,3-, 1,4-, 1,5-distances) and intermolecular contacts below 4 Å were reported. Error-free structures showing no disorder and with $R<0.06$ were considered. (*View this art in color at www.dekker.com.*)

for example, the angle D···X–C formed by the covalent and noncovalent bonds around the halogen atom (approximately 180°) and the value of the D···X distance for halogen bondings involving the same donor and acceptor atoms. The CSD scatterplots of N···X halogen-bonding distance versus N···X–C angle for X=I (left, 522 structures) and Br (right, 2107 structures) are reported in Fig. 2.

These plots show how the halogen bonding occurs both intra- and intermolecularly. Clearly, it may play a key role in understanding the conformational preferences of molecules and in designing the construction of supramolecular architectures.

Hundreds of supramolecular structures grounded on halogen bonding were reported since the seminal work of Hassel. The following part of this article will survey some

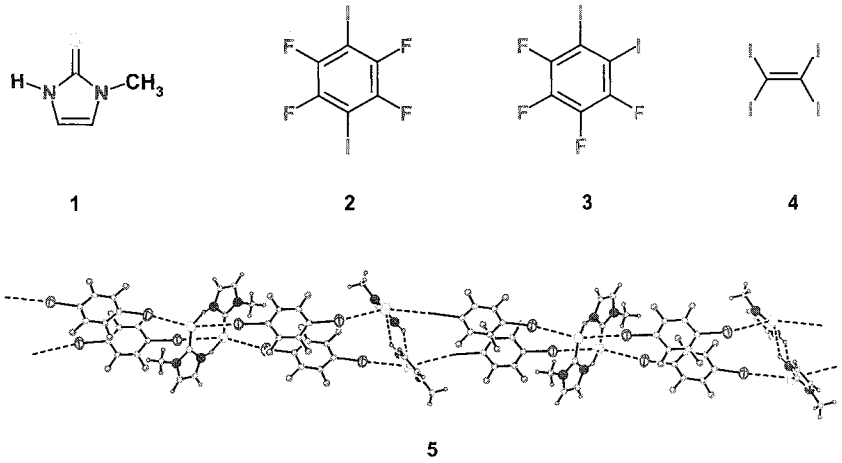

Fig. 3 Double-stranded chain structure in the halogen-bonded co-crystal **5** between 2-mercapto-1-methylimidazole (**1**) and 1,4-diiodotetrafluorobenzene (2). Halogen-bonding distances S···I=3.314(1) Å, 3.342(1) Å. Colors are as follows: black 70%—nitrogen; black 50%—iodine: black 30%—fluorine and hydrogen: black 10%—sulfur and carbon. Dashed lines represent intermolecular halogen and hydrogen bondings. (*View this art in color at www.dekker.com.*)

specimen examples proving the great potential of halogen bonding in the design of new and high-value functional materials, interpenetrated architectures,[16] etc.

2-Mercapto-1-methylimidazole (1) functions as an iodine sponge forming a stable halogen-bonded complex with the I_2.[17] Pennington et al. recently reported the preparation of new complexes of 1 with the organic iodides 1.4-diiodotetrafluorobenzene (2), 1,2-diiodotetrafluorobenzene (3). and (4) tetraiodoethylene.[18] All of these structures are characterized by the simultaneous presence of remarkably similar N–H···S hydrogen-bonding patterns and I···S halogen-bonding patterns. Endless one-dimensional (1D) chains of alternating donor 1 and acceptor 2 are present in cocrystal 5. which is formed through I···S···I interactions where sulfur works as a bidentate donor (Fig. 3).

These chains are then joined into supramolecular double strands through N–H···S interactions that link two molecules of 1 into a dimer. The other two complexes given by 1 show a similar supramolecular organization. This demonstrates the great potential of these components for crystal design. Moreover, hydrogen and halogen bondings can be seen as competing noncovalent interactions.[19] They can, however. also cooperate in the building of remarkably complex supramolecular structures.

The research for organic conductors in the last two decades revealed that if interesting electronic properties, such as superconductivity. are pursued, the design and control of the supramolecular arrangement in the crystal structure are as important as the design of an individual donor or acceptor molecule. For instance. the introduction on tetrathiofulvalene donor molecules (TTFs) of specific substituents able to be engaged in weak intermolecular interactions was extensively used in numerous molecular organic conductors with the aim of controlling the supramolecular arrangement of molecules in their crystal structures. The application of the hydrogen bond to TTFs was examined, but the intrinsic flexibility of the hydrogen bond was found to hinder reliable control of the organization of the crystal matrix. T. Imakubo et al. found that the N···I halogen bonding is suitable for this purpose, and they reported several unique crystal systems of supramolecular organic conductors based on the iodine-bonded TTFs.

Presented in Fig. 4 is the crystal structure of 8, which is the $Au(CN)_4^-$7 salt of diiodo(ethylenedithio)diselenadithiafulvalene (DIETS, 6),[20] with a 6/7 ratio of 2.

The two modules 6 and 7 stack separately into different layers that are joined by halogen bonding between each iodine atom of and the cyano groups of two different and adjacent $Au(CN)_4$ anions. The N···I halogen bonding distance is approximately 3 Å. These materials showed an onset temperature of the superconductivity under uniaxial strain parallel to the crystallographic c-axis.

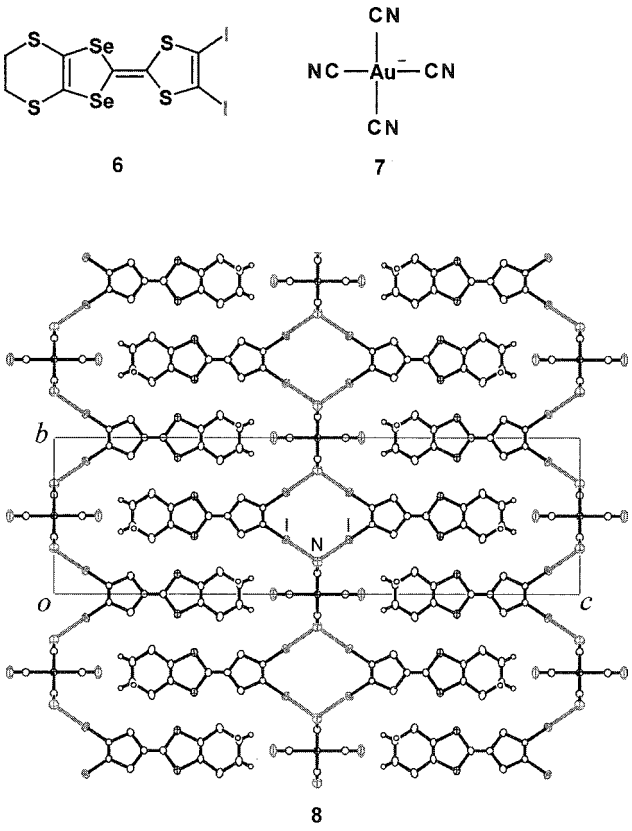

Fig. 4 Crystal structure of the salt 8 compounded by two molecules of diiodo(ethylenedithio)diselenadithiafulvalene (DIETS. 6) and one anion $Au(CN)_4^-$7 viewed along the a-axis. Halogen-bonding distance N···I=3.018(7) Å. Colors are as follows: black 70%—nitrogen: black 50%—iodine. Continuous gray lines represent halogen bonding?. (*View* this art *in* color *at www.dekker.com.*)

which is the highest among the known superconductors based on unsymmetrical organic π-donors. There seems to be no doubt that the strong halogen bonding between the layers of DIETSs and counteranions is stronger than the side-by-side chalcogen···chalcogen contacts in conductors based on TTFs. This affects the distortion manner under the uniaxial strain and. consequently, increases superconductivity.

Halogens, mainly I_2 and Br_2 but also Cl_2, interhalogens, such as ICl and IBr, and pseudohalogens, like ICN, have traditionally played a key role in the identification of the structural aspects of the halogen bonding. Nevertheless, these molecules may not be the ideal modules for defining the inherent characteristics of this intermolecular interaction. For instance, one or both of the iodine atoms of I_2 can work as electron acceptors, depending on the strength of the electron-donor species. Because of this, it is difficult to control the supramolecular architecture of the formed cocrystals. In other cases, I_2 can even work as

an amphoteric species, where one iodine atom functions as electron acceptor and the other as electron donor. More recently. particular attention was paid to triiodo- and tribromomethanes, as well as their tetrasubstituted analogues. and diiodobenzene derivatives.[21]

Resnati and Metrangolo et al. introduced dihaloperfluorocarbons, which are compounds of technological relevance. as new tectons for the construction of supramolecular systems, where halogen bonding could be studied free from interference of other interactions. Fluorine atoms and perfluorinated residues are strongly electronegative. As a consequence, the electron-accepting ability of halogen atoms in perfluorocarbon (PFC) halides is definitely higher than in the corresponding hydrocarbon (HC) halides. Different from C–H groups in HC halides, C–F groups in PFC derivatives have a weak tendency to give rise to any attractive interactions. As a consequence, the use of PFC halide5 minimizes possible interaction interferences in a pattern controlled by halogen bonding. Moreover, unlike the zigzag organization of the alkyl chains of their HC parents, PFC chains adopt an all-trans, rigid, rod-like twisted conformation that causes their typical alignment in parallel bars. Due to this behavior, telechelic dihaloperfluorocarbons can be considered ideal ditopic 180° tectons for halogen-bonding-based crystal engineering, with metrics that can be tuned by simply

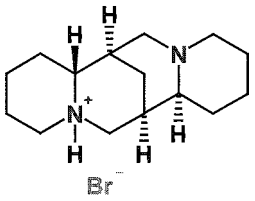

9

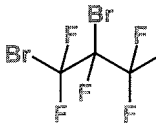

10

11

Fig. 5 Perspective view of co-crystal 11 between (*S*)-1,2-dibromohexafluoropropane and (−)-sparteine hydrobromide (9) along the crystallographic *b* direction. Colors are as follows: black 70%—nitrogen; black 50%—bromine: black 30%—fluorine. Dashed black lines represent halogen bondings. (*View this art in color at www.dekker.com.*)

choosing perfluoroalkyl chains of different lengths. The peculiar properties of perfluorocarbons along with the precise geometrical features of the halogen bonding allow a degree of architectural design that is unusual for supramolecular chemistry.[22]

The optical resolution of racemic molecules with a basic or an acidic functional group is frequently performed by resorting to hydrogen bonding to form diastereoisomeric salts with one of the numerous acid or basic resolving agents available in the literature. The use of halogen bonding as the driving force in the diastereoisomeric adduct formation for the resolution of chiral but racemic halocarbons was also reported.[23] Specifically, chiral haloperfluorocarbons are a virtually unknown class of compounds, and racernic 1,2-dibromohexafluoropropane (10) was resolved for the first time through cocrystallization with enantiopure (−)-sparteine hydrobromide (9). The driving force toward the cocrystallization is the $Br^{-}\cdots Br–C$ halogen bonding between bromide ions, which function as electron donors, and carbon-bound bromine atoms, which work as electron acceptors. Each bromide ion bridges the primary and secondary bromine of two distinct PFC units 9, each of which is bound to two adjacent bromide ions. Enantiopure infinite twofold helices develop parallel to the *b* axis (Fig. 5).

The resolution of 9 is the result of the highly specific inclusion of solely the (S) enantiomer in the chiral crystal 11 with a "halogen-bonded" helical arrangement. This arrangement maximizes the transfer of information from the HC to the PFC units.

From a supramolecular point of view, anionic species play a key role in many mineral or biological routes. Despite this, however, anion-centered self-assembly processes were little explored. Recently. anion coordination was addressed mainly through the design of *endo*-receptors; on the contrary, the electron-poor organic halides work effectively as *exo*-receptors of anions. The ability described here of the halide anions to act as electron donors to carbon-bound halogens may develop as a general protocol for halide-centered supramolecular chemistry.

Finally, the ability of the neutral halogen atoms to function as electron-pair donors toward other halogen atoms should be mentioned. Price et al. demonstrated the importance of the nonspherical atomic charge distribution on the halogens in directing the halogen–halogen interactions.[24] Desiraju convincingly argued that the halogen–halogen interaction, while weaker and less directional than other halogen bondings, is an attractive force that can be used for manipulating and organizing the supramolecular structure within a crystal.[25] In particular, triangular X_3 (X=Cl, Br, I) supramolecular synthons were extensively used in the design of hexagonal networks based on tritopic 120° tectons. such as 1,3,5-trihalobenzenes. Interesting examples of two-dimensional (2D) sheet-like structures[26] and hexagonal nanoporous architectures, also capable of hosting guest species with chiral discrimination,[27] were obtained.

12

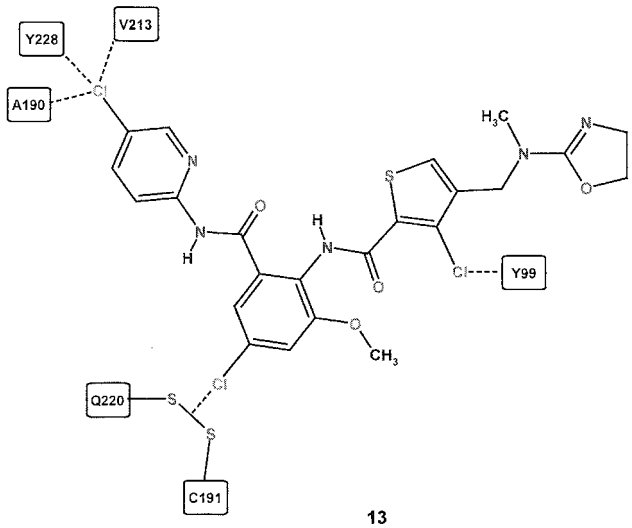

13

Fig. 6 Chemical structures of halotane 12 and inhibitor of the human *Xa* factor 13. For the latter. the major contacts between the inhibitor and aminoacidic residues in the receptorial pocket of the *Xa* factor. which can be rationalized as O···Cl and S···Cl halogen bondings. were reported. (*View this art in* color *at www.dekker.com.*)

CONCLUSION

"Does the concept of halogen bonding *contribute* to an *explanation* of *some* aspects *of* reactivity or *biological activity?*"

Reactions between dihalogen molecules XY and simple Lewis bases are of fundamental interest in organic and inorganic chemistry. Legon et al. demonstrated that the formation of prereactive halogen-bonded complexes D···XY characterizes the gas-phase chemistry of these reactions.[28] Thus, the halogen bonding may evolve into a covalent-bond-making reaction.

The use of halogell-substituted organic compounds as general anesthetics led to the investigation of the

mechanism of this activity. A nonspecific mechanism was proposed[1''' following the unitary theory of Overton. Halotane (1-bromo-1-chloro-2,2,2-trifluoroethane, 12) is a common volatile anesthetic used in therapy in the racemic form. The two enantiomers have different pharmacological activities: and the measured eudismic ratio was attributed to the specific binding with proteinaceous receptor sites. The enantioselective recognition of the drug in vivo may be mediated by the formation of halogen-bonded complexes with electron-pair donors present in the receptor pockets. This hypothesis is also supported by the evaluation of haiogen-bonding mediated intermolecular recognition in solution through the use of synthetic receptors.[30]

The x-ray crystal structures of complexes between halogen atoms containing drugs and their specific proteinaceous receptors have unequivocally proven the existence of halogen bondings that optimize the receptorial fitting. For example, short contacts were found between the iodine atoms of thyroid hormone thyroxin (T4) and the carbonyl oxygens of the aminoacidic residues in the pocket of transthyretin (TTR). which is the major transporter of T4 in the human body.[31] Short O···Cl and S···Cl contacts were detected in the crystal structure of the coinplex between the factor *Xa* of the human blood coagulation cascade and the inhibitor **13** (Fig. 6). which is used in the treatment of thrombotic diseases.[32]

The halogen bonding was also proposed to be involved in the toxicity mechanism of polyhaiogenated aromatic compounds, which are persistent environmental pollutants.[33]

''Does halogen bonding *open new perspectives in supramolecular chemistry?''*

The careful control of the overall architecture of crystalline organic solids is a topic of current intense interest, with the aim of obtaining desirable and useful properties. Metal coordination and hydrogen bonding are, by far, the most studied noncovalent interactions that drive the self-organization of inorganic and organic supramolecular structures, respectively. New interactions will have to he searched actively. because future crystal engineering projects will require full utilization of various methodologies. Halogen bonding represents an effective and reliable tool for crystal engineering. It can be considered a new item on the palette of noncovalent interactions at the disposal of the chemist to be used as the cement for assembling molecules into supramolecular structures.

New protocols based on halogen bonding were exploited to overcome the low affinity between perfluorocarbons and hydrocarbons. to design new molecular conductors, to prepare pseudopolyhalide salts,[34] to resolve racemic mixtures, to control polymorph interconversion,[35] and to tune the reactivity in the solid state.[36]

These results open new opportunities in the design and manipulation of molecular aggregation processes. The implications extend to diverse fields, such as organic chemistry, biopharmacology. and materials science.

ACKNOWLEDGMENTS

The authors gratefully acknowledge the contribution of Ms. Hannele Primetta in the preparation of the manuscript.

ARTICLES OF FURTHER INTEREST

The Cambridge Structural Database, p. *161*
Concepts in Crystal Engineering, p. 319
Crystal Engineering with Hydrogen Bonds, p. 357
Crystal Structure Prediction, p. 371
Hydrogen Bonding, p. 658
Hydrogen Bonds to Metals and Metal Hydrides, p. *666*
Nomenclature in *Crystal Engineering*, p. 967
π–π Interactions: Theory and Scope. p. 1076
Soft and Smart Materials, p. 1302
Strong Hydrogen Bonds. p. 1379
van der Waals Forces, p. 1550
Weak Hydrogen Bonds, p. 1576

REFERENCES

1. Dumas. J.M.; Gomel, L.: Guerin, M. Molecular Interactions Involving Organic Halides. In *The Chemistry of Functional Groups, Supplement D*; Wiley: New York, *1983: 985–1020.*
2. Mulliken, R.S.; Person. W.B. *Molecular Complexes: A Lecture and Reprint Volume*; Wiley-Interscience: New York. *1969.*
3. Prout. C.K.; Kamenar, B. *Molecular Complexes*; Elek Science: London, *1973:* Vol. 1, *151–207.*
4. Cuthrie, *F.* On the iodide of iodammonium. J. Chem. Soc. 1863, *16*, 239–244.
5. Remsen, I.: Norris, J.F. The action of halogens on the methylamines. Am. Chem. J. 1896. *18.* 90–95.
6. Hassel, O. Structural aspects of interatomic charge-transfer bonding. Science 1970, *170*. 497–502.
7. Bent, H.A. Structural chemistry of donor-acceptor interactions. Chem. Rev. 1968, *68*, 587–648.
8. Metrangolo. P.: Resnati. G. Halogen bonding: A paradigm in supramolecular chemistry. Chem. Eur. J. 2001. 7. 2511–2519.
9. Farnham. W.B.; Dixon, D.A.: Calabrese. J.C. Novel fluorine-bridged polyfluorinated iodine structures. Presence of fluorine as the central atom in a five-center, six-electron bond. J. Am. Chem. Soc. 1988. *110. 8453–8461.*
10. Burdeniuc. J.: Sanford, M.: Crabtree. R.H. Amine charge transfer complexes of perfluoroalkanes and an application

to poly(tetrafluoroethylene) surface functionalization. J. Fluorine Chem. 1998. *91.* 49–54.
11. Landrum. G.A.; Goldberg, N.; Hoffmann, R. Bonding in the trihalides (X_3^-), mixed trihalides (X_2Y^-) and hydrogen bihalides (X_2H^-). The connection between hypervalent. electron-rich three-center. donor-acceptor and strong hydrogen bonding. J. Chem. Soc., Dalton Trans. 1997, *19,* 3605–3613.
12. Lommerse, J.P.M.; Stone, A.J.: Taylor. R.; Allen. F.H. The nature and geometry of intermolecular interactions between halogens and oxygen or nitrogen. J. Am. Chem. Soc. 1996. *118,* 3108–3116.
13. Metrangolo, P.; Panzeri, W.: Recupero, F.; Resnati, G. Perfluorocarbon-hydrocarbon self-assembly part 16. ^{19}F NMR study of the halogen bonding between halo-perfluorocarbons and heteroatom containing hydrocarbons. J. Fluorine Chem. 2002, *114.* 27–33.
14. Romaniello. P.; Lelj. F. Halogen bond in $(CH_3)_nX$ (X=N, P, $n=3$. X=S. $n=2$) and $(CH_3)_nXO$ (X=N, P, $n=3$, X=S. $n=2$) adducts with CF_3I. Structural and energy analysis including relativistic zero-order regular approximation approach in a density functional theory framework. J. Phys. Chem.. A 2002. *106.* 9114–9119.
15. Liantonio, *R.:* Metrangolo. P.: Pilati, T.; Resnati, G. Fluorous interpenetrated layers in a three-component crystal matrix. Cryst. Growth Des. 2003, *3,* 355–361.
16. Thaimattam, R.; Sharma, C.V.K.; Clearfield. A.; Desiraju. G.R. Diamondoid and square grid networks in the same structure. Crystal engineering with the iodonitro supramolecular synthon. Cryst. Growth Des. 2001.1. 103–106.
17. Laurence, C.; El Ghomari, M.J.: Le Questel, J.-Y.: Berthelot, M.: Mokhlisse. R. Structure and molecular interactions of anti-thyroid drugs. Part 3'. Methimazole: A diiodine sponge. J. Chem. Soc., Perkin Trans. 2 1998. *7.* 1545–1551.
18. Jay. J.I.; Padgett. C.W.: Walsh, R.D.B.: Hanks, T.W.; Pennington, W.T. Noncovalent interactions in 2-mercapto-1-methylimidazole complexes with organic iodides. Cryst. Growth Des. 2001, *1.* 501–507.
19. Corradi, E.; Meille, S.V.; Messina, M.T.: Metrangolo, P.: Resnati, G. Halogen bonding versus hydrogen bonding in driving self-assembly processes. Angew. Chern., Int. Ed. 2000. *39* (10). 1782–1786.
20. Imakubo, T.: Tajima, N.; Tamura. M.; Kato, R.; Nishio, Y.; Kajita K. Supramolecular organic conductor-(DIET s)-, $[Au(CN)_4]$: Unique crystal structure and superconductivity under uniaxial strain. Synth. Met. 2003. *133–134.* 181–183.
21. Allen, F.W.: Biradha. K.; Desiraju, G.R.: Hoy, V.J.; Howard, J.A.K.; Sarma, J.A.R.P.; Thaimattam. R. Design of an SGH-active crystal. 4-iodo-4'-nitrobiphenil: The role of supramolecular synthons. Chem. Commun. 1997, *1,* 101–102.
22. Cardillo, P.; Corradi, E.: Lunghi, A.; Meille. S.V.; Messina, M.T.: Metrangolo, P.; Resnati. G. The N···I intermolecular interaction as a general protocol for the formation of perfluorocarbon-hydrocarbon supramolecular architectures. Tetrahedron 2000. *56.* 5535–5550.
23. Farina, A.: Meille, S.V.; Messina, M.T.: Metrangolo, P.; Resnati, G.; Vecchio. G. Resolution of racemic 1.2-dibromohexafluoropropane through halogen-bonded supramolecular helices. Angew. Chem.. Int. Ed. 1999, *38.* 2433–2436.
24. Price, S.L.: Stone. A.J.; Lucas. J.; Rowland, R.S.; Thornley, A.E. The nature of –Cl···Cl-intermolecular interactions. J. Am. Chem. Soc. 1994. *116.* 4910–4918.
25. Desiraju, G.R. Supramolecular synthons in crystal engineering—A new organic synthesis. Angew. Chem., Int. Ed. Engl. 1995. *34.* 2311–2327.
26. Barnes, C.L.; Bosch, E. Triangular halogen-halogen interactions as a cohesive force in the structures of trihalomesitylenes. Cryst. Growth Des. 2002, 2, 299–302.
27. Tanaka. K.; Fujimoto, D.; Oeser, T.; Imgartinger, H.; Toda, F. Chiral inclusion of tetra(*p*-bromophenyl)ethylene by exposure to the vapor of achiral guest molecules: A novel racemic-to-chiral transformation through gas-solid reaction. Chem. Commun. 2000, *5,* 413–414.
28. Legon, A.C. Prereactive complexes of dihalogens XY with Lewis bases B in the gas phase: A systematic case for the halogen analogue B···XY of the hydrogen bond B···HX. Angew. Chem., Int. Ed. 1999, *38.* 2686–2714.
29. Kaufman, R.D. Biophysical mechanisms of anesthetic action: Historical perspective and review of current concepts. Anesthesiology 1977. *46.* 49–62.
30. Wash, P.L.; Shihong, M.; Obst, U.: Rebek, J.. Jr. Nitrogen-halogen intermolecular forces in solution. J. Am. Chem. Soc. 1999. *121.* 7973–7974.
31. Steinrauf, L.K.; Hamilton, J.A.; Braden, B.C.; Murrel, J.R.: Benson. M.D. X-ray crystal structure of the ala-109→thr variant of human transthyretin which produces euthyroid hyperthyroxinemia. J. Biol. Chem. 1993, *268.* 2425–2430.
32. Adler. M.; Kochannp. M.J.; Ye. B.: Rumennik, G.; Light, D.R.; Biancalana, S.; Whitlow, M. Crystal structures of two potent nonamidine inhibitors bound to factor Xa. Biochemistry 2002, *41,* 15514–15523.
33. Chana, A.: Concejero, M.A.; de Frutos, M.; González, M.J.: Herradón, B. Computational studies on biphenyl derivatives. Analysis of the conformational mobility, molecular electrostatic potential, and dipole moment of chlorinated biphenyl: Searching for the rationalization of the selective toxicity of polychlorinated biphenyls (PCBs). Chem. Res. Toxicol. 2002, *15.* 1514–1526.
34. Grebe, J.; Geiseler. G.; Harms, K.: Dehnicke, K. Donor-akzeptor-komplexe von halogenidionen mit 1.4-diiodtetrafluorbenzol. Z. Naturforsch. 1999, *54.* 77–86.
35. Bailey, R.D.; Grabarczyk. M.; Hanks, T.W.; Pennington, W.T. Synthesis. structure and thermal decomposition of tetra(2-pyrydyl)pyrazine I_2 charge-transfer complexes. J. Chem. Soc., Perkin Trans. 2 1997, *12,* 2781–2786.
36. Sanrame. C.N.: Suhrada, C.P.; Dang. H.; Garcia-Garibay, M.A. Photochemistry of crystalline chlorodiazirines: The influence of conforrnational disorder and intermolecular Cl···N=N interactions on the solid-state reactivity of singlet chlorocarbenes. J. Phys. Chern., A 2003, *107,* 3287–3294.

Hemoglobins: O_2 Uptake and Transport

J. Timothy Sage
Northeastern University, Boston, Massachusetts, U.S.A.

INTRODUCTION

Enormous protein molecules containing many thousands of atoms execute the fundamental processes of life. In several remarkable cases. these molecular behemoths are designed to interact with the smallest molecules known, consisting of only two atoms. In particular, following the development of an oxygen atmosphere; many organisms evolved more efficient metabolisms based on reduction of O_2 to H_2O. In large organisms, specialized proteins enhance the transport of molecular oxygen.

These oxygen-binding proteins occupy an important place in the field of supramolecular chemistry. Because of the relative simplicity of diatomic ligand-binding reactions, these proteins provide outstanding laboratories for exploring the control of reactions by a highly organized local environment. The reaction takes place at a transition metal, and a number of highly selective spectroscopic probes can specifically monitor the electronic and vibrational properties of the active site. Molecular variants of naturally occurring proteins can test the influence of individual amino acids on the reactivity of the active site.

HEMOGLOBINS

The adult human body typically contains 3–4 g of Fe.[1] Approximately two-thirds of this Fe is bound to the oxygen transport protein hemoglobin,[2,3] located in red blood cells. Hemoglobins are also found in muscles and in the nervous system,[4] and in a wide range of species, including bacteria, plants. and animals.[5]

Hemoglobins share a common molecular architecture, composed of a polypeptide backbone and an iron porphyrin, as illustrated in Fig. 1. Molecular oxygen binds to the Fe at the center of the planar heme b (Fe protoporphyrin IX). The polypeptide adopts the globin fold constructed primarily from a-helices, customarily labeled with the letters A–H.[2] The heme group binds tightly to a hydrophobic pocket formed primarily from the E- and F-helices. and a bond between the heme Fe and the ε-nitrogen of a histidine in the F-helix (His F8) provides the only covalent link between the polypeptide and the heme.

The structure shown in Fig. 1. with a molar mass near 17.000 g, can form a building block for more complex molecules. The hemoglobin found in red blood cells is a tetramer formed from chemically distinct x- and β-subunits (two of each), which both adopt a globin fold. In common usage, hemoglobin (Hb) usually refers to the form of this tetrameric molecule found in adult humans. The monomeric hemoglobin from muscle tissue depicted in Fig. 1 is called myoglobin (Mb) to distinguish it from the Hb in blood.

The polypeptide matrix surrounding the heme active site plays an essential role, because iron porphyrins can participate in a wide variety of reactions other than simple binding, transport, and release of O_2. Burial of the active site in the protein interior restricts access to the immediate vicinity of the iron and protects the heme from possible reactions with larger ligands. including other hemes. The local environment of the oxygen-binding site must also enhance the selectivity of the heme for O_2 binding and release relative to undesirable side reactions. Possible heme reactions that must be guarded against include poisoning of the O_2-binding capability of the heme by other small ligands such as CO and activation of the bound O_2, which could lead to the irreversible oxidation of the heme or to the generation of reactive oxygen species such as peroxide and superoxide.

The reactivity of the active site is controlled not only by the chemical identity of amino acids in the active site but also by the positions of these groups. Moreover, these atomic positions are modulated by the dynamics of the global protein conformation. The characteristic dynamics of proteins allow their functional behaviors to respond to changing metabolic demands. Hb is a classic illustration, because the change in the arrangement of the four subunits on oxygen binding in the lungs permits the efficient cooperative release of oxygen from all four hemes in oxygen-poor tissues.'" The inaccessibility of the oxygen-binding site from solvent in the static structure of Fig. 1 also underlines the need for dynamical fluctuations to allow O_2 to penetrate and escape.

Summarized in Fig. 2 are some of the key geometrical factors and groups involved in controlling O_2 transport by hemoglobins. Protein influences on the active site of heme proteins are conventionally classified as proximal or distal. Proximal mechanisms for protein control of heme reactivity involve the covalent link with the protein through the histidine (His F8) ligand *trans* to the oxygen-binding site. Distal interactions involve direct interactions of

Encyclopedia of Supramolecular Chemistry
DOI: 10.1081/E-ESMC 120012684

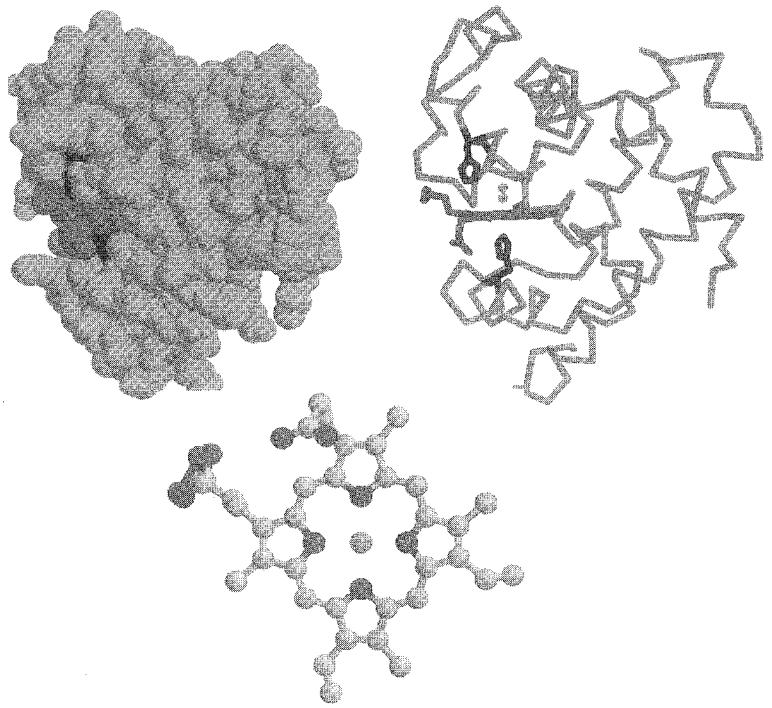

Fig. 1 The CO complex of sperm whale myoglobin determined from refinement of x-ray diffraction data to 1.15 A resolution.[22] A space-filling model (upper left) emphasizes the compact packing of atoms in the molecular structure. while a series of tubes connecting the α-carbons (upper right) reveals the underlying structure. The heme group is shown in red in both structures, and an expanded view of the heme group is shown below. The proximal histidine (below the heme) and the distal histidine (above the heme) are highlighted in blue. Note that CO (orange. upper right) is not visible in the space-filling structure. Atomic coordinates for this structural model of MbCO were obtained from the Protein Data Bank file 1bzr. (*View* ***this*** *art* in color *nt www.dekker.com.*)

amino acid residues in the oxygen-binding pocket, such as the distal histidine (His E7), with the bound ligand.

Mb and Hb were the first proteins for which x-ray diffraction provided structural models with atomic detail.[6,7] As a result. they were investigated in great depth,[8] and textbooks often use these proteins to illustrate fundamental biochemical principles.[9] Many fundamental questions remain unanswered, but an understanding of some effects is beginning to emerge. For example, the physiologically crucial mechanism by which these proteins avoid being poisoned by endogenously produced CO was clarified in the 1990s, and new observations continue to refine the understanding of cooperative oxygen binding by Hb. Mb and Hb remain models for detailed investigations of protein dynamics,[8] and significant progress is now being made in understanding dynamical processes that allow for the penetration of small molecules to the buried active site.

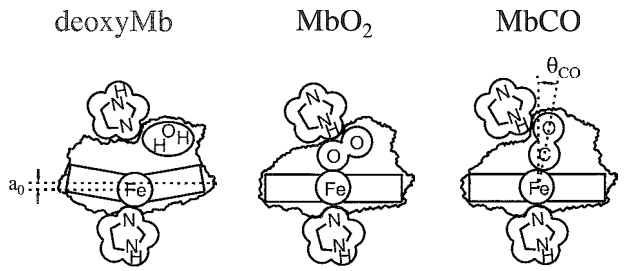

Fig. 2 Factors controlling diatomic ligand binding to hemoglobins. The Fe atom is displaced from the mean plane of the heme in deoxyMb (left) and moves into the heme plane on binding O_2 (center) or CO (right) Through the proximal histidine the protein may influence the Fe displacement a_0 and thus the energetic barrier to ligand binding. The shape and polarity of the proximal pocket stabilize O_2 binding through hydrogen bonding with the distal histidine (center) and destabilize CO binding by angular displacement θ_{CO} of the bound CO from its equilibrium geometry perpendicular to the heme plane (right).

DISTAL CONTROL OF REACTION SPECIFICITY

Interaction with residues in the heme pocket is the most direct means for the protein to influence the free energy of ligand binding. These interactions depend on the nature of the bound ligand and allow the protein environment to

selectively discriminate between the binding of O_2 and other small molecules. In particular, the binding affinity of CO is approximately 20,000 times the affinity of O_2 for free heme, but the CO/O_2 affinity ratio is reduced to about 25 for Mb.[10] This highly efficient discrimination between CO and O_2 is essential to prevent poisoning of the oxygen-binding site by endogenous CO, produced in the breakdown of heme.[11] Electronic and geometric differences in the nature of bound CO and O_2 allow distal residues to discriminate between these ligands.

Electrostatic Stabilization of Bound Oxygen

Binding of O_2, but not CO, is accompanied by substantial transfer of charge from the heme, giving rise to distinct charge distributions for the O_2 and CO complexes. Pauling [12] originally suggested that hydrogen bonding with the evolutionarily conserved distal histidine residue stabilized the bound O_2. This is now recognized as an essential factor. Crystallographic and spectroscopic evidence support the presence of a strong hydrogen bond between His E7 and O_2 in Mb and Hb,[13,14] and NMR data confirm hydrogen bonding to O_2 in both α- and β-chains of Hb.[15]

Extensive studies of mutant proteins establish a quantitative basis for stabilization of O_2 binding by the distal histidine. When His E7 is replaced with nonpolar residues, the oxygen affinity of Mb or the α-hemes in Hb drops by two orders of magnitude. largely because of an enhanced rate for O_2 dissociation.[10] Spectroscopic evidence also suggests hydrogen bonding of the distal histidine with CO in Mb.[16] Computational studies confirm these conclusions but estimate that the hydrogen bond to O_2 is 7–21 kJ/mol stronger than that to CO,[17,18] in reasonable agreement with the mutant studies.

Another distal factor is the presence of a water molecule bound to the distal histidine in deoxyMb, which is displaced upon ligand binding. The energetic cost of displacing the bound water. and thus its proposed influence on ligand binding,[10] is unclear. However, because CO or O_2 binding displaces the distal water, it has no influence on discrimination between these ligands.

Steric Discrimination Against CQ Binding

Significant differences in the energetically favored binding geometries of the bound ligands provide another possible criterion for discriminating between O_2 and CO binding. In the absence of the protein. bound CO is oriented perpendicular to the heme plane, while the O—O bond of bound O_2 lies approximately 60° from the heme normal. Thus, distal pocket residues could sterically discriminate against CO binding by displacing bound CO away from its energetically preferred structure.[11] In the 1990s, a semiquantitative reevaluation of the importance of steric destabilization of CO binding relative to electronic stabilization of O_2 binding was seen.

On one hand; more precise structural information from infrared crystallography[19,20] and ultrafast infrared photoselection measurements,[21] subsequently confirmed by high-resolution x-ray diffraction,[22] showed that the displacement θ_0 of the C—O bond from the perpendicular (Fig. 2) was smaller than previously believed. On the other hand, calculations revised downward the force constant κ for displacing CO from linearity.[23] Current estimates of the energetic cost $(1/2)\kappa\theta_0^2$ for the small displacement of bound CO from linearity observed in high-resolution x-ray structures of MbCO lie in the range 1–4 kJ/mol.[24] The additional energetic cost associated with displacement of distal pocket residues to accommodate the upright CO geometry[19] or with reorientation of the E- and F-helices[22] on ligand binding is more difficult to evaluate. Assuming that the latter contribution from protein distortion is equal to that of the heme-CO distortion yields an estimate[12] consistent with mutant studies,[10] indicating that the steric destabilization of CO binding is smaller than the enhancement of O_2 binding by the H-bond with the distal histidine. However, it is worth noting that approximately 1% of the Hb in the body of a nonsmoker is saturated with CO,[25] and a 2–8 kJ/mol enhancement of discrimination against CO binding may be a significant factor in maintaining this low level.

PROXIMAL INFLUENCE OM HEME REACTIVITY

In addition to interacting with the bound ligand, the protein can directly modulate heme reactivity by influencing atomic motion along the reaction coordinate connecting the ligated and deligated structures. Early structural data on porphyrin model compounds, as well as Hb, identified motion of the Fe into the plane of the heme, accompanied by adoption of a more planar porphyrin structure, as the most apparent structural change upon binding O_2 or other ligands.[26,27] The proximal histidine, which links the protein F-helix directly to the heme Fe. provides a natural conduit for influencing the "doming" of the heme. and thus for controlling ligand binding and dissociation *trans* to the histidine. In particular, changes in the positioning of the proximal histidine and the F-helix can control the affinity for O_2 and other exogenous ligands by influencing the energetic cost of changes in heme geometry that take place on ligation.

The largest effect attributed to this proximal influence is probably the control of ligand-binding affinity in Hb. Two distinct quaternary structures were identified for Hb (see next section). The R-state has a ligand-binding affinity between two and three orders of magnitude higher than that of T-state Hb, depending on solution conditions.[28] The rupture of the Fe–His bond of the r-hemes upon NO binding to deoxyHb or CN^- binding to metHb in the *T*-state strikingly illustrates the protein restraint on Fe motion into the heme plane.[29,30] The approximate $10\,cm^{-1}$ reduction of the Fe–His bond-stretching frequency in the T-state was also attributed to protein-induced strain in this bond.[31,32]

A particularly incisive method for evaluating the contribution of ihe covalent link with the protein is to sever the bond connecting the histidine imidazole ring and the protein backbone.[33] In these "proximally detached" hernoglobins, the electronic character of the heme–irnidazole complex is unchanged, but the protein can no longer control the heme conformation through the Fe–His link. In Hb. removal of the bond connecting the imidazole to the F-helix increases the T-state ligand-binding affinities, and quantitative comparison of CO binding and dissociation rates with R- and T-state native Hb confirins that the difference in affinity of the α-hemes is primarily controlled by the proximal linkage.[33]

In addition to restraining the motion of the imidazole toward the heme piane. the protein may also control the orientation and electronic character of the imidazole. In Hb and Mb, residues surrounding the proximal histidine restrain it in an eclipsed orientation relative to the pyrrole nitrogens. Because the imidazole ring follows the Fe into the heme plane on ligand binding. steric repulsion between the pyrrole nitrogens and the 6- and c-carbons of the irnidazole ring may influence the relative energy of the ligated and deligated hemes. Hydrogen bonding of the histidine N_δ with the backbone carbonyl at F4. as well as with the serine located at F7 (in Mb, but not in Hb) could also help stabilize this orientation or perturb the electronic character of the imidazole. In fact. mutations that remove the hydrogen bond to the imidazole or change its orientation lead to modest changes in ligand affinity.[34]

In summary, there is considerable evidence that the protein can influence the ligand-binding affinity through the proximal histidine. Mutant studies provide sorne information on the strength of such effects. However, further investigation is needed to bring the understanding of proximal effects to the same quantitative level that is beginning to be achieved for distal interactions. The hypothesis that the energetic cost $(1/2)ka_0^2$ of Fe displacement relative to the heme plane quantitatively determines variations in the free energy of ligand binding[35] is compelling, but quantitative tests will require experimental input on the effective force constant k for Fe displacement perpendicular to the heme. Emerging techniques may yield this information.[36,37]

COOPERATIVE OXYGEN BINDING IN HEMOGLOBIN

Hb is responsible for transporting molecular oxygen from the lungs to the tissues. The hemes of Hb are almost completely saturated with oxygen at typical alveolar oxygen pressures but are able to unload this oxygen over a narrower range of oxygen pressures than monomeric hemoglobins (Fig. 3). This facilitates efficient oxygen transport by minimizing the drop in oxygen pressure from the lungs to the tissues. This characteristic oxygen-binding curve reflects the fact that oxygen binds cooperatively, that is, binding of oxygen at one site enhances the affinity of the remaining sites. Perutz proposed a detailed stereochemical model for cooperative oxygen binding by hemoglobin,[27,38] and many predictions of this model were confirmed quantitatively.[38,39] Textbooks often use Hb to illustrate interactions among spatially separated active sites in rnultimeric proteins.[2,9,40]

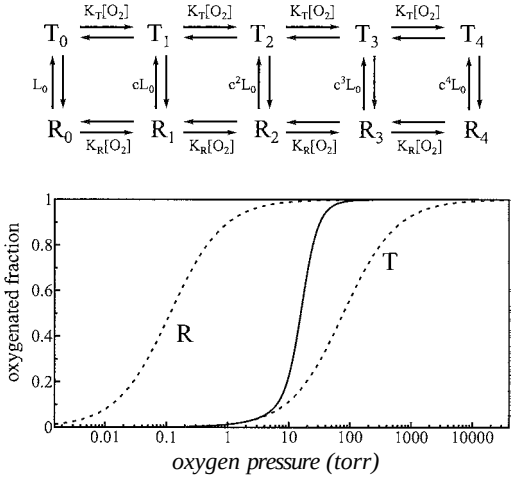

Fig. 3 *Monod–Wyman–Changeux model for cooperative* O_2 *binding to* human *hemoglobin.* T_k *and* R_k *denote hemoglobin in the low-affinity T-state and high-affinity R-states. respectively. with* O_2 *bound to k of the four hemes. Binding of each subsequent* O_2 *decreases the equilibrium constant* $L_k = [T_k]/[R_k]$ by *the ratio* $c = K_T/K_R$ of *the* O_2 *affinities. The resulting* O_2 *binding curve (solid line) allows binding and release* of O_2 *over a narrow range of* O_2 *partial pressures. For reference. dashed curves labeled R and T illustrate* noncooperative O_2 *binding with R- and T-*state *affinities.corresponding to* $L_0 \ll 1$ *and* $c^4L_0 \gg 1$. *respectively. Parameter values* ($L_o = 2.56 \times 10^8$, $K_T^{-1} = 78.1$ *torr.* $K_R^{-1} = 0.115$ *torr) from Ref.* [70] *for native* Hb *at* pH *7.4 in 2* mM *diphosphoglycerate are provided.*

The mechanism outlined by Perutz[27,38,39] builds on the allosteric model proposed by Monod. Wyman, and Changeux[41] (see Fig. 3). The fundamental assumption is that there are distinct high-affinity and low-affinity conformations, called R and *T*, respectively. Oxygen binding to any of the hemes does not directly influence the affinity of the other hemes but thermodynamically stabilizes the high-affinity R-state relative to the T-state. The resulting gradual shift from the *T*-state to the R-state as the protein becomes oxygenated is paralleled by an increase in the average affinity of the unbound sites. This two-state model describes the oxygen-binding curve of Hb in terins of three parameters: the oxygen affinities K_R and K_T of the R- and T-states and the equilibrium constant $L_0 = [T_0]/[R_0]$ between the unligated *R*- and T-states.

Perutz identified the *R*- and T-states of the MWC model with structural models for HbO_2 and deoxyHb, respectively, and proposed a plausible mechanism by which oxygen binding would destabilize the T-state relative to the R-state. Rigid-body rotation of one heterodimer ($\alpha_1\beta_1$) relative to the other ($\alpha_2\beta_2$) provides an approximate description of the structural differences between the *R* and T structures. which are stabilized by a distinct set of salt bridges at the $\alpha_1\beta_2$ and $\alpha_2\beta_1$ interfaces in these two limiting structures. Binding of oxygen to the T conformation leads not only to local structural changes at the heme but also to a shift of the F-helix that weakens salt bridges at the subunit interfaces, thus destabilizing the T-state relative to the R-state. Perutz also provided a plausible account of the mechanism of heterotropic effectors. including protons. CO, chloride ions; and diphosphoglycerate. which stabilize the *T*-state and thus reduce oxygen affinity.[27,38,39]

Increasingly detailed quantitative tests continue to refine the original MWC model but have not altered the fundamental scientific picture. The simple MWC model neglects differences in the binding affinity of the two hemes and assumes no direct interaction among the hemes in *R*- or T-states. In fact, differences in the binding affinity of α- and β-hemes are detected in elegant oxygen-binding measurements on T-state hemoglobin crystals,[42] and measurements of tetramer/dimer dissociation for all ligation microstates suggest that the binding of one ligand slightly enhances the affinity of the other site within the same dimer.[43] However. these effects partially cancel each other and are both less than an order of magnitude, in contrast to the several hundred-fold difference in affinity of the *R*- and *T*-states.[44]

Many questions remain unanswered. A simple thermodynamic consequence of the MWC model is that binding of each subsequent oxygen decreases the *R*/*T* equilibrium constant L_0 by the ratio $c = K_T/K_R$ of the oxygen affinities of the two conformations. Qualitatively. the reduced affinity of the *T*-state can be attributed to proximal restraint on the α-hemes,[33] while distal interactions may play a larger role in the low affinity of the β-hemes.[38,45] However, although some aspects of the energetics of the R–T transition can be explored theoretically,[46] it remains a challenge to account quantitatively for the large magnitude of the free energy of cooperativity:

$$\Delta\Delta G = -k_B T \ln c = 15 \text{ kJ/mol}$$

A related question is what exactly are the structures of the R- and the *T*-states? Perutz originally identified these states with structural models derived from x-ray diffraction measurements on ligated and deligated Hb crystals grown from concentrated salt solutions. However, the report of a fully ligated Hb with an *R*-like quaternary structure distinct from the R-state conformation identified in earlier structures suggests that crystallization selects only a subset of the conformations that comprise the R-state of the MWC model.[47] In the absence of a quantitative understanding of the large difference in oxygen affinity for the R- and T-states, the possibility exists that the oxygen-affinity varies significantly among R and among T substates. If so, then mechanistic understanding of RIT differences in oxygen affinity may require knowledge of the relative populations and oxygen affinities of different *R* substates present in solution.

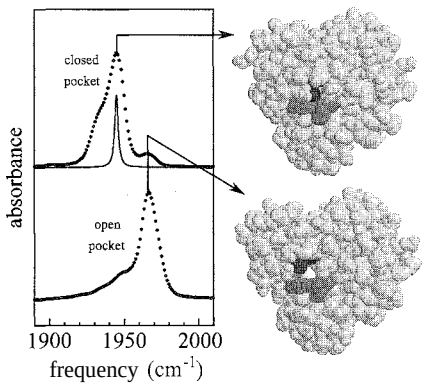

Fig. 4 Structure (right) and spectra (left) of open and closed conformations of myoglobin. Both x-ray diffraction and infrared absorption data were recorded on single crystals of MbCO at pH 6 (top) and pH 4 (bottom). Displacement of the distal histidine (blue) from the heme pocket in the open structure leads to a shift of the C-O stretch frequency from 1945 cm^{-1} to 1966 cm^{-1}, and may facilitate entry and exit of small molecules. The solid curve represents the contribution of an individual protein conformer to the IR band, based on the 2.7 cm^{-1} homogeneous linewidth expected from IR photon echo measurements.[55] The heme is rendered in red. the bound CO in white. the distal histidine in blue. and the remainder of the protein in green. Atomic coordinates for structural models of MbCO at pH 6 and pH 4 were obtained from the Protein Data Bank files 1vxf and 1spe, respectively.[52] (*View this art in* color *at www.dekker.com.*)

DYNAMICAL CONTROL OF GLOBIN REACTIONS

Proteins are necessarily dynamic objects. The relatively weak noncovalent interactions stabilizing the highly organized three-dimensional structure are constantly disrupted by thermal fluctuations. In fact, operation of these molecular machines relies on this dynamical behavior. Myoglobin is a "poster child" for the functional importance of protein dynamics, because the inaccessibility of the oxygen-binding site from solvent in the static structure derived from x-ray crystallography (Figs. 1 and 4) highlights the need for structural fluctuations that allow O_2 migration to and from the binding site. The dynamical behavior of proteins and its relation to physiological function was probably investigated in greater depth for Mb than for any other protein.[8,48]

Conformational Heterogeneity

Numerous observations show that in thermal equilibrium, an ensemble of chemically identical proteins samples a wide distribution of conformations. Early measurements found that recombination of photolyzed CO to Mb at cryogenic temperatures was highly nonexponential, because the conformational substates have rebinding rates distributed over many orders of magnitude.[49] These substates correspond to a large number of local minima on the complex energy surface of the protein, which are sampled during molecular dynamics simulations.[50] These conformational distributions also inhomogeneously broaden spectral lines of protein-associated chromophores.[51]

In some cases. such as the *R* and Tstructures of Hb. it is possible to characterize distinct conformations. As discussed above. the O_2 affinities of these structures differ by more than two orders of magnitude: and form the starting point for modeling the allosteric behavior of Hb.[39] Another example is the open and closed pocket conformations of MbCO with peak C–O stretch frequencies near 1960 and 1945 cm^{-1}, respectively (Fig. 4).[19,52,53] In the open conformation, the distal histidine is displaced from the heme pocket, and the O_2 dissociation rate increases by approximately three orders of magnitude,[54] similar to the effect of His E7 mutations.[10] However, the population of the open state is only 3–5% in vitro at neutral pH, and a physiological role for this conformation remains to be established.

In general. structural models based on x-ray diffraction from protein crystals represent an average over many conformational substates. Because the homogeneous line width of the C–0 stretch is only 2.7 cm ' at room temperature,[55] the broad C–O stretch bands observed in the crystalline state (Fig. 4) for open and closed states reflect contributions from a distribution of conformational substates with differing C–O frequencies. Furthermore, these substates are kinetically as well as spectroscopically distinct.[56] These observations suggest a fundamental challenge: conformational changes too small to distinguish with available structural techniques nevertheless result in reaction rates that vary by more than an order of magnitude.

Conformational Dynamics

At low temperatures, each protein is trapped in a particular conformational substate, and dynamics are nearly harmonic. Qualitatively different dynamical behavior appears above a dynamical transition near 180 K, where the mean square displacement of the Fe atom in myoglobin, as determined using Mossbauer spectroscopy, strongly deviates from a harmonic extrapolation of low-temperature behavior[48,57] (Fig. 5). Hydrogen fluctuations

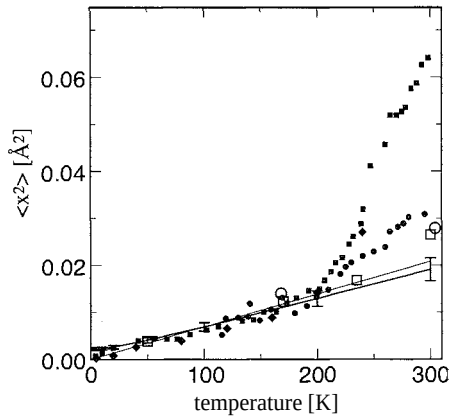

Fig. 5 Mean square displacement (MSD) of Fe in Mb as a function of temperature. illustrating the dynamical transition near 200 K. All values are determined from measurements of the 14.4 keV nuclear resonance of ^{57}Fe. Filled symbols. derived from measurements of recoilless absorption using Mossbauer spectroscopy, indicate the total Fe mean square displacement (MSD) averaged over the 140 ns nuclear-excited state lifetime. Above the dynamical transition, the 140 ns MSD of Mb solutions (filled squares) clearly deviates from a linear extrapolation of low-temperature measurements (thin solid line) or from the MSD calculated from the density of vibrational states (thick solid line). In contrast; the dynamical transition is not apparent in Fe MSD measurements averaged over a 5 ps time scale (open squares). determined from vibrational transitions near the nuclear resonance with 0.85 meV energy resolution. In constrast. 5 ps and 140 ns MSD values (filled and open circles, respectively) measured for dry oxidized Mb agree; suggesting that dehydration suppresses the dynamical transition. The dynamical transition signals the activation of protein conformational dynamics on time scales longer than a few picoseconds. (Reprinted with permission from Ref. [57]. Copyright 2001, American Physical Society.)

observed using inelastic neutron scattering reveal the same dynamical transition.[58] This characteristic change in atomic dynamics is believed to signal the onset of interconversion among conformational substates. Suppression of this dynamical behavior in the lyophilized protein[58] (Fig. 5) illustrates the essential role of solvent in activating protein dynamics.

Reaction kinetics also change above the dynamical transition, because the time scale of conformational interconversion becomes comparable to or faster than ligand binding. In contrast to the broad distribution of rebinding rates at low temperatures,[49] only two kinetically distinct conformational states contribute to CO rebinding to Mb at high temperatures."'" The rate of interconversion depends strongly on solvent viscosity and has a value of $\sim 10^6$ s^{-1} in aqueous solvent at 273 K. Analysis of double-pulse kinetic measurements,[59] in agreement with direct IR measurements in glycerol/water solutions."'" shows that the populations of these states correspond to the spectroscopically distinguishable open and closed pocket states shown in Fig. 4.

The rate of geminate CO rebinding to open or closed states represents an average over many substates, which interconvert more rapidly than 100 ns at physiological temperatures.[59] Thus, the kinetic properties of the structurally distinguishable open and closed states represent an average over many structurally indistinguishable substates. On the other hand, these substates are spectroscopically distinguishable on the 4 ps dephasing time of the C–O oscillator at room temperature[55] (Fig. 4). Measurements of the ^{57}Fe nuclear resonance are consistent with these bounds on conformational interconversion, because the Fe fluctuations activated above the dynamical transition (Fig. 5) take place faster than the 141 ns lifetime of the excited ^{57}Fe nucleus but slower than the 5 ps time scale of vibrational measurements[57]

Ligand Entry, Migration, and Escape

As noted above. it is apparent from x-ray structures that conformational fluctuations must take place to allow diatomic ligands to migrate between the active site and solvent. The pathways that the ligand follows, and the dynamical processes required to permit ligand migration. remain the focus of active investigation. An early suggestion that displacement of the distal histidine from the heme pocket would open a channel between the active site and solvent,[61,62] similar to the open-pocket structure shown in Fig. 4, found some theoretical support.[63] However. later calculations found that a CO molecule released at the heme migrated to various internal cavities before escaping from the protein.[64]

Time-resolved x-ray structures find electron density associated with a photolyzed CO approximately parallel to the heme group following photolysis with a 7.5 ns laser pulse.[65] Interestingly, electron density attributed to the photolyzed CO gradually develops in a cavity on the proximal side of the heme, bounded in part by the heme and the proximal histidine, with a maximum occupancy at 100 ns that decays to half the peak value in several microseconds.[65] The possible relevance of this proximal cavity to ligand migration under physiological conditions is uncertain because of the possibility that the crystal lattice perturbs the protein dynamics.

Spectroscopic probes provide a more precise determination of the time constant for CO escape from the heme pocket, approximately 200 ns at 20°C.[66] Temperature-dependent measurements of the rate for entry of water following NO photolysis from metMb find a 42 kJ/mol Arrhenius barrier, identical to the barrier for CO escape from photolyzed Mb, suggesting a common mechanism for ligand exit and entry.[67] Approximate equality of the rates for CO escape and interconversion of the open and closed conformations (Fig. 4) at 273 K is consistent with escape via the pathway created by displacement of the histidine in the open conformation.["] Detailed kinetic analysis of various mutant Mbs led to the conclusion that photolyzed ligands escape along classical pathway.[68] A reported transient volume change, interpreted as the entry of photolyzed CO into solvent, with a rate three to four times slower than the rate for CO escape,[69] indicates that some ligands may remain in the protein interior after leaving the heme pocket. However, observation of the same 42 kJ/mol barrier for the transient volume change[69] implicates the same fundamental process in escape of the ligand from the heme pocket and from the protein.

ARTICLES OF FURTHER INTEREST

The Allosteric Effect, p. 20
Biological Ligands, p. *88*
Biological Models and Their Characteristics, p. 101
Hydrogen Bonding, p. 658
Induced Fit. p. *7 17*
Molecular-Level Machines, p. 931
O_2 Uptake and Transport, Models of, p. 1023
Porphyrin Derivatives, Functional, p. *1139*
Protein Supramolecular Chemistry, p. 1161
Vitamin B_{12} and Heme Models, p. 1569

REFERENCES

1. Lindley. P.F. Iron in biology: A structural viewpoint. Rep. Prog. Phys. 1996, *59*. 867–993.
2. Dickerson, R.E.: Geis, I. *Hemoglobin: Structure, Function,*

Evolution, and Pathology; Benjamin/Cummings: Menlo Park. NJ. 1983.
3. Antonini, E.: Brunori. M. *Hemoglobin* and Myoglobin *in Their* Reactions *with Ligands*; North-Holland: Amsterdam, 1971.
4. Burmester, T.; Welch, B.: Reinhardt, S.: Hankeln, T. A vertebrate globin expressed in the brain. Nature 2000. *407,* 520–523.
5. Hardison. R.C. A brief history of hemoglobins: Plant, animal. protist. and bacteria. Proc. Natl. Acad. Sci. U. S. A. 1996. *93,* 5675–5679.
6. Kendrew. J.C.: Dickerson, R.E.: Strandberg. R.E.: Hart. R.G.; Davies. D.R.: Phillips. D.C.: Shore, V.C. Structure of myoglobin. A three-dimensional Fourier synthesis at 2 A resolution. Nature 1960. *185.* 422–427.
7. Perutz. *M.F.* Structure and function of haemoglobin. I. A tentative atomic model of horse oxyhaemoglobin. J. Mol. Biol. 1965. *13.* 646–668.
8. Sage, J.T.: Champion, P.M. Small Substrate Recognition in Heme Proteins. In *Comprehensive Supramolecular Chemistry*; Suslick, K.S.. Ed.; Pergamon: Oxford. 1996; Vol. 5.
9. Stryer. L. *Biochemistry*, 3rd Ed.; W. H. Freeman: San Francisco. 1988.
10. Springer, B.A.: Sligar, S.G.: Olson. J.S.: Phillips. G.N., Jr. Mechanisms of molecular recognition in myoglobin. Chern. Rev. 1994. *94.* 699–714.
11. Collman. J.P.; Brauman. J.I.; Halbert, T.R.; Suslick. K.S. Nature of O_2 and CO binding to metalloporphyrins and heme proteins. Proc. Natl. Acad. Sci. U. S. A. 1976. *73.* 3333–3337.
12. Pauling, L. Nature of the iron-oxygen bond in oxyhaemoglobin. Nature 1964. *203.* 182.
13. Phillips. S.E.; Schoenborn. B.P. Neutron diffraction reveals oxygen-histidine hydrogen bond in oxymyoglobin. Nature 1981, *292.* 81–82.
14. Kitagawa, T.; Ondrias. M.R.: Rousseau. D.L.: Ikeda-Saito, M.; Yonetani, T. Evidence for hydrogen bonding of bound dioxygen to the distal histidine of oxycobalt myoglobin and haemoglobin. Nature 1982. *298.* 869–871.
15. Lukin. J.A.; Simplaceanu, V.: Zou. M.; Ho. N.T.; Ho, C. NMR reveals hydrogen bonds between oxygen and distal histidines in oxyhemoglobin. Proc. Natl. Acad. Sci. U. S. A. 2000. *97.* 10354–10358.
16. Unno. *M.:* Christian. J.F.: Olson, J.S.: Sage. J.T.: Champion, P.M. Evidence for hydrogen bonding effects in the iron ligand vibrations of carbonmonoxymyoglobin. J. Am. Chem. Soc. 1998. *120.* 2670–2671.
17. Sigfridsson. E.: Ryde, U. Theoretical study of the discrimination between O_2 and CO by myoglobin. J. Inorg. Biochem. 2002. *91.* 101–115.
18. Rovira, C.: Schulze, B.; Eichinger. M.: Evanseck, J.D.; Parrinello, M. Influence of the heme pocket conformation on the structure and vibrations of the Fe-CO bond in myoglobin: A QM/MM density functional study. Biophys. J. 2001. *81.* 435–445.
19. Sage. J.T.; Jee, W. Structural characterization of the myoglobin active site using infrared crystallography. J. Mol. Biol. 1997, *274,* 21–26.
20. Ivanov, D.: Sage. J.T.: Keim, M.: Powell. J.R.: Asher, S.A.: Champion, P.M. Determination of CO orientation in myoglobin by single-crystal infrared linear dichroism. J. Am. Chem. Soc. 1994. *116.* 4139–4140.
21. Lim. M.: Jackson, T.A.: Anfinrud. P.A. Binding of CO to myoglobin from a heme pocket docking site to form nearly linear Fe-C-O. Science 1995. *269.* 962–966.
22. Kachalova, G.S.; Popov, A.N.; Bartunik, H.D. A steric mechanism for inhibition of CO binding to heme proteins. Science 1999. *284.* 473–476.
23. Ghosh, A.: Bocian. D.F. Carbonyl tilting and bending potential energy surface of carbon monoxyhemes. J. Phys. Chem. 1996. *100.* 6363–6367.
24. Spiro, T.G.: Kozlowski, P.M. Is the CO adduct of myoglobin bent. and does it matter? Acc. Chern. Res. 2001, *34.* 137–144.
25. Zander, R. Concentrations of Carboxylhemoglobin in the Blood of Smokers and Non-smokers. In The *Oxygen Status* qf Arterial Blood; Zander. R., Mertzlufft. F.. Eds.: Karger: Basel. 1991; Vol.
26. Hoard. J.L.: Scheidt, W.R. Stereochemical trigger for initiating cooperative interaction of the subunits during the oxygenation of cobaltohemoglobin. Proc. Natl. Acad. Sci. U. S. A. 1973. 70. 3919–3922.
27. Perutz. M.F. Stereochemistry of cooperative effects in haemoglobin. Nature 1970, *228.* 726–739.
28. Mathews. A.J.: Olson. J.S. Assignment of rate constants for O_2 and CO binding to alpha and beta subunits within R- and T-state human hemoglobin. Methods Enzymol. 1994, *232.* 363–386.
29. Maxwell, J.C.; Caughey, W.S. An infrared study of NO bonding to heme B and hemoglobin A. Evidence for inositol hexaphosphate induced cleavage of proximal histidine to iron bonds. Biochemistry 1976, *15.* 388–396.
30. Paoli, M.: Dodson. G.: Liddington, R.C.; Wilkinson. A.J. Tension in haemoglobin revealed by Fe-His(F8) bond rupture in the fully liganded T-state. J. Mol. Biol. 1997, *271.* 161–167.
31. Rousseau, D.L.: Friedman. J.M. Transient and Cryogenic Studies of Photodissociated Hemoglobin and Myoglobin. In Biological *Applications of Raman Spectroscopy*; Spiro. T.G.. Ed.; Wiley-Interscience: New York, 1988; Vol. 3, 133–215.
32. Kitagawa. T. The Heme Protein Structure and the Iron Histidine Stretching Mode. In Biological *Applications of Raman Spectroscopy*; Spiro. T.G., Ed.; Wiley-Interscience: New York, 1988; Vol. 3. 133–215.
33. Barrick. D.: Ho, N.T.: Simplaceanu, V.: Dahlquist, F.W.: Ho. C. A test of the role of the proximal histidines in the Perutz model for cooperativity in hemoglobin. Nat. Struct. Biol. 1997. *4,* 78–83.
34. Kundu, S.; Snyder, B.; Das. K.: Chowdhury, P.: Park. J.: Petrich. J.W.; Hargrove. M.S. The leghemoglobin proximal heme pocket directs oxygen dissociation and stabilizes bound heme. Proteins 2002. *46.* 268--277.
35. Šrajer, V.; Reinisch, L.; Champion, P.M. Protein fluctuations, distributed coupling. and the binding of ligands to heme proteins. J. Am. Chem. Soc. 1988, *110,* 6656–6670.

36. Zhu. L.: Sage. J.T.: Champion. P.M. Observation of coherent reaction dynamics in heme proteins. Science 1994, 266.
37. Sage. J.T.: Durbin. S.M.; Sturhahn, W.: Wharton. D.C.: Champion. P.M.: Hession. P.: Sutter, J.: Alp, E.E. Long-range reactive dynamics in myoglobin. Phys. Rev. Lett. 2001, *86*, 4966–4969.
38. Perutz. M.F.: Wilkinson. A.J.; Paoli. M.; Dodson, G.G. The stereochemical mechanism of the cooperative effects in hemoglobin revisited. Annu. Rev. Biophys. Biomol. Struct. 1998, 27. 1–34.
39. Eaton, W.A.: Henry, E.R.; Hofrichter, J.; Mozzarelli, A. Is cooperative oxygen binding by hemoglobin really understood? Nat. Struct. Biol. 1999. 6. 351–358.
40. Wyman, J.: Gill. S.J. Binding *and Linkage: Functional Chemistry of* Biological Macromolecules; University Science Books. 1990.
41. Monod. J.; Wyman. J.: Changeux. J.-P. On the nature of allosteric transitions: A plausible model. J. Mol. Biol. 1965. 12. 88–118.
42. Rivetti. C.: Mozzarelli, A.; Rossi. G.L.: Henry. E.R.: Eaton, W.A. Oxygen binding by single crystals of hemoglobin. Biochemistry 1993. 32. 2888–2906.
43. Ackers. G.K. Deciphering the molecular code of hemoglobin allostery. Adv. Protein Chern. 1998, 51. 185–253.
44. Mathews, A.J.; Olson. J.S. Assignment of rate constants for O_2 and CO binding to alpha and beta subunits within R- and T-state human hemoglobin. Methods Enzymol. 1994. 232. 363–386.
45. Khachfe. H.: Mylrajan, M.: Sage, J.T. Infrared crystallographic investigation of T-state hemoglobin. Cell. Mol. Biol. 1998. 44. 39–52.
46. Gelin, B.R.: Lee. A.W.: Karplus. M. Hemoglobin tertiary structural change on ligand binding. Its role in the co-operative mechanism. J. Mol. Biol. 1983. 171. 489–559.
47. Silva, M.M.: Rogers, P.H.: Arnone, A. A third quaternary structure of human hemoglobin at 1.7 A resolution. J. Biol. Chern. 1992. 267. 17248–17256.
48. Parak, F.; Frauenfelder, H. Protein dynamics. Physica A 1993. 201. 332–345.
49. Austin. R.H.: Beeson. K.W.; Eisenstein, L.: Frauenfelder. H.: Gunsalus. I.C. Dynamics of ligand binding to myoglobin. Biochemistry 1975, 14. 5355–5373.
50. Elber. R.: Karplus. M. Multiple conformational states of proteins: A molecular dynamics analysis of myoglobin. Science 1987. 235, 318–321.
51. Srajer, V.; Schomacker. K.T.: Champion. P.M. Spectral broadening in biomolecules. Phps. Rev. Lett. 1986, 57. 1267–1270.
52. Yang, F.; Phillips. G.N., Jr. Crystal ctructures of CO-, deoxy- and met-myoglobins at various pH values. J. Mol. Biol. 1996. 256. 762–774.
53. Sage. J.T. Myoglobin and CO: Structure, energetics. and disorder. J. Biol. Inorg. Chern. 1997. 2. 537–543.
54. Tian. W.D.; Sage, J.T.: Champion. P.M. Investigations of ligand association and dissociation rates in the ''open'' and "closed" states of myoglobin. J. Mol. Biol. 1993. 233. 155–166.
55. Rella, C.W.; Kwok, A.; Rector. K.; Hill. J.R.; Schwettman. H.A.; Dlott, D.D.: Fayer, M.D. Vibrational echo studies of protein dynamics. Phys. Rev. Lett. 1996, 77. 1648–1651.
56. Ormos. P.: Ansari, A.; Braunstein. D.: Cowen, B.R.; Frauenfelder, H.: Hong. M.K.; Iben. I.E.T.: Sauke. T.B.; Steinbach. P.J.: Young. R.D. Inhomogeneous broadening in spectral bands of carbonmonoxymyoglobin. The connection between spectral and functional heterogeneity. Biophys. J. 1990. 57, 191–199.
57. Achterhold. K.; Keppler, C.: Ostermann, A.; van Burck. U.: Sturhahn. W.: Alp, E.E.; Parak, F.G. Vibrational dynamics of myoglobin determined by the phonon-assisted Mossbauer effect. Phys. Rev. E 2002, 65, 051916.
58. Doster. W.: Cusack, S.: Petry. W. Dynamical transition of myoglobin revealed by inelastic neutron scattering. Nature 1989. *337*, 754–756.
59. Tian, W.D.: Sage, J.T.; Champion. P.M.; Chien, E.; Sligar. S.G. Probing heme protein conformational equilibration rates with kinetic selection. Biochemistry 1996. 35. 3487–3502.
60. Young. R.D.; Frauenfelder. H.: Johnson, J.B.; Lamb. D.C.: Nienhaus. G.U.: Phillip. R.; Scholl. R. Time- and temperature-dependence of large-scale conformational transitions in myoglobin. Chem. Phys. 1991. 158, 315.
61. Perutz. M.F.; Mathews. F.S. An x-ray study of azide methaemoglobin. J. Mol. Biol. 1966, 21. 199–202.
62. Chance, B.: Ravilly, A.; Rumen, N.J. Reaction kinetics of a crystalline hemoprotein: An effect of crystal structure on reactivity of fei-rimyoglobin. J. Mol. Biol. 1966. 17. 525–534.
63. Case. D.A.; Karplus. M. Dynamics of ligand binding to heme proteins. J. Mol. Biol. 1979, 132. 343–368.
64. Elber. R.: Karplus, M. Enhanced sampling in molecular dynamics: Use of the time-dependent Hartree approximation for a simulation of carbon monoxide diffusion through myoglobin. J. Am. Chem. Soc. 1990, 112. 9161–9175.
65. Šrajer. V.: Ren. Z.; Teng. T.-Y.; Schmidt. M.: Ursby, T.: Bourgeois. D.: Pradervand. C.: Schildkamp, W.; Wulff. M.: Moffat. K. Protein conformational relaxation and ligand migration in myoglobin: A nanosecond to millisecond molecular movie from time-resolved Laue x-ray diffraction. Biochemistry 2001, 40. 13802–13815.
66. Henry. E.R.: Sommer, J.H.; Hofrichter. J.; Eaton. W.A. Geminate recombination of carbon monoxide to myoglobin. J. Mol. Biol. 1983, 166, 443–451.
67. Cao. W.: Christian, J.F.: Champion, P.M.: Rosca, F.: Sage. J.T. Water penetration and binding to ferric myoglobin. Biochemistry 2081. 40. 5728–5737.
68. Scott, E.E.: Gibson. Q.H.: Olson, J.S. Mapping the pathways for O_2 entry into and exit from myoglobin. J. Biol. Chem. 2001, 276. 5177–5188.
69. Ogilvie. J.P.; Plazanet, M.; Dadusc, G.: Miller. R.J.D. Dynamics of ligand escape in myoglobin: Q-band transient absorption and four-wave mixing studies. J. Phys. Chern. B 2002. 106. 10460–10467.
70. Imai. K. Analyses of oxygen equilibria of native and chemically modified human adult hemoglobins on the basis of Adair's stepwise oxygenation theory and the allosteric model of Monod. Wyman, and Changeux. Biochemistry 1973, 12. 798–807.

Hofmann-Type Clathrates

Toschitake Iwamoto
Iwaki Meisei University, Iwaki, Fukushima, Japan

H

INTRODUCTION

A group of the clathrate compounds formed between the metal complex host diamminemetal(II) tetracyanometallate(II) and aromatic guest molecules (G), $[M(NH_3)_2M'(CN)_4]\cdot 2G$, is named a Hofmann-type clathrate.''' after German chemist K. A. Hofmann (1870–1940), who discovered the prototype $Ni(CN)_2\cdot NH_3\cdot C_6H_6$, by chance, in 1897.[2] The formula was revised as $[Ni(NH_3)_2Ni(CN)_4]\cdot 2C_6H_6$ based on the crystal structure determined by Powell in 1949–1952.[3,4] The host metal complex involves two kinds of nickel(II) atoms different in coordination geometry, octahedral and square planar, linked successively by ambidentate cyano ligands to form a two-dimensional (2D) network. The octahedral nickel(II) is coordinated with a pair of the ammine ligands at *trans* positions. Thus, the host network can be divided into the two building blocks. square planar $[Ni(CN)]_4^{2-}$ and *trans*-$[Ni(NH_3)_2]^{2+}$, respectively. The guest benzene molecule is entrapped between the metal complex networks in cavities formed by the protrusion of the ammine ligands. A wide variety of Hofmann-type host structures were subsequently derived by means of crystal engineering. i.e., replacement of the nickel(II) in either one or both metal sites, by the appropriate metal species and that of the ammines by other unidentate or ambidentate ligands.

HISTORICAL BACKGROUND

A remarkable amount of progress in chemistry. particularly in inclusion and coordination chemistry, was made by fortuitous discovery of something new. as in the case of chlorine clathrate hydrate, quinol-host clathrates, Prussian blue, ferrocene, etc. The formation of complex compounds between metal salts and organic molecules can be traced to the year 1827 and the discovery of Zeise's salt $KCl\cdot PtCl_2\cdot C_2H_4\cdot H_2O$ (=$K[PtCl_3(C_2H_4)]\cdot H_2O$), as an incidental product of a redox reaction between platinum(IV) chloride and ethanol. The discovery stimulated chemists in the nineteenth century to seek novel inorganic–organic molecular complexes. Hofmann and Küspert tried to pass coal gas through an amrnoniacal solution of nickel hydroxide. The product they reported in 1897 showed the coinposition $Ni(CN)_2\cdot NH_3\cdot C_6H_6$; the cyanide and benzene were afforded from the coal gas used for lighting at the time.''' The apparently anomalous behavior of the $Ni(CN)_2\cdot NH_3$ salt was reported in 1903: namely, that the salt yielded the molecular complex $Ni(CN)_2\cdot NH_3\cdot G$ with an aromatic G. neutral C_6H_6, basic $C_6H_5NH_2$, and acidic C_6H_5OH, respectively.[5] Further examination revealed that the aromatic G was limited to that with a molecular volume not larger than that of aniline, i.e., pyrrole, furan, thiophene, benzene, phenol, or aniline. From these observations, Hofmann concluded that the aromatic molecule G was not combined by any covalent or coordination bond through certain atoms but as a whole with the inorganic moiety to fill up a space upon the formation of the complex compound.[6] His view should be evaluated in the context of the earlier and excellent insight into the formation of inclusion compound. which requires a fitness of size and shape between the host and the guest. His view is a bit different in concept from Fischer's ''Key-and-Lock'' theory. Fischer persisted in the interaction between functional molecules fitting each other in shape and size, but Hofmann pointed out that the geometrical fitness is dominant regardless of the functional group on the guest. as exemplified by the isostructural clathrates of benzene. aniline. and phenol. Furthermore. Hofmann's host is not an Avogadro molecule but an infinite lattice of coordination polymer. Avogadro molecule here denotes a discrete chemical species built of a definite number of atoms belonging to certain elements. i.e., an ordinary molecule or molecular ion, the simplest examples being BH_4^-, CH_4, and NH_4^+, discriminated from those polymeric ones giving no definite molecular weight but only a formula weight, as in solid NaCl, SiO_2, etc.

A half century after the discovery of Hofmann's benzene compound. Powell verified Hofmann's view by determining the crystal structure of the complex,[3,4] a modernized sketch of which is shown in Fig. 1. The host has a layer structure involving stacking of 2D networks linked by cyano ligands, in which a network of square planar $[Ni(CN)_4]^{2-}$ anions play the role of an N-connected cross-shaped linker to four octahedral Ni(II) cations at the respective N ends; a pair of the ammine ligands protrude up and down from the octahedral Ni(II) cation in the

Encyclopedia of Supramolecular Chemistry
DOI: 10.1081/E-ESMC 120012727

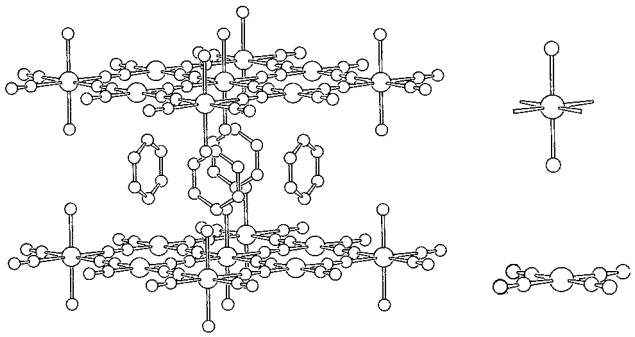

Fig. 1 A view of Hofmann-type benzene clathrate $[M(NH_3)_2M'(CN)_4]\cdot 2C_6H_6$: diamminemetalM(II) (right upper) and tetracyanometallateM′(II) (right lower) as building blocks of the host.

network. The *stacking of the flat network with the* ammine *protrusion* makes *an interlayer cavity for a guest benzene* molecule, *which is surrounded by four* ammine *ligands. The* limited *size of the square-mesh of the network, about 5.3* Å *edge length, allows the aromatic guest to have a* substituent *no* more *voluminous than an* amino *group.*

A primitive attempt at crystal engineering was tried by Baur *and* Schwarzenbach:[7] *an apparently* systematic *series was obtained by replacing the octahedral* Ni(II) *by* Cd(II), Cu(II), *and* Zn(II), *respectively. as* $[Cd(NH_3)_2Ni(CN)_4]\cdot 1.5C_6H_6$, $[Cu(NH_3)_2Ni(CN)_4]\cdot C_6H_6$, *and* $[ZnNi(CN)_4]\cdot 0.5C_6H_6$, *for the last of which the* ammine *ligands was lost. The apparently systematic but* nonstoichiometric *compositions were caused* from *the inappropriate drying of the products over concentrated sulfuric acid under reduced pressure. An extensive investigation by* Iwamoto *et al. since* 1966[8–15] *clarified that the series could be formulated as substantially stoichiometric* $[M(NH_3)_2M'(CN)_4]\cdot 2G$ *for octahedral* M=Mn, *Fe. Co.* Ni, Cu, Zn, *or Cd; square planar* M'=Ni, *Pd. or Pt: and aromatic* G=C_4H_4S, C_4H_4NH, C_6H_6, C_6H_5OH, or $C_6H_5NH_2$. *Iwamoto proposed naming the series Hofmann-type* clathrates[1] *in recognition of* K. *A. Hofmann's remarkable foresight into molecular inclusion phenomena.*

So-called Werner clathrates are another prominent series of clathrate compounds formed between a metal complex host and an aromatic *guest molecule. The name Werner originates* from *A. Werner. who established the coordination theory of metal complex compounds. The host of the series has* a *general formula* $[M(NCS)_2(4\text{-}Mepy)_4]$, *and in fact, the series is obtained conceptually by replacement of C N and* NH_3 *in the* Hofmann-type *host by SCN and 4-Mepy* (4-methylpyridine), *respectively. This was done in order to increase the* inclusion *capability* for *bulkier substituted aromatic molecules, in particular. those related to the petroleum industry. However. the host does not* have a *polymeric structure like that of the Hofmann-type but comprises a discrete metal-complex molecule. The name Werner was used to differentiate the host as a coordination complex from other kinds of complexes,* e.g., *organic–organic or organic–inorganic molecular complex, charge–transfercomplex, etc. Hence, the name of Werner* is *independent of molecular inclusion phenomena.*

STRUCTURAL FEATURES

The metal complex layer in the Hofmann-type hosts is not only a typical GN-linked 2I9 network but also a singular example of a regular structure with a flat and orthogonal (crystallographically tetragonal) square mesh. as well as the Prussian blue framework that is orthogonal, cubic, and three-dimensional (3D). *The Hoffman-type clathrates represent an* isomorphous *series of octahedral transition metal* M(II) *cations in a high-spin state* Mn(d^5), Fe(d^6), Co(d^7), Ni(d^8), Cu(d^9), *and* Zn(d^{10}) *or* Cd(d^{10}), *while the square planar* d^8 M′(II) *ions. Ni.* Pd, *and* Pt, *are in a low-spin state and are always diamagnetic. likely to* Tutton's *salts* $M(I)_2[M(II)(H_2O)_6](SO_4)_2$ *and alums* $M(I)[M(III)(H_2O)_6](SO_4)_2\cdot 6H_2O$.

As for the crystal engineering of the Hofmann-type hosts, the two building blocks, the trans-$[M(II)(NH_3)_2]^{2+}$ *rod with four equatorial extensions fi-om the* M(II) *center and the* $[M'(II)(CN)_4]^{2-}$ *cross are important; their alternating array gives a network. The topological features of the network are conserved in the Hofmann-type derivatives, in which the* NH_3 *is replaced by other unidentate ligands. such as* H_2O, NH_2CH_3 *(mmaj.* $NH(CH_3)_2$ *(dma),* $N(CH_3)_3$ (tma), *or unidentate coordinated* $NH_2(CH_2)_2OH$ *(mea).* $NH(CH_2CH_2)_2NH$ *(piperazine: den). The substituted network possesses a more lipophilic or hydrophilic surface than the original Hofmann-type compounds. Moreover, the flat network* becomes *corrugated and shifts to a certain* extent in *stacking so that the size of the cavity* and *the number of cavities per formula unit of the host complex change one by one. Examples are* $[Cd(H_2O)_2Ni(CN)_4]\cdot 4H_2O$, $[Fe(H_2O)_2Ni(CN)_4]\cdot 2C_4H_8O_2$, $[Cd(mma)_2Ni(CN)_4]\cdot 1.5(o\text{-}CH_3C_6H_4NH_2)$, $[Cd(dma)_2Ni(CN)_4]\cdot 0.5C_6H_6$, $[Cd(tma)_2Ni(CN)_4]$ *(no cavity).* $[Cd(mea)_2Ni(CN)_4]\cdot C_4H_4NH$, *and* $[Cd(den)_2Ni(CN)_4]\cdot 2C_6H_5OH$.

The stacking of the 2D network in *the Hofrnann-type hosts is extended to a* 3D *lattice work by linking the octahedral* M(II) *sites in adjacent networks with an* ambidentate *ligand such as an* α,ω-diaminoalkane $NH_2(CH_2)_nNH_2$ *(diam:* $n=2$–9*). mea,* $NH_2CH(CH_3)CH_2NH_2$ *(pn), den. etc. In the case of* α,ω-diaminoalkanes $NH_2(CH_2)_nNH_2$, *en* ($n=2$; *Hofmann-en-type). as well as mea and* pn, the *original Hofmann-type structure is retained,*

but adjacent networks are spanned by the ambidentate en, mea, or pn in place of the contacting pair of NH_3 ligands protruding into the interlayer space. In the case of pn, the methyl groups occupy a cavity so as to give the stoichiometry of $[Cd(pn)Ni(CN)_4]\cdot 1.5C_4H_4NH$. The bridging diam with the longer methylene chain ($n \geq 3$) keeps the host topology the same as that of the Hofmann-en-type—$[Cd(en)Ni(CN)_4].2C_6H_6$—but the size and shape of the cavities, and accordingly, the number of guest molecules in the chemical formula, change one by one. as well. Examples include the following: $[Cd(tn)Ni(CN)_4]\cdot 0.5(o\text{-}CH_3C_6H_4NH_2)$ (n=3), $[Cd(dabtn)Ni(CN)_4]\cdot C_6H_5N(CH_3)_2$ (n=4), $[Cd(daptn)Ni(CN)_4].1.5(p\text{-}C\cdot H_3C_6H_4NH_2)$ (n=5), $[Cd(dahxn)Ni(CN)_4]\cdot m\text{-}CH_3C_6H_4NH_2$ (n=6), $[Cd(dahpn)Ni(CN)_4]\cdot 1.5$(2-methylquinoline) ($n$=7), $[Cd(daotn)Ni(CN)_4].C_6H_{13}OH$ (n=8), and $[Cd(danon)Ni(CN)_4]\cdot 0.5(o\text{-}C_6H_4(CH_3)_2$ (n=9). In general, longer aliphatic chains increase the flexibility of the host lattice structure and the lipophilic character of the inclusion cavity.

STRUCTURAL DEVELOPMENTS

Replacement of the square planar $[M'(II)(CN)_4]^{2-}$ in the Hofmann-type host by a tetrahedral tetracyanometalate(II), e.g., $[Cd(CN)_4]^{2-}$ or $[Hg(CN)_4]^{2-}$, gives another series of clathrates with apparently the same chemical composition. i.e., the Hofmann-Td-type—$[Cd(NH_3)_2Cd(CN)_4]\cdot 2C_6H_6$. The structure of the host involving the tetrahedral moiety is closely related to that of the original Hofmann-type, given the change of point group from D_{4h} of the square planar moiety to T_d of the tetrahedral one, as shown in Fig. 2. As an idealized representation. the square planar moiety is twisted at the central atom by 90° upon replacement by the tetrahedral one. Half of the number of the tetragonal cavities in the Hofmann-type host are twisted along the body-diagonal plane by 90° with respect to one another. but the volume of the cavity remains unchanged. Actually, the unit cell of the Hofmann-Td-type becomes twice the size of the Hofmann-type: generally $Z = 1$ for the Hofmann-type but $Z = 2$ for the Hofmann-Td-type.

A number of compounds with chemical compositions that are similar to that of the original Hofinann-type ciathrates were reported. However. as usual for other inclusion compounds. similarity in composition does not necessarily co relate with similarity of structure. For example, in the $[Cd(pn)Ni(CN)_4]\cdot G$ series with aliphatic guests, the host structure is entirely different from the Hofmann-pn-type pyrrole clathrate $[Cd(pn)Ni(CN)_4].(3/2)C_4H_5N$. Two subseries of structures were observed for the channel cavities. one being a snake-like extension similar to chat observed for the urea–host inclusion compounds and the other a nodal extension similar to that observed for the thiourea-clathrates. Many cyanometal-complex-host clathrates and cyanometal complexes were observed with similar compositions and entirely different structures.

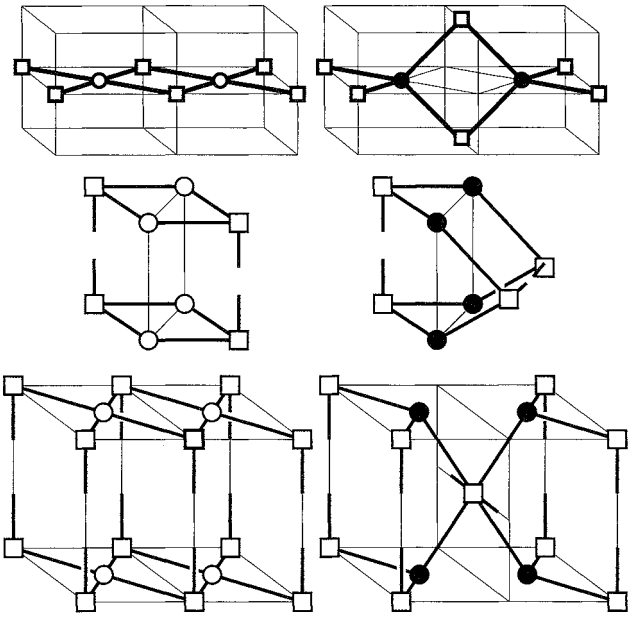

Fig. 2 The replacement of a square planar center (open circle) by a tetrahedral (solid circle) one; the open square denotes an octahedral center. (Left top) Flat network in the Hofmann-type. (Right top) Twisted network in the Hofmann-Td-type. (Left middle) A rectangular box cavity in the Hofmann-type. (Right middle) A twisted biprismatic cavity in the Hofmann-Td-type. (Bottom) A couple of Hofmann-type unit cells (left) makes a unit cell (right) of the Hofmann-Td-type.

CONCLUSION

During the earlier stages of research on Hofmann-type clathrates, Hofmann's benzene clathrate was applied to purify benzene produced probably by the coal chemical industry; at the time, the elimination of trace amounts of thiophene was a problem. Syntheses of polythiophenes, polypyrroles, etc., examined in a few cases, appear to have been unsuccessful. However. if the Hofmann-type structure is seen as a system composed of robust metal complex host and guest molecules entrapped discretely in the cavity, it may act as a reservoir of unstable species as the guest. An example is the long-lived cyclohexadienyl radicals generated in $[Cd(en)Hg(CN)_4]\cdot 2C_6H_6$ by γ-ray irradiation; the thermally stable $C_6H_7\bullet$ radicals survive up to 423 K in a vacuum-sealed tube.[16,17]

Almost all important contributions to the chemistry of Hofmann-type and related inclusion compounds and host cyanometal complexes were revicwcd in the literature.[12–15]

ARTICLES OF FURTHER INTEREST

Channel Inclusion Compounds, p. *223*
Isostructurality of Inclusion Compounds, p. *767*
Layered Supramolecular Solids and Their Intercalates, p. 791
Mineralomimetic Structures, p. 868
Molecular Squares, Boxes, and Cubes, p. *909*
Zeolites: Structures and Inclusion Properties, p. *1623*

REFERENCES

1. Iwamoto, T.; Nakano, T.; Morita, M.; Miyoshi, T.; Miyamoto, T.; Sasaki, Y. The Hofmann-type clathrate: $M(NH_3)_2M'(CN)_4 \cdot 2G$. Inorg. Chim. Acta **1968,** 2, 313–316.
2. Hofmann, K.A.: Küspert, F.A. Verbindungcn von Kohlenwasserstoffcn mit Metallsalzen. Z. Anorg. Allg. Chem. **1897**. *5*, 204–207.
3. Powell, H.M.; Rayncr, J.H. Clathrate compound formed by benzene with an ammonia-nickel cyanide complex. Nature (Lond) **1949,** *163*, 566–567.
4. Rayner, J.H.; Powell. H.M. Structure of molecular compounds. Part X. Crystal structure of the compound ol' benzene with an ammonia-nickel cyanidc complex. **1952.3**19–328.
5. Hofmann, K.A. Höchtlen. Abnormc Vcrbindungcn des Nickels. Bcr. Dtsch. Chern. Ges. **1903,** *33*, 1149–1151.
6. Hofmann, K.A.: Arnoldi, H. Auffällige Unterschiedc homologcr cyclischer Moleküle im Vcrhalten gegen Nickelcyanürammoniak. Ber. Dtsch. Chcm. Ges. **1906,** *36*, 339–344.
7. Baur, R.: Schwarzenbach, G. Ncue Einschlussverbindungen vom Typus dcs Nickelcyanid-Ammoniak-Benzols. Helv. Chim. Acta **1960,** 43, 842–847.
8. Miyamoto, T.; Iwamoto. T.; Sasaki, Y.: Fujiwara, S. Long T_1 of NMR in thc isolated benzene molecule. J. Chem. Phys. **1966,** *45*. 752.
9. Iwamoto, T.: Miyoshi, T.: Miyamoto. T.; Sasaki, Y. The metal amminc cyanide aromatics clathrate. 1. The preparation and stoichiomctry of diammincmetal(II) tetracyanoniccolate(II) dibenzene and dianiline. Bull. Chem. Soc. Jpn. **1967,** 40. 1174–1178.
10. Iwamoto, T. The aromatic guest molecules cnclathrated in Hofmann type and the analogous clathrates. Isr. J. Chcm. **1979,** *18*, 240–245.
11. Iwamoto, T. Recent dcvclopmcnts in thc chemistry of Hofmann-type and the analogous clathrates. J. Mol. Struct. **1981.** *75*. 51–65.
12. Iwamoto, T. The Hofmann-Type and Rclatcd Inclusion Compounds. In *Inclusion Compounds,* I: Atwood. J.L., Davies. J.E.D., MacNicol. D.D., Eds.; Academic Press: London, 1984: 29–57.
13. Iwamoto, T. Inclusion Compounds of Multi-Dimensional Cyanometal Complex Hosts. In *Inclusion Compounds,* 5; Atwood. J.L., Davies, J.E.D.. MacNicol, D.D., Eds.; Oxford University Press: Oxford. 1991; 177–212.
14. Iwamoto, T. Past. present and future of the clathrate and inclusion compounds built of cyanometallate hosts. J. Incl. Phenom. Mol. Recognit. Chem. **1996,** 24, 61–132.
15. Iwamoto, 'I. Supramolecular Chemistry in Cyanometallate Systems. In *Comprehensive Supramolecular Chemistry, 6, Solid-State Supramolecular Chemistry: Crystal Engineering;* MacNicol. *D.D.,* Toda, F., Bishop, R., Eds.; Pergamon. 1996; 643–690.
16. Iwamoto, T.; Kiyoki. M.; Matsuura, N. Thermally stable cyclohcxadicnyl radicals produced in thc benzene clathrates with metal complex host latices. Chem. Lett. **1975,** 847–848.
17. Iwamoto; T.; Kiyoki, M.; Matsuura, N. Cyclohexadienyl radicals in γ-irradiated *catena*-μ-ethylenediaminecadmium (II) *catena*-tetra-μ-cyanomercurate(II)-benzene(1/2) and the analogous clathrates. Bull. Chcm. Soc. Jpn. **1978,** *51*, 390–393.

Homocalixarenes

Peter J. Cragg
University of Brighton, Brighton, United Kingdom

INTRODUCTION

Of all the macrocycles encountered in supramolecular chemistry, two are predominant: calixarenes and crown ethers. Conventionally, calixarenes are 2,6-metacyclophanes derived from phenols, with a single CH_2 group separating each phenolic moiety (see *Calixarenes: Synthesis and Historical Perspectives*). It is possible to introduce variation into the calixarene framework by extending the bridge between phenols to create a range of "homocalixarenes." This bridge majj consist solely of alkyl groups or may have heteroatoms. such as nitrogen or oxygen, incorporated in the chain. Introduction of heteroatoms has the additional interesting effect of combining crown ether (or azacrown ether) features with those of calixarenes. The potential of homocalixarenes and their derivatives to form a wide range of supramolecular complexes is therefore vast and as yet largely untapped.

NOMENCLATURE

The term "homocalixarene" was coined by Brodesser and Vogtle in 1994 to describe calixarene analogues containing two or more CH_2 groups between the aromatic moieties.[1] Homocalixarenes in which all the bridges were expanded to the same degree are termed all-homocalixarenes; those in which bridges of differing lengths occur are usually given names based on cyclophane nomenclature (see *Cyclophanes: Definition and* Scope).

An additional subgroup of these compounds contains combinations of CH_2 groups and heteroatoms such as oxygen ("hornooxacalixarenes") or nitrogen ("homoazacalixarenes"). The presence of heteroatoms is reflected in the nomenclature, thus a calix[4]arene in which one CH_2 was replaced by CH_2OCH_2 is described as a dihomooxacalix[4]arene.[2] The "dihomo" element of the name implies two additional atoms in the cyclic framework; "oxa" implies that one of these is oxygen: and "calix[4]arene" is the class of the parent compound. Other structural features that contribute to nomenclature include the "lower-rim" substituents (if any) attached to the phenolic oxygens, the "upper-rim" substituents found in the 4-position of the phenols. and, in the case of homoazacalixarenes. the substituents on the nitrogens.

HOMOCALIX[*N*]ARENES

The simplest member of this group is calix[2]arene, 8,16-dihydroxy[2.2]metacyclophane, comprised of two *p-t*-butylphenols linked through ethylene bridges.[3] Larger *all*-homocalixarenes containing three phenols with all ethyl[4] and all propyl[5–7] linkers have been prepared. Trimers with combinations of methyl and ethyl[8] and methyl and propyl[9] bridges, tetramers linked by two methyl and two propyl bridges,[10,11] and *all*-homocalix[4]arenes[12] are also known.

Synthesis

Two main procedures were used to prepare homocalixarenes. The first uses the sulfone extrusion route (Fig. 1) initially developed by Vogtle to prepare [2.2.2.2]biphenylophane and extended by Tashiro and Yamato to synthesize dihomocalix[3]arenes, dihomocalix[4]arenes, and homocalixarenes with differing lengths of bridges.[12,13] Typically. this method combines 2,6-(chloromethyl)-4-*t*-butylanisole with *bis*(3-thiomethyl-5-*t*-butylanisole)methane to prepare the sulfur-containing intermediate. This is transformed into the dihomocalix[3]-arene through pyrolysis under reduced pressure followed by hydrolysis. The second synthetic route owes much to the work of Yamato,[14] who pioneered an approach that employs base-catalyzed (Fig. 1) condensation of linked phenols with formaldehyde to prepare the asymmetric homocalixarenes. A typical example involves the preparation of 1,3-*bis*(5-*t*-butyl-2-hydroxyphenyl)propane from 4-t-butylanisole. and its subsequent reaction with paraformaldehyde under basic conditions to form the tetrahomocalix[4]arene. Variations on this method are used to synthesize 4-*t*-butylhexahomocalix[3]arene through cyclization of 2,6-(bromomethyl)-4-*t*-butylanisole.[13] An indication of the success of these synthetic methods may be given by the observation that bishomocalix[3]-, [4]-, [5]-, [6]-, [7]-, and [8]arenes are all available.

Derivatives

Alkylation of the lower rims of these compounds was largely restricted to methyl substituents. with the notable

Encyclopedia of Supramolecular Chemistry
DOI: 10.1081/E-ESMC 120019188

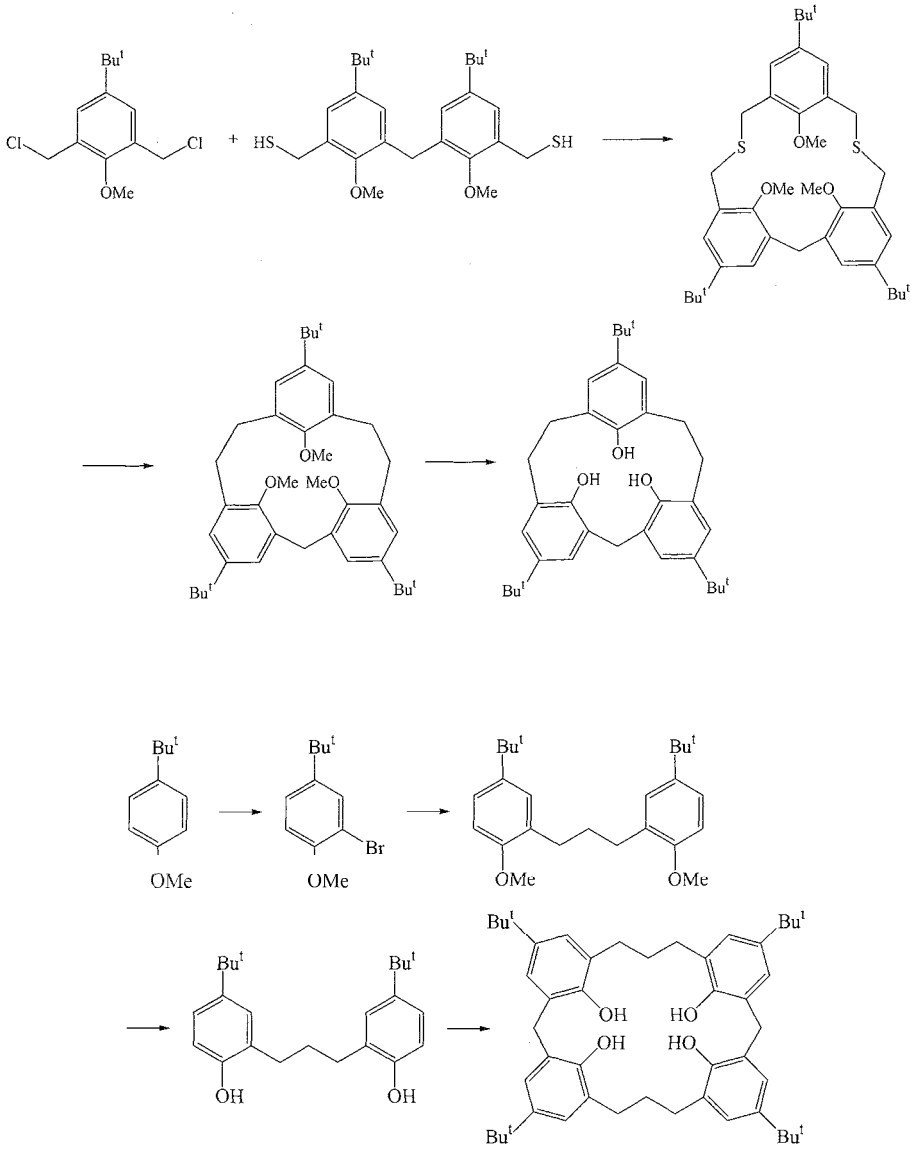

Fig. 1 Homocalixarene synthesis: sulfone extrusion (top) and base-catalyzed (bottom) methods.

exception of hexahomocalix[3]arenes and tetrahomocalix[4]arenes. Methyl-, benzyl-, and diethylacetamide and ethylacetate derivatives of both were prepared.[5,15] In addition, the tripyridyl derivative of the hexahomocalix[3]arene was prepared.[5] Unlike the calix[*n*]arene family. where many conformers may be formed, the homocalix[3]arenes can only adopt cone conformers and the less sterically demanding partial cone conformers. Unfortunately. the partial cone conformers of these derivatives tend to collapse on the macrocyclic cavity, thus reducing the potential for host–guest interactions. Statistically, only 25% of *O*-alkylated products should form in the generally more useful cone conformer, however, this may be improved by correctly choosing reagents. For example, the choice of base can influence the ratio between cone and partial cone conformers of the products formed from *O*-alkylation of hexahomocalix[3]-arene. The ester and amide derivatives may be synthesized as the cone conformer or partial cone with 95% or 67% specificity, respectively. More striking is the reaction of 4-*t*-butylhexahomocalix[3]arene with 2-(chloromethyl)pyridine. Use of sodium hydride as the base, in tetrahydrofuran, gives the cone conformer exclusively; however, if cesium carbonate is substituted as the base, only the partial cone conformer is formed. Free rotation of the aromatic groups through the annulus allows the cone conforiner to form readily when the lower-rim substituents are relatively small: however, as these groups become

larger. the macrocycles can no longer interconvert between conformers through rotation alone.

Complexes

The importance of the cone conformer for guest binding may be illustrated through the extensive investigation of binding carried out on the pyridyl derivative of hexahomocalix[3]arene, which is selective for Ag^+ over alkali metals and the butylaminonium cation. This is true in either the cone or. surprisingly, partial cone conformer; nevertheless, the strongest binding occurs with the cone conformer.[6] Unsubstituted homocalixarenes display metal extraction profiles that unusually reflect their flexibility and number of phenolic binding sites rather than the size of the cavity they form: *bis*homocalix[5]arene binds Ca^{2+}, Sr^{2+}, and Ba^{2+} to an equal extent. whereas the larger *bis*homocalix[8]arene is specific for Ba^{2+} over all other alkaline earths. Incorporation of lower-rim amido groups further enhances the discrimination of the latter for Ba^{2+}. There are other consequences of metal–homocalixarene interactions: cation–π interactions between alkali metals and the aromatic rings of *bis*homocalix[2]arene were cited as reasons for difficulties in its selective demethylation.[15]

HOMOOXACALIX[*N*]ARENES

Homooxacalix[*n*]arenes (oxacalixarenes) are members of the calixarene family of macrocycles that incorporate one or more ethereal bridges (CH_2OCH_2) in place of CH_2 groups, which link phenol moieties through the 2- and 6-positions. The first members of the family to be reported were hexahomotrioxacalix[3]arenes,[16–19] however. many others are now known. The synthesis of the entire series of expanded calix[4]arenes (dihomooxa-, both isomers of tetrahomodioxa-. hexahornotrioxa-, and octahomotetraoxacalix[4]arenes) as the corresponding methyl ethers was described in detail by Masci.[20] Oxacalix[4]arenes, notably dihomodioxacalix[4]arene, enjoyed some success as chelators for lanthanides and actinides; nevertheless, the oxacalix[3]arenes remain the focus of attention.[''']

HEXAHOMOTRIOXACALIX[3]ARENES

Synthesis

Hexahomotrioxacalix[3]arenes (oxacalix[3]arenes) were first reported in 1962,[16] but it took another two decades until a reliable synthetic method appeared.[17] Additional routes and refinements continue to make these coinpounds more accessible.[18,19] The most straightforward synthesis involves the acid-catalyzed condensation of 2,6-*bis*(hydroxymethyl)-4-*t*-butylphenol in refluxing o-xylene. Mixtures of hexahomotrioxacalix[3]arenes and octahomotetraoxacalix[4]arenes are usually formed, however, if *p*-toluenesulfonic acid is used as the catalyst, the hexahomotrioxacalix[3]arene is the sole product[''' ((Fig. 2).

Derivatives

The attractive threefold symmetry of the oxacalix[3]arenes and potential for modification at upper and lower rims led to their application as models for ion channel filters,[22] chiral recognition agents,[23] sensors for neurotransmitters, rotaxanes, and molecular capsules.[24] Derivatization generally takes place at the lower rim through reaction of phenolic oxygens with a variety of species. including alkyl iodides, *N*, N-diethylchloroacetamide, ethylbromoacetate, and 2-(chloromethyl)pyridine. As with hexahomocalix[3]arenes in general. the main drawback of lower-rim substitution is that statistically only 25% of the product forms in the cone conformation. Likewise. careful control of alkylating conditions can direct the product conformer: reaction of 4-*t*-butylhexahomotrioxacalix[3]arene with *N*, N-diethylchloroacetamide using sodium hydride in tetrahydrofuran gives the cone product. whereas cesium carbonate in acetone gives the partial cone product. Once *O*-alkylation occurred. the macrocycle is frozen into the conformation it adopted. unless the substituent is a propyl group or smaller. Interestingly, the hexahomotrioxacalix[3]arene derivatives are more conformationally mobile than their hexahomocalix[3]arene analogues. The propyl ether derivative of the latter cannot rotate through the macrocyclic annulus, and the ethyl ether derivative inverts at 90°C compared to 50°C for the oxygen-containing homologue.

Complexes

The parent oxacalix[3]arenes show little ability to bind alkali metals,[18] however, a range of quaternary ammonium cations are attracted to the symmetric cavity. Deprotonation of the phenol moieties allows them to bind to transition metals (scandium, titanium, vanadium. rhodium. molybdenum. gold. etc.), lanthanides (lutetium. yttrium, and lanthanum), and actinides (uranium: as uranyl). Oxacalix[3]arenes derivatized on the lower rim can complex gallium, mercury. and alkali metals, including sodium, in a manner reminiscent of natural transmembrane cation filters. One major use was to purify crude samples of fullerenes. The pseudo-C_3 symmetry of the macrocyclic cavity is complementary to threefold symmetry elements of C_{60}, which binds preferentially in

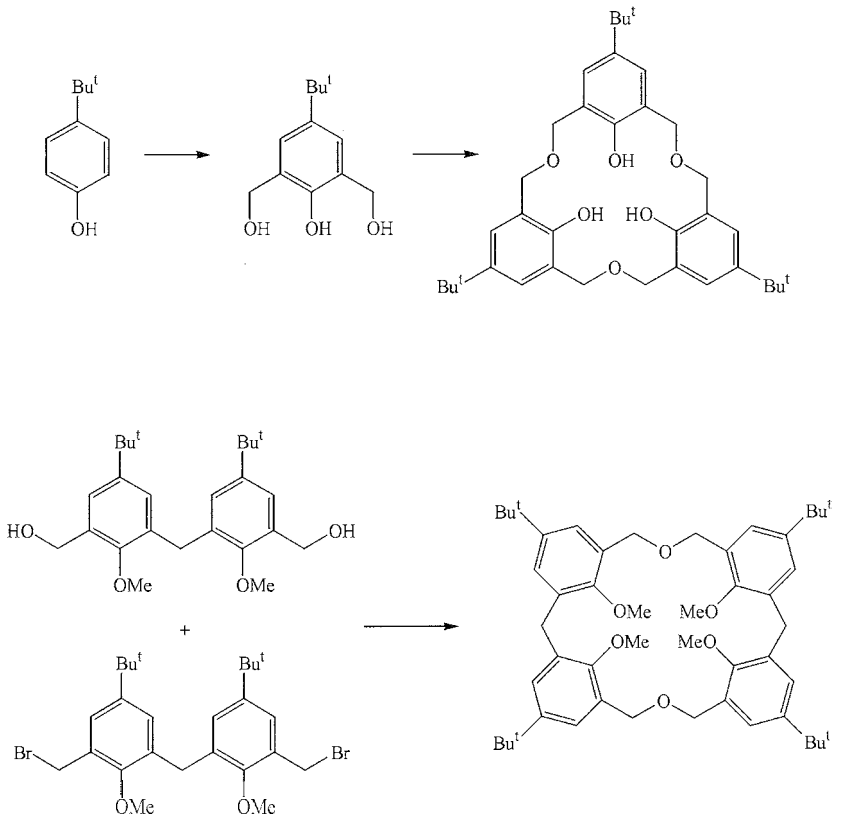

Fig. 2 Homooxacalixarene syntheses: hexahomotrioxacalix[3]arene (top) and tetrahomodioxacalix[4]arene (bottom)

aromatic solventr. The oxacalixarene-C_{60} coinplex can be isolated and the pure fullerene liberated through dissolution in dichloromethane.[25]

DIHOMOOXACALIX[4]ARENES, TETRAHOMODIOXACALIX[4]ARENES, AND OTHER DERIVATIVES

Synthesis

Initially, the expanded oxacalix[4]arenes were obtained as trace products from the preparation of calix[4]arenes:[26,27] however, high-yielding routes have since been reported in which the expanded calix[4]arenes are the major products.[20] For example. optimized synthetic methods are now available to prepare cone and partial cone conformers of tetrahomodioxacalix[4]arene (as their methyl ethers) through the reaction of a *bis*(hydroxymethyl)phenol methyl ether dimer or trimer with a *bis*(bromomethyl)phenol methyl ether dimer or monomer, respectively, via Williamson ether syntheses.

Derivatives

The majority of examples of expanded calix[4]arenes in the literature are 4-*t*-butyl derivatives of dihomooxa- or tetrahomodioxacalix[4]arenes, as parent compounds or as phenyl ethers and esters,[28,29] although *p*-methyl- and p-phenyl-containing compounds were reported.[30,31]

Complexes

X-ray crystallographic determinations illustrate a range of complexes exhibiting inclusion of m-xylene, dimethylformamide, tetrahydrofuran. triethylamine, dimethylsulfoxide. or acetone. iThe expansion of the calix[4]arene framework is particula ly suited. however. to europium and uranyl complexation by phenolic oxygens.[21]

HOMOAZACALIX[*N*]ARENES

Analogous to the homooxacalixarenes. the homoazacalixarenes contain nitrogen bridge heads with an array of

substituents. Homoazacalix[4]arenes may be prepared through cyclization of methylene-bridged 4-substituted phenol dimers or tetramers in the presence of amines. Homoazacalix[3]arenes are synthesized through acid-catalyzed cyclization of 2,6-*bis*(hydroxymethyl)phenols with arnines followed by thermal dehydration or base-catalyzed cyclization of 2,6-di(chloromethyl)phenols with amines (Fig. 3).

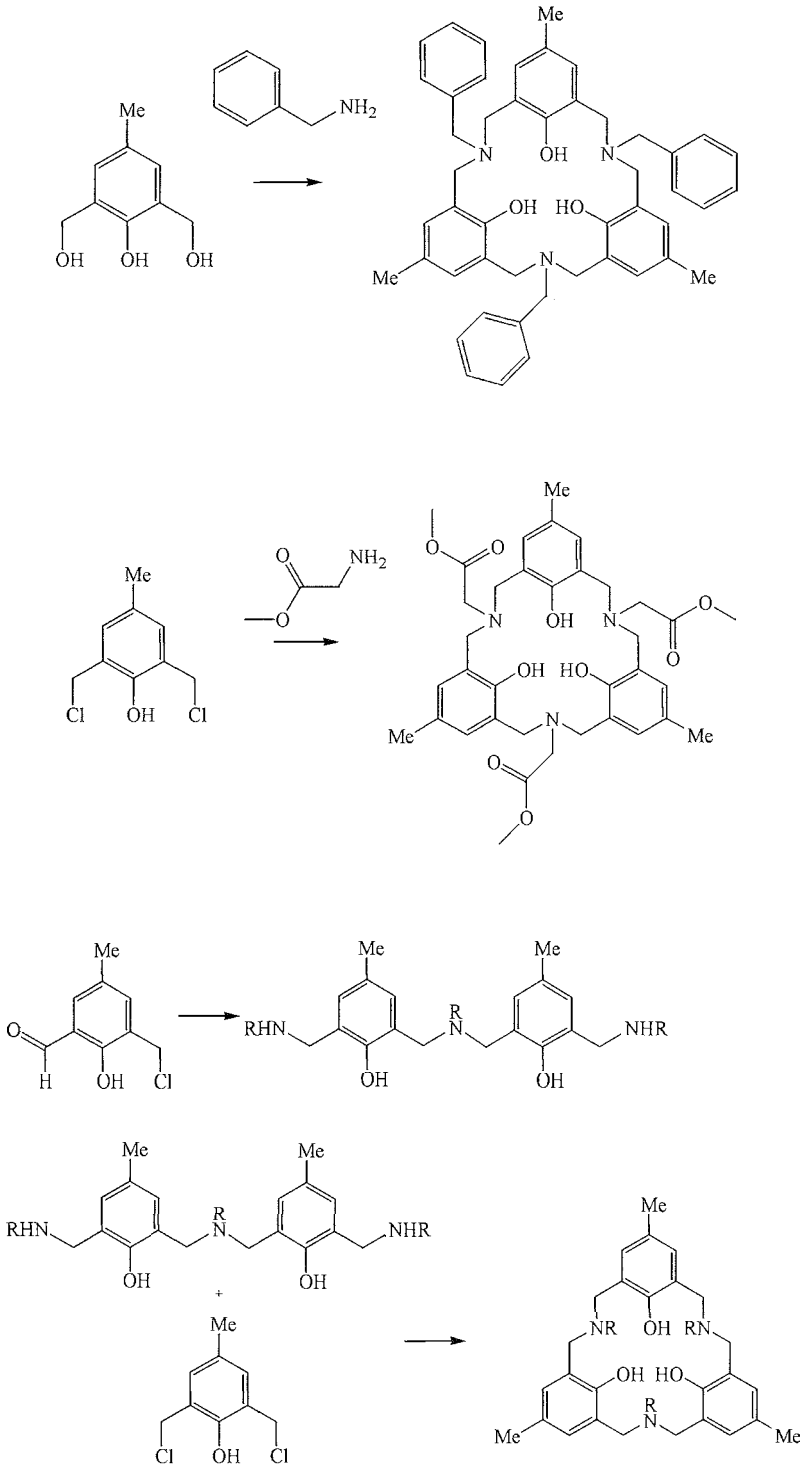

Fig. 3 Homoazacalixarene syntheses high-temperature (top), base-catalyzed (center). and convergent (bottom) methods

Synthesis

The first hornoazacalixarene was reported by Hultsch,[16] who prepared hexahomotriazacalix[3]arene through direct reaction of 4-t-butylphenol with hexamethylenetetramine, however, his method has yet to be verified. The first practical synthesis was that of tri(4-methyl-*N*-benzyl)hexahomotriazacalix[3]arene by Takemura.[32] In the two-step process, 2.6-bis(hydroxymethy1)-4-methylphenol was first refluxed in toluene with benzylamine, solvent was removed. and the residue was thermally dehydrated at 135°C to give the azacalix[3]arene in 38% yield. A convergent synthesis was developed by Hampton based on the reaction of 2-(chloromethyl)-5-methylbenzaldehyde with benzylamine (to form a dimer), followed by the addition of *bis*(chloromethyl)-4-methylphenol to give the compound in 95% yield.[33] Characterization of the product prepared by Hampton's method indicates that Takemura's procedure generates a mixture of oligomers, predominantly the azacalix[3]arene and its azacalix[4]arene homologue.

An alternative to this method. and one by which a variety of *N*-substituents may be introduced, is through the base-catalyzed reaction of a suitable amine, such as an amino acid ester with 2,6-*bis*(chloromethyl)phenols.[34] The advantage of this method is that the *N*-substituents

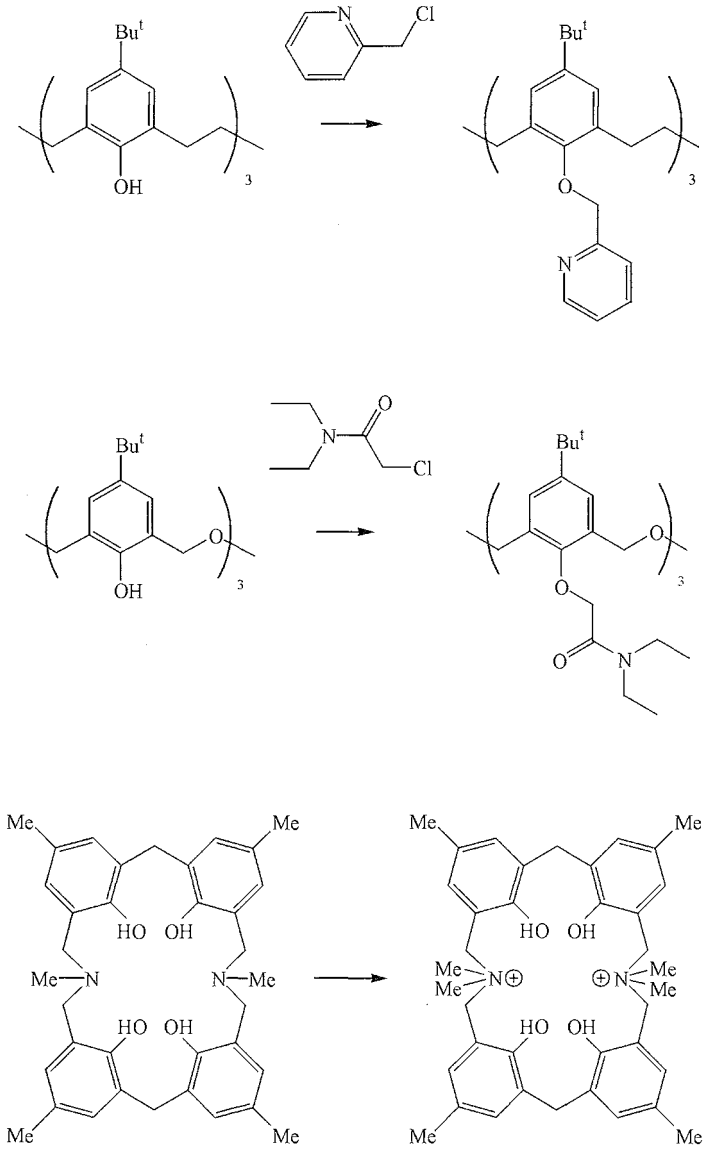

Fig. 4 Derivatives of the parent macrocycles: *O*-alkylation of hexahomocalix[3]arenes (top) and hexahomotrioxacalix[3]arenes (center): formation of tetrahomodiazacalix[4]arene betaine (bottom).

may be derived from volatile amines that would not be stable in refluxing o-xylene. Other azacalixarenes are made through condensation of benzylamine with *bis*(hydroxymethyl)phenol dimers or tetramers to yield tetrahomodiazacalix[4]arenes and dihomoazacalix[4]arenes.[35] Reaction of the *bis*(hydroxymethyl)phenol dimers with methylamine produces a dibishomoazacalix[4]arene that can be quaternarized to form the cationic azacalix[4]arene betaine.[36]

Derivatives

Unlike homocalixarenes and homooxacalixarenes, little was done to derivatize the lower, phenolic rim of the homoazacalixarenes. Upper-rim substituents, thus far, are limited to chloro, methyl. and t-butyl groups. The greatest scope for variation came in the groups appended to the bridging nitrogen. Early examples include benzyl and glycine methyl ester derivatives. but this range has since extended to include pyridyl, acetyl, i-butyl, allyl, and the N-unsubstituted derivative first reported by Hultsch (Fig. 4).

Complexes

Crystal structures of dihomoazacalix[3]arene containing *N*-glycyl methyl ester substituents and its trimethylsiloxy derivative show that the former adopts the cone and the latter the partial cone conformer, though neither includes solvent in the solid state. Structures of tri(4-chloro-*N*-benzyl)hexahomotriazacalix[3]arene complexed to ytterbium nitrate and neodymium nitrate show that the metal is centrally coordinated to ail three phenolic oxygens. This provides an interesting contrast with the dimeric structures determined for hexahomooxacalix[3]arenes. Di(4-methyl-*N*-benzyl)tetrahomodiazacalix[4]arene complexes the uranyl cation in two distinct modes that may involve all four phenolic groups or just two (Figs. 5,6).

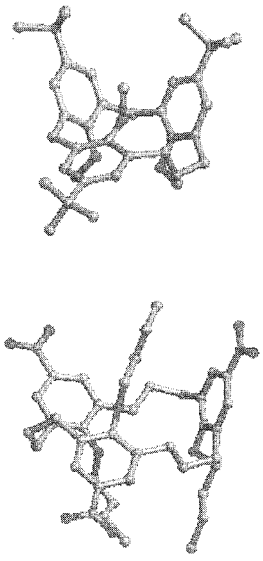

Fig. 5 Structures of homocalixarenes: 4-I-butyldihomocalix[3]arenetrimethyl ether (top) and 4-nitrohexahomocalix[3]arenetributyl ether (bottom). with solvents and hydrogen atoms removed for clarity. (*View this art in* color *at www.dekker.com.*)

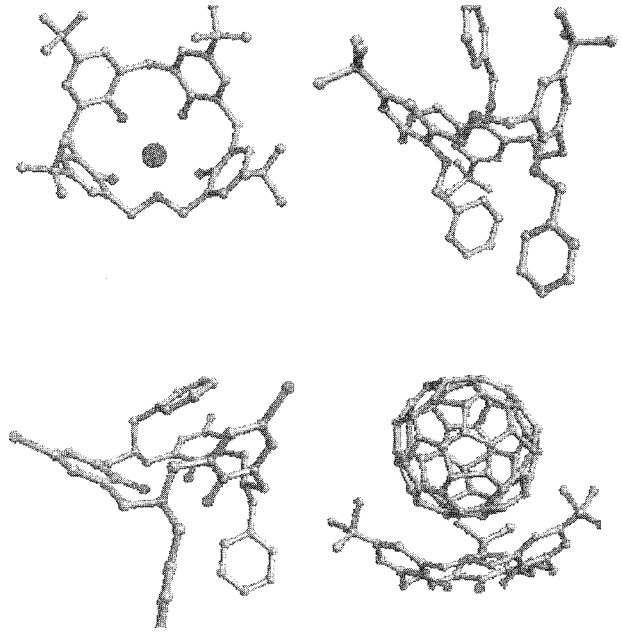

Fig. 6 Structures of homooxa- and azacalixarenes: 4-*t*-butyldihomooxacalix[4]arene-europium complex (top left), 4-*t*-butylhexahomotrioxacalix[3]arenetripyridyl ether (top right), chlorohexahomotriazacalix[3]arenetribenzyl ether (bottom left). and 4-*t*-butylhexahomotrioxacalix[3]arene-C_{60} complex (bottom right), with solvents and hydrogen atoms removed for clarity. (*View this art in* color *at www.dekker.com.*)

CONCLUSION

Expansion of the calix[*n*]arene framework, thus increasing the interphenolic separation by homo- or heteroatomic moieties: yields homocalixarenes with increased flexibility over the parent macrocycles. This. in turn, gives rise to novel inclusion complexes, particularly where oxqgen or nitrogen heteroatoms are incorporated in the macrocycle. The expanded macrocyclic cavities present in homocalixarenes give the compounds the potential to complex large guests. as evidenced by the oxa- and azacalixarene complexes of lanthanides and actinides. Modification of the upper and, more importantly, lower rims of the phenolic groups allows for even greater functionality to be

added to the compounds. Unlike the parent calix[*n*]arenes, the derivatized homocalixarenes are less constrained in the range of conformers that they can adopt and readily interconvert, as long as the lower-rim substituents are not too bulky.

Much of the early research into homocalixarenes focused on simply extending the intesphenolic bridges. however, the current trend is to exploit the binding properties of heteroatoms incorporated in the macrocyclic framework. To this end, research into the synthesis and inclusion chemistry of oxa- and azacalixarenes has now become the main area of interest for those working on homocalixarenes.

ACKNOWLEDGMENTS

The use of the EPSRC's Chemical Database Service at Daresbury is gratefully acknowledged.

ARTICLES OF FURTHER INTEREST

Alkali Metal Cations in Biochemistrj, p. *1*
Cnlixarenes and Their Analogues: Cation Complexation, p. 137
Calixarenes and Their Analogues: Molecular Complexation, p. *145*
Cnlixarenes: Synthesis and Historical Perspectives, *p.* 153
Cation–π Interactions, p. 214
Complexation of Fullerenes, p. 302
Crown Ethers. p. 326
Cyclophanes: Definition and Scope, p. 414
Cyclophanes: Endoacidic, Endobasic, and Endolipophilic Cavities, p. 424
Macrocycle Synthesis, p. *830*

REFERENCES

1. Brodesser. G.; Vogtle. F. Homocalixarenes and homocalixpyridines. J. Incl. Phenom. Mol. Recog. Chem. 1994, 19 (1–4), 111–135.
2. Gutsche. C.D.; Bauer. L.J. Calixarenes 13. The conformational properties of calix[4]arenes, calix[6]arenes, calix[8]-arenes, and oxacalixarenes. J. Am. Chem. Soc. 1985, *107* (21), 6052–6059.
3. Tashiro, M.: Koya. K.; Yamato, T. Metacyclophanes and related compounds 7. Preparation and reduction of [2.2]metacyclophanequinone. J. Am. Chem. Soc. 1982, *104* (13), 3707–3710.
4. Vogtle, F.: Schmitz. J.; Nieger, M. Many-membered and donor-substituted hydrocarbon rings. Chem. Ber.-Recl. 1992, *125* (11), 2523–2531.
5. Yamoto. T.: Doamekpor, L.K.: Koizumi, K.; Haraguchi, M.; Tashiro. M. Synthesis and conformational studies of calixarene-analogous trihydroxy[3.3.3]metacyclophanes and their 0-alkylated derivatives. Liebigs Ann. 1995, (7), 1259–1267.
6. Yamato, T.; Haraguchi, M.; Nishikawa, J.; Ide. S. Synthesis, conforniational studies and inclusion properties of *O*-benzylated calixarene analogues of trihydroxy[3.3.3]-metacyclophanes. J. Chem. Soc., Perkin Trans. 1 1998. (3), 609–614.
7. Yamato, T. Synthesis, conformations and inclusion properties of homocalix[3]arenes. J. Incl. Phenom. Mol. Rec. Chem. 1998. *32* (2–3). 195–207.
8. Tsuge, A.; Sawada. T.; Mataka, S.: Nishiyama. N.: Sakashita, H.: Tashiro, M. Preparation and structural properties of hydroxy- and alkoxy[2.2.1]metacyclophanes. J. Chem. Soc., Perkin Trans. 1 1992, (12). 1489–1494.
9. Yamato, T.; Doamekpor, L.K.; Tsuzuki. H.; Tashiro. M. A novel calixarene-analogous macrocyclic metacyclophane, molecular pendulum. Chem. Lett. 1995, 89–90.
10. Yamato, T.; Saruwatari, Y.: Nagayama, S.; Maeda, K.: Tashiro. M. Preparation and confonnational properties of tetrahydroxy[3.1.3.1]metacyclophanes. J. Chem. Soc., Chem. Commun. 1992, (11), 681–682.
11. Yamato, T.; Saruwatari, Y.: Yasumatsu, M. Synthesis and conformational studies of regio- and conformational isomers derived by 0-alliylation of tetrahydroxy[3.1.3.1]metacyclophane. J. Chem. Soc., Perkin Trans. 1 1997. (11), 1731–1737.
12. Tashiro. M.; Yamato. T. Metacyclophanes and related compounds 1. Preparation and nuclear magnetic resonance spectra of 8,16-disubstituted [2.2]metacyclophanes. J. Org. Chem. 1981. *46* (22), 1541–4562.
13. Tashiro, M.: Tsuge. A.; Sawada. T.: Makishima, T.: Horie, S.: Arimura. T.: Mataka, S.; Yamato, T. Metacyclophanes and related compounds 26. Tetrahydroxy[2.n.2.n]metacyclophanes — Preparation. reactions and spectra. J. Org. Chem. 1990. *55* (8). 2404–2409.
14. Yamato. T.: Saruwatari. Y.; Doamekpor. L.K.: Hasegawa, K.-I.; Koike. M. Preparation and conformational studies of ethylene-bridged calixarene-analogous macrocyclic metacyclophanes. Chem. Ber.-Recl. 1993. *126* (11), 2501–2504.
15. Yamato. T.: Yamada. Y.; Hirahara, M. Medium-sized cyclophanes. Part 49. 0-alkylation of 8,16-dihydroxy[2.2]-metacyclophane. J. Chem. Res.-S 1999. (12). 724–725.
16. Wultzsch. K. Ring-kondensate in alkylphenolharzen. Kunststoffe 1962, *52* (1). 19–24.
17. Dhawan. D.; Gutsche, C.D. Calixarenes 10. Oxacalixarenes. J. Org. Chem. 1983. *48* (9). 1536–1539.
18. Hampton. P.D.; Bencze, Z.: Tong, W.D.: Daitch. C.E. A new synthesis of oxacalix[3]arene macrocycles and alkali-metal-binding studies. J. Org. Chem. 1994. *59* (17), 4838–4843.
19. Miah, M.; Romanov. N.N.: Cragg, P.J. Acid-catalyzed formation of hexahomooxacalix[3]arenes. J. Org. Chem. 2002. *67* (9). 3124–3126.
20. Masci. B.; Finelli. M.; Varrone, M. Fine tuning of the

cavity size in calixarene-like cyclophanes: A complete series of homooxacalix[4]arene ligands for quaternary ammonium ions. Chern. Eur. J. 1998. 4 (10), 2018–2030.
21. Hanowfield. J.M.; Ogden. M.I.: White, A.H. Actinide complexes of the calixarenes. Part 1. Syntheses and crystal structure of bis(homo-oxa)-*p-tert*-butylcalix[4]arene and its uranyl ion complex. J. Chem. Soc., Dalton Trans. 1991. (4). 979–985.
22. Cragg, P.J.: Allen, M.C.: Steed, J.W. A 'toothpaste tube' model for ion transport through trans-membrane channels. Chern. Commun. 1999. (6). 553–554.
23. Araki. K.: Inada. K.: Shinkai. S. Chiral recognition of α-amino acid derivatives with a homooxacalix[3]arene: Construction of a pseudo-C_2-symmetrical compound from a C_3-symmetrical macrocycle. Angew. Chem.. Int. Ed. Engl. 1996. *35* (1), 72–74.
24. Zhong, Z.; Jkeda, A.: Shinkai. S. Triple linkage of two homooxacalix[3]arenes creates capsular molecules and self-threaded rotoxanes. J. Am. Chem. Soc. 1999, 121 (50). 11906–11907.
25. Atwood. J.L.: Barbour. L.J.; Nichols, P.J.: Raston. C.L.: Sandoval, C.A. Symmetry-aligned supramolecular encapsulation of C_{60}: [C_{60}⊂(L)$_2$], L=*p*-benzylcalix[5]arene or *p*-benzylhexahomooxacalix[3]arene. Chem. Eur. J. 1999.5 (3), 990–996.
26. Gutsche, C.D.: Dhawan. B.; No. K.H.: Murthukrishnan, R.J. Calixarenes 4. The synthesis, characterization and properties of the calixarenes from para-tert-butylphend. J. Am. Chem. Soc. 1981. 103 (13). 3782–3792.
27. Asfari, Z.; Vicens. J. Isolation and characterization of bishomooxacalix[4]arene from the condensation product of 4-octadecylphenol with formaldehyde. Makromol. Chem., Rapid Commun. 2989. 10 (4), 177–179.
28. Perrin. M.; Bavoux. C.: Lecocq. S. Change of conformation induced by complexation in *p-tert*-butyldihomooxacalix[4]arene. Supramol. Chem. 1996, *8* (1). 23–29.
29. Marcos. P.M.; Ascenso. J.R.; Segurado, M.A.P.; Pereira, J.L.C. Synthesis. NMR conformational analysis. complexation and transport studies of an inherently chiral dihomooxacalix[4]arene ester. Tetrahedron 2001. *57* (32), 6977–6984.
30. Masci, B.; Gabrielli. M.; Mortera. S.L.: Nierlich. M.; Thuéry, P. Hydrogen bonded supramolecular assemblies from uranyl ion complexes of tetrahomodioxacalix[4]arenes with various counterions. Polyhedron 2002, 21 (11). 1125–1131.
31. No, K.; Lee. J.H.: Yang, S.H.: Yu, S.H.: Cho. M.H.; Kim, M.J.: Kim, J.S. Syntheses and conformations of tetrahomodioxacalix[4]arene tetraamides and tetrathioamides. J. Org. Chem. 2002. 67 (9). 3165–3168.
32. Takemura. H.; Yoshimura, K.: Khan. I.U.: Shinmyozu. T.: Inazu. T. The first synthesis and properties of hexahomotriazacalix[3]arene. Tetrahedron Lett. 1992, 33 (39), 5775–5778.
33. Chirakul. P.: Hampton, P.D.; Bencze, Z. A convergent synthesis of hexahomotriazacalix[3]arene macrocycles. J. Org. Chem. 2000. *65* (24). 8297–8300.
34. Hampton. P.D.: Tong. W.: Wu, S.: Duesler, E.N. Synthesis, X-ray structure and alkali-metal binding properties of a new hexahomtriazacalix[3]arene. J. Chem. Soc., Perkin Trans. 2 1996. (6). 1127–1130.
35. Khan, I.U.; Takemura. H.; Suenaga, M.; Shinmyozu, T.; Inazu. T. Azacalixarenes: New macrocycles with dimethyleneaza-bridged calix[4]arene systems. J. Org. Chem. 1993. *58* (11), 3158–3161.
36. Takemura, H.; Kozima, Y.: Inazu. T. Synthesis of azacalix[4]arene betaine. Tetrahedron Lett. 1999, *40* (35). 6431–6434.

Hydrogen Bonding

Gautam R. Desiraju
University of Hyderabad, Hyderabad, Andhra Pradesh, India

INTRODUCTION

The hydrogen bond, which in its simplest form may be abbreviated as X–H···A (*X*, donor; A, acceptor) is an intermolecular interaction of fundamental importance.[1] It is of great significance in molecular association. because it is common. strong enough, and sufficiently directional. No other interaction has ail three of these attributes, and supramolecular assemblies constructed with hydrogen bonds are structurally robust and orientationally specific. An additional feature of hydrogen bonding is that it is also weak enough to be dissociated in solution. In effect, the hydrogen bond with its intermediate energy (0.540 kcal/mol) can be formed easily. and it can also be broken easily. It is, therefore, of importance in supramolecular processes in solution, where kinetics and reversibiiity are critical issues. The hydrogen bond is a complex interaction and also a composite interaction.[2] It is complex, because it involves at least three atorns. one of which is the all-important bridging H-atom. It is composite in character, because it may be dissected into four main components — electrostatic. covalency. dispersion–repulsion. and polarization — that have widely differing attributes and consequences. Hydrogen bonding has been studied for about a century, and the literature on the subject is vast. The phenomenon constantly lends itself to new research and reinterpretation.[3] In this article, the subject of hydrogen bonding is sketched with respect to supramolecular chemistry. and with an emphasis on how present-day ideas in structural chemistry have evolved. The treatment given here is necessarily abbreviated and subjective.

WHAT IS A HYDROGEN BOND?

Surprisingly, this is stiil debated. A geometrical definition is easier than a chemical one. The hydrogen bond X–H $\cdot\cdot A$ is constituted with a donor X–H and an acceptor A. Readers will note that this convention is exactly the opposite as that used in the rest of the chemical literature, wherein donors are electron-rich species, and acceptors are electron deficient. The hydrogen bond may be described in terms of the d, D, θ, and r as shown in Fig. 1. and certain limits and ranges are well accepted for these geometrical parameters. With the ever-increasing quality of modern diffraction data, H-atoms can be identified accurately, and the distance d and the angle θ are most commonly used. If the hydrogen bond is extended on the acceptor side as X–$H\cdot\cdot A$–Y, an acceptor angle ϕ, $H\cdot\cdot A$–Y may also be defined. Often, a donor group will present itself to two or more distinct acceptors (say, A_1 and A_2), or an acceptor will likewise interact with several donors (X_1–H and X_2–H). These multifurcated interactions are common, especially if both strong and weak donors and acceptors are considered. Multi-atom acceptors like double and triple bonds and aromatic rings were also identified and are of general significance.

A hydrogen bond, X–$H\cdot\cdot A$, is an interaction wherein a hydrogen atom is attracted to two atoms. X and A. rather than just one, and so acts like a bridge between them. What is the nature of this attraction? Chemists are in agreement that all hydrogen bonds are electrostatic interactions. and that the attraction always increases with the increasing electronegativity of X and A. Disagreements arise as to the extent of electrostatic character required to term an interaction X–$H\cdot\cdot A$ as a hydrogen bond. By "eiectrostatic" is meant an interaction with an r^{-1} to r^{-3} energy–distance dependence, so that dipole–dipole interactions are included, and a distinction is drawn between electrostatic and van der Waals interactions, which are interactions between dipoles or induced dipoles with an r^{-6} dependence. During the first 50 years of this phenomenon. the term '-hydrogen bond" was restricted to interactions like N–H···O, O–H···O, and F–H···F, in which the donors and acceptors are activated.[4] Today, the concept of the hydrogen bond extends to weaker interactions like C–H···O and O–H···π, which have hardly any covalent character and are only marginally electrostatic."[5] The domain of the hydrogen-bond phenomenon expanded even more with the inclusion of interactions like C–H···π, which is more of the dispersion–repulsion type (van der Waals) with oniy residual electrostatic character.[6] This conceptualization and extension was largely the handiwork of suprarnolecular chemists who found it convenient to define a hydrogen bond as an interaction capable of maintaining a certain regular suprarnolecular organization.[7] The operational definition of a hydrogen bond for a supramolecular chemist is then functional; rather than geometrical.

Encyclopedia of Supramolecular Chemistry
DOI: 10.1081/E-ESMC 120012654

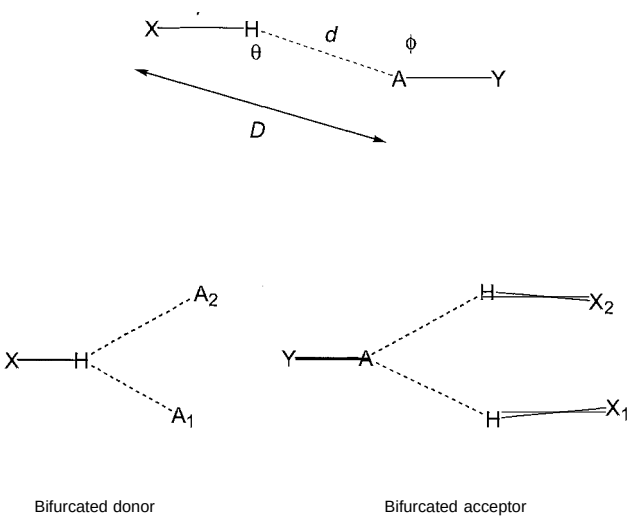

Fig. I (Top) Definition of the terms D, d, r, θ, and ϕ in a hydrogen bond X–H· ·A–Y. (Bottom) Bifurcated donor (left) and bifurcated acceptor (right) arrangements. The hydrogen bond in each case consists of all the atoms X, H. A,, and A_2, or Y. A. H. X_1, H, and X_2.

energetic, or spectroscopic. although all of these definitions have large common intersections. The functional criterion of a hydrogen bond still has its basis in electrostatics—the more long-range an interaction, the more specific will be its orienting effect during crystallization and self-assembly. So, it was proposed that any interaction X–H· ·A with an r^{-4} or shallower energy–distance dependence should be termed a hydrogen bond.[5] According to such a definition, all O–H· ·π interactions are hydrogen bonds, as is the C–H· ·π interaction in acetylene. but the C–H· ·π interaction in benzene is not. However, any criterion to define a hydrogen bond will be, in the end, simplistic, because hydrogen bonding is a complex phenomenon and does not lend itself easily to a simple and accurate definition. Considering the chemical connotations of the word bond, it was suggested that the term "hydrogen bridge" may be more suitable for the phenomenon than "hydrogen bond."[2]

TYPES OF HYDROGEN BONDS

Hydrogen bonds may be classified as very strong, strong. and weak based on their ability to determine and control supramolecular structure.[1,5] Listed in Table 1 are pertinent geometrical, energetic, thermodynamic. and functional attributes. The table provides a rough guide and is not intended to divide hydrogen bonds into watertight compartments. The reader will easily recognize the differences among the three categories. To assign a hydrogen bond in the borderline regions, chemical considerations are more advisable than numerical criteria and cutoff definitions.

Very strong hydrogen bonds occur in an energy range of 1540 kcal/mol and are formed by unusually activated donors and acceptors. Frequently, they are formed between an acid and its conjugate base, X–H· ·X^-, or

Table 1 Some properties of very strong, strong, and weak hydrogen bonds. *X–H· ·A*

	Very strong	Strong	Weak
Bond energy (−kcal/mol)	15–40	4–15	<4
Examples	$[F\cdots H\cdot\cdot F]^-$	O–H· ·O=C	C–H· ·O
	$[N\cdot\cdot H\cdot\cdot N]^+$	N–H· ·O=C	O–H· ·π
	P–OH· ·O=P	O–H· ·O–H	Os–H· ·O
IR ν_s relative shift	>25%	5–25%	<5%
Bond lengths	H–A ≈ X–H	H· ·A>X–H	H· ·A≫X–H
Lengthening of X–H	0.05–0.2 A	0.01–0.05 A	≤0.01 A
X· ·A (D) range	2.2–2.5 Å	2.5–3.2 Å	3.0–4.0 Å
H· ·A (d) range	1.2–1.5 Å	1.5–2.2 Å	2.0–3.0 Å
Bonds shorter van der Waals cutoff	100%	Almost 100%	30–80%
Angle (θ) range	175–180°	130–180°	90–180"
kT (room temperature)	>25	7–25	<7
Effect on crystal packing	Dominant	Distinctive	Variable
Utility in crystal engineering	Unknown	Useful	Partly useful
Relevance in biological structures	Unknown	Important	Ubiquitous
Covalency	Pronounced	Weak	Vanishing
Electrostatics	Significant	Dominant	Moderate

Source: Adapted From Ref. [5]

between a base and its conjugate acid, X^+–H···X. They are often intramolecular and assisted by resonance. A distinctive characteristic of very strong hydrogen bonds is their substantial covalent character so that the X–H and H···A distances are comparable. Very strong hydrogen bonds are of great importance in the context of chemical reactivity and biological mechanisms.

Strong hydrogen bonds (4–15 kcal/mol) are largely electrostatic. They are certainly the most familiar (ice. DNA, proteins) and well studied of hydrogen bonds. To many structural chemists and biologists, the properties associated with this category exemplify hydrogen bonding as a whole.[8] Molecules that contain functional groups capable of forming strong hydrogen bonds always do so, unless there are adverse steric factors. Their ability to control and modulate supramolecular structure means that they are reliable agents of intermolecular architecture. The strong hydrogen bond is the master-key of molecular recognition, and full control of this interaction will lead to mastery of supramolecular chemistry in general.

Weak hydrogen bonds (<4 kcal/mol), although numerous, were not identified in a general sense until recently.[5] These bonds are electrostatic, but this characteristic is modified by variable dispersive and covalency (charge-transfer) components that depend substantially on the nature of the donor and the acceptor group. The strongest of these, say bonds such as O–H···Ph and C≡C–H···O, are electrostatic and comparable to a bond like O–H···O–H. They lie in the energy range of 2–4 kcal/mol. The weakest of these are formed by unactivated methyl groups and are barely stronger than van der Waals interactions (about 0.5 kcal/mol). Bonds formed by weak donors with strong acceptors have been studied the longest. This set includes C–H···O/N and more recently M–H···O, where *M*=Tr.[9] The second set is constituted with strong donors like O–H and N–H and weak acceptors like C≡C, Ph, and M. Bonds formed with weak donors and weak acceptors (C–H···π, S–H···π. C–H···M, C–H···F–C) are at the end of the hydrogen-bonding regime.

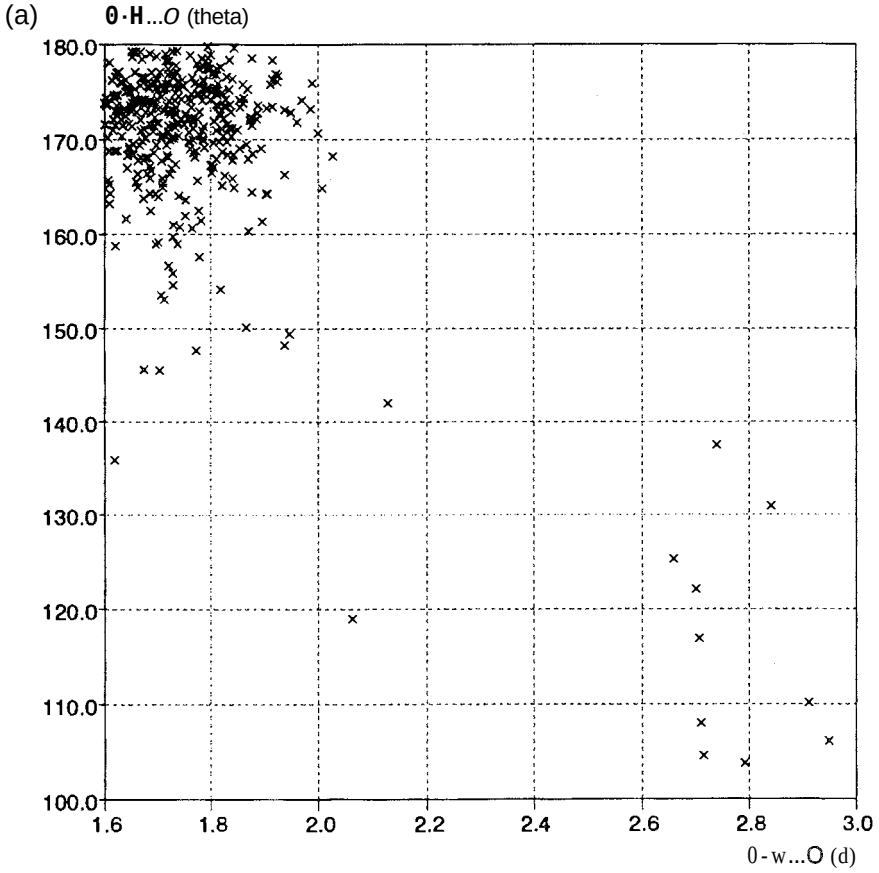

Fig. *2* Difference between strong and weak hydrogen bonds. θ–d scatterplots for (a) O–H···O and (b) C–H···O hydrogen bonds in representative crystal structures (CSD data). The weak hydrogen bonds span a much wider range of angles and distances than the tightly grouped sample of the strong hydrogen bonds. Note. however, the roughly inverse θ–d correlation that is characteristic of all hydrogen bonds for the C–H···O data. (From Ref. [5].)

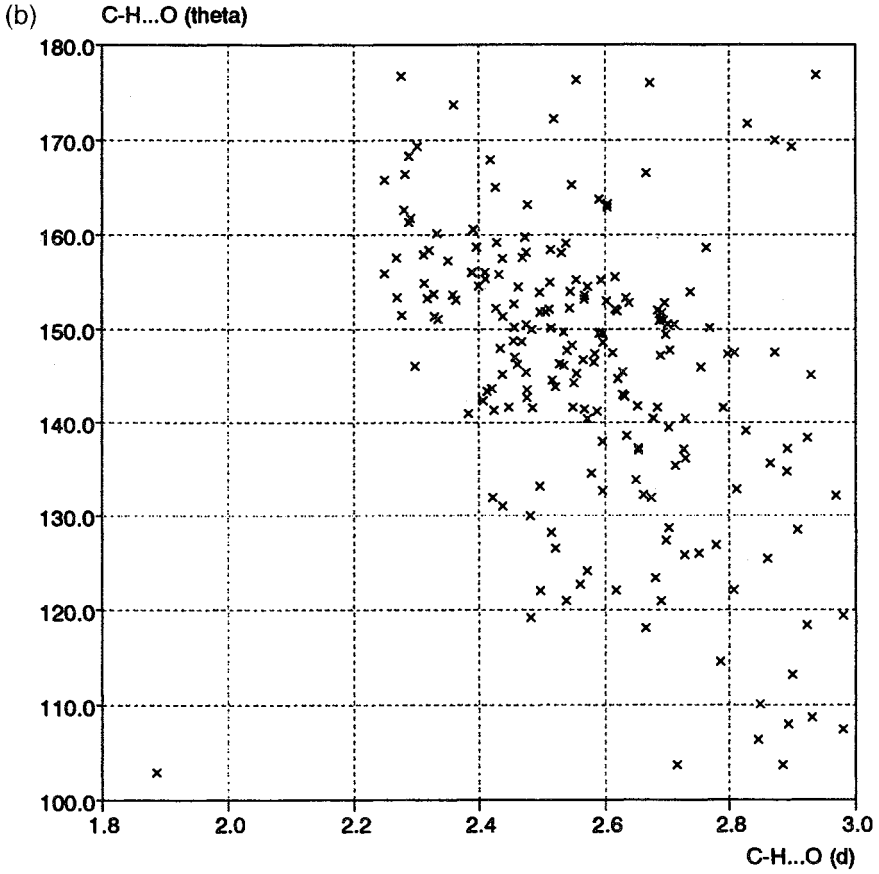

Fig. 2 (*Continued*).

DETECTION OF HYDROGEN BONDS

A number of methods and techniques are available. and the most appropriate needs to be chosen for the system in hand. Diffraction methods are especially important, because they are easy, fast, and accurate, and they may be applied to the weakest of hydrogen bonds. Advances in crystallographic hardware and software and automated methods of crystal growth of biological crystals means that we may reasonably expect a very large number of accurate crystal structure determinations in the near future. The number of organic and organornetallic crystal structures has grown to around 300,000 during the last 75 or so years. It is expected that this number will touch nearly 500,000 in less than a decade from now. A great majority of these structures will contain some type of hydrogen bond. Neutron diffraction is closely associated with the field of hydrogen bonding, because only with this technique is the crystallographer able to accurately establish the position of the most crucial atom in the interaction. namely, hydrogen.

An important consequence of the ever-growing number of small-molecule crystal structure determinations has been the development of methods for the storage and retrieval of crystallographic data. This has. in turn, led to the widespread use of crystallographic databases, and this was a development of great significance in the study of hydrogen bonding.[10] The Cambridge Structural Database (CSD) and the Protein Data Bank (PDB) are especially relevant. As a representative example, the reader's attention is directed to Fig. 2, which presents d–8 scatterplots for strong (O–H· . ·O) and weak (C–H· · ·O) hydrogen bonds obtained from around 500 and 150 accurately determined and representative crystal structures. The geometrical parameters of the strong O–H· . ·O bonds cluster within a narrow d–θ region, but this is certainly not the case for the weak C–H· . ·O bonds. However, as shown in Fig. 2, despite their scatter, these interactions have the inverse length–angle correlation that is characteristic of an electrostatic interaction like hydrogen bonding. So, the C–H . ·O interaction is a hydrogen bond. but it is "soft." Crystallographic databases also permit the analysis of more extended supramolecular patterns and networks in crystals. This was realized early in the development of databases, and this is of much utility in subjects such as crystal engineering[11] and structural genomics.[12]

Vibrational spectroscopy is the classical method for the study of hydrogen bonding in condensed phases."] Its applicability ranges from the strongest to the weakest hydrogen-bond types, and in both solution and in the solid state. The probe here is the vibrational frequencies of the atomic groups involved in hydrogen bonding, and because these frequencies can be measured accurately, subtle effects can be detected. Correlations of structural and vibrational parameters were established for various strong hydrogen-bond types. Despite the many benefits, the spectroscopic method is not free from drawbacks. Even for relatively simple systems, spectral complexity can prevent proper interpretation; this is the case: in particular, for systems exhibiting vibrational coupling. Furthermore, it is not always easy to distinguish between intra- and intermolecular effects based on vibrational spectra. Recent improvements in instrument technology and. parallel growth of interest in weak hydrogen bonds led to a renaissance of IR techniques in the hydrogen-bonding field, in particular: for solid samples.

Quantum chemistry complements crystallography and spectroscopy in the study of weak intermolecular interaction~.''~Theoretical methods can provide benchmark values for the energies of intermolecular interactions without the complicating effects of the solid-state or solution environment. Crystallography and spectroscopy provide information on equilibrium geometries, as many experimental techniques do. Computational methods, on the other hand, can be used to study domains of the potential energy surface, which are far from the equilibrium structure. Because of the widespread availability of powerful and yet low-cost computers, theoretical methods are now accessible to a large number of structural chemists, including experimentalists. Theory coupled with database research emerged as an effective way to study weak intermolecular interactions. Theory enables one to compartmentalize the various contributions to hydrogen-bond energy and also to dissect and study the important phenomenon of cooperativity. Of more recent interest is the computational treatment of small molecular clusters, or supramolecular synthons, and to examine their roles in crystal growth and stabilization. In the biological area, molecular dynamics (MD) may be useful, because it enables study of the dynamics of the breaking and making of weak hydrogen bonds. In this way, not only the energetics but also the lifetimes of weak hydrogen bonds may be studied.

THE HYDROGEN **BOND** IN SUPRAMOLECULAR CHEMISTRY

Strength and directionality render the hydrogen bond of critical importance in establishing and maintaining supramolecular structure. Hydrogen bonds are simpler to detect and their manifestations easier to demonstrate in the solid state than in solution. Most definitive studies are, therefore, based on crystal structure determinations. Robertson was the first to enunciate the principle of maximum hydrogen bonding.[14] In his words:

> *all the available hydrogen atoms attached to* electronegative *groups. are generally employed* in *hydrogen bond formation. Some of the bonds* formed *may be weaker than others. but the molecular packing is generally capable of adjustment in such a way as to permit the fulfillment of this condition.*

This principle appears to be of universal application. Donohue, in suggesting to Crick and Watson that the DNA bases are hydrogen bonded and in pointing out the appropriate tautomeric structures, paved the way for the double helix structure, and incidentally provided a blueprint for multipoint recognition in biological molecules." Powell described the structures of the clathrate compounds of β-hydroquinone (Fig. 3a) and introduced the network depiction for hydrogen-bonded arrays.[15] Many years later. Herbstein[16] described the crystal structure of benzene-1,3,5-tricarboxylic acid (trimesic acid) in terms of a 2D network (Fig. 3b). The main impetus to visualization of a crystal structure as a network came later from the important paper of Ermer[17] on the crystal structure of adamantane-1,3,5,7-tetracarboxylic acid (Fig. 3c). In this paper, a 3D hydrogen-bonded network was described, and a specific discussion of network interpenetration, which is multiple catenation, was included. Although interpenetration was not new (it occurs in the β-quinol clathrates of Powell and in trimesic acid), Ermer's vivid description of this structure was one of the key events that led to the establishment of crystal engineering as a distinct subject.

It was always well recognized that hydrogen bonding plays an important role in crystal engineering. the design and synthesis of solid-state supramolecular structures.''"] Schmidt and Eeiserowitz realized early the need to develop guidelines by examining the packing systematics of organic molecules, and they carried out a survey of amide crystal structures.[18] Leiserowitz subsequently provided a detailed analysis of the crystal packing of carboxylic acids.[19] Desiraju showed that weak hydrogen bonds could be brought into the scope of crystal engineering.[7] A comparison of the strong hydrogen bonds in the Whitesides rosette structure of melamine-cyanuric

"Surprisingly. the special supplement of *Nature* commemorating the 50th anniversary of the DNA structure, 23rd January. 2003 (reprinted from vol. 421. no. 6921) makes no mention of Donohue.

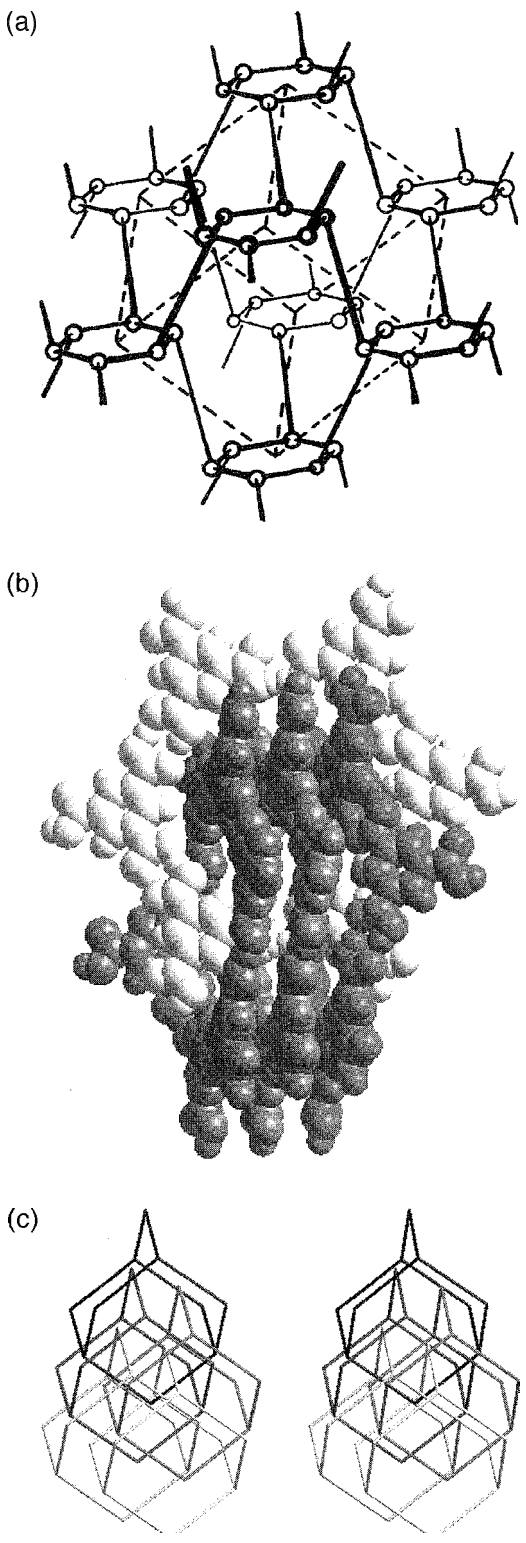

Fig. *3* (a) Network structure in the β-quinol structure (after Powell). The solid lines represent hydrogen bonds. (b) Interpenetrated two-dimensional networks in trimesic acid. (c) Interpenetrated three-dimensional networks in adamantane-1,3,5,7-tetracarboxylic acid. (*View this* ***art in*** *color at www.dekker.com.*)

acid[20] and the weak hydrogen bonds in the molecular complex of 2,5-dibenzylideneacetone and *sym*-trinitrobenzene[''] is illustrative (Fig. 4). Etter reformulated the principles set forth by Roberston and Donohue with an added stipulation that the best hydrogen-bond donors and acceptors form intermolecular hydrogen bonds with each other.[22] A number of rules for specific classes of functional groups were also provided. In retrospect, much of this is more by way of guidelines rather than rules. Exceptions are common, and today's exceptions become tomorrow's rules as the number and variety of crystal structure determinations increase. As the subject of crystal engineering has grown in breadth and scope, a very large number of crystal structures that were designed using the principles of hydrogen bonding have been reported. As stated previously, hydrogen bonding is the interaction of choice in crystal design strategies, and the reader is directed to the general and specialist literature on this topic. It would be impossible to provide even partial coverage here.

Hydrogen bonding is also extremely important in the construction of supramolecular aggregates in solution. Because issues of kinetics and reversibility need to be considered. it is important that the assembling interactions be as strong and as numerous as possible.[23] Typically, O–H···O, O–H···N, N–H···O, and N–H···N interactions are employed, and many systems, derived from the melamine–cyanuric acid recognition; were investigated. This system, which is based on three-point hydrogen-bonded recognition (Fig. 4), is archetypical. The need for multiple binding sites follows from the fact that the individual interactions are not robust enough to maintain supramolecular organization in solution. Reinhoudt described the formation of large aggregates that display suprarnolecular chirality.[''] Stoddart used hydrogen bonding in supramolecular-assisted molecular synthesis, in which the noncovalent interaction has a templating

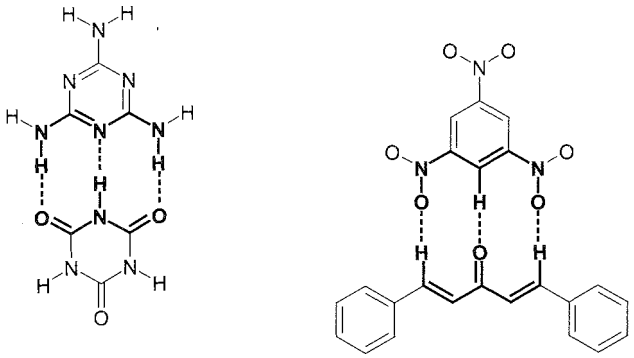

Fig. 4 Three-point recognition motifs consisting of strong and weak and hydrogen bonds.

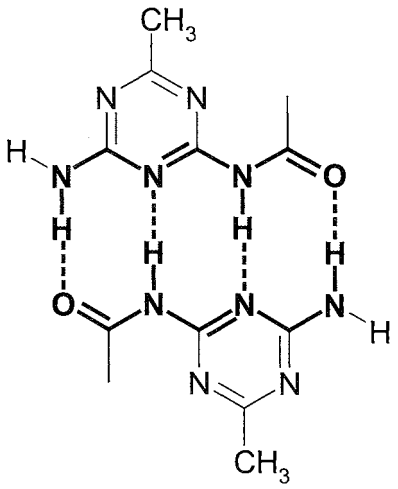

Fig. 5 Four-point recognition in a supramolecular polymer (after Meijer).

function and brings together molecular components for a covalent bond-forming process.[25] Meijer used four-point recognition in the synthesis of supramolecular polymers (Fig. 5). Hydrogen bonding is strong enough to maintain the polymer structure and weak enough to confer flexibility. thereby bringing a new element of variety to polymer chemistry.[26] By attaching hydrophobic residues to hydrogen-bonding functionalities, Fenniri et al. showed how entropic assistance from hydrophobic groups may favor the formation of supramolecular hydrogen-bonded aggregates.[27] Supramolecular reactions in solution are subject to thermodynamic control, and while this may confer benefits in subsequent dynamic applications, it is clear that molecules need to be designed with a clear perception of their supramolecular characteristics, the chief among which is their propensity for hydrogen bonding.

CONCLUSION

The great versatility of hydrogen bonding in supramolecular design and construction will ensure that this interaction will be used in many interesting and diverse chemical systems. An anonymous referee report on the paper by Taylor and Kennard[10] was included by the authors as the conclusion of their paper. It is worthwhile to ponder, with pleasure and anticipation, 20 years down the line, the statement made: ''*there have been some heroic attempts and a few minor advances but rationalization of crystal structure—hydrogen bonding patterns is still at the foot of the rainbow.*''

ACKNOWLEDGMENTS

Continuing financial support from the Department of Science and Technology and the Council of Scientific and Industrial Research. Government of India. toward my research programs is gratefully acknowledged.

ARTICLES OF FURTHER INTEREST

The Cambridge Structural Database. p. 161
Cation–π interactions: p. 214
Concepts in Crystal Engineering, p. 319
Crystal Engineering with Hydrogen Bonds. p. 357
DNA Nanotechnology, p. 475
Halogen Bonding, p. 628
Hydrogen Bonds to Metals and Metal Hydrides, p. 666
Neutron Diffraction, p. 959
π–π Stacking: Theory and Scope, p. 1076
π–π Stacking as a Crystal Engineering Tool, p. 1093
Self-Assenzbling Capsules, p. 1231
Self-Assembly in Biochemistry, p. 1257
Strong Hydrogen Borzds, p. 1379
Weak Hydrogen Borzds, p. 1576
X-Ray Crystallography, p. 1586

REFERENCES

1. Jeffrey, *G.A. An Introduction to Hydrogen Bonding*; Oxford University Press: New York, 1997.
2. Desiraju, *G.R.* Hydrogen bridges in crystal engineering: Interactions without borders. Acc. Chem. Res. 2002, *35.* 565–573.
3. Steiner. T. The hydrogen bond in the solid state. Angew. Chem. Int. Ed. 2002. 41. 48–76.
4. Pauling, L. *The Nature of the Chemical Bond;* Cornell University Press: Ithaca, NU, 1939.
5. Desiraju. G.R.; Steiner. T. *The Weak Hydrogen Bond in Structural Chernistn and Biology;* Oxford University Press: Oxford, 1999.
6. Nishio. M.; Hirota, M.; Umezawa, Y. *Tlie CH/π Interaction. Evidence, Nature and Consequences*; Wiley-VCH: New Uork, 1998.
7. Desiraju, G.R. The C–H···O hydrogen bond: Structural implications and supramolecular design. Acc. Chem. Res. 1996. 29. 565–573.
8. Jeffrey. G.A.; Saenger, W. *Hydrogen Bonding in Biological Structures:* Springer-Verlag: Berlin. 1991.
9. Brammer. L. Hydrogen Bonds in Inorganic Chemistry: Applications to Crystal Design. In *Crystal Design. Structure and Function*; Desiraju. G.R., Ed.; Wiley: Chichester. *2003;* 1–75.
10. Taylor, *R.:* Kennard. O. Hydrogen-bond geometry in organic crystals. Acc. Chem. Res. 1984, *17*, 320–326.

11. Desiraju, G.R. Crystal Engineering. The Design *of* Organic Solids; Elsevier: Amsterdam, 1989.
12. *Structural Genomics*; Bertini, I.. Ed.: Special Issue of Acc. Chem. Res., American Chemical Society (ACS), 2003; Vol. 36 (3), 157–221.
13. Scheiner, S. Hydrogen Bonding. A *Theoretical* Perspective; Oxford University Press: Oxford. 1997.
14. Robertson, J.M. Organic *Crystals* and Molecules; Comell University Press: Ithaca, NY. 1953: 239.
15. Powell, H.M. The structure of molecular compounds. Part IV. Clathrate compounds. J. Chem. Soc. **1948,** 61–73.
16. Herbstein. F.H. Topics in Current *Chemistry*; Weber, E., Ed.; Springer-Verlag: Berlin, 1987; Vol. 140, 107–140.
17. Ermer, O. Five-fold diamond structure of adamantane-1,3,5,7-tetracarboxylic acid. J. Am. Chem. Soc. **1988,** *110*, 3747–3754.
18. Leiserowitz. *L.;* Schmidt, C.M.J. Molecular packing modes. Part III. Primary amides. J. Chem. Soc., A **1969.** 2372–2382.
19. Leiserowitz, L. Molecular packing modes. Carboxylic acids. Acta Crystallogr. **1976**, *B32*, 775–802.
20. Zerkowski, J.A.: Seto. C.T.; Wierda, D.A.; Whitesides, G.M. The design of organic structures in the solid state: Hydrogen-bonded molecular "tapes." J. Am. Chem. Soc. **1990**. *112*. 9025–9026.
21. Desiraju, G.R. Designer crystals: Intermolecular interactions. network structures and supramolecular synthons. Chem. Commun. **1997.** 1475–1482.
22. Etter, M.C. Hydrogen bonds as design elements in organic chemistry. J. Phys. Chem. **1991.** *95*, 4601–4610.
23. Whitesides, G.M.; Simanek. E.E.: Mathias. J.P.; Seto, C.T.; Chin, D.N.; Mammen, M.; Gordon. D.M. Noncovalent synthesis: Using physical–organic chemistry to make aggregates. Acc. Chem. Res. **1995.** *28*. 37–44.
24. Reinhoudt. D.N.; Crego-Calama, M. Synthesis beyond the molecule. Science **2002,** *295*, 2403–2406.
25. Fyfe. M.C.T.: Stoddart, J.F. Synthetic supramolecular chemistry. Acc. Chem. Res. **1997,** *30*. 393–401.
26. Sijbesma, R.P.; Meijer. E.W. Quadruple hydrogen bonded systems. Chem. Commun. **2003.** 5–17.
27. Fenniri, H.; Deng, B.-L.; Ribbe, A.E.; Hallenga, K.; Jacob. J.; Thiyagarajan, P. Entropically driven self-assembly of multichannel rosette nanotubes. Proc. Natl. Acad. Sci. **2002.** *99*. 6487–6492.

Hydrogen Bonds to Metals and Metal Hydrides

Robert H. Crabtree
Yale University, New Haven, Connecticut, U.S.A.

INTRODUCTION

Classical hydrogen bonds[1] of general type A–H...B (**1**) have a weak acid A–H as hydrogen bond donor and lone pairs of electronegative atoms like F, O, and N as the hydrogen bond acceptor or weak base component, B (see "Hydrogen Bonding"). Since 1990. two new classes of hydrogen bonds have emerged, 2 and 3, that both retain the usual A–H donor component but differ in the nature of the acceptor. In the first class,[2] an electron pair in a nonbonding orbital on transition metal atoin of a metal complex plays the role of B (2). In the second,[3,4] the proton acceptor is the σ bonding electron pair of an M–H bond (3). The first type differs from classical hydrogen bonding only in that the nonbonding electron pair of B is located on an unusual element. In the second case. no nonbonding electron pair is involved, so in that sense. the situation is fundamentally different from that in classical hydrogen bonds.

A—H- - - -B

1

A—H- - - -M

2

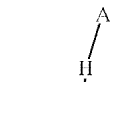

3

From another point of view, the situation in 2 or **3** is not so different from the classical case, **1.** If we regard a hydrogen bond as an interrupted proton transfer, any base capable of being protonated by a strong acid should form a hydrogen bond with a suitable weak acid. Metals in neutral complexes can often be protonated with strong acids to give cationic hydrides. Also, M–H bonds in neutral complexes $[L_nMH]$ can protonate to give dihydrogen complexes, $[L_nM(H_2)]^+$, where the molecular hydrogen ligand is bound side-on. In this view, hydrogen bonding between M or M–H and weak acids A–H is an incomplete proton transfer just as is the case for **1.** Any proton transfer implies the existence of such an intermediate form. even if only as a transient. Other basic element hydride bonds such as B–H can also give Type 3 hydrogen bonds. so a transition metal is not required, just an element E that is sufficiently electropositive to give a hydridic E–H group.

Other H-bridged metal complexes that seem at first sight to be hydrogen bonded are, in fact. very different. Complexes and compounds with 2-coordinate H bridging between two metals are coinmon in inorganic chemistry, but the great majority are not hydrogen bonded. Typical examples are $[(OC)_5Cr–H–Cr(CO)_5]^-$ and $H_2B(H)_2$-BH_2. Unlike the near-linear situation in the A–H...B fragment of a hydrogen bond, in these bridging hydrides, the E–H–E bonds are strongly bent (E = element). They are classified as σ-complexes[5] and can be considered as consisting of an H^- ion simultaneously donating two valence electrons to each of two sixteen-valence electron metal fragments by bridging to form three center two-electron bonds. In a σ-complex, the bridging H often shows a high-field NMR shift on bridging in contrast with the low-field shift normally seen for **1–3**.

A–H...M HYDROGEN BONDING

This area developed from the x-ray and neutron diffraction work of Brammer,[2,6,7] who first drew attention to the N–H...Pt interactions in a complicated square planar Pt(II) amine structure in 1991. In this work, also cited were prior structures proposed as examples of the same type of interaction. Starting from a square planar Pt(II) complex, an N–H bond is typically located in the otherwise vacant fifth coordination position of a square pyramid (4) with d(H...Pt) near 2.25 Å. The H...O distance in a classical hydrogen bond is often around 1.8 Å, or 0.4 Å longer than the van der Waals radii of O. If

Encyclopedia of Supramolecular Chemistry
DOI: 10.1081/E-ESMC 120012758

the van der Waals radius of a metal like Pt is ca. 2 Å, 2.4 A would be reasonable for an H...Pt hydrogen bonding distance.

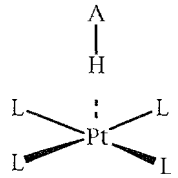

4

In a more straightforward example. Brammer[6,7] recognized that an ammonium counterion of type R_3NH^+ could form N–H...M hydrogen bonds with $[Co(CO)_4]^-$ anions (5). Having 18 valence electrons, $[Co(CO)_4]^-$ ion is unable to form three center two-electron bonds, which would require <18 e. Taken together with the linearity of the NHCo system, the hydrogen bonded character of the system was clearly demonstrated. As expected, a more basic metal, achieved by replacing one CO by PPh_3[7] gave a stronger interaction, N...Co decreasing from 3.437 to 3.294 Å. In this case. the tetrahedral $[Co(CO)_4]^-$ ion was minimally distorted by the interaction, the N–H approaching along a C_3 axis of the tetrahedron. The N–H bond is slightly elongated, and the NH stretching frequency in the IR spectrum is shifted to a low-energy shift on adduct formation, as is also the case for classical N–H...B hydrogen bonds.

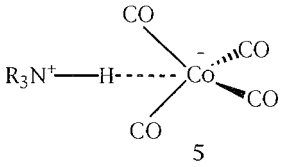

5

Like the classical A–H...B interaction, a predominantly electrostatic origin was proposed. In line with this idea, the presence of the following features[2] was suggested for identification of an A–H...M hydrogen bond: 1) protonic AH; 2) basic M; 3) a downfield proton NMR shift on bridging (the opposite situation from σ-complexes); and 4) linear A–H...M. The metal could be electronically saturated (e.g., $[Co(CO)_4]^-$) or not [e.g., square planar Pt(II)].

Whenever proton transfer takes place in an A–H...M system, an $A^-...H–M^+$ hydrogen bonded group must be considered as a stable form or transient intermediate. Because A^- is a base, this is equivalent to a classical A–H...B hydrogen bond with an acidic M–H replacing the usual A–H. Spectroscopic evidence shows that cationic metal hydrides interact in this way with bases such as O = PPh_3.[8] Such a situation is probably best considered a classical hydrogen bond of Type **1.**

A-H...H–M HYDROGEN BONDING

In spite of its relatively recent development. hundreds of A–H...H–M hydrogen-bonded species of Type **3** are now known. These are said to contain a dihydrogen bond, often shortened to DHB to avoid confusion with the IUPAC term. dihydrogen (H_2). DHBs have proven to be attractive to the computational chemistry community because they prominently involve hydrogen atoms. The field has implications for inorganic and organic chemistry, and perhaps also biochemistry, because some enzymes involve metal hydrides. In addition, a variety of physical and spectroscopic techniques were successfully applied to the problem. Reviews of the field are available.[3,4]

The first suggestion of an A–H/H–M attractive interaction was in a 1990 proposal that invoked them to explain the close contact (H...H, 2.4 Å) between the IrOH proton and the Ir–H hydrogen found in the neutron diffraction structure of *cis*-$[Ir(OH)H(PMe_3)_4]$.[9] The H...H distance is long and about equal to the sum of the van der Waals radii for two H atoins (2 × 1.2 Å), and so the interaction may be relatively weak and better considered a dipole–dipole interaction. A short d(H...H) of 1.86 Å was found by neutron diffraction[10] in mer-$[Fe(H)_2(H_2)(PEt_2Ph)_3]$, a study originally carried out to test the author's earlier spectroscopic assignment[11] of this species as an H_2 complex. The orientation of the H_2 ligand that brings it close to a terminal FeH hydride was explained by Eisenstein on theoretical grounds[10] as involving a proton–hydride attraction termed the "*cis*-effect." Now, it can be considered as a dihydrogen bond, because of the very short H...H distance (1.86 Å). Here the role of A–H is taken by a proton of a molecular hydrogen complex, known to act as a weak acid in most cases.

Structures that are more representative of typical DHBs (e.g., 6–7) came from the author's and Morris' groups in the form of an extensive series of metal hydrides in which a DHB is formed with OH or NH protons (= A–H) as the weak acid partners, both intramolecularly and intermolecularly. The characteristics of the DHB proved to be a short H...H distance (ca. 1.8 Å versus the sum of the van der Waals radii of 2.4 Å) found from x-ray and neutron diffraction work in the solid state and by NMR relaxation time studies in solution. Theoretical and experimental studies led to a typical A–H...H–M interaction strength of ca. 4–8 kcal/mol.

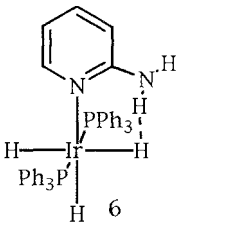

6

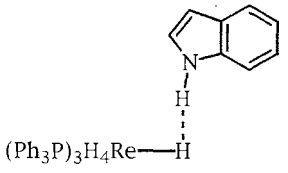

7

Unlike classical hydrogen bonds,[1] A–H...B, where A and B are electronegative atoms or groups, in A–H...H–M, M and H are much less electronegative than the N, O, or F atoms common in the classical type. Morris[4] used an alternative descriptive term: proton–hydride interaction.

Rather than the linear arrangement of the classical hydrogen bond, dihydrogen bonds show a different conformational preference, such that the N–H or O–H bond approaches the M–H bond in a side-on direction (8 but as also seen in 6–7), although linear examples were also found in cases where conformational or steric effects disfavor a bent geometry. Eisenstein found in DFT calculations that the potential energy surface is flat, so distortions from the ideal geometry are not very costly.[12] The A–H...H is roughly linear, however, A–H points to the M–H bond rather than directly toward M or H.

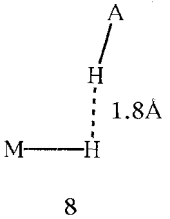

8

The A–H group shows the same spectroscopic trends compared to the free A–H group in all of the hydrogen bonds 1–3: a reduced ν(A–H) stretching frequency in the IR spectrum and a deshielding of the AH proton leading to a low-field shift of the resonance. The effect of hydrogen bonding of Type 2 on the spectroscopic properties of the metal fragment is still insufficiently understood. although H...M coupling was seen in certain cases. Two proton NMR effects were recognized for **3:** an H...H coupling of 2–9 Hz is sometimes seen, together with a significant increase in the T_1 relaxion rate of the two hydrogens as a result of their close proximity.[3,4]

INTRAMOLECULAR INTERACTIONS

Complex 6, an intramolecular case of DHB. was chosen to get some idea of the energetics of the interaction. By a VT NMR method, one can estimate the H...H bond energy from the C–NH_2 rotation barrier in 6. In the transition state for **6**→**6′**, (Eq. 1), the H...H bond is broken. and the resonance energy of the NH_2 group with the pyridine ring is lost. The intrinsic C–N rotation barrier in the absence of dihydrogen bonding can be estimated at ca. 6 kcal/mol using a combination of experimental data and Hartree–Fock calculations by Eisenstein and Clot. By measuring the barrier for **6**/**6′** and subtracting 6 kcal/mol, we arrive at an apparently reasonable estimate of the H...H bond energy: 5.0 kcal/mol for **6**.[13]

When one hydride in 6 is replaced by any of a variety of anions, Y, to give 9, the strength of the DHB varies strongly. When Y is a weak *trans* effect ligand like F, the DHB is very weak, but it becomes strongest when Y is a high *trans* effect ligand. Because H ligands *trans* to high *trans* effect ligands tend to be particularly hydridic,[14] this implies that a basic hydride is best for dihydrogen bonding, in accord with the electrostatic bonding model mentioned above. The high *trans* effect nitrosyl ligand causes particularly strong dihydrogen bonding to H *trans* to NO.[15]

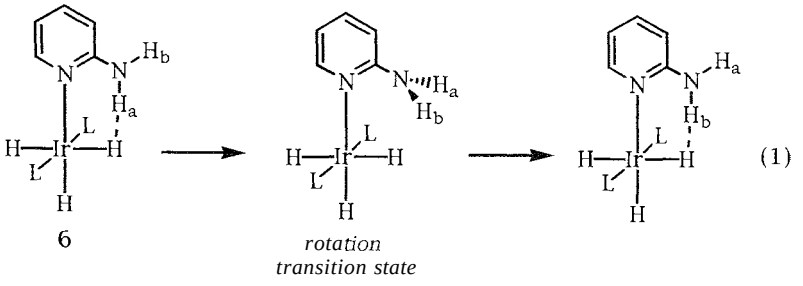

6 *rotation transition state* (1)

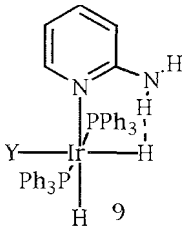

9

When Y = F^-, often considered the best hydrogen bond acceptor. a classical NH...F hydrogen bond is formed in 8. Using the NMR method of Eq. 1, the bond strength was found to be just a little more (5.2 kcallmol) than that for the N–M...H–Ir bond in the Y = H^- analogue (5.0 kcallmol). This illustrates the unexpectedly high DHB interaction strength, at least for Y = H.

This finding was paradoxical. because hydrogen bonding energies'" decrease on moving from the classical lone pair H-bond, N–H...(lone pair) (4–8 kcallmol). to the N–H...(π bond) case, in which the proton acceptor is usually an arene π system. ($\leq$ 2 kcallmol). so one might expect that any N–H...(σ bond) type, where the acceptor is an σ bond, would have a negligible bond energy (<1 kcal/mol). In contrast, N–H...H–E interaction energies can be up to 4–8 kcallmol, which are almost as large as for the N–H...(lone pair) case. This requires E to be an electropositive element such as boron or a transition metal, so that the hydride has significant hydridic character. and even then we usually need to have a high *trans* effect ligand *trans* to the H in question. It is still not clear why the dihydrogen bonding energies in species such as 6 are so large. The H...H distance of 1.8 Å is essentially the same as the H...B distance in the classical hydrogen bond. so an unusually close approach of donor and acceptor atoms is not the critical factor. Possibly, the ready polarization of the soft L_nM–H system by the AH dipole may be a factor.

THE MATURE OF A–H...H–E HYDROGEN BONDING

In the first A–H...H–M hydrogen bonds.'" AH was NH or OH. and M was a d^6 metal (as in 6–7). This raised a possible ambiguity; because a d^6 metal's d_π nonbonding electrons could; in principle. interact with the A–PI proton. considering this orbital points between the ligands and therefore directly toward an NH_2 proton as seen in diagram 10. A typical H...M distance in such a case was found to be 2.8 A. Admittedly, the AH proton is always close to the MH hydride, but this may have nothing to do with a proton–hydride interaction. Instead, the AH might interact with the d, electrons adjacent to the M–H bond simply because PI is the sterically smallest ligand present that allows the NH to approach the metal d_π orbital closely. In that case. the A–H...H–E system becomes just another example of the A–H...M hydrogen bond of Type 2, and the H...H interaction would be repulsive.

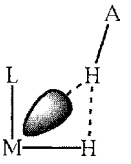

10

Because neither B nor N have nonbonding electrons, the case of BH_3NH_3 was useful to resolve this A–H...M/H...H ambiguity. BH_3NH_3, a solid, has a m.pt. of + 104°C or almost 300 degrees higher than that of its isoelectronic analogue ethane (m.pt., –183°C). This elevation might have been due to polar effects, but the polar molecule CH_3F, having a dipole moment about 0.4 of that for BH_3NH_3, has a m.pt. of –140°C, suggesting that polar effects alone should lead to a m.pt. for BH_3NH_3 of about –100°C. The 200" additional m.pt. elevation seemed likely to be associated with hydrogen bonding.

Cambridge Structural Database (CSD) data on intermolecular N–H...H–B hydrogen bonds[116] showed that the structures were essentially identical in the transition metal and boron examples. Therefore, the nature of the interaction was taken to be similar. If that is true, the d, nonbonding electrons play no more than a supporting role. The range of H...H distances is similar in both cases [1.7–2.2 Å versus 2.4 Å.[16] the sum of the van der Waals (vdW) radii for two hydrogens]. In BH_3NH_3, only true dihydrogen bonding was possible, resolving the ambiguity mentioned above. Therefore, dihydrogen bonding is real.

According to the reported x-ray crystallographic coordinates, BH_3NH_3 had an entirely different configuration from that shown in **3.**

The B–H...H–N configuration found was the reverse of the one in 3: B–H...HN appeared to be almost linear, and N–H...HB appeared strongly bent. A subsequent neutron diffraction structure of BH_3NH_3, carried out to resolve this problem. showed that the B and N were previously misassigned; the true assignments produced a normal BHHN configuration as expected.

A DFT caiculation on $[BH_3NH_3]_2$[116] shows a BH...HN conformation similar to that in **3** and an H...H bond energy of 4.6 kcal/mol per bond, comparable to the transition metal analogues. The calculation also suggested

that the BPI bonds polarize on forming the H...H interaction. which may help explain the relatively high interaction energy, and that the boron is more negatively charged than the hydride. The entire B–H bond should probably be considered as being the true proton acceptor. The $^1J(H^-...H^+)$ coupling in the range 2–7 Hz is seen in the ^1H NMR spectrum of cornpounds such as **5–6**, so the H...H bonding is not entirely electrostatic. Small $^1J(H,B)$ couplings were recently seen for classical A–FI...B hydrogen bonds.[17]

In other theoretical work,[18] Calhorda et al.[19] found a large number of complexes in the CSD database with short MH...H(O,N) distances. Their DFT study on $[(H_3P)_4IrH(OH)]PF_6$ showed that the counterion needed to be included to obtain agreement with experimental results.

INTERMOLECULAR INTERACTIONS

The metric parameters and interaction energies in **6** and **9** might be artefacts if the NH bond is held too rigidly. Intermolecular systems were used to resolve this problem. In such cases. an acid AH cocrystallizes with a metal hydride (L_nMH). Normally, however, AH and L_nMH crystallize separately. To favor cocrystallization, one needs an acid such as indole, which as a liquid cannot crystallize, and a base, $ReH_5(PPh_3)_3$, which forms poor quality powders on attempted crystallization (see Crystal Engineering with Hydrogen Bonds). An x-ray structure of the 1:1 cocrystal **(7)** gave a short (<2 Å) H...H distance. High-quality crystals allowed a high-quality neutron diffraction structure to be obtained.[18] The same conformation (4) was seen as previously, so the constraints of chelation were not dominant. The H...H distance of 1.73 Å for (7), the smallest reliably determined, is much smaller than the sum of the van der Waals radii for two hydrogens (2.4 Å).

Approximate energetics for adducts of $ReH_5(PPh_3)_3$ with indole (3.6 kcallmol) and with a hindered phenol, ArOH (5.6–5.8 kcallmol), were estimated[18] by IR spectroscopy with a modified Iogansen[20] equation, relating the Δν(NH) or Δν(OH) to the interaction energy.

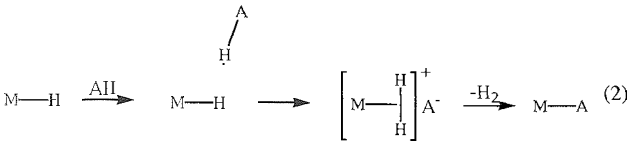

(2)

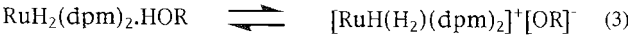

(3)

Full equilibrium studies[18] by UV/Vis give a ΔG of 5 kcallmol for $ReH_5(PPh_3)_2(C_5H_5N)$ and indole. Adducts[14] between acidic alcohols such as $(CF_3)_2CHOH$ and the hydridic hydride, $[WH(CO)_2(NO)(PMe_3)_2]$ give association energies of ca. 5.5 kcallmol by the Iogansen method: full equilibrium studies gave an interaction energy of 4.9 kcallmol.

REACTIVITY

Protonation of metal hydrides may often go via the pathway of Eq. 2. which also shows the side-on binding of the H_2 ligand resulting from proton transfer.

In one case,[22] an equilbrium was seen between $RuH_2(dpm)_2$ (dpm = $Ph_2PCH_2PPh_2$), and a dihydrogen complex formed as a result of proton transfer from an alcohol such as $(CF_3)_2CHOH$ (Eq. 3). Other related cases are known.[21–23]

OTHER CONSEQUENCES OF H...H BOND FORMATION

Many metal hydrides protonate to give H_2 complexes,[24] but kinetic protonation can take place on M–H to give an M–(H_2) complex, even when protonation is thermodynamically favored at the metal. Protonation of CpFeH(dppe) gave the dihydrogen complex at −80°, followed by rearrangement to the dihydride at 25°.[25] Kinetic protonation by A–H at M–H is consistent with the presence of a dihydrogen bonded A–H...H–M precursor adduct as intermediate. Proton transfer in the adduct gives the H_2 complex, and conversion to the *trans* dihydride is slower, because motion[26] of the heavy atoms is needed.

Gatling and Jackson[27] showed how dihydrogen bonding to an –OH group of a hydroxyketone can direct the attack of borohydride to one face of the molecule; indeed, the product is 99.7% *trans* (Eq. 4). The effect was suppressed by addition of F^-, an additive that interrupts the hydrogen bonding. Under the conditions used, formation of an intermediate borate ester could be excluded.

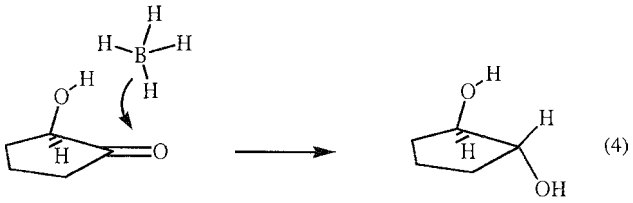

(4)

The role of dihydrogen bonding in stabilizing the transition states for solid state reactions involving loss of H_2, such as in the thermal decomposition of triethanolamine/$LiBH_4$ or of BH_3NH_3 was emphasized recently in experimental[29] and theoretical[29] work.

CONCLUSION

A combination of computational and experimental approaches gives an understanding of the proton–hydride interaction in the DHB.[30] This new type of hydrogen bond influences the physical properties and reactivities of a number of main group and transition metal compounds and seems to be important in cases of protonation of hydrides by acids AH.

ARTICLES OF FURTHER INTEREST

Crystal Engineering with Hydrogen Bonds, p. *357*
Hydrogen Bonding, p. 658

REFERENCES

Jeffrey. G.A.; Saenger, W. *Hydrogen Bonding in* Biological Structures; Springer: Berlin, 1994.

Brammer. L.: Zhao. D.: Ladipo, F.T.: Braddock--Wilking, J. Hydrogen-bonds involving transition-metal centers—A brief review. Acta Crystallogr., B 1995. *51*, 632–640.

Crabtree. R.H.: Siegbahn. P.E.M.: Eisenstein, O.; Rheingold. A.L. A new intermolecular interaction: Unconventional hydrogen bonds with element-hydride bonds as proton acceptor. Acc. Chem. Res. 1996. 29. 348.

Morris, R.H. 1995 Alcan award lecture—New intermediates in the homolytic and heterolytic splitting of dihydrogen. Can. J Chem. 1996. 74, 1907.

5. Crabtree. R.H. Sigma complexes. Angew. Chem. **1993**, *32*, 789.
6. Brammer. L.; McCann. M.C.; Bullock. R.M.: McMullan, R.K.: Sherwood, P. $Et_3NH^+Co(CO)_4^-$ hydrogen-bonded adduct or simple ion-pair—Single-crystal neutron-diffraction study at 15 K. Organometallics 1992. 11. 2339.

Brammer, L.: Zhao, D.; Ladipo, F.T.: Braddock-Wilking, J. Hydrogen-bonds involving transition-metal centers—A brief review. Acta Crystallogr.. B **1995**, 51. 632–640.

Epstein. L.M.: Shubina, E.S.: Krylov, A.N.; Kreindlin. A.Z.; Rybinskaya, M.I. Interaction between $[(\eta^5\text{-}C_5Me_5)_2OsH]^+PF_6^-$ and nitrogen or oxygen bases—Hydrogen-bonds of the type $[OsH]^+ \ldots B$. J. Organometal. Chem. 1993,447. 277.

9. Stevens, R.; Bau, R.; Milstein. D.: Blum, O.: Koetzle, T.F. Concept of the proton–hydride interaction—A low-temperature neutron-diffraction study of *cis*-$[IrH(OH)(PMe_3)_4]PF_6$. J.C.S. Dalton **1990**. 1429.
10. Van der Sluys, L.S.: Eckert. J.: Eisenstein. O.; Hall. J.H.: Huffinan, J.C.; Jackson, S.A.: Koetzle, T.F.; Kubas, G.J.: Vergamini, P.J.; Caulton. K.G. An attractive cis-effect of hydride on neighbor ligands—Experimental and theoretical studies on the structure and intramolecular rearrangements of $Fe(H)_2(\eta\text{-}^2\text{-}H_2)(PEtPh_2)_3$. J. Am. Chem. Soc. 1990. 112. 4831.
11. Crabtree. R.H.: Hamilton. D.G. Classical (M = Os) and nonclassical (M = Fe, Ru) polyhydride structures for the complexes $MH_4(PR_3)_3$. J. Am. Chem. Soc. 1986. 108, 3124.
12. Sini, G.; Eisenstein. O.: Yao, W.: Crabtree. R.H. Intermolecular Re–H...H–X hydrogen bonding (X = N, C) involving $ReH_5(PPh_3)_3$. Inorg. Chim. Acta 1998. 280, 26.
13. Peris, E.: Lee. J.C.. Jr.; Rambo, J.R.: Eisenstein. O.; Crabtree. R.H. Factors affecting the strength of X–H–...–H–M hydrogen- bonds. J. Am. Chem. Soc. 1995.117, 3485.
14. Shubina, E.S.; Belkova, N.V.; Krylov, A.N.; Vorontsov, E.V.; Epstein, L.M.: Gusev. D.G.: Niederniann. M.; Berke. H. Spectroscopic evidence for intermolecular M–H...H–OR hydrogen bonding: Interaction of $WH(CO)_2(NO)L_2$ hydrides with acidic alcohols. J. Am. Chem. Soc. 1996, 118. 1105.
15. Belkova. N.V.: Shubina, E.S.; Ionidis, A.V. Intermolecular hydrogen bonding of $ReH_2(CO)(NO)L_2$ hydrides with perfluoro-tert-butyl alcohol. Inorg. Chem. **1997**, 36 (7). 1522–1525.
16. Klooster, W.T.: Koetzle. T.F.: Siegbahn. P.E.M.: Richardson, T.B.; Crabtree, R.H. Study of the N–H...H–B dihydrogen bond including the crystal structure of BH_3NH_3 by neutron diffraction. J. Am. Chem. Soc. 1999. 121. 6337.
17. Benedict, H.: Shenderovich, I.G.: Malkina, O.L.: Malkin, V.G.; Denisov. G.S.; Golubev. N.S.; Limbach. H.H. Nuclear scalar spin–spin couplings and geometries of hydrogen bonds. J. Am. Cheni. Soc. 2000. 122. 1979.
18. Maseras. F.; Lledós. A.; Clot, E.: Eisenstein. O. Transition metal polyhydrides: From qualitative ideas to reliable computational studies. Chem. Rev. 2000, 100. 601.
19. Braga. D.: Grepioni. F.; Tedesco, E.: Calhorda. M.J.: Lopes. P.E.M. The effect of the counter ion on M–H(H–X (X = O,N) interactions in crystalline transition metal hydrides. New J. Chern. 1999. 23. 219.
20. Iogansen, A.V.; Kurchi, G.A.: Furman. V.M.; Glazunov, V.P.: Odinokov. S.E. Zh. Prikl. Spectrosk. **1980**. 33. 460.
21. Desmurs. P.: Kavallieratos. K.: Yao. W.; Crabtree, R.H. Intermolecular Re–H...H–N and Re–H...base hydrogen

bonding estimated in solution by a UV-VIS spectroscopic method. New J. Chem. **1999.** *23.* 1111.

22. Ayllon, J.A.: Gervaux. C.; Sabo-Etienne, S.; Chaudret, B. First NMR observation of the intermolecular dynamic proton transfer equilibrium between a hydride and coordinated dihydrogen. Organometallics **1997**, *16.* 2000.
23. Toner, A.J.: Grundemann, S.; Clot, E.; Limbach, H.H.: Donnadieu, B.: Sabo-Etienne, S.; Chaudret. B. Ruthenium assisted reversible proton transfer from an aromatic carbon to a hydride. J. Am. Chem. Soc. **2000.** *122.* 6777.
24. Jessop, P.G.: Morris, R.H. Reactions of transition-metal dihydrogen complexes. Coord. Chem. Rev. **1992,** 121, 155.
25. Hamon, P.; Toupet. L.: Hamon. J.-R.; Lapinte, C. Protonation of an iron hydride. J. Organometal. Chem. **1992.** *428.* 49.
26. Crabtree, R.H.; Luo. X.-L.: Michos. D. Hydrogen bonding in metal complexes. Chemtracts Inorg. Chem. **1991.** *3.* 245.
27. Gatling, S.C.; Jackson. J.E. Reactivity control via dihydrogen bonding: Diastereoselection in borohydride reductions of a-hydroxyketones. J. Am. Chem. Soc. **1999,** *121,* 8655.
28. Custelcean. R.; Jackson. J.E. Topochemical dihydrogen to covalent bonding transformation in $LiBH_4$.TEA: A mechanistic study. J. Am. Chem. Soc. **2000**, *122.* 5251.
29. Kulkarni. S.A. Intramolecular dihydrogen bonding in main group elements. Connection with dehydrogenation reactions. J. Phys. Chem.. A **1999.** *103.* 9330.
30. Custelcean. R.: Jackson. J.E. Dihydrogen bonding: Structures, energetics. and dynamics. Chein. Rev. **2001**, *101.* 1963.

Hydrophobic Effects

Hans-Jörg Schneider
Universität des Saarlandes, Saarbrücken, Germany

INTRODUCTION

Hydrophobic interactions are considered to be essential in many systems, be it micelles, vesicles. colloids. membranes and transport; self-organization, polymer interactions, protein folding and ligand binding, nucleic acids, drug action. water-mediated organic reactions,[1–4] and in the last decades. also synthetic host–guest complexes. Hydrophobic effects belong to the most often cited intermolecular forces: chemical abstracts already cite 2735 reviews on the topic, and there is a large number of books[5–7] and reviews[3,4,8–14] on the topic. In this article. only a short introduction can be given, which is eased by the increasing evidence that hydrophobic binding, at least in the sense of entropic contributions, plays a small role in most synthetic host–guest complexes.

FUNDAMENTALS

Hydrophobic binding cannot be understood without understanding the special properties and structure of water. Liquid water can best be viewed as a fluctuating mixture of loose "open" iceberg structures, favored by Coulombic hydrogen bonds, and more dense ice-type structures. favored by dispersive interactions of the oxygen atoms. Solid-state structures of ice ("ice II") show each water molecule surrounded in a tetrahedral arrangement by four other molecules, each of which is linked with each other by hydrogen bonds. For liquid water. x-ray and neutron diffraction studies give radial distribution functions. with about 90% of all molecules having, on the average, the oxygen atoms in relatively close contact. and allowing for many hydrogen bonds. Water structure and energetics change dramatically with the state. Solvation of cations and anions leads to special structures around the charged species that were recently elucidated, also with neutron inelastic scattering methods.[15,16] Salts like sodium chloride have little effect on the water structure, whereas. e.g., guanidinium halide or urea slightly increase the excess self-association of water; the effect of a solvent like trifluorethanol depends on concentration—at low values, there is a strong increase in the self-association of water.[17]

The hydrophobic effect is thought to arise from the exceptionally high energy needed to form a cavity in a solvent, which in a very small space has more interactions between the solvent molecules than any others, and which is characterized by low expandability. Water has an exceptionally high internal cohesion energy density, resulting in a large vaporization enthalpy and a high surface tension. The classical Frank–Evans hypothesis[18] explains the hydrophobic effect mainly by the loss of freedom of water molecules involved in solvation of nonpolar solutes. In this description, solvation requires specific orientation of water molecules toward the solute surface as a "clathrate" (sometimes called "iceberg" structure). in order to maintain a large number of hydrogen bonds between the water molecules. The number of water inolecules suffering from entropic disadvantage is higher, if two cavities must be formed for the accommodation of two separate solute molecules *A* and *B*, than the number obtained by forming one larger cavity that accominodates both A and *B* (Fig. 1A).

The Frank–Evans model has come under debate recently, mainly as the transfer free energy of unpolar solutes to water can be quantitatively described by the so-called scaled particle theory (SPT) on the basis of molecular size, density, and pressure of water alone. without the need to introduce hydrogen-bond functions to account for special water structures.[19] The low solubility of hydrocarbons in water can be due to the small volume of water molecules: with the consequence that a large number of solvent molecules are involved in the creation of a cavity of sufficient volume.[4] Also, neutron diffraction shows no evidence of enhancement of water–water interactions in the presence of unpolar solutes over that in pure water,[20] which speaks like recent computational results[21–23] against the clathrate hypothesis of a particular structure-making effect by solute solvation. A recent description of the hydrophobic effect is based on the high activity coefficient of the aggregating solute in water. while that of the bulk water is close to one.[24] As an alternative to the Frank–Evans model, one can consider the formation of two cavities in water, which reduces translational motions of the solvent molecules, with a subsequent entropy disadvantage (again, the disadvantage is smaller for one larger cavity than for two smaller cavities). The solvation of the solute can then

DOI: 10.1081/E-ESMC 120012669

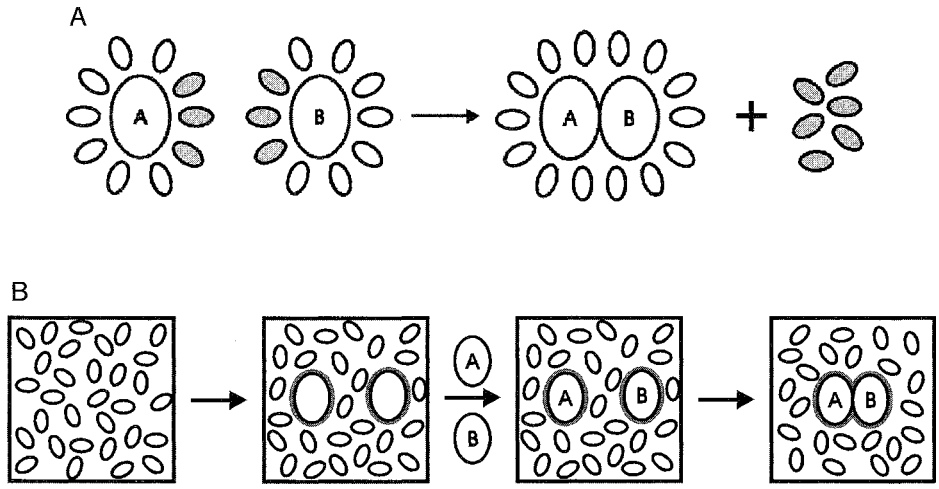

Fig. 1 (A) Liberation of solvent molecules by association of two solute molecules A and B. (B) Creation of cavities in solvent and association of two solute molecules A and B. (*View* this *art in color at www.dekker.com.*)

be accompanied by favorable enthalpic contributions (Fig. 1B). One often observes entropy–enthalpy compensation in hydrophobic binding. At higher temperatures, solute clustering becomes less entropy driven than enthalpy driven. The energy needed to form cavities in a cohesive solvent like water explains the low solubility of lipophilic solutes in water. and their preference for lipophilic media. In addition, a distinction was introduced between ''bulk'' and "pairwise" hydrophobic interactions.[4,25] Bulk interactions stand for the association of a large nuinber of nonpolar molecules, as occurs in micelle formation or protein folding. Each nonpolar molecule in such a process changes its aqueous surroundings to a completely (or nearly completely) nonaqueous environment, in the same way as with the transfer of nonpolar solutes from water to organic solvent.

A so-called nonclassical hydrophobic effect,[26] which can have an enthalpic origin. is based on the consideration of disruption of cohesive forces in the solvent by forming cavities. again with an advantage of one larger rather than two smaller cavities.'"' Another driving force due to the special tendency of water molecules to form many hydrogen bonds can result if the few water molecules inside a host cavity are unable to form as many hydrogen bonds as the outside bulk water. Such "unhappy" water molecules were experimentally located in crystal structures of cyclodextrins[28] and of peptides.[29] Replacement of such water molecules by a guest molecule will lead to a gain of additional hydrogen bonds of the expelled water and would show as enthalpic advantage.

With all models. hydrophobic interactions will increase with the size of those surface parts that are no longer exposed to water but are buried in a nonpolar environment. Quantification of the hydrophobic interaction free energy ΔG_{hp} is, therefore, usually based on calculations of this excluded surface ΔA by an equation with a factor γ describing the cohesive force by the surface tension of the solvent, or by the inicroscopic free energy related to the interfacial tension between a lipophilic solute and water:

$$\Delta G_{hp} = \text{const } \gamma \Delta A$$

For the hydrophobic contribution, measurements of solvent transfer give ΔG values of 80–140 J/(mol Å^2).[11] Studies with engineered proteins indicate similar numbers, but in some cases. values as high as 500 J/(mol Å^2) are given. Experimental data from associations of about 50 different aromatic compounds, which are noticeably independent of heteroatoms and charges within the π-systems, lead to a value of 430 J/(mol Å^2).[30] The size exclusion ΔA can be conveniently assessed by computer-aided evaluation of the surface difference for the host and guest molecules before and after association.

The most direct way to factorize interaction energies of unpolar solutes with water is based on thermodynamic measurements of the solute transfer from gas or from a hydrocarbon medium to water. Such measurements with the transfer of linear alkanes from hexane to water yield. as increments for a CH_2 group, $\Delta\Delta G = 3.85$, $\Delta\Delta H = 2.75$ kJ/mol. respectively; the enthalpic contribution dominates for the CH_2 group; in contrast to the CH_3 group, for which one observes AAC = 8.4, AAH = −5.4 and $T\Delta\Delta S = -13.8$ kJ/mol, respectively.[31] Another often-used way to evaluate hydrophobic contributions of solutes is based on measurements of distribution coefficients between water and a lipophilic solvent, for which one traditionally

used *n*-octanol.[32] The method is of prime importance in medicinal chemistry for determining the lipophilicity of potential drugs. and therefore. it was applied to thousands of compounds. Based on these partition constants (P), one can derive corresponding substituent values $\pi_X = \log(P_{R-X}/P_{R-H})$ that also allow the hydrophobicity of many compounds to be estimated.

CYCLODEXTRIN COMPLEXES

The best-studied examples for hydrophobic interactions in host–guest chemistry are cyclodextrin complexes, although it is often not clear to what degree they are really dominated by a solvophobic force. Obvious examples of solvophobic effects are found if the substrates have a high polarizibility and if the cavity allows a tight fit, in which case calorimetric data speak for a dispersive binding mechanism (see the entry on van der Waals interactions in this *Encyclopedia*). For cyclodextrin complexes with hydrocarbons, one observes a similarity of thermodynamic parameters to those of transfer of the same hydrocarbons from water to a hydrocarbon medium (Table 1). The a-cyclodextrin complexes are more exothermic, with unfavorable AS values, which speaks for van der Waals and not hydrophobic interactions in these tightly fitting systems. Generally. one observes large negative heat capacity changes ΔC_P that. however, were found to be strongly temperature dependent.[33] This is typical for the transfer heat capacity,[13,34] e.g., binding of *n*-heptane to β-cyclodextrin is endothermic at 273 K (AN = 6.3kJ/mol) but is exothermic at 323 K (AN= −8.8 kJ/mol).[35] This illustrates that arguments based on the relative values of AH and TAS are questionable. Also, AS can give either favorable or unfavorable contributions to AG, depending on the chosen standard state. because AC and AS, in contrast to AN, are concentration-dependent units (cf. Table I).

Complexes of aliphatic alcohols with α-cyclodextrin show a linear correlation between lg K and the number of carbon atoms, n_C in normal alcohols, yielding binding increments for the methylene group of AAG = −3.0 kJ/mol, $\Delta\Delta H = -3.83$ kJ/mol, and $T\Delta\Delta S = -0.83$ kJ/mol.[36] These numbers are close to the increments obtained from the transfer of methylene group from hexane to water, discussed above. In contrast, the complexation of a whole molecule, e.g., I-hexanol, is totally "enthalpy driven" in sharp contrast to the more entropy-driven transfer thermodynamics of *n*-hexane.[13] Similar thermodynamics were found for the complexation of alicyclic carboxylic acids, such as admantanecarboxylic acid, bicyclo[2.2.2]-octanecarboxylic acid, etc., and β-cyclodextrin,[37–39] with AG = −3.3 kJ/mol for neutral acids and −2.5 kJ/mol for their anions per methylene group. Again, complexation is enthalpy driven and is characterized by large negative ΔC_P values [−440 and −397 J/(mol K) for adamantanecarboxylate binding to a- and β-cyclodextrins, respectively]. There are many calorimetric data on cyclodextrin complexes in water,[36] and they are all enthalpy driven, in contrast to expectations on the grounds of the Frank–Evans principle.

There is, however. indication that complexation in cavities too wide for a tight fit. and with substrates of smaller polarizibility, is accompanied by some less-entropic

Table 1 Thermodynamic parameters for the complexation by cyclodextrins and transfer from water to hydrocarbon media of heptane cyclohexane, and benzene at 298 K

	ΔG			ΔS		
Solute	**M**	**m.f.**	**ΔH**	**M**	**m.f.**	**ΔC_P**
Complexation with a-cyclodextrin						
cyclo-Hexane	−15.1	−25.1	−19.2	−13.8	19.8	−303
n-Heptane	−21.6	−31.6	−21.3	1.0	34.6	−492
Benzene	−8.6	−18.6	−13.1	−15.1	18.5	−272
Complexation with β-cyclodextrin						
n-Heptane	−19.7	−29.7	−0.6	64	97.6	−305
cyclo-Hexane	−21.4	−31.4	−5.4	53.6	87.2	−316
Benzene-12.8	−22.8	−1.9	36.6	70.2	−498	142
Transfer from water to hydrocarbon						
n-Heptane		−28.6	−0.7		94	
cyclo-Hexane		−28.2	0.1		95	−360
Benzene		−19.4	−2.1		58	−225

Units: kJ/mol for AG and AN and J/(mol K) for AS and ΔC_P. Values of AG and AS are given for two standard states: 1 M solution (Column M) and unit mole fraction solution (Column m.f.).
(From Refs. [31, 33].)

disadvantage than those with tight fits and with substrates of higher polarizibilities, such as nitrophenolate, which is dominated by van der Waals interactions. With, e.g., nitrophenole or adamantane carboxplic acid and β-cyclodextrin, there is a favorable entropic contribution, which. however, is still small compared to the enthalpic driving force (e.g., AN=−21.6 kJ/mol. $T\Delta S$=+2.9 kJ/mol for adamantane carboxyiic acid).[37–39] With less-polarizable substrates, there is a noticeable preference for loose binding that would lead to smaller entropic restrictions. This is evident from NMR studies of complexes with substrates offering alternative smaller phenyl rings or larger naphthyl moieties for complexation. Although the cavity of β-cyclodextrin is geometrically well disposed to take up naphthalene rings, one observes its intracavity inclusion only with the wider γ-CD cavity.[40] A similar preference for loose binding in an aqueous medium is observed with cycloveratrylene complexes.[41]

CYCLOPHANE COMPLEXES

Calorimetric measurements with Cyclophane 1 (Scheme I) and several benzene derivatives show a rough correlation with the lipophilicity parameters lgP of the substrates, but always with dominating AH values against large $T\Delta S$ disadvantages (Table 2).[42] Noticeably, studies with similar complexes in many different solvents exhibit the same enthalpic origin of complexation, with no special entropic advantage in water or. e.g., in methanol. Complexes of lipophilic compounds with the Cyclophane 2 (Scheme 1) show like those with **1,** an affinity decrease with an increasing amount of organic solvents in aqueous solutions.[43] The observed lgK values are a linear function of the solvent polarity parameters, even more so of a solvent hydrophobicity parameter. The sensitivity against solvent change is as expected. larger for complexes with more hydrophobic cavities, such as cyclodextrins.[43] These changes seem to be characteristic of a hydrophobic binding mechanism but would also agree with dispersive interactions. because the higher polarizibility of organic solvent molecules would lead to a similar affinity change.

Table 2 Selected thermodynamic parameters (kJ/mol) for the complex formation between cyclophane **I** and 1,4-disubstituted benzene guests (1,4-X-C_6H_4-X) in water at 293 K

X	ΔG	AH	TΔS	A	logP[b]
COOMe	−28.5	−49.4	−20.9	−251	2.6
MeO	−22.5	−41.8	−19.3	−84	2.2
Me	−22.3	−30.1	−7.8	−84	3.15
CN	−21.9	−43.1	−21.2	−126	1.0
NO_2	−21.8	−41.0	−19.2	−167	1.5
OH	−15.4	−43.1	−27.7	−251	0.6

[a]J/(mol K).
[b]Logarithms of partition constants of guest molecules between octanol and uater.
(From Ref. [42].)

As mentioned above, a possible explanation of the always-dominating enthalpic force in the complexation with synthetic hosts may be the unusual water configuration in the corresponding cavities. Molecular modeling shows that, e.g., inside Cyclophane 2, only five water molecules can be accommodated. which on the average can only materialize two hydrogen bondr.

CONCLUSION

In summary, the evidence for classical hydrophobic effects in supramolecular complexes is often missing. Careful investigations with model compounds. where one can measure the balance of conformations. show that stacking interactions, e.g., with more hydrophilic heterocyclic aromatic moieties, are stronger than with more hydrophobic arenes.[44] This (as well as the small effects of alkyl in comparison to aryl ligands in associations with. for instance, porphyrins) evidence supports the finding

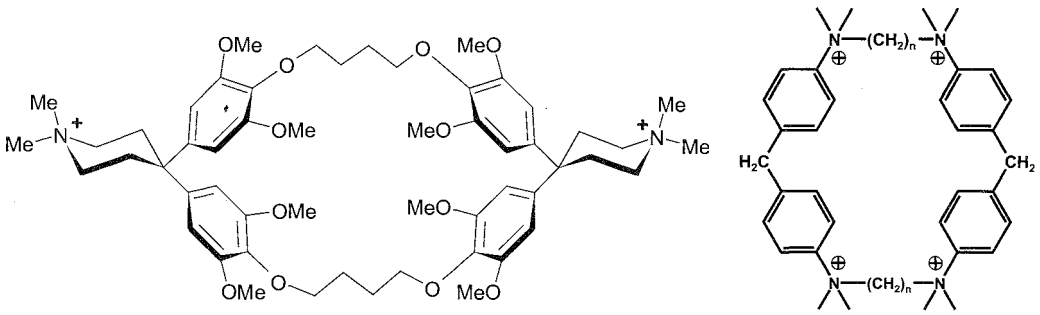

Scheme 1. Cyclophanes 1 and 2.

that many interactions believed to be solvophobic are, in fact, dispersive (see entry on van der Waals interactions in this *Encyclopedia).* The stability decrease of stacked aggregations in model compounds[45] or in nucleic acid components[46] upon addition of organic solvents does not necessarily imply that solvophobic forces dominate. as the high polarizibility of organic molecules leads at the same time to decreased van der Waals attractions between host and guest. It should be noted that other interactions in supramolecular complexes, like ion pairing in water, are entirely entropy driven but are not usually considered to be of hydrophobic nature.

ARTICLES OF FURTHER INTEREST

Artificial Enzymes, p. 76
Biological Ligands, p. 88
Biological Models, Clzaracteristics. p. 101
Calixarenes and Their Analogues: Molecular Complexation, p. 145
Carbohydrates, Recognition of, p. 169
Carbonic Anhydrase Models, p. 178
Carcerands and Hemicarcerands, p. 189
Cation–n Interactions, p. 214
Cavitands, p. 219
Chiral Guest Recognition, p. 236
Classical Descriptions of Inclusion Compounds, p. 253
Classification and Nomenclature of Supramolecular Compounds, p. 261
Clathrate Hydrates, p. 274
Conzplexation of Fullerenes, p. 302
Concepts in Crystal Engineering, p. 319
Crown Ethers, p. 326
Cryptands, p. 334
Cryptophanes, p. 340
Cyclodextrins, p. 398
Cyclophanes: Definition and Scope, p. 414
Cyclophanes: Endoacidic, Endobasic, and Endolipophilic Cavities, p. 424
Dendrimers, p. 432
Deoxycholic, Cholic, and Apocholic Acids, p. 441
Drug Design, p. 490
Enzyme Mimics, p. 546
Enzymes: Clzaracteristics and Mechanisms, p. 554
Halogen Bonding, p. 628
Hydrogen Bonding, p. 658
Inclusion Compounds: Selectivity, Thermal Stability, and Kinetics. p. 696
Micelles and Vesicles, p. 861
π–π Interactions: Theory and Scope, p. 1076
Podands, p. 1106
Porphyrin Derivatives, Functional. p. 1139
Protein Supramolecular Chemistry, p. 1161
Self-Assembly: Definition and Kinetic and Thermodynamic Considerations, p. 1248
Self-Assembly in Biochemistry, p. 1257
Soft and Smart Materials, p. 1302
Solvation Effects in Guest Binding, p. 1322
Stability Constants: Definition and Determination, p. 1360
Steroid-Based Anion Conzplexation Agents, p. 1365
Supramolecular Chemistry: Definition, p. 1401
Supramolecular Stabilization, p. 1453
Surfactants, Part I: Fundamentals, p. 1458
Surfactants, Part 11: Applications. p. 1470
van der Waals Forces. p. 1550
Weak Hydrogen Bonds, p. 1576

REFERENCES

1. *Organic Synthesis in Water;* Grieco, P.A., Ed.; Thomson Science: London. 1998.
2. Li, C.-J.; Chan. T.H. *Organic Reactions* in *Aqueous Media;* Wiley: New York, 1997.
3. Engberts. J.B.F.N.: Blandamer. M.J. Chem. Commun 2001, 18, 1701–1708.
4. Blokzijl, W.; Engberts, J.B.F.N. Angew. Chem.. Int. Ed. Engl. 1993, *32.* 1545.
5. Ben-Naim. A. *Hydrophobic Interactions:* Plenum Press: New York. 1980.
6. Tanford. C. *The Hydrophobic Effect,* 2nd Ed.; Wiley: New York. 1980.
7. *Water, A Comprehensive Treatise;* Franks, F.. Ed.: Plenum Press: New York, 1973–1982: Vol. 1–7.
8. Muller, N. Acc. Chem. Res. 1990, 23. 23–28.
9. Muller, N. Trends Biochem. Sci. 1994. *17.* 459.
10. Schellman, J.A. Biophys. J. 1997, 73. 2960–2965.
11. Makhatadze. G.I.; Privalov, P.L. Adv. Protein Chem. 1995, 47, 307–425, and references cited therein.
12. Schmid. R. Monatsh. Chem 2001. *132,* 1295–1326.
13. Privalov, P.L.: Gill, S.J. Adv. Protein Chem. 1988. 39, 191.
14. Lazaridis, T. Acc. Chem. Res. 2001. 34 (12). 931–937.
15. Enderby, J. Chem. Soc. Rev 1995. *95.* 159.
16. Neilson, G.W.; Enderby, J.E. Adv. Inorg. Chem. 1989, 34, 195.
17. Chitra, R.: Smith, P.E.J. Phys. Chem., B 2002, 106 (6), 1491–1500, and references cited therein.
18. Frank. H.S.: Evans; M.W. J. Chem. Phys. 1945, *13.* 507.
19. Kodaka, M. J. Phys. Chem., B 2001,105 (24), 5592–5594. and references cited therein.
20. Turner. J.; Soper, A.K.; Finney, J.L. Mol. Phys. 1992. 77. 441.
21. Silverstein. K.A.T.: Haymet, A.D.J.: Dill, K.A. J. Am. Chem. Soc. 2000. 122, 8037.
22. Bagno, A. J. Chem. Soc., Faraday Trans. 1998; 94. 2501.
23. Graziano. G. J. Chem. Soc., Faraday Trans. 1998. 94,3345.
24. Marmur. A. J. Am. Chem. Soc. 2000, 122, 2120–2121.

25. Wood. R.H.; Thompson, P.T. Proc. Natl. Acad. Sci. U. S. A. 1990. *87.* 946.
26. Jencks. W.P. *Catalysis* in *Chemistry* and *Enzymology*; McGraw Hill: New York. 1989.
27. Sinanoglu, O. Molecular *Associations* in Biology: Pullman, B., Ed.; Academic Press: New York, 1968: 427.
28. Steiner, T.; Mason, S.A.; Saenger, W. J. Am. Chem. Soc. 1990, *112.* 6184. and references cited therein.
29. Karle, I.R.; Balaram, P. Biochem. 1990, *29.* 6747.
30. Cohen, J.L.: Connors. K.A. J. Pharm. Sci. 1970, 59, 1271.
31. Abraham, M.H. J. Am. Chem. Soc. 1982. *104.* 2085.
32. Hansch, C.: Leo, A. *Substituent* Constants for *Correlation Analysis* in *Chemistry* and Biology; Wiley: New York. 1979.
33. Wishnia, A.; Lappi, S.J. J. Mol. Biol. 1974, *82,* 77.
34. Dill. *K.A.* Science 1990, *250,* 297–298.
35. Tucker, E.E.; Christian, S.D. J. Am. Chern. Soc. 1984, *106.* 1942.
36. Rekharsky. M.V.: Inoue, Y. Chem. Rev. 1998, *98,* 1875, and references cited therein.
37. Eftink. M.R.: Andy. M.L.: Bystrom, K.; Perlmutter, H.D.: Kristol. D.S. J. Am. Chem. Soc. 1989; *111,* 6765.
38. Harrison, J.C.: Eftink, M.R. Biopolymers 1982, *21,* 1153.
39. Riidiger. *V.;* Eliseev. A.; Svetlana. S.: Schneider, H.-J.: Blandamer, M.J.; Cullis, P.M.: Meyer. A. J. Chem. Soc., Perkin Trans. 2 1996. 2119–2123.
40. Schneider. H.-J.: Blatter, T.; Simova, S. J. Am. Chem. Soc. 1991. *113.* 1996.
41. Bartik, K.: Luhmer, M.; Dutasta, J.-P.: Collet. A.; Reisse. J. J. Am. Chem. Soc. 1998. 120, 784.
42. Smithrud, D.B.; Wyman, T.B.; Diederich. F. J. Am. Chem. Soc. 1991, *113,* 5420.
43. Schneider, H.-J.; Kramer. R.; Simova, S.; Schneider, U. J. Am. Chem. Soc. 1988. *110,* 6442.
44. McKay, S.L.: Haptonstall, B.; Gellman, S.H. J. Am. Chem. Soc. 2881, *123,* 1244–1245, and references cited therein.
45. Pang. Y.-P.: Miller, J.L.; Kollman, P.A. J. Am. Chem. Soc. 1999. *121,* 1717–1725.
46. Guckian, K.M.: Schweitzer, B.A.; Ren, R.X.F.; Sheils, C.J.: Tahmassebi, D.C.; Kool. E.T. J. Am. Chem. Soc. 2000, *122* (10), 2213–2222.

Hydroquinone

Thomas C. W. Mak
Chi-Keung Lam
The Chinese University of Hong Kong, Hong Kong SAR, People's Republic of China

INTRODUCTION

Hydroquinone, p-$C_6H_4(OH)_2$, also known as quinol in the older literature) exists in three polymorphic forms (or crystalline modifications). a-Hydroquinone is the stable form at room temperature, whereas the metastable monoclinic γ-form can be prepared by sublimation or rapid evaporation of a solution in ether. Crystallization of hydroquinone from a common solvent such as methanol generally yields a clathrate with guest solvent inolecules trapped inside cavities of the β-hydroquinone host lattice.''.''The existence of the β polymorph of hydroquinone (empty β-hydroquinone clathrate), which can be obtained by crystallization from n-octane, was reported in 1981.[3] Described in this article are the structural features of these compounds. and some recent developments are also covered.

CRYSTAL STRUCTURE OF β-HYDROQUINONE AND TOPOLOGICAL EQUIVALENCE

The salient symmetry aspects of the crystal structure of β-hydroquinone, or equivalently the β-hydroquinone host lattice, are best understood with reference to the structural archetype of polonium.[4] In its low-temperature α-form, polonium is the only element known to have a simple cubic crystal structure (a = 335.9 pm) in which each atom has six near neighbors. At ∼ 36°C, the α form transforms to a rhombohedral β modification (Fig. 1a. a_1 = 336.8 pm, α = 98.24"; also isostructural with ReO_3). Now consider an assembly of six hydroquinone molecules with their terminal OH groups H-bonded into an $[OH]_6$ ring in accordance with 3 symmetry. Replacement of each atom in the β-polonium structure by an $[OH]_6$ ring, such that each edge of the rhombohedral unit cell is matched by a p-phenylene moiety (i.e., the C_6H_4 aromatic ring plus its two para C – 0 bonds) linking a pair of $[OH]_6$ rings. gives rise to the idealized *single* P-hydroquinone host network shown in Fig. 1b. The topological equivalence of this open-meshed three-dimensional network with the host-water framework of hexamethylenetetramine hexahydrate, with an O—H· ·O hydrogen bond replacing each p-phenylene moiety. was noted several decades ago,[5,6] and Ermer described the structure of β-hydroquinone as superpoloniuin and its building blocks as supercubes (or, more precisely. superrhombohedra).[7,8]

The hypothetical single β-hydroquinone structure is inherently unstable, as it has a large unoccupied cavity at the center of the unit cell. In fact a second. translation-equivalent network (displaced by one-half of the vertical body diagonal of the supercube) can be introduced such that the spacious voids of each network are filled by [OH], rings of the other. This system of two mutually interpenetrating, but unconnected, networks constitutes the basis of the β-hydroquinone host lattice, which can accommodate small guest species such as Xe,[9] H_2S,[10,11] SO_2,[12] or MeOH[13] in cavities that are each sandwiched between a pair of $[OH]_6$ rings belonging to different networks (Fig. 2). Entrapment of a guest molecule in a β-hydroquinone clathrate is represented schematically in Fig. 1c, which shows a pair of interlocking supercubes with vertices and edges that represent the $[OH]_6$ rings and the p-phenylene groups, respectively.

β-HYDROQUINONE CLATHRATES

The classical studies of Powell and coworkers established that all three cystallographically distinguishable types of β-hydroquinone clathrates (designated I. II, and 111) have the same general formula 3 $C_6H_4(OH)_2$·x G, where G represents an encaged guest species, and x is a site occupancy factor that depends on the conditions of adduct formation (e.g., Xe, x = 0.866; H_2S, x = 0.874).[14–18] In Table 1, the first entry is empty β-hydroquinone, with unit-cell dimensions that are the smallest in the series.'']

Encyclopedia of Supramolecular Chemistry
DOI: 10.1081/E-ESMC 120012834

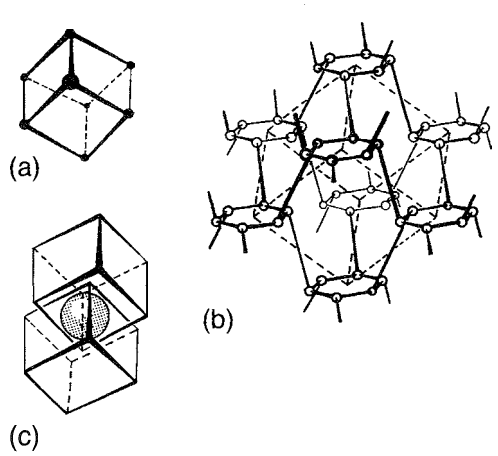

Fig. 1 (a) Perspective view of a rhombohedral unit cell of P-polonium with its principal symmetry axis drawn vertically. (b) Single β-hydroquinone network constructed from the linkage of $C_6H_4(OH)_2$ molecules by O—H···O hydrogen bonds. Each corner of the rhombohedra1 unit cell is occupied by a nearly planar $[OH]_6$ ring, and the *p*-phenylene groups are represented by slant lines. (c) Enclosure in the β-hydroquinone host lattice. The enclosed molecule is represented by a sphere imprisoned between two interlocking supercubes. Each vertex of a supercube represents an $[OH]_6$ ring and each edge a *p*-phenylene group. The crystal structure consists of an infinitely extended three-dimensional array of this cagework.

Structure of Type I Clathrates

In Type I clathrates. cavities with *3* site symmetry are present. In Fig. 2a, a stereoview of such a centrosyinmetric cage of the unsolvated form is shown. The top and bottom of the void are formed by nearly planar hexagons of H-bonded oxygen atoms; an ordered arrangement of hydrogen atoms is apparent in the $[OH]_6$ rings, and the host molecules point alternately above and below the mean plane of the oxygen atoms. The hexameric units forming the ceiling and floor of a given cage belong to two identical, but displaced, three-dimensional interlocking networks (Fig. 2b).

In the Type I xenon[9] and hydrogen sulfide[10,11] clathrates, the encaged guest species occupies an approximately spherical cavity of mean free diameter ~480 pm. The H_2S guest molecule undergoes pronounced thermal motion, particularly in the direction of the centers of the $[OH]_6$ rings. The results are consistent with rotational disorder of the guest molecule.

Recent *ah initio* calculations showed that when small guest molecules (either nonpolar Ne or polar HF) are accommodated in the β-hydroquinone cage structure, the unit cell parameters of the empty host lattice remain largely unaffected. Moreover, the magnitudes of the host–guest interaction energies were estimated as ~ −2 kcallmol with Ne and −7 to −9 kcallmol with HF as the guest species.[19]

Structure of Type II Clathrates

In Type II clathrates, the space group symmetry is lowered from *R 3* (in Type *I)* to R3, and guest accommodation is provided in cages that are still trigonal, although no longer centrosymmetric. For the linear guest molecule methyl isocyanide, the cage length, corresponding to the c-spacing. is markedly increased compared with that of a Type I system. Illustrated in Fig. 3a is the alignment of MeNC molecule along the c-axis in its Type II clathrate.[20] In the methanol clathrate,[13] the encaged MeOH molecule exhibits three preferred orientations related by C_3 rotation about the c-axis; in each orientation, the C — 0 bond is tilted by 35° from the c-axis to facilitate interaction of its hydroxy group with each of three phenolic oxygen atoms of the adjacent $[OH]_6$ ring (Fig. 3b). Host–guest interaction is reflected by unequal O—H···O hydrogen bonds in the $[OH]_6$ ring, a feature also found in the Type II hydrogen chloride clathrate studied by x-ray and neutron diffraction methods.[21]

Structure of Type III Clathrate

In the acetonitrile clathrate of hydroquinone, the only authenticated Type III system, a further reduction in space group symmetry from R3 (in Type II) to P3 occurs. There are now three distinct clathration cavities in the shape of prolate spheroids. The three symmetry-independent MeCN molecules fit snugly inside these cavities, one guest molecule being aligned in the opposite sense to the other two.[19]

CRYSTAL STRUCTURES OF α-HYDROQUINONE

α-Hydroquinone belongs to space group $R\bar{3}$, with a_h = 3846(2) pm. c = 565.0(3) pin, and 54 $C_6H_4(OH)_2$ molecules in the triple primitive hexagonal unit cell.[22,23] As shown in Fig. 4a, two crystallographically independent hydroquinone molecules in the asymmetric unit are involved in forming two interpenetrating. open. H-bonded networks similar to those in β-hydroquinone and capable of enclathrating small molecules, such as carbon dioxide.[" sulfur dioxide,[24] and argon,[17] whereas the third forms double helices consisting of H-bonded chains of $C_6H_4(OH)_2$ molecules about a threefold screw axis.

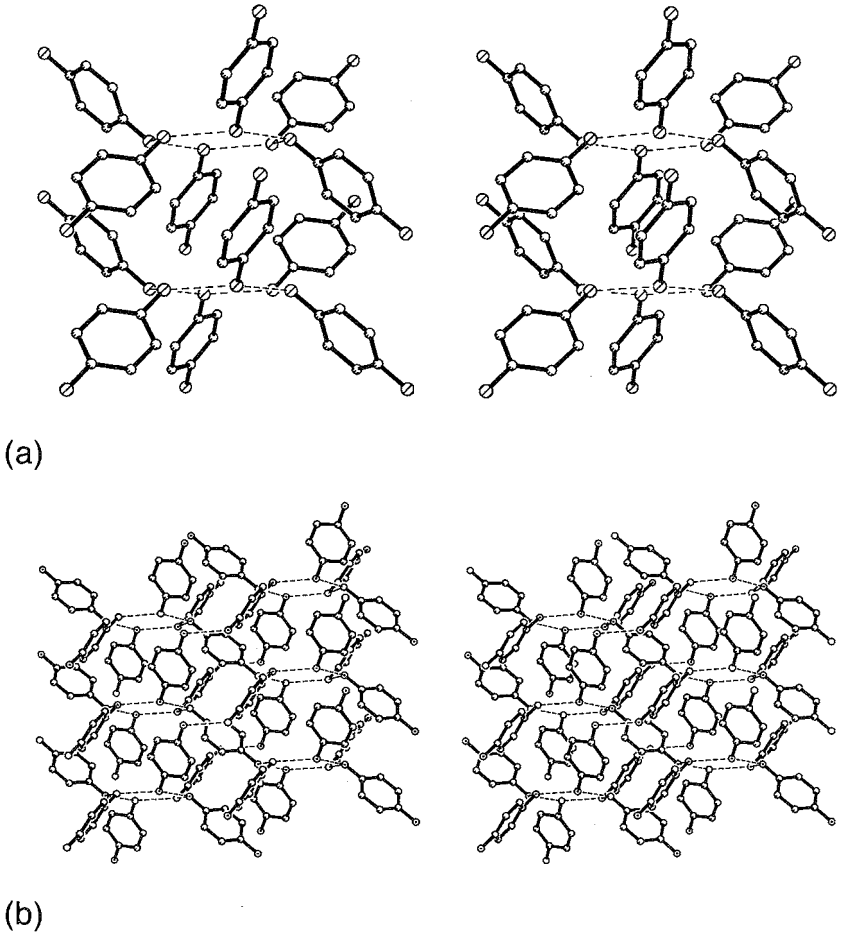

Fig. 4 Stereoviews illustrating (a) the construction of a clathration cage in unsolvated β-hydroquinone, and (b) more extended portions of two identical, but displaced, three-dimensional networks that constitute the β-hydroquinone host structure.

The networks and helices are Fa-bonded together in such a way that the interpenetrating networks are directly linked to each other (in contrast to the unconnected, complementary networks of β-hydroquinone), as are two strands of the double helix. With the presence of three cages (similar in size to those of the β form) per unit cell, the maximum host:guest molar ratio expected for an α-hydroquinone clathrate is 18:1.

Table 1 Crystal data for β-hydroquinone clathrates*

Type	Space group	a	c	Guest species	Interatomic O···O distance(pm) in $[OH]_6$ ring
I	*R*3 (No 148)	1661 3 (3)	547.46 (5)	None	267.8 (3)
		1661 0 (3)	552.4 (1)	Xe	270.5 (2)
		1661 6 (3)	548.9 (1)	H_2S	269.6 (1)
II		1631 (5)	582.1 (1)	SO_2	272.7 (6). 273.3 (6)
	R3 (No 146)	1662 1 (2)	556.2 (1)	MeOH	265.3 (5), 277.9 (5)
		1665 0 (1)	545.3 (1)	HCl	261 (1), 277 (1)
		1594 6 (2)	634.8 (2)	MeNC	277.9 (6), 280.0 (6)
III	*P*3 (No 143)	1600 3 (2)	624.5 (2)	MeCN	277.8 (mean)
Super-polonium	*R*3m (No 166)	1621 5 (2)	1384.6 (2)	C_{60}	279.9 (5)

*Lattice parameters (pm) are given for a hexagonal unit cell

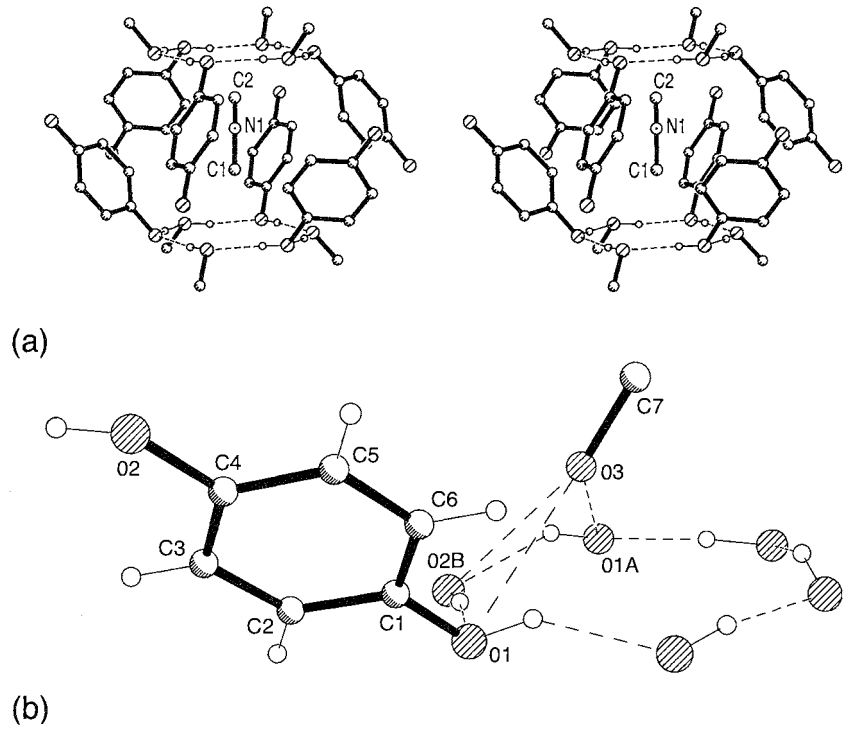

Fig. **3** (a) Stereoview showing a MeNC guest molecule trapped inside a cage in the structure of a Type II β-hydroquinone clathrate. For clarity. all hydrogen atoms were omitted; (b) host–guest interactions in the Type II methanol clathrate of β-hydroquinone; the disordered MeOH guest molecule is inclined at an angle of 35° to the c-axis.

CRYSTAL STRUCTURES OF γ-HYDROQUINONE

Crystals of the γ-form of hydroquinone are monoclinic, space group $P2_1/c$, with a = 807. b = 520, c = 1320 pm, β = 107°. and Z = 4.[25] The structure is built from sheets of H-bonded hydroquinone molecules (Fig. 4b). There are no H-bonded hexameric units, and the inclusion properties are still not well-linown. In accord with the instability and pronounced cleavage of the γ-form, these sheets are apparently held together only by van der Waals forces.

HYDROQUINONE HOST LATTICES WITH ENCLATHRATED FULLERENES

Ermer noted that the edge length of a supercube (−1000 pm) in the single β-hydroquinone (HQ) host framework closely matches the diameter of buckminsterfullerene, C_{60}, and predicted that the resulting supramolecular host–guest complex would have the stoichiometric formula $3C_6H_4(OH)_2{\cdot}C_{60}$, with enclathration being favored by the π-donating properties of HQ and the unusually strong electron-acceptor character of C_{60}. Guided by these considerations. the 3:1 complex was successfully prepared as black dendritic crystals by dissolving stoichiometric amounts of the two components in hot benzene and conducting subsequent crystallization.[7] A similar preparation using a 6:1 molar mixture of HQ and high-purity C_{70} yielded black shiny hexagonal plates of the complex $9C_6H_4(OH)_2{\cdot}2C_{70}{\cdot}2C_6H_6$, which appeared brownish-red in transmitted light.[8] The crystal structures of complexes have been determined using MoK_α data collected at room temperature.

Crystal Structure of $3C_6H_4(OH)_2{\cdot}C_{60}$

The 3:1 adduct of HQ with C_{60} crystallizes in space group $R\bar{3}$ m (No. 166) with Z = 3 in a hexagonal unit cell of dimensions a_h = 1621.5(2) pm and c = 1384.6(2) pm.[7] The corresponding rhombohedra1 unit cell has a, = 1043.8(3) pm and $\alpha = 2\sin^{-1}(a_h/2a_r) = 101.92(2)°$. The HQ molecule occupies a site of symmetry $2/m$. whereas the C_{60} molecule is highly disordered, with relatively shallow electron-density maxima smeared out tangentially over a sphere of radius 351 pm.

The architecture of the single β-hydroquinone host lattice of $3C_6H_4(OH)_2{\cdot}C_{60}$ may be compared with that of empty β-hydroquinone, with hexagonal unit cell edges

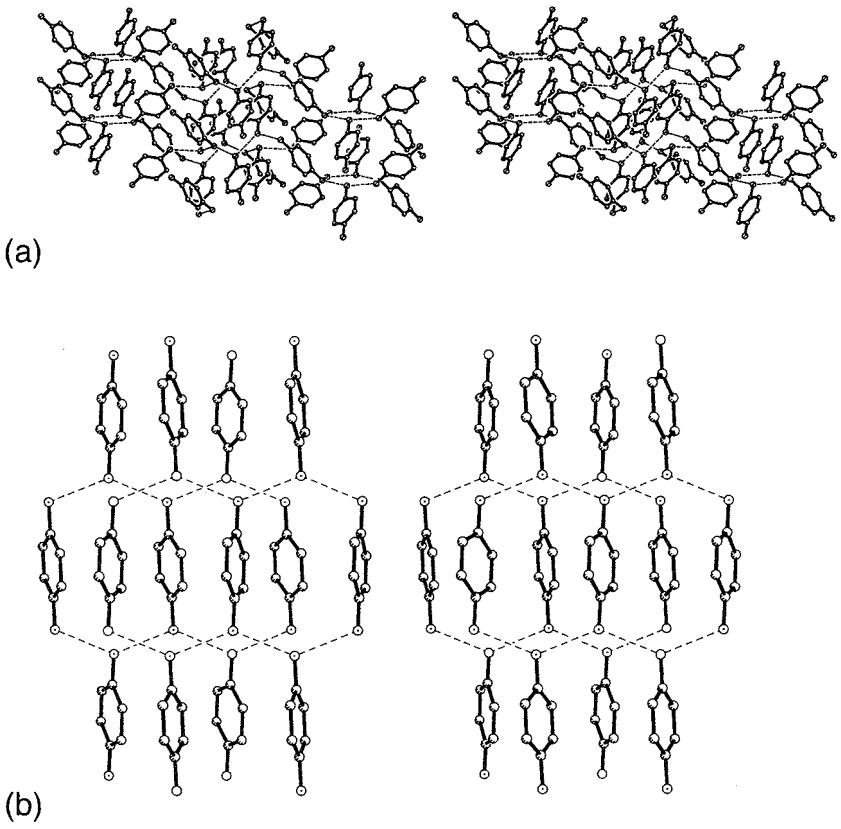

Fig. 4 Stereoviews: (a) the structure of α-hydroquinone, in which two crystallographically distinct $C_6H_4(OH)_2$ molecules are used to construct the unoccupied cages. while a third independent molecule forms double helices around a threefold screw axis in the middle; (b) the crystal structure of γ-hydroquinone built from sheets of H-bonded molecules.

that are a_h = 1661.3 pm and c = 1094.9 pm (the c-axis is doubled to allow for twofold interpenetration). The considerable trigonal elongation (with concomitant contraction of its "waist" as measured by a_h) of the HQ supercube in $3C_6H_4(OH)_2 \cdot C_{60}$, compared to β-hydroquinone, is a consequence of the highly puckered $[OH]_6$ ring, which takes a cyclohexane-like chair conformation with O···O = 279.9 pm, O···O···O = 112.9°, and dihedral angle O··O··O··O = 50.5°. Accordingly. the C_{60} molecules fit tightly inside the cavities of the rather strained single HQ host network. Furthermore, the distance between the centers of a C_{60} cluster and a polar face-to-face orientated HQ molecules is 657.4 pm (Fig. 5a), leading to a distance of 310 pm between the C_{60} surface and the HQ plane, which matches the interplanar stacking distance in the 1:1 charge transfer (CT) complex of HQ with quinone (quinhydrone).[26,27] The implied host–guest charge transfer interaction in $3C_6H_4(OH)_2 \cdot C_{60}$ is consistent with the high electronegativity of C_{60} and the π-donor properties of HQ, as well as the deep color and metallic luster of the crystals.

The orientational disorder of the enclathrated C_{60} in the single β-hydroquinone host network was studied using MoK_α data at four different temperatures, 100, 200, 293, and 373 K. The results showed that the two independent bond lengths of the buckminsterfullerene. d_{56} common to a pentagon and a hexagon and d_{66} common to two hexagons, changed smoothly by −0.03 Å as functions of temperature between 100 and 373 K: the higher the temperature, the longer was d_{56} and the shorter was d_{66}, while the molecular diameter remained almost constant between 7.072 and 7.075 Å.[28]

Crystal Structure of $9C_6H_4(OH)_2 \cdot 2C_{70} \cdot 2C_6H_6$

This inclusion complex $9C_6H_4(OH)_2 \cdot 2C_{70} \cdot 2C_6H_6$ crystallizes in space group P $\bar{3}$ m1 (No. 164). with a_h = 1710.2(5) pm, c_h = 2390.4(9) pm. and Z = 2.[8] There are three types of independent HQ molecules of site symmetry *m*: Types 1 and 2 each with a crystallographic mirror plane containing the C — 0 bonds and orthogonal to the molecular plane, and Type 3, with the mirror plane normal to the C — 0 bonds. The C_{70} molecules occupy two nonequivalent 3*m* sites (Types A and B) and exhibit orientational disorder such that their principal molecular C_5 axes are normal to the c-axis. The

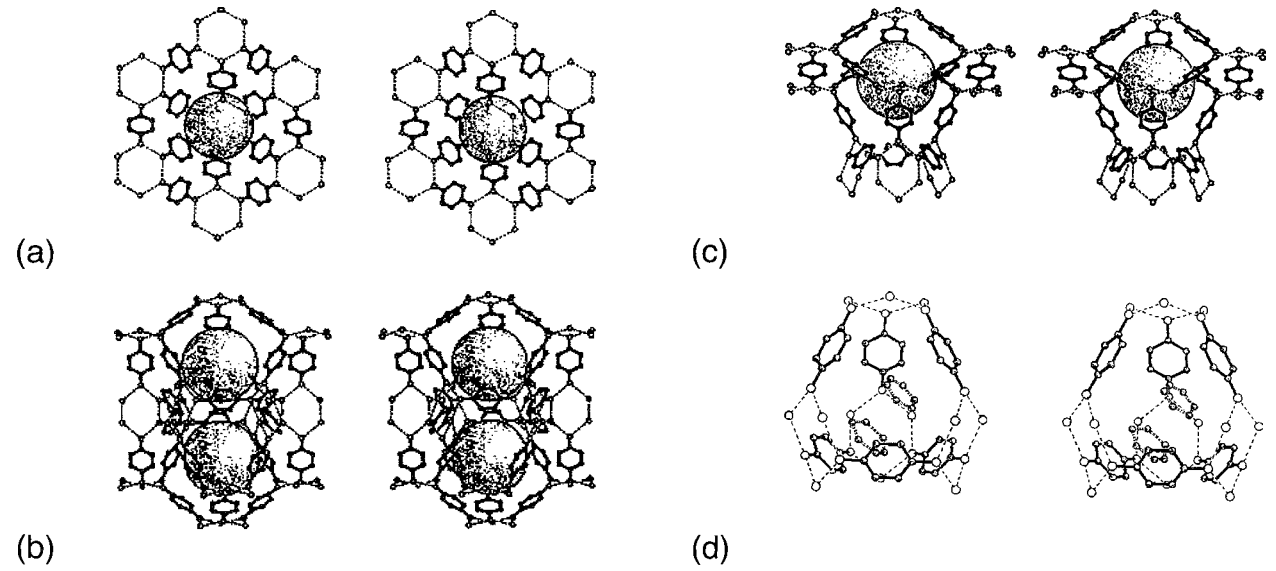

Fig. 5 (a) Stereoview of the crystal structure of $3C_6H_4(OH)_2{\cdot}C_{60}$ viewed parallel to the c-axis. Stereoviews of the disordered C_{60} molecule is depicted as a large sphere, and the O—H···O hydrogen bonds are represented by broken lines. The b-axis is horizontal and orthogonal to a vertical mirror plane containing the c-axis. The crystal structure of $9C_6H_4(OH)_2{\cdot}2C_{70}{\cdot}2C_6H_6$; (b) the peanut-shaped twin cage viewed in the [210] direction. The h-axis is horizontal, and the c-axis is vertical. The two disordered Type A C_{70} guest molecules in the cage are represented as large spheres, and the O—H···O hydrogen bonds are shown as broken lines; (c) the medium-size cage containing a Type B C_{70} guest niolecule viewed along [210]; and (d) the small tetrahedral cage viewed in the [210] direction. the encaged pair of face-to-face benzene molecules being shown in one of the six possible orientations.

enclathrated benzene molecules are grouped in pairs around a $3m$ site and are less well characterized in the x-ray analysis.

The HQ host architecture of the $9C_6H_4(OH)_2{\cdot}2C_{70}{\cdot}2C_6H_6$ complex contains three nonequivalent chair-like $[OH]_6$ rings located in sites of symmetry $3\,m$, $3m$, and $2/m$, respectively. The three-dimensional HQ host network contains three kinds of cavities: 1) large cage of site symmetry m accommodating a pair of C_{70} clusters of Type A (see Fig. 5b); 2) medium-size cage of symmetry $3m$ containing a C_{70} cluster of Type B (see Fig. 5c); and 3) small cage of symmetry $3m$ enclosing a pair of benzene molecules (see Fig. 5d).

In the first type of cage, the large cage is bounded by 14 $[OH]_6$ rings and 24 p-phenylene units. It has the shape of a peanut shell, with each equivalent half-filled by one Type A C_{70} molecule, such that the principal symmetry axis of C_{70} lies perpendicular to the 3 axis of the cage. The two enclosed C_{70} molecules are 1010 pm apart center-to-center, and each is additionally involved in six face-to-face and nine edge-to-face contacts with the enclathrating HQ molecules: three face-to-face with HQ (Type 1) at 697 pm near a polar cap, six edge-to-face with FIQ (Type 2) at 963 pm, and three face-to-face plus six edge-to-face at 706 pm and 863 pm, respectively, with HQ (Type 3) that constitute the equatorial waist of the cage. Conceptually, this large cage may be generated from the single HQ host cage of 3 $C_6H_4(OH)_2{\cdot}C_{60}$ by elongation along the trigonal axis and equatorial insertion of a macro-ring of six H-bonded HQ (Type 3) molecules.

The second type of cage, the medium-size cage: is surrounded by 10 $[OH]_6$ rings and 15 p-phenylene connectors. Starting with the simple HQ supercube of $3C_6H_4(OH)_2{\cdot}C_{60}$, the medium-size cage may be obtained by replacing a vertex on the trigonal axis by an equilateral arrangement of three linked vertices.

The third cage, the small cage, takes the shape of a trigonal pyramid assembled from four $[OH]_6$ rings and six p-phenylene linkers. Electron-density distributions from difference Fourier maps suggest that this approximately tetrahedral cage encloses a pair of face-to-face benzene molecules. which are necessarily subject to orientational disorder around the C_3 axis of the cage. However. the quality of the x-ray intensity data is insufficient to establish this staggered benzene sandwich model as unequivocal.

CONCLUSION

A comparative study of the crystal structures of tetrafluoro-, tetrachloro-, and tetrabro~nohydroquinone showed that they are built of an almost invariant network of O—H···O hydrogen bonds that is analogous to that of γ-hydroquinone, indicating the robustness of this kind of hydrogen-bonding pattern. Both Cl and Br atom, tend to

form a polarization-induced X···X contact to interconnect adjacent layers. but the F atom does not manifest this type of interaction.[29]

The crystal structure of 2.5-di-tert-butylhydroquinone is topologically equivalent to the α-form of arsenic.[30] Introduction of the bulky *tert*-butyl substituents next to the phenolic groups of the hydroquinone leads to the polar stacking of nonpolar, puckered hydrogen-bonded sheets with trigonal symmetry. Similar to the case of β-hydroquinone, the novel layer structure constructed by 2,5-di-tert-butylhydroquinone may be developed from *r*-. As through replacement of the As atoms by H-bonded three-meinbered rings of oxygen atoms, and the As–As bonds by covalent 2.5-di-tert-butyl-p-phenylene links. The formation of the three-membered rings of H-bonded oxygen atoms are rare but are rendered favorable by the presence of a bulky alkyl group close to the hydroxyl group (e.g., tertiary alcohols).

In the presence of bridging water molecules. calix[4]-hydroquinone can self-assemble to form a linear tubular polymeric structure, having an infinitely extended one-dimensional hydrogen-bonded array that can be suspended in aqueous solution and also be grown to very thin tubes as well as a bundle of well-ordered three-dimensional chessboard-like rectangular arrays. These arrays possess useful electrochemical/photochemical properties and can function as an organic nanotube template for designing molecular electronics components.[31] For example, ultrathin silver wires with 0.4 nanometer width can be grown up to micrometer-scale length inside the pores of these self-assembied calix[4]hydroquinone nanotubes by electro/photochemical redox reaction in an ambient aqueous phase.[32]

ARTICLES OF FURTHER INTEREST

Concepts in Crystal Engineering, p. 319
Crystal Engineering with Hydrogen Bonds, p. 357
Hydrogen Bonding, p. 658
Hydroquinone, p. 679
Inclusion Compounds: Selectivity, Thermal Stability, and Kinetics. p. 696
Interpenetration, p. 735
Isostructurality of *Inclusion Compounds*, p. 767
Supramolecular Stabilization. p. 1453
X-Ray Crystallography, p. 1586

REFERENCES

1. MacNicol, D.D. Inclusion Compounds: Atwood. J.L., Davies, J.E.D.. MacNicol, D.D.. Eds.: Academic Press: London. 1984: Vol. 2. 1–45. chap. 1.
2. Mali. T.C.W.: Bracke, B.R.F. Comprehensive Supramolecular Chemistry: MacNicol, D.D.. Toda. F.. Bishop, R., Eds.: Pergamon: New York. 1996: Vol. 6. 23–60. chap. 2.
3. Lindeman. S.V.; Shklover. V.E.: Struchkov. Yu.U. The β-modification of hydroquinone, $C_6H_6O_2$. Cryst. Struct. Commun. 1981. *10* (4). 1173–1179.
4. DeSando. R.J.; Lange, R.C. The structures of polonium and its compounds. I. α-and β-polonium metal. J. Inorg. Nucl. Chem. 1966. 28 (9). 1837–1846.
5. Mak. T.C.W. Hexamethylenetetrainine hexahydrate: A new type of clathrate hydrate. J. Chem. Phys. 1965. *43* (8). 2799–2805.
6. Jeffrey. G.A.; Mak, T.C.W. Hexamethylenetetralnine hexahydrate-new type of clathrate hydrate. Science (Washington) 1965. *149* (3680). 178–179.
7. Ermer, O. 3:1 Molecular complex of hydroquinone and C60. Helv. Chim. Acta 1991. *74* (6). 1339–1351.
8. Ermer, O.: Röbke. C. New host architecture of hydroquinone with enclathrated C70. J. Am. Chem. Soc. 1993. *115* (22), 10077–10082.
9. Birchall, T.: Frampton, C.S.; Schl-obilgen, G.J.: Valsdóttir, J. β-Hydroquinone xenon clathrate. Acta Crystallogr., Sect. C 1989. *45* (6). 944–946.
10. Mak. T.C.W.: Tse, J.S.; Tse, C.-S.; LeeK.-S.; Chong, Y.-H. Crystal structure of a clathrate inclusion coinpound of hydroquinone and hydrogen sulfide. J. Chem. Soc., Perkin Trans. 2 1976. (10). 1169–1172.
11. Ho, W.C.: Mak. T.C.W. Refinement of the crystal structure of hydroquinone-hydrogen sulfide clathrate. Z. Kristallogr. 1982, *161* (1–2). 87–90.
12. Polyansltaya. T.M.; Alekseev, V.I.: Bakakin. V.V.; Chekhova. G.N. Crystal structure determination of a clathrate compound of β-hydroquinone with sulfur dioxide. Zh. Strukt. Khim. 1982. 23 (1). 123–127.
13. Mak, T.C.W. Orientation of methanol enclathrated in the β-hydroquinone lattice: An x-ray crystallographic study. J. Chem. Soc., Perkin Trans. 2 1982. (11). 1435–1437.
14. Palin, D.H.; Powell. H.M. Hydrogen-bond linking of quinol molecules. Nature (London) 1945, *156*. 334–335.
15. Palin, D.E.; Powell. H.M. Structure of molecular compounds. III. Crystal structure of addition complexes of hydroquinone with certain volatile compounds. J. Chem. Soc. 1947. 208–221.
16. Palin, D.E.: Powell, H.M. Structure of molecular compounds. IV. Clathrate compounds. J. Chem. Soc. 1948. 61–73. 815–821.
17. Powell, H.M. The structure of molecular compounds. VII. Compounds formed by inert gases. J. Chem. Soc. 1950, 298–301. 468–469.
18. Wallwork. S.C.; Powell. H.M. The structure of molecular compounds. XI. Crystal structure of the addition complex of quinol and methyl cyanide. J. Chem. Soc. 1956. 4855–4858.
19. Hermansson. K. Host-guest interactions in an organic crystal: β-hydroquinone clathrate with Ne and HF guests. J. Chern. Phys. 2000, *112* (2). 835–840.
20. Chan, T.-L.; Mak, T.C.W. X-ray crystallographic study of guest-molecule orientations in the β-hydroquinone clathrates of acetonitrile and methyl isocyanide. J. Chem. Soc., Pel-kin Trans. 2 1983. (6). 777–781.

21. Boeyens. J.C.A.: Pretorius, J.A. X-ray and neutron diffraction studies of the hydroquinone clathrate of hydrogen chloride. Acta Crystallogr., Sect. B 1977, 33. 2120–2124.
22. Wallwork. S.C.; Powell. H.M. The crystal structure of the α form of quinol. J. Chem. Soc., Perkin Trans. 2 **1980.** (4). 641–646.
23. Powell. H.M. Inclusion Compounds: Atwood. J.L., Davies. J.E.D.. MacNicol. D.D.. Eds.: Academic Press: London, 1954: Vol. 1. 1–28. chap. 1.
24. Chekhova. G.N.; Polyanskaya, T.M.: Dyadin, Yu.A.: Alekseev. V.I. Hydroquinone clathrates. II. Chemical and x-ray phase analysis of solid phases in the hydroquinone-water-sulfur dioxide system. Zh. Strukt. Khim. 1975, 16 (6). 1054–1060.
25. Maartmann-Moe, K. Crystal structure of γ-hydroquinone. Acta Crystallogr. 1966. 216. 979.
26. Sakurai. T. The crystal structure of the triclinic modification of quinhydrone. Acta Crystallogr. **1965,** *19* (3). 320–330.
27. Sakurai. T. On the refinement of the crystal structures of phenoquinone and monoclinic quinhydrone. Acta Crystallogr., Sect. B **1968.** *24* (3). 403–412.
28. Blanc. E.; Restori. R.: Schwartzenbach, D.; Bürgi, H.-B.; Fortsch. M.; Venugopalan, P.; Ermer. O. Orientational disorder as a function of temperature in the clathrate structure of hydroquinone and C60. Acta Crystallogr., Sect. B 2000, *56* (6), 1003–1010.
29. Thalladi, V.R.; Weiss. H.-C.; Boese. R.; Nagaia. A.; Desiraju, G.R. A comparative study of the crystal structures of tetrahalogenated hydroquinones and -hydroquinone. Acta Crystallogr.. Sect. B **1999.** 55 (6). 1005–1013.
30. Ermer. O.; Robke, C. Crystal structure of 2,5-di-tert-butylhydroquinone: Polar stacking of nonpolar H-bridged layers with trigonal symmetry. Angew. Chem.. Int. Ed. Engl. **1994.** 33 (17). 1755–1757.
31. Hong, B.H.; Lee. J.Y.: Lee. C.-W.; Kim, J.C.: Bae. S.C.; Kim, K.S. Self-assembled arrays of organic nanotubes with infinitely long one-dimensional H-bond chains. J. Am. Chem. Soc. **2001,** 123 (43). 10748–10749.
32. Hong, B.H.; Bae. S.C.; Lee, C.-W.; Jeong, S.; Kim. K.S. Ultrathin single-crystalline silver nanowire arrays formed in an ambient solution phase. Science (Washington) **2001.** *294* (5541). 348–351.

Imaging and Targeting

Stephen Faulkner
Rebecca J. Aarons
University of Manrhester, Manchester, United Kingdom

INTRODUCTION

The twin fields of imaging and targeting developed rapidly over the last quarter of a century. Both exploit the interactions between discrete species. albeit in very different ways. This brief overview examines the two concepts separately, covering the broad range of techniques being used at the beginning of the twenty-first century. with particular emphasis on the exploitation of molecular recognition and metal binding.

IMAGING

Noninvasive imaging of biological systems has the potential to provide information relating to the structure and function of tissue without resort to surgery. Traditionally, this relied on the use of x-rays for hard-tissue imaging. However. a range of soft-tissue imaging techniques were developed in the last quarter of a century that extends the range of options for clinical diagnosis and opens the possibility of specific and functional imaging. In the three key areas. advances in detection and data–processing techniques were applied and combined with exploitation of biological and chemical supramolecular processes.

Magnetic Resonance Imaging

Magnetic resonance imaging (MRI) is the dominant form of soft-tissue imaging. MRI uses the principles of gradient field NMR spectroscopy to build contrast between tissue types. It relies on the relaxation properties of water protons in a magnetic field." These vary naturally from one tissue type to another. depending on the freedom of movement of water protons. Protons tumbling rapidly relax more quickly than those tumbling slowly. so the signal obtained from fluid media is different than that obtained from viscous media (e.g., water protons associated with protein molecules will relax more slowly than bulk water). These differences in relaxation rates are used to create a tissue map.

Paramagnetic species are of increasing importance in MRI. because they enhance the relaxation rates of water protons in the medium surrounding them. giving rise to improved contrast.[2,3] Such species are known as contrast agents. A variety of classes of paramagnetic contrast agent exist, and one of the most important is that consisting of paramagnetic ions. particularly gadolinium ions. Gadolinium(III) is an ideal species for use as a contrast agent. It possesses seven unpaired electrons combined with a long electron spin relaxation time. while bound water niolecules are in rapid exchange with bulk solvent. The free ion is toxic, making it unsuitable for use as a contrast agent. Instead, gadolinium complexes are used. The ideal gadolinium complex should have high kinetic stability to minimize toxicity. while still allow close approach of water molecules and facile exchange of inner- and outer-sphere solvent molecules with the bulk solvent. These two aims must be balanced, because they are. in part, contradictory: kinetic stability is best achieved in rigid complexes that exclude solvent from the inner coordination sphere, while rapid exchange of solvent molecules is best achieved with significant numbers of coordinated water molecules.

Shown in Fig. 1 are some typical contrast agents. These all have hard donor atoms and, with one exception, are eight coordinate ligands. The exception. a texaphyrin,[4] a five-coordinate ligand, trades some kinetic stability in favor of increased inner-sphere coordination of water molecules. Of the other molecules, two (DTPA and BOPTA)[2] are acyclic and derived from diethylenetriamine. This makes them relatively simple to prepare but results in lower kinetic stability of the gadolinium complexes relative to ligands based on a rigid inacrocyclic backbone (DOTA, DO3AHP. and GADOBENZ).[2,5] The increased stability of the macrocyclic complexes arises as a result of preorganization of the ligands combined with restricted rotational freedom in the ligand backbone. $[Gd.DTPA]^{2}$, $[Gd.BOPTA]^{2}$, $[Gd.DOTA]^{-}$, and [Gd.DO3AHP] allow the close approach of one water molecule to the metal center. Contrast arises from the inner and the outer coordination spheres of solvent molecules. By contrast, GADOBENZ has bulky (and hydrophobic) benzyl groups appended to the phosphinate donor groups. These prevent the close approach of water, and the contrast

"For a more detailed discussion of the techmque. see Ref [1]

DOI: 10.1081/E-ESMC 120012799

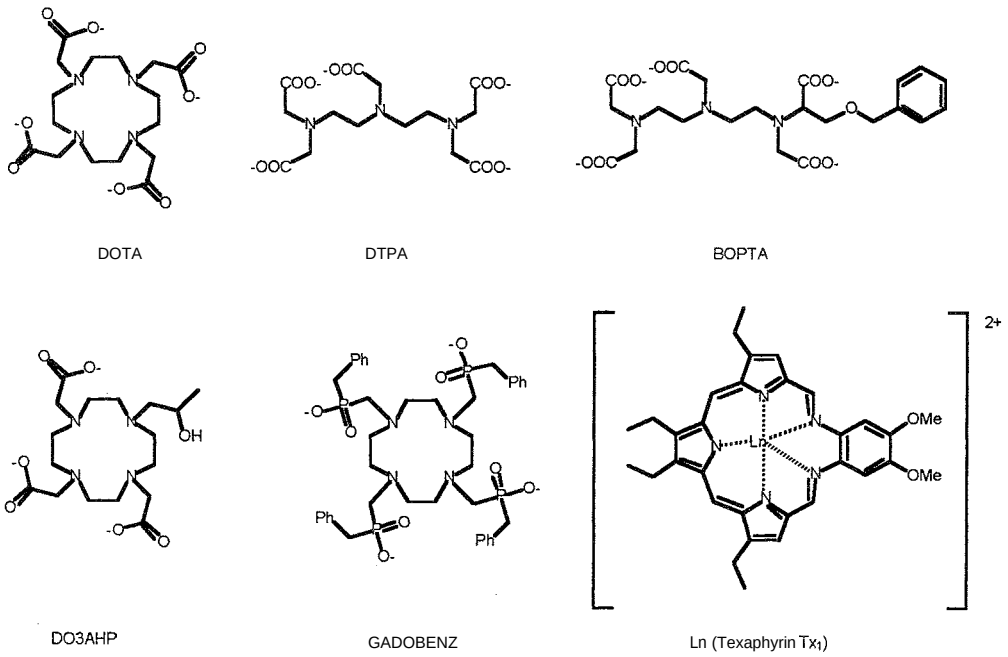

Fig. I Ligands and complexes used as MRI contrast agents

properties of this species arise solely as a result of exchange of outer-sphere solvent.[5] The nature of the inner- and outer-sphere solvation for a particular complex can be determined by field cycling relaxometry[3] or by luminescence measurements on analogous lanthanide complexes.[6]

Current interest centers on the possibility of developing smart contrast agents. targeted to particular cell lines and to cell surface receptors. There is some debate as to whether the use of targeting vectors (vide infra) to specify cell surface receptors will prove an effective means of generating contrast, because agents such as those described above give rise to reasonable contrast at concentrations well above those of typical cell surface receptors.[7]

Accordingly. it becomes necessary to improve the effectiveness of the contrast agent. One approach to this problem is to increase the number of gadolinium ions present. for instance, by preparing dendrimers bearing many gadolinium ions.[8] The effectiveness of a contrast agent is measured by its relaxivity, the paramagnetic relaxation rate enhancement caused by a 1 mM solution of the complex. This may be regarded as the sum of the inner- and outer-sphere relaxivities, with the inner-sphere contribution dominating for systems where there are bound water molecules. The chief determinant of the inner-sphere relaxivity is the rotational correlation time of the complex. This can be exploited for inononuclear complexes by placing the complex at the hub of a much larger molecule or by utilizing the binding of the contrast agent by albumin proteins and the consequent reduction in rotational freedom.''' Dendritic systems achieve higher relaxivities by increasing the effective gadolinium concentration. The inner- and outer-sphere contributions for individual ions in surface-functionalized dendrimers are comparable to those for mononuclear complexes.

Positron Emission Tomography and Single-Photon Emission Tomography

While smart imaging with MRI contrast agents still represents a challenge. other imaging techniques have achieved the goals of smart. or functional, imaging. Tomographic imaging with radioisotopes represents a useful alternative, particularly where the goal involves imaging species at low concentrations. Because background radiation in vivo is generally very low, radioisotopes can be detected at very low concentrations. At such low concentrations. the risk to health is minimal.

There are two main techniques. each of which utilizes different types of radioisotopes to obtain an image:

1. Single-photon emission tomography (SPET),[9] also known as single-photon emission computer tomography (SPECT). depends on the emission of gamma rays by appropriate isotopes. These gamma rays can be detected by a gamma camera; and images are then obtained using conventional mapping techniques.
2. Positron emission tomography (PET)[10] uses positron (β^+)-emitting isotopes as signaling moieties. Positrons are antimatter and annihilate when they encounter an electron, giving rise to two photons,

each of 511 keV. This annihilation occurs almost instantly when the positron is produced, i.e., before it can travel through tissue. The production of such photon pairs can be detected using a technique called coincidence detection, which registers a signal every time two photons of appropriate energy arrive simultaneously at an array of detectors. These signals can then be deconvoluted to give rise to images showing the localization of the isotope.

Both SPET and PET use isotopes with short half-lives to optimize image contrast while minimizing dose.

Considered to be among the best choices for SPET are ^{99m}Tc (half-life 6 h) and ^{123}I (half-life 13 h), as they have monoenergetic emissions (141 kev and 159 keV, respectively) that make them easy to detect, and they provide a lower radiation dose to the patient.

We can pass over iodine in a few words. The iodide ion is not an option, as it tends to localize in the thyroid, so covalently linked species are the best. These tend to be prepared at the hospital by iodination of a suitable organic molecule (usually one containing a double bond). Such reactions need to be fast. given the short half-life of the nuclide.

Suitable isotopes of metal ions are more readily used in complexes. Among others, gallium (^{67}Ga), technetium (^{99m}Tc), and indium (^{111}In) complexes have been used.

Positron-emitting isotopes are more numerous and more varied. They also tend to have a wide range of half-lives, although all have the same photon energy owing to the way in which the photons are produced. Among the isotopes commonly used for PET are ^{11}C (half-life 0.3 h), ^{18}F (half-life 2 h), ^{55}Co (half-life 18 h), ^{64}Cu (half-life 13 h), ^{66}Ga (half-life 9.5 h), ^{83}Sr (half-life 33 h), ^{94g}Tc (half-life 5 h), and ^{120}I (half-life 1.4 h).

It is important to consider how quickly the radionuclide can be delivered to the patient from the source (including the time taken for any complex or compound preparation). Unless the hospital has a cyclotron and the chemistry is simple, half-lives of the order of minutes are too short. There is an alternative, in that nuclides that are not positron emitters may produce them by radioactivative decay. Such nuclides, called generators, can have longer half-lives and, thus, provide a ready source of short-lived positron emitters. It is also important that the parent and daughter nuclides be easily separated, so that the parent can produce more daughter nuclides while the first batch is being used. Examples of such systems include the use of ^{134}Ce (half-life 3 days) to produce ^{134}La (half-life 7 min). and the use of ^{68}Ge (half-life 271 days) to produce ^{68}Ga (half-life 68 min).

The choice of radionuclide depends on the type of imaging envisaged. For simple imaging, isotopes with short half-lives are suitable. For targeted imaging, the localization process may take up to 72 h, meaning that short-lived isotopes will decay before they can be used.

As a result of the short half-lives of the nuclides described above, the complexes chosen for their delivery are, of necessity, simple. In Fig. 2, complexes A through C are designed for use with technetium ions.[11–13] Pertechnetate is readily available but must be reduced in situ to Tc(V) or Tc(I) before complexation is possible. Ligands D and E are suitable for the complexation of ^{64}Cu for positron emission tomography.[14,15] In all cases, it is

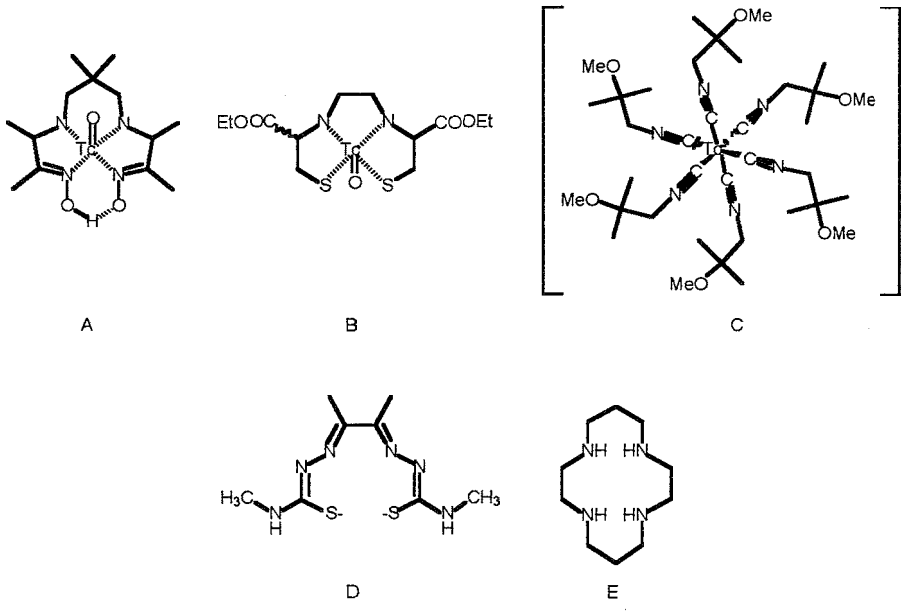

Fig. 2 Ligands and complexes used in radioisotope-based imaging techniques

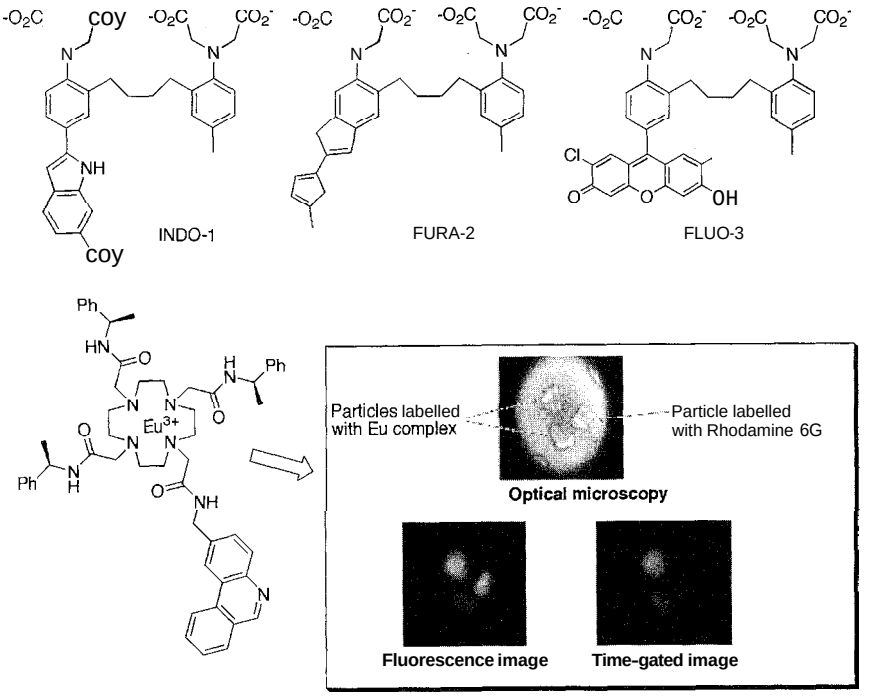

Fig. 3 Ligands and complexes used in luminescent imaging

essential that the manipulation and purification of the complex can be achieved with minimal effort in as short a time as possible, because such manipulations are generally performed at the hospital by nonchemists.

Luminescence-Based Imaging Techniques

MRI and radiochemical imaging techniques are both highly effective for whole-body imaging but tend to offer limited spatial resolution when applied to systems where a degree of magnification is necessary. Both techniques are capable of resolution to the millimeter level but offering higher resolution is difficult. For many physiological applications. for example, the study of subcellular processes, higher resolution is essential. Optical microscopy offers the desired resolution but suffers some disadvantages—chief among these is the nature of the technique. Contrast in optical microscopy arises from differing degrees of light absorption by the sample. and as such, the potential of the technique for specific imaging is limited by the absorbance of the tissue.

Fluorescence offers one route around this problem. The emission of light by an electronically excited molecule can occur in any direction and need not necessarily be colinear with the absorbed photon. The sample can thus be observed perpendicular to the probe beam. This results in an enormous improvement in sensitivity, because any signal represents an increase on a zero background. By contrsst. absorption must be detected as a small decrease in a large signal—a much less sensitive approach. Biological samples are fluorescent in their own right (a phenomenon known as autofluorescence), as a result of the presence of naturally occurring chromophores. However, most biological absorption occurs in the UV, and most autofluorescence occurs in the blue region of the spectrum. Thus. autofluorescence can be avoided by using fluorescent compounds (or fluorophores) that absorb light at longer wavelengths than biological absorption.[b]

Smart fluorescent indicators are widely used in fluorescent imaging microscopy. INDO-1,'''' FURA-2,[17] and FLUO-3[18] (Fig. 3) belong to the same family of calcium indicators. All share a binding site derived from BAPTA, comprising two amine and four carboxylate moieties (at the top of the molecule). which is selective for calcium ions over other endogenous metal ions. The acyclic binding site has considerable rotational freedom, allowing rapid binding and release of metal ions and minimizing the degree to which low concentrations of ligand will buffer metal ion concentrations. In each case. the left-hand side of the molecule also constitutes an extended conjugated system in which one of the amine groups in the binding site acts as an electron donor. Because this amine performs a dual function, the availability of the nitrogen lone pair to the conjugated system will vary depending on whether or not a metal ion is bound. This, in turn, will affect the photophysical

[b]For a detailed treatment of fluorescence microscopy. see Ref. [16]

properties of the system. In the case of INDO-1 (for the free ligand λ_{ex} = 349 nm. λ_{em} = 485 nm; for the calcium complex λ_{ex} = 331 nm, λ_{em} = 410 nm),[17] little change is observed in the absorption spectrum, but the emission spectrum is shifted considerably. The reverse is true for FURA-2 (for the free ligand λ_{ex} = 362 nm, λ_{em} = 512 nm; for the calcium complex λ_{ex} = 335 nm, λ_{em} = 505 nm).[17] Because the free and bound systems can thus be distinguished without difficulty, the calcium concentration may be quantified easily. Both INDO-1 and FURA-2 absorb light at relatively short wavelengths. similar to those associated with biological absorption. This gives rise to a significant fluorescent bacliground. FLUO-3 attempts to overcome this problem by shifting the excitation band to lower energy and longer wavelength. However. the increase in conjugation and the presence of another donor unit in the fluorescein-like chromophore conspire to ensure that, while the intensity of fluorescence changes on binding calcium, the shift in excitation and emission wavelength between the free and the bound species is so small as to be negligible (for the free ligand λ_{ex} = 556 nm. λ_{em} = 576 nm; for the calcium complex λ_{ex} = 553 nm. λ_{em} = 576 nm).[18] Quantification of the calcium ion concentration therefore becomes more complicated, requiring the use of ratio experiments.

An alternative approach can be used to remove background fluorescence, allowing accurate imaging even when autofluorescence occurs. Because fluorescent compounds have short luminescence lifetimes. typically of the order of 0.1–10 ns, it is easy to envisage using a probe molecule that has a much longer luminescence lifetime (of the order of 500 ns–1 s). The fluorescent emission will have decayed almost completely 100 ns after an excitation pulse, while any longer-lived luminescence will still be present. It is easy to envisage a system in which a period of time is allowed to elapse after the excitation pulse, ensuring that only the desired luminescence is collected, while fluorescence is rejected. This approach is called time-gated imaging. Organic phosphors tend to be unsuitable for this approach to imaging, because their luminescence is quenched by dissolved oxygen in solution. Lanthanide complexes. such as the europium complex shown in Fig. 3. are ideal—particularly when an organic chromophore is used to harvest light and transfer energy to the metal center.[19] Lanthanides have low extinction coefficients and absorb light weakly, but they have long luminescence lifetimes (0.1–5 ms for europium and terbium complexes[20] and 0.1–10 μs for ytterbium[21] and neodymium complexes[22]). They are also well established as acceptors of energy from aromatic donor chromophores, which can be used to solve the problem of extinction coefficient.

The europium complex in Fig. 3 bears a phenanthridine chromophore on the ligand. which absorbs light effectively. The images show three particles. The two on the left were labeled with the europium complex, while that on the right was labeled with rhodamine 6G, a fluorescent dye that absorbs and emits light at the same wavelengths as the europium complex (λ_{ex} = 355 nm, λ_{em} = 615 nm).[19] It is clearly seen that it is impossible to differentiate the particles by conventional optical microscopy or fluorescence imaging. However, time-gated imaging completely rejects the rhodamine fluorescence. illustrating how the technique can dramatically improve signal-to-noise ratios in systems where background fluorescence is problematic.

TARGETING

Selective therapy or chemotherapy of disease states has long been a challenge for medical science. Chemotherapy for cancer and genetic disorders represents the greatest challenge. because both disease states arise within the patient and are thus difficult to differentiate from normal tissue. The development of such techniques concentrates on the delivery of drugs or genetic material to specific sites. Targeting of this kind is achieved by incorporating a targeting vector specific to sites on or within the cells being targeted, into the assembly being used for therapy. Such assemblies may be covalently linked,[23] may rely on coordination of a metal ion,[24] or may be noncovalent assemblies held together by supramolecular interaction~.''Supramolecular chemistry interactions remain important regardless of the nature of the assembly; all rely on noncovalent interactions between the targeting vector and the targeted site.

Antibodies

It is possible to raise antibodies to specific cell types (e.g., cancer cells.)" The strategy is simple in its early stages and involves implanting a foreign tumor into an animal. The immune system then fights this tumor, raising antibodies to it. that recognize any unusual proteins on the surface of the cells. These antibodies can then be expressed in cultures. However, the process is not finished. because the animal's body system. with the original tumor. will recognize the antibodies as foreign. This means that the antibodies then have to be humanized, by modifying their structures to retain selectivity but suppressing the immune response.

In general. while vectors derived from antibodies offer high specificity. they have drawbacks. They are difficult to make and tend to have much larger molecular weights

"Details of monoclonal antibody-based technique? can be found in Ref. [26].

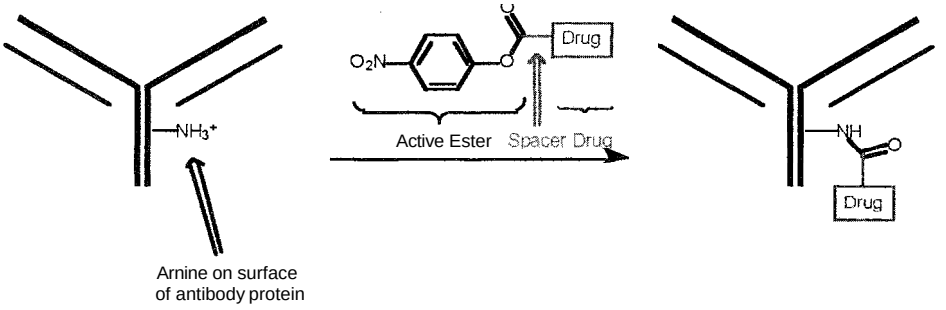

Fig. 4 Formation of an antibody conjugate.

than the rest of the BFCA. meaning that the amount of drug delivered is small relative to the molecular mass of the antibody conjugate.

Shown in Fig. 4 is a cartoon representation of the preparation of an antibody conjugate from a monoclonal antibody. The antibody surface is covered with hydrophilic residues. Some of these. particularly side chains containing amines and thiols. are nucleophilic. The cartoon illustrates the use of an active ester to form an amide. covalently linking the antibody to the drug, though other

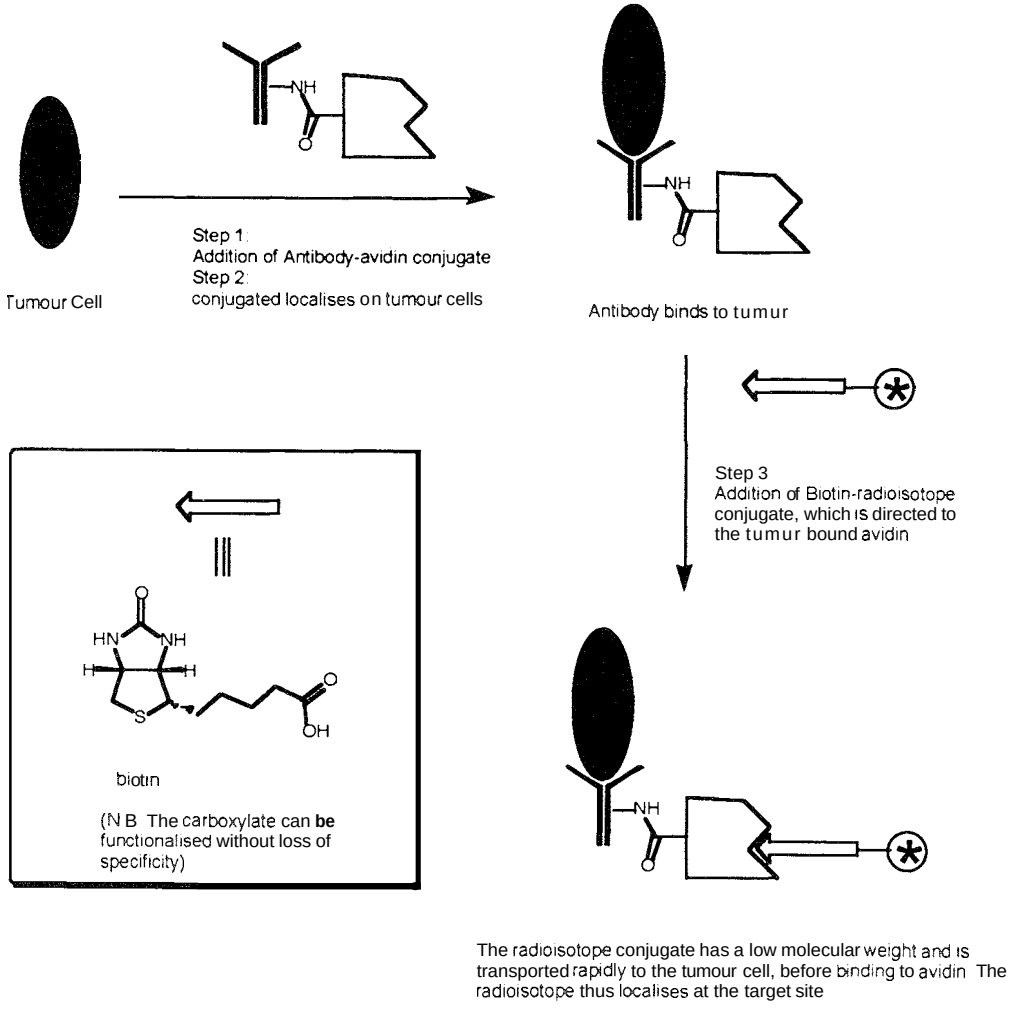

Fig. 5 A tumor pretargeting with an antibody–avidin conjugate

approaches using isothiocyanates or thiol reactive maleimides are equally valid. All of these reactive groups must be used in aqueous solution at ambient temperatures to avoid denaturing the antibody.

bow-Molecular-Weight Targeting Vectors

Low-molecular-weight targeting vectors are much simpler to prepare than antibodies. Such targeting vectors are derived from bioactive peptides (e.g., in the chelating agent octreotide)[27] and small molecules such as biotin, which bind strongly to biological receptors or proteins. While they are easier to prepare, there are two potential problems with using low-molecular-weight vectors. First, the vector and the therapeutic agent are likely to be of similar size; the presence of the drug inay thus alter the specificity of the targeting vector, particularly where a metal complex is being delivered. Second. small targeting vectors, particularly peptides. inay be metabolized in vivo: this problem is often overcome by using cyclic peptides as delivery vectors. In such systems. the lack of terminal residues reduces the susceptibility of the peptide to hydrolysis.

Small conjugates also have one great advantage over antibody conjugates in that they localize rapidly. whereas antibody conjugates, being large, are transported slowly through the body. This is particularly important when delivering radioisotope conjugates, where the slow localization of an antibody conjugate can represent several half-lives of the isotope being delivered. To avoid minimizing the dose in this way, the two approaches can be combined using a technique known as tumor pretargeting.[28] In this approach, a monoclonal antibody is used to deliver a nonendogenous protein to the tumor cell. This can then be targeted using a low-molecular-weight conjugate. Illustrated in Fig. 5 is this approach. The antibody is used to deliver avidin to the tumor cell. Because both components are unstable, the long localization time is relatively unimportant. The avidin is then used as the substrate for a low-molecular-weight conjugate between biotin and a metal complex. This approach allows the unstable component to localize quickly and combines the best aspects of antibody-based techniques with those of techniques using low-molecular-weight vectors.

Gene Targeting

From the supramolecular chemist's viewpoint, gene therapy is an exercise in drug delivery. In this case, the drug in question is DNA, which must be directed to appropriate cells. then be internalized by the cell and subsequently by the nucleus—a process commonly called

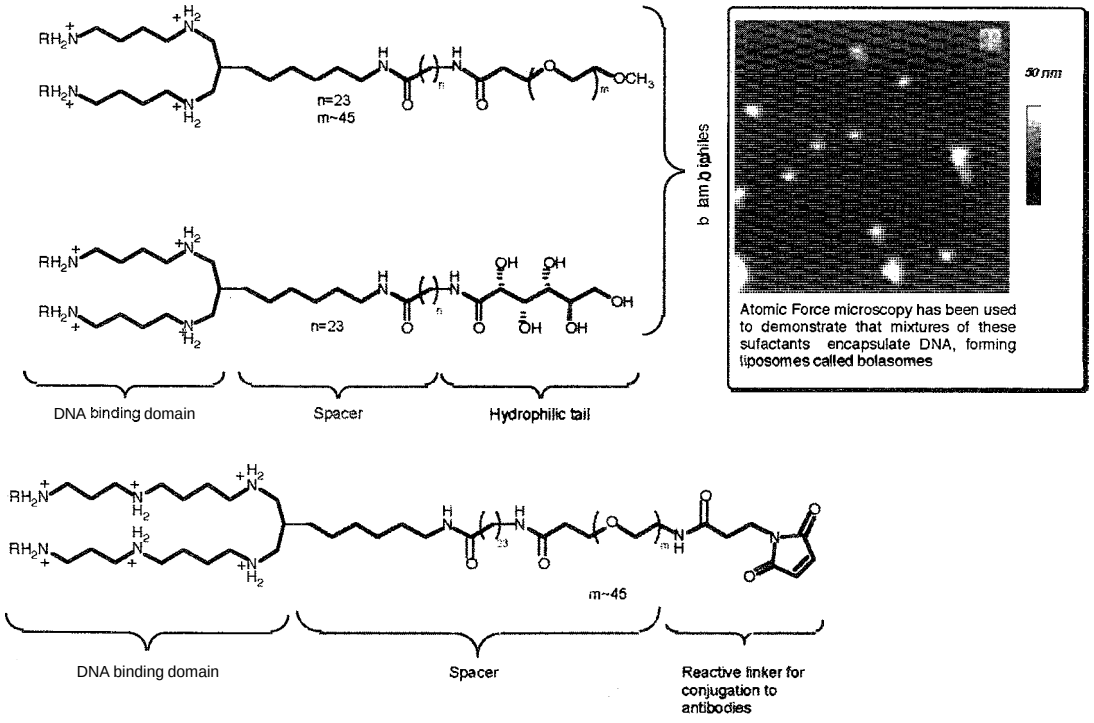

Fig. 6 The use of bolaamphiphiles as DNA-encapsulating agents

transfection. To do this, the drug DNA must be stabilized throughout its passage through the body.

The vast majority of approaches to DNA delivery use DNA enveloped in the coat proteins of adenoviruses or retroviruses.[29] This approach uses a biological delivery system without modification. An alternative approach is rapidly gaining in popularity and offers a solution based on chemistry and self-assembly using surfactants to form micelles or liposomes that encapsulate the DNA.[25,30]

An example of this approach is illustrated in Fig. 6. The surfactants shown consist of polyamine groups linked via a spacer group to hydrophilic sugar moieties.[25] In aqueous solution at physiological pH. the amine groups are protonated and can bind to DNA through electrostatic interaction with the minor groove. Mixtures of these surfactants can be self-assembled around the DNA, forming a liposome, sometimes referred to as a bolasome, that can transport the DNA into cells without difficulty. Furthermore, self-assernbled structures like these can be directed to specific cell lines using monoclonal antibodies. The maleimide-bearing surfactant molecule can be linked to an antibody once the bolasome is formed, providing a large targeting vector conjugate. In this way, targeting methodologies are being applied to a new and burgeoning area.

ARTICLES OF **FURTHER** INTEREST

Biological Ligands, p. *88*
Biological Models and Their Characteristics. p. 101
Biosensors, p. 115
Cyclodextrins: Applications, p. 405
Drug Delivery, p. *484*
Fluorescent Sensors. p. 572
Imaging and Targeting, p. *687*
Luminescent Probes, p. *821*
Nuclear Magnetic Resonance Spectroscopy, p. *981*
Photochemical Sensors, p. *1053*
Self-Assembly in Biochemistry, p. 1257

REFERENCES

1. Andrew. E.R.; Bydder. G.; Criffiths. J.: Iles, R.; Styles. P. *Clinical Magnetic* Resonance *Imaging and* Spectroscopy: John Wiley and Sons: Chichester, 1990.
2. Caravan, P.: Ellison, J.J.; McMurry, T.J.: Lauffer. R.B. Gadolinium(III) chelates as MRI contrast agents: Structure, dynamics, and applications. Chem. Rev. **1999,** 99. 2293.
3. Aime. S.: Botta, M.: Fasano, M.; Terreno. E. Lanthanide(III) chelates for NMR biomedical applications. Chem. Soc. Rev. **1998,** *27,* 19.
4. Young, S.W.: Qing. F.: Harriman. A.: Sessler. J.L.; Dow. W.C.: Mody. T.D.; Hemmi. G.W.: Hao. Y.P.; Miller. R.A. Gadolinium(III) texaphyrin: A tumor selective radiation sensitizer that is detectable by MRI. Proc. Natl. Acad. Sci. U. S. A. **1996.** *93,* 6110.
5. Aime, S.: Batsanov, A.; Beeby, A.; Botta. M.: Dickins, R.S.: Faulkner, S.: Foster. C.E.; Howard. J.A.K.: Norman, T.J.; Parker, D.; Williams, J.A.G. Structural investigations of benzyl phosphinate bearing complexes of lanthanides. J. Chem. Soc., Dalton Trans. **1997.** 3623.
6. Beeby, A.; Clarkson. I.M.; Dickins. R.S.; Faulkner. S.; Parker, D.: de Sousa. A.S.; Williams, J.A.G. The effect of X-H oscillators on luminescence quenching in lanthanide complexes. J. Chem. Soc., Perkin Trans. 2 **1999.** 493.
7. Ranganathan, R.S.; Fernandez, M.E.; Kang, S.I.: Nunn, A.D.: Ratsep. P.C.; Pillai. K.M.R.: Zhang. X.: Tweedle. M.F. New multimeric magnetic resonance imaging agents. Invest. Radiol. **1998,** *33.* 779.
8. Toth. E.: Pubanz. D.: Vauthey, S.: Helm. L.: Merbach, A.E. The role of water exchange in attaining maximum relaxivities for dendrimeric MRI contrast agents. Chem. Eur. J. **1996.** *2.* 1607.
9. Dilworth. J.R.: Parrott. S.J. The biomedical chemistry of technetium and rhenium. Chem. Soc. Rev. **1998.** *27,* 43.
10. Anderson, C.J.: Welch. M.J. Radiometal labeled agents (non-technetium) for diagnostic imaging. Chem. Rev. **1999.** *99,* 2219.
11. Leonard, J.P.: Novotmik. D.P.; Neirinckx. R.D. Technetium-99m-d.1-hm-pao—A new radiopharmaceutical for imaging regional brain perfusion using spect—A comparison with I-123 hipdm. J. Nucl. Med. **1986.** *27.* 1819.
12. Cheesman, E.H.: Blanchette. M.A.; Caney, M.V.: Maheu. L.J.; Miller, S.J.: Watson, A.D. Technetium-99m ECD for brain perfusion imaging—Ester-derivatized diamine-dithiol Tc complexes. Eur. J. Nucl. Med. **1988,** *14*, 304.
13. Holman, B.I.: Sporn. Y.; Benjamin-Sin. S.T.: Perez-Balino. N.; Davison. A.: Lister-James. J.: Kronauge. J.F.: Mitta. A.E.A.: Camin. L.L.; Camell. S.; Williams. S.J.; Carpenter. A.T. Myocardial imaging with Tc-99m CPI—Initial experience in the human. J. Nucl. Med. 1987, *28*, 13.
14. Lewis. J.S.: McCarthy, D.W.: McCarthy, T.J.; Fujibayashi. Y.: Welch, M.J. Evaluation of Cu-64-ATSM in vitro and in vivo in a hypoxic tumor model. J. Nucl. Med. **1999.** *40.* 177.
15. Kukis. D.L.; Diril, H.; Greiner, D.P.: De Nardo, G.L.: Salako. Q.A.; Meares. C.F. A comparative study of copper-67 radiolabeling and kinetic stabilities of antibody-macrocycle chelate conjugates. Cancer 1994, *73*, 779.
16. Herman. *B*. Fluorescence Microscopy: Bios Scientific Publishers: Oxford, 1997.
17. Grynkiewicz, G.; Poenie. M.; Tsien, R.Y. A new generation of Ca^{2+} indicators with greatly improved fluorescence properties. J. Biol. Chem. 1985, *260.* 3440.
18. Minta. A.; Kao, J.P.Y.; Tsien. R.Y. Fluorescent indicators for cytosolic calcium based on rhodamine and fluorescein chromophores. J. Biol. Chem. 1989, *264*, 8171.
19. Beeby, A.: Botchway, S.W.; Clarkson, I.M.; Faulkner. S.: Parker. D.: Parker, A.W.: Williams, J.A.G. Luminescence imaging microscopy and lifetime mapping using kinetically stable lanthanide(III) complexes. J. Photochem. Photobiol.. B Biol. 2000, *57*, 83.

20. Parker, D.; Williams. J.A.G. Getting excited about lanthanide complexation chemistry. J. Chem. Soc., Dalton Trans. 1996. 3613.
21. Beeby, A.: Dickins. R.S.; Faulkner, S.: Parker, D.: Williams. J.A.C. Luminescence from ytterbium(III) and its complexes in solution. Chem. Commun. 1997. 1401.
22. Beeby, A.; Faulkner, S.; Parker, D.: Williams, J.A.G. Sensitised luminescence from phenanthridine appended lanthanide complexes: Analysis of triplet mediated energy transfer processes in terbium. europium and neodymium complexes. J. Chem. Soc. Perkin Trans. 2 2001, 1268.
23. Colcher. D. Centralized radiolabeling of antibodies for radioimmunotherapy. J. Nucl. Med. 1998, *39S*. 11.
24. Anderson, C.J.; Pajeau, T.S.: Edwards, W.B.: Sherman, E.L.; Rogers. B.E.: Welch, M.J. In vitro and in vivo evaluation of copper-64-octreotide conjugates. J. Nucl. Med. 1995. *36*, 2315.
25. Eaton. M.A.W.; Baker, T.S.: Catterall. C.F.: Crook, K.; Macaulay, G.S.; Mason, B.; Norman. T.J.; Parker, D.; Perry. J.J.B.; Taylor. R.J.: Turner, A.; Weir, A.N. A new self-assembling system for targeted gene delivery. Angew. Chem. Int. Ed. 2000, *39*. 4063.
26. Peters, J.H.: Baumgarten, H. *Monoclonal Antibodies;* Springer Verlag: Berlin, 1992.
27. Heppeler, A.; Behe. M.; Froidvaux, S.: Hennig, M.; Jermann, E.; Maecke, H.R. Metal coordination chemical aspects and tumor targeting of a promising somatostatin analogue. J. Nucl. Med. 1998, *39*, 63P.
28. Barbet, J.; Peltier. P.; Bardet, S.; Vuillez, J.P.: Bachelot, L.: Denet, S.: Olivier, P.: Leccia, F.; Corcuff, B.; Huglo, D.: Proye, C.; Rouvier, E.; Meyer, P.; Chatal. J.F. Radioimmunodetection of medullary thyroid carcinoma using indium-111 bivalent hapten and anti-CEA X anti-DTPA-indium bispecific antibody. J. Nucl. Med. 1998, *39*. 1172.
29. Lyddiatt, A.; O'Sullivan, D.A. Biochemical recovery and purification of gene therapy vectors. Cum. Opin. Biotechnol. 1998, *9*, 177.
30. Ronsin, G.; Perrin. C.; Guedat, P.; Kremer, A.; Camilleri. P.; Kirby. A.J. Novel spermine-based cationic gemini surfactants for gene delivery. Chem. Commun. 2001. 2234.

Inclusion Compounds: Selectivity, Thermal Stability, and Kinetics

Luigi R. Nassimbeni
University of Cape Town, Rondebosch, Western Cape Province, South Africa

INTRODUCTION

The history of inclusion compounds dates back to the early nineteenth century, with Humphrey Davy's discovery of chlorine hydrate. but the field of inclusion phenomena, or host–guest chemistry, a subfield of supramolecular chemistry, is growing dramatically, particularly in the last 10 years. This can be seen at a glance in Fig. 1, which shows the number of abstracts appearing in *Chemical Abstracts* under the term "clathrate" and "inclusion compound" (Fig. 1a) and "supramolecular chemistry" (Fig. 1b).

It is instructive to list some of the main discoveries in this field, and listed below are 10 significant events:[1]

• 1811	Sir Humphrey Davy prepares chlorine hydrate.
• 1823	Michael Faraday confirms Davy's observation and determines the composition of chlorine hydrate.
• 1849	F. Wohler prepares a β-quinol•H_2S molecular complex.
• 1894	E. Fischer introduces the "lock and key" principle.
• 1947	D. E. Palin and H. M. Powell publish the crystal structures of β-quinol•H_2S compound.
• 1948	H. M. Powell coins the word "clathrate."
• 1967	C. J. Pedersen prepares crown ethers.
• 1969	J.-M. Lehn and coworkers synthesize cryptands.
• 1974	D. J. Cram and J. M. Cram introduce the terms "host." "guest." and "host–guest complexation."
• 1978	J. -M. Lehn introduces the concept and term "Supramolecular Chemistry."
• 1987	The Nobel prize for Chemistry was awarded to D. J. Cram. J. -M. Lehn. and C. J. Pedersen for their nork in the field of supramolecular chemistry.

CLASSIFICATION

Host inolecules may be broadly classified into two main types: those that form molecular complexes by fitting convex guests into the concave cavity of the host (examples include cyclodextrins, cyclophanes. calixarenes, cycloveratrylenes, and various carcerands[2]); and those that form lattice inclusion compounds by packing in such a manner as to leave cavities, channels. or layers in the crystal structure so as to accommodate various guest molecules.[3] Many of the compounds that act as hosts in the inclusion compounds were discovered by chance, but in the last 20 years, considerable effort has gone into the synthesis of host molecules with specific properties, and Weber reviewed the principles of directed host design.[4] He showed that a successful molecule should be bulky and rigid in order to provide suitable space so as to accommodate a guest. In addition, it is helpful for the host to have a high-affinity functional group that can engage in specific host–guest interactions, such as hydrogen bonding.

The templating effect of the guest in the formation of a given crystalline lattice inclusion compound is a subject currently under debate. What. for example, is the role of a "noncompetitive" solvent in the crystallization of a given compound? The fact that it can give rise to a different polymorph of the compound in question. suggests that there is a molecular recognition step involving the solvent during crystallization.[5] The guest may template the reaction, forming an inclusion compound that retains its structure even when the guest is removed, as occurs in the case of gossypol with dichloromethane.[6] This occurs infrequently with organic host molecules. and in most cases; the host compound reverts to its nonporous, α-phase, upon desorption.[7] The synthesis of an inclusion compound is carried out by dissolving the host in a liquid guest and allowing concentration of the solution. In the case of a solid guest, a noncompetitive solvent may be employed. The powdered host compound may also be exposed to vapors of the guest, and single crystals of diffraction quality may sometimes be prepared in this way.[8] Host–guest compounds may also be synthesized by direct grinding of two solids, although the mechanism of such reactions is not clearly understood and may involve partial melting.[9]

The general formation of the inclusion compound may be as follows:

$$H_{(s\,\alpha)} + nG_{(l)\text{ or }(g)} \rightarrow H \bullet Gn_{(s\,\beta)}$$

where a represents the nonporous phase of the pure host; H is the apohost, and β is the phase of the host–guest compound with guest :host ratio n, and l = liquid. g = gas, and s = solid.

Encyclopedia of Supramolecular Chemistry
DOI: 10.1081/E-ESMC 120012852

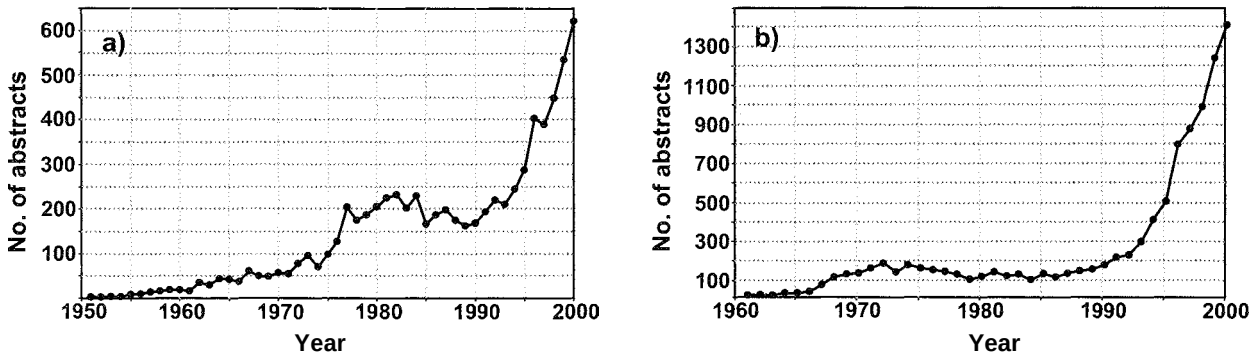

Fig. 1 (a) Number of abstracts found for the terms ''clathrate'' and ''inclusion compound,'' for the years 1950–2000 (b) Number of abstracts found for the term ''supramolecular,'' for the years 1950–2000

When the β-phase decomposes upon heating, it may do so in multiple steps:

$$H \bullet Gn_{(s,\beta)} \rightarrow H \bullet G(n - m)_{(s,\gamma)} + mG_{(g)} \uparrow$$

$$H \bullet G(n - m)_{(s,\gamma)} \rightarrow H_{(s,\alpha)} + (n - m)G_{(g)} \uparrow$$

The intermediate γ-phase, $H \bullet G(n-m)_{(s,\gamma)}$, may be stable over a wide teinperature range, but single crystals of $H \bullet Gn_{(s,\beta)}$ generally break up to form fine powders of the intermediate γ-phase, making it impossible to subject the latter to single-crystal structure analysis. However. demonstrated in recent work was the possibility of controlling the guest : host ratio of an inclusion coinpound by changing the crystallization temperature.[10] In this regard. Ibragimov formulated a rule that predicts the topology of inclusion compounds.[11] In essence, this states that at low crystallization temperatures. one may expect high guest : host ratios with layer or tubulate structures, and that by raising the temperature, the guest: host ratio decreases, giving rise to cryptates (true clathi-ates). When the temperature is sufficiently high and close to the boiling point of the guest. its thermal mobility is too great to allow entrapment. and the host crystallizes in its nonporous a-phase. This technique was employed to control the selectivity of xylene isomers by a dicarboxylic host.[12] A proper thermodynamic analysis, linking the guest–host ratio with the crystallization temperature has yet to be made.

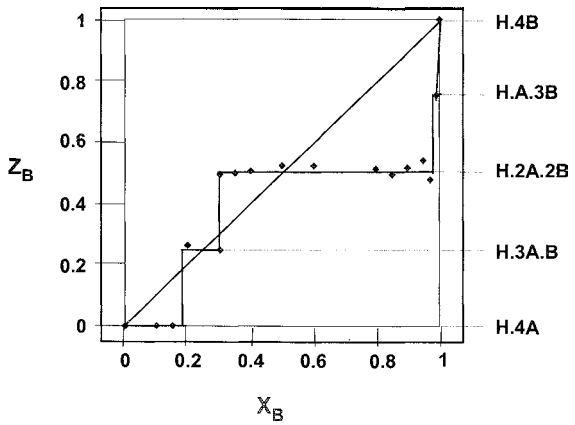

Fig. 2 Results of the competition experiments for the system $H \bullet nA \bullet (4-n)B$. *H* = *trans*-9,10-dihydroxy-9,10-*bis*(*p*-*tert*-butylphenyl)-9,10-dihydroanthracene; A = dimethylformamide; *B*=dimethylsulfoxide. (Reproduced by permission of the Royal Society of Chemistry.)

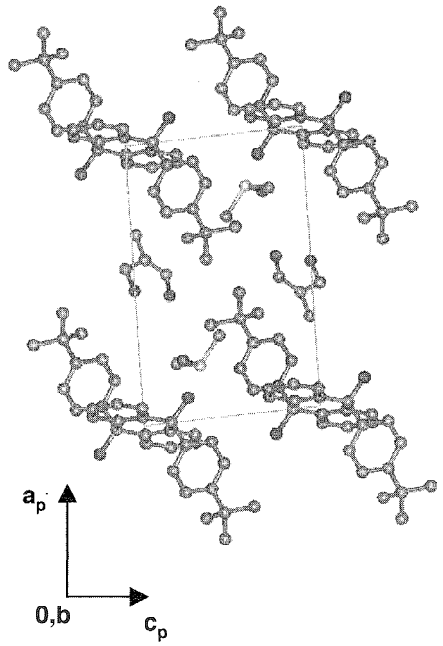

Fig. 3 Projection of the $H \bullet 2A \bullet 2B$ structure. viewed along [010]. (Reproduced by permission of the Royal Society of Chemistry.) (*View this art in color at www.dekker.com.*)

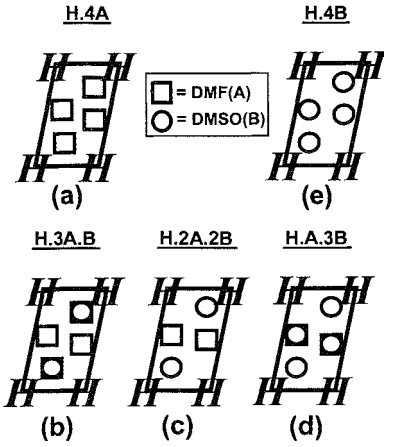

Fig. 4 The location of Guests A and B in the system H • 4A • (4 − n)B. (Reproduced by permission of the Royal Society of Chemistry.)

Recently, a clathrate system was announced in which the host entraps mixed guests. and the stoichiometry is controlled by the relative concentrations of the guests in the starting mixture. The host, *trans*-9,10-dihydroxy-9,10-*bis*(*p*-*tert*-butylphenyl)-9,10-dihydroanthracene (N) forms inclusion compounds with dimethylformanide (A) and dimethylsulfoxide (B) of the type H • nA • (4 – n)B, such that n varies from 0 to 4.[13] The results of competition experiments are given in Fig. 2, which shows that the stoichiometry of the inclusion compounds varies in discrete steps, giving rise to five distinct compounds: H • 4A, H • 3A • B, H • 2A • 2B, H • A • 3B, and H • 4B.

The compounds are isostructural with respect to the locations of the host atoms, shown in Fig. 3. The changes that occur in the positions of the guests are summarized in Fig. 4a–e.

This system, which allows control of the ratio of mixed guests, has implications in crystal engineering.[14] Thus, the physical and chemical properties of such compounds can be governed, which is significant for fields such as chemical sensors. optical and electronic properties of organic crystals, as well as their thermal stabilities and kinetics of decomposition.

SELECTIVITY

Selectivity Coefficient, Competition Experiments

The complementarity of molecular shape defines the process of molecular recognition. and the strength and directionality of the various intermolecular interactions are responsible for the stability of a given host–guest compound. In their account of the nature of supramolecular interactions, Steed and Atwood[15] discussed the full range of forces that impinge on a molecular assembly. They vary from strong ion–ion interactions ($\sim$250 kJmol^{-1}) to weak van der Waals forces (<5 kJmol^{-1}). Of these, the hydrogen bond is particularly important, and its properties were extensively reviewed.[16,17]

A quantitative measure of the selectivity of a given host compound for a given guest in a mixture is obtained by competition experiments. For a pair of competing guests, these involve the setting up of a series of vials in which the concentrations of the guest mixtures are varied systematically, and the dissolved host is allowed to crystallize under controlled conditions. The relative quantities of the enclathrated guests and of the mother liquors are analyzed with a suitable analytical technique, such as gas chromatography. thermal gravimetry, or NMR spectroscopy. In general, three kinds of selectivity curves arise. as shown in Fig. 5. The term X_A is the mole fraction of Guest A in the liquid mixture, and Z_A is that of Guest A entrapped in the crystal. The diagonal line represents zero selectivity; Curves b_1 and b_2 occur when Guest A is strongly selected over B for the whole concentration range.

Following Ward,[18] we may define a selectivity coefficient:

$$K_{A:B} = (K_{B:A})^{-1} = Z_A/Z_B{*}X_B/X_A \quad (x_A + x_B = 1)$$

Thus, $K_{A:B} = 1$ yields Curve a; $K_{A:B} = 2$ and 5 yield Curves b_1 and b_2, respectively; while Curve c results

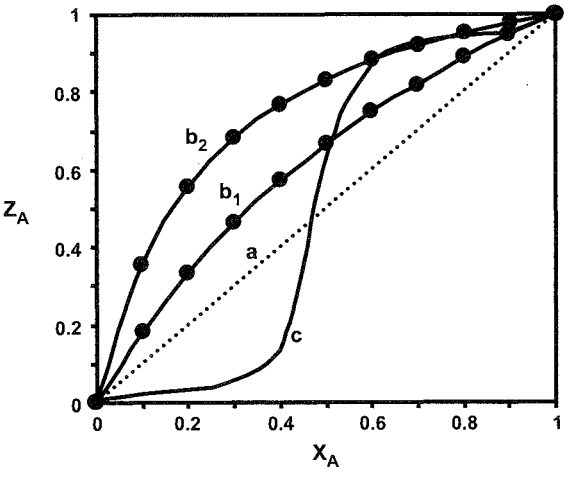

Fig. 5 Selectivity curves obtained from competition experiments. X_A = mole fraction of Guest A in the liquid; Z_A = mole fraction of Guest A in the crystal: Curve a represents zero selectivity. $K_{A:B} = 1$; Curves b_1, and b_2 represent selectivities with $K_{A:B} = 2$ and 5. respectively: and Curve c represents concentration-dependent selectivity.

when the selectivity is concentration dependent. These experiments can be extended to analyze simultaneous competition by three guests. The results are displayed on an equilateral triangle in which each apex represents a pure guest. Consider three guests A. B. and *C*, that compete in pairs for enclathration by a host *H*, such that $K_{A:B} = 5$, $K_{A:C} = 2$. and $K_{C:B} = 1$. A complete selectivity profile is shown in Fig. 6.

Three-component samples taken from the area represented by the circle centered at $X_A = X_B = X_C = 1/3$ will move toward the upper apex, showing an enrichment of Guest A by enclathration. When one of the pair-wise competition experiments gives rise to a concentration-dependent selectivity, the three coinponent experiments are more difficult to predict, because the synergistic effects of the third guest are difficult to estimate. They require a judicious sampling of the three component mixtures and generally result in a split of the enrichment process.[''] interestingly, it was demonstrated that competition experiments can also be carried out with solid guests by grinding appropriate mixtures with the solid host. This was shown in the inclusion by the host 1,1,6,6-tetraphenyl-hexa-2.4-diyne- 1.6-diol of the isomers aminobenzonitrile (ABN). Competition experiments showed that this host selected the guests in the preference of 2ABN > 3ABN > 4ABN, and the result of the solid–solid reactions yielded results that were remarkably similar to those carried out in solution using 1-butanol as a noncoinpetitive solvent.[8]

Competition experiments by enclathration can be employed to separate isomers with similar boiling points, and if we consider the selectivity diagram of the two-component systeins A–B with $K_{A:B} = 5$, discussed earlier, we can employ a McCabe–Thiele-type plot[18] to show that by starting with an initial mixture of $X_A = 0.1$, we can achieve an enrichment $X_A = 0.93$ in three successive crystallization steps (Fig. 7).

This technique has industrial implications. Guanidium organosulfonates were employed to separate isomeric mixtures of xylenes and dimethylnaphthalenes[18] as well as mixtures of xylenols.[19]

THERMAL STABILITY

Thermal Gravimetry (TG), Differential Scanning Calorimetry (DSC), Lattice Energies

Thermal gravimetry (TG) and differential scanning calorimetry (DSC) are the most accessible tools for the

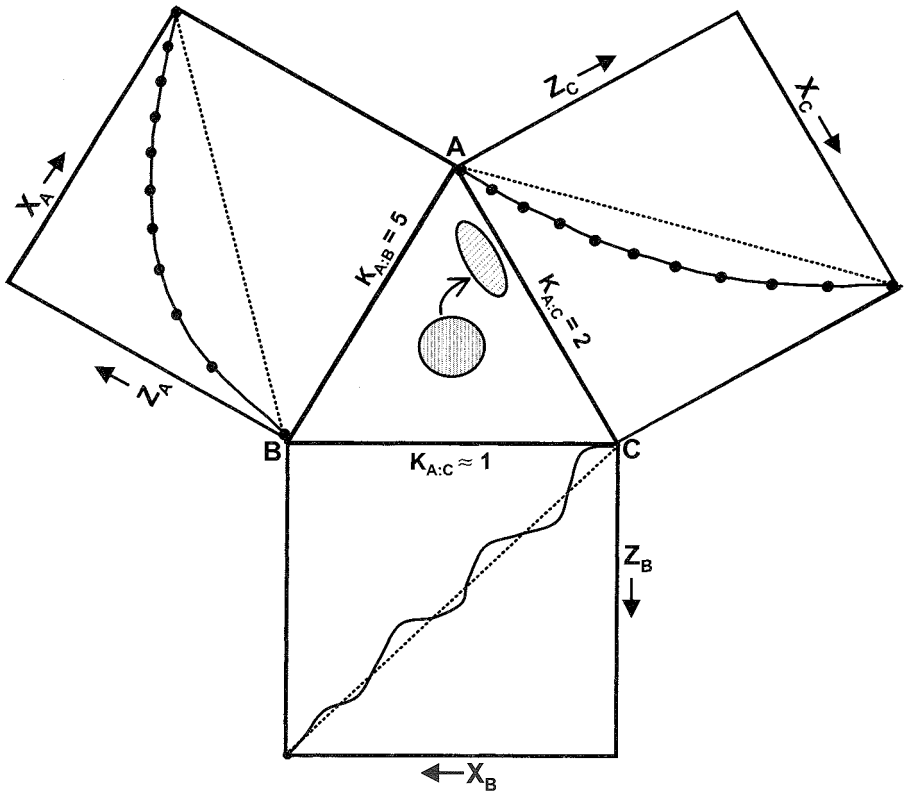

Fig. **6** Selectivity curves for a three-guest system A. B. C, such that $K_{A:B} = 5$. $K_{A:C} = 2$. and $K_{A:C}$

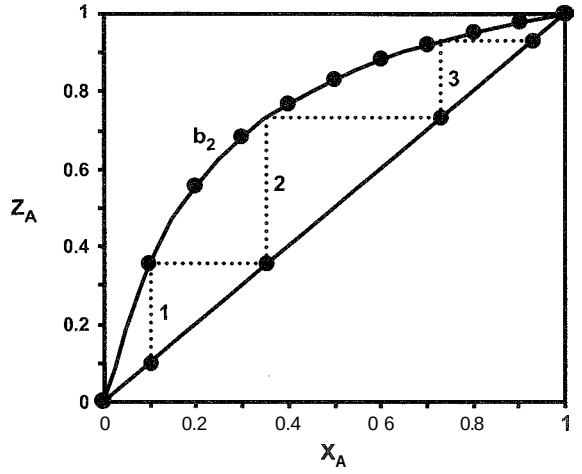

Fig. 7 McCabe–Thiele-type plot foı a txo-component system with $K_{AB}=5$ showing that Guest 4 ıs enriched from $X_A=0\,1$ to $X_A=0\,93$ ın three successıve crystallization steps

quantitative study of the thermal stability of inclusion compounds. When the guest is relatively volatile. TG is a suitable method for obtaining accurate host–guest ratios of inclusion compounds, and mass losses with an accuracy of 1–2% can be routinely obtained with modern commercial thermal balances. It should be emphasized that this is important, because inclusion compounds are often non-stoichiometric, and crystal structure analysis is not a suitable analytica! tool in this instance. This is because. in the refinement process, the site occupancies and temperature factors of the guest atoms are correlated. The DSC measurements yield the onset temperatures of the guest release reaction. T_{on}, and their associated enthalpy change *AN*. Such a measurement should be treated with caution. and accurate values can only be achieved if care is taken with regard to instrument calibrations, flow rate of the purging gas. heating rate. and the particle size distribution of the sample. The latter is crucial and is sometimes difficult to achieve, because the inclusion compound may be labile and not lend itself to crushing or sieving. A recommended technique is to prepare a sample of the host–guest system under conditions of fast stirring, which yields powders with small particles with a narrow size distribution. It should be noted however, that crystals grown under different conditions may yield inclusion compounds with different host : guest ratios; with differing structures, or different polymorphs of the same compound. It is thus important to monitor each preparation by x-ray powder diffraction to ensure consistency. Shown in Fig. 8 are the idealized curves of an inclusion compound $H\bullet G_n$ with a volatile guest that decomposes in a single step. The DSC shows two distinct endotherms: the first corresponding to guest loss followed by the second, due to melting of the host.

The multistep thermal decompositition of a host–guest system can be followed in this way. An illustrated example is given in Fig. 9, which shows the decomposition of the clathrate formed between the inorganic host tetrakis(4-aminopyridine)diisothiocyanatonickel(II) and dimethylsulfoxide. The TG shows four distinct steps: A. corresponding to the loss of two DMSO guests per host molecule: followed by B, corresponding to the loss of two 4-aminopyridine ligands; and C and D, due to the loss of single 4-aminopyridines. The DSC yields endotherms corresponding to B and C, but the trace for D is complex due to ligand decomposition.[20]

In order to obtain accurate. reproducible results for the desorption step, an apparatus was devised that measures the vapor pressure of a volatile guest over a large temperature range. The device comprises a transducer, which converts pressure to a voltage signal, which is amplified and fed to a computer. The inclusion compound is placed in a small flask, open to the transducer, both of which are immersed in a water bath. The temperatures of the compound and the water bath are monitored by thermocouples; and the heating rate is controlled. The method is fully automated and yields curves of P versus T under equilibrium conditions. The semilogarithmic plot of ln P versus $1/T$ has a slope of $-\Delta H/R$ and yields values of the enthalpy change of desorption to a precision of approximately 2%. This was employed in the study of the thermodynamics of decomposition of *bis*-(9,9′-dihydroxy-9.9'-difluorene)$\bullet$0.5 ethanol over the temperature range 30–80°C. yielding a AH=17.9 kJmol^{-1}.[21] When an inclusion compound decomposes, the guest release reaction is made up of two components: the desorption of the guest. and the rearrangement of the "empty cage" or β_0

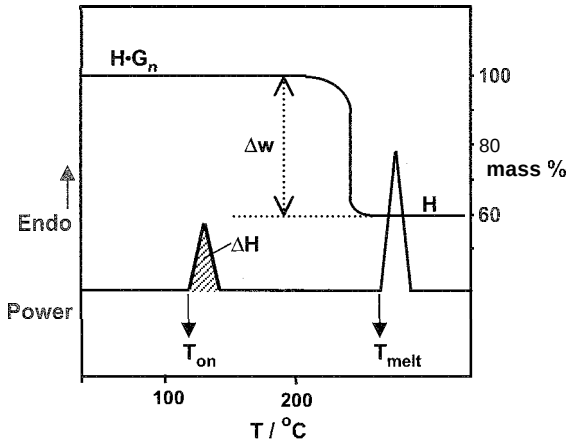

Fig. 8 The TG and DSC curves for the decomposition of an inclusion compound $H\bullet Gn_{,,\beta)} \rightarrow H_{,,\alpha)} + nG_{(g)}\uparrow$

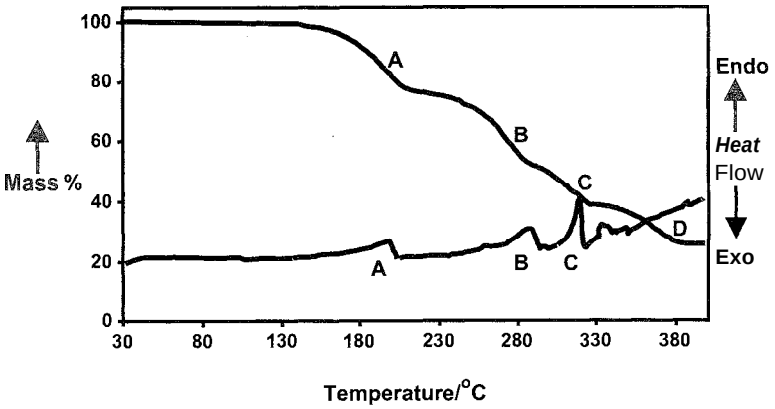

Fig. **9** Multistep decomposition of the inorganic clathrate tetrakis(4-aminopyridine)diisothiocyanatonickel (II) • 2 DMSO. (Reproduced by permission of the Royal Society of Chemistry.)

structure of the host to its nonporous α-phase.[22] The DSC endotherm measures the sum of these, generally with a precision of about 10%. The onset temperature T_{on} and the AH of the guest release reaction are measures of the thermal stability of the host–guest compound. To compare the stabilities of a series of compounds with different guests. one may calculate T_{on}/T_b, where T_b is the normal boiling point of the guest. High values of T_{on}/T_b and of AH are indicative of high thermal stability and of strong host–guest interactions. A quantitative measure of thermal stability is the lattice energy of the compound in question. This may be evaluated by the method of atom–atom potentials using the refined positions of accurate crystal structure determinations.

One may employ force fields of the following type:

$$V(r) = a\exp(-br) - c/r^6$$

where r is the interaction distance. and the coefficients a. b, and c are those given by Gavezzotti.[23] Care must be taken to incorporate a suitable hydrogen-bonding potential, such as that of Vedani and Dunitz,[24] which is formulated as $V\ (H\text{-bond}) = (A/R^{12} - C/R^{10})\ \cos'\ \theta$, where R is the distance between the donor hydrogen and acceptor atom.

θ is the Donor–H .... Acceptor angle, and the $\cos^2\theta$ term is the energy penalty paid by the bond in order to take nonlinearity into account. Such lattice energy calculations often correlate well with enthalpies of the guest release reaction and with onset temperatures.[8]

In cases where the guest is a high-temperature boiling liquid, the DSC may yield a single endotherm corresponding to the dissolution of the host in the escaping guest. In such cases. the AH and the dissolution temperatures may be correlated to the lattice energies of the compounds.

KINETICS

Kinetics of Desorption

The kinetics of desorption of a host–guest compound with a volatile guest may be monitored by measuring the mass as a function of time. The fraction decomposed. α, is evaluated from the mass loss:

$$\alpha = (m_o - m_t)/(m_o - m_f)$$

where m_o is the initial mass, m_t is the mass at time t, and m_f is the final mass. A generalized α-time curve is shown in Fig. 10. It comprises an initial step A, often attributed to the decomposition of impurities or superficial materials. followed by B, an induction period during which nucleation takes place. This is followed, in turn. by an acceleration period C, a deceleration period D, and finally completion, Step E.

Various models can be fitted to the α-time curves that correspond to particular mechanisms of the desolvation reaction.[25] The most common are as follows:

$$-\ln(1 - \alpha) = kt \quad \text{(First order—F1)}$$

$$1 - (1 - \alpha)^{1/2} = kt \quad \text{(Contracting area—R2)}$$

$$1 - (1 - \alpha)^{1/3} = kt \quad \text{(Contracting volume—R3)}$$

The best way to obtain the activation energy for the desorption reaction is to carry out a reries of isothermal runs at selected temperatures, finding the appropriate rate law and deriving the corresponding rate constants that can be employed in the Arrhenius equation:

$$k = \exp(-Ea/RT)$$

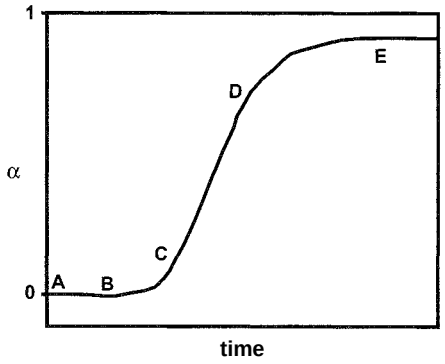

Fig. 10 Generalized α-time curve for a decomposition reaction.

The application of this equation to heterogeneous reactions is controversial, but Galway and Brown discuss this topic and give theoretical justification for its use.[26,27]

Kinetics of Enclathration

The kinetics of enclathration between a solid host and guest vapor received relatively little attention. This is because measurements are experimentally difficult, and the inclusion compounds formed are often unstable under ambient conditions. A suitable suspension balance, which allows measurement of mass change with time under controlled conditions of guest vapor and temperature, was constructed for this purpose.[28] An interesting aspect of these reactions is that they give rise to anti-Arrhenius behavior, in that for a given vapor pressure of the guest, the rate of the reaction decreases with increasing temperature. This arises from the fact that a threshold pressure, P_o, is required to initiate the reaction of the gaseous guest uptake by the host. This was noted for the enclathration of acetone vapor by the host *trans*-9,10-dihydroxy-9,10-diphenyl-9,10-dihydroanthracene,[29] when a plot of k_{obs} versus p at two different temperatures gives rise to two straight lines, as shown in Fig. 11.

Thus, when we consider the rate constant at a fixed pressure of (say) 100 mmHg, we obtain a value of 0.57 s^{-1} at *284* K. which decreases to 0.10 s^{-1} at 303 K.

Guest Exchange

The question of guest exchange in inclusion compounds received little attention, despite that fact that such processes are important for sensing and catalysis based on inclusion. However, a number of host–guest systems with organic and metal-containing hosts that entrap volatile guests were recently studied.[20,30] The host 1,1,6,6-tetraphenyl-2,4-diyne-1.6-diol (*H*) forms inclusion compounds with tetrahydrofuran (THF), and thiophene (THIO), and we analyzed the dynamics of the reaction:

$$H \bullet THF_{(s)} + 2\ THIO_{(g)} \rightarrow H \bullet 2\ THIO_{(s)} + 2\ THF_{(g)}$$

This was performed by exposing a powdered sample of $H \bullet 2\ THF_{(s)}$ to thiophene vapor in a closed vessel at 25°C. The resultant product was analyzed periodically by *DSC*, and the results are given schematically in Fig. 12.

In such reactions, there are two possible mechanisms for the exchange between guests G1 and 62:

1. The host–guest system retains its structure throughout the exchange and so behaves like a zeolite, with the

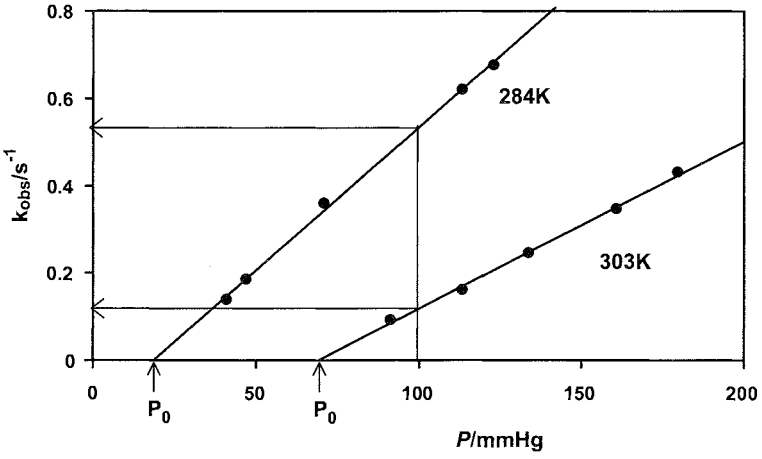

Fig. 11 Plot of k_{obs} versus guest pressure for the enclathration of acetone vapor by *trans*-9,10-dihydroxy-9,10-diphenyl-9,10-dihydroanthracene. Note the existence of threshold pressures P_o at both temperatures.

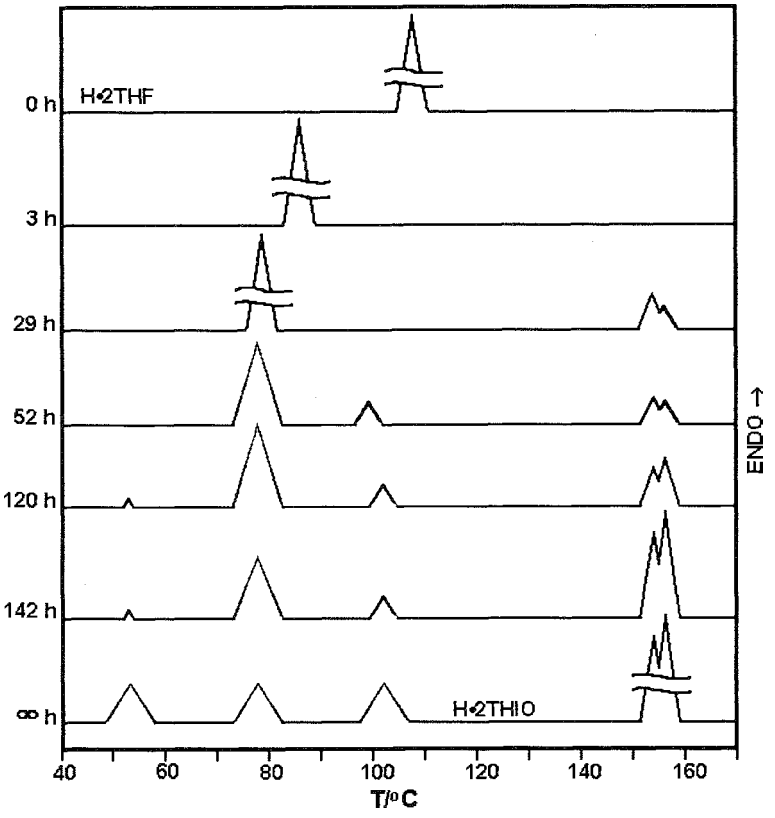

Fig. 12 The DSC curves for the guest exchange in the reaction Ha2 $THF_{(s)}$ + 2 $THIO_{(g)} \rightarrow H \bullet 2$ $THIO_{(s)}$ + 2 $THF_{(g)}$, with *H*=1.1.6. 6-tetraphenyl-2.4-diyne-1,6-diol (Reproduced by permission of the Royal Society of Chemistry)

channels remaining open to incoining and outgoing guest molecules:

$$H \bullet nG_{1(s)} + nG_{2(g)} \rightarrow H \bullet nG_{2(s)} + nG_{1(g)}$$

2. The host–guest system desorbs to yield the apohost (a-phase), which in turn, absorbs the incoming guest and forms the new structure:

$$H \bullet nG_{1(s,\beta)} \rightarrow H_{(s,\alpha)} + nG_1 \uparrow$$

$$H_{(s,\alpha)} + nG_{2(g)} \rightarrow H \bullet nG_{2(s,\beta)}$$

In the second mechanism, there would be a small but detectable amount of the apohost present throughout the time of guest exchange. We showed this to be the case in the study of the diol host *H* and its inclusion compounds, with G_1, G_2=furan, tetrahydrofuran, and thiophene.[30] It was noted that the kinetics of these exchange reactions depend on such factors as the particle size distribution of the $H \bullet nG_1$ solid, the vapor pressure of the incoming guest, and the strength of the host–guest interactions of both the reactant and the product.

In conclusion, the structures and topologies of inclusion compounds form the basis of their reactivities and their physico-chemico properties. An understanding of the molecular recognition process occurring in these compounds forms the basis of predicting their behavior.

ACKNOWLEDGMENTS

The author is indebted to Prof. M.R. Caira (Cape Town) for constructive comments. Thanks are due to Tanya le Roex and Dejana Vujovic for technical assistance. Research funding from the University of Cape Town and the National Research Foundation (Pretoria) is gratefully acknowledged.

ARTICLES OF FURTHER INTEREST

Channel Inclusion Compounds, p. *223*
Classical Descriptions of Inclusion Compounds, p. *253*
Isostructurality of Inclusion Compounds. p. *767*

Kinetics of Complexation, p. 776
Selectivity: *Thermodynamic* and Kinetic, p. 1225
Self-Assembly: Definition *and* Kinetic and *Thermo*-dynamic Considerations, p. 1248

REFERENCES

1. Nassimbeni, L.R. Thermodynamics and Kinetics of Crystalline Inclusion Compounds. In Crystal Engineering. From *Molecules and* Crystals to Materials; Braga. D., Grepioni. F.. Orpen, A.G., Eds.; Kluwer Academic Publishers: Dordrecht. 1999; 163–179.
2. Cram, D.J.: Cram, J.M. Container *Molecules* and *Their* Guests; Royal Society of Chemistry: Cambridge, 1994.
3. Vogtle, F. *Supramolecular* Chemistry; Wiley: Chichester. 1991: ch. 5.
4. Weber. E. Scissor-Type Hosts: Molecular Design and Inclusion Behaviour. In *Inclusion Compounds*; Atwood, J.L.. Davies, J.E.D., MacNicol, D.D., Eds.; Oxford University Press: Oxford, 1991: Vol. 4. 188–262.
5. Caira, M.R. Crystalline Polymorphism of Organic Compounds. In Design of Organic Solids: Weber, E.. Ed.: Springer: Berlin, 1998; 163–208.
6. Ibragimov. B.T.: Talipov. S.A.; Aripov, T.F. Inclusion complexes of the natural product gossypol—Recognition by gossypol of halogeno methanes—Structure of the dichloromethane complex of gossypol and single crystal conservation after decomposition. J. Incl. Phenom. 1994. *17*, 317–324.
7. Bond, D.R.; Caira, M.R.: Harvey. G.A.: Nassimbeni. L.R. Complexation with diol host compounds. 5. Structures and thermal analysis of inclusion compounds of *trans*-9.10-dihydroxy-9.10-diphenyl-9.10-dihydroanthracene with 2-butanone. 4-vinylpyridine, 4-methylpyridine and 2-methylpyridine. Acta Crystallogr. 1990. *B46*. 771–780.
8. Caira. M.R.: Nassimbeni, L.R.: Toda. F.; Vujovic, D. Inclusion of aminobenzonitrile isomers by a diol host compound: Structure and selectivity. J. Am. Chem. Soc. 2000. *122* (39). 9367–9372.
9. Rothenberg, G.: Downie, A.P.: Raston. C.L.; Scott. J.L. Understanding solidsolid organic reactions. J. Am. Chem. Soc. 2001, 123. 8701–8708.
10. Nassimbeni, L.R.: Su, H. Controlled host:guest ratio in an inclusion compound. J. Phys. Org. Chem. 2000, *13*. 368–371.
11. Ibragimov. B. A simple correlation between the structures of different crystal modifications of a given host–guest complex and their crystallisation temperatures. J. Incl. Phenom. Macrocycl. Chem. 1999. *34*. 345–353.
12. Beketov, K.: Weber, E.; Seidel. J.: Kohnke, K.: Makhkamov, K.; Ibragimov, B. Temperature controlled selectivity of isomeric guest inclusion: Enclathration and release of xylenes by 1,1′-binapthyl-2,2′-dicarboxylic acid. Chem. Commun. 1999. 91–92.
13. Caira. M.R.: le Roex, T.; Nassimbeni. L.R. Tunable clathrates. Chem. Commun. 2001. 2128–2129.
14. Desiraju. G.R. *Crystal* Engineering; Elsevier: Amsterdam, 1989.
15. Steed, J.W.: Atwood. J.-L. *Supramolecular Chemistry*; Wiley: Chichester. 2000; 19–29.
16. Jeffrey. G.A. *An Introduction* to *Hydrogen Bonding*; Oxford University Press: Oxford, 1997.
17. Desiraju, G.R.: Steiner. T. The Weak Hydrogen Bond; Oxford University Press: Oxford, 1999.
18. Pivotar, A.M.; Holman, K.T.; Ward. M.D. Shape selective separation of molecular isomers with tunable hydrogen-bonded host frameworks. Chem. Mater. 2001. *13*. 3018–3031.
19. Caira. M.R.; Nassimbeni, L.R.; Vujovic, D.; Toda. F. Separation of xylenols by inclusion. J. Phys. Org. Chem. 2000: *13*, 75–79.
20. Nassimbeni, L.R.; Kilkenny. M.L. Tetrakis(4-aminopyridine)diisothiocyanatonickel(II) and its clathrates with EtOH. Me_2CO and DMSO: Structures, thermal stabilities and guest exchange. J. Chem. Soc. Dalton Trans. 2001. 1172–1175.
21. Barbour. L.J.; Caira. M.R.: Nassimbeni. L.R.; Wierig, A.; Weber, E. Complexation with diol host compounds. Part 17. Structures and thermal analysis of 9.9'-dihydroxy-9.9'-bitluorene with ethanol. 1-butanol and pyridine. Supramol. Chern. 1995. *5*, 153–158.
22. Lipkowski, J. Werner Clathrates. In *Comprehensive Supramolecular* Chemistry: MacNicol, D.D.. Toda, F.. Bishop. R.. Eds.; Pergamon: Oxford, 1996; Vol. 6. 691–714.
23. Gavezzotti. A. The crystal packing of organic molecules: Challenge and fascination below 1000 Da. Crystallogr. Rev. 1998. 7. 5–121.
24. Vedani, A.; Dunitz. J.D. Lone-pair directionality in hydrogen-bond potential functions for molecular mechanics calculations: The inhibition of human carbonic anhydrase II by sulfonamides. J. Am. Chem. Soc. 1985. *107*, 7653–7658.
25. Galway, A.K.: Brown. M.E. Kinetic Background to Thermal Analysis and Calorimetry. In Handbook of *Thermal Analysis* and Calorimetry. *Vol. I*, Principles *and* Practice: Brown, M.E.. Ed.; Elsevier Science B.V.: Amsterdam, 1998; 147–225.
26. Brown, M.E.; Galway, A.K. Arrhenius parameters for solid-state reactions from isothermal rate–time curves. Anal. Chem. 1989. 61, 1136–1139.
27. Galway, A.K.; Brown. M.E. A theoretical justification for the application of the Arrhenius equation to kinetics of solid state reactions (mainly ionic crystals). Proc. R. Soc. Lond.. A 1995. *450*. 501–512.
28. Barbour. L.J.; Achleitner. K.: Green. J.R. A system of studying gas–solid reaction kinetics in controlled atmospheres. Thermochim. Acta 1992. 205, 171–177.
29. Barbour. L.J.; Caira, M.R.: Nassimbeni. L.R. Kinetics of inclusion. J. Chem. Soc., Perkin Trans., 2 1993. 2321–2322.
30. Caira, M.R.; Nassimbeni, L.R.: Toda, F.; Vujovic; D. Inclusion by a diol host compound: Structure and dynamics of volatile guest exchange. J. Chem. Soc., Perkin Trans., 2 2001, 2119–2124.

Inclusion Reactions and Polymerization

Mikiji Miyata
Osaka University, Osaka, Japan

INTRODUCTION

A variety of monomers can be trapped in the inclusion spaces at the inolecular level and polymerized under suitable conditions. Such a reaction is called inclusion polymerization.[1–10] The study of inclusion polymerization started soon after the discovery of a honeycomb structure of urea inclusion compounds. The early study aimed to obtain highly stereoregular and asymmetric polymers in the spaces. Further studies brought about a profound understanding of the space effects from various viewpoints. Now. inclusion polymerization is classified between bulk or solution polymerization and solid state polymerization. In other words. it may be situated as low-dimensional and space-dependent polymerizations. Such a polymerization closely relates to supramolecular chemistry from a viewpoint of molecular information and expression.

GENERAL FEATURES

Cyclic Process

In Fig. 1, a cyclic process for inclusion polymerization is shown. The process consists of four steps: 1) hybridization of a host assembly with a solvent; 2) complexation of the host with a guest monomer; 3) polymerization of the monomer; and 4) separation of the resulting polymer from the host. This cycle is based on spontaneous and noncovalent phenomena, such as intermolecular association and dissociation among host–host, host–guest, and guest–guest components.

The host components (Fig. 1a) are first recrystallized from usual solvents for isolation and purification. This operation produces host assemblies with or without the solvents (Fig. Ib). There are two methods for obtaining inclusion compounds with the monomers (Fig. 1c): by the addition of monomers into the solvents and by replacement of the guests with retention of the host assemblies, called intercalation.

The polymerization should consist of four elementary reactions: an initiation. a propagation, a termination. and a chain transfer. γ-Ray and UV irradiation are preferably employed for the initiation, although conventional free-radical initiators are also available. The propagation reaction can be accelerated at elevated temperatures. because molecular motions of the included monomers are constrained in the inclusion spaces. The termination reaction is inhibited due to isolation of the active species in the spaces. Any transfer reaction might take place between the host and guest components.

Inclusion polymerization usually results in host–polymer composites (Fig. 1d). The addition of suitable solvents induces separation of the resulting polymers from the hosts. The separated polymers sometimes involve the host component even after thorough solvent treatment. This may be explained by the fact that the initiating radicals come from the hosts in some cases. The separated host components assemble together by recrystallization to give original inclusion compounds with solvents (Fig, 1a).

Effects of the Inclusion Spaces

Inclusion polymerization may be reasonably distinguished from other polymerizations by various effects of the inclusion spaces. as mentioned below. Shown in Fig. 2 is a general relation in size between the inclusion spaces and guest molecules. A macroscopic flask (Fig. 2a) in a chemical laboratory practically has an infinite space as compared with a monomeric molecule. enabling us to neglect any effects of the space. Monomer molecules freely move in the space at moderate temperatures. In contrast. a molecular flask at a nanometer level (Fig. 2b. c) has spaces nearly equal to guest molecules in size. Because electromagnetic forces work among the host and guest molecules. monomer molecules are constrained in the spaces, even at relatively high temperatures, leading to the observation of various space effects. On the other hand; assemblies composed of the monomers only (Fig. 2d) have no inclusion spaces in the solid state, meaning that the space effects may be ignored. In this case. the monomer molecules can move slightly below their melting temperatures.

A comparison among the polymerizations in the different states is summarized in Table 1. The monomer molecules form low-dimensional and anisotropic assemblies in the inclusion and solid states; although they form three-dimensional and isotropic assemblies in the solution

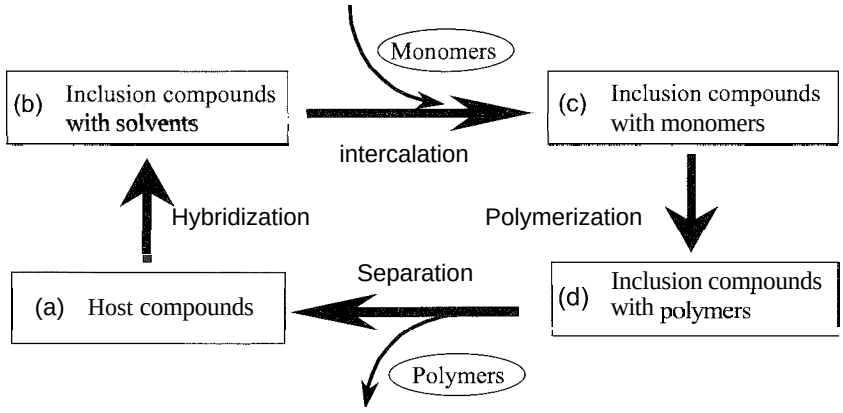

Fig. 1 A cyclic process for the study of inclusion polymerization. Parts (a) through (d) show products of the inclusion process.

or bulk state. One- or two-dimensional assemblies are formed in a channel (canal) or an interlayer, where corresponding one- or two-dimensional inclusion polymerization may take place. respectively. The inclusion spaces vary in size, shape, polarity, and chirality. The use of a set of the different spaces enables us to observe different inclusion polymerizations, leading to interpretation of the space effects.

ONE-DIMENSIONAL INCLUSION POLYMERIZATION

Hosts and Monomers

Inclusion polymerization is now recognized as a general polymerization that is useful for over 100 different monomers. Shown in Figs. 3 and 4 are some hosts and monomers employed so far for one-dimensional inclusion polymerization, respectively. First, a pair of hosts, urea (Fig. 3a) and thiourea (Fig. 3b), were used for the polymerization of 1,3-butadiene and 2,3-dimethyl-1,3-butadiene, respectively. Perhydrotriphenylene (Fig. 3c) was applied to many methyl-substituted butadiene derivatives, yielding the corresponding polymers with 1,4-*trans* units. Pioneering work was accomplished for optical resolution of the racemic host. leading to the first asymmetric inclusion polymerization of 1,3-pentadiene.

A chiral host could readily be available from a naturally occurring compound. The use of steroidal acid, deoxycholic acid (Fig. 3d), yielded coinprehensive polymers, particularly, optically active polymers from prochiral monomers. Many derivatives of deoxycholic acid have the corresponding characteristic inclusion abilities. For example, use of apocholic acid (Fig. 3e), cholic acid (Fig. 3f), and chenodeoxycholic acid (Fig. 3g) enabled us to perform one-dimensional inclusion polymerization of various diene and vinyl monomers.

Other effective hosts are cyclophosphazenes, such as *tris*(*o*-phenylenedioxy)cyclotriphosphazene (Fig. 3h) and

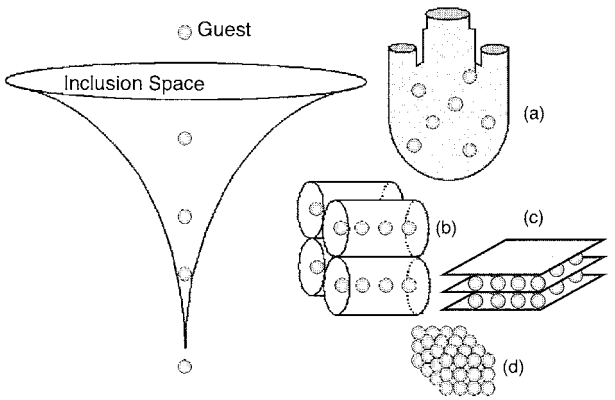

Fig. 2 A relative relationship between spaces and guest molecules: (a) a container with a macroscopic space: containers with molecular-level spaces called (b) channels and (c) interlayers: and (d) a molecular assembly without containers. (View *this art in* color *at www.dekker.com.*)

Table 1 Space effects among the polymerizations in different states

Polymerization	Solution or bulk	Inclusion	Solid stale
Space size	Macroscopic	Molecular-level	None
Assembly	Isotropic	Anisotropic	Anisotropic
Space effect	Negligible	Not negligible	Negligible
Dimensionality	Three-dimensional	Low-dimensional	Low-dimensional

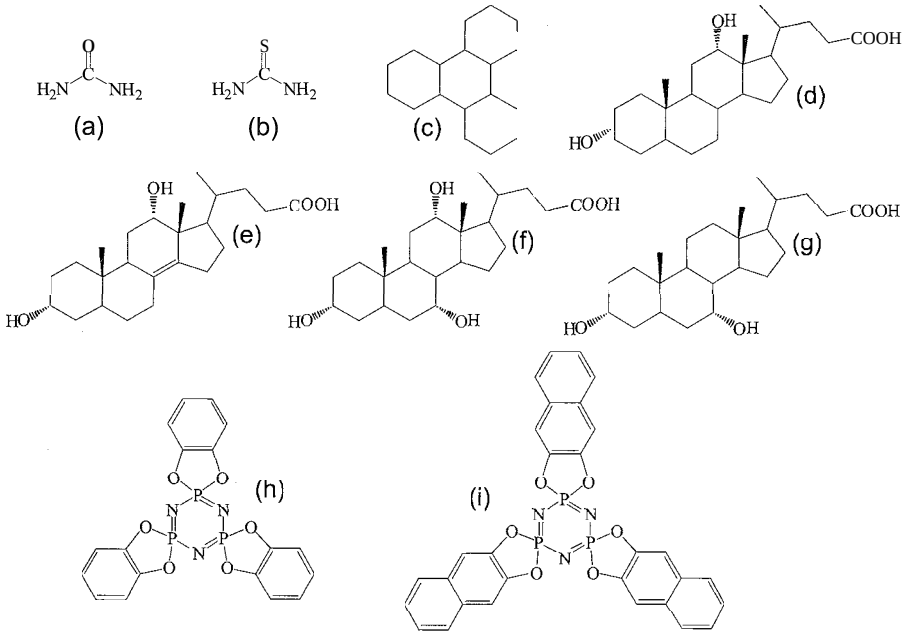

Fig. **3** Organic hosts used for one-dimensional inclusion polymerization: (a) urea: (b) thiourea; (c) perhydrotriphenylene; (d) deoxycholic acid; (e) apocholic acid; (f) cholic acid; (g) chenodeoxycholic acid; (h) *tris*(*o*-phenylenedioxy)cyclotriphosphazene; and (i) *tris*(2,3-naphthalenedioxy)cyclotriphosphazene.

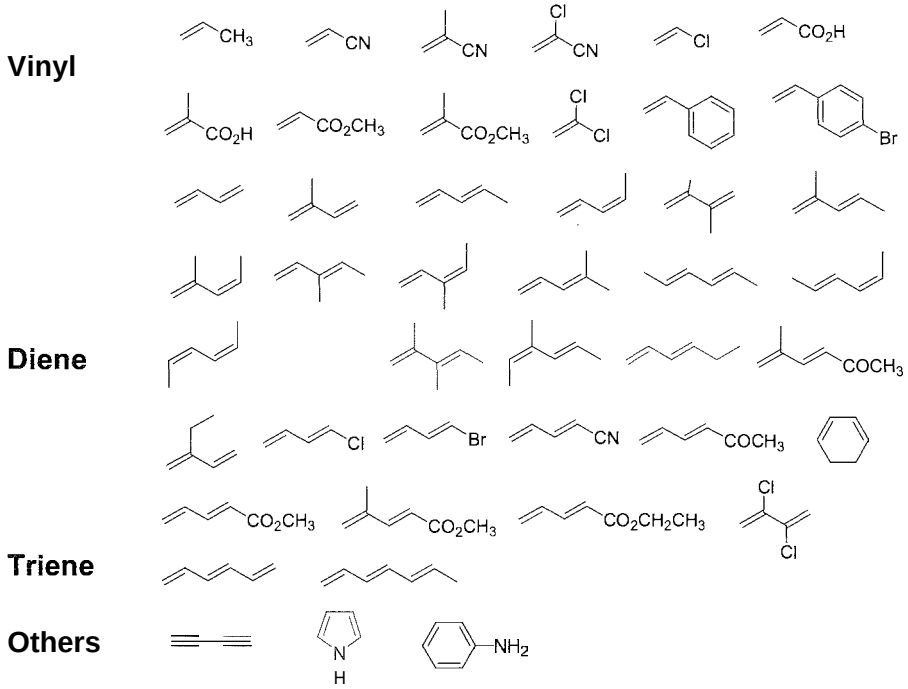

Fig. 4 Various monomers used for one-dimensional inclusion polymerization

tris(2,3-naphthalenedioxy)-cyclotriphosphazene (Fig. 3i). They were utilized for inclusion polymerization of many diene and vinyl monomers. Cyclodextrins were used for addition polymerization as well as polycondensation. Some kinds of inorganic polymers were used for one-dimensional polymerization. For example, a novel zeolite ZSM-5 was employed for the polymerization of vinyl monomers, such as propylene and 1-hexene.

It can be seen from Fig. 4 that many diene monomers were polymerized using various hosts. It might be possible to polymerize multiconjugated monomers, such as trienes and tetraenes, in one-dimensional spaces. Diacetylene spontaneously polymerized in channels of three hosts: perhydrotriphenylene, deoxycholic acid, and apocholic acid. On the other hand, there are not so many studies of the polymerization of vinyl monomers, because highly stereoregular polymers are not obtained.

Reaction Mechanism

Direct evidence for polymerization in the channels is given by crystal structure analysis. We can compare crystal structures before the polymerization and after the polymerization. Computed tomography works well in simulating whether or not inclusion polymerization will take place. Comparison of cross sections of channels with those of polymers enables us to consider whether or not the resulting polymers can be accommodated in the channels.

Radical species during inclusion polymerization can readily be detected by ESR spectroscopy, indicating that the radicals are thermally stable in the channels. The reason is that the radicals in the channels do not meet with each other due to the host walls. y-Irradiation produces radicals of the host component as well as the monomers. Monomeric and propagating radicals were observed in the case of urea. while only the propagating radicals were observed in the case of perhydrotriphenylene, deoxycholic acid, and apocholic acid. Simulation of the spectra clarified that the propagating radicals do not rotate freely, indicating that mobilities of the radicals are constrained in the channels.

Molecular motions are much smaller in channels than in solution at the same temperature. This indicates that the polymerization may proceed slowly. But the neighboring monomers are located very near, suggesting that the reaction may proceed rapidly. This is how the reversed effects work during the propagation reaction. It is known that inclusion polymerization smoothly occurs at low temperatures in the channels of urea, thiourea, and perhydrotriphenylene. However, in the case of steroidal hosts, we observed a decrease in polymerization rates. For example. in one case, the polymerization reached a saturated state after 1 month.

Table 2 Parameters for the inclusion and solution polymerizations

Parameter	Inclusion	Solution
*k*p	10^{-3} kg mol^{-1} s^{-1}	10^{0}–10^{3} L mol^{-1} s^{-1}
kt	10^{-9} kg mol^{-1} s^{-1}	10^{7}–10^{10} L mol^{-1} s^{-1}
[M]	10^{-3} mol kg^{-1}	10^{-7}–10^{-8} mol L^{-1}
Lifetime of M	$>10^{6}$ s	0.1–1 s

Shown in Table 2 are the rate constants for the polymerization of *trans*-1-chloro-1,3-butadiene in the channels of deoxycholic acid. The rate constant of the propagation (kp) was about 10^{-3} kg mol^{-1} sec^{-1}, less than 10^{-3} of that for the solution. The termination rate constant is extremely small: about less than 10^{-10} of that for solution. Another important finding is that the concentration of radicals in the channels amounted to about 10^{-3} mol per 1 kg of the host by means of ESR spectroscopy. This concentration exceeds that for usual solution polymerizations by a factor of 10'. These results indicate that decrease of the propagation rate may be compensated for by a decrease of termination reaction and by an increase of radical concentration.

Steric Control

There are many possible schemes for addition reactions of diene monomers from electronical and steric viewpoints. Because the monomer molecules arrange along the direction of the channels, α,ω-addition may selectively take place in one-dimensional inclusion polymerization. Therefore, conjugated polyenes, such as dienes and trienes, may selectively polymerize by 1,4- and 1,6-addition, respectively. 1,3-Butadiene polymerized via 1,4-addition exclusively in the channels of urea and perhydrotriphenylene. while the same monomer polymerized via both 1,2- and 1,4-additions in the channels of deoxycholic acid and apocholic acid. Moreover, we have to evaluate head-to-tail or head-to-head (tail-to-tail) additions in the case of dissymmetric conjugated diene monomers such as isoprene and 1.3-pentadiene.

Tacticities of the polymers were estimated. For example, poly(l.3-pentadiene) was highly isotactic in the channels of perhydrotriphenylene, while it was preferentially isotactic (meso:racemic = 2:1) in the channels of deoxycholic acid. A completely isotactic polymer was utilized to prepare a unique polymer. hemitactic polypropylene, by hydrogenation of a completely 1,4-*trans* isotactic poly(2-methyl-1,3-pentadiene).

Chiral hosts provide chiral molecular-level spaces, where asymmetric inclusion polymerization may occur. A

requirement is that the polymerization proceed via head-to-tail and isotactic addition along a one-dimensional array in a chiral channel. So far, many optically active polymers were prepared from prochiral diene monomers by using chiral hosts. For example, optically resolved perhydrotriphenylene gave asymmetric polymers from *trans*-1,3-pentadiene. while deoxycholic acid gave those from *cis*-1,3-pentadiene. These polymers were ozonolyzed to give optical yields over 10% e.e. and about 20%, respectively.

Space-Size Effects

It is considered that the motion of guest molecules depends on the space sizes even at the same temperature. That is, the molecules can move more freely in a larger space than in a smaller space. Such a difference would affect polymerization behaviors. Such space effects can be observed on the basis of subtle changes of polymerization behaviors by using a suitable set of hosts. Use of a set of the hosts, deoxycholic acid, apocholic acid, cholic acid, and chenodeoxycholic acid, enables us to observe the effects of one-dimensional polymerization in detail. On the other hand, a pair composed of urea and thiourea is not suitable for such an aim, because the pair does not include identical monomers at the same temperatures.

The following three points were ascertained: 1) polymerizabilities of the monomers; 2) motion of polymer chains around the ends of the propagating radicals; and 3) microstructures of the resultant polymers. These space-size effects are summarized in Table 3.

Only a definite scope of monomers can be polymerized in a given host. This indicates that inclusion polymerization displays a sterically different boundary condition from other polymerizations. That is, an increase of one methylene unit of one monomer can induce an inhibition of the polymerization in a given channel (Fig. 5a,b). Moreover, the relative sizes of the channels change the polymerizabilities of the identical monomers. Even though a monomer does not polymerize in a small channel, the same monomer polymerizes in a larger channel, (Fig. 5b,c). For example, 4-methyl-1,3-pentadiene polymerized in the smaller channels of deoxycholic acid,

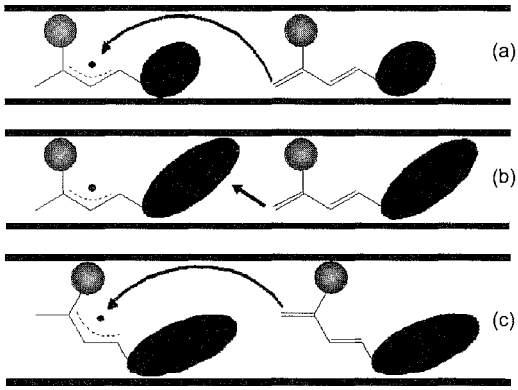

Fig. **5** Polymerizabilities of the monomers in the channels: (a) smaller monomers in a smaller channel can be polymerized; (b) larger monomers in a smaller channel are not polymerized: and (c) larger monomers in a larger channel can be polymerized.

while 2,4-dimethyl-1,3-pentadiene did not. However, the latter polymerized in the larger channels of apocholic acid.

The radicals can move depending on space sizes and shapes. So, it is considered that the propagating radicals are tightly included in the smaller channels and loosely in the larger channels. This means that an identical monomer exhibits different ESR spectra in various channels. A set of steroidal hosts enabled us to detect a large amount of such slightly different ESR spectra of the propagating radicals from various vinyl and diene monomers having alkyl and polar substituents. Simulation studies showed that such spectra may be explained by different conformations of the polymer chain ends.

Stereoregularities of the resulting polymers depend on the sizes of the host channels. Moreover, the space effect in chirality was observed in asymmetric inclusion polymerization of *trans*- or cis-2-methyl-l,3-pentadiene by using a pair of hosts, deoxycholic acid and apocholic acid. We obtained optically active polymers with predominant absolute configurations (R). Optical yields varied with the polymerization conditions and the hosts. A maximum optical yield of the *trans* monomer was *36%* in the channel of apocholic acid.

Table **3** Space-size effects on one-dimensional inclusion polymerization

Inclusion *space*	Polymerizability	*Propagating radicals*	*Selectivity* of *reaction*
Large space	Large scope	Large motion	Low selectivity
↓	↓	↓	↓
Small space	Small scope	Small motion	High selectivity

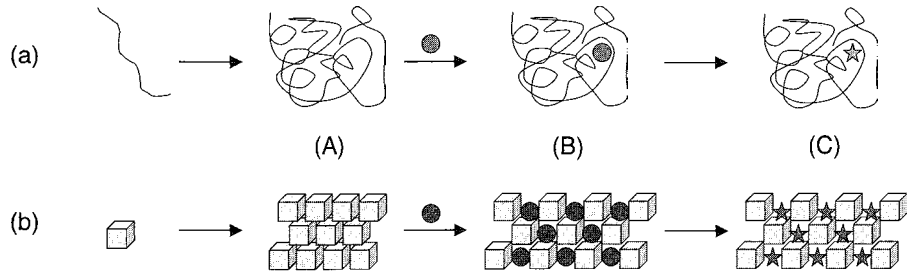

Fig. 6 Conceptual comparison of the processes for enzymatic reaction of proteins (a) and inclusion polymerization (b). The chiral and sequential carbon chains express their information through their architectures (A), host–guest compounds (B), and reactions of the guests (C). *(View this art in color at www.dekker.com.)*

TWO-DIMENSIONAL INCLUSION *POLYMERIZATION*

Some two-dimensional inclusion polymerizations are known. For example. montmorillonite and graphite were used for the polymerization of vinyl monomers such as methyl methacrplate and styrene, respectively. Polymerization of salts of 6-amino-2,4-*trans*,*trans*-hexadienoic acid was performed using perovskite-type layered compounds on UV or γ-ray irradiation, resulting in stereoregular polymers with a high head-to-tail, 1,4-*trans* structure. Many organic long-chain compounds form bilayered membranes to form a matrix for the two-dimensional polymerization. For example, photopolymerization was carried out using cast films composed of double-chain ammonium amphiphile involving a cross-linked acrylate polymer. Extraction of the amphiphile with methanol left a multilayered film.

Recently, it was found that crystalline organic salts of unsaturated carboxylic acids with aromatic amines were polymerized by UV irradiation to yield highly stereoregular polymers.[11,12] The bilayered polymeric aggregates were ascertained to replace amine components through intercalation. So. the polymerization is considered to correspond to one of the two-dimensional inclusion polymerizations. In this assembly, the aromatic part of the amines corresponds to the host component, while the alkyl part of the acids corresponds to the guest component. The amines employed are benzylamine, 1-naphthylmethylamine, long-alkylamines and their derivatives, and so on.

The polymerization of sorbic acid was found to proceed highly selectively to give a 1,4-*trans*, *erythro*-diisotactic structure, because ^{13}C-NMR spectrum of the polymer exhibits simple and sharp absorptions. Although the resulting polymers showed no optical rotation. crystal structural analysis tells us the following interesting feature of the polymerization. The molecules in one array polymerize to give a chiral polymer with (*R*,*R*) absolute configuration. while that in the neighboring array do so with (*S*,*S*). This means that we obtained a racemate of chiral polymers.

INCLUSION *POLYMERIZATION BASED ON MOLECULAR INFORMATION*

The study on inclusion polymerization by using steroidal hosts led us to the concept of molecular information and expression. as follows. It is theoretically considered that molecular information at a nanometer level may originate from sequential and chiral carbon chains, like proteins and steroidal molecules. As shown in Fig. 6a, the proteins express their molecular information through noncovalent bonds by the following processes: molecular architecture (Fig. 6A). host–guest compounds (Fig. 6B), and reactions of the included guest components (Fig. 6C). Similarly. the steroidal molecules express their information through the noncovalent processes (Fig. 6b). Therefore, inclusion polymerization corresponds to one step of the expression process of molecular information that the sequential and chiral carbon-chains store.

CONCLUSION

Starting from the synthesis of stereoregular and optically active polymers, we reached the idea that inclusion polymerization constitutes one of supramolecular chemistry from a viewpoint of the space effects. Now such a study might be connected to nanotechnology. because the polymerization can produce molecular composite materials, such as molecular wires; layers, and so on. The bottom-up technology would be constructed through various

noncovalent processes that are based on the principle of molecular information and expression.

ARTICLES OF FURTHER INTEREST

Channel Inclusion Compounds, p. *223*
Chiral Induction, p. *245*
Concepts in Crystal Engineering, p. *319*
Deoxycholic, Cholic, and Apocholic Acids, p. *441*
Electron Paramagnetic Resonance Spectroscopy, p. *520*
Solid-Stnte Reactivity/Topochemistry, p. *1316*

REFERENCES

1. Chatani. Y. Prog. Polym. Sci.. Jpn. 1974. 7. 149.
2. Takemoto. K.; Miyata, M. J. Macromol. Sci., Rev. Macromol. Chem. 1980. 618, 83.
3. Farina. M. Makromol. Chem. Suppl. 1981, 4. 21.
4. Farina, M.: Di Silvestro, G.; Sozzani. P. Mol. Cryst. Liq. Cryst. 1983. 93, 169.
5. Farina, M. Inclusion Compounds: Atwood. J.L.. Davies. J.E.D.. MacNicol. D.D.. Eds.: Academic Press: London, 1984: Vol. 3. 297–329.
6. Farina. M.: Di Silvestro. G. Encyclopedia *in* Polymer *Science and* Engineering, 2nd Ed.: Mark. H.F., Bikales, N.M.. Overberger, C.G., Menges, G., Eds.: Wiley & Sons: New York. 1988: Vol. 12. 486–504.
7. Miyata. M. *Polymerization* in *Organized Media*; Paleos, C.M., Ed.: Gordon and Breach Science Publishers: New York. 1992: 327–367.
8. Takemoto. K.; Miyata, M. Advances *in Supramolecular Chemistry*; Gokel, G.W.. Ed.: JAI Press Inc.: Greenwich. 1993: Vol. 3. 37–63.
9. Miyata, M. *Comprehensive Supramolecular Chemistry;* Volume 10 Special Topics Related to Supramolecular Chemistry: Reinhoudt. N.D., Ed.: Pergamon Press: Oxford. 1996: 557–582.
10. Miyata, M.: Sada, K. *Soft Chemistry* Leading to *Novel Materials*: Agarwala. R.P.. Ed.; Scitec Publications: Switzerland. 2001: 99–123.
11. Matsumoto, A.; Odani. T. Macromol. Rapid Commun. 2001. 22, 1195.
12. Matsumoto, A. Prog. React. Kinet. Mech. 2001. 26. 59.

Incommensurate and Commensurate Structures

Kenneth D. M. Harris
Cardiff University, Cardiff, Wales

INTRODUCTION

It is convenient to regard a crystalline solid inclusion compound to be composed of two chemically distinguishable substructures: the host and guest substructures. In many cases. the guest molecules are disordered within the crystalline host structure, but in those cases for which the guest molecules are ordered (at least sufficiently well ordered that an average lattice periodicity may be defined),an important concept is the degree of structural registry between the two periodic (host and guest) substructures. Here. we focus only on the simplest case of one-dimensional (1D) tunnel host structures in which both host and guest substructures have well-defined periodicities along the tunnel (Fig. 1). The periodic repeat distance of the guest molecules along the tunnel (c-axis) is denoted c_g, and the periodic repeat distance of the host substructure along the tunnel is denoted c_h. The degree of structural registry between the two periodic substructures is assessed by considering the relationship between c, and c_h.

Conventionally, the ratio c_g/c_h is used as a basis for dividing these systems into two categories—commensurate and incommensurate. The ciassical definition assigns the inclusion compound as commensurate if c_g/c_h is a rational number and as incommensurate if c_g/c_h is an irrational number. However. because experimental measurements of c_g and c_h can never be made with absolute precision, it is more practical to define an inclusion compound as commensurate if (and only if) c_g/c_h is sufficiently close to a rational number with low denominator. This is equivalent to stating that, for a commensurate system, small integers p and q can be found that satisfy the relationship $pc_h = qc_g$. If no sufficiently small integers p and q can be found, the inclusion compound is incommensurate.

An important consequence of an incommensurate relationship between the host and guest substructures is that, in principle, each guest molecule within a given tunnel samples a slightly different environment with respect to the host structure. For a commensurate material, on the other hand, the guest molecules in the tunnel sample only one or a small number of different local environments within the host structure. Clearly, several chemical and spectroscopic properties of the guest molecules may reflect these differencesin the distribution of local environments for commensurate and incommensurate structures.

X-ray diffraction studies of the inclusion compound can be used to measure the values of c_g and c_h. For example, as shown in Fig. 2, a single-crystal x-ray diffraction oscillation photograph recorded for the crystal oscillating about the tunnel axis shows distinguishable sets of layer lines for the host and guest substructures in an incommensurate system, and the values of c_g and c_h may be determined from the spacing of the layer lines within each set. In the case of a commensurate inclusion compound, separate layer lines due to the host and guest substructures cannot be distinguished, and all layer lines are described by a single periodicity along the c-axis.

We now consider in more detail the consequences of the incommensurate/commensurate nature of a tunnel inclusion compound in terms of diffractionand structural properties, and then energetic aspects and vibrational properties are discussed.

DIFFRACTION PROPERTIES AND STRUCTURAL ASPECTS

In terms of diffraction properties and structural properties, a commensurate inclusion compound behaves as a conventional crystal. The periodicities of the host and guest molecules within the inclusion compound are described by a common three-dimensional (3D) periodic lattice, and the symmetry of the structure is described by a conventional 3D space group. Correspondingly, all diffractionmaxima in the diffraction pattern are described by a single 3D periodic reciprocal lattice. As discussed in more detail below. the inability to rationalize all diffraction maxima in the diffraction pattern of an inclusion compound by a single 3D periodic reciprocal lattice often provides the first indication that the structure rnay be incommensurate.

For a tunnel inclusion compound in which the host and guest substructures have an incommensurate relationship along the tunnel (c-axis). the host and guest substructures are generally commensurate in other directions by virtue of the fact that the guest molecules are constrained to occupy the tunnels within the host

Encyclopedia of Supramolecular Chemistry
DOI: 10.1081/E-ESMC 120012729

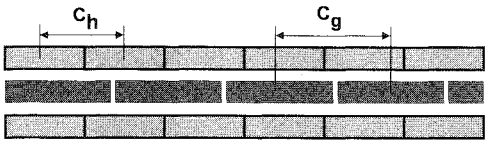

Fig. 1 Two-dimensional representation of a tunnel inclusion compound viewed perpendicular to the tunnel axis. The definitions of c_g and c_h are shown. (View this art in color at *www.dekker.com.*)

substructure. This implies that when the structure is projected onto a plane perpendicular to the tunnel axis, there is a commensurate relationship between the host and guest substructures, and corresponds to the host and guest substructures having a common a^*b^* reciprocal lattice plane.

Each substructure in the inclusion compound can be considered in terms of an incommensurately modulated "basic" structure. The basic structure has 3D lattice periodicity and crystallographic symmetry described by a 3D space group. The incommensurate modulation to a given basic structure represents the structural perturbations that arise from its interaction with the other substructure. Thus, the basic structure is an hypothetical entity and represents the structure to which the real substructure would relax if there were no interaction with the other substructure (i.e., in the absence of host–guest interaction). Clearly, the incommensurate modulation in one subsystem has the same periodicity as the basic structure of the other subsystem. In summary, the incommensurate inclusion compound can be considered as an intergrowth of two incommensurately modulated substructures.

The lattice describing the periodicity of the basic host structure is (a_h, b_h, c_h), and the corresponding reciprocal lattice is (a_h^*, b_h^*, c_h^*). The lattice describing the periodicity of the basic guest structure is (a_g, b_g, c_g), and the corresponding reciprocal lattice is (a_g^*, b_g^*, c_g^*). The vectors c_h and c_g are parallel to each other and are directed along the tunnel axis. As a consequence of the incommensurate relationship between c_h and c_g, the complete diffraction pattern from the inclusion compound cannot be rationalized on the basis of a single 3D periodic reciprocal lattice. Thus, it is not possible to express the positions (S^*) of all diffraction maxima within the diffraction pattern in terms of a linear combination

$$S^* = H\,a_1^* + K\,a_2^* + L\,a_3^*$$

of three reciprocal lattice vectors (a_1^*, a_2^*, a_3^*) with integer coefficients H, K, and L. For an incommensurate tunnel inclusion compound of the type described above, one additional reciprocal lattice vector (a_4^*) is required in order

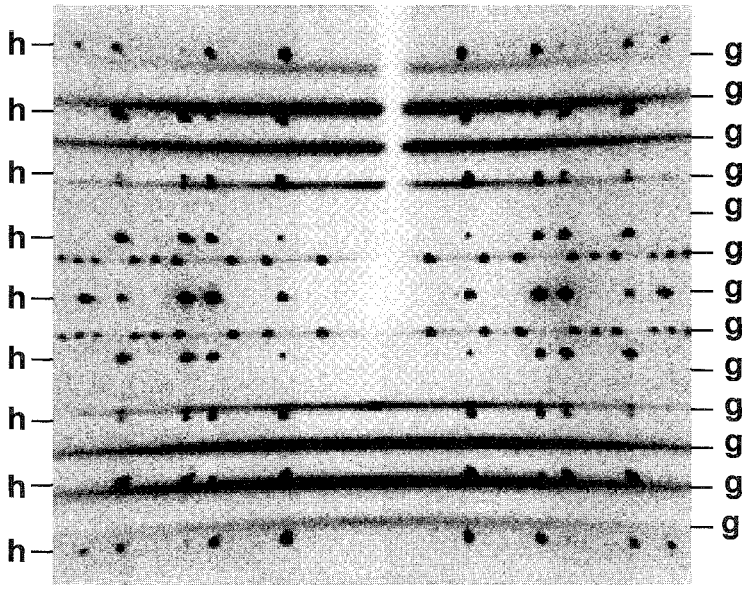

Fig. 2 Single-crystal x-ray diffraction oscillation photograph for an incommensurate tunnel inclusion compound (the 1,9-diiodononane/urea inclusion compound), recorded for a single crystal oscillating about its tunnel axis. The layer lines (horizontal) from the host component are indicated (h) on the left-hand side. The layer lines from the guest component are indicated (g) on the right-hand side. In this case, the guest layer lines contain discrete scattering (sharp spots) and diffuse scattering. The fact that separate sets of layer lines are observed for the host and guest components is a consequence of the incommensurate relationship between c_h and c_g.

to have integer indexing of all diffraction maxima in the diffraction pattern. Thus,

$$S^* = H\,a_1^* + K\,a_2^* + L\,a_3^* + M\,a_4^*$$

with integer coefficients H, K, L, and M.

In practice, one possible choice for the set (a_1^*, a_2^*, a_3^*, a_4^*) is (a_h^*, b_h^*, c_h^*, c_g^*) (note that; as discussed above, the host and guest substructures have a common a^*b^* reciprocal lattice plane, and hence: $a_h^* = a_g^*$ and $b_h^* = b_g^*$). The diffraction maxima (H, K, L, M) can be subdivided as follows:

1. $M = 0$: "Main reflections" from the host substructure, which primarily contain information on the basic host structure and also contain information on the incommensurate modulations within the guest substructure.
2. $L = 0$: "Main reflections" from the guest substructure, which primarily contain information on the basic guest structure and also contain information on the incommensurate modulations within the host substructure.
3. $L \neq 0$ and $M \neq 0$: "Satellite reflections" due to the intermodulations of the two substructures.

Clearly, the (H. K, 0, 0) reflections are a superposition of main reflections from both substructures, representing the common a^*b^* reciprocal lattice plane discussed above. A more detailed discussion of these concepts relating to the diffraction properties of incommensurate 1D inclusion compounds has been given elsewhere.[1–4]

Corresponding to the requirement for four reciprocal lattice vectors to describe the positions of all diffraction maxima. the structural periodicity of the incommensurate inclusion compound in direct space requires four lattice vectors, and the symmetry of the composite inclusion compound requires a four-dimensional (4D) superspace group.[5] Methods have been developed[6–11] and applied for deriving the superspace group symmetry of incommensurate intergrowth materials. Examples include a general discussion of superspace concepts for urea inclusion compounds,[2] as well as the development of superspace descriptions for the specific cases of the *n*-heptadecane/urea,[12] octane/urea,[13] octanedioic acid/urea,[14] and suberic acid/urea[15] inclusion compounds.

It is important to emphasize the benefits of understanding the symmetry properties (and structural properties) of the composite inclusion compound in a superspace group, rather than restricting the structural description of such materials at the level of the separate basic structures. Knowledge of the structural properties of the separate basic structures contains no information on the modulations that each subsystem experiences in the real inclusion compound. The modulations may have an important bearing on properties of the inclusion compound. even though they may, in some cases, represent rather small structural perturbations.

ENERGETIC **ASPECTS**

To understand the commensurate versus incommensurate nature of 1D inclusion compounds at a more fundamental level, a commensurate/incommensurate classification that reflects a division in the energetic "behavior" of the inclusion compounds within each category has been developed.[16] This theoretical approach considers the magnitude of fluctuations in the average host–guest interaction energy per guest molecule as the guest substructure is moved along the tunnel keeping the guest periodicity c_g fixed. If these fluctuations are sufficiently small (i.e., within $\pm\varepsilon$. where ε is some physically meaningful energy term), the inclusion compound is said to exhibit incommensurate behavior, whereas if these fluctuations are sufficiently large (i.e., larger than $\pm\varepsilon$), the inclusion coinpound is said to exhibit commensurate behavior. In the commensurate case. a significant energetic "lock-in" between the host and guest substructures will occur for a specific position of the guest substructure relative to the host substructure. whereas for the incommensurate case, the energy of the inclusion compound is essentially independent of the position of the guest substructure relative to the host substructure.

Methodology has been developed[17] for applying these concepts to predict structural properties of 1D inclusion compounds from knowledge of potential energy functions for the inclusion compound (with known host structure and fixed c_h). Fundamental to this approach is the definition of an appropriate energy expression—the "characteristic energy" of the inclusion compound—that directly indicates the relative energetic favorability of inclusion compounds with different guest periodicities. The optimum guest structure for the inclusion compound corresponds to minimum characteristic energy, and the methodology allows the following structural properties to be established from computed potential energy functions (describing host–guest interaction, guest–guest interaction. and intramolecular potential energy of the guest molecules) for the inclusion compound of interest: the optimum guest periodicity *(c,).* whether this value of c_g corresponds to commensurate or incommensurate behavior, and the optimum conformation of the guest molecules within the host structure. The method has been applied successfully to predict structural properties of alkane/urea inclusion compounds[18] in agreement with experimental results.

VIBRATIONAL PROPERTIES

We now consider the question of obtaining direct experimental evidence of incommensurateness in solid inclusion compounds. recalling that from consideration of values of c_g and c_h measured experiinentally from diffraction data, it may be ambiguous whether the st ucture is genuinely incominensurate or whether it represents a commensurate superstructure. The vibrational properties of a crystal depend directly on its energetic properties, and as now discussed, the energetic reasons that underlie incommensurate behavior in a solid inclusion compound have a direct manifestation in terms of the acoustic vibrational modes of the material. First. we recall that conventional crystals (including commensurate inclusion compounds) have three translation invariances (i.e., a translation of the crystal with no change of energy), corresponding to translation along the x, y, and z axes in 3D space. An incommensurate 1D inclusion compound. on the other hand, has four translation invariances. The extra translation invariance is an internal translation invariance and corresponds to the shift of the guest substructure relative to the host substructure along the incommensurate direction (as discussed above, the energy of an incommensurate inclusion compound is, in principle, independent of the shift of the guest substructure relative to the host substructure along this direction). There is an acoustic phonon corresponding to each translation invariance in a crystal, and therefore, an incommensurate 1D inclusion compound should have four acoustic phonons and a commensurate inclusion compound should have three acoustic phonons. The additional acoustic mode in the incommensurate system is called the "sliding mode,'' and observation of the sliding mode can be taken as direct experimental evidence for incominensurate behavior of the inclusion compound (unfortunately. the converse is not true. as there are experimental reasons that the sliding mode may be difficult to detect, even if the material is incommensurate). Brillouin scattering investigations may be used to assess the existence of the sliding mode, and there have been several reports of the quest to observe the sliding mode in solid inclusion compounds.[19–23]

CONCLUSION

The opportunity for certain classes of solid inclusion compounds, such as the 1D tunnel structures discussed in this article. to form structures that may be commensurate or incommensurate represents an intriguing aspect of these materials. both with regard to understanding the fundamental energetic reasons underlying commensurate versus incommensurate behavior and with regard to establishing a detailed characterization of the properties of the incommensurate systems. The diffraction properties of incommensurate materials and the corresponding structural descriptions in direct space present challenges that extend beyond the normal crystallographic principles encountered for conventional crystals.

ARTICLES OF FURTHER INTEREST

Brillouin Scattering. p. *129*
Modulated Structures, p. 873
Urea Inclusion Compounds, p. 1538

REFERENCES

1. Harris. K.D.M.: Thomas, J.M. Structural aspects of urea inclusion compounds and their investigation by X-ray diffraction: A general discussion. J. Chem. Soc., Faraday Trans. 1990. *86.* 2985.
2. van Smaalen, S.; Harris, K.D.M. Superspace group descriptions of the symmetries of incommensurate urea inclusion compounds. Proc. R. Soc., A 1996, *452.* 677.
3. Lefort. R.: Etrillard. J.; Toudic, B.: Guillaume, F.; Breczewski, T.; Bourges, P. Incommensurate intermodulation of an organic intergrowth compound observed by neutron scattering. Phys. Rev. Lett. 1996. 77.4027.
4. Hollingsworth, M.D.; Harris, K.D.M. *Comprehensive Supramolecular Chemistry*; MacNicol. D.D., Toda, F., Bishop. R., Eds.; Pergamon Press, 1996; Vol. 6. 177.
5. de Wolff. P.M.; Janssen, T.; Janner, A. The superspace groups for incommensurate crystal structures with a one-dimensional modulation. Acta Crystallogr. 1981. *437.* 625.
6. Janner. A.: Janssen, T. Symmetry of incommensurate crystal phases. I. Commensurate basic structures. Acta Crystallogr. 1980. *A36,* 399.
7. Janner, A.: Janssen, T. Symmetry of incommensurate crystal phases. II. Incommensurate basic structures. Acta Crystallogr. 1980. *A36*. 408.
8. van Smaalen. S. Symmetry of composite crystals. Phys. Rev., B 19911. *43.* 11330.
9. van Smaalen, S. Superspace description of incommensurate intergrowth compounds and the application to inorganic misfit layer compounds. In *Incommensurate Sandwiched Layered Compounds*, Materials Science Forum. 100 & 101; Meerschaut, A., Ed.: Trans Tech Publications, 1992: p. 173 .
10. van Smaalen, S. Renormalization of bond valences: Application to incommensurate intergrowth crystals. Acta Crystallogr. 1992, *A48.* 408.
11. van Smaalen, S. Incommensurate crystal structures. Crystallogr. Rev. 1995. 4, 79.

12. Weber. T.; Boysen, H.; Frey, F.; Neder, R.B. Modulated structure of the composite crystal urea/*n*-heptadecane. Acta Crystallogr. 1997. *B53*, 544.
13. Peral. I.: Madariaga. G.; Petricek. V.: Breczewski, T. Superspace description of the structure of the composite crystal urea/*n*-octane at room temperature. Acta Crystallogr. 2001. *B57.* 378.
14. Peral. I.: Madariaga. G.; Petricek. V.: Breczewski. T. Average structure of the composite crystal urea/octanedioic acid at room temperature within the superspace formalism. Acta Crystallogr. 2001, *B57.* 386.
15. Peral, I.; Madariaga. G.; Petricek. V.; Breczewski, T. Superspace description of the structure of the suberic acid + urea inclusion compound at room temperature. Ferroelectrics 2001, *250.* 27.
16. Rennie. A.J.O.: Harris, K.D.M. A mathematical model of one-dimensional inclusion compounds: A new approach towards understanding commensurate and incommensurate behaviour. Proc. R. Soc., A 1990. *430,* 615.
17. Rennie. A.J.O.: Harris. K.D.M. A quantitative analysis of guest periodicity in one-dimensional inclusion compounds. J. Chem. Phys. 1992. 96. 7117.
18. Shannon. I.J.: Harris. K.D.M.: Rennie. A.J.O.; Webster. M.B. Theoretical prediction of the guest periodicity of alkane/urea inclusion compounds. J. Chem. Soc., Faraday Trans. 1993, *89,* 2023.
19. Schmicker. D.; van Smaalen. S.; Haas, C.; Harris, K.D.M. Elastic constants of the dioctanoyl peroxide/urea inclusion compound determined by Brillouin scattering. Phys. Rev.. B 1994. *49.* 11572.
20. Schmicker, D.: van Smaalen, S.; de Boer, J.L.; Haas, C.; Harris, K.D.M. Observation of the sliding mode in incommensurate intergrowth compounds: Brillouin scattering from the inclusion compound of urea and heptadecane. Phys. Rev. Lett. 1995. *74,* 734.
21. Schmicker. D.: van Smaalen. S. Dynamical behaviour of aperiodic intergrowth crystals. Int. J. Mod. Phys. B 1996. *10.* 2049.
22. Ollivier, J.: Ecolivet. C.: Beaufils, S.: Guillaume. F.; Breczewski. T. Light scattering by low-frequency excitations in quasiperiodic n-alkanelurea adducts. Europhys. Lett. 1998. *43,* 546.
23. Brussaard, L.A.; Fasolino, A.; Janssen, T. Phason mode in *n*-alkane/urea composites. Physica, B 2002, *316.* 174.

Induced Fit

Yan Liu
Li Li
Heng-Yi Zhang
Nankai University, Tianjin, People's Republic of China

INTRODUCTION

It is well known that the induced-fit mechanism exists widely in biological and chemical processes, and is also an important characteristic of molecular recognition in supramolecular chemistry. Based on the general concept of induced fit derived from interactions between enzyme and substrate, mainly described in this article is the induced-fit mechanism of molecular selective binding of guests by artificial receptors. including binding and assembly behaviors induced by ionic and molecular guests. as well as the thermodynamic origin of induced-fit. Therefore, the induced-fit concept is not only of theoretical interest for understanding selective molecular-binding behaviors but also of practical importance in designing novel receptors to achieve biological functions.

BACKGROUND

The induced-fit theory first described by Daniel E. Koshland. Jr., in 1958[1] is one of the most fundamental discoveries of our age and is a development of Emil Fischer's well-known lock and key theory.[2,3] it should be noted that an important characteristic of the key–lock theory is that the enzyme accommodates the substrate without having to change the shape of the active site; however, in the induced-fit model, the enzyme changes shape when it reacts, like a glove into which a hand is thrust. To visualize the concepts of induced fit and key–lock, two binding models are illustrated in Fig. 1.

Early in the development of induced-fit theory. it was mainly utilized in biological systems, especially enzymes. to describe the phenomenon of interactions between the enzyme and the substrate. In such a case. enzyme action first requires the precise orientation of catalytic groups. and then the substrate causes an appreciable change in the three-dimensional relationship of the amino acids at the active site, organizing the catalytic groups into the proper alignment.[4] This induced-fit process was validated by more experiment results,[5,6] and now it is proven that almost all enzymes show ligand-induced structural changes during interactions with substrates.[7] Along with the acceptance of induced-fit theory by numerous scientists, it was extensively applied not only for enzymes but also in the control and regulation of biological and chemical systems. One of the most important purposes of supramolecular chemistry research is to mimic the interactions between enzyme and substrate, and induced-fit theory is therefore applied to describe the phenomenon of interactions between host and guest in supramolecular systems.

CURRENT STUDIES IN SUPRAMOLECULAR CHEMISTRY

The importance of host–guest chemistry and supramolecular chemistry, developed by Cram and Lehn. respectively, from the fundamental discovery of crown ethers by Pedersen, was recognized since the 1980s. From then on, supramolecular chemistry made considerable progress, and different host molecules were employed, such as crown ethers, cyclodextrins, calixarenes, porphyrins, etc., in this field for examining their binding behaviors along with a variety of guest molecules and then for mimicking enzyme–substrate interactions. Because some of these host molecules have flexible structures and may change their conformations during guest binding, the induced-fit theory, derived from biological systems, serves as one of the basic concepts for illustrating and understanding some interesting binding behaviors in supramolecular chemistry. Induced fit can be understood in a broad sense by the way in which the introduction of the guest (substrate) induces the conformational changes of the host (synthetic receptor), and by the way the changed conforination of the host or guest becomes much fitter for guest binding.

Binding Behavior induced by Ionic Guests

The selective binding of ions by synthetic receptors (hosts) attracted significant attention over the past 30 years. Among the synthetic receptors, macrocyclic polyethers (crown ethers and csyptands) were extensively utilized to cooperate with metal ions in forming a stable host–guest complex. In the ion-binding processes of

Encyclopedia of Supramolecular Chemistry
DOI: 10.1081/E-ESMC 120019161

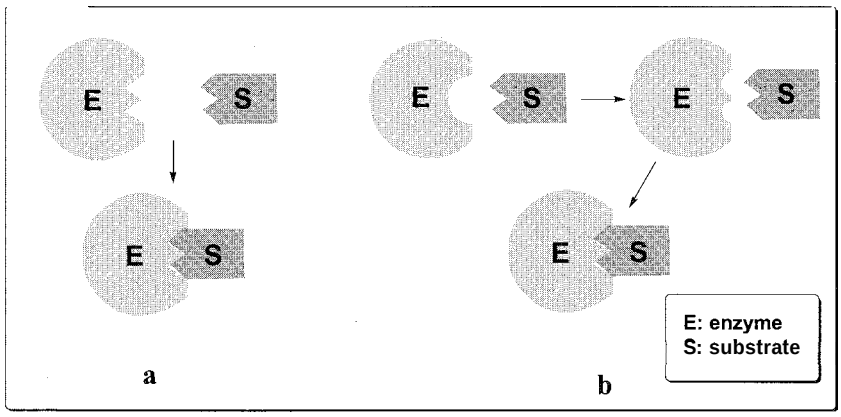

Fig. 1 The *(a) lock-and-key and (b) induced-fit models. (View this art in color at www.dekker.com.)*

crown ethers, the size and shape fit combination between host *and guest gives high complex stability based on the strong ion–dipole interactions of the oxygen atoms or nitrogen as well as other* heteroatoms *in the general case. For example. 15-crown-§ is* known *to fit the size of the* Na^+ *ion, and 18-crown-6 is a size* match *for the* K^+ *ion. In the case of large-sized crown ethers, such as 24-crown-8 and 30-crown-10, though their ring sizes are apparently too large to* fit Na^+ *and* K^+ *ions, they can be induced by the guest cations to give bent conformations forming three-dimensional complexes (Fig.* 2).[8] *On the other hand, in the lariat ethers possessing a side-arm group covalently bonded to a crown macroring developed by C.W.* Gokel,[9] *more recognition sites are appended, and sometimes the binding behavior cannot be explained simply by the coordination of the ring.* It *is found, consequently. that the induced-fit* mechanism *appears to play an important role in such processes of binding ion guests (Fig. 3).* Liu *and Inoue et al. reported the complexation behavior of aza-16-crown-5 lariat ethers with light* lanthanoid *nitrates and found that* the *size of the induced three-dimensional cavity of lariat ether is an important factor in binding trivalent lanthanoid* ions.[10] In *the two lariat ethers they employed (Fig. 4), a* nitrogen-*pivot 16-crown-§ 1 lariat possessing the flexible conformation showed an exceptionally high relative cation selectivity for* Nd^{3+}*, eight to nine times the neighboring* Pr^{3+} *and* Sm^{3+}*, which indicates that only the most* size-*fitting lanthanoid ion* accommodated *in the cavity of* 16-*crown-5 fully enjoys further ligation by the donating side arm with relatively large structural flexibility, making the operation of exact size-matching easy. That is to say, the host molecule* examined *could be induced to change its conformation by many kinds of guests. but the binding modes of the resulting complexes are not always as stable as the perfect induced-fit model. In the* same *way, through investigating the interaction of* polyether dicarboxylic *acids and heavy metal ions,* Hayashita *and coworkers found that a pseudo-18-crown-6 structure is formed based on the induced-fit mechanism, and it is predominant for* Pb(II) recognition.[11] *These* examples *described one important character of the induced-fit mechanism, that is, though it emphasizes the* conformational *change during the binding process in contrast to the key–lock theory,* it *also exhibits the* enzyme *specificity, similar to the* key–*lock theory to* some *extent.*

Among the ion-binding behavior mechanisms, cation–π *interaction* is *an important* kind *of driving force in molecular recognition. Even here, the induced-fit concept is reportedly an important mechanism for understanding the structures of* cation–π *complexes. Yoshida et* al.[12]

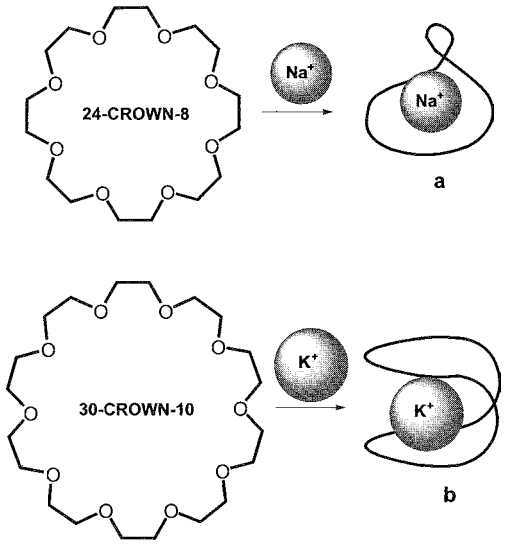

Fig. 2 *Three-dimensional complexes of (a)* 24-crown-8/Na^+ *and (b)* 30-crown-10/K^+. *(View this art in color at www. ilekker.com.)*

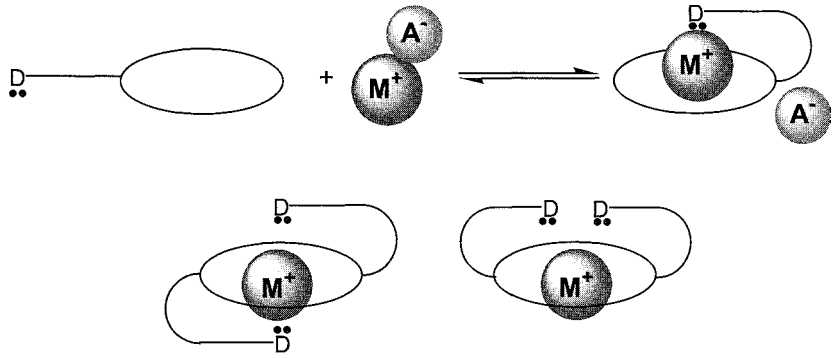

Fig. 3 The induced three-dimensional cavity of lariat ether by metal ion. ***(View** this art in color at www.dekker.com.)*

reported that the most stable conformation in the uncomplexed form is not always the preferred conformation of the π-complexes (Fig. 5). This is found to be the general condition in induced-fit systems, namely, there always exist several probable conformations for the host molecule, and one of them is most suitable for binding with the guest. Then, the different conformations will be induced by the guest binding to change to the complexed geometry. In this case, the action of the induced-fit mechanism breaks the original equilibrium and creates a new equilibrium distribution between the different states (conformations) of the host.

On the other hand, the induced-fit mechanism not only operates in the spontaneous process but also could be utilized for the special cases, for controlling the binding behavior. Wolte et al.[13] showed a bis-crown-ether analogue that could be induced by metal ion complexation to a conformation preorganized for binding with certain guests. In this case, induced-fit theory was expanded to a more specific understanding and became a two-step process involving an "induced step" and a "fit step" (Fig. 6). The "induced step" refers to the conformational change of receptor induced by metal ion binding. However, the "fit step" refers to the binding behavior of another guest, but not metal ion, with the same receptor. It means that three components are included in this induced-fit system by introducing an additional inducing agent (metal ion, here) besides the original host and guest.

Upon the ionic guest-induced binding behavior, most changes are caused by the direct interactions between ion and host (coodination. cation–π, etc.) but not size or shape factors. though size or shape sometimes controls the effect of induced fit to a certain degree.

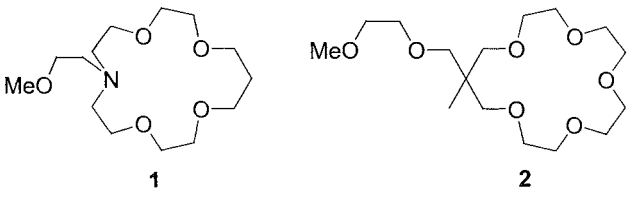

1 2

Fig. 4 The structures of *N*-methoxyethylaza-4,7,11,14-tetraoxacyclohexadecane (aza-16-crown-5 lariat, **1**) and 15-(2,5-dioxahexyl)-15-methyl-1,4,7,10,13-pentaoxacyclohexadecane (16-crown-5 lariat, 2).

Binding Behavior Induced by Molecular Guests

Molecular recognition is a central concept in supramolecular chemistry and generally refers to the selective binding of guests (substrates) by the host (receptor).

For example, the macrocyclic sugars called cyclodextrins (CDs) (see entry on *Cyclodextrins*) are important receptors for organic and inorganic guests via their hydrophobic cavities. To expand the binding ability and selectivity of native CDs, chemical modification is performed to introduce different substituents to the primary or secondary side of CDs, which provides the possibility for the operation of an induced-fit mechanism in this field. Ueno et al. reported many chromophore-modified CDs[14–16] that change fluorescence and absorption intensities upon accommodation of a guest molecule and, consequently, can be used as the photosensors. The studies indicated that the spectral variations are due to decomplexation of the chromophore moiety upon guest binding, and the induced-fit mechanism plays an important role in controlling the conformational change of the hosts. Similar examples were also found by Liu et al. concerning the binding behavior of chromophore-modified β-CDs.[17,18] These studies pointed out that conformers involving a free or a self-included chromophore tethered to CD are in a dynamic equilibrium. The addition of a guest leads to further equilibrium with the inclusion complex, as is illustrated in Fig. 7. The induced-fit mechanism herein is to choose the predominant conformation

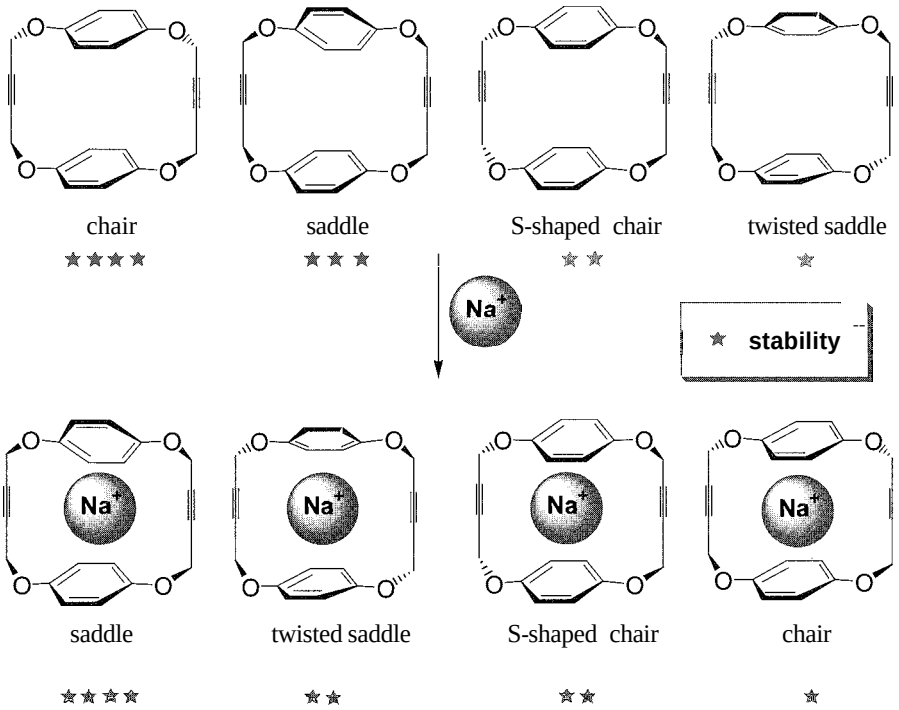

Fig. 5 Stability comparison of conformations of n-receptors and their cation–n complexes. (*View this art in color at www.dekker.com.*)

and then make the equilibrium shift. Simultaneously, it could be seen that in these instances, the size and shape of the guest become a key factor influencing the induced-fit mode finally formed between host and guest.

Recently, the induced-fit theory was utilized to explain the binding behavior arising upon the complexation of bridged *bis*(cyclodextrin)s and guest molecules. Because the *bis*(cyclodextrin)s possess two hydrophobic cavities in close proximity to one another and a relatively flexible spacer to link them together; these elements could cooperate to achieve a conformational change induced by guest binding.[19,20] For example, induced-fit behavior is exhibited by fluorescence investigations on the inclusion complexation of 2,2′-biquinoline-4,4′-dicarboxamide-bridged *bis*(β-cyclodextrin)s with sterols (Fig. 8).[21] The enhancement of fluorescence intensity of the *bis*(cyclodextrin)s proves the important function of the induced-fit mechanism. indicating that a subtle change in conformation may significantly alter the binding behavior.

The induced-fit mechanism exists not only in the molecular recognition process of cyclodextrins but also in that of other synthetic receptors. Rebek and coworkers introduced a family of receptors designed to bind adenosine derivatives within a pocket formed through induced fit.[22] Also, Schneider et al. described a configurational isomer with three different forms as a function of pH[23] (Fig. 9). On complexing with ammonium derivatives, the configurational isomer could change from one form to the other. accompanied by deprotonation via an induced-fit mechanism. Though only a few molecular recognition processes are presented, it is clear that the molecule-induced conformational change is different from the ion-induced conformational change due to the variability and complexity of the size and shape of the molecular guest. More interactions between host and guest are incorporated into the induced-fit mode formed. including hydrophobic interaction, hydrogen bond, van der Waals interaction, etc.. and thus the understanding of the induced-fit mechanism from the molecular aspect should be more helpful and give insight into the interaction between enzyme and substrate in biological systems.

Supramolecular Assembly by Induced Fit

If molecular recognition is regarded as the foundation of supramolecular chemistry for investigating the interactions between host and guest, then the molecular assembly or aggregation function could be considered to be the aim of these investigations. Because supramolecular assembly consists of many transformable factors, the induced-fit theory becomes necessary for understanding the relationships among the complicated elements forming the supramolecular assembly.

It was discussed that the lariat ether can serve as an induced-fit receptor. Gokel et al.[24] described a ditopic receptor system termed a "molecular box." in which the

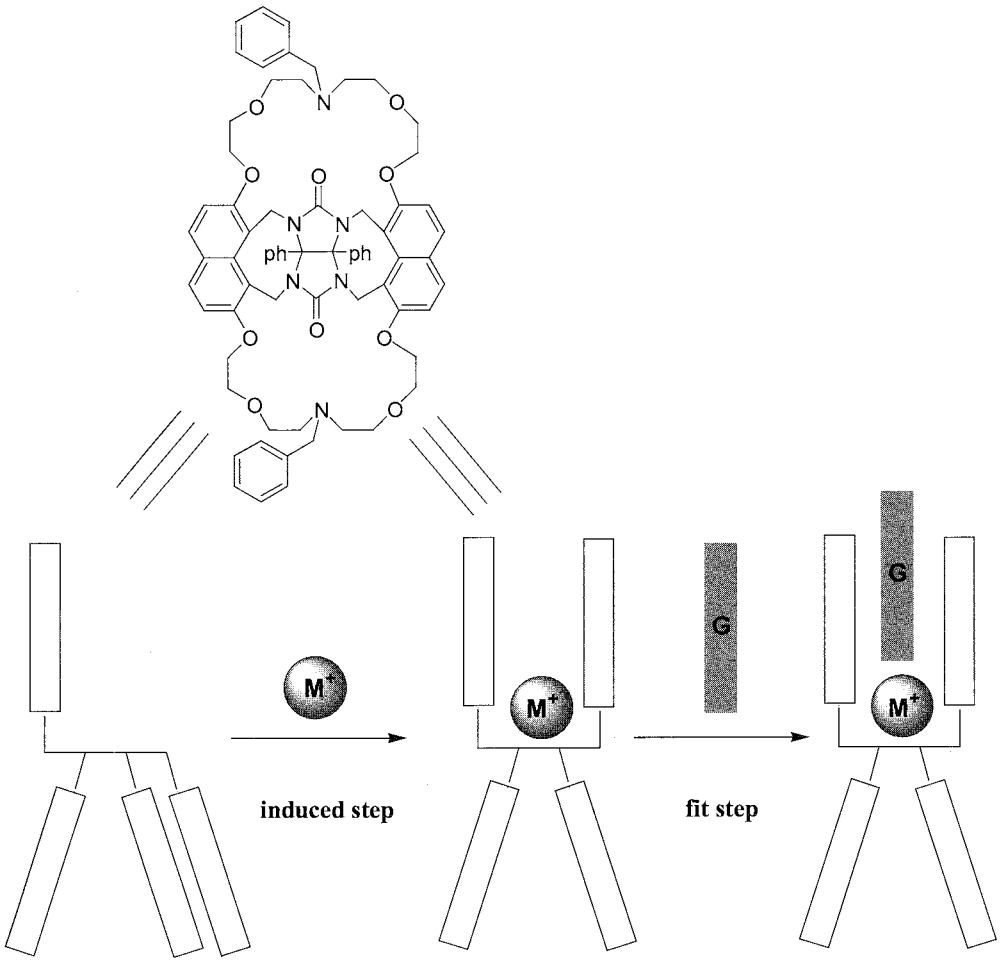

Fig. 6 The "induced step" and "fit step" of a his-crown-ether analogue in the guest-binding process. (*View this art in color. at www.dekker.com.*)

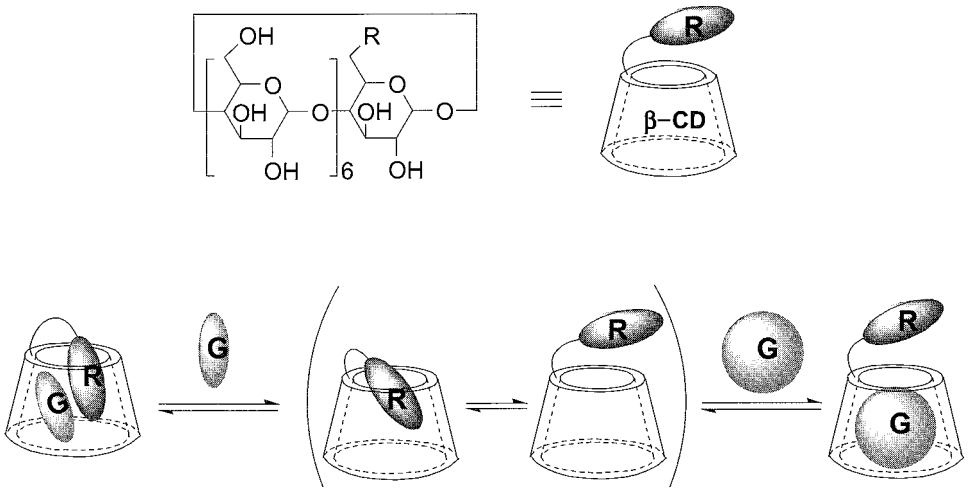

Fig. 7 Conforniational equilibria and guest-induced conformational change of modified cyclodextrin. *(View* this *art in color at www.dekker.com.*)

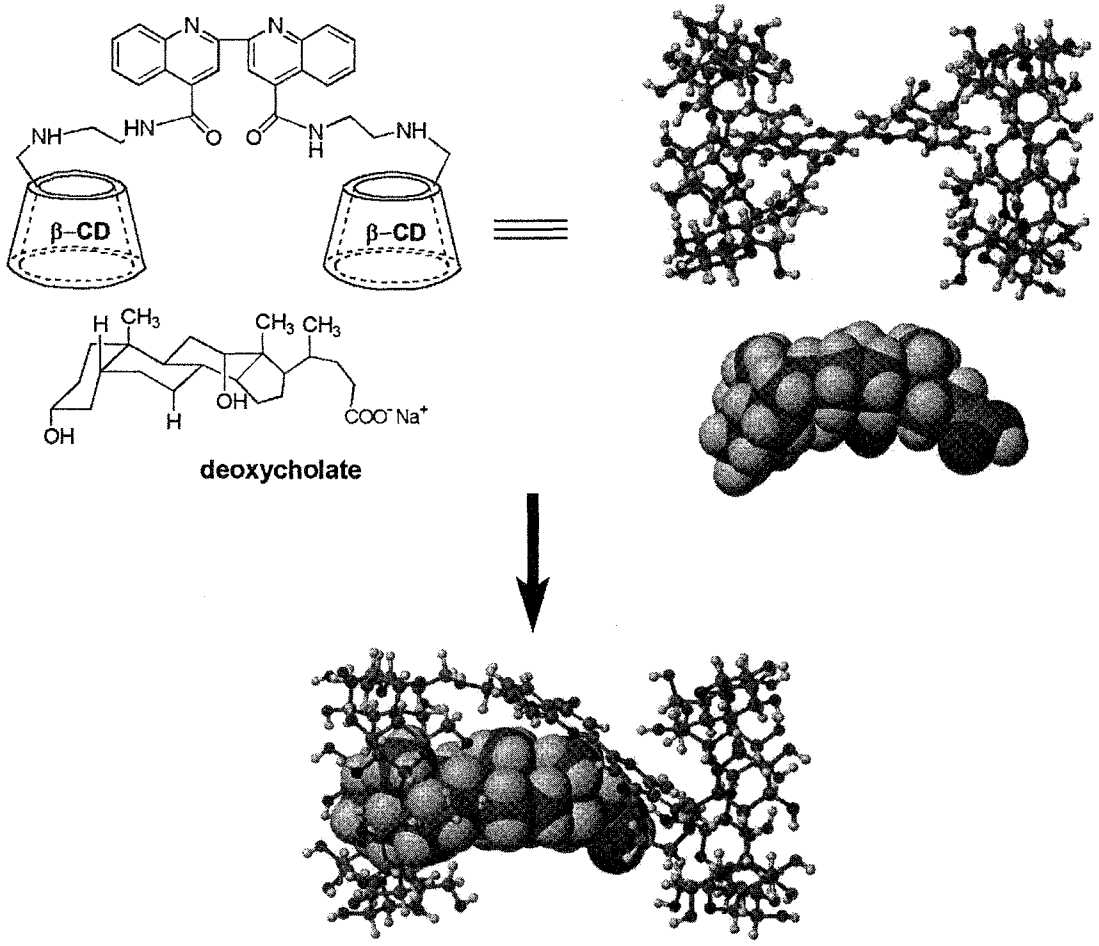

Fig. 8 The induced-fit model formed by *bis*(*β*-cyclodextrin)s and sterol.

sides of the box are Adenine::Thymine pairs, and the ends are crown ethers that serve as the induced-fit receptor. The system forms a three-component assembly in the presence of appropriately sized diammonium salts by means of an induced-fit mechanism. The compound represents a low-molecular-weight "induced-fit receptor model." As the size of a system increases. the induced fit in assembly becomes more complicated and precise due to the increased number of recognition sites. In this case, the appropriate length of the guest and the organized H-bonding or z-stacking are incorporated into the formation of the assembly. so the cooperativity of these factors should be a precondition for the good performance of the induced-fit process. In other words, it may be said that the process of assembly formation is just the process in which all components induced fit with each other in a certain mode. From this point of view, induced fit can also be utilized as a way to construct the assemblies and then to control their behavior. Chen et al. presented a K^+-induced aggregation via sandwich complexation of IS-crown-5 functionalized gold nanoparticles in a sodium-containing solution (Fig. 10).[25] Here, the crown-thiol molecule was induced to change its conformation from a 1:1 complex with Na^+ to a sandwich complex of 2:1 with K^+, again demonstrating the specificity of induced-fit processes.

In recent years, a new concept in molecular recognition, "molecular imprinting," was advanced and developed extensively. Many investigations indicate that the molecular imprinting displays characteristics of induced fit to a certain degree. It is the process in which the guest (substrate) induces the host to aggregate in accordance with guest size and shape. In this process, sometimes the host does not change its conformation, but several hosts cooperatively form a new assembly with a particular conformation different from the monomer. It could be said from this viewpoint that the molecular-imprinting technique expands the induced-fit mechanism to a more complicated and ordered system with many elements accompanied. For instance, induced fit was mentioned to occur upon the inclusion complexation between guest and

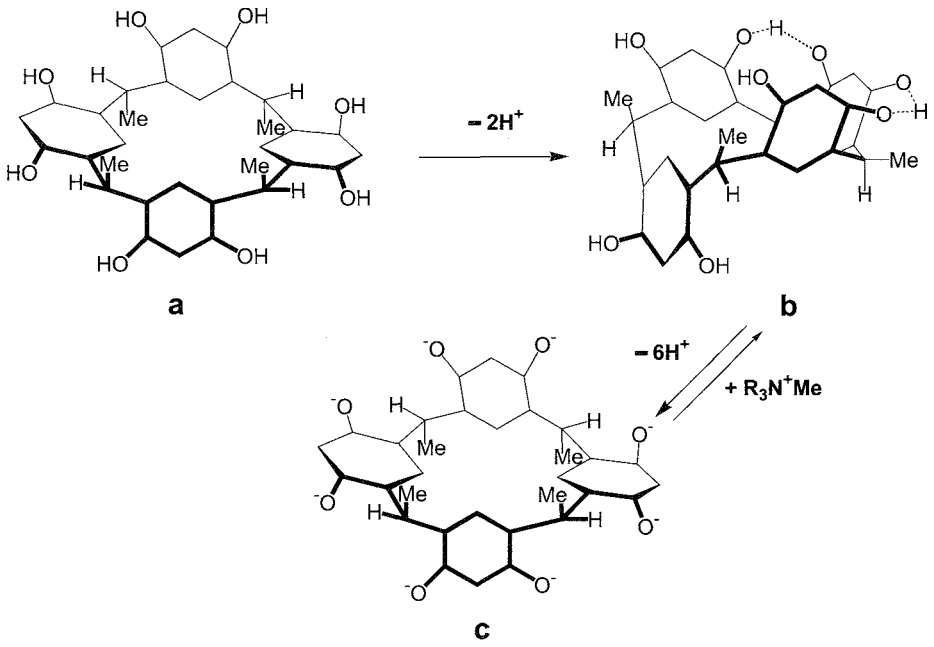

Fig. 9 The three different forms of cyclophane as a function of pH

cyclodextrin derivatives. However, for some special guests with large size and shape, even if induced-fit processes occur, the binding ability of cyclodextrin could not be improved in a general instance. However, in the molecular-imprinting process, when induced fit is worked to collect several cyclodextrins together using a large-sized guest as the template, the aggregate obtained might be favorable by virtue of recognizing the corresponding template molecule (Fig. 11).[26] It should be emphasized that the induced fit only exists in the process of preparing (assembling) the imprinting molecule but not in the recognition process. which would be more reasonably described as a lock and key recognition process.

Thermodynamic **Origin of** Induced Fit

In the classical lock and key model, complementary groups are rigidly positioned for maximal interaction with the substrate, which usually implies that the shape and nature of the cavity will provide good, close van der Waals contacts, and then the local free energy belonging to each active site will sum to the overall free energy of binding.[27] In contrast, in the induced-fit model, the complexation between host and guest is usually accompanied by the formation of a new configuration or sometimes a shift of equilibrium between different conformations of the host, and therefore, the contribution of this rearrangement to the overall free energy of binding must be entropically unfavorable. At the same time, as the result of induced fit, the rearrangement of the host conformation should achieve much stronger van der Waals contacts as well as other interactions between host and guest, such as ion–dipole, dipole–dipole, π–π, hydrogen-bond interactions. etc., which means favorable free-energy contributions from an enthalpic viewpoint. It is relatively straightforward to demonstrate the existence of entropy–enthalpy compensation effects in induced-fit binding.[28,29] Sanders and coworkers rationalized the conformational changes and binding between porphyrin hosts and *bis*-amine ligands in terms of the sum of the entropic and enthalpic contributions of each individual interaction to the overall binding energy, providing insight to the important features of the thermodynamics of conformational switching and the behavior of induced-fit enzyme models.[30] It could be deduced that the thermodynamics of induced fit involves a balance between the energetic penalty for conformational change and the gain in binding energy as a result of the chelate effect and any other favorable interactions. That is to say, only the induced-fit structure possessing the lower energetic penalty for conformational change or much larger binding energy compensated for by favorable interactions from confonnational change, displays the highest affinity. Consequently, for the formation of such a perfect induced-fit complex, a guest with suitable size and shape is necessary for complexation with a given host, which explains the specificity of induced fit thermodynamically. Furthermore. Murakami et al. presented their

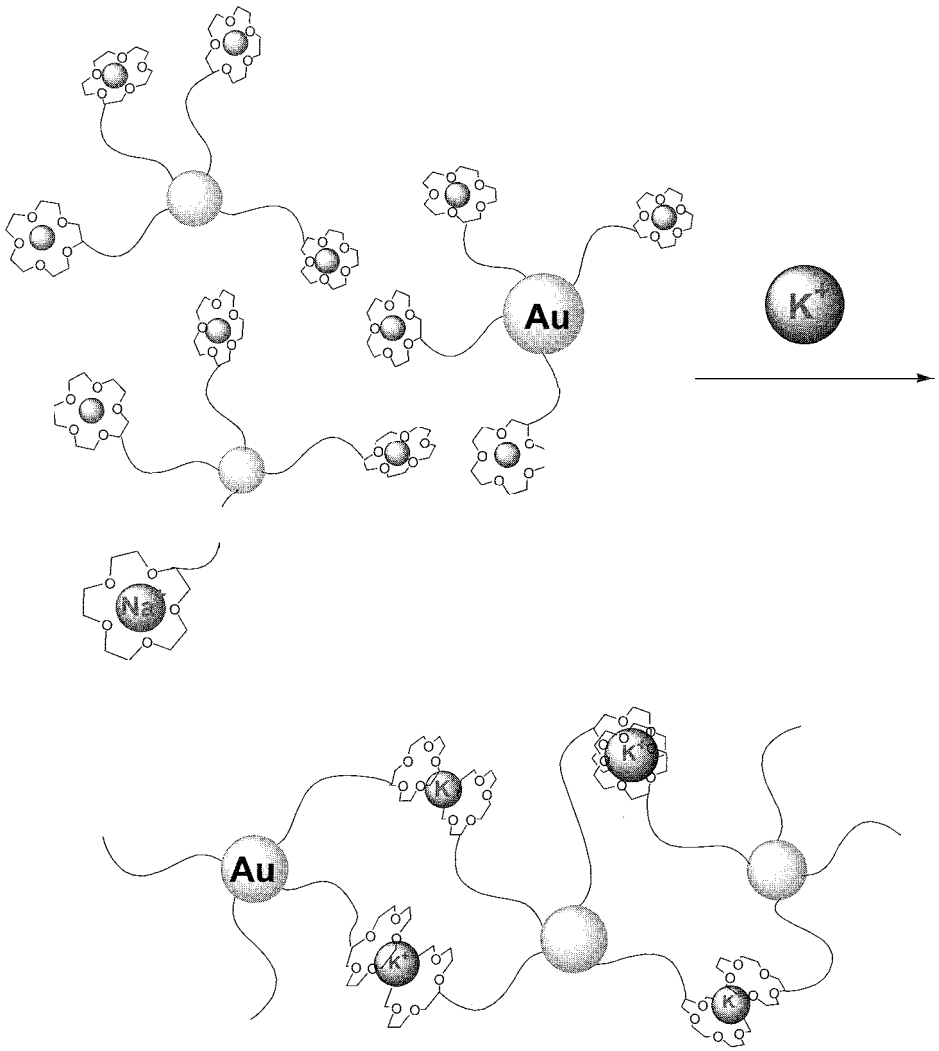

Fig. 10 The K^+-induced conformational changes of 15-crown-5 functionalized gold nanoparticles. *(View this art in color at www.dekker.com.)*

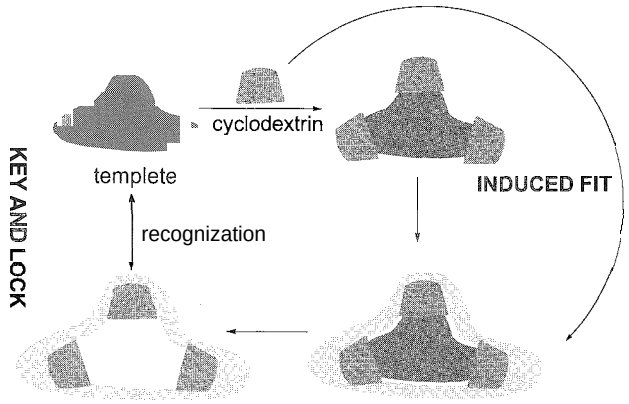

Fig. 11 The molecular-imprinting process of cyclodextrin. *(View this art in color. at www.dekker.com.)*

observations of dynamic features of an induced-fit complexation in artificial host–gueot systems,[31] which provides a useful guidepost for designing functionalized hosts as artificial receptors and enzyme models

CONCLUSION

It was demonstrated that the induced-fit concept of the interaction between an enzyme and a substrate was introduced from biological processes to supramolecular systems for explaining the molecular-binding behavior of artificial receptors, including crown ethers, cyclodextrins. calixarenes, porphyrins, etc. The induced-fit mechanism was utilized to explore the binding behavior of ions and molecules, and was adopted to accurately describe

supramolecular aggregates bearing more complicated structures. In the molecular recognition and assembly processes, when a guest (ion or molecule) induces a host (artificial receptor) to fit its size and shape, unavoidable conformational changes of the host sometimes exist; which is the essential characteristic of an induced-fit interaction. Thermodynamic investigations of induced-fit processes for molecular selective binding are not only of theoretical interest as the direct quantitative measures of the conformational change but are also of practical importance as the guiding principle in designing novel receptors to achieve biological functions.

ACKNOWLEDGMENT

This work was supported by NNSFC (No. 29992590-8 and 20272028), the Tianjin Natural Science Fund (No. 013613511), and the Special Fund for Doctoral Program from the Ministry of Education of China (No. 20010055001), which are gratefully acknowledged.

ARTICLES OF FURTHER INTEREST

The Allosteric Effect, p. 20
Anion-Directed Assembly, p. 51
Calixarenes and Their Analogues: Cation Complexation, p. 137
Crown Ethers, p. 326
Cyclodextrins, p. 398
Hemoglobins: O_2 Uptake and Transport, p. 636
The Lock and Key Principle, p. *809*
Self-Assembly: Definition and Kinetic and Thermodynamic Considerations, p. 1248

REFERENCES

1. Koshland. D.E., Jr. Application of a theory of enzyme specificity to protein synthesis. Proc. Natl. Acad. Sci. U. S. A. 1958, *44*. 98–104.
2. Fischer. E. Ueber die optischen isomeren des traubenzuckers, der gluconsäure und der zuckersaure. Ber. Dtsch. Cheni. Ges. 1890. 23 (2). 2611–2624.
3. Fischer, E. Einfluss der configuration auf die wirkung der enzyme. Ber. Dtsch. Chem. Ges. 1894. 27 (2). 2985–2993.
4. Koshland. D.E.. Jr. The key–lock theory and the induced fit theory. Angew. Chem.. Int. Ed. Engl. 1994. *33* (23). 2375–2378.
5. Blake. C.C.: Koenig, D.F.; Mair, G.A.: North. A.C.; Phillips. D.C.: Sarma. V.R. Structure of hen egg-white lysozyme. A three-dimensional Fourier synthesis at 2 Angstrom resolution. Nature 1965, *206* (986). 757–761.
6. Anderson, C.M.; Zucker, F.H.; Steitz, T.A. Space-filling models of kinase clefts and conformation changes. Science 1979, *204* (4391), 375–380.
7. Gerstein, M.: Lesk. A.M.; Chothia. C. Structural mechanisms for domain movements in proteins. Biochemistry 1994, 33 (22). 6739–6749.
8. Tsukube, H. Cation Binding by Natural and Modified Ionophores: From Natural Ionophore to Synthetic Ionophore. In Cation *Binding* by *Macrocycles: Complexation of Cat*ionic Species by *Crown Ethers*; Inoue. Y., Gokel, G.W., Eds.; Marcel Dekker, Inc.: New York. 1990; 497–522.
9. Gokel, G.W.; Dishong. D.M.; Diamond, C.J. Lariat ethers. Synthesis and cation binding of macrocyclic polyethers possessing axially disposed secondary donor groups. J. Chem. Soc., Chem. Commun. 1980. (22), 1053–1054.
10. Liu, Y.: Han, B.-H.; Li, Y.-M.: Chen, R.-T.; Ouchi, M.; Inoue, Y. Molecular design of crown ethers. 13. Complexation thermodynamics of light lanthanoid nitrates with aza-16-crown-5 lariat in acetonitrile: Enhanced selectivity for Nd^{3+}. J. Phys. Chem. 1996. *100* (43). 17361–17364.
11. Hayashita. T.; Sawano, H.; Higuchi, T.; Indo. M.: Hiratani, K.; Zhang, Z.-Y.: Bartsch, R.A. Molecular design of acyclic polyether dicarboxylic acids possessing pseudo-18-crown-6 frameworks for selective lead(II) extraction. Anal. Chem. 1999. 71 (4), 791–795.
12. Yoshida. M.; Tsuzuki. S.; Tamaoki, N. Induced-fit conformational changes in the cation–π complexes of pyxophane: A DFT study. J. Chem. Soc., Perkin Trans. 2 2001, (7). 1021–1023.
13. Sijbesma, R.P.: Nolte. R.J.M. A molecular clip with allosteric binding properties. J. Am. Chem. Soc. 1991, 113 (17), 6695–6696.
14. Ueno, A.; Moriwaki, F.; Osa. T.; Harnada. F.; Murai, K. Association; photodimerization, and induced-fit types of host–guest complexation of anthracene-appended γ-cyclodextrin derivatives. J. Am. Chem. Soc. 1988. *110* (13), 4323–4328.
15. Ikeda. H.; Nakamura, M.: Ise, N.: Ogurna. N.: Nakamura, A.: Ikeda, T.; Toda, F.: Ueno, A. Fluorescent cyclodextrins for molecule sensing: Fluorescent properties. NMR characterization. and inclusion phenomena of *N*-dansylleucine-modified cyclodextrins. J. Am. Chem. Soc. 1996, *118* (45). 10980–10988.
16. Uenc, A.; Ikeda, A.: Ikeda. H.: Ikeda, T.; Toda, F. Fluorescent cyclodextrins responsive to molecules and metal ions. Fluorescence properties and inclusion phenomena of N^{α}-dansyl-L-lysine-β-cyclodextrin and monensin-incorporated N^{α}-dansyl-L-lysine-β-cyclodextrin. J. Org. Chem. 1999. *64* (2). 382–387.
17. Liu, Y.: Han, B.-H.: Sun, S.-X.; Wada. T.; Inoue. Y. Molecular recognition study on supramolecular systems. 20. Molecular recognition and enantioselectivity of aliphatic alcohols by L-tryptophan-modified β-cyclodextrin. J. Org. Chem. 1999, *64 (5)*. 1487–1493.
18. Liu, Y.; You. C.-C.; Wada, T.: Inoue, Y. Molecular recognition studies on supramolecular systems. 22. Size, shape. and chiral recognition of aliphatic alcohols by organoselenium-modified cyclodextrins. J. Org. Chem. 1999. *64* (10). 3630–3634.

19. Liu. Y.; You, C.-C.; Chen. Y.: Wada, T.: Inoue, Y. Molecular recognition studies on supramolecular systems. 25. Inclusion complexation by organoselenium-bridged bis(β-cyclodextrin)s and their platinum(IV) complexes. J. Org. Chem. **1999.** *64* (21). 7781–7787.
20. Liu. Y.; Li, B.: You. C.-C.; Wada. T.; Inoue, Y. Molecular recognition studies on supramolecular systems. 32. Molecular recognition of dyes by organoselenium-bridged bis(β-cyclodextrin)s. J. Org. Chem. **2001;***66* (1), 225–232.
21. Liu. Y.; Song, Y.: Wang. H.; Zhang. H.-Y.; Wada, T.: Inoue. Y. Selective binding of steroids by 2,2′-biquinoline-4.4'-dicarboxamide-bridged bis(β-cyclodextrin): Fluorescence enhancement by guest inclusion. J. Org. Chem. **2003.** *68* (9), 3687–3690.
22. Conn, M.M.: Deslongchamps, G.; de Mendoza, J.; Rebek, J.. Jr. Convergent functional groups. 13. High-affinity complexation of adenosine derivatives within induced binding pockets. J. Am. Chem. Soc. **1993,** *115* (9). 3548–3557.
23. Schneider, H.-J.; Güttes, D.; Schneider. U. Host–guest complexes with water-soluble macrocyclic polyphenolates including induced fit and simple elements of a proton pump. J. Am. Chem. Soc. **1988.** *110* (19), 6449–6454.
24. Schall. O.F.; Gokel, G.W. Molecular boxes derived from crown ethers and nucleotide bases: Probes for Hoogsteen vs. Watson–Crick H-bonding and other base–base interactions in self-assembly processes. J. Am. Chem. Soc. **1994**, *116* (14). 6089–6100.
25. Ein. S.-Y.; Liu, S.-W.: Lin. C.-M.; Chen. C.-H. Recognition of potassium ion in water by IS-crown-5 functionalized gold nanoparticles. Anal. Chem. **2002.** *74* (2). 330–335.
26. Hishiya, T.; Asanuma. H.; Komiyama, M. Spectroscopic anatomy of molecular-imprinting of cyclodextrin. Evidence for preferential formation of ordered cyclodextrin assemblies. J. Am. Chem. Soc. **2002.** *124* (4). 570–575.
27. Wishnia, A. On the thermodynamic basis of induced fit. Specific alkane binding to proteins. Biochemistry **1969.** **8** (12), 5070–5075.
28. Liu, Y.: Han. B.-H.; Chen, Y.-T. The complexation thermodynamics of light lanthanides by crown ethers. Coord. Chem. Rev. **2008.** *200–202.* 53–73.
29. Inoue. Y.; Hakushi, T.: Liu, Y. Thermodynamics of Cation–Macrocycle Complexation: Enthalpy–Entropy Compensation. In *Cation Binding by Macrocycles: Complexation of Cationic Species by Crown Ethers*; Inoue, Y., Gokel, G.W., Eds.; Marcel Dekker. Inc.: New York, 1990; 1–110.
30. Anderson, H.L.: Hunter. C.A.; Meah, M.N.: Sanders, J.K.M. Thermodynamics of induced-fit binding inside polymacrocyclic porphyrin hosts. J. Am. Chem. Soc. **1990**, *112* (15). 5780–5789.
31. Murakami, Y.; Kikuchi, J.; Ohno, T.; Hayashida, O.; Kojima, M. Syntheses of macrocyclic enzyme models. 7. Octopus cyclophanes having L-aspartate residues as novel water-soluble hosts. Aggregation behavior and induced-fit molecular recognition. J. Am. Chem. Soc. **1990.** *112* (21). 7672–7681.

Inelastic Neutron Scattering

Marc Bée
Université J. Fourier, Grenoble, France

INTRODUCTION

Inelastic neutron scattering is a well-established and powerful technique used to study elementary excitations in condensed matter on the atomic scale, including local vibrational modes and single-particle diffusive modes as well as collective modes such as phonons and magnetic excitations.[1–5] The theoretical foundations were developed in the 1950s. Van Hove[L6] expressed the differential scattering cross section in terms of time-dependent pair cosrelation functions, and Glauber and Zemach developed the theory of neutron vibrational spectroscopy for solids and diluted molecular gases.[7,8] Then the availability of large fluxes of low-energy neutrons from nuclear reactors permitted the design of spectrometers for accurate investigation of diffusive motions in disordered materials.[9–11] In the course of time, inelastic neutron scattering has been applied to more complex systems, such as polymers[12] and biological macromolecules.[13,14]

BASIC ASPECTS OF NEUTRON INELASTIC SCATTERING

Neutrons are particles liberated in fission of ^{235}U in nuclear reactors or by pelting heavy nuclei with GeV protons in spallation sources. They propagate with a finite velocity v. and according to the laws of kinematics, a neutron with mass rn= 1.675 10^{-24} g has a kinetic energy

$$E = \frac{1}{2}mv^2$$

Typical velocities of neutrons used in condensed matter research vary from 500–14.000 m/sec, corresponding to energies from E=1.3 meV to 1.0 eV.

At the same time, a neutron can be considered a wave, with wavelength, λ. related to its velocity by the De Broglie relation:

$$\lambda = \frac{h}{mv} = \frac{2\pi}{|\boldsymbol{k}|}$$

where h is the Planck's constant (h=6.62 10^{-34} J.s), and $\boldsymbol{k}$ is the wave vector. The kinetic energy is then

$$E = \frac{\hbar^2 k^2}{2m}$$

Neutron wavelengths are of the order of crystallographic spacings. Therefore. neutrons obey Bragg's law when diffracted by single crystals. The relationship between wavelength, λ. lattice parameters, d_{hkl}, and diffraction angle θ, is as follows:

$$\lambda = 2d_{hkl}\sin\theta$$

Experimental techniques make use of these two features to select the required energy of a neutron beam. The neutron flight time is easily determined on sufficiently large lengths: a 5 Å wavelength neutron has a flight time, τ [L(m)/v(ms^{-1})] of 1264 s m ^{1}.

The neutron energy range encompasses a wide range of dynamical processes in condensed matter. Typical energies are 100 meV (1.2 10^{13} Hz) for molecular vibrations, 0–50 meV (6 10^{12} Hz) for lattice vibrations (phonons) or spin waves in solids, 0.01–1 meV (characteristic times τ=10^{-10} 10^{-12} s) for reorientations of inner chemical groups in molecules (e.g., polymer side groups) or for whole molecule reorientations in disordered phases (liquid crystalline phases or rotator phases), and a few μeV (τ=10^{-9} s) for long-range translational diffusion of molecules in the liquid state or in intercalation compounds (zeolites).

It can be found in standard textbooks that the neutron nuclear scattering is isotropic and characterized by a single parameter, b, the scattering length, independent of the neutron energy. Theory also attributes to each nucleus a coherent bound cross section:

$$\sigma_{coh} = 4\pi b^{coh} = 4\pi\langle b^2\rangle$$

together with an incoherent bound cross section:

$$\sigma_{inc} = 4\pi b^{inc} = 4\pi(\langle b^2\rangle - (b)')$$

where the brackets hold for an average over all the isotopes and spin states.

Encyclopedia of Supramolecular Chemistry
DOI: 10.1081/E-ESMC 120012833

Coherent and incoherent b^{coh} and b^{inc} scattering lengths are properties of the neutron–nucleus interaction and play an important role in the analysis of the dynamics of solids and liquids. They are fundamentally different in nature. Coherent scattering is the scattering that would be observed if all the atoms of the same chemical species had the same scattering length (b). The neutron would see an average uniform potential. which could give rise to interference effects. Coherent scattering involves the correlation between the positions of different nuclei and enables the study of collective excitations like phonons or spin waves, where all atoms or spins move in concert. Because deviations from the average potential are distributed at random, they cannot yield interference effects. Incoherent scattering describes the correlation between the positions of the same atom at different times. This scattering is added to the coherent scattering to obtain the scattering of the real system. Depending on the isotopes present in the sample, it is possible to select between coherent and incoherent scattering processes. The incoherent scattering cross section of hydrogen, in particular [σ_{inc}(H)=80 10^{-24} cm^2], is larger than that of all other atoms by a factor of 20. Incoherent neutron scattering is a powerful method for investigating motions in hydrogenated organic compounds like polymers or biological macromolecules. Moreover. isotopic substitution of deuterium [σ_{inc}(D)=2 10^{-24} cm^2] for hydrogen allows some chemical groups to be hidden and can be of considerable help in the identification of observed motions.

Through its spin. the neutron interacts with the magnetic moment (spin and orbital) of unpaired electrons. Inelastic magnetic scattering probes the dynamics of spin systems like spin waves (magnons). The use of polarized neutrons and the analysis of their polarization after scattering allows the differentiation of magnetic fluctuations from positional fluctuations and separation of coherent nuclear scattering from incoherent.

The neutron spectroscopy method consists of the measurement of changes in energy and momentum of neutrons interacting with matter in order to obtain information about the dynamics and the geometry of constituent atoms. Let us denote by indexes i and f the initial and final states of the physical quantities attached to the neutron. In the scattering process, the sample transfers momentum $\hbar\boldsymbol{Q}$ and energy $\hbar\omega$ to the neutron according to

$$\boldsymbol{Q} = \boldsymbol{k}_f - \boldsymbol{k}_i$$

($\boldsymbol{Q}$ is the scattering vector) and

$$\hbar\omega = E_f - E_i = \frac{\hbar^2 k_f^2}{2m} - \frac{\hbar^2 k_i^2}{2m}$$

The general double differential cross section for neutron nucleus scattering is as follows:[1–5]

$$\frac{\partial^2\sigma}{\partial\Omega\partial E_f} = \frac{1}{\hbar}\frac{\partial^2\sigma}{\partial\Omega\partial\omega} = \frac{\sigma_{coh}}{4\pi\hbar}\frac{k_i}{k_f}S(\boldsymbol{Q},\omega) + \frac{\sigma_{inc}}{4\pi\hbar}\frac{k_i}{k_f}S_{inc}(\boldsymbol{Q},\omega)$$

The scattering functions $S(\boldsymbol{Q},\omega)$ and $S_{inc}(\boldsymbol{Q},\omega)$ measure the response of the atomic number density to the external driving potential caused by the neutron interaction. They are expressed as the space and time Fourier transforms:

$$S(\boldsymbol{Q},\omega) = \frac{1}{2\pi}\int_{-\infty}^{+\infty} dt \int_{-\infty}^{+\infty} d\boldsymbol{r} G(\boldsymbol{r},t)\exp(-i\boldsymbol{Q}\cdot\boldsymbol{r}) \times \exp(-i\omega t)$$

$$S_{inc}(\boldsymbol{Q},\omega) = \frac{1}{2\pi}\int_{-\infty}^{+\infty} dt \int_{-\infty}^{+\infty} d\boldsymbol{r} G_s(\boldsymbol{r},t)\exp(-i\boldsymbol{Q}\cdot\boldsymbol{r}) \times \exp(-i\omega t)$$

where $G(\boldsymbol{r},t)$ and $G_s(\boldsymbol{r},t)$ are the pair and self-correlation functions, respectively, according to the formalism first introduced by Van Hove.[6] The notation $G(\boldsymbol{r},t)$ represents the conditional probability for a relative displacement r of a scatterer with respect to another within time t. $G_{inc}(\boldsymbol{r},t)$ is the conditional probability for the same scatterer to undergo a displacement $\boldsymbol{r}$ within time t. Thus, the two basic quantities to be measured are ω and $\boldsymbol{Q}$ (or simply $Q=|\boldsymbol{Q}|$ in the case of isotropic samples like liquids or powders).

INSTRUMENTS IN NEUTRON INELASTIC SCATTERING

Atomic motions cause the energies of scattered neutrons to be changed. Depending on the time scale of motion, one needs to cover an energy range from *10* neV–1 eV and to span wave vectors from *0.01–10* $Å^{-1}$. This wide time scale of analysis is covered by different classes of instruments. The phase space region (ω,Q) accessible to the various types of neutron spectrometers is schematized in Fig. 1.

Any spectrometer must perform three functions:

1. The incident neutrons must be selected in a small energy range between E_i and E_i+dE_i and in a small solid angle about the direction of k,.
2. The final energy E_f of the scattered neutrons must be analyzed to determine the energy change $\hbar\omega=E_f-E_i$.

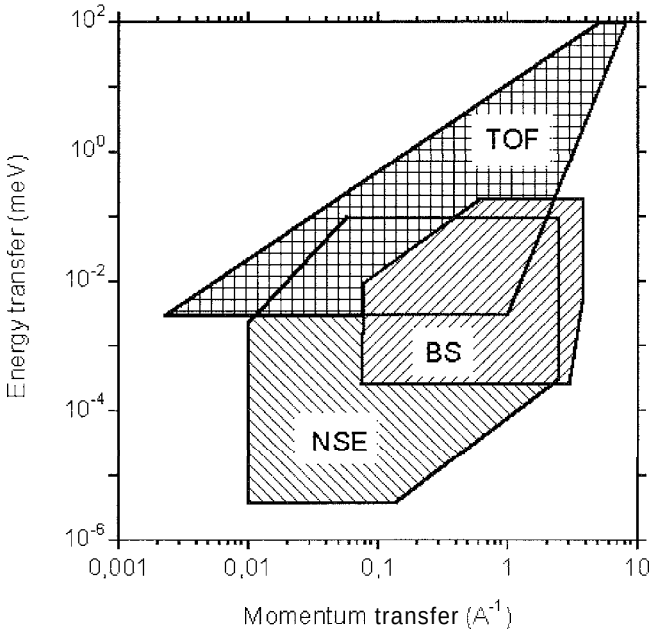

Fig. 1 The energy and momentum transfer regions accessible to different types of neutron spectrometers: time of flight (TOF), backscattering (BS). and neutron spin echo (NSE).

3. The scattering angle with respect to the incident beam and with respect to the sample orientation must be measured to determine the momentum transfer $Q = k_f - k_i$.

In practice, these three functions are achieved using the wave/particle duality of the neutron. The incident and scattered wave vectors can be determined by Bragg reflection from single crystals or by time of flight analysis of their velocity.

Triple-Axis Spectrometers

The triple-axis spectrometer (TAS) was invented by Brockhouse in 1962. This type of instrument is cominon in reactor centers. It is used to investigate well-defined excitations such as phonons or spin waves in single crystals. Since their first appearance, these instruments have changed little and can be schematically sketched as in Fig. 2. Incident and final wave vectors are determined by Bragg reflection of the neutron beam by suitable single crystals: a monochromator determines the magnitude and the orientation of the incident wave vector, k_i. Another crystal, the analyzer. determines the final wave vector k_f. Adjustment of the sample orientation allows the neutron wave vector transfer to be positioned at will in the reciprocal lattice of the sample and the phonon dispersion curves to be investigated. The best energy or wave vector resolution can be achieved in several ways. The most general method is the constant-Q mode, in which the scattering vector is kept equal to $\boldsymbol{Q}=\boldsymbol{G}+\boldsymbol{q}$, where G is a vector of the reciprocal lattice around which the dispersion curves are analyzed. Then, the initial energy can be fixed, and the final energy is scanned; conversely, the initial energy can be scanned, and the final energy kept fixed. The simultaneous collection of data over a range of (Q,ω) requires the use of a position-sensitive detector, as with DFTAS at NIST (Gaithersburg, USA[''']).

Time-of-flight and Backscattering Spectrometers

In contrast to TAS, time-of-flight (TOF) spectrometers and backscattering (BS) spectrometers are adapted to simultaneously record neutrons scattered into a wide range of wave vectors and energies. They are used to measure $S(Q,\omega)$ for liquids or disordered samples or magnetic energy spectra that vary only little with Q. A detailed review of existing instruments can be found in Ref. [16].

Neutron TOF spectroscopy is a powerful method for the study of dynamic processes over a wide dynamical range for polycrystalline and disordered solids. The continuous neutron flux is chopped into short bursts to set a time mark $t=0$ for the flight time of the neutrons. A

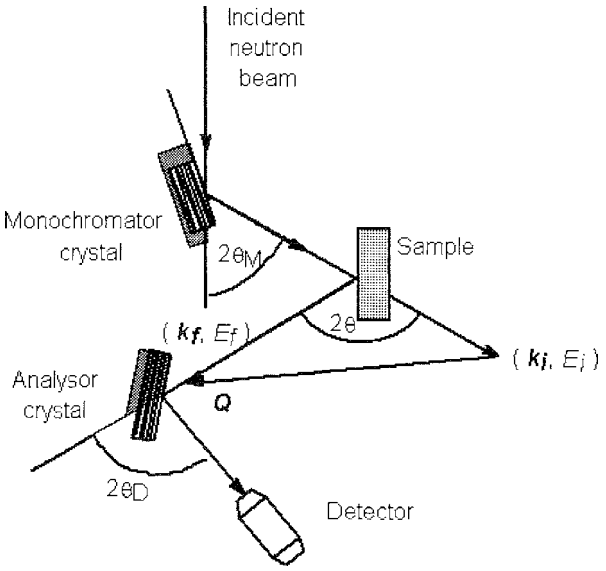

Fig. 2 A triple axis spectrometer.

large assay of several hundred detectors is placed to simultaneously collect counts for several final wave vectors in the scattering plane and also above and below. The first instrument of this type has been IN5 at ILL (Grenoble, France[17]). It uses several disk choppers separated from each other for pulsing the neutron beam and selecting a particular energy from it. Later, new TOF instruments were also built: MIBEMOL at LLB (Saclay, France[18]), NEAT at HMI (Berlin, Germany[19]), and DCS at NIST, with a number of technical improvements. Other TOF spectrometers use a crystal monochromator in combination with a Fermi chopper. Numerous instruments of this type exist for thermal neutrons. For cold neutrons, the use of focusing techniques permitted a substantial gain in intensity: IN6 at ILL. FOCUS at PSI (Villigen. Switzerland[20]), and FCS at NIST.

Neutrons inelastically scattered from the target gain or lose energy and then suffer a speed change. Obviously, the part of the spectrum corresponding to neutron energy loss is limited by the time interval between two bursts. The energy resolution of a TOF spectrometer is determined from the flight time and the energy uncertainty proportional to the burst duration. Accurate measurements are obtained with machines having large diinensions (several meters) and rapidly rotating disks.

Due to kinematic limitations: it is clear that at a constant angle between k_i and k_f, the scattering vector, $\boldsymbol{Q}$, is a function of the energy transfer, $\hbar\omega$. This point has to be taken into account in the data analysis.

Inverted TOF spectrometers are often used at spallation sources. IRIS at ISIS (RAL, United Kingdom[21]) is the first spectrometer of this type. Its main advantage is that it is flexible. with a wide dynamic range. The design of IRIS inspired many similar instruments on other spallation sources. A polychromatic neutron burst hits the sample. The repetition rate of the neutron bursts is directly determined by the period of the neutron pulses from the source. After the scattering process, crystal analyzers reflect only neutrons with well-defined energies into the detectors, where they are counted into different TOF channels.

BS spectrometers can be described as a particular case of TAS in which Bragg scattering angles on the monochromator and on the analyzers are equal or close to 90°. Differentiation of the Bragg's law gives

$$\frac{\Delta\lambda}{\lambda} = \frac{\Delta d}{d} + \frac{\Delta\theta}{\tan\theta}$$

The best resolution is obtained for $\theta = 90°$, where only the spread of the lattice spacing contributes. Typical energy resolutions of 1 μeV are obtained with $\Delta d/d$ of the order of 10^{-5}. Neutron backscattering spectroscopy is an important scattering technique for probing dynamical processes with long characteristic times. The analysis is made at constant final energy. The incident energy is varied by fast translational motion (Doppler effect) of the monochromator or by thermal expansion of the lattice parameters, the monochromator being cooled or heated in a cryofurnace. BS can operate over a wide momentum-transfer range simultaneously and can potentially access a time range between 0.01 μs and 100 ps. The resolution is mainly determined by the divergence of the neutron beam.

Molecular spectroscopy stimulated the development of especially dedicated spectrometers. At ISIS, the accessible energy range is spanned through the traditional spectroscopy region (2–500 meV) with TOSCA up to high energies (>5 eV) with eVS. The latter uses a filter technique. A filter instrument also exists at ILL (IN1-BeF) over a different energy range.

Neutron **Spin-Echo** Spectrometers

Neutron spin-echo (NSE) spectroscopy is somewhat different from the time-of-flight or BS techniques. The principle was introduced by F. Mezei in 1972.[22,23] NSE spectrometers use the Larmor precession of the neutron magnetic moment in an external magnetic field as an internal clock and directly compare the incident and scattered velocities of each individual neutron. Angular precession of the neutron spin is related to their velocities. After scattering by the sample, the direction precession axis of the spins is reversed. Analyzers measure the difference of the two precession angles and, hence, their energy exchange. The energy resolution becomes basically independent of the beam monochroinatization and

intensity. While BS and TOF spectrometer5 measure in frequency space. and thus determine $S(\boldsymbol{Q},\omega)$, neutron spin-echo spectroscopy measures in time space and directly determines the intermediate scattering function $S(\boldsymbol{Q},t)$ that is both the space Fourier transform of the pair correlation function and the inverse time Fourier transform of the scattering function:

$$S(\boldsymbol{Q},t) = \int_{-\infty}^{+\infty} G(\boldsymbol{r},t)\exp(-i\boldsymbol{Q}\cdot\boldsymbol{r})d\boldsymbol{r}$$

$$S(\boldsymbol{Q},t) = \frac{1}{2\pi}\int_{-\infty}^{+\infty} S(\boldsymbol{Q},\omega)\exp(+i\omega t)d\omega$$

In 1987 Gähler and Golub suggested a new type of spectroineter designed as "neutron resonance spin echo" or on "zero field neutron spin echo" that uses radio-frequency coils directly inspired from nuclear magnetic resonance.[24] Instruments of this type have been built at HMI and LLB or are under development (Munich).

Fourier times accessible to spin-echo spectroscopy range from 1 ps–100 ns. i.e., the energy resolution is better by two orders of magnitude than with the backscattering technique. The scientific fields under interest are polymer dynamics, glass transitions, dynamics of magnetic disordered compounds, colloids, microemulsions, or inelastic excitations (rotons in ^{3}He).

COHERENT NEUTRON SCATTERING

Phonons

Atoms in a crystal are not at rest. They execute small displacements about their equilibrium positions. The theory of crystal dynamics describes the crystal as a set of coupled harmonic oscillators. Atomic motions are considered a superposition of the normal modes of the crystal, each of which has a characteristic frequency $\omega(\boldsymbol{q})$ related to the wave vector of the propagating mode, $\boldsymbol{q}$, through dispersion relationships. Neutron interaction with crystals proceeds via two possible processes: phonon creation or phonon annihilation with. respectively, a simultaneous loss or gain of neutron energy. The scattering function $S(\boldsymbol{Q},\omega)$ involves the product of two delta functions. The first guarantees the energy conservation of the neutron phonon system and the other that of the wave vector. Because of the translational symmetry. these processes can occur only if the neutron momentum transfer, $\boldsymbol{Q}$, is such that

$$\boldsymbol{Q} = \boldsymbol{K} \pm \boldsymbol{q}$$

K being a vector of the reciprocal lattice. Coherent inelastic neutron scattering remains a powerful method for investigating collective motions in condensed matter. It allows for a complete determination of the dispersion curves in a Brillouin zone (BZ), as a function of the mode polarization. Other techniques, such as Brillouin scattering for the acoustic modes and Raman scattering for the optic modes are sensitive to phonon branches close to the Γ point in the reciprocal lattice.

Magnetic Scattering

Inelastic neutron scattering is a powerful tool for measuring inelastic magnetic excitations. Because the magnetic response is often spread over a wide energy range (from a fraction of μeV to several meV), a combination of several spectroscopy methods with different resolution (NSE, BS, and TOF) is required. Collective modes yield dispersion curves that can be investigated in detail with TAS. On the other hand, as long as the excitations are localized modes. they can be observed with TOF instruments. but dispersion smears the peaks. The study of itinerant magnetism requires spectrometers working with high incident energies (IN4 at ILL or MARI at ISIS). Recent developments in neutron instrumentation (^{3}He neutron spin filters, polarizing super-mirrors) make feasible new experiments on inelastic neutron scattering with simultaneous analysis of the polarization of the scattered neutrons.

INCOHERENT NEUTRON SCATTERING

Inelastic Scattering

Incoherent scattering is related to the self-correlation function and, therefore, does not contain any interference terms. Unlike in the case of coherent scattering. there is no momentum selection rule. Incoherent one-phonon scattering occurs for a continuous range of k_f wave vectors, each corresponding to a phonon mode fulfilling the energy conservation.

The relevant quantity is the density of states (DOS), $g(\omega)$. In the case of cubic crystals composed of a single type of atoms of mass M, measurement of the energy distribution of the scattered neutrons directly yields the DOS:

$$S(Q,\omega) = \exp[-2W(Q)] \times \left[\delta(\omega) + \frac{\hbar Q^2}{4M\omega}\frac{\exp\left(-\frac{\hbar\omega}{2k_BT}\right)}{\sinh\left(\frac{\hbar\omega}{2k_BT}\right)}g(\omega)\right]$$

k_B is the Boltzman constant. and $2W(Q)$ is the Debye–Waller factor that takes into account atomic vibrations.

For completely incoherent scatterers, such as vanadium, $g(\omega)$ is the only information about phonons that can be obtained from neutron scattering. Nevertheless, a singular behavior can be observed at critical phonon frequencies at the limits of the Brillouin zone (BZ) and in the center of the BZ. Large maxima appear in the scattered intensity, providing a rough estimation of the phonon dispersion curves.

For noncubic crystals or when there are several atoms in the unit cell, one can access only to a weighted DOS. $G(\omega)$, with a polarization term involving the polarization vectors of the normal modes with respect to the scattering vector $\boldsymbol{Q}$. This DOS can be obtained by extrapolation to small Q of the purely inelastic part of the scattering.

The theory of neutron scattering from vibrating molecules was developed by Zemach and Glauber.[8] Recently, the method was applied to complex biological substances (bovine pancreatic trypsin inhibitor).[13]

Quasi-Elastic Neutron **Scattering**

Quasi-elastic neutron scattering (QENS) is related to stochastic particle motions. Because the displacements are random, the diffusive motion of particles in liquids cannot be quantized, and the energies are continuously distributed. Unlike the case of cooperative motions like phonons in solids or molecular vibrational excitations, in the dynamic scattering function $S(\boldsymbol{Q},\omega)$, there are no δ-functions at finite momentum and energy transfers. Instead. the dynamic scattering function is centered at zero-energy transfer with a characteristic quasielastic line width proportional to the diffusivity of the particles.

One looks at the motion of an individual atom. Therefore, the relevant quantity is the incoherent scattering function. Because of the large incoherent cross section of hydrogen, quasielastic scattering is particularly suited and mostly used for the investigation of hydrogenated organic compounds with dynamical disorder, like rotator phases; liquids. polymers, and biological macromolecules.

Coherent quasi-elastic neutron scattering due to the pair-correlation of atomic motions is more complex than incoherent scattering from single particle motion. Therefore, the theory of coherent scattering function is not yet fully developed. However, approximate expressions for the coherent scattering function exist (incoherent approximation).

Translational long-range diffusion

Long-range diffusion of particles in solids and liquids was investigated for many years using the neutron scattering techniques,[11,25] and several types of descriptions were stimulated. The most simple is the continuous diffusion model according to Fick's law:

$$\frac{\partial G_s(\boldsymbol{r},t)}{\partial t} = D \cdot \nabla^2 G_s(\boldsymbol{r},t)$$

where D is the self-diffusion constant, and ∇^2 is the Laplace operator with respect to r. On the microscopic scale. it corresponds to the Brownian motion of large molecules immersed in a viscous solvent. The mean square displacement

$$\langle r^2(t)\rangle = 6Dt$$

corresponds to the Einstein free diffusion law.[26]

The incoherent scattering function $S(Q,\omega)$ exhibits a Lorentzian shape with a parabolic increase of its full-width at half-maximum (fwhm), Γ, as a function of Q:

$$\Gamma = 2DQ^2$$

At large momentum transfer, systematic deviations to this law are observed, because on distances smaller than several molecular diameters, the medium is no longer continuous, and underlying microscopic mechanisms intervene. Several jump models were developed. The Chudley–Elliott model[10,11] assumes a diffusion by successive jumps. It is successful in the description of hydrogen diffusion in metals or molecules in porous media. In their description of the dynamics of water molecules in the liquid state, Singwi and Sjolander[10,11] take into account successive oscillatory and diffusive states. At small Q values, both models yield the macroscopic DQ^2 law, the diffusion constant, D, being related to the mean residence time on a given site τ, by Einstein's relation:

$$D = \frac{l^2}{6\tau}$$

Localized motions

A large majority of solids is composed of molecules in crystal lattices or in amorphous phases. Then under the influence of thermal fluctuations, atoms can sometimes undergo displacements toward a limited number of other sites, by well-defined reorientations of chemical groups or of the whole molecule.[9,10] Also in liquid crystal phases, rotations of the molecules about their long axes were evidenced.

Because the motion of the scatterers is essentially restricted in space, the scattering function comprises a Dirac function $\delta(\omega)$ and a series of Lorentzian functions; the forms of which are directly related to the characteristic times of the relevant motions. Experimentally, one

observes a purely elastic peak with zero width (actually widened by the instrument energy resolution), superimposed on a broader quasi-elastic contribution. Their relative importance provides direct information on the geometry of the relevant motions.[10]

Numerous IQNS studies of organic chemical groups reorienting on several sites exist. Scattering laws were derived for proton two-site exchange mechanisms and rotations about symmetry axes like methyl groups or aromatic rings. When reorientation jumps occur about several axes, calculation of the scattering law is greatly simplified by using group theory. When the number of equilibrium sites becomes large, rotations approach axial or spherical rotational diffusion.

In recent years, many studies of biological samples carried out on TOF or BS spectrometers addressed the question of how the activities or functions of biological macromolecules are related to their local dynamics. It seems established that systems become active when their atoms are sufficiently mobile and the macromolecule can explore several conformational substates.[27]

Quantum tunneling

At low temperature, when the thermal energy of the rotating group becomes smaller than the energy barrier between equilibrium sites, a classical system freezes. However, there is a quantum mechanical probability of tunneling through the barrier, due to the overlap of the wave functions: the librational ground state is split due to tunneling, and direct observations of the transitions between these states are possible by high-resolution inelastic scattering. Tunnel splitting is sensitive to the mass of the tunneling atoms and to the strength of the potential. Inelastic neutron scattering permits probing of the force fields applied in molecular dynamic simulations. Earlier investigations were carried out with crystalline samples. Recently, tunneling excitations could also be observed in amorphous polymers poly(vinyl acetate) and poly(methyl methacrylate).[29]

CONCLUSION

Inelastic neutron scattering is a powerful technique for investigating atomic and molecular motions in condensed phases. Several types of instruments permit a time range from typically 10^{-13}–10^{-9} s to be covered and thus vibrations (collective or individual) as well as diffusive displacements to be investigated. The technique also provides geometrical information about the relevant motions. For the study of vibrations, it is complementary of Raman or IR spectroscopy with the advantage of an absence of selection rules, in spite of a worse resolution. For diffusive motions. it can be profitably associated to NMR, with both methods providing an inspection of the dynamical mechanisms on the same microscopic scale. Inelastic neutron scattering data are also directly comparable with computer molecular simulations. Finally, inelastic neutron scattering should benefit the development of new intense neutron sources.

ARTICLES OF FURTHER INTEREST

Brillouin Scattering, p. 129
Light Scattering, p. 799
Neutron Diffraction, p. 959
Nuclear Magnetic Resonance Spectroscopy, p. 981
Solid-State Nuclear Magnetic Resonance Spectroscopy. p. 1307
Vibrational Spectroscopy, p. 1557

REFERENCES

1. Lovesey. S.W. *Theory of Neutron Scattering from Condensed Matter. Nuclear Scattering*; Clarendon Press: Oxford, *1984;* Vol. 1, 1–329.
2. Egelstaff, P.A. *Thermal Neutron Scattering*; Academic Press: New York. *1965:* 1–522.
3. *Introduction to the Theory of Thermal Neutron Scattering:* Squires. G.L.. Ed.; Cambridge University Press: Cambridge. *1978:* 1–260.
4. Willis. B.T.M. *Chemical Applications of Thermal Neutron Scattering:* Oxford University Press: London. *1973* 1–*312.*
5. Kostorz, G. *Treatise on Materials Science and Technology. Neutron Scattering;* Academic Press: New York, *1979:* Vol. *15.* 1–523.
6. Van Hove. L. Correlations in space and time and Born approximation in systems of interacting particles. Phys. Rev. 1954, 95 (1), 249–262.
7. Glauber, *R.* Time-dependent displacement correlations and inelastic scattering by crystals. Phys. Rev. 1955, 98 (6). *1692–1698.*
8. Zemach. A.J.; Glauber, R. Dynamics of neutron scattering by molecules. Phys. Rev. 1956. *101* (1), *118–136.*
9. Springer. T. *Quasielastic Neutron Scattering for the Investigation of Diffusive Motions in Solids and Liquids*; Springer Tracts in Modern Physics, Springer-Verlag: Berlin. *1972:* Vol. 64, 1–100.
10. Bée, M. *Quasielastic Neutron Scattering: Principles and Applications in Solid State Chemistry, Biology and Materials Science:* Adam Hilger: Bristol. *1988;* 1–437.
11. Hempelmann. R. *Quasielastic Neutron Scattering and Solid State Diffusion*; Lovesey, S.W.. Mitchell. E.W.J..

Eds.: Oxford Series on Neutron Scattering in Condensed Matter. Clarendon Press: Oxford. 2000: Vol. 13, 1–304.
12. Higgins. J.S.; Benoît, H.C. Oxford Series on Neutron Scattering in Condensed Matter. *Polymers and Neutron Scattering*; Lovesey, S.W., Mitchell, E.W.J.. Eds.; Clarendon Press: Oxford. 1996; Vol. 8, 1–436.
13. Smith, J. Protein dynamics: Comparison of simulations with inelastic neutron scattering experiments. Q. Rev. Biophys. 1991, 24 (3), 227–291.
14. Doster. W.; Cusack. S.; Petry. W. Dynamical transition of myoglobin revealed by inelastic neutron scattering. Nature 1989. 337, 754–756.
15. http://rddjazz.nist.gov (accessed May 2002).
16. Frick, B.; Farago, B. Neutron Spectroscopy by Time-of-Flight, Backscattering and Spin-Echo Techniques. In *Scattering; Scattering and Inverse Scattering in Pure and Applied Science:* Pike. *R.*, Sabatier. P.. Eds.: Academic Press: San Diego, 2002: 1209–1241.
17. http://www.ill.fr (accessed May 2002).
18. http://www-llb.cea.fr (accessed May 2002).
19. http://www.hmi.de (accessed May 2002).
20. http:l/www.psi.ch (accessed May 2002).
21. http:/lwww.isis.rl.ac.uk (accessed May 2002).
22. Mezei, F. Neutron spin echo: A new concept in polarized thermal neutron techniques. Z. Phys. 1972, *255*. 146–160.
23. *Lecture Notes in Physics: Neutron Spin Echo;* Springer-Verlag: Berlin, 1980; Vol. 128. 1–253.
24. Colub, R.; Gähler, R. A neutron resonance spin-echo spectrometer for quasielastic and inelastic scattering. Phys. Lett.. A 1984. 123, 13–48.
25. Egelstaff, P.A. Oxford Series on Neutron Scattering in Condensed Matter. *An Introduction to the Liquid State.* 2nd Ed.: Lovesey. S.W., Mitchell, E.W.J.. Eds.; Clarendon Press: Oxford. 1992; 1–390.
26. Einstein, A. Investigation of motions in condensed matter by inelastic neutron scattering. Ann. Phys. 1905, 17. 349.
27. Zaccai', G. How soft is a protein? A protein dynamics force constant measured by neutron scattering. Science 2000, *288*. 1604–1607.
28. *Neutron. and Numerical Methods—N2M. Grenoble, France 1998;* Johnson, M., Biittner, H., Kearley, G.. Eds.; AIP Conference Proceedings, American Institute of Physics: New York, 1999: Vol. 479. 1–238.
29. Colmenero. J.; Mudkhopadhyay. R.; Alegria, A.; Frick. B. Quantum rotational tunneling of methyl groups in polymers. Phys. Rev. Lett. 1998. SO (11), 2350–2353.

Interpenetration

Stuart R. Batten
Monash University, Clayton, Victoria, Australia

INTRODUCTION

Crystal engineering is of great current interest and can be thought of as "the supramolecular chemistry of the solid state." A common theme is the analysis of crystal structures and the application of the knowledge gained to the design of new structures.

A particularly useful approach to the analysis and design of crystal structures is to reduce the structures to simple topological networks.[1,2] These networks are basically descriptions of multiply connecting nodes and the ways they connect, and are usually named after simple chemical examples of the net (e.g., diamond, NbO, α–Po) or are given numerical descriptions [e.g., (6,3), (4,4), (10,3)-*a*].

This approach is particularly useful for structures containing coordination polymers or molecules that are connected by hydrogen bonding into infinite arrays, and the structures examined here will be described in terms of their topological networks. One application of this network approach has been in the design of structures with large, open frameworks that might potentially include guest species. Often, however, this results in structures with multiply interpenetrating networks, as nature seeks to maximize crystal packing efficiency. Interpenetrating networks can be thought of as polymeric analogues of molecular catenanes and rotaxanes, and they involve the intimate entanglement of two or more polymeric networks.[1,3,4]

An important and defining feature of interpenetration is the condition that the entanglement of the topological nets is such that, although there is no direct connection between the networks, they cannot be separated (in a topological sense) without requiring the breaking of network connections. Any amount of bending or distortion of the nets is allowed: but breaking of the connections is not permitted—connectivity and not geometry is important in topological descriptions. Thus, cooked spaghetti is not interpenetrating, but links in a chain are. Alternatively, the chemical example of simple linear one-dimensional (1D) chains penetrating through the windows of a stack of two-dimensional (2D) sheets is not interpenetration if, in an imaginary, topological sense, the chains could be simply drawn out without requiring any connections of any of the networks to be broken.

Although the 1D chains penetrate the 2D networks. the 2D nets do not penetrate the 1D chains; so it is not interpenetration. If, however, the 1D nets possessed windows that were penetrated by the 2D nets (for example, if they had a ladder-like motif), then the term interpenetration would apply.

When describing interpenetrating systems, it is important to describe not just the topology of the interpenetrating networks but also the topology of interpenetration.[1,4] This is analogous to describing not only the molecular geometry in a simple molecular crystal structure but also the way the molecules pack together. The way the networks interpenetrate can have important structural consequences. For example. interpenetration of low-dimensional networks can give entanglements with the same or higher dimensions [interpenetration of 2D nets, for example, can give overall 2D or three-dimensional (3D) entanglements]. A notation for partially describing the topology of interpenetration was developed".'' and is used at various stages in the following discussion to help illustrate not only the network topologies but also the interpenetration topologies.

1D NETS

The importance of describing interpenetration topology, as well as dimensional increase through interpenetration. can be illustrated by looking at 1D networks. The structure of $[\{HO_2CC_6H_4CH_2)(Bu_2bipy)Me_2Pt\}_3(tpt)](PF_6)_3$ [*Bu_2bipy* = 4.4'-di-tertbutyl-2.2'-bipyridine, *tpt* = 1,3,5-tri(4-pyridyl)-2,4,6-triazine], consists of trimeric species connected by hydrogen-bonding carboxylate dimers to generate 1D nets that consist, topologically, of alternating windows and links.[5] The chains entangle in parallel pairs such that the links of one chain penetrate the windows of the other and vice versa, generating 1D entanglements of pairs of nets (Fig. 1a). The mean vectors of propagation of each chain in the interpenetrating pairs are both parallel and coincident, and the 1D entanglement of 1D nets is called "1D → 1D interpenetration."

The structure of $[Cu_2L_3(MeCN)_2](PF_6)_2$ [*L* = 1.4-bis (4-pyridyl)butadiyne] contains 1D ladder-like networks that interpenetrate such that each Ladder interpenetrates

DOI: 10.1081/E-ESMC 120012732

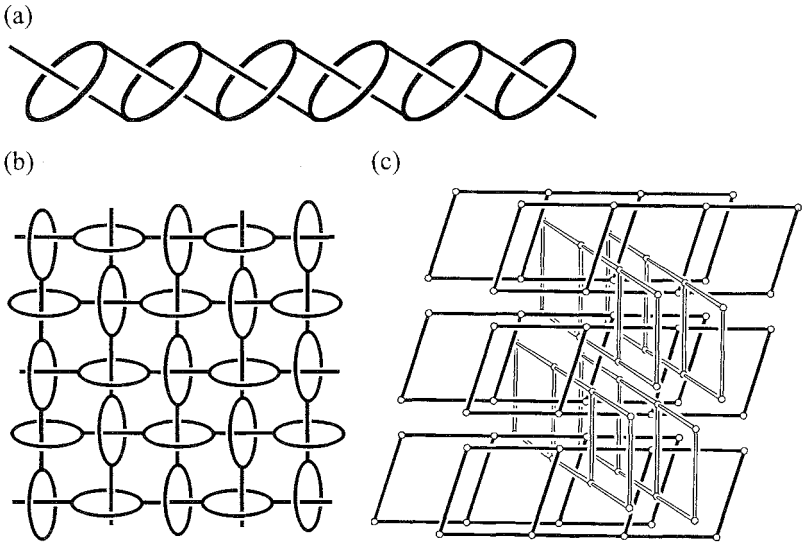

Fig. 1 Interpenetration of ID nets: (a) 1D — 1D interpenetration in the structure of $[\{HO_2CC_6H_4CH_2)(Bu_2bipy)\text{-}Me_2Pt\}_3(tpt)](PF_6)_3$;[5] (b) 1D → 2D inclined interpenetration in the structure of $Ag_2(bix)_3(NO_3)_2$;[8] and (c) 1D → 3D inclined interpenetration in the structure of $CdL_{1.5}(NO_3)_2$, *L* = 1,4-*bis*(4-methylpyridyl)benzene.[9]

with four others.[6,7] As in the previous example, the mean vectors of propagation of the interpenetrating networks are parallel; however, they are no longer coincident. As a result, the interpenetration is such that 2D layers of interpenetrating 1D ladders are formed. This is 1D → 2D parallel interpenetration.

1D → 2D inclined interpenetration is illustrated by the structure of $Ag_2(bix)_3(NO_3)_2$ [*bix* = 1,4-*bis*(imidazol-1-ylmethyl)benzene].[8] Like the example of 1D → 1D interpenetration discussed above. this structure contains 1D chains that consist of alternating windows and links. The mean vectors of propagation of the interpenetrating nets are. however, no longer all parallel but rather occur in two sets of parallel directions inclined to each other. The interpenetration results in an overall 2D entanglement (Fig. 1b). An interesting feature of this structure and the first compound mentioned in this section is that they are rare examples of structures in which there are only rotaxane-like interactions and no catenane-like interactions.

The generation of a 3D entanglement from the interpenetration of 1D networks is displayed by the structure of $CdL_{1.5}(NO_3)_2$ [*L* = 1,4-*bis*(4-methylpyridyl)benzene].[9] Each window of each 1D ladder-like net is penetrated by four other ladders at an inclined angle to the first (Fig. lc), resulting in an overall 3D entanglenlent (1D → 3D inclined interpenetration). Another possible topology of interpenetration. 1D → 3D parallel interpenetration, is yet to be observed.

2D NETS

As for 1D nets, there are a number of different ways for 2D networks to interpenetrate. The compound Ag(tcm) (*tcm* = tricyanomethanide), $C(CN)_3^-$ is a coordination polymer composed of 2D chicken-wirelike (6,3) networks.[10,11] The networks are corrugated and interpenetrate such that discrete layers of doubly interpenetrating networks are formed (Fig. 2a). The mean planes of the interpenetrating sheets in each layer are parallel and coincident, and the topology of interpenetration can be described as 2D → 2D parallel interpenetration. The topology of interpenetration can and should be described further (see Ref. [1] for further descriptions of different possible interpenetration topologies).

When the mean planes of the interpenetrating networks are parallel but no longer coincident, an overall 3D entanglement is achieved (2D → 3D parallel interpenetration). An example of this is the structure of $Cu_4(dca)_4(bipy)_3(MeCN)_2$ [*dca* = dicyanamide, $N(CN)_2^-$, *bipy* = 4,4′-bipyridine].[12] Each coordination network is polymeric in only two directions but has a certain "thickness" in the third. Each net is penetrated by four others that are parallel but offset in the third, nonpolymeric direction. Two layers penetrate the first toward the edges of the layer (one on either side), and two others penetrate toward the middle of the layer (again, one each propagating out either side). Each layer is identical; and thus, a 3D entanglement results.

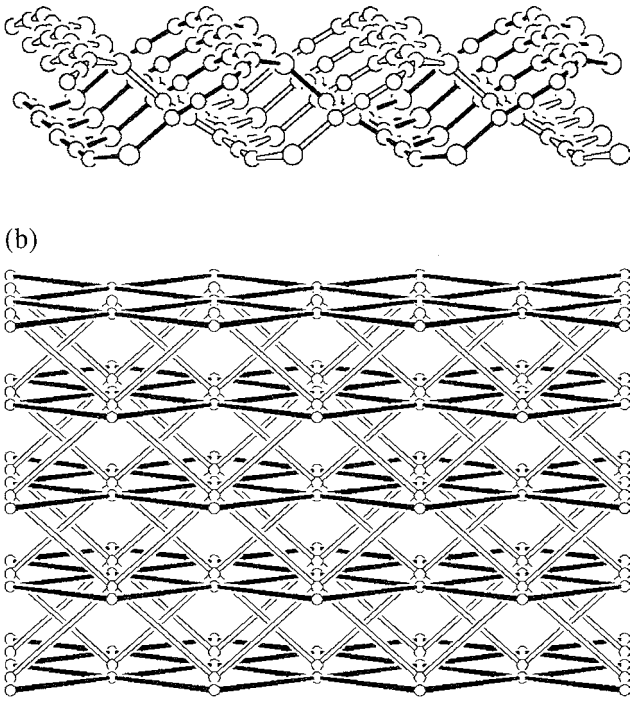

Fig. 2 Interpenetration of 2D nets: (a) 2D → 2D parallel interpenetration in the structure of Ag(tcm);[10,11] and (b) 2D → 3D inclined interpenetration in the structure of $[Zn(bipy)_2(H_2O)_2]SiF_6$.[13]

The structure of $[Zn(bipy)_2(H_2O)_2]SiF_6$, *bipy*=4,4′-bipyridine (Fig. 2b) contains two sets of parallel (4,4) sheets that interpenetrate each other at an inclined angle (2D inclined interpenetration).[13] The interpenetration is such that each window of each sheet contains a node of an interpenetrating sheet. Zaworotko[14] recently categorized three of the likely interpenetration topologies for inclined (4,4) sheets as parallel/parallel, parallel/diagonal, and diagonal/diagonal; the structure described here has the latter topology.

Another long-known example of 2D inclined interpenetration is the structure of trimesic acid (1,3,5-benzenetricarboxylic acid).[15] It contains hydrogen-bonded (6.3) sheets that interpenetrate such that each window of each sheet is penetrated by three other inclined sheets. It is also possible for more than two stacks of parallel sheets to show inclined interpenetration—the remarkable structure of $Co_2(azpy)_3(NO_3)_4 \cdot Me_2CO \cdot 3H_2O$ [*azpy*=4,4′-azo*bis*-(pyridine)] contains four separate stacks of parallel (6,3) sheets that all interpenetrate at mutually inclined angles.[16] Combinations of network and interpenetration topologies are also possible. Inclined interpenetration between (4,4) and (6.3) sheets has been reported,[17] and the structure of $[AgL_2]SbF_6$ (L = 3-cyanophenyl 4-cyanobenzoate) has 2D layers of doubly interpenetrating parallel sheets; these layers then show inclined interpenetration.[18]

3D NETS

A simple 3D network composed of three-connecting nodes is the (10,3)-*a* net.[19,20] The (10.3)-a net is inherently chiral, and this chirality has interesting consequences for interpenetration. The structure of $Ni_3(btc)_2(py)_6(eg)_6 \cdot solv$ (*H_3btc* = trimesic acid, *py* = pyridine. eg = ethylene glycol). for example, has four interpenetrating (10,3)-*a* networks, all of the same hand.[21] The structure of $Zn(tpt)_{2/3}(SiF_6)(H_2O)_2(MeOH)$ (*tpt* = 1,3,5-tri(4-pyridyl)-2,4,6-triazine), however. contains eight interpenetrating networks: four of either hand.[22] Thus, interpenetration can retain the chirality of the individual networks or can result in an overall racemic structure. The largest class of interpenetrating networks is that with the diamondoid topology. Some of the oldest examples are the structures of $M(CN)_2$ (M = Zn, Cd),[2,23,24] which contain two interpenetrating diamondoid networks (Fig. 3a). Other long-known examples of twofold interpenetration of diamond-like nets are Cu_2O[25] and certain high-pressure forms of ice.[26,27] An interesting series of compounds contains the derivatives of $Cu(DCNQI)_2$ (*DCNQI* = *N*,*N*′-dicyanoquinodiimine).[28] These materials show metal-like electrical conductivity that can be related to the way their seven diamondoid networks interpenetrate. Curiously. of all the known examples of interpenetration of diamondoid networks, all but a few[12,29,30] show the same topology of interpenetration.

The PtS network consists of equal numbers of tetrahedral and square-planar centers. Two such networks interpenetrate in the structure of $[\{Cu^{II}(tcp)\}Cu^{I}]BF_4 \cdot 17C_6H_5NO_2$ [Cu^{II}(tcp) = 5,10,15,20-tetrakis(4-cyanophenyl)-21H,23H-porphine copper(II)].[31] The networks interpenetrate in an asymmetric fashion, i.e., the second net does not lie in the center of the channels and cavities of the first, but rather lies to one side. Attractive internet porphyrin...porphyrin interactions are the likely cause, and it produces larger channels and cavities, which contain large amounts of essentially liquid solvent, than would normally be expected.

The α–Po network contains octahedral 6-connecting nodes: two such networks interpenetrate in the structure of α–$M(dca)_2(pyz)$ (*dca* = dicyanamide, $N(CN)_2^-$, *pyz* = pyrazine), as shown in Fig. 3b.[32] Another structure that can be related to two interpenetrating α–Po nets is the structure of $Zn(CN)(NO_3)(tpt)_{2/3} \cdot solv$ [tpt = 1,3,5-tri

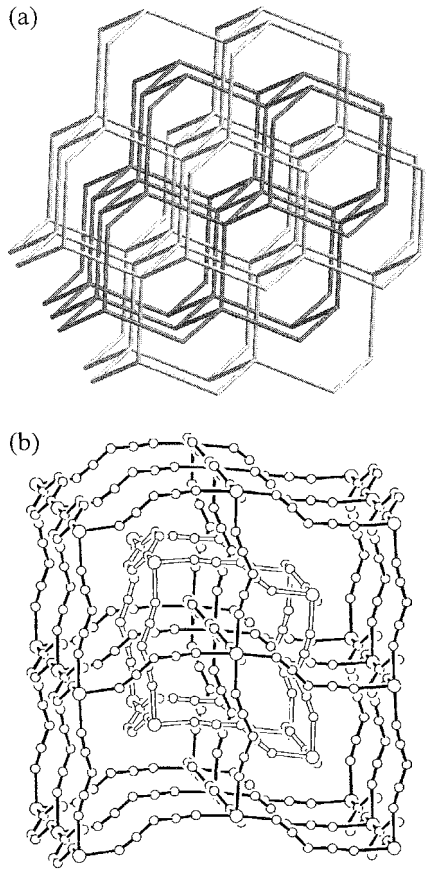

Fig. *3* Interpenetration of 3D nets: (a) two interpenetrating diainondoid networks; and (b) two interpenetrating α-Po nets in the structure of α-M(dca)$_2$(pyz).[32] ***(View this** art in color at www.dekker.com.)*

(4-pyridyl)-2,4,6-triazine].[33] The octahedral connectors are [{$Zn_4(CN)_4(NO_3)_4$}$_6$(tpt)$_8$] cages that share Zn_4-$(CN)_4(NO_3)_4$ squares with adjoining cages. Remarkably, the interpenetration of the two networks is such that the second network wraps around the aforementioned cages of the first network (and vice versa). creating large (>1290 A') completely sealed-off cavities that can contain up to 22 molecules of liquid solvent.

The Pt_3O_4 net contains four-connecting square-planar centers and three-connecting trigonal centers. The structure of $Cu_3(BTB)_2(H_2O)_3\cdot 9DMF\cdot 2H_2O$, *$H_3BTB$* = 4,4′,4″-benzene-1,3,5-triyl-tribenzoic acid contains two networks with Pt_3O_4 topology that interpenetrate in an asymmetric fashion.[''] Thus: despite the interpenetration, the structure is highly porous, containing large cavities and channels. and was shown to reversibly sorb large amounts of gases and organic solvents. The interpenetration is thought to reinforce the frameworks against structural collapse upon removal of solvent.

NETS OF DIFFERENT COMPOSITION, TOPOLOGY. AND DIMENSIONS

While the vast majority of interpenetrating structures involve interpenetration of identical networks, an increasing number of examples of heterogeneous interpenetration are being reported. The structure of $K_2[PdSe_{10}]$ contains two interpenetrating diamondoid networks, one of composition $Pd(Se_4)_2^{2-}$ and one of composition $Pd(Se_6)_2^{2-}$.[35] The Se_6^{2-} bridges are considerably more twisted than the Se_4^{2-} bridges, allowing both nets to have the same intranet Pd...Pd separation.

$[Ni(azpy)_2(NO_3)_2]_2[Ni_2(azpy)_3(NO_3)_4]\cdot 4CH_2Cl_2$ [*azpy* = 4,4′-azo*bis*(pyridine)] shows 2D inclined interpenetration of (4,4) and (6,3) sheets.[17]

The structure of $[Cu_5(bpp)_8(SO_4)_4(EtOH)(H_2O)_5]$-$SO_4\cdot EtOH\cdot 25\cdot 5H_2O$ [bpp = 1,3-*bis*(4-pyridyl)propane] contains 1D polymers that interpenetrate at an inclined angle with (4,4) 2D sheets (1D/2D→3D inclined interpenetration).[36] Two sheets penetrate each window of each 1D net. while each window of the 2D sheets is penetrated by one 1D net. The structures of $Ni(bipy)_2(H_2$-$PO_4)_2\cdot C_4H_9OH\cdot H_2O$ (*bipy* = 4,4′-bipyridine)[37] and $[Cu_2L_4\cdot 3H_2O][Cu_2L_4\cdot 2H_2O]\cdot 2H_2O$ (L = isonicotinate)[38] both contain interpenetrating 2D (4,4) sheets and 3D $CdSO_4$-like nets (2D/3D interpenetration). In the former case, both nets have the same composition, whereas in the latter example; they differ.

SELF-PENETRATION

A self-penetrating network is one in which the smallest topological circuits are penetrated by other parts of the same network.['''] The smallest topological circuits are the shortest pathways (in terms of the number of nodes) that can be taken which form a circuit that contains any two links from a given node. It is therefore important to note that the smallest topological circuits are not necessarily all the same size. For example, the smallest circuits for the 3D rutile network, which contains 3-connecting nodes and 6-connecting nodes, are four-membered rings and six-membered rings, depending on which pairs of links from which node are used to define the circuit.

An interesting series of structures based on the rutile net illustrates the relationship between interpenetration and self-penetration. The compounds are constructed using octahedral metal ions and the trigonal ligands tcm [tricyanomethanide, $C(CN)_3^-$] and dca [dicyanamide, $N(CN)_2^-$]. It is iinportant to note that dca is a smaller ligand than tcm. Thus. while the compounds $M(tcm)_2$ have two interpenetrating rutile-related networks,[39] the

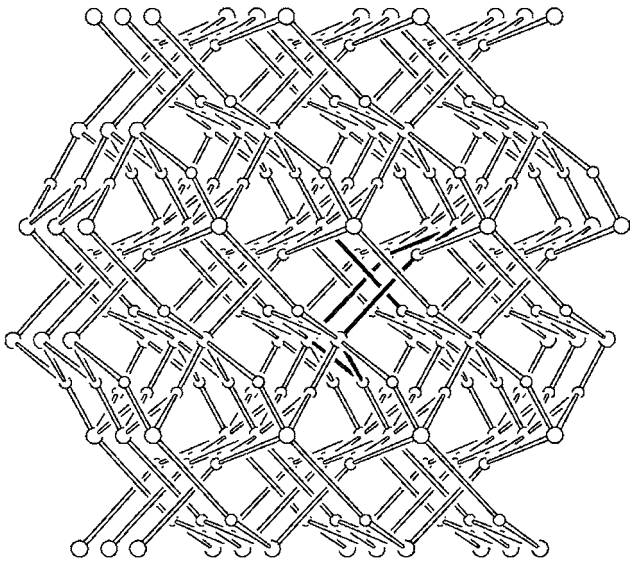

Fig. 4 The self-penetrating network of M(dca)(tcm), with the penetration of a rod through a ring highlighted.[''']

compounds α–M(dca)$_2$ have only a single rutile network.[40] In the tcm complexes, each net penetrates through the six-membered rings of the other, while the four-membered rings are left untouched. Interestingly. when only half the large tcm ligands are replaced by the smaller dca ligand. as in the structures of M(dca)(tcm), a single, self-penetrating network is formed (Fig. 4).[41] Again, it is the six-membered rings that are penetrated. this time by rods from other parts of the same network. The structure of this network is closely related to the rutile net, with the two nets having the same Schlafli notation.[1,19,20] The magnetic properties of these mixed-ligand complexes were also studied, and like their structures. their magnetic properties are a compromise between the two ''parent'' compounds.

Another self-penetrating network is the (12,3) net, of which two examples were recently reported.[42,43] If interpenetrating networks can be related to catenanes and rotaxanes, then self-penetrating networks can be considered to be polymeric equivalents of molecular knots.

CONCLUSION

Interpenetration of networks is becoming an increasingly more common phenomenon, with any structure containing networks that account for less than 50% of the crystal volume being open to interpenetration. The effects of interpenetration vary — examples were given of compounds in which interpenetration reinforced highly porous structures,[34] structures that contained unique sealed-off cavities containing essentially minute droplets of liquid,[33] or materials that had metal-like conductivities.[28]

In order to understand such systems, it is important not only to describe the network topology but also the topology of interpenetration. A number of examples of different interpenetration topologies were given above. Further details on the numerous examples of interpenetration can be found in a number of recent reviews,[1,3,4] and also on the author's Web site, which contains a regularly updated table of all known interpenetrating structures, sorted according to network and interpenetration topologies.[44]

ARTICLES OF FURTHER INTEREST

Catenanes and Other Interlocked Molecules, p. *206*
Crystal Engineering with Hydrogen Bonds. p. 357
Rotaxanes and Pseudorotaxanes, p. *1194*

REFERENCES

1. Batten, S.R.: Robson, R. Interpenetrating nets: Ordered, periodic entanglement. Angew. Chem. Int. Ed. 1998. 37. 1460–1494.
2. Hoskins, B.F.; Robson, R. Design and construction of a new class of scaffolding-like materials comprising infinite polymeric frameworks of 3D-linked molecular rods. A reappraisal of the $Zn(CN)_2$ and $Cd(CN)_2$ structures and the synthesis and structure of the diamond-related frameworks $[N(CH_3)_4][Cu^{I}Zn^{II}(CN)_4]$ and Cu^{I}[4,4′,4″,4‴-tetracyanotetraphenylmethane]$BF_4 \cdot xC_6H_5NO_2$. J. Am. Chem. Soc. 1990. 112. 1546–1554.
3. Batten, S.R.: Robson. R. Catenane and Rotaxane Motifs in Interpenetrating and Self-penetrating Coordination Polymers. In *Molecular Catenanes, Rotaxanes and Knots, A Journey Through the World of Molecular Topology;* Sauvage, J.-P., Dietrich-Buchecker. C., Eds.: Wiley-VCH: Weinheim, 1999: 77–105.
4. Batten, S.R. Topology of interpenetration. CrystEngComm 2001. 3. 67–73.
5. Fraser. C.S.A.; Jennings, M.C.; Puddephatt, R.J. An organometallic polyrotaxane and a new type of polyrotaxane architecture. Chem. Commun. 2001. 1310–1311.
6. Blake, A.J.; Champness, N.R.; Khlobystov, A.; Lemenovskii. D.A.: Li. W.-S.; Schroder, M. Polycatenated copper(I) molecular ladders: A new structural motif in inorganic co-ordination polymers. Chem. Commun. 1997, 2027–2028.
7. Maekawa, M.: Konaka. H.; Suenaga, Y.: Kuroda-Sowa, T.: Munakata. M. A variety of one-. two- and three-dimensional copper(I) and silver(I) co-ordination polymers

assembled by 1,4-*bis*(4-pyridyl)butadiyne and 1.4-bis(2-pyridyl)butadiyne. J. Chem. Soc., Dalton Trans. 2000, 4160–4166.
8. Hoskins, B.F.: Robson, R.: Slizys. D.A. An infinite 2D polyrotaxane netuork in $Ag_2(bix)_3(NO_3)_2$ (bix = 1,4-bis-(imidazol-1-ylmethyl)benzene). J. Am. Chem. Soc. 1997. *119*, 2952–2953.
9. Fujita. M.; Kwon. Y.J.: Sasaki, O.: Yamaguchi, K.: Ogura, K. Interpenetrating molecular ladders and bricks. J. Am. Chem. Soc. 1995, 117. 7287–7288.
10. Konnert. J.: Britton. D. The crystal structure of $AgC(CN)_3$. Inorg. Chem. 1966. 5. 1193–1196.
11. Batten, S.R.; Hoskins. B.F.; Robson, R. The structures of [Ag(tcm)], $[Ag(tcm)(phz)_{1/2}]$ and [Ag(tcm)(pyz)] (tcm = tricyanometliaaide, $C(CN)_3^-$, phz = phenazine. pyz = pyrazine). Neu· J. Chem. 1998. *22*. 173–175.
12. Batten. S.R.: Harris. A.R.: Jensen, P.; Murray, K.S.: Ziebell. A. Copper(I) dicyanainide coordination polymers: Ladders, sheets. layers, diamond-like networks and unusual interpenetration. J. Chem. Soc., Dalton Trans. 2000. 3829–3836.
13. Gable. R.W.: Hoskins, B.F.; Robson. R. A new type of interpenetration involving enmeshed independent square grid sheets. The structure of diaquabis-(4,4′-bipyridine)-zinc hexafluorosilicate. J. Chem. Soc., Chem. Commun. 1990, 1677–1678.
14. Zaworotko. M.J. Superstructural cliversity in two dimensions: Crystal engineering of laminated solids. Chem. Commun. 2001. 1–9.
15. Herbstein. F.H.; Kapon. M.: Reisner. G.M. Trimesic acid. its hydrates, complexes and polymorphism. VIII. Interstitial complexes of α- and (the hypothetical) *I-trimesic acid. Acta Crystallogr. Sect. B 1985. 41, 348–354.
16. Kondo. M.: Shimamura, M.; Noro. S.: Minakoshi, S.: Asami. A.; Seki. K.; Kitagawa. S. Microporous materials constructed from the interpenetrated coordination networlis. Structures and methane adsorption properties. Chem. Mater. 2000. *12*, 1288–1299.
17. Carlucci, L.: Wilson, S.R.: Proserpio, D.M. Three-dimensional architectures of intertwined planar coordination polymers: The first case of interpenetration involving two different bidimensional polymeric motifs. Neu J. Chern. 1998, *22*. 1319–1321.
18. Hirsch. K.A.; Wilson. S.R.: Moore, J.S. Crystallization of 3-cyanophenyl 4-cyanobenzoate with $AgSbF_6$: A polar coordination network based on the crisscrossing of intertwined helices. Chem. Commun. 1998. 13–14.
19. Wells. A.F. *Three-Dimensional* Nets *and Polyhedra*; Wiley-Interscience: New York, 1977.
20. Wells. A.F. Further Studies *of Three-Dimensional* Nets; ACA Monograph, American Crystallographic Association. 1979: Vol. 8.
21. Kepert. C.J.: Rosseinsky. M.J. A porous chiral framework of coordinated 1,3,5-benzenetricarboxylate: Quadruple interpenetration of the (10.3)-a network. Chem. Commun. 1998. 31–32.
22. Abrahams. B.F.: Batten. S.R.; Hamit. H.: Hoskins. B.F.: Robson. R. A Wellsian '3D racemate': Eight interpenetrating, enantiomorphic (10.3)-a nets, four right handed and four left handed. Chem. Coinmun. 1996. 1313–1314.
23. Zhdanov. H.S. Crystalline structure of $Zn(CN)_2$. C. R. Acad. Sci. URSS 1941. 31, 352–354.
24. Shugam, E.: Zhdanov. H. The crystal structure of cyanides. II. The structure of $Cd(CN)_2$. Acta Phpsiochim. URSS 1945. *20*. 247–252.
25. Niggli, P. The crystal structure of several oxides. Z. Krist. 1922, 57. 253–299.
26. Kamb. B.; Davis, B.L. Ice VII. the densest form of ice. Proc. Natl. Acad. Sci. U. S. A. 1964, 52. 1433–1439.
27. Whalley, E.; Davidson, D.W.: Heath. J.B.R. Dielectric properties of ice VII. Ice VII: A new phase of ice. J. Chem. Phys. 1966. *45*. 3976–3982.
28. Sinzger, K.; Hunig, S.: Jopp. M.; Bauer. D.; Bietsch, W.; von Schutz, J.C.; Wulf. H.C.; Kremer, R.K.; Metzenthin, T.; Bau, R.: Khan, S.I.; Lindbaum. A.; Lengauer, C.L.: Tillmanns. E. The organic metal $(Me_2\text{-}DCNQI)_2Cu$: Dramatic changes in solidstate properties and the crystal structure due to secondary deuterium effects. J. Am. Chem. Soc. 1993, 115. 7696–7705.
29. Ermer, O. Five-fold diamond structure of adamantane-1.3.5.7-tetracarboxylic acid. J. Am. Chem. Soc. 1988. *110*, 3747–3754.
30. Chen, Z.-F.: Xiong. R.-G.: Abrahams. B.F.: You, X.-Z.; Che. C.-M. An unprecedented six-fold anion-type chiral diamondlike eight-coordinate Cd(II) coordination polymer with a second-order nonlinear optical effect. J. Chern. Soc., Dalton Trans. 2001, 2453–2455.
31. Abrahams. B.F.; Hoskins. B.F.: Michail, D.M.; Robson. R. Assembly of porphyrin building blocks into network structures with large channels. Nature 1994. 369. 727–729.
32. Jensen, P.: Batten, S.R.: Moubaraki, B.: Murray. K.S. Synthesis, structural isomerism and magnetism of the coordination polymers $[M(dca)_2pyz]$, M = Mn, Co, Ni and Zn, dca = dicyanamide $(N(CN)_2^-)$ and pyz = pyrazine. J. Solid State Chem. 2001. *159*, 352–361.
33. Batten, S.R.; Hoskins, B.F.; Robson. R. Two interpenetrating 3D networlis which generate spacious sealed-off compartments enclosing of the order of 20 solvent molecules in the structures of $Zn(CN)(NO_3)(tpt)_{2/3}\cdot solv$ (tpt = 2,4,6-tri(4-pyridyl)-1,3,5-triazine, solv = $\sim 3/4C_2H_2Cl_4\cdot 3/4CH_3OH$ or $3/2CHCl_3\cdot 1/3CH_3OH$). J. Am. Chern. Soc. 1995. 117. 5385–5386.
34. Chen, B.; Eddaoucli. M.: Hyde. S.T.; O'Keeffe, M.: Yaghi. O.M. Interwoven metal–organic framework on a periodic minimal surface with extra-large pores. Science 2001, *291*. 1021–1023.
35. Kim. K.W.: Kanatzidis. M.G. Hydrothermal synthesis of K_2PdSe_{10}. Coexistence of two large interpenetrating frameworks of $[Pd(Se_4)_2]^{2-}$ and $[Pd(Se_6)_2]^{2-}$. J. Am. Chem. Soc. 1992. *114*. 4878–4883.
36. Carlucci. L.; Ciani. G.; Moret. M.: Proserpio, D.M.; Rizzato. S. Polymeric layers catenated by ribbons of rings in a three-dimensional self-assembled architecture: A

nanoporous network with spongelike behaviour. Angew. Chem. Int. Ed. 2000, *39*, 1506–1510.

37. Jiang, U.-C.: Lai, Y.-C.: Wang. S.-L.; Lii, K.-H. [Ni(4,4′-bpy)$_2$(H_2PO_4)$_2$]·C_4H_9OH·H_2O: A novel metal phosphate that exhibits interpenetration of 2D net into 3D framework. Inorg. Chem. 2001. 40. 5320–5321.
38. Lu, J.Y.; Babb. A.M. An unprecedented interpenetrating structure with two covalently bonded open-frameworks of different dimensionality. Chem. Commun. 2001. 821–822.
39. Batten, S.R.: Hoskins. B.F.: Moubaraki. B.; Murray, K.S.: Robson, R. Crystal structures and magnetic properties of the interpenetrating rutile-related compounds M(tcm)$_2$ [M = octahedral, divalent metal: t c m = tricyanomethamethanide, $C(CN)_3^-$] and the sheet structures of [M(tcm)$_2$-(EtOH)$_2$] (M = Co or Ni). J. Chem. Soc., Dalton Trans. 1999. 2977–2986.
40. Batten, S.R.: Jensen. P.: Moubaraki. B.: Murray, K.S.: Robson. R. Structure and molecular magnetism of the rutile-related compounds M(dca)$_2$, M = Co^{II}, Ni^{II}, Cu^{II}, dca = dicyanamide, $N(CN)_2^-$. Chem. Commun. 1998, 439–440.
41. Jensen. P.; Price. D.J.: Batten, S.R.: Moubaraki. B.: Murray. K.S. Self-penetration—A structural compromise between single networks and interpenetration: Magnetic properties and crystal structures of [Mn(dca)$_2$(H_2O)] and [M(dca)(tcm)], M = Co. Ni, Cu. dca = dicyanamide. $N(CN)_2^-$, tcm = tricyanomethanide. $C(CN)_3^-$. Chem. Eur. J. 2000, 6. 3186–3195.
42. Abraharns. B.F.; Batten. S.R.: Grannas, M.J.: Hamit, H.; Hoskins, B.F.; Robson, R. Ni(tpt)(NO_3)$_2$—A three-dimensional network with the exceptional (12.3) topology: A self-entangled single net. Angew. Chem. Int. Ed. 1999. *38*, 1475–1477.
43. Schareina. T.; Schick. C.: Abrahams. B.F.; Kempe. R. Coordination polymers of bipyridyldicarhorcylates—A cobalt containing 12,3-net with potential reactive sites. Z. Anorg. Allg. Chem. 2001. 627. 1711–1713.
44. http://web.chem.monash.edu.au/Department/Staff/Batten/Intptn.htm. (accessed November 2001).

Ion Channels and Their Models

Karycia D. D. Mitchell
Thomas M. Fyles
University of Victoria, Victoria, British Columbia, Canada

INTRODUCTION

Ion channels, which control the movement of ions across lipid membranes. are essential to the function of many biological systems.[1] Ion transport across membranes can occur via one of two broadly defined mechanisms: transport via channels or transport via carriers.[1] The former suggests a tubular or helical membrane-spanning structure that is stationary and allows ion translocation through or along the transporter. The latter suggests a smaller. encapsulating structure that forms a complex with the ion and moves through the membrane via diffusion.

In molecular terms, the movement of an ion across a membrane via a channel can best be described as a series of "hops" along the stationary channel molecule. The ion–transporter interactions that facilitate ion translocation replace ion–water interactions on either side of the membrane. The energy barrier for direct ion diffusion across the membrane is directly due to the instability of the ion in the nonpolar membrane interior. Ion–channel interactions significantly lower the barrier and thus facilitate diffusion.[1] A similar argument applies to carrier-mediated transport. with the result that channels and carriers are kinetically indistinguishable. However. activation barriers for channel-mediated diffusion are expected to be much lower than the activation barrier for carriers."' with the result that the maximum transport rates of channels are typically several orders of magnitude higher than those of carriers.

Another important distinction between carriers and channels is the ability to regulate or "gate" channels. The nature of channels is such that they could be pliysically switched "on" and "off" by altering the binding of the ion with the transporter: either through altering the conformation of the channel or by plugging the channel orifice."'

BILAYER CLAMP TECHNIQUE

Experimental deiection of the formation of ion channels is best achieved using the bilayer clamp technique.[2] In this experiment. a freestanding bilayer membrane is interposed in a small orifice separating two pools of aqueous electrolyte. The bilayer is an effective insulator. so no current is passed under applied potentials in the range of ±150 mV. An ion channel in the bilayer will significantly increase the transmembrane current in an abrupt "all-or-nothing" fashion. The resulting trace of current shows sharp transitions between a nonconducting "off" condition and a conducting "on" condition. Shown in Fig. 1 is the bilayer conductance of the peptide channel gramicidin under different applied potentials. Note that at a given potential, the step heights of the conductance changes are the same, indicating a single type of channel structure. in this case, a dimer. Step conductance changes are the unique experimental signature of channel activity; carriers provoke a general increase in the bilayer conductance but do not show abrupt "on–off" behavior. The bilayer clamp technique is a powerful method with which to elucidate ion selectivity, channel lifetime. and voltage gating properties of single channels.[1]

CHANNEL TRANSPORT MEASUREMENT

Indirect methods of measuring channel transport are based on measurements of indicators trapped within a vesicle bilayer membrane."' These measurement methods include ^{23}Na–NMR; UV/Vis or fluorescence spectroscopy of pH. metal ion concentration, or concentration of environment-sensitive indicators; radiochemical techniques; and pH stat techniques to monitor proton efflux. These methods give evidence that an active compound can alter membrane permeability, but it is difficult to establish a distinction between channel function, transport via carriers. or a nonspecific membrane disruption.[1]

NATURAL ION CHANNELS

Natural ion channels are high-molecular-weight membrane-spanning proteins that are believed to act via multiple α-helical strands that cross the membrane repeatedly.[3] While much about protein channels is still not understood, it is believed that several helices arrange into an ion-selective pore. with ion transport occurring

Encyclopedia of Supramolecular Chemistry
DOI: 10.1081/E-ESMC 120012685

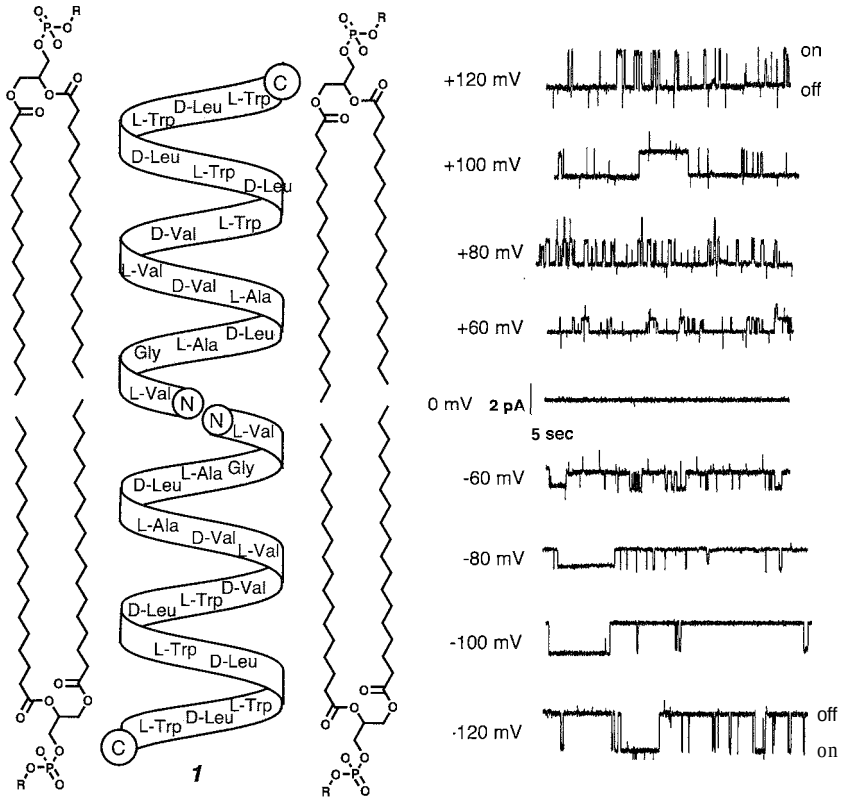

Fig. 1 (left) Schematic structure of a gramicidin dimer in a phospholipid bilayer. (right) Bilayer conductance exhibited by gramicidin in a phospholipid bilayer at various applied potentials.

via the hydrated spaces adjacent to the bundles of helices. The most detailed insights into the structural origins of specificity stem from the crystal structures of the KcsA channel from *Streptomyces lividans*[4] and of *CLC* chloride channels from *Salmonella enterica* serovar *typhimurium* and *Escherichia coli,*[5] for which McKinnon was awarded the *2003* Nobel Prize in Chemistry.

The best-studied natural ion channels are peptides, which act as aggregates comprised of peptide monomers. The most well-known examples are alamethicin and gramicidin.

The aminoisobutyric acid containing peptide alamethicin[6] is a naturally occurring ion-channel compound that acts via a cluster of α-helices without the support of additional proteins. Produced by the fungus *Trichodevrna viride,* it is an antibiotic peptide, known to affect the quality of pastureland through its effects on ruminant animal stomach bacteria. Side-by-side association of several alamethicin molecules to form a barrel-stave aggregate occurs. The membrane-spanning aggregate possesses a net transmembrane dipole; thus producing voltage-gated behavior. Alamethicin pores also have short lifetimes, showing ''burst'' activity of only a few milliseconds duration.

Gramicidin[1,6] is one of the most well-studied ion channels. It is naturally synthesized by *Bacillus brevis* and derives its name from its antibiotic properties against gram-positive bacteria. Gramicidin, **1** (Fig. 1), is a pentadecapeptide derivative, composed of alternating D- and L-amino acid residues, that forms a monovalent–cation–selective tubular helix channel in lipid membranes. Ion translocation occurs via cation interactions with carbonyl oxygens on the inside of the helix. Two molecules of gramicidin span the membrane via formation of an end-to-end dimer held together by hydrogen bonding. Due to its unique mechanism, in which the ion transfer occurs within a single helix, the gramicidin channel has limited relevance to channels in the natural world, but it has inspired numerous synthetic mimics.

SYNTHETIC MIMICS

An example of such a synthetic mimic is the hydraphile channel system developed by Gokel.[13] The system is based on the 4,13-diaza-18-crown-6 macrocycle **3** (Fig. *2),* with an inner crown ether believed to be embedded in the

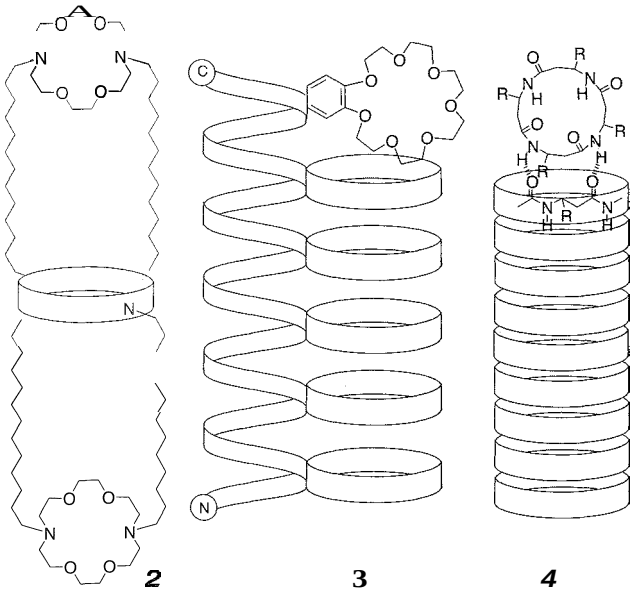

Fig. *2* Schematic structures of synthetic transporters incorporating macrocyclic ion binding units.

bilayer as the central relay group. The other crown ethers lie near the bilayer surface and can regulate cation entry to the membrane interior. The sodium transport rate of these channels is about 100-fold lower than gramicidin but substantially faster than a single crown ether acting as a carrier.

Unimolecular channel compounds have also been formed using an α-helical peptide scaffold to support an assay of 21-crown-7 moieties, **4**.[7] Models suggest that the structure formed is about 3.2 nm long, and that the crown ethers stack to form the channel. Compound 4 showed transport ability similar to that of gramicidin and displayed bilayer-dependent single-channel features.

Self-assembling transmembrane peptide nanotubes were formed from cyclic peptides composed of an even number of alternating D- and L-α-amino acids. These macrocycles adopt flat, ring-shaped conformations, with the backbone amides positioned perpendicular to the plane of the ring. Hydrogen-bonding conditions, such as adsorption onto a lipid membrane, are ideal for stacking the peptides, forming open-ended β-sheet-like tubular structures, 5. Cyclic hexapeptide channels showed transport rates for Na^+ and K^+ that rival those of gramicidin,[8,9] and larger structures will allow transport of small molecules, such as glutamate. Cyclic peptides of this type are antibacterial agents; as demonstrated against Staphylococcus *aureus*,[8] and antibiotic activity was correlated with enhanced membrane permeability to ions.

Alternatives to tubular channels are transmeinbrane aggregates that enclose a hydrophilic pore. One example is based on poly-p-phenylene oligomers bearing side arms

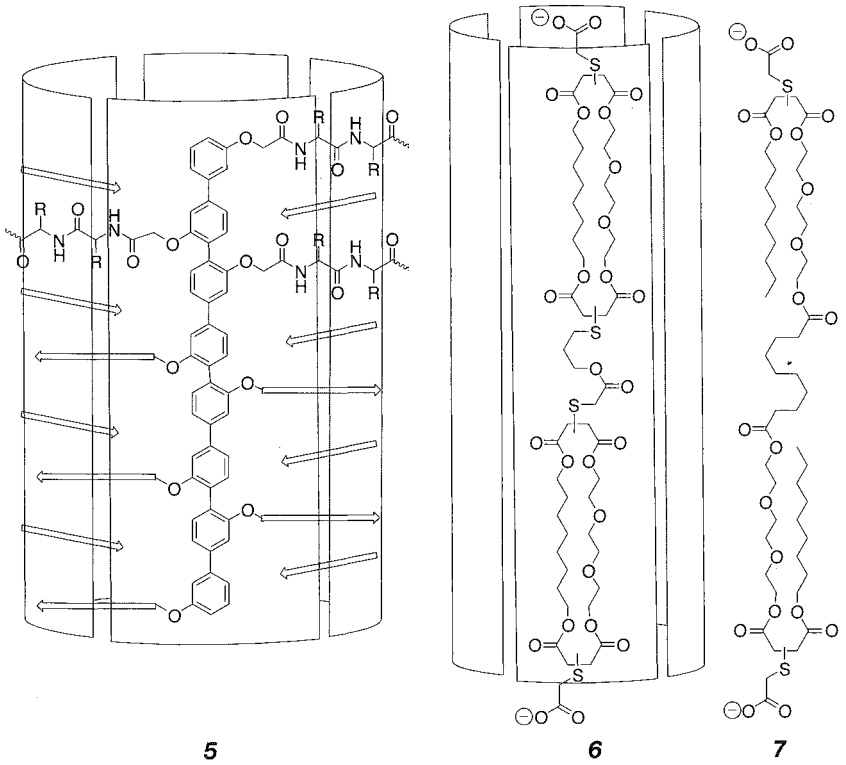

Fig. *3* Schematic structures of synthetic transporters that act via transmembrane aggregates.

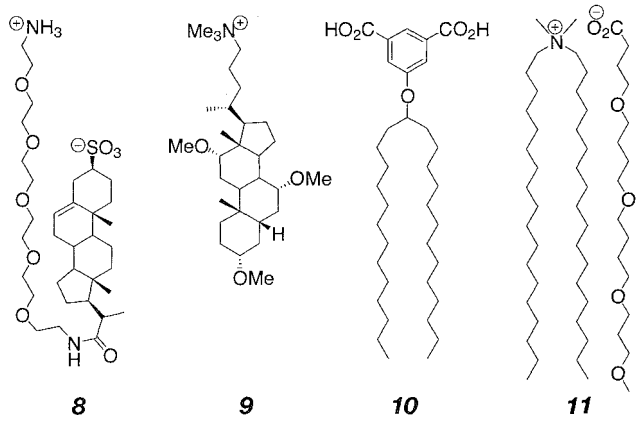

Fig. 4 Simple compounds that form transmembiane ion channels.

to promote the formation of side-to-side and tubular aggregates. 6 (Fig. 3).[10] This system produces stable hexameric pores with an "infinite" lifetime, i.e., the conductance is always in the "on" state.

Specific intermolecular interactions between components may not be essential, as macrocyclic bolaamphiphiles 4 form specific channels composed of a few molecules.[11] The association of the components is presumed to be driven by microphase separation in the lipid. Voltage-gated pores based on this system were also designed.[12] This group of compounds demonstrated a specific activity dependent on the structure of the core regions of the molecule, while ion selectivity and voltage switching appeared to be controlled by the polar head groups. The macrocyclic components are not essential for activity, as related acyclic compounds **7** are virtually indistinguishable from the bismacrocyclic compounds.[13]

Even simpler compounds form defined ion channels. Sterol conjugates 8 (Fig. 4) were prepared by steroid derivatization. as well as from cholic acid–spermine conjugates in which the hydrophilic face of each sterol was altered to incorporate methoxy. hydroxy, carbamate. or sulfate groups.[14,15] Another example is 9. a cholic-acid-based ion conductor that was altered to incorporate rnethoxy groups in place of the sterol hydroxyl groups.[16] These channel compounds were found to exist as membrane-spanning dimers, capable of Na^+ transport. with the rate of ion transport dependent on the bilayer membrane thickness. Similar structures with cholate groups appended to a resorcin[4]arene core formed long-lived K+ selective channels.[17]

The simplest compounds known to form defined ion channels are the isophthalate derivative **10**[18] and the ion-pair transporter **11**.[19] Single channels were observed for both systems, although incorporation and activity are somewhat erratic in both cases.

CONCLUSION

Attempts to mimic naturally occurring channels yielded a wide range of compounds of many shapes, sizes. and structures. Each group of cornpounds synthesized has a basic structure, which appears in every case to be subject to structure-activity control. Clearly, a wide range of basic structural types will support channel formation. making it unlikely that structurally specific interactions between the channel compound and the transient ion are essential.

Note that many of the molecules produced have few internal polar functional groups to which ions may bind. Instead, it is more likely that ion–water–channel interactions escort the ion through the pore. To that end. many of the models can then be viewed as methods to pull water into the lipidic core of a bilayer membrane and thereby stabilize ions in transport. Recent studies of molecular dynamics simulations of ion transportation in human aquaporin-1 and in the bacterial glycerol facilitator GlpF revealed the key role of water in the stabilization of ions in transit and in the molecular selectivity of channels.[8,20] Synthetic compounds form less-defined structures than these complex proteins but apparently act as efficiently as more complex natural materials. It is likely that continued study of synthetic systems will continue to reveal the general details underlying all transport processes.

ARTICLES OF FURTHER INTEREST

Biological *Ligands*, p. 88
Crown Ethers, p. 326
Cryptands, p. 334
Enzyme Mimics, p. 546
Ionophores, p. 760
Micelles *and Vesicles*, p. 861

REFERENCES

1. Fyles, T.M.: Van Straaten-Nijenhius, W.F. Ion Channel Models. In *Comprehensive Supramolecular Chemistry*; Atwood. J.L.. Davies, J.E.D., MacNicol, D.D., Vogtle, F.. Eds.; Elsevier Science Ltd.: Tarrytown, NY. 1996: Vol. 16, 53–77.
2. Fyles. T.M. Bilayer membranes and transporter models. Curr. Opin. Chern. Biol. **1997**, *1*. 497–505.
3. Gokel. G.W.; Ferdani, R.: Liu, J.: Pajewski. R.: Shabany. H.; Uetrecht, P. Hydrophile channels: Models for transmembrane, cation-conducting transporters. Chem. Eur. J. 2001. 7 (1). 33–39.
4. Doyle. D.A.: Cabral. J.M.; Pfuetzner, R.A.: Kuo. A.; Gulbis, J.M.: Cohen. S.L.; Chait, B.T.; MacKinnon, R. The structure of the potassium channel: Molecular basis of K^+ conduction and selectivity. Science 1998, 280. 69–77.

5. Dutzler. R.: Campbell, E.B.; Cadene. M.; Chait, B.T.; MacKinnon, R. X-ray structure of a ClC chloride channel at 3.0 Å reveals the molecular basis of anion selectivity. Nature 2002, *415*, 287–294.
6. Woolley. G.; Wallace. B.A. Model ion channels: Gramicidin and alamethicin. J. Membr. Biol. 1992, *129*. 109–136.
7. Meillon, J.C.: Voyer. N. A synthetic transmembrane channel active in lipid bilayers. Angew. Chem. Int. 1997, *36* (9), 967–969.
8. Fernandez-Lopez, S.; Kim, H.; Choi. E.C.: Delgado, M.; Granja, J.R.; Khasanov, A.; Kraehenbuehl. K.: Long, G.; Weinberger, D.A.: Wilcoxen, K.M.; Ghadiri, M.R. Antibacterial agents based on the D,L-α-peptide architecture. Nature 2001. *412*. 452–455.
9. Sanchez-Quesada, J.; Kim. H.S.; Ghadiri, M.R. A synthetic pore-mediated transmembrane transport of glutamic acid. Angew. Chem.. Int. Ed. 2001. *40* (13), 2503–2506.
10. Baurneister, B.: Sakai, N.; Matile. S. Giant artificial ion channels formed by self-assembled, cationic rigid-rod β-barrels. Angew. Chem., Int. Ed. 2000.39 (11), 1955–1958.
11. Fyles, T.M.; Loock. D.; Van Straaten-Nijenhius, W.F.; Zhou, X. Pores formed by his-macrocyclic bola-amphiphiles in vescile and planar bilayer membranes. J. Org. Chem. 1996, *61*, 8866–8874.
12. Fyles. T.M.: Loock, D.; Zhou. X. Ion channels based on *bis*-macrocyclic bolaamphiphiles: Effects of hydrophobic substitutions. Can. J. Chem. 1998. 76, 1015–1026.
13. Fyles, T.: Hu, C.; Knoy, R. Transmembrane ion conductance by an acyclic bolaamphiphile. Org. Lett. 2001. *3* (9). 1335–1337.
14. Bandyopadhyay, P.; Janout, V.: Zhang, L.: Regen, S.L. Ion conductors derived from cholic acid and spermine: Importance of facial hydrophilicity on Na^+ transport and membrane selectivity. J. Am. Chem. Soc. 2001. *123*, 7691–7696.
15. Bandyopadhyay, P.: Janout, V.; Zhang. L.: Sawko. J.A.: Regen, S.L. An ion conductor derived from spermine and cholic acid. J. Am. Chem. Soc. 2000, *122*, 12888–12889.
16. Kobuke. Y.: Nagatani. T. A supramolecular ion channel based on alnphiphilic cholic acid derivatives. Chem. Lett. 2000, *4*, 298–299.
17. Yoshino, N.; Satake, A.: Kobuke. Y. An artificial ion channel formed by a macrocyclic resorcin[4]arene with amphiphilic cholic acid ether groups. Angew. Chem., Int. Ed. 2001. *40* (2), 457–459.
18. Fyles. T.M.; Knoy, R.; Mullen, K.; Sieffert. M. Membrane activity of isophthalic acid derivatives: Ion channel formation by a low molecular weight compound. Langmuir 2001. *17* (21). 6669–6674.
19. Kobuke. Y.: Ueda, K.: Sokabe, M. Totally synthetic voltage dependent ion channel. Chem. Lett. 1995, *6*. 435–436.
20. De Groot, B.L.; Grubmuller. H. Water permeation across biological membranes: Mechanism and dynamics of aquaporin-1 and GlpF. Science 2001. *294*. 2353–2356.

Ion-Selective Electrodes

Yoshio Umezawa
University of Tokyo, Tokyo, Japan

INTRODUCTION

Ion-selective electrodes (ISEs) are among chemical methods of analysis, and one of the major chemical sensors that include bioaffinity-, gas-, ion- and other molecular sensors. A common feature for these chemical sensors is that molecular recognition of analytes takes place chemically by. e.g., bioreceptors, and various synthetic supramolecular receptors, immobilized in many cases on solid substrates. The molecular recognition process is followed by appropriate signal transductions. such as electrochemical, optical, and gravimetric methods. The YSE chemistry involves permselective transport of analyte ions from adjacent aqueous sample solutions into ionophore-incorporated organic liquid membranes. This process leads to ion-selective charge separation at the aqueous/organic interface. and the change in boundary potentials becomes a measure for the analyte ion concentrations (activities). The development of the liquid-membrane ISEs owes much to the progress of supramolecular chemistry and has played an important role in bridging supramolecular chemistry with analytical chemistry.

BACKGROUND

Methods of analysis based on immiscible aqueous/organic-solution interfaces include solvent extraction, liquid–liquid partition chromatography, and ionophore-incorporated liquid-membrane ion-selective electrodes (ISEs). A common feature for these analytical methods is partitioning of analyte ions between the two phases, aqueous and organic. Of these, solvent extraction is based on the occurrence of electroneutrality in the bulk phases. On the contrary. the ISE is based on the occurrence of ion-selective charge separation at the interface of the two phases. The analyte-ion-selective charge separation at the aqueous/organic interface occurs as a result of permselective transfer of analyte ions from aqueous to organic phases upon their complexation with the corresponding ionophore at the surface of the organic phase; it leaves hydrophilic counterions in the aqueous phase. This forms an electrical double layer at the interface, while the electroneutrality in the bulk organic and aqueous phases is still satisfied. The partitioning of the analyte ions between aqueous and organic phases is described as follows:

$$K = a_0/a_a = e^{-\Delta G\ kT} \quad (1)$$

where K is the partition coefficient, a_a the activity of the analyte in the aqueous phare, a_o the activity of the analyte ion in the organic phase. and k the Boltzmann constant. The AC is the chemical potential change of analyte ions between the two phases, as expressed

$$\Delta G = nF\phi + \Delta G_{dehyd} + G_{solv} + \Delta G_{compl} + \Delta G_{ionpair} \quad (2)$$

where n is the charge number of the analyte ions. F the Faraday constant, o the electrochemical potential, ΔG_{dehyd} the dehydration energy of the ion, ΔG_{solv} the ion-solvation energy in the organic phase, ΔG_{compl} the complexation energy of the ion with the relevant ligand or ionophore. and $\Delta G_{ionpair}$ the ion-association energy between the complexed ion and its counterion in the organic or membrane phase.

The first term in Eq. 2 is responsible for the generation of membrane potentials: the liquid-membrane ion-selective electrode targets only charged ionic analytes in contrast to solvent extraction and partition chromatography.

PHENOMENA WITH IONOPHORE-BASED ION-SELECTIVE ELECTRODES

The most representative ISEs are valinomycin (VM)-based liquid membrane ISEs. W. Simon pioneered the development of liquid membrane ISEs incorporating natural ionophores such as VM and nonactin (1967). The first VM-based ISE was constructed by dissolving VM in diphenyl-ether that was supported in a cellulose membrane. which then gave selective response to K^+ over Na^+ in the concentration range of 10^{-5}–10^{-1} M K^+ ion.

At the surface of ionophore-incorporated liquid membranes; ion-selective charge separation occurs as a result of permselective analyte ion transfer from the aqueous organic phase. This phenomenon is illustrated in Fig. 1.

Hydrophilicity of counterions is important for primary ion-dependent charge separation to occur at the interface. If counterions are more or less hydrophobic, such as

Encyclopedia of Supramolecular Chemistry
DOI: *10.1*081/E-ESMC 120012872

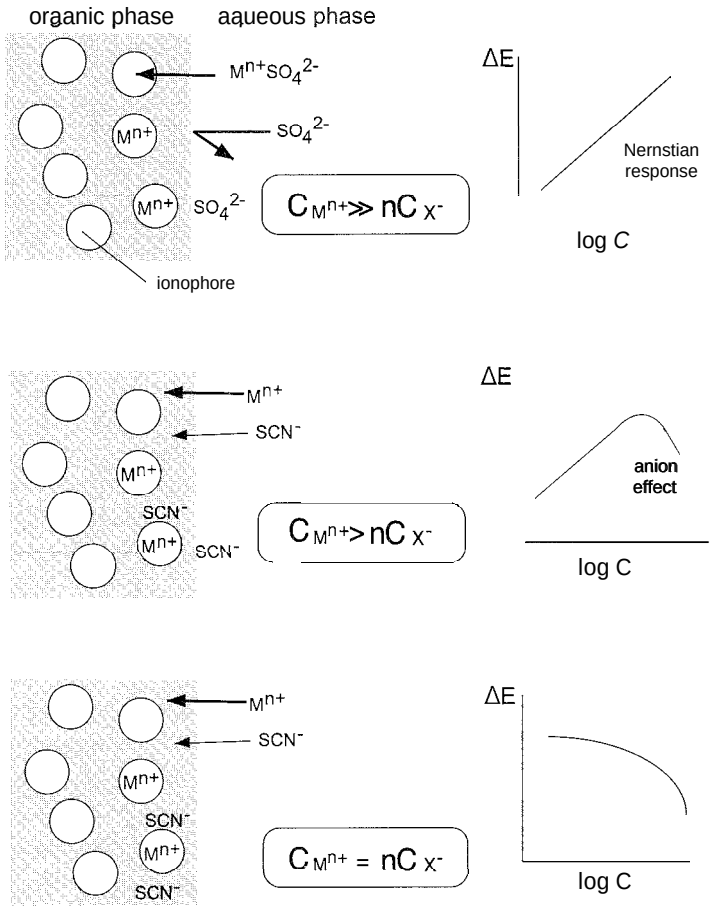

Fig. 1 Partition of metal ions and counterions at the polymer (PVC)-supported ionophore liquid-membrane/aqueous-solution interface: relation with interfacial boundary potentials. $C_M n+$ and C_{X^-} are concentrations of the ionophore-metal-ion complex and its counterions. respectively. These concentrations were measured with FT-IR-ATR to a depth of μm range in the organic phase near the interface. When $C_M n+ > nC_{X^-}$, the observed membrane potential *(AE)* exhibits a Nernstian response that meets Eq. 2. When the value of $C_M n+$ is small but still greater than nC_{X^-}, the anion effect distorted the log C–ΔE relation observed for a non-Nernstian response. When permselectivity was completely lost. i.e.. $C_M n+ = C_{X^-}$, *AE* showed no M^{n+} concentration dependence. Hydrophilic SO_4^{2-} ion and hydrophobic S C N ion made the observed difference. (From Ref. [1].) *(View this art in color* at *www.dekker.com.)*

SCN^-, ClO_4^-, *and* picrate *ions, salt extraction* (coextraction) *rather than* charge *separation results. This is called the* anion *effect, and the activity (concentration)-dependent potential changes, which are a requisite for analytical purposes, are not* fulfilled.[1]

In *the case of hydrophilic counterions. the analyte ions transported into the organic phase* form *an electrical double layer together with hydrophilic counterions left behind in the aqueous phase. The thickness of this double layer is of the order* of *50–100* Å. *From the charge density and charge distribution (Boltzmann distribution is assumed) at this electrical double layer, the membrane boundary potential is obtained from the Poisson* law.[2,3] *In thermodynamics. this process is described as follows:*

$$E = E_0 + RT/nF \log a_0/a_a \quad (3)$$

This relation is *derived* from *the free-energy change, including the term of the activity* (a_0/a_a) *dependent* free-*energy change. Eq. 4* sums *up of each free energy term in Eq. 2:*

$$\Delta G = \Delta G^0 + RT \log a_0/a_a \quad (4)$$

where ΔG^0 is the standard free-energy change.

In Eq. 3, E corresponds to the related electrochemical potential. and the standard potential E_0 corresponds to ΔG^0. When the observed potential with an ISE fulfills Eq. 4, the response is called a Nernstian response.

After the success of VM-based ISEs, *a number of synthetic ionophores were applied for the* developments *of respective* ISEs. *For alkali metal ions, crown-ether derivatives and calixarene derivatives were employed*

for developing excellent Li^+, Na^+, and K^+ ion ISEs. For alkaline earth ions, Ca^{2+} and recently Mg^{2+} ion ISEs were developed. These ISEs were applied for the analysis of serum electrolytes. For ISEs for heavy metal ions, thiocrown-ether derivatives comprise a major ionophore. The ISEs for inorganic anions, such as sulfate and chloride, are also available based on, e.g., recently developed ionophores based on multitopic hydrogen-bond interactions to these ions. For organic cations and anions, recently developed supramolecular chemistries helped in the development of many novel ISEs,[4] which include ISEs for guanosine nucleotide with a cytosine-pendant triamine derivative, dopamine cation sensing with a calix[6]arene derivative, and ATP^{4-} with a macrocyclic polyamine-derivative ionophore. The ionophore-based liquid-membrane ISEs are, in principle, applicable to any target ions, with the development of appropriate new ionophores continuing for many years.

MOLECULAR MECHANISMS FOR ISE RESPONSES

Liquid membranes for ionophore-based ISEs contain not only ionophores but also ion exchangers (ionic sites). If no ionic sites are added in the membrane, coextraction or salt extraction of ionophore/primary ion complexes with counterions occurs, thereby causing no charge separation at the interface.

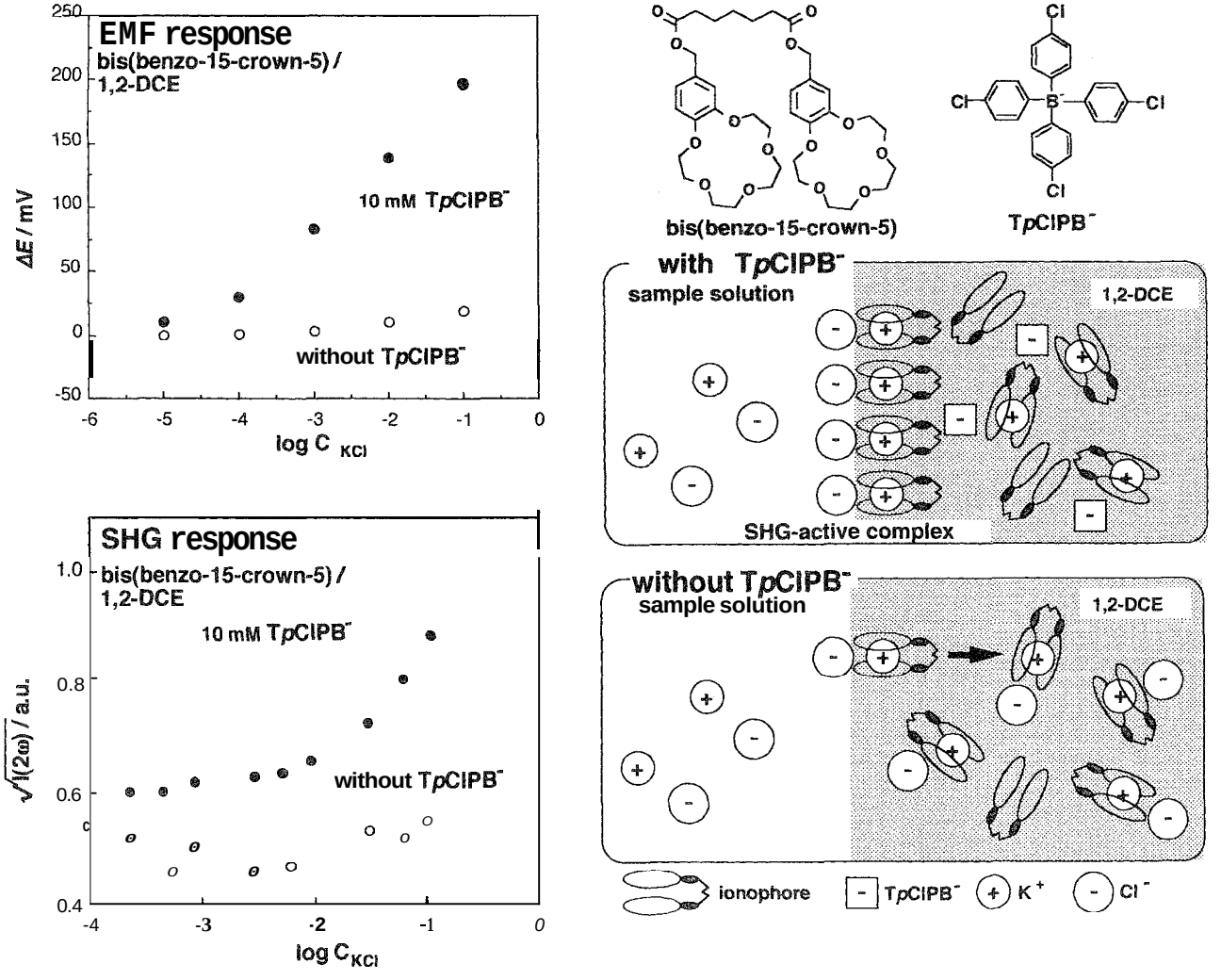

Fig. 2 Dependence of membrane potential change ΔE and second-harmonic generation (SHG) response, $\sqrt{I(2\omega)}$, on the concentration of added lipophilic anionic sites [tetrakis (*p*-chlorophenyl) borate (T*p*ClPB)] (left), and the corresponding surface model that shows orientation of SHG-active K^+-ionophore complexes across the aqueous/1,2-dichloroethane (1,2-DCE) interface in the presence of the added anionic sites in the membrane phase (right). (From Refs. [5,6].)

As shown in Fig. 2. the charge separation is the result of the occurrence of an oriented layer for ionophore/analyte ion complexes at the organic/aqueous interface in the organic side of the interface, leaving their hydrophilic counterions in the aqueous side at the interface. The extent of this charge separation is dependent on the activity (concentration) of respective analyte ions and is measurable as changes in the membrane boundary potentials.

The ionic sites [tetrakis (p-chlorophenyl) borate. T*p*ClPB$^-$] work to reject counterions from being coextracted into the organic phase and are, therefore. requisite for the generation of analyte-ion activity (concentration)-dependent membrane potential changes. This molecular mechanism for the potential response process of ISEs was recently revealed experimentally by simultaneous measurements of laser-induced second-harmonic generation (SHG) and membrane potentials, in which it was found that the observed membrane potentials originate from the SHG-active surface-oriented charged chemical species of the order of a few molecular layers (Fig. 2).[5,6]

On the basis of this mechanism, a great number of ionophore-based ISEs were developed. It should also he noted here that polyvinyl chloride (PVC) has been used since the early 1970s to support liquid membranes, and the term ''plasticized liquid membrane'' has been coined to describe these systems. In those days, the addition of ionic sites was not explicitly realized, but instead. impure ionic sites in the PVC (anionic sites) played virtually the same role. However, the membrane including such an impurity does not allow quantitative control of the optimized amounts of ionic sites, and therefore, it was supplemented later by deliberately added ionic sites.

MEASUREMENT WITH ION-SELECTIVE ELECTRODES

The performance characteristics for ISEs are evaluated in terms of ion selectivity, detection limit, dynamic range [measurable concentration (activity) range]. and response time.

The selectivity and detection limit for each ISE are basically determined by the magnitude of formation constants (K_f) of ionophores with analyte ions under otherwise identical conditions. including cornpositions of respective membrane and inner-filling solutions. In many ionophore-based liquid-membrane ISEs developed so far. the lower detection limit is reported to be around 10^{-6}–10^{-7} M.

The response time for ISEs to attain equilibrium potentials is around 3 minutes or less. Therefore, this technique is suited for high-throughput rapid analysis. The ion selectivity of ISEs is exemplified by one of the best examples involving VM-based ISEs, in which Na^+ ion

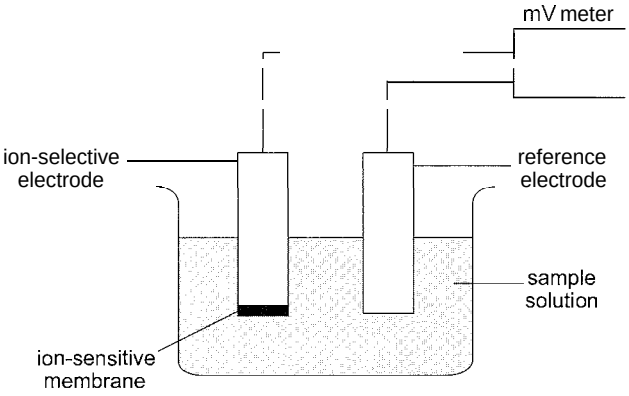

Fig. 3 Potentiometric measurement with ion-selective electrodes. (*View this art in color at www.dekker.com.*)

interference is minimized so as to allow its coexistence in up to 10' times higher concentration than K^+ ion.

To evaluate the extent of such selectivity for each ISE, the selectivity coefficient defined by the following equation is experimentally determined:

$$E = E_0 + RT/(z_A F) \ln \left[a_A + \Sigma K^{pot}_{A,B} (a_B)^{z_A/z_B}\right] \quad (5)$$

where E is the measured potential; E_0 is a constant that includes the standard potential of the electrode. the reference electrode potential, and the junction potential: z_A and z_B are charge numbers of the primary ion. A, and of the interfering ion. B: a_A and a_B are the activities of the primary ion, A, and the interfering ion, B: and $K^{pot}_{A,B}$ is the potentiometric selectivity coefficient for the primary ion *A* against the interfering ion *B*, *R*, *T*, and F have the usual meanings. If $K^{pot}_{A,B}$ is larger than 1. the ISE responds to the interfering ions more selectively than to the primary ions. In most cases, $K^{pot}_{A,B}$ is smaller than 1, which means that such ISEs respond to the primary ions more selectively than to interfering ions.

The experimental methods for measuring selectivity coefficients and the values of selectivity coefficients thus obtained are given in the references for a large number of ISEs developed during the past three decades.[7–12]

The measurements of ISEs are achieved by potentiometry. Potentiometry is an electrochemical method that measures changes relative to a reference electrode of observed potentials at the indicator electrode. ISE under a condition of no net current flow (Fig. 3).

A PROBLEM FOR LIQUID-MEMBRANE ISES

For comparison and better understanding of the ISE response, ion-channel mimetic sensing for phosphate ion using the receptor (I) was examined.[14]

A hydrogen bond-forming *bis*(thiourea) (Compound 1) is strongly bound to $H_2PO_4^-$ (K_{11}=55,000 M^{-1} for 1:1 binding in DMSO-d_6) and shows the selectivity sequence $H_2PO_4^- > CH_3COO^- > Cl^-$ by formation of hydrogen bonds to the thiourea groups of the receptor.

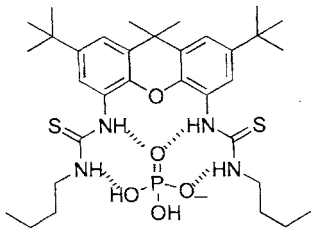

1

The response of the ISE with receptor 1 was highest for Cl^-, not for $H_2PO_4^-$, and the selectivity sequence was of the order of $Cl^- > SO_4^{2-} > CH_3COO^- > HPO_4^{2-} \sim H_2PO_4^-$. This leads to a high-quality Cl^- ISE.[13] The phosphate ion is located at the end in the Hofmeister series; indicating its high hydrophobicity. Pulling phosphate ion out of aqueous phases and putting it into organic phases is therefore difficult: C l ion has, on the contrary, relatively lower dehydration energy than phosphate, although its coinplex formation constant with host 1 is less than that of phosphate. As a result, the Cl^- ion is transferred from the aqueous to the organic phase, thereby generating the corresponding charge separation and membrane potential.

A receptor (1) monolayer was formed at the air–water interface and subsequently contacted with a highly oriented pyrolytic graphite electrode (Fig. 4). Horizontal touch cyclic voltammetry was performed with subphase solutions containing various electroinactive analyte anions and with $[Fe(CN)_6]^{4-}$ as the electroactive marker. The binding of analyte anions to the receptor monolayer was found to inhibit $[Fe(CN)_6]^{4-}$ oxidation. The influences of the analyte anions on the cyclic voltammograms were largest for HPO_4^{2-} and decreased in the order of $HPO_4^{2-} > F^- \sim SO_4^{2-} > CH_3COO^- > Cl^-$, in contrast to the selectivity of the ISE containing the same Receptor (1) as described above. Because the *bis*(thiourea) receptor does not bind to all potentially hydrogen-bonding sites of most of these anions, it is apparent that several of the larger anions, and in particular, phosphate and sulfate, are substantially hydrated while being bound to the interfacial receptor layer. This distinct feature of interfacial molecular recognition seems to explain why the selectivities of these ion-channel-mimetic sensors differ strongly from the selectivities for the complete anion transfer from aqueous to organic phases. as represented by the ISE selectivity.

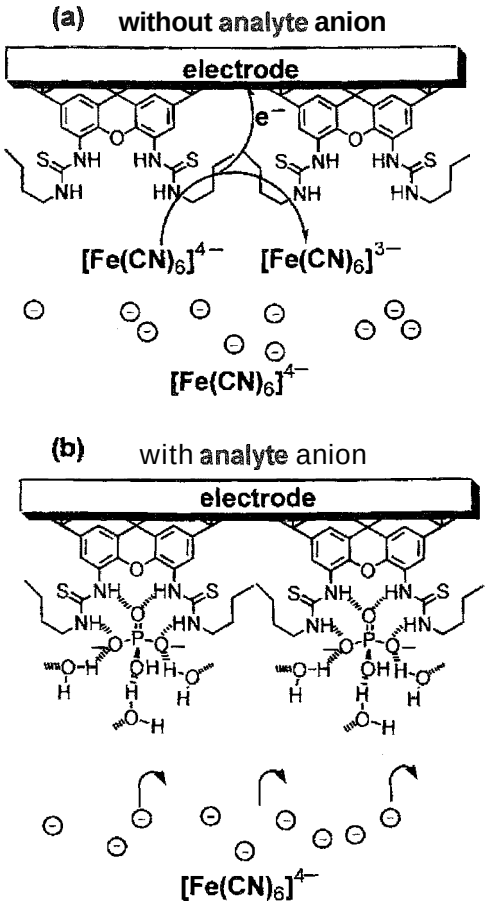

Fig. 4 The marker oxidation at the surface of an oriented monolayer of Receptor 1: (a) oxidation of $[Fe(CN)_6]^4$ at the electrode surface coated with a monolayer of Receptor I in the absence of analyte anions: (b) oxidation of $[Fe(CN)_6]^{4-}$ is hampered by the binding of the phosphate ion to the monolayer. (From Ref. [14].)

The results suggest that the ionophore-based liquid-membrane ISEs are not suited for the analysis of hydrophilic, relatively large analyte ions, for which hosts that encapsulate the analyte and remove its hydration sphere are difficult to synthesize.[14]

ARTICLES OF FURTHER INTEREST

Anion-Directed *Assembly*, p. 51
Biosensors, p. 115
Crown Ethers, p. 326
Electrochemical Sensors, p. 505
Fluorescence Sensing of Anions, p. 566
Fluorescent *Sensors*, p. 572
Guanidium-Based Anion Receptors, p. 615
Hydrogen Bonding. p. 658

Ion Channels and Their Models, p. 742
Ion-Selective Electrodes, p. *747*
Ionophores, p. 760
Photochemical Sensors, p. 1053

REFERENCES

1. Umezawa, K.: Lin, X.M.: Nishizawa. S.; Sugawara, M.; Umezawa, Y. Cation permselectivity in the phase boundary of ionophore-incorporated solvent polymeric membranes as studied by fourier transform infrared attenuated total reflection spectrometry. Anal. Chim. Acta 1993. 282. 247–257.
2. Tohda, K.; Yoshiyagawa, S.; Kataoka. M.: Odashima. K.: Umezawa, Y. Photoswitchable azobis(benzo-15-crown-5) derivatives as a molecular probe for phase boundary potentials at ion-selective poly (vinyl chloride) liquid membranes. Anal. Chem. 1997. 69, 3360–3369.
3. Umezawa, Y. Liquid Membrane Ion-Selective Electrodes: Response Mechanisms Studied by Optical Second Harmonic Generation and Photoswitchable Ionophores as a Molecular Probe. In Liquid *Interfaces in* Chemical, Biological, and *Pharmaceutical Applications*; Volkov. A.G.. Ed.: Marcel Dekker, Inc.: New York, 2000; 439–468.
4. Biihlmann, P.; Amemiya. S.; Nishizawa, S.: Xiao. K.P.: Umezawa, Y. Hydrogen-bonding ionophores for inorganic anions and nucleotides and their application in chemical sensors. J. Incl. Phenom. Mol. Recognit. Chem. 1998. *32*, 151–163.
5. Tohda. K.; Umezawa. Y.: Yoshiyagawa. S.; Hashimoto, S.: Kawasaki. M. Cation permselectivity at the phase boundary of ionophore-incorporated solvent polymeric membranes as studied by optical second harmonic generation. Anal. Chem. 1995. *34*, 570–577.
6. Yajima, S.; Tohda, K.; Buhlmann. P.; Umezawa. Y. Donnan exclusion failure of neutral ionophore-based ion-selective electrodes studied by optical second-harmonic generation. Anal. Chem. 1997. 69. 1919–1924.
7. CRC *Handbook* of Ion-Selective Electrodes: *Selectivity* Coefficients: Umezawa, Y.. Ed.; CRC Press: Florida. 1990.
8. Umezawa. Y.; Umezawa, K.; Sato. H. Selectivity coefficients for ion-selective electrodes: Recommended methods for reporting $K^{pot}_{A,B}$ values. Pure Appl. Chem. 1995. *67*, 507–518.
9. Tohda, K.; Dragoe. D.; Hibata. M.; Umezawa. Y. Studies on the matched potential method for determining the selectivity coefficients of ion-selective electrodes based on neutral ionophores: Experimental and theoretical verification. Anal. Sci. 2001, 17, 733–743.
10. Umezawa, Y.; Biihlmann, P.: Umezawa. K.; Tohda, K.; Amemiya, S. Potentiometric selectivity coefficients of ion-selective electrodes. Part I. Inorganic cations. Pure Appl. Chem. 2000. 72. 1852–2082.
11. Umezawa. Y.; Umezawa. K.; Biihlmann. P.: Hamada. N.: Nakanishi, J.; Aoki, H.: Sato, M.: Nishimura, Y.: Xiao. K.P. Potentiometric selectivity coefficients of on-selective electrodes. Part II. Inorganic anions. Pure Appl. Chem. 2002, 74. 923–994.
12. Umezawa, Y.: Buhlmann, P.: Umezawa, Y.; Hamada, N. Potentiometric selectivity coefficients of ion-selective electrodes. Part III. Organic ions. Pure Appl. Chem. 2002. 4. 995–1099.
13. Xiao. K.P.: Biihlmann, P.: Nishizawa. S.: Umezawa. Y. A chloride ion-selective solvent polymeric membrane electrode based on a hydrogen bond forming ionophore. Anal. Chem. 1997. 69 (6). 1038–1044.
14. Xiao. K.P.; Biihlmann. P.: Umezawa. Y. Ion-channel mimetic sensing of hydrophilic anions based on monolayers of a hydrogen bond forming receptor. Anal. Chem. 1999. 71. 1183–1187.

Ionic, Dipolar, and Interfacial Processes

Gyan P. Johari
McMaster University, Hamilton, Ontario, Canada

INTRODUCTION

Absorption of an electromagnetic wave's energy in a homogeneous liquid and solid is determined by two thermally activated occurrences: diffusion of ions and reorientation of dipolar units. These are referred to as ionic and dipolar processes, respectively. Both contribute to a measured dielectric property and are regarded as part of molecular dielectrics. When a liquid or solid is, in addition. heterogeneous. and the conductivity of inclusions is ohmic. the buildup of electrical charges at the interface of the inclusions also causes absorption of energy. This absorption process also occurs in a polycrystalline solid with abundant grain boundaries. and it is called the interfacial process or Maxwell–Wagner process. Finally, a further absorption of energy results from an accumulation of ions on the electrodes and the consequent formation of a double layer that acts like an electrical capacitor. This process is present in all dielectric measurements on homogeneous and heterogeneous materials. It is extrinsic to the liquid or solid, and its effect varies with the type of metal used as electrodes.

These four processes—diffusion, dipolar reorientation, interfacial charge buildup, and double layer formation—appear in different parts of the dielectric spectra of materials. The frequency range in which each process dominates varies with temperature and pressure, as do their magnitudes. Several monographs[1–4] and reviews[5,6] on dielectric properties and molecular structure provide brief descriptions of these processes and references to research articles on this subject. These overviews may be consulted and applied to the dielectric study of supramolecular structures. It is to be noted that dipolar processes are often ignored in the description of ionic processes in crystals and glasses, and the subject is treated as impedance spectroscopy.[7] The formalism underlying this description is also useful for interpreting the electrical properties of highly conducting supramolecular structures. But because only the capacitance and conductance are measured as a function of frequency in all cases, separate names for the spectroscopy seem unnecessary, and only the term ''dielectric spectroscopy'' will be used here.

Dielectric spectroscopy is now performed over a range of frequencies from 1 μHz to 10 THz, i.e., over 19 decades of frequency, which include the far-infrared region of the spectra.[8] The measurements yield the real and imaginary components e' and e'', respectively. of the complex relative permittivity ε^*. The term permittivity is used for c'. and the term dielectric loss is used for e''. Although the temperature and pressure can be chosen such that the spectral features arising from the ionic. dipolar, and interfacial processes and from electrode polarization appear in different frequency regions of the ε' and ε'' spectra. these features often overlap at ambient conditions. These are then analytically resolved by using formalisms specific to a process.

THE IONIC PROCESS

The diffusion of ions produces flow of a direct current through a liquid or solid. For an applied field strength given by E in Volts/m and the current density, **J.** in Amperes/m, the dc conductivity is given by the ratio, $J/E=\sigma_{dc}=\omega\varepsilon_0\varepsilon''_{dc}$, where ω is the angular frequency ($=2\pi f$, with f being the frequency in Hz), ε_0 is the permittivity of free space (vacuum) and is equal to 8.8514 pF/m, and ε''_{dc} is the loss due to dc conductivity. Thus. for a given ω. the magnitude of ε''_{dc} is directly proportional to ad,. For example, for water with $\sigma_{dc}=100$ μS/m, ε''_{dc} is 1.8 at 1 MHz frequency and 1800 at 1 kHz frequency. and for hydrated cyclodextrin with $\sigma_{dc}=1$ mS/m, ε''_{dc} is 18 at 1 MHz frequency and 18×10^3 at I kHz frequency.

In a wide variety of organic materials; σ_{dc} arises from the presence of impurity ions and is. therefore, extrinsic. In those supramolecular structures in which it is intrinsic, σ_{dc} arises from one or a combination of the following: diffusion of ions, as in hydrated crystals, gels, and liquids; transfer of protons along a hydrogen bond. as in the ices and ice clathrates, cyclodextrins, and proteins; and displacement of ions in a crystal lattice. Irrespective of its extrinsic or intrinsic origin, σ_{dc} is determined by the number of mobile ions n, electronic charge on the ions e. and their mobility μ, according to the equation, $\sigma_{dc}=ne\mu$. On decreasing the temperature T, the mobility of ions decreases and, hence, σ_{dc} decreases. In hydrated states or aqueous solution. ions can also form ion pairs, thereby

Encyclopedia of Supramolecular Chemistry
DOI: 10.1081/E-ESMC 120012655

reducing their number. This decrease is described by the ion–ion-pair equilibrium constant:[9]

$$K_A = \frac{4\pi N a^3}{3000} \exp\left(\frac{z_1 z_2 e^2}{a\varepsilon_s k_B T}\right) \quad (1)$$

where N is the Avogadro number; a is the ion size parameter; z_1 and z_2 are the ionic charges; e is the electronic charge: ε_s is the equilibrium or static dielectric permittivity of the medium; k_B is the Boltzmann constant: and T is the temperature. The quantity K_A or, equivalently, the concentration of ion pairs, increases sensitively as T in the exponential term in Eq. 1 decreases, because a for an unsolvated ion is expected to remain constant with changing T. The quantity n in the equation, $\sigma_{dc}=ne\mu$, therefore, decreases on cooling when diffusing ions associate to form ion pairs. Thereby, they are effectively removed from the material. Because K_A also varies as $\exp(1/\varepsilon_s T)$ in Eq. 1, a decrease in the product $\varepsilon_s T$ of the material resulting from deviations from the Curie law (i.e., the product $\varepsilon_s T$ remains constant on cooling) would lead to a decrease in n. Such deviations from the Curie law often result from short-range interactions between the molecular dipoles. According to the Stokes–Einstein relation and Arrhenius equation.

$$\sigma_{dc} = ne^2 D_{ions}/RT,$$
$$D_{ions} = D_{0,ions} \exp(-\Delta E_{ions}/RT) \quad (2)$$

where D_{ions} is the diffusion coefficient of the ions; $D_{0,ions}$ is the preexponential factor; ΔE_{ions} is the Arrhenius energy for ionic diffusion; and R is the gas constant. It follows that σ_{dc} would decrease with T not only because D_{ions} decreases but also because n decreases.

Studies of a number of supramolecular materials showed that a logarithmic plot of their σ_{dc} against $1/T$ curves downwards, particularly at low T values, i.e., the decrease in σ_{dc} is much larger than expected. This means that σ_{dc} does not merely follow the Arrhenius variation of D_{ions} with T: other processes contribute. One such process is ion-pair formation, which decreases n.

THE DIPOLAR PROCESS

A dipolar process is described in terms of three quantities: the orientation polarization, the vibrational polarization. and the relaxation time. The first of the three is expressed as $\Delta\varepsilon=\varepsilon_s-\varepsilon_\infty$, where ε_s is as defined earlier, and ε_∞ is the limiting high-frequency permittivity. The vibrational polarization is expressed as $\Delta\varepsilon_{vib}=\varepsilon_\infty-n_{op}^2$, where n_{op} is the refractive index of the material, usually at the frequency of the Na–D line; and n_{op}^2 is a measure of the electronic polarization. These properties are described in phenomenological terms as well as molecular structure terms involving the dipole moment. any short-range interactions between the neighboring molecules and motion of molecular segments of different chemical structures, and of whole molecules.

The Orientation Polarization

In the statistical mechanical theories of a dipolar orientation process,[10–12]

$$\varepsilon_s - \varepsilon_\infty = \left(\frac{3\varepsilon_s}{2\varepsilon_s + \varepsilon_\infty}\right)\left(\frac{\varepsilon_\infty + 2}{3}\right)^2 \frac{4\pi N_d}{3k_B T} g\mu^2 \quad (3)$$

where N_d is the number of dipoles per unit volume, and μ_0 is the dipole moment of an isolated molecule, i.e, the value in the vapor phase. The quantity g is referred to as the orientational correlation factor. It is given by the following:

$$g = 1 + \sum_{j,(j\neq i)}^{\cdot\cdot} \cos\gamma_{ij}$$

where γ_{ij} is the angle between the i,j pair of dipole vectors, i and j, of the neighboring segments within a molecule or the neighboring molecules. It is a measure of the short-range interactions between the neighboring molecules that may represent intermolecular hydrogen bonding or strong dipolar forces. For a completely random arrangement of dipolar molecular segments and of dipolar molecules, $g=1$. In the extreme of an antiferroelectric arrangement, $g=0$, and in that of a ferroelectric arrangement, $g=\infty$. From the knowledge of measured ε_s and ε_∞, it is therefore possible to determine the dipolar alignment as a result of short-range interactions. For example; such an analysis showed that on cooling cyclodextrin undecahydrate crystals, the dipoles tend to align in an antiparallel manner.[13] Thus, variation in g with T also indicates the occurrence of an ordering–disordering transformation in a supramolecular structure. Short-range interactions of this type are important aspects of such structures, particularly because electrostatic interaction often determines their stability conditions as well as their practical use as intercalation compounds and templates for chemical reactions.

It was also possible to calculate g by first presuming a near-neighbor structure, as originally done for water.[14] and then to compare the calculated value from that determined from Eq. 3 by using the measured ε_s. This leads to information on the arrangement of molecules when intermolecular hydrogen bonding determines their dipole vectors, or when their dipolar segments are connected by flexible covalent bonds. Alternatively, g may be determined from the known positions of dipolar molecules in the crystal structure of a material. In this procedure, the orientation of one molecule is fixed, and the vector sum of all possible orientations of the

neighboring molecules is computed. Computation is done for all orientations of a given molecule and then for all molecules. Such cornputations for g of ice clathrates of Type I and Type II, which contain foreign molecules confined to the cages of 0.39–0.47 nm radius in their structures' hydrogen-bonded networks,[15] were provided, and the results were compared with the experimentally determined ε_s.[16] Similar computations also yielded the electrostatic field strength at a molecular site arising from its dipolar neighbor. the magnitude of increase in the dipolar moment, and the Coulombic interaction energy. The now available faster and more elegant computational procedures can help in such calculations on an irregularly shaped supramolecule in all its possible configurations. This may lead to not only their configurational thermodynamics but also the relative stability of molecular configurations at a given T and P.

The Vibration Polarization and Poley Absorption

Contribution from vibrational polarization in a material is given by the following:

$$\Delta\varepsilon_{\text{vib}} = \varepsilon_\infty - n_{\text{op}}^2 = (\Delta n_{\text{vib}} + n_{\text{op}})^2 - n_{\text{op}}^2 = \Delta n_{\text{vib}}^2 + 2\Delta n_{\text{vib}} n_{\text{op}} \tag{4}$$

$$\Delta n_{\text{vib}} = \sum (2\pi^2)^{-1} \int_0^\infty \frac{K(\nu)}{\nu^2}\,\partial\nu \tag{5}$$

where the absorptivity K at a frequency ν is given by

$$K(\nu) = -\frac{1}{l}\log_e\left[\frac{I(\nu)}{I_0(\nu)}\right] \tag{6}$$

where I_0 and I are the intensities of a radiation before and after traversing a distance l in the medium. The summation is for all absorption bands. The quantity Δn_{vib} is more when the vibrational frequencies are low, which occurs when the structure is relatively loose or floppy, and intermolecular forces are weak.

Molecules of different types confined to a regular or irregular cage-like structure, a doughnut-shaped, or a channel-like structure, undergo librations (rotational oscillations) in the THz frequency range and, hence, contribute significantly to Δn_{vib} and to $\Delta\varepsilon_{\text{vib}}$. This is similar to the effect observed for dipolar liquids at ambient temperatures by Poley,[17] which was attributed to rotational oscillations of a molecule inside a temporary. irregular cage formed by the neighboring molecules — a subject recently discussed in relation to the so-called Boson peaks.[18] A discussion of the magnitude of $\Delta\varepsilon_{\text{vib}}$ in the supramolecular structures of ice clathrates may be found in Refs. [15] and [16]. Because $\Delta\varepsilon_{\text{vib}}$ is the fastest dipolar process, its study should be useful in determining how configurational statistics of inclusion compounds, with lamellar, channel-like, cage-like, or toroidal structures, determine the chemical reactivity of its confined molecules.

The Dipolar Relaxation and its Characteristics

In general, the frequency-dependent complex permittivity $\varepsilon^*(\omega)$, and time-dependent complex permittivity $\varepsilon^*(t)$ are related by a Fourier transform according to

$$\frac{\varepsilon^*(\omega) - \varepsilon_\infty}{\varepsilon_0 - \varepsilon_\infty} = 1 - i\omega\int_0^\infty \phi(t)\exp(-i\omega t)dt \tag{7}$$

where ϕ is the normalized relaxation function given by

$$\phi(t) = \frac{\varepsilon^*(t) - \varepsilon_\infty}{\varepsilon_0 - \varepsilon_\infty} \tag{8}$$

where $\varepsilon^*(t)$ describes the evolution of the apparent permittivity with time when a static electric field is removed as a step at $t=0$ from the polarized material. The magnitude of $\phi(t)$ decays from 1 to 0, in the absence of any contribution to the permittivity from ionic, interfacial: or electrode polarization effects. Therefore, a discussion of the dielectric relaxation may be carried out only after the dipolar contributions are isolated from other contributions. The function $\phi(t)$ is closely related to the dipole time correlation function, which describes the randomization of the dipole vector in time consequent to molecular motions.

The simplest form of $\phi(t)$ is a single exponential decay, $\phi(t)=\exp[-(t/\tau)]$, where τ is the relaxation time. Such a single relaxation time decay was observed for some ice clathrates, hydrogen-bonded liquids and amides, and simple molecules at high temperatures. But. in general, supramolecular structures showed a variation of ε' and ε'' that yielded $\phi(t)$ spread over a broader range than expected from a single exponential decay.[13,15] In such cases. empirical equations for the ε^* were used as described in Refs. [1–4]. These include the following:

- The Cole–Cole equation:[19]

$$\frac{\varepsilon^*(\omega) - \varepsilon_\infty}{\varepsilon_0 - \varepsilon_\infty} = \frac{1}{1 + (i\omega\tau)^\alpha}; \quad \text{where } 0 < \alpha < 1 \tag{9}$$

- The Davidson–Cole equation:[20]

$$\frac{\varepsilon^*(\omega) - \varepsilon_\infty}{\varepsilon_0 - \varepsilon_\infty} = \frac{1}{[1 + (i\omega\tau)]^\beta}; \quad \text{where } 0 < \beta < 1 \tag{10}$$

- The Fuoss and Kirkwood equation:[21]

$$\frac{\varepsilon''(\omega)}{\varepsilon_0 - \varepsilon_\infty} = m\frac{(\omega\tau)^{2m}}{1 + (\omega\tau)^{2m}}, \quad (11)$$

where $0 < m < 1$

- A combination of Eqs. 9 and 10:

$$\frac{\varepsilon^*(\omega) - \varepsilon_\infty}{\varepsilon_0 - \varepsilon_\infty} = \frac{1}{[1 + (i\omega\tau)^\alpha]^\beta}, \quad (12)$$

where $0 < \alpha < 1$ and $0 < \beta < 1$

The shape of the ε' and ε'' relaxation spectra was also described by writing $\phi(t)$ in an empirical form; $\phi(t)=\exp[-(t/\tau)^{\beta KWW}]$, where $0<\beta_{KWW}<1$.[5,6] A wide variety of dielectric studies have attempted to determine the significance of β_{KWW}. It was interpreted in terms of hierarchically controlled dynamics of a dipolar process,[22] i.e., the existence of a strong degree of correlations between the molecular degrees of freedom, and the occurrence of dipolar reorientation in series, rather than in a parallel fashion—faster degrees of freedom successively controlling the slower ones and: thus. generating a wide range of relaxation times. More recent studies demonstrated that the distribution of relaxation times arises from microscopic heterogeneity,[23] and further. that the broadness of the spectra results from overlapping single relaxation time processes.[24] Thus, in supramolecular structures of ice clathrates, analysis of the relatively broad ε' and ε'' spectra in terms of a sum of several single relaxation time processes[15] seems to be reliable. The interpretation is that the number of dielectric relaxation times and the broadness of the ε' and ε'' spectra is a reflection of the presence in the lattice of crystallographically nonequivalent sites and energetically different orientations of the water molecules. With a decrease in temperature, thermal energy decreases. With the consequent increase in the number of energetically different orientations, the relaxation spectra are further broadened. Analysis of broad dielectric spectra observed for cyclodextrins[13] and other structures in such terms is now easily possible by using computation algorithms.

In most supramolecular structures, the temperature dependence of the characteristic dielectric relaxation time follows the Arrhenius equation, $\tau=\tau_0\exp(\Delta E_{dip}/RT)$, where τ_0 is the preexponential factor that is often of the magnitude of the vibrational time scale; and ΔE_{dip} is the activation energy of the dipolar process.[6,15] The dipolar process of the host lattice and the trapped molecules follows this behavior, but ΔE_{dip} for the trapped molecules is less than that for the host lattice molecules. In ice ciathrates, the dipolar processes of the water molecules that form the host lattice and the guest molecules inside the cages of this lattice occur at widely different time scales. This allows for a reliable attribution of the dielectric spectra features to water molecules and to the guest molecules. As an example of the magnitude of the dielectric properties of suprainolecular structures, the data on selected ice clathrates and other inclusion compounds are summarized in Tables 1 and 2.

THE INTERFACIAL PROCESS

When a liquid or solid is heterogeneous. i.e.. it consists of conglomerates of macroscopic volume elements with different ε_0 and σ_{dc} and the wavelength of the frequency

Table 1 The various properties of the dipolar processes in the two types of host lattices of some clathrate structures

Guest molecule	ε_s (233.2 K)	ε_∞ (165.2 K)	τ (233.2 K)	ΔE_{dip} (kJ/mol)	μ_0 (Debye)
Ice Clathrate Type I structures					
Cyclopropane	≥53	2.90 (233.2 K)	310	47.6	0
Ethylene oxide	62	10.8	0.33	32.2	1.90
Trimethylene oxide	≥49	≥11.1	0.03	24.2	1.93
Ice Clathrate Type II structures					
Nitrogen	61	2.85 (233.2 K)	180		0
Argon	62	2.85 (233.2 K)	96		0
SF_6	63	2.9	780	51.4	0
1.3-Dioxolane	69	4.57	5.4	36.4	1.47
Propylene oxide	70	5.94	2	33.4	2
2,5 Dihydrofuran	68	5.03	1.5	31.3	1.54
Tetrahydrofuran	67	5.06	1	30.9	1.63
Acetone	≥47	≥8.6	0.57	27.2	2.88
Cyclobutanone	71	9.85	0.49	27.2	2.89
Trimethylene oxide	65	5.63	0.48	29.3	1.93

Note: ε_s is the equilibrium permittivity; ε_∞ is the high-frequency permittivity: τ is the dielectric relaxation time; ΔE_{dip} is the activation energy; and μ_0 is the dipole moment of the guest molecule in the vapor phase.
Source: (From Ref. [6], Table 2).

used is large compared with the dimension of the congloinerates or inclusions, energy dissipation can occur by scattering of radiation at the interfacial boundaries. This is similar to the loss of energy by the scattering of light by colloidal solutions; but it occurs in the range of dielectric absorption frequencies. Maxwell's[25] treatment of this situation and Wagner's[26] and Sillars'[27] development of this subject may be found in Refs. [1], [2] and [28].

Briefly, the relaxation time and permittivity corresponding to the effects arising from interfacial boundaries from a heterogeneous material can be calculated from the knowledge of σ_{dc} and of ε_s values of the two phases in the heterogeneous system. In a general discussion of the dielectric effect arising from interfacial polarization, Wagner considered an even distribution of spherical particles of Phase 2 material with a small volume fraction f_2, permittivity ε_2, and conductivity σ_2 in Phase 1 of permittivity ε_1 and negligibly small conductivity. The expressions for the resulting permittivity and loss are then given by the following:[2]

$$\varepsilon'_{\text{interfacial}} = \chi\left(1 + \frac{\psi}{1 + \omega^2\zeta^2}\right);$$

$$\varepsilon''_{\text{interfacial}} = \left(\frac{\chi\psi\omega\zeta}{1 + \omega^2\zeta^2}\right) \tag{13}$$

where

$$\chi = \varepsilon'_1\left\{1 + \frac{3f_2(\varepsilon'_2 - \varepsilon'_1)}{2\varepsilon'_1 + \varepsilon'_2}\right\}$$

$$\psi = \left(\frac{9f_2\varepsilon'_1}{2\varepsilon'_1 + \varepsilon'_2}\right)$$

$$\zeta = \frac{(2\varepsilon'_1 + \varepsilon'_2)\varepsilon_0}{\sigma_2}$$

Because χ, ψ, and ζ are fixed quantities at a given T, the form of Eq. 13 corresponds to a frequency dependence

Table 2 The various properties of the dipolar processes of the guest (or included) inolecules in the lattice of selected clathrate structures

Guest molecule	T (K) (for τ=1.59 μs)	ΔE_{dip} (kJ/mol)	ε_s (168 K)	ε_∞ (4 K)
Ice Clathrate Type I structure				
Methyl chloride	20.3	3.34	2.9	
Ethylene oxide	34.2	5.89	10.8	4
Trimethylene oxide	66.4	8.8	$\geq$11.1	3.4
Ice Clathrate Type II structure				
1.3-Dioxolane	23	3.8	4.5	
Tetrahydrofuran	27.6	3.8	5.06	3.5
Acetone	24.3	4.26	$\geq$8.6	3.9
Cyclobutanone	39.9	6.02	9.84	3.6
Trimethylene oxide	16.2	1.92	5.63	3.7
β-Quinol clathrate				
Methanol		9.78, 0.96, 2.5[a]		
Acetonitrile		75, 67[a]		
Hydrogen cyanide		16.3, 5.27[a]		
Fomic acid		13.96		
Urea clathmte				
Didodecyl ether		4.2	3.80	
n-Octadecyl bromide		10.1	3.79	
9-Heptadecanone		7.6	5.53	
Dianin's compound clathrate				
Methyl chloride		12.1		
Ethyl alcohol		20, 16.5, 10.3[a]		
Acetonitrile		8.8		
Cyclodextrin clathrate				
11.Water (8-form)		51.8	38	
p-Nitrophenol (α-form)		56.8	6	
Manganese squarate				
Acetic acid–water		11.5, 4[a]	5.15, 4.17[a]	

Note: T is the temperature at uhich the relaxation time of the guest molecule is 1.59 its; ΔE_{dip} is the activation energy of the dielectric relaxation of the guest molecules: ε_s is the equilibrium permittivity; and ε_∞ is the high-frequent) perinittivity at the indicated temperatures

"See Table 4. Ref. [6], for details.

Source: From Ref. [6], Tables 3 and 4.

of the interfacial polarization process identical to that of the Debye single relaxation time process. Its spectra shifts with change with T only in as much as the quantity ζ changes with T.

Interfacial processes in the dielectric data obtained for biological systems were described by Pethig.[4] He summarized the formalisms for different shape particles and mixtures of particles in a medium, for porous heterogeneous systems, for emulsions of various types. and for the surface ion conductivity and counterion effects. Then, he compared the interfacial processes observed for synthetic polymers and biopolymers suspended in electrolytic solutions. In general, the E' and c" spectrum from an interfacial process is broadened as a result of effects arising from the particle shape, intra- and interparticle interactions, electrical and structural interactions (coalescence/division) between particles, heterogeneity of morphological and electrical properties of particles, and frequency dependence of their dielectric behavior; etc. This broadness at high frequencies makes $\varepsilon''_{\text{interfacial}}$ become proportional to $(\omega)^s$ when $\omega\zeta \gg 1$, with the empirical parameter, $s<1$. In contrast, s=1 when the dipolar process has a single relaxation time and $\omega\tau \gg 1$, and when σ_{dc} of the ionic process dominates the ε'' spectra.

The ε' and ε''contributions from an interfacial process provide no molecular insight. even though such data contain information on ε_{s} and σ_{dc} of the component phases. Often. the magnitudes of $\varepsilon'_{\text{interfacial}}$ and $\varepsilon''_{\text{interfacial}}$ are overwhelmingly large,[1–4] and need to be subtracted from the measured ε' and ε'' before attempting a molecular interpretation of the dielectric spectra.

THE ELECTRODE POLARIZATION EFFECT

In this process, ions migrate to the electrode surfaces. producing localized concentrations that increase with a decrease in ω. If a chemical reaction between the electrode material and the ions also occurs, an irreversible, nonequilibrium process sets in, and the effects of the reaction products begin to contribute. Such effects are observed in liquids and solids and are relatively small at high ω or low σ_{dc} values. But when σ_{dc} from the ionic process exceeds 1 μS/m, the electrode polarization effects begin to contribute significantly to the e' and e" values in the low-frequency part of the spectrum. and its magnitude needs to be determined.

The electrode impedance, z_{el}, resulting from this polarization is written as a complex function: $z^*_{\text{el}}=z_0(i\omega)^{-n}$, where z_0 is a characteristic of the electrode/dielectric interface. and the exponent n is usually taken to be 0.5.[2,29] This is equivalent to a constant phase element in series with the bulk dielectric properties of a material. The expression for the measured conductance G_{meas} (in Siemens), for an electrode impedance z_{el} in series with the dielectric sample,[2,29] is as follows:

$$\frac{G_{meas}}{C_0} + i\omega\varepsilon'_{meas} = \frac{(G_{bulk}/C_0) + i\omega\varepsilon'_{bulk}}{1 + z^*_{el}[(G_{bulk}/C_0) + i\omega\varepsilon'_{bulk}]}$$

where C_0 is the capacitance of the empty dielectric cell; ε'_{meas} is the measured permittivity; ε'_{bulk} is the true (bulk) permittivity from the dipolar process; and G_{bulk} is the true (bulk) conductance, which is the sum of the ionic and dipolar processes. For frequencies when $G_{bulk} \gg \omega\varepsilon' C_0$ and $|z^*_{\text{el}}|=z_0 G_{bulk}\omega^{-n}$, Eq. 14 is expanded as a Taylor series. After truncating at the first order. it was written as

$$\frac{G_{meas}}{C_0} = \frac{G_{bulk}}{C_0} - \left[z_0 \cos\left(\frac{n\pi}{2}\right)\frac{G^2_{bulk}}{C_0}\right]\omega^{-n} \tag{15}$$

and its transformation to

$$\varepsilon'_{meas} = \varepsilon'_{dip} + \left\{\left[z_0 \sin\left(\frac{n\pi}{2}\right)\right]\frac{(\sigma_{dc} + \sigma_{dip})C_0}{\varepsilon_0^2}\right\}\omega^{-(n-1)} \tag{16}$$

and

$$\varepsilon''_{meas} = \varepsilon''_{dc} + \varepsilon''_{dip} - \left\{\left[z_0 \cos\left(\frac{n\pi}{2}\right)\right]\frac{(\sigma_{dc} + \sigma_{dip})C_0}{\varepsilon_0^2}\right\}\omega^{-(n+1)}$$

In Eqs. 16 and 17, the last term is the magnitude of electrode polarization. It contributes to ε' and ε'' values. and its magnitude depends upon that of σ_{dc}. This term is evaluated by using a reiterative procedure.[30] This polarization can also be treated empirically in terms of $(\omega)^s$, the frequency dependence of the measured conductivity.[31]

CONCLUSION

In practice, electrical measurements do not distinguish between conduction and polarization currents, because only the total current that appears in Maxwell's equation, $J_{\text{total}}=J_0+(\partial P/\partial t)$, is measured. The conduction cunent J_0 and the polarization current $(\partial P/\partial t)$ need to be separated into the electrode polarization, dc conduction, and dipolar orientation contributions by using suitable procedures. This is particularly the case for a majority of highly conducting suprainolecular structures of all types at ambient temperatures, with ε' and e" data that do not show features directly attributable to a molecular dielectric process. In such cases, Eqs. 16 and 17 are used to determine contributions from electrode polarization and dc conductivity. On subtraction from the measured ε' and

ε'' data. the spectrum of the dipolar process is obtained by an analysis described earlier.[30]

Studies of the dielectric properties will certainly provide greater insight into the molecular processes that determine the applications of supramolecular structures. The onset of ferroelectric and antiferroelectric behavior and the ordering–ordering transitions in supramolecular structures. as well as the dynamics of molecular segments in such structures, can be investigated by studying their dielectric spectra.

ARTICLES OF FURTHER INTEREST

Biomaterials, p. 110
Clathrate Hydrates, p. 274
Cyclodextrins, p. 398
Drug Delivery, p. 484
Hydrogen *Bonding*, p. 658
Hydroquinone, p. 679
Inclusion Compounds: Selectivity, Thermal Stability, and Kinetics, p. 696
Liquid Clathrates, p. 804
Supramolecular Electrochemistry, p. 1412
Vibrational Spectroscopy. p. 1557
Weak *Hydrogen Bonds*, p. 1576

REFERENCES

1. Daniel, V.V. Dielectric *Relaxation*; Academic Press: London, 1967.
2. Mill. N.E.; Vaughan. W.E.; Price. A.H.: Davies. M. Dielectric Properties *and* Molecular *Behaviour*; Van Nostrand Reinhold: London. 1969.
3. Masted. J.B. *Aqueous* Dielectrics; Chapman and Hall: London. 1973.
4. Pethig, R. Dielectric *and* Electronic Properties *of* Biological Materials: John Wiley: New York. 1979. Chap. 5.
5. Williams, G. Theories of Dielectric Properties. In *Dielectric Relaxation* Spectroscopy of Polymers. *Fundamentals and* Application; Runt. J.P., Fitzgerlad. J.J.. Eds.: American Chemical Society Series: Washington. DC. 1997. Chap. 1.
6. Johari. G.P. Dielectric Methods in Studying Supramolecular Structures. In *Comprehensive Supramolecular Chemistry, Vol. 8,* Physical Methods *in Supramolecular Chemistry*; Davies. J.E.D.. Ripmeester. J.A., Eds.: Elsevier: Oxford. 1996. Chap. 3.
7. Macdonald, J.R. *Impedance* Spectroscopy: John Wiley. 1987.
8. Lunkenheimer. P.; Schneider. U.: Brand, R.; Loidl, A. Glassy dynamics. Contemp. Phys. 2000, 41. 15.
9. Davies. C.W. *Ion Association*; Butterworths: London. 1962.
10. Onsager. L. Electric moments of molecules in liquids. J. Am. Chem. Soc. 1936. *58.* 1486.
11. Kirkwood, J.G. The dielectric polarization of polar liquids. J. Chem. Phys. 1939. *7.* 911.
12. Frohlich, H. *Theory* of Dielectrics: Oxford University Press: Oxford. 1949.
13. Pathmanathan. K.: Johari, G.P.; Ripmeester. J.A. Dielectric and calorimetric studies of β-cyclodextrin undecahydrate. J. Phys. Chem. 1989. *93*, 7391.
14. Oster, *G.;* Kirkwood, J.G. The influence of hindered molecular rotation on the dielectric constants of water, alcohols and other polar liquids. J. Chem. Phys. 1943, 11. 175.
15. Davidson. D.W. Clathrate Hydrates. In *Water—A Comprehensive* Treatise: Franks. F.. Ed.: Plenum Press: New York, 1973; Vol. 2. Chap. 3.
16. Johari. G.P. The dipolar correlation factor. the electrostatic field. the dipole moment and the Coulombic interaction energy of water molecules in clathrate hydrates. J. Chem. Phys. 198%.*74.* 1326.
17. Poley, J. Ph. Microwave dispersion of some polar liquids. J. Appl. Sci. Res.. B 1955, 4. 337.
18. Johari. G.P. Molecular inertial effects in liquids: Poley absorption. collision-induced absorption, low-frequency Raman spectrum and Boson peaks. J. Non-Cryst. Solids 2002. *307–310.* 114.
19. Cole, K.S.: Cole. R.H. Dispersion and absorption in dielectrics. J. Chem. Phys. 1941, *9,* 341.
20. Davidson. D.W.: Cole. R.H. Dielectric relaxation in glycerol, propplene glycol and n-propanol. J. Chem. Phys. 1951, *19*, 1484.
21. Fuoss, R.M.: Kirkwood. J.C. Electrical properties of solids. VIII. Dipole moments in polyvinyl chloride-diphenyl systems. J. Am. Chem. Soc. 1941. *63.* 385.
22. Palmer. R.G.; Stein. D.L.; Abrahams, E.; Anderson. P.W. Models of hierarchically constrained dynamics of glassy relaxation. Phys. Rev. Lett. 1984. *53.* 958.
23. Schmidt-Rohr, K.: Speiss, H.W. Nature of nonexponential loss of correlation above the glass transition investigated by multidimensional NMR. Phys. Rev. Lett. 1991, 66. 3020.
24. Schiener. B.: Bohmer. R.; Loidl. A.; Chamberlin, R.V. Non-resonant spectral hole-burning in the slow dielectric response of supercoolecl liquids. Science 1996. *274.* 752.
25. Maxwell, J.C. *Electricity and Magnetism,* 3rd Ed.: Oxford University Press: Oxford. 1892: 452.
26. Wagner, K.W. Explanation of the Dielectric Fatigue Phenomenon on the Basis of Maxwell's Concept. In *Arkiv. fur Electrotechnik*: Schering, H., Ed.: Springer Verlag: Berlin, 1914: 371.
27. Sillars. R.W. Properties of dielectric containing semiconducting particles of various shapes. J. Inst. Electr. Eng. 1937. *80.* 378.
28. Van Beek. L.K.H. Dielectric Behavior of Heterogeneous Systems. In Progress *in* Dielectrics: Birks, J.B., Ed.: Heywood Press: London, 1965; Vol. 7, 69.
29. Johnson. J.F.: Cole. R.H. Dielectric polarization of liquid arid solid formic acid. J. Am. Chem. Soc. 1951. *73,* 4536.
30. Parthun. M.G.; Johari. G.P. Analysis for a dipolar relaxation in the featureless dielectric spectrum and a comparison between the permittivity. modulus and impedance formalisms. J. Chem. Soc.. Faraday Trans. 1995, 91. 329.
31. Lunkenheimer. P.: Bobnar, V.: Pronin. A.V.; Ritus, A.I.; Volkov, A.A.; Loidl, A. Origin of apparent colossal dielectric constants. Phys. Rev.. B 2002, 66. 052105.

Ionophores

Riccardo Ferdani
George W. Gokel
Washington University School of Medicine, St. Louis, Missouri, U.S.A.

INTRODUCTION

Ionophore (literally "ion bearer") is a name given to the family of compounds with the principal characteristic that is to "promote the transfer of ions from aqueous medium into a hydrophobic phase."[1–4] The Shorter *Oxford English* Dictionary gives the following definition: "An agent which is able to transport ions across a lipid membrane, in a cell." By extension, ionophores are host molecules that bind ionic guests and transport them across a membrane, such as a bulk organic phase or a phospholipid bilayer. In the latter case, the bilayer may be present in a cell or subcellular organelle.

The name was coined to describe the activity of compounds. such as valinomycin, a naturally occurring cyclic depsipeptide that transports K^+ ions across membranes efficiently and selectively.[5,6] A number of natural ion transport agents have been identified. They regulate the concentrations of the predominant biological cations (Na^+, K^+, Mg^{2+}, and Ca^{2+}).[7] Artificial ionophores were first prepared to serve as models for their natural but more complex counterparts. They now comprise a broad family of compounds that includes inter alia, podands, crown ethers. lariat ethers: and cryptands.

The name ionophore suggests a "bearer" or carrier function. Cations are typically transported across a membrane by a carrier or a channel mechanism. Channel function is less well understood but is generally thought to involve the formation of a transmembrane pore through which ions pass. Effectively, a channel is a scaffold or superstructure that facilitates this process. In contrast, the ionophores discussed here typically function by a carrier mechanism. An ionophore is usually soluble in a hydrophobic or membrane phase. The ionophore (host) captures the guest ion at the aqueous–hydrophobic interface. The complex diffuses across the hydrophobic membrane or barrier phase. At the opposite interface, guest release occurs, passing the ion into the second aqueous phase. The ionophore or host molecule then diffuses back to the opposite interface. where the process is repeated until equilibrium is reached.

In one sense, ionophores comprise a superfamily that includes all compounds that bind a charged (ionic) species, screen its charge so that transport across a highly hydrophobic phase becomes feasible, and release it at the end of the transport process. Taken together, the number of compounds that are more or less effective at transporting cations is large. We briefly describe this family below, but the reader is directed to other, more specific entries that deal with individual compound groups.

CLASSES OF IONOPHORES

Any classification scheme is necessarily arbitrary, but ionophores are often divided into two groups: naturally occurring and synthetic. A subclassification distinguishes on the basis of open-chained (noncyclic) versus cyclic. Examples of the latter typically exceed the former because binding site preorganization and geometric complementarity are usually easier to achieve or ensure in a cyclic structure when the goal is to complex a spherical ion.

Natural Cyclic Ionophores

Valinomycin

Valinomycin[8–13] is probably the best known and characterized of the natural ionophoretic, antibiotic compounds. It is a K^+-selective carrier molecule that is produced by *Streptomyces fulvissimus*.[14] It is a dodecadepsipeptide comprised of 12 alternating amino and hydroxy acids to form a neutral, macrocyclic ionophore (Fig. 1).

The macrocyclic ring of valinomycin contains 36 atoms and is flexible. It is too large to complex a K^+ ion. for which it is selective, in a two-dimensional fashion. Instead, it wraps about the cation in what has been called a "tennis ball seam" conformation. Because of the conformational flexibility, this host molecule readily binds and releases the cation. This is a critical issue for transport because both complexation at one interface and cation release at the opposite interface must take place with reasonable rates or strong complexation and fast diffusion will be to little avail.

When complexation takes place, two water molecules may be included in the K^+ coordination sphere, giving a coordination number of eight. As the carbonyl groups turn inward to complex the cation, the nine isopropyl and three

Encyclopedia of Supramolecular Chemistry
DOI: 10.1081/E-ESMC 120012686

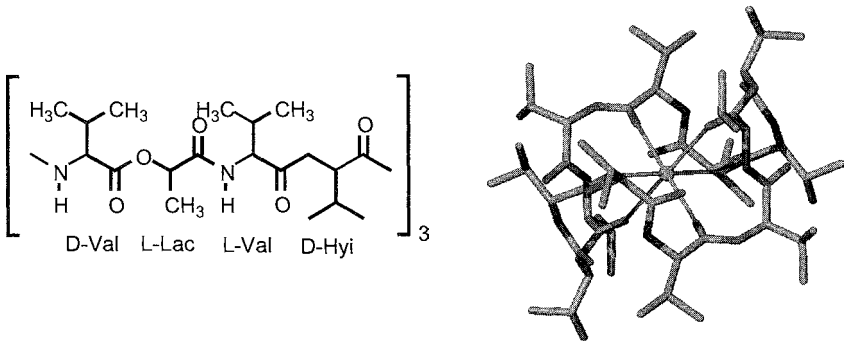

Fig. 1 Chemical structure of valinomycin (left). D-Val and L-Val are the D- and L-enantiomers of valine. D-Hyi is D-hydroxyisovaleric acid. and L-Lac is L-lactic acid. A solid-state structure of the potassium complex is shown on the right. *(View this art in color at www.dekker.com.)*

methyl groups turn outward to interact with the hydrophobic medium. This conformation effectively creates a solvent gradient from the nonpolar exterior to the polar coordination site. As such, the complex is soluble in hydrophobic membranes. and transport is effective.

Enniatins

Enniatins A (also called lateritiin I) (Fig. 2), B, C, D, E, and F[15] are antibiotics synthesized by various strains of the genus *Fusarium*.[16–20] Like valinomycin, they are cyclic compounds, but they differ in several respects. First, the enniatins are cyclohexadepsipeptides, so they are half the size of valinomycin. Second, their ring nitrogen atoms are methylated. In contrast to valinomycin, they show poor ion selectivity. The prototype of this family is enniatin B, a cyclohexadepsipeptide assembled by threefold repetition of the L-N-methylvaline D-hydroxyisovaleric acid subunit. When L-*N*-methylvaline is replaced by L-N-methylphenylalanine in this repeating sequence, beauvericin results.

Enniatins form 1:1 and 1:2 complexes with cation~. [~ Structures were obtained for the Na^+, K^+, Rb^+, and Ba^{2+} complexes. Complexation occurs as a result of carbonyl donor groups interacting with the bound cation. The conformations of Na^+- and K^+-bound enniatin B complexes differ little in overall conformation. This fact may account for the poor cation selectivity.

Nactins

Nonactin (Fig. 2) is a macrotetrolide antibiotic comprised of four nonactic acid groups that have alternating chirality. Nonactin is of historical interest. as its potassium complex was the first solid-state structure of an ionophore complex to be resolved.[23] The resulting structural insights were valuable in explaining the formation of such complexes and in understanding transmembrane transport. It is interesting to note that the macrotetrolides[24–29] exhibit a broad range of biological activities. including antibacterial, antifungal, antitumor, and immunosuppressive activity.

Natural Noncyclic Ionophores

Nigericin and related compounds

Nigericin, monensin, grisorixin, ionomycin, and many other compounds are structurally related and may be grouped into a family.[30–37] All are carboxylic acid ion-

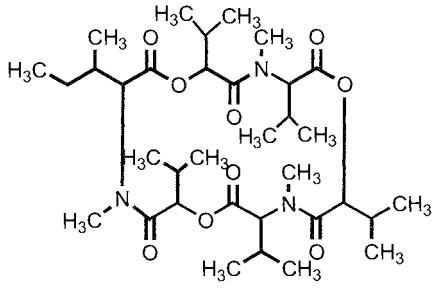

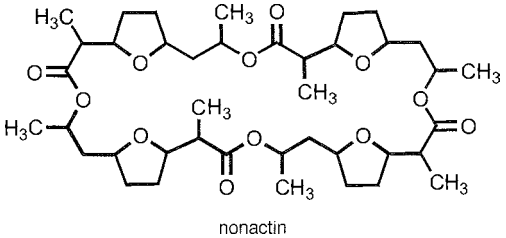

Fig. 2 Structures of enniatin A and nonactin.

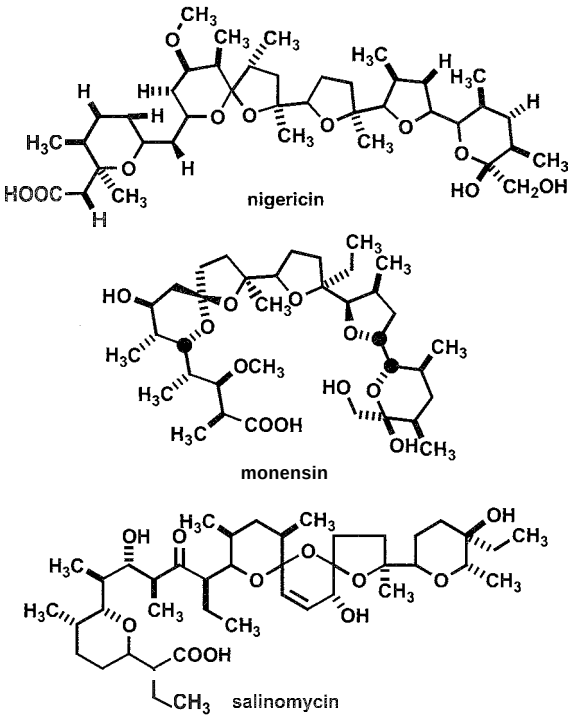

Fig. 3 Structures of nigericin, monensin. and salinomycin.

ophores that contain tetrahydrofuran and tetrahydropyran structural units. Nigericin,[38] the structure of which is shown in Fig. 3. contains three five-membered and three six-membered rings in a noncyclic array.

Although these compounds are acyclic,[39] they adopt semicircular conformations in which the oxygen heteroatoms are focused for cation binding.[40] The uncomplexed forms may adopt a cyclic conformation as a result of hydrogen-bond formation between the molecule's head and the tail. It is interesting to note that valinomycin transports cations (typically K^+) into mitochondria: the carboxylic ionophores in this family typically transport in the opposite direction. The ionophores in this group are deprotonated at physiologic pH (7.4), so their complexes with alkali metal cations are ordinarily neutral. Nigericin has 11 oxygen atoms, all of which could potentially interact with a bound cation. Typically. however, only five to seven donors coordinate. The donor number has been attributed to the lack of symmetry in these ionophores and to conformational restrictions caused by, inter alia. the spiro ring junctions.

Several other natural, acyclic carboxylic ionophores are known. Among these, salinomycin is notable for its unusual tricyclic spiroketal ring system. Further, the ester of salinomycin affords complexes that have a helical, rather than "circular," conformation.[41] Ionomycin[42] is likewise notable as the first example of a dibasic ionophore to be discovered. Ionomycin has a high affinity for divalent cations such as Ca^{2+} and Cd^{2+}, owing to the presence of an enolized β-diketone.

Artificial Noncyclic Ionophores

Crown ethers are two-dimensional, cyclic, cation-complexing agents. The corresponding three-dimensional analogues are called cryptands. The open-chained (noncyclic) analogues of crown ethers are generally referred to as podands. Like the crowns and cryptands. their structures include oxygen. nitrogen, sulfur, or other donors typically separated by ethylene units. The donors may be part of a small ring. such as tetrahydrofuran, and the ethylene or other carbon spacer units may be part of other structures. such as a benzene ring.

Polyethylene glycols

Polyethylene glycols. acyclic compounds having the repeating (OCH_2CH_2) units, have been known for many

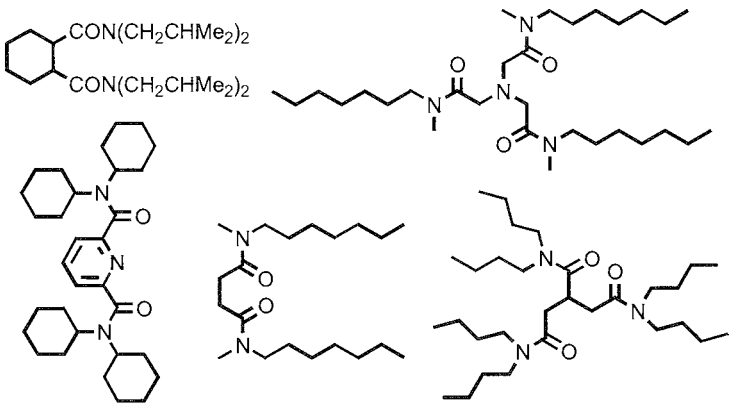

Fig. 4 Structures of open-chained ''podand'' cation complexing agents

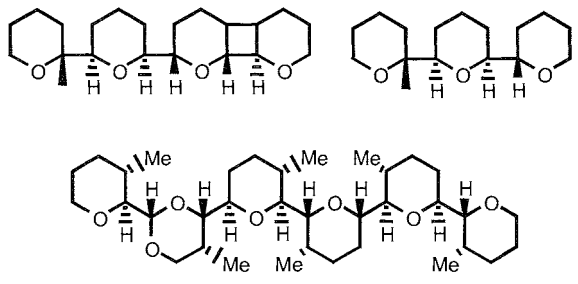

Fig. 5 Synthetic, pyran-containing open-chained ionophores.

years. The chains may be terminated by hydroxyl groups [HO-$(CH_2CH_2O)_nH$], by one alkyl group [$RO(CH_2CH_2O)_nH$], or by two alkyl residues [$R^1O(CH_2CH_2O)_n R^2$]. In the latter case, R^1 and R^2 may be the same or different, but the most common examples are mono- and dimethyl ethers. The molecular weights known for these compounds range from hundreds to millions of Daltons. The polyethylene glycols are commonly referred to as ''PEGs,'' and the methylated derivatives as ''MPEGs.'' Polyethylene glycols are available commercially under a variety of trade names, including "Carbowax," typically followed by a number indicating the molecular weight. For example, Carbowax 300 is a liquid having approximately seven repeating ethyleneoxy units. The designation PEG-2000 refers to a polymer mixture of the type $HO(CH_2CH_2O)_nH$, in which n is about 45. MPEG-2000 has the formula $CH_3O(CH_2CH_2O)_nH$, but n remains about the same.[43]

Attachment of a polyethylene glycol chain to, for example, a protein, is called ''PEGylation.'' The covalent attachment of PEG chains to drugs, peptides. proteins, and other substances often has the effect of increasing the derivative's circulation time in the bloodstream. This derivatization was also found to reduce the immunogenicity of the conjugate in some cases.[44,45]

Polyethylene glycols are similar to crown ethers except that they are linear rather than cyclic oligomers.[44] Accordingly, they can bind cationic species, just as do crown ethers.[45–47] An important difference is that crowns are preorganized in a cyclic conformation that PEGs must adopt with a corresponding entropy cost. Thus, a crown ether will typically bind a cation more strongly than will a PEG of corresponding molecular weight.[48,49]

Ion-selective, open-chained ionophores

Simon and coworkers prepared numerous novel open-chained compounds that exhibited cation selectivity.[50–57] Some of these compounds were incorporated into ion-selective electrodes. An especially successful application is their use in the detection of divalent calcium cation. Several of the structures developed in the Simon laboratory are shown in Fig. 4.

Oligotetrahydropyrans

Still and coworkers prepared a family of polytetrahydropyran derivatives such as those depicted in Fig. 5.[58–60] These compounds are preorganized by virtue of their stereochemistries into conformations that are appropriate for cation binding. These conformations confer upon them ionophoretic abilities that sometimes exceed those of crown ethers containing the same number of donor atoms.

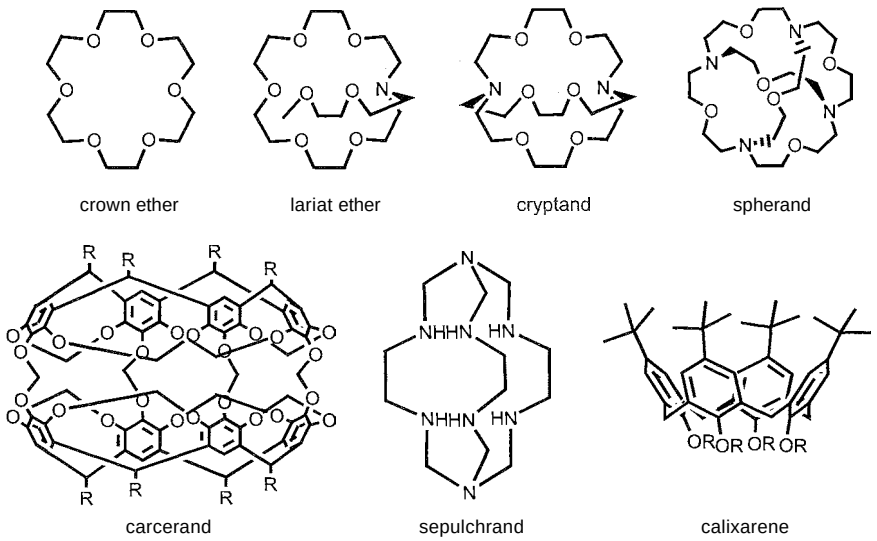

Fig. 6 Structures representing major classes of ionophores.

Compounds such as the one shown in the bottom of Fig. 5 are conformationally locked; the oxygens are held in the same geometry observed in the solid-state structure of the 18-crown-6 potassium complex.[61] Most of these compounds are chiral and are capable of enantioselectively complexing chiral ammonium ions.[62–64]

Artificial Cyclic Ionophores

The ion-bearer concept applies to cyclic and bicyclic molecules as well as to the open-chained counterparts described above. Complexing agents such as crown ethers comprise such an enormous class. however, that they are usually referred to by the more specific cognomen. This tradition applies to lariat ethers. spherands. cryptands, carcerands, calixarenes, sepulchrands, and numerous other compounds that are dealt with separately in this *Encyclopedia*. Structures exemplifying these various families are shown in Fig. 6.

CONCLUSION

Ionophores are ion-bearers. In order to bear or carry ions, they must also complex them. The complexation and transport of cations depends to an appreciable extent on the ion, the medium. the ionophore's structure, the counterion, and other variables. The reader is referred to other articles in this *Encyclopedia* for information concerning structures that encapsulate ions. For a more detailed discussion of complexation and complexing agents, the reader should consult Ref. [65] and information therein.

ARTICLES OF FURTHER INTEREST

Crown Ethers, p. *326*
Cryptands, p. *334*
Lariat Ethers, p. *782*

REFERENCES

1. Dobler. M. *Ionophores and Their* Structures: Wiley: New York. 1981; 379.
2. Dobler, M. Natural *Cation Binding* Agents: Compr. Supramol. Chem., Pergamon. 1996; Vol. 1. 267–313.
3. Hilgenfeld, R.: Saenger, W. Structural chemistry of natural and synthetic ionophores and their complexes with cations. Top. Curs. Chem. 1982. 101. 1–82.
4. Dietrich. B.; Viout, P.: Lehn, J.-M. *Macrocyclic Chemistry:* Aspects of *Organic and Inorganic Supra Molecular Chemistry*; VCH: Weinheim. 1993: 384.
5. Moore. C.; Pressman, B.C. Mechanism of action of valinomycin on mitochondria. Biochem. Biophys. Res. Commun. 1964. *15*. 562–567.
6. Pressman. B.C.: Harris. E.J.: Jagger, W.S.: Johnson, J.H. Antibiotic-mediated transport of alkali ions across lipid barriers. Proc. Natl. Acad. Sci. U. S. A. **1967**. 58. 1949–1956.
7. Urry, D.W. Chemical basis of ion transport specificity in biological membranes. Top. Curs. Chem. 1985, 128, 175–218.
8. Ohnishi. M.: Urry. D.W. Solution conformation of valinomycin–potassium ion complex. Science 1970. 168. 1091–1092.
9. Duax, W.L.; Hauptman, H.; Weeks. C.M.: Norton, D.A. Valinomycin crystal structure determination by direct methods. Science **1972**. *176*. 911–914.
10. Neupert-Laves, K.: Dobler, M. Crystal structure of potassium(+) ion complex of valinomycin. Helv. Chim. Acta 1995. *58*, 432–442.
11. Easwaran. K.R.K. Interaction between valinomycin and metal ions. Met. Ions Biol. Syst. 1985. 19. 109–137.
12. Duax. W.L.; Griffin. J.F.; Langs, D.A.; Smith, G.D.: Grochulski. P.; Pletnev, V.; Ivanov, V. Molecular structure and mechanisms of action of cyclic and linear ion transport antibiotics. Biopolymers 1996, 40. 141–155.
13. Dobler, M. X-ray diffraction studies of peptide ionophores and related compounds. Biochem. Soc. Trans. 1973, *1*. 828–832.
14. Brockmann, H.: Schmidt-Kastner. G. Antibiotics from actinomycetes. XXVII. Valinomycin I. Chem. Ber. 1955, 88. 57–61.
15. Tomoda, H.: Nishida, H.; Huang. X.H.: Masuma. R.: Kim. Y.K.; Omura. S. New cpclodepsipeptides. enniatins D, E, and F produced by Fusarium sp. FO-1305. J. Antibiot. 1992. 45. 1207–1215.
16. Steinrauf. L.M. Beauvericin and the other enniatins. Met. Ions Biol. Syst. **1985**. *19*, 139–171.
17. Benz. R. Alkali ion transport through lipid bilayer membranes mediated by enniatin A and B and beauvericin. J. Membr. Biol. **1978**. 43. 367–394.
18. Ovchinnikov, Yu.A.: Ivanov, V.T.; Evstratov, A.V.: Mikhaleva, I.I.: Bystrov, V.F.; Portnova, S.L.; Balashova, T.A.; Meshcheryakova. E.N.; Tul'chinskii. V.M. Enniatin ionophores. Conformation and ion binding properties. Int. J. Pept. Protein Res. 1974. 6. 465–498.
19. Ovchinnikov, Yu.A. Membrane-active complexones. Chemistry and biological function. FEBS Lett. **1974**, 44. 1–21.
20. Dobler. M.: Dunitz, J.D.; Krajewski, J. Structure of the potassium ion complex with enniatin B, a macrocyclic antibiotic with potassium ion transport properties. J. Mol. Biol. 1969, 42. 603–606.
21. Ivanov. V.T. 'Sandwich' complexation in cyclopeptides and its implications in membrane processes. Ann. N. Y. Acad. Sci. 1995, 264. 221–243. (Carriers Channels Biol. Syst.).
22. Ivanov, V.T.; Evstratov. A.V.: Sumskaya, L.V.: Mel'nik. E.I.; Chumburidze. T.S.: Portnova. S.L.; Balashova, T.A.:

Ovchinnikov. Yu.A. Sandwich complexes as a functional form of the enniatin ionophores. FEBS (Fed. Eur. Biochem. Soc.) Lett. 1973. 36. 65–71.
23. Kilbourn, B.T.; Dunitz. J.D.: Pioda, L.A.R.; Simon, W. Structure of the K+ complex with nonactin. a macrotetrolide antibiotic possessing highly specific K+ transport properties. J. Mol. Biol. 1967. *30.* 559–563.
24. Nawata, Y.; Iitaka. Y. The conformation of the macrotetrolide ring system from x-ray and molecular mechanics studies. Tetrahedron 1983, 39. 1133–1140.
25. Sakamaki, T.: Iitaka. Y.; Nawata. Y. The crystal and molecular structures of cesium(+) complexes of tetranactin and nonactin. Acta Crystallogr., Sect. B **1977**, *B33*, 52–59.
26. Asher, I.M.; Phillies, G.D.J.; Kim. B.J.: Stanley. H.E. Ion complexation in nonactin, monactin, and dinactin: A Raman spectroscopic study. Biopolyrners 1977. *16,* 157–185.
27. Eisenman, G.; Krasne. S.: Ciani, S. The kinetic and equilibrium components of selective ionic permeability mediated by nactin- and valinomycin-type carriers having systematically varied degrees of methylation. Ann. N. Y. Acad. Sci. 1975. *264*, 34–60. (Carriers Channels Biol. Syst.).
28. Phillies, G.D.J.: Asher, I.M.; Stanley, H.E. Nonactin. monactin, dinactin. trinactin. and tetranactin. Raman spectroscopic study. Biopolyrners **1975**, *14*, 2311–2327.
29. Nawata, Y.; Ando. K.: Iitaka, Y. Nactins: Their complexes and biological properties. Met. Ions Biol. Syst. 1985. *19.* 207–227.
30. Steinrauf, L.K.; Czerwinski. E.W.: Pinkerton, M. Comparison of the monovalent cation complexes of monensin. nigericin, and dianemycin. Biochem. Biophys. Res. Commun. 197%.*45*. 1279–1283.
31. Agtarap. A.; Chamberlin, J.W. Monensin. a new biologically active compound. IV. Chemistry. Antimicrob. Agents Chernother. 1968. 359–362. (Volume Date 1967).
32. Gorman, M.: Chamberlin. J.W.; Hamill. R.L. Monensin. a new biologically active compound. V. Compounds related to monensin. Antirnicrob. Agents Chemother. 1968. 363–368. (Volume Date 1967).
33. Duax. W.L.: Smith. G.D.; Van Roey, P. Ion selectivity and mechanism of ion capture by carboxylic ionophores. Stud. Phys. Theor. Chem. 1983. *24.* 217–233. (Phys. Chem. Transmembr. Ion Motions).
34. Painter. G.R.: Pressman, B.C. Cation complexes of the monovalent and polyvalent carboxylic ionophores: Lasalocid (X-537A). monensin, A23187 (calcimycin). and related antibiotics. Met. Ions Biol. Syst. **1985**. *19.* 229–294.
35. Mitani, M.: Otake, N. Studies on the ionophorous antibiotics. XV. The monovalent cation selective ionophorous activities of carriomycin. lonomycin. and etheromycin. J. Antibiot. **1978**, 31. 750–755.
36. Pressman. B.C.; Fahim. M. Pharmacology and toxicology of the monovalent carboxylic ionophores. Annu. Rev. Pharmacol. Toxicol. 1982. *22.* 465–490.
37. Lutz, W.K.: Frueh. P.U.: Simon. W. Microcalorimetric determination of AH°. ΔG°. and AS° for the interaction of the carrier antibiotics nigericin and monensin with sodium and potassium ions. Helv. Chim. Acta 1971. *54.* 2767–2770.
38. Steinrauf. L.K.; Pinkerton, M.; Chamberlin. J.W. The structure of nigericin. Biochem. Biophys. Res. Commun. 1968. *33.* 29–31.
39. Rodios. N.A.; Anteunis. M.J.O. Non-closed forms of monensin and nigericin free-acid in protic solvents. Bull. Soc. Chim. Belg. 1980, *89,* 537–550.
40. Anteunis. M.J.O. Application of simple rules for the prediction of the conformation of carboxylic ionophores. Bull. Soc. Chim. Belg. **1981**, *90.* 449–470.
41. Kinashi, H.: Otake, N.: Yonehara, H.: Sato. S.: Saito. Y. Ionophorous antibiotics. I. Crystal and molecular structure of salinomycin p-iodophenacyl ester. Acta Crystallogr., B **1975**, *B31*, 2411–2415.
42. Toeplitz. B.K.; Cohen. A.I.: Funke. P.T.; Parker. W.L.: Gougoutas. J.Z. Structure of ionomycin—A novel diacidic polyether antibiotic having high affinity for calcium ions. J. Am. Chem. Soc. 1979, *101*. 3344–3353.
43. *Poly(ethylene glycol) Chemistry:* Biotechnicnl and *Biomedical Applications*; Harris, J.M.. Ed.: Plenum: New York, 1992.
44. Gokel, G.W.: Murillo, O. Podands. In *Comprehensive Supramolecular Chemistry*; Gokel, G.W.. Ed.: Pergamon Press: Oxford. 1996; 1. 1–34.
45. Weber, E.: Voegtle. F. Crystalline 1:1 complexes of alkali metals with noncyclized neutral ligands. Tetrahedron Lett. 1975. *29.* 2415–2418.
46. Saenger, *W.:* Suh. I.H.: Weber. G. Structures of polyether complexes. Part XIII. Wrapping of metal cations by linear polyethers. Isr. J. Chem. **1980**, *18,* 253–258. (Volume Date 1979).
47. Hilgenfeld, R.: Saenger, W. Structural chemistry of natural and synthetic ionophores and their complexes with cations. Top. Curr. Chem. 198%.*101*. 1–82.
48. Gokel, G.W.; Goli, D.M.: Schultz. R.A. Binding profiles for oligoethylene glycols and oligoethylene glycol monomethyl ethers and an assessment of their abilities to catalyze phase transfer reactions. J. Org. Chem. 1983. *48.* 2837–2842.
49. Xu. W.Y.: Smid, J. Affinities of crown ethers, glymes, and polyamines for alkali picrates in toluene. Application of polymer-supported linear polyethers. J. Am. Chem. Soc. 1984. *106.* 3790–3796.
50. Ammann, D.: Bissig, R.: Gueggi, M.: Pretsch, E.: Simon, W.; Borowitz. I.J.: Weiss. L. Preparation of neutral ionophores for alkali and alkaline earth metal cations and their application in ion selective membrane electrodes. Helv. Chim. Acta 1975. *58*, 1535–1548.
51. Morf. W.E.: Ammann, D.; Bissig. R.; Pretsch. E.; Simon. W. Cation selectivity of neutral macrocyclic and nonmacrocyclic complexing agents in membranes. Prog. Macrocyclic Chem. **1979**, *1*, 1–61.
52. Vuilleumier, P.; Gazzotti. P.: Carafoli, E.: Simon. W. The translocation of calcium ion across phospholipid bilayers induced by a synthetic neutral calcium ion-ionophore. Biochirn. Biophys. Acta **1977**, 467. 12–18.
53. Simon. W.: Carafoli. E. Design. properties. and applications of neutral ionophores. Methods Enzymol **1979**, *56.* 439–448. (Biomernbranes. Part G).
54. Maj-Zurawska, M.: Erne. D.: Ammann. D.: Simon, W.

Lipophilic synthetic monoamides of dicarboxylic acids as ionophores for alkaline earth metal cations. Helv. Chim. Acta 1982. *65*. 55–62.
55. Erne, D.: Ammann, D.: Zhukov, A.F.; Behm, F.; Pretsch. E.: Simon, W. Lipophilic diamides as ionophores for alkali and alkaline earth metal cations. Helv.Chim. Acta 1982. *65*, 538–545.
56. Erne, D.: Stojanac, N.: Ammann, D.; Hofstetter. P.; Pretsch, E.; Simon. W. Lipophilic di- and triamides as ionophores for alkaline earth metal cations. Helv. Chim. Acta 1980, *63*, 2271–2279.
57. Erne, D.; Stojanac, N.: Ammann, D.; Pretsch, E.; Simon, W. Lipophilic amides of EDTA, NTA and iminodiacetic acid as ionophores for alkaline earth metal cations. Helv. Chim. Acta 1980. *63*, 2264–2270.
58. Iimori, T.: Still, W.C.; Rheingold, A.L.; Staley, D.L. Podand ionophores. A new class of nonmacrocyclic yet preorganized hosts for cations. J. Am. Chem. Soc. 1989. **111.** 3439–3440.
59. Erickson, S.D.; Ohlmeyer, M.H.J.: Still, W.C. Enhancing the binding properties of a conformationally rigid podand ionophore. Tetrahedron Lett. 1992. *33.* 5925–5928.
60. Burger, M.T.; Still, W.C. Improved synthesis of functionalized podand ionophores. J. Org. Chem. 1996. 61. 775–777.
61. Li, G.; Still. W.C. A podand analog of 18-crown-6. Tetrahedron Lett. 1993. 34, 919–922.
62. Wang. X.; Erickson. S.D.; Iimori. T.: Still. W.C. Enantioselective coinplexation of organic ammonium ions by simple tetracyclic podand ionophores. J. Am. Chem. Soc. 1992. *114*. 4128–4137.
63. Armstrong, A.; Still, W.C. Enantioselective cation binding with a functionalized podand ionophore. J. Org. Chem. 1992, *57*. 4580–4582.
64. Li. G.; Still, W.C. Dipeptidic ammonium ion binding by a synthetic receptor. Bioorg. Med. Chem. Lett. 1992. 2. 731–734.
65. *Cation Binding by Macrocycles: Complexation of Cationic Species by Crown Ethers;* Inoue. Y., Gokel, C.W., Eds.: Marcel Dekker: New York, 1990.

Isostructurality of Inclusion Compounds

Mino R. Caira
University of Cape Town, Rondebosch, Western Cape Province, South Africa

INTRODUCTION

Crystal isostructurality refers to identical or nearly identical packing arrays of chemically distinct compounds and is inversely related to the phenomenon of polymorphism, which, instead. refers to the ability of a single compound to crystallize in different packing arrays.[1] A series of isostructural inclusion compounds is typically based on a common host framework with voids that may be occupied by different guest molecules. The constant guest environment provided by such a series is a factor that facilitates interpretation of the mechanisms of processes such as thermal decomposition and guest exchange.

GENERAL SIGNIFICANCE OF CRYSTAL ISOSTRUCTURALITY

Description of Isostructurality and Its Implications in Supramolecular Chemistry

''Crystal isomorphism'' is a term used to indicate similarity in crystal morphology and, as such, is inappropriate for describing two or more crystals containing essentially the same three-dimensional arrangement of geometrically similar structural units. For such systems, the term ''isostructural'' is appropriate.[1] Crystal isostructurality of organic compounds was initially recognized as an interesting aspect of the packing of structurally similar molecules. In recent years, with the explosive increase in the number of published crystal structures, its increasing frequency of occurrence, especially among inclusion compounds, has generated renewed interest. In a strict definition, isostructural compounds crystallize with similar unit cell dimensions, the same space group, and almost identical atomic coordinates for common atoms. This implies that the entire atomic array of one crystal is virtually superimposable on the array of its isostructural partner. Crystallographers have for many years used isostructurality to advantage in the solution of crystal structures by the so-called isomorphous replacement technique.

A series of isostructural inclusion compounds presents a unique opportunity to investigate structure and property relationships, because one structural degree of freedom, namely the host arrangement, is effectively constant. If the guests are volatile, thermal analysis can be used to establish whether the guest loss event has common or widely disparate thermodynamic and kinetic parameters. Interpretation of such data can lead to postulation of a mechanism for desolvation, especially if the structure of the resulting polymorphic form has also been established. In principle, two members of a series of isostructural inclusion compounds may yield the same or different polymorphs on desolvation. Guest exchange processes are most easily interpreted in the case of isostructural inclusion compounds; because the exchangeable guests in these species occupy voids or channels of virtually identical topology, and the complicating appearance of new solid phases is eliminated.

Two isostructural inclusion compounds are most conveniently identified as such from close correspondence between their powder x-ray diffraction (PXRD) patterns. Shown in Fig. 1 are representative crystal structures of three members of an isostructural series of inclusion compounds with their corresponding PXRD patterns.[2] The angular positions of the diffraction peaks are dictated by the respective lattice constants, which for isostructural compounds frequently differ by very small percentages, resulting in near coincidence of peak positions. Peak intensity differences, however, reflect differences in the structures and orientations of the guest molecules present. These features of PXRD patterns may be exploited in developing a reference pattern for a series of isostructural clathrates, useful for identifying and characterizing clathrates of new guests of the same host unequivocally. More than one series of isostructural clathrates may exist for a given host, and their reference patterns may permit a finer level of structural characterization, including space group discrimination.

DEFINITION AND QUANTIFICATION OF ISOSTRUCTURALITY

Isostructurality and Homeostructurality

Since the 1980s, Kálmán and his rchool have been largely responsible for systematizing the notion of isostructurality for organic compounds[3] and for developing numerical

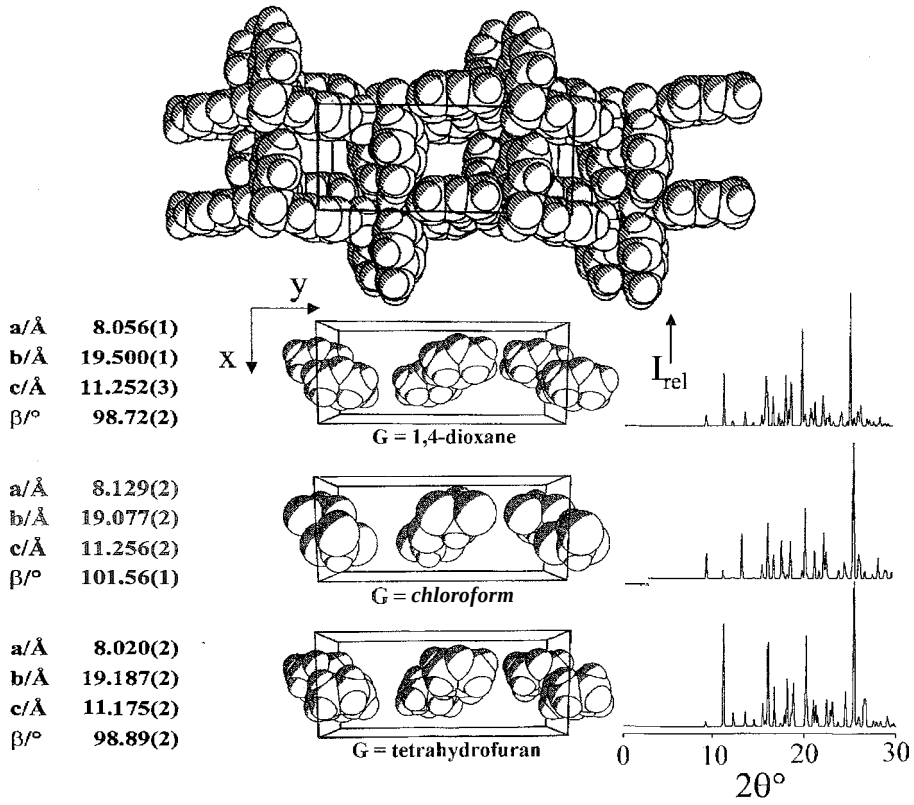

Fig. 1 Space-filling representation of the common host framework adopted by 5-methoxysulfadiazine in three isostructural clathrates (space group $P2_1/c$) and cavity occupation by the respective guests. Also shown are the unit cell data and PXRD patterns for the clathrates. (Adapted from Ref. [2] with permission from Gordon and Breach Publishing and Taylor & Francis.)

indices[i]'' with which to quantify the extent of isostructurality shared by two or more crystal structures. A synopsis of their classification follows. Distinction is made between ''isostructural'' and ''homeostructural'' crystals. In the former, crystals are characterized by having small differences on the surfaces of their respective molecules. which are otherwise isometric (''main part isostructuralism''). a pre-requisite for the formation of identical packing motifs. Small molecular differences include a substituent difference at a common site. e.g., $H \rightarrow CH_3$ substitution as in digitoxigenin→(21S)-methyldigitoxigenin,[1] or chirality differences at a common site. The term ''homeostructural'' allows for more relaxed forms of isostructurality, in which substitution occurs at more than one atomic site on the related molecules. As regards molecular associates, such as clathrates with similar host substructures but containing different guest molecules in coinmon cavities, crystal pairs of this type may be isostructural to a greater or lesser extent. and in the latter case, are included among the homeostructural cases. Ideally. classification can be based upon computed values of the various isostructurality indices available (see below), but this is not yet common practice. Instead, recent literature abounds with the term ''isostructural,'' even for systems that should properly be called ''homeostructural.'' In the absence of quantitative data for most systems, the term ''isostructurality'' is used here henceforth, but the finer distinctions recommended by Kálmán and coworkers[i]'' should be borne in mind.

Indices of Isostructurality

Indices for measuring the extent of isostructurality of two or more organic crystal structures can be applied not only to homomolecular crystals but also to molecular associates. such as inclusion compounds. A qualitative summary of these descriptors follows, and the reader is referred to a recent account for explicit mathematical definitions.[4] Earlier descriptors of isostructurality included the ''''degree of isostructurality'' $I_i(n)$ (based on the distance differences ΔR_i between the crystal coordinates of identical nonhydrogen atoms within the same section of the asymmetric units of two or more related structures); the packing coefficient increment. $\Delta(pc)$; and the unit cell similarity index Π.[3]

Recently; Fábián and Kálmán highlighted certain limitations in the above indices. proposing that the degree of isostructurality of two or more structures be based instead on the extent of their volume overlap.[4] They accordingly defined a "volume isostructurality index" represented by the ratio of the volume overlap of the two compared fragments and their average volumes. This parameter, computed over the entire unit cell, has merit in that it can be used selectively on two or more related inclusion compounds to measure the levels of isostructurality between the entire crystal structures, the hosts alone, or the guests alone.

OCCURRENCE AND CONSEQUENCES OF ISOSTRUCTURALITY

Classes of inclusion Compounds Exhibiting Isostructurality

Isostructurality occurs frequently in many classes of inclusion compounds. Here, selected examples are drawn from several classes displaying this tendency, starting with clathrate hydrates and metal-containing inclusion compounds. The inherent stabilities of many host frameworks are conducive to the formation of isostructural series. At the other extreme, however, isostructurality may also arise in situations where the host is unstable, originating only within the clathrate phase, which self-assembles in the presence of guest molecules.

Isostructurality among clathrate hydrate phases is common. the known isostructural types being based on different but well-defined combinations of polyhedral water frameworks that accommodate guest molecules of different sizes. From diffraction data, it is known that, e.g., the hydrates of N_2, O_2, and air are isostructural. belonging to "structure Type II'' with cubic symmetry ($Fd\bar{3}m$) and unit cell dimensions in the range of 17.07–17.24 Å.[5] The voids occupied by the guest molecules in this series are pentagonal dodecahedra and hexakaidecahedra. Clathrate hydrates containing substantially larger guest molecules (e.g., methylcyclohexane, t-butyl ether) belong to a different isostructural series crystallizing in the hexagonal system. These and other clathrate hydrates are known to have isostructural counterparts among the clathrasils (clathrates based on the SiO_2 host framework).

Numerous instances of isostructurality among Hofmann clathrates. $M(NH_3)_2M'(CN)_4\cdot 2G$, are known. the high frequency of occurrence probably owing to the fact that this family of inclusion compounds has been studied extensively over a long period. In addition. isostructurality can manifest itself in different ways, e.g., with either M. M' fixed and guest G variable or with M, M′ variable and a common guest. An example in the former category is the pair $Fe(NH_3)_2Ni(CN)_4\cdot 2G$ with G=benzene and pyrrole[6] crystallizing in the tetragonal system with similar unit cell dimensions. The clathrate with the more symmetrical guest, benzene, crystallizes in the space group P4/mmm, while the pyrrole clathrate crystallizes in P4/m. The isostructural host frameworks, however, share the high symmetry of P4/mmm. Isostructurality in a system of the second type occurs in the series $M(NH_3)_2Ni(CN)_4\cdot 2C_6H_6$, where M=Mn. Ni, Cd, and Cu.[7] Here, a linear increase in the lattice constant a of the common tetragonal unit cell is observed and is attributed to the increasing ionic radius of M.

Isostructurality is maintained in variants of the classic Hofmann clathrates, in which the host ammonia ligands are replaced by N-substituted α,ω-diaminoalkanes,[8] e.g., *N*-methyl-1,3-diaminopropane (mtn). Thus, the host $H=Cd[CH_3NH(CH_2)_3NH_2]Ni(CN)_4$ forms a series of isostructural clathrates $2H\cdot G$ with no fewer than 27 guests. Isostructurality was deduced from close correspondence among the PXRD patterns, all of which could be indexed as tetragonal. based on the single crystal x-ray structure of one member of the series (G=cyclohexane). When the ligand mtn is replaced by N, *N*-dimethyl-1,3-diaminopropane and 2-hydroxyethylmethylamine, the resulting hosts form several clathrates each, also isostructural with the series based on mtn. Despite a wide variety of guests incorporated in the three host frameworks, the *a* and c unit cell dimensions for all of the clathrates are in the narrow ranges of 14.12–14.33 and 7.69–7.85 Å, respectively, suggesting that a high level of host isostructurality is maintained throughout.

Werner complexes, MA_4X_2, and their variants[9] also form numerous series of isostructural clathrates, but in contrast to the Hofmann clathrates, the host substructure comprises discrete molecules rather than being polymeric. In limiting cases, such host molecules may be so unstable that they do not exist as a separate phase but arise only inside the clathrate phase during its formation (the phenomenon of "contact stabilization''[10]). Isostructurality may also occur in such systems. A case in point is the isostructural pair $[M(Py)_4(NO_3)_2]\cdot 2Py$, M=Zn,Cd, and Py=pyridine. A common space group (Ccca) and similar unit cell dimensions were deduced for these clathrates from single crystal x-ray data.[10] The existence of the host molecules within the clathrates as well as their essential structural features were inferred by analogy with the isostructural species $[Ni(Py)_4(NO_3)_2]\cdot 2Py$ on which complete x-ray analysis had been performed earlier. Isostructurality in the space group Ccca is maintained when the nitrate ion of the previous series is replaced by cyanate to yield a series of seven clathrates $[M(Py)_4(NCO)_2]\cdot 2Py$, M=Mn–Zn,Cd.[11] Their isostructural nature was deduced by comparison of space group and unit cell data, with those for $[Ni(Py)_4(NCO)_2]\cdot 2Py$, whose

structure in space group Ccca was determined fully. These seven coinpounds represent the longest known row of isostructural clathrates of type $[M(Py)_4X_2]\cdot 2Py$ containing the same ligand X. Introduction of the slightly longer azido ligand in the hosts of the clathrates $[M(Py)_4(N_3)_2]\cdot 2Py$, M=Ni.Co leads to a change in the crystal structure from space group Ccca to Pnna, which is common to this isostructural pair.[12] This illustrates that apparently small chemical variations in Werner compounds can induce significant morphotropic shifts. The host $[Ni(MePy)_4(NCS)_2]$, MePy=4-methylpyridine, is a versatile clathrate former giving rise to cage, organic zeolite, and layered structures, and including guests ranging from rare gases to organic molecules the size of naphthalene.[9] The clathrates of, e.g., benzene, p-xylene. and MePy, form a well-known isostructural series crystallizing in the tetragonal space group $I4_1/a$. Inclusion of larger molecules (e.g., naphthalene derivatives) by the host $[Ni(MePy)_4(NCS)_2]$ involves a change in structure from tetragonal to triclinic with an accompanying change in the topologies of the voids occupied by guests.[''''] The clathrates $[Ni(MePy)_4(NCS)_2]\cdot 2G$, G=2-methylnaphthalene and 2-bromonaphthalene are isostructural, crystallizing in the space group $P\bar{1}$ with similar unit cell dimensions. Not surprisingly, isostructurality extends even to the guest molecules, and this was exploited in the structure solution of the 2-bromonaphthalene clathrate by isomosphous replacement.

Isostructurality among inclusion compounds of organic hosts and guests occurs widely, and selected cases are highlighted here. An isostructural series derived from a specific host cocrystallizing with a range of guests represents the most common situation. The bile acids, cholic acid (CA) 1 and deoxycholic acid (DCA) 2, exemplify such hosts.[''''] Their inclusion compounds generally feature an assembly of host bilayers with the guest molecules enclosed within cavities or helical channels. CA cocrystallizes with the aliphatic esters ethylacetate and ethylpropionate to yield an isostructural pair of I:1 host–guest stoichiometry in the space group $P2_1$.[15] Inclusion of *n*-propylacetate, i-propylaceiate, and n-butylacetate results in a rnorphotropic change to a new isostructural series, again crystallizing in $P2_1$ but with distinctly different unit cell dimensions. The structural change involves a shift in the relative positions of the host bilayers, yielding channels with different cross-sectional shapes to accommodate the new guests.

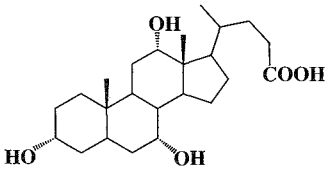

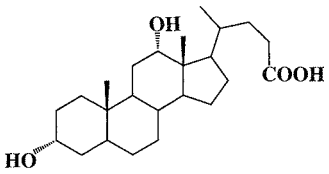

2

Synthetic diol host compounds are prolific clathrate formers.[16] Among these are the alicyclic diols (e.g., **3)** that cocrystallize with a large variety of guests to form helical tubulate inclusion compounds.[17] Here, isostructurality may occur within a series of inclusion compounds containing a common host and variable guests, while homeostructurality is evident between some clathrates in which both the host and the guest differ. Kálmán used several of these compounds as models to illustrate the use of indices to quantify individually the levels of isostructurality among hosts, guests, and the entire clathrate structures.[''] The diol 4, which was used to separate close isomers of several organic compounds,[18] forms an isostructural series with guests methanol, ethanol, 2-propanol. and n-butanol of 1:1 H:G stoichiometry in the space group $P\bar{1}$. The host framework is a double ribbon motif, and guests are located in channels formed by host layers. The unit cell parameter normal to the layers shows a steady increase from 12.9 to 14.8 Å as guests of increasing size are accommodated.

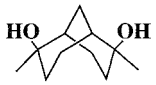

3

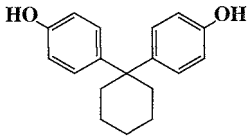

4

The host tri-o-thymotide 5 was reported to form over 140 clathrates with guests of the most varied shapes.[19] These clathrates crystallize in about a dozen isostructural series, the most populous belonging to space group $P3_121$. For several of these series, a linear relationship between unit cell size and guest molecular volume was observed.

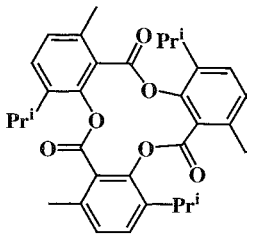

5

Clathrates of tetraphenylene 6 form a single isostructural series ($P4_2/n$) with H:G ratio 2:1, in which guests range in size from dichloromethane to cyclohexane.[20] Guests occupy common spheroidal cavities generated by the isostructural host framework. Elaboration of the host 6 to the more bulky tetrabenzo[*b*,*h*,*n*,*t*]tetraphenylene 4 produce, no fewer than three distinct isostructural series of clathrates (two triclinic, one monoclinic).

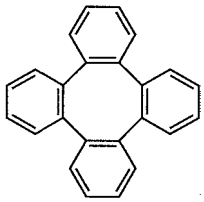

6

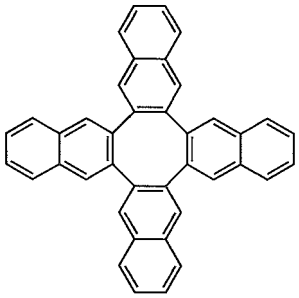

The prototype hexa-host 8 forms an isostructural series of H:G ratio 1:2 with halogenated species (e.g., CCl_4, CCl_3Br) crystallizing in space group $R\bar{3}$.[21] The latter space group and those derived by lowering its symmetry are characteristic of phenolic clathrates; isostructural series of β-hydroquinone clathrates crystallizing in R3 and R3 are familiar examples.[22]

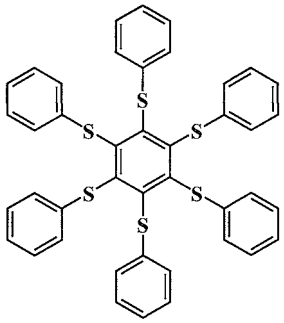

8

The yellow polyphenol pigment gossypol 9 is undiscriminating in its formation of inclusion compounds with organic guests and was recently dubbed the "universal clathrate-forming agent."[23] Over 100 crystalline forms of gossypol, including clathrates and polymorphs, have been identified. Single crystal and powder x-ray diffraction studies enabled the classification of these species into 24 groups of isostructural crystals represented in the space groups P1, $P2_1$, $P2_1/c$, C2, C2/c, and Pbcn. Such diversity in the types of supramolecular associates formed by gossypol is attributed to the presence of several polar functional groups in the molecule, as well as conformational mobility and its racemic nature. These permit the existence of a variety of centrosyinmetric host dimeric motifs from which the substructures in the various isostructural clathrate series are constructed.

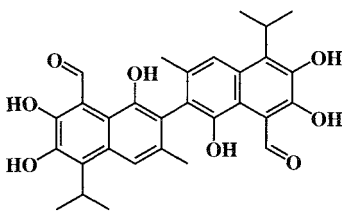

9

The cyclodextrins represent another group of hosts giving rise to numerous isostructural series of clathrates. Crystalline cyclodextrin complexes are generally ternary systems, containing host, guest, and water molecules. A recent survey of crystal structures of cyclodextrin inclusion complexes with organic guests[C2] showed that for β-cyclodextrin 10, at least eight isostructural series can be identified. This host can form monomeric complexes but more frequently yields dimeric complexes in which the guest is encapsulated within a hydrogen-bonded

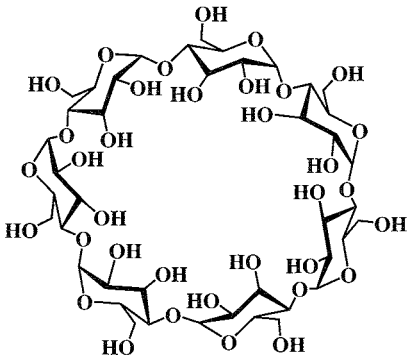

10

host dimer. Three of the eight isostructural series are represented by sets of monomeric complexes (all crystallizing in space group $P2_1$ but with distinctly different unit cell dimensions), while the remaining five isostructural series occur in P1, $P2_1$, C2. and $C222_1$ and are based on distinct modes of packing of dimeric complex units. Reference PXRD patterns for these and other isostructural series of cyclodextrin inclusion complexes have been generated. and their utility in identifying new complexes has unequivocally been demonstrated.[24] Shown in Fig. 2 is an empty β-cyclodextrin dimer that occurs in the isostructural series in space group $P2_1$, a cutaway view revealing the topology of the channel available for guest accommodation and channel occupation by two different guests in this series.[25] Assignment of a new inclusion compound to a particular isostructural series using PXRD is valuable. because this immediately defines the host arrangement as well as the void topology.

Isostructurality–Reactivity Correlations

Although isostructurality of inclusion compounds is frequently identified, published accounts of its role in reactivity (e.g., formation. thermal decomposition, selective enclathration, guest exchange) are generally lacking. Several topical aspects of isostrucrurality are illustrated by the following recent case studies.

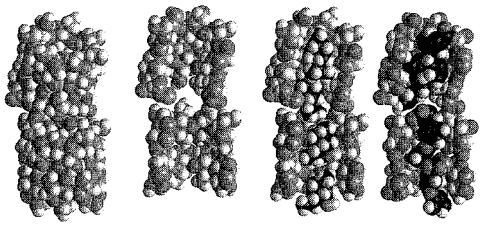

Fig. 2 Space-filling representations of (from left to right): empty β-cyclodextrin dimers, a sectioned view showing the empty channel. and sectioned views showing channel occupation by (L)-menthol and (R)-fenoprofen guest molecules in the isostructural clathrates. (Prepared from data in Ref. [25].) (View this *art in color at www.dekker.com.*)

Isostructural clathrates based on certain metal molecular complexes display different thermal properties.[11] For the isostructural series $[MPy_4(NCO)_2]\cdot 2Py$, M=Mn–Zn,Cd, the thermal stability order of the first four members is Mn<Fe<Co<Ni, and they desolvate to give the host phase $[MPy_4(NCO)_2]$. The Cu clathrate, however, loses all four moles of pyridine in a single step, with no subsequent evidence for the host phase, while the Cd clathrate shows intermediate behavior. sometimes revealing the host phase during incongruent melting of the clathrate. Consideration of similar trends occurring in related series led to the conclusion that the thermal stabilities of these clathrates depend on those of the coordination bonds in the host molecule and therefore upon the nature of the metal center. Only in cases where the host phase is sufficiently stable to remain intact during all processes is clathrate stability governed by host–guest complementarity.

Nonuniform behavior during therinal decomposition was also reported for isostructural organic inclusion compounds. The "wheel-and-axle" host **11** forms isostructural clathrates $H\cdot(THF)_2$ and $H\cdot(1,3\text{-dioxolane})_2$, in which one set of guest molecules is sandwiched between host phenyl rings.[26] Thermal desolvation of the clathrates is a one-step process, but despite the higher volatility of the pure solvent THF, the onset temperatures for desolvation are 116 and 87°C, respectively. It was argued that in the THF clathrate, there is net stabilization due to attractive host–guest π···HC(methylene) interactions that outweigh the π···O(ether) repulsive interactions. The reverse is obtained for the guest 1,3-dioxolane with the larger complement of oxygen atoms, accounting for the lower stability of its clathrate phase.

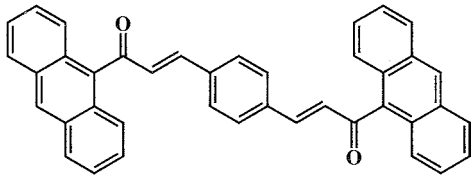

11

Host–guest hydrogen bonding differences underlie the anomalous thermal stabilities of the isostructural clathrates $H\cdot(MeOH)_{0.5}$, $H\cdot(EtOH)_{0.5}$, and $H\cdot(H_2O)_{0.67}$, where H=tetroxoprim **12**.[27] These likewise desoivate in a single step with onset temperatures in the order $t(H_2O)<t(EtOH)<t(MeOH)$, which is unexpected in view of the

relative volatilities of the guests. X-ray studies subsequently showed that the guest –OH group in MeOH acts as both donor and acceptor in hydrogen bonding to the common host framework, whereas for EtOH, the hydroxyl group acts as donor only. In the hydrate, guest disorder and low partial occupancy account for the weakest host–guest interactions. On the other hand, normalized enthalpy changes for desolvation increase in the order H_2O<MeOH<EtOH relative to the enthalpies of vaporization of the pure solvents. This was attributed to the increasing energy required to effect diffusion of guest molecules of increasing steric bulk through the transforming solid phase.

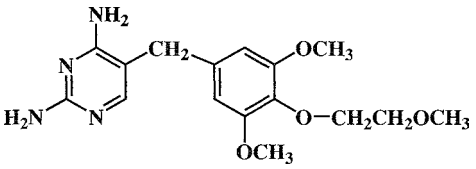

12

In contrast to the above cases. uniform behavior was observed for the thermodynamics as well as the kinetics of desolvation of the system shown in Fig. 1, namely, the isostructural 1:1 clathrates of 5-sulfamethoxydiazine (SMD) 13 with chlorofom, THF, and 1.4-dioxane as guests.[2] This was ascribed to the presence of uniformly weak host–guest interactions within the identical guest-filled cavities of the SMD framework and the similarities in guest steric bulk. These clathrates yielded the same SMD polymorph on desolvation.

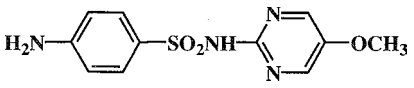

13

The question of the influence of isostructurality on the identity of the polymorph resulting from clathrate desolvation is an important one. because this process is a potential route for obtaining new polymorphs. One example is cited here, namely. that of gossypol 9 for which each of six isostructural groups of tubulate clathrates yields a distinct polymorph on desolvation.[23]

Unusual control of host–guest stoichiometry in isostructural clathrates of mixed guests was recently reported.[28] The diol 14 forms isostructural clathrates H·4A and H·4B (A=dimethylformamide, B=dimethyl sulfoxide). Investigation of the selectivity of H in mixtures of A and B spanning the entire concentration range $0 \leq x_A \leq 1$ yielded the stepwise competition profile shown in Fig. 3, leading to isolation of three intermediate clathrates H·3A·B, H·2A·2B, and H·A·3B, which are isostructural with those containing the pure solvents.

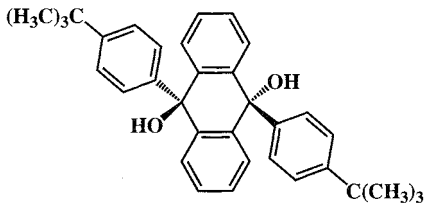

14

Exchange of similarly sized guests molecules should be facilitated if they form isostructural inclusion compounds with a particular host. This was demonstrated using diol 15, which forms isostructural clathrates H·2G [G=tetrahydrofuran (THF) and thiophene].[29] The exchange was carried out by exposing a powder of H·2THF to thiophene vapor in a closed system and monitoring the products periodically by the DSC technique. The facility of guest exchange was ascribed to the isostructurality of the clathrates and the fact that their computed lattice energies are comparable. The presence of apohost could, however, be detected during the exchange process. Guest exchange via gas–solid contact also occurs in isostructural clathrates of 16 with compositions H·$(EtOH)_2$, H·$(n\text{-PrOH})_2$, and H·$(i\text{-PrOH})_2$.[30] These clathrates contain an isostructural host framework with the guests located in channels. Exposure of, e.g., H·$(EtOH)_2$ to *n*-PrOH vapor results in gradual, but complete: replacement of ethanol by n-propanol. In this system, guest exchange does not proceed via the apohost, because pure H does not form these clathrates by a gas-sorptive mechanism. Guest

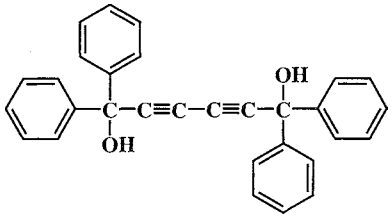

15

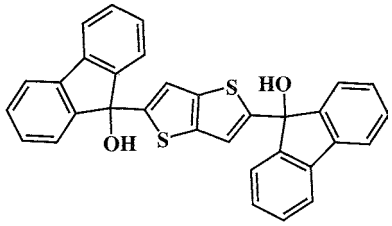

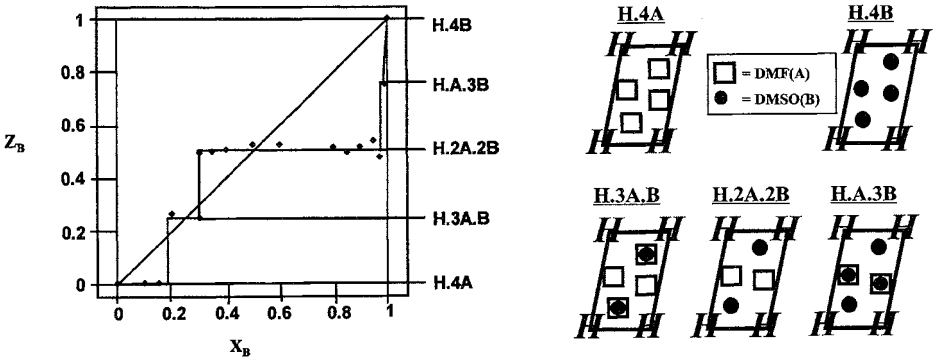

Fig. 3 Left: Results of competition experiments. The symbol X_B represents the mole fraction of Guest B in the liquid mixture and Z_B that of Guest B enclathrated in the inclusion compound. The diagonal line represents zero selectivity. Right: The five isostructural species isolated. H represents the host molecule (on a center of symmetry), and guest disorder is implied in H.3A.B and H.A.3B. (From Ref. [28]. Reproduced by permission of the Royal Society of Chemistry.)

elimination was also observed in this system. Recrystallization of host **16** from MeOH does not yield an inclusion compound but rather a polymorph of the host. Accordingly, when the three clathrates containing ethanol and the propanol isomers were exposed to methanol vapor, guest-free host solids resulted in all cases. An explanation for guest elimination is that while MeOH molecules are able to enter the crystals and displace the respective guests, their small size prevents them from stabilizing the wide channel (originally "designed" for larger guest molecules), and the structure collapses to that of the apohost.

The examples above serve to illustrate that both uniform and diverse behaviors may be observed in different series of isostructural inclusion compounds. In the latter case, anomalous behavior can often be traced to subtle host–guest interactions.

CONCLUSION

The occurrence of an isostructural series of inclusion compounds is informative, indicating the structural integrity of a particular type of host array but also reflecting a degree of flexibility to accommodate small to moderate structural modifications in the guest. This information can be carried over to the design of analogous host systems.

The finding that a new inclusion compound has an isostructural counterpart is readily achieved by the PXRD technique and represents an enormous return in terms of structural information, because it immediately defines the host substructure and the topology of the voids. This is useful for crystal structure solution of the new species by either single crystal x-ray diffraction or high-resolution PXRD. Systematic investigation of the physical and chemical properties of isostructural inclusion compounds can reveal novel phenomena in supramolecular chemistry that have practical implications for crystal engineering and polymorphism.

ACKNOWLEDGMENTS

The author is indebted to Professor Alajos Kálmán (Budapest) for his inspirational studies of isostructurality and to Professor Luigi Nassimbeni (Cape Town) for constructive comments. Thanks are due to Vincent Smith for his able technical assistance. Research funding from the University of Cape Town and the NRF (Pretoria) is gratefully acknowledged.

ARTICLES OF FURTHER INTEREST

Channel Inclusion Compounds, p. 223
Clathrate Hydrates, p. 274
Cyclodextrins, p. 398
Deoxycholic, Cholic, and Apocholic Acids, p. *441*
Gossypol, p. *606*
Hofmann-Type Clathrates, p. 645
Polymorphism, p. 1129
Space Groups and Crystal Packing Modes, p. 1337
X-Ray and Neutron Powder Diffraction, p. 1592

REFERENCES

1. Kálmán, A. On the Isostructurality of Supramolecules: Packing Similarities Governed by Molecular Complementarity. In *Fundamental Principles of Molecular Modeling*; Cans. *W.*, Ammon, A.. Boeyens, J.C.A., Eds.; Plenum Press: New York, 1996: 209–221.
2. Caira, M.R.; Mohamed, R. Inclusion compounds with the

drug 5-methoxysulfadiazine: Structures, thermodynamics of decomposition and relationship to polymorphism of the sulfonamide. Supramol. Chem. 1993.2 (2–3). 201–207.
3. Kálmán, A.: Párkányi, L.: Argay. G. Classification of the isostructurality of organic molecules in the crystalline state. Acta Crystallogr.. Sect. B: Struct. Sci. 1993. *B49* (6). 1039–1049.
4. Fábián. L.: Kálmán, A. Volumetric measure of isostructurality. Acta Crystallogr., Sect. B: Struct. Sci. 1999, *B55* (6). 1039–1049.
5. Davidson. D.W.; Gough, S.R.: Handa. Y.P.: Ratcliffe, C.I.; Ripmeester, J.A.: Tse, J.S. Some structural studies of clathrate hydrates. Can. J. Phys.. Colloq. **1987**, (C1), C1-537–C1-542.
6. Kitazawa, T.; Sato. Y.; Gomi. Y.: Takahashi. M.: Takeda, M. Crystal structure and ^{57}Fe Mössbauer spectra of Hofmann-type pyrrole clathrate, $Fe(NH_3)_2Ni(CN)_4\cdot 2C_4H_5N$. Mol. Cryst. Liq. Cryst. Sci. Technol. Sect A **1996**, *286*, 431–436.
7. Kuroda. R.; Sasaki, Y. The crystal structure of a Hofmann-type clathrate. $Mn(NH_3)_2Ni(CN)_4\cdot 2C_6H_6$. Acta Crystallogr., Sect. B 1974. *30* (3), 687–690.
8. Nishikiori. S.; Takahashi-Ebisudani. Y.; Iwamoto, T. Novel series of clathrate compounds of the three-dimensional metal complex hosts (*N*-methyl-1,3-diaminopropane) cadmium(II) tetracyanonickelate(II), (*N,N*-dimethyl-1,3-diaminopropane) cadmium(II) tetracyanonickelate(II) and (2-hydroxyethylinethylamine) cadmium(II) tetracyanonickelate(II). J. Inclusion Phenom. Mol. Recognit. Chem. **1990**, *9* (2), 101–112.
9. Lipkowski. J. Werner Clathrates. In *Comprehensive Supramolecular Chemistry*; Atwood, J.L.. Davies. J.E.D., MacNicol. D.D., Eds.; Pergamon: Oxford. 1996: Vol. 6. 691–714.
10. Dyadin, Y.A.: Soldatov. D.V.; Logvinenko, V.A.; Lipkowski, J. Contact stabilization of host complex molecules during clathrate formation: The pyridine–zinc nitrate and the pyridine–cadmium nitrate systems. J. Coord. Chem. 1996. *37* (1–4), 63–75.
11. Soldatov. D.V.; Logvinenko. V.A.; Dyadin, Y.A.: Lipkouski. J.: Suwinska. K. $[M(py)_4(NCO)_2]\cdot 2Py$ clathrates (M=M(II)=Mn, Fe, Co. Ni, Cu, Zn, Cd): Py=pyridine). J. Struct. Chem. 1999. *40* (5). 757–771.
12. Soldatov, D.V.: Lipkouski. J. Crystal structure of nickel- and cobalt-diazidotetrapyridinemetal(II)-2(pyridine) clathrates. J. Inclusion Phenom. Mol. Recognit. Chem. 1998. *30* (2). 99–109.
13. Lipkowski, J.: Sgarabotto. P.; Andreetti. G.D. Clathrate inclusion compounds of *bis*(isothiocyanato)*tetrakis*(4-methylpyridine) nickel(II). I. Compounds with 2-methyl- and 2-bromonaphthalene as guest components. Acta Crystallogr.. Sect. B 1988. 36 (1). 51–57.
14. Miyata. M.: Sada, K. Deoxycholic Acid and Related Hosts. In *Comprehensive Supramolecular Chemistry*; Atwood, J.L., Davies, J.E.D.. MacNicol. D.D., Eds.: Pergamon: Oxford. 1996; Vol. 6, 147–176.
15. Caira, M.R.; Nassimbeni. L.R.; Scott. J.L. Inclusion compounds of cholic acid with aliphatic esters. J. Chem. Soc., Perkin Trans. 2 **1994**, (3), 623–628.
16. Toda. F. Diol, Bisphenol, and Diamide Host Compounds. In *Comprehensive Supramolecular* Chemistry; Atwood, J.L., Davies, J.E.D.. MacNicol, D.D., Eds.: Pergamon: Oxford. 1996; Vol. 6, 465–516.
17. Bishop, R. Helical Host Lattices Formed by Alicyclic Diols. In Comprehensive *Supramolecular* Chemistry: Atwood, J.L., Davies, J.E.D.. MacNicol. D.D.. Eds.: Pergamon: Oxford. 1996: Vol. 6. 85–115.
18. Caira, M.R.; Horne, A.; Nassirnbeni, L.R.: Toda, F. Selective inclusion of aliphatic alcohols by a diol host compound. J. Mater. Chem. 1998, *8* (6), 1481–1484.
19. Gerdil, R. Tri-o-Thymotide and Related Hosts. In Comprehensive *Supramolecular Chemistry*; Atwood, J.L., Davies, J.E.D., MacNicol, D.D.. Eds.: Pergamon: Oxford. 1996: Vol. 6. 239–280.
20. Mak. T.C.W.: Wong, H.N.C. Tetraphenylene and Related Hosts. In Comprehensive *Supramolecular Chemistry*; Atwood. J.L., Davies, J.E.D.. MacNicol. D.D., Eds.; Pergamon: Oxford. 1996: Vol. 6, 351–369.
21. MacNicol. D.D.; Downing, G.A. Symmetry in the Evolution of Host Design. In *Comprehensive Supramolecular* Chemistry; Atwood. J.L., Davies, J.E.D., MacNicol, D.D., Eds.: Pergamon: Oxford, 1996; Vol. 6. 421–464.
22. Mak, T.C.W.: Bracke, B.R.F. Hydroquinone Clathrates and Diamondoid Lattices. In *Comprehensive Supramolecular Chemistry*; Atwood, J.L., Davies, J.E.D., MacNicol, D.D.. Eds.: Pergamon: Oxford. 1996: Vol. 6, 23–60.
23. Ibragimov, B.T.: Talipov. S.A. Supramolecular association of gossypol in the crystalline state. J. Struct. Chem. 1999. *40* (5). 686–704.
24. Caira. M.R. On the isostructurality of cyclodextrin inclusion complexes and its practical utility. Rev. Roum. Chim. 2001. 46, 371–386.
25. Cambridge *Structural* Database and *Cambridge* Structural Database *System,* Version 5.22; Cambridge Crystallographic Data Centre. University Chemical Laboratory: Cambridge. England, October 2001.
26. Hayashi, N.; Yamaguchi, K.; Matsumoto, K. Correlation between structure and thermal behavior in isostructural clathrates. Mol. Cryst. Liq. Cryst. Sci. Technol.. Sect. A **2001**, *356*, 407–411.
27. Caira, M.R.: Bettinetti, G.; Sorrenti, M. Structural relationships, thermal properties and physicochemical characterization of anhydrous and solvated crystalline forms of tetroxoprirn. J. Pharm. Sci. **2002**, *91*, 467–481.
28. Caira. M.R.: le Roex. T.: Nassimbeni. L.R. Tunable clathrates. J. Chem. Soc.. Chem. Commun. **2001**, (20), 2128–2129.
29. Caira. M.R.: Nassimbeni, L.R.: Toda. F.: Vujovic, D. Inclusion by a diol host compound: Structure and dynamics of volatile guest exchange. J. Chem. Soc., Perkin Trans. 2 **2001**, 2119–2124.
30. Kuruma, K.: Nakagawa, H.: Imakubo, T.: Kobayashi. K. Guest-exchange and guest-release via gas–solid contact in clathrate crystals based on 2.5-bis(9-hydroxyfluoren-9-yl)thieno[3,2-b]thiophene as a host compound. Bull. Chem. Soc. Jpn. 1999. 72 (6), 1395–1401.

Kinetics of Complexation

Donal H. Macartney
Queen's University, Kingston, Ontario, Canada

INTRODUCTION

While generally overshadowed by structure determinations and the measurements of thermodynamic stability constants, the determination of rate constants and activation parameters ($\Delta H^{\ddagger}$, $\Delta S^{\ddagger}$, $\Delta V^{\ddagger}$) for the assembly of supramolecular host–guest complexes in solution provide vital information in understanding the properties of these systems.[1,2] These studies, which began in the early 1970s involving alkali metal ion complexation by crown ethers and cryptands, were extended in more recent years to include anionic and neutral guest molecules in a myriad of natural and synthetic hosts. Using a variety of physical and spectroscopic techniques, through kinetic investigations of host–guest formation and dissociation reactions, as a function of temperature and pressure, several reaction mechanisms in operation were identified. Extensive compilations of rate and activation parameters for host–guest complexations. along with the corresponding thermodynamic stability constants. regularly appeared in the literature.[3]

MECHANISMS

The ligand exchange and substitution reactions of the first coordination sphere of transition metal ions with unidentate ligands, with rate constants that span close to 20 orders of magnitude (10^{-10}–10^{10} s^{-1}), were well studied and are understood in terms of a range of mechanisms from purely dissociative (D), involving an intermediate of lower coordination number, to purely associative (A), with an intermediate of higher coordination number.[4,5] In a majority of ligand substitution reactions, no such intermediate is present, and a concerted interchange (I) mechanism (Eigen–Wilkins mechanism[''])>with dissociative (I_d) or associative (I,) activation, is operating. For the multistep complexation reactions of metal ions with polydentate acyclic and macrocyclic ligands, the rate of the reaction and the position of the rate-determining step in the overall mechanism are dependent on Iigand properties such as acyclic versus cyclic. the presence and placement of strong donor atoms, and the degree of substitution and flexibility of the chains.[5,6] While a flexible acyclic tetraamine permits a facile stepwise substitution of coordinate aqua ligands on a copper(II) ion, for example, the increased rigidities of the corresponding saturated tetraazamacrocycle and aromatic porphyrin ligands result in decreases of two and eight orders of magnitude, respectively, in complexation rate constants.[5,6]

For the complexation of guests by more elaborate macrocyclic ligands with preformed three-dimensional cavities, such as crown ethers, cryptands, calixarenes, etc., the Eigen–Wilkins mechanism was modified slightly to give the Eigen–Winkles mechanism.[7] In the latter mechanism, shown below (Eqs. 1 and 2), the macrocyclic ligand may undergo required conformational changes prior to the complexation process. With cryptands, for example, equilibria between *endo–endo*, *endo–exo*, and exo–exo conformers exist, with *endo–exo* species (C) being reactive toward the solvated metal ion (MS^+). A preassociation of the metal ion and the macrocycle generates a solvent-separated complex (M^+--C), from which the first metal–ligand bond formation leads to an ''exclusive'' complex, in which the metal ion is outside the macrocyclic ring. The formation of the remaining bonds between the cation and the ligand donor atoms yields the ''inclusive'' complex. $(MC)^+$, in which the metal ion resides inside the ring:[1,2]

$$*C \rightleftharpoons C \tag{1}$$

$$MS^+ + C \underset{k_{-0}}{\overset{k_0}{\rightleftharpoons}} M^+ \text{--} C \underset{k_{-1}}{\overset{k_1}{\rightleftharpoons}} MC^+ \underset{k_{-2}}{\overset{k_2}{\rightleftharpoons}} (MC)^+ \tag{2}$$

The transformation of M^+--C to $(MC)^+$ in Eq. 2 may be further divided into individual elementary steps, $MC_{i-1}{}^+ \rightarrow MC_i{}^+$, representing the successive replacements of the solvent molecules associated with the cation by the donor atoms of the ligand.[8] As with ligand substitution reactions on transition metal ions, there are two limiting hypothetical mechanisms: dissociative and associative.[1,2] The first mechanism is a dissociative or pseudomonomolecular process with consecutive dissociation (Eq. 3) and recombination (Eq. 4) steps:

$$(MC)^+ \underset{k_1}{\overset{k_{-1}}{\rightleftharpoons}} M^+ + C \tag{3}$$

Encyclopedia of Supramolecular Chemistry
DOI: 10.1081/E-ESMC 120012657

$$(M)^{+*} + C \underset{k_{-2}}{\overset{k_2}{\rightleftharpoons}} (M^*C)^+ \quad (4)$$

The second is an associative or bimolecular exchange reaction in which the dissociation of the macrocyclic complex is initiated by a free metal cation M^{*+} present in excess (Eq. 5). This was also identified as the metal cation interchange mechanism and assigned the symbol I_M.[9]

$$(MC)^+ + M^{+*} \overset{k_2}{\rightleftharpoons} (M^*C)^+ + M^+ \quad (5)$$

$$\begin{aligned}(MC)^+ + M^{+*} &\rightleftharpoons [M^+ - - C - - M^{*+}] \\ &\rightleftharpoons (M^*C)^+ + M^+\end{aligned} \quad (6)$$

An associative exchange, accompanied by large negative entropies of activation, is primarily controlled by changes in the conformation of the macrocycle with a concerted decomplexation of one cation and partial complexation of the second cation (Eq. 6).[10]

A third mechanism, a ligand associative mechanism (Eq. 7). may be applicable to systems where a 1:2 guest:host stoichiometry is important:[1]

$$(MC)^+ + C^* \rightleftharpoons (MC^*)^+ + C \quad (7)$$

The mechanisms shown above do not consider the possibility of ion pairing between the metal ion and the spectator anion, a feature observed in relatively nonpolar solvents.[1] In solvents of low dielectric constant, the metal ion species available for complexation is not a lone solvated MS^+ cation but rather a solvated ion pair MS^+X^-. In solvents with a low Gutmann donor number. the solvent competes poorly for positions in the first coordination sphere of the metal ion. In these solvents. ion pairings of the counteranion with the metal cation (MX) and the resulting metal–host complexes become important. The complexation processes, such as the Eigen–Winkles mechanism (Eq. 2), must be modified to include ion pairing, where XM--C, XMC, and X(MC) are the solvent-separated, exclusive, and inclusive species. respectively:[1]

$$MSX + C \underset{k_0}{\overset{k_0}{\rightleftharpoons}} XM - - C \underset{k_{-1}}{\overset{k_1}{\rightleftharpoons}} XMC \underset{k_{-2}}{\overset{k_2}{\rightleftharpoons}} X(MC) \quad (8)$$

TECHNIQUES

There are two basic categories of kinetic experiments that may be performed on the complexation reactions in solution." [2,5] The first is the direct monitoring of the approach of the system to equilibrium. involving rapid mixing of reagents or perturbation of an existing equilibrium. The second type of measurement uses competitive methods in which excess of a competing guest or host is added, and the exchange process is monitored. The physical or spectroscopic technique most conveniently employed depends primarily on the time scale of the formation or dissociation of the guest–host complex in solution (see Table 1).[5,9–19] Three of the most commonly employed techniques for determining the kinetics of complexation of supramolecular entities are conventional and dynamic NMR spectroscopy,[10–12] a variety of stopped-flow"'' methods (conductivity,[14] variable pressure,"'' etc.), and ultrasonic absorption relaxation spectrometry.[16] Recently, techniques such as fluorescence[17] and EPR line shape analysis,[18] along with appropriate guest probes; were successfully applied to the kinetics of complexation and served to fill in the time domains that were not as easily accessible by the other techniques. Fluorescent probes, such as the fluorazophores[17] (with excited state fluorescence lifetimes in the 300–800 ns range), and persistent radical probes, such as benzyl tert-butyl nitroxide,[18] are ideal for the submicrosecond time scales commonly associated with guest complexation of the macrocyclic hosts described herein.

CROWN **ETHERS** AND **CRYPTANDS**

The complexation reactions of alkali metal cations by crown ethers and cryptands generally exhibit competition between the dissociative (Eqs. 1 and 2) and associative (Eqs. 3 and 4) processes, with the preferred mechanism determined by the nature of the solvent and the temperature of the reaction.[10,19,20] In low dielectric solvents, such as nitromethane (DN = 2.7) an associative

Table 1 Some techniques for kinetic studies of guest–host complexation reactions in solution

Technique	Time domain(s)[5,17]	*References*
Classical mixing	$\geq 10^2$	[5]
Stopped-flow methods	10^{-3}–10^3	[5,13–15]
Temperature jump	10^{-9}– $\geq 10^3$	[5]
NMR—saturation transfer and 2D EXSY methods	10^{-2}–10^2	[12]
NMR — dynamic line shape analysis	10^{-5}–10^{-2}	[10,11,19]
EPR	10^{-10}–10^{-5}	[18]
Ultrasonic absorption	10^{-11}–10^{-4}	[16]
Fluorescence	10^{-12}–10^{-6}	[17]

mechanism is generally preferred, while in higher dielectric solvents such as acetonitrile (DN = 14.1) the dissociative pathway is favored.[20] Similarly, at lower temperatures the associative process is dominant. with an increase in the temperature leading to a more competitive dissociative mechanism. This may be attributed to the importance of comformational changes of the ligand during the concerted partial decomplexation of one cation and the partial complexation of the second ion in the associative mechanism.[10] In the dissociative process. the solvation of the metal ion places a major role in the barrier to complexation.[20]

Cryptands are macrobicyclic or macrotricyclic hosts, of which the cryptands [221] and [222] have been the most widely studied. The reactions of cryptands with metal cations are generally slower than observed with crown ethers because of more extensive confosmational changes, and are slow enough to allow for the use of stopped-flow kinetic methods.[14] The mechanism of the complexation reactions of cryptands depends on the natures of the cryptand, the cation and the solvent. With alkali earth cations, for example, a three-step mechanism is reported involving an initial change in the conformation of the metal-free host (*exo–exo* to endo–endo), followed by a slow external binding of the cation and a slower conversion to internal binding in the host cavity.[14] For cryptands, the thermodynamic stability constants correlate quite strongly with the dissociation rate constants, with each dependent on the structure of cryptand, the number and type of macrocycle donor atoms, and the nature of the metal ion.[21,22] It is also observed that an increase in the solvent dielectric constant results in an increase in the magnitude of k_d (decrease in K), with k_f being much less sensitive to changes in the nature of the solvent.

CYCLODEXTRINS, CALIXARENES, AND CUCURBITURILS

Cyclodextrins (CD) are naturally occuring toroidal-shaped cyclic oligimers of commonly six (α-CD), seven (β-CD), or eight (γ-CD) a-D-glucose possessing a hydrophobic interior cavity with hydroxyl-rimmed portal~.'They are capable of including a variety of guest molecules. and the kinetics of the complexation and dissociation of host–guest systems was widely investigated using many different techniques. While in general the inclusion of the guest proceeds rapidly (10^7–10^9 M^{-1} s^{-1} for many small anions and organic guests[18,23,24]), some complexation reactions are significantly slower. For the complexation of many guests in cyclodextrins, such as the well-studied aromatic azo dyes (L), a two-step mechanism is evident,[25] with the formation of a transient complex (CD·L) followed by relaxation to the final form of the guest–host speciec (CD·L), as in Eq. 9:

$$CD + L \underset{k_{-1}}{\overset{k_1}{\rightleftharpoons}} CD \cdot L^* \underset{k_{-2}}{\overset{k_2}{\rightleftharpoons}} CD \cdot L$$

The technique of variable-pressure stopped-flow kinetic studies, of great benefit in mechanistic investigations of ligand substitution reactions of transition metal complexes,[4,5] was recently applied to complexation reactions of α-CD by diphenyl azo dye guest molecules.[15] The inclusion of the dye in α-CD. with the sulfonate group passing through the wide rim exclusively, proceeds in the two steps, as above (Eq. 9). The rapid first step is attributed to the formation of an encounter complex between the dye and α-CD and results in partial desolvation of the sulfonate head group of the dye and a corresponding negative volume of activation [$\Delta V_1^{\ddagger} = -24 - (-8)$ cm^3 mol^{-1}]. In the slower second step, as the guest moves further through the cavity, the head group interacts with two internal "activated" waters, and their expulsion from the cavity is delayed by the primary hydroxyls on the narrow rim [$\Delta V_2^{\ddagger} = -15 - (-2)$ cm^3 mol^{-1}]. A subsequent rehydration of the sulfonate group occurs as it emerges from the cavity. With more extended guest molecules, with bulky head groups, threading of the cyclodextrin by the guest leads to the formation of pseudorotaxanes (head groups not sufficiently bulky to prevent dissociation) and rotaxanes. The threadings of α-CD by 1,10-*bis*(trimethylammonium)decane (k_1 = 1.6 x 10^{-1} M^{-1} s^{-1} at 25°C) and 1,10-*bis*(trimethylphosphonium)decane (k_1 = 2 x 10^{-7} M^{-1} s^{-1} extrapolated to 25°C) proceed slowly, with the latter guest forming rotaxanes, by the "slippage" mechanism. only above 50°C.[26]

Calix[*n*]arenes are synthetic macrocyclic oligomers formed from the condensation of phenol and formaldehyde (*n* is most commonly 4, 5, and 6). The calixarenes are easily modified on the phenolic lower rim to permit versatile recognition of cationic, anionic. and neutral guests,[1–3] with the presence of aromatic groups in the cavity walls allowing for cation–π interactions to contribute to guest–host binding of metal and organic cations. The cavities of calixarenes are less rigid than the cyclodextrins and the calix[4]arenes, for example, exist in four conformations with the interconversion of the conformers proceeding via the partial cone structure. The alkali metal cations form a complex exclusively with the cone conformation of the tetramethoxy calix[4]arenes, with cation exchange following a dissociative mechanism.[27] The low stability constants of these calixarenes, compared with crown ethers or cryptands, originate mainly in a poor preorganization of the ligand for the complexation.[1] The sulfonated calix[5]arene and calix[6]arene are exceptional uranophiles in terms of their stability

constants ($\approx 10^{19}$ M^{-1}) and selectivity for the UO_2^{2+} cation.[28] The complexation reactions. however. are very slow, owing to the energy barrier between the initial exo (the UO_2^{2+} lies flat on the calixarene rim) and final *endo* conformers of the complexes.

Cucurbit[*n*]urils (CB*n*, *n* = 5–10) are macrocycles, prepared by the condensation of gycoluril and formaldehyde under acidic conditions, which were only recently studied in detail.[29] The rigid cavity of CB6 (5.5 Å wide by 6 Å in depth), which is capable of including nonpolar guests through van der Waals interactions, is accessible through 4 Å portals, surrounded by two rims of six carbonyl oxygen atoms capable of complexing cations through hydrogen bonding and ion–dipole interactions. To date, kinetic studies of the complexation of cucurbiturils were limited to CB6 and a series of alkyl- and arylammonium cations; with a dissociative mechanism operative.[29,30] The rate constants for the formation of inclusion complexes with alkylammonium cations [e.g., $\geq 10^6$ M^{-1} s^{-1} for cyclopropylmethylamine[29] versus 8.8×10^{-4} M^{-1} s^{-1} for cyclohexylmethylamine[30] at 40°C], but not the thermodynamic stability constants. correlate with the molecular diameters of the cations and are slower than the corresponding complexation reactions with cyclodextrins and calixarenes, which possess larger and unobstructed openings to their cavities. The rate constants for the reaction of CB6 with cyclohexylmethylamine exhibit a pH dependence attributed to two inclusion pathways. The unprotonated amine guest is able to pass directly through the portal into the cavity. whereas the protonated ammonium guest initially forms an association complex with the CB6, which positions the methylcyclohexyl group away from the portal, necessitating a slower. rate-determining "flip-flop" of the group through a distorted portal. With the advent of new methods for synthesizing and separating the larger CB7 and CB8 hosts (analogous to β- and γ-CD, respectively). kinetic studies of the cucurbiturils with a wider range of guests are warranted.[31]

LARGE-CAVITY ENCAPSULATING HOSTS

The efforts to synthesize host molecules with larger. noncollapsing cavities for specific guest molecules resulted in the production of several families of hosts, including the cavitands, hemicarcerands. carcerands, cryptophanes, and calixarene capsules. etc.[32] These molecules have well-defined portals for entry and exit of the guest molecules and the possibility of functionalization of the cavity interior to control the orientation and fluxionality of the guest, and the binding forces for complexation. While the cavitands provide no steric hindrance to complexation and decornplexation processes and the carcerands permanently entrap guest molecules, the hernicarcerands contain equatorial portals for guests to slowly enter and exit the host cavity.[32] In addition to the numerous modes of noncovalent interactions between guest and the interior of the host cavity, an additional form of binding termed "constrictive binding" was coined by Cram.[33] Defined as the difference between the activation energy for dissociation and the free-energy of complexation (intrinsic binding), the constrictive binding free-energy term represents the physical barrier to escape of the guest from the hemicarceplex. Constrictive binding of guests to the hemicarcerands is comparable to the process of "slippage" described above for the assembly of cyclodextrin pseudorotaxanes.[27]

The majority of kinetic studies was performed on hemicarcerands and related molecular capsules in which the two halves of the host are joined by variable bridging units. The rate-determining processes of the entry and exit of guests in hemicarcerands rely on conformational changes in the bridging units to open and close the "gates," respectively.[34] Varying the number, length, flexibility, and composition of the bridging units allows for control of the shapes and sizes of the gates, and this may be correlated with the decomplexation rate constant~.~'" ~Houk proposed two gating processes, a '-sliding door" (increased separation between the bridges) mechanism and a "French door" (bridge components swing open) mechanism, to account for the conformational changes involved in guest complexation and decomplexation.[36] For hemicarcerands containing o-xylyl gates, the "sliding door" pathway is important for all guests, while the contribution of the "French door" mechanism is dependent on the steric nature of the guest. More recently, Stoddart and Cram designed dynamic hemicarcerands containing diimine bridges capable of reversible formation/hydrolysis allowing a "bar-opening1 bar-closing" mechanism to provide entry and escape (with a decrease in the decomplexation half-life by an order of magnitude) of a fesrocene guest.[37]

CONCLUSION

Several mechanisms, based on dissociative and associative limits, were identified for the guest complexation reactions with a variety of cyclic host molecules. Kinetic studies have considerable potential for providing greater insight into the details of these mechanisms. Further investigations of the hosts described above and others, using a wider range of guests, will allow for a greater understanding of the processes that lead to the selective formation of the guest–host complexes and the forces that hold them together. The use of variable-pressure kinetic methods and the advent of new guest probes for accessing

specific time domains. along with continued design and syntheses of new hosts and guests, will assist in this ongoing endeavor.

ARTICLES OF FURTHER INTEREST

Alkali Metal Cations in Biochemistry, p. 1
Calixarenes and Their Analogues: Cation Complexation, p. 137
Calixarenes and Their Analogues: Molecular Complexation, p. 145
Carcerands and Hemicarcerands, p. 189
Cavitands, p. 219
Crown Ethers, p. 326
Cryptands, p. 334
Cucurbituril, Its Homologues, and Derivatives, p. 390
Cyclodextrins, p. 398
Inclusion Compounds: Selectivity, Thermal Stability, and Kinetics, p. 696
Lariat Ethers, p. 782
Nuclear Magnetic Resonance Spectroscopy, p. 981
Podands, p. 1106
Selectivity: Thermodynamic and Kinetic, p. 1225
Self-Assembly: Definition and Kinetic and Thermodynamic Considemtions, p. 1248
Solvent Effects in Guest Binding, p. 1322
Spherands, p. 1344
Zwitterion Receptors, p. 1639

REFERENCES

1. Detellier, C. Complexation Mechanisms. In *Comprehensive Supramolecular Chemistry*; Atwood. J.L., Davies, J.E.D.. MacNicol. D.D., Vogtle. F., Szejtli, J.. Osa. T.. Eds.; Permagon: Oxford, 1996; Vol. 8, 357–375, and references therein.
2. Petrucci, S.; Eyring. E.M.: Konya, G. Kinetics of Complexation. In *Comprehensive Supramolecular Chemistry*; Atwood, J.L., Davies, J.E.D., MacNicol. D.D.. Vogtle, F., Szejtli, J., Osa. T.. Eds.; Permagon: Oxford, 1996: Vol. 8. 483–497, and references therein.
3. Izatt, R.M.; Pawlak, K.; Bradshaw, J.S.; Bruening, R.L. Thermodynamic and kinetic data for macrocycle interaction with cations, anions, and neutral molecules. Chem. Rev. 1995, *95* (7). 2529–2586, and references therein.
4. Tobe. M.L.; Burgess. J. Inorganic Reaction Mechanisms: Addison Wesley Longman: New York. 1999; 271–307. and references therein.
5. Wilkins, R.C. The Study *of* Kinetics and Mechanisms *of Reactions of Transition* Metal Complexes, 2nd Ed.: VCH: Weinheim, 1991: 131–256, and references therein.
6. Lindoy, L.F. The *Chemistry* of Macrocyclic *Ligand Complexes*; Cambridge University Press: Cambridge. 1989: 192–208.
7. Eigen. M.; Winkles, R. Alkali–Ion Carriers: Dynamics and Selectivity. In *Neurosciences:* Second *Study Program*; Schmitt, F.O., Ed.: Rockefeller University Press: New York. 1970: 685–696.
8. Cox. B.C.; Schneider, H. Kinetics and mechanism of macrocyclic complex formation. Pure Appl. Chem. 1990. 62 (12). 2259–2268.
9. Schneider, H.-J.; Yatsimirsky, A.K. Principles and Methods *in Supramolecular* Chemistry; Wiley: Chichester. 2000: 259–266. and references therein.
10. Bribre, K.M.; Detellier, C. Metal interchange of crown ether–alkali metal cation complexes in solution. ^{7}Li Nuclear magnetic resonance study of the exchange kinetics of lithium 15-crown-5 and lithium monobenzo-15-crown-5 in nitromethane. J. Phys. Chem. 1992. *96* (5), 2185–2189.
11. Detellier. C. Reaction Kinetics and Exchange. In Modern NMR *Techniques* and Their *Applications* in *Chemistry*; Popov. A.I., Hallenga, K.. Eds.; Practical Spectroscopy Series. Dekker: New York, 1986: Vol. 11, 521–566.
12. Perrin, C.L.; Dwyer, T.J. Application of two-dimensional NMR to kinetics of chemical exchange. Chem. Rev. 1990, *90* (6), 935–967.
13. Robinson, B.H. Rapid Flow Methods. In *Investigation of* Rates *and* Mechanisms of *Reactions,* Part *II,* 4th Ed.; Bernasconi, C.F.. Ed.; Techniques of Chemistry Series. Wiley: New York. 1986: Vol. VI. 9–26.
14. Kitano, H.; Hasegawa, J.; Iwai, S.; Okubo, T. Kinetic study of the complexation of cryptand 222 with alkaline earth ions by the conductance stopped-flow method. J. Phys. Chem. 1986, *90* (23). 6281–6284.
15. Abou-Hamdan, A.; Bugnon. P.; Saudan, C.; Lye, P.G.; Merbach, A.E. High-pressure studies as a novel approach in determining inclusion mechanisms: Thermodynamics and kinetics of the host–guest interactions for α-cyclodextrin complexes. J. Am. Chem. Soc. 2000. 122 (4). 592–602.
16. Stuehr, J.E. Ultrasonic Methods. In *Investigation* of Rates and Mechanisms of Reactions. Part *II,* 4th Ed.; Bernasconi, C.F., Ed.: Techniques of Chemistry Series. Wiley: New York. 1986; Vol. VI, 247–304.
17. Nau. W.M.; Wang, X. Biornolecular and supramolecular kinetics in the submicrosecond time range: The fluorazophore approach. Chem. Phys. Chem. 2002, 3 (5). 393–398.
18. Lucarini, M.: Luppi, B.: Pedulli, C.F.; Roberts. B.P. Dynamic aspects of cyclodextrin host–guest inclusion as studied by an EPR spin-probe technique. Chem. Eur. J. 1999, *5* (7). 2048–2054.
19. Detellier. C.; Graves. H.; Brière, K.M. Alkali Metal NMR Studies of Synthetic and Natural Ionophore Complexes. In *Isotopes* in the Physical and *Biomedical* Sciences: Buncel, E.. Jones. J.R., Eds.: Elsevier: Amsterdam, 1991: Vol. 2, 159–211.
20. Bribre. K.M.; Detellier. C. Solvent effects in the metal interchange of crown ether–alkali metal cation complexes. Transition from an associative exchange in nitromethane to a dissociative exchange in acetonitrile studied by ^{23}Na

nuclear magnetic resonance. Can. J. Chem. 1992. *70* (10), 2536–2543.
21. Cox, B.G.; Garcia-Rosas, J.: Schneider, H. Solvent dependence of the kinetics of formation and dissociation of cryptate complexes. J. Am. Chem. Soc. 19811, *103 (5)*. 1053-–1059.
22. Lincoln. S.F.: Rodopoulos, T. Complexation of lithium(I), sodium(I), silver(I) and thallium(I) by 4.7.13.16-tetraoxa-1,10-diazabicyclo[8.8.5]tricosane and 4,7,13,-rioxa-1,10-diazabicyclo[8.8.5]tricosane in trimethyl phosphate. A potentiometric titration and ^{7}Li and ^{23}Na nuclear magnetic resonance study. Inorg. Chim. Acta 1991. *190* (2). 223–229.
23. Connors, K.A. The stability of cyclodextrin complexes in solution. Chem. Rev. 11997. *97* (5). 1325–1357; and references therein.
24. Cramer, F.: Saenger, W.: Spatz, H.-Ch. Inclusion compounds. XIX. The formation of inclusion compounds of α-cyclodextrin in aqueous solutions. Thermodynamics and kinetics. J. Am. Chem. Soc. 1967. 89 (1). 14–20.
25. Yoshida. N.: Hayashi, K. Dynamics aspects in host–guest interactions. Part 2. Directional inclusion reactions of some azo guest molecules with α-cyclodextrin. J. Chern. Soc., Perkin Trans. 2 11994. (6). 1285–1290.
26. Lyon, A.P.: Banton. N.J.; Macartney, D.H. Kinetics of the self-assembly of a-cyclodextrin [2]pseudorotaxanes with polymethylene threads bearing quaternary ammonium and phosphonium end groups. Can. J. Chem. 1998. *76* (6). 843–850. and references therein.
27. Meier. U.C.: Detellier. C. Mechanisms of formation and dissociation of a cesium-calix[4]arene acetamide complex in solution: A Cs-133 dynamic NMR study. J. Phys. Chem.. A 1999. *103* (20), 3825–3829. and references therein.
28. Nagasaki, T.; Kamano. K.; Araki, K.: Shinkai. S. Kinetic studies of calixarene-based cyclic and non-cyclic 'super-uranophiles'. J. Chem. Soc.. Perkin Trans. 2 1991, (9). 1325–1327
29. Mock. W.L. Cucurbituril. Top. Curr. Chern. 11995, *175*. 1–24. and references therein.
30. Marquez, C.; Nau, W.M. Two mechanisms of slow host–guest complexation between cucurbit[6]uril and cyclohexylmethylamine: pH-Responsive supramolecular kinetics. Angew. Chem.. Int. Ed. 2001, *40* (17). 3155–3160.
31. Day. A.; Arnold, A.P.: Blanch. R.J.: Snushall. B. Controlling factors in the synthesis of cucurbituril and its homologues. J. Org. Chem. 2001, *66* (24). 8094–8100.
32. Container Molecules *and Their* Guests: Cram. D.J., Cram, J.M., Stoddart, J.F.. Eds.; Supramolecular Chemistry Monographs. The Royal Society of Chemistry: Cambridge, 1994.
33. Cram, D.J.: Blanda. M.T.; Paek. K.; Knobler. C. Constrictive and intrinsic binding in a hemicarcerand containing four portals. J. Am. Chem. Soc. 1992, *114* (20). 7765–7773.
34. Yoon. J.: Cram. D.J. Decomplexation rate comparisons of hemicarceplexes whose single unique host bridge is change in length and blocking power. Chem. Commun. 1997. (16). 1505–1506.
35. Ihm. C.; Kim. M.; Ihm, H.: Paek. K. Molecular engineering. Part 5. Tuning the constrictive binding of container host by the atomic order of portal pillars. J. Chem. Soc., Perkin Trans. 2 1999. (8), 1569–1575.
36. Houk, K.N.: Nakamura. M.: Sheu, C.; Keating, A.E. Gating as a control element in constricutive binding and guest release by hemicarcerands. Science 1996. *273*. 627–629.
37. Ro, S.; Rowan. S.J.: Pease, A.R.; Cram, D.J.: Stoddart, J.F. Dynamic hemicarcerands and hemicarceplexes. Org. Lett. 2000, 2 (6), 2411–2414.

Lariat Ethers

George W. Gokel
Washington University School of Medicine, St. Louis, Missouri, U.S.A.

INTRODUCTION

Lariat ethers *are crown-ether derivatives in which one or* more *side arms is appended to the macrocycle. The term* ''lariat *eiher" was coined in* 1980,[1] *but a number of macrocyclic* compounds *that possessed side arms were prepared* previously.[2] *The purposes inherent in these earlier* preparations *varied considerably. The early development of lariat ethers had a specific goal.*

Crown ethers readily complex a variety of metals. The binding of spherical cations generally occurs within the hole of the crown ether. The latter is "doughnut" shaped, i.e., *essentially two-dimensional with a central void. Entry and egress of the cation are sterically unencumbered. The complexation process may be represented as follows: crown + cation* $\leftrightarrows$ *complex. The position of the equilibrium* is *given by the equilibrium constant, K. sometimes written as* K_{eq}. *The value of* K *depends on the two rate constants that characterize the forward and reverse rates symbolized by the arrows. Thus,* $K = k_f/k_r = k_1/k_{-1} = k_{complex}/k_{release}$. *Typically, the rates for crown* complexation *and release are fast. Thus, the equilibrium or binding constant (also written as* K_S) *may be modest. but cation complexation and release* may *both be rapid. For three-dimensional* complexing *agents such as cryptands: the cornplexing and release rates are typically slower. As a result, the binding constant is greater for cryptands than for crowns. but the* dynamics *of the process are typically slow.*

The transport of cations across membranes requires binding at the first interfacial boundary. diffusion of the complex *across the barsier, and release of the cation at the other interface.* If *cation release is slow, transport will be inefficient. The natural ionophore valinomycin binds* K^+ *selectively* and *transports it effectively.* Valinomycin *is a* cyclododecadepsipeptide. It *is a 36-membered ring comprised of amino and hydroxyacids. It seems to be* too *large to effectively* complex K^+, *but* it *does so by folding over to* assume *the shape of a tennis ball seam. Thus,* K^+ *is solvated three-dimensionally by the host, but the* complexation *and release processes remain dynamic owing to the macrocycle's inherent flexibility.*

Lariat ethers were designed to incorporate a *macroring and* one *or more side arms. The crown ether was expected to provide binding and some selectivity. The flexible side arm was designed to augment the complexation by positioning a donor group in a third dimension. This would* mimic valinomycin *in the sense that the host is flexible but it can complex the cation in a three-dimensional arrangement. Because the side-armed* macrocycles *resembled a looped rope in overall shape, and because the ring and side* arm *could "rope and tie" the cation: the* name *"lariat'' ether seemed appropriate.*

When more than one arm *was present, the Latin word for arm,* i.e., *bracchium, was used in the name.* Two-*armed and three-armed lariat ethers were called* bibracchial *and tribracchial lariat ethers, respectively. These names were shortened to* BiBLEs[3] *and* TriBLEs.

Related complexing agents for inorganic ions were also developed in the 1970s and 1980s. These compounds generally contained nitrogen atoms as donors and were often described as "macrocycles having pendant arms." Although coinage and transition metals were the complexation *targets: many of the concepts are* similar *to those developed in the lariat ether area. Kaden reviewed this work in* 1984.[4]

SYNTHETIC ACCESS TO LARIAT ETHERS

Flexibility and *rigidity are important elements of the lariat ether concept,* and *each* may *be used to advantage, depending on the situation. The means by which the side arms are attached is, therefore, an important consideration. For a compound such as 18-crown-6. the side arm can be attached only at carbon. The carbon junction is inherently inflexible. because carbon is noninvertable. Carbon is chiral so attachment of a side arm to the* macroring's *ethyleneoxy unit introduces stereochemical issues. The lower flexibility and the fixed stereochemistry may be desirable properties in certain situations.*

These two issues can be circumvented, however, by replacing one ring-oxygen by nitrogen and attaching the side arm *to* it. *Nitrogen undergoes facile inversion. so* the *side-arm stereochemistry is not fixed. Further, side arms attached at nitrogen have higher overall mobility than do arms attached at carbon. The attachment atoms were called "pivots," and C- and N-pivot lariat ethers are shown in Fig.* 1.

Encyclopedia of Supramolecular Chemistry
DOI: 10.1081/E-ESMC 120012706

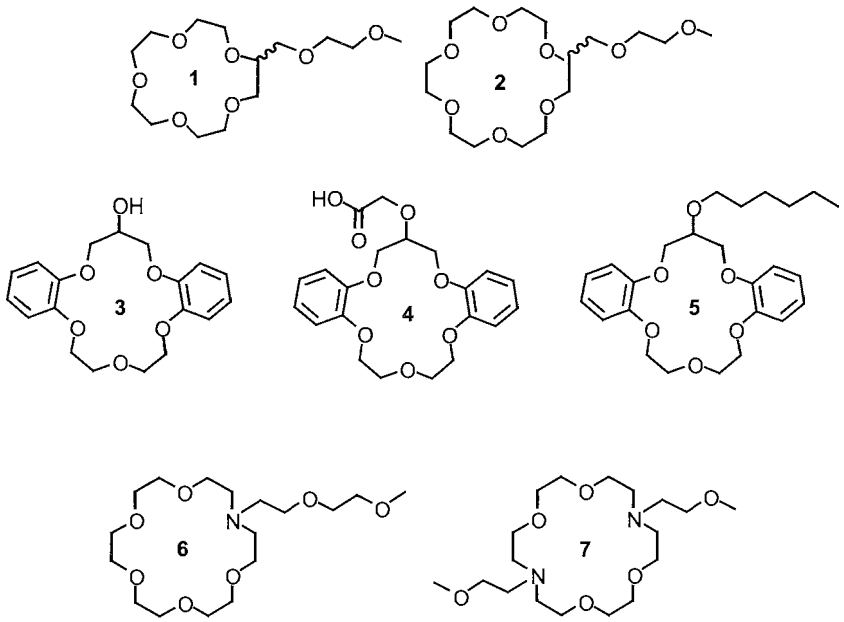

Fig. 1 Examples of one- and two-armed lariat ethers. The wavy line in structures 1 and 2 indicates that the sidearm may occupy isomeric positions.

Two types of C-pivot compounds were prominent during the past decades. These are shown in Fig. 1 as compounds 1–2 and 3–5. Both classes use glycerol as the pivot element, but in 1 and 2, the side arms are attached to the 1- and 2-positions, respectively. The former group was developed independently by Okahara and Gokel and their coworkers. The coinpounds represented by the 16-crown-5 structures 3–5 were studied extensively by Bartsch and his colleagues. The importance of the glycerol subunit for K^+ binding was recently demonstrated in the 16-crown-5 case.[5]

The earliest work by Okahara and colleagues involved cornpounds that possessed side arms but did not necessarily contain donor groups.[6] Okahara also developed approaches to N-pivot compounds at an early stage[7] and to C-pivot compounds in which the side arms bore geminal substituents.[8,9]

The syntheses of C-pivot molecules are generally accomplished by opening the epoxide residue of epichlorohydrin with an aliphatic alcohol or phenol. This affords a substituted diol of the type RO–CHOH–CH_2OH. Reaction of the diol with, for example, tetraethylene glycol ditosylate, TsO($CH_2CH_2O)_4$Ts, under basic conditions will afford 15-crown-5, in which one ring carbon is substituted by CH_2OR. The carbon to which the side arm is attached is chiral. Both enantiomers are typically formed. Pentaethylene glycol. which would lead to 18-crown-6 derivatives, is less readily available than is tetraethylene glycol, the 15-crown-5 precursor. This and the stereochemical issue limit the versatility of carbon-pivot molecules of this type.

Bartsch and coworkers developed an alternate approach to C-pivot lariats. Epichlorohydrin is treated with a *bis*(phenol) in aqueous base to give lariat ethers in which a hydroxyl group is attached to the crown-ether ring.[10] This is a single-step process in which one phenoxide opens the epoxide ring to form an ether, while the epoxide reforms on the other side. The newly formed three-membered ring is then opened by the other phenoxide to form the macrocycle **(3).** The hydroxyl group may be capped by an alkyl substituent **(5)** or by another functional group (4). Nearly 50 examples of this family were recently reported by Bartsch and coworkers.[11] Synthetic and conformational studies on asymmetric dibenzo-16-crown-5 derivatives were undertaken by Kim, Bartsch, and Ramesh.[12] This group also described synthetic approaches to a large family of dibenzo lariats having pendant *N,N*-dialkyl oxyacetamide residues.[13] Marchand and Chong reported "cage-functionalized diaza(17-crown-5) ethers" that were used to complex alkali metal picrates (see below).[14]

One-, two-, and three-armed derivatives of azacrown ethers were formed by relatively straightforward synthetic approaches. Alkylation of diethanolainine. HN(CH_2CH_2 OH)$_2$ with an alkyl or benzyl group gives RN(CH_2CH_2 OH)$_2$. Treatment of RN(CH_2CH_2OH)$_2$ with TsO(CH_2-$CH_2O)_3$Ts or TsO($CH_2CH_2O)_4$Ts gives an alkylaza-15-crown-5 or -18-crown-6 derivative.

The molecule is flexible because of nitrogen's rapid inversion; this also obviates the potential stereochemical issue.[''''] A single-step condensation affords two-armed, diaza-18-crown-6 derivatives such as 7.[3] An alternate approach affords 18- and 15-membered ring BiBLEs.[16]

Although the family of simple lariats was developed early, numerous variants were reported that were designed for a variety of purposes. The N-(2-methoxy-I-naphthy1)-methyldiaza-18-crown-6 BiBLEs were produced by templated reactions and complexation was confirmed by x-ray analysis.[17] Pyridine side chains[18] and 8-hydroxyquinoline[i''''] side chains were incorporated. and binding strengths and selectivities as well as chromophoric properties were studied. In another study, five single-armed. chiral D-glucose-substituted aza-15-crown-5 ethers having a phosphonoalkyl side chain were developed for potential use in phase-transfer catalysis.[20]

EVIDENCE FOR SIDE-ARM PARTICIPATION

Early studies in the lariat ether area required confirmation of the design principles. There were several key questions concerning side-arm participation. The first was simply whether or not the side arm(s) interacted with the ring-bound cation in accord with the design. Second, if the side-arm interaction occurred. to what extent was binding enhanced? Third, was there evidence that this arrangement was more flexible than the corresponding cryptand?

Confirmation that the side arm participated in complexation when appropriately placed was obtained by comparing the complexation strengths of 8 and 9. Sodium cation is bound in the center of the macrocycle. The side arm of 8 or 9 can reach over the ring, but only 8 has an oxygen donor (methoxy) positioned appropriately to interact. The equilibrium binding constant (K_S) for Na' by 15-crown-5 at 25°C in methanol solution is 1860. Because complexation constants can be large. especially in less-polar solvents, they are usually expressed as decadic logarithms. Thus, $\log_{10}K_S$ for this reaction is 3.24. The binding constant for 8 is 3.27, or no different from 15-crown-5. This appears to contradict the concept of side-arm participation. However, the 4-isomer (9) has a binding constant of only 2.90, identical to the 3-isomer (not shown). It was concluded[1] that although the presence of the side arm engendered some hindrance, a side arm having an appropriately placed donor enhanced binding.

An alternate demonstration of side-arm interaction involved ammonium cation, NH_4^+. In this case: the more flexible azacrown compounds were used. Molecular models suggested that when tetrahedral ammonium ion formed three hydrogen bonds to macroring donors. the fourth N–H bond would be perpendicular to the ring's plane. The three N–H to macroring bonds would be optimal for 18-membered crowns and poorer for the smaller 15-membered rings. Models suggested that the fourth N–H bond would interact optimally with the distal oxygen when the side arm was $-(CH_2CH_2O)_2CH_3$. This is shown in Fig. 2. All of the required lariat ethers were prepared. and these expectations were confirmed by measuring ammonium ion bisiding constants.[21]

Convincing as these results were, solid-state structural evidence was sought for confirmation.[22] Two structures are shown in Fig. 3. At the top is the KI complex of *N*-(2-methoxyethyl)aza-18-crown-6, abbreviated $CH_3OCH_2CH_2\langle N18)$. The potassium cation is 8-coordinate and fonns a hexagonal bipyramid. One apical position is occupied by the side-arm oxygen and the other by iodide anion. The lower structure is of the NaI complex of *N,N'-bis*(2-hydroxyethyl)-4,13-diaza-18-crown-6 ($HOCH_2CH_2\langle N18N\rangle CH_2CH_2OH$). In this case, Na^+ is 8-coordinate, and the side arms interact with the bound cation from the same side. Iodide anion. an excellent donor. is excluded from the cryptate-like solvation sphere.

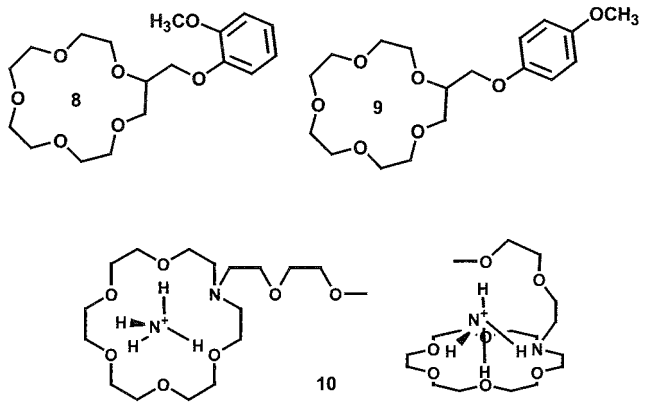

Fig. 2 Lariat ether compounds used to demonstrate side-arm participation in guest binding.

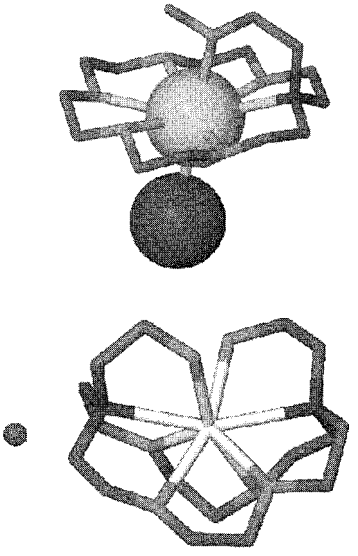

Fig. 3 Solid-state structures of 1- and 2-armed lariat ethers showing sidearm participation in cation complexation. (*View this art in color at www.dekker.com.*)

Numerous solid-state structures are available of 1- and 2-armed lariat ether compounds. Extensive structural data were obtained as part of an effort to demonstrate that side-arm participation occurred as inferred from solution studies.[23] More recently, structural data for the 16-crown-5, C-pivot lariats were reported. Liu and coworkers reported the preparation of a derivative of 3 in which the hydroxyl group (OH) was elaborated to OCH_2CH_2-OCH_3.[24] Data showed side-arm participation in binding for Na and Pb complexes.

The final issue of overall flexibility was addressed by use of NMR.[25] Longitudinal relaxation times (^{13}C-NMR, T_1) were determined for C- and *N*-pivot lariat ethers alone and in the presence of Na^+, K^+, and Ca^{2+}. Structural changes that occur when complexation takes place are reflected in the relaxation times. It was found that the macroring in C-pivot compounds became more rigid. suggesting a greater importance in cation complexation. The *N*-pivot compounds became more uniformly rigid, suggesting a nearly equal contribution to binding by ring and side arm(s). The dynamics of the side-arm interaction were also confirmed by ultrasonic relaxation studies.[26]

A single-armed lariat ether. N-heptylaza-18-crown-6, was crystallized as its *KSCN* complex. Although the side arm was aligned in a vertical arrangement, its lack of donors precluded a secondary donor interaction.[27] The two dodecyl side arms of *N,N'-bis*(dodecyl)-4,13-diaza-18-crown-6 were found not only to align but also to form an extended bilayer in the solid state when complexed to sodium cation. The bilayer formed could be correlated to the formation of liposomes by this compound in aqueous suspension.[28]

In recent work, x-ray crystal structures were obtained for La(III), Ce(III), and Pr(III) complexes of *N,N'-bis*(2-salicylaldiminobenzyl)-4,13-diaza-18-crown-6. The deprotonated host afforded a dianionic, 10-coordinate *syn*-side-armed arrangement for the cations.[29] Lariats were used as the experimental vehicle to demonstrate cation-x complexation with alkali metal ions.[30]

APPLICATIONS

The key difference in applications between crown ethers and lariat ethers is that the side chain(s) may possess residues that confer unique properties on the system. The crown ether continues to be important as a complexation site, but the chemistry of the molecule may actually be dominated by the side-arm substituents.

Complexation

The original goal in developing lariat ethers was to obtain a cooperative interaction between the ring and side arm to enhance binding strength and selectivity. For the aza-crown compounds. binding was dependent on the total number of donors rather than on their arrangement. *N*-(2-Methoxyethyl)aza-18-crown-6 ($CH_3OCH_2CH_2\langle N18\rangle$) contains one nitrogen and six oxygen atoms that can serve as donors to bind a cation.

The same number and types of donors are available in 12-, 15-, and 18-membered rings, which have three. two, and one side-arm donors, respectively. The binding profiles for there compounds are shown in Table 1 along with all-oxygen crowns. Nitrogen is a poorer donor for an alkali metal than is oxygen. Still, the Na^+ binding constants for all of the lariats exceed the values observed for the corresponding side-arm-free macrocycles. The

Table 1 Cation cornplexation constants determined in CH_3OH at *25°C*

Macrocycle	log K_S Na^+	log K_S K^+
12-crown-4	1.7	1.74
15-crown-5	3.24	3.43
18-crown-6	4.35	6.08
$\langle 12N\rangle(CH_2CH_2O)_3CH_3$	3.64	3.85
$\langle 15N\rangle(CH_2CH_2O)_2CH_3$	4.54	4.68
$\langle 18N\rangle CH_2CH_2OCH_3$	4.58	5.67

differences are generally less dramatic for K^+ binding, but side-arm enhancement of cation complexation is clear. Extensive binding studies were reported for N-pivot lariat ether compounds.[31]

Cation binding was also studied in detail for the 16-crown-5 family of *C*-pivot lariats. Inoue and coworkers studied the effects of donor groups in 1,4,7,10,13-pentaoxacyclohexadecane (16-crown-5), which lacked benzo substituents.[32] As with some other C-pivot lariats, it was found that although cation extractabilities were improved by the presence of a side arm, stability constants showed less effect. Similar mixed results were observed for 19-crown-6 derivatives.[33] A series of G-pivot [3_n-methylene-(3_n + 1)-crown-n (n = 5,6,7)] lariat ethers having an oxyquinoline as the side-arm donor was found to exhibit considerable cation selectivity. As might be expected, this was dependent on ring size and side-arm position.[34] Alkali metal, alkaline earth, and ammonium ion complexation selectivities were measured for nearly a dozen dibenzo-16-crown-5 compounds bearing a variety of side arms. These compounds were adapted for use in ion-selective electrodes.[35,36] Two studies reported lariat ethers that possess Ag^+ ion selectivity.[37,38] Bartsch recently reviewed metal ion separations accomplished by use of proton-ionizable lariat ethers.[39] Complexation thermodynamics were assessed for two-armed dibenzo-15-crown-5 lariats[40] and for azalariats.[41] A recent report described the complexation behavior of lariat ethers in supercritical CO_2.[42] Finally, urea complexation by lariat ethers has been studied.[43]

Mass spectrometry proved to be a fast and reliable method for assessing coinplexation by crowns when appropriate controls are done. This proved to be the case for lariat ethers as well, especially using electrospray (ES-MS) techniques.[44,45] The dibenzo-16-crown-5 compounds were the focus of these studies. Related compounds were examined by Brodbelt, Bartsch, and their coworkers using the ES-MS method.[46] In the latter case, selectivity data obtained in the gas and solution phases were compared. A combination of HPLC and ES-MS was proposed as a method for rapidly screening host metal-binding selectivities in various mixtures.[47]

Chromoionophores

Ionophores are compounds that transport ions. Compounds that have this capability and exhibit spectroscopic changes on binding are called chromoionophores. A cation is typically bound in the macroring that does not contain spectroscopically active groups. Fluorescent or UV-active side arms are positioned so that they may interact with the bound cation in a fashion that induces spectral change. Misumi,[48] Vögtle,[49] Takagi,[50] and Shinkai[51] reported chromogenic crown ethers at about the same time. Takagi and coworkers were especially important contributors in this area and reviewed it in 1984.[52] An example of an azalariat that exhibits complexation-induced UV shifts is shown as **11**[49] in Fig. 4. Recent chromoionophores include macrocycles having pendant phenanthridine units,[53] *N*-pivot lariats complexing luminescent Eu(II),[54] and 2,2′-bipyridine lariat calix crowns that complex Eu(III) and Tb(III).[55]

Chemical Switching

Chromogenic lariat ethers show cation-induced shifts upon complexation. The binding is often enhanced by

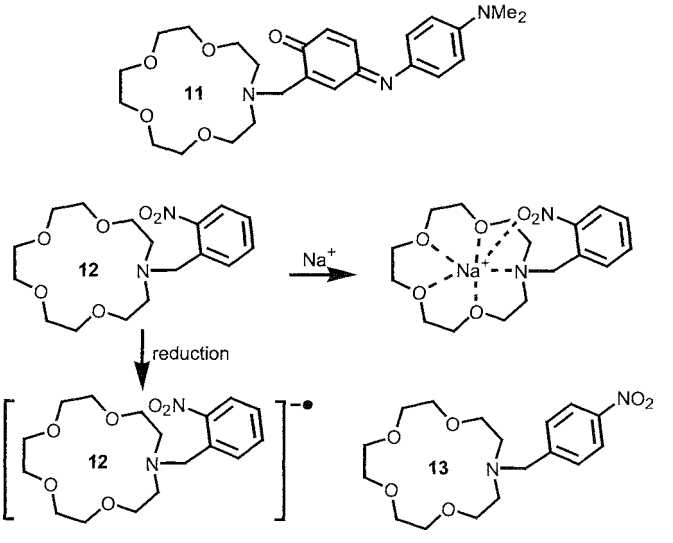

Fig. 4 *Lariat ethers with chromophonc and redox-switchable side arms.*

the side-arm interaction, but this is a benefit rather than a goal of the design. It is possible to use the side arm to enhance binding. Dibenzo-lariat 4 accomplishes this by loss of a proton. The carboxylate group may serve as a donor for the ring-bound cation when it is appropriately positioned. If the position is inappropriate for complexation, the carboxylate may still serve as an internal counterion.[39]

An alternate means for enhancing side arm binding efficacy is shown for **12**. The nitro group of **12** is positioned to interact with a ring-bound cation, whereas **13** is not. Some binding enhancement for **12** is expected, but nitro is a weak donor. When reduced to the nitrobenzene radical anion. however: the nitro group's binding potential is greatly enhanced. Moreover. complexation can be reversed on demand by oxidation. which restores the nitro group to its weaker. neutral state.[56]

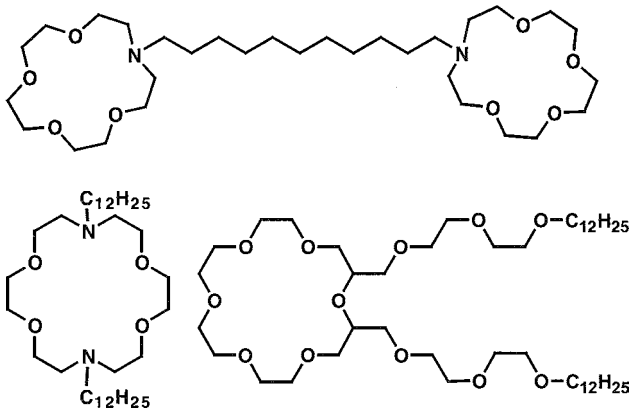

Fig. 5 Lariat ethers that form aggregates in water.

Membrane Formation

Crown ethers are polar and are known to interact effectively with water. When a hydrocarbon tail is appended. the lariat ether becomes amphiphilic. Typically. amphiphilic lariat ethers do not possess donor groups in the side arm (tail), as this would make the latter more polar. When a hydrocarbon tail of sufficient length is present. the lariats will organize when suspended in water. They may form micelles. vesicles. or other aggregates with structures that are more difficult to define. A miceile is typically a loosely organized. 100 Å structure in which the hydrocarbon tails interact with each other, and the head groups form the boundary by interacting with water. Micelles are usually small, dynamic structures of ill-defined size and shape. Vesicles (also called liposomes) normally have diameters greater than 100 Å and an aqueous compartment bounded by an amphiphile bilayer.

Vesicles may be characterized by light scattering, which gives the distribution of their sizes. by electron microscopy, and other methods. Once formed, vesicles will often be stable for significant time periods, although they may collapse or fuse to form larger structures. The membrane of a vesicle encloses space. so it is important to demonstrate encapsulation. Vesicles may be formed in the presence of a fluorescent dye such as carboxyfluorescein. Exchange of the aqueous solution in which the vesicles are suspended leaves only the dye present within the liposomes. If the dye is detected after rupture of the vesicles, it must have been encapsulated. Three examples of vesicle-forming lariat ethers are shown in Fig. 5.

A wide variety of vesicles (liposomes) were formed and characterized to varying degrees.[57] The factors that control whether micelles or vesicles form, what sizes will result, and how stable they will be are not completely understood. Much remains to be explored in this area.

Other **Applications**

As noted above, a goal of the lariat ether work was to develop compounds that might function in a fashion similar to valinomycin. A dozen crown ethers, including two 1.3-xylyl-21-crown-6 macrocyclic polyether 2-carboxylic acid lariat ethers, were prepared and tested in vitro for biological activity. Several of the compounds showed activity and are thought to be functional mimics of ionophore antibiotics.

Crown and lariat ethers formed the basis of several synthetic channel model systems. These involved multiple crown ethers separated by fixed spacers and macrocycles having flexible side arms. Polymers and peptides were also used as backbones to organize multiple crowns that inserted into phospholipid bilayers.[58]

Lariat ethers proved to be an effective vehicle for demonstrating alkali metal cation–π interactions. When either Na^+ or K^+ is bound in the macroring, interactions are possible with neutral side arms. Indole. benzene, and phenol were studied. because these arenes are present on the side chains of tryptophan, phenylalanine, and tyrosine. respectively.[30] Additional studies were reported of cation–x interactions between neutral double and triple bonds with these same alkali metal cations.[59] Lariat ethers were also explored as ion-regulated DNA cleavage agents. Monomeric propargylic sulfone-armed lariat ethers were found to cleave DNA. Modest increases in DNA cleavage efficiency were observed in the presence of Na^+ and K^+.[60]

CONCLUSION

The lariat ethers are a *growing branch of the crown ether family. The appended side arms may cooperate with the macrocycle or may perform important independent* functions. *The study of lariat ethers* is *an active area. and this is expected to remain the case* for *the foreseeable future.*

ARTICLES OF FURTHER INTEREST

Crown Ethers. p. 326
Cryptands, p. *334*
Ionophores, *p. 760*

REFERENCES

1. Gokel. C.W.: Dishong. D.M.: Diamond, C.J. Lariat ethers. Synthesis and cation binding properties of macrocyclic polyethers possessing axially disposed secondary donor groups. J. C. S. Chem. Commun. 1980. 1053–1054.
2. Gokel. G.W.: Koraeniowski, S.H. *Macrocyclic Polyether Syntheses*; Springer-Verlag: Berlin. 1982: 410 pp.
3. Gatto, V.J.; Gokel. G.W. Syntheses of calcium-selective, substituted diazacrown ethers: A novel. one-step formation of bibracchial lariat ethers (BiBLES). J. Am. Chem. Soc. 1984, *106*, 8240–8244.
4. Kaden, T.A. Synthesis and metal complexes of aza-macrocycles with pendant arms having additional ligating groups. Top. Curr. Chem. 1984. *121*. 157–180.
5. Kita. K.; Kida. T.; Nakatsuji, Y.: Ikeda. I. Importance of the glycerol structure of C-pivot lariat ethers containing a 16-crown-5 ring for effective complexation toward alkali metal cations. Chern. Lett. 1997. 405–406.
6. Ping-Lin, K.; Miki. M.; Okaliara. M. General synthesis of substituted and unsubstituted crown ethers. J. Chem. Soc., Chem. Commun. 1978. 504–505.
7. Kuo. P.-L.; Miki, M.: Ikeda, I.; Okahara. M. New synthesis of N-alkyl monoaza crown ethers. Tetrahedron Lett. 1978. 4273–4276.
8. Mizuno. T.: Nakatsuji, Y.; Yanagida. S.; Okahara, M. The synthesis and cation-complexing ability of alkyl crown ethers. Bull. Chem. Soc. Jpn. 1980. *53*. 481–484.
9. Nakatsuji, Y.: Nakamura. T.: Okahara. M.; Dishong. D.M.: Gokel. G.W. Crown cation complex effects. 22. Enhancement of cation binding in lariat ethers bearing a methyl group at the quaternary. pivot carbon atom. J. Org. Chem. 1983. 48. 1237–1242.
10. Heo, G.S.: Bartsch. R.A.: Schlobohm. L.L.: Lee. J.G. Preparation of hydroxy crown ethers by reactions of diphenols with epichlorohydrin. J. Org. Chem. 1981, 46. 3574–3575.
11. Bartsch. R.A.: Cowey, C.L.; Elshani. S.: Goo, M.-J.: Huber. V.J.; Ivy, S.N.: Johnson, R.J.: Kim. J.S.; Luboch. E.; McDonough, J.A.: Pugia, M.J.; Son. B.; Zhao. Q. Synthesis of lariat ether carboxylic acids based on dibenzo-16-crown-5. J. Heterocycl. Chern. 2001. *38*, 311–332.
12. Kim. J.S.; Bartsch, R.A.: Ramesh. V. Synthesis and conformational studies of an asymmetrical dibenzo-16-crown-5 carboxylic acid. J. Incl. Phenom. Macrocycl. Chem. 2000. 36, 287–299.
13. Huang, X.: Jang, Y.; Collier. J.J.; Hwang. H.-S.; Bartsch. R.A. Synthesis of lariat ethers with pendent N,N-dialkyl oxyacetamide groups. J. Heterocycl. Chem. 1996, 33, 223–228.
14. Marchand, A.P.: Chong, H.-S. Synthesis and alkali metal picrate extraction capabilities of novel. cage-functionalized diaza(17-crown-5) ethers. Tetrahedron 1999. *55*. 9697–9706.
15. Schultz, R.A.: White, B.D.: Dishong. D.M.; Arnold. K.A.; Gokel. G.W. 12-, 15-, and 18-Membered-ring. nitrogen-pivot lariat ethers: Syntheses. properties, and sodium and ammonium cation binding properties. J. Am. Chem. Soc. 1985. 107. 6659–6668.
16. Gatto, V.J.; Arnold, K.A.; Viscariello. A.M.; Miller. S.R.; Gokel, G.W. Novel synthetic access to 15- and 18-membered ring diaza-bibracchial lariat ethers (BiBLEs) and a study of sidearm-macroring cooperativity in cation binding. Tetrahedron Lett. 1986, 327–330.
17. Wang, D.; Ge, Y.: Hu, H.; Yu. K.; Zhou. Z. The synthesis and binding properties of bibracchial lariat ethers. J. Chem. Soc., Chem. Commun. 1991. 685–687.
18. Tsukube. H.; Uenishi, J.: Higaki, H.: Kikkawa, K.; Tanaka, T.; Wakabayashi. S.: Oae. S. Side arm effects on cation binding. extraction. and transport functions of oligopyridine-fuactionalized aza-crown ethers. J. Org. Chem. 1993. *58*. 4389–4397.
19. Su. N.; Bradshaw. J.S.: Zhang. X.X.; Song. H.; Savage. P.B.: Xue, C.: Krakowiak. K.E.: Izatt. R.M. Syntheses and metal ion complexation of novel 8-hydroxyquinoline-containing diaza-18-crown-6 ligands and analogues. J. Org. Chem. 1999. 64. 8855–8861.
20. Bako. P.: Novak. T.: Ludanyi. K.; Pete. B.; Toke. L.: Keglevich, G. D-glucose-based aza-crown ethers with a phosphonoalkyl side chain: Application as enantioselective phase transfer catalysts. Tetrahedron: Asymmetry 1999. 10. 2373–2380.
21. Schultz. R.A.: Schlegel, E.; Dishong. D.M.; Gokel, G.W. Effect of chain length and heteroatom position on ammonium ion binding in nitrogen-containing lariat ethers. J. Chem. Soc., Chem. Commun. 1982. 242–243.
22. Gandour. R.D.; Fronczek. F.R.; Gatto, V.J.; Minganti. C.; Schultz. R.A.: White. B.D.: Arnold. K.A.; Mazocchi. D.: Miller. S.R.: Gokel, G.W. Solid-state structural chemistry of lariat ether and bible cation complexes: Metal ion identity and coordination number determine cavity size. J. Am. Chem. Soc. 1986. *108*. 4078–4088.
23. Gandour. *R.D.*: Fronczek, F.R.: Gatto, V.J.: Minganti. C.: Schultz. R.A.; White. B.D.: Arnold. K.A.: Mazzocchi. D.; Miller. S.R.; Gokel. G.W. Solid-state structural chemistry of lariat ether and BiBLE cation complexes: Metal ion

identity and coordination number determine cavity size. J. Am. Chem. Soc. 1986. *108,* 4078–4088.
24. Liu, L.K.; Lin. C.-S.: Young. D.-S.: Shyu, W.-J.: Ueng. C.-H. X-ray crystal structure of a new PbII-selective carbon-pivot lariat ether. Chem. Commun. 1996, 1359–7345.
25. Kaifer. A.; Echegoyen. L.: Durst. H.: Schultz, R.A.: Dishong. D.M.; Goli, D.M.; Cokel, G.W. Dynamics of lariat ether cation complexation assessed by C-13 NMR relaxation times. J. Am. Chem. Soc. 1984, 106. 5100.
26. Echegoyen. L.: Cokel, G.W.: Kim. M.S.: Eyring, E.M.: Petrucci. S. Mechanism of complexation of sodium cation by nitrogen-pivot lariat 15-crown-5 ethers in methanol at 25°C. J. Phys. Chem. 1987. *91*. 3854–3862.
27. He, G.X.; Kikukawa, M.: Nishiyama, N.: Ohe, H.: Matsuda. T. New applications of crown ethers. IX. Crystal structure of KSCN complex of N-heptylmonoaza-18-crown-6. and conformational features of the pivot nitrogen. Bull. Chem. Soc. Jpn. 1988. *61*. 3785–3787.
28. De Wall. S.L.: Barbour. L.J.: Gokel, G.W. Solid state bilayer formation from a dialkyl-substituted lariat ether that forms stable vesicles in aqueous suspension. J. Phys. Org. Chem. 2001. 14. 383–391.
29. Platas, C.; Avecilla, F.: de Blas, A.; Rodriguez-Blas, T.; Bastida, R.; Macias. 4.: Rodriguez, A.; Adams, H. A Schiff-base bibracchial lariat ether selective receptor for lanthanide(III) ions. J. Chem. Soc., Dalton Trans. 2001. 1699–1705.
30. Meadows. E.S.: De Wall. S.L.: Barbour. L.J.; Gokel. G.W. Alkali metal cation-π interactions observed by using a lariat ether model system. J. Am. Chem. Soc. 2001. *123,* 3092–3107.
31. Cokel. G.W.; Trafton, J.E. *Cation Binding* by *Macrocycles:* Gokel, G.W.. Inoue. Y., Eds.: Marcel Dekker. Inc.: New York. 1990: 253–310.
32. Inoue, Y.: Ouchi. M.: Hososyama, K.: Hakushi. T.: Liu, Y.: Takeda. Y. Molecular design of crown ethers. Part 8. Substitution and lariat effect upon cation complexation with 1,4,7,10,13-pentaoxacyclohexadecane (16-crown-5) derivatives in solvent extraction and in homogeneous solution. J. Chem. Soc., Dalton Trans. 1991. 1291–1293.
33. Ouchi. M.: Inoue, Y.: Wada, K.; Iketani, S.: Hakushi, T. Molecular design of crown ethers. 4. Syntheses and selective cation binding of 16-crown-5 and 19-crown-6 lariats. J. Org. Chem. 1987, *52*. 2420–2427.
34. Kita, K.: Kida. T.: Nakatsuji. Y.; Ikeda. I. Synthesis and complexation properties of C-pivot lariat ethers containing 16-crown-5, 19-crown-6 and 22-crown-7 rings toward alkali metal cations. J. Chem. Soc., Perkin Trans. 1 1998. 3857–3866.
35. Ohki, A.; Lu. J.P.: Huang. X.: Bartsch, R.A. Alkali metal. alkaline earth metal. and ammonium ion selectivities of dibenzo-16-crown-5 compounds with functional side arms in ion-selective electrodes. Anal. Chem. 1994. *66,* 4332–4336.
36. Ohki, A.; Lu. J.P.: Hallman, J.L.: Huang. X.: Bartsch. R.A. Sodium ion-selective electrodes based on dibenzo-16-crown-5 compounds with pendent ester groups. Anal. Chem. 1995. *67,* 2405–2408.
37. Nabeshima, *T.;* Nishijima, K.; Tsukada, N.: Furusawa. H.: Hosoya, T.: Yano. Y. Remarkably selective binding of silver ion by thiolariat ether with a 15-crown-5 ring. J. Chern. Soc., Chem. Commun. 1992, 1092–1094.
38. Prince. P.D.; Cragg. P.J.; Steed, J.W. Formation of an organonietallic coordination polymer from the reaction of silver(I) with a non-complinientary lariat ether. Chem. Commun. 1999. 1179–1180.
39. Bartsch, R.A. Metal ion separations with proton-ionizable lariat ethers. ACS Symp. Ser. Metal-Ion Separ. Preconcentration 1999, *716,* 146–155.
40. Liu. Y.: Zhang, H.-Y.; Bai, X.-P.: Wada, T.: Inoue. Y. Molecular design of crown ethers. 21. Synthesis of novel double-armed benzo-15-crown-5 lariats and their complexation thermodynamics with light lanthanoid nitrates in acetonitrile. J. Org. Chem. 2000. *65*. 7105–7109.
41. Arnold. K.A.: Echegoyen. L.; Gokel, G.W. Determination of thermodynamic parameters in lariat ether complexes using ion-selective electrodes. J. Am. Chem. Soc. 1987, 109. 3713–3715.
42. Elshani, S.; Du. H.: Laintz, K.E.; Natale, N.R.: Wai, C.M.: Elkarim, N.S.A.; Bartsch, R.A. Lariat ether carboxylic acids, O-benzylhydroxamates and hydroxamic acids with fluorinated substituents: Synthesis. metal ion complexation and solubility in supercritical carbon dioxide. Tetrahedron 2000. *56*. 4651–4657.
43. Aarts, V.M.L.J.; Grootenhuis. P.D.J.; Reinhoudt. D.N.: Czech, A.; Czech. B.P.; Bartsch. X.A. Macrocyclic receptor molecules with a pendant carboxylic acid group for the complexation of urea. Recl. Trav. Chim. Pays-Bas 1988. *107*. 94–103.
44. Young. D.-S.: Hung, H.-Y.: Liu, L.K. An easy and rapid method for determination of stability constants by electrospray ionization mass spectrometry. Rapid Commun. Mass Spectrom. 1997. *11*. 769–773.
45. Young. D.-S.; Hung, H.-Y.: Liu, L.K. Estimation of selectivities and relative cationization efficiencies of different [crown + M]$^+$ by electrospray mass spectrometry. J. Mass Spectrom. 1997, 32. 432–437.
46. Kempen. E.C.; Brodbelt. J.S.: Bartsch, R.A.: Jang. Y.; Kim. J.S. Investigation of alkali metal cation selectivities of lariat ethers by electrospray ionization mass spectrometry. Anal. Chem. 1999. *71*. 5493–5500.
47. Kempen. E.C.: Brodbelt. J.S.; Bartsch. R.A.; Blanda. M.T.: Farmer, D.B. Screening metal binding selectivities of macrocycle mixtures by HPLC-ESI-MS and postcolumn reactions. Anal. Chem. 2881. *73*. 384–390.
48. Yamashita. I.: Fujii, M.: Kaneda. T.; Misumi. S.: Otsubo, T. Synthetic macrocyclic ligands. II. Synthesis of a photochromic crown ether. Tetrahedron Lett. 1980. *21*. 541–544.
49. Dix. J.P.; Voegtle. F. Ligand structure and complexation. L. Ion-selective crown ether dyes. Chem. Ber. 1980. *113*. 457–470.
50. Yamashita, T.; Nakamura. H.: Takagi. M.: Ueno. K. Synthesis of crown ether dyes. Bull. Chem. Soc. Jpn. 1980. *53*. 1550–1554.

51. Shinkai. S.; Shigematsu, K.: Kusano, Y.; Manabe. O. Photoresponsive crown ethers. Part 3. Photocontrol of ion extraction and ion transport by several photofunctional bis(crown ethers). J. Chem. Soc., Perkin Trans. 1 1981. 3279–3283.
52. Takagi, M.: Ueno, K. Crown compounds as alkali and alkaline earth metal ion selective chromogenic reagents. Top. Curr. Chem. 1984, *121,* 39–66.
53. Alihodzic. S.; Zinic. M. Lariat ethers with pendant phenanthridine units. Synthesis and complexation of Na- and K-picrate. Croat. Chem. Acta 1999. 72. 803–817.
54. Higashiyama, N.; Takemura. K.; Kimura, K.; Adachi. G. Luminescence of divalent europium complexes with N-pivot lariat azacrown ethers. Inorg. Chim. Acta 199%.194. 201–206.
55. Fischer. C.: Sarti, G.: Casnati. A.; Carrettoni. B.; Manet, I.: Schuurman. R.: Guardigli, M.; Sabbatini, N.: Ungaro, R. 2,2′-Bipyridine lariat calixcrowns: A new class of encapsulating ligands forming highly luminescent Eu^{3+} and Tb^{3+} complexes. Chem. Eur. J. 2000. *6*, 1026–1034.
56. Kaifer, A.: Echegoyen, L.; Gustowski, D.; Goli. D.M.; Gokel. G.W. Enhanced sodium cation binding by electrochemically-reduced, nitrobenzene-substituted lariat ethers. J. Am. Chem. Soc. 1983, *105,* 7168–7169.
57. Gokel, G.W.; Echegoyen. L. Lariat Ethers in Membranes and as Membranes. In Advances in Bio-organic *Frontiers*; Dugas, H., Ed.: Springer Verlag: Berlin, 1990: Vol. 1, 116–141.
58. Gokel, G.W.; Mukhopadhyay, A. Synthetic models of cation-conducting channels. Chem. Soc. Rev. 2901, 30. 274–286.
59. Urban, F.J.; Chappel, L.R.; Girard, A.E.: Mylari, B.L.; Pimblett, I.J. Lipophilic 1,3-xylyl-21-crown-6 macrocyclic polyether 2-carboxylic acids as biological mimics of the ionophore antibiotics. J. Med. Chem. 1990. 33. 765–771.
60. McPhee. M.M.; Kern, J.T.: Hoster. B.C.; Kerwin. S.M. Propargylic sulfone-armed lariat crown ethers: Alkali metal ion-regulated DNA cleavage agents. Bioorg. Chem. 2000, *28.* 98–118.

Layered Supramolecular Solids and Their Intercalates

George K. H. Shimizu
University of Calgary, Calgary, Alberta, Canada

INTRODUCTION

The number of examples of functional extended solids based upon weaker interactions increased dramatically in recent years in the scientific literature. This is more of a reflection of a change in perception of the potential functionality of "soft" solids rather than any single chemical breakthrough. The predominant thinking in the past. certainly among inorganic chemists. equated the utility of a framework with its structural rigidity and thermal stability. The explosion of research in the domain of coordination assays yielded exquisite examples of extended metal-organic networks. In this research domain, the "Holy Grail' ` is largely regarded as a permanently porous solid with functionality beyond that offered by a zeolitic analogue, whether the enhancement is in respect to pore size,[1–3] chiral catalysis,[4] or tunability.[5] The cited recent works demonstrate these properties, however, this science is not yet at a stage of growth where these desirable qualities may be selected a priori from the components of a framework.

To continue along the same avenue of thought. that is, extended solids based upon weaker interactions. one arrives at frameworks that do not possess high thermal stability and are not rigid in their structures. These are solids based on weaker metal–ligand interactions or even noncovalent interactions. By the criteria of, for example, metal oxide chemistry, these compounds would be described as lacking potential utility. A different frame of reference is required for these "softer" extended solids. If one considers that a living animal relies upon weak interactions for its abilities to grow, think, and reproduce. the validity of these interactions in the construction of functional extended architectures becomes self-evident.

There are undoubtedly benefits to a solid with a more flexible structure. Prospects range from selective sorbents, which can be dissolved to liberate included guests, to networks. which swiich between distinctly different physical forms upon inclusion. To elaborate on the latter point. a flexible network may possess one form, where magnetic centers are in proximity, yielding a ferromagnetic response. This signal could then be lost upon guest inclusion as a result of conversion to a second structural form, either antiferromagnetic or simply paramagnetic.[6] Similar prospectus may be discussed for conductivity, optical activity. luminescence, or any other physical response that may be incorporated into a solid network.[7] Thus. extended solids based upon weaker interactions can be viewed as complements to highly robust inorganic solids, rather than replacements.

This short review deals with supramolecular intercalates. Supramolecular intercalates is a term open to considerable breadth of definition. Within the scope of this article. the author chose to focus on two-dimensional solids. based upon weak interactions, that demonstrate intercalation ability. An emphasis is placed on frameworks that demonstrate flexibility of structure and the benefits of such compounds. This short review is not meant to be comprehensive, as many systems that may fall under the broad umbrella of "supramolecular intercalates" were reviewed elsewhere.[8–14] This review is meant simply as an overview of some examples in this topical field that readily illustrate the potential of soft networks.

ORGANIC LAYERED SOLIDS AS HOSTS

Guanidinium Sulfonates

The most extensively studied intercalation solids based upon weak interactions are the guanidinium sulfonate (GS) frameworks of Ward et al.[14,15] These structures are assembled into undulating layers, describable as cross-linked ribbons: via the complementary charge-assisted hydrogen bonding between the NH_2 groups of guanidinium cations and the oxygen atoms of organosulfonate anions (Fig. 1). A structural comparison may be drawn between this family and metal phosphonates.[8] In metal phosphonates, a rigid and robust inorganic backbone serves as a scaffolding for a wide range of organic groups, the pendant group of the phosphonate. In a homophosphonate structure. space for guest inclusion is minimal due to the efficient packing of phosphonate R groups. One of the main assets of the GS system is that the guanidinium cation is considerably larger than a metal ion, and hence. at hydrogen-bonding distances. the sulfonate organic groups are situated in a inanner to welcome guest inclusion. Two framework types are typically observed in this family, a bilayer motif and a continuous layer, depending on the nature of the included guest and sulfonate R group. With

DOI: 10.1081/E-ESMC 120012726

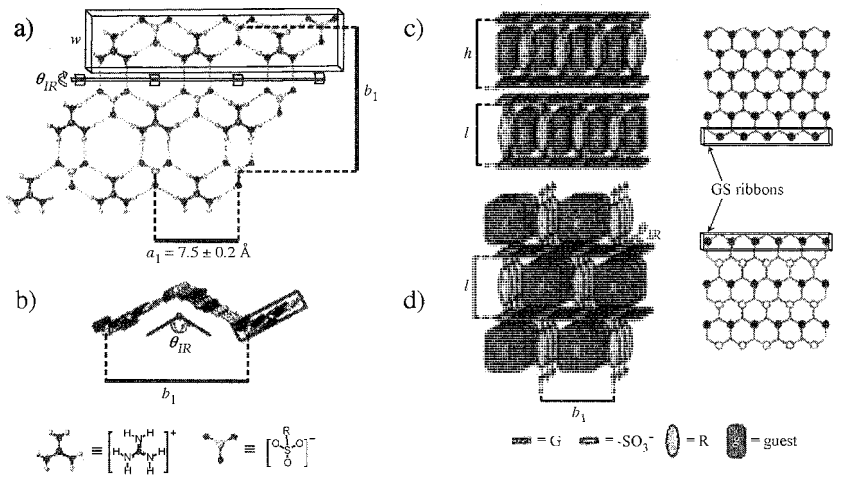

Fig. 1 A single layer of a guanidiniuin sulfonate framework showing the cross-linked ribbon motif. Also shown are the two general structures observed: bilayer and continuous layer motifs. Reprinted with permission from Ref. [14]. Copyright 2001 by American Chemical Society.

the skeleton being maintained by noncovalent forces, the solid has an inherent flexibility. In general, for the GS networks. this flexibility is manifested as ''accordion-like'' puckering of the cross-linked ribbons and ''turn-stile-like'' rotation of the organic pillars. This is a good recipe for a network capable of adjusting to accommodate a wide range of guest molecules. Indeed, the number of variations of host and guest in this family number in the hundreds. Remarkably, despite the dependence on weak interactions, in these numerous compounds. the basic structural unit persists. Recently, Ward reported GS inclusion frameworks that exhibit second harmonic generation.[16] The optical properties of the framework result from ordering guests within a polar channel resulting from ''banana-shaped'' sulfonate pillars.

The most significant feature of the GS family cannot be ascertained from any single compound. The body of work illustrates the role of subtle intermolecular interactions in dictating structure, as well as how a material can be tuned to exploit these features to advantage. A tantalizing prospect is that of a highly selective bulk separations agent, where the guest and host need only be partitioned between organic and aqueous phases for quantitative separation and recovery of all components. The extent of structural variation was pushed to a new extent with the recent report of tubular GS arrays formed.[17]

Secondary Ammonium/ Tricarboxylate Assemblies

Keeping with organic solids, Zaworotko et al. reported a series of intercalate complexes based upon hydrogen bonding between secondary ammonium cations and trimesate or trimellitate anions.[18,19] In these complexes, the tricarboxylate anions form a layer and are linked by hydrogen bonds to the protons of the dialkyl amsnonium salts. The organic moieties of the ammonium ion are projected above and below the hydrogen-bonded plane to ''pillar'' an interlayer region. Guest inclusion is highly dependent on the nature of the organic group of the ammonium cation. For dibenzylammonium. the resultant interlayer is lined with aromatic groups, and accordingly. the framework has a tremendous ability to include aromatic guests. ranging from nitrobenzene to pyrene. Shown in Fig. 2 are two views of a typical dibenzylammonium–trimesate assembly. As with the GS compounds, the flexibility of the scaffolding once again allows for the network to adjust to accommodate different guests of varying steric and electronic properties.

An analogy was made of this family of compounds to clays. This is a good illustration of the complementarity of soft networks to metal oxides mentioned in the introduction. Whereas clays typically consist of anionic, aluminosilicate layers, these ''supramolecular laminates'' represent a neutral alternative. Clays. owing to the array of oxygen atoms lining the interlayer, favor inclusion of polar species. In contrast. the Zaworotko networks represent a system that favors inclusion of nonpolar aromatic guests. For the Zaworotko structures, in the absence of guests, the interlayer is compacted with benzyl groups interdigitated. Thus, as in clays, the framework can swell to accommodate guests. If the benzyl groups are substituted for straight-chain alkyl groups, neither swelling nor guest inclusion take place, as the solid remains in a compact interdigitated form. This observation illustrates

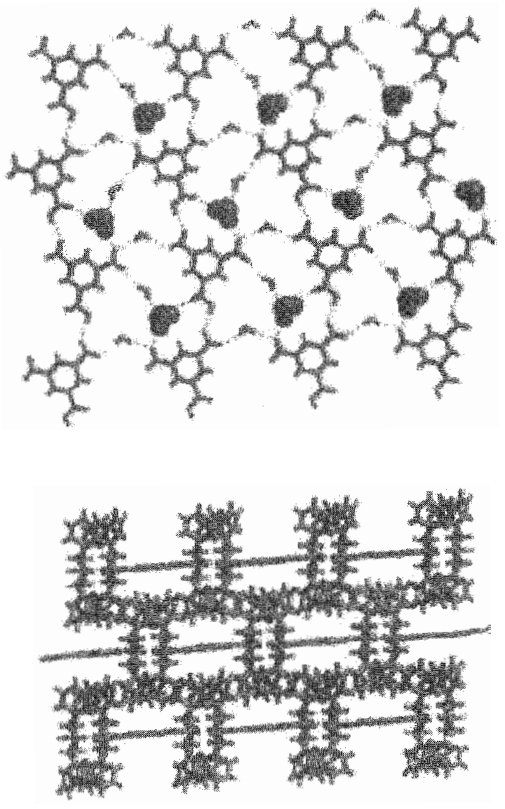

Fig. *2* Views perpendicular (top) and parallel (bottom) to a single layer showing trimesate–ammonium units hydrogen bonding in the Zaworotko clay mimics. Interlayer guests are shown in a space-filling representation. In the lower figure, the 8.3 A separation is between layers. as depicted in the upper figure. Reprinted with permission from Ref. [19]. Copyright 1998 by American Chemical Society.

the potential for adjustable framework properties with the softer network.

A Catalytic Bisresorcinol Host

The two previous examples concerned organic frameworks sustained by charge-assisted hydrogen bonds. Aoyama et al. reported a system of interacting neutral organic molecules chat form a layered network that functions as a catalytic host.[20,21] The complementary interaction in this case is a self-association between anthracenebisresorcinol units. Initially, the authors observed that this system had the ability to include different types of guest molecules within its cavities simultaneously, for example, ethyl acetate and benzene. In an elegant extension of this work. the authors generated the same host network in the presence of an acrylic ester and 1.3-cyclohexadiene, in place of ethyl acetate and benzene, respectively (Fig. 3). The relevance of these included components is their ability to undergo intermolecular Diels–Alder reactions. The product of the cyclization is a bicyclooctene isomer. where endocyclic and exocyclic products are possible with respect to the orientation of the ester group. Of major significance is that the host framework enhances selectivity for the endoisomer over the exoproduct. In the absence of the host, these reactions typically proceeded with a preference for the endoisomer (87:13). but in some cases, the presence of the host would push the selectivity to the point where virtually only the endoisomer was obtained.

LAYERED COORDINATION SOLIDS AS HOSTS

A Highly Guest-Selective Metal–Trimesic Acid Network

Yaghi et al. reported a copper(II) network with trimesate as the counterion,[22] isolated via a slow diffusion of pyridine into an ethanolic solution of $Cu(NO_3)_2$ and trimesic acid. As might be expected with a trigonally symmetric building block. this compound adopted a layered honeycomb structure. The axial coordination sites on the Cu center, not bound to the trimesate ions, were ligated by pyridine and directed into the interlayer region. Typically, a monodentate pyridine ligand may be readily removed upon heating. In this example. that was not the case, as the stability of the pyridine molecules was

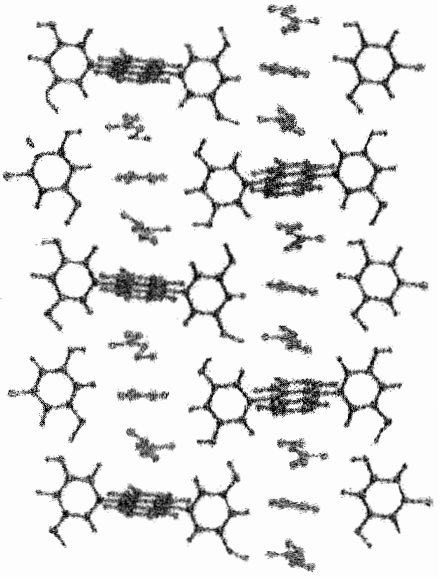

Fig. **3** A portion of a single layer in Aoyama's anthracene-bisresorcinol host that catalyzes Diels–Alder reactions. Note the stacking of two acrylic esters and the cyclohexadiene unit prior to cyclization. Reprinted with permission from Ref. [20]. Copyright 1997 by American Chemical Society.

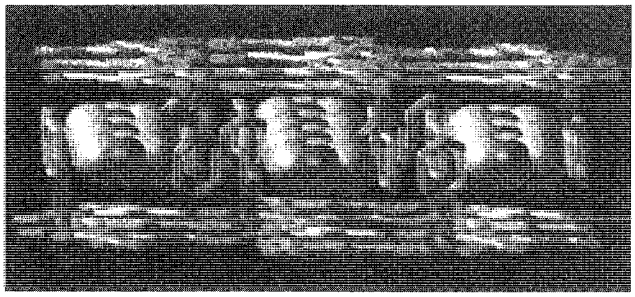

Fig. 4 Vieu parallel to the honeycomb layers of Yaghi's Cu(II) trimesic acid framework that is selective for aromatic inclusion. Shown is the efficient n-stacking of guests by the pyridine pillars. Reprinted with permission from Ref. [22]. Copyright 1995 by Nature Publishing Group. (*View this art in color at www.dekker.com.*)

augmented by interpyridine n-stacking interactions. These supramolecular interactions served to pillar the interlayer and, along with the trimesate core as a spacer, generated cavities for inclusion of other extensively hydrogen-bonded guest pyridine molecules (Fig. 4). The truly remarkable feature of this network was that the guest pyridine molecules could be liberated. while the ligated pyridine molecules were retained. This generated a porous interlayer lined with aromatic groups from the coordinated pyridine units and the benzene cores of the trimesate anions. The work was extended to show that the partially desolvated network was then selective for the uptake of aromatic over structurally similar. nonaromatic guests.

Tunable Frameworks Based upon Silver Organonitrile interactions

The Lee group reported some elegant and thorough work on networks hinged on silver(I) nitrile interactions. Even relative to other interactions used to form coordination solids. the silver nitrile interaction can be considered weak. Additional structural stability in these networks is undoubtedly imparted by the observed layer formation, which essentially functions as an extended chelate. Lee et al. synthesized a family of layered honeycomb structures with tris(nitrile)benzene organic cores linked by silver(I).[23] Channels in these solids include a range of organic guests. The elegance of the Lee work is illustration of the variety of modifications, both with respect to the dimensions and functionality of the organic skeleton. which could be tolerated in a solid sustained by presumably weaker interactions.[24] In Fig. 5, the range of functionality is shown, including chiral groups for enantioselective separations that were incorporated into the honeycomb nets. Impressively. this system even includes an example (esterification of a pendant alcohol group) where functionalization of the organic skeleton was after assembly of the silver framework. Thus, in addition to thermal stability. this postassembly modification demonstrated that the system possessed chemical stability. In

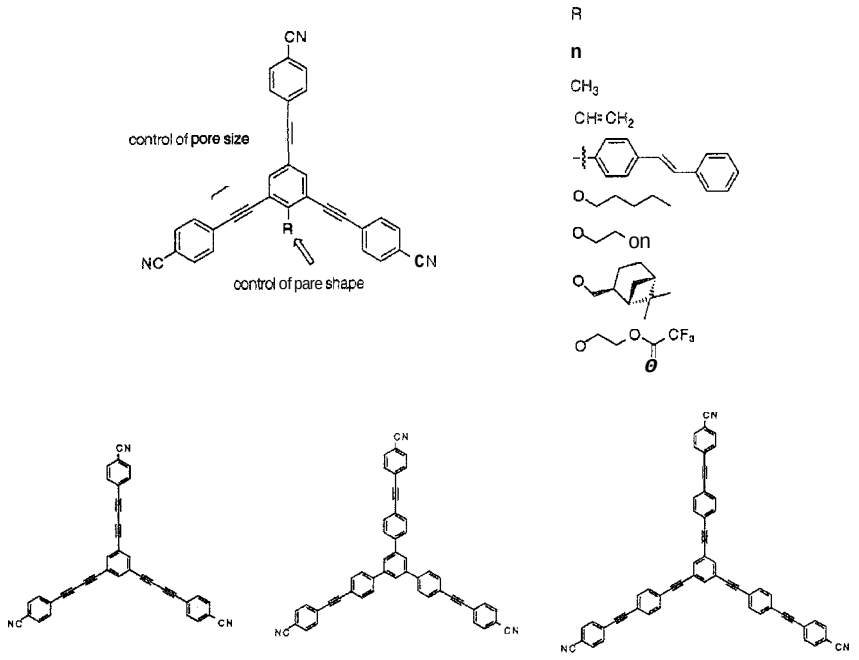

Fig. 5 Designed diversity in the silver organonitrile frameworks of Lee while still maintaining a honeycomb-type layered structure. Reprinted with permission from Ref. [24]. Copyright 1999 by American Chemical Society.

more recent work, Lee extended these studies to append longer chains of a well-defined hydroaffinity to a series of different organonitrile cores and used hydrophobic interactions to assemble different structural motifs.[25] This example of soft chemistry exists in a domain interinediate to block copolymer chemistry and surfactant-templatea inorganic synthesis. It is an excellent illustration of the complementary status of this science relative to existing materials.

Chloroanilic Acid Networks

Kitagawa et al. reported layered coordination polymers based upon chloranilic acid which exhibit intercalation phenomena.[26,27] These frametvorks have a formula $\{[M(CA)(H_2O)_2](guest)\}_\infty$, where $M = Fe^{2+}$, Co^{2+}, Mn^{2+}, Cu^{2+}. The chloroanilic acid adopted a doubly chelating coordination mode to the metal ions to form a one-dimensional ribbon. The metal ions were all six-coordinate and contained two sites not occupied by the CA ligands. These two sites were ligated by water molecules, which were in a cis or a *trans* orientation, depending on the nature of the complex. The extension of the ribbon to a layer is the reason for the inclusion of this system in this review. The ribbons were further joined via hydrogen-bonding interactions between one hydrogen atom of each metal-bound aquo ligand and the oxygen atoms of the CA^{2-} ligands of the adjacent ribbon, thus forming supramolecular layers. The remaining hydrogen atoms of each aquo ligand also functioned as a hydrogen-bond donor to a range of intercalate guest molecules. Guests that were intercalated included phenazine. dimethylpyrazine (Fig. 6). and water. With regards to materials properties, an appealing prospect is that the metal centers in these structures are, for the large part. paramagnetic. Thus, the size of the intercalate could regulate the degree of interlayer interaction and, hence, the extent of ferromagnetism. Interestingly, using these building blocks. frameworks of general formula. $\{(guest)[M(CA)_2(H_2O)_2]\}_\infty$, were also attainable.[28] The key alteration is that the ratio of divalent metal to CA^{2} . which was I:1. is now halved, resulting in an overall anionic framework. Thus, the regulation of the structures was achievable by the variation of countercations rather than neutral guests.

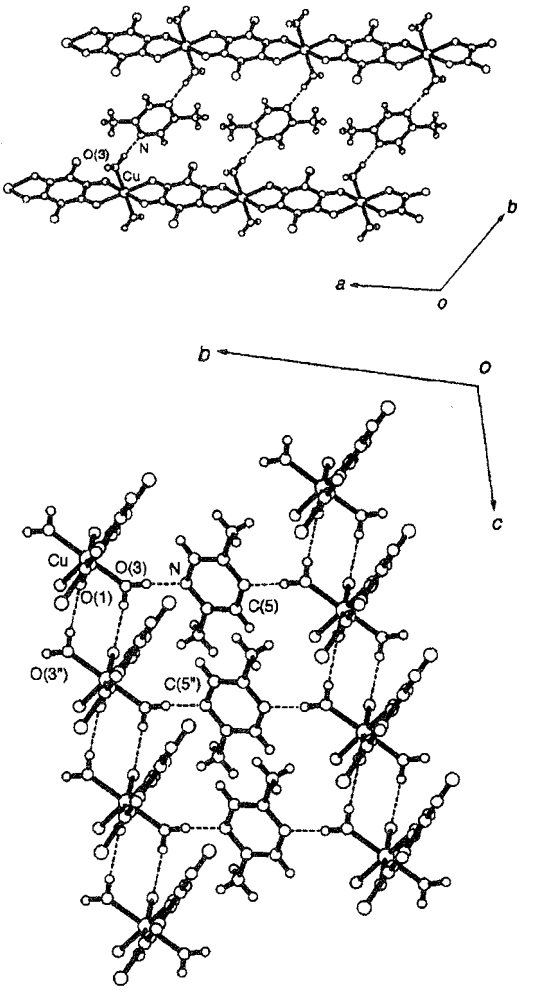

Fig. 6 Structure of a copper chloranilic acid framework reported by Kitagawa. The top figure shows the intercalation of dimethylpyrazine. and the bottom figure shows hydrogen bonding between Cu(CA) units to form the layers. Reprinted with permission from Ref. [26]. Copyright 1996 by American Chemical Society.

Silver Sulfonate Frameworks

Our research group has been studying the chemistry of silver(I) sulfonate frameworks. These two components offer an interesting compatibility with respect to structural pliancy. Silver(I) is noted, among transition metal ions. for having a flexible coordination sphere due primarily to its d^{10} electronic configuration. Sulfonate ions can bridge metal centers in modes ranging from bonding to a single metal to μ^6. Sulfonates are largely ignored in transition metal coordination chemistry owing to the perception that they are weakly interacting ligands. While this is true. when this fact is coupled with their potential for multiple interactions: the silver sulfonate interactions have potential as useful synthons in a supramolecular sense. With simple organosulfonate groups, silver sulfonates exist as layered solids structurally reminiscent of metal phosphonates,[29] which typically form rigid inorganic layers with a broad range of R group on the phosphonates.[8] In contrast to their divalent cousins, silver sulfonates hate more flexible layers. For example, going from R = phenyl to tolyl results in a change of the sulfonate bridging mode from μ^6 to μ^5. This led us to draw the

analogy of the sulfonate group to a "ball of Velcro" when considering its interactions with silver(I).

An example of a silver-sulfonate-layered network with intercalation properties is that of silver triflate ($CF_3SO_3^-$). In studies of layered metal phosphonates, intercalation typically requires thermal pretreatment of the solid to generate a site on the metal by liberating a coordinated solvent.[30] At this stage, the compound is usually highiy air and moisture sensitive. Silver triflate. in contrast, underwent facile coordinative intercalation of straight-chain alcohols under ambient conditions in air.[31] No thermal pretreatment was required, and no hypersensitive intermediate was generated. This was enabled due to the ''ball of Velcro" coordination ability of the sulfonate group. Whereas the phosphonate group is rigidly fixed in its bonding. the sulfonate group simply reorients to accommodate the alcohol group. This flexibility does not come at a sacrificial price with respect to lamellar stability, as the intercalation of straight-chain alcohols was topotactic over the range from ethanol (C_2) to eicosanol (C_{20}).

A second example of silver sulfonate interactions facilitating a supramolecular intercalation event is the complex, Ag(3-pyridinesulfonate). This framework existed as a dense pure compound and also as an acetonitrile intercalate.[32] The acetonitrile intercalate can be viewed as one-dimensional 24-membered rings linked in one dimension to form layers, as represented on the left side of Fig. 7. Upon desorption of the MeCN guests, the framework converted to a dense three-dimensional structure shown on the right side of Fig. 7. The reintroduction of acetonitrile was facile. as was the reconversion of the network to the layered structure. In virtually all extended solids, this structural reversion comes with a loss of long-range order reflected in broadening of peaks in the powder X-ray diffraction pattern. In this fi-amework. as all the connectivities lost and regained were weaker contacts (i.e., Ag–O bonds ranging from 2.6–2.8 Å), it was a facile process for the network to reorient and find its energetic minimum. Notably, no broadening of peaks was observed, even after 20 sorption/desorption cycles. Another significant observation concerning this system was the selectivity with which the guest inclusion took place. It was coordination of MeCN to the metal center that triggered the structural reorganization. Therefore, larger nitriles were excluded on a steric basis. while poorer Lewis bases, such as methanol, were excluded, as they likely did not displace the sulfonate group from the silver center. While it is difficult to describe a solid as porous when it never actually contains a void, this framework exhibits selective and reversible guest sorption. it may be stated that the most selective pore is. in fact. the pore that only exists in the presence of the guest.

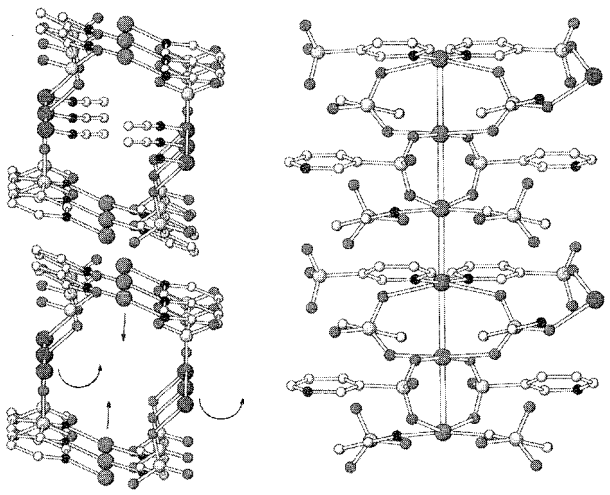

Fig. 7 Interconversion of MeCN intercalated (left) and the dense form (right) of silver 3-pyridinesulfonate, enabled by a "ball of Velcro'. rotation of the sulfonate group. Reprinted with permission from Ref. [32]. Copyright 2001 by John Wiley and Sons. (*View this art in color at www.dekker.com.*)

CONCLUSION

This short review has not. by any means, been meant as a comprehensive survey of layered solids and intercalates or supramolecular inclusion, as there are many studies that have not received mention here. Within the context of this review, the focus was specifically on two-dimensional solids. where the structure is sustained, in whole or in part, by weak interactions and that exhibit some intercalation phenomenon.

The incorporation of organic units into an extended structure cannot but bring more structural diversity. This point is indisputable. The cloud to this silver lining has always been the question as to whether frameworks incorporating organic moieties can possess the stability to enable any functionality. This point is even more poignant for two-dimensional architectures. as they are inherently less stable than their three-dimensional counterparts. The examples discussed in this review illustrate the potential utility as materials of networks based upon weaker interactions. These soft frameworks can be thought of as solids that bend but do not break. They offer more options for tunable diversity, and this will ultimately translate to greater and, importantly, different functionality. Thus. the point that cannot be overemphasized, is that soft solids should be perceived as a complement to existing inorganic materials rather than as an alternative. In an article prophesizing materials challenges for the twenty-first century, W. M. Tolles. the former Director of Strategic Planning for the U.S. Naval Research Laboratory.

is quoted as saying; *"The field of chemistry evolved by understanding the consequences of bonding forces, leading to a vast array of materials today. An extension of the same approach to weaker ,forces is envisionecl. Materials having properties not heretofore available may he expected."*[33]

ARTICLES OF FURTHER INTEREST

Channel Inclusion Compounds, p. 223
Classical Descriptions of Inclusion Compounds, p. 253
Clathrate Inclusion Compounds, Phase Transitions in, p. 289
Concepts in Crystal Engineering, p. 319
Crystal Engineering with Hydrogen Bonds, p. 357
Crystal Structure Prediction. p. 371
Crystalline Microporous Silicas, p. 380
Dye Inclusion Crystals, p. 497
Hofmann-Type Clathrates, p. 645
Mineralomimetic Structures, p. 868
Molecular Squares, Boxes, and Cubes, p. 909
Organic Zeolites, p. 996
Soft/Smart Materials, p. 1302
Strict Self-Assembly and Self-Assembly with Covalent Modifications, p. 1372
Swelling Clays (Smectites) and Nanofilms, p. 1478
X-Ray Crystallography, p. 1586
Zeolites in the Petroleurn Industry, p. 1599
Zeolites: Catalysis, p. *1610*
Zeolites: Separation Science, p. *1617*
Zeolites: Structures and Inclusion Properties, p. 1623

REFERENCES

1. Chen, B.L.: Eddaoudi. M.; Hyde. S.T.: O' Keeffe, M.: Yaghi, O.M. Interwoven metal–organic framework on a periodic minimal surface with extra-large pores. Science 2001, *291*. 1021–1023.
2. Li. H.: Eddaoudi. M.; O' Keeffe. M.; Yaghi. O.M. Design and synthesis of an exceptionally stable and highly porous metal-organic framework. Nature 1999. *402*, 276–279.
3. Noro. S.; Kitagawa. S.; Mondo. M.; Seki, K. A new methane adsorbent porous coordination polymer [{$CuSiF_6$-(4,4′-bipyridine),),,]. Angew. Chern. Int. Ed. 2000. *39*. 2082–2084.
4. Seo, J.S.; Whang, D.; Lee, H.; Jun, S.I.; Oh, J.; Jeon, Y.J.; Kim. K. A homochiral metal–organic porous material for enantioselective separation and catalysis. Nature 2000. *404*, 982–986.
5. Chui. S.S.Y.: Lo. S.M.F.: Charmant, J.P.H.: Orpen, A.G.; Williams, I.D. A chemically functionalizable nanoporous material [$Cu_3(TMA)_2(H_2O)_3]_n$. Science 1999, *283*, 1148–1150.
6. Kahn, O. Chemistry and physics of supramolecular magnetic materials. Acc. Chem. Res. 2000. *33*. 647–657.
7. Gaudry, J.B.; Capes. L.; Langot. P.: Marcen, S.: Kollmannsberger, M.: Lavastre, **O.:** Freysz. E.: Letard. J.F.; Kahn. **O.** Second-order non-linear optical response of metallo-organic compounds: Towards switchable materials. Chem. Phys. Lett. 2000. *324*. 321–329.
8. Clearfield. A. Metal phosphonate chemistry. Prog. Inorg. Chem. 1998. *47*. 371–510.
9. Kryszewski, *M*. Nanointercalates—Novel class of materials with promising properties. Synth. Met. 2000. *109*. 47-- 54.
10. Kaschak. D.M.: Johnson, S.A.; Waraksa. C.C.: Pogue, J.: Mallouk, T.E. Artificial photosynthesis in lamellar assemblies of metal poly(pyridyl) complexes and metalloporphyrins. Coord. Chem. Rev. 1999, *186*. 403–416.
11. Atwood, J.L.; Barbour, L.J.; Hardie, M.J.: Raston. C.L. Metal sulfonatocalix[4,5]arene complexes: Bi-layers, capsules. spheres, tubular arrays and beyond. Coord. Chern. Rev. 2001. *222*, 403–416.
12. Moulton. B.: Zaworotko. M.J. From molecules to crystal engineering: Supramolecular isomerism and polymorphism in network solids. Chem. Rev. 2001. *101*. 1629–1658.
13. Nangia. A. Organic nanoporous structures. Curr. Opin. Solid State Mater. Sci. 2001. *5*. 115–122.
14. Holman, K.T.; Pivovar. A.M.: Swift, J.A.: Ward, M.D. Metric engineering of soft molecular host frameworks. Acc. Chern. Res. 2001. *34*. 107–118.
15. Russell, V.A.: Evans, C.C.: Li. W.J.; Ward, M.D. Nanoporous molecular sandwiches: Pillared two-dimensional hydrogen-bonded networks with adjustable porosity. Science 1997. *276*. 575–579.
16. Holman. K.T.: Pivovar. A.M.: Ward. M.D. Engineering crystal symmetry and polar order in molecular host frameworks. Science 2001. *294*. 1907–1911.
17. Horner, M.J.; Holman. K.T.: Ward. M.D. Lamellae-nanotube isomerism in hydrogen-bonded host frameworks. Angew. Chem. Int. Ed. 2001. *40*. 4045–4048.
18. Melendez, R.E.: Sharma. C.V.K.; Zaworotko. M.J.: Bauer, C.; Rogers, R.D. Toward the design of porous organic solids: Modular honeycomb grids sustained by anions of trimesic acid. Angew. Chem. Int. Ed. 1996, *35*. 2213–2215.
19. Biradha, K.: Dennis, D.: MacKinnon. V.A.: Sharma. C.V.K.: Zaworotko, M.J. Supramolecular synthesis of organic laminates with affinity for aromatic guests: A new class of clay mimics. J. Am. Chem. Soc. 1998, *120*, 11894–11901.
20. Endo. K.; Koike, T.: Sawaki, T.; Hayashida, O.; Masuda. H.: Aoyama. Y. Catalysis by organic solids. Stereoselective Diels-Alder reactions promoted by microporous molecular crystals having an extensive hydrogen-bonded netu-ork. J. Am. Chem. Soc. 1997. *119*. 4117 -4122.
21. Endo. M.: Sawaki. T.: Koyonagi. M.: Kobayashi. K.: Masuda. H.; Aoyama, Y. Guest binding properties of organic crystals having an extensive hydrogen-bonded network—An orthogonal anthracene-*bis*(resorcinol) derivative as a functional organic analog of zeolites. J. Am. Chem. Soc. 1995, *117*, 8341–8352.
22. Uaghi. O.M.: Li. G.: Li, H. Selective binding and removal

of guests in a miroporous metal–organic framework. Nature 1995. *378.* 703–706.
23. Gardner. G.B.; Venkataraman, D.; Moore, J.S.; Lee. S. Spontaneous assembly of a hinged coordination network. Nature 1995. *374*, 792–795.
24. Kiang. Y.H.; Gardner, G.B.; Lee. S.; Xu, Z.T.: Lobkovsliy. E.B. Variable pore size, variable chemical functionality. and an example of reactivity within porous phenylacetylene silver salts. J. Am. Chem. Soc. 1999. *121.* 8204–8215.
25. Xu, Z.T.: Kiang, Y.H.: Lee, S.: Lobkovsky. E.B.; Emmott, N. Hydrophilic-to-hydrophobic volume ratios as structural determinant in small-length scale amphiphilic crystalline systems: Silver salts of phenylacetylene nitriles with pendant oligo(ethylene oxide) chains. J. Am. Chem. Soc. 2000. 122. 8376–8391.
26. Kawata. S.; Kitagawa, S.; Kumagai. H.: Kudo. C.; Kamesaki, H.: Ishiyama. T.: Suzuki. R.; Kondo, M.; Katada, M. Rational design of a novel intercalation system. Layer-gap control of crystalline coordination polymers, $\{[Cu(CA)(H_2O)_m](G)\}_n$ (m = 2. G = 2.5-diinethylpyrazine and phenazine; m = 1, G = 1,2,3,4,6,7,8,9-octahydrophenazine). Inorg. Chem. 1996. *35*, 4449–4461.
27. Kawata. S.: Kitagawa. S.; Kumagai, H.; Ishiyama, T.; Honda. K.: Tobita. H.; Adachi, K.: Katada. M. Novel intercalation host systems based on transition metal (Fe^{2+}, Co^{2+}, Mn^{2+})–chloranilate coordination polymers. Single crystal structures and properties. Chem. Mater. 1998. *10.* 3902–3912.
28. Kabir, M.K.; Miyazaki, N.; Kawata, S.; Adachi. K.; Kumagai, H.: Inoue, K.; Kitagawa. S.; Iijima, K.: Katada, M. Novel layered structures constructed from iron-chloranilate compounds. Coord. Chem. Rev. 2000, *198*, 157–169.
29. Shimizu, G.K.H.; Enright, G.D.; Ratcliffe. C.I.: Rego, G.S.; Reid, J.L.: Ripmeester, J.A. Silver sulfonates: An unexplored class of layered solids. Chem. Mater. 1998. 10, 3282–3283.
30. Johnson, J.W.: Jacobson, A.J.; Butler, W.M.; Rosenthal. S.E.; Brody. J.F.; Lewandowski, J.T. Molecular recognition of alcohols by layered compounds with alternating organic and inorganic layers. J. Am. Chem. Soc. 1989. *111*. 381–383.
31. Côté, A.P.: Ferguson, M.J.; Khan. K.A.; Enright, G.D.: Kulynych, A.D.; Dalrymple. S.A.; Shimizu, G.K.H. Intercalation of alcohols in Ag sulfonates: Topotactic behavior despite flexible layers. Inorg. Chem. 2002. *41*, 287–292.
32. Mäkinen, S.K.: Melcer. N.J.; Parvez, M.; Shimizu, G.K.H. Highly selective guest uptake in a silver sulfonate network imparted by a tetragonal to triclinic shift in the solid state. Chem. Eur. J. 2001, *7*. 5176–5182.
33. Tolles. W.M. Self-assembled materials. Mater. Res. Soc. Bull. October 2000. *25.* 36–38.

Light Scattering

Robin E. Westacott
Heriot-Watt University, Edinburgh, United Kingdom

Carolyn A. Koh
King's College London, London, United Kingdom

INTRODUCTION

Light and matter interact in such a way that the electric field of the light induces an oscillating polarization of the electrons in the constituent atoms or molecules of the matter. These interactions cause the light to be scattered by the atoms or molecules with and without absorption of energy by the material. This scattering causes frequency shifts, angular distribution, and changes in polarization and intensity of the light, all of which provide information on the size, shape, and interactions of the material. This information, when combined with classical electrodynamics and statistical mechanics, provides details on the structure and molecular dynamics of the system. The structure and dynamics of a wide range of systems such as solids,[1] liquid crystals,[2] gels,[3] solutions of macromolecules,[4] simple fluids and electrolyte solutions,[5] dispersions of microorganisms,[6] viruses,[7] membrane vesicles,[8] and colloidal dispersions[9] can be investigated using light-scattering techniques. Light-scattering has seen a rapid increase in use and applicability over the last 20 years due to the dramatic advances in laser technology.

THEORY

When a monochromatic beam of light is incident on a sample, the light is scattered at an angle θ with respect to the incident beam. The volume defined by the intersection of the incident and scattered beams is called the scattering volume. Atoms and molecules in the scattering volume experience the electric field of the incident light, and charged species are accelerated due to the force they experience. The accelerated charge emits light, which can be collected by a detector placed at the scattering angle, θ. The light reaching the detector is the sum of the light scattered by all the charges in the scattering volume and is thus dependent on the position of the scattering bodies (see Fig. 1).

Atoms or molecules in the scattering volume are constantly moving, so that the total scattered electric field constantly changes and therefore looks like noise. But, it contains all the information, structural and dynamic, on the atoms and molecules in the scattering volume. If the wavelength of the incident light is large compared to the size of the scattering bodies, the same electric field is experienced by each body. Destructive interference of the scattered waves leads to most of the transmitted light being observed in the same direction as the incident light, and only very small amounts of scattered light can be observed. The intensity of light scattered over directions other than that of the incident light increases with increasing size of the scatterer. For scatterers of larger dimensions, this leads to the well-known Tyndall effect observed when light is passed through an emulsion or solution of macromolecules.

If the scattering volume is composed of many small units, where each unit is small compared to the wavelength of the incident light, the total scattered electric field is the sum of the scattered electric fields from each unit. If the optical properties of each unit are different, then light is scattered in directions other than forward, otherwise light is only scattered in the forward direction.

When monochromatic light is incident on a single molecule having anisotropic polarizability α, a dipole moment is induced that varies with time:

$$\mu(t) = \alpha \cdot \mathbf{E}(t) \tag{1}$$

A time-varying dipole moment emits light. The light scattered from a collection of molecules is simply the sum of the amplitudes of light scattered from each of the individual molecules, i.e., proportional to

$$\sum_j{}' \alpha_j(t) \exp i\mathbf{q} \cdot \mathbf{r}_j(t) \tag{2}$$

where j indicates each individual molecule, q is the scattering vector, r_j is the position of the center of mass of molecule j, and the $'$ indicates that the sum is only over the molecules in the scattering volume. The intensity of the scattering field is then proportional to

$$I(\mathbf{q}, \omega) = \frac{1}{2\pi} \int_{-\infty}^{+\infty} \mathrm{d}t \exp^{-i\omega t} I(\mathbf{q}, t) \tag{3}$$

Encyclopedia of Supramolecular Chemistry
DOI: 10.1081/E-ESMC 120012814

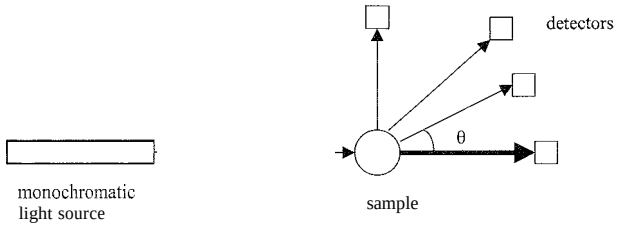

Fig. 1 Simplified light-scattering experiment. Commonly, there is a focusing lens between the light source and the sample.

where

$$I(\mathbf{q},t) = \langle \partial\alpha_j^{*}(\mathbf{q},0)\partial\alpha_j(\mathbf{q},t)) \tag{4}$$

and

$$\partial\alpha_j(\mathbf{q},t) = \sum_{j=1}^{N} {}'\alpha_j(t)\exp^{i\mathbf{q}\cdot\mathbf{r}(t)} \tag{5}$$

is the spatial Fourier component of the polarizability density,

$$\partial\alpha_j(\mathbf{r},t) = \sum_{j=1} {}'\alpha_j(t)\partial(\mathbf{r}-\mathbf{r}_j(t)) \tag{6}$$

This approach is only approximate, because the incident light is directed on a collection of molecules rather than a single molecule. These molecules are subject to collisions with one another, and this causes disturbances in the electric field around the molecules, which persist for as long as it takes for the molecules to separate to a distance outside the influence of each other's electric fields.

The polarizability term in Eq. 5 can be split into two terms: a polarizability term for the nuclear configuration and a term dependent on vibrations. The expression for intensity contains four terms: rigid molecule polarizability, two linear cross terms for vibrational modes. and one quadratic cross term for vibrational modes. The linear terms generally average to zero. The quadratic term leads to the vibration-rotation Raman spectrum. Light scattering is only concerned with those terms that contain the pure rotations and translations of molecules with the rigid molecule polarizability. often referred to as Rayleigh–Brillouin scattering.

Difficulties arise in understanding results when applying light scattering to complicated systems. Thus, model systems are used to aid interpretation. The simplest example of this is the use of spherical molecules. because the induced dipole moment is always parallel to the incident electric field, and exact solutions can be derived. Model solutions can also be derived for dilute solutions and low-density gases when the sizes of the particles being analyzed approach the wavelength of the incident light, and the interior and surface of the particle are different, such as during crystallization. Again. exact solutions are available for simple model systems such as spheres (Mie theory[10]), and some are available for cylinders. Light scattering was also used to study the mobility of microorganisms.[11] The reader is referred to the text of Berne and Pecora,[12] and references therein, for further details of the uses of light scattering.

APPLICATIONS

Some recent examples of light scattering in fields of supramolecular chemistry are provided in the remainder of this article.

Moradian-Oldak[13,14] studied amelogenin proteins, which are hydrophobic in nature and exhibit reversible temperature coacervation (gel conversion from a translucent state at 4°C to an opaque form at room temperature). The bulk of the amelogenin is enriched in amino acids: Pro, Leu, His, and Gln, while the terminal region is composed of a sequence of hydrophilic-charged amino acids. Amelogenin distribution in the extracellular matrix of enamel is believed to be due to alternative splicing of primary mRNA transcript as well as the presence of the proteolytic product. Interestingly, the amelogenin structure self-assembles to generate nanosphere structures, which were recognized as being the main structural component of secretary-stage enamel matrix. The self-assembly of amelogenin proteins to form a supramolecular structural framework is a major extracellular event in enamel formation. Dynamic light scattering was used to study the amelogenin self-assembly process, which is one of the key factors in controlling some processes of the crystal growth of enamel. The light-scattering measurements detected nanospheres of 5-100 nm diameter.[13] These nanospheres are considered the basic building blocks of the amelogenin matrix and may be the supramolecular st uctures responsible for organizing this matrix. These measurements also indicated that the self-assembly process is hydrophobically driven and is sensitive to the pH and temperature of the solution.

In particular, temperature variation studies gave the following results:[14] at low temperature (5–25°C) and pH 8, full-length recombinant amelogenin forms aggregates in a narrow size distribution between 15 and 18 nm. Between 27–35°C, the size distribution becomes bimodal and multimodal. with average particles having up to four times the hydrodynainic radius of those at the lower temperatures . At higher temperatures (37–40°C), particles are larger and better defined. suggesting that amelogenin changes conformation and reassembles in a new arrangement.

Modified amelogenins, with systematic domain deletion or substitution. were also investigated.[15] This work showed that there are substantial differences in the size distributions of the aggregates, depending on the modifications made to the pure amelogenin. Time-dependent dynamic light-scattering measurements also showed that altering the hydrophillic B-domain in the amelogenin sequence results in a significant shift in the size distribution of the amelogenin nanospheres.[13]

There is increasing interest in DNA suprainolecular complexes for nonviral gene therapy. Nonviral DNA complexes may be important as alternative gene-delivery vectors for treating genetic disorders. Most studies of nonviral gene-delivery systems focus on new condensing agent synthesis, expression vector development, and characterization and structure of the supramolecular complex. In contrast, there have been few studies on the formation kinetics of this supramolecular complex. Understanding the kinetics of the complexation process is important to achieve an optimal formulation of the DNA complex dispersion (i.e., having an optimal size and composition). Lai and van Zanten[16] used time-resolved multiangle laser light scattering to measure the kinetics of formation of a DNA/poly-L-lysine polyplex and to monitor the time evolution of the supramolecular complex. as well as changes in the mass and geometric size. The light-scattering results showed that the primary polyplexes of a smaller geometric size than individual DNA molecules in solution form rapidly when DNA is mixed with poly-L-lysine. After a certain tiine, the primary polyplexes then aggregate into larger structures. where the size is dependent on the relative conceritration of DNA to poly-L-lysine. It was found that at relatively high or low DNA/poly-L-lysine mass concentration ratios. the polyplex mass and geometric size remain almost constant with time after initial aggregation. The results also indicated that aggregation is rapid and yields polyplexes that remain stable for at least a few hours.

Resonance light scattering (RLS) is a valuable technique for detecting and characterizing extended aggregates of chromophores. Scattering intensities of such species are significantly enhanced at or near the wavelength of absorption when strong electronic coupling exists among chromophore units. This means that RLS is extremely sensitive and selective for monitoring such molecular assemblies and for studying their sizes and shapes. However. the interpretation of data obtained from RLS are complicated by the large amount of absorption present. Collins et al.[17] reported an empirical method for making absorption corsections to RES spectra obtained using a 90° fixed scattering angle spectrofluorimeter. The supramolecular assembly of the chromophore, tetrakis (4-sulfonatophenyl) porphine (H_4TPPS), was studied using RLS by considering the absorption and scattering of the sample: thus separating the extinction measurement into the individual components.

Chromic materials are present in many materials, such as drugs, dyes. nucleic acids, and antibodies. The driving force for self-association of these chromic molecules in aqueous solution is enthalpically driven. with attractive interactions occurring between π-systems leading to the formation of stacks of molecules. A well-known assembly of this kind is formed by certain cyanine and merocyanine dyes. also known as J-aggregates, because they give a sharp optical absorption band (*J*-band) shifted to longer wavelengths compared to the long wavelength absorption band of monomers. This unusual spectroscopic phenomenon was attributed to a stacking of the chromophores into polymer-like assemblies. The relationship between molecular structure and the mesoscopic properties of these materials is complex. In addition, their aggregation number, geometric size, and morphology are not well understood. Light scattering was used by von Berlepsh et al.[18] to characterize 5,5′,6,6′-tetrachlorobenzimidacarbocyanine dyes with 1,1′-dioctyl and 3,3′-*bis*(3-carboxypropyl) substituents that form distinct supramolecular aggregates in solution. The light-scattering results revealed that there was nonuniformity in aggregate diameter. The particles in solution were rod-shaped. Small-angle light-scattering measurements also showed that the scattering behavior was unchanged over the whole accessible scattering vector range down to Q of around 5×10^{-3} nm^{-1}, suggesting that particles remained a particular length. which could be on the order of a few microns.

Alloisio et al.[19] used light scattering to investigate a soluble polydiacetyiene (PDA), poly[1,6-*bis*(3,6-dihexadecyl-*N*-carbazoyl)-2,4-hexadiyne]. It was possible to create thin films of some of this polymer that have good optical quality. Dilute solutions of this polymer in benzene and toluene were characterized using light scattering. which showed that this specific polymer behaves differently than other soluble PDAs. Specifically, the results indicated that the polymer behaves as a rod-like chain. and it is this property that potentially allows preparation of thin films with good optical quality using spin coating. Gelatin forms a physical rather than a chemical gel; that is, direct chemical cross-linking of the polymer strands does not occur. This process is well understood. but chemical cross-linking of gelatin is required for some applications, such as surgical absorbents and drug capsule casings. In order to understand the effects of chemical cross-linking. Sharma and Bohidar[20] used light scattering to study the interactions between glutaraldehyde and gelatin in aqueous solution at concentrations less than that required for physical gelation or gelatin. The results suggest that there are two possible supramolecular structures for the gelatin–glutasaldehyde

complexes—a random coil with glutaraldehyde bound to lysine *residues in the gelatin chain and also pairing of gelatin molecules using glutaraldehyde bridges.*

Andjelić *and* Richard[21] *used depolarized light scattering to study* the *effects of* γ-irradiation *on the crystallization of ultrahigh* molecular *weight polyethylene. This material is important, as it is used for the manufacture of bearings in human total joint replacements. Recentiy, it was shown that the method of sterilization of the joint replacements has a significant effect on their wear characteristics, because free radicals* that *are produced can react with oxygen. leading to weakening, but if they react with each other, it* can *actually strengthen the bearing. Depolarized light scattering showed that the* nonirradiated *polymer is characterized by individual* spherulites *and their clusters, whereas for the irradiated samples. there was no evidence of ordered* supramolecular *structures.*

Zeng et al.[22] *studied the* self-assembly *of dendrimers based* on *tetraacid systems. Eight scattering allowed* them *to determine the molecular weight of the dendrimers, with results* that *compared well with other methods. including size exclusion chromatography. mass* spectrometry, *and vapor pressure* osmometry.

Eecollinet et al.[23] *investigated the self-assembly of tetraether glycolipid analogues representative of those found* in *the membranes of archaehacteria. and they used light scattering to show the stability of vesicles produced.*

Larger Systems—Crystallization

Light scattering was also used to study crystal growth. In *particular, size distributions for crystals growing* in *the nascent liquid were obtained. This is of particular interest in the pharmaceutical industry. where controlling particle size is often important. However, in many applications, dilution of the suspension is required, as the concentration of particles often exceeds the limits of conventional* light-*scattering equipment. One* method *to avoid this is to use* spectral *extinction that can cope with higher* concentrations.[24] *One field of particular interest in the area of* supramolecular *chemistry is that of clathrate (or gas) hydrates (for more* details *on clathrate hydrates. see the article Clathrate Hydrates and Ref.* [25]). *Several researchers* in *this area measured particle sizes, but the technique* is *notoriously* difficult *to use for these systems.* Monfort[26] used laser light *scattering to monitor* cyclo*propane hydrate* formation *and observed particles in the* 6–564 μm range. Yousif[27] also *used light scattering, but* only *to detect the* onset *of crystallization. which gives rise* to *a spike* in *the scattered light intensity. Moh and* Westacott[28] *also used* dynamic *light scattering to study the effect of chemical inhibitors on the* THF *hydrate formation process.* Nerheim[29] indicated *a critical* cluster *size* for *Structure* II *hydrates* in *the range* 3–80 nm *using dynamic light scattering. More recently, Bishnoi and* coworkers[30] *used light scattering to study the nucleation and growth of ethane hydrate on latex spheres. The approach has the advantage that hydrate* nucleates *on the* latex *particles, which overcomes some of the difficulties associated with water and hydrate having similar refractive indices. However, it complicates the issue by having an extra component in the system, and* more *work will need to be performed to increase the understanding of this system.*

CONCLUSION

Light scattering is clearly an important *tool for studying the structural characteristics and kinetics of formation of a wide range of materials, including proteins, polymers, chromophores. microorganisms. and inclusion compounds. such as gas hydrates. More specifically, information on particle size distributions of aggregates can be* determined from *laser* light *scattering. Depending on the* system *being studied, particle sizes of about a few nanometers to a few microns can be detected as a function of time, temperature. and composition. Such* information *is important in a* wide *range of industrial and medical applications, including self-assembly of amelogenin proteins, which is a major stage in enamel formation: crystallization of* ultrahigh-molecular-weight *polyethylene, which is used in bearings in* human *joint* replacements; *and control of crystal growth of gas hydrates, which is important in gas production and transportation.*

ACKNOWLEDGMENTS

Funding from Chevron Texaco *and the Gas Research Institute are gratefully acknowledged.*

ARTICLES OF FURTHER INTEREST

Classification and Nomenclature of Supramolecular Compounds, p. 261
Clathrate Hydrates, p. 274
Crystal Growth Mechanisms, p. 364
Self-Assembly: Definition and Kinetic and Thermodynamic Considerations, p. 1248
Self-Assembly in Biochemistry, p. 1257
Supramolecular Polymers, p. 1443

REFERENCES

1. Rerge. B.: Sudholz, M.: Steiner. B.: Rohmann, J.; Ruhl, E. In-site determination of single levitated solid aerosols. Phys. Chem. Chem. Phys. 1999. 24. 5485–5489.

2. Benmouna, F.: Peng, B.; Gapinski, J.: Patkowski. A.; Ruhe. J.; Johannsmann, D. Dynamic light scattering from liquid crystal polymer brushes swollen in a nematic solvent. Liq. Cryst. 2001, *28,* 1353–1360.
3. Ikkai. F.: Naito, S. Dynamic light scattering and circular dichroism studies on heat-induced gelation of hard-keratin protein aqueous solutions. Biomacromolecules 2002. 3, 482–487.
4. Bernocco, S.: Ferri, F.; Profurno, A.: Cuniberti, C.; Rocco. M. Polymerization of rod-like rnacromolecular monomers studied by stopped-flow, rnultiangle light scattering: Set-up. data processing. and application to fibrin formation. Biophys. J. 2000, 79. 561–583.
5. Ruso. J.M.: Attwood, D.; Taboada, P.; Mosquera, V.; Sarmiento, F. Light scattering and NMR studies on the self-aggregation of sodium *n*-hexyl sulfate in aqueous electrolyte solution. Langmuir 2000, *16.* 1620–1625.
6. Bagayev, S.N.: Gusev, V.A.; Orlov. V.A.: Panov. S.V. Investigation of moving species of microorganisms by laser light scattering spectroscopy. Laser Phys. 1996. *6*. 596–599.
7. Baetens. D.G.A.; Van Renterghem. L.M.L. Coupled particle light scattering: A new technique for serodiagnosis of epstein-barr virus infection. J. Med. Virol. 2001. *64,* 519–525.
8. Strawbridge. K.B.; Palmer. L.R.: Merrill, A.R.; Hallett, F.R. Integrated light-scattering spectroscopy, a sensitive probe for peptide-vesicle binding—Application to the membrane-bound colicin El channel peptide. Biophys. J. 1995. *68.* 131–136.
9. van der Zande, B.M.I.: Dhont. J.K.G.; Bohmer. M.R.; Philipse, A.P. Colloidal dispersions of gold rods characterized by dynamic light scattering and electrophoresis. Langmuir 2000. *16.* 459–464.
10. Mie. G. Ann. Phys. 1908, *25.* 377.
11. Bronk. B.V.; Li. Z.Z.; Czege. J. Polarized light scattering as a rapid and sensitive assay for metal toxicity to bacteria. J. Appl. Toxicol. 2001. *21,* 107–113.
12. Berne. B.J.; Pecora. R. *Dynamic Light Scattering with Applications to Chemistry, Biology and Physics*; Wiley: New York. 1976.
13. Moradian-Oldak. J. Amelogenins: Assembly, processing and control of crystal morphology. Matrix Biol. 2001, *20.* 293–305.
14. Moradian-Oldak. J.; Leung, W.; Fincham, A.C. Temperature and pH-dependent supramolecular self-assembly of amelogenin molecule: A dynamic light scattering analysis. J. Struct. Biol. 1998. *122.* 320–327.
15. Moradian-Oldak, J.: Paine. M.L.; Lei. Y.P.: Fincham. A.G.: Snead, M.L. Self-assembly properties of recombinant engineered amelogenin proteins analyzed by dynamic light scattering and atomic force microscopy. J. Struct. Biol. 2000. *131,* 27–37.
16. Lai, E.: van Zanten. J.H. Monitoring DNA/Poly-L-Lysine polyplex formation with time-resolved multiangle laser light scattering. Biophys. J. 2001. *80.* 864–873.
17. Collings, P.J.: Gibbs, E.J.; Starr, T.E.; Vafek, O.; Yee, C.; Pomerance, L.A.: Pasternack, R.F. Resonance light scattering and its applications in determining the size. shape, and aggregation number for supramolecular assemblies of chromophores. J. Phys. Chem.. B 1999. *103.* 8474–8481.
18. von Berlepsch. H.; Bottcher. C.: Ouart. A.; Burger. C.; Dahne. S.: Kirstein, S. Supramolecular structures of J-aggregates of carbocyanine dyes in solution. J. Phys. Chern., B 2000. *104.* 5255–5262.
19. Alloisio. M.; Moggio, I.: Cornoretto, D.; Cnniberti, C.; Dell'Erba. C.; Dellepiane, G. Soluble polydiacetylenes: Molecular properties and solid state organisation. Synth. Met. 2001. *124.* 253–255.
20. Sharma, J.; Bohidar. H.B. Gelatin-glntaraldehyde supramolecular structures studied by laser light scattering. Eur. Polym. J. 2000. 36. 1409–1418.
21. Andjelić, S.; Richard, R. Crystallization behaviour of ultrahigh molecular weight polyethylene as a function of in vacuo γ-irradiation. Macromolecules 2001, *34,* 896–906.
22. Zeng, F.: Zimmerman, S.C.: Kolotuchin. S.V.; Reichert. D.E.C.; Ma. Y. Supramolecular polymer chemistry: Design. synthesis. characterization. and kinetics, thermodynamics. and fidelity of formation of self-assembled dendrimers. Tetrahedron 2002, *58.* 825–843.
23. Lecollinet. G.; Gulik, A.; Mackenzie. G.; Goodby, J.W.: Benvegnu, T.; Plusquellec. D. Supramolecnlar self-assembling properties of membrane-spanning achaeal tetraether glycolipid analogues. Chem. Eur. J. 2002. *8.* 585–593.
24. Li. *M.:* Wilkinson. D. Particle size distribution determination from spectral extinction using evolutionary programming. Chem. Eng. Sci. 2001. *56.* 3045–3052.
25. Koh. C.A. Towards a fundamental understanding of natural gas hydrates. Chem. Soc. Rev. 2002. *31.* 157–167.
26. Monfort. J.P.; Nzihou. A. Light scattering kinetics study of cyclopropane hydrate growth. J. Cryst. Growth 1993. *128,* 1182–1186.
27. Yousif, M.H.: Dorshow, R.B.; Young. D.B. Testing of hydrate kinetic inhibitors using laser light scattering technique. Ann. N. Y. Acad. Sci. 1994. *715.* 330–340.
28. Koh. C.A. *Gas Research Institute Report:* Gas Research Institute: Chicago. 1996.
29. Rigmour-Nerheim, A. PhD Thesis: University of Trondheim, Department of Physics, 1993.
30. Servio. P.; Englezos. P.; Bishnoi. P.R. In *Kinetics of Ethane Hydrate Growth on Latex Spheres Measured by a Light Scattering Technique*. Proceedings of the New York Academy of Science, 2000: Vol. 912. 576–582.

Liquid Clathrates

Scott K. Spear
John D. Holbrey
Robin D. Rogers
The University of Alabama, Tuscaloosa, Alabama, U.S.A.

INTRODUCTION

Clathrates are a class of crystalline compounds formed from two different stable compounds that exhibit no covalent bond between them. A clathrate can be obtained when one compound. the host, crystallizes in such a way that holes or cavities within the lattice trap a second compound, the guest. This concept of a host matrix trapping a guest molecule can easily be extended from solid to liquid phases. Since their initial discovery in 1969, liquid clathrates have proven to be an interesting and growing area of research.''''

In the following sections, the distinction between air-sensitive and air-stable liquid clathrate systems will be discursed. We will also present typical synthesis and characterization procedures as well as a number of interesting applications for these nonconventional solvents.

BACKGROUND

''Liquid clathrate'' is a term coined by Professor Jerry L. Atwood, then at The University of Alabama.[4] This term was used to describe the serendipitous discovery of the biphasic behavior of a wide selection of salts with aromatic solvents. such as toluene and benzene. These semiordered liquids containing complex salt hosts and aromatic hydrocarbons represent the most common examples of liquid clathrates.[2]

The first examples of materials that supported liquid clathrate phase formation, in contact with aromatic hydrocarbons, were highly reactive air-sensitive salts containing alkylaluminum anions, first described by Atwood.[1,2] Their applications for separations of aromatics from hydrocarbons[5] and in coal liquefaction[6] were extensively explored. However, a drawback of the initial systems studied was their air-sensitivity and reactivity.

More recent research established that a much greater range of organic salts can form liquid clathrates when contacted with aromatic solvents,[3] including liquid salts now known as ''ionic liquid.''[7] Formation of liquid clathrates is observed most often with halide and pseudohalide anions. Regardless of cation or anion, these materials can be expressed as ''nonstoichiometric liquid inclusion compounds'' forming complexes in conjunction with aromatic solvents ranging between 1.3–42.2 molecules of solvent.[3]

Liquid clathrate phases are formed when large regions of liquid order exist, in which cations and anions exhibit strong interactions with aromatic molecules. Aromatic molecules acting as guests within the salt ions serve to support and stabilize the structure resulting from the cation–anion packing interactions. With too little interaction between aromatics and cation–anion hosts, the salts are simply completely miscible or immiscible with the aromatics, whereas, if the ion–ion interaction5 are too great, then the salt will simply crystallize. Provided in Fig. 1 is a simplistic view of the phenomenon.

SYNTHESIS, ANALYSIS, AND EXAMPLES OF LIQUID CLATHRATES

Preparation of the First Liquid Clathrates

Liquid clathrates may be prepared by two different methods. These methods can best be illustrated by the preparation of $K[Al_2(CH_3)_6N_3]$.[8] In an N_2 atmosphere dry box, approximately 0.010 mol $Al(CH_3)_3$ was added to 0.005 mol KN_3 to give solid $K[Al_2(CH_3)_6N_3]$ (1). The addition of toluene (0.10 mol) to 1 produced the liquid clathrate $K[Al_2(CH_3)_6N_3] \cdot 3.8\ C_6H_5CH_3$.

A second method for the production of liquid clathrates involves the addition of 0.005 mol KN_3 and 0.010 mol $Al(CH_3)_3$ to 0.10 mol toluene in an N_2 atmosphere dry box. This procedure yields a liquid clathrate identical in composition to the one prepared in the previous method. Note that liquid clathrate formation is a visually dramatic event. As the reaction proceeds, separation of two distinct liquid layers becomes obvious.

Analysis of Aromatic Stoichiometries

Molar miscibility and saturation point measurements describing liquid clathrate behavior are commonly analyzed by the integration of NMR spectra. In most cases. the aromatic stoichiometries are the average of three preparations and integrations with an acceptable standard deviation result of ±0.2 molecules. A common feature of all liquid clathrate NMR spectra is the shifting of the entire spectrum 0.2–0.5 ppm downfield relative to the pure aromatic substance.

Encyclopedia of Supramolecular Chemistry
DOI: 10.1081/E-ESMC 120012800

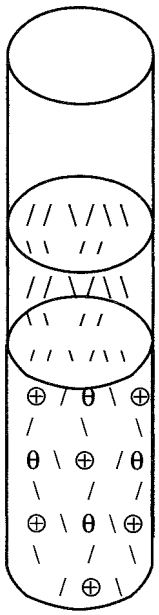

Fig. 1 Excess aromatic molecules (top phase) with a liquid clathrate (bottom phase).

Air-Sensitive Liquid Clathrates

Since the initial discovery of liquid clathrate systems, hundreds of compounds having the structure $M[Al_2R_6X]$ were found to exhibit liquid clathrate behavior.[1,2] While these highly reactive air-sensitive salts are useful in such applications ranging from separations of aromatics from hydrocarbons to coal liquefaction. their air-sensitivity and reactivity posed drawbacks to further study.

Liquid clathrate systems are characterized by a maximum aromatic-to-parent compound ratio (A/A ratio). The A/A ratio has proven to be constant for each liquid clathrate system. regardless of the presence of excess aromatic. In order to illustrate three important trends of liquid clathrates, a partial listing is shown in Table 1.

Table 1 Some representative alkylaluminum liquid clathrates"

Compound	A/A Ratio[b]
$K[Al_2(CH_3)_6N_3]$	5.8
$Rb[Al_2(CH_3)_6N_3]$	6.1
$Cs[Al_2(CH_3)_6N_3]$	7.4
$K[Al_2(CH_3)_6NO_3]$	7.0
$Cs[Al_2(CH_3)_6NO_3]$	12.0
$[N(CH_3)_4][Al_2(CH_3)_6Cl]$	8.1
$K[Al_2(CH_3)_6N_3]$	3.8[c]
$[N(CH_3)_4][Al_2(CH_3)_6Cl]$	5.6[c]

"From Ref. [2].
[b]Maximum aromatic-to-parent compound ratio for benzene.
[c]Maximum aromatic-to-parent compound ratio for toluene.

From such data as shown in Table 1, Atwood suggested the following observations:[2,3]

- For a given anion and aromatic. the larger the cation, the larger the A/A ratio.
  For a given cation and anion, the larger the anion, the larger the A/A ratio.
  For a given anion and cation. the larger the aromatic, the smaller the A/A ratio.

These observations appear to hold for all known alkylaluminum-based liquid clathrates. For example, a selenonium ion-based liquid clathrate having the inclusion formula $[(CH_3)_3Se][ClAl(CH_3)_2(Cl)Al(CH_3)_3]$.(aromatic solvent), can accommodate 8.5 benzene molecules or 8.3 toluene molecules per parent compound.[9]

Extensive research was conducted on liquid clathrates formulations using crown-ether complexes of oxonium ions.[3] One such reaction of interest arises from the interaction of 18-crown-6 with HCl in toluene with a little moisture. which results in a liquid clathrate layer having composition $[H_3O \cdot 18\text{-crown-6}][HCl_2] \cdot 3.6\ C_6H_5Me$.[10] While having a "measurable" stability, these liquid clathrates eventually deposit crystals over hours or days, and crystals of $[H_3O \cdot 18\text{-crown-6}1[HCl_2]$ were isolated.[10] Listed in Table 2 are several oxonium ion-liquid clathrates along with their reported A/A ratios and corresponding reference.

Air-Stable Liquid Clathrates and Ionic Liquids

For a rationalization of the similar physical behavior of liquid clathrate formation with aromatics. for a chemically dissimilar set of materials. Zaworotko et al.[16] suggested that liquid clathrate formation was chiefly dependent on the physical properties of the organic salts. rather than on their chemical natures. Thus, an approach to developing other systems capable of sustaining liquid clathrates would be to investigate organic salts with low melting points (or even salts that were liquid at room temperature). This is clearly a description of ionic liquids.[17,18]

In studies to determine the miscibility of ionic liquids with aromatic solvents, Holbrey et al. found that ionic liquid-aromatic mixtures form liquid clathrate systems.[7] For example, ionic liquids of current interest, such as hydrophobic 1-alkyl-3-methylimidazolium salts ($[C_n$-mim]X) with hexafluorophosphate, *bis*(trifyl)imide, and tetrafluoroborate anions were observed to form liquid clathrates with benzene. toluene, and xylenes (Fig. 2). In

Table 2 Some oxonium ion–crown ether liquid clathrates

Compound	A/A Ratio	Reference
$[H_3O$ 18-crown-6$][Cl\text{-}H\text{-}Cl]$	4.8[a]	[10]
$[H_3O$ 18-crown-6$][Cl\text{-}H\text{-}Cl]$	3.6[b]	[10]
[K 18-crown-6$][Cr(CO)_5Cl]$	1.7[b]	[11]
$[H_3O$ 18-crown-6$][W(CO)_5Cl]$	3.1[b]	[11]
$[H_3O$ 18-crown-6$][W(CO)_4Cl_3]$	2.3[a]	[11]
$[H_2O$ *bis-aza*-18-crown-6 $(H)_2][W(CO)_4Cl_3]_2$	2.2[a]	[11]
$[H_3O$ 18-crown-6$][I_7]$	3.6[b]	[12]
$[H_3O$ 18-crown-6$][MoOCl_4(H_2O)]$	1.9[b]	[13]
$[H_3O$ 18-crown-6$][WOBr_4(H_2O)]$	3[b]	[13]
$[H_2O$ *aza*-18-crown-6 (H)$][MoOCl_4(H_2O)]$	1.9[b]	[13]
$[H_2O$ *aza*-18-crown-6 $(H)]_2[WOCl_4(H_2O)][Cl]$	2.1[b]	[13]
$[H_3O$ 18-crown-6$][CrCl_4(H_2O)_2]$	1.67[b]	[14]
$[H_3O$ 18-crown-6$]_2[H_5O_2\ Mo_2Cl_9]$	1.9[b]	[14]
$[H_3O$ 18-crown-6$][WOCl_4(H_2O)]$	2.3[b]	[14]
$[H_3O$ 18-crown-6$][TiCl_5(H_2O)]$	2.1[b]	[15]

[a]Maximum aromatic-to-parent compound ratio for benzene
[b]Maximum aromatic-to-parent compound ratio for toluene.

the system [1-butyl-3-methylimidazolium][*bis*(trifyl)imide] ($[C_4mim][NTf_2]$)/benzene, the upper phase is wholly benzene, whereas the lower ionic liquid clathrate phase contains ca. 1:3.5 ratio of ionic liquid:benzene, i.e., has an excess of aromatic solvent.

Other air- and water-stable liquid clathrates based on boronic acid derivatives were also shown to possess water-dependent liquid clathrate formation.[19] These phosphonium cyanoborates. *bis*(methyltriphenylphosphonium)*B*,*B*′-dicyano-*B*,*B*′-hexamethylenebis(9)-borata-bicyclo[3.3.1]nonane, when anhydrous, did not dissolve in furan, but adding one equivalent of H_2O and warming resulted in rapid formation of a yellow liquid clathrate below a colorless furan layer. Some average A/A ratios included benzene (0.8), o-, *m*-, p-xylene (all 0.3), and mesitylene (0.2).

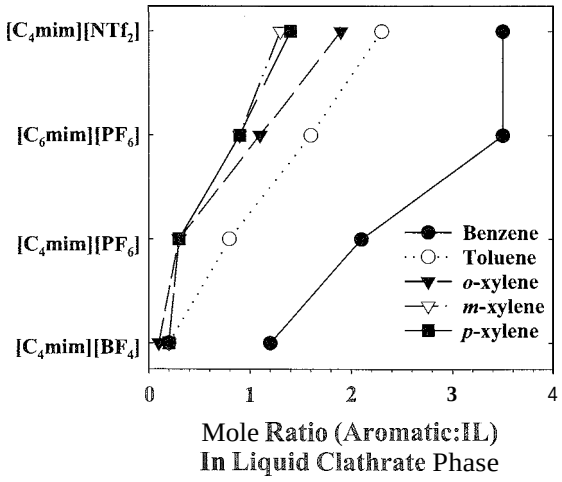

Fig. 2 Ratio of aromatic to ionic liquids in the lower phase of the liquid clathrate biphasic systems. The data shown for *n*-alkyl-methylimidazolium ionic liquids is from Ref. [7]. Connecting lines are a visual guide to changes in the liquid clathrate phase composition.

APPLICATIONS

Separations

The potential application of liquid clathrates to separation science is of continuing interest. in particular, the separation of closely related aromatic hydrocarbons such as benzene and toluene, or o. *m*. and p-xylene [2] Organic nonquaternary clathrate salts were successfully applied as useful materials for separating hydrocarbon feed streams into aromatics-rich fractions and aromatics-lean fractions [5]

Coal Liquefaction

Another interesting application of liquid clathrates that was explored is in coal liquefaction. This patented application resulted in the rapid partitioning of 23% of the coal mass into the liquid clathrate phase of a toluene-based liquid clathrate system at 50°C.[6] It is reported that no chemical reaction is believed to occur between the liquid clathrate and the coal.[2]

Catalysis

The liquid clathrate phase will dissolve substances that act as olefin hydrogenation catalysts, creating homogeneous hydrogenation catalysts.[2] Polymerization catalysts comprised of stable liquid clathrate aluminoxane, aromatic solvents. and organic. inorganic, or organometallic compounds were described.[20,21] Liquid clathrate compositions comprised of a metal halide, a quaternary ammonium salt, a quaternary phosphonium salt. or a ternary sulfonium salt: an aluminum trihalide; and an aromatic hydrocarbon have proven useful as reusable aluminum catalysts in Friedel–Crafts reactions.[22]

The support for liquid clathrate formation under biphasic conditions in ionic liquid-aromatic systems is an important and underrecognized phenomena. As the use of ionic liquids as solvents and catalyst immobilization phases for transition metal catalyzed reactions becomes increasingly commonplace, the importance of understanding liquid clathrate formation as an activation and

Table 3 Oxonium ion–crown ether complexes crystallized from liquid clathrates

Compound	Ref.
$[Ti(\eta\text{-}C_5H_5)Cl \cdot 18\text{-crown-}6][AlCl_2Me_2]$	[15]
$[ZrCl_2 \cdot (OCH_2CH_2)_5OCH_2CH_2Cl][ZrCl_5(thf)]$	[15]
$[Na \cdot 18\text{-crown-}6][HfCl_5(thf)]$	[15]
$[H_3O \cdot 18\text{-crown-}6]_2[ReCl_6]$	[26]
$[H_2O \cdot 12\text{-crown-}4 \cdot Co][(CoCl_3)\mu\text{-}Cl]$	[27]

separations tool will become crucial. Differences in chemistry can be achieved in IL-aromatic biphasic systems and IL-hydrocarbon, or other biphasic systems, are almost certain, because the former example supports formation of liquid clathrate phases, whereas in the latter, the biphases are truly ionic liquid-molecular liquid.

It was recognized that Lewis acid Friedel–Grafts alkylation of benzene in $Cl/AlCl_3^-$ containing ionic liquids was occurring under liquid clathrate conditions. and that from the reactive chemistry perspective, these systems were identical to liquid clathrates that formed with higher melting alkylammonium salts. Liquid clathrate formation with ionic liquids was also applied as a separations technique for aromatic/aliphatic hydrocarbon mixtures,[23] with the advantage that all components are liquid at room temperature, which precludes formation of precipitants. Most recently, Dixneuf and coworkers described olefin metathesis reactions catalyzed by ruthenium allenylidene catalysts under biphasic ionic liquid-toluene systems, that is in a liquid clathrate supporting reaction media.[24,25] The authors reported that the biphasic systems formed were stable. with the ruthenium catalysts remaining in the lower (salt-rich) phase, allowing facile product extraction by transfer of the upper, toluene phase. It would be interesting to compare reactivity in this system with an analagous ionic liquid/hexane or other aliphatic upper-phase system to examine whether the reaction productivity and mass transport effects are enhanced in a liquid clathrate system over a solely ionic liquid biphasic system.

Crystallizations

Liquid clathrates as crystallization media have resulted in many new structures. Crystals of crown ether,[26,27] cryptand,[28,29] and tetramethylethylenediammonium and triphenylphosphonium[30] complexes were prepared. Presented in Table 3 is a short list of some oxonium ion crown-ether crystal complexes which deposited from the liquid clathrate mixture. Oxonium ion complexes with crown ethers from a liquid clathrate media were formed of a suitable size and shape to crystallize lanthanides and actinides.[31]

CONCLUSION

Liquid clathrates represent an interesting area of supramolecular chemistry. Over the years. the move from air-sensitive to air-stable liquid clathrate systems greatly simplified their handling procedures. Also, with the emergence of air-stable liquid clathrate systems, their possible applications broadened beyond early useful applications of coal liquefaction and hydrocarbon separations to include aqueous separations and catalytic systems.

The field of liquid clathrates can also aid in our understanding of new fields; such as ionic liquids, where many ionic liquid compositions are being observed to behave as liquid clathrates. The ionic liquid researchers are searching for new and varied liquid salt compositions, and thus, one may predict that a plethora of new liquid clathrate hosts will soon appear in the literature. It will be incumbent on researchers in liquid clathrates and ionic liquids to make the connections between the two fields.

ARTICLES OF FURTHER INTEREST

Cation–π Interactions, p. *214*
Classical Descriptions of Inclusion Compounds, p. *253*
Clathrate Hydrates, p. *274*
Clathrate Inclusion Compounds, Phase Transitions in, p. 289
Crown Ethers, p. *326*
Hydrogen Bonding. p. 658
Inclusion Compounds: Selectivity, Thermal Stability, and Kinetics, p. *696*
Nuclear Magnetic Resonance Spectroscopy. p. 981
n–n Interactions: Theory and Scope. p. *1076*
n–n Stackirzg as a Crystal Engineering Tool. p. 1093

REFERENCES

1. Atwood, J.L.; Atwood, J.D. Non-Stoichiometric Liquid Enclosure Compounds ("Liquid Clathrates"). In *Inorganic Compounds with Unusual* Properties; King. R.B., Ed.: American Chemical Society: Washington, 1976: 112–127.
2. Atwood, J.L. Liquid Clathrates. In *Inclusion Compounds*; Atwood, J.L., Davies. J.E.D., MacNicol, D.D., Eds.: Academic Press: London, 1984; Vol. 1, 375–405.
3. *Supramolecular* Chemistry: Steed. J.W., Atwood, J.L., Eds.: John Wiley & Sons: New York. 2000: 707–714.
4. Atwood, J.L. Liquid Clathrates. U.S. Patent 4,024,170, May 17, 1977.
5. Boate. D.R.: Zaworotko. M.J. U.S. Patent 5,220,106. Jun. 15, 1993.
6. Atwood, J.L. Coal Liquefaction Using Liquid Clathrates. U.S. Patent 4,321,127. Mar. 23, 1982.
7. Flolbrey. J.D.: Reichert. W.M.: Nieuwenhuyzen, M.:

Sheppard, O.: Hardacre. C.: Rogers, R.D. Liquid clathrate formation in ionic liquid-aromatic mixtures. Chem. Commun. 2003. 476–477.
8. Atwood, J.L.; Newberry, W.R. Solid state structure and solution behavior of compounds of the type $M[Al_2(CH_3)_6X]$. J. Organomet. Chem. 1972. 42. C77–C79.
9. Sangokoya, S.A.: Robinson, G.H. Reaction of trimethylaluminum with selenium tetrachloride. Synthesis of $[(CH_3)_3Se][ClAl(CH_3)_2(Cl)Al(CH_3)_3]$. The first selenium-based liquid clathrate. J. Incl. Phenom. Mol. Recognit. Chem. 1990. 9. 85–88.
10. Atwood, J.L.; Bott. S.G.; Coleman, A.W.: Robinson, K.D.; Whetstone, S.B.; Means, C.M. The H_3O^+ cation in aromatic solvents. Synthesis. structure, and solution behavior of $[H_3O^+ \cdot 18\text{-crown-}6][Cl\text{-}H\text{-}Cl]$. J. Am. Chem. Soc. 1987. *109*, 8100–8101.
11. Atwood, J.L.: Bott. S.G.; Junk, P.C.: May, M.T. Liquid clathrate media containing transition metal halocarbonyl anions; formation and crystal structures of $[K^+ \cdot 18\text{-crown-}6][Cr(CO)_5Cl]$, $[H_3O^+ \cdot 18\text{-crown-}6][W(CO)_5Cl]$, $[H_3O^+ \cdot 18\text{-crown-}6][W(CO)_4Cl_3]$, and $[H_2O \cdot \text{bis-aza-}18\text{-crown-}6 \cdot (H^+)_2][W(CO)_4Cl_3]_2$. J. Organomet. Chem. 1995. *487*, 7–15.
12. Junk. P.C.; MacGillivray. L.R.; May. M.T.; Robinson. K.D.; Atwood. J.L. Synthesis and x-ray structure of $[H_3O^+ \cdot 18\text{-crown-}6][I_7^-]$. A new infinite sawhorse geometry for I_7^- crystallized from a liquid clathrate medium. Inorg. Chem. 1995. *34*. 5395–5396.
13. Atwood. J.L.; Bott, S.G.: Junk. P.C.: May. M.T. Anionic coordination complexes of Mo and W which crystallize from liquid clathrate media with oxonium ion-crown ether cations. J. Coord. Chem. 1996. *37*. 89–105.
14. Atwood, J.L.; Junk, P.C.; May, M.T.: Robinson, K.D. New. simple coordination compounds of Cr. Mo, and W from liquid clathrate media. J. Coord. Chem. 1996, *40*. 247–251.
15. Alvanipour, A.; Atwood. J.L.; Bott. S.G.: Junk. P.C.; Kynast. U.H.; Prinr, Pi. Some crown ether chemistry of Ti, Zr, and Hf derived from liquid clathrate media. J. Chem. Soc., Dalton Trans. 1998. 1223–1228.
16. Gaudet. M.V.: Peterson. D.C.: Zaworotko, M.J. Ternary hydrogen halide/base/benzene mixtures: A new generation of liquid clathrates. J. Incl. Phenom. Mol. Recognit. Chern. 1988. 6. 425.
17. *Ionic Liquids: Industrial Applications to Green Chemistry*; Rogers. R.D.. Seddon. K.R., Eds.; ACS Symposium Series. American Chemical Society: Washington, 2002; Vol. 818.
18. Ionic Liquids in *Synthesis*; Wasserscheid. P., Welton. T., Eds.; Wiley–VCH: Weinheim. 2003.
19. Hunter. R.: Haueisen, R.H.; Irving, A. The first water-dependent liquid clathrate: X-ray evidence in the solid for a C–H···π(heteroarene)···H–C interaction. Angew. Chem.. Int. Ed. Engl. 1994, *33*, 566–568.
20. Sangokoya. S.A. Liquid Clathrate Aluminoxane Compositions. U.S. Patent 5,670.682, Sep. 23, 1997.
21. Sangokoya. S.A. Liquid Clathrate Aluminoxane Compositions as Co-Catalysts with Transition Metal Catalyst Compounds. U.S. Patent 5,922,631. Jul. 13. 1999.
22. Park, W.S. Liquid Clathrate Compositions. U.S. Patent 6,096,680, Aug. 1. 2000.
23. Selvan. M.S.; McKinley, M.D.; Dubois. R.H.; Atwood. J.L. Liquid–liquid equilibria for toluene + heptane + 1-ethyl-3-methylimidazolium triiodide. and toluene + heptane + 1-butyl-3-methylimidazolium triiodide. J. Chem. Eng. Data 2000, *45*. 841–845.
24. S¿meril, D.: Olivier-Bourbigou. H.; Bruneau, C.; Dixneuf, P.H. Alkene metathesis catalysis in ionic liquids with ruthenium allenylidene salts. Chem. Commun. 2002. 146–147.
25. Csihony, S.; Fischmeister. C.: Bruneau, C.; HorvÏth, I.T.: Dixneuf. P.H. First ring-opening metathesis polymerization in an ionic liquid. Efficient recycling of a catalyst from a ruthenium allenylidene complex. New J. Chem. 2002, 26, 1667–1670.
26. Barbour, L.J.; MacGillivray, L.R.: Atwood. J.L. Crystal and molecular structure of $[H_3O \cdot 18\text{-crown-}6]_2[ReCl_6]$ isolated from a liquid clathrate medium. J. Chern. Crystallogr. 1996, 26. 59–61.
27. MacGillivray, L.R.; Atwood. J.L. Synthesis and structure of (H_2O)(12-crown-4)-Co(II)(Co(II)(μ-Cl) isolated from a liquid clathrate medium. J. Chern. Crystallogr. 1997, *27*, 453–456.
28. MacGillivray, L.R.; Atwood, J.L. Proton-induced chirality: Proton complexation in the chiral cryptand 222-$2H^+$ dication isolated from a liquid clathrate medium. J. Org. Chem. 1995. *60*, 4972–4973.
29. MacGillivray, *L.R.;* Atwood. J.L. Insight into the mechanism of the protonation of cryptand 222 within a liquid clathrate medium: Synthesis and x-ray crystal structure of $[H_3O][222\text{-}2H][(CoCl_3)_2(\mu\text{-}Cl)]$. Chem. Commun. 1996. 735–736.
30. Junk. P.C.; Atwood. J.L. Hydrogen-bonded tetramethylethylenediammonium and triphenylphosphonium complexes derived from liquid clathrate media. J. Coord. Chem. 1999, *46*. 505–518.
31. Hassaballa. H.; Steed. J.W.: Junk. P.C.; Elsegood, M.R.J. Formation of lanthanide and actinide oxonium ion complexes with crown ethers from a liquid clathrate medium. Inorg. Chern. 1998. *37*. 4666–4671.

The hock and Key Principle

Anatoly K. Yatsimirsky
Universidad Nacional Autónoma de México, Mexico City, Mexico

INTRODUCTION

More than one century ago, Emil Fisher introduced the lock-and-key analogy for the specificity of enzyme action, thus providing the first description of the molecular recognition phenomenon.[1–3] In terms of modern concepts, the lock-and-key principle describes the binding strength and specificity as a result of a number of complementary interactions between rigid preorganized host and guest molecules. Discovery of high flexibility of proteins and observations of significant conformational changes accompanying binding of ligands to proteins led to an extension of the lock-and-key principle by the induced fit mechanism, which was initially proposed to explain some anomalies in the catalytic action of enzymes transforming sugar substrates.[''] Binding via the induced-fit mechanism may be accompanied by free energy losses due to the shift of the receptor conformation from that which corresponds to the energy minimum. On the other hand, the induced-fit mechanism gives a way of understanding such important phenomena as allosteric regulation and cooperativity. Organic ligands also undergo substantial conformational changes upon complexation, which also may be energetically unfavorable due to such factors as restrictions of internal rotations, induced torsional strain, etc. These energy losses will be minimal if the ligand is prepared in a rigid binding conformation and, therefore. will interact with the receptor by the lock-and-key mechanism.

PROTEIN–PROTEIN AND PROTEIN–LIGAND ASSOCIATIONS

A large number of x-ray structures of proteins and protein–ligand as well as protein–protein complexes accumulated since the mid-1970s. In some cases, e.g., for complexes of proteolytic enzymes with small protein inhibitors as well as for the first reported structure of an antigen–antibody complex,[5] the results agree with the classical lock-and-key principle. but in general. modest to strong conformational changes in protein and ligand molecules are observed.[6,7] Recent analysis of 39 pairs of structures of protein complexes and respective individual proteins revealed that the general model of binding is induced fit. In many cases, however, conformational changes are relatively small and often do not involve functionally important residues, so it is suggested that the binding can be considered in terms of the lock-and-key principle as a first approximation.[8]

Detailed analysis of protein–ligand binding was performed for interaction of Fab fragments of affinity-matured antibody 28B4 and its germline precursor with hapten **1**.[9] The affinity-matured antibody forms ca. 1000 times more stable complex with **1** than the germline antibody: $K_d = 37$ nM and 25 μM, respectively. Shown in Fig. 1 are structures of haptene complexes with both antibodies. Comparison of these structures with those of respective unligated proteins shows only minor differences in the case of 28B4. consistent with the classical lock-and-key mechanism, but significant binding-induced changes in the structure of the germline antibody in accordance with the induced-fit mechanism. However, lower affinity of the germline antibody probably is not due to a possible energetic cost of the induced fit. As one can see from Fig. 1, there are several mutations in the active site of the affinity-matured antibody that provide additional binding interactions with the hapten. As a result, the hapten gains two additional hydrogen bonds to the phosphonate group with $Lys53^H$, which substitute $Asn53^H$ of the germline antibody, and a higher degree of stacking interaction with the aromatic groups of $Trp95^H$, $Phe50^H$, and $Tyr32^L$, the first of which substitutes $Asp95^H$ of the germline antibody. The mutation of $Trp95^H$ to Asp in the affinity-matured antibody reduces its affinity essentially to the level of the germline antibody ($K_d = 20$ μM). And, the germline antibody with mutations $Asn53^H$Lys/$Asp95^H$Trp has the affinity increased to a level that is only three times less than that of the affinity-matured antibody ($K_d = 110$ nM). It seems, therefore, that at least in this case, the number of pairwise binding interactions is more important than preorganization.

The problems of optimum geometry, conformational rigidity/flexibility, and binding mechanism of organic ligands to proteins are extensively studied with respect to the design of new drugs.[10,11] We will discuss some of these aspects, taking as an example detailed studies reported on thermolysin phosphonamide inhibitors.[12,13] In Fig. 2, the structures of inhibitors and the dissociation constants of their complexes with thermolysin are shown.

Encyclopedia of Supramolecular Chemistry
DOI: 10.1081/E-ESMC 120012666

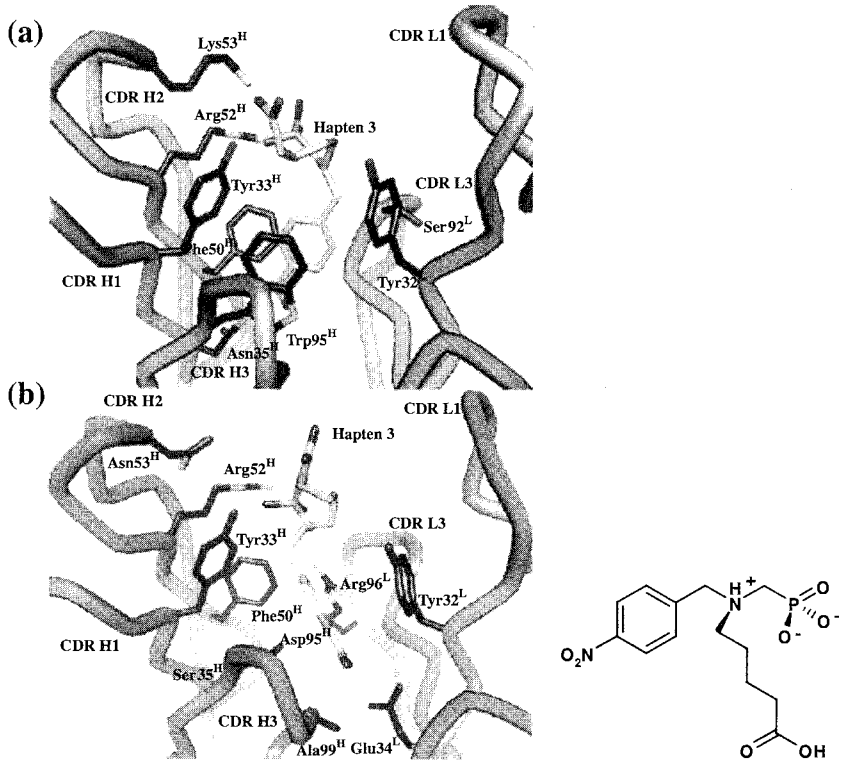

Fig. 1 The active site of the affinity-matured 28B4 Fab–hapten I (**Hapten 3** on the figure) complex (a) and the germline Fab–hapten **1** complex (b).[9] The backbone of the affinity-matured 28B4 Fab is in light brown, and its active site residues are in dark brown. The backbone of the germline Fab is in light blue. and the active site residues are in dark blue. Both haptens are shown in yellow. Reprinted with permission from Ref. [9]. Copyright 2001 by American Chemical Society.

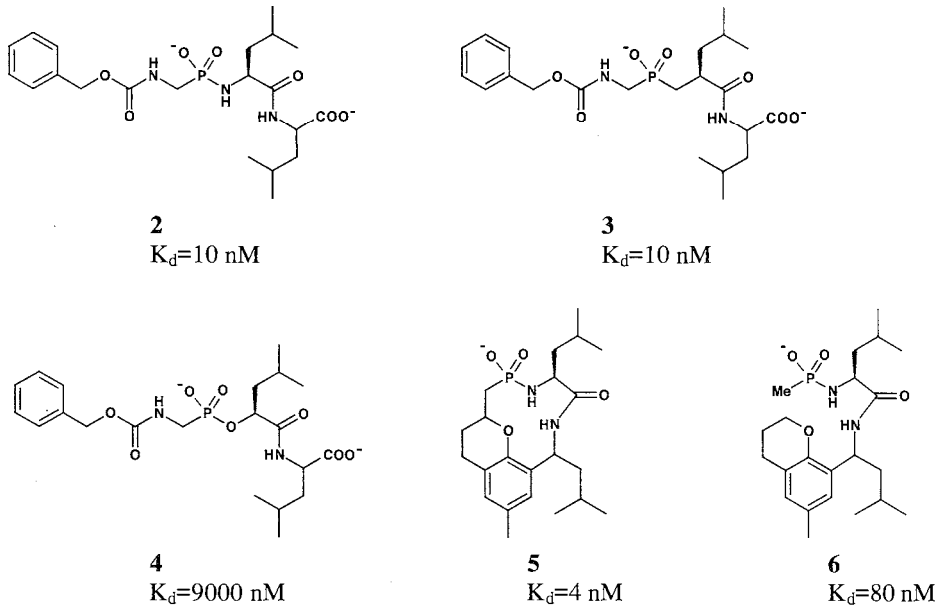

Fig. 2 Therrnolysin phosphonamide and analog inhibitors with dissociation constants of enzyme-inhibitor complexes

The binding site of the enzyme involves a Zn(II) cation, which interacts with an anionic phosphate group, and a number of functional groups, which participate in hydrogen bonding. In particular, the carbonyl oxygen of Ala-113 forms a hydrogen bond with the phosphonamidate NH group in 2. Substitution of this NH group with CH_2 in **3** does not affect binding, but the phosphonate 4 in which this group is substituted with O has much lower affinity. The structure of the thermolysin complex with 4 is the same as with 2. Therefore. the negative effect of oxygen replacement can be attributed to the repulsive interaction of partial negative charges on oxygen atoms of 4 and Ala-113. (In other cases, the replacement of an amide group of the ligand with an ester group leads to a misfit between guest and host molecules and to a strong inhibitory effect. For example, this was observed in the comparison of structures of vancomycin complexes with N-Ac-D-ala and O-Ac-D-lac.[14] This simple and efficient '.mutation'' of the ligand structure is used by bacteria to develop resistance to the vancomycin antibiotic.) Similar stability constants for 2 and **3** were interpreted as a result of hydration effects: the methylene group of inhibitor **3** does not form a hydrogen bond with the enzyme or with a water molecule, in contrast to the NH group of 2; therefore, the balance of ruptured and formed hydrogen bonds is the same for both inhibitors.

Cyclic inhibitor (S,S)-**5** was designed on the basis of the structure of the enzyme complex with 2 in such a way that it would adopt the conformation observed in the crystal structure but would be conformationally rigid and avoid unfavorable steric interactions with the enzyme.[13] Also, chemically and conformationally similar, but acyclic, inhibitor (S)-**6** was prepared. Crystal structures of the complexes between these inhibitors and thermolysin confirmed the anticipated mode of binding. The stability of the thermolysin complex with rigid (S,S)-**5** is 2.5 times stronger than with 2 and, more importantly, 20 times stronger than with acyclic analog (S)-**6**.

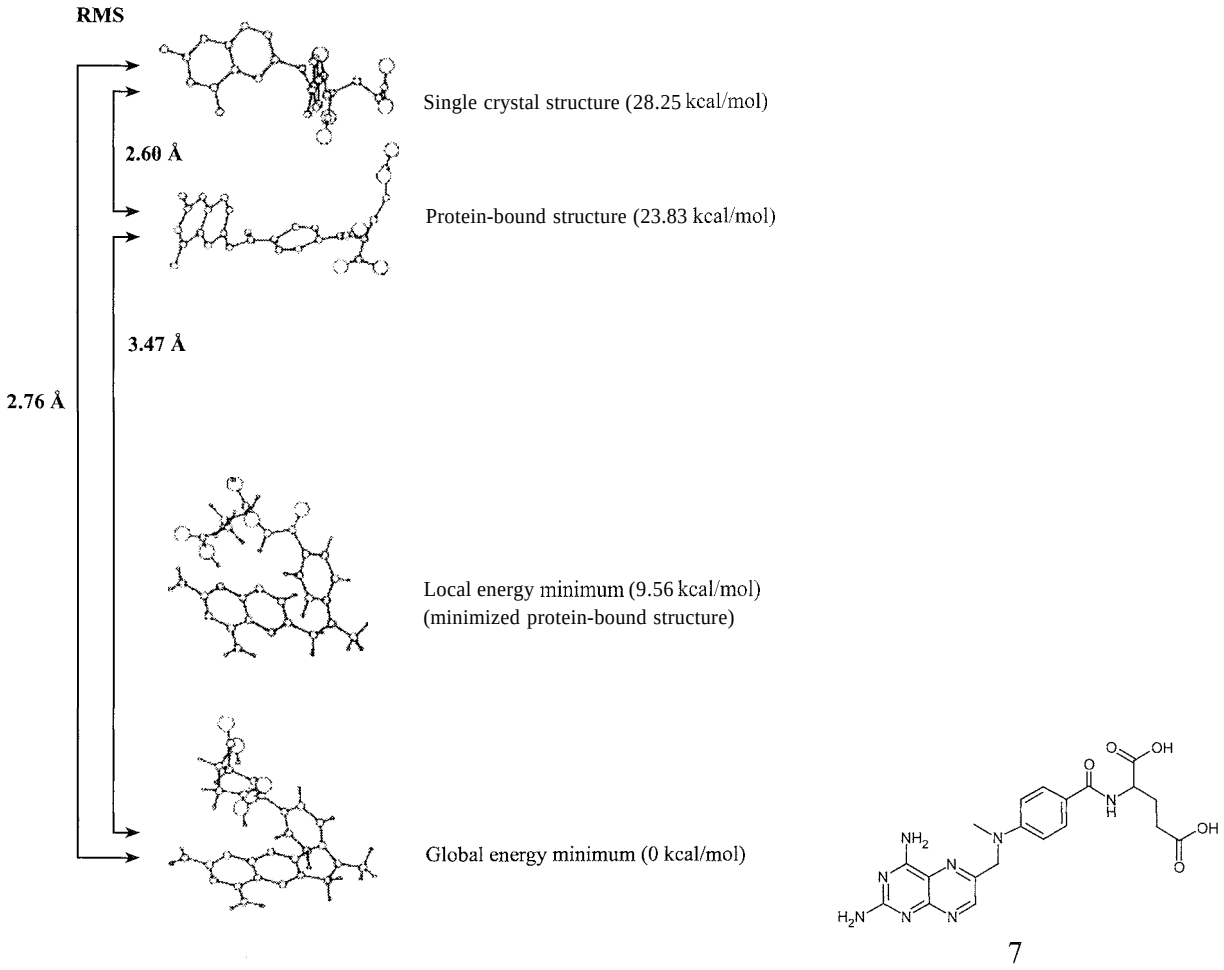

Fig. 3 Conformational changes of methotrexate **7**.[16] Reprinted from Ref. [16]. Copyright 1995, with permission from Elsevier

It is worth noting that rigidification of a flexible ligand often leads to the loss of affinity,[10] but the reason for this is the fixing of a conformation different from the optimum for binding or the appearance of some repulsive steric interactions with fragments used for rigidification. Another factor, which should be taken into account, is that some flexibility of the ligand and the receptor persists even in their complex, reducing interaction enthalpy but increasing the entropy.[13] For example; the binding constant of 2-[(4′-hydroxyphenyl)azo]benzoate to streptavidine increases from $7.3 \times 10^3\ M^{-1}$ to $2.0 \times 10^5\ M^{-1}$ and then to $1.2 \times 10^6\ M^{-1}$ on going from unsubstituted dye to its 3'-methyl and 3′,5′-dimethyl derivatives, exclusively due to the increase in the complexation entropy.'''' High-resolution x-ray structural studies suggest that the positive complexation entropy is due to two factors: displacement of water from the binding site and retention of ligand flexibility in the bound state. Therefore, rigidification is expected to improve the interaction enthalpy but may be unfavorable for the interaction entropy.[13]

Interesting results were obtained by molecular mechanics calculations of conformational changes of small molecules accompanying their binding to proteins.[16,17] The analysis of crystal structures of 33 small molecules as pure compounds and as protein-bound compounds showed considerable differences in their conformations.[16] Both conformations are also different from the global energy minimum conformation. and the degree of deformation depends on the number of bonds around which free rotation exists. Interrelations between different structures of a ligand are illustrated in Fig. 3 for methotrexate (**7**).[16] Both pure compound and protein-bound compound structures are well above the global minimum structure and do not correspond to a local energy minimum structure. However, the important question is how essential are these differences for binding? Comparisons of minimized solution conformations and protein-bound conformations of 10 small molecules showed that if the criterion is the values of torsion angles, the structures can be considered different, but if one compares the positions of ''anchor points'' (several key atoms responsible for tight binding), they appear to be similar in the free and bound ligand conformations.'''' On this basis, it was concluded that despite obvious conformational changes. the binding essentially follows the lock-and-key mechanism, and the low-energy structure in solution correctly represents the positions of importance for binding groups.

HOST–GUEST ASSOCIATION

Synthetic receptors of different types (crown ethers. podands, cyclophanes, calixarenes) possess large degrees of conformational mobility. The binding mode to these receptors is the induced-fit mechanism that. in particular, leads to a possibility of allosteric regulation of the ligand binding to these receptors. This aspect and the respective conforinational changes are discussed in the article. *The Allosteric Effect.* Rigidification of these receptors, usually considered preorganizaiton. in several instances was found

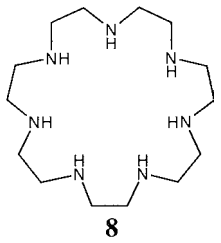

8

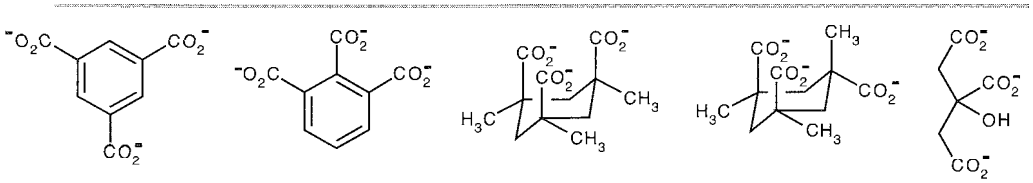

$H_4 8^{4+}$	4.6	5.2	5.2	4.0	2.7
$H_7 8^{7+}$	10.0	12.7	15.7	11.7	8.1

Fig. 4 *Logarithms of the association constants of some tricarboxylate anions with differently protonated* forms *of a* macrocycle *8. (From Ref.* [24].)

to improve the binding selectivity and affinity, see, e.g., Refs. [18,19]. The binding mode to such preorganized receptors is essentially the lock-and-key mechanism.

Cyclodextrins are an important class of rigid receptors. although molecular modeling predicts some degree of flexibility.[20] A modified mono-*altro*-β-cyclodextrin, in which one of the seven glucose units is changed to an altrose. was prepared to achieve the induced-fit mechanism of binding.[21] Complexation of adamantancarboxylate to this host induced a conformational change in the altropyranose unity.

It was pointed out that the degree of complementarity between interacting atoms and the losses due to restrictions of internal rotations depend on the interaction strength, and for weak and nondirectional interactions, such as ion pairing and hydrogen bonding. may be small.[22,23] The conclusion was based on observations that the association constants between dicarboxylate dianions and diamides (hydrogen bonding) or between dicarboxylate dianions and diammonium cations (ion pairing) are insensitive to the rigidity of a spacer between the interacting groups, e.g., the difference in the association constants with isophthalate and glutarate dianions is only ca. 50% in favor of the rigid isophthalate. Nevertheless, even pure ionic binding may lead to fairly strong shape selectivity in molecular recognition. Shown in Fig. 4 are logarithms of the association constants of a series of tricarboxylate anions with two protonated forms of macrocycle **8**.[24] There are several points of interest in these results. Binding of all rigid tricarboxylate anions is stronger by two to three orders of magnitude than that of flexible citrate. The binding of rigid carboxylates is strongly shape dependent. in particular. for isomeric cyclohexanetricarboxylates. The degree of discrimination increases with an increase in affinity — going from a less-charged tetraprotonated receptor to a highly charged heptaprotonated macrocycle. Apparently, for stronger interacting host and guest species, the geometrical requirements become progressively important. and the binding mode becomes closer to the lock-and-key model.

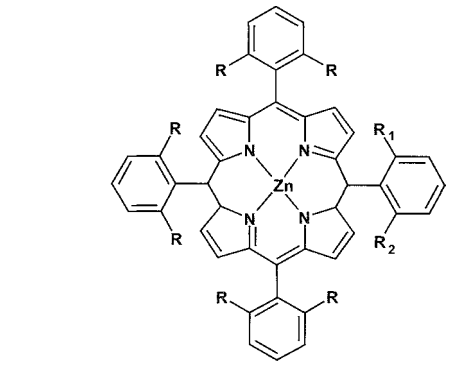

Fig. 5 Chemical structures and molecular models of shape-selective receptors for recognition of amine guests.[25] Reprinted with permission from Ref. [25]. Copyright 2000 by American Chemical Society.

Shape selectivity of molecular recognition is one of the direct consequences of the lock-and-key mechanism. It may result from complementarity of interacting atoms: as is the case in the system described in Fig. 4, or from steric restrictions in the binding pocket of the receptor. The latter principle is illustrated by shape-selective binding of amines to Zn(II) porphyrin complexes shown in Fig. 5.[25] The binding of three groups of ligands was studied with these sterically encumbered porphyrins and with sterically undemanding Zn(II) tetraphenylporphyrin [Zn(TPP)]: aliphatic primary and secondary amines, alicyclic secondary amines. and aromatic amines. Within each group of ligands, binding constants vary unsystematically and in limits of only one order of magnitude for Zn(TPP). Some steric discrimination is observed for $Zn(Si_6PP)$, and stronger selectivity is observed for $Zn(Si_8PP)$: binding constants vary in limits of three to four orders of magnitude for ligands of different structures. Molecular models shown in Fig. 5 explain the difference in steric requirements for these two guests.

CONCLUSION

In many cases, ligand binding to proteins and low-molecular-weight receptors follow, at least at first approximation. the lock-and-key mechanism. A more general binding mechanism is induced fit. Binding-induced conformational changes in the receptor are important for the allosteric regulation and cooperativity, but they may be unfavorable for the binding free energy. Similarly, ligand flexibility can be unfavorable due to losses of internal rotations and induced torsional strain. In several instances, the "freezing" of a ligand in its binding conformation by rigidification. e.g., via cyclization, significantly improves binding, which proceeds in this case by the lock-and-key mechanism. In general, however. it is difficult to give a real estimate of losses due to flexibility of the ligand and the receptor; in particular. taking into account solvent effects. It should be noted that the importance of the lock-and-key principle extends beyond the ligand–receptor complexation discussed above. It applies to a certain degree to all types of supramolecular interactions, e.g., one easily recognizes the lock-and-key principle in self-assembly of synthons in crystal engineering."" in chiral discrimination,[27] and in zeolite catalysis.[28]

ARTICLES OF FURTHER INTEREST

The Allosteric Effect, p. 20
Induced ***Fit.*** p 717
Preorganization and Complementarity, p. 1158

REFERENCES

1. Ficher. E. Einfluss der gonfiguration auf die wirkung der enzyme. Ber. Dtsch. Chem. Ges. 1894. 27. 2985–2993.
2. Lichtenthaler, F.W. 100 years "Schliissel-Schloss-Prinzip": What made Emil Fisher use this analogy? Angew. Chem.. Int. Ed. Engl. 1994. *33* (23 24). 2364–2374.
3. *The Lock-and-Key Principle, Vol. I, The State of the Art—100 Years On;* Behr. J.-P.. Ed.: Wiley: Chichester, 1995.
4. Koshland, D.E., Jr. The key-lock theory and the induced fit theory. Angew. Chern., Int. Ed. Engl. 1994. *33* (23 24). 2375–2378. and references therein.
5. Amit, A.G.; Mariuzza, R.A.; Phillips; S.E.V.: Poljak, R.J. Three-dimentional structure of an antigen-antibody complex at 2.5 resolutions. Science 1986. *233* (4765). 747–753.
6. Jorgensen. W.L. Rusting of the lock and key model for protein-ligand binding. Science 1991. 254 (5034). 954–955.
7. Gershtein. M.: Lesk. A.M.; Clothia, C. Structural mechanism for domain movements in proteins. Biochemistry 1994. *33* (22). 6739–6749.
8. Betts, M.J.; Sternberg. M.J.E. An analysis of conformational changes on protein-protein association: Implications for predictive docking. Protein Eng. 1999. 12 (4). 271–283.
9. Yin. J.; Mundorff. E.C.; Yang, P.L.: Wendt, K.U.; Hanway. D.: Stevens. R.C.: Schultz, P.G. A comparative analysis of the immunological evolution of antibody 28B4. Biochemistry 2001. 40 (36). 10764–10773.
10. Kubinyi. H. Lock and key in the real world: Concluding remarks. Pharm. Acta Helv. 1995. *69* (4). 259–269.
11. Bohm. H.-J.: Klebe. G. What can we learn from molecular recognition in protein-ligand complexes for the design of new drugs'? Angew. Chern., Int. Ed. Engl. 1996, *35* (22). 2588–2614.
12. Morgan. B.P.: Scholtz. J.M.; Ballinger. M.D.: Zipkin, I.D.; Bartlett. P.A. Differential binding energy: A detailed evaluaiton of the influence of hydrogen-bonding and hydrophobic groups on the inhibition of thermolysin by phosphorus-containing inhibitors. J. Am. Chem. Soc. 1991. *113* (1). 297–307.
13. Morgan. B.P.; Holland. D.R.; Matthews, B.W.; Bartlett. P.A. Structure-based design of an inhibitor of zinc peptidase thermolysin. J. Am. Chem. Soc. 1994. *116* (8). 3251–3260.
14. Loll. P.J.: Kaplan. J.: Selinsky. B.S.: Axelsen, P.H. Vancomycin binding of low-affinity ligands: Delineating a minimum set of interactions necessary for high-affinity binding. J. Med. Chem. 1999, 42 (22). 4714–4719.
15. Weber. P.C.; Pantoliano. M.W.; Simons, D.M.; Salemme, F.R. Structure-based design of synthetic azobenzene ligands for streptavidin. J. Am. Chem. Soc. 1994. *116* (7), 2717–2724.
16. Nicklaus. M.C.; Wang, S.: Driscoll, J.S.: Milne, G.W. Conformational changes of small molecules binding to proteins. Bioorg. Med. Chem. 1995. *3* (4), 411–428.
17. Vieth, M.; Hirst. J.D.; Brooks, C.L.. III Do active site conformations of small ligands correspond to low free-energy

solution structures? J. Cornput.-Aided Mol. Des. 1998. 12 (6). 563–572.
18. Li. G.: Still, W.C. An 18-crown-6 derivative with only one conformation. J. Am. Chem. Soc. 1993, *115* (9). 3804–3805.
19. Casnati. A.; Pochini, A.: Ungaro, R.: Ugozzoli, F.; Arnaud. F.: Fanni. S.: Schwing, M.-J.; Egbernik, R.J.M.: Jong, F.: Reinhoudt, D.N. Synthesis, complexation, and membrane transport studies of 1,3-alternate calix[4]arene-crown-6: A new class of cesium selective ionophores. J. Am. Chem. Soc. 1995, 117 (10). 2767–2777. and references therein.
20. Connors, K.A. The stability of cyclodextrin complexes in solution. Chem. Rev. 1997, *97* (5), 1325–1357.
21. Fujita. K.: Chen, W.-H.; Yuan, D.-Q.; Nogami, Y.; Koga, T.; Fujioka, T.; Minashi. K.; Immel. S.: Lichtenthaler. F.W. Guest-induced conformational change in a flexible host: Mono-*altro*-β-cyclodextrin. Tetrahedron: Asymmetry 1999. *10* (9). 1689–1696.
22. Hossain, M.A.: Schneider, H.-J. Supramolecular chemistry, part 85. Flexibility, association constants. and salt effects in organic ion pairs: How single bonds affect molecular recognition. Chem. Eur. J. 1999, *5* (4). 1284–1290.
23. Eblinger, F.; Schneider, H.-J. Stabilities of hydrogen-bonded supramolecular complexes with various numbers of single bonds: Attempts to quantify a dogma in host-guest chemistry. Angew. Chem.. Int. Ed. Engl. 1998. *37* (6), 826–829.
24. Bencini, A.; Bianchi, A.: Bmguete, M.I.; Garcia-Espaiia, E.; Luis, S.V.: Ramirez, J.A. Remarkable shape selectivity in the molecular recognition of carboxylate anions in aqueous solution. J. Am. Chem. Soc. 1992. 114 (5). 1919–1920.
25. Sen, A.; Suslick, K.S. Shape-selective discrimination of small organic molecules. J. Am. Chem. Soc. 2000, 122 (46). 11565–11566.
26. Desiraju, G.R. Supramolecular synthons in crystal engineering—A new organic synthesis. Angew. Chem., Int. Ed. Engl. 1995, 34, 2311–2327.
27. Landis, C.R.; Feldgus, S. A simple model for the porigin of enantioselection and the anti "lock-and-key" motif in asymmetric hydrogenation of enamides as catalyzed by chiral diphosphine complexes of Rh(I). Angew. Chem., Int. Ed. Engl. 2001. *39* (16), 2863–2866.
28. Martens. J.A.; Vanbutsele, G.; Jacobs, P.A.; Denayer, J.; Ocakoglu, R.; Baron. G.; Muños Arroyo, J.A.; Thybaut, J.; Marin, G.B. Evidences for pore mouth and key-lock catalysis in hydroisomerization of long n-alkanes over 10-ring tubular pore bifunctional zeolites. Catal. Today 2001, *65*. 111–116.

Luminescent Materials

Suning Wang
Corey Seward
Queen's University, Kingston, Ontario, Canada

INTRODUCTION

Luminescence is the emission of light from any substance and involves electronic transitions from excited states (excitons) to the ground state. Luminescence is formally divided into two categories, fluorescence and phosphorescence, depending on the nature of the excited state.[1] Luminescent materials are capable of performing certain tasks/functions via emitting light, changing the emitted light (intensity or energy), or converting light to other energy forms, such as chemical energy. There are three classes of luminescent materials — inorganic solids, organic polymers, and small molecules. Supramolecular luminescent materials involve mostly small organic or coordination molecules. The most important current applications of supramolecular luminescent materials are their uses as sensors and probes for certain chemicals or biological molecules, and as emitters or hole/electron transport materials in light-emitting diodes.

CLASSIFICATION OF LUMINESCENT MATERIALS BASED ON THE ORIGIN OF THE EMISSION

bigand-Based Emission

This category contains two classes of lnolecules (organic molecules and coordination compounds) in which the emission involves electronic transitions of the ligands. There are many luminescent organic molecules, most of which are aromatic molecules. Examples include 9,10-diphenylanthracene, 1,4-*bis*(5-phenyloxazol-2-yl)benzene, perylene, acridine, and fluorescein.[1] Many luminescent main-group coordination compounds are luminescent due to electronic transitions that involve ligands only. Typical examples are Alq_3 (q = 8-hydroxyquinolinolato), $Al(POP)_3$, (POP = 2-(5-phenyl-1,3,4-oxadiazolyl)phenonate), BPh_2q and BPh_2(2-py-azain), (2-py-azain = 2-(2-pyridyl)-7-azaindolyl).[2,3] The common features of these main group complexes are that they all contain chelate ligands that are luminescent and that the complexes are all much brighter emitters than the corresponding free ligands. Enhancement of the luminescent efficiency is attributable to the chelation of the ligand to the central atom. increasing the rigidity of the chromophore, and hence, the emission efficiency. A number of luminescent zinc(II) complexes also belong to this category.

Metal Center-Based Emission

This category consists of two classes of molecules: I) molecules that emit color due to electronic transitions localized on one metal center; and 2) molecules that emit color due to electronic transitions involving more than one metal center:

1. A few transition metal complexes such as Mn^{2+} and Cr^{3+} complexes are known to display luminescence that originates from d → d transitions. However, the most important class of luminescent molecules involving a single metal center-based emission is that of lanthanide compounds. Many lanthanide ions with a partially filled *4f* shell are emissive due to $f \rightarrow f$ transitions. Depending on the lanthanide ion, blue, green, or red emission can be achieved. Lanthanide luminescence is usually weak due to the forbidden nature of the $f \rightarrow f$ transitions. In order to achieve relatively bright luminescence, ligands that can function as activators for lanthanide emission are required.[" The role of the ligand is to harvest photons and transfer the energy of the photons to the lanthanide center. The requirement for the ligand is that its band gap be greater than the band gap of $f \rightarrow f$ transitions of the lanthanide ion, and the triplet energy level of the Iigand should be comparable to that of the excited state of the lanthanide ion. Many lanthanide complexes that display bright luminescence, facilitated by ligands, are known. Two well-known examples are Eu(tta)$_3$(phen), a red emitter and Tb(benzoate)$_3$, a green emitter.
2. Luminescent complexes that involve multiple metal centers are most well-known for dinuclear and multinuclear Au(I) complexes, where weak metal–metal bonding interactions are present.[5] Examples

Encyclopedia of Supramolecular Chemistry
DOI: 10.1081/E-ESMC 120012502

are $[Au_2(dppm)_2]^{2+}$, where *dppm* = *bis*(diphenylphosphino)methane, and $[Au_3(dmmp)_2]^{3+}$, where *dmmp* = *bis*(dimethylphosphinomethyl)methylphosphine, both of which have emission bands in the 570–590 nm region that were attributed to the transition of Au–Au σ^* $(d–d)\leftarrow$Au–Au σ $(p–p)$. A number of $d^{10}–d^8$ mixed metal complexes, such as $[AuIr(CH_3CN)_2(dppm)]^{2+}$, display a similar luminescence due to the Au–Ir σ^* $(d–d)\leftarrow$Au–Ir σ (p–p) transition.[6] The most impressive are heteronuclear molecules that involve both $5d^{10}$ and 6s' metal ions:[7] two examples are $[Tl(OPPh_3)_2][Au(C_6F_5)_2]$ and $Au_2Pb(mtp)_4$, where *mtp* = $(CH_2P(S)Ph_2)^-$. While neither of the molecular components in $[Tl(OPPh_3)_2][Au(C_6F_5)_2]$ are emissive. the linear solid-state aggregate with alternating Tl···Au units is luminescent. a consequence of weak Tl···Au bonding interactions. The luminescence of $Au_2Pb(mtp)_4$ changes dramatically from solution (λ = 555 nm) to the solid state (λ = 752 nm) due to the formation of infinite one-dimensional Au···Pb···Au chains in the solid state. A trinuclear Au(I) complex, [Au3(MeN = COMe)$_3$], was recently demonstrated to exhibit an unusual phenomenom termed solvoluminescence. When the solid of the complex is irradiated with near-UV light, it appears to undergo a charge separation. When contacted by a solvent in which the complex is soluble, the separated charge recombines. and a yellow light with $\lambda \cong 560$ nm is emitted. It is currently unclear, however, exactly where the emission originates.[8]

Intramolecular Charge-Transfer Emission

Charge-transfer emission refers to luminescence originating from electronic transitions from one center to another. This can occur within a molecule (intramolecular charge transfer. ICT) or between molecules (e.g., exciplexes and excimers).[1] Compounds that display intramolecular charge-transfer emission belong to two categories: 1) charge transfer within the ligand and 2) charge transfer between ligand and metal centers. Many organic molecules that display charge-transfer emission belong to the first category. The well-established examples include (4-dimethylamino)benzonitrile, arylanilines, carboxamide quinoline derivatives, and biaryls. ICT emissions are often solvent dependent. Charge-transfer emissions that involve a metal center and a ligand can originate from metal-to-ligand transitions (MECT) or ligand-to-metal transitions (LMCT), depending on the relative energy levels. The most well-known examples of MLCT emissions are $[Ru(bpy)_3]^{2+}$and $[Ru(bpy')_3]^{2+}$ complexes, where bpy = 2,2′-bipyridine, bipy' = derivatives of 2,2′-bipyridine.[1] The highest-filled orbital in the Ru(II) complexes is mostly *d* character, while the lowest unoccupied empty orbital is ligand-based π^* orbital. A number of Pt(II) diimine complexes also display MLCT emission.[9] Cp_2TiX_2, $Cp^*_2TiX_2$, $CpTiX_3$, and Cp^*TiX_3, where Cp = cyclopentadienyl anion, Cp^* = substituted cyclopentadienyl anion: and X = halide known to display charge-transfer transitions from the filled *Cp* or Cp^* π orbital to the empty d orbital of the Ti(IV) center.[10]

Intermolecular Charge-Transfer Emission

Two commonly used terms for intermolecular charge-transfer emission materials are exciplex and excimer. The former refers to an excited state charge-transfer complex and the latter to an excited state dimer. For example, anthracene and diethylaniline form an exciplex that has a broad emission band at $\lambda \cong 485$ nm. The best-known excimer is pyrene, which displays an intense excimer emission band at $\lambda \cong 470$ nm in a relatively concentrated solution ($\sim 10^{-3}$ M). Excimers formed by aromatic molecules such as pyrene typically display a stacked dimer structure.[11] Excimer and exciplex emission are useful for probing morphology and intermolecular interactions of luminescent molecules.

APPLICATIONS OF LUMINESCENT COMPOUNDS

Luminescent compounds have versatile applications in many different areas of materials sciences. Below is a brief summary of some of the important applications of luminescent compounds.

Displays

Intense research efforts for the past two decades were devoted to the development of light-emitting diodes (LEDs). The ultimate goal of LEDs is their use in display devices, such as computer and TV monitors. LEDs are based on electroluminescence, where excitons are created through electron and hole injections and charge recombination processes. LEDs are devices that convert electrical energy to light and typically have a three-layer structure, i.e., hole-transport. emitter, and electron-transport layers. Traditionally, inorganic semiconductors (Group 14 elements, Group 13/15 compounds) were used for this purpose. Small luminescent molecules (organic or coordination compounds) and organic polymers were recently demonstrated to be useful emitters in LEDs.[12,13] The display devices based on molecular compounds (small molecules or polymers) can be fabricated readily and relatively cheaply in comparison to semiconductor-based devices. In addition, large and flexible display

devices, which are difficult to achieve by using inorganic semiconductors, are possible by using molecular compounds. Alq_3, $Eu(tta)_3(Phen)$, and $Ir(ppy)_3$ (*ppy* = 2-phenylpyridine) are among the most widely used molecular emitters in LEDs. The structure of a typical three-layer light-emitting device is shown in Fig. 1.

Sensors and Probes

Luminescent sensors and probes (see also fluorescent sensors and luminescent probes) are based on the change of luminescent signal upon interaction with an analyte (Fig. 2). Analytes can be metal ions, oxygen molecules. organic molecules, or biomolecules, and the change can be intensity or energy. The intensity change can be an increase or decrease of emission intensity. The increase of emission intensity is often observed in lanthanide compounds, where the analyte enhances the energy transfer to the lanthanide center via specific interactions with the coordination sphere of the lanthanide ions, and, hence, increasing the emission intensity from the lanthanide center. This type of interaction was used for the detection of benzene by lanthanide compounds.[14] The more commonly used strategy in chemical sensing is fluorescent quenching by the analyte via direct or indirect interaction of the analyte with the chromophore. Direct nonbonding interactions between benzene molecules and an aromatic chromophore in a trinuclear Zn(II) complex were demonstrated to be responsible for the highly selective detection of benzene.[15] Similar nonbonding interactions were also used for probing the structure of DNA molecules and for fluorescent labeling of DNA molecules.[16,17] Many examples of indirect interaction of the analyte with the chromophore that results in the quenching of luminescence involve photoinduced electron transfer (PET). The commonly used system for sensors based on PET involves a chromophore that is attached to a

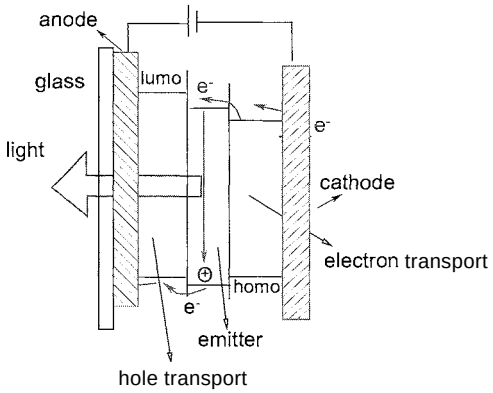

Fig. **I** A typical three-layer light-emitting device. (*View this art in color at www.dekker.com.*)

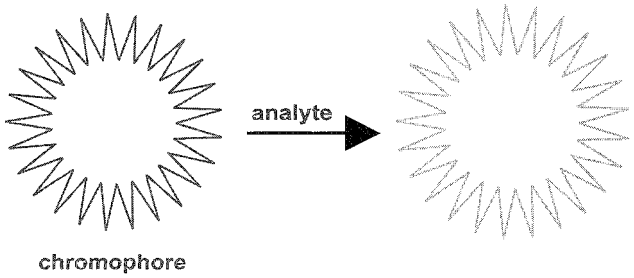

Fig. **2** Luminescent sensors/probes. *(Weir this art in color at www.dekker.coin.)*

nonemissive macrocyclic or multidentate ligand.[18] The binding of a metal ion or a proton to the nonemissive ligand induces the PET process and fluorescent quenching, hence the detection of the metal ion or protons. Long-range PET processes were also used in the investigation of DNA structures by using Ru(II) complexes as the probes.[19] The change of emission energy upon interaction with the analyte is a common occurrence when the analyte forms a covalent bond or a coordination bond with the chromophore, due to the change in energy levels. Formation of an exciplex or excimer between the chromophore and the analyte is also known to lead to a dramatic change of emission energy. Due to the large separation of excitation and emission energy in Eu(III) and Tb(III) compounds and their persistent luminescence in aqueous solutions, Eu(III) and Tb(III) compounds were demonstrated to be useful probes, stains. and markers for biological systems.[20] When Eu(III) or Tb(III) compounds are used as reagents for luminescent imaging of tissues, the background fluorescence from the tissue can be readily eliminated. For example, several classes of Tb(III) complexes were demonstrated to be effective contrasting reagents in the fluorescent imaging of cancer tissues.[21] Luminescent compounds are also widely used as imaging reagents for mechanical structmes such as airplanes and for the study of fluid-flow dynamics.[22]

Switches

Molecular switches based on luminescence are devices that change the luminescent signal reversibly by an external input, such as change of pH, variation of redox potential. or illumination (Fig. 3) (see also molecular switches and molecular logic gates).[23] A typical molecular switch contains a control unit that exists in two states of comparable stability. which can be interconverted reversibly by an external input. Each state interacts to a different extent or in a different manner with another active subunit of the system via bonding interaction/isomerization, of electron or energy transfer processes. The different

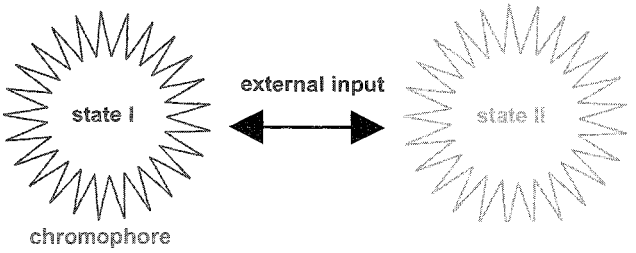

Fig. **3** Luminescent switches. (*View this art in color at www.dekker.com.*)

extent or different manner of interaction between the control subunit and the active subunit in each state provides the on/off function of the molecular switch. Redox switches modulate the luminescence by changing the oxidation state of the metal ion, an example of which is a Ni(II) complex of a naphthalene-containing macrocyclic ligand. The complex undergoes a reversible one-electron reduction process that switches the fluorescence of the naphthyl component off and on via electron transfer.[24] Switches modulated by illumination were demonstrated by a phosphorus(V) porphyrin compound with an axially bound azobenzene subunit. Irradiation by light causes a reversible $Z \leftrightarrow E$ isomerization of the azobenzene subunit, which leads to the modulation of the fluorescence from the basal porphyrin chromophore.[25]

PHOTOCHEMICAL REACTIONS

Numerous luminescent compounds were demonstrated for their potential uses as centers/catalysts for photochemical syntheses—syntheses catalyzed by light (see also photochemical techniques and supramolecular photochemistry). Catalysts for photochemical reactions and syntheses are devices that convert photon energy to chemical energy (Fig. 4). In order to achieve a working photochemical system, several key components are required, such as a chroinophore for electron-hole creation, antennae for harvesting and transferring photons. and redox couples, etc. The most well-known example is the photochemical splitting of water using derivatives of $[Ru(bpy)_3]^{2+}$ as the catalysts.[''''] A number of derivatives of Pt(II) complexes of diimines and dithiolates were recently shown to be promising candidates for photochemical reactions.[9] The research in effective photochemical systems remains to be one of the most challenging and potentially most rewarding areas in sciences.

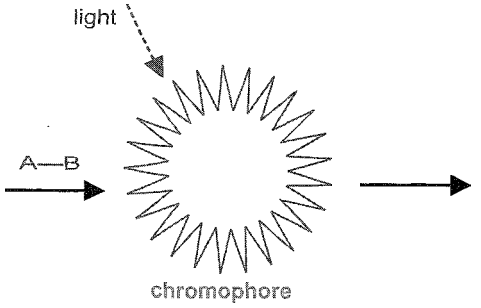

Fig. **4** Photochemical reactions. (*View* this art *in color at www.dekker.com.*)

CONCLUSION

In summary, the combination of luminescence and supramolecular structures gives luminescent supramolecular materials many advantages over other types of materials. By controlling the supramolecular structures. it is possible to achieve selective and highly effective guest–host interactions that can be recorded or monitored by luminescent signal change. Using supramolecular interactions, it is possible to assemble luminescent molecules or charge transport molecules to form the desired molecular layers and architectures on an appropriate substrate so that the resulting surface can perform the desired optoelectronic or photonic functions effectively. These are perhaps some of the most exciting and most challenging tasks in supramolecular materials research.

ARTICLES OF **FURTHER** INTEREST

Fluorescent Sensors, p. 572
Luminescent Probes, p. 821
Molecular Logic Gates. p. 893
Molecular Switches, p. 917
Supramolecular Photochemistry, p. 1434

REFERENCES

1 Lakowicz, J R *Principles of Fluorescence Spectroscopy*, 2nd Ed . Kluwer Academic/Plenum Publishers New York. 1999
2 Chen. C H , Shi J Metal chelates as emitting materials for organic electroluminescence Coord Chem Rev **1998** 171. 161
3. Wang, S. Luminescence and electroluminescence of Al(III), B(III), Be(II) and Zn(II) complexes with nitrogen donors. Coord. Chem. Rev. **2000**, 215. 79.
4. Crosby, G.A.; Whan. R.E.: Alire. R.M. Intramolecular

energy transfer in rare earth chelates. Role of the triplet state. J. Chem. Phys. 1961, *34*. 742.
5. Forward, J.M.: Fackler. J.P., Jr.; Assefa, Z. *Photophysical and Photochemical Properties of Gold(I) Complexes in Optoelectronic Properties of Inorganic Compounds;* Roundhill, D.M., Fackler, J.P., Jr.. Eds.: Plenum Press: New York, 1999. chapter 6.
6. Balch, A.L.; Catalano. V.J. Ligation-induced changes in metal–metal bonding in luminescent binuclear complexes containing gold(I) and iridium(I). Inorg. Chem. 1991, *30*, 1302.
7. Fernández. E.; Laguna, A.: López-de-Luzuriaga, J.M. Luminescent gold-heterometal complexes. Gold Bull. 2001. *34*. 14.
8. Fung, E.Y.; Olmstead. M.M.; Vickery, J.C.: Balch. A.L. Glowing gold rings: Solvoluminescence from planar trigold (I) complexes. Coord. Chem. Rev. 1998. *171*. 151.
9. Paw, W.; Cummings, S.D.; Mansour. M.A.: Connick, W.B.; Geiger. D.K.: Eisenberg, R. Luminescent platinum complexes: Tuning and using the excited state. Coord. Chem. Rev. 1998. *171*. 125.
10. Kenney, J.W., III; Boone. D.R.; Striplin, D.R.: Chen, Y.H.: Hamar. K.B. Electronic luminescence spectra of charge transfer states of titanium(IV) metallocenes. Organometallics 1993. *12*, 3671.
11. Winnik, F.M. Photophysics of preassociated pyrenes in aqueous polymer solutions and in orther organized media. Chem. Rev. 1993. 93. 587.
12. Sibley. S.: Thompson, M.E.: Burrows, P.E.; Forrest, S.R. *Electroluminescence in Molecular Materials in Optoelectronic Properties of Inorganic Compounds*; Roundhill. D.M., Fackler. J.P.. Jr., Eds.: Plenum Press: New York, 1999. chapter 6.
13. Tsutsui, T. Progress in electroluminescent devices using molecular thin films in. Mater. Res. Soc. Bull. 1997, June. *22*. 39.
14. Mortellaro. M.A.: Nocera. D.G. A turn-on for optical sensing. Chemtech 1996, February. *26*, 17.
15. Pang, J.; Marcotte. E.J.-P.; Seward. C.: Brown. R.S.; Wang. S. A blue luminescent starburst Zn(II) complex that can detect benzene. Angew. Chemie.. Int. Ed. Engl. 2001, *40*. 4042.
16. Arkin. M.R.; Stemp, E.D.A.: Turro. C.; Turro, N.J.; Barton, J.K. Luminescent quenching in supramolecular systems: A comparison of DNA- and SDS micelle-mediated photoinduced electron transfer between metal complexes. 9. Am. Chem. Soc. 1996, 118. 2267.
17. Davies, M.J.; Shah. A.; Bruce. I.J. Synthesis of fluorescently labeled oligonucleotides and nucleic acids. Chem. Soc. Rev. 2000, *29*, 97.
18. de Silva, A.P.: Gunaratne. H.Q.N.; Gunnlaugsson. T.; Huxley, A.J.M.; McCoy, C.P.; Rademacher. J.T.: Rice, T.E. Signaling recognition events with fluorescent sensors and switches. Chem. Rev. 1997. *97*, 1515.
19. Jenkins, Y.: Friedman. A.E.; Turro. N.J.: Barton, J.K. Characterization of dipyridophenazine complexes of ruthenium(II): The light switch effect as a function of nucleic acid sequence and conformation. Biochemistry 1992. *31*, 10809.
20. Richardson, F.S. Terbium(III) and europium(III) ions as luminescent probes and stains for biomolecular systems. Chem. Rev. 1982. 82. 541.
21. Bornhop, D.J.; Hubbard, D.S.; Houlne. M.P.; Adair, C. Fluorescent tissue site-selective lanthanide chelate, Tb-PCTMB for enhanced imaging of cancer. Anal. Chem. 1999, *71*, 2607.
22. Pang. *Z.;* Gu. X.; Yekta. A.; Masoumi, Z.; Coll, J.B.; Winnik, M.A.: Manners, I. Phosphorescent oxygen sensors utilizing sulfur–nitrogen–phosphorus polymer matrixes. Adv. Mater. 1996. *8*, 768.
23. de Silva. A.P.; Gunaratne, H.Q.N.; Gunnlaugsson, T.: Huxley, A.J.M.; McCoy. C.P.; Rademacher. J.T.; Rice, T.E. Supramolecular photonic devices: Photoinduced electron transfer (PET) systems with switchable luminescence output. Adv. Supramol. Chem. 1997, *4*. 1.
24. Fabbrizzi. L.; Licchelli. M.: Pallavicina, P. Transition metals as switches. Acc. Chem. Res. 1999. *32*, 846.
25. Reddy. D.R.: Malya, B.G. A molecular photoswitch based on an 'axial-bonding' type phosphorus(v) porphyrin. Chem. Commun. 2001, 117.
26. Miller. D.S.; Bard, A.J.: McLendon, G.; Ferguson, J. Catalytic water reduction at colloidal metal ''microelectrodes''. 2. Theory and experiment. J. Am. Chem. Soc. 1981, *103*, 5336.

Luminescent Probes

Dmitri B. Papkovsky
Tomás C. O'Riordan
University College Cork, Cork, Ireland

INTRODUCTION

Luminescent probes represent a substantial segment of supramolecular structures. They are widely used in the design and investigation of physicochemical and structural properties of supramolecular compounds and in various bioanalytical applications based on luminescence detection. In general, a luminescent probe contains a luminophoric structure, functional moiety, ancillary units (such as linkers connecting these fragments), and peripheral groups used to adjust properties of the probe as a whole. Such a probe produces a traceable luminescent signal, and it may also respond to certain events involving the probe or its environment, such as the presence of particular compounds, recognition processes, conversion into different conformations, chemical and spectral forms, changes in environment, etc.

The main advantages of luminescent probes and detection include the following:

- High selectivity due to efficient wavelength discrimination (excitation and emission). which can be further enhanced by lifetime discrimination: potential for multiplexing.
- High sensitivity, down to single-molecule detection, and a broad range of concentrations measurable by luminescence spectroscopy.
- Multiple detection formats, including spectral, intensity, lifetime, polarization. quenching, energy transfer, time-resolved, and phase-resolved measurements.
  Imaging capability with submicrometer spatial resolution. two- and three-dimensional (with confocal optics); sensitive visual detection.
- Temporal resolution spanning from picosecond to second scale for studies of inter- and intramolecular dynamics and processes.
- On/off switching by means of an excitation source.
- Low hazard, chemical stability, robustness, low cost.

Below we describe the basics of luminescence and examples of some common types of luminescent probes, their organization and functioning, applications, and information obtainable with such probes. A general outline of a luminescent probe is given in Fig. 1.

PRINCIPLES AND PARAMETERS OF LUMINESCENCE

The photophysics of photoluminescence (other types of luminescence are outside the present scope) is represented in Fig. 2, commonly called a Jablonski diagram.[1] The absorption of light by a molecule promotes its electrons from the ground singlet state S_o to the vibrational levels of excited singlet states (S_1, S_2,...). In this excited state, the molecule will quickly lose its energy to the lowest vibrational level of the first singlet state. Some molecules can change their spin to the triplet state (T_1) by the process known as intersystem crossing. These processes are rapid and proceed on a scale of 10^{-15}–10^{-12} s. At this point, nonluminescent molecules will lose energy nonradiatively by internal conversion to vibrational levels of the ground state overlapping with excited state levels or as heat in collisions with solvent molecules (external conversion). For luminescent molecules, a substantial energy gap between the excited and ground states limits radiationless deactivation pathways, such that return to the ground state partly occurs via the emission of photons: as fluorescence ($S_1 \rightarrow S_o$) or phosphorescence ($T_1 \rightarrow S_o$).[2]

Excitation and Emission Spectra

These allow for the identification of luminophores and their selective detection in complex mixtures using spectral discrimination. Main spectral characteristics are location, shape, width, peak wavelength of excitation and emission bands, and spectral integrals. For simple molecular structures, excitation spectra are close to their absorption spectra, while emission spectra resemble a mirror image of the excitation spectrum (Frank–Condon rule)[3] and are independent of the excitation wavelength. Because some energy is lost before a molecule can emit light (see Fig. 1), the emission spectrum is shifted toward longer wavelength (Stokes' shift). For more complex structures, spectra of individual chromophoric moieties usually superimpose and reflect photophysical interactions between them, such as internal quenching, complex formation, and energy transfer. Spectral changes may indicate chemical or physical transformations occurring with the luminescent probe or changes in its environment.

Encyclopedia of Supramolecular Chemistry
DOI: 10.1081/E-ESMC 120012875

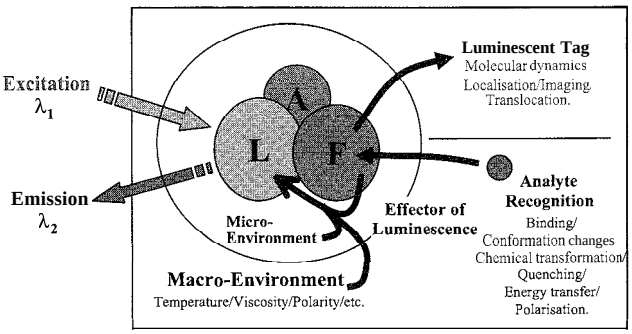

Fig. 1 General outline of a luminescent probe, showing luminescent (*L*), functional **(F).** and ancillary *(A)* groups and various sensing mechanisms. *(View this art in color at www.dekker.coin.)*

Luminescence **Intensity**

Luminescence intensity (I_L) is the main measured parameter that depends on a number of factors related to the instrument, measurement conditions, luminophore characteristics, and sample properties. In dilute solutions, its relationship with the concentration of luminophore is as follows:

$$I_L = I_o * k * \phi * \varepsilon * l * [C] + I_b \quad (1)$$

where **I,,** = intensity of excitation: k = instrumental factor; o = emission yield: E = molar absorptivity: 1 = optical path; [C] = concentration; and I_b = background signal on the photodetector (i.e., without the luminophore). Luminescence intensity is measured in arbitrary units, but measurements performed on different instruments can be easily compared using appropriate standards or relative values. The product of E and Φ is called the "absolute spectral sensitivity." and it estimates the efficiency of different luminophores.[2]

Emission Yield

The emission yield *(h)* defines the quantum efficiency of luminescence: the ratio of the number of emitted and absorbed photons ($0<o<1$). Changes in emission yield can indicate quenching and other photophysical and chemical processes occurring with the luminophore.

Luminescence Lifetime

The luminescence lifetime (τ) is a kinetic characteristic that gives an estimate of luminescence duration and time profile once the excitation source is switched off:

$$I(t) = I_o * \exp(-t/\tau) \quad (2)$$

where t is the time after the excitation pulse. Luminescence lifetime relates to the structure of the luminophore and the presence of other processes (quenching. RET, see below). Compared to the steady-state (averaged) luminescence intensity, lifetime measurements provide additional information about luminescent supramolecular structures and their intra- and intermolecular interactions. Most fluorescent dyes have nanosecond lifetimes. Phosphorescent dyes have millisecond lifetimes and even longer. Such long-lived excited states are prone to nonradiative deactivation and quenching processes, and for many dyes; phosphorescence vanishes at room temperature. A few compounds have bright long-decay luminescence at room temperature. including transition-metal complexes (lanthanides, ruthenium(II), osmium(II)) erythrosine, metalloporphyrins, with lifetimes 1 μs–1 ms. Probes on their basis are becoming increasingly popular, as they allow sensitive time-resolved luminescence detection and some special applications.[4]

Luminescence Quenching

This originates from various internal and external processes involving luminescent probes and other molecular structures called quenchers. Changes in molecular organization, dynamics, environment affecting the luminophore-quencher interactions; or chemical transformations can cause luminescence quenching. Physical quenching encompasses two mechanisms. Static quenching includes formation of a dark complex between the quencher and the luminophore. Dynamic quenching proceeds via collisions of quencher molecules with luminophore excited states deactivating them and also quenching the emission lifetime. Both processes are described by the Stern–Volmer equation:

$$I_o/I = 1 + K_{s-v} * [Q] \quad (3)$$

For static quenching. K_{s-v} corresponds to the binding conrtant. whereas for dynamic quenching. K_{s-},$=k\tau_o$, where k is the bimolecular quenching rate constant. and τ_o

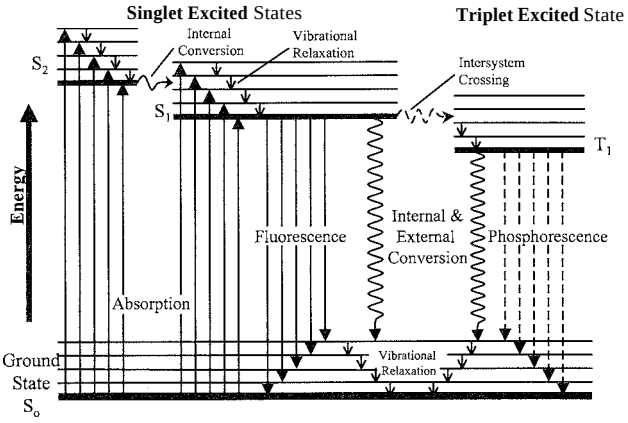

Fig. 2 Jablonski diagram showing transitions giving rise to absorption. fluorescence, and phosphorescence spectra

is the emission lifetime in the absence of the quencher. Long emission lifetime, high temperature, and low solvent viscosity favor dynamic quenching but not static. The opposite process, luminescence enhancement, is usually associated with the elimination of quenching or with the transfer of energy from other specie to the luminophore. Quenching facilitates the study of various nonluminescent structures with luminescent probes.

Polarization of Luminescence

This is the consequence of photoselective excitation of luminophores by polarized light, which selectively excites a population of molecules oriented with respect to the electrical vector of excitation. Emission also occurs with the light polarized along a fixed axis in the luminophore. The angle between these moments determines the maximal polarization of fluorescence.[5] Luminescence polarization is defined as follows:

(4)

where $I_{\parallel}$ and $I_{\perp}$ are the intensities of the vertically and horizontally polarized emission, respectively. Rotational diffusion occurring during the lifetime of the excited state is the most common cause of depolarization of luminescence. Even short-lived fluorescent probes of small size are almost completely depolarized in solution; but their binding to macromolecules or translocation to viscous environments, such as lipid membranes, can partly restore their polarized emission. For these reasons: fluorescence polarization is widely used to study (bio)molecular interactions and molecular and conformational dynamics.

Resonance Energy Transfer

From the excited state of a luminophore, resonance energtransfer (RET) can occur as a result of dipole–dipole interaction with another chemical structure (acceptor). The RET proceeds without the emission of a photon by the donor, and its efficiency is determined by the spectral overlap between the donor emission and absorption of the acceptor and by the distance between them.[6] Distance dependence of RET efficiency is as follows:[7]

$$E = \frac{R_o^6}{R_o^6 + r^6} \tag{5}$$

where R_o is the distance at which RET efficiency is 50%, called the Forster radius. Remarkably. for the majority of donor–acceptor pairs, R_o is about 30–50 Å, which is comparable with the size of molecules including DNA and proteins. The steep distance dependence of RET facilitates its use as a "spectroscopic ruler''[8] with which to measure distances between chemical and molecular structures and to monitor intra- and intermolecular interactions, molecular dynamics, etc.

These features provide luminescent probes with versatility and a broad range of applications. A variety of luminescent dyes and probes were described (e.g., *Molecular* Probes) and the number continues to grow rapidly. A small cross section of common luminescent structures is given in Table 1 and Fig. 3. Examples of typical luminescent probes, their organization, and their properties are discussed below.

MAIN CLASSES OF LUMINESCENT PROBES

Natural Fluors

The majority of naturally occurring compounds are nonluminescent, including nucleic acids (DNA/RNA), mono- and polysaccharides, lipids, and most of the small biomolecules. Proteins contain in their structure three amino acids — phenylalanine, tyrosine, and tryptophan — that fluoresce in the UV range. Due to its long-wave emission and relatively low abundance, tryptophan is commonly used as an intrinsic luminescent probe to study proteins. Tryptophan also exhibits phosphorescence at room temperature.

Some natural pigments, including chlorophylls, porphyrins. riboflavin. bilirubin, carotene, NADH, and FAD. have strong fluorecence in the UV and visible ranges. They were exploited for studies of enzyme active sites (NADH, FAD), enzyme kinetics, photosynthesis, and electron-transport processes (chlorophylls. porphyrins).

Luminescent Labels

Fluorescent compounds are commonly used as labels, which allows other molecules and structures to be traced and quantified by luminescence spectroscopy. Such labels, which usually do not change their luminescent characteristics during the assay, are conjugated to the molecules of interest via functional groups of the latter, such as $-NH_2$, -OH. -COOH, and -SH groups. To facilitate the conjugation. the fluorophore is often functionalized with reactive groups: aldehyde, isothiocyanate, sulfony! chloride, *N*-hydroxysuccinimide for labeling via amino groups; and iodoacetamide and malemide for labeling via sulfhydryl residues. Other groups such as carboxylic acids may require additional activating or condensing reagents for conjugation.[9] Fluorescently labeled reagents are used for the detection of DNA. proteins, hormones; cells, etc., in applications such as binding assays (immuno, hybridization, and receptor based): fluorescent microscopy,

Table *1* Some common luminescent structures and their properties

Probes	λ *Abs* (nm)	ε ($mM^{-1}cm^{-1}$)	λ Em (nm)	*Quantum yield* (%)	τ (nsec)
Natural					
Tyrosine (amino acid)	275	1.42	304	14	3.6
Tryptophan (amino acid)	295	5.6	353	13	3.1
NADH (enzyme cofactor)	290, 340	6.2	440, 460		0.4
FAD (enzyme cofactor)	450	11	535		2.3
Chlorophyll (pigment)	430		665		2–6
Allophycocyanin (protein)	650	700	660	70	3
R-phycoerythrin (protein)	565	1960	578	82	
Fluorescent proteins					
Green (GFP)	489	55	508	60	
Blue (BFP)	380	31	440	18	
Cyan (CFP)	434	26	477	40	
Yellow (YFP)	514	84	527	61	
Red (RFP)	558	22.5	583	29	
Fluorescent					
Umbelliferone	316	14	376		
ANS	372	7.8	480	40	8
DNS-Cl	340–350	4.3	510–560	30	10–15
Pyrene	340	44	375, 392	70	100
Fluorescamine	394	6.3	475	10	7
FITC	492	77	520	85	4.5
Alexa family	346–749	19–250	445–782		1.2–4.1
Bodipy family	495–646	60–142	503–665		5
Cy family	489–743	150–250	506–767	20	
Long-lived luminescent					
Tryptophan	295	5.6	450		30×10^6
Eu-$Bipy_3$ cryptate	337	27	613	2	3.4×10^5
Pt-coproporphyrin	380	200	650	40, 20	1×10^5
Ru (II)-*tris*-bipyridine	475		610–625	4.2	460
Erythrosin	540	90	690		2.6×10^3

fluorescence in situ hybridization (FISH), and fluorescence-activated cell sorter (FACS).

For complex samples. the presence of proteins and other fluorescent compounds results in high optical background, basically in the range of 250400 nm. Probes working in this spectral region are prone to interference and limited sensitivity. Therefore. research focused on the design of luminophores with long-wave spectral characteristics (above 500 nm). large Stokes' shifts, and long luminescence lifetimes. Such Iabels can overcome interference by scattering and autofluorescence and provide higher selectivity and sensitivity.

Fluorescein isothiocyanate (FITC) and dansyl-chloride were among the first extrinsic fluorescent labels for proteins used for immunofluorescence microscopy and polarization measurements.[10,11] Fluorescein and rhodamine labels were extensively employed due to their bright emission in the visible range. These probes have drawbacks: including hydrophobicity, small Stokes' shifts, and sensitivity to pH and photobleaching, which led to the development of new dyes such as Alexa, Bodipy, and cyanine dye families (see Table 1). These dyes cover a broad spectral range and are represented by derivatives with various functionalities and physical chemical properties suitable for conjugation to various molecular structures.

The phycobiliproteins are a group of light-harvesting proteins derived from algae and composed of a polypeptide chain enclosing the chromophoric bilin (open-chain tetrapyrrole) groups. The *R*-phycoerythrin and allophycocyanin, which display large extinction coefficients and emission yields, long-wave absorption and emission, and high photostability, were exploited as labels in immunoassays[12] and flow cytometry.[13]

Green fluorescent protein (GFP) is a conserved polypeptide fragment isolated from the bioluminescent jellyfish *Aequorea Victoria.* It displays bright visible fluorescence upon processing of the polypeptide structure, where a β-sheet conformation encloses a central α-helix, which forms the fluorophore. Such polypeptide labels can be produced by recombinant techniques and used as "intrinsic tags," both in vivo and in vitro. The sequences encoding the polypeptide can be incorporated into donor DNA. which is then translated to a protein-bearing GFP tag. Several variants of GFP were developed, giving a

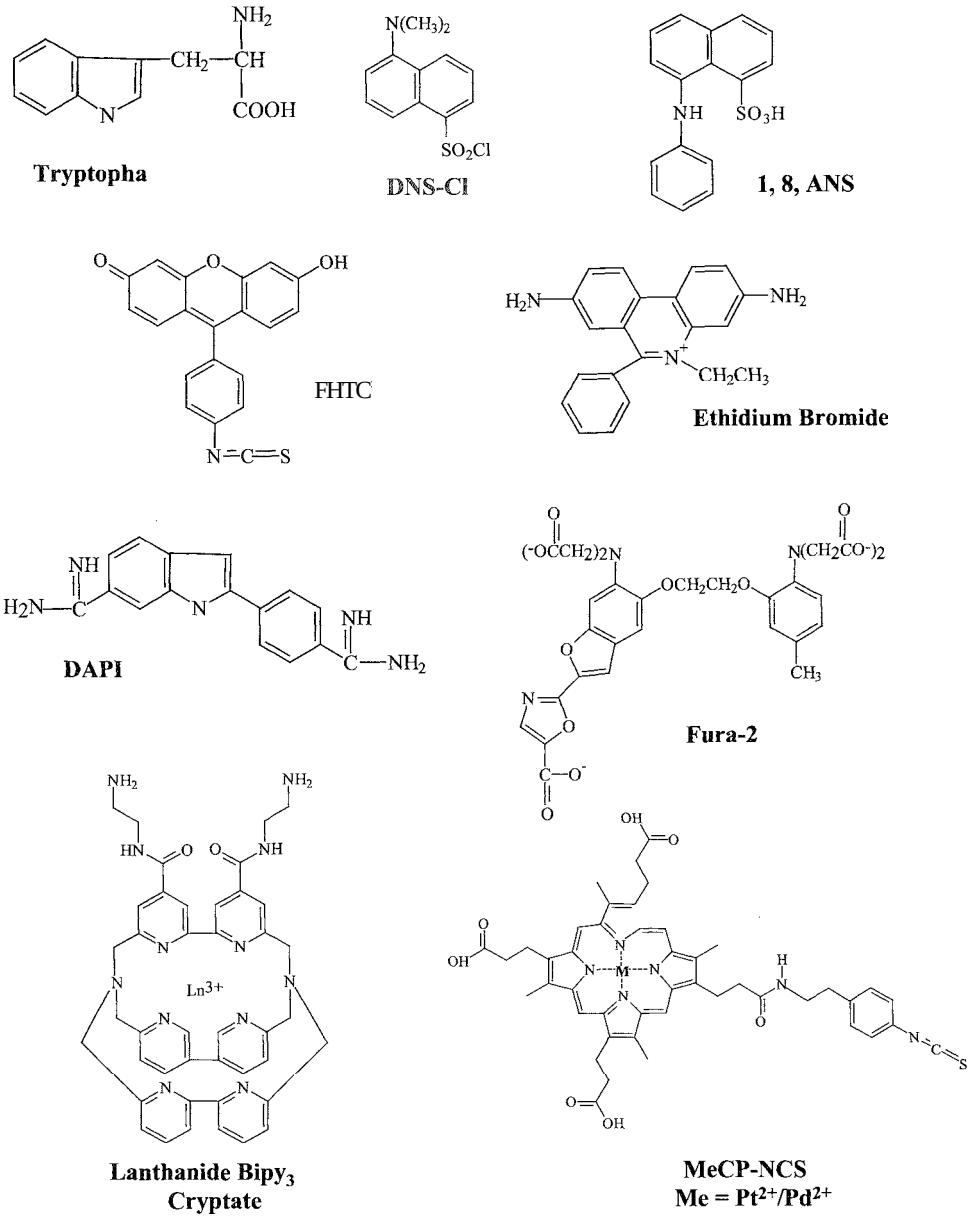

Fig. 3 Chemical structures of some fluorescent and phosphorescent compounds.

color palette of fluorescent proteins (see Table 1) available as labeling reagents and tags. They are actively used to study gene expression, synthesis and localization of protein markers, co-localization using FRET pairs, and multicolor detection.[14,15]

Probes for Micro- and Macroenvironments

The complex photophysics of luminescence makes luminophores sensitive to their immediate and macro-environments, so they can change emission characteristics in response to minor changes in the environment. Intrinsic fluorescence of amino acids was used to monitor the conformational dynamics and protein folding in vitro. Hydrophobic tryptophan residues tend to be buried within the core of folded proteins, thus shielded from an aqueous environment. Unfolding exposes tryptophan residues to an aqueous environment, which quenches their emission. These effects may be augmented by the presence of quenchers located within protein structures, e.g., a methionine residue, or a second tryptophan[11,16] or external quenchers present in or added to the sample.[17] The dynamics of protein folding, conformational change, or interactions with other molecules can be monitored in this way by measuring intensity, lifetime, or polarization of tryptophan fluorescence.

Similarly, 1-anilinonaphthalene-8-sulfonic acid (ANS) only emits in a hydrophobic environment, being almost completely quenched in aqueous solution. ANS and some other dyes, including 6-(*p*-toluidinyl)naphthalene-2-sulfonate, pyrene, 1,6-diphenyl-1,3,5–hexatriene, fluorescein, and rhodamine derivatives attached to long acyl chains or to fatty acids that localize in the cellular membranes were used as probes for hydrophobic sites in proteins, protein folding, imaging of membranes of the cell, and solvent polarity. Pyrene-labeled fatty acids were used to detect the fusion of two membranes. When prcscnt in a membrane at sufficiently high concentrations, pyrene excimers (excited-state dimers) are formed that emit at 470 nm. Upon fusion with other membranes, probe concentration decreases, and excimer fluorescence is replaced by monomer fluorescence at 400 nm. This process can be monitored by ratiometric detection of pyrene labels.[18]

The dyes that alter their emissions on binding to nucleic acids have high utility in molecular and cell biology. The mechanism of binding is intercalation of the planar aromatic dye structure into double-helical DNA, which is favored and stabilized by multiple electrostatic and hydrophobic interactions between the two matching chemical structures (see Fig. 4). Such an interaction has significant impact on the electronic structure of the dye,

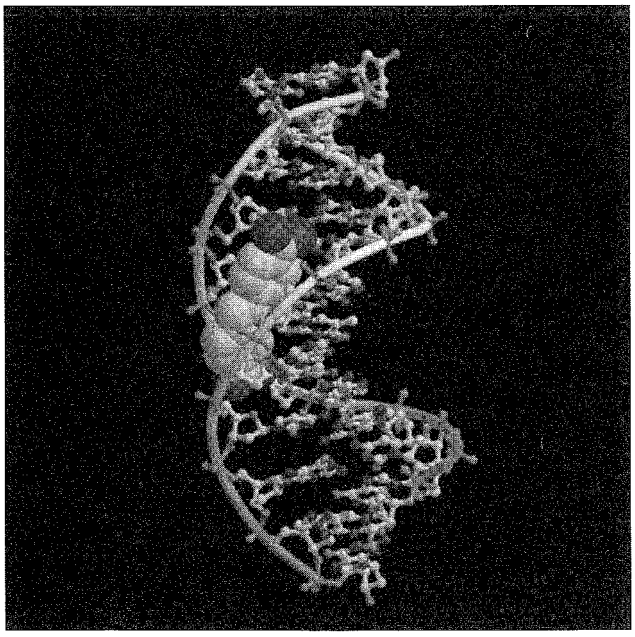

Fig. 4 X-ray crystal structure of DAPI intercalating with DNA. The image was obtained from the Protein Data Bank (*www.rcsb.org/pdb*, Nucleic Acids Res., 2000, 28, 235–242, no. PDR 1D30) with permission. The original structure was described in J. Biomol. Struct. Dyn, 1989, 7, 477. *(View this art in color at www.dekker.com.)*

its microenvironment, and its availability to quenchers, thus causing changes in luminescence. Ethidium bromide, a common fluorescent DNA stain, displays weak fluorcscscence in solution. On binding to double-stranded DNA, there is a 30-fold increase in intensity, with an increase in lifetime from 1.7 ns to approximately 20 ns. Some other fluorescent stains for DNA, RNA (acridine orange, Hoechst, DAPI), proteins (MDPF, SYPRO), and specific proteins (albumin blue 580) have found use for the detection and imaging of these biomolecules, e.g., in electrophoretic gels under UV excitation and in fluorescccnce microscopy.

Luminescent indicators

Luminescent indicators were used for a quantifying variety of biological and chemical specie and also ions such as $H^{\cdot}$, Ca^{2+}, K^{+}, I^{-}, Mg^{2+}, Cl , and Na^{+}. The basis of such probes is a change in luminescence properties in the presence of the analyte, which affects the luminophoric moiety.

Fluorogenic dyes are used as probes and reagents for particular chemical compounds. Nonfluorescent fluorescamine, when reacting with free amino groups, gives highly fluorescent products. A variety of fluorogenic enzyme substrates were also developed, such as β-methylumbelliferryl-β-D-galactopyranoside, which is cleaved by β-D-galactosidase enzyme, releasing highly fluorescent umbelliferrone. Such probes are employed in the detection of amino acids, proteins, sugars, and enzyme activity, with high sensitivity.

The ion-selective probes usually exist in two interchangeable chemical and spectral forms (free and bound) having different luminescent charactcristics. By determining the ratio of the two forms by luminesccncc measurements, the analyte concentration in a sample can be quantified, based on the known binding constant and probe concentration. Such indicators usually have limited dynamic range, which is detcrmincd by the binding constant:

$$0.1{*}K_{\mathrm{d}} < [C] < 10{*}K_{\mathrm{d}}$$

Fluorescent pH indicators are based on the protonation of some dyes. The phenolic moiety of fluorescein derivatives, such as 2′, 7′-*bis*-carboxyethyl-5(6)-carboxyfluorescein (pH range 6.5–7.5) is in the anionic form at higher pH, resulting in a longer wavclcngth absorbance band. On protonation of this group, the absorbance maximum is shifted to lower wavelengths. Other fluorescent pH indicators, such as the seminaphthorhohafluors and scminaphthofluoresceins (pH ranges 6.0–8.0 and 7.2–8.2, respectively), display changes in absorption and

emission maxima on protonation. Fluorescent pH indicators respond to minor changes in pH within the range of protonation (pK_a).[19]

Fluorescent indicators for ions are based on corresponding chelators. The Ca^{2+} indicators usually mimic the structure of ethyleneglycol-*bis*(β-aminoethylether)-*N*,*N*,*N*′,*N*′-tetraacetic acid (EGTA), which also contains an adjacent fluorophore moiety affected by the binding. The most popular intracellular Ca^{2+} indicator, Fura-2, displays a shift in excitation maximum between 300–400 nm when monitoring emission at 510 nm, thus allowing ratiometric measurements. Calcium Green displays an increase in emission at 530 nm on addition of calcium but displays no spectral shift. Other fluorescent calcium indicators with different affinities and spectral characteristics are available that allow for the measurement of Ca^{2+} from nano- to submillimolar concentrations.[19]

Long-decay luminescent dyes and probes that are effectively quenched by molecular oxygen can be used for its quantitation. Examples of such probes include ruthenium(II)-*tris*(diphenyl phenanthroline) and phosphorescent platinum(II) porphyrins. Their long emission lifetimes facilitate quantitation by lifetime or intensity measurements.[20] Other chemical specie, such as heavy-metal ions and heterocyclic compounds, can be quantified by luminescence quenching, according to Eq. 3.

Molecular Switches

Some probes containing luminophoric fragments may be switched into "on" or "off" luminescence modes in the presence of certain analytes. such as H^+, Cu^{2+}, and Ca^{2+}, by a process termed photoinduced electron transfer (PET). This sensing mechanism of such molecular switches uses the ability of certain chemical structures to quench the excited states of adjacent luminophoric moiety by electron transfer. On the recognition and binding of the analyte, the PET process may be curtailed, resulting in fluorescence off-to-on switching, or initiated, resulting in on-to-off switching. Molecular switches bearing two recognition sites for the same analyte facilitate production of off-on-off switches. Where PET is initially occurring, low concentrations of analyte terminate the process, and higher concentrations cause it to resume.[21] Potential applications for such probes include molecular electronics, computing, and data storage systems.

Polyfunctional and Long-Decay Luminescent Probes

A luminescent probe may contain more than one luminescent. functional, or chemical moiety in its structure. For example, for monitoring chemical specie intracellularly, it is essential to have a cell-permeant probe that can easily be loaded into the cell and then stay inside it. This is achieved with acetoxymethyl derivatives of the fluorescent indicators (AM-esters), which are nonluminescent and hydrophobic and tend to accumulate in cell membranes. where the ester groups are cleaved by cellular esterases, producing a water-soluble fluorescent probe that is trapped inside the cell.[22]

Dual-labeled luminescent probes contain pairs of dyes attached to a functional chemical or biological structure, such as specific oligonucleotide or peptide sequence. The detection is based on the monitoring of close-proximity quenching of the reporter dye, which is dependent on the probe conforination. Chemical or biological recognition or transformation alters the effective distance and the degree of interaction between the dyes, thus producing positive or negative luminescent response.

The molecular beacon probe contains an internal oligonucleotide sequence specific to target DNA, short self-complementary sequences at both 3'- and 5'-ends, and the donor and quencher dyes attached to these ends. Such a probe exists in two main conformations. In the absence of a target, it forms a hairpin structure ("dark" complex), with the dyes close to each other. The self-hybridization and quenching can be eliminated by the target sequence, which hybridizes to the probe with greater affinity, or by exposing the probe to high temperatures (melting). Opening the hairpin structure increases the distance between the two dyes, thus eliminating proximity quenching. Such probes were coupled with DNA amplification in polymerase chain reaction (PCR), so that they produce a luminescence response proportional to the amount of a target DNA. Such closed-tube format is called real-time PCR.[23] Mechanism of action of these probes is shown in Fig. 5.

Similar principles are employed in the fluorogenic peptide substrates and TaqMan® DNA probes, in which the luminescent label is quenched due to close proximity of the other dye. Enzymatic cleavage of the probe during the assay separates the two dyes. thus causing enhancement of the luminescence of the reporter. Pairs of single-labeled RET probes are used for sensing molecular interactions in solution, such as immuno, receptor, or DNA-binding assays.[23] Similar approaches were used for cell-based assays for proteases, such as proapoptotic caspases. where the fluorphor and quencher are conjugated on opposite sides of a specific amino acid recognition sequence. Upon cleavage, energy transfer terminates. and the signal is enhanced. Luminescent labels employed for these schemes include xanthene dyes (FITC, rhodamines, TAMPRA), coumarin derivatives, and lanthanide chelates.

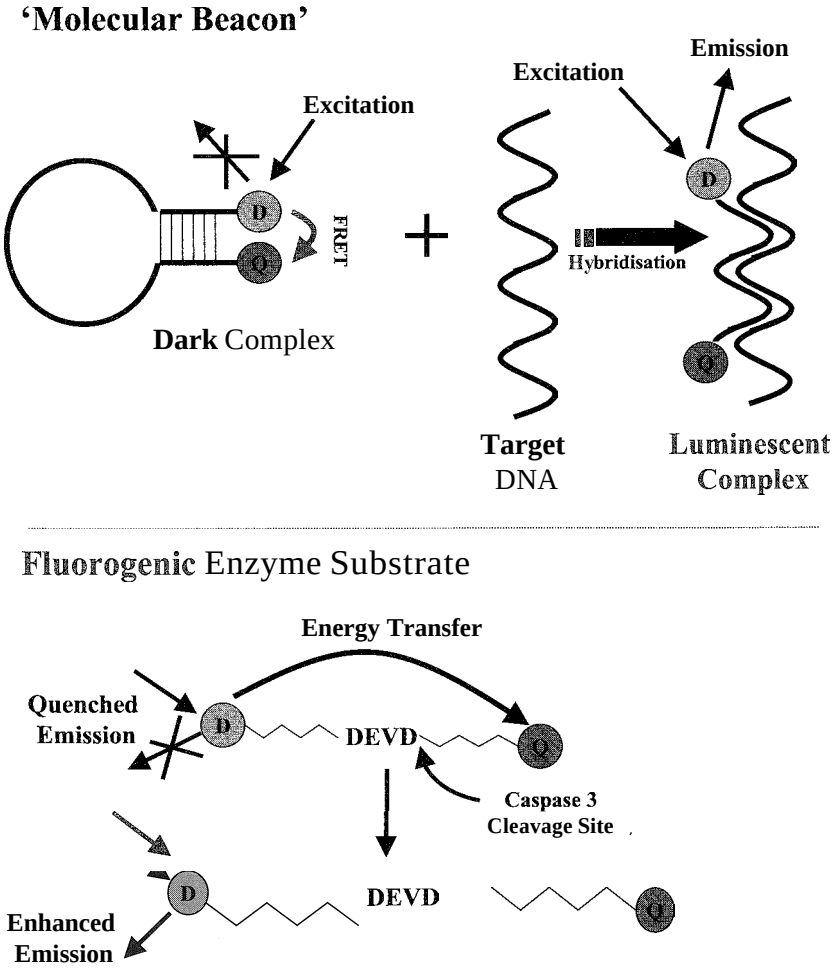

Fig. 5 Two RET-based sensing schemes. A molecular beacon structure with a fluorescent donor (D) and a quenches (Q) enhances emission upon target hybridization. A protease substrate with donor and acceptor conjugated to an amino acid recognition sequence (DEVD) enhances emission upon enzymatic cleavage. (*View* this *art in color at www.dekker.com.*)

Probes based on long-decay luminescent complexes of lanthanides (Eu^{3+}, Tb^{3+}, Sm^{3+}) and transition metals (Ru^{2+}, Os^{2+}) usually contain a central metal ion responsible for luminescence but with weak intrinsic absorbance; aromatic ligands serving as "light antennae" that absorb UV-light and transfer its energy via their excited triplet states to the metal ion; ancillary chemical groups and ligands shielding the luminophore from quenching by water and other molecules; and a linker arm, a functional chemical group for covalent attachment, and a chemical or biological moiety that recognizes the target analyte.[4,24] In contrast, the luminescence of metalloporphyrin dyes originates from the tetrapyrrolic macrocycle, but it is greatly affected by the nature of the central metal ion coordinated by the porphyrin ring and by axial ligands.[25] Pt^{2+}- and Pd^{2+}-porphyrins are particularly interesting because of their bright short-decay phosphorescence at room temperatures, and practically no fluorescence. They were used as sensitive labels for binding assays based on time-resolved luminescent detection[12] and as probes for oxygen sensing.[20] Other porphyrin complexes can be fluorescent (metal-free, Mg^{2+}), fluorescent and phosphorescent (Zn^{2+}, Al^{3+}), or nonluminescent (Fe^{3+}, Co^{2+}, Ni^{2+}). Structures of lanthanide chelates and metalloporphyrins are given in Fig. 3.

CONCLUSION

Overall, luminescent probes provide a powerful and versatile tool for studying supramolecular structures and their practical uses. Multiple intrinsic and extrinsic parameters of chemical and biological samples are measurable by their means. Accompanying multiple detection formats facilitate the collection of large amounts of information about supramolecular structures, their macro- and micro-

environments, and their interactive processes. Such probes allow for a variety of (bio)analytical applications, and they are actively being exploited in many areas of research and human practice.

ARTICLES OF FURTHER INTEREST

Biosensors, p. *115*
DNA Nanotechnology, p. 475
Fluorescence Sensing of Anions. p. 566
Fluorescent Sensors, p. *572*
Imaging and Targeting. p. 687
Luminescent Materials. p. 816
Photochemical Sensors. p. 1053
Supramolecular Photnchernistn, p. 1434

REFERENCES

1. Jablonski. A. Uber den mechanisms des photolumineszenz von farbstoffphosphoren. Z. Phys. 1935. *94*, 38–46.
2. Parker, C.A. *Photoluminescence of Solutions*; Elsevier: Amsterdam, 1968.
3. Condon, E.U. The Franck-Condon principle and related topics. Am. J. Phys. 1947, *15* (5), 365–374.
4. Hemmila, I.; Mukkala, V-M. Time-resolution in fluorometry technologies. labels. and applications in bioanalytical assays. Crit. Rev. Clin. Lab. Sci. 2001. *38* (6), 441–519.
5. Lakowicz, J.R. *Principles of Fluorescence Spectroscopy*, 2nd Ed.; Kluwer Academic/Plenum Publishers: New York, 1999.
6. Van Der Meer, B.W.; Colter, G.; Chen, S.-Y. *Resonance Energy Transfer Theory and Data:* VCH: New York. 1994.
7. Forster, T. Intermolecular energy migration and fluorescence. Ann. Phys. (Leipz.) 1948, *2*. 55–75.
8. Stryer, L. Fluorescence energy transfer as a spectroscopic ruler. Ann. Rev. Biochem. 1978. *47*, 819–846.
9. Hermanson. G.T. *Bioconjugate Techniques:* Academic Press: San Diego, 1996.
10. Coons. A.H.; Creech. H.J.: Jones. R.N.; Berliner. E. The demonstration of pneumococcal antigen in tissues by the use of fluorescent antibody. J. Immunol. 1942. *45*. 159–170.
11. Weber, G. Polarisation of the fluorescence of macromolecules. Biochem. J. 1951. *51*, 155–167.
12. Bazin, H.; Préaudat. E.; Trinquet, E.: Mathis. G. Homogeneous time resolved fluorescence resonance energy transier using rare earth cryptates as a tool for probing molecular interactions in biology. Spectrochim. Acta. Part A 2001. *57*. 2197–2211.
13. Baumgarth, N.: Roederer, M. A practical approach to multicolour flow cytometry for immunophenotyping. J. Immunol. Methods 2000, *243*. 77–97.
14. Chalfie, M.; Tu, Y.: Euskirchen, G.: Ward. W.W.: Prasher, D. Green fluorescent protein as a marker for gene expression. Science 1994, *263*, 802–805.
15. Kain, S.R. Green fluorescent protein (GFP): Applications in cell-based assays for drug discovery. Drug Discov. Today 1999. *4* (7), 304–312.
16. Eftink, M.R. The use of fluorescence methods to monitor unfolding transitions in proteins. Biophys. J. 1994, 66. 482–501.
17. Petrich, J.W.; Longworth, J.W.; Fleming, G.R. Internal motion and electron transfer in proteins. Biochemistry 1987. *26*, 2711–2722.
18. Orsel, J.G.; Bartoldus, I.: Stegmann. T. Kinetics of fusion between endoplasmic recticulum vesicles in vitro. J. Biol. Chem. 1997, *272* (6). 3369–3375.
19. Haugland, R.P. *Handbook of Fluorescent Probes and Research Products*. 9th Ed.; 2002.
20. Demas, J.N.; DeGraff. B.A.; Coleman, P.B. Oxygen sensors based on luminescence quenching. Anal. Chem. 1999. 71 (23), 793A–800A.
21. de Silva, A.P.; Fox, D.B.: Moody, T.S.; Weir, S.M. The development of molecular fluorescent switches. Trends Biotechnol. 2001. *19* (1), 29–34.
22. Dive, C.; Cox. H.; Watson. J.V.; Workman, P. Polar fluorescein derivatives as improved substrate probes for flow cytoenzymological assay of cellular esterases. Mol. Cell. Probes 1988. *2*. 131.
23. Didenko. V.V. DNA probes using fluorescence resonance energy transfer (FRET): designs and applications. BioTechniques 2001, *31*, 1106–1121.
24. Hemmila, I.A. *Applications of Fluorescence in Immunoassays*; Winefordner, J.D., Ed.; Wiley & Sons: New York, 1991.
25. Gouterman, M. *The Porphyrins Volume 3:* Dolphin, D., Ed.; Academic Press: New York, 1978.
26. O'Riordan, T.C.; Soini, A.E.; Soini. J.T.; Papkovsky, D.T. Performance evaluation of the phosphorescent porphyrin label: Solid-phase immunoassay of a-fetoprotein. Anal. Chem. 2002, *74* (22). 5845–5850.

Macrocycle Synthesis

Bernard Dietrich
ISIS—Université Louis Pasteur, Strasbourg, France

INTRODUCTION

Over the past decades, the number of macrocyclic compounds have increased in an explosive manner. This fast-growing phenomenon is due to the discovery of an impressive number of new macrocyclic families of natural. seminatural, or artificial origins: porphyrins, phthalocyanins, cyclodextrins, calixarenes, coronands, cryptands, spherands. etc. Special mention has to be given to the impressive number of natural bioactive macrocycles isolated from soil bacteria and, more recently, from marine organisms. The importance of these metabolites may be illustrated by their medical applications as antibiotics (nonactin, erythromycin), immunosuppressants (cyclosporin, FK506), and an anticancer agent (cytovaricin), to mention just a few. Thus. the macrocyclic type of structure is constantly supplied by two main sources: 1) the supramolecular chemistry field. for which the macrocyclic arrangement is of fundamental importance and which still plays a major role in the design of specific (macrocyclic) targets; and natural sources: which give access to new macrocycles, usually exhibiting complicated chemical skeletons and requiring sophisticated tools for elucidation of their structures. The most extravagant and the a priori most complicated target molecule will invariably fascinate some (high-rank) chemists who do not hesitate to rush in the gambling of total synthesis. As an almost general rule in macrocycle synthesis, the methodology consists of a step-by-step building of a linear precursor, followed by the macrocyclization event, which usually takes place in one of the final seeps. The necessity of obtaining a high yield in this crucial step has been, and still is. the major stimulus for efforts to improve existing macrocyclization methods or to discover new ones.

In this article, we will first present some general considerations of cyclization and then concentrate on some of the various synthetic approaches. The synthesis of macrocyclic families will not be covered here. as this topic is treated in detail in other entries of this Encyclopedia (see articles on calixarenes. cyclodextrins, porphyrins, etc.)

HISTORY

The emergence of macrocyclic chemistry came surprisingly late and was beset with difficulty, because for a long time, it was a common belief that macrocyclic compounds did not exist. The story of the macrocycle started at the beginning of the nineteenth century when Walbaum isolated from natural musk the odor principle, which he called muscone, and then a few years later, Sack isolated the odor principle from civet (civetone). But elucidation of the chemical constitutions of these compounds was accomplished only in the mid-1920s by L. Ruzicka, who presented in his Nobel Lecture a description of the difficulties he encountered: ''I was hindered less by the caprices of the substance itself than by the general prejudice, shared by myself, against the probability of the existence of a 15- and a 17-membered ring.''[1] The above-mentioned compounds were indeed identified as being 15- and 17-membered macrocyclic ketones.

Shortly after these investigations. he described a method for the synthesis of macrocyclic ketones by thermolysis of thorium or cerium salts of dicarboxylic acids. Unfortunately, the yields were poor. Between 1930 and 1950, several efficient methods were devised: the use of high dilution conditions (K. Ziegler); depolymerization methods (W. H. Garothers); and acyloin condensation (V. Prelog, M. Stoll). With the start of the supramolecular chemistry field in the 1960s, and the simultaneous growing interest in natural macrocyclic compounds, a large number of new synthetic methods were developed. A select and, due to space limitations. restricted number of procedures will be described here.

GENERAL CONSIDERATIONS

For the past 70 years or so. the cyclic compounds have been divided into four families depending on the number (n) of atoms in the ring: small rings ($n = 3,4$); normal rings (n = 5,6,7); medium rings ($n = 8$–11); and large rings or macrocycles ($n \geq 12$). This classification is the result of several empirical and experimental facts. The ease (or

Encyclopedia of Supramolecular Chemistry
DOI: 10.1081/E-ESMC 120012658

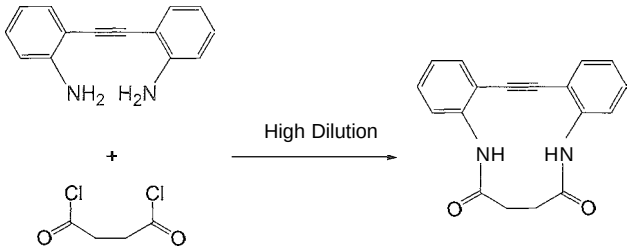

Fig. 1 First macrocycle synthesized in 1912 by the high dilution method.

difficulty) of cyclization as a function of ring size was recognized a long time ago, and the first classification was based on these results. More elaborate is the classification established from the heats of cornbustion of cycloalkanes per CH_2 group. with cyclohexane acting as the reference. These values reflect the ring strain, which is maximum for small rings (angular strain) and high for medium rings (transannular repulsive interactions). It should be noted that in macrocycles, there is no more ring strain, and the difficulty of the syntheses rests on other factors, as will be shown below.

HIGH DILUTION

The story of this fundamental technique used in many macrocycle syntheses is odd. In 1912, P. Ruggli was interested in the synthesis of cyclic compounds containing a triple bond in their ring. He realized that because of the intrinsic properties of a triple bond, the ring had to be large. He estimated that a 12-membered ring would be appropriate to fulfill his expectations. So, trying to afford such a 12 membered ring, he discovered that operating in ''normal conditions'' leads essentially to an insoluble polymer, and that in order to obtain the target molecule, the reaction should be carried out in high dilution conditions[2] (Fig. 1). This publication came too early and did not attract attention, mainly because at that time. nobody was interested in macrocycles.

Elegantly, in a large footnote of one of his publications K. Ziegler admitted that he ''rediscovered'' the high dilution principle 20 years later.[3]

In the reaction described in Fig. 1. the reactants are bifunctional, and the first step is intermolecular and does not present any difficulty. The problems arise in the second intramolecular step (see Fig. 2a). The long chain formed by the first connection between X and Y can be assumed to exist in a large number of shapes, but the specific conformations required for ring closure are limited. Expressed in another way, one has to assume that in a long chain there exists only a low probability of encountering the two remaining reactive centers X and Y. Therefore, in order to allow this reaction to occur, the competitive intermolecular reaction should be avoided. This can be achieved by operating in high dilution conditions, i.e., leaving the reactive molecule ''alone'' for the time necessary for the intramolecular encounter of the reactive ends X and *Y*. This type of high dilution reaction involving bifunctional reactants was largely used, for example, for the first cryptand synthesis. The one-component cyclization (Fig. 2b) is another common alternative that was used, for example, in the amide formation from a carboxylic acid and a terminal amine. This is the type of reaction mainly used in the synthesis of the elaborate natural compounds. Here again, high dilution will favor the intramolecular reaction between X and *Y*, thus affording a single macrocycle and minimizing the intermolecular reactions leading to a dimer or various oligomers. A schematic summary of the two major types of macrocyclization methods requiring high dilution conditions is given in Fig. 2.

One may note that in both methods, valuable side products can be obtained (formation of larger rings by 2+2 or 1+1 condensations in Fig. 2a and 2b, respectively). In a more practical viewpoint, several comments have to be made. In the one-component cyclization the two reactive centers are present on the same molecule. What arises, therefore, is the need to hide the reactivity of the two centers (or at least one of the centers) until the ultimate moment. This is usually realized in the following way: 1) one end of the reactive center is activated, while the other center is maintained in an unreactive form; 2) then, a solution of the linear precursor is slowly added to a well-stirred solution containing the substance that is able to activate the protected site (bases often play this role). For

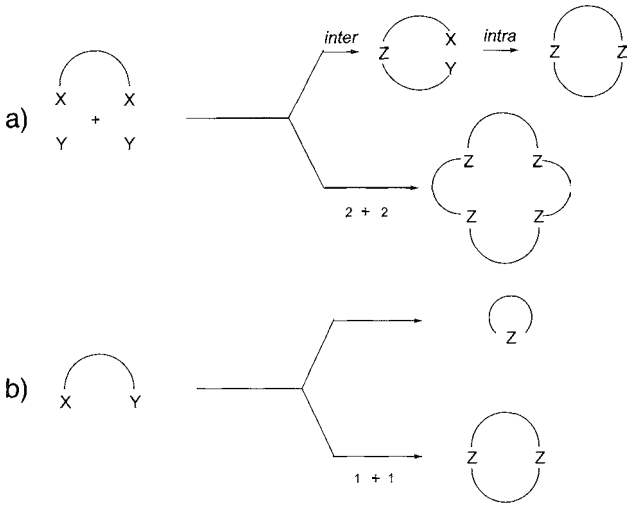

Fig. 2 Two-components (a) and one-component (b) cyclizations.

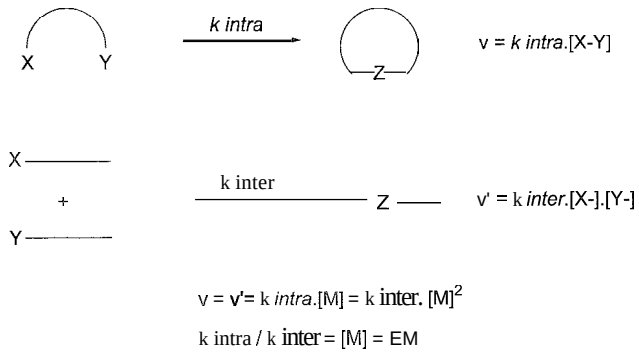

Fig. 3 Intramolecular cycliration and intermolecular reaction between two model reactants—the effective molarity (EM) definition.

the two-components cyclization. the procedure is simpler: solutions of the two reactants are introduced into two precision dropping funnels, and the two solutions are added very slowly to a well-stirred large volume of solvent. As noticed above, the two-components method becomes, after the initial intermolecular reaction, a one-component reaction with its specific requirements. We will, therefore, concentrate our attention on this type of reaction.

Going more deeply into the subject, the first question we can ask is: what is really a reaction conducted in high dilution conditions? Rigorous studies are rare, so we will mention one of the most studied, developed by Mandolini and Illurninatti. in which they introduce the concept of effective molarity.[''] They defined the effective molarity (EM) as being the concentration at which the rate of intramolecular reaction is similar to the rate of intermolecular reaction (Fig. 3).

Thus, at this concentration equal amounts of cyclic and open products are formed. A significantly more diluted solution will, therefore, give predominantly the desired macrocycle. Conversely, a solution that is too concentrated will afford almost exclusively polymers. This rigorous procedure is, in practice, not used, and the cyclization reactions are conducted on the basis of more empirical considerations that, nevertheless, respect the necessity to operate in low concentrations.

Several other factors also play a role: the presence of heteroatoms (oxygen, nitrogen, sulfur) in the chain or the presence of rigid groups (aromatic ring) usually favors the formation of macrocycles.

We will turn our attention toward the synthesis of macrocyclic lactones, macrocyclic lactams, cyclopeptides, and macrocarbocycles, which are abundant in nature. Retrosynthetic cleavage of the lactone function, lactam function, and cycloalkanes provides an ω-hydroxy-acid, an ω-amino-acid, and an open-chain hydrocarbon derivative, respectively, which can therefore be considered a good precursors for the formation of the parent cyclic compounds (Fig. 4).

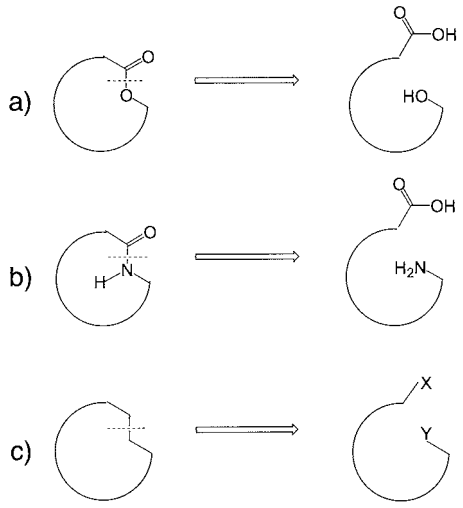

Fig. 4 Retrosynthetic cleavage of (a) rnacrocyclic lactone, (b) rnacrocyclic lactam, and (c) macrocarbocycles.

The intramolecular esterification of simple ω-hydroxy-acids (for example, those containing only a saturated hydrocarbon chain) or of its ω-halogeno derivative can be realized easily (Fig. 5), but the harsh reaction conditions are not compatible with the numerous sensitive functions present in the seco ω-hydroxyacids of natural origin. The necessity to perform the lactonization in a smoother way has been an efficient motor for progress. The same considerations apply for the macrolactamization or the formation of macrocarbocycles of natural origins.

The development of activating groups for acid and alcohol functional groups led to great advances in macrolide chemistry.[5] Many such activating groups for acids or alcohols were developed to improve macrocyclization. Some examples of activating groups for carboxylic

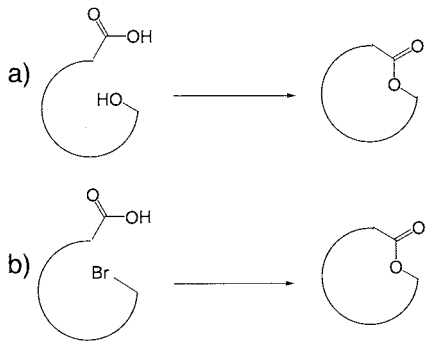

Fig. 5 Lactone synthesis from (a) ω-hydroxy- or (b)ω-bromo-acids.

acids are given in Fig. 6: thiol esters (1,2): 2-acyloxypyridinium or 2-acyloxybenzothiazolium (3,4); and mixed anhydrides (5,6). One may be surprised by the large number of activating groups. But, the screening of total synthesis of natural macrolides reveals that in each case. one group is the most efficient. This may be due to the stereochemistry of the linear precursor, which plays a crucial role. The best conforination of the linear precursor is the conformation that brings the two reactive sites in close proximity. Nevertheless. the conformation is an intrinsic property of the precursor. on which the operator has little influence (by change of solvent, for example). Also important are the relative orientations of the interacting sites, the steric hindrance, the lipophilicity, etc. The prolific production of activating agents has been realized by talented chemists such as Corey, Nicolaou, Mukaiyama, Masamune. Roush, and Yamaguchi among many others.

Two other important methods are described in Fig. 7. The first is a macrolactonization mediated by the Mitsunobu reaction. In this case, in contrast with the preceding examples. the hydroxyl functional group is activated, and the carboxylate group behaves as a nucleophile. The reaction of the hydroxy acid with diethyl azodicarboxylate and triphenylphosphine leads to ring closure via an alkoxyphosphonium carboxylate intermediate (Fig. 7a).

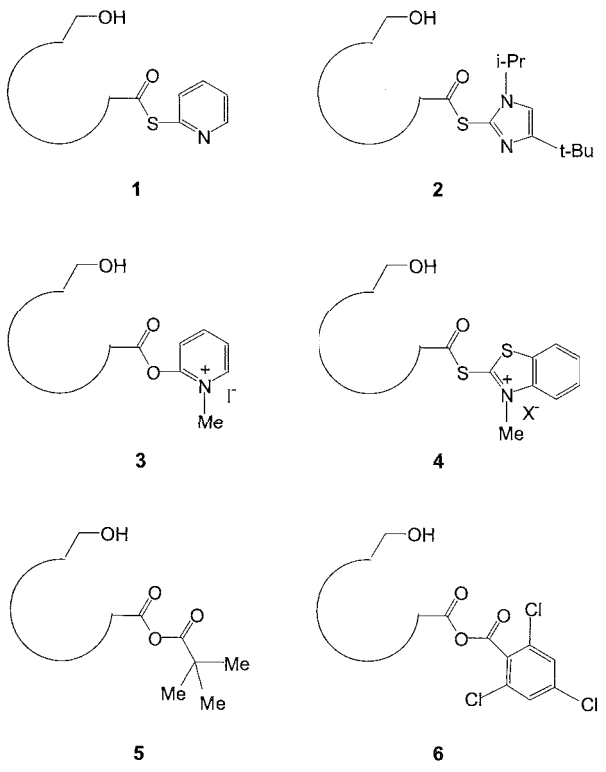

Fig. 6 Activating groups for an acid functional group: 1 and 2, thiol esters; **3,** 2-acyloxypyridinium; 4, 2-acyloxybenzothiazolium: and **5,** and 6, mixed anhydrides.

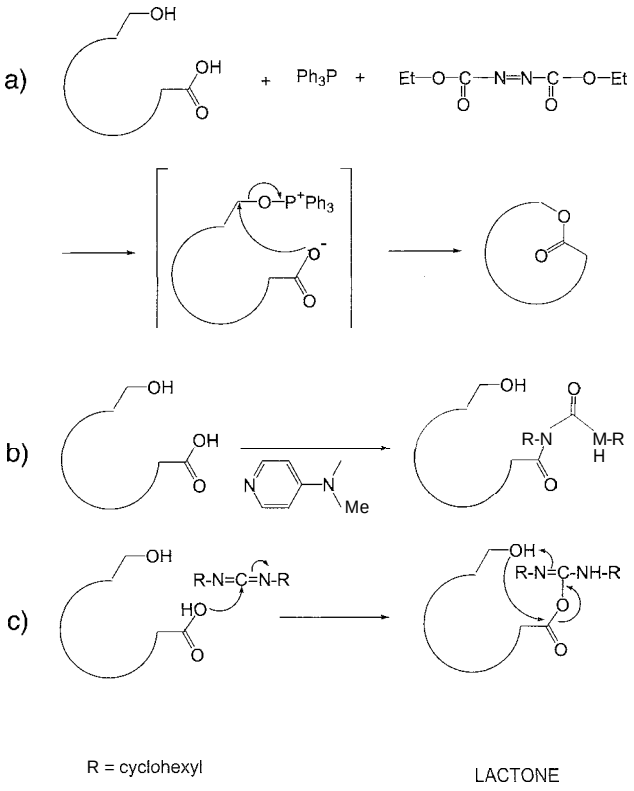

Fig. 7 Macrolactonizations mediated by (a) the Mitsunobu reaction; (b) the Steglich esterification run in the presence of DMPA, which gives only an urea derivative; and (c) high yields of lactones, which are obtained in the presence of a proton source (DMPA, HCl).

The second example is based on Steglich esterification, for which it was shown that the yield of esterification reaction using dicyclohexylcarbodiimide is greatly increased by the addition of 4-dimethylarninopyridine (DMPA). However, in the case of w-hydroxyacids under these reaction conditions, the N-acylurea derivative is formed almost exclusively (Fig. 7b), with almost no lactone formation. The reason for this failure appears to lie in the proton-transfer steps. By operating in the presence of a proton source (DMPA-HCl), the lactonization occurred in excellent yield (Fig. 7c).

Many other activating groups have been elaborated. and further examples can be found in a review on synthesis of natural macrocyclic compounds.[6]

The lactam functional group is encountered in numerous macrocyclic lactams like, for example, the inacrocyclic polyamine alltaloids and the ansamycin antibiotics. Lactam formation can be achieved by intramolecular reaction between acyl chloride and amine functional

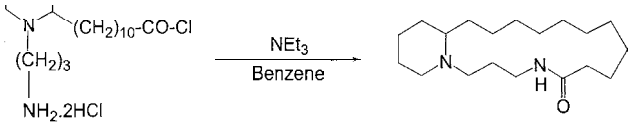

Fig. **8** Macrolactam synthesis by intramolecular reaction of an ω-acyl chloride-amine

groups. Tne reaction can be carried out by slow addition of the precursor **1** into a large volume of benzene containing triethylamine (Fig. 8).

Several methods of activation of the acid functional group have been described (hydroxypiperidine, thiophenol, thiazolidine-2-thione.).[7] Mixed anhydride methods (phosphonic, phosphoric. sulfonic, carbonic anhydrides) have been used in the final steps of many impressive total syntheses (rifamycin S for example).

The biological importance of cyclopeptides is widely known (oxytocin. vasopressin: cyclosporin, etc.). During the syntheses of these compounds. several problems were encountered. In particular, good protecting groups are needed for the amino acid side chain functionality, and efficient coupling methods are needed.[8] The general principles governing macrocyclization, which were covered extensively above, can be applied in this case (Fig. 9). The methodology consists of constructing the linear precursor step by step. At this point, the acid moiety is activated using classical reagents for peptide synthesis, while keeping the amine moiety protected (by

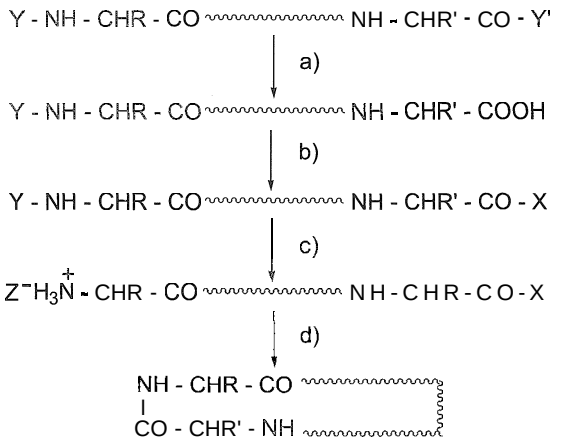

Fig. **9** Macrocyclopeptide synthesis: *Y*, Y are protecting groups; X is an activating group. (a) Deprotection of the carboxyl group; (b) activation of the carboxyl group: (c) acidic deprotection of the terminal amine; and (d) cyclization in a basic medium. The high dilution conditions are obtained by the slow addition of the protonated amine into a large volume of pyridine.

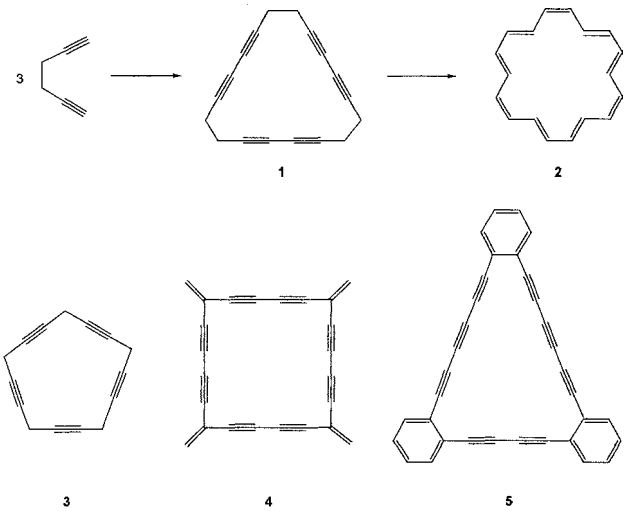

Fig. 10 Formation of carbomacrocyles by oxidative coupling of diacetylenes. 2: [18] annulene: **3.** 4, and **5,** macrocyclic-oligoacetylenes.

protonation) after removal of Y. The cyclization reaction takes place during the slow addition of the activated precursor to a basic medium (pyridine, for example).

Among compounds containing only carbon atoms in the macrocyclic framework, the macrocarbocycles, we will first mention the annulenes that were important synthetic targets in the 1960s. An important method

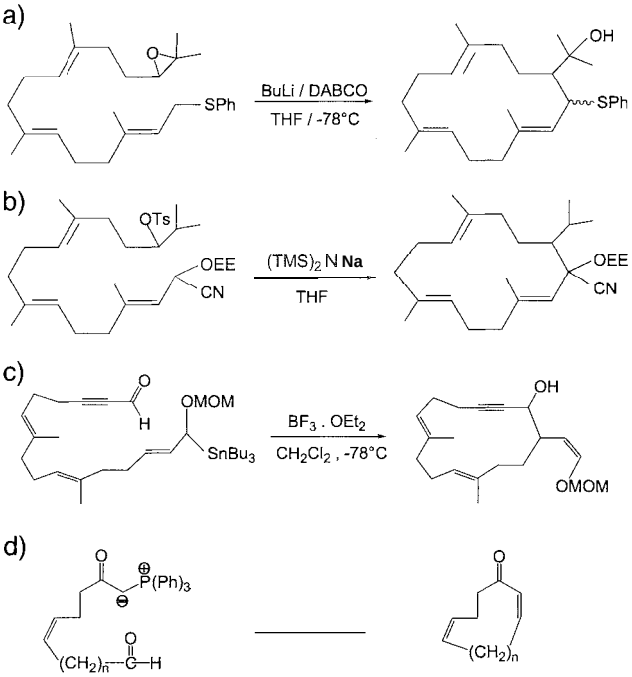

Fig. 11 (a–d) Natural macrocpcles syntheses via carbon–carbon bond formations.

allowing the preparation of macrocarbocycles relies on the oxidative coupling of terminal diacetylenes in the presence of copper acetate (Fig. 10). Thus, the coupling of the hexadiyne gave the cyclic trimer **1,** which on rearrangement and partial hydrogenation afforded 2. This method was extended to the formation of many annulenes. In recent years, the field of macrocyclic oligoacetylenes has exploded. Hundreds of these compounds have been synthesized by carbon–carbon bond formation often using the oxidative coupling described above or closely related reactions[9–11] (3. 4, and *5,* in Fig. 10). The interest in these compounds rests on their potential applications as advanced materials.

In the field of synthesis of natural macromolecular carbocycles, macrocyclization through formation of a carbon–carbon bond has been intensively investigated. We will give just a few examples: the alkylation of carbanions (Fig. 11a, 11b); the addition of allylstannane to aldehyde (Fig. 11c); and the intramolecular Wittig reaction (Fig. 11d).[6 9–11]

Powerful methods make use of metal-catalyzed macrocyclization. We mention the following: the allylic alkylations catalyzed by palladium[12] (Fig. 12a); the reductive coupling of dicarbonyl compounds[13] (Fig. 12b); the Stille coupling[14] (Fig. 12c); and ring closing metathesis[15] (Fig. 12d).

SOLID-PHASE SYNTHESIS

The macrocyclizations using the high dilution method described above were carried out in an homogeneous medium. Heterogeneous conditions have also been explored. A long-known example is the acyloin cyclization developed by Prelog and Stoll. The diester was added to a suspension of liquid sodium in boiling xylene and was efficiently stirred (Fig. 13a). The high yields were attributed to coordination of the diester to the surface of the metal, hence, isolating the molecules from each other and bringing the chain ends in close proximity.

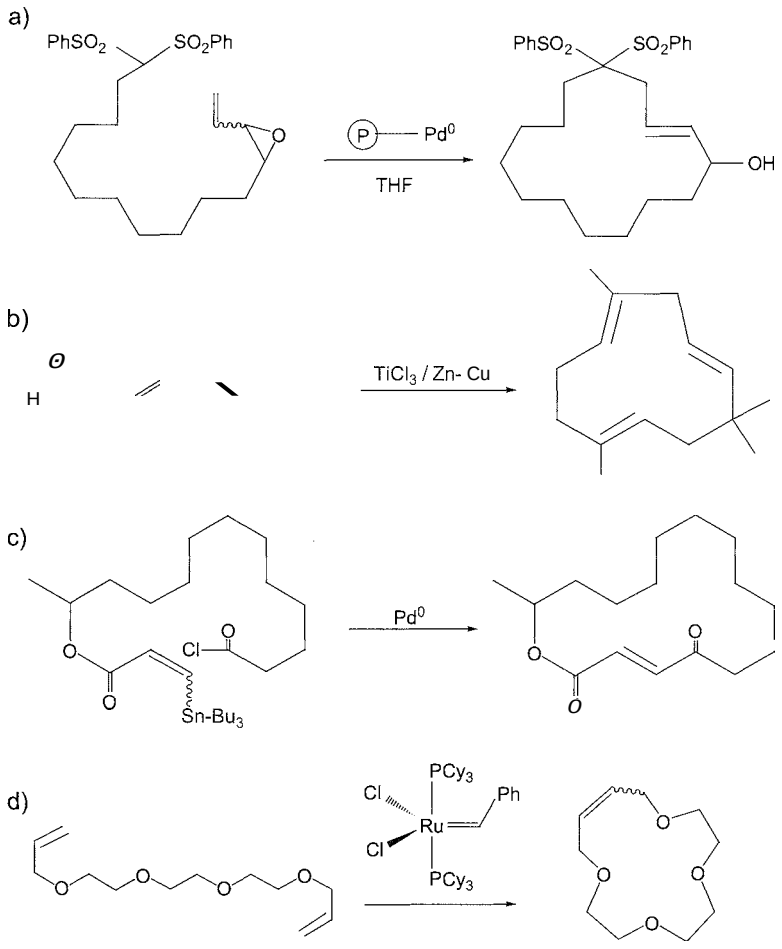

Fig. 12 (a–d) Examples of metal-catalyzed macrocyclizations.

Solid-phase synthesis[16] offers a more rational approach toward high dilution in a solid–liquid heterogeneous medium by using a polymer support to bind the reactant, which leads to site isolation on a solid matrix (Fig. 13b). The loading of the beads should be accomplished in order to ensure real site isolation. Solid-phase synthesis was initially designed for peptide syntheses, and the solid-phase methodology was largely used in the preparation of cyclopeptides.[8] The principle of the procedure is illustrated in Fig. 13c. The first step consists of binding amino acid 5 (which had to be trifunctional, such as glutainic acid: asparagine, tyrosine, serine, and cysteine) onto the polymer. By using the amine and carboxylate functional groups of 5, two linear chains are elaborated in parallel to afford polypeptides having amino acids 1 and 9 at the two chain ends as end-products. This is followed by cyclization and then cleavage of the cyclopeptide from the polymer support.

The necessity to have practically quantitative coupling is required, because the separation of the target peptide from the side products is almost impossible when the number of peptide residues becomes large. This requirement is still a significant problem in the synthesis of the numerous existing cyclosporins which are characterized by a large number of N-methyl amino acids that have weak reactivity toward activated acids due to their steric hindrance. One may note that in this series of compounds, the cyclization was not accomplished on the resin but on the linear undecapeptide precursor after its cleavage from the resin.[17]

In recent years, combinatorial synthesis has become a powerful tool in organic synthesis, in particular; in the field of drug research.[18] This methodology has also been efficiently applied on solid-phase support. Two examples make use of the intramolecular Heck reaction, and large libraries of peptides or nonpeptides have been prepared. The first example (Fig. 14a) concerns the synthesis of various derivatives containing the Arg-Gly-Asp (RGD) sequence—a biologically important tripeptide unit.[19] In the second example, a large number of macrocycles of the type described in Fig. 14b were obtained in good yields.[20] In both cases, the libraries were elaborated by

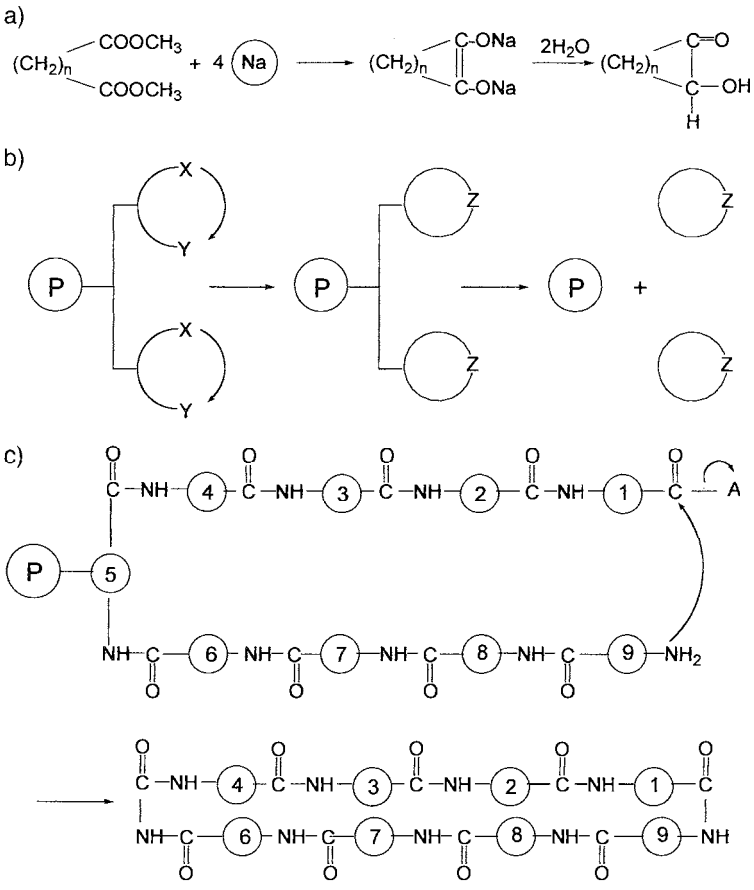

Fig. 13 (a) Acyloin cyclization, an example of macrocyclization in an heterogeneous medium: (b) scheme for cyclization on a polymer support; (c) and synthesis of a cyclopeptide on a polymer support.

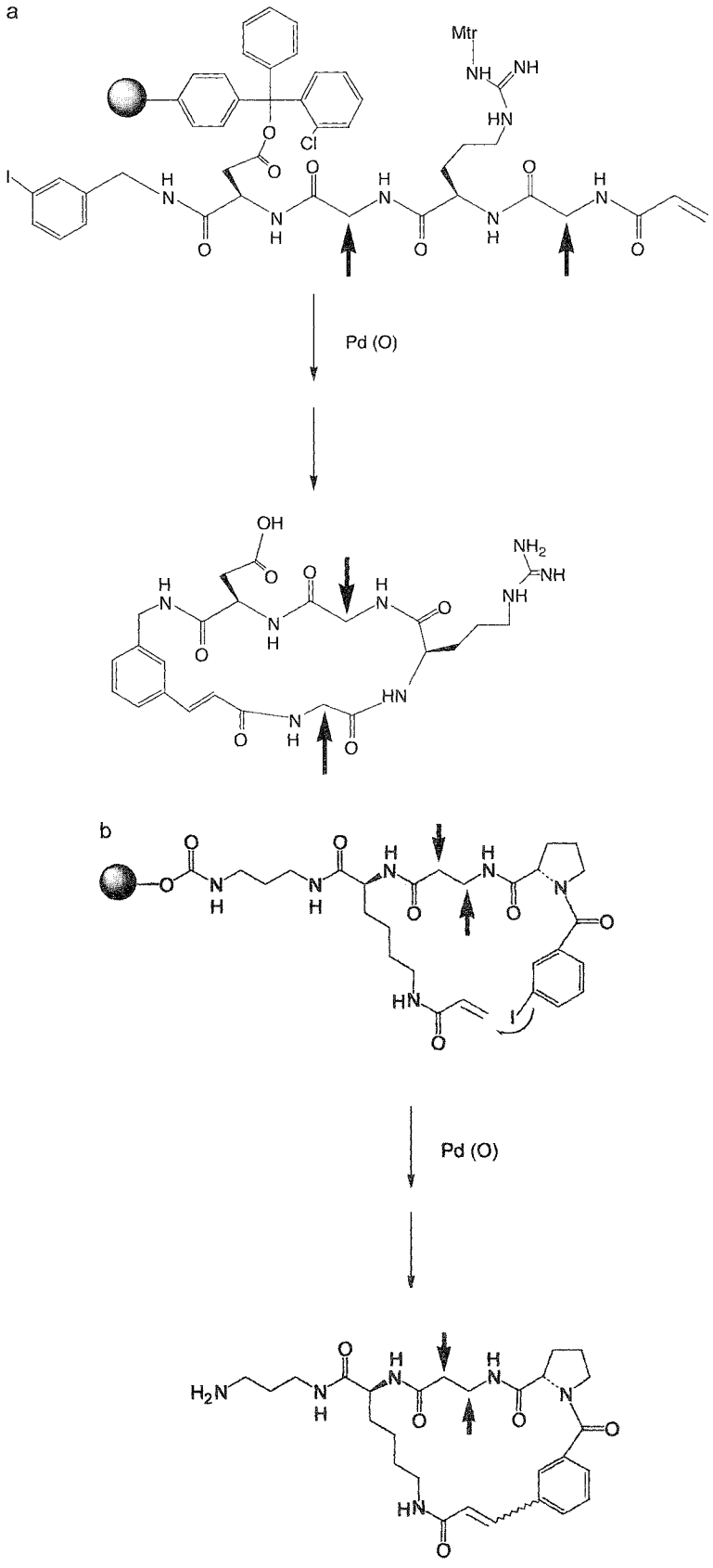

Fig. 14 (a,b) Intramolecular macrocyclizations on a solid support using the Heck reaction.

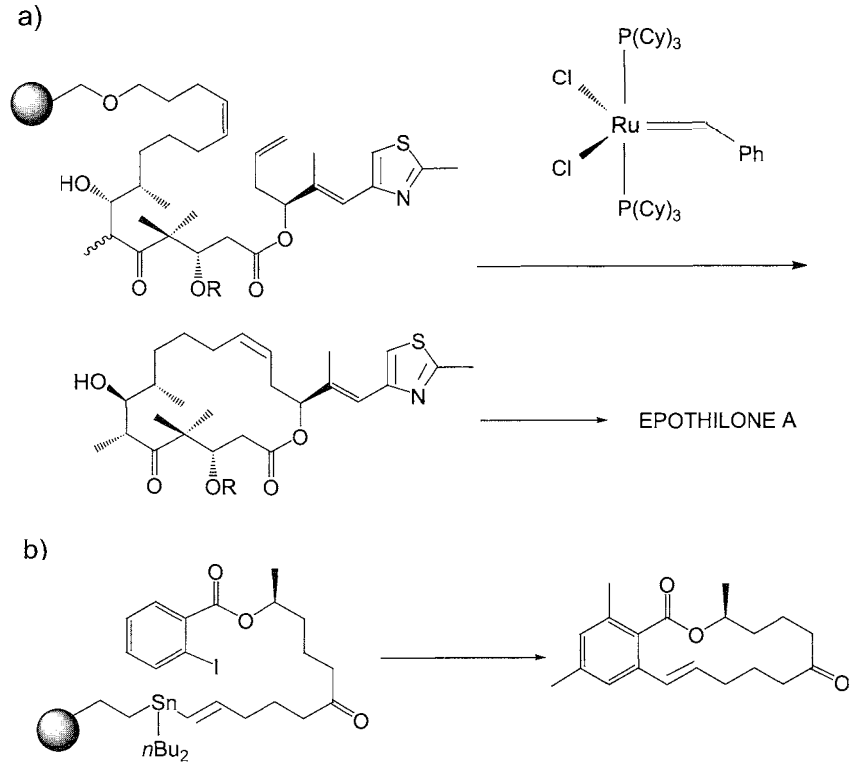

Fig. 15 Examples of cyclorelease: (a) ring-closing metathesis (this reaction afforded several macrocycles, among which we describe only one) and (b) Stille coupling.

the introduction of various substituents in the positions indicated by arrows.

To complete this short treatment on solid-phase synthesis, let us be mention the efforts made by several groups to obtain methods that allow a cyclorelease (also called cyclative cleavage) of the macrocycle, in other words. the cyclization reaction and the release from the polymer support occur simultaneously. The methods developed so far involve the metathesis reaction (Fig. 15a);[21] the Stille coupling (Fig. 15b);[22] and sulfur ylides (Fig. 16a).[23]

In the strategy described in Fig. 16b, the linear precursor is not built on the polymer, but the final cyclization reaction using the Suzuki–Miyaura coupling takes place on a polymer. The aryl boronic acid is captured on a Dowex ammonium hydroxide resin. leading to the polymer ionically bonded borate, which is subsequently treated in the appropriate conditions to give the final macrocyle. This methodology is called "resin capture–release.."[24]

PHASE-TRANSFER CATALYSIS

In classical phase-transfer catalysis (PTC), the catalyst (often a quaternary ammonium salt) transfers the reagent (the associated anion) from the aqueous phase into the organic phase containing the substrate. Another alternative is the solid–liquid phase-transfer catalysis in which the insoluble salt incorporating the active anionic species is in suspension in the organic solvent containing the substrate and the phase-transfer catalyst. This method has been applied to the synthesis of macrolides. The catalytic cycle affording various lactones is shown in Fig. 17.

It should be noted that this reaction is a special case of solid–liquid catalysis, because the anionic species, solubilized by the catalyst, is both reactant and substrate. Also of importance is the fact that because the tetrabutylammonium salt is used in catalytic quantities, the concentration of active species (the tetrabutylammonium carboxylate) remains very low throughout the reaction, which is therefore conducted in high dilution conditions. As expected, the yields are excellent.[25] Another type of PTC is the triphase catalysis,[26] having as a peculiar feature, the catalyst immobilized on a polymer (solid phase), which is in contact with the aqueous and organic phases containing the reactant and the substrate. respectively. This method presents the major advantage of avoiding the problem of catalyst and product separation. Various macrolides have been synthesized by this procedure.

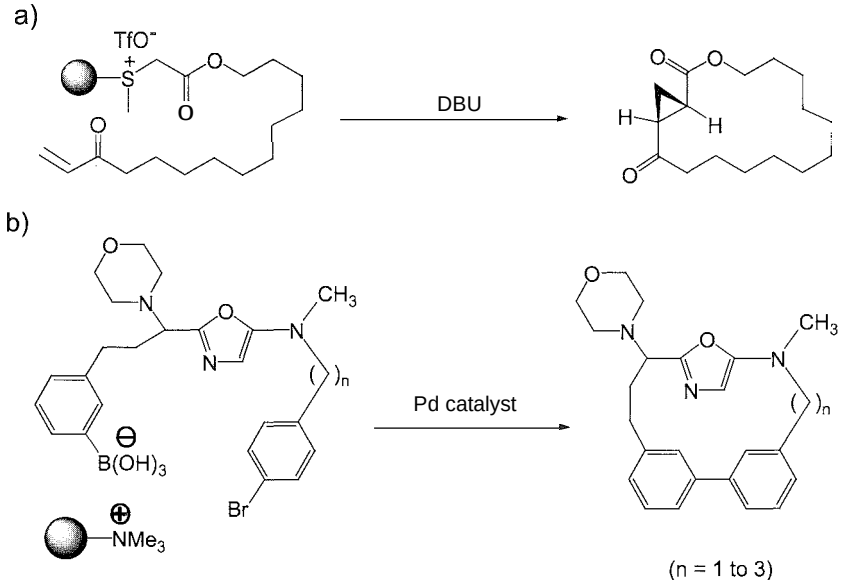

Fig. 16 (a) macrocyclic lactone synthesis by cyclorelease via a sulfur ylide and (b) macrocyclization via intramolecular Suzuki–Miyaura coupling: an example of resin capture–release.

HIGH PRESSURE

High-presrure chemistry has been applied in many fields, including organic synthesis. The method is based on the volume of activation $\Delta V^{\neq}$ that characterizes each reaction. Depending on the type of reaction. $\Delta V^{\neq}$ can be positive, negative, or close to zero. Reactions occurring with a negative volume of activation are favored by an increase of pressure. Formation of a quaternary ammonium salt from a tertiary amine and an alkylating agent is a reaction with a negative $\Delta V^{\neq}$. Jurczak et al. made use of this property in the synthesis of cryptands (Fig. 18a). The yields of diquaternary salts are very high (80–100%), and the demethylation step occurs in lower yields (50–90%).[27] High-pressure conditions were applied more recently to the synthesis of chiral macrocyclic tetraamides (Fig. 18b). These compounds are obtained in various yields (7–61%) by reaction of chiral diesters with α,ω-diamines under 10 kbar pressure.[28]

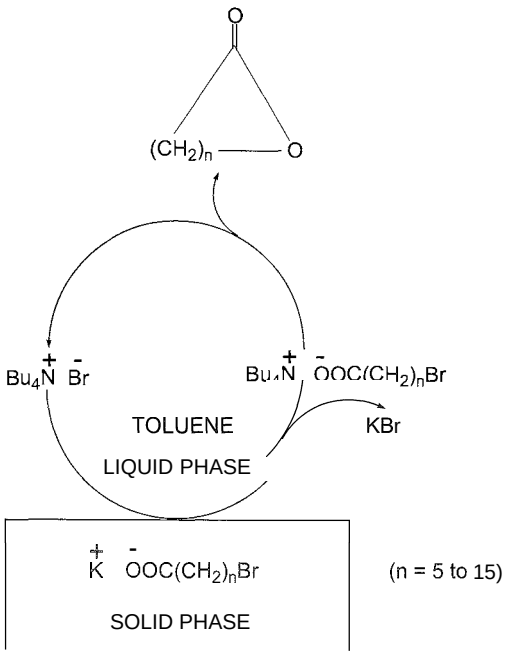

Fig. 17 Lactone synthesis by solid–liquid phase-transfer catalysis.

The Diels–Alder reaction has a negative $\Delta V^{\neq}$, and high-pressure conditions are particularly well adapted for this reaction. Using these conditions, Stoddart et al. synthesized, by successive Diels–Alder reactions, a[14] cyclacene derivative (Fig. 19).[29]

TEMPLATED MACROCYCLE SYNTHESIS

The synthesis of a macrocyclic ligand in the presence of a metal cation has been used since the mid-1960s. N.F. Curtis and D.H. Busch should be mentioned as pioneer workers in the field.[30] The so-called "template effect" is simple to understand. The presence of a metal cation leads to positioning of the reactants (by virtue of the presence of coordinating sites) such that macrocyclization is highly favored (Fig. 20).[30]

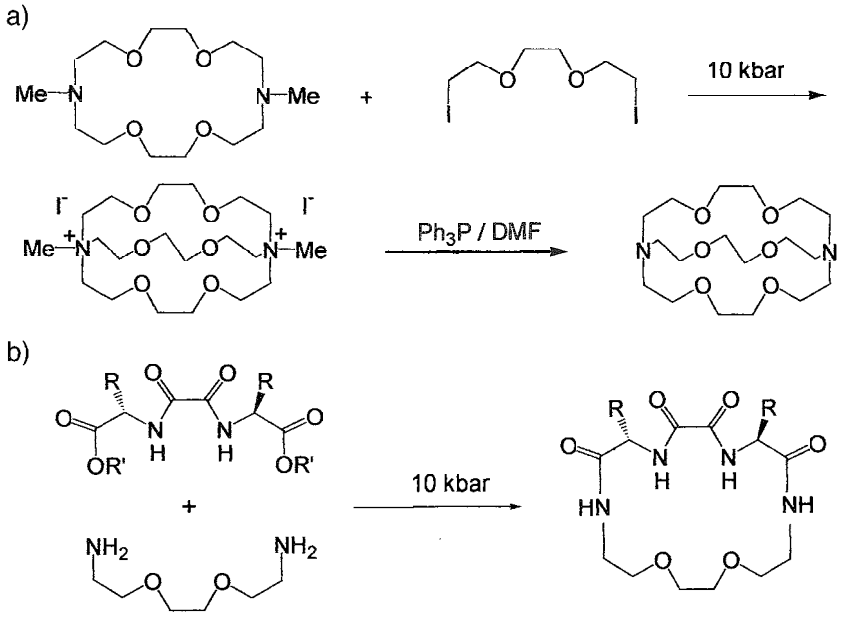

Fig. **18** High-pressure synthesis (a) of cryptands and (b) of chiral macrocyclic tetraamides.

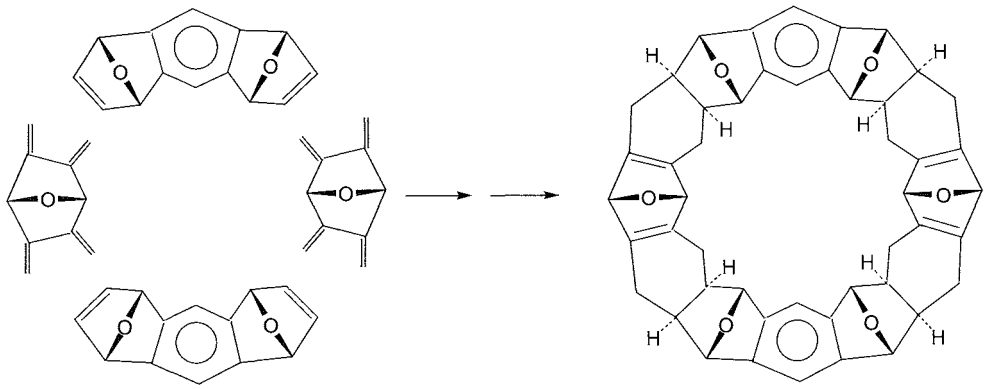

Fig. 19 Synthesis of a [12]-cyclacene derivative by a series of Diels–Alder reactions performed under high pressure

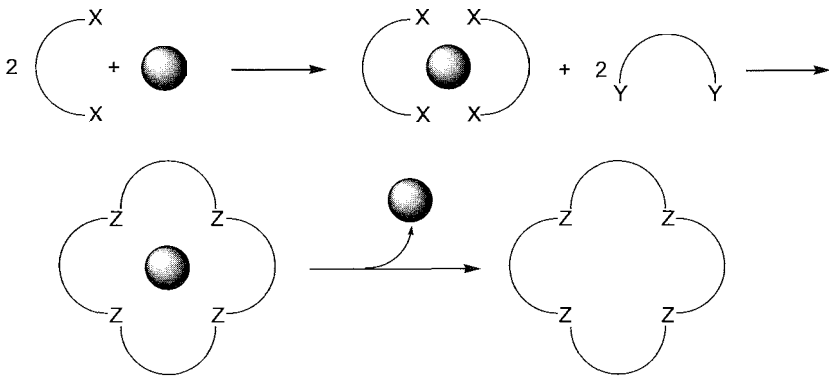

Fig. **20** Metal-templated cyclization using two subunits X–X and Y–Y. The free macrocycle may be obtained by demetallation (which can be difficult in some cases).

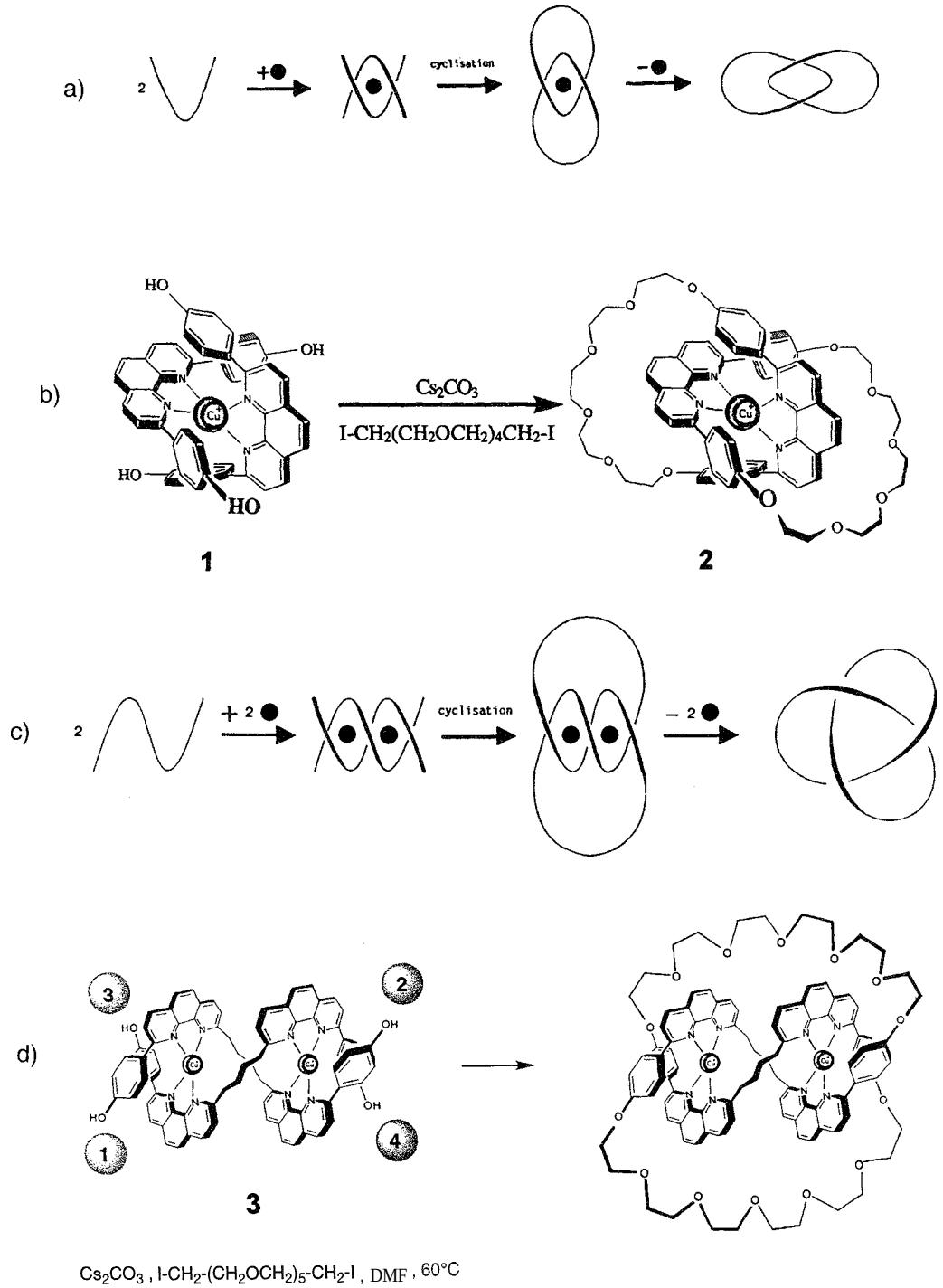

Fig. 21 (a) Principle for the synthesis of a [2] catenane. (b) Key-steps of the formation of the metallocatenane. (c) Principle for the synthesis of a trefoil knot. (d) Key-steps of the formation of the trefoil knot: formation of the double-helix 3, and cyclization by reaction of the diido compound—the coupling should occur between the phenol functions 1 and 4. 2 and 3. respectively. (The author thanks J.-P. Sauvage and C.O. Buchecker-Dietrich for supplying these figures.)

An elegant extension of the template effect is catenane (interlocked macrocycles) synthesis, which is based on the formation of a stable tetrahedral precursor complex between Cu(I) and the diphenolic derivative of 1,10-diphenylphenanthroline. This property has been used in the construction of a catenate, as shown in the synthetic scheme of Fig. 21a.

The key step in this approach is the formation of the precatenate **1** from the diphenolic derivative of 1,10-diphenylphenanthroline in presence of Cu(I). It can be seen that in structure **1,** the four phenol groups are in good position for subsequent attack and hence cyclization by the diiodo compound giving the catenate 2 (Fig. 21b). The Cu(I) ion can be easily removed by treatment with potassium cyanide, affording the catenane.[31] The tridimensional template effect induced by Cu(I) was extended to the formation of a trefoil knot (Fig. 21c,d).

Finally, dynamic combinatorial chemistry (DCC) opens new perspectives for templated syntheses. Early work was accomplished by the late M. Nelson, who studied in detail the condensations between diamines and 2.6-diacetyl-pyridine in the presence of various metal cations. To conclude, he found that the macrocyciic compounds formed depend on the overall proportions of the reactants and the type of cation used as the template. Related studies were accomplished using pyridine dialdehyde and several diamines (Fig. 22).[32]

The macrocyles formed depend on the overall proportions of 1 and 2, the diamine chain length and the type of cation used as the template. Of importance is the fact that the imine formation is a reversible reaction. Expressed in the DCC sense, one can say that all products. the macrocycies and the nonrepresented oligomers and polymers. are in constant equilibrium. and that all the species represented in Fig. 22 constitute a virtual combinatorial library (VCL). From this library, the high proportion of a specific macrocycle can be obtained by the use of the appropriate conditions (type of metal template, relative proportion of reactants).[32]

To conclude this part on dynamic combinatorial chemistry, we will mention the use of a polymer bound N-methyl ammonium ion as a template. The library is generated from the pseudopeptide building block mPro, which gives a dynamic library of hydrazones (Fig. 23). Depending on the conditions, the following will be formed at equilibrium: in the absence of a template, 85% of the cyclic dimer and 7% of the cyclic trimer: in the presence of the template BTA, 47% of the dimer and 50% of the trimer; and in the presence of the immobilized template. 40% of pure trimer can be isolated by washing the resin.[33]

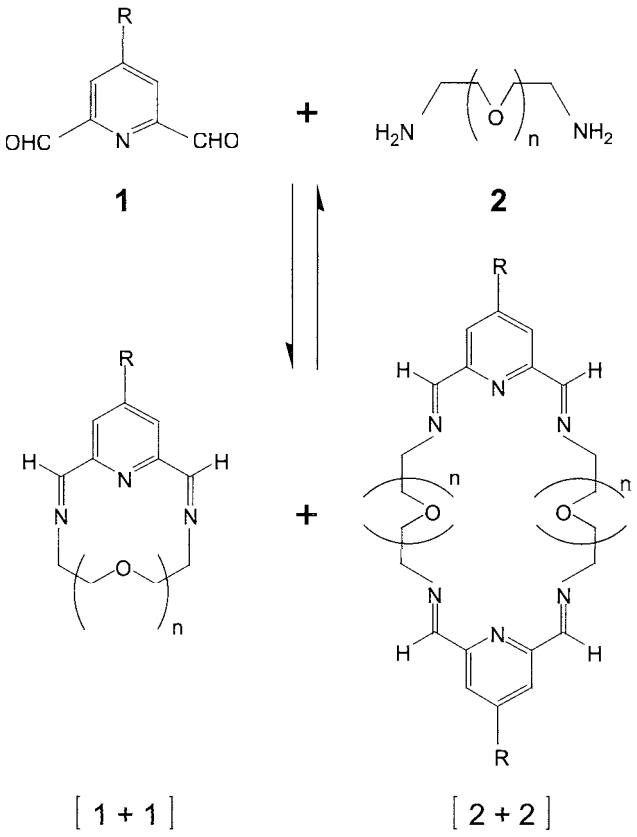

Fig. 22 Condensation of diamines with a dicarbonyl compound. The size and nature of the macrocycles thus obtained are strongly related to the relative overall proportion of the two reactants, the chain length of the diamine, and the template cation used.

CONCLUSION

Before concluding this limited survey of macrocyclic synthesis, the author would like to mention a few other aspects. For several important purposes. the syntheses of isotopically labeled macrocycles have been described.[34] Strategies leading to very large macrocycles were developed.[35] And, promising perspectives can be expected by elucidation of the biosynthetic mechanisms of the numerous natural macrocyclic compounds.[36,37]

ARTICLES OF FURTHER INTEREST

Amino Acids: Applications, p. 42
Anion-Directed Assembly, p. 51
Anticrowns, p. 68
Catenanes and Other Interlocked Molecules. p. 206
Chiral Guest Recognition, p. 236

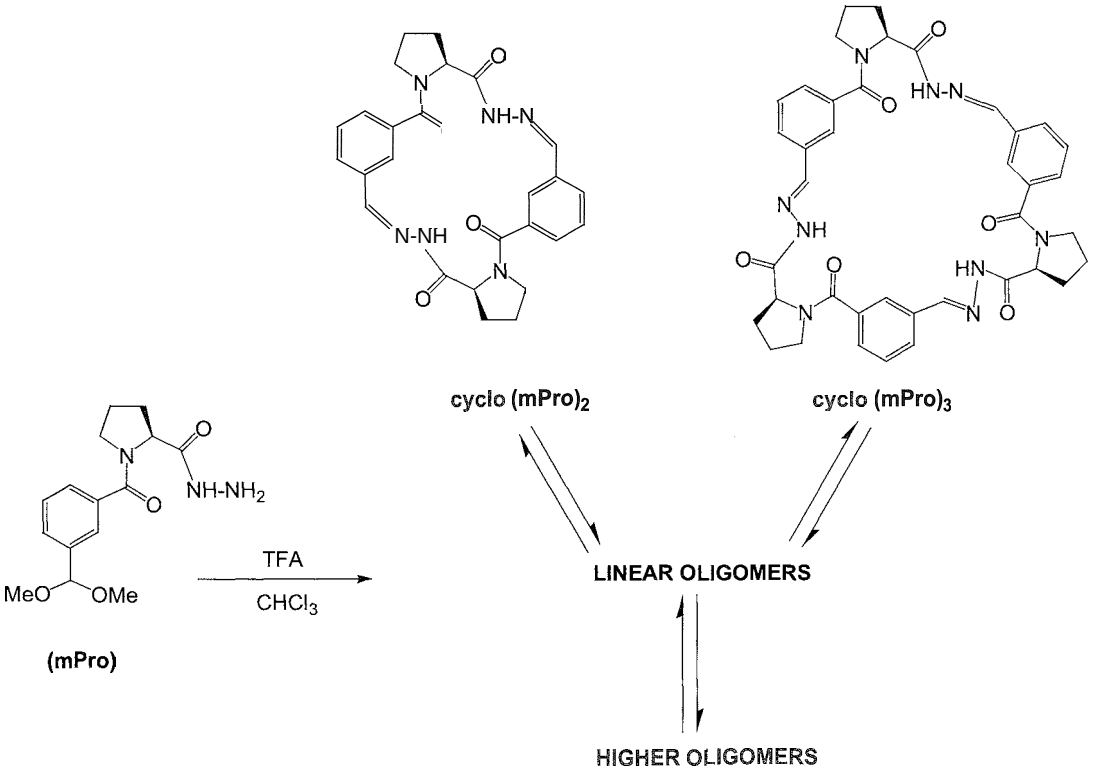

Fig. *23* Dynamic combinatorial chemistry. Library generated from the building block mPro.

Crown Ethers, p. 326
Cryptands, p. 334
Cyclophanes: Definition and Scope, p. 414
Inclusion Reactions and Polymerization, p. 705
Macrocycle Synthesis, p. *830*
Naked Anion effect, p. 939
Phase-Transfer Catalysis in *Environmentally Benign Reaction Media*, p. 1042
Self-Assembly: Definition and Kinetic and Thermodynamic Considerations, p. 1248
Supramolecular Libraries, p. 1427
The Ternplate Effect, p. 1493

REFERENCES

1. Ruzicka. L. Multimembered Rings, Higher Terpene Compounds and Male Sex Hormones. In *Nobel Lectures;* Chemistry. Elsevier Publishing Company: Amsterdam, 1964–1970; 468–492.
2. Ruggli, P. Über einen Ring mit dreifacher Bindung. Annalen **1912**, *392*, 92–100.
3. Ziegler. K. Über ringschluss-reaktionen. Ber. Dtsch. Chem. Ges. 1934. *67A*. 139–149.
4. Illuminati, G.: Mandolini, L. Ring closure reactions of bifunctional chain molecules. Acc. Chem. Res. **1981**, *14*, 95.
5. Nicolaou. K.C. Synthesis of macrolides. Tetrahedron **1977**. 33, 683–710.
6. Meng. Q.; Hesse. M. Ring closure methods in the synthesis of macrocyclic natural products. Top. Curr. Chem. **1991**. 161, 107–176.
7. Dietrich. *R.:* Viout. P.: Lehn, J.-M. *Macrocyclic Chemist??—Aspects of Organic and Inorganic Supramolecular Chemist?:* VCH Publishers: Weinheim, 1993.
8. Bodanszky, M. *Principles* of *Peptides Synthesis;* Springer-Verlag: Berlin. 1984.
9. de Meijere, A.; Kozhushkov, S.I. Macrocyclic structurally homoconjugated oligoacetylenes: Acetylene- and diacetylene-expanded cycloalkanes and rotanes. Top. Curr. Chem. **1999**. *201*. 1–42.
10. Diederich, F.: Gobbi, L. Cyclic and linear acetylenic molecular scaffolding. Top. Cum. Chem. 1999. *201*. 43–79.
11. Haley, M.M.: Pak. J.J.: Brand, S.C. Macrocyclic oligo-(phenylacetylenes) and oligo(phenyldiacetylenes). Top. Curr. Chern. 1999. *201*. 81–130.
12. Trost, *B.M*. Cyclizations via palladium-catalyzed allylic. alkylations. Angew. Chem. Int. Ed. Engl. **1989**, *28*. 1173–1192.
13. Fiirstner, A.; Bogdanovic, B. New developments in the chemistry of low-valent titanium. Angew. Chern. Int. Ed. Engl. 1996. *35*. 2442–2469.
14. Stille. *J.K.* The palladium-catalyzed cross-coupling reac-

tions of organotin reagents with organic electrophiles. Angew. Chem. Int. Ed. Engl. 1986, *25*, 508–524.
15. Grubbs. R.H.; Chang, S. Recent advances in olefin metathesis and its application in organic synthesis. Tetrahedron 1998. *54*, 4413–4450.
16. Merrifield. *B*. Solid phase synthesis. Science 1986, *232*, 341–347.
17. Sewald. N. Efficient. racemization-free peptide coupling of *N*-alkyl amino acids by using amino acid chlorides generated in situ. Total syntheses of the cyclopeptides cyclosporin *O* and omphalotin A. Angew. Chem. Int. Ed. Engl. 2002. *41*, 4661–4663.
18. Balkenhohl, F.: von dem Bussche-Hiinnefeld, C.; Lansky, A.; Zechel, C. Combinatorial synthesis of small organic molecules. Angew. Chem. Int. Ed. Engl. 1996, *35*, 2289–2337.
19. Akaji, K.; Teruya. K.: Akaji, M.: Aimoto. S. Synthesis of cyclic RGD derivatives via solid phase macrocyclization using the Heck reaction. Tetrahedron 2001. *57*. 2293–2303.
20. Hiroshige, M.; Hauske. J.R.: Zhou, P. Palladium-mediated macrocyclization on solid support and its applications to combinatorial synthesis. J. Am. Chem. Soc. 1995, *117*. 11590–11591.
21. Nicolaou, K.C.; Winssinger, N.; Pastor, J.; Ninkocic. S.; Sarabia, F.: He. Y.: Vourloumis. D.; Yang, Z.; Li, T.; Giannakakou. P.: Hamel. E. Synthesis of epothilones A and B in solid and solution phase. Nature 1997, *387*, 268–272.
22. Nicolaou, K.C.: Winssinger, N.; Pastor. J.: Murphy, F. Solid-phase synthesis of macrocyclic systems by a cyclorelease strategy: Application of the Stille coupling to a synthesis of (*S*)-Zearalenone. Angew. Chem. Int. Ed. Engl. 1998. *37*. 2534–2537.
23. La Porta, E.: Piarulli, U.; Cardullo, F.; Paio, A.; Provera, S.: Seneci, P.; Gennari. C. Cyclative cleavage via solid phase supported stabilized sulfur ylides: Synthesis of macrocyclic lactones. Tetrahedron Lett. 2002. *43*. 761–766.
24. Lobrégat, V.; Alcaraz, G.; Bienaymé, H.; Vaultier. M. Application of the 'resin-capture-release' methodology to macrocyclisation via intramolecular Suzuki-Miyaura coupling. J. Chem. Soc. Chem. Commun. 2001. 817–818.
25. Kimura, Y.; Regen, S.L. High dilution via solid-liquid phase-transfer catalysis. A practical approach to the synthesis of macrolides. J. Org. Chem. 1983, *48*, 1533–1534.
26. Regen, S.L. Triphase catalysis. Angew. Chem. Int. Ed. Engl. 1979. *18*. 421–429.
27. Jurczak, J.: Pietraszkiewicz, M. High-pressure synthesis of cryptands and complexing behaviour of chiral cryptands. Top. Curr. Chem. 1983. *130*. 150–204.
28. Zielinski, T.: Achmatowicz, M.; Jurczak, J. A simple synthesis of chiral macrocyclic tetraamides derived from α-amino acids. Tetrahedron: Asymmetry 2002, *13*, 2053–2059.
29. Ashton, P.R.; Brown. G.R.: Isaacs, N.S.; Giuffrida. D.: Kohnke, F.H.: Mathias. J.P.: Slawin, A.M.Z.: Smith, D.R.: Stoddart. J.F.: Williams, D.J. Molecular LEGO. 1. Substrate-directed synthesis via stereoregular Diels–Alder oligomerizations. J. Am. Chem. Soc. 1992, 114, 6330–6353.
30. Hoss, R.; Vogtle, F. Template syntheses. Angew. Chem. Int. Ed. Engl. 1994, *33*, 375–384.
31. Dietrich-Buchecker. C.: Rapenne. G.; Sauvage, J.-P. Molecular Knots—From Early Attempts to High-Yield Template Synthesis. In Molecular *Catenanes, Rotaxanes and Knots*: Sauvage, J.-P., Dietrich-Buchecker, C., Eds.; Wiley-VCH: Weinheim. 1999; 107–142.
32. Storm, O.; Lüning, U. How to synthesize macrocycles effitiently by using virtual combinatorial libraries. Chem. Eur. J. 2002. *8*. 793–798.
33. Roberts, S.L.; Furlan, R.L.E.: Cousins. G.R.L.; Sanders, J.K.M. Simultaneous selection, amplification and isolation of a pseudo-peptide receptor by an immobilized N-methyl ammonium ion template. Chem. Comm. 2002, 938–939.
34. Filer, C.N. The preparation of isotopically labeled macrocyclic compounds by organic synthesis. J. Labelled Compd Radiopharm. 2001, *44*. 931–945.
35. Prautzsch. V.; Ibach, S.: Vogtle, F. Very large cyclic compounds. J. Incl. Phenom. Macrocycl. Chem. 1999. *33*. 427–457.
36. Katz, L. Manipulation of modular polyketide synthases. Chem. Rev. 1997. *97*. 2557–2575.
37. Khosla, C. Harnessing the biosynthetic potential of modular polyketide synthases. Chem. Rev. 1997, *97*, 2577–2590.

Mesoporous Materials

Sheng Dai
Oak Ridge National Laboratory, Oak Ridge, Tennessee, U.S.A.

Craig E. Barnes
University of Tennessee, Knoxville, Tennessee, U.S.A.

INTRODUCTION

Recent breakthroughs in catalyst synthesis resulted in the development of a number of novel methodologies for the preparation of mesoporous inorganic materials with extremely high surface areas and ordered mesostructures. These "nanostructured" materials are of great interest to scientists in many disciplines, with potential applications as catalysts, separation media. and advanced electronic materials. Although improvements and new variations continue to be developed for all of the methods described below, the range of applicability and pace with which new mesoporous materials were described in the past decade are evidence of interest in this area as a continuing source of new, technologically relevant materials.

BACKGROUND

Briefly reviewed in this article are the current methodologies available for preparing mesoporous inorganic materials other than silicon oxides and their properties. Currently. the most important general synthetic approach utilizes mixtures of aqueous surfactants or amphilic block copolymers to create high-surface-area solids containing organized arrays of mesoscopic channels. This method, commonly referred to as "surfactant templating" or "liquid crystal templating" is the main focus of this article. A brief survey of mesoporous materials other than oxides is also included at the end of this article. For more comprehensive overviews of this area, the reader is directed to several reviews and monographs that recently appeared.[1–5]

The preparation of mesoporous silicas and aluminosilicates using aqueous mixtures of surfactants and solgel chemistry was first described by scientists at Mobil Oil.[6] The essence of this new methodology involves the use of molecular assemblies of surfactants or related substances as structure directors during formation of oxides. The mechanism for the organization of such mesostmctures involves electrostatic interactions and charge matching between micellar assemblies of quaternary ammonium cations and anionic silicate oligomer species.[5] Complex mesoscopic silicon oxides are produced by fluctuating chemical affinities and local perturbations of self-assembled surfactant molecules at the organic–inorganic interface during oxide formation processes. Here, the surfactant assemblies are used as scaffold-like templates to direct mineralization along. around, and between the organic–inorganic interfaces through "organized reaction fields." Illustrated in Fig. 1 is a simplified view of the original mechanism for synthesizing mesoporous silicon oxide based on this method.[7] From this mechanism, it can be seen how the principal methodology can be extrapolated to prepare mesophases with different metal oxides. as long as there is an interacting complementarity between the inorganic ions in solution and the surfactant head groups.

Stucky and coworkers proposed a general model for surfactant templating based upon the cooperative organization of inorganic and organic molecular species into three-dimensional mesoscopic arrays.[7] They divided the global surfactant-directed ordered porous material synthesis process into three reaction steps: multidentate binding of the inorganic oligomers to the cationic surfactant assemblies, preferential polymerization of the inorganic species in the interface region. and charge density matching between the organic and inorganic interfaces. The interaction between inorganic precursors and organic surfactants is not limited to electrostatic interactions but also includes hydrogen and dative bonding interactions or may be mediated by countercharged ions. The surfactants used in synthesis can be cationic, anionic, or neutral, depending on the charge of the inorganic precursors. Basic guiding principles in rationally synthesizing mesoporous metal oxide materials were developed.[7] In general, there are six main methodologies for synthesizing high-surface-area mesoporous metal oxide materials:

1. I^-S^+, where positively charged surfactant (S^+) interact with negatively charged inorganic (I^-) oxide precursors via coulombic interactions.
2. I^+S^-, where negatively charged surfactant interact with positively inorganic oxide precursors via coulombic interactions.
3. $I^+X^-S^+$, where positively surfactant molecules interact with positively charged inorganic oxide precursor, through a negatively charged mediator (X^-).

Encyclopedia of Supramolecular Chemistry
DOI: 10.1081/E-ESMC 120012687

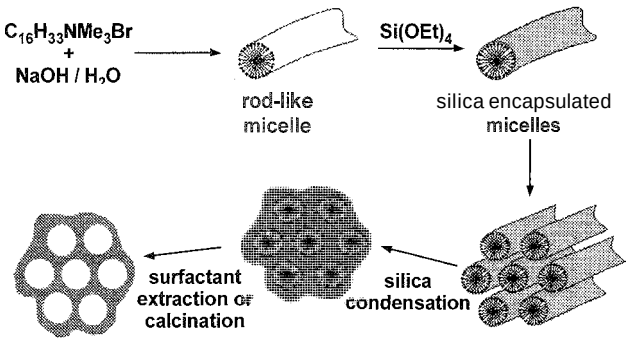

Fig. I Simplified illustration of the process of surfactant ternplating of silica based sol-gels. (*View this art in color at www.dekker.com.*)

4. I←S. where inorganic precursors interact via dative bonds with surfactant templates.
5. I^0S^0, where neutral template molecules such as amine and block copolymer surfactants interact with inorganic oxide precursors via hydrogen bonds or coordination bonds.
6. Phase transformation from a lamellar materials.

The as-synthesized mesostructures obtained from these six methods consist of spatially and chemically well-defined arrays containing inorganic species and organic template molecules which are not porous. Ordered pore structures result when the surfactant templates are removed from the channels between metal oxide domains. Removal of the surfactant templates is commonly achieved by calcination at 400–800°C or by extraction with solvents that have high solubilities for the corresponding surfactant templates. When porosity is maintained, calcination provides a measure of the chemical and thermal robustness to the matrix.

The ordered structures formed in the case of metal oxides other than silica are more susceptible to the collapse of pore structures with high-temperature treatments. This destruction of the ordered mesoscopic structures was ascribed to the crystallization of the metastable amorphous metal oxide phase, frequently leading to solids with no ordered mesophases. Although a majority of the metal oxides can be prepared in high-surface-area mesoporous forms with the above methodologies, few robust. ordered mesoporous materials with crystalline wall structures have been obtained to date. Accordingly, one of the remaining challenges in this area is to develop generally applicable synthetic approaches that yield thermally and chemically robust mesoporous metal oxides.

A second synthetic challenge is to make the walls of mesoporous materials out of mixed oxides (binary and ternary oxide systems). The key difficulty associated with syntheses in this case lies in control over different hydrolysis rates of the different metal species, which may cause the sequential precipitation and phase segregation. In addition to the mixed oxides, the mixed valent mesoporous metal oxides are also interesting because of their unique semiconducting and catalytic properties. So far, these oxide materials are derived from the corresponding parent mesoporous metal oxides through redox reactions.

In all of the methodologies listed above, the basic components of each system consist of a metal oxide precursor, similar to those used in solgel syntheses, a surfactant templating agent, water, and frequently a cosolvent. The size and organization pores in the final material can be predicted and controlled through a consideration of the molecular properties of the surfactant and its phase diagram in aqueous solutions. The size of the micelles is the most important factor defining the position of the pore size maximum. Within a series of similar surfactants having different tails, the pore size maximum increases with tail length. The addition of nonpolar, "swelling" reagents provides one means of adjusting the pore size maximum over significant ranges without changing surfactant.[5]

The most commonly observed ordered pore arrangements are lamellar and hexagonal close packed, both of which have nonintersecting mesopores (Fig. 2), and a cubic arrangement of intersecting pores that has overall cubic symmetry. Less-ordered "wormhole" arrangements of mesopores are sometimes observed in systems involving nonionic surfactants. It should be borne in mind, however, that surfactant-templated solids do not display the same order as crystalline microporous zeolites. The walls of the pores, whether crystalline or amorphous, frequently exhibit significant microporosity, presumably due to the presence of cracks and defects in the walls that can connect mesopores within the solid. Furthermore, the diameter along the length of the mesopore may have irregularly spaced bottlenecks or bulges, which effect access and transport in the matrix.

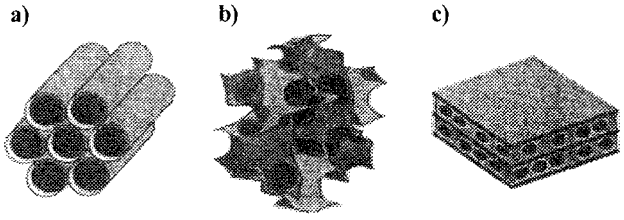

Fig. 2 Illustrations of mesoporous M41S materials: (a) hexagonal MCM-41, (b) cubic MCM-48. and (c) lamellar MCM-50.[1] *(View this art in color at www.dekker.com.)*

Although fundamentally the same approach is used to prepare mesoporous silica and aluminosilicates, what distinguishes the syntheses of mesoporous metal oxides from silicas is that the hydrolysis and condensation rates involved in the formation of the oxide phase are much faster and thus more difficult to control. Developing methods and adjusting conditions (e.g., amount of water present, pH. complexing agents) that bring these two processes under control so that continuous, robust oxide matrices are formed around the micelles was a ''rate-limiting'' step in the general development of mesoporous metal oxides. In the following. we try to summarize the recent results in using the above six methodologies to synthesize nonsiliceous mesoporous materials.

SYNTHESIS METHODOLOGIES FOR MESOPOROUS NONSILICEOUS METAL OXIDES

Nonsiliceous Mesoporous Materials via Cationic Surfactants (I^-S^+)

As is clear from the suggested mechanism, the interacting inorganic precursors should be negatively charged. Accordingly, the reaction pH values involved in this methodology should be above the isoelectric points of the corresponding oxides.[8] The hydrolysis reactions under these conditions are usually very fast, so that only powder morphologies are obtained. The most common cationic surfactants used in this inethodology are alkylainmonium salts such as cetyltrimethyl ammonium halides $(C_{16}H_{33}NMe_3)X$ (X = Cl, Br). An earlier example of synthesizing mesoscopic metal oxides using cationic surfactant templates is the work by Stucky and coworkers.''] They showed that anionic metal oxide clusters [e.g., ammonium metatungstate $(NH_4)_6H_2W_{12}O_{40}$] can interact with cationic surfactant templates to form the hexagonal mesoscopic composites. The metal oxide precursors usually do not form a connected oxide framework. Accordingly, removal of the templates by calcination usually results in the collapse of the mesopores, as found in the case of tungsten oxide. Su and coworkers''' recently successfully obtained mesoporous zirconium oxides with the I^-S^+ methodology. consistent with an earlier investigation by Knowles and Hudson.[10] The calcined mesoporous zirconium oxide exhibits mesopores with wormhole-like channels. Thermally stable zirconia (sulfate and oxophosphate) was also prepared through the use of cationic ammonium-based surfactants.[11] Mesoporous iron oxide was prepared using CTAB and sonochemical acceleration of the reaction.[12] Sayari and coworkers succeeded in preparing the mesoporous hafnium oxide in the presence of a cationic surfactant (CTAB).[13]

Suib and coworkers demonstrated that a mesoporous mixed-valent manganese oxide can be successfully synthesized by the direct precipitation of manganese hydroxide precursors in basic conditions.[14] The ordered mesoporous structure with crystalline pore walls was retained after calcination: as confirmed by powder x-ray diffraction (XRD) and transmission electron microscope (TEM). Such mixed-valent mesoporous oxides are semiconducting and possess catalytic activity in the oxidation of alkanes. The mixed oxidation states of manganese (III/IV) in these materials were introduced by the direct oxidation of the metal precursor [Mn(II)]. Both hexagonal and cubic phases of such mesoporous materials can be synthesized.

Ozin and coworkers recently extended the supramolecular I^-S+ assembly into the synthesis of binary mesoporous yttrium oxide-stabilized-zirconium oxide materials.[15] These materials were synthesized by a modified sol-gel method under basic conditions. where zirconium ethoxide and yttrium acetate were used as the precursors for the transition metal oxides. and CTAB was used to form the supramolecular templates. The use of ethylene glycol with coordinating capability as a cosolvent may play a role in controlling the hydrolysis rate and solubility of zirconium(IV) and yttrium(III). This synthesis strategy is similar to that of so-called polymerizable-complex method, which was widely used to prepare multicoinponent single-phase oxides.[16] The yttrium content in these binary materials can be tuned from 12–56 wt%, and no phase segregation of yttrium and zirconium oxides was observed. These materials could be applied in designing new solid oxide fuel-cell electrode materials.

Nonsiliceous Mesoporous Materials via Anionic Surfactants (I^+S^-)

In contrast to the above methodology. pH conditions used in this synthesis methodology should be below the isoelectric point of the corresponding oxides and above the pK_a of the anionic surfactant for strong interaction on the interface between the anionically charged template and the developing positively charged oxide. Because most of the oxides have significant solubilities in low pH conditions. this methodology requires more control over synthesis conditions. Typical surfactants used in this methodology are dodecyl sulfate[17] and phosphate.[18] Huo et al. synthesized mesostructured lead and iron oxides by the supramolecular assembly of iron and lead polycations and anionic surfactants (dodecyl sulfate).[7] Mesoporous zirconium oxide. yttrium oxide,[19] and rare earth oxides[20] were synthesized using dodecyl sulfate and dodecyl phosphate as templates. In several cases. however, no ordered mesostructures were observed via TEM and XRD studies after calcination.

This destruction of the ordered mesostructures can be attributed to the crystallization of zirconium oxide in the calcination step.

Nonsiliceous Mesoporous Materials via Mediated Coloumbic Interaction ($I^+X^-S^+$)

Stucky and coworkers[17] proposed that under certain conditions (usually strongly acidic), an electrical double layer develops between the surface of the oxide and surfactant head groups (i.e., $I^+X^-S^+$). The templates used in this synthesis methodology can be cationic surfactants or neutral surfactants with hydrophilic head groups that can be charged through protonation under strong acid conditions. Syntheses are, therefore, conducted below isoelectric points, and the rate of hydrolysis reactions can be tuned to be slow so that thin films or other morphologies (e.g., monoliths) can be synthesized via this methodology. Because the surface charge on the oxide is balanced by the presence of the mediating anion (X halide), removal of the surfactant does not require replacement by a new cation. Therefore, the surfactant template can be effectively removed by simple leaching with solvent rather than calcination, but both methods are used.

There are many well-documented examples of the methodology having been applied to nonsiliceous mesoporous materials. For example, mesoporous aluminophosphates using CTAB in acidic media were described.[21] Recently, Bhaumik and Inagaki successfully used a similar methodology to prepare ordered mesoporous titanium phosphates.[22] The ammonium-based surfactant templates were removed via ion-exchange processes. The unique property of the resulting mesoporous materials is their ion-exchange capability. Similar mesoporous materials can also be synthesized by the S^-I^+ methodology.

One of the most versatile methodologies for the preparation of nonsiliceous ordered mesoporous materials involves the use of nonionic, block copolymer surfactants in alcoholic or mixed solvent systems under highly acidic conditions. This general procedure is thought to involve a combination of electrostatic, H-bonding, and van der Waals forces as the forces behind the self-assembly and templating process. Stucky and coworkers described that over 25 nonsiliceous, ordered mesoporous metal, and main group oxides were prepared using this approach.[23] In general, metal chlorides or metal alkoxides were used as metal oxide precursors that, when contacted with alcoholic solutions of a variety of block copolymers, formed mesostructured solids. To limit the rates of hydrolysis and condensation, the above mixtures were simply allowed to stand in air for variable times (1–30 days), whereby moisture was absorbed, thus providing a "controlled" source of water. High surface area (100–800 m^2/g), thermally robust, mesoporous (3–12 nm pore diameter maxima) samples of pure and mixed metal oxides were obtained using this method. All retained mesoporosity and long-range order in their mesopore structures after calcination. Shown in Fig. 3 is a TEM image of a typical mesoporous titanium oxide prepared by this methodology.

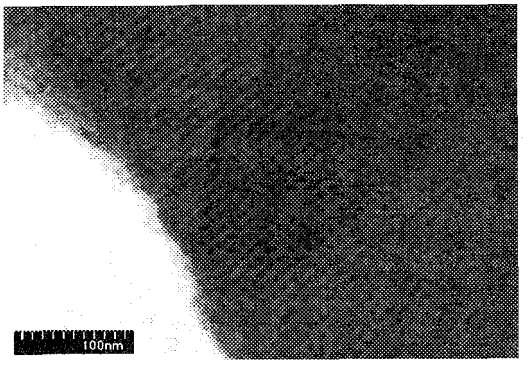

Fig. 3 TEM image of mesoporous TiO_2 synthesized at ORNL. *(View this art in color at www.dekker.com.)*

This methodology enjoys the merits of other approaches and exhibits several additional advantages: 1) it has proven applicable to a wide range of transition metal and main group oxides; 2) the metal precursors studied so far are readily available, being either alkoxide or halide complexes; 3) in many cases, syntheses can be run in alcoholic solvents in essentially nonhydrolytic conditions, which aids in controlling hydrolysis and condensation rates; 4) the critical micelle concentrations required for polyethylene-oxide–polypropylene-oxide di- and triblock copolymers are usually much lower than the concentrations needed for ionic surfactants;[5] and 5) because of the neutral, nonaqueous conditions used in these preparations, control of pH is not required, and the surfactant can be removed from the mesostructured material by calcination or milder solvent extraction methods with nonpolar solvents.

Two recent variations of this methodology are the synthesis of single crystals of mesoporous niobium and tantalum oxides[24] and the rapid preparation of titanium dioxide solids using sonochemistry.[25]

Nonsiliceous Mesoporous Materials via Complexing Surfactants (I^0S)

An approach that does not rely on electrostatic interactions between charged groups at the oxide–surfactant interface involves precomplexing surfactant ligands to the oxide precursors before exposing them to water. The metal precursors are generally alkoxide complexes [e.g., $Ti(Oi-Pr)_4$, $Nb(OEt)_5$] that are typically mixed with the surfactant in alcohol solution. Control of the mesostructure phases can be accomplished by adjusting the

surfactant:metal ratio. while the rate of hydrolysis can be controlled by regulating the vapor diffusion rate of water into mixtures. Both neutral (aliphatic amines such as dodecylamine) and charged (e.g., alkylphosphates) amines proved successful in this "ligand-assisted" methodology for preparing mesoporous oxides of titanium, niobium, and tantalum.[26–28] Although amine surfactants are usually preferred due to the ease with which they can be removed cleanly by simple solvent extraction. carboxylate surfactants were also used with sonication to shorten reaction times.[29]

Nonsiliceous Mesoporous Materials via Neutral Surfactants (I^0S^0)

The interactions between surfactant and oxide responsible for mesostructuring are primarily hydrogen bonding or simply hydrophilic/hydrophobic interactions between the various polymer blocks of the copolymer. An important drawback of this methodology is that the mesostructures of the resulting materials frequently exhibit long-range order. Instead, they have mesopore assemblies that resemble disordered, interconnecting, wormhole-like channels. Examples of this methodology include the preparation of mesoporous alumina,[30] aluminophos-phates,[21] and tungstated zirconia.[31]

Tilley's group recently showed that this method of surfactant templating can be extended to high-temperature pyrolysis of organometallic silicates to produce mesoporous, high-surface-area, metal–silicon oxides with narrow pore size maxima.[32]

Nonsiliceous Mesoporous Materials via Phase Transformation from a Lamellar Phase

Neeraj and Rao demonstrated an interesting lamellar-to-hexagonal-to-cubic phase transformation for an as-synthesized zirconium oxide ternplated by a neutral amine surfactant.[33] This methodology is based on the facile precipitation synthesis of the lamellar oxides in basic conditions and subsequent removal of some of the surfactant templates. The latter process induces the curling of the surfactant bilayer in order to minimize the surface/interface energy, as shown in Fig. 4. This mechanism is similar to the formation of mesoporous silica FSM-16.[34] The curled surfactant bilayers gradually change to cylindrical rods, which further assemble to the ordered hexagonal mesostructures.

This elegant methodology can be exploited to synthesize other nonsiliceous mesoporous materials. In fact. Yada et al. observed several similar transformations of lamellar yttrium-based mesophases teinplated by dodecyl sulfate to the corresponding hexagonal phases.[19] In this case, no cubic inesophases were observed. even after long reaction times Mesoporous magnetic materials based on rare earth oxides[20] and a binary mesoporous yttrium aluminium oxide[17] were also successfully synthesized through this phase transformation methodology

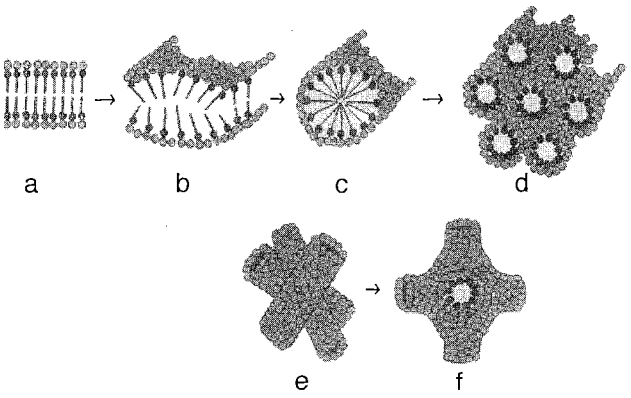

Fig. **4** Schematic representation of lamellar 4 hexagonal phase transforination (a through d) and the hexagonal 6 cubic transformation (e and f). The shaded circles around the surfactant aggregates represent the inorganic species (generally metal alkoxides or other metal-oxo species).[33] (*View* this *art in color. at www.dekker.com.*)

MESOPOROUS MATERIALS OTHER THAN METAL OXIDES

The micellar template approach to mesoporous oxides was generalized to make nonoxide mesoporous materials. Attard et al. prepared mesoporous metals with hexagonal ordered structures, where redox reactions and the general mesoscopic templating synthesis were employed to generate the metallic mesosti-uctures. The materials are typically obtained as powders composed of nanoparticles. Attard et al. also succeeded in adapting the above methodology to synthesize mesostructured metallic thin films through the electrodeposition under liquid-crystal environments.[35] More recently, a high-surface-area graphitized carbon with uniform mesopores was synthesized by the group of Jaroniec through a colloidal imprinting methodology.[36,37]

A recent approach that uses mesoporous silicas to produce mesoporous replicate templates of other materials appears to hold some promise as a general methodology in this area. In essence, a precursor to the desired material is diffused into the pores of ordered mesoporous silica and then chemically transformed into a homogeneous solid filling the pores. The silica is then removed by exposing the solid to HF or NaOH solutions. leaving a porous solid that is an "inverse replica" of the original pore structure of the silica. Mesoporous carbon solids were prepared via this method using a variety of simple precursors. such as sucrose. furfuryl alcohol, or in situ

polymerized phenol resins as the carbon precursors.[38–41] Carbonation is accomplished by heating the filled pore silicas to ~ 1000°C. The mesoporous carbon replicates exhibit surface areas; pore size distributions, and pore orderings that closely resemble those measured in the original silica matrix. as long as the original silica pore system is interconnected though pore intersections or via micropore channels between mesopores. A similar approach starting with platinum and other metal precursors led to intertwined platinum and other metal wire assemblies,[42–44]

CHARACTERIZING MESOPOROUS MATERIALS

The general characteristics of a material's porosity and pore ordering are determined via three types of measurements: isothermal gas adsorption behavior, small-angle x-ray scattering (SAXS) experiments, and electron microscopy. The overall surface area of the solid, the pore volume, and pore size distribution information are provided by gas adsorption measurements.[45] After removal of the surfactant, templated, mesoporous solids exhibit well-defined maxima in their pore distribution curves between 2–50 nm with widths (half-height) typically less than 1 nm. Mesoporous metal oxides usually have total surface areas from 100 to over 1000 m^2/g. When the pores of a templated inaterial are ordered (e.g., hexagonal or cubic ordering): SAXS data will show Bragg diffraction peaks that characterize the ordering and can give values for the interpose separation. SAXS measurements can be done on mesostructured material before removal of the templating surfactant to determine if pore ordering survives calcination. Finally. because of the size range for mesopores, TEM was used extensively to image pores in templated materials and can provide an independent measurement of pore ordering and wall thickness. Simultaneous electron dispersive x-ray (EDX) measurements can also be used to provide spatially resolved elemental analysis data on these solids.

CONCLUSION

The general field of nonsiliceous mesoporous materials is still in its infancy. A variety of surfactant-templating approaches were developed that can be used to prepare a wide variety of mesoporous metal oxide solids. Early problems concerning the thermal stability of these porous materials are slowly being overcome but remain obstacles in some cases. Promising replicate-templating procedures where the pore systems of ordered. mesoporous silicas are used to produce mesoporous carbons and metals were recently described. Although few applications of non-siliceous mesoporous materials have appeared to date,[3 46 47] the field is young and holds great promise.

ARTICLES OF FURTHER INTEREST

Crystalline Microporous Silicas. p. 380
Incommensurate and Commensurate Structures, p. 712
Mesoporous Silica and Silica-Organic Hybrids. p. 852
Nanocasting Strategies and Porous Materials. p. 950
Organic Zeolites, p. 996
Scanning Tunneling Microscopy, p. 1202
Structural Engineering in Organic–Inorganic Perovskites, p. 1387
Zeolites in the Petroleum Industry, p. 1599
Zeolites: Catalysis. p. 1610
Zeolites: Seperntion Science, p. 1617
Zeolites: Structures and Inclusion Properties. p. 1623

REFERENCES

1. Ying. J.Y.; Mehnert. C.P.: Wong. M.S. Synthesis and applications of supramolecular-templated rnesoporous materials. Angew. Chem., Int. Ed. 1999, *38.* 56.
2. Schuth. F. Non-siliceous mesostructured and mesoporous materials. Chem. Mater. 2001. *13.* 3184.
3. He, X.: Antonelli, D. Recent advances in synthesis and applications of transition metal containing rnesoporous molecular sieves. Angew. Chem. Int. Ed. 2002, *41,* 214.
4. Ma, Y.: Tong. W.: Zhou. H.: Suib. S.L. A review of zeolite-like porous materials. Microporous Mesoporous Mater. 2000. 37. 243.
5. Stein, A.: Melde. B.J. The role of surfactants and amphiphiles in the synthesis of porous inorganic solids. Surfactant Sci. Ser. 2001. 100. 819.
6. Kresge, C.T.; Leonowicz, M.E.: Roth. W.J.; Vartuli. J.C.: Beck. J.C. Ordered rnesoporous molecular sieves synthesized by a liquid–crystal template mechanism. Nature 1992. 359. 710.
7. Huo. Q.; Margolese. D.I.: Ciesla. U.; Feng. P.: Gier, T.E.: Sieger. P.: Leon, R.: Petroff. P.M.: Schuth. F.: Stucky, G.D. Generalized synthesis of periodic surfactant/inorganic composite materials. Nature 1994. 368, 317.
8. Park. G.A. Isoelectric points of metal oxides. Chem. Rev. 1965, *65.* 177.
9. Blin. J.L.; Gigot. L.: Leonard. A.: Su. B.L. Mesoporous zirconium oxides: An investigation of physical–chemical synthesis parameters. Stud. Surf. Sci. Catal. 2002, *141.* 257.
10. Knowles, J.A.; Hudson, M.J. Preparation and characterization of mesoporous, high surface area zirconium(IV) oxides. Chem. Commun. 8995, 2083.
11. Ciesla. U.: Froba. M.; Stucky, G.: Schuth. F. Highly ordered porous zirconias from surfactant-controlled syntheses: Zirconium oxide-sulfate and zirconium oxo phosphate. Chem. Mater. 1999. *11.* 227.
12. Srivastava. D.N.: Perkas. N.; Gedanken, A.: Felner. I. Sonochemical synthesis of rnesoporous iron oxide and

accounts of its magnetic and catalytic properties. J. Phys. Chein.. B 2002. *106*, 1878.
13. Liu, P.: kiu, J.: Sayari. A. Preparation of porous hafnium oxide in the presence of a cationic surfactant. Chem. Commun. 4994. 577.
14. Tian, Z.-R.; Tong, W.: Wang, J.-Y.; Duan, N.-G.; Krishnan. V.V.: Suib. S.L. Manganese oxide mesoporous structures: Mixed-valent semiconducting catalysts. Science 1997, *276*. 926.
15. Mamak. M.: Coombs. N.; Ozin. G. Mesoporous yttria-zirconia and metal-yttria zirconia solid solutions for fuel cells. Adv. Mater. 2000, *12*, 198.
16. Kakiliara. M.; Kazunari. D. The synthesis of photocatalysts using the polynierizable complex method. MRS Bull. 2000, September, 27.
17. Yada. M.: Ohya, M.: Ohe, K.; Machida. M.; Kijirna, T. Porous yttrium aluminum oxide templated by alkyl sulfate assemblies. Langmuir 2000, 16. 1535.
18. Pacheco. G.: Zhao. E.; Garcia. 4.; Sklyarov, A.: Fripiat, J.J. Synthesis of mesoporous zirconia with anionic surfactants. J. Mater. Chem. 1998. *8*. 219.
19. Yada. M.; Kitamura. H.; Machida. M.: Kijima, T. Yttrium-based porous materials templated by anionic surfactant assemblies. Inorg. Chem. 1998. 37. 6470.
20. Yada. M.: Kitamura. H.; Ichinose. A.; Machida. M.: Kijima, T. Mesoporous magnetic materials based on rare earth oxides. Angew. Chem. Int. Ed. 1999. *38*. 3506.
21. Tiemann. M.: Fröba, M. Mesostructured aluminophosphates synthesized with supramolecular structure directors. Chem. Mater. 2001, *13*, 3211.
22. Bhaumik, A.: Inagaki, S. Mesoporous titanium phosphate molecular sieves with ion-exchange capacity. J. Am. Chem. Soc. 2001. *123*. 691.
23. Yang. P.: Zhao, D.; Margolese. D.I.; Chmelka, B.F.; Stucky. G.D. Block copolymer templating syntheses of mesoporous metal oxides with large ordering lengths and semicrystalline framework. Chem. Mater. 1999, *11*. 2813.
24. Lee. B.: Yamashita, T.; Lu, D.: Kondo, J.N.: Domen. K. Single-crystal particles of mesoporous niobium-tantalum mixed oxide. Chern. Mater. 2002. *14*, 867.
25. Wang, Y.; Tang. X.: Yin, L.: Huang, W.: Hacohen, Y.R.: Gedanken. A. Sonochemical synthesis of mesoporous titanium oxide with wormhole-like framework structures. Adv. Mater. 2000. *12*, 1183.
26. Antonelli. D.M.; Nakahira. A.; Ying, J.Y. Ligand-assisted liquid crystal templating in mesoporous niobium oxide molecular sieves. Inorg. Chem. 1996, *35*. 3126.
27. Wang, Y.-Q.; Chen. S.-G.; Tang, X.-H.; Palchik. O.; Zaban, A.; Koltypin, Y.: Gedanken. A. Mesoporous titanium dioxide: Sonochemical synthesis and application in dye-sensitized solar cells. J. Mater. Chem. 2001. *11*. 521.
28. Mondo. J.N.: Takahara, Y.: Lu, D.: Domen. K. Mesoporous ta oxide. 2. Improvement of the synthetic method and observation of rnesostructure formation. Cliem. Mater. 2001. *13*. 1200.
29. Wang. Y.Q.; Yin. L.X.; Palchik, O.; Hacohen, Y.R.: Koltypin. Y.; Gedanken. A. Rapid synthesis of mesoporous yttrium-zirconium oxides with ultrasound irradiation. Langmuir 2001. *17*, 4131.
30. Zhang. Z.; Hicks. R.W.: Pauly, T.R.; Pinnavaia. T.J. Mesostructured Forms of γ-Al_2O_3. J. Am. Chem. Soc. 2002. *124*. 1592.
31. Wong, M.S.; Jeng, E.S.: Ying. J.Y. Supramolecular templating of thermally stable crystalline mesoporous metal oxides using nanoparticulate precursors. Nano Lett. 2001, *1*. 637.
32. Kriesel, J.W.: Sander. M.S.: Tilley. T.D. Block copolymer-assisted synthesis of mesoporous. multicomponent oxides by nonhydrolytic, thermolytic decomposition of molecular precursors in nonpolar media. Chem. Mater. 2001. *13*. 3554.
33. Neeraj, S.: Rao. C.N.R. Phase transformations of mesoporous zirconia. J. Mater. Chem. 1998. *8*. 1631.
34. Inagaki. S.: Fukushirna. Y.; Kuroda. K. Synthesis of highly ordered mesoporous materials from a layered polysilicate. Cliem. Commun. 1993. 680.
35. Attard. G.S.: Bartlett. P.N.: Coleman, N.R.B.; Elliott. J.M.: Owen, J.R.; Wang. J.H. Mesoporous platinum films from lyotropic liquid crystalline phases. Science **1997**, *278*, 838.
36. Li. Z.J.: Jaroniec. M.: Lee. Y.J.: Radovic, L.R. High surtace area graphitized carbon with uniform mesopores synthesized by a colloidal imprinting method. Chem. Commun. 2002. 1346.
37. Li. Z.J.: Jaroniec, M. Colloidal imprinting: A novel approach to the synthesis of mesoporous carbons. J. Am. Chem. Soc. 2001. *123*. 9208.
38. Ryoo. R.; Joo. S.H.: Kruk, M.: Jaroniec, M. Ordered mesoporous carbons. Adv. Mater. 2001. *13*. 677.
39. Jun, S.; Joo. S.H.; Ryoo. R.: Kruk, M.; Jaroniec. M.: Liu. Z.: Ohsuna. T.; Terasaki. O. Synthesis of new. nanoporous carbon with hexagonally ordered mesostructure. J. Am. Chem. Soc. 2000. *122*. 10712.
40. Lee. J.-S.: Joo. S.H.: Ryoo. R. Synthesis of mesoporous silicas of controlled pore wall thickness and their replication to ordered nanoporous carbons with various pore diameters. J. Am. Chem. Soc. 2002. *124*. 1156.
41. Kim, S.-S.: Pinnavaia. T.J. A low cost route to hexagonal mesostructured carbon molecular sieves. Chem. Commun. 2001, 2418.
42. Shin. H.J.: Ryoo, R.; Liu, Z.: Terasalti, O. Template synthesis of asymmetrically mesostructured platinum networks. J. Am. Cliem. Soc. 2001. *123*. 1246.
43. Shin. H.J.; Ko, C.H.: Ryoo. R. Synthesis of platinum networks with nanoscopic periodicity using mesoporous silica as template. J. Mater. Chern. 2001. *11*, 260.
44. Zhang. Z.T.: Dai. S.; Blom. D.A.; Shen, J. Synthesis of ordered metallic nanowires inside ordered mesoporous materials through electroless deposition. Chem. Mater. 2002. *14*. 965.
45. Kruk, M.; Jaroniec. M. Gas adsorption characterization of ordered organic-inorganic nanocomposite materials. Chem. Mater. 2001. *13*, 3169.
46. Hayward, R.C.: Alberius-Henning, P.: Chmelka. B.F.: Stucky. G.D. The current role of mesostructures in composite materials and device fabrication. Microporous Mesoporous Mater. 2001. *44–45*. 619.
47. Scott. B.J.; Wirnsberger, G.: Stucky, G.D. Mesoporous and rnecostructured materials for optical applications. Chern. Mater. 2001. *13*. 3140.

Mesoporous Silica and Silica–Organic Hybrids

Abdelhamid Sayari
University of Ottawa, Ottawa, Ontario, Canada

INTRODUCTION

Since the breakthrough discovery of the so-called M41S *family of silica* mesophases some 10 *years ago.[1] research on periodic mesoporous inaterials grew so dramatically that it developed into a distinct field. During this short period of* time, *remarkable progress was achieved in many directions, including synthesis* strategies. *materials diversity. and innovative applications. The original work described three silica mesophase structures,* namely, *MCM-41 (hexagonal, p6mm*), *MCM-48 (cubic,* I*a3d*), *and* MCM-50 *(lamellar). They were* synthesized *via a supramolecular templating mechanism under basic conditions using long-chain alkyltrimethylammonium surfactants. Currently. periodic* mesoporous *silicas* may *be readily synthesized under a wide* range *of pH and temperature conditions. in the presence of a large* variety *of* amphiphile *molecules, including cationic, anionic, neutral. zwitterionic,* bolaamphiphile, *geinini.* and diva*lent surfactants. as well as many* commercially *available* oligomers *and block copolymers. This effort led to* the *discovery of numerous* new silica *mesophases including* SBA-1 *and* SBA-6 (*Pm3n*), *SBA-2 and SBA-12* ($P6_3/mmc$), SBA-8 (*cmm*), *SBA-11* (P*m3m*), *SBA-16* (I*m3m*),[2] *disordered* HMS,[3] MSU-n,[4] *and* MSU-V. *Extensive* work was *also carried out to develop strategies for controlling the pore size. the morphology. the surface properties, and the hydrothermal stability of such materials. In addition to* silica-based mesoporous *materials, the* supramolecular *templating approach was extended to numerous other materials, including transition* metal *oxides[1] and* chalcogenides,[6] organosilicates,[7,8] metallophosphates,[9] *metals.* alloys,[10] *and zeolite* nanocrystals.[11,12] *Furthermore. silica* meso*phases were. in turn, used as* templates *for the synthesis of a variety of other materials. such as* nanoporous *carbons[1] and polymers. and* metallic[14] and semiconductor[15] *nanowires. This extensive* effort *in the area of synthesis was paralleled by the* development *of innovative applications. not* only in *conventional areas such as adsorption, separation. and catalysis,[1,19] but also as advanced* materials *such as electrodes for solid oxide* fuel cells,[20] *or as hosts* for *quantum dots* and *sensing species for electronic and optical* applications.[21,22]

The short review *will be* limited *to periodic* mesoporous *silica and silica–organic hybrids. Because of their relevance to the subject of the current Encyclopedia, the supramolecular templating mechanisms leading to ordered mesoporous materials will be one of the* main *thrusts of this contribution. Authoritative reviews on nonsilica periodic* mesoporous *materials are available in the* literature.[5,10,22]

SYNTHESIS MECHANISMS OF PERIODIC MESOPOROUS MATERIALS

Synthesis of Periodic Mesoporous Silica Under Basic Conditions in the Presence of Alkyltrimethylammonium Surfactants

The synthesis mechanism of M41S *silica mesophases was originally referred to as the liquid crystal* templating mechanism. *This may erroneously suggest that silica mesophases are simple replicas of preexisting liquid crystalline phases. While direct transcription of existing* liquid *crystals may occasionally take place under high concentrations of* surfactant,[23] *in practice. this* is *seldom the case. The following observations are consistent with the fact that the occurrence of a liquid crystalline phase is not a prerequisite for the* formation *of the corresponding silica mesophase: 1) it is possible to synthesize any of the three* M41S *silicas only by changing the relative amount of silica precursor. everything else being the same: 2) mesoporous materials* may *be prepared using surfactant concentrations well below those required for the formation of liquid crystals, and even below the* critical *concentration for the formation of rod-like micelles; 3)* MCM-41 *silica inay be synthesized in the presence of short-chain surfactants, such as* $C_{12}H_{25}N(CH_3)_3OH$, *that do not form rod-like micelles in water: 4) MCM-41 and MCM-48 silicas may* form *at temperatures above* 70°C, *where rod-like micelles are not stable.*

Stucky et al.[24] *provided* compelling *evidence that in addition to amphiphile molecules. inorganic species play a key role in driving the supramolecular* assembly *process to take place. As shown* schematically *in Fig. 1,*

Encyclopedia of Supramolecular Chemistry
DOI: 10.1081/E-ESMC 120012759

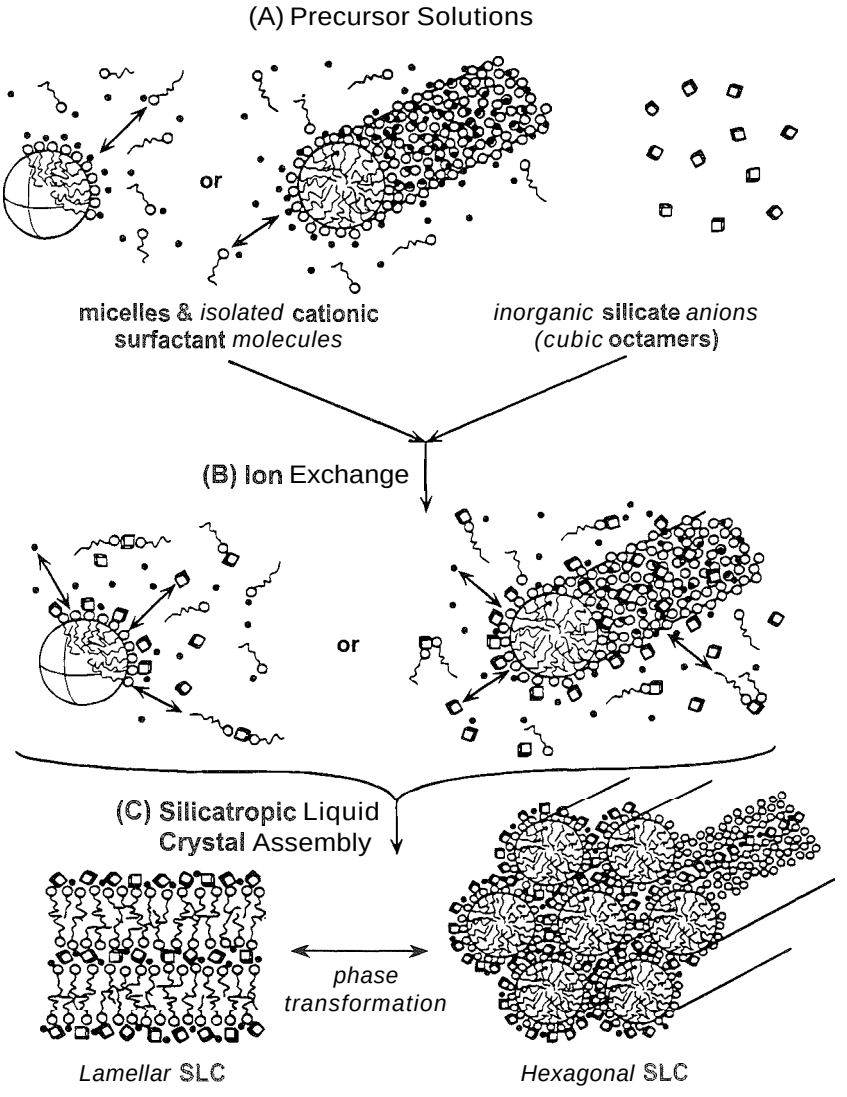

Fig. 1 Cooperative templating mechanism. (From Ref. [24].)

this so-called cooperative organization mechanism is a three-step process. The first step, driven by electrostatic interactions, is the displacement of the surfactant counterions by polydentate and polycharged inorganic anions leading to organic–inorganic ion pairs. The latter then self-organize into a liquid crystal-like mesophase with a structure that depends ultimately on controllable synthesis parameters such as the composition of the mixture. the pH. and the temperature. The final step is the cross-linking of the inorganic species, giving rise to a rigid shell with a structure that is a replica of the underlying liquid crystalline phase. The structure of such a mesophase is determined by dynamic interplay among organic–inorganic ion pairs: the charge density, coordination. and steric requirements of organic and inorganic species at the interface are the main controlling factors.

As a first approximation, the mesophase structure can be linked directly to the packing factor $g = V/a_0 l$, where V is the total volume of the surfactant chain plus any cosolvent organic molecules between the chains, a_0 is the effective head group area at the micelle surface. and 1 is the kinetic length of the surfactant tail. As the g value decreases. transitions to higher curvature mesophases occur at the following critical values: g = 1 (lamellar mesophase), $1/2 < g < 213$ (cubic. $Ia3d$), g = 1/2 (hexagonal, $p6mm$), and $g = 1/3$ (cubic, $Pm3n$). This factor was introduced earlier to rationalize the

aggregation behavior of ainphiphile molecules in water. Despite its simplicity. the concept of packing factor proved to be very useful not only to explain experimental findings but also; more importantly. to design mesoporous materials via direct manipulation of the g factor. For example, the addition of cosolvents or polar molecules was found to increase the volume V of the hydrophobic tail.[25] In turn. this decreases the packing factor and affects the nature of the mesostructure obtained. Another simple and effective way to fine tune the packing factor is through the use of surfactant blends. In a recent study, Kim et al.[26] prepared high-quality silica mesophases having two-dimensional hexagonal ($p6mm$), three-dimensional hexagonal ($P6_3/mmc$), and cubic ($Im3m$) structures through systematic variation of the effective head- and tail-group sizes via appropriate mixtures of amphiphilic block copolymers.

Generalization sf Electrostatically Driven Synthesis Mechanisms

The cooperative organization mechanism driven by electrostatic interactions described above is not limited to ion pairs between cationic surfactants (S^+) and anionic inorganic species (I^-), but can be generalized to include three other routes.[27] Pathway S^-I^+ involves direct electrostatic interaction between anionic surfactants and cationic inorganic species. The synthesis of mesostructured antimony or tungsten oxide under acidic conditions is a typical example for this pathway. In the two other routes. the interactions occur between similarly charged organic and inorganic species with the mediation of small counterions of opposite charges. These pathways are referred to as $S^+X^-I^+$ (X^- = Cl^-, Br^-) and $S^-M^+I^-$ (M^+ = Na^+, K^+). The synthesis of silica mesophase at pH < 2, and that of mesostructured zinc oxide at pH>12.5, are examples of these two routes, respectively.

Other Supramolecular Templating Mechanisms

Pinnavaia et al.[3,4] introduced a neutral (N^0I^0) and a nonionic (S^0I^0) templating mechanism using alkylamines and polyethyleneoxide surfactants, respectively. The obtained silicas. referred to as HMS and MSU-n. respectively, exhibited nonordered systems of cylindrical nanopores with narrow size distributions. Instead of the electrostatic interactions. in the presence of neutral surfactants, hydrogen bonding becomes the predominant factor in pairing organic and inorganic species. As seen in Fig. 2. the neutral species formed by partial

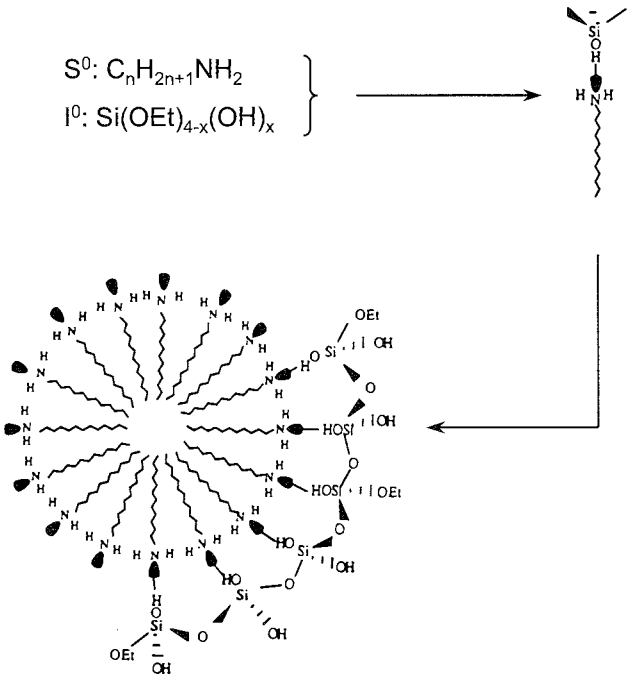

Fig. *2* Neutral templating mechanism. (From Ref. [3].)

hydrolysis of tetraethyl orthosilicate interacts with the surfactant amine head group via hydrogen bonding. The obtained organic–inorganic complex may be considered as an amphiphile with a bulky head group leading to a small packing factor. As mentioned earlier, decreasing the g value increases the likelihood for the forination of high-curvature micelles such as rod-like micelles. which exhibit a natural tendency to self-assemble into a hexagonal lyotropic mesophase. This is followed by condensation of silanol groups and formation of rigid silica walls.

For completeness, it should be mentioned that in addition to the electrostatically driven cooperative assembly pathways, and the nonionic routes based on van der Waals interactions, Antonelli and Ying[28] introduced the so-called ligand-assisted templating mechanism to explain the formation of a number of periodic mesoporous transition metal oxides. This mechanism is based on the formation of a covalent bond between organic and inorganic species. Using the synthesis of mesoporous Nb_2O_5 for illustration (Fig. 3), it is seen that the initial step, which takes place in the absence of water. is the formation of a Nb–N covalent bond between $Nb(OEt)_5$ and the long-chain amine surfactant. This is followed by intermolecular condensation of these species in the presence of water with simultaneous self-organization into micelles. and ultimately into a mesophase (Route *a'*, b' in Fig. 3). Alternatively. the

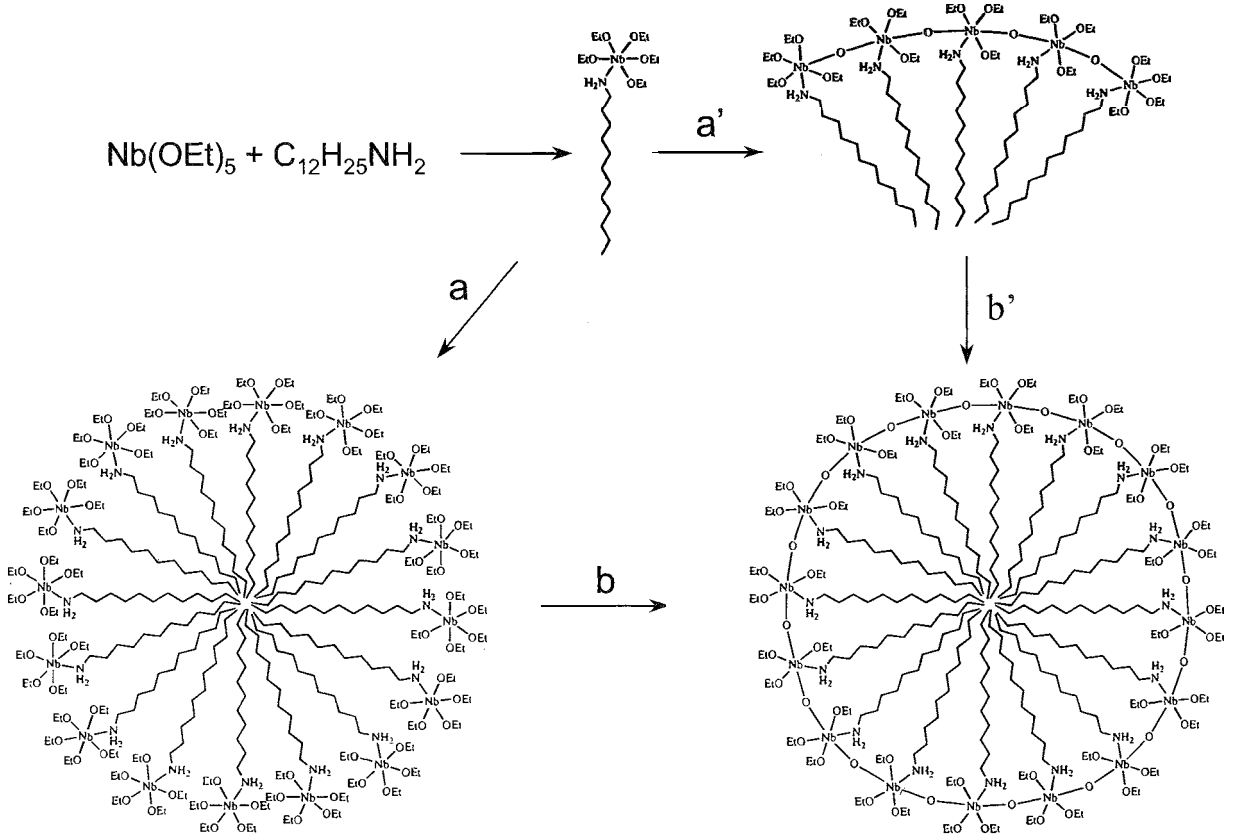

Fig. 3 Ligand-assisted templating mechanism. (From Ref. [28].)

formation of the micelles may precede the condensation step (Route *a*, *b* in Fig. 3). The key feature of this mechanism, i.e., the formation of a covalent M–N bond, was inferred from nuclear magnetic resonance (NMR) studies on 100% ^{15}N-enriched dodecylamine niobium ethoxide precursor in [D_8]toluene and the corresponding as-synthesized Nb_2O_5 mesophase.[28]

CHARACTERIZATION OF PERIODIC MESOPOROUS SILICA-BASED MATERIALS

Characterization of periodic mesoporous silicates involved a wide range of techniques. One of the first realizations made was that despite their long-range order, these materials were amorphous in nature. as conclusively demonstrated by Raman spectroscopy, solid-state NMR, and other techniques.[1,17] As a result, their x-ray diffraction (XRD) patterns were dominated by a limited number of peaks at low angles (Fig. 4), often providing insufficient information with regards to the structure of the materials under investigation. In this respect, transmission electron microscopy (TEM) (Fig. 5) and, more importantly, electron crystallography[29] played a key role in elucidating the structure of various silica mesophases. Because they are readily available to most researchers, adsorption techniques were, along with XRD, the most frequently used methods for characterizing periodic mesoporous materials.[30] This simple technique provides essential information regarding structural and textural properties of mesoporous materials, such as the surface area, the pore volume, the pore size distribution, the occurrence of micropores, the surface hydrophobicity, etc. Moreover, in combination with XRD data, nitrogen adsorption measurements provide an estimate for the pore wall thickness. In Fig. 6. a representative example of nitrogen adsorption–desorption isotherms for a MCM-41 silica is shown. Such isotherms are usually of Type IV in the IUPAC classification and exhibit characteristic steps on both branches, corresponding to the condensation and evaporation of the adsorbate from mesopores with narrow size distributions. They are usually reversible for MCM-41 silicas with mesopores less than ca. 4 nm in diameter and exhibit hysteresis loops of different shapes for two-dimensional hexagonal (*p6mm*) silica with pores larger

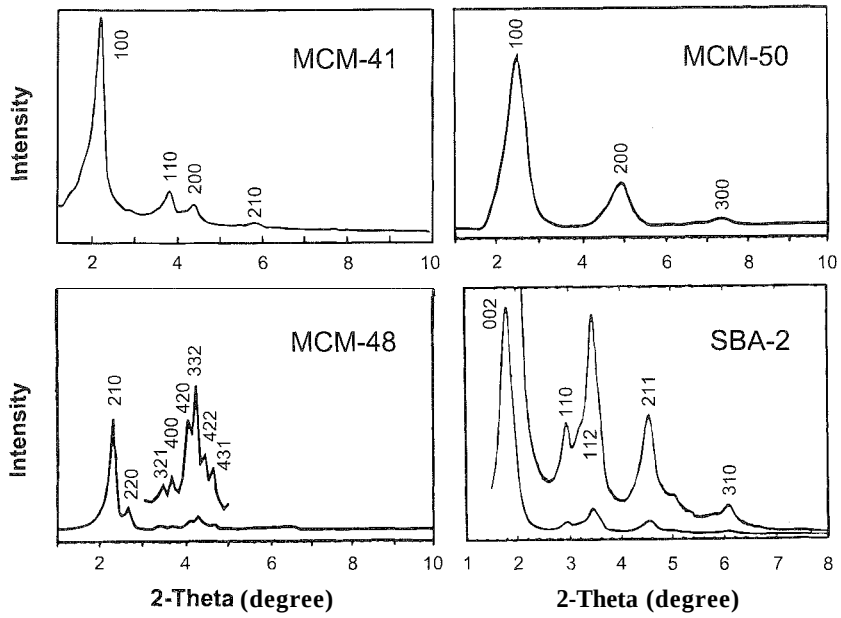

Fig. 4 X-ray diffractograms for typical silica mesophases. (From Refs. [1, 25].)

than 4 nm, mesocellular silica foams, ac well as the three-dimensional hexagonal ($P6_3/mmc$) and the cubic ($Im3m$), such as *SBA-2* and *SBA-16,* respectively, which both exhibit cage-like mesopores

PERIODIC MESOPOROUS SILICA–ORGANIC HYBRIDS

Combining organic and inorganic species within the same periodic mesoporous material offers added flexibility to control an extended range of surface properties such as catalytic activity, hydrophobicity, and hydrophilicity, as well as bulk properties such as density, dielectric constant, hardness, and mechanical strength. Sayari and Hamoudi[7] divided these materials, based on their structures, into five categories, namely: I) as-synthesized amphiphile/silica mesophases; *2)* expanded mesoporous silicas; *3)* mesoporous silicas with organically modified surfaces; 4) mesoporous organosilicates; and 5) mesoporous silicas with occluded organic materials such as polymers. This contribution will deal only with surface

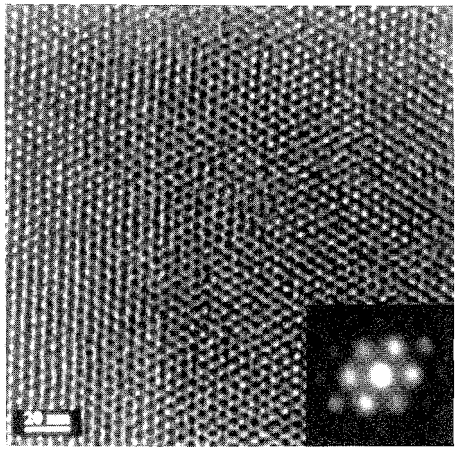

Fig. 5 TEM image and the corresponding electron diffraction pattern for a typical MCM-41 silica.

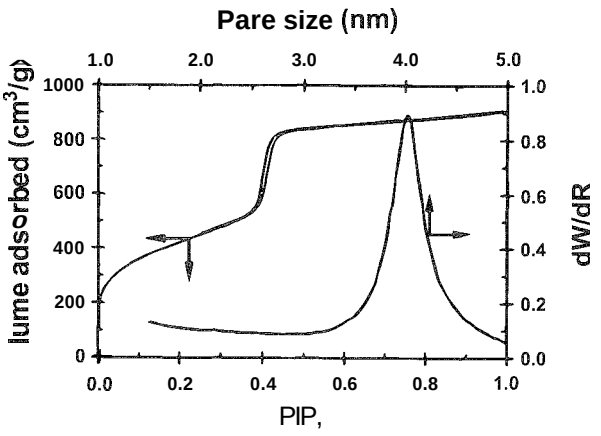

Fig. 6 Typical nitrogen adsorption–desorption isotherm and pore size distribution for MCM-41. (From Ref. [17].)

and framework organically modified silicas, i.e., Classes 3 and 4 silica–organic hybrids. As for the other categories of hybrid materials, the reader rnay refer to two recent reviews.[7,8]

Periodic Mesoporous *Silicas* with *Organically* Modified Surfaces

Surface modification of periodic mesoporous silicas via covalent bonding of organic molecules may be achieved using a postsynthesis procedure or directly via cocondensation procedures. In addition to the obvious changes in chemical properties of the inaterials upon surface modification with organic functionalities, improvement of physical properties may also occur. It was reported that surface silylation of inesoporous silica improves not only the chemical stability of the hybrid materials against moisture, but also enhances mechanical stability compared to their pure silica counterparts. Moreover; incorporation of $-CH_2-CH_2-$ groups within the walls of the silica mesopores was found to increase the Young's modulus and hardness of the material, and decrease its dielectric constant.

The two-step method was described in the Mobil group's early work.''' It consisted of coupling a suitable organosilane reagent with the silica surface hydroxyl groups using an appropriate solvent under reflux. This could be followed by higher-order modifications that involve further reactions to create new functionalities. To achieve selective functionalization of the internal surface. it was suggested to first passivate the external surface using dichlorodiphenylsilane Ph_2SiCl_2, then carry out the grafting process. In some instances. surface-functionalized mesoporous silica may also be prepared using the as-synthesized silica mesophase by simultaneously removing the surfactant and grafting the organic species. The two-step approach to organically surface-modified mesoporous silica was used to incorporate many functionalities. including alkyl groups, amine. thiol, and sulfonic acid functions, as well as more elaborate structures such as coordination complexes and chiral ligands.

As an alternative to the two-step approach, mesoporous silica with organic moieties covalently linked to their internal surface could be obtained in a single-step cocondensation of siloxane and organosiloxane precursors using similar supramolecular templating techniques as those for the synthesis of pure silica. Successful one-step syntheses of MCM-41 silicas modified with alkyl, phenyl, vinyl. cyanoethyl, amine. thiol, and propylsulfonic acid moieties were reported in the literature.[7] Similar preparations were extended to MCM-48 silica and to mesoporous materials prepared via nonionic and polymeric surfactants. i.e., HMS, MSU, and SBA-15 silicas.

Surface-functionalized mesoporous materials were characterized using numerous techniques. Solid-state ^{29}Si-. ^{13}C-, and ^{1}H-MAS-NMR (MAS = magic angle spin) measurements were used to investigate changes in the local environment of silicon atoms and to determine the degree of surface functionalization of mesoporous silicas. infrared spectroscopy. sometimes in combination with ^{1}H-NMR. was used to monitor the consumption of silanol groups and the functionalization of the silica surface through the development of characteristic vibrations. Thermogravimetric analysis was used to probe the thermal stability as well as the hydrophobic or hydrophiiic character of the hybrid materials. Structural ordering of organically modified mesoporous silicas was characterized by TEM, XRD, and nitrogen adsorption measurements. These studies revealed that postsynthesis surface modification had limited effect on the periodic structure of the starting material. However, the structural ordering of hybrid mesoporous silicas synthesized in a single step via cocondensation, was found to decrease progressively as the relative amount of the organic precursor present in the synthesis mixture increased. The upper limit for the organosiloxane-to-tetsaethoxysilane (TEOS) ratio in the synthesis gel, above which no structural ordering occurred, was typically 10–25%.

Periodic Mesoporous Organosilicates

Unlike surface-fiinctionalized silica. in periodic mesoporous organosilicates (PMOs), the organic component is built in the pore walls instead of protruding from the surface into the internal channels. This recent development in the area of periodic nanoporous materials opens a wide range of new and exciting opportunities for designing materials with controlled surface properties at the molecular level. The fact that the organic moieties constitute an integral part of the inesoporous framework allows the formation of pure silica–organic hybrids using bridged silsesquioxanes without addition of any other source of silica. This is in contrast with surface-functionalized mesoporous silica prepared via cocondensation. which requires large amounts of silica precursor, such as TEOS for the formation of rigid walls, to take place. In the latter case, the TEOS to organotrialkoxysilane is typically higher than 75%.

Mesoporous organosilicates are synthesized using similar self-assembly approaches as pure silica mesophases: the main difference being the silicon-containing precursors that consist of bridged silsesquioxanes, $(RO)_3Si-R'-Si(OR)_3$. Different types of amphiphile molecules, including cationic (alkyltrimethylammonium),

anionic (dodecylsulfate), nonionic (Brij-56), and block copolymer (P123) surfactants were used as supramolecular templates. Successful syntheses of periodic mesoporous organosilicates with organic spacers R' originating from methane. ethane. ethylene, acetylene, butene, benzene, toluene, xylene, dimethoxybenzene, thiophene, bithiophene, and ferrocene were reported in the literature. Similar to silica mesophases, the formation of mesoporous organosilicates was found to occur under acidic and basic conditions. The removal of the templating surfactants was generally performed by acid solvent extraction. Most organosilicates reported in the literature exhibited cubic, and two- or three-dimensional hexagonal structures.

X-ray diffraction, nitrogen adsorption, SEM, TEM, and solid-state NMR are some of the techniques used for characterizing periodic mesoporous organosilicates. Of particular importance was the role of NMR spectroscopy in confirming the preservation of the Si–R′–Si unit's integrity during the precipitation process, thus providing direct evidence that the organic–inorganic moiety constituted the building block of the mesoporous channel walls. For instance, ^{29}Si-MAS-NMR for ethane–silica mesophases showed mainly two peaks at $\delta \approx -57.0$ and -66.0 ppm attributable to T^2 [C*Si*(OSi)$_2$(OH)] and T^3 [C*Si*(OSi)$_3$] Si species covalently bonded to carbon atoms. Similar chemical shifts were also obtained for the methylene–silica material. The T^2 resonance was observed at -75 and -71 ppm. for ethylene and phenylene–silica mesophases, respectively: whereas the corresponding T^3 resonances occurred at -83 and -78.2 ppm, respectively. In all cases. no Q^n [*Si*(OSi)$_n$OH$_{4-n}$] species were observed. indicating that no Si–C bond hydrolysis took place. Likewise. ^{13}C-CP-MAS-NMR for surfactant-free materials were consistent with these conclusions. For example, the ethane–silica mesophase exhibited a peak with chemical shift at ca. 5–6 ppin assigned to methylene convalently bound to Si as in Si–CH_2CH_2–Si. The ethylene–silica materials exhibited a strong resonance at ca. 145 ppm, while the phenylene-bridged system gave rise to a ^{13}C resonance at 133.4 ppm. The methylene-containing material generated a single peak at ca. 0 ppm. All these data indicate that the Si–R′–Si units were preserved during the organic–inorganic mesophase formation.

APPLICATIONS OF PERIODIC MESOPOROUS SILICA-BASED MATERIALS

These materials were found to be useful in many potential applications. particularly in the areas of catalysis.[16–18] Catalytically active acid sites were generated using different approaches, including framework modification with trivalent cations as in aluminosilicates; surface modification. for example. with propylsulfonic acid; and addition of acid ingredients such as heteropolyacids. More recently. highly stable mesoporous materials were prepared via supramolecular templating of strongly acidic zeolite *Y*, β, and ZSM-5 nanocrystals. All these types of materials were found to be effective acid catalysts. Al-MCM-41 was used in oligomerization of propene, alkylation of bulky aromatic molecules, cracking of cumene, and straight run naphtha, as well as in hydroisomerization and hydrocracking of n-hexadecane. Phosphotungstic acid containing mesoporous aluminosilica was found to be more efficient than H_2SO_4 or bulk phosphotungstic acid in liquid-phase alkylation of 4-tert-butylphenol by isobutene and styrene. Similarly, sulfonic acid containing MCM-41 silicas exhibited excellent performance in acid-catalyzed reactions involving large molecules. such as esterification of glycerol with fatty acids. Materials with SAB-15 structure prepared via assembly of MFI aluminosilicate nanoclusters were also found to be powerful catalysts for the cracking of cumene and 1,3,5-triisopropylbenzene.[12] Similar progress was made in the area of base-catalyzed reactions. Mesoporous materials with basic properties were prepared via Na^+ or Cs^+ ion exchange using MCM-41 aluminosilica as starting materials, or via grafting of organic moieties containing basic functions such as amines. Such materials were found to be effective catalysts in esterification, Knoevenagel condensation, and Michael reaction.

Like their zeolitic counterparts, mesoporous titano- and vanadosilicates were also found to be excellent catalysts for selective oxidation of organic substrates, such as alkenes, ketones, aromatic or aliphatic hydrocarbons, and fatty esters, using dilute hydrogen peroxide or tert-butylhydroperoxide, under mild conditions. Because of their large pores. they had the added advantage of being able to accommodate bulky molecules. Further silylation of periodic mesoporous titanosilicates was found to improve their activities and selectivities. Another important catalytic application of functionalized mesoporous silica is chiral catalysis. For example, optically active secondary alcohols. often used for the manufacture of drugs and other biologically active compounds, were obtained in very high yield via asymmetric addition of diethyl zinc to benzaldehyde using MCM-41 and SBA-15 silica modified by prolinol-based ligands. In many instances. capping unreacted surface siianol groups with hexamethyldisiiazane was found to improve the catalyst selectivity.[7]

In addition to catalysis, mesoporous silicas were used as hosts for a wide variety of advanced materials, such as metallic and semiconductor nanoparticles and

nanowires with unique optical and electronic properties. They were also employed as templates for the synthesis of porous polymers and carbons. Another important area of application, particularly for surface-functionalized mesoporous materials, is protection of the environment. For example, mercaptopropyls bearing MCM-41, HMS, MSU, and SBA-15 silicas were successfully tested for scavenging heavy-metal cations such as mercury and lead from wastewaters. Likewise, mesoporous silicas with appropriate functionalities were used to adsorb harmful metallic anions and organic pollutants from water.

ARTICLES OF FURTHER **INTEREST**

Channel Inclusion Compounds, p. 223
Crystal Growth Mechanisms, p. 364
Crystalline Microporous Silicas, p. 380
Gels, p. 586
Mesoporous Materials, p. 845
Organic Zeolites, p. 996
The Template Effect, p. 1493
Zeolites: Catalysis, p. 1610
Zeolites: Separation Science, p. 1617
Zeolites: Structures and Inclusion Properties, p. 1623

REFERENCES

1. Beck. J.S.; Vartuli. J.C.; Roth, W.J.: Leonowicz, M.E.; Kresge, C.T.: Schmitt, K.D.: Chu. C.T.-W.; Olson, D.H.: Sheppard, E.W.: McCullen, S.B.; Higgins, J.B.; Schlenker. J.L. A new family of mesoporous molecular sieves prepared with liquid crystal templates. J. Am. Chem. Soc. **1992,** *114* (27), 10834–10843.
2. Zhao, D.; Huo, Q.: Feng, J.; Chmelka, B.F.: Stucky, G.D. Nonionic triblock and star diblock copolymer and oligomeric surfactant syntheses of highly ordered. hydrothermally stable. mesoporous silica structure. J. Am. Chem. Soc. **1998,** *120* (24). 6024–6036.
3. Tanev, P.T.; Pinnavaia, T.J. A neutral templating route to mesoporous molecular sieves. Science **1995.** *267* (5199), 865–867.
4. Bagshaw. S.A.: Prouzet. E.: Pinnavaia. T.J. Templating of mesoporous molecular sieves by nonionic polyethylene oxide surfactant. Science **1995.** *269* (5228), 1242–1244.
5. Sayari, A.; Liu. P. Non-silica periodic rnesostructured materials: Recent progress. Microporous Mater. **1997.** *12* (3), 149–177.
6. Trikalitis. P.N.; Rangan, K.K.: Kanatzidis. M.G. Platinum chalcogenido MCM-41 analogues. High hexagonal order in mesostructured semiconductors based on Pt2 + and [Ge4Q10]4- (Q = S, Se) and [Sn4Se10]4-adamantine clusters. J. Am. Chem. Soc. **2002.** *124* (11), 2604–2613.
7. Sayari. A.; Hamoudi. S. Periodic mesoporous silica-based organic–inorganic nanocomposite materials. Chem. Mater. **2001.** *13* (10). 3151–3168.
8. Stein, A.; Melde, B.J.: Schroden, R.C. Hybrid inorganic-organic mesoporous silicates—Nanoscopic reactors coming of age. Adv. Mater. **2000.** *12* (19). 1403–1419.
9. Tiemann. M.: Froba, M. Mesostructured aluminophosphates synthesized with supramolecular structure directors. Chem. Mater. **2001.** *13* (10). 3211–3217.
10. Schiith, F. Non-siliceous rnesostructured and mesoporous materials. Chem. Mater. **2001,** *13* (10), 3184–3195.
11. Liu, Y.: Pinnavaia, T.J. Assembly of hydrothermally stable aluminosilicate foams and large-pore hexagonal mesostructures from zeolite seeds under strongly acidic conditions. Chem. Mater. **2002.** *14* (1), 3–5.
12. Han, Y.; Wu, S.: Sun, Y.: Li. D.; Xiao. F.S.: Liu. J.: Zhang. X. Hydrothermally stable ordered hexagonal mesoporous aluminosilicates assembled from a triblock copolymer and preformed aluminosilicate precursors in strongly acidic media. Chem. Mater. **2002,** *14* (3). 1144–1148.
13. Lee, J.S.; Joo, S.H.; Ryoo. R. Synthesis of mesoporous silicas of controlled pore wall thickness and their replication to ordered nanoporous carbons with various pore diameters. J. Am. Chem. Soc. **2002,** *124* (7). 1156–1157.
14. Zhang. Z.: Dai, S.; Blom, D.A.: Shen, J. Synthesis of ordered metallic nanowires inside ordered mesoporous materials through electroless deposition. Chem. Mater. **2002.** *14* (3). 965–968.
15. Coleman, N.R.B.; O'Sullivan, N.: Ryan, K.M.: Crowley, T.A.: Morris. M.A.; Spalding, T.R.: Steytler. D.C.; Holmes. J.D. Synthesis and characterization of dimensionally ordered semiconductor nanowires within mesoporous silica. J. Am. Chem. Soc. **2001.** *123* (29). 7010–7016.
16. Sayari. A. Catalysis by crystalline mesoporous molecular sieves. Chem. Mater. 1996. *8* (8). 1840–1852.
17. Sayari, A. Periodic Nanoporous Materials: Synthesis. Characterization and Potential Applications. In *Recent Advances and New Horizons in Zeolite Science and Technology;* Chong. H., Woo. S.I., Park. S.E., Eds.; Elsevier: Amsterdam, 1996; 1–46.
18. Corma, A. From microporous to mesoporous molecular sieve materials and their use in catalysis. Chem. Rev. **1997,** 97 (6). 2373–2420.
19. Ying, J.Y.; Mehnert, C.P.; Wong, M.S. Synthesis and applications of supramolecular-templated mesoporous materials. Angew. Chem., Int. Ed. **1999,** *38* (1–2), 56–77.
20. Mamak. M.; Coombs. N.; Ozin, C. Self-assembling solid oxide fuel cell materials: Mesoporous yttria–zirconia and metal–yttria–zirconia solid solutions. J. Am. Chem. Soc. **2000.** *122* (37). 8932–8939.
21. Scott. B.J.: Wirnsberger, G.: Stucky. G.D. Mesoporous and mesostructured materials for optical applications. Chem. Mater. **2001.** 13 (10). 3140–3150.
22. He, X.: Antonelli. D. Recent advances in synthesis and applications of transition metal containing mesoporous

molecular sieves. Angew. Chem.. Int. Ed. 2002. 41 (2), 214–229.

23. Attard. C.A.; Glyde, J.C.: Goltner, C.G. Liquid crystalline phases as templates for the synthesis of mesoporous silica. Nature 1995. *378* (6555). 366–368.
24. Firouzi. A.; Monnier. A.; Bull. L.M.; Besier, T.; Sieger. P.; Huo, Q.: Walker. S.A.; Zasadzinski, J.A.: Glinka. C.; Nicol, J.: Margolese. D.; Stucky, G.D.; Chmelka, B.F. Cooperative organization of inorganic–surfactant and biomirnetic assemblies. Science 1995, 267 (5201), 1138–1143.
25. Huo, Q.; Margolese. D.I.: Stucky, G.D. Surfactant control of phases in the synthesis of rnesoporous silica-based materials. Chem. Mater. 1996. *8* (5), 1147–1160.
26. Kim, J.M.: Sakamoto. Y.: Hwang, Y.K.; Kwon. Y.U.; Terasaki. O.; Park, S.E.; Stucky, C.D. Structural design of mesoporous silica by micelle-packing control using blends of amphiphilic block copolymers. J. Phys. Chem., B 2002. *106* (10), 2552–2558.
27. Huo, Q.; Margolese, D.I.; Ciesla. U.: Feng. P.; Cier, T.E.; Sieger, P.; Leon, R.: Petroff, P.M.; Schiith, F.: Stucky. G.D. Generalized synthesis of periodic surfactant/inorganic composite materials. Nature 1994. *368* (6469); 317–321.
28. Antonelli. D.M.; Ying, J.Y. Synthesis of a stable hexagonally packed rnesoporous niobium oxide molecular sieve through a noble ligand-assisted ternplating mechanism. Angew. Chem.. Int. Ed. Engl. 1996. *35* (4). 426–430.
29. Sakamoto. Y.; Díaz. I.; Terasaki, O.; Zhao. D.; Pérez-Pariente. J.: Kim, J.M.; Stucky, G.D. Three-dimensional cubic mesoporous structures of SBA-12 and related materials by electron crystallography. J. Phys. Chem.. B 2002. 106 (12), 3118–3123.
30. Kruk, M.: Jaroniec, M.: Sayari. A. Application of large pore MCM-41 molecular sieves to improve pore size analysis using nitrogen adsorption measurements. Langmuir 1997. *13* (23). 6267–6273.

Micelles and Vesicles

Raoul Zana
Institut Charles Sadron (CNRS-ULP), Strasbourg, France

INTRODUCTION

Surfactant molecules are made up of two moieties *that have antagonistic properties, a polar or electrically charged hydrophilic moiety and a hydrophobic moiety, most often an alkyl chain. In aqueous solution, most surfactants self-assemble and* form *micelles when their concentration* becomes *larger* than *the so-called critical micellization concentration* (CMC). *In micelles (from the Creek mica, which means "grain"), the alkyl chains are in contact and form an oily core that is coated by the polar head groups. The outer layer that contains head groups, counterions (in the case of ionic surfactants), water and the first methylene group of the alkyl chain is called the palisade layer. The* formation *of* micelles *is a cooperative process that is spontaneous and reversible. Micelles* are *thermodynamically stable species that are in chemical equilibrium with free* surfactants.

Some surfactants *self-assemble into closed bilayers called vesicles (or* liposomes *when formed from phospholipids). Vesicles are often spherical but can take other shapes and* can *be unilamellar or multilamellar. In contradistinction to micelles, vesicles may not be thermodynamically stable. Another* important *difference between vesicles and micelles is that vesicles have an inside that encloses* some *of the aqueous phase and an outside. The existence of a critical vesiculation concentration, above which some surfactants would form vesicles. is sometimes mentioned. This is probably incorrect.* At *very low* concentrations, *surfactants always start* forming *micelles that* may *turn into vesicles at higher concentrations. Given in Fig. 1 are* schematic *representations of a* micelle *and a vesicle, both of spherical shape.*

Micelles are important in many uses of surfactants for their capacity to solubilize water-insoluble compounds. Vesicles are model systems for biological cells and can be used for entrapping active compounds in their insides. Besides. vesicles and micelles are used as microreactors for performing chemical reactions and *preparing solid* nanoparticles *of varied shapes.*

Reviewed in *this article are some important properties of micelles and vesicles: formation and stability. size and shape. internal organization. dynamics, and vesicle-to-micelle transition. Only few* of *the most significant papers* in *the immense* literature *dealing with micelles and vesicles are cited due to the lack of space. Also due to lack of space, this article presents no mathematical development.*

FORMATION OF MICELLES AND VESICLES: EXPERIMENTAL ASPECTS

Micelles are obtained by solubilizing a surfactant in water at a concentration $C > \mathrm{CMC}$. *The CMC is the most important property of a surfactant. It is not a single concentration but rather a narrow range of concentrations. Its value slightly depends on the method of determination, reflecting differences in the way each method weighs micelles and free surfactants. The CMC decreases by a factor of 2 for ionic surfactants and 3 for nonionic* surfactants *for each additional* methylene *group in the* surfactant *alkyl* chain.[1,2] *For ionic surfactants, the CMC also decreases upon increasing concentration* C_e *of an added electrolyte having a common ion with the* surfactant, *according to:* $\log \mathrm{CMC} = A - B\log(\mathrm{CMC}_0 + C_e)$. Terms *A and B are two constants, and* CMC_0 *is the* CMC *in the absence of* salt.[1] *The value of B is close to the degree of counterion association to the micelle. Thermodynamic studies showed that the formation of micelles is entropy* driven.[2] *The large positive value of the entropy of* micellization *reflects a change affecting the water molecules surrounding the surfactant alkyl chains when the chains are transferred from the aqueous phase to the micelle core.*

Aqueous vesicles are commonly *observed with phospholipids and with their synthetic analogues, which are two-chain* surfactants *having alkyl chains with 10 or more carbon atoms. Different methods were used to prepare* vesicles.[3] *For instance, dispersions of appropriate sparingly water-soluble surfactants or phospholipids give rise to vesicles upon* sonication. *Vesicles may also be obtained by solubilizing an appropriate amphiphile in an organic solvent, depositing the solution on a glass plate. evaporating the organic solvent; and exposing the resulting film to water. Vesicle-forming surfactants can also be* solubilized *in an aqueous solution of a hydrotrope or of a* micelle-forming surfactant. *Dilution of this solution with water gives rise to vesicles. Sonication, extrusion through Millipore filters. and other methods were used to transform large* multilamellar *vesicles into small unilamellar vesicles. Vesicles prepared by these methods* can *have* long-

Encyclopedia of Supramolecular Chemistry
DOI: 10.1081/E-ESMC 120012804

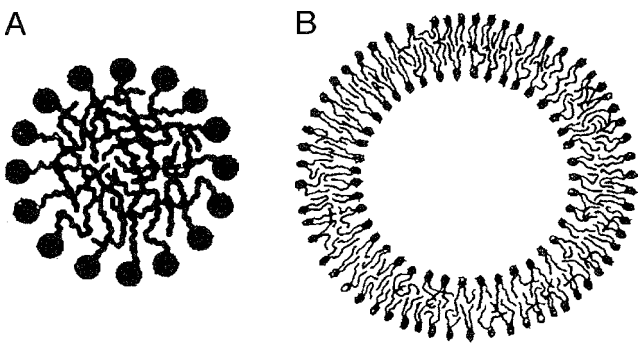

Fig. 1 (A) A micelle (diameter: 5 nm): and (B) a vesicle (diameter: 20–1000 nm. thickness: 4–5 nm) of spherical shape. The alkyl chains were represented in a disordered state reminiscent of the liquid-like structure of the aggregate core. Such a representation is closer to reality than that where the alkyl chains are represented straight and normal to the assembly surface.

term stabilities. Nevertheless, vesicles made of a single surfactant or phospholipid are unstable and revert to liquid crystalline aggregates after a time that can be long. Unilainellar vesicles obtained by mixing aqueous solutions of two surfactants of appropriate structure and of different electrical charge may be different. Such vesicles appear to form spontaneously and reproducibly and can have long-term stabilities.[4]

FORMATION OF MICELLES AND VESICLES: THEORETICAL ASPECTS

The driving force for surfactant self-assembly into micelles or vesicles is the so-called hydrophobic (attractive) interaction between surfactant alkyl chains.[2,5] The origin of this interaction lies in the strong attractive interaction that exists between water molecules. When alkyl chains are immersed into water, some water-molecule–water-molecule contacts are replaced by alkyl-chain–water-molecule contacts. Even though interactions between water molecules and alkyl chains are attractive; they are energetically less favorable than interactions between water molecules. As a result. the system tends to minimize its free energy by eliminating contacts between alkyl chains and water molecules. This is achieved by having the alkyl chains get together. With surfactants, this results in the formation of micelles, where the alkyl chains are bunched together forming the micelle core. The hydrophilic head groups remain at the surface of the core, further reducing alkyl-chain–water-molecule contacts.

The main repulsive interactions involved in micelle formation are the electrostatic interaction between head groups, steric interactions arising from the packing of head groups at the micelle surface and of the alkyl chains in the micelle core, and an interaction associated with residual alkyl-chain–water-molecule contacts at the micelle surface. The balance between attractive and repulsive interactions results in micelles of finite size.

The molecular thermodynamic theory for micelle formation was worked out with increasing sophistication following the pioneering work of Israelachvili, Mitchell, and Ninham.[6] The most comprehensive reports on micelle formation are those of Ruckenstein and Nagarajan[7] and of Blankschtein et al.[8] Many other theoretical approaches were used in recent years to account for the forination of micelles and their properties: thermodynamics of small systems, self-consistent field lattice model, scaled particle theory, Monte Carlo simulations, and molecular dynamics (MD) simulations.[9] The last two approaches are presently much in favor due to the increased calculating capacity of modern computers. A common prediction of all of these theories is that micelles represent a therinodynamically stable state, and that micellar solutions are single-phase systems. Many of the recent results of MD and Monte Carlo simulations are in agreement with experimental results.

The consensus about the existence of thermodynamically stable vesicles remains to be reached. A surfactant monolayer takes a curvature equal or close to its spontaneous curvature. which is determined by the surfactant chemical structure and the interaction between surfactants. Considerations based on the bending energy of a surfactant monolayer led to the conclusion that only flat (zero curvature) bilayers can be thermodynamically stable.[10] The curvatures of the inner and outer layers of a vesicle are finite. Their values are nearly equal in value but opposite in sign. Thus, vesicles (curved bilayers) formed from a single surfactant or phospholipid cannot be thermodynamically stable.[10] The situation may be different for vesicles made from a binary mixture of surfactants. Safran et al.[11] showed that for mixtures of two interacting surfactants forming monolayers with large bending constants. the free energy of the system can be a minimum for vesicles with different concentrations of the two surfactants in the inner and outer monolayers. The spontaneous curvatures of the two layers are then equal but have opposite signs. Systems containing such vesicles would be single-phase systems, like micellar solutions. However, Laughlin[12] pointed out that binary mixtures of surfactants are complex. because they contain up to five components. He concluded that the phase behavior of binary mixtures of water and cationic surfactants, which are made of two oppositely charged surfactant ions, in the absence of other small ions, must be investigated before a conclusion can be reached on the stability of vesicles formed in such mixtures.

SIZE AND SHAPE OF MICELLES AND VESICLES

The technique of transmission electron microcopy at cryogenic temperature (cryo-TEM) allowed for the direct visualization of micelles and vesicles of all shapes described below.[13,14]

At a concentration close to the CMC, the micelles are generally spherical or close to spherical (see Fig. 2). As the concentration is increased. the micelles may remain spheroidal or grow and become oblate (disk-like) or prolate (rod-like). The giant worm-like or thread-like micelles represent an extreme case of growth into elongated micelles. The worm-like micelles can be linear or branched (see Fig. 2). The hemispherical end caps of thread-like micelles have a larger diameter than the cylindrical body,''' a result correctly predicted by theory. Micelles can also be ring-like.[14]

At moderate surfactant concentration. the micelle shape is determined by the value of the surfactant packing parameter $P=v/a_0l$, where v and l are the volume and length of the hydrophobic moiety (alkyl chain), and a_0 is the optimal surface area occupied by one surfactant at the micelle–water interface.[6] It is important to realize that the value of a_0 is determined by the cross-sectional area of the surfactant head group and also by the various interactions at play in micelle formation.[6] Surfactants characterized by values of $P<113$ give rise to spherical1 spheroidal micelles. Surfactants with $1/3<P<1/2$ tend to form elongated micelles. Surfactants with $1/2<P<1$ form disk-like micelles that can be viewed as precursors of surfactant bilayers. Last, surfactants with $P>1$ form reverse micelles. The packing parameter concept is extremely powerful and useful. In particular. it permits one to understand or predict changes of micelle shape induced by changes of experimental conditions. It can also be extended to surfactant mixtures. Besides, the packing parameter is related to the curvature of the surfactant monolayer.[15]

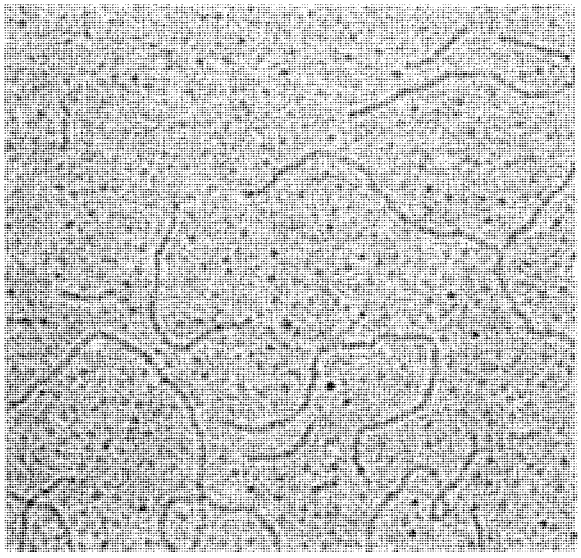

Fig. 2 Cryo-TEM micrograph of a 0.62 wt% solution of the gemini surfactant 12-2-12 that shows spherical micelles (black dots) and thread-like micelles. A branched thread-like micelle can be seen at the right side of the micrograph. Bar=100 nm. Reproduced from Ref. [14] with permission of the American Chemical Society.

The micelle size increases with the carbon number m of the surfactant alkyl chain. For conventional surfactants, the aggregation number of the maximum spherical rnicelle can be estimated from $N_S=4\pi l^3/3v$ using the reported expressions of the length l and volume v of the hydrophobic moiety.[2] The micelle growth with the surfactant concentration is well explained by different models that assume that the free energy of a surfactant in a spherical micelle is higher than in a cylindrical or disk-like micelle.[6–8,16] The free energy difference ΔG_{CS} per surfactant is small, -0.2–0.5 kT per surfactant, as compared to a free energy of micellization of about -15 kT per surfactant with a dodecyl chain. The larger the value of ΔG_{CS}, the steeper the increase of micelle size with increasing surfactant concentration.[6–8] Surfactants with $P>113$ show micelle growth. Ionic surfactants with $P<1/3$ may show moderate micelle growth, because the ionic strength of the solution and. in turn. P increase slightly with the surfactant concentration. The size polydispersity of spherical micelles is small. while that of prolate and oblate micelles can be very large.

Theoretical[16] and experimental[17] studies demonstrated the existence of rapid (10^{-10}–10^{-6} s) and important fluctuations of micelle shape. Substantial shape deformations can take place at a low cost of free energy. For instance. a spherical micelle of diameter 4 nm can be distorted into a prolate rnicelle 4.8 nm long and 3.6 nm wide at a cost of about 1 kT.[16] Surfactants giving rise to vesicles are also those giving rise to disk-like micelles, that is, surfactants with $1/2<P<1$. Such values of P are easily obtained with phospholipids or two-chain surfactants for which l and a_0 are nearly the same as for the corresponding one-chain surfactants, whereas v is two times larger. A disk-like micelle can be thought of as a fragment of a surfactant bilayer having its edge coated by a half of a cylindrical micelle. Disk-like-shaped micelles become rapidly energetically unfavorable as they grow in size and may turn into vesicles (or liposomes when formed from phospholipids) where the edge is eliminated. when some mechanical energy is provided to the system. Vesicles can be large (diameter of several microns) or small (diameter of 20 nm) and unilarnellar or multilamellar. An extreme case of large multilamellar vesicles

Fig. 3 Freeze-fracture TEM of the onion phase in the system tetradecyltrimethylammonium bromide-tetradecyldimethylamineoxide-hexanol, showing large multilamellar vesicles (bar=1 μm). Reproduced from Ref. [18] with permission of Academic Press.

(LMV) is encountered in the so-called onion phase, where each LMV includes tens to hundreds of concentric vesicles and where the LMVs are in contact, as seen in Fig. 3.[18] The onion phase is used in slow-release formulations of active compounds. Vesicles and liposomes are often spherical, particularly those of small size. However, faceted and tubular vesicles were reported.[19]

INTERNAL ORGANIZATION OF MICELLES AND VESICLES

It is now generally accepted that the alkyl chains forming the micellic core are in a quasi-liquid state. Three types of results support this conclusion. First, the viscosity of the core (microviscosity) is only slightly larger than that of alkanes.[20] Second, the order parameter of the alkyl-chain carbon atoms decreases from a finite value for the α-carbon atom (methylene group adjacent to the head group) to a value close to zero for the ω-carbon atom (terminal methyl group) (see Fig. 4). This variation reveals the progressively increasing disorder in alkyl-chain packing as one goes from the micelle surface to its center.[21] Last, extensive chain looping occurs in the core, thereby permitting tight packing of the chains. Any methylene group or terminal methyl group in an alkyl chain has a finite probability to be found at a given distance from the micelle center.[17] In fact, a few terminal methyl groups are present close to or at the micelle surface.

Another important feature of the micellic core is that it is practically devoid of water. Thus, the core of sodium dodecylsulfate micelles contains less than one water molecule per dodecyl chain.[17] Nevertheless, extensive contacts between alkyl chains and water still occur at the micelle surface or in the micelle palisade layer due to three features of micelles. First, surfactant head groups cover only part of the micellic surface. A typical head group covers about 0.25 nm^2, whereas the surface area available per head group at the surface of a spherical micelle may be of about 0.7 nm'. The uncovered parts constitute "fatty patches" that are in contact with water. Second, the surfactants making up a micelle have a radial motion that makes them move out of the micellic and temporarily protrude in the aqueous phase (see next paragraph). Although these surfactants may not leave the micellic, protrusion favors alkyl-chain–water contacts. Third, the penetration of water in the core, even over a relatively small length, results in the wetting of a significant fraction of the methyl and methylene groups making up the core. For instance, water penetration over a length equivalent to one carbon–carbon bond results in the wetting of 20% and 14% of the core of a spherical and a cylindrical micelle, respectively, made with a surfactant with a dodecyl chain.

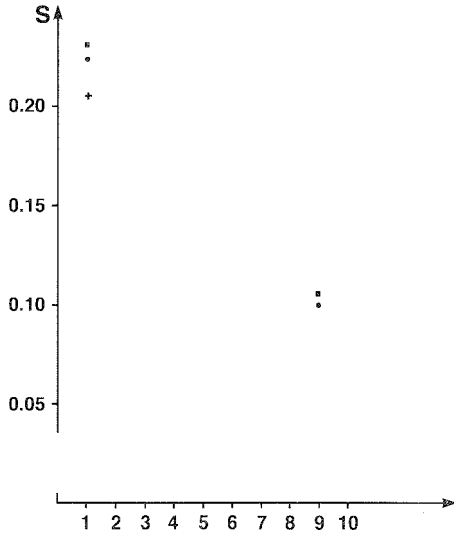

Fig. 4 Variation of the order parameter S with the position of the carbon atom on the alkyl chain of decylammonium chloride for spherical (s) and elongated (s) micelles. Reproduced from Ref. [21] with permission of the American Chemical Society.

Packing is tighter in vesicles than in micelles. It is thus likely that water penetration in vesicles is even less than that in micelles. The viscosity reported by various probes solubilized in vesicles is not significantly larger than in micelles when the measurements are performed at above the transition temperature of the system.[22] Disorder within bilayers and vesicles was evidenced.[23]

DYNAMICS OF MICELLES AND VESICLES

Micelles are not frozen objects. They are in dynamic equilibrium with the free (nonmicellized) surfactant. Surfactants are constantly exchanged between micelles and the intermicellar solution (exchange process), and the residence time of a surfactant in a micelle is finite.[24] Besides, micelles have a finite lifetime.[25] They constantly form and break up via two identified pathways: by a series of stepwise entry/exit of one surfactant A at a time into/from a micelle (Reaction 1) or by a series of fragmentation/coagulation reactions involving aggregates A_i and A_j (Reaction 2).[26]

$$A_i + A \leftrightarrow A_{i+1} \quad (1)$$

$$A_i + A_j \leftrightarrow A_{i+j} \quad (2)$$

The reaction of entry of a surfactant in a micelle is controlled for conventional surfactants with an alkyl chain containing up to 14 carbon atoms.[24,26] This means that the rate of entry is essentially determined by the number of collisions between micelles and free surfactants. The values of the entry rate constant k^+ are all around 10^9 $M^{-1}s^{-1}$, irrespective of the surfactant nature and length of its alkyl chain.[24] On the contrary, the exit rate constant k^- is an exponentially decreasing function of the alkyl chain carbon number m (hydrophobicity), as expected from theoretical considerations,[24] whereas the surfactant residence time $T_R = N/k^-$ increases exponentially with m (N = micelle aggregation number; see Fig. 5). The approximate relationship: $T_R \approx 10^{-9} N/\mathrm{CMC}$ holds for conventional surfactants. The micelle lifetime is relatively long (milliseconds and more) when micelles form and break up via reactions (1) but can become much shorter when reactions (2) dominate the kinetics.

For conventional surfactants with a long alkyl chain ($m > 16$) and dimeric (gemini) surfactants with $m > 8$, the entry of a surfactant in a micelle is slower than for a diffusion-controlled process.[26] The surfactant residence time and the micelle lifetime can become long with respect to the values found for conventional surfactants.[26]

Vesicles also exchange surfactants or phospholipids with the surrounding solution. These exchanges are much slower, probably by several orders of magnitude, than in micellar solutions. essentially because the surfactant or lipids making up vesicles are much more hydrophobic than those giving rise to micelles.[26] Besides, because the number of surfactants making up a vesicle are 10 to 1000 times larger than for a micelle, the lifetime of a vesicle must be extremely long, and vesicles can probably be considered frozen on the laboratory time scale (month to year).

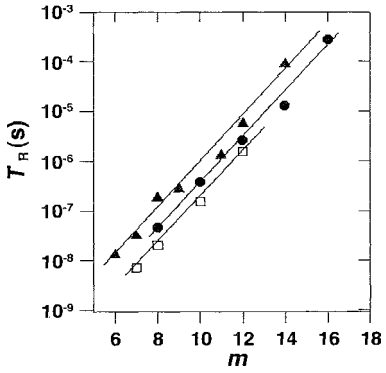

Fig. 5 Residence time T_R of surfactants in micelles. Variation with the carbon number m of the surfactant alkyl chain for sodium alkylsulfates (▲), potassium alkylcarboxylates (○) and alkylpyridinium chlorides (●). Reproduced from Ref. [26].

Many studies investigated the kinetics of the process of vesicle break up upon addition of a micelle-forming surfactant and the reverse process of vesicle formation when a system containing a micelle-forming surfactant is appropriately perturbed.[26–28] In most reports, the kinetics is complex and involves several steps. Also, the rates of the processes are dependent on the system investigated, stretching from fractions of seconds to hours or days.[26–28]

VESICLE-TO-MICELLE AND MICELLE-TO-VESICLE TRANSITIONS

In most instances, the vesicle-to-micelle transition is induced by the addition of a micelle-forming surfactant to a vesicular system.[19,31] The micelle-to-vesicle transition is often induced by mixing two oppositely charged surfactants[27,28] or removing a micelle-forming surfactant or a hydrotrope from a mixed micellar solution of this surfactant and of a vesicle-forming surfactant. The transitions can also be induced by a change of pH, temperature, or ionic strength of a micellar solution or of a vesicular system, or by shearing the system.[29]

Various studies[10,27,28] suggested the existence of structures intermediate between micelles and vesicles. These structures—perforated vesicles, bilayer fragments, giant worm-like micelles, ring-like micelles, and disk-like micelles, depending on the investigated system—were

visualized by cryo-TEM.[13,19,30] Some of these structures are shown in Fig. 6. However, some systems show no intermediate structure.[31] The course of the vesicle-to-micelle and micelle-to-vesicle transition has obviously much to do with the packing parameter of the mixture of the two surfactants and its variation with composition. In a study where the vesicle-to-micelle transition was induced by an increase of the temperature, the vesicles gave rise to giant worm-like micelles.[29] The increase of vesicle size induced by the addition of a micelle-forming surfactant to a vesicular system, at low content of surfactant, was also visualized by cryo-TEM.[19]

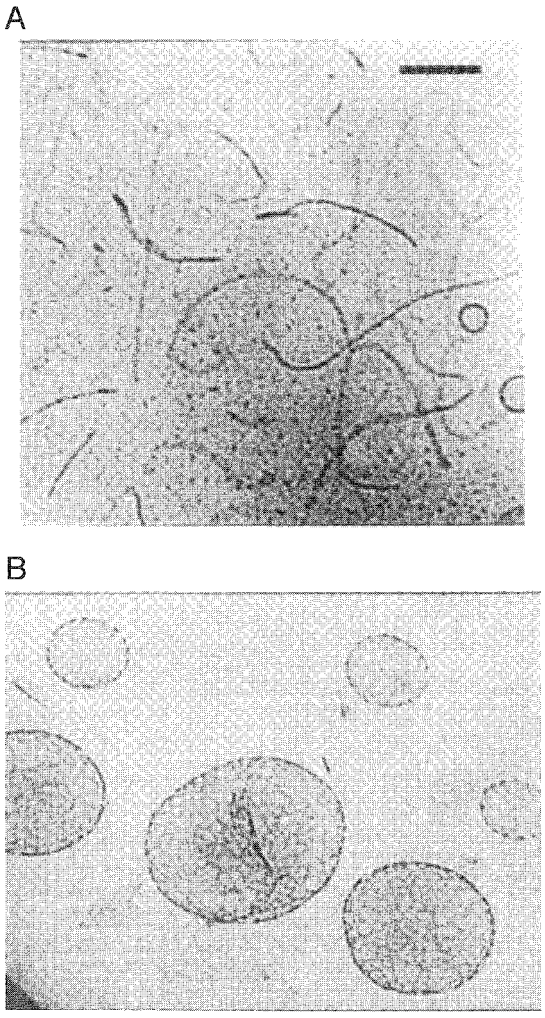

Fig. 6 Cryo-TEM micrographs show the shape of the aggregates in the course of the vesicle-to-micelle transformation in the MGO/CTAB mixture. (A) Coexistence of globular micelles. elongated micellcs that are probably ribbon-like, and vesicles (lipid mole fraction 0.47). (B) Perforated vesicles (lipid mole fraction 0.64). Reproduced from Ref. [30] with permission of the American Chemical Society.

CONCLUSION

Our knowledge of micelles is presently satisfactory thanks to a huge number of experimental studies and increasingly sophisticated methods of investigations. Molecular dynamics and Monte Carlo simulations of the self-association behavior of surfactants into micelles are becoming increasingly accurate. Hopefully, these simulations will become useful tools for predicting micellar properties of new surfactants in the coming years. The situation is still not satisfactory for vesicles on a theoretical level. The problem concerning the thermodynamic stability of vesicles is still unresolved and is the topic of much discussion in the recent literature. However, vesicles continue to be actively investigated, particularly those made from surfactant mixtures. Many of these studies aim at discovering vesicular systems that are nontoxic and have a long stability for future use in drug delivery. The onion phase (see Fig. 3) holds much promise in this respect.

ARTICLES OF FURTHER INTEREST

Drug Delivery, p. 484
Hydrophobic Effects, p. 673
Self-Assembly in *Biochemistry,* p. *1257*
Supramolecular Polymers, p. 1443

REFERENCES

1. Mukerjee, P. The nature of the association equilibria and hydrophobic bonding in aqueous solutions of association colloids. Adv. Colloid Interface Sci. **1967,** *1*, 241–275.
2. Tanford, C. *The* Hydrophobic *Effect*; Wiley: New York, 1980.
3. Lasic, D. The mechanism of vesicle formation. Biochem. J. **1988,** *256*, 1–11.
4. Kaler, E.M.: Murthy, A.K.; Rodriguez, B.E.; Zasadzinski, J.A. Spontaneous vesicle formation in aqueous mixtures of single-tailed surfactants. Science **1989**, 245, 1371–1374.
5. Chandler, D. Two faces of water. Nature 2002, *417,* 491.
6. Israelachvili. J.N.: Mitchell, D.J.; Ninham, B.W. Theory of self-assembly of hydrocarbon amphiphiles into micelles and bilayers. J. Chem. Soc., Faraday Trans. **1976.** 72. 1525–1567.
7. Nagarajan, R.; Ruckenstein, E. Theory of surfactant self-assembly: A predictive molecular thermodynamic approach. Langmuir **1991.** 7, 2934–2969.
8. Shiloah, A.; Blankschtein, D. Measurements and predictions of ionic/nonionic mixed micelle formation and growth. J. Langmuir **1998.** *14*, 7166–7182, and references therein.
9. Bruce, C.D.; Berkowitz, M.L.; Perera, L.; Forbes, M.D. Molecular dynamics simulation of sodium dodecylsulfate

micelles in water. J. Phys. Chern., B 2002. *106*. 3788–3793. and references therein.
10. Lichtenberg, D. Micelles and Liposomes. In *Biomembranes: Physical Aspects*; Shinitzky. M.. Ed.: VCH: New York. 1993; Chapter 3.
11. Safran. S.A.; Pincus, P.; Andelman. D. Theory of spontaneous vesicle formation in surfactant mixtures. Science 1990. *248*. 354–356.
12. Laughlin, R.C. Equilibrium vesicles: Fact or fiction. Colloids Surf.. A 1997. *128*, 27–38. and references therein.
13. Talmon, Y. Cryogenic Temperature Transmission Electron Microscopy in the Study of Surfactant Systems. In *Modern Characterization Methods of Surfactant Systems*; Binks. B., Ed.; M. Dekker. Inc.: New York. 1999: 147–178.
14. Bernheim-Groswasser. A.; Zana. R.; Talmon, Y. Sphere-to-cylinder transition in aqueous micellar solutions of a dimeric (gemini) surfactant. J. Phys. Chem., B 2000, *104*, 4005–4009.
15. Hyde, S.T. On the variation of microstructure within surfactant solutions. Prog. Colloid Polym. Sci. 1990, *82*, 236–242.
16. Halle. B.; Landgren, M.: Jönsson, B. The shape of ionic micelles. J. Phys. France 1988, *49*, 1235–1259.
17. Cabane. B.; Duplessix, R.; Zemb, T. High resolution neutron scattering on ionic surfactant micelles: SDS in water. J. Phys. France 1985, *46*. 2161–2178.
18. Hoffmann, H.: Munkert. U.: Thunig, C.; Valiente, M. Lyotropic mesophases in dilute surfactant mixtures of TDMAB, TTAB and hexanol: Influence of ionic charge on mesophase. J. Colloid Interface Sci. 1994, 163. 217–228.
19. Bernheim-Groswasser. A.; Zana, R.; Talmon, Y. Microstructures in aqueous solutions of mixed dimeric surfactants: Vesicle transformation into networks of thread-like micelles. J. Phys. Chern.. B 2000. *104*. 12192–12201. and references therein.
20. Turley. W.D.; Offen, H.W. Micellar microfluidities at high pressure. J. Phys. Chern. 1985, 89, 2933–2937.
21. Néry, H.; Soderman. O.; Canet, D.; Walderhaug, H.; Lindman, B. Surfactant dynamics in spherical and nonspherical micelles. A nuclear magnetic resonance study. J. Phys. Chem. 1986. *90*, 5802–5808.
22. Turley. W.D.; Offen. H.W. Lipid microviscosity of DMPC vesicles at high pressure. J. Phys. Chem. 1986, *90*, 1967–1970.
23. Czarniecki, M.; Breslow, R. Photochemical probes for model membrane structures. J. Am. Chem. Soc. 1979, *101*. 3675–3676.
24. Aniansson, E.A.G.; Wall, S.N.; Almgren. M.; Hoffmann, H.; Kielman. I.; Ulbricht, W.; Zana, R.: Lang, J.; Tondre, C. Theory of the kinetics of micellar equilibria and quantitative interpretation of chemical relaxation studies of micellar solutions of ionic surfactants. J. Phys. Chem. 1976, *80*. 905–922.
25. Aniansson, G.E.A. The mean lifetime of a micelle. Prog. Colloid Interface Sci. 1985, *70*, 2–5.
26. Zana, R. Dynamics of Micellar Systems. In Encyclopedia *of Surface and* Colloid Science; Hubbard, A., Ed.; M. Dekker, Inc.: New York. 2002: 1515–1528. and references therein.
27. Robinson, B.H.; Bucak. S.: Fontana, A. On the concept of driving force applied to micelle and vesicle self-assembly. Langmuir 2000, *16*. 8231–8237, and references therein.
28. Shioi. A.; Hatton, T.A. Model for formation and growth of vesicles in mixed anionic/cationic surfactant systems. Langmuir 2002. *18*, 7341–7348.
29. Mendes, E.; Narayanan, J.; Oda, R.; Kern. F.; Candau, S.J.; Manohar, C. Shear-induced vesicle-to-wormlike rnicelle transition. J. Phys. Chem., B 1997, *101*, 2256–2258.
30. Gustafsson. J.; Orädd, G.; Nyden, M.; Hansson, P.; Almgren, M. Defective lamellar phases and micellar polyinorphism in mixtures of glycerol monooleate and CTAB in aqueous solution. Langmuir 1998, 14. 4987–4996, and references therein.
31. Danino, D.: Talmon. Y.; Zana, R. Vesicle-to-micelle transformation in systems containing dimeric surfactants. J. Colloid Interface Sci. 1997, *185*. 84–93.

Mineralomimetic Structures

Toschitake Iwamoto
Iwaki Meisei University, Iwaki, Fukushima, Japan

INTRODUCTION

A number of natural minerals have structures comprised of infinite linkages of coordination polyhedra building up multidimensional arrays, as exemplified by chains. networks, and frameworlis in silicate minerals. Clays and zeolites are, respectively, typical two-dimensional (2D) and three-dimensional (3D) materials and give supramolecular systems with organic or inorganic guests, systems that might have played important roles in the generation of well-organized assemblies of prebiotic compounds in the earlier stages of terrestrial evolution. The linkage structure of inorganic coordination polyhedra, mainly that of cyanometallate tetrahedra, mimics the behavior of silicate or other tetrahedral moieties in natural minerals. Countercations of the cyanometallate, mainly octahedral Cd^{2+}, also mimic the behavior of octahedral moieties in minerals. The mineralomimetic crystal engineering strategy, applied to the systems of cadmium cyanide. tetracyanocadmate, polycyanopolycadmate, polycyanopolycuprate(I), secondary ligands other than the primary CN^-, and organic guest and ligand molecules gave a number of self-assembled mineralomimetic crystalline structures under ambient conditions. In comparison with the multidimensional silicate structures. appropriate guest and secondary ligands are necessary to stabilize the whole crystal structures of these mineralomimetic systems by filling the void generated owing to the longer M–CN–M' span length (ca. 5.5 Å), cornpared to Si–O–Si (ca. 3.2 Å). The term mineralomimetic was used as the counterpart of biomimetic. The term rnineralomimetic chemistry was proposed to denote the chemistry of the building-up of mineral-like structures using materials that never give stable minerals in nature. The concept extended to a new aspect of inorganic coordination chemistry developing novel compounds comprised of infinite linkages of coordination polyhedra.[1]

GENERAL CONCEPT

One of the group I4 elements silicon. placed just below C in the conventional periodic table. plays an important role in the lithosphere of the Earth's crust, just as carbon does in the biosphere. The composition of the Earth's crust may be denoted to SiO_2 to the zeroth-order approximation. The relative abundance of O is 6.47 as the exponent normalized to log(abundance of Si) = 6.00; 6.30 of O is formally spent to form SiO_2. Both Si and C share an ability to make multidimensional structures by catenation. but the mode is different (the term catenation is used to denote linking the same moiety repeatedly: not for ''catenane'' formation). Carbon makes –C–C–, –C=C–. and –C≡C– linkages in bio- and organic materials, but Si forms –Si–O–Si– in minerals. In the multidimensional silicate structures, SiO_4 tetrahedra share some portion of O atoms to extend one-dimensional (1D) chains, 2D networks, 3D frameworks. etc. Silica, SiO_2, is formed by the limiting extension of the 3D framework of SiO_4 tetrahedra in the same way as the diamond skeleton results from the succeeding replacement of H atoms of quarternary C_nH_{2n+2} by CH_3 groups. Indeed. the high-temperature-phase cristobalite (H-cristobalite), one of the polymorphs of silica, has a diamondoid structure.

The structure of cadmium cyanide $Cd(CN)_2$ is comparable to those of silica SiO_2 and ice H_2O (=OH_2) with respect to the AB_2 composition, A taking a tetrahedral position linked infinitely by B to form a 3D framework (Table 1). In addition, polycyanopolycadmate $[Cd_x(CN)_y]^{-y+2x}$ resembles polyoxopolysilicates $Si_xO_y^{-2y+4x}$ in its catenation behavior to form multidimensional infinite structures. Hence. silicate and other mineral structures are mimicked by cadmium cyanide and polycyanopolycadmates: in the latter, the tetrahedral Cd can be replaced by such tetrahedral centers as Cu(I) to extend infinite catenation structures with cyanide anions.

The skeletons of the mimicked structures are combined through coordination and covalent bonds. The accommodation of bulky guest species or ligands in the void is essential to stabilize the crystal structures in several cases. The field of mineralomimetics does not include merely copying, imitating, or reproducing natural minerals; it also excludes modifying the structures of natural minerals by using compositional materials identical or similar to those of natural minerals. A number of structures were found to have no counterparts in natural minerals but comprise unprecedented inultidimensional fraineworks made of infinite linkages of coordination polyhedra. The chemistry of coordination polyhedra linkages forms a key part of mineralomimetic chemistry.[1]

Encyclopedia of Supramolecular Chemistry
DOI: 10.1081/E-ESMC 120012805

Table I Structural similarities among ice, silica. and cadmium cyanide host

Space group	H_2O	SiO_2	$Cd(CN)_2$ host
$Fd\bar{3}m$	I_c	H-cristobalite	$[Cd(CN)_2].C(CH_3)_4$
$P4_12_12$		L-cristobalite	$[Cd(CN)_2].CHCl_2CH_2Cl$
	III. IX	heatite	
$P6_3/mmc$	I_h	H-tridymite	$[Cd(CN)_2]\cdot 0.5(n\text{-}Bu_2O\cdot H_2O)$
$C222_1$, etc.		L-tridymite	
$P6_2(6_4)22$		H-quartz	
$R3_1(3_2)21$		L-quartz	
Pm3m	Clathrate hydrate I[a]	Melanophlogite[b]	
$Fd\bar{3}m$	Clathrate hydrate II[c]		
$Pn\bar{3}m$	VII. VIII	(Cu_2O: cuprite)	Neat $Cd(CN)_2$
$P4_2/mnm$		Stishovite	$[Cd^{(o)}\{Cd(CN)_3(Him)\}_2].G$[d]

[a]General formula: $46H_2O\cdot[6X\cdot 2Y]$.
[b]General formula: $46SiO_2\cdot 8G$.
[c]General formula: $136H_2O\cdot[8X\cdot 16Y]$.
[d]Him = imidazole, G = *p*-xylene.

CADMIUM CYANIDE AND ANALOGOUS HOSTS

Cadmium cyanide has an anticuprite (cuprite: Cu_2O; space group $Pn\bar{3}m$) structure of doubly interpenetrating diamondoid frameworks. in which one framework appears to be the host of another as the guest forming a self-clathrate structure. The formal replacement of the guest framework by appropriate guest (G) molecules affords a clathrate, with a structure that is isomorphous to H-cristobalite (Fig. 1). A group of clathrate compounds was obtained with the chemical formula $[Cd(CN)_2]\cdot G$, which is the simplest formula of the clathrate compounds so far discovered.[1–5]

The thermal phase transition observed for silica was mimicked chemically by appropriately choosing the geometry of the guest molecules. Tetrahedral and pseudotetrahedral guests select the H-cristobalite-like host (space group $Fd\bar{3}m$).[2–4] However. guests that have a molecular shape considerably distorted from tetrahedral, such as $CHCl_2CH_2Cl$, $(CH_3)_2CHBr$, and $(CH_3)_2CHCN$, deform the host to an L-cristobalite-like structure ($P4_12_12$: isomorphous to the low-temperature phase of cristobalite). Aliphatic long-chain guest molecules, such as $\{CH_3\text{-}(CH_2)_3\}_2O$, are included by the H-tridymite-like host ($P6_3/mmc$: high-temperature phase of tridymite) with channel cavities.[1,2]

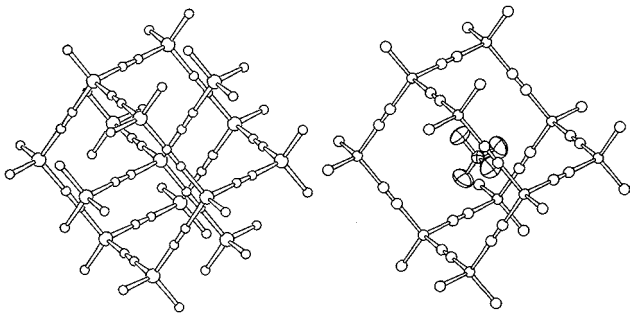

Fig. 1 Doubly interpenetrating diamondoid lattices (self-clathrate) of $Cd(CN)_2$ (left) and the clathrate structure of $[Cd(CN)_2]\cdot C(CH_3)_4$.

Mixed metal cyanide hosts. $[CdHg(CN)_4]$ and $[CdZn(CN)_4]$, are also isomorphous to H-cristobalite, but the formula unit is effectively doubled, e.g., $[CdHg(CN)_4]\cdot 2CCl_4$.[4] When one tetrahedral center is replaced by Cu(I), the host acquires a negative charge that is neutralized by an accompanying cationic guest, such as $N(CH_3)_4^+$, along with a neutral guest as observed for $[N(CH_3)_4].[CdCu(CN)_4].CCl_4$.[4] The assembly of smaller secondary ligands such as $(H_2O)_4$ plays the role of guest in $[Cd_5(CN)_{10}(H_2O)_4].4(cyclo\text{-}C_6H_{11}OH)$.[6] Four of the five Cd^{2+} are five-coordinate with an aqua ligand. four of which form a tetrahedral hydrogen-bonded $(H_2O)_4$ assembly in one of the five cavities per formula. The cyclohexanol guests in the four cavities surrounding the cavity tetrahedrally accommodating $(H_2O)_4$ extend OH groups to the tetramer to form hydrogen bonds. Such spanning of guest molecules between two cavities was also observed for the two H-cristobalite-like host clathrates $[Cd(CN)_2]\cdot 0.5(i\text{-}C_4H_9)_2O$ and $[Cd(CN)_2]\cdot 0.5(i\text{-}C_5H_{11})_2O$,[5] and others.

LINKAGE OF COORDINATION POLYHEDRA

Cadmium(II) and copper(I) are typical central atoms with tetrally coordinated cyanide groups. giving not only a discrete tetracyanometallate anion but also several kinds

of polycyanopolymetallate anions analogous to those observed for natural silicate minerals. Silicate structures are roughly *classified into neso-silicates with a discrete or isolated* SiO_4 *(orthosilicate) units: soro-silicates or coupling silicates with* a *dimeric* Si_2O_7 *(pyrosilicate) or trimeric* Si_3O_{10} *unit: ino-silicates or* chain *silicates extending a* 1D $(SiO_3)_n$ *(metasilicate) chain:* cyclo-silicates *or ring silicates with a ring unit of* $(SiO_3)_n$*; phyllo-silicates or layer silicates extending a* 2D *layer; and tecto-silicates or framework silicates extending a* 3D *framework; ionic charges were neglected. All of these structures were mimicked* in *the* (poly)cyano(poly)cadmate *structures, as shown in Fig.* 2;[7–10] *topologically, the same structures were also seen for* cyanocuprate(I).[11]

A spinel (Al_2MgO_4)-like $K_2[Cd(CN)_4]$ *contains a discrete tetracyanocadmate,* although *spinel is not a silicate.* It *appears there is not a particularly strong interaction between the N-end of* $[Cd(CN)_4]^{2-}$ *and* K^+ [N–K: 2.930(2) Å], *in contrast to the spinel* in *which no isolated* MgO_4 *units* exist.[12]

In the other linking structures, almost always the terminal *N*-ends *of* CN *groups coordinate to other octahedral centers, mainly of* Cd^{2+} (=$Cd^{(o)}$). *The way of* linking to *the* $Cd^{(o)}$ *center is* either *similar to that observed in silicate structures, for example, to* Mg^{2+}, Fe^{2+}, etc., *or different. depending on the components involved with the whole structure.*

Pyrosilicate-like $Cd_2(CN)_7$, *eclipsed and staggered forms, and trimeric* $Cd_3(CN)_{10}$ *moieties are seen as the building blocks of several host structures that were classified into clay-like layers, zeolite-like cages,* and *other* 3D frameworks.[1,3,7,10,13] The *anion of* $[P(C_6H_5)_4]_3[Cd_2(CN)_7]$ *is discrete,* taking *a staggered* form.[14] *A* tetraphenylstibinium *salt* $[Sb(C_6H_5)_4]_2$ $[Cd(CN)_3]_2$ *(there are two* crystallographically *independent chains and cations, respectively, in the unit cell) is* pyroxene($A^{II}B^{II}Si_2O_6$)–mimetic, *but the ino-silicate-like chain is* comprised *of* a *dimeric unit in a staggered form in comparison with the eclipsed form in pyroxenes.*[7,9]

A tetrameric *ring of* $[Cd(CN)_3]_4$, *like the* cyclo-silicate *ring in* tetramellite $Ba_2(Fe,Ti,Mg)_2(OH)_2(Si_4O_{12})$, *is found as the building block in the 319 host* of $[\{Cd^{(o)}(piperazine)\}_2\{Cd(CN)_3\}_4]\cdot 4C_6H_5OH$ *clathrate*[11] *and others. A* beryl($Al_2Be_3Si_6O_{18}$)–mimetic *host* $[Cd^{(o)}(Him)_2\{Cd(CN)_3\}_2]$ (Him = *imidazole) involving the hexameric ring of* $[Cd(CN)_3]_6$ accommodates *m*-xylene *as the guest in its channel cavity, similar to the water molecules of crystallization in beryl."] The trans*-bis *coordination of* Him ligands *to the* $Cd^{(o)}$ *makes it a square planar four-hand linkage builder in place of the tetrahedral Be in beryl. However, if the guest is p*-xylene *in the host of the* same *composition. the host skeleton changes its topology and coordination structure to a* rutile(TiO_2)–mimetic $[Cd^{(o)}\{Cd(CN)_3(Him)\}_2]$.[16] *The Him ligands move to the tetrahedral Cd, which mimics the* three-*coordinate* O^{2-} *in rutile. As exemplified for these structures, the structural variations are complicated and delicate in mineralomimetic structures as well as in natural minerals.*

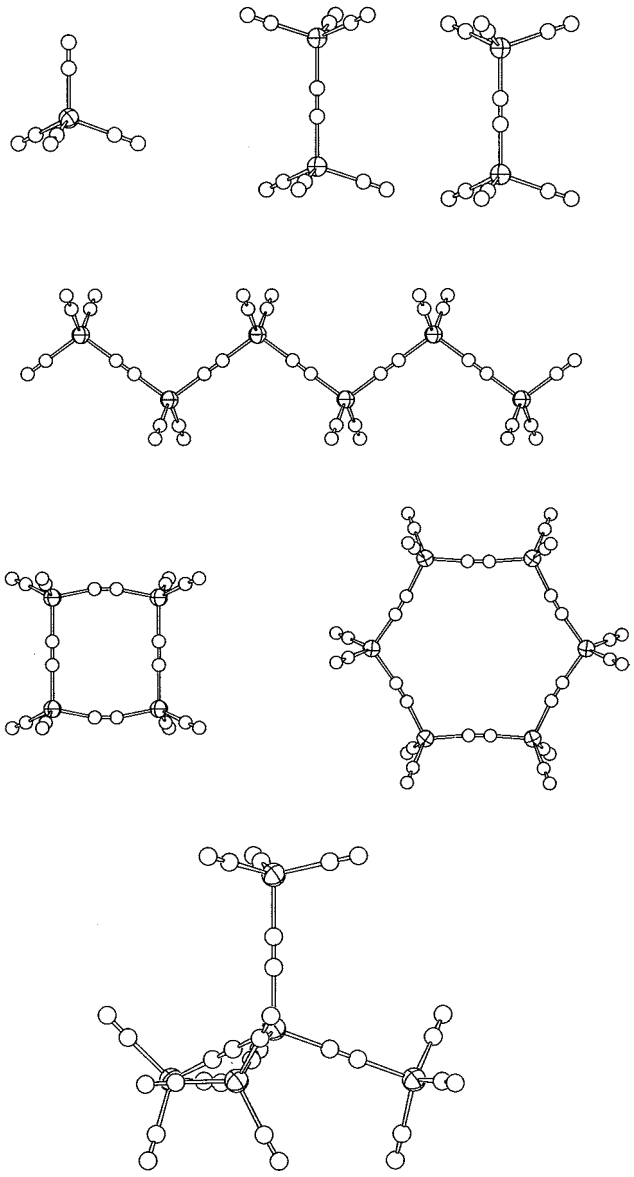

Fig. 2 Silicate–mimetic arrays of $Cd(CN)_4$ and $Cd(CN)_3$ moieties in mineralomimetic structures. From top left to bottom: discrete $Cd(CN)_4$, dimeric $Cd_2(CN)_7$ in a staggered form. dimeric $Cd_2(CN)_7$ in an eclipsed form, $[Cd(CN)_3]_n$ chains, tetrameric $[Cd(CN)_3]_4$ ring, hexameric $[Cd(CN)_3]_6$ ring, and pentameric $[Cd\{Cd(CN)_4\}_4]$ tetrahedron.[7,9]

A number *of clay-* and *zeolite–mimetic structures also show some differences from the natural ones. Layers of the clay–mimetic structures are comprised of the unit of tetrahedral* (T), *octahedral (O), and tetrahedral (T) Cd*

atoms linked successively by CN, Cd–CN–$Cd^{(o)}$–NC–Cd, similar *to the* T–O–T *unit linkage sharing oxide anion in natural clays. However, the* –CN *(or* $-OH_2$, *–OH,* –Cl) *vertices of the tetrahedra are arranged on the surface of the layer instead of the tetrahedra! faces in natural* clays.[7] *Although few natural zeolites involve octahedral coordination centers in their skeletons, the zeolite–mimetic structures are built up of the* T–O–T *units as well as the clay–mimetic* ones.[7,13] To *avoid misunderstanding, it should be noted that in zeolite chemistry,* ''T–O–T'' *is generally used to denote the connection of tetrahedral centers sharing an oxide anion. Some clay–mimetic structures have intralayer cavities. that is, the layer itself generates a void to* accommodate *guest species as a layer zeolite.*

MISCELLANEOUS

The Mofmann-Td-type host (see Hofmann-Type Clathrate) $[Cd(NH_3)_2M'(CN)_4]$ (M'=Cd, Hg) *has a skeleton topologically the* same *as that of cooperite* (PtS), *for which the square planar Pt is mimicked by trans-*$[Cd(NH_3)_2]$ *and the tetrahedral* S *by* $[Cd(CN)_4]$.

The solid acid with apparently a curious cornposition $3HCN \cdot Cd(CN)_2 \cdot 2CuCN \cdot 14H_2O$ *should be* formulated *as* $[H_3(H_2O)_{14}] \cdot [Cd^{(o)}\{Cu_2(CN)_7\}]$ *according to its cubic crystal structure isostructural to pyrite* (FeS_2) *with the same space group* $Pa\bar{3}$.[11] *The dimeric anion* $Cu_2(CN)_7$ *in a staggered form mimics the* S_2 *moiety in pyrite. Three terminal CN groups are linked to three different* $Cd^{(o)}$ *corresponding to Fe in pyrite, respectively. The octahedral coordination of the* $Cd^{(o)}$ *is accomplished by six N-terminals* from *six different* dimeric *anions. Fourteen* H_2O *molecules, three of which should be protonated, extend a 3D hydrogen-bonded framework with a topology the* same *as that of rutile* (TiO_2). *A crown ring of the 12* H_2O *molecules encircles the* –Cu–(CN)–Cu– *axis of the dimeric* $Cu_2(CN)_7$ *to form a rotaxane structure. Six* H_2O molecules *in the dodecameric ring are connected to another kind of six* H_2O *molecules, respectively, which extend the hydrogen bond to three different rings of the dodecamer. The ring mimics* Ti, *and the three-hand* H_2O mimics O *in the rutile structure.*

Finally, an experimental problem should be noted for the discrimination of C *and* N atoms *in x-ray crystallography. The* C *and* N *in ordered structures are clearly discriminated through the processes of structure refinement when the applied space group is appropriate. In some cases, inappropriate space groups are selected by assuming* that *discrimination is possible without any supporting evidence;* the *systematic absences of reflections should be carefully checked. In general, the* CN *group coordinates to a tetrahedral center at* C *and an octahedral center at* N *in the link. The CN* link *between a couple of tetrahedral centers* is *usually disordered. Solid-state NMR of the coordination center nucleus,* e.g., ^{113}Cd,[6] *is* useful *to judge whether the disorder is real or apparent due to the space group applied—a determination which is often ruled by the arrangement of heavy metal coordination centers.*

CONCLUSION

Precise molecular chemistry has developed based on the structures of Avogadro molecules, which are discrete chemical species comprised of definite numbers, as small as H_2 *or as large as DNA, of atoms belonging to distinct elements regardless of electronic charge. Biomimetic chemistry is essentially the chemistry of Avogadro molecule. albeit some with polymeric structure. On the other hand, many inorganic solid materials are substantially* nonstoichiometric *with an infinite range of structures. A relatively simple chemical composition of a species never necessarily means that the species has a simple and unique structure of Avogadro molecules, as exemplified by* C_2H_6O. *The inorganic chemistry of a* non-*Avogadro molecule, paid less attention to in comparison with that of an Avogadro molecule, has yet been less explored as precise structural chemistry.* Mineralomimetic *chemistry is a spike struck artificially into the lithosphere, apparently with a hoary look, in order to reveal another harmony of nature. For more details, refer to a few comprehensive works in the* literature.[1,8–10]

ARTICLES OF FURTHER INTEREST

Chemical Topology, p. 229
Concepts in Crystal Engineering, p. 319
Crystalline Microporous Silicas, p. 380
Hofmann-Type Clathrates, p. 645
Interpenetration, p. 735
Isostructurality of Inclusion Compounds, p. 767
Mesoporous Materials, p. 845
Mesoporous Silica and Silica–Organic Hybrids, p. 852
Organic Zeolites. p. 996
Supramolecular Isomerism, p. 1420
Zeolites: Structures and Inclusion Properties, p. 1623

REFERENCES

1. Iwamoto, T.; Nishikiori. S.; Kitazawa. T.: Yuge, H. Mineralomimetic chemistry as a modern aspect of coordination chemistry. J. Chem. Soc., Dalton Trans. 1997, 4127–4136.
2. Kitazawa, T.; Nishikiori, S.: Kuroda. R.; Iwamoto. T.

Novel clathrate compound of cadmium cyanide host with an adamantane-like cavity. Cadmium cyanide–carbon tetrachloride(1/1). Chem. Lett. 1988, 1729–1732.
3. Kitazawa, T.; Nishikiori, S.; Yamagishi, A.; Kuroda, R.; Iwamoto. T. Tetrahedral guest in a tetrahedral cavity: A neopentane molecule encaged in a three-dimensional cadmium cyanide framework. J. Chem. Soc., Chem. Commun. 1992. 413–415.
4. Kitazawa. T.: Nishikiori. S.; Kuroda. R.: Iwamoto. T. Clathrate compounds of cadmium cyanide and related hosts with cristobalite-like lattice structures. J. Chem. Soc., Dalton Trans. 1994. 1029–1036.
5. Kitazawa. T.: Kikuyama. T.; Takeda. M.; Iwamoto, T. Silica–mimetic polymorphism of the $Cd(CN)_2$ host lattice depending on the guest G in $Cd(CN)_2 \cdot x$G clathrates. J. Chem. Soc., Dalton Trans. 1995. 3715–3720.
6. Nishikiori, S.; Ratcliffe. C.I.; Ripmeester. J.A. Crystal structure of $Cd_5(CN)_{10}(H_2O)_4 \cdot 4C_6H_{11}OH$ studied by x-ray diffraction and solid-state ^{113}Cd NMR. A new type of cristobalite-like framework host with a site interaction with cyclohexanol by hydrogen bonding. J. Am. Chem. Soc. 1992. *114*. 8590–8595.
7. Kitazawa. T.: Nishikiori. S.; Kuroda. R.: Iwamoto. T. Two novel metal-complex host structures consisting of cyanocadmate coordination polyhedra. Clay-like and zeolite-like structures. Chem. Lett. 1988. 459–462.
8. Iwamoto. T. Inclusion Compounds of Multi-dimensional Cyanometal Complex Hosts. In *Inclusion Compounds, 5;* Atwood, J.L., Davies, J.E.D., MacNicol, D.D., Eds.; Oxford University Press: Oxford. 1991: 177–212.
9. Iwamoto. T. Past, present and future of the clathrate and inclusion compounds built of cyanometallate hosts. J. Incl. Phenom. Mol. Recognit. Chem. 1996, *24*. 61–132.
10. Iwamoto. T. Supramolecular Chemistry in Cyanometallate Systems. In *Comprehensive Supramolecular Chemistry, 6, Solid-State Supramolecular Chemistry: Crystal Engineering;* MacNicol. D.D.. Toda. F.. Bishop, R.. Eds.: Pergamon, 1996: 643–690.
11. Nishikiori. S.: Iwamoto, T. Ring of 12 hydrogen-bonded water molecules in a pyrite-like framework of heptacyanodicuprato(I)cadmate(II) $[CdCu_2(CN)_7]^{3-}$. J. Chem. Soc., Chem. Commun. 1993, 1555–1556.
12. Ziegler, B.: Babel, D. Die Kristallstruktur des Cyanospinells $K_2Cd(CN)_4$. Z. Naturforsch. 1991. *46b*, 47–49.
13. Kitazawa. T.: Nishikiori. S.; Iwamoto, T. Three-dimensional framework structures built of heptacyanotricadmate(II) units providing polyhedral cavities for guests: Classification of the zeolite-like structures. J. Chem. Soc., Dalton Trans. 1994. 3695–3710.
14. Kitazawa. T.: Takeda. M. Synthesis and structural characterization of a new mineralomimetic ion, $[Cd_2(CN)_7]^{3-}$. J. Chem. Soc., Chern. Commun. 1993. 309–310.
15. Kitazawa, T.: Akiyama. M.; Takahashi, M.; Takeda, M. $Cd(CN)_3^-$: A novel mineralomimetic infinite chain-like polycyanopolycadmate anion. J. Chem. Soc., Chem. Commun. 1993. 1112–1113.
16. Kim, C.-H.; Iwamoto. T. Crystal structure and rutile–mimetic framework in cyanocadmate chlathrate $[Cd\{Cd(CN)_3(imH)\}_2] \cdot p\text{-}C_6H_4Me_2$ involving unidentate imidazole ($imH = C_3H_4N_2$) ligand. Bull. Korean Chem. Soc. 199'7, *18*, 791–793.
17. Kitazawa. T.: Kikuyama, T.: Takahashi, M.: Takeda. M. Cadmium cyanide–ether- clathrates: Crystal structures of $Cd_8(CN)_{16}(H_2O)_6 \cdot 6G$ ($G = Et_2O$ or Pr^i_2O) and $Cd_3(CN)_6(H_2O)_2 \cdot 2Pr^n_2O$. J. Chem. Soc., Dalton Trans. 1994, 2933–2937.

Modulated Structures

Gervais Chapuis
University of Lausanne, Lausanne, Switzerland

INTRODUCTION

The three-dimensional periodic arrangement of atoms or molecules was believed to be one of the most fundamental and indisputable aspects of crystalline architectures. The direct consequences of this periodicity were manifold. Perhaps the most important was that any crystal face could be uniquely characterized, i.e., indexed by three integers, the so-called Miller indices. Prior to the discovery of x-ray diffraction, many generations of mineralogists dedicated a large amount of effort to identify the Miller indices of all possible crystalline faces occurring in nature. Later, the discovery of x-rays was instrumental in providing a clear picture of the three-dimensional arrangements of individual atoms in condensed matter. It was soon discovered that any crystal, placed in an incident x-ray beam, deviates the intensities and redirects them in selected directions covering all the space. Here again, it appeared that each diffracted beam could be uniquely characterized by three integers, the Bragg indices.

At this point, it seems natural to associate each integer index of a crystalline face or a diffracted beam with one dimension of space. In other words, the periodic arrangement of the atoms along the three independent space dimensions explains the property that each face or diffracted intensity can be characterized by three integers.

The paradigm of the three-dimensional (3D) periodic arrangement of atoms was so anchored in the minds of scientists that most ignored some obvious signs pointing to a deviation from this model. Already in the 1930s, Goldschmidt, Palache, and Peacock,[1] following a careful study of more than 100 crystalline samples from different origins, concluded that Calaverite, a mineral of composition $Au_{1-p}Ag_pTe_2$ ($p < 0.15$) did not follow the rule stating that each face could be indexed with three Miller indices. The solution of this troublesome finding had to wait until the late 1980s, when Janner and Dam[2] published their interpretation of the Calaverite crystal form. These authors succeeded in completely reindexing all of the faces, providing the use of four integers to characterize each.

Another interesting phenomenon was discovered in the 1960s by Brouns, Visser, and De Wolff,[3] who studied the room-temperature phase of sodium carbonate. After many efforts, they were unsuccessful in indexing the lines of the powder diagram according to the admitted procedure, i.e., by assigning three integers only. However, they succeeded in completely indexing the diffraction pattern of a single crystal provided the use of four integers. From this period on, other examples of crystal structures requiring more than three indices were discovered, which culminated in 1984 in the discovery of quasicrystals by Shechtman and coworkers.[4] In this material, the full diffraction pattern could only be indexed provided the use of six integers.

In analogy with the rule that we introduced before, can we postulate that (some) crystals are periodic objects in dimensions higher than three? We will show in this article that this is the case and how we can reinterpret a crystal structure in the 3D space in which we live.

DESCRIPTION OF CRYSTALS IN SUPERSPACE

The most direct approach to study any crystalline structure is to place the crystal in an incident x-ray beam and to observe its diffraction pattern following a rotation or any other type of displacement of the sample in the beam. In the introduction, we saw that for a classical crystal, each possible diffracted intensity $I(\boldsymbol{h})$ can be associated with three integers (h_1, h_2, h_3) forming a vector $\mathbf{h} = h_1\mathbf{a_1}^* + h_2\mathbf{a_2}^* + h_3\mathbf{a_3}^*$, a so-called reciprocal vector. The reciprocal basis vectors $\mathbf{a_1}^*$, $\mathbf{a_2}^*$, $\mathbf{a_3}^*$ are linked to the basis vector $\mathbf{a_1}$, $\mathbf{a_2}$, and $\mathbf{a_3}$, forming the unit cell of the periodic structure in three dimensions by the scalar product relation $\mathbf{a_i}\,\mathbf{a_j}^* = \delta_{ij}$, i.e., = 1 if $i = j$ and = 0 if $i \neq j$.

Let us suppose now that the number of integers required to fully index the diffraction pattern is larger than three. We can, of course increase the number of reciprocal basis vectors and form a new vector $\mathbf{H} = \mathbf{h} + h_4\mathbf{q_1} + \ldots$. In this context and without losing generality, we will limit the total number of integer needed to characterize the pattern to four. The vector $\mathbf{q_1}$ becomes $\mathbf{q}$ and is subject to the following restriction $\mathbf{q} = q_1\mathbf{a_1}^* + q_2\mathbf{a_2}^* + q_3\mathbf{a_3}^*$, where at least one of the q_i is irrational. If this condition is not imposed, it would be possible to select another set of bases so that the three-dimensional vector $\mathbf{h}$ could index all the possible reflections. Revealed in Fig. 1 is the way the vector $\mathbf{q}$ and hence $\mathbf{H}$ are reinterpreted in a four-dimensional (4D) space. In this figure, the subscript S refers to

Encyclopedia of Supramolecular Chemistry
DOI: 10.1081/E-ESMC 120019158

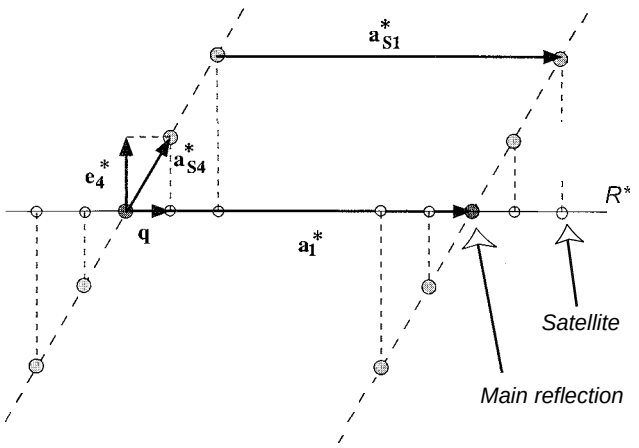

Fig. 1 Four-dimensional extension of the reciprocal space.

the higher dimensional space, i.e., the superspace. The reciprocal vectors $\mathbf{a_{S1}}^*$ to $\mathbf{a_{S3}}^*$ are identical to $\mathbf{a_1}^*$ to $\mathbf{a_3}^*$, respectively. whereas vector $\mathbf{a_{S4}}^*$ includes two parts and is equal to $\mathbf{q} + \mathbf{e_4}^*$. In this 4D example, we classify a reflection as a main reflection if its coefficient h_4 is 0. Otherwise, it is called a satellite reflection. In this model, the observed diffraction pattern (line R^* in Fig. 1) is interpreted as a 3D projection of the superspace.

Now that we learned how to extend the dimension of the reciprocal space, it is legitimate to ask the following: What is the direct space description of a crystal that corresponds to the extension of the reciprocal space? Illustrated in Fig. 2 is the concept of embedding a crystal structure in a space of higher dimension.[''] The basic principle behind this embedding is that the 3D crystal observed in the world in which we live, is a 3D cut out of a higher-dimensional periodic arrangement called superspace. In Fig. 2, a_{S1} and a_{S4} refer to the lattice parameters in superspace. Atoms are characterized by atomic modulation functions that repeat periodically in all dimensions. In this particular 4D case, each atom is represented by a string. In five-or six-dimensional superspace, atoms are represented by surfaces and volumes, respectively. In our figure, the line indicated by R represents the 3D space in which the atoms are located (A, B, and C in this example). In general, this cut is not periodic (AB $\neq$ BC), and in this case. the resulting structure is aperiodic. From Fig. *2*, we can also see that the atoms are displaced along the modulation function relative to an average position (vertical dotted line in the figure). If this is the case, the structure is called modulated. If at least one of the components q_i is irrational, the structure is incommensurately modulated, whereas in the other cases, the structure is commensurately modulated.

With this model in hand, the challenge of the diffraction specialist is to fully characterize the structure, in other words, determine the shape of the modulation curve on the basis of the experimental observations. For classical periodic crystals, the determination of the periodic crystalline structure consists, in a first step, of locating each atomic position in the unit cell, i.e., the unit volume repeated periodically in the three spatial dimensions and determined by the three basis vectors. The diffracted intensities of a crystal structure are related to the atomic positions by the structure factor expression. For aperiodic crystals, the structure factor $F_{\mathbf{H}}$ includes a term describing the modulation and is given by the following relation:

$$F_{\mathrm{H}} = \sum_{\mu} f_{\mathrm{H}}^{\mu} \exp(2\pi i \mathbf{H} \cdot \mathbf{r}^{\mu}) \times \int_0^1 \mathrm{d}t \; p^{\mu}(t) \exp\{2\pi i(\mathbf{H} \cdot \mathbf{u}^{\mu}(t) + h_4 t)\}$$

The summation is over all the μ atoms in the unit cell with atomic scattering factor $f^{\mu}_{\mathbf{H}}$. The modulation $\mathbf{u}^{\mu}$ describes the individual atomic displacement relative to its basic position $\mathbf{r}^{\mu}$. The integration variable t is related to the fourth dimension by the expression $x_4 = \mathbf{q} \cdot \mathrm{r} + t$ (see Fig. *2)*. The first line of this expression corresponds to the structure factor of a conventional crystal (h_4 is equal to zero, and thus $\mathbf{H} = \mathbf{h}$). The second line of the expression is specific to aperiodic structures and contains the information related to the atomic modulation function in superspace. In addition to a displacement parameter, the modulation can also be affected by a variable occupation parameter p^{μ}.

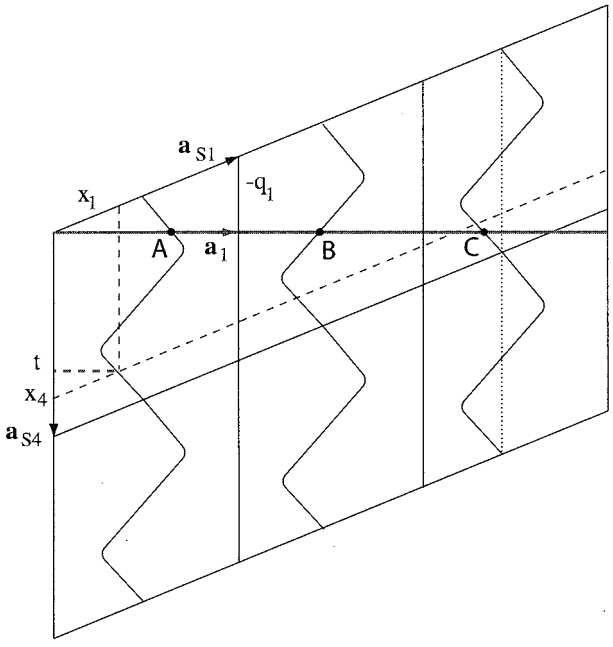

Fig. 2 Four-dimensional extension of a crystal in direct space. *(View this art in color at www.dekker.com.)*

EXAMPLE OF AN INCOMMENSURATELY MODULATED ORGANIC STRUCTURE

In order to illustrate the principles of superspace extension, we will present one example of an organic aperiodic structure that was recently studied. Quininium (*R*)-mandelate, $C_{20}H_{25}N_2O_2^+ . C_8H_7O_3^-$, (Fig. 3) is an organic salt that exhibits a complex x-ray diffraction pattern schematically illustrated in Fig. 4.[6] All the satellites can be uniquely associated to main reflections with the modulation vector q. Without entering into the details of the structure solution, we will describe in this context only some specific stereochemical features of the resulting aperiodic structure determination.

Shown in Fig. 5 is a selection of electron-density maps related to N13 and C10, with the vertical axis representing the x_4 coordinate. We observe that the modulation function is specific for each atom. For N13, the atomic modulation function is continuous along the x_4 axis with extrema lying approximately 1.8 Å apart in the b direction. This deviation indicates that the departure from the average structure is particularly important throughout the crystal structure. The modulation of C10 describes another aspect of the diversity of aperiodic structures. In the crystal, this atom exhibits two stable positions a and b which are best represented in superspace by slightly modulated crenel functions. Thus, the domain of existence of C10a and C10b is colnplementary and mutually exclusive.

Once the refinement of the structure in superspace converged to a satisfactory solution, the nonperiodic structure can be obtained from the appropriate 3D cut. Illustrated in Fig. 6 are some of the features deduced from the structure solution. As an example, the orientation of the quinoline double ring varies continuously in space. This is not the case for the vinyl part that exhibits essentially two different orientations if we neglect the wavy modulation.

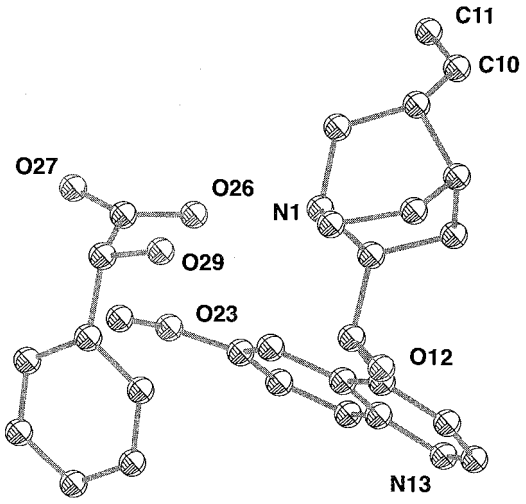

Fig. **3** Quininium (*R*)-mandelate with oxygen atoms (red, indicated with ''O'') and nitrogen atoms (magenta, indicated with ''N''). Mandelic acid is the entity containing 026 and 027. (View *this* art in color at *www.dekker.com.*)

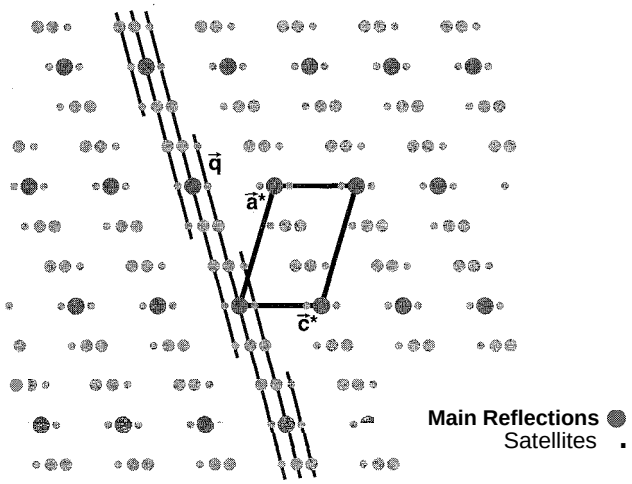

Fig. 4 A reciprocal layer of quininium (R)-mandelate. (*View* this art *in* color at *www.dekker.com.*)

What are the essential features of the refined modulated structure? Most of the effect of the modulation is observed in the H-bond network. The most significant change concerns the alternate intermolecular bonds O29–H···N13 and 029–H..·027. These bonds are mutually exclusive and are equally distributed in space. Obviously, the displacement of the quinoline illustrated above is directly linked to the H-bond formation with N13. The modulation with the shape of a crenel function is associated to a weak H-bond C11–H···O23. The two H atoms bonded to C11 of the vinyl group form alternatively a link to 023. which explains the two conformations observed in Fig. 6.

We should stress at this point that the existence of pairs of possible H–bonds should not be assimilated with any type of disorder. The sharp peaks observed in the diffraction pattern indicate long-range ordering, which means that the distribution in space of one or the other bond satisfies strict rules.

SIMULATION OF MODULATED STRUCTURES

The origin of the modulations is mostly due to competing interactions at the atomic level. The crystal attempts to resolve this frustration by favoring, alternatively. each type of interaction. The periodicity of the alternating interactions is, in general, independent of the 3D periodicity

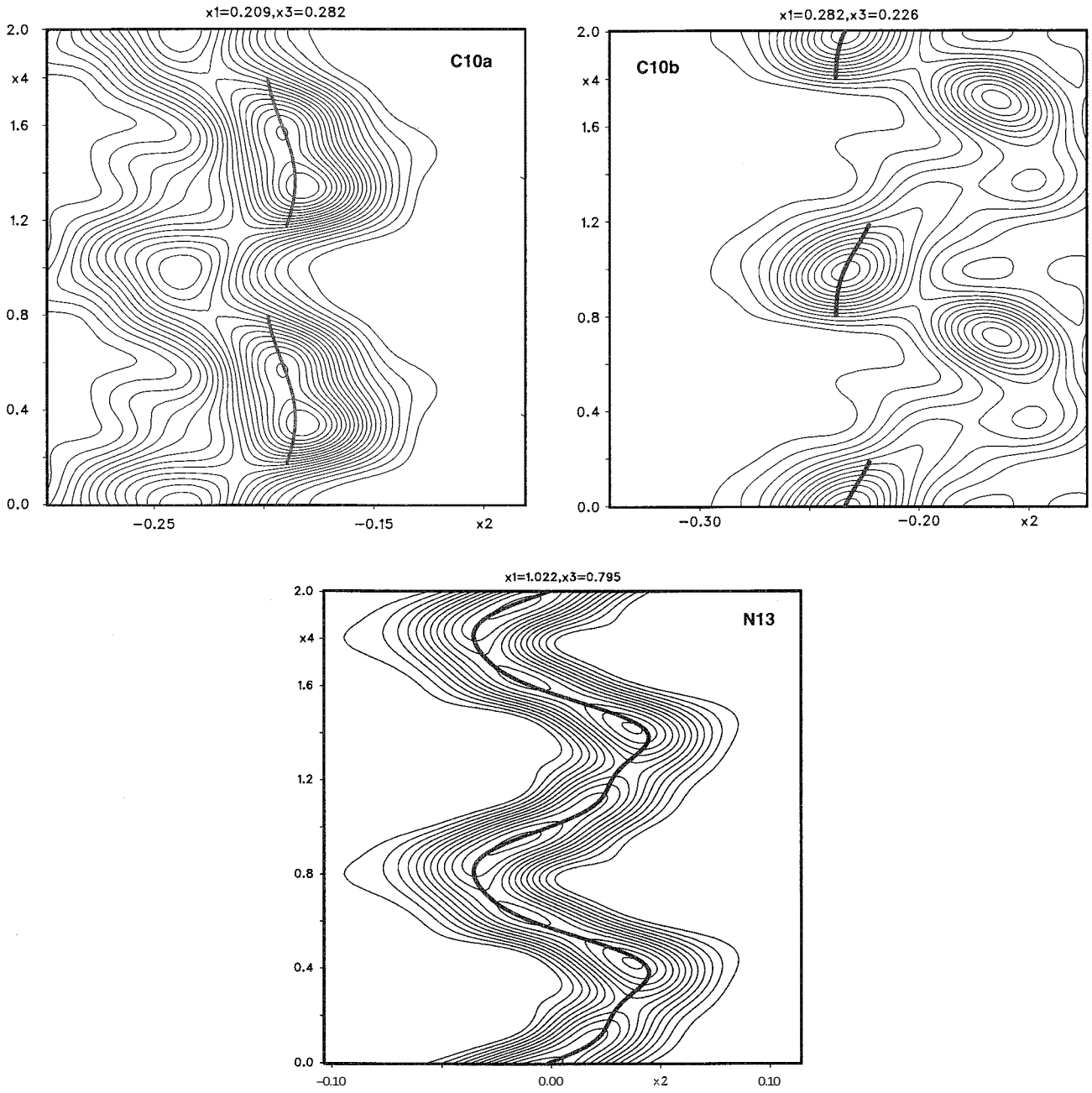

Fig. 5 Electron density of atoms C10 and N13 in the (x_2, x_4) plane. (See Fig. 3). (*View this art in color at www.dekker.com.*)

of the structure and. therefore, is incommensurately modulated. It often varies with pressure or temperature.

In this context, we propose to illustrate the formation of modulated structures by molecular dynamical simulation. As an example, we will consider a molecular crystal structure under various temperature conditions. As nonbonded pair potentials. we apply the Lennard–Jones (LJ) 9–6 potential and the Coulombic potential. Bonded potentials include terms to describe bond stretching. bond angle bending, torsional rotations, and out-of-plane deformations. All potential parameters are taken from a second-generation force field. the consistent force field (CFF91).[7] This force field is commonly used to maintain proper intramolecular geometry coupled with van der Waals and electrostatic interactions between atoms. It was used to successfully predict lattice parameters, root-mean-square (rms) atomic coordinates, and sublimation energies for crystals.

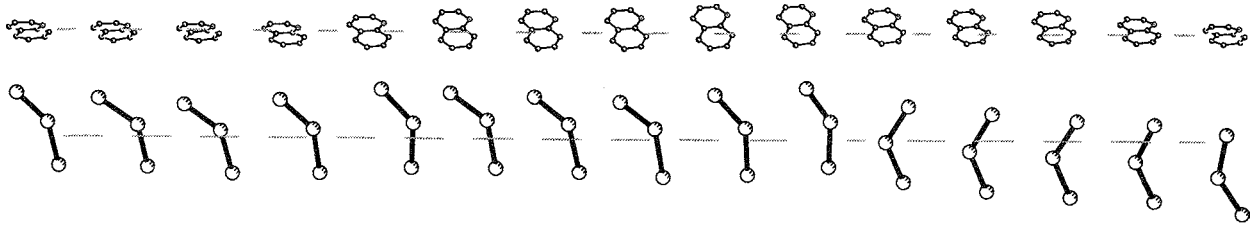

Fig. 6 Sequence ot identical elements of the structure along a particular direction Examples of the orientation variation of the quinoline and the vinyl parts

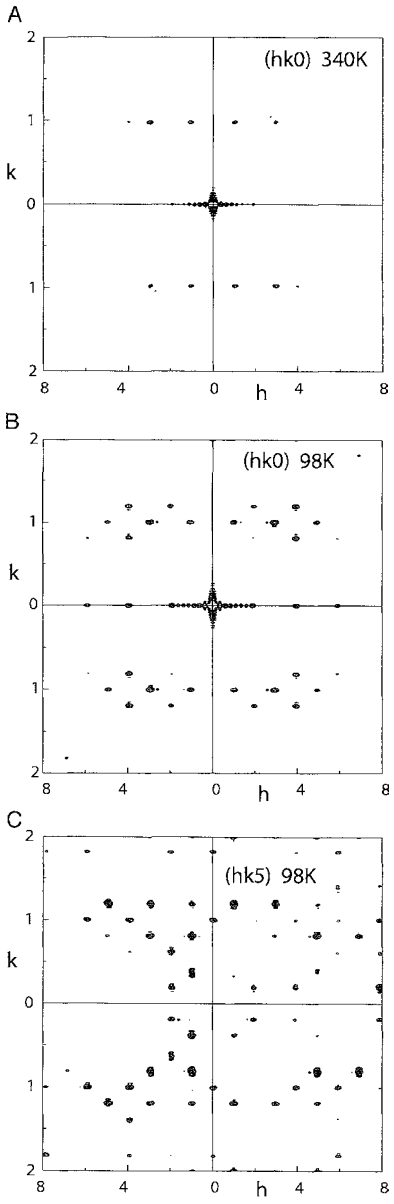

Big. 7 Simulated diffraction patterns of the high-(340 K) and low-temperature phases (98 K) of DCPS resulting from the MD calculations.

The organic compound 4.4'-dichlorodiphenyl sulfone (DCPS) presents an incommensurate structure below 150 K. The structure is periodic above this temperature.[8] The MD simulation starts with an equilibrated system that was first optimized under NVT conditions (constant number of atoms, volume, and temperature) from x-ray data at 90 K. In order to compensate for the imperfections of the CFF and match the MD results with the experimental lattice parameters. a pressure tensor is introduced in the calculation. The evolution of the temperature dependence of the system is obtained by NPT conditions (constant pressure). The results of the simulation are best illustrated by simulating the diffraction pattern of the structures at specific temperatures. Illustrated in Fig. 7 are the phases of DCPS above and below the phase transition. At 340 K, the diffractogram indicates that the structure is periodic. Moreover. it also indicates systematic absences pointing to the presence of specific symmetry characteristics in the crystal. The 98 K diffractograms reveal the presence of satellite reflections, indicating the existence of a modulated structure from which the modulation vector q can be deduced. Note that in this structure, its nonperiodicity requires the use of a single-unit cell containing more than 100.000 atoms, the magnitude of which is only limited by the capacity of the high-performance computer.

Hence, the method of MD simulations is able to reproduce the characteristic modulations that occur in DCPS under specific temperature conditions. The modulation vector obtained by MD exceeds only slightly the experimental value measured by x-ray diffraction. This method was also successfully applied to other organic crystals results,'" reinforcing the results obtained by diffraction and confirming them by an independent method.

CONCLUSION

Modulated crystal structures are by no means a rarity. Since the Calaverite mineral. many other examples of modulated structures and more generally aperiodic crystals were and continue to be discovered. They occur in all types of

crystalline structures, from metals to alloys, from minerals to organic materials, covering the full range of crystalline structures. They often occur in pressure-or temperature-induced phase transitions with variable ranges of stability. As mentioned above, these phases should not be considered as disordered material as was often the case in the past. The discrete nature of their diffractograms, i.e., the presence of sharp peaks is a direct proof of the long-range ordering of the atoms in the crystal. Of course, disorder can occur as well in aperiodic as in periodic structures.

The structural study of aperiodic material is a field that is still evolving. Their detailed study at the atomic level will possibly deliver the origin of the mechanism leading to aperiodicity rather than periodicity. We can also expect to use the structural properties of incoinmensurabilities as a probe to improve our knowledge of the chemical and physical aspects of atomic interactions. In addition, we can also expect to discover and take advantage of some specific properties associated with the aperiodicities of crystalline material. A series of studies on the NMR and NQR properties of incommensurate crystals already revealed some specific characteristics[10] of these systems.

At this point, one may wonder why the studies on modulated structures only recently acquired some momentum. One obvious answer lies in the availability of the tools required to perform these studies. The discovery of the 3D space groups that are fundamental for the symmetry description of crystalline material preceded by a quarter of a century the discovery of x-ray diffraction by crystals. Shortly after, a selected number of crystal structures were described for the first time by W.H. and W.L. Bragg. For aperiodic crystals and, in particular, modulated ones, all the tools and methodologies necessary to study chis new type of materials had to be developed before further progress could be made. The development of the mathematical theory of superspace was instrumental for further success. After more than three decades of development, the availability of good performing tools is just starting to appear and explains the relatively belated development of this speciality.

ACKNOWLEDGMENTS

The contributions of Drs. Yuansheng Pan and Andreas Schonleber are gratefully acknowledged.

ARTICLES OF FURTHER INTEREST

The Cambridge Structural Database, p. 161
Crystal Structure Prediction, p. 371
Disorder and Diffuse Scattering, p. 457
Hydrogen Bonding, p. 658
Incommensurate and Commensurate Structures, p. 712
Modulated Structures, p. 873
Molecular Modeling and Related Computational Techniques, p. 901
Solid State Nuclear Magnetic Resonance Spectroscopy, p. 1307
Weak Hydrogen Bonds, p. 1576
X-Ray Crystallography, p. 1586

REFERENCES

1. Goldschmidt. V.; Palache, Ch.: Peacock, M. Ueber calaverit. Neues Jahrb. Mineral. 1931. 63, 1–58.
2. Janner, A.; Dam. B. The morphology of calaverite ($AuTe_2$) from data of 1931—Solution of an old problem of rational indexes. Acta Cryst., A 1989. *45,* 115–123.
3. Brouns, E.: Visser, J.W. An anomaly in the crystal structure of Na_2CO_3. Acta Cryst. 1964, 17. 614.
4. Shechtman. D.; Blech. I.; Gratias, D.; Cahn, J.W. Metallic phase with long-range orientational order and no translational symmetry. Phys. Rev. Lett. 1984, *53* (20), 1951–1953.
5. De Wolff, P.M. Pseudo-symmetry of modulated crystal-structures. Acta Cryst., A 1944. *30.* 777–785.
6. Schonleber, A.; Chapuis, G. The superspace description of the incommensurately modulated structure of quininium (R)-mandelate. Ferroelectrics 2001, *250* (1-4), 91–94.
7. Hwang, M.J.: Stockfisch, T.P.; Hagler, A.T. Derivation of class-II force-fields. 2. Derivation and characterization of a Class-I1 force-field. Cff93, for the alkyl functional-group and alkane molecules. JACS 1994, 116 (6). 2515–2525.
8. Kasano. H.; Koshiba, T.; Kasatani, H.; Terauchi, H. Incommensurate phase-transition in 4,4′-dichlorodiphenyl sulfone. J. Phys. Soc. Jpn. 1990, *59* (2), 408–411.
9. Pan, Y.S.; Chapuis, G.; Mechanism of the incommensurate phase in hexamethylene- tetramine suberate: A molecular-dynamics study. Phys. Rev., B 2002. 65 (18). art. no.-184205.
10. Blinc. R. Magnetic-resonance and relaxation in structurally incommensurate systems. Phys. Rep. -Rev. Sect. Phys. Lett. 1981, 79 (5). 331–398.

Molecular Biomimetics

Philip **Ball**
Nature, London, United Kingdom

INTRODUCTION

The idea of nature as engineer is an old one. but only recently have its engineering principles begun to be uncovered at the molecular and supramolecular scales. The cell is now imagined as a production plant in which molecular machinery works in precise orchestration to generate complex products from raw materials. This mechanism is self-assembling, self-repairing, and self-replicating. Meanwhile, advances in microfabrication have made us accustomed to the idea that engineering can be conducted at microscopic scales while employing principles familiar from the macroscopic world.

Reviewed in this article are some of the consequences of this convergence in scale and perspective of biology and engineering. Many of nature's principles and practices at the molecular and nanometer scales can be adapted for developing synthetic chemical and materials systems sharing the kind of superior properties and special functions that natural systems exhibit.

NANOSCALE MECHANISMS

Catalysis

With thousands of enzyme structures now solved and the number growing daily, Emil Fischer's "lock and key" mechanism of enzyme action is embroidered with ever more elegant detail. Fischer's idea. that the enzyme has a cleft at the active site within which its substrate makes a good geometrical fit, is basically sound but in need of refinement in some important ways. At least as important as the considerations of a good geometric fit is the nature of the microenvironment inside the binding cavity. Carboxylic acid groups that will be wholly ineffective at hydrolyzing polysaccharides in aqueous solution are adequate for the job within the active site of lysozyme. because they are not solvated and screened as they are in water. Thus, the active site can provide an effectively different (often hydrophobic) solvating medium that profoundly alters the reactivity of its functional groups relative to their behavior in aqueous solution. In the same way, the internal space of the microporous aluminosilicate zeolites is superacidic—hydroxy groups attached to the silicate framework will protonate alkanes—even while zeolites can be handled safely.

One aim of supramolecular chemistry is to devise molecules that bind substrates according to exacting geometric requirements, through the precise placement of interacting groups. For example, water-soluble cyclodextrins possess hydrophobic cavities reminiscent of enzyme-binding pockets, within which small hydrophobic molecules can be bound strongly. Breslow et al. developed a cyclodextrin-based mimic of the enzyme ribonuclease (which breaks down RNA by catalyzing the selective hydrolysis of a cyclic phosphate) based on a cyclodextrin molecule functionalized with imidazole groups.[1] There is now a broad range of cyclodextrin-based mimics of biomolecules.[2]

Hydrogen bonds often play a role in the binding of substrate to enzyme and are particularly valuable for shape-selective binding because of their directional nature. The use of hydrogen bonding in artificial receptor molecules was studied by Hamilton and coworkers,[3] who reported receptors exquisitely sculpted to bind their targets and stabilize a particular transition state during catalytic transformation (Fig. 1).

Antibodies can provide tailor-made molecular catalysts (although so far lacking enzyme-like rate enhancements) by using transition-state analogues as the antigens.[4] The same kind of sculpting of an active site around a small-molecule template affords catalytic activity via molecular imprinting of polymers.[5]

Self-Assembly

Self-assembly and replication, the paradigms of molecular and cell biology, are being increasingly seen as desirable goals for engineering. The alternative—laborious fabrication of individual structures "by hand"—is still the way that electronic and micromechanical devices are made today. by a sequence of deposition. patterning, etching or mechanical manipulating that becomes harder as the scales shrink and the device areal density increases.

To build a structure as complex as the Golgi apparatus, the chloroplast or the chromosome-charged mitotic

Encyclopedia of Supramolecular Chemistry
DOI: 10.1081/E-ESMC 120019312

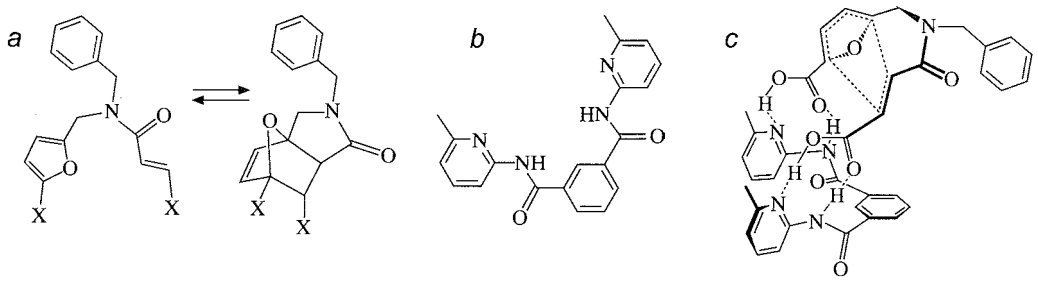

Fig. I The use of hydrogen bonding for enzyme mimicry. The intramolecular Diels–Alder reaction *a* is catalyzed by *b*, which has hydrogen-bonding functionality disposed to stabilize the transition state *c*.

spindle. the cell programs its molecular components with the information needed to bring them together in the right configuration. This is proof of the principle of the kind of "informed chemistry" advocated by Lehn.[6]

Thus. the hydrophilic head group and hydrophobic tail of lipids ensure assembly into the oriented bilayer array of cell membranes. The amphiphilic sheet, bilayer, and vesicle are now familiar mofits in biomimetic materials and structures. Synthetic liposomes are employed as biocompatible, biodegradable drug-delivery vehicles. Amphiphile assemblies may serve as templates: monodisperse nanoparticles are synthesized inside reverse micelles, and inorganic structures and materials such as ceramic tubules[L7] or mesoporous silica[8] are formed around tubular micelles, rather as inorganics are patterned by vesicles in the formation of the exoskeletons of radiolarians and diatoms.

A more sophisticated self-assembly process in nature is the folding of a protein to its native state. The linear polypeptide chain is preprogrammed to adopt and maintain its compact, three-dimensional form. One of the principal programmed motifs of protein folding is the β-sheet. a secondary structural component that was designed into some synthetic molecules.[9] As well as providing a model system for making molecules with well-defined higher-order structures, understanding β-sheet formation might lead to new antibiotics and treatments for diseases in which this process plays a role.

Using noncovalent interactions to guide the assembly of many molecules into organized structures is the major focus of supramolecular chemistry. Hydrogen bonding is used extensively for supramolecular organization; but so are metal-ion coordination chemistry, donor–acceptor interactions, π–π stacking, and other forces that might guide the recognition process. Metal ions, for example. were deployed by Sauvage and coworkers as organizing centers around which ligands are draped in geometries characteristic of the metal's oxidation state, so as to prearrange the organic components for forging into supramolecular topologies such as linked rings (catenanes) or knots.[10] Donor–acceptor interactions furnished a different breed of catenanes and threaded molecular assemblies called rotaxanes.[11]

One self-assembly strategy much used in biology is templating. The idea of using noncovalent supramolecular interactions to assist covalent synthesis is inherent in the formation of proteins on messenger RNA, catalyzed by the ribosome, as well as the formation of mRNA on DNA (transcription) and the replication of DNA. In all these cases, a template molecule helps to bring the components of the product into the right juxtaposition via base pairing. Liu et al. used the same principle — DNA templating — to catalyze the reactions between small molecules.[12] Here the DNA strands provide exquisite recognition groups that plug the reactants together, holding them in close proximity.

More dramatically. biology reveals how templating is the key to chemical replication, which is now achieved in a number of synthetic systems.[13] Templating must be exploited catalytically, requiring eventual separation of the product from the template, so that the bonds holding the two together while assembly takes place must eventually be broken. In the same way, if molecular recognition and self-assembly are the agents of some dynamical process such as ion transport [for example, when ionophores such as valinomycin selectively bind metal (potassium) ions and carry them across a cell membrane (see below)], then the substrate must be able to leave the receptor as well as to bind to it. This need for reversibility is common in biological self-assembly and recognition: it is characteristic of cell-surface signaling, neurotransmission, and the mechanisms of the immune response. High binding affinities favor strong selectivity but at the expense of reversibility. In proteins such as hemoglobin, a conformational change might alter the substrate binding affinity, highlighting the relationship between rigidity and selectivity on the one hand, and flexibility and reversibility on the other.

Energy Conversion

The conversion of photonic to chemical energy is what powers nearly every ecosystem on Earth. because it drives primary production. And yet this ubiquitous process is, at face value. not obviously one that warrants mimicry in solar-energy research. Even commercial solar cells based on polycrystalline silicon exceed the efficiency (at most 8–9%) of the chloroplast. the light-harvesting organelle of plants.

But this does not mean that nature's design for solar cells is poor. The rate of primary *production is generally limited by the availability not of solar energy but of nutrients such as phosphate and iron. Moreover, commercially viable solar energy is not about achieving record-breaking energy-conversion figures but about lowering the unit cost of solar cells. If devices could be produced as cheaply as green leaves, they would have no need of outstanding efficiency. So in asking whether solar-cell technology can usefully learn from nature, the right question is whether there are aspects of photosynthesis that might be gainfully employed to create cheaper devices?*

One *of the key differences between the chloroplast and a silicon solar cell is that the former is modular, and the latter is more or less monolithic. Tasks that are performed by different molecular entities in the chloroplast are subsumed into a single silicon matrix in the artificial devices. In the chloroplast, this division of labor reduces the possibility of recombination of charge carriers: a molecular relay produces quick, long-lived. and long-distance charge separation across the thylakoid* membrane. It is *a trick that was exploited in the nanocrystalline solar cells developed by* Grätzel *and* coworkers,[14] *in which charge generation takes place in ruthenium-based dye molecules, while charge transport is effected by the* titania *nanocrystals on which the dye is bound. The electronics* company *Toshiba is now aiming to commercialize these cells.*

Other systems *may, like the chloroplast. be concerned not with the generation of electricity per se but with the use of solar energy to drive a chemical reaction. Moore, Gust. and their coworkers developed a biomimetic system that derives a kind of artificial metabolism from sunlight (Fig. 2). Photon absorption by a porphyrin-containing molecular triad embedded in a* liposome *membrane stimulates the shuttling of an electron into the interior, accompanied by the simultaneous transmeinbrane movement of a proton. Thus, the pH inside the* liposome *decreases, just as it does within the thylakoid membrane in photosynthesis. The resulting electrochemical potential is used to power the enzyme ATP synthase, incorporated into the liposome* wall.[15]

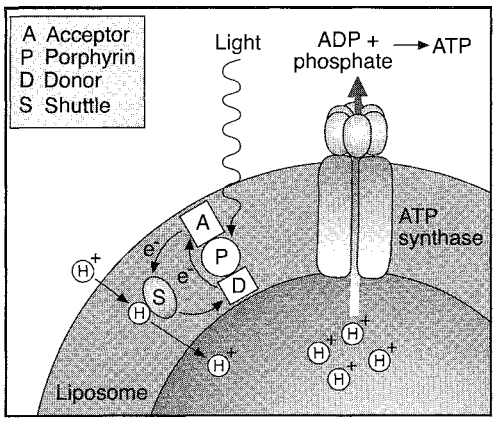

Fig. 2 A biomimetic system for solar-energy conversion. A molecular triad embedded in the bilayer membrane allows photoexcited electrons to be transported across the membrane to acceptor species in the interior. This charge transport is accompanied by the transmembrane flow of hydrogen ions. leading to a decrease in pH inside the compartment. This proton-motive force is then used to drive ATP synthesis by the membrane protein ATP synthase, as it is in photosynthesis.

Light-harvesting in the chloroplast's photosystems is not reliant on absorption by chlorophyll alone. Several accessory photopigments *increase the absorbing area and the wavelength sensitivity while channeling the energy of absorbed photons onto the photosynthetic reaction center down an energy gradient. This concept of an "antenna" system that acts as a funnel for captured energy was mimicked* in *synthetic light-harvesting systems, such as the* dendrimers *prepared by Shortreed et* al.[16] *The arms of these highly branched macromolecules are made of rod-like conjugated groups that absorb visible light.* A *progressive shortening of the arms* in *successive generations of the dendrimer's structure blueshifts their absorption maximum; so that the energy captured by all the light-absorbing groups is funneled into the* dendrimer's *center.*

For storing and transmitting captured photochemical energy, the molecular engineer cannot but be inspired by the elegance of ihe scheme used by photosynthetic bacteria. The light is absorbed by a toroidal protein complex called LH2, *which stores the energy before passing it on to the similarly shaped but larger* LH1 *complex, where it is used to create an electrochemical potential. The* LH2 complex *is a* supramolecular *storage ring in which 18 porphyrin groups are stacked face to face around the* circumference *(Fig.* 3a).[17] *The energy. passing freely between the porphyrin groups, can be tapped off at any point around the ring. This elegant structure inspired the synthesis of porphyrin rings that*

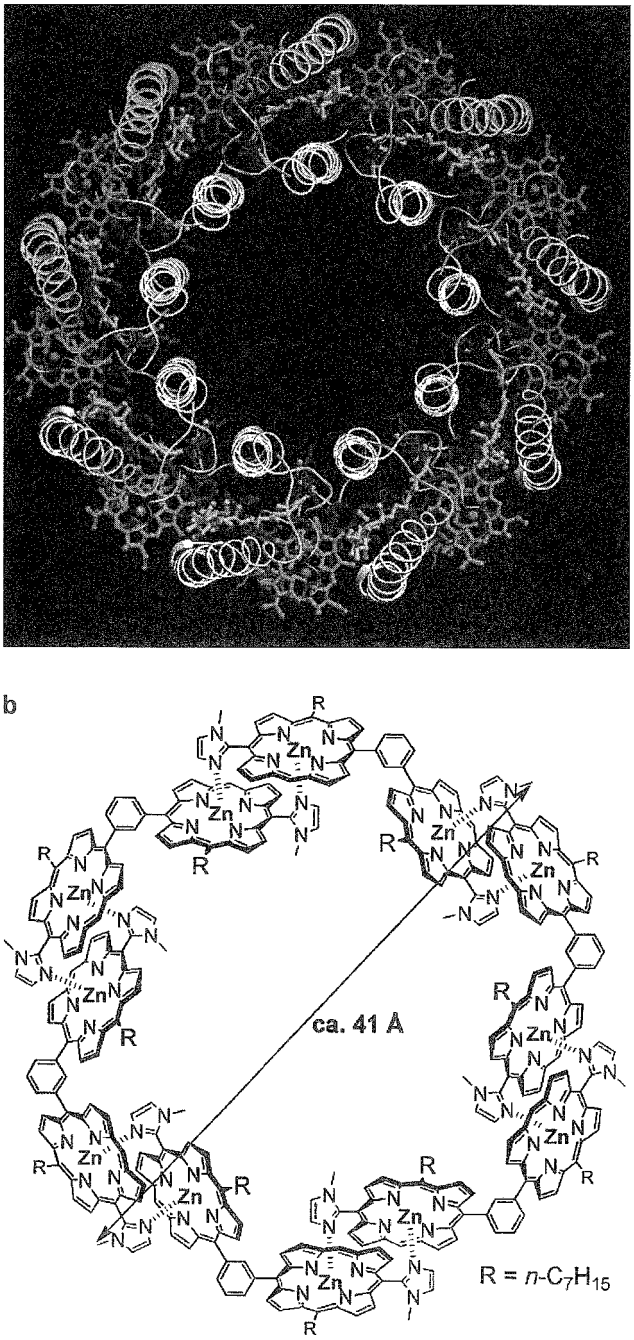

Fig. 3 (a) The light-harvesting LH2 complex of photosynthetic bacteria is a molecular "storage ring" in which absorbed energy is delocalized around a ring of 18 stacked porphyrins. (From Ref. [17].) (b) Such a supramolecular ring structure was mimicked in a hexameric assembly of porphyrin dimers. (From Ref. [19].) (***Virw*** *this art in color at www.dekker.com.*)

might act as antenna arrays or as energy-storage systems. For example, Li et al. made an oligomcric ring of three free-base porphyrins and three zinc porphyrins and saw photoinduced transfer of energy and charge carriers from the former to the latter.[18] Takahashi and Kobuke made a 4 nm ring of 12 zinc porphyrin units from six overlapping dimcr units (Fig. 3b).[19]

Sensing and Transduction

Essential to any sensing device is the process of transduction or signaling. In engineering, this is typically conducted electronically or, increasingly, optically. But it is rare in biology for electrons to represent the charge carriers of electrical signaling, at least in the sense of their being mobile in extended electron states. Electrons are typically passed between molecules in a series of redox reactions. Attempts to develop molecular wires — molecules such as polyacetylene and carbon nanotubes that transport electrons through conjugated systems — are, therefore, still based firmly in the electronics paradigm rather than in the biological.

Electronic signals in nerve cells travel by means of metal-ion transport laterally in and out of the axon. Such transmembrane transport of ions is fundamental to cell biology, and attempts to mimic it artificially laid the foundation of supramolecular chemistry. Early studies in molecular recognition by Lehn in the 1970s explored the use of crown ethers as mimics of cyclic peptide ionophores like valinomycin, which bind cations selectively in their internal cavities. Natural ionophores act as antibiotics by upsetting the ionic balance across bacterial cell walls.

Another way to transport ions is to provide them with a polar channel — in cells, a protein pore embedded in the membrane with a lipophilic outer face and a hydrophilic inner face. Artificial mimics of ion channels include peptide nanotubes — cyclic peptide inolecules designed to stack into cylindrical channels by the suitable placement of hydrogen-bonding groups around their edges (Fig. 4).[20] Thcsc peptides induce transmcmbrane ion transport at rates comparable to those of natural ion-channel proteins, such as gramicidin A, and show considcrablc promise as antibiotics.

Natural ion-channel proteins were used in single-molecule sensors, where the change in transmembrane ion current due to molecules partially blocking the pore provides a signature of the obstructing species. Bayley and coworkers used α-hemolysin as a molecular sensor, its pore neck tailored with a cyclodextrin "collar" to recognize various hydrophobic molecules.[21] Branton and coworkers use the same pore protein for single-molecule DNA sequencing: as each of the four types of

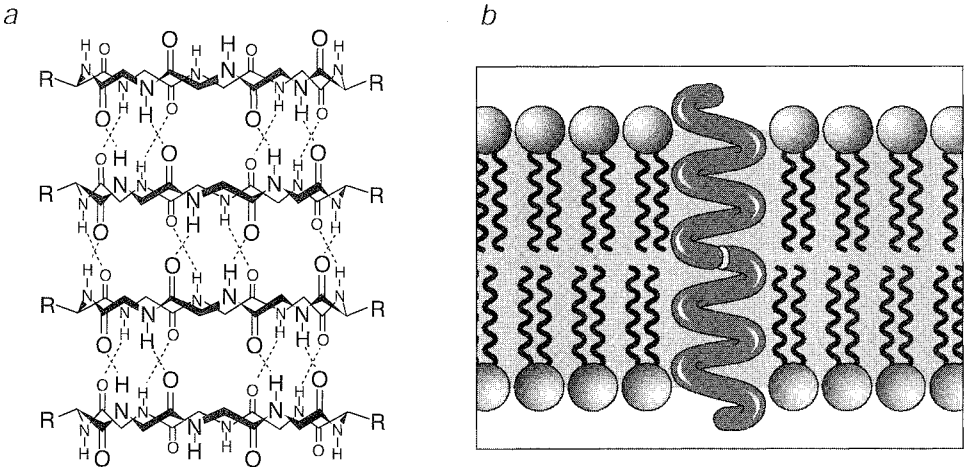

Fig. 4 Biomimetic and natural pore-forming systems for transferring ions across membranes. Tubes assembled from hoop-shaped molecules, such as cyclic peptides (a); mimic tubular ion channels such as the protein gramicidin A (b).

nucleotide is pulled through the pore, it has a distinct effect on the ion current.[22]

In macroscale engineering, transduction is often conducted mechanically. The generation of linear mechanical force and torque is widespread in the cell too: in the rotary motors of bacterial flagella, the rotary head of ATP synthase, and the ratcheting motion of the ribosome along mRNA during protein synthesis, for example. The paradigmatic examples of molecular force generation in biology are the molecular motors myosin, which powers the contraction of muscle tissue, and kinesin and dynein, which drive motion along cytoskeletal microtubules.

Controlled molecular motion was achieved in several synthetic systems,[23] including DNA machines that use a conformational change of the double helix to develop torque, and propeller-like molecules that can be rotated in a specific direction on a molecular axle by a sequence of chemical transformations. The hybridization and dissociation of DNA strands was also used to make DNA motors that extend and contract like pistons in response to DNA "fuel." One such device, unlike many artificial molecular motors, is capable of free running rather than requiring intervention at different points in the duty cycle.[24]

Materials

The extraordinary properties of natural materials, and their mimicry in artificial ones, have been amply advertised.[25] What are the guiding principles that, in determining the properties of natural materials at the nanoscale, are regarded as attractive targets for the materials chemist'?

While optimizing a particular material parameter tends to involve the fine-tuning of a specific feature of the structure, the combination of several desirable properties is typically a matter of controlling structure and organization across several different length scales. That is why natural materials generally display hierarchical structure, as evident in bone, wood, tendon, cartilage, and silk.

Related to the idea of hierarchy is the use of modular structure: building up materials through the assembly of identical smaller units. The stepwise unfolding of the muscle protein titin is due to a kind of modular domain structure and gives it a sawtooth stress–strain curve, very different from a purely elastic filament. Similar force curves were measured for the polymeric filaments that are pulled out from the organic binder between the aragonite plates of nacre as the plates are separated (Fig. 5).[26] This gives the composite a high work of fracture.

Spider capture silk, which can withstand extensions of up to 1000%, shows analogous behavior. The threads dissipate energy strongly as they stretch, minimizing the risk that a captured flying insect will be catapulted free again on the rebound. The capture silk proteins collapse into more or less helical coils that act as "molecular springs" (perhaps entropic). The jumps in the force curve presumably reflect hydrogen-bond breaking as these springs are progressively extended.

Biological materials are, almost by definition, self-assembling—which generally also implies that there are active control systems to provide self-repair, self-reinforcement, and disassembly when needed. Self-assembly has become an objective of much of materials chemistry: for example, in the formation of mesoporous silica and of colloidal crystals with potential uses in photonic tech-

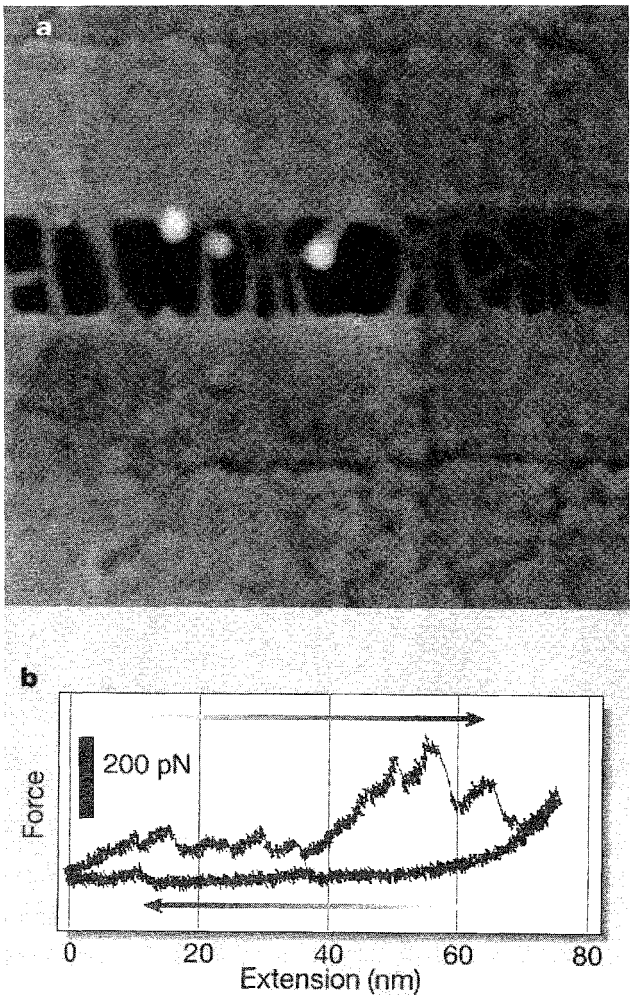

Fig. 5 The proteinaceous filaments that are pulled out of the organic binding layer between separated sheets of aragonite in nacre (a) extend in a stepwise manner, as revealed by force measurements with the atomic force microscope (b). The sawtooth stress–strain curve creates a greater work of fracture (area below the curve) than that for either a short, stiff adhesive strand or a long. smoothly elastic one. (After Ref. [26].) (*View this art in color at www.dekker.com.*)

nology. The sequence-specific ligation of DNA strands was used to create topologically complex self-assembling molecular architectures.[27]

Materials synthesis in biology is often conducted in compartments that delimit the extent of growth as well as provide a microenvironment in which parameters such as supersaturation of a precipitating phase can be delicately controlled by active transport of ions. This is how many biomineralization processes take place—for example, the formation of exquisitely patterned mineral plates in the soft tissues of coccolithophores. Mimesis of this principle is exemplified by the formation of monodisperse iron oxide nanoparticles inside the iron-storage protein ferritin, and the casting of inorganic particles inside the empty protein coats (virions) of viruses.

BIOSYNERGY

While the use of natural systems as guides to design at the molecular scale will surely continue to be exploited in creative ways in the coming years, biomimetic molecular engineering is also starting to employ a somewhat different philosophy in which "learning from nature" becomes a matter of adapting nature's existing machinery for technological ends. There need be no sharp distinction between the natural world and artificial mimics of it; instead, a hybridization of the two might reconfigure the cell's machinery to serve subtly different ends. There is a potential synergy in combining the natural with the artificial to achieve engineering objectives at the molecular scale.

For example, the rotary motion of ATP synthase was commandeered by Montemagno and coworkers to drive a nanoscale metal propeller at a rate of around five revolutions per second.[28] Protein engineering was used to insert a zinc-operated chemical switch into the enzyme to turn it on and off (Fig. 6).

Vogel and coworkers transported microtubules directionally across a surface, propelled by rows or linear channels of surface-bound kinesin.[29] Nanoparticle "cargo" was propelled in this way, and the motion was

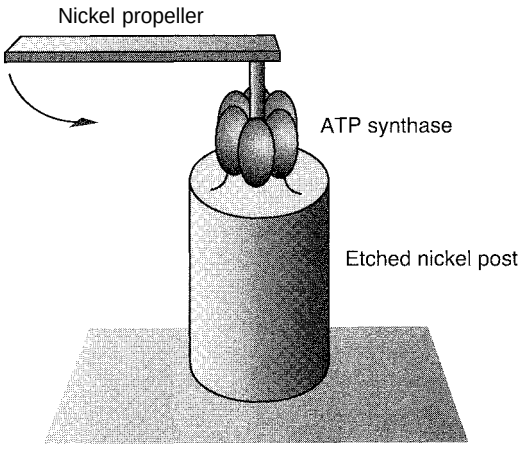

Fig. 6 A molecular-scale propeller representing a hybrid of the synthetic and the natural: the enzyme ATP synthase was attached to a metal post and modified to allow the attachment of a nanoscale "blade" of nickel metal.

switched on and off photochemicaliy using "caged" ATP as the fuel.

Phage transfection was used to transfer DNA into a wholly synthetic polymer vesicle containing the appropriate docking protein in its wall.[30] Modified phages might be used as "nanomachines" for loading genetic material into synthetic polymer nanoparticles used as vectors in gene therapy.

CONCLUSION

Biomimetics has become so popular a buzzword that there is a risk of it becoming its own justification, as if mimicking biology will undoubtedly turn out for the good. Yet nature offers little guidance for designing many technological processes and products, which operate under extreme conditions using materials alien to the living world. This article has illustrated, however, that the benefits accrue when our aim shares more in common with the exigencies of nature. If we wish to conduct chemistry at room temperature in aqueous media or to make organic compounds with complex architectures and precisely defined stereochemistry, nature reveals an astonishing repertoire of useful tricks. The materials engineer who requires a combination of low cost, light weight, and toughness, will probably already be using nature's fabrics in more or less modified forms, such as wood, leather, and paper. And as chemistry's synthetic targets become more sophisticated, embracing many-molecule supramolecular assemblies rather than simple small molecules, they often share features in common with the multi-molecular nanoscale structures of the cell.

A nanotechnology based on a literal downsizing of mechanical engineering. with every nanoscale device fabricated from hard moving parts, fails to acknowledge that there may be better, more inventive ways of engineering at this scale—ways that take advantage of the opportunities that chemistry and intermolecular interactions offer. Traditional engineering is often about trying to eliminate chemistry. At the molecular scale, we shall make life easier by embracing it. On the other hand, the cell's objectives are not necessarily the engineer's. For cellular information processing, accuracy is more important than speed. "Cost" to the cell does not equate with "cost" to manufacturing through a tidy conversion table. The materials of the cell need not be prescriptive. And perhaps most importantly, there is no justification for assuming that nature is optimized for any particular function. Biomimetics, at the nano- or any other scale, cannot afford a rose-tinted view of nature.

ARTICLES OF FURTHER INTEREST

Alkali Metal Cations in Biochemistry, p. *1*
Amino Acids: Applications, p. 42
Artificial Enzymes, p. *76*
Biomaterials, p. *110*
Biosensors, p. 115
Catenanes and Other Interlocked Molecules. p. 206
Cyclodextrins, p. 398
Dendrimers, p. 432
DNA Nanotechnology, p. 475
Drug Delivery, p. 484
Enzyme Mimics, p. 546
Ion Channels and Their Models, p. 742
The Lock and Key Principle, p. 809
Mesoporous Materials, p. 845
Peptide Nanotubes, p. 1035
Porphyrin Derivatives, Functional, p. 1139
Protein Supramolecular Chemistry, p. *1161*
Self-Assembly in Biochemistry, *p.* 1257
Supramolecular Photochemistry, p. 1434
The Template Effect, p. 1493

REFERENCES

1. Breslow. R.; Doherty, J.B.; Guillot, G.; Lipsey. C. Beta-cyclodextrinyl-bisimidazole, a model for ribonuclease. J. Am. Chem. Soc. 1978. *100.* 3227.
2. Breslow. R.: Dong, S.D. Biomimetic reactions catalyzed by cyclodextrins and their derivatives. Chem. Rev. 1998. 98. 1997–2012.
3. Xirst, S.C.; Hamilton. A.D. Complexation control of pericyclic reactions: Supramolecular effects on the Diels–Alder reactions. J. Am. Chem. Soc. 1991, *113.* 882.
4. Schultz. *P.G.;* Lerner. R.A. From molecular diversity to catalysis: Lessons from the immune system. Science 1995, *265,* 1835–1842.
5. Rarnstrom. O.: Mosbach, K. Synthesis and catalysis by molecularly imprinted materials. Cun. Opin. Chem. Biol. 1999. *3*, 759.
6. Lehn. J.-M. *Supramolecular Chemistry*; VCH: Weinheim. 1995.
7. Archibald, D.D.;Mann. S. Template mineralization of self-assembled anisotropic lipid microstructures. Nature 1993. 364. 430–433.
8. Kresge, C.T.: Leonowicz, M.E.: Roth. W.J.: Vartuli, J.C.; Beck, J.S. Ordered mesoporous molecular sieves synthesized by a liquid-crystal template mechanism. Nature 1992, *359*, 710–712.
9. Nowick. J.S. Chemical models of protein β-sheets. Acc. Chem. Res. 1999. *32*, 287.
10. Sauvage, J.-P. Interlacing molecular threads on transition metals: Catenands, catenates. and knots. Acc. Chem. Res. 1990. *23.* 319.

11. Fyfe. M.C.T.: Stoddart. J.F. Synthetic supramolecular chemistry. Acc. Chem. Res. 1997, *30,* 393.
12. Gartner, Z.J.; Kanak, M.W.; Liu, D.R. Expanding the reaction scope of DNA-templated synthesis. Angew. Chem., Int. Ed. 2002, *41,* 1796–1800.
13. Orgel, L.E. Molecular replication. Nature 1992, *358.* 203–209.
14. O'Regan, B.: Grätzel, M. A low-cost, high-efficiency solar cell based on dye-sensitized colloidal TiO_2 films. Nature 1991, *353,* 737–740.
15. Steinberg-Yfrach, G.: Rigaud, J.-L.; Durantini, E.N.: Moore, A.L.: Gust, D.; Moore. T.A. Light-driven production of ATP catalysed by F_0F_1-ATP synthase in an artificial photosynthetic membrane. Nature 1998, *392,* 479–482.
16. Shortreed. M.; Swallen. S.F.; Shi, Z.-Y.; Tan, W.; Xu, Z.; Devadoss. C.; Moore, J.S.; Kopelman, R. Directed energy transfer funnels in dendrimeric antenna supermolecules. J. Phys. Chem.. B 1997. *101,* 6318.
17. McDermott. G.: Prince. S.M.; Freer. A.A.; Hawthornethwaite-Lawless. A.M.; Papiz, M.Z.; Cogdell, R.J.; Isaacs. N.W. Crystal structure of an integral membrane light-harvesting complex from photosynthetic bacteria. Nature 1995. *374.* 517–521.
18. Li. J.: Ambroise. A.; Yang, S.I.; Diers. J.R.; Seth, J.: Wack. C.R.; Bocian. D.F.; Holten. D.; Lindsey, J.S. Template-directed synthesis. excited-state photodynamics, and electronic communication in a hexameric wheel of porphyrins. J. Am. Chem. Soc. 1999, *121,* 8927–8940.
19. Takahashi, R.; Kobuke. Y. Hexameric macroring of gable-porphyrins as a light-harvesting antenna mimic. J. Am. Chem. Soc. 2003. *125,* 2372–2373.
20. Chadiri. M.R.; Granja, J.R.; Milligan, R.A.: McRee. D.E.; Khazanovich, N. Self-assembling organic nanotubes based on a cyclic peptide architecture. Nature 1993, *366;* 324–327.
21. Gu. L.-Q.; Braha, O.; Conlan, S.; Cheley. S.: Bayley, H. Stochastic sensing of organic analytes by a pore-forming protein containing a molecular adapter. Nature 1999. *398,* 686–690.
22. Meller, A.: Nivon. L.; Brandin, E.; Golovchenko, J.: Branton. D. Rapid nanopore discrimination between single polynucleotide molecules. Proc. Natl. Acad. Sci. U. S. A. 2000, *97,* 1079–1084.
23. Balzani, V.: Credi, A.: Venturi, M. Molecular Devices *and Machines*; Wiley-VCH: Weinheim. 2003.
24. Turberfield, A.J.; Mitchell, J.C.; Yurke, B.: Mills, A.P., Jr.; Blakey, M.I.: Simmel. F.C. DNA fuel for free-running nanomachines. Phys. Rev. Lett. 2003, *90,* 118102.
25. *Biomimetics—Design and* Processing of Materials; Sarikaya, M.. Aksay, I.A., Eds.; AIP Press: New York, 1995.
26. Smith, B.L.; Schaffer, T.E.; Viani, M.: Thompson, J.B.; Frederick, N.A.: Kindt, J.; Belcher, A.; Stucky, G.D.; Morse, D.E.: Hansma, P.K. Molecular mechanistic origin of the toughness of natural adhesives. fibres and composites. Nature 1999, *399.* 761–763.
27. Seeman, N.C. DNA in a material world. Nature 2003, *421,* 427–431.
28. Soong, R.K.: Bachand G.D.; Neves, H.P.; Olkhovets. A.G.; Craighead, H.G.; Montemagno. C.D. Powering an inorganic nanodevice with a biomolecular rotor. Science 2000, *290.* 1555–1558.
29. Dennis, J.; Howard. J.: Vogel, V. Molecular shuttles: Directed motion of microtubules along nanoscale kinesin tracks. Nanotechnology 1999. *10.* 232–236.
30. Graff. A.; Sauer. M.; Van Gelder. P.; Meier. W. Virus-assisted loading of polymer nanocontainer. Proc. Natl. Acad. Sci. U. S. A. 2002. 99, 5064–5068.

Molecular Clefts and Tweezers

M

Michael Harmata
University of Missouri—Columbia, Columbia, Missouri, U.S.A.

INTRODUCTION

The phenomenon of molecular recognition has been studied through a number of synthetic hosts of various shapes and sizes—hosts being chosen to exhibit complementarity to various guests on the bases of size, shape, and specific, directional, molecular interactions.[1–3] One class of hosts is the molecular tweezers, defined by Whitlock as receptors in which two, flat. generally aromatic "pincers" or chromophores are linked by a rigid spacer to provide an approximately two-dimensional cleft into which a guest can bind.[4] This guest is generally a flat, aromatic system, but the term "molecular tweezer" was applied to other hosts that can bind other types of guests.

A more general class of receptors is called molecular clefts. These are hosts, that have pockets or indentations in a molecular surface, into which a guest can fit but is not completely encapsulated. They are often, if not always, characterized by convergent functional groups directed toward each other but separated by a spacer. The space between the functional groups provides the cleft into which a guest can bind. Molecular tweezers are examples of molecular clefts. Binding in molecular clefts may be mediated by a number of interactions, including dispersion forces, stacking, hydrogen bonding, and salt bridging, among others.

ACHIRAL MOLECULAR TWEEZERS

Perhaps the most critical factor associated with the design and synthesis of a molecular tweezer is the nature of the spacer separating the two aromatic chromophores that play a key role in guest binding. The molecular tweezers introduced by Whitlock were constructed from caffeine molecules linked by a diyne linker. An example is shown in Fig. 1. This linker provides for a space between the caffeine moieties of about 7 Å, an ideal size for the inclusion of another π system. This compound and related species demonstrated binding in aqueous solution to theophylline derivatives that exceeded that based on simple additivity. Analogues with spacers that consisted of simple aliphatic chains bound the guests with much lower binding constants.

While this seminal work set the stage for further developments in the area, one problem was that the linker, despite its rigidity, still afforded the possibility of conformational isomerism such that the caffeine moieties were free to adopt orientations in which they were not *syn* and did not create a cleft into which binding could occur. The entropic demand associated with producing conformers with a *syn* orientation of binding elements certainly lowered the efficiency of molecular tweezers of this type.

This problem was addressed by Zimmerman and coworkers, who introduced a class of molecular tweezers in which a *syn* orientation between the binding elements was enforced by the nature of the spacer and the linkage between the spacer and the binding elements."' The spacer used by the Zimmerman group was based on dibenz [*c*,*h*]acridine. This was linked at the 2 and 12 positions to various aromatic systems like anthracene and various heterocyclic analogs to produce a class of molecular tweezers represented by Compound 2, shown in Fig. 2. While these species are largely constrained, rotation about the bonds connecting the chromophores to the spacer is possible, but they can readily adopt a conformation in which both chromophores are parallel. as shown. Further. such rotation actually provides for slight changes in the distance between the chromophores, providing the opportunity for finding an optimum fit for a guest through rotation about carbon–carbon bonds. Such tweezers have high affinity for polynitro aromatic species.[6,7] In fact. a stationary phase based on a molecular tweezer in this class was developed for the separation of nitroaromatics.[8]

The binding potentials of molecular tweezers of this class were enhanced by the incorporation of a carboxylic acid functionality within the cavity of the molecular tweezer. Such species were used to bind nucleotide bases with extremely high affinities. Studies as to the origin of the strength and selectivity of the binding were conducted.[9–11]

Another class of rigid molecular tweezers introduced by Klärner and coworkers is represented by Structure **3.** shown in Fig. 3.[12,13] This compound was shown to bind certain secondary ammonium salts. viologen analogues, tropylium ion. and other electron-deficient π systems. Two possible mechanisms for the binding process were

DOI: 10.1081/E-ESMC 120012735

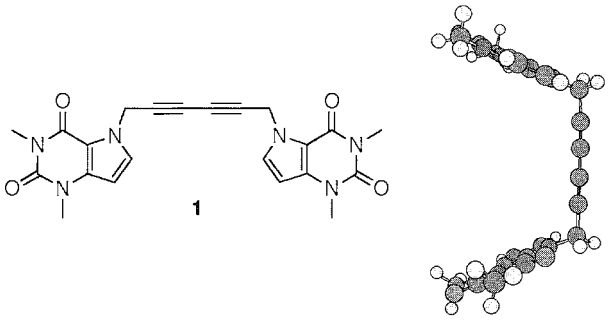

Fig. 1 *Two- and three-dimensional representations of a molecular tweezer prepared by* Whitlock *and* coworkers. *(From Refs.* [1–3].) *(View this art in color at www.dekker.com.)*

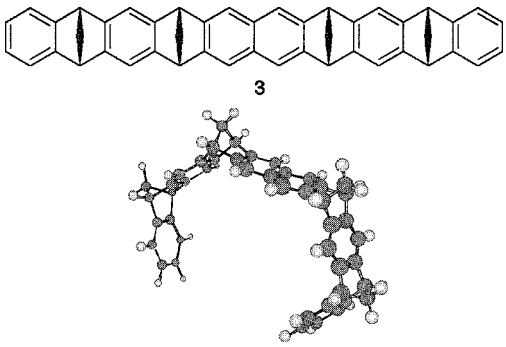

Fig. 3 *Rigid molecular tweezer prepared by Klarner and coworkers. (From Refs.* [12,13].) *(View this art in color at www.dekker.com.)*

identified, in which a guest enters through the holes on the open sides of the molecule or through the gap between the pincers of the tweezer. Studies involving the effect of temperature and pressure on the binding process were conducted.''] This molecular tweezer was also incorporated into a stationary phase and shown to be effective in separating n-deficient aromatic systems.[15]

Another class of molecular tweezers based on the *trans*,*trans*,*trans*-perhydronapththacene spacer was prepared by Nemoto and coworkers and was shown to bind to x-deficient aromatic guests.[16]

Notwithstanding the good results obtained with rigid molecular tweezers, the synthesis of more flexible systems continues to be of importance, as such systems offer adaptability not found in rigid systems. A recent example comes from the work of Fukazawa, who showed that polyether systems such as 4 in Fig. 4 could bind electron-deficient π systems in solution and in solid state.[17] The distance between the binding chromophores of the molecular tweezer shown containing tetracyanoquinomethane as a guest was 6.54 A. It was postulated. as in studies conducted on derivatives of Kagan's ether (vide infra), that π-stacking and edge–face interactions were important in the binding process.

Warrener and coworkers developed an approach to molecular tweezers that are largely rigid but contain a hinge or hinges to allow limited flexibility, which might prove important in providing a better fit to guest molecules.[18] This approach is a part of the so-called ''Lego'' approach to the construction of rigid and flexible molecular tweezers and clefts.[19]

Recent work by Reed. Boyd. and coworkers led to the development of a series of tweezers, called ''jaws porphyrin'' hosts, that can bind fullerenes.[20]

CHIRAL MOLECULAR TWEEZERS

Among the first molecular tweezers. which were also chiral, were those prepared by the Karmata group. This

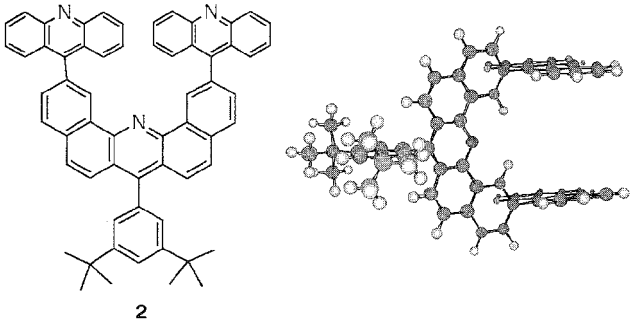

Fig. 2 *Two- and three-dimensional* represntations *of a* molecular *tweezer prepared by Zimmerman* and *coworkers. (From Ref.* [5].) *(View this art in color af www.dekker.com.)*

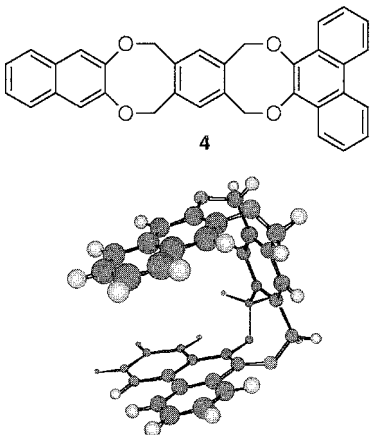

Fig. 4 *Flexible* molecular tweezer *synthesized by Fukazawa and* coworkers *(From Ref* [17]) *(View this art in color at www dekker com)*

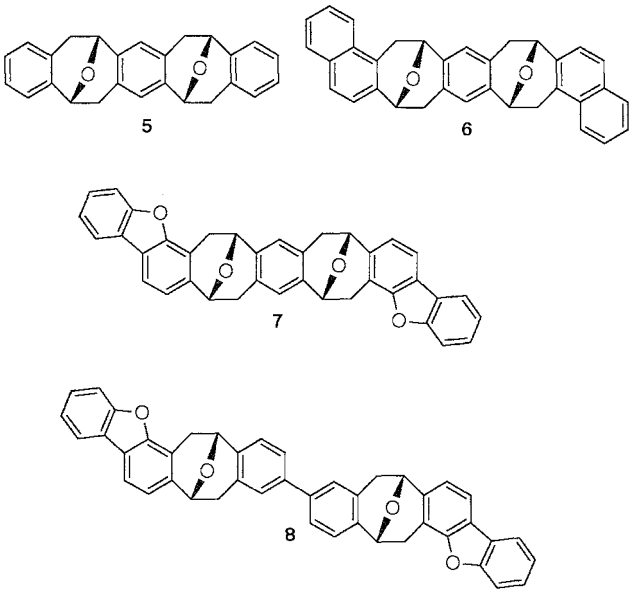

Fig. *5* Three different classes of chiral molecular tweezers prepared by Harmata and coworkers. (From Refs. [20–23].)

class of molecular tweezers was based on the framework provided by Kagan's ether, a C-2 symmetric structure built upon a dibenzobicyclo[3.3.1]octadiene skeleton. Two classes of tweezers thus far were reported, and these are shown in Fig. 5. It was reported that the smallest tweezer *(5)* did not form complexes with various n acids but formed a relatively stable clathrate with ethyl acetate in the solid state.[20] This demonstrated that the depth of the cleft is an important variable in the design of functional molecular tweezers.

In support of this idea. both 6 and 7 showed binding to 1.3.5-trinitrobenzene (TNB). in the solid state and in solution. as evidenced by shifts observed in the proton nuclear magnetic resonance (NMR) spectra of mixtures of

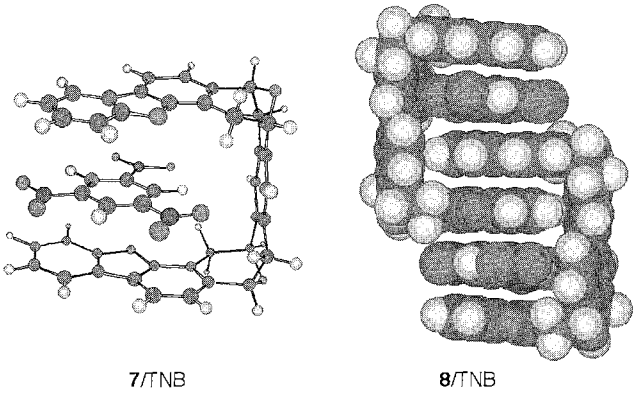

Fig. *6* Crystal structures for the 7/TNB and 8/TNB inclusion complexes. (*View this art in color at www.dekker.com.*)

the hosts and TNB.[22,23] Titration experiments indicated that 7 bound TNB more strongly than 6 by more than an order of magnitude. Enantiomer recognition with 7 was examined via variable temperature high-perforiuance liquid chromotography (HPLC) studies using a Whelk-Q 1 chiral HPLC column. The results demonstrated that discrimination of the two enantioiners of **7** was possible; with binding of the two species differing by 0.5 kcal/mol, differences in enthalpy changes being the exclusive basis for the binding differences.

The tweezer **8** was introduced as an analogue of echinomycin (vide infra). As such. the distance between the two binding chromophores is 10.4 Å, large enough to accommodate two π systems. It was shown that in the solid state. two π systems can be bound in the cleft of **8**.[24] Shown in Fig. 6 are crystal structure data for the inclusion complexes of 7 and 8 with TNB. Both n-stacking and edge–face interactions between guest and host are evident from these structures. The 8/TNB complex indicates clearly that two π systems can be accommodated within the cleft of 8.

Other chiral inolecular tweezers are known. including one based on Tröger's base. which is exactly analogous to **5**,[25] as well as several based on a steroidal spacer to which are appended aromatic acids via an ester linkage.[26,27]

NATURAL MOLECULAR TWEEZERS

Nature "beat mankind to the punch" with respect to molecular tweezers. For example, echinomycin (Fig. 7) is

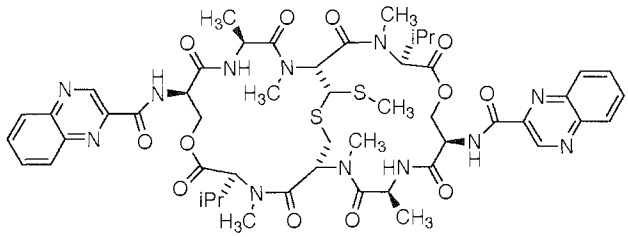

Echinomycin

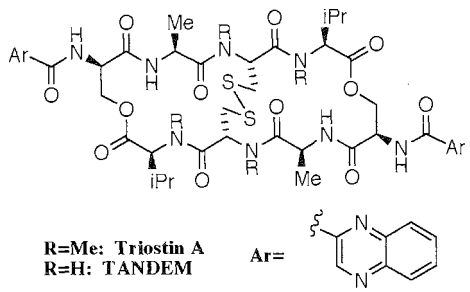

Fig. 7 A selection of natural molecular tueerers

the first representative of a growing class of cyclic depsipeptide antitumor antibiotics that includes the octadepsipeptides triostin A. the synthetic drug TANDEM, UK-63502 and BE-22179, the decadepsipeptides sandramycin, and the luzopeptins (Fig. 7), as well as the decapeptide quinaldopeptin.[28–37] These compounds exhibit a variety of interesting biological activities, including antibacterial, antiviral, and antitumoral.

The solid-state and solution structures of echinomycin and triostin complexes of DNA were studied.[38–40] These indicate that the drugs interact with DNA by "tweezing" two base pairs in GC-rich regions of double-stranded DNA. In the solid state and often in solution with an oligonucleotide target, this results in a twist of the helix to give Hoogsteen base pairing in base pairs flanking the binding site.

Other studies showed that binding affinity and specificity involve the octadepsipeptide and chromophores of echinomycin. One key to affinity and selectivity are hydrogen bonds between the N3 nitrogen and N2 amino of guanines in the CpG step and the NH and CO of the alanines of the octadepsipetide backbone of echinomycin. Replacement of *G* by hypoxanthine (G minus 2-amino) obliterates binding between echinornycin and a normally bound DNA fragment.[41] The synthetic intercalator TANDEM prefers AT regions of DNA, because its alanine CO groups are not available for hydrogen bonding with the 2-amino groups of guanine.[42,43] Further, the bias of echinomycin for the CpG step can be changed by substituting of adenine by 2-aminopurine.[44] The bottom iine is that the spacer of a his-intercalator can be significant in strong and selective DNA binding. Other work suggests that the chromophores of the intercalator are of some significance. Theoretical studies conclude, in particular, that the chromophore interactions with the DNA contribute at least 50% to the binding of the drug and that the electrostatic interactions between the chrornophores and flanking base pairs are important.[45] A balance between repulsive and attractive interactions involving the spacer and chromophores is important to the selectivity observed and, as important, can be changed by appropriate structural modifications.

Solution NMR and footprinting studies of DNA–drug interactions for some other naturally occurring ***Dis***-intercalators led to a grossly similar picture for the event: minor groove binding mediated by hydrogen bonding and van der Waals interactions. with stacking interactions involving dispersion. and electrostatic interactions no doubt being of importance.[46,47] In all cases, two base pairs are "tweezed," but the hydrogen bonding motif varies, as might be expected due to changes in the depsipeptide backbone.

ACHIRAL MOLECULAR CLEFTS

Molecular clefts that bear convergent functionality are of major interest. In systems of this type, a rigid spacer is used to create a scaffold onto which functional groups can be placed. These functional groups are often, but not always, directed toward each other but are held apart by the spacer. Guest binding takes place in the space between the functional groups, and selectivity is determined in part by the size of this aperture.

Many examples of molecular clefts of this type come from the labs of Rebek.[48] Many other structural types are known, including terpyridyl systems introduced by Bell[49] and the "molecular clips" from the group of Nolte.[50]

CHIRAL MOLECULAR CLEFTS

There are a number of examples of chiral molecular clefts. Among the most interesting are those introduced by Wilcox and coworkers, which involve derivatives of Tröger's base.[51,52] Such systems were used as hosts for various guests and as tools for the evaluation of edge–face interactions between π systems. Related molecular clefts are known.[53,54]

NATURAL MOLECULAR CLEFTS

Large biological molecules contain indentations, cavities, and pockets. Essentially all proteins and polynucleotides possessed of even simple tertiary structures have a portion of their structure that forms a gully into which a molecule might fall and bind. The major and minor grooves of DNA come to mind as obvious and important examples. Many enzyme-active sites and receptor-binding sites are essentially molecular clefts.[55] Our attempts tomimic these structural types are responsible for a great dealof the development of bioorganic and molecular cleft chemistry.

CONCLUSION

Design and application of molecular tweezers, particularly those that are chiral and those that can bind multiple π systems within their clefts, are only beginning to be explored. Molecular tweezers and other molecular clefts have the potential to dimerize to produce molecular

capsules; which are currently of great interest. Chiral species with reactive functionality directed toward the inside of the cavity still offer opportunities for creating new catalysts. drug-delivery systems, and perhaps materials for molecular electronics and computing. New directions for molecular recognition and supramolecular chemistry remain to be found or invented in this area, and new breakthroughs are to be expected.

ARTICLES OF FURTHER INTEREST

Biological Ligands, p. 88
Chiral Guest Recognition, p. 236
Complexation of Fullerenes, p. 302
Concave Reagents, p. 311
Cyclophanes: Definition arzd Scope, p. 414
Drug Delivery, p. 484
Glycoluril-Based Hosts, p. 597
Podands, p. 1106
Preorganization and Complementarity, p. 1158

REFERENCES

1. Vogtle. F. *Supramolecular Chemistry*; Wiley: Chichester. 1991.
2. Lehn. J.-M. *Supramolecular Chemistry*; VCH: Weinheim. 1995.
3. Steed. J.W.: Atwood. J.L. *Supramolecular Chemistry:* Wiley: Chichester. 2000.
4. Chen. C.-W.; Whitlock, H.W., Jr. J. Am. Chem. Soc. 1978. *100*, 4921.
5. Zimmerman, S.C. Top. Curr. Chem. 1993, *165*, 71.
6. Zimmerman, S.C.: VanZyl, C.M. J. Am. Chem. Soc. 1987. *109*. 7894.
7. Zimmerman, S.C.; VanZyl, C.M.: Hamilton. G.S. J. Am. Chem. Soc. 1989. *111*. 1373.
8. Zimmerman, S.C.: Saionz. K.W. J. Am. Chem. Soc. 1995. *117*. 1175.
9. Zimmerman. S.C.; Wu. W. J. Am. Chem. Soc. 1989. *111*, 8054.
10. Zimmerman. S.C.; Zeng, Z.: Wu, W.; Reichert. D.E. J. Am. Chem. Soc. 1991. *113*. 183.
11. Zimmerman. S.C.: Wu. W.; Zeng. Z. J. Am. Chem. Soc. 1991. 113. 196.
12. Kamieth, M.; Klarner. F.-G. J. Prakt. Chem. 1999,341,245.
13. Klärner. F.-G.; Benkhoff. J.: Boese. R.: Burkett. U.: Karnieth. M.: Naatz. U. Angew. Chern.. Int. Ed. Engl. 1996. *35*. 1130.
14. Ruloff. R.: Seelbach. U.P.: Merbach, A.E.: Klarner. F.-G. J. Phys. Org. Chem. 2002. *15*. 189.
15. Karnieth, M.: Burkert. U.: Corbin, P.S.: Dell, S.J.; Zimmennann, S.C.; Klarner, F.-G. Eur. J. Org. Chem. 1999, *64*. 2741.
16. Nemoto. H.; Kawano, T.; Ueji, N.; Bando. M.: Kido, M.; Suzuki, I.; Shibuya, M. Org. Lett. 2000, 2, 1015.
17. Kurebayashi. H.; Haino, T.; Usui. S.; Fukazawa. Y. Tetrahedron 2001. *57*, 8667.
18. Warrener, R.N.; Butler, D.N.; Liu, L.; Margetic, D.; Russell, R.A. Chem. Eur. J. 2001. 7. 3406.
19. Warrener, R.N.; Margetic. D.: Amarasekara, A.S.: Butler, D.N.; Mahadevan. I.B.; Russell, R.A. Org. Lett. 1999; 1, 199.
20. Sun, D.; Tham. F.S.; Reed. C.A.: Chaker. L.; Boyd. P.D.W. J. Am. Chem. Soc. 2002, 124. 6604.
21. Harmata. M.; Barnes. C.L. Tetrahedron Lett. 1990, 31, 1825.
22. Harmata. M.; Barnes, C.L. J. Am. Chem. Soc. 1990. *112*. 5655.
23. Harmata, M.: Kahraman. M.; Tyagarajan, S.: Barnes. C.L.; Welch. C.J. Molecular Recognition and Inclusion. Proceedings of the International Symposium on Molecular Recognition and Inclusion, 9th, Lyon, Sept. 7–12, 1996; 1998; 109.
24. Harmata, M.: Barnes, C.L.; Karra, S.R.: Elahmad, S. J. Am. Chem. Soc. 1994. *116*, 8392.
25. Pardo. C.; Sesmilo, E.; Gutierrez-Puebla, E.; Monge. A.; Elguero. J.; Fruchier. A. J. Org. Chem. 2001. *66*, pp. 1607. 4104.
26. Potluri. V.K.: Maitra. U. J. Org. Chem. 2000, *65*. 7764.
27. D'Souza, L.J.; Maitra. U. J. Org. Chem. 1996. *61*. 9494.
28. Waring, M.J. *Molecular Aspects of Anticancer Drug–DNA Interactions:* Neidle, S., Waring. M.J.. Eds.: CRC: Boca Raton, 1993: Vol 1: 213–242. Chapter 7.
29. Waring. M.J. Pathol. Biol. 1992, *40*. 1022–1034.
30. Waring, M.J. Antibiotics 1949. *5*, 173–194.
31. Viswamitra, M.A.: Kennard. O.; Cruse. W.B.T.; Egert, E.: Sheldrick, G.M.: Jones, P.G.; Waring, M.J.: Wakelin. L.P.G.: Olsen, R.K. Nature 1981, *289*. 817–819.
32. Hossain. M.B.; Van der Helm. D.; Olsen. R.K.: Jones. P.G.: Sheldrick. G.M.; Egert, E.: Kennard, O.: Waring. M.J.; Viswamitra. M.A. J. Am. Chem. Soc. 1982. *104*, 3401–3408.
33. Rance. J.J.; Ruddock. J.C.: Pacey, M.S.: Cullen, W.P.: Huang. L.H.: Jefferson. M.T.: Whipple, E.B.; Maeda. H.: Tone, J. J. Antibiot. 1989. *42*, 206–217.
34. Okada, H.; Suzuki. H.; Yoshinare, T.: Arakawa, H.; Okura. A.; Suda. H. J. Antibiot. 1994, 47. 129–135.
35. Boger, D.L.; Chen. J.H. J. Am. Chem. Soc. 1993. *115*, 11624–11625.
36. Konichi. M.; Ohkuma, H.; Sakai. F.: Tsuno. T.; Koshiyama. H.: Naito, T.; Kawaguchi. H. J. Am. Chem. Soc. 1981. *103*. 1241–1243.
37. Soichiro. *T.*: Sugawara, K.: Nishiyama, Y.: Ohbayashi, M.; Ohkusa, N.: Yamamoto. H.: Konishi, M.: Oki, T. J. Antibiot. 1990. *43*. 796–808.
38. Wang. A.H.J.: Ughetto, G.; Quigley, G.J.; Rich, A. J. Biomol. Struct. Dyn. 1986. 4. 319–342.
39. Wang, A.H.J.; Ughetto. G.: Quigley. G.J.; Hakoshima, T.:

Van der Marel, G.A.: Van Boom. J.H.; Rich, A. Science 1984, *225.* 1115–1121.
Ughetto. G.; Wang, A.H.J.: Quigley, G.J.; Van der Marel, G.A.: Van Boom. J.H.: Rich. A. Nucleic Acids Res. 1985, *13.* 2305–2323.
Marchand. C.: Bailly. C.: McLean, M.J.; Moroney, S.E.; Waring. M.J. Nucleic Acids Res. 1992. *20.* 5601–5606.
Addess, K.J.: Feigon. J. Biochemistry **1994**, *33.* 12397–12404.
Addess. K.J.: Gilbert. D.E.; Olsen, R.K.; Feigon, J. Biochemistry 1992. *31.* 339–350.
Bailly, *C.:* Marchand. C.; Waring, M.J. J. Am. Chem. Soc. 1993, *115.* 3784–3785.
Gallego, J.; Luque, F.J.; Orozco. M.; Burgos, C.; Alvarez-Builla. J.: Rodrigo. M.M.; Gago. F. J. Med. Chem. 1994. *37,* 1602–1609.
Chen. H.: Patel, D.J. Biochem. J. 1994, *304.* 967–979.
Zhang. X.: Patel. D.J. Biochemistry 1991. *30.* 4026–4041.
48. Shimizu. K.D.: Dewey. T.M.; Rebek, J.. Jr. J. Am. Chem. Soc. 1994. *116.* 5145–5149.
49. Bell, *T.W.;* Cragg, P.J.: Firestone, A.; Kwok, A.D.-I.; Liu, J.; Ludwig. R.; Sodoma. A. J. Org. Chem. 1998, *63,* 2232–2243.
50. Reek. J.N.H.: Rowan. A.E.: Crossley, M.J.: Nolte. R.J. M. J. Org. Chem. 1999, 64. 6653–6663, and references therein.
51. Wilcox, C.S.: Greer, L.M.; Lynch. V. J. Am. Chem. Soc. 1987. *109,* 1865–1867.
52. Kim, E.: Paliwal, S.; Wilcox, C.S. J. Am. Chem. Soc. 1998. *120.* 11192–11193.
53. Field, J.D.; Turner. P.; Harding, M.M.: Hatzikominos, T.; Kim. L. New J. Chem. **2002.** *26,* 720–725.
54. Kimber, M.C.; Try, A.C.: Painter. L.; Harding, M.M.: Turner, P. J. Org. Chem. **2000,** 65. 3042–3046.
55. Taylor. S.S.: Radzio-Andzelm. E.; Madhusudan, X.: Cheng, L.; Ten Eyck, N. Pharmacol. Ther. 1999, 82, 133–141.

Molecular Logic Gates

Gareth J. Brown
A. Prasanna de Silva
Sheenagh M. Weir
The Queen's University of Belfast, Belfast, Northern Ireland

INTRODUCTION

The forces that drive research in molecular logic gates are identified as neural science and computer technology. The longest established design relies on chemical (usually ionic) inputs and fluorescence outputs. This design also incorporated chemical input–transmittance (or absorbance) output situations. Light and chemical input–fluorescence (or absorbance) output situations involving chemically switched photochromism can also be a valuable design approach. All-optical methods involve electron transfer or two-photon absorption. After decades of discussion and effort; ail-electronic methods are recently making the transition from wires and switches into logic gates. Examples are provided for each design. This article illustrates all of the single-input logic gates and a substantial number of the double-input family.

WHY BOTHER WITH MOLECULAR LOGIC GATES?

None of us are immune to the effects of the modern information technology revolution.[1] Nevertheless; how many of us as chemists helped to start or even drive it? Very few, would be the answer. Chemists were behind the purification of silicon to the exacting levels required for the construction of semiconductor devices, but most of these developments essentially laid in the hands of physicists. mathematicians, and engineers.

There is. however. an arguably more vital and far oider information revolution: the one still functioning in our genes, nerves. and brains.[2] Chemical processes start and drive it. even though the complexities are best examined by biologists. Chemists certainly played their role here. This role is set to grow as the semiconductor revolution runs out of space. After all. molecules gladly go to spaces where semiconductors fear to tread. It therefore falls on chemists to explore the information-handling capabilities of molecules. As far as this article is concerned. information processing is what we are after. That is where molecular logic gates come in.

HOW ARE MOLECULAR LOGIC GATES DESIGNED?

Logic gates are the workhorses of modern information technology. because computation relies on arithmetic and logic units. Arithmetic units can be dissected into simpler logic gate arrays.[1] So, the challenge is to pass on these properties and capabilities to molecules. This challenge has been accepted with increasing frequency since 1993. when we demonstrated that molecular fluorescence signals can be switched under the influence of simple chemical species.[3] Chemical inputs and fluorescence/optical outputs (photoionic schemes) circumvent problems of wiring between molecular and macro worlds. The ease of detecting fluorescence output allows for the operation of such devices at the single-molecule limit.[4] Optical inputs are also useful. High and low signal levels are taken as binary 1 and 0, respectively. whether chemical concentrations or light intensities are under discussion. Of course. the same applies when electric voltages are used as input and output signals. A huge amount of effort was expended to miniaturize existing electronic devices, where the semiconductors were replaced by molecules or at least molecular ensembles. Different logic gates produce different output signal patterns as a small set of input signals are applied. So. let us begin at the beginning, however trivial it may seem at first. For one thing, valuable generalizations emerge early on. For another, the field is young. and consolidation of early material is necessary for progress.

SINGLE-INPUT LOGIC GATES

Shown in Fig 1 are the truth tables of all possible output patterns triggered by a single input These four are now discussed in turn. with the emphasis laid on molecular implementation

PASS 0

Pass 0 is an instance where the output remains switched "off." whatever the input situation. In the electronic case.

Encyclopedia of Supramolecular Chemistry
DOI: 10.1081/E-ESMC 120012827

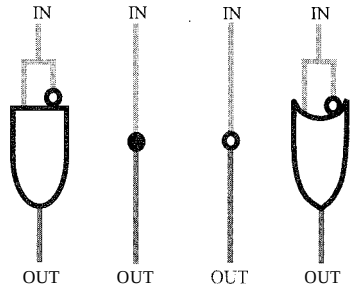

	PASS 0	YES	NOT	PASS?
IN	OUT	OUT	OUT	OUT
0	0	0	1	1
1	0	1	0	1

Fig. 1 Truth tables and physical electronic representations of the four single-input logic gates: PASS 0, YES, NOT. and PASS 1. (*View this art in color at www.dekker.com.*)

all chis requires is an earthed output unconnected to the input. The same outcome can be arranged by employing common digital electronic components—NOT and AND gates (see below)—as shown in Fig. 1. A molecular implementation with chemical input and fluorescence output would be any molecule without a fluorophore or observation at a wavelength remote from the emission band of a fluorophore. say **1.** If transmittance of light (during an absorption experiment) is employed as output instead of fluorescence. the molecular implementation would require observation at a wavelength near the absorption band maximum of a simple chromophore devoid of receptors. **1** would fit the bill.

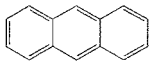

1

PASS 1

Pass 1 would be the opposite extreme. where the output stays switched "on," uncontrolled by the input. Again in the electronic case, a live output unconnected to the input line would achieve this result. Common electronic logic gates—NOT and OR (see below)—can be wired together, as shown in Fig. 1. to give PASS 1 action. A simple fluorophore devoid of receptors would be a molecular implementation. Say that **1** would give a high fluorescence signal if observed within its emission band, while being excited within its absorption band(s), whether or not. say. H^+ was present. If the emphasis is on transmittance rather than fluorescence. the molecular implementation requires observation well away from absorption bands. Better still. one can avoid using a chromophore.

YES

YES requires the output to follow the input. In fact, the electronic case simply corresponds to any point along a wire. Single molecular electronic implementation of a wire[5] was neatly accomplished by planting **2** via its thiol moiety at a grain boundary of a self-assembled monolayer of **3** on a gold surface and then contacting the distal terminus with the tip of a scanning tunnelling microscope.[6] Photoionic implementation can be illustrated by **4**[7] and many other ion sensors (both fluorometric and absorptiometric). We discuss such systems in more depth within a companion article.[8] The choice of **4** is driven by its structural relationship to **1** and by the general utility of its photochemical design. The straightforward observation concerning **4** is that the presence of high levels of H^+ triggers strong fluorescence, whereas there is almost no emission if H^+ concentrations are kept low. All this happens because the fluorophore (9-chloroanthracene. in this case) leads to photoinduced electron transfer (PET) from the amine lone electron pair to the fluorophore. Thus; fluorescence is not an option. The arrival of high enough levels of H^+ blocks the lone electron pair of the amine and lets fluorescence reassert itself. The switching behavior of **4** hinges on the receptor action of the amine toward the H^+ input. Such fluorophore–spacer–receptor systems and relatives often appear in molecular logic implementations, as the following pages will show. A particular feature of these is the switching "on" or "off" of the fluorescence output right across the range of observation wavelengths. Thus, the logic type is robust with respect to variation or fluctuation of observation conditions such as wavelength. Furthermore. fluorescent PET systems are designable with a substantial degree of quantitative predictability.[9]

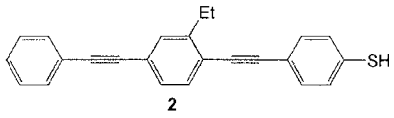

2

$CH_3(CH_2)_{11}$— SH

3

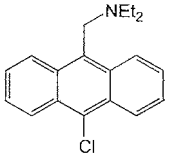

4

NOT

NOT logic naturally has the output behaving opposite to the input. Now the electronic case takes on significance, even having its own (and much used) symbol (Fig. 1). Such inversion of a voltage signal received a molecular implementation recently within a single bundle of carbon nanotubes.[10] Avouris' team treats part of this intrinsically p-doped bundle with potassium metal to leave it *n*-doped. This forms the twin hearts of connected. but complementary, field-effect transistors, which produces NOT logic behavior in the same way as currently seen in common semiconductor devices. While this achievement has been quite rightly feted,[11] we must not lose sight of the fact that the full NOT gate occupied an area about 1 μm^2, i.e. about the size of current semiconductor gates. The low-budget photoionic approach is represented by **5**,[12] which is a fluorescent PET fluorophore–spacer–receptor system like 4 but with opposite characteristics. A key difference is that 5 contains a pyridine receptor for H^+ that becomes more reducible when bound, whereas 4 had an amine receptor that becomes less oxidizable upon protonation. So. **5** galvanizes fluorescence-quenching PET from the fluorophore to the pyridine receptor only when H^+ arrives. On the other hand. PET was only seen in 4 when H^+ was absent at the amine receptor.

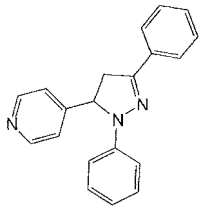

5

DOUBLE INPUT LOGIC GATES

We could work our way systematically through all 16 of the double-input logic gates. except that space restrictions on this article will stop us well short of that objective. Instead. we will consider six types frequently encountered in the computer literature.

AND

AND is the logic type many people recognize, perhaps because its human analogy embraces those universal values of cooperation and unity. Any one input is powerless to fire the output. But, the output comes alive when both inputs are applied at the same time (Fig. 2). Our 6 is a molecular photoionic implementation and is a fluorophore–$spacer_1$–$receptor_1$–$spacer_2$–receptor: system relying on PET.[3] In fact. each receptor can engage the fluorophore to quench the fluorescence. As in the case of 4, each receptor needs to he blocked by its own target species before the fluorescence can be switched "on." H^+ is the input chosen by the amine group. while Na^+ is selected by the benzo-15-crown-5 ether moiety. Eight and ions can serve as mixed inputs for AND gates. An example by Pina. Balzani, and colleagues is 7, where ultraviolet light allows isomerization of **7** to its *cis*-form.[13] H^+ then cyclizes the latter to a fluorescent product.

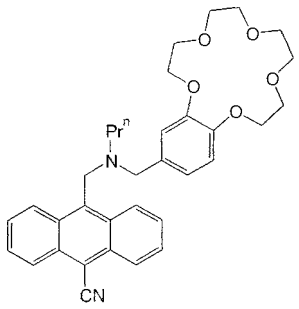

6

All-optical examples of AND logic recentiy became available,[14,15] even though an old claim of this kind in the conference literature seems not to have crossed into the refereed literature.[16] Due to the teams of Wasielewski and Levine. 8 and 9, respectively, achieve their objectives by very different means. Compound 8 shows a tetrachromophore system held together by *m*-substituted benzene rings. The 4-amino-1,8-naphthalimide is initially pumped at 420 nm to cause PET from it to the 1,4:5,8-naphthalenediimide. The other chrornophores become involved only if the naphthalenediimide radical anion is pumped at 480 nm. Now, the extra electron within the napthalenediimide is passed to the 1,8-naphthalimide and then on to the 1,2:4,5-benzenediimide. So. the absorption signature of the benzenediimide radical anion at 720 nm (the output) is only observed if the two femtosecond laser pulses at 420 nm (IN_1) and at 480 nm (IN_2) are applied sequentially (2 ns separation). It is notable. however. that conventional AND gates require simultaneous. and not sequential. application of inputs (a 2 ns delay would matter in devices running near gigaHertz rates). Nevertheless. **8** is a fast gate. because it resets in 25 ns.

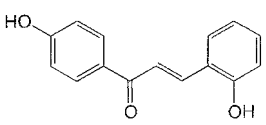

Levine noticed that two-photon processes in general could be candidates for two-input AND logic. especially when the output of the process is a detectable fluorescence. This has additional utility. as discussed later. if the

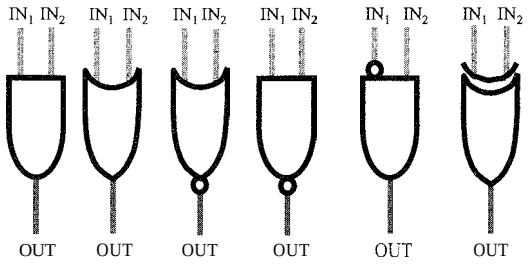

IN_1	IN_2	OUT	OUT	OUT	OUT	OUT	OUT
0	0	0	0	1	1	0	0
0	1	0	1	0	1	0	1
1	0	0	1	0	1	1	1
1	1	1	1	0	0	0	0

Fig. 2 Truth tables and physical electronic representations of six of the 16 double-input logic gates: *AND, OR. NOR. NAND,* INHIBIT. and XOR. (*View this art in color at www.dekker.com.*)

fluorescence is from an upper-level excited state. A fundamental photochemical generalization—the Vavilov–Kasha rule—stands in the way of this requirement, though thankfully it makes a few exceptions.[17] The common laser dye **9** is a suitable example. where a relatively low-intensity laser beam at 532 nm (IN,) would allow one-photon absorption to the lowest excited state. Another laser beam of similar intensity (and color) (IN_2) is then directed onto the sample such that the combined intensity enables two-photon absorption that populates the next higher excited state. This obviously requires judicious choice of the beam intensities. Now. a weak but detectable fluorescence is seen at 430 nm. AND and all 15 other two-input logic gates are recently described by Zhang et al., with bacteriorhodopsin as the active medium; two laser beams (blue and yellow) as inputs, and a chosen transmittance as the output.[18] Another laser beam is required for biasing purposes. The rich photochemical cycle of bacteriorhodopsin is the source of this versatility.

Conventional semiconductor logic gates, such as AND, are produced by wired arrays of simpler switches, such as diodes or (in newer systems) transistors. Molecular electronic implementations can therefore do the same with a good chance for success. Heath, Stoddart, and colleagues use a monolayer of **10** sandwiched between metal and metal oxide layers and outer metallic contacts to produce diode behavior,[19] several of which are known.[20,21]

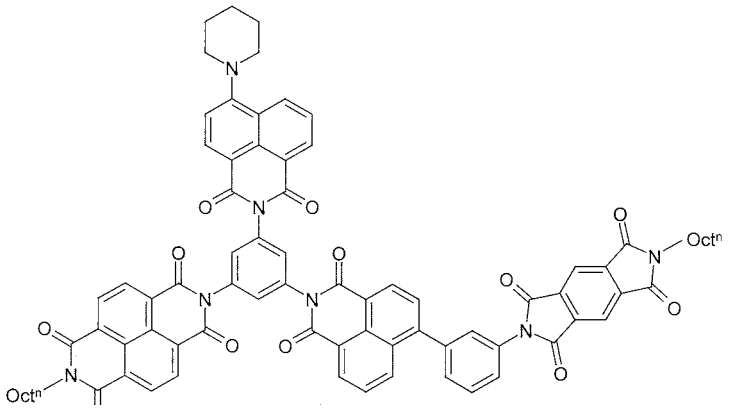

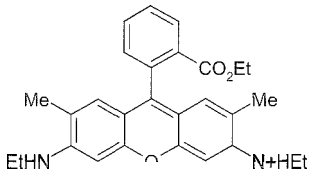

9

These diodes can now be wired conventionally to give logic behavior. AND logic arises when a power supply leads via a resistor to the output unless diverted through two diodes, each of which would conduct only if the inputs applied to their distal end are zero. If both inputs are high, both diodes cease to conduct, and the output takes on the voltage of the power supply.

OR

OR logic gates (Fig. 2) also receive a molecular electronic implementation in Ref. [19], with a conventional wiring of diodes. OR logic happens when two diodes lead to the output. Each of the diodes conducts only if the inputs applied to their distal ends are high. If both inputs are zero, the output takes on zero, the value of earth to which it is also connected via a resistor. Our **11** shows the photoionic approach to OR logic. Ca^{2+} and Mg^{2+} inputs are sufficiently unselective to produce essentially identical extents of switching "on." Scheme **11** shows a fluorophore–spacer–receptor PET system, where the aromatic amino acid receptor acts as an electron donor toward the excited diarylpyrazoline fluorophore. resulting in negligible emission. Ca^{2+} or Mg^{2+} binding blocks the electron-rich sites of the receptor and cuts off PET. It is notable that a single-receptor system is sufficient in this case to achieve a two-input logic gate.

NOR

Though NOR logic (Fig. 2) is as legitimate as any of the other 15 double-input logic gates. common computer literature represents it as a particular integration of NOT and OR gater (as its name also suggests). Such physical integration requires additional wiring that throws more obstacles toward molecular implementation. This challenge can be mitigated by remembering that even OR gates (already implemented at the molecular scale) are commonly physical integrations of wires, resistors, and diodes (or transistors), as mentioned in the previous paragraph. Furthermore, a functional integration of NOT and OR logic operations would be sufficient to achieve the same objective. In a fluorescent photoionic context, we can argue as follows. NOT logic represents the switching "off" of fluorescence when an ionic species arrives. Two-input OR logic represents unselective switching "on" of fluorescence when either of two ionic species arrive. So, NOR logic corresponds to the switching "off" of fluorescence when either of two ionic species arrive. Our **12**[22] fits the bill if the two ionic species are H^+ and Hg^{2+}. H^+ kills the fluorescence of this internal charge transfer (ICT) fluorophore, a 1,3-di(2′-pyridyl) pyrazoline, by launching a transfer of electronic excitation into vibrational quanta of N ··H–O bonds. The latter are formed when H_3O^+ docks into the bay region with its three nitrogen lone electron pairs. Hg^{2+} quenches the fluorescence of 12 in a different, but equally efficient, way. Hg^{2+} binds to the 2.2': 6'. 6" - terpyridyl look-alike, and the excited state of the complex takes on a ligand-to-metal charge transfer (LMCT) character verging on a PET process.

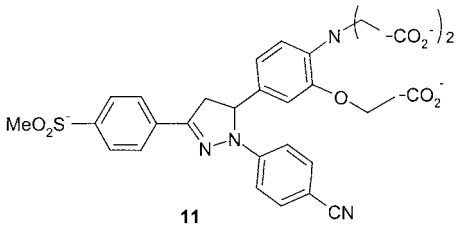

11

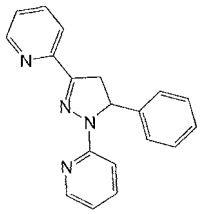

12

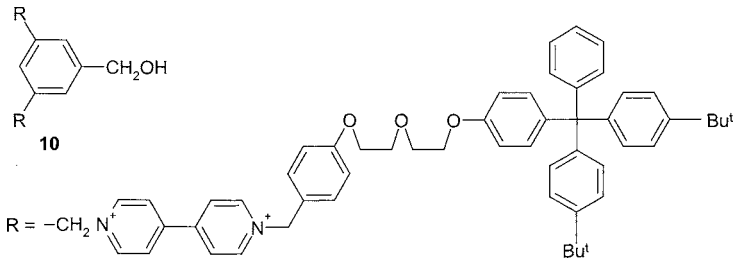

NAND

NAND logic (Fig. 2) can be discussed in much the same way as NOR logic was considered in the previous paragraph. While several molecular NAND gates exist,[23–25] we highlight Akkaya and Baytekin's **13**[25] here. because the entire experiment requires no new syntheses. Because 13 is a well-known fluorescent reagent in DNA research, it even binds to a single mononucleotide pair, such as the one involving adenine and thymine bases. In fact, it is likely that **13** stabilizes the Watson–Crick base pair via two amidine–phosphate interactions as well as some degree of aromatic π–π stacking. Nevertheless. the experiment requires substantial dilution of water with dimethylsulfoxide in order to be successful. Then, a significant drop in the intensity of the fluorescence spectrum is seen at 455 nm. No such drop is found if the mononucleotides are applied singly. Several other delights await readers of Ref. [25].

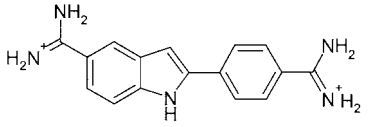

13

INHIBIT

INHIBIT logic is another type that can be viewed as an integration of NOT and AND operations. though in a different connectivity than seen with NAND logic. The NOT operation is only applied to IN_2 (Fig. *2)*. So, IN_2 is really a disabling input that kills the output, irrespective of the state of IN_1. Though three-input INHIBIT logic is known,[22] a two-input case comes from the work of Gunnlaugsson and colleagues that is based on the Tb^{3+} complex of **14**.[26] O_2 is the disabling input IN_2, which quenches the delayed, line-like emission. The role of IN_1 is taken by H^+, which tunes the absorption spectrum into the range of the excitation wavelength. Once excited. strong emission arises only if O_2 is barred.

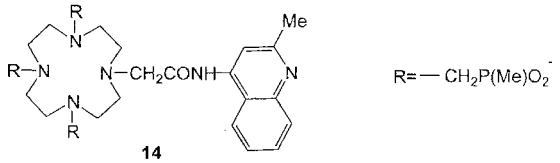

14

R= — $CH_2P(Me)O_2^-$

XOR

XOR logic (Fig. *2)* received a higher than normal amount of attention. because it is an essential part of semiconductor numeracy. Arithmetic units within computers are composed of XOR and AND gates running in parallel. Though an earlier example of a fluorescent molecular XOR gate driven by chemical inputs is available,[27] we put the spotlight on a recent fluorescent case driven by optical inputs.[28] Compound 15 shows a close structural and functional analogue of 7. One novel twist introduced by Pina, Balzani. and colleagues is that $[Co(CN)_6]^{3-}$ costars alongside 15. While **15** rapidly leads to a fluorescent cyclized product under the influence of light and H'. $[Co(CN)_6]^{3-}$ slowly hydrolyzes and ties up H^+ in the form of HCN. So when suitably high photon numbers are absorbed. the fluorescent cyclized product is turned back to 15 in the alkalinized solution. The second novel twist is the design of an experiment with two light flashes such that either flash alone produces a large amount of fluorescent product, whereas the flashes together lead to the alkalinized solution where the amount of the fluorescent product is very low. The latter situation of low fluorescence almost corresponds to the preirradiative condition. i.e., XOR logic applies. Ref. [28] contains more information.

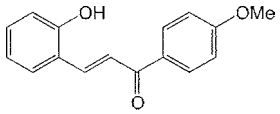

15

Our photoionic approach to XOR logic uses Ca^{2+} and H^+ inputs applied to **16**,[29] while transinittance is monitored at a wavelength close to the ion-free absorption band maximum. The chromophore within 16 is of the ICT type and has the two ion receptors attached at the opposite ends. The excited-state dipole arising from the cha ge transfer will suffer opposite energetic influences when each ion arrives. The monitored transmittance rises in each case, because the absorption band moves away from the monitoring wavelength. These two ionic influences virtually cancel each other when simultaneously applied. So. the monitored transmittance falls again to the original ion-free level. This XOR gate can be run in parallel with an optically and ionically compatible AND gate to produce a numerate molecular system for the first time outside of our brains.[29] Such a half-adder can "comprehend" the decimal numbers 0, 1, 2 but no higher.

Compound 9. discussed above with respect to AND logic, also contains an XOR logic gate within.[15] Whereas the fluorescence output at 430 nm from the second excited state produced AND logic from two *532* nm inputs, the emission output at 571 nm from the lowest excited state corresponds to XOR logic. The latter is naturally zero when both inputs are absent. Provision of a relatively low-intensity laser beam at *532* nm leads to strong fluorescence at 571 nm. A combination of input beams gives sufficient intensity to kick-start two-photon absorption to populate the second excited state at the expense of the lowest. So. the 571 nm emission is less than might have been expected (on the basis of one-photon

processes, exclusively). Overall, this means that **9** on its own can serve as a half-adder.

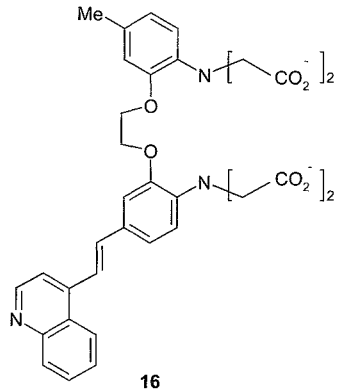

16

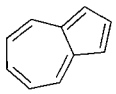

17

The results from Ref. [15] continue. The 571 nm emission of **9**, or the output from the XOR gate component, can be used to feed a second half-adder **17**, with a lowest excited state that is suitably lower than that of **9**. Electronic energy transfer (EET) is the link. The additional input (IN_3) required to run **17** is a third relatively low-intensity laser beam at 694 nm. As seen with **9**, Compound **17**'s lowest and higher excited state emissions at 746 and 375 nm, respectively, produce XOR and AND logic, respectively. Together, **9** and **17** constitute a full-adder if the outputs of the AND gate parts of **9** and **17** at 430 and 375 nm are put through a final OR gate. The authors suggest that this can be done with a one-photon broadband absorber, though guaranteeing a uniformly high signal in the "on" state may not be easy. Nevertheless, the numerical "comprehension" of this system does not meet a glass ceiling at decimal 2. Amazingly, all this is achieved with two compounds that are available from virtually any chemical supply house.

The numerical operations highlighted in the previous paragraphs underline the fact that several molecular logic systems now available involve the integration of gates as components. Of course, it must not be forgotten that even a two-input AND logic gate of the electronic variety, which can be emulated by a single molecular gate of the photoionic kind, consists of several wires, transistors, and resistors joined in an array. Some of these molecular logic systems involve integration of functions rather than physical components, e.g., **12**. Others involve a degree of physical component integration, as in the case of the parallel operation of **16** and its partner AND gate or in the case of the serial operations of **9** and **17**. Furthermore, **9** and **17** involve functional integrations within. So, molecular logic arrays containing parallel and serial links between components are growing. Dabestani's team[30] as well as Raymo and Giordani[31–33] recently consolidated this growth with some excellent examples.

CONCLUSION

After being in the realm of science fiction for a considerable time, molecular logic gates are now among us for real. Virtually all of the simpler logic types now have molecular implementations. Chemical, optical, and electrical interfaces proved successful for communication across the billion-fold size difference between molecules and ourselves. When we appreciate that these successes arrived in less than a decade, it is clear that the future will be fun.

ACKNOWLEDGMENTS

We thank the Department of Employment and Learning, Northern Ireland, and Avecia Ltd. for support of our efforts in this area.

ARTICLES OF FURTHER INTEREST

Alkali Metal Cations in Biochemistry, p. 1
Calixarenes and Their Analogues: Cation Complexation, p. 137
Crown Ethers, p. 326
Cryptands, p. 334
Cyclodextrins: Applications, p. 405
DNA Nanotechnology, p. 475
Electrochemical Sensors, p. 505
Energy and Electron Transfer in Supramolecular Systems, p. 535
Fluorescence Sensing of Anions, p. 566
Fluorescent Sensors, p. 572
Guanidium-Based Anion Receptors, p. 615
Imaging and Targeting, p. 687
Ion-Selective Electrodes, p. 747
Ionophores, p. 760
Lariat Ethers, p. 782
Luminescent Materials, p. 816
Luminescent Probes, p. 821
Molecular Logic Gates, p. 893
Molecular Switches, p. 917
Molecular Wires, p. 925
Molecular-Level Machines, p. 931
Photochemical Sensors, p. 1053
Simultaneous Binding of Cations and Anions, p. 1291
Simultaneous Binding of Cations and Neutral Molecules, p. 1295
Solvatochromism, p. 1330

Supramolecular Electrochemistry, p. 1412
Supramolecular Photochemistry, p. 1434
Torands, p. 1508
Zwitterion Receptor;., p. 1639

REFERENCES

1. Malvino A.P.: Brown J.A. Digital Computer Electronics. 3rd Ed.; Glencoe: Lake Forest, 1993.
2. *Principles of Neural Science*, 3rd Ed.: Kandel E.R.. Schwartz J.H.. Jessell T.M., Eds.; Elsevier: New York, 1991.
3. de Silva A.P.: Gunaratne H.Q.N.; McCoy C.P. A molecular photoionic and gate based on fluorescent signalling Nature 1993. 364. 42–44.
4. Brasselet S.: Moerner W.E. Fluorescence behaviour of single-molecule pH sensors. Single Mol. 2000, *1*, 17–23.
5. Molecular Wires. In *Encyclopedia of Supramolecular Chemistry*; Atwood J.L., Steed J.W., Eds.; Dekker, 2002.
6. Bumm L.A.: Arnold J.J.: Cygan M.T.: Dunbar T.D.; Burgin T.P.; Jones L.; Allara D.L.: Tour J.M.: Weiss P.S. Are single molecular wires conducting? Science 1996. 271. 1705–1707.
7. de Silva A.P.; Rupasinghe R.A.D.D. A new class of fluorescent pH indicators based on photoinduced electron-transfer. J. Chem. Soc.. Chern. Cornmun. 1985. 1669–1670.
8. de Silva A.P.; McClean G.D.; Moody T.S. Fluorescent Sensors. In *Encyclopedia of Supramolecular Chemistry*; Atwood J.L.. Steed J.W.. Eds.; Dekker. 2002.
9. Bissell R.A.; de Silva A.P.: Gunaratne H.Q.N.: Lynch P.L.M.: Maguire G.E.M.; McCoy C.P.: Sandanayake K.R.A.S. Fluorescent PET (photoinduced electron-transfer) sensors. Top. Curr. Chern. 1993. 168. 223--264.
10. Derycke V.: Martel R.; Appenzeller J.: Avouris P.H. Carbon nanotube inter- and intramolecular logic gates. Nano lett. 2001. *1*, 453–456.
11. Service R.F. Molecules get wired. Science 2001, 294. 2442–2443.
12. de Silva A.P.; Gunaratne H.Q.N.; Lynch P.L.M. Luminescence and charge-transfer. 4. On–off fluorescent PET (photoinduced electron-transfer) sensors with pyridine receptors—1,3-diaryl-5-pyridyl-4,5-dihydropyrazoles J. Chem. Soc.. Perkin Trans. 1995. 2, 685–690.
13. Pina F.; Roque A.; Melo M.J.; Maestri I.; Belladelli L.: Balzani V. Multistateimultifunctional molecular-level systems: Light and pH switching between the various forms of a synthetic flavylium salt. Chem. Eur. J. 1998, 4. 1184–1191.
14. Lukas A.S.; Bushard P.J.: Wasielewski M.R. Ultrafast molecular logic gate based on optical switching between two long-lived radical ion pair states. J. Am. Chem. Soc. 2001, *123*, 2440–2441.
15. Remacle F.: Speiser S.: Levine R.D. Intermolecular and intramolecular logic gates. J. Phys. Chem.. B 2001. 105. 5589–5591.
16. Birge R.R. Molecular electronics. In *Nanotechnology: Research and Perspectives*; Crandall B.C.. Lewis J., Eds.; MIT Press: Cambridge. MA, 1992: 149–170.
17. Turro N.J.: Ramamurthy V.: Cherry W.; Farneth W. The effect of wavelength on organic photoreactions in solution: Reactions from upper excited states. Chern. Rev. 1978. 78. 125–145.
18. Zhang T.H.; Zhang C.P.; Fu G.H.: Li Y.D.; Gu L.Q.: Zhang G.Y.; Song Q.W.; Parsons B.: Birge R.R. All-optical logic gates using bacteriorhodopsin films. Opt. Eng. 2000. 39. 527–534.
19. Collier C.P.: Wong E.W.: Belohradsky M.; Raymo F.M.: Stoddart J.F.: Kuekes P.J.; Williams R.S.: Heath J.R. Electronically configurable molecular-based logic gates. Science 1999. *285*. 391–394.
20. Metzger R.M. Electrical rectification by a molecule: The advent of unimolecular electronic devices. Acc. Chem. Res. 1999, 32. 950–957.
21. Brady A.C.: Hodder B.; Martin A.S.: Sambles J.R.: Ewels C.P.; Jones R.: Briddon P.R.: Musa A.M.; Panetta C.A.F.; Mattern D.L. Molecular rectification with M/(D-sigma-A LB film)/M junctions. J. Mater. Chem. 1999. *9*, 2271–2275.
22. de Silva A.P.: Dixon I.M.: Gunaratne H.Q.N.; Gunnlaugsson T.; Maxwell P.R.S.: Rice T.E. Integration of logic functions and sequential operation of gates at the molecular-scale. J. Am. Chem. Soc. 1999. 121. 1393–1394.
23. Iwata S.; Tanaka K. A novel cation and anion recognition host having pyrido[1′,2′/1,2]imidazo[4,5-*b*]pyrazine as the fluorophore. J. Chern. Soc.. Chem. Cornmun. 1995. 1491–1492.
24. Parker D.; Williams J.A.C. Taking advantage of the pH and pO(2) sensitivity of a luminescent macrocyclic terbium phenanthridyl complex. Chem. Cornmun. 1998. 245–246.
25. Baytekin H.T.; Akkaya E.U. A molecular NAND gate based on Watson–Crick base pairing. Org. Lett. 2080. 2, 1725–1727.
26. Gunnlaugsson T.; Mac Donaill D.A.: Parker D. Luminescent molecular logic gates: The two-input inhibit (INH) function. Chem. Commun. 2000. 93–94.
27. Credi A.; Balzani V.; Langford S.J.; Stoddart J.F. Logic operations at the molecular level. An XOR gate based on a molecular machine. J. Am. Chem. Soc. 1997. 119. 2679–2681.
28. Pina F.: Melo M.J.: Maestri M.: Passaniti P.; Balzani V. Artificial chemical systems capable of mimicking some elementary properties of neurons. J. Am. Chem. Soc. 2000. 122. 4496–4498.
29. de Silva A.P.; McClenaghan N.D. Proof-of-principle of molecular-scale arithmetic. J. Am. Chern. Soc. 2000. 122. 3965–3966.
30. Ji H.F.: Dabestani R.; Brown G.M. A supramolecular fluorescent probe. activated by protons to detect cesium and potassium ions. mimics the function of a logic gate. J. Am. Chem. Soc. 2000, 122. 9306–9307.
31. Raymo F.M.; Giordani S. Signal processing at the molecular level. J. Am. Chem. Soc. 2001, *123*, 4651–4652.
32. Raymo F.M.; Giordani S. Digital communication through intermolecular fluorescence modulation. Org. Lett. 2001, 3. 1833–1836.
33. Raymo F.M.: Giordani S. Multichannel digital transmission in an optical network of communicating molecules. J. Am. Chem. Soc. 2002.124.

Molecular Modeling and Related Computational Techniques

M

Manuela Grotjahn
Torsten Rambusch
Karsten Gloe
Technische Universitat Dresden, Dresden, Germany

Leonard F. Lindoy
The University of Sydney, Sydney, New South Wales, Australia

INTRODUCTION

The evolution of computational chemistry, facilitated by the development of ever more powerful computers in conjunction with more efficient computational methods, has increasingly contributed to a better understanding of structural and thermodynamical features of chemical systems.[1] In this context, computational studies of supramolecular systems became increasingly popular in order to interpret processes of molecular recognition and supramolecular organization.[''']

Typically, supramolecular systems incorporate noncovalent interactions, such as hydrogen bonding, electrostatic. van der Waals, and donor–acceptor interactions — all of which are amenable to simulation. Thus, even though normal characterization by physical methods may lead to supramolecular systems that are chemically well defined, coinputational studies often provide the means with which to obtain additional complementary structural and electronic information about the system. This, in turn, can help rationalize experimental data and lead to predictions concerning the outcomes of future experiments.

Generally, molecular modeling studies provide deeper insights into conformational and recognition properties and enable questions concerning preorganization. complementarity, and binding selectivity to be addressed. In addition to the countless calculations of individual molecules in the gas phase, increasingly. the influence of solvent and environinental effects on the precise structure and dynamics of molecular systems has been considered.

MOLECULAR MODELING — THE MAIN TECHNIQUES

Several computational methods are routinely employed for the study of molecular systems.[1 3–5] However, due to limitations of space, it is not possible here to discuss each of these in detail. Rather, a brief overview is presented of the common techniques employed in computational studies, with some important features of each type highlighted. Reviews covering the use of computational methods, in particular, supramolecular applications, have appeared. These include studies concerned with sulfur-containing host–guest systems,[6] cyclodextrins[7] (in each case using methods that range from molecular mechanics to ab initio quantum mechanics), macrocycles,[8,9] calixarenes[10] and anion-binding receptors[''' (all mainly molecular mechanics), cyclophanes[12] (Monte Carlo methods). and siinulations of the complexation dynamics and phase-transfer behavior of synthetic ionophores[13] (molecular dynamics).

Molecular Mechanics (MM)

Molecular mechanics or force field methods are empirical procedures widely used for studying molecular structure — particularly of medium-sized molecules, although the technique was also employed for larger systems; including supramolecular host–guest design. One important advantage of this method is its high calculation speed.

A force field is a set of energy functions that describes the potential energy surface of the investigated system. It includes functions for bond lengths and angles. torsion angles. out-of-plane coordinates, van der Waals interactions, and electrostatic interactions. Typically, parameterization based on a large amount of experiinental data is required for the development of a reliable force field. Although different force fields frequently involve different potentials. reflecting differences in their calibration procedures, they, nevertheless. usually give rise to similar calculated geometries. Allinger's MM2 and MM3 force fields. AMBER, GHARMM, and MMFF, are examples of widely used force fields, although a number of others also exist.''' It needs to be noted that the calculated energies

Encyclopedia of Supramolecular Chemistry
DOI: 10.1081/E-ESMC 120012817

from MM have no direct physical meaning but are useful in a relative sense.

MM calculations involving metal-containing species are usually not as straightforward as those for organic species,[14] especially when transition metals are involved. Special care needs to be exercised when considering the relative energies of such species, as these can be force field dependent.[15–17] Where possible, in such cases, it is prudent to interpret any result in the context of appropriate experimental data for the system.

Quantum Mechanics (QM)

An objective of quantum mechanical methods is to describe the positions of all electrons and nuclei that occur in a molecular system.[1] Using these methods, the calculation of molecular geometries. electron density distributions, and some other molecular properties is possible. with electrons and nuclei treated explicitly. The starting point and basis of quantum mechanics is the Schrodinger equation, which can be solved using the Hartree–Fock formalism. Quantum mechanical methods include ab initio and semiempirical procedures. Ab initio methods range from the simplest Hartree–Fock, self-consistent field inethod to methods that include some treatment of the effects of electron correlation, such as those based on Moller–Plesset perturbation theory, without ignoring or approximating any of the integrals or terms in the Hamiltonian operator.

Semiempirical methods. for example, MNDO. AM1. and PM3. are simplifications of ab initio molecular orbital theory and employ empirically determined parameters; in essence, they only differ in the approximations being made. These methods involve adjustable parameters associated with molecular properties that are calibrated against experimental data. The chief advantage of semiempirical calculations over ab initio calculations is that they are several orders of magnitude faster. Thus, calculations for systems of up to c. 200 atoms are currently possible. whereby with ab initio methods, the limit is a moderately sized molecule (about 50 atoms at the time of writing), if rational results are to be obtained. Frequently, semieinpirical methods have proved to be the computational procedures of choice for studying relatively large molecules.

Density Functional Theory (DFT)

Density functional theory is now an established alternative to conventional ab initio methods. It is well documented that with DFT calculations. geometries, bonding energies. and spectral characteristics of a wide range of molecular systems can accurately be predicted. The advantage of DFT over ab initio calculations is that calculations for systems of up to c. 100 atoms are possible. The DFT approach is based upon a strategy of modeling electron correlation via general functionals of the electron density instead of a wave function. There are now many different functionals. each containing a functional for exchange and a functional for correlation. Currently, the B3LYP hybrid functional is commonly used for inolecular calculations.

Hybrid Methods (QM/MM)

An interesting approach used for the treatment of particular systems has been to employ a combination of MM and QM methods. In such a case. the information about molecular structure and therinodynarnic properties obtained by MM. and on the electronic behavior. bond breaking. and bond formation resulting from QM, can be brought together. Hybrid methods have been employed to investigate chemical processes in large molecular systems and in condensed phases. For example. in such a study. a solute molecule is treated quantum mechanically. while the solvent molecules are approximated by a force field procedure. It is noted that hybrid methods of the present type have the potential advantage of being able to describe the role of the electrons as a natural part of the overall simulation.

Molecular Dynamics (MD)

Molecular dynamics simulations emerged as an important tool for the study of motion in inolecular systems. During a MD simulation. the classical Newtonian equations of motion for interacting atoms are solved interactively. The force on an atom is given by the negative gradient of the potential. which is derived from the same force field employed in MM calculations. The solution of the differential equations gives the position of each atom at each time step over a total time interval limited by the computational speed of the computer. the force field, and the size of the molecular system. Trajectories can be used to investigate time-dependent phenomena, as in conformational transitions, and thermodynamic averages. Further. use of the method gives a high probability that a given conformational search will be complete. Because MD is capable of overcoming the energy barriers between different conformations, it is possible to locate local minima. provided the simulation time and temperature protocol are appropriate.

The application of MD to liquids or solvent–solute systems allows for the computation of properties such as diffusion coefficients or radial distribution functions for use in statistical mechanical treatments.

Monte Carlo (MC) Methods

Monte Carlo simulations are inherently of a statistical nature and provide an alternative to MD. They involve the generation of a sequence of molecular configurations showing a Boltzmann distribution in the potential energies of the selected configurations. The calculation starts with an optimized structure, and new Cartesian coordinates are assigned randomly. The resulting conformation is then minimized using MM, and this procedure is repeated. The minimized conformation obtained is compared with the previously generated one and only saved if it is unique. This method can be employed to treat most molecules. however, for larger, highly flexible species, the conformational space may be too large for convergence to occur. Ab initio MD simulations (Carr Parinello, CPMD), which are based on Newtonian dynamics and where the interaction potential is handled quantum mechanically,[18] tend to be important for the treatment of large systems.

MC simulations (as for MD simulations) are often more difficult than running single-molecule calculations. The input must specify not only the molecular structure but also the temperature, pressure, density, boundary conditions, time steps, and more.

Conformational Analysis

Molecules are not rigid, with the atoms in a molecule moving continuously. The conformational space of a

Table 1 Comparison of commercial computational packages

Programs	MM	MC	MD	QM	DFT	Graphic interface	Possible types of calculations
GAUSSIAN	+	—	—	+	+	GAUSSVIEW MOLDEN CERIUS	NMR chemical shifts, nonlinear optical properties. transition structures. IRC, frequency. etc.
http://208.192.129.32/index.htm							
GAMESS http://www.msg.ameslab.gov/GAMESS/GAMESS.html	—	—	—	+	—	MOLDEN	Transition structures; reaction coordinates. vibrational frequencies, etc.
ADF http://www.scm.com/	—	—	—	—	+	CERIUS	Transition structures. IRC. frequency, electronic excited states, etc.
AMBER 6.0 http://www.amber.ucsf.edu/amber.html	+	—	+	—	—	VMD	MM studies in solution
MOPAC 2000 http://www.fqspl.com.pl/mopac2000/	—	—	–	+	—	+	Molecular properties
SPARTAN http:llwww.\vavefun.com/	+	—	—	+	+	+	Transition structures, conformational searches. etc.
HYPERCHEM http://www.hyper.com/	+	+	+	+	+	+	Transition structures, vibrational frequencies, electronic excited states, etc.
MATERIAL EXPLORER http://www.addlink.es/product/fujitsu/MaterialExplorer.htm	+	—	+	—	—		MM studies in solution
SYBYL http://ww\v.tripos.com	+	—	+	+	—	+	Conformational searches, etc.
MOMEC 97 http://www.chemcad.fr/en/produits/chemische/momec.html	+	—	—	—	—	HYPERCHEM	Inorganic compounds
CHEM3D http://www.camsoft.com/	+	—	+	+	—		Transition structures, dipole moments, population analysis, polarizability. etc.

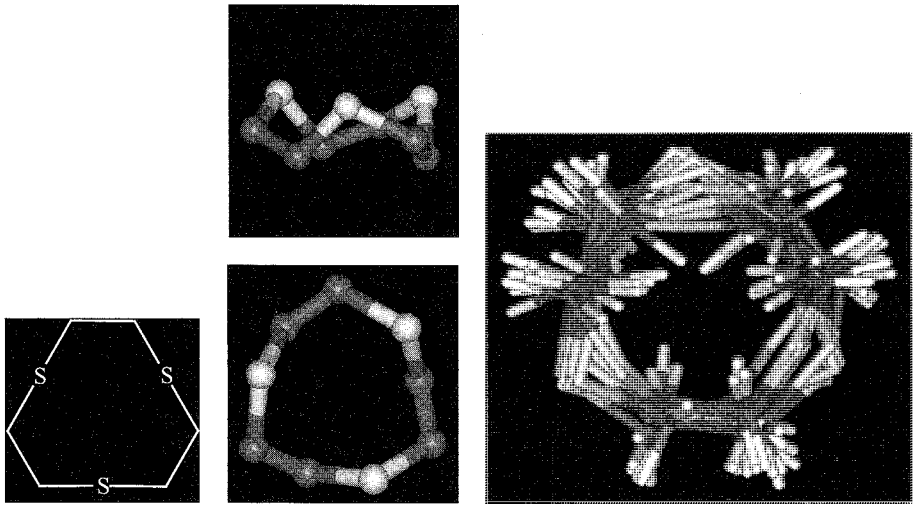

Fig. 1 (a) Formula. (b) x-ray structure. and (c) calculated conformers of the 1.4.7-trithiacyclononane 9S3 using a systematic search. *(View this art in color at www.dekker.com.)*

system can be calculated using QM or MM methods. However, because QM calculations are so time consuming, they are normally not employed for conformational analysis of large and flexible molecules. In such cases, MM, MD, and MC methods or a systematic search of conformational space may be more appropriate tools for undertaking conformational analysis. In the latter case. torsion angles are systematically varied in order to generate all possible configurations. The number of generated structures depends on the chosen step size and the number of rotatable bonds *n* (with the number increasing with the nth power).

COMMERCIAL PACKAGES

Most of the computational techniques so far discussed are available as commercial software packages. which differ in cost, functionality. efficiency, ease of use, and automation. Some widely used computational chemistry software packages and their Internet addresses are listed in Table 1.

COMPARISON OF SELECTED METHODS

The relative quality of structure calculations by different computational techniques was assessed using the small macrocycle 1,4,7-trithiacyclononane 9S3 (Fig. 1a.b)—a ligand showing a complexation preference for soft transition and post-transition metal ions.[6] Given in Fig. 2 is a compilation of the deviations (represented by the respective RMS values) of the calculated structures from the corresponding crystal structure.[19] It is clearly shown that the force field MMFF, the ab initio method MP2 [basic set 6-311G(2d,p)], and the DFT method BP86 [basic set GGA-IV(TZ+P)] lead to comparable results in this case.

A conformational analysis using the MM or MD techniques allowed the identification of 11 conformers with small energy differences separating them (Fig. lc). For the structure calculation of the corresponding Ag(I) and Hg(II) complexes[iG1] with 9S3. only the DFT method using the BP functional yielded satisfactory results.

FURTHER CONSIDERATIONS

Each of the methods discussed has its strengths and weaknesses (Table 2), and one needs to be careful when selecting the calculation method in order to ensure the validity of the results. Indeed. it seems as important to know the limitations of a method as it is to know its capabiiities. Further, it is also important to be aware of the theoretical basis underlying the procedure as well as the nature and role of the type of paramete ization used.

A common problem in many calculations revolves around obtaining adequate sampling of the possible configurations accessible to a molecular system under investigation. Similarly. there are often difficulties associated with correctly evaluating the potential energies of these configurations. For a given system, there usually needs to be a compromise between the chosen level of

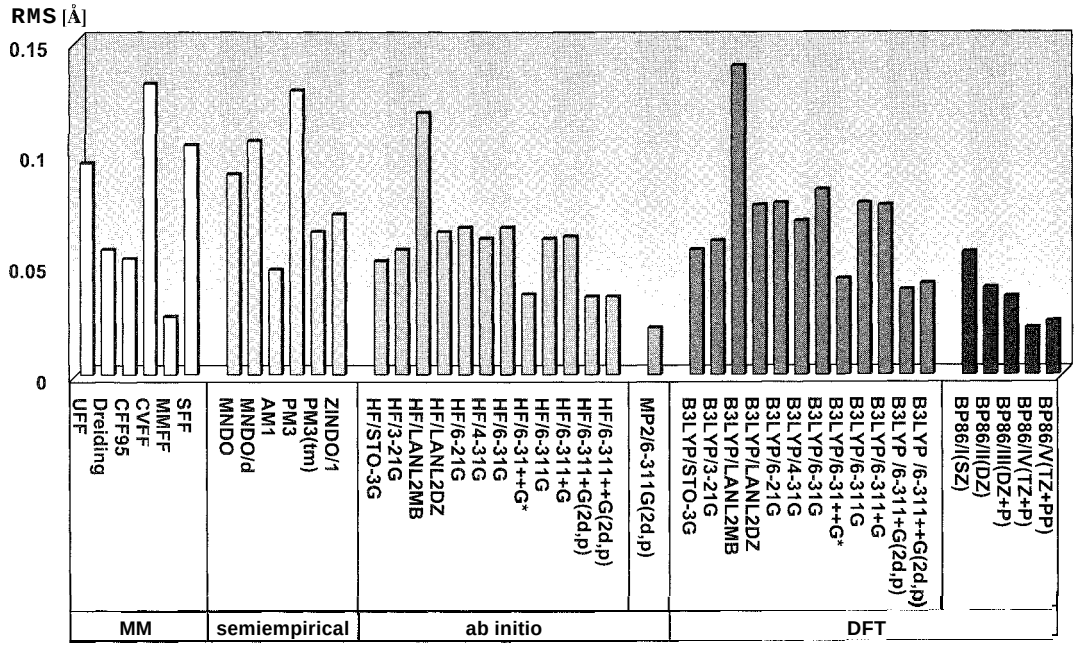

$$RMS\,[\text{Å}] = \sqrt{\sum \frac{(x_a - x_b)^2 + (y_a - y_b)^2 + (z_a - z_b)^2}{N}}$$

N is the number of atoms over which the *Root Mean Square* is measured;
x, y and *z* are the Cartesian coordinates of the calculated and the X-ray structures.

Fig. 2 Compilation of the deviations of the calculated structures of **9S3** from the corresponding crystal structure using MM, QM, and DFT methods.

computation employed and the available computer resources. In practice, such a consideration may effectively limit the size of a molecular system that can be investigated by a given technique, if the results are to be meaningful.

While X-ray diffraction studies of supramolecular systems yield solid-state structures directly, they are frequently of additional utility by providing the "starting" structures for computer simulations. In this context, it is noted that the relevance of solid-state structural data to solution behavior is often not straightforward, because the statistical presence of conformers and of various host–guest species (and their associated time-dependent dynamic processes) may then come into play. As already mentioned, these features are amenable for investigation

Table 2 Comparison of methods

Method	*Advantage*	*Disadvantage*
MM	Modeling of giant molecules (proteins, segments of DNA)	Many chemical properties not defined (electronic excited states)
QM—semiempirical	Good for predicting molecular geometry and energetics, predicting vibrational modes and transition structures (but does so less reliably than ab initio methods)	Poor results for van der Waals and dispersion intermolecular forces (lack of diffuse basic functions)
QM—ab initio	Very good qualitive results	Expensive (computer CPU time, memory and disk space)
DFT	Less computationally intensive than ab initio (similar accuracy), optimal accuracy versus CPU time	Some classes of problems not yet explored

by computational means, even though the situation in solution is usually different from that in the gas phase and in the solid state. For example. MD or MC simulations may be employed to provide statistical representations of the solvent shell around a solute. Such studies met with various degrees of success: in many cases, they were successful in providing insight into explicit solvation behavior, as well as in yielding a microscopic view of host–guest complexes and their solvation. However, the inclusion of solvation (either implicitly or explicitly) increases the computational expense, and this, in turn. may limit the level of sophistication of the solvation model that can be employed.

SOME CASE STUDIES

Examples of molecular modeling studies that exemplify the use of individual calculation types will now be discussed in order to further illustrate the manifold applications of such calculations.

An MD Study

Although variable temperature line-broadening NMR investigations are frequently employed to obtain conformational and dynamic information for supramolecular systems, for a number of reasons. such measurements are not always possible. As an alternative, dynamic processes of this type can sometimes be investigated using computational techniques. An example is given by an investigation of the maleonitrile-dithiacrown ether **mn-S_2O_{n+1}** (n=1–4) (Fig. 3) ligands and their interaction with Pt(II).[20] Simulations using molecular dynamics of processes involving the **mn-S_2O_{n+1}** (n=1–3) ligands and their Pt(II) complexes were performed at different temperatures. and these investigations were also coupled to search calculations. Different ground-state conformations for the ligands and their Pt(II) complexes were obtained, where the exodentate orientation of the *S* atoms proved to be preferred. Sulfur inversion was observed at *500* K for [**$PtCl_2$(mn-$15S_2O_3$)**] and at 373 K for [**$PtCl_2$(mn-$18S_2O_4$)**]. The localization of the transition state proved difficult, because simultaneous changes of more than one dihedral angle were involved in the search. The semiempirical (PM3) energy barriers were found to be about *5* kcal/mol (21 kJ/mol). These calculated low barriers are in accordance with the high flexibility of the ring systems and with the experimental results.

An MC Simulation Study

In order to obtain insight into the conformational influences affecting the stronger Ca^{2+} selectivity of *p-t*-butylcalix[4]arene-ethyleneoxydiphenylphosphine oxide **1** relative to *p-t*-butylcalix[4]arene-methyleneoxydiphenylphosphine oxide 2 (Fig. 3), MC conformational searches in conjunction with Merck Molecular Force Field calculations were performed.[21] From these studies, it appears that the selectivity of **1** toward Ca^{2+} lies in the adoption of a unique eight-fold coordinate complex that involves close interaction of all four phenoxy and four phosphine oxide oxygen atoms with the Ca^{2+} ion. In contrast, for 2, the closeness of the phenoxy oxygen atoms and the phosphine oxide oxygen atoms appears to allow a number of metal ions to form stable eight-coordinate complexes.

Computational Studies of Host–Guest Complexation in Solution

The behavior of a hexaprotonated aminocryptand **3** (Fig. 3) toward 1:1 halide inclusion in aqueous solution was investigated using MD simulations. Structural aspects,

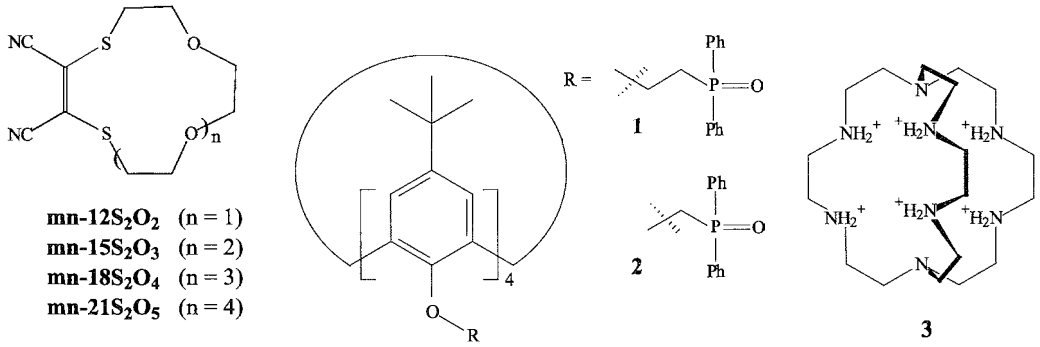

Fig. *3* The host compounds discussed in the text.

hydration properties, and status of external halide counterions were probed in order to gain microscopic insight into the host–guest complexes and their environments.[22] This represented the first reported study of spontaneous ion binding by a polycyclic ligand.

The nature of the 1:1 inclusion complexes of **3** with the fluoride or chloride ion in water were described and compared with the X-ray structure of the relevant compound. Furthermore, simulations involving the uncomplexed ligand and both anions led to the experimentally observed F^- over Cl^- binding selectivity. which was reproduced quantitatively by free-energy perturbation (FEP) calculations.[23] The latter provide a thermodynamic measure of the relative interaction and binding free energies in solution, these are, of course. of particular interest in supramolecular chemistry, where molecular association is of paramount importance.

FUTURE PROSPECTS

Molecular modeling is an essential tool in supramolecular chemistry. A significant number of computational studies of macrocyclic compounds continue to be directed toward understanding molecular structural features in the gas and liquid phases. These include the geometry. charge distribution, lipophilicity pattern. energetics of host–guest binding, as well as an assessment of the structure and dynamics of individual host–guest complexes. Such data are often useful for explaining observed molecular recognition behavior. for predicting the structure of a flexible receptor in solution, for assessing the binding and extraction properties of a given ionophore, as well as for understanding the self-assembling properties of monomer units. The computational tools used are typically both quantum mechanical and force field based.

With the further development of hardware and improvements in theory and algorithms, molecular modeling will undoubtedly be employed increasingly as a useful tool for solving problems in supramolecular chemistry in a rapid and effective way. Clearly. it will increasingly aid in the interpretation of experimental results as well as allow for the prediction of an extended range of supramolecular properties and behavior.

What is the prognosis for the future of computational chemistry? Computing hardware is nowadays stellar. Even commonplace computers are capable of handling calculations of systems containing thousands of particles and simulation times in the range of nanoseconds on a single processor. As the power of modern computers continues to grow. it is only a matter of time before computational techniques are used more routinely for problems of interest to supramolecular chemists. Calculations that are more accurate and able to handle a wider range of compounds will be possible.

ARTICLES OF **FURTHER INTEREST**

Calixarenes: Synthesis and Historical Perspectives, p. *153*
Crown Ethers, p. *326*
Cryptands, p. *334*
Cyclodextrins, p. *398*
Cyclophanes: Endoacidic, Endobasic, and Endolipophilic Cavities, p. *424*

REFERENCES

1. *Encyclopedia of Computational Chemistry*; Schleyer, P.v.R., Allinger. N.L.. Clark, T., Gasteiger, J.. Kollman, P.A.. Schaefer. H.F.. III. Schreiner. P.R., Eds.: John Wiley & Sons: Chichester. UK, 1998: Vol. 1–5. and references therein.
2. *Computational* Approaches *in Supramolecular Chemistry*; Wipff. G., Ed.; Kluwer Academic Publishers: Dordrecht. 1994.
3. Young, D. *Computational* Chemistry: A Practical *Guide for Applying Techniques* to Real *World Problems*; Wiley-Interscience: New York. 2001.
4. Leach. A.R. *Molecular* Modeling: Principles *and Applications*; Longman: Harlow. 1996.
5. Harrison. P. *Computational* Methods *in* Physics, *Chemistry* and *Biology: An Introduction*: Wiley: Chichester. 2001.
6. Rambusch. T.: Hollmann-Gloe. K.: Gloe. K. Molecular modeling studies of sulfur containing host/guest systems. J. Prakt. Chem. **1999**, 341 (3), 202–217.
7. Lipkowitz, K.B. Applications of computational chemistry to the study of cyclodextrins. Chem. Rev. 1998. **98.** 1829–1873.
8. Comba. P. Metal ion selectivity and molecular modeling. Coord. Chem. Rev. **1999**, *186*. 81–98.
9. Hay, B.P.: Hancock. R.D. The role of donor group orientation as a factor in metal ion recognition by ligands. Coord. Chem. Rev. 2001. 212. 61–78.
10. Van Veggel, F.C.J.M. Molecular Modeling of Calixarenes and Their Host–Guest Complexes. In *Calixarenes in* Action; Mandolini, L.. Ungaro, R.. Eds.; Imperial College Press: Singapore. 2000: 11–36.
11. Wiorkiewicz-Kucrera. J.: Bowman-James, K. Anion Binding Receptors: Theoretical Studies. In *Supramolecular Chemistry of Anions*; Bianchi. A.. Bowman-James, K., Garcia-Espana, E.. Eds.; Wiley-VCH: New York, 1997: 335–354.
12. Jorgensen. W.L.: Nguyen, T.B. Structure and Binding for Cyclophane-Arene Complexes in Water from Monte Carlo Simulations. In *Supramolecular* Chemistn: Balzani. V.. De Cola, L.. Eds.: Kluwer Acad. Pub.: Dordrecht, 1992; 383–394.

13. Wipff. G. Molecular Dynamics Simulations on Cation Complexation and Extraction. In *Calixarenes 2001;* Harrowfield, J., Vicens. J., Asfari. Z.. Bohmer. V.. Eds.: Kluwer Acad. Pub.: Dordrecht. 2001: 312–333.
14. Comba. P.; Hamhley, T.W. *Molecular Modeling of Inorganic Compounds*; Wiley-VCH: Weinheim. 2000.
15 Adam. K.R.; Antolovich. M.; Brigden, L.G.: Lindoy, L.F. Comparative molecular mechanics study of the low-spin nickel(II) complexes of an extended series of tetraaza macrocycles. J. Am. Chem. Soc. **1991**, *113* (9). 3346–3551.
16. Adam, K.R.: Atkinson, I.M.: Antolovich, M.: Brigden, L.G.: Lindoy. L.F. Comparative molecular mechanics study of the high-spin nickel(II) complexes of an extended series of tetraaza macrocycles. J. Mol. Struct. **1994**, 323 (9). 223–231.
17. Bygott, A.M.T.: Sargeson. A.M. Critical evaluation of metal complex molecular mechanics. Part I. Cobalt(III) hexaarnines. Inorg. Chem. **1998**, 37, 4795–4806.
18. Rothlisberger, U. 15 Years of Car–Parrinello Simulations in Physics, Chemistry and Biology. In *Computational Chemistry: Reviews* qf *Current Trends*; Leszczynski. J.. Ed.; World Scientific: Singapore. 2001: Vol. 6.
19. Glass. R.S.: Wilson, G.S.: Setzer. W.N. Crystal and molecular structure of 1,4,7-trithiacyclononane. J. Am. Chem. Soc. 1980. *102* (15). 5068–5069.
20. Grotjahn. M.: Jager. N.: Drexler, H.-J.; Holdt. H.-J.; Kleinpeter, E. Molecular modeling study of the $PtCl_2$ complexes of unsaturated S_2O_{n+1} coronands: Dynamic simulations and investigation of the ring interconversion. J. Mol. Model. 1999. *5*. 72–77.
21. Kane. P.; Kincaid, K.: Fayne, D.: Diamond. D.: McKervey, M.A. Modelling metal complexes of calixarene esters and phosphine oxides using molecular mechanics. J. Mol. Model. 2000. 6. 272–281.
22. Pierre. P.: Schurhammer, R.: Wipff. G. Halide anion recognition in water by a hexaprotonated octaaza-crypt-and: A molecular dynamics investigation. Chem. Eur. J. **2000**, 6 (23). 4257–4264.
23. Kollman. P. Free energy calculations: Applications to chemical and biochemical phenomena. Chem. Rev. **1993**, *93* (7). 2395–2417.

Molecular Squares, Boxes, and Cubes

Peter H. Dinolfo
Shih-Sheng Sun
Joseph T. Hupp
Northwestern University, Evanston, Illinois, U.S.A.

INTRODUCTION

Molecular squares, boxes, and cubes featuring transition-metal corners are the focus of tremendous activity in contemporary synthetic coordination chemistry. Their design and study comprise a promising subfield of inorganic and organometallic supramolecular chemistry. The interest in these objects is partly aesthetic: they are beautiful high-symmetry assemblies. The interest is also functional: the assemblies contain cavities that are capable, in principle, of encapsulating, and then sensing, processing, or transporting useful molecules or atomic ions—in other words, all the functions associated with organic host–guest chemistry.

Why coordination chemistry? And why discrete molecules? Actually. metal-free squares and boxes exist, albeit, without the ubiquity of the metal-containing systems. Notable examples include the various viologen-derived cyclophanes or boxes of Stoddart and coworkers,[1]—clear antecedents of many molecular squares. What metal ions offer are a readily accessible range of angles for ligand-metal-ligand subunits (including right angles, which is difficult to achieve with carbon chemistry), structural predictability based on well-known metal-ion coordination motifs (linear. octahedral. square planar, etc.), a range of charges, a range of ligand-binding capacities, and, perhaps most importantly, a propensity to engage in highly efficient directed assembly. Metals, of course, can also usefully expand the range of redox, photophysical, and catalytic properties displayed by supramolecular assemblies. In principle, squares and other structures can be assembled not only as discrete molecules, but also as porous two- and three-dimensional arrays or coordination polymers. While the array strategy clearly works[2], a common complication is the formation of interpenetrating grids that eliminate most of the void volume associated with isolated cavities. Preassembly of discrete squares and related structures avoids the problem; indeed, to date there are no examples of extended catenation. the molecular equivalent of grid interpenetration.

An important idea suggested by the chemistry of coordination polymers is higher-order assembly of squares and other structures into large void-volume, high-porosity molecular materials. This can be done surprisingly easily using van der Waals interactions (which, of course, are large for large molecules), although more elaborate and controllable strategies are emerging. In any case, the notion of porous molecular materials and the stacking of cavities to make uniformly sized channels is one that is receiving increasing attention as supramolecular coordination chemistry evolves from a mainly synthetic effort toward one that also strongly focuses on function.

Finally, the connection to nanotechnology cannot be overlooked. The cavity sizes of existing molecular squares, boxes, and cubes extend from about 0.4–5 nm, as measured along the cavity edges. These, of course, are the right dimensions to couple to other nanoscale objects or simply to function as building blocks for periodically nanostructured thin films or other materials. In these contexts, descriptions of functional suparamolecular assemblies as nanoreactors, nanofactories, nanogates, nanotemplates, and so on, are appropriate.

MOLECULAR SQUARES

Some Early Examples

The first metal-containing molecular squares appeared in 1983.[3] They featured $M(CO)_4$ (M=Cr, W, or Mo) corners and $P(OCH_2)_3P$ ligand edges, **1** (Fig. 1). While these compounds are potentially capable of behaving as hosts for small molecular guests, interest in squares as receptors or hosts really did not take hold until 1990 when an ethylenediamine Pd(II) square featuring 4,4′-bipyridyl edges, **2**, was shown to function as a hydrophobic host for organic guests in water as solvent.[4,5] Aqueous solubility was engendered by the square's 8+ charge and by the use of nitrate as a counterion. Nuclear magnetic resonance (NMR) titrations revealed association constants on the order of 10^2 for planar, electron-rich aromatic species. while aliphatic compounds showed little propensity to associate. The difference was attributed to the ability of the electron-rich, aromatic guests to form charge-transfer complexes with the bridging bipyridine ligands of the molecular square. Extension of the chemistry to Pt(II) was

DOI: 10.1081/E-ESMC 120012772

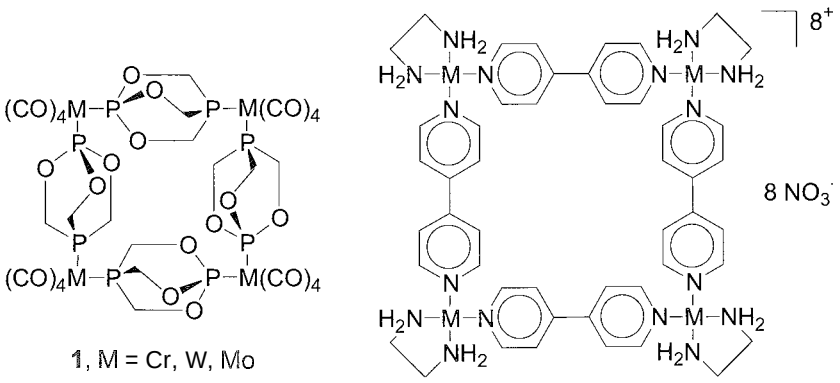

Fig. 1 Two of the earliest examples of tetrametallic molecular squares

followed by the observation that for longer edges. closely related square and triangle structures can coexist in dynamic equilibrium. The equilibrium is concentration-dependent, with entropy favoring triangles, because they assemble from fewer components.[6] A related transformation, observed with a Pd(II) square and a pair of dimeric Pd(II) loops in D_2O as solvent. is formation of two copies of a nonsquare catenated assembly.[7] The driving force for catenation is primarily the enhancement of dispersion interactions accompanying van der Waals contact of pairs of ligands.[8] Formation of the catenated species should occur most readily in solvents that offer comparatively little stabilization via dispersion interactions.

Another early approach, since generalized to more than 70 different squares, triangles, prisms, rectangles, and dodecahedra, also relies upon Pd(II) and Pt(II) as corners but with chelating diphosphine ligands in place of ethylenediamine to provide solubility and enforce subsequent ***cis*** coordination.[9] The combination of corner units with difunctional imine edges leads to octa-cationic squares. The variety of ligand edges used ranges from porphyrins, luminescent perylene diimides,[10] and redox-active ferrocene derivatives,[9] to chiral linkers, such as phosphine-functionalized binaphthols.[9] With chiral squares, one could easily envision applications such as enantioselective catalysis, separation, or sensing. Indeed, several examples of moderately enantioselective sensing with a chiral-ligand-containing square were reported."[1] Elaboration of squares via functionalization of the phosphine ligands is also possible. In one instance. squares featuring pendent crown ethers were prepared.[9]

What about neutral squares? By using acetylides or phenylides as edges. and forming metal(II)-carbon linkages, squares lacking net charges can be formed.[12] Other routes to neutral squares are described below.

Assembly Principles

Why has the square motif proven so popular in supramolecular coordination chemistry? First. with the right set of ancillary ligands. octahedral and square planar coordination geometries provide pairs of ligation sites oriented at 90° with respect to each other. Second, square formation is typically accomplished with high efficiency, usually in a one-pot reaction. The one-pot forination process is often termed ''self assembly,'' although a more accurate term might be "directed assembly." which is the combination of ***cis*** coordination sites and edge-ligand rigidity. providing the necessary initial directions or instructions.

There is more to the process. however. In nearly every case. the square represents a thermodynamic rather than kinetic product. The reasons are several. The open ligation sites that characterize dimeric. trimeric, and noncyclic oligomeric species are temporarily filled by weakly coordinated solvent molecules; this, in turn. tends to keep these intermediates in solution. In addition. coordinate–covalent bonds tend to be labile, at least at elevated temperatures. Mistakes in the assembly process can be corrected, and assembly can continue until formation of the desired square molecule is complete (Fig. 2).[13] If the completed tetrametallic cycles are less soluble than open oligomers (often the case), precipitation of the cycles can pull the reaction toward completion. Also favoring reaction completion (i.e., high yields) is the enthalpy released upon replacement of a weak metal–solvent bond with a somewhat stronger metal–ligand (edge) bond. For several reasons, therefore, the choice of solvent is important in square synthesis.

Ignoring occasional complications due to triangle formation, the directed assembly approach works well with rigid difunctional ligands. What about flexible

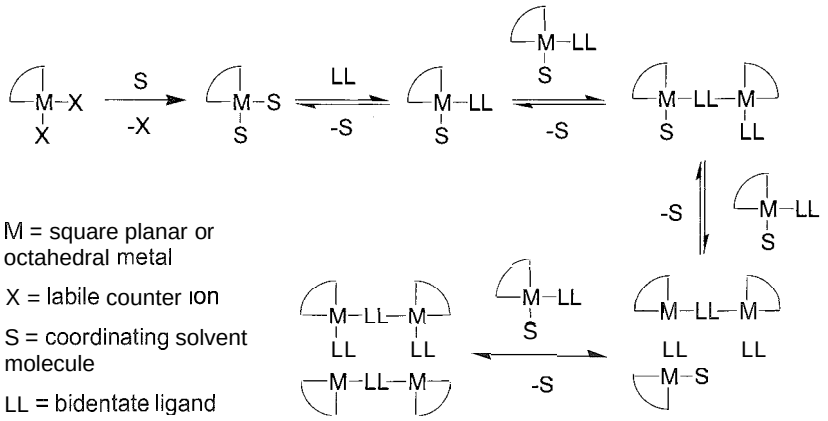

Fig. *2* Proposed mechanism of molecular square formation

ligands? If the ligands are long. the standard assembly approach tends to yield cyclic dimers instead of squares. consistent with simple entropy considerations. While no examples were reported, presumably, in some cases, templating methods could be used to generate flexible-walled squares.

Other Structural Motifs

Squares can also be obtained by linearly coordinating bent (right-angle-containing) difunctional ligands. A metal ion then occupies the center of each edge, and the bent ligands comprise the corners. One example is trans coordination of Pt(II) by 5,10-pyridyl-porphyrins, **3** (Fig. 3).[14] Notably, construction of the square in this way configures the four porphyrin ligands in a coplanar fashion. The alternative assembly featuring linear ligand edges (5,15-pyridyl porphyrin species) and cis-coordinated metal ions as corners configures alternating pairs of porphyrins in a nominally cofacial arrangement. **4**.[9] The two motifs obviously suggest different applications and different ways of assembling multisquare structures.

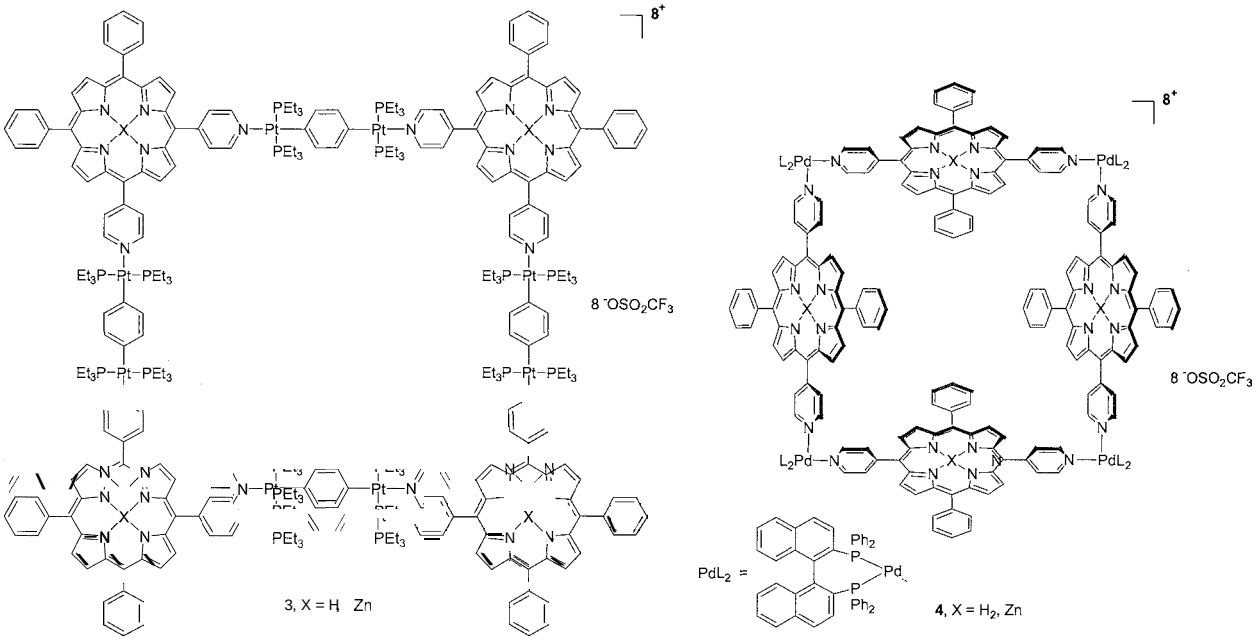

Fig. 3 Two examples of porphyrinic molecular squares. In 3. the cis orientation of pyridyl groups, combined with the *trans* binding of the Pt metal units, leads to a coplanar orientation for the four porphyrins. The *trans* configuration of dipyridyl porphyrins in 4 leads to a nominally cofacial arrangement of opposing pairs of porphyrins. For the particular example shown, however, steric demands force the porphyrins to fold in to yield an almost flat structure.

Another alternative square motif is based on carboxylate coordination of triply and quadruply bonded dimetallic corner units.[15] The coordination geometry requires the metal–metal bond axis to be oriented normal to the plane of the square or, in some cases, triangle. An interesting consequence is that monodentate ligand coordination sites at the ends of the dimetallic units can often be accessed, permitting squares to be linked ''vertically'' in extended structures. Examples of squares based on Mo_2^{4+}, Ir_2^{4+}, and Rh_2^{4+} were reported. In solution, several show multistep metal redox reactivity that is reversible on an electrochemical time scale. Unfortunately, on a longer time scale. the ease of oxidation together with further chemical reactions renders some of the squares structurally unstable in air or in oxygen-containing solutions.

A third alternative simply uses ferrocenes as walls in cyclophane-like structures.[16] The ferrocenyl units typically are linked via flexible hydrocarbon chains appended to cyclopentadiene ligands. In other words, covalent carbon–carbon bonds rather than coordinate–covalent metal–nitrogen, –carbon, –oxygen, or –phosphorous bonds are used.

Porous Molecular Solids

Remarkably, almost all molecular squares crystallize as one-dimensional channel-containing materials, with square cavities defining the channel width. For smaller squares, microcrystallinity typically persists when the squares are cast as thin films. For larger squares, such as porphyrin squares, thin films are more typically amorphous. Films of both kinds, however, can display good microporosity. Obviously, facilitating porosity for neutral squares is the absence of potentially channel-blocking counterions. Many charged squares, however, also feature open channels with counterions positioned above and below metal corners rather than within cavities. (An interesting idea yet to be examined is that the cavity fields generated by the spatially separated charges may engender catalytic activity in a fashion reminiscent of many reactions in zeolites.)

An important characteristic of molecular materials based on squares is their ability to withstand solvent removal without cavity collapse or loss of porosity. The stability reflects the strength of coordinate–covalent bonds. These bonds are often four to 10 times stronger than typical hydrogen bonds.

Explored in most detail with respect to porosity were molecular materials based on neutral tetrarhenium squares {$[Re(CO)_3Cl(\mu\text{-diimine})]_4$ species) as described further below. One step beyond strictly molecular materials are ones composed of covalently or coordinatively linked square units. Interesting examples here are the dimetallic-cornered squares mentioned above, although their behavior as porous materials has yet to be explored. Another approach involves liquid–liquid interface polymerization. Acid-chloride functionalized linkers (short alkane chains) in one phase react with hydroxyl-functionalized porphyrin squares in another phase to generate high-porosity thin-film polymers.[17] Film growth is self-limiting (a few microns), and the density of pinhole defects that fully penetrate the films is low. A third approach uses phosphonate-functionalized porphyrin squares and makes use of the enormous affinity of Zr(IV) for phosphonates. Layer-by-layer porous film assembly can be done on glass, conductive glass, or ceramic platforms. The approach provides exceptional control over film thickness and yields films with channels strongly preferentially oriented in the direction normal to the platform.[18]

Functional Squares

Thin films of tetrarhenium squares {$[Re(CO)_3Cl(\mu\text{-diimine})]_4$ species} can function as molecular sieves, in the form of coatings on macroporous membrane supports or as overlayers on electrode surfaces. Sieving can be followed by spectrally observing the passage of dye molecules, via the coated membrane, from a reservoir solution to a receiving solution or by monitoring the electrochemical cunent produced by passage of a redox-active probe molecule through a porous square coating.[19] Sharp size cutoffs for probe molecules are observed, with the cutoffs corresponding to the sizes of cavities for isolated squares. Quantitative studies with films as thin as 20 nm show that molecular flux scales inversely with film thickness. demonstrating that rates of transport in these cases are limited by film-based diffusion rather than solution-to-film partitioning. For small- and medium-sized squares, known to form microcrystalline films, the observed molecular transport rates exceed by 20- to 50-fold rates of transport through related amorphous metallopolymers featuring similar size cutoffs. These observations point to the importance of the one-dimensional channels created by alignment of squares and their cavities. Films of larger squares featuring metalloporphyrin walls are amenable to cavity functionalization via axial ligation of porphyrin-embedded metal ions. Extensions of this kind readily permit size cutoffs for film sieving to be rationally altered. In principle, chemical selectivity could also be engendered in this way.

Facilitated transport of sodium tosylate across a chloroform solution separating two aqueous phases was demonstrated. The carrier was a Pt(II)-bipyridine square featuring calixarene receptors as corner appendages.[9]

Advantage was taken of the luminescence of small- and medium-sized rhenium squares to accomplish chemical sensing: anions in solution[20] and volatile aromatic

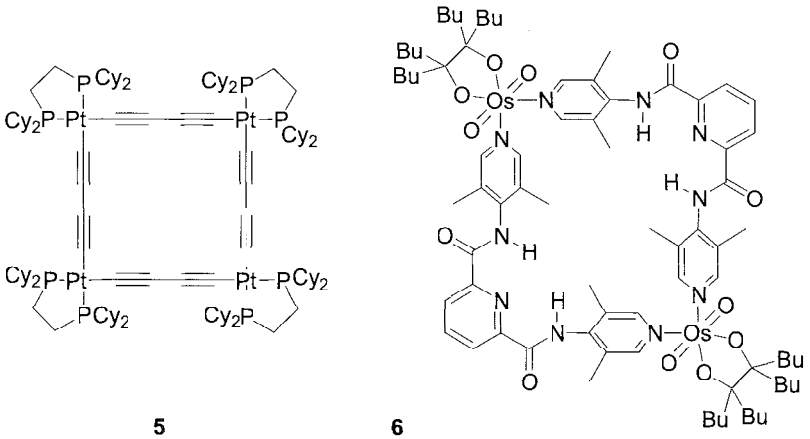

5 6

Fig. 4 Two examples of molecular squares designed for enhanced host–guest binding interactions. Structure 5 is able to bind Ag^+ ions between adjacent alkyne ligands via a n–tweezer effect. The corner receptor groups in 6 allow for enhanced binding of various amides through hydrogen-bonding contacts.

compounds in the vapor phase.[21] Quartz crystal microgravimetry and modulated visible-light diffraction schemes were also used to report on selective uptake of analytes by porous molecular square films.[22] By expanding the number of potential host sites available, porous thin films of squares offer sensitivity advantages over simple monolayers of host compounds. Nevertheless, squares are usually of limited effectiveness in sensing schemes. Few, if any, candidate guest molecules (analytes) are square shaped, ruling out efficient sensing based on shape complementarity, and simple squares lack the requisite functionalities to bind analytes in a highly cheinically selective fashion. (The examples described above depend on comparatively weak and nonspecific electrostatic, donor/acceptor, and dispersion interactions.)

Interesting exceptions are Pt-acetylide-based squares such as 5, that bind Ag^+ strongly based on specific interactions with pairs of ethynyl groups (Fig. 4).[9,23] Another involves a square featuring OsO_4 units as two diagonal comers and pyridine-2,6-dicarboxamides as the other corners (6). This assembly selectively binds appropriately sized amides via multiple hydrogen-bonding interactions.[24]

A potentially more general solution is to decorate the interiors of large molecular squares with receptor ligands, for example. by anchoring them to metal ions embedded in porphyrins (Fig. 5). More than 100 cavity-modified squares were described. Nevertheless, only a handful were exploited for selective chemical sensing (e.g., iodine sensing with tethered thiols, alkali metal ion sensing with cavity-confined crown ethers, and zinc ion sensing with a cavity-confined polyamine ligand).[25]

Encapsulation of metalloporphprin-based epoxidation catalysts by a porphyrin square was described.[26] By largely preventing the catalysts from destructively encountering other catalyst molecules, the square substantially extends catalyst lifetimes. At the same time, it creates a spatially restricted reaction environment that translates into substrate size selectivity in the epoxidation reaction. In one case, a dipyridylporphyrin catalyst was encapsulated within a Zn(II)-containing square. leaving two of the four porphyrinic zinc sites available for further ligation. By binding sterically demanding ligands to these sites, the substrate size selectivity was shown to be tunable. The degree of selectivity engendered in this way, however, is limited, because the putative cavity-modifying ligands are apparently sometimes bound to the square exterior.

MOLECULAR BOXES AND CUBES

In contrast to the vast assortment of molecular squares now in existence, relatively few examples of molecular boxes or cubes were synthesized, unless one views squares having tall edges (for example, porphyrinic squares) as open-ended flexible boxes. As defined here; molecular boxes are right-angle-containing complexes, where the metal coordination units are arranged in three dimensions. instead of two.

A ruthenium-based molecular cube was described.[27] Comprising its corners are $\{([9]aneS_3)Ru\}^{2+}$ ([9]aneS$_3$ = 1,4,7-trithionane) units, Iinked by 4,4′-bipyridine edges. The assembly was obtained by reaction of stoichometric amounts of $\{([9]aneS_3)Ru\}^{2+}$ and 4.4'-bpy (8:12) in a noncoordinating solvent for 4 weeks. Key to the cube synthesis is the sulfurcontaining macrocycle. By occupying three coordination sites in a facial fashion, it

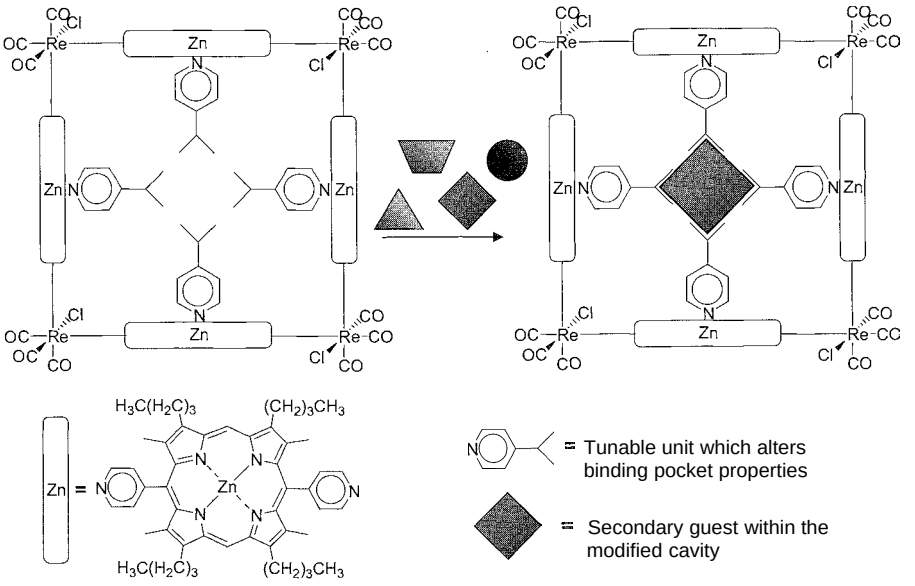

Fig. 5 Porphyrin square functionalization for selective guest binding. (*View* this *art* in color *at www.dekker.com.*)

leaves open three additional sites (also facially arranged) for ligation of the cube's rigid edges. A crystal structure of a cube fragment. $\{([9]aneS_3)(4,4'\text{-bpy})_3Ru\}^{2+}$, clearly illustrates the anticipated mutually perpendicular arrangement of the three *bpy* ligands. Although an x-ray crystal structure of the cube was not reported. ^{1}H-NMR of the sample reveals two sets of 4,4′-bpy resonances. consistent with the formation of the highly symmetrical product.

Two types of molecular boxes featuring (ethylenediamine)Pd(II) corners and polypyridyl linkers were described.[28,29] One uses roughly rectangular tetrapyridyl ligands as walls for an open-ended cube. (7) Multiple isomers were obtained. and one is shown in Fig. 6. By carrying out the synthesis in the presence of an appropriate guest molecule, the isomer distribution can be

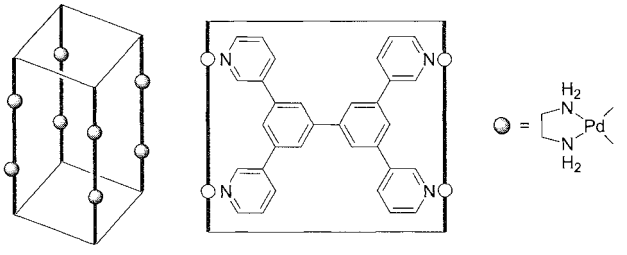

Fig. 6 One of three isomeric boxes that can be obtained from the combination of 3.3′,5,5′-tetrakis(3-pyridyl)biphenyl and (en)Pd$(NO_2)_2$

controlled; as can an equilibrium between competing prisin and cube assemblies. The second type comprises a family of elongated boxes. The wails here consist of 3,5-linked terpyridine, tetrapyridine. and pentapyridine ligands with 6, 8, or 10 (en)Pd(II) units serving as connectors along the box seams. Remarkably. box formation is efficiently templated by rod-like guest molecules. In the absence of templates. either no supramolecular complex formation is seen, or a range of complexes (trimers, tetramers. and pentamers) are present. presumably in dynamic equilibrium. These observations clearly point toward the idea of employing dynamic combinatorial libraries to generate optimal supramolecular inorganic hosts for specific molecular guests. In addition to x-ray crystallography and solution-phase NMR spectroscopy. cold-spray ionization mass spectroscopy was shown to be useful for identifying reaction products. including thermodynamically unstable products in these initial synthesis studies.

A series of mixed-metal molecular cubes, based on the coordination chemistry of Prussian blue and other polymeric cyanometalates, was described. The cubes feature Rh and either Co or Mo on alternating corners, with edges consisting of bridging CN groups.[30] The cubes are formed by the binary combination of molecular squares, subsequent to removal of axially bound chloride ligands. The intermediate molecular squares species are formed by the reaction of $[Cp^*M(CN)_3]^-$ (*Cp** = pentamethyl cyclopentadienyl, *M* = Rh, Co) with either $\{[(R)MCl_2]_2\}$ (*R* = Cp*, $C_{10}H_{14}$; *M* = Rh, Ru) or $(\eta^6\text{–}C_6H_3Me_3)Mo(CO)_3$. The *Cp** ligands serve to block three of the six octahedral

sites, thereby precluding polymer formation. Recently, however, the controlled formation of a double cube (one shared corner) was described.[31]

An interesting property of cyanide-bridged molecular cubes is their ability to bind alkali metals (especially K^+ and Cs^+) selectively within the cube interior.[30] Crystallographic analysis of a Rh–Mo molecular cube indicates bond formation between the cationic guest and the cube's CN edges. When K^+ is encapsulated, the ion is distributed over two equivalent positions, both slightly displaced from the cube center. Encapsulated cesium ions, on the other hand, occupy a central position. The locational differences reflect differences in ionic radii: 2.02 and 1.78 Å for Cs^+ and K^+, respectively, with coordination numbers of 12 for each. The structural differences translate into a nearly 4000-fold preference for uptake of Cs^+ versus K^+ from salt solutions, where the difference was evaluated competitively via ^{133}Cs-NMR measurements.

CONCLUSION

Inorganic supramolecular chemistry yielded an enormous number of discrete assemblies having square or box-like structures and ranging in size from several angstroms to several nanometers. Many of these compounds feature accessible, well-defined voids, rendering them useful, or at least viable, for several applications, including ones involving host–guest chemistry, mesoporous materials, or catalysis. Substantial possibilities for expansion upon applications in selective chemical catalysis, in particular, appear to exist. Applications yet to be fully realized include transport functions in which assemblies serve as artificial pores for natural or biomimetic membranes, as electron or energy transfer for solar energy conversion, and service as components of molecular electronic devices. Also yet to be exploited is the use of channels for templated growth of polymeric or other materials. If the square or cube templates were retained after polymer growth: new classes of nanocomposites, potentially having exceptional or even unique materials properties, might be obtained. Obviously, further advances in molecular and higher-order assembly chemistry will facilitate these developments and likely stimulate others.

ARTICLES OF FURTHER INTEREST

Classification and Nomenclature of Supramolecular Compounds, p. *261*
Mesoporous Materials, p. 845
Self-Assembly: Definition and Kinetic and Thermodynamic Considerations, p. 1248
Supramolecular Chemistry: Definition, p. 1401
Supramolecular Electrochemistry, p. 1412
Supramolecular Photochemistry, p. *1434*

M

REFERENCES

1. Odell, B.; Reddington, M.V.; Slawin, A.M.Z.; Spencer, N.: Stoddart, J.F.: Williams, D.J. Cyclobis(paraquat-p-phenylene), a tetracationic general-purpose receptor. Angew. Chem. **1988**, *100* (11). 1605–1608.
2. Eddaoudi, M.; Li, H.; Yaghi, O.M. Highly porous and stable metal-organic frameworks. Structure design and sorption properties. J. Am. Chem. Soc. 2000, *122* (7), 1391–1397.
3. Stricklen, P.M.; Volcko, E.J.; Verkade. J.G. Novel homo and heterometallic coordination macrocycles. J. Am. Chem. Soc. 1983, *105* (8), 2494–2495.
4. Fujita. M.; Yazaki, J.; Ogura, K. Preparation of a macrocyclic polynuclear complex, [(en)Pd(4,4′-bpy)]4(NO3)8 (en=ethylenediamine, bpy=bipyridine), which recognizes an organic molecule in aqueous media. J. Am. Chem. Soc. 1990, *112* (14), 5645–5647.
5. Fujita, M.; Yazaki, J.; Ogura. K. Macrocyclic polynuclear complexes [(en)M(4,4′-bpy)]4(NO3)8 (M=palladium or platinum) as "inorganic cyclophane." Their ability for molecular recognition. Tetrahedron Lett. 1991, *32* (40), 5589–5592.
6. Fujita, M.; Sasaki, O.; Mitsuhashi, T.: Fujita, T.; Yazaki, J.: Yamaguchi, K.: Ogura, K. On the structure of transition-metal-linked molecular squares. Chem. Commun. **1996**, (13), 1535–1536.
7. Fujita, M.; Ibukuro, F.; Yamaguchi, K.; Ogura. K. A molecular lock. J. Am. Chem. Soc. 1995. *117* (14), 4175–4176.
8. Hori, A.; Kumazawa, K.; Kusukawa, T.; Chand, D.K.; Fujita, M.; Sakamoto, S.; Yamaguchi. K. DOSY study on dynamic catenation: Self-assembly of a [3]catenane as a meta-stable compound from twelve simple components. Chem.-Eur. J. 2001. 7 (19), 4142–4149.
9. Stang, P.J.; Olenyuk. B. Self-assembly, symmetry, and molecular architecture: Coordination as the motif in the rational design of supramolecular metallacyclic polygons and polyhedra. Acc. Chem. Res. **1997**, *30* (12), 502–518.
10. Wurthner, F.; Sautter, A. Highly fluorescent and electroactive molecular squares containing perylene bisimide ligands. Chem. Commun. 2000, (6). 445–446.
11. Lee. S.J.; Lin, W. A chiral molecular square with metallocorners for enantioselective sensing. J. Am. Chem. Soc. **2002**. *124* (17), 4554–4555.
12. Leininger. S.; Olenyuk, B.; Stang, P.J. Self-assembly of discrete cyclic nanostructures mediated by transition metals. Chem. Rev. **2000**, *100* (3), 853–907.
13. Davis, A.V.; Yeh, R.M.; Raymond. K.N. Supramolecular assembly dynamics. Proc. Natl. Acad. Sci. U. S. A. 2002, 99 (8), 4793–4796.
14. Drain, C.M.; Lehn, J.-M. Self-assembly of square

multiporphyrin arrays by metal ion coordination. J. Chem. Soc.. Chem. Commun. 1994. (19). 2313–2315.
15. Cotton, F.A.; Lin, C.; Murillo, C.A. Supramolecular arrays based on dimetal building units. Acc. Chem. Res. 2001. *34* (10), 759–771.
16. Beer. P.D.: Gale, P.A. Anion recognition and sensing: The state of the art and future perspectives. Angew. Chem.. Int. Ed. Engl. 2001. *40* (3), 486–516.
17. Keefe, M.H. Ph.D. Dissertation; Northwestern University, 2001.
18. Wightman, M. M.S. Thesis: Northwestern University, 2001.
19. Williams, M.E.; Hupp, J.T. Scanning electrochemical microscopy assessment of rates of molecular transport through thin films of mesoporous films of porphyrinic 'molecular squares.' J. Phys. Chem.. B 2001. *105* (37). 8944–8950.
20. Slone. R.V.: Yoon, D.I.; Calhoun. R.M.; Hupp. J.T. Luminescent rhenium/palladium square complex exhibiting excited state intramolecular electron transfer reactivity and molecular anion sensing characteristics. J. Am. Chem. Soc. 1995, *117* (47). 11813–11814.
21. Sun. S.-S.: Lees, A.J. Self-assembly triangular and square rhenium(I) tricarbonyl complexes: A comprehensive study of their preparation, electrochemistry, photophysics. photochemistry, and host–guest properties. J. Am. Chem. Soc. 2000. *122* (37). 8956–8967.
22. Keefe, M.H.; Slone. R.V.: Hupp, J.T.: Czaplewski, K.F.: Snurr, R.Q.: Stern, C.L. Mesoporous thin films of ''molecular squares'' as sensors for volatile organic compounds. Langmuir 2000. *16* (8), 3964–3970.
23. Alqaisi, S.M.; Galat, K.J.: Chai. M.H.: Ray, D.G.; Rinaldi. P.L.: Tessier, C.A.; Uoungs, W.J. Synthesis of neutral tetranuclear and octanuclear macrocyclic platinum-butadiyne heterocyclynes. J. Am. Chem. Soc. 1998. *120* (46). 12149–12150.
24. Jeong, K.-S.: Cho. Y.L.; Song, J.U.; Chang. H.-Y.; Choi. M.-G. Neutral macrocyclic boxes spontaneously assembled from osmium tetraoxide, olefin, and pyridyl ligand. J. Am. Chern. Soc. 1998. *120* (42). 10982–10983.
25. Mines. G.A.; Tzeng. B.-C.; Stevenson, K.J.; Li, J.; Hupp, J.T. Microporous supramolecular coordination compounds as chemosensory photonic lattices. Angew. Chem., Int. Ed. Engl. 2002. 41 (1), 154–157.
26. Merlau, M.L.; Mejia, M.d.P.: Nguyen, S.T.: Hupp, J.T. Artificial enzymes formed through directed assembly of molecular square encapsulated epoxidation catalysts. Angew. Chem., Int. Ed. Engl. 2001. *40* (22), 4239–4242.
27. Roche, S.: Haslam. C.: Heath. S.L.; Thomas, J.A. Self-assembly of a supramolecular cube. Chem. Commun. 1998. (16). 1681–1682.
28. Yamanoi. U.: Sakamoto, U.: Kusukawa. T.: Fujita. M.: Sakamoto. S.: Yamaguchi, K. Dynamic assembly of coordination boxes from (en)Pd(II) unit and a rectangular panel-like ligand: NMR. CSI-MS. and x-ray studies. J. Am. Chem. Soc. 2001. *123* (5), 980–981.
29. Aoyagi, M.; Biradha. K.: Fujita, M. Quantitative formation of coordination nanotubes templated by rodlike guests. J. Am. Chem. Soc. 1999. *121* (32). 7457–7458.
30. Klausmeyer, K.K.: Wilson. S.R.; Rauchfuss, T.B. Alkali metal-templated assembly of cyanometalate ''Boxes'' (NEt4)3{M[Cp*Rh(CN)3]4[Mo(CO)3]4} (M=K, Cs). Selective binding of Cs+. J. Am. Chern. Soc. 1999. *121* (12), 2705–2711.
31. Contakes, S.M.; Kuhlman. M.L.: Ramesh. M.: Wilson, S.R.: Rauchfuss. T.B. Systematic assembly of the double molecular boxes: {CsC[CpCo(CN)3]4[Cp*Ru]3} as a tridentate ligand. Proc. Natl. Acad. Sci. U. S. A. 2002. 99 (8). 4889–4893.

Molecular Switches

Ruud G. E. Coumans
Alan E. Rowan
University of Nijmegen, Nijmegen, The Netherlands

INTRODUCTION

In nature. control and regulation of enzymes in biological pathways are of fundamental importance.[1] The switching "on" and "off" of processes is principally carried out by the binding of ions or molecules, which. in turn. influences the conformation of the enzyme and its activity and materials properties. These types of enzymes can therefore be viewed as nanosized switches, e.g., their activities can be turned on or off under the influence of external chemical or physical stimuli. These so-called "allosteric" interactions[2] play a key role in life and inspired many chemists to mimic these systems using simpler building blocks.'" The innovative designs and creative thinking of numerous scientists led to artificial molecular switches that do not serve only a role as biomimetic models but are of interest in their own right and. in some cases: are on the verge of being used in device applications.[4] Moreover. with the arrival of nanotechnology, there is even more interest in the design, synthesis, and characterization of artificial molecular machine~.[~This interest can contribute greatly to the bottom-up approach in nanoscience. Molecular switches comprise an interesting class of artificial molecular machines and can be defined as molecules that can be switched between two or more different states. In this article, several examples of such switches will be presented; ranging from relatively simple molecular switches to more complex (macromolecular) switches based on DNA. It is impossible to give a thorough overview of all the molecular switches described in the literature. Consequently, we chose to highlight only a few exciting examples.

A SIMPLE PHOTOREDOX MOLECULAR SWITCH

A simple but illustrative example of a molecular switch is shown in Fig. 1a and was developed by Lehn and coworkers.[6] It consists of a quinone/hydroquinone moiety covalently attached to a luminescent Ru$(bpy)^{2+}$ core (bpy = 2,2′-bipyridine).

The luminescence of the excited metal complex **1** is quenched by the lower-energy quinone moiety. Once the quinone is electrochemically reduced to hydroquinone, the luminescence is restored. because the hydroquinone is unable to quench the luminescence of the excited metal complex. In turn, the hydroquinone can be switched back by oxidation to the quinone, and quenching of the luminescence is restored. The electrochemical interconversion of both species was shown to be fully reversible, and both the oxidized and reduced forms are isolable and stable. In the simplest form, this system can be regarded as a bistable (on/off) electrophotoswitch.

SWITCHES BASED ON PHOTOCHEMICAL *CIS–TRANS* ISOMERIZATION

An important example of a molecular switch in nature is the *cis–tmns* isomerization of retinal in the retina.'" This isomerization is the primary event in the process of vision, in which, through a cascade of enzymatic reactions, the light signal is eventually converted to generate a nerve signal. A considerable part of the molecular switches described in the literature rely on the photoinduced *cis–trans* isomerization of olefinic bonds and azobenzenes. One example of the use of azobenzenes as switches is in the switching of the alignment mode of a nematic liquid-crystalline (LC) phase.[7] The switching is achieved by attaching functionalized azobenzenes to quartz surfaces. These surfaces were then used to construct nematic LC cells. Irradiation of the azobenzenes with visible light results in a *trans* configuration of the azobenzenes and an alignment of the LC molecules perpendicular to the surface. Irradiation with UV light results in *trans–cis* isomerization of the azobenzenes, and concomittantly, the LC molecules are aligned parallel to the surface. An elegant example of a molecular system based on *cis–trans* isomerization was reported by Inoue and coworkers, who used the photochemical *cis–tmns*

Encyclopedia of Supramolecular Chemistry
DOI: 10.1081/E-ESMC 120011789

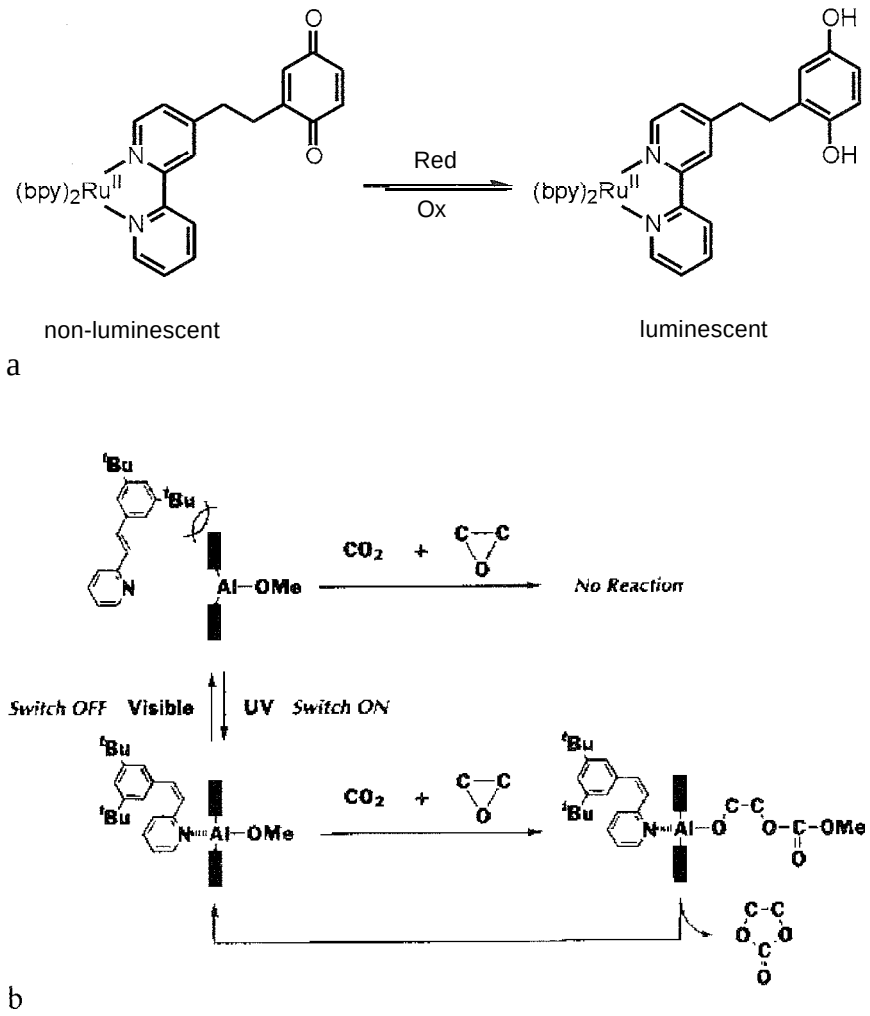

Fig. 1 (a) A photoredox molecular switch. (b) A photoswitchable catalyst. Reprinted with permission from Ref. [8]. Copyright 1999 by American Chemical Society.

isomerization to switch a catalyst on and off (Fig. 1b) and chemically fixate CO_2.[8] It is known that under the influence of methoxyaluminum tetraphenylporphyrin 2, carbon dioxide and an epoxide can be coupled and converted to a five-membered cyclic carbonate. However, coordination of a nitrogen-containing base to the aluminum center is necessary to achieve high catalytic activity. By using 3′,5′-di-*tert*-butyl-2-stilbazole as the base in this system. the catalyst could be switched on and off by irradiation at an appropriate wavelength. Upon irradiation with UV light, the stilbazole exists predominantly in its ***cis*** form; and the catalyst exhibits high activity. By irradiation of the system with visible light, the stilbazole moiety isomerizes to its *trans* form, blocking the coordination of the nitrogen to the metal center due to unfavorable steric interaction between the tert-butyl groups and the porphyrin, and the catalyst loses its activity and is in its off slate.

MOLECULAR SWITCHES BASED ON DIARYLETHENES

Diarylethenes emerged recently as versatile building blocks for several types of molecular switches. The switching mechanism of these compounds is based on a photocyclization with UV light of the colorless, open form **3,** resulting in a colored, conjugated species 4. This

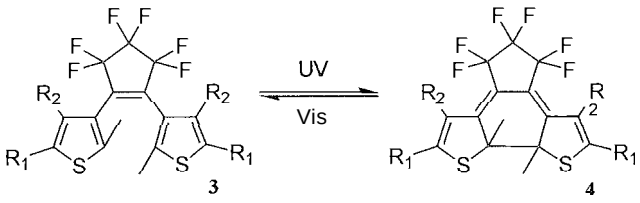

Fig. 2 Switching of diarylethenes with light

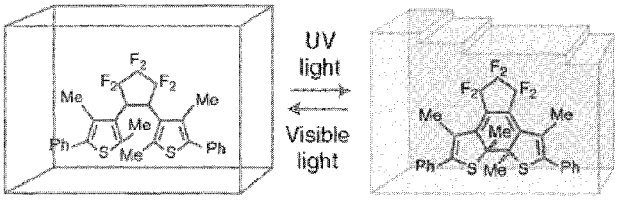

Fig. 3 Reversible surface morphology change of crystals of **5** upon irradiation with light. Reprinted with permission from Ref. [11]. Copyright 2000 by American Association for the Advancement of Science. (*View this art in color. at www.dekker.com.)*

process can be reversed by a visible-light-induced cycloreversion (Fig. 2). The diarylethenes based on the perfluoro-cyclopentenebisthien-3-yl framework were found to be ideal due to their excellent thermal and chemical stabilities (Fig. 2).

Irie and coworkers utilized this aryl framework in a wide variety of molecular switches, ranging from photoelectrochemical switches to liquid-crystalline switches.[9] One outstanding example is the reversible switching of surface morphology in single crystals of **5** (R_1 = Ph, R_2 = Me)[10,11] (Fig. 3).

It was shown that the surface morphology of these crystals can be altered by irradiation at an appropriate wavelength. Upon irradiation with UV light, the colorless crystals turned blue, and 1 nm steps appeared on the surface. Upon irradiation with visible light, the crystals decolored. and a flat surface was obtained. It was shown that these crystal are structurally resistant. because the crystal integrity remained intact through thousands of irradiation cycles. The surface morphological changes are related to the molecular structural changes of **5,** which are regularly packed in the single crystal. These small atomic molecular changes are amplified by the crystal packing. This exciting result demonstrates the potential for this as a photodriven nanometer-size actuator.

MORE COMPLEX SWITCHES: OVERCROWDED ALKENES AND UNIDIRECTIONAL ROTORS

The group of Feringa developed the concept of overcrowded alkenes as potential molecular switches.[12] These alkenes adopt a helical conformation due to steric interactions between the bulky groups attached at either end of the double bond. This approach was used in several examples of molecular switches. Compound 6 exists as two equal enantiomers. This racemic mixture can be enriched in P or *M* enantiomers, by irradiation at 313 nm with either left or right circular polarized light (*l*- or *r*-CPL) (Fig. 4a).[13] This chiral bias can be removed by irradiation with linear polarized light (LPL), which results in a racemic mixture. Doping of 4′-(pentyloxy)-4-biphenylcarbonitril with 20 wt% of racemic 6 resulted in a stable nematic liquid-crystalline phase. If a thin film of this LC material was irradiated at 313 nm, with *l*-CPL for 90 min, a chiral cholesteric LC phase was obtained. Irradiation of the nematic phase with *r*-CPL resulted again in the formation of a cholesteric phase but now with the opposite screw sense. Both cholesteric phases could be switched back to the nonchiral nematic phase by irradiation with LPL at 313 nm (Fig. 4b), because then racemization of the dopant occurs. It is now possible to

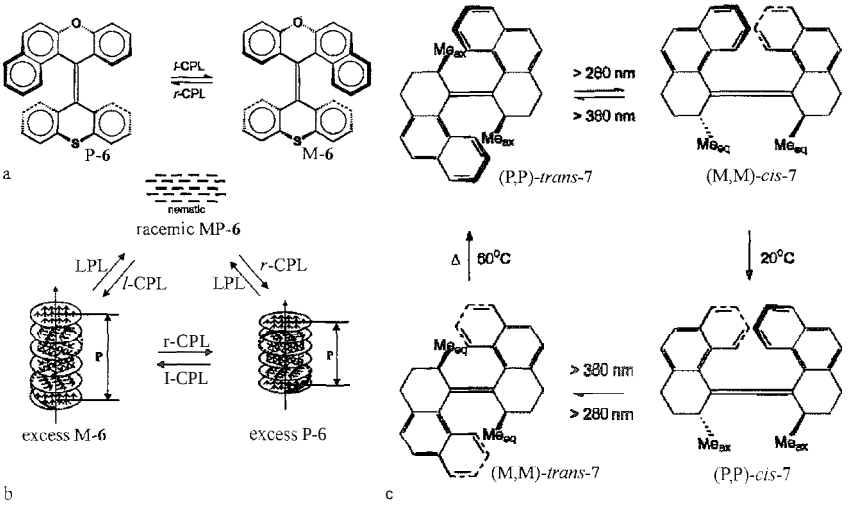

Fig. 4 (a) Photochemical switching between P-6 and M-6. (b) Photochemical switching between three different LC phases. (c) Light-driven molecular rotor. Reprinted with permission from Ref. [12]. Copyright 2000 by American Chemical Society.

switch between three different LC phases by irradiation with LPL or CPL.

Another application of the overcrowded alkene framework is in a light-driven unidirectional molecular rotor, also described by Feringa and coworkers.[14] It was demonstrated that at $-55°C$, compound (*P*,*P*)-*trans*-7, with two helical substituents attached to the olefinic bond, could be converted to a mixture of (*P*,*P*)-*trans*-7 and (*M*,*M*)-*cis*-7 in a 5:95 ratio by irradiation at $\lambda > 280$ nm. The process can be reversed by irradiation at $\lambda > 380$ nm. Helix inversion of the less-stable (*M*,*M*)-*cis*-7 to (*P*,*P*)-*cis*-7 occurred irreversibly at 20°C. Irradiation of (*P*,*P*)-cis-7 at $\lambda > 280$ nm resulted in a mixture of (*P*,*P*)-*cis*-7 and (*M*,*M*)-*trans*-7 in a 10:90 ratio: which also can be reversed by irradiation at $\lambda > 380$ nm. Helical (*M*,*M*)-*trans*-7 could be thermally inversed back to (*P*,*P*)-*trans*-7 (Fig. 4c) at 60°C. By using circular dichroism (CD) spectroscopy. the unidirectionality of the rotor was established. Every step of the rotary motion could be identified spectroscopically. and full cycles of the rotary motion can be followed at 217 nm. The unidirectionality of this rotor arises from the thermal interconversion of the less-stable forms. with equatorial Me substituents. to the more stable forms, with axial Me substituents. Compound 7 can rotate a full 360° unidirectional rotation in two photochemical steps and two thermal steps. This unique rotor can be regarded as an optical switch with four distinct states. Switching between these states depends on the wavelength of the light and the temperature used. A chemically driven unidirectional rotor was described by Kelly and coworkers (Fig. 5).[15,16] The operating mechanism of this rotor consists of several stepwise chemical modifications on triptycyl[4]helicene 8. Reaction of **8** with carbamoylchloride resulted in isocyanate 9. which rotates to give urethane 10. This relatively high-energy conformation rotates further to give **11.** Cleavage of the urethane bond results in Compound 12, completing a 120" rotation. To achieve a full 360° rotation, each of the blades of the triptycene needs to be functionalized with amino groups and by repeated reaction, rotation. and cleavage. a chemically driven rotor can be obtained.

MOLECULAR SWITCHES BASED ON ROTAXANES AND CATENANES

Rotaxanes are systems in which one or more macrocyclic molecules encircle a linear molecule that is terminated at both ends with bulky substituents, preventing the macrocycles from sliding off the thread. With the expansion of the field of supramolecular chemistry, several interesting rotaxanes systems were assembled, making use of different kinds of ternplating effects, e.g., noncovalent interactions and metal coordination.[17] Members of the Stoddart group were the first to demonstrate that rotaxanes can be switched between two different states. chemically (acid/base controlled) or electrochemically. One example is benzocrown ether/bipyridinium [2]-rotaxane 13 that can be switched chemically and electrochemically (Fig. 6).[18] It consists of a π-electron-accepting tetracationic cyclophane as the macrocycle that encircles a dumbbeli-shaped component that contains two diffe ent π-donating sites, a benzidine. and a biphenol unit. The cyclophane unit can bind to the benzidine and the biphenol unit on the

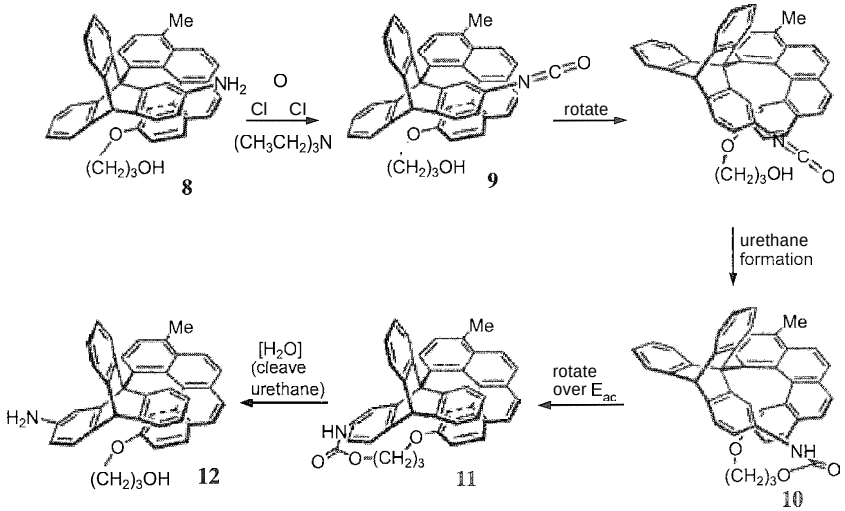

Fig. 5 A chemically driven unidirectional rotor. Reprinted with permission from Ref. [16]. Copyright 2000 by American Chemical Society.

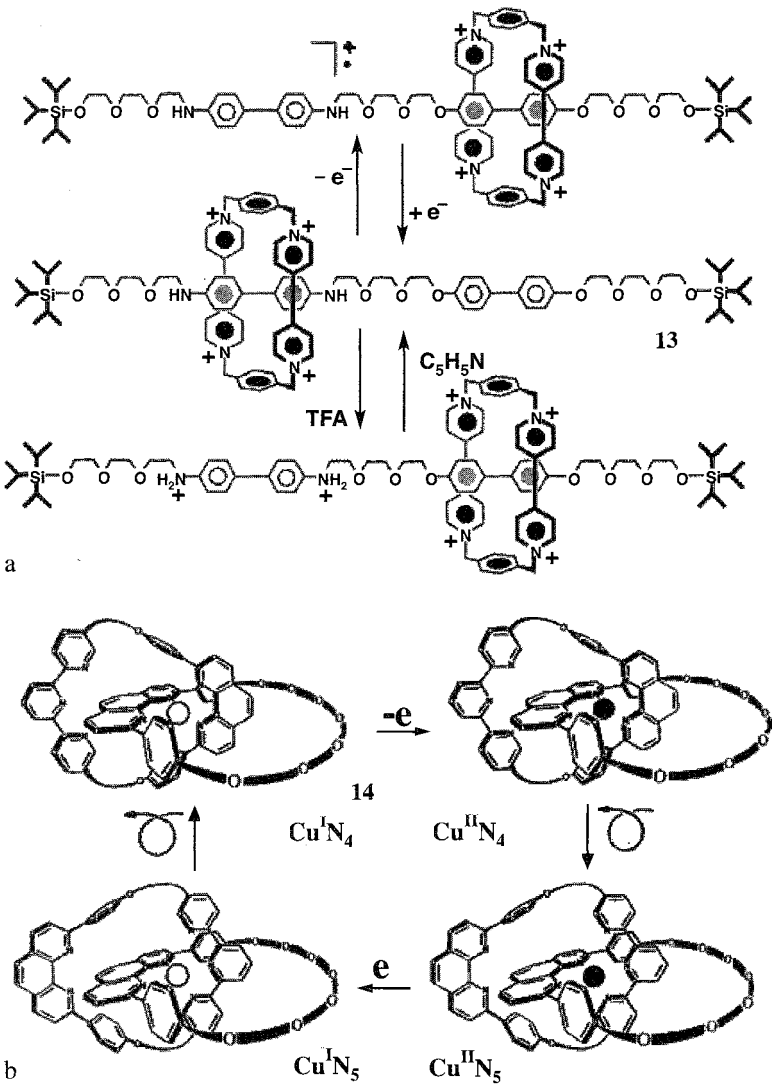

Fig. 6 (a) Electrochemical and chemical switching in a molecular shuttle. Reprinted with permission from Ref. [17]. Copyright 1998 by American Chemical Society. (b) Electrochemical switching in a [2]-catenane. Reprinted with permission from Ref. [22]. Copyright 1997 by American Chemical Society.

dumbbell because of attractive $\pi-\pi$ interactions and [CH—O] hydrogen bonds between the α-bipyridinium hydrogen atoms and the poiyether oxygen atoms.

At room temperature, the cyclophane was shown to shuttle between the benzidine and the biphenol unit. At 229 K, an equilibrium was established in which 84% of the cyclophane encircles the benzidine unit, because the cyclophane has a higher binding affinity for the benzidine group than for the biphenol group. Upon protonation of the nitrogen atoms of the benzidine group, the cyclophane shuttles away from the protonated benzidine groups, due to electrostatic repulsion of the protonated nitrogens and the tetracationic cyclophane. Only binding to the biphenoi unit is observed. The addition of base resulted in re-establishment of the aforementioned equilibrium. The same results can be obtained by electrochemical oxidation of the benzidine unit to its radical cation. Again because of electrostatic repulsion, the cyclophane reside5 at the biphenol unit. Electrochemical reduction regenerates the neutral dumbbell. and preferentially, binding to the benzidine group is observed. More recent derivatives, e.g., a bistable pseudorotaxane incorporating a tetrathiafulvalene (TTF) unit and a naphtalene unit in the dumbbell part. were incorporated in material devices.[19,20]

Catenanes are molecules similar to rotaxanes in that they consist of interlocked components. Instead of using linear molecules that are encircled by macrocyclic compounds, circular molecules can also be used, resulting in

interlocked macrocycles. The group of Sauvage developed a template-directed strategy based on metal coordination for the synthesis of switchable electrochemical catenanes.[21] An example is the switchable copper–catenate 14, i.e., a copper complex with an organic [2]catenane backbone (Fig. 6).[22] The organic [2]catenane backbone consists of one macrocycle containing a bidentate phenantroline unit interlocked with another macrocycle that contains a bidentate phenantroline and a terdentate terpyridine unit. The switching mechanism depends on the preferred coordination number accompanying the mono- or divalency of copper. Monovalent copper prefers to be 4-coordinate, while divalent copper prefers to be 5-coordinate. In the red-brown catenate 14, a tetrahedral coordination geometry is obtained by the coordination of the two bidentate phenanthroline units to the monovalent Cu center. Oxidation to the divalent species leads to a metastable complex that rearranges to the give the stable, deep green 5-coordinate copper(II) complex, coordinated by one bidentate phenantroline unit and one terdentate terpyridine unit. Reduction of this 5-coordinate species results in a metastable complex that rearranges back to catenate 14. The first step in the cycle can also be initiated by photochemical oxidation with p-nitrobenzylbromide. Unfortunately, the reduction step could not be initiated with light, because the 5-coordinated species is not photosensitive.

MACROMOLECULAR SWITCHES

Switches based on polymer arrays are of great general interest, because polymers often already exhibit interesting application-directed macroscopic properties. These properties could, in principle, be switched on or off, if switchable polymers could be utilized. One interesting example of such an approach is based on the chiroptical switching of polyisocyanates. Polyisocyanates are helical macromolecules in which an enantiomeric excess of a certain helical conformation (*P* or *M*) can be obtained by incorporating small amounts of chiral isocyanates during the polymerization of achiral isocyanate monomers. This so-called "sergeants and soldiers" effect, which is basically an amplification of chirality, was first reported by Green and coworkers.[23] And, this principle was used by the group of Zentel in the preparation of chiral photoswitchable polyisocyanates **15** (Fig. 7a).

The incorporation of chiral azobenzenes, containing two chiral centers, in the backbone of a polyisocyanate

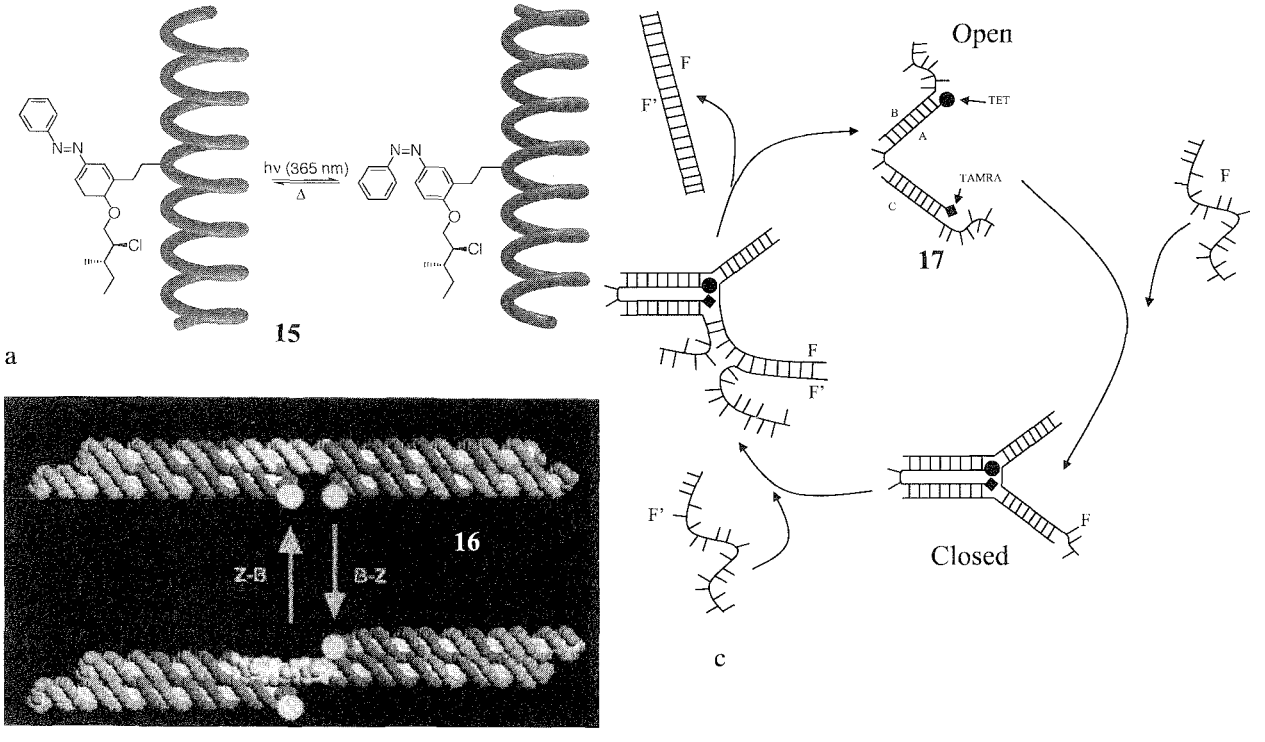

Fig. 7 (a) Chiral photoswitchable polyisocyanates. (b) DNA-based switch by Seeman. Reprinted with permission from Ref. [28]. Copyright 1999 by Macmillan Magazines Limited. (c) DNA-based switch by Yurke.

resulted in amplification of chirality, and a preference in the polyisocyanates for an *M*-helix was observed.[24] Irradiation of the azobenzene moieties at 365 nm resulted in a *trans–cis* isomerization of the azobenzene with a concomitant isomerization. The helical twist sense of the macromolecules was inversed, and a preference for the P-helical conformation was obtained. Further studies revealed that an increase of chiral azobenzenes in the polymer backbone resulted in an even higher stereoselectivity.[25] The incorporation of other azobenzenes, with only one chiral center, resulted in a change in the occupation of helical segments within one polymer but left the preferred helical twist sense of the overall polymer unchanged.[26]

Not only have synthetic polymers been used as a scaffold for macromolecular switches, but also nature's polymers, e.g., polypeptides and DNA, have also been used as a basis for macromolecular switches. Seeman et al. pioneered the use of DNA as a building block for a variety of topological objects, e.g., cubes and truncated octahedron and DNA arrays.[27] Because the DNA used is flexible; they developed the use of the DNA double-crossover (DX) system. This DX-DNA is much stiffer than normal DNA and was shown to be an ideal building block for a DNA-based molecular switch.[28] Switch **16** consists of two DX molecules connected to each other by 4.5 turns of DNA. At the free ends of the DX molecules, two dye molecules (a donor and an acceptor) are attached (Fig. 7b). The actual switching of the DNA-based switch relies on the B–Z transition of DNA, which can be regulated by adjusting the solution conditions favoring either B or Z forms of DNA. Under conditions that favor right-handed B-DNA, the two dye molecules are on the same side of the central helix. If conditions are used that favor left-handed Z-DNA, the dye molecules lie on opposite sides of the central helix. The fluorescence resonance energy transfer between the two dye molecules was monitored, and by observing the donor and acceptor energy transfers it could be shown that upon switching between conditions that favor B- or Z-DNA, energy transfer between the dyes was less in Z-DNA than in *B*-DNA. This can be explained by the fact that in Z-form DNA, the dyes are further apart, and electron transfer is less efficient.

An alternative DNA-based molecular switch **17**, developed by Yurke and coworkers.[29] consists of three strands of DNA (A, B, and *C*), and it has the form of a pair of tweezers. As shown in Fig. 7c, the DNA-based switch can be switched between an open form and a closed form. Adding an additional DNA strand **F** results in a hybridization of *F* with the dangling ends of strands B and *C*. This results in a closed form, with a dangling end of *F*. Addition of DNA strand **F'** results in the hybridization with **F**, and the duplex DNA strand *FF'* is removed from the tweezers. This again creates the open form of the tweezers. The whole process can be followed by monitoring the fluorescence intensity between the two dyes (a donor and an acceptor) at both ends of the A strand. Addition of *F* to the tweezers leads to a decrease of fluorescence intensity, because the dyes come in close proximity to each other, and fluorescence is quenched. Addition of *F'* leads to an increase in fluorescence intensity, corresponding to the open form. The process can be cycled by alternating additions of **F** and **F'**. Not only is this switch based on DNA, but also the ''fuel'' to operate it is made of DNA.

CONCLUSION

Throughout millions of years, nature developed subtle protein architectures that can alter conformation upon some forms of stimuli. It is amazing how only a limited amount of building blocks available for the biosynthesis of these architectures can lead to such a diverse range of switches. Using nature as an inspiration, physicists, biologists, and chemists are only now constructing a wide variety of synthetic switches with possible applications in the areas of microelectronics and materials sciences. With availability of a much wider range of building blocks and increasing insight into how to design, synthesize, and implement synthetic molecular switches, scientists are on the way to more closely mimicking the elegant switches found in nature. It has yet to be seen if they can rival the natural switches or perhaps even out-perform them. Toward this goal, there are already several exciting examples of the incorporation of switches in device applications,[''''the next step in the development of nanomachines.

ARTICLES OF FURTHER INTEREST

Catenanes and Other Interlocked Molecules, p. *206*
DNA Nanotechnology, p. *475*
Rotaxanes and Pseudorotaxanes, p. *1194*

REFERENCES

1. Stryer. L. *Biochemistry*, 4th Ed.; Freeman: New York. 1995.
2. Livitzki, A. *Quantitative Aspects of Allosteric Mechanisms*; Springer-Verlag: Berlin. *1978.*
3. Takeuchi, M.; Ikeda, M.; Sugasaki, A.; Shinkai, S. Molecular design of artificial molecular and ion recognition systems with allosteric guest responses. Acc. Chem. Res. **2001**, 34 (11), 865–873.

4. Feringa. B.L. *Molecular Switches*; Wiley-VCH: Weinheirn. 2001.
5. Balzani. V.: Credi, A.; Raymo, F.M.: Stoddart, J.F. Artificial molecular machines. Angew. Chem.. Int. Ed. 2000, *39* (19). 3348–3391.
6. Goulle, V.: Harriman. A.; Lehn. J.M. An electro-photoswitch: Redox switching of the luminescence of a bipyridine metal complex. J. Cheni. Soc., Chem. Commun. 1993, 1034–1036.
7. Ichimure. K.: Suzuki, Y.: Seki. T. Reversible change in alignment mode of nematic liquid crystals regulated photochemically by 'command surfaces' modified with an azobenzene monolayer. Langmuir 1988. *4* (5), 1214–1216.
8. Sugirnoto, H.: Kimura. T.; Inoue, S. Photoresponsive molecular switch to control chemical fixation of CO_2. J. Am. Chem. Soc. 1999. *121* (10). 2325–2326.
9. Irie, M. Diarylethenes for memories and switches. Chem. Rev. 2000. *100* (5). 1685–1716.
10. Irie. M.; Kobatake, S.: Horichi, M. Reversible surface morphology changes of a photochromic diarylethene single crystal by photoirradiation. Science 2800. *291* (5509), 1769–1772.
11. Scheffer, J.R.; Scott, C. Solid state organic chemistry: Stepping it up. Science 2008. *291* (5509), 1712–1713.
12. Feringa, B.L.; van Delden. R.A.; Koumura, N.: Geertsema, E.M. Chiroptical molecular switches. Chem. Rev. 2000. *100* (10). 1789–1816.
13. Huck, N.P.M.: Jager, W.F.: de Lange, B.; Feringa, B.L. Dynamic control and amplification of molecular chirality by circular polarized light. Science 1996. *273* (5282), 1686–1688.
14. Koumura, N.: Zijlstra, R.W.J.: van Delden, R.A.: Harada. N.: Feringa. B.L. Light-driven monodirectional molecular rotor. Nature 1999. *401* (6749), 152–155.
15. Kelly. T.R.; De Silva, H.; Silva. R.A. Unidirectional rotary motion in a molecular system. Nature 1999. *401* (6749). 150–152.
16. Kelly. T.R.: Silva, R.A.: De Silva. H.; Jasmin. S.: Zhao, Y. A rationally designed prototype of a molecular motor. J. Am. Chem. Soc. 2000. *122* (29). 6935–6949.
17. Balzani. V.: Gómez-López, M.; Stoddart, J.F. Molecular machines. Acc. Chem. Res. 1998. *31* (7), 405–414.
18. Bissel. R.A.: Cordova. E.; Kaifer. A.E.; Stoddart. J.F. A chemically and electrochemically switchable molecular shuttle. Nature 1994. *369* (6476). 133–137.
19. Pease, A.R.; Jeppesen, J.O.: Stoddart. J.F.; Luo. Y.; Collier. C.P.: Heath, J.R. Switching devices based on interlocked molecules. Acc. Chem. Res. 2001, *34* (6), 433–444.
20. Collier, C.P.: Jeppesen. J.O.: Luo, Y.: Perkins. J.: Wong, E.W.; Heath. J.R.; Stoddart. J.F. Molecular-based electronically switchable tunnel junction devices. J. Am. Chem. Soc. 2001, *123* (50). 12632–12644.
21. Sauvage, J.P. Transition metal-containing rotaxanes and catenanes in motion: Toward molecular machines and motors. Acc. Chern. Res. 1998. *31* (10), 611–619.
22. Livoreil, A.; Sauvage. J.P.; Armaroli, N.; Balzani, V.: Flamigni, L.: Ventura, B. Electrochemically and photochemically driven ring motions in a disymmetrical copper [2]-catenate. J. Am. Chem. Soc. 1997. *119* (50), 12114–12124.
23. Green. M.M.; Peterson. N.C.; Dato, T.; Teramoto. A.; Cook. R.: Lifson. S. A helical polymer with a cooperative response to chiral information. Science 8995, *268* (5219), 1860–1866.
24. Maxein, G.; Zentel. R. Photochemical inversion of the helical twist sense in chiral polyisocyanates. Macromolecules 1995. *28* (24). 8438–8440.
25. Mayer. S.: Maxein, G.: Zentel, R. Correlation between the isomerisation of side groups and the helical main chain in chiral polyisocyanates. Macromolecules 1998. *31* (24). 8522–8525.
26. Miiller. M.; Zentel, R. Photochemical amplification of chiral induction in polyisocyanates. Macromolecules 1994. *27* (15), 4404–4406.
27. Seeman. N.C. Nucleic acid nanostructures and topology. Angew. Chem., Int. Ed. 1998. *37* (23). 3220–3238.
28. Mao. C.; Sun. W.: Shen, Z.: Seeman. N.C. A nanomechanical device based on the B–Z transition of DNA. Nature 1999. *397* (6715), 144–146.
29. Yurke, B.: Turberfield. A.J.; Mills, A.P., Jr.; Simmel. F.C.: Neumann, J.L. A DNA-fueled molecular machine made of DNA. Nature 2000. *406* (6796). 605–608.
30. Collier. C.P.; Mattersteig, G.; Wong. E.W.: Luo. Y.: Beverly. K.; Sampaio. J.; Raymo, F.M.: Stoddart, J.F.;

Molecular Wires

Franco Scandola
Università degli Stodi di Ferrara, Ferrara, Italy

INTRODUCTION

The origin of molecular electronics can be traced back to 1974, when Aviram and Ratner[1] suggested that a single molecule could perform as a current rectifier. The paradigm of molecular electronics[2–6] is that typical functions of electronic devices can be emulated by individual molecules or by suitable assemblies thereof (supramolecular systems). The ultimate objective of this research field is the construction of electronic circuits (and computers) from molecules, in a bottom-up approach.

The simplest component of an electrical circuit is a wire, and the design of molecular wires has received a great deal of attention. In a broad sense. this term can be used to designate any molecular" structme able to mediate the transfer of electrons between appropriate electron donor and acceptor sites (electrodes, photoactive, and redox-active molecular components). In practice. different "conduction" mechanisms may apply, depending on the molecular structure of the wire and on the type of experimental setup used (see below). Molecular wires were studied in a variety of experimental conditions, depending on the nature of the donor and acceptor terminals the wire is connected to. and on the method used to detect the electron flow. Available methods can be broadly divided into the following (Fig. 1): photoinduced eiectron transfer in donor-wire-acceptor systems (dyads), fast electrochemistry of adsorbed wire-electroactive group asseinblies, and conductance $[I(V)]$ measurements on metal-wire-metal junctions.

PHOTOINDUCED ELECTRON TRANSFER

Some examples of donor–acceptor dyads for studies of photoinduced electron transfer across molecular bridges are shown in Fig. 2.[10–12] These systems are usually studied by exciting the chromophore (left component in Fig. 2) with appropriate light pulses and by observing electron transfer to the acceptor (right component in Fig. 2) by means of time-resolved spectroscopy. The time resolution of such techniques is generally limited by the light pulse duration. extending now into the ultrafast (femtosecond) regime.

In many of the systems investigated (e.g., in those of Fig. 2a–c), the energy levels of the bridge are far apart from those of the donor and acceptor sites (Fig. 3a. middle). Therefore, the electron tunnels in a single coherent step from donor to acceptor, without being localized at any time on the bridge (Fig. 3a. top). These processes are described by standard nonadiabatic electron transfer theory,[13–18] where the transfer probability is proportional to the square of the donor–acceptor electronic coupling. The role of the connecting bridge is actually that of a mediator of donor–acceptor electronic coupling. The phenomenon is conveniently described in terins of superexchange,[19–22] whereby "virtual" bridge states (i.e., high-energy excited states of electron transfer character involving the bridge) mix into the initial and final wave functions. as represented schematically in Fig. 3a (bottom) (where a donor-to-bridge state is shown. and possible bridge-to-acceptor states are omitted for clarity). According to this mechanism. the electron transfer probability k_{ET} decreases exponentially with donor–acceptor distance r_{DA} (Eq. 1).

$$k_{ET} = k(0)\exp(-\beta r_{DA}) \quad (1)$$

Thus, in the superexchange regime, the bridges behave differently from macroscopic ohmic conductors. In such cases, the term "molecular wire" can only be used in a broad sense. to emphasize the fact that bridges play an important role in eiectron transfer processes. Different bridges give different β attenuation factors. and measurements of photoinduced electron transfer rates as a function of bridge length can be used to characterize the "conducting" properties of the bridge. For modular bridges. made of a sequence of individual weakly coupled units (e.g., like those shown in Fig. 2a–c), the value of β depends on the following: 1) the energy of the virtual states localized on each module: and 2) the magnitude of the coupling between adjacent modules. As a consequence of 1 (above). fully saturated bridges usually give high β values (e.g., $\beta = 1.0 \pm 0.2$ Å^{-1} for the bridges in Fig. 2a–b),[10] while

"This restricts the Geld to discrete molecular systems. Thus. some very interesting work carried out with more extended wires, such as carbon nanotubes (Refs. [7,8]) and one-dimensional semiconductors (Ref. [9]), will not be dealt with in this entry.

Encyclopedia of Supramolecular Chemistry
DOI: 10.1081/E-ESMC 120017790

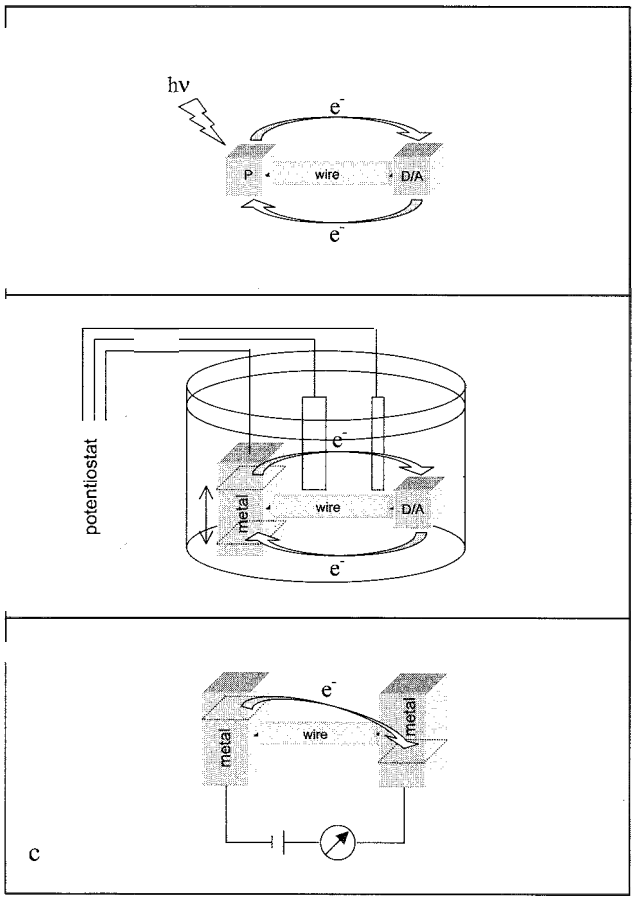

Fig. 1 Schematic representation of three types of experiment used to study electron transfer across molecular wires.

bridges with unsaturated units are characterized by lower values (e.g., $\beta = 0.5$ Å^{-1} for the bridge in Fig. 2c).[11] As an example of the effect of 2 (above), photoinduced electron transfer in the dyad of Fig. 2c is slowed by a factor of 50, simply by introducing alkyl substituents (R = hexyl instead of H) in the central ring. This is a consequence of the increased torsion angle and decreased electronic coupling between adjacent phenyl rings.[11]

A different situation may be encountered when the molecular wire connecting the donor and acceptor molecular components is a highly delocalized organic bridge. In such a case, the wire levels may become energetically accessible (Fig. 3b, middle). The bridge-localized states are no longer "virtual" (Fig. 3b, bottom), and the electron transfer proceeds via real injection of electrons into the wire (Fig. 3b, top). In such cases, the term "molecular wire" applies in a more strict sense, and the bridge is expected to approach the behavior of a conventional ohmic conductor, with a simple inverse dependence of the electron transfer rate on distance. An example of such a situation is represented by the dyad of Fig. 2d, based on a poly-p-phenylenevinilene bridge.[12] In fact, an interesting switch in mechanism was observed when the length of this type of bridge was changed systematically, by increasing the number of phenylenevinylene units from 0 to 4. For short bridges (0 and 1 repeating units), the distance dependence expected for superexchange ($\beta = 0.57$ Å^{-1}) was obtained. But then, an abrupt change in mechanism occurred, and the systems containing 2, 3, and 4 repeating units exhibited higher electron transfer rates and a true molecular wire behavior (apparent $\beta = 0.04$ Å^{-1}). This was explained by the decrease in energy of the LUMO of the bridge with increasing length of the conjugated system: beyond a critical bridge length, the LUMO bridge becomes thermally accessible from the donor level, and the mechanism switches from superexchange to molecular wire.[12]

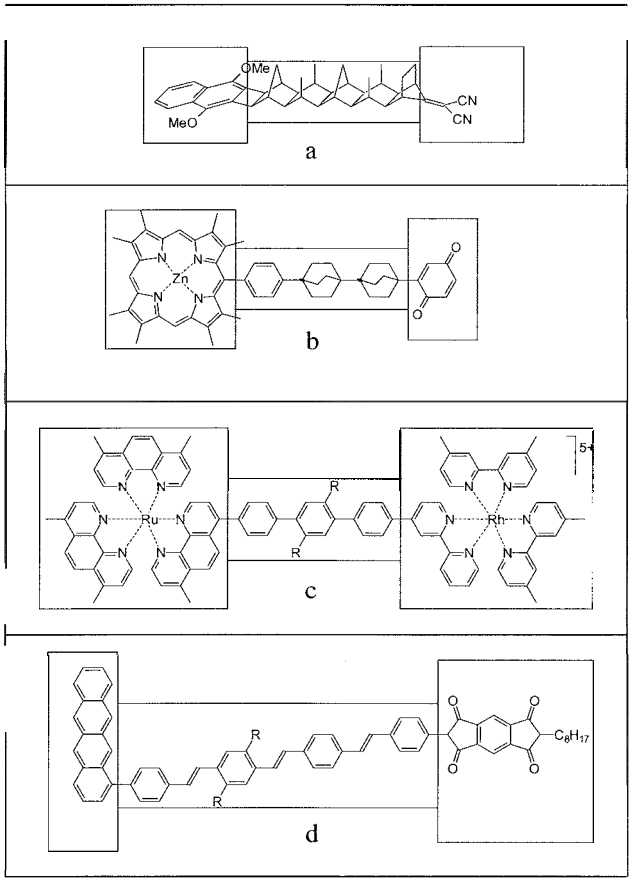

Fig. 2 Examples of covalently linked donor-acceptor systems (dyads) used for the study of photoinduced electron transfer across organic spacers. Boxes are drawn to identify the photoexcitable chromophore (left), the bridge (center), and the acceptor unit (right).

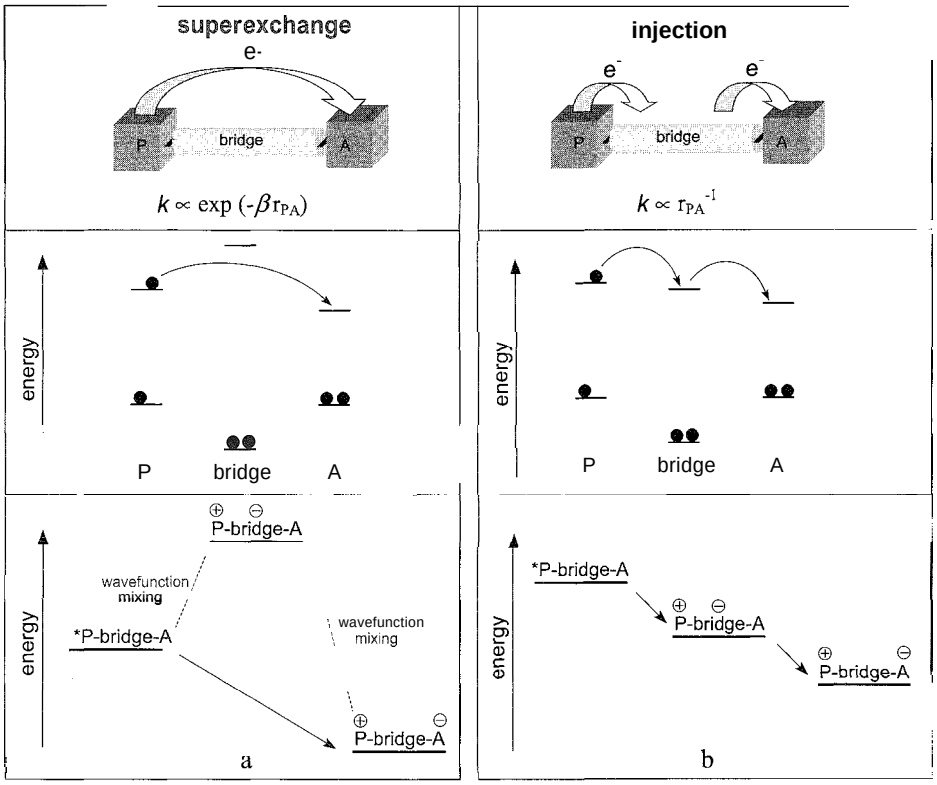

Fig. **3** Schematic representation of two limiting mechanisms for photoinduced electron transfer across a bridge: superexchange (a) and electron injection (b).

ELECTROCHEMISTRY IN SELF-ASSEMBLED MONOLAYERS

One-dimensional organic molecules with head groups suitable for metal binding (e.g., –SH, pyridyl) form self-assembled monolayers (SAMs) at metal surfaces (e.g., Au. Ag. Hg. Pt). Particularly well-characterized stable SAMs are those formed by alkanethiols.[23] Several interesting studies were carried out with SAM-forming molecules that comprise a binding group. an organic spacer, and an electroactive group (Fig. 1b). In such systems. various types of electrochemical techniques (e.g., fast-scan cyclic voltammetry,[24] AC voltammetry,[25] coulostatic T-jump methods,[26,27] and potential step chronoamperometry,[28]) can be used to measure heterogeneous electron transfer rates between the electrode and the electroactive group. Pure SAMs of the electroactive species or mixed SAMs. where the electroactive species is diluted in a monolayer of inactive molecules, can be studied by such techniques. The time scales of the electron transfer processes that can be observed depend on the technique, with rates as fast as 10^7 s^{-1} being presently accessible.

Representative examples of such types of measurement involve thiol-based SAMs on gold, with ferrocene as the electroactive group, and hydrocarbons of varying degrees of conjugation (alkanes[25] phenylethynyl,[25] and phenylenevinylene oligomers,[27]) as spacers. The length of the spacer can be systematically changed by varying the number of modular units (Fig. 4). With the alkane and phenylethynyl spacers, the experimental rates were found to fall off exponentially with distance, as required for an electron tunneling mechanism (Eq. 1). The damping factor is much higher for the saturated systems (β = 0.9 $Å^{-1}$ for the alkane spacers) than for the unsaturated ones (β = 0.36 $Å^{-1}$ for the phenylethynyl spacers),[25] again in agreement with the predictions of a superexchange mechanism. For the systems involving phenylenevinylene oligomers as spacers, electron transfer is so fast that the rates are not limited by eiectronic coupling (adiabatic limit) for bridges up to 28 Å long.[27] Interestingly, the β values obtained by these electrochemical techniques are similar to those obtained from photoinduced electron transfer in dyads with similar types of spacers.

METAL-MOLECULE-METAL JUNCTIONS

Toward the objective of molecular electronics. i.e.. to use molecules as components of electronic circuits, a

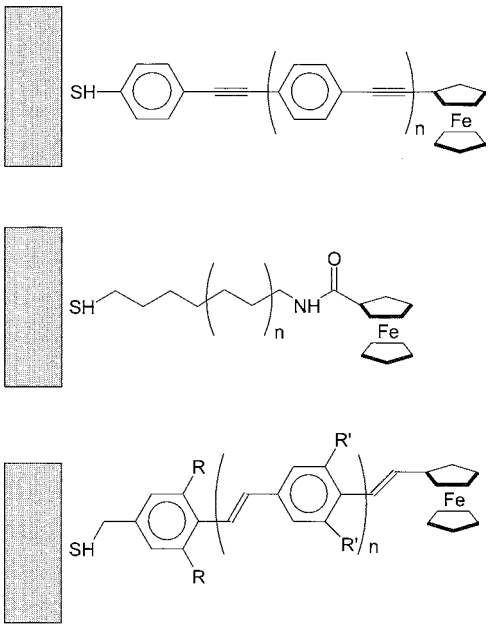

Fig. 4 Examples of molecules used for studies on electroactive SAM.

key step is the possibility to effectively wire molecules to solid (metal or semiconductor) contacts, so as to measure, e.g., their electrical conductivity. In recent years, this is becoming a feasible goal, thanks to the progress made in nanotechnology and scanning microscopy techniques. Several ingenious techniques are currently being applied to this problem. They include, among others, the following: probing conjugated molecules inserted into an isolating SAM by scanning tunneling miscroscopy (STM);[29] binding dithiolated molecules within a break junction;[30] using nanopores to build metal-SAM-metal junctions;[31,32] touching molecules in an isolating matrix with a conducting atomic force microscope (AFM);[33] contacting two SAMs together using a mercury drop electrode;[34,35] and attaching gold nanoparticles to dithiolated molecules inserted into a SAM and probing with STM[36] or conducting atomic force microscopy (AFM).[37]

Among such techniques, the last seems to be particularly reliable in terms of generating reproducibile single-molecule contacts. In a recent example,[37] molecules of 1.8-octanedithiol were inserted into an octanethiol SAM on Au(111). The thiol groups at the surface of the monolayer were derivatized with gold nanoparticles (less than 2 nm in diameter). A gold-coated conducting AFM tip was used to locate and contact individual particles bonded to the monolayer (Fig. 5). Current-voltage [$I(V)$] measurements made on a large number of nanoparticles (> 4000) produced only five distinct types of curves. These curves correspond to integer multiples of a fundamental one, that is thus assigned as the $I(V)$ characteristics of a single-molecule contact. The resistance of a single octanedithiol molecule, measured in this way, is 900 ± 50 MR. On the other hand, the resistance of the molecules of the octanethiol layer (which are probed via nonbonded contacts) are at least four orders of magnitude larger and much less reproducible.[37]

An experimentally simple, but versatile, approach is that based on M-SAM(1)SAM(2)-Hg junctions (M = Ag, Au).[34,35] These junctions are formed by depositing a first SAM on a solid metal surface (e.g., Ag, Au), a second SAM on a hanging drop of Hg, and then by bringing into contact the two monolayers (Fig. 6). This junction takes advantage of the smooth, compliant, defect-free nature of the Hg surface to minimize the effects of irregularities of the solid surface and the potential for shosting. A variety of experiments can be performed with such a simple experimental setup, by systematically changing the length of the SAM-forming molecules, their chemical natures, the natures of the chemical groups that consitute the interface between the two SAMs, or by inserting appropriate chemical species at this interface (Fig. 6). When the length of the molecules in the Au-supported SAMs are varied systematically, the $I(V)$ curves show exponential decreases in current density with distance, with potential-independent β values that depend on the chemical nature of the molecules. Again. the β values for saturated SAMs (0.87 $Å^{-1}$ for alkanethiols) are larger than those for unsaturated ones (0.61 $Å^{-1}$ for oligophenylene thiols),[35] in agreement with the trends found by studying photoinduced electron transfer in molecular dyads and electrochemical processes in SAMs with electroactive groups.

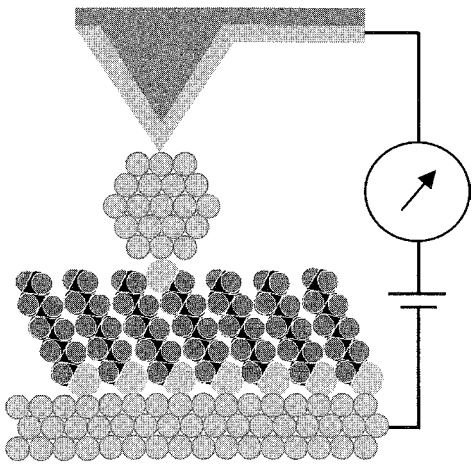

Fig. **5** Schematic representation of the AFM experiment described in Ref. 37.

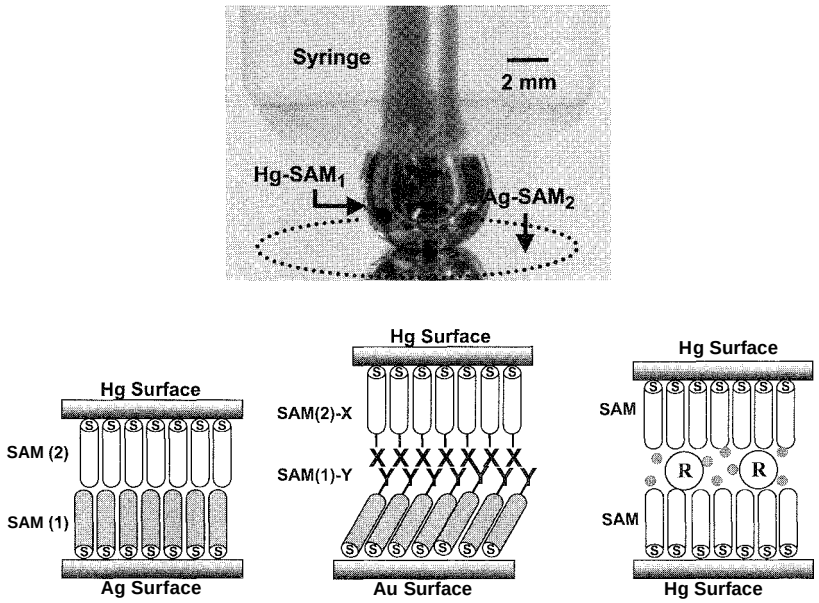

Fig. 6 Schematic representation of double-SAM junctions between a metal surface and a mercury drop (adapted from Ref. 35)

CONCLUSION

The techniques employed to characterize the behavior of molecular wires are so varied that extreme care should be used in comparing data between different experiments, especially absolute values of electron transfer rates, resistance, etc. Nevertheless, some general features can be noticed. In particular. in most of the experiments, the rate of electron transfer is found to decrease exponentially with the length of the wire, consistent with a coherent electron tunneling process. The interesting point is that the damping factor of this exponential decrease, β, is appreciably constant for a given type of bridge, regardless of the type of experiment from which it is derived. Thus, β emerges from these studies as a characteristic property of the bridge, suitable to describe its electron-transmitting (''conducting'') ability in a variety of experimental contexts.

The study of electron transport through molecules (especially at the single-molecule level) is a forefront scientific field that deserves considerable experimental and theoretical efforts. However, the fact that a variety of methods for wiring molecules and studying their electrical characteristics is now available should be regarded as an exciting breakthrough on the way to the ambitious goals of molecular electronics. Indeed, a number of interesting functions, reminiscent of those of conventional electronic devices, were recently observed by studying metal-molecule-metal junctions (e.g., rectification,[38] negative differential resistance,[31,32] conductance switching,[29] electromechanical amplification,[39] and field-effect transistor behavior.[''''])

ARTICLES OF FURTHER INTEREST

Energy and Electron Transfer in Supramolecular Systems, p. 535
Molecular Switches, p. 917
Supramolecular Electrochemistry, p. 1412
Supramolecular Photochemistry, p. *1434*

REFERENCES

1. Aviram, A.; Ratner, M.A. Molecular rectifiers. Chem. Phys. Lett. 1974, 29, 277.
2. Molecular *Electronics*; Jortner, J., Ratner, M., Eds.: Rlackwell Science: London. 1997.
3. Aviram, A., Ratner, M.A., Eds. Annu. N. Y. Acad. Sci. **1998**, *852*. (Special volume on Molecular Electronics).
4. Joachim, C.; Gimzewski, J.K.; Aviram, A. Electronics using hybrid-molecular and mono-molecular devices. Nature 2000. 408, 541.
5. Tour, J.M. Molecular electronics. Synthesis and testing of components. Acc. Chem. Res. 2000, 33, 791–804.
6. Pease, A.R.: Jeppcsen, J.O.; Stoddart, J.F.; Luo, Y.; Collier, C.P.; Heath, J.R. Switching devices based on interlocked molecules. Acc. Chem. Res. 2001, 34, 433.
7. Dresselhaus, M.S.; Dresselhaus, G.; Avouris, P. *Carbon Nanotubes*: Springer-Verlag, 2000.

8. Bachtold. A.; Hadley, P.; Nakanishi, T.: Dekker. C. Logic circuits with carbon nanotube transistors. Science 2001, 294. 1317.
9. Huang. Y.: Duan. X.: Cui, U.: Lauhon. L.J.: Kim, K.: Lieber. C.M. Logic gates and computation from assembled nanowire building blocks. Science 2001. 294, 1313.
10. Paddon-Row, M.N. Covalently Linked Systems Base on Organic Componente. In *Electron* Transfer in *Chemistry*; Balzani, V.. Ed.: Wiley-VCH: Weinheim, 2001; Vol. III, 337. Chapter 2.3.
11. Scandola. F.: Chiorboli. C.: Indelli, M.T.: Rampi, M.A. Covalently Linked Systems Containing Metal Complexes. In Electron Transfer *in Chemistry*; Balzani. V., Ed.; Wiley-VCH: Weinheim, 2001: Vol. III, 179. Chapter 2.1.
12. Davis. W.B.: Svec, W.A.; Ratner, M.A.; Wasielewski, M.R. Molecular wire behaviour in p-phenylenevinylene oligomers. Nature 1998, 396. 60.
13. Marcus, R.A. Chemical and electrochemical electron-transfer theory. Annu. Rev. Phys. Chem. 1964. *15*, 155.
14. Sutin, N. Theory of electron transfer reactions: Insights and hindsights. Prog. Inorg. Chem. 1983. *30*, 441.
15. Marcus. R.A.: Sutin, N. Electron transfers in chemistry and biology. Biochim. Biophys. Acta 1985. *811*. 265.
16. Jortner, J. Temperature dependent activation energy for electron transfer between biological molecules. J. Chem. Phys. 1936. 64. 4860.
17. Bixon, M.: Jortner. J. Electron transfer—From isolated molecules to biomolecules. Adv. Chem. Phys. 1999. *106*. 35.
18. Newton. M.D. Quantum chemical probes of electron-transfer kinetics: The nature of donor-acceptor interactions. Chem. Rev. 1991. 91. 767.
19. Halpern, J.: Orgel, L.E. The theory of electron transfer between metal ions in bridged systems. Disc. Faraday Soc. 1960. 29. 32.
20. McConnell, H.M. Intramolecular charge transfer in aromatic free radicals. J. Chem. Phys. 1961, 35. 508.
21. Miller. J.R.; Beitz. J.V. Long-range transfer of positive charge between dopant molecules in a rigid glassy matrix. J. Chem. Phys. 1981, 74. 6746.
22. Richardson, D.E.: Taube. H. Electronic interactions in mixed-valence molecules as mediated by organic bridging groups. J. Am. Chesn. Soc. 1983. 10, 540.
23. Ulman, A. Formation and structure of self-assembled monolayers. Chem. Rev. 1996. 96. 1533.
24. Weber, K.: Creager, S.E. Voltammetry of redox-active groups irreversibly adsorbed onto electrodes. Treatment using the marcus relation between rate and overpotential. Anal. Chern. 1994, 66, 3164.
25. Creager. S.: Yu. C.J.; Bamad, C.: O'Connor. S.; MacLean, T.; Lam. E.: Chong. Y.: Olsen, G.T.: Luo, J.: Gozin. M.; Kayyem, J.F. Electron transfer at electrodes through conjugated rnolecular wire bridges. J. Am Chem. Soc. 1999. 121. 1059.
26. Sachs. S.B.: Dudek. S.P.; Hsung. R.P.: Sita. L.R.; Smalley. J.F.; Newton. M.D.; Feldberg. S.W.; Chidsey. C.E.D. Rates of interfacial electron transfer through π-conjugated spacers. J. Am. Chern. Soc. 1993. 119. 10563.
27. Sykes, H.D.: Smalley. J.F.: Dudek, S.P.: Cook, A.R.; Newton. M.D.; Chidsey. C.E.D.: Felberg, S.W. Rapid electron tunneling through oligophenylenevinylene bridges. Science 2001. 291. 1519.
28. Chidsey, C.E.D. Free energy and temperature dependence of electron transfer at the metal-electrolyte interface. Science 1991. 251, 919.
29. Donhauser, Z.J.: Mantooth. B.A.: Kelly. K.F.: Bumm. L.A.: Monnell, J.D.; Stapleton, J.J.; Price. D.W., Jr.; Rawlett, A.M.: Allara, D.L.; Tour. J.M.; Weiss, P.S. Conductance switching in single molecules through conformational changes. Science 2001. 292, 2303.
30. Reed, M.A.; Zhou. C.: Muller. C.J.; Burgin, T.P.; Tour, J.M. Conductance of a molecular junction. Science 1997, 278, 252.
31. Chen. J.; Reed, M.A.; Rawlett. A.M.; Tour. J.M. Large on–off ratios and negative differential rersistance in a molecular electronic device. Science 1999. 286. 1550.
32. Tour, J.M.; Rawlett, A.M.; Kozaki, M.: Yao, U.: Jagessar. R.C.; Dirk, S.M.: Price, D.W.; Reed, M.A.; Zhou, C.-W.: Chen. J.: Wang. W.: Campbell. I. Synthesis and preliminary testing of molecular wires and devices. Chem. Eur. J. 2001, 7. 5118.
33. Leathermann. G.; Durantini. E.N.: Gust. D.: Moore. T.A.: Moore, A.L.; Stone, S.: Zhou, Z.: Rez. P.: Liu. Y.Z.: Lindsay. S.M. Carotene as a molecular wire: Conducting atomic force microscopy. J. Phys. Chem.. B 1999, 103. 4006.
34. Haag, R.: Rampi, M.A.; Holmlin. R.E.: Whitesides, G.M. Electrical breakdown of aliphatic and aromatic self-assembled monolayers used as nanometer thick organic dielectrics. J. Am. Chem. Soc. 1999. 121, 7895.
35. Holmlin. E.H.; Ismagilov, R.F.: Haag, R.; Mujica. V.; Ratner. M.A.: Rampi, M.A.: Whitesides. G.M. Correlating electron transport and molecular structure in organic thin films. Angew. Chem., Int. Ed. 2001. 40, 2316.
36. Andreas, R.P.: Bein, T.: Dorogi. M.: Feng, S.; Henderson, J.I.; Kubiak, C.P.; Mahoney, W.: Osifchin. R.G.; Reifenberger. R. Coulomb staircase at room temperature in a self-assembled molecular nanostructure. Sience 1996, 272. 1323.
37. Cui. X.D.: Primak. A.: Zarate, X.: Tomfohr. J.; Sankey, O.F.; Moore, A.L.; Moore. T.A.: Gust. D.: Harris, G.: Lindsay. S.M. Reproducible measurement of single-molecule conductivity. Science 2001. 294. 571.
38. Metzger. R.M.: Xu, T.: Peterson, I.R. Electrical rectification by a monolayer of hexadecylquinolinium tricyanoquinodimethanide measured between macroscopic gold electrodes. J. Phys. Chem.. B 2001, 105. 7280.
39. Joachim. C.; Gimzewski. J.K. An electromechanical amplifier using a single molecule. Chesn. Phys. Lett. 1997. 265. 353.
40. Park. J.: Pasupathy, A.N.: Goldsmith, J.I.: Chang. C.; Yaish. Y.; Petta, J.R.: Marie Rinkoski. M.; Sethna, J.P.: Abruna, H.D.; McEuen, P.L.: Ralph. D.C. Coulomb blockade and the Kondo effect in single-atosn transistors. Nature 2002. 417. 722.

Molecular-Level Machines

Vincenzo Balzani
Alberto Credi
Università di Bologna, Bologna, Italy

INTRODUCTION

The concept of "machine," which is so familiar in our macroscopic world, can be extended to the molecular level."] A molecular-level machine can be defined as an assembly of a discrete number of molecular components (i.e., a supramolecular system) designed to perform mechanical-like movements under the control of appropriate energy inputs. Molecules have nanometer dimensions and are the smallest entities exhibiting well-defined structures and shapes. Therefore, molecular-level machines represent the ultimate limit of miniaturization of the mechanical-machine concept.

In order to generate motion, a molecular-level machine requires an energy source. Therefore; spontaneous molecular movements caused by thermal energy; including the demonstration of the rotation of a single molecule on a surface,[2] have nothing to do with the concept of a molecular-level machine.

NATURE'S MOLECULAR MACHINES

Living organisms represent the synergistic integration of functionally diverse molecular machines.[3] The molecular machines produced by nature are extremely complicated assemblies of proteins with structures at the atomic and molecular levels that are not yet determined. In most cases, biological machines use chemical energy produced by ATP or proton gradients to perform their fucntions. How these biological fuels ultimately cause mechanical motions is still largely unknown.

In the last few years, however, the outstanding development of single molecule manipulation and observation, particularly by fluorescence spectroscopy, has thrown some light on the operational mechanism of several biological machines. For example, it was shown[4–6] that ATP synthase. the enzyme that manufactures adenosine triphosphate (ATP) from adenosine diphosphate (ADP) and inorganic phosphate (Pi) is powered by a rotary motor fueled by a proton gradient (Fig. 1). The asymmetric membrane-spanning F_0 portion of the enzyme contains a proton channel. and the soluble F_1 portion contains three catalytic sites that cooperate in the synthetic reactions. The catalytic region is made up of nine protein subunits with the stoichiometry $3\alpha{:}3\beta{:}1\gamma{:}1\varepsilon$. approximating to a flattened sphere. 10 nm across and 8 nm high. The flow of protons through F_0 generates a torque that is transmitted to F_1 by an asymmetric shaft, the coiled-coil y-subunit. This subunit acts as a rotating "cam" within F_1, sequentially releasing ATPs from the three active sites. The F_0F_1-ATP synthase is reversible, i.e.. the full enzyme can synthesize or hydrolyze ATP; F_1 in isolation, however, can only hydrolyze it. The spinning of F_1-ATPase, i.e., the rotary motor nature of this enzyme. was directly observed[7] during ATP hydrolysis by attaching a fluorescent actin filament to the γ subunit as a marker.

Enzymes such as myosin. kinesin, dynein, and their relatives are linear rnotors that convert the energy of ATP hydrolysis into mechanical work along polymer substrates: myosin along actin filaments in muscle and other cells, and kinesin and dynein along microtubules.[3] Motion derives from a mechanochemical cycle during which the motor protein binds to successive sites along the substrate in such a way as to move forward on the average. For myosin II (skeletal muscle myosin). the working stroke was observed[8,9] by optical methods. but the motor mechanism is still unknown. Several other biological processes are based on motions. For example, RNA polymerase moves along DNA while carrying out transcriptions, acting as a molecular motor. The force and velocity of single molecules of RNA polymerase were measured."] The folding and unfolding of proteins is also subjected to intensive investigations.

ARTIFICIAL MOLECULAR-LEVEL MACHINES

The idea of constructing artificial molecular-level machines is recent. This topic was first discussed by R. P. Feynman,[10] Nobel Laureate in Physics. in his famous address. "*There is plenty of room at the bottom*," to the American Physical Society in 1959. His idea was that of constructing nanoscale machines "atom by atom." a concept later expanded with fascinating perspectives but almost no practical progress, by K. E. Drexler.[11,12] With the advent of supramolecular chemistry."] it became

Encyclopedia of Supramolecular Chemistry
DOI: 10.1081/E-ESMC 120012829

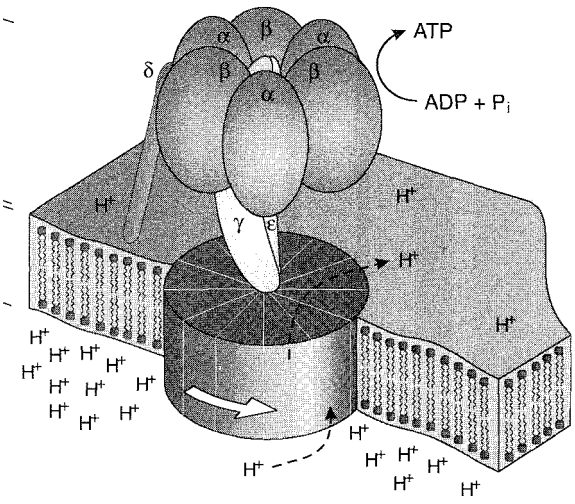

Fig. 1 Structure of F_0F_1-ATP synthase. (*View* this *art in color at www.dekker.com.*)

clear that molecules are by far more convenient building blocks than atoms for constructing molecular-level devices,[13–15] and in recent years, research on molecular-level machines has grown vigorously.[1,16–21]

Molecular-level machines operate through chemical reactions that cause electronic and nuclear rearrangements. Like macroscopic machines, they are characterized by the kind of cnergy input supplied to make them work, the kind of movement performed by their components, the way in which their operation can be controlled and monitored, the possibility to repeat the operation at will, the time scale needed to complete a cycle of operation, and the function performed.

The Energy Problem

The problem of the cnergy supply to make artificial molecular machines work is of greatest importance.[22] The most obvious way to supply energy to a chemical system is through an exergonic chemical reaction. In his address to the American Physical Society, R. P. Feynman observed the following:[10]

> An internal combustion engine of molecular size is impossible. Other chemical reactions, liberating energy when cold, can be used instead.

This is exactly what happens in our body, where the chemical energy supplied by food is used in a long series of slightly cxergonic reactions to power the biological machines that sustain life.

If an artificial molecular-level machine has to work by inputs of chemical energy, it will need the addition of fresh reactants (''fuel'') at any step of its working cycle, with the concomitant formation of waste products. Accumulation of waste products, however, will compromise the operation of the machine unless they are removed from the system, as happens in our body as well as in macroscopic internal combustion engines. The need to remove waste products introduces noticcable limitations in the design and construction of artificial molecular-level machines based on ''chemical fuel'' inputs.

Chemists have long known that photochemical and electrochemical energy inputs can cause endergonic and reversible reactions. In recent years, the outstanding progress made in supramolecular photochemistry[23] and electrochemistry[24] has thus led to design and construction of molecular machines powered by light or electrical energy that work without formation of waste products. In the case of photoexcitation, the commonly used endergonic and reversible reactions are isomerization and redox processes. In the case of electrochemical cnergy inputs, the induced endergonic and reversible reactions are, of course, heterogeneous electron transfer processes. Photochemical and electrochemical techniques offer further advantages, because lasers provide the opportunity to work in very small spaces and in very short time domains, and electrodes represent one of the best ways to interface molecular-level systems with the macroscopic world.

Needless to say, the operation of a molecular machine is accompanied by partial conversion of free energy into heat, regardless of the chemical, photochemical, and electrochemical natures of the energy input.

Other Features

The motions performed by the component parts may imply rotations around covalent bonds or the making and breaking of intercomponent noncovalent bonds. In order to control and monitor the machine operation, the motions of the component parts should cause readable changes in some properties of the system; any kind of chemical or physical technique can be useful, particularly the various types of spectroscopies. Because a machine has to work by repeating cycles, an important requirement is that any chemical reaction involved in the operation has to be reversible. The time scale needed to perform a cycle can range from less than picoseconds to hours, depending on the nature of the molecular components and the types of rearrangements involved. Finally, the functions that can be performed by exploiting the movements of the component part in artificial molecular-level machines are varied and, to a large extent, still unpredictable. In this regard, it should be pointed out that the mechanical movements taking place in molecular-level machines, and the related changes in the spectroscopic and electrochemical properties, usually obey binary logic and can thus be taken as a basis for

information processing at the molecular level. Artificial molecular machines capable of performing logic operations have already been reported.[25]

In the following. we illustrate a few examples of molecular-level machines powered by chemical. electrochemical, or light energy.

MOLECULAR MACHINES **POWERED** BY **CHEMICAL FUELS**

Chemical energy inputs are used[1,16–22] to induce rotary motions in specially designed molecules, to control threading/dethreading processes in pseudorotaxanes. to govern ring shuttling in rotaxanes, and to cause ring motions in catenanes. Two among the most significant examples are illustrated below.

Unidirectional Rotation

The unidirectional rotation illustrated in Fig. 2 from structure 1a to 1b is an important step toward the realization of a chemically powered molecular motor.[26,27] Compounds 1a and 1b are two of three low-energy rotamers about the axle connecting the triptycene and helicene components. Rotamer 1a is activated by reaction with phosgene to give isocyanate 2. Isocyanate 2 is chemically armed to react with the OH group in the hydroxypropyl tether attached to helicene. but, in the rotational ground state 2, the isocyanate and the OH group are too far apart to interact. However, at those instants when a clockwise rotation of the triptycene (not possible with a comparable counterclockwise rotation) brings the isocyanate and the OH group sufficiently close to react (see 3), urethane formation can then result (4). This irreversibly traps the triptycene in a relatively high-energy conformation around the triptycene/helicene axle. Ambient thermal energy then drives the exoergonic, but very slow, unidirectional rotation from 4 to 5. Finally, 5 is cleaved to 1b, thereby completing the chemically driven rotation of 1a to 1b. After this proof of principles, much work still has to be done to obtain a system that can undergo a full, continuous, and fast rotation.

A pH-Controllable Molecular Shuttle

Rotaxanes are made of dumbbell-shaped and ring components that exhibit some kind of interaction originating from complementary chemical properties. In rotaxanes containing two different recognition sites in the dumbbell-shaped component, it is possible to switch the position of the ring between the two stations by using an external stimulus. A system that behaves as a chemically controllable molecular shuttle[28] is shown in Fig. 3. It is made of a dibenzo[24]crown-8 (DB24C8) macrocycle and a dumbbell-shaped component containing a dialkylammonium center and a 4,4′-bipyridinium unit. An anthracene moiety is used as a stopper, because its absorption, luminescence: and redox properties are useful to monitor the state of the system. Because the hydrogen bonding interaction between the DB24C8 macrocycle and the ammonium center is much stronger than the charge–transfer interaction of the macrocycle with the bipyridinium unit, the rotaxane exists as only one of two possible translational isomers. Deprotonation of the ammonium center, however, causes 100% displacement of the macrocycle to the bipyridiniuin unit; reprotonation directs the macrocycle back onto the ammonium center (Fig. 3).

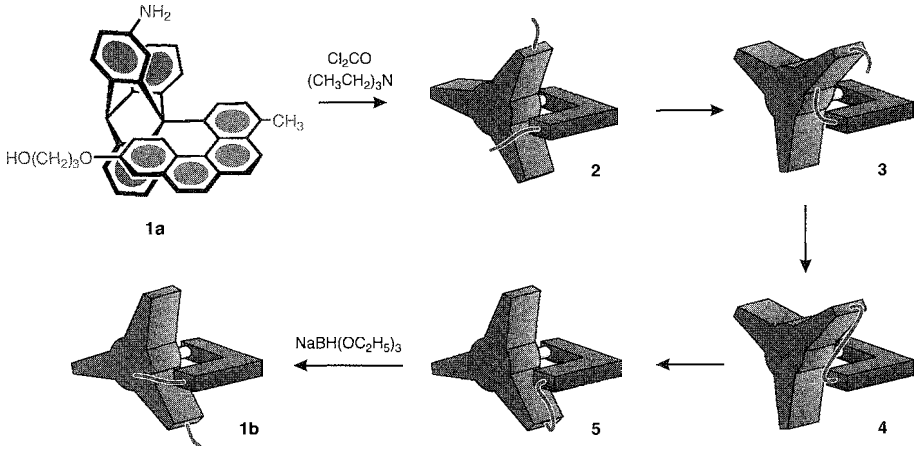

Fig. **2** Sequence of events involved in the chemically powered unidirectional rotation of a compound made of triptycene and helicene components. (*View this art in color at www.dekker.com.*)

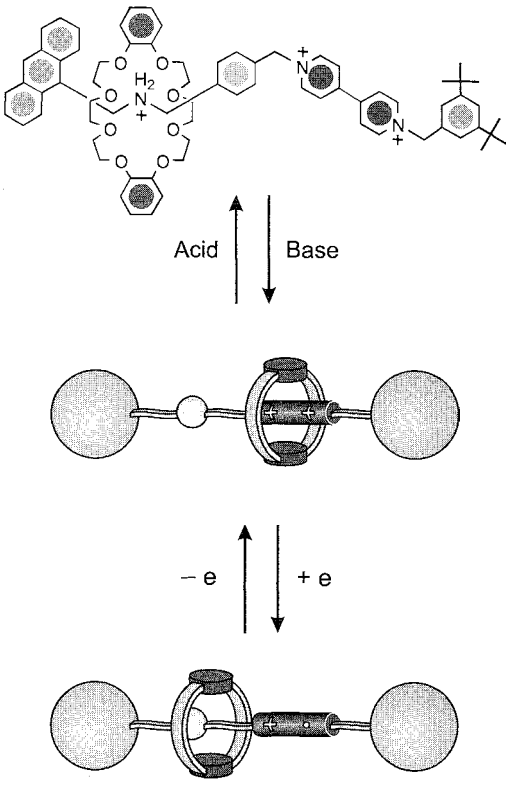

Fig. **3** A chemically controllable molecular shuttle: the macrocyclic ring can be switched between the two stations of the dumbbell-shaped component by base/acid inputs. Additionally, in the deprotonated rotaxane, the ring can be displaced from the bipyridinium station through reduction of such unit. (*View this art in* color *at www.dekker.com.*)

Such a switching process was investigated by ^{1}H-NMR spectroscopy and by electrochemical and photophysical measurements. The full chemical reversibility of the energy-supplying acid/base reactions guarantees the reversibility of the mechanical movement, in spite of the formation of waste products. Notice that this system could be useful for information processing,[29] because it exhibits a binary logic behavior. It should also be noted that in the deprotonated rotaxane. it is possible to displace the crown ring from the bipyridinium station by destroying the charge–transfer interaction through reduction of the bipyridinium station (Fig. 3) or oxidation of the crown ring. Therefore, in this system. mechanical movements can be induced by two different types of stimuli (acid/base and electron/hole).

MOLECULAR MACHINES POWERED BY ELECTROCHEMICAL ENERGY

Electrochemical energy inputs are used[1,16–22,23] to control threading and dethreading in pseudorotaxanes, ring shuttling in rotaxanes, and ring motions in catenanes. An example of the last type of motion is illustrated below.

Controllable Ring Motions in Catenanes

In a catenane, structural changes caused by circumrotation of one ring with respect to the other can be clearly evidenced when one of the two rings contains two nonequivalent units. In the catenane shown in Fig. 4, the electron-acceptor tetracationic cyclophane is symmetric, whereas the other ring contains two different electron-donor units, namely, a tetrathiafulvalene (TTF) unit and a 1.5-dioxynaphthalene (DON) unit.[30] In a catenane structure, the electron donor located inside the cavity of the electron-acceptor ring experiences the effect of two electron-acceptor units, whereas the alongside electron donor experiences the effect of only one electron acceptor. Therefore; the better electron donor (i.e., TTF) enters the acceptor ring and the other (i.e., DON) remains alongside. On electrochemical oxidation, the first observed process concerns TTF, which thus loses its electron donating properties. Fusthermore, an electrostatic repulsion arises between TTF^+ and the tetracationic macrocycle. These effects cause circumrotation of one ring to yield the translational isomer with the DON moiety positioned inside the acceptor. Upon reduction of TTF^+, the initial configuration is restored. However, this may happen without the occurrence of a full rotation. because it is equally probable that the reset caused by reduction of TTF^+ occurs by a reverse rotation compared to that which occurred in the forward switching caused by TTF oxidation. In order to obtain a full rotation, i.e., a molecular-level rotary motor, the direction of each switching movement should be controllable. This goal can likely be reached by introducing appropriate functions in one of the two macrocycles.[22] When this goal is reached, it will be possible to convert alternate electrical potential energy into a molecular-level mechanical rotation.

MOLECULAR MACHINES POWERED BY LIGHT ENERGY

Light is the most appealing energy source with which to make molecular-level machines work.[22] A variety of such machines using light as a partial or exclusive energy source were described.[1,15–23,31] They include tweezers. controllable doors and boxes. piston–cylinder systems, ring motions; rotary motors, and linear motors. A rotacatenane was also designed that should be able to couple a linear and a rotary motion upon a photosensitized electron-transfer reaction.[32]

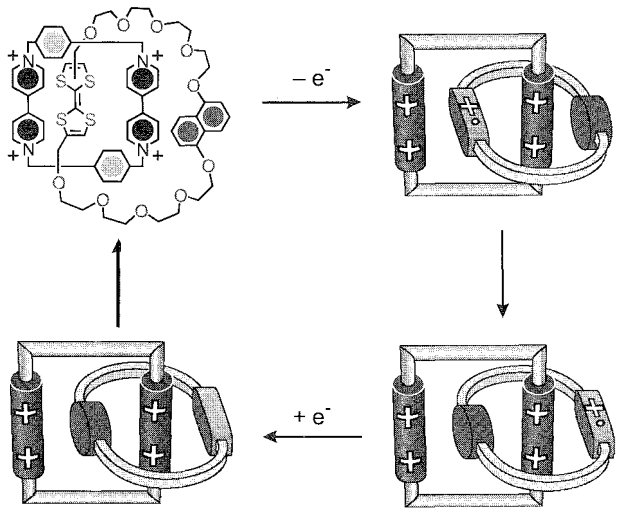

Fig. 4 Electrochemically controlled movements of the ring components upon one-electron oxidation/reduction of a TTF unit in a catenane containing a nonsymmetric ring. *(View this art in color at www.dekkcr.com.)*

A Light-Driven Molecular Rotary Motor

Photochemical *trans-cis* isomerization around a carbon–carbon double bond is a well-known reversible reaction.[123] Exploitation of this photochemical reaction in a suitably designed compound that contains two chiral elements has led to a photoinduced unidirectional rotary

In the methyl-substituted phenanthrylidcne 6, shown in Fig. 5, each one of the two helical subunits linked by a double bond can adopt a right-handed (P) or a lest-handed (M) helicity. As a result, a total of four stereoisomers are possible for this compound. The cis-trans photoisomerization reactions are reversible and occur upon irradiation at appropriate wavelengths. By contrast, the inversions of helicities, while maintaining a *cis* or a truns conliguration, occur irreversibly under the influence of thermal energy. Upon irradiation ($\geq$280 nm, 218 K) of a solution of (*P*,*P*)-*trans*-**6**, a mixture of (*P*,*P*)-*trans*-**6** and (*M*,*M*)-*cis*-**6** is obtained in a ratio of 5:95. By warming the solution to 293 K, (*M*,*M*)-*cis*-**6** interconverts irreversibly to (*P*,*P*)-*cis*-**6**. Subsequent irradiation ($\geq$280 nm) of the solution produces a mixture of (*P*,*P*)-*cis*-**6** and (*M*,*M*)-*trans*-**6** in a ratio of 10:90. Upon increasing the temperature further (333 K), (*M*,*M*)-*trans*-**6** interconverts irreversibly to the original isomer (*P*,*P*)-*trans*-**6**. Thus, a sequence of light- and temperaturc-induced isomcrizations can bc exploited to move this molecular rotor in one direction only (Fig. 5). When (*P*,*P*)-*trans*-**6** is irradiated ($\geq$280 nm) at a high temperature (293 K), a clockwise 360° rotation occurs spontaneously. The overall process can be followed by monitoring the change in the intensity of the absorption band at 217 nm in the circular dichroism trace. The unidirectional motion in this system is dictated by the stereogenic centers associated with the two methyl substituents. As a result of a trans ›*cis* isomerization, the axial methyl substituents of (*P*,*P*)-*trans*-**6** are forced to adopt a less favorable equatorial orientation in (*M*,*M*)-*cis*-6. However, the strain associated with the equatorial methyl susbstituents is released upon thermal interconversion of (*M*,*M*)-*cis*-**6** in the more stable isomer (*P*,*P*)-cis-6. The subsequent cis-–)trans isomerization forces the methyl groups to adopt, once again, equatorial orientations in the isomer (*M*,*M*)-*trans*-**6**. Finally, the thermal interconversion of (*M*,*M*)-*trans*-**6** into the original isomer (*P*,*P*)-*trans*-**6** is accompanied by a change from equatorial to the more stable axial orientations for the methyl substituents (Fig. 5). Morc recently, this molecular motor was redesigned to improve its performance, and it was shown that unidirectional rotation can be controlled by a single stereogenic center.[''']

A Photocontrollable Molecular Shuttle

In order to achieve photoinduced ring switching in rotaxanes containing two different recognition sites in the dumbbell-shaped component, the designed compound 7^{6+} shown in Fig. 6 was synthesized.[''''] This rotaxane is made of macrocycle **R** and a dumbbell component that contains the following: 1) a photoactive Ru(II) polypyridine complex (**P**) as a stopper; 2) a 4,4′-bipyridinium unit ($\mathbf{A_1}$) and a 3,3′-dimethyl-4,4′-bipyridinium unit ($\mathbf{A_2}$) as electron accepting stations; 3) a p-terphenyl-type ring system as a rigid spacer (**S**); and 4) a tetraarylmethane group as the second stopper (**T**). The stable translational isomer is the one in which the **R** component encircles the better electron-acceptor $\mathbf{A_1}$ unit. In order to obtain the

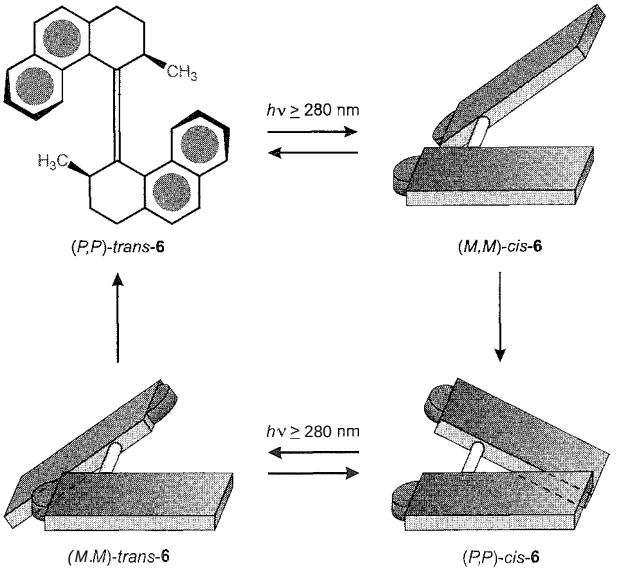

Fig. 5 The light-fueled rotary motor 6 undergoes unidirectional rotation in *n*-hexane at 333 K upon irradiation at appropriate wavelengths. (View *this art in color at www.dekker.com.*)

photoinduced abacus-like movement of macrocycle $\mathbb{R}$ between the A_1 and A_2 stations. two strategies were devised: one is fully based on processes involving the rotaxane components (intramolecular mechanism), while the other requires the help of external reactants (sacrificial mechanism).

The intramolecular mechanism, which implies the conversion of light energy into mechanical energy without generating waste products,[34] is based on the four operations illustrated in Fig. 6.

1. *Destabilization of the stable translational isomer:* Light excitation of $\mathbb{P}$ (Step I) is followed by the transfer of an electron to the A_1 station (Step 2), which is encircled by ring $\mathbb{R}$; such a photoinduced electron-transfer process, which competes with the intrinsic excited-state decay (Step 3), deactivates the A_1 station.
2. *Ring displacement*: The ring movement from A_1^- to A_2 (Step 4) has to compete with the back electron-transfer process from A_1 (still encircled by $\mathbb{R}$) to the oxidized photoactive unit $\mathbb{P}^+$ (Step 5).
3. *Electronic reset*: The back electron-transfer process from the free reduced station A_1 to $\mathbb{P}^+$ (Step 6) restores the electron-acceptor power to the A_1 station.
4. *Nuclear reset:* As a consequence of the electronic reset. back movement of the ring from A_2 to A_1 occurs (Step 7).

It is worthwhile noticing that in a system which behaves according to the intramolecular mechanism shown in Fig. 6. each light input causes the occussence of a forward and back ring movement (i.e., a full cycle) without generation of any waste product. In some way, it can be considered a four-stroke cyclic linear motor powered by light. For another example of photocontrollable molecular shuttle, see Ref. [35].

CONCLUSION

In the last few years. several examples of inolecular-level machines have been designed and constructed.[1,16–22] It should be noted. however, that the described systems work in solution, i.e, incoherently. For most applications, they need to be interfaced in some way with the macroscopic world by ordering them, so that they can behave coherently either in parallel or in series. Research on this topic is developing at a growing rate.[19,21]

The extension of the concept of a device to the molecular level is of interest not only for the development of nanotechnology but also for the growth of basic research. Looking at supramolecular chemistry from the viewpoint of functions with references to devices of the macroscopic world is an interesting exercise that introduces novel concepts into chemistry as a scientific discipline.

ACKNOWLEDGMENTS

Support from the European Union, the Ministero dell'Istruzione, Università e Ricerca. and the University of Bologna is gratefully acknowledged.

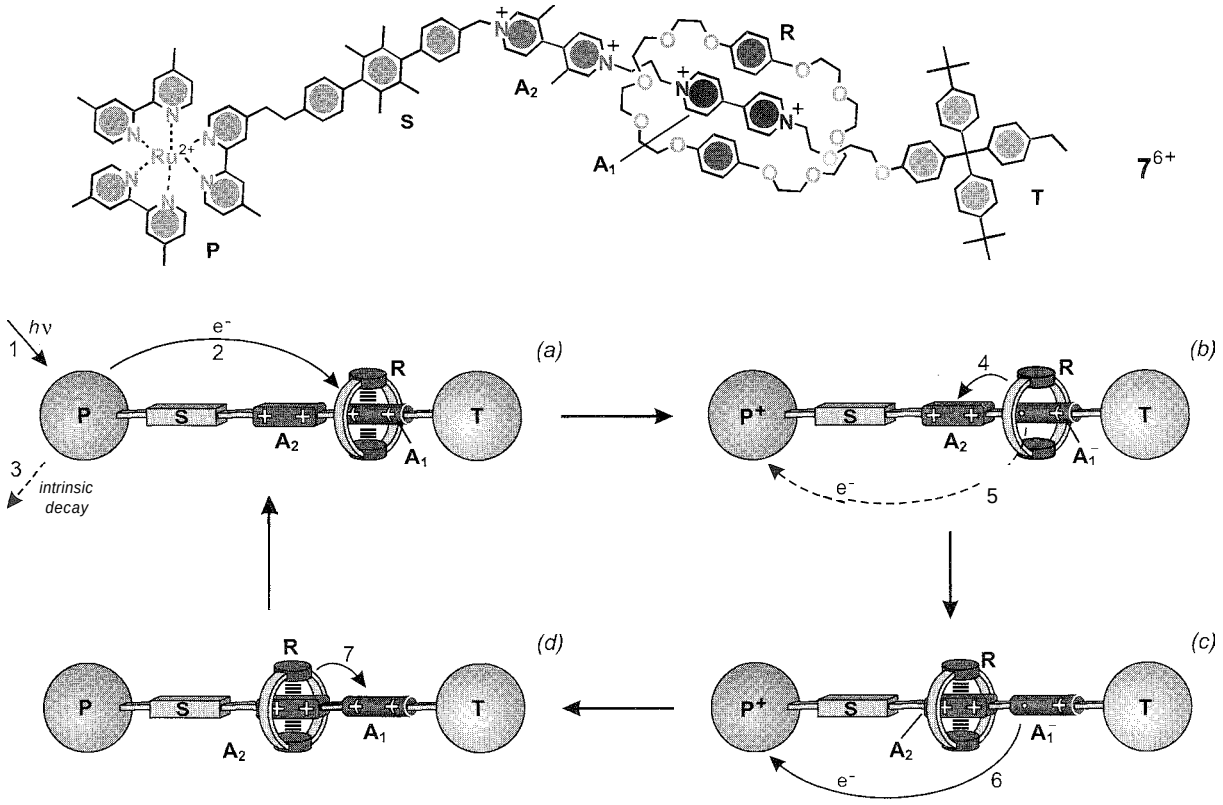

Fig. 6 The intramolecular mechanisms for the photoinduced shuttling movement of macrocycle **R** between the two stations $\mathbf{A_1}$ and $\mathbf{A_2}$ in rotaxane $\mathbf{7}^{6+}$. (*View* this *art in color at www.dekker.com.*)

ARTICLES OF FURTHER INTEREST

Catenanes and Other *Interlocked* Molecules. p. 206
Crown Ethers, p. 326
Energy and Electron Transfer in Supramolecular Systems, p. 535
Rotaxanes and Pseudorotaxanes, p. 1194
Supramolecular Photochemistry, p. 1334

REFERENCES

1. Balzani. V.; Credi. A.: Raymo. F.M.: Stoddart. J.F. Artificial molecular machines. Angew. Chem.. Int. Ed. *2000. 39* (19). 3348–3391.
2. Gimzewski. J.K.: Joachim. C.: Schlittler, R.R.; Langlais, V.: Tang. H.: Johannsen. I. Rotation of a single molecule within a supramolecular bearing. Science 1998, *281* (5376). 531–533.
3. Goodsell. D.S. *Our Molecular Nature: The* Body's Motors, Machines, *and* Messages: Copernicus: New York. 1996.
4. Boyer, P.D. Energy. life, and ATP (Nobel lecture). Angew. Chem.. Int. Ed. 1998. *37* (17). 2296--2307.
5. Walker. J.E. ATP synthesis by rotary catalysis (Nobel lecture). Angew. Chem.. Int. Ed. 1998. *37* (17). 2308–2319.
6. Skou. J.C. The identification of the sodium-potassium pump (Nobel lecture). Angew. Chem.. Int. Ed. 1998, 37 (17). 2320–2328.
7. Yasuda. R.: Noji, H.; Kinoshita. K.. Jr.: Yoshida. M. F_1-ATPase is a highly efficient molecular motor that rotates with discrete 120 degrees steps. Cell 1998. 93 (7). 1117–1124.
8. Finer. J.T.: Simmons. R.M.: Spudich. J.A. Single myosin molecule mechanics—Piconewton forces and nanometer steps. Nature 1994. *368* (6467). 113–119.
9. Wang. M.D.: Schnitzer, M.J.; Yin. H.: Landick. R.: Gelles. J.; Block. S.M. Force and velocity measured for single molecules of RNA polymerase. Science 1998. 282 (5390). 902–907.
10. Feynman, R.P. There's plenty of room at the bottom. Enp. Sci. 1960. *23* (5). 22–36. See also: http://www.zyvex.com/nanotech/feynman.html (accessed July 2003).
11. Drexler, K.E. *Engines of Creation*: Doubleday: New York, 1986.
12. Drexler. K.E. *Nanosystems: Molecular Machinery, Manufacturing,* and *Computation*; Wiley: New York, 1992.
13. Lehn. J.-M. *Supramolecular Chemistry; Concepts and Perspectives*; VCH: Weinheim. 1995.

14. Molecular *Electronic* Devices; Carter, F.L., Siatkowski, R.E., Wohltjien, H.. Eds.; Elsevier: Amsterdam. 1988.
15. Balzani, V.: Moggi, L.; Scandola, F. Towards a Supramolecular Photochemistry: Assembly of Molecular Components to Obtain Photochemical Molecular Devices. In Siipramolecular *Photochemistry*; Balzani, V., Ed.; Reidel: Dordrecht, 1987; 1–28.
16. Balzani, V.; Gbmez-Lopez, M.; Stoddart. J.F. Molecular machines. Acc. Chem. Res. **1998,** *31* (7). 405–414.
17. Sauvage, J.-P. Transition metal-containing rotaxanes and catenanes in motion: Toward molecular machines and motors. Acc. Chem. Res. **1998.** *31* (10), 611–619.
18. Balzani, V.; Credi. A.; Venturi. M. Molecular-Level Devices. In *Supramolecular* Science: Where it Is *and Where* it Is Going: Ungaro, R.. Dalcanale, E., Eds.; Kluwer: Dordrecht, 1999: 1–22.
19. Acc. Chem. Res. **2001.** *34* (6). 409–522. (Special issue on Molecular Machines).
20. Balzani. V.: Credi. A.: Venturi, M. Molecular-Level Devices and Machines. In *Stimulating* Concepts in *Chemistry*; Shibasaki. M., Stoddart. J.F., Vogtle, F., Eds.: Wiley-VCH: Weinheim. 2001; 255–266.
21. *Structure and* Bonding; Sauvage, J.-P., Ed.; Springer: Heidelberg, 2001; Vol. 99, 1–281. (Volume devoted to Molecular Machines and Motors).
22. Ballardini. R.: Balzani. V.: Credi, A.; Gandolfi. M.T.; Venturi. M. Artificial molecular-level machines: Which energy to make them work? Acc. Chem. Res. **2001.** *34* (6). 445–455.
23. Balzani. V.: Scandola. F. *Supramolecular Photochemistry*; Horwood: Chichester, 1991.
24. Kaifer, A.E.; Gómez-Kaifer, M. *Supramolecular Electrochemistry*; Wiley-VCH: Weinheim. 1999.
25. de Silva. A.P.: McClenaghan, N.D.; McCoy, C.P. Molecular Logic Systems. In Molecular *Switches*: Feringa, B.L., Ed.; Wiley-VCH: Weinheim. 2001: 339–361.
26. Kelly. T.R.; De Silva, H.; Silva, R.A. Unidirectional rotary motion in a molecular system. Nature **1999,** *401* (6749), 150–152.
27. Kelly, T.R.; Silva, R.A.; De Silva, H.; Jasmin, S.; Zhao, Y.J. A rationally designed prototype of a molecular motor. J. Am. Chem. Soc. **2000.** *122* (29), 6935–6949.
28. Ashton, P.R.; Ballardini. R.; Balzani, V.: Baxter. I.; Credi. A.; Fyfe, M.C.T.; Gandolfi, M.T.; Gómez-López, M.; Martinez-Diaz, M.V.; Piersanti, A.; Spencer, N.: Stoddart, J.F.: Venturi. M.: White, A.J.P.: Williams, D.J. Acid-base controllable molecular shuttles. J. Am. Chem. Soc. **1998,** *120* (46). 11932--11942.
29. Scientific *Computing World*; Cambridge Publishers Ltd., February/March 1999; p. 11.
30. Asakawa, M.; Ashton, P.R.; Balzani, V.; Credi, A.; Hamers, C.; Mattersteig. G.; Montalti, M.: Shipway, A.N.: Spencer, N.; Stoddart, J.F.; Tolley, M.S.: Venturi, M.; White, A.J.P.; Williams, D.J. A chemically and electrochemically switchable [2]catenane incorporating a tetrathiafulvalene unit. Angew. Chem., Int. Ed. **1998.** *37* (3). 333–337.
31. Ballardini, R.; Balzani; V.: Credi, A.; Gandolfi. M.T.; Venturi, M. Artificial molecular-level machines with $[Ru(bpy)_3]^{2+}$ as a "light-fueled motor." Int. J. Photoenergy **2001,** *3* (2). 63–77.
32. Koumura. N.: Zijlstra, R.W.J.: van Delden, R.A.: Harada, N.; Feringa. B.L. Light-driven monodirectional molecular rotor. Nature **1999**, *401* (6749), 152–155.
33. Koumura, N.: Geertsema, E.M.: Meetsma, A.; Feringa. B.L. Light-driven molecular rotor: Unidirectional rotation controlled by a single stereogenic center. J. Am. Chem. Soc. **2000.** *122* (48). 12005–12006.
34. Ashton, P.R.; Ballardini, R.; Balzani, V.; Credi, A.: Dress. R.; Ishow. E.; Kleverlaan, C.J.: Kocian, O.: Preece. J.A.; Spencer, N.; Stoddart, J.F.: Venturi, M.; Wenger, S. A photochemically driven molecular shuttle. Chem. Eur. J. **2000,** 6 (19). 3558–3574.
35. Brouwer, A.M.: Frochot, C.: Gatti. F.G.: Leigh. D.A.; Mottier. L.; Paolucci. F.; Roffia, S.; Wurpel, G.W.H. Photoinduction of fast, reversible translational motion in a hydrogen-bonded molecular shuttle. Science **2001,** *291* (5511). 2124–2128.

Naked Anion Effect

Dario Landini
Angelamaria Maia
Università degli Studi di Milano, Milano, Italy

INTRODUCTION

The fundamental role that the interactions with the solvent as well as with the counterion play in determining the rate of anion-promoted reactions is well known. This class of reactions is of primary importance in organic and industrial chemistry. The effect of the medium can be quantified by comparing the reactivity in the condensed phase with that in the gas phase. where in the absence of any solvation, the "intrinsic" reactivity of the "naked" anion is observed. The goals of this entry are to briefly summarize the research on anion activators and activation. The scope of the article is necessarily limited and readers are urged to use the citations for more information.

NAKED ANION CONDITIONS

The anion reactivity (nucleophilicity and basicity) in solution can differ greatly according to the strength of the interaction with the surrounding molecules, the stronger the bond with the molecules of the solvent shell. the higher the Gibbs energy of activation and the lower the reaction rate. A typical example is represented by the S_N2 ion–molecule reaction (Eq. 1). where when going from a hydrogen-bond donor (HBD) solvent (water) that specifically solvates the anion through hydrogen bonds to a dipolar aprotic non-HBD solvent (DMF), where interactions are minimized, and then to the gas phase. the chloride anion reactivity increases by 5 and 15 powers of 10, respectively.[1,2] Comparison of the activation energy of this reaction in the gas phase (12.5 kJ mol ') with that in water (104.5 kJ mol^{-1}) indicates that the reaction rates in solution are mainly determined by the amount of energy necessary to destroy the solvation shell of the nucleophile in the activation process and: to a lesser extent. by the intrinsic properties of the reactants:[1]

$$Cl^- + CH_3Br \longrightarrow Br^- + CH_3Cl \qquad (1)$$

The association of the anion with the corresponding cation is another important factor in determining anionic reactivity. In general, the ion-paired anion is found to be less reactive than the corresponding free nonassociated ion.[3] According to Coulomb's law, the energy of interaction between cation and anion depends on the nature of the ionophores, decreasing on increasing the dielectric constant of the solvent. Depending on the ability of the medium to separate charges, the ionic species in solution range from scarcely solvated ion-pair aggregates to solvated free ions (Eq. 2):[4]

$$\underset{\text{Aggregate ion pairs}}{[(M^+Y^-)_n]_{solv}} \rightleftharpoons \underset{\text{Contact ion pairs}}{n(M^+Y^-)_{solv}} \rightleftharpoons \underset{\text{Solvent–separated ion pairs}}{n(M^+//Y^-)_{solv}} \rightleftharpoons \underset{\text{Free ions}}{n(M^+)_{solv} + n(Y^-)_{solv}} \qquad (2)$$

The interaction with the cation noticeably affects the reactivity of the anion in media of low dielectric constant. Thus. on switching from the large tetra *n*-butylammonium to the small lithium cation, the reactivity sequence of the corresponding halides in the nucleophilic substitution of *n*-butyl 4-bromobenzenesulfonate in the weakly dissociating acetone is completely reversed (Eq. 3).[5] Whereas the order obtained with bulky quaternary onium salts ($Cl^- > Br^- > I^-$) corresponds to that of free, nonassociated halides in dipolar non-HBD solvents (e.g., acetone). the sequence of the lithium halides ($Cl^- < Br^- < I^-$), typical of protic solvents, is mainly due to the increasing deactivation of the anion in the ion pair on increasing the cation charge density:[5]

$$nC_4H_9OBs + M^+Hal^- \xrightarrow{\text{Acetone}} nC_4H_9Hal + M^+OBs^-$$
$$M^+ = Bu_4N^+, Li^+; \quad Hal^- = Cl^-, Br^-, I^-; \quad Bs = 4BrC_6H_4SO_2 \qquad (3)$$

Main Anion-Activating Systems

The highest values of anion reactivity are obtained in the condensed phase. when the anions are less solvated and associated with the cation. Both of these conditions can be realized at the same time by using bulky quaternary onium salts; electron pair donor (EPD) solvents of high Lewis

Encyclopedia of Supramolecular Chemistry
DOI: 10.1081/E-ESMC 120012707

basicity (specific cation solvators); or cation complexing agents. such as polyether ligands (cyclic and open-chain).

The EPD solvents of high Lewis basicity include the most common dipolar non-HBD solvents (e.g., DMSO. acetonitrile, DMF, acetone, HMPA, etc.) and some open-chain polyethers (oligoethylene glycol dialkyl ethers **1** (''glymes''). They specifically solvate the cation but weakly interact with the anion and, for this reason, are found to enhance nucleophilicity and basicity of anion-promoted reactions in comparison with the reactivity realized in protic HBD media.[1,2]

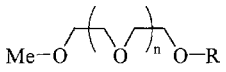

R = Me
$n \geq 3$

1

Cyclic and open-chain polyethers (polyethylene glycols. crown ethers, cryptands, polypodands, such as **1–10**) are known for their unique abilities to specifically bind inorganic salts. giving rise to stable inclusion complexes. In the complexation process. such ligands coordinate, through ion–dipole interactions, a relatively small metal ion M^{n+} and transform it into a large. more lipophilic cationic species. This allows the solubilization, even in weakly polar nonaqueous media, of a number of metal salts. as $(M^{n+} \subset \text{Lig})\ nY^-$ ion pair, and their transfer from an aqueous to an immiscible organic phase. As a consequence. anion-promoted reactions can be performed in the presence of these ligands under homogeneous and heterogeneous conditions.[1,6–17] Whereas in the first case the ligand is used in stoichiometric quantity. only catalytic amounts of it are required in two-phase systems, such as solid–liquid (SL) or liquid–liquid (LL) phase-transfer catalysis (PTC).[1,6–17] In these complexes, the anion is remarkably activated due to the reduced interaction with the bulky complexed cation and the small stabilization by the weakly polar medium.

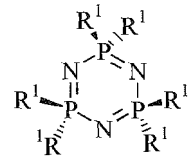

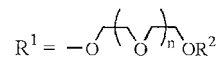

(a) $n = 2$ $R^2 = Bu$
(b) $n = 3$. $R^2 = C_{12}H_{25}$
(c) $n = 4$ $R^2 = 4C_8H_{17}C_6H_4$

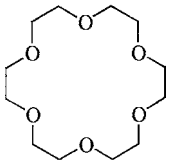

18-crown-6
(18C6)

3

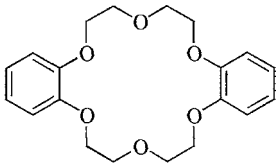

Dibenzo-18-crown-6
(DB18C6)

4

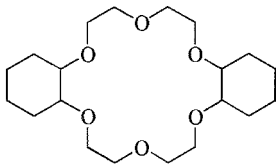

Dicyclohexano-18-crown-6
(DCH18C6)

5

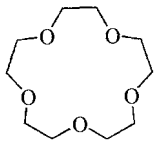

15-crown-5
(15C5)

6

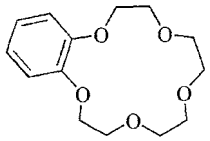

Benzo-15-crown-5
(B15C5)

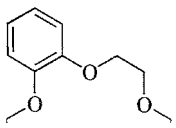

Benzo-18-crown-6
(B18C6)

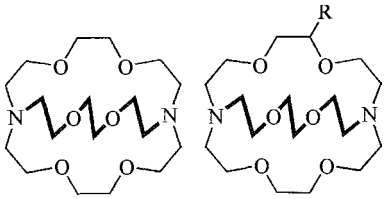

[2.2.2] R = $(CH_2)_9Me$

9 [2.2.2,C_{10}]

10

POLYETHER LIGANDS AND QUATERNARY ONIUM SALTS AS ANION ACTIVATORS

Liotta and coworkers were among the first to utilize 18-crown-6, ***3*** for solubilizing inorganic salts in polar and nonpolar aprotic solvents.[18] In particular, they studied the relative nucleophilicities in a typical S_N2 reaction (Eq. 4) of a series of potassium salts dissolved in acetonitrile by 18-crown-6, **3**. The sequence ($N_3^- > MeCO_2^- > CN^- > F^- > Cl^- \geq Br^- > I^- > SCN^-$) and the narrow nucleophilicity range found, different from those in polar protic media; were attributed to a much weaker solvation of the anion in acetonitrile that does not modify anionic intrinsic reactivity. Because this behavior is typical of the gas phase. the authors claimed the complexes formed by crown ethers with potassium salts in acetonitrile as sources of "naked" anions:[18]

$$C_6H_5CH_2OTs + [K^+ \subset \mathbf{3}]Y^- \xrightarrow{\text{Acetonitrile}} C_6H_5CH_2Y + [K^+ \subset \mathbf{3}]OTs^-$$
$$Y = N_3, MeCO_2, CN, F, Cl, Br, I, SCN \quad (4)$$

In a systematic kinetic study,[19] Thomassen and coworkers compared the effect of the addition of cyclic and acyclic polyethers on the rate of alkylation of potassiuin phenoxide with bromobutane in dioxane, a solvent of low cation-solvating power and low dielectric constant (ε=2.2, at 25°C) (Eq. 5):

$$n\text{BuBr} + \text{PhOK} \xrightarrow{\text{Dioxane}} \text{PhBu}n + \text{KBr} \quad (5)$$

As reported in Table 1, the addition of one molar equivalent of DCH18C6. ***5,*** produced a reaction rate increase of 8700-fold , while a reactivity enhancement of only 11 times resulted from the addition of the same amount of tetraethylene glycol dimethyl ether, **1**.

Table 1 Effect of the addition of polyether ligands on the alkylation rate of potassium phenoxide with n-butyl bromide in dioxane at 25°C[a]

Additive	[Additive]/[phenoxide]	k_{rel}
None	0	1
Tetraglyme **1**	0.054	1.5
	0.62	7.1
	1	11
DCH18C6 **5**	0.054	280
	1	8700
	1.53	11,200
	2.06	11,700

[a]From Ref. [19]

In addition, especially in the case of crown ethers, the rate constant depends strongly on the ligand–potassium phenoxide molar ratio, reaching a maximum value for the complete salt complexation, e.g., DCH18C6 **5**/PhOK=2.06. Under these conditions, the rate increased 11,700-fold, an enhancement similar to that observed by using tetraglyme **1** as a pure solvent. Because kinetic evidence showed that in dioxane the **5**/PhOK complex reacts as a single ion pair, these data clearly indicate that crown ethers are much better metal-cation-solvating ligands than acyclic polyethers with a comparable number of oxygen atoms, producing highly reactive solvent-separated ion pairs. Interestingly, the reactivity of these ion pairs approaches that of bulky tetrabutylammoniurn phenoxide ion pairs in the same solvent and is only 10 times lower than that of free ions in DMF and DMSO.[19] In line with these data. Hirao and coworkers reported[i''''] that the alkylation rate of sodium phenoxide with bromobutane in dioxane was strongly accelerated (about 100 times) by the addition of 5.4 molar equivalents of DB18C6, 4. A comparable rate increase was only obtained in the presence of the same amount of polyethylene glycol dimethyl ethers **1** of molecular weight $\geq 10^4$. Analogue results (Table 2) were obtained upon addition of DCH18C6. ***5,*** in the alkylation rate of diethyl sodium n-butylmalonate with bromobutane in both THF and benzene[12''] (Eq. 6):

$$n\text{BuBr} + n\text{BuC}(CO_2Et)_2^-Na \longrightarrow (n\text{Bu})_2C(CO_2Et)_2 + \text{NaBr} \quad (6)$$

Table 2 Effect of the addition of DCH18C6 5 on the alkylation rate of diethyl sodium *n*-butylmalonate with *n*-butyl bromide in various reaction media at 25°C[a]

Solvent	Additive	(M)	k_{rel}
THF			1
	DCH18C6 5	0.01	3
		0.04	6
		0.10	11
		0.20	14
		0.50	17
Benzene	DCH18C6 **5**	0.0116	1
		0.0358	6
		0.1015	12
		0.2020	19
		0.5270	28
DMF			65

"From Ref. [21]

Also. in this case, a rate plateau is reached when the sodium enolate is totally complexed by the ligand (≈4 molar equivalents of 5). Under these conditions, the crown-ether-separated ion pair is only 3.8 in THF and 2.3 times in benzene less reactive than the kinetically active species in DMF. Once again. these results highlight the remarkable ability of crown ethers to specifically solvate cations activating counterions.

A systematic study was performed by our group on the anion activation realized by complexes of different polyether ligands 2c, 5. 10 with alkali salts and the corresponding tributylhexadecylphosphonium salts in the low polar chlorobenzene (Eq. 7).[13,22] As reported in Table 3, the anion reactivity increases when going from the open-chain polypodand 2c to the cyclic crown ether **5** to the bicyclic cryptand 10 in parallel with the increasing cation–anion separation induced by the ligand. The nucleophilicity scale found with cryptates of 10. the same as for quaternary salts, is slightly modified with the complexes of crown ether 5. In addition, with the latter ligand. the reactivity spans a narrow range, particularly for halide ions (Cl:Br:I=1.3:1.4:1). Such behavior is mainly due to the different topologies of these ligands:

$$n\mathrm{C_8H_{17}OMs} + \mathrm{Q^+Y^-} \longrightarrow n\mathrm{C_8H_{17}Y} + \mathrm{Q^+OMs^-}$$

$$\mathrm{Q} = \mathrm{C_{16}H_{33}P^+Bu_3}\ \ \mathrm{Octyl_4N^+}\ \ (\mathrm{M^-}\ \mathrm{C}\ \mathrm{lig})$$

$$\mathrm{M^+} = \mathrm{K^+}.\mathrm{Li^-}\ \ \mathrm{lig} = \text{polypodand 2c DCH18C6 5}$$

$$[2\,2\,2\ \mathrm{C_{10}}]\mathbf{10} \qquad (7)$$

Cryptates, where the metal cation is completely included in the cavity of the tridimensional ligand, give rise to "solvent-separated" ion pairs particularly reactive in low-polarity media. Conversely, in the crown ether complexes, the ligand does not induce a large cation–anion separation, and the complexed anion is still accessible for interaction with the anion in a "crown-separated" ion pair. As a consequence, by increasing the charge density of the cation or the anion, the ion pair becomes progressively more intimate and. hence, less reactive. This is confirmed by the trend obtained with the complexes of the lithium halides (Table 3).[13]

In this case. in fact, the nucleophilicity sequence is reversed on switching from the complexes of crown ether **5** to the corresponding cryptates. Interestingly. the same trend of crown ether **5** is found with the corresponding complexes of cyclophosphazenic polypodand **2c**. As shown in Table 3. cyclophosphazenic polypodands like **2c** have a reactivity only slightly lower (three to four times) than that of the corresponding crown ethers and, hence, can be considered a valid alternative to the more sophisticated cyclic ligands.

Crown ether/cryptand effects were also revealed by Buncel et al. in the oximate-promoted 1,2-elimination from β-phenylmercaptoethyl *p*-nitrophenolate in tetraglpme (Eq. 8).[23] The addition of cryptand [2.2.2], 9, in fact. greatly enhanced (654 times) the oximate reactivity in comparison with the potassium oximate ion-paired, whereas the effect was much lower with crown ether DCH18C6, **5** (only 11 times): (see equation below)

The use of lipophilic crown ethers and cryptands in catalytic instead of stoichiometric amounts (LL-PFC or SL-PTC) revealed considerable improvement for synthetic applications due to the relatively high cost of these cyclic ligands in comparison with the cheaper quaternary onium salts and the open-chain analogues.[6–13]

Under LL-PTC conditions. the anions associated with bulky lipophilic cations (quaternary onium salts, macrocyclic and macrobicyclic polyethers, etc.) are extracted into the organic medium specifically solvated by a limited number (1–11 moles per mol of Q^+Y^-) of water molecules. Furthermore. two additional molecules of water are found to accompany the cyclic polyethers 5, 10, as both free and complexed ligands.[13] This hydration sphere, characteristic of each anion, always reduces, more or less remarkably. anionic reactivity. As shown in Table 4, when changing from LL-PTC to anhydrous homogeneous

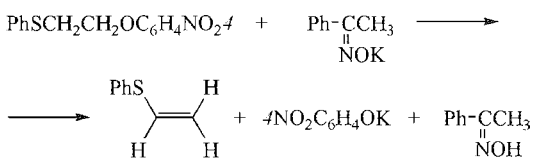

Table *3* Anionic reactivity of complexes $(M^+ \subset Lig)Y^-$ ($M^+ = K^+$, Li^+; Y = N_3, Cl^-, Br^-, I^-, SCN^-, Lig = **2c**, **5**, **10**) and quaternary phosphonium salts $C_{16}H_{33}P^+Bu_3Y^-$ in the S_N2 reaction with *n*-octylmethanesulfonate in chlorobenzene, at 60°C[a]

	$10^3 k$ ($M^{-1}s^{-1}$)			
		($M^+ \subset$Lig)		
Y^-	$C_{16}H_{33}P^+Bu_3$	Polypodand **2c**	Crown ether **5**	Cryptand **10**
N_3^-	70		89[b]	150[b]
Cl^-	20		12[b]	51[b]
Br^-	8.10		13[b]	37[b]
I^-	3.00	5.0[b]	9.2[b]	8.7[b]
SCN	0.75		1.1[b]	1.5[b]
Cl^-		0.37[c]	1.5[c]	
Br^-		3.3[c]	12.7[c]	43[c]
I^-		27[c]	26.3[c]	15[c]

"From Refs. [13,22].
[b]$M^+ = K^+$.
[c]$M^+ = Li^+$.

conditions, the nucleophilicity of a representative series of tetraoctylammonium saits increases: particularly in the case of anions with high charge density and more hydration (Eq. 7).[22,24] It is worth noting that the reactivity of the homogeneous anhydrous phase can be reproduced under LL-PTC conditions by using concentrated aqueous alkaline solutions (50% aq NaOH, 60% aq KOH). These solutions. where the water activity tends to zero, are found to be efficient systems for having anions largely or even completely "nonhydrated" in the organic phase (Table 4).[22,24]

Once again. crown ethers behave differently from quaternary salts and cryptates. With the complexed crown ethers. removal of the hydration sphere of the anion in going from two-phase to anhydrous conditions is balanced by a larger cation–anion interaction in the ion pair. thus resulting in a small variation of anionic reactivity. This is another proof that, unlike cryptates, complexed crown ethers can hardly be considered as a source of "naked anions."[24]

In low-polarity media, specific interaction with protic species (water) dramatically affects the reactivity (nucleophilicity or basicity) of anions with high charge density (OH . F . oxanions. carbanions, etc.). Basicity of OH in the Hofmann elimination reaction of $(hexyl)_4N^+OH^- \cdot nH_2O$ (Eq. 9), carried out in a chlorobenzene–water two-phase system, increases 50.000 times by reducing the hydration number *n* of the anion from 11 to 3. The enhancement is extrapolated to be more than nine powers of 10 for the hypothetical anhydrous hydroxide.[22,24] This indicates that the largely dehydrated hydroxide. extracted in a low-polarity solvent (chlorobenzene) from concentrated alkaline soluiions. is an extremely powerful base. Results account for the dramatic effect produced by an increase of base on the rate of reactions promoted by alkali hydroxides under LL-PTC conditions, such as carbanion formation and alkylation. alkene isomerization, H/D exchanges in carbon acids. and acid–base equilibria:

$$hexyl_4N^+OH^- \xrightarrow{\text{PhCl-aq NaOH}} hexyl_3N + \text{hex-1-ene} \qquad (9)$$

In a recent kinetic study. we investigated the ability of macrocyclic polyethers to activate enolates in the alkylation of deoxybenzoin with butyl derivatives *n*BuY (*Y*=Br, I, OMes) catalyzed by crown ether 5 or cryptand **10** under EL- and SL-PTC conditions with strong bases (NaOH, KOH) (Eq. 10).[25] The enolate reactivity increases; up to 40 times. on going from crown ether **5** to cryptand **10** in line with the better anion activation realized by the latter. The regioselectivity of the reaction (O/C ratio) is also reinarkably affected by the ligand.

Table 4 Effect of the anion hydration *n* of $octyl_4N^+Y^- nH_2O$ on the second-older rate constant of reaction (5) under LL-PTC and anhydrous homogeneous (PhCl) conditions, at 35°C

	LL-PTC conditions			
	PhCl–H_2O		PhCl—50% aqNaOH	
Y^-	Hydration state *n* of **octyl$_4$N$^+$Y$^-$ *n*H$_2$O**	10^3 k ($M^{-1}s^{-1}$)	$10^3 k$ ($M^{-1}s^{-1}$)	Homogeneous conditions anydrous PhCl
N_3^-	3.0	2.9	11.6	11.7
Cl^-	3.4	0.26	3.4	3.4
Br^-	2.1	0.42	1.1	1.1
I^-	1.0	0.29	0.42	0.45

With crown ether **5**, the preferential association of the complexed cation with oxygen favors the alkylation of the less-electronegative center, the carbon, and hence, only the C-alkylation product is obtained. Conversely, cryptand **10**, which realizes a better cation–anion separation, leads to an increase in the nucleophilicity of the enolate 0-center. resulting in a greater quantity of *O*-alkylated product and, hence, lower regioselectivity:[25]

$$\mathrm{PhCH_2COPh} + n\mathrm{BuY} \xrightarrow[\text{PhCl-conc MOH (or solid)}]{\text{catalyst (5 or 10)}} \mathrm{PhCHBuCOPh} + \mathrm{PhCH{=}COBuPh} \quad (10)$$

GENERATION AND ACTIVATION OF ANIONS FOR SYNTHETIC APPLICATIONS

Since the appearance of Pedersen's work on the discovery of crown ethers in late 1967,[26] the special ability of polyether ligands, in particular crown ethers, to activate anionic reagents in homogeneous and heterogeneous systems was exploited in a huge number of applications on both laboratory and industrial scale (many of them were already reviewed).[6–17] Some recent examples among the most relevant ones are presented and discussed here.

The K_2CO_3/18C6, **3,** system is widely used for in situ generating oxa- and azanions, and promoting their reactions under homogeneous and heterogeneous condition~.[~It'wa]s the base of choice in the synthesis of an important class of dendrimers, i.e., poly(benzyl ether) dendrimers, 17. via an elegant "convergent-growth" methodology[27] (Scheme 1).

The procedure, based on the 3,5-dihydroxybenzyl alcohol **11** as the monomer unit, involves a repetitive two-step process: reaction of **11** with benzyl bromide 12 in the presence of K_2CO_3/18C6, **3,** gives the next generation of alcohol **13,** that is converted to the corresponding bromide 14. Repetition of the two-step process affords successive generations up to the sixth-generation dendron **15**. The synthesis of final poly(benzyl ether) dendrimers, e.g., 17, involves the Williamson coupling of bromide **15** with a polyfunctional phenolic core, in this case, 1,1,1-*tris*(4′-hydroxyphenyl) ethane **16,** once again promoted by K_2CO_3/18C6, 3. In this procedure, the Williamson reaction is the key step of the overall process. In particular, the appropriate power of the base is the crucial factor for the reaction outcome. Solid potassium carbonate, activated by even catalytic amounts of 18C6 in dry acetone, fulfills this requirement.[27] The K_2CO_3/18C6 couple is widely used in the synthesis of other dendrimer structures bearing traditional and chiral[28] segments, and in the preparation of linear-dendric copolymers and dendronized linear polymers.[27]

Similarly, K_2CO_3/18C6 was the base of choice for selectively performing mono- and dialkoxylation of cyanuryl chloride, affording the corresponding 2-alkoxy-4,6-dichloro- and 2,4-dialkoxy-6-chloro-1,3,5-triazines, valuable intermediates for the organic synthesis[i''' (Eq. 11).

Recently,[30] anhydrous K_2CO_3 in the presence of catalytic quantities of 3 in toluene was used as the base for the in situ generation of ylides from the corresponding phosphonium salts. This reaction is the first step of an one-pot eco-safer protocol for the preparation of olefins directly from phosphonium salts under oxygen atmosphere in the presence of $VO(acac)_2$ as the oxidation catalyst (Eq. 12).

The efficient activation of poor nucleophilic acetate by crown ethers was exploited for introducing this versatile group in organic valuable molecules. For example, Nakata and coworkers developed an efficient method for the

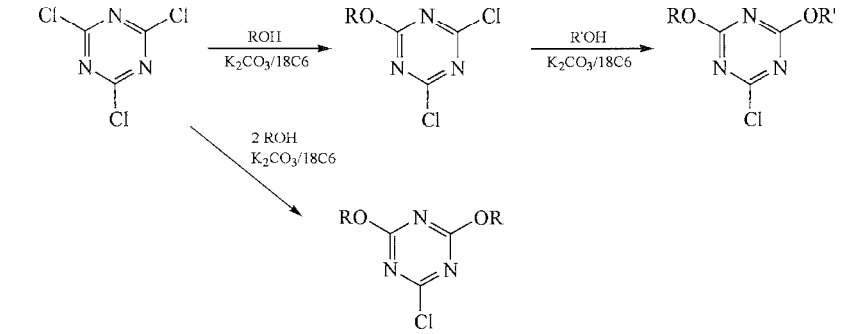

(11)

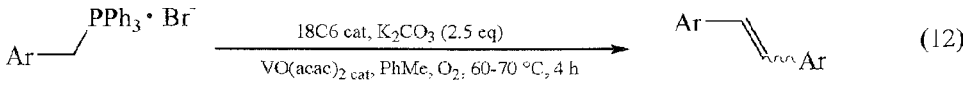

(12)

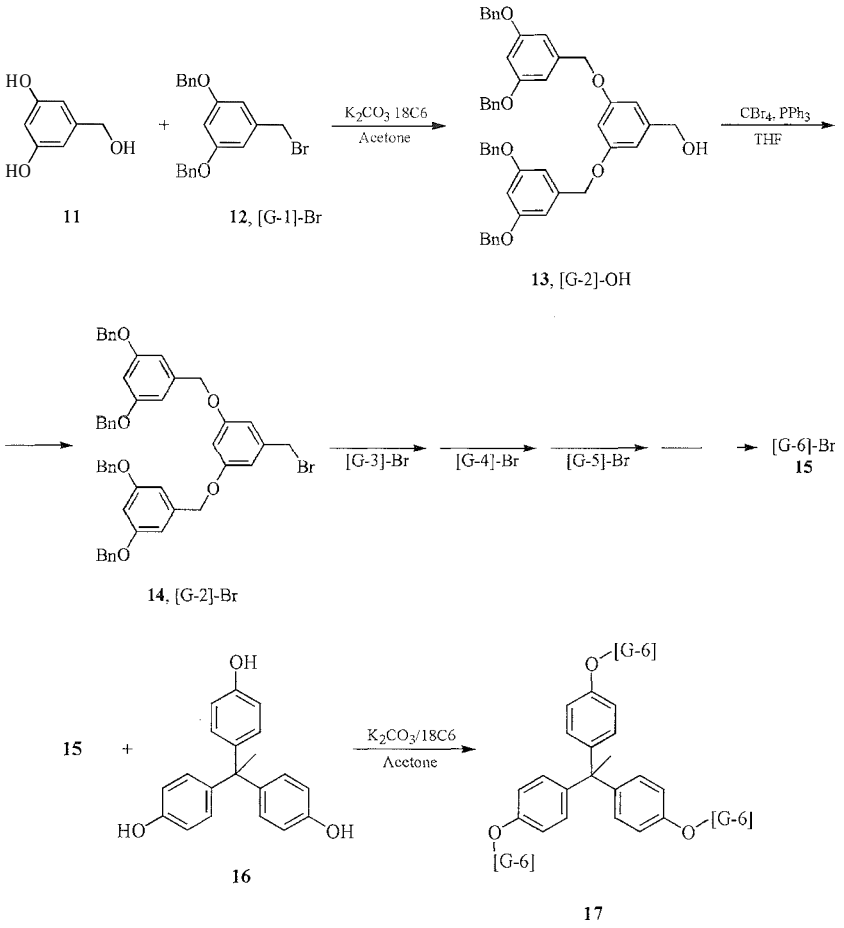

Scheme 1 Synthesis of poly(benzyl) ether dendrimers.

inversion of secondary alcohols by reaction of the corresponding chloromethanesulfonates with cesium acetate. activated by 18C6 in benzene (Eq. 13).

The reaction smoothly proceeds, affording the inverted *sec*-alkyl acetates in excellent yields, via a clean S_N2 reaction.[31] Recently. a similar protocol, i.e., KOAc/18C6/toluene. was applied by Wengel et al.[32] in interconverting C2′-epimeric nucleosides. key intermediates for the preparation of α-L-*ribo*-configured nucleic acids (Eq. 14).

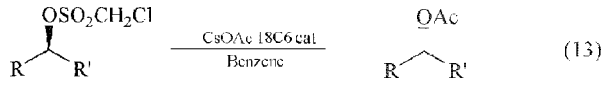

(13)

The N-alkylation of "naked" nitranions of 2-nitroimidazole and theophylline, generated from their alkaline salts in the presence of 18C6 or 15C5. was usefully applied to the synthesis of nitroimidazolylbutyltheophylline 18.

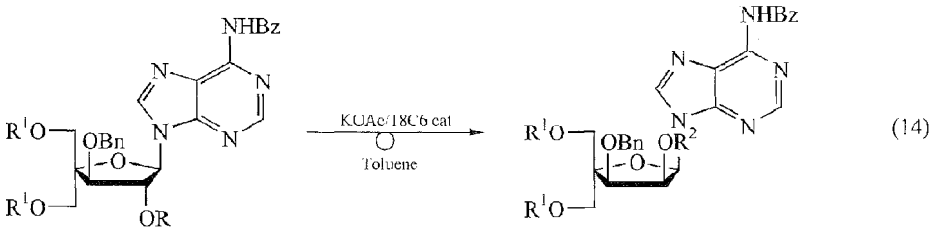

(14)

R^1 = Bz or Ms; R = Tf; R^2 = Ac

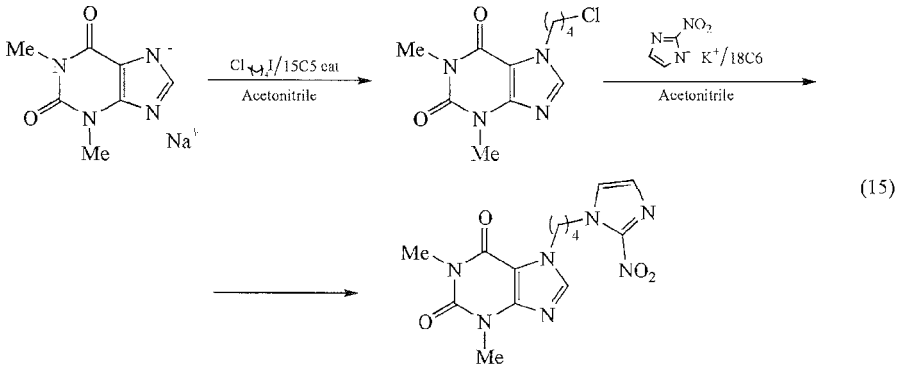

(15)

18

which is a probe to identify. locate. and quantify hypoxia in sections from solid tumors[33] (Eq. 15).

We found that K_2CO_3/DCH18C6 is an effective basic system for the in situ generation and reaction of activated trifluoroacetoamidide with 2-bromo carboxylic esters, affording the corresponding *N*-(trifluoroacetyl)-α-amino esters, valuable precursors of natural and unnatural a-amino acids[33] (Eq. 16). The reactivity of nitroanion activated by crown ether 5 was found to be comparable to that obtained by using bulky onium salts as anion activators:[34]

$$CF_3CONH_2 + RCH(Br)CO_2R^1 \xrightarrow[\text{Acetonitrile}]{K_2CO_3 \text{ solid/DCH18C6}} R(CF_3CONH)CHCO_2R^1 \quad (16)$$

The N-anions. generated in situ from aryl and hetero-arylamines and NaH/DCH18C6 5 in toluene. smoothly reacted with 4-chloronitrobenzene to give the corresponding diarylamines, the protocol being a possible alternative for the synthesis of diarylamines[35] (Eq. 17). Interestingly. kinetic data showed that the reactivity of (DCH18C6 ⊃ Na^+)$ArNH^-$ species in toluene is more than two orders of magnitude lower than that of $ArNH^-Na^+$ in DMSO in the absence of crown ether. The UV/Vis evidence indicates that such a behavior is mainly due to the different reacting species in these two media: mostly free ions in dipolar DMSO and ion pairs in the low-polarity toluene:[35]

$$4NO_2C_6H_4Cl + ArNH_2 \xrightarrow[\text{Toluene}]{\text{NaH/DCH18C6}} 4NO_2C_6H_4NHAr \quad (17)$$

Leckta et al. recently described an efficient procedure for the in situ generation of reactive monosubstituted ketenes through dehydrochlorination of acid chlorides promoted by NaH/15C5 in THF. This new methodology was applied to a cost-effective, catalytic asymmetric synthesis of β-lactams and α-chloroesters, pharmaceutically useful classes of compounds[36] (Eq. 18).

The last step of an efficient protocol for the one-pot synthesis of biologically important (*Z*)-γ-substituted-α, β-didehydroglutamates 21 starting from *N*-alkylidene-glycinates 19, involves the C-alkylation of intermediate alkaline dienolates 20 in THF. However, capture of 20 with an excess of electrophiles. such as MeI, failed even in the presence of DMPU as an anion activator. The generation of "naked" enolates by using 18C6 allowed for a smooth and efficient reaction[37] (Eq. 19).

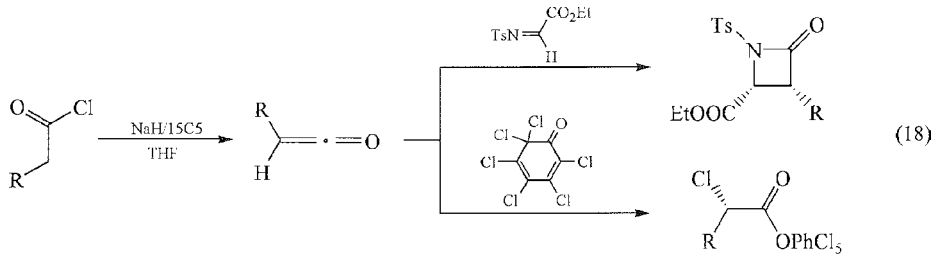

(18)

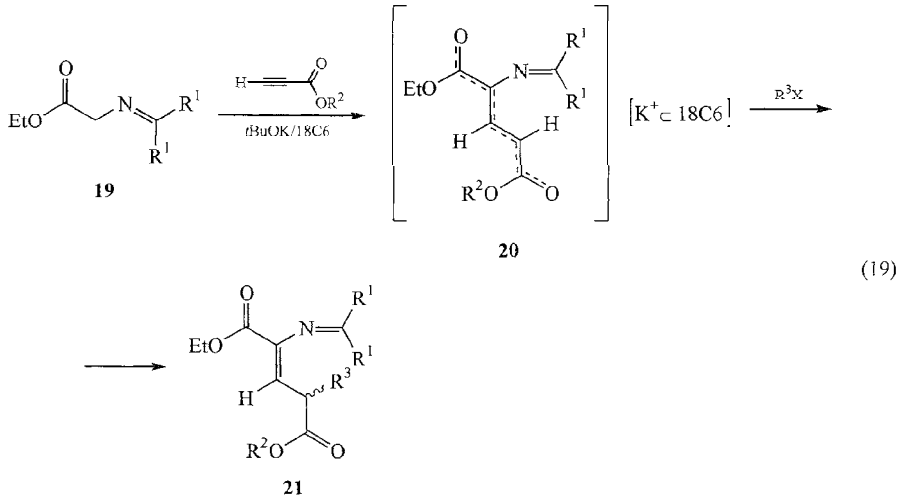

(19)

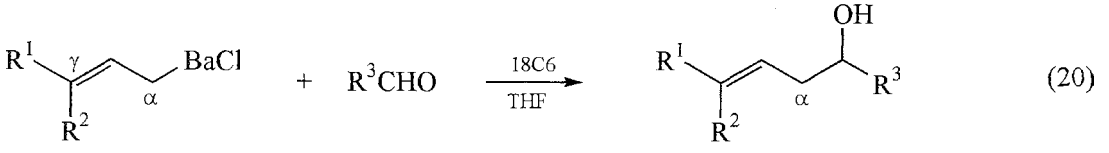

(20)

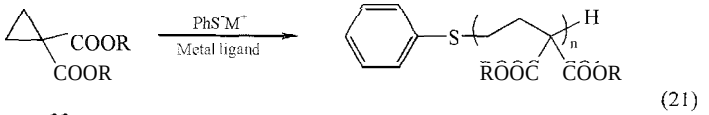

22

(21)

$M^+ = Na^+, K^+, [K^+ \subset 18C6], [K^+ \subset (2.2.2)]$

Similar results were obtained only in the presence of bulky Schwesinger's base.[37]

Yamamoto and coworkers reported that the complexation of allylic barium reagents with crown ethers, in particular 18C6. substantially improved the reactivity toward electrophiles. e.g., aldehydes, and α-regioselectivity of these organoalkyl derivatives in THF[38] (Eq. 20). By contrast. only a negligible effect of acyclic polyethers on the reaction was observed.[38]

The ability of polyether ligands to activate alkoxyde anions was checked in the etherification of primary alcohols with alkyl bromides, by using solid potassium hydroxide as a base. Results showed that the efficiency of the open-chain PEG2000 dimethylether 1 is similar to that of cryptand 9 and DCH18C5.[39]

In anionic ring-opening polymerization of cyclopropane-1,1-dicarboxylates 22 using sodium and potassium thiophenolates as initiators, the nature of the cation was found to play an important role in the rate and selectivity of the polymerization. In particular, reaction rate increased in the order $Na^+ < K^+ < [K^+ \subset DCH18C6] < [K^+ \subset (2.2.2)]$, relative rates being ≈1, 2. 6, and 15, respectively (Eq. 21).[40] According to the authors. these results suggest that the anionic polymerization involves ceveral kinds of propagating species in equilibrium with each other (aggregates, contact ion pairs. solvent-separated ion pairs, and free ions), the relative contribution of each depending on the nature of the counterion. As expected. the complexation of the potassium ion bicyclic polyether ligands, in particular, cryptands, gives rise to highly reactive "naked" carbanions.[40]

CONCLUSION

Lipophilic polyether ligands, like crown ethers, cryptands, polypodands. and quaternary onium salts. proved to be efficient activators of anions ("naked anions") in low-polarity media. In these solvents. they give rise to ion pairs particularly reactive due to the low stabilization by the solvent and the low interaction with the bulky cation. The reactivity of these ion pairs is even higher than that

observed in dipolar aprotic media, where mostly free ions are present. It *mainly depends on the ability of the ligand to induce cation–anion separation. increasing in the following order: open-chain < cyclic < bicyclic polyether. The use of these complexing agents in catalytic amounts (LL-PTC or* SL-PTC) *revealed considerable improvement for synthetic applications due to the high cost of these cyclic polyethers, especially cryptands. in comparison with the open-chain analogues and quaternary* onium *salts. The LL-PTC conditions with concentrated aqueous alkaline solutions allow the transfer into the organic phase of the anions largely or completely* nonhydrated, *so obtaining the same reactivity of the anhydrous homogeneous phase. This is particularly useful for high-charge-density anions* (OH^-, F^-, *oxanions, carbanions, etc.). with reactivities that are* dramatically *reduced by the specific interaction with a limited number of water molecules. Anion activation realized by lipophilic polyether ligands and quaternary* onium *salts in anhydrous low-polarity media is probably the highest obtainable in solution. approaching that of the gas phase.*

The application examples, here discussed, clearly indicate that anion activation remarkably improves *several synthetic procedures and is often essential for the outcome of certain reactions. From a practical point of view. the criteria for selecting an anion-activating system (quaternary* onium *salts.* PEGs, *crown ethers, cryptands, etc.), especially in* industrial *applications, include considerations dealing with efficiency. stability. availability. recycling. and cost. Quaternary* onium *salts and crown ethers appear to be the best compromise; indeed, they fulfill many of* these *requirements. The high cost and the scarse availability of lipophilic cryptands are strong limitations to the use of these very active anion activators. The cheap PEG* dimethyl *ethers can be the ligands of choice when a limited anion activation is required.*

ACKNOWLEDGMENTS

This work was supported by MURST (Progetto Nazionale Stereoselezione in Sintesi Organica. *Metodologie e* Applicazioni) *and CNR.*

ARTICLES OF FURTHER INTEREST

Crown Ethers, *p. 326*
Cryptands, *p. 334*
Phase-Transfer Catalysis in Environmentally Benign Reaction Media, *p.* 1042
Podands, p. *1106*

REFERENCES

1. Reichardt, C. Solvent Effects on the Rate of Homogeneous Chemical Reactions. In *Solvents and Solvent Effects in Organic Chemistry,* 3rd Ed.; VCH: Weinheim, *2003:* 147–320.
2. Parker. A.J. Protic–dipolar aprotic solvent effects on rates of bimolecular reactions. Chem. Rev. **1969**. 69 (1). 1–32.
3. Gordon, J.E. *The Organic Chemistry of Electrolyte Solutions;* Wiley: New York. 1975.
4. Marcus, Y. *Ion Solvation*; Wiley: Chichester, 1985.
5. Winstein. S.; Savedoff. L.G.; Smith. S.: Steven. I.D.R.; Gall, J.S. Ion pairs, nucleophilicity and salt effects in bimolecular nucleophilic substitution. Tetrahedron Lett. **1960**, (9). 24–30.
6. Gokel. G.W.: Durst, H.D. Principles and synthetic applications in crown ether chemistry. Synthesis **1976**, (3). 168–184.
7. Vogtle. F.: Weber, E. *Host Guest Chemistry–Macrocycles—Synthesis, Structures, Applications*; Springer: Berlin. 1985.
8. Weber. W.P.: Gokel, G.W. *Reactivity Concepts in Organic Chemistry-Phase Transfer Catalysis*; Springer: Berlin. 1972: Vol. 4.
9. Starks. C.M.: Liotta, C.L.: Halpern, M. *Phase-Transfer Catalysis—Fundamentals, Applications and Industrial Perspectives*; Chapman and Hall: New York. 1994.
10. Montanari. *F.:* Landini, D.: Rolla. F. Phase-transfer catalyzed reactions. Top. Curr. Chem. 1982, *101.* 147–200.
11. De Jong. *F.;* Reinhout. D.N. Stability and reactivity of crown-ether complexes. Adv. Phys. Org. Chem. 1980. 17. 279–433.
12. Dehmlow. E.W.: Dehmlow, S.S. *Phase Transfer Catalysis,* 3rd Ed.: VCH: Weinheim, 1993.
13. Landini. D.; Maia. A.; Penso, M. Anion Activation. In *Comprehensive Supramolecular Chemistry—Molecular Recognition: Receptors for Cationic Guests*: Gokel. G.W., Ed.: Pergamon: Oxford. 1996; Vol. 1. 417–464.
14. Lehn, J.M. Supramolecular chemistry—Scope and perspectives molecules. supramolecules. and molecular devices. Angew. Chem., Int. Ed. Engl. **1988**. 27 (1), 89–112.
15. Totten. G.E.; Clinton. N.A. Poly(ethylene glycol) derivatives as phase transfer catalysts and solvents for organic reactions. JMS-REV. Macromol. Chem. Phys. 1988. *C28* (2). 293–337.
16. Kron. T.E.: Tsvetkov, E.K. Neutral acyclic analogues of crown-ethers and cryptands and their complex-forming properties. Russ. Chem. Rev. 1990. *59* (3). 283–298.
17. Bartsch, R.A. Stereochemical and base species dichotomies in olefin-forming E2 eliminations. Chem. Rev. 1980. *80.* 453–494.
18. Liotta. C.L.; Grisdale, E.E.: Hopkins, H.P., Jr. Chemistry of "naked" anions. IV. Relative nucleophilicities of "naked" anions. Tetrahedron Lett. **1975**. (48). 4205–4208.
19. Thomassen. L.M.: Elligsen, T.: Ugelstad, J. The effect of the solvent on the reactivity of potassium phenoxide in

nucleophilic substitution reactions. Acta Chem. Scand. 1971. 25 (8), 3024–3030.
20. Hirao. A.; Nakahama, S.: Takahashi. M.: Yamazaki, N. Additive effect of poly(ethylene oxide), 2. An acceleration effect of poly(ethylene oxide) in a Williamson reaction. Makromol. Chem. 1978. *179* (7). 1735–1741.
21. Zaugg, H.E.: Ratajczyk, J.F.: Leonard. J.E.; Schaefer. A.D. Specific solvent effects. VII. Ion-pair processes in the alkylation of alkali enolates. J. Org. Chem. 1972, *37* (14). 2249–2253.
22. Maia. A. Anion activation by quaternary onium salts and polyether ligands in homogeneous and heterogeneous systems. Pure Appl. Chem. 1995. 67 *(5)*. 697–702. and references therein.
23. Buncel. E.; Kuniar. A.: Xie. H.: Moir. R.Y.; Purdon, J.G. Solvent and crown ether/cryptand effects on the oximate-promoted 1,2-elimination from β-(phenylthio)ethyl *p*-nitrophenyl ether. Formation and reactivity of a crown ether-complexed potassium oximate ion pair. Can. J. Chem. 1994. *72* (2). 437–447.
24. Albanese. D.; Landini. D.: Maia. A.: Penso, M. Key role of water for nucleophilic substitutions in phase-transfer-catalyzedprocesses: A mini-review. Ind. Eng. Chem. Res. 2001. *40* (11). 2396–2401. and references therein.
25. Maia, A.; Landini. D.: Petricci, S. Macrocyclic polyethers as enolate activators in homogeneous and heterogeneous systems. Supramol. Chem. 2000. *11* (4). 289–292.
26. Pedersen. C.J.: Frensdorff. H.K. Macrocyclic polyethers and their complexes. Angew. Chem.. Int. Ed. Engl. 1972, *11* (1). 16–25. and references therein.
27. Grayson, S.M.; Frechet. J.M. Convergent dendrones and dendrimers: From synthesis to applications. Chem. Rev. 2001. *101* (12). 3819–3867. and references therein.
28. Junge. D.M.: Wu, M.J.; McElhanon, J.R.; McGrath. D.V. Synthesis and chiroptical analysis of optically active shell dendrons. J. Org. Chem. 2000. *65* (17). 5306–5314.
29. Menicagli. R.: Malanga, C.; Peluso. P. Selective mono- or dialkoxylation of 2,4,6-trichloro-1,3,5-triazine in solid–liquid phase transfer conditions. Synth. Commun. 1994. *24* (15). 2153–2158.
30. Shi, M.: Xu. B. $VO(acac)_2$-catalysed oxidative coupling reactions of phosphonium salts. J. Org. Chem. 2002. *67* (1). 294–297.
31. Shimizu. T.: Hiranuma. S.: Nakata. T. Efficient method for inversion of secondary alcohols by reaction of chloromethanesulfonates with cesium acetate. Tetrahedron Lett. 1996, *37* (34). 6145–6148.
32. Sorensen, M.D.: Kvrno. L.; Bryld, T.; Hakansson, A.E.; Verbeure. B.: Gaubert. G.; Herdewijn, P.: Wengel, J. EL-ribo-Configured locked nucleic acid (α-L-LNA): Synthesis and properties. J. Am. Chem. Soc. 2002. *124* (10). 2164–2176.
33. Long, A.: Parrick. J.: Hodgkis. R.J. An efficient procedure for the 1-alkylation of 2-nitroimidazoles and the synthesis of a probe for hypoxia in solid tumours. Synthesis 1991. (9), 709–713.
34. Albanese. D.: Landini. D.: Maia. A.: Penso. M. Phase transfer catalysis: Some recent applications in organic synthesis. J. Mol. Catal. A: Chem. 1999, *150* (1–2). 113–131.
35. Landini. D.; Maia. A.; Secci. D.; Vlasov. V.M.: Os'kina. I. Nucleophilic aromatic substitution reactions promoted by aryl and heteroaryl amine nitranions. New J. Chem. 1998. 22 (1), 71–74.
36. Taggi. A.E.: Wack, H.: Hafez. A.M.: France. S.: Lectka. T. Generation of ketenes from acid chlorides using NAH/crown ether shuttle-deprotonation for use in asymmetric catalysis. Org. Lett. 2002. *4* (4). 627–629.
37. Alvarez-Ibarra. C.; Csaky. A.G.; Martin. M.El.; Quiroga. M.L. Study of the asymmetric synthesis of (Z)-γ-substituted-α,β-didehydroglutamates from *N*-alkylideneglycinates. Tetrahedron 1999. *55* (23). 7319–7330.
38. Yanagisawa, A.; Yamada. Y.; Yamamoto. H. Effect of crown ethers on the regioselectivity of allylation of benzaldehyde with allylic barium reagents. Synlett 1997. (9). 1090–1092.
39. Abribat. B.; Le Bigot. Y. Selective etherification of hydroxylated functions in the absence of solvent. II. Polyethylene glycol as catalyst. Tetrahedron 1993. *53* (6). 2119–2124.
40. Penelle. J.: Xie. T. Ring-opening polymerization of diisopropyl cyclopropane-1.1-dicarboxylate under living anionic conditions: A kinetic and mechanistic study. Macromolecules 2000.33 (13). 4667–4672

Nanocasting Strategies and Porous Materials

Sebastian Polarz
Ruhr-University Bochum, Bochum, Germany

INTRODUCTION

Recent efforts of scientists worldwide concentrate on structuring all sorts of matter on a nanoscale. This structuring process is the key to nanotechnology. One fascinating class of nanornaterials are those with pores of the order of just several nanometers in width, possessing a mutual correlation *to each other (order), so-called ordered nanoporous materials. Therefore, methods to obtain control over pore size, pore shape. pore correlation,* and *ultimately pore surface are highly desired. A process enabling this superior level of* materials *design is the so-called* nanocasting *technique.* Nanocasting *is related to a method known to all of us in the macroscopic world transferred into the nanoscale dimensions, namely. the molding technique as used for the production of church bells.*

Organic template structures derived by self-assembly processes of amphiphiles *are imprinted into cross-linked networks. mostly of the inorganic type. The* template *morphology determines the structure and morphology of the entire pore system. Furthermore, detailed investigation of the pore structure allows inferences to be dl-awn about the template, and therefore. about the* self-assembly *process.*

Many applications of nanoporous materials relate to more than pure size-sieving effects. One interesting field is the use of nanopores *as nanoreactors.*

THE PRINCIPLES AND RULES OF NANOCASTING

Template⟶Materials Relationship

One goal of nanoscience *in* general *and in the field of* nanoporous *materials''' in particular is to achieve control over the architecture of matter on the nanoscale* (1–*100* nm). *Because porous materials are divided into the subgroups* microporous *(voids* smaller *than 2 nm).* mesoporous (voids *between 2–50 nm). and macroporous (voids larger than 50 nm), it becomes obvious that these materials are raw* models *for nanostructured matter. Three criteria can be formulated to* evaluate *the ultimate goals in the synthesis of* porous *materials:*

Criterium I: *Control over pore size.*
Criterium II: Control *over pore shape.*
- Criterium *IIH: Control over pore-surface* functions.

If one *considers how* to *fulfill these three criteria: it seemed to be beneficial if* it *was possible to apply a* bell-*casting process on the* nanoscale *(Fig. la).*

At first. a suitable template *structure needs to be provided, as demonstrated in Fig.* 1b. *This template can range from molecules* (i, ii) *to* assemblies *of molecules* (ii–iv, *v) to colloidal* particles *(v) or even to* assemblies *of colloidal particles* (vi). *The template* is *then surrounded by liquid (or dissolved) network precursors that are subsequently cross-linked. After* removal *of the template (depending* on *the network materials and template. this is done by calcination. liquid–liquid extraction.* ion-exchange, *or etching), a void is left over with a structure that is fully determined by the template. Normally. when single molecules are used as templates. microporous materials are derived. Famous examples for this case are zeolites or* moleculary imprinted polymers.[1] *Colloidal crystals as templates lead to* macroporous solids *with photonic properties. However. for this article. templates made from* self-assembling *molecules are of special importance. These* molecules. *so-called amphiphiles, contain one hydrophilic and one hydrophobic part. as* shown *in Fig.* 1b(ii). *In aqueous systems.* these *chemically different molecular parts tend to microphase separate, and depending on concentration. self-assembly to* micelles *(iii) or* lyotropic liquid crystals *(iv) occurs (see Fig.* 1). *Typically. these* templates *lead to* mesoporous *structures.*

Boundaries sf Nanocasting

It was indicated *in the previous* section *that the promise of nanocasting is* that the template morphology *will* fully *determine* the *structure of the porous system. However. certain conditions have to be fulfilled* in *the template–network combinations in order to make the* nano-*casting process work.*

Encyclopedia of Supramolecular Chemistry
DOI: 10.1081/E-ESMC 120019195

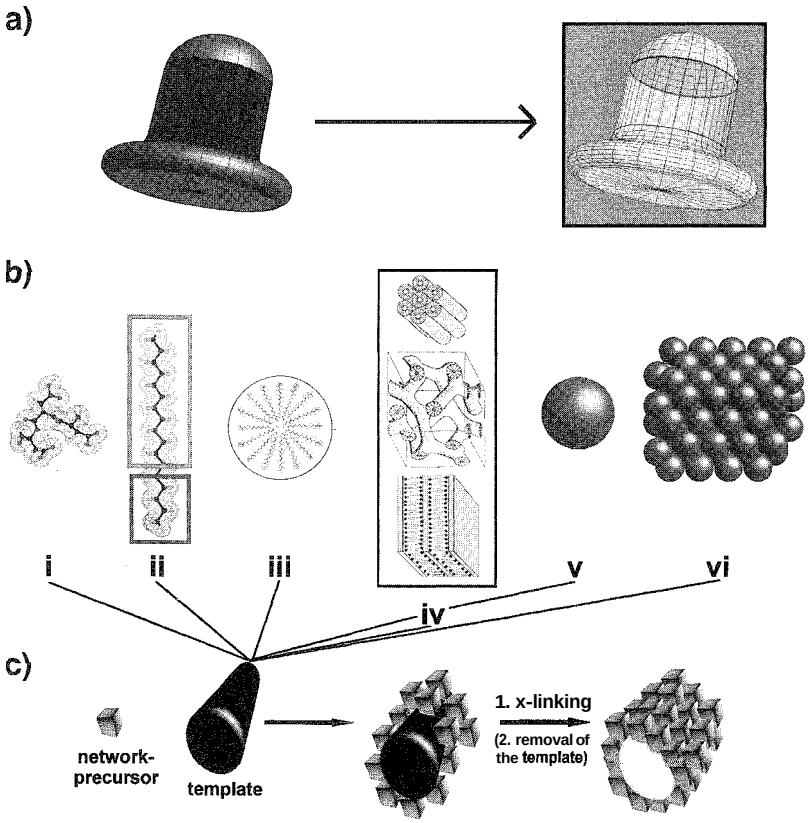

Fig. 1 It is shown how ideas from the ancient bell-casting technique (a) are transferred to obtain nanoporous materials (b–c). This process, accordingly named nanocasting, uses nanoseale template structures (b) ranging from molecules (i) to colloidal crystals (vi). This template structure is imprinted into a solid hybrid material (c). Finally, after removal of the template, one ideally achieves a pore resembling the template. (*View this art in color at www.dekker.com.*)

The template structure needs to be compatible and dispersion-stable in the solvcnt–network precursor system throughout the entire nanocasting process and during the solidification of the network phase (via polycondensation or cross-linking, for instance). Macrophase separation has to be avoided at all times. Therefore, repulsive forces between the template and the network precursors must be avoided. However, in cases where the forces between these components are strongly attractive as, for instance, between a positively charged template and negatively charged network species, cooperative effects are likely to occur, which restrict the direct relation between the template morphology and the pore. A typical example for this case is the preparation of the well known MCM-41[2] material, where cylindrical pores resembling a hexagonal liquid crystal are obtained, although the concentration of the cationic surfactant CTAB is even lower than the CMC (critical micelle concentration). It can be concluded that providing weak attractive interactions between the template and the network source is the key for the nanocasting method. Hydrogen-bonding interactions are ideally suited for this purpose.

Simple considerations make it obvious that the porous materials created arc characterized by high surface area and, therefore, also high surface energy. The porous materials are only metastable in comparison to the corresponding bulk state due to this vast interface energy. 'A high degree of cross-linking as observed for most silica materials demands such a high activation energy for restructuring processes that the pore structure is stable practically infinitely. Additionally, it should be noted that the pore walls represent a confined situation. If amorphous phases or entropically restricted phases are thermodynamically significantly less stable than the bulk or crystalline counterparts, nanocasting is restricted. Two examples should elucidate this point. Crystallization processes often occur for porous transition-metal-oxide materials, and it is hard to maintain the full integrity of the pore structure at higher temperatures. Many attempts were also made to produce ordered mesoporous polymer materials via nanocasting procedures.[3] The high flexibility and the entropically unfavorable situation of limiting the polymer conformation inside the thin walls make it practically impossible to nanocast polymers with

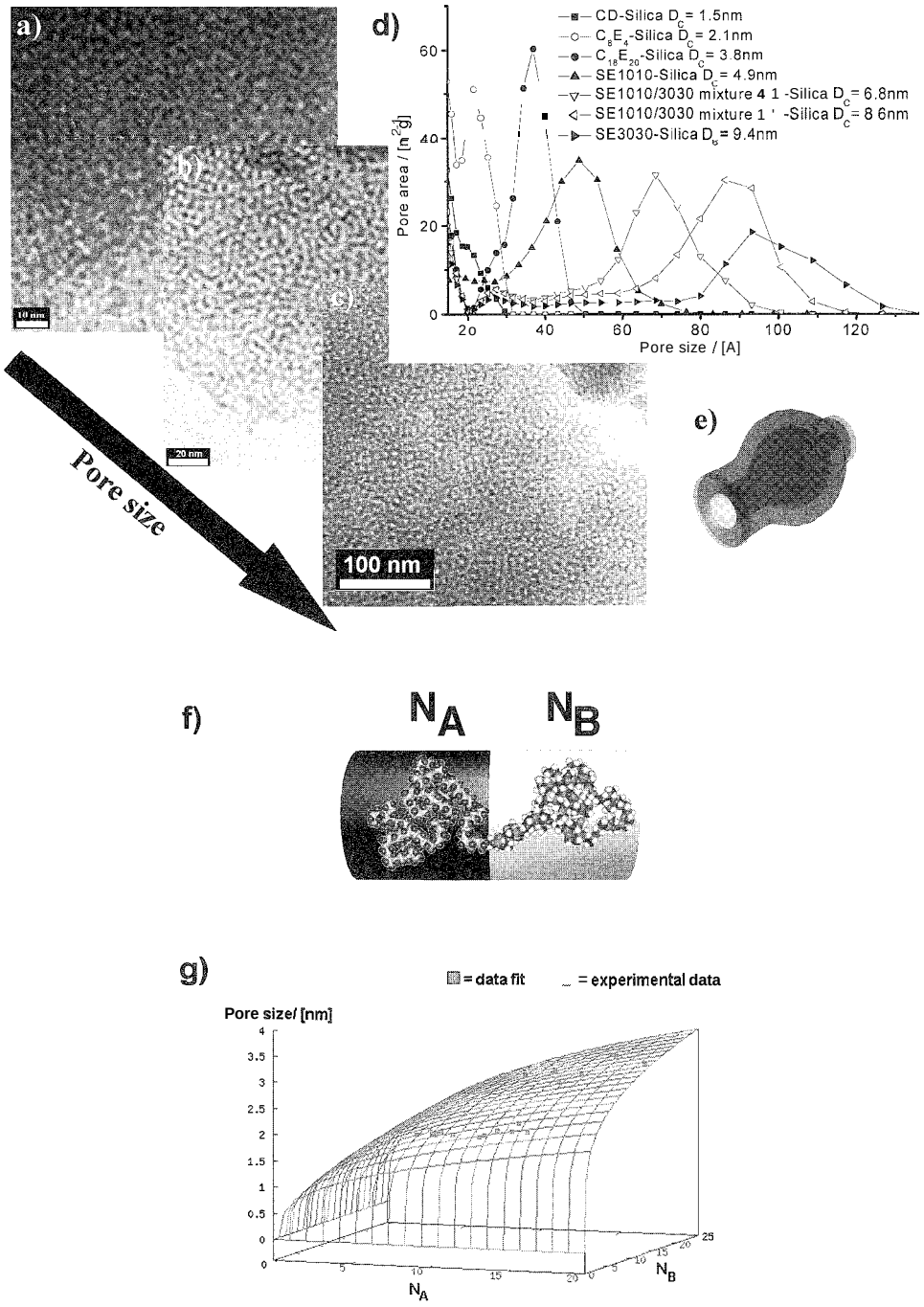

Fig. 2 (a–c) Transmission electron microscopy (TEM) images of mesoporous materials obtained via nanocasting of self-assernbled structures of amphiphiles of different sizes. The smallest type of templates CDs (cyclodextrins will be mentioned later) lead to the smallest pores of 1.5 nm in diameter, as also determined by N_2-sorption experiments and correlating pore-size distributions (d). Block copolymer systems such as SE (polystyrene–polyethlylencoxide) lead to larger pores of the order of 5–10 nm. A model for the obtained pores is given in (e). The amphiphilic molecules can be described by the number of monomeric units in each of the amphiphile chains (f). The hydrophobic block is characterized by N_A, and the hydrophilic block is characterized by N_B. (g) This part shows how the pore sizes correlate to N_A and N_B for Brij [alkyl-poly(ethylene oxide)] surfactants. (*View* ***this*** *art in color at* www.dekker.com.)

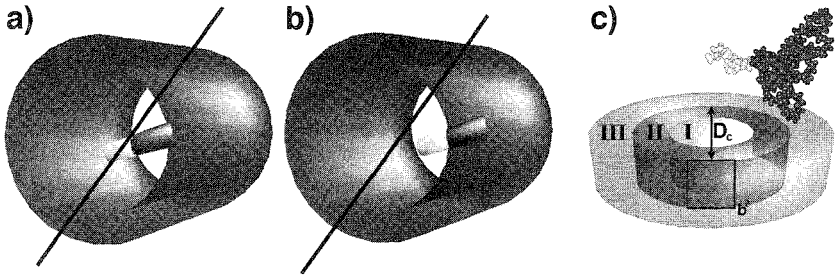

Fig. 3 The three possible scenarios of how the amphiphilic molecule (yellow–blue units) create a pore. (a) The "one-phase" scenario, where both blocks, hydrophilic and hydrophobic (yellow), contribute with full length to the pore. The classical view (b) expects a microphase separation, whcrc the hydrophobic core would determine the pore size, while the hydrophilic shell would be dissolved in the aqueous network-precursor medium. (c) The "three-phase" scenario proved to represent thc results most accurately."[7] (View this *art* in color *at* www.rlekker.com.)

amphiphilic templatc structures. Only when the templates are much bigger, which results in thicker walls, can successful nanocasting be achieved. For instance, inverted polymer opals exist.[4]

DESIGNER MATERIALS VIA NANOCASTING

It will be demonstrated in this section how the Criteria I–III mentioned in the first section of this article, desirable for porous nanostructures can be controlled via nanocasting. Therefore, it is not unrealistic to state that nanocasting materials are "designer materials."

Gaining Control over Pore Size

Within thc philosophy of nanocasting, it is straightforward to expect that the size of the template will directly influence the size of the pores. As larger amphiphilic molecules will lead to larger self-assembled structures (lyotropic phases with respectively larger periodicities), a correlation should be shown as well.

Howcvcr, at first it is important to know if, in principle, larger pore sizes are possiblc, as it is known, for instance, for zeolithes (with crystalline alumosilicate walls) that there is a natural limitation. Navrotsky et al. were able to show that there is, in principle, no limitation for accessible pore sizes in amorphous silica materials.[5] They demonstrated that the amorphous silica in materials like MCM-41 is only marginally less stable than the most stable form of SiO_2, crystallinc quartz. This means that suitable experimental pathways have to bc found to reach a certain pore size. Then, the materials are stable. One of these pathways, and maybe the best one, is nanocasting.

A series of experiments with different-sized templates proves that this assumption is correct (see Fig. 2). Larger amphiphiles lead to larger templates and, thus, to larger pores.

However, more details would be desirable. It is possible to express the architecture of an amphiphilic moleculc by the number of units in the molecular chain. For instance, N_A would denote the number of CH_2 atoms, and N_B would denote the number of ethylene oxidc units in so-called Brij surfactants (see Fig. 2f). It is then possible to relate the sizc of the pores to the molecular architecture of the templatc molecules for a row of compositions (see Fig. 2g). Interestingly, the pore size depends on the size of both blocks. Classically (Fig. 3b), a microphase separation of the hydrophilic parts and hydrophobic parts into separate domains is expected. In this case, the pore-size dependence on both molecular parts is impossible. A "one-phase" scenario as depicted in Fig. 3a can also be excluded due to many reasons, which will not be further discussed here.[6]

It seems in Fig. 2g that all the experimental points are lying on a master surface, which is a first indication that there might be a physical law describing the correlation between the pore size and the molecular architecture of the amphiphile. However, because neither the one-phase nor the two-phase model was appropriate to describe the data (as shown elsewhere),"[7] a new model was needed. It seems that in addition to the hydrophobic core (bright yellow), a certain fraction of the hydrophilic poly(ethylene oxide) (PEO) chain contributes to thc size of the mesopore D_c (areas I and II in Fig. 3c). Only the remaining fraction of PEO is imbedded in the pore wall. By considering the total volume given by the number of units in the amphiphile chain and the stabilization of thc interface I + II/III, it was finally possible to derive an equation that relates the mesopore size D_c to the molecular composition of the amphiphile expressed as $N_{A/B}$ (see Eq. 1):

$$D_C = \frac{c}{N_A^{0.16} N_B^{0.40}} \{K_I [N_A]_I + K_{II}([N_B]_{II} - [0.26N_A + 0.24N_B]_{III})\}$$

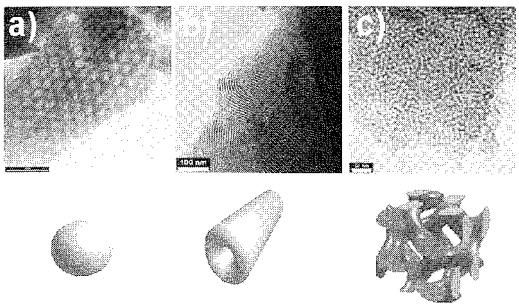

Fig. 4 Three alternative pore shapes are shown schematically and in TEM images for spherical pores (a); cylindrical pores (b), and bicontinuous, "worm-type" pores (c). (View this *art* in color *at www.dekker.com.*)

The constants $K_{I/II}$ contain molecular parameters, and a more detailed description of the derivation of this equation is given in Ref. [6]. Surprisingly, pore sizes can be adjusted by applying mixtures of chemically similar but different-sized amphiphilic molecules, as shown in Fig. 2d. This is a key result, because it is now possible to obtain every pore size between two borders determined by the "parent templates." Nevertheless, it is worth mentioning alternative ways to influence and control pore size. It was already demonstrated that a possible way would be to select an amphiphilic molecule with a suitable molecular composition in order to obtain the desired pore size. However, it is practically impossible to get all of these amphiphiles, or at least it is tedious to synthesize them. The dependence of the pore size on the length of ammonia-based surfactants was demonstrated by the first works of Beck, Vartuli, Kresge, et al.[2]

Two additional routes to change pore size are as follows:

- Swelling of the lyotropic phase by adding selective solvents.[7]
- Changes in reaction parameters like temperature or electrolyte concentration.[8]

It can be concluded that nanocasting allows for control over pore size.

Gaining Control over Pore Shape

The analogy between nanocasting and bell-casting can be further used to influence the shape of the pore. Spherical templates (micelles) lead to spherical pores, cylindrical templates to cylindrical pores, and bicontinuously interwoven templates to bicontinuous and highly curved pore systems. This is shown in Fig. 4.

Therefore, nanocasting allows for control of the pore shape.

Gaining Control Over the Pore-Wall Surface

The ultimate goal in materials design would be achieved if in addition to size and shape the properties of the pore surfaces could be chosen by demand. Thus, one needs to overcome the limitation of SiO_2 as the network material. Either the silica is modified with organic groups or other network compositions are treated with nanocasting.

Organic modification of the pores without affecting pore size and shape was realized recently. Here, silica-network precursors with bridging organic ligands $(OEt)_3Si–R–Si(OR)_3$ are used for the preparation of ordered mesoporous materials. The organic groups practically cover the pore walls, as can be seen in Ref. [9]. Neither pore shape nor pore size are altered due to the use of the modified precursors. Furthermore, nanocasting (as, for instance, creating pores of different sizes) is fully applicable (see Fig. 5). It also brings the benefits of preparing monolithic materials.

This tool allows coverage of the walls of the pores with functional groups R, and thus control of the properties of the pore walls.''' For instance, the pore wall can be adjusted to show $Si–CH_2–Si$, $Si–CH_2CH_2–Si$, $Si–CH{=}CH–Si$, $Si–C_6H_4–Si$ motifs, and many more. Crystallinity in the otherwise amorphous walls was also achieved.[10]

Many experiments were designed to obtain ordered mesoporous materials with completely different compositions of the network no longer correlated to silica. Also here, nanocasting is beneficial. Due to their high relevance in many areas of catalysis and their variable redox- and magnetic properties. much work was devoted to the creation of stable ordered mesoporous transition-metal oxides. In the meantime, many compositions with Ti, Zr, V, Ta, Mo, W, Mn, and Y, as the central element were introduced."[11]

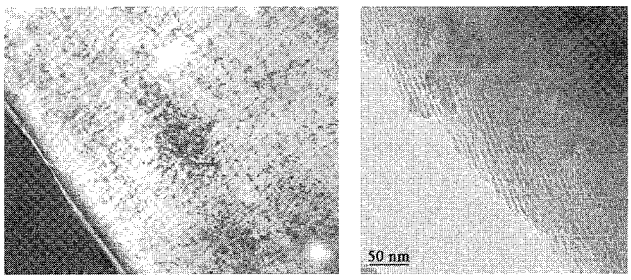

Fig. 5 Ordered mesoporous materials with double bonds (C=C) covering the pore walls obtained via nanocasting a Pluronic liquid crystal. The high degree of ordered nanostructure is shown by polarization optical microscopy (left) and TEM (right). (*View* this art in color *at* www.dekker.com.)

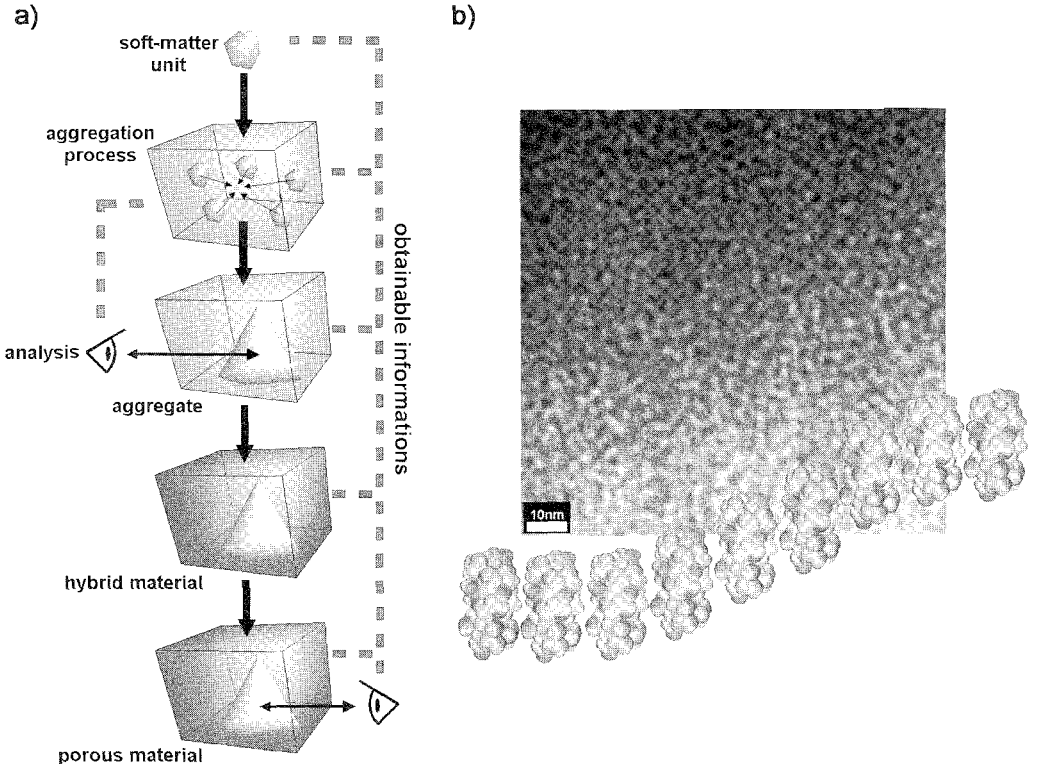

Fig. 6 (a) Shown is how the nanocasting principle may be applied as a new technique to investigate soft-matter aggregation in water. Instead of investigating the soft-mattcr aggregate directly, those aggregated are as templates cast into a solid silica mold, and the porc structure is finally investigated. Under nanocasting conditions. it is possiblc to relate the pore to the shape and size of the template. (b) Shown is how this concept was successfully applied to elucidate the aggregation behavior of cyclodextrin molecules in water.[12] Worm-type pores as presented in the TEM image allowed for the conclusion that cyclodextrin molecules self-assemble to aggregates. where the exterior hydrophilic domain shields the interior hydrophobic domain (see schematic). (View *this* art in color *at www.dekker.com.*)

NANOCASTING AS AN ANALYTICAL TECHNIQUE

So far, nanocasting was presented as a method to produce innovative and state-of-the-art materials. It would bc interesting to explorc if it is possible to invert this idea, namely to discover something about the self-assembly of a sort-matter unit by investigating the nanocast pore structure. The idea behind this concept is shown in Fig. 6a. Here, soft-matter aggregates are interpreted as templates for the nanocasting process. Accordingly, the size and shape of the pore is determined by the template. Instead of investigating the soft-matter structure in water directly, the pore structure can be used to yield information about the guest template aggregates. The analytical processing of a solid, porous material is easier to achieve than for the correlating dispersed aggregate. The electron contrast between void space and porc wall is very high, which increases the contrast for any scattering technique. The porous silica is stable against most conditions, such as ultrahigh vacuum uscd in electron microscopy, excluding solvents The pores are fixed in position and, therefore, do not represent a time average The last point is somewhat problematic, because dynamic information is lost It is, for instance, not possible to determine the weight of the aggregate via nanocasting

Some examples should elucidate the use of nanocasting as an analytical technique

Nanocasting and the Conformation of Amphiphiles

The reader might have been wondering about the origin of the following term in Eq. 1:[6]

$$\frac{1}{N_A^{0.16} N_B^{0.40}}$$

This relation stems Pi-om the description of amphiphiles in polymer physics, as follows:

$$b^2 = b_0^2 N_A^{\alpha} N_B^{\beta} \qquad (2)$$

and describes how the interface area per amphiphile scales with the molecular composition. The exponents α=0. 16 and β=0.40 are the outcomes of the experiments described in the section "Gaining Control over Pore Size" and in Ref. [6]. However, if one realizes that the volume of the molecular chain X in general scales with $V \propto L \cdot b^2 \propto N_X^1$, it is possible to conclude that the length l of the hydrophobic chain A scales as $L \propto N_A^{0.86}$. In comparison to this, the hydrophobic chain in a micellar system (diluted situation) scales with $L \propto N_A$ (stretched conformation),"" while chains in a polymer melt scale with $L \propto N_A^{0.66}$ (coiled chain).[14]

In conclusion, nanocasting gives detailed information about the formation and structure of molecules in lyotropic liquid crystals. without having investigated organic matter. Just the fine details of the pore structure reveal these secrets: It seems that a classical two-phase separation model is not fully applicable to lyotropic liquid crystals (high-concentration situation). but it seems that a fraction of the hydrophilic block belongs to the micellar core. Furthermore. it was seen that the chain conformation is an intermediate between stretched (micelles) and coiled (polymer melt).

Nanocasting end the Aggregation of Cyclodextrins

Cyclodextrins (CDs) are cyclic oligosaccharides, and it is known that they possess a hydrophilic shell and a hydrophobic core. Despite their high technical potential and academic importance, little is known about the structure of cyclodextrins in water.[12] Both opinions of aggregated modes and nonaggregated states were discussed in the literature. Nanocasting aqueous CD solutions were used to approach this problem (Fig. 6b). Interestingly, no disordered materials were found. Instead. the experiment revealed materials with a well-defined pore size and a worm-type structure. The size of the pores inatched the size of a single-CD molecule, and the order of the materials was highly dependent on the hydrophilic–hydrophobic difference of outer and inner CD moieties. It was, therefore. reasonable to argue that cyclodextrins self-assemble to worm-type aggregates in water.[12]

Nanocasting end Polyoxometalates

As pointed out before, it can be hard to investigate supramolecular species in solution. This is true for a particula inorganic system, the so-called giant polyoxometalates prepared by Müller et al.[15] Although these fascinating compounds are fully characterized, it was an open question as to if these large clusters can be dissolved and if crystallization is a driving force for their formation. In other words, it was questioned if these giants exist only in the solid state or also in solution. Again. nanocasting was able to shed some light onto this problem. Aqueous solutions of giant polyoxometalates were nanocasted into a solid silica material. and in both cases studied, the spherical keplerate and the disk-like giant wheels were found to be dispersed in the material.[16] Therefore. it was clear that giant polyoxoinetalates exist in solution. and new materials were prepared.

Nanocasting and Swelling of Lyotropic Phases

Another interesting phenomenon is observed via nanocasting when trimethylbenzene (TMB) is added to the lyotropic phase of a Pluronic block copolymer for the preparation of SBA-15[17] to increase the pore size by swelling. At a certain ratio. mesocellular foams are obtained. as Stucky et al. pointed out.[17] The ideal hexagonal structure of SBA-15 is maintained only for relatively low concentrations of TMB. When the oil-to-polymer ratio is 0.2–0.3. the silica walls begin to buckle, forming nodes accompanied by an increase in pore size. If the amount of oil is increased further, the nodes undergo a transition to spherical pores ($d \approx 20$ nm), the so-called mesocellular foam. The explanation for this phase transition lies in the reaction of the iyotropic phase due to a change in the surfactant parameter by adding a hydrophobic solvent. The TMB Is located in the hydrophilic PPO regions of the amphiphilic assemblies. which changes the packing pararneter of ihe surfactant and finally leads to the transition of micelles to microemulsions.[7]

NANOCHEMICAL APPLICATIONS OF NANOCASTING MATERIALS

As nanocasting allows us to obtain porous materials with desired pore sizes and shapes. these materials are ideal candidates to act as nanoreactors[18] or to study host–guest relationships. However, the latter is a topic in its own right and is not mentioned here in further detail.

But. the analogy given previously that nanocasting is a bell-casting technique on the nanometer scale is not absolutely correct. Because for bell-casting, the first hollow replica is filled again to get the desired material in its desired shape. Therefore. it would be tempting to be able to use mesopores as a cast for new materials. showing the structure of the original organic liquid crystal.

Many scientists successfully realized this goal. The pore system can be infiltrated with precursors for metals. semiconductors. or polymers. and afterwards, a suitable reaction is carried out. and the empty pore space is

transformed into a metal, for instance. It was shown that the pore determines the shape and size of the new nanoparticle.[19] A lot of work was done in the field of polymerization in ordered mesoporous hosts.[20] Just one example among many should be mentioned.[21] Kageyama et al. connected a titanocence catalyst covalently to the pore walls of MCM-41. When the polymerization of ethylene is performed, the poly(ethylene) chain is hindered to bend backwards. so it has to grow along the channel axes. This results in the situation that hexagonally aligned polymer fibers leave the MCM-41 "crystals." Finally. bundles of several polymer fibers with diameters 30–50 nm form. The obtained molecular weight is extremely high (M_n=62,000,000).

As described earlier. the other important subfield of nanochemistry in ordered mesoporous materials is the creation of nanoparticles. Due to the high interface energy, once-nucleated nanosized crystals tend to grow by Ostwald ripening. This growth can be restricted by performing the crystallization inside the pore system of a mesoporous host. Often, caused by quantum size effects, interesting composite materials are created. Therefore, much of the work was devoted to the preparation of semiconductor nanoparticles via this route. Examples are gallium nitride, cadmium selenide. cadmium sulfide. silicon, titanium dioxide, germanium, gallium arsenide, zinc sulfide, and indium phosphide.[1,22] Ordered mesoporous silica materials, especially of the MCM-41 type, were also used as matrices for the preparation of metal colloids. In this way, for example, metal nanowires were produced with Pd, Pt, or Ag.[23,24]

A different, interesting topic is one where the whole pore system is transformed into carbon. This interesting area of producing ordered porous carbon materials was reviewed elsewhere.[25,26]

CONCLUSION

Reviewed in this article was the so-called nanocasting process. which is the three-dimensional transformation of self-assembled organic structures (templates) into hollow inorganic replicas. This process allows for significant control over the morphological features of the resulting porous materials. Most importantly. pore size can be controlled via mixed-template routes. Furthermore. the pore size was rationalized as a dependence on the molecular compositions of the template. Additionally, pore shape can be tuned by selecting different-shaped templates. Nanocasting still holds when network precursors other than those leading to pure SiO_2 are used. Organically modified materials or other porous inorganic oxides can be achieved. Furthermore, nanocasting allows for the production of porous materials of different macroscopic appearance as monoliths or thin films.

This high level of materials design enables researchers to go one step further. to use the cavities (pores) of well-defined sizes, shapes. and surface functionalities to perform chemistry under confined conditions.

ARTICLES OF FURTHER INTEREST

Cyclodextrins, p. 398
Cyclodextrins: Applications, p. 405
Mesoporous Silica and Silica–Organic Hybrids, p. 852
Micelles and Vesicles. p. 861
Zeolites: Structures and Inclusion Properties, p. 1623

REFERENCES

1. Polarz, S.; Smarsly. B. Nanoporous materials. J. Nanosci. Nanotechnol. **2003**, 2. 581.
2. Kresge. C.T.; Leonowicz. M.; Roth. W.J.: Vartuli, J.C.; Beck, J.S. Ordered mesoporous molecular sieves synthesized by liquid–crystal template mechanism. Nature 1992. *359*, 710.
3. Hentze, H.P.: Antonietti, M. Template synthesis of porous organic polymers. Curr. Opin. Solid State Mater. Sci. 2001. *5.* 343.
4. Stein. A. Sphere templating methods for periodic porous solids. Microporous Mesoporous Mater. 2001. *44.* 227.
5. Navrotsky, A.; Petrovic, I.; Hu, Y.: Chen. C.; Davies, M.E.J. Energetics of microporous materials. J. Non-Cryst. Solids **1995**. *192–193.* 474.
6. Smarsly, B.; Polarz. S.; Antonietti. M. Preparation of porous silica materials via sol–gel nanocasting of nonionic surfactants: A mechanistic study on the self-aggregation of amphiphiles for the precise prediction of the mesopore size. J. Phys. Chem., B **2001**, *105.* 10473.
7. Lettow, J.S.; Han. Y.J.; Schmidt-Winkel, P.; Yang, P.; Zhao, D.: Stucky. G.D.: Ying, J.Y. Hexagonal to mesocellular foam phase transition in polymer-templated mesoporous silicas. Langmuir 2000. *16.* 8291.
8. Corma, A.; Kan. Q.; Navarro. M.T.: Pérez-Pariente, J.: Rey, F. Synthesis of MCM-41 with different pore diameters without addition of auxiliary organics. Chem. Mater. **1997**. 9. 2123.
9. Asefa. T.; MacLachan, M.J.: Coombs, N.: Ozin. G.A. Periodic mesoporous organosilicas with organic groups inside the channel walls. Nature 1999. *402.* 867.
10. Inagaki. S.: Guan. S.; Ohsuna. T.: Terasaki, O. An ordered mesoporous organosilica hybrid material with a crystal-like wall structure. Nature 2002. *416.* 304.
11. Schuth, F. Non-siliceous mesostructured and mesoporous materials. Chem. Mater. **2001**, 13. 3184.
12. Polarz. S.; Smarsly, B.: Bronstein. L.; Antonietti, M. From

cyclodextrin assemblies to porous materials by silica templating. Angew. Chem., Int. Ed. 2001, *40*, 4417.
13. Forster, S.; Zisenis. M.; Wenz. E.; Antonietti, M. Micellization of strongly segregated block copolymers. J. Chem. Phys. 1996. *104*. 9956.
14. Bates. F.S.; Fredrickson, C.H. Block copolymer thermodynamics—Theory and experiment. Annu. Rev. Phys. Chem. 1990. *41*. 525.
15. Müller, A.; Shah. S.Q.N.; Bogge. H.: Schmidtmann, M. Molecular growth from a Mo176 to Mo248 cluster. Nature 1999. *397*. 48.
16. Polarz, S.: Smarsly, B.; Göltner, C.: Antonietti. M. The interplay of colloidal organization and 0x0-cluster chemistry: Polyoxometalate-silica hybrids—Materials with nanochemical function. Adv. Mater. 2000. *12*. 1503.
17. Zhao, D.; Feng. J.; Huo. Q.; Melosh. N.: Fredrickson. G.H.: Chmelka. B.F.: Stucky. G.D. Triblock copolymer synthesis of rnesoporous silica with periodic 50 to 300 angstrom pores. Science 1998. *279*, 548.
18. Antonietti. M.; Landfester. K.: Mastai, Y. The vision of ''Nanochemistry,'' or is there a promise for specific chemical reactions in nano-restricted environments? Israel J. Chem. 2001. *41*. 1.
19. Bronstein. L.M.: Polarz, S.: Smarsly, B.: Antonietti, M. Sub-nanometer noble-metal particle host synthesis in porous silica monoliths. Adv. Mater. 2001, 13. 1333.
20. Wu, C.G.: Bein, T. Conducting polymer wires in mesopore hosts. Zeolites and Related Microporous Materials: State of the Art 1994 1994, *84*. 2269.
21. Kageyama, K.: Tamazawa, J.: Aida. T. Extrusion polymerization: Catalyzed synthesis of crystalline linear polyethylene nanofibers within a mesoporous silica. Science 1999. *285*, 2113.
22. Ozin, G.A.; Chomski. E.: Khushalani, D.; Maclachlan. M. Mesochemistry. J. Curr. Op. Coll. Interf. Sci. 1998. 3. 181.
23. Han. J.; Kim. J.M.: Stucky, G.D. Preparation of noble metal nanowires using hexagonal rnesoporous silica SBA-15. Chem. Mater. 2000. 12, 2068.
24. Lee. K.B.: Lee. S.M.; Cheon, J. Size-controlled synthesis of Pd nanowires using a mesoporous silica template via chemical vapor infiltration. Adv. Mater. 2001, *13*, 517.
25. Ryoo. R.; Joo, S.H.: Kruk, M.: Jaroniec. M. Ordered mesoporous carbons. Adv. Mater. 2001. *13*. 677.
26. Kyotani. *T*. Control of pore structure in carbon. Carbon 2000. *38*. 269.

Neutron Diffraction

Chick C. Wilson
University of Glasgow, Glasgow, United Kingdom;
Central Laboratory of the Research Councils (CLRC) Rutherford Appleton Laboratory, Oxon, United Kingdom

INTRODUCTION

The general characteristics of neutron diffraction as applied to studies of condensed matter are summarized, along with their means of production in steady-state reactor and pulsed spallation sources. Techniques for single-crystal neutron diffraction are discussed, and the application of these techniques in the study of molecular systems is summarized. A short review of applications in the field of molecular crystals is given. A more detailed account of this area was recently published.[1]

NEUTRON SCATTERING

Neutrons are, in many ways, unique probes of condensed matter. In many cases, the information available from neutron scattering is not only conveniently measured using the technique but is also the only method with which to obtain the information. In contrast to other techniques such as x-ray or electron diffraction. neutrons are scattered by the nucleus, rather than by the electrons in an atom. As a consequence, the scattering power, given by the scattering length, b, does not vary monotonically with Z (Fig. 1). This means that neighboring elements in the periodic table generally have substantially different scattering cross sections, offering a direct method of distinguishing neighboring elements. The dependence of the scattering on the nucleus also allows isotopes of the same element to have substantially different scattering lengths for neutrons, thus allowing the technique of isotopic substitution to be used to yield structural and dynamical details. In the area of organic and biological molecular structures, the most relevant isotopic substitution is that of ^{2}H (deuterium, scattering length 6.67 fm) for ^{1}H (hydrogen, scattering length -3.74 fm). The use of contrast variation, where the scattering density of different parts of a molecule or of an H_2O–D_2O mixture is altered. is powerful and has been key to many successful applications of neutron scattering in chemistry and biology.

In addition, with neutrons it is easier to sense light atoms, such as hydrogen. in the presence of heavier ones. For example. in the presence of relatively light carbon atoms, a hydrogen contributes around 0.32 of the measured neutron scattering intensity (proportional to b_2) for a carbon atom. The equivalent ratio for x-rays is less than 0.03, meaning that hydrogen atoms are determined around 12 times more accurately with neutrons than x-rays in the presence of carbon atoms. This factor increases as the atomic number of the "heavy" atom increases.

The lack of a fall-off in scattering power as a function of scattering angle also gives us the ability to study structures to very high resolution with neutron diffraction.

Among the other properties of the neutron that make it a successful probe of structure is the fact that neutrons interact weakly with matter and are therefore nondestructive, even to complex or delicate materials. Similarly, neutrons allow probing of the interior of materials, not merely the surface layers as probed by x-rays, electron microscopy, or optical methods. Neutrons also have a magnetic moment, allowing magnetic structure (the distribution of magnetic motnents within a material) and magnetic dynamics (how these moments interact with each other) to be studied in a way not possible with other forms of radiation.

There are also some drawbacks, however, largely due to sample size and data collection time requirements. With the relatively low flux of neutron sources and the weak scattering of most materials, usually crystals of several mm' are required to allow for the collection of a good data set in a reasonable data collection time. The limit is usually regarded as being around 1 mm^3, but there are significant efforts being made by source and instrument designers to allow this to be reduced further, as we shall see below. Assuming an appropriate sample is available, the choice between neutron and x-ray diffraction in the study of molecular systems is often clear cut. If there are one or more hydrogen atoms in the structure, of which location is critical to a complete understanding of the system, its configuration, and its interactions, then neutron diffraction should be the method of choice. In general; hydrogen atoms can be treated on an equal basis with the other atoms in a neutron diffraction experiment. More subtly, if some or all of the hydrogen atoms can be exchanged for deuterium, the use of contrast variation methods renders neutron diffraction still more powerful.

Encyclopedia of Supramolecular Chemistry
DOI: 10.1081/E-ESMC 120013818

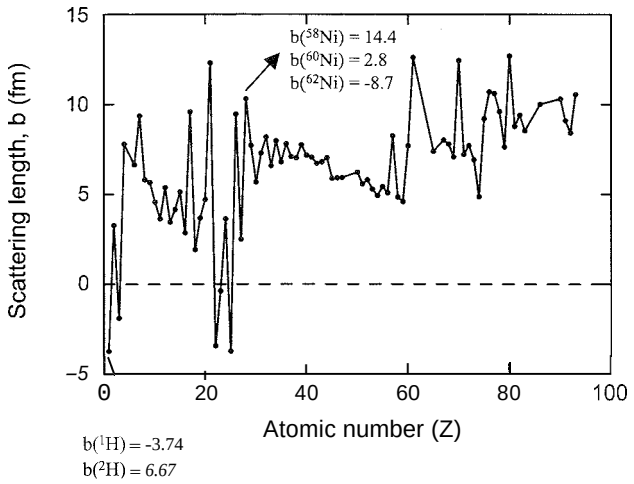

Fig. I Neutron scattering lengths vary randomly as a function of atomic number. In addition, isotopes of the same element can have substantially different scattering lengths, two representative examples. H and Ni, being shown here.

Neutron Sources

The characteristics of the two types of neutron sources (nuclear reactors and accelerator-driven spallation sources) used for condensed matter research are very different. A reactor is a steady-state source, in which neutron production is continuous. The neutrons produced are slowed (moderated) for use in neutron scattering experiments. Typically these neutrons are then passed through a monochromator. or filter. to select a wavelength, or wavelength range, to be used in the experiment. The 58 MW high flux reactor at the ILL. Grenoble, France. operational since 1973, is the highest flux research reactor in the world dedicated to neutron scattering and the study of condensed matter. Details can be found on the Web page http://www.ilI.fr/.

In a spallation source. the neutron production is normally pulsed, and all neutrons are effectively produced at the same time, when the proton beam hits the target. This leads to a tight pulse that must be retained for use of the white-beam time-of-flight technique, essential at such a source. The high-energy neutrons are thus slowed to thermal energies by using small hydrogenous moderators that retain the pulse structure. The use of pulsed spallation sources for neutron scattering science was largely established in the past two decades or so. The highest flux pulsed neutron source is currently the 160 kW ISIS facility at Rutherford Appleton Laboratory in the U.K. Details can be found on the Web page http://www.isis.rl.ac.uk/.

Future Neutron Sources

For practical technological reason, it is difficult to achieve substantially higher flux at a reactor-based steady-state source. The inherent limits of reactor technology mean that a factor of five in flux is the most one could realistically hope to achieve, though there is a vigorous program of instrument optimization and upgrading to ensure optimal use of the available flux. For pulsed sources, the situation is different. The ISIS will remain the brightest pulsed neutron source for several more years. and its capacity is likely to double in the next few years. as a second target station is constructed to host a further suite of neutron scattering instruments. There are currently in construction 1–2 MW pulsed sources in the U.S. and Japan. These will be six to 12 times more powerful than ISIS. Looking forward. the proposed European Spallation Source would provide a 5–10 MW pulsed neutron source, 30–60 times the power of ISIS. which would combine the time-averaged flux of the best reactor source (produced at 1/10th of the power consumption) with the benefits of the pulsed structure from a spallation source—a true next-generation source.

SINGLE-CRYSTAL NEUTRON DIFFRACTION

In order to meet the needs of scientists working on modern aspects of structural molecular science, such as supramolecular chemistry, the instrumentation used for neutron diffraction determinations has developed enormously over the last few years. This was an essential advance, because neutron diffraction is intrinsically a flux-limited technique, due to the relatively low neutron fluxes available from even the most advanced sources. For the structural determination of a sample under a set of variable conditions, experiment times of a few hours per determination are becoming the norm. This also allows for the screening of larger numbers of different materials. further increasing the power of the technique in this area.

On a steady-state neutron source, traditional four-circle diffractometer techniques[2] are normally used for single-crystal diffraction, with a monochromatic beam and a single detector. Rotations of the crystal (and detector) are used to allow measurement of each reflection sequentially. For each Bragg reflection, it is necessary to set up a scan in order for the reflection intensity to be recorded. In such cases, all reflections are observed with the same neutron wavelength. eliminating the need for wavelength-dependent corrections. The constant wavelength nature of the data collection and the steady state of the source also remove the need for correcting data for the incident flux profile and lead to more straightforward error analysis. It is possible to increase the region of reciprocal space accessed in a single measurement by using an area detector, but when this is combined with a monochromatic incident beam, it is still necessary to scan the crystal or the detector to observe the diffracted intensity. Alternatively. an area detector can be combined with a polychromatic

beam and used for Laue or quasi-Laue diffraction, with a stationary crystal and detector. The time-averaged flux at current high-flux steady-state sources is substantially higher than at present-day pulsed sources, allowing better counting statistics to be obtained at the same time, and allowing the study of smaller crystals or larger unit cells. particularly in the Laue diffraction technique.

All of these factors tend to lead to more accurate structure factors, better internal agreement, and ultimately to lower crystallographic *R* factors and somewhat more precise atomic parameters, hence: the best accuracy for neutron single-crystal structure determination. Constant wavelength single-crystal diffraction is the method of choice if ultimate precision is required in an individual structure determination. The high-flux reactor sources are currently favored for larger unit cells or smaller crystals.

The time-of-flight Laue diffraction technique used at pulsed sources samples a large three-dimensional volume of reciprocal space in a single measurement with a stationary crystal and detector. This is due to the combination of the wavelength sorting inherent in the time-of-flight (TOF) technique with large area position-sensitive detectors (PSDs).

For structural studies, there are advantages to collecting the structure factor data on an instrument with a PSD on a pulsed source. Many Bragg reflections are collected simultaneously in the detector, allowing for the accurate determination of crystal cell and orientation from a single data frame (collected in one fixed crystal/detector geometry). The nature of the Laue method also allows greater possibilities for the rapid collection of data sets by removing the need to measure each reflection individually. This flexibility, long appreciated in synchrotron Eaue methods for studying protein structures,[3] recently became recognized as a great strength of TOF neutron Eaue diffraction methods.'" For some applications, a single frame may be the only data required. The high flux of useful epithermal neutrons from the undermoderated beams thus enables collection of data to potentially high sinθ/λlues. which can allow more precise parameters to be obtained. thus enabling subtle structural features to be examined.

The TOF single-crystal diffraction method is ideal for surveying reciprocal space. rapidly determining large numbers of reflections, and following structural changes using a subset of reflections. It also provides accuracy and precision in standard structural refinements, while not matching the ultimate performance of a constant wavelength instrument in this area. It is worth noting in this context that large electronic area detectors can lead to systematic deviations caused by fluctuations of detector response and can also be more difficult to shield; hence it is more difficult to obtain low background levels.

The Future Potential of Laue and TOF Laue Diffraction

The relative lack of flux of neutron sources compared with x-ray sources means that in spite of the large amount of high-quality work achieved to date, the full potential of the unique ability of neutrons to look at structure and dynamics in different ways has not as yet been fully exploited. The solution to this in terms of instrumentation is to collect large amounts of data as efficiently as possible — hence. using larger detector arrays.

The quasi-Laue diffractometer LADI at the ILL[5] exploits newly developed neutron image plate detectors wrapped around a cylinder surrounding the sample to give more than 2π solid angle coverage (Fig. 2). In order to reduce the problems of accidental reflection overlap, and more importantly to prevent the accumulation of a large background in the Laue pattern from the hydrogenous samples of interest to the supramolecular chemist. LADI operates with a relatively narrow wavelength range of around 1 Å (typically $3.2 < \lambda < 4.2$ Å). hence. the term "quasi-Laue." This instrument has already demonstrated

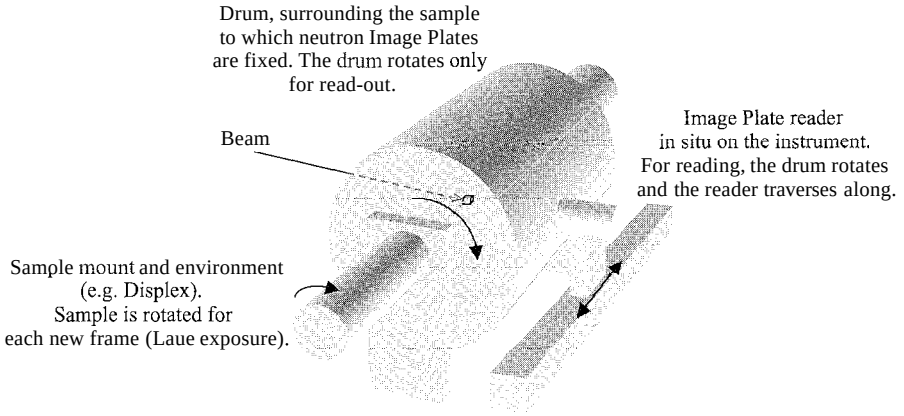

Fig. 2 The LADI diffractometer at ILL. with its large cylindrical image plate detector.

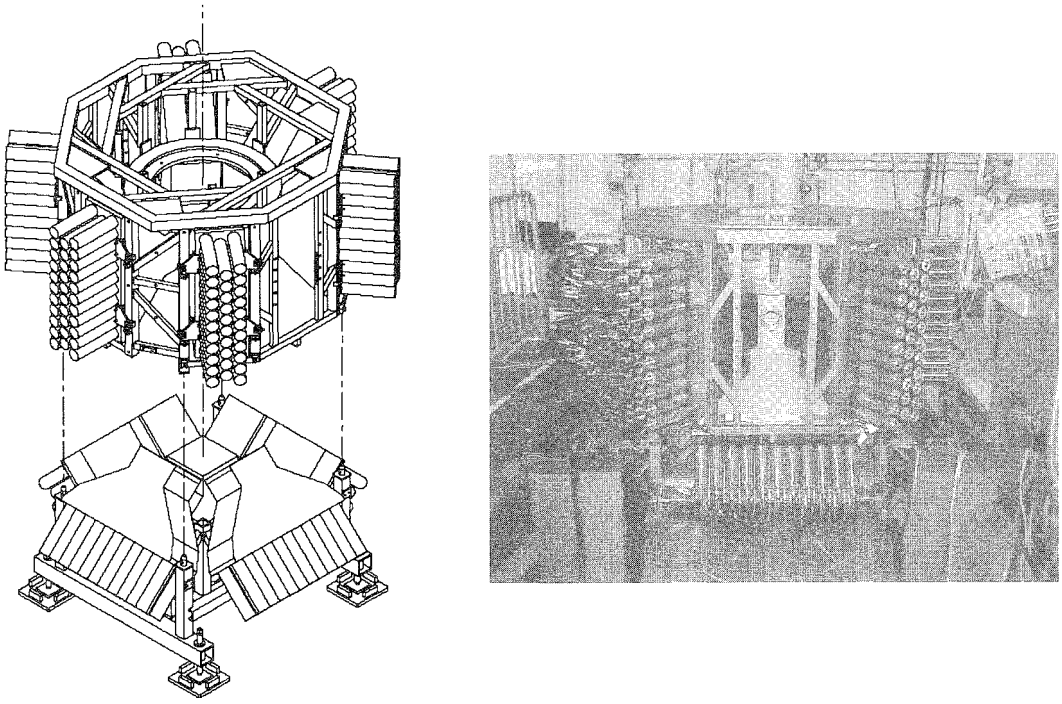

Fig. 3 The newly upgraded SXD at ISIS provides an instrument with 11 area PSDs arranged around a sphere surrounding the sample and over 50% solid angle coverage. Shown here arc an exploded view of the detector array (left) and a view of the detector assembly prior to installation (right).

its potential to revolutionize neutron protein crystallography with dramatically reduced data collection times.[6,7] In addition to these exciting applications in biological crystallography. the LADI concept has obvious applications in the study of smaller molecular systems, including supramolecular chemistry. The thermal LADI instrument VTVALDT, also at the ILL, promises to expand capability in this area.

There is also a tremendous opportunity for the exploitation of neutron TOF diffraction using single-crystal samples. As we have seen, the combination of polychromatic incident neutron beam and large area detector coverage results in a simultaneous measurement of a three-dimensional portion of reciprocal space. If the detector coverage is sufficiently great, a complete collection of the unique portion of reciprocal space is possible to good resolution with a minimal number of crystal orientations. An upgrade recently undertaken to the single-crystal diffractometer SXD at ISIS begins to realize this potential. This upgraded instrument has detectors covering over 50% of the solid angle, with a total of 11 PSDs placed on a sphere centered on the sample (Fig. 3), and thus offers fast collection of Bragg intensities.

These new instruments will benefit all areas of structural science, including chemical crystallography, drug structure, phase transitions, magnetism, and structural disorder, and will be of particular relevance to supramolecular chemists wishing to build up systematic patterns of structural information from a range of samples.

POWDER NEUTRON DIFFRACTION

Modern high-resolution powder diffraction, particularly with neutrons, is a powerful method for structure determination and refinement. particularly for inorganic materials and systems. for which it is very difficult to obtain single crystals. The information in a powder pattern, overlapped as it is, is increasingly being used to allow the refinement of detailed structural parameters, particularly using the method of Rietveld refinement.[8,9] Increasingly more complex structures have been examined and successfully refined using the method, and the iinproved resolution of modern day diffractometers can be combined with Rietveld refinement to further expand these horizons.[10]

There are limits, of course. and particularly relevant here is the fact that powder diffraction is not ideal for studying molecular systems. This is due to several factors. Molecular structures frequently have large, low symmetry unit cells. which leads to much peak overlap in the powder pattern. The structures under study also frequently

contain many atoms and are flexible, leading to many parameters in a refinement. and to difficulty in obtaining stability, even in geometrically constrained refinements. These factors are true for both x-ray and neutron powder diffraction. There is an additional technical problem in measuring neutron powder diffraction from a hydrogen-containing material. due to the large incoherent scattering cross section of ^{1}H, which leads to very high background levels. This problem can be minimized by deuterating the material under study, but this is often chemically unfeasible and expensive. There is, in general. no need to deuterate an organic structure for study by single-crystal neutron diffraction. The advent of very high count-rate neutron powder diffractometers may give new opportunities for neutron powder diffraction to make an impact in the study of molecular systems and become of more relevance to the supramolecular chemist, but for now, single-crystal neutron diffraction is clearly the method of choice.

NEUTRON CRYSTALLOGRAPHY OF MOLECULAR MATERIALS

Neutron diffraction played a major role in developing an understanding of how structure affects the properties of crystalline materials, in areas of relevance in much of modern structural chemistry.[11] Areas accessible to single-crystal and powder neutron diffraction include organic materials, pharmaceuticals, small biological macromolecules, zeolites, polymer electrolytes, battery materials, catalysts. superconductors, time-resolved and in situ studies, and chemical magnetism.[12] Neutron diffraction experiments are often carried out under extreme conditions of sample environment. such as high and low temperature, under controlled atmospheres, high pressure, and in chemical reaction cells. The combination of x-rays and neutrons is powerful in many studies. including the characterization of host–guest interactions in, for example, zeolites. and in determination of charge distributions in crystal structures.

Specifically in molecular systems, neutron diffraction is essential for obtaining the most definitive answers to structural problems. The technique is especially powerful in providing accurate positional and thermal parameters of all atoms. It is unparalleled in its ability to locate hydrogen atoms and refine their positions and thermal parameters. Hydrogen atoms (e.g., hydride ligands) can be located in organometallic complexes[13–20] far more reliably than by any other method (Fig. 4). Much of the structural work on hydrogen-bonded systems (e.g., amino acids, nucleic acid components, carbohydrates. cyclodextrins) used neutron diffraction.[21–32] In addition, determination of the hydrogen anisotropic displacement parameters in short **O**...O hydrogen bonds allows, for example, the deduction of the shape of the potential well in which the atom sits.[33–36] Neutron single-crystal diffraction has an important role in defining the patterns of "weak" intermolecular interactions in complex molecular and supramolecular structures, as these often crucially involve hydrogen atoms.[37–39] This leads directly to a strong impact in the expanding area of supramolecular chemistry and crystal engineering. (Fig. 5)[1,11] Neutron diffraction also gives complementary information to x-ray diffraction for charge density studies.[40–45] In joint x-ray/neutron studies, the neutron parameters fix the nuclear positions, and with the x-ray data. the electron density involved in bonding and nonbonding interactions is determined.

Neutron diffraction also has a prominent role in the determination of thermal parameters, in particular, their interpretation and analysis and the implications of this for interatomic potentials. The accuracy of single-crystal neutron diffraction studies of molecular structure, along with the complete description of positional and vibrational parameters of all atoms in a structure, has led to many examples of its use in this area. These applications include the accurate determination of thermal parameters for

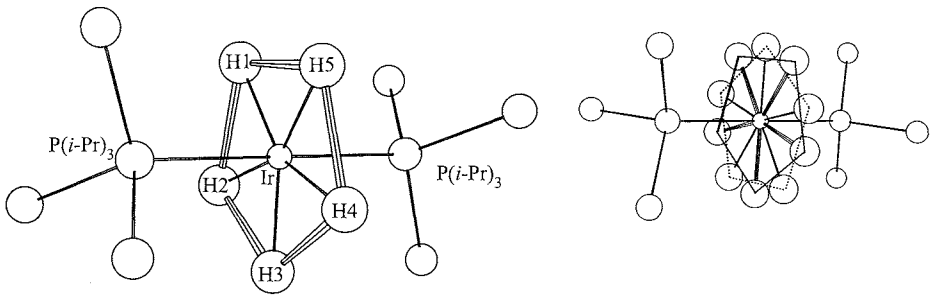

Fig. 4 Determination of the disposition of the terminal hydride ligands in $H_5Ir[P(i\text{-}Pr)_3]_2$ by single-crystal neutron diffraction shows these to adopt an equatorial pentagonal arrangement (left).[20] Disorder in the structure means that there are actually two superimposed pentagons (right), each comprising half-occupancy hydrogen sites.

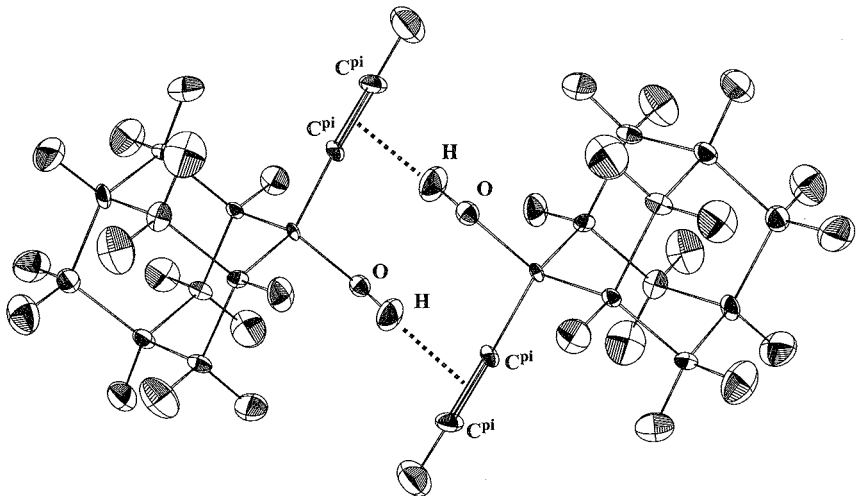

Fig. 5 The dimeric synthon in 2-ethynyl-adamantan-2-01, formed via O–H···π interactions between symmetry-related copies of one of the two molecules in the asymmetric unit.[38] The neutron study allows the full directionality of the O–H···π interaction forming this synthon to be determined.

hydrogen atoms,[46] allowing the comparison between x-ray and neutron diffraction determinations,[47] allowing for understanding of the effect of thermal vibrations on apparent molecular geometry,[48] allowing for the study of the effect of temperature on structure.[49] and in many other areas. Accurate single-crystal neutron diffraction is also well suited to the study of disorder and is particularly important where there are disordered hydrogen atoms present in a structure.[50,51]

Neutron diffraction is an important, complementary structural tool for the supramolecular chemist. The facilities available are developing in directions that are well suited to applications in this area. and the technique can have an increasing impact.

CONCLUSION

Modern neutron diffraction is becoming an increasingly relevant tool for supramolecular chemistry. Allied to its natural advantages for the determination of hydrogen atom parameters, and thus for the fuller description of many nonbonded interactions, improvements in sources and instrumentation for neutron diffraction are now enabling these advantages to be realized in a wider range of systems.

ARTICLES OF FURTHER INTEREST

Crystal Engineering with Hydrogen Bonds, p. 357
Hydrogen Bonding, p. 658
Hydrogen Bonds to Metals and Metal Hydrides, p 666
Inelastic Neutron Scattering, p 727
Nonlinear Optical Materials, p. 973
Strong Hydrogen Bonds, p 1379
Weak Hydrogen Bonds, p. 1576
X-Ray Crystallography, p 1586
X-Ray and Neutron Powder Diffraction, p 1592

REFERENCES

1. Wilson, C.C. Single *Crystal Neutron Diffraction from Molecular* Materials; World Scientific: Singapore. 2000.
2. Arndt. U.W.: Willis, B.T.M. Single *Crystal Diffractometry*; Cambridge University Press: Cambridge, 1966; 82–88.
3. Time-Resolved Diffraciion: Helliwell. J.R.. Rentzepis, P., Eds.: Oxford University Press: Oxford, 1997.
4. Wilson. C.C.; Smith. R.I. Puised Neutron Diffraction: New Opportunities in Time-Resolved Crystallography. In *Time-Resolved* Diffraction; Helliwell. J.R.. Rentzepis, P., Eds.; Oxford University Press: Oxford. 1997; 401–435.
5. Wilkinson. C.; Lehmann. M.S. Quasi-Laue neutron diffractometer. Nucl. Instr. Methods. A **1991**, 310. 411–415.
6. Niimura. N.: Minezaki. Y.; Nonaka. T.; Castagna. J.C.: Cipriani. F.: Hoghoj, P.: Lehmann. M.S.: Wilkinson. C. Neutron Laue diffractometry with an imaging plate provides an effective data collection regime for neutron protein crystallography. Nat. Struct. Biol. **1997**. 4. 909–914.
7. Helliwell, J.R. Neutron Laue diffraction does it faster. Nat. Struct. Biol. **1997.** 4. 874–876.
8. Rietveld, H.M. Line profiles of neutron powder-diffraction peaks for structure refinement. Acta Crystallogr. **1967.** 22. 151–152.
9. Rietveld. H.M. A profile refinement method for nuclear

and magnetic structures. J. Appl. Crystallogr. 1969. 2. 65–71.
10. *The* Rietveld Method: Young, R.A.. Ed.; IUCr Monographs on Crystallography, Oxford University Press: New York, 1995; Vol. 5.
11. Wilson. C.C. Modern Neutron Diffraction. In *Implications* of *Molecular and Materials Structure* for *New* Technologies; Howard, J.A.K.. Allen. F.H.. Shields, G.P.. Eds.: NATO Science Series E. Kluwer: Dordrecht, 1999; Vol. 360. 11–21.
12. Wilson. C.C. Achievements and Future Prospects for Neutrons in Chemistry. In *Contribution* to the *Royal Society* of *Chemistry* Scientific *Forward* Look for Chem*istry*; http:/lwww.rsc.org/pdf/forwardlooWneutrongrp,pdf (accessed 1998).
13. Orpen, A.G.: Pippard, D.: Sheldrick, G.M.: Rouse. K.D. Decacarbonyl-μ-hydrido-μ-vinyl-*triangulo*-osmium: A combined x-ray and neutron diffraction study. Acta Crystallogr. Sect.. B 1978. 34, 2466–2472.
14. Stevens, R.C.: McLean. M.R.: Bau, R.; Koetzle, T.F. Neutron diffraction structure analysis of a hexanuclear copper hydrido complex, $H_6Cu_6[P(p\text{-tolyl})_3]_6$: An unexpected finding. J. Am. Chem. Soc. 1989, **111.** 3472–3473.
15. Ricci, J.S.; Koetzle, T.F.: Bautista. M.T.; Hofstede. T.M.; Morris, R.H.: Sawyer. J.F. Single crystal x-ray and neutron diffraction studies of an η^2-dihydrogen transition-metal complex: *Trans*-$[Fe(\eta^2\text{-}H_2)(H)(PPh_2CH_2CH_2PPh_2)_2]BPh_4$. J. Am. Chem. Soc. 1989. 111. 8823–8827.
16. Heinekey, D.M.; Millar, J.M.; Koetzle, T.F.: Payne. W.G.: Zilm, K.W. Structural and spectroscopic characterisation of iridium trihydride complexes: Evidence for proton–proton exchange coupling. J. Am. Chem. Soc. 1990. 112. 909–919.
17. van der Sluys. L.S.: Eckert. J.: Eisenstein. O.; Hall, J.H.; Huffman. J.C.; Jackson, S.A.: Moetzle. T.F.; Kubas, G.J.; Vergamini. P.J.: Caulton, K.G. An attractive "cis-effect" of hydride on neighbor ligauds: Experimental and theoretical studies on the structure and intramolecular rearrangements of $Fe(H)_2(\eta^2\text{-}H_2)(PEtPh_2)_3$. J. Am. Chem. Soc. 1990. 112. 4831–4841.
18. Howard, J.A.K.: Johnson, O.; Koetzle. T.F.; Spencer. J.L. Crystal and molecular structure of bis(diisopropylphenylphosphine)hexahydridoosmium. $[OsH_6(PC_{12}H_{19})_2]$: Single crystal neutron diffraction study at 20 K. Inorg. Chem. 1987, 26. 2930–2933.
19. Wei. C.-Y.; Garlaschelli, L.: Bau. R.; Koetzle. T.F. X-ray and neutron diffraction analysis of the structures of $H_3Re_3(CO)_{11}[P(C_6H_5)_3]$ and $H_4Os_4(CO)_{11}[P(OCH_3)_3]$. J. Organomet. Chem. 1981. 213. 63–78.
20. Garlaschelli, L.: Khan. S.I.; Bau. R.; Longoni. G.; Koetzle. T.F. X-ray and neutron diffraction study of $H_5Ir[P(i\text{-}Pr)_3]_2$. J. Am. Chem. Soc. 1985. 107. 7213–7214.
21. Jeffrey, G.A.: McMullan, R.K.; Takagi. S. A neutron diffraction study of the hydrogen bonding in the crystal structures of methyl-α-D-mannopyranoside and methyl-α-D-glucopyranoside. Acta Crystallogr. Sect.. B 1977. 33. 728–737.
22. Lehmann. M.S.; Verbist. J.J.; Hamilton, W.C.: Koetzle. T.F. Precision neutron diffraction structure determination of protein and nucleic acid components. Part V. Crystal and molecular structure of the amino acid L-arginine dihydrate. J. Chem. Soc., Perkin Trans., II 1973. 133–137.
23. Takagi. S.: Jeffrey, G.A. Neutron diffraction refinement of the crystal structures of methyl α-D-galactopyranoside monohydrate and methyl β-D-galactopyranoside. Acta Crystallogr. Sect.. B 1979. *35*, 902–906.
24. Takusagawa, F.; Koetzle, T.F.; Srikrishnan. T.; Parthasarathy, R. C–H···O interactions and stacking of water molecules between pyrimidine bases in 5-nitro-1-(β-D-ribosyluronic acid)-uracil monohydrate [1-(5-nitro-2,4-dioxopyrimidinyl)- β-D-ribofuranoic acid monohydrate]: A neutron diffraction study at 80 K. Acta Crystallogr. Sect., B 1979. 35. 1388–1394.
25. Takagi, S.; Jeffrey, G.A. α-L-xylopyranose: A neutron diffraction refinement. Acta Crystallogr. Sect., B 1979. 35. 1482–1486.
26. Kvick, Å.; Thomas, R.: Koetzle, T.F. Hydrogen bond studies. CI. A neutron diffraction study of 2-amino-5-chloropyridine. Acta Crystallogr.. B 1976. 32. 224–231.
27. Mighell. A.: Santoro, A.; Prince, E.: Reimann, C. Neutron diffraction structure determination of dichlorotetrapyrazolecopper(II), $Cu(C_3H_4N_2)_4Cl_2$. Acta Crystallogr.. B 1975. *31*, 2479–2482.
28. Jones. D.D.; Bemal, I.; Frey, M.N.: Koetzle, T.F. Precision neutron diffraction structure determination of protein and nucleic acid components. XIV. Crystal and molecular structure of the amino acid L-cystine dihydrochloride. Acta Crystallogr., B **1974**. 30. 1220–1227.
29. Koetzle, T.F.; Hamilton. W.C.: Parthasarathy, R. Precision neutron diffraction structure determination of protein and nucleic acid components. II. The crystal and molecular structure of the dipeptide glycylglycine monohydrochloride inonohydrate. Acta Crystallogr., B 1972, 28. 2083–2090.
30. Wei. C.H.; Hingerty, B.E.: Busing. W.R. Structure of tetrakis(pyridine)platinum(II) chloride trihydrate: Unconstrained anisotropic least squares refinement of hydrogen and non-hydrogen atoms from combined x-ray–neutron diffraction data. Acta Crystallogr., C 1989. 45, 26–30.
31. Depmeier, W.: Heger. G. Structure of β-bis(ethylammonium) tetrachloromanganate(II): A neutron refinement. Acta Crystallogr.. B 1978. 34. 1698–1700.
32. Roziere. J.; Williams. J.M. The hydrated proton $H^+(H_2O)_n$. VII. A neutron diffraction study of the isolated diaquooxonium ion $H_3O^+\cdot 2H_2O$ in 2,5-dichlorobenzenesulphonic acid dihydrate. J. Chem. Phys. **1978**, *68*. 2896–2901.
33. Schlemper, E.O.; Hamilton, W.C.; La Placa. S.J. A short, slightly asymmetrical, intramolecular hydrogen bond: A neutron diffraction study of bis(2-amino-2-methyl-3-butanone oximato)nickel(II) chloride monohydrate $\{Ni(C_5H_{11}N_2O)_2H\}^+Cl^-\cdot H_2O$. J. Chem. Phys. 1971.54. 3990–4000.
34. Kostansek. E.C.: Busing, W.R. A single crystal neutron diffraction study of urea-phosphoric acid. Acta Crystallogr., B 1972, *28*, 2454–2459.
35. Kiippers. H.; Takusagawa, F.; Koetzle. T.F. Neutron diffraction study of lithium hydrogen phthalate monohydrate: A material with two very short intramolecular

O···H···O hydrogen bonds. J. Chem. Phys. 1985, 82. 5636–5647.
36. Roziere. J.; Belin. C.: Lehmann, M.S. A strong symmetrical N–H–N bond. A 120 K neutron diffraction study of hydrogen diquinuclidinone perchlorate. J. Chem. Soc., Chem. Commun. 1982. 388–389.
37. Howard. J.A.K.; Bilton. C.: Desiraju, G.R.; Wilson. C.C. Designer Molecules. In *ISIS Annual* Report 1998; RAL-TR-050. Rutherford Appleton Laboratory: Oxon, 1998; 42–43.
38. Allen, F.H.: Howard, J.A.K.; Hoy, V.J.: Desiraju, G.R.: Reddp. D.S.; Wilson, C.C. First neutron diffraction analysis of an O–H...π hydrogen bond: 2-ethynyl-2-adamantanol. J. Am. Chem. Soc. 1996, 118. 4081–4084.
39. Bilton. C.; Howard, J.A.K.; Madhavi. N.N.L.; Nangia. A.; Desiraju, G.R.: Allen, F.H.: Wilson. C.C. When is a polymorph not a polymorph? Helical trimeric O–H···O synthons in *trans*-1,4-diethynylcyclohexane-diol. Chem. Comm. 1999, 1675–1676.
40. He, X.M.: Swaminathan, S.: Craven. B.M.: McMullan, R.K. Thermal vibrations and electrostatic properties of parabanic acid at 123 and 298 K. Acta Crystallogr., B 1988. 44. 271–281.
41. O'Connor, B.H.; Moore. F.H. Neutron diffraction refinement of the crystal structure of 1,3,5-triacetylbenzene. Acta Crystallogr.. B 1973. *29.* 1903–1909.
42. Tellgren, R.: Thomas, J.O.: Olovsson, I. Hydrogen bond studies. CX. A neutron diffraction and deformation electron density study of sodium hydrogen oxalate monohydrate. $NaHC_2O_4 \cdot H_2O$. Acta Crystallogr.. B 1977. 33. 3500–3504.
43. Thomas. J.O.; Tellgren. R.: Almlöf, J. Hydrogen bond studies. XCVI. X-N maps and ab initio MO-LCAO-SCF calculations of the difference electron density in non-centrosymmetric lithium formate monohydrate. $LiHCOO \cdot H_2O$. Acta Crystallogr.. B 1975. 31. 1946–1955.
44. Craven, B.M.: McMullan. R.K. Charge density in parabanic acid from x-ray and neutron diffraction. Acta Crystallogr.. B 1971, *35.* 934–945.
45. Coppens, P.; Vos. A. Electron density distribution in cyanuric acid. II. Neutron diffraction study at liquid nitrogen temperature and comparison of x-ray and neutron diffraction results. Acta Crystallogr.. B 1971, 27. 146–158.
46. Koetzle. T.F.: Lehmann, M.S.: Hamilton. W.C. Precision neutron diffraction determination of protein and nucleic acid components. IX. The crystal and molecular structure of 4-hydroxy-L-proline. Acta Crystallogr.. B 1973. 29. 231–236.
47. Sequeira. A.; Berkebile. C.A.: Hamilton, W.C. Structure and dynamics in hydrogen bonding systems. I. A neutron diffraction study of potassium hydrogen diaspirinate [bis-acetylsalicylate]. J. Mol. Struct. 1967–68. 1, 283–294.
48. McMullan, R.K.: Craven, B.M. Crystal structure of 1-methyluracil from neutron diffraction at 15. 60 and 123 K. Acta Crystallogr.. B 1989. *45.* 270–276.
49. Kvick, Å.: Canning, W.M.: Koetzle. T.F.; Williams. G.J.B. An experimental study of the influence of temperature on a hydrogen bonded system: The crystal structure of *J*-glycine at 83 K and 298 K by neutron diffraction. Acta Crystallogr.. B 1980, *36.* 115–120.
50. Craven. B.M.; Sabine, T.M. The 5-hydroxyl configuration in dialuric acid monohydrate by neutron crystal structure determination. Acta Crystallogr., B 1969. *25.* 1970–1978.
51. Nimmo. J.K.: Lucas, B.W. Solid-state phase transition in triethylenediamine. $N(CH_2CH_2)_3N$. I. The crystal structure of phase II at 298 K. Acta Crystallogr.. B 1976. 32. 348–353.

Nomenclature in Crystal Engineering

Ashwini Nangia
University of Hyderabad, Hyderabad, India

INTRODUCTION

The definition of the term "csystal engineering" evolved since its inception over three decades ago. Gerhard Schmidt (1971) used this term in the context of engineering crystal structures having intermolecular contact geometry appropriate for photodimerization in the solid state."' He noted that the introduction of a dichlorophenyl group in unsaturated molecules steers crystallization into a unit cell with a shortest axis of ca. 4 Å, a distance optimal for photoreaction of alkenes. Gautam Desiraju (1989) widened the meaning of crystal engineering as "the understanding of intermolecular interactions in the context of crystal packing and in the utilisation of such understanding in the design of new solids with desired physical and chemical properties.''[2] In 1996, Kenneth Seddon stated that the subject "now hovers on the edge of maturity, a scientific discipline establishing its own unique identity, developing a distinctive profile, and with a promising future ahead."'" Rapid developments in supramolecular chemistry in the 1990s and the realization that a crystal is a supermolecule par excellence. led to the idea that crystal engineering is the synthesis of supramolecular structures in the solid state.[4,5] Today, crystal engineering is an interdisciplinary subject dealing with the self-assembly of molecular crystals. metal–organic architectures, nanostructures, and coordination polymers using hydrogen bonding, electrostatic, and van der Waals interactions. and metal coordination bonding. It brings together chemists of different specialization (synthetic. physical, computational. theoretical, analytical) to work in collaboration with crystallographers and physicists for the design of organic, inorganic, and hybrid systems. In order that such a diverse group of scientists interact and communicate effectively, the meaning of commonly used terms must be uniformly understood and accepted by all. This justifies the need for the present article. I now present a glossary of terms in crystal engineering.

GLOSSARY

Cambridge Structural Database (CSD)

A storehouse of over 290,000 organic, organometall~c. and coordination polymer crystal structures (April 2003 update) maintained and distributed by the Cambridge Crystallographic Data Centre (CCDC). The reason for archiving crystal structures is that while a structure may have been determined for one reason (e.g., to confirm the stereochemistry), it may provide valuable data on intermolecular interactions and close packing to a crystal engineer at a subsequent date. The CSD is now routinely employed as an empirical database for supramolecular retrosynthesis—to use what is known to predict what is unknown.

Cone Correction

The D–H···A hydrogen bond has a preference for linearity ($\theta=180°$). The N versus θ histogram of O–H . ·O hydrogen bonds shows a peak at $\theta=160$–$170°$. The departure from linearity for strong H-bonds is actually an artefact, because the solid angle covered by an angular interval $\Delta\theta$ is smaller for linear than for bent geometry. If this bias is corrected by plotting Nlsin θ versus 8. the histogram has a sharp maximum at 170–180° indicating hydrogen bond linearity. Cone correction is an obligatory step in the statistical analysis of hydrogen bond data.

Cooperativity

Hydrogen bonds possess the important property of cooperativity (synergy). The energy of an array of n hydrogen bonds is greater than the sum of isolated hydrogen bonds, $(O–H\cdot\cdot O–H\cdot\cdot O–H\cdot\cdot)_n > n \times (O–H\cdot\cdot O)$. Cooperativity in effect represents the difference between calculating energies using atom-pair potentials and many-atom potentials. This nonadditive property tapers off at about $n=5,6$ and arises because the ability of donor and acceptor groups to form hydrogen bonds is enhanced by the polarization of hydrogen and lone-pair electron densities in a collective ensemble. Hydrogen bond arrays may have resonance-assisted H-bonding (RAHB) in P-diketones, π-bond cooperativity in carboxylic acids and amides, σ-bond cooperativity in carbohydrate crystal structures, and polarization-enhanced H-bonding in homodromic, antidromic, and heterodromic arrays of alcohols/phenols.

Encyclopedia of Supramolecular Chemistry
DOI: 10.1081/E-ESMC 120012708

Crystal Structure

A crystal is a solid having a regularly repeating internal arrangement of atoms. Crystal structure is the mutual arrangement of atoms. molecules, or ions packed together on a lattice to form a crystal.[6] In the context of this volume, crystals are ordered supramolecular systems, and crystallization is an impressive display of supramolecular self-assembly in a periodic arrangement.

Crystal Structure Prediction

This is an ab initio prediction of the crystal structure from computation and theory given the molecular structure. The CCDC conducted blind tests in 1999 and 2001 to assess the progress in this challenging goal that lies at the heart of crystal engineering. Given our present understanding of molecular conformations and intermolecular interactions in crystals and despite the progress in accurately computing atom–atom potentials. a general solution to this problem is impossible to very difficult at the moment. but conditional success is likely in the foreseeable future.

Disordered Structure

A crystal structure in which ions or molecules pack in alternate ways in different unit cells is a disordered structure. Such disorder may be revealed by the presence of diffuse scattering, either as halos or streaks. around intense reflections. Guest molecules in crystals tend to be disordered. at times in a liquid-like state. Disorder is of two types. Static disorder occurs when a molecule is located in different orientations/conformations in syrnmetry-related positions in the unit cell. When molecules are fluxional at the same position in the crystal. the disorder is dynamic (e.g., perchlorate anion. *tert*-butyl group). Dynamic disorder can be dampened or frozen at low temperature. whereas static disorder persists even if x-ray data is collected at cryogenic conditions.

Graph Set

This is a geometrical description of hydrogen-bond patterns to encode complicated networks as combinations of four simple patterns: chains (*C*), rings (R). intramolecular H-bonds (*S*), and other finite motifs (D). The number of atoms (n) is the degree of the pattern. Specification of a pattern is augmented by the number of hydrogen bond donors (d) and acceptors (a). e.g., $G_d^a(n)$. Basic graph sets are of the lowest degree, and complex graph sets describe patterns of higher degree. Unitary or first-level graph set N_1 is a list of all motifs (one type of H-bond) in the structure, binary or second-level N_2 describes patterns of two H-bonds. and N_3 describes patterns of three H-bonds. The same hydrogen bond array may be analyzed in more than one graph set notations. e.g., α-glycine has $C_2^2(6)$, $C_2^2(10)$. and $R_4^4(16)$ graph set patterns depending on the complexity with which the structure is analyzed. Graph sets are useful in identifying different hydrogen-bond patterns in polymorphs.

Helix

A helix is characterized by a helical axis. a screw sense (i.e., chirality). and pitch (rate of axially linear to angular movement). Ideally, the axis is a straight line. and the two kinds of tnotion are circular and linear at a constant distance r from the axis, producing a cylindrical (constant radius), palindromic (constant pitch) helix. A helix may be right-handed (designated *P*) or left-handed (*M*) according to whether the rotation is clockwise or anticlockwise when the helix is considered to wind from the viewer's eye toward a point distant from the viewer.

Herringbone Motif and π···π Interactions

Recognition between phenyl groups is mediated by numerous interactions that have two extreme geometries: edge-to-face herringbone T-motif (dipole–quadrupole interaction, energy 1–2 kcailmol). and parallel-stacked arrangement of phenyl rings with face-to-face interaction between π-electron clouds (quadrupole–quadrupole interaction, energy 1 kcal/mol). Possible variations in these geometries are the vertex-to-face approach, and the presence of offset or slight inclination between π-stacked rings.

Host–Guest Compound

The inclusion of small guest molecules in the open framework of a host molecule constitutes a host–guest compound. They are of two major types: cavitands. or molecular host compounds with intramolecular cavities—the cavity is an intrinsic property of the molecule and exists in solution and in the solid state. e.g., calixarenes. cyclodextrins: clathrands are hosts with extramolecular cavities that result from the aggregation of two or more molecules—lattice inclusion hosts exist only in the crystalline or solid state, e.g., hydroquinone and urea. The corresponding host–guest adducts are referred to as cavitates and clathrates. Tuning the pore sire and shape and controlling the hydrophobic/hydrophilic nature of a host cavity are major endeavors in crystal engineering. The distinction between a host–guest adduct H•G and a binary molecular complex A•B is that in H•G, there are either no specific H···H and G···G interactions. or H···H interactions along with weak H···G association stabilize

the structure; in A•B there are A···B interactions, or A···B is comparable in strength to A···A aggregation. When the guest molecule is the solvent of crystallization, the structure inay also be referred to as solvate or pseudopolymorph. The overlap of meaning for these terms makes the classification of multicomponent crystals difficult. For example, the 1:1 sulfathiazole•acetonitrile adduct is a clathrate, while 1:1 sulfathiazole•*N*-formylpiperidine is a cocrystal.[7] The difference between a cocrystal and a molecular complex was never outlined clearly. Borderline cases can be difficult to classify with the above terminologies, because they are somewhat subjective.

Hydrogen Bond

A hydrogen bond D–H···A is formed when the electronegativity of donor *D* relative to *H* in the D–H covalent bond is such as to withdraw electrons and leave the proton partially unshielded so that it can interact with the lone-pair or polarizable π electrons on the acceptor A. Hydrogen bonds are of three types: strong or conventional H-bonds (O–H···O, O–H···N, N–H···O) with energy of 4–15 kcal/mol, weak or unconventional H-bonds (C–H···O, C–H···N, O–H···π) with energy of 2–4 kcal/mol, and very strong or ionic H-bonds ($O–H\cdots O^-$, $O^+–H\cdots O$) with partial covalent character and energy of 15–40 kcal/mol. The total energy of the hydrogen bond may be partitioned into electrostatic, charge transfer, polarization. dispersion, and electron repulsion with the major contribution varying, depending on whether the H-bond is strong (mostly electrostatic), weak (electrostatic); and very strong (mostly covalent). The strongest hydrogen bond is comparable in strength to the weakest covalent bond.

Hydrogen Bond Rules

Formulated by Margaret Etter, these rules correlate functional groups in neutral organic molecules with hydrogen-bond patterns in crystals. 1) All good proton donors and acceptors are used in H-bonding. 2) Six-membered-ring intramolecular H-bonds form in preference to intermolecular PI-bonds. 3) The best proton donors and acceptors remaining after intramolecular hydrogen-bond formation will form intermolecular H-bonds to one another. There is a ranking of hydrogen-bond donors and acceptors in a crystal; and pairing takes place in an hierarchical fashion. These rules inay be exploited in the design of cocrystals.

Interpenetration

Open or porous networks minimize the empty space between them (nature abhors a vacuum). Interdigitation, interpenetration. interweaving, or catenation of two or more networks can occur to fill the empty space in crystals. Intercalation or inclusion of guest molecules (solvent, ligand) is another route to close packing. Self-penetrating nets have two types of topology: parallel interpenetration of corrugated layers leading to a two-dimensional network (generally) and inclined interpenetration of laminated nets resulting in a three-dimensional structure. Thus, interpenetration topology is a way to increase the dimensionality of the structure. The number (n) of independent interweaving networks defines n-fold interpenetration. e.g., trimesic acid is fourfold inclined interpenetrated, and its 2:3 adduct with 4,4′-bipyridine has a threefold parallel interpenetrated network.

isomorphism and Isostructurality

Isomorphism is similarity of crystal shape, unit-cell dimensions. and structure between substances of similar chemical composition. Ideally, the substances are so closely similar that they can generally form a continuous series of solid solutions. The degree of similarity between crystals can be calculated using Kálmán's parameters: the unit cell similarity index, Π. and isostructurality index $I_i(n)$:

$$\Pi = \left|\frac{a+b+c}{a'+b'+c'}\right| - 1$$

where a. b, *c* and a', b', c' are the orthogonalized lattice parameters of related crystals.

$$\mathrm{I_i(n)} = \left[1 \quad \left(\frac{\sum \Delta R_i^2}{n}\right)^{1/2}\right] \times 100$$

where n is the number of distance differences (ΔR_i) between the absolute coordinates of identical nonhydrogen atoms within the same section of the asymmetric units of related structures. For an isostructural pair of crystals, Π must be close to 0, and $I_i(n)$ should approach 100%. These parameters were derived in the context of steroid crystals but are now used for all classes of molecules.

Isotropic and Anisotropic Interactions

Intermolecular interactions in organic solids are of two types: short- to medium-range isotropic or van der Waals interactions; long-range anisotropic interactions and hydrogen bonds. Dispersive forces are attractive, their magnitudes are proportional to the sizes of the molecules, and they vary as r^{-6} (r=interatomic distance). Exchange repulsion (varies as r^{-12}) balances the attractive forces to define the arrangement of molecules in the crystal based on the close-packing principle of Mitaigorodskii. Anisotropic interactions define directional preferences in the

mutual recognition of molecules during crystallization. They are electrostatic in nature and operate at long range (fall off as r^{-1}). These include ionic interactions ($K^+ \cdots O$), strong and weak hydrogen bonds (O–H···O, C–H···O), and interactions between heteroatoms (halogen . .halogen). The crystal structure of a molecule is the free-energy minimum resulting from the optimization of attractive and repulsive intermolecular interactions with varying strengths, directional preferences, and distance-dependence properties.

Molecular Network

A supramolecular structure, theoretically composed of an infinite number of molecules (tectons) capable of mutual recognition; is termed a molecular network. Complicated structures that contain repeating arrays of molecules joined by strong and directional metal–ligand or hydrogen bonds can be reduced to simple topological networks of multiple connecting nodes (molecules) and the rods that connect them (intermolecular interactions). The network representation facilitates analysis and design of crystal structures, e.g., a three-dimensional diamondoid network from tetrahedral molecules, and a two-dimensional honeycomb network of trigonal molecules.

Neutron Normalization

The D–H distance in a typical organic molecule (D=O, N. C) is systeinatically underestimated by x-ray diffraction, because the one-electron of H is polarized toward the heavy atom to which it is bonded and also because of the librational motion of the D–H bond, even at low temperature. Because x-ray crystallography relies upon electron density to locate atoms. the D–H bond is artificially shortened by up to 0.2 Å. The accurate location of a proton is paramount in hydrogen-bond studies. This error is corrected by lengthening the D–H bond vector to the standard distance determined by neutron diffraction. The H···A distance is slightly shorter in normalized geometry. and the angle is lower. Neutron scattering depends upon the atomic nuclei and not the electron density to locate atoms. and so the coordinates of both H and D are determined with near-equal precision (±0.002 Å, ±0.2°). The precision of locating an H-atom with a cryogenic x-ray diffractometer is 10 times lower (k0.02 Å).

Polymorphism

A solid crystalline phase of a coinpound resulting from the possibility of at least two different arrangements of the molecules of that compound in the solid state. Polymorphs are like supramolecular isomers in the spontaneous organization from molecule → nucleus → crystal. Polymorphism is the antithesis of crystal engineering. Yet. this phenomenon is of fundamental and commercial importance, because polymorphs have different physical and chemical properties. About 10% of compounds are estimated to be polymorphic, though the percentage could be higher for pigments, dyes, explosives. and pharmaceuticals. When polymorphs occur, kinetic factors are deemed to be important during crystallization. Some related terms are concomitant polymorphs (crystals from the same flask under identical crystal growth and solvent conditions), conformational polymorphs (different conformations of the same molecule in different crystals), conformational isomorphs (multiple conformations of the same molecule in the same crystal), configurational polymorphs (different configurations of the same molecule, e.g., Z, E, in different crystals), and pseudopolymorphs (crystals formed by the same substance crystallized with different amounts or types of solvent molecules).

Porous Solids

Organic zeolite analogues are commonly referred to as porous solids. These materials promise a new range of applications. e.g., in pharmaceutical manufacture and in molecular sieves, sensors. and devices. They are crystalline or amorphous materials that permit the reversible passage of molecules through holes on their surface. Porous solids are classified according to pore diameter: nanoporous or microporous (<15 Å), mesoporous (15–500 A) and macroporous (>500 Å). The natural and synthetic inorganic zeolites with uniform pore sizes of 10–20 Å are the classical examples of microporous materials with widespread use in industry.

Site Occupancy Factor (SOF)

The SOF is the partial occupancy of a given site by a particular atom. It is most frequently used to describe disorder in a portion of a molecule or for describing nonstoichiometric situations. e.g., in solid solution.

Structure Solution and Refinement

The intensity data from 1000–100,000 reflections (depending on molecular size) collected on x-ray diffractometers is solved by direct methods or by Patterson function to "guess" approximate phases. This gives the outline of the molecule with bond lengths to ±0.1 Å precision. The structure is refined by the least squares method

to minimize the difference between experimental and calculated electron density maps. The optimized model of coordinates and thermal parameters is converted to display the molecular structure (bond distances, angles, torsions) with hydrogen-bonding interactions. The structure solution and refinement process is complete when the agreement between calculated and observed data is as good as possible. For a good structure determination; the estimated standard deviation or standard uncertainty, or errors in bond lengths and angles, should be t0.002 Å and $\pm 0.2^{\circ}$. respectively, and the residual R factor should be <5%. Structure solution and refinement are almost automated now with programs like SHELX.

Supramolecular Chemistry

This is the chemistry of molecular assemblies. intermolecular bonds, noncovalent interactions, and hydrogen bonds. The original meaning of "supramolecular" is "beyond the molecule."[8] '"Supramolecular" currently has three different meanings: intermolecular interactions. coordination chemistry, and a strategy for the controlled organization of multiple components. Supramolecular chemistry is a philosophy and strategy for the controlled grand assembly of complex matter.[9]

Supramolecular Chiron

This is a suprainolecular synthon involving recognition between chiral molecules and leading to enantio- or diastereopure architectures. The term, suggested by Hanessian. may also be used to designate the minimum hydrogen bond ensemble leading to chiral or polar crystals of racemic molecules.

Supramolecular Isomerism

The existence of more than one type of network superstructure for the same molecular building block represents supramolecular isomerism. Therefore, it is related to structural isomerism at the molecular level. Supramolecular isomerism is the existence of different architectures (i.e., architectural isomerism) or superstructures. Polymorphism is a type of supramolecular isomerism but not vice versa. Supramolecular isomerism can be classified as structural (the same components result in different network superstructures). conformational (different conformations of a flexible molecule generate different. but often related. network architectures). catenane (the different manner and degrees in which networks interpenetrate or interweave), and optical (chirai networks that crystallize in enantiomorphous space groups. or the spontaneous resolution of chiral solids).

Supramolecular Synthon

Structural units within supermolecules (crystals) that can be formed and/or assembled by known or conceivable synthetic operations involving intermolecular interactions. most often hydrogen bonds, are supramolecular synthons. The goal of crystal engineering is to design robust synthons that can be exchanged from one structure to another and then incorporate recurring synthons in retrosynthesis to anticipate (predict) the one-, two-, or three-dimensional structure of novel target architectures. Desiraju suggested that this exercise may be referred to as crystal synthesis in analogy with target molecule synthesis. However. because hydrogen bonds are an order of magnitude weaker than covalent bonds. the robustness of a synthon is reliably derived from statistical trends, i.e., the probability of occurrence of a particular structural motif in the CSD. The prediction of crystal packing through such an empirical-cum-chemical intuition approach was reasonably successful. This is distinct from crystal structure prediction, i.e., to know the unit cell and space group of a given molecule without any experimental data. Synthon interchange is the exchange of one functional group with another (e.g., halogen; ethynyl, hydroxy) to generate topologically identical structures.

Synthon Interference and Structural Insulation

Crystal structures are a result of a subtle balance of forces between various intermolecular interactions with different distance-dependence and directional properties. When the geometrical requirements of two interactions can be met in isolated regions of the crystal. the two interactions are said to be structurally insulated. If the geometric demands of two interactions come into conflict, optimization of one interaction changes the normal pattern of the other, and this phenomenon is termed as interaction interference. The challenge in crystal engineering is that it is difficult to anticipate when a particular chemical modification will conserve the synthon and when the structure will be disturbed.

Tecton

(Greek word τεκτων for builder) Molecules with sticky surfaces with interactions that are dominated by specific attractive forces that induce the assembly of aggregates with controlled geometries are tectons. Wuest suggested

molecular tectonics as the art and science of supramolecular construction using tectonic subunits.

Twinned Crystal

This is a composite crystal built from two or more crystal specimens that grow together in a specific manner. so that there is at least one plane and a direction perpendicular to it that are related in the same manner to the crystallographic axes of both parts of the twin.

CONCLUSION

Today, crystal engineering covers a wide palette spanning organic, inorganic, and organometallic structures in the solid-state; crystal growth and morphology; pharmacophore mapping and drug design; and materials science and nanoscience.[10,11] The importance of this subject is increasing and its scope diversifying, as it lies at the intersection of engineering-down and synthesis-up technologies. The present article gives working definitions of some terms that were selected based on the personal experience of this author, who entered crystal engineering from an organic synthesis background. Exact definitions are all but impossible in chemistry, and working definitions should not be taken too literally. For example. the accepted definition of organometailic chemistry as "the chemistry of cornpounds with metal-to-carbon bond" rules out the coinmon industrial compound, Wilkinson's catalyst, $RhCl(PPh_3)_3$. I conclude my glossary on this sobering note.

ACKNOWLEDGMENTS

I thank the Departinent of Science and Technology, Council of Scientific and Industrial Research, and University Grants Commission, Government of India, for their continued support of my research in crystal engineering and supramolecular chemistry.

ARTICLES OF FURTHER INTEREST

The Cambridge Structural Database, p. 161
Disorder and Diffuse Scattering, p. 457
Hydrogen Bonding, p. 658
Interpenetration, p. 735
Isostructurality of Inclusion Compounds, p. 767
Neutron Diffraction, p. 959
π–π *Interactions: Theory and Scope,* p. 1076
Polymorphism, p. 1129
Supramolecular Isomerism. p. 1420
Tectons: Definition and Scope, p. 1484

REFERENCES

1. Schmidt, G.M.J. Photodimerization in the solid state. Pure Appl. Chem. 1971, *27,* 647–678.
2. Desiraju, G.R. *Cnstal Engineering. The Design of'Organic Solids*: Elsevier: Amsterdam. 1989.
3. *Crystal Engineering: The Design and Application of Functional Solids*: Seddon, *K.R.*. Zaworotko. M.J., Eds.: NATO ASI Series, Kluwer: Dordrecht. 1999.
4. *The Crystal as a Supramolecular Entity; Perspectives in Supramolecular Chemistry*; Desiraju. G.R., Ed.; Wiley: Chichester. 1996; Vol. 2.
5. *Solid-State Supramolecular Chemistry: Crystal Engineering; Comprehensive Supramolecular Chemistry*; MacNicol. D.D.. Toda. F., Bishop, R., Eds.; Pergamon: Oxford, 1996: Vol. 6.
6. Clusker, J.P.: Trueblood, K.N. *Crystal Structure Analysis. A Primer,* 2nd Ed.: OUP: Oxford. 1985.
7. Hushes, D.S.; Hursthouse. M.B.: Lancaster. R.W.: Tavener. S.: Threlfall, T.L. Over one hundred solvates of sulfathiazole. Chem. Commun. 2001. 603–604.
8. Lehn. J.-M. *Supramolecular Chemistry: Concepts and Perspectives;* VCH: Weinheim, 1995.
9. Dance, I. What is supramolecular? New J. Chem. *2003.27.* 1–2.
10. Sharma. C.V.K. Crystal engineering—Where do we go from here? Cryst. Growth Des. 2002. 2, 465–474.
11. Weissbuch. I.; Lahav. M.: Leiserowitz. L. Toward stereochemical control, monitoring, and understanding of crystal nucleation. Cryst. Growth Des. 2003. 3, 125–150.

Nonlinear Optical Materials

Ravi Mosurkal
University of Massachusetts Lowell, Lowell, Massachusetts, U.S.A.

Lynne A. Samuelson
U.S. Army RDECOM, Natick, Massachusetts, U.S.A

Jayant Kumar
University of Massachusetts Lowell, Lowell, Massachusetts, U.S.A.

INTRODUCTION

There has been a growing interest in fundamental and scientific research in the area of molecule-based nonlinear optical (NLO) inaterials with large second- and third-order nonlinearities. The research was primarily motivated by applications of optical and electro–optical devices based on these materials in the telecommunications and optical data-processing industries.'" In particular, second-order NLO inaterials offer many attractions, such as large nonresonant ultrafast response times, low dielectric constants, and intrinsic architectural tailorability.[2] The noncentrosymmetric organization of chromophores is an essential requirement for efficient bulk second-order nonlinear optical materials. Thus. the controlled construction of supramolecular assemblies has become a popular method in the design and synthesis of NLO materials. A variety of methods such as electric field poling,[3–6] Langmuir–Blodgett assembly.'".'' and crystal engineering'''''] were employed to prepare second-order NLO materials. In the last decade. the layer-by-layer molecular self-assembly approach was tremendously active in the development of new NLO materials.'''' In this article, we discuss the concept of optical nonlinearity and the strategies for design and synthesis of nonlinear optical chromophores and supramolecular structures.

THE CONCEPT OF OPTICAL NONLINEARITY

When the electric field of electromagnetic radiation interacts with a material, it induces a dipole moment in the material. The dipole moment induced per unit volume is called "polarization." At low electric fields, the inacroscopic polarization or polarization of the bulk medium. P. is linearly related to the field by the proportionality constant, $\chi^{(1)}$, known as the linear electric susceptibility. At high fields, typically those associated with lasers. contribution of the nonlinear (second- and higher-order) terms becomes significant.[15] Higher-order susceptibilities $\chi^{(n)}$ $(n>1)$ are inherently inuch smaller than $\chi^{(1)}$, and progresrively become smaller as n increases. The polarization component along the i^{th} axis can. therefore, be generally represented as follows:

$$P_i = \chi_{ij}^{(1)} E_j + \chi_{ijk}^{(2)} E_j E_k + \chi_{ijkl}^{(3)} E_j E_k E_l + \ldots \quad (1)$$

Because the electric field and the polarization are vectors. the n^{th}-order macroscopic electric susceptibility ($\chi^{(n)}$) that relates the components of the polarization to the applied field; is an $(n + 1)$-order tensor. The microscopic polarization in molecules is defined by the induced dipole moment pi, which depends on the molecular polarizability, α, and hyperpolarizabilities, β, γ, etc., as follows:

$$\rho_i = \alpha_{ij} E_j + \beta_{ijk} E_j E_k + \gamma_{ijkl} E_j E_k E_l + \ldots \quad (2)$$

In Eqs. 1 and 2. the indices i, *j*. *k*. and I refer to the coordinate system of the bulk material and molecule. respectively. Illustrated in Fig. 1 are the linear and nonlinear polarizations with respect to electric field. The Fourier decomposition of this nonlinear polarization comprising components of zero frequency, the fundamental frequency, the second-harmonic frequency, the third-harmonic frequency. etc.. is shown in Fig. 2. The effects up to the second order. which are easily observed experimentally, are called the optical rectification. $P(0)$; linear electro–optic effect $P(\omega)$; second-harmonic generation $P(2\omega)$, and third-harmonic generation $P(3\omega)$.

Second-Harmonic Generation (SHG)

The phenomenon of frequency doubling or second-harmonic generation can be visualized as follows. If the applied electric field is of frequency ω, it can be represented as $\sin\omega t$. and the quadratic terms are seen to have a 2ω dependence.

$$E \propto \sin \omega t$$

$$E^2 \propto \sin^2 \omega t \left(= \frac{1}{2}(1 - \cos 2\omega t) \right)$$

Encyclopedia of Supramolecular Chemistry
DOI: 10.1081/E-ESMC 120012826

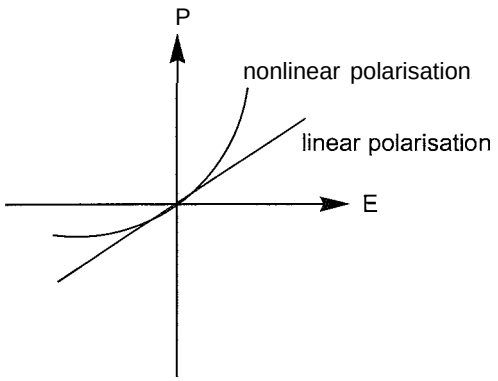

Fig. 1 Linear and nonlinear polarization versus electric field.

There is an important symmetry constraint for observing second-harmonic generation or other quadratic (in general any even order) *NLO* effects. The quadratic and other even-order effects are possible only in noncentrosymmetric systems. In a gaseous or liquid state where random fluctuations create a center of symmetry, one needs an alignment of molecules using an external field to break the center of inversion and observe second-order effects. However, in the case of third-order nonlinearities. there is no such symmetry constraint. Thus, in this article, we deal exclusively with second-order nonlinear optical properties of organic materials because of the important role of supramolecular chemistry in designing noncentrosymmetric systems.

SECOND-ORDER NONLINEAR OPTICAL MATERIALS

Most of the materials developed initially for *NLO* applications were based on inorganic systems. Ferroelectric materials lacking a center of symmetry were prime candidates. With inorganic materials, the optical and acoustic phonons as well as the electronic polarization contribute to the *NLO* effects. The NLO effects in inorganics can be interpreted only at a bulk level; extension of the atomic or ionic polarizabilities to the bulk *NLO* properties is complicated. There is growing interest in developing π-conjugated organic molecules for *NLO* applications.

The molecular structures of some well-known systems are presented in Fig. 3. It was established that push–pull organic molecules have very high values of β_{ijk} (Eq. 2) and when they crystallize in a non-centrosymmetric space group, they possess large nonlinear susceptibility. The nonlinearity in these systems is dominated by electronic polarization effects. In the solid state, these organic compounds form molecular crystals in which the molecules interact through weak intermolecular forces and retain their individual identity to a high degree.

The quadratic *NLO* active molecules are mostly based on donor–acceptor substituted aromatics; benzene, stilbenes, diaryl acetylenes, diacetylenes, and biaryls are commonly used frameworks. In addition to the above materials, many more organic and organometallic compounds were examined by the powder SHG method, or their molecular hyperpolarizabilities were measured using EFISHG/HRS techniques, or both.[16–19]

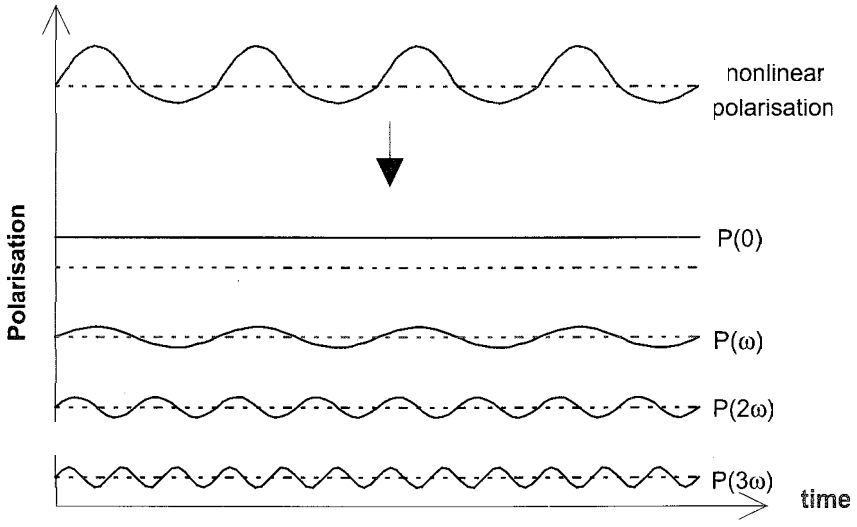

Fig. 2 The Fourier decomposition of nonlinear polarization and the components of $P(x)$ at frequencies 0. ω, 20, and 30. (*View this art in color at rv+t,w.dekker..com.)*

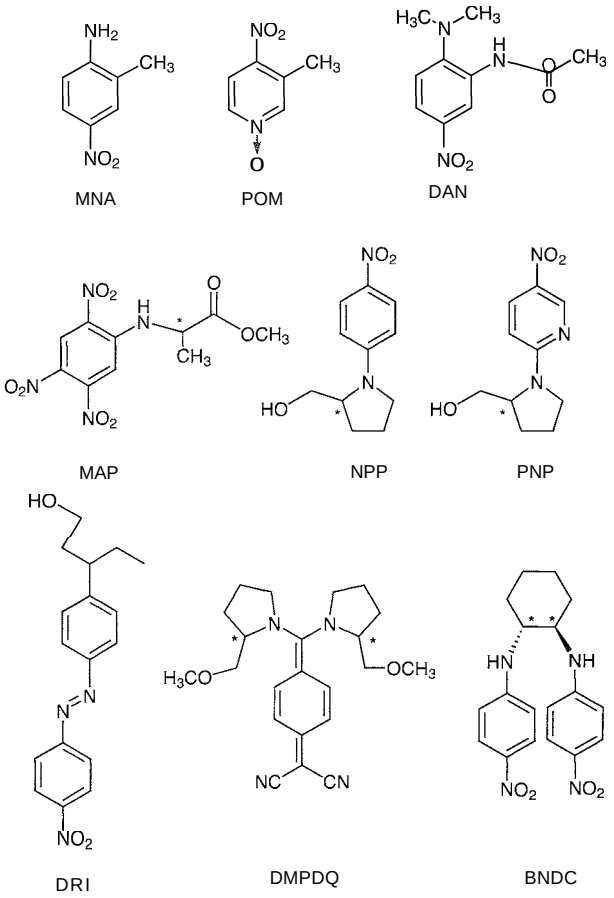

Fig. **3** Well-known organic NLO molecules

STRATEGIES TO OBTAIN NONCENTROSYMMETRIC STRUCTURES FOR QUADRATIC NLO APPLICATIONS

In the previous section, we already noted that a noncentrosymmetric structure is essential for a material to show second-order NLO properties. Amorphous and glassy solids are, in general. centrosymmetric. A majority of crystalline organic materials are also centrosymmetric. A variety of techniques were attempted to induce a noncentric lattice formation. Thin films can be prepared as noncentrosymmetric structures, using special techniques. Some of the popular strategies developed to induce noncentrosymmetry in bulk structures are as follows: inclusion of chirality in the molecule: utilization of crystal engineering techniques that exploit weak intermolecular forces; electric field poling of thin films or polymer films in which the mclecules of interest are bound physically or chemically: preparing *X*, *Z*, or alternate-type Langmuir–Blodgett (LB) films; and layer-by-layer molecular self-assembly for generating intrinsically noncentric super lattices. These methods are discussed in some detail below.

Crystal Engineering

Inclusion of chirality

The utility of chirality for the fabrication of NLO organic materials was recognized very early in the case of amino acids and sugars.[1] Molecular chirality guarantees the crystallization of a pure enantiomer in one of the 21 noncentrosymmetric space groups. Achiral molecules generally crystallize in a centric lattice, though some important exceptions are known, e.g., urea ($P42_1m$), benzil (P32), *m*-nitroaniline. mNA ($Pbc2_1$), MNA (Cc), POM ($P2_12_12_1$), and 3-acetamido-4-dimethylaminonitrobenzene, DAN ($P2_1$). On the other hand, a pure enantiomer must crystallize in an enantiomorphous space group, and there are plenty of examples of such systems. Some well-known cases are MAP ($P2_1$), NPP ($P2_1$), and PNP ($P2_1$) and TCNQ-based push–pull quinonoid molecule, DMPDQ (Fig. 4).[24] Though a mixture of equal quantities of a pair of enantiomers, i.e., a racemate, usually crystallizes in centrosymmetric space groups. some cases of crystallization in enantiomorphous space groups are also known. We note that the optical activity of a molecule only guarantees a noncentric lattice structure, but does not guarantee usefulness as a material for SHG. This is because the polarizable part of the molecules may still be aligned almost antiparallel, resulting in near cancellation of the NLO response of the molecules that are so aligned. It is important to have the NLO chromophores turned away from an antiparallel alignment to generate good SHG capability. In spite of this. the utilization of optical activity appears to be one of the most successful techniques for the generation of noncentric crystal structures, especially when used in conjunction with one of the following techniques. From Fig. 4, the effect of inclusion of

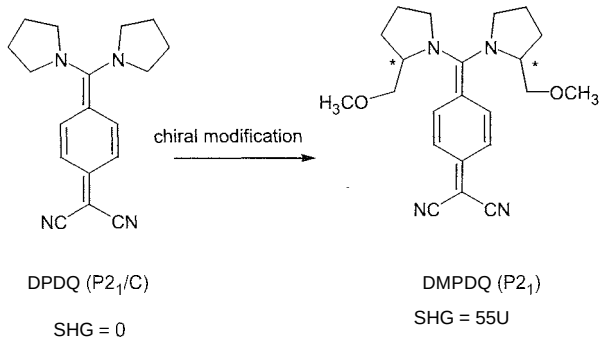

Fig. 4 Chirality-induced noncentrosprnmetry and nonlinearity

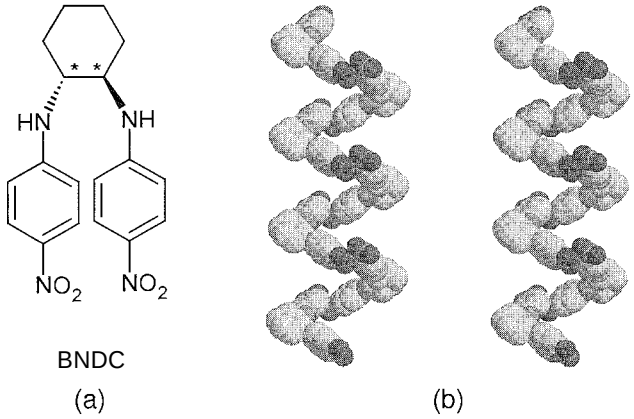

Fig. 5 (a) Molecular structure of BNDC and (b) helical superstructures of BNDC formed during crystallization. Reprinted with permission from Ref. [28]. Copyright (2001) Wiley-VCH. (*View this art* in color *at www.dekker.com.*)

chirality in a molecule on its crystal space group and bulk NLO property is clearly seen.[20]

Intermolecular H-bonding

Hydrogen bonding is a well-known crystal engineering tool used to obtain desired crystal packing.[21] In the field of NLO. it was also used to get optimized noncentric structures in the organic crystals. The hydrogen bond bridges two atoms that have high electronegativities (such as O, N), and this can strongly influence the crystal structure and the spectroscopic properties of the molecules. Some examples of NEO systems where H-bonding has been crucial are, *o*-nitroaniline and its derivative, MAP, and urea. Urea is an extreme case of a hydrogen-bonded network.[1] The urea molecule that has eight atoins is involved in eight hydrogen bonds (four to each carbonyl and one each from each of the hydrogens). In urea, the hydrogen bonding played a crucial role in evolving a noncentric crystal structure.[10] Even though W-bonding affects the crystal structure in many significant ways. it is known to have a negligible effect on the molecular hyperpolarizabilities. Some theoretical investigations[11] do, however, indicate that in special cases molecular βs are influenced mildly by H-bonding. The weak interactions between iodo and nitro groups that form supramolecular synthons were also exploited for designing materials for SHG.[22]

Recently, Radhakrishnan et al. reported the formation of a perfectly polar lattice in the crystal of (4-dimethylaminopyridyl) *bis*(acetylacetonato) zinc (II) (ZNDA).[23] This is one of the best examples of molecular assemblies that aligned noncentrosymmetrically in the lattice and is useful as a prototype for engineering polar supramolecular assemblies for NLO applications. In another article: they also reported[i2''] the formation of helical superstructures (Fig. 5b) from a simple crystallization of the C_2-symmetric and chiral *N,N′-bis*(4-nitrophenyl)-(1R-2R)-diaminocyclohexane (BNDC. Fig. 5a), which showed strong second-harmonic generation comparable to that of a well-known NLO compound, WPP. This study suggests that the control of supramolecular organization by molecular structure and symmetry can be a useful strategy in induction and enhancement of solid-state SHC in molecular materials.[25]

Poling of Doped Polymer Films

Polymer films with exceptionally large second-order nonlinearities can be produced by the corona poling (Fig. 6) process.[26] An efficient NLO chrornophore molecule is either doped in a host polymer matrix or covalently linked as pendant groups on a polyrner backbone. The polymer is then cast as a film. usually by spin-coating techniques. Subsequently, the film is subjected to a strong external dc electric field and heated to the glass transition temperatures of the polymer. At this point, the chromophores are aligned parallel by the field and locked into position when the film is cooled to room temperature with the external field on.

The poling thus leads to the alignment of doped molecules in the polymer films according to the Boltzmann distribution law. The oriented molecular dipoles produce a polarization. $P=N\mu\langle\cos\theta\rangle$, where N is the number density of the molecules, μ, the ground state dipole moment, and 0, the angle between the dipole and the direction of the poling field. This method can

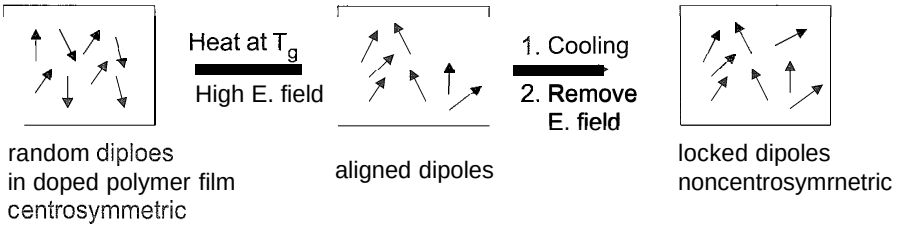

Fig. 6 Orientation of chromophoric dipoles under high electric field using corona poling in doped polymer films

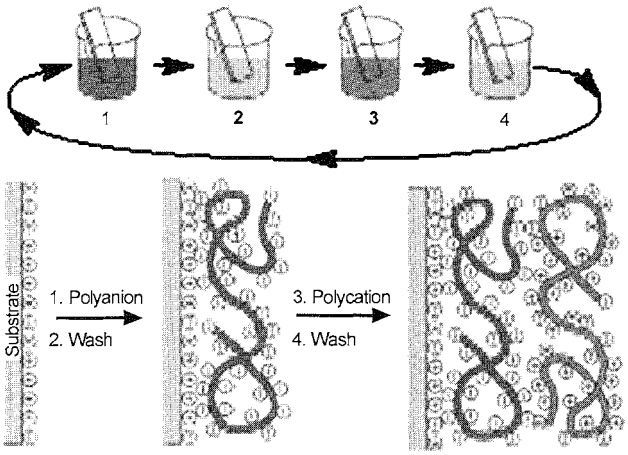

Fig. 7 Procedure for electrostatic layer-by-layer assembly. Reprinted with permission from Oliveira et al. (Ref. [29]). (View this art *in* color *at www.dekker.com.*)

also be used for functionalized and cross-linkable polymer matrices. The resulting polymeric material is of high optical quality and suitable for wave-guided electro–optic devicec. The main problem associated with the poled polymer is the metastability of the system. After the external field is removed, the poled orientation of the chromophores slowly gets randomized over a period of time, and hence, the noncentrosymmetry geneiated is lost This destroys the quadratic NLO capability Post-poling treatments such as cross-linking have to be undertaken to arrest the depoling process

Langmuir–Blodgett (LB) Films

Another approach to the construction of efficient thin-film-based SHG materials has been to incorporate NLO chromophores into acentric X- or Z-type LB films.[1] This approach offers far greater net chromophore alignment than is possible in a poling field (where the net alignment is statistical). LB films are built up from amphiphilic molecules: i.e., molecules having a hydrophilic part and a hydrophobic part. The preparation of the LB film consists of the following steps. The amphiphilic molecule is first dissolved in a solvent immiscible with water, and the solution is spread onto the clean water surface in a Langmuir trough. The solvent is left to evaporate. leaving the molecules spread on the water surface. The Langmuir trough is equipped with a mobile barrier to compress the film laterally. The film is gradually compressed to a surface pressure just below its collapse pressure. Because of their long aliphatic chains: the molecules cannot

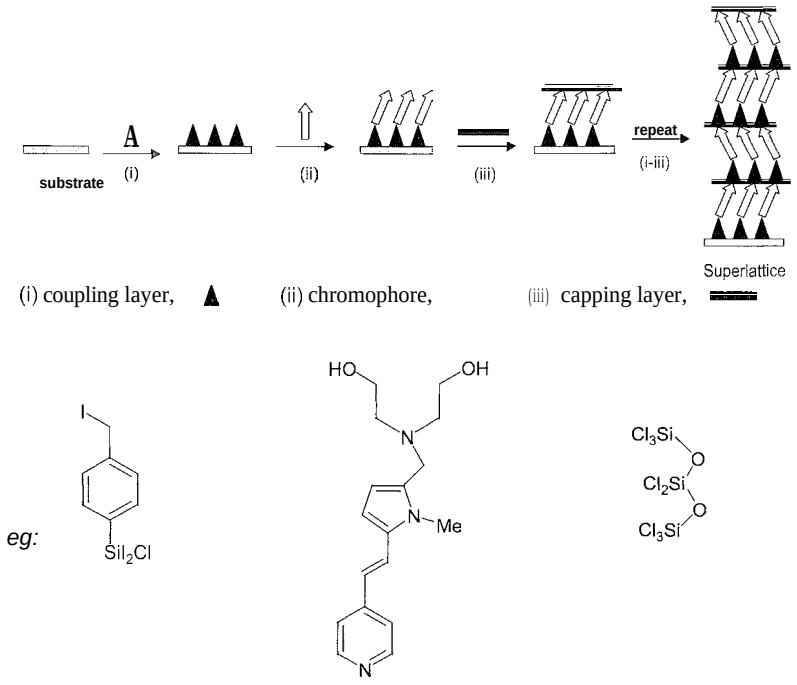

Fig. 8 Assembly of chromophoric super lattices by an iterative sequence of (i) covalent chemisorption of (*p*-iodomethyl)-phenyl-diiodochlorosilane onto hydrophobic substrates to form a "coupling" layer, (ii) spin-coating of a methanol solution of chromophore precursor followed by vacuum oven treatment, and (iii) reaction of the quaternized-chrornophore-based monolayer with octachlotrisiloxan. Reprinted with permission from Ref. [31b]. Copyright (2003) American Chemical Society. (*View this art in color at www.dekker.com.*)

dissolve in water. and due to their hydrophilic group, they cannot leave the water surface. Hence, they form a compact. monomolecular, and in many instances. stable film at the water–air interface. When a hydrophilic substrate previously immersed is slowly raised through the monolayer, deposition takes place with the hpdrophilic group attached to the substrate and the hydrophobic part sticking out. Subsequent dipping creates a head-to-head or tail-to-tail assangement of the amphiphiles deposited as multilayers on the substrate. By the above method, one prepares an EB film that is basically centrosymmetric (called Y-type). Such films are not suitable for optical second-harmonic generation. The X- and Z-type films with a head-to-tail arrangement and. hence, a noncentric bulk arrangement can be prepared with relatively low-polarity hydrophilic groups or with special functionalization of the hydrophobic chain ends.

Another approach is to prepare alternate layered films of the type A–B–A–B–A–B, wherein one of the molecules A or *B* is the active NLO chromophore and the other is just a binding spacer unit.

Layer-by-layer (LBL) Molecular Assembly

Orientation of nonlinear optical active dyes in electrostatically self-assembled polymer films containing cyclodextrins was studied.[27] The concept of molecular recognition of organic chromophores by coordinating polymers was another novel approach in the construction of nonlinear optical supramolecular assemblies.[28]

Electrostatic layer-by-layer (LBL) self-assembly techniques based on oppositely charged poipelectrolytes can be useful to create stable noncentrosymmetric order in thin films. Using this interesting technique. thermodynamically stable noncentrosymmetric multilayer films can be prepared without any need for poling. Tripathy et al. reported the fabrication stable multilayer films of epoxy-based side chain azo polymers for second-order nonlinear optics.[29] The second-order NLO coefficients of the five-bilayer LBL films of these polymers were found to be comparable to those of spin-coated poled films. A schematic view of the procedure to fabricate polyelectrolyte-based LBL films is shown in Fig. 7.

Since 1990, self-assembly techniques involving covalent linkages and layer-by-layer fabrication were reported to yield robust noncentric super lattices highly suited for applications such as SHG and electro–optic effects.[30–33] Spontaneous and sequential adsorption of appropriately derivatized adsorbates onto substrates in a self-limiting fashion can yield thin films with uniform polar orders in individual layers. This represents an attractive approach to the construction of intrinsically acentric chromophoric super lattices. Li et al.[30] reported synthetic routes to the first SHG-active multilayer structures using an attractive covalent siloxane self-assembly approach, highly regular and highly nonlinear [$\chi^{(2)} \sim 200$ pm/v at $\omega = 1064$ nm] self-assembled stilbazolium multilayers were constructed in a regular, layer-by-layer fashion. Recently. the synthesis of super lattices of pyrrole-based diethanolamino methyl functionalized derivatives was reported and is described in Fig. 8.[31] The key feature to self-assembled multilayers is that the microstructural acentricity is maintained, and thus. they show the quadratic dependence of the SHG response on the number of assembled layers. These multilayers have good structural reproducibility and are suitable for efficient NLO properties as was reported for the second-order nonlinear optical susceptibility [$\chi^{(2)} \sim 150$ pm/v at w = 1064 nm] for the chromophore in Fig. 8.

CONCLUSION

In this article. we discussed the basic concept of nonlinearity and fabrication of noncentrosymmetric structures using well-known strategies like crystal engineering, corona poling, LB films, and molecular assembly of acentric structures. The role of supramolecular chemistry in developing efficient NLO materials is clearly delineated. Though physical methods like poling and LB techniques are successful strategies for creating noncentrosyrnmetric materials for NEO. the design of molecular chromophores with specific groups and functionalities for creating noncentrosyminetric materials through crystal engineering is still a fascinating subject to chemists and material scientists. Molecular assembly via synthesis is also a well-accepted strategy for fabricating covalent. robust, noncentrosymmetric structures for electro–optics and many other controlled structures for applications like light-emitting diodes. sensors and photovoltaics, etc. In the forthcoming years. the approaches of creating layer-by-layer molecular assemblies synthetically or by ionic adsorption may lead to other approaches and provide new methodologies for materials chemistry.

ACKNOWLEDGMENT

We thank U.S. Army RDECOM. Natick and Office of Naval Research.

ARTICLES OF FURTHER INTEREST

Concepts in Crystal Engineering, p. 319
Crystal Engineering with Hydrogen Bonds, p. *357*

Hydrogen Bonding, p. 658
Hydrophobic Effects, p. 673
Layered Supramolecular Solids and Their Intercalates, p. 791
Molecular Switches, p. 917
Molecular Wires, p. 925
Space Groups and Crystal Packing Modes, p. 1337
Strict Self-Assembly and Self-Assembly with Covalent Modifications, p. 1372
van der Waals Forces, p. 1550
X-Ray Crystallography, p. 1586

REFERENCES

1. Singer. K.D.; Lalama. S.L.: Sohn. J.E.; Small, R.D. Nonlinear *Optical* Properiies of Organic *Molecules and Crystals*; Chemla, D.S.. Zyss. J., Eds.: Academic Press: New York, 1987: Vol. 1. 437.
2. Prasad. P.N.: Williams. D.J. *Introduction* to *Nonlinear* Optical *Effects in Organic Molecules and Polymers*; Wiley: New York. 1991.
3. Miyata. S.: Sasabe. H. Poled Polymers and Their Applications to SHG and EO Devices. In *Advanced Nonlinear* Optics: Miyata. S.. Sasabe, H.. Eds.: Gordon & Breach: Amsterdam. 1997: Vol. 4. 279.
4. Choi, D.H.: Wijekoon. W.M.K.P.: Kim, H.M.: Prasad, P.N. Second-order nonlinear optical effects in novel polymethacrylates containing a molecular-ionic chromophore in the side chain. Chem. Mater. 1994. *6* (2). 234.
5. Hsiue. G.H.: Kuo. J.K.: Jeiig. R.J.: Chen. J.I.: Jiang, X.L.; Marturunkakul, S.: Kumar, J.: Tripathy. S.K. Stable second-order nonlinear optical polymer network based on an organosoluble polyimide. Chern. Mater. 1994. *6* (7). 884.
6. Zhang, Y.: Prasad, P.N.: Burzynslci. R. Second-order nonlinear optical properties of N-(4-nitrophenyl)-(s)-prolinol-doped sol–gel-processed materials. Chem. Mater. 1992. *4* (4), 851.
7. Ashwell. G.J.: Dawnay, E.J.C.; Kuczynski. A.P.: Szablewski, M.: Sandy, I.M.: Bryce. M.R.: Grainger. A.M.: Hasan. M. Langmuir–Blodgett alignment of zwitterionic optically non-linear D–π–A materials. J. Chem. Soc., Faraday Trans. 1990, *86* (7), 1117.
8. Miller. L.S.: Walton. D.J.: Stone. P.J.W.: McRoberts. A.M.; Sethi, R.S. Langmuir–Blodgett films for nonlinear optical applications. J. Mater. Sci.. Mater. Electron. 1994. *5* (2). 75.
9. Ravi. M.: Rao. D.N.: Cohen. S.; Agranat. I.; Radhakrishnan, T.P. Push–pull quinonoid compounds: Enhanced SHG utilizing the effect of the chiral centre on dipole alignment. Chem. Mater. 1997. 9, 830.
10. Zyss, J.: Berthier. G. Nonlinear optical properties of organic crystals with hydrogen-bonded molecular units: The case of urea. J. Chem. Phys. 1982. 77 (7). 3635.
11. Sarma. J.A.R.P.: Laxmikanth Rao, J.; Bhanuprakash, K. Role of intermolecular hydrogen bonding in some supramolecules: An AM1 study of the binding energies and hyperpolarizabilities. Chem. Mater. 1995. 7 (10). 1843.
12. Cangopadhyay, P.: Rao, S.V.: Rao. D.N.: Radhakrishnan. T.P. N-Alkyl-p-nitroanilines — Impact of alkyl chain length on crystal structures and optical SWG. J. Mater. Chern. 1999. 9 (8), 1699.
13. Sharma. S.: Radhakrishnan, T.P. Control of crystal packing in SHG active 7,7-bis(n-pentylamino)-8,8-dicyanoquinodimethane by intermolecular H-bonds and alkyl chain interactions. Mol. Cryst. Liq. Cryst. 2000. 338, 257.
14. Marks, T.J.: Ratner. M.A. Design. synthesis, and properties of molecule-based assemblies with large second-order optical nonlinearities. Angew. Chem. Int. Ed. Engl. 1995. *34* (2), 155.
15. Kanis. D.R.: Ratner, M.A.; Marks. T.J. Design and construction of molecular assemblies with large second-order optical nonlinearities. Quantum chemical aspects. Chem. Rev. 1994. *94* (1), 195.
16. Long. N.J. Organometallic compounds for nonlinear optics—The search for en-light-enment! Angew. Chem. Int. Ed. Engl. 1995. *34* (1). 21.
17. Verbiest. T.: Clays. K.: Samyn, C.: Wolff. J.: Reinhoudt. D.: Persoons. A. Investigations of the hyperpolarizability in organic molecules from dipolar to octopolar systems. J. Am. Chem. Soc. 1994. *116* (20), 9320.
18. Ray. P.C.: Das, P.K. First-order hyperpolarizabilities of octupolar aromatic molecules: Symmetrically substituted triazines. Chem. Phys. Lett. 1995. 244 (1–2). 153.
19. Bahl. A.; Grahn. W.: Stadler. S.; Feiner. F.; Bourhill. G.; Bräuchle. C.; Reisner. A.: Jones. P.G. Novel. blue-transparent frequency doublers based on 1,8-di(hetero)-arylnaphthalenes. Angew. Chem. Int. Ed. Engl. 1995, 34 (13–14), 1485.
20. Ravi, M.: Rao, D.N.: Cohen, S.: Agranat. I.: Radhakrishnan. T.P. Strong optical second harmonic generation in a chiral diaminodicyano-quinodimethane system. J. Mater. Chem. 1996. *6* (7). 1119.
21. Desiraju. C.R. *Crystal* Engineering: *The* Design *of* Organic Solids: Elsevier: Amsterdam. 1989.
22. Sarma, J.A.R.P.; Allen. H.A.: Hoy. V.J.: Houard, J.A.K.; Thaimattam. R.: Biradha. K.; Desiraju. G.R. Design of an SHG-active crystal. 4-iodo-4'-nitrobiphenyl: The role of supramolecular synthons. J. Chem. Soc., Chem. Commun. 1997. 101.
23. Philip Anthony. S.: Radhakrishnan. T.P. Perfectly polar assembly of molecular dipoles in crystals of Zn(II)(DMAP)-(acac)2—A case of self-poling. J. Chern. Soc.. Chem. Commun. 2001. 931.
24. Gangopadhyay, P.: Radhakrishnan, T.P. Helical superstructures of a C_2-symmetric molecule exhibiting strong second harmonic generation in the solid state. Angew. Chem. Int. Ed. 2001. 40 (13). 2451.
25. Gangopadhyay. P.: Naga Srinivas. N.K.M.: Rao. D.N.; Radhakrishnan. T.P. Control of supramolecular organization by molecular structure and symmetry leading to the

induction and enhancement of solid state SHC. Opt. Mater. 2002; 21, 55.

26. Burland. D.M.; Miller. R.D.: Walsh, C.A. Second-order nonlinearity in poled-polymer systems. Chem. Rev. **1994.** 94 (1), 31.
27. Fischer, P.; Koetse. M.; Laschewsky, A.; Wischerhoff, E.; Jullien, L.; Persoons, A.; Verbiest, T. Orientation of nonlinear optical active dyes in electrostatically self-assembled polymer films containing cyclodextrins. Macromolecules 2000. *33* (26). 9471.
28. Huang, S.D.; Xiong, R.G. Molecular recognition of organic chromophores by coordination polymers: Design and construction of nonlinear optical supramolecular assemblies. Polyhedron **1997.** 16 (22). 3929.
29. Oliveira. O.N., Jr.; He, J.-A.; Zucolotto, V.; Balasubramanian. S.; Li, L.; Nalwa, H.S.; Kumar, J.: Tripathy, S.K. *Handbook of Polyelectrolytes and Their Applications;* Tripathy. S.K., Kumar. J., Nalwa, H.S., Eds.; American Scientific Publishers: Stevenson Ranch. 2002; Vol. 1, 1.
30. Li, D.: Ratner, M.A.; Marks, T.J.; Zhang, C.Yang, J.; Wong. G.K. Chromophoric self-assembled multilayers. Organic superlattice approaches to thin-film nonlinear optical materials. J. Am. Chem. Soc. **1990.** *112* (20), 7389.
31. Facchetti, A.; Abbotto. A.: Beverina, L.: van der Boom, M.E.; Dutta, P.: Evmenenko. G.; Pagani. G.A.: Marks, T.J. Layer-by-layer self-assembled pyrrole-based donor-acceptor chromophores as electro–optic materials. Chem. Mater. 2003. *15* (5), 1064.
32. Wenbin, L.: Weiping, L.: Wong, K.W.: Marks, T.J. Supramolecular approaches to second-order nonlinear optical materials. Self-assembly and microstructural characterization of intrinsically acentric [(Aminophenyl)azo)]-pyridinium superlattices. J. Am. Chem. Soc. **1996.** 118 (34), 8034.
33. Yitzchaik, S.; Marks, T.J. Chromophoric self-assembled superlattices. Acc. Chem. Res. **1996.** 29 (4), 197.

Nuclear Magnetic Resonance Spectroscopy

Arvin Moser
Christian Detellier
University of Ottawa, Ottawa, Ontario, Canada

INTRODUCTION

The 1952 Physics Nobel prizewinners Bloch and Purcell independently carried out the first nuclear magnetic resonance (NMR) experiments during the 1940s.[1,2] In the following decades, NMR spawned several major breakthroughs. During the 1960s, NMR sensitivity was strongly improved with the use of short, intense, radio frequency pulses. which led to the development of Fourier transform NMR. In the 1970s, two-dimensional (2D) NMR emerged as a revolutionary technique. Ernst, 1991 Chemistry Nobel prizewinner, played a key role in these developments."' In the same years, one could start exploring the NMR spectroscopy of a large amount of nuclei in the Periodic Table. all those possessing a nonzero spin quantum number. NMR was becoming multinuclear,[4] while the field of kinetics in NMR was expanding through the analysis of different patterns of line shapes.[5,6] Consequently, in addition to providing a powerful structural characterization tool. NMR spectroscopy was becoming invaluable in providing access to dynamic information. leading to essential mechanistic interpretations.

In the 1970s, a major medical breakthrough came with magnetic resonance imaging (MRI), a technique relying on the water content of the sample to provide detailed images without invasion.[7] This technique can be applied to a large variety of soft, amorphous, inorganic. or organic supramolecularly organized materials. For example. it can be applied to the human body to provide detailed images without invasive surgery or harmful radiation exposure to the patient.

In parallel, more sophisticated materials were used in the design of the magnets, allowing access to continuously higher magnetic fields. Fields of 21.6 T are becoming available in 2003. compared to 0.7 T available in the first commercial spectrometer proposed by Varian in 1953.

The development in the 1960s–1970s of magic angle spinning NMR (MAS NMR),[8] following the construction of probes capable of containing high-speed rotors for solid samples. allowed for the recording of high-resolution, liquid-like spectra for solid samples. Nowadays, a large variety of nuclei are routinely studied, for structural, dynamic, and mechanistic information. The availability of Fourier transform techniques, high magnetic fields. powerful signal processing and magic angle spinning techniques, led to the development of this extremely versatile spectroscopy, finding applications in a broad range of disciplines, from chemistry to biology. from biochemistry to earth sciences, and from materials sciences to medicine.

Because NMR is capable of distinguishing minute changes in the geometric and stereoisomeric properties of a structure and is also capable of obtaining qualitative as well as quantitative information, which includes information on dynamic processes of chemical exchange within the molecule or with other molecules, it is an essential, invaluable, technique for the study of aggregation phenomena, of self-assemblies, and of supramolecular structures. both in solution and in the solid state.

BRIEF OVERVIEW OF THE TECHNIQUE

The observation of a signal in NMR spectroscopy necessitates a nucleus with a nonzero spin quantum number, that is. a nucleus with either an odd mass number or an even mass number and an odd atomic number. The resulting nuclear spin produces a magnetic moment. When the nucleus is placed inside a static magnetic field, B_0, the magnetic moment of the nucleus interacts with the external field, the Zeeman interaction, yielding different energy levels for the nucleus.

When a specific radio frequency pulse is applied to the nucleus in the field B_0, the magnetic moment precessing about B_0 at a frequency called the Larmor frequency, is perturbed. That is, energy is transferred to the spin system via the radio frequency pulse. and the state of the system changes: transitions between the allowed magnetic energy levels are induced. The system subsequently relaxes and emits a signal or free induction decay (FID) as a function of time that is recorded. The FPD is converted to frequency domain data using a Fourier transformation.

The Larmor (ω_0) frequency of precession is denoted by the equation $\omega_0 = |\gamma/(2\pi)|B_0$, where γ is the gyromagnetic

Encyclopedia of Supramolecular Chemistry
DOI: 10.1081/E-ESMC 120012819

ratio and is specific to the nucleus being studied. The effective field (B_{eff}) received by the nucleus under study depends on the density and on the spatial distribution of the electronic clouds in its close proximity ($B_{eff} = B_0 - \sigma B_0$, where σ is a screening constant). This is the origin of the chemical shift. The value of B_{eff} received by the nucleus under study will also depend on the presence in its close proximity of other nuclei with magnetic moments, resulting generally in splittings of the signal. This is the origin of the coupling constants.

The acquisition of the signal in the time domain allowed for the development of spectra recorded in two dimensions. indicating, generally more clearly than in one dimension. the various relations existing between nuclei, such as, among others, coupling and exchange.

In addition to signal intensities, to chemical shifts, and to coupling constants, the relaxation times, T_1 and T_2, are essential characteristics of a nuclear spin system. The T_1 is the longitudinal or spin-lattice relaxation time. It is related to the relaxation of M_z, the magnetic moment component in the B_0 direction. the z direction. The relaxation process occurs as a result of the nucleus transferring the absorbed energy to its surrounding. The T_2 is the transverse or spin–spin relaxation time. It involves the mutual exchange of spins between two precessing nuclei that are in close proximity. That is, the energy transfer occurs from one nucleus to the other and results in line broadening. As such, the T_2 (excluding the effects of B_0 inhomogeneity and of chemical exchange) is inversely proportional to the line width at half intensity of the corresponding peak.

These brief considerations demonstrate the extreme sensitivity of the NMR parameters to the electronic environment of the nucleus being examined. Minute modifications of the electronic densities and distribution can result in large effects on the spectrum. This is particularly true for quadrupolar nuclei. whose signals' linewidths can vary by several orders of magnitude depending upon the nature of their closest neighbors. The reader is referred to monographs and textbooks for complete description and development of the theory of NMR spectroscopy and of its parameters and techniques. Just two examples are suggested[9,10] among a number of other excellent books and recent reviews, giving an overview of current solid-state NMR methods.[8,11]

NMR PROBES OF SUPRAMOLECULAR STRUCTURES

The aim of research in supramolecular chemistry is to interpret, rationalize. and design new chemical systems beyond the covalent bond, developing complex supramolecular architectures with specific new properties in, for example, molecular recognition, catalysis, separations, sensors, and, perhaps, ultimately, in the simulation of living, self-replicating systems.

Supramolecular systems result from organized molecular associations: aggregations. and assemblies. Any agglomeration of molecules constitutes a supramolecular system. because, at the minimum, weak dispersion forces are present, organizing the distribution of the molecular components among themselves: a liquid solvent is structured and is a supramolecular host system for the solute, and a crystal is a supramolecular assembly. The forces responsible for the supramolecular organization, ranging from H-bonding and ion–dipole to induced dipole–induced dipole, are then responsible for the directionality of the assemblies. such as in multiple H-bonds[12] or in π-stacking.[13,14]

In that context. NMR spectroscopy provides essential tools for the characterization of supramolecular organizations. The chemical shifts are sensitive to the nucleus' electronic environment: ^{1}H, ^{13}C, or ^{15}N chemical shifts, for example, are affected by H-bonding involving their molecule. and the magnitude of the ^{1}H chemical shift is indicative of the strength of the H-bond. Also, ^{1}H chemical shifts are strongly dependent upon anisotropic shielding effects, which can provide information on relative molecular orientations involving aromatic rings, for example.[15,16] Metal ion chemical shifts (^{23}Na, for example) can vary considerably with the molecular nature of the first coordination sphere of the cation.[17] With the demonstration that scalar couplings across the hydrogen bond are observable for Watson–Crick base pairs in ^{15}N-labeled RNA, Dingley and Grzesiek gave. for the first time, direct evidence of H-bonding, which. otherwise. must come from a variety of indirect observations.[18]

The relaxation times. T_1 and T_2, among other factors, depend upon the size of the supramolecular entity, and, consequently, can constitute an invaluable tool for the characterization of its size, giving information about the number of assembling units.[19,20]

Nuclear Overhauser enhancement (NOE) experiments, both in one-dimensional (1D) and 2D domains; can give information on the proximity of noncovalently bonded nuclei, and, consequently, to spatial relationships between molecules in an assembly.[21]

In addition to thermodynamic measurements. NMR spectroscopy provides an invaluable tool for kinetics and mechanistic measurements, giving access to a time range from the picosecond to years.[6] The dynamic NMR studies of supramolecular complexes were recently reviewed.[22]

This short review, which cannot be exhaustive, will give examples of applications of these NMR tools to structural determinations and mechanistic elucidations of supramolecular systems.

STRUCTURES AND MECHANISMS OF SUPRAMOLECULAR ASSEMBLIES

Large Network Assemblies

In recent years, the number of noncovalent synthesis of sophisticated systems has strongly increased. One example is the report by the group of Reinhoudt of the spontaneous and reversible assembly of similar to 20kDa synthetic hydrogen-bonded assemblies via the formation of 144 cooperative hydrogen bonds. In connection with other techniques, ^{1}H-NMR spectroscopy clearly showed the formation of the "eight-floor" assembly, named so because eight singlets between 12 and 15 ppm are observed fo the N–^{1}H signals of the 5,5-diethylbarbituric acid building blocks. Moreover, the N–^{1}H signals for the outside floors are significantly different from the signals of the other floors.[23] Another example is the assembly of calix[4]hydroquinones in nanotube bundles. In this case, the ^{1}H-NMR large chemical shifts of the phenolic protons are indicative of the presence of short H-bonds.[24] Hydrogen-bonded supramolecular complexes were prepared by self-assembly of a proton donor (diacid) and an acceptor (bipyridyl ethylene) through the formation of intermolecular hydrogen bonds.[25] An upfield shift of the ^{13}C-CP/MAS NMR (where CP stands for cross-polarization) carbonyl carbon resulted from the forination of intermolecular hydrogen bonds. The natural abundance of ^{15}N-CP/MAS NMR chemical shifts was in agreement with the formation of hydrogen-bonded molecular complexes.[25]

In the context of large assemblies resulting from multiple hydrogen bonds. one cannot resist mentioning an example from the mineral world. Kaolinite is a remarkable, dissymmetric. 1:1 layered aluminosilicate composed of repeating layers of a tetrahedral silicate sheet sharing oxygens with an octahedral aluminate sheet in an extended 2D network. The surface silicate sheet is coinprised of hexagonal-(SiO-)$_6$ macrorings, and the surface aluminate sheet is covered with aluminol groups. The layers are held together by van der Waals attractive forces. electrostatic interactions, and a large network of hydrogen bonds between the aluminol groups of a layer and the silicate sheet of another layer. A chemistry of intercalation and of interlamellar grafting could be developed in the interlayer spaces of reduced diinensionality, by the rupture of the H-bonds network.[26,27] The 2D confinement of poly(ethylene glycols) (PEG) was achieved in kaolinite.[28] The interlayer structure and dynamics of the intercalated PEGs could be probed by ^{13}C-CP/MAS NMR. Dipolar dephasing experiments were particularly useful in showing that the polymer chains in the kaolinite interlamellar spaces are more constrained and less mobile than in the bulk form (Fig. 1).

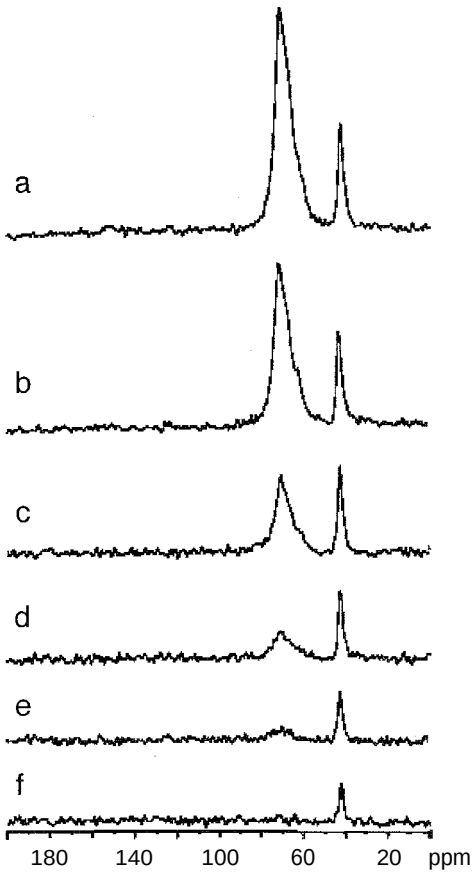

Fig. I Solid-state ^{13}C-CP/MAS NMR spectra of a kaolinite-polyethyleneglycol intercalate: (a) no dipolar dephasing: (b–f) with dipolar dephasing. (From Ref. [28]. Reproduced with permission from the American Chemical Society.)

A series of 1D and 2D NMR experiments performed on nanocomposites of hectorite, a smectite clay mineral. showed new opportunities for studying large assemblies of layered minerals with polymeric materials.[29] In particular. rotational-echo double-resonance (REDOR) experiments afforded ^{1}H–^{29}Si distances with precision, and a mobility gradient of intercalated polyethyleneoxide (PEO) segments was demonstrated in ^{1}H–^{29}Si wideline separation (WISE) experiments.[29]

Nucleotide Aggregation

The structure of the most celebrated supramolecular structure was published more than 50 years ago, in the April 2, 1953, issue of *Nature*, when Watson and Crick proposed "a structure for Deoxyribose Nucleic Acid," the current paradigm for the structure of life.[30] While the ability of the guanine moiety to form tetrameric. planar assemblies. called "G-quartets," was recognized for a while,[31,32] it is more recently that G-quartets were shown

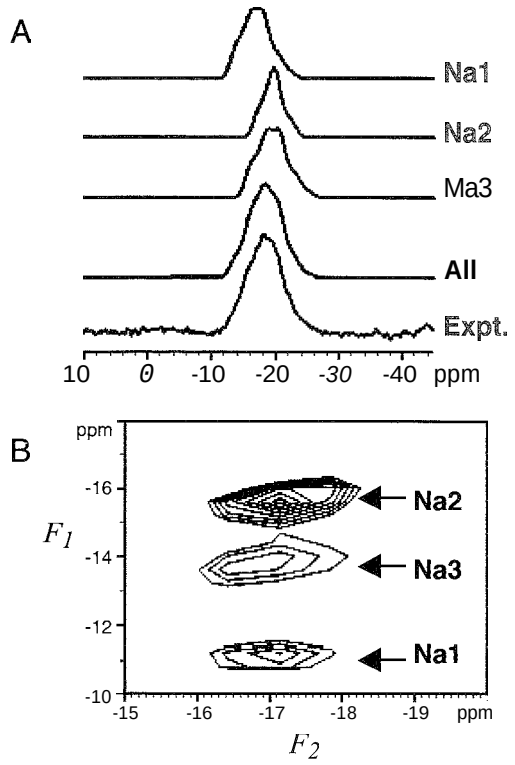

Fig. 2 (A) Experimental and simulated 1D ^{23}Na-MAS spectra and (B) 2D ^{23}Na-MQMAS spectrum of a G-quadruplex channel. (Frorn Ref. [40]. Reproduced with permission from the American Chemical Society.)

to form from various C-rich DNA or RNA sequences.[33] The G-quartets further aggregate in the presence of various monovalent cations.[33]

The NMR provided invaluable information on the structures of a variety of assemblies of 6-quartets. In the presence of $Na^+$and K^+. an octameric structure of 5'-CMP is formed in water.[34–38] The analysis of the non-Lorentzian line shapes of the ^{23}Na-NMR signals afforded a measurement of the correlation time of the reorienting. rigid, supramolecular entity, confirming the size of the aggregate. in complement to the ^{1}H- and ^{31}P-NMR structural data.[19,37,38]

Among the numerous recent studies on various G-quartet structures, two examples will be given, one in a nonpolar organic solvent and one in the solid state. A lipophilic derivative of deoxyguanosine, soluble in chlorinated solvents, can transfer alkali metal salts from the aqueous to the organic phase. An in-depth NMW study, including 1D and a variety of 2D experiments, elucidated the solution structure of the K^+ octameric assembly, demonstrating that a well-defined structure, resulting from the stacking of two tetramers sandwiching a potassium cation, is obtained in $CDCl_3$ solution. The glycosidic bonds have a *syn* conformation in one tetramer and an all-*anti* conformation in the other.[39]

Another illustration of how powerful structural NMR tools can be is found in the ^{23}Na multiple quantum MAS (MQMAS) NMR study of a G-quadruplex channel. A guanine nucleoside derivative forms tetramers, G-quartets. which. in the presence of monovalent cations, assemble to result in a G-quadruplex channel consisting of the stacking of four 6-quartets, coordinating in the channel four cations: in this case, three Na^+ and one Cs^+.[40] While the 1D ^{23}Na-MAS NMR spectrum exhibits only a broad, unresolved signal; the 2D MQMAS spectrum gives a clear and neat separation for the three crystallographically distinct Na^+sites (Fig. 2).

Polymer Associations

Supramolecular polymers, made of polymeric chains associated by noncovalent interactions such as H-bonding, are expected to display new types of properties, different from the classical covalently cross-linked polymers. These systems could be seen as softly cross-linked polymers. The NMR spectroscopy is routinely used to characterize the formation of hydrogen-bonding networks, such as in supramolecular polymer networks based on ureido-pyrimidone subunits.[41] These subunits, when taken as molecular entities in chloroform solutions, dimerize, forming different isomers.[42] Rotational nuclear Overhauser enhancement spectroscopy (ROESY) experiments elucidated the structure in solution of one of these isomers: not obtained from x-ray crystallography. The mutual rates of exchange between the isomers could be determined from a combination of exchange spectroscopy (EXSY) experiments and of integration of the ^{1}H-NMR signals.[42] The ^{1}H-NMR is also invaluable in following the thermal reversibility of these systems. the formation and dissociation of H-bonds in the network, such as in the assemblies of polystyrene-bearing nucleic acid bases.[43]

Other forces than H-bonding can lead to supramolecular polymer associations. Polymers such as PEO and sodium poly(α,L-glutamate) (PCNA) form complexes by ion–dipole and hydrophobic interactions.[44] A quantitative analysis of the ^{23}Na-NMR spectra in D_2O showed that only 6% of the sodium cations was complexed by PEO, while the majority of Na^+ was in the solvated form. In nonaqueous media. a combination of ^{23}Na and 2D-nuclear Overhauser enhancement spectroscopy (NOESY) ^{1}H-NMR suggests that the sodium ions are completely complexed by PEO through ion–dipole interactions.[44]

Using conventional solid-state NMR and double-quantum (DQ) techniques, the helical structure of small linear peptides, composed of alternating leucine and lysine residues. was confirmed when they were adsorbed onto highly porous hydrophobic polystyrene surfaces.[45] Moreover, the absence of chemical shift anisotropy averaging led to the conclusion that there is no detectable

motion of the peptides in the timescale of the experiment (<1 kHz). The fact that 2D DQ experiments allow such high-resolution determination of secondary structures in heterogeneous environments is another illustration (see also Ref. [40]) of the power of the structural tools offered by solid-state NMR.

Host–Guest Associations and Inclusion Compounds

A large number of host molecular architectures with internal cavities adapted to the recognition of guest ionic or molecular entities were designed. The recognition properties of inacrocyclic hosts such as crown ethers or calixarenes, for example. depend largely upon their preorganization in solution. Consequently. it is essential to analyze the conformational structures and their dynamics as a prerequisite to the interpretation of the recognition mechanisms. This will be exemplified in the following case, illustrating bow EXSY spectroscopy can be applied to the analysis of the conformational dynamics of a calix[4]arene[46] and to the mechanism of its complexation of the sodium cation.[47]

Tetramethoxycalix[4]arene (1) interconverts between four conformers: cone; partial cone. 1.2-alternate. and 1.3-alternate. The rate constants for the various conformational exchanges were obtained from 2D ^{1}H-EXSY NMR spectra (Fig. 3) on the basis of the exchange scheme shown on Scheme 1. A complete thermodynamic and kinetic picture of the various conformational exchanges could be drawn.[46]

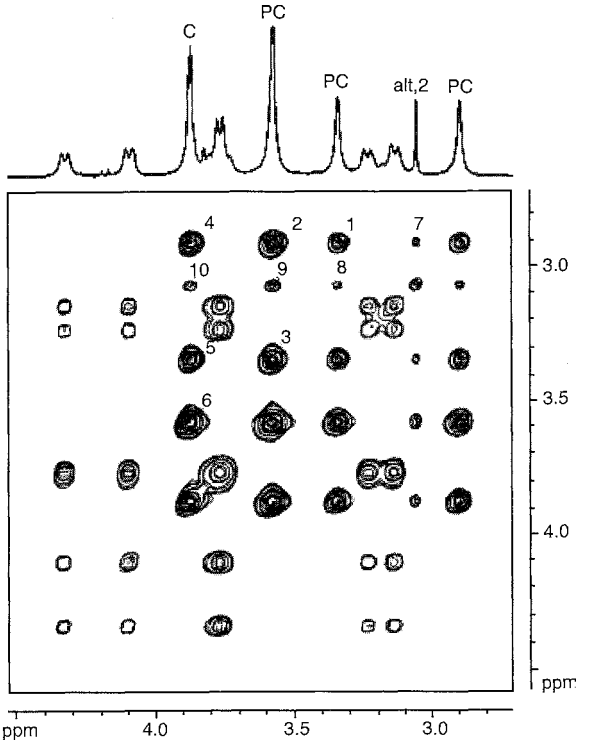

Fig. *3* The 1D ^{1}H- and 2D ^{1}H- EXSY NMR spectra of the methoxy and methylene regions of calixarene 1 at 280 K in a binary mixture of chloroform and acetonitrile. (From Ref. [46]. Reproduced with permission from the American Chemical Society.)

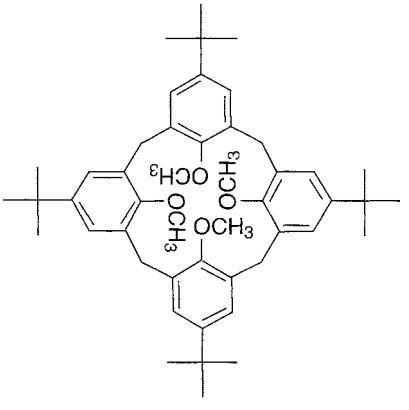

1

The main findings are the demonstration that the conformational exchanges proceed through one-step processes, as shown in Scheme 1, and the fact that the interconversion processes are kinetically controlled by the entropies of activation. This effect was tentativeiy attributed to a larger organization of the solvation cage

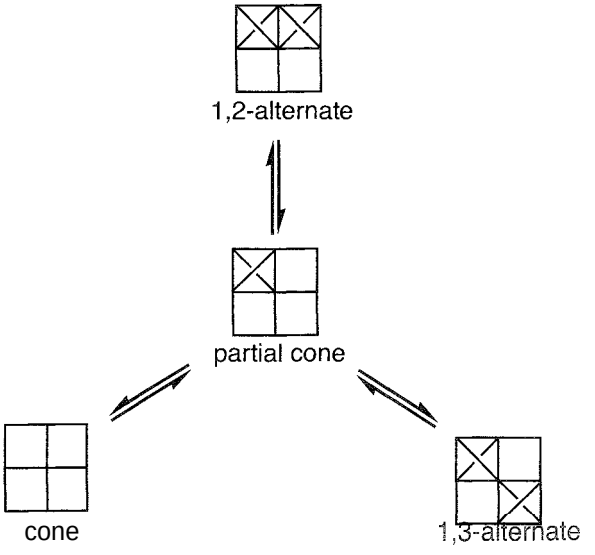

Scheme 1 (From Ref. [46]. Reproduced with permission from the American Chemical Society.)

in the transition state, in the case of the most kinetically stable 1,2 conformer.[46]

As sodium tetraphenylborate is added to a solution of (1), three new ^{1}H-NMR peaks appear in the range of 3–4.5 ppm.[47] As [Na^+]>, [I] only the peaks attributed to $(Na,1)^+$are present, with (I) exclusively in the cone conformation. demonstrating a slow exchange and a strong affinity of the sodium cation for the cone conformation. Similar studies using cesium triiodide showed the formation of 1:1 complexes of 1, with the cesium, cation in the 1,3 alternate and partial cone conformations.[48]

The calixarene cavity can also host neutral molecules. An example of co-complexation of the sodium cation and acetonitrile is provided by the *p-tert*-butylcalix[4]arene tetraacetamide receptor.[49] The p-tert-butyl calixarenes also show selectivity in the recognition of aromatic molecules, which can be attributed to weak attractive forces between the CH_3 groups and the π-system. A noticeable and interesting microdynamics experience, using NMR relaxometry measurements (T_1), was performed on *p-tert*-butyl-calix[4]arene (1:1) toluene systems in the solid state[50] to give information on the activation energy of the calixarene methyl group's reorientation in the presence of toluene in the cavity and to give information on CH_3–π interactions. The experimentally determined activation energy of reorientation of the methyl group pointing toward the interior of the cage is increased in the presence of a toluene guest, from 2.1 to 3.2 kcal/mol. This is not the case for the other two methyl

Aromatic ring electronic currents create large diamagnetic anisotropies resulting in chemical shift variations for the nuclei in the proximity of the aromatic ring. Given the relatively small chemical shift range of ^{1}H, the effect is particularly noticeable for this nucleus. Because of the spatial anisotropy of the effect. the observed chemical shifts can give indications of the relative positions of nuclei and aromatic rings. This property can be used as an indication of the inclusion of a guest in a cavity and of the resulting host–guest geometry.[15,16] The ^{1}H DQ techniques can now be applied to host–guest aromatic systems in the solid state. An example can be found in the application of rotor-synchronized ^{1}H DQ/MAS NMR to the complex formed by a molecular tweezer encaging 1, 4-dicyanobenzene.[51]

CONCLUSION

The spectacular development of NMR spectroscopy in the last decades provided invaluable, necessary tools for the precise determination of chemical structures not always accessible through x-ray single crystal analysis. It also provides the tools to reliably determine supramolecular levels of organization, in solution and in the solid state. It gives access to information on the dynamics and the kinetics of molecular assemblies, and, consequently, to the mechanisms by which they are created, they evolve, and they dissociate. Access to the new generation of ultrahigh-field NMR spectrometers will allow precise determination of faster exchange kinetics.

With the adaptation of NMR techniques for larger molecules, it becomes possible to analyze proteins with molecular weights reaching 50 kDa. These techniques include 'H-, ^{15}N-TROSY (transverse relaxation-optimized spectroscopy, with the mutual cancellation of ^{1}H-, ^{15}N-dipole–dipole coupling and the ^{15}N chemical shift anisotropy) and CRINEPT (Cross-correlated Relaxation-Enhanced Polarization Transfer, combining insensitive nuclei enhanced by polarization transfer (INEPT) transfer with cross-correlated relaxation-induced polarization transfer). They are used in conjunction with the ^{15}N-, ''c-labeling of the protein for increased sensitivity.

Consequently, the emerging field of proteomics will immensely benefit from the new; constantly developing multidimensional techniques and from increasing magnetic fields. Functional proteomics will rely on NMR tools to unravel supraproteinic interactions and dynamics and the structures of associating proteins in solution.

Access to ultrahigh fields will also allow the detection of quadrupolar nuclei bound on large structures. See, for example, the recent direct detection by ^{39}K solid-state NMR of potassium cations bound to G-quadruplex structures.[52] The ^{67}Zn or ^{25}Mg NMR, for example, will become more accessible in biological systems,[53] an achievement that was still a dream only 20 years ago. The main challenge in the development of new nanohybrid materials is their characterization, many being amorphous. The precise characterization of nanostructures will also strongly rely on the current developments of NMR spectroscopy.

ACKNOWLEDGMENTS

The Natural Sciences and Engineering Research Council of Canada is gratefully acknowledged for a Discovery Grant to CD. Part of this review was written during a sabbatical leave of CD, and Dr. Eduardo Ruiz-Hitzky is warmfully thanked for the hospitality provided in his laboratory of the CSIC in Madrid (Spain). The ''Secretaria de Estado de Educacidn y Universidades'' of Spain is gratefully thanked for financial support.

ARTICLES OF FURTHER INTEREST

Alkali *Metal Cations* in *Biochemistry*, p. 1
Alkalides and Electrides, p. *12*

Calixarenes and Their. Analogues: Cation Complexation, p. 137
Calixarenes and Their Analogues: Molecular Complexation, p. 145
Carcerands and Hemicarcerands, p. 189
Cation–π Interactions, p. 214
Cavitands, p. 219
Classification and Nomenclature of Supramolecular Compounds, p. 261
Crown Ethers, p. 326
Cryptands, p. 334
Hydrogen Bonding. p. 658
Ionophores, p. 760
Kinetics of Complexation, p. 776
Lariat Ethers, p. 782
Layered Supramolecular Solids and Their Intercalates, p. 791
Podands. p. 1106
Protein Supramolecular Chemistry, p. 1161
Rotaxanes and Pseudorotaxanes, p. 1194
Selectivity: Thermodynamic and Kinetic, p. 1225
Self-Assembly: Definition and Kinetic and Thermodynamic Considerations, p. 1248
Solid-State Nuclear Magnetic Resonance Spectroscopy, p. 1307
Supramolecular Chemistry: Definition, p. 1401
Supramolecular Polymers, p. 1443
Swelling Clays (Smectites) and Nanofilms, p. 1478

REFERENCES

1. Bloch. F.; Hansen, W.W.; Packard, M. The nuclear induction experiment. Phys. Rev. 1946, 70. 474–485.
2. Purcell. E.M.: Ton-ey, H.C.: Pound. R.V. Resonance absorption by nuclear magnetic moments in a solid. Phys. Rev. 1946. 69. 37–38.
3. Ernst. R.R.; Bodenhausen, G.; Wokaun, A. Principles of *Nuclear Magnetic Resonance in* One rind *Two Dimensions*: Clarendon: Oxford. 1987.
4. *NMR of Newly Accessible Nuclei*: Laszlo. P.. Ed.: Vols. I & TI, Academic Press: New York. 1983.
5. Sandstrom. J. *Dynamic NMR Spectroscopy*; Academic Press: New York. 1982.
6. Detellier. C. Reaction Kinetics and Exchange. In *Modern NMR Techniques and* Their *Applications* to *Chemistry*; Popov. A.I.. Hallenga. K., Eds.: Practical Spectroscopy Series. Marcel Dekker Inc.: New York. 1990: 521–564. Chapter 9.
7. Lauterbur. P.C. Image formation by induced local interactions: Examples employing nuclear magnetic resonance. Nature 1973. 242, 190–191.
8. Brown, S.P.; Spiess. H.W. Advanced solid-state NMR methods for the elucidation of structure and dynamics of molecular. macromolecular. and supramolecular systems. Chem. Rev. 2001. *101*, 4125–4155.
9. Harris. R.K Nuclear Magnetic Resonance *Spectroscopy—A Physicochemical View*; Longman Scientific and Technical: Essex. 1994.
10. Sanders. J.K.M.; Hunter, B.K. Modern NMR Spectroscopy: *A Guide for* Chemists. 2nd Ed.: Oxford Univ. press: New York. 1993.
11. Bryce. D.L.; Bernard, G.M.: Gee, M.: Lumsden, M.D.; Eichele. K.: Wasylishen, R.E. Practical aspects of modern routine solid-state multinuclear magnetic resonance spectroscopy: One-dimensional experiments. Can. J. Anal. Sci. Spectrosc. 2001, 46. 46–82.
12. Prins. L.J.; Reinhoudt, D.N.: Timmerman, P. Noncovalent synthesis using hydrogen bonding. Angew. Chem.. Int. Ed. 2001, 40. 2383–2426.
13. Gilbert. M.; Claverie. P. *Molecular Associations in* Biology; Pullman. B.. Ed.: Academic Press: New York. 1968: 245.
14. Yamamoto. T.; Kornarudin. D.: Arai, M.; Lee, B.-L.: Suganurna. H.: Asakawa. N.; Inoue. Y.; Kubota. K.: Sasaki. S.: Fukuda, T.; Matsuda. H. Extensive studies on n-stacking of poly(3-alkylthiophene-2,5-diyl)s and poly(4-alkylthiazole-2,5-diyl)s by optical spectroscopy. NMR analysis. light scattering analysis. and x-ray crystallography. J. Am. Chem. Soc. 1998, 120. 2047–2058.
15. Chapman, R.C.: Sherman, J.C. Study of templation and molecular encapsulation using highly stable and guest-selective self-assembling structures. J. Am. Chem. Soc. 1995, 117. 9081–9082.
16. Tucci. F.C.; Rudkevich, D.M.: Rebek. J., Jr. Stereochemical relationships between encapsulated molecules. J. Am. Chem. Soc. 1999. *121*. 4928–4929.
17. Detellier, C. Alkali Metals. In NMR of *Newly Accessible Nuclei*: Laszlo. P., Ed.; Academic Press: New York. 1983; Vol. II, 105–151. Chapter 5.
18. Dingley. A.J.; Grzesiek. S. Direct observation of hydrogen bonds in nucleic acid base pairs by internucleotide $^{2}J_{NN}$ couplings. J. Am. Chem. Soc. 1998, 120. 8293–8297.
19. Delville. A.: Detellier. C.: Laszlo, P. Determination of the correlation time for a slowly reorienting spin-312 nucleus: binding of Na^{+} with the 5'-GMP supramolecular assembly. J. Magn. Reson. 1979. 34. 301–315.
20. Israeli, Y.: Detellier. C. Complexation of the sodium cation by a calix[4]arene tetraester in solution. Formation of a 2:1 calixarene:sodium complex. J. Phys. Chem.. B 1997. 101. 1897–1901.
21. Feller. S.E.: Brown. C.A.: Nizza. D.T.; Gawrisch. K. Nuclear overhauser enhancement spectroscopy cross-relaxation rates and ethanol distribution across membranes. Biophys. J. 2002, 82. 1396–1404.
22. Pons. M.; Millet, O. Dynamic NMR studies of supramolecular complexes. Progr. Nucl. Magn. Reson. Spectrom. 2001. 38. 267–324.
23. Paraschiv. V.: Cregocalama, M.; Fokkens. R.H.: Padberg, C.J.: Timmerman, P.: Reinhoudt. D.N. Nanostructures via noncovalent synthesis: 144 hydrogen bonds bring together 27 components. J. Org. Chem. 2001, *66*. 8297–8301.
24. Kim, K.S.: Suh, S.B.: Kim. J.C.; Hong, B.H.: Lee, E.C.: Yun, S.: Tarakeshwar. P.; Lee. J.Y.; Kim. Y.: Ihm. H.; Kim, H.G.: Lee. J.W.: Kim. J.K.;Lee. H.M.; Kim. D.; Cui,

C.Z.: Youn, S.J.: Chung. H.Y.: Choi. H.S.; Lee. C.W.: Cho. S.J.: Jeong. S.: Cho, J.-H. Assembling phenomena of calix[4]hydroquinone nanotube bundles by one-dimensional short hydrogen bonding and displaced π–π stacking. J. Am. Chem. Soc. 2002. *124.* 14268–14279.

25. Xu. J.W.; He, C.B.: Toh. K.C.; Lu. X.H. Intermolecular interaction in multicomponent supramolecular complexes through hydrogen-bonding association. Macromolecules 2002. *35,* 8846–8851.
26. Tunney. J.J.; Detellier, C. Preparation and characterization of two distinct ethylene glycol derivatives of kaolinite. Clays Clay Miner. 1994. *42.* 552–560.
27. Tunney, J.J.; Detellier. C. Chemically modified kaolinite. Grafting of inethoxy groups on the interlamellar aluminol surface of kaolinite. J. Mater. Chem. 1996. 6, 1679.
28. Tunney. J.J.: Detellier, C. Aluminosilicate nanocornposite materials. Poly(ethylene glycol)- kaolinite intercalates. Chem. Mater. 1996. *8.* 927–935.
29. Hou. S.S.; Beyer. F.L.: Schmidt-Rohr, K. High-sensitivity multinuclear NMR spectroscopy of a smectite clay and of clay-intercalated polymer. Solid State Nucl. Magn. Reson. 2002. *22.* 110–127.
30. Watson, J.D.; Crick. F.H.C. Molecular structure of nucleic acids. A structure for deoxyribose nucleic acid. Nature 1953. *171.* 737–738.
31. Gellert. M.; Lipsett. M.N.: Davies. D.R. Helix formation by guanylic acid. Proc. Natl. Acad. Sci. U. S. A. 1962. *48.* 2013–2018.
32. Guschlbauer. W.: Chantot. J.F.: Thiele. D. Four-stranded nucleic acid structures 25 years later: from guanosine gels to telomer DNA. J. Biomol. Struct. Dyn. 1990, *8.* 491–511.
33. Williamson. J.R. G-quartet structures in telomeric DNA. Ann. Rev. Biophys. Biomol. Struct. 1994, *23,* 703–730.
34. Pinnavaia. T.J.: Marshall, C.L.: Mettles, C.M.: Fisk. C.L.; Miles, H.T.: Becker. E.D. Alkali metal ion specificity in the solution ordering of a nucleotide, 5'-guanosine monophosphate. J. Am. Chem. Soc. 1978, *100.* 3625–3627.
35. Detellier. C.: Paris. A.: Laszlo. P. L'auto-assemblage du 5′-GMP: nucléation par les ions potassium. C. R. Acad. Sci. Paris, D 8978. *286.* 781–783.
36. Borro. M.: Detellier. C.: Laszlo. P.; Paris. A. ^{1}H, ^{23}Na, and ^{31}P NMR studies of the self-assembly of the 5'-guanosine monophosphate dianion in neutral aqueous solution in the presence of sodium cation. J. Am. Chem. Soc. 11980, *102.* 1124–1134.
37. Detellier, C.: Laszlo. P. Role of alkali metal and ammonium cations in the self-assembly of the 5'- guanosine monophosphate dianion. J. Am. Chem. Soc. 1980. *102,* 1135–1141.
38. Detellier. C.: Laszlo. P. Influence of amino acids, ammonium and potassium cations on the self-assembly of 5'-GMP. Helv. Chim. Acta 1979, *62.* 1559–1565.
39. Marlow. A.L.: Mezzina. E.; Spada, G.P.: Masiero, S.: Davis. J.T.: Gottarelli. G. Cation-templated self-assembly of a lipophilic deoxyguanosine: solution structure of a K^{+}-dG_8 octamer. J. Org. Chem. 1999, *64.* 5116–5123.
40. Wong. A.: Fettinger. J.C.: Forman. S.L.: Davis. J.T.: Wu, G. The sodium ions inside a lipophilic G-quadruplex channel as probed by solid-state ^{23}Na NMR. J. Am. Chem. Soc. 21002. *124.* 742–743.
41. Lange. R.F.M.: Van Gurp, M.: Meijer, E.W. Hydrogen-bonded supramolecular polymer networks. J. Polym. Sci., A. Polym. Chem. 1999, *37.* 3657–3670.
42. Folmer. B.J.B.: Sijbesma. R.P.: Kooijman, H.; Spek. A.L.: Meijer, E.W. Cooperative dynamics in duplexes of stacked hydrogen-bonded moieties. J. Am. Chem. Soc. 1999. *121;* 9001–9007.
43. Yamauchi, K.: Lizotte, J.R.; Long. T.E. Synthesis and characterization of novel complementary multiple-hydrogen bonded (CMHB) macromolecules via a Michael addition. Macromolecules 2002. *35.* 8745–8750.
44. Pemawansa. K.P.: Thakur. A.; Karikari. E.K.; Khan. I.M. Preparation and characterization of sodium poly(α,L-glutamate)/poly(ethylene oxide) macromolecular complexes. Macromolecules 1999. *32.* 1910–1917.
45. Long. J.R.; Oyler. N.: Drobny. G.P.: Stayton, P.S. Assembly of α-helical peptide coatings on hydrophobic surfaces. J. Am. Chem. Soc. 2002. 124, 6297–6303.
46. Blixt, J.; Detellier. C. Conformational dynamics of calixarenes. Kinetics of conforinational interconversion in 5.11,17,23-tetra-*p-tert*-butyl-25,26,27,28-tetramethoxy-calix[4]arene under entropic control. J. Am. Chem. Soc. 1994, *116.* 11957–11960.
47. Blixt, J.: Detellier. C. Kinetics and mechanism of the sodium cation complexation by 5,11,17,23-tetra-*p-tert*-butyl-25,26,27,28-tetramethoxy-calix[4]arene in solution. J. Am. Chem. Soc. 1995. *117.* 8536–8540.
48. Meier. U.C.: Detellier, C. Kinetics and mechanisms of complexation of the cesium cation by 5,11,17,23-tetra-*p-tert*-butyl-25,26,27,28-tetramethoxycalix[4] arene in solution. J. Phys. Chem.. A 1998. *102,* 1888–1893.
49. Moser. A.; Yap, G.A.P.: Detellier. C. Concurrent insertion of cationic guest and solvent molecules in molecular receptors. Co-complexation of the sodium cation and acetonitrile by a calix[4]arene tetraacetamide. J. Chem. Soc. Dalton Trans. 20102. 428–434.
50. Caciuffo. R.: Galeazzi, R.; Horsewill, A.J.; Ikram, A.; Ugozzoli. F. Measurements of host–guest interaction energies in a calixarene supramolecular complex. Phys. Rev.. B Condens. Matter 1999. *60.* 11867–11870.
51. Brown. S.P.; Schaller, T.; Seelbach. U.P.: Koziol. F.; Ochsenfeld, C.: Klarner, F.G.; Spiess, H.W. Structure and dynamics of a molecular tweezer host–guest complex: Coupling synthesis. solid-state NMR and quantum chemical calculations. Angew. Chem.. Int. Ed. Engl. 2001. *40.* 717–720.
52. Wu, G.: Wong. A.: Gan. Z.: Davis. J.T. Direct detection of potassium cations bound to G-quadruplex structures by solid-state 39K NMR at 19.6 T. J. Am. Chem. Soc. 2003. *125.* 7182–7183.
53. Larsen. F.H.; Lipton, A.S.: Jakobsen. H.J.; Nielsen. N.C.: Ellis, P.D. ^{67}Zn QCPMG solid-state NMR studies of zinc complexes as models for metalloproteins. J. Am. Chern. Soc. 1999. *121.* 3783–3784.

Nuclear Quadrupole Resonance Spectroscopy

John A. S. Smith
King's College London, London, United Kingdom

INTRODUCTION

Nuclear quadrupole resonance (NQR) is a technique in radiofrequency (RF) spectroscopy in which the energy levels originate in an electric interaction between the nuclear electric quadrupole moment (Q), and the electric field gradient (q) at the nuclear site. The observed frequencies cover a wide range, from 100 kHz–1 GHz, depending on the nucleus; the nuclear spin quantum number, **I.** must satisfy the condition $I \geq 1$, but the frequencies and relaxation times are specific to a given compound and enable a study to be made of electronic structure and molecular motion in a wide range of materials, both crystalline and amorphous. Signals are usually seen only in solids. but in compensation. no static magnetic field is required, so portable instruments can be envisaged. and samples remote from the RF antenna can be studied.

PRINCIPLES

NQR is a branch of magnetic resonance spectroscopy concerned with the absorption of RF radiation by matter in a zero static magnetic field.[1] Like its close counterpart. nuclear magnetic resonance (NMR), the transitions are excited by interaction of the RF magnetic field B_1 with the magnetic moment of the nucleus, but the energy levels depend on electric rather than magnetic interactions. However. signals are only observed in the solid state, in single crystals and in polycrystalline or amorphous samples. Such signals may be observed when the nucleus possesses an electric quadrupole moment, a property of nonspherical charge distributions: the nuclear electric quadrupole moment. Q, may be defined as follows:

$$eQ = \int \rho_n (3z_n^2 - r_n^2) d\tau_n \quad (1)$$

in which ρ_n is the nuclear charge density in a volume element $d\tau_n$, e is the electronic charge, and the integration extends over the nuclear volume in the state in which the maximum component of the nuclear magnetic moment lies along the z axis, that is $I=I_z$. This integral and. hence. the nuclear electric quadrupole moment, can be positive or negative, depending on whether the nucleus has the shape of a prolate (elongated) spheroid or an oblate (flattened) spheroid. Approximately half of the elements in the Periodic Table have one or more isotopes with a quadrupolar nucleus, subject to the general condition that their spin quantum number $I \geq 1$. so that all quadrupolar nuclei also have a magnetic moment. Some of the more important of these are listed in Table 1. together with recent values of Q in units of mb (the unit of 10^{-28} m^2 is often referred to as a "barn"). Note that the reliability of these values is constantly improved by calculation and experiment; however. the accuracy of the isotopic ratios, that is the ratio of the electric quadrupole moments of two isotopic nuclei. is usually considerably higher.

In NQR spectroscopy, the energy of the quadrupole levels depends on the interaction between the nuclear electric quadrupole moment and the electric field gradient produced by neighboring charges. both electrons and nuclei. The electric field gradient behaves as a second-rank tensor: in its principal axis representation. it may be defined by its three principal components q_{xx}, q_{yy}, q_{zz}, where. for example.

$$q_{xx} = -\partial E/\partial x = \partial^2 V/\partial x^2 = V_{xx} \quad (2)$$

and V is the electric potential at the nuclear site (strictly speaking, the electric field gradient is $-q_{xx}$). Because Laplace's equation

$$V_{xx} + V_{yy} + V_{zz} = 0 \quad (3)$$

is assumed to hold, only two quantities are required to define the electric field gradient, in addition. of course. to the direction cosines of the principal axes with respect to some set of axes embedded in the molecule or crystal. By convention, these are taken to be the maximum principal component. defined to be $q=q_{zz}$ (where $|V_{zz}| > |V_{yy}| > |V_{xx}|$) and the so-called asymmetry parameter, η, defined by

$$\eta = (V_{xx} - V_{yy})/V_{zz} \quad (4)$$

a positive number lying in the range between zero and unity η may be regarded as measuring the departure of the electric field gradient at the nucleus from axial symmetry On the other hand. q. the maximum principal component, can be negative and positive, and is zero only at sites of high symmetry, e g . tetrahedral (T_d) or octahedra1 (O_h) It

Encyclopedia of Supramolecular Chemistry
DOI: 10.1081/E-ESMC 120012820

Table 1 Nuclear electric quadrupole moments

Nucleus	Natural abundance (%)	I	Q/mb[a] ($\times 10^{-31}$ m^2)	Isotopic ratio
^{2}H	0.0156	1	2.86	
^{6}Li	7.43	1	−0.82	
^{7}Li	92.57	3/2	−40.1	0.0204
^{9}Be	100	3/2	52.9	
^{10}B	18.83	3	84.6	
^{11}B	81.17	3/2	40.6	2.084
^{14}N	99.64	1	20.2	
^{17}O	0.037	5/2	−25.6	
^{27}Al	100	5/2	140.3	
^{35}Cl	75.4	3/2	−81.6	
^{37}Cl	24.6	3/2	−64.4	1.269
^{45}Sc	100	7/2	−220	
^{55}Mn	100	5/2	330	
^{59}Co	100	7/2	410	
^{63}Cu	69.09	3/2	−220	
^{65}Cu	30.91	3/2	−204	1.081
^{75}As	100	3/2	314	
^{79}Br	50.57	3/2	298.9	
^{81}Br	49.43	3/2	276	1.197
^{113}In	4.16	9/2	799	
^{115}In	95.84	9/2	810	0.9843
^{121}Sb	57.25	5/2	−360	
^{123}Sb	42.75	7/2	−490	0.7845
^{127}I	100	5/2	−651	
^{135}Ba	6.59	3/2	160	
^{137}Ba	11.32	3/2	245	0.6500
^{185}Re	37.07	5/2	2180	
^{187}Re	62.93	5/2	2070	1.057
^{197}Au	100	3/2	547	
^{209}Bi	100	9/2	−500	

[a]Values were taken from P. Pyykkö and J. Li, Report HUKI 1-92. Helsinki. 1992. and were updated to 2002 values.

will. therefore, be zero at the nuclei of the chlorine and sodium ions in crystalline NaCl. unless their immediate environments are perturbed by strains or defects in the crystal. In many solids, however, such ions will not be at sites of high symmetry, and nonzero values of q are to be expected.

It should be noted that the quadrupole interaction is only the first nonzero term in the mathematical expression governing the variation of the electric potential V over the nuclear volume: the second is the nuclear hexadecapole interaction.[''] which depends on the coupling between the nuclear electric hexadecapole moment H and the fourth derivative of the electric potential $V^{(4)}$. The nuclear hexadecapole coupling constant, $e^2HV^{(4)}/h$. is only observable when $\mathbf{I} \geq 5/2$, e.g., for ^{127}I in MI. In this example of a strain-free single crystal. the quadrupole interaction can be ignored. in which case a small hexadecapole coupling constant of 2.8 kHz is derived for ^{127}I. Its small value makes it difficult to measure experimentally. but it should be assumed to be present for all heavy high-spin quadrupolar nuclei.

Experimentally, it is the product of the nuclear electric quadrupole moment, Q, and the electric field gradient, q, that is usually measured. The quantity e^2qQ/h, where h is Planck's constant. is often referred to as the quadrupole coupling constant and has units of frequency. It is positive or negative, according to the product of the signs of q and (2. As an illustration, consider the H^{35}Cl molecule in the vapor phase; assume $r_e = 0.127_8$ nm, and $Q(^{35}\text{Cl}) = -81.6$ mb. The neighboring proton generates a positive electric field gradient at the chlorine nucleus given by $+0.862 \times 10^{40} e$ m^{-2}J C^{-2} (see Eq. 9). The electronic contribution is also expected to be positive; assuming a value of $+20.61 \times 10^{40} e$ gives a net value for eq of $21.47 \times 10^{40} e$, and from Table 1. the product (e^2qQ/h) is then negative with a value of −67.85 MHz. However, the actual value observed in the solid will normally differ significantly. first because of solid-state effects (presumably hydrogen bonding in this example) and the averaging effects of thermal vibrations, which render q and η dependent on temperature and, to a lesser extent. on pressure.

In "pure" or zero-field NQR, the energy levels are obtained by solution of the quadrupolar Hamiltonian.[3] which in the principal axis representation may be written as follows:

$$\hat{H}_Q = eQ/[4I(2I-1)] \cdot [3I_z^2 - I(I+1) + 1/2\eta(I_+^2 + I_-^2)] \quad (5)$$

For a nuclear spin of **I**, there are $21+1$ levels in total, and the way in which these are arranged depends on whether **I** is half-integral or integral. By far the majority of quadrupolar nuclei have half-integral spin, in which case. the energy levels occur in $\mathbf{I} + {}^1/_2$ sets of degenerate pairs. irrespective of the value of η. For $I = 3/2$, for example. as in ^{35}Cl or ^{79}Br, two degenerate levels are obtained (as in Fig. 1a), and just one transition is observed of frequency:

$$\nu_Q = 1/2\ (e^2qQ/h)(1 + \eta^2/3)^{\frac{1}{2}} \quad (6)$$

according to the selection rule $\Delta m_I = \pm 1$, where m_I is the nuclear magnetic quantum number. It is customary to classify the two levels in terms of the two sets of degenerate values of m_I, namely, $\pm {}^1/_2$ and $\pm 3/2$. but strictly speaking, this distinction is only correct when $\eta = 0$. When this is not the case. the eigenfunctions of $_Q$ are linear combinations of $|+{}^1/_2\rangle$ with $|-3/2\rangle$ and $|-{}^1/_2\rangle$ with $|+3/2\rangle$, which are mixed because of the last term on the right-hand side of Eq. 5. For $I = 3/2$, the quadrupole coupling constant cannot, therefore, be derived unless η is

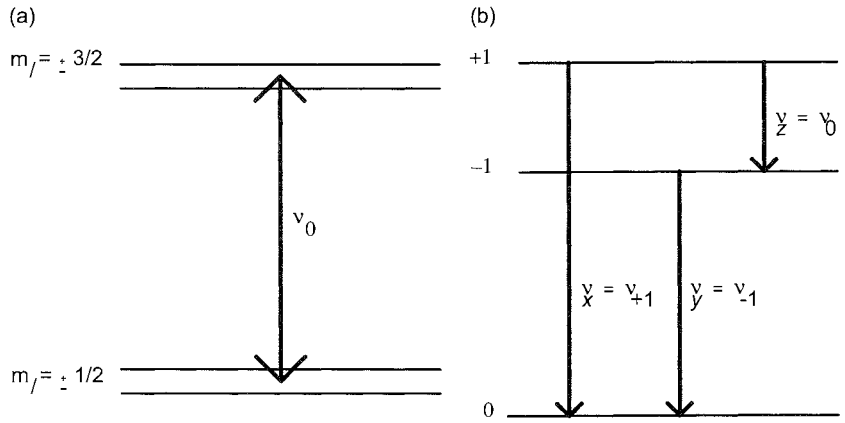

Fig. 1 Quadrupolar energy levels for (a) $I=3/2$ and (b) $I=1$.

known: the latter, however. can be obtained by experiments in weak magnetic fields or by quadrupole nutation spectroscopy.[4] For higher half-integral values of I, three or more sets of degenerate energy levels are obtained, and the existence of two or more allowed transitions following the selection rule $\Delta m_I=\pm 1$ means that values of the quadrupole coupling constant and asymmetry parameter can be separately derived by direct solution of the secular equation or by the use of tables listing frequency ratios as a function of η. In fact. because of the admixture of states when η is nonzero, transitions following the selection rule $\Delta m_I=\pm 2$ can also be weakly observed. In all cases. however, the sign of the quadrupole coupling constant is not usually derived. because changing its sign simply inverts the order of the energy levels. The sign can be obtained if other couplings of known sign, such as dipolar interactions. are present in the spectrum; alternatively, one can work at low temperatures [e.g., 100 μK for ^{45}Sc ($I=7/2$) in scandium metal],[5] when the substantial differences in populations cause deviations in the intensity ratios of adjacent transitions. For these higher-spin nuclei, when η is zero, the higher frequencies are all harmonics of the lowest, $\pm 1/2 \rightarrow \pm 312$. which equals 3/20 ($e^2qQ/h$) for spin 512, 1/14 ($e^2qQ/h$) for 712. and 1124 ($e^2qQ/h$) for 912. Thus, in $[Co(C_5H_5)_2]^+ ClO_4^-$ at room temperature. the three ^{59}Co frequencies expected for a spin −712 nucleus are detected near 12, 24. and 36 MHz, showing that the cobalticinium ion has axial symmetry and that the ^{59}Co quadrupole coupling constant is close to 170 MHz.

The situation is simpler for integral-spin nuclei, for which the degeneracy of the $2I+1$ levels is always resolved, except when η is zero. Typical examples are the spin-1 nuclei ^{2}H and ^{14}N, which in the general case, have three observed transitions. as in Fig. 1b, one of which is the sum of the other two, facilitating assignments when all three can be observed. The quadrupole coupling constant and asymmetry parameter can be separately determined from any pair of the three transitions. correctly assigned. from the following equations:

$$\begin{aligned} \nu_x &= \nu_+ = 3/4\ (e^2qQ/h)(1 + \eta/3) \\ \nu_y &= \nu_- = 3/4\ (e^2qQ/h)(1 - \eta/3) \\ \nu_z &= \nu_0 = 1/2\eta(e^2qQ/h) \end{aligned} \tag{7}$$

Many of the comments in the previous sections apply equally to single crystals as to polycrystalline samples, hut the advantage of the former is that they also allow the direction cosines of the quadrupole tensor to be determined. For spin-312 nuclei, such as ^{35}Cl or ^{79}Br, a weak magnetic field. B_0, is usually needed, which splits the $\pm 1/2$ and $\pm 3/2$ levels in Fig. 1 into a doublet and a quadruplet. respectively. Four transitions are now observed, symmetrically located about the original resonance frequency, the inner pair labeled α and the outer β. Their splitting varies with the orientation of the crystal with respect to B_0; the locus of zero splitting of the α doublet defines a geometric shape from which η and the direction cosines of V_{zz} and V_{xx} with respect to the crystal axes can be determined. Such measurements are relatively uncommon: the increasing use of high-field NMR spectrometers enables similar measurements to be made, often with a higher sensitivity and smaller single crystals. provided. of course. that the quadrupole splitting frequencies are considerably smaller than the NMK frequency.

EXPERIMENTAL METHODS

Experimentally, NQR measurements may be conducted on essentially the same instruments used for solid-state NMR, except that no static magnetic field is needed.

Unfortunately, the frequency range required is extremely large, stretching from less than 100 kHz or so for ^{2}H to 600 MHz or more for the high-frequency lines of heavy nuclei such as ^{127}I. A variety of RF probes has been designed to cover this range, from simple RF coils at low frequencies to butterfly capacitors and transmission lines up to and above 300 MHz. Because no static magnetic field is necessary, NQR experiments can be conducted with samples located inside much larger volumes of up to 600 liters or more, or in remote locations, tens of centimeters away from the RF antenna.[6] Most modern spectrometers use pulsed-RF techniques, which have the advantage of measuring relaxation times as well as frequencies. Whereas the latter give information on molecular structure and electron distribution, the former are an important source of information on molecular dynamics. Noise or stochastic excitation can also be used to observe spectra and has the advantage of requiring considerably smaller RF powers than conventional pulsed techniques used for solids.[7]

An advantage of pulse techniques is that they allow ready measurement of the quadrupole relaxation times, which are important in the investigation of molecular motion in solids. One useful quantity is the spin-lattice relaxation time. T_1, which as in NMR governs the time taken for the spin system to return to equilibrium following an RF pulse, and which can be measured, for example, by a pulsed steady-state sequence, in which a string of 90° RF pulses of variable spacing τ is applied to the sample, the signals being detected between pulses (the term 90° refers to that pulse width that generates the maximum signal). As τ is lengthened from values much less than T_1 to much longer, the recovered signal between pulses increases exponentially according to T_1, eventually reaching its equilibrium value.

The probes for pulsed RF spectrometers are usually difficult to tune over a sufficiently wide range to be suitable for searching for new resonances. Variable frequency continuous wave or superregenerative oscillator spectrometers are better adapted for this purpose, but they give little information on relaxation times. The same is true of NMR methods, which, however, may give problems when the solid to be studied contains several nonequivalent nuclei with different quadrupole parameters. Double-resonance techniques based on magnetic field cycling are also useful. provided the solid contains suitable magnetic nuclei, such as ^{1}H. with strong NMR signals.[8] However, if the structure of the solid is known, e.g., from x-ray or neutron diffraction, theoretical calculations can be employed to give a good estimate of the magnitudes and signs of the quadrupole parameters. Essentially, they are one-electron properties of the ground electronic state of the molecule; their significance can be understood from Fig. 2, which represents a volume

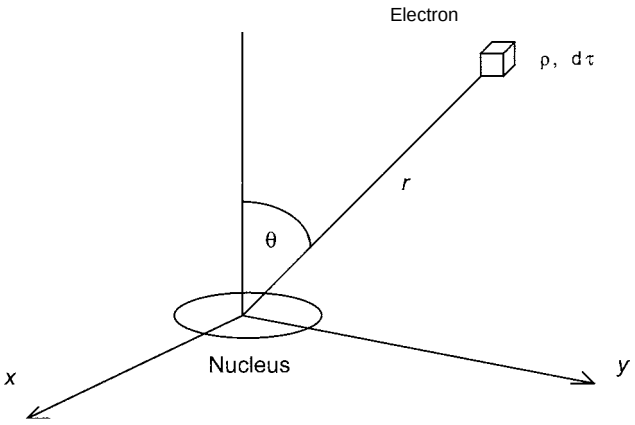

Fig. 2 A volume element, $d\tau$. of charge density p, distance r from the nucleus at the origin.

element $d\tau$ of the molecular charge density p (including sign) generating at the origin the electric potential:

$$V = \rho d\tau/\{(4\pi\varepsilon_0)r\} \tag{8}$$

where ε_0 is the vacuum permittivity, from which it is easy to show that

$$\partial V/\partial z = -\rho(4\pi\varepsilon_0)^{-1}(z/r^3)d\tau$$
$$= -\rho(4\pi\varepsilon_0)^{-1}(\cos\theta/r^2)d\tau$$

and

$$q_{zz} = \partial^2 V/\partial z^2 = \rho(4\pi\varepsilon_0)^{-1}(\{3\cos^2\theta - 1\}/r^3)d\tau \tag{9}$$

Separating out the nuclear charge contribution of nuclei at a distance R_i from the nucleus under study (which behave as point charges) and replacing ρ for the electrons by the product $\psi\psi^*$ gives the following equation for eq:

$$eq = V_{zz} = (4\pi\varepsilon_0)^{-1}\{-e\int \psi^*([3\cos^2\theta - 1]/r^3)\psi d\tau + \sum Z_i e([3\cos^2\theta_i - 1]/R_i^3)\} \tag{10}$$

To evaluate the first term on the right-hand side of Eq. 10 one needs good ground-state wave functions. for the second one needs the molecular geometry or crystal structure. Similar equations can be used to calculate the asymmetry parameter η from V_{xx} and V„. Modern, a priori, programs that include all electrons are now being used[9] and give quadrupole parameters that agree with experiment to better than 20%. They do not. however. always include corrections for vibrational and translational motions of the atoms and molecules in the solid state, which are largely responsible for the observed temperature variation of the quadrupole parameters.

There are several approximate methods often useful in understanding the trends in the quadrupole parameters in a related series of molecules containing the same quadrupolar nucleus. One. due to Townes and Dailey,[10] *is essentially a localized orbital approach. in which attention is focused on changes in the orbital populations of the atom containing the quadrupolar nucleus. and polarization of the core electrons (the so-called Sternheimer polarization factor) is assumed to vary negligibly from one molecule to another. In the case of* ^{14}N, *for example, the* $2p$ *electron distribution is the dominant factor; in a molecule such as* NH_3, *the lone pair is the major contributor, so that* q_{zz} *lies along the lone pair direction, the electronic term from Eq. 9 is negative. and because* Q *is positive (Table* I), *the quadrupole coupling constant is negative. Donation of the* N *lone pair, as in coordination to an electron acceptor, reduces the* $2p$ *lone-pair population* and *hence makes the quadrupole coupling constant less negative. Such a model, however. contains many approximations; it neglects, for example. changes in the H–N–H angle that may occur on coordination.*

APPLICATIONS

Almost all quadrupolar nuclei in the Periodic Table have been studied experimentally in one or more of their compounds. A *current list of these results is available in a database published by the JAICI (Japan Association for International Chemical Information, Tokyo, Japan). Biennial International Symposia on nuclear quadrupole interactions are also excellent sources of the latest experimental and theoretical works. As an illustration of the kind of solid-state problems that may be studied, we give some recent examples of such investigations. Sensitivity. or signal-to-noise ratio (SNR) in WQR spectroscopy, as well as NMR, depends on the observed frequency, which in turn, depends, inter alia, on the value of* Q. *The lighter* elements *tend to have low values of Q and low NQR frequencies and low sensitivities.* ^{2}H, *for example. a spin-1 nucleus, has NQR frequencies less than 200* kHz, *and most measurements are therefore* made *by high-field* NMR *methods. The* ^{14}N, *another spin-I nucleus, resonates from below 0.4 to 6 MHz, an intermediate region where both NQR and NMR methods are used. Because they are governed predominantly by electric interactions. NQR frequencies and relaxation times are sensitive to phase changes and the numbers of lines to changes in the crystal symmetry. For example,* ^{14}*N-NQR was used*[i''] *to study the inclusion compound of thiourea and carbon tetrachloride, which undergoes a second-order phase transition near 67 K, the low-temperature phase having three signals for the* ν_+ *transition from the host, whereas above 67 K, only a singlet is observed. Over a range of about* 1 *K, signals can be observed from both phases near 2.5 MHz.*

At higher frequencies of 40–41 MHz, ^{35}Cl-NQR *signals can be* observed[12] *in the guest molecules, which show two resonance lines with an intensity ratio of* 1:3, *indicating that they lie at sites of threefold symmetry in the channels of the host. Above 27 K, the* ^{35}Cl *lines disappear, due to gross reorientation of the* CCl_4 *molecules. The favorable sensitivity at these higher* radio-*frequencies has led to a number of notable experiments, including NQR imaging and two-dimensional (2D) exchange spectroscopy. In the* former,[13] *the experiments were conducted at* 116 MHz, *the* ^{75}As-NQR *frequency in arsenolite. and the imaging technique was based on the* use *of gradients in the RF* B_1 *field (rotating-frame* NQR *imaging). Two cylinders of this material of diameter 3.5 cm, and placed* 5.5 cm *apart, were easily resolved in two* dimensional *images. In the latter. the phrase "exchange" should be interpreted in a general sense, to include not only chemical exchange of atoms or groups but also molecular rearrangements or rotation of atoms or groups within molecules. For example, a three-pulse, 2D sequence was used to study molecular rotation of the* $-CCl_3$ *group in p-*chlorobenzotrichloride.[14] *The first pulse excites all quadrupole resonances within the excitation* width *of the pulse. which are allowed to evolve in a time* t_1; *the second pulse restores some of the longitudinal magnetization, which now changes as the exchange process takes place. Finally,* a *third pulse generates the exchange-modified NQR signals that are sampled over a* time t_2. A *double Fourier transform with respect to* t_1 *and* t_2

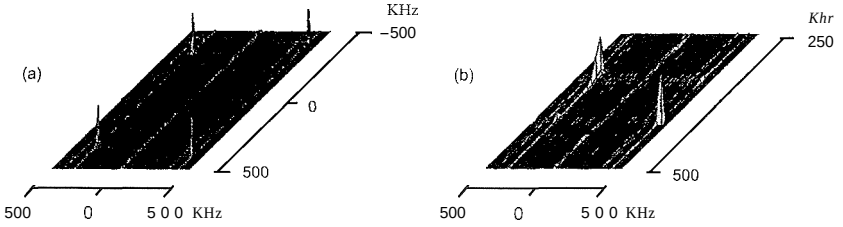

Fig. **3** A two-dimensional exchange ^{35}Cl-NQR spectrum of *p*-chlorobenzotrichloride at 208 K. (a) Whole spectrum and (b) lower part in more detail.

then generates a 2D spectrum in which the off-diagonal or cross peaks represent a transfer of magnetization at frequency coordinates corresponding to the sites between which exchange occurred. In the example selected, the ^{35}Cl-NQR spectrum of the $-CCl_3$ group consists of two lines at frequencies close to 38.07 and 38.82 MHz at 207 K (Fig. 3): the cross peaks on either side of the diagonal arise from hindered rotation of the $-CCl_3$ group. which interchanges the two sites of different frequencies. At a temperature of 201 K. jump times are of the order of a ms or so.

Pulsed NQR measurements of the spin-lattice relaxation time, T_1, also give detailed information on the mechanisms and dynamics of molecular motion in solids. For example, ^{14}N quadrupole relaxation times for solid triethylenediamine show a T_1 minimum at a temperature close to 260 K. when T_1 equals 0.048 s.[15] On either side of the minimum, T_1 depends exponentially on temperature, according to an Arrhenius-type equation with an activation energy of 34 kJ mol^{-1}. The mechanism of the relaxation is shown to be hindered rotation of the triethylenediamine molecule about its threefold symmetry axis, which modulates the dipolar coupling between ^{14}N and the adjacent CH_2 protons.

NQR can be used to study the electronic structure of a wide variety of inorganic compounds and complexes. As an example. ^{63}Cu and ^{65}Cu, both spin-312 nuclei, have been investigated in a variety of Cu(I) complexes.[16] In a number of halocuprate ions, for example, the ^{63}Cu-NQR frequencies lie between 26–31 MHz according to the halogen atoms (Cl. Br, I) attached to the Cu(I) atom: in such cases. by using the Townes–Dailey theory. it is possible to interpret the variation in terms of the 3*d*, 4s. and 4*p* orbital populations of the Cu atom in the complex.

Intercalated compounds can also be studied by WQR methods, typical examples being amine intercalates of the layered structures of CdI_2 and PbI_2,[17] in which the ^{127}I (I= 512) resonances lie close to 80 (112→312) to 90 (3/2→512) MHz for the former and 17 (112→312) to 75 (3/2→512) MHz for the latter. depending on the chemical nature of the amine intercalate and its chemical interaction with the host.

Finally. crystalline and amorphous phases can be studied by NQR methods, the expected distinction between the two being that much broader lines are encountered in the latter. Despite line widths of 1 MHz or more. NQR signals can still be seen. provided suitable frequency-swept pulse sequences are used. An example is ^{75}As-NQR in arsenic-chalcogen glasses, such as As_2S_3 and As_2Se_3, in which the resonance lines can be 8–10 MHz in width.[18] In Fig. 4, the dotted line shows ^{75}As-NQR in annealed glassy As_2S_3 in bulk, with the two lines at the top of the diagram denoting the experimental frequencies in crystalline As_2S_3. The triangles (dashed line) are for the fast-evaporated film. which shows new peaks close to 80 and 94 MHz, close to the ^{75}As-frequencies in crystalline As_4S_3. These new lines are attributed to the presence of As—As bonds in the film, which are broken when the sample is irradiated for 30 h with radiation of wavelength 5145 Å.

Two-dimensional NQR methods give further information on the broadening mechanisms by the use of 2D correlation methods.[19] In a coherence transfer experiment, for example, a pair of 90° pulses separated by a variable delay t_1 is applied to (say) one transition ν_1 of a half-integral spin nucleus (such as ^{123}Sb, for which $I=7/2$), followed by a 90°-τ-180° pulse pair at a second connected transition ν_2, the signal being detected at a time t_2 following the 180° pulse (a 180° pulse is approxiinately twice the width of a 90" pulse). A double Fourier transform with respect to t_1 and t_2 gives a 2D spectrum correlating the two transitions ν_1 and ν_2, from an analysis of which the individual broadening components of the electric field gradient tensor. Δq_{xx}, Δq_{yy}, Δq_{zz} can be derived, giving information on the anisotropy of the line-broadening mechanisms.

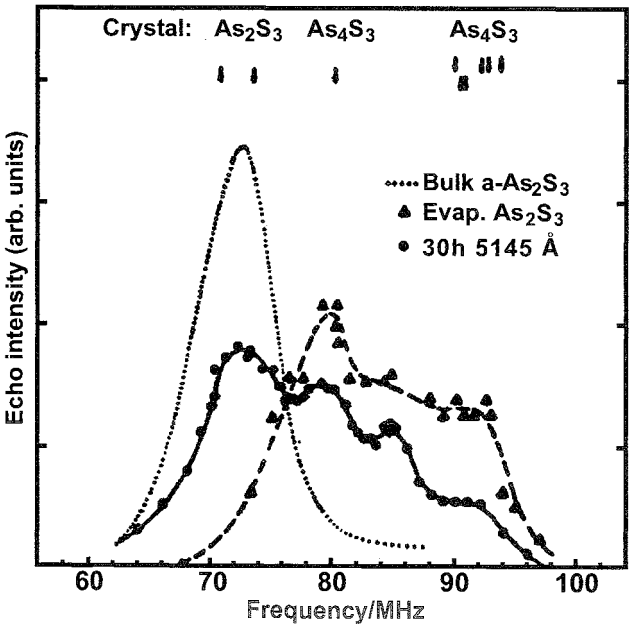

Fig. 4 ^{75}As-NQR in bulk glassy A_2S_3 (dotted line) and in rapidly evaporated film (dashed line). Irradiation for 30 h with light of wavelength 5145 Å produces the NQR response shown by the continuous line. The frequencies of ^{75}As-NQR signals in selected crystals are shown at the top of the figure.

CONCLUSION

NQR spectroscopy is a powerful method for studying the electronic structure of molecules and their dynamic

behavior in the solid state. A wide range of nuclei has an electric quadrupole moment and can be studied in crystalline and amorphous phases. The frequencies and relaxation times are related to the electronic structure and dynamic behavior, respectively, enabling the electron distribution in inorganic complexes. host and guest molecules in inclusion and intercalated compounds, and any molecular motion therein, such as chemical exchange and molecular rearrangements as well as phase changes, to be investigated. NQR spectra are usually inhomogeneously broadened, and experimental methods are available with which to study the magnitude and anisotropy of these effects. Illustrative examples are given of NQR studies in a range of materials containing one or more of the quadrupolar nuclei ^{14}N, ^{35}Cl, ^{59}Co, $^{63\,65}$Cu, ^{75}As, and ^{127}I.

ARTICLES OF **FURTHER** INTEREST

Inelastic Neutron Scattering, p. *727*
Neutron Diffraction, p. *959*
Solid-State Nuclear Magnetic Resonance Spectroscopy, p. 1307
X-Ray Crystallography, p. *1586*

REFERENCES

1. Smith. J.A.S. Nuclear quadrupole interactions in solids. Chem. Soc. Rev. 1984, *15.* 225–260.
2. Ni. Q.W.; Sears. R.E.J. Quadrupole echoes and the ^{127}I nuclear hexadecapole interaction in KI. J. Chem. Phys. 1991, *95.* 4796–4801.
3. Slichter, C.P. *Principles* of *Magnetic Resonance;* Springer-Verlag: Berlin, 1990: Chapter 10.
4. Maćkowiak, M.; Kątowski, P. 2D off-resonance nutation spectroscopy of spin 3/2 nuclei. Z. Naturforsch. 1998, *53a.* 285–292.
5. Pollack. L.: Smith. E.M.: Parpia. J.M.: Richardson. R.C. Determination of the electric field gradient and relaxation time measurements in scandium metal at very low temperature. J. Low Temp. Phys. 1992. *87.* 753–772.
6. Peirson. N.F.; Rowe. M.D.; Smith, J.A.S. In *State* of *the Art in NQR Mine Detectiorz—An Overview,* Proceedings of a Joint Workshop on Research on Demining Technologies, European Commission, JRC–Ispra. Italy, July 2000; 91–93.
7. Liao, M.-Y.; Zax, D.B. Analysis of signal-to-noise ratios for noise excitation of quadrupolar nuclear spins in zero field. J. Phys. Chem. 1996, *100.* 1483–1487.
8. Stephenson, D.; Smith. J.A.S. Nitrogen-14 quadrupole cross-relaxation spectroscopy. Proc. Royal Soc. Lond. 1988. *416A,* 149–178.
9. Soldner. T.: Troger. W.; Butz, T.; Blaha. P.; Schwarz, K. ISOLDE collaboration. Measurement and calculation of electric field gradients in Hg-mercaptides. Z. Naturforsch. 1998; *53a,* 404–410.
10. Lucken, *E.A.C. Nuclear Quadrupole Coupling Constants*; Academic Press: London, 1969: Chapter 7.
11. Ghallali, J.El.; Courdji. M.; Guibé, L.; Péneau. A. Investigation of the phase transition at 67.17 K in the thiourea-CCl_4 compound as studied by ^{14}N NQR. Z. Naturforsch. 1994. *49a,* 433–438.
12. Matsuo, *T.;* Sekii, M.: Suga, H.; Nakamura. N. ^{35}Cl NQR study of guest dynamics in thiourea-CCl_4 inclusion complex. Z. Naturforsch. 1990, *45a,* 519–522.
13. Kimmich, R.; Rommel. E.; Nickel, P.; Pusiol, D. NQR imaging. Z. Naturforsch. 1992. *47a,* 361–366.
14. Kimmich. R. Multidimensional NQR: Imaging and exchange spectroscopy. Z. Naturforsch. 1996. *51a,* 330–336.
15. Zussman, A.; Alexander, S. Pure nuclear quadrupole resonance in triethylene diamine. J. Chem. Phys. 1968, *48,* 3534–3539.
16. Lucken, E.A.C. The nuclear quadrupole resonance of the $^{63.65}$Cu nuclei in Cu(I) complexes. Z. Naturforsch. 1994, *49a.* 155–166.
17. Babushkina, T.A.: Seryukova, I.V. NQR ^{127}I spectroscopy of layered inorganic compounds intercalated with aromatic amines. Z. Naturforsch. 1998. *53a,* 585–589.
18. Boolchaud, P. Nuclear quadrupole interactions as a probe of glass molecular structure. Z. Naturforsch. 1996, *51a.* 572–584.
19. Liao. M.-Y.; Harbison, G.S. Two-dimensional nuclear magnetic resonance correlation spectroscopy at zero field. J. Chem. Phys. 1999, *111,* 3077–3082.

Organic Zeolites

Tino Hertzsch
Jürg Hulliger
University of Berne, Berne, Switzerland

Edwin Weber
Technische Universitat Bergakademie Freiberg, Freiberg, Germany

Piero Sozzani
Universitd di Milano—Bicocca, Milan, Italy

INTRODUCTION

Since 1756, when the Swedish mineralogist Cronstedt described a group of silicate minerals as zeolites, this area developed immensely. In early times, observations were limited to the fact that these minerals lose water while heating (zeolithos: *steaming stones). An ever-increasing number of other properties are known today. Zeolites were found to show outstanding ion exchange and sorption properties for all kinds of small-diameter molecules.'" The most well known are topochemical applications for large-scale cracking of olefins. Essentially, zeolites are* somehow *porous materials. A great number of synthetic zeolite frames were synthesized over the years. Most of these structures are formed by use of a template and are obtained by kinetic control. Many inclusion compounds survive the removal of guest molecules upon heating and under vacuum conditions, although they are not* thermodynamically *stable thereafter. Recently, much effort was devoted to obtaining materials that feature zeolite properties, however, exclusively involving molecular units and supramolecular interactions in the solid* state.[2] *Although a tuning of pore sizes may give rise to materials featuring the potential of zeolites, a* main *drawback of molecular crystals may be that the chemical and thermal stabilities are inferior to inorganic counterparts. Impressively: at present. organic network structures can show porosity up to about 91% of the total* volume *and are capable of undergoing selective guest inclusion.'"* Such *supramolecular* materials *yield significantly more open space than classical inorganic* zeolites.[4,5]

A p omising strategy for assembling porous organic networks refers to the stability of some supramolecular *interactions. As a result of strong bonding by metal coordination or hydrogen bonding. some networks are robust enough to withstand the total removal of guests. All* kinds *of driving forces that can induce* self-assembly *to access zeolite-like organic compounds are thus of great interest.*

CRYSTAL DESIGN

Prediction of Porous Networks

The main molecular strategy to structure materials uses supramolecular synthons.[6]

Despite the effect of packing constraints given by molecular shape and symmetry, organic solids may be designed by using directional or anisotropic interactions (hydrogen bonding or halogen–halogen or metal–*ligand interactions).*

The Cambridge Structural Database (CSD) *is a comprehensive source for intermolecular motifs.* In *view of the fact that structural predictions became more* successful *in the last few years. open framework materials are nevertheless difficult to predict correctly, because they often represent thermodynamically nonstable states.*

The avoidance of close packing in *a crystal structure is thus a major aim in creating nanoporous organic materials.*

A *basic principle for the prediction of crystal structures was described by Kitaigorodskii:*

> We must first of all deduce all possible methods of constructing chains of molecules (formations extending in one dimension) and then demonstrate what layers are possible (formations extending in two dimensions). followed finally by considering layer stacking in the crystal (a formation extending in three dimensions).[7]

The occurrence of porosity in crystals may be generated by molecules. which prevent close packing by their constitution, the molecular bulkiness or rigidity in suitable positions. Hexahosts, *molecules of the* ''wheel *and axle" type and coordinatoclathrates are representative*

Encyclopedia of Supramolecular Chemistry
DOI: 10.1081/E-ESMC 120012806

examples of nanoporous structures exhibiting guest inclusion.[8–11]

More often, geometrical approaches prove useful. Molecules or metal ions in crystals may be considered as nodes and the intermolecular interactions as connectors.[12,13] This widely accepted concept facilitates a design of one-dimensional (1D), two-dimensional (2D), and three-dimensional (3D) networks by the "building block" principle (Fig. 1a).[14,15] However, there is a significant problem associated with this concept. Because of a gain in lattice energy by n-fold interpenetration, many attempts result in densely packed structures.

Some of the basic principles leading to a large number of zeolite-type materials are summarized below. In view of what is known today, the series of examples is by no means complete.

Avoiding Close Packing: A Delicate Issue

Giving a concise definition for an organic zeolite remains an ambiguous task. In inorganic zeolites, the crystal structure is determined by ionic and covalent bonding. Directional and nondirectional forces play the important role for design of organic crystal structures.

Porous organic lattices may thus be designed, using the idea of nodes and connectors similar to inorganic networks. This principle is used above all in coordination polymers. Compared to these, in organic compounds; much weaker interactions are responsible for the assembly of a porous network. Therefore, structures tend to be flexible, being unstable in many cases and not able to maintain empty cavities after removal of a template. However, cavity-type channel systems exist that can be obtained free of guests, featuring reversible exchange.

In some cases, a polymorphic modification referred to as apohost (host without guest) is left after desorption of guests. Apparently, network topologies are interesting, which after desolvation and collapse of their cavity structure can restore porosity. Other networks allow a partial desorption of guests or guest exchange, without passing through a solvent-free stage. A delicate issue is, thus, the avoidance of interpenetration.

POTENTIAL ORGANIC ZEOLITES: STRUCTURAL AND KINETIC ASPECTS OF THEIR FORMATION

The fundamental questions in view of structural and kinetic aspects of organic zeolites are reduced to the following: How can structures with stable voids be generated, and by which mechanism can guest exchange occur?

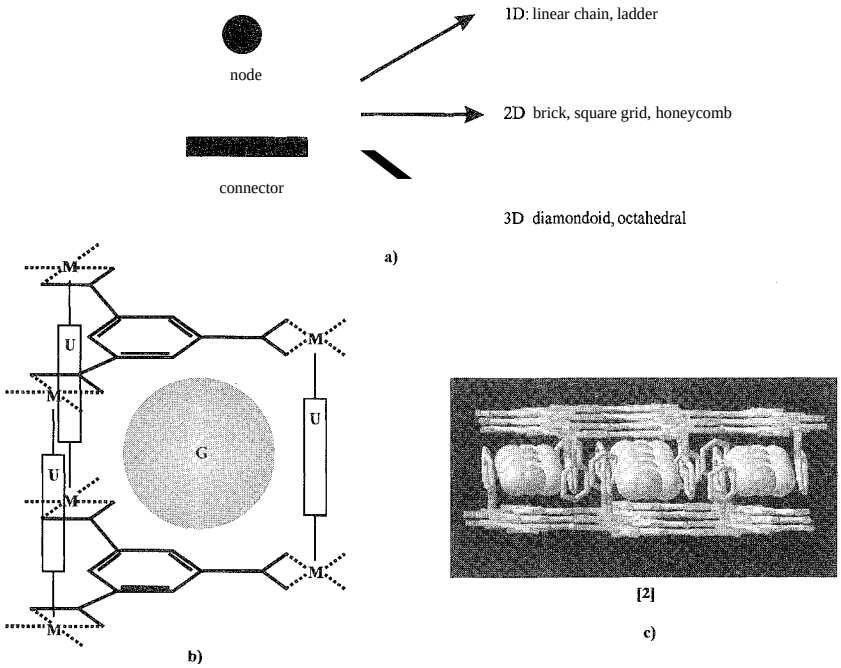

Fig. 1 Node and connector principle for metal–organic networks design. (a) Basic approach to form 1D, 2D, and 3D architectures using the principle of nodes and connectors. (From Refs. [14, 15].) (b) BTC-ligand occupying the vacant metal sites perpendicular to layers. This can produce a porous metal–organic framework with large channels. A variation of the metal ion (M) and the molecular unit (U) provided many options for the design of networks (G: guest). (From Ref. [16].) (c) Structure of $CoC_6H_3(COOH_{1/3})(NC_5H_5)_2(NC_5H_5)_{2/3}$ [2] with a rigid disk-like conformation, where pyridine is incorporated in the free space of the metal–organic framework (Co: green, O: red, N: blue. C: gray). (From Ref. [16].) (View this *art* in *color at www.dekker.com.*)

Structural Aspects of Stability

Metal–organic frameworks (MOF) and coordination polymers

A known strategy to prevent interpenetration is based on symmetry and functionality. Coordination polymers are built from ligand-to-metal bonding between transition metals and suitable organic ligand types. It is noteworthy that the geometry of the metal environment reproduces itself over the bridging ligands, i.e., by its network topology. Benzenetricarboxylate (BTC) offers three equally spaced carboxylate groups linked to an aromatic ring to form a rigid disk-like conformation. Metal–carboxylate (MC) layers result with first-row-transition metal–ions, being altered by molecular units (U) to produce alternating MC and *U* layers (Fig. Ib). Depending on the nature of *U*, a suitable environment for selective inclusion of guests between layers was achieved.''' Upon exchange, the crystal lattice is preserved, and the distance between the MC layers remains constant. The dimension of the metal-BTC-porous framework depends on the solvent used for synthesis and on the strength of the base applied for the deprotonation of trimeric acid (TMA).[17] In $Zn_2(BTC)(NO_3)(H_2O)(C_2H_5OH)_5$ [**1**], the triple-bidentate functionality of BTC promotes rigidity for the Zn-BTC-network, in which the metal centers can undergo unsaturated coordination. In $CoC_6H_3(COOH_{1/3})_3(NC_5H_5)_2(NC_5H_5)_{2/3}$ [**2**], rectangular channels (7 x 10 Å^2) are developed (Fig. 1c).[16]

By means of copolymerization of Zn(II) with the bidentate ligand 1,4-benzenedicarboxyl (BDC) a 3D porous framework of the composition $Zn_3(BDC)_3(CH_3OH)_6$ [**3**] was formed. The unsaturated zinc centers are able to coordinate guests selectively.[18]

After desorption of water in $Zn(BDC)(DMF)(H_2O)$ [**4**], only O···Zn interactions are responsible for stabilization of the remaining guest-free rnicroporous network (Fig. 2a).[19]

A further prominent strategy is based on the metal carboxylate chemistry, where an organic dicarboxylate linker is used to yield octahedral clusters being capped with monocarboxylate. $Zn_4O(BDC)_3(DMF)_8(C_6H_5Cl)$ [**5**] consists of $Zn_4(O)(CO_2)_6$ clusters, which spawn a pore sphere as large as 8 Å in diameter (Fig. 2b).[20] The bidentate linkers can be varied and functionalized, whereby crystalline materials are obtained with an open space up to 91.1% of the crystal volume. The diameter of the pores can be varied from 3.8–28.8 A. Some compounds reveal densities of 0.21 g/cm^3 and thus represent the lowest densities for crystalline materials.'''

In the polymer of $CuSiF_6(bipy)_2$ [**6**], Cu^{II}-ions are coordinated by four 4,4-bipyridyl (bipy) ligands forming a

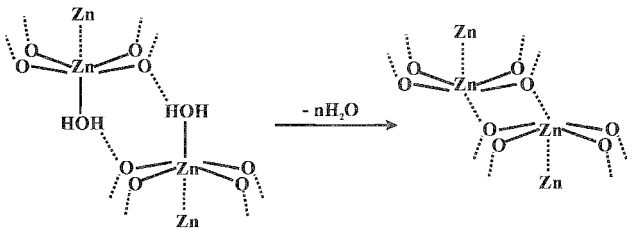

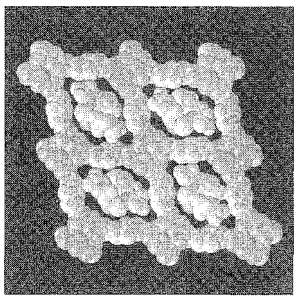

[4]

a)

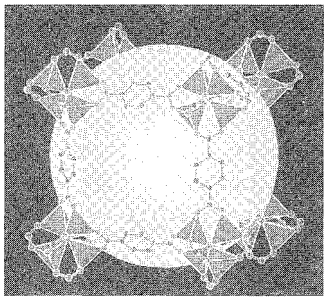

[5]

b)

Fig. 2 Stabilized Zn(BDC) networks due to cluster formation. (a) Formation of strong O···Zn interactions was obtained in the absence of water in the Zn(BDC) framework. The crystal structure of $Zn(BDC)(DMF)(H_2O)$ [**4**] showed 1D channels, which are occupied by DMF molecules (Zn: blue. C and H: gray, 0 : green, and N: red). (From Ref. [19].) (b) Eight clusters of $Zn_4(O)(CO_2)_6$ in the metal–organic framework of compound $Zn_4O(BDC)_3(DMF)_8(C_6H_5Cl)$ [**5**] surrounding a large cavity (yellow sphere). Approximately 55–61% of the space is accessible to guest species. The color scheme is the same as that in Fig. 2a. (From Ref. [20].) (*View* ***this*** *art in color at www.dekker.com.*)

3D network. Here, SiF_6 anions connect layers, preventing interpenetration. Channels with pore sizes of 8 x 8 Å^2 along the c-axis. and 6 x 2 Å^2 along the h-axis are formed (Fig. 3a).[21]

The elongation of the spacer enables variation of the void structures as well as the pore sizes. A noninterpenetrated square-grid arrangement with 4,4-*bis*(4-pyridyl)biphenyl [**7**] and Ni(II) was obtained. In this network, channels are stretched and offer a pore dimension of about 20 x 20 Å^2.

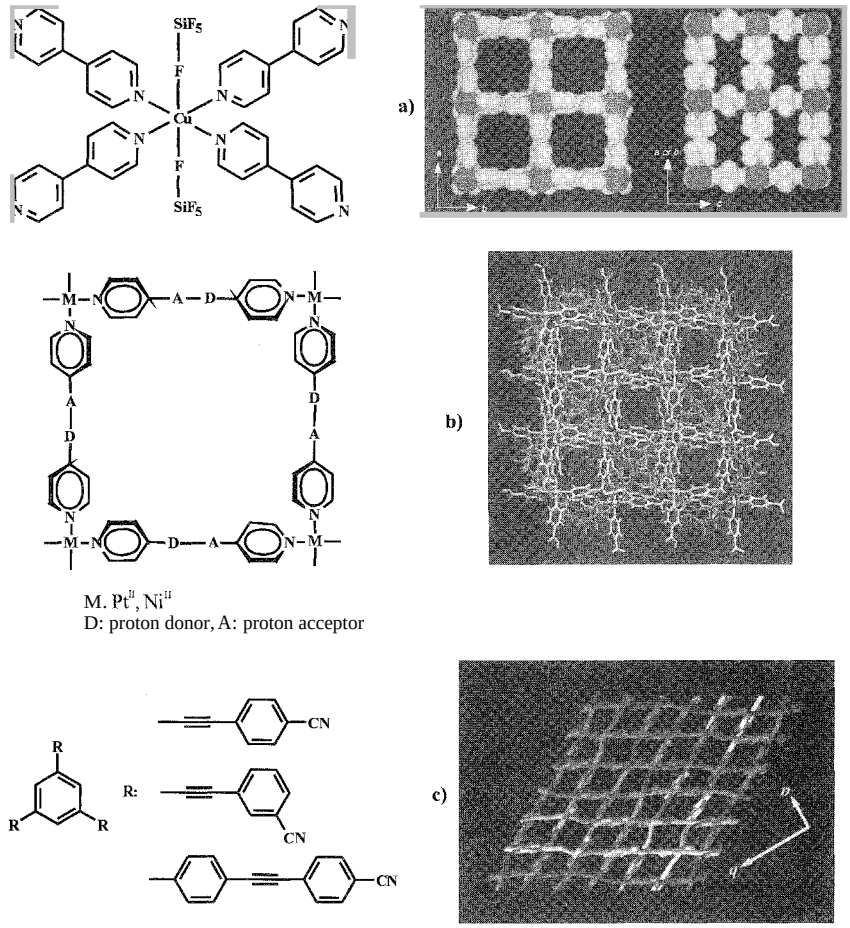

Fig. 3 Coordination polymers—a successful approach to permanent voids. (a) The porous coordination polymer $[CuSiF_6(4,4'\text{-bipyridine})_2]_n$ [**6**] produced a 3D network with channels in all directions in the crystal (Cu: blue, N: red, Si: green; F and C: gray). (From Ref. [21].) (b) Pt^{II}- and Ni^{II}- metal ions coordinating pyridine and forming a square arrangement stabilized by donor–acceptor interactions. (From Ref. [23].) (c) Trigonal rigid arrangements of the phenylacetylene nitrile molecules producing a honeycomb channel structure. Despite six interpenetrating networks (different colors) in the (*a,b*)-plane of benzene-1,3,5,-TEB-silvertriflate [**8**], a channel with a diameter of 15 Å was obtaincd along the c-axis. (From Refs. [24–26, 45].) (*View this* art in color at *www.dekker.*corn.)

Therein, guest molecules occupy more than 50% of the crystal volume, thus providing high porosity.[22]

Because of donor–acceptor interactions through hydrogen bonding between pyridinc derivatives and coordination to Pt or Ni, a square-planar cavity structure was obtained that showed decomposition above 300°C (Fig. 3b).[23] Mutual penetration of individual networks can give rise to an increase in thermal stability, even though empty cavities still exist.

Guest removal and exchange were investigated for benzene-1,3,5,-TEB-silvertriflate [TEB=*tris*(4-cthynyl-benzonitrile)] [**8**] (Fig. 3c).[24] The nitrile functionality of the trigonal phenyl-acetylene-derived ligand coordinates to silver cations forming a (3,3)-connected 3D network. A honeycomb-like structure with a channel dimension of 15 x 22 $Å^2$ was obtaincd. Further examples appeared in the literature involving coordination of Ag by CN ions. Here, the length and shape of the rigid axle appear to diversify, and thus, the channel diameter of the networks becomes variable (Fig. 3c).[25,26]

In the zeolite-like material, 4,6-di(1-imidazolyl)-1,3,5-triazin-2-one (dimto) [**9**], large pores were found in which a dimto anion can act as a threefold ligand forming a continuous box-like unit with Zn(II) featuring a pore size of 9.6 x 5.5 $Å^2$ (Fig. 4a).[27]

The 1,2-dipyridylglycol (dpgy) acts as a functional pillar in the case of $Cu_2(pzdc)_2(dpyg)(H_2O)_8$ (pzdc: pyrazine-2,3-dicarboxylate) [**10**]. A 3D pillared-layer structure was obtained, whereby the resulting microchannels show a cross section of 4 x 6 $Å^2$ (Fig. 4b).[28]

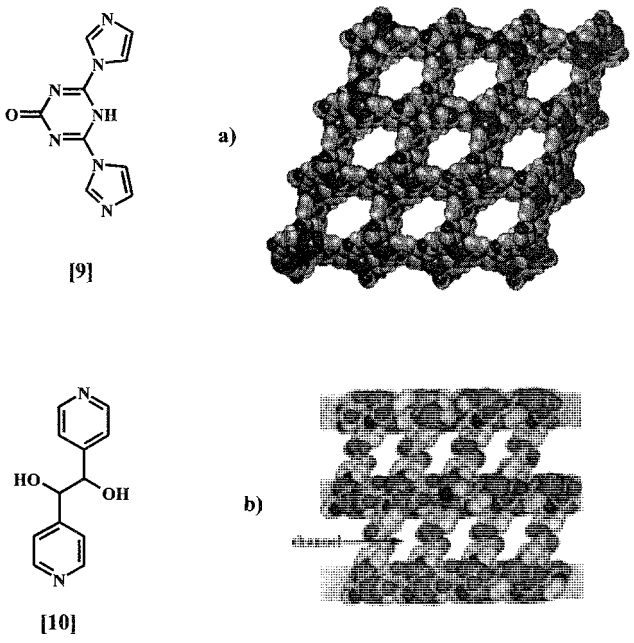

Fig. *4* Slight deformation of the lattice in coordination polymers after removal of the guests. (a) The 4,6-di(1-imidazolyl)-1,3,5-triazin-2-one [**9**] can form a counterion-free framework with channels of a cross section of 9.5 x 5.5 Å^2.[27] (b) In compound $Cu_2(pzdc)_2(dpyg)(H_2O)_8$ [**10**], the 1,2-dipyridylglycol acts as a flexible and functional pillar to form a 3D pillared-layer structure. Channels with a dimension of 4×6 Å^2 undergo a slight change after removing guests. (From Ref. [28].)

Porphyrins

Disk-like molecules such as porphyrins can be modified to form porous network architectures. Porphyrins and their derivatives yield large pores and show excellent thermal and oxidative stabilities. In addition to these properties, porphyrins represent an extremely versatile platform for tailoring porous solids. On the one hand, they can easily be "programmed" by adding various substituents and, on the other hand. by introducing recognition sites.[29] Starting from meso-tetraphenylporphyrins (in which π–π interactions occur between aromatic metalloporphyrins), many compounds were synthesized. In the lattice of Zn(TCPP) [**11**] (TGPP = tetra (4-carboxyphenyl) porphyrin) (Fig. 5a), self-penetration due to large interporphyrin voids is present (16 x 21 A'). To prevent interpenetration. different auxiliary species. such as nitrobenzene and potassium or sodium 18-crown-6, were introduced to sustain the lattice by a concerted ion-paired coordination. Further structural stability can be achieved by coordination through bidentate ligands, e.g., bipy. whereby bridge formation of adjacent layers stabilizes the networks. The cross sections of resulting pillars are 8 x 10 and 8 x 12.5 Å^2. The framework lattice occupies just 42% of the total crystal volume. Porphyrins gives access to coordination polymers. which are shaped by metal–ligand interactions and by a variation of substituents.[30]

Coordination polymers with a composition [{M(tpyp)}$_6$]guest (M: Co^{II}, Mn^{II}; tpyp: tetrapyridylporphyrin) were obtained by hydrothermal reactions. Their structures

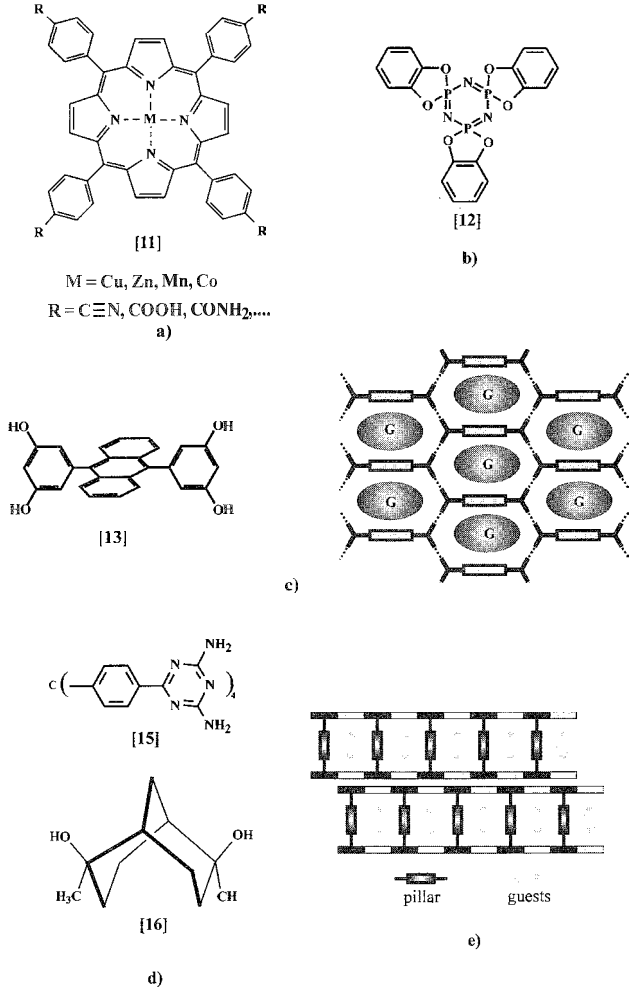

Fig. 5 Porphyrin and formation of hydrogen bonds for stabilizing empty channels. (a) The variation of metal ions and substituents in metalloporphyrin is a basic approach to tailoring networks.[30] (b) The trigonal spirocyclophane *tris*(*o*-phenylenedioxy)cyclotriphosphazene [**12**] yields a hexagonal channel topology.[33,34] (c) *Bis*(resorcinol)anthracene [**13**] forms a 2D network, in which hydrogen bonding occurs between the guest (G) and host molecules.[35-37] (d) A tecton of 2.4-diarninotriazine [**15**] and the helical diol 2,6-dimethylbicyclo[3.3.1]nonane-exo-2-exo-6-diol [**16**] give access to organic zeolites. in which the porous network is merely stabilized on the basis of hydrogen bonding.[39,40] (e) Bilayer structure in which two opposing hydrogen-bonded sheets are linked by organodisulfonate pillars. (From Refs. [42, 43].)

indicate a hexagonal cage showing an effective pore size of 13 x 16 Å^2.[29]

Hydrogen bonds and other weak interactions

Is it possible to produce stable porous channel structures. held together only by hydrogen bonds?

A trigonal symmetry of host molecules provides a typical template for obtaining cavities or channels. In the crystal structure of α-TMA (TMA=trimeric acid, the parent acid of the BTC anion), mutual triple catenation of hydrogen-bonded TMA was found.[''] However, self-penetration is preventable, if the TMA was crystallized with template molecules or is functionalized with bulky substituents to obtain a rigid arrangement.[32]

Another well-known trigonal rigid-structure motif is given by *tris*(*o*-phenylenedioxy)cyclotriphosphazene (TPP) [**12**] (Fig. 5b). The crystallization from different solvents results in a hexagonal channel structure of an average diameter of 5 Å. An empty channel-like structure was obtained by removing volatile guests. Formation of a pseudohexagonal crystal structure was observed.[33,34]

Compared to rigid derivatives of compounds featuring trigonal symmetry in which a planar arrangement can produce a channel system, a flexible *bis*(resorcinol)anthracene [**13**] motif (Fig. 5c) is known as well to generate a stable pore system, essentially being structured by hydrogen bonds.[35,36] A widespread 2D hydrogen-bonding network results from an orthogonal aromatic-triad strategy, with sheets layered in a staggered manner. thus preventing close packing. Anthracene and resorcinol rings are oriented nearly perpendicular to each other and form an extensive hydrogen-bonded network showing zigzag polyresorcinol chains and face-to-face stacked anthracene columns. This channel system undergoes no interpenetration and offers a pore diameter of 10 Å (Fig. 5c).

The intermolecular hydrogen bonding between derivates of 2-pyridone [**14**] rings forms a diamond-like network structure featuring rectangular channels able to accommodate guest molecules. However: this diamond architecture collapses after complete removal of guests, whereas the network is porous enough for an exchange of guest, retaining the lattice.[37,38]

A tecton of 2,4-diaminotriazine [**15**] (Fig. 5d) consists of 16 intertectonic hydrogen bonds supplying a 3D network that is stable enough, even if most guest molecules were desorbed. The resulting network defines channels of 11.8 Å diameter.[39]

A chiral bicyclic diol and its derivatives crystallize in a series of hydrogen-bonded species surrounding parallel channels in which guest molecules can be trapped by a cross section as large as 35 Å^2.[40] An example for a helical tubuland is 2,6-dimethylbicyclo[3.3.1]nonane-exo-2-exo-6-diol [**16**] (Fig. 5d), which contains parallel channels with a triangular pore size of roughly 20 Å^2. The guest-free diol was obtained in different ways: sublimed twice under reduced pressure, inclusion compounds heated (100°C) under reduced pressure, and recrystallized from mesitylene.

A channel-type organic material providing a stable empty nanoporous architecture was found by extracting gossypol (Gp), 2,2′-[1,1′,6,6′,7,7′-hexahydroxy-3,3′-dimethyl-5,5′-diisopropyl-8,8′-diformyl]-naphthalene [**17**], from cotton plants.[41]

A similarly remarkable arrangement of molecular sheets is formed by alkane- or arensulfonate anions (RSO_3^-) (S) and the guanidinium cation (G) [**18**].[42,43] This quasihexagonal 2D GS network sustains strong (G) N–H···O (S) hydrogen bonds and forms nanoporous galleries with 1D channels (Fig. 5e). A method was devised of manipulating the gallery in terms of their height, shape, and chemical environment through a choice of the disulfonate pillars. As a result of the size of the pillars, two basic structural motifs were obtained: a single-layer motif of large pillars: which favors large guests; and sterically undemanding pillars preferring small guests by a bilayer motif. The gallery heights are given by the size of the organodisulfonate, ranging from 5.5–11.5 Å. If guest molecules are removed from the host lattice, a new crystalline phase forms.

Kinetic **Aspects and** Properties

Guest-free cavities are obtained by removing volatile guests for materials when heated or put into vacuum. In many cases, the crystal structure collapses and forms more densely packed arrangements. However, due to strong

Table 1

Coordination polymer	Type of adsorption isotherm	Guest sorption
Zn(BDC)(DMF)(H_2O) [**4**]	I	N_2, CO_2
$Zn_4O(BDC)_3(DMF)_8(C_6H_5Cl)$ [**5**]	I	N_2
{[$CuSiF_6$(4,4′-bipy)$_2$]$_n$} [**6**]	I	CH_4
Tb(bdc)NO_3 [**20**]	I	CO_2, CH_2Cl_2, different alcohols
$Cu_2(pzdc)_2(dpyg)(H_20)_8$ [**10**]	II, hysteresis	CH_3OH, H_2O
[(**13**)$^{4-}$ 2Zr(O^{t}Bu)$_4$] [**19**]	II, hysteresis	N_2, AcOEt. hexane, benzene

intermolecular interactions, remarkably stabile guest-free crystals may arise in some networks, up to 300°C.

X-ray powder diffraction (XRPD), thermo gravimetric (TGA) analysis, solid-state nuclear magnetic resonance (NMR), and measurements of adsorption isotherms are key methods for characterizing zeolite-like behavior. However. a simple proof for observing structural changes during the sorption processes is XRPD.

Evidence for solvent-free pores can also be gained by ^{129}Xe-NMR spectroscopy. This was first applied for Dianin's clathrate. It is particularly suited for the study of void spaces. including amorphous materials.[44]

Stable voids in crystal networks

Stuctural stability of a supramolecular network after complete removal of guest molecules representing a significant part of the volume is an astonishing phenomenon.

In Zn(BDC)(DMF)(H_2O) [4] for example, one water molecule is released at 65°C followed by the evaporation of DMF at 160°C.[19] Empty pores (5 Å) remain because of an increase of the O···Zn bonding in the absence of guests.

A promising designs strategy of the architecture and functionalization of the pores stems from metal carboxylate cluster chemistry. Noninterpenetrated empty

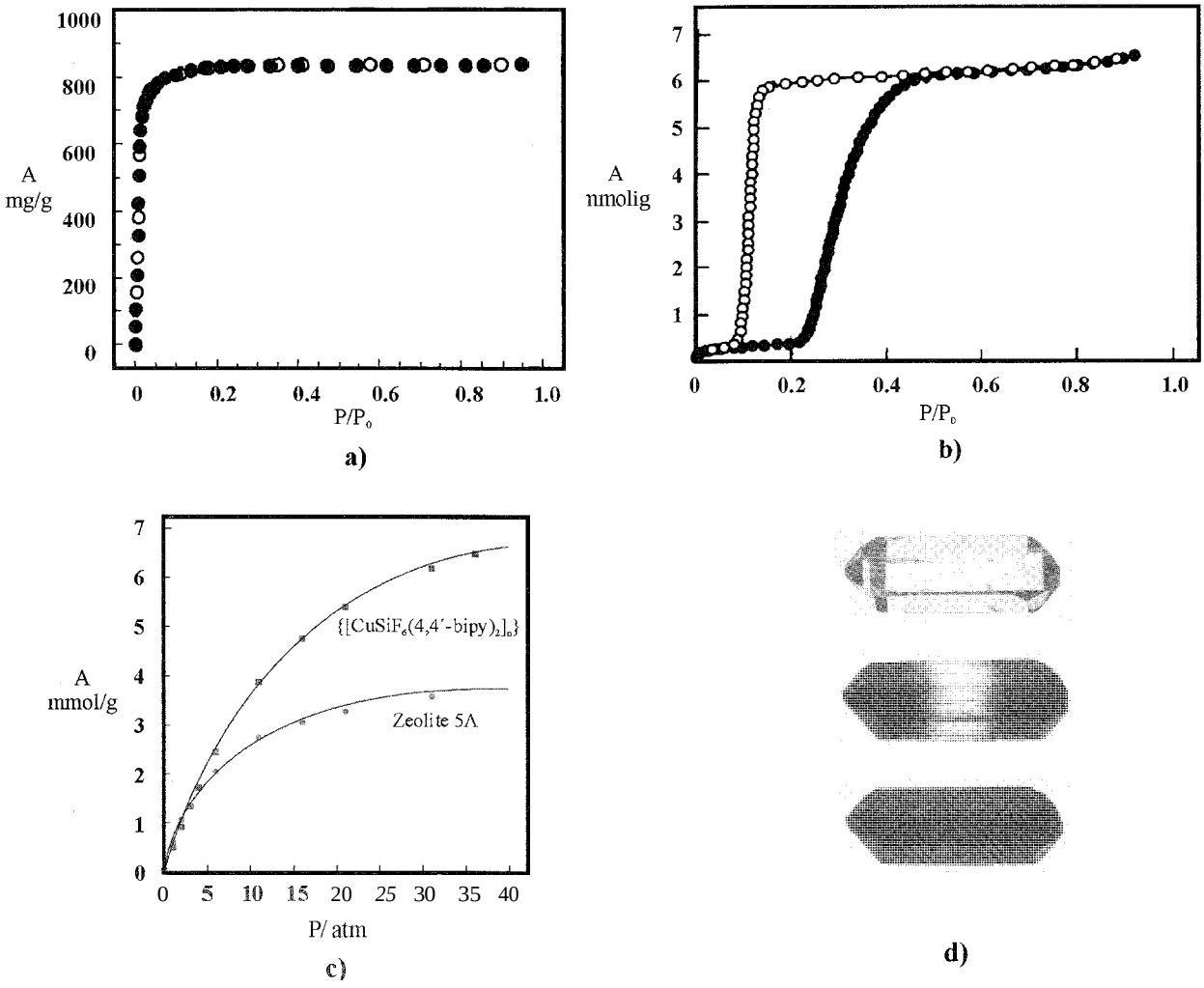

Fig. 6 Demonstration of zeolite-like properties by means of selected examples. (a) Nitrogen gas sorption at 78 K for $Zn_4O(BDC)_3(DMF)_8(C_6H_5Cl)$ [**5**] showed a Type I adsorption isotherm. (From Ref. [20].) [P/P_0 (P: gas pressure; P_0: saturation pressure).] (b) Adsorption and desorption investigations for methanol in the crystal structure of $Cu_2(pzdc)_2(dpyg)(H_20)_8$ [**10**] (298 K). Isotherm with hysteresis loop (A: absolute absorption, P/P_0 is the same as in Fig. 6a). (From Ref. [28].) (c) Comparison of the adsorption isotherm for methane by the inorganic zeolite 5A as compared to $[CuSiF_6(4,4'\text{-bipyridine})_2]_n$ [**6**], demonstrating a larger affinity of the organic compound (A: absolute absorption). (From Ref. [21].) (d) TPP shows a remarkable affinity to include iodine by *in*-diffusion. The staining started from capping faces, extending continuously into the volume (from top to bottom). (From Ref. [48].) (*View this art in* color *at www.dekker.com.*)

networks with a modifiable pore sire up to 28.8 Å were obtained. Despite the large empty voids and the low density of this crystalline material, the crystal structure is maintained after evaporation of the inclusion solvents.[3]

Structures 5–7 show similar behavior. The solvents can be fully removed or exchanged by other guests without destruction of the pores and are stable up to 300°C.

Guest molecules were exchanged for $[Ag(TEB)CF_3SO_3](C_6H_6)$ [**8**] in the liquid state while the framework remained intact. Complete substitution with C_6D_6 was confirmed by NMR spectroscopy.[45] Here. guest exchange does not seem to be limited to benzene because of a preference for selective sorption of aromatic alcohols and, to lesser extent, for unfunctionalized aromatics or aliphatic molecules.[24]

Flexible network structures

After heating the inclusion adducts of Structure [**13**] in vacuum. a polycrystalline guest-free apohost was obtained. This apohost is capable of reversibly binding ketones and esters. The uptake of guests in various liquids is fast (completed within seconds).

Solid–solid complexation of an apohost with compounds in the solid state. such as benzophenone or 1,2-cyclohexandiol, is feasible as well. Host–guest formation in the solid state may be considered a heterogeneous equilibrium, where guest molecules are bonded at the surface of the apohost and by translocation enter the host pores. However, the mechanism is not yet understood.

A bidentate ligand is similarly a candidate for the coordination to metal ions. Polycondensation with $Zr(O^tBu)_4$ provided an insoluble, amorphous. and microporous powder [$\mathbf{13}^{4-} \cdot 2Zr(O\text{-}^tBu)_4$] [**19**] that forms a stable 0-Zr-Q network with a pore size of 7 Å. The completely insoluble Zr-host system allows for Diels–Alder reactions. In this case, a batch flow system was set up for continuous processing.[46]

An empty channel-like structure and formation of a pseudohexagonal crystal structure is shown by TPP [**12**], which can be obtained by removing volatile guests. In these crystals, a reversible gas transport of xenon in 1D channels was reported and analyzed by laser-polarized ^{129}Xe-NMR spectroscopy.[33,34]

After slow removal of dichloromethane from the inclusion co pounds of gossypol, a polymorph was formed with an ink-bottle-like empty space of an average diameter of 5 Å.[41]

CONCLUSION

Organic zeolites are interesting material, for an application in catalysis. gas storage, separation, or implementation of some physical properties.

The effectiveness of organic pore systems is generally explored by measuring adsorption isotherms. Most examples for reversible sorption properties are reported for coordination polymers. Two types of adsorption-isotherms were found: reversible Type I adsorption isotherms (Table 1) were observed for guest-free metal–organic networks (Fig. 6a). Isotherms showing a hysteresis loop (Type II) provide evidence for the crystal structure undergoing a slight deformation during the sorption process (Fig. 6b).

In comparison to inorganic zeolites, organic porous networks show a considerably higher uptake of different guests. $CuSiF_6(bipy)_2$ features a higher affinity to methane than that found for the inorganic zeolite 5A (Fig. 6c).

In addition to the reversible uptake of CO_2, the solvent-free derivative $Tb(bdc)NO_3$ [**20**] revealed a further application potential in view of a sensor technology, where lanthanides play an important role.[47]

An efficient guest exchange was observed for TPP and iodine (Fig. 6d). Here, a dark conductivity along the channels in the order of pure $I_2(s)$ was reported.[48]

The completely insoluble Zr host system [**19**] allows for Diels–Alder reactions. In this case. a batch flow system was set up for continuous processing.[46]

To summarize. present examples reflect a great variety of different materials opening space for a tailoring of the pore size, the sorption, and other properties.

ARTICLES OF FURTHER INTEREST

Channel Inclusion Compounds, p. 223
Concepts in Crystal Engineering, p. 319
Gossypol, p. 606
Guanidinium-Based Anion Receptors, p. 615
Inclusion Compounds: Selectivity, Thermal Stability, and Kinetics, p. 696
Zeolites: Structures and Inclusion Properties, p. 1623

REFERENCES

1. Vaughan. D.E.W. Molecular Sieves Zeolites: A Historical Perspective. In *Comprehensive Supramolecular Chemistry*, 1st Ed.: Atwood, J.L.. Davis. J.E.D.. MacNicol. D.D., Vogtle, F.. Eds.; Elsevier Science Ltd.: Oxford, 1996; Vol. 7. 379–391.
2. Cheetham, A.K.: Day, P. *Solid State Chemistry Compounds*, 1st Ed.: Oxford University Press, Inc.: New York. 1992.
3. Eddaoudi. M.; Kim. J.: Rosi. N.: Vodak. D.: Wachter. J.: O'Keeffe. M.: Yaghi, O.M. Systematic design of pore size and functionality in isoreticular MOFs and their application in methane storage. Science 2002. 295. 469–472.

4. Cheetham. A.K.: Ferey. G.; Loiseau. T. Open-framework inorganic materials. Angew. Chem., Int. Ed. 1999. 38. 3268–3292.
5. Davis. M.E.: Robo. R.F. Zeolite and molecular sieve synthesis. Chem. Mater. 1992; 4. 756–768.
6. Desiraju, G.R. *Crystal Engineering: The Design of Organic Solids,* 1st Ed.: Desiraju, G.R.. Ed.: Elsevier Science Publishers B.V.: Amsterdam, 1989.
7. Kitaigorodskii, A.I. Theory of Close Packing of Molecules. In *Organic Chemical Crystallography,* 1st Ed.; Kitaigorodskii. A.I.. Ed.; Consultants Bureau Enterprises. Inc.: New York, 1961; 65–112.
8. MacNicol. D.D.; Mc Kendrick. J.J.; Wilson. D.R. Clathrates and molecular inclusion phenomena. Chem. Soc. Rev. 1978. 7. 65–87.
9. Toda. F.: Akagi. K. Molecular complexes of acetylene with *n*- and χ-donors. Tetrahedron. Lett. 1968. 9, 3695–3698.
10. Weber, E.: Josel, H.P. A proposal for the classification and nomenclature of host-guest-type compounds. J. Incl. Phenom. 1983, *1*, 79–85.
11. Weber. E. Shape and Symmetry in the Design of New Hosts. In *Comprehensive Supramolecular Chemistry,* 1st Ed.: Atwood. J.L., Davis, J.E.D.. MacNicol, D.D.. Vogtle, F., Eds.: Elsevier Science Ltd.: Oxford, 1996; Vol. 6, 535–592.
12. Desiraju. G.R. Supramolecular synthons in crystal engineering—A new organic synthesis. Angew. Chem.. Int. Ed. 1995. 34, 2328–2361.
13. Wells. A.F. Polyhedra and Nets. In *Structural Inorganic Chemistry,* 5th Ed.: Wells, A.F., Ed.; Oxford University Press Inc.: New York. 1984: 63–140.
14. Abrahams, B.F.: Hoskins, B.F.: Michall. D.M.: Robson, R. Assembly of porphyrin building blocks into network structures with large channels. Nature 1994. 369. 727–729.
15. Moulton, B.: Zaworotko, M.J. From molecules to crystal engineering: Supramolecular isomerism and polymorphism in network solids. Chem. Rev. 2008. 101. 1629–1658.
16. Yaghi. O.M.; Li. G.; Li. H. Selective binding and removal of guests in a microporous metal–organic framework. Nature 1995. 378. 703–706.
17. Yaghi. O.M.: Davis, C.E.; Li. G.: Li. H. Selective guest binding by tailored channels in a 3-D porous zinc(II)-benzenetricarboxylate network. J. Am. Chem. Soc. 1997. *119,* 2861–2868.
18. Li, H.: Davis. C.E.; Groy, T.L.: Kelly, D.G.: Yaghi. O.M. Coordinatively unsaturated metal centers in the extended porous framework of $Zn_3(BDC)_3 \cdot 6CH_3OH$. J. Am. Chem. Soc. 1998. *120.* 2186–2187.
19. Li. H.; Eddaoudi, M.: Groy. T.L.: Yaghi. O.M. Establishing niicroporosity in open metal–organic frameworks: Gas sorption isotherms for Zn(BDC). J. Am. Chem. Soc. 1998. 120. 8571–8572.
20. Li, H.: Eddaoudi. M.; O'Keeffe. M.: Yaghi. O.M. Design and synthesis of an exceptionally stable and highly porous metal–organic framework. Nature 1999. 402. 276–279.
21. Noro. S.: Kitagawa. S.: Kondo. M.: Seki. K. Anew, methane adsorbent. porous coordination polymer [$\{CuSiF_6(4,4'$-bipyridine$)_2\}_n$]. Angew. Chem., Int. Ed. 2000. 39. 2081–2084.
22. Biradha. K.: Hongo. Y.: Fujita, M. Open square-grid coordination polymers of the dimensions 20 x 20 A: Remarkably stable and crystalline solids even after guest removal. Angew. Cheni., Int. Ed. 2000. 39. 3843–3845.
23. Aakeroy, C.B.: Beatty. A.M.: Leinen, D.S. A versatile route to porous solids: Organic–inorganic hybrid materials assembled through hydrogen bonds. Angew. Chem.. Int. Ed. 1999. 38. 1815–1819.
24. Gardner. G.B.: Kiang, Y.H.; Lee. S.: Asgaonkar, A.: Venkataraman, D. Exchange properties of the three-dimensional coordination compound 1.3.5-tris(4-ethynylbenzonitrile)benzene. AgO_3SCF_3. J. Am. Chern. Soc. 1996. *118,* 6946–6953.
25. Venkataraman. D.: Gardner. G.B.: Lee. S.; Moore. J.S. Zeolite-like hehaviour of a coordination network. J. Am. Chern. Soc. 1995. 117. 11600–11601.
26. Xu. Z.: Lee. S.: Kiang. Y.-H.: Mallik. A.B.: Tsomaia. N.; Mueller, K.T. A cross-linked large channel organic coordination solid. Adv. Mater. 2001. 13. 637–641.
27. Goodganie. D.M.L.; Grachvogel, D.A.; Williams. D.J. A new type of metal–organic large-pore zeotype. Angew. Cheni.. Int. Ed. 1999. 38. 153–156.
28. Kitaura. R.: Fujimoto, K.: Noro. S.: Kondo. M.; Kitagawa, S.A. Pillared-layer coordination polymer network displaying hysteretic sorption: $[Cu_2(pzdc)_2(dpyg)]_n$. Angew. Chern., Int. Ed. 2002. 41. 133–135.
29. Goldberg. I. Metalloporphyrin molecular sieves. Chern. Eur. J. 2000. 112. 3863–3870.
30. Dislcin-Posner. Y.: Goldberg. I. From porphyrin sponges to porphyrin sieves: A unique crystalline lattice of aquazinc tetra(4-carboxyphenyl)porphyrin with nanosized channels. Chem. Commun. 1999. 19. 1961–1962.
31. Herbstein, F.H.: Kapon, M.: Reisner, G.M. Trimesic acid. its hydrates. complexes and polymorphism. Acta Crystallogr.. B 1985. 41. 348–354.
32. Kolutuchin, S.V.: Fenlon. E.E.: Wilson. S.R.: Loweth. C.J.: Zimmerman. S.C. Self-assembly of 1,3,5-benzenetricarboxylic acids (trimesic acids) and their analogues in the solid state. Angew. Chern.. Int. Ed. 1995. 34. 2654–2657.
33. Sozzani. P.: Comotti. 4.: Simonutti, R.: Meersmann, T.: Logan, J.W. A porous crystalline molecular solid explored by hyperpolarized xenon. Angew. Chem.. Int. Ed. 2002. 39. 2695–2699.
34. Meersmann, T.: Logan, J.W.: Simonutti. R.: Caldarelli. S.: Comotti. A.: Sozzani. P.: Kaiser. L.G.: Pines. A. Exploring single-file diffusion in one-dimensional nanochannels by laser-polarized ^{129}Xe NMR spectroscopy. J. Phys. Chem.. A 2000. *104,* 11665–11670.
35. Endo. K.; Sawaki. T.: Koyanaghi, M.: Kobayashi, K.: Masuda. H.: Aoyama, Y. Guest-binding properties of organic crystals having an extensive hydrogen-bonded network: An orthogonal anthracene-bis(resorcinol) derivates as a functional organic analog of zeolite. J. Am. Chem. Soc. 1995. 117. 8341–8352.
36. Aoyama, Y. Functional organic zeolite analogues. Top. Curr. Chem. 1998, 198, 132–161.
37. Simard, M.: Su. D.: Wuest. J.D. Use of hydrogen bonds to control molecular aggregation. Self-assembly of three-dimensional networks with large chambers. J. Am. Chem. Soc. 1991. 113. 4696–4698.

38. Wang. X.; Simard. M.: Wuest, J.D. Molecular tectonics. Three–dimensional organic networks with zeolite properties. J. Am. Chern. Soc. 1994, 116. 12119–12120.
39. Brunet. P.: Simard, M.: Wuest, J.D. Molecular tectonics. Porous hydrogen-bonded networks with unprecedented structural integrity. J. Am. Chem. Soc. 1997. 119. 2737–2738.
40. Ung, A.T.; Gizachew. D.: Bishop. R.: Scudder. M.L.: Dance. I.G.: Craig, D.C. Structure and analysis of helical tubulate inclusion compounds formed by 2,6-dimethylbicyclo[3.3.1]nonane-*exo*-2,*exo*-6-diol. J. Am. Chem. Soc. 1995. 117. 8745–8756.
41. Ibragimov, B.T.; Talipov. S.A. Inclusion complexes of the natural product gossypol. Recognition by gossypol of halogeno methanes. Structure of the dichloromethane complex of gossypol and single crystal conservation after decomposition. J. Incl. Phenom. Mol. Recognit. 1994, 17. 317–324.
42. Russell. V.A.: Evans, C.C.: Li, W.: Ward, M.D. Nanoporous molecular sandwiches: Pillared two-dimensional hydrogen-bonded networks with adjustable porosity. Science 1997. 276, 575–579.
43. Swift, J.A.; Russell. V.A.; Wuest, M.D. Organoporous hosts with adjustable molecular environments. Adv. Mates. 1997, 9. 1183–1186.
44. Lee, F.; Gabe. E.; Tse, J.S.; Ripmeester, J.A. Crystal structure. CP/Mas ^{129}Xe, and ^{13}C NMR of local ordering in Dianin's compound clathrates. J. Am. Chem. Soc. 1988, 110. 6014–6019.
45. Gardner, C.B.: Venkataraman. D.; Moore. J.S.; Lee, S. Spontaneous assembly of a hinged coordination network. Nature 1995, *374*. 792–795.
46. Sawaki. T.; Aoyama. Y.J. Immobilization of a soluble metal complex in an organic network. Remarkable catalytic performance of a porous dialkoxyzirconium polyphenoxide as a functional organic zeolite analogue. J. Am. Chern. Soc. 1999. *121*. 4793–4798.
47. Reinecke, T.M.; Eddaoudi. M.: Keeffe, M.O.; Yaghi, O.M. A rnicroporous lanthanide-organic framework. Angew. Chern., Int. Ed. 1999. *38*, 2590–2594.
48. Hertzsch. T.: Budde, F.: Weber. E.; Hulliger, J. Supramolecular-wire confinement of I_2 molecules in channel of the organic zeolite tris(*o*-phenylenedioxy)cyclotriphos-phazene. Angew. Chem., Int. Ed. 2002, *41*, 2281–2284.

Organometallic Anion Receptors

Paul D. **Beer**
Elizabeth **J.** *Hayes*
University of Oxford, Oxiord, United Kingdom

INTRODUCTION

Anions are ubiquitous species, and therefore. their sensing is of considerable interest. Anion receptors containing redox-active organometallic groups such as ferrocene or cobaltocenium allow the binding of anions to be detected by an electrochemical response of the metallocene redox couple. These systems were incorporated into various acyclic, macrocyclic, and calix[4]arene frameworks. many of which include an arnide hydrogen-bonding group. Receptors can operate in a range of environmental conditions, including aqueous solution.

COBALTOCENIUM-BASED ANION RECEPTORS

The cobaltocenium moiety was studied extensively in the context of redox-responsive anion receptors.[1,2] The first class of anion receptor based on this system was reported by Beer and Keefe in 1989.[3] The ester functionalized *bis*-cobaltocenium macrocyclic Receptor 1 bound and electrochemically sensed bromide in acetonitrile via favorable electrostatic interactions.

Amide functionalities were appended to the cobaltocenium moiety to provide hydrogen bond donors capable of coordinating anions, such as in Receptors 2 and 3 in Fig. 1.[4] Proton NMR anion titration studies in d_6-DMSO reveal considerable downfield shifts. particularly for the arnide protons. indicative of a strong hydrogen-bonding interaction. Receptors 2 and 3 selectively bind dihydrogenphosphate over chloride in CD_3CN, with differences in stability constant of approximately an order of magnitude [$K(H_2PO_4^-)$ 1200 M^{-1} and $K(Cl^-)$ 100 M^{-1} for 2, $K(H_2PO_4^-)$ 320 M^{-1} and $K(Cl^-)$ 35 M^{-1} for **3**].[5] This selectivity may be attributed to the greater basicity of the $H_2PO_4^-$ anion. The importance of the amide hydrogen-bonding interaction was highlighted by studies with cobaltocenium receptors containing tertiary amides.[6] These receptors exhibit negligible anion binding. Crystal structure analysis of the bromide complex of Receptor 2 clearly shows hydrogen bonds to the arnide proton. as well as to Cp and aryl protons.

These receptors are also capable of electrochemically recognizing anions. Complexation of an anionic guest stabilizes the positively charged cobalt center, making it more difficult to reduce. and results in substantial cathodic shifts of the reversible Cp_2Co^+/Cp_2Co redox couple. Dihydrogenphosphate induces cathodic shifts of 200 and 240 mV, respectively, for Receptors 2 and 3, whereas chloride produces shifts of lower magnitude, 30 and 85 mV, respectively. This complements the higher binding constants obtained via NMR for the $H_2PO_4^-$ anion. Macrocyclic compounds also provided evidence for an anion chelate effect.[7]

A variety of novel calix[4]arene receptors 4–6 were prepared,[8–10] and it was shown that the anion-coordination properties are dependent upon the degree of upper-rim preorganization. For instance, 4 binds acetate much better than dihydrogenphosphate in DMSO, whereas the trend is reversed with the isomeric **5.** The bridged cobaltocenium calix[4]arene **6** forms thermodynamically more stable complexes with carboxylate and $H_2PO_4^-$ than either 4 or 5, with notable selectivity for acetate. The upper-rim bidentate amide group of **6** provides a hydrogen-bond cavity suitable for complexing bidentate anions such as carboxylates.

Ditopic *bis*-cobaltocenium receptors such as molecule 7 were synthesized in an attempt to enhance selectivity and complex stability.[7] Various spacer groups separate the two metallocenes. ^{1}H-NMR titrations revealed that the receptors with ethyl, propyl, and butyl spacers bound halide anions in CD_3CN in a 1:1 complex, with a preference for chloride. However, increasing the length of the alkyl chain leads to an overall decrease in the stability constant and in the degree of selectivity. Longer aromatic spacers gave 2:1 complexes with anions, presumably due to the increased size of the cleft cavity. Electrochemical measurements for all receptors showed considerable cathodic shifts in the cobaltocenium redox wave with a variety of anions.

A novel cobaltocenium porphyrin receptor 8 was synthesized,[11] in which four metallocenes were appended to the porphyrin. The selectivity is atropisomer dependent. and the *cis*-$\alpha,\alpha,\alpha,\alpha$-atropisomer shown exhibits the selectivity trend $Cl^- > Br^- \gg NO_3^-$. Proton NMR titrations in acetonitrile showed shifts of up to 0.7 ppm

Encyclopedia of Supramolecular Chemistry
DOI: 10.1081/E-ESMC 120012719

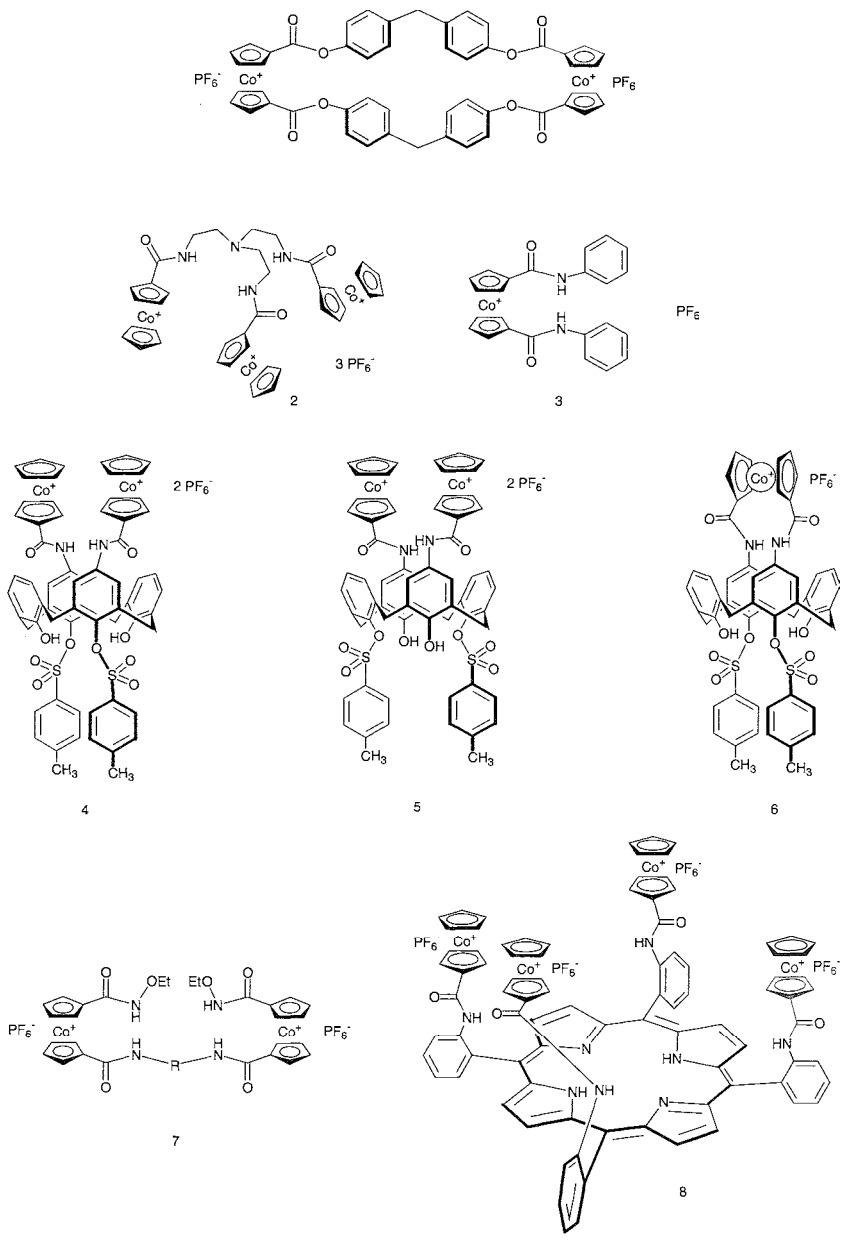

Fig. 1 Cobaltocenium-based receptors.

for the amide. Cp, and pyrrole protons upon addition of halide anions. Chloride and bromide bound in 1:1 stoichiometry and gave stability constants of 860 M^{-1} and 820 M^{-1}, respectively, whereas nitrate exhibited weaker binding with $K=190\ M^{-1}$. The molecule exhibits complicated electrochemistry, with multiple redox waves due to the cobaltocenium and the porphyrin. The addition of anions to acetonitrile solutions of 8 resulted in cathodic shifts of the cobaltocenium redox couple of 35–75 mV for chloride, bromide, and hydrogensulfate, and 225 mV for dihydrogenphosphate. Smaller shifts were observed for the porphyrin oxidation redox couple.

FERROCENE-BASED ANION RECEPTORS

The ferrocene moiety was also used in the sensing of anions, with many of the receptors similar in design to the cobaltocenium molecules.[7,8] One of the significant differences is that the ferrocene analogues are neutral and. therefore, have no inherent electrostatic interaction.

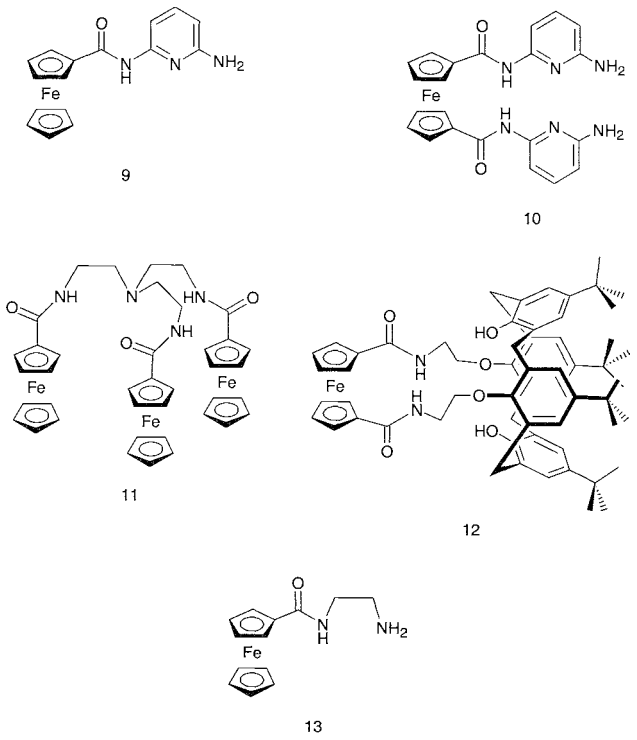

Fig. 2 Ferrocene-amide-based receptors.

NMR-determined stability constants are therefore lower in magnitude. The ferrocene does not directly interact with the anion until it is oxidized to ferrocenium, when electrostatic interactions are '.switched on."[12]

A range of receptors incorporating ferrocene units with secondary amides is shown in Fig. 2.[12,13] Molecules **9**–**12** exhibited $H_2PO_4^-$ induced cathodic shifts of up to 240 mV in acetonitrile in the presence of a 10-fold excess of HSO_4^- and Cl^-. Receptor **13**, on the other hand, exhibits selectivity for HSO_4^- in the presence of $H_2PO_4^-$, with a shift of 220 mV. The HSO_4^- anion protonates the basic amine functionality, which then binds the SO_4^{2-} anion.

A ferrocene-zinc metalloporphyrin analogous to 8 was prepared, in which anions are bound via the Lewis acidic zinc center and amide hydrogen bonding.[14] As with the cobaltocenium analogue, the atropisomer dictates the selectivity, and anion complexation in 3:2 CH_2Cl_2/CH_3CN results in cathodic electrochemical perturbations of the porphyrin and ferrocene redox processes. Lower-rim polyferrocene-substituted calixarenes were aiso synthesized and shown to electrochemically sense Cl^-. HSO_4^-, and $H_2PO_4^-$ anions in CH_2Cl_2, with shifts of up to 160 mV being observed with $H_2PO_4^-$.[15]

The relative ease of synthesis and substitution of ferrocene led to its widespread use. In particular. it has been attached to various well-known anion-binding structures in an attempt to introduce a responsive element. For example, Astruc and coworkers produced dendriiners containing up to 18 ferrocene units and found evidence for a dendritic effect in the anion recognition process.[16] $H_2PO_4^-$ induces the largest cathodic shifts, from 110–315 mV. Recently. this group synthesized functionalized gold nanoparticles containing (amidoferrocenyl) alkanethiol (AFAT) ligands for the purpose of redox recognition of oxoanions. These compare favorably to the

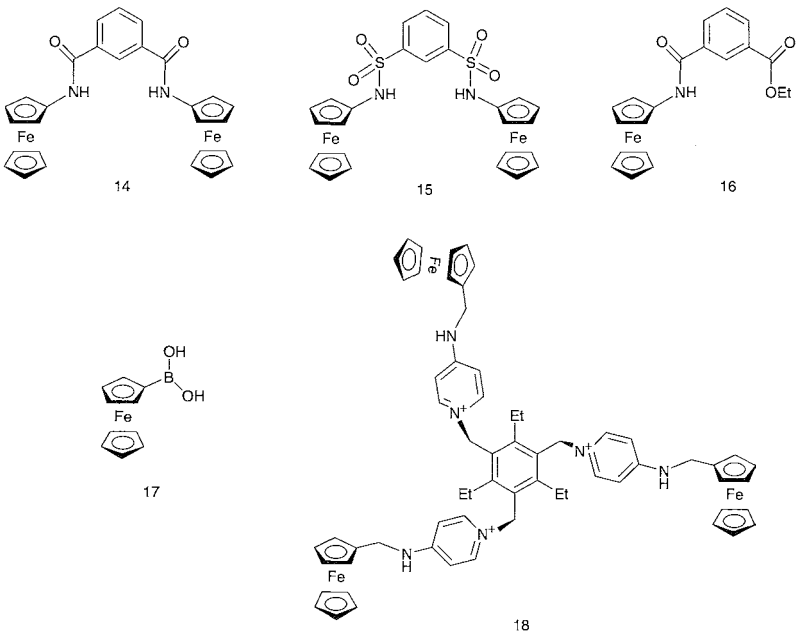

Fig. **3** Other ferrocene-based receptors.

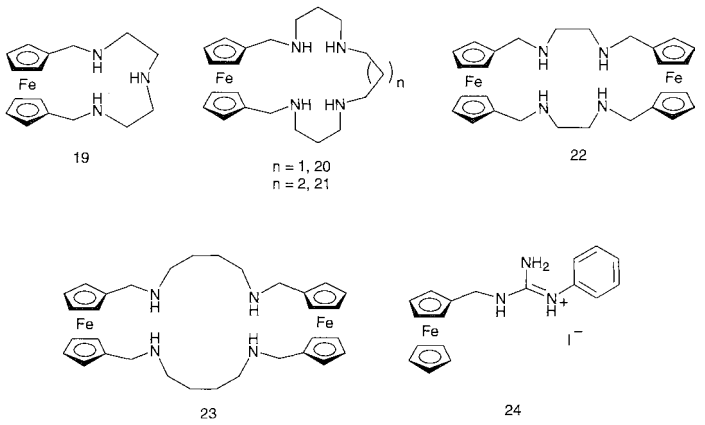

Fig. 4 Water-soluble ferrocene-amine receptors.

dendrimers in terms of selectivity for $H_2PO_4^-$ over HSO_4^-, with $H_2PO_4^-$ induced shifts of around 200 mV in CH_2Cl_2, and 100–175 mV in the presence of HSO_4^- and Cl^-.[17]

Crabtree and coworkers incorporated ferrocene subunits into isophthaliinide and disulfonamide frameworks.[18] The addition of Cl^- anions to CD_2Cl_2 solutions of **14** and **15** (Fig. 3) resulted in large chemical shift changes, up to 3.13 ppm for the amide N–H proton of 15. The stability constant for 15 was found to be 9500 M^{-1}, whereas that for the monamide 16 was only 30 M^{-1}, demonstrating the importance of the two convergent hydrogen-bonding groups. Disappointingly. relatively low cathodic electrochemical shifts of 20 and <5 mV were observed for 15 and 16, respectively. after addition of one equivalent of Cl^-. Ferrocene was also attached to imidazolium salts[19] and calix[4]pyrroles.[20]

Shinkai and coworkers reported that ferroceneboronic acid 17 (Fig. 3) acts as an electrochemical anion sensor.[21] It exhibits excellent selectivity for fluoride ions in the presence of other halides and anions such as SCN^-, SO_4^{2-}, and $H_2PO_4^-$. A K_{ox} value of 1000 M^{-1} in $MeOH/H_2O$ was found for fluoride, compared to values of less than 2 M^{-1} for chloride and bromide. The fluoride ion is a hard base and. therefore. interacts considerably with the hard boron atom. Oxidation results in the ferrocene group becoming more electron withdrawing. The electron density of the boron atom decreases; therefore, the strength of the fluoride complex increases. A bidentate *bis*(boronate) Lewis acid was also shown to act as a fluoride sensor.[22]

Steed and coworkers synthesized a series of "Venus flytrap'' anion sensors; such as 18 (Fig. 3), based on podands with a hexasubstituted core and arms with hydrogen-bonding and cationic pyridinium groups, with ferrocene attached to the pyridinium.[23,24] The host is preorganized into a cone conformation and shows considerable affinity for halides. and chloride in particular. with complexation-induced chemical shifts of up to 1.54 ppm for the NH protons in CD_3CN. The selectivity trend is $Cl^- > Br^- > I^-$, and some selectivity is also shown for acetate. Preliminary electrochemical studies suggest relatively poor coupling between binding and signaling moieties, but the observed selectivity sequence is in agreement with that obtained by NMR.

Receptors capable of operating under aqueous conditions are obviously important, given the prevalence of anions in biological and environmental systems. However, the large hydration energies of anions make their sensing in water a challenging task.[25] Beer et al. synthesized a series of acyclic and cyclic ferrocene-amine ligands, as shown in Fig. 4. These were shown to selectively bind and electrochemically sense phosphate and sulfate as well as nucleotide ions in aqueous solution.[26–28]

In general: the selectivity of these receptors is dependent upon pH. Results from ^{31}P-NMR imaging showed that Receptors 19, 20, and 21 (Fig. 4) bind adenosine triphosphate and hydrogenphosphate in water. At pH 6.5. where at least two of the nitrogen atoms are protonated. 1:1 complexes were formed. Electrochemical experiments at the same pH showed cathodic shifts with the phosphate anions of 60–80 mV. Receptor 22 discriminates for sulfate over phosphate at pH 4 in 70:30 THF/H_2O, with cathodic shifts of 54 and <10 mV, respectively. Compound 23 shows shifts of 23 mV with sulfate at pH 4 and 30 mV with phosphate at pH 8.

Molecule 20 shows a perturbation of the Fc^+/Fc redox couple by 50 mV upon addition of phosphate at pH 7 in water. Sulfate, on the other hand, results in a negligible shift. Calibration curves of the change in the half-wave potential $\Delta E_{1/2}$ versus the $[A^-]/[L]$ ratio at a certain pH value showed that the concentrations of phosphate and sulfate in the presence of competing anions can be quantitatively determined using Receptors 20 and 22.

This demonstrates their potential for use as prototype anion sensors.

The ferrocene-appended guanidinium receptor 24 senses pyrophosphate in methanol/water mixtures. exhibiting cathodic shifts of up to 70 mV.[29] Azamacrocycles functionalized with ferrocene arms were also shown to possess anion-binding properties and are capable of electrochemically detecting sulfates, phosphates, and ATP in 70:30 THF/H_2O solutions.[28,30]

OPTICAL SENSORS CONTAINING METALLOCENES

An acyclic $[Ru(bpy)_3]^{2+}$-ferrocene receptor 25 was prepared (Fig. 5).[31] The ferrocene units quench the emission of the ruthenium center in the free receptor. but addition of $H_2PO_4^-$ ions increases the emission by 20-fold in acetonitrile. This increase is not observed with Cl^- or HSO_4^- ions. Competition experiments in the presence of these anions gives rise to an emission increase identical to that obtained upon addition of $H_2PO_4^-$. Receptor 25 can therefore be considered a $H_2PO_4^-$ selective luminescent anion receptor. Particularly noteworthy are Receptors **26**–**27**, synthesized by Beer and coworkers. that exhibit a marked selectivity for chloride ions.[32] Stable 1:1 complexes are formed in DMSO, with stability constants of up to $4 \times 10^4\ M^{-1}$. No evidence of $H_2PO_4^-$ binding was shown with ^1H- and ^{31}P-NMR. Luminescence studies show a blue-shift of the MECT emission band with significant intensity enhancement in response to the addition of chloride anions but no response to $H_2PO_4^-$. Anion-induced cathodic shifts of the metallocene redox-couple of up to 110 mV were observed upon addition of chloride anion. The rigidity of the inacrocycle is thought to contribute to its selectivity. because acyclic analogues tend to prefer $H_2PO_4^-$. The larger size and tetrahedral shape of this anion make it incompatible with the macrocycle's cavity. However, increasing the size of the cavity by two or four methylene units dramatically reverses the trend in anion selectivity.

ARENE AND OTHER ORGANOMETALLIC RECEPTORS

Atwood and coworkers made considerable progress in the synthesis of new anion hosts by directly attaching cationic organometallic arene moieties to the calixarene aromatic rings.[33,34] Of note is Receptor 28 (see Fig. 6), which is capable of binding anions in aqueous solution. Nitrate and halide anions give binding constants in the range 100–550 M^{-1}, as determined by ^1H-NMR. Binding constants decrease in the order $Cl^- > Br^- > I^-$ and are significantly increased in nonaqueous media. This approach was also used to synthesize $[CpFe(arene)]^+$-derivatized cyclotriveratrylenes. such as 29. that bind halides and PF_6^-. The upper-rim charge preorganization allows anion binding within the host cavity.'''' Astruc also used different metallocenes. having synthesized a cationic metallodendrimer with 24 $[CpFe(\eta^6\text{-}N\text{-alkylaniline})]^+$ termini. This molecule is capable of recognizing chloride and bromide.[36]

Beer and coworkers made several simple receptors by substituting one cyclopentadienyl ring of a ferrocene with a benzene ring. to give the amide arene CpFe 30 in Fig. 6. The same article also described the synthesis of the arnide arene tricarbonyl chromium compound 31.[37] Downfield shifts of the arnide N–H protons are observed for both receptors upon addition of chloride or bromide in CD_3CN. For instance, with chloride, Receptor 30 exhibits a shift of 2.5 ppm and 31 a shift of 0.9 ppm. Negligible shifts are observed with unsubstituted metallocene and nonmetallated aromatic molecule.

Gale and coworkers synthesized Receptor 32 in Fig. 6.[38] Electron-withdrawing $Cr(CO)_3$ groups were attached in order to increase the acidity of the NH protons.'''' ^1H-NMR titrations of 32 in CD_3CN showed a

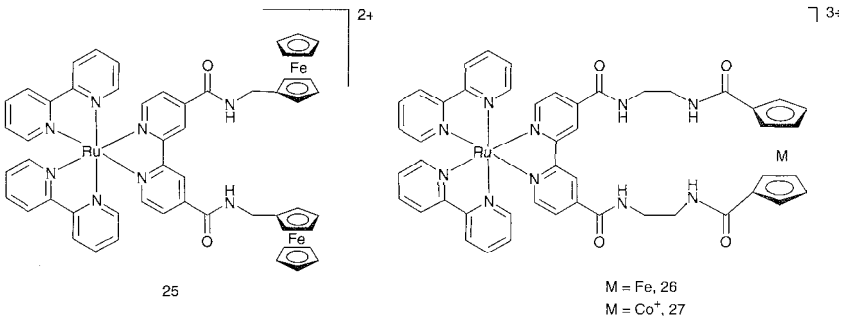

Fig. 5 Fluorescent organornetallic anion receptors.

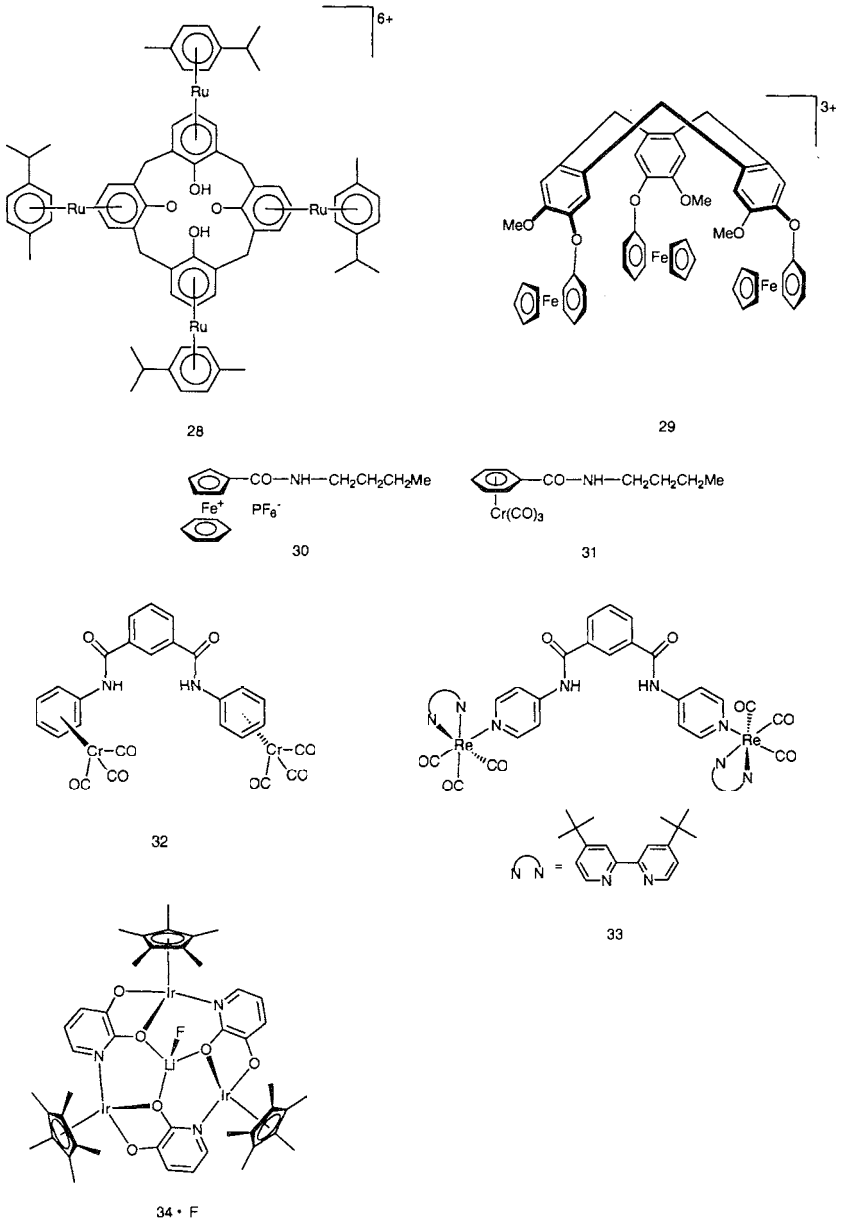

Fig. 6 Other organometallic receptors

selectivity for chloride over other anionic guests. with a log K value of greater than four. Selectivity for chloride over dihydrogen phosphate is high. perhaps reflecting the steric bulk of the $Cr(CO)_3$ moieties, which may hinder the approach of the bulky $H_2PO_4^-$ to the amide cleft. Receptor 33 was shown to have high affinities for halides, cyanide, and acetate anions.[39] The addition of anions results in a significant downfield shift of the N–H protons in $CDCl_3$ and quenching of the luminescent intensities in CH_2Cl_2. Binding constants as high as 10^4–10^5 M^{-1} and a detection limit as low as 10^{-8} M were observed.

Severin and coworkers synthesized an organometallic metallacrown complex **34**.[40] The receptor was found to be highly selective for fluoride, even in the presence of an excess of other anions. Electrochemical ineasurements in 2:1 $CHCl_3/CH_3CN$ showed a cathodic shift in oxidation potential of 203 mV upon addition of fluoride. whereas other anions induced rhifts of less than 24 mV.

CONCLUSION

Organometallic groups such as ferrocene and cobaltocenium lend themselves extremely well to the synthesis of anion receptors Their relative ease of substitution led

to the inclusion of them in acyclic. macrocyclic, calix[4]arene, and many other receptor systems. Anion-induced cathodic shifts in the redox potential of the metallocene provide a physical means of monitoring the anion-binding process. These two metallocenes. as well as other organometallic moieties. are continually being used in new classes of redox-responsive anion receptor, and it is apparent that this strategy is highly effective.

ARTICLES OF **FURTHER** INTEREST

Calixarenes: Synthesis and Historical Perspectives, p. 153
Dendrimers, p. 432
Electrochemical Sensors. p. 505
Fluorescence Sensing of Anions, p. 566
Stability Constants: Definition and Determination. p. 1360

REFERENCES

1. Beer, P.D.; Cadman, J. Electrochemical and optical sensing of anions by transition metal based receptors. Coord. Chern. Rev. 2000. *205.* 131.
2. Beer, P.D.: Gale. P.A. Anion recognition and sensing: The state of the art and future perspectives. Angew. Chem. Int. Ed. Engl. 2001. *40*. 486.
3. Beer, P.D.: Keefe. A.D. A new approach to the coordination of anions, novel polycobalticinium macrocyclic receptor molecules. J. Organomet. Chem. 1989. *375.* C40.
4. Beer. P.D. Anion selective recognition and optical/electrochemical sensing by novel transition-metal receptor systems. Chem. Commun. 1994. *6.* 689.
5. Beer. P.D.: Hesek, D.: Kingston. J.E.: Smith, D.K.: Stokes, S.E.; Drew, M.G.B. Anion recognition by redox-responsive ditopic bis-cobaltocenium receptor molecules including a no\el calix[4]arene derivative that binds a dicarboxylate dianion. Organometallics 1995. *14.* 3288.
6. Beer, P.D.; Hazlewood, C.; Hesek, D.: Hodacova. J.: Stokes. S.E. Anion recognition by acyclic redox-responsive amide-linked cobaltocenium receptors. J. Chern. Soc. Dalton Trans. 1993, *8*, 1327.
7. Beer, P.D.: Drew. M.G.B.: Hodacova. J.; Stokes. S.E. Synthesis, structure and anion co-ordination chemistry of a novel macrocyclic cobaltocenium receptor. J. Chem. Soc. Dalton Trans. 1995, *21.* 3447.
8. Beer. P.D.; Drew, M.G.B.; Hesek. D.; Shade. M.: Szemes. F. Anion recognition properties of new upper-rim bis[rhenium(I) bipyridyl. ruthenium(II) bis(bipyridyl), cobaltocenium]calix[4]arene receptors dictated by lower-rim substituents. Chern. Commun. 1996, *18*, 2161.
9. Beer. P.D.; Drew. M.G.B.; Hesek. D.; Nam, K.C. A new carboxylate anion selective cobaltocenium calix[4]arene receptor. Chem. Cornmun. 1997. 1. 107.
10. Beer, P.D.; Drew. M.G.B.: Hesek. D.: Nam, K.C. Anion recognition properties of new upper-rim cobaltocenium calix[4]arene receptors. Organometallics 1999. *18*. 3933.
11. Beer. P.D.: Drew, M.G.B.: Hesek. D.; Jagessar. R. Spectral and electrochemical anion sensing by a novel 5,10,15,20-tetrakis(R-substituted) porphyrin receptor ($R=C_6H_4NHC(O)C_5H_4CoC_5H_5+PF_6-$). Chem. Commun. 1995, *11,* 1187.
12. Beer. P.D.: Graydon, A.R.: Johnson, A.O.M.: Smith. D.K. A calix[4]arene with diethylthiocarbamoylmethyloxy substituents in the 1,3 positions. Inorg. Chem. 1997. *36.* 2112.
13. Beer. P.D.; Chen. G.Z.: Goulden. A.J.: Graydon, A.R.: Stokes. S.E.; Wear, T. Selective electrochemical recognition of the dihydrogen phosphate anion in the presence of hydrogen sulfate and chloride ions by new neutral ferrocene anion receptors. Chem. Commun. 1993, *24.* 1834.
14. Beer. P.D.: Drew. M.G.B.: Jagessar. R. Selective anion recognition by novel 5,10,15,20-tetrakis(o-ferrocenylcarbonylaminophenyl-substituted) zinc metalloporphyrin receptors. J. Chem. Soc. Dalton Trans. 1997. *5,* 881.
15. Gale. P.A.: Chen. Z.: Drew. M.G.B.: Heath. J.A.: Beer. P.D. Lower-rim ferrocenyl substituted calixarenes: New electrochemical sensors for anions. Polyhedron 1998. *17*, 405.
16. Valero. C.; Fillaut, J.-L.; Ruiz. J.: Guittard. J.: Blais. J.-C.: Astruc. D. The dendritic effect in molecular recognition: Ferrocene dendrimers and their use as supramolecular redox sensors for the recognition of small inorganic anions. J. Am. Chem. Soc. 1997. *119.* 2588.
17. Labande. A.; Ruiz, J.; Astruc. D. Supramolecular gold nanoparticles for the redox recognition of oxoanions: Syntheses. titrations, stereoelectronic effects. and selectivity. J. Am. Chem. Soc. 2002. *124* (8). 1782.
18. Kavallieratos. K.: Hwang. S.: Crabtree. R.H. Aminoferrocene derivatives in chloride recognition and electrochemical sensing. Inorg. Chern. 1999. *38.* 5184.
19. Thomas. J.-L.: Howarth. J.: Hanlon. K.: McGuirk. D. Fen-ocenyl imidazolium salts as a new class of anion receptors with C–H···X hydrogen bonding. Tetrahedron. Lett. 2000, *41*. 413.
20. Gale, P.A.: Hursthouse. M.B.; Light, M.E.; Sessler, J.L.: Warriner. C.N.; Zimmerman. R.S. Ferrocene-substituted calix[4]pyrrole: A new electrochemical sensor for anions involving CH···anion hydrogen bonds. Tetrahedron. Lett. 2001, *442.* 6759.
21. Dusemuncl. C.: Sandanayake, M.R.A.S.: Shinkai. S. Selective fluoride recognition with ferroceneboronic acid. Chem. Commun. 1995. *3.* 333.
22. Aldridge. S.; Bresner. C.: Fallis. I.A.: Coles. S.J.; Hursthouse, M.B. Multidentate Lewis acids: Synthesis. structure and mode of action of a redox-based fluoride ion sensor. Chem. Commun. 2002, *7.* 740.
23. Abouderbala. L.O.: Belcher. W.J.: Boutelle. M.G.: Cragg. P.J.; Dhaliwal. J.: Fabre. M.: Steed, J.W.; Turner, D.R.: Wallace. MJ. Anion sensing 'venus flytrap' hosts: A modular approach. Chem. Commun. 2002. *4.* 358.
24. Abouderbala, L.O.: Belcher. W.J.: Boutelle, M.G.: Cragg, P.J.: Steed, J.W.; Turner. D.R.: Wallace. K.J. Cooperative anion binding and electrochemical sensing by modular podands. Proc. Nat. Acad. Sci. U.S.A. 2002. *99* (8). 5001.
25. Bianchi, A.: Bowman-James. K.; Garcia-Espana. E.

Supramolecular Chemistry of Anions; Wiley VCH: New York, 1997.

26. Beer, P.D.; Chen, Z.; Drew, M.G.B.; Kingston, J.E.; Ogden, M.; Spencer, P. New polyaza and polyammonium ferrocene macrocyclic ligands that complex and electrochemically recognize transition metal cations and phosphate anions in water. Chem. Commun. **1993**, *13*, 1046.
27. Beer, P.D.; Chen, Z.; Drew, M.G.B.; Johnson, A.O.M.; Smith, D.K.; Spencer, P. Transition metal cation and phosphate anion electrochemical recognition in water by new polyaza ferrocene macrocyclic ligands. Inorg. Chim. Acta **1996**, *246*, 143.
28. Beer, P.D.; Cadman, J.; Lloris, J.M.; Martinez-Manez, R.; Padilla-Tosta, M.E.; Pardo, T.; Smith, D.K.; Soto, J. Selective electrochemical recognition of sulfate over phosphate and phosphate over sulfate using polyazo ferrocene macrocyclic receptors in aqueous solution. J. Chem. Soc. Dalton Trans. **1999**, *2*, 127.
29. Beer, P.D.; Drew, M.G.B.; Smith, D.K. Selective electrochemical recognition of bidentate anionic guests in competitive solvents using novel ferrocenyl thiourea and guanidinium receptors. J. Organomet. Chem. **1997**, *543*, 259.
30. Lloris, J.M.; Martinez-Manez, R.; Padilla-Tosta, M.E.; Pardo, T.; Soto, J.; Garcia-Espana, E.; Ramirez, J.A.; Burguete, M.I.; Luis, S.V.; Sinn, E. 1,4,8,11-tetrakis(4-ferrocenyl-3-azabutyl)-1,4,8,11-tetraazacyclotetradecane as a ferrocene-functionalized polyammonium receptor for electrochemical anion sensing. J. Chem. Soc. Dalton Trans. **1999**, *11*, 1779.
31. Beer, P.D.; Graydon, A.R.; Sutton, L.R. Luminescent anion recognition: Selective induced emission by binding of dihydrogenphosphate. Polyhedron **1996**, *15*, 2457.
32. Beer, P.D.; Szemes, F.; Balzanni, V.; Sala, C.M.; Drew, M.G.B.; Dent, S.W.; Maestri, M. Anion selective recognition and sensing by novel macrocyclic transition metal receptor systems. ^{1}H NMR, electrochemical, and photophysical investigations. J. Am. Chem. Soc. **1997**, *119*, 11864.
33. Staffilani, M.; Hancock, K.S.B.; Steed, J.W.; Holman, K.T.; Atwood, J.L.; Juneja, R.K.; Burkhalter, R.S. Anion binding within the cavity of *p*-metalated calixarenes. J. Am. Chem. Soc. **1997**, *119* (27), 6324.
34. Atwood, J.L.; Holman, K.T.; Steed, J.W. Laying traps for elusive prey: Recent advances in the non-covalent binding of anions. Chem. Commun. **1996**, *12*, 1401.
35. Holman, K.T.; Orr, W.; Steed, J.W.; Atwood, J.L. Deep cavity [CpFe(arene)]+ derivatized cyclotriveratrylenes as anion hosts. Chem. Commun. **1998**, *19*, 2109.
36. Valerio, C.; Alonso, E.; Ruiz, J.; Blais, J.-C.; Astruc, D. A polycationic metallodendrimer with 24 [Fe(h_5-C_5Me_5)(h_6-*N*-alkylaniline)]+termini that recognizes chloride and bromide anions. Angew. Chem. Int. Ed. Engl. **1999**, *38* (12), 1747.
37. Beer, P.D.; Dickson, C.A.P.; Fletcher, N.; Goulden, A.J.; Grieve, A.; Hodacova, J.; Wear, T. New classes of anion receptor containing charged and neutral transition-metal Lewis acidic recognition sites. Chem. Commun. **1993**, *10*, 828.
38. Camiolo, S.; Coles, S.J.; Gale, P.A.; Hursthouse, M.B.; Mayer, T.A.; Paver, M.A. Hydrogen bonding networks and anion coordination in (h_6-arene)$Cr(CO)_3$ complexes: Metal carbonyls as hydrogen bond acceptors. Chem. Commun. **2000**, 275.
39. Sun, S.-S.; Lees, A.J. Anion recognition through hydrogen bonding: A simple, yet highly sensitive, luminescent metal-complex receptor. Chem. Commun. **2000**, *17*, 1687.
40. Lehaire, M.-L.; Scopelleti, R.; Piotrowski, H.; Severin, K. Selective recognition of fluoride anion using a Li^+-metallacrown complex. Angew. Chem. Int. Ed. Engl. **2002**, *41* (8), 1419.

Organometallic Oligomers and Polymers

Alaa S. Abd-El-Aziz
The University of Winnipeg, Winnipeg, Manitoba, Canada

INTRODUCTION

Historically, metal-containing oligomers and polymers have been utilized for hundreds of years; however, it was not until the development of ferrocene in the early 1950s that organometallic polymers emerged as a focused area of research. Despite the fact that these materials were only developed within the past 50 years, there have been significant advances in this field, most importantly, within the past two decades. Organometallic oligomers and polymers are currently the focus of considerable attention in light of their electrical, magnetic, optical, catalytic, and biological properties.[1–3]

Brganometallic polymers are often classified according to the types of o- or π- (metal–carbon) bonds within their structures. Within this classification, these macromolecules can be further divided based on the placement of the metallic moieties in the polymer backbone or side chain. This review will highlight some of the main families of organotransition metal-containing oligomers and polymers, focusing on the most widely studied organornetallic systems; namely, metallocene-based polymers and their closely related transition-metal-coordinated arene- and cyclobutadiene-containing oligomers and polymers. In addition to these n-coordinated systems, there are also a number of examples of materials with metals o-bonded to carbon in the polymer backbone and polymers incorporating metal–metal bonds.

METALLOCENE-BASED POLYMERS

The first example of a metallocene-based polymer, polyvinylferrocene, was described in 1955.[4] This macromolecule was synthesized via the radical and cationic chain growth polymerization of vinylferrocene and incorporated the ferrocenyl unit pendent to the polymer backbone. Over the next 20 years. a multitude of reports detailed the mechanistic features of the addition polymerization of vinyl-substituted fessocene derivatives. In the 1960s, heteroannularly substituted ferrocenes were subjected to polycondensation reactions, which resulted in polymers with the ferrocenyl units in the backbone. Early investigations also described the direct polymerization of ferrocene and its derivatives; these reactions produced homo- and heteroannularly substituted polyferrocenylenes, in which the cyclopentadienyl rings were directly bonded to one another.[1,2]

The polymerization of vinyl metallocene-containing monomers is still an active area of research. In particular. current research is focused on new types of catalysts, copolymer synthesis, and the development of polymers with interesting biological, nonlinear optical: liquidcrystalline, electrical, and optical properties. Polyiner 1 is an example of a liquid-crystalline polymethacrylate containing ferrocenyl moieties in its side chains.[5] This polymethacrylate exhibited enantiotropic smectic C and smectic A phases with a weight average molecular weight of 100,000. Other classes of polymers containing metallocenes in their side chains were prepared by ring-opening polymerization reactions. For example, Allcock and coworkers reported the synthesis of fessocene- and ruthenocene-functionalized polyphosphazenes such as Polymer 2. which is a polyphosphazene with transannular and pendent ferrocene moieties.[6] It was possible to prepare this class of polymer either by ring-opening the metallocene-substituted cyclic phosphazene monomers or by reacting metallocene complexes with preformed polyphosphazenes. Ring-opening metathesis polymerization of norbornene monomers substituted with fessocenyl moieties also allowed for the

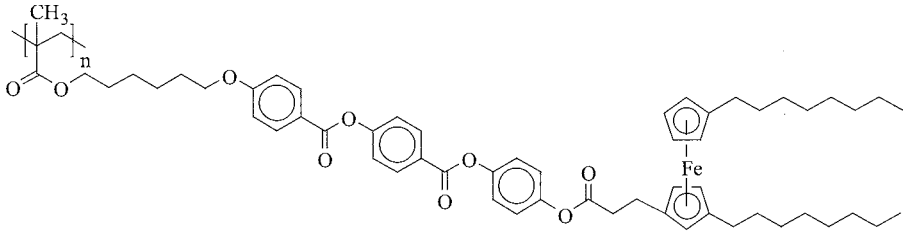

1

Encyclopedia of Supramolecular Chemistry
DOI: 10.1081/E-ESMC 120019202

production of metallocene-based polynorbornenes such as **3** using well-defined transition metal catalysts.[7]

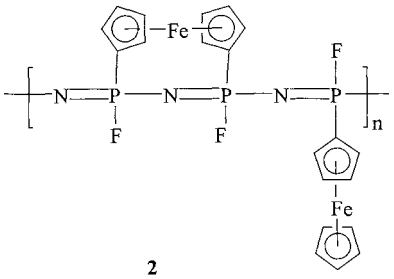

2

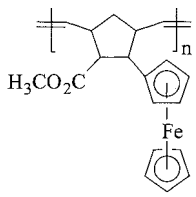

3

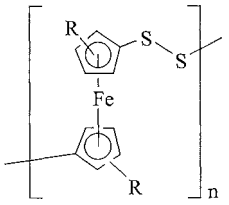

4

There continue to be developments in the synthesis of functional polymers, most importantly from the ring-opening polymerization (ROP) of ferrocenophanes. In the early 1990s, Rauchfuss reported the desulfurization- and deselenization-induced ring-opening polymerization of [trithiaferrocenes and [3]selenaferrocenes using PBu_3.[8] Reduction of the resulting high-molecular poly(ferrocenylene persulfide) 4 with $LiBHEt_3$ resulted in cleavage of the disulfide linkages in the polymer and the production of a monometallic complex; however, the polymer could be regenerated upon oxidation with iodine. Manners and coworkers pioneered one of the most important developments in metallocene-based polymers.[9,10] It was reported that high-molecular-weight polyferrocenylsilanes could be prepared by the thermal ring-opening polymerization of [1]silaferrocenophanes. Since that time, a number of research groups have been active in this area, and a number of reports detailed the syntheses, properties. and applications of polymers prepared via ROP of [1]ferrocenophanes.[11,12] These polymers. **5**. have since been prepared where the bridging element is silicon. germanium, tin, phosphorus. and boron.[9–13] [2]Ferrocenophanes containing carbon. sulfur. and phosphorus bridges were also polymerized. Initiation of ring-opening reactions was achieved thermally, using anionic and cationic initiators and using */-irradiation. A number of copolymers and cross-linked polymers were also synthesized.[13]

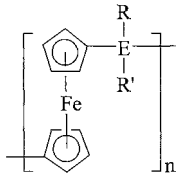

5

The synthesis of cobaltoceniurn-based polymers has also been described since the 1970s; however, there are only a limited number of reports on these cationic polymers in light of the difficulties involved in the derivatization of cobaltocene. As well, there are a number of reports detailing the synthesis of metallocenes, where the polymer chain propagates through the metal atoms rather than the cyclopentadienyl rings. These polymers include polyethers, thioethers, amines. and esters of metallocenes (M = Ti, Zr, Hf). Polymer 6 is an example of a mixed-metal polymetallocene in which the cobaltocenium complex is substituted via the cyclopentadienyl rings. and the titanocene complex is bonded through the titanium atoms.[14]

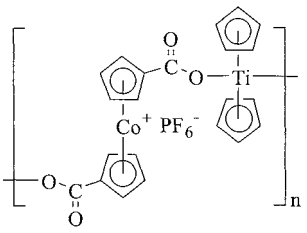

6

There has also been considerable interest directed toward the synthesis of conjugated polymetallocenes due to the electronic communication that these materials may possess. Many polymetallocenes were produced via polycondensation reactions of I,1'-disubstituted metallocenes. More rare are examples that describe the polycondensation of 1.3-disubstituted metallocenes. The synthesis of an optically active homoannularly substituted conjugatedpolyferrocene **7** was recently reported by Plenio and coworkers.[15]

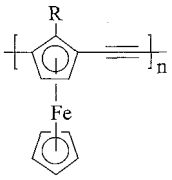

An interesting class of metallocene-based macromolecules is the face-to-face and stacked polymetallocenes.

Rosenblum and coworkers described the synthesis of oligomeric and polymeric materials, 8, using iron, ruthenium, cobalt. and nickel complexes.[16] Closely related are the metailocarborane oligomers that were produced by Grimes and coworkers.[17] *Bis*(cobaltocarborane) complexes were deprotonated and, subsequently, underwent coordination reactions with cobalt or nickel complexes to produce the pentainetallic complex 9. This oligomer could be further reacted using the same strategy to produce higher molecular weight materials.

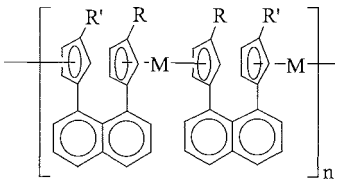

8

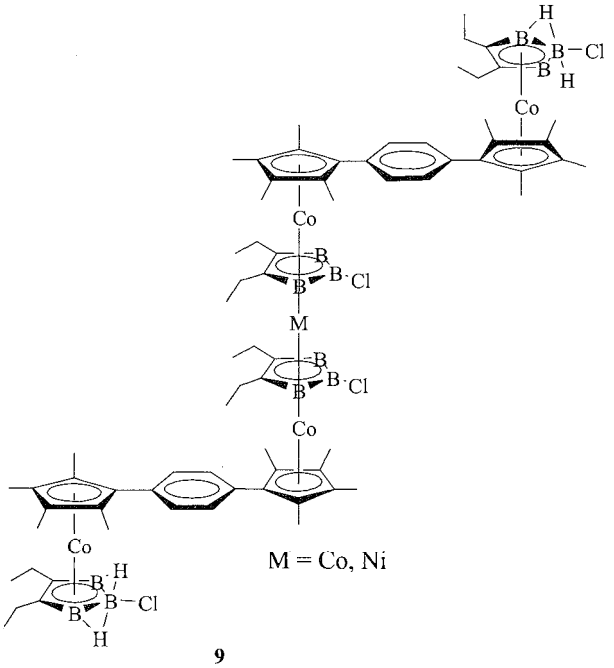

9

POLYMERS CONTAINING ARENES COORDINATED TO TRANSITION METAL COMPLEXES

The coordination of transition metal moieties to arenes alters the reactivity of the aromatic ring. making it more susceptible to nucleophilic addition and substitution reactions and also making substituents on the arene more readily deprotonated. Some of the first examples of polyiners containing arenes n-coordinated to transition metal moieties were described by Pittman and coworkers.[17] Acrylate and methacrylate monomers containing arenes coordinated to chromium tricarbonyl moieties were hoino- and copolymerized using a radical initiator to yield polymers such as 10. More recently. cationic cyclopentadienyliron-functionalized methacrylate monomers were synthesized using a metal-mediated strategy.[18] These monomers were subsequently polymerized to yield the cationic organoiron poly(methyl methacrylate); 11. Abd-El-Aziz et al. also prepared polynorbornenes such as 12 with arene complexes of cyclopentadienyliron pendent to the side chains.[20] The incorporation of azobenzene chromophores into the side chains of these polynorbornenes, polyarornatic ethers. and ether-thioethers allowed for the formation of orange and red materials. Photobleaching of azobenzene-substituted polyethers was achieved in the presence of hydrogen peroxide.[19]

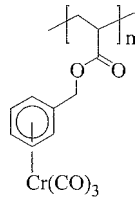

10

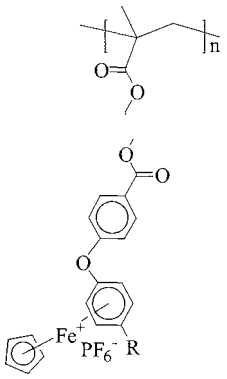

11

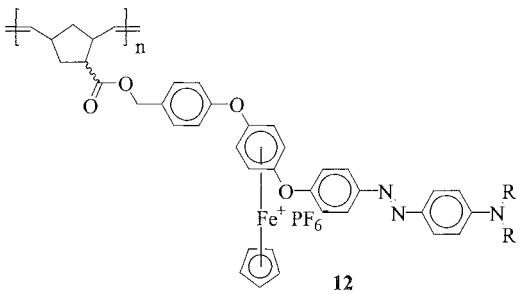

12

A number of polymers containing transition-metal moieties coordinated to arenes in the polymer backbone were synthesized by polycondensation reactions. Polymer 13 shows the general structure of this class of polymer. in which the linkages between the complexed arenes include esters. amides, imines, amines, ethers, thioethers. and acetylene groups. It was found, in most cases, that the incorporation of the chromium, iron, and ruthenium complexes pendent to the backbones of these aromatic polymers increased their solubilities significantly.[''' The coordination of electron-withdrawing $CpFe^+$, $CpRu^+$, and Cp^*Ru^+ moieties to dichloroarenes also allowed for the preparation of polyaromatic ethers and thioethers via nucleophilic aromatic substitution reactions using mild reaction conditions. The cationic polymers were found to exhibit polyelectrolyte effects in polar organic solvents.[19] The synthesis of oligomers and polymers with structures such as 14, with pendent cyclopentadienyliron cations and skeletal ferrocenyl moieties were also recently reported.[22] Another strategy utilized to produce transition-metal-coordinated aromatic polyiners is to use complexation reactions of organic polymers with transition-metal complexes. Nishihara reported the isolation of poly(hexyl phenylenes), 15, coordinated to cyclopentadienyliron. molybdenum tricarbonyl, and chromium tricarbonyl moieties using this methodology.[23]

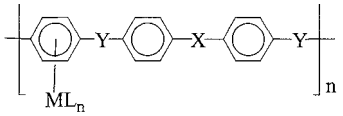

ML_n = $Cr(CO)_3$, $CpFe^+$, $CpRu^+$, Cp^*Ru^+

13

The production of supramolecular polymers containing chromium tricarbonyl and manganese tricarbonyl moieties was described.'''' Sweigart recently reported the self-assembly of η^4-quinone and η^5-semiquinone complexes derived from hydroquinone coordinated to cationic manganese tricarbonyl moieties.''''' The metal-mediated deprotonation of these complexes allowed for the production of polymers such as 16.

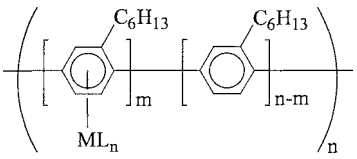

ML_n = $CpFe^+$, $Mo(CO)_3$, $Cr(CO)_3$

15

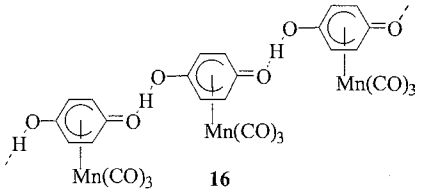

16

POLYMERS CONTAINING METALLACYCLOPENTADIENE RINGS AND CYCLOBUTADIENE RINGS COORDINATED TO CYCLOPENTADIENYL METAL COMPLEXES

Tilley and coworkers synthesized a number of linear polymers and macrocycles containing zirconacyclopentadiene units in the backbone.[25] Polymers such as 17 were synthesized by the intramolecular coupling of zirconocene with poly(*p*-phenylenediyne)s. Metallacycling polymerization was also utilized to prepare polymers with cobaltacyclopentadiene moieties in the main chain. For example. Polymer 18 was synthesized by reacting (η^5-cyclopentadienyl)bis(triphenylphosphine)cobalt with bifunctional diynes.[26] Thermal rearrangement of this class of polymer results in the formation of polymers containing main-chain cyclobutadiene rings coordinated to cyclopentadienylcobalt moieties. An alternative approach to the synthesis of polymers with complexed cyclobutadiene units in the main chain is to react monomers already containing these complexes in their structures. Liquid-crystalline polymers such as 19 were prepared by nickel-catalyzed debromination polycondensation of a complex containing terminal bromophenyl groups.[27] Oligomers containing cyclobutadiene rings coordinated

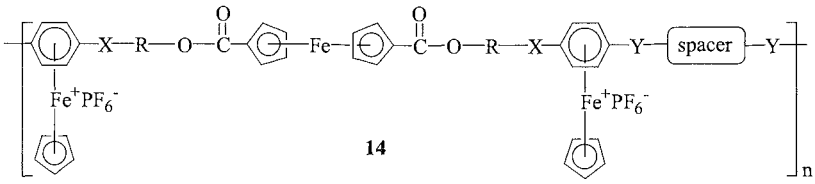

14

to cyclopentadienylcobalt and iron tricarbonyl moieties **20** were synthesized by Bunz and coworkers.[28]

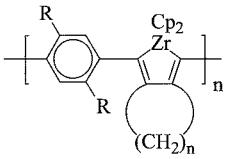

17

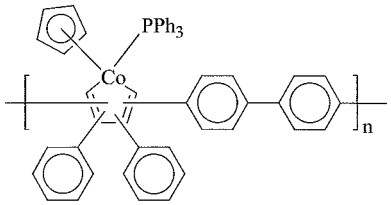

18

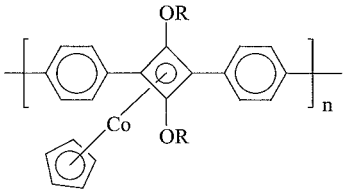

19

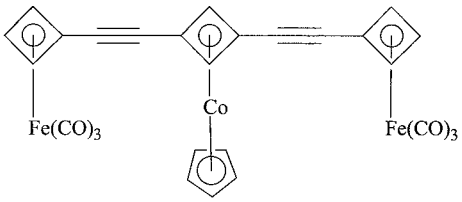

20

METAL CARBONYLS PENDENT TO POLYMER BACKBONES AND SIDE CHAINS

There are a number of different types of polymers that contain metal carbonyl complexes attached to polymer backbones and side chains. In the 1970s, Pittman and coworkers reported the synthesis and polymerization of a wide range of vinyl monomers containing transition-metal-coordinated cyclopentadienyl rings. Polymer **21** is an example of a copolymer containing chromium and manganese complexes in the side chain.[29] Another class of polymer incorporates iron tricarbonyl moieties π-coordinated to dienes in the side chains of polyacrylate homo- and copolymers.[30] The copolymer with styrene **22** could be converted to π-allyliron tri- and tetracarbonyl derivatives. Oxidative polymerization of dicarbonyl(η^5-cyclopentadienyl)(η^1-pyrrolyl)iron using dodecylbenzenesulfonic acid and tetrabutylammonium persulfate gave a polymer, **23**, with a conductivity of 7×10^{-3} S/cm.[31] This polymer lost its carbonyl ligands in solution upon heating to yield an azaferrocene derivative.

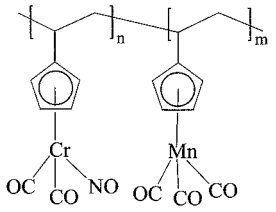

21

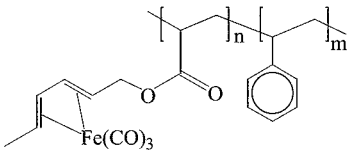

22

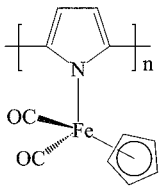

23

Mapolie and coworkers prepared metal-containing polyesters via polycondensation of iron- or rhenium-containing diols.[32] The organometallic monomer [(η^5-C_5H_5)$(CO)_2Fe(CH_2)_3O$–{2,6–$(CH_2OH)_2$–4–CH_3–C_6H_2}] was synthesized via the reaction of 2,6-*bis*(hydroxymethyl)-*p*-cresol with an iodopropyl complex. Polycondensation of this monomer with terephthaloyl chloride in toluene in the presence of triethylamine gave Polymer **24**. Molecular weight analysis of the toluene-soluble fraction of the iron-containing polyester showed that it consisted of low-molecular-weight oligomers. The tricarbonylmanganese-coordinated Polymer **25** was synthesized via Suzuki coupling of substituted diiodocyclopentadienylmanganesetricarbonyl with *p*-phenylenediboronic acid.[33]

This manganese-based polymer had a number-average molecular weight of 11 x 10^3, with a polydispersity of 6.4.

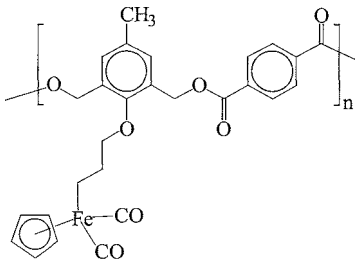

24

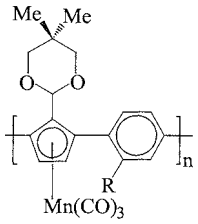

25

One of the few articles on metal-carbene-containing poiymers was authored by Masuda and coworkers.[34] Polycondensation reactions of a bifunctional alkoxycarbene with diamines allowed for the preparation of polymers such as 26. with metal-carbene units attached directly to the polymer backbone. The polymers were air stable but were unstable in solution. These polymers had number-average molecular weights in the range of 3900–8800 and polydispersity indices between 2.15–2.90.

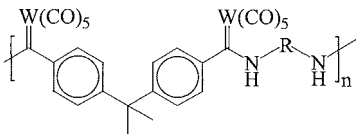

26

POLY(METAL ACETYLIDES)

In the 1970s, Hagihara and coworkers reported the synthesis of oligomeric and polymeric poly(metal acetylides), also called poly-ynes. containing transition metals in the main chain.''] Conjugated poly-ynes containing platinum or palladiuin complexes in their backbones were prepared by polycondensation of a metal chloride and an acetylene monomer in the presence of CuI. Platinum and palladium complexes were introduced into the backbones of these rigid polymers via reaction of *trans*-$(PBu_3)_2$-$Pt(C{\equiv}C{-}C{\equiv}CH)_2$ with *trans*-$(PBu_3)_2PdCl_2$ or via reaction of *trans*-$(PBu_3)_2Pd(C{\equiv}C{-}C{\equiv}CH)_2$ with *trans*-$(PBu_3)_2PtCl_2$ to give the alternating metal Polymer **27**.

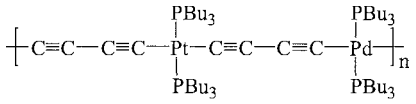

27

The rigid-rod linear ruthenium poly-yne 28 was prepared via the reaction of *trans*-$[Ru(PMe_3)_4Cl_2]$ with $Me_3Sn{-}C{\equiv}C{-}R{-}C{\equiv}C{-}SnMe_3$ in a 1:1 stoichiometric ratio.''' Using similar strategies, polymers containing a vast array of transition-metal complexes in their backbones were synthesized. This class of rigid-rod polymer exhibits interesting electrical and optical properties, and research is currently focused on optimizing these features. For example. platinum polyacetylides. such as 29, containing bithiazole units functionalized with electron-donating and electron-withdrawing substituents, were recently reported.[37] These soluble platinurn polyacetylides showed photoconducting behavior.

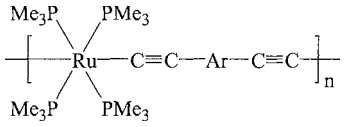

28

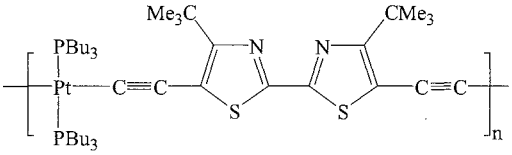

29

Interesting zirconocene polyacetylides such as 30 were synthesized by reaction of *bis*(pentamethylcyclopentadienyl) zirconium(IV) dichloride with dilithiated acetylene monomers.[38] These polymers had weight average molecular weights between 55.000 and 68,000, as measured by gel permeation chromotography (GPC). Acetylide complexes of platinum and palladium functionalized with cyano groups were polymerized by hydroboration to produce Polymer 31 with cyclodiborazane units in the backbone.[39] The platinum and palladiuin polymers showed enhanced solubility and had number average molecular weights around 6000. This class of polymer

exhibited π-conjugation via the transition-metal atoms and the boron atoms.

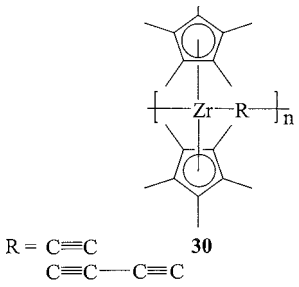

30

POLYMERS WITH METAL–METAL BONDS

There are relatively few reports on organometallic polymers with metal–metal bonds in their structures. Tyler and coworkers synthesized a number of polyurethanes, 32, amides, and ureas containing photodegradable metal–metal bonds in their backbones by polycondensation reactions.[40] Cross-linked polymers. 33, were also produced by the radical polymerization of vinyl monomers containing Fe—Fe bonds.[40] Cuadrado described the synthesis of silicon-based polymers with iron–iron bonds either within the polymer backbone, as shown in 34, or pendent to the polymer backbone by reaction of polysiloxanes with $Fe(CO)_5$.[41] These polymers had lower solubility compared to the dimer precursors. The thermal gravimetric analysis of Polymer 34 showed initial weight loss at 300°C, however, analogous polymers with Fe—Fe moieties pendent to the polymer backbone showed higher thermal stability due to cross-linking. Puddephatt reported the synthesis of a number of organometallic oligomers and polymers containing Pt–Pt bonds in their backbones.[42] These polymers, containing acetylide, phosphine, or isocyanide. 35, bridges in their backbones exhibited poor solubilities in organic solvents.

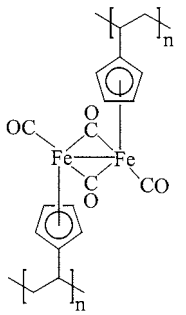

33

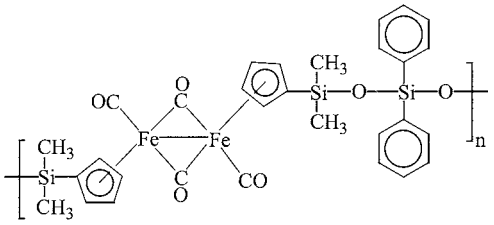

34

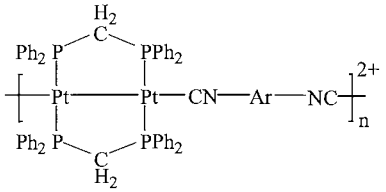

35

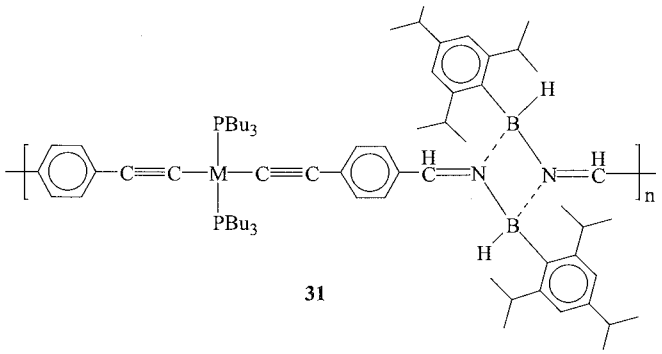

31

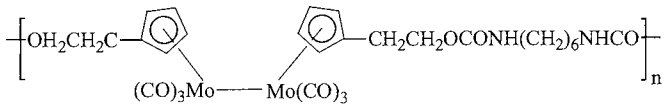

CONCLUSION

The field of organometallic oligomers and polymers received considerable attention over the past two decades. The transition-metal-containing oligomers and polymers described in this article were produced using well-established methodologies. which include olefin, condensation, coordination. and ring-opening polymerizations. While the discovery of new classes of organometallic macromolecules continues to be an important area of research. the focus of many investigations is currently on tailoring the properties of these materials for specific applications. Some of the most widely studied of these properties include electrical, magnetic. and optical properties. There is also considerable interest devoted to exploring the biological properties of organometallic oligomers and polymers.

ARTICLES OF FURTHER INTEREST

Dendrimers, p. 432
Molecular Wires, p. *925*
Soft and Smart Materials, p. 1302

REFERENCES

1. Abd-El-Aziz, A.S. Organometallic polymers of the transition metals. Macromol. Rapid Commun. 2002. *23*. 995–1031.
2. Nguyen, P.: Gomez-Elipe. P.: Manners. I. Organometallic polyrners with transition metals in the main chain. Chem. Rev. 1999. 99 (6), 1515–1548.
3. Archer. R.D. *Inorganic* and *Organometallic Polymers*; Wiley-VCH: New York. 2001.
4. Arimoto. F.S.: Haven. A.C.. Jr. Derivatives of dicyclopentadienyliron. J. Am. Chein. Soc. 1955. 77. 6295–6297.
5. Deschenaux, R.: Turpin, F.: Guillon. D. Ferrocene-containing therniotropic side-chain liquid-crystalline polymethacrylate from a mesomorphic trisubstituted ferrocene monomer. Macromolecules 4997. 30. 3759–3765.
6. Allcock. H.R.: Riding. G.H.: Lavin. K.D. Polymerization of new metallocenylphosphazenes. Macromolecules 1987. *20*. 6–10.
7. Albagli. D.: Bazan. G.C.; Schrock. R.R.: Wrighton, M.S. Surface attachment of well-defined redox-active polymers and block polymers via terminal functional groups. J. Am. Chem. Soc. 1993. 115. 7328–7334.
8. Compton. D.L.: Brandt. P.F.: Rauchfuss, T.B.: Rosenbaum, D.F.: Zukoski. C.F. Organometallic polymers based on S–S and Se–Se linked *n*-butylferrocenes. Chem. Mater. 1995. 7. 2342–2349.
9. Kulbaba. K.: Manners, I. Polyferrocenylsilanes: Metal-containing polyrners for materials science, self-assembly and nanostructure applications. Macromol. Rapid Commun. 2001. *22*. 711–724.
10. Manners, I. Polymer science with transition metals and main group elements towards functional. supramolecular inorganic polymeric materials. J. Polym. Sci., Part A: Polym. Chem. 2002, *40*. 179–191.
11. Hempenius. M.A.; Peter. M.: Robins. N.S.: Kooij. E.S.; Vancso, G.J. Water-soluble poly(ferrocenylsilanes) for supramolecular assemblies by layer-by-layer deposition. Langmuir 2002, *18*, 7629–7634.
12. Espada. L.: Pannell. K.H.: Papkov. V.; Leites. L.; Bukalov, S.; Suzdalev. I.; Tanaka, M.; Hayashi. T. Iodine-doped ferrocenylene-silylene and -germylene polymers. Organometallics 2002. *21*. 3758–3761.
13. Kulbaba. *K.*: Cheng. A.: Bartole, A.: Greenberg, S.; Resendes. R.: Coombs, N.: Safa-Sefat. A.; Greedan. J.E.: Stover. H.D.H.: Ozin, G.A.: Manners, 1. Polyferrocenylsilane rnicrospheres: Synthesis. mechanism of formation, size and charge tunability, electrostatic self-assembly. and pyrolysis to spherical magnetic ceramic particles. J. Am. Chem. Soc. 2002. *124*. 12522–12534.
14. Carraher. C.E., Jr.: Sheats, J.E. Synthesis of poly [bis(oxycarbonylcyclopentadienyl)cobalt(III)(dicyclopentadienyltitan(IV)) hexafluorophosphate]. Makromol. Chem. 1973. 166. 23–29.
15. Plenio, H.; Hermann. J.; Schring. A. Optically and redox-active ferrocenylacetylene polymers and oligomers. Chem. Eur. J. 2000. 6 (10). 1820–1829.
16. Rosenblum. M.: Nugent, H.M.: Jang. K.-S.: Labes. M.M.: Cahalane. W.; Klemarczyk, P.: Reiff. W.M. The synthesis and properties of face-to-face metallocene polymers. Macromolecules 1995. *28*. 6330–6342.
17. Meng, *X*.: Sabat. M.: Grimes, R.N. Metallacarborane staircase oligomers. Stepwise assembly via tetradecker stacking reactions. J. Am. Chem. Soc. 1993. *115*. 6143–6151.
18. Pittman, C.U., Jr.: Voges. R.L.: Elder. J. Organometallic polymers. XIII. Addition polymerization of π-(benzyl acrylate)chromium tricarbonyl. Macromolecules 1971. *4*, 302–308.
19. Abd-El-Aziz. A.S. Monomers, oligomers and polymers containing arenes with pendent transition metal moieties. Coord. Chem. Rev. 2002. *233–234*. 177–191.
20. Abd-El-Aziz. A.S.; Okaslia. R.M.; Afifi. T.H.: Todd. E.K. A new class of cationic organoiron polynorbornenes containing azo dyes. Macromol. Chem. Phys. 2003. *204*, 555–563.
21. Abd-El-Aziz. A.S.: Afifi. T.H.; Budakowski, W.R.; Friesen, K.J.; Todd. E.K. The first example of cationic iron-coordinated polyaromatic ethers and thioethers with azo dye-functionalized side chains. Macromolecules 2002. *35*. 8929–8932.
22. Abd-El-Aziz. A.S.: Todd. E.K.: Okasha, R.M.: Wood. T.E. Novel approach to oligomers and polymers containing neutral and cationic iron moieties within and pendent to their backbones. Macromol. Rapid Commun. 2002. *23*. 743–748.
23. Nishihara. H. Organometallic Conductive Polymers. In *Handbook of Organic Conductive Molecules and Poly-*

mers. Conductive Polymers: Synthesis and Electrical Properties: Nalwa. S.H.. Ed.: John Wiley & Sons Ltd.: New York. 1997; Vol. 2, 799–832. Chapter 19.

24. Oh, M.; Carpenter, G.B.: Sweigart. D.A. (η^5-Semiquione and η^4-quinone complexes of manganese tricarbonyl. Intermolecular hydrogen bonding in the solid state and in solution. Organometallics 2002. *21*, 1290–1295.
25. Lucht. B.L.; Mao. S.S.H.; Tilley, T.D. A zirconocene-coupling route to substituted poly(*p*-phenylenedienylene)s: Band gap tuning via conformational control. J. Am. Chem. Soc. **1998.** *120*, 4354–4365.
26. Lee. J.-C.; Nishio, A.: Tomita, I.; Endo, T. Synthesis of organometallic polymers containing cobaltacyclopentadiene moieties in the main chain. Synthesis of organocobalt polyiners from various diynes. Macromolecules **1997.** *30.* 5205–5212.
27. Sawada, Y.; Tomita, I.; Rozhanskii, I.L.; Endo, T. Synthesis of liquid crystalline organometallic poly(arylene)s containing 1,3-type ((η^4-cyclobutadiene)cobalt moieties in the main chain. J. Inorg. Organomet. Polym. 2000. *10* (4). 221–230.
28. Bunz. U.H.F.; Wiegelmann-Kreiter, J.E.C. Alkynyl-substituted tricarbonyl(cyclobutadiene)iron complexes: Stille coupling of iodocyclobutadiene complexes with stannylalkynes. Chem. Ber. **1996,** 129. 785–797.
29. Pittman. C.U., Jr.: Rounsefell, T.D.; Lewis, E.A.: Sheats, J.E.; Edwards, B.H.; Rausch, M.D.; Mintz. E.A. The vinyl reactivity of (η^5-vinylcyclopentadienyl)dicarbonylnitrosylchromium. A novel vinyl organometallic monomer. Macromolecules **1978,** *11.* 560–565.
30. Pittman, C.U.. Jr. Functionaiization of polymers via π-allyliron tetracarbonyl cations. Macromolecules **1974.** 7, 396–397.
31. Martin. K.F.: Hanks, T.W. Soluble organoiron derivatives of polypyrrole. Qrganoinetallics **1997,** 16, 4857–4860.
32. Mapolie, S.F.: Mavunkal. I.J.; Moss, J.R.: Smith. G.S. The synthesis, characterization and polycondensation of metal-containing diols: Crystal structure of [(η^5-C_5H_5)(CO_2Fe(CH_2)$_3$O-{2,6-(CH_2OH)$_2$-4-CH_3–C6H_2}]. Appl. Organomet. Chem. 2002. 16. 307–314.
33. Setayesh, S.; Bunz, U.H.F. Synthesis of cymantrene-containing organometallic polymers using the Suzuki coupling. Organometallics **1996.** 15. 5470–5472.
34. Nomura, R.: Watanabe, K.; Masuda, T. Synthesis of metal-carbene containing polymers by polycondensation of a bifunctional alkoxycarbene with diamines. Macromolecules 2000, 33, 1936–1939.
35. Sonogashira, K.; Kataoka, S.: Takahashi. S.; Hagihara, N. Studies of poly-yne polymers containing transition metals in the main chain. J. Organomet. Chem. **1978.** *160*, 319–327.
36. Davies, S.J.; Johnson. B.F.G.; Lewis, J.: Raithby, P.R. Synthesis of mononuclear and oligomeric ruthenium(II) acetylides. J. Organomet. Chem. **1991,** 414. C51–C53.
37. Wong, W.-Y.; Chan. S.-M.; Choi, K.-H.; Cheah, K.-W.; Chan, W.-K. Synthesis. optical and photoconduction properties of platinum poly-yne polymers functionalized with electron-donating and electron-withdrawing bithiazole units. Macromol. Rapid Commun. 2000, 21, 453–457.
38. Sahoo. P.K.; Swain. S.K. Synthesis of zirconocene-acetylene and zirconocene-diacetylene polymer. J. Polym. Sci., Part A: Polym. Chem. **1999.** 37, 3899–3902.
39. Matsumoto, F.; Matsumi, N.; Chujo, Y. Synthesis of novel poly(cyclodiborazane)s containing transition metal complexes in the main chain and their properties. Polym. Bull. 2002, 48. 119–125.
40. Tyler, D.R.: Wolcott, J.J.: Nieckarz, G.W.; Tenhaeff, S.C. New Class of Photochemically Reactive Polymers Containing Metal–Metal Bonds Along the Polymer Backbone. In *Inorganic and Organometallic Polymers II*; Wisian-Neilson, P.. Allcock, H.R., Wynne, K.J., Eds.; ACS Symposium Series 572, American Chemical Society: Washington, DC, 1994; 481–496. Chapter 36.
41. Moran, M.; Pascual. M.C.; Cuadrado, I.; Losada. J. (Dimethylamino)dimethylsilyl-substituted dimeric and siloxanyl polymeric compounds containing [(η^5-C_5R_4)-Fe(CO)(μ-CO)]$_2$ (R = H. Me) moieties. Synthesis, characterization, and electrochemistry. Organometallics **1993.** *12* 811–822.
42. Irwin, M.J.: Jia, *G.;* Vittal, J.J.; Puddephatt. R.J. Rigid-rod polymers, oligomers, and complexes with Pt–Pt bonds in the backbone. Organometallics **1996.** *15.* 5321–5329.

O_2 Uptake and Transport, Models of

James P. Collman
Katja E. Berg
Stanford University, Stanford, California, U.S.A.

INTRODUCTION

The three classes of blood-oxygen carriers that reversibly bind and store oxygen are hemoglobin(Hb)/myoglobin(Mb), hemocyanin(Hc), and hemerythrin(Hr). Heme, copper. and nonheme iron models, respectively, of these proteins were utilized to target structure and function relationships of the respective active sites for a better understanding of properties and biological functions. Although biomimetic studies need not duplicate the structural or the physical characteristics of the native enzyme, past research shows that careful design of tunable systems helped identify important factors (coordination geometry, nature of ligands, potentials, cooperativity), which in turn have contributed to an understanding of the protein structure. spectroscopy. and mechanism of oxygen binding.[1,2]

In this article. a brief background to oxygen-binding proteins will be presented and recent development of their models highlighted. Reasons underlying differences in dioxygen binding affinities will be emphasized. Particular attention will be given to the hemoglobin family. which has been studied in more detail than any other group of proteins. Although CO binding acts in conjunction with oxygen binding, this matter is not in the scope of this review. and the reader is encouraged to read one of the reviews portraying that subject (e.g., Refs. [3–5]).

BIOLOGY: STRUCTURE, FUNCTION, AND O_2 BINDING OF OXYGEN CARRIERS

Myoglobin and Hemoglobin

The most common reversible oxygen-binding proteins in biological systems are Mb and Hb. This family of globins is found in all vertebrates (except in the Antarctic fish *Cyclostomata*), many invertebrates (including molluscs, annelid worms, and insect larvae). and some plants (leghemoglobin in *Leguminosae*).[3] In 1960, the first high-resolution x-ray crystallographic structures of sperm whale myoglobin[6] and horse hemoglobin A were determined.[7,8] The active site heme in Mb (16 kDa), an iron(II) protoporphyrinIX, is encapsulated in a pocket, where hydrophobic interactions from protein residues hold the heme in place. Iron(II) (high-spin, S=2), coordinated to four pyrrole nitrogens, is bound to the protein via a fifth ligand, a proximal histidine (HisF8), and is located about 0.5 Å from the heme plane in the direction of the histidine. Although invertebrate Hb may have as many as 192 subunits, Mb contains only one heme prosthetic group, while mammalian HbA holds four structurally analogous subunits ($2\alpha + 2\beta$), each with one heme prosthetic group; these four hemes are involved in cooperative dioxygen binding.[3,4]

The most significant property of Hb is its allosteric (cooperative) O_2 binding[3,8] where the Hill constant n is a measure of the degree of cooperative binding. The value for Hb is 2.8. Due to these allosteric interactions of tetrameric hemoglobin, dioxygen binds cooperatively under high O_2 concentrations (--20 mM), allowing the globin to become nearly saturated in the lungs. Oxy-Hb is transported via the bloodstream to areas of low oxygen concentration in muscle tissue, where a thermodynamically favorable O_2 transfer occurs from hemoglobin to myoglobin. The monomeric, predominantly α-helical globular protein Mb stores oxygen during rest until short bursts are required for oxidative phosphorylation, at rates higher than would be provided by the venous oxygen flow. Relative to a noncooperative system. at low O_2 availability, dioxygen release is facilitated; at high O_2 availability, dioxygen binding is facilitated. Binding of O_2 to the vacant sixth coordination site modifies the structure and electronic configuration of the heme. Careful studies indicate that the so-called T or tense state is a low O_2 affinity structure, and the R or relaxed state is a high O_2 affinity structure. The out-of-plane iron atom in the deoxy form is restrained in a T state until the successive O_2 binding relieves the tension as the oxygenated protein adopts the relaxed R state. This cooperativity between heme centers is propagated via structural changes associated with the $T \rightarrow R$ states. The geometry of the bent (120°), end-on O_2 binding mode to the six-coordinate nearly centered (low-spin) iron atom in oxy-Hb was proposed as early as 1936 by Pauling.[9] Crystallographic and spectroscopic studies of native HbO_2 *(2)* and MbO_2 provided evidence for H-bonding between the imidazole N–H of the distal histidine (HisE7) and the bound O_2 of

Encyclopedia of Supramolecular Chemistry
DOI: 10.1081/E-ESMC 120012688

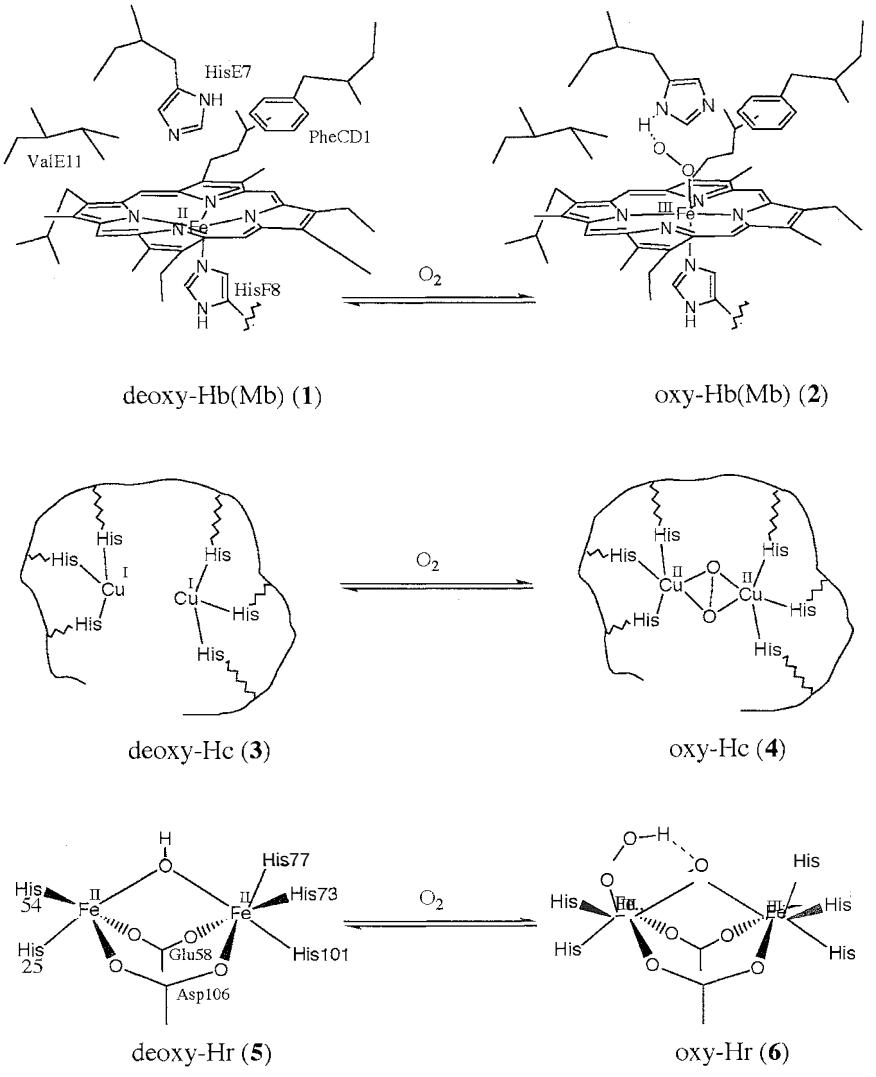

Fig. 1 Active site deoxy and oxy forms of the biological oxygen carriers hemoglobin (Hb), hemocyanin (Hc). and hemerythrin (Hr).

the polarized $Fe\delta^+-O_2\delta^-$ unit (Fig. 1). The proximity of the terminal O_2 atom to N^{ε} of HisE7 was found to be 2.6 Å in MbO_2, 2.8 Å in HbO_2-α, and 3.5 Å in HbO_2-β subunits. Whereas binding of dioxygen to Mb or to isolated a or β subunits of Hb shows 1:1 association ($Mb + O_2 \rightarrow MbO_2$), the equilibrium uptake of O_2 by tetrameric hemoglobin is more complex due to the cooperative effect of oxygen binding. In addition, the extent of O_2 binding to Mb/Hb depends on several factors: pH (Bohr effect), temperature, partial pressure of oxygen, the proximal ligand, and the phosphate effect (O_2 binding is altered by the binding of an organic phosphate to Hb).

Hemocyanin

Hemocyanins. found in arthropods (e.g., lobsters and scorpions) and molluscs (e.g., octopi and snails), are large multisubunit proteins capable of transporting oxygen. Although the spectral features of the two types of Hc are similar, arthropod Hc is composed of −75 kDa subunits (assembled into hexamers or multiple hexamers), whereas the molluscan Hc consists of −350−450 kDa subunits (assembled into cylinders of five- or 10-fold symmetry). In the arthropod Hc, each subunit contains a single oxygen binding site, while in mollusc Hc. multiple oxygen binding sites are found. In both Hc types, oxygen is reversibly bound at a dinuclear dicopper active site (Cu_A and Cu_B), ligated to N-atoms of three histidines in the protein side chains (**4**).[3,10]

Similar to Hb. hernocyanins demonstrate a high degree of cooperativity in oxygen binding. Chemical and spectroscopic similarities of the mollusc and arthropod forms indicate a closely related active site structure and binding mode. Oxygenation of the dinuclear center alters

the oxidation states from Cu(I) (dl^0, colorless) to Cu(II) (blue) with a consequent geometry modification from trigonal to square planar arrangement. In oxy-Hc, the two closest histidines and two oxygen atoms ($\mu-\eta^2:\eta^2O_2^{2-}$) are coordinated to the copper centers (Fig. 1) (d_{Cu-Cu} = 3.6 Å; $\nu(O-O) \sim 750\ cm^{-1}$; EPR-silent).[10]

Hemerythrin

Hemerythrin is a relatively rare oxygen-carrier protein in marine invertebrates, including sipunculids (nonsegmented worms), annelids (segmented worms), priapulids, and brachiopods (shrimps). It parallels the functions of mammalian Hb and Mb as an O_2 transport and storage protein for invertebrates. Hr exists mostly as an octamer of ~14 kDa subunits. although monomers (myohemerythrin) and oligomers are known with active sites of four-helix bundles. In its asymmetric deoxy-Hr form (Fig. 1), the two Fe atoms, roughly 3.3 A apart. are held in the protein by seven amino acid side-chain residues (five histidines and two carboxylic acid residues). Three histidines are bound to one Fe(II) center and two to the remaining Fe(II). Glutamic acid. aspartic acid. and hydroxide bridge the two metals, yielding an antiferromagnetic coupling between the metals ($J \sim -15\ cm^{-1}$).[3,11]

Upon oxygenation, the colorless protein becomes purple-red. and an asymmetric tribridged diiron(III) is formed with novel features; an oxobridged (Fe–0–Fe) unit ($J \sim -120\ cm^{-1}$), and a terminal end-on Fe(III)–O–O–H unit (6) (hydrogen-bonded to the bridging oxygen atom; $\nu(Fe-OO) = 503\ cm^{-1}$, $\nu(O-O) = 844\ cm^{-1}$). A Bohr effect (release or uptake of protons) is absent in oxygen binding to Hr, ruling out hydroxo-bridged oxy-Hr.[12]

SYNTHETIC ANALOGUES OF O_2 TRANSPORT PROTEINS

Models for Myoglobin and Hemoglobin

Synthetic requirements

Necessary conditions for synthetic models to mimic oxyhemoglobins are formation of a five-coordinate heme precursor with a proximal base (e.g., imidazole, pyridine), prevention of μ-peroxo/μ-oxo (M–O_2–M/M–O–M) dimer formation upon oxygenation (i.e., reversible oxygenation). and exclusion of protons and nucleophiles. Model systems should be easily modified and allow probing of distal and proximal influences. Tetraphenylporphyrins (TPP) serve as the basis of numerous model complexes, because they are less susceptible to oxidation and relatively easy to synthesize. derivatize, and crystallize. Other *meso*- and pyrrole-substituted models have also proven valuable.

The six-coordinate low-spin (d^6) iron(II) gains electronic stabilization relative to the high-spin five-coordinate species due to ligand field stabilization energy. As a consequence, there is a larger equilibrium constant for the addition of the second ligand than for the first, causing the heme to be predominantly six-coordinated. Many approaches were presented to limit six-coordinate formation in models: 1) steric hindrance of the axial base; 2) covalent attachment of the proximal base to the heme backbone; 3) steric hindrance of one (or both) of the heme faces: and 4) preparation of "integrated hemes''—a combination of two or more of these features. Whichever method is utilized, the axial base needs to be a strong σ donor to increase dioxygen affinity at the metal center.

Heme models

The high-spin complexes Fe(TPP)(2-MeIm) (7) and Fe(TpivPP)(1,2-diMeIm) (10) are examples of five-coordinate Fe(II) with sterically hindered axial bases (Fig. 2). Both porphyrins show similarity to the globins (10–11° off-axis tilt of the proximal ligand; 0.5–0.6 Å out-of-plane iron displacement), suggesting that 2-MeIm gives a good model for axial ligation in T-state deoxy-Hb.[8,13] Formation of *bis*(2-MeIm) adducts is never observed at room temperature, even at high ligand concentrations. Another successful approach to five-coordination was achieved by covalent attachment of the axial base to the periphery of the heme (Fig. 2). In these models. an imidazole or a pyridine ligand is often covalently attached through ester or amide linkages to either the propionic acid side chains of the porphyrin sing to the β-pyrrole position of a TPP ring or to the *ortho* position of a *meso* phenyl ring of TPP. Although five-coordination is enhanced via covalent attachment of base to porphyrin, a disadvantage is the possible dimerization into mixed 416-coordinate dimers favored at low temperatures and high concentrations. Chain length and position of attachment have dramatic effects on the ligand-binding properties. A more recent tactic to obtain five-coordinated hemes is the preparation of sterically encumbered porphyrins, wherein the obtained cavity leaves one face of the porphyrin protected and the other open for coordination. A plethora of architecturally distinct model porphyrins following this approach have been studied. e.g., picket fence (10), pocket (BP), *bis*-pocket (17), cyclophane (16), cofacial (two covalently bridged porphyrins). strapped (aliphatic chains). cross-strapped (13), capped (14), crowned (crownether cap). hybrid (combination of picket fence and strap with one

A Structures of hemes with a steric base or with covalently attached axial ligands:

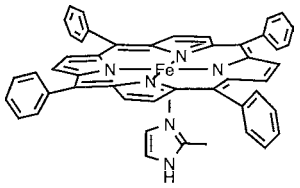

Fe(TPP)(2-MeIm) (7)

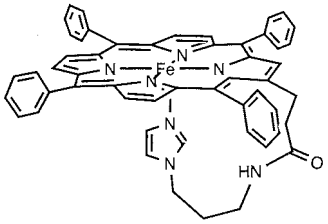

Fe(TPP-Im) (8)
[Momenteau, 1979]

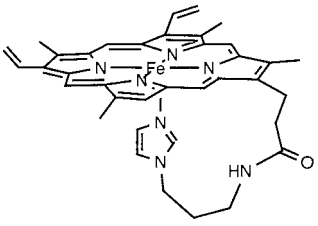

Fe(PPIX-Im) (9)
[Traylor, 1973]

Structures of single-face hindered hemes:

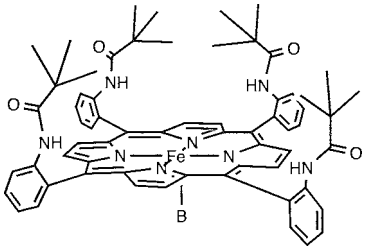

Picket Fence Porphyrin:
Fe(TpivPP)(Base) (10)
[Collman, 1975]

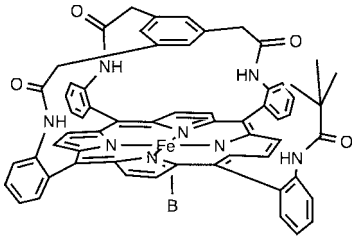

Pocket Porphyrin:
Fe(PocPiv)(Base) (PI)
[Collman, 1983]

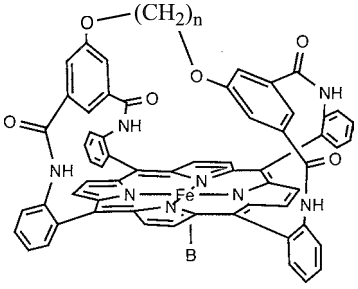

Picnic Basket Porphyrin:
Fe(PicnicPP)(Base) (12)
n=2,4,6,8,10
[Collman. 1988]

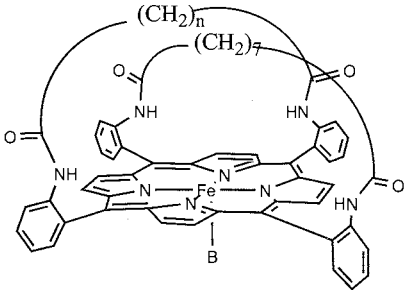

(Cross-)Strapped Porphyrin:
Fe(bis-StrapPP)(Base) (13)
n=14,18
[Uemori, 1987]

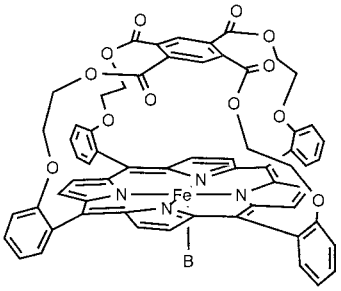

Capped Porphyrin:
Fe(C_2CapPP)(Base) (14)
[Baldwin, 1975]

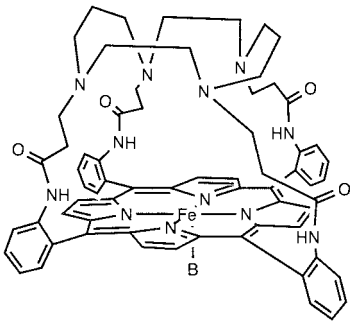

Capped Porphyrin:
Fe(CyclamCapPP)(Base) (IS)
[Collman, 1999]

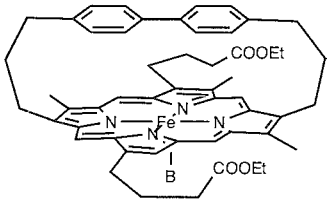

Cyclophane Porphyrin:
Fe(CphPP)(Base) (16)
[Traylor, 19711

Fig. 2 Structures of hemoglobin models.

B Structures of both-faces hindered hemes:

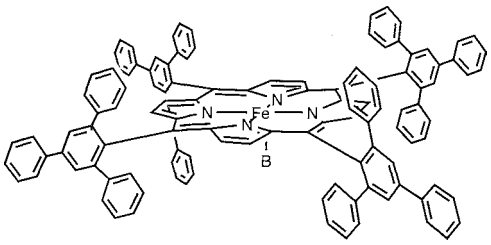

Fe(bis-PocPP)(Base) (**17**)
[Suslick, 1983]

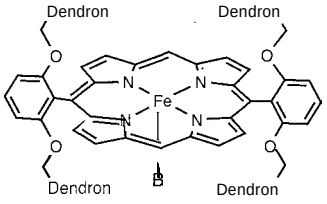

Fe(dendron)$_4$PP(Base) (**18**)
[Diederich, 2002]

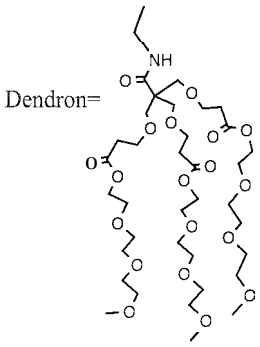

Structures of "integrated" hernes:

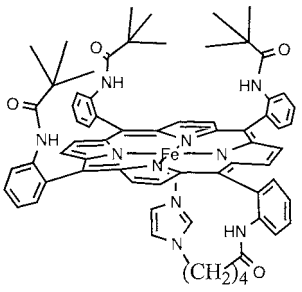

Picket Fence:
Fe(Piv$_3$PP-Im) (19)
[Collman, 1983]

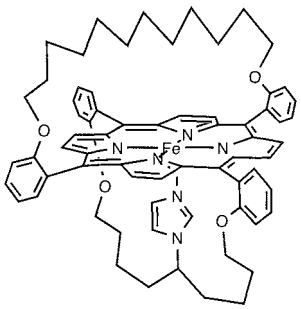

Bridged:
Fe(C12StrapPP-Im) (**20**)
[Momenteau, 1985]

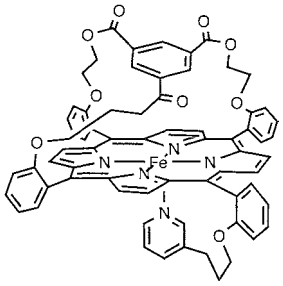

Pocket:
Fe(PocPP-Py) (21)
[Orth, 1986]

Fig. 2 (*Continued*)

face open), jellyfish (combination of picket fence and strap on opposite faces). picnic basket (**12**), reverse picket fence (both faces picket fence substitution), and dendritic (18) porphyrins.[8,14,15] The binding of the external base highly depends on the size of the host cavity. A large and constrained steric group near the axial position lowers affinity of ligand binding. resulting in a five-coordinate iron. However, formation of a six-coordinate species prior to oxygenation cannot be excluded. because dioxygen is able to replace an axial base in hemochromes. Whereas Fe(II) complexes with 2-MeIm may be considered good analogs of the T state. the Fe(Piv$_2$C8PP) is a reasonable model for the R state of hemoglobin.

Today. the most effective mimics of deoxy-Hb(Mb) are the integrated complexes, which use the both-faces-hindered concept. Within this design, an endogenous nitrogenous base (pyridine or imidazole) is inserted into a proximal strap ensuring a high degree of five-coordinated iron(II). The other sterically hindered distal face inhibits *inter*molecular association. Although synthetic procedures were known, efficient preparation and isolation of the required $\alpha_3\beta$ atropisomer was first reported in 1998. As depicted in Fig. 2, high-spin. five-coordinate ferrous porphyrins were synthesized following this both-faces-hindered concept, including the picket-fence (**19**), capped (**15**), pocket (**21**), and bridged (also called hanging-base, where the base is integrated into the strap; in some instances chiral bridges are used) (**20**). In some cases, distal pickets were designed to accommodate a second metal, thereby modeling bimetallic enzymes such as C*c*O. In other examples, distal *N*-donor caps such as TACN. cyclam, cyclen,[16] or tren were utilized. Studies of these complexes show that the iron(II) coordination environment can be satisfactorily modeled, but that the corresponding O_2 binding strongly depends on the distal and proximal features of the porphyrin.

Oxygen binding

It is essential to understand that oxygen binding to a metal center involves a redox process whereby one electron is transferred to O_2, yielding a superoxide complex. Correspondingly, when two metal centers bind O_2, a bridging peroxide complex is formed. Only appropriate redox centers such as Fe(II), Co(II), and Cu(I) form dioxygen complexes; dioxygen is not a simple Lewis base.

In hemoproteins, dioxygen is bound and released at a rapid rate, and the polypeptide chain surrounding the heme prevents irreversible autoxidation of iron(II). Simple ferrous porphyrins tend to undergo rapid and irreversible autoxidation upon oxygenation (usually yielding an inactive metal in a higher oxidation state), which limits their use as models for hemoprotein active sites. This review portrays reversible models of O_2 binding, thus, only models that undergo repeated oxygenation1 deoxygenation cycles without appreciable loss of activity will be discussed.

The first thoroughly studied iron porphyrin model was picket fence porphyrin (10), which binds O_2 reversibly and yields dioxygen equilibrium affinities values similar to those exhibited by Hb/Mb. Other systems that reversibly bind dioxygen at room temperature with limited oxidation over several cycles are the capped (14) and *bis-pocket*[17] porphyrins. Although O_2 affinities in biological carriers span five orders of magnitude, the same wide range of O_2 affinities has not yet been paralleled in synthetic systems, which is demonstrated in Tables 1 and 2. However, the numerous iron and cobalt porphyrin mimics prepared during the past 30 years have played an important role in developing the understanding of dioxygen binding in the two native enzymes.

Structural and environmental effects on dioxygen binding

Electronic and Polar Effects. Electron-donating groups on the porphyrin ring or on the proximal base increase

Table 1 Thermodynamic and kinetic data for O_2 binding to biological oxygen carriers (at 20–25°C, buffered at pH 6.5–8.5)

Carrier	$P_{1/2}(O_2)$ (Torr)	ΔH (kcal/mol)	ΔS (eu)	k_{on} ($\mu M^{-1}s^{-1}$)	k_{off} (s^{-1})
Hemoglobins:					
Hb *Ascaris*	0.0047	–		1.5	0.0041
Leg Hb	0.047	−18.9		156	1
Whale Mb	0.51	−14.9		14	12
+(E7His→Gly)	–			140	1600
HbA, α:					
Isolated chains	0.74	−14.2	−21	50	28
R	0.15–1.5	−18	−30	29	10
(E7His→Gly)	–	–	–	220	620
T	9–160	−12	−35	2.9	183
HbA, β:					
Isolated chains	0.42	−16.9	−29	60	16
R	0.15–1.5	−18	−30	100	21
(E7His → Gly)	–	–	–	100	3
T	9–160	−12	−35	11.8	2500
Hemocyanins:					
Molluscan Hc					
Helix Pomatia R	2.7	−11.5	−12.6	3.8	10
Helix Pomatia T	55	−15.4	−31.1	1.3	300
Arthropod Hc					
Panulirus interruptus R	1.0			31	60
P. interruptus inonomer	9.3	–	–	57	100
Leirus quinquestris R	1.7	−7.4	0		
Leirus quinquestris T	117	+3.1	+27		
Hemerythrins:					
Phascolopsis gouldii	2.0	−12.4	−18	7.4	56
Themiste zostericola 8-*mer*	6.0	–	–	7.5	82
T. zostericola monomer	2.2	–		78	315

Source: From Ref. [3].

Table 2 Thermodynamic and kinetic data for O_2 binding to heme models

Porphyrin	$P_{1/2}(O_2)$ (TORT)	AH (kcal/mol)	AS (eu)	k_{on} ($\mu M^{-1}s^{-1}$)	k_{off} (s^{-1})
Fe(TPP)(Py)[a] (7)	0 0015	–	–	0 59	110.000
Fe(TPP-Im)[b] (8)	84 3	–	–	0 5	25.000
Fe(PPIX-Im)[c] (9)	5 6	62	–	–	4,200
Fe(TpivPP)(1,2-diMeIm)[c] (10)	38	−14 3	−42	106	46.000
Fe(PocPiv)(1-MeIm)[c] (11)	0 36	–	–	2 2	9
Fe(PocPiv)(1,2-diMeIm)[c] (11)	12 6	−13 9	−28	1 9	280
Fe(Piv_2C8PP)(1-MeIm)[b]	0 10	–	–	0 022	2
Fe(Piv_2C8PP)(1,2-diMeIm)[b]	3 9	–	–	0 0054	14 7
Fe(C2PicnicPP)(1 2-diMeIm)[b] (12)	25	–	–	–	–
Fe(*bis*-StrapPP)(1,5-DCIm)[b] (13)	15	–	–	1 7	250
Fe(C2CapPP)(1-MeIm)[c] (14)	23	1 0 5	2 8		
Fe(CyclamCapPP)(1,2-diMeIm)[d] (15)	22	–	–	–	–
Fe(CyclamCapPP)(1,5-DCIm)[d] (15)	−3	–	–	–	–
Fe(TACNCapPP)(1,2-diMeIm)[d]	2 3	–	–	–	–
Fe(TACNCapPP)(1,5-DCIm)[d]	<0 2	–	–	–	–
Fe(Piv_8PP)(1,2-diMeIm)[b]	870	–	–	–	–
Fe(*bis*-PocPP)(1,2-diMeIm)[c] (17)	508	1 4 4	4 7	–	–
Fe(dendron)$_4$PP(1,2-diMeIm)[e,f] (18)	0 035				
Fe(Piv_3PP-Im)[c] (19)	0 58	−16 3	4 0	430	2,900
Fe(C12StrapPP-Im)[c] (20)	18	–	–	300	40.000

Solubility of O_2 in toluene (–benzene) at 22°C is 1.02×10^{-5} M/torr.
[a]From Ref. [4].
[b]From Ref. [8].
[c]From Ref. [3].
[d]From Ref. [5].
[e]From Ref. [15].
All measurements were performed in toluene/20–25°C, except: [f]: benzene/25°C

dioxygen affinity, principally by slowing the dioxygen dissociation rates. The dipolar nature of $Fe\delta^+-O_2\delta^-$ is stabilized by polar solvents (nearby the reaction center) and by covalently bound polar groups near the iron center, indicating that O_2 affinities are enhanced by polar environments and by hydrogen bonding to neighboring X–H groups (Fig. 3). For instance, the two sterically similar models Fe(TpivPP)(1,2-diMeIm) (10) and Fe(*bis*-Poc)(1,2-diMeIm) (17), show $P_{1/2}(O_2)$ values of 38 torr and 508 torr (toluene). respectively. The higher O_2 affinity of Fe(TpivPP) is attributed to local polar effects (and B-bonding) arising from the picket amide groups. In recent studies of dendritic ferrous porphyrin models,[15] derivatives with and without H-bond donor functionality were prepared. Dendrons with amide groups show strong O_2 binding affinity [$P_{1/2}(O_2) = 0.035$ torr/toluene], whereas dendrons with ester groups lead to rapid irreversible decomposition. In structurally characterized oxyhemoglobins, the coordinated dioxygen ligand is hydrogen bonded to the distal histidine or a water molecule. This O_2–HN interaction was supported by EPR spectroscopy measurements of cobalt oxyhemoglobin.[17] An estimate of 1.5 kcal/mol for the free energy associated with hydrogen bonding was reported when O_2 binding constants were compared between native and mutant myoglobins.[18]

Proximal and Distal Steric Effects. Similar to Hb, R and T states can be induced in heme models by intentional choice of proximal bases. If 1-MeIm is replaced with 2-MeIm or 1,2-diMeIm, the planar heme

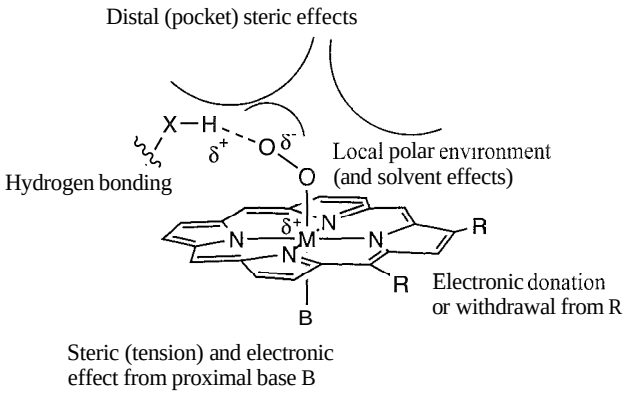

Fig. 3 Environmental effects on dioxygen binding to a heme model.

geometry is deformed due to steric interaction between the 2-methyl groups and the porphyrin ring. A steric deformation also occurs with a short chain in a chelated heme, which causes tilting of the proximal base and thus strain in the iron–imidazole bond. Such strain decreases association rates. increases dissociation rates, and, consequently, decreases dioxygen affinity. For example, Fe(C2Cap)(1-MeIm) (14) has 10^2 higher affinity for dioxygen than does Fe(C2Cap)(1,2-diMeIm) [$P_{1/2}(O_2)$ = 23 and 4000 toss, respectively].[3] In hemoglobins, low-affinity O_2 binding appears to be associated with the inability of the Fe-histidine(proximal) unit to move toward the plane of the porphyrin.

In addition, when dioxygen is absent, x-ray structural studies of heme proteins reveal that nearby lying side-chains occupy some of the space that would otherwise be required by O_2. Hence, O_2 binding rate constants decrease according to the distal sizes of the heme pockets: hemoglobin (R state) > myoglobin (domed T state) > horseradish peroxidase.[4] Comparable results were found for heme models, where O_2 binding rates are influenced by distal sterics. Typically, pocket, strapped, and capped porphyrins exhibit lower rates of O_2 binding than open-faced and picketed ones. In comparison. Fe(TpivPP)(1,2-diMeIm) (10) binds dioxygen 50 times faster than Fe(PocPiv)(1,2-diMeIm) (11).[3]

Other hemoglobin models

Paralleling the Fe(II) systems, studies of Co(II)Mb and Co(II)Hb reveal reversible dioxygen binding [CoMb (sperm whale): $P_{1/2}(O_2)$ = 33 torr/20°C], a similar degree of cooperativity (n ~ 2.5), and retaining of Bohr and phosphate effects. Cobalt porphyrin complexes prove useful in understanding factors that determine oxygen binding in Hb and Mb. The advantages of choosing cobalt over iron include a small equilibrium constant for addition of a second axial base, no **O–O** bond cleavage and dimerization to form a μ-oxo species, and stable paramagnetic $Co–O_2$ adducts characterized by EPR. These differences simplify the interpretation of spectral changes upon oxygenation. The O_2 affinity is generally lower for cobalt than for iron but increases with greater axial ligand basicity or electron-donating groups on the porphyrin ring. The same effects that influence dioxygen affinity in cobalt systems are often found for iron. These effects and many examples thereof are discussed in comprehensive reviews.[19,20] Other synthetic $Co–O_2$ models were used to obtain thermodynamic and kinetic parameters that may be extrapolated to iron systems. Among these. the "lacunas" complexes, i.e., compounds with a cavity or void to accommodate O_2 or another small ligand, were studied.[21] Macrocyclic Schiff-base (bridged or non-bridged) Co and Fe complexes of salen, cyclidene, malen, and oxime were investigated. and their dioxygen affinities were shown to be influenced by cavity size (bridging length/group/location; causing doming), macrocycle substituents (steric and electronic effects), and nature of base (the stronger the base, the higher the O_2 affinity) in a similar manner to porphyrin systems.

Models for Hemocyanin

During the past 20 years, the dicopper active site of Hc attracted the attention of inorganic and bioinorganic chemists. In order to understand the complex behavior of copperldioxygen chemistry, synthetic dicopper models were prepared, and their spectroscopic and magnetic properties were elucidated upon oxygenation (e.g., Refs. [22,23]). Whereas μ-oxo and *bis*-μ-oxo dicopper centers are frequently observed in $Cu(I)/O_2$ chemistry. the μ-peroxo dicopper adducts are more difficult to obtain. In 1992, the unusual $Cu_2[HB(3,5\text{-}i\text{Pr}_2\text{pz})_3]_2(O_2)$ (22) complex was synthesized and characterized.[24] The peroxo-dicopper(II) adduct is generated at reduced temperatures by reacting O_2 with $Cu(I)[HB(3,5\text{-}i\text{Pr}_2\text{pz})_3]\text{-}CH_3CN$, or via an acid-base reaction of hydrogen peroxide with $Cu(II)[HB(3,5\text{-}i\text{Pr}_2\text{pz})_3]\text{-}bis\text{-}\mu\text{-}(OH)_2\text{-}Cu(II)[HB(3,5\text{-}i\text{Pr}_2\text{pz})_3]$. An unprecedented side-on-bound $\mu\text{–}\eta^2\text{:}\eta^2$ bridged O_2 binding mode was observed. The physical and spectroscopic properties of 22 [d_{Cu-Cu} = 3.56 A: $\nu(O–O) = 741\ cm^{-1}$ ($^{16}O_2$), 698 cm^{-1} ($^{18}O_2$)] were found to be almost identical to those in oxy-Hc. In a series of functionalized TACN-capped Cu(I) complexes, the binuclear complex (1,4,7-*i*Pr$_3$-TACN)-Cu(II)-($\mu\text{–}\eta^2\text{:}\eta^2$–$O_2$)-Cu(II)-(1,4,7-*i*Pr$_3$-TACN)$^{2+}$ was formed when treated with O_2 at −80°C in dichloromethane [$\nu(O–O) = 722$ cm ' ($^{16}O_2$), 680 cm^{-1} ($^{18}O_2$)].[25] Dioxygen binding could be reversed by warming under vacuum or by purging with N_2 or Ar. A reversible scission and formation of the **O–O** bond was observed between the two cores $[Cu\text{-}(\mu\text{-}O)_2\text{-}Cu]^{2+}$ and $[Cu\text{-}(\mu\text{–}\eta^2\text{:}\eta^2\text{–}O_2)\text{-}Cu]^{2+}$. It is unclear how different solvents, counterions, and TACN ligand substituents induce preferential stabilization of these forms. Reversible dioxygen binding was reported for the Cu(I)TMPA system.[26] A structurally characterized trans-1.2-peroxo dicopper(II) complex (23) was isolated [d_{Cu-Cu} = 4.359 Å; $\nu(O–O) = 832\ cm^{-1}$. $\nu(Cu–OO) = 561\ cm^{-1}$]. An initial transient adduct, $[(TMPA)Cu–O_2]^+$, is formed at 183 K ($k_1 = 2 \times 10'\ M^{-1}\ s^{-1}$; $K_1 = 1.9 \times 10^3\ M^{-1}$), which yields the final stable product 23 upon reaction with another $[(TMPA)Cu–CH_3CN]^+$ complex ($K_{formation} = 4.3 \times 10^{11}\ M^{-2}$). Compound 23 is not stable at room temperature due to an unfavorable entropy term. The $[LCu(II)\text{-}(\mu\text{–}\eta^2\text{:}\eta^2\text{–}O_2)\text{-}Cu(II)L]^{2+}$ complex (24) (E = 1,2-*bis*{2-[*bis*(6-methyl-2-

Structures of hemocyanin models:

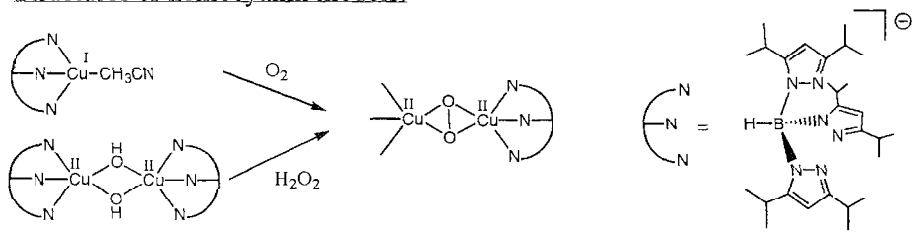

{Cu[HB(3,5-*i*Pr$_2$pz)$_3$]}$_2$(O_2) (**22**)
[Kitajima, 1992]

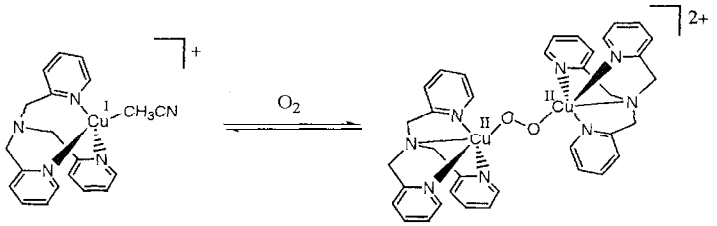

[(TMPA)Cu-(O_2)-Cu(TMPA)]$^{2+}$ (**23**)
[Tyeklar, 1993]

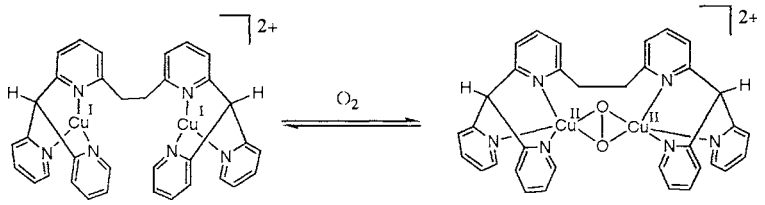

[LCu-O_2-CuL]$^{2+}$ ((24)
[Kodera, 1999]

Structures of hemerythrin models:

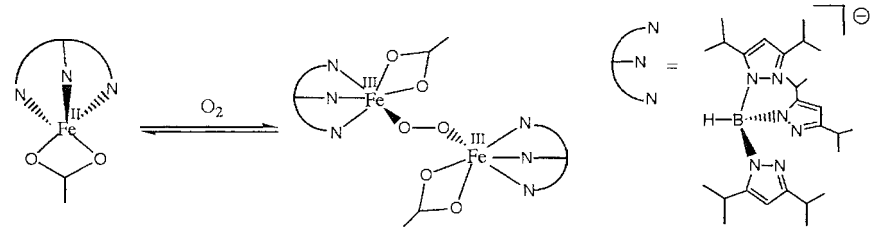

{Fe[HB(3,5-*i*Pr$_2$pz)$_3$](Ac)}$_2$(O_2) (**25**)
[Kitajima, 1995]

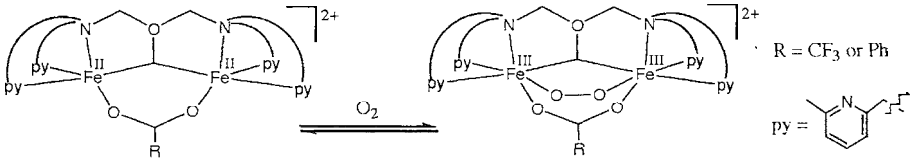

{Fe$_2$(HPTMP)(RCOO)}(O_2) (**26**)
[Hayashi, 1994]

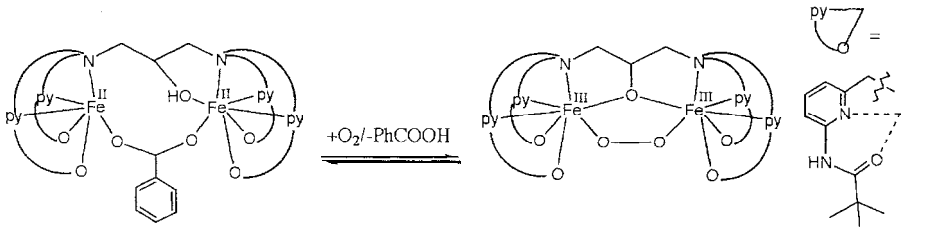

{Fe$_2$(HTPPDO)(O_2)} (**27**)
[Arii, 2000]

Fig. **4** Structures of hernocyanin and hemerythrin models

pyridyl)methyl]-6-pyridyl}ethane) (25°C, dichloromethane), which shows reversible dioxygen binding, is presently the most stable peroxo-bridged dicopper species at room temperature ($t_{1/2} = 25.5$ h).[27] Other dinucleating ligands show reversible dioxygen binding, but usually at low temperatures (e.g., Ref. [10]). To conclude, temperature. solvent, counterion, and steric effects strongly influence the oxygenation of copper complexes. Tridentate ligands tend to facilitate side-on O_2 binding, while tetradentate donor ligands promote *trans*-μ-1,2-peroxo coordination. Changes in reactivity upon modification of donor atoms, chelate ring sizes, and bulky substituents indicate the importance of ligand effects in copper(I)/O_2 chemistry.

Models for Hemerythrin

The protein backbone in Hr has an important role of bringing together the asymmetric diiron(III) nucleus. Although many μ-oxodiiron(III) complexes exist, only a few are asymmetric (e.g., Ref. [28]) due to synthetic challenges. Few nonporphyrinic ferrous complexes were found to react with dioxygen to form stable adducts, and only a handful of these exhibit reversible dioxygen binding. One of the more robust nonheme iron dioxygen complexes is the peroxo-bridged {Fe(III)[HB(3,5-*i*Pr_2pz)$_3$]}$_2$(O_2) biscarboxylate adduct (25), which exhibits O_2 binding reversibility between −50 and −20°C in noncoordinating solvents (Fig. 4).[29] The resonance Raman spectrum of 25 shows an O–O stretch at 876 cm^{-1} ($d_{Fe-Fe} = 4.3–4.4$ Å; $J = -33$ cm^{-1}) and is supported by $^{18}O_2$ isotope shifts. The steric bulk of the tridentate ligand is believed to be responsible for the added stability. Another complex, the diiron HPTMP (26). exhibits reversible dioxygen binding [$P_{1/2}(O_2) = 42$ torr and 6 torr for the CF_3COO^- and $PhCOO^-$ complexes. respectively] at −35°C in dichloromethane.[30] From stopped-flow measurements. internal ligand rearrangement is postulated to open a coordination site for dioxygen coordination prior to peroxide bridge formation. Moreover, small amounts of DMSO or other polar aprotic solvents have a stabilizing influence on 26, although the reason for this effect is uncertain. The diiron complex of the dinucleating ligand MTPPDO (27) creates hydrophobic pockets via *tert*-butyl groups, mimicking the hydrophobic peripheral structure of the active site of Hr.[31] Fe(II)$_2$HTPPDO and benzoate in acetone manifest reversible O_2 binding at −50°C, where the peroxo anion binds to the Fe_2 core in a μ-1,2 bridging mode [ν(O–O) = 873, 887 cm^{-1}; Δν($^{16}O_2$/$^{18}O_2$) = 48, 48 cm^{-1}]. The thermodynamic stability and reversible O_2 binding of this rare asymmetric Hr model are proposed to depend on the hydrophobic environment over the diiron center rather than the iron redox potentials.

CONCLUSION

In order to enhance dioxygen delivery and storage in respiratory and metabolic processes. biological systems developed O_2 carriers that reversibly coordinate O_2 to a transition metal (Fe or Cu) bound to a protein. Many of the attributes of the oxygen-binding proteins have been reproduced with well-designed functional models. Hemoglobin and myoglobin are fairly well understood due to significant development in model studies. Additional work can be anticipated in nonheme iron and copper synthetic analogues.

ACKNOWLEDGMENTS

The authors would like to thank NIH (Grant CHE 9612725), NSF (Grant GM 17880), and STINT (The Swedish Foundation for International Cooperation in Research and Higher Education) for financial support, and Dr. Christopher J. Sunderland for aid in preparing the manuscript.

ABBREVIATIONS

1-MeIm	1-methylimidazole
1,2-diMeIm	1,2-dimethylimidazole
1,4,7-*i*Pr_3-TACN	1,4,7-triisopropyl-1,4,7-triazacyclononane
1,5-DCIm	1,5-dicyclohexylimidazole
2-MeIm	2-methylimidazole
allosieric binding	when binding or release of dioxygen at one site may affect the affinity and kinetics of ligand binding and release at a neighboring site
C*c*O	cytochrome *c* oxidase
cyanin	from *cyanos*, Greek for blue
cyclam	1,4,8,11-tetraazacyclotetradecane
cyclen	1,4,7,10-tetraazacyclododecane
cyclidene	ligands derived from Jaeger's dianionic tetraazamacrocycle
DMSO	dimethylsulfoxide
EPR	electron paramagnetic resonance spectroscopy
ΔH	enthalpy
Hb	hemoglobin
HB(3,5-*i*Pr_2pz)$_3$	hydrotris(3,5-diisopropyl-pyrazolyl)-borate anion
Hc	hemocyanin
heme	iron(II) porphyrin
hemochrome	six-coordinate heme(III) center
HPTMP	*N,N,N′,N′-tetrakis*((6-methyl-2-pyridyl)methyl)-2-hydroxy1,3-diaminopropane

Hr	hemerythrin
HTPPDO	*N,N,N′,N′-tetrakis*(6-pivalamido-2-pyridylmethyl)-1,3-diaminopropan-2-ol
lacunar	applied in anatomy and biology to indicate the presence of a space or cavity where there would ordinarily be none
M	arbitrary metal
inalen	ligands derived from β-diketone and 1.3-dialdehyde Schiff bases
Mb	myoglobin
myo	from the Greek root *mys* for muscle
oxime	ligands derived from *bis*(α-dioxime); adjacent oxime oxygens bridged
$P_{1/2}(O_2)$	pressure of dioxygen necessary to oxygenate one half of the available sites
PPIX	protoporphyrin IX
py	ppridine
pz	pyrazole
R-state	relaxed-state porphyrin: Fe atom in the plane of the porphyrin
AS	entropy
salen	ligands derived from ethylenediamine and salicylaldehyde Schiff bases
TACW	1,4,7-triazacyclononane
TMPA	*tris*-((2-pyridyl)methyl)amine
TPivPP	*meso*-α,β,γ,δ-*tetrakis*(*o*-pivalamidophenyl)-porphyrin
TPP	nzeso-tetraphenylporphyrin
tren	*tris*(2-aminoethyl)amine
T state	tense-state porphyrin; Fe atom out of the plane of the porphyrin

ARTICLES OF FURTHER INTEREST

The Allosteric Effect. p. 20
Biological Ligands, p. 88
Biological Models and Their Characteristics, p. 101
Dendrimers, p. 432
Enzyme Mimics, p. 546
Hemoglobins: O_2 Uptake and Transport, p. 636
Hydrogen Bonding, p. 658
Pyrrole- and Polypyrrole-Based Anion Receptors, p. 1176
Selectivity: Thermodynamic and Kinetic, p. 1225
Stability Constants: Definition and Determination, p. 1360
Strong Hydrogen Bonds, p. 1379

REFERENCES

1. Hay. R.W. *Bio-Inorganic Chemistry*; Ellis Horwood Limited: Chichester. 1984.
2. Liang, H.-C.: Dahan, M.: Karlin, K.D. Dioxygen-activating bio-inorganic model complexes. Curr-. Opin. Chern. Biol. 1999. 3. 168–175.
3. Jameson. G.B.; Ibers, J.A. Biological and Synthetic Dioxpgen Carriers. In *Bioinorganic Chemistry*; Bertini. I.. Gray, H.B.. Lippard, S.J., Valentine. J.S.. Eds.; University Science Books: Mill Valley. 1994: 167–252.
4. Traylor, T.G.: Traylor, P.S. Reactions of Dioxygen and Its Reduced Forms with Heme Proteins and Model Porphyrin Complexes. In *Active Oxygen in Biochemistry*; Valentine, J.S.. Foote. C.S.. Greenberg. A., Liebman, J.F., Eds.: Blackie Academic & Professional: London, 1995: Vol. 3, 84–187.
5. Collman, J.P.; Fu. L. Synthetic models for hemoglobin and myoglobin. Acc. Chem. Res. **1999**. 32. 455–463.
6. Kendrew, J.C.: Dickerson. R.E.; Strandberg. B.E.; Hart. R.G.: Davis. D.R.; Phillips. D.C.: Shore. V.C. Structure of myoglobin. Three-dimensional Fourier synthesis at 2 A resolution. Nature **1960**, *185*, 422–427.
7. Perutz, M.F.: Rossman, M.G.: Cullis. A.F.: Muirhead. H.; Will. G.: North. A.C.T. Structure of hemoglobin. A three-dimensional Fourier synthesis at 5.5 A resolution, obtained by x-ray analysis. Nature **1960.** *185*. 416–422.
8. Momenteau, M.: Reed. C.A. Synthetic heme dioxygen complexes. Chern. Rev. **1994**. 94. 659–698.
9. Pauling. L.: Coryell. C.D. Magnetic properties and structure of hemoglobin. oxyhemoglobin and carbonmonoxyhemoglobin. Proc. Natl. Acad. Sci. U. S. A. **1936**. 22. 210–216.
10. Fox. S.; Karlin, K.D. Dioxygen Reactivity in Copper Proteins and Complexes. In Active *Oxygen* in *Biochemistry*: Valentine. J.S.. Foote. C.S.. Greenberg. A.. Liebman, J.F.. Eds.: Blackie Academic & Professional: London. 1995; Vol. 3. 188–231.
11. Que. L.J. Oxygen Activation at Nonheme iron Centers. In Active *Oxygen in Biochemistry*; Valentine. J.S.. Foote. C.S.. Greenberg. A.. Liebman. J.F.. Eds.: Blackie Academic & Professional: London. 1995; Vol. 3. 232–275.
12. Feig. A.L.: Lippard, S.J. Reactions of non-heme iron(II) centers with dioxygen in biology and chemistry. Chem. Rev. **1994.** 94. 759-–805.
13. Collman, J.P.; Brauman. J.I.: Iverson. B.L.: Sessler, J.L.; Morris, R.M.: Gibson. Q.H. O_2 and CO binding to iron(II) porphyrins: A comparison of the picket fence and pocket porphyrins. J. Am. Chem. Soc. 1983. *105*. 3052–3064.
14. Collman, J.P.: Halbert. T.R.: Suslick. K.S. O_2 Binding to Heme Proteins and Their Synthetic Analogs. In Metal *Ion Activation of Dioxygen: Metal* Ions *in* Biology; Spiro, T.G., Ed.: John Wiley & Sons: New York. 1980; Vol. 2. 1–72.
15. Zingg. A.; Felber. B.: Gramlich. V.: Fu. L.; Collman. J.P.: Diederich. F. Dendritic iron(II) porphyrins as models for hemoglobin and myoglobin: Specific stabilization of O_2 complexes in dendriiners with H-bond-donor centers. Helv. Chim. Acta 2002. *85*. 333–351.
16. Collman. J.P. Functional analogs of heme protein active sites. Inorg. Cliem. **1997**. 36. 5145–5155.
17. Walker. F.A.: Bowen. J. EPR evidence for hydrogen bond donation to the terminal oxygen of cobalt–oxygen model compounds and cobalt oxymyoglobin. J. Am. Chem. Soc. **1985.** 107. 7632–7635.
18. Olson. J.S.; Mathews. A.J.; Rohlfs. R.J.: Springer. B.A.;

Egeberg, K.D.; Sligar, S.D.: Tame, J.; Renaud, J.P.; Nagai, K. The role of distal histidine in myoglobin and hemoglobin. Nature **1988,** 336, 265–266.

19. Jones, R.D.: Summerville, D.A.; Basolo, F. Synthetic oxygen carriers related to biological systems. Chem. Rev. 1979, *79*. 139–179.
20. Niederhoffer, E.C.; Timmons, J.H.; Martell, A.E. Thermodynamics of oxygen binding in natural and synthetic dioxygen complexes. Chem. Rev. **1984,** *84*, 137–203.
21. Busch, D.H.; Alcock, N.W. Iron and cobalt "lacunar" complexes as dioxygen carriers. Chem. Rev. **1994,** *94*. 585–623.
22. Blackman, A.G.: Tolman, W.B. Copper–dioxygen and copper–0x0 species relevant to copper oxygenases and oxidases. Struct. Bond. **2000.** *97*, 179–211.
23. Karlin, K.D.: Tyeklár, Z.; Zuberbiihler, A.D. Formation, Structure, and Reactivity of Copper Dioxygen Complexes. In *Bioinorganic* Catalysis; Reedijk, J., Ed.: Marcel Dekker, Inc.: New York, 1993; 261–315.
24. Kitajima, N.; Fujisawa, K.: Fujimoto, C.: Moro-oka, Y.; Hashimoto. S.; Kitagawa. T.; Toriumi, K.; Tasumi, K.; Nakamura, A. A new model for dioxygen binding in hernocyanin. Synthesis, characterization and molecular structure of the $\mu-\eta^2:\eta^2$ peroxo dinuclear copper(II) complexes $[CuHB(3,5\text{-}R_2pz)_3]O_2$ (R = i-Pr and Ph). J. Am. Chem. Soc. **1992,** *114*, 1277–1291.
25. Tolman. W.B. Making and breaking the dioxygen **O–O** bond: New insights from studies of synthetic copper complexes. Acc. Chem. Res. 1997, 30, 227–237.
26. Tyeklár, Z.; Jacobson, R.R.: Wei, N.; Murthy, N.N.; Zubieta. J.; Karlin. K.D. Reversible reaction of O_2 (and CO) with a copper(I) complex: X-ray structures of relevant mononuclear Cu(I) precursor adducts and the *trans*-(μ-1,2-peroxo)-dicopper(II) product. J. Am. Chem. Soc. **1993,** *115*. 2677–2689.
27. Kodera, M.; Katayama, K.; Tachi, Y.; Kano. K.; Hirota, S.; Fujinami, S.; Suzuki, M. Crystal structure and reversible O_2 binding of a room temperature stable $\mu-\eta^2:\eta^2$–peroxodicopper(II) complex of a sterically hindered hexapyridine dinucleating ligand. J. Am. Chem. Soc. **1999.** *121*, 11006–11007.
28. Mizoguchi, T.J.; Lippard, S.J. Synthetic models of the deoxy and oxy forms of the non-heme diiron–O_2 adduct: Insight into the mechanism of oxygen activation. J. Am. Chem. Soc. **1998,** *118*. 11022–11023.
29. Kitajima, N.; Tamura, N.; Amagai, H.: Fukui, H.; Moro-oka, Y.; Mizutani. Y.; Kitagawa, T.; Mathur. R.; Heerwegh, K.; Reed, C.A.: Randall, C.R.; Que, L., Jr.; Tatsumi, K. Monomeric carboxylate ferrous complexes as models for the dioxygen binding-sites in non-heme iron proteins: The reversible formation and characterization of μ-peroxo diferric complexes. J. Am. Chem. Soc. **1994,** *116*, 9071–9085.
30. Hayashi, Y.; Kayatani, T.; Sugimoto. H.; Suzuki, H.; Inomata, K.; Uehara, A.: Mizutani. Y.: Kitagawa, T.; Maeda. Y. Synthesis, characterization and reversible oxygenation of μ-alkoxo diiron(II) complexes with dinucleating ligand *N,N,N′,N′*-tetrakis((6-methyl-2-pyridyl)-methyl)-1,3-diaminopropan-2-olate. J. Am. Chem. Soc. **1995.** *117*, 11220–11229.
31. Arii, H.; Nagatomo, S.: Kitagawa, T.: Miwa, T.; Jitsukawa, K.: Einaga. H.; Masuda, H. A novel diiron complex as a functional model for hemerythrin. J. Inorg. Biochem. **2000.** 82, 153–162.

Peptide Nanotubes

Carl Henrik Görbitz
University of Oslo, Oslo, Norway

INTRODUCTION

The first peptide that formed a tubular arrangement in the crystal structure was the cyclic tetrapeptide L-Ser(*O*-*t*-But)-β-Ala-Gly-L-β-Asp(OMe), presented as far back as in 1975,[1] but it was the breathtaking image on the front page of the November 25 issue of *Nature* in 1993, showing self-assembly of cyclic octapeptides by β-sheet-like hydrogen bonds[2] that made the scientific community aware of the new class of nanotube-forming compounds. In the years that passed. further research on these systems revealed a series of intriguing properties, including membrane incorporation that leads to antibacterial activity.[3] Construction of channels as models for membrane pores is one of the key issues in studying peptide nanotubes, but they may also find use as transport vehicles, in catalysis, and as artificial receptors. Such a diversity is possible due to the subsequent discovery of yet other classes of nanotube-forming peptides. with internal van der Waals' diameters ranging from 3–10 Å for hydrophobic dipeptides up to 10,000 Å (1 μm) for surfactant-like peptides and peptide derivatives.

CLASSIFICATION OF PEPTIDE NANOTUBES

Peptide-based nanotubes can be constructed in several different manners depending on the sizes and types of molecular building blocks:

- Nanotubes from the rtacking of cyclic peptides
- Nanotubes from dipepiides
- Naturally occurring peptide membrane channels
- Amphiphilic surfactant-like nanotubes
- Bolamphiphilic peptide nanotubes

NANOTUBES FROM THE STACKING OF CYCLIC PEPTIDES

Cyclic peptides with an even number of α-amino acids can adopt a flat. low-energy conformation in which all backbone amide functionalities are oriented approximately perpendicular to the plane of the molecule. If. furthermore, an alternating sequence of D- and L-amino acids is used. all peptide side chains lie on the outside of the ensemble, allowing formation of a hollow tubular structure through formation of intermolecular β-sheet-like hydrogen bonds as shown in Fig. 1. The first evidence of nanotube formation by stacking of cyclic α-peptides was provided by Ghadhiri and coworkers for cyclo[(D-Ala-L-Glu-D-Ala-L-Gln)$_2$-], a structure that was going to coin the expression ''peptide nanotube.''[2] Early work on these systems was reviewed in Ref. [4].

A wide range of applications was predicted for cyclic D,L-α-peptide nanotubes. Theoretical calculations have, for instance, indicated a wide HOMO–LUMO gap (−5 eV), which suggests that this material can be engineered to yield useful microelectronic devices.[5] Still. the most important property is undoubtedly their ability to be integrated into lipid membranes and thus act as models for biological transmembrane channels. With recent results from experiments on bacteria, this research has taken a dramatic step forward by demonstrating that appropriately designed peptides may be able to selectively target and self-assemble in bacterial membranes and create extensive damage by increasing the membrane permeability.[3] Each peptide was designed to bear at least one basic residue to enhance its target specificity toward negatively charged bacterial membranes. Systematic exchange of amino acids showed that it was possible to fine-tune the biological activity. For example, cyclo(D-Lys-L-Lys-D-Leu-L-Trp-D-Leu-L-Trp) displayed broad-spectrum antibacterial activity in vitro, while cyclo(D-Lys-L-His-D-Leu-L-Trp-D-Leu-L-Trp) (L-Lys substituted by L-His) showed a high degree of specificity against methicillin-resistant *Staphylococcus aureus* (MRSA). Cyclo(D-Arg-L-Arg-D-Leu-L-Trp-D-Leu-L-Trp), on the other hand, was particularly active against *Escherichia coli*. In these experiments, essentially no disruptive effect on red blood cells was observed. Moreover, the bacteria were killed in minutes, in contrast to the timescale of hours for most antibacterial agents. Experimental in vivo results showed that mice infected with a lethal dose of MRSA were protected by a 10 mg k g ^{1} dose of cyclic peptide. Toxicity studies in mice indicated that high doses were tolerated with no or limited, temporary signs of toxicity.[3]

The remarkable pores of the cyclic octapeptides have a van der Waals' internal diameter between 7 and 8 A,

Encyclopedia of Supramolecular Chemistry
DOI: *10.1081*/E-ESMC 120022254

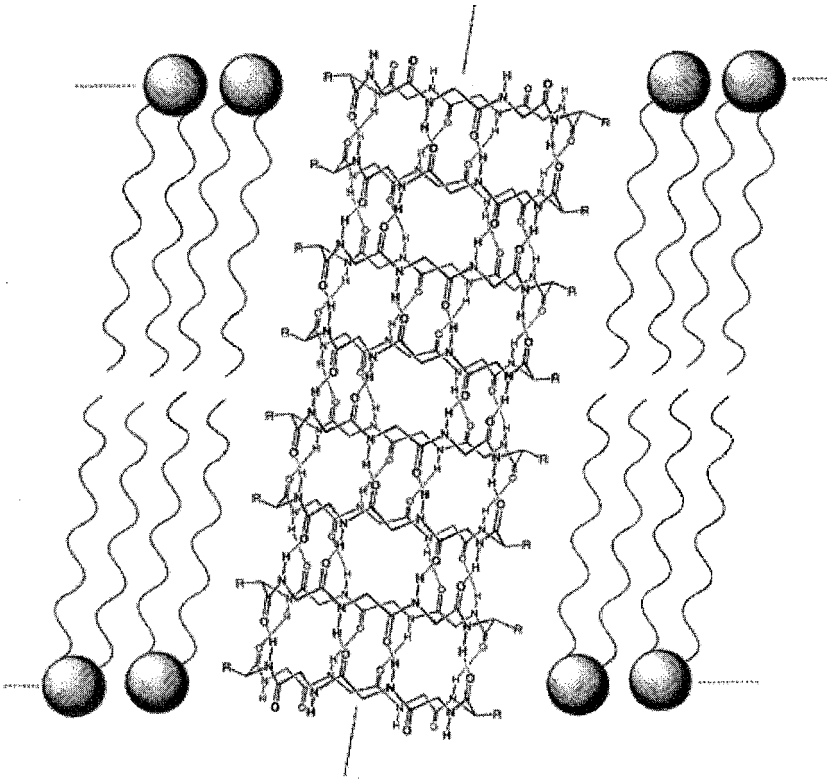

Fig. 1 The assembly of cyclic D,L-α-octapeptides in a lipid bilayer. Antiparallel β-sheet-like hydrogen bonds are shown as dotted lines. Reprinted with permission from Ref. [9]. Copyright 1998 American Chemical Society.

enough to allow efficient, size-selective transport of small ions[6] and water molecules. The organization and diffusion of water molecules through the channels were studied by molecular dynamics simulation of a stack of 10 peptide molecules.[7] During the simulation, an average of 33 water molecules were found inside the tube. while the diffusion constant was $0.44 \times 10^{-5}\ cm^2\ s^{-1}$: one sixth of the self-diffusion constant of bulk water and much faster than diffusion through the structurally related gramicidin A transmembrane channel (see below). Transmembrane transport of larger molecules. like glutamate and glucose, is not possible with a 7–8 Å pore size, but they are transported through channels formed by decapeptides with a 10 Å van der Waals' diameter.[8]

In the first models of incorporation of cyclic peptide stacks in membranes, a perpendicular orientation of the central axis of the nanotubes relative to the bilayer plane was assumed. Subsequent investigations of cyclo[(L-Trp-D-Leu)$_3$-L-Gln-D-Leu-] in functionally relevant lipid membranes by polarized attenuated total reflectance (ATR), grazing angle reflection–absorption and transmission Fourier transform infrared (FT-IR) techniques showed that this is not quite so.[9] In fact, their central axes are aligned parallel to the hydrocarbon chains of the lipid and are. thus. tilted approximately 7° from the axis normal to the bilayer plane, as shown in Fig. 1.

The two subunits at the ends of the channel assembly. termed "caps," differ from other subunits by their mode of interaction and the microenvironment in which they reside, which should make it possible to incorporate structurally distinct peptides as cap units.[10] Various experimental observations derived from single-channel conductance measurements support formation of such heteromeric noncovalent assemblies. It was suggested that such an approach may find utility in the design of ligand-gated channels and stochastic sensing.[10]

Cyclic tetramers of α-unsubstituted-β-chiral-β-amino acids (β^3-amino acids) can also adopt flat-ring conformations and stack in solid state through backbone–backbone hydrogen bonding.[11] The resulting hollow tubular ensembles are structurally analogous to those formed by the cyclic D,L-α-peptides, but because all C=O groups are aligned in the same direction (and vice versa for the N–H groups), the tubes have a dipole moment. Cyclic β^3-peptides with appropriately chosen hydrophobic side chains can self-assemble in lipid bilayers to form highly efficient transmembrane ion channels.[12]

A recent development of hybrid systems utilizes cyclic peptides in which (1*R*,3*S*)-3-aminocyclohexanecarboxylic acid alternates with D-x-amino acids. In such structures. the β-methylene moiety of each cyclohexane constitutes a part of the inner surface of the cylinder. creating a partially hydrophobic cavity with an approximate van der Waals' internal diameter of 5.4 Å.[13] By adding functional groups to C2, it should be possible to prepare nanotubes with greater selectivity as ion channels, catalysts, or receptors, a possibility that is precluded for a- and β-nanotubes, because all side chains lie on the exterior of the ensemble.

The very low solubility of the cyclic peptides has frustrated all attempts to grow crystals of a useful size for single-crystal x-ray diffraction investigations; structures have, in general, been characterized by electron microscopy. electron diffraction, calculations, FT-IR spectroscopy, and x-ray powder diffraction. The need for a high-resolution structural model was addressed by designing cyclic peptides with a selectively *N*-alkylated (usually *N*-methylated) backbone that blocks peptide aggregation. Several of these compounds were shown to self-assemble into discrete soluble cylindrical dimers in nonpolar organic solvents (Fig. 2a).[14,15]

The inherent solubility problem of the cyclic peptides was overcome by construction of special cyclic tripeptides made from unsaturated δ-amino acids. The resulting lipophilic lactams could easily be crystallized by diffusion (ethanol and diethyl ether). X-ray data[16] confirmed the expected tubular structure (Fig. 2b). with all the carbonyl groups pointing in the same direction. giving, as for the cyclic β^3-peptides,[11,12] a dipole arrangement. Furthermore. the highly polarized tubes orient in the same direction in the whole crystal, yielding an extremely strong dipole.

Incorporation of small aromatic units into the backbone of a cyclopeptide constitutes an alternative approach in creating flat-ring peptides. Thus, 18-membered macrocycles containing an alternating sequence of L-serine and aromatic (Phe or Pyr) units were demonstrated to self-assemble into tubular structures using aromatic Phe-Pyr and Pyr-Pyr π–π interactions as the main organizing force.[17] New classes of cystine-based nanotubes were constructed by closing polymethylene chains by -X-Cys-S-S-Cys-X- bridges, where the link X may be urea functionalities (cyclic bisureas.[18]) or simple amide bonds (cyclobisamides[19]).

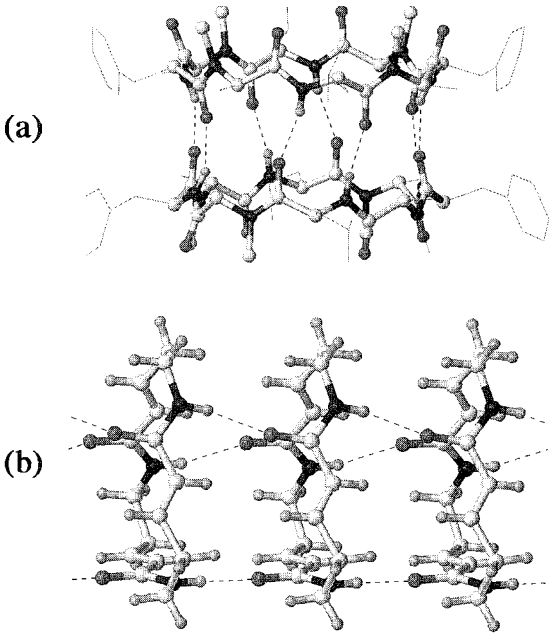

Fig. *2* (a) Dimeric β-sheet assembly formed by cyclo[(L-Phe-D-^{Me}*N*-Ala-L-Leu-D-^{Me}*N*-Ala)$_2$-].[15] For clarity. stick drawings were used for heavy atoms in the side chains. (b) Alignment of dipoles by stacking cyclic tripeptides built from 6-amino acids. (From Ref. [16].)

NANOTUBES FROM DIPEPTIDES

Crystal structures of dipeptides are often divided into distinct hydrophilic and hydrophobic layers. the former containing two $-NH_3^+\cdots{}^-OOC$ head-to-tail hydrogen-bonded chains. The essential third amino H atom is accepted by a functional group in one of the side chains or in a cocrystallized solvent molecule. In solvent-free crystals of dipeptides with two hydrophobic residues. neither alternative is available. which raises an inherent packing problem: How can three acceptors still be positioned around each amino group? A series of crystal structures revealed a number of ways to solve this problem. one of them being the surprising formation of nanotubes.

The first dipeptide nanotube system was L-Val-L-Ala (VA), which forms crystals with narrow hydrophobic channels (diameter about 5 Å) lined by peptide side chains.[20] This structure is conceptually different from those of the cyclic peptides in that the pores are generated from self-assembly of small molecules. which are hydrogen bonded. head-to-tail, into helices (Fig. 3a). The extremely robust three-dimensional hydrogen-bonding scaffold was since observed for a series of other hydrophobic dipeptides.[21] Pore size can be regulated from 3.3 Å (L-Ile-L-Val) to 5.2 Å (L-Ala-L-Val) by adjusting the bulk of the hydrophobic side chains. Furthermore, L-Ala-L-Val has pores that can adapt their shapes and sizes to absorb large solvent molecules like 2-butanol.[22]

Dipeptides with L-Leu and L-Phe residues also form nanotubes, but these structures are completely different from those in the VA class. In a sense. the basic construction of the VA class was wrapped inside-out. giving a

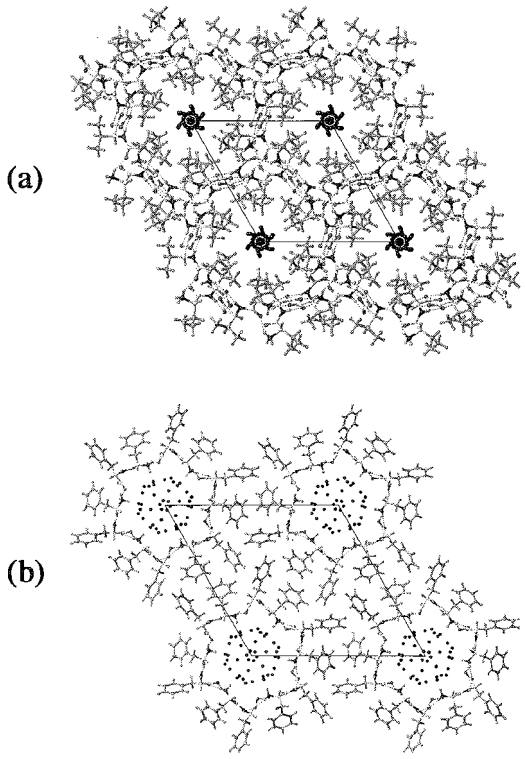

Fig. 3 Views along the hexagonal axes (space group $P6_1$) of (a) L-Val-L-Val[21] and (b) L-Phe-L-Phe.[23] Atoms in the side chains are shown in a grey tone; refined positions for oxygen atoms of disordered water molecules are shown in black.

one-dimensional hydrogen-bonding pattern in the shape of cylinders. as shown for L-Phe-L-Phe (FF) in Fig. 3b.[23] It follows that the tubes have hydrophilic inner surfaces, and one of the amino H atoms points straight into the channel interior, where it is accepted by a disordered solvent water molecule. Because the interior is chiral, it was suggested that these structures may act as chiral receptors or selectors.[23] For L-Trp-Gly·H_2O (WG), which forms crystals with tecragonal symmetry also belonging to the FF class, an unusual negative thermal expansion (NTE) for the axis parallel to the channels was observed.[24]

NATURALLY OCCURRING PEPTIDE MEMBRANE CHANNELS

Biological membrane channels are formed not only by integral membrane proteins like porine but also by certain peptides antibiotics called ionophores that vastly increase the permeability of membranes to particular ions.[25] The antibiotic properties of ionophores arise from their tendency to discharge vital concentration gradients. The principal channel-forming peptides are gramicidin A and the peptaibol peptides.

Gramicidin A

Gramicidin A is a linear 15-residue hydrophobic peptide produced by the bacterium *Bacillus brevis* that permits passage of protons and alkali cations but is blocked by Ca^{2+}. The amino acid sequence is HCO-L-Val-Gly-L-Ala-D-Leu-L-Ala-D-Val-L-Val-D-Val-L-Trp-D-Leu-L-Trp-D-Leu-L-Trp-$NHCH_2CH_2OH$. The unique alternating L- and D-configurations make gramicidin A an obvious reference and benchmark for the properties of the cyclic D,L-α-peptides discussed previously. There was some discussion about the structure of the peptide in its conducting, membrane-bound state. Previously, most models involved a head-to-head dimer of two single-stranded helices, but the most recent crystallographic investigations report gramicidin A to occur as right-handed double-stranded double-helical dimers, as shown in Fig. 4.[26] The ion-conducting channel has a van der Waals' diameter of no more than 4.6 Å.

Peptaibol Peptides

Alamethicin is a 20-residue peptide from the fungus *Trichoderma viride* that contains a high proportion of the unusual amino acid x-aminoisobutyric acid (Aib). As for gramicidin A. both termini are blocked, and the amino acid sequence is Ac-Aib-L-Pro-Aib-L-Ala-Aib-L-A~~-L-Gln-Aib-L-Val-Aib-Gly-L-Leu-Aib-L-Pro-L-Val-Aib-Aib-L-Glu-L-Glu-L-Phl (Phl=phenylalaninol). Peptides with high Aib (and Pro) content have a marked propensity to form helices. Indeed, crystal structure determinations of alamethicin and the related peptaibol peptides Leu-zervamincin and antiamoebin[27] show that these molecules are predominately x-helical. It follows from the secondary structure of the peptide chains that the mechanism of channel formation must be completely different from that of gramicidin A. In the crystal structure of antiamoebin,[27] three symmetry-related peptide molecules in bent conformations apparently form hourglass-shaped channels. One cocrystallized octanol molecule mimics a membrane segment along the exterior of the channel assembly, while a second octanol molecule resides inside the channel.

AMPHIPHILIC SURFACTANT-TYPE NANOTUBES

While all peptide nanotubes considered thus far have fairly small pores (up to 13 Å van der Waals diameter for cyclic D,L-α-dodecapeptides[4]), nanotubes in a completely

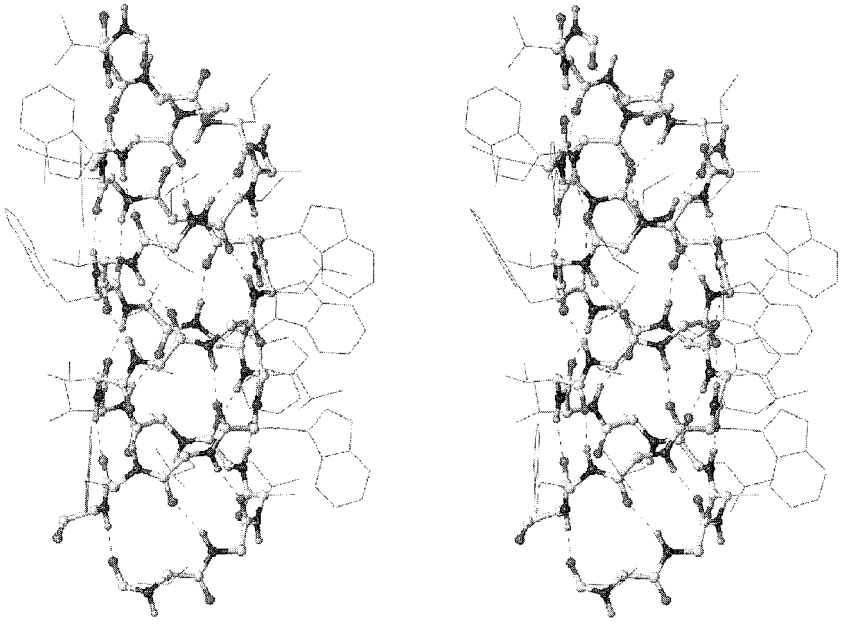

Fig. 4 Stereo illustration of the right-handed double-stranded helical dimer of the pentadecapeptide antibiotic gramicidin A.[27] The inner channel has a diameter of approximately 4.6 A. For clarity, heavy atoms in the side chains are shown in a stick representation.

different size range with typical diameters of *300–500* Å can be formed by several surfactant-like peptides. thus broadening the diversity of building blocks of self-assembling peptides for scaffolds and biological materials.[28,29] The peptide monomers contain seven or eight residues. with a hydrophilic head composed of aspartic acid and a tail of hydrophobic amino acids. such as alanine. valine, and leucine. The length of each peptide is the same as that of biological phospholipids, about 20 A. A model for nanotube formation by the heptapeptide Ac-(L-Val)$_6$-L-Asp is shown in Fig. 5. Studies of peptide surfactant molecules may have significant implications for the development of scaffolds and biologically inspired materials.

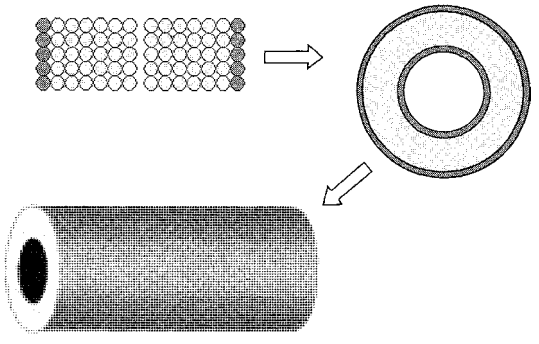

Fig. 5 Suggested pathway of Ac-(L-Val)$_6$-L-Asp peptide nanotube formation Peptide molecules interact with one another to form closed rings. which ultimately yield nanotubes upon stacking

BOLAAMPHIPHILIC PEPTIDE NANOTUBES

Molecules like *bis*(*N*-α-amido-Gly-Gly)-1,7-heptane dicarboxylic acid (Fig. 6) belong to a class of compounds called bolaamphiphiles that form tubular aggregates at low pH.[30,31] These peptide nanotubes have diameters in the range of 200–10,000 Å (1 μm) and are thus comparable in size to those of the surfactant molecules, but hydrogen bonds rather than hydrophobic interactions are responsible for self-assembly (Fig 6). Each bolaamphiphile peptide contains at least one free ainide site in the tubule assembly. which may interact with protein molecules. At high pH. the carboxpl groups gradually lose their acidic H atoms, and the acid–acid dimer is replaced by anion–acid hydrogen bonds (COO –H– OOC). This hydrogen-bonding modification triggers a molecular rearrangement that eventually leads to transformation of tubes into helical ribbons. These observations suggest that the bolaamphiphiles could be useful in controlled release applications. with the pH-dependent structural transformations serving as simple release mechanisms.[31] In the presence of Ni^{2+} ions. macroscopic bundles of well-ordered peptide nanotubes are assembled,[32] probably driven by the ability of adjacent nanotubes to form metal coordination bridges.

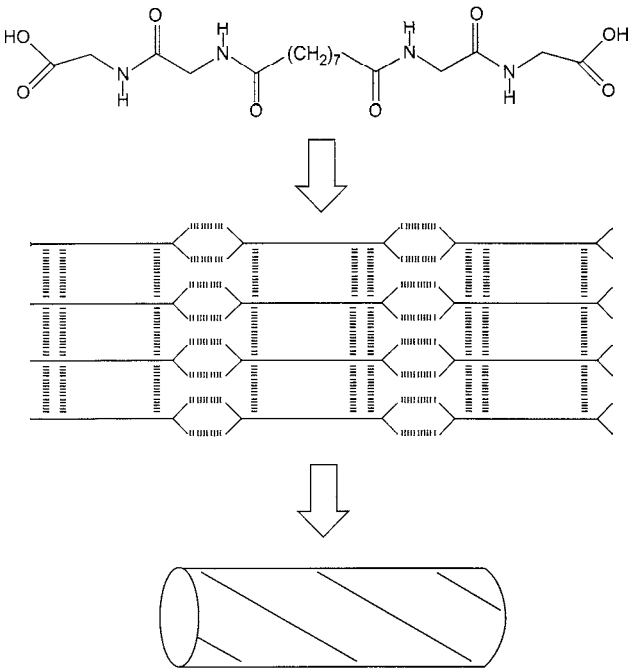

Fig. 6 Self-assembly of *bis*(*N*-α-amido-Gly-Gly-1,7-heptane dicarboxylic acid) into sheets and then into nanotubes by formation of acid diiners and amide–amide hydrogen bonds. (From Refs. [31,32].)

CONCLUSION

Nanotubes constructed by peptides comprise a promising group for development of membrane-mimics, antibiotics, carriers, electronic devices, sensors, scaffolds, and biological materials. Future areas of interest may include catalysis and use as chiral selectors. Except for the surfactant-like peptides, the driving force in the self-assembly process is formation of hydrogen bonds. As the knowledge of and experience with hydrogen bonds as design tools are developed further, new avenues will open to the development of classes of materials different than those discussed here. in the solid phase (crystal engineering) as well as in solution.

ARTICLES OF FURTHER INTEREST

Amino Acids: Applications, p. 42
Concepts in Crystal Engineering, p. 319
Crystal Engineering with Hydrogen Bonds, p. 357
Cyclodextrins, p. 398
Ion Channels and Their Models, p. 742
Ionophores, p. 760
Micelles and Vesicles, p. 861
Self-Assembly in Biochemistry, p. 1257
Supramolecular Chemistry: Definition, p. 1401

REFERENCES

1. Karle, I.L.; Handa, B.K.: Hassall, C.H. The conformation of the cyclic tetrapeptide L-Ser(O-t-Bu)-β-Ala-Gly-L-β-Asp(OMe) containing a 14-membered ring. Acta Crystallogr. 1975, *B31* (2), 555–560.
2. Ghadiri, M.R.: Granja, J.R.; Milligan. R.A.; McRee, D.E.; Khazanovich, N. Self-assembling organic nanotubes based on acyclic peptide architecture. Nature **1993**, *366*, 324–327.
3. Fernandez-Lopez, S.; Kim, H.-S.: Choi, E.C.: Delgado. M.; Granja, J.R.; Khasanov, A.; Kraehenbuehl, K.; Long, G.; Weinberger, D.A.: Wilcoxen, K.M.: Chadiri. M.R. Antibacterial agents based on the cyclic D,L-α-peptide architecture. Nature **2001**, *412*. 452–455.
4. Hartgerink. J.D.: Clark, T.D.; Ghadiri, M.R. Peptide nanotubes and beyond. Chem. Eur. J. 1998, *4* (8), 1367–1372, and references therein.
5. Lewis, J.P.: Pawley. N.H.: Sankey, O.F. Theoretical investigation of the cyclic peptide system cyclo[(D-Ala-Glu-D-Ala-Gln)$_{m=1-4}$]. J. Phys. Chem., B 1997, *101* (49), 10576–10583.
6. Ghadiri, M.R.; Granja, J.R.: Buehler. L.K. Artificial transmembrane ion channels from self-assembling peptide nanotubes. Nature 1994, 369. 301–304.
7. Engels, M.; Bashford, D.; Ghadiri, M.R. Structure and dynamics of self-assembling peptide nanotubes and the channel-mediated water organization and self-diffusion. A molecular dynamics study. J. Am. Chem. Soc. 1995. *117* (36), 9151–9158.
8. Sánchez-Quesada, J.: Kim, H.S.; Ghadiri, M.R. A synthetic pore-mediated transmembrane transport of glutamic acid. Angew. Chem. Int. Ed. 2001, *40* (13). 2503–2506. and references therein.
9. Kim, H.S.; Hartgerink. J.D.; Ghadiri, M.R. Oriented self-assembly of cyclic peptide nanotubes in lipid membranes. J. Am. Chem. Soc. 1998. *120* (18). 4417–4424.
10. Sanchez-Quesada, J.; Isler. M.P.: Ghadiri. M.R. Modulating ion channel properties of transmembrane peptide nanotubes through heterorneric supramolecular assemblies. J. Am. Chem. Soc. 2002, *124* (34). 10004–10005.
11. Seebach. D.; Matthews, J.L.: Meden, A.; Wessels, T.; Baerlocher. C.: McCusker, L.B. 15. Cyclo-β-peptides: Structure and tubular stacking of cyclic tetramers of 3-aminobutanoic acid as determined from powder diffraction data. Helv. Chim. Acta 1997, *80* (1), 173–182.
12. Clark, T.D.: Buehler, L.K.; Ghadiri, M.R. Self-assembling cyclic β^3-peptide nanotubes as artificial transmembrane ion channels. J. Am. Chem. Soc. 1998, *120* (4), 651–656.
13. Amorín, M.; Castedo. L.; Granja, J.R. New cyclic peptide assemblies with hydrophobic cavities: The structural and thermodynamic basis of a new class of peptide nanotubes. J. Am. Ghem. Soc. 2003. *125* (10). 2844–2845.

14. Clark. T.D.: Buriak. J.M.: Kobayashi, K.: Isler, M.P.; McRee. D.E.; Ghadiri. M.R. Cylindrical β-sheet peptide assemblies. J. Am. Chern. Soc. 1998,120 (35).8949–8962.
15. Bong. D.T.; Ghadiri. M.R. Self-assembling cyclic peptide cylinders as nuclei for crystal engineering. Angew. Chem. Int. Ed. 2001, 40 (11). 2163–2166.
16. Gauthier, D.; Baillargeon, P.: Drouin, M.; Dory. Y.L. Self-assembly of cyclic peptides into nanotubes and then into highly anisotropic crystalline materials. Angew. Chem. Int. Ed. 2001. 40 (24). 4635–4638.
17. Ranganathan, D.: Haridas, V.: Gilardi. R.; Karle. I.L. Self-assembling aromatic-bridged serine-based cyclodepsipeptides (serinophanes): A demonstration of tubular structures formed through aromatic π–π interactions. J. Am. Chern. Soc. 1998. 120 (42), 10793–10800.
18. Ranganathan. D.; Lakshmi. C.: Karle. I.L. Hydrogen-bonded self-assernbled peptide nanotubes from cystine-based macrocyclic bisureas. J. Am. Chem. Soc. 1999. 121 (26), 6103–6107.
19. Ranganathan, D.; Haridas, V.: Sundari. C.S.; Balasubramanian, D.; Madhusudanan. K.P.: Roy. R.; Karle, I.L. Design. synthesis, crystal structure, and host–guest properties of polymethylene-bridged cystine-based cyclobisamides: A facile entry to hydrogen-bonded peptide nanotubes. J. Org. Chern. 1999, 64 (25), 9230–9240.
20. Gorbitz. C.H.: Gundersen, E. L-Valyl-L-alanine. Acta Crystallogr. 1996. *C52* (7), 1764–1767.
21. Gorbitz. C.H. Nanotubes from hydrophobic dipeptides: Pore size regulation through side chain substitution. New J. Chem. 2003, submitted.
22. Gorbitz, C.H. An exceptionally stable peptide nanotube system with flexible pores. Acta Crystallogr. 2002. *B58* (5), 849–854.
23. Gorbitz, C.H. Nanotube formation by hydrophobic dipeptides. Chem. Eur. J. 2001. 7 (23). 5153–5159.
24. Birkedal, H.; Schwarzenbach, D.: Pattison. P. Observation of uniaxial negative thermal expansion in an organic crystal. Angew. Chem. Int. Ed. 2002, 41 (5), 754–756.
25. Marsh. D. Peptide models for membrane channels. Biochem. J. 1996. *315* (2). 345–361.
26. Burkhart, B.M.; Li, N.: Langs, D.A.; Pangborn, W.A.: Duax, W.L. The conducting form of gramicidin A is a right-handed double-stranded double helix. Proc. Natl. Acad. Sci. U. S. A. 1998, *95* (22). 12950–12955.
27. Karle, I.L.; Perozzo, M.A.: Mishra, V.K.: Balaram. P. Crystal structure of the channel-forming polypeptide antiamoebin in a membrane–mimetic environment. Proc. Natl. Acad. Sci. U. S. A. 1998, *95* (10). 5501–5504.
28. Vauthey, S.: Santoso. S.; Gong, H.: Watson, N.; Zhang, S. Molecular self-assembly of surfactant-like peptides to form nanotubes and nanovesicles. Proc. Natl. Acad. Sci. U. S. A. 2002. 99 (8), 5355–5360.
29. Zhang, S.: Marini, D.M.: Hwang, W.; Santoso. S. Design of nanostructured biological materials through self-assembly of peptides and proteins. Curr. Opin. Chern. Biol. 2002. 6 (6), 865–871.
30. Kogiso, M.: Ohnishi. S.: Yase. K.: Masuda, M.: Shimizu. T. Dicarboxylic oligopeptide bolaamphiphiles: Proteon-triggered self-assembly of microtubes with loose solid surfaces. Langmuir 1998, 14 (18), 4978–4986.
31. Matsui, H.: Gologan, B. Crystalline glycylglycine bolaamphiphile tubules and their pH-sensitive structural transformation. J. Phys. Chem.. B 2000. 104 (15). 3383–3386.
32. Matsui, H.: Douberly, G.E.J. Organization of peptide nanotubes into macroscopic bundles. Langmuir 2001. 17 (25). 7918–7922.

Phase-Transfer Catalysis in Environmentally Benign Reaction Media

Silvio Quici
Amedea Manfredi
Gianluca Pozzi
CNR-Istituto di Scienze e Tecnologie Molecolari, Milano, Italy

INTRODUCTION

Phase-transfer catalysis (PTC) was discovered more than 30 years ago,[1-3] but this powerful means of conducting reactions between two or more reactants present in two or more immiscible phases still attracts considerable scientific and practical interest. Nowadays, the term PTC encompasses several effective techniques of which typical advantages are simplicity, mild conditions, high reaction rates, high selectivities, and the use of inexpensive reagents. The interested reader is encouraged to refer to some books[4-7] and reviews[8-14] for a thorough survey. which is far beyond the scope of this brief article, where the basic principles of PTC and a few recent advances toward the use of safe and environmentally acceptable reaction media in combination with PTC will be outlined.

GENERAL PRINCIPLES

Liquid–Liquid PTC

Anionic reactivity can be promoted by dipolar aprotic solvents such as hexamethylphosphoramide (HMPA), dimethylsulfoxide (DMSO), and dimethylformamide (DMF), which dissolve inorganic salts by selectively solvating the cation. while the unsolvated anion becomes highly reactive.[15] This traditional approach is no longer appealing due to the considerable pressure to replace toxic and environment-detrimental reaction media. Dipolar aprotic solvents can be highly toxic and generally exhibit high boiling points and water solubility. making their recovery and product separation difficult. From its emergence, PTC aimed to perform anion-promoted reactions under mild multiphase conditions. usually in liquid/liquid "aqueouslorganic" or solid/liquid "solid salt/organic'' two-phase systems, thus avoiding the use of hazardous solvents. The basic idea is that solubilization of the anion in a low-polarity organic solvent and activation by decreasing the coulombic interaction with the cation are two primary requisites for high anionic reactivity. The PT catalyst fulfills both functions, forming lipophilic ion pairs A^+B^-, in which A^+ is a large organic or organometallic cation (e.g., tetraalkylammonium, tetraalkylphosphonium, or alkali metal complexes of cryptands and crown ethers), and B is the anion. The large size accounts for the low charge density on the surface of the cations: accordingly, interactions with the anion are strongly reduced, and this leads to increased anionic reactivity.

The first PTC mechanism proposed by Starks assumed that the catalyst, an ammonium or phosphonium salt (Q^+X^-), is partitioned between two immiscible liquid phases. In this way, the reacting anion X^- is transferred from the aqueous to the organic phase. where the reaction occurs, and the product anion Y^- is released in the aqueous phase (Fig. 1).[3]

Subsequently. it was found that the catalytic efficiency of a quaternary salt is directly related to its solubility in the organic phase, other conditions being the same. This and other observations support the mechanism reported in Fig. 2, in which anion transfer does not necessarily require the partitioning of the quaternary cation, the charge parity in both phases being ensured by the quaternary and the metal cation. respectively.[16,17]

This mechanism also applies when lipophilic crown ethers or cryptands are used as catalysts. The extent of anion extraction into the organic phase and its reactivity depend on the combination of many parameters, including the nature of the anion (its charge. size. polarizability, etc.). the concentration of the inorganic salt in the aqueous phase. the dielectric constant of the organic solvent: the separation between cation and anion in the ion pair. and the number of water molecules associated with the anion in the organic phase. The influence of these parameters on the reaction rate was exhaustively discussed.[18]

Solid–Liquid and Gas–Liquid Phase-Transfer Catalysis

Under classical aqueouslorganic PTC. a small amount of water is also extracted into the apolar organic phase. mainly as a specific solvation sphere of the anion. The

Encyclopedia of Supramolecular Chemistry
DOI: 10.1081/E-ESMC 120012709

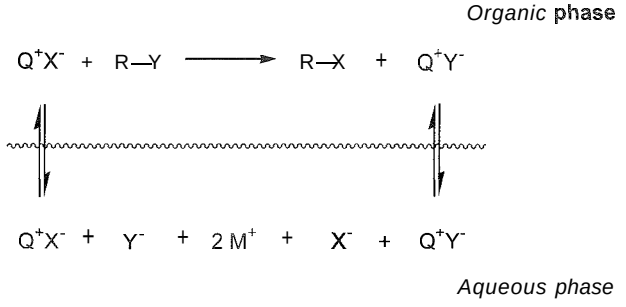

Fig. 1 Basic PTC mechanism. Adapted from Ref. [3].

presence of water. besides reducing reaction rates. may produce undesired side reactions that can be avoided by using a solid salt suspended in an anhydrous organic solution of the substrate as a source of the nucleophile. Under these conditions. the PTC catalysts transfer the anion as a reactive ion pair from the surface of the solid into the organic phase. Solid–liquid conditions are particularly suitable for reactions involving strong basic reagents such as carbenes and carbanions generated in situ. Eipophilic crown ethers and cryptands are the catalysts of choice in this case, because they show higher chemical stability in comparison to onium salts, and. more importantly. they interact more efficiently with the solid surface, thus promoting the collapse of the crystal lattice.[19] Diffusion can play a critical role in solid–liquid PTC, and in many cases. mass transfer is the limiting step of the overall process. This drawback can be partly overcome by using organic solvents such as acetonitrile or acetone. in which most solid salts used as sources of nucleophiles are slightly soluble.

Gas–liquid phase-transfer catalysis (GL-PTC) relies on the use of thermally stable PT catalysts adsorbed onto a solid support, which can also act as a source of the desired nucleophile. Reactions are carried out at a temperature that ensures that the catalyst is in a molten state and that reagents are in the vapor phase. and that the chemical transformation occurs in the organic microphase of molten catalyst. The products are recovered after condensation outside the reaction vessel. Only catalysts having melting points lower then the process temperature <180°C are active. but despite this limitation, GL-PTC is a versatile technique that has been applied to a number of chemical transformations.[20]

Inverse PTC

Liquid–liquid PTC typically involves the extraction of an anionic reactive species from the aqueous phase to the organic solution where the reaction occurs. However. a different approach based on the transport of a lipophilic reactant into the aqueous phase. named inverse phase-transfer catalysis (IPTC), was expressly introduced in 1986.[''''] In the presence of 4-(dimethylamino)pyridine, the reaction of aqueous alanine with acyl chlorides was greatly accelerated. Analogously. 4-pyrrolidinopyridine and a polymeric analogue were found to catalyze the hydrolysis of p-nitrophenyl caproate, although 4-pyrrolidinopyridine had to be used in excess with respect to the substrate. Further studies proved that IPTC includes an interphase component. as evidenced by competitive transacylation experiments carried out in the presence of 4-(dimethylamino)pyridine, pyridine N-oxide, or Et_3N in CH_2Cl_2-water.[22] Moreover, in the pyridine-catalyzed reaction of benzoyl chloride with aniline in $CHCl_3$-water, the rate of Cl^- appearance exceeded the sum of the rates of aniline transport (from water) and benzoylpyridinium chloride transport (into water), indicating that reaction occured in both phases.[23] Several factors, including the concentration of reactants and catalyst, the ionic strength of the aqueous phase. stirring rate, and, above all, the nature of the organic solvent, greatly influence the mechanism of IPTC reactions catalyzed by pyridine derivatives.[24–26] Also, when simple onium salts are used, as in the case of the epoxidation of chalcone with H_2O_2 catalyzed by dodecyltrimethyl ammonium bromide (DTAB) in water/heptane, interfacial processes are involved in IPTC. in addition to the transport of the lipophilic reactant into the aqueous phase.[27]

TOWARD PTC WITHOUT VOLATILE ORGANIC SOLVENTS

The advent of PTC had a positive impact on the need to eliminate some hazardous solvents and reagents from the laboratory and industrial practice. However, many PTC reactions still involve the use of volatile organic solvents, which are partly discharged into the atmosphere with a host of negative environmental effects. Replacement of these solvents with reaction media such as water,

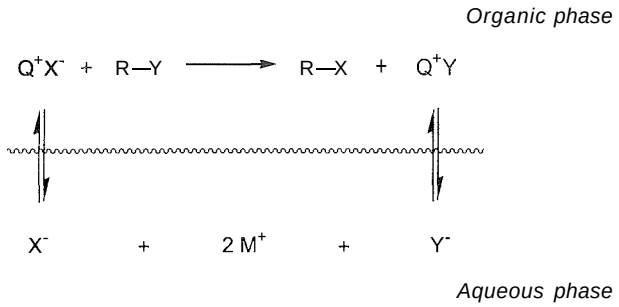

Fig. 2 PTC inechanisrn without partitioning of the onium salt. Adapted from Ref. [17].

supercritical fluids,[28] and ionic liquids,[29,30] brings about potential advantages, such as the opportunity for environmentally benign processing, lower costs, and easy separation of the catalysts from the reaction medium.

PTC in Water as Bulk Solvent

Although the understanding of IPTC is still limited in comparison to that of normal PTC, it is clear that this method is apt to effect organic reactions in water. As discussed in the introduction: simple pyridine derivatives were introduced mainly in connection to kinetic and mechanism studies. but more recently. it was shown that the use of host compounds; such as cyclodextrins[7,8] and water-soluble calix[*n*]arenes,[32] offers the opportunity to combine IPTC, molecular recognition, and transition metal catalysis, with additional economic and environmetal advantages deriving from the use of water as a bulk solvent.

Cyclodextrins are cyclic glucose oligomers. and the 6-. 7-, and 8-units terms are commercially available under the names of α-, β-, and γ-cyclodextrin, respectively. These compounds are characterized by a typical shape that can be described as barrel-like (Fig. 3). The inner cavity is essentially hydrophobic and can host organic guests, whereas hydrophilic-OH groups span from the upper and the lower rim, ensuring water solubility to the molecule. The free hydroxyl groups can be selectively functionalized. thus making possible the fine-tuning of the inclusion and solubility properties of these compounds.

It is interesting to note that unmodified α-and β-cyclodextrins were investigated as carriers of organic molecules into water before the concept of IPTC was rationalized. For instance, Trifonov and Nikiforov reported that in the presence of β-cyclodextrin, the rate of the nucleophilic displacement of neat octyl bromide with aqueous cyanide, iodide, and thiocyanate anions was considerably increased.[7,8] After the IPTC concept was established, commercially available cyclodextrins found applications as inverse PT agents in several important organic reactions catalyzed by transition metals. including the aerobic oxidation of olefins to ketones in water, in the presence of $PdCl_2$ and $CuCl_2$ (Wacker process),[34] the $IrCl_3$ catalyzed isomerization of 4-allylanisole,[35] the hydrogenation of conjugated dienes to monoolefins catalyzed by $HCo(CN)^{5-}$, generated in situ from $CoCl_2$, KOH, and KCN. and promoted by lanthanide halides.[36] In 1994 Mortreux and coworkers reexamined the application of IPTC to the Wacker process and found that 1-decene could be oxidized to 2-decanone with excellent yield (98%) in water; using $O_2/PdSO_4/CuSO_4/H_9PV_6Mo_6O_{40}$ as the redox system. The organic substrate was transferred into the aqueous phase containing the catalytic system by an amphiphilic β-cyclodextrin, in which about 60% of the free-OH groups were methylated.[37] Other cyclodextrins (native α-, β-, y-, fully acetylated β-cyclodextrin or 2-hydroxypropyl-β-cyclodextrins with different degrees of substitution) were tested with limited success. The correct balance between lipophilic and hydrophilic character had an overwhelming importance. but the results obtained pointed also to the possible role of molecular recognition based on reversible interactions between the cyclodextrins' host cavity and 1-decene. The same modified β-cyclodextrin was successfully used as inverse PT catalysts for the rhodium-catalyzed hydroformylation of water-insoluble olefins in an aqueous two-phase system free of organic solvent (Fig. 4).[38] In the case of 1-decene, conversion reached 100%, with 95% selectivity and a ratio nliso-aldehyde = 1.9. Other terminal olefins gave similar

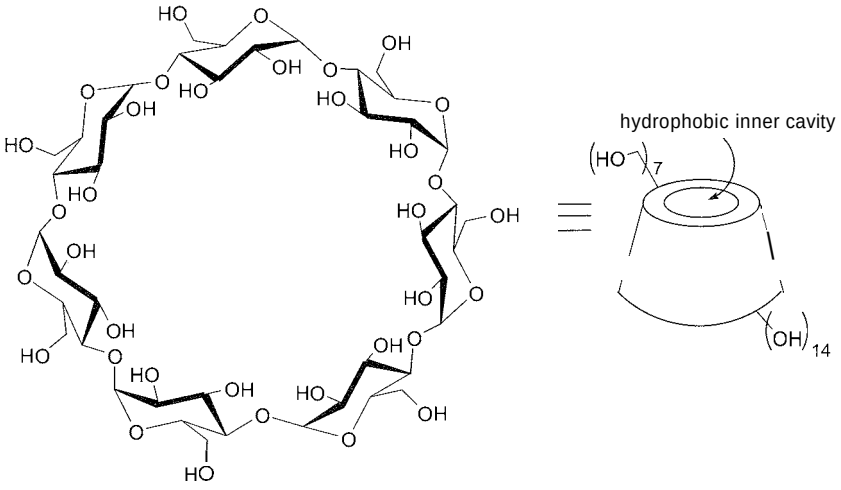

Fig. *3* β-cyclodextrin

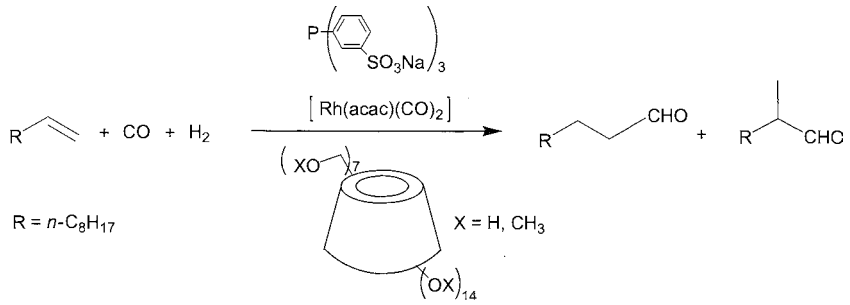

Fig. 4 Hydroformylation of 1-decene in the presence of methylated β-cyclodextrins. Adapted from Ref. [38]

results, but less-reactive internal olefins were found to be almost inert.[39]

A common picture emerged from these studies: the amphiphilic cyclodextrin acts as a host, wrapping the hydrophobic substrate and transferring it into the water phase, where the reaction occurs. The stability constant of the new host–guest complex is lower. and the product is then released into the organic phase (Fig. 5).

The validity of these working hypotheses was tested in other catalytic organometallic reactions. Interesting results were obtained in the biphasic hydrogenation of water-insoluble aldehydes to alcohols catalyzed by $RuCl_3$/$P(C_6H_4SO_3Na)_3$,[40] the cleavage of allylic substrates in the presence of $Pd(OAc)_2$/$P(C_6H_4SO_3Na)_3$,[41,42] and the hydrocarboxylation of olefins catalyzed by $PdCl_2$/$P(C_6H_4SO_3Na)_3$ to give carboxylic acids.[43] Deeper insight into the effective role of cyclodextrins in the catalytic system was thus achieved. In two recent independent studies, the influence of partly methylated β-cyclodextrins on the other component of the catalytic system was been evidenced in the case of the hydroformylation of alkenes. Kalck and coworkers proposed that a gradual supramolecular organization in the interphase occurs for the catalytically active rhodium complex. which should involve at least two cyclodextrin molecules.[44] Monflier and coworkers refined their previous model, taking into account the formation of inclusion complexes between the cyclodextrin and some components of the catalytic system. in particular, $P(C_6H_4SO_3Na)_3$. It was concluded that chemically modified cyclodextrins influence the biphasic reaction not only by acting as inverse phase-transfer agents but also by modifying the equilibria between the components of the catalytic system.[45]

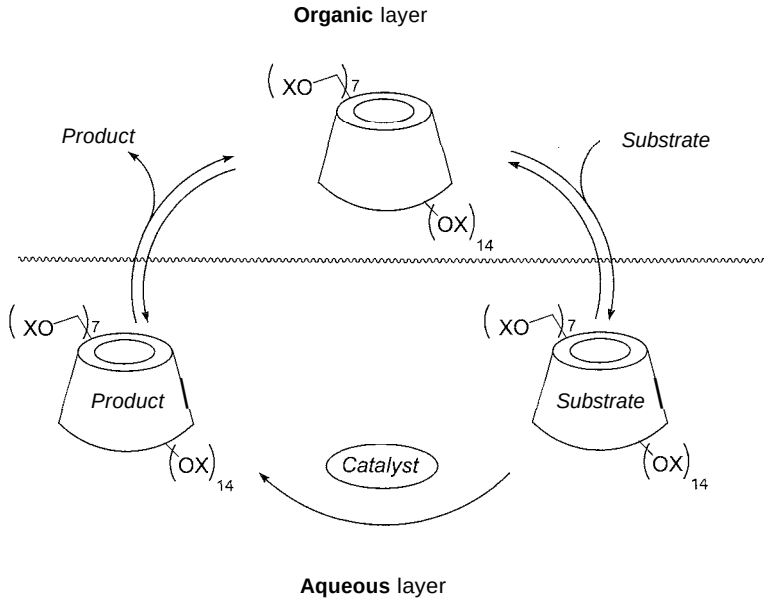

Fig. 5 Proposed role of chemically modified cyclodextrins as carriers in aqueous-phase organometallic catalysis. Adapted from Ref. [43].

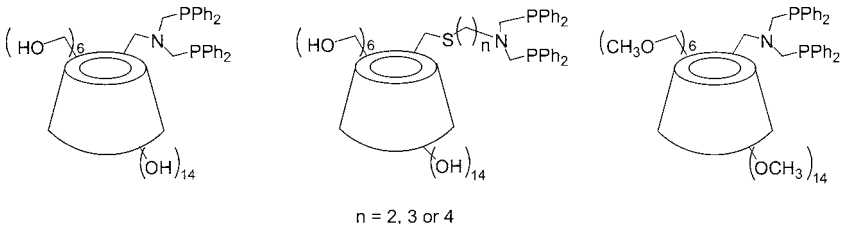

Fig. 6 Multicomponent ligands for organometallic catalysis Adapted from Ref [46]

A more sophisticated β-cyclodextrin-based catalytic system combining different functions in the same molecule was also conceived. Rhodium complexes of multicomponent ligands featuring a chelating diphosphine covalently linked to the upper riin of β-cyclodextrin (Fig. 6) were used as catalysts for the hydrogenation and the hydroformylation of alkenes in water–organic two-phase systems.[46]

These supramolecular catalysts showed high substrate selectivity in competition hydrogenation experiments and exceptional activity in the hydroformylation reactions. In contrast to the simple methylated β-cyclodextrin previously mentioned, even internal and cyclic olefins were converted into aldehydes. Such improvements were explained with the formation of an inclusion complex at the phase boundary. with the cylodextrin host fixing the substrate in the proximity of the catalytically active metal center (Fig. 7).[47]

In contrast to cyclodextrins, water-soluble calix[*n*]arrenes (*n* = 4, 6, 8) were proposed as inverse PT catalysts only a few years ago.[48] Shimizu and coworkers reported the use of previously known calix[n]arenes bearing trimethylarninonioinethyl groups **1–3** (Fig. 8) in the nucleophilic displacement of alkyl and arylalkyl halides with NaCN, KI, KSCN in water. The catalytic activity of these compounds exceeded that of β-cyclodextrin, whereas (4-methoxybenzyl)trimethylammonium chloride **4** (the monomeric unit of the calix[*n*]arene catalysts) did not show any activity. It was also found that the efficiency of the calix[*n*]arenes varied depending on the sizes and shapes of the substrates. and it was proposed that they behave similarly to cyclodextrins. forming inclusion compounds with the substrate that is thus transferred into the aqueous phase.

Calix[*n*]arenes **1–3** were used as inverse PT catalysts in the alkylation of active methylene compounds with alkyl halides in aqueous NaOH solutions,[49] and in aldol-type condensation and Michael addition reactions.[50] In the aikylation of phenylacetone with octyl bromide. the IPTC procedure enhanced the alkylation versus hydrolysis and *C* versus *O* alkylation selectivities with respect to those observed under classical PTC reactions in the presence of tetrabutylammonium bromide (TBAB) or hexadecyltributylammonium bromide (HTPB). Moreover, the aqueous catalyst solution was easily separated from the organic phase containing the products, and no organic solvent was required. In the case of the aldol-type condensation of benzaldehyde with indene or acetophenone in aqueous NaOH (Fig. 9), IPTC reactions catalyzed by **1** were compared with those conducted in aqueous micelles in the presence of cetyltrimethylammonium bromide (CTAB) as the sufactant. Although selectivities and yields were similar. the IPTC procedure avoided the formation of emulsions, thus facilitating product separation and catalyst recovery. In the light of the results obtained. water-soluble calix[*n*]arenes **1–3** were proposed

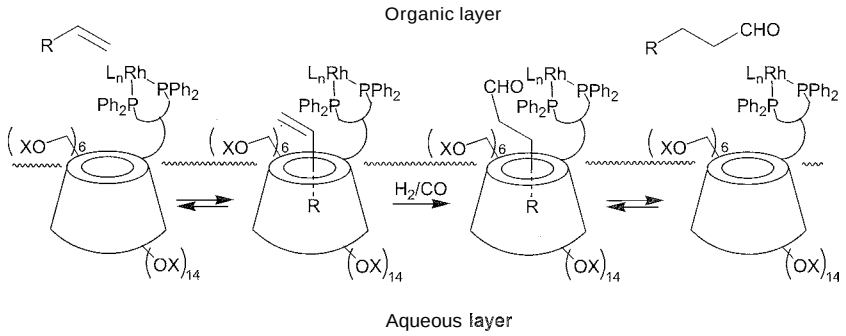

Fig. 7 Proposed mode of action of rhodium complexes of chelating phosphines tethered to β-cylodextrins. Adapted from Ref. [47].

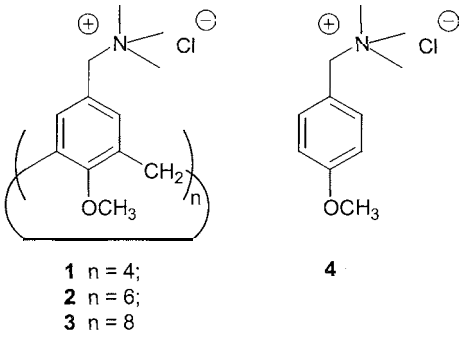

1 n = 4;
2 n = 6;
3 n = 8

4

Fig. 8 Water-soluble calix[*n*]arenes and their monomeric units. Adapted from Ref. [48].

to form host–guest complexes in the aqueous phase with the carbanions that arise from the deprotonation of the active methylene compounds. The nucleophilic attack of the hosted anion on the acceptor would then take place at the interface.

Analogously to cyclodextrins, water-soluble calixarenes were integrated into catalytic systems, where the ability to perform IPTC and organometallic catalysis are combined in a single molecule. Phosphacalix[4]arenes **5** and **6** (Fig. 10) were synthesized and used as dual functional ligands in the rhodium-catalyzed hydroformylation of I-octene and I-decene.[51] Both ligands afforded better conversions and yields than $P(C_6H_4SO_3Na)_3$ or $P(C_6H_4SO_3Na)_3$/2,6-di-*O*-methyl-β-cyclodextrin, and **8** proved to be particularly effective [nonanals (73%) and undecanals (52%) were obtained with linear/branched aldehyde ratio = 1.7 and 2.3. respectively]. Moreover, the aqueous layer was recycled twice with no apparent decrease of activity and selectivity. The beneficial effect of **5** and 6 was reasonably explained with the improvement in the mass transfer of the substrate and products between the phases. but neither formation of inclusion

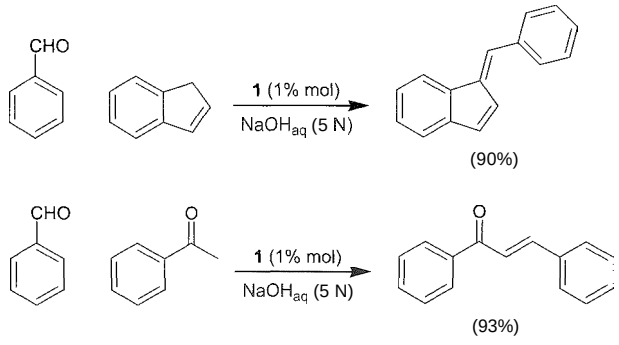

Fig. 9 Condensation of benzaldehyde with indene or acetophenone catalyzed by the water-soluble calix[4]arene **1.** Adapted from Ref. [50].

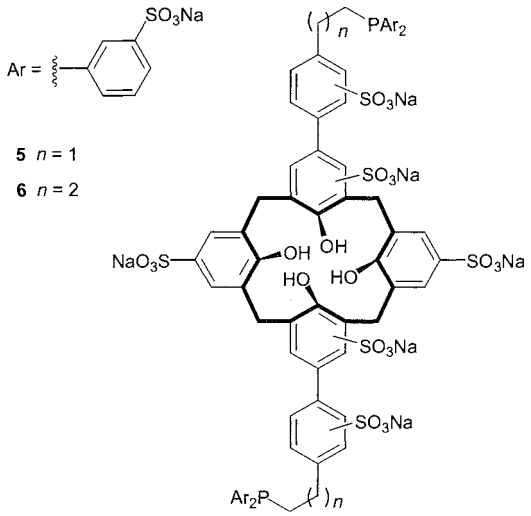

Fig. 10 Water-soluble phosphacalix[4]arenes. Adapted from Ref. [51].

complexes nor transport ability of the ligands were specifically investigated.

The inclusion of aromatic guests in the hydrophobic pocket of the water-soluble calixarenes 7–9 (Fig. 11) was recently studied by ^{1}H-NMR titration experiments in aqueous buffered solutions and molecular modeling studies combined with ab initio NMR shift calculations.[52]

Association constants of various aromatic compounds with **7** and 8 were found to be close to those observed with β-cyclodextrin, with the exception of iodobenzene, which showed a remarkable higher affinity to β-cyclodextrin than to the calixarenes (K_{ass} > 1000 M^{-1} versus about 60 M^{-1}). Under acidic conditions, the association

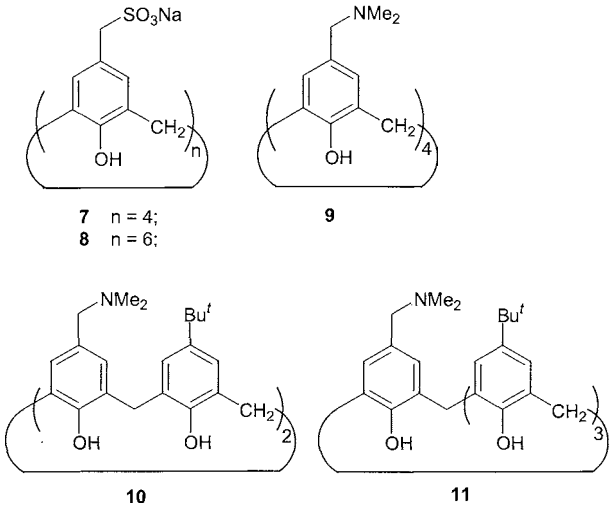

7 n = 4;
8 n = 6;

9

10

11

Fig. 11 Water-soluble calix[*n*]arenes. Adapted from Ref. [52].

constants with the amino methyl-substituted calixarene 9 were also higher than those measured with 7 and 8 at pH 7.4. Calix[4,6]arenes 7–11 were then evaluated as IPT catalysts in the Suzuki coupling of phenylboronic acid and iodobenzene in water, yielding diphenyl as a product. The influence of 7–11 was studied at low levels of conversions (10–15%) in order to compare initial reaction rates (t = 30 min) and to exclude product inhibition effects. Amino-substituted calix[4]arenes 9–18 gave better results. with increases of initial yields up to a factor of 12.7 in the case of 10.

PTC in Supercritical Fluids

Besides environinental and separation advantages, the use of supercritical fluids associated with PTC provides the extra benefit of an increased mass transfer. Viscosities and solute diffusivities of supercritical fluids are gas-like, and this can avoid the mass transfer limitations often encountered in liquid PTG systems.

The first reported example of a PTC reaction carried out in a supercritical fluid was the nucleophilic displacement of benzyl chloride with solid potassium bromide, in the presence of tetraheptylammoniurn bromide (THAB) or 18-crown-6 as catalysts.[53] Supercritical CO_2 ($scCO_2$) was used as a bulk solvent, with variable amounts of acetone added in order to increase the solubility of the catalyst. The kinetics of the nucleophilic displacement was studied, and the reaction was found to follow first-order, reversible kinetics in the case of THAB and zero-order kinetics for reactions catalyzed by 18-crown-6.

A detailed mechanistic study of the nucleophilic displacement of benzyl chloride with potassium cyanide catalyzed by THAB in $scCO_2$ was reported.[54] This simple, irreversible S_N2 model reaction is also of practical interest, and it was thoroughly investigated in a liquid

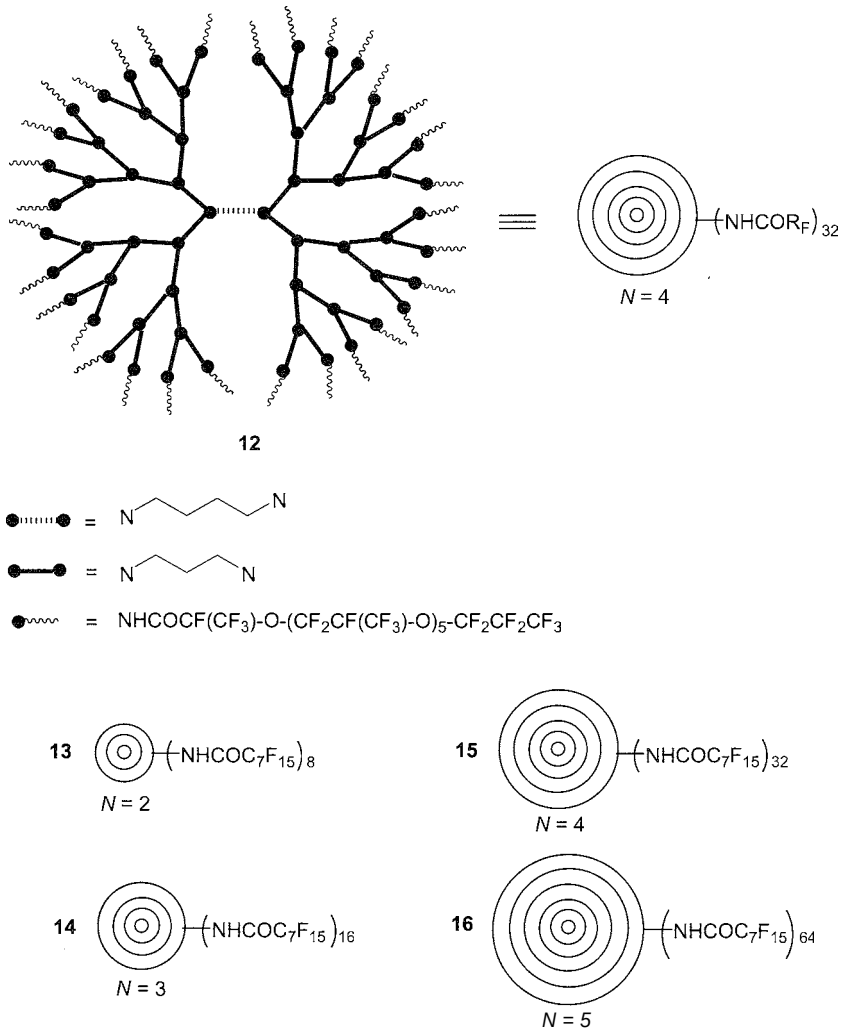

Fig. 12 Fluorinated poly(propylene imine) dendrimers. Adapted from Refs. [55,56].

system. thus making the comparison particularly interesting. The kinetic data together with catalyst solubility measurements clearly showed that three phases (a $scCO_2$ phase, a catalyst-rich phase. and a solid potassium salt phase) exist in the reaction system, and that the nucleophilic displacement proceeds in the catalyst-rich phase. The observed decrease of reaction rate upon addition of acetone is consistent with this particular phase behavior, which also partly justifies the lower efficiency of two nonionic catalysts [18-crown-6 and poly(ethylene glycol)] with respect to THAB.

Although the low solubility of TMAB in $scCO_2$ does not seem to be a major issue in the case of the above-mentioned reactions. better control of the solubility of PT catalysts could considerably extend the scope of PTC in supercritical fluids. Dendritic surfactants featuring perfluorinated ponytails attached to a polar interior are able to extract hydrophilic compounds from water into liquid CO_2. It was found that the apolar fluorous layer surrounding the unimolecular micellar-like structure of 12 (Fig. 12) shows a great affinity for CO_2, whereas the aqueous-soluble dye methyl orange is confined to the inner cavities of the dendritic host.[55] On the basis of this observation, perfluoroalkyl-functionalized poly(propylene imine) dendrimers 13–16 (second-. third-, fourth-, and fifth-generation, respectively) were synthesized and used as phase-transfer catalysts for the halogen exchange reaction of benzyl chloride into benzyl bromide and for the esterification of oxalic acid with pentafluorobenzyl-bromide in a biphasic system $H_2O/scCO_2$.[56]

The dendrimer extracts the bromide ions or oxalic acid from the aqueous phase to the $scCO_2$ phase, and the tertiary amine groups in the dendrimer core are responsible for the extraction. Dendrimers of different generations were compared, keeping the concentration of the tertiary amine groups constant. It was found that the rate of reaction strongly depends on the generation number N of the dendrimer. In the case of the halogen exchange. second-and third-generation dendrimers 13 and 14 afforded similar reaction rates. while in the presence of the fourth-generation dendrimer 15 (bearing 32 fluorinated ponytails). conversion of benzyl chloride proceeded essentially at the same rate as without a PT catalyst. This indicates that mass-transfer limitations occur within the unimolecular micellar-like structure of the higher-generation dendrirners, with cores that are almost completely shielded from the bulk $scCO_2$ phase. Similar behavior was observed in the case of the esterification of oxalic acid.

Beside modification of the PT catalyst by incorporation of ''CO_2-philic'' groups, other approaches to the problem of the poor solubility of polar compounds in $scCO_2$ were envisaged. Fluorinated surfactants (perfluoropolyether ammonium carboxylates) were used as stabilizers of $H_2O/scCO_2$ microemulsions.[57] The nucleophilic displacement of benzyl chloride with aqueous potassium bromide in $H_2O/scCO_2$ microemulsions[58] or emulsions[59] was reported. Reaction yields in the case of $H_2O/scCO_2$ emulsions were slightly better than those obtained with dendritic PT catalysts. A third approach was recently described that takes advantage of immobilized onium salts.[60] The S_N2 displacement of n-octyl methanesulfonate by bromide and iodide anions was performed using silica-supported ammonium or phosphonium phase-transfer catalysts in $scCO_2$, both under solid–liquid (stoichiometric amounts of functionalized silica) and liquid–liquid PTC (added aqueous KBr or KI) conditions. Although the anionic reactivity was found to be comparable to that observed in conventional organic solvents: the use of $scCO_2$ has no environmental impact and simplifies recovery of the catalyst.

Due to the low critical temperature and pressure (T_c = 31°C, P_c = 74 bar), $scCO_2$ is certainly the most investigated supercritical medium, as also witnessed by the examples reported here . However, alternative supercritical fluids must be explored in cases where the intrinsic reactivity of CO_2 cannot be neglected. As recently reported, the PT-catalyzed alkylation of phenylacetonitrile with ethyl bromide can be conveniently carried out in supercritical ethane in the presence of tetrabutylammonium bromide (TBAB) and solid potassium carbonate as a base (Fig. 13).[61] Under classical liquid–liquid PTC conditions, this reaction typically requires the use of strong aqueous bases (sodium amide, 50% NaOH), leading to the formation of significant amounts of diethylated product. Under solid-supercritical fluid PTC, only traces of this by-product were detected. Moreover, the use of a weak solid base presents evident advantages in view of an industrial application of the method. It should be noted that the use of $scCO_2$ as a bulk solvent led to the formation of an undesired cyanoester as the main product (Fig. 13), because the carbanion formed by deprotonation of phenylacetonitrile quickly reacts with CO_2, forming a carboxylate anion that is then alkylated by ethyl bromide.

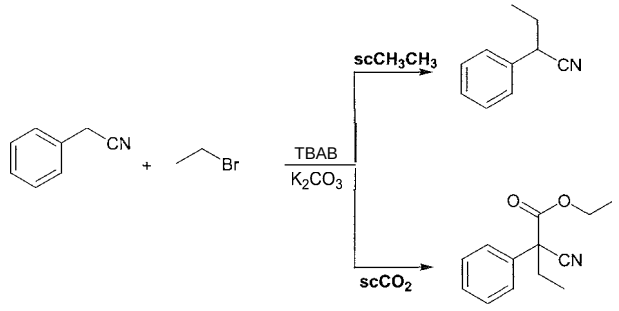

Fig. 13 Alkylation of phenylacetonitrile in supercritical fluids Adapted from Ref. [61].

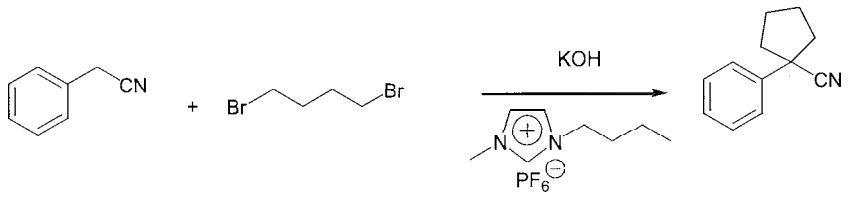

Fig. 14 Cycloalkylation of phenylacetonitrile in ionic liquids. Adapted from Ref. [64].

Nucleophilic Substitution in Ionic Liquids

The use of ionic liquids comprised of bulky organic cations as novel reaction media is gaining a great deal of attention due to the remarkable properties of these compounds. which include low-temperature melting point, negligible vapor pressure. high thermal stability, and inertness to air and water. Examples of their applications are appearing at an increasing rate in the literature, ranging from catalytic reactions[62] to enhanced product recovery.[63]

Room-temperature ionic liquids are generally salts of tetraalkylammonium, tetraalkylphosphonium. *N*-alkylpyridinium. and 1,3-dialkylimidazolium containing a wide variety of anions (Cl^-, NO_3 . BF_4 , PF_6 , $CH_3CO_2^-$, $CF_3CO_2^-$, etc.). the nucleophilicity of which can be enhanced by the lack of solvation. Therefore, it was recently proposed that ionic liquids could act as reaction media and anion activators in some organic transformations. The use of 1-*n*-butyl-3-methylimidazolium hexafluorophosphate, one of the most widely used room-temperature ionic liquids. as a solvent for reactions between organic compounds and inorganic salts, was demonstrated.[64] The displacement of benzyl chloride with solid potassiuin cyanide and the KOH-promoted cycloalkylation of phenylacetonitrile (Fig. 14) were carried out in the absence of any classical PT catalyst, relying on the ability of the ionic liquid to act as a catalyst for the activation of the anion.

Kinetic data for the benzyl chloride displacement indicated that at 40°C. the mass transfer of KCN into the solvent is the rate-limiting step. However, at 60°C and 80°C. reaction rates were high, and pseudo-first-order kinetic behavior was observed in agreement with an efficient transfer of the salt into the liquid, which is faster than the reaction step.

n-Butanol, *sec*-butanol, *tert*-butanol, and n-octanol were converted to their corresponding alkyl halides at room temperature using 1-*n*-butyl-3-methylimidazolium halides in the presence of a Brønsted acid (typically H_2SO_4).[65] Reaction conditions are significantly milder than those required by classical methods. and the products are easily removed from the reaction mixture. The proposed mechanism involves protonation of the alcohol followed by nucleophilic displacement by the halide anion. This step is accelerated by the effective charge separation in the transition state, which is ensured by the lack of extensive solvation in ionic liquids. The assessment of the role of these peculiar reaction media on the reaction mechanism is still underway.

CONCLUSION

PTC is now an established branch of catalysis, and applications for it are found in the laboratory as well as in large-scale processes. The design of PTC systems able to work in the absence of common volatile organic solvents is a promising field of research that deserves investigation in order to better understand manifold factors (solubility of the catalyst. formation of new phases, influence of the reactants on the physical state of the bulk fluid. etc.) that could influence the outcome of the reaction. However, as shown by the examples discussed here, the combined utilization of PTC and nontraditional reaction media affords new opportunities for improving numerous chemical processes while reducing emissions to the environment.

ARTICLES OF FURTHER INTEREST

Crown Ethers, p. 326
Cryptands, p. 334
Cyclodextrins, p. 398

REFERENCES

1. Makosza, M.: Serafin. B. Reactions of organic anions I. Catalytic ethylation of phenplacetonitrile in aqueous medium. Rocz. Chem. **1965**. 39. 1223–1230.
2. Brändstrom. A.: Gustavii. K. Ton pair extraction in preparative organic chemistry. A convenient method for the preparation of salts of amines. Acta Chem. Scand. **1969,** 23. 1215–1218.
3. Starks, C.M. Phase-transfer catalysis I. Heterogeneous reactions involving anion transfer by quaternary ammoni-

um and phosphonium salts. J. Am. Chem. Soc. 1971. *93*, 195–199.
4. Dehmlow. E.V.; Dehmlow. S.S. Phase-Transfer *Catalysis*; VCH: Weinheim, Germany. 1993.
5. Phase-Ti-aizsj'er *Catalysis: Fundamentals, Applications, and Industrial Perspectives*; Starks, C.M., Liotta, C.L.. Halpern, M., Eds.; Chapman and Hall: New York. 1994.
6. *Phase-Transfer* Catalysis; Halpern, M.E., Ed.: American Chemical Society: Washington. 1997.
7. *Handbook* of *Phase Transfer* Catalysis: Sasson, Y., Neumann, R.. Eds.; Blackie Academic & Professional: London. 1997.
8. Dehmlow, E.V. On the Borderline of Aqueous-Phase Catalysis. Phase-transfer Catalysis. In *Aqueous-Phase Organometallic Catalysis*: Cornils, B., Herrmann. W.A., Eds.; Wiley-VCH: Weinheim. Germany, 1998: 207–221.
9. Naik. S.D.; Doraiswamy. L.K. Phase transfer catalysis: Chemistry and engineering. AIChE J. 1998. *44*, 612–646.
10. Totten, G.E.; Clinton. N.A.: Matlock, P.L. Poly(ethylene glycol) and derivatives as phase transfer catalysts. J. Macromol. Sci.. Rev. Macromol. Chern. Phys. 1998. C38, 77–142.
11. Albanese. D.; Landini. D.: Maia, A.; Penso, M. Phase transfer catalysis: Some recent applications in organic synthesis. J. Mol. Catal. A Chem. 1999. *150*, 113–131.
12. Makosza, M. Phase-transfer catalysis. A general green methodology in organic synthesis. Pure Appl. Chem. 2000, *72*. 1399–1403.
13. Wolff, M.O.: Alexander, K.M.: Belder, G. Uses of quaternary phosphonium compounds in phase transfer catalysis. Chini. Oggi 2000. *18*. 29–32.
14. Albanese. D.: Landini, D.: Maia. A.; Penso, M. Key role of water for nucleophilic substitutions in phase-transfer-catalyzed processes: A mini-review. Ind. Eng. Chem. Res. 2001. *40*. 2396–2401.
15. Parker. A.J. Protic-dipolar aprotic solvent effects on rates of bimolecular reactions. Chem. Rev. 1969, *69*, 1–32.
16. Brandstrom. *A*. Principles of phase-transfer catalysis by quaternary ammonium salts. Adv. Phys. Org. Chem. 1977, *15*. 267–330.
17. Landini, D.: Maia. A.: Montanari, F. Phase-transfer catalysis. Nucleophilicity of anions in aqueous organic two-phase reactions catalyzed by onium salts. A comparison with homogeneous organic systems. J. Am. Chem. Soc. 1978. *100*, 2796–2801.
18. Montanari. *F.*: Landini. D.: Rolla. F. Phase-transfer-catalyred reactions.. Top. Curr. Chem. 1982. *101*. 147–200.
19. Montanari. F.: Quici, S.: Banfi, S. Phase-Transfer Catalysis. In *Comprehensive Supramolecular Chemistry*; Atwood, J.L., Davies, J.E.D.. Macnicol. D.D.. Vogtle, F., Eds.: Pergamon Elsevier: Oxford, United Kingdom. 1996: Vol. 10. 389–416.
20. Selva. M.: Tundo. P. Gas-liquid phase-transfer catalysis (GL-PTC). Chim. Ind. (Milan) 1995, *77*, 411–414.
21. Mathias. L.J.: Vaidya. R.A. Inverse phase transfer catalysis. First report of a new class of interfacial reactions. J. Am. Chern. Soc. 1986. *108*. 1093–1091.
22. Fife. W.K.: Xin. Y. Inverse phase-transfer catalysis: Probing its mechanism with competitive transacplation. J. Am. Chem. Soc. 1987. *109*, 1278–1279.
23. Wamser. C.C.; Yates. J.A. Kinetics and mechanisms for the two-phase reaction between aqueous aniline and benzoyl chloride in chloroforni, with and without pyridine catalysis. J. Org. Chem. 1989, *54*. 150–154.
24. Kuo. C.S.: Jwo. J.J. Inverse phase transfer catalysis. Kinetics and mechanism of the pyridine 1-oxide catalyzed substitution reaction of benzoyl chloride and benzoate ion in a two-phase waterldichloromethane medium. J. Org. Chem. 1992. *57*, 1991–1995.
25. Wang, M.-L.: Ou, C.-C.: Jwo, J.-J. Effect of organic solvents on the pyridine 1-oxide-catalyzed reaction of benzoyl chloride and acetate ion in a two-phase medium. Ind. Eng. Chem. Res. 1994, *33*, 2034–2039.
26. Wang. M.-L.; Ou. C.-C.: Jwo. J.-J. Study of the reaction of glycine and benzoyl chloride under inverse phase transfer catalysis. Chem. Eng. Commun. 2000, 179. 233–252.
27. Boyer. B.; Hambardzoumian. A.; Roque, J.-P.; Beylerian. N. Reaction in biphasic water/organic solvent sy ctem in the presence of surfactant: Inverse phase transfer catalysis versus interfacial catalysis. Tetrahedron 1999, *56*, 303–307.
28. *Chemical Synthesis* in *Supercritical Fluids*; Jessop. P.J.. Leitner. W., Eds.; Wiley-VCH: New York. 1999.
29. Welton, T. Room-temperature ionic liquids. Solvents for synthesis and catalysis. Chem. Rev. 1999, *99*. 2071–2083.
30. Wasserscheidt. P.; Keim, W. Ionic liquids—New "solutions" for transition metal catalysis. Angew. Chem.. Int. Ed. 2080. 39. 3772–3789.
31. D'Souza, V.T.; Lipkowitz, K.B. Cyclodextrins: Introduction. Chem. Rev. 1998. *98*. 1741–1742.
32. Gutsche, C.D. *Calixarenes* Revisited: Royal Society of Chemistry: Letchworth, United Kingdom. 1998.
33. Trifonov, A.; Nikiforov, T. Cyclodextrins as phase-transfer catalysts in a nucleophilic clisplacenient reaction. J. Mol. Catal. 1984, *24*. 15–18.
34. Zahalka, H.A.: Januszkiewicz, K.: Alper, H. Olefin oxidation catalyzed by palladium chloride using cyclodextrins as phase-transfer agents. J. Mol. Catal. 1986. *35*, 249–253.
35. Barak. G.: Sasson, Y. β-Cyclodextrin as a reverse phase transfer catalyst in the isornerization of 4-allylanisole. Bull. Soc. Chim. Fr. 1988. 584.
36. Lee. J.T.; Alper. H. Regioselective hydrogenation of conjugated dienes catalyzed by hydridopentacyanocobaltate anion using β-cyclodextrin as the phase transfer agent and lanthanide halides as promoters. J. Org. Chern. 1990, *55*. 1854–1856.
37. Monflier, E.; Blouet, E.: Barbaux. Y.; Mortreux. A. Wacker oxidation of I-decene to 2-decanone in the presence of a chemically modified cyclodextrin system: A happy union of host–guest chemistry and homogeneous catalysis. Angew. Chern.. Int. Ed. 1994. *33*. 2100–2102.
38. Monflier, E.: Fremy, G.: Castanet. Y.: Mortreux. A. Molecular recognition between chemically niodifiecl β-cylodextrin and 1-decene: New prospects for biphasic hydroformylation of water-insoluble olefins. Angeu. Chem.. Int. Ed. 1995, *34*. 2269–2271.

39. Monflier, E.: Tilloy, S.; Fremy, G.: Castanet, Y.; Mortreux, A. A further breakthrough in biphasic rhodium-catalyzed hydroformylation: Use of per(2,6-di-*o*-methyl)-β-cyclodextrin as inverse phase transfer catalyst. Tetrahedron Lett. 1995. 36. 9481–9484.
40. Monflier, E.: Tilloy. S.: Castanet, Y.; Mortreux. A. Chemically modified β-cyclodextrins—Efficient supramolecular carriers for the biphasic hydrogenation of water-insoluble aldehydes. Tetrahedron Lett. 1998. *39*. 2959–2960.
41. Lacroix. T.: Bricout. H.; Tilloy. S.; Monflier. E. Chemically modified β-cyclodextrins as supramolecular carriers in the biphasic palladium-catalyzed cleavage of allylic substrates: Activity enhancement and substrate-selective catalysis. Eur. J. Org. Chem. 1999. 3127–3129.
42. Widehem, R.: Lacroix. T.; Bricout, H.; Monflier. E. Convenient cleavage of water-insoluble allylic substrates in the presence of per(2,6-di-*o*-methyl)-β-cyclodextrin. Synlett 2000. 722–724.
43. Tilloy, S.: Bertoux. F.; Mortreux. A.; Monflier, E. Chemically modified β-cyclodextrins in biphasic catalysis: A fruitful contribution of the host-guest chemistry to the transition-metal catalyzed reactions. Catal. Today 1999. *48*, 245–253.
44. Dessoudeix. M.; Urrutigoity. M.: Kalck, P. Catalytic activity enhancement of a cyclodextrin/water-soluble-rhodium complex system due to its gradual supramolecular organization in the interphase. Eur. J. Inorg. Chem. 2001. 1797–1800.
45. Mathivet, T.: Meliet. C.; Castanet. Y.: Mortreux. A.: Caron, L.: Tilloy. S.: Monflier, E. Rhodium catalyzed hydroformylation of water insoluble olefins in the presence of chemically modified β-cyclodextrins: Evidence for ligand-cyclodextrin interactions and effect of various parameters on the activity and the aldehydes selectivity. J. Mol. Catal., A Chern. 2001, 176. 105–116.
46. Reetz, M.T.; Waldvogel. S.R. β-Cyclodextrin-modified dipliosphane as ligands for supramolecular rhodium catalysis. Angew. Chem., Int. Ed. 1997. *36*. 865–867.
47. Reetz, M.T. Supramolecular transition metal catalysts in two-phase systems. Catal. Today 1998, 42, 399–411.
48. Shimizu. S.: Kito, K.: Sasaki. Y.; Hirai. C. Water-soluble calixarenes as new inverse phase-transfer catalysts. Nucleophilic substitution of alkyl and arylalkyl halides in aqueous media. Chem. Conimun. 1997, 1629–1630.
49. Shimizu, S.; Suzuki, T.: Sasaki. Y.: Hirai, C. Water-soluble calixarenes as new inverse phase-transfer catalysts. Their application to C-alkylations of active methylene compounds in water. Synlett 2000, 1664–1666.
50. Shimizu, S.: Shirakawa. S.: Suzuki. T.: Sasaki, Y. Water-soluble calixarenes as new inverse phase-transfer catalysts. Their application to aldol-type condensation and Michael addition reactions in water. Tetrahedron 2001. *57*, 6169–6173.
51. Shimizu. S.: Shirakawa, S.: Sasaki, Y.: Hirai. C. Novel water-soluble calix[4]arene ligands with phosphane-containing groups for dual functional metal-complex catalysts: The biphasic hydroformylation of water-insoluble olefins. Angew. Chern., Int. Ed. 2000. *39*, 1256–1259.
52. Baur. M.; Frank, M.; Schatz. J.; Schildbach, F. Water-soluble calix[*n*]arenes as receptor molecules for non-polar substrates and inverse phase transfer catalysts. Tetrahedron 2001. *57*. 6985–6991.
53. Dillow, A.K.; Yun. S.L.J.; Suleiman. D.; Boatright. D.L.; Liotta, C.L.: Eckert. C.A. Kinetics of a phase-transfer catalysis reaction in supercritical fluid carbon dioxide. Ind. Eng. Chem. Res. 1996. *35*. 1801–1806.
54. Chandler. K.: Culp, C.W.: Lamb, D.R.: Liotta. C.L.; Eckert. C.A. Phase-transfer catalysis in supercritical carbon dioxide: Kinetic and mechanistic investigations of cyanide displacement on benzyl chloride. Ind. Eng. Chem. Res. 1998, 37, 3252–3259.
55. Cooper. A.I.; Londono. J.D.: Wignall, G.; McClain. J.B.: Samulski. E.T.: Lin. J.S.; Dobrynin. A.: Rubinstein, M.: Burke. A.L.C.: Frechet. J.M.J.: DeSimone. J.M. Extraction of a hydrophilic compound from water into liquid CO_2 using dendritic surfactants. Nature (Lond.) 1997, *389*. 368–371.
56. Goetlieer. E.L.V.: Baars. M.W.P.L.: van den Broeke, L.J.P.; Meijer, E.W.; Keurentjes. J.T.F. Functionalized poly(propylene imine) dendrimers as novel phase transfer catalysts in supcrcritical carbon dioxide. Ind. Eng. Chem. Res. 2000, *39*, 4634–4640.
57. Clarke. M.J.: Harrison. K.L.: Johnston. K.P.: Howdle. S.M. Water in supercritical carbon dioxide microemulsions: Spectroscopic investigation of a new environment for aqueous inorganic chemistry. J. Am. Chem. Soc. 1997. *119*. 6399–6406.
58. Jacobson. G.B.: Lee. C.T., Jr.: Johnston. K.P. Organic synthesis in water/carbon dioxide microemulsions. J. Org. Chem. 1999. 64. 1201–1206.
59. Jacobson. G.B.: Lee. C.T.. Jr.: daRocha. S.R.P.: Johnston. K.P. Organic synthesis in water/carbon dioxide emulsions. J. Org. Chem. 1999. *64*. 1207–1210.
60. DeSimone. J.: Selva. M.; Tundo. P. Nucleophilic displacements in supercritical carbon dioxide using silica-supported phase-transfer agents. J. Org. Chem. 2001. *66*. 4047–4049.
61. Wheeler, C.: Lamb. D.R.: Jayachandran, J.P.; Hallett. J.P.; Liotta. C.L.: Eckert, C.A. Phase-transfer-catalyzed alkylation of phenylacetonitrile in supercritical ethane. Ind. Eng. Chem. Res. 2002. 41. 1763–1767.
62. Sheldon, R. Catalytic reactions in ionic liquids. Chern. Commun. 2001. 2399–2407.
63. Brennecke. J.F.: Maginn, E.J. Ionic liquids: Innovative fluids for chemical processing. AIChE J. 2001. 47. 2384–2389.
64. Wheeler. C.: West, K.N.: Eckert. C.A.; Liotta, C.L. Ionic liquids as catalytic green solvents for nucleophilic displacement reactions. Chem. Commun. 2001. 887–888.
65. Ren, R.X.; Wu. J.X. Mild conversion of alcohols to alkyl halides using halide-based ionic liquids at room temperature. Org. Lett. 2001. *3*. 3727–3728.

Photochemical Sensors

Luigi Fabbrizzi
Università di Pavia, Pavia, Italy

INTRODUCTION

A sensor is a device that responds to an external input by generating a measurable signal. The most common sensor in chemistry is probably the glass electrode, which responds to a change of H^+ concentration with a variation of the eiectrical potential, and, following appropriate calibration, directly communicates pH units. Other devices respond to physical inputs; for instance. a thermocouple is a temperature sensor, and the generated signal is still a variation of potential. Noticeably, the definition of a sensor can be brought to the molecular level. In this case, the sensor is a discrete molecule (or, better, a multitude of single molecules) that responds to a chemical or physical stimulus by generating a signal detectable and measurable by an external operator. In particular, the molecule constituting the sensor has to be equipped with two basic subunits: 1) a fragment capable of selectively interacting and recognizing the desired analyte (e.g., H^+, Ca^{2+}, Cl^-, CO_2); and 2) a functionality that signals the occurrence of the recognition. The signal can have a different instrumental nature. For instance, it can be the shift of an NMR line. the displacement of a voltammetric wave, a color change with the associate modification of the absorption spectrum, or a change of luminescent activity. Luminescence, in particular, is a convenient property for sensing purposes. for a variety of reasons: it is visual, it can be measured with not-too-expensive instrumentation (a spectrofluorimeter). and it can be detected with remarkable sensitivity. As an essential requirement, the interaction of the recognizing moiety (the receptor) with the analyte must activate a mechanism that substantially modifies the light-emitting properties of the luminophore.

FLUORESCENT MOLECULAR **SENSOR**

An efficient fluorescent molecular sensor is available for the determination of intracellular calcium(II) concentration, $[Ca^{2+}]$.[1] The molecular system, **1**, has as a receptor moiety, a fragment reminiscent of ECTA, a ligand displaying a special affinity toward alkaline-earth metal ions. In particular; ECTA gives with Ca^{2+} a 1:1 complex, with a stability constant K that is about 10^{11}, i.e., five orders of magnitude higher than that of the corresponding complex with the competing ion Mg^{2+}. This feature is important, because intracellular $[Mg^{2+}]$ can be up to 10^4 times higher than $[Ca^{2+}]$. In system **1.** an indole fragment is covalently Iinked to the EGTA framework as a light-emitting subunit. In particular, this subunit, when excited with ultraviolet light (λ = 338 nm), emits light in the full visible region (λ_{max} of the emission band is 500 nm). Ca^{2+} complexation induces a drastic structural rearrangement of **1**, which causes a modification of the energy of the π orbitals of the indole fragment, and as a consequence, the emission band is displaced to λ_{max} = 400 nm. This spectral shift is especially useful, as the ratio of the emission intensities at the two wavelengths provides a measure of $[Ca^{2+}]$ independently upon the concentration of the fluorescent probe and the length of the optical path. After the fluorescent sensor **1** (commercially known as indo-1), other fluorescent molecules were developed by following the same approach. They are currently employed in the laboratories of cell physiology for the determination of $[Ca^{2+}]$, in real time and real space, by using a fluorescence microscope.[2]

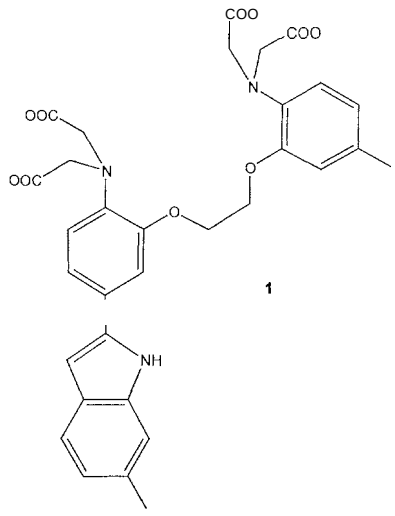

1

LUMINOPHORE–SPACER–RECEPTOR PARADIGM

The previously outlined approach—covalently link a luminescent fragment to the receptor of the envisaged

DOI: 10.1081/E-ESMC 120012791

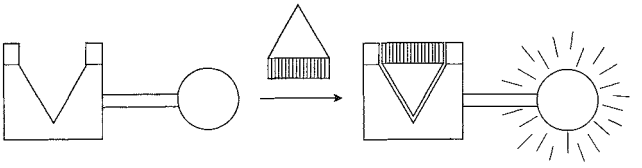

Fig. 1 The fluorophore–spacer–receptor paradigm. It is expected that the interaction of the desired analyte with the receptor portion drastically modifies the emission of the nearby fluorophore. In the case illustrated, the recognition process restores the quenched fluorescence. Alternatively, the fluorescence before recognition may be on and after recognition be off.

analyte––is known as the luminophore–spacer–receptor paradigm and is pictorially illustrated in Fig. 1. Such an approach was utilized for the design of sensors for a variety of substrates, both electrically charged and neutral.''

As an example, the two-component system 2 in Fig. 2 was developed for the fluoriinetric determination of the K^+ ion.[4] In system 2, the receptor moiety belongs to the family of crown ethers: in particular, the macrocycle can be considered as deriving from the 18-crown-O_h macrocycle, in which an ethereal oxygen atom was replaced by a secondary amine group; –NH–. The 18-crown-NO_5 ring of 2 possesses the right size to selectively include (''recognize'') the K^+ cation, in the presence of the other alkali metal ions. The problem is now to communicate to the outside that recognition has taken place. To this purpose, the classical fluorescent fragment anthracene was linked. through a $-CH_2-$ spacer, to the nitrogen atom of the macrocycle. It has to be noted that in spite of the presence of a powerful fluorophore, molecular system 2 is not fluorescent. In fact, one of the two electrons of the lone pair on the nitrogen atom of the macrocycle is transferred on the half-filled HOMO π orbital of the photoexcited anthracene fragment, a process that fully quenches fluorescence. However: when K^+ is included within the macrocycle. the lone pair on the nitrogen atom is fully engaged in the metal–ligand interaction with K^+, and no electron can be transferred to the excited fluorophore. Then. in the absence of electron transfer, the photoexcited anthracene fragment deactivates in its typical radiative way. As a consequence. K^+ recognition is clearly signaled by the revival of the blue fluorescence of anthracene. System 2 is an ingenious device, because a typically redox-inactive substrate, K^+. is able to promote an electron-transfer process. This was made possible by the presence of the amine nitrogen atom, that behaves as an electron relay.

The design of a luminescent sensor for transition metal ions based on photoinduced electron transfer is, at least in principle, easier, because d-block metals exhibit a natural tendency to uptake/release electrons. Thus, a transition metal ion should be able to promote the transfer of one electron from/to an excited luminophore in the absence of any relay. An example is provided by system **3.** shown in Fig. 3, in which (following again the luminophore–spacer–receptor approach) an anthracene fragment was linked, through a $-CH_2-$ group. to the carbon framework of a quadridentate chelating agent containing two secondary amide groups and two primary amine groups.[5] In its neutral form. ligand **3**, in view of the poor coordinating tendencies of the amide groups. does not coordinate any metal ion. However. in the presence of divalent metal ions late in the 3d series. i.e., Cu^{II} and Ni^{II}, at pH values close to the neutrality, the two amide groups deprotonate, and the ligand coordinates the metal according to a square-planar stereochemistry. In each deprotonated amide fragment. the negative charge is distributed on both nitrogen atoms via a π-delocalization mechanism. Opportunely for sensing purposes. metal complexation modifies the light-emitting properties of the anthracene subunit and can be followed through spectrofluorimetric titration experiments.

Titration of **3** in the absence of metals does not modify the emission intensity of the anthracene fragment, I_F,

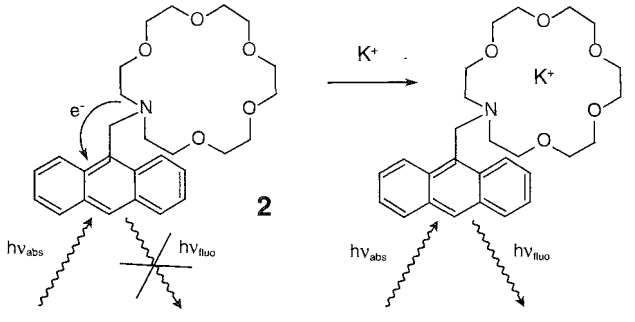

Fig. 2 Fluorescent sensing of the K^+ ion. Metal inclusion within the macrocycle interrupts a preexisting quenching mechanism (due to a nitrogen-to-tluorophore electron-transfer process) and revives anthracene fluorescence.

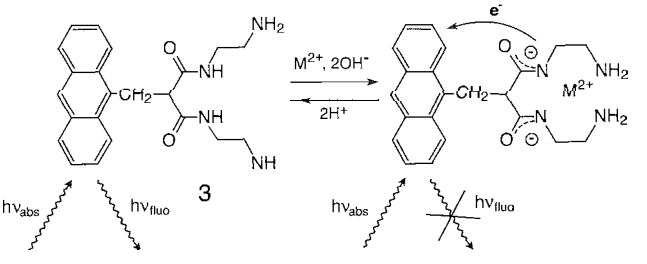

Fig. **3** Fluorescent sensing of transition metal ions (M = Ni, Cu). Following complexation. an intramolecular metal-to-fluorophore electron-transfer process takes place that quenches anthracene fluorescence.

which remains constant on moving from pH = 2 to pH = 12 (diamonds in Fig. 4). However, if an equimolar amount of Cu^{II} is added to the solution, a sharp decrease of I_F is observed beyond pH = 5, and complete fluorescence quenching takes place at pH = 7 (full triangles in Fig. 4). Sigmoidal I_F decrease is to be associated with the complexation of Cu^{II} by **3.** In particular. the fluorescent emission is quenched due to the occurrence of an electron-transfer process from the Cu^{II} center to the excited fluorophore, An^*. The occurrence of such a process can be accounted for on a thermodynamic basis.

In particular, the free-energy change value associated with the Cu^{II}-to-An^* electron transfer, ΔG_{eT}°, can be calculated taking profit from the thermodynamic cycle illustrated in Fig. 5. by combining pertinent photophysical and electrochemical quantities. The obtained value is distinctly negative (– 0.50 eV) and accounts for the observed quenching efficiency. Thus, in contrast to that previously observed for K^+, Cu^{II} recognition is signaled through quenching. rather than from revival, of anthracene fluorescence. A careful examination of the varying contribution to ΔG_{eT}° indicates that the signal controlling mechanism; i.e., the metal-to-fluorophore electron transfer, results from easy access to the Cu^{III} state. Such an access is favored by the strongly donating donor set consisting of two amine groups and, in particular, from two deprotonated amide groups. The intense in-plane interactions exerted by the four nitrogen atoms raise the energy of the antibonding level. essentially centered on the metal, from which the electron is abstracted on Cu^{II}-to-Cu^{III} oxidation. The presence of a double negative charge on the coordinating system further facilitates the oxidation process that involves a moderate increase of the

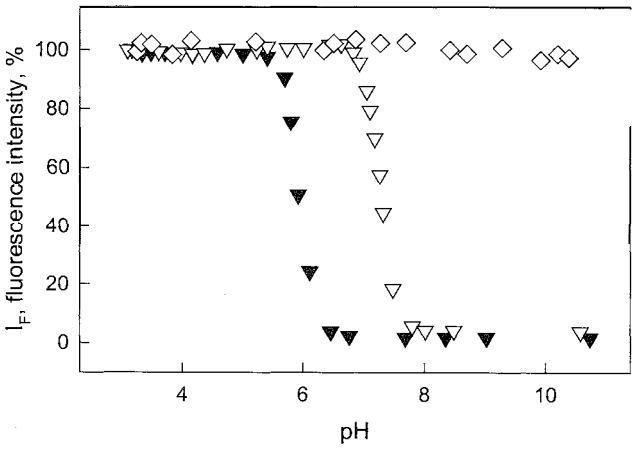

Fig. 4 The pH dependence of the fluorescence intensity of system 3 in the absence (open diamonds) and in the presence of an equimolar amount of transition metal ions (full triangles: Cu^{II}; open triangles: Ni^{II}). Other metal ions (Mn^{II}, Fe^{II}, Co^{II}, Zn^{II}) do not affect the emission of the anthracene fragment.

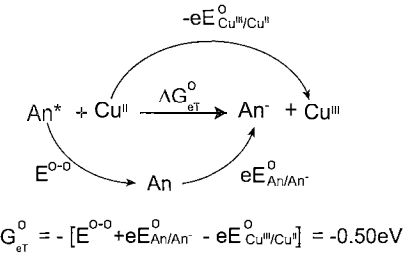

Fig. 5 Thermodynamic cycle suitable for calculating the free-energy change value, ΔG_{eT}°, associated with the copper(II)-to-anthracene electron transfer within system Cu^{II}-**3**. ΔG_{eT}° is obtained from the appropriate combination of photophysical and electrochemical quantities.

overall electrical charge from *0* to *+1*. It derives that a judicious choice of the coordinating tendencies of the ligating subunit allows for the transduction mechanism of the sensing system to be determined.

An analogous behavior is observed with Ni^{II}. In particular, it is observed that the sigmoidal decrease of I_F (in Fig. 4) is centered at pH = 7.5, i.e., two units higher than that observed for Cu^{II}. This reflects the lower stability of the Ni^{II} complex with the deprotonated amide–amine ligand, compared to Cu^{II}. In this case too, fluorescence quenching has to be ascribed to the formation of the complex with the doubly negatively charged ligand and to the thermodynamically favored Ni^{II}-to-An^* electron-transfer process (ΔG_{eT}° = – *0.35* eV). Noticeably, if analogous pH-titration experiments are carried out in the presence of other divalent cations of the *3d* series (Mn^{II}, Fe^{II}, Co^{II}, Zn^{II}), the anthracene emission is not modified over the 2–12 pH interval. This behavior is to be ascribed to failure in the formation of the corresponding metal complexes, even in a distinctly basic solution. In particular. the deprotonation of the two amide groups of **3** is an endoergonic process that can be compensated for only by the formation of strong metal–ligand interactions. This is the case of Cu^{II} and Ni^{II} but not of the other metal ions. which do not profit too much (or do not profit at all) from ligand field stabilization effects. Thus, system **3,** among *3d* cations, recognizes Cu^{II} and Ni^{II} and signals the occurrence of the recognition process through fluorescence quenching.

Let us now consider the case of polyatomic analytes. The analyte can be multifunctional, i.e., it can contain distinct groups of different natures and electrical charges—in this case. the receptor must provide distinct binding sites of appropriate characteristics. A representative case is that of amino acid in their zwitterionic forms: NH_3^+–CH(R)–COO^-. The first example of a molecular fluorescent sensor amino acid was presented by de Silva.[6]

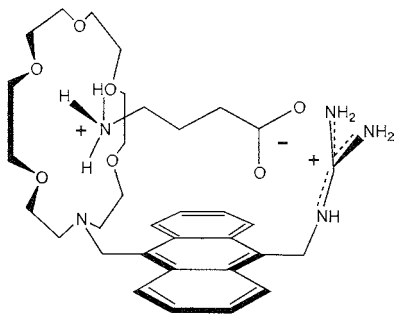

4

In the ditopic system 4, the light-emitting anthracene fragment also displays the function of a spacer, as it links the two binding sites for the bifunctional substrate—a guanidinium subunit, suitable for electrostatic interaction with the carboxylate group of the amino acid: and the 18-crown-NO_5 moiety, which can establish hydrogen-bonding interactions with the ammonium residue. As outlined with the K' sensor 2, also in this case; the presence of a tertiary amine nitrogen atom in the crown, close to the anthracene subunit, is essential for the sensing behavior. Prior to substrate binding, the amine group undergoes the thermodynamically feasible transfer of an electron to the nearby excited fluorophore, thus quenching its emission. Therefore, one would expect that, following the amino acid recognition, and, in particular, after the nonbonding electron pair of the nitrogen in the crown becomes engaged in a hydrogen-bonding interaction with the ammonium group of the amino acid; the eT process is interrupted. and the fluorescence is revived. Actually, the interaction of 4 with a series of amino acids of general formula NH_3^+-$(CH_2)_n$-COO^- in an aqueous methanol solution is signaled through a significant enhancement of the anthracene emission. Interestingly, system 4 displays linear recognition features, the highest binding constant, and the more significant increase of the emission intensity being observed with $n = 4$. It appears that in the case of the latter amino acid (-/-amino butyric acid, GABA), the distance between the carboxylate and the ammonium residues fits well the separation of the binding sites provided by the heteroditopic receptor 4. Interestingly, the natural amino acid glycine. as well as glutamic acid [NH_3^+–CH(COO^-)– $(CH_2)_2$–COO^-, the physiological precursor of GABA], induces a negligible fluorescence response. even if added in large excess with respect to the sensor.

However, if one is interested in sensing natural amino acids, with the general formula NH_3^+–CH–(**R**)–COO^-, and in which the distance between the charged groups to be recognized, $-NH_3^+$ and $-COO^-$, is the same. sensing systems of the type of 4 cannot be used. But. in order to obtain the most selective recognition of the desired α-amino acid, one should try to ignore the common $-NH_3^+$ and $-COO^-$ fragments and center attention on the **R** residue. In particular, a receptor subunit should be designed exclusively for the **R** moiety of the substrate. This case is illustrated by the design of a fluorescent sensor for histidine, with an **R** group that is an imidazolyl fragment. An effective receptor for imidazole can be designed by taking advantage of its tendency to deprotonate and to act as an ambidentate ligand. Imidazole, ImH. $pK_a = 14.5$, is a weaker acid than H_2O and does not deprotonate in aqueous solution. However, in the presence of two prepositioned metal ions M^{II} (M = Cu, Zn), the ImH molecule deprotonates, and the I m anion that forms bridges the two metal centers, according to the equilibrium:

$$[M^{II}_2]^{4+} + ImH = [M^{II}(Im^-)M^{II}]^{3+} + H^+ \quad (1)$$

A basic requirement for reaction (1) to proceed is that the two M^{II} centers occupy predetermined positions, in a rather rigid coordinative framework, at the correct distance. This is the case of system ***5*** in which two tripodal tetramine subunits of the *tren* type are linked to an anthracene fragment that acts both as a spacer and as a fluorophore.[7]

Each *tren* subunit binds a metal ion, e.g., Zn^{II}, according to a trigonal bipyramidal stereochemical arrangement, in which the fifth coordination site is left available for a further ligand, either a solvent molecule or an anion (see structural sketches in Fig. 6). At pH = 9–10, the dizinc(II) complex 6 forms that behaves as a specific receptor for imidazole, to give the bridged imidazolate complex 7. In particular, titration with imidazole of an aqueous solution of the dimetallic complex 6 induces quenching of the anthracene fluorescence, thus providing a visual mechanism for recognition. Noticeably, titration with 1-methyl-imidazole, which cannot undergo deprotonation, does not induce any modification of the anthracene fluorescent emission. confirming that signaling is promoted by Zn^{II}–Zn^{II} bridging of the imidazolate fragment. Quenching in the dimetallic complex 7 has to be ascribed to the occurrence of an intracomplex electron-transfer

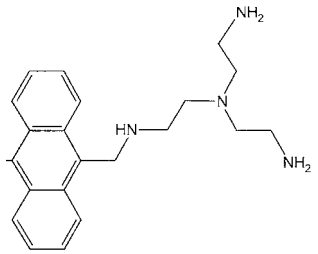

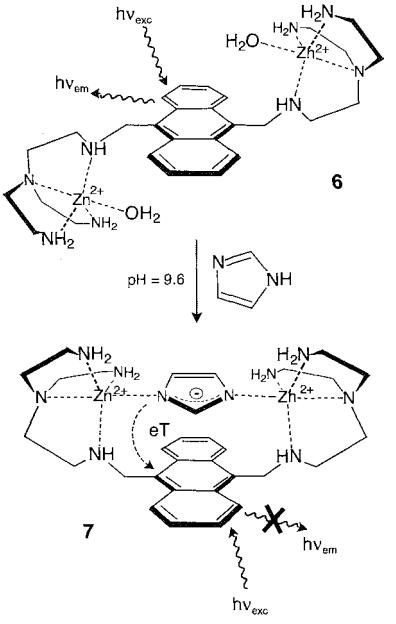

Fig. **6** Recognition of the imidazole fragment (e.g., from L-histidine) by a dizinc(II) polyamine receptor. Recognition is signaled by quenching of the emission of the anthracene subunit, which results from an electron-transfer process from the bridged imidazolate anion to the excited fluorophore.

process from a π orbital of the electron-rich im^- moiety to a π^* orbital of the photoexcited anthracene fragment.

Spectrofluorimetric titration of complex **6** with the natural amino acid L-histidine induces a similar, even if slightly less pronounced, fluorescence quenching. Interestingly, the titration profile is not modified when the solution contains even a large excess of any other amino acid. As an example, the addition of L-histidine to a solution buffered at pH = 9.6 and containing the receptor 6 plus 10 equivalents of any other natural amino acid gave the same titration profile. The lack of interference is due to the fact that the only anionic group any amino acid other than histidine can offer, i.e., the carboxylate fragment, does not display bridging tendencies toward the dimetallic core of receptor 6. Thus, 6 recognizes and senses L-histidine in the presence of any other natural amino acid.

CHEMOSENSING ENSEMBLE APPROACH

Other approaches than the luminophore–spacer–receptor paradigm exist, illustrated in the preceding examples, for designing a molecular system for sensing analytes in solution. An efficient one—the chemosensing ensemble approach—is reminiscent of the antibody-based competition test in immunoassays.[8] According to this approach, the plain receptor interacts in solution with a fluorescent indicator, i.e., a light-emitting substrate. Two main requirements have to be fulfilled: 1) the receptor/indicator interaction must not be too strong; and 2) the indicator must show significantly different emissive properties when bound to the receptor and when dispersed in solution. Thus, on titration with the desired analyte, the indicator is displaced from the host cavity and released back to the solution, where it displays drastically different emission features. An example of a chemosensing ensemble suitable for determining of inorganic anions is described below.[9]

The receptor, 8, consists of a bistren octamine cage that includes two Cu^{II} ions. Each metal ion is coordinated by the four nitrogen atom of each *tren* subunit and. as it likes five-coordination, offers a binding site available for the interaction with a further donor atom. Thus, in the intermetallic cavity, there is room for an ambidentate anion, i.e., an anion presenting two distinct donor atoms. The chosen fluorescent indicator is coumarine 343, 9, which, in its anionic form, should be capable of bridging the two Cu^{II} ions of 8, with the carboxylate group. In fact, titration of a solution of coumarine 343, buffered at pH = 7, with a solution of the dicopper(II) cage complex 8, induces quenching of the intense coumarine emission at λ_{max} = 487 nm. Quenching is associated with the bridging of the two metal ions by the carboxylate group of coumarine 343 and with the occurrence of an electronic energy transfer involving the metal center(s) and the excited fluorophore. Thus, the desired chemosensing ensemble can be generated by making a degassed aqueous solution 2 x 10^{-4} M in **8** and 10^{-7} M in the fluorescent indicator, i.e., two thousands times less concentrated.

Titration of the resulting cheinosensing ensemble solution with a standard solution of carbonate (Fig. 7, full triangles) results in an almost complete recovery of the coumarine emission. This result indicates that there is successful competitive binding of the HCO_3^- ions and displacement of the indicator from the intermetallic cavity of complex 8. Full restoration of the coumarine emission is also observed when the solution of the chemosensing ensemble is titrated with N_3^- and with

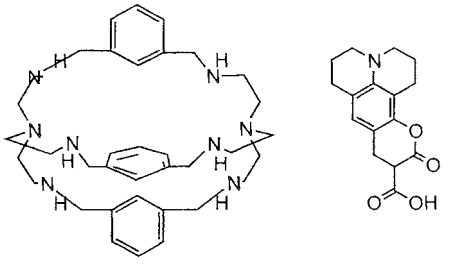

8

9

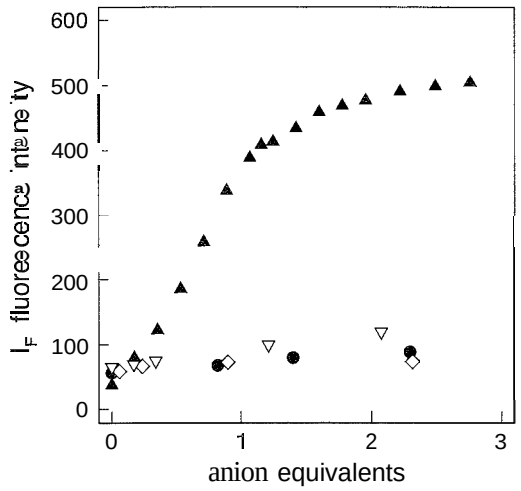

Fig. 7 Titration of the chemosensing ensemble [**8** + 9] with some inorganic anions. HCO_3^- is able to displace the indicator from cape **8.** an event signaled by fluorescence revival of the released indicator 9 (full triangles). Other anions do not displace the indicator and do not make fluorescence revive: phosphate (open triangles); acetate (full circles): and sulfate (open diamonds).

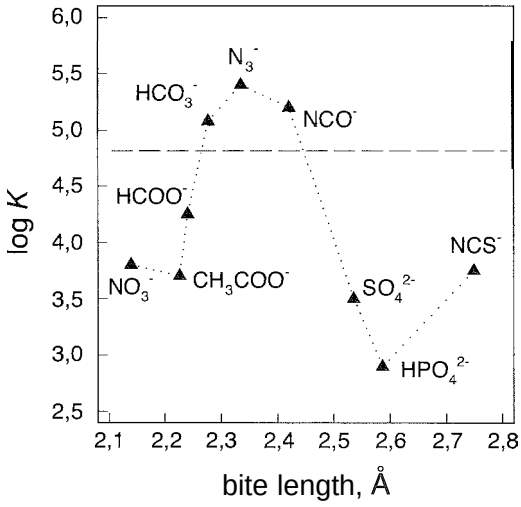

Fig. 8 Selective inclusion of ambidentate anions into the dimetallic cage 8. Log*K* values refer to the anion inclusion equilibrium at pH = 7. The bite is the distance of two consecutive donor atoms of the anion (see Fig. 9 for examples). Only anions with an inclusion constant K that is higher than $10^{4.8}$ (which corresponds to the inclusion of indicator 9, value indicated by the dashed horizontal line) are able to displace the indicator from the cage. with consequent fluorescence revival. Anions with a lower K are neither recognized nor sensed.

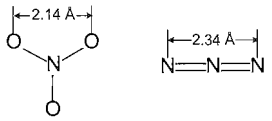

Fig, 9 The definition of anion bite: the distance of two consecutive donor atoms of an ambidentate anion. For linear anions like N_3^- . bite coincides with anion length.

NCO . However. titration with a variety of ambidentate anions induces only a slight enhancement of the fluorescence. As an example. fluorescence intensity data for phosphate (open triangles). acetate (full circles), and sulfate (diamonds) are shown in Fig. 7.

The behavior described above can be interpreted on the basis of the diagram shown in Fig. 8. In this diagram. the log*K* values for the equilibrium for the anion inclusion into the dimetallic cage **8**. at pH = 7 (full triangles). are plotted versus the anion bite length, i.e., the distance between two consecutive donor atoms of the arnbidentate anion. As an example, bite length for N_3^- and NO_3^- anions is shown in Fig. 9.

The diagram in Fig. 8 displays a well-defined selectivity peak pattern, the highest inclusion affinity being observed with the N_3^- anion. In particular. N_3^- has the correct bite length with which to place its donor atoms in the positions required by the two Cu^{II} centers. without inducing any endoergonic rearrangement of the cage. Almost ideal bite length values are exhibited by HCO_3^- and NCO^- . with inclusion affinities slightly slower than those for N_3^-. On the other hand. anions like NO_3^- and N C S exhibit bite lengths that are too short or too long, respectively. and their incorporation within the cage induces an endoergonic rearrangement of the host cavity. either contraction or expansion. which makes inclusion affinity drastically decrease. The horizontal dashed line at log*K* = 4.8 corresponds to the inclusion affinity of the coumarine 343 indicator.

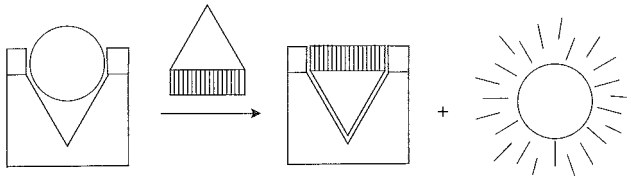

Fig. P0 The chemosensing ensemble paradigm. A fluorescent indicator occupies the cavity of a receptor. and its emission is quenched. When displaced by an analyte showing a higher affinity for the receptor, it displays its full fluorescence, so signaling the occurrence of analyte recognition.

Such a line defines the anions that can be revealed through the chemosensing ensemble procedure. by using coumarine 343 as an indicator. In particular, those anions with log$K$ values that stay above the dashed line are able to displace the indicator from the cage and can be fluorimetrically detected. On the other hand, anions with log$K$ values that stay below the dashed line are not able to displace the indicator from the host cavity and cannot be fluorimetrically detected.

CONCLUSION

The principle of the chemosensing ensemble approach is pictorially illustrated in Fig. 10. It has to be noticed that, compared to the luminophore–spacer–receptor paradigm, the chemosensing ensemble approach presents a significant benefit: it does not involve any tedious synthetic step for covalently linking together the luminophore and the receptor, which can be used as such. Moreover, a further element of selectivity is introduced, in addition to that related to the analyte–receptor interaction. This selectivity term is associated with the choice of the indicator. The indicator's higher or lower affinity toward the receptor (i.e., the height of the dashed line in a diagram like that shown in Fig. 8) determines which analytes can be detected and which cannot.

ARTICLES OF FURTHER INTEREST

Fluorescence Sensing of Anions. p. 566
Fluorescent Sensors, p. 572
Luminescent Probes, p. 821

REFERENCES

1. Tsien, R.Y. New calcium indicators and buffers with high selectivity against magnesium and protons: Design, synthesis, and properties of prototype structures. Biochemistry **1980.** *19* (11). 2396–2404.
2. Grynkiewicz, G.; Poenie, M.: Tsien. R.Y. A new generation of calcium indicators with greatly improved fluorescence properties. J. Biol. Chem. **1985**, 260 (6), 3440–3450.
3. de Silva. A.P.: Gunaratne, H.Q.N.: Gunnlaugsson, T.; Huxley, A.J.M.; McCoy, C.P.; Rademacher. J.T.; Rice, T.E. Signaling recognition events with fluorescent sensors and switches. Chem. Rev. **1997,** 97 (5), 1515–1566.
4. de Silva, A.P.; de Silva, S.A. Fluorescent signaling crown ethers: Switching on of fluorescence by alkali metal ion recognition and binding in situ. J. Chem. Soc., Chem. Cornmun. **1986.** 1709–1710.
5. Fabbrizzi, L.; Licchelli, M.; Pallavicini, P.; Perotti, A.; Sacchi, D. A fluorescence sensor for transition metal ions based on anthracene. Angew. Chem., Int. Ed. Engl. **1994**, *33* (19). 1975–1977.
6. de Silva, A.P.; Gunaratne, H.G.N.: McVeigh, C.: Maguire. G.E.M.: Maxwell, P.R.S.; O'Hanlon, E. Fluorescent signaling of the brain neurotransmitter γ-aminobutyric acid and related amino acid zwitterions. Chem. Commun. **1996;** 2191–2192.
7. Fabbrizzi, L.: Francese, G.: Licchelli, M.; Perotti. A.: Taglietti, A. Fluorescent sensor of irnidazole and histidine. Chem. Commun. **1997,** 581–582.
8. Wiskur, S.L.; Ait-Haddou, H.: Lavigne, J.J.; Anslyn. E.V. Teaching old indicators new tricks. Acc. Chem. Res. **2001**, 34 (12). 963–972.
9. Fabbrizzi. L.: Leone. A.; Taglietti, A. A chemosensing ensemble for selective carbonate detection in water based on metal–ligand interactions. Angew. Chem., Int. Ed. Engl. **2001**, 40 (16). 3066–3069.

Photophysical and Photochemical Methods

Pavel Anzenbacher, Jr.
Michael A. J. Rodgers
Bowling Green State University, Bowling Green, Ohio, U.S.A

INTRODUCTION—TYPICAL ADVANTAGES OF PHOTOPHYSICAL METHODS

During the last two decades, there has been an enormous increase in the use of photophysical methods in supramolecular chemistry. Until recently, photophysical methods, such as transient spectrometry and time-resolved fluorescence spectrometry, were primarily research tools in the arenas of photokinetics of small molecules. materials physics, and biophysics. This situation changed dramatically with the introduction of commercial. user-friendly electro-optical components such as charge-coupled detector (ED)-based spectrometers, solid-state pulsed lasers, and other instrumentation necessary for time-resolved measurements. As a result. time-resolved spectrometry became more available to the community of supramolecular chemists, who now reached the level of sophistication that can benefit from the new horizons offered.

Photophysical methods generally offer numerous advantages of crucial importance for suprainolecular chemists. particularly high sensitivity. i.e., reliable output at low concentration. Also important is the possibility of selectively probing individual chromophoric parts of molecules and supramolecules. The accessibility of the information from dilute samples (typically 10^{-5}–10^{-7} mol/l) is important to a supramolecular chemist. as the typical features studied in supramolecular chemistry, such as receptor–substrate association and formation and dissociation of supramolecular associates and complexes, typically suffer from side effects such as receptor–receptor self-association and component homoassociation at higher concentrations ($>10^{-4}$ mol/l). Additional advantages of photophysical methods are the usually nondestructive nature of the measurements and the small sample volume required for the experiments.

Most importantly. however, photoexcitation methods allow the detection of transient species. While an entity with a lifetime of 50 ns or less can be comfortably analyzed by transient absorption or fluorescence spectrometry, other physical inethods of steady-state character are likely to fail. For example, the timescale of most NMR experiments is longer than ca. 100 ms. which renders this method unsuitable for studies of short-lived species. Moreover. the typical tools of supramolecular chemistry. such as NMR spectrometry. require concentrations usually in excess of 10^{-4} mol/l. and other favorite methods such as mass spectroscopy [fast-atom bombardment (FAB), electrospray ionization (ESI), matrix-assisted laser desorption ionization (MALDI)], and vapor-pressure osmoinetry do not directly provide information about supramolecular behavior in solution. The most favorite method, x-ray analysis. suffers from the limitation posed by the ultimate requirement of being able to grow single crystals. While this is. in numerous instances, possible in the case of pure molecular entities. supramolecules, being mixed molecular objects by nature, are usually difficult to grow in the form of a single crystal.

These statements are not meant to be demeaning of the classical tools of supramolecular chemistry. rather to point out that photo-techniques offer researchers in this field another level of information. The previous paragraphs are meant to define the areas where photophysical techniques may be particularly useful. and a major purpose of this article is to alert the supramolecular chemistry coinmunity to the potential of photo-methodology and to provide encouragement for its utilization.

SUPRAMOLECULAR BEHAVIOR OF CHROMOPHORES

The focus of supramolecular chemistry is on the development and application of molecules with highly selective structure-specific interaction. i.e., molecules that can "recognize" each other and form complexes or supramolecular associates together. A typical object of study investigated using photophysical methods is the association of chromophoric species. The requirements for this are that at least one of the entities forming the associate has to be a chromophore, or contain a chromophoric residue, and that the process of association must be accompanied by an observable perturbation of the photophysical properties of the chromophore. If this is the case, photophysical methods are able to provide invaluable information about the behavior and environment of the chromophore. simply by observing the absorption and emission patterns and their changes with time.

Encyclopedia of Supramolecular Chemistry
DOI: 10.10811%-ESMC 120012842

Luminescence Methods

The most common methods of measuring excited state lifetimes involve monitoring the time dependence of the sample emission after exciting it with pulsed excitation. From the sample response relative to the excitation pulse, information about the decay kinetics and about the amount of species generated (quantum yield) can be obtained. One such instrument used by these authors is depicted in Fig. 1. This apparatus is based on a nitrogen-pumped broadband dye laser [2–3 nm full width at half maximum (FWHM)] (PTI GL-3300 N_2 laser; GL-301 dye laser). The N_2-laser fundamental output at 337.1 nm can be employed directly, or it can be used to pump the dye laser to obtain the excitation pulses. For example, the authors used Coumarin 460 (440–480 nm) for excitation of Ru(II) diimine complexes, see below. Pulse energies were typically attenuated to ~100 μJ/pulse. The luminescence was recorded at 90° to the incident beam via a long-pass optical filter to cut out scattered laser light, focused through a lens system onto the entrance slit of an *f*/3.4 monochromator (± 4 nm). The emission was detected with a Hamamatsu R928 photomultiplier tube (PMT), wired for fast response, and was negatively biased with a Stanford Research PS325 power supply. The PMT signal was terminated through a 50 ohm resistor to a Tektronix TDS 380 digital oscilloscope (400 MHz). The CRO data, representing an average of 128 laser shots collected at 2–3 Hz, were transferred to a computer and processed using Microcal™ Origin™ software. This system, depicted in Fig. 1, allows measurement of luminescence lifetimes from a few ns upwards, with excellent signal-to-noise and data reproducibility. Such an instrument is an excellent choice for studies involving various luminescent metallocomplexes that display relatively long-lived excited states.[1,2] One can find countless examples of supramolecular structures utilizing the photophysical properties of diimine and other complexes of Ru(II), Os(II), and Re(I). An important advantage of such an instrument is that it can be straightforwardly assembled from parts by nonexperts at relatively low cost. The dye laser allows excitation tuning over a wide variety of visible wavelengths (*v.i.*).

The instrument described above may be conveniently used to investigate supramolecular association of species with long-lived excited states. A typical example of such a situation is the binding of a substrate to an optical sensor. In principle, one can consider two possible situations: quenching of the fluorescence intensity or an increase in fluorescence intensity. In the first, the fluorescence intensity is quenched as a result of decreases in the fluorescence lifetime or quantum yield on binding. The fluorescence quantum yield may decrease because of dynamic or static quenching, depending on whether the quenching of the excited state is due to diffusion of the luminescent entity and the quenches, or whether the

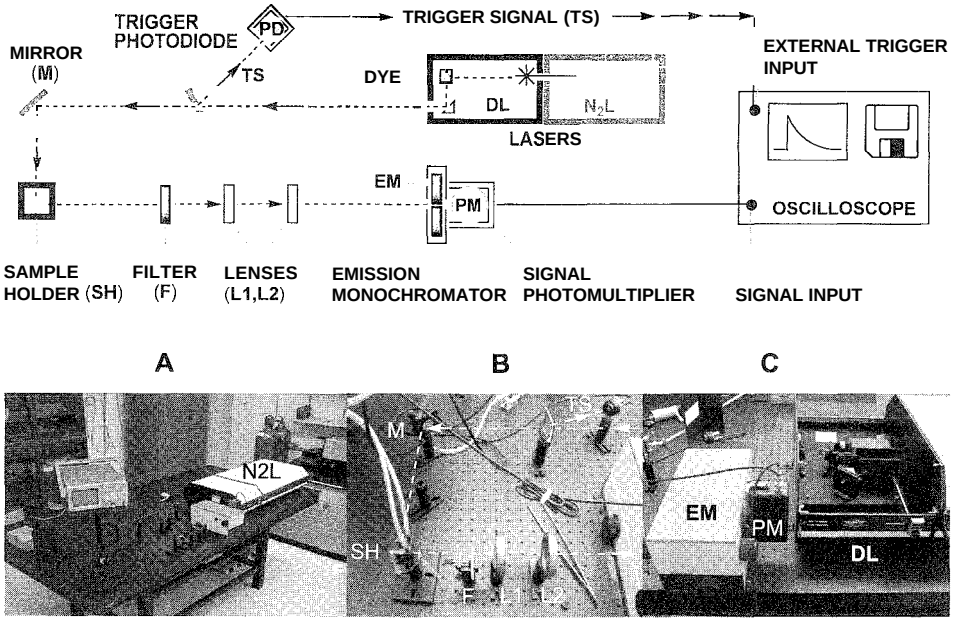

Fig. 1 General outline of the dye laser lifetime instrument. (Upper panel) The instrumental scheme. (Panel A) The whole instrument setup and the nitrogen laser housing (N2L) and the digital oscilloscope. (Panel B) The optical path. (Panel C) The emission monochromator (EM). photomultiplier (PM), and dye laser (DL). (Courtesy of Dr. F.N. Castellano, Center for Photochemical Sciences. BGSU.) (*View this art in color at www.dekker.com.*)

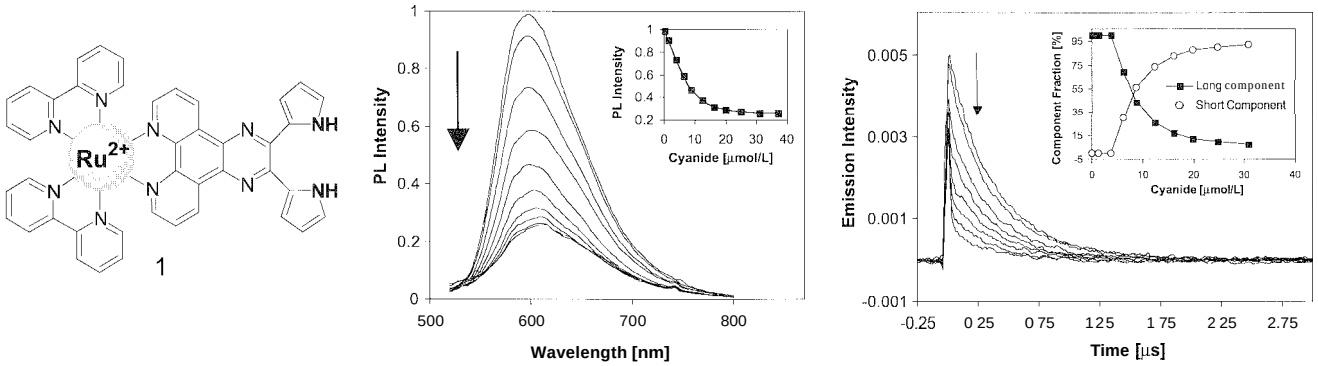

Fig. 2 (Left pancl) Structure of sensor **1.** (Center pancl) Changes in lumincsccncc intensity of sensor 1 upon the addition of cyanide. [(Inset) Binding isotherm monitored by the integrated luminescence intensity.] (Right pancl) Changes in the time-resolved PL decay of sensor 1 upon the addition of cyanide. [(Inset) Shifts in fractional intensity of the two lifctimc components obtained from bicxponential analysis.]

qucnchcr forms a weakly (or non-) luminescent complex with the luminophore in the ground state. The concentration quenching process is utilized in so-called lifetime-based sensing. The lifetime here is used to observe the degree of saturation of the sensor by the substrate. Such lifctime measurements are most effectively performed using compounds with long-lived excited states, making for a higher degree of sensitivity to added substrate concentration, for example, sensors incorporating *tris*(phenanthroline)Ru(II) or *tris*(bipyridine)Ru(II) complexes that exhibit long-lived metal-to-ligand charge-transfer (MLCT) excited states with lifetimes up to 150 ns,[3] e.g., complex **1.** Complex **1** is an efficient sensor for fluoride and cyanide anions, which are bound to the sensor presumably via hydrogen bonding to the pyrrole NH groups (Fig. 2).[4]

Shown in Fig. 2 is the luminescence lifetime quenching of sensor **1** as a function of the cyanide concentration. Prior to cyanide addition, **1** exhibits a single exponential lifetime (τ=380 ns). At low [CN], the decay profiles could be adequately fit by a single exponential function, with a slightly reduced lifetime (340 ns). At higher [CN], the time profiles exhibit biexponential kinetics. Both exponential components remain effectively constant, ranging from 320–370 ns (long ?) and 13 to 17 ns (short ?). The average lifetimes shorten as a function of the CN concentration, because the fractional intensity shifts from an initial dominant long lifetime component to the short lifetime component as the C N concentration increases (Fig. 1, right panel, inset). These data suggest that there are at least two distinct luminescent species, consisting of anion-bound **1** (short τ) and free **1**, the sum of which results in the observed lifetime qucnching. In this case, the shift in fractional intensity makes **1** a suitable lifetime-based sensor for anions.

While the above-described instrumentation is an excellent choice for long-lived excited states such as the Ru^{2+} and Os^{2+} polypyridyl complexes, organic-based chromophores and fluorescence labels frequently used by supramolecular chemists require higher time resolution. Commercially available time-correlated single photon counting (TCSPC) instruments can readily access

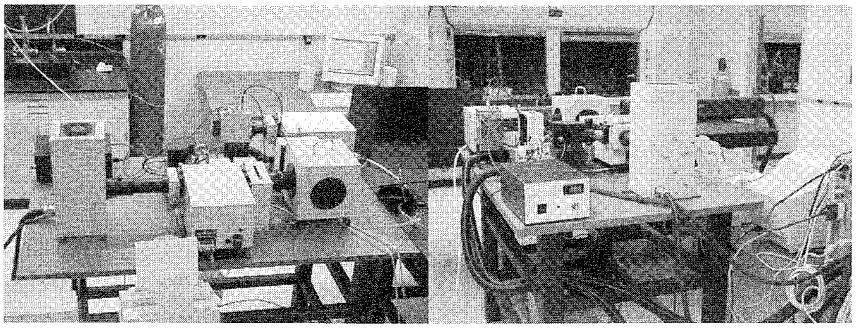

Fig. 3 Two views of a TCSPC spectrofluorimcter from Edinburgh Analytical Instruments (FL/FS 900). ***(View*** this *art in color at* www.dckkev.com.)

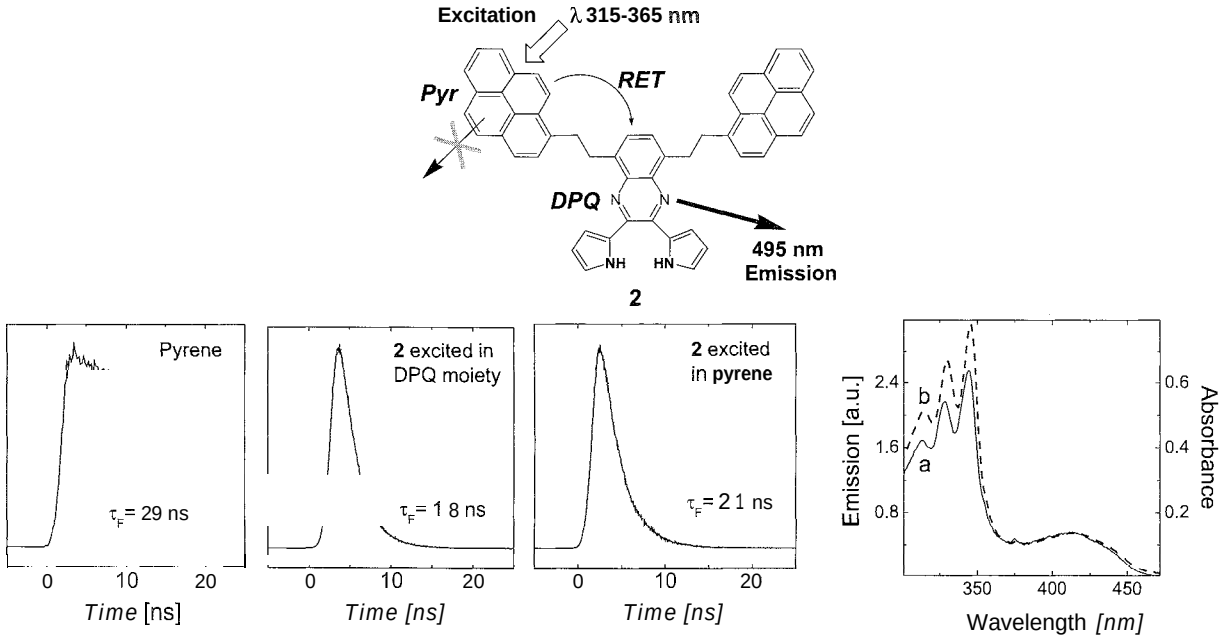

Fig. **4** *Sensor* **2**. *Excited state decays of pyrene and Sensor 2 when excited in DPQ moiety and in the pyrene antennae. (Right-bottom) The excitation (trace a, left axis,* emission *at 490 nm) and absorbance (trace b, right axis) spectra of* **2.**

lifetimes as short as 500 ps, and longer than 1 μs. Such instruments are relatively expensive, but their great advantage is modularity. Commercial instruments may be purchased as turnkey lifetime/continuous wave (CW) instruments, and their modularity allows for continuous upgrading and adding of different excitation sources, thus providing avenues for development of the instrument to suit the increasing needs of the users. The price of such instruments (see. for example, Fig. 3) is in the U.S. $70.000–100.000 range, depending on the accessories required.

An example of a commercially available TCSPC instrument used by the authors is shown in Fig. 3. The excitation source in the steady-state configuration is a 450 W Xe lamp optically coupled to a monochromator (2 nm). The emission is gathered at 90" and passed through a second monochromator (2 nm). The emitted light is detected with a Peltier-cooled (−30°C), R955 red-sensitive photomultiplier tube (PMT). This same instrument can also be configured for TCSPC measurements, when the excitation source is a nanosecond flash lamp operating under an atmosphere of H_2 gas (0.50–0.55 bar, 0.7 nm FWHM, 40 kHz repetition rate), the output of which is dispersed with a monochromator prior to sample excitation. This particular setup allows access to lifetimes as short as 300 ps. It should be noted, however, that with an alternative light source and detector, TCSPC can measure lifetimes as short as a few ps. The data from time-correlated experiments are analyzed by iterative convolution of the luminescence decay profile with the instrument response function using software packages that are usually provided by the manufacturer.

One example of the use of this instrument is in the investigation of the resonance-energy-transfer-amplified sensing of inorganic anions by Compound *2*. The dipyrrolylquinoxaline (DPQ) moiety of Compound 2 is an efficient energy acceptor for the two pyrene antennae inolecules present in the structure. The excitation of pyrene does not result in emission from pyrene moiety ($\lambda_F = 395$ nm, τ = ca 30 ns). Instead, the energy of the pyrene excited state is rapidly transferred into the DPQ residue of the sensor, which emits ($\lambda_F = 495$ nm. $\tau = 1.8$ ns). This behavior is schematically shown in Fig. 4. The kinetic experiments together with the steady-state excitation spectrum of *2* (which shows remarkable resemblance to the absorption spectrum of 2, including the well-resolved bands of pyrene) were recorded using the above-described TCSPC instrument.

Transient Absorption Spectrometry

The observation of luminescence. in general. and fluorescence, in particular, requires that the excited state being monitored undergo a radiative decay process that is significant with respect to all the other deactivation processes. If this is not the case, then techniques based on light emission become useless. However. most excited states, radicals, and other transient species of potential

interest to the supramolecular chemist absorb light to some degree. It is this property that is harnessed in transient optical absorption spectrornetry. In the so-called flash photolysis instrument, the absorption spectra and the kinetic behaviors of transient entities are recorded by monitoring their electronic absorption spectra before, during, and after photoexcitation of the sample with a short laser pulse. While this technique is not routinely used in the supramolecular chemistry community, we anticipate that it has the potential to become one of the favorite spectrometric methods for study of the behavior of multichromophoric supramolecular systems.

Instrumentation

Experiments that do not require resolution below a few ns have a distinct advantage in terms of the relative simplicity of instrumentation, because they can be carried out using "real-time" detection. In those cases, a suitable continuous or pseudocontinuous probe source is generated, and the intensity of the probe beam transmitted by the sample can be monitored as a function of time using a photomultiplier tube or suitable photodiode. A typical response time of a PMT+amplifier combination is of the order of 3 ns, and its output can be digitized in real time by a digital storage oscilloscope; currently, oscilloscopes capable of digitizing at 1 Gsamples/s are found. The oscilloscope records the time profile of transmitted light intensity (measured as voltage). The construction details of laser flash photolysis instruments vary between research groups. In recent years, commercial units became available.[5] The schematic layout of a typical nanosecond laser flash spectrometer used by the authors is shown in Fig. 5.

The instrument uses an excitation source of one of the harmonics (266 nm/355 nm/532 nm, 7 ns FWHM) of a Nd:YAG laser (Continuum Surelite I) or tunable visible light from an optical parametric oscillator (OPO) (Opotek). Other pulsed lasers can be employed, the criteria being that a short pulse of light (<20 ns) be produced, with sufficient per pulse energy to generate enough absorbance to rise above the noise inherent in the spectrometer. During the experiment, the laser beam excites the sam-

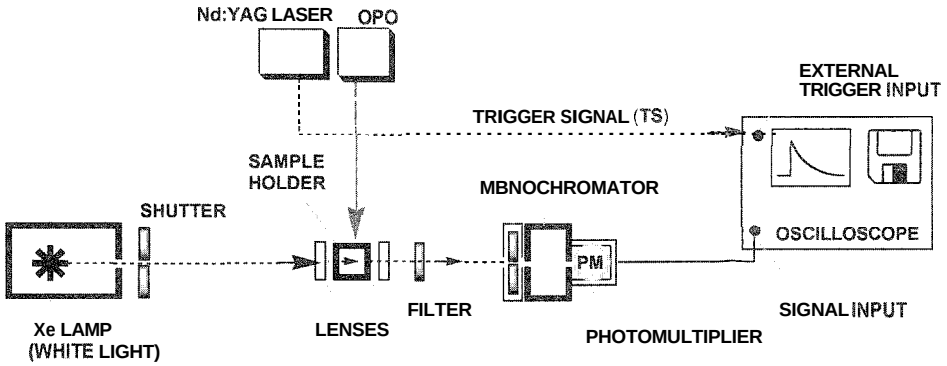

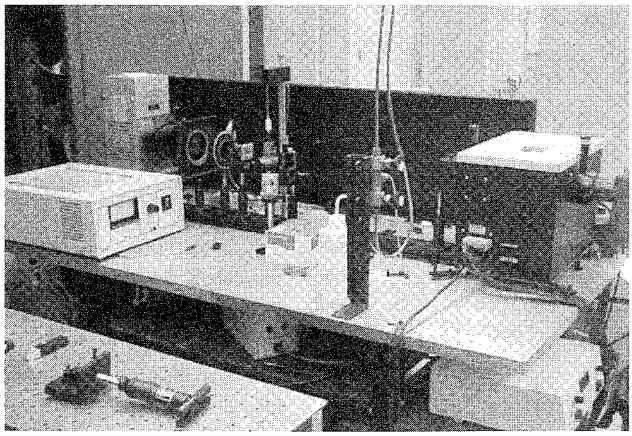

Fig. 5 Nanosecond time-resolved absorption spectrometer located in the author's laboratory. The excitation source is one of the harmonics (355 nm/532 nm, 7 ns FWHM) of a Nd:YAG laser (Continuum Surelite I) or tunable visible light from an OPO (Opotek). Data are acquired at 5 Hz and analyzed with programs assembled using LabView (National Instruments) software. (View *this art in* color at w+vw.dekker.com.)

ple generating the transient species. In many instruments, the pump and the probe beams are perpendicular to each other, but collinear and counterpropagating configurations are also employed. Continuum light sources such as the xenon arc or quartz-halogen lamp are most often used for a probe beam source. These lamps in CW mode provide useful output across the ranges 200–800 nm and 300–1000 nm, respectively. In some cases, it is advantageous to briefly pulse the monitoring lamp to high intensity.

The CW white light transmitted by the sample contains embedded information on the time-dependent absorption spectrum of the generated transients. One method of extracting the information is to select a wavelength of interest with a monochromator, placing a photo-detector at the exit slit. The most widely used detectors are photomultiplier tubes (PMT), chosen for their high sensitivity and fast time response. Solid-state devices, based on Si (200–1100 nm), InGaAs (700–1800 nm) and Ge (800–1800 nm), were also employed. but their lack of dynode amplification necessitates coupling them to high-bandwidth, high-gain amplifiers.

The electrical charge collected by the anode of the detector is caused to run to ground through a load resistance (most often the input impedance of a waveform processing device). This generates a voltage across the resistance. which is processed by a digital storage oscilloscope, or other analog-to-digital converter. These devices can also be used to filter and average signals. The digitized voltage-time profile (at one wavelength) is transfened to a PC for processing and data analysis. Then, the wavelength can be changed by a chosen interval and the data acquisition process repeated sufficient times until sufficient data are accumulated to assemble an absorbance wavelength time, or $A(\lambda,t)$, surface (see Fig. 8). In practice, some signal treatment is required, because often the difference between the amplitudes of the incident and transmitted monitoring beams is very small. of the order of <1% of the total signal, and severely distorted by the intrinsic noise in the spectrometer. In such cases. data acquisition is repeated many times at each wavelength step, and signal averaging techniques are employed. Described above is a method termed "continuous photoelectric recording."

Instead of using the monochromator–detector combination and collecting time profiles at single wavelengths, a spectrographic technique can be employed. In this method, the exit slit of the monochromator is removed, and an anay detector (e.g., a CCD) is placed at the focal plane of the grating/mirror. In this way. the dispersed white light spectrum illuminates the array and each pixel views a given narrow wavelength region, depending on the dispersion of the grating. Thus, the whole transmitted light spectrum is recorded simultaneously. This is termed the multiplex, or Felgett, advantage. Array detectors are limited in time resolution, so to use this method for microsecond and shorter-lived species, a gating method must be used to restrict the time for which the detector views the probe beam to short durations. For example, if dealing with a transient state having a 500 ns lifetime, in order to obtain a time profile with sufficient resolution, it would be necessary to sweep the profile with gate widths of no more than 50 ns.

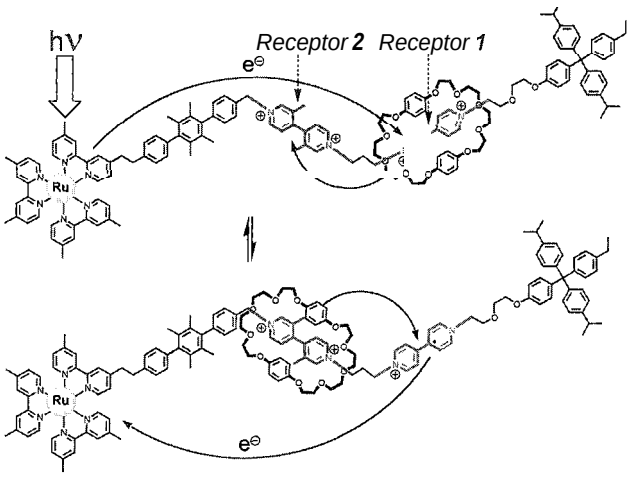

Fig. **6** A photochemically driven translation isomerism in a [2]rotaxane supramolecular machine according to Ashton et al. The flash photolysis data, together with electrochemistry observations, allowed the authors to obtain a complete electronic picture of the processes governing the switching mechanism in this [2]rotaxane, from both energy and kinetic perspectives.

For a supramolecular chemist who wants to investigate the association processes between several chromophores capable of interaction, such as donor–acceptor pairs in resonance energy transfer (RET) or photoinduced electron transfer (PET), laser flash photolysis is an indispensable technique. A particular example is given in a report of a light-driven molecular machine by Ashton et al.[6] The authors studied a [2]rotaxane system consisting of a π-electron-donating macrocyclic polyether bis-*p*-phenylene-34-crown-10 and a dumbbell-shaped component that contains a Ru^{II} trisbipyridine complex as one of its stoppers in the form of a photoactive unit; a *p*-terphenyl-type ring system as a rigid spacer; a 4,4′-bipyridinium unit and a 3,3′-dimethyl-4,4′-bipyridinium unit as π-electron-accepting receptors; and a tetraarylmethane group as the second stopper. The stable translation isomer is the one in which the crown-ether macrocycle is docked in the 4,4′-bipyridinium unit. Upon excitation of the Ru^{II} trisbipyridine moiety of the rotaxane, the photochemical reduction of the 4.4'-bipyridinium takes place. As a result, the polyether macrocycle is shifted to the second receptor site, the 3,3′-dimethyl-4,4′-bipyridinium unit. The reverse electron transfer from Receptor 1 to the Ru^{II} trisbipyridine complex results in a polyether macrocycle shift back from receptor

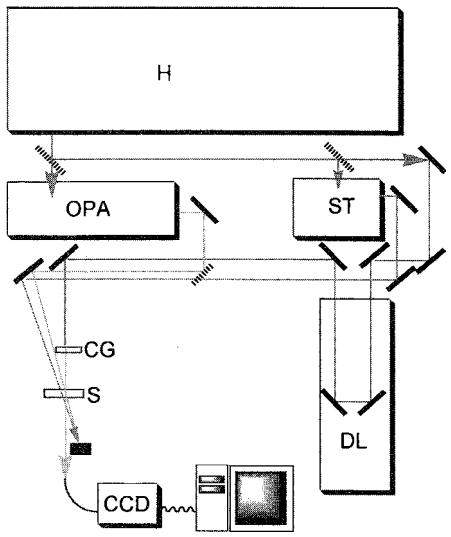

Fig. 7 An ultrafast transient spectrograph used by authors. *(View this art in color at www.dekker.com.)*

1 to Receptor 2. This mechanism of photochemical switching is shown in Fig. 6. The photochemical behavior of the rotaxane. as well as model compounds, was thoroughly investigated by laser flash photolysis, which allowed the authors to observe growth and decay of the individual excited states of the [2]rotaxane components, thus allowing for study of the sequential character of the processes involved.

Ultrafast Techniques

The major limitation of the photoelectric recording widely used for flash photolysis studies on the suprananosecond timescale is what can be thought of as the nanosecond bawier. This limitation arises because of the intrinsic time response of the electronic devices that must be used to acquire and process the photon-generated cathode current of the PMT or photodiode. All such devices have impedance, and even the best-designed circuitry has stray capacitance of typically 20 pF, which, when combined with the 50 Ω industry standard of electronic amplifiers, yields a RC time constant of 1 ns. Hence. instruments built from conventional electronic units will have minimum rise times in the ns region. and therefore. chemical changes that have lifetimes less than 5 ns. say, will be severely deformed. Of course other reasons may intervene (e.g., 10 ns wide laser pulses) that make the instrument response even poorer than implied by the nanosecond barrier.

It is important to find a way around the nanosecond barrier problem if reactions occurring in the subnanosecond regime are to be investigated, and the pump-probe method provides the path. In this, two light pulses are generated: one to excite the sample and one to probe the system at a given time postexcitation. Early pump-probe experiments used high-energy flash lamps for generating the transients and lower energy flash sources as interrogating beams. The two flashes were electronically delayed, one with respect to the other. This procedure stems from the methodology employed by Norrish and Porter in 1949 as part of their invention of flash photolysis leading to the Nobel prize in Chemistry in 1967 and which revolutionized the study of short-lived transient species.[7,8]

Flash lamps were superceded by pulsed laser sources, which are monochromatic, highly collimated, and have a much higher repetition rate. Using a single laser source. the probe pulse can be a small amount split from the main pump beam and sent to the sample via a variable length delay line. Because the pump and probe pulses are of the same wavelength. this experiment is restricted to measuring the kinetics of repopulation of ground state absorption removed (bleached) by the pump pulse. In spite of this restriction, this method was fruitfully employed in several laboratories.[9–12] Significantly more information is available when the probe pulse is a white light continuum coupled to spectrographic dispersion. Coherent continua are generated by taking a few μJ of the laser output, sending it around an optical delay line with a step resolution of 6.6 fs, and focusing it into a suitable liquid or crystal to generate self-phase modulation (a nonlinear optical process involving stimulated Raman and multiwave mixing within the waist of a high-peak-power laser beam). The resulting white light is directed through the irradiated sample, where it picks up the absorption information, and from there it is dispersed in the spectrograph and finally incident on a CCD detector at the focal plane of the spectrograph. Under these conditions. one obtains an absorption spectrum of transient species formed or ground-state species removed by the initiating pulse. This spectrum will be registered at a time that is given by the difference in arrival times of the pump and probe pulses at the sample, and it will be an average over the temporal width of the probe pulse. An alternative method of obtaining spectral information is to employ a probe beam of a selected, but changeable wavelength. Such a beam can be isolated from a continuum by one of a set of interference filters, or it can be generated by an optical parametric amplifier that can be scanned to provide spectral coverage.[13,14] In both instances. the detector is a commonplace photodiode.

Repetition of the spectrum acquisition sequence at different probe pulse arrival times provides a series of spectra delayed with respect to each other. Thus. time resolution of the reaction is achieved in a point-by-point manner, whereby the $A(\lambda,t)$ surface can be produced. In this experiment type, the detector of the transmitted probe

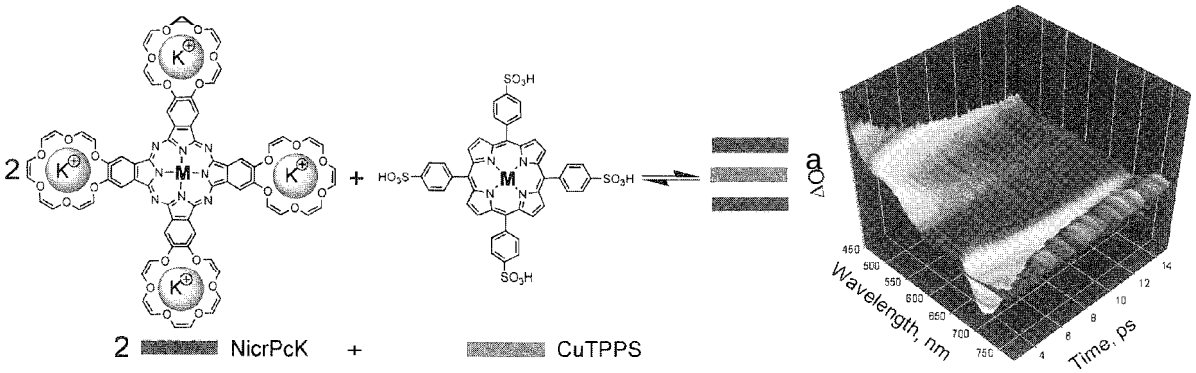

Fig. 8 The dynamic surface shows the first 15 ps postexcitation of the complex formed between NicrPcK and CuTPPS (*View this art in color at www dekker com*)

light (CCD) behaves as a photon integrator only, and the time resolution derives from the instrument's capability for measuring the difference in the time of arrival of the pump and probe pulses. This capability provides an intrinsic limitation to the pump-probe method, which depends critically on the width of the pulses being employed. These days, light pulses as short as 20 fs or less are available.

A schematic layout of the ultrafast system extant at the Ohio Laboratory for Kinetic Spectrometry at Bowling Green State University is shown in Fig. 7. The excitation source (H) is a mode-locked, amplified Ti-S laser (SpectraPhysics, Hurricane). The output (red line) is typically 1 mJ per pulse at a repetition rate of 1 kHz (1 W average power). To obtain useful excitation wavelengths (400 nm, 266 nm) the output of the amplifier is coupled to a harmonic generator (CSX, SuperTripler, ST). To achieve tunable excitation wavelengths in the visible and near 111, the 800 nm beam is employed as a pump for an optical parametric amplifier (OPA-400, SpectraPhysics). The white light probe is generated (CG) by focusing a few μJ of the 800 nm beam into a thin sapphire plate. It is delayed with respect to the pump beam with the variable delay line (DL). It is overlapped with the appropriate pump beam in the sample cuvettc (S) steered into a fiber optic cable, then to the spectrograph (CCD). The PC controls all aspects of data acquisition and processing.

This instrument was employed to examine the excited state dynamics of supramolecular systems generated from self-asseinblies between metal-substituted 18-crown-6 tetra-substituted phthalocyanines (McrPc) with K^+ ions contained in the crown sites (McrPcK) and metal-substituted *meso*-tctrakis(4-sulfonatophenyl)porphyrin (MTPPS) or *meso*-(4-carboxylphenyl)porphyrin (MTPPC). In the absence of added potassium ions, no hetero-complexes were formed. In the presence of K^+, absorption spectral changes indicated the formation of a ligand-to-ligand charge transfer (LLCT) state between the constituent π-systems. Excitation could be carried out at 400 nm, which populated the porphyrin-localized S_2 state or directly into the CT band (690 nm).[15]

Each complex studied showed transient features and kinetics that were independent of the excitation wavelength. The dynamic surface depicted in Fig. 8 shows the first 15 ps postexcitation of the complex formed between NicrPcK and CuTPPS. Subsequent to 400 nm excitation, all coinplexes displayed rapid (sub-ps) conversion to the low-lying LLCT state, deactivation of which involved metal-centered states. In many complexes, the metal-centered states were formed within 2 ps, with lifetimes that varied somewhat with the metal center. In the case of the complex in Fig. 8, repopulation of the ground state occurred with a lifetime of 8 ps. In the figure, the immediate bleaching of the 690 nm LLCT absorption can be seen as a rapidly recovering negative absorption. This is accompanied by a growing spectral band to the red side of the bleach and at shorter wavelengths by the positive absorption assigned to the LLCT state.

Ultrafast fluorescence techniques such as up-conversion and streak camera methods were not described in this article, as these were recently reviewed elsewhere.[''''']

CONCLUSION

After three decades of rapid development, time-resolved absorption and luminescence spectrometry emerged as powerful tools for studying the supramolecular behavior of molecules and materials Such techniques provide complementdry information to steady state UV/Vis nuclear infrared spectroscopy, which may be used to study the supramolecular behavior in the ground state The general sensitivity ot time-correlated techniques combined with insight into the process dynamics and low

amounts of samples required for experiments make these the methods of choice for investigation of supramolecular behavior of chromophores or chromophore-containing materials. With the exception of ultrafast methods, the experimental setups are, in most instances, relatively straightforward and commercially available to supramolecular chemists. At this point, the studies reviewed in this article illustrate how transient and time-resolved luminescence spectrometry can be used to observe and understand the processes of association between molecules and ions in solution. The authors believe that future trends in applications of photochemical techniques would involve. among others, the development of instrumentation and experiments for application to multicomponent (multichromophore) systems and supramolecular behavior on interfaces between solid and liquid. liquid and liquid, etc. Most notably, with the growing accessibility of instrumentation and widening scope of applications, we envision that photochemical methods in conjunction with microscopy will constitute the cutting edge in the transition from bulk-material to supramolecular chemistry on a single-chromophore level.

ARTICLES OF FURTHER INTEREST

Crown Ethers, p. 326
Energy and Electron Transfer in Supramolecular Systems, p. 535
Fluorescence Sensing of Anions, p. 566
Fluorescent Sensors, p. 572
Hydrogen Bonding, p. 658
Luminescent Materials, p. 816
Luminescent Probes, p. 821
Photochemical Sensors, p. 1053
Pyrrole- and Polypyrrole-Based Anion Receptors, p. 1176
Rotaxanes und Pseudorotaxanes, p. 1194

REFERENCES

1. Kalyanasundaram. K. *Photochemistry of Polypyridine and Porphyrin Complexes. Academic Press, London,* 1992.
2. Vogler. A.; Kunkely, H.: Luminescent Metal Complexes: Diversity of Excited States. In *Topics in Current Chemistry, Vol. 213: Transition Metal and Rave Earth Compounds: Excited States, Transitions, Interactions I:* Yersin, H.. Ed.: Springer: Berlin. 2001.
3. Tyson. D.S.; Bialecki. J.; Castellano. F.N. Ruthenium(II) complex with a notably long excited state lifetime. Chem. Commun. 2000. 2355–2356.
4. Anzenbacher. P.. Jr.; Tyson, D.S.: Jursíková, K.: Castellano, F.N. Luminescence lifetime-based sensor for cyanide and related anions. J. Am. Chem. Soc. 2002. 124, 6232–6233.
5. See http://www.ultrafastsystems.com.
6. Ashton. P.R.; Ballardini, R.: Balzani, V.; Credi, A.; Dress. K.R.; Ishow. E.; Kleverlaan. C.J.; Kocian, O.: Preece, J.A.: Spencer. N.: Stoddart. J.; Venturi, M.: Wenger, S. A photochemically driven molecular-level abacus. Chem. Eur. J. 2000, 6. 3558–3574.
7. Porter. G. Flash photolysis and spectroscopy. A new method for the study of free-radical reactions. Proc. R. Soc. Lond. **1950**, *A200*. 284–300.
8. Norrish. R.G.W.; Poster, G. Chemical reactions produced by very high light intensities. Nature **1949**. 164, 658.
9. Ippen. E.P.; Shank. C.V.; Berginan, A. Picosecond recovery dynamics of malachite green. Chem. Phys. Lett. 1976. *38*. 611.
10. Gillbro, T.; Sundström, V.P. *Picosecond Phenomena III*; Eisenthal. K.B.. Hochstrasser. R.M.. Kaiser. W.. Laubereau, A., Eds.: Springer: Berlin, 1982: 315–318.
11. Spears, K.G.: Gray, T.H.: Huang. D. *Picosecond Phenomena III*; Eisenthal, K.B.. Hochstrasser, R.M.. Kaiser, W.. Laubereau, A., Eds.; Springer: Berlin. 1982: 278–281.
12. Chuang, T.J.; Hoffman, C.W.: Eisenthal, K.B. Picosecond studies of the cage effect and collision induced predissociation of iodine in liquids. Chem. Phys. Lett. **1974**, *25*. 201–205.
13. Kobayashi, T. Ultrafast spectroscopy with broad probe spectral range extending from near ultraviolet to near infrared. Bull. Chem. Soc. Jpn. **1997**, 70. 1211–1224.
14. Schweitzer. G.: Xu. L.; Craig, B.B.: Deschryver. F.C. A double OPA femtosecond laser system for transient absorption spectroscopy. Opt. Commun. **1997**. *142*, 283–288.
15. Gusev, A.; Danilov. E.O.: Rodgers. M.A.J. Association complexes between cationic metallophthalocyanines and anionic metalloporphyrins II: Ultrafast studies of excited state dynamics. J. Phys. Chem.. A 2002. 106. 1993–2001.
16. Mialocq. J.-C.: Gustavsson. T.: Investigation of Molecular and Suprarnolecular Systems. In *New Trends in Fluorescence Spectroscopy:* Applications to Chemical and Life Sciences; Valeur. B.. Brochon, J.-C., Eds.: Springer: Berlin. Heidelberg. 2001; 61–77.

Phthalocyanines

Marco Evangelisti
Leiden University, Leiden, The Netherlands

INTRODUCTION

Porphyrin-like structures received considerable attention because of their interesting chemical and physical behaviors, and because of nature's ubiquitous use of porphyrins in electron-transfer processes. The phthalocyanine (hereafter referred to as Pc) is a porphyrin-like dye that has been known for many years. The word phthalocyanine, from the Creek for naphtha (rock oil) and cyanine (blue), was first used by Linstead in 1933 to describe a new class of organic compounds.[1] Phthalocyanine was probably discovered by accident in 1907. as a by-product during the synthesis of o-cyanobenzamide, but it was not until almost 20 years later that a patent was filed describing a manufacturing process. Linstead and coworkers showed that a vast range of phthalocyanines, the metal (M)-substituted forms of the molecules (hereafter referred to as MPcs), were all based on the structure depicted in Fig. 1. In a classic series of papers, starting in 1935, Robertson and coworkers showed that the environment of the metal atom in MPcs was square planar and coordinated with four pyrrolic *N* atoms, and moreover, that the entire Pc-molecule was flat within the limits of uncertainty.[2,3]

To date, a large number of different MPcs were synthesized and studied. with a concomitant huge literature of thousands of publications. The impact of the phthalocyanines is so high that. since 1997. John Wiley & Sons Ltd. publishes in regular issues *The Journal of Porphyrins and Phthalocyanines.* Also. monographs on phthalocyanines and their derivatives can be found in the literature.[4] Ill academic laboratories, MPcs received extensive attention for the reasons that follow. They provide a versatile chemical system, and they can be easily crystallized and sublimed, resulting in materials of very high purity. Crystals of phthalocyanines are exceptionally stable in a huge range of temperature and pressure variations. Also. strong acids or bases do not affect conventional MPcs. The conjugated π-system, containing 18 electrons in the macrocyclic ring, leads to reinarkable electronic and optical properties.[5] Especially intriguing is the ability to adjust the phthalocyanine's structural and electrical properties by synthetic means. thus making them ideal model compounds. They are. moreover. of great interest for their magnetic properties, because manganese phthalocyanine (MnPc) was one of the first molecular magnets,[6] and iron phthalocyanine (FePc) has one of the largest internal hyperfine fields ever reported for iron coordination compounds. regardless of the spin value.[7]

USES OF METALLOPHTHALOCYANINES

As a consequence of their chemical and physical properties, phthalocyanines are widely exploited in industry in a variety of applications.[8,9] For example. the English Royal Mint uses the popular copper-substituted variety (CuPc) as a blue dye in £5 notes. Besides as conventional dyestuffs. MPcs are commercially used as coatings for read/write CD-ROMs, with obvious implications for the coinputer and communications industries. Moreover, many types of chemical sensors based on phthalocyanines were proposed, including thin-film resistive devices, FET sensors; and Langmuir–Blodgett films. They are also used for electrochromic display devices, photovoltaic and electrophotographic devices, shields against electromagnetic interference, germicides. and deodorants. In addition, cobalt phthalocyanine is used as a homogeneous catalyst in the industrial desulfurization of crude petroleum (the Merox process), while iron phthalocyanine (FePc) is a useful laboratory catalyst for several oxidation reactions: including hydrocarbon oxidations.[10] Particularly important, in this respect. is that FePc is currently used to prepare arrays in large-scale production of carbon nanotubes[11] that have electronic properties currently of great interest for promising technological applications. Also, in medicine, the fluoroaluminum phthalocyanine was extensively studied for potential use as a target molecule in anticancer treatments. For these purposes, more than 50,000 tons of Pcs are used per year.

A VERSATILE CHEMICAL SYSTEM

The methods of synthesis. originally described by Linstead, are still the most widely used for preparing phthalocyanines. Effective solvents to obtain metal-free Pc (M = 2H) from 1,2-dicyanobenzene are found to be dialkylalkanolamines. Many MPcs are obtained by reacting a derivative of 1,2-dicyanobenzene with a finely

DOI: 10.1081/E-ESMC 120019177

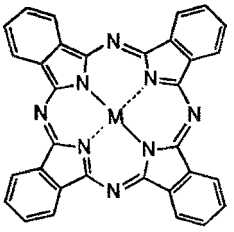

Fig. 1 Chemical structure of metallophthalocyanines.

dispersed metal or a metal salt. The reactants are usually heated in high-boiling-point solvents like *o*-dichlorobenzene and chloronaphtalene. The nature of the sequestered metal ions has an influence on the physicochemical properties of the MPc. For example, the oxido-reduction behavior of the molecular unit or the nature of the photochemical excited state may be altered by changing the metal ion in the complex. By varying substituents on the ring, the range of properties of MPcs may be expanded even further. In recent years, many reports appeared on the synthesis of new phthalocyanine derivatives. These experiments are aimed at the development of materials with specific properties. Of the numerous compounds based on Pcs. some selected examples are reported in what follows.

SELECTED EXAMPLES OF PHTHALOCYANINES AND THEIR DERIVATIVES WITH SPECIFIC PROPERTIES AND POSSIBLE APPLICATIONS

Indium Phthalocyanines as Optical Limiters

Phthalocyanines have interesting optical properties that may be useful for nonlinear optical applications of these complexes. In this respect, optical limiting of indium phthalocyanines (InPcs) is particularly promising, as evidenced by the research activity of Hannack and coworkers in the last few years.[12] They succeeded in optimizing InPc for optical limiting using different axial and peripheral substituents and expanding the ring to naphthalocyanines. Among the phthalocyanines, the materials with tetra-tert-butyl peripheral substitution and (*para*-trifluoromethyl)phenyl-, and perfluorophenyl- axial substituents

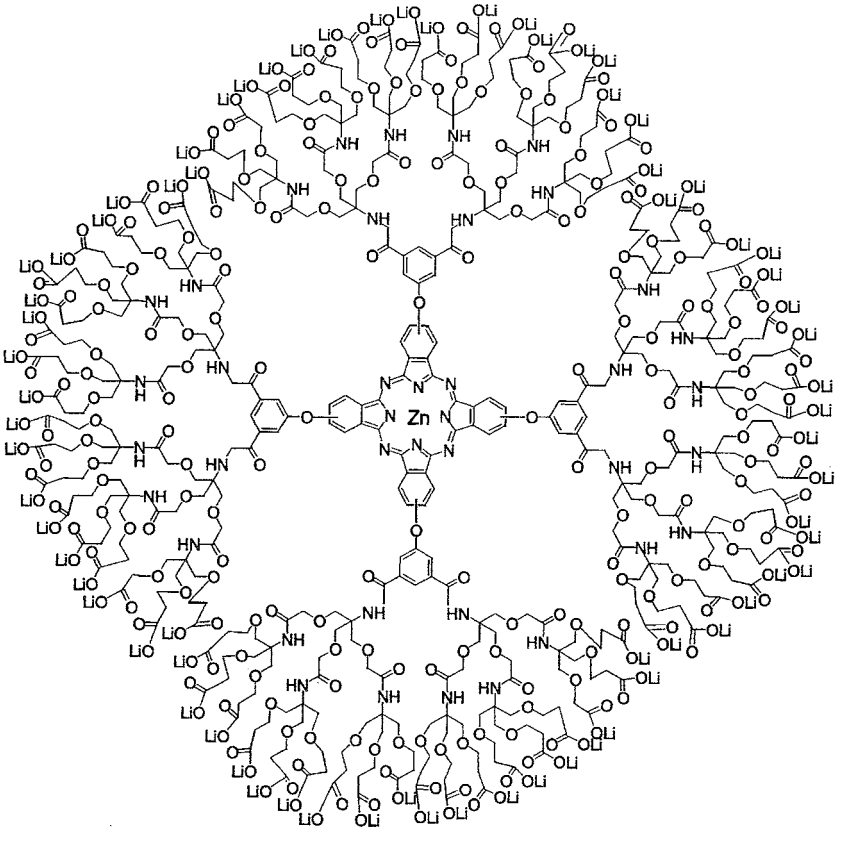

Fig. 2 The first reported and water-soluble dendritic phthalocyanine. (After Ref. [13]. Reproduced by permission of The Royal Society of Chemistry.)

were found to be useful materials for optical limiters in the 480–580 nm range.

A Phthalocyanine-Based Dendrimer for Harvesting Low-Energy Photons or for Photoinduced Electron Transfer Reactions

Metallophthalocyanines are poorly soluble in water. A way to increase their solubility is by introducing substituents onto the aromatic rings. This is the case, for example. of the first dendritic phthalocyanine that was reported in 1998 by Kobayashi's group.[13] The octakis[3,5-(dicarboxy)-phenoxy] ZnPc was first synthesized and eight triply-branched carboxyethylesters containing amino groups were reacted in the presence of dicyclohexylcarbodiimide. The 23 terminal ester groups were hydrolyzed with LiOH in MeOH–H_2O. A repeat of this reaction gave the second-generation dendrimer. After hydrolysis, the compound became the first water-soluble dendritic phthalocyanine (Fig. 2) with an approximate diameter of 5 nm. Dendrimers are of great interest for their possible uses, because they function for harvesting low-energy photons[14] or giving a hydrophobic environment in aqueous solutions.[15] Because Pcs are robust. dendrimers of MPcs are promising candidates for future research.

Electronic Conductors Based on Phthalocyanine Complexes

Similarly, the solubility of Pcs in organic solvents is increased by introducing bulky substituents on the ring. For example, Pc derivatives substituted with crown ether macrocycles[16] are soluble enough in organic solvents to be deposited from solutions and arranged in thin films. which may, thus, be used for electrical devices and sensors. Even if these materials are insulators when undoped (as are conventional MPcs), they possess, however, accessible π and π^* orbitals that make at least partial oxidation or reduction of the macrocycle possible with gases such as NO_2. This yields more or less conductive molecular materials. The presence of the metal ion is not a prerequisite for high electrical conductivity. For example, room temperature measurements on the 15-crown-5 metal-free Pc derivative showed that the conductivity increases notably (with satisfactory reversibility) when the layers are exposed to NO_2 in the range of 1–5 ppm.[16] Of importance here there is that there are, also, Pc complexes of rare-earth ions,[17] which are far more easily oxidized and reduced than the Pc derivatives substituted with crown ether macrocycles. These rare-earth-containing derivatives are most often

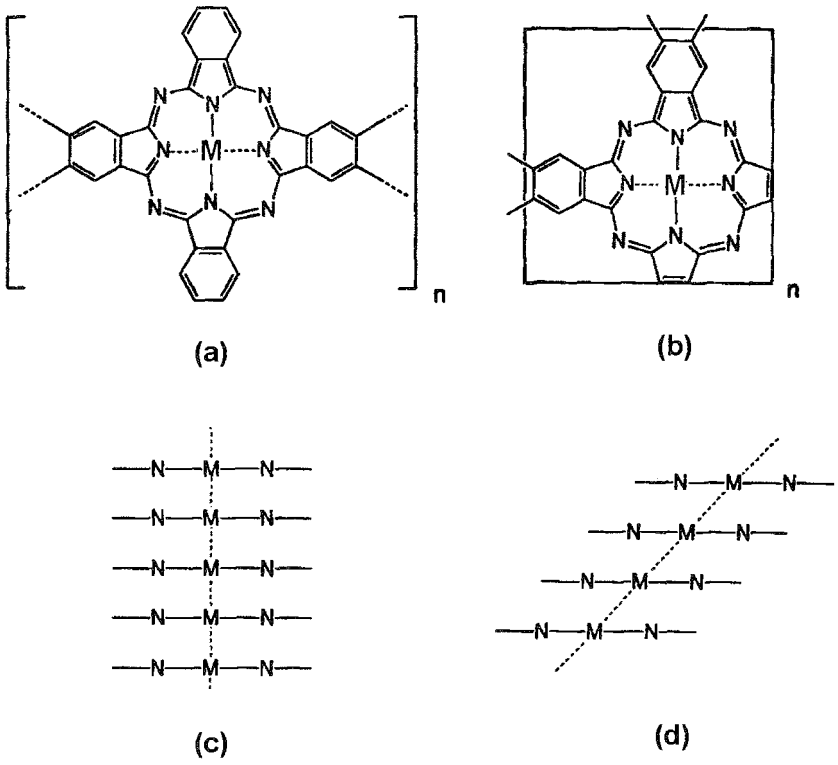

Fig. *3* Different ways of assembling phthalocyanines: (a) a ladder polymer: (b) a plane polymer; (c) and (d) stacked arrangements

dimeric, with the metal "sandwiched" between the two Pc rings. Rare-earth ions are normally in the 3+ state, and the dimer is a neutral molecular radical. This radical was reported to be the first intrinsic molecular semiconductor.[18] For a recent review on dimers of phthalocyanines and related compounds, we refer the reader to Ref. [19]. Organic conductors based on Pcs were investigated extensively (see. i.e., Ref. [20]). Large systems of these metal complexes can be assembled in three different ways (Fig. 3). A first a rangement is that of the ladder polymers and a second one that of the plane polymers.[21] The latter type, e.g., polyCuPc, has conductivity 10"" times higher than that of monomeric CuPc. A third possible way of assembling MPcs is via the stacked arrangement. This arrangement leads to low-dimensional materials and permits electron delocalization by π–π overlap of the macrocycles. This stacking is thought to be a prerequisite for facile electrical conduction.

Network Planar Polymers of Phthalocyanines as Catalysts or Adsorbents

Network planar polymers of phthalocyanines (Fig. 3) are a subject of ongoing research: because they have potential technological applications, such as catalysts and adsorbents. Because phthalocyanines are highly stable toward low pressure, a range of solvents. and elevated temperatures; they are desirable in applications. The drawback is that, in comparison with catalysts and adsorbents made by inorganic nanoporous materials, with surface areas as high as 1200 m^2/g, phthalocyanine-based network polymers usually have low porosity, with low values of surface areas ($\approx$1 m^2/g). However, promising preliminary studies of novel phthalocyanine-based network polymers showed that the surface area may be notably increased (450–950 m^2/g) by using *bis*(phthalonitrile), which provides a rigid spirocyclic linker for the phthalocyanine molecules.[22]

MAGNET16 PROPERTIES OF METALLOPHTHALOCYANINES

Polymorphism and Magnetic Interactions

From the discussion above, it is, thus, clear that the packing of the Pc molecules has a strong influence on the physical properties of the materials. Pcs seldom crystallize in the stacked arrangement shown in Fig. 3. Generally. the packing is as illustrated in Fig. 4, for the so-called α- and β-forms. These two forms were first reported in the early days for the CuPc and. subsequently. for other MPcs. A detailed description of the early research on the polymorphism of MPcs can be found in Ref. [23]. In more recent

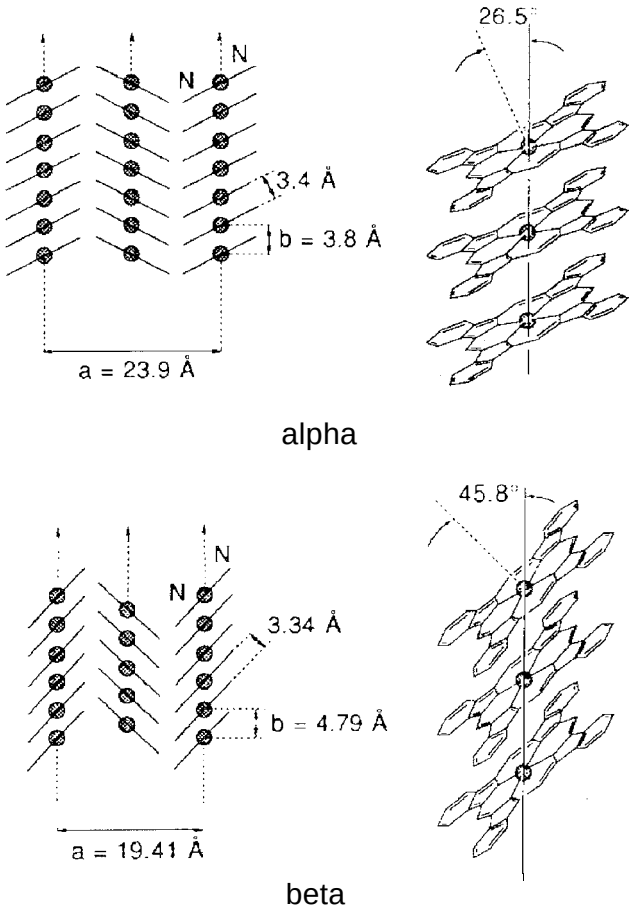

Fig. 4 Structural arrangements of macrocycles in the α- and 8-forms.

years, several new forms were reported." The main differences between the polymorphic structures are, for example, different angles of the Pc molecules with respect to the stacking axis, linear or slipped arrangement of the molecules along the stacking axis, and, consequently. different overlapping of the neighboring molecules. In what follows. we will consider only the a- and β-forms, which are the most well known. We will see how they determine the magnetic properties of some selected examples of MPcs. nominally manganese and iron phthalocyanines.

Manganese Phthalocyanines

In the a- and β-forms, the molecules are tilted by a substantial angle with respect to the chain axis (Fig. 4): in the a-form. the angle between the stacking axis and the molecular plane of MPc is about 65°. while in the β-form,

"For a detailed description of crystal structures of Pc complexes. see Refs. [4,24].

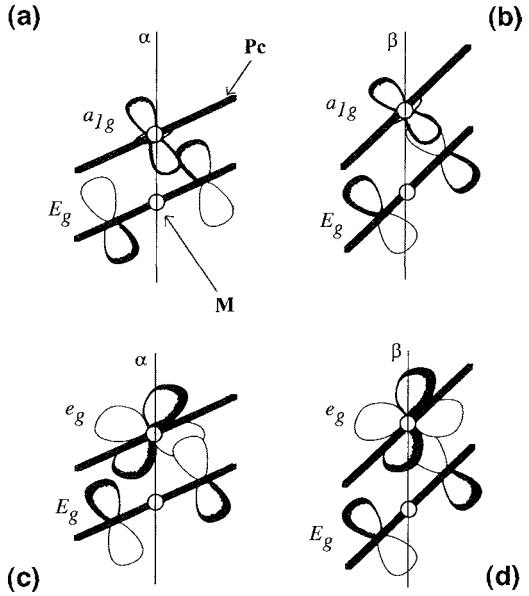

Fig. 5 The a_g–E_g interaction for α-form (a) and β-form (b), and the e_g–E_g interaction for α-form (c) and β-form (d).

it is about 45°. The angle at the parallel adjacent chain is opposite. thus constructing a so-called "herringbone" structure. The particular structure in the β-form of manganese phthalocyanine (β-MnPc) is thought to cause the Mn–Mn ferromagnetic interactions that make this compound one of the first molecule-based magnets.[6] Upon cooling below 8.6 K, β-MnPc undergoes a phase transition to a canted ferromagnetic state. The magnetic moment associated with each molecule is essentially perpendicular to the macrocyclic plane, and, hence, is canted with respect to the stacking axis. On the contrary, the a-form of MnPc is antiferromagnetic.[25] To understand these different behaviors, we will examine the spin correlation between Mn ions in adjacent molecules, because the orbital overlaps determine the magnitude of the magnetic interaction (Fig. 5). Here we must notice that the orthogonal metal $3d^5$ and Pc π orbitals in the same molecule make the ferromagnetic interaction. Under the assumption that the electronic configuration of the $3d^5$ electrons is $(d_{xy})^2(d_{xz})^1(d_{yz})^1(d_{z2})^1$, the ferromagnetic interaction is caused by the overlap between the d_{z2} unpaired electron (a_g symmetry) with the π orbital of E_g symmetry of the adjacent aromatic ring, which is orthogonal to the d_{z2} orbital of its metal ion. The antiferromagnetic interaction is due to the overlap of the $d_{xz}d_{yz}$ orbitals (e, symmetry) with the same π orbital of E_g symmetry. If the angle between the stacking axis and the Pc-ring increases from 45" to 65°, the overlap of the d_{z2} and the adjacent π orbital moves from the electron-rich N atom towards the node. Consequently, the ferromagnetic interaction will become weak. Thus. in the β-MnPc, the ferromagnetic mechanism dominates, while in the α-MnPc. the antiferromagnetic path prevails over the much weaker ferromagnetic path.

A Ferromagnetically Ordered Metalloporphyrin

The search for molecular magnets is. at present. a subject of intense investigation.[26] It follows that the observation of ferromagnetic correlations in the β-form of manganese phthalocyanine stimulated the research on the magnetic properties of this kind of material. Nevertheless, the most interesting results were obtained only recently. Structurally similar to the phthalocyanines, the metalloporphyrins may also stack in different forms, giving rise to different magnetic properties. In 1998, it was reported that iron(II) octaeihyitetraazaporphyrin crystallizes in two structures: the α-form, which is a canted molecular ferromagnet. with a critical transition temperature $T_c = 5.6$ K, and the β-form, which remains paramagnetic down to I K.[27] Thus, iron(II) square coordinated complexes also seem prone to show different magnetic behavior depending on the stacking structure.

Iron Phthalocyanines

In view of these experimental findings. a detailed characterization of the magnetic properties of iron phthalocyanines (FePc) was recently carried out.[7] There are two forms of FePc described in the literature. The a-form is metastable and obtained either as a polycrystalline powder or as a thin film formed by vacuum deposition onto a cold substrate. The β-form is the most stable and may be obtained from the sublimation technique in the form of a single crystal. Since 1935, the β-form of this compound has been repeatedly reported to behave as a paramagnet down to the lowest measured temperatures. Instead, detailed magnetic studies of the a-form of iron phthalocyanine (α-FePc) showed the onset of strong ferromagnetic correlations within the Fe ions along the stacking axis.[7] For comparison. the magnetic susceptibilities of the a- and the β-forms are shown together in Fig. 6. It can be seen that the two susceptibilities are coincident at high temperatures, but that they strongly differ once the temperature is lowered below 100 K. The fact that the susceptibility of β-FePc goes to zero at very low temperatures was explained in terms of zero-field splitting of the $S = 1$ triplet state of the Fe ion. leaving a nonmagnetic singlet as the lowest energy level occupied. Differently, the susceptibility of α-FePc increases strongly by lowering the temperature, indicating the presence of ferromagnetic correlations among the Fe ions. Only at

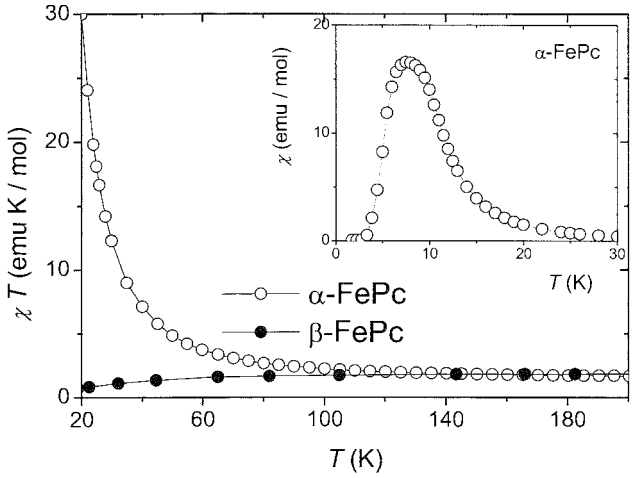

Fig. 6 Experimental $\chi_m T$ versus T curves for α-FePc (O) and β-FePc (●). In the inset: the low-temperature variation of the molar magnetic susceptibility of α-FePc.

about 10 IS does the susceptibility show a change of slope, and a rounded maximum is found at still lower temperatures (inset of Fig. 6). The decrease below the maximum was explained in terms of increasing domain-wall stiffness of the ferromagnetically coupled Fe ions along the stacking axes with decreasing temperature. which is common in molecularly based ferromagnets exhibiting anisotropy and low magnetic density. By means of alternate-current magnetic susceptibility measurements, it was also reported that the maximum in the susceptibility depends strongly on the frequency of the alternate current."' Such a behavior was already observed in metalloporphyrins,[27,28] which have similar structures to the FePc, and implies that a fully ferromagnetic ordered state is not achieved in these systems. The reason is again intrinsic to the magnetic structure. The low-temperature properties of anisotropic ferromagnetically coupled Fe (or Mn) ions along the stacking axes are dictated by the thermal excitation of domain walls. It follows that if the metal ions belonging to neighboring axes are weakly magnetically correlated. the establishment of a fully ordered magnetic state can become a delicate process that is readily disturbed by the presence of lattice defects. i.e.. stacking faults of the molecular arrangement along the axes. The presence of structural disorder was already directly observed by means of high-resolution transmission electron microscopy in several metalloporphyrins and metallophthalocyanines.[29] The magnetic behavior of α-FePc strongly resembles that of a glassy system, in which a freezing of the magnetic components is formed below a certain temperature into a state of random magnetic disorder.

Curiously, the magnetic phenomenology of the FePc forms is opposite that reported above for the MnPc forms: i.e., FePc is ferromagnetic when it is in its α-form, while MnPc is ferromagnetic when it is in its 6-form. To explain such a difference, we should again consider Fig. 5 and Fig. 4. Using the same arguments that we used for the MnPc forms. it is easy to show that the only possible electronic configuration of the Fe ions giving rise to ferromagnetic correlations is given by $E_gB\ (d_{z2})^2(d_{xz})^2(d_{yz})^1(d_{xy})^1$. However, the intensity of the ferromagnetic exchange should probably be weak: because it is in the *xy* plane, and the overlap is small. Thus. most likely, the ferromagnetic coupling present in the a-form does not originate from exchange interactions. On the other hand. the condition for enhancement with respect to the β-form of the direct Fe–Fe interaction is fulfilled. because the Fe–Fe distance is reduced from 4.8 Å (6-form) to 3.8 Å (a-form). In this respect, the overlap between a half-filled and a full orbital gives rise to ferromagnetic coupling. It follows that if the orbital configuration is $E_gA\ (d_{xy})^2(d_{xz})^2(d_{yz})^1(d_{z2})^1$, as proposed by Coppens and coworkers for the β-form from accurate x-ray diffraction,[30] the overlap may take place between two $(d_{xz})^2(d_{yz})^1$ orbitals. Of course, this overlap will decay strongly when the atoms are separated further by 1 Å, and so the fe romagnetic interaction weakens to the extent of being negligible in the β-form.

CONCLUSION

The β-MnPc and the α-FePc are the only known examples of phthalocyanine-based magnets. A strategy to achieve molecular magnetic ordering was to couple in three dimensions ferromagnetically coupled chains. The β-MnPc compound. having the Mn ions ferromagnetically correlated along the stacking axes of the molecules, belongs to this class, with $T_c = 8.6$ K.[6] Other attempts to obtain ferromagnets with this strategy, such as α-FePc and the metalloporphyrine electron transfer salts. have in common the incomplete achievement of magnetic long-range order at low temperatures.[7,26,27] This is inconvenient in the search for molecular magnets. The reason for this shortcoming is that the building elements are ferromagnetic linear chains. and they are sensitive to defects, because a single defect breaks long-range magnetic order in a chain. So, the shortcorning is inherent to the approach. However, and for the same reason, they provide new phenomenology to clarify the interesting field of coexistence of ferromagnetism and glassy behavior.

ACKNOWLEDGMENTS

I am indebted to Prof. J. Bartolome and Prof. L.J. de Jongh for fruitful discussions on the magnetism of metallophthalocyanines.

ARTICLES OF FURTHER INTEREST

Crown Ethers. p. 326
Dendrimers, p. 432
Energy and Electron Transfer in Supramolecular Systems, p. 535
Hemoglobins: O_2 Uptake and Ti-ansport. p. 636
Molecular-Level Machines, p. 931
O_2 Uptake and Transport, Models of, p. 1023
π–π Stacking as a Crystal Engineering Tool, p. 1093
Porphyrin Derivatives, Functional, p. 1139
Porphyrin-Based Clathrates, p. 1150
Pyrrole- and Polypyrrole-Based Anion Receptors. p. 1176
Supramolecular Photochemistry, p. 1434

REFERENCES

1. Linstead. R.P.J. Phthalocyanines. Part I. A new type of synthetic colouring matters. Chem. Soc. 1934, 1016–1017.
2. Robertson, J.M.: Linstead. R.P.: Dent. C.E. Molecular weights of the phthalocyanines. Nature 1935, 135, 506–507.
3. Robertson. J.M. *Organic Crystals and* Molecules: Cornell Univ. Press: Ithaca, NY, 1953, and references therein.
4. The *Porphyrin Handbook*: Kadish. K.M., Smith. K.M.. Guilard. R.. Eds.: Academic Press: Oxford. 2003: Vols. 15–20.
5. Cook. M.J. Thin film formulation of substituted phthalocyanines. J. Mater. Chem. 1996, 6 (5), 677–689.
6. Mitra. S.; Gregson, A.; Hatfield. W.; Weller, R. Single-crystal magnetic study on ferromagnetic manganese (II) phthalocyaninate. Inorg. Chern. 1983. 22. 1729–1732.
7. Evangelisti. M.: Bartolomé. J.; de Jongh. L.J.: Filoti, G. Magnetic properties of α-iron(II) phthalocyanine. Phys. Rev. B. 2002. 66 (14). 114410 1–11.
8. *Phthalocyanines: Properties and Applications*; Leznoff. C.C., Lever. A.B.P.. Eds.: VCH Publishers: New York. 1996: Vol. 4.
9. McKeown. N.B. *Phthalocyanine Materials—Synthesis,* Structure *and Function*: Cambridge Univ. Press: Cambridge. 1998.
10. Parton. R.F.: Vankelecom. I.F.J.: Casselman. M.J.A.: Bezoukhanova. C.P.: Uytterhoeven, J.B.R.: Jacobs. P.A. An efficient mimic of cytochrome-p-450 from a zeolite encaged iron complex in a polymer membrane. Nature 1994. 370. 541–544.
11. Huang. S.: Dai, L.: Mau. A. Synthesis and structures of aligned branches carbon nanotubes produced by pyrolysis of iron(II) phthalocyanine. Physica. B 2002. 323. 336–338 and references therein.
12. Hanack, M.: Schneider. T.: Barthel, M.; Shirk, J.S.: Flom, S.R.: Pong, R.G.S. Indium phthalocyanines and naphthalocyanines for optical limiting. Coord. Chem. Rev. 2001. 219–221. 235–258.
13. Kimura. M.: Nakada. M.: Yainaguchi, Y.: Hanabusa. K.: Shirai. H.; Kobayashi. N. Dendric metallophthalocyanines: Synthesis and characterization of a zinc(II) phthalocyanine[8]^3-arborol. J. Chem. Soc. Chem. Commun. 1997, (13). 1215–1216.
14. Jiang, D.L.: Aida, T. Photoisomerization in dendrimers by harvesting of low-energy photons. Nature 1997, *388*, 454–456.
15. Sadamoto, R.; Tomioka, N.; Aida. T. Photoinduced electron transfer reactions through dendrimer architecture. J. Am. Chem. Soc. 1996. 118, 3978–3979.
16. Roisin, P.: Wright. J.D.: Nolte. R.J.M.: Sielcken. O.E.: Thorpe, S.C. Gas-sensing properties of semiconducting-films of crown-ether-substituted phthalocyanines. J. Mater. Chem. 1992. 2 (1). 131–137.
17. Ishikawa, N.; Kaizu, Y. Synthetic, spectroscopic and theoretical study of novel suprainolecular structures composed of lanthanidephthalocyaninedouble-deckercomplexes. Coord. Chem. Rev. 2002,226.93–101 and references therein.
18. Maitrot, M.: Guillaud. C.: Boudjema, B.; André, J.-J.; Strzelecka, H.: Simon. J.: Even. R. Lutetium bisphthalocyanine: The first molecular semiconductor. Conduction properties of thin films of *p*- and n-doped materials. Chem. Phys. Lett. 1987. 133 (1). 59–62.
19. Kobayashi. N. Dimers. trimers and oligomers of phthalocyanines and related compounds. Coord. Chem. Rev. 2002. 227. 129–152.
20. Guillaud, G.; Simon. J.; Germain, J.P. Metallophthalocyanines: Gas sensors. resistors and field effect transistors. Coord. Chem. Rev. 1998. *178–180*. 1433–1484 and references therein.
21. Wohrle. D. Phthalocyanines in macromolecular phases—Methods of synthesis and properties of the materials. Macromol. Rapid Commun. 2001. 22 (2). 68–97.
22. McKeown. N.B.; Makhseed. S.; Budd. P.M. Phthalocyanine-based nanoporous network polymers. Chem. Commun. 2002. (23). 2780–2781.
23. Moser, F.H.;Tomas. A.L. The *Phthalocyanines*; CRC Press: Boca raton. 1983; Vol. 1, 21–33. Vol. 2. 105.
24. Engel, M.K. Single-crystal and solid-state molecular structures of phthalocyanine complexes. Report Kawamura Inst. Chem. Res. 1997. 8, 11–54.
25. Yarnada. H.: Shimada, T.: Koma. A. Preparation and magnetic properties of manganese(II) phthalocyanine thin films. J. Chem. Phys. 1998. 108, 10256–10261.
26. Luneau. D. Molecular magnets. Curr. Opin. Solid State Mater. Sci. 2001. 5 (2–3), 123–129.
27. Sellers, S.P.: Korte, B.J.: Fitzgerald, J.P.; Reiff, W.M.: Yee, C.T. Canted ferromagnetism and other magnetic phenomena in square–planar. neutral manganese(II) and iron (II) octaethyltetraazaporphyrins. J. Am. Chem. Soc. 1998. 120 (19). 4662–4670.
28. Griesar. K.: Athanassopoulou, M.A.; Soto Bustamante, E.A.: Tomkowicz, Z.: Zaleski. A.J.; Haase. W. A ferrimagnetically coupled liquid crystal. Adv. Mater. 1997. 9 (1), 45–48.
29. Kobayashi, T.: Isoda, S. Lattice images and molecular images of organic materials. J. Mater. Chem. 1993. 3 (1). 1–14.
30. Coppens, P.: Li. L.: Zhu. N.J. Electronic ground state of iron(II) phthalocyanine as determined from accurate diffraction data. J. Am. Chem. Soc. 1983.105.6173–6174.

π–π interactions: Theory and Scope

Ban *Dance*
University of New South Wales, Sydney, New South Wales, Australia

INTRODUCTION

Intermolecular interactions involving aromatic sections of molecules are common in chemistry, biology, and materials science. The prototypical properties and conceptual framework for these interactions are introduced first, then the scope of the interaction will be surveyed, followed by more detailed description of key current fields of investigation and application.

FUNDAMENTALS

An aromatic hydrocarbon molecule, usually flat, contains a cyclic or polycyclic carbon framework that supports π-delocalized electron density. The n-electron density is polarizable, and this enhances the stabilizing dispersion interactions between the aromatic molecule and its neighbors. In addition, if there are more polarizable (larger Z) atoms or groups involved in the n-delocalized bonding, these dispersion stabilizations are further enhanced. In these ways, the underlying van der Waals contributions to intermolecular stabilization energy are more favorable for π-delocalized aromatic molecules than for analogues without this bonding.

There is also an electrostatic component of the intermolecular stabilization, and this provides directionality. In an aromatic hydrocarbon, there is small polarization of C–H bonds, yielding a slightly negative charge over the n-bonded core, relative to the slightly positive rim of hydrogen atoms on the edge of the molecule. This may or may not introduce a molecular dipole, depending on the structure of the molecule, but it will introduce higher multipoles: benzene, for example, possesses a quadrupole moment.

Maximization of the electrostatic stabilization energy between multipoles is the source of directionality in aromatic–aromatic interactions. The concepts of multipoles can be substituted with the more chemically intuitive concepts of favorable orientation of the relatively positive and negative sections of the molecule. Consistent with these fundamental properties, there are two commonly observed geometrical relationships between adjacent aromatic molecules. These are illustrated for benzene in Fig. 1, and they are known as the offset-face-to-face (OFF) motif, and the edge-to-face (EF) motif. In the OFF geometry, the molecules are exactly or closely parallel but are offset so that the oppositely charged regions of the molecules are closest. In the EF motif (sometimes vertex-to-face, sometimes called T-shaped) the relatively positive hydrogenic rim is directed toward the central negative π-electron density.

There is a third geometrical type, in which parallel aromatic molecules are parallel but not offset, i.e., face-to-face (FF) or eclipsed. For the electrostatic reasons just outlined, this is not an energy minimum for a pair of identical molecules in a symmetrical motif and is rarely observed. However, if the two aromatic molecules in a motif are different, with complementary electron distributions, the FF motif can be the energy minimum. One of the better-known instances of this is the intermolecular interaction between a hydrous arene and a perfluorous arene. Due to the opposite polarization of the C–H and C–F bonds, the molecular quadrupoles of C_6H_6 and C_6F_6 are oppositely signed, and so the electrostatic intermolecular stabilization between them is maximized with FF geometry.

In this article. the adjective "aromatic" is generally used to encompass many chemical types characterized by delocalized n-bonding and relatively flat local geometry.

The term "n-stacking" is commonly used for aromatic–aromatic interactions. This is sometimes appropriate. but often is not because only two molecules are involved, or because there is EF geometry. Throughout this article, the generic description "aromatic–aromatic interactions" is used, and the term "stack" is used only for legitimate sequences of parallel molecules.

The content of this article is restricted to systems with at least two aromatic molecules: there are other sets of intermolecular interactions involving cations, or hydrogen-bonding molecules,[1] interacting with the π-delocalized aromatic molecules.

At the outset, it is important to appreciate the energies of aromatic–aromatic intermolecular interactions. The stabilizing energy for a pair of benzene molecules in either the OFF or EF arrangement is about 2.2 kcal mol^{-1} (9 kJ mol^{-1}), which is about 40% of the energy of a hydrogen bond between two water molecules. Further energy information is provided later in this article in the section entitled "Geometries and Energies of Intermolecular Aromatic Interactions."

Encyclopedia of Supramolecular Chemistry
DOI: 10.1081/E-ESMC 120012670

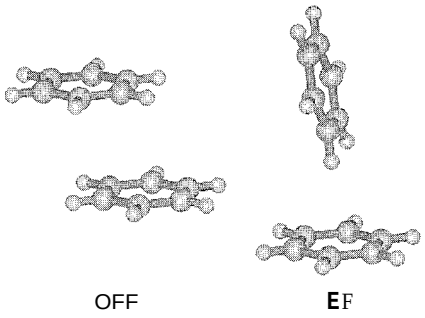

Fig. 1 The offset-face-to-face *(OFF)* and edge-to-face *(EF)* motifs for benzene. *(View this art in color at www.dekker.com.)*

The primary concept for aromatic–aromatic interactions is nondirectional van der Waals stabilization, enhanced by π-polarizability, plus electrostatic stabilization that is directional. This concept needs to be expanded, because there are additional sources of stabilization. Where two aromatic molecules have different electron affinities, such that there is a complementary relationship of electron-donor–electron-acceptor, then there is a stabilizing charge-transfer component to the interaction (see section below entitled "Polarizable π-Donors and n-Acceptors and Significant Charge-Transfer Solids"). As an extension of this, if one of the aromatic entities is charged, there is additional electrostatic stabilization of the interaction. and if two adjacent aromatic entities have opposite charges, there is strong electrostatic stabilization that dominates the other intermolecular energies. Partial charging of aromatic entities in opposite directions occurs when there is substantial difference in electron affinities or redox potentials, and electron transfer occurs from donor to acceptor.

In addition, the general hydrophobic character of aromatics (at least of aromatic hydrocarbons) leads to a solvophobic stabilization in polar and hydrogen-bonding solvent systems: the concept is that segregation of hydrophobic and hydrophilic components in the condensed phases is thermodynamically advantageous.

Another basic determinant of aromatic–aromatic interactions is molecular shape. The aromatic sections of molecules are generally flat and disc shaped. Purely geo-

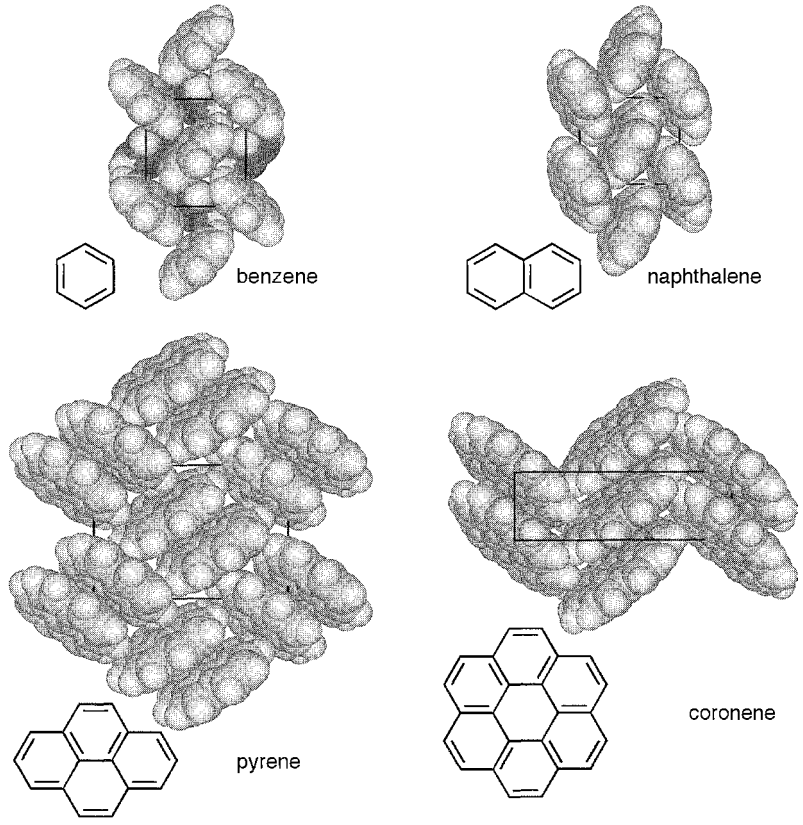

Fig. 2 Comparable representations of the crystal structures of benzene, naphthalene. pyrene, and coronene. Each projection is along the appropriate crystallographic axis. and in all structures except benzene, the molecular arrangement is simply translated along the projection axis. The different packing of benzene is illustrated by inclusion of part of the layer behind. with carbon colored blue. (*View this art in color ut www.dekker.com.*)

metric factors are involved in considerations of the modes of association. A stacking of discs is clearly efficient but also generates substantial intermolecular space around the edges of the discs. The area of the disc relative to its thickness influences the modes of association of aromatics. For relatively small areas, the EF motif can be developed more effectively than the OFF motif, and the herringbone pattern that contains only EF motifs is commonly observed. As the area of the aromatic face increases, the OFF motif becomes more prevalent. This trend in geometrical structure for aromatic–aromatic interactions is manifest in the crystal structures of polycyclic arenes, as exemplified in Fig. 2 for benzene. naphthalene. pyrene. and cossolene. In benzene and naphthalene, the crystal packing is herringbone, with no OFF motifs. In crystalline pyrene, pairs of molecules in the OFF motif are repeated in herringbone fashion, while in the larger corrolene molecular crystal, there are infinite offset stacks of aromatics, with the maximum number of OFF motifs. This analysis was applied to a larger number of polycyclic arenes.[2]

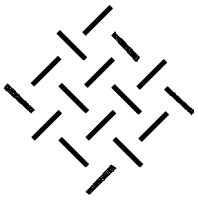

herringbone pattern

In Fig. 2. it is noticeable that there is variation in the angle between arene planes in the EF motifs. This is characteristic of aromatic–aromatic intermolecular motifs: there is little variation in energy with angle, and the concept of a continuous range of stability between the parallel OFF motif and the angled EF motif is valid. Aromatic–aromatic intermolecular potentials are soft.

At the upper size limit of aromatic systems, nonmolecular graphite, the structure is completely π-stacked. and offset. The shearing softness of graphite manifests the soft energy variation with the degree of offset in parallel motifs. (Further information on this is provided in the section below entitled "Geometries and Energies of Intermolecular Aromatic Interactions.") Offset stacks are also named "slipped π-stacks'' or "skew stacks."

THE SCQPE OF AROMATIC–ARBMATE INTERACTIONS

In this section. some of the diversity and scope of aromatic–aromatic interactions is illustrated. For example, the curved surfaces of C_{60} and other fullerenes are known to engage in parallel and oblique interactions with other arenes, mimicking the OFF and EF motifs.[3]

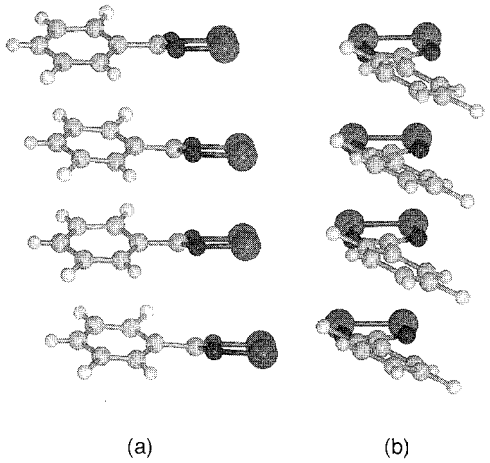

Fig. *3* The stacking of the difluorophenyl diselenadiazolyl radicals (2. E = Se) showing (a) the almost eclipsed stacking of diselenadiazolyl rings and (b) the offset stacking of the difluorophenyl rings: Se. red: N, blue; F, yellow. (Adapted from Ref. [5].) (View *this art* in color *at www.dekker.com.*)

Heteroarornatic molecules. and particularly polycyclic arenes with N, O, or S substitution for carbon. are prone to aromatic–aromatic interactions. As the size of the x-delocalized system increases, the OFF motif prevails over EF, but because the charge distribution and occurrence of dipoles and higher electrostatic multipoles can be variable in heteroaromatics, the nature of any offset between parallel planar molecules can similarly be variable. Net charges that can occur on heteroaromatic molecules also influence intermolecular energy and geometry.

Odd-electron aromatic systems, such as the thiazolyl radicals **1**[4] and **2**[5] form x-stacks. Shown in Fig. 3 are details of the stack formed by 2 (Se). revealing that the diselenadiazolyl rings are stacked in almost eclipsed FF geometry. while the difluorophenyl ring is twisted from the plane of the diselenadiazolyl ring so that the stack of difluorophenyl rings has the normal offset geometry. Some radical species undergo a weak dimerization and pairing of the electrons. which results in irregular stacking: these effects are significant for the magnetic properties and applications of these paramagnetic aromatic materials.

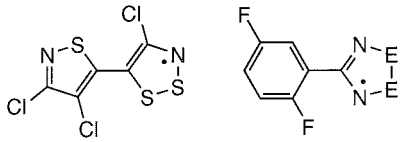

1 **2** E = S, Se

Metalloporphyrins **3** and metal phthalocyanine complexes 4, as well as the metal-free ligands, commonly engage in aromatic–aromatic interactions.

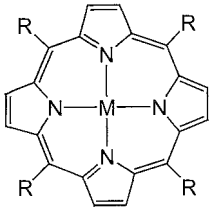

3

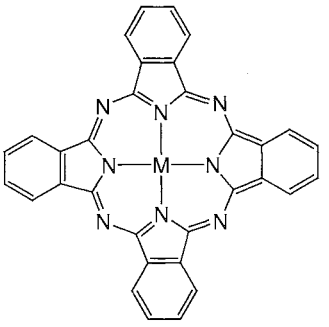

4

Metallocene molecules, such as the prototype ferrocene 5. pack in crystals mainly with EF motifs, similar to the crystal packing of benzene.

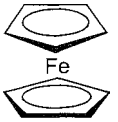

5

Organometal compounds like 6 form π-stacks[6] as illustrated in Fig. 4.

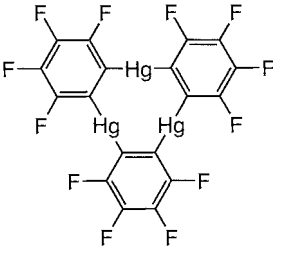

6

A significant property of Structure 6 is the intercalation of polycyclic arenes to form binary stacks of alternating 6 and arene.[6,7] The structure of the mixed stack of **6** and pyrene is shown in Fig. 5. The photophysical properties of these compounds are significant. and the binary stacked compounds with pyrene. naphthalene. and biphenyl exhibit strong phosphorescent emissions in the red. green, and blue regions. respectively.[7]

Aromatic interactions occur between conducting partially oxidized polyheteroarene polymers. such as polythiophene.[8]

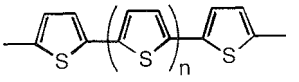

polythiophene

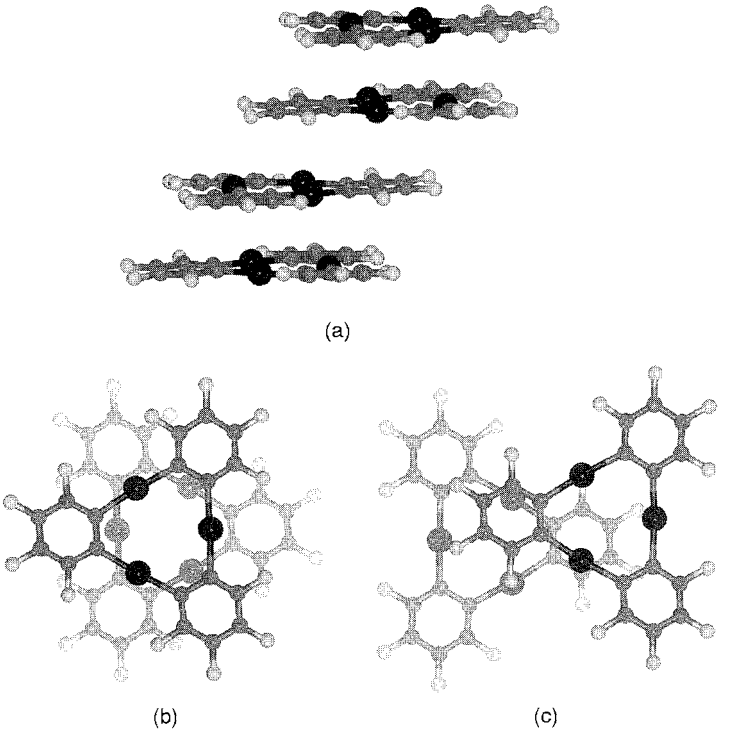

Fig. 4 Aspects of the crystal structure of Structure 6, which forms stacks with two different offset motifs. Motif (b) with plane separation ca. 3.3 Å is that of the outer pairs of (a). and motif (c) (plane separation ca. 3.45 A) is the inner pair in (a). (*View* ***this*** *art in color at www.dekker.com.*)

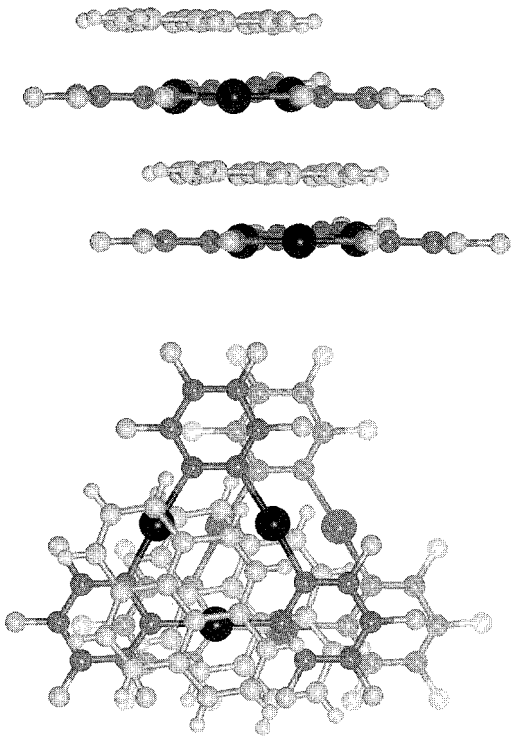

Fig. 5 The alternating π-stack of 6 and pyrene. (*View this art in color at www.dekker.com.*)

The stacking of the hydrogen-bonded base pairs of helical DNA is well-known and is described, together with the intercalation of heteroaromatics into the stack. in the section entitled "DNA Base Stacking" below,

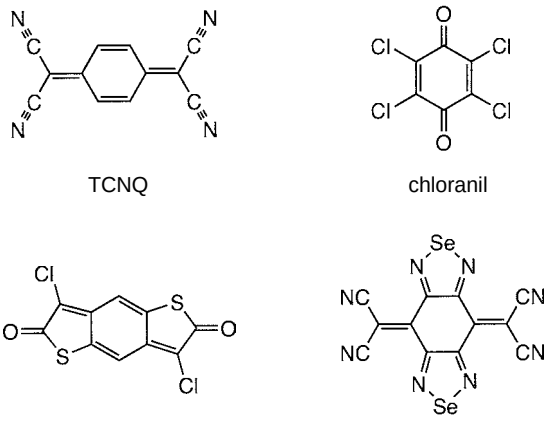

Chart 2 n-Acceptors

The influences of aromatic–aromatic interactions between the side chains of amino acids phenylalanine. tyrosine, and tryptophan affecting protein structure and folding were reported.[9 10]

POLARIZABLE κ-DONORS AND κ-ACCEPTORS AND SIGNIFICANT CHARGE-TRANSFER SOLIDS

Aromatic molecules containing high-Z heteroatoms are more polarizable than corresponding molecules containing carbon or nitrogen. and this increases the disper-

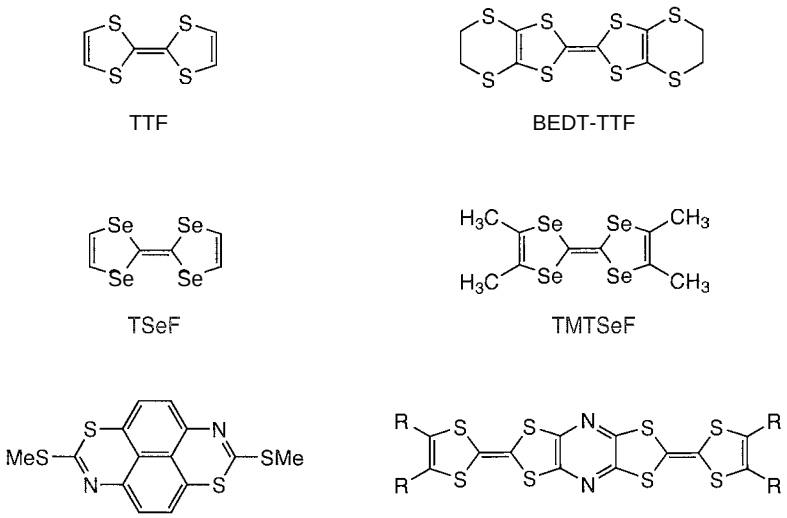

Chart I n-Donors

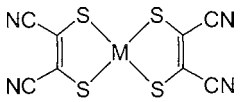

$[M(mnt)_2]^z$

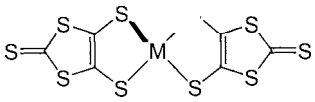

$[M(dmit)_2]^z$

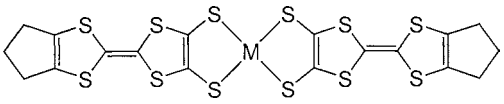

$[M(tmdt)_2]$

Chart 3 Some metal–dithiolene complexes.

sion stabilization of intermolecular interactions. Further, substitution of electron-donating or electron-withdrawing atoms or groups at appropriate locations in a molecule can change its overall electronegativity. This leads to π-delocalized heteroaroniatic molecules with distinct donor and acceptor properties, which then leads to partial charge transfer when donors and acceptors are combined. This charge transfer influences the electrostatics of the heteroaromatic–heteroaromatic interactions. Donor properties correspond to relatively low ionization potential (or favorable electrochemical oxidation potential), and are enhanced by electron-releasing substituents or negative charge, while acceptor properties are the opposite. Many combinations of polarizable π-donors and polarizable n-acceptors are now known in condensed phase materials, mainly crystals. Extensive investigation of these compounds has been stimulated by discoveries so that a number of them have enhanced electron conductivity and are regarded as "organic metals."

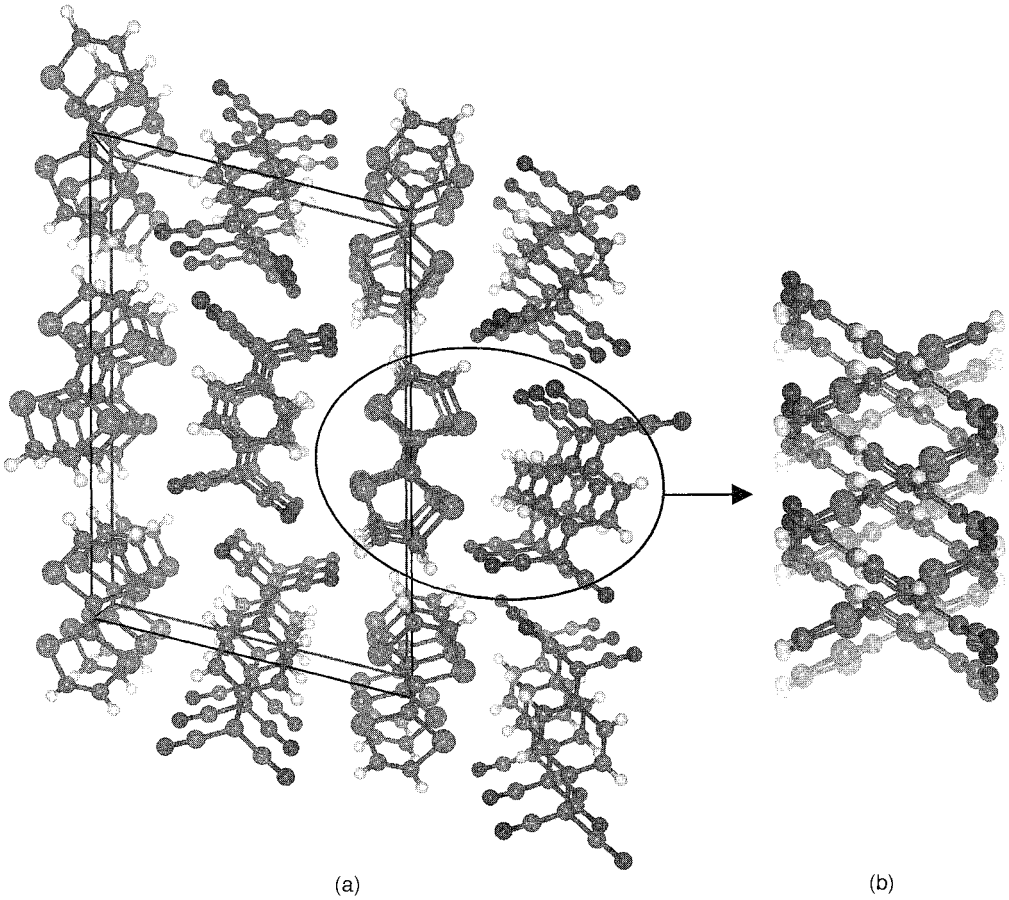

Fig. 6 Aspects of the crystal structure of TSeF–TCNQ [14] (a) The tuo components. TSeF (Se. led) and TCNQ, occur in segregated stacks. drawn with perspectıve (b) The stacks of TSeF and TCNQ are oppositely inclined to the stacking axıs (25° TSeF, 34° TCNQ). and within each stack, the molecules are OFF (*Vieu this aıt ın colo1 at www dekker coin*)

A few typical examples of the hundreds of such donor and acceptor heteroaromatic molecules[11,12] are shown in Charts 1 and 2.

Metal dithiolene complexes[13] such as $[M(mnt)_2]^z$ and $[M(dmit)_2]^z$ (see Chart 3) are electron-transfer active and can be readily generated in oxidized or reduced forms with variable charge z and can be used as either donors or acceptors.

One of the most studied donor–acceptor complexes is TTF–TCNQ, and its selenium homoiogue TSeF–TCNQ. Shown in Fig. 6 are aspects of the crystal structure of TSeF–TCNQ.[14] It is estimated that the degree of charge transfer in this solid is 0.63,[15] i.e., the species are $TSeF^{+0.63}$ or $TCNQ^{-0.63}$. The n-interactions occur within the stacks of homo-charged species, and the interplanar spacings are relatively small. 3.52 Å for TSeF and 3.21 Å for TCNQ. TTF–TCNQ and TSeF–TCNQ are one-dimensional conductors along the stack direction.

In Fig. 7, part of the structural chemistry of a different example is shown, with the composition $(BEDT\text{-}TTF)_2[Br_{1.3}I_{1.1}Cl_{0.6}]$.[16] The anion component is a mixture of the mixed trihalides I_2Br^-, IBr_2^-, $BrICl^-$, and ICl_2^-, which is specifically required to form this material that has three crystal phases. One phase. β″, is metallic and occurs in two separate temperature ranges; <185 K and >395 K, and is shown in Fig. 7. It contains stacks of $BEDT\text{–}TTF^{+1.5}$ cations, separated by layers of trihalide monoanions. The other phases have different geometrical relationships between the $BEDT\text{–}TTF^{+1.5}$ stacks.[16]

There are numerous examples of donor–acceptor complexes involving components like those in Charts 1 and 2 and dithiolene complexes. While there is considerable structural diversity, n-stacking is a common feature. Another common property is partial charge transfer from donor to acceptor, and anions such as $(TCNQ)_3^{2-}$ occur. As intimated in the previous example: small variations in structure can have large effects on physical properties.

Metallic conductivity, superconductivity, and cooperative magnetic properties are the most significant attributes of these donor–acceptor (and partial charge transfer) solids.[15] These properties derive from the partially occupied delocalized n-orbitals of the donor and acceptor species. which overlap to form energy bands along the stacks. Interactions between the stacks are less important, as the conductivities are usually anisotropic. Enlargement of the donor and acceptor species diminishes the coulombic destabilization of stacks of homo-(partially)-charged molecules.

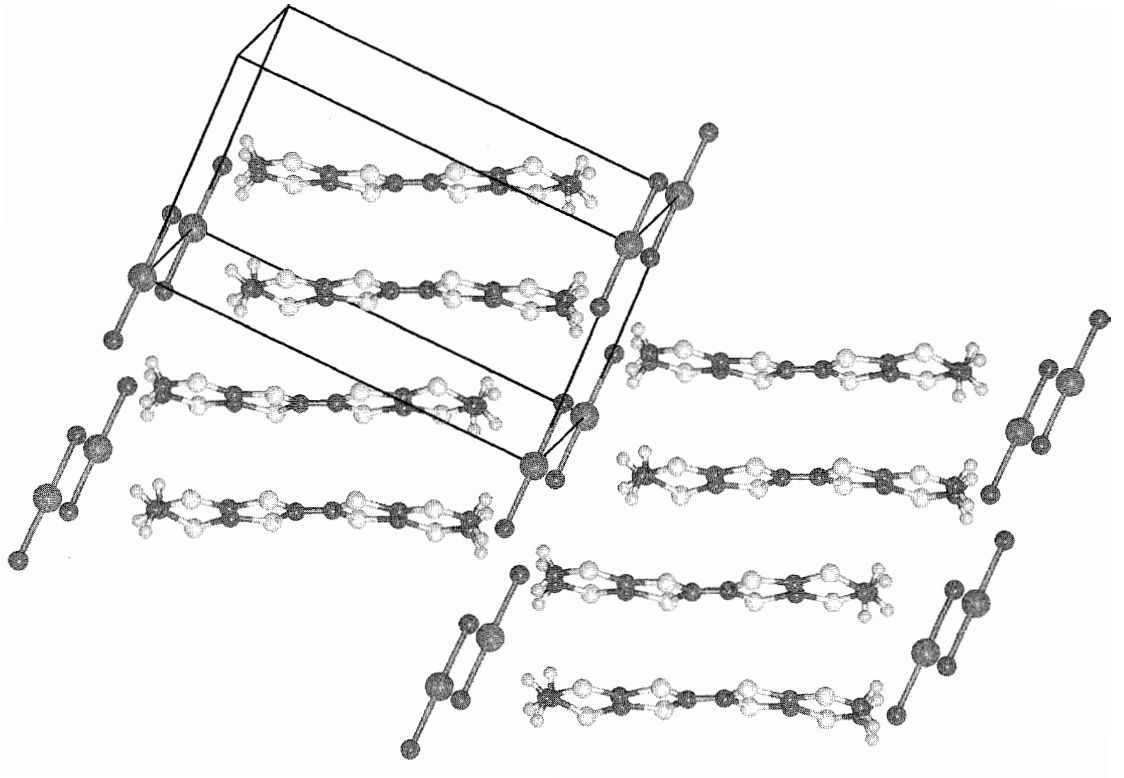

Fig. 7 The crystal structure of the metallic β″ phase of $(BEDT\text{-}TTF)_2[Br_{1.3}I_{1.1}Cl_{0.6}]$,[16] illustrating the stacking of $BEDT\text{-}TTF^{+1.5}$ cations. The trihalide ion represented in magenta and brown is a disordered mixture of I_2Br^-, IBr_2^-, $BrICl^-$ and ICl_2^-. (*View this art in color at www.dekker.com.*)

SINGLE-MOLECULE π-STACKED METALLIC CONDUCTION

Most of the molecular compounds with significant electrical conductivity or magnetic properties contain donor–acceptor pairs or are comprised of partially charged n-delocalized molecules. The two solids described in the previous section exemplify these two types. The generation of these properties in a single molecule, desirable from the practical perspective of sure fabrication. is more difficult. The strategy is to choose a molecule with small separation between the highest occupied and lowest unoccupied molecular orbitals (HOMO and LUMO), such that they form partially occupied bands. A molecule that achieves this is uncharged Wi-$(tmdt)_2$,[17] (Chart 3) which is metallic down to 0.6 K. The important aspects of the crystal structure are shown in Fig. 8.

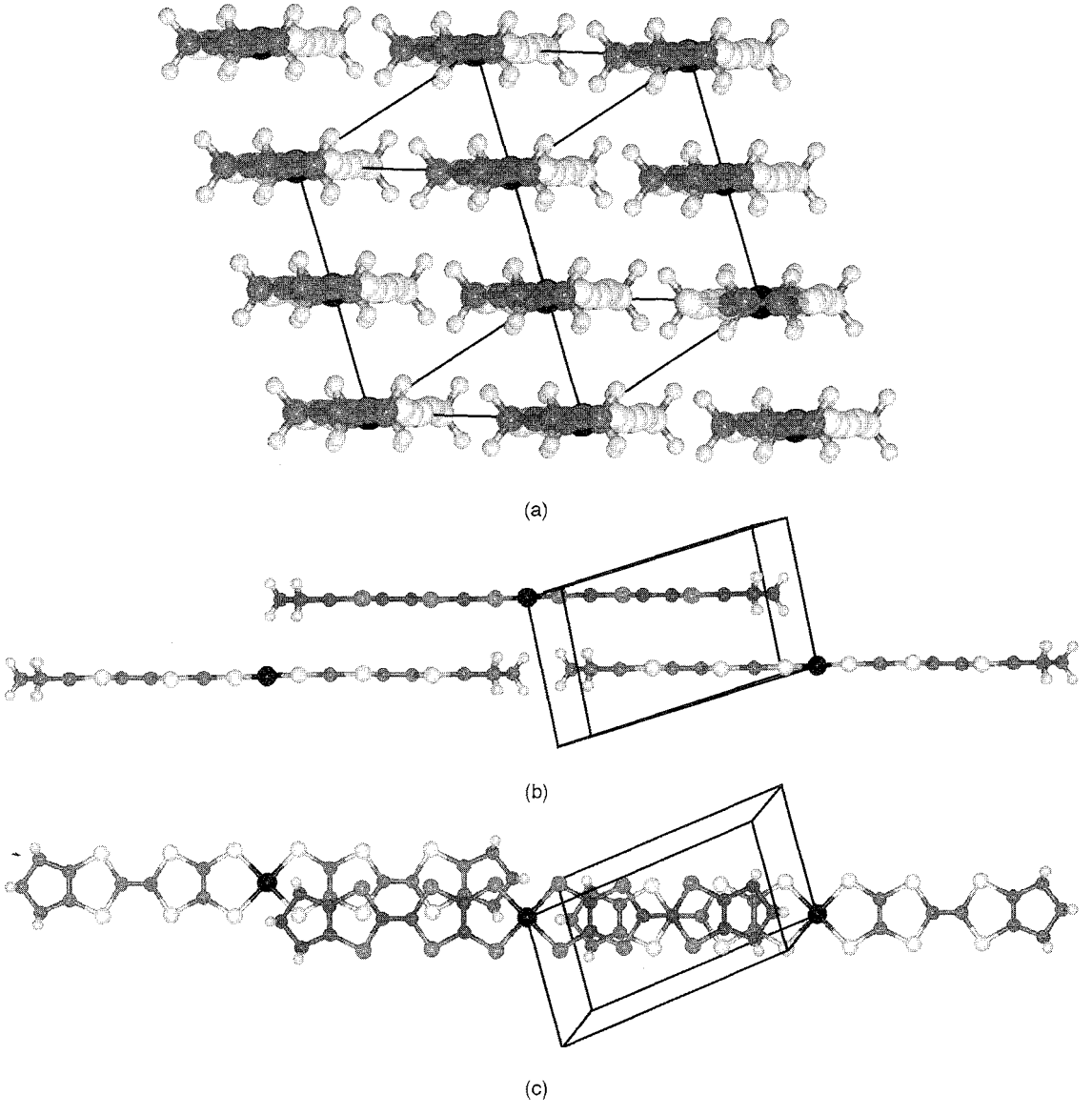

Fig. 8 The crystal structure of $Ni(tmdt)_2$,[17] space-group $P\bar{1}$. (a) End view of the chains of molecules. and their occurrence as slightly offset stacks of chains. Near chains are almost coplanar. (b) The stepped relationship between molecules adjacent in one stack. (c) Detail of the offsets between molecules [colored as in (b)] in a stack: the view direction is perpendicular to the molecules. The C (blue)/S (red) molecule is offset laterally relative to one greenlyellow underlying molecule, and offset longitudinally relative to the next green/yellow underlying molecule. Note also that molecules (greenlyellow) in a chain are slightly twisted relative to the chain axis in order to reduce interference between the propylene ends of each molecule and increase packing density. (*View this art in color at www.dekker.com.*)

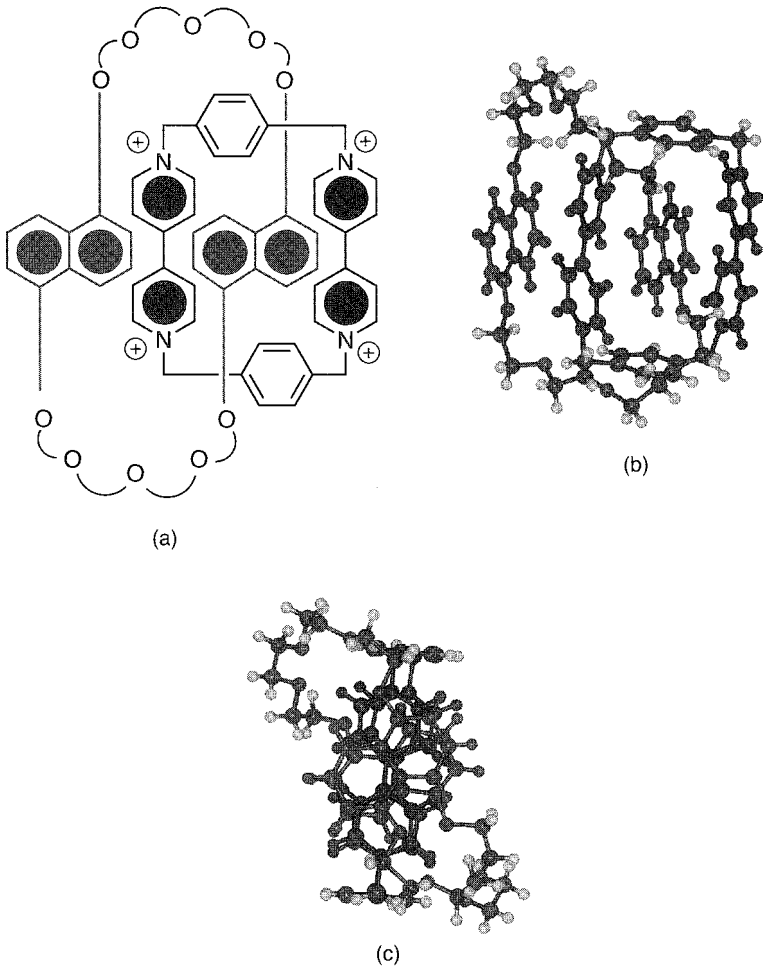

Fig. 9 The [2]catenane formed by donor–acceptor interactions between a *bis*-1,5-dioxynaphthalene cycle (red, donor) and a *bis*-4,4′-bipyridinium cycle (blue, acceptor). (a) Molecular connectivity: the curved lines represent $-(CH_2CH_2)-$. (b) The catenane as it occurs in the crystal. (c) View of (b) normal to the planes of the 1,5-dioxynaphthalene and 4,4′-bipyridinium rings. showing the FF geometry of red and blue components. (Adapted from Ref. [18].) (*View this* urt in color *nt www.dekker.com.*)

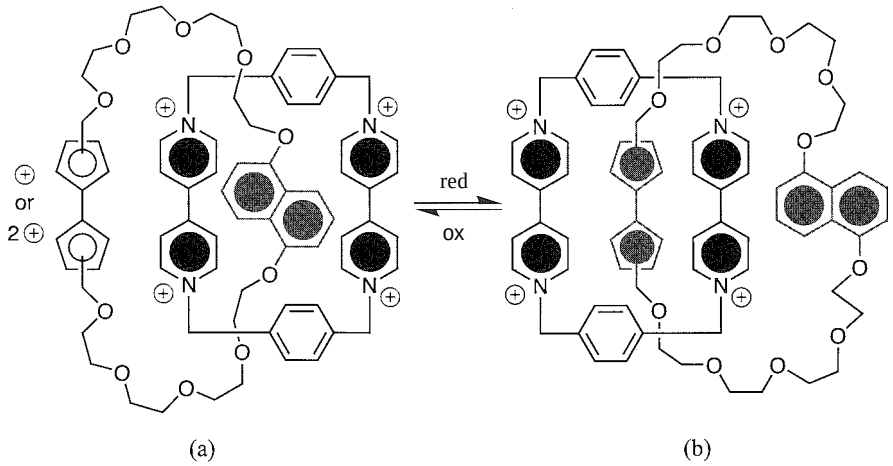

Fig. 10 A switchable [2]catenane, using a TTF function. (a) The TTF oxidized by one or two electrons outside the positively charged 4,4′-bipyridinium acceptor sandwich. (b) This is the reduced form. in which TTF is the better π-donor, inside the sandwich. (Adapted from Ref. [19].) (*View this art in* color *at www.dekker.com.*)

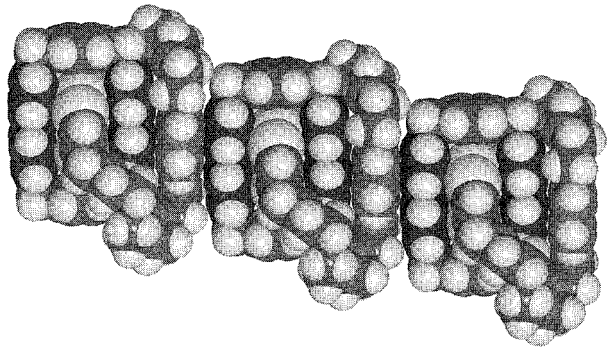

Fig. **11** The donor–acceptor stacking of the [2]catenane moiecules shown in Fig. 10b. The 4,4′-bipyridinium carbon atoms are coloured blue; 1.5-dioxynaphthalene carbon atoms are red; sulfur atoms of TTF are yellow. (View *this art in* color *at www.dekker.com.*)

DONOR–ACCEPTOR π-INTERACTION IN CATENANES

An extensively studied and deployed donor–acceptor π-interaction occurs between a 1,5-dioxynaphthalene system (as donor) and a 4,4′-bipyridinium (also known as paraquat) acceptor. The association of these two species can be used as a template for the cyclization reactions involved in the synthesis of mechanically linked chemical structures,[18] such as the [2]catenane shown in Fig. 9.

The augmented electrostatic contributions to a donor–acceptor interaction such as this can override the electrostatic influences that cause a parallel n-aromatic interaction to be offset. and so the geometry of the motif can be FF, as illustrated in Fig. 9c. to maximize the electrostatic component of the stabilization.

The TTF molecule (Chart 1) is a π-delocalized system with readily accessible redox states. TTF. TTF^{+}, and TTF^{2+}. The reduced form functions as a n-donor in FF interactions, but the oxidized forms have n-acceptor character. Incorporation of one TTF moiety into a donor cycle also containing 1.5-dioxynaphthalene, and catenation with a *bis*-4,4′-bipyridinium n-acceptor cycle. leads to a switchable [2]catenane (Fig. 10). In the reduced TTF form (Fig. 10b), the TTF molecule, as donor, is sandwiched between the two 4,4′-bipyridinium acceptors. When oxidized (chemically or electrochemically). so that the TTF has a positive or 2+ charge (Fig. 10a), electrostatics cause rotational translation of one cycle relative to the other to displace the positive TTF to the outer section of the catenane. This switching is reversible.[19]

In crystals. [2]catenane molecules, such as those in Fig. 9 and Fig. 10b, stack in order to further use n-donor and n-acceptor motifs between catenane molecules, as illustrated in Fig. 11.

MULTIPLE AROMATIC EMBRACES

The examples so far involve independent aromatic moieties, freely able to arrange into OFF and EF motifs. There are also chemical systems in which the aromatic component is a substituent or is part of a more elaborate molecule. In these; the mutually dependent configurations and conformations of the aromatic groups influence the intermolecular interactions they can form. A considerable number of classes of compounds allow synergy of individual aromatic–aromatic interactions. and the generation of concerted sets of OFF or EF motifs. These are termed embraces, because they are multi-armed, mutual, concerted. and attractive. Some of the principal types of embrace are outlined here for representative molecules.

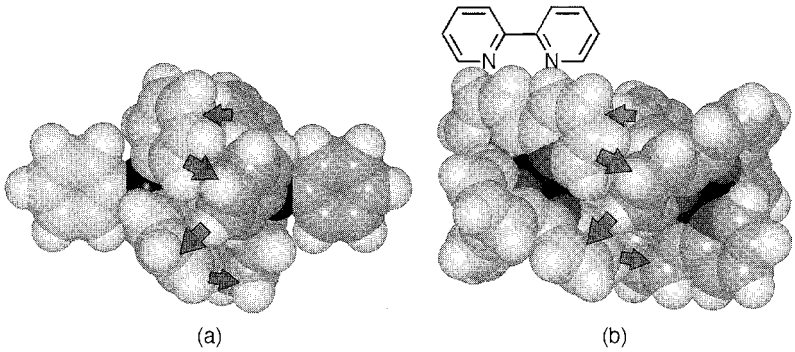

Fig. 12 The concerted $(EF)_6$ embrace (a) between a pair of Ph_4E molecules, involving six phenyl groups. and (b) between a pair of $[M(bipy)_3]$ octahedral inetal complexes. involving six pyridyl groups. The arrows point to the EF primary motifs. two of which are obscured in each example. Different colors are used for the carbon atoms of the inversion-related molecules in each embrace. (*View this art in* color. *at www.dekker.com.*)

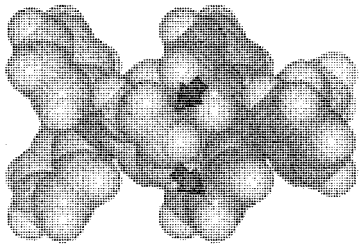

Fig. 13 The $(EF)_4$ embrace between a pair of Ph_4E molecules (*View this art in color at www.dekker.com*)

Concerted $(EF)_6$, Sixfold Aryl Embrace

Molecules with a threefold rotor conformation of three phenyl groups can engage across a center of inversion (exact or approximate) to form a concerted cycle of six intermolecular EF motifs (Fig. 12a). This multi-armed mutually favorable concert is called a sixfold phenyl embrace motif: there are six phenyl rings and a cycle of six EF motifs between heterochiral rotors. This embrace occurs frequently for molecules of type Ph_4E and type Ph_3EX. A similar embrace motif forms between end pyridyl groups of $[M(bipy)_3]^z$ octahedral metal complexes (Fig. 12b) Again a concerted cycle of six pyridyl-edge to pyridyl-face motifs occurs, between heterochiral complexes

A tetrahedral molecule Ph_4E can have more than one threefold rotor set of phenyl groups and can form more than one $(EF)_6$ embrace. There are many instances in crystals of zigzag chains based on two such embraces per Ph_4E molecule, especially between Ph_4P^+ ions: $–Ph_4E–(EF)_6–Ph_4E–(EF)_6–Ph_4E–$[20] A $[M(bipy)_3]$ complex has

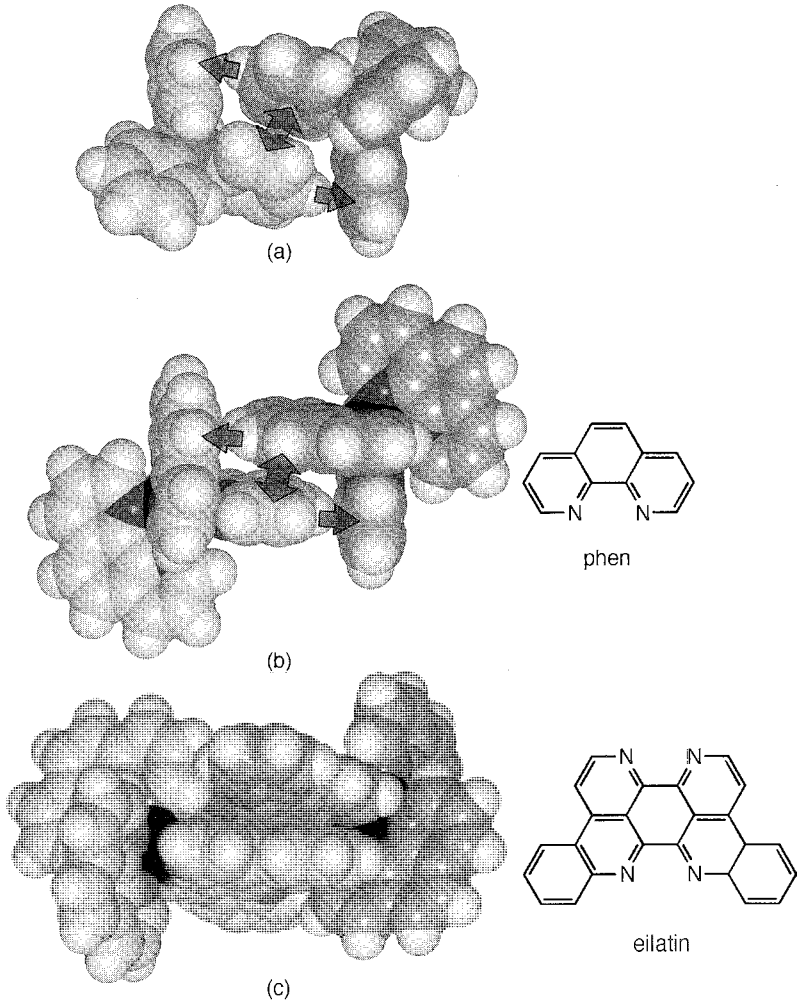

Fig. 14 The concerted $(OFF)(EF)_2$ embrace as it occurs for (a) a pair of Ph_4E molecules and (b) a pair of $[M(phen)_3]^z$ complexes. (c) This shows the embrace between two complexes $[Ru(phen)_2(eilatin)]^{2+}$,[23] emphasizing the OFF motif. Each example is centrosymmetric. (*View this art* in *color at www.dekker.com.*)

equivalent ends along its (pseudo) threefold axis and. thereby. forms linear chains of $(EF)_6$ embraces: –[M(bipy)$_3$]–$(EF)_6$–[M(bipy)$_3$]–$(EF)_6$–.[21]

Concerted $(EF)_4$, Fourfold Phenyl Embrace

The fourfold analog of the sixfold embrace just described is shown in Fig. 13: four phenyl rings are engaged in a concerted cycle of four EF motifs. This occurs mainly with Ph_4E systems, for which the relationship between the two molecules involved is simple translation, and infinite chains with a repeat of just one molecule occur in crystals.

Concerted $(OFF)(EF)_2$ Embrace

This involves two aryl groups on each molecule, and usually it is centrosyminetric. As shown in Fig. 14a,b, there is an OFF motif between two groups, each of which is also donor in an EF motif. The $(OFF)(EF)_2$ embrace is also named the parallel fourfold phenyl(aryl) einbrace, to differentiate it from the orthogonal fourfold phenyl embrace. $(EF)_4$.[22] As the size of a heteroaromatic ligand increases, as in eilatin. the OFF motif in the embrace becomes dominant (Fig. 14c), and the association of the complexes $[Ru(phen)_2(eilatin)]^{2+}$ in acetonitrile is measurable.[23]

This $(OFF)(EF)_2$ embrace and variants commonly occur for $M(phen)_2$ and $M(phen)_3$ complexes,[24] as shown diagrammatically in Chart 4.

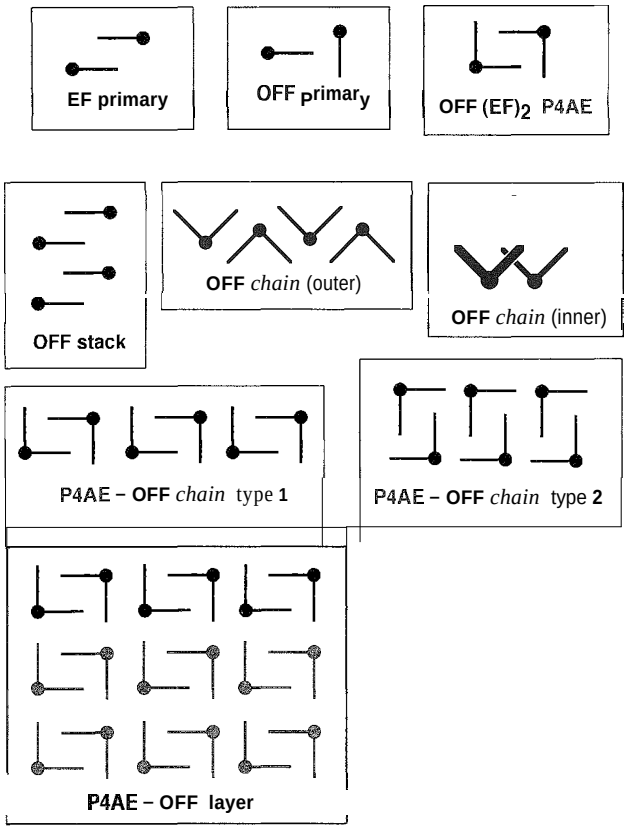

Chart 4 Diagrams of OFF, EF. and $OFF(EF)_2$ motifs that occur for $M(phen)_2$ and $M(phen)_3$ complexes (Adapted from Ref [25].)

The Terpy Embrace Motifs

Octahedral metal coinplexes with two planar heterocyclic tridentate ligands, such as [M(terpy)$_2$] (Fig. 15a), can form an $OFF(EF)_2$ embrace like that already described, involving the outer ligand heterocycles. Because the two ligand planes arc orthogonal. this embrace is propagated to generate a two-dimensional net, shown in Fig. 15b. with actual or approxiinate fourfold symmetry.[26] This close-packed terpy embrace layer contains deep and shallow grooves on each surface, as illustrated in Fig. 15c.

GEOMETRIES AND ENERGIES OF INTERMOLECULAR AROMATIC INTERACTIONS

The benzene pair has been the subject of a number of experimental investigations in the gas phase, and the subject of numerous theoretical studies. There is experimental evidence (summarized in Ref. [27].) for the less symmetric EF geometry and more symmetric OFF structures. and for structural variability. The estimates of the dissociation energy (D_0) are 1.6 ± 0.2[28] 1.6 a 0.5.[29] and 2.4 ± 0.4[30] kcal mol^{-1}. The more accurate theoretical calculations are converging toward values of 2–3 kcal mol^{-1} for the binding energy (D,) at the energy minimum, for both the OFF and EF geometries. The zero-point vibrational energy ($ZPE = D_e - D_o$) for the benzene pair is estimated to be 0.3–0.5 kcal mol^{-1}. The general consensus of experimental and theoretical work is that the dissociation energy of a pair of benzene molecules in the OFF and EF geometries is in the range of 2–2.5 kcal mol^{-1}.

The rich crystallographic databases for organic and organometallic compounds and for biological macromolecules enable statistical analyses of the metrical relationships between aromatic functionalities. The metrical properties of main interest are the separation and offset of the aromatic planes in the OFF motif. and the separation of the ring centroids and the angle of inclination of the rings in the EF motif. The most commonly observed properties of the OFF motif are a plane separation of 3.4–3.6 Å, with an in-plane offset of ca. 1.8 Å, while the EF motif for a pair of phenyl groups has a centroid–centroid separation of ca. 5 A. A useful reference point for the OFF motif is the graphite layer separation of 3.6 A.

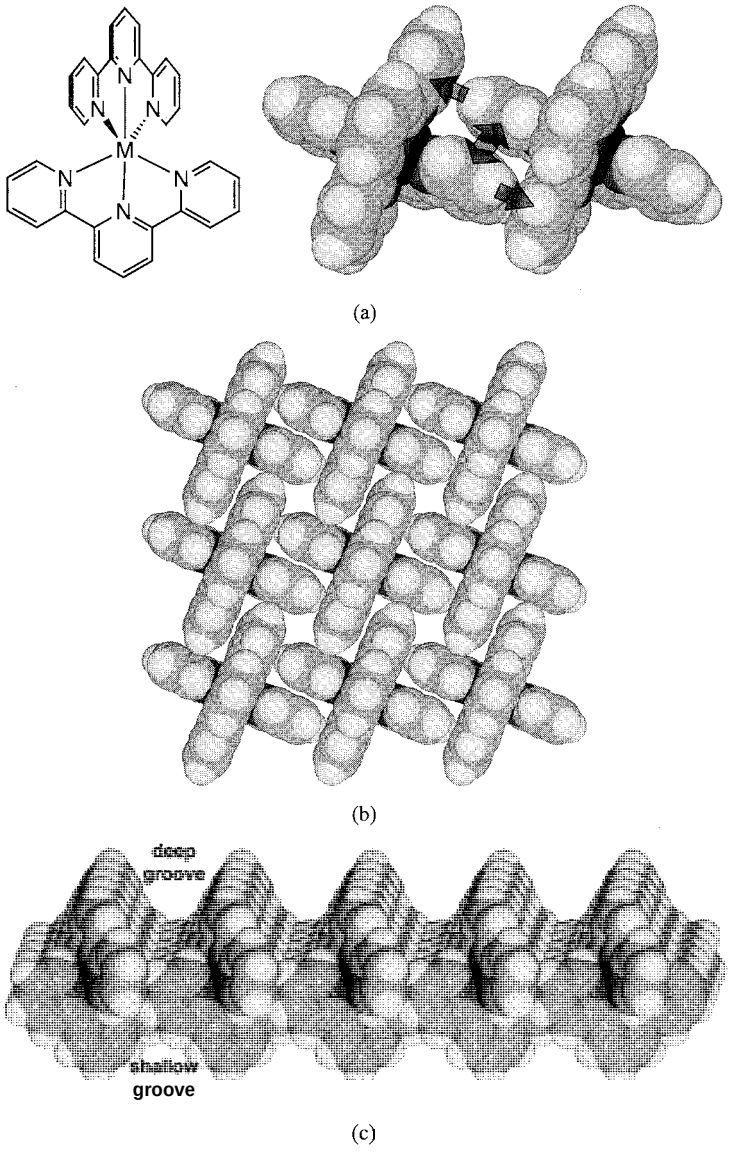

Fig. 15 (a) The OFF(EF)$_2$ embrace, or terpy embrace, formed by a pair of [M(terpy)$_2$] complexes. (b) The two-dimensional net generated by the propagation of terpy embraces. (c) The deep and shallow grooves that occur on both sides of an infinite terpy embrace layer. (View *this art* in *color at www.dekker.com.*)

In this context, it is important to recognize that the intermolecular potentials for aromatic–aromatic interactions are very soft, meaning that relatively large variations in geometry are associated with relatively small changes in energy. This is illustrated in Fig. 16 for the OFF motif of a pair of naphthalene molecules. showing the effect of offset or sliding of one naphthalene molecule over the other, in the direction pictured.[31] For electrostatic reasons, the stabilization decreases strongly when the molecules are eclipsed, and energy minima occur in the potential when there is overlap of H and C atoms. Note that significant intermolecular energy remains when the molecules slide away from each other. The interactions between aromatic molecules operate over long ranges. Analyses of the principal contributions to the intermolecular energy indicate that the dispersion energy is the principal component, and that longer-range electrostatic interactions are also significant and provide the directionality.[32] Since the potentials are soft, interpretations of aromatic–aromatic interactions should not necessarily attach significance to deviations from standard geometries.

In solution; the aromatic–aromatic interactions are ameliorated by solvation and subject to entropic influences. Modeling calculations give the free energy of association of the benzene pair as -0.4 kcal mol^{-1} in benzene solvent, -1.0 kcal mol^{-1} in chloroform: and

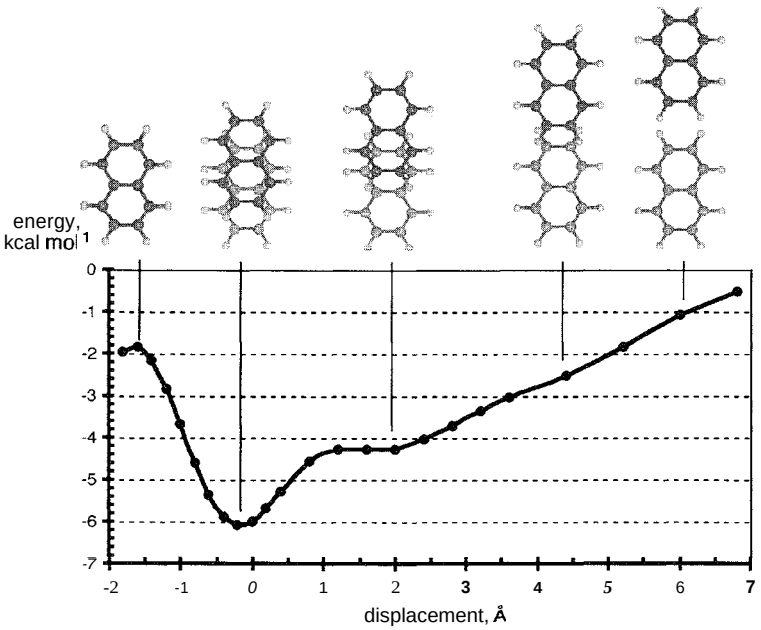

Fig. 16 An intermolecular potential for the OFF motif between a pair of parallel naphthalene molecules and interplanar separation 3.35 Å, illustrated as the energy variation according to the degree of in-plane displacement pictured. (*View* this art *in* color *at www.dekker.com.*)

-1.5 kcal mol^{-1} in water.[''''] This sequence illustrates the hydrophobic stabilization of aromatic–aromatic aggregates in hydrogen-bonding solvents.

A considerable number of chemical systems designed to probe aromatic–aromatic interactions were reported.[10,34] Many of these are host–guest combinations. in which designed host molecules with one or more exposed aromatic surfaces are used to measure the thermodynamics of inclusion of aromatic guests. This approach was also used to assess the influence of substituents on aromatics. In general, the association energies are determined to be ca. 1–2 kcal mol^{-1}.

The involvement of charged species in aromatic–aromatic interactions increases the stabilization energy. For the benzene pair radical cation. $(C_6H_6)_2^+$, experimental values of the dissociation energy are 17, 15, 8. >10 and 14.8 kcal mol^{-1}.[35] Similarly. for the C_6F_6 pair, experimental dissociation energies[36] of 7.2 ± 1 kcal mol^{-1} for $(C_6F_6)_2^+$ and 10.4 ± 1 kcal mol^{-1} for $(C_6F_6)_2^-$ are larger than the estimated 4 kcal mol^{-1} for the uncharged pair $(C_6F_6)_2$.[37]

An unusual interaction occurs for $TCNE^-$ radical anions, which associate as an eclipsed pair $(TCNE)_2^{2-}$ in a number of crystals, with a distance of about 2.9 Å between the central C atoms of the two molecules. This is interpreted in terms of competition between the electrostatic destabilization of the two anions and weak stabilization of nascent C–C bonds.[38]

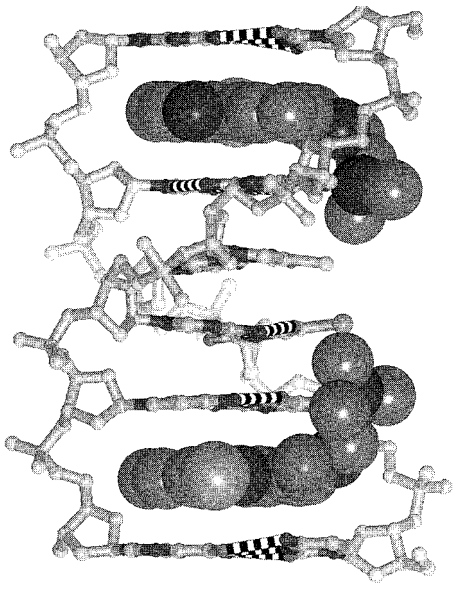

Fig. 17 The crystal structure of the centrosymmetric double intercalation of DACA molecules (large spheres) into a d(CG(5-BrU)ACG)$_2$ duplex. (Adapted from Ref. [40].) Black and white stripes are the hydrogen bonds of base pairs: Br, orange: **O.** red; and N. blue. (*View* ***this*** art in color at *www.dekker.com.*)

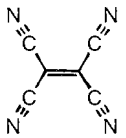

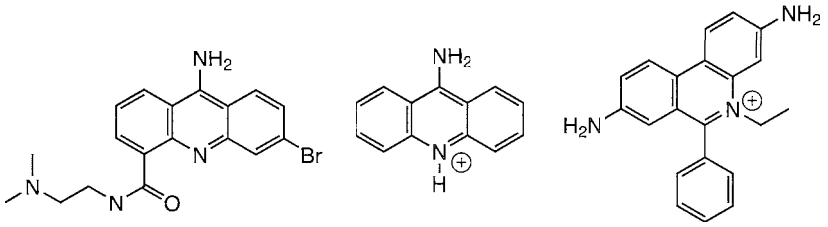

DACA 9-aminoacridine ethidium

Chart 5

DNA BASE STACKING

An essential characteristic of DNA is x-stacking. The base pairs are separated by 3.4 Å, which is the rise of the double helix per base pair. The stacking is not offset: and the different base pairs are essentially coaxial with the local stacking axis. The stacking stabilizations per single base in DNA were measured via the effects of additional nucleoside bases at the end of a DNA sequence. These experiments, on realistic condensed phases (1 M aqueous NaCl, 10 mM sodium phosphate buffer, pH 7, 37°C), yield stacking free energies of 1–2 kcal mol^{-1}.[39] There is considerable compensation of favorable enthalpies and unfavorable entropies in the stacking of nucleotide base pairs.

Many polycyclic heteroaromatic molecules with essentially planar geometry and extensive n-delocalization are able to intercalate the base pair stack, separating the base pairs, and then functioning like an extraneous base pair in the stack. This is an expanded modification of the n-stacking of DNA. An example of such intercalation is shown in Fig. 17, where two DACA molecules are inserted into a six-base duplex.[40] Other examples of well-studied DNA intercalating molecules are 9-aminoacridine and ethidium (Chart 5). This intercalation interferes with the normal functions of the DNA and attracts pharmaceutical interest. There is a substantial electrostatic component of the stabilizing energies of the base stacking and the intercalation.[41,42]

CONCLUSION

Identifiable interinolecular interactions and motifs between molecules with n-delocalized bonding are ubiquitous. The essence of the interaction is dispersion stabilization, enhanced by the polarizability of the π-electronic structure. In addition. there is electrostatic stabilization, the magnitude of which can vary widely, from relatively small in the prototypical aromatic hydrocarbons, to dominant when partially or fully charged molecules are involved. The electrostatic component of the intermolecular energy provides directionality to the interaction.

The geometries of these interactions are also influenced by the molecular planarity associated with x-delocalization. Planar molecules (or parts of molecules) usually arrange with parallel or steeply inclined geometry. and for pairs of equivalent molecules, the OFF and EF primary motifs are prevalent. These geometries are favored by the electrostatic components of intermolecular energy. Dissimilar n-delocalized molecules. particularly pairs with complementary electron-donor and electron-acceptor properties, are commonly arranged face-to-face: in order to maximize the electrostatic energy between them. The parallel primary motifs, OFF, and FF. favor continuous stacking (n-stacking).

The π–π interactions occur in all areas of chemistry and for chemically diverse molecules. The stacking of π-delocalized molecules favors cooperative phenomena. such as electron conduction. The n-stacking motifs are key components of the design of molecular materials with ensemble properties. Nucleotide base-pair stacking is fundamental to molecular biology. and aromatic interactions between amino-acid side chains influence protein structure.

The x–n interactions are valuable fundamental components of contemporary research in the frontier fields of molecular engineering. molecular machines, and crystal engineering.

ARTICLES OF FURTHER INTEREST

Catenanes and Other Interlocked Molecules. p. *206*
Cation–n Interactions. p. 214
π–π Stacking as a Crystal Engineering Tool. p. 1093

REFERENCES

1. Kim. K.S.: Tarakeshwar. P.: Lee. J.Y. Molecular clusters of π systems: Theoretical studies of structures. spectra. and

origin of interaction energies. Chem. Rev. 2000. 100 (11), 4145–4186.
2. Desiraju. G.R.: Gavezzotti, A. Crystal structures of polynuclear aromatic hydrocarbons. Classification, rationalization and prediction from molecular structure. Acta Crystallogr. 1989. *B45*, 473–482.
3. Olmstead, M.M.; Ginwalla. A.S.; Noll. B.C.; Tinti, D.S.: Balch. A.L. Supramolecular aggregation of Pd_6Cl_{12}, a cluster of comparable size to a fullerene, with aromatic donors and with C_{60}. J. Am. Chem. Soc. 1996, *118*. 7737–7745.
4. Beer, L.; Cordes, A.W.: Haddon. R.C.; Itkis, M.E.: Oakley. R.T.: Reed, R.W.: Robertson, C.M. A x-stacked 1,2,3-dithiazolyl radical. Preparation and solid state characterization of $(Cl_2C_3NS)(ClC_2NS_2)$. Chem. Commun. 2082. 1872–1873.
5. Beer. L.: Cordes, A.W.: Myles, D.J.T.; Oakley. R.T.: Taylor. N.J. 1,2,3,5-Dithiadiazolyls and 1,2,3,5-diselenadiazolyls: stacking and packing of π-dimers. CrystEngComm 2008. *2* (20).
6. Haneline, M.R.: Tsunoda. M.; Gabbai, F.P. π-Complexation of biphenyl, naphthalene. and triphenylene to trimeric perfluoro-ortho-phenylene Mercury. Formation of extended binary stacks with unusual luminescent properties. J. Am. Chern. Soc. 2002. *124* (14). 3737–3742.
7. Omary, M.A.: Kassab, R.M.: Haneline, M.R.: Elbjeirami, O.: Gabbai. F.P. Enhancement of the phosphorescence of organic luminophores upon interaction with a mercury trifunctional Lewis acid. Inorg. Chem. 2803. *42*. 2176–2178.
8. Miller. L.R.: Mann, K.R. π-Dimers and n-stacks in solution and in conducting polymers. Acc. Chem. Res. 1996. 29. 417–423.
9. Aravinda, S.: Shamala. N.; Das, C.; Sriranjini, A.: Karle. 1.: Balaram. P. Aromatic–aromatic interactions in crystal structures of helical peptide scaffolds containing projecting phenylalanine residues. J. Am. Chem. Soc. 2003, 125 (18); 5308–5315.
10. Meyer, E.A.; Castellano, R.K.; Diederich. F. Interactions with aromatic rings in chemical and biological recognition. Angew. Chem.. Int. Ed. 2003. *42* (11). 1210–1250.
11. Yamashita. Y.: Tomura. M. Highly polarized electron donors, acceptors and donor–acceptor compounds for organic conductors. J. Mater. Chem. 1998. *8* (9). 1933–1944.
12. Bryce. M.R. Tetrathiafulvalenes as π-electron donors for intramolecular charge-transfer materials. Adv. Mater. 1999. 11 (1). 11–23.
13. Robertson, N.: Cronin. L. Metal *bis*-1,2-dithiolene complexes in conducting or magnetic crystalline assemblies. Coord. Chem. Rev. 2002. *227* (1). 93–127.
14. Corfield, P.W.R.: La Placa, S.J. Structure of the charge-transfer salt 2,2′,5,5′-tetraselenafulvalene-7,7,8,8-tetracyano-p-quinodimethane (TSeF-TCNQ). Acta Crystallogr., B 1996. *52* (2). 384–387.
15. Jerome. D.: Schulz, H.J. Organic conductors and superconductors. Adv. Phys. 2002. *51* (1). 293–479.
16. Laukhina, E.: Vidal-Gancedo. J.: Laukhin. V.: Veciana. J.: Chuev. I.: Tkacheva, V.: Wurst, K.; Rovira. C. Multistability in a BEDT-TTF based molecular conductor. J. Am. Chem. Soc. 2003, *125* (13), 3948–3953.
17. Tanaka. H.; Okano, Y.: Kobayashi. H.; Suzuki, W.; Kobayashi. A. A three-dimensional synthetic metallic crystal composed of single-component molecules. Science 2001. *291* (5502), 285–287.
18. Stoddart. F.J.; Tseng, H.-R. Chemical synthesis gets a fillip from molecular recognition and self-assembly processes. Proc. Natl. Acad. Sci. U. S. A. 2002. *99* (8). 4778–4781.
19. Asakawa, M.; Ashton, P.R.; Balzani. V.; Credi. A.; Hamers. C.: Mattersteig. G.; Montalti. M.; Shipway, A.N.; Spencer. N.; Stoddart. F.J.: Tolley, M.S.: Venturi, M.; White, A.J.P.; Williams. D.J. A chemically and electrochemically switchable [2]catenane incorporating a tetrathiafulvalene unit. Angew. Chem., Int. Ed. 1998, *37*. 333.
20. Dance. *I.*: Scudder, M. Concerted supramolecular motifs: Linear columns and zig-zag chains of multiple phenyl embraces involving Ph_4P^+ cations in crystals. J. Chem. Soc., Dalton Trans. 1996. 3755–3769.
21. Dance, I.: Scudder. M. Supramolecular motifs: Sextuple aryl embraces in crystalline $[M(2,2'\text{-bipy})_3]$ and related complexes. J. Chem. Soc.. Dalton Trans. 1998. 1341–1350.
22. Dance, I.: Scudder, M. Supramolecular motifs: Concerted multiple phenyl embraces between Ph_4P^+ cations are attractive and ubiquitous. Chem. Eur. J. 1996. *2* (5). 481–486.
23. Gut. D.: Rudi, A.; Kopilov, J.: Goldberg. I.: Kol. M. Pairing of propellers: Dimerization of octahedral ruthenium(II) and osmium(II) complexes of eilatin via π–π stacking featuring heterochiral recognition. J. Am. Chem. Soc. 2002, *124*, 5449–5456.
24. Russell. V.: Craig, D.: Scudder. M.: Dance. I. Crystal packing motifs for mixed oxalate/phenathroline metal complexes. CrystEngComm 2002. *3* (24). 96–106.
25. Russell. V.M.: Scudder. M.L.; Dance, I.G. The crystal supramolecularity of metal phenanthroline complexes. J. Chem. Soc.. Dalton Trans. 208%.789–799.
26. Scudder. M.L.: Goodwin. H.A.: Dance. I.G. Crystal suprarnolecular motifs: Two-dimensional grids of terpy embraces in $[ML_2]^z$ complexes (L=terpy or aromatic N3-tridentate ligand). New J. Chem. 1999. *23*, 695–705.
27. Tran, F.: Weber. J.: Wesolowski. T.A. Theoretical study of the benzene dimer by the density-functional-theory formalism based on electron-density partitioning. Helv. Chim. Acta 2001, *84* (6), 1489–1503.
28. Krause, H.: Ernstberger. B.: Neusser. H.J. Binding energies of small benzene clusters. Chem. Phys. Lett. 1991, *184* (5,6), 411–417.
29. Kiermeier, A.; Ernstberger. B.; Neusser. H.J. Multiphoton mass spectrometry of clusters: Dissociation kinetics of the benzene cluster ions. J. Phys. Chem. 1988, *92*. 3785–3789.
30. Grover. J.R.: Walters. E.A.: Hui. E.T. Dissociation energies of the benzene dimer and dimer cation. J. Phys. Chem. 1987. *91*. 3233–3237.

31. Dance. I.G. 2003. In preparation for publication.
32. Tsuzuki, S.: Honda. K.; Uchimaru. T.; Mikami, M.; Tanabe, K. Origin of attraction and directionality of the π/π interaction: Model chemistry calculations of benzene dimer interaction. J. Am. Chem. Soc. 2002. *124* (1). 104–112.
33. Jorgeasen. W.L.; Severance. D.L. Aromatic–aromatic interactions: Free energy profiles for the benzene dimer in water. chloroform, and liquid benzene. J. Am. Chem. Soc. **1990**, *112*. 4768–4774.
34. Hunter, C.A.; Lawson, K.R.: Perkins. J.; Urch, C.J. Aromatic interactions. J. Chem. Soc., Perlcin Trans. 2 2001, 651–669.
35. Moet-Ner, M.; Hamlet. P.; Hunter, E.P.: Field, F.H. Bonding energies in association ions of aromatic compounds. Correlation with ionisation energies. J. Am. Chem. Soc. **1978**. *100* (17). 5466–5471.
36. Hiraoka, K.: Mizuse. S.: Yamabe, S. Stabilities and structures of $C_6F_6^-$ (C_6F_6) and $C_6F_6^+$ (C_6F_6). J. Phys. Chem. 1990. *94*. 3689–3694.
37. Lorenzo. S.: Lewis, G.R.: Dance. I.G. Supramolecular potentials and embraces for fluorous aromatic molecules. New J. Chem. 2000. 24. 295–304.
38. Novoa. J.J.; Lafuente. P.; Del Sesto. R.E.; Miller, J.S. On the existence of long C–C bonds between pairs of anions which repel: When and why? A test case on the $[TCNE]_2^{2-}$ dimers found in ionic crystals. CrystEngComm 2002. 4 (65). 373–377.
39. Guckian. K.M.; Schweitzer, B.A.: Ren. R.X.-F.: Sheils, C.J.; Tahmassebi, D.C.; Kool, E.T. Factors contributing to aromatic stacking in water: Evaluation in the context of DNA. J. Am. Chem. Soc. **2000**, *122*, 2213–2222.
40. Todd. A.K.; Adams, A.; Thorpe, J.H.; Denny, W.A.; Wakelin. L.P.G.; Cardin, C.J. Major groove binding and 'DNA-induced' fit in the intercalation of a derivative of the mixed topoisomerase 1/11 poison N-(2-(dimethylamino)ethyl)acridine-4-carboxamide (DACA) into DNA: X-ray structure complexed to *d*(CG(5-BrU)ACG)2 at 1.3 Å resolution. J. Med. Chem. 1999. *42*, 536–540.
41. Medhi, C.; Mitchell. J.B.O.; Price. S.L.: Tabor, A.B. Electrostatic factors in DNA intercalation. Biopolymers 1999. *52*. 84–93.

π–π Stacking as a Crystal Engineering Tool

Stuart L. James
Queen's University Belfast, Belfast, Northern Ireland

INTRODUCTION

Although it is widely realized that significant attractive interactions can occur between aromatic molecules, and they are often described as such in the discussions of new *crystal structures. their deliberate exploitation as tools for controlling crystal structure has lagged behind that of hydrogen bonding. However, positive developments are now occurring, with crystal packing "synthons"* (i.e., *reliable. recurring crystal packing arrangements) being identified and beginning to be exploited. This article is divided into two sections. First, examples of potentially useful structural trends and actual crystal packing* synthons, *which were identified through crystal structure database searches or through new synthetic studies, are reviewed. Second, some examples of deliberate crystal engineering that rely on the exploitation of n – π synthons to control crystal structure, and so control solid-state reactivity, are described. For discussion of the fundamental nature of aromatic interactions. readers should consult the article entitled ''π – π Stacking:Theory and Scope" in this Encyclopedia.*

STRUCTURAL TRENDS IN MOLECULAR **CRYSTALS**

Aromatic Hydrocarbons

Crystalline benzene adopts a packing arrangement that is widely referred to as the "herringbone" pattern'" and that is characterized by intermolecular edge-to-face contacts (Fig. 1). That benzene molecules adopt this geometry in the crystal is consistent with the theoretical prediction that the most stable arrangement for the benzene dimer *is edge-to-face.'" Molecular beam dipole moment measurements also suggest that the benzene* dimer *adopts this T-shaped geometry in the gas* phase.[3] *For crystals of larger aromatic hydrocarbons (a group of 32, including napthalene,* pyrene, *etc.). three additional packing modes were identified (called stacked* herringbone, γ *and* β), *each exhibiting edge-to-face or offset face-to-face stacking between* neighboring molecules.[4] *The different packing modes were correlated by the authors with the C:H ratios of the compounds involved: those with high values favoring face-to-face stacking* (i.e., *C...C contacts) and those with low* C:H *ratios favoring* herringbone (i.e., *C–C and C–H contacts).*

Multiple Aromatic "Embraces"

Dance and coworkers extensively searched the Cambridge Crystallographic Database to identify recurring packing motifs in compounds that contain multiple aromatic groups in the form of pyramidal EAr_3 *units* (E = P, *As, B,* etc.).[5,6] *Such species include transition metal complexes of triarylphosphines as well as salts containing such ions as* EPh_4^+ (E = P, *As) and* BPh_4^-. *A number of motifs were classified, the most symmetrical being the so-called sixfold phenyl embrace, or* 6PE. *illustrated in Fig. 2. In this multiple aromatic interaction, two* X-PPh_3 *groups make contact through six edge-to-face contacts. so that the interaction has local approximate* C_3 *symmetry and the two* P–X *bonds are approximately colinear. The frequencies with which* 6PEs *occur was been found to vary greatly according to the precise chemical species involved: however, it was found to be highest for* PPh_4^+ *cations. occurring at a probability level of ca.* 60%.[5,7] *It should be borne in mind, however. that* PPh_4^+ *can engage simultaneously in more than one 6PE. and the 60% probability value does not refer precisely to* a *60% likelihood per cation. However, this fairly high probability suggests that the 6PE may be a usable crystal engineering synthon for this cation. whereas for other species (such as metal complexes* M-PPh_3), which *statistically engage* in 6PEs *significantly less often, it seems less likely to be useful. Despite this, the 6PE provides an interesting pointer for further research: for example, it is quite likely that synthetic derivatization can increase the predictability of packing in* PAr_3 *complexes. Attractive energies as large as* -60 kJmol^{-1} *were calculated for certain* 6PEs. *corresponding to 9–12* kJ mol^{-1} *per* phenyl–phenyl *contact.*

Porphyrins

Hunter and Sanders correlated the experimentally determined packings of porphyrins *with an essentially electrostatic* model *of the* n – x *interaction between two molecules.'"* The *optimum geometry predicted by the model*

DOI: 10.1081/E-SMC 120012766

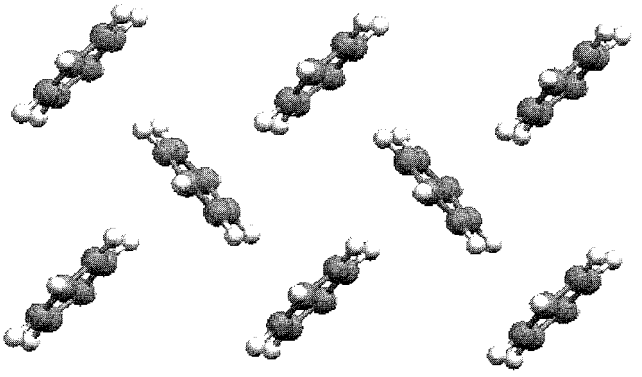

Fig. 1 The 'herringbone' crystal packing in benzene showing the edge-to-face interactions.

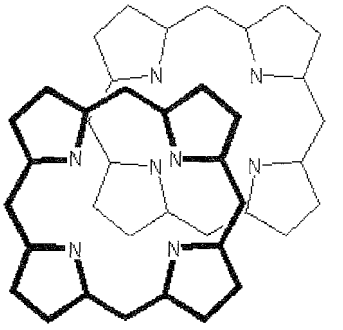

Fig. 3 The predicted preferred mutual orientation of two porphyrins.[8]

is with one pyrrole ring over the π-cavity of its neighboring porphyrin, and with the porphyrins not rotated with respect to each other (Fig. 3). The database study was intended to ascertain the accuracy of the electrostatic model, and so porphyrins with packings that were constrained, for example. with bulky side groups or axial ligands, were not included.

Packing Involving Hydrocarbyl and Fluorinated Aromatics—$Ar^H...Ar^F$ Interactions

In 1960, Patrick and Prosser reported that when benzene and hexafluorobenzene were mixed under ambient conditions, 1.1 cocrystalr formed, which had a melting point significantly higher (23.7°C) than that of either of the pure components (5.4 and 5.0°C for benzene and hexafluorobenzene, respectively).[9] The 1:1 cocrystal exhibits temperature-dependent behavior. The lowest temperature phase consists of columns in which equispaced face-to-face benzene and hexafluorobenzene molecules alternate (Fig. 4).[10] The face-to-face interactions are slightly offset. or in other words. the planes of the molecules are not perfectly orthogonal to the propagation direction of the column, tilting away from this "ideal" by 23° for benzene and 27" for hexafluorobenzene. The distance between the molecular centroids is *3.77* A. The formation of this type of $Ar^H...Ar^F$ stacked motif was since found to be fairly general.[11–22,24,25] A crystallographic study was made of hexafluorobenzene and its complexes with a range of methyl-substituted aromatics.[10] A structural trend within this series was identified. in that the inter-planar separations were generally lower for the greater number of methyl subsiituents on the electron-rich aromatic. This was noted to be in contrast to the general lack of structural trends identified for π–π* charge-transfer complexes. Vangala et al.[12] studied the crystal structures of diaryl azines that

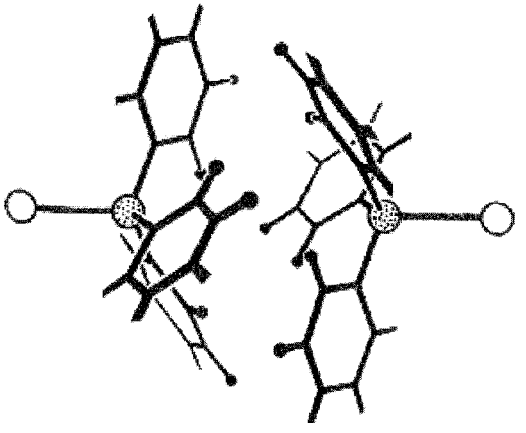

Fig. 2 The sixfold phenyl embrace (reproduced with permission from Ref. [5]). (*View this art in color at www.dekker.com.*)

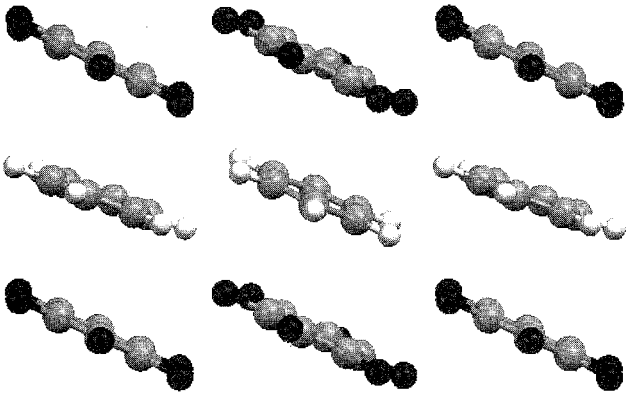

Fig. 4 Crystal packing in the cocrystal $C_6H_6C_6F_6$, showing the alternating stack5 (H = white, F = black). *(View this art in color at www.dekker.com.*)

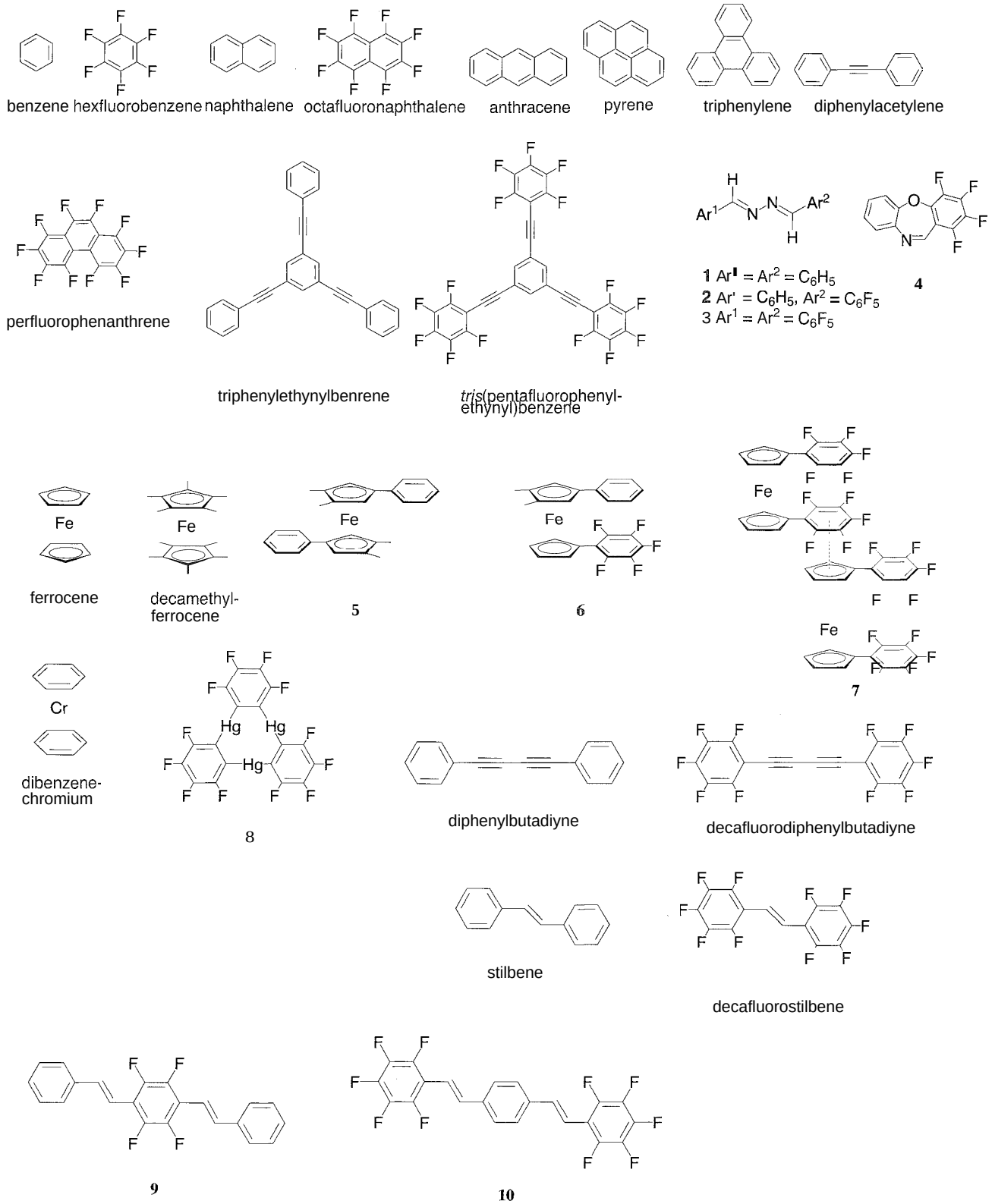

Fig. 5 Hydrocarbon and fluorinated molecules used to investigate $Ar^H...Ar^F$ interactions

contained C_6H_5 or C_6F_5 groups (**1**, **2**, and **3**—Fig. 5). It was concluded that the cofacial stacking of C_6H_5 and C_6F_5 groups dominated in determining the crystal packing over other potentially competing stabilizing interactions such as C–H...F, herringbone, and F...F contacts. Vangala's molecules were effectively planar. and the crystal packing ''synthon'' involves fivefold fluorine substitution on the aromatic group. The 1,2,3,4-tetrafluorodibenzoxazepine (**4**—Fig. 5), characterized by Saunders and Nieuwenhuyzen,[13] has a curved shape (due to buckling of the central seven-membered ring) and involves only fourfold fluorine substitution on one of the rings. Nevertheless, this compound also stacked in columns with head-to-tail packing so that again, alternating $Ar^H...Ar^F$ stacks occurred.

A series of investigations by Batsanov. Marder, and coworkers. into 1:1 cocrystals of perfluorinated aromatics and hydrocarbon aromatics, where each component was varied over a range of molecular sizes and shapes. showed that the basic alternating stack motif occurred in all the cocrystals obtained.'''' Thus. octafluoronaphthalene formed alternating stacks with anthracene, phenathrene, pyrene, and triphenylene. Even the smaller hexafluorobenzene reliably formed alternating stacks with hydrocarbons as large as pyrene and triphenylene. as well as with naphthalene and anthracene.[15] The planes of neighboring aromatics within the stacks were all almost parallel, however, the ''slip angles'' (the angles made by the normals to the molecular planes to the direction of propagation of the stack) within stacks and the three-dimensional packings varied, and no simple relationship between these aspects of the packing and the molecular sizes and shapes was identified. Clearly, though. the basic alternating stack motif can be expected to occur widely and may, therefore, be exploited in controlling the solid-state structures of molecules containing diverse hydrocarbyl and fluorocarbyl aromatic groups. A 1:1 cocrystal structure of octafluoronaphthalene and diphenylacetylene was also described.[16] Although this formed the expected alternating stack. with an interplanar separation of 3.6 Å, the octafluoronaphthalene interacted with the alkyne fragment as well as the phenyl rings, so that the fluorinated and nonfluorinated rings were not actually eclipsed.

The examples above relied on either one or two intermolecular ArH...ArF contacts per molecule. Seigel et al. showed that 1,3,5-*tris*(pentafluorophenylethynyl)-benzene and its nonfluorous analogue 1,3,5-triphenylethynylbenzene (Fig. 5) also formed a 1:1 cocrystal via three ArH...ArF stacks, forming slipped stacks of alternating molecules.[17]

The effect of phenyl and pentafluorophenyl substituents on the inter-and intramolecular structures of crystalline ferrocene derivatives (**5–7**, Fig. 5) was investigated by Hughes and coworkers.[18] In the crystal structure of the homoleptic purely hydrocarbyl ferrocene $Fe(Me_2PhCp)_2$ **5**, the phenyl groups were found to be in *anti* positions about the central Fe. However, the mixed-ligand compound $Fe(Me_2PhCp)(C_6F_5Cp)$ **6** adopted an eclipsed conformation with inter-and intramolecular stacking between the C_6H_5 and C_6F_5 groups. The $Fe(C_6F_5Cp)_2$ **7** crystallized again with eclipsed stacked rings. Intermolecular stacking in this case occurred between the C_6F_5 groups and Cp rings. It was concluded that $Ar^H...Ar^F$ stacking was the dominant crystal packing interaction in these compounds. and that it could be of further use as a crystal packing synthon.

Ferrocene was found to form a 1:1 cocrystal with octafluoronaphthalene.[15] Interestingly, in this case. only half of the octafluoronaphthalene molecules in the crystal actually formed face-to-face contacts with the cyclopentadienyl groups of ferrocene, and the structure was not a straightforward alternating stack. These workers found that hexafluorobenzene did not cocrystallize with ferrocene. The bulky decamethylferrocene was found by other workers to form 1:1 cocrystals with fluoroaromatics, for example, perfluorophenanthrene.[19] Despite the presence of the bulky methyl groups on the ferrocene, the interplanar separation between molecules was still only 3.7 A. Short F...C(methyl) distances of ca. 3.36 A suggested that there may also have been significant F...H contacts. The bond lengths within the molecules suggested that the structure was not of the charge transfer $[Fe(Cp^*)_2]^+[C_{10}F_{14}]^-$ type. However, Perutz et al. found a different situation when yellow-green dibenzenechromium $[Cr(\eta^6\text{-}C_6H_6)_2]$ reacted with C_6F_6 to give the cocrystal $[Cr(\eta^6\text{-}C_6H_6)_2].C_6F_6$ as claret-or yellow-colored crystals.[20] The claret crystals consisted of stacks of alternating $[Cr(\eta^6\text{-}C_6H_6)_2]$ and C_6F_6 units with an interplanar distance between stacked rings of ca. 3.5 Å. The rings were almost eclipsed with the angle between ring normals being 5.9''. Bands in the UV were assigned. in this case, to charge-transfer transitions, and EPR spectra were consistent with the formation of $[Cr(\eta^6\text{-}C_6H_6)_2]^+$ to some extent (3.3% in the presence of a fivefold excess of C_6F_6 in toluene solution).

Gabbai and coworkers[21] found that the perfluorinated planar metallotrimer $[Hg(o\text{-}C_6F_4)]_3$ **8** (Fig. 5) could cocrystallize with hydrocarbon aromatics to form alternating stack structures. For the naphthalene and biphenyl cocrystals. it was actually Hg(II)...arene interactions that were established in the crystal, rather than arene–fluoroarene contacts, but for the triphenylene complex, arene–fluoroarene contacts were also present. All three compounds exhibited luminescence associated with the nonfluorinated arene component. but the emission from the triphenylene complexes was shifted to longer wavelengths than normal for this chromophore. This was tentatively correlated with the presence of $Ar^H...Ar^F$ interactions.

DELIBERATE EXPLOITATION OF AROMATIC INTERACTIONS AS TOOLS FOR DESIGNING CRYSTAL STRUCTURE AND REACTIVITY

Desiraju and coworkers cocrystallized cinnamic acids bearing electron-withdrawing NO_2 or electron-donating OCH_3 groups, relying on the formation of charge-transfer face-to-face interactions between the electron-poor and electron-rich aromatic rings (Fig. 6a).[22,23] Although in all cases the expected packing occurred: and the alkene groups were separated by less than 4.2 Å, a distance criterion for allowing photochemical 2+2 additions, the substitution pattern on the rings of the electron-poor aromatics was crucial to the solid-state reactivity. Only when NO_2 groups were in the 3,5 positions, i.e., unable to conjugate with the alkene, did photochemical cyclization occur.

Some successful synthetic crystal engineering was also based on the ArH...ArF synthon.[24,25] Daugherty and Grubbs et al.[23] exploited phenyl–pentafluorophenyl stacking interactions to control the arrangement of diaryldiynes in the solid state. and by this method, also controlled their solid-state polymerization behavior (Fig. 6b). Solid-state polymerization of diynes to give *trans*-polybutadiynes was well documented, but it is sensitive to the solid-state packing geometry of the diyne. By inducing strictly cofacial orientation of the aromatic diyne substituents, through $Ar^H...Ar^F$ stacking at an intermolecular separation of 3.4–3.6 Å, these workers anticipated that solid-state polymerization should be able to occur, and further that polybutadiynes with novel ***cis*** geometry might result (Fig. 6b). Diphenylbutadiyne and decafluorodiphenylbutadiyne were successfully cocrystallized from ethanol solution to give a 1:1 adduct with packing of the two molecules in the expected alternating stack. While neither of the pure diynes were susceptible to UV-induced polymerization, UV irradiation of the alternating 1:1 cocrystal gave up to 50% yield of oligomers, making them markedly more active. The *cis*/*trans* geometry of the polymeric product was not established.

In related work,[25] alkenes and dienes bearing phenyl or pentafluorophenyl groups were similarly investigated

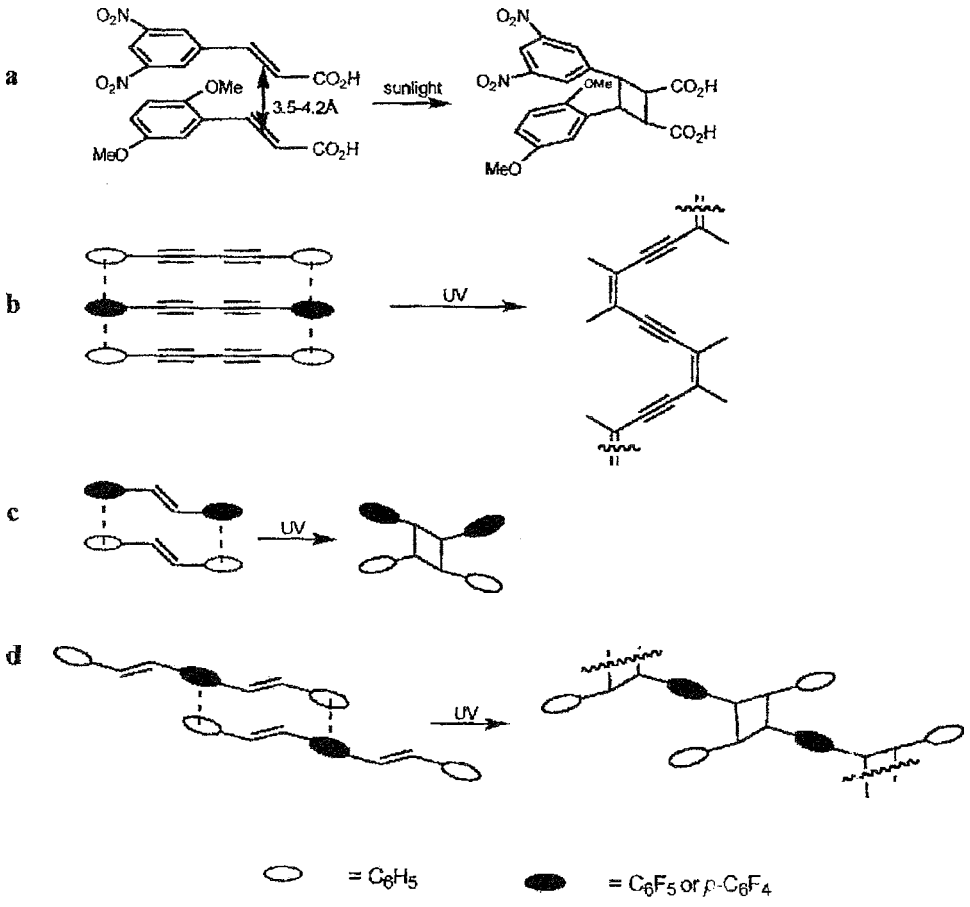

Fig. 6 *Solid-state organization* of *alkenes,* alkynes, *and dienes through* $Ar^H...Ar^F$ *interactions for photoinduced dimerization and polymerization reactions.*

by Coates and Grubbs et al. for their crystal packing arrangements and associated photoactivity toward [2+2] reactions in the solid state. When phenyl and perfluorophenyl groups were present, they directed the crystal packing to give geometries and distances generally conducive to the photoinduced reaction. In particular, the 1:1 cocrystal of trans-stilbene and *trans*-decafluorostilbene exhibited the expected stacked structure with C...C separations of the alkene groups of 3.784 and 3.749 Å. Whereas the pure components were not susceptible to solid-state dimerization, under UV irradiation, this cocrystal gave the photodimerization product quantitatively after 5 h (Fig. 6c). The studies were extended to the photopolymerization of diolefins such as 1,4-*bis*(2-phenylethenyl)-2,3,5,6-tetrafluorobenzene, **9** (Fig. 5 and Fig. 6d). This diolefin packs in strongly slanted stacks because of the expected cofacial arrangement of the central fluorinated group with the outer nonfluorinated groups of its two nearest neighbors. The intermolecular separation of the double bonds was 3.823 Å. Irradiation produced in 15% a mixture of soluble dimer and tetramer, and the insoluble remainder was taken to be higher oligomers. However, the "inverse" analogue of this diene, trans,trans-1,4-*bis*(2-pentafluorophenylethenyl)benzene, **10**, was completely photostable. Correspondingly. x-ray analysis showed that the packing was not as anticipated, with the pentatluorophenyl groups face-to-face with the *trans*-alkenes, rather than with the 1,4-phenylene group, resulting in an alkene–alkene separation of 4.86 Å—too great for the photoreaction. However, when this compound was cocrystallized with o-xylene, the structure exhibited face-to-face packing of Ar^H and Ar^F units, both between the diene units and between the diene and included solvent. Irradiation gave dimerization, to which the crystal structure was predisposed. The cocrystal **9**·**10** was also susceptible to photoreaction, but its crystal structure was not determined.

CONCLUSION

The field of crystal engineering based on π–π interactions is now changing from the initially necessary surveying of crystal structures (in order to determine packing trends and recurring packing arrangements), to include the application of synthons to control crystal structure and properties. The fundamental natures of these interactions are also becoming clearer (see *n-n* Stacking: Theory and Scope, p. 000), which will aid their further application in control and prediction of crystal structure. The identification and design of further synthons and the more detailed testing and application of existing ones. in order to demonstrate control over material properties, are likely to be important aspects for future research. Synthetic studies aimed at deliberately increasing the reliability of some identified synthons will also provide stimulating research challenges.

ARTICLES OF FURTHER INTEREST

The *Cambridge Structural* Database, p. 161
Cation–n Interactions, p. 214
Concepts in Crystal Engineering, p. 319
Crystal Engineering *with Hydrogen Bonds*, p. 357
Crystal Structure Predictiorz, p. 371
Cyclophanes: Definition and Scope, p. 414
Hydrogen Bonding, p. 658
Nomenclature *in Crystal* Engineering, p. 967
π–π Interactionr: Theory and Scope, p. 1076
Polymorphism, p. 1129
Porplzyrin Derivatives, Functional, p. 1139
Porphyrin-Based Clnthrates, p. 1150

REFERENCES

1. Bacon, G.E.; Curry, N.A.; Wilson, S.A. A crystallographic study of solid benzene by neutron diffraction. Proc. R. Soc. Lond. Ser.. A 1964, *279*, 98.
2. Pawliszyn. J.; Szczesniak, M.M.; Scheiner, S. Interactions between aromatic systems—Dimers of benzene and *s*-tetrazine. J. Phys. Chem. 1984, *88*. 1726–1730.
3. Janda, K.C.: Hemminger, J.C.; Winn, J.S.; Novick, S.E.: Harris. S.J.: Klemperer, W. Benzene dimer: A polar molecule. J. Chem. Phys. 1975. 63, 1419–1421.
4. Desiraju, G.R.: Gavezzotti, A. From molecular to crystal-structure—Polynuclear aromatic-hydrocarbons. J. Chem. Soc., Chem. Commun. 1989, 621–622.
5. Dance; I.; Scudder, M. Supramolecular motifs: Concerted multiple phenyl embraces between Ph_4P^+ cations are attractive and ubiquitous. Chem. Eur. J. 1996, 2. 481–486.
6. Dance, I.; Scudder. M. High symmetry crystal supramolecularity: -XPh_3 molecules in rhombohedral lattices, using multimolecular rather than bimolecular sixfold phenyl embraces. New J. Chem. 2001, *25*. 1510–1515, and references therein.
7. Steiner. T. Multiple phenyl interactions. Part 1: Relative frequencies of six-fold phenyl embraces (6PE) in crystalline compounds containing the fragment XPh_3 (X=any tetrahedral atom). New J. Chem. 2000. 24. 137–142.
8. Hunter. C.A.: Sanders. J.K.M. The nature of π–π interactions. J. Am. Chem. Soc. 1990. 112, 5525–5534.
9. Patrick. C.R.: Prosser, G.S. A molecular complex of benzene and hexafluorobenzene. Nature 1960, 1021.
10. Wiiliams. J.H.; Cockcroft. J.K.: Fitch. A.N. Structure of the lowest temperature phase of the solid benzene hexafluorobenzene adduct. Angew. Chem.. Int. Ed. Engl. 1992. 31, 1655–1657.
11. Dahl, T. Crystallographic studies of molecular-complexes

containing hexafluorobenzene. Acta Chem. Scand. 1988. A *42*. 1–7.
12. Vangala, V.R.: Nanpia. A.: Lynch, V.M. Interplay of phenyl-perfluorophenyl stacking. C-H...F. C-F...π and F...F interactions in some crystalline aromatic azines. Chem. Commun. 2002. 1304–1305.
13. Allaway, C.L.; Daly, M.: Nieuwenhuyzen, M.; Saunders, G.C. Synthesis of polyfluorodibenz[b,f][1,4]oxazepines by the cyclization of 2-[(polyfluorobenzylidene)amino]phenols. J. Fluorine Chem. 2002. *115*, 91–99.
14. Collings, J.C.; Roscoe. K.P.; Robins. E.G.; Batsanov, A.S.: Stimson. L.M.: Howard, J.A.K.; Clark, S.J.; Marder. T.B. Arene-perfluoroarene interactions in crystal engineering 8: Structures of 1:1 complexes of hexafluorobenzene with fused-ring polyaromatic hydrocarbons. New J. Chem. *2002. 26.* 1740–1746.
15. Clyburne, J.A.C.: Hamilton, T.: Jenkins. H.A. The molecular quadrupole moment: Solid state architectures containing organic and organometallic molecules. Cryst. Eng. 2001. *4.* 1–9.
16. Collings, J.C.; Roscoe. K.P.: Thomas, R.Ll.; Batsanov, A.S.: Stimson. L.M.: Howard, J.A.K.; Marder. T.B. Arene-perfluoroarene interactions in crystal engineering. Part 3. Single-crystal structures of 1:I complexes of octafluoronaphthalene with fused-ring polyaromatic hydrocarbons. New J. Chem. 2001, 25. 1410–1417.
17. Ponzini, F.: Zagha, R.; Hardcastle, K.: Siegel, J.S. Phenyll pentafluorophenyl interactions and the generation of ordered mixed crystals: Sym-triphenethynylbenzene and sym-tris(perfluorophenethynyl)benzene. Angew. Chem., Int. Ed. *2000.* 39. 2323–2325.
18. Blanchard, M.D.: Hughes. R.P.: Concolino. T.E.: Rheingold. A.L. n-Stacking between pentafluorophenyl and phenyl groups as a controlling feature of intra- and intermolecular crystal structure motifs in substituted ferrocenes. Observation of unexpected face-to-face stacking between pentafluorophenyl rings. Chern. Mater. *2000.12.* 1604–1610.
19. Beck. C.M.; Berdeniuc, J.: Crabtree. R.H.; Rheingold. A.L.; Yap, G.P.A. A ferrocene-perfluoroarene molecular complex. Inorg. Chim. Acta 1998, 270, 559–562.
20. Aspley, C.J.; Boxwell, C.: Buil. M.L.: Higgitt. C.L.; Long, C.: Perutz. R.N. A new combination of donor and acceptor: Bis(η^6-benzene)chromium and hexafluorobenzene form a charge-transfer stacked crystal. Chem. Commun. 1999, 1027–1028.
21. Haneline, M.R.: Tsunoda. M.; Gabbai, F.P. π-complexation of biphenyl, naphthalene, and triphenylene to trimeric perfluoro-ortho-phenylene mercury. Formation of extended binary stacks with unusual luminescent properties. J. Am. Chem. Soc. 2002, *124.* 3737–3742.
22. Sharma. J.A.R.P.; Desiraju, G.R. C–H...O hydrogen-bonding and topochemistry in crystalline 3,5-dinitrocinnamic acid and its 1-1 donor-acceptor complex with 2,5-dimethoxycinnamic acid. J. Chem. Soc., Chem. Commun. 1991. 1239–1241.
23. Sharma. C.V.K.: Panneerselvam. K.; Shimoni. L.: Katz, H.: Carrell. H.L.: Desiraju, G.R. 3-(3′,5′-dinitrophenyl)-4-(2′,5′-dimethoxyphenyl)cyclobutane-1,2-dicarboxylic acid—Engineered topochemical synthesis and molecular and supramolecular properties. Chem. Mater. 1994. 6. 1282–1292.
24. Coates. G.W.; Dunn. A.R.: Henling. L.M.: Dougherty. D.A.; Grubbs, R.H. Phenyl-perfluorophenyl stacking interactions: A new strategy for supermolecule construction. Angew. Chem., Int. Ed. Engl. 199'7. 36, 248–251.
25. Coates. G.W.: Dunn. A.R.: Henling. L.M.; Ziller. J.W.: Lobkovsky. E.B.: Grubbs, R.H. Phenyl-perfluorophenyl stacking interactions: Topochemical[2+2] photodimerization and photopolymerization of olefinic compounds. J. Am. Chern. Soc. 1998, *120.* 3641–3649.

Platonic and Archimedean Solids

Leonard R. MacGillivray
University of Iowa, Iowa City, Iowa, U.S.A.

INTRODUCTION

A molecular host that completely surrounds its guest provides a means to stabilize reactive and transient chemical intermediates, to transfer biologically active molecules to target cells, and to construct molecular-scale devices.[1–2] To design such a host, such a shell requires positioning of organic and/or *inorganic chemical subunits in space such that the topological relationship of its subunits approximates a hollow spherical shell S capable of packaging single or multiple guests (Fig. 1).*[1] *A simple design strategy for the construction of such a host involves utilizing principles of solid geometry, wherein the chemical subunits positioned along the surface of S conform to either a Platonic or an Archimedean* solid.[1–3]

SPHERICAL HOSTS

A spherical virus (e.g., *rhinovirus) is a* familiar *example of a spontaneous process of self-assembly that gives rise to a spherical shell with a closed cavity able to host atoms and molecules as* guests.[1] *Such a spherical structure is desirable. because it employs an economy of information. providing access to a shell with chemical subunits in identical chemical environments where surface area is at a minimum and strain energy is distributed evenly along the surface. Whereas nature utilizes identical chemical subunits in the form of proteins. which assemble by way of* noncovalent *forces* (e.g., *hydrogen bonds), to construct a spherical virus. chemists have a wide variety of organic and inorganic building blocks at their disposal that may be used to design atomic- and nanometer-scale shells held together by* noncovalent *or covalent bonds.* In *a similar way to a spherical virus. such a shell may be designed to exhibit a targeted property* (e.g., *catalysis). The targeted property* may *be less available, or completely inaccessible. by nature.*

SPHEROID DESIGN

To construct a molecular host with a spherical structure. the framework must *be derigned so that the guest is centralized within a hollow spherical shell S.*[1] *From a chemical standpoint, such a framework, however. is impossible to design, because atoms and molecules are discrete entities. whereas the surface of S is uniform. Thus, to construct a spherical molecular host, one must consider the number of identical chemical subunits n for spheroid design and their placement along the surface of the shell.*

SUBUNITS FOR SPHEROID DESIGN

The simplest host chat may be constructed using chemical *subunits that approximate a sphere is a shell based on* $n=4$ *subunits with a structure that conforms to a tetrahedron.[1,3] Such* a *shell consists of four identical subunits in the form of equilateral triangles. where edge-sharing by the triangular faces provides the curvature along the surface of the shell. The polygonal subunits of the tetrahedron are related by combinations of twofold and threefold rotation axes such that the* framework *is of cubic symmetry* (i.e., *32 symmetry).*

PLATONIC SOLIDS

The tetrahedron belongs to a closed family of five convex uniform polyhedra known *as the Platonic solids (Fig. 2).* named *after the ancient Greek philosopher* Plato *(circa 427–347* BC),[5] *who speculated that the five solids were the shapes of the* fundamental *components of the universe. Each member of this family possesses cubic symmetry* (i.e., *32, 432. or 532 symmetry) and is* made *of the same regular polygons* (e.g., *equilateral triangle. square) arranged* in *space so that* its *vertices and edges, and* three *coordinate directions. are equivalent. That there is a* finite *number of such polyhedra* is *a consequence of the fact that a limited number of* ways *exist in which identical regular polygons may be* adjoined *to construct a convex corner. Equilateral triangles* may *be adjoined in three ways. while squares and pentagons* may be *adjoined* in *only a single manner. These principles give rise to* five *isometric polyhedra that are achiral.* with *polygons that are related by* combinations *of* n-fold *rotation axes. The Platonic solids include the tetrahedron, which belongs to the point group* T_d *and possesses 32 symmetry; the* cube *and octahedron,*

Encyclopedia of Supramolecular Chemistry
DOI: 10.1081/E-ESMC 120012767

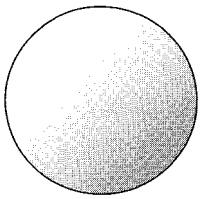

Fig. 1 Hollow spherical shell *S*.

which belong to the point group O_h and possess 432 symmetry; and the dodecahedron and icosahedron, which belong to the point group I_h and possess 532 symmetry.

ARCHIMEDEAN SOLIDS

In addition to the Platonic solids, a family of 13 convex uniform polyhedra known as the Archimedean solids (Fig. 3) exist, first described by the Greek philosopher Archimedes (287–211 or 212 BC).[6] The original work was lost and was reported second-handedly by Pappus of Alexandria (290–350), a Greek geometer. Each member of this family of solids is made up of at least two different regular polygons and may be derived from at least one Platonic solid through either truncation or twisting of faces. In the case of the latter, two chiral members, the snub cube and the snub dodecahedron, are realized. Like the Platonic solids. the Archimedean solids possess identical vertices and exhibit 32, 432, or 532 symmetry. The Archimedean solids exhibit a larger variety of polygons than the Platonic solids. These include the equilateral triangle, square. pentagon, hexagon, octagon. and decagon.

MODELS FOR THE DESIGN OF SPHERICAL MOLECULAR HOSTS

With a synthetic scheme for designing spherical shells based on principles of solid geometry realized, chemists exploited such geometric principles for the synthesis of spherical hosts that encapsulate atoms and molecules as guests.[1–3] In serving as models for the construction of spherical hosts, the Platonic and Archimedean solids provide a means with which to determine where chemical subunits should be placed along the surface of S and the bonding arrangements they should adopt. To demonstrate these principles. examples of spherical inolecular hosts derived from the laboratory and nature will be described.

Platonic Solids

As stated, the Platonic solids constitute a family of five convex uniform polyheda made up of the same regular polygons and possessing 32. 432. or 532 symmetry.

Tetrahedral hosts

The macrotricyclic spherand designed by Lehn was the first tetrahedral host (Fig. 4a).[7] The bridgehead nitrogen atoms and ethyleneoxy units supply the threefold and twofold rotation axes, respectively. This molecule, and its tetraprotonated form, was shown to bind an ammonium and chloride ion, respectively.

Saalfrank was the first to introduce metal-based tetrahedral cages by using metal ions as corner units and bridging malonate ligands as edges (Fig. 4b).[8] Owing to a bend in each ligand, these cages are adamantane-like. In terms of host–guest behavior, an iron-based system was shown to complex a single ammonium ion.

Octahedral hosts

A cyclophane-based system reported by Murakami was shown to conform to a structure of a cube (Fig. 4c).[9] The sides of the host consist of tetraaza-[3.3.3.3]paracyclophane units, and its octaprotonated cation was shown to bind anionic guests. A polyoxovanadate. $(VO_6)(RPO_3)_8]^+$ (R=*t*Bu,$OSiMe_3$), reported by Zubieta[10] and Thorn,[11] was also shown to adopt an octahedral framework (Fig. 4d). The vanadium atoms of the shell are located at the vertices of an octahedron, while the phosphorus atoms are located at the corners of a cube. A cube with a structure based on deoxyribonucleic acid (DNA) was described by Seeman (Fig. 4e).[12] The directionality and ability of the double helix to form branched junctions were exploited for the edges and vertices, respectively.

Icosahedral hosts

Spherical viruses, found in nature, are examples of molecular hosts related to an icosahedron (Fig. 4f).[11] Possessing identical copies of proteins that assemble by

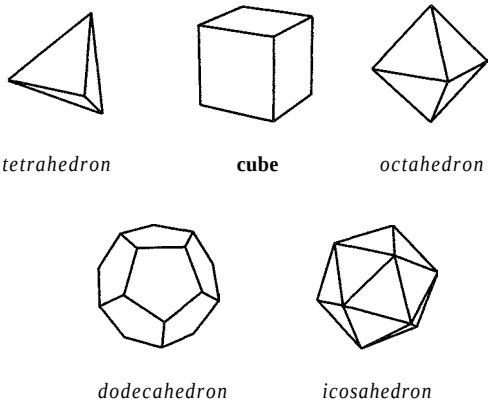

Fig. *2* The five Platonic solids

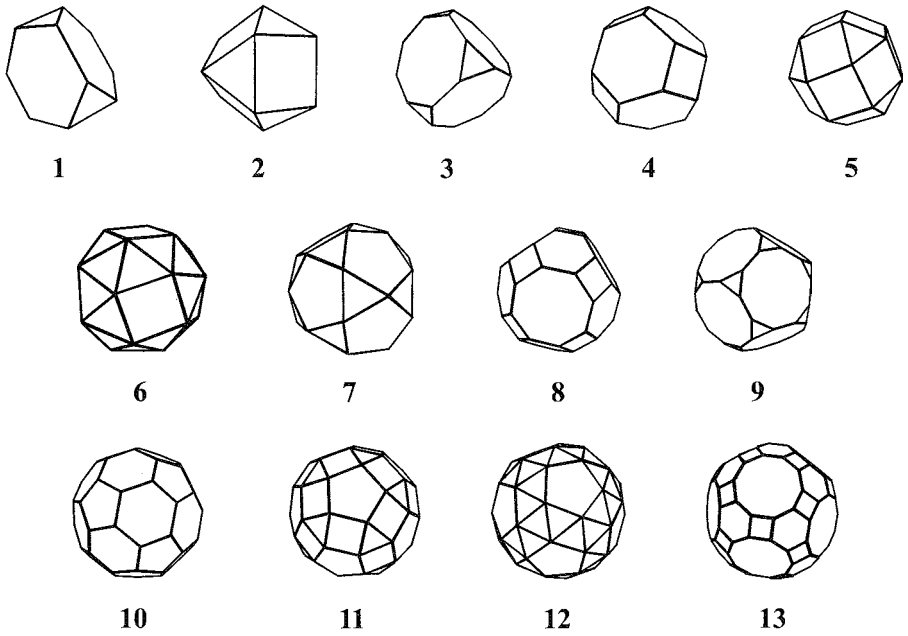

Fig. **3** The 13 Archimedean solids Truncated tetrahedron (1), cuboctahedron (2), truncated cube (3). truncated octahedron (4). rhombicuboctahedron (5), snub cube (6). icosidodecahedron (7), rhombitruncated cuboctahedron (8), truncated dodecahedron (9). truncated icosahedron (10). rhombicosidodecahedron (11). snub dodecahedron (12), and rhombitruncated icosidodecahedron (13)

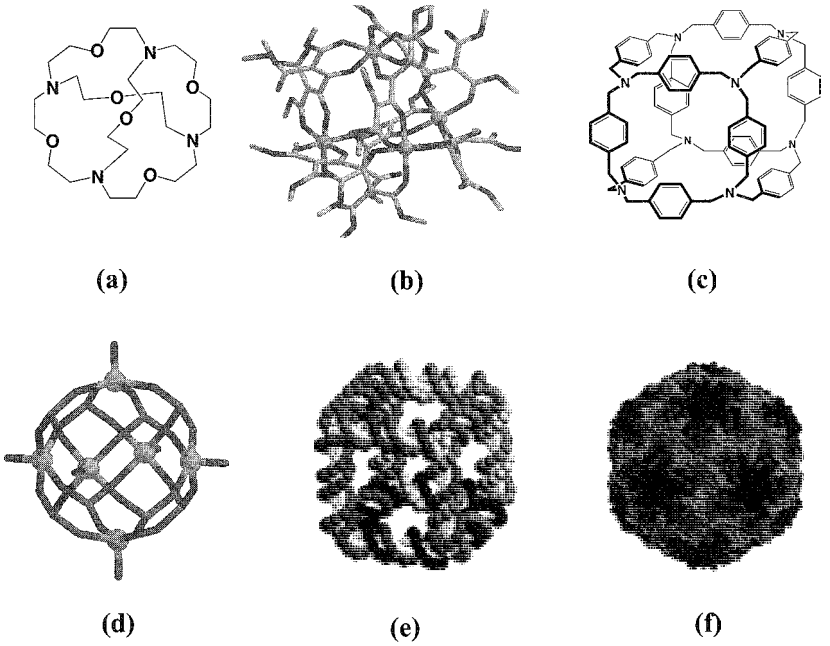

Fig. **4** Spherical hosts based on the Platonic solids: (a) spherand (tetrahedron): (b) metal-organic cage (tetrahedron); (c) cyclophane-based cube (cube): (d) the $[(VO_6)(RPO_3)_8]^+$ ion (R=*t*Bu, $OSiMe_3$) (octahedron and cube): *(e)*DNA-based cube (printed with permission by Professor Nadrian Seeman) (cube); and (f) the rhinovirus (icosahedron). (*View this art* in color *at www.dekker.com.*)

way of noncovalent forces (e.g., hydrogen bonds), these hosts range from 15–90 nm in diameter and encapsulate strands of ribonucleic acid.

Archimedean Solids

As stated. the Archimedean solids constitute a family of 13 convex uniform polyhedra made up of two or more regular polygons and, like the Platonic solids. possess 32, 432, or 532 symmetry.

Truncated tetrahedron

Fujita,[13] Stang,[14] and Steel[15] described metal-organic cages that are topologically analogous to a truncated tetrahedron (Fig. 5a). These systems consist of metal ions and aromatic-based bridging ligands that constitute the twofold and threefold rotation axes. respectively. In terms of host–guest behavior, x-ray crystallographic studies revealed the assembly reported by Fujita to form a complex with four adamantyl carboxylate ions, while that reported by Steel to encapsulate a molecule of dimethylsulfoxide. According to mass spectrometric data, the cage described by Stang associates with four triflate ions.

Cuboctahedron

Gonzalez-Duarte described the ability of eight cadium ions and 16 thiolate ligands to assemble to form a highly charged cage. $[ClCd_8\{SCH(CH_2CH_2)_2N(H)Me\}_{16}]^{15+}$, the sulfur atoms of which sit at the vertices of a cuboctahedron.[16] The host contains a central chloride ion and an inner tetrahedral array of cadmium ions. A large metal-organic shell that conforms to a cuboctahedron and is based upon Cu(II) ions that assemble with a triazo ligand was described by Robson.[17] The shell possesses a cavity with a volume of approximately 816 $Å^3$ and is speculated to accommodate five to six molecules of dimethylformamide.

Truncated octahedron

Seeman constructed a DNA-based shell analogous to a truncated octahedron.[18] The edges of this molecule, each of which contains two turns of the double helix, contain 1440 nucleotides. The molecular weight of the structure, which is an overall 14-catenane, is 790,000 Daltons. The design strategy relied on a solid support approach, where a net of squares is ligated to give the polyhedron.

Rhombicuboctahedron

Müller showed that 24 oxygen atoms of the polyoxometalate $[As_4Mo_6V_7O_{39}]^{2-}$ may be attributed to the structure of a rhombicuboctahedron.[19] A strong "tetrahedral distortion" of each ion is required to correspond each host to the polyhedron. This shell was shown to complex a sulfate ion in the solid state.

Snub cube

MacGillivray and Atwood demonstrated the ability of six resorcin[4]arenes and eight water molecules to assemble in apolar media to form a spherical molecular assembly that conforms to a snub cube (Fig. 5b).[20] Each resorcin[4]arene lies on a fourfold rotation axis and each H_2O molecule on a threefold axis. The vertices of the square faces of the polyhedron correspond to the corners of the resorcin[4]arenes and the centroids of the eight triangles that adjoin three squares correspond to the water molecules. The assembly, which exhibits an external diameter of 2.4 nm, possesses an internal volume of about 1400 $Å^3$ and is held together by 60 O–H···O hydrogen bonds.

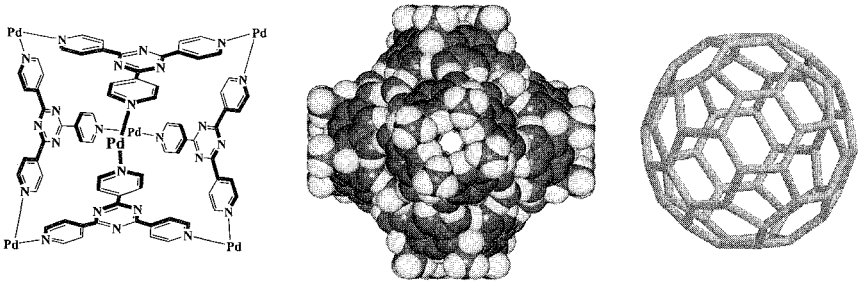

Fig. 5 Spherical hosts based on the Archimedean solids: (a) metal-organic cage (truncated tetrahedron), (b) calix[4]resorcinarene spheroid (snub cube), and (c) buckminsterfullerene (truncated icosahedron). (*View* this *art in* color *at www.dekker.com.*)

Truncated icosahedron

Buckminsterfullerene. an allotrope of carbon, is topologically equivalent to a truncated icosahedron, an Archimedean solid based on 12 pentagons and 20 hexagons (Fig. 5c).[21] Each carbon atom of the framework corresponds to a vertex of the polyhedron. As a result, C_{60} is held together by 90 covalent bonds. the number of edges of the solid.

CONCLUSION

Although chemists demonstrated an ability to utilize principles of solid geometry to design spherical hosts that encapsulate atoms and molecules, it is clear that much work remains to be accomplished. Indeed, although there exists a limited number of ways (i.e., Platonic and Archimedean solids) in which polygons may be arranged to enclose space. that chemists are able to mimic such structures chemically means that, in principle, an unlimited number of shells. with sizes that range from the angstrom — to the nanometer-scale level. and beyond (i.e., >10 Å), may be constructed. Moreover, a recent report by Swiegers illustrated that a classification system that accounts for different assembly processes available for a given polyhedron is feasible, meaning that a variety of routes to Platonic and Archimedean structures remain unexplored.[22] Notably. whereas nature utilizes template-directed synthesis to form the polypeptide chains that assemble to form a spherical virus, chemists utilized a fundamentally different approach to synthesis that relies on diffusion-controlled synthesis to construct the subunits of spherical hosts.[23] Moreover, an ability of chemists to mimic such template-controlled processes could provide access to spherical hosts with properties not accessible using a more classical approach synthesis. The imagination of the chemist, concomitant with an understanding of principles of biology and geometry, will lead to further advances in this area.

ARTICLES OF FURTHER INTEREST

Anion-Directed Assembly, p. 51
Calixarenes and Their Analogues: Cation Complexation, p. 137
Calixarenes and Their Analogues: Molecular Complexation, p. 145
Carcerands and Hemicarcerands, p. 189
Cavitands, p. 219
Chiral Guest Recognition, p. 236
Crown Ethers, p. 326
Cryptands, p. 334
Cryptophanes, p. 340
Cucurbituril, Its Homologues, and Derivatives, p. 390
Cyclodextrins, p. 398
Cyclophanes: Endoacidic, Endobasic, and Erzdolipophilic Cavities, p. 424
DNA Nanotechnology, p. 475
Fullerenes as Encapsulating Hosts: Prepamtion, Detection, and Structures of Endohedral Fullerenes, p. 579
Glycoluril-Based Hosts, p. 597
Homocalixarenes, p. 649
The Lock and Key Principle. p. 809
Macrocycle Synthesis, p. 830
Molecular Squares, Boxes, and Cubes, p. 909
Platonic and Archimedean Solids, p. 1100
Preorganization and Complementarity, p. 1158
Self-Assembling Capsules, p. 1231
Self-Assembly: Terminology, p. 1263
Solvation Effects in Guest Binding, p. 1322
Spherands, p. 1344
Viruses as Host Assemblies, p. 1563

REFERENCES

1. MacGillivray, L.R.; Atwood. J.L. Structural classification and general principles for the design of spherical molecular hosts. Angew. Chem., Int. Ed. Engl. 1999; *38.* 1018–1033.
2. Leininger. L.; Olenyuk, B.; Stang, P.J. Self-assembly of a discrete cyclic nanostructure mediated by transition metals. Chem. Rev. **2000**, 100, 853–908.
3. Caulder. D.L.; Raymond. K.N. The rational design of high symmetry coordination clusters. Dalton Trans. 1999. 1185–1200.
4. Holden, A. Shapes, Space, and *Symmetry*; Columbia University Press: New York. 1971.
5. Plato. *Timaeus*: Warrington, J., Ed.; Dent: London, 1965. Original c. 360 B.C.
6. Wenninger. M.J. *Polyhedron Models;* Cambridge University Press: New York. 1971.
7. Graf, E.; Lehn, J.-M. Cryptates. XVII. Synthesis and cryptate complexes of a spheroidal macrotricyclic ligand with octahedrotetradral coordination. J. Am. Chem. Soc. **1975**, 97. 5022–5024.
8. Saalfrank, R.W.; Stark. A.; Peters, K.; von Schnering, H.G. Adamantanoid chelate complexes. 1. The first adamantanoid alkaline earth metal chelate complex: Synthesis, structure, and reactivity. Angew. Chem., Int. Ed. Engl. **1988**, 27. 851–853.
9. Murakami. Y.; Hayashida, O. Supramolecular effects and molecular discrimination by macrocyclic hosts embedded in synthetic bilayer membranes. Proc. Natl. Acad. Sci. U.S.A. 1993, 90, 1140–1145.
10. Salta, J.; Chen, Q.: Chang, Y.D.; Zubieta, J. The

oxovanadium organophosphonate system: $(VO)_6$(*tert*-$C_4H_9PO_3)_8Cl]$, $[(VO)_4\{PhP(O)_2OP(O)_2Ph\}_4Cl]$-, and $[V_{18}O_{25}(H_2O)_2(PhPO_3)_{20}Cl_4]^{4-}$, complex cluster structures with chloride ions inclusion from simple precursors. Angew. Chem.. Int. Ed. Engl. **1994.** *33.* 757–760.

11. Thorn, D.L.: Harlow, R.L.: Herron, N. Phosphatovanadium chemistry: New conipounds. including an example of "Tenne's prospect,." and oxidation of cyclohexadiene. Inorg. Chem. **1995**, *34*. 2629–2638.
12. Chen. J.: Seeman, N.C. Synthesis from DNA of a molecule with the connectivity of a cube. Nature **1991**, *350*, 631–633.
13. Fujita, M.; Oguro. D.: Moyazawa. M.: Oka. H.: Yamaguchi, K.: Oguro. K. Self-assembly of ten molecules into nanometre-sized organic host frameworks. Nature **1995,** 378, 469–471.
14. Stang. P.J.; Olenyuk, B.; Muddiman, D.C.: Smith, R.D. Transition-metal-mediated rational design and self-assembly of chiral, nanoscale supramolecular polyhedra with unique T symmetry. Organometallics **1997.** *16.* 3094–3096.
15. Hartshorn. C.M.: Steel. P.J. Self-assembly and x-ray structure of a ten-component. three-dimensional metallosupramolecular cage. Chern. Commun. **1997.** 541–542.
16. Gonzalez-Duarte. P.: Clegg. W.; Casals, I.; Sola, J.; Rius, J. Unprecedented polycrystal structure of a new cadmium thiolate containing an unusually highly charged $[ClCd_8\{SCH(CH_2CH_2)_2N(H)Me\}_{16}]^{15+}$ core. J. Am. Chem. Soc. **1998,** *120.* 1260–1266.
17. Abrahams. B.F.: Egan. S.J.; Robson. R. A very large metallosupramolecular capsule with cube-like 43 topology assembled from twelve Cu(II) centers and eight tribidentate tri-anionic ligands derived from 2,4,6-triphenylazo-1,3,5-trihydroxybenzene. J. Am. Chem. Soc. **1999.** *121.* 3535–3536.
18. Zhang, Y.; Seeman, N.C. Construction of DNA-truncated octahedron. J. Am. Chem. Soc. **1994,** *116*. 1661–1669.
19. Müller, A.: Krickemeyer. E.; Dillinger, S.; Bogge, H.: Stammler, A. $As_4Mo_6V_7O_{39}(SO_4)^{4-}$: A species with an unusual structure and a model for the different host–guest properties of poly-vanadates and -molybdates. J. Chem. Soc. Chem. Commun. **1994,** 2539–2540.
20. MacGillivray, L.R.: Atwood. J.L. A chiral spherical molecular assembly held together by 60 hydrogen bonds. Nature **1997.** 369, 469–472.
21. Kroto, H.W.: Heath. J.R.; O'Brien, S.C.; Curl. R.F.; Smalley. R.E. C_{60}: Buckminsterfullerene. Nature **1985.** 318. 162–163.
22. Swiegers. G.F.: Malefetse. T.J. Classification of coordination polygons and polyhedra according to their mode of self-assembly. Chem. Eur. J. **2001**. 7. 3637–3643.
23. Branden. C.: Tooze. J. *Introduction* to Pmtein Structure: Garland: New York, 1991.

Podands

Edwin Weber
Technische Universität Bergakadernie Freiberg, Freiberg, Germany

INTRODUCTION

The discovery of crown ethers and their unique complexation properties in the 1960s[1–3] initiated an explosive development of the field that is now called "host–guest chemistry''[4] or, within a broader scope of understanding, "supramolecular chemistry.''[5] This gave rise to an enormous number and structural variety of compounds all tracing back to the original crown ethers. Apart from the parent-type crown compounds, they range over the monocyclic coronands, the bi- and oligocyclic cryptands, the spherands, cavitands, carcerands, and even more sophisticated structures showing the course of evolution to very complex systems.[6] Weighing the advantages and disadvantages of such complicated structures. e.g., high selectivity and high stability of complexation on the one hand, but high expenditure of preparation and low kinetics of complexation on the other hand. contributed to the opposite course of development. that is to say, design of less-complicated acyclic structures. This process resulted in the synthesis of the so-called "podands." which are by definition open-chained analogues of crown compounds and cryptands. Podands now exist in a great many structural variations ranging from single-chained basic compounds to multiarmed dendrimers like inolecules and from highly flexible to rather rigidly preorganized molecular architectures.[7–9] However, it should also be noted at the beginning that compounds of the podand type were well known, long before the discovery of crown ethers, because many of the traditional ligands. e.g., oligoamines, salens, etc., used to form chelate complexes of metal ions are podands in their structural features.[10] Other long-known compounds of podand type are the commercial oligo- and polyethylene glycols (PEGs) and their dimethyl ethers (glymes).[11,12] Moreover, certain natural cation-binding ionophores (antibiotics. siderophores) are also close to the structure of podands,[13,14] giving a foretaste of the diversity of compound types classified among the podands with a broad range of occurrence and applications being discussed in the following sections.

DEFINITION, BASIC STRUCTURE, AND TERMINOLOGY

Coming from supramolecular. coordination, or host–guest chemistry, the podands are classified as multidendate organic ligands or multidonor-site host compounds.[15] Within the general class specification of supramolecular ligands and host compounds. the structural feature characteristic of a podand are the alignment of donor atoms (D) in an open-chain framework[16] (Fig. 1a). Thus, within the most generalized system of nomenclature for organic ligands, the podands represent noncyclic structures, coinpared to the monocyclic coronands (Fig. 1b) and bi- or oligocyclic cryptands (Fig. 1c). Referring to the noncyclic backbone of a podand that can be a simple line of atoms or a branched or multibranched structural arrangement. a subdivision is made into mono-, di-, tetra-. oligo-. or multipodands.[16] Exemplary cases of general construction representative of these structural types are shown in Fig. 1. e.g., mono- (Fig. 1a). di- (Fig. 1d), tri- (Fig. 1e). tetra- (Fig. If). podandobridged tetra- (Fig. 1g), or multibranched (Fig. Ih) podands. While the single-strand monopodands do not involve a so-called anchor group (A in Fig. I). the branched oiigo- and inultipodands. beginning with the dipodands, have at least one such anchor group or branching point incorporated in their structure. The anchor groups or branching points refer to any construction element or branching unit to which the podand segments are attached, mostly being an aromatic unit or an oligovalent atom (often N, P. or C).[7–9] Because the donor atoms, as well as the bridging units (ethylene, 1,2-phenylene) of ordinary podands are mostly the same as used for the construction of the crown ethers, coronands. and cryptands, it is understandable that the podands are sometimes compared with the cyclic or bicylic counterpart structures of crown ethers[7,8] and cryptands and are called open-chain crown ethers (cf. Fig. 1d with Fig. 1b) or open-chain cryptands[17,18] (cf. Fig. 1e with Fig. 1c). Although the name podand comes from the Greek meaning "foot,.' it is also spoken of "arms" in this structural context.'"']So. mono-. oligo-, and multipodands

Encyclopedia of Supramolecular Chemistry
DOI: 10.1081/E-ESMC 120012710

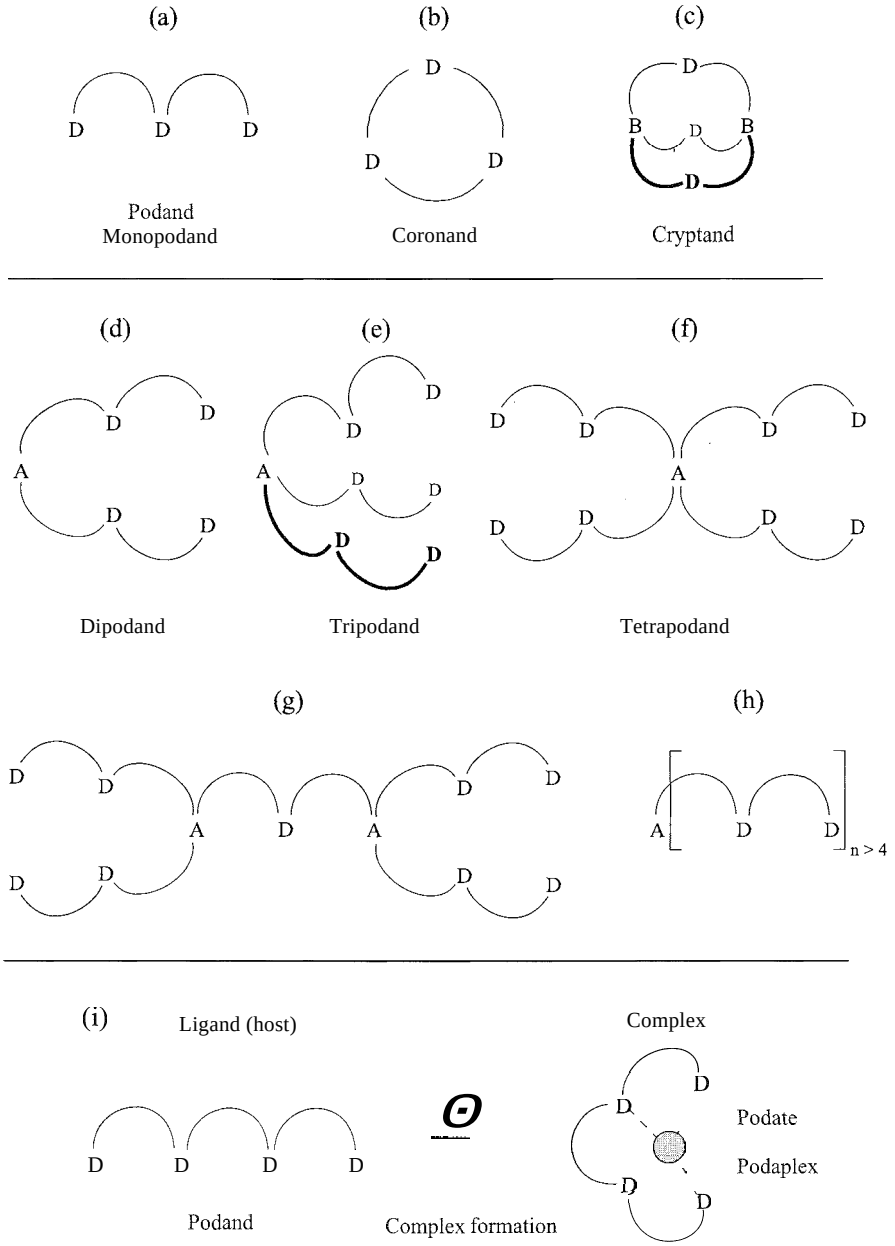

Fig. 1 (a)–(h) Definition, specification, and nomenclature of podands. including (i) podand complexes.

are synonymous with mono-, oligo-, and multiarmed open-chain ligands or host compounds, rerpectively.

Finally, most of the podands were synthesized with the formation of complexes (mostly with metal cations, see below) in mind. These complexes are termed "podates,''[15,16] or sometimes ''podaplexes''[19,20] (Fig. 1i).

REPRESENTATIVE COMPOUNDS AND SPECIFIC NOMENCLATURE

Because the acyclic podands were developed by imitating the crown ethers to a large extent, the podands featuring an open-chain framework with alignment of oxygen atoms bridged via ethylene units and having hydroxyl (Fig. 2a, R=OH) or alkoxy (especially methoxy) terminal groups (Fig. 2a, R=OCH_3, OAlkyl) are perhaps the most commonly known conventional podands.[7–9] According to their structures, they are oligoethylene (di-, tri-, tetraethylene, etc.), polyethylene glycols (polymers of ethylene oxide) or their dialkylether derivatives. Although many names were applied to the higher polymers of ethylene oxide (Carbowax, Jeffox, Nycolene, rnacrogol). they are conveniently designated as PEG followed by a number (e.g., PEG-200), where PEG is the abbreviation for polyethylene glycol. and the number designates the

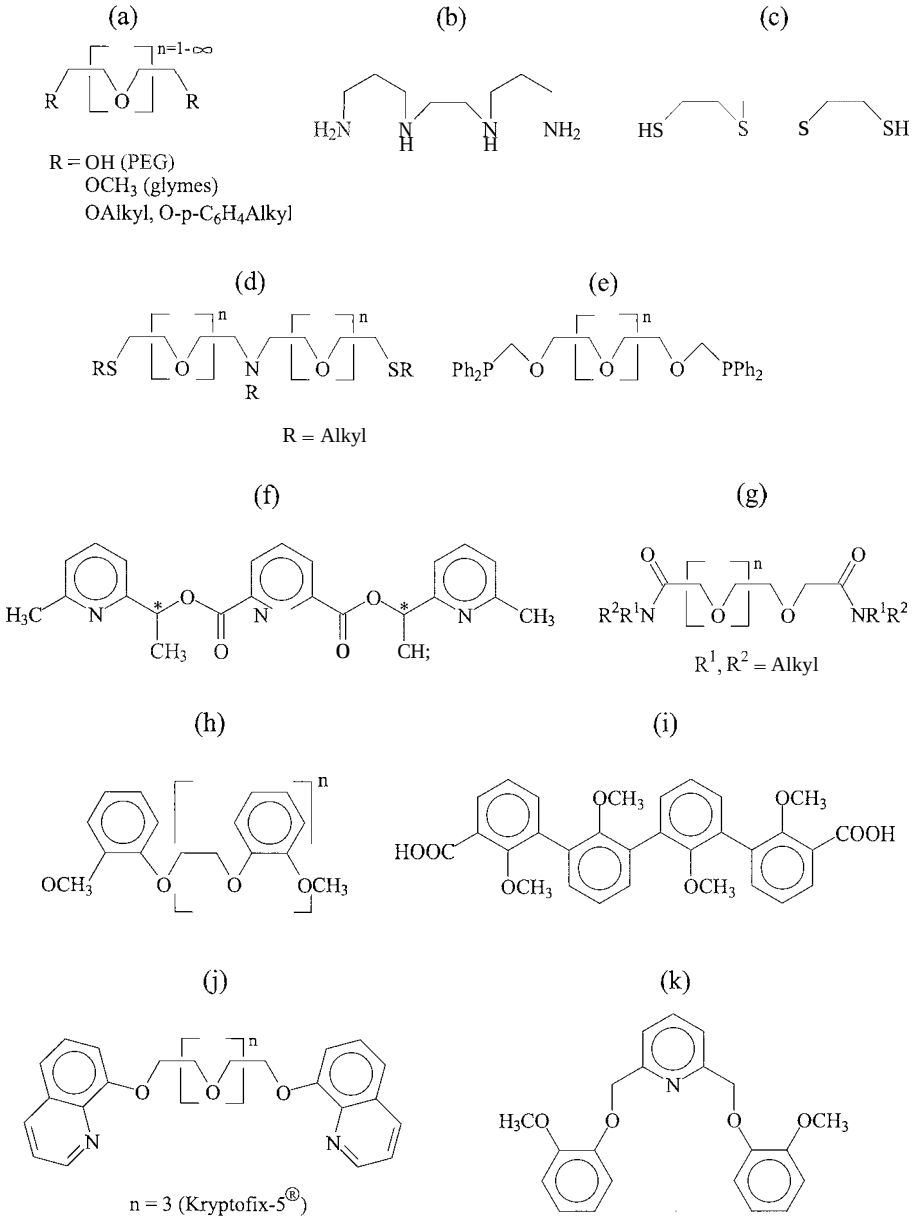

Fig. *2* Exemplary cases of linear podand types (monopodands. open-chain crown compounds): (a) conventional: (b,c) modified donor atoms: (d)–(g) mixed donor groups: (h,i) rigid building blocks; and (j,k) specific donor end groups.

molecular weight. which is an average molecular weight for commercial compound mixtures (e.g., 190–210 Da for PEG-200).[11] The dimethylether derivatives of the oligoethylene glycols are called ''glymes'',[12] which is short for glycol methyl ethers. or more specifically, diglyme (Fig. 2a, R=OCH_3, n=1), triglyme (n=2), tetraglyme (n=3), or oligoglyme (n being a higher number). In another naming of these compounds, the number following the class name glyme denotes the total number of ether oxygens connected with the ethylene glycol linkages, e.g., glyme-4 is tantamount to triglyme.[7,8] Moreover, numerous polyethylene glycol relatives exist in which only one of the terminal hydroxyl groups of polyethylene glycol is replaced by an alkoxy residue[1''] (cf. Fig. 2a). Important industrial representatives of this compound type[11,12] contain a long alkoxy chain as the terminal group. e.g., ''Laureth 9,'' which is short for nonaethylene glycol monododecyl (lauryl) ether. In addition. the family of industrial compounds known as ''nonoxynols'' are also mcnosubstituted derivatives of PEGs, but they possess a p-nonylphenyloxy residue at one end of the PEG chain (e.g., an undecaethylene glycol in the case of ''nonoxynol 11'') (cf. Fig. 2a). Similar compounds derived from polypropylene glycols are also in existence but play a less

important part compared to the PEGs and their derivatives.'" A block copolymer of ethylene oxide and propylene oxide having a molecular weight of $\sim 3 \cdot 10^3$ Da is termed ''poloxalene.''

On the other hand, open-chain analogues of the coronands featuring donor atoms different from oxygen are known in an immense variety,[7–10] including among all nitrogen and sulfur podands any mixed arrangement of potential donor atoms (O, N, S, P, As). Examplary cases are given in Fig. 2b–e. As for the crown compounds and cryptands, the donor atoms of podands may also be an integral part of a heterocyclic ring, a composite functional group, or a substituent (Fig. 2f,g). Although the most common bridging element connecting the donor atoms of podands is the aliphatic ethylene unit, the 1,2-phenylene (Fig. 2h) and analogous groups as aromatic counterparts are also in use. providing conformational rigidity of the podand framework and thus enhancing the overall organization or preorganization of the podand. For the same reason, the rigid all aromatic1 heteroaromatic group containing podands (Fig. 2i) may be referred to as open-chain spherands.[19,20] A further alternative to achieve organized podands is based on the so-called "end group concept''.[21,22] Here, use is made of a well-considered combination of strong donor sites and rigid building blocks to yield the end groups that are attached to the termini of a podand chain. The 8-oxyquinoline (Fig. 2j), 2-methoxyphenoxy (Fig. 2k) and analogous units (cf. Fig. 3e) were often used in this respect.

In most published cases of the tripodands (tripodes),[7–9] the three podand subunits are attached to nitrogen as the branching point and are usually the same in structure, but may be different. making the compounds symmetrical triamines (Fig. 3a.b). Also, in many representative cases of this compound class. rigidifying terminal groups according to the end-group concept are a particular feature of the structure (Fig. 3b). Nevertheless, many tripodands differing significantly from this structural principle were reported,[7–9] such as the derivatives of glycerol with carbon as the branching point (Fig. 3c). Others contain a central benzene or a 1,3,5-triazine nucleus (Fig. 3d) as the branching unit. Tetrapodands and higher polypodal ligands are similarly constructed,[7–9] using ethylenediamine (Fig. 3e), pentaerythritol, benzene units. or a calixarene framework (Fig. 3f) as the multibranching elements. Compounds of the latter type are called .'calixpodands.''[23,24] A striking example of a hexapodand is shown in Fig. 2g. Because of the pictorial parallelism to an octopus (in the strict sense a hexapus), benzene and other derivatives of this general structure are termed "octopus molecules."[25,26] However, as it may have appeared. podands are not exclusively manmade but also originate from nature. A variety of nonmacrocyclic ionophore antibiotics, such as grisorixin and nigericin[13] or the acyclic siderophlores[14] are podands in their overall structures. It is a common feature of the antibiotic structures that many of the donor atoms are located in tetrahydrofuran or tetrahydropyran rings (Fig. 3h). Another typical feature of the podal antibiotics is their chirality effected by a multitude of chiral centers. This structural property was also imitated by artificial podands, of which an example is shown in Fig. 2f.[27]

Finally, it is worth mentioning that in the same way as for the crown compounds and cryptands. a specific notation system was developed for podands.[16] However, because of the broad structural range of the podands: it is complex in layout and rules and is, therefore, only scarcely in use. For instance, applying this notation system to the simple compounds of Fig. 2a (R=OCH_3, n=2) and Fig. 2j (n=3) would result in the designations ''1,10-dimethyl<O_4 podand-4>'' and ''<(8)quinolino, O_5 (8)quinolinopodand-7>.'' respectively. The latter compound is sold under the tradename Kryptofix-5®; the names more common in use for the former compound (see above) are triglyme or glyme-4.

SYNTHESIS OF PODANDS

Most of the conventional podands, including the oligo-/polyethylene glycols and their rich variety of simple derivatives (glymes. PEG monoalkyl ethers, nonoxynols, etc.) are industrial products: usually obtained by polymerization of ethylene oxide (oxirane) or from oxirane and alcohols or oxirane and phenols, respectively.[11,12] Unfortunately, the polymerization process results in a mixture of compounds (oligomers of oxirane). causing difficulties when pure compounds are required, but the reactions per se are without problems. Indeed, even the bench synthesis of more specific acyclic podands is, by far, less problematic as for the macrocyclic crown compounds and macrobicyclic/oligocyclic cryptands.[28] This is mainly a consequence of their noncyclic structure, making superfluous laborious and other specific preparative methods (high dilution techniques, template support), usually required for the synthesis of macrocyclic ligands.[29] Hence, the podands are generally obtained by using conventional synthetic methods including common ether. sulfide, ester, or amide bond formation.[7–9]

However, certain difficulties may arise from the substrates that are often bi- or even oligofunctional in their structures: thus causing problems with respect to the control of the reactive sites. In order to eliminate these problems. protective group techniques are used. in particular, when hydroxyl or amino functions are involved. For that purpose, the interfering functions are temporarily

paralyzed through transformation into the corresponding labile ether, acetal, ester, or urethane derivatives. In this context, it is interesting to note that the purely accidental discovery of the first crown ether, dibenzo-18-crown-6, by Pedersen is the result of an incompletely protected substrate (catechol), while he aimed at preparing a bisphenolic podand.[1–3] Mention should also be made that many of the podands are simply intermediates of a crown ether, coronand, or cryptand synthetic sequence.[28,29] Here. they are mostly found at the level before final ring closure and may contribute to the accomplishment of a template effect.[30]

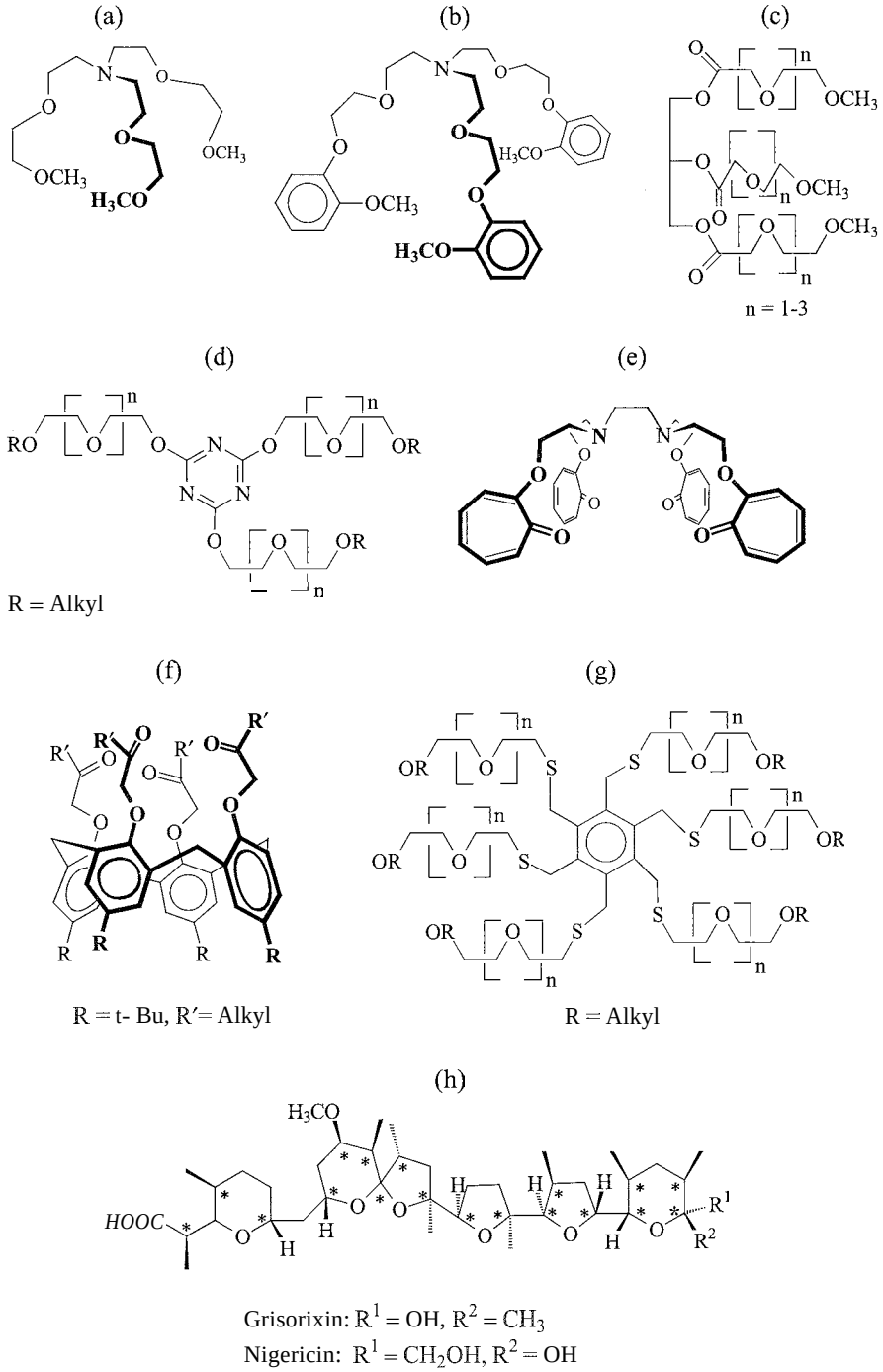

Fig. **3** Representatives of (a)–(d) tripodands: (e,f) tetrapodands; (g) a hexapodand (oligopodands): and (h) podal natural ionophores.

COMPLEXATION PROPERTIES AND HOST BEHAVIOR OF PODANDS

Because the podands were developed from the crown compounds and are seen as their open-chain analogues, properties similar to the crown compounds are to be expected for the podands. This is most evidently shown by the ability to form complexes.[4,5] In case of the podands, they are called "podates''[15,16] or sometimes ''podaplexes.''[19,20] This behavior of the podands to act as open-chained multidonor ligands was assessed with a variety of metallic and organic cations.[7–9] However, due to the acyclic structure of the podands. as contrasted with the macrocyclic crown compounds, there are also differences in the behaviors of the two compound types. including pros and cons.

Complexation of Cations (Metal Ions)

To begin with the simple polyethylene glycols and glymes. they both were found to form complexes with alkali metal cations (Na^+, K^+) of increasing stability with increasing chain length of the podand.[7–9] Incorporation of an organizing 1,2-benzo unit into the glyme structure does not fundamentally alter the facts. These observations accord nicely with the general understanding of the complexation phenomenon accepted for crown ethers.[29,31] However, when making a comparison between crown ethers and the open-chained relatives, the macrocyclic crown ethers generally exhibit much higher cation affinity than their acyclic podand analogues.[32] To set an example, the stabilities of the potassium cation complexes of pentaglyme (glyme-6) (Fig. 4a) and 18-crown-6 (Fig. 4b) differ by about four orders of magnitude in favor of 18-crown-6, depending on the solvent (e.g., methanol). The enormous binding difference is said to result from a so-called "macrocyclic effect" and may be explained by enthalpic and entropic effects, unfavorable in case of the podand.[33] The potassium complex of cryptand [2.2.2] is still more stable (again by about four orders of magnitude; Fig. 4c), as a consequence of the macrobicyclic effect or cryptate effect.[33] Thus, with reference to the three basic types of oligodentate organic ligands (Fig. la–c). one may reach the conclusion that the podands give the weakest complexes of the series. Nevertheless, the podands profit from the well-known chelate effect,"' which relates to the observation that metal complexes of bidentate or oligodentate ligands are significantly more stable than closely related materials that contain unidentate ligands (such as diethyl ether or ammonia). When drawing a comparison between the cation complexes of simple monopodands or dipodands and the topologically higher tripodands (open-chain cryptands). the tripod complexes are somewhat more stable than the analogous complexes of the mono- or dipodands.[7,8] On the other hand, the complex stabilities for the tetrapodands were generally found to be somewhat lower than for the tripodands. which is attributed to potential steric hindrance of the terminal groups in the complex arrangement (an effect also believed to affect the complexation of higher oligopodands).

However. the affinity for metal cations is also regulated by the character of the donor atoms contained in the podand framework.[7–9] While the all-oxygen podands, in keeping with the hard nature of the oxygen donor atoms, favor the formation of complexes with alkali and alkaline earth metal cations: incorporation of nitrogen and sulfur donor atoms into the podand framework is attractive, as it alters the binding tendency of all-oxygen podands so that they may more readily complex cations of the transition metals, such as Ag, Cd, Hg, Co, or Ni.[33] Several other donor atoms (P, As) and types of donor groups, including functional units (ester, amide, etc.) may stabilize specific podand cation complexes. including complexes with NH_4^+ and organic (chiral) ammonium ions."' But probably the most general effect of complex stabilization in this context is produced by the end-group concept mentioned above, which is effective when sufficiently rigidifying donor end groups are present.[21,22] A complex stability constant typical of an end-group-assisted podand is exhibited by the 1:1 K^+ complex of Kryptofix-5® (cf. Fig. 2j, $n=3$) with log $K_s=3.5$ (in methanol).[34]

Another typical feature of the podands is that the stability constants of their complexes are largely independent of the metal cation radius, resulting in relatively small discriinination factors $K(M_1^+)/K(M_2^+)$, i.e., relatively low cation selectivity, as compared to the more preorganized crown compounds and cryptands [cf. $K(K^+)/K(Na^+)$ in Fig. 4a–c].[32] This is a consequence of the flexible podand chain that can more readily adapt to the various ions. Nevertheless. when circumstances meet the structural requirements, podands may definitely achieve useful metal cation selectivities, most distinctly manifested by the natural ionophores (e.g., nigericin significantly prefers K^+ over Na^+, while monensin is in the reverse order)[13] or the so-called ''stereognostic ligands''[35] detigned for specific target cations such as $[UO_2]^{2+}$ or $[VO]^{2+}$.

However, in one important respect, the podands are undoubtedly superior to the cyclic analogues, which is the kinetics of complexation and decomplexation of cations.[32] In fact, it is a general phenomenon that the more rigidly preorganized a host is for cation binding, the slower the kinetics of the process are. The same is true for decomposition of the complex. Thus, both the forward (k_1) and reverse complexation rates (k_{-1}) of the podands are high, while the rates for the forward and back reactions of the macrocycles are slower, in practice, 10^2–10^3 times slower than with open-chain ligands. The complex

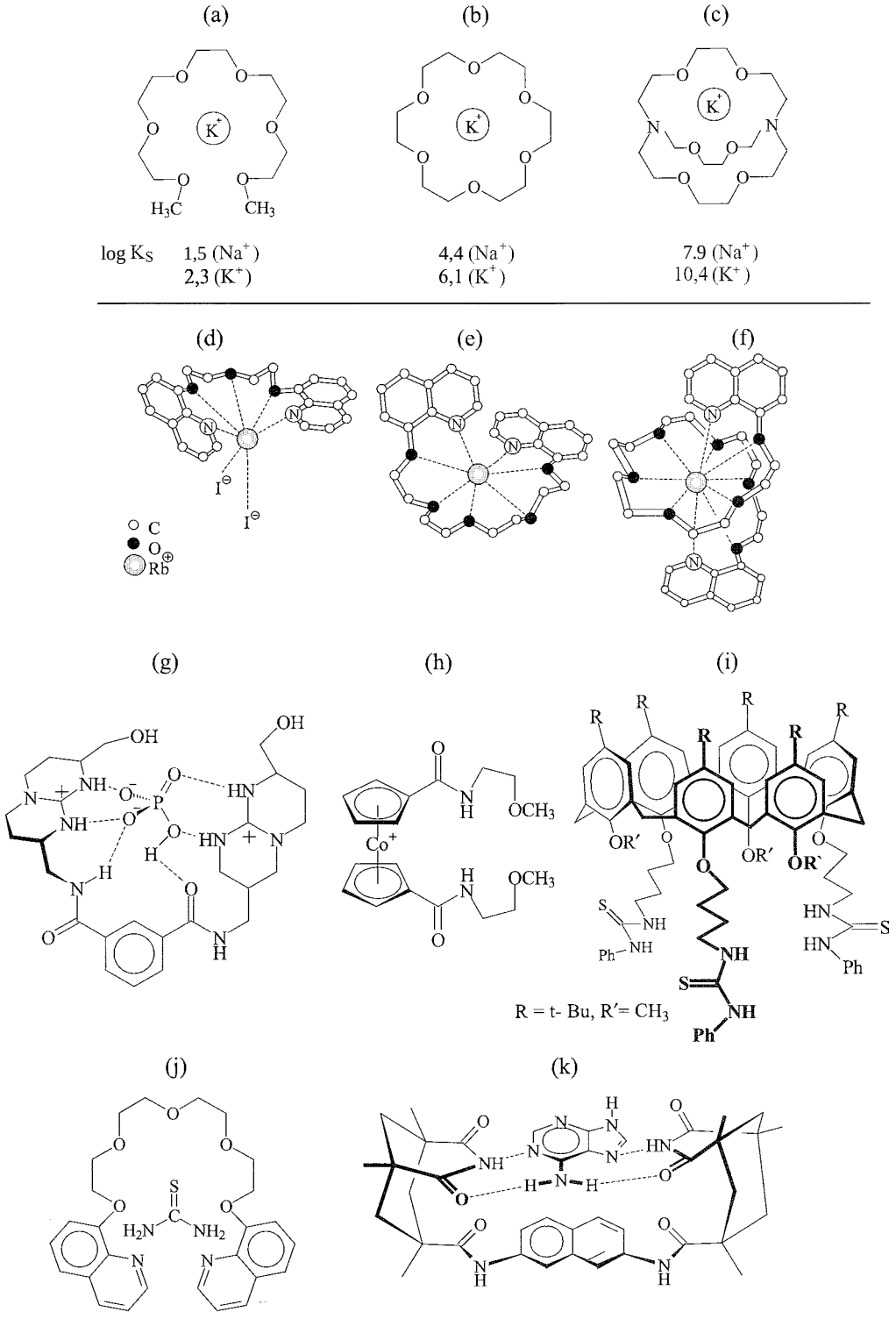

Fig. 4 Complex formation of podands: (a)–(c) log K_s of the Na^+ and K^+ complexes of (a) pentaglyme, (b) 18-crown-6, and (c) [2.2.2] cryptand demonstrating the macrocyclic and cryptate effects: (d)–(f) Rb^+ coordination spheres in the solid-state structures of the RbI complexes of bisquinolino podands of different chain length (cf. Fig. 2j); (g)–(i) podand anion complexation: (g) podand HPO_4^{2-} complex, and podands for (h) halide (Cl^-, Br^-) and (i) carboxylate (benzene-1.3.5-tricarboxylate) complexation: and (j,k) complexes of podands with uncharged molecules involving (j) thiourea and (k) adenine.

stability per se then results from the rates for complexation and decomplexation ($K_s = k_1/k_{-1}$), giving rise to a static or dynamic complex stability. The podand complexes are mostly affected from kinetics. This is an important point in the use of podands (see below).

Solid-state structures of complexes between podands and metal cations were solved in great number, including the complexes of simple glymes[36] and of the natural acyclic ionophore antibiotics,[13] but perhaps most of the structures that have become known relate to the complexes of podands involving rigid donor end groups of which three representative examples are illustrated in Fig. 4d–f.[7,8] In all three cases, the podand chain is wrapped around the cation (Rb^+), and all donor atoms coordinate. Nevertheless, the conformation of the ligands reveals significant differences dependent on the chain length, being approximately planar and folded like a butterfly (Fig. 4d), helically arranged (Fig. 4e), or spherically wrapped (Fig. 4f) for the penta-, hepta-, and decadentate podands, respectively, giving an impression of the flexible structure and adaptability of the podand chains. Moreover, as shown with the pentadentate ligand, if the solvation sphere of the cation is not satisfied by the donor atoms of the podand, anions are alternatively used to fill the coordination sphere. While most of the complexes are of mononuclear 1:1 stoichiometric type, the long-chain multidentate podands were also found to form dinuclear 1:2 stoichiometric or polymeric complexes.[7,8,32]

Complexation of Anions

In comparison to the complexes of cations, complexation between podands and anions is a rather recent development.[5] Nonetheless, different types of anion-complexing podands were designed.[37] Due to the special features of the anions that must be addressed, they include positively charged, organometallic, coordination interaction, or hydrogen-bonding structures of which representative examples are illustrated in Fig. 4(g–i). Anions often complexed by these hosts range from simple inorganic halide ions to the biologically relevant phosphate or carboxylate ions. Among the cationic podand structures, the guanidinium-based receptors are certainly the most important. One of these compounds that incorporates two guanidinium pendant arms attached to a 1,3-phenylene unit, e.g., allows effective complex formation of hydrogenphosphate, even in water (Fig. 4g). The organometallic cobaltocenium receptor of Fig. 4h endowed with additional amide hydrogen-bonding functionality in the podand subunits, developed for halide (Cl^-, Br^-) complexation, makes possible the electrochemical detection of anion binding [e.g., $K_s(Cl^-) = 20\ M^{-1}$ in DMSO]. The high affinity of actinide metals such as uranium for oxoanions is used in a ditopic coordination-type receptor to bind two $H_2PO_4^-$ anions, while the podand hosts not bearing any positive charge but based mainly on hydrogen-bonding interactions are mostly ureas of rigid-cleft structure or tripods derived from the *tren*, 2, 2′, 2″-*tris*(aminoethyl)amine, motif. A particular example of complementary anion complexation is shown by a tripodal thiourea receptor featuring a trifold symmetric calix[6]-arene scaffold that binds the trianion of trimesic acid markedly well in chloroform ($K_s = 2 \cdot 10^5\ M^{-1}$), while halides are only moderately bound (Fig. 4i). Other uncharged hydrogen-bonding podands, comprising a chiral framework, show chiral discrimination in the complexation of carboxylates (tartrate, amino acid anions). Thus, the podands are capable of selective anion complexation, although the complexes are only of moderate stability.

Complexation of Uncharged Molecules

The complexation between podands and uncharged molecules appears to be even less strongly explored than between podands and anions.[5] To this day, complexes of simple glymes with neutral molecules have not successfully been isolated. Only when the podands have a somewhat more specific or rigid structure are complexes with uncharged molecules formed or isolated in crystalline state. In most cases, these podands are of rigid-cleft type or contain rigidifying donor end groups.[38] Conventional guest molecules are water, urea, and thiourea, but relatively complex neutral guest molecules, such as nucleic acid bases or sugars, are also efficient in complex formation.[5] The main interactions that hold these complexes together are hydrogen bonds and π-stacking. Remarkable cases of complexes are illustrated in Fig. 4j,k. On the other hand, the so-called solid-state complexes of multiarmed podands (e.g., hexahosts) with neutral molecules are more likely to be classed with clathrates (crystal void inclusion compounds).[39]

APPLICATION OF PODANDS

Considering the properties of podands, as demonstrated in the previous section, several important applications can be deduced. They relate to utilization of podands or to molecular classes that evolved in part from podand chemistry.[7–9]

Chemical Synthesis

Due to cation complexation and aftereffects relating to the increased solubility of inorganic salts in low-polarity organic media and enhanced activity of the counterion reactant (quasi-naked anion), the podands, just as the crown compounds and cryptands, are promising catalysts in the synthetic methodology of phase-transfer catalysis,

both in liquid–liquid or solid–liquid systems.[40] Although the crown compounds and cryptands are more active in complexation and surpass the podands in anion activation; these agents also show deficiencies: as compared to the podands. In the first place, they are relatively expensive, being an obstacle to industrial use, and second, they are much slower in the kinetics of the complexation/decomplexation process (see above), which is of general disadvantage for the catalysis. Hence, making use of the podands as a PT-catalyst saves costs and time. thus affording a reasonable alternative to the crown compounds and cryptands. and in some respect, also to the conventional quaternary ammonium salts. This is, in particular, true for the siinple oligo-/polyethylene glycols (PEGs) and their methyl ethers (glymes) (Fig. 2a). They proved to be effective catalysts in a variety of anion-proinoted reactions, involving nucleophilic substitutions with anions such as fluoride, cyanide, acetate. azide, thiocyanate, and sulfide or eliminations using hydroxide as a base, both under liquid–liquid and solid–liquid PT-conditions.[7–9] Mostly. the reactivity increases by increasing the molecular weight of the ligands, however, the catalytic activity does not appear to be generalizable for any kind of anion-promoted reaction. For instance, when considering the dehydrobromination of 2-bromoethylbenzene with 60% aqueous KOH, pentaethylene glycol (Fig. 2a. R=OH, n=3) was found to be the optimum PT-catalyst, while higher and lower glycols, and even 18-crown-6 (cf. Fig. 4b). proved to be less effective. This specific behavior is presumably attributed to the self-solvating behavior of PEG, unlike the crown ether. Because the PEGs are so inexpensive, they may even be used as solvents in processes of this type. Moreover, particular end-group-assisted linear podands (Fig. 2j) and tripods (Fig. 3b), as well as oligopodands, derived from trisubstituted triazine (Fig. 5a), respectively, hexasubstituted benzene (Fig. 3g). cyclotriphosphazene, or cyclotriveratrylene, are. in part, very good catalysts, mainly in solid–liquid PTC. showing superiority to similar commercial ligands like the ''Trident'' (Fig. 3a).[7–9] Finally; the possibility of solving the catalyst recovery problem by attaching active catalyst centers to insoluble polymeric matrices (''three-phase-catalysis''), which is of high interest from the industrial point of view. was also used with podands.''''' And last but not least, glymes are excellent solvents in the laboratory use of organometallic reactions. while the PEGs and other simple podands of this type are useful starting materials in the preparation of crown compounds and cryptands[28–30] as well as in the synthesis of many other commercial products of the chemical industry.''''' A few out of this wide range of compounds were mentioned in earlier passages.

Another field of application where the flexible podand structure offers advantages to chemical reactions is enzyme modeling.[41] Without going into detail, this has given rise to a variety of catalysts being inspired of enzyme activity, such as the Zn^{2+} complex of the tripodand shown in Fig. 5b. which is an esterase mimic.

Chemical Analytics

Compound separation and concentration determination are important processes in analytical chemistry. In both respects, the podands are useful tools.[42] Considering the so-called ''solvent extraction'' of metal ions, which uses a water/organic solvent two-phase system for separation and enrichment of metal ions, suitable ligands operate as carriers.[43] Their effectiveness not only depends on their complexation ability but also on the partitioning between the two phases. This factor is taken into account by modification of the podand with lipophilic substituents to a balanced degree, such as butyl or higher alkyl groups at the termini of an oligoethylene glycol chain (Fig. 2a, R=OAlkyl). Nevertheless. due to their flexible structures, these lipophilic derivatives of glymes were found to be much less efficient in the extraction and separation of alkali metal ions as compared to lipophilic crown compounds. However. amido analogues of this compound type (Fig. 2g) show clear preferences in the extraction of rare earth [Yb(III), La(III)] and alkaline earth [Ca(II), Sr(II)] metal ions, while certain aza and thia derivatives of the lipophilic glymes (Fig. 2d) show good carrier properties for the extraction of Hg(II), Cu(II), Ag(I), Au(III), and other ions of polluting or precious transition metals. On the other hand, as compared to the macrocyclic hosts, the podands have only scarcely been used as carriers in membrane transport, which is another technique used to accumulate and separate chemical species such as metal cations''''] (e.g., the podand of Fig. 2f being selective for Ag^{+}), though most of the natural podands (nonmacrocyclic ionophore antibiotics)[13] are typical of this behavior.

Owing to the fast complexatioddecomplexation kinetics. podands have found wide applications in chemical sensing, such as in ion-selective liquid-membrane electrodes: which in some relevant cases contain a lipophilic podand as the sensor component.[44] These podands mostly possess an amide structure and have long alkyl chains that are needed to retain the compounds in the lipophilic medium of the membrane. Based on this strategy, ion-selective membrane carriers are available for nearly all cations of interest in concentration analytics (metal ions, ammonium ions), including clinical. biological, and environmental fields. Remarkable cases with indication of the ions to be determined are illustrated in Fig. 5c–e. Also, among the immense variety of fluoroionophores designed for cation-sensitive fluorescent sensors. the fiuorogenic podands rank high.[45] These podand structures contain a fluorogenic subunit that tranduces the chemical information of the ion–podand interaction, ion

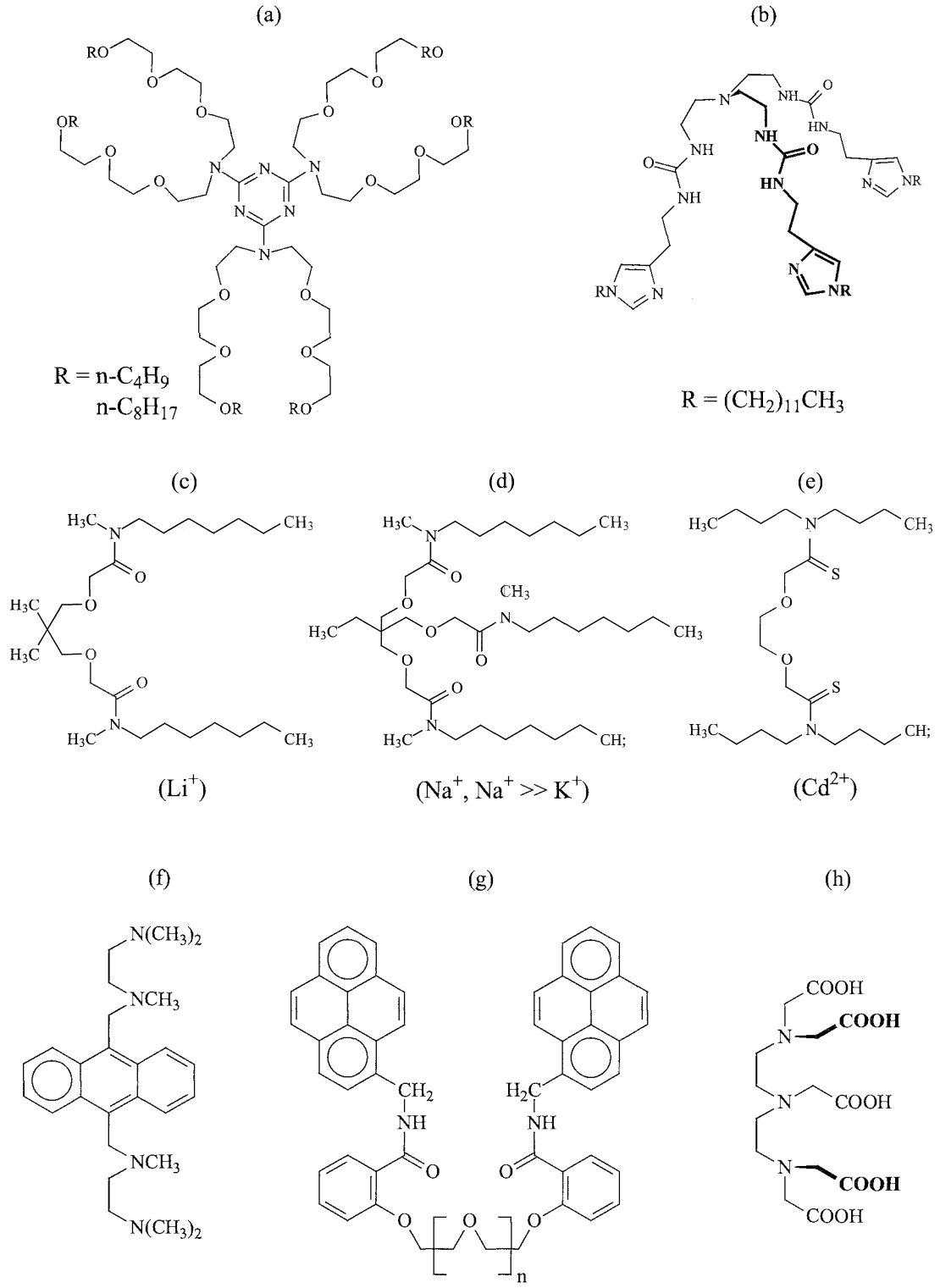

Fig. 5 Podands with reference to practical uses: (a) PT-catalyst: (b) enzyme model: (c)–(e) selective membrane carriers (ions to be determined in parentheses); (f,g) fluoroionophores: and (h) imaging agent.

selective and in dependence of concentration, in an optical signal. Often. the fluorophore unit is an anthracene or pyrene derivative. while the podand donor sires are oxygen or nitrogen atoms with affinity for hard alkali and alkaline earth or soft transition metal ions, respectively. Relevant examples are shown in Fig. 5f,g. Moreover, certain paramagnetic lanthanide complexes of oligopodands (Fig. 5h) are in clinical use as contrasting agents for magnetic resonance imaging.[46]

Other Uses and Potential Applications

Although the podands classify a particular compound type, including numerous structural variations,[7–9] certain other molecular types that have grown into separate compound classes trace, in part. back to the chemistry of podands. This holds, in particular. for the so-called "lariat ethers" or more general ''lariat compounds'. (from the Spanish "la reata" meaning "the rope," due to their graphic resemblance to a lasso) featuring a coronand (crown ether) ring with one or more podand side chains attached to it[47] (Fig. 6a–c). Because the "rope and tie" analogy is less satisfactory for the two- and higher-armed macrocyles (Fig. 6b,c), the term ''bracchial'' (from the Latin ''bracchium'' meaning ''arm'') was adopted. Thus, leading to names bibracchial lariat ether (BiBLE) or tribracchial lariat ether (TriBLE) for a two- or three-armed system. and so on.[47] Referring to the general class specification of supramolecular ligands elaborated with the terminoiogy of podands. the lariat compounds go by "podandocoronands," e.g., monopodando- or dipodandocoronand. and so on."'' Moreover, following the previous designation open-chain cryptand for the tripodands, the podandocoronands are occasionally called "half-open" or "semi-closed" cryptands. The overall goal in developing the lariat ether (podandocoronand) structures was to prepare a class of flexible but selective alkali and alkaline earth metal cation complexing agents. Another inspiration came from the naturally occurring TriBLE enterobactin, which is an iron-sequestering compound.[14] Heterodederivatives of the side-armed structures were also pursued with interest in the complexation of different transition metal ions.'" These compounds are of particular use for imaging and targeting purposes[46] as well as for supramolecular catalysis.[41]

In recent years, the tree-like molecular constitutions. being a logical extension of the oligopodands. developed explosively, thus now being classed under new general terms. Those multibranched structures consisting entirely of branched repeat units are usually called "dendrimers" or "hyperbranched polymers." The hyperbranched polymers are usually the product of a noniterative polymerization procedure and exhibit an irregular structure with incompletely reacted branch points throughout the structure. Dendrimers, on the other hand, are highly ordered, regularly branched. globular macromolecules prepared by a stepwise iterative approach with ''dendrons'' (cascade branching subunits) being part of it.[48] Numerous examples of this class of compounds are relevant to polypodands. of which typical illustrations are given in Fig. 6d.e. Because of their well-defined, unique macromolecular structures, dendritic architectures are attractive scaffolds for a variety of high-end applications, including nanoscale electronics. energy harvesting and conversion, nanoreactors, or highly targeted drugs.'"'

Another unique type of podands constituting a separate class of compounds are the helicands. They feature molecular threads containing a number of discrete metal-binding domains separated by spacer groups that give rise to the formation of helical complexes termed ''helicates.''[50] The majority of helicands contain nitrogen donor atoms, often incorporated in heterocyclic rings such as pyridine or 1,10-phenanthroline. In pasticular cases. double and triple helicates are created via self-assembly (Fig. 6f). Similar preorganized compounds, closely related to the podands. showed remarkable ability in the construction of molecular cages, grids, and rods through metal coordination, having advanced the new field of metallosupramolecular chemistry.[51] In addition, podands of PEG-type, bearing voluminous stoppers at the ends, brought new efficient approaches to rotaxanes to fruition.[52] Here. podands are used as the rod-like component for threading of the macrocyclic components. which are held together by mechanical bonds (Fig. 6g). All of these fascinating compounds and appealing structures suggest the possibility of generating electrochemically responsive and photochemically active molecular and supramolecular devices and materials at the nanoscopic level with precise functions and shapes. thus being promising to future high-tech applications.[53]

Finally, mention should be made that podands were in use long before the term was coined and one began to take notice of their complex formation property.[9] Strictly speaking, the conventional PEGs and glyme-type compounds (Fig. 2a, R=OH, OCH_3) are broadly used as solvents, solubilizers. emulsifiers. lubricants; finishings, sizings, softeners, wetting agents. and binders in technical products including varnishes. colors and oils, or cosmetics and pharmaceutics (such as face lotions. lipsticks, crèmes, ointments. and pills).[11,12] Others involving the PEG monoethers with one long alkyl chain or alkylphenyi residue as the terminal group (Fig. 2a, R=OAlkyl, O-p-C_6H_4Alkyl)) generally exhibit amphiphilic, detergent. or surfactant properties, and, accordingly, many are used industrially, including pharmaceutical preparations and emulsifying agents used in foods.[54] This may indicate that the ordinary podands are probably harmless for health. unlike the crown compounds and cryptands.

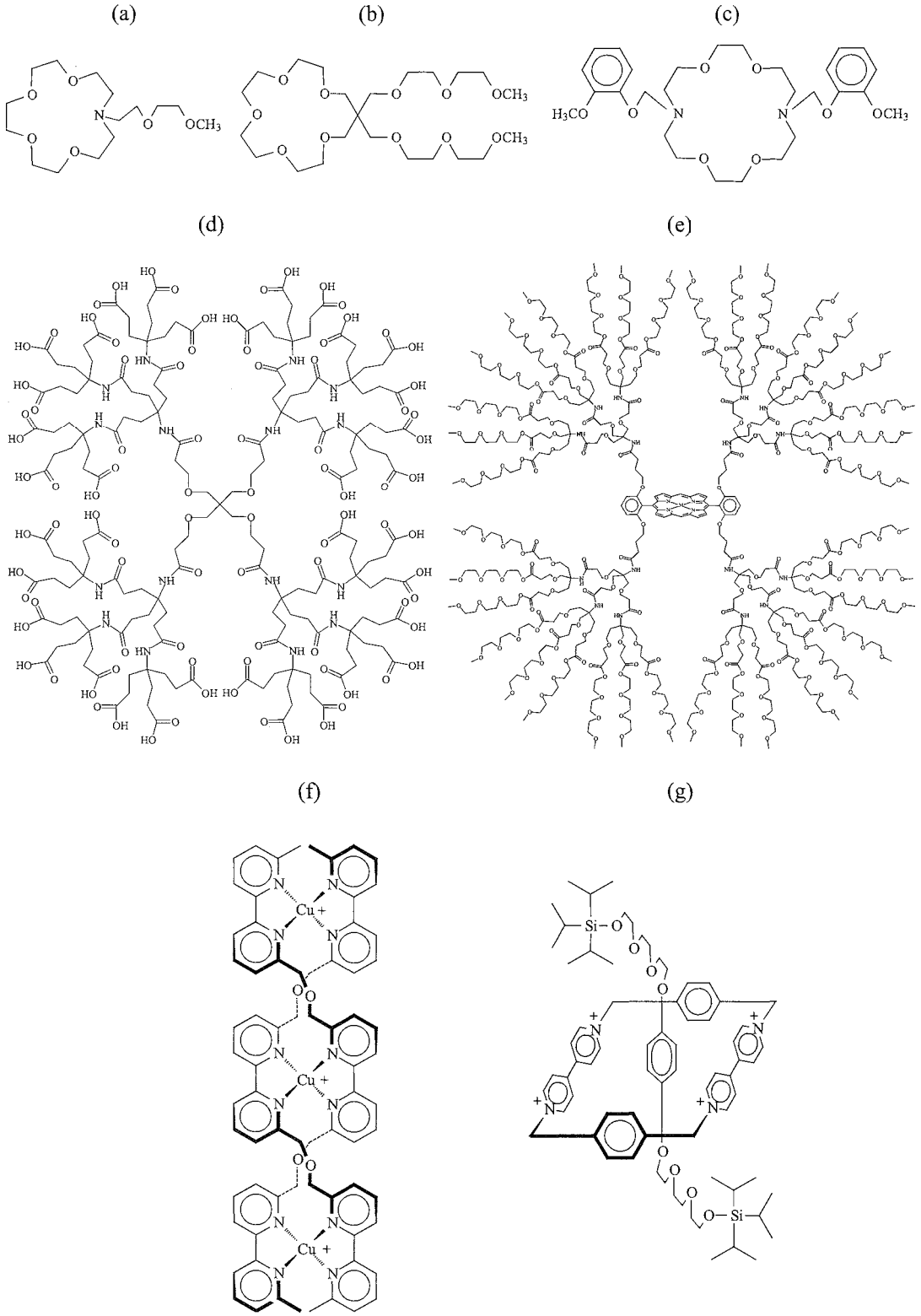

Fig. 6 Typical examples of (a)–(c) podandocoronands (lariat and bibracchial ethers); (d,e) dendrimers; (f) a helicate (double helicate); and (g) a rotaxane.

CONCLUSION

Despite the fact that the podands were well known before crown compounds and cryptands were recognized. it was only when the particular cation-binding ability of the latter was discovered that the study of podands took on a new impetus. This development has given rise to a vast array and enormous variety of novel structures of podands. which still continues. Beyond that, the podands inspired new structural variations such as those given by the lariat ethers. dendrimers, helicands, or rotaxanes that have grown into separate compound classes. Although the fundamental property of podands is to complex metal ions, other species, including organic cations, anions, or neutral molecules, are also bound. However, in comparison with the crown compounds and cryptands, the complexes of the podands are less stable and, as a rule, also less selective but kinetically much faster in formation and decomposition, which is advantageous in phase transfer, ion transport, sensing, and other promising fields of application. The most important advantage podands have. however, is their inherent inexpensiveness. The synthesis of podands is a comparatively simple one, not requiring high dilution or template processes, and is thus economic and enhances their commercial utility. Hence, there is little doubt that podand frameworks are versatile building blocks that will be used increasingly in a variety of real and innovative applications, indicated in the text, in addition to the ordinary use of podands, e.g., as solubilizers and detergents. But these latter properties, in the true sense, are not explained by the term ''podand'' and are, thus. beyond the scope of this article.

ARTICLES OF FURTHER INTEREST

Amide- and Urea-Based Anion Receptors, p. 31
Artificial Enzymes, p. 76
Calixarenes and Their Analogues: Cation Complexation, p. 137
Calixarenes: Synthesis and Historical Perspectives, p. 153
Chiral Guest Recognition, p. 236
Classification and Nomenclature of Supramolecular Compounds, p. 261
Crown Ethers, p. 326
Cryptands, p. 334
Dendrimers, p. 432
Electrochemicul Sensors, p. 505
Enzyme Mimics, p. 546
Fluorescent Sensors, p. 572
Imaging and Targeting, p. 687
Ion-Selective Electrodes, p. 747
Ionophores, p. 760
Kinetics of Complexation, p. 776
Lariat Ethers. p. 782
Molecular Clefts and Tweezers, p. 887
Organometallic Anion Receptors, p. 1006
Phase-Transfer Catalysis in Environmentally Benign Reaction Media. p. 1042
Siderophores, p. 1278
Surfactants, Part I: Fundamentals. p. 1458
Surfactants, Part 11: Applications. p. 1470
The Template Effect, p. 1493

REFERENCES

1. Pedersen, C.J. Die Entdeckung der Kronenether (Nobel-Vortrag). Angew. Chem. 1988. 100, 1053–1059.
2. Pedersen. C.J. The discovery of crown ethers (Nobel Lecture). Angew. Chem. Int. Ed. Engl. 1998. 27. 1021–1027.
3. Pedersen, C.J. The discovery of crown ethers (Nobel Lecture). J. Incl. Phenom. 1988. *6*, 337–350.
4. *Host–Guest Complex Chemistry*; Vogtle. F., Weber, E., Eds.: Springer-Verlag: Berlin; Germany, 1985.
5. Steed, J.W.: Atwood, J.L. *Supramolecular Chemistry;* Wiley: Chichester. UK, 2000.
6. *Comprehensive Supramolecular Chemistry*; Atwood, J.L., Davies, J.E.D., MacNicol; D.D., Vogtle. F.. Eds.; Elsevier Science: Oxford. UK. 1996; Vols. 1–10.
7. Vogtle. F.: Weber, E. Vielzähnige nichtcyclische Neutralliganden und ihre Komplexierung. Angew. Chem. 1979; *91*, 813–837.
8. Vogtle, F.: Weber, E. Multidendate acyclic neutral ligands and their complexation. Angew. Chem. Int. Ed. Engl. 1979, *18*, 753–776.
9. Gokel, G.W.: Murillo, O. Podands. In *Comprehensive Supramolecular Chemistry*; Atwood. J.L., Davies, J.E.D., MacNicol. D.D., Vogtle. F.. Eds.; Elsevier Science: Oxford, UK, 1996; Vol. 1, 1–33.
10. Black, D.St.C.; Hartshorn, A.J. Ligand design and synthesis. Coord. Chem. Rev. 1972. 9. 219–274.
11. Rebsdat, S.: Mayer. D. Ethylene Glycol. In *Ullmann's Encyclopedia of Industrial Chemistry*, 5th Ed.: Cerhartz, W.. Ed.; VCH: Weinheim, Germany, 1987; Vol. A 10. 101–115.
12. Weissermel. K.; Arpe, H.-J. *Industrial Organic Chemistry*, 3rd Ed.; VCH: Weinheim, Germany, 1997.
13. Dobler, M. Natural Cation Binding Agents. In *Comprehensive Supramolecular Chemistry*; Atwood. J.L.. Davies. J.E.D., MacNicol. D.D.. Vogtle, F., Eds.; Elsevier Science: Oxford. UK, 1996: Vol. 1267–313.
14. Telford. J.R.; Raymond, K.N. Siderophores. In *Comprehensive Supramolecular Chemistry*; Atwood. J.L., Davies, J.E.D., MacNicol. D.D., Vogtle. F.. Eds.; Elsevier Science: Oxford. UK, 1996; Vol. 1. 245–266.
15. Weber. E.; Josel, H.-P. A proposal for classification and nomenclature of host–guest-type compounds. J. Incl. Phenom. 1983. *1*. 79–85.
16. Weber. E.: Vogtle, F. Classification and nomenclature of coronands, cryptands, podands. and their complexes. Inorg. Chim. Acta 1980. *45*. L65–L67.
17. Vogtle. F.: Müller, W.; Wehner, W.; Buhleier, E. Nichtcyclische Cryptate. Angew. Chem. 1977. *89*. 564–565.

18. Vögtle, F.; Müller, W.; Wehner, W.; Buhleier, E. Noncyclic cryptates. Angew. Chem. Int. Ed. Engl. **1977**, *16*, 548–549.
19. Cram, D.J. Präorganisation—von Solventien zu Sphäranden. Angew. Chem. **1986**, *98*, 1041–1060.
20. Cram, D.J. Preorganization—From solvents to spherands. Angew. Chem. Int. Ed. Engl. **1986**, *25*, 1039–1057.
21. Vögtle, F.; Sieger, H. Nichtcyclische Kronenether: Das Endgrappen-Konzept. Angew. Chem. **1977**, *89*, 410–412.
22. Vögtle, F.; Sieger, H. Noncyclic crown ethers: The end group concept. Angew. Chem. Int. Ed. Engl. **1977**, *16*, 396–398.
23. Gutsche, C.D. *Calixarenes*; Monographs in Supramolecular Chemistry, The Royal Society of Chemistry: Cambridge, UK, 1989; Vol. 1.
24. Gutsche, C.D. *Calixarenes Revisited*; Monographs in Supramolecular Chemistry, The Royal Society of Chemistry: Cambridge, UK, 1998; Vol. 6.
25. Vögtle, F.; Weber, E. Krakenmoleküle. Angew. Chem. **1974**, *86*, 896–898.
26. Vögtle, F.; Weber, E. Octopus molecules. Angew. Chem. Int. Ed. Engl. **1974**, *13*, 814–816.
27. Tsukube, H.; Shinoda, S.; Uenishi, J.; Hiraoka, T.; Imakoga, T.; Yonemitsu, O. Ag^{+}-specific pyridine podands: Effects of ligand geometry and stereochemically controlled substitution on cation complexation and transport functions. J. Org. Chem. **1998**, *63*, 3884–3894.
28. Gokel, G.W.; Korzeniowski, S.H. *Macrocyclic Polyether Syntheses*; Springer-Verlag: Berlin, Germany, 1982.
29. Dietrich, B.; Viout, P.; Lehn, J.-M. *Macrocyclic Chemistry*; VCH: Weinheim, Germany, 1993.
30. Gerbeleu, N.V.; Arion, V.B.; Burgess, J. *Template Synthesis of Macrocyclic Compounds*; Wiley-VCH: Weinheim, Germany, 1999.
31. Gokel, G.W. *Crown Ethers and Cryptands*; Monographs in Supramolecular Chemistry, The Royal Society of Chemistry: Cambridge, UK, 1991; Vol. 3.
32. Vögtle, F.; Weber, E. Crown Ethers—Complexes and Selectivity. In *Crown Ethers and Analogs*; Patai, S., Rappoport, Z., Eds.; Wiley: Chichester, 1989; 207–304.
33. Schneider, H.-J.; Yatsimirsky, A. *Principles and Methods in Supramolecular Chemistry*; Wiley: Chichester, UK, 2000.
34. Tümmler, B.; Maass, G.; Weber, E.; Wehner, W.; Vögtle, F. Noncyclic crown-type polyethers, pyridinophane cryptands, and their alkali metal ion complexes: Synthesis, complex stability, and kinetics. J. Am. Chem. Soc. **1977**, *99*, 4683–4690.
35. Powers, R.E.; Fuller, W.L., III; Raymond, K.N. Stereognostic Coordination Chemistry. In *Comprehensive Supramolecular Chemistry*; Atwood, J.L., Davies, J.E.D., MacNicol, D.D., Vögtle, F., Eds.; Elsevier Science: Oxford, UK, 1996; Vol. 10, 537–555.
36. Rogers, R.D.; Bauer, C.B. Structural Chemistry of Metal–Crown Ether and Polyethylene Glycol Complexes Excluding Groups 1 and 2. In *Comprehensive Supramolecular Chemistry*; Atwood, J.L., Davies, J.E.D., MacNicol, D.D., Vögtle, F., Eds.; Elsevier Science: Oxford, UK, 1996; Vol. 1, 315–355.
37. Seel, C.; De Mendoza, J. From Chloride Katapinates to Trinucleotide Complexes: Developments in Molecular Recognition of Anionic Species. In *Comprehensive Supramolecular Chemistry*; Atwood, J.L., Davies, J.E.D., MacNicol, D.D., Vögtle, F., Eds.; Elsevier Science: Oxford, UK, 1996; Vol. 2, 519–552.
38. Vögtle, F.; Sieger, H.; Müller, W.M. Complexation of Uncharged Molecules and Anions by Crown Type Host Molecules. In *Host Guest Complex Chemistry I*; Vögtle, F., Ed.; Topics in Current Chemistry, Springer-Verlag: Berlin, Germany, 1981; Vol. 98, 107–161.
39. Weber, E. Inclusion Compounds. In *Kirk–Othmer Encyclopedia of Chemical Technology*, 4th Ed.; Kroschwitz, J.I., Ed.; Wiley: New York, 1995; Vol. 14, 122–154.
40. Starks, C.M.; Liotta, C.L.; Halpern, M. *Phase Transfer Catalysis: Fundamentals, Applications, and Industrial Perspectives*; Chapman & Hall: New York, USA, 1994.
41. Dugas, H. *Bioorganic Chemistry—A Chemical Approach to Enzyme Action*, 3rd Ed.; Springer-Verlag: New York, 1999.
42. Blasius, E.; Janzen, K.-P. Analytical Applications of Crown Compounds and Cryptands. In *Host–Guest Complex Chemistry I*; Vögtle, F., Ed.; Topics in Current Chemistry, Springer-Verlag: Berlin, Germany, 1981; Vol. 98, 163–189.
43. Moyer, B.A. Complexation and Transport. In *Comprehensive Supramolecular Chemistry*; Atwood, J.L., Davies, J.E.D., MacNicol, D.D., Vögtle, F., Eds.; Elsevier Science: Oxford, UK, 1996; Vol. 1, 377–416.
44. Spichiger-Keller, U.E. *Chemical Sensors and Biosensors for Medical and Biological Applications*; Wiley-VCH: Weinheim, Germany, 1998.
45. Valeur, B.; Leray, I. Design principles of fluorescent molecular sensors for cation recognition. Coord. Chem. Rev. **2000**, *205*, 3–40.
46. Parker, D. Imaging and Targeting. In *Comprehensive Supramolecular Chemistry*; Atwood, J.L., Davies, J.E.D., MacNicol, D.D., Vögtle, F., Eds.; Elsevier Science: Oxford, UK, 1996; Vol. 10, 487–536.
47. Gokel, G.W.; Schall, O.F. Lariat Ethers. In *Comprehensive Supramolecular Chemistry*; Atwood, J.L., Davies, J.E.D., MacNicol, D.D., Vögtle, F., Eds.; Elsevier Science: Oxford, UK, 1996; Vol. 1, 97–152.
48. Newkome, G.R.; Moorefield, C.N.; Vögtle, F. *Dendrimers and Dendrons*; Wiley-VCH: Weinheim, Germany, 2001.
49. Grayson, S.M.; Fréchet, J.M.J. Convergent dendrons and dendrimers: From synthesis to applications. Chem. Rev. **2001**, *101*, 3819–3867.
50. Piguet, C.; Bernardinelli, G.; Hopfgartner, G. Helicates as versatile supramolecular complexes. Chem. Rev. **1997**, *97*, 2005–2062.
51. Fujita, M. Metal directed self-assembly of two- and three-dimensional synthetic receptors. Chem. Soc. Rev. **1998**, *27*, 417.
52. *Molecular Catenanes, Rotaxanes and Knots*; Sauvage, J.P., Dietrich-Buchecker, C., Eds.; Wiley-VCH: Weinheim, Germany, 1999.
53. *Supramolecular Materials and Technologies*; Reinhoudt, D.N., Ed.; Perspectives in Supramolecular Chemistry, Wiley: Chichester, UK, 1999; Vol. 4.
54. Kosswig, K.; Stache, H. *Die Teuside*; Hauser Verlag: München-Wien, 1993.

Polarity Formation: Markov Chain Model

Jürg Hulliger
University of Berne, Berne, Switzerland

INTRODUCTION

In nature. polarity (defined as a nonvanishing vector sum of dipolar moments) is widely present in living systems. It has been known for more than 35 years that bones. teeth, tendons, and other connective tissues show effects of macroscopic polarity. i.e., a pyroelectric effect. Later, it was shown that host–guest compounds[3] can feature a high occurrence of the effect of polarity, and that crystals grown from dipolar molecules[4–6] can show polarity, although the packing is found to be centrosymmetric by x-ray diffraction. The unifying principle behind these phenomena was recently recognized[7,8] as a Markov-chain mechanism of polarity formation by polar building blocks subjected to unidirectional growth.

The review is arranged as such to first provide an introduction to polarity. followed by drawing attention to aspects of crystal design and to supramolecular systems explicitly found to match the conditions for a Markov process of polarity formation. Theoretical aspects are reviewed in a separate section. Techniques for mapping grown-in polarity are briefly introduced as well. A generalization to polarity formation in single-component molecular crystals, mechanical objects; and collagen fibril fusion in tendon is given at the end.

POLARITY: DEFINITION AND MACROSCOPIC EFFECTS

Molecules or crystals can show spatial distribution of electrical charge giving rise to a dipolar moment. In physics, electrical polarity is described by a vector pointing from the negatively to the positively charged part of a system. Because of charge separation. polarity can only exist in point groups classifying molecules and crystals that preserve a vector property. For crystals,[9,10] there are 10 polar point groups called the pyroelectric groups (1. m, 2. mm2. 3, 3m. 4, 4mm. 6. 6mm). In cases where the orientation of the macroscopic polarization vector can be changed (inverted or tilted) by action of an external electrical field. we have ferroelectricity. or in case of stress, we speak of ferroelasticity. These properties are known for many inorganic compounds, however, so far. they have not been frequently observed for crystals grown from neutral molecules.[1,12]

Because species carry positive or negative charges, crystals classified by polar group do not show a permanent macroscopic polarization at constant temperature (T), electrical field (E), or stress (σ), respectively. As a matter of existing charges in the environment of a crystal, the negative and the positive ends of the polar axis are likewise covered by compensating charges. Here we notice a fundamental difference of magnetic systems, for which no compensation of the spontaneous magnetization by monopoles exists. A rapid change of temperature (AT) or stress ($\Delta\sigma$) thus induces a spontaneous polarization $\boldsymbol{P}$, which can be detected by an electrometer for crystals placed into a capacitor. In case of AT. we observe a pyroelectric effect. In the case of $\Delta\sigma$, a piezoelectric effect is observed:

$$P_i = p_i \Delta T \quad i = 1, 2, 3 \tag{1}$$

$$P_i = \sum_{j=1}^{3} \sum_{k=1}^{3} d_{ijk}\, \Delta\sigma_{jk} \quad i, j, k = 1, 2, 3 \tag{2}$$

where p_i are the pyroelectric vector components, d_{ijk} are the elements of the piezoelectric tensor (third rank), σ_{jk} are the elements of the stress tensor (second rank). and A indicates that a change is necessary in order to induce a macroscopic polarization $\boldsymbol{P}$.

At this point. we will make an amendment concerning the piezoelectric effect. Piezoelectricity[9,10] is found for 20 of the 32 point groups describing crystals, 10 of them also belonging to the pyroelectric class. Piezoelectricity is not a vector property, it is defined by a third-rank tensor. Given by symmetry. there are piezoelectric groups that are not polar. although effects of polarity can occur (e.g., charged faces). Other effects of polarity are represented by a third-rank tensor—the second-order nonlinear optical and the linear electrooptical effect.[11,13] A summary of noncentrosymmetric point groups is provided in Table 1. allowing for some solid-state properties of crystals.[9,10]

Are there further manifestations of a polar axis in crystals? Obviously, the morphology,[15] the crystal growth speed,[16,17] the form of etch figures,[18] and the chemical reactivity[11] of faces are properties that can express a polar symmetry.

Encyclopedia of Supramolecular Chemistry
DOI: 10.1081/E-ESMC 120012843

Table 1 Some symmetry-allowed physical properties

Point group	Enantiomorphism	Pyroelectricity *(vector property)*	*Piezoelectricity, second-order optical nonlinearity* **(third** *rank tensor property)*
1. C_1	+	+	+
2, C_2	+	+	+
m. C_s		+	+
222. D_2	+		+
mm2. C_{2v}		+	+
4. C_4	+	+	+
4. S_4			+
422. D_4			+
4mm. C_{4v}			+
42m D_{2d}			+
3. C_3	+		+
32, D_3	+		+
3m. C_{3v}		+	+
6. C_6	+	+	+
6 C_{3h}			+
622. D_6	+		+
6mm. C_{6v}			+
6 m2 D_{3h}			+
23, T	+		
432, O	+		
43m T_d			+
Number	11	10	20

(See Refs. [9,10].)

Along the present review, we will focus on polarity in the strict sense, thus being a vector property.

ASPECTS OF CRYSTAL DESIGN: HOW TO OBTAIN A POLAR CRYSTAL?

> We consider this approach [supramolecular approach by inclusion formation] to be an important achievement that points to new methodology. a paradigm of guest–host induced dipolar alignment that can be used by chemists to engineer solid-state materials with specific properties.[11]

Present crystallographic data on the crystal structures of molecular compounds show that polar structures represent a minority, even among noncentrosymmetric (~24%, n.c.) ones. The main reason for this may be found in the electrostatic contribution to the packing energy of molecules, tending to align polar subunits (molecules, chains. planes) in antiparallel fashion. There are a few structures featuring perfectly aligned dipoles,[20–22] however, in most packings of polar structures, dipole moments are inclined by an angle θ to the polar axis. The field of nonlinear optics[13,14] generated a large number of compounds crystallizing in noncentrosymmetric structures. From the point of view of crystal design,[11] it is clear how to align dipolar, functionalized molecules into polar chains or planes (driven by synthon interactions[11]). however, the striking difficulty enters in preserving polarity in the bulk.

Classically. there is only one way to obtain a noncentrosymmetric crystal packing. The use of enantiomerically pure dipolar cornpounds ensures crystallization in one of the 11 enantiomorphic groups, whereof 10 show a piezoelectric effect. Only five (namely, those featuring an unique rotational axis: 1, 2, 3, 4. 6) of the enantioinorphic groups that are piezoelectric also allow for pyroelectricity (see Table 1). At present. there is no design concept with which to obtain a polar point group by spontaneous nucleation.

In the following, we review a supramolecular concept[3,25] that demonstrates that the idea of supramolecular interactions, may provide an answer. Essentially, this is achieved by aligning dipolar molecules into a parallel array provided by an inclusion lattice, in which guest molecules are subjected to orientational selectivity of the dipoles

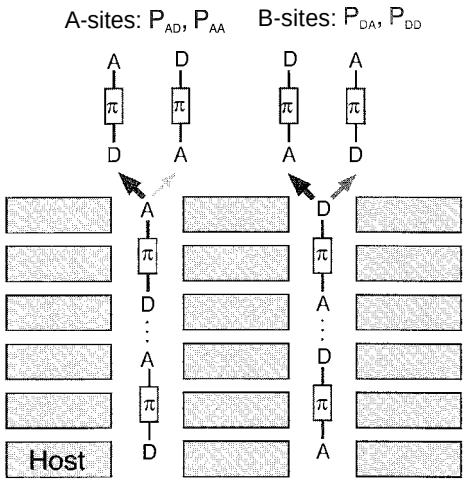

Fig. 1 Polarity formation for channel-type inclusion compounds. where A–D molecules enter channels, while the crystal grows in the direction of the channels. Orientational selectivity for A–D molecules is assumed to occur independently for each channel (A-and D-sites). *(View this art in color at www.dekker.com.)*

when included (Fig. 1). A further important effect of a channel-type architecture is to weaken lateral interactions between dipolar molecules, which frequently tend to an antiparallel packing. Examples from the literature are inclusion compounds of thiourea,[26] perhydrotriphenylene,[26,27] *tris*(*o*-phenylenedioxy)cyclotriphosphazene,[28] and others,[29] including polar molecules, into their channels.

THE MARKOV GROWTH MODEL OF POLARITY FORMATION

In case dipolar molecules A–D (A: acceptor-type, D: donor-type molecular fragment) and a symmetrical host molecule H are self-assembling into a channel-type inclusion compound $(A–D)_xH$, where A–D entities are aligned into chains in channels made up by H molecules, we may model the system as shown in Fig. 1. Spontaneous nucleation has only to create the inclusion-type lattice, where existing chains of A–D molecules in channels may at this early state show no bulk polarity. If such a seed is growing lo macroscopic size. molecular recognition (synthon interactions[24]) taking place during individual channel formation can provide conditions for orientational selectivity, irrespective of the type of interactions of guest molecules to the channel wall made up by H entities. Generally speaking, interactions of guest to guest and guest to surface (wall at entry of a channel) can contribute to polarity formation.

During further attachment (growth), the orientation of the incoining guest molecule is subjected to probabilities P. For the channel to the left, continuation of the preexisting polarity is given by P_{AD}, whereas inversion is induced by P_{AA}. Similar arguments hold for the channel to the right (P_{DA}, P_{DD}). Because we can assume here that the process of orientational selectivity is taking place independently at all channels exposed to growth. there is polarity formation. if $P_{AA} \neq P_{DD}$. The queuing system we have here can be modeled by a Markov-chain:[25,30,31]

$$\begin{bmatrix} X_A\ (q) \\ X_D\ (q) \end{bmatrix} = \begin{bmatrix} P_{AD} & P_{DD} \\ P_{AA} & P_{DA} \end{bmatrix}^q \begin{bmatrix} X_A\ (0) \\ X_D\ (0) \end{bmatrix}$$

where X_A, X_D are the molar fractions of the functional groups A or D appearing at the growing surface: q is the index for the actual layer of growth. starting at $q=0$ (seed) and rising to $q=\infty$, the macroscopic crystal. Note that $P_{AD}+P_{AA}=1$, $P_{DA}+P_{DD}=1$, and $X_A+X_D=1$.

Because of the ergodic property of a Markov chain. the result at $q=x$ is independent of the initial state of seeding. i.e., the initial values $X_A(q=0)$, $X_D(q=0)$. This means that the supramolecular approach generating polarity through a process of growth is circumventing the basic difficulty of creating polarity by spontaneous nucleation.

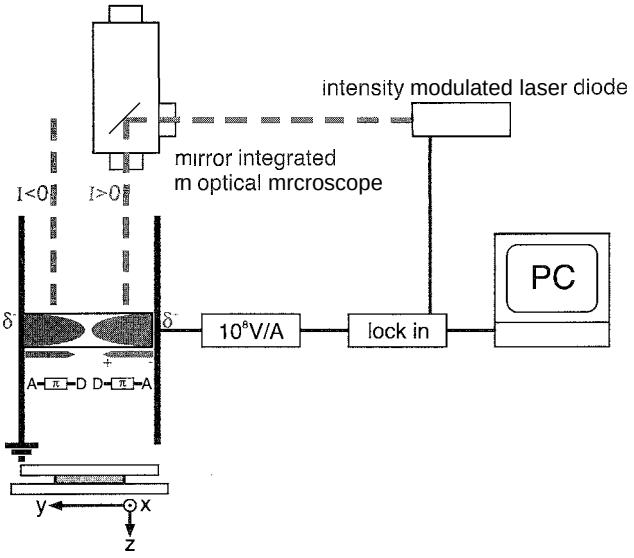

Fig. 2 Experimental setup for scanning pyroelectric microscopy (SPEM). As indicated, the sample may consist of two domains of opposite polarization. Local heating in either domain of polarization produces excess charges at both ends of the polar axis. This induces a current flow in the outer circuit. Opposite polarity is seen because of a change in the current direction.[33,36] *(View this art in color at www.dekker.com.)*

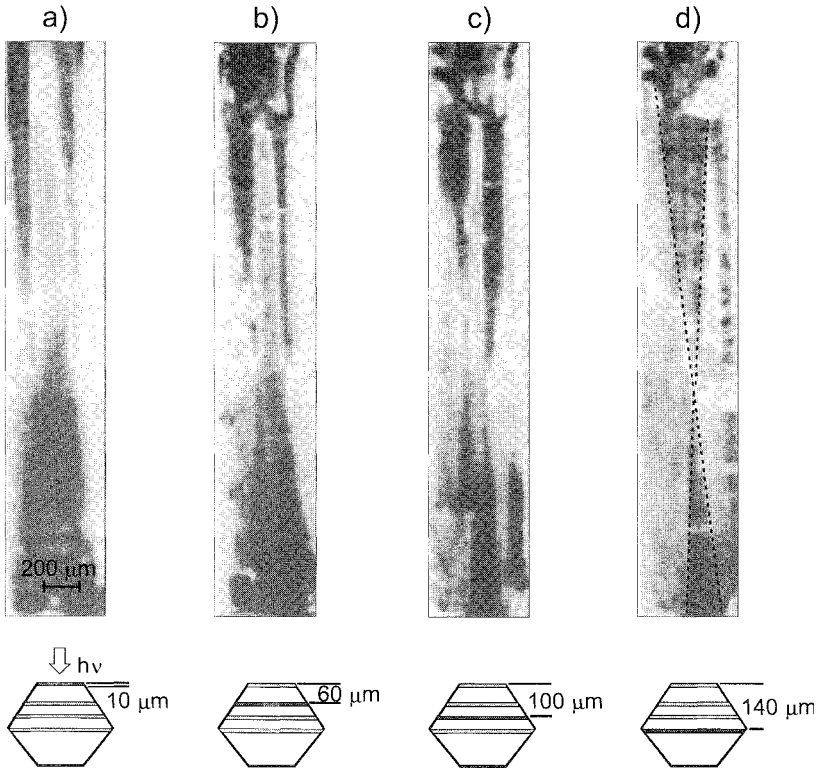

Fig. 3 SPEM images of perhydrotripenylene inclusion crystals[26] with a dipolar guest molecule [1-(4-nitrophenyl)piperazine], thinned in three steps. A two-dimensional mapping of the pyroelectric response in the channel direction is shown for a constant modulation frequency of the heating laser source of 415 Hz. Color code: red=positive current; blue=negative current. Low color intensity: no current.[3336] Moving from the outer to the inner part of the needle-shaped crystal shows that at all depths, there are two main domains of opposite polarization: although somehow interpenetrating. In the middle of the needle, a cone-shaped structure of polarity distribution is seen, which is typical for a Markov-type growth in two dimensions. Qualitative agreement with stochastic simulations is obtained. *(View this art in color at www.dekker.com.)*

The net fraction X_{net} (where A groups preferably cover the surface) of polarity may be defined by

$$X_{net} = X_A(q=\infty) - X_D(q=\infty) = \frac{1-e^{-\Delta E_f/RT}}{1+e^{-\Delta E_f/RT}+2e^{-\Delta E_A/RT}} \quad (4)$$

where $\Delta E_A = E_{AA} - E_{AD}$, $\Delta E_f = E_{AA} - E_{DD}$; with E_{AA}, E_{DD}, E_{AD} being the three basic interaction energies for a collinear geometry of A, D functional fragments of guest molecules A–D (additionally, we define $\Delta E_D = E_{DD} - E_{AD}$, see Fig. *6)*. Possible interactions to the surface other than to groups A, D are not explicitly introduced here, although they may exist.

From the point of view of optimizing the extent of polarity formation,[32] we may ask for the best type of A–D molecules in order to obtain X_{net} close to 1 at lowest possible q. The Markov model gives the answer. Guest molecules providing an A–R structure (R: fragment undergoing no typical synthon interactions) featuring $E_{AR} \approx E_{RR} \approx 0$, $E_{AA} > 0$, can develop an X_{net} of more than about 0.95 just after about six steps of attachments, if a strongly repulsive-A···A-interaction between A-fragments is the dominant contribution at a typical van der Waals distance when supposed to enter a growing channel.

We should emphasize here that Markov-grown polarity is not the result of a kinetically controlled growth process (i.e., fast grow), although we assume kinetic stability for the grown-in state of polarity. This means that guest molecules do not reverse their dipolar direction if definitively included in a channel.

As growth may be allowed along both directions of the channels, bipolar crystals are obtained, showing an inhomogeneous polarity distribution essentially because of the lateral growth by newly formed channels (see scetion on Physical *Methods)*. The interplay of growth along channels and in the lateral direction can result in a cone-like distribution of polarity (see Fig. 3).

PHYSICAL METHODS FOR A SPACE-RESOLVED MAPPING OF THE MACROSCOPIC POLARIZATION IN POLAR MATERIALS

Scanning Pyroelectric Microscopy (SPEM)

The compensation of the macroscopic polarization by outer charges in polar materials can be disturbed by a rapid change in. e.g., the temperature producing excess surface charge because of the pyroelectric effect. A two-dimensional mapping of the polarization distribution is possible when an intensity-modulated beam of a laser is scanning over the sample surface coated by a thin absorption layer (black). The lateral resolution in surface SPEM is limited by the spot size of the laser. An experimental setup is shown in Fig. 2. Tomographic information is obtained by layered thinning of a sample (Fig. 3). In the case of channel-type inclusion crystals, SPEM was the first technique to reveal the bipolar structure, the cone-shaped distribution of polarity (Fig. 3d) because of effects of lateral growth,[33] and the sign of polarization.

Phase-Sensitive Second Harmonic Microscopy (PS-SHM)

Norinal second-harmonic microscopy (SHM) may show that polarity is present in certain growth sectors, however. 180° domains cannot be resolved. Sectors featuring an opposite average polarity can be made visible by a phase sensitive technique,[34] introduced in Fig. 4. Provided the crystal thickness is in the range or below the coherence length of the second harmonic generation (SHG) effect, a reference beam of a polarized second-harmonic (SH) wave will undergo a constructive or destructive interference with an SH wave generated by the sample. By adjusting the phase difference between the fundamental and the SH reference wave. all parts of a bipolar crystal with the proper sign of the nonlinear optical tensor element allowing constructive interference will appear bright, whereas the adjacent domain will release an SH signal of much lower intensity (ideally zero). Keeping all optical settings constant but rotating the crystal around an angle of 180° (perpendicular to the incident beam), will interchange the brightness of the macrodomains, where enhanced or attenuated SH waves are released. Essentially. the contrast is due to inversion symmetry, changing the sign of the nonlinear optic (NLO) coefficient when transforming the tensor from one coordinate system into the other (Side I into Side II; Fig. 4).

In Fig. 5 we show the SHG response of a micrometer thin plate of a single component organic crystal, releasing green light only from the + and – b-sector (Fig. 5a). Phase-sensitive inforination is retrieved from Figs. 5b, c demonstrating that this crystal grew into a bipolar state. This is the first experimental demonstration that centrosymmetric molecular crystals can feature a grown-in bipolar state.[35]

For further details on the SPEM and the PS-SHM techniques, see a review in Ref. [36].

GENERALIZATION TO MECHANICAL OBJECTS, CRYSTALS, AND NATURAL TISSUES

The Markov growth model is generalized in the following way.[7] When polar building blocks attach to a surface, there is, by symmetry, a difference in the probabilities of attaching "tip-first" or "back-first." This difference drives polarity formation, irsespective of lateral interactions that may suppress a parallel alignment of vectors. However, if a packing energetically tends to arrange

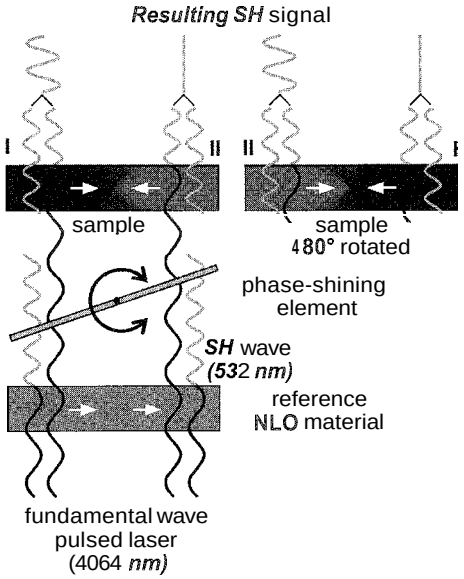

Fig. 4 Far-field phase-sensitive second-harmonic microscopy (PS-SHM).[34] Oppositely oriented domains (colored in blue. red) in a sample with uniform thickness below the coherence length emit SH light with a phase shift of π. Domain contrast is achieved by using the interference effect between the sample and a homogeneous SHG reference crystal. Angle-tuned phase shifting is used to adjust the phase between the fundamental wave and the SH wave from the reference in order to achieve a maximum interference of the green light of the reference and green light produced by the sample in, e.g., Domain I (blue). Keeping optical settings constant but rotating the sample by 180° leads to an interchange of the interference contrast. For clarity. it should be noticed that the laser beam direction is perpendicular to what is shown about the sample. (View *this* art in color *at www.dekker.com.*)

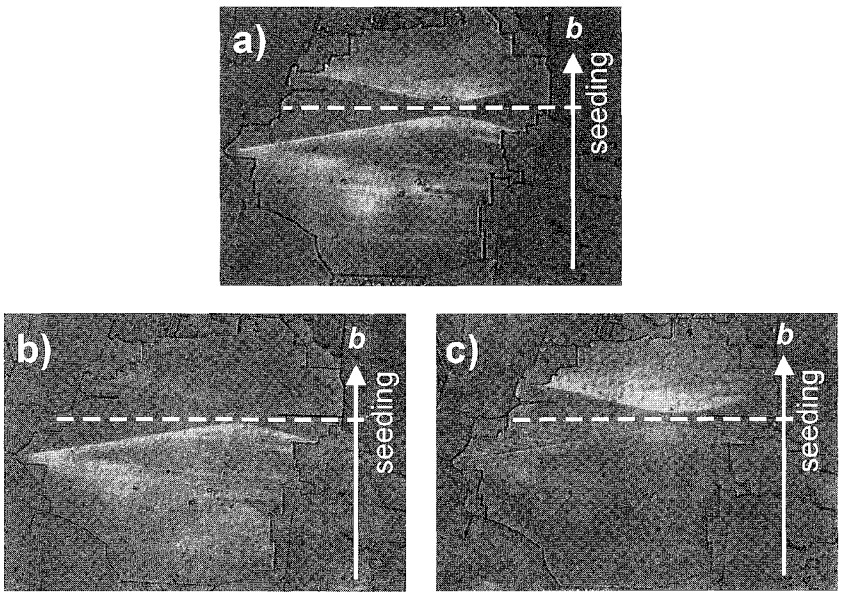

Fig. 5 Second-harmonic generation analysis[7,35] to show polarity formation in the centrosymmetric crystal structure of 4-chloro-4′-nitrostilbene. Micromctcr thin crystal plate with (001) orientation, grown from the melt. (a): Polarization of the fundamental wave (1064 nm) parallel to the *b*-axis. Both the upper and lower h-sectors emit green light. (b): Effect of phase contrast for the lower b-sector. (c): Correspondingly, upper *b*-sector. The change in contrast within sectors allows us to conclude that the average polarization in the lower (b) sector is opposite that in the upper (c) one. (*View this art in* color *at www.dekker.com.*)

building blocks in a centrosymmetric fashion, the Markov mechanism of polarity formation represents just a perturbation to a crystal. Examples include crystals of dipolar compounds refined to, e.g., $P2_1/c$, for which SHG techniques (see previous section), nevertheless, may reveal some polarity.[5,6,37] In 4-chloro-4'-nitro-stilbene (CNS), crystallizing in $P2_1/c$, with phase-sensitive second-harmonic microscopy (Fig. 5) a bipolar structure was found. Polarity in agreement with theoretical predictions develops in the + and – h-sectors.

In centrosymmetric structures, there are at least two different growth sites (similar to those shown in Fig. 1) for which we may assume independent Markov chains,[5,6,37] such as to describe polarity formation by taking into account longitudinal ($\Delta E_A, \Delta E_D$) and transversal (E„: parallel packing, E_{ap}: antiparallel packing; $\Delta E_\perp = E_p - E_{ap}$) interaction parameters. The general case for crystals calculated by a Markov model is summarized in Fig. 6: Assuming typical values for ΔE_A, ΔE_D, net polarity X_{net} is shown as a function of the transversal parameter $\Delta E_\perp$ at 300 K.

For a structure strongly preferring antiparallel packing (AP, to the right). only little polarity may appear. On the other hand, if A E is negative (P, to the left), the stochastic process may to some extent reduce X_{net} from being 1. In between (P', middle), we find a window, where polarity strongly depends on $\Delta E_\perp$. At $\Delta E_\perp{}^c$, a phase transition separates structures being centrosymmetric but perturbed (*AP*) from those being highly disordered but polar (P'). Note that polarity can well exist at $\Delta E_\perp = 0$ (case of inclusion compounds.[326–29] To the left, there is a second border given by $\Delta E_\perp(T_c)$. Below a certain value for $\Delta E_\perp$, a polar crystal may become metastable with respect to growth along one direction of the polar axis (for details, see Refs. [5,6,36,37], for which most of the dipoles should invert their orientations.

The Markov-type analysis lets us conclude that polarity in molecular crystals built up by dipolar coinpounds is a general property, however, X_{net} depends strongly on specific parameters given by intermolecular interactions. A further example is given by solid-solution formation[38–40] of A–D (crystallizing in a centrosymmetric lattice) with A–A or D–D (centrosymmetric as well). The $(A–D)_1$,(A–A), and $(A–D)_{1\ x}(D–D)_x$ crystals can develop polarity for the same reasons discussed above.

Finally, we can extend our view further in demonstrating that the stochastic growth of heaps (1D, 2D, 3D) using polar mechanical objects is yielding polarity as well.[7] Surprisingly; the existing pyroelectricity[1] in connective tissues was recently explained[7,8] by the following theory. Driven by chemical recognition, collagen fibrils during the process of self-assembly into tendon (Fig. 7) show the property of fusing[41,42] in a way that can produce macroscopic polarity. This occurs because the fusion probabilities P_{CC} for C-termini differ from that for N-termini (P_{NN}). Polarity evolution at the level of the early state of a piece of tendon may start with an

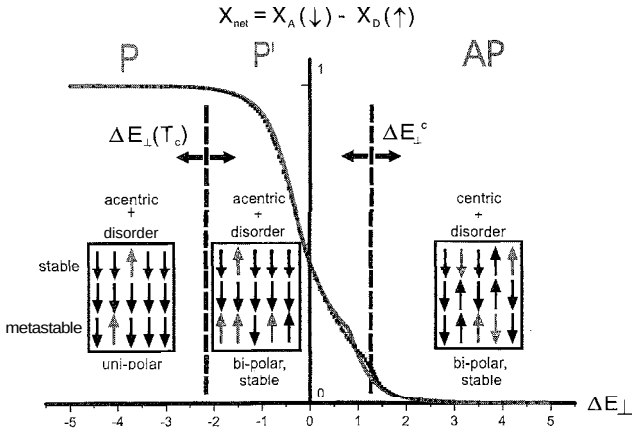

Fig. 6 Summary[37] of the behavior of stochastic polarity formation in crystals. showing the influence of $\Delta E_\perp$ (lateral interactions) on net polarity X_{net} for given values $\Delta E_A = 5$ kJ/mol and $\Delta E_D = 2$ kJ/mol at 300 K and a square lattice. Points: Monte Carlo simulation (periodic boundary conditions): red curve: Markov-chain model taking into account lateral interactions. P: structure with polar order showing some defects reducing polarity: P': polar order with many orientational defects; AP: centrosyrnmetric structure showing some orientational defects. For an explanation of boundaries separating AP. P'. and P, see Ref. [37]. (*View this* art *in color at www.dekker.com.*)

equal number of "up" and "down" fibrils exceeding elongation (see Fig. 7) in extracytoplasmic channels. Following ideas developed for inclusion compounds (see Fig. 1), we model polarity formation in growing tendon by two independent Markov chains (I, II; see Fig. 7). Driving forces for the lateral aggregation may support or work against macroscopic polarity formation. As a result of the interplay of all interactions, in principle. polarity can evolve if a difference in P_{CC} and P_{NN} is effected by a stochastic mechanism of self-assembly. A stochastic delivery of small aggregates of procollagen to extracytoplasmic channels (secretion: see Fig. 7) is provided because of a translocation time along the cell that is larger than the rotational diffusion of small aggregates. In agreement with experimental findings, only a small percentage of collagen fibrils in the bulk of tendon show polar order for a reasonably small ratio[7,8] of P_{NN} and P_{CC}. As found experimentally[1] in tendon, N-termini are preferably oriented in the direction of growth.

Summarizing. we can say that polarity is a property that can arise in systems showing unidirectional stochastic growth by use of polar building blocks. In other words, an average $<P>$ of the pertinent polar property P of building blocks is preserved by a stochastic process of growth,

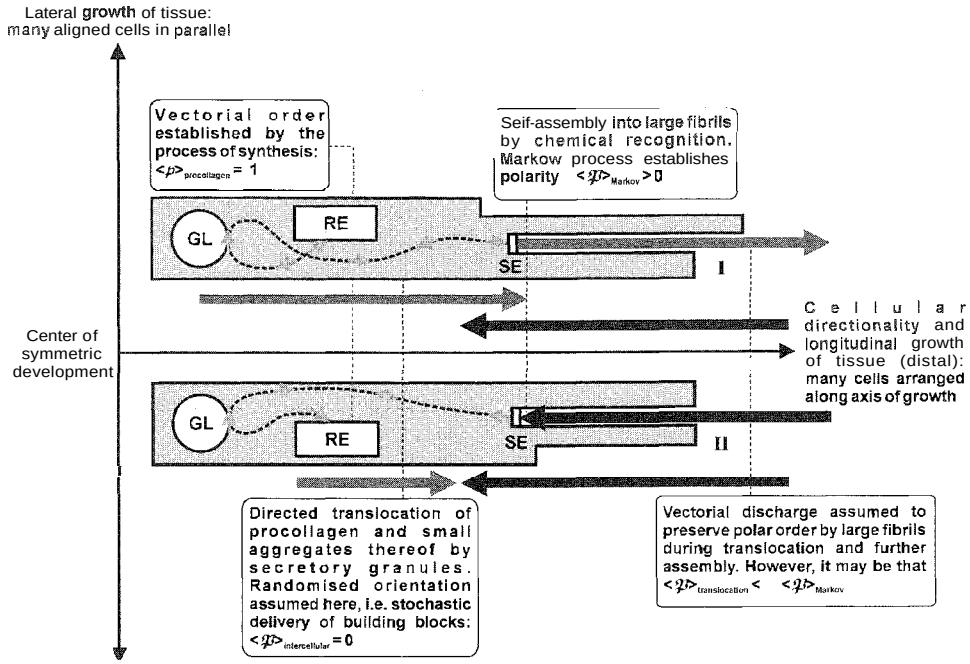

Fig. 7 How cells (green part) aligned in the direction of longitudinal growth of tendon produce fibrils (red and blue arrows) from small segments secreted (SE) into extracytoplasmic channels. Self-assembly is assumed to occur in the channels. Cells and produced fibrils are interwoven. RE: endoplasmatic recticulum: GL: Golgi apparatus; and SE: secretion. I and II refer to the basic orientations of the polarity of fibrils starting growth (compare with channels in Fig. 1). $P_{procollagen}$: polarization of the molecule: $<P>$: macroscopic polarization. As a result of the Markov process,[8] the sum of red vectors is larger than that of blue vectors, because here $P_{CC} > P_{NN}$.[41,42] Small pink arrows: intercellular translocation of procollagen and aggregates thereof. (*View this art in color at www.dekker.com.*)

because the growing system represents polar symmetry as well. In essence: there is always some bulk polarity $<P>$, although in most real cases; it may not reach the maximum extent. The extent of stochastic polarity depends on the ratio of P_{AA} and P_{DD}, both of which may be functions of longitudinal and transversal intermolecular interactions. Interesting to see that. particularly, a supramolecular system (e.g., channel-type inclusion compounds) can reach X_{net} values close to unity. This is because the negative influence of transversal interactions can be strongly reduced by any approach that succeeds in shielding guest molecules, as they do not prefer to align in an antiparallel fashion.

ACKNOWLEDGMENTS

I thank all of my collaborators and colleagues who over the years contributed to this work: O. Konig, P. Rogin, A. Quintel, M. Wiibbenhorst, P. Rechsteiner, T. Müller, H. Bebie, B. Trusch, S. Kluge, T. Hertzsch, F. Budde, and others. This work received support from the national priority program "Functional Supramolecular Materials," NFP 47, grant no. 4047-0574761.

ARTICLES OF FURTHER INTEREST

Biomaterials, p. 110
Channel Inclusion Compounds, p. 223
Collagens, p. 295
Space *Groups and Crystal* Packing Modes. p. 1337

REFERENCES

1. Athenstaedt, H. Permanent longitudinal electric polarisation and pyroelectric behaviour of collagenenous structures and nervous tissue in man and other vertebrates. Nature 1970. 228, 830–834.
2. Freund. I.: Deutsch, M.: Sprecher. A. Connective tissue polarity. optical second-harmonic microscopy, crossed-beam summation. and small-angle scattering in rat-tail tendon. Biophys. J. 1986. *50*, 693–712.
3. Ramamurthy. V.; Eaton. D.F. Perspectives on solid-state host-guest assemblies. Chem. Mater. 1994. 6. 1128–1136.
4. Hulliger; J. On an intrinsic mechanism of surface defect formation producing polar, multidomain real-structures in molecular crystals. Z. Kristallogr. 1998. *213*, 441–444.
5. Hulliger, J.; Alaga-Bogdanovic, M.; Bebie, H. Growth-induced effects of polarity in molecular crystals: Comparison of Schottky-and Markov-type models with Monte Carlo simulations. J. Phys. Chem., B 2001. 36. 8504–8512.
6. Bebie. H.; Hulliger. J.; Eugster, S.; Alaga-Bogdanovic. M. Ising model of polarity formation in molecular crystals: From the growth model to the asymptotic equilibrium state. Phys. Rev., E 2002, 66, 021605.
7. Hulliger, J. On a stochastic evolution into a polar state of materials. Chem. Eur. J. 2002, 8. 4578–4586.
8. Hulliger. J. Connective tissue polarity unravelled by a Markov-chain mechanism of collagen fibril segment self-assembly. Biophys. J. 2002, *84*. 3501–3507.
9. Nye. J.F. Physical *Properties of* Crystals, their Representations by Tensors *and* Matrices; Clarendon Press: Oxford, 1992.
10. Kleber, W.; Bautsch, H.J.; Bohm, J.; Kleber, I. *Einführung* in die *Kristallographie,* 17th Ed.: Verlag Technik: Berlin, 1990.
11. Kamishina, Y.; Akishige, Y.; Hashimoto, M. Ferroelectric activity of organic crystal trichloroacetamide. J. Phys. Soc. Jap. 1991. 60. 2147–2150.
12. Brown, M.E.; Hollingsworth. M.D. Stress-induced domain reorientation in urea inclusion compounds. Nature 1995, 376, 323–327.
13. Nonlinear Optics of Organic *Molecules and* Polymers: Nalwa, H.S., Miyata, S., Eds.: CRC Press: London. 1997.
14. Zyss, J.: Ledoux. I. Nonlinear optics in multipolar media: Theory and experiments. Chem. Rev. 1994, *94*. 77–105.
15. Groth, P. *Chemische Krystallographie*; Verlag Engelmann: Leipzig, 1919: Vols. III–IV.
16. Davey, R.J.; Milisavljevic, B.; Bourne, J.R. Solvent interactions at crystal surfaces: The kinetic story of α-resorcinol. J. Phys. Chem. 1988, *92*. 2032–2036.
17. Chen. B.D.: Garside, J.; Davey, R.J.; Maginn, S.J.: Matsuoka, M. Growth of nz-chloronitrobenzene crystals in the presence of tailor-made additives: Assignment of the polar axis from morphological calculations. J. Phys. Chern. 1994. 98. 3215–3221.
18. Heimann, R.B. *Auflösen* von *Kristallen, Theorie und technische Anwendung*; Springer-Verlag: Wien, 1975.
19. Curtin. D.Y.: Paul, I.C. Chemical consequences of the polar axis in organic solid-state chemistry. Chem. Rev. 1981. *81*, 525–541.
20. Sarma, J.A.R.P.: Allen. F.H.Hoy, V.J.: Howard. J.A.K.; Taimattam, R.: Biradha. K.: Desiraju, G.R. Design of an SHG-active crystal 4-iodo-4′nitrobiphenyl: The role of supramolecular synthons. Chern. Comm. 1997. 101–102.
21. Anthony, S.P.: Radhakrishnan. T.P. Perfectly polar assembly of molecular dipoles in crystals of Zn(II)(DMAP) $(acac)_2$: A case of self-poling. Chem. Comm. 2001. 931–932.
22. Wong, M.S.: Pan. F.: Bösch, M.: Spreiter. R.; Bosshard. C.; Giinter, P.: Gramlich. V. Novel electro-optic molecular crystals with ideal chromophoric orientation and large second-order nonlinearities. J. Opt. Soc. Am. B 1998. 15. 426–431.
23. The *Crystal as* a *Supramolecular Entity,* Perspectives in *Supramolecular* Chemist??: Desiraju. G.R., Ed.: Wiley: New York. 1995: Vol. 2.
24. Desiraju. G.R. Supramolecular synthons in crystal engineering—A new organic synthesis. Angew. Chem. Int. Ed. Engl. 1995, *34*. 2311–2327.
25. Hulliger, J.: Rogin. P.; Quintel, A.; Rechsteiner. P.: Konig, O.; Wiibbenhorst. M. The crystallization of polar. channel-

type inclusion compounds: Property-directed supramolecular synthesis. Adv. Mater. 1997. 9. 677–680.
26. Hulliger. J.: Monig, O.; Hoss, R. Polar inclusion compounds of perhydrotriphenylene (PHTP) and efficient nonlinear optical molecules. Adv. Mater. 1995. 7. 719–721.
27. Hoss. R.: Konig, O.; Kramer-Hoss, V.: Berger. U.: Rogin. P.; Hulliger. J. Crystallization of supramolecular materials: Perhydrotriphenylene (PHTP) inclusion compounds with nonlinear optical properties. Angew. Chem. Int. Ed. Engl. 1996. *35*. 1664–1666.
28. Hertzsch. T.: Kluge, S.: Weber, E.: Budde. F.: Hulliger, J. Surface recognition of dipolar molecules entering channels of the organic zeolite *tris*(*o*-phenylenedioxy)cyclotriphosphazene. Adv. Mater. 2001. *13*. 1864–1867.
29. Müller, T.; Hulliger. J.: Seichter. W.: Weber, E.: Weber, T.; Wiibbenhorst. M. A new organic nanoporous architecture: Dumb-bell-shaped molecules with guests in parallel channels. Chem. Eur. J. 2000, 6, 54–61.
30. Harris. K.D.M.; Jupp. P.E. Mathematical analysis of the alignment of guest molecules in solid one-dimensional inclusion compounds: The design of materials for applications in nonlinear optic. Chem. Phys. Lett. 1997. *274*. 525–534.
31. Harris, K.D.M.; Jupp. P.E. Stochastic models for guest-guest interactions in one-dimensional inclusion compounds. Proc. R. Soc. Lond., A 1997. *453*. 333–352.
32. Quintel, A.; Hulliger. J. A theoretical base for optimising intermolecular interactions driving polarity formation in channel-type host-guest materials. Chem. Phys. Lett. 1999. *312*. 567–571.
33. Quintel, A.; Hulliger. 3.: Wiibbenhorst, M. Analysis of the polarization distribution in a polar perhydrotriphenylene inclusion compound by scanning pyroelectric microscopy. J. Phys. Chem.. B 1998, *102*. 4277–4283.
34. Rechsteiner. P.; Hulliger. 3.: Florsheimer, M. Phase-sensitive second harmonic microscopy reveals bipolar twinning of Markov-type molecular crystals. Chem. Mater. 2000. *12*, 3296–3300.
35. Kluge, S.; Budde, F.: Dohnke. I.; Rechsteiner, P.: Hulliger. 3. Phase-sensitive second-hannonic microscopy reveals polarity of topologically centrosymmetric molecular crystals. Appl. Phys. Lett 2002, *81*. 247–249.
36. Hulliger, J. New physical methods for a space resolved mapping of the macroscopic polarisation in molecular crystals and a stochastic theory for understanding. Chimia 2001. *55*, 554–561.
37. Hulliger. J.: Bebie. H.; Kluge. S.: Quintel, A. Growth-induced evolution of polarity in organic crystals. Chem. Mater. 2002. *14*. 1523–1529.
38. Vaida, M.; Shimon. L.J.W.: Weisinger-Lewin, Y.: Frolow. F.; Lahav. M.: Leiserowitz. L.: McMullan. R.M. The structure and symmetry of crystalline solid solutions: A general revision. Science 1988, *241*, 1475–1479.
39. Weissbuch, *I.*; Lahav. M.: Leiserowitz. L.: Meredith, G.R.: Vanherzeele, H. Centrosymmetric crystals as host matrices for second-order optical nonlinear effects. Chem. Mater. 1989, *1*. 114–118.
40. Weissbuch, I.; Popovitz-Biro, R.; Lahav. M.: Leiserowitz. L. Understanding and control of nucleation. growth. habit, dissolution and structure of two-and three-dimensional crystals using "tailor-made" auxiliaries. Acta Cryst. 1995. *B51*. 115–148.
41. Graham. H.K.; Holmes. D.F.: Watson. R.B.; Kadler. M.E. Identification of collagen fibril fusion during vertebrate tendon morphogenesis. The process relies on unipolar fibrils and is regulated by collagen–proteoglycan interaction. J. Mol. Biol. 2000. *110*. 245–249. (part *A)*.
42. Kadler. K.E.: Holmes, D.F.: Trotter, J.A.: Chapman, J.A. Collagen fibril formation. Biochem. J. 1996. *316*. 1–11.

Polymorphism

Mino R. Caira
University of Cape Town, Rondebosch, Western Cape Province, South Africa

INTRODUCTION

Purification of a solid organic compound is achieved principally by crystallization, a process involving the successive formation of prenuclear aggregates of the molecules in question. crystal nuclei: and eventually, mature crystals. Altering the experimental conditions of crystallization of a given substance can lead to its isolation in different crystalline forms, or polymorphs, each of which is unique in terms of its thermodynamic stability and physical properties. Two polymorphs of a given compound may exhibit properties as different as those displayed by two distinct compounds. This versatile aspect of solids. particularly insofar as it presents opportunities for selecting an appropriate crystalline form for a specific application, continues to be exploited in all areas of chemical and materials research. In a systematic experimental study of the polymorphism of a given compound, investigators are likely to encounter not only polymorphs but also solvated crystal forms (sometimes called pseudopolymorphs) and amorphous forms, ail of which are unique and of practical relevance because of their possible interconversion and potential utility.

OCCURRENCE AND GENERAL IMPACT

Polymorphism and polymorphic transformations are phenomena encountered during the manufacture, handling, processing. and storage of solid materials, both in small-scale operations in academic laboratories and in bulk processing in commercial establishments. The challenges they present are considerable. the foremost being those of establishing the conditions for reproducible preparation of a specific solid form with desired properties (for application in areas such as suprarnolecular chemistry, crystal engineering. explosives manufacture, food chemistry. agrochemicals, and pigment and pharmaceutical manufacture) and retention of that form during the lifetime of its application. Patent litigation hinging on the polymorphism and pseudopolymorphism of commercially or strategically important materials is becoming more frequent as companies strive to protect their intellectual property.

CRYSTALLIZATION DYNAMICS AND POLYMORPHIC STABILITY RELATIONSHIPS

Understanding the origin of polymorphism and ultimately controlling the outcome of crystallization processes require consideration of the thermodynamic and kinetic factors involved.'" At specified temperature and pressure, only one polymorph of a given compound is thermodynamically stable (i.e., has the minimum Gibbs free energy): and all other polymorphs are metastable to varying degrees. If this factor alone determined the outcome of crystallization. then only one polymorph (the most stable) should appear. However. because the nuclei of different polymorphs have unique structural and interfacial properties, their free energies of activation differ, and hence, the nucleation rates of different polymorphs of the same compound generally differ. Consequently, if conditions are such that the nucleation rate of a metastable polymorph exceeds that of a more stable polymorph, crystallization of the former will be favored. The successive crystallization and dissolution of increasingly more stable (less-soluble) forms from a solution of a compound, described by Ostwald's Rule of Stages, is a manifestation of the interplay between the thermodynamic and kinetic factors operating in such a system. Each polymorph has an associated "occurrence domain," i.e., solvent medium, temperature range, and other conditions under which it will crystallize.[2] Simultaneous crystallization of two or more polymorphs ("concomitant polymorphism") is not uncommon[3] and may occur if the occurrence domains of these species intersect. Establishing the limits of this intersection provides a rational basis for polymorphic control in crystallization.

Thermodynamic stability relationships between polymorphs are conveniently represented in schematic energy–temperature diagrams.[4] Shown in Fig. 1 is such a diagram for the system comprising three polymorphs of the hypocholesterolemic drug lifibrol (4-{4-[4-(1,1-dimethyl)phenyl]-2-hydroxybutoxy} benzoic acid) **1,** established on the basis of measured thermal, solubility, and spectroscopic data.'" Focusing first on the curves G_{I}, G_{II}, and G_{liq}, which represent the temperature variations of the Gibbs free energies of polymorphs I, II, and their common liquid phase. respectively, it is evident that

Encyclopedia of Supramolecular Chemistry
DOI: 10.1081/E-ESMC 120012844

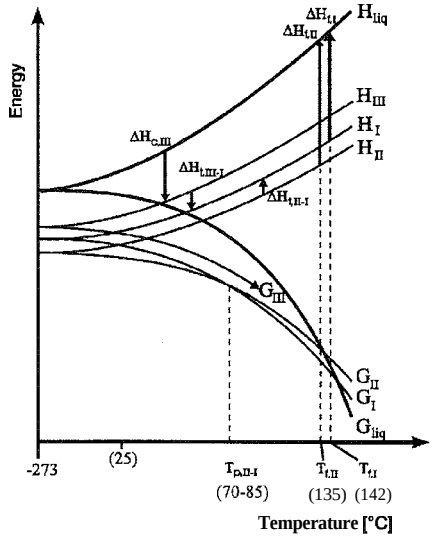

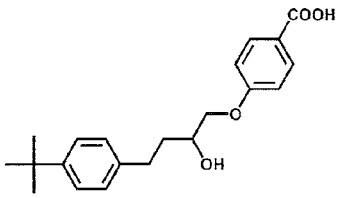

1

Fig. 1 Semischematic energy–temperature diagram for three polymorphic modifications of lifibrol 1. (Reprinted from the European Journal of Pharmaceutics & Biopharmaceutics, Vol. 49. A. Burger and A. Lettenbichler. Polymorphism and preformulation studies of lifibrol, pp. 65–72. 2000 (Ref. [5]), with permission from Elsevier Science.)

polymorphs I and 11 melt at the temperatures $T_{f,I}$ and $T_{f,II}$, where each solid phase is in equilibrium with the liquid. The curves G_I and G_{II} intersect at the temperature $T_{p,II-I}$, which represents their transition point. At temperatures less than $T_{p,II-I}$, the curve G_{II} lies below curve G_I, indicating that polymorph II is more stable in this temperature region. In the temperature range between $T_{p,II-I}$ and $T_{f,I}$, however, polymorph I is the more stable form. Thus. heating polymorph II above $T_{p,II-I}$ will result in its conversion to the more stable polymorph I, and conversely, cooling polymorph I below $T_{p,II-I}$ will yield polymorph II. These features are the hallmarks of enantiotropy, and polymorphs I and II are said to be enantiotropically related. Because the curve G_{III} (for the third polymorph of lifibrol) lies above those of G_I and G_{II}, polymorph III is evidently metastable with respect to both polyrnorphs I and II. Owing to its metastable nature, polymorph III has a natural tendency to convert (irreversibly) to I or II and will do so under favorable conditions (e.g., via solution-mediated transformation or by mechanical treatment). The polymorphs I and III are accordingly said to be related monotropically, as are 11 and III. Establishing whether polymorphs are enantiotropically or monotropically related is of practical significance, because it guides crystallization strategy.[6] For example. in order to isolate one of the polymorphs in an enantiotropic system. it is necessary to maintain the temperature and pressure conditions at which the Cibbs free-energy curve of the desired polymorph is below that of the undesired one. Included in Fig. 1 are the enthalpy (H)–temperature variations for the various phases present, from which the relative magnitudes of the enthalpy changes for possible solid–solid and solid–liquid transformations can be deduced. Ideally, the construction of an energy–temperature diagram for each new polymorphic system encountered is desirable, as such a diagram summarizes a considerable amount of thermodynamic data for the system and enables prediction of phase stability and possible phase transformations. The conclusion of the study on lifibrol[5] was that polymorph 11 (stable at both room temperature and body temperature) is suitable for pharmaceutical formulation.

Consideration of the general features of energy–temperature diagrams has enabled us to formulate several practical guidelines (Burger's rules) for distinguishing monotropic and enantiotropic systems.[4] The heat-of-transition rule and the heat-of-fusion rule are especially useful. The second, for example, states that if the enthalpy of fusion of the lower melting form is greater than that of the higher melting form, the polymorphs are enantiotropically related. (This is evident in Fig. 1 for polymorphs I and II, for which $\Delta H_{f,II} > \Delta H_{f,I}$). Extension of the theory underlying energy–temperature diagrams has led to formulae for calculating $\Delta G(T)$, the difference in the Gibbs free energy for two polymorphs as a function of temperature.[7] Extrapolation of this quantity to zero enables estimation of their transition temperature.

GENERATION AND CHARACTERIZATION OF POLYMORPHS

Preparative Methods

A thorough practical investigation of the propensity for the existence of different solid forms of a new compound

should follow the type of systematic program that has become mandatory for drug substances.[8] This involves isolation of all possible forms of the compound (including polymorphs. solvates, and amorphous phases), followed by application of physicochemical methods of analysis to establish the identity of each form as well as the stability and structural relationships among the various forms. Both steps in this procedure are outlined here.

Methods for generating polymorphs. hydrates, solvates, and amorphous phases have been reviewed.[9] Starting with the raw material (in whatever form available), polymorphs may be obtained by sublimation. crystallization from solvents (single or mixed), precipitation from solution by pH adjustment (for acidic or basic compounds). vapor diffusion, thermal treatment, crystallization from the melt. seeding. thermal desolvation of crystalline solvates, and grinding. As regards pseudopolymorphs, hydrates may be obtained by crystallization of the anhydrous compound from water or by exposure of water vapor. Analogous procedures using organic solvents may yield the corresponding solvates.

Because crystallization from a given solvent may yield either a polyrnorph or a solvate, some guideline is desirable for predicting the likely outcome. A useful recent study assessed the tendency for different solvent molecules to be incorporated in the crystallized product.[10] Mere, account was taken of the frequency of occurrence of solvates as well as the frequency of usage of specific solvents in crystallization experiments. This enabled a ranking of common solvents according to their probabilities of leading to solvate formation. Thus. despite the fact that diethyl ether is used much more frequently as a recrystallization medium than 1.4-dioxane. it has a inuch lower tendency to form solvates. These observations can be rationalized on the basis of solvent–solute interactions. Retention of organic solvents in the product crystal is facilitated for solvents such as 1,4-dioxane that can interact with appropriate polar functions of the solute molecule through multiple-point recognition, e.g., via strong O(solvent)···H–O, O(solvent)···H–N as well as weak O(solvent or solute)···H–C hydrogen bonds. The practical significance of pseudopolymorphs should not be underestimated. If the parent compound has a tendency to solvate. it may crystallize in only one or two polymorphs but generate a large number of pseudopolymorphs. On desolvation. the latter produce polymorphs, among which hitherto unobserved forms might be present. The versatile drug sulfathiazole 2 is remarkable in forming over 100 solvates.[11] Structurally, these crystal modifications fall into the classes of clathrates, cocrystals, and salts.

Finally, to generate amorphous phases from the parent compound, the various methods include rapid cooling of the melt, particle size reduction (by milling. with or without additives), spray-drying. freeze-drying, eliminating solvents from solvated phases, and adjusting solution pH. Amorphous phases are thermodynamically metastable and, therefore, more soluble than polymorphs of the same compound. As such, they may be useful pharmaceutically to enhance bioavailability provided their tendency to revert to more stable forms can be prevented.

Physicochemical Characterization

A wide range of physicochemical techniques is available for the characterization of polymorphs and pseudopolymorphs. A brief description of the most widely used methods follows, but it should be noted that numerous other techniques have been employed in special cases. and the ingenuity of future investigators will no doubt lead to the application of novel methods. X-ray diffraction remains unique in its ability to distinguish different polyrnorphs of the same compound, because each species yields its own characteristic x-ray powder pattern.[12] Shown in Fig. 2 are the distinctly different experimental patterns for the polymorphs I–III of lifibrol **1**[5] that permit their unequivocal identification. The technique is also used dynamically and variable-temperature powder x-ray diffraction is being increasingly employed to identify polymorphic phase transforinations and to determine transition temperatures. When single crystals of a polymosph are available, x-ray analysis permits complete elucidation of the molecular and crystal structures. enabling the investigator to correlate bulk properties of the polymorph with details of the molecular conformation. crystal packing. and hydrogen-bond interactions. The refined crystal data (atomic positions, displacement parameters. unit cell dimensions) and space group data for any structure are also required for the computation of the idealized x-ray powder pattern of that crystalline phase. Such a pattern is invaluable as a fingerprint for future phase identification.

Standard thermal methods of analyzing polymosphs include differential scanning calorimetry (DSC). thermogravimetric analysis (TGA), and hot-stage inicroscopy (HSM). These methods are applied routinely in the pharmaceutical industry to monitor the integrity of specific polymorphs intended for formulation and to detect and characterize solvated forms.[10] Whereas polymorphs yield zero mass loss upon heating up to the melting point, solvates usually lose their included solvent. as indicated by an accurately measurable mass loss on TGA (enabling calculation of the solvate stoichiometry). an endothermic peak in the DSC trace. and the formation of bubbles of released solvent when the crystals are heated under an inert medium in HSM. DSC traces for various forms of lifibrol **1**[5] are also shown in Fig. 2. Primary data from DSC include characteristic onset and peak temperatures of thermal events (polymorphic transitions:

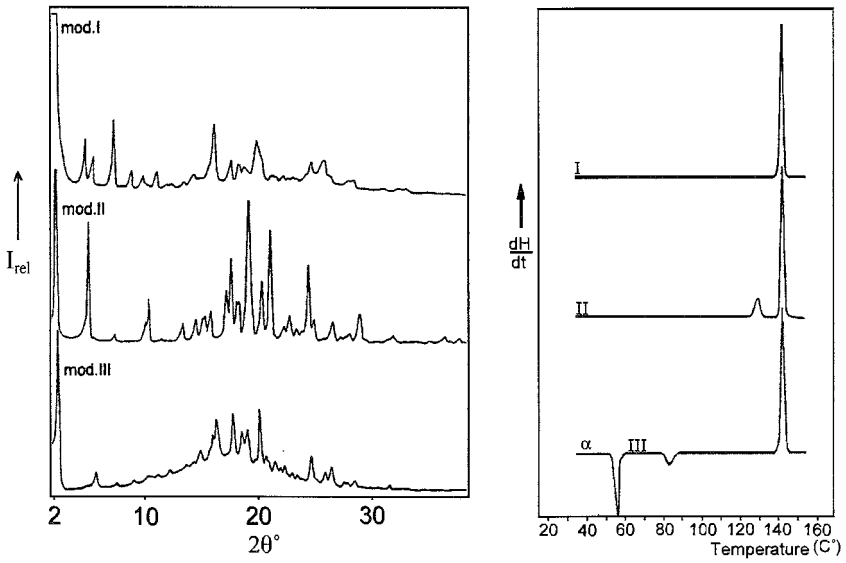

Fig. *2* Powder x-ray diffraction patterns (left) for three polymorphs of lifibrol I and DSC traces (right) for modifications I and II as well as the amorphous α-modification that transforms into modification III. (Reprinted from the European Journal of Pharmaceutics & Biopharmaceutics, Vol. 49. A. Burger and A. Lettenbichler, Polymorphism and preformulation studies of lifibrol. pp. 65–72, 2000 (Ref. [5]), with permission from Elsevier Science.)

fusion). as well as their associated enthalpy changes. Accurate enthalpies of fusion for different polymorphs are used in conjunction with Burger's rules to distinguish enantiotropic and monotropic behaviors.[4]

FTIR and Raman spectroscopy are frequently used to characterize polymorphs.[12] Both the molecular conformation and the crystal packing may lead to differences in the FTIR spectra of polymorphs; the differences are more pronounced for compounds capable of hydrogen bonding. Characteristic shifts in C=O, N–H, and O–H stretching frequencies often lead to unequivocal polymorphic identification. Differences in fine structure and in the positions and intensities of IR bands enabled seven crystalline forms of the steroid prasterone 3 to be distinguished.[9,11] The presence of characteristic absorption bands due to included solvent molecules allows ready distinction between polymorphs and pseudopolymorphs.

Solid-state WMR (mainly ^{13}C) is rapidly gaining popularity as a method for distinguishing polymorphs.[12] The existence of different crystal-packing schemes inherent in a series of polymorphs implies that specific nuclei of the parent molecule will generally experience different local magnetic environments in the various crystals, yielding characteristic shifts in resonance positions. The method allows for detection of subtle structural features. including differences in molecular conformation, crystallographically independent molecules, and molecular disorder. It is. however, desirable to confirm the presence of such features using x-ray analysis.[12] It should be emphasized that thorough and unambiguous characterization of polymorphic systems usually requires application of several techniques in combination, and that all of these should be conridered as supporting the definitive technique of x-ray diffraction.

STRUCTURAL ASPECTS OF POLYMORPHIC SYSTEMS

Rigid or Semirigid Molecules

For a system comprising two or more polymorphs, x-ray crystal structure analyses of the various forms are highly desirable, because they reveal, at an extraordinary level of accuracy and precision; how chemically identical molecules can be accoinmodated in different crystalline architectures. This knowledge is indispensable for establishing and interpreting structure–property relationships. The vast majority of polymorphic crystal structures were determined using single-crystal x-ray techniques. but there is an increasing incidence of successful structural elucidation from high-resolution powder x-ray diffraction data, especially for metastable phases and in cases where the crystallite size is very small.

Molecules possessing few conformational degrees of freedom frequently crystallize in different polymorphic forms with retention of a common. low-energy conformation but with different intermolecular relationships, reflected in their space group symmetries. Examples

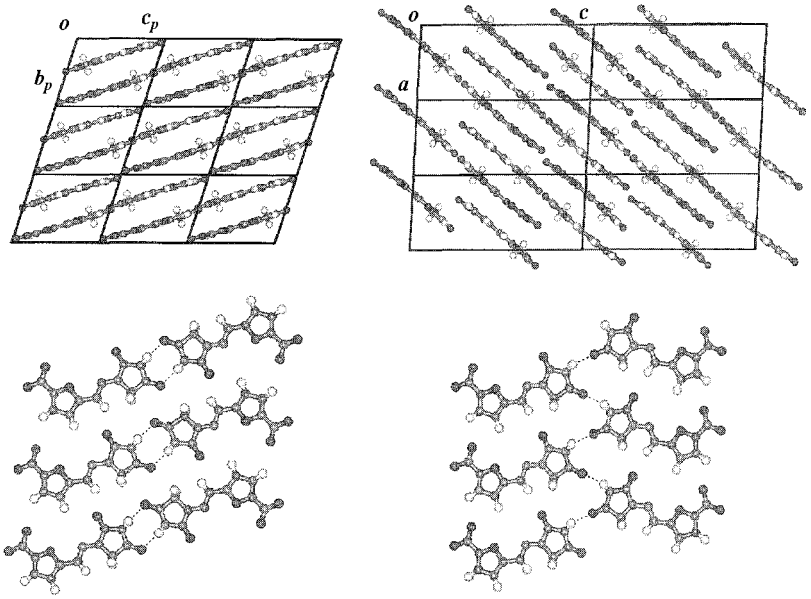

Fig. 3 Crystal structures of nitrofurantoin polymorphs: layer stacking (top left) and hydrogen bonding within a layer (lower left) for the a-polymorph; and layer stacking (top right) and hydrogen bonding within a layer (lower right) for the β-polymorph. Only the N–H···O hydrogen bonds are indicated. (Adapted from E.W. Pienaar, M.R. Caira and A.P. Lotter, Journal of Crystallographic and Spectroscopic Research. 23(10), 1993, 785–790. with permission from Kluwer Academic/Plenum Publishers.) (*View* this *art in color at www.dekker.com.*)

include the compounds maltol 4, sulfamerazine **5,** nitrofurantoin 6.[14] and acetaminophen (paracetamol) **7**.[15] Shown in Fig. 3 are the crystal packings in the α-polymorph (triclinic, space group $P\bar{1}$) and the β-polymorph (monoclinic, $P2_1/c$) of nitrofurantoin 6, both of which are based on the stacking of molecular layers.''''' The same types of hydrogen bonds (N–H.·O, C–H···O) occur in both phases, but their arrangements within the layers of the two polymorphs differ substantially. One consequence of the structural difference is that the dissolution rates of the two polyrnorphs differ significantly. Two polymorphs of acetaminophen **7** provide a striking example of such a structure–property relation.''''' The crystal structure of the stable monoclinic polymorph ($P2_1/c$) is based on a complex molecular array stabilized by intermolecular hydrogen bonds that assume a variety of spatial directions, whereas the less-stable orthorhombic crystal (Pbca) contains hydrogen-bonded molecules assembled in layers that lack strong cohesion. As a consequence, the crystals respond differently to the application of pressure. The monoclinic polymorph resists compaction in the absence of excipients, while the orthorhombic polpmorph may be tabletted without additives, owing to the presence of graphite-like slip planes in the crystal. Numerous polymorphic structure–property relationships are documented.''''' Other bulk properties that were correlated with crystal structures of polymorphic systems include electrical conductivity. magnetism, photovoltaic and photoconductive effects. nonlinear optical (NLO) activity, photochromism, thermochromism, and mechanochromism. Such properties are intimately associated with special structural features of the polymorphs displaying them (e.g., NLO activity, occurring exclusively with noncentrosymmetric polymorphs).

Conformational Polymorphs

Conforrnationally flexible molecules frequently possess several low-energy conformations, two or more of which may appear in different crystal structures. giving rise to ''conformational polymorphism.''[14] Examples of compounds crystallizing as conforrnational polymorphs and the variety of space groups represented include dichloro-N-benzylideneaniline 8 ($P\bar{1}$, Pccn), iminodiacetic acid **9** (trimorphic, with two polymorphs in $P2_1/c$, one in $Pbc2_1$), spironolactone **10** (two polymorphs in $P2_12_12_1$), and probucol **11** (two polymorphs in $P2_1/c$). Two enantiotropically related polymorphs of piroxicam pivalate **12** fall into this category.[17] Form 1 is orthorhombic (Pbca), with one molecule in the asymmetric unit. Form 2 is inonoclinic ($P2_1/c$), with two molecules (A. B) in the asymmetric unit. As shown in Fig. 4. the molecular conformations differ significantly for all observed conformers. Examination of the crystal structures revealed that the arrays of A and B molecules in Form 2 are located in separate domains, each with a distinct hydrogen-

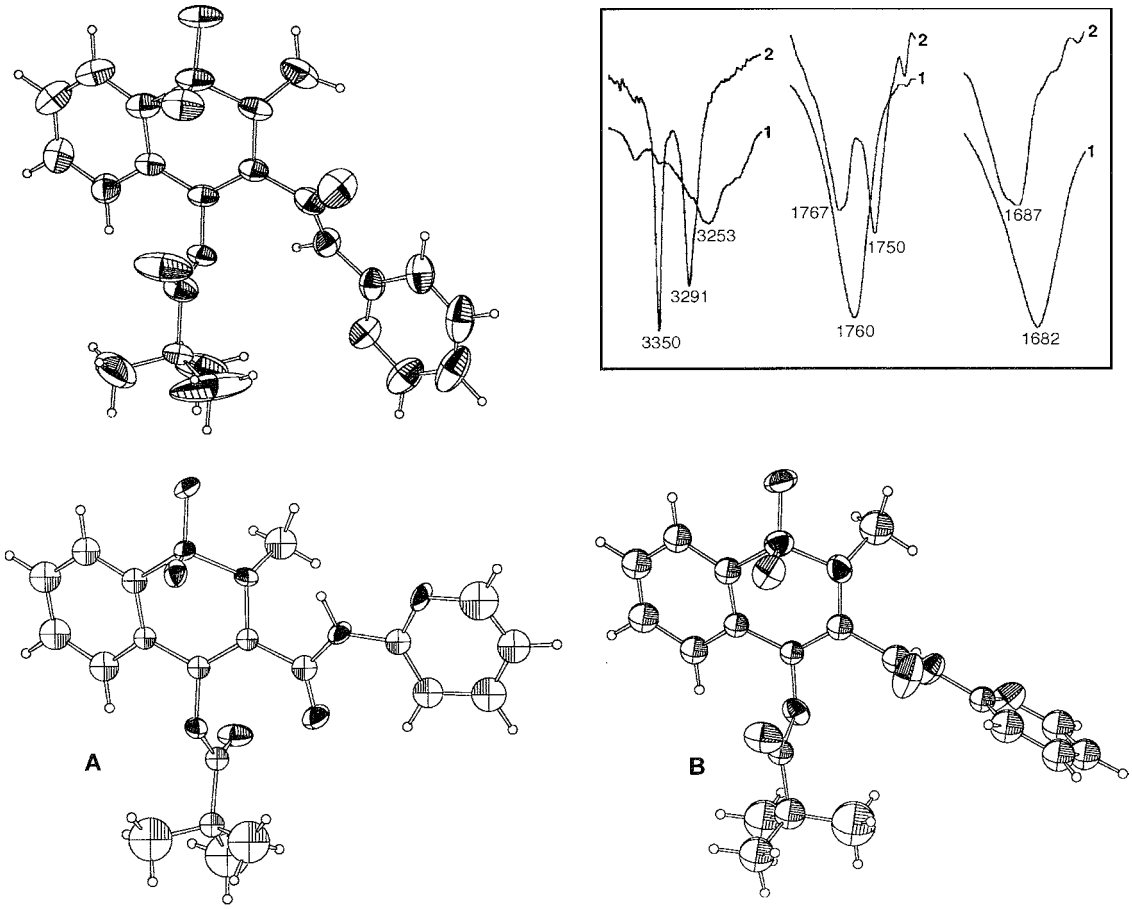

Fig. 4 Conformational polymorphism in piroxicam pivalate **12**: the single conformer occurring in Form 1 (top left). two independent conformers (A. B) found in Form 2 (lower left, lower right). and the IR absorption bands (c m $^{-1}$) in Forms 1 and 2 in the amide N–H. ester C=O. and amide C=O stretching regions (upper right). (Adapted from the Journal of Pharmaceutical Sciences. Vol. 87. M.R. Caira, M. Zanol. T. Peveri, A. Gazzaniga. and F. Giordano. Structural characterization of two polymorphic forms of piroxicam pivalate, pp. 1608–1614. 1998 (Ref. [17]), with permission from Wiley-Liss, Inc., A Wiley Company.)

bonding arrangement. These structural features could be reconciled with the appearance and positions of the IR absorption bands for the amide N–H, ester C=O, and amide C=O stretching vibrations (Fig. 4), the Form 2 spectra accordingly showing higher peak multiplicities.

Conformational polymorphs have been exploited for structure–property relationships. A recent study of the color polymorphism (red. orange. yellow) displayed by six conformational polymorphs of 5-methyl-2-[(2-nitrophenyl)amino]-3-thiophenecarbonitrile 13 showed that this phenomenon could be explained by conformational differences that change the extent of π-conjugation between the *o*-nitroaniline chromophore and the thiophene ring.[18] This thorough investigation employed optical crystallography, polarized single-crystal absorption spectroscopy, and computational methods. In the context of polymorphic control (see below). in comparison with rigid molecules, the crystallization of conformationally flexible molecules is especially challenging[19] because of the reduced tendency for such molecules to crystallize and the possibility of their crystallizing in a variety of structural arrangements.

CHALLENGES AND REGENT DEVELOPMENTS

Polymorphic Control

Several challenges in the area of polymorphism continue to be the focus of intensive research. These include polymorphic control in crystallization, structural elucidation of polymorphs available only as powders, and the central problem of crystal structure prediction by theoretical methods from a knowledge of the molecular structure only. Here, the essential features of these challenges are described, and some recent developments that attempt to address them are outlined.

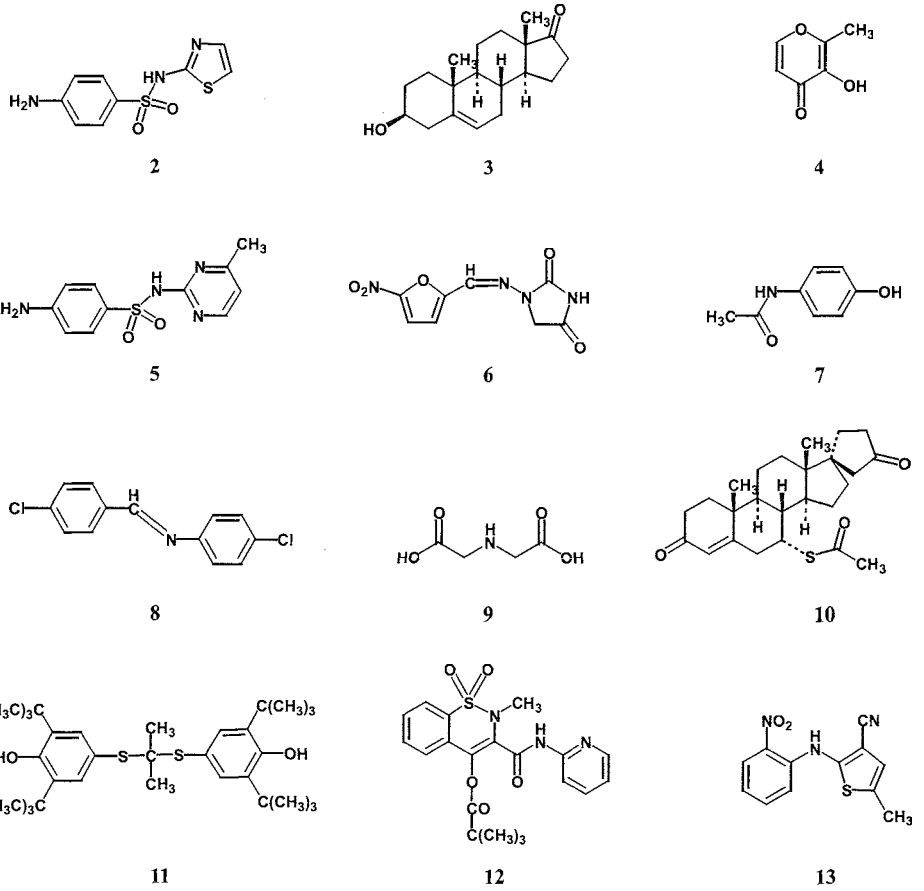

2 3 4

5 6 7

8 9 10

11 12 13

The crucial need to control the outcome of crystallization of a polymorphic compound was alluded to above. Failure to manufacture the desired polymorph reproducibly can lead to massive financial loss and, in the case of pharmaceutical compounds, to the more serious risk of compromising human health. A recent dramatic case involved the anti-AIDS drug ritonavir **14** that failed dissolution requirements in mid-1998.[20] The cause was traced to the sudden appearance of a new, thermodynamically more stable polymorph with a solubility only ~ 25% that of the known polymorph (measured in hydroalcoholic solvents. at the required formulation storage temperature of 5°C). The original polymorph temporarily "disappeared," having been "displaced" by the more stable form. Only after extensive investigation were manufacturing processes developed for selective crystallization of the two polymorphs. Some of the strategies for polymorphic control include recrystallizing from specified solvent systems, altering the crystallization conditions from "thermodynamic" to "kinetic" or vice versa, using of seeding, and employing designed additives to induce crystallization of a desired polymorph. The use of specific solvents or mixtures of solvents does not guarantee isolation of a particular polymorph unless other experimental conditions are carefully controlled. Critical factors include the degree of solvent purity, solute concentration, temperature program, and the time of harvesting the crystals. Increasing emphasis is being placed on the need to accurately record these conditions to ensure reproducibility of the outcome.[21] Metastable polymorphs may generally be obtained under kinetic (i.e., far from equilibrium) conditions of crystallization (e.g., rapid cooling of the solution, conditions of high supersaturation), whereas more stable forms tend to crystallize under thermodynamic conditions (e.g., slow cooling. slow evaporation). The latter may also be obtained by solvent-mediated transformation, as a result of spontaneous dissolution of metastable forms and subsequent recrystallization. The seeding technique is commonly employed in industrial batch crystallizations and enables control of the polymorphic outcome.[22] Its rational application does, however, rely on a thorough knowledge of the stabilities and relative solubilities of the polymorphs involved. Exclusive crystallization of a metastable polymorph is a desirable goal in industry. A novel batch crystallizer was recently employed to exclusively isolate the metastable form of L-glutamic acid **15** from aqueous solution.[23] This was achieved

through separate control of the crystallization temperature and the nucleation temperature. Another strategy for stabilizing and isolating a metastable polymorph from solution involves preventing its transformation to a more stable polymosph by deliberately adding a trace amount of another compound. The latter may be found serendipitously or by design, and its role is one of inhibiting the nucleation and crystal growth of the more stable form. Polymorph I of sulfamerazine **5** normally undergoes a solvent-mediated transformation to the more stable polymorph II in acetonitrile medium. If, however, any of the structurally related species N^4-acetylsulfamerazine **16**, sulfadiazine **17**, or sulfamethazine 18 is present as an impurity. it retards this transformation significantly.[24] For this system. it was found that the rank order of the inhibitory effect of the three additives corsesponded with the rank order of the calculated binding energy of the additive to the crystal surface of polymorph II. These results, incidentally. also serve to highlight the possibility that discovery of a polymorph might actually be delayed due to the presence of unknown impurities in a crystallizing system. Rational design of inhibitors is possible. provided that detailed knowledge of the relationships between crystal structure and crystal morphology for both the desired and undesired polymorphs are known.[25] This again underscores the constant need for x-ray structural elucidation of polymorphs.

Polymorphic Structures from X-ray Powder Data

Many industrially important polymorphs can be prepared in microcrystalline form only, preventing their crystal structure solution by conventional single-crystal x-ray techniques. However, considerable progress in elucidating crystal structures from high-resolution powder x-ray diffraction data was achieved in recent years. The essential steps in the procedure include indexing of the powder diffraction pattern; optimization of the molecular unit by modeling methods, generation of trial structures. and Rietveld refinement. Developments that improved the success rate in this area include the use of synchrotron radiation for rapid data capture, superior treatment of overlapping reflections. more reliable indexing routines, and more flexible methods of obtaining trial structures. As an illustration of the power of the method, the crystal structures of two polymorphs of telrnisartan **19** (an angiotensin II receptor antagonist with considerable conformational flexibility) were solved from high-resolution x-ray powder diffraction data.[26] Structure solution required the determination of 13 degrees of freedom in each case (three translational, three orientational, and seven torsion angles) and was achieved on a personal computer (Pentium II 350 MHz) in about 2 hours using the method of simulated annealing. One limitation of the method, however. is that while molecular conformations in different polymorphs may be determined with high precision, the same is not true for bond lengths and angles.

Polymorphs and Crystal Structure Prediction

Finally, what may be considered as a central goal in this research area is the complex problem of prediction of the crystal structure of a compound, given only its molecular connectivity. The problem is better formulated as computer generation of a set of potential polymorphs of the compound: detection of the most stable one at a given temperature, and modeling of the nucleation kinetics to determine which phase will actually appear under given conditions.[27] This is a vast and rapidly developing subject in its own right, and only a brief outline of the challenges that this problem presents can be given here. Two general approaches to crystal structure prediction are discussed in a recent review.[28] The first step in one established approach[27] is the generation of trial crystal structures by utilizing the known, limited number of symmetry operations that relate molecules spatially in crystals. Frequently, the more populous space groups of the 230 theoretically possible are selected for structure generation. Structures with the highest possible packing efficiencies are accepted as the most plausible, and these are further optimized by minimization of the lattice energy. Crystal structures predicted in this way have similar energies, so that several candidates ensue, and ranking their likelihood of representing realizable structures is thus difficult. (On the other hand, if the x-ray powder pattern of a polymorph is available. its coincidence with a pattern generated from one of the predicted structures immediately characterizes it structurally). Conformationally flexible molecules are especially challenging for crystal structure prediction. as no general algorithms enabling simultaneous optimization of molecular conformation and crystal structure are available. In such cases, the most stable conformations are usually determined. each then being treated as a rigid model in the approach described above. Pseudopolymorphs clearly present a severe challenge for crystal structure prediction, as the correct relative positions and orientations of host and guest molecules must be established before trial structure generation can proceed.

The factors leading to correct structure prediction are not easily defined. Examples of molecules with predicted (i.e., computed) crystal structures that coincide with their observed x-ray structures are shown as **20**, 21, and 22. On the other hand: for the molecules 23. 24. and 25, which superficially do not appear to be any more challenging, the observed x-ray crystal structures are very different from the most stable computed models. These anomalies

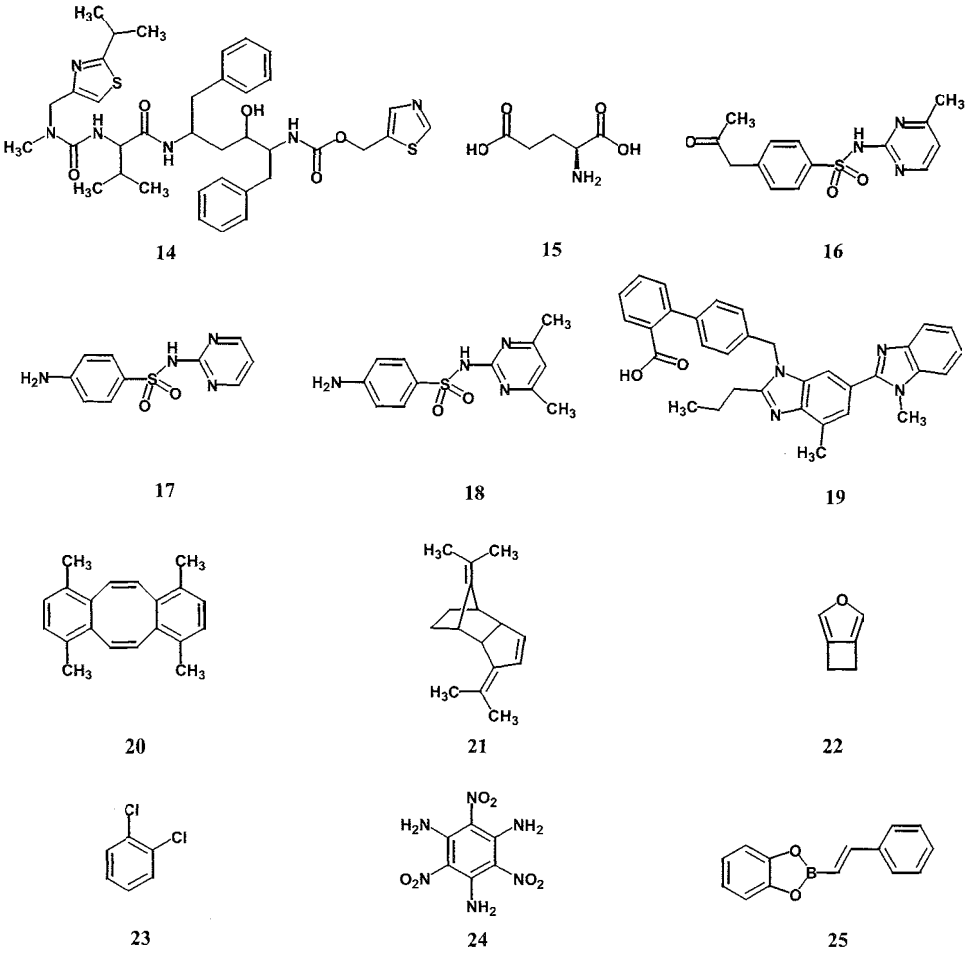

14 15 16 17 18 19 20 21 22 23 24 25

and other concerns (e.g., the inaccuracy or inadequacy of current empirical force fields, neglect of dynamic effects) were recently brought into perspective by a pioneer in the field.[29] and the successes and failures of current approaches were highlighted. Incorporation of molecular dynamics is suggested as a promising adjunct to current strategies.

CONCLUSION

Crystal polymorphism is assuming ever-increasing importance in the solid-state chemistry of materials. Every newly synthesized compound has the potential for existing in multiple crystalline forms as polymorphs or pseudopolymorphs. If advantage is to be gained from exploiting the physical properties of a specific crystalline form of a compound. it will be necessary to manufacture it reproducibly and ensure that it maintains its integrity. Major research challenges in the area of crystal polymorphism include control of the crystallization process, routine determination of crystal structures of polymorphs available as powders. and accurate prediction of crystal structures by computational methods. Different levels of success were attained in each area. Perhaps the most important outcome of the increasing volume of scientific literature relating to polymorphism is the creation of an awareness of its ubiquity and its enormous practical significance in the science of solids.

ACKNOWLEDGMENT

The author thanks the University of Cape Town and the National Research Foundation (Pretoria) for financial support and Mr. Vincent Smith for technical assistance.

ARTICLES OF FURTHER INTEREST

Clathrate Inclusion Compounds, Phase Transitions in, p. 289
Concepts in Crystal Engineering, p. *319*
Crystal Growth Mechanisms, p. *364*

Crystal Structure Prediction, p. 371
Nonlinear Optical Materials, p. 973
Solid-State Nuclear Magnetic Resonance Spectroscopy. p. 1307
Space Groups and Crystal Packing Modes. p. *1337*
X-Ray Crystallography, p. *1586*
X-Ray and Neutron Powder Diffraction, p. 1592

REFERENCES

1. Bernstein. J. Fundamentals. In *Polymorphism in Molecular Crystals,* 1st Ed.; Oxford University Press Inc.: New Uork. 2002; 29–65.
2. Sato. K.: Boistelle, R. Stability and occurrence of polymorphic modifications of stearic acid in polar and nonpolar solutions. J. Cryst. Growth 1984, 66 (2), 441–450.
3. Bernstein, J.: Davey, R.J.; Henck, J.-O. Concomitant polymorphs. Angew. Chem.. Int. Ed. 1999.38 (23). 3441–3461.
4. Grunenburg. A.; Kenck. J.-O.; Siesler, H.W. Theoretical derivation and practical application of energy/temperature diagrams as an instrument in preformulation studies of polymorphic drug substances. Int. J. Pharm. 1996, 129 (1. 2). 147–158.
5. Burger, A.: Lettenbichler. A. Polymorphism and preformulation studies of lifibrol. Eur. J. Pharm. Biopharm. 2000. 49 (1). 65–72.
6. Bernstein, J. Controlling the Polymorphic Form Obtained. In *Polymorphism in Molecular. Crystals,* 1st Ed.: Oxford University Press Inc.: New York. 2002: 66–93.
7. Yu. L. Inferring thermodynamic stability relationship of polymorphs from melting data. J. Pharm. Sci. 1995. 84 (8). 966–974.
8. Byrn, S.R.: Pfeiffer, R.R.; Stowell, J.G. Regulatory Aspects of the Solid-State Chemistry of Drugs. In *Solid-State Chemistry of Drugs,* 2nd Ed.; SSCI Inc: West Lafayette. IN, USA. 1999; 489–503.
9. Guillory. J.K. Generation of Polymorphs, Hydrates, Solvates. and Amorphous Solids. In *Polymorphism in Pharmaceutical Solids,* 1st Ed.; Brittain. H.G.. Swarbrick. J., Eds.; Drugs and the Pharmaceutical Sciences. Marcel Dekker Inc.: New York. 1999: Vol. 95, 83–226.
10. Nangia, A.; Desiraju. G.R. Pseudopolymorphism: Occurrence of hydrogen bonding solvents in molecular crystals. J. Chem. Soc.. Chem. Commun. 1999. (7). 605–606.
11. Bingham. A.L.: Hughes. D.S.: Hursthouse, M.B.; Lancaster. R.W.; Tavener. S.; Threlfall. T.L. Over one hundred solvates of sulfathiazole. J. Chem. Soc.. Chem. Commun. 2001. (7), 603–604.
12. Brittain, H.G. Methods for the Characterization of Polymorphs and Solvates. In *Polymorphism in Pharmaceutical Solids,* 1st Ed.; Brittain. H.G.. Swarbrick, J.. Eds.: Drugs and the Pharmaceutical Sciences. Marcel Dekker Inc.: New York, 1999: Vol. 95, 227–278.
13. Caira. M.R. Crystalline Polymorphism of Organic Compounds. In *Design of Organic Solids;* Weber. E.. Ed.: Springer-Verlag: Berlin. 1998; Vol. 198. 163–208.
14. Brittain, H.G.; Bym. S.R. Structural Aspects of Polymorphism. In *Polymorphism in Pharmaceutical Solids,* 1st Ed.: Brittain. H.G.. Ed.: Drugs and the Pharmaceutical Sciences. Marcel Dekker Inc.: New York, 1999: Vol. 95. 73–124.
15. Nichols. G.: Frampton. C.S. Physicochemical characterization of the orthorhombic polymorph of paracetamol crystallized from solution. J. Pharm. Sci. 1998. 87 (6). 684–693.
16. Bernstein. J. Polymorphism and Structure–Property Relations. In *Polymorphism in Molecular Crystals,* 1st Ed : Oxford University Press Inc.: New York, 2002: 188–239.
17. Caira, M.R.: Zanol, M.; Peveri, T.: Gazzaniga. A.; Giordano. F. Structural characterization of two polymorphic forms of piroxicam pivalate. J. Pharm. Sci. 1998. 87 (12). 1608–1614.
18. Yu. L. Color changes caused by conformational polymorphism: Optical-crystallography. single crystal spectroscopy. and computational chemistry. J. Phys. Chem.. A 2002. 106 (3). 544–550.
19. Uu. L.: Reutzel-Edens, S.M.; Mitchell, C.A. Crystallization and polymorphism of conformationally flexible molecules: Problems. patterns and strategies. Org. Process Res. Dev. 2000. 4 (5). 396–402.
20. Bauer, J.; Spanton, S.; Henry. R.: Quick, J.; Dziki, W.; Porter, W.: Morris, J. Ritonavir: An extraordinary example of conformational polymorphism. Pharm. Res. 2001, 18 (6). 859–866.
21. Rodriguez-Hornedo. N.; Murphy, D. Significance of controlling crystallization mechanisms and kinetics in pharmaceutical systems. J. Pharm. Sci. 1999. 88 (7). 651–660.
22. Beckman. W. Seeding the desired polymorph: Background. possibilities. limitations, and case studies. Org. Process Res. Dev. 2000, 4 *(5).* 372–383.
23. Shan, G.; Igarashi. K.; Noda. H.: Ooshima, H. Control of solvent-mediated transformation of crystal polymorphs using a newly developed batch crystallizer (WWDJ-crystallizer). Chem. Eng. J. 2002, 85 (2–3). 169–176.
24. Gu. C.-H.; Chatterjee, K.: Young. V.: Grant. D.J.W. Stabilization of a metastable polymorph of sulfamerazine by structurally related additives. J. Cryst. Growth 2002, *235* (1–4). 471–481.
25. Weissbuch. I.: Popovitz-Biro, R.: Lahav. M.: Leiserowitz. L. Understanding and control of nucleation, growth, habit, dissolution and structure of two- and three-dimensional crystals using 'tailor-made' auxiliaries. Acta Crystallogr.. B: Struct. Sci. 1995. *B51* (2). 115–148.
26. Dinnebier. R.E.; Sieger. P.; Nar, H.: Shankland. K.; David, W.I. Structural characterization of three crystalline modifications of telmisartan by single crystal and high-resolution x-ray powder diffraction. J. Pharm. Sci. 2000, *89* (11). 1465–1479.
27. Gavezzotti, A. Are crystal structures predictable? Acc. Chem. Res. 1994. 27 (10). 309–314.
28. Desiraju, G.R. Cryptic crystallography. Nat. Mater. 2002. *1* (2). 77–79.
29. Gal-ezzotti, A. The chemistry of intermolecular bonding: Organic crystals. their structures and transformations. Synlett 2002. (2). 201–214.

Porphyrin Derivatives, Functional

Mladen Žinić
Rudjer Bošković Institute, Zagreb, Croatia

INTRODUCTION

Porphyrins, named "molecules of life," constitute active sites of bacterial photosynthetic systems and important groups of enzymes such as cytochrome P450, cytochrome C. oxygen carriers (hemoglobin), etc. In supramolecular chemistry. posphyrins and metalloposphyrins are frequently used building blocks for construction of systems with energy- and electron-transfer properties aimed at preparation of artificial antenna systems, photosynthetic center mimics, photonic wires, gates. and redox switches with potential applications in supramolecular devices and machines. Due to the well-established synthetic methodologies and favorable photophysical properties, posphyrins are frequently used for construction of receptor molecules with a high degree of constitutional and chiral recognition properties. Metalloporphyrin (MP) derivatives with peripheral binding and recognition functionalities and catalytically active metal ions bound in the macrocycle endow new organic oxidation catalysts or cytochrome P450 mimics working in bilayer membranes. The advantage of coordinative binding of nitrogen and other ligands by metalloposphyrins combined with additional peripheral binding or coordination functionalities enables construction of a wealth of impressive supramolecular architectures and organized multiporphyrin arrays by self-assembly processes of predesigned supramolecular synthons. This article gives a brief outline of the supramolecular chemistry of functional porphyrins and presents some selected examples illustrating the impressive achievements associated with this topic.

PHOTOINDUCED ELECTRON AND ENERGY TRANSFER

The covalently linked or self-assembled systems constructed from free-base porphyrins or metalloposphyrins and various quenchers and related studies of excited-state energy-transfer and electron-transfer processes in such systems are a widely studied topic of contemporary supramolecular chemistry.[1,2] There are two major reasons for the exceptional interest in the topic: a challenge to synthesize artificial systems for harvesting solar energy of efficacy comparable to natural photosynthetic membranes of bacteria,"." and the more recent one, directed toward preparation of photo- or electroactive organized systems suitable for application in the fast-emerging field of nanotechnology.[5,6] The building block approach to the synthesis of covalently linked posphyrin architectures allowed "in depth" studies of the mechanisms of electronic communications such as excited-state energy transfer and ground-state hole/electron hopping.[7,8] Both processes occur predominantly via a through-bond mechanism, and their rates can be tuned over a wide range by varying structural and conformational characteristics of the linkers joining the posphyrin–acceptor dyads or by changing metal ions present in the metalloposphyrin units. The numerous studies resulted in successful design of a light-harvesting antenna (Fig. 1a), photonic wires, optoelectronic gates, and gates with redox-switching sites. Different examples of covalently linked dyads, triads, and polyads constructed, in most cases, from a free-base porphyrin as an electron donor and various electron acceptors, were prepared and studied to date. aiming to mimic the natural photosynthetic reaction center (see selected reviews: Refs. [9–12]). Major problems in the artificial systems with porphyrins involve the short-lived donor–acceptor charge-separated states disabling efficient conversion of photonic to chemical energy. Besides quinone as the biomimetic electron acceptor, which is present in natural photosynthetic systems, fullerenes were also used in combination with porphyrins. The lifetime of initial charge-separated states in fullerene-based dyads is, in general. considerably longer than in similar systems with quinones, and the photoinduced electron-transfer processes can take place in nonpolar solvents at low temperatures. Remarkably, the charge recombination reaction occurs in a fullerene-based dyad with a rate constant of ≈ 25 times lower than in a quinone-based dyad.[13] The latter is of the highest importance for designing new, more efficient, artificial systems for conversion of photonic energy. The following example describes another successful strategy based on competing donor systems. The carotenoid (C)–FbP–C_{60} molecule (Fig. 1b) presents the triad, with prolonged lifetime of the final charge-separated state and a quantum yield of 0.88. In the system, the carotenoid acts as the second electron donor unit by giving an electron to the initially formed C–FbP^{+}–C_{60}^{-}

Encyclopedia of Supramolecular Chemistry
DOI: 10.1081/E-ESMC *120019176*

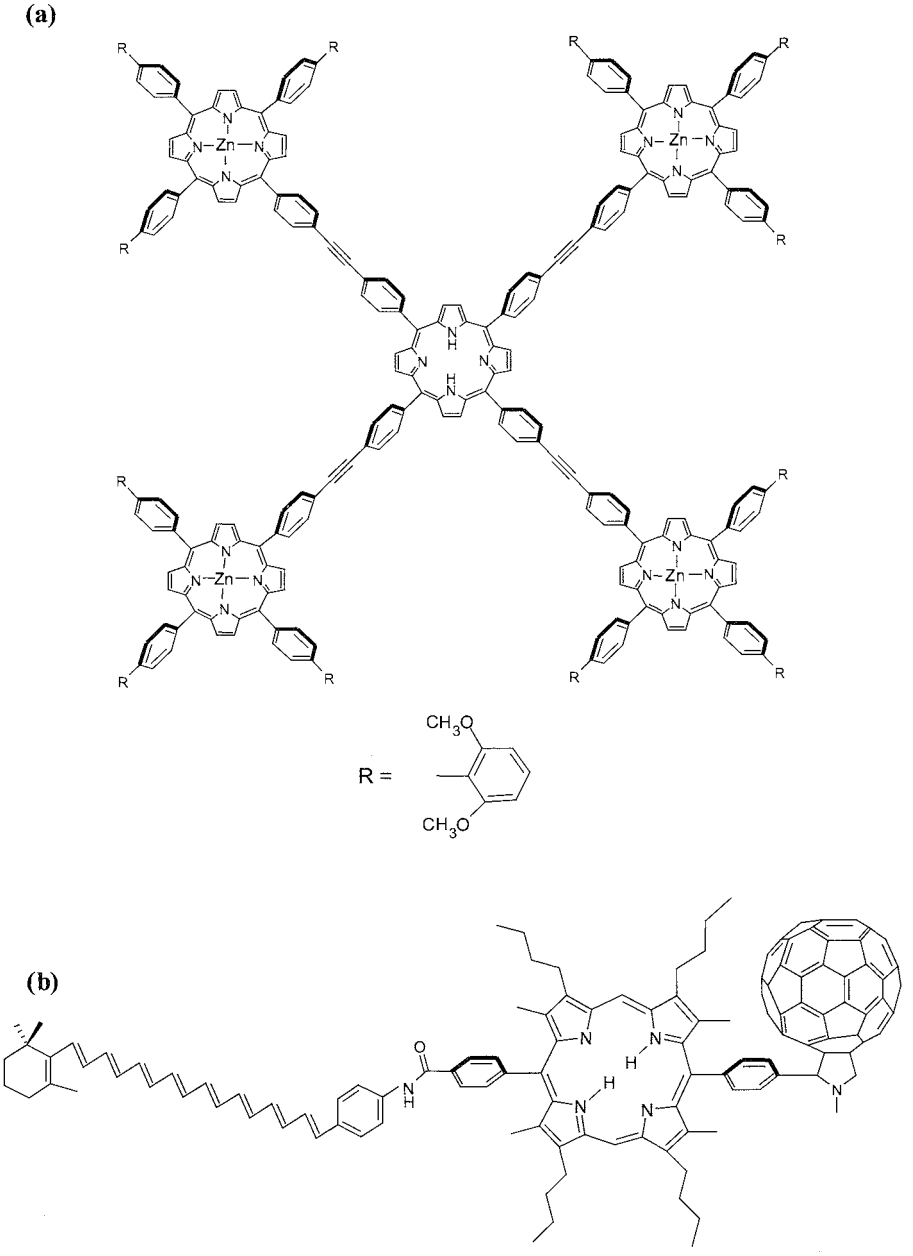

Fig. 1 (a) A star-like light-harvesting array (antenna) synthesized by modular approach (Ref. [8]). (b) The carotene-free-base porphyrin–fullerene [(C)–FbP–C_{60}] triad (Ref. [13]).

charge-separated state; this process successfully competes with C–FbP^{+}–C_{60}^{-} charge recombination and gives the final long-lived C^{+}–FbP–C_{60}^{-} charge-separated state.[14] Besides the covalently linked porphyrin–electron–acceptor molecules, there are numerous recent examples of supramolecular systems in which weak intermolecular forces hold the components in the complex. The linking forces (supramolecular bonds) in the majority of such complexes are hydrogen bonds. coordinate bonds with MP, hydrophobic, and aromatic π–π-stacking interactions or their combinations (see selected recent reviews from Refs. [3,10–12] for examples). The hydrogen-bonded and the covalently bonded dyads shown in Fig. 2a are constructed by having the ZnP as electron donor and the FeP as an electron acceptor; for the supramolecular and the covalently linked dyad. the electron-transfer rate constants, k_{ET} of 8.1×10^{9} s^{-1} and 4.4×10^{9} s^{-1} were measured. respectively. The results reveal that the double-hydrogen-bond interface between the components is more effective in mediating electron transfer than

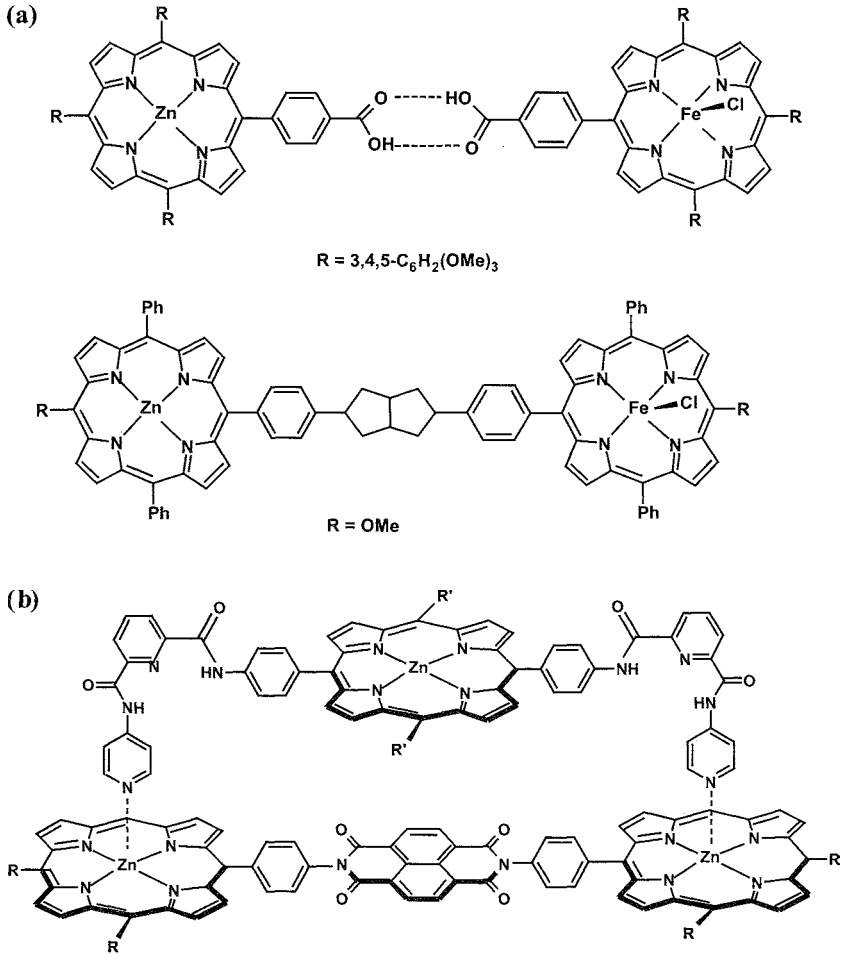

Fig. *2* (a) Hydrogen-bonded and covalently linked ZnP donor and FeP electron-acceptor dyads (Ref. [15]). (b) The self-assembled donor–acceptor system exhibiting through-space electron transfer (Ref. [16]).

is the interface of comparable length consisting of C–C σ-bonds.[15] Examples of protort-coupled electron-transfer processes were also found in the hydrogen-bonded dyads. Besides covalent and hydrogen-bond interfaces for electron transfer. it was shown that in the properly designed supramolecular coinplexes that ensure close spatial proximity of electron donor and acceptor units (Fig. 2b), the electron transfer occurs through space, or more accurately. through the solvent molecules occupying the cavity between the donor and acceptor units.[16] Electron-transfer processes were also observed to occur in the supramolecular systems of a high level of complexity, which include protein complexes or artificial bilayers. Zinc porphyrin bearing ta·o side arms with altogether eight carboxylate groups can be inserted into the horse heart apomyoglobin as an artificial prosthetic group. Such reconstituted Zn inyoglobin was shown to bind positively charged viologen. and the singlet electron-transfer process from zinc myoglobin to viologen acceptor was encountered via intermolecular interaction.[17] In another remarkable achievement. the cholenyl Mn(II)P–imidazolyl trianionic ZnP complex of linear shape was shown to span the artificial bilayer membrane locating trianionic porphyrin at the membrane surface. Cytochrome C binds the trianionic site. The electron-transfer process occurs by electron movement from cholenyl Mn(II)P via trianionic ZnP to Cytochrome C bound at the membrane surface.[18] Recently. the artificial photosynthetic reaction center became a reality; the carotenoid (C)–porphyrin–(P)–quinone (Q) triad and free quinone (Q_f) constitute a proton pump inserted in the lipid bilayer membrane of a liposome vesicle. Upon absorption of light. the charge-separated C^+–P–Q^- state is generated, which upon subsequent redox loop on Q_f produces the proton motive force across the bilayer. Remarkably. the addition of ATP synthase and ADP into this system results in production of ATP and presents a biomimetic nanoscale machine capable of converting sunlight into chemical energy.[19]

MOLECULAR RECEPTORS

A porphyrin system provides an excellent platform for construction of molecular receptors with well-defined geometry. because diverse binding functionalities can be introduced at porphyrin *meso*-positions by using well-established synthetic procedures.[20,21] The favorable spectroscopic features of porphyrins, such as the typical molar extinction coefficients in the range of 250,000 M^{-1} cm^{-1} for the Soret band (B band, $S^{o} \rightarrow S_2$) and 5000 to 35.000 M^{-1} cm^{-1} for the Q bands ($S^{o} \rightarrow S_1$) are due to the conjugation of 18π electrons and provide the advantage of easy and precise monitoring of guest-binding processes by spectroscopic methods (UV, CD. fluorescence, and NMR). The binding and photophysical properties of porphyrins can be varied by selecting metals bound in the macrocyclic ring or by increasing the number of pyrrole units, the latter giving the important family of expanded porphyrins (sapphyrins, rubyrins. and texaphyrins).[22,23] An exhaustive review of porphyrin and metalloporphyrin receptors and their binding and recognition properties toward different guest molecules (carbohydrates; amino acid derivatives, and nucleotides) was written by Ogoshi et al., and four recently published reviews are focused on zinc(II)-porphyrin receptors. allosteric and cooperative effects.[24–27] and analytical applications of porphyrin receptors.[28] Several basic structural types of porphyrin receptors were prepared to date: the monoporphyrinic receptors of the picket-fenced. strapped, and basket-handled types and acyclic and macrocyclic types incorporating two or more porphyrin units. In the vast majority of cases. the Zn(II)-5,10,15,20-tetraphenyl- or -5,10-diphenylporphyrin systems are used for the construction of receptors by introducing various binding functionalities at the ortho-positions of the phenyl rings. The tetracoordinated square planar Zn(II) serves for strong axial ligation of nitrogen base guests and also for much weaker ligation of the oxygenated ligands. Some remarkable examples of the picket-fence, strapped, and basket-handle receptors[29–31] are shown in Fig. 3a, b. and

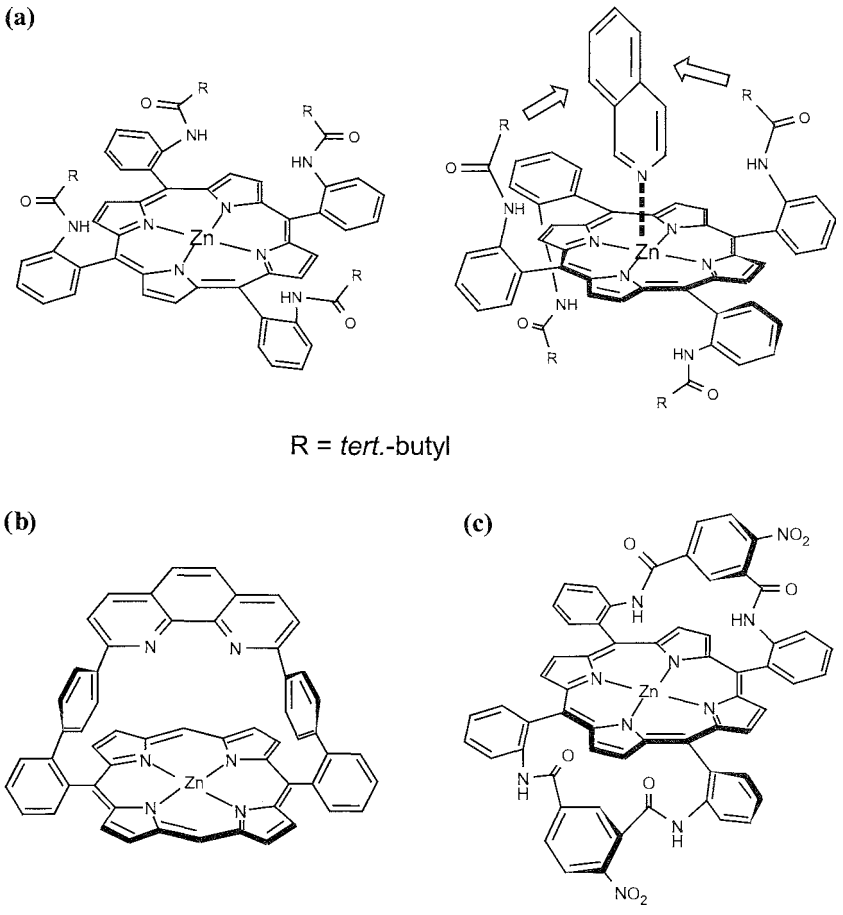

Fig. *3* (a) The α^4- (left) atropisomer and *trans*-α^2-atropisomer (right) with bound isoquinoline in the picket-fence porphyrin receptor (Ref. [29]). (b) The strapped porphyrin receptor with a rigid phenanthroline strap (Ref. [30]). (c) Chiral basket-handle receptor exhibiting a high degree of chiral recognition of amino acid derivatives (Ref. [31]).

c, respectively. The picket-fence receptor synthesized by Imai and Kyuno illustrates the importance of atropisomerism [32] the α^4-atropisomer binds isoquinoline from the open porphyrin face only by axial ligation to Zn(II) ($\Delta G^0 - 25.5$ kJ mol^{-1}), while the *trans*-α^2 isomer exhibits stronger binding ($\Delta G^0 = -34.1$ kJmol^{-1}) due to additional CH–π interactions between *tert*-butyl groups and isoquinoline.[29] A highly rigid posphyrin receptor containing phenanthroline strap strongly binds 2-methylimidazole in dichloromethane with the association constant (K_{ass}) close to 2 x 10^7 M^{-1} as a consequence of axial ligation to Zn(II) and two equivalent hydrogen bonds formed with phenanthroline nitrogens.[30] Chiral recognition of amino acid guests is achieved. by successfully designed chiral porphyrin receptors. The selected example of the chiral basket-handle receptor shows that a high degree of chiral recognition can be achieved giving the ratio of K_{ass}L/K_{ass}D of 7.5 for (–)-isomer of the receptor and L- and D-Val methyl esters.[31] An important class of receptors constructed by capping Zn(II)-porphyrins with the chiral cavity of cyclocholate was synthesized by Sanders.[33–35] The bowl-shaped receptor with four steroid units (Fig. 4a) exhibits high affinity for morphine and codeine derivatives in dichloromethane due to hydrogen bonding with four converging hydroxyl groups. The receptors capped with cyclocholate units on one (Fig. 4b) or both sides of the porphyrin were also prepared and shown to exhibit recognition of axial nitrogen bases. Remarkably. the anhydride of 3-carboxypyridine in the presence of 2,6-dichlorobenzoic acid binds and reacts inside the receptor cavity, giving selectively the monoacylated derivative of doubly capped steroid Zn(II)-porphyrin.[34,35] Exclusively aromatic κ–n interactions could be operative in some receptor–substrate complexes; the flexible macrocyclic receptor with two Zn(II)-porphyrin units (Fig. 4c) is capable of binding fullerene due to strong π–π interactions between surfaces of Zn(II)–posphyrin and fullerene. The complex is so stable that

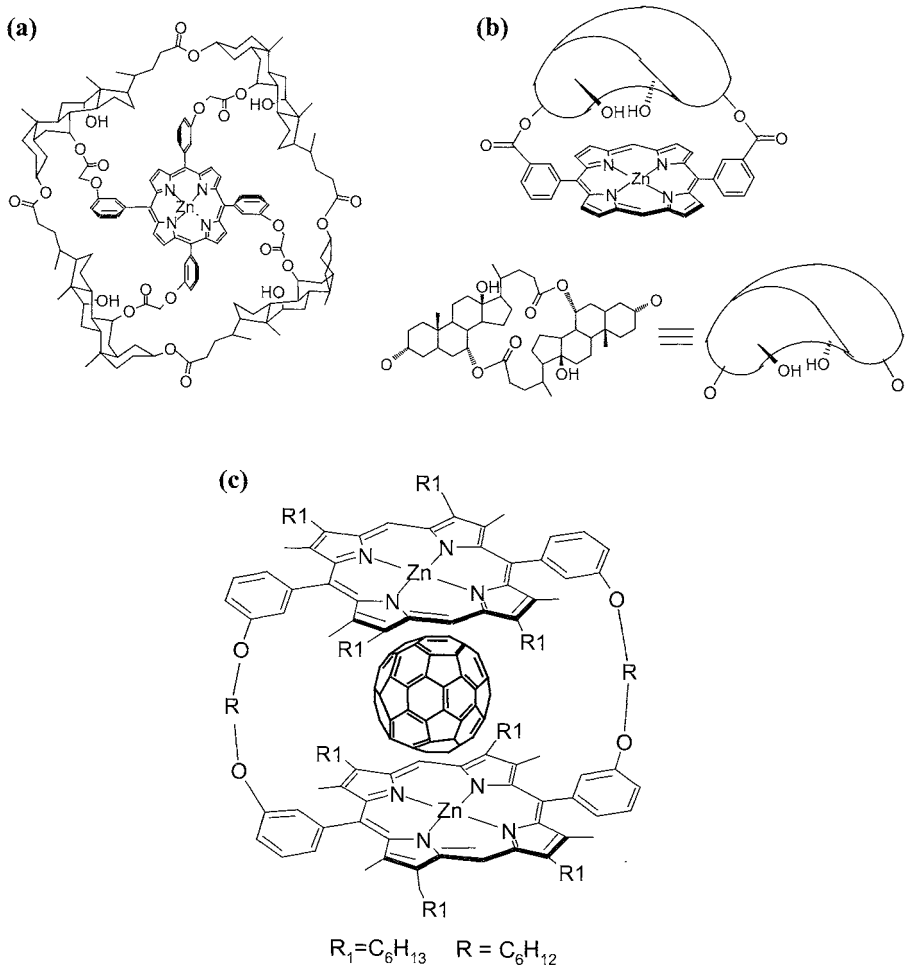

Fig. 4 (a) The bowl-shaped receptor with four steroid units (Ref. [33]). (b) Singly capped cyclocholate-porphyrin receptor (Ref. [34]) (c) Macrocyclic *bis*-ZnP receptor capable of strongly binding C_{60} (Ref. [36]).

chromatographic separation is possible.[36] Chiral as well as achiral porphyrin receptors were used as chromophoric chirality probes for amine guests. Binding of chiral amino acid in an achiral porphyrin receptor or chiral diamine with the acyclic bisposphyrin derivative results in induced circular dichroism (ICD), with the sign directly related to absolute configuration on the chiral center.[37–39]

CATALYSTS AND **ENZYME** MODELS

Cytochrome P450-dependent monooxygenases are membrane-bound enzymes that incorporate Fe(III) protoporphyrin IX as the active site and catalyze many oxidative transformations including epoxidation of alkenes and hydroxylation of alkanes and aromates. Successful preparation of porphyrin receptors with guest recognition properties inspired supramolecular chemists to consider the construction of new organic oxidative catalysts based on metalloporphyrin receptor structures with catalytically active metal ions, most frequently Fe(III) and Mn(III), bound in the posphyrin ring. Several recent reviews are available presenting in-depth coverage of this topic.[27,40–42] Some remarkably successful supramolecular oxidation catalysts are shown in Fig. 5. Chiral Fe(III)-tetraphenylporphyrin bearing two binaphtyl bridges in the α–α–β–β arrangement (Fig. 5a) gives high e.e.s (80–90%) and yields (80–95%) in catalytic epoxidation of styrene derivatives with iodosylbenzene at the rate of 40 turnovers/min [43] Taking advantage of the chiral cyclodextrin cavity for binding of lipophilic substrates. the cyclodextrin–porphyrin models were prepared;[27] the porphyrin with four cyclodextrin units prepared by Breslow[44] (Fig. 5b) is capable of binding cholesterol and alkene derivatives in a specific orientation and can perform site-specific and stereoselective hydroxylations and epoxydations of alkene derivatives in the presence of iodosylbenzene as the single oxygen donor. The Diederich group[45] prepared a water-soluble Fe(III)-porphyrin–azacyclophane catalyst (Fig. 5c) capable of oxidizing acenaphtylene to acenaphtylen-I-on in the presence of iodosylbenzene. A number of impressive self-assembled model systems of cytochrome P450 functioning in bilayer vesicle membranes were reported.[40] For example, the lipophilic Mn(III)-tetraphenylporphyrin bearing four cholesteryl units in α–α–β–β arrangement can be incorporated into DMPC bilayers, and in the presence of flavoprotein pyruvate oxydase and aniphiphilic flavine. the reductive activation of molecular oxygen is

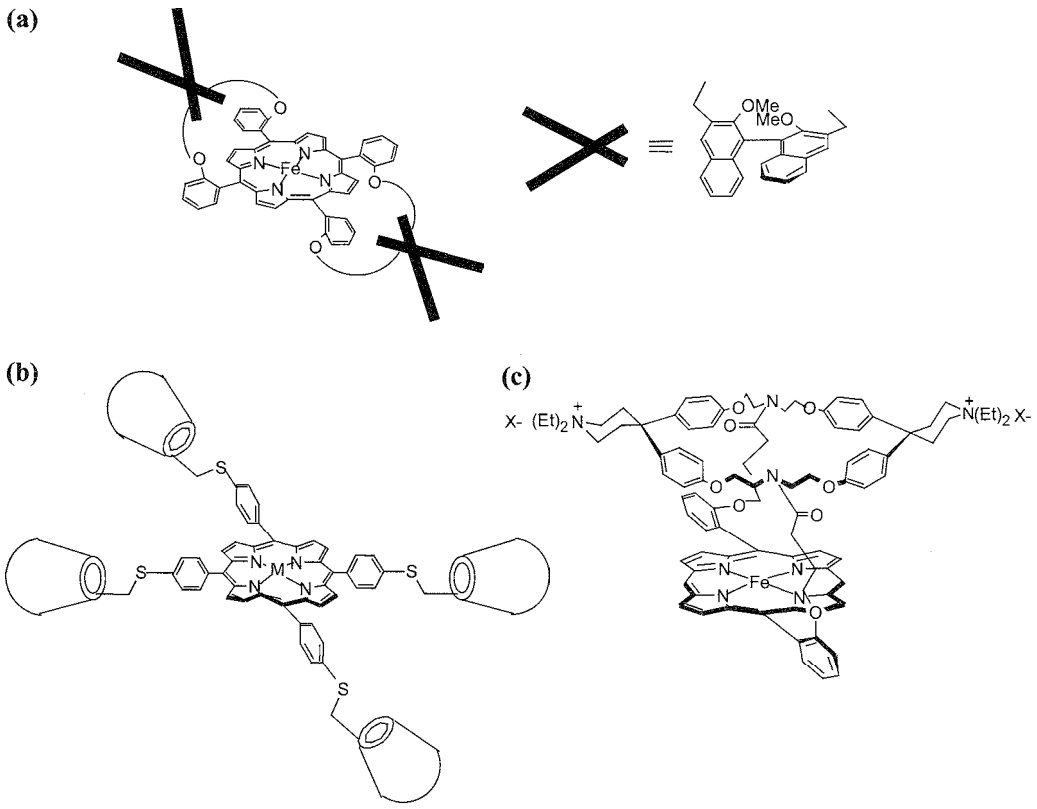

Fig. 5 (a) Chiral Fe(III)–tetraphenylporphyrin catalyst bearing two binaphtyl bridges (Ref. [43]). (b) The porphyrin catalyst with four cyclodextrin units prepared (Ref. [44]). (c) Water-soluble Fe(III)-porphyrin–azacyclophane catalyst (Ref. [45]).

achieved. The self-assembled system is capable of producing 20 mol of acetophenone per I mol of porphyrin derivative from ethylbenzene within 15 h at 30°C.[46] Also, the amphiphilic rhodiuin bipyridine complex Mn(III)-porphyrin–DHP vesicle system described by Nolte[47] is capable of oxidizing α-pinene with turnover numbers comparable to those of Cytochrome P450 at room temperatnre.

SELF-ASSEMBLED MULTIPORPHYRIN ARRAYS

Porphyrins and metalloporphyrins represent a highly advantageous class of building blocks for the construction of large functional supramolecular architectures. These architectures have potential applications as new photonic materials, molecular wires. switches, photon funnels,

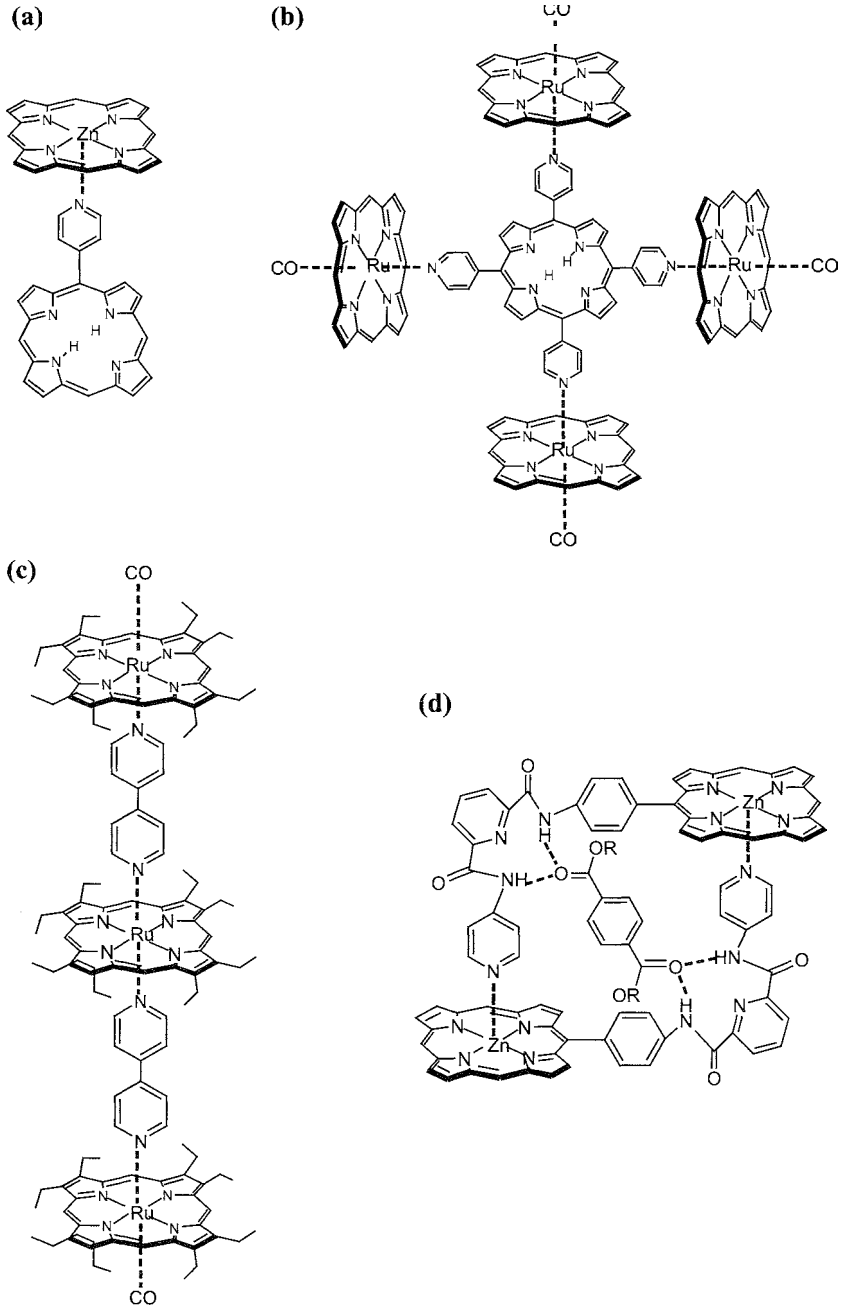

Fig. 6 Examples of stable dimer (a) and pentamer (b) prepared by coordinative assembly of free-base *meso*-pyridylporphyrins and metalloporphyrins (Refs. [52,53]). (c) A triple-decker complex with 4,4′-bipyridine (Ref. [56]). (d) The coordinatively self-assembled receptor exhibiting strong binding of terephthalic acid derivatives in chloroform (Ref. [57]).

elements for information storage, new magnetic materials, catalysts. etc., due to their favorable and tunable photophysical and redox properties and established synthetic methodologies enabling the introduction of a diversity of binding functions at the periphery of the porphyrin ring.[48] Selected recent reviews present a wealth of impressive self-assembled architectures based on porphyrin building blocks and methods of their construction.[49–51] Starting with the simplest self-assembly based on one free-base porphyrin with an attached single donor group at the periphery interacting with a metalloporphyrin having a five-coordinate metal (e.g., Zn) or a six-coordinate metal with one position occupied by a kinetically inert ligand [e.g., Ru(II) or Os(II) coordinated to CO] stable dimeric[52] to pentameric[53] porphyrin complexes could be prepared (Fig. 6a,b). In such systems, the porphyrins are mutually perpendicular, and there is no interaction between their π-systems. The UV spectra are the sum of monomer absorptions. Cyclic voltammetry confirms that there is no electrochemical communication between monomers so that they are oxidized and reduced independently. Combining the described coordination approach with covalently linked Ru(II)CO-porphyrine oligomers, Sanders succeeded in preparing large

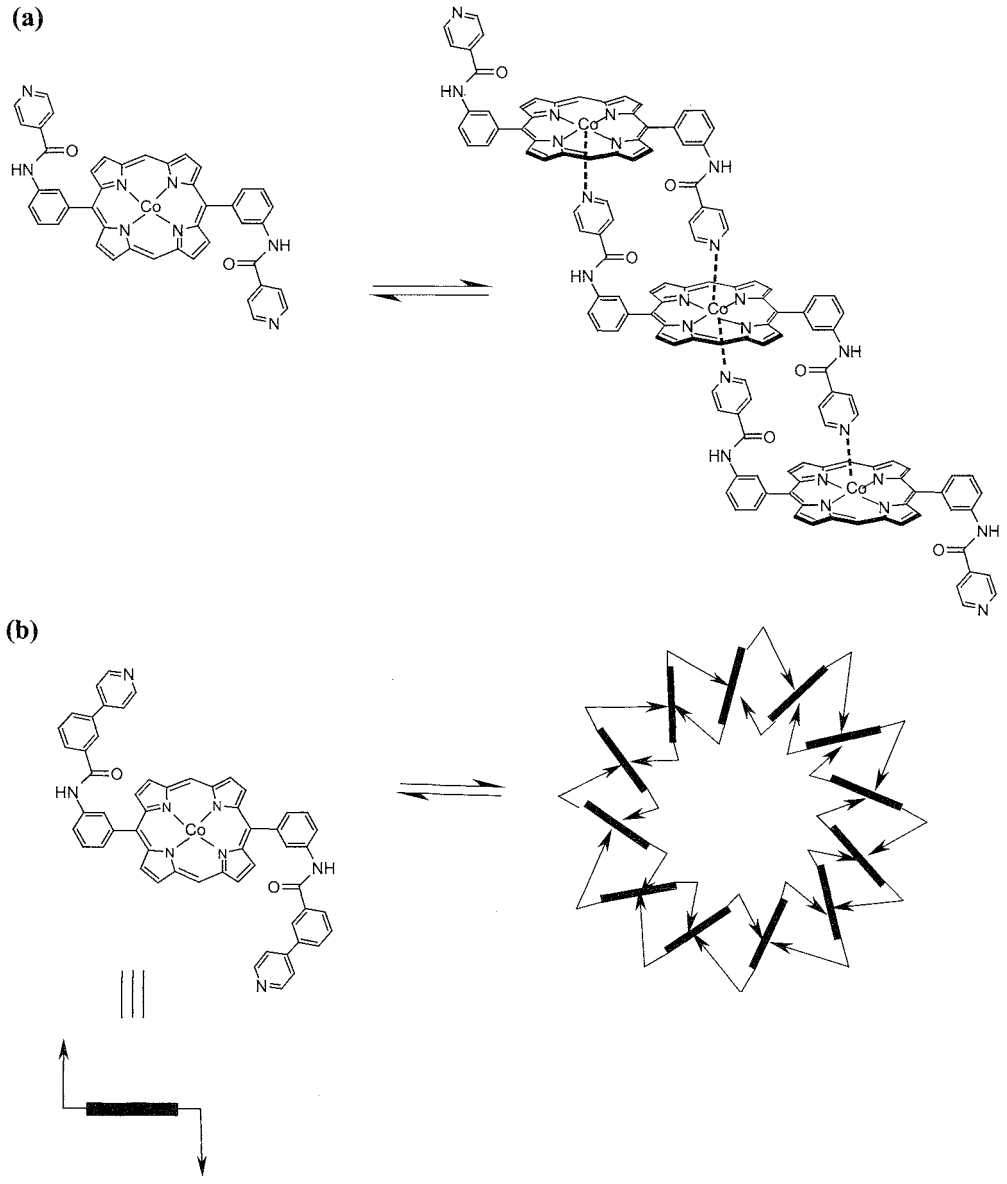

Fig. 7 Controlled coordinative self-assembly giving a linear supramolecular polymer (a) or a macrocyclic dodecamer (b) achieved by altering geometry and length of ligating arms of self-complementary porphyrin monomers (Ref. [60]).

assembled assays containing up to 21 porphyrins.[54,55] In another approach, the use of bidentate ligands with metalloporphyrins led to formation of the complexes with parallel arrangement of porphyrins: for example, the triple-decker complex with 4,4′-bipyridine (Fig. 6c) was prepared, and electrochemical studies proved that terminal porphyrins could interact with each other.[56] Diaza compounds such as 1,4-diazabicyclo[2,2,2]-octane (DABCO). pyrazine, 4.4'-bipyridine. 1,2-*bis*(4-pyridyl)-ethane, and *trans*-1,2-*bis*(4-pyridyl)ethylene were most frequently used as bidentate ligands with Ru- or Fe-porphyrins. Zn-porphyrins also interact with diaza ligands, however, giving kinetically and thermodynamically less stable complexes. The strategy based on the combination of the coordination approach with the self-complementary metalloporphyrin components possessing various binding functionalities at the periphery (hydrogen bonding, salt bridges, other metal coordination sites) endows the self-assembled receptors with a higher level of complexity, capable of binding and recognizing various guests. Impressively, the self-assembled dimer shown in Fig. 6d forms with a high association constant (K_{ass} of 2×10^8 M^{-1}) and strongly binds terephthalic acid derivatives in chloroform.[57] Organized porphyrin arrays of diverse geometries could be prepared by heterocoordination-driven self-assembly of appropriately designed porphyrin units bearing additional metal coordination sites at the periphery.[49–51] Linear supramoleclar polymers named ''shish kebab'' are formed when a bidentate ligand bridges two inetalloporphyrins with hexacoordinated metals. Supramolecular structures of this type were studied mostly with regard to their conductivity properties.[58] The Co(II)-porphyrins bearing two arms with pyridyl groups at meso-positions form supramolecular polymers by pyridine–cobalt coordination. Importantly, the Co(II)-porphyrin with a single pyridine arm can be used as a chain capping agent to control the average chain length.[59] Supramolecular self-assembly can also be controlled by tuning structural and conformational properties of the ligating arms of self-complementary porphyrin monomers. By altering the lengths and geometries of pyridine-containing arms. the process can be directed toward unidirectional self-assembly, giving linear polymers, or toward formation of a closed macrocyclic dodecarner (Fig. 7a,b).[60]

CONCLUSION

The most vivid research activity in supramolecular chemistry of functional porphyrin derivatives in the last two decades resulted in the preparation of many impressive supramolecular systems of high complexity. These include artificial light conversion systems. photonic wires. switches and gates, efficient receptor molecules exhibiting a high degree of constitutional and chiral recognition. new organic oxidation catalysts, the artificial ATP-producing nanomachine. and a diversity of remarkable supramolecular architectures possessing well-organized multiporphyrin assays. The success achieved is becoming of the utmost importance for the present and future scientific and technological activities aiming to prepare supramolecular systems of an even higher level of structural and functional complexity, necessary for the development of nanotechnology. The utmost advantage of functional porphyrin derivatives as building blocks relies on their favorable photophysical properties, the advantage of using coordinative self-assembly, the acceptable complexity of synthetic methods that enable introduction of a variety of additional binding functionalities, and the possibility of modifying and fine-tuning their propertiesby an almost unlimited variation of metals bound inthe macrocyclic ring and binding functionalities at their periphery.

ARTICLES OF FURTHER INTEREST

Biological Models and Their *Characteristics*, p. 101
Emergence of Life, p. 528
Energy and Electron *Transfer in Supramolecular Systems*, p. 535
Enzyme Mimics, p. 546
Hemoglobins: O_2 Uptake and Transport, p. 636
Molecular Logic Gates, p. 893
Molecular-Level Machines, p. 931
Phthalocyanines, p. 1069
π–π Stacking: Theory and Scope, p. 1076
Porphyrin-Based Clathrates, p. 1150
Self-Assembly: Definition and Kinetic and Thermodynamic Considerations, p. 1248
Self-Assembly: Terminology, p. 1263
Strict *Self-Assembly* and *Self-Assembly with Covalent Modifications*, p. 1372
Supramolecular Photochemistry, p. 1434
Vitamin B_{12} and Heme Models, p. 1569

REFERENCES

1. Lehn. J.M. *Supramolecular Chemistry. Concepts and Perspectives*; VCH: Weinheim. 1995.
2. Balzani. V.: Scandola. F. *Supramolecular Photochemistry*; Ellis Horwood Limited: New York. 1991.
3. Ward, M.D. Photo-induced electron and energy transfer in non-covalently bonded supramolecular assemblies. Chem. Soc. Rev. 1997, 26. 365.

4. Kurreck, H.: Huber, M. Model reactions for photosynthesis-photoinduced charge and energy transfer between covalently linked porphyrin and quinone units. Angew. Chem.. Int. Ed. Engl. 1995. 34, 849.
5. Liu, C.-Y.; Bard. A.J. Optoelectronic properties and memories based on organic single-crystal thin films. Acc. Chem. Res. 1999, 32. 235.
6. Li. F.: Gentemann. S.; Kalsbeck. W.A.: Seth. J.; Lindsey, J.S.: Holten. D.: Bocian, D.F. Effects of central metal ion (Mg, Zn) and solvent on singlet excited-state energy flow in porphyrin-based nanostructures. J. Mater. Chem. 1997, 7. 1245.
7. Holten, D.; Bocian. D.F.: Lindsey. J.S. Probing electronic communication in covalently linked multiporphyrin arrays. A guide to the rational design of molecular photonic devices. Acc. Chem Res. 2002, 35. 57.
8. Wagner. R.W.; Johnson. T.E.; Lindsey. J.S. Soluble synthetic multi-porphyrin arrays. 1. Modular design and synthesis. J. Am. Chem. Soc. 1996. *118*, 11166.
9. Gust. D.: Moore, T.A.: Moore. A.L. Mimicking photosynthetic solar energy transduction. Acc. Chem. Res. 2001, *34*, 40.
10. Chambron, J.-C.: Collin. J.-P.; Dalbavie, J.-O.; Dietrich-Buchecker, C.O.: Odobel. V.H.C.; Solladie. N.: Sauvage, J.-P. Rotaxanes and other transition metal-assembled porphyrin arrays for long-range photoinduced charge separation. Coord. Chem. Rev. 1998. *178–180*. 1299.
11. Hayashi, T.: Ogoshi. H. Molecular modelling of electron transfer systems by noncovalently linked porphyrin–acceptor pairing. Chem. Soc. Rev. 1997. *26*, 355.
12. Guldi. D.M. Fullerene–porphyrin architectures; photosynthetic antenna and reaction center models. Chem. Soc. Rev. 2002. 31. 22.
13. Gust. D.: Moore. T.A.: Moore. A.L. Photochemistry of supramolecular systems containing C_{60}. J. Photochem. Photobiol., B: Biol. 2000. *58*. 63.
14. Kuciauskas. D.; Liddell. P.A.; Lin. S.; Stone. S.G.: Moore. A.L.; Moore. T.A.: Gust, D. Photoinduced electron transfer in carotenoporphyrin–fullerene triads: Temperature and solvent effects. J. Phys. Chem. 2000, 140, 4307.
15. DeRege, P.J.F.; Williams, S.A.; Therien. M.J. Direct evaluation of electronic coupling mediated by hydrogen bonds — Implications for biological electron transfer. Science 1995. *269*. 1409.
16. Hunter, C.A.; Hyde. R.K. Photoinduced energy and electron transfer in supramolecular porphyrin assemblies. Angew. Chem.. Int. Ed. Engl. 1996. *35*. 1936.
17. Hayashi, T.: Takimura, T.; Ogoshi. H.J. Photoinduced singlet electron transfer in a complex formed from zinc myoglobin and methyl viologen — Artificial recognition by a chemically modified porphyrin. J. Am. Chem. Soc. 1995, 117. 11606.
18. Lahiri, J.; Fate, F.D.; Ungashe, S.B.: Groves. J.T. Multiheme self-assembly in phospholipid vesicles. J. Am. Chem. Soc. 1996. 118. 2347.
19. Steinberg-Yfrach, G.: Rigaud. J.-L.; Durantini. E.N.; Moore, A.L.; Gust, D.; Moore, T.A. Light-driven production of ATP catalysed by F_oF_1–ATP synthase in an artificial photosynthetic membrane. Nature 1998. 392. 479.
20. *The Porphyrin Handbook, Vol.* I. *Synthesis and Organic Chemistry*; Kadish, K.M., Smith. K.M., Guilard. R.. Eds.; Academic Press: San Diego, 2000.
21. Slianmugathasan. S.: Edwards, C.: Boyle, R.W. Advances in modern synthetic porphyrin chemistry. Tetrahedron 2000, *56*. 1025.
22. Sessler. J.L. Expanded Porphyrins. In *The Porphyrin Handbook*: Kadish. K.M.. Smith. K.M., Guilard, R., Eds.; Academic Press: San Diego, 2000; Vol. 2.
23. Sessler, J.L.: Hemmi, G.; Mody, T.D.; Murai, T.: Burrell, A.; Young, S.W. Texaphyrins: Synthesis and applications. Acc. Chem. Res. 1994, 27. 43.
24. Ogoshi. H.: Mizutani, T.: Hayashi, T.; Kuroda. Y. Porphyrins and Metalloporphyrins as Receptor Models in Molecular Recognition. In *The Porphyrin Handbook*; Kadish. K.M., Smith, K.M., Guilard, R.. Eds.: Academic Press: San Diego, 2000: Vol. 6. 279.
25. Weiss. J. Zinc(II)-porphyrin receptors in multi-point molecular recognition: Recent progress. J. Incl. Phenom. Macrocycl. Chem. 2001. 40. 1.
26. Shinkai. S.; Ikeda, M.; Sugasaki. A.; Takeuchi. M. Positive allosteric systems designed on dynamic supramolecular scaffolds: Toward switching and amplification of guest affinity and selectivity. Acc. Chem. Res. 2001, 34. 494.
27. Shinkai. S.: Robertson, A. Cooperative binding in selective sensors. catalysts and actuators. Coord. Chern. Rev. 2000, 205. 157.
28. Zaruba, K.: Setnička, V.; Charvatova, J.: Rusin, O.: Tomankova. Z.; Hrdlička, J.: Sykora, D.; Kral. V. Analytical application of oligopyrrole macrocycles. Collect. Czech. Chem. Commun. 2001, 66. 693.
29. Imai, H.: Kyuno. E. Base binding to zinc picket fence porphyrins. Attractive intramolecular interactions in organic solvents. Inorg. Chem. 1990. 29. 2416.
30. Froidevaux. J.: Ochsenbein. P.: Bonin. M.; Schenk. K.; Maltese, P.: Gisselbrecht. J.-P.: Weiss. J. Side selection of the fifth coordinate with a single strapped zinc(II) porphyrin host — Full characterization of two imidazole complexes. J. Am. Chem. Soc. 1997. 119. 12362.
31. Kuroda. Y.; Kato, Y.: Higashioji, T.; Hasegawa, J.; Kawanami, S.: Takahashi, M.; Shiraishi, N.; Tanabe, K.: Ogoshi. H. Chiral amino acid recognition by a porphyrin based artificial receptor. J. Am. Chem. Soc. 1995, *117*. 10950.
32. Collman. J.P.: Gagne, R.R.: Reed. C.A.: Halbert. T.R.; Lang, G.; Robinson, W.T. "Picket fence porphyrins." Synthetic models for oxygen binding hemoproteins. I. Am. Cheni. Soc. 1975. 97. 1427.
33. Bonar-Low. R.P.: Mackay, L.G.; Sanders. J.K.M. Morphine recognition by a porphyrin cyclocholate molecular bowl. J. Chem. Soc.. Chern. Commun. 1993. 456.
34. Bonar-Low. R.P.: Sanders. J.K.M. Synthesis. binding properties and self-functionalization of a steroid capped porphyrin. J. Chem. Soc.. Chem. Commun. 1991. 574.
35. Bonar-Low, R.P.: Mackay, L.G.; Walter, C.J.; Marvaud, V.: Sanders, J.K.M. Towards synthetic enzymes based on

porphyrins and steroids. Pure Appl. Chem. 1994. 66, 803.
36. Tashiro, K.; Aida, T.: Zheng. J.-Y.; Kinbara, K.: Saigo, K.; Sakamoto, S.; Yamaguchi, K. A cyclic dimer of metalloporphyrin forms a highly stable inclusion coniplex with C-60. J. Am. Chem. Soc. 1999. 121. 9477.
37. Mizutani, T.; Ema, T.: Yoshida, T.; Kuroda, Y.; Ogoshi, H. Recognition of α-amino acid esters by zinc porphyrin derivatives via coordination and hydrogen bonding interactions. Evidence for two-point fixation from thermodynamic and induced circular dichroism spectroscopic studies. Inorg. Chern. 2993, *32.* 2072.
38. Mizutani, *T.;* Ema, T.; Yoshida, T.: Renn, T.: Ogoshi, H. Mechanism of induced circular dichroism of amino acid ester–porphyrin supramolecular systems—Implications to the origin of the circular dichroism of hemoprotein. Inorg. Chern. 1994, *33,* 3558.
39. Huang, *X.;* Rickman, B.H.; Borhan. B.: Berova. N.; Nakanishi. K. Zinc porphyrin tweezer in host–guest complexation—Determination of absolute configurations of diamines, amino acids, and amino alcohols by circular dichroism. J. Am. Chem. Soc. 1998. *120.* 6158.
40. Feiters. M.C.: Rowman, A.E.; Nolte, R.J.M. From simple to supramolecular cytochrome P450 mimics. Chem. Soc. Rev. 2000, 29. 375.
41. Murakami, U.; Kikuchi, J.; Hisaeda. Y.; Hayashida, O. Artificial enzymes. Chem. Rev. 1996. 96. 721.
42. Gonsalves, A.M.d'A.R.; Pereira. M.M. State of the art in development of biomimetic oxidation catalysts. J. Mol. Catal.. A: Cheni. 1996, *113,* 209.
43. Collman, J.P.: Wang. Z.: Straumanis. A.; Quelquejeu. M. An efficient catalyst for asymmetric epoxydation of terminal olefins. J. Am. Chem. Soc. 1999, 121. 460.
44. Breslow. R.: Huang. Y.; Zhang. X. Selective catalytic hydroxylation of a steroid by artificial cytochrome P450 enzyme. J. Am. Chem. Soc. 1997. *199.* 4535.
45. Benson, D.R.: Valentekovich. R.; Diederich, F. Cyclophane catalysts. A cyclophane containing bridging porphyrin as a model for cytochrome P450 enzyme. Angew. Chem., Int. Ed. Engl. 1990. 29. 191.
46. Groves. J.T.; Ungashe. S.B. Biocompatible catalysis. Enzymic reduction of metalloporphyrin catalysts in phospholipid bilayers. J. Am. Chem. Soc. 1990, *112,* 7796.
47. Schenning. A.P.H.J.: Lutje Spelberg, J.H.: Hubert. D.H.W.; Feiters, M.C.; Nolte. R.J.M. Control of aggregation and tuning of the location of porphyrins in synthetic membranes as mimics for cytochrome P450. Langmuir 1996. *12.* 1572.
48. The *Porphyrin* Handbook, Vol. *6,* Applications: Past, Present and *Future;* Kadish. K.M., Smith. K.M., Guilard, R., Eds.: Academic Press: San Diego, 2000.
49. Baldini, L.; Hunter, C.A. Self-Assembly of Porphyrin Arrays. In Advances *in* Inorganic *Chemistry;* Elsevier Science: USA, 2002; Vol. 53. 213.
50. Wojaczynski. J.: Latos-Grazynski. L. Poly- and oligometalloporphyrins associated through coordination. Coord. Chem. Rev. 2000, 204, 113.
51. Sliwa, W.: Mianowska, B. Metalloporphyrin arrays. Transit. Met Chem. 2000, 25. 491.
52. Fleischer, E.B.: Shachter. A.M. Coordination oligomers and a coordination polymer of zinc tetraarilporphyrins. Inorg. Chem. 1991, *30,* 3763.
53. Kariya. *N.;* Imamura. T.; Sasaki, Y. Synthesis, characterization, and spectral properties of new perpendicularly linked osmium(III) porphyrin. Inorg. Chem. 1997, 36. 833.
54. Mak, C.C.; Bampos, N.; Sanders. J.K.M. Ru(II)-centred porphyrin pentamers as coordination building blocks for large porphyrin arrays. J. Chem. Soc., Chem. Commun. 1999. 1085.
55. Darling, S.L.: Mak, C.C.: Bampos, N.; Feeder, N.: Teat, S.J.: Sanders, J.K.M. A combined covalent and coordination approach to dendritic multiporphyrin arrays based on ruthenium(II) porphyrins. New J. Chem. 1999, *23,* 359.
56. Endo, A.; Tagami. U.: Wada, Y.; Saito. M.; Shimizu, K.: Sato, G.P. Triple-decker trinuclear porphinatoruthenium-(II) complexes bridged with pyrazine or 4,4′-bipyridine preparation and electrochemical oxidation. Chem. Lett. 1996. 243.
57. Hunter. C.A.; Sarson, L.D. Self-assembly of a dimeric porphyrin host. Angew. Chem.. Int. Ed. Engl. 1994, 33. 2313.
58. Hanack, M.; Deger, S.; Lange, A. Bisaxially coordinated macrocyclic transition metal complexes. Coord. Chem Rev. 1988, *83.* 115.
59. Michelsen, U.; Hunter, C.A. Self-assembled porphyrin polymers. Angew. Chem.. Int. Ed. Engl. 2000. 39, 764.
60. Haycock, R.A.: Hunter; C.A.; James, D.A.; Michelsen, U.; Sutton. L.R. Self-assembly of oligomeric porphyrin rings. Org. Lett. 2000. *2,* 2435.

Porphyrin-Based Clathrates

Israel Goldberg
Tel Aviv University, Tel Aviv, Israel

INTRODUCTION

The term "clathrate," in its modern version, is defined in the Oxford and Webster's English Dictionaries as a compound formed by the inclusion of chemical species of one kind (guests) within the crystal lattice (host) constructed by molecules or ions of another kind. An effective building block of such host lattice is often characterized by noncomplementary molecular shape or by specific coordination or molecular recognition features that prevent a compact intermolecular organization of these entities in the condensed crystalline phase. The favored aggregation of the host components in the form of an open lattice, along with the requirement to minimize void space in solids, provide the driving force for their cocrystallization with additional species that are present in the crystallization environment. Inclusion of a guest or solvent in an ordered crystalline lattice (i.e., formation of clathrates or solvates) is a commonly observed, though less-frequently predictable; phenomenon in the formation of organic and inorganic crystals. It was generally considered a by-product of the crystallization process and deserved little attention. However, a systematic study of clathrate chemistry, which started with the pioneering publication by H. M. Powell in 1948,[1] revealed a number of host compounds with consistently high propensity to yield clathrate materials with interesting properties. These include, for example, the β-quinol, tri-o-thymotide, urea and thiourea. choleic acids, Dianin's compound. cyclodextrins. and a number of other species, some of which are discussed in other entries of this Encyclopedia *of Supramolecular Chemis-tn*. More recent investigations revealed and characterized the fascinating clathrate features of the *meso*-tetraaryl derivatives of porphyrins and metalloporphyrins. The porphyrin platform provides excellent building blocks for the design of porous solids with tunable nanosized pores (typically between 0.5–2.0 nm in diameter) and a wide variety of new solid receptors for the effective inclusion or clathration of other species. With the rapid development of the chemistry of the intermolecular bond in the last two decades, the search after, and deliberate design of, new clathrate solids with attractive properties lies in the focus of materials science.

THE UNIQUE FEATURES OF THE TETRAPHENYLPORPHYRIN SYSTEM

The porphyrin macrocycle is one of the most widely studied chemical systems in solution and in the solid state due to its high relevance to catalysis, as well as to electron- and energy-transfer processes and related biological functions. It is characterized by an extensive conjugation, a nearly square-planar symmetry, and a considerable thermal as well as oxidative stability. The synthetic compound is most readily available in the forms of alkyl or aryl derivatives, with the corresponding aliphatic or aromatic substituents attached to the *beta-* or *meso*-positions of the macrocycle, respectively. In this context, the 2,3,7,8,12,13,17,18-octaethylporphyrin and the 5,10,15,20-tetraphenylporphyrin (TPP) provide leading examples. The latter is characterized by a more rigid. flat conformation and remarkable structural robustness, particularly when given in its metallated MTPP form (Fig. 1). Insertion of a bivalent metal ion within the porphyrin core is associated with elimination of the two inner *N*-pyrrole protons, yielding a neutral species; when metals at other oxidation states are applied, the presence of suitable counterions in the crystal lattice is required to balance the charge. The peripheral aryl groups substituted at the *meso* positions of the porphyrin macrocycle are oriented in a roughly perpendicular manner with respect to the central aromatic core and introduce roughness and the desired noncomplementary packing features to the molecular shape of this unit. Then, the coordination properties of the metal entity in the center of the porphyrin ring, provide an element of "programming." by allowing association through coordinative metal–ligand interactions with additional species along the axial directions. Fmther activation of the lipophilic TPP framework can be achieved readily by substituting polar functional groups on it during the porphyrin synthesis. In a typical system, functionalities with coordination or hydrogen-bonding capacity are symmetrically placed at the peripheral positions of the aryl rings and may control, to a considerable extent: the intermolecular organization of the TPP units along the lateral directions. Representative examples include replacement of the phenyl substituents by 4-pyridyl groups [to yield tetra(4-pyridyl)porphyrin—TPyP], and

Encyclopedia of Supramolecular Chemistry
DOI: 10.1081/E-ESMC 120013478

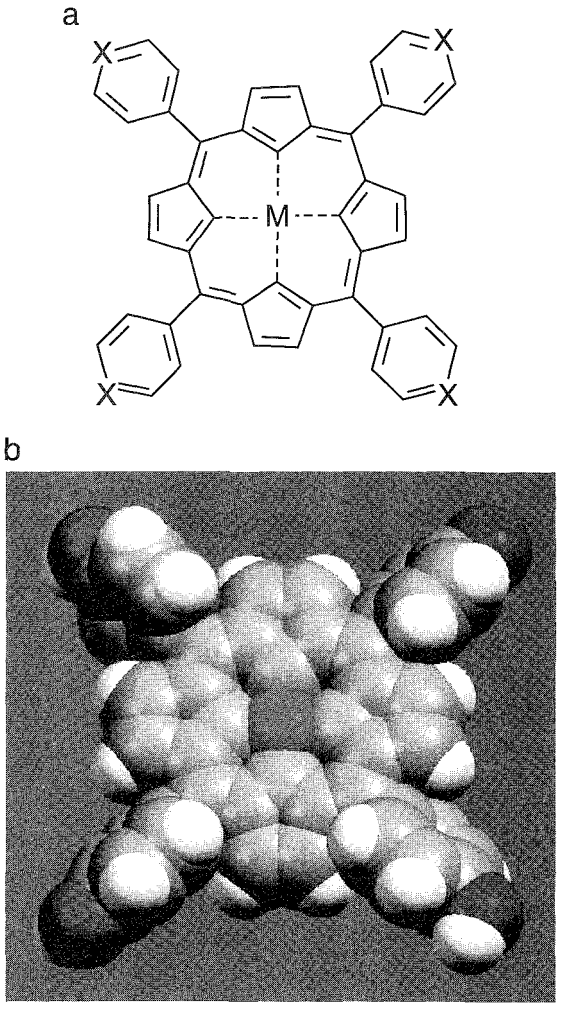

Fig. 1 (a) The tetraarylmetalloporphyrin building block. For MTPP, MTPyP, and MTCPP, X=C—H, N: and C—COOH, respectively. M represents a metal ion inserted into the porphyrin core (M=H_2 for the free-base porphyrin). (b) Space-filling model of the MTPP moiety substituted with OH polar groups at the 4-position of the peripheral phenyl ring. The M and OH sites symbolize here the molecular recognition features active in directional interactions with the surrounding species. Note that the aryl groups are oriented nearly perpendicular to the central porphyrin macrocycle. Fig 1b and all the following illustrations of molecular and crystal structures were produced with the aid of the relevant crystallographic information freely available from the Cambridge Crystallographic Database.[2] (View this art in color *at www.dekker.com.*)

substitution of the phenyl rings at their 4-positions by carboxylic [to yield tetra(4-carboxyphenyl)porphyrin—TCPP] or hydroxylic (Fig. 1b) functions. The above features make the TPPs versatile and attractive building blocks (termed "tectons") for the assembly of open multi-porphyrin lattice arrays through diverse interaction motifs/molecular recognition algorithms (termed "synthons").

THE "PORPHYRIN SPONGES" AS TYPICAL CLATHRATE SYSTEMS

Numerous publications in the scientific literature confirm that the TPP and MTPP molecules provide remarkably attractive building blocks for the formulation of lattice clathrates. Due to a poor packing efficiency in three dimensions, the vast majority of their crystal structures was found to contain solvate/guest molecules incorporated within the porphyrin lattice. These clathrate structures, which are stabilized primarily by weak dispersion forces, form readily. The large base of available structural information with major contributions from the groups of Scheidt and Strouse now amounts to several hundreds of TPP-based crystal structures.[2] The TPP clathrates were structurally systematized by Strouse and coworkers.[3–5] It was observed that in many of the materials studied, the porphyrin host structure is strongly conserved in two dimensions. These materials could be characterized in terms of an intercalation-type pattern in which corrugated sheets of stacked porphyrin molecules are interspaced by sheets of the included guest species (Fig. 2). Two main features characterize the intermolecular architecture in the

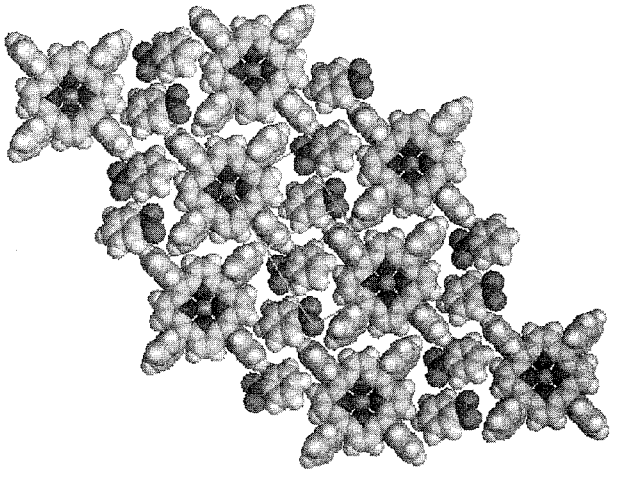

Fig. 2 A typical "porphyrin sponge" clathrate formed by MTPP, with nitrobenzene as the included guest, viewed perpendicular to the porphyrin plane.[3–5] Note the alternating arrangement of the MTPP and the nitrobenzene species. In the third dimension, the clathrate structure is characterized by an offset-stacked arrangement of such mixed porphyrin-guest layers. The interporphyrin organization in the "porphyrin sponges" expands upon the inclusion of larger guest species. (View this art in color at www.dekker.com.)

layered TPP-based crystalline solids: 1) An offset stacking of the square-planar aromatic molecules along a direction normal to the porphyrin plane at regular intervals (ca. 4.0–5.0 Å). This pattern appears to be a fundamental property of the porphyrin–porphyrin interaction required to optimize van der Waals stabilization in these solids. 2) Face-to-face as well as edge-to-face interaction modes between the peripheral phenyl rings within the layered arrangement of the TPP frameworks in a direction parallel to the porphyrin plane (Fig. 2). The intralayer interaction mode between the phenyl rings is similar to that observed in solid benzene and other structures containing aryl derivatives.

The lack of specific interactions between the porphyrin building blocks (other than by dispersion) allows for little constrained expansion of the porphyrin arrays by inclusion of guest components of versatile nature, size, and shape in different molar ratios, giving rise to the classification of these clathrate materials as "porphyrin sponges."[3–5] The guests included in such TPP clathrates vary from small species such as methanol and water, through medium-size aromatic moieties or metallic complexes such as anthracene and ferrocene, to the very large C_{60} and C_{70} fullerene entities.[6,7] In the latter case, the interaction of the curved π surface of a fullerene with the planar π surface of a porphyrin macrocycle were found to stabilize unique supramolecular porphyrin/fullerene aggregation modes (Fig. 3). Smaller guests (e.g., nitrobenzene or pyrene) can also associate strongly or weakly with the porphyrin building blocks through coordination to the metal center or by π overlapping the delocalized porphyrin core. The structures of these clathrates tend to be centrosymmetric due to the high symmetry of the individual tecton unit, with symmetric disposition of the guest components with respect to the porphyrin core. Potential applications of the porphyrin sponges include molecular separations by occasionally preferential inclusion of a given component from solvent mixtures. and controlled guest release of volatile organics from the porphyrin lattice voids.[3–5] A practical example of the latter in the area of pest control involves incorporation and slow release of fly sex pheromones.[5]

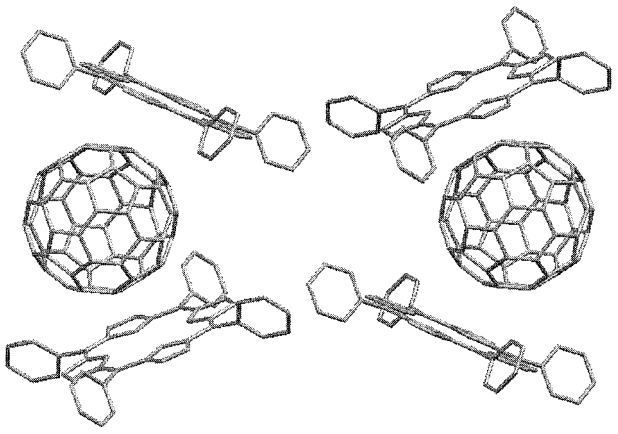

Fig. 3 Characteristic inclusion mode of Buckminsterfullerenes (C_{60} is shown) within the crystal lattice of TPP.[6,7] (*View this art in color at www.dekker.com.*)

FROM "PORPHYRIN SPONGES" TO THE "PORPHYRIN SIEVES" CONCEPT

It is well known that the intermolecular organization in organic solids usually reflects molecular recognition features (i.e., a scheme of specific and directional interactions) between the component species.[8,9] In the last decade, this paradigm was also applied effectively to the porphyrin-based solids, by activating the porphyrin framework, on its periphery, with polarized aryl groups. It involved the use of diverse molecular recognition algorithms to modify and direct the spontaneous buildup of the porphyrin lattice,[10–12] leading to more rigidly assembled molecular arrays and to porphyrin-lattice architectures with better-defined dimensionality than that in the common porphyrin clathrates (see above). For example, the addition of functional substituents at the four peripheral phenyl groups, capable of forming specific directional noncovalent links with the neighboring building blocks, allows directed aggregation of the porphyrin species in the form of porous layered networks. On the other hand. the introduction of polar groups capable of axial ligation to metal ions placed in the porphyrin center enhances formation of multiporphyrin oligomers and polymers by axial coordination of one porphyrin species to the metal centers of the neighboring moieties. Formation of other kinds of enforced supramolecular porphyrin arrays was achieved by the use of external auxiliaries that may readily associate with the functional groups of several neighboring units at the same time. This includes external metal ions and organic ligands that can mediate extended connectivity by coordinating to, and linking between, the metal centers of the peripheral functional groups of adjacent metalloporphyrins. A combined expression of the various molecular recognition algorithms along the lateral as well as axial directions in the same structure represents the most desirable approach to the design and construction of multiporphyrin architectures with high structural integrity. As opposed to the sponge character of the simple porphyrin-based clathrates, which are little sensitive to the nature and size of the guest component (see above), the intermolecularly linked lattices based on the functionalized porphyrin building

blocks are characterized by a better-defined pore structure and guest selectivity features.

REALIZATION OF CLATHRATES WITH ENFORCED PORPHYRIN LATTICE MOTIFS

Different types of lattice clathrates based on two-dimensionally or three-dimensionally interconnected posphyrin units were developed. As mentioned earlier, the use of peripherally substituted TPPs dictates, in many cases, the formation of open-layered porphyrin assemblies (β-molecular networks) sustained by lateral interactions between adjacent tecton units. In the crystal, these layers are arranged in an offset-stacked manner. The presence of intra- as well as interlayer voids drives incorporation of suitably sized guest components into the lattice during crystallization. Formulations of such flat-layered porphyrin anays can be effected by direct dipolar attractions[10] and by multiple hydrogen bonds'"' between adjacent posphyrin units. Depending on the type of the functional groups involved in these interaction synthons, the observed widths of the guest-accessible open space within the porphyrin layers may vary from 0.4 nm (with halogen and hydroxyl substituents) to 1.O–1.5 nm (with nitrile and carboxylic substituents). An example of a molecular-sieve-type structure coinposed of hydrogen-bonded two-dimensional porphyrin layers in which the flat networks stack in an almost overlapping manner along the normal direction at an average interlayer distance of 4.7 Å is illustrated in Fig. 4. The posphyrin lattice in this material occupies less than 40% of the crystal volume and contains 1.5 nm-wide guest-accessible channels propagating through the crystal. It is perfectly suited for guest transport applications.

Structures based on stacked porphyrin networks with larger interporphyrin voids are difficult to obtain. When the size of the individual building block is smaller than that of the interporphyrin cavity, interpenetration of the Rat networks occurs to partly fill the void space.[14] The crystallization template also plays an important role in directing the preferred intermolecular organization, when the functional porphyrin units can self-assemble in more than one mode.[11,12] Formation of clathrate structures, which consist of open-layered porphyrin assemblies aided by external metal ion auxiliaries. is also feasible.[15–17] The metal ions can coordinate to. and bridge between, theperipheral functional groups (e.g., pyridyl. hydroxyphenyl, or carboxyphenyl) of neighboring porphyrins, thus yielding robust two-dimensional structural motifs with open voids conveniently accommodated by suitable guest species. Conespondingly. it is possible to control to a considerable extent the porosity of the porphyrin layers. and thus the nature of guest components preferably

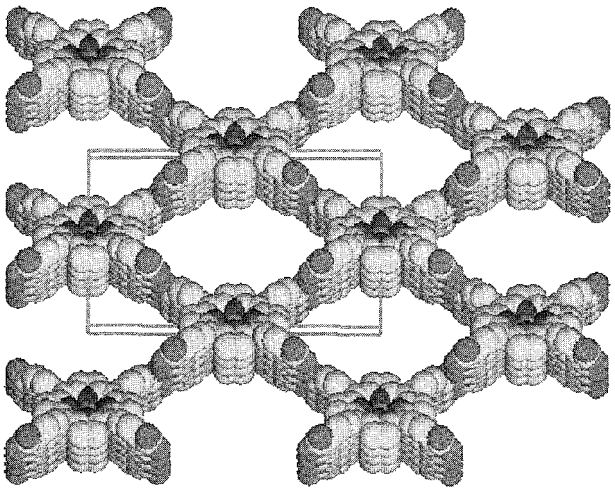

Fig. 4 Porphyrin-sieve-type clathrate consisting of stacked networks of hydrogen-bonded MTCPP moieties, showing four to 5 overlapping layers. The van der Waals width of the interporphyrin channels propagating through the crystal and accessible to other species is about 1.5 nm.[13] (*View* ***this*** *art in color at www.dekker.com.*)

incorporated within the interporphyrin cavities. This tuning can be accomplished by changing the type of the sensor group bound to the porphyrin framework as well as by introducing an external bridging template.

Association of the porphyrin moieties aiong the axial direction (i.e., roughly perpendicular to the porphyrin plane) provides another useful tool for constructing enforced supramolecular porphyrin aggregates. Columnar motifs of the porphyrins are readily achieved, for example, by means of axial coordination interaction of a bidentate bridging moiety (e.g., of the binitrile or bipyridyl type) to transition metal ions (with either five or six-coordination preference) inserted into the posphyrin core.[16,18,19] Theу can also be constructed by using multiple hydrogen bonds between peripheral polar groups oriented in a direction perpendicular to the porphyrin plane.[20,21] The void space created between and within such one-dimensional porphyrin columns leads to the incorporation of guest species into the crystal lattice and creation of clathrates. Some materials of this type were found potentially useful as molecular magnets'"' or solid-state catalysts.[20]

The columnar one-dimensional, or network two-dimensional, polymeric motifs can be further varied in different ways to construct three-dimensional lattices of interlinked porphyrin species with better-defined pore sizes. One way to achieve this goal is to apply external transition metal-bridging auxiliaries with three-dimensional coordination features. These include, for example, zinc,'"' copper,[22] and molybdenum,[23] metal ion bridges that can associate

simultaneously with several neighboring porphyrin units. Another way to effect extended supramolecular architectures is to bring to expression a concerted mechanism of the lateral (i.e., parallel to the porphyrin planej as well as axial (i.e., approximately perpendicular to the porphyrin plane) interaction schemes between the porphyrin building blocks. Different combinations are possible: 1) direct interporphyrin hydrogen bonding in the equatorial directions combined with axial coordination through a bridging organic ligand: 2) equatorial intercoordination through metal ion auxiliaries combined with axial coordination through a bridging organic ligand; 3) equatorial as well as axial interporphyrin coordination through an organic ligand; and 4) self-assembly of multiporphyrin coordination polymers without resorting to external auxiliaries, in which the peripheral functional groups (e.g., pyridyl) of one porphyrin associate with the transition metal center (e.g., zinc or molybdenum) of neighboring metalloporphyrin units.[11,12,24] The geometric restrictions imposed by directionality and specificity of the intermolecular interactions lead, in most of the known cases, to the formation of architectures with intralattice voidr of restricted dimensions and are. thus. characterized by selective guest-entrapment features.

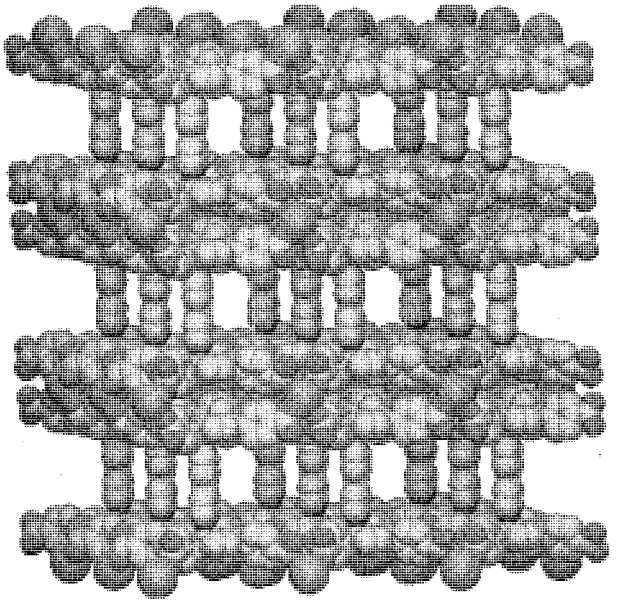

Fig. 6 Porphyrin zeolite analogue utilizing the MTCPP building blocks. along with bipyridyl and external metal ion auxiliaries.[27] The nearly 1 nm-wide channel voids propagate in the crystal in two perpendicular directions parallel to the porphyrin planes. *(View this art in color at www.dekker.com.)*

DESIGN OF PORPHYRIN-BASED ZEOLITE ANALOGUES

Formulation of porphyrin clathrates, which resemble to a significant extent the structure and function of the naturally occurring zeolites, represents one of the highlights of the porphyrin clathrate chemistry. Pioneering publications came out simultaneously from the research groups of Robson[22] and Goldberg[25] in 1994. The two groups reported the first porphyrin materials of this kind that represent single-framework open architectures based on coordination polymerization, either direct or through an external auxiliary. between the porphyrin tectons. Robson et al. used the Cu^{II}TPyP units tessellated together by Cu^{I} external transition metal auxiliaries to prepare a solid network structure with wide channels (diameter >1 nm). However, these frameworks did not survive solvent removal and were found to deteriorate rapidly in open air at ambient conditions. On the other hand. and in order to eliminate the need to use an external auxiliary along with its counterion, Goldberg et al. used the Zn^{II}TPyP building blocks to induce direct interporphyrin coordination. These efforts led to successful formulation of a homogeneous multiporphyrin honeycomb architecture of trigonal symmetry. which contains an array of parallel −0.6 nm-wide channels centered around the threefold rotation axes and propagating through the structure (Fig. 5). The inner walls of these channels are hydrophilic. facilitating an easy absorption of small polar guests in a reversible manner. More recent evaluations of identical Co^{II}TPyP and

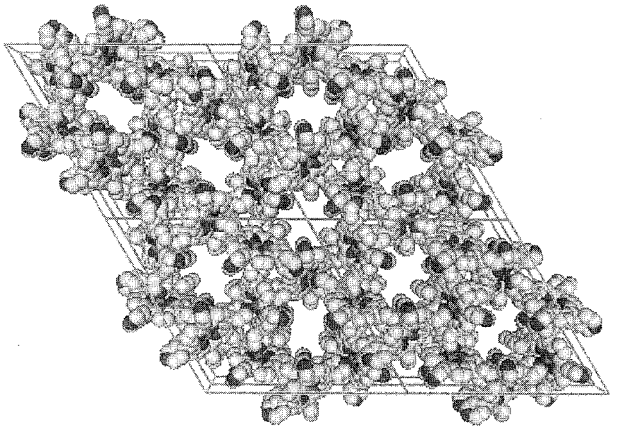

Fig. 5 Channel-type molecular-sieve structure based on the self-assembly via coordination of MTPyP building blocks. View down the channel axis. The width of the parallel one-dimensional channels is 0.6 nm. suitable for the storage and transport of small molecules.[25,26] *(View this art in color at www.dekker.com.)*

$Mn^{III}TPyP$ architectures confirmed the high structural integrity and thermal stability (up to ca. 400°C) of this material, its sorption capacity, and its potential utility in shape-selective catalysis.[26]

The two other examples of successful construction of stable metalloporphyrin zeolite involve the MTCPP building blocks and external organic and metal ion auxiliaries. The first represents a single-framework three-dimensional coordination polymer fully sustained by a specific and directional interaction scheme (Fig. 6). The structure consists of porphyrin bilayers held together via coordination, through their carboxylic functions, by bridging sodium metal ion auxiliaries. These layers are then cross-linked in the axial directions by bipyridyl ligands. which associate to the central zinc ions of successive bilayers. The crystal lattice thus formed is perforated by wide-open galleries (0.8×1.2 nm^2 and 1.0×1.2 nm^2), which extend between the bipyridyl pillars.[27] The polymeric framework occupies less than 40% of the crystal volume, the remaining space being accessible to the guest component, and maintains it stability up to ca. 150°C.

The second example relates to a functional nanoporous material based on the supramolecular assembly of the CoTCPP tectons, which was fabricated by Suslick et al. with the aid of solvothermal techniques.[28] Its structure is based on peripheral coordination of the porphyrin building blocks to each other, into a three-dimensional coordination polymer, with the aid of external cobalt ion auxiliaries (Fig. 7). The bending of the CoTCPP units allows formation of a three-dimensionally intercoordinated single-framework architecture, without the organic bridging ligand applied in the previous example. The resulting solid is thermally robust, and 74% of its total crystal volume is accessible to solvent and guest species. It contains large, refillable tridirectional channels (with cross section dimensions of 0.7×0.9 nm^2 and 0.7×1.4 nm^2), exhibiting extraordinary hydrophilic character. It also reveals selective guest absorption properties with considerable preference for water and amines, highlighted by its remarkable ability to remove water from common organic solvents. In the latter context, this porphyrin system was found to outperform common zeolites.

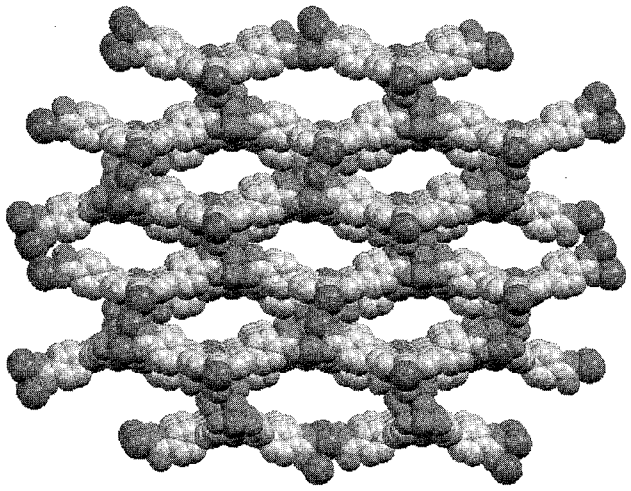

Fig. 7 Suslick's porphyrin zeolite, based on a Co-bridged CoTCPP self-assembled framework, showing its open architecture.[28] This structure is also perforated by smaller channels that propagate roughly perpendicular to the porphyrin planes. *(View this art in color at www.dekker.com.)*

CONCLUSION

The intensive research on porphyrin-based clathrates over the past decade led to interesting formulations of novel materials. The properties of the porphyrin sponges and their potential applications as slow guest release agents were extensively explored. It was further shown that suprainolecular chemistry along with crystal engineering provide useful concepts and synthetic tools for the designed construction of enforced lattices with genuine molecular-sieve properties.[13,25–28] These methods involve the generation of high-order structures with controlled geometries from robust molecular building blocks, by exploring diverse interaction motifs that can exist between the functionalized porphyrin molecules. The design of organic molecular solids with structural and functional similarity to inorganic zeolites and high structural integrity remains an exciting challenge in materials chemistry.

Nanoporous solids in general, and the porphyrin sieves materials in particular, provide an increasingly important class of materials for potential applications in the areas of enantioselective separations, molecular sorption and sensing, heterogeneous catalysis, and as possible nanoscale reaction chambers. Until the end of 2002, only a small fraction of the newly designed porphyrin-based solids were found to exhibit unprecedented nanoporosity and structural rigidity at high temperatures. Most of these materials still lose their crystallinity upon expulsion of the intercalated guest and are not suitable for practical uses. Further effort is required to optimize the porphyrin building blocks, reveal more specific and stable interaction synthons, and improve the preparative techniques in order to formulate new zeolite-type materials that can rivai the naturally occurring aluminosilicates. The remarkable achievements in nanoscale supramolecular

synthesis of molecular sieve architectures achieved thus far establish strong potential for the successful development of a new generation of useful functional materials in the near future.

ACKNOWLEDGMENT

This research was supported in part by The Israel Science Foundation founded by the Israel Academy of Sciences & Humanities, as well as by Grant No. 1999082 from the United States-Israel Binational Science Foundation (BSF), Jerusalem, Israel.

ARTICLES OF FURTHER INTEREST

Concepts in Crystal Engineering, p. 319
Inclusion Compounds: Selectivity, Thermal Stability, and Kinetics, p. 696
Mesoporous Materials, p. 845
Nomenclature in Crystal Engineering, p. 967
Organic Zeolites, p. 996
Phthalocyanines, p. 1069
π–π Stacking as a Crystal Engineering Tool. p. 1093
Porphyrin Derivatives, Functional, p. 1139
Pyrrole- and Polypyrrole-Based Anion Receptors, p. 1176
Soft and Smart Materials, p. 1302
Solid-State Reactivity/Topochemistry, p. 1316
X-Ray Crystallography, p. 1586
Zeolites: Structures and Inclusion Properties. p. 1623

REFERENCES

1. Powell, H.M. The structure of molecular compounds. Part IV. Clathrate compounds. J. Chem. Soc. 1948. 61–69.
2. Allen. F.H. The Cambridge structural database: A quarter of a million crystal structures and rising. Acta Crystallogr.. Sec. B 2002. *58.* 380–388.
3. Byrn, M.P.; Curtis, C.J.: Coldberg, I.: Hsiou. Y.; Khan. S.I.; Sawin, P.A.: Tendick. S.K.: Strouse, C.E. Porphyrin sponges: Strucral systematics of the host lattice. J. Am. Chem. Soc. 1991. *113*, 6549–6557.
4. Byrn. M.P.; Curtis, C.J.; Hsiou, Y.: Khan. S.I.; Sawin, P.A.; Tendick, S.K.: Terzis. A.; Strouse, C.E. Porphyrin sponges: Conservation of host structure in over 200 porphyrin-based lattice clathrates. J. Am. Chem. Soc. 1993. *115.* 9480–9497.
5. Byrn, M.P.; Curtis. C.J.; Hsiou. Y.; Khan, S.I.: Sawin. P.A.; Terzis, A.; Strouse, C.E. Porphyrin-Based Lattice Clathrates. *In Comprehensive Supramolecular Chemistry*; MacNicol. D.D.. Toda, F., Bishop. R., Eds.: Elsevier: Oxford, UK. 1996: Vol. 6, 715–732. chap. 21.
6. Boyd. P.D.W.: Hodgson. M.C.; Rickard, C.E.F.; Oliver. A.G.; Chaker, L.: Brothers, P.J.; Bolskar. R.D.: Tham. F.S.; Reed. C.A. Selective supramolecular porphyrin/fullerene interactions. J. Am. Chem. Soc. 1999, 121. 10487–10495.
7. Ishii. T.: Kanehama, R.; Aizawa. N.; Yamashita. M.; Matsuzaka. H.; Sugiura. K.-I.; Miyasaka. H.; Kodama. T.; Kikuchi, K.: Ikemoto. I.: Tanaka. H.: Marumoto. K.: Kuroda. S.-I. Fullerene C_{60} exhibiting a strong intermolecular interaction in a cocrystallite with C_4 symmetrical cobalt tetrakis(di-tert-butylphenyl)porphyrin. J. Chem. Soc. Dalton Trans. 200%.2975–2980.
8. Desiraju, G.R. Supramolecular synthons in crystal engineering—A new organic synthesis. Angew. Chern. Int. Ed. 1995.34. 2311–2327.
9. Etter. M.C. Hydrogen bonds as design elements in organic chemistry. J. Phys. Chem. 1991. *95,* 4601–4610.
10. Krishna Kumar, R.: Balasubramanian. S.; Goldberg. I. Supramolecular multiporphyrin architecture. Coordination polymers and open networlis in crystals of tetrakis(4-cyanophenyl)- and tetrakis(4-nitrophenyl)-metalloporphyrin. Inorg. Chem. 1998, 37. 541–552.
11. Coldberg. I. Metalloporphyrin molecular sieves. Chem. Eur. J. 2000, 6, 3863–3870.
12. Goldberg. I. Design strategies for supramolecular porphyrin-based materials. Cryst. Eng. Comm. 2002. 4. 109–116.
13. Diskin-Posner, Y.: Goldberg. I. From porphyrin sponges to porphyrin sieves: A unique crystalline lattice of aquazinc tetra(4-carboxyphenyl) porphyrin with nanosizecl channels. Chem. Commun. 1999, 1961–1962.
14. Dahal. S.: Goldberg. I. Solid-state supramolecular chemistry of porphyrins. Hydrogen-bonded networks and porous crystals of meso-tetra[4-(3,5-diaminotriazino)phenyl]porphyrin. J. Phys. Org. Chem. 2000. 13. 382–387.
15. Diskin-Posner. Y.; Dahal. S.: Goldberg. I. New effective synthons for supramolecular self-assembly of meso-carboxyphenylporphyrins. Chem. Commun. 2000. 585–586.
16. Diskin-Posner. Y.; Goldberg, I. Porphyrin sieves. Designing open networks of tetra(carboxyphenyl)porphyrins by extended coordination through sodium ion auxiliaries. New J. Chem. 2001, *25.* 899–904.
17. Sharma. C.V.K.; Broker, G.A.: Huddleston. J.A.: Baldwin, J.W.: Metzger. R.M.; Rogers. R.D. Design strategies for solid-state supramolecular arrays containing both mixed-rnetalated and freebase porphyrins. J. Am. Chem. Soc. 1999. 121, 1137–1144.
18. Diskin-Posner, Y.: Patra. C.K.: Goldberg. I. Crystal engineering of 2-D and 3-D multiporphyrin architectures—The versatile topologies of tetracarboxyphenylporphyrin-based materials. Eur. J. Inorg. Chem. 2001. 2515–2523.
19. Brandon. E.J.: Rittenberg. D.K.: Arif, A.M.: Miller. J.S. Ferrimagnetic behavior of multiple phases and solvates of

[meso-tetrakis(4-chlorophenyl)porphinato]manganese(III) tetracyanoethenide, $[MnTClPP]^+$ [TCNE]. Enhancement of magnetic coupling by thermal annealing. Inorg. Chem. 1998, 37, 3376–3384.

20. Bhyrappa, P.; Wilson, S.R.; Suslick. K.S. Hydrogen-bonded porphyrinic solids: Supramolecular networks of octahydroxy porphyrins. J. Am. Chem. Soc. 1997. *119*. 8492–8502.
21. Kobayashi, K.: Koyanagi. M.; Endo. K.; Masuda. H.: Aoyama, Y. Self-assembly of porphyrin arrays by hydrogen bonding in the solid state: An orthogonal porphyrin-bisresorcinol system. Chem. Eur. J. 1998, 4, 417–424.
22. Abrahams, B.F.; Hoskins. B.F.; Michail. D.M.: Robson, R. Assembly of porphyrin building-blocks into network structures with large channels. Nature 1994. 369. 727–729.
23. Hagrman, D.; Hagrman, P.J.: Zubieta. J. Solid-state coordination chemistry: The self-assembly of microporous organic-inorganic hybrid frameworks constructed from tetrapyridylporphyrin and bimetallic oxide chains or oxide clusters. Angew. Chem. Int. Ed. 1999, *38*. 3165–3168.
24. Diskin-Posner, Y.: Patra. G.K.; Goldberg. I. Crystal engineering of metalloporphyrin assemblies. New supramolecular architectures mediated by bipyridyl ligands. Chem. Commun. 2002. 1420–1421.
25. Krupitsky, H.; Stein. Z.: Goldberg, I. Crytalline complexes, coordination polymers and aggregation modes of tetra(4-pyridyl)porphyrin. J. Incl. Phenom. 1994. *18*, 177–192.
26. Lin, K.-J. SMTP-1: The first functionalized metalloporphyrin molecular sieves with large channels. Angew. Chem. Int. Ed. 1999, *38*, 2730–2732.
27. Diskin-Posner. Y.; Dahal, S.; Goldberg. I. Crystal engineering of metalloporphyrin zeolite analogues. Angew. Chem. Int. Ed. 2000, 39. 1288–1292.
28. Kosal, M.E.; Chou, J.-H.; Wilson, S.R.; Suslick, K.S. A functional zeolite analogue assembled from metalloporphyrins. Nat. Mat. 2002, *1*, 118–121.

Preorganization and Complementarity

John C. Sherman
University of British Columbia, Vancouver, British Columbia, Canada

INTRODUCTION

Chemists have long been entranced by nature's example of sophistication in recognition. Our drive as scientists has been to understand how nature manages such exquisite specificity, and how we can use such information to our own ends. Biologists are mostly concerned with elucidation of natural processes, with hope that such understanding may lead, for example, to new therapies, better control in agriculture, and perhaps even to "more useful" organisms. Chemists too have been interested in elaborating on how such recognition is manifested, usually on a more fundamental molecular level. Our approach has included mimicry, and this has led us further, to create new systems that can potentially perform tasks that nature cannot or simply does not. As chemists, we are interested in understanding the fundamentals of recognition processes and in applying this knowledge to our synthetic bent. Thus, we seek to create nonnatural supramolecular assemblies that are limited in scope only by our imagination.

Our ability to synthesize complex molecules and to characterize their structure, conformation, and dynamics continues to grow. So does our appetite for grander schemes. With enzymes and receptors as nature's examples of billions of years of honing recognition, chemists sought to capitalize. and perhaps even leap-frog nature. Key transitional compounds were available in the 1950s: cyclodextrins are naturally occurring compounds that are capable of recognizing and binding a variety of organic molecules.[1] Although naturally occurring cyclodextrins manifest some specificity, they do not compare to enzymes or receptors in this regard. In the 1960s came cyclophanes, which are synthetic compounds that are macrocyclic in structure, but they lacked the elements needed for binding of guest molecules.[2,3]

A hallmark in supramolecular chemistry came in 1967, when Pedersen created the first crown ethers.[4] These were entirely synthetic, macrocyclic, and capable of recognizing and binding small ions. Crowns opened the door to many possibilities. Most importantly, new ideas began to flood, and a new field was created. called host–guest chemistry. Donald J. Cram was among the first to recognize the potential of crowns, and he assimilated his knowledge of cyclophanes, crowns. cyclodextrins. as well as recognition in biology, including concepts such as the lock and key theory of Emil Fischer, to create the field of host–guest chemistry.[2,3,5,6] Charles Pedersen, Jean-Marie Lehn, and Donald J. Cram won the Nobel Prize in Chemistry for their work in host–guest chemistry.

COMPLEMENTARITY

The synthesis of host–guest chemistry from the above elements began with the definitions of the terms that title this chapter. Complementarity in simple terms refers to host and guest complementing each other, again akin to the lock and key model of Fischer. The shape and size of the cavity of the host must match that of the guest. The electronic interactions between host and guest must be attractive. Of all the possible interactions between host and guest, including ion–ion, ion–dipole. dipole–dipole, hydrogen bonds, π–π, and van der Waals interactions, the more complementary the host and guest, the stronger will be their binding. Or as Cram put it, "to complex, hosts must have binding sites which can simultaneously contact and attract the binding sites of guests without generating internal strain or strong nonbonded repulsions."[3]

Two striking early examples of complementarity from the lab of Jean-Marie Lehn are cryptands 1 and 2 (Fig. 1).[7] Cryptand 1 shows selective binding of Li^+ over Na^+ by a factor of 4800, and cryptand 2 shows selective binding of Na^+ over Li^+ by a factor of 440,000. Both hosts are complementary to small spherical cations. The inwardly pointing lone pairs of electrons on the oxygens and nitrogens donate into the alkali cations. and thus. they electronically complement the guests. The lone pairs form an essentially spherical cavity, which is complementary in shape to the spherical cations. This is an electronic conlplementarity as well, because such cations do not have stringent structural or electronic requirements for ligand arrangements, such as a square planar geometry. Finally, there is size complementarity, which is clearly switchable from the smaller to the larger, as demonstrated by the two examples (vide infra).

Encyclopedia of Supramolecular Chemistry
DOI: 10.1081/E-ESMC 120012660

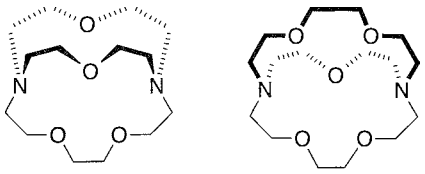

Cryptand 1 Cryptand 2

Fig. I

PREORGANIZATION

Preorganization essentially comes down to "you can pay me now or you can pay me later." The currency of payment in this case is energy. Energy in terms of binding affinity and energy in terms of synthetic labor. As Cram stated, "the more highly hosts and guests are organized for binding and low solvation prior to their complexation, the more stable will be their complexes."[3] A highly flexible host is not well preorganized. It will show weak binding, because there will be only one or perhaps a few similar conformations that are optimal for guest binding. Although many other conforinations are available to the free host. most of these conformations are denied access upon binding. This costs energy in terms of entropy, and will be reflected in the low energy of binding. As well, a poorly preorganized host will be highly solvated. Desolvation will be required before binding can take place. This will cost energy in terms of enthalpy and entropy and again will be reflected in the weak binding of host and guest.

The classic example of preorganization is the contrast between podand **3** and spherand 4 (Fig. 2).[3,8,9] The difference in the binding constants for these two compounds for Li^+ is $>10^{12}$. The electronics of the molecules are nearly identical. For the podand, a multitude of conformations must be denied, which costs energy in terms of entropy. The conformation that is most complementary for binding is likely a relatively high energy conformation. so there is an enthalpic price to be paid as well. And there is the problem of desolvation of each of the ether oxygens. In contrast. the spherand pays these prices up front, before coming in on binding day. The synthesis of spherand 1 is an arduous one,[8,9] and the host must possess a reasonable amount of strain. This up front payment brings to the table a host with its six oxygens fully preorganized for binding small cations. The lone pairs (one from each oxygen) point into the cavity toward the guest, and the methyl groups effectively preclude solvation. No conformations need to be frozen out, and any strain that there may be in the binding conformation is already present in the free host. so there is no additional price to pay. All advanced payment. i.e., energy, goes to binding. In boxing terms. the spherand has come to the bout well trained and at the proper weight (preorganized), so it performs with astounding strength. In contrast, the podand did not prepare well and is overweight (i.e., is not preorganized). It must work off some weight on the day of the bout (i.e., it must arrange itself into a binding geometry) and is thus left with little energy for the bout.

One might expect such highly preorganized species to slow the process of binding. What is affected considerably is the rate of decomplexation. The rates of complexation are not as affected." In principle, a fully preorganized host could shut down the rate of complexation to the point where binding is no longer reversible. This is the case for carcerands, which are discussed in another article. In cases of highly preorganized spherands such as 4. a guest can be slowed considerably. to as low as $10^{-12}s^{-1}$.[3]

One final comment on complementarity. One can intuit that it is possible to create a host with a cavity that is selective to Li^+ over Na^+ by making the cavity small, such that Na^+ will cause strain: either host and guest occupying the same space or host will have to adjust to a high-energy conformation to avoid occupying the same space as the

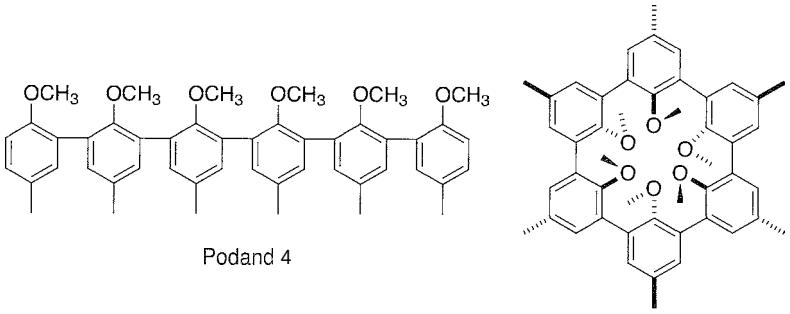

Podand 4 Spherand 4

guest. This is illustrated in the example of cryptand **1** showing selective binding of Li^+ over Na^+ by a factor of 4800. as stated earlier. What is even more challenging is the reverse. The complementarity and preorganization must be very high for cryptand 2 to show selective binding of Na^+ over Li^+ by a factor of 440,000. The host must be unable to shrink its cavity to accommodate the Li^+, or if the host can. it must cost a lot of energy. In this regard, this is an amazing example. But it is not unique.

CONCLUSION

There are many exainples of complementarity and preorganization. Essentially every article in this encyclopedia contain5 examples. After all, complementarity and preorganization are precepts to supramolecular chemıstry, and thus, these concepts are integral to all supramolecular assemblies.

ACKNOWLEDGMENT

This article ıs dedicated to the memory of Donald J Cram. whom I thank for creating the field of host–guest chemistry, for teaching and supporting me, and for promotıng the field ın general I hope such articles help to keep Cram's energy and spırıt with us

ARTICLES OF FURTHER INTEREST

Chiral Guest Recognition, p. 236
Classification and Nomenclature of Supramolecular Compounds, p. 261
Crown Ethers; p. 326
Cryptands, p. 334
Hydrogen Bonding, p. *658*
Induced Fit, p. 717
The Lock and Key Principle. p. 809
Selectivity: Thermodynamic and Kinetic, p. 1225
Self-Assembly: Definition and Kinetic and Thermodynamic Considerations, p. 1248
Stability Constants: Definition and Determination, p. 1360
The Template Effect, p. 1493

REFERENCES

1. Szejtli. J. introduction and overview of cyclodextrin chemistry. Chem. Rev. 1998. 98. 1743–1753.
2. Cram. D.J. *From Design to Discovery*; Ainerican Chemical Society: Washington. DC. 1990.
3. Cram. D.J.; Cram, J.M. Container Molecules and Their Guests. In *Monographs in Supramolecular Chemistry*; Stodclart. J.F., Ed.: Royal Society of Chemistry: Cambridge, 1990; 39–41.
4. Pedersen. C.J. Cyclic polyethers and their complexes with metal salts. J. Am. Chem. Soc. 1963. *89*, 7017–7036.
5. Cram, D.J.: Cram. J.M. Design of complexes of synthetic hosts and organic guests. Acc. Chem. Res. 1978. *11*. 8–*14*.
6. Cram. D.J. The design of molecular hosts. guests. and their complexes. Science 1988. *240*, 760–767.
7. Dietrich. B.; Lehn. J.-M.; Sauvage, J.P. Les cryptates. Tetrahedron Lett. 1969. *10*. 2888–2892.
8. Cram. D.J.; Lein. G.M.: Kaneda. T.: Helgeson. R.C.: Knobler. C.B.: Maverick, E.: Trueblood. K.N. Augmented and diminished spherands and scales of binding. J. Am. Chern. Soc. 1981. *103*. 6228–6232.
9. Cram, D.J.: Lein. G.M. Host–guest complexation. 36. Spherand and lithium and sodium ion complexation rates and equilibria. J. Am. Chem. Soc. 1985. 107. 3657–3668.

Protein Supramolecular Chemistry

Jörg Andrä
Research Center Borstel, Leibniz-Center for Medicine and Biosciences, Borstel, Germany

Patrick Garidel
Martin-Luther-Universitat Halle/Wittenberg, Halle/Saale, Germany

Klaus Brandenburg
Research Center Borstel, Leibniz-Center for Medicine and Biosciences, Borstel, Germany

INTRODUCTION

Proteins fulfill a variety of functions in biological systems. They serve as biocatalysts, inolecular motors, signal receptors. building material of cellular structures, and much more. Although the strategy of protein chemists was the functional characterization of high-purity isolated proteins, most proteins seem to act not in an isolated but rather in an organized manner, at least from time to time, whether they be supramolecular assembled multiprotein complexes or aggregates. In this article, we summarize the recent contributions to the field of suprarnolecular protein chemistry. including the new methods used for the structural characterization of high-molecular-weight assemblies.

METHODS FOR THE ANALYSIS OF SUPRAMOLECULAR PROTEIN COMPLEXES

Nuclear Magnetic Resonance (NMR)

New techniques for solution nuclear magnetic resonance (NMR) studies of molecular and supramolecular structures were described by Riek et al.[1,2] The authors combined TROSY (transverse relaxation-optimized spectroscopy) and CRIPT (cross-correlated relaxation-induced polarization transfer) or CRINEPT (cross-correlated relaxation-enhanced polarization transfer) for the two-dimensional (2D) NMR analysis of ^{15}N-, ^{1}H-labeled homo-oligomeric macromolecules with masses ranging from 110–800 kDa. Practical applications of these methods are, for instance; analyses of intermolecuiar interactions in supramolecular complexes or conformational changes of a single macromolecule upon interactions with other molecules.

Electron Paramagnetic Resonance (EPR)

As a new method for the investigation of the structure and conformational switching in soluble and membrane proteins, site-directed spin labeling (SDSL) was presented as a general method.[3] In the SDSE technique, a nitroxide side chain is introduced into the protein by reacting an engineered cysteine with a selective nitroxide reagent, and the shape of the electron paramagnetic resonance (EPR) signal is determined by the motion of the nitroxide ring on the nanosecond timescale. It is known that the motion is a superposition of the rotary diffusion of the protein. internal dynamic modes of the side chain, and local backbone fluctuations. Usually, however, the experimental conditions can be arranged so that contributions from the rotary diffusion are negligible. Thus, if the internal side chain motions are known at particular sites. the local backbone fluctuations can be deduced. In a similar way, collective modes in α-helices of soluble proteins and other internal motions can be detected.''

Electron Cryomicroscopy

The applicability of electron cryomicroscopy methods on biological macromolecules and their supramolecular assemblies was reviewed by Unger.[4] Examples were presented comprising the membrane protein aquaporin, the herpes-virus capsid, and the small nuclear ribonucleoprotein complex. Developments in electron cryomicroscopy and image analysis in combination with x-ray crystallography allow scientists to investigate structure, assembly. and dynamics of biological supramolecular assemblies.[5] This is particularly interesting with regard to viral proteins and receptor proteins as, for example, the coxsackievirus-adenovirus receptor (Fig. I). Thus, the authors were able to resolve the structure of human herpes simplex virus 1 capsid at 8.5 Å resolution by combining 5860 images of particles from 130 micrographs.

Light Scattering

Some supramolecular structures are sensitive to external perturbations. which can result from sample preparation and ''harsh'' conditions during fixation of the

DOI: 10.1081/E-ESMC 120019170

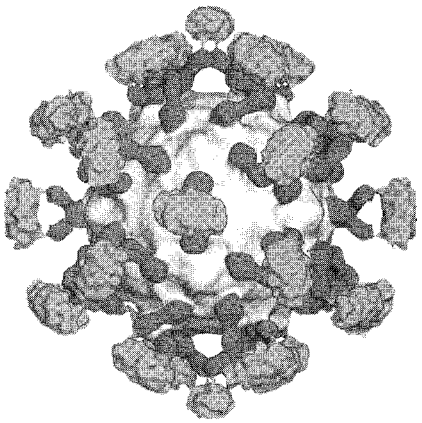

Fig. 1 Cryo-EM map of the coxsackievirus-adenovirus receptor (CAR. red and green) bound to coxsackievirus B3 (CVB3, grey). Adapted from Ref. [51] with permission from Nature Publishing Group. (*View this* urt in color *at www.dekker.com.*)

sample (e.g., electron microscopy). Static light scattering (SLS) and dynamic light scattering (DLS) are two techniques based on the analysis of hydrodynamic properties. These methods permit the characterization of protein supramolecular structures as they exist in unperturbed solutions. Ehrlich et al.[6] showed by DLS that the HIV-1 capsid protein CA is able to form spherical and tubular structures. However, using electron microscopy, they found that some protein assemblages were inherently sensitive to perturbations.

Mass Spectrometry

Matrix-assisted laser desorption/ionization mass spectrometry (MALDI-MS) can be used for primary structure verification and protein identification. Belghazi et al.[7] described the application of MALDI-MS for the analysis of yeast mitochondrial proteins in a supramolecular complex exhibiting NADH dehydrogenase activity. Protein complexes were isolated by 2D gel electrophoresis, fragmented by Lys C digest and analyzed by MALDI-MS. Protein identification was done in a multistep procedure: first, a database search was performed with the monoisotopic masses; second, peptide peaks corresponding to promising candidates were analyzed by postsource decay; and finally, a search was performed with the postsource decay fragments to confirm the first identification. Of 38 proteins identified in this approach, most were known mitochondrial proteins.[8]

Classical Assays

The most routinely used methods in pharmaceutical research for the characterization of protein aggregations are the HP-SEC (high-performance size exclusion chromatography) and native and denaturated PAGE (poly acryl amide gel electrophoresis) techniques (for more details, see any of a number of classical biophysical and biochemical textbooks).

UNDERSTANDING THE FORMATION OF SUPRAMOLECULAR PROTEIN STRUCTURES

The term ''amyloid'' was used originally to describe certain deposits found postmortem in organs and tissues, which gave a positive reaction when stained with iodine.'" Later. it was realized that the material was predominantly proteinaceous when obtained from many ex vivo sources. Amyloids are observed when proteins self-assemble into large oligomers that are visible by, e.g., electron microscopy, as fibrils. Amyloid deposits are associated with several neurodegenerative diseases, including Alzheimer's disease and the prion diseases. The amyloid fibrils isolated from these different diseases share similar structural features. In the late 1950s, Cohen and Calkins[10] demonstrated that all forms of amyloids studied exhibit a comparable fibrillar ultrastructure: bundles of straight, rigid fibrils ranging in width between 6–13 nm (average 7.5–10 nm) and in length from 100–1600 nm.[11,12] Perutz et al.[13] described amyloid fibers as water-filled nanotubes. However, the protein sequences that assemble into these fibrils differ substantially from one disease to another. To understand the relationship between the amino acid sequence and the propensity to form higher aggregates and protein misfolding[14,15] like the amyloid structure,[16] different research groups employed an approach based on the de novo design of synthetic protein structures[17–20] by using combinatorial libraries. Basically, two different secondary structures are found in most proteins: α-helical and β-sheet structures. Both are quite different. In contrast to an isolated β-strand, which is not stable: an individual a-helix can exist in isolation, and thus a-helices can be considered independent structural modules and used as ''building blocks'' for the design of new proteins. This contrast between secondary structures stems from the fundamental difference in hydrogen-bonding characteristics. In the α-helix, the backbone hydrogen bonding is intrasegmental, in which the carbonyl of an amino residue *j* interacts with the amino group of residue $j+4$. This arrangement induces the formation of a self-contained structure. by satisfying most of its backbone hydrogen-bonding interactions without the help of an ''external'' partner. In β-strands, however. the situation for fulfilling maximum hydrogen bonds is different. The carbonyl and amino groups in β-sheets form a hydrogen-bonding network to amino and carbonyl

groups of neighboring strands. Thus, an "external partner" is usually required and, as a consequence, β-sheet strands tend to form higher supramolecular structures via the formation of defined structures to amorphous aggregates. Another issue to consider is hydrophobic interactions with other molecules with nonpolar surfaces. This is especially an issue for β-strands. Both the formation of backbone hydrogen bonds and the burial of hydrophobic surfaces require a β-strand to interact with neighboring elements of the structure. As an example, for a 0-strand going into the page, the neighboring strands on its right and left sides can form hydrogen bonds with the backbone of the amino and carbonyl groups. Amino acid side chains will point up and down, enabling hydrophobic residues to interact with neighbors above and below the original strand. Thus, the 0-strand can form favorable interactions with neighbors in four directions. This neighborliness has significant practical implications: β-strands have a tendency to aggregate and to form a precipitate in solution. However: nature developed strategies to avoid protein aggregations. Richardson and Richardson[21] analyzed a number of synthetic proteins, and from their studies, they concluded that natural β-sheet proteins use a negative design[17,18] to avoid edge-to-edge aggregation. Naturally occurring 0-sheet proteins are mostly stable and aggregate only after a longer period of time, as is observed for various diseases, whereas synthetically derived peptides and proteins with β-sheet structures have the tendency to form higher molecular arrangements of often unknown structure, and insoluble aggregates are formed. Nature, therefore, knows something and uses strategies we do not know or are actually not able to understand.[21] From their investigations, Xiong et al.[22] deduced that the periodicity of polar and nonpolar amino acids is the major determinant of secondary structure in self-assembling oligomeric peprides and is thus responsible for the formation of protein supramolecular structures.

Proteins with regular 0-sheet edges have a pronounced tendency to form aggregates, because they are already in the correct conformation to interact with any other β-strand they encounter. In their study, Richardson and Richardson[L2]" surveyed edge strands in a large sample of all-0-proteins to tabulate features that could protect against further β-sheet interactions. Of course. β-barrels avoid edges by performing continuous H-bonding around the barrel cylinder. Parallel a-helix proteins protect their 0-sheet ends by covering them with loops of other structures. The β-propeller and single-sheet proteins use a combination of 6-bulges, prolines, strategically placed charges, very short edge strands, and loop coverage. The β-sandwich proteins favor placing an inward-pointing charged side chain on one of the edge strands, where it would be buried by dimerization; they also use bulges, prolines, and other mechanisms.[21] One recent β-hairpin design has a constrained twist too great for accommodation into a larger β-sheet, whereas some β-sheet edges are protected by the bend and reverse twist produced by a glycine residue. All free edge strands were protected, usually by several redundant mechanisms. In contrast, edge strands that natively form x-H-bonded dimers or rings have long, regular stretches without such protection. The results presented by Richardson and Richardson[21] are relevant to understand how proteins may assemble into β-sheet amyloid fibers.[23,24] The possible strategies as summarized"" for the protection of β-sheet edges are shown in Table 1. Many edge-protection strategies used by natural proteins are beyond our current abilities to constrain by design, but one possibility stands out as especially useful: a single charged side chain near the middle of what would ordinarily be the hydrophobic side of the edge β-strand. This minimal negative-design strategy changes only one residue, requires no backbone distortion, and is easy to design. Wang and Hecht[25] showed with great success how to apply the concept of the inward-pointing charge strategy to turn highly aggregated β-sandwich designs into soluble monoiners. Nesloney and Kelly described another method for achieving monomeric 0-sheet designs[26] by the methylation of exposed backbone amino groups in edge β-strands to prevent aggregation. However, this strategy is only applicable for the design of synthetic peptides and not for biological protein synthesis. Thirumalai et al.[27] recently reviewed the various concepts on the molecular

Table 1 Various design strategies for the protection of β-sheet edges

Used strategy	*Frequently found?*	*Suitability as designable strategy?*
Continuous H-bonding	+ + +[a]	No
Covering loop	+ + +[a]	No
β-Bulge	+ + +[a]	Perhaps[d]
Proline	+ + +[a]	perhaps[d]
Inward point charge	+ + +[a]	Yes
Sheet edge rolls in	+ +[b]	No
Very short	+ +[b]	No
Very twisted	+ +[b]	Only for two strands parts
Lβ-Gly bend, reverse twist	+[c]	No
Switch between sheets	+[c]	No

'Refened strategy 1S frequently found and common
[b]Referred rtrategy 1S found and common
'Referred strategy 1S rarely found
[d]Used strategy 1nvol\es understanding effects on backbone conformation
(Adapted from Ref [21])

basis that govern protein and peptide aggregation, identifying the two global ''blocking'' strategies that nature utilizes to prevent edge-to-edge aggregation as the most important the minimization and protection of dangling hydrogen bonds. and inward pointing charged residues that block protein aggregation.

DESIGN OF PROTEIN ASSEMBLIES

The design of new proteins that can assemble into filaments, symmetric cages, and regular assays was described by Yeates and Padilla.[28] These investigations are based on the consideration that proteins self-assemble to fulfill their biological functions and also as part of a pathogenic process. For example, natural linear protein assemblies are, in most cases, tubular structures, such as filamentous viruses and microtubules, but this is not the case for the protein actin, which is one of the well-studied examples of a linear filament. Engineered proteins comprise head-to-tail, head-to-head, and tail-to-tail designed protein filaments. For example, two unrelated dimeric proteins were fused genetically, and the 44 kDa designed protein could self-assemble into filaments that were also seen to associate in bundles and networks (Fig. 2). A particular procedure of producing nanofibers is presented by Hartgerink et al.,[29] who reported about the self-assembly of peptide-amphiphiles, in which the supramolecular aggregation is caused by lipid chains. These fibers can reversibly be polymerized to enhance their stability,

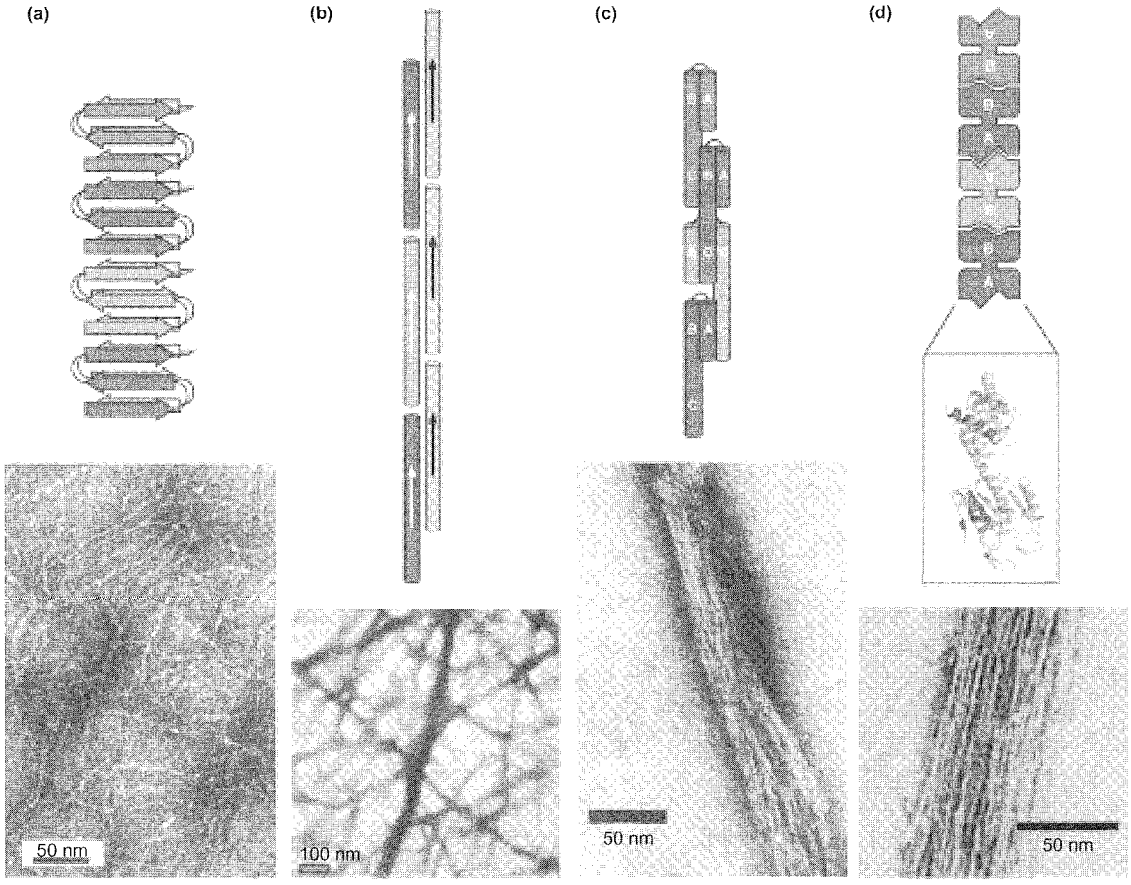

Fig. 2 Various strategies for the design of linear protein assemblies. (a) Beta-sheet polypeptides and proteins tend to associate at their edges to form fibrils that may be related to amyloid structure. (b) Protein filaments are formed by two polypeptides designed to form a parallel heterodimeric coiled coil with 'sticky ends.' (c) Protein filaments are formed by a domain-swapping mechanism from a designed protein created as a variation on a three-helix-bundle protein. (d) Filaments are formed by a fusion protein between two distinct, naturally dimeric proteins (carboxylesterase (A) and influenza virus matrix protein MI (B)). Figure is adapted from Ref. [28] and reprinted with permission from Elsevier, copyright (2002). Electron micrographs (from left to right) are reprinted with permission from Ref. [52], copyright (1999) National Academy of Science. USA; Ref. [53], copyright (2000) American Chemical Society; Refs. [54] and [55], both copyright (2001) National Academy of Science, USA. (View *this* art in color *at www.dekker.com.*)

and the formation of supramolecular structure and polymerization produces a remarkably versatile material. Variants of the peptide-amphiphiles with variations in alkyl chain length, the polymerizable region, and the C-terminal peptide sequence were shown to self-assemble into a one-dimensional fibrous motif.

STRUCTURE PROTEINS

Fibrillins are found throughout the connective tissue of humans as integral components of extended fibrils, which may occur isolated or together with elastin. These polymeric structures were named microfibrils, which are particularly abundant in skin, blood vessels, tendons, and the ciliary zonules of the eye. Handford et al.[30] reviewed existing literature on fibrillins and presented information on the elucidated molecular structure and the effects of mutations on structural and functional properties. In particular, studies of functional domains in fibrillin are discussed that are important in assembling microfibrils. Immunolocalization of fibrillins can be performed within the microfibrils, residing in all tissue locations. Furthermore, immunolocalization experiments suggest an ordered arrangement of fibrillin molecules within the microfibrils. The authors conclude, however, that many questions were not answered, for example, which regions of fibrillin are rigid or flexible, which domains in fibrillins participate in the assembly of microfibrils, and whether fibrillin interacts with other molecules in the assembly process.

An important class of aggregate-forming proteins is the collagen family, a main component of connective tissues. The amino acid sequence of all collagens is now known in detail. The sequence shows a distinct domain organization, with the dominant occurrence of the amino acid glycine and of the posttranslational hydroxylation of proline and lysine residues. Although the primary, secondary, and tertiary structures of the collagens are well known, the different models of supramolecular arrangement, deduced among others from freeze-fracture or "normal" transmission electron microscopy (TEM) and atomic force microscopy (AFM), within the collagen fibers proposed in literature are far from being accepted generally (see review in Ref. [31]). The basic models are comprised of five- or eight-stranded helical microfibrils; smectic or hexagonal crystals: micelles; cylindrical or spiral lattices; compressed microfibrils; and several other arrangements (an example is given in Fig. 3).

Amelogenins are tissue-specific proteins of developing dental enamel. Regarding the biomineralization of the teeth, amelogenins seem to have an important role as a space-filling gel or an intercrystallite packing substance.[32,33] No clear definitive secondary structure is known; and unusual reversible aggregation properties

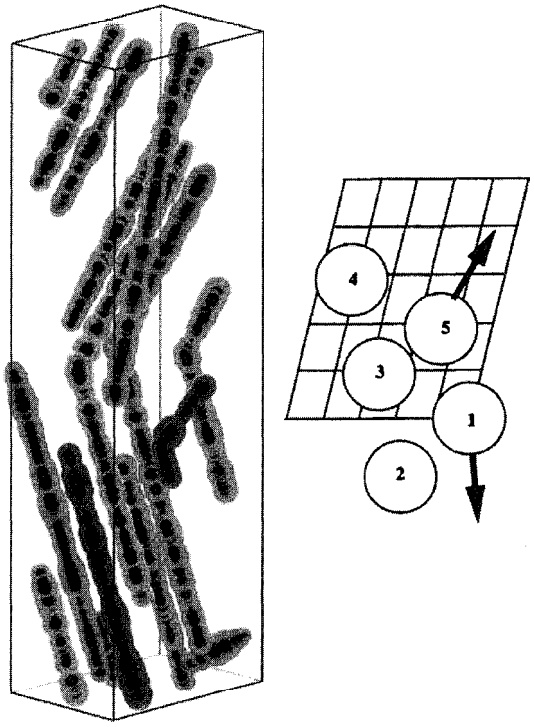

Fig. **3** 3D representation of the molecular arrangement of type I collagen according to Ref. [56] (left). The molecule is divided into five successive segments, identified with different colours. On the right. cyclic set of the final model and the telopeptide directions. Reprinted from Ref. [56], copyright (1998) with permission from Elsevier. (View this art in color *at www.* dekker.com.)

reminiscent of liquid crystal mesophases were observed. The application of dynamic light scattering and AFM exhibited an extreme dependence of the hydrodynamic radius of the major compound with a strong increase around the physiological temperature.

Another example of supramolecular protein structures is an extracellular aggregation factor (AF), a proteoglycan, from the marine sponge Microcionn *prolifera*.[34] The species-specific cell adhesion consists of the AF and a corresponding cell membrane receptor. Because the sponges were the first animals faced with multicellularity, it can be suggested that proteoglycan-like macromolecules belonged to the first extracellular matrix molecules, which originally were designed to allow precise modulation of their adhesive properties. Although early work suggested a self-association of AF due to a Ca^{2+}-dependent interaction of its carbohydrate moiety, the finding that glycan-free recombinant AF provoked specific cell aggregation of *Microciona* cells in the absence of Ca^{2+} proved a direct role of the protein moiety of AF in sponge cell adhesion.

VIRAL CAPSID PROTEINS

The viral genome and replicative enzymes of various viruses [such as the human immunodeficiency virus (HIV)] are encased in a conical shell that is assembled from a single protein subunit, the capsid protein.[35] The core shell of the virus forms a stable, effective protective barrier.[36,37] However. the shell must permit dissolution to allow transmission of the viral genome into its new host. The stability of the capsid protein depends on environmental factors like pH. The pH-dependency of some viral proteins reflects the requirement for a pH-dependent alteration in the conformation of the fusion protein (found at the outside protein core of viral systems) in order to render the protein competent for membrane fusion with the host.[38] The HIV-1 capsid protein can assemble in tubular structures and is also capable of forming spheres, depending on the pH of the protein solution. The switch from formation of one to the other occurred within a narrow physiological pH range (i.e., pH 7–6.8).[6] Below and above this range, only dimers and tubular structures were detected, respectively. Ehrlich et al.[6] found that the CA protein possesses the inherent ability to form metastable structures, the morphology of which is regulated by an environmentally sensitive molecular switch. Such metastable structures may exist as transient intermediates during the assembly and disassembly of the virus core. Icosahedral particles were found for the assembly of physalis mottle virus capsid protein in *Escherichia coli*. Amino acid carboxy termini play a role in the formation of these supermolecular protein structures.[39] Ou and collaborators[40] analyzed the minimal sequences on human JC virus, which belongs to the family polyomaviridae, VP1 required for capsid assembly. They found that the viral capsid is composed of 72 capsomers and that five VP1 molecules make up each capsomer structure. Twelve amino terminal and 16 carboxy terminal amino acids of VP1 are dispensable for the formation of virus-like particles, and further truncation at either end of VP1 leads to the loss of this property. Herpes simplex virus-1 (HSV-1) virions are large, complex, enveloped particles containing a proteinaceous tegument layer connected to an icosahedral capsid. The major capsid protein, VP5 (149 kDa), makes up both types of capsomere, pentons and hexons. Bowman et al.[37] found that alterations in the geometrical arrangements of the VP5 subunits in the capsomeres exposes different residues, resulting in the differential association of the tegument and VP26 with the pentons and hexons, respectively. The rearrangements of VP5 subunits required to form pentavalent and hexavalent capsomeres result in structures that exhibit different electrostatic properties. These differences may mediate the binding and release of other structural proteins during capsid maturation. Also; rotaviruses, a major pathogen of infantile gastroenteritis, are made of a large (100 nm) and complex icosahedral assembly, which is formed by three concentric capsid layers. However, in contrast to rotavirus, Norwalk virus, a causative agent of epidemic gastroenteritis in humans, has a simple architecture with an icosahedral capsid made of 180 copies of a single protein.[41,42] Recently, the crystal structure of the major capsid protein VP6 of rotavirus was determined. It revealed a trimer containing a central zinc ion, which is coordinated by histidine from each of the three subunit~.[~From their investigations. Erk et al.[43] were able to demonstrate that under conditions in which the histidine residues are not charged, the properties of VP6 depend on the presence of the centrally coordinated zinc atom in the trimer.

ENZYME COMPLEXES

The photosystem I (PSI) is one of the two pigment-containing reaction centers of oxygenic photosynthesis found in cyanobacteria and plants. The main function is to catalyze the light-dependent transfer of electrons from reduced plastocyanin or cytochrome c_6 to soluble ferredoxin or flavodoxin across the thylalkoid membrane. The functional reaction center, for thermophilic cyanobacteria, consists of 11 protein subunits and 90 chlorophyll molecules within a 340 kDa complex. Fotiadis et al.[44] performed surface relief reconstructions from electron micrographs and AFMs, and defined the lumenal and stromal PSI surfaces. They obtained precise information on the integration of the PSI reaction center in the lipid bilayer and determined the heights for the stromal and lumenal protrusion, which allowed for definition of the boundaries of the membrane-embedded complex.

An impressive approach to identify supramolecular protein complexes was done by Gavin et al.[45] and Ho et al.[46] They used labeled proteins as bait to capture and identify protein complexes in the budding yeast. Tags were added to the protein cDNA of interest, and these constructs were expressed in the yeast, and physiological complexes were formed. These complexes were thus easily isolated by exploiting the bait and were analyzed further by mass spectrometry. In summary, the authors reported more than 1000 proteins within several hundred supramolecular complexes in yeast, meaning the identification of several thousands of protein interactions. However, this approach: although powerful, has to deal with false positive and false negative results, and the authors failed to identify known interactions.

Grandier-Vazeille et al.[8] reported the analysis of the supramolecular organization of mitochondria1 dehydrogenases by isolation of the complex by non-denaturating electrophoresis (first dimension). Further identifications

of the complex proteins were made by SDS-PAGE analysis (second dimension). Endoproteinase Lys C digest in the gel resulted in fragments suitable for MALDI-MS and database searching. In a first screening, top-ranked protein candidates were identified by mono-isotopic mass searching. These candidates were further analyzed by postsource decay. The authors identified a supramolecular protein complex of five intermembrane space-facing dehydrogenases (Nde1p, Nde2p, Gut2p, Cyb2p, Dld1p), and the matrix-facing NADH-ubiquinone oxidoreductase Ndi1p, as well as the malate dehydrogenase Mdh1p. Three other enzymes of the tricarboxylic acid cycle were associated with this complex: fumarate dehydrogenase (Fum1p), citrate synthase (Cit1p), and succinate dehydrogenase (Sdh1p). Acetaldehyde dehydrogenase (Ald4p), a major component of the complex, implies the function as a channeling complex for matricidal NADH. The sensitivity of the method allows for the identification of physiological protein–protein interactions,[47] here NADH-producing enzymes, although some contaminants may be identified as well.

SUPRAMOLECULAR STRUCTURES ASSOCIATED WITH DISEASES

Atherosclerosis is a progressive disease of the large arteries, where lipids and proteins derived from circulating low-density lipoprotein (LDL) accumulate within cells and in the extracellular space. Ursini et al.[48] hypothesized that atherosclerosis might result from protein misfolding. Normally, protein folding into the correct secondary structure and conformation is indispensable for the biological function of proteins and is achieved during or immediately following protein synthesis. The secondary structure of apo-B 100, the protein moiety within LDL, is determined by lipid–protein interaction and dynamics, and may be affected by the addition or removal of lipids during lipoprotein metabolism. As a consequence of a change of the lipid–water interface, for example due to the oxidation of lipids, a misfolding of apo-B 100 may take place, which leads to a modified lipoprotein with several atherogenic properties. The authors conclude that atherogenesis can be considered as a disease produced by the accumulation of cytotoxic and proinflammatory misfolded lipoproteins.

Amyloid fibrils, formed by the β-amyloid peptide, are the hallmarks of Alzheimer's disease. Lakdawala et al.[49] and Antzutkin et al.[50] used molecular dynamics simulation and electron microscopy as well as NMR spectroscopy, respectively, to investigate fibril formation. Electron microscopy and solid-state NMR investigations were done with peptides Aβ(1–42) and Aβ(10–35). Fibril morphology was strongly dependent on pH. Aβ(10–35) forms single protofilaments at pH 3.7, but pairs or higher-ordered bundles of protofilaments were formed at pH 7.4. Aβ(1–42)-formed protofilaments were single or pairs at pH 7.4. Solid-state NMR revealed an in-register parallel β-sheet organization for both types of fibrils [Aβ(10–35) and Aβ(1–42)], suggesting that the supramolecular structures of both peptides are similar. However, the energetic constraints that contribute to fibril dynamics and stability are still not well understood and were investigated by molecular dynamic simulation based on the peptide Aβ(10–35). These calculations revealed high flexibility and dynamics of the fibrils, particularly in the formation of H-bonds within the in-register parallel β-strands. Therefore, the fibril interior should adopt an indefinite ensemble with ''molten globule-like'' properties.

CONCLUSION

Protein supramolecular arrangements varied widely in their molecular masses, ranging from two or more peptide chains in proteins with quarternary structures, over temporary or permanent interactions of a handful of proteins in multienzyme complexes, up to hundreds or thousands of protein subunits in structure proteins like viral capsid proteins or collagen. It is, therefore, impossible to give a comprehensive overview about this topic, so we picked out some interesting examples of the recent literature. Because most proteins are arranged in complexes and aggregate structures, supramolecular structures are an important issue to consider when discussing protein function.

ARTICLES OF FURTHER INTEREST

The Allosteric Effect, p. 20
Amino Acids: Applications, p. 42
Collagens, p. 295
Emergence of Life, p. 528
Enzymes: Characteristics and Mechanisms, p. 554
Peptide Nanotubes, p. 1035
Self-Assembly: Definition and Kinetic and Thermodynamic Considerations, p. 1248
Self-Assembly in Biochemistry, p. 1257
Viruses as Host Assemblies, p. 1563

REFERENCES

1. Riek, R.; Fiaux, J.; Bertelsen, E.B.; Horwich, A.L.; Wüthrich, K. Solution NMR techniques for large molecular and supramolecular structures. J. Am. Chem. Soc. **2002**, *124*, 12144–12153.

2. Riek. R.: Pervushin. K.: Wiithrich, K. TROSY and CRINEPT: NMR with large supramolecular structures in solution. Trends Biochem. Sci. 2000. *25*, 462–468.
3. Columbus. L.; Hubbell, W.L. A new spin on protein dynamics. Trends Biochem. Sci. 2002. *27*, 288–295.
4. Unger, V.M. Electron cryomicroscopy methods. Curr. Opin. Struct. Biol. 2001. *11*. 548–554.
5. Tang. L.: Johnson, J.E. Structural biology of viruses by the combination of electron cryomicroscopy and X-ray crystallography. Biochemistry 2002. *41*. 11517–11524.
6. Ehrlich. L.S.: Liu, T.; Scarlata. S.: Chu. B.: Carter, C.A. HIV-1 capsid protein forms spherical (immature-like) and tubular (mature-like) particles in vitro: Structure switching by pH-induced conformational changes. Biophys. J. 2001, *81*. 586–594.
7. Belghazi, M.; Bathany, K.: Hountondji, C.: Grandier-Vazeille, X.; Manon. S.; Schmitter, J.M. Analysis of protein sequences and protein complexes by matrix-assisted laser desorption/ionization mass spectrometry. Proteomics 2001. *1*, 946–954.
8. Grandier-Vazeille, X.; Bathany, K.: Chaipnepain, S.; Camougrand, N.; Manon. S.; Schmitter. J.M. Yeast mitochondrial dehydrogenases are associated in a supramolecular complex. Biochemistry 2001. *40*, 9758–9769.
9. Virchow. R. Zur Cellulose-Frage. Virchows Arch. 1854, *6*, 415–426.
10. Cohen, A.S.; Calkins. E. Electron microscopic observation on a fibrous component in amyloid of diverse origins. Nature 1959. *183*. 1202–1203.
11. Cohen. A.S.: Shirahama. T.: Skinner. M. Electron Microscopy of Amyloid. In *Electron Microscopy of Proteins*: Harris, J.R., Ed.: Academic Press: New York. 1982; Vol. 3, 165–205.
12. Sunde, M.; Blake. C.C.F. From the globular to the fibrous state: Protein structure and structural conversion in amyloid formation. Q. Rev. Biophys. 1998. *31*, 1–39.
13. Perutz, M.F.; Finch, J.T.: Berriman, J.; Lesk. A. Amyloid fibers are water-filled nanotubes. Proc. Natl. Acad. Sci. U. S. A. 2002. *99*. 5591–5595.
14. Dobson, C.M. Protein misfolding, evolution and disease. Trends Biochem. Sci. 1999, *24*. 329–332.
15. Gazit, E. "Korrekt gefaltete" Proteine—ein metastabiler Zustand? Angew. Chem. 2002. *114*, 267–269.
16. Rochet. J.C.: Lansbury. J.P.T. Arnyloid fibrillogenesis: Themes and variations. Curr. Opin. Struct. Biol. 2000. *10*. 60–68.
17. Hecht. M.H.; Richardson. J.S.; Richardson. D.C.; Ogden, R.C. De novo design, expression, and characterization of Felix: A four-helix bundle protein of native-like sequence. Science 1990. *249*. 884–891.
18. Hecht. M.H.: Richardson. J.S.; Richardson, D.C.: Ogden, R.C. De novo design. expression, and characterization of Felix: A four-helix bundle protein of native-like sequence. Science 1990, *249*, 973.
19. Mamtekar. S.: Hecht, M.H. The four-helix bundle: What determines a fold'? FASEB J. 1995. *9*. 1013–1022.
20. Kamtekar, S.: Schiffer. J.M.; Xiong. H.; Babik. J.M.; Hecht. M.H. Protein design by binary patterning of polar and nonpolar amino acids. Science 1993. *262*, 1680–1685.
21. Richardson, J.S.: Richardson, D.C. Natural beta-sheet proteins use negative design to avoid edge-to-edge aggregation. Proc. Natl. Acad. Sci. U. S. A. 2002, *99*. 2754–2759.
22. Xiong, H.: Bucliwalter. B.L.; Shieh. H.M.; Hecht. M.H. Periodicity of polar and nonpolar amino acids is the major determinant of secondary structure in self-assembling oligomeric peptides. Proc. Natl. Acad. Sci. U. S. A. 1995. *92*. 6349–6353.
23. West, M.W.; Wang, W.; Patterson, J.; Mancias, J.D.; Beasley, J.R.; Hecht, M.H. De novo amyloid proteins from designed combinatorial libraries. Proc. Natl. Acad. Sci. U. S. A. 1999, *96*, 11211–11216.
24. Xu, G.; Wang. W.; Groves. J.T.: Hecht. M.H. Self-assembled monolayers from a designed combinatorial library of the novo beta-sheet proteins. Proc. Natl. Acad. Sci. U. S. A. 2001, *98*, 3652–3657.
25. Wang, W.: Hecht, M.H. Rationally designed mutations convert de novo amyloid-like fibrils into monomeric beta-sheet proteins. Proc. Natl. Acad. Sci. U. S. A. 2002. *99*. 2760–2765.
26. Nesloney, C.L.: Kelly, J.W.A. 2,3′-Substituted biphenyl-based amino acid facilitates the formation of a monomeric beta-hairpin-like structure in aqueous solution at elevated temperature. J. Am. Chem. Soc. 1996. *118*, 5836–5845.
27. Thirumalai. D.; Klimov. D.K.: Dima, R.I. Emerging ideas on the molecular basis of protein and peptide aggregation. Curr. Opin. Struct. Biol. 2003. *13*, 146–159.
28. Yeates. T.O.: Padilla, J.E. Designing supramolecular protein assemblies. Curr. Opin. Struct. Biol. 2002. *12*. 464–470.
29. Hartgerink. J.D.; Beniash. E.: Stupp, S.I. Peptide-amphiphile nanofibers: A versatile scaffold for the preparation of self-assembling materials. Proc. Natl. Acad. Sci. U. S. A. 2002, 99. 5133–5138.
30. Handford, P.A.; Downing. A.K.; Reinhardt, D.P.; Sakai. L.Y. Fibrillin: From domain structure to supramolecular assembly. Matrix Biol. 2000. *19*. 457–470.
31. Ottani, *V.*; Martini, D.: Franchi. M.: Ruggeri. A.; Raspanti. M. Hierarchical structures in fibrillar collagens. Micron 2002. *33*, 587–596.
32. Moradian-Oldak, J.: Leung. W.: Fincham. A.G. Temperature and pH-dependent supramolecular self-assembly of ameiogenin molecules: A dynamic light-scattering analysis. J. Struct. Biol. 1998, *122*. 320–327.
33. Moradian-Oldak. J.: Paine. M.L.; Lei. Y.P.; Fincham, A.G.: Snead, M.L. Self-assembly properties of recombinant engineered amelogenin proteins analyzed by dynamic light scattering and atomic force microscopy. J. Struct. Biol. 2000, *131*. 27–37.
34. Jarchow, J.: Fritz, J.; Anselmetti. D.: Calabro. A.; Hascall, V.C.: Gerosa. D.: Burger, M.M.: Fernandez-Busquets, X. Supramolecular structure of a new family of circular proteoglycans mediating cell adhesion in sponges. J. Struct. Biol. 2000. *132*. 95–105.
35. Welker, R.; Hohenberg. H.: Tessmer, U.; Huckhagel, C.: Kraeusslich, H.-G. Biochemical and structural analysis of isolated mature cores of human immunodeficiency virus type 1. J. Virol. 2000, *74*, 1168–1177.

36. Lu, M.W.; Lin, C.S. Involvement of the terminus of grouper betanodavirus capsid protein in virus like particle assembly. Arch. Virol. 2003. *148*, 345–355.
37. Bowman, B.R.; Baker, M.L.; Rixon. F.J.; Chiu, W.; Quiocho, F.A. Structure of the herpesvirus major capsid protein. EMBO J. 2003. *22*, 757–765.
38. Duncan, R. The low pH dependent entry of avian reovirus is accompanied by two specific cleavages of the major outer capsid protein m2C. Virology 1996, *219*. 179–189.
39. Sastri, M.; Kekuuda, R.; Gopinath, K.; Kunar. C.T.R.; Jagath, J.R.; Savithri, H.S. Assembly of Physalis mottle virus capsid protein in *Escherichia coli* and the role of amino acid carboxy termini in the formation of icosahedral particles. J. Mol. Biol. 1997, *272*, 541–552.
40. Ou, W.C.; Chen, L.H.; Wang, M.; Hseu. T.H.; Chang. D. Analysis of minimal sequences on JC virus VP1 required for capsid assembly. J. Neurovirology 2001, *7*. 298–301.
41. Prasad, B.V.; Crawford, S.; Lawton, J.A.; Pesavento, J.; Hardy. M.; Estes, M.K. Structural studies on gastroenteritis viruses. Novartis Found. Symp. 2001. *238*, 26–37.
42. Suzuki. H. A hypothesis about the mechanism of assembly of double-shelled rotavirus particles. Arch. Virol., Suppl. 1996, *12*, 79–85.
43. Erk, I.; Huet, J.C.; Duarte, M.; Duquerroy. S.; Rey, F.; Cohen, J.; J, L. A zinc ion controls assembly and stability of the major capsid protein of rotavirus. J. Virol. 2003, *77*, 3595–3601.
44. Fotiadis. D.; Müller, D.J.; Tsiotis, G.; Hasler, L.; Tittmann, P.; Mini. T.; Jeno, P.; Gross, H.; Engel, A. Surface analysis of the photosystem I complex by electron and atomic force microscopy. J. Mol. Biol. 1998. *283*, 83–94.
45. Gavin, A.C.; Bosche. M.; Krause, R.; Grandi, P.; Marzioch, M.; Bauer, A.; Schultz, J.; Rick, J.M.; Michon. A.M.; Cruciat, C.M.; Remor. M.; Hofert, C.; Schelder. M.; Brajenovic. M.; Ruffner, H.; Merino, A.; Klein. K.; Hudak, M.; Dickson. D.; Rudi, T.; Gnau, V.; Bauch, A.; Bastuck, S.; Huhse, B.; Leutwein, C.; Heurtier, M.A.; Copley. R.R.; Edelmann, A.; Querfurth, E.; Rybin, V.; Drewes. G.; Raida. M.; Bouwmeester. T.; Bork, P.; Seraphin, B.; Kuster, B.; Neubauer, G.; Superti-Furga, G. Functional organization of the yeast proteome by systematic analysis of protein complexes. Nature 2002. *415*, 141–147.
46. Ho, Y.; Gruhler, A.; Heilbut, A.; Bader, G.D.; Moore, L.; Adams, S.L.; Millar, A.; Taylor, P.; Bennett, K.; Boutilier, K.; Yang, L.; Wolting, C.; Donaldson, I.; Schandorff. S.; Shewnarane, J.; Vo, M.; Taggart, J.; Goudreault, M.; Muskat. B.; Alfarano, C.; Dewar, D.; Lin. Z.; Michalickova, K.; Willems, A.R.; Sassi, H.; Nielsen, P.A.; Rasmussen, K.J.; Andersen. J.R.; Johansen, L.E.; Hansen. L.H.; Jespersen. H.; Podtelejnikov, A.; Nielsen, E.; Crawford, J.; Poulsen, V.; Sorensen, B.D.; Matthiesen. J.; Hendrickson. R.C.; Gleeson, F.; Pawson, T.; Moran, M.F.; Durocher, D.; Mann, M.; Hogue, C.W.; Figeys. D.; Tyers, M. Systematic identification of protein complexes in *Saccharomyces cerevisiae* by mass spectrometry. Nature 2002. *15*, 180–183.
47. Kakey, J.H.; Raggett, E.M. Measuring protein–protein interaction. Curr. Opin. Struct. Biol. 1998, *8*, 119–123.
48. Ursini. F.; Davies, K.J.; Maiorino, M.; Pal-asassi, T.; Sevanian. A. Atherosclerosis: Another protein misfolding disease? Trends Mol. Med. 2002, *8*, 370–374.
49. Lakdawala, A.S.; Morgan. D.M.; Liotta, D.C.; Lynn. D.G.; Snyder, J.P. Dynamics and fluidity of amyloid fibrils: A model of fibrous protein aggregates. J. Am. Chem. Soc. 2002. *124*, 15150–15151.
50. Antzutkin, O.N.; Leapman, R.D.; Balbach, J.J.; Tycko. R. Supramolecular structural constraints on Alzheimer's β-amyloid fibrils from electron microscopy and solid-state nuclear magnetic resonance. Biochemistry 2002. *41*. 15436–15450.
51. He, Y.; Chipman, P.; Howitt, J.; Bator, C.; Whitt. M.; Baker. T.; Kuhn, R.; Anderson, C.; Freimuth, P.; Rossmann. M. Interaction of coxsackievirus B3 with the full length coxsackievirus-adenovirus receptor. Nat. Struct. Biol. 2002, *8*, 874–878.
52. West, M.W.; Wang. W.; Patterson, J.; Mancias. J.D.; Beasley, J.R.; Hecht. M.H. De novo amyloid proteins from designed combinatorial libraries. Proc. Natl. Acad. Sci. USA 1999. *96*. 11211–11216.
53. Pandya. M.J.; Spooner, G.M.; Sunde, M.; Thorpe. J.R.; Rodger. A.; Woolfson, D.N. Sticky-end assembly of a designed peptide fiber provides insight into protein fibrillogenesis. Biochemistry 2000, *39*, 8728–8734.
54. Ogihara, N.L.; Ghirlanda, G.; Bryson. J.W.; Gingery, M.; deGrado, W.F. Design of three-dimensional domain-swapped dimers and fibrous oligomers. Proc. Natl. Acad. Sci., USA 2001, *98*. 1404–1409.
55. Padilla, J.E.; Colovos, C.; Yeates, T.O. Nanohedra: Using symmetry to design self-assembling protein cages. layers, crystals, and filaments. Proc. Natl. Acad. Sci., USA 2001. *98*, 2217–2221.
56. Wess, T.J.; Hammersley, A.; Wess. A.; Miller, A. Molecular packing of type I collagen in tendon. J. Mol. Biol. 1998, *275*, 255–267.

Protonated Aza-Macrocycles for Anion Complexation

José M. Llinares
Kristin *Bowman-James*
University of Kansas, Lawrence, Kansas, U.S.A.

INTRODUCTION

Anions are notoriously intractable targets for selective binding. Nonetheless, the field of anion coordination chemistry continues to grow after its early beginnings in the late 1960s, with the discovery by Park and Simmons that simple bicyclic diazakatapinands could encapsulate halide ions.'" Binding in the liatapinands and in polyammonium receptors. in general, is governed by electrostatic and hydrogen-bonding interactions between protonated amines and the anion guest. In the decades ensuing the initial discovery. many elegantly designed azamacrocycles were examined for various types of anion-binding properties. These cyclic receptors can be divided into three main categories: monocyclic, bicyclic, and polycyclic. Structures for various receptors cited are depicted in Chart 1 and are labeled numerically in the sequence in which they appear in the text.

MONOCYCLIC POLYAZAMACROCYCLES

Substrates for monocyclic receptors mainly include the following: I) simple inorganic anions—oxoanions, halides, pseudohalides, and other halo anions; 2) organic anions—dicarboxylates and nucleotides: and 3) anionic metal complexes.

Simple Inorganic Anions

Monocyclic polyamines are not especially selective in the binding of simple oxoanions and halides. Binding constants for singly charged anions with monocycles are usually small. if even measurable, as seen for a simple monocycle derived from a Schiff base condensation followed by reduction, **1**, Ar=*m*-xylyl (Fig. 1). However, affinity increases with increasing charge on the anion.[2] A layered structural motif consisting of alternating anions and cations is typical of many of the observed crystal structures.[2,3] In keeping with these findings, molecular dynamics studies indicate that monocycles tend to be somewhat flexible and subject to hydration effects,[4–6] thereby decreasing their effectiveness in selective anion binding. On the other hand. structural results for certain flexible. linear oxoanions. such as pyrophosphate and triphosphate, with monocycles such as **1** (Ar=*m*-furan and *m*-xylyl) indicate a tendency for these ions to thread the macrocycle.[7–9] High affinity is also observed, e.g., log $K_{[H_6L\,PP]/[H_6L][PP]}$=13.07 for **1** (Ar=*m*-xylyl, PP=$P_2O_7^{4-}$).[8]

Organic Anions

Monocyclic polyamines are considerably better receptors for more complex organic ions.[10–13] Even simple penta- and hexa-amine macrocycles were found to bind polycarboxylates and to show selectivity for certain dicarboxylates as opposed to monocarboxylates.[11] This binding preference for dicarboxylates was improved by linking two such macrocycles together to achieve a tethered ditopic receptor (**2**).[12] An effective strategy for selective binding of dicarboxylates of varying chain lengths was also found by placing spacer chains between two diethylenetriamine units, **3,** and by matching the length of the spacers to the $-(CH_2)_m-$ chain in the dicarboxylate. In this manner. the complementarity of the receptor can be fine-tuned to a targeted dicarboxylate, as demonstrated for α-dicarboxylates with chain length, m (Fig. 2). For m=3. the most stable complex was formed with a $-(CH_2)_7-$ chain; for m=5. a chain length of $-(CH_2)_{10}-$ was best. The binding constant, log K_s, was 4.4 in both cases.[13]

Nucleotide binding was also studied extensively after the 1981 report that polyammonium macrocycles bind nucleotides with high affinity.[10] Subsequent studies indicated that, in addition to binding nucleotides, monocyciic macrocycles such as 4 cataiyze the dephosphorylation of nucleotides. Certain metal ions such as Mg(II), Ca(II), and La(III) were found to provide regulation by stabilizing or increasing an observed phosphorylated macrocyclic (phosphoramidate) intermediate.[14] These findings, coupled with the observation that the attack of 4 on formyl phosphate led to *N*-formylation instead of *N*-phosphorylation of the macrocycle led to the use of this simple ligand in a multistep reaction involving formate activation, mimicking N^{10}-formyltetrahydrofolate synthetase.[14] Further studies of the chemistry between ATP and polyammonium macrocycles of varying ring

Encyclopedia of Supramolecular Chemistry
DOI: 10.1081/E-ESMC 120012720

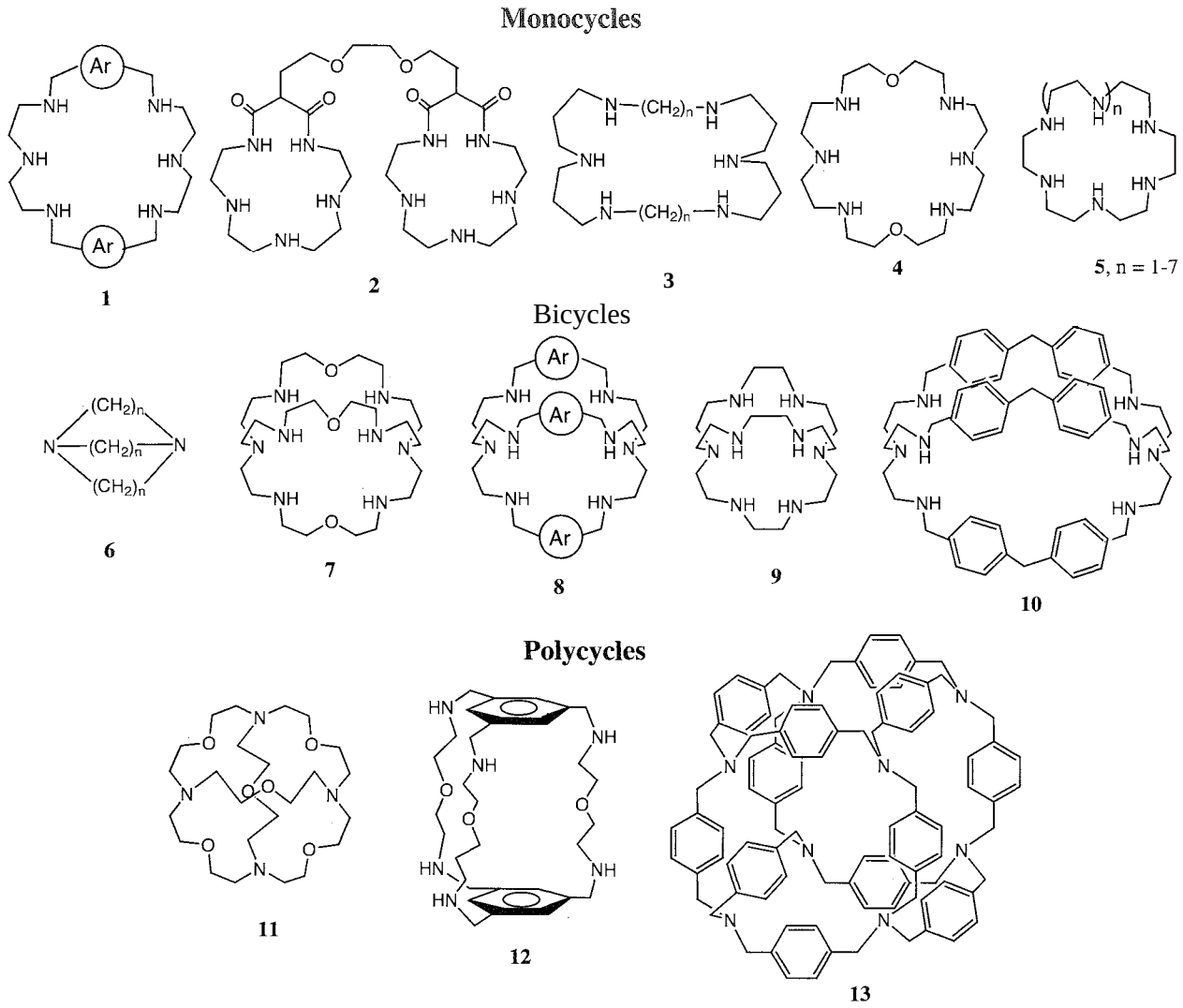

Scheme 1

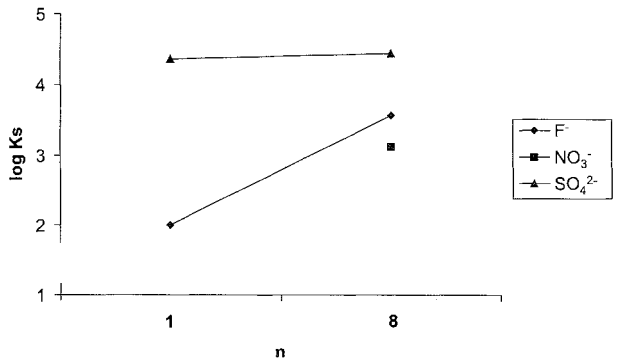

Fig. 1 Stability constants, log K_s, for binding of F^- (spherical), NO_3^- (trigonal planar), and SO_4^{2-} (tetrahedral) with monocycle **1** and bicycle **8**, $^-$(Ar = m-xylyl) in H_2O. No observable binding was observed for NO_3^- with **1**. Data were taken from Refs. [2] (NO_3^- and SO_4^{2-}) and [24] (F^-).

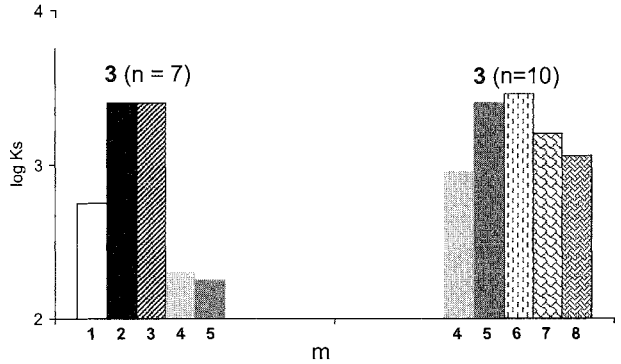

Fig. **2** Stability constants, log K_s, for dicarboxylate, $-O_2C-(CH_2)_m-CO_2-$, binding by **3**. The number in the legend *(m)* is the number of atoms separating the two terminal carboxylate groups, following this formula, $-O_2C-(CH_2)_m-CO_2$. Data were taken from Ref. [13].

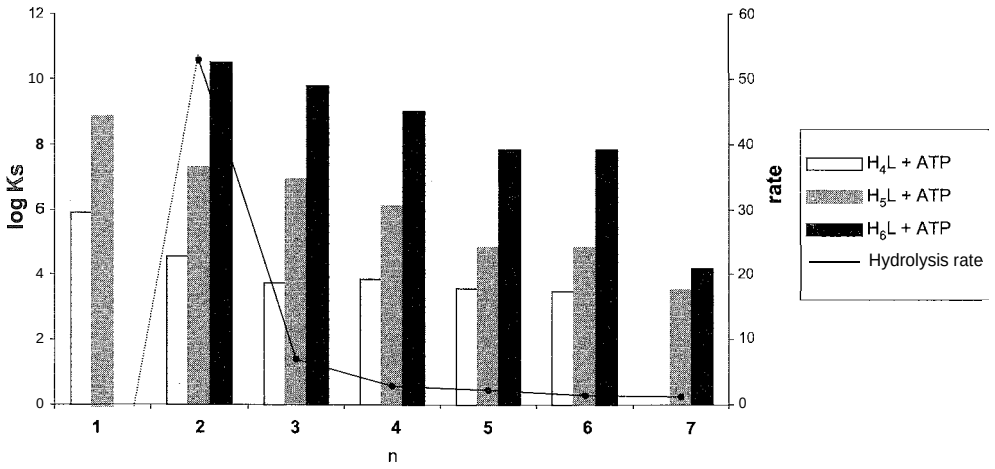

Fig. 3 Stability constants, log K_s, for ATP in H_2O with ***5*** (n=1–7). The solid line represents the first-order rate constant (min^{-1} x 10') for the hydrolysis of ATP catalyzed by ***5*** (n=2–7) at pH 7.0 and 70°C. The dotted line indicates the slow rate observed for 5, rz= 1, which was so slow as to not appear on the scale under those conditions. Data were taken from Ref. [15].

sizes (5) indicated an important correlation between size of the macrocycle and hydrolysis rate"'' (Fig. 3). By covalently attaching an additional recognition site consisting of a pendant acridine unit to enhance binding via a π-stacking effect, higher recognition for nucleotides was achieved. but catalysis was diminished.[16] Recognition of more complex anions such as dinucleotides, NAD, and NADP, was reported for 5 (n=2) and is proposed to occur by virtue of interaction of the receptor with the negatively charged phosphate portion of the dinucleotide.[17]

Anionic Metal Complexes

Large ring polyammonium monocycles also form complexes with a variety of transition metal anionic complexes.[10] Both square planar [e.g., $PdCl_4^{2-}$ and $Pt(CN)_4^{2-}$], and octahedral [e.g., $M(CN)_6^{n-}$; M=Fe, Co, Cr; and Ru: n=3 and 4] complexes were studied. Structural findings often indicate layered structures with protonated polyammonium macrocycles alternating with the anions in linear arrays.[18,19] However, an inclusion complex was observed for a $PdCl_4^{2-}$ complex with ***5***, n=5.[20] As anticipated, affinity tends to increase with increasing charge on the complex and increasing degree of protonation of the macrocycle (Fig. 4). For a given degree of protonation, however, the smaller macrocycles bind more effectively. Binding also tends to influence electrochemical[21] and photochemical[22] properties of these supercomplexes.

BICYCLIC POLYAZAMACROCYCLES

Binding constants for the azacryptands with anions are often two or more orders of magnitude higher than that observed for the corresponding monocycles. Even monoanions show significant affinities (Fig. 1).[1,22–29]

Halides and Pseudohalides

The first examples of bicyclic receptors forming inclusion complexes with anions were the katapinand halide complexes, 6. An equilibrium constant of K>10 was observed for the binding of the $-(CH_2)_{10}-$ bridged receptor with chloride.[1]

The field expanded with the introduction of the linear bis-tren azacryptand **7**,[23] which was found to be exceptionally complementary for encapsulating the linear azide ion, with an aqueous stability constant of log K_s=4.3. Crystallographic studies also indicated halide inclusion within the cavity of 7. While chloride and bromide were observed to be centrally located, fluoride was found to sit off-center, closer to one of the tren units.[23] This latter finding was attributed to the small size of the fluoride as being mismatched with that of the large azacryptand.

More recently, receptors derived from simple Schiff base synthetic strategies were found to bind fluoride and water in the cavity 8 (Ar=*m*-xylyl).[24] In a slightly larger cavity derived from a p-xylyl spacer, two fluorides were bound inside the cavity, bridged by a single water molecule in a type of cascade complex (Ar=*p*-xylyl).[25] The latter motif is reminiscent of the ditopic metal ion cascade complexes observed for these ligands.[30]

A very small azacryptand, 9, binds fluoride with almost unprecedented anion affinity and selectivity, log K=8.8 and log K_F/K_{Cl}=7.6 at pH 5.9.[26] The high binding constant was attributed to a perfect match of cryptand cavity and fluoride size, and it was speculated that the cavity was too small to admit other anions. Subsequent

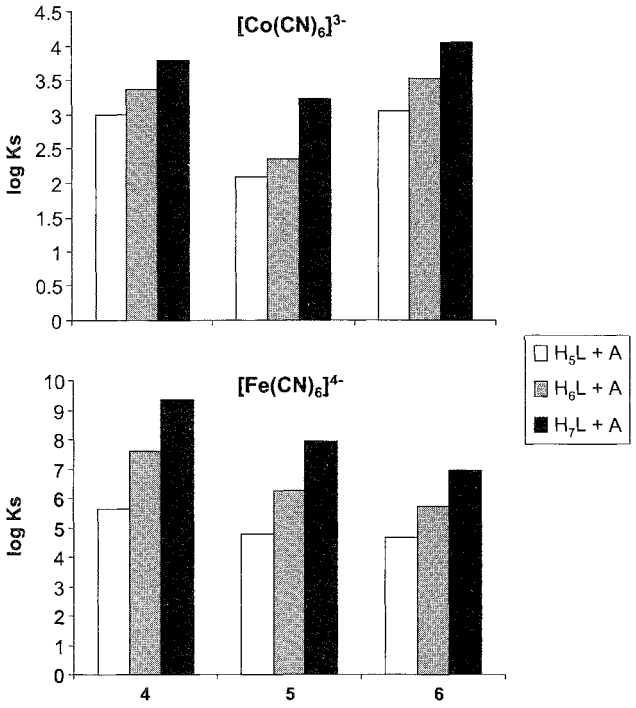

Fig. 4 Coinparison of stability constants, log K_s, for binding of $Co(CN)_6^{3-}$ (top graph) and $Fe(CN)_6^{4-}$ (bottom graph) with 5. as a function of size (n=4–6) and degree of protonation. Data were taken from Ref. [18].

studies, verified crystallographically, showed that the 9 also binds chloride internally at pHs below 2.5, presumably the point of addition of the sixth proton.[31]

Oxoanions

The first example of internal binding of an oxoanion was reported for a perchlorate encapsulated in 8 (Ar=furan).[28] Azacryptands display a variety of binding propensities with oxoanions. Even ditopic nitrate binding was observed with these versatile receptors (8, Ar=*m*-xylyl).[2,29]

Organic Anions

Azacryptands also bind nucleoiides strongly.[31] However, the bicycles are unlike the monocycles in that they are not effective hydrolysis catalysts. This inactivity was attributed to the presence of the steric constraints imposed by the cryptand cavity that might result in a lessened probability of forming a phosphorylated receptor intermediate. As noted, such an intermediate appears to be a key pathway in dephosphorylation, at least in some monocycles.

Dicarboxylates can also be encapsulated as reported for the crystal structure of terphthalate in 10.[32] In a series of linear chain dicarboxylates. $-O_2C(CH_2)_mCO_2-$, PO was found to bind adipate (m=4) better than the longer or shorter dicarboxylates of the series.

POLYCYCLIC POLYAZAMACROCYCLES

The macrotricyclic "soccer ball" ligand, 11, is perhaps the most famous of the polycyclic systems because of its versatility in binding cations such as NH_4^+, anions such as halides; and even a neutral water molecule, depending on its degree of protonation. It is especially well-suited for spherical recognition, incorporating halides inside its cavity with high affinities (log K=4.0) for Cl^-. A number of crystallographic and theoretical studies have been performed,[33] and the latter indicate a complex interplay involving anion and receptor hydration and dehydration, steric effects, and electrostatic interactions.[34]

Another structural motif effective in binding anions is that of two face-to-face 1,3,5-trisubstituted benzenes with bridges containing amines (12). These receptors were observed to bind small anions with some selectivity. In the majority of binding studies, monovalent species such as nitrate and chloride bind more weakly (log $K_s \sim 2.5$) compared to dianions such as sulfate (log $K_s \sim 6.0$).[35] This structural motif was expanded even further in the elegant azaparacyclophane (13). At pH 4, this cubane is tetraprotonated and binds anionic fluorescent molecules such as 1-anilinonaphthalene-8-sulfonate (ANS).[36]

CONCLUSION

The field of anion coordination chemistry has grown tremendously during the last three decades, from the discovery of the simple katapinand receptors to complex. cleverly designed polycyclic systems. Much of the current understanding of the chemistry of anion recognition is the result of key contributions provided by protonated aza-macrocycles, only some of which have been described in this overview. While many types of ligand frameworks now exist for anion recognition and binding, the role of the aza-macrocycles in the early development of this field will always be acknowledged.

ARTICLES OF FURTHER INTEREST

Halogen Bonding, p. 628
Macrocycle Synthesis, p. 830
Supramolecular Chemistry: Definition, p. 1401

REFERENCES

1. Park, C.H.: Simmons. H.E. Macrobicyclic amines. III. Encapsulation of halide ions by in, in-1. (*k*+2)-diazabicylo[*k.l.m*]alkane-ammonium ions. J. Am. Chem. Soc. 1968, *90*, 2431–2433.
2. Clifford. T.: Danby, A.; Llinares, J.M.: Mason, S.: Alcock. N.W.: Powell. D.; Aguilar. J.A.; Garcia-Espaiia, E.; Bowman-James. K. Anion binding with two polyammonium macrocycles of different dimensionality. Inorg. Chem. 2001. *40*. 4710–4720.
3. Cullinane, J.: Gelb, R.I.; Margulis, T.N.: Zompa, L.J. Hexacyclen complexes of inorganic anions: Bonding forces. structure, and selectivity. J. Am. Chem. Soc. 1982. *104*. 3048–3053.
4. Papoyan. G.; Gu, K.: Wibrkiewicz-Kuczera. J.; Kuczera. K.: Bowman-James. K. Molecular dynamics simulations of nitrate complexes with polyammonium macrocycles: Insight on phosphoryl transfer catalysis. J. Am. Chem. Soc. 1996. *118*. 1354–1364.
5. Boudon. S.: Decian. A.: Fischer. J.; Hosseini, M.W.: Lehn. J.-M.: Wipff. G. Structural and anion coordination features of macrocyclic polyammonium cations in the solid solution and computational phases. J. Coord. Chem. 1991.23. 113–135.
6. Wiórkiewicz-Kuczera, J.; Kuczera, K.: Bazzicalupi, C.: Bencini, A.: Valtancoli, B.: Bianchi. A.; Bowman-James, K. Solid state to solution: Crystal structure and molecular dynamics simulations of a polyammonium nitrate host. New J. Chem. 1999. *23*. 1007–1013.
7. Lu, Q.; Motekaitis. R.: Reibenspies. J.J.; Martell, A.E. Molecular recognition by the protonated hexaaza macrocyclic ligand 3,6,9,16,19,22-hexaaza-27,28-dioxatricyclo[22.2.$2^{11,14}$]octacosa-1(26),11.13.24-tetraene. Inorg. Chem. 1995. *34*. 4958 - 4964.
8. Nation, D.A.: Reibenspies, J.; Martell, A.E. Anion binding of inorganic phosphates by the hexaaza macrocyclic ligand 3,6,9,17,20,23-hexaazatricyclo[23.2.1.$1^{11,15}$]triaconta-1(29),11(30),12,14,25,27-hexaene. Inorg. Chern. 1996. *35*. 4597–4603.
9. Lu. Q.; Reibenspies, J.H.; Carroll, R.I.; Martell, A.E.; Clearfield. A. Interaction of mono- and triphosphate anions uith a protonated polyaza macrocycle and its Cu(II) complexes. Inorg. Chim. Acta 1998, 270. 207–215.
10. Dietrich, B.: Hosseini. M.W.; Lehn. J.-M.: Sessions, R.B. Anion receptor molecules. Synthesis and anion-binding properties of polyammonium macrocycles. J. Am. Chem. Soc. 1981. *103*. 1282–1283.
11. Kimura, E.; Sakonaka. A.; Yatsunamic, T.; Kodama, M. Macrocyclic polyamines as specific receptors for tricarboxylate-cycle anions. J. Am. Chem. Soc. 1981. *103*, 3041–3045.
12. Kimura. E.: Kuramoto. Y.: Koike, T.; Fujioka. H.; Kodama, M. A study of new *bis*(macrocyclic polamine) ligands as inorganic and organic anion receptors. J. Org. Chem. 1990. *55*. 42–46.
13. Hosseini. M.W.: Lehn, J.-M. Anion coreceptor molecules—Linear molecular recognition in the selective binding of dicarboxylate substrates by ditopic polyammonium macrocycles. Helv. Chim. Acta 1986, *69*, 587–603.
14. Mertes, M.P.; Mertes. K.B. Evolution of an enzyme mimic. Acc. Chem. Res. 1990. *23*, 413–418.
15. Bencini, A.; Bianchi. A.; Garcia-Espaiia. E.; Scott, E.C.; Morales, E.; Wang, B.; P. Mertes. M.; Bowman Mertes. K. Potential ATPase mimics by polyammonium macrocycles: Criteria for catalytic activity. Bioorg. Chem. 1992. *20*, 8–29.
16. Hosseini. M.W.; Blacker, A.J.: Lehn. J.-M. Multiple molecular recognition and catalysis. A multifunctional anion receptor bearing an anion site, an intercalating group. and a catalytic site for nucleotide binding and hydrolysis. J. Am. Chem. Soc. 1990, *112*, 3896–3904.
17. Doménech. A.: Garcia-Espaiia, E.; Ramirez. J.A.: Celda, B.: Martinez. M.C.; Monlebn, D.: Tejero, R.; Bencini. A.: Bianchi. A. A thermodynamic, electrochemical and molecular dynamics study of NAD and NADP recognition by 1,4,7,10,13,16,19-heptaazacyclohenicosane ([21]ane N_7). J. Chem. Soc., Perkin Trans. 2 1999. 23–32.
18. Bianchi. A.: Micheloni. M.: Paoletti. P. Large polyazacycloalkanes: Ligational properties and anion coordination chemistry. Pure Appl. Chem. 1988. *60*. 525–532.
19. Bencini; A.; Bianchi. A.; Dapporto. P.: Garcia-Espafia. E.; Micheloni. M.; Ramirez. J.A.: Paoletti, P.: Paoli. P. Thermodynamic and structural aspects of the interaction between macrocyclic polyammonium cations and complexed anions. Inorg. Chem. 1992, *31*. 1902–1908.
20. Bencini, A.; Bianchi, A.; Dapporto, P.; Garcia-Espaiia, E.; Micheloni, M.: Paoletti. P.; Paoli. P. $(PdCl_4)^{2-}$ Inclusion into the deca-charged polyammonium receptor (H_{10}[30]aneN_{10}=1,4,7,10,13,16,19,22,25,28-deca-azacyclotriacontane). J. Chem. Soc., Chem. Commun. 1990, 753–755.
21. Peter, F.: Gross. M.: Hosseini. M.W.: Lehn, J.-M. Redox properties of metalhexacyanide anions complexed by macrocyclic polyammonium receptor molecules. J. Electroanal. Chem. 198%. *144*, 279–292.
22. Pina. *F.;* Parola, A.J. Photochemistry of supramolecular species involving anionic coordination compounds and polyammonium macrocyclic receptors. Coord. Chem. Rev. 1999. *185–186*. 159–165.
23. Dietrich. B.: Guilhem, J.: Lehn. J.-M.: Pascard, C.: Sonveaux, E. Molecular recognition in anion coordination chemistry. structure. binding constants and receptor-substrate complementarity of a series of anion cryptates of a inacrobicyclic receptor molecule. Helv. Chim. Acta 1984. 67. 91–104.
24. Aguilar, J.A.: Clifford. T.; Danby, A.; Llinares. J.M.: Mason, S.: Garcia-Espafia. E.: Bowman-James. K. Fluoride ion receptors: A comparison of a polyammoniurn monocycle versus its bicyclic corollary. Supramolec. Chem. 2001, *23*. 405–417.
25. Hossain. M.A.; Llinares, J.M.: Mason, S.: Morehouse, P.: Powell, D.: Bowman-James, K. Parallels in cation and anion coordination: A new class of cascade complexes. Angew. Chem.. Int. Ed. 2002. *41*. 2335–2338.
26. Reilly, S.D.; Khalsa. G.R.K.; Ford. D.K.; Brainard. J.R.:

Hay, B.P.: Smith, P.H. Octaazacryptand complexation of the fluoride ion. Inorg. Chem. **1995,** 34, 569–575.
27. Hossain, M.A.: Llinares, J.M.; Miller, C.; Bowman-James, K. Further insight to selectivity issues in halide binding in the tiny octaaza cryptand. Chem. Commun. 2000. 2269–2270.
28. Morgan, G.; McKee, V.: Nelson, J. Caged anions: Perchlorate and perfluoroanion cryptates. J. Chern. Soc., Chern. Commun. **1995.** 1649–1652.
29. Mason. S.: Clifford, T.; Seib, L.: Kuczera, K.; Bowman-James, K. Unusual encapsulation of two nitrates in a single bicyclic cage. J. Am. Chem. Soc. **1998,** *120.* 8899–8900.
30. Lehn. J.-M. Dinuclear cryptates: Dimetallic inclusion complex concepts—Design-prospects. Pure Appl. Chem. **1980.** *52,* 2441–2459.
31. Hosseini, M.W.; Lehn, J.-M.: Mertes, M.P. Efficient molecular catalysis of ATP hydrolysis by protonated macrocyclic polyamines. Helv. Chim. Acta **1984.** 66, 2454–2466.
32. Lehn, J.-M.; Méric, R.; Vigneron, J.-P.: Bkouche-Waksman, I.: Pascard. C. Molecular recognition of anionic substrates. Binding of carboxylates by a macrobicyclic coreceptor and cryrtal structure of its supramolecular cryptate with the terephthalate ion. J. Chern. Soc., Chem. Commun. **1991.** 2762–2771.
33. Graf, E.; Lehn, J.-M. Anion cryptates: Highly stable and selective macrotricyclic anion inclusion complexes. J. Am. Chem. Soc. **1976.** *98.* 6403–6405.
34. Owenson. R.D.; MacElkro. R.D.; Pohorille, A. Molecular dynamics study of ion capture from water by a model ionophore. tetraprotonated cryptand SC24. J. Am. Chem. Soc. **1988,** *110.* 6992–7000.
35. Fujita, T.; Lehn, J.-M. Synthesis of dome-shaped cyclophane-type macrotricyclic anion receptor molecules. Tetrahedron Lett. **1988,** 29, 1709–1712.
36. Murakami. Y.: Hayashida. O.; Ito. T.; Hisaeda, Y. Molecular recognition by novel cage-type azaparacyclophanes bearing chiral binding sites in aqueous media. Pure Appl. Chem. **1993.** *65.* 551–556.

Pyrrole- and Polypyrrole-Based Anion Receptors

Philip A. **Gale**
University of Southampton, Southampton, United Kingdom

Jonathan L. Sessler
University of Texas at Austin, Austin, Texas, U.S.A

Salvatore **Camiolo**
University of Southampton, Southampton, United Kingdom

INTRODUCTION

Pyrrole is an attractive hydrogen bond donating moiety that has a unique role to play in the design of anion receptors. Unlike amides, ureas, and similar functional groups that often self-associate via C=O···HN interactions, pyrrole does not contain a hydrogen bond acceptor. As such. it does not compete with itself for the hydrogen bonds used to bind potential anionic guests. In spite of this attractive feature, it is only in the last decade that pynoies and pyrrole-containing systems have begun to see application in the area of anion recognition. The first hint that this class of compounds could prove useful as anion receptors came in 1990. when Sessler and Ibers[1] succeeded in crystallizing the diprotonated form of sapphyrin, a pentapyrrolic expanded porphyrin, first prepared by Woodward and coworkers.[2] While expecting to obtain the *bis*-PF_6-salt, what Sessler and Hbers actually found was a mixed F^--PF_6^- complex, wherein the fluoride anion was centrally bound within the diprotonated sapphyrin core. Following this initial serendipitous finding. considerable effort was devoted to developing first sapphyrin and other expanded porphyrins as anion-binding agents and then, subsequently. a range of other pyrrole-based systems.

This work, which has flourished as the result of contributions from numerous research groups. served to establish that pyxole-containing entities far less complex than expanded porphyrins can act as effective anion receptors. In fact, Gale and coworkers recently demonstrated that pyrrole can stabilize an anion complex, at lease in the solid state. Specifically, these latter workers succeeded in elucidating the crystal structure of a pyrrole-chloride complex prepared by crystallizing tetramethylammonium chloride from pyrrole (Fig. 1a).[3] In this structure, direct hydrogen bonding interactions between the chloride anion and two pyrrole NH protons were seen (N···Cl=3.241 Å), as well as ones involving the tetramethylammonium cation. Unfortunately, these interactions were found not to persist in dichloroinethane solution for simple pynoles, at least not to an appreciable extent,[4] underscoring the need to incorporate pyrrole into a complementary host framework in order to bind anions effectively in solution. In this entry, the chemistry of pyrrole-based anion receptors is reviewed, starting from the simplest and moving to the more complex. While this presentation order deviates from that in which many of the systems in question were first introduced historically, we think it provides a better backdrop against which the current state-of-the-art in the field may be most fully appreciated.

ACYCLIC PYRROLIC AND POLYPYRROLIC RECEPTORS

In some respects, the simplest approach to generating pyrrole-based anion receptors involves modifying the pyrrole ring with groups capable of increasing the strength of the receptor-anion interaction. Not surprisingly. this approach attracted the interest of a number of research groups in the last decade. For instance. recently, Gale and coworkers prepared and studied a variety of simple 2,5-diamidopyrrole derivatives, including **1** and **2**.[5] Compounds **1** and 2 proved selective for oxoanions in polar organic solvent. However. they displayed some differences in their individual binding characteristics, with peak association constants of 2500 M^{-1} being

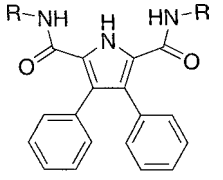

1 R = n-Bu
2 R = Ph

Encyclopedia of Supramolecular Chemistry
DOI: 10.1081/E-ESMC 110012773

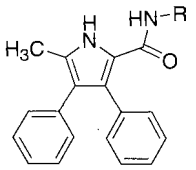

3 R = n-Bu
4 R = Ph

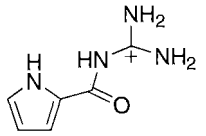

5

displayed by Compound 1 when binding benzoate anions in acetonitrile-d_3 while a corresponding K_a value of 1450 M^{-1} was observed for the binding of dihydrogenphosphate by Compound 2 in DMSO-d_6/H_2O 0.5%.

In order to confirm the participation of the two amide groups and the pyrrolic NH group in the complexation process, Gale also produced a series of monoamide pyrrole derivatives (compounds 3 and 4).[6] Solution studies revealed that these compounds, while still binding

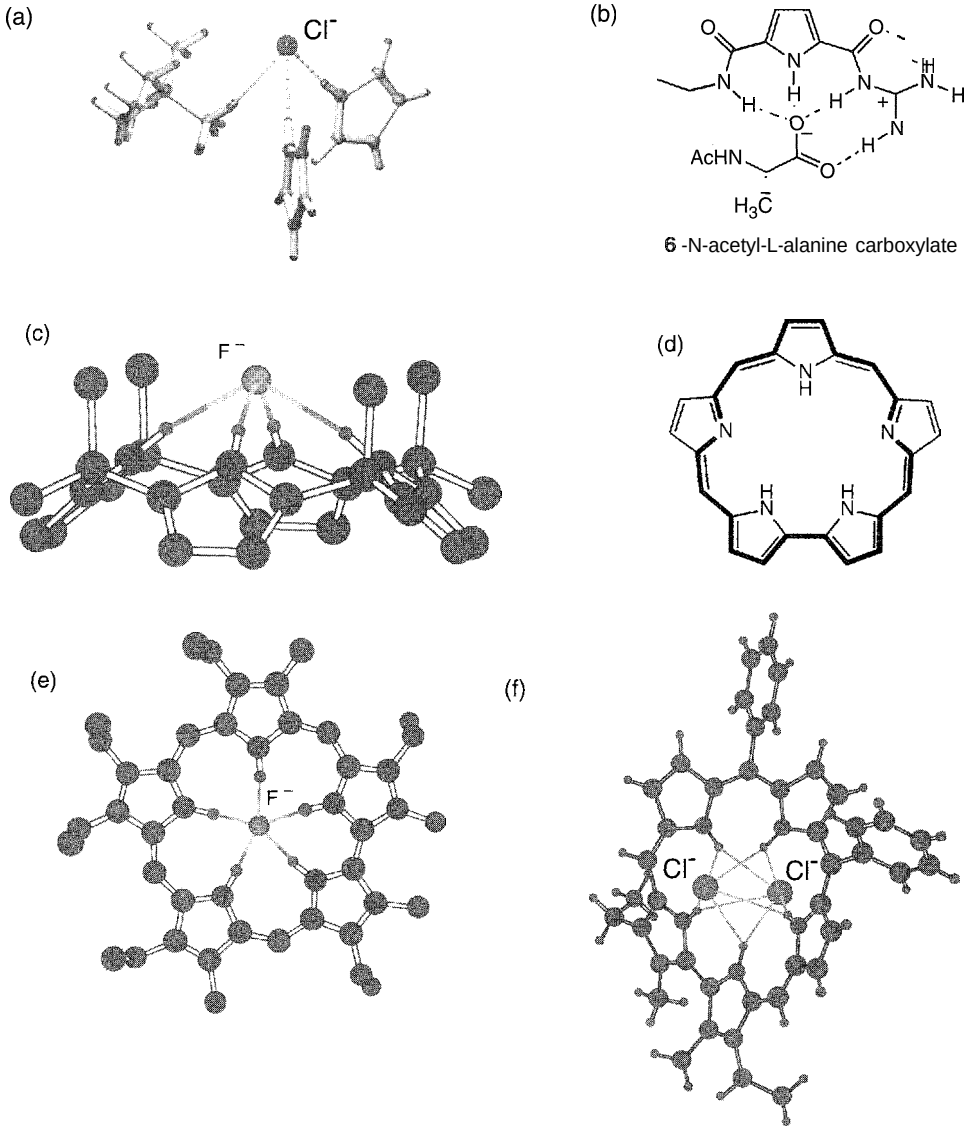

Fig. 1 (a) Chloride coordination environment in tetramethylammonium chloride-(pyrrole)$_2$ (Copyright Royal Society of Chemistry 2001, reproduced with permission); (b) the structure of 6-N-acetyl-L-alanine carboxylate: (c) the fluoride complex of *meso*-octamethylcalix[4]pyrrole; (d) the sapphyrin skeleton: (e) a fluoride-sapphyrin complex: and (f) a bis-chloride sapphyrin complex illustrating the perching binding mode. (View *this art* in color *at www.dekker.com.*)

oxoanions selectively over halides, displayed association constants for the binding of benzoate that were at least an order of magnitude lower did their *bis*-amide analogues, 1 and 2. This finding thus provided important support for the postulate that cooperation between the three NH groups present in 1 and 2 serves to enhance the anion-binding process.

Schmuck and coworkers reported a series of pyssole-functionalired guanidinium species (e.g., Compound **5**)[7] that are excellent receptors for carboxylates. In DMSO solution, the association constant for the formation of the acetate complex of receptor **5**, proved too high to measure accurately ($K>10^6\ M^{-1}$). By moving to a more polar solvent mixture (50% water-DMSO), however, it proved possible to determine the association constant; it was found to be approximately $10^3\ M^{-1}$.[7]

Schmuck also reported the synthesis of a pyrrole-based receptor 6 for *N*-acetyl-α-amino acid carboxylates that functions in aqueous solution.[8] Compound 6 consists of a pyrrole ring substituted in the 2-and 5-positions by an amide group and a guanidinium moiety (Fig. lb). In this case, acetate was found to be the best bound of all the carboxylate anions studied (presumably due to the absence of unfavorable steric interactions). A number of *N*-acetyl-α-amino acid carboxylate anions were also studied (Fig. lb). The identity of the side chain present in these amino acid derivatives presumably serves to modulate the strength of the anion-receptor complex with, for instance, p-stacking interactions between the acylguanidinium residue of the receptor and the aromatic ring of phenylalanine serving to enhance the stability of the 6-Ac-L-Phe complex.

Acyclic pyrrolic optical sensors were recently reported by Sessler and coworkers. Specifically, these researchers investigated the anion complexation properties of dipyrrolylquinoxaline 7 using a variety of anionic guest species including fluoride, chloride, and dihydrogenphosphate.[9] While the addition of 100 molar equivalents of the latter two anionic species to a dichloromethane solution of Compound 7 did not elicit any evident color change. the addition of fluoride anion led to a dramatic yellow to purple color change not only in dichloromethane, but also in DMSO solution. This phenomenon, which is accompanied by a quenching of the fluorescence. was rationalized in terms of the orbital overlap between the pyrroles and the quinoxaline subunits being changed upon complexation of the fluoride anion. The use of 3,4-difluoropyrrole in the synthesis leads to compound 8 that showed an increased affinity for the same anions and a higher selectivity for dihydrogenphosphate over chloride.[10] Hence, Compound **8** shows a naked-eye yellow-to-orange color change upon addition of 100 molar equivalents of fluoride or dihydrogenphosphate anions in dichloromethane solution, and does not undergo any change of color in the presence of the same concentration of chloride anion.

In nature, pyssole also plays a role in the chemistry of anionic species. A class of tripyrrolic linear oligomers (the prodigiosins, e.g., 9), red pigments produced by microorganisms like *Streptomyces* and *Serratia*, and some of its derivatives, are believed to symport HCl and so raise intralysosomal pH.[11] Currently, prodigiosins are being explored for their potentials in treating neoplastic disease and for their potential immunosuppressive activity.[12,13]

MACROCYCLIC PYRROLIC AND POLYPYRROLIC RECEPTORS

Pyrrole-containing macrocycles represent a class of compounds that are widely studied by an increasing number of researchers. In addition to the work with expanded porphyrins and other polypyrrolic systems discussed further in this entry, Sessler and coworkers generated a number of macrocyclic systems containing more isolated pyrrolic subunits. One of the more interesting of these is the bridged dipyrrole *ansa*-ferrocene **10**.[14] This compound contains two pyrrolic NH and two amidic NH groups that combine to make it and its analogues efficient anion receptors. In the specific case of 10, Sessler reported that the binding stoichiometry was dependent on the size of the anionic guest: Job plots highlighted a 2:1 ratio (anion-to-host) for fluoride and a 1:1 ratio for the other anions (chloride, bromide, hydrogensulfate, and dihydrogenphosphate). Quantitative

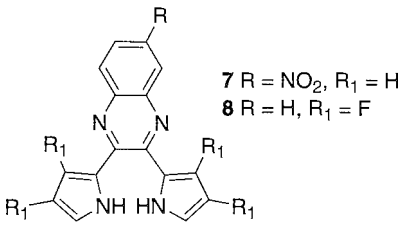

7 R = NO_2, R_1 = H
8 R = H, R_1 = F

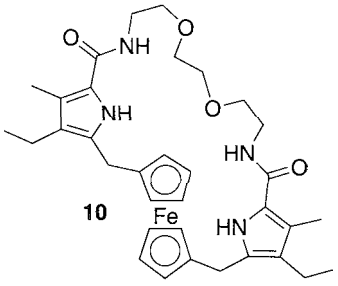

10

^{1}H-NMR titration experiments also revealed that this macrocyclic receptor possessed an inherent affinity for dihydrogenphosphate, fluoride and chloride over a range of other studied anions. These findings were corroborated by electrochemistry studies that allow detection of a coordinated anionic species through specific cathodic shift of the ferrocene–ferrocenium redox couple. The largest shift was observed in the presence of dihydrogenphosphate anions (136 mV) followed by fluoride and chloride (80 and 24 mV, respectively). Because these observed shifts reflect a number of chemical events. including relative binding to the oxidized ferrocenium and neutral ferrocene forms of the macrocycle, they are not a direct measure of binding per se. Nonetheless, the qualitative correspondence between the electrochemical and NMR analyses is gratifying and is inspiring a range of further work. Simple polypyrrole films were recently prepared and shown to respond electrochemically to the presence of substoichiometric quantities of anions.[15]

Porphyrinogens are a well-known class of compound that have been in the literature for more than a century. However. in the last decade. these molecules emerged as a particularly useful and important class of anion receptors, in part, because they are incredibly easy to make. Specifically. acid catalyzed condensation of pyrrole with a ketone leads to the formation of a tetrapyrrolic macrocycle that is reasonably stable to oxidation and therefore cannot be regarded as a precursor to porphyrin. Rather, they bear a strong structural similarity to calix[4]arenes, a congruence that prompted the authors to re-name these systems as calix[4]pyrroles.[4,16,17] In contrast to the calix[4]arenes, however. meso-octamethylcalix[4]pyrrole **11** and other structurally similar calix[4]pyrroles were found to bind anions such as fluoride and chloride via the formation of four convergent pyrrole-anion hydrogen bonds (Fig. 1c). Wow extensively reviewed, calix[4]pyrroles are used for a variety of applications, including sensing and anion separation technologies.[18]

Acid-cataiyzed condensation of 3,4-difluoropyrrole with acetone produces octailuorinated calix[4]pyrrole that shows enhanced affinity and selectivity for anionic species.[10] Compound **12**, for example, proved to be a better anion receptor than **11**. binding fluoride, chloride,

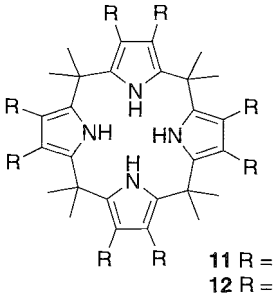

11 R = H, n =1
12 R = F, n =1

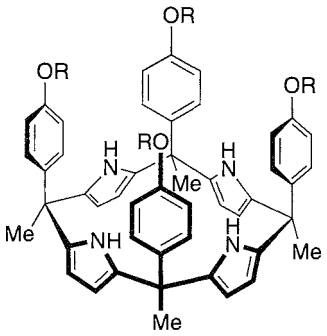

13 R = H
14 R = CH_2COOEt
15 R = CH_2CONEt_2

and dihydrogenphosphate anions with higher association constants than the corresponding unsubstituted systems; they also displayed an increased selectivity for chloride anion over hydrogenphosphate.

In 1999, Sessler and coworkers and, independently, Floriani and coworkers, reported the synthesis of deep-cavity calixpyrroles (e.g., **13**) formed from the condensation of 4-hydroxyacetophenone and pyrrole.[19,20] The $\alpha\alpha\alpha\alpha$-isomer of this species may be isolated by column chromatography or by fractional crystallization. Gale and coworkers recently reported the synthesis of ''super-extended cavity'' calix[4]pyrroles **14** and 15 in which the selectivity for fluoride is considerably increased in DMSO solution.''' No other anion is bound in this solvent, even in high concentrations (i.e., substoichiometric quantities of fluoride are bound in the presence of 100 equivalents of chloride that do not interact with the receptor).

In contrast to what is true in the case of the non-fluorinated calix[*n*]pyrroles where it has proven difficult to isolate species with $n > 4$. the synthesis of Compound 12 led to the two isolable and kinetically stable higher-order

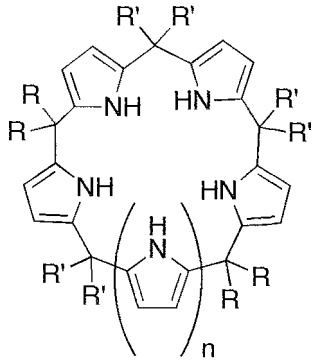

16 R = R' = F, n = 1
17 R = R' = F, n = 4
18 R = R' = H, n = 4
19 R = Ph, R' = Me n = 2

by-products, namely. the calix[5]pyrrole **16** *and the* calix[8]pyrrole **17**.[22] *Chloride was selectively* co-ordi*nated by compound* **16** *with an association constant of* 41.000 M^{-1} *in acetonitrile containing* 0.5% D_2O, *a value that proved to be a factor of four greater than recorded using the* corresponding *(but smaller)* octafluorocalix[4]-pyrrole **12**.

*Other approaches to the synthesis of higher-order calixpyrroles were pursued. For instance. the synthesis of meso-*dodecamethylcalix[6]pyrrole *18 from the previously known furan-based analogue was reported by Kohnke and coworkers."''* This *higher-order calixpyrrole was found to be a better receptor for chloride than the corresponding meso-*octamethylcalix[4]pyrrole *11, probably due to the larger core size of the macrocycle. Transport experiments from an aqueous solution to a DCM solution also revealed Compound 18 to be ca. 10 times more selective for chloride anion than Compound 11. Meanwhile, Eichen used a step-wise procedure to prepare the* calix[6]pyrrole **19** *and demonstrated that it shows a selectivity for larger anions. Specifically,* ^{1}H-NMR *titration experiments carried out in* acetonitrile-chloroform (1:9) *revealed that this system shows a preference for iodide anion over the other* halides.[24]

Recently, Sessler and coworkers reported the first example of cryptand-like calix[4]pyrrole (**20**).[25] *Compound 20 provides three identical binding cavities, leading to the consideration that it could stabilize* anion-*receptor complexes of* 1:1, 1:2, *or 1:3 stoichiometry in solution. In point of fact,* ^{1}H-NMR *experiments carried out in* dichloromethane-d_2 *and* THF-d_8 *revealed* host–*guest* stoichiometries *that* were *even more complicated and depended directly upon the anion considered. For instance. fluoride. when added as an anionic guest, was found to be bound to six of the nine pyssolic subunits.* presumably *in a* 1:1 *fashion. By contrast, it was proposed that the chloride anion interacts with two molecules of Receptor 28 in* solution (i.e., 2:1 *host-to-anionic guest binding stoichiometry)* and is *bound with a stability constant of 3.08 x 106* M^{-2} *in* dichloromethane-d_2 so*lution. Finally. a* 1:2 *(host-to-guest) stoichiometry was observed* upon *addition of nitrate with the stability constants* K_1 *and* K_2 *being* 1740 *and 420* M^{-1}, *respectively, in* dichloromethane-d_2 *solution.*

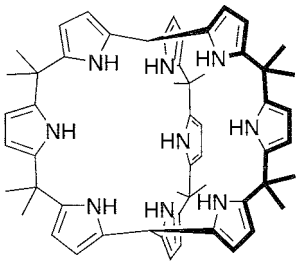

20

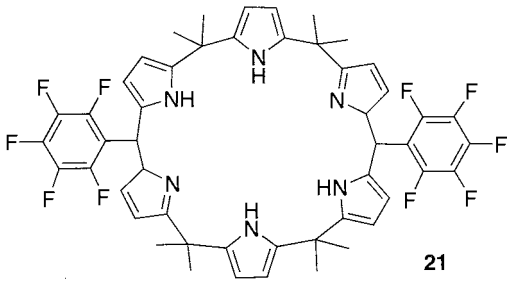

21

In the year 2000. Sessler et al. reported the synthesis of several so-called calix[*n*]phyrins, *macrocyclic compounds that may be regarded as hybrids of* calixpyrroles *and* porphyrins.[26] *Compound 21, a novel hexapysrolic system, was generated by reaction of* pentafluorobenzalde*hyde with an appropriate* tripyrrane *precursor (obtained, in turn, from the TFA acid-catalyzed condensation of pyrrole and acetone). The crystal structure of this compound reveals a molecule of water bound to the pysrolic NH protons, a finding that led to the suggestion that this system could* function *as* an *anion receptor. However. no interaction was observed between Compound* **21** *and any of a range of targeted anions (chloride. bromide, iodide, nitrate. hydrogensulfate), at least when this putative receptor was studied in its neutral form. On the other hand, both the mono- and bis-*protonated *forms were found to interact with chloride,* bromide, *and iodide anions. Unfortunately, only in the case of the latter anion and only when 21 was fully* (i.e., *di-) protonated was evidence for the formation of a clean* 1:1 *host–guest complex obtained; in this instance. an association constant of ca. 8 x* 107 M^{-1} *was estimated for a binding process involving the interaction between iodide anion and diprotonated* **21** *in acetone solution.*

Modified porphyrins have *been used to bind* anions *selectively. In* 2001, *Swager and coworkers reported the synthesis of the doubly strapped* porphyrin **22**;[27] *this compound proved to be able to coordinate two fluoride*

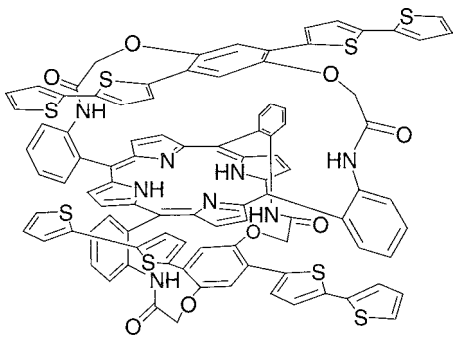

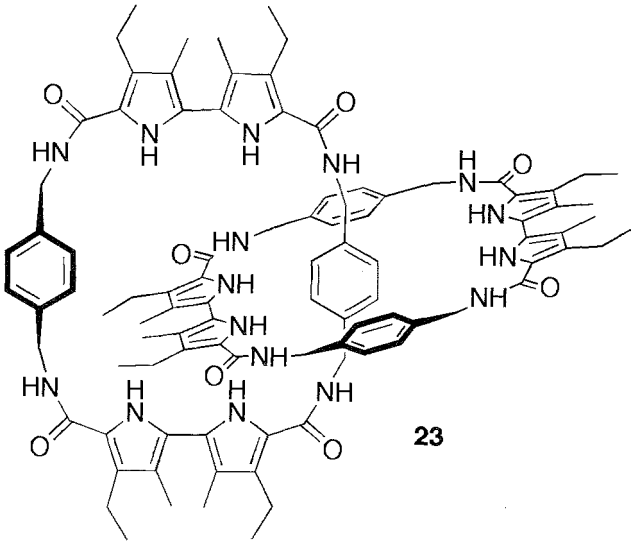

23

anions via a cooperative binding process in dichloromethane solution. Addition of larger anion such as chloride, bromide, iodide, acetate. cyanide, and dihydrogen phosphate, did not lead to perturbation of the UV spectrum. leading to the suggestion that they were not appreciably bound.

Sessler. Vogtle. and coworkers reported the first example of a dipyrrole-based[2]catenane.[28] Compound 23 was synthesized from the appropriate bipyrrole acyl chloride and p-xylenediamine building blocks. ^{1}H, ^{13}C, and ^{19}F-NMR studies carried out in 1,1,2,2-tetrachloroethane-d_2 provided evidence consistent with this compound being able to bind fluoride anions effectively as the result of changing its conformation in solution to accommodate the guest anionic species. Even more interesting results came from the coordination studies carried out in 1,1,2,2-tetrachloroethane-d_2. In this solvent. it was found that anionic species, such as chloride and dihydrogenphosphate, are bound to Compound 23 with a stability constant higher than that of fluoride. These findings led to the suggestion that these larger anions may be binding between the two rings of the catenane.

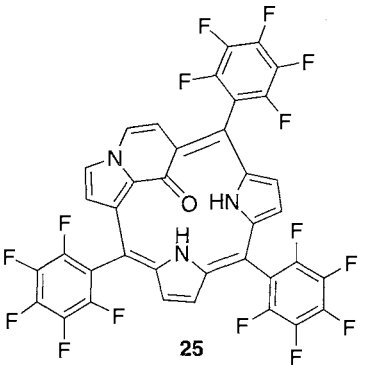

25

The tetrapyrrolic macrocycles discussed so far all contain an arrangement of inward-pointing nitrogens within the molecule core. Recently, N-confused porphyrins. tetrapyrrolic macrocycles in which some of the pyrrolic subunits are linked through at least one β position, were studied by a number of groups including Latos-Gražyński,[29] and the team of Osuka, Furuta, and coworkers.[30] One example of this class of compounds. tetrapyrrole 24, was synthesized via the acid-catalyzed condensation of an N-confused dipyrromethane with pentafluorobenzaldehyde. While this product proved to be stable in air at room temperature, treatment of 24 with $SnCl_2$ for 8 h while heating in benzene at reflux was found to give rise to the fused system 25 in 6% yield. This latter compound proved capable of coordinating anionic species with association constants comparable to those of typical: unsubstituted calix[4]pyrroles (e.g., $K_a \approx 10^4\ M^{-1}$ for fluoride anion in dichloromethane-d_2).

The potential advantages associated with the presence of a large central binding core containing a large number of potentially coordinating heteroatoms led to a renewed interest in expanded polypyrrolic macrocycles. Sapphyrin (Fig. Id). the first pyrrole-based anion receptor to be characterized as such (c.f., "Introduction"), belongs to this class of compound and remains one of the better studied of all anion-binding agents.[31] The synthesis of

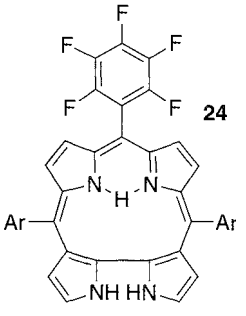

24

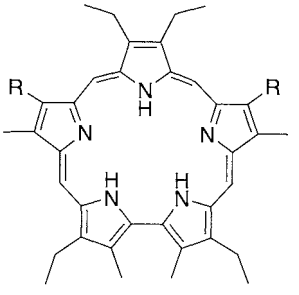

26 R = Et
27 R = $(CH_2)_2CH_2OH$

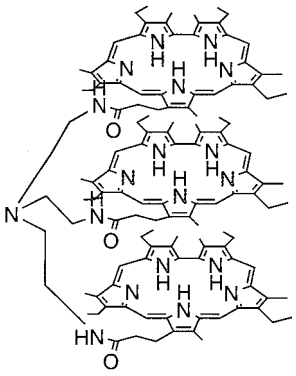

28

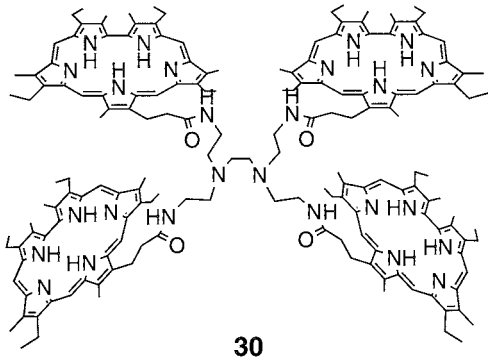

30

these compounds (e.g., 26, 27), which was recently reviewed,[31] was achieved by a variety of means, with those based on direct condensations of pyrrole and appropriately chosen linear oligopyrroles remaining the most popular. Sapphyrins are planar, rigid molecules that possess an aromatic 22 x-electron periphery. Sessler and coworkers reported a complete structural and solution study of this class of compound.[32,33] As noted in the introduction. the diprotonated forms of sapphyrins are capable of encapsulating fluoride in the solid state, holding the anion by a pentagonal array of N–H···F hydrogen bonds within a ca. 5.5 Å diameter core (Fig. 1e). Other anions are also coordinated by the diprotonated formo f sapphyrin but are not centrally bound. as is true for fluoride anion. For example, solid-state studies of the *bis*-HCl salt of sapphyrin revealed the presence of a 2:1 (chloride-to sapphyrin) complex with the two anions being held by N–H···Cl hydrogen bonds ca. 1.8 Å above and below the rnacrocycle (Fig. 1f). Presumably as a result of this structural difference and the enhanced ability of fluoride anion to act as a hydrogen bond acceptor relative to other anions, the diprotonated form of sapphyrin acts as an unique and selective fluoride anion receptor, exhibiting a selectivity at least $\geq 10^3$ relative to chloride or bromide.

The selectivity displayed for F-relative to other halide anions encouraged Sessler and coworkers to investigate whether sapphyrin would act as a fluoride anion carrier in a model three-phase H_2O-CH_2Cl_2-H_2O bulk liquid membrane transport system.[34] When two aqueous solutions; with different fluoride anions concentrations, were separated by a dichloromethane solution, slow transfer of fluoride anions from the more concentrated to less concentrated aqueous phases was observed, due to simple diffusiono f the anionic species. The addition of an organic-soluble sapphyrin to the dichloromethane phase. however. led to a considerable increase in F-transport flux o (greater than 100-fold in the best of cases), at pH 7.0. a regime wherein sapphyrin is known to be mono-, not di-, protonated.

Diprotonated sapphyrins were also found to bind rnonobasic phosphate anions in solution and in the solid state.[32] The same proved true for monoprotonated sapphyrins, at least in polar protic solvents. This led Sessler and Iverson to consider the possibility that sapphyrins might interact with DNA.[35] Consistent with this proposition, it was found that addition of an excess of calf thymus dsDNA (ca. 200 phosphate anion equivalent) to an aqueous solution of the water-solubilized sapphyrin 26. produced an 11 nm bathochromic shift in the sapphyrin Soret band. This spectroscopic change gave an apparent stability constant of 25,000 M^{-1}. A range of follow-up experiments, including ones based on ^{19}P-NMR spectroscopy, circular dichroism studies, and DNA topoisomerase I unwinding analyses, led to the conclusion that protonated sapphyrin gives rise to a new type of small-molecule-DNA interaction that involves the specific chelation of the anionic phosphate diester group by the protonated sapphyrin. Of particular interest is the fact that this kind of interaction differs substantially from other previously reported DNA-binding motifs, including the intercalation-based ones most often invoked in the case of porphyrins.

In 1995. Sessler and coworkers reported the synthesis of several novel oligosapphyrins and highlighted the efficiency of these species as potential carriers for the

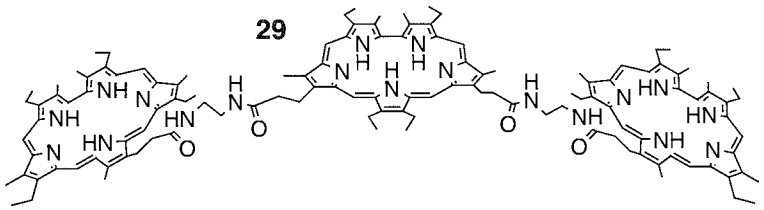

29

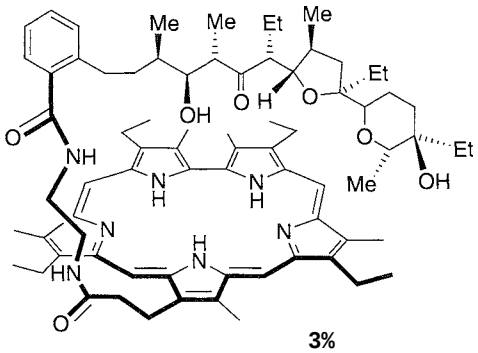

3%

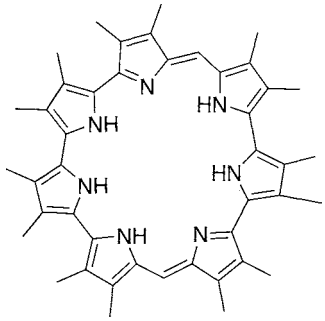

32

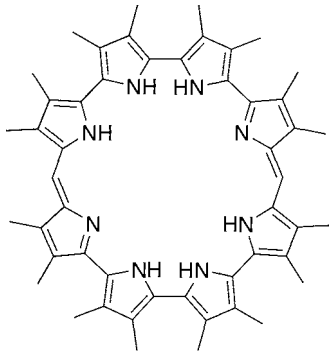

33

transport of phosphorylated nucleotides.[36] The trimers 28 and 29 (linear and branched) and the tetramer **30,** showed two distinct Soret bands in the UV spectrum, a clear sign of considerable aggregation. Addition of phosphate anion was found to induce an increase in the intensity of the higher wavelength portion of the split Soret-like band at the expense of the one at the lower wavelength. This behavior may be explained by considering the encapsulation of the anionic species followed by the de-aggregation of the oligomer in solution.

The next step was the employment of Compounds 28, 29, and 38 as carriers for the transport of nucleotides across bulk liquid membranes. This was done using the same kind of U-tube setup used to study halide anion transport. Under these condiditions, Compounds 28 and 29 were found to be efficient carriers for nucleotide diphosphates. However, they failed to effect the transport of nucleotide triphosphates. By contrast, Compound **38** proved to be an effective carrier for all the phosphorylated species under consideration.

In 1996 Sessler and coworkers reported the synthesis of a new Lasalocid modified sapphyrin **31**[37] that acts as an efficient carrier for the transport of aromatic amino acids in their zwitterionic form. Again, a standard H_2O-CH_2Cl_2-H_2O U-tube transport model was used to determine the transport efficiency of Compound **31**. This receptor showed not only a high selectivity for phenylalanine and tryptophan (K_t=20 for L-Phe), but was also found to be capable in some cases of discriminating between the different chiral homologues.

More expanded pyrrole-based macrocyles were recently reported in the literature. In 1999. Sessler and coworkers presented the synthesis of[30] heptaphyrin *(1.0.0.1.0.0.0)* 32 and of[13] octaphyrin(1.0.0.0.1.0.0.0) **33**.[38] These compounds, synthesized via a directed oxidative ring closure of linear polipyrrolic species, were crystallized in their diprotonated forms in the presence of

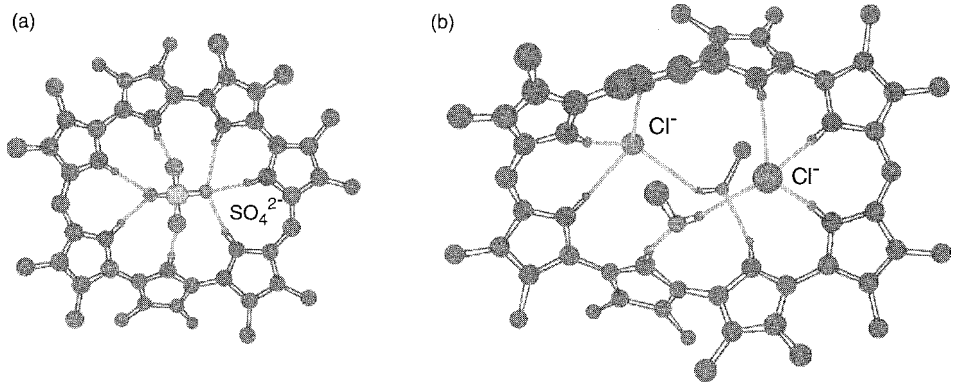

Fig. 2 (a) The crystal structure of the sulfate complex of Compound 32 (note that sulfate is bound by seven hydrogen bonds) and (b) the chloride complex of Compound **33** (including methanols involved in the hydrogen-bonding array). (View *this art* in *color at www.dekker.com.*)

sulfate and chloride anions, respectively. While compound 32 was found to encapsulate a sulfate anion within the macrocyclic core via seven hydrogen bonds in a manner reminiscent of the sulfate-binding protein,[''] and to assume a planar conformation (Fig. 2a), Compound **33,** larger and more flexible, was found to bind two chloride anions while deviating substantially from planarity (Fig. 2b). The latter binding mode is reminiscent of what is seen in the solid state for various anion complexes of a range of other protonated expanded posphyrins, including ones with rather fanciful names such as rubyrin,[40] rosarin,[41] amethyrin,[42] and turcasarin.[43] Unfortunately, as yet, there is little in the way of solution phase K_a information to support these recently reviewed solid-state analyses.[44]

CONCLUSION

Over the last decade. pyrrole has emerged as an important structural motif that may be used to construct receptor systems capable of interacting effectively and, in many instances, selectively with a range of anionic substrates. While early work concentrated on the use of so-called expanded porphyrin systems to impart a high degree of preorganization and provide systems with intrinsic, protonation-derived positive charge, increasingly it has come to be recognized that a range of simpler pyrrole-containing systems can be used to bind and recognize anions, but often at the price of selectivity or affinity. As a result. effort continues to be devoted to the synthesis and study of increasingly elaborate macrocyclic and polycyclic systems, just as attention continues to be focused on finding easier-to-make pyrrole-based anion receptors that can be readily exploited in a range of real-world applications running the gamut from sensing and transport to perhaps ultimately waste remediation and tailored drug development.

ACKNOWLEDGMENTS

P.A.G. would like to acknowledge the Royal Society for a University Research Fellowship and the EPSRC for a project studentship (to S.C.). J.L.S. thanks the National Institute of Health (GM 58907 and CA 68682), the National Science Foundation (CHE 9725399), and the Texas Advanced Research Program for support.

ARTICLES OF **FURTHER** INTEREST

Amide- and Urea-Based Anion Receptors, p. *31*
Anion-Directed Assembly, p. 51
Guanidinium-Based Anion Receptors, p. 615
Hydrogen Bonding, p. 658
Organometallic Anion Receptors, p. 1006
Protonated Aza-Macrocycles for Anion Complexation, p. 1170

REFERENCES

1. Sessler, J.L.: Cyr. M.J.; Lynch, V.; McGhee. E.: Ibers, J.A. Synthetic and structural studies of sapphyrin, a 22 π-electron pentapyrrolic 'Expanded Porphyrin'. J. Am. Chem. Soc. 1990, *112* (7), 2810–2813.
2. Bauer. V.J.: Clive, D.L.J.; Dolphin, D.: Paine. J.B., III; Harris. F.L.; King, M.M.; Loder, J.; Wang, S.W.C.; Woodward, R.B. Sapphyrins: Novel aromatic pentapyrrolic macrocycles. J. Am. Chem. Soc. 1983, *105* (21). 6429–6436.
3. Coles, S.J.; Gale, P.A.; Hursthouse, M.B. The first example of an anion-pyrrole complex. Cryst. Eng. Comm. 2001, 53.
4. Gale, P.A.: Sessler, J.L.: Král. V.: Lynch, V. Calix[4]pyrrole: Old yet new anion binding agents. J. Am. Chem. Soc. **1996**. *118* (21), 5140–5141.
5. Gale, P.A.: Camiolo. S.; Chapman. C.P.: Light, M.E.; Hursthouse, M.B. Hydrogen-bonding pyrrole amide cleft anion receptors. Tetrahedron Lett. **2001**, *42* (30). 5095–5097.
6. Gale, P.A.: Camiolo. S.; Tizzard, G.J.; Chapman, C.P.; Light. M.E.; Coles, S.J.: Hursthouse, M.B. 2-Amidopyrroles and 2.5-diamidopyrroles as simple anion binding agents. J. Org. Chern. **2001**, 66 (23). 7849–7853.
7. Schmuck, C.; Lex. J. Acetate binding within a supramolecular network forrned by a guanidiniocarbonyl pyrrole cation in the solid state. Org. Lett. 1999, *1* (11), 1779–1781.
8. Schmuck. C. Side chain selective binding of *N*-acetyl-α-amino-acid carboxylates by a 2-(guanidiniocarbonyl)pyrrole receptor in aqueous solvents. Chem. Commun. 1999. (9), 843–844.
9. Black. C.B.; Andrioletti. B.: Try, A.C.; Ruiperez, C.: Sessler, J.L. Dipynolylquinoxalines: Efficient sensor for fluoride anion in organic solution. J. Am. Chem. Soc. 1999. *121* (44). 10438–10439.
10. Anzenbacher, P.. Jr.: Try. A.C.; Miyaji, H.; Jursíková. K.: Lynch, V.M.; Marquez, M.; Sessler. J.L. Fluorinated calix[4]pyrrole and dipyrrolequinoxaline: Neutral anion receptors with augmented affinities and enhanced selectivities. J. Am. Chem. Soc. 2000. *122* (42). 10268–10272.
11. Fiirstner, A.; Grabowski, J.; Lehmann. C.W.: Kataoka. T.; Nagai, K. Synthesis and biological evaluation of nonylprodigiosin and macrocyclic prodigiosin analogues. Chembiochem 2001. 2 (1), 60–68.
12. Montaner, B.: Pérez-Tomás, R. Prodigiosin-induced apoptosis in human colon cancer cells. Life Sci. **2001**. *68* (17). 2025–2036.
13. Ohkuma, S.; Sato, T.; Okamoto. M.; Matsuya, H.; Arai. K.: Kataoka, T.: Nagai, K.; Wassermann. H.H. Prodigiosins uncouple lysosomal vacuolar-type ATPase through promotion of H^+/Cl^- symport. Biochem. J. **1998**. 334 (Part 3). 731–741.

14. Scherer, M.; Sessler. J.L.: Gebauer. A.: Lynch, V. A bridged pyrrolic *ansa*-ferrocene. A new type of anion receptor. Chern. Commun. 1998, (1). 85–86.
15. Gale, P.A.; Bleasdale. E.R.; Chen, G.Z. Synthesis and electrochemical polymerisation of calix[4]pyrroles containing *N*-substituted pyrrole moieties. Supramol. Chem. 2001, I 3 (4), 557–563.
16. Sessler. J.L.: Gale. P.A. Calixpyrroles: Novel Anion and Neutral Substrate Receptors. In The *Porphyrin Handbook*; Kadish. K., Smith. K.M., Guilard. R.. Eds.; Academic Press: San Diego, CA. 2000; Vol. 6, 257–278.
17. Camiolo, S.; Coles. S.J.: Gale, P.A.: Hursthouse. M.B.; Sessler. J.L. Tetrabutylammonium *meso*-octamethylcalix[4]pyrrole fluoride dichloromethane solvate. Acta Cryst. 2001. *E57* (9). o816–o818.
18. Gale. P.A.: Anzenbacher, P., Jr.: Sessler, J.L. Calixpyrroles II. Coord. Chem. Rev. 2001. 222. 57–102.
19. Anzenbacher, P.. Jr.: Jursíková. K.; Lynch, V.M.: Gale. P.A.: Sessler. J.L. Calix[4]pyrroles containing deep cavities and fixed walls. Synthesis. structural studies, and anion binding properties of the isomeric products derived from the condensation of p-hydroxyacetophenone and pyrrole. J. Am. Chem. Soc. 1999. 121 (47). 11020–11021.
20. Bonomo, L.; Solari. E.; Toraman, G.: Scopelliti. R.: Latronico. M.: Floriani, C. A cylindrical cavity with two different hydrogen-bonding boundaries: The calix[4]arene skeleton screwed onto the meso-position of calix[4]pyrrole. Chem. Commun. 1999; (23). 2413–2414.
21. Camiolo. S.; Gale, P.A. Fluoride recognition in "super-extended cavity" calix[4]pyrrole. Chern. Commun. 2000. 13. 1129–1130.
22. Sessler. J.L.: Anzenbacher, P., Jr.: Shrives. J.A.; Jursikova, K.; Lynch, V.: Marquez, M. Direct synthesis of expanded fluorinated calix[*n*]pyrroles: Decafluorocalix[5]pyrrole and hexafluorocalix[8]pyrrole. J. Am. Chem. Soc. 2000, 122 (48). 12061–12062.
23. Cafeo. G.; Kohnke, F.H.: La Tome. G.L.: White. A.J.P.; Williams. D.J. The complexation of halides ions by a calix[6]pyrrole. Chem. Commun. 2000. (13). 1207–1208.
24. Turner. B.; Shterenberg, A.: Kapon, M.: Suwinska. K.; Eichen, Y. Selective anion binding and solid-state host-guest chemistry of an extended cavity calix[6]pyrrole. Chem. Commun. 2001. (1), 13–14.
25. Bucher, C.; Zimmerman. R.S.: Lynch. V.: Sessler. J.L. First cryptand-like calixpymole: Synthesis, x-ray structure, and anion binding properties of a bicyclic[3,3,3] nonapyrrole. J. Am. Chem. Soc. 2001. 123 (39). 9716–9717.
26. Bucher. C.: Zimmerman. R.S.; Lynch, V.; Král. V.; Sessler. J.L. Synthesis of novel expanded calicphyrin: Anion binding properties of a calix[6]phyrin with a deep cavity. J. Am. Chem. Soc. 200%.123 (39), 2099–2100.
27. Takeuchi. M.: Shioya, T.: Swager, T.M. Allosteric fluoride anion recognition by doubly strapped porphyrin. Angew. Chem. Int. Ed. 2001, 40 (18). 3372–3376.
28. Andrievsky. A.: Ahuis. F.: Sessler. J.L.; Vögtle, F.: Gudat, G.; Moini, M. Bipyrrole-based [2]catenane: A new type of anion receptor. J. Am. Chem. Soc. 1998. 120 (37). 9712–9713.
29. Latos-Grażyński, L. Core-Modified Heteroanalogues of Porphyrins and Metalloporphyrins. In The *Porphyrin Handbook*: Kadish. K.M.. Smith. K.M., Guilard, R., Eds.; Academic Press: San Diego, CA. 2000: 361–416. Chapt. 14.
30. Furuta. H.: Maeda, H.; Osuka, A. Oxyindolophyrin: A novel fluoride receptor derived from *N*-confused corrole isomer. J. Am. Chem. Soc. 2001. 123 (26), 6435–6436.
31. Sessler. J.L.: Davis. J.M. Sapphyrins: Versatile anion binding agents. Acc. Chem. Res. 2001. 34 (12), 989–997.
32. Sessler. J.L.; Cyr, M.; Furuta. H.: Král. V.: Mody, T.; Morishima. T.; Shionoya, M.: Weghorn. S. Anion binding: A new direction in porphyrin-related research. Pure Appl. Chem. 1993, *65* (3), 393–398.
33. Shionoya. M.; Furuta. H.; Lynch. V.: Harriman, A.; Sessler, J.L. Diprotonated sapphyrin: A fluoride selective halide anion receptor. J. Am. Chem. Soc. 1992. 114 (14). 5714–5722.
34. Sessler. J.L.; Ford. D.A.: Cyr, M.J.: Furuta, H. Enhanced transport of fluoride anion effected using protonated sapphyrin as a carrier. Chem. Commun. 1991. (24). 1733–1735.
35. Iverson. B.L.; Shreder, K.: Kral, V.; Sessler, J.L. Phosphate recognition by sapphyrin. A new approach to DNA binding. J. Am. Chem. Soc. 1993.115 (23), 11022–11023.
36. Král. V.: Andrievsky. A.: Sessler, J.L. Oligosapphyrins: Receptors for the recognition and transport of nucleotide Di-and Tri-phosphate. Chem. Commun. 1995. (22), 2349–2351.
37. Sessler. J.L.: Andrievsky, A. Sapphyrin-lasalocid conjugate: A novel carrier for aromatic amino acid transport. Chem. Commun. 1996, (10), 1119–1120.
38. Sessler, J.L.: Seidel. D.; Lynch, V. Synthesis of [28]heptaphyrin(1.0.0.1.0.0.0) and [32]octaphyrin(1.0.0.0.1.0.0.0) via a direct oxidative ring closure: The first expanded porphyrins containing a quaterpyrrole subunit. J. Am. Chem. Soc. 1999. 121 (48). 11257–11258.
39. Pflugrath, J.W.: Quicho, F.A. Sulphate sequestered in the sulphate-binding protein of salmonella typhimurium is bound solely by hydrogen bonds. Nature 1985, 314 (21 March). 257–260.
40. Sessler, J.L.: Morishima. T.: Lynch, V. Rubyrin: A new hexapyrrolic expanded porphyrin. Angew. Chem. Int. Ed. Engl. 1991, 30 (8). 977–980.
41. Sessler. J.L.: Weghorn. S.J.; Morishima. T.; Rosingana. M.: Lynch. V.; Lee. V. Rosarin: A new, easily prepared hexapyrrolic expanded porphyrin. J. Am. Chem. Soc. 1992. 114 (21). 8306–8307.
42. Sessler. J.L.: Weghorn, S.J.: Hiseada. Y.; Lynch, V. Hexaalkyl terpyrrole. A new building block for the preparation of expanded porphyrins. Chem. Eur. J. 1995, *1* (1), 56–67.
43. Sessler. J.L.: Weghorn. S.; Lynch, V.; Johnson. M.R. Turcasarin. the largest expanded porphyrin prepared to date. Angew. Chem. Int. Ed. Engl. 1994.33 (14), 1509–1512.
44. Sessler, J.L.; Gebauer, A.; Weghorn. S.J. Expanded Porphyrins. In The *Porphyrin Handbook*: Kadish. K.M., Smith. K.M.. Guilard. R., Eds.: Academic Press: San Diego, CA, 2000: 55–124. Chapt. 9.

Racks, Ladders, and Grids

Marius Andruh
University of Bucharest, Bucharest, Romania

INTRODUCTION

The self-assembly processes of metal complexes into highly organized architectures (racks. ladders, grids, helicates, cages) represent one of the most important topics in supramolecular chemistry. Beyond the beauty of these supermolecules. the various topologies of the metal arrays generate interesting optical, redox, magnetic, or catalytic properties, with potential applications in nanotechnology.

Two components are necessary in every synthetic approach leading to inorganic supramolecular architectures: the suitable designed organic ligand and the metal ion. The spontaneous generation of the supramolecular entities is based on metal-ion-directed self-assembly. In the language of supramolecular chemistry, the ligand is a programmed species. that is, an organic molecule with binding sites in a correct arrangement. with encoded information that is read by the metal ion according to its coordination algorithm (stereochemical preference).[1] The main feature of the instructed polytopic ligand consists of the position and the high selectivity of its coordination sites (a polytopic ligand contains at least two coordination sites). The identity of the coordination sites (''pockets'') is given by their ability to selectively interact with metal ions having a dominant coordination geometry. For example. tetrahedral pockets (with bidentate coordination site) will recognize metal ions with a marked preference for the tetrahedral stereochemistry (Ag^{+}, Cu^{+}), while the octahedral pockets (with tridentate coordination sites) prefer transition metal ions such as Ni^{2+}, Fe^{2+}, Ru^{2+}, Os^{2+}, which currently exhibit the octahedral coordination geometry.

Racks, $[n]\boldsymbol{R}$, ladders, $[2n]\boldsymbol{L}$, and grids, $[m \times n]\boldsymbol{G}$, (Fig. 1) are examples of inorganic superstructures, which are obtained through the spontaneous and correct sequential interaction between different and highly instructed components ($[n]$, $[2n]$, and $[m \times n]$ specify the number of the metal ions in the R. $\boldsymbol{L}$, and $\boldsymbol{G}$ structures). All these architectures are the result of the thermodynamic driving force. which leads to discrete species. rather than to coordination polymers. They have in common linear polytopic ligands as building elements, which can bridge a preestablished number of metal ions. Several ligands of this type are depicted in Fig. 2.

In the realm of supramolecular synthesis. the construction of rack, ladder. and grid architectures represents a particular case of self-assembly. which relies on the three basic levels of operation of a programmed supramolecular system: recognition (selective interaction of complementary components): orientation (building up the structure through the correct spatial disposition of the components): and termination. that is, the formation of the desired discrete supramolecular entity.''

RACKS

A molecular rack. $[n]\boldsymbol{R}$, is constructed from linear n-topic ligands, which connect n metal ions in a linear arrangement. as well as from ancillary ligands attached to the metal ions, playing the role of platforms (Fig. la). If the polytopic ligand contains octahedral pockets. that is, tridentate moieties. than the ancillary ligand must be tridentate as well, in order to fulfill the octahedral stereochemistry of the metal ion. The first dinuclear and trinuclear racks (Fig. 3) were obtained by coordination of linear ligands of type **L5** (octahedral pockets) to $Ru(terpy)^{2+}$(terpy stands for 2,2′:6′,2″-terpyridyl) (Fig. 3a).[2] Complexes of this type are redox active. For the ruthenium trirnetallic complex. $[3]\boldsymbol{R}$, the cyclic voltammogram indicates the inequivalency of the Ru sites: the central ruthenium atom, located between two dipositive centers, is more difficult to oxidize (+1.88 V) than the terminal ones (+1.47 V).

The rack-type architecture can be assembled also from tetrahedral metal ions, e.g., Cu^{+}. linear polytopic ligands with tetrahedral pockets (E1). and bidentate ligands such as phenathroline or 2.2'-bipyridyl. One example is illustrated in Fig. 3b. It is a rigid rack of rotaxane-type. the ancillary ligand being a macrocyclic molecule with a 1.10-phenathroline moiety.[3]

LADDERS

The ladder topology. $[2n]\boldsymbol{L}$ (Fig. lb) can be obtained by using. as ladder sides. two linear polytopic ligands

Encyclopedia of Supramolecular Chemistry
DOI: 10.1081/E-ESMC 120019181

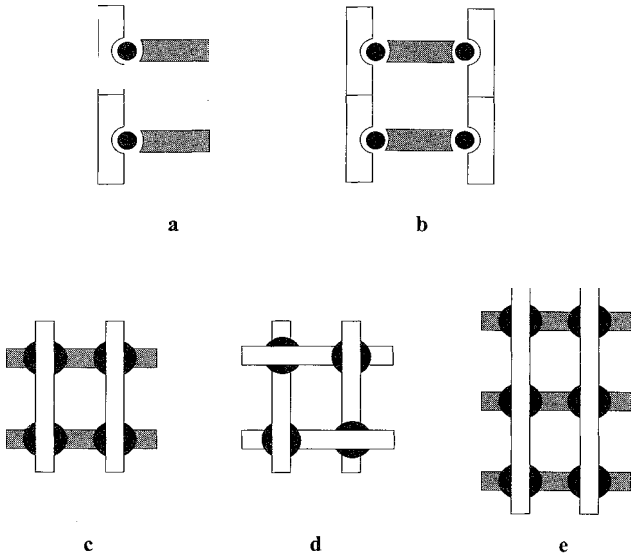

Fig. 1 Inorganic supramolecular architectures of (a) rack, [2]*R*; (b) ladder. [2·2]*L*; (c) square grid. [2 x 2]*G*; (d) chiral [2 x 2] grid; ie) rectangular [2 x 3] grid.

arranging the metal ions in parallel chains, which are further interconnected by ancillary bridging ligands (ladder steps). If the assembling cation is Cu^+, then linear polytopic ligands of type **L1** (Fig. 2a) are suited. Bipyrimidine derivatives are used as bridging ligands connecting the metal ions from two different chains (Fig. 4).[4] The orthogonality of the ligand components. which gives the orthogonality between the ladder sites and the inner "rungs," is provided here by the tetrahedral geometry of the metal ions. The formation of the [2*n*]*L* architecture, by reacting the three components (metal ions, rod-like and ancillary bis-chelating ligands) in the 2*n*:2:*n* molar ratio, illustrates a key concept in the supramolecular synthesis, namely the multicomponent self-assembly, which means that the well-defined superstructures are spontaneously generated from a larger set of components (at least two types of ligands, metal ions)."]

By mixing in the same solution two different linear ligands (**L1**, with $x=0$, and E1 with $x=1$), tetraphenylbipyrimidine, and $[Cu(MeCN)_4](PF_6)$ in the molar ratio 1:1:2.5:5, after 72 h only two products were formed, namely, the [2·2]*L* and [2·3]*L* species. This means that the 19 particles of four different types strictly follow the operations of two programs, which generate the two well-defined nanoarchitectures. each constructed from two different ligands. This is an example of an instructed mixture. with components that assemble according to two parallel programs, without crossover between the two superstructures. The instructed mixture paradigm opens wide perspectives in supramolecular synthesis.[1]

Molecular ladders with finite dimensions are still scarce. Much more numerous are the one-dimensional. infinite ladder structures. Such architectures, which are obtained serendipitously rather than intentionally, are constructed from metal ions and *exo*-bidentate ligands. From the most popular ligands. we recall here the *bis*-(4-pyridyl)-derivatives.[5,6] Both homo-and heterometallic systems with one dimensional ladder structures are characterized.

GRIDS

The molecular grid. [in x *n*]*G*, consists of a square ($m=n$) or a rectangular-matrix array of metal centers (Fig 1c,d,e) Square grids. [*n* x *n*]*G*, based on metal ions with tetrahedral coordination geometry (Cu^+, Ag^+), are constructed from n-topic, rigid, rod-like ligands with tetrahedral pockets and n^2 metal ions Alternatively, polytopic ligands with octahedral pockets may generate grids by interacting with octahedral metal centers In general, the ligands are divided into two sets, one above and one below the plane of the metal ions

Square Grids

One of the first square grids was obtained by combining a tritopic rigid ligand (**L2**, $x=2$) with tetrahedral Ag^+ ions: $[Ag_9(L2, x=2)_6](CF_3SO_3)_9$. The correct self-assembly of the 15 particles into a [3 x 3] grid was proved by means of NMR spectroscopy (^1H, ^{13}C, ^{109}Ag) and x-ray diffraction studies.[7] The ^{109}Ag-NMR spectrum recorded in D_3-nitromethane (566.06. 507.56, 406.13 ppm) is consistent with the three types of Ag^+ ions in a molar ratio 4:4:1 (four silver ions located at the corners, four silver ions at the four edge mid-positions, and the last one located at the central site).

If the cavity within a square grid is enlarged. then it can accommodate a guest molecule with appropriate size. The dimensions of the cavities can be tuned by using ligands with a larger separation between binding sites. Such a ligand. **L4** (R=C_6H_5), is represented in Fig. 2a. It contains tetrahedral pockets. The tetracopper grid is obtained almost quantitatively in nitromethane.[8] Single crystals were obtained by slow diffusion of benzene into a nitromethane solution of the tetrametallic system. The cationic grid possesses an internal box-shaped void with the dimensions: 4.2 x 3.8 Å, and 12.5 Å depth. The internal box of the grid is sufficiently large to accommodate six guests: four benzene and two nitromethane molecules.

Oligophenathrolines (**L3**, Fig. 2a) are also suited as scaffolds for the construction of grids. The reaction of ligands of type **L3** (R=anisyl, *p*-C_6H_4-OCH_3, or tolyl, p-C_6H_4-CH_3) with Cu^+ led to interesting tetranuclear square grids.'" Two additional uncoordinated ligands are hosted. one above and one below the interstitial space. generating

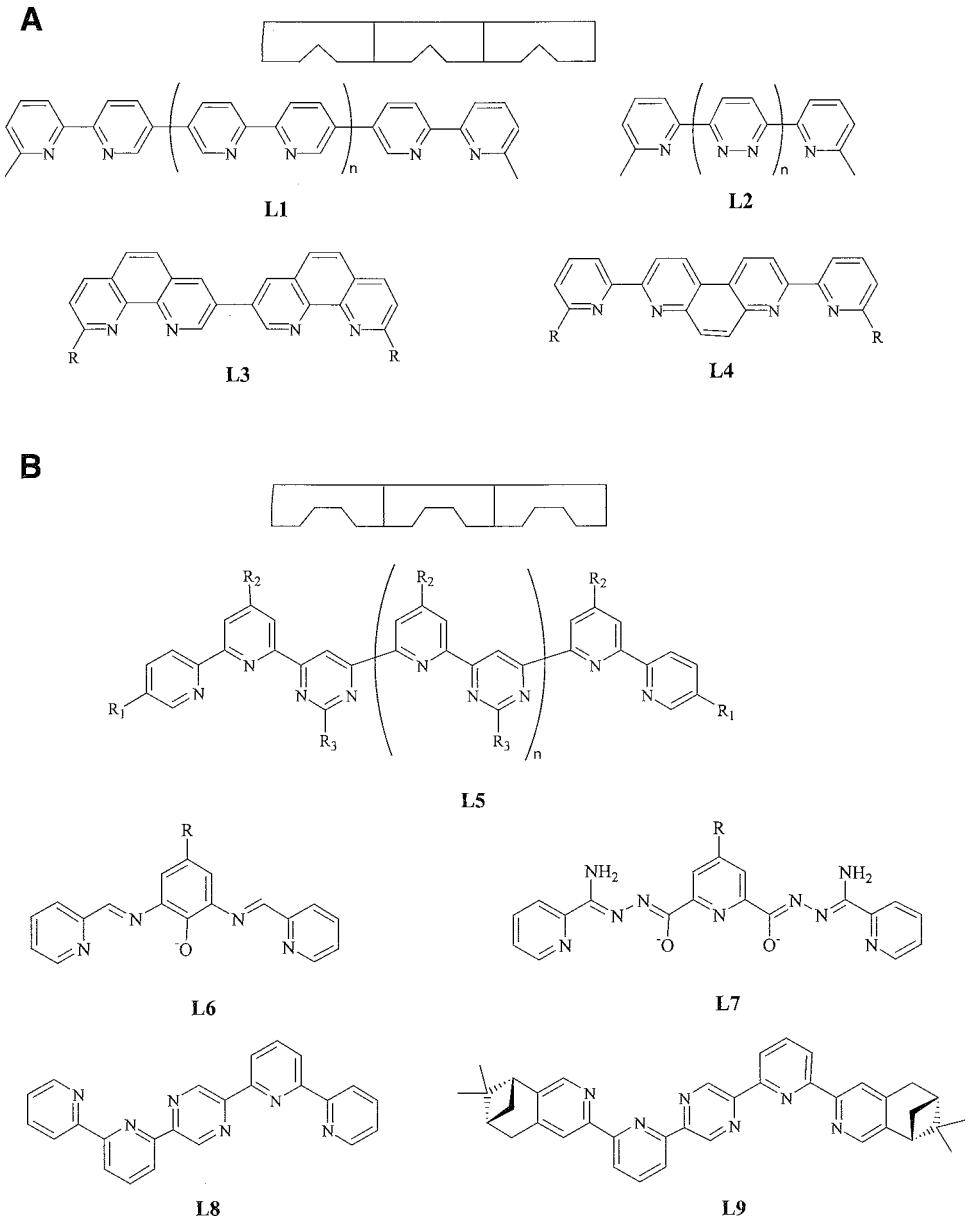

Fig. 2 Linear ligands used to generate racks. ladders, and grids: (a) polytopic ligands with tetrahedral pockets; (b) polytopic ligands with octahedral pockets.

r

a 3 x 3 grid (3 here means the number of rods). The hosted biphenathroline molecules (R=anisyl) can be reversibly exchanged with two molecules of the tolyl derivative. The use of the mesityl derivative did not lead to the expected grid architectu e.

Numerous square grids were obtained by using linear ligands with octahedral pockets. **L5** (Fig. 2b) and appropriate assembling cations: Fe^{2+}[2 x 2],[10] Co^{2+}[2 x 2],[11] Zn^{2+}[2 x 2],[11] Pb^{2+}[2 x 2], [3 x 3], [4 x 4].[12] The crystal structures of all these grids were solved. The Zn^{2+} and Co^{2+} ions display a distorted octahedral stereochemistry. The Zn···Zn distances vary between 6.584 and 6.767 Å, while the Co···Co distances lie in the range 6.453–6.570 A. In both compounds. the ditopic ligand is of type **L5** with x=0, R_1=R_2=H; R_3=C_6H_5. The phenyl ring attached to the pyrimidine moiety plays an important role in the high stability of the tetranuclear complexes, being involved in interligand n – n stacking interactions. The tetrazinc grid exhibits a strong luminescence at 450 nm upon irradiation at 335 nm. at room temperature, while the uncoordinated ligand shows only a weak emission at about 410 nm, when irradiated at 272 nm. The strong

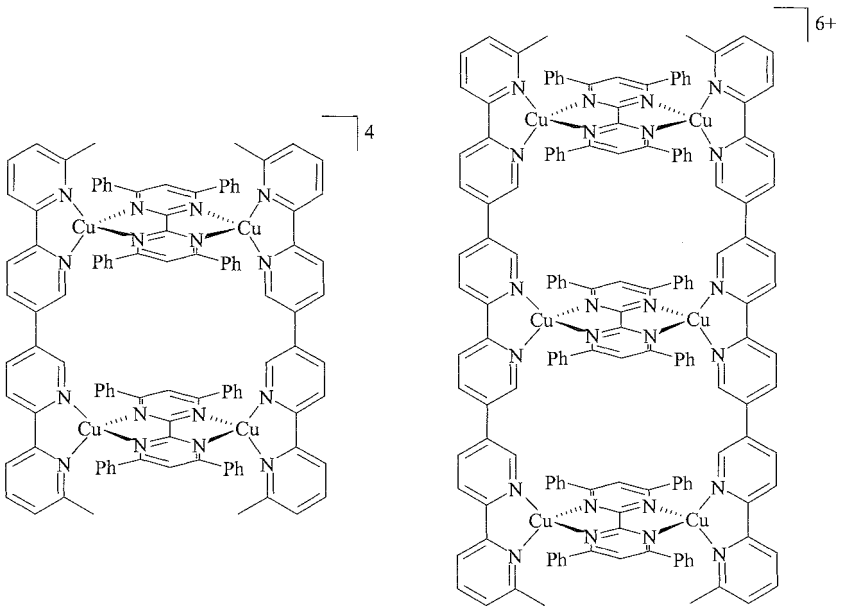

a b

Fig. **3** Racks: (a) rack constructed from octahedral Ru(II) ions; (b) rotaxane-type rack constructed from tetrahedral Cu(I) ions.

luminescence of the tetrametallic grid is due to the rigidity of the complex, which decreases the radiationless decay. The tetracobalt grids are redox active. A unique electrochemical behavior was emphasized for the above-discussed [Co^{II}_4] grid: the cyclic voltammogram recorded at $-20°C$ shows 10 well-resolved, completely reversible reduction steps (from -0.59 to -2.73 V) involving 11 electrons.[13] These are ascribed to $Co^{2+} \rightarrow Co^{1+}$ processes. as well as to ligand localized reductions. A similar system (**L5**, $x=0$. $R_1=R_2=R_3=H$) was investigated.[14] The reduction processes of the cobalt(II) ions (-0.14, -0.24. -0.44. -0.83 V) occur at less negative potentials than, for example. $[Co(terpy)_2]^{2+}$. One of the reasons is the high charge of the tetranuclear grid, which makes it easier to reduce.[14]

The stereochemistry of Pb^{2+} in the corresponding [2 x 2] grid is interesting: it is a hemidirected structure. in which the nitrogen atoms from the ligands (**L5**, $x=0$. $R_1=R_2=R_3=H$) are coordinated to only one part of the coordination sphere of the lead ions. This is due to the presence of the stereochemically active electronic lone pair in the Pb^{2+} ions. The average distance between the lead atoms is 6.51 Å. The structure of the [4 x 4]-Pb_{16} grid was established by means of ES mass spectrometry and NMR spectroscopy. The ^{207}Pb-NMR spectrum shows three signals in a 1:2:1 ratio, corresponding to three types of lead cations: four at the corners; eight at positions 2 and 3 on the edges. and four in the interior. It is a spectacular case. where 24 components self-assemble through the formation of 96 coordination bonds, leading to the exclusive formation of the hexadecanuclear complex in the solution.

The case of the tetrairon(II) grid (**L5**, $x=0$, $R_1=R_2=H$; $R_3=C_6H_5$) is particularly interesting: at room temperature (293 K). three out of the four iron(II) ions are in high-spin (HS) state ($S=2$), with Fe–N distances ranging between 2.086(5) and 2.287(4) Å. For the fourth iron(II) ion, the Fe–N distances are shorter [1.977(5)–2.162(4) Å], values which are intermediate between those expected for HS and LS (low-spin, $S=0$) Fe(II) ions. At 100 K, three out of the four iron(II) ions display distances intermediate between LS and HS but closer to LS state [Fe–N: 1.895(6)–2.117(5) Å], while the fourth ion is in HS state [Fe–N: 2.116(6)–2.282(5) Å]. This is an indication that the iron(II) ions here are subject of a spin-transition phenomenon. Clear information on the spin state of the iron(II) ions, both at room and low temperatures. is obtained from Mössbauer spectroscopy and from the magnetic measurements. At room temperature. the value of the $\chi_M T$ product (10.0 $cm^3 mol^{-1} K$) corresponds to three HS iron(II) ions and one LS iron(II) ion (χ_M is the molar magnetic susceptibility). By lowering the temperature. $\chi_M T$ decreases. reaching a value of 5.6 $cm^3 mol^{-1} K$ at 30 K. The spin transition of the tetrairon grid was induced also by light (LIESST effect) or by pressure.

Other ligands displaying octahedral pockets and able to generate [2 x 2] and [3 × 3] grids are presented in Fig. 2b: **L6** and **L7**. They have in common the presence of the

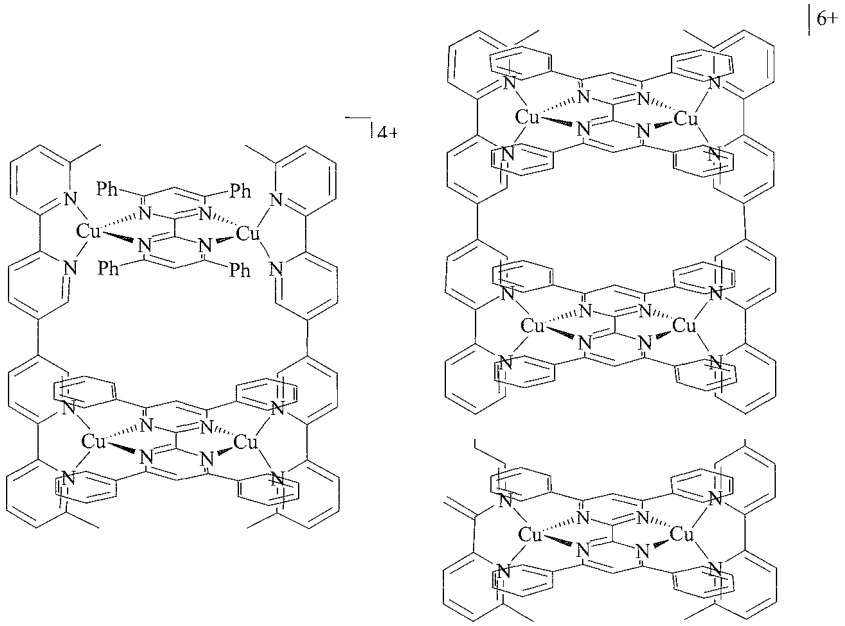

a **b**

Fig. 4 Ladders: (a) a [2·2]***L*** architecture: (b) a [2·3]***L*** architecture.

mononegatively charged oxygen atoms, which can bridge two metal ions. The self-assembly process involving ligand **L6** (Fig. 2b) and Cu^{2+} ions leads to a tetranuclear complex of [2 x 2] grid type.[15] The copper(II) ions are connected through phenoxo bridges and adopt a distorted bipyramidal stereochemistry. The exchange interaction between the copper(II) ions located on the edge of the square described by the inetal ions was found to be weak antiferromagnetic ($J = -0.4$ cm^{-1}). The heptadentate ligand **L7** (R=H) combines with Mn^{2+}, Fe^{3+}, or Zn^{2+} ions. resulting in a nonanuclear [3 x 3] grid system with alkoxo-bridged metal ions.[16,17] The cryomagnetic investigation of the manganese(II) derivative reveals an antiferromagnetic exchange interaction between the metal ions within the nonanuclear $[Mn_9(\mu\text{-}O)_{12}]$ grid ($J = -4.6$ cm^{-1}). The crystal structure of this nonanuclear complex is represented in Fig. 5.

An alternative way to design grids (Fig. 1d) consists of the use of ligands of **L8** type (Fig. 2b). They have an important peculiarity: the orientation of the "binding vectors" of the two terpyridine moieties is antiparallel, so they coordinate to the two metal ions once above and once below the plane of the four metal ions. Moreover, the resulting grid, with a D_4 symmetry, is chiral. The self-assembly process between **L8** and Zn^{2+} ions leads to a racemic, crystallizing in the centrosymmetric *C2/c* space group."'' In order to obtain only one enantiomer, the ligand **L9** was "chiralized" by introducing pinene moieties (**L9**). The combination of **L9** with Zn^{2+} ions results in a chiral grid. The crystal contains only one diastereomer (space group *P*1).[18]

A more complex case is that of the grids containing different metal ions. For a [2 x 2] grid constructed by using two different inetal ions; two topoisomers are possible: *syn* (two identical metal ions on the same edge of the square) and *anti* (identical inetal ions disposed diagonally). The synthetic strategy must fulfill an important condition: it has to avoid the scrambling of the metal ions. The problem was solved by introducing the metal ions in a sequential way, namely. in order of the increasing lability of the coordination centers which are formed. Two $[M^{II}_2Fe^{II}_2]$ grids (*M*=Ru, Os) were obtained by using ligands of type **L5**(*x*=0; R1=R3=H, R2=S−^{n}Pr).[19] The first step was to protect one of the binding sites of the ditopic ligand. by methylating the nitrogen atom from one of the two peripheral pyridyl rings. Consequently. only one pocket is available to interact with the metal ion. The reaction of the methylated ligand with $RuCl_3$ or ammonium hexachloroosmate leads to chiral mononuclear precursors, which result as racemic mixtures. The [2 x 2] grid structure (the *anti*-topoisomer) is assembled in the presence of a second metal ion (e.g., Fe^{2+}), which combines with mononuclear precursors of the same chirality (R + *R* or S + *S*). In other words. the process is diastereoselective. the connection of an *R* and an S precursor into a *meso* diastereoisomer being precluded for geometric reasons.

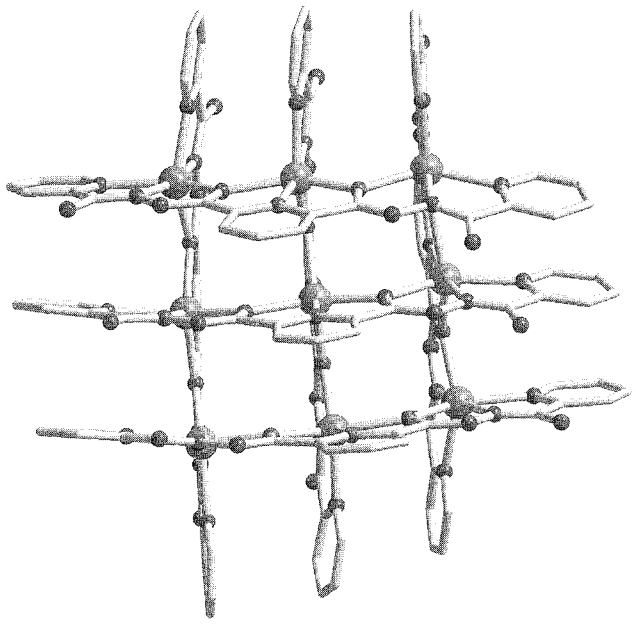

Fig. 5 Crystal structure of a $[Mn^{II}_9(\mu\text{-}O)_{12}]$ grid (adapted from Ref. [17]).

Rectangular Grids

The self-assembly of rectangular grids, $[n \times m]\boldsymbol{G}$ (Fig. 1e), needs two types of linear ligands, for example, a ditopic and a tritopic ligand. The first $[2 \times 3]$ rectangular grid was obtained by combining two ligands of the type **L2** and Ag^+as an assembling cation, in a molar ratio **L2**(x=1):**L2**(x=2):Ag^+=1.5:1:3.[20] The rectangular grid was formed in solution and in the solid state. Although the two square grids, $[2 \times 2]$ and $[3 \times 3]$, can also result, the $[2 \times 3]$ grid is formed preferentially, as indicated by ^{109}Ag-and ^{1}H-NMR spectroscopy. The $[2 \times 3]$ rectangular grid coexists in solution (nitromethane) with only 8% $[2 \times 2]$ and 2% $[3 \times 3]$ grids. (If the three grids were formed nonpreferentially, their statistical distribution, following the 1.5:1:3 molar ratio between the starting components, would have been 36% $[2 \times 2]$, 16% $[3 \times 3]$, and 48% $[2 \times 3]$.) The preferential formation of the heteroligand grid arises from the lower stability of the $[3 \times 3]$ grid in comparison with the $[2 \times 3]$ one. [In the $[3 \times 3]$ grid, the central Ag(pyridazin)$_4$ unit is less stable than the Ag(bipy) moieties.]

In the attempt to obtain a $[5 \times 5]$-Ag_{25} grid, by using a pentatopic ligand of type **L2**(x=4), two unexpected polynuclear architectures were obtained: a $[4 \times 5]$ grid, $[Ag_{20}\{\mathbf{L2}(x=4)\}_9](CF_3SO_3)_{20}$, and an Ag_{10} quadruple helicate, $[Ag_{10}\{\mathbf{L2}(x=4)\}_4](CF_3SO_3)_{10}$.[21] The two compounds crystallize simultaneously from the same reaction mixture. Actually, the $[4 \times 5]$ grid can be described as a $[2 \times (2 \times 5)]$ grid of grids. The particular topology of the metal array arises from the possibility of the ligand to adopt a *transoid* conformation (twisting around the central C—C bond). Five out of the nine ligands have this *transoid* conformation and form a parallel row, while the remaining four ligands display the all-*cis* arrangement of the nitrogen atoms (*cisoid* conformation). These four ligands are arranged into two parallel sets lying on the opposite sides of the grid, one above and one below the mean plane of the silver atoms (Fig. 6). The four outer corner silver atoms describe a rhombus with inner angles of 70 and 109°.

The grid motif is also encountered in a plethora of two-dimensional extended structures, either noninterpenetrating or interpenetrating nets, constructed from metallic ions as nodes, and various *exo*-bidentate ligands.[6,22,23]

Mechanistic aspects

The above results highlight the important role that can be played in the self-assembly process by the different conformations of the **L2**-type ligands. The reaction between **L2**(x=2) and Ag^+ was reinvestigated, with a special emphasis on the kinetic species that may or may not be direct intermediates toward the thermodynamically stable $[3 \times 3]$ grid.[24] The $[3 \times 3]$-Ag_9 grid forms immediately, as the only reaction product, when the two components are mixed in the correct stoichiometric ratio

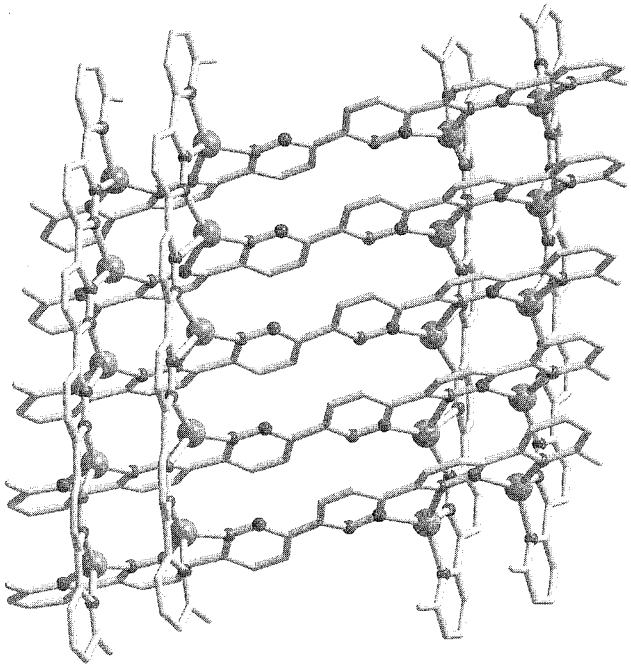

Fig. 6 Crystal structure of the $[Ag_{20}\{\mathbf{L2}(x=4)\}_9]^{20+}$ $[2 \times (2 \times 5)]$ grid (adapted from Ref. [21]).

(Ag^+:L2=9:6). The progressive addition of $AgCF_3SO_3$ to the solution of the ligand leads to a series of species that were identified by means of NMR (^1H, ^{109}Ag) spectroscopy. These are complexes of $[(L2)_nAg_n]^{n+}$ type (n=3,4-, probably triangular and square intertwined structures, with all ligands in the *transoid* conformation) and grid-like species having the composition $[(L2)_5Ag_6]^{6+}$. Two of these hexanuclear complexes are particularly important. In both of them, the L2(x=2) molecules are disposed into two sets of parallel ligands: a set of three. and another one of two ligands, their superposition making an incomplete grid, with the six metal ions disposed on the opposite edges. One of the two complexes is made up only of ligands in the *cisoid* form, *c*-$[(L2)_5Ag_6]$, while in the second one, *t*-$[(L2)_5Ag_6]$, three parallel ligands present a *transoid* conformation around the central C—C bond, and the other two are in the *cisoid* form. Ligand exchange reactions occur between the $[(L2)_nAg_n]^{n+}$ and *t*-$[(L2)_5Ag_6]^{6+}$ species, leading to *c*-$[(L2)_5Ag_6]^{6+}$, which is a prerequisite process in the way toward the [3 x 3] grid. The *c*-$[(L2)_5Ag_6]^{6+}$ entity displays three coordination sites available to bind, in a single overall step, three Ag^+ ions and one ligand molecule. completing the [3 x 3] grid architecture (termination). The process is favored by high cooperativity between the binding sites of the hexanuclear species and those of the incoming sixth ligand. The [3 x 3]-Ag_9 grid remains the only reaction product, even in a large excess of Ag^+ions, that is, above the 9:6 metal/ligand ratio.

CONCLUSION

The cases discussed here show that the self-assembly process represents a direct, efficient. and economic inethod for the construction of supramolecular inorganic architectures. Because such processes involve highly chemically informed systems, they can better be described as "informational assembly processes."[25] They are of interest for scientific and technological reasons. The emerging fields of nanoscience will benefit from the ability of chemists to create arrays of metal ions with predetermined topologies and useful physicochemical properties arising from the electronic communication between the metallic centers (redox activity. luminescence. spin-transitions, single-molecule inagnet behavior). The grid architectures are particularly attractive, because they might serve as a basis for high-density information storage devices.

A further step in programming inorganic supramolecular systems consists of the use of ligands with a double-code program, that is, ligands with two complexation subunits that code the assembly of two different structures within the same supramolecular entity. for example. a double helicate and a [2×2] grid. Each code may be viewed as a subroutrne. and the process is viewed as a "double-subroutine self-assembly "[26–28]

The implementation of information features in constructing supramolecular architectures as those described here represents a higher level in understandrng cheinistry. getting chemical synthesis closer to the complexity of the processes occurring in the living cell

ARTICLES OF FURTHER INTEREST

Chemical Topology. p. 229
Molecular Squares, Boxes, *and Cubes*, p. 909
Self-Assembly: Definition and Kinetic *and Thermodynamic Considerations*, p. 1248
Self-Assembly: Terminology, p. 1263

REFERENCES

1. Lehn. J.-M. *Supramolecular Chemistry—Concepts and Perspectives*; VCH: Weinheim. 1995.
2. Hanan, G.S.: Arana. C.R.: Lehn. J.-M.; Fenske, D. Synthesis. structure. and properties of dinuclear and trinuclear rack-type Ru^{II} complexes. Angel?;.Chem.. Int. Ed. Engl. **1995**, *34*, 1122–1124.
3. Sleiman. H.: Baxter. P.: Lehn, J.-M.; Rissansen. K. Self-assembly of rigid-rack multimetallic complexes of rotaxane type. J. Chem. Soc., Chem. Commun. 1995. 715–716.
4. Baxter. P.N.W.: Hanan, G.S.; Lehn, J.-M. Inorganic arrays via multicomponent self-assembly: The spontaneous generation of ladder architecture. Chem. Commun. 1996. 2019–2020.
5. Power. K.N.; Hennigar, T.L.: Zaworotko. M.J. Crystal structure of the coordination polymer $[Co(bipy)_{1.5}(NO_3)_2]\cdot CS_2$ (bipy=4,4′-bipyridine), a new motif for a network sustained by "T-shape" buiding blocks. New. J. Chem. **1998**. *22*, 177–181, and references therein.
6. Roesky, H.W.; Andruh. M. The interplay of coordinative, hydrogen bonding and π-π stacking interactions in sustaining supramolecular solid-state architectures. A study case of bis(4-pyridyl)-and bis(4-pyridyl-N-oxide) tectons. Coord. Chem. Rev. 2003. 236. 91. and references therein.
7. Baxter. P.N.W.: Lehn. J.-M.; Fischer. J.; Youinou. M.-T. Self-assembly of a 3 x 3 inorganic grid from nine silver ions and six ligand components. Angew. Chem.. Int. Ed. Engl. 1994. 33. 2284–2287.
8. Baxter. P.N.W.; Lehn. J.-M.: Kneisel. B.O.; Fenske. D. Self-assembly of a symmetric tetracopper box-grid with guest trapping in the solid state. Chem. Commun. 1997. 2231–2232.
9. Toyoya, S.: Woods, C.R.: Benaglia, M.; Haldimann, R.; Wärnmark, K.: Hardcastle. K.: Siegel. J.S. Tetranuclear copper(I)-biphenanthroline gridwork: Violation of the principle of maximal donor coordination caused by

intercalation and CH-to-N forces. Angew. Chem.. Int. Ed. 2001, *40*, 751–754.

10. Breuning. E.; Ruben. M.; Lehn, J.-M.: Renz, F.: Garcia, Y.; Ksenofontov. V.: Gütlich, P.; Wegelius, E.: Rissanen. K. Spin crossover in a supramolecular Fe^{II}_4 [2 x 2] grid triggered by temperature, pressure, and light. Angew. Chem., Int Ed. 2000. 39. 2504–2507.
11. Rojo, J.: Romero-Salguero, J.; Lehn, J.-M.: Baum, G.; Fenske. D. Self-assembly, structure, and physical properties of tetranuclear Zn^{II} and Co^{II} complexes of [2 x 2] grid-type. Eur. J. Inorg. Chem. 1999, 1421–1428.
12. Garcia. A.M.: Romero-Salguero, J.; Bassani, D.M.; Lehn. J.-M.: Baum. G.; Fenske. D. Self-assembly and characterization of multimetallic grid-type lead(II) complexes. Chem. Eur. J. 1999. *5*, 1803–1808.
13. Ruben. M.; Breuning, E.; Gisselbrecht, P.; Lehn. J.-M. Multilevel molecular electronic species: Electrochemical reduction of a [2 x 2] Co^{II}_4 grid-type complex by 11 electrons in 10 reversible steps. Angew. Chem., Int. Ed. 2000. 39, 4139–4142.
14. Hanan. G.S.: Volkmer, D.; Schubert. U.S.; Lehn, J.-M.; Baum. G.; Fenske. D. Coordination arrays: Tetranuclear cobalt(II) complexes with [2 × 21-grid structure. Angew. Chem.. Int. Ed. 1997. 37, 1842–1844.
15. Rojo, J.; Lehn, J.-M.; Baum. G.; Fenske. G.; Waldmann. O.; Müller, P. Self-assembly, crystal structure, and magnetic properties of a phenoxo-bridged tetranuclear Cu^{II} complex of the [2 x 2] grid type. Eur. J. Inorg. Cheni. 1999, 517–522.
16. Zhao. L.; Matthews, C.J.: Thompson, L.K.; Heath. S.L. A novel magnetically coupled nonamanganese(II) 3 x 3 portcullis-like grid involving just oxygen bridges, generated by strict self assembly of the metal cation and a single heptadentate ligand. Chem. Commun. 2000, 2656–266.
17. Thompson. L.K.; Zhao. L.; Xu, Z.; Miller, D.O.: Reiff, W.M. Self-assembled supramolecular M_9 (Mn(II), Fe(III), Zn(II)), M_5 (Fe(III)), and $[M_3]_2$ (Pb(II)) complexes: Structural. magnetic. and Mossbauer properties. Inorg. Chem. 2003, *42*, 128–139.
18. Bark, T.: Düggeli, M.; Stoeckli-Evans. H.: von Zelevsky, A. Designed molecules for self-assembly: The controlled forination of two chiral self-assembled polunuclear species with predetermined configuration. Angew. Chem., Int. Ed. 2001. 40. 2848–2851.
19. Bassani. D.: Lehn. J.-M.: Fromm. K.; Fenske, D. Toposelective and chiroselective self-assembly of [2 x 2] grid-type inorganic arrays containing different octahedral metallic centers. Angew. Chein.. Int. Ed. 1998, 37, 2364–2367.
20. Baxter. P.N.W.; Lehn, J.-M.; Kneisel, B.O.; Fenske. D. Multicomponent self-assembly: Preferential generation of a rectangular [2 x 3] grid by mixed ligand recognition. Angew. Chein., Int. Ed. 1997, 36. 1978–1981.
21. Baxter, P.N.W.; Lehn. J.-M.; Baum. G.: Fenske, D. Self-assembly and structure of interconverting multinuclear inorganic arrays: A [4 x 5]-Ag^{I}_{20} grid and an Ag^{I}_{10} quadruple helicate. Chein. Eur. J. 2000. 6. 4510–4517.
22. Zaworotko. M.J. Superstructural diversity in two dimensions: Crystal engineering of laminated solids. Chem Commun. 2001. 1–9.
23. Batten. S.R.: Robson, R. Interpenetrating nets: Ordered, periodic entaglement. Angew. Chem.. Int. Ed. 1998. 37. 1460–1494.
24. Marquis. A.: Kintzinger. J.-P.: Graff. R.: Baxter. P.N.W.; Lehn, J.-M. Mechanistic features, cooperativity and robustness in the self-assembly of multicomponent silever(I) grid-type metalloarchitecture. Angew. Chem., Int. Ed. 2002. 41. 2760–2764.
25. Baxter. P.N.W. Metal Ion Directed Assembly of Complex Molecular Architectures and Nanostructures. In *Comprehensive Supramolecular Chemistry:* Atwood, J.L.. Davies. J.E.D.. Macnicol. D.D.. Vogtle, F., Eds.: Pergamon, 1996; Vol. 9. 165–211.
26. Funeriu, D.P.: Lehn, J.-M.: Baum. G.; Fenske, D. Double subroutine self-assembly; Spontaneous generation of a nanocyclic dodecanuclear Cu^{I} architecture. Chem. Eur. J. 1997, 3. 99–104.
27. Lehn, J.M. Programmed chemical systems: Multiple subprograms and multiple processing/expression of molecular information. Chem. Eur. J. 2000. 6. 2097–2101.
28. Funeriu, D.P.: Lehn. J.M.: Fromm, K.M.; Fenske, D. Multiple expression of molecular information: Enforced generation of different supramolecular inorganic architectures by processing of the same ligand information through specific coordination algorithms. Chem. Eur. J. 2000. 6. 2103–2111.

Rotaxanes and Pseudorotaxanes

Petra Linnartz
Christoph A. Schalley
Kekulé-Institut für Organische Chemie und Biochemie der Universitat, Bonn, Germany

INTRODUCTION

In the early 1960s, chemists set out to investigate mechanically interlocked molecules, among them, catenanes and rotaxanes (Fig. 1a,b). Catenanes are two intertwined macrocycles, while rotaxanes are made from an axle threaded into a wheel.[1,2] The axle is restrained to remain inside the wheel by suitable stopper groups that prevent deslipping. In contrast, a pseudorotaxane (Fig. 1c) is formed when noncovalent forces bind an axle inside a macrocycle without the help of stoppers. The idea of threading one molecule through the cavity of a second macrocyclic one was not only appealing with respect to molecular geometry and topology but also promised insight into fundamental chemical questions: How would it be possible to efficiently synthesize these molecules? What would their properties be? Appropriately substituted. one envisaged a new form of chirality based only on the topology of the molecule, without the necessity of implementing chiral centers. However, the first attempts to synthesize such architectures by low-yield statistical methods[3,4] or by a tedious multistep procedure[5] involving a covalent junction between the two subunits and subsequent cleavage of the covalent bond between them quickly showed how difficult their preparation was.

Starting in the mid-1980s, the use of noncovalent templates[6] greatly facilitated the formation of rotaxanes. and the field gained fresh impetus. For years, the focus of researchers in this field was the realization of new, more complex topologies. such as oligocatenanes, rotaxanes with more than one wheel, pretzelanes, and knots (Fig. I). Because many of these architectures are chiral without bearing a chiral center. topological chirality received increasing attention.[7] However. the aesthetics of beautiful molecules lost importance as the driving force for new developments, and for modern rotaxane chemistry, functionality is of major interest. Because mechanical bonding provides ideal features with respect to the mobility of the two components relative to each other, many reports appeared on controlled motions within these complexes.[8,9] Many researchers in this area ultimately aim for the construction of molecular motors and functional molecular devices at a nanometer scale.

TEMPLATED ROTAXANE SYNTHESIS

A rotaxane can. in principle: be built by slipping the wheel over one of the stoppers at an elevated temperature. by threading the axle center piece into the wheel and capping it with stoppers, by trapping a stopper in the wheel's cavity and reacting it with the other half of the axle, or by clipping the wheel around the axle and subsequent ring closure.[10] All of these pathways only give high yields of rotaxanes if attractive forces between wheel and axle are operative. This idea led to the development of several different template effects based on noncovalent bonding between axle and wheel, which greatly reduced the synthetic demands of rotaxane synthesis. With the help of template effects, the reaction of the rotaxanes' subunits can be directed toward the formation of these interlocked molecules and avoid, more or less efficiently, undesired side reactions. In the next sections, several template effects will briefly be discussed as examples for synthetic pathways to rotaxanes. Others exist. which we cannot describe in such detail, e.g., rotaxanes with cyclodextrin wheels,[11] which are based on the use of hydrophobic effects, or Crignard-type R-Mg-R compounds[12] bearing a crown ether wheel around the central magnesium ion.

Let us start the discussion with a metal ion template,[13] which was introduced by Sauvage and his coworkers in the mid-1980s (Fig. 2, top left). A Cu(I) ion with its preferred tetrahedral coordination geometry is capable of binding two phenanthroline units. If one of the phenanthrolines is incorporated in a macrocycle, which later will become the wheel, the second ligand is drawn into the cavity by the copper ion and can be easily equipped with two stoppers. The rotaxane precursor can then be dernetallated by treatment with cyanide ions to yield the desired rotaxane. Similarly, catenanes and other mechanically bound molecules can be synthesized. Also, other transition metals were used. some of which had an octahedral coordination geometry and were reacted with terpyridine instead of phenanthroline units.

Stoddart and his group utilized π-donor, n-acceptor interactions between electron-poor paraquat (*N*-,*N*-dimethyl 4.4'-bipyridinium) and electron-rich hydroquinone or napthoquinone moieties in order to preorganize a

Encyclopedia of Supramolecular Chemistry
DOI: 10.1081/E-ESMC 120012775

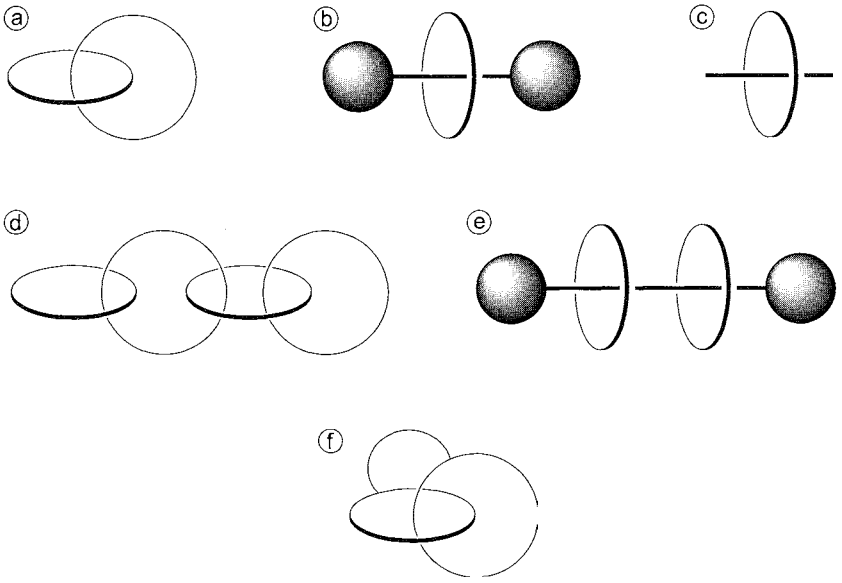

Fig. 1 Different topologies of mechanically interlocked molecules: (a) catenane, (b) rotaxane. (c) pseudorotaxane, (d) oligocatenane, (e) [3]rotaxane, and (f) pretzelane.

pseudorotaxane that can then be functionalized with appropriate stopper groups.[14] A large number of synthetic variations using this strategy are available. For example. the hydroquinone axle center piece can be threaded into a bis-paraquat wheel. and a paraquat center piece also binds inside a *bis*-hydroquinone wheel. Furthermore, a complete axle can be converted into a rotaxane by clipping the macrocycle around its centerpiece (Fig. 2, top right). Many other combinations are possible, and all of the synthetic strategies (slipping, threading, trapping. and clipping) were used.

Of course, hydrogen bonding is an excellent candidate for noncovalent templating, in particular because hydrogen bonds are directional in nature and thus may help to appropriately position two building blocks for a rotaxane relative to each other. Secondary ammonium ions can be inserted into crown ethers by hydrogen bonds and stoppered to yield a rotaxane.[14] However, hydrogen bonding also permits the use of nonionic templates. For example, amide groups incorporated in the rotaxane axle bind in the cavity of a tetralactam macrocycle with three hydrogen bonds (Fig. 2, bottom left). X-ray structures give insight into the pattern. Two hydrogen bonds form between amide NH protons of the wheel and the carbonyl group in the axle. and the third one can be considered as "backbonding" of the axle's NH proton to one of the carbonyl groups of the wheel. With this type of template effect, a large variety of different axles can be incorporated in the wheel.[15,16]

As a last example, an anion template should be mentioned that was recently discovered by Vogtle and his coworkers.[17,18] A phenolate ion is bound with its oxygen inside the cavity of the tetralactarn macrocycle by two strong hydrogen bonds ($K > 10^5\ M^{-1}$ in CH_2Cl_2). In other words, the macrocycle serves as an anion receptor strongly binding one part of the axle. This supramolecular. "wheeled" nuclophile can react with an electrophilic semiaxle through the wheel trapping it on the axle between two stoppers and thus giving access to rotaxanes with yields of up to 95% (Fig. 2. bottom right).

These examples of template effects illustrate the close relationship between host–guest and rotaxane chemistry. Appropriate concave host molecules bind convex guests in such a way that they can be equipped with two stoppers that mechanically prevent dissociation of the host–guest complex. Any macrocyclic receptor may thus be suitable for the formation of rotaxanes.

STABILITY OF ROTAXANES

For any application of rotaxanes, as. for example. the constuction of machines at a molecular scale. stability is a major issue. Stoppers too small in size permit the wheel to deslip from the axle so that the rotaxane decays into its two free components (Fig. 3).[19] A region of metastable rotaxanes exists between pseudorotaxanes without stopper groups on one side and stable rotaxanes on the other, where the barrier for the deslipping process is so high that cleavage of a covalent bond in the axle or wheel would be energetically favored.[20] In some cases, the transition from stable rotaxanes to their quickly deslipping

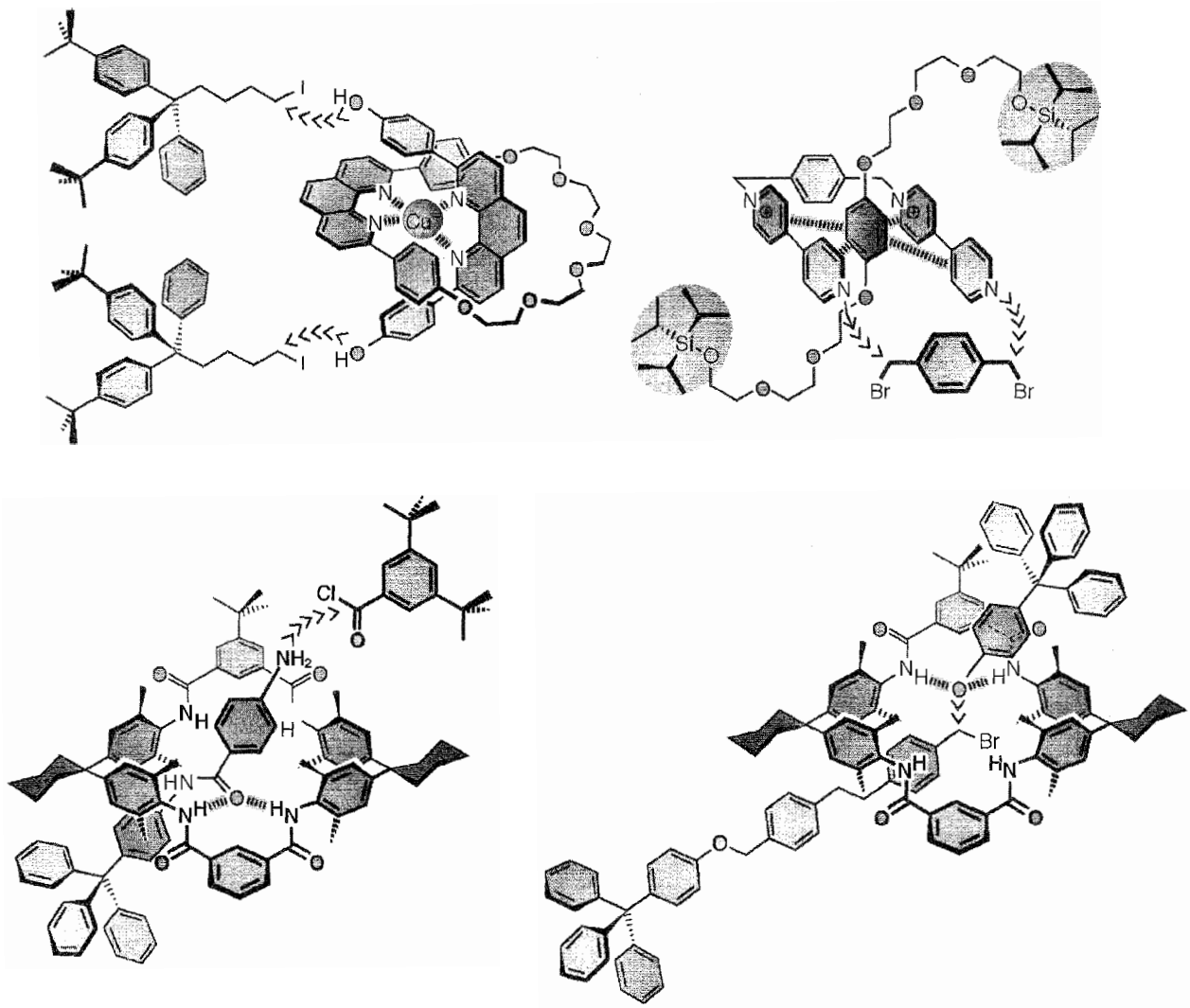

Fig. 2 Template syntheses of rotaxanes: the Cu(I) ion binds a phenanthroline ligand inside a macrocycle (top left). A *bis*-paraquat macrocycle is clipped around an axle bearing a hydroquinone center piece (top right). Hydrogen bonding permits the use of nonionic template effects for the preparation of amide-type rotaxanes (bottom left). Phenolate anions bound to the macrocycle react as a supramolecular nucleophile (bottom right).

counterparts is abrupt. and only slight changes in the rotaxane structures cause huge differences in the deslipping rates. Stoddart et al. reported an all-or-nothing effect,[21] where a simple methyl group decided the fate of the rotasane. With a *tri*-(*t*-butylphenyl) methane stopper, no deslipping occurred, while the same stopper with one i-propyl instead of a *t*-butyl group easily permitted decomposition into axle and wheel. Similarly surprising is the increase in half-life for the rotaxanes shown in Fig. 3. Replacing just a CH-group in the wheel by an isoelectronic nitrogen atom causes the'half-life at 333 K to jump from ca. 60 h to more than 10^6 h.[22] Here, the analysis of the activation enthalpies and entropies indicates that this effect is almost exclusively enthalpic. This points to a significantly more unfavorable size complementarity of stoppers and wheel. which is due to hydrogen bonding. Molecular modeling yields the geometrical parameters given in Fig. 3. A significant decrease of the space available inside the wheel's cavity is iliustrated by the N–N distances that shrink by about 10% for the pyridine wheel relative to that bearing two isophthalic acid amide units. Of course, a smaller-diameter wheel corresponds to an energetically more demanding barrier for deslipping.

Deslipping can also be used to determine the steric demand of a group of atoms. Vögtle and his group measured the effective size of dendrons by comparing the

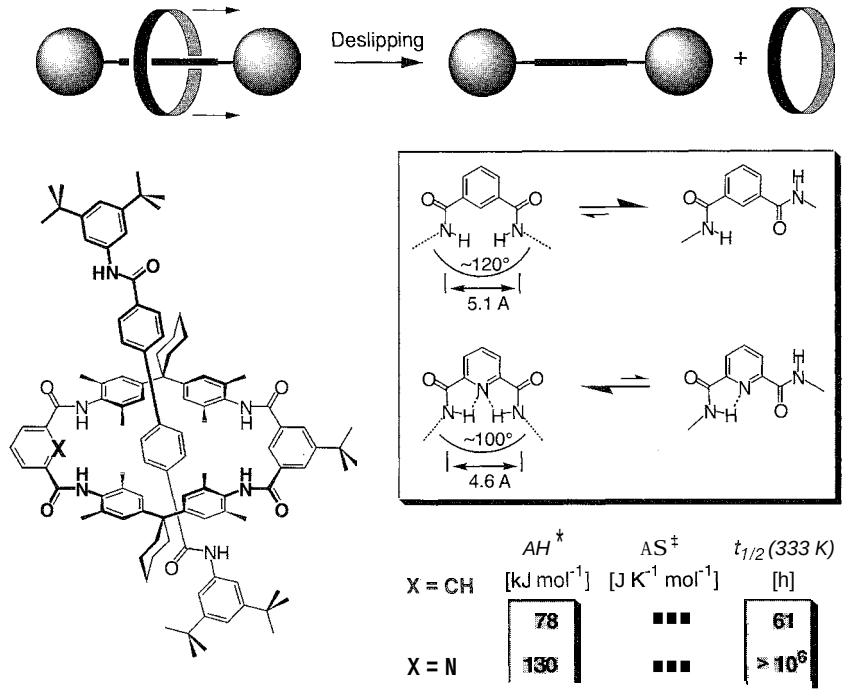

Fig. **3** Top: The deslipping process. Bottom: Intramolecular hydrogen bonding significantly decreases the ring size of the tetralactam inacrocycle bearing a pyridine dicarboxamide relative to that of a wheel with two isophthalic acid amides. This provokes a more than 10,000-fold increase in half-life. The activation parameters are given for both rotaxanes, and the effect can be almost exclusively attributed to enthalpic contributions. i.e.. the size complementarity between stoppers and wheel. Shown in the inset are the preferred conformations of the two differing building blocks and some parameters from molecular modeling, confirming the reduction of the wheel's inner diameter due to hydrogen bonding.

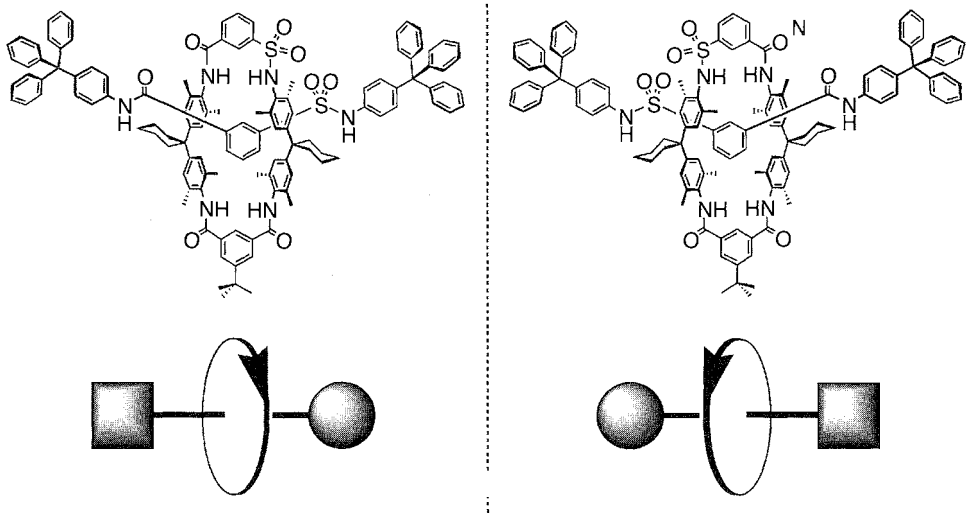

Fig. **4** Two enantiomers of an amide rotaxane. showing their overall structures. Note that the sulfonamide group in the wheel defines an atom sequence (indicated by the arrows in the bottom drawings). The sulfonamide incorporated in the axle permits the two stoppers to be distinguished. Such rotaxanes can be separated into the two enantiomers by HPLC on chiral stationary phases. and their CD spectra were measured.

half-life of several rotaxanes with dendritic stoppers to those with tritylphenol or di-t-butyl phenyl stoppers.[23,24] Dendritic stoppers appear smaller than a static, computer-generated model would imply, because their high flexibilities probably permit them to deslip in a branch-by-branch fashion. Consequently, deslipping experiments not only yield information about the stability of rotaxanes but also at the same time allow us to address fundamental questions in organic chemistry, such as that of spatial demand of functional groups. from a new point of view.

TOPOLOGICAL CHIRALITY

Let us assume that a rotaxane is formed from an axle with two different stoppers and a wheel that bears a directionality defined by the sequence of atoms in the macrocycle. Both of these subunits are achiral, both are identical to their mirror images. Nevertheless. the corresponding rotaxane exists in two enantiomeric forms, although no chiral center is present in the molecule (Fig. 4). It is the molecular topology that makes these species chiral. and consequently. this phenomenon was coined "topological chirality..' It also exists for catenanes, knots. and other mechanically bound molecules. Shown in Fig. 4 is a detailed structure of such a rotaxane. The wheel contains one sulfonamide group that provides the directionality of the atom sequence. The two enantiomers of the rotaxane can be separated and studied by CD spectroscopy.[25]

For [3]rotaxanes, i.e., an axle with two wheels, even diastereomers exist, if both wheels have a directionality with respect to their atom sequence.[26,27] Both wheels can then display the same clockwise atom sequence yielding a mirror symmetrical species that can be regarded as the supramolecular analogue of the *meso* form of tartaric acid. If the two wheels assemble on the axle with opposing directionality. diastereomers are formed.

MOLECULAR MACHINES, NANOMUSCLES, AND **OTHER** DEVICES

Nature has often been a model for scientists. and the functions of many enzymes were mimicked by chemists with the help of much less complicated model systems. A particularly fascinating enzyme is ATP synthase, a molecular motor that converts the energy stored in a proton gradient into mechanical rotation. The rotation is then coupled to the production of ATP. the major source of energy for most cellular processes. Although we can give only a sketchy description of this enzyme here. its features are interesting with respect to the construction of artificial inolecular motors.[28] First. there is geometric resemblance. The F_0 ATP synthase consists of a cyclic

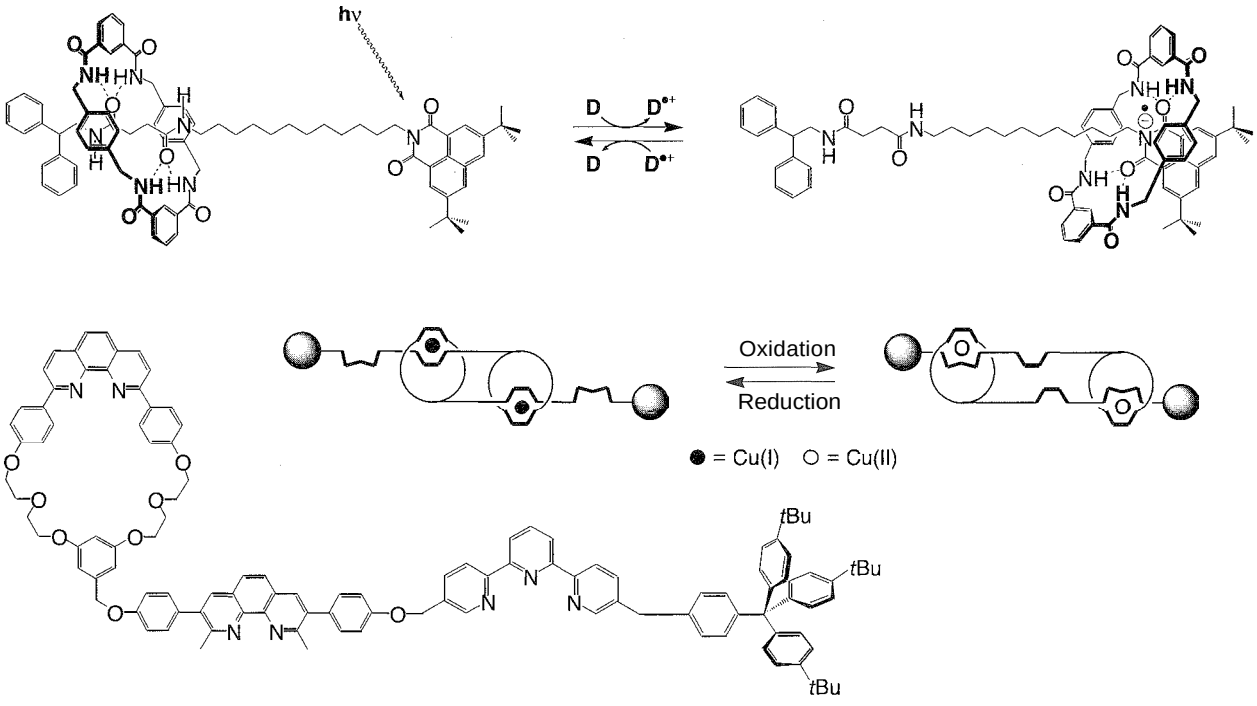

Fig. 5 Controlled molecular motion in rotaxanes: light-driven shifting of the wheel along the rotaxane axle (top); and contraction of a molecular ''muscle'' stimulated by electrochemical Cu(I)–Cu(II) interconversion (bottom).

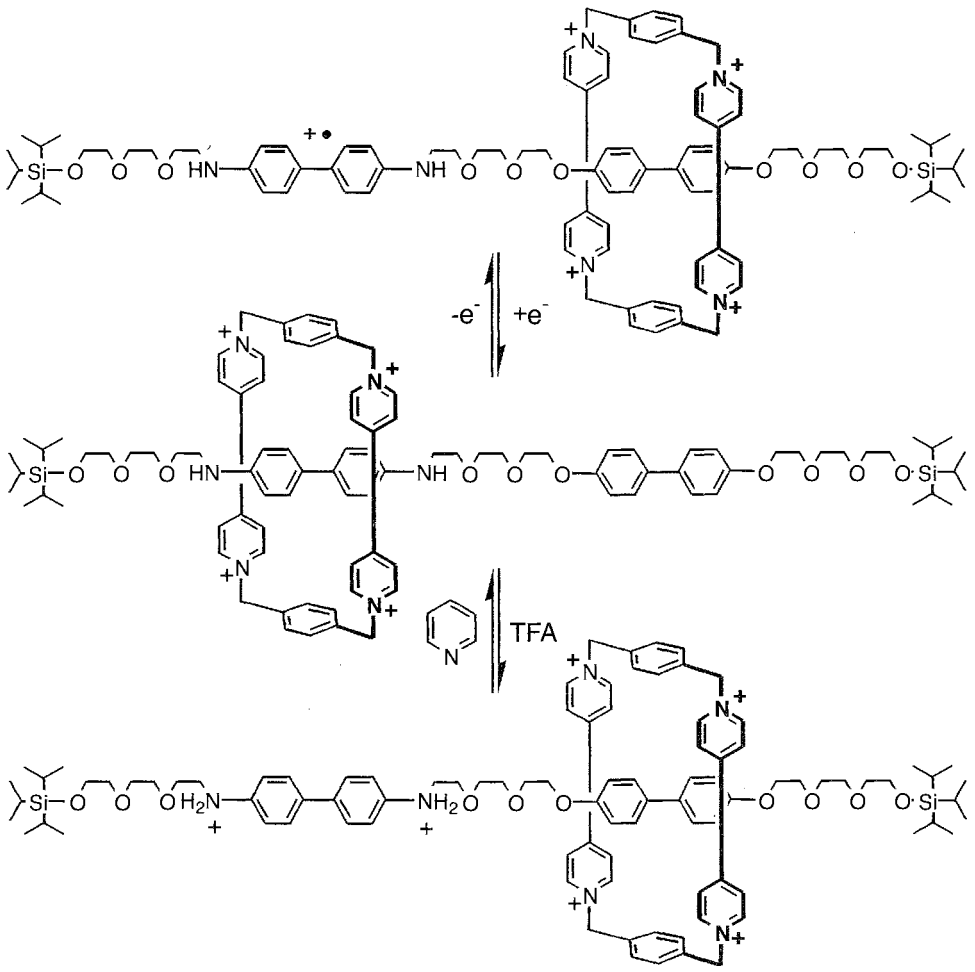

Fig. 6 A molecular shuttle controllable either chemically or electrochemically. In the resting state, the wheel is located on the left. Oxidation or protonation force the wheel to travel to the other side of the axle due to unfavorable charge–charge interactions. Considering oxidation and protonation as the two inputs and the motion of the wheel as the output. this system resembles a logic OR gate.

arrangement of membrane-inserted proteins (the stator) in which a rod-like protein (the rotor) can rotate. The source of energy for rotation comes from differences in the proton concentration inside and outside of the membrane. Thus; it is clear that the membrane separates the two compartments and prohibits immediate equilibration of the proton concentrations on both sides. Unidirectional rotation is achieved by a helical proton channel inside the membrane part of ATP synthase and by a defined orientation of the enzyme in the membrane. Axle rotation and the proton migration through the channel are coupled to each other, and immediately, it becomes clear that the chiral element of a helical proton channel is mandatory for unidirectionaiity. Finally. the rotating rod induces conformational changes in the F_1 part consisting of an $\alpha_3\beta_3$ protein hexamer. These changes in structure are the basis for the production of ATP from ADP and phosphate.

Based on these considerations. several groups attempted to construct artificial molecular motors on the basis of rotaxanes, the macrocyclic wheel being the stator. and the axle representing the rotor. The topic of controlled molecular motion was studied intensely. Several types of motion are feasible besides rotation.[29] namely, shuttling along the axle[30] and pivotal rocking of the axle. With respect to the energy sources for such movements, let us discuss two examples in which motion is induced by exposure to light of appropriate wavelengths and by redox reactions. Recently. Brower. Leigh. and coworkers published a study describing the light-controlled shuttling of a wheel along the axle (Fig. 5).[31] In its resting state. the rotaxane wheel is bound to the left side by hydrogen bonding. A light-induced electron transfer from a donor present in solution to the stopper on the right generates an anion radical with better hydrogen bond acceptor

qualities, and consequently. the wheel moves to this side surprisingly quickly. Backconversion to the resting state by reduction of the anion radical causes the wheel to shift back to the left. The second example from the group of Sauvage may be considered as a molecular analog of a muscle.[''''] Two filaments are each connected to a macrocycle. By the Cu(I) ion template, two of these molecules are threaded into each other, as depicted in Fig. 5. One of the particular features of copper is that it changes its preferred coordination geometry upon oxidation from Cu(I) (tetrahedron) to Cu(II) (trigonal bipyramid). Incorporation of one phenanthroline unit in each of the wheels and both a phenanthroline and a terpyridine in each of the filaments permits a switch between an extended form and a contracted form. Cu(I) prefers to be bound to two phenanthroline ligands. but oxidation to Cu(II) provokes preferential binding to the terpyridine unit. This change necessarily involves an increase of the distance between the two macrocycles. Reduction of the Cu(II) ion to Cu(I) reverts the process.

Other applications in nanoscale electronics can be envisaged. A molecular shuttle with two different states—despite all technical difficulties involved in writing and reading information into or from one molecule—may be considered as one bit of a miniaturized computer chip.[33] If the switching between two states can be controlled by two different stimuli, logic gates can be constructed that combine two different input signals to one output (Fig. 6).[30]a Such electronic devices at a molecular level are one of the chemists' potential answers to the visions of Feynman's bottom-up approach.[35] Because the ongoing reduction of the size of conventional electronic devices (the top–down approach) has limitations that cannot be overcome with current technology. it seems promising to start with molecules and construct electronic devices at a nanometer level.

Although the goal of perfectly functional molecular motors or electronic building blocks has not yet been reached, these examples illustrate how far the development in rotaxane chemistry and the art of controlling it has gone. For the future. we expect the field to shift more to applications, which might be the focus of the next decade.

ARTICLES OF FURTHER INTEREST

Amide- and Urea-Based Anion Receptors. p. 31
Anion-Directed Assembly, p. 51
Catenanes and Other Interlocked Molecules, p. 206
Chemical Topology, p. 229
Cucurbituril, Its Homologues, and Derivatives, p. 390
Cyclodextrins, p. 398
Hydrogen Bonding, p. 658
Hydrophobic Effects, p. 673
Interpenetration, p. 735
Molecular Logic Gates, p. 893
Molecular-Level Machines, p. 931
π–π Interactions: Theory and Scope. p. 1076
The Template Effect. p. 1493

[a]For an example of an XOR gate, see Ref [34]

REFERENCES

1. Schill, G. *Catenanes, Rotaxanes and Knots*; Academic Press: New York. USA. 1971.
2. *Molecular Catenanes, Rotaxanes, and Knots:* Sauvage. J.-P., Dietrich-Buchecker. C.. Eds.: Wiley-VCH: Weinheirn, Germany. 1999.
3. Wasserman, E. The preparation of interlocked rings: A catenane. J. Am. Chem. Soc. 1960. *82,* 4433.
4. Harrison. I.T.; Harrison. S. The synthesis of a stable complex of a macrocylce and a threaded chain. J. Am. Chem. Soc. 1967. *89,* 5723.
5. Schill. G.; Zollenkopf. H.; Rotaxan-Verbindungen I. Liebigs Ann. 8969. 721. 53.
6. *Teinplated Organic Synthesis;* Diederich. F.. Stang. P.J., Eds.; Wiley-VCH: Weinheim. Germany. 2000.
7. Chambron. J.-C.; Dietrich-Buchecker. C.: Sauvage. J.-P. From classical chirality to topologically chiral catenands and knots. Top. Curr. Chem. 1993. *165*, 131.
8. Balzani, V.; Credi. A.; Raymo. F.M.: Stoddart, J.F. Artificial molecular machines. Angew. Chem. 2000. 112. 3484.
9. Balzani, V.; Credi. A.; Raymo, F.M.: Stoddart, J.F. Artificial molecular machines. Angew. Chem. Int. Ed. *2000. 39.* 3348.
10. Seel. C.: Vogtle. F. "Wheeled reagents." and a new route to rotaxanes by anion complexation: The trapping method. Chem. Eur. J. 2000. 6. 21.
11. Onagi. H.: Easton, C.J.: Lincoln. S.F. An hermaphrodite [2]rotaxane: Preparation and analysis of topology. Org. Lett. 2001. *3*. 1041.
12. Markies, P.R.: Akkerman, O.S.: Bickelhaupt, F. Complexation of *bis*(*p*-tert-butylphenyl)magnesium with 1.3-xylene crown-ethers and glymes. Organornetallics 1994, 13. 2616.
13. Chambron. J.-C.: Dietrich-Buchecker, C.O.; Nierengarten, J.-F.; Sauvage. J.-P. Transition-metals as assembling and templating species—From catenanes and knots to strings threaded through molecular rings. Pure Appl. Chem. 1994. *66*, 1543.
14. Raymo, F.M.; Stoddart. J.F. Organic Template-Directed Syntheses of Catenanes. Rotaxanes, and Knots. In *Molecular Catenanes, Rotaxanes, and Knots*: Sauvage. J.-P.. Dietrich-Buchecker. C.. Eds.: Wiley-VCH: Weinheiin, Germany. 1999; 143.
15. Jäger, R.: Vogtle, F. A new synthetic strategy towards molecules with mechanical bonds: Nonionic template

synthesis of amide-linked catenanes and rotaxanes. Angew. Chem. 1997. *109*, 966.
16. Jager. R.: Vogtle, F. A new synthetic strategy towards molecules with mechanical bonds: Nonionic template synthesis of amide-linked catenanes and rotaxanes. Angew. Chem. Int. Ed. 1997, *36*, 930.
17. Reuter. C.; Wienand. W.: Hiibner, G.M.: Seel. C.; Vogtle, F.F. High-yield synthesis of ester. carbonate. and acetal rotaxanes by anion template assistance and their hydrolytic dethreading. Chem. Eur. J. 1999. *5*. 2692. and literature cited.
18. Schalley, C.A.: Silva, G.; Nising, C.-F.; Linnartz, P. Analysis and improvement of an anion-templated rotaxane synthesis. Helv. Chim. Acta, 2002. *85*. 1578.
19. Heim. C.: Affeld, A.; Nieger, M.: Vogtle, F. Size complementarity of macrocyclic cavities and stoppers in amide-rotaxanes. Helv. Chim. Acta 1999. *82*, 746.
20. Ashton. P.R.; Baxter. I.; Fyfe, M.C.T.; Raymo, F.M.; Spencer, N.: Stoddart, J.F.: White, A.J.P.: Williams, D.J. Rotaxane or pseudorotaxane? That is the question! J. Am. Chem. Soc. 1998. *120*, 2297.
21. Raymo, F.M.: Houk, K.N.; Stoddart, J.F. The mechanism of the slippage approach to rotaxanes. Origin of the ''all-or-nothing'' substituent effect. J. Am. Chem. Soc. 1998, 120, 9318.
22. Affeld. A.; Hiibner, G.M.: Seel, C.Schalley, C.A. Rotaxane or pseudorotaxane? Effects of small structural variations on the deslipping kinetics of rotaxanes with stopper groups of intermediate size. Eur. J. Org. Chem. 2001. 2877.
23. Hiibner, G.; Nachtsheiin, G.; Li. Q.-Y.; Seel, C.; Vogtle, F. The spatial demand of dendrimers: Deslipping of rotaxanes. Angew. Chem. 2000, *112*. 1315.
24. Hiibner. G.: Nachtsheim, G.; Li, Q.-Y.; Seel, C.; Vogtle, F. The spatial demand of dendrirners: Deslipping of rotaxanes. Angew. Chem. Int. Ed. 2000. *39*. 1269.
25. Yamamoto. C.; Okamoto, Y.: Schmidt. T.: Jager. R.; Vogtle. F. Enantiomeric resolution of cycloenantiomeric rotaxane, topologically chiral catenane, and pretzel-shaped molecules: Observation of pronounced circular dichroism. J. Am. Chem. Soc. 1997. 119. 10547.
26. Schmieder, R.; Hubner. G.; Seel, C.: Vogtle, F. The first cyclodiastereomeric [3]rotaxane. Angew. Chem. 1999, **111,** 3741.
27. Schmieder. R.: Hiibner, G.; Seel, C.: Vogtle. F. The first cyclodiastereomeric [3]rotaxane. Angew. Chem. Int. Ed. 1999. *38*, 3528.
28. Schalley, C.A.; Beizai, K.; Vogtle. F. On the way to rotaxane-based molecular motors: Studies in molecular mobility and topological chirality. Acc. Chem. Res. 2001, *34*, 465.
29. Bermudez, V.; Capron, N.; Gase. T.; Gatti, F.G.; Kajzar, F.: Leigh, D.A.; Zerbetto. F.: Zhang. S. Influencing intramolecular motion with an alternating electric field. Nature 2000. *406*. 608.
30. Bissell. R.A.: Córdova, E.; Kaifer. A.E.; Stoddart. J.F. A chemically and electrochemically switchable molecular shuttle. Nature 1994, *369;* 133.
31. Brouwer. A.M.: Frochot, C.: Gatti. F.C.; Leigh. D.A.: Mottier. L.; Paolucci, F.; Roffia. S.: Wurpel. G.W.H. Photoinduction of fast, reversible translational motion in a hydrogen-bonded molecular shuttle. Science 2001.291. 2124.
32. Collin, J.-P.; Dietrich-Buchecker. C.: Gaviña, P.: Jimenez-Molero, M.C.: Sauvage. J.-P. Shuttles and muscles: Linear molecular machines based on transition metals. Acc. Chem. Res. 2001. *34*. 477.
33. Balzani, *V.*: Gómez-López, M.: Stoddart. J.F. Molecular machines. Acc. Chem. Res. 1998. *31*. 405.
34. Credi, A.: Balzani. V.; Langford, S.J.: Stoddart. J.F. Logic operations at the molecular level. An XOR gate based on a molecular machine. J. Am. Chem. Soc. 1997. 119. 2679.
35. Feynman, R.P. There is plenty of room at the bottom. Sat. Rev. 1960. *43*. 45.

Scanning Tunneling Microscopy

Lucidalva S. Pinheiro
Instituto de Química da Universidade de Sdo Paulo, São Paulo, Brazil

INTRODUCTION

Scanning tunneling inicroscopy (STM) was used successfully to image and propose the molecular packing of several small molecules adsorbed on surfaces. In supramolecular chemistry. a large assembly of small molecules can take place via weaker forces than covalent bonds. Supramolecular structures or their building blocks adsorbed on a surface can also be studied with STM. Physisorption or chemisorption can take place for each system. The forces acting in these two types of adsorption are important and can govern the final arrangement of the species on the surface. The range of molecular interactions observed in the solid inight be transferred to the adsorbed molecular layer. STM also offers the possibility of manipulation of the adsorbed species. This could be useful in host–guest complexation in situ. STM tip functionalization opens the possibility of recognition between species that act as hosts and guests in traditional supramolecular chemistry.

THE STM TECHNIQUE

G. Binnig and H. Rohrer[1,2] developed STM in the early 1980s. The technique is used in the study of conductive and semiconductive solid surfaces. It is based on a tunneling current between a sensor. the tip, and a sample.

The tunneling current is an exponential function of the separation between tip and sample. An approximate form of the tunneling current in the limit of low-bias voltage is given by the following:

$$I \propto Ve^{-2\kappa S} \quad (1)$$

V is the bias voltage: $\kappa=[2m(V_0-E)]^{1/2}/\hbar$; and s is the distance between tip and sample. A discussion of the tunneling cur-sent can be found elsewhere.[3,4]

STM presents a very high lateral resolution, and soon it was realized that it could be employed to study modified surfaces. The microscope can be used in ultrahigh vacuum (UHV), air, and under solutions. which makes it a very powerful technique. The STM instrument comprises a control unit and a piezoelectric device responsible for the displacements of the sample or tip. These components are interfaced to a computer.[5]

STM images are a mixture of topography and electronic information The contribution of each factor depends on the system under study Some approaches to analyze molecular layers were made, such as identifying chemical marker groups,[6] tunneling spectroscopy and fluorescence,[7,8] shape of the adsorbed species,[9] and image simulation [10 11]

STM Operation Modes

Constant current mode

In this mode, a current is chosen, and the feedback loop of the STM makes the tip track the surface to maintain this preset current. In this condition, the tip moves up and down in the z direction, while it scans in the x–y direction, rendering a tridimensional map of the surface. Scan speed in this mode is low due to the need to track the surface features.

Constant height mode

In this mode, the feedback loop of the STM is disabled. This way. the tip does not move in the z direction while scanning, keeping a constant height from the surface. The overlap between the tip states and those of the surface renders a tunneling current that is compared to that of the preset. Surfaces areas where there is effective overlap appear bright in the image. while those where the process is not so efficient appear darker in the image. Scan speed can be high in this mode, as there is no need to track the surface topography.

Tips

Tips are normally made of thin metal wires (ca. 0.25 mm), such as tungsten, platinum. or alloys (such as platinum-iridium and platinum-rhodium). Gold and silver tips can also be useful in some systems. To obtain the desired high resolution of the STM. it is necessary to have a very sharp tip with which to acquire the images. Tips can be prepared electrocheinically by etching the metal in a convenient solution, such as potassium hydroxide for W or basic aqueous cyanide solution for Pt-Ir tips. They can also be

Encyclopedia of Supramolecular Chemistry
DOI: 10.1081/E-ESMC 120019172

prepared mechanically by cutting the wire. This method also produces tips capable of providing atomic and molecular resolutions. More details of tip etching and sharpening techniques were reviewed by Chen.[4]

Electrochemical STM (ECSTM)

In ECSTM, a cell with four electrodes replaces the conventional three-electrodes cell, the tip being the fourth one. In this case. a convenient design of the STM is required to allow for the inclusion of the potentiostat.[12] In ECSTM, care should be taken with the tip. The tunneling current used in STM ranges from the picoampere to the nanoampere regime. The tip can suffer electrochemical redox processes in the potential window sampled during the experiment. The current deriving from tip redox processes can overshadow the tunneling current. This problem is minimized by insulating the tip, leaving the smallest surface area exposed to solution. Tips are normally coated before the ECSTM experiment using nail varnish. wax, or polymers.

SUBSTRATES

Metals

A very flat surface without defects is normally desired when performing molecular adsorption. The condition for large terraces suitable for molecular adsorption is met by using the face-centered cubic metal surfaces of low Miller index.

The Au(111) is often employed in air and ECSTM due to its inertness. The Au(111) can be prepared as a thin film grown on mica or glass.[13] Gold beads can also be used as substrates. They are formed by melting the end of a wire on a torch following the method of Clavilier.[13] The beads present flat areas suitable for molecular adsorption. The Au surfaces are cleaned by thermal annealing in a flame before molecular adsorption. When well prepared, the Au(11I) surface presents a reconstruction known as 22 x *J3*. This structure is characterized by a pair of dislocation lines[13] and is sometimes preserved upon molecular adsorption. Other compounds promote the lifting of the reconstruction. The other low Miller index faces of Au. namely, Au(110) and Au(100), normally employed as monocrystals, were also studied.

Silver is often used in UHV STM and is also employed in air STM as a substrate to adsorb molecules. It can be used as a single crystal or as a thin film.[14,15] Single crystals of Cu. Rh, and Pt were also employed as substrates in many STM experiments for molecular adsorption.[16,17]

Layered Materials

Highly oriented pyrolitic graphite (HOPG) is one of the substrates most used for molecular adsorption. The material consists of a layered structure of carbon atoms arranged in a honeycomb lattice.[18] The atomic structure sampled with STM should be carefully analyzed. The surface atomic arrangement of HOPG imaged by STM was studied. and the conclusion is that a true hexagonal structure is not always sampled by the microscope.[18]

A characteristic of molecular adsorption on HOPG is the possibility of imaging the adsorbed layer with one set of tunneling parameters and the substrate surface by modifying these parameters. In general, the adsorbed layer is seen with high resistance in the gap, while the substrate structure can be imaged by decreasing the tunneling resistance.[19] This mechanism allows the overlay of the molecular structure on the HOPG lattice, giving information on surface site adsorption.

A layered material with semiconducting behavior, MoS_2, was used as substrate for STM. A discussion of the metals dichalcogenides structures and analyses of STM images was presented by Anselmetti and Wiesendanger.[18]

SUPRAMOLECULAR STRUCTURES

The chemistry and properties of supramolecular building blocks were presented and discussed in specialized texts.[20,21] The next topics highlight some of the STM results reported in the literature for the building blocks used in supramolecular chemistry.

Calixarenes

Adsorption of a calix[4]arene and calix[4]diquinone disulfide was carried out on Au(111) and analyzed with ECSTM.[22] The molecules form organized layers on the metal. The calix[4]arene is supposed to bind through hydroxyl groups, while the calix[4]diquinone disulfide is expected to interact with the gold through the sulfur atom. Calix[4]arenes with different functional groups were adsorbed on Au(111).[23] The molecules form large ordered adlayers. The presence of groups such as NO_2 and tert-butyl in the upper rim of the calix[4]arenes are supposed to reduce lateral interaction between the molecules.

Calix[4]resorcinarene functionalized with a thiol head was self-assembled on Au(111) from several different solvents.[24] The UHV STM was used to acquire the images of the layers. The thiol head is thought to bind to the surface, leading to molecular-ordered regions, which also depends on the preparation method.

Catenanes

Benzylic amide[2]catenanes were studied on HOPG by air STM.[25] Molecular adsorption is supposed to take place on the surface through the carbonyl groups present in the backbone. The authors comment on the possibility of molecular diffusion during imaging and also on molecular degradation upon adsorption as contributor factors to the very few features observed with submolecular resolution in the STM images.

The adsorption from solution of larger [2]catenanes consisting of two 87-membered rings was studied on HOPG.[26] The STM image shows with submolecular resolution that the [2]catenane adsorb on the HOPG forming domains. The authors discuss the thermodynamics reasons for adsorption and the dynamics of the adsorbed layer.

Crown Ethers, Cryptands, and Cyclophanes

The diaza-15-crown-5 molecule adsorbed on Cu(111) was studied by ECSTM.[27] The molecule forms a well-ordered layer on the metal under a certain range of potentials. The molecular interaction with the substrate is thought to be responsible for the adlayer formation. Dibenzo-18-crown-6-ether and its inclusion cornpound with potassium were studied on Au(111). The STM images obtained with submolecular resolution show that the species arrange in a two-dimensional (2D) supramolecular structure under potential control.[28]

A crown ether substituted phthalocyanin was adsorbed on HOPG, presenting several orientations. The molecules can be manipulated with the STM tip to adopt different orientations on the substrate.'''' The STM images of an aromatic cryptand adsorbed on HOPG show the formation of chains of molecular nanoclusters and areas with a 2D arrangement of the molecules.[29]

A cyclophane was studied on HOPG, and the authors concluded that the molecule stands upright on the surface, forming one-dimensional (1D) tubes.[30]

Cyclodextrins

The STM studies of cyclodextrins ranged from imaging to molecular manipulation. The basic units of α-cyclodextrin and β-cyclodextrin adsorbed on HOPG were imaged with submolecular resolution.[31] An inclusion compound of a-cyclodextrin and adamantane-methanol was also studied; the images showing a pattern similar to the empty α-cyclodextrin.[31] An inclusion complex between β-cyclodextrin and a triphenylphosphine sodium salt was analyzed by STM with submolecular resolution. The authors assign the STM contrast observed to the two phenyl rings of the guest molecule, while the β-cyclodextrin structure would not contribute to it.[32] An inclusion compound of a β-cyclodextrin and calix[4]arene was studied on HOPG.[33] The STM images show stripes with submolecular resolution for the inclusion compound. The adsorption of cyclodextrins functionalized with side groups such as thiol and Iipoamide was also pursued with the STM.[34,35] The final ordering of the molecules on the surface was shown to be dependent on the intermolecular interactions that are controlled by the side groups. The β-cyclodextrin, adsorbed on Au(111) and studied with the ECSTM. was found to form a nanotube-like structure on some potentials.[36] Aggregates of β-cyclodextrin threaded to polymers chains were studied on HOPG. The STM images are used to confirm the formation of pseudorotaxanes on the surface.[37] Molecular necklaces of α-cyclodextrin with poly(ethyleneglycol) adsorbed on MoS_2 were manipulated with the STM tip. The cyclodextrin units can be shuttled along the polymer thread reversibly.[38]

Polycyclic Aromatic Hydrocarbons (PAH) and barge Shape-Persistent Macrocycles

One of the methods used to grow layers on the substrate surface is molecular sublimation at low pressure.[39] However, for very large molecules this process does not work well. To adsorb the very large PAHs, such as $C_{42}H_{18}$ and $C_{132}H_{34}$, on HOPG, a wet technique with careful choice of solvent was presented.[39] The molecules are then adsorbed through self-assembly on HOPG. The air STM images were obtained with submolecular resolution, allowing the proposal of the molecular packing structure. Coronene adlayers were studied by STM on Au(111).[40] The adsorbed layer was grown by adsorption from a molecular solution. The STM imaging was then carried out under potential control. The molecules form a well-organized adlayer, and the authors suppose that there are multilayers on the surface.[40]

Large shape-persistent macrocycles containing thiophene- and pyridine-derivatived moieties were adsorbed on HOPG and imaged by STM.[41] The adsorbed layers of these large macrocycles present an interesting structure. because the large cavities of the molecules can be used to trap other molecules or ions on the surface.[41]

Porphyrins and Phthalocyanines

Several article\ dealing with the imaging of porphyrins and phthalocyanines were recently published. The key factor to image these layers by STM appears to be the adsorption step. In UHV, the layers are formed by vaporization of the molecules on the chosen substrate.[42,43] Structural defects on the layers, such as missing molecules, and the domain boundary arrangement are well

resolved in the STM images. It was possible to identify the ion core of phthalocyanines and porphyrins with high molecular resolution.[42,43] The chemical identification of the porphyrin or phthalocyanine by its central ions enables its identification in mixed layers of these molecules.[43]

STM imaging of layers of porphyrins and phthalocyanines assembled from solutions was harder to perform. Some methodologies were developed to enable this process. A porphyrin was found to adsorb on an Au surface previously modified with iodine or sulfur.[44,45] The resulting STM images showed fourfold structures assigned to the porphyrin. He et al. showed that it is possible to adsorb a porphyrin on a gold surface using only the electrochemical potential to promote the growth of the molecular layer.[46] A Co porphyrin molecule was imaged in the electrochemical environment. The molecule shows a bright central core that is assigned to the Co ion due to its dz^2 orbital, in agreement with the UHV results.[47]

HYDROGEN BONDS AS A TOOL FOR BUILDING SUPRAMOLECULAR ARCHITECTURES ON THE SURFACE

Some molecules carrying functional groups that can interact via hydrogen bonds were used to grow well-defined structures on surfaces. In this category, the molecule 2-mercaptopyriinidine (2MPy) was found to form a bidiinensional structure made of molecular dimers that align in chains separated by channels. The coadsorption of electron-rich molecules leads to the formation of mixed layers.[48,49] The structure of the 2MPy molecule opened the possibility of imaging arenes on Au(111).[48] The images of Figs. 1A,B show the coadsorption of 2MPy and azulene. The bilobed features (marked by B) seen in the images were assigned to azulene that adopts two different positions in the mixed layer. The features marked by *A* represent the 2MPy molecular dimers.

Molecules derived from benzoic acid showing optical isomerism and with application on nonlinear optics were adsorbed on Ag(111) and analyzed in UHV with STM.[14] The molecules form an ordered surface and bind through hydrogen bonds forming dimeric and trimeric rows and ribbons, depending on the surface coverage.[14] Molecules having several groups able to form hydrogen bonds can present a variety of adsorption behaviors on surfaces. Examples include molecules such as trimesic acid (1,3,5-benzenetricarboxylic acid), which was adsorbed on Cu(100) and studied by UHV STM at different temperatures. The trimesic acid is found to adopt two different structures on the surface, depending on the adsorption temperature. Adsorption at low temperatures leads to a planar arrangement of the molecules, and they bind to

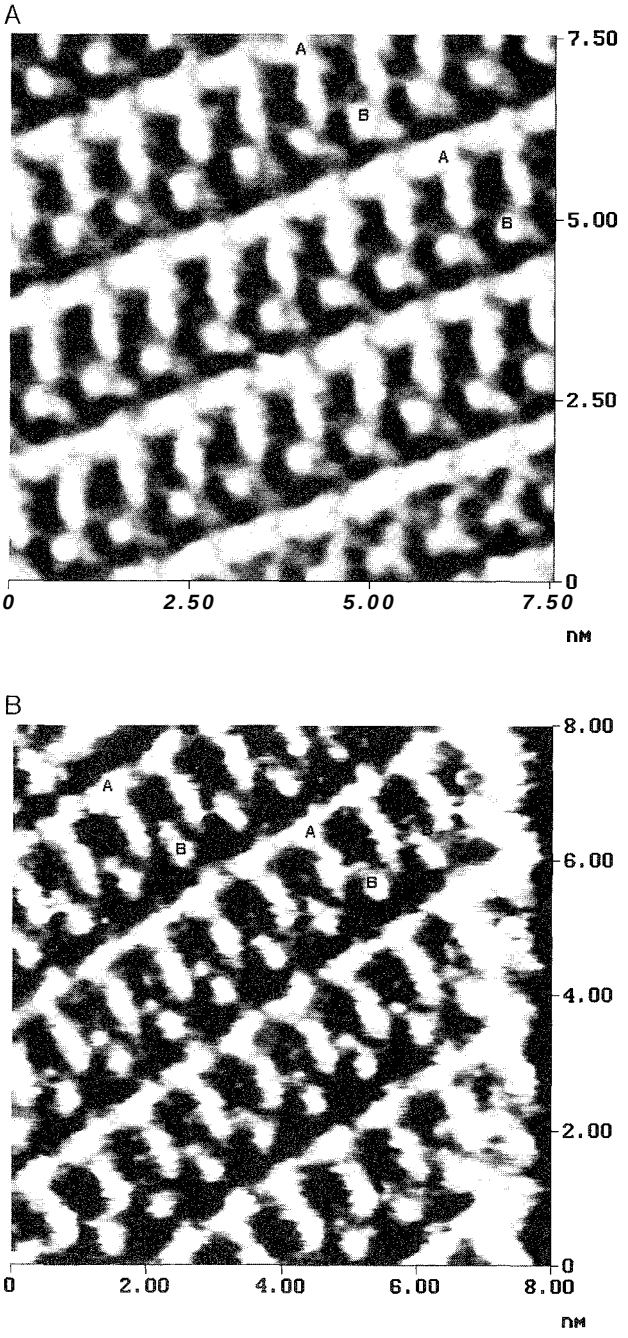

Fig. 1 (A) Air STM image of a mixed layer of 2-mercaptopyrimidine and azulene adsorbed on Au(111). Bias voltage: 400 mV; tunneling current: 3.0 nA; and area 76×76 Å^2. (B) Air STM image of a mixed layer of 2-mercaptopyrimidine and azulene adsorbed on Au(111). Bias voltage: 400 mV; tunneling current: 3.0 nA; and area 80×80 Å^2. (Parts A and B were reprinted from Curr. Appl. Phys. 2. Pinheiro, LS; Tempcrini, M.L.A. 2-mereaptopyrimidine as a suitable matrix to trap arenes on Au(111): STM probing of the modified surface. 145–153. Copyright 2002, with permission from Elsevier.)

each other through hydrogen bonding. At room temperature, the molecules are supposed to stand on the surface through their carboxylate groups. The STM data with submolecular resolution show that trimesic acid adsorbed on Au(111) forms dimers on the surface.[51]

The DNA bases, guanine, thymine, cytosine, and adenine, were studied by STM on several substrates. Some authors report hydrogen bonding or stacking of the molecules on Au(111).[52] The Cu surfaces are often used as substrates for adsorption of the DNA bases. Hydrogen-bond patterns were analyzed on this surface.[53,54]

Amino acids are molecules that can interact via hydrogen bonding in the solid state. The STM studies were performed on adsorbed layers on several substrates. The adsorption manner is governed by the substrate and also by the preparation method.[55–57] The use of electrochemical potential control enables the formation of different phases on the surface. Lysine adsorbed on Cu(001) was studied by UHV STM and found to form different phases.[55] The amino acids, with the exception of glycine, are chiral molecules, and the STM was used to examine this property along with the adsorption mode of the structure.[55,57]

MODIFIED TIPS

Some reports in the literature proposed the use of modified tips to image specific surfaces, aiming to improve the STM contrast. These reports use small molecules[58] or conductive polymers such as doped polypyrrole,[59] organic molecules that are able to hydrogen bond with the adsorbed molecule on the substrate.[60] Iodine and sulfur atoms were also tried as tips to image a thiol layer on HOPG.[61] Using this approach, it is expected that some areas of the adsorbed layer will appear brighter in the image. This is assigned to a specific interaction of a functional group on the adsorbed molecule recognizing the molecule or atom working as the tip. Carbon nanotubes were also used as tips to probe the surface and improve the adsorbed layer contrast.[62] The tip can also be modified in situ and used to form molecule–atom species, such as in the case of the interaction between Xe and Cu(II) etioporphyrin studied in UHV.[63]

CONCLUSION

The STM has proven to be useful in the study of supramolecular structures such as those formed by the traditional building blocks or hydrogen-bound layers. The results are still "new," and the best conditions for molecular deposition and imaging are being developed. The STM data for porphyrins and phthalocyanines are encouraging. because the microscope presents high-definition image5 of the internal features of individual molecules.

It was pointed out that intermolecular interactions should predominate over substrate–molecule interactions to enable the formation of supramolecular structures.[43,51] The expectation is that the STM data in two dimensions for the supramolecular structures can reach a point where the host–guest interaction can be analyzed in situ.

ACKNOWLEDGMENTS

The author is grateful to the editors for giving me this opportunity. Thanks to Dr. M.L.A. Temperini and Dr. E.P.G. Areas for their help with the manuscript.

ARTICLES OF FURTHER INTEREST

Calixarenes and Their Analogues: Cation Complexation, p. 137
Calixarenes and Their Analogues: Molecular Complexation, p. *145*
Crown Ethers, p. 326
Crystal Engineering with Hydrogen Bonds, p. 357
Cyclodextrins, p. 398
Hydrogen Bonding, p. *658*
Nanocasting Strategies and Porous Materials, p. 950
Phthalocyanines, p. 1069
Supermicroscopy: AFM, SNOM, and SXM. p. 1394

REFERENCES

1. Binnig. C.: Rohrer. H. Scanning tunneling microscopy. Helv. Phys. Acta 1982. *55*. 726–735.
2. Binnig. G.: Rohrer, H. Scanning tunneling microscopy. Surf. Sci. 1983. 126, 236–244.
3. Tersoff, J.; Lang. N.D. Theory of Scanning Tunneling Microscopy. In *Scanning Tunneling Microscopy;* Stroscio, J.A., Kaiser, W.J., Eds.; Methods of Experimental Physics. Academic Press: USA. 1993; Vol. 27. 1–29.
4. Chen, J.C. *Introduction to Scanning Tunneling Microscopy:* Oxford University Press: Oxford Series in Optical and Imaging Sciences: Oxford, 1993.
5. Park, S.-I.; Barret, R.C. Design Consideration for an STM System. In *Scanning Tunneling Microscopy:* Stroscio. J.A.. Kaiser, W.J.. Eds.: Methods of Experimental Physics. Academic Press: USA. 1993: Vol. 27. 31–76.
6. Ciancarlo. L.; Flynn, C.W. Raising flags: Application of chemical marker groups to study self-assembly, chirality,

and orientation of interfacial films by scanning tunneling microscopy. Acc. Chem. Res. 2000, 33, 491–501.
7. Stipe. B.C.: Rezaei, M.A.; Ho, W. Single molecule vibrational spectroscopy and microscopy. Science 1998.280. 1732–1735.
8. Qiu. X.H.; Nazin. G.V.; Ho, W. Vibrationally resolved fluorescence excited with submolecular precision. Science 2003. 299, 542–546.
9. Jung, T.A.; Himpsel, F.J.: Schlittler. R.R.; Gimzewski. J.K. Chemical Information From Scanning Probe Microscopy and Spectroscopy. In *Scanning* Probe *Microscopy (Annlytical Methods)*; Wiesendanger. R., Ed.; Nanoscience and Technology: Springer, 1998: 11–48.
10. Sautet. P. Images of adsorbates with the scanning tunneling microscope: Theoretical approaches to the contrast mechanism. Chem. Rev. 1997, 97, 1097.
11. Hallmark. V.M.: Chiang. S. Predicting STM images of molecular adsorbates. Surf. Sci. 1995, 329. 255–268.
12. Zhang. J.; Chi, Q.; Kuznetsov. A.M.: Hansen. A.G.: Wackerbath. H.: Christensen, H.E.M.: Andersen, J.E.T.; Ulstrup. J. Electronic properties of functional biomolecules at metal/aqueous solution interfaces. J. Phys. Chem., B 2002. 106, 1131–1152.
13. Kolb, D.M. Reconstruction phenomena at metal-electrolyte interfaces. Prog. Surf. Sci. 1996, *51*, 109–173.
14. Barth, J.V.; Weckesser. J.; Trimarchi, G.; Vladimirova, M.: De Vita. A.; Cai, C.; Brune, H.: Giinther, P.; Kern, K. Stereochemical effects in supramolecular self-assembly at surfaces: 1-D versus 2-D enantiomorphic ordering for PVBA and PEBA on Ag(111). J. Am. Chem. Soc. 2002. 124, 7991–8000.
15. Baski, A.A.: Fuchs. H. Epitaxial growth of silver on mica as studied by AFM and STM. Surf. Sci. 1994, 313,275–288.
16. Wan. L.-J.; Itaya, K. In situ scanning tunneling microscopy of Cu(110): Atomic structures of halide adlayers and anodic dissolution. J. Electroanal. Chern. 1999, 473, 10–18.
17. Yau, S.-L.: Kim. Y.-G.: Itaya. K. In situ scanning tunneling microscopy of benzene adsorbed on Rh(111) and Pt(111) in HF solution. J. Am. Chem. Soc. 1996. 118, 7795–7803.
18. Wiesendanger, R.; Anselmetti, D. STM on Layered Materials. In Scanning *Tunneling Microscopy* I, 2nd Ed.; Giintherodt, H.-J., Wiesendanger. R., Eds.: Springer Series in Surface Science. Springer-Verlag: Germany, 1994: 131–179.
19. Samori. P.: Engelkamp. H.: de Witte, P.: Rowan, A.E.; Nolte. R.J.M.: Rabe, J.P. Self-assembly and manipulation of crown ether phthalocyanines at the gel-graphite interface. Angew. Chem., Int. Ed. 2001, 40. 2348–2350.
20. Beer. P.D.: Gale. P.A.; Smith, D.K. *Supramolecular* Chemistry: Oxford University Primers. Oxford University Press: Great Britain. 1999.
21. *Comprehensive Supramolecular Chemistry*, 1st Ed.: Atwood. J.L.. Davies. J.E.D., MacNicol. D.D.. Vögtle, F., Eds.: Pergamon: New York. 1996.
22. Pan, G.-B.: Wan. L.-J.: Zheng. Q.-Y.; Bai, C.-L.; Itaya. K. Self-organized arrays of calyx[4]arene and calyx[4]arene diquinone disulfide on Au(111). Chem. Phys. Lett. 2002. 359. 83–88.
23. Pan. G.-B.; Wan. L.-J.: Zheng. Q.-Y.; Bai. C.-L. Highly ordered adlayers of three calyx[4]arenes derivatives on Au(111) surface in $HClO_4$ solution: In situ STM study. Chem. Phys. Lett. 2003. 367, 711–716.
24. Raible, S.; Pfeiffer, J.: Weiss, T.: Clauss. W.; Goepel, W.: Schurig. V.: Kern, D.P. Scanning tunneling microscopy on self-assembled calix[4]resorcinarene monolayer adsorbates on Au(111). Appl. Phys., A 2000. *70*, 607–611.
25. Biscarini. F.: Gebauer, W.; Di Domenico. D.; Zamboni, R.: Pascual, J.-I.; Leigh, D.A.: Murphy, A.; Tetard, D. STM investigations of flexible supramolecules: Benzylic amide [2] catenanes. Synth. Met. 1999, 102, 1466–1467.
26. Samori, P.; Jäckel, F.: Unsal, O.; Godt, A.; Rabe. J.P. Ordered nanostructures of a [2] catenane through self-assembly at surfaces-an STM study with sub-molecular resolution. Chem. Phys. Chem. 2001. 7, 461–464.
27. Wang, D.: Xu. Q.-M.; Wan. L.-J.: Wang, C.; Bai, C.-L. In situ scanning tunneling microscopy study of adsorption of diaza-15-crown-5 on Cu(111). Surf. Sci. 2001.489. L568–L572.
28. Ohira. A.; Sakata, M.: Hirayama, C.; Kunitake, M. 2-D supramolecular arrangements of dibenzo-18-crown-6-ether and its inclusion complex with potassium ion by potential controlled adsorption. Org. Biomol. Chem. 2003, 1, 251–253.
29. Markey, L.; Stievernard, D.: Devos. A.: Lannoo, M.; Demol. F.; de Backer, M. STM observations of self-assembled 1D and 2D nanoclusters of aromatic cryptand molecules deposited on highly oriented pyrolitic graphite. Supramol. Sci. 1997. 4, 375–379.
30. Laitenberger. P.; Claessens, C.G.; Kuipers. L.: Raymo, F.M.; Palmer. R.E.; Stoddart, J.F. Building supramolecular nanostructures on surfaces: The influence of the substrate. Chem. Phys. Lett. 1997, 279, 209–214.
31. Shigekawa. H.: Morozumi, T.; Komiyama. M.: Yoshimura. M.: Kawazu, A.; Saito. Y. Scanning tunneling microscopy on cyclodextrin inclusion complexes. J. Vac. Sci. Technol., B 1991, 9, 1189–1192.
32. Da Costa. A.; Monflier. E.; Landy. D.: Fourmentin. S.: Surpateanu, G. Scanning tunneling microscopy investigation of an inclusion complex between the β-cyclodextrin and the sodium salt of the trisnlfonated triphenylphosphine. Surf. Sci. 2001. 470. 275–283.
33. Liu, Y.; Li, L.; Fan. Z.: Zhang. H.-Y.: Wu, X.: Guan, X.-D.: Liu, S.-X. Supramolecular aggregates formed by intermolecular inclusion complexation of organo-selenium bridged bis(cyclodextrin)s with calyx[4]arene derivative. Nano Lett. 2002, 2. 257–261.
34. Yasuda, S.: Futaba, D.N.; Takeuchi, O.; Suzuki, I.: Yase. K.: Sumaoka. J.: Komiyama. M.: Shigeliawa, H. Monolayer formation of 6-deoxy-6-thiol-P-cyclodextrin on a Au(111) surface studied by scanning tunneling microscopy. J. Vac. Sci. Technol.. A 2001. 19. 1266–1269.
35. Yasuda. S.; Shigekawa, H.; Suzuki, I.: Nakamura. T.; Matsumoto. M.: Komiyama, M. Scanning tunneling microscopy on the formation of lipoamide-cyclodextrin monolayer on Au(111). Appl. Phys. Lett. 2000. 76, 643–645.
36. Ohira. A.; Ishizaki. T.; Sakata. M.: Taniguchi. I.:

Hirayama, C.: Kunitake, M. Formation of the 'nanotube' structure of β-cyclodextrin Au(111) surfaces induced by potential controlled adsorption. Colloids Surf., A: Physicochem. Eng. Asp. *2000. 169,* 27–33.

37. Liu. Y.: Li, L.; Zhang, H.-Y.: Zhao. Y.-L.; Wu. X. Bis(pseudopolyrotaxane)s possessing copper (II) ions formed by different polymer chains and bis(β-cyclodextrin)s bridged with a 2,2′-bipyridine-4,4′-dicarboxy tether. Macromolecules *2002. 35,* 9934–9938.
38. Shigekawa, H.: Miyake. K.; Sumaoka. J.; Harada. A.; Komiyama. M. The molecular abacus: STM manipulation of cyclodextrin necklace. J. Am. Chem. Soc. *2000. 122.* 5411–5412.
39. Samori, P.; Severin, N.; Simpson, C.D.; Müllen. K.: Rabe. J.P. Epitaxial composite layers of electron donors and acceptors from very large polycyclic aromatic hydrocarbons. J. Am. Chem. Soc. *2002. 124,* 9454–9457.
40. Uemura. S.: Sakata, M.: Taniguchi, I.: Hirayama. C.; Kunitake. M. In situ observation of coronene epitaxial adlayers on Au(111) surfaces prepared by the transfer of Langmuir films. Thin Solid Films *2002. 409.* 206–210.
41. Grave, C.; Schliiter, A.D. Shape-persistent, nano-sized macrocycles. Eur. J. Org. Chem. *2002,* 3075–3098.
42. Scudiero. *L.*: Barlow. D.E.: Hipps, K.W. Physical properties and metal ion specific scanning tunneling microscopy images of metal(II) tetraphenylporphyrins deposited from vapor onto gold (111). J. Phys. Chem.. B *2000. 104,* 11899–11905.
43. Scudiero. L.: Hipps, K.W.: Barlow, D.E. A self-organized two-dimensional bimolecular structure. J. Phys. Chem.. B *2003. 107.* 2903–2909.
44. Batina. N.: Kunitake. M.: Itaya, K. Highly ordered molecular arrays formed on iodine-modified Au(111) in solution: In situ STM imaging. J. Electroanal. Chem. 1996. *405,* 245–250.
45. Wan. L.J.; Shundo. S.: Inukai. J.; Itaya. K. Ordered adlayers of organic molecules on sulfur-modified Au(111): In situ scanning tunneling microscopy study. Langmuir 2000, *16.* 2164–2168.
46. He. Y.: Ye. T.: Borguet. E. Porphyrin self-assembly at electrochemical interfaces: Role of potential modulated surface mobility. J. Am. Chem. Soc. *2002, 124.* 11964–11970.
47. Yoshimoto. S.: Tada, A.: Suto. K.; Narita. R.; Itaya. K. Adlayer Structure and electrochemical reduction of O_2 on self-organized arrays of cobalt and copper tetraphenyl porphynes on a Au(111) surface. Langmuir 2003. *19.* 672–677.
48. Pinheiro, L.S.: Temperini, M.L.A. 2-Mercaptopyrimidine as a suitable matrix to trap arenes on Au(111): STM probing of the modified surface. Curr. Appl. Phys. *2002. 2,* 145–153.
49. Pinheiro. L.S.: Temperini. M.L.A. Coadsorption of 2-mercaptopyrimidine and 1,10′-phenanthroline on Au(111) as seen by STM. Surf. Sci. 1999. *441.* 53–64.
50. Dimitriev. A.: Lin. N.; Weckesser. J.: Barth. J.V.; Kern. K. Supramolecular assemblies of trimesic acid on a Cu(111) surface. J. Phys. Chem.. B *2002. 106,* 6907–6912.
51. Ishikawa, Y.; Ohira. A.: Sakata. M.; Hirayama. C.: Kunitake, M. A twc-dimensional molecular network structure of trimesic acid prepared by adsorption-induced self-organization. Chem. Commun. *2002.* 2652–2653.
52. Tao. N.J.: De Rose. J.A.: Lindsay, S.M. Self-assembly of molecular superstructures studied by in situ scanning tunneling microscopy: DNA bases on Au(111). J. Phys. Chem. 1993. *97.* 910–919.
53. Furukawa, *M.*: Tanaka. H.: Kawai, T. The role of dimmer formation in the self-assemblies of DNA base molecules on Cu(111) surfaces: A scanning tunneling microscope study. J. Chem. Phys. *2001. 115.* 3419–3423.
54. Chen. Q.; Frankel. D.J.; Richardson. N.V. Self-assembly of adenine on Cu(110) surfaces. Langmuir *2002, 18,* 3225–3319.
55. Zhao. X.; Zhao. R.G.: Yang. W.S. Scanning tunneling microscopy investigation of L-lysine adsorbed on Cu(001). Langmuir *2000. 16.* 9812–9818.
56. Zhang. J.: Chi, Q.: Nielsen. J.U.; Friis. E.P.: Andersen. J.E.T.: Ulstrup, J. Two-dimensional cysteine and cystine cluster networks on Au(111) disclosed by voltammetry and in situ scanning tunneling microscopy. Langmuir 2000. 16. 7229–7237.
57. Wang, D.; Xu, Q.-M.: Wan. L.-J.: Bai, C.-L.; Jin, G. Adsorption of enantiomeric and racemic tyrosine on Cu(111): A scanning tunneling microscopy study. Langmuir *2003. 19.* 1958–1962.
58. Bartels, L.; Meyer, G.: Rieder. K.-H. The evolution of CO adsorption on Cu(111) as studied with bare and CO-functionalized scanning tunneling tips. Surf. Sci. 1999. *432.* L621–L626.
59. Ito. T.: Biihlmann. P.: Umezawa. Y. Polypyrrole-modified tips for functional group recognition in scanning tunneling microscopy. Anal. Chem. 1999. *71.* 1699–1705.
60. Olson. J.A.: Buhlmann, P. Scanning tunneling microscopy with chemically modified gold tips: In situ reestablishment of chemical contrast. Anal. Chem. *2003. 75,* 1089–1093.
61. Xu, Q.-M.; Wan. L.-J.: Yin. S.-X.; Wang. C.: Bai. C.-L. Effect of chemically modified tips on STM imaging of 1-octadecanethiol molecule. J. Phys. Chem. *2001. 105.* 10465–10467.
62. Nishino. T.: Ito. T.: Umezawa. Y. Carbon nanotube scanning tunneling microscopy tips for chemically selective imaging. Anal. Chem. *2002. 74.* 4275–4278.
63. Qiu. X.: Nazin, G.V.; Hotzel, A.: Ho. W. Manipulation and characterization of xenon–metalloporphyrin complexation with a scanning tunneling microscope. J. Am. Chem. Soc. *2002, 124.* 14804–14809.

Second-Sphere Coordination

Derek A. Beauchamp
Stephen J. Loeb
University of Windsor, Windsor, Ontario, Canada

INTRODUCTION

The concept that a transition metal complex can interact orderly with neutral molecules to give an outer-sphere complex dates back some 90 years to Alfred Werner's original description of coordination chemistry. Werner found this idea, that we now call second-sphere coordination, essential to explain such simple phenomena as the dependence of optical rotation on the nature of the anion and solvent. the formation of adducts between amines and saturated complexes. and solvents of crystallization. The modern focus of second-sphere coordination varied from simple topics such as stability and solubility.[1] to biological concerns.[2] as diverse as transport properties.[3] and the relaxivity of MRI contrast agents.[4] Reviews by Stoddart in 1996,[5] Loeb in 1996,[6] and Steed in 2001[7] described the second-sphere coordination chemistry of transition metal complexes and alkali metals with crown ethers. This particular entry updates that published by Loeb in Volume 1 of *Comprehensive Supramolecular Chemistry* and is primarily focused on cationic transition metal complexes in which second-sphere coordination is provided by a host/receptor/ligand with an organized set of donors, such as a crown ether or macropolycyclic ligand rather than the many examples that contain second-sphere interactions with simple rnonodentate ligands or solvents. In particular, a transition metal complex that contains hydrogen-bond donor groups (i.e., NH_3 or H_2O) in its primary coordination sphere can be considered a guest capable of binding to a hydrogen-bond acceptor host via second-sphere coordination.

METAL AMMINE COMPLEXES AS GUESTS

Ando investigated the interaction of a variety ot ruthenium(II) ammine complexes[8,9] with crown ethers (Fig 1) and documented the effect ot second-sphere coordination on a variety of structural and physical properties.[10] Initially, pentammineruthenium(II) complexes **1d**, **1h**. and **1l** (Fig 2) were shown to form adducts with 18-crown-6 ether, 18C6, through NH O hydrogen bonds between the ammine ligands coordinated to the metal and crown ethei oxygen atoms.[11] Spectrophotometric, electrocheinical, and ^{1}H-NMR spectroscopic data showed that Ru(II) and Ru(III) ammine complexes form adducts with 18C6 that differ in the mode of hydrogen bonding. The crown ether binds to tmns-positioned NH_3 groups for Ru(II) but cis-oriented ammines for Ru(III). The binuclear complex **1i** was shown to form 1:2, 1:3, and 1:4 adducts in a stepwise fashion. lit was reasoned from electrochemical and ^{1}H-NMR experiments that mixed valence Ru(II)–Ru(III)-ammine complexes interact with three molecules of 18C6 in acetonitrile solution. In a mixed-valence complex, an asymmetric adduct implies the possibility of valence trapping and trapping/untrapping of the delocalized valence by adjusting the concentration of the crown ether.[11,12]

Studies involving Ru(II) complexes with fewer ammine ligands. **2a–d**, **3c–f**. and 4, demonstrated that the stoichiometry is the same as for pentammine complexes, **1c–g**, however, the electrochemical behavior is different because of the lower stability of the host–guest interaction and the steric difficulty of forming a 1:2 complex:crown adduct.[12,13]

It was found that binuclear complexes with delocalized mixed-valence states form an asymmetric 1:3 adduct to 18C6, in which there is a 1:1 stoichiometry at one ruthenium moiety and 1:2 stoichiornetry at the other. From the results of this study, it was clear that the valence of the metal center significantly affects the composition of crown ether adducts of metal complexes.[14]

In general, formation of ruthenium complexes with crown ethers was controlled by the valence of the metal center and the size of the crown ether. The change in redox potential of the ruthenium complexes was affected by the number of ammine ligands coordinating to the ruthenium, the n-electron acceptability of a ligand not interacting with the 18-crown-6. and the flexibility of the crown ether rings.[11–14] A combination of these factors makes it possible to design supramolecular adducts that possess a range of redox potentials.

In a series of papers,[15–17] Crumbliss illustrated that the siderophore ferrioxamine-B can be selectively recognized through second-sphere complexation of the protonated amine side chain by different ionophore host molecules.

The initial study focused on second-sphere coordination between Fe(III) complexes of deferriferrioxamine-B.

Encyclopedia of Supramolecular Chemistry
DOI: 10.1081/E-ESMC 120012712

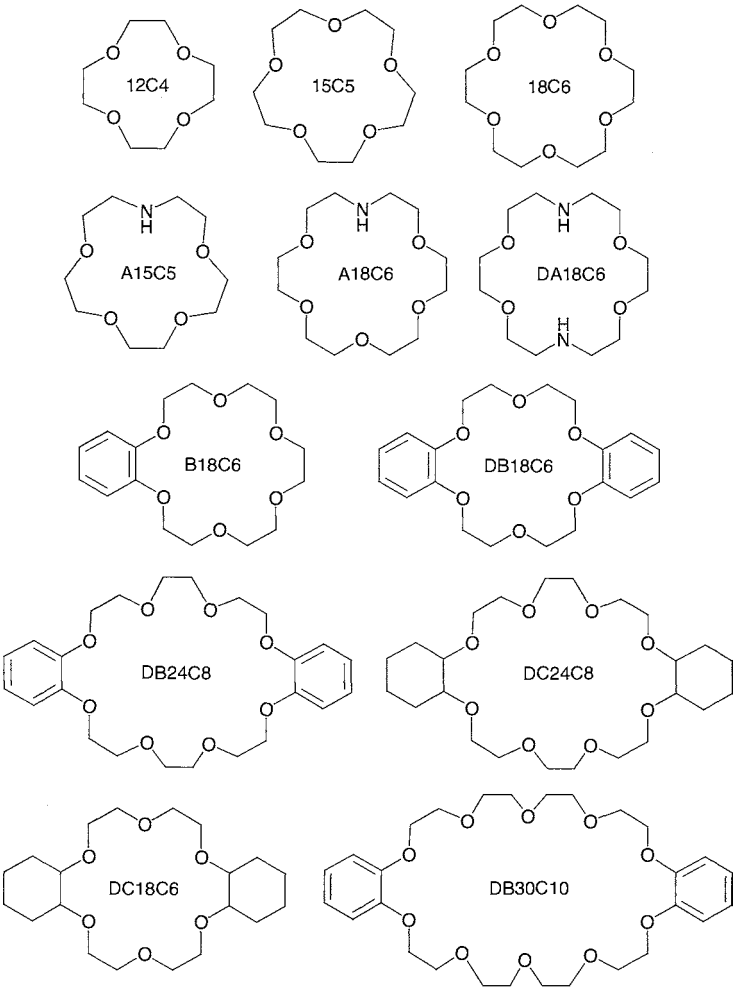

Fig. 1 Crown ether hosts used as second-sphere ligands for transition metal complex guests

$MHDFB^+$, and DC18C6.[15] The deferriferrioxamine-B complex has a distinct side chain containing an ammonium group, which is not involved in first-sphere coordination to the metal. It was shown that crown ethers could be involved in second-sphere coordination with this ammonium group by hydrogen bonding and electrostatic interactions to form a second-sphere adduct **5,** as illustrated in Fig. 3. The positive charge was demonstrated to be important, as no adduct formation was observed when the metal complex was deprotonated. Metal ion selectivity in a chloroform medium was experimentally determined to be Al(III) < Fe(III) < Ga(III) < In(III). The effect of counterion was also studied.

Although siderophore cell receptors are more complex than simple crown ethers; these studies are relevant as to how ionophores, such as antibiotics. affect the biodistribution of Fe carriers in the body. The influence of the host crown ether substituent and ring size on ferrioxamine **B** host–guest stability was studied.[16] The hosts investigated were crown ethers 18C6. B18C6, DB18C6, DB24C8. DB30C10. DC18C6. and DC24C8, as well as the natural cyclic ionophores valinomycin and nonactin. It was concluded that host–guest formation for ferrioxamine-B with synthetic crown ethers decreases in stability with increasing cavity size. These second-sphere complexes allowed for a thorough investigation of the relative efficiency of various ionophores to effect bulk ligand membrane transport of ferrioxamine.[16]

Additionally, functional groups (–RCOOH) were added to a crown ether to probe the influence of tethering the counterion to the macrocyclic host and to determine the optimum tether length for stable host–guest complex formation.[17] At an elevated pH, the substituted crown ether serves as host and counterion. It was experimentally

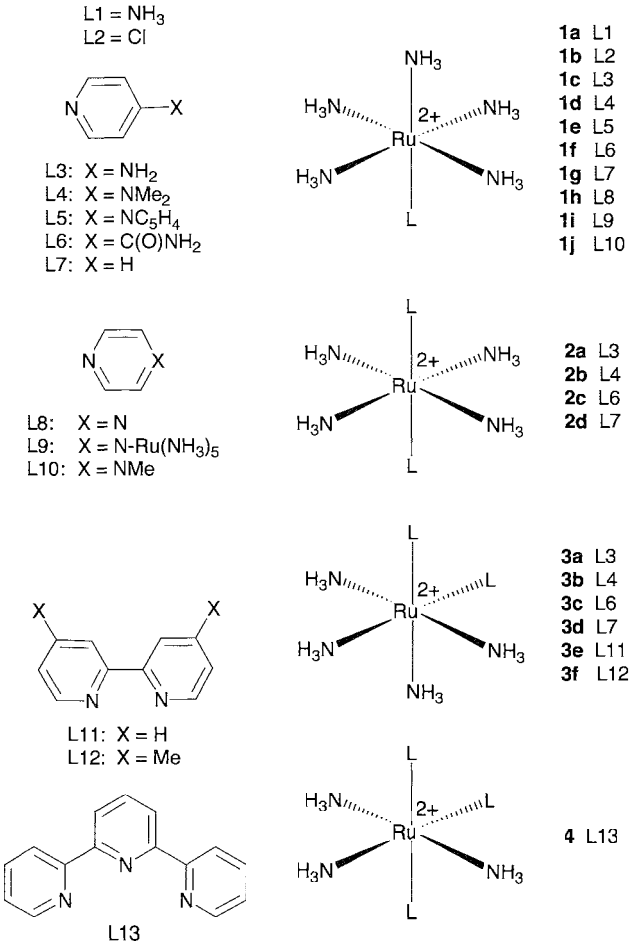

Fig. 2 Ruthenium complexes investigated as guests for crown ethers.

determined that a tethered, ionized carboxylate functional group significantly enhances host–guest formation. Moreover, with increased length of the side chain, the stability of the complex increased.

A new class of transition metal containing host or metalloreceptor was reported by Loeb, in which $PtCl_2(PEt_3)$ units were coordinated to the nitrogen donors of mono- and diazacrown ethers, A15C5, A18C6, and DA18C6.[18] These hosts behaved much like crown ethers, forming hydrogen-bonded adducts with alkylammonium salts. Binding could be measured by ^1H- or ^{31}P-NMR spectroscopy. One unique adduct reported in this series was 6, the second-sphere adduct formed between the monoamine complex $[PtCl_2(PEt_3)(NH_3)]$ and the azacrown ether containing complex $[PtCl_2(PEt_3)(A18C6)]$. This adduct was the first example of a host–guest complex in which both the host and the guest are transition metal complexes. As in alkylammonium adducts of crown ethers, the $[M\text{-}NH_3]$ guest perches over

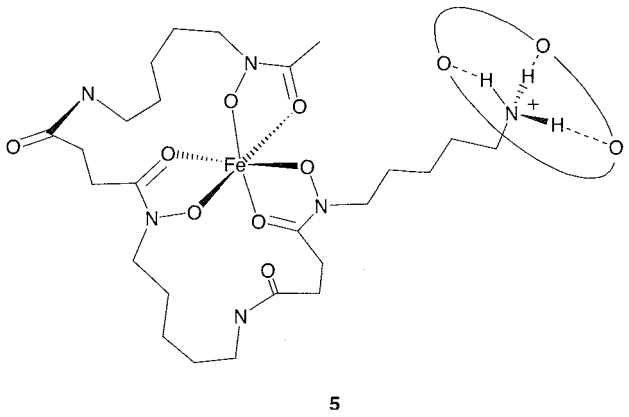

5

Fig. **3** The second-sphere adduct between a ferrioxammine B guest and an ionophore or crown ether host.

the crown ether ring and forms a three-point hydrogen-bonding scheme with alternating oxygen atoms of the crown ether host. as shown in Fig. 4.

METAL **AQUA COMPLEXES** AS **GUESTS**

The unique second-sphere coordination of 1,10-phenanthroline to aquabromotri-p-tolyltin 7, was studied by Ng.[19] In this structure, the 1,10-phenanthroline ligand is coordinated in a second-sphere fashion through hydrogen bonds from the water molecule to the nitrogen atoms of the heterocycle. In contrast, the water molecules in the crystal structure of 1,10-phenanthroline hydrate are bonded to only one of the nitrogen atoms. It was suggested that electronic effects and packing forces influence

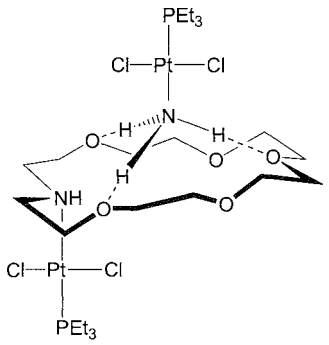

6

Fig. **4** A second-sphere. hydrogen-bonded, host–guest adduct in which both the host and the guest are transition metal complexes.

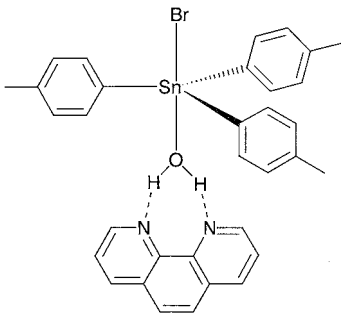

7

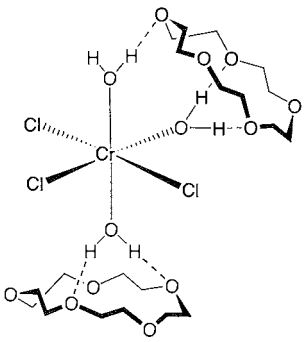

8

Fig. 5 Hydrogen-bonded second-sphere adducts involving aqua metal complexes.

the formation of second-sphere adducts in these compounds (Fig. 5).

Junk and Atwood recently synthesized a new structural isomer of $CrCl_3(H_2O)_3$, in which this species exhibits second-sphere coordination to a molecule of 15C5.[20] Crystals were obtained after irradiation with UV radiation and the addition of HCl(g) to a refluxing toluene solution of 15C5, H_2O, and $Cr(CO)_6$. This complex did not crystallize as discrete cations and anions but rather as a neutral Cr(III) complex, 8. The complex is coordinated in a second-sphere fashion to two molecules of 15C5 that are hydrogen bonded to the three water ligands to generate a polymeric array.[20] Interestingly, the 15C5 molecules only successively bridge the mer-isomer of $CrC_3(H_2O)_3$, and when the metal center was changed from Mo or W, one-dimensional hydrogen-bonded arrays were formed, but second-sphere coordination did not occur.

CONCLUSION

It is now well established that second-sphere adducts can be formed between transition metal guests containing hydrogen-bond donor ligands such as ammonia or water and hydrogen-bond acceptor ligands such as crown ethers. The question for the future is as follows: "How can the concept of second-sphere coordination be systematically applied to modern areas of interest in suprarnolecular chemistry." Two avenues of investigation are briefly discussed herein as examples of where second-sphere coordination might be applied in the future.

Metalloreceptors Utilizing Simultaneous First- and Second-Sphere Coordination

Loeb reported a series of macrocyclic organopalladium complexes **9a–f** that were shown to act as efficient hosts or metalloreceptors. Studies showed that these complexes can selectively distinguish between primary, secondary, and tertiary alkylamines,[21] ammonium ions,[21] isomers of aminopyridines,[22] and even DNA nucleobases.[23,24] In each case, the substrate was bound to a labile Pd(II) center by σ-donation, while noncovalent interactions such as hydrogen bonding and π-stacking to peripheral receptor sites on the ligand were used to selectively bind a particular substrate. This was extended to include the cavity of a calix[4]arene as the second-sphere binding unit that selectivity bound *para*-phenylpyridine over the *ortho* and *meta* isomers (Fig. 6).[25–27]

Solid-State Inorganic Materials

Shimizu showed the complete encapsulation of hexaqua metal ions by 12 hydrogen bonds to the second spheres of sulfonate ligands.[28] The complexes **10a–c** were prepared by mixing $M(NO_2)_3$ [M = Fe(III), Cr(III), Al(III)] and the sodium salt of 1,3,5-*tris*(sulfomethyl)-

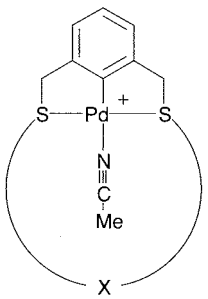

9a: X = $(CH_2)_{11}$
9b: X = $(CH_2)_2O(CH_2)_2$
9c: X = $(CH_2)_2O((CH_2)_2O)_2(CH_2)_2$
9d: X = $(CH_2)_2O((CH_2)_2O)_4(CH_2)_2$
9e: X = *p*-$CH_2(C_6H_4)O((CH_2)_2O)_3(C_6H_4)CH_2$
9f: X = *m*-$CH_2(C_6H_4)O((CH_2)_2O)_3(C_6H_4)CH_2$
9g: X = (*p*-$CH_2(C_6H_4)OCH_2C(O)NH)_2$-calix[4]arene(O*i*Pr)$_4$

Fig. 6 Organopalladium complexes used as metalloreceptors to bind substrates via first- and second-sphere coordination.

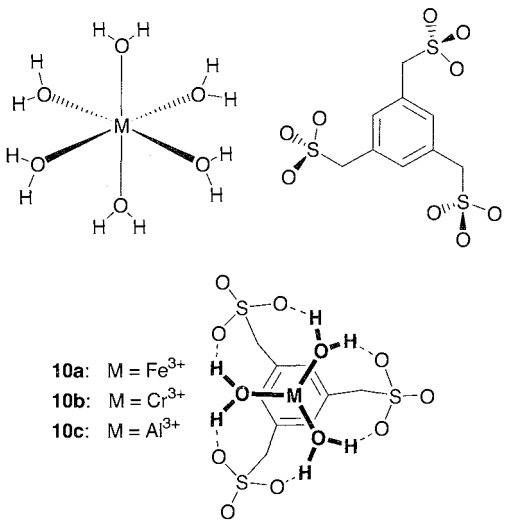

Fig. 7 A trisulfonate host forms multiple hydrogen bonds to encapsulate hexaqua transition metal coinplexes by second-sphere coordination.

benzene in aqueous media. In the crystal st ucture of **10a**, there are two types of (hexaqua)Fe(III) centers, one that is completely encapsulated by two molecules of the sulfonate ligand to give $[Fe(H_2O)_6(L)_2]^{3-}$ and one that simply acts as a second-sphere adduct held together by *12* hydrogen bonds: six to each sulfonate ligand, as shown in Fig. 7. Thermogravimetric analysis (TGA) of the solid showed that the coordinated water molecules involved in second-sphere coordination were only lost at temperatures −100°C above normal. This demonstrated that second-sphere coordination can be purposefully applied to provide thermal stability to a polymeric material.

ARTICLES OF FURTHER INTEREST

Crown Ethers, p. *324*
Hydrogen Bonding, p. *458*
Hydrogen Bonds to Metals and Metal Hydrides, p. 666
Lariat Ethers, p. *782*
Protein Supramolecular Chemistry, p. 1161
Secondary Bonding, p. *1215*
Weak Hydrogen Bonds. p. *1576*

REFERENCES

1 Zamaraev. K Chemistry in the 2nd coordination spheie of metal complexes New J Chem 1994. IS 3–18
2 Williams, D R *The Metals of Life The Solution Chemistry of Metal Ions in* Biological *Systems*; Van Nostrand Reinhold: London. 1971.
3. Crumbliss, A.L.; Batinic-Haberle. I.: Spasojevid. I. Molecular recognition of stable metal complexes through second-sphere coordination by macrocycles. Pure Appl. Chem. 1996. *68*, 1225–1230.
4. Botta, M. Second coordination sphere water molecules and relaxivity of gadolinium (III) complexes: Implications for MRI contrast reagents. Eur. J. Inorg. Chem. 2000. 3. 399–407.
5. Raymo. M.; Stoddart. J.F. Second-sphere coordination. Chem. Ber. 1996. 129. 981–990.
6. Loeb. S.J. *Comprehensive Supramolecular Chemistry*; Atwood. J.L., Davies. J.E.D.. MacNicol, D.D.. Vogtle. F.. Eds.: Elsevier Science: New York. 1996: Vol. 1, 733–753.
7. Steed, J.S. First- and second-sphere coordination chemistry of alkali metal crown ether complexes. Coord. Cheni. Rev. 2001. 215. 171–221.
8. Ando, I.; Ishimura. D.; Mitsumi. M.: Ujimoto. K.: Kurihara Adduct formation between $[Ru(NH_3)_5L][PF_6]_n$ (n = 2 and 3) and 18-crown-6 ether in solution and the effect on redox behavior. Polyhedron 1992. 11. 2335–2340.
9. Zhang, X.L.: Kankel. C.R.: Hupp, J.T. Solvent effects of amminemetal complexes by macrocyclic ethers—111 situ probes of extent of encapsulation. Inorg. Chem. 1994. 33. 4738–4743, and references therein.
10. Ando. I.; Kurihara. H. Second-sphere coordination of crown ethers to ruthenium–ammine complexes. Fukuoka Daigaku Rigaku Shuho 2001. 31. 83–113.
11. Ando. I.: Ishimura. D.: Ujimoto. K.; Kurihara. H. Effect of second-sphere coordination 3. Adduct formation of mononuclear and binuclear ruthenium-ammine complexes with 18-crown-6 ether. Inorg. Chem. 1994. *33*, 5010–5014.
12. Ando. I.: Ishimura. D.: Ujimoto. K.: Kmihara. H. Effect of second-sphere coordination 4. Factors influencing the electrochemical behavior of ruthenium-ammine coinplexes caused by second-sphere coordination of crown ethers. Inorg. Chem. 1996. *35*. 3504–3508.
13. Ando, I.: Ishimura. D.; Mitsunii. M.: Ujimoto, K.: Kurihara. H. Effect of second-sphere coordination 6. Adduct formation of monoammine-, diammine-. triammine-, and tetraammineruthenium(II) complexes with 18-crown-6 ether. Inorg. Chim. Acta 1996. 249, 201–205.
14. Ando. I.: Higashi, M.: Ujimoto. K.: Kurihara. ti. The effect of second-sphere coordination 7. Isolation of 18-crown-6 ether adducts of ruthenium-ammine complexes. Inorg. Chim. Acta 1998. 282. 247 -251.
15. Batinic-Haberle. I.; Crumbliss. A.L. Influence of the anion on the stability of second-sphere coordination of ferrioxamine B with cis-dicyclohexano-18-crown-6 in chloroform. Inorg. Chem. 1995. 34, 928–932.
16. Batinic-Haberle, I.: Spasojevid, I.; Crumbliss. A.L. Second-sphere coordination of ferrioxamine B and association of deferriferrioxamine B. $CH_3(CH_2)_4NH_3^+$, NH_4^+, and Mg^{2+} with synthetic crown ethers and the natural ionophores valinomycin and nonactin in chloroform. Inorg. Chem. 1996. *35*. 2352–2359.
17. Batinic-Haberle, I.: Spasojevid. I.: Hang, Y.; Bartsch. R.A. :

Crumbliss, A.L. Lariet ether carboxylic acids as ionizable hosts in the second coordination sphere of the siderophore ferrioxamine B in chloroform. Inorg. Chem. 1998. 37, 1438–1445.

18. Cameron, B.R.; Corrent, S.S.; Loeb, S.J. Transition metal complexes as both host and guest: Second-sphere coordination between a Pt-azacrown ether host and a Pt-NH_3 guest. Angew. Chem.. Int. Ed. Engl. 1995.34, 2689–2691.
19. Ng, S.W.; Yap, C.K.; Chen, W.; Kumar Das, V.G.; Sinn, E. Outer-sphere coordination of o-phenanthroline in aquabromotri-p-tolyltin-o-phenanthroline. Main Group Met. Chem. 1997, 20. 531–534.
20. Junk, P.C.; Atwood, J.L. Use of metal carbonyls in the formation of $[H_5O_2^+$.15-crown-5][$MOCl_4(H_2O)^-$], (M = Mo, W), and a second-sphere coordination complex in [*mer*-$CrCl_3)(H_2O)_3$.15-crown-5]. J. Organomet. Chem. 1998, 565. 179–186.
21. Kickham, J.E.; Loeb, S.J. Simultaneous first- and second-sphere coordination. Organopalladium metalloreceptors for water. ammonia, amines, hydrazine, and the hydrazinium ion. Inorg. Chem. 1995, 34, 5656–5665.
22. Kickham, J.E.; Loeb, S.J. Simultaneous first- and second-sphere coordination. Organopalladium crown ether complexes as metalloreceptors for o-aminopyridine derivatives. Inorg. Chem. 1994, 33, 4351–4359.
23. Kickham, J.E.; Loeb, S.J.; Murphy, S.L. Molecular recognition of nucleobases via simultaneous first- and second-sphere coordination. J. Am. Chem. Soc. 1993. 115. 7031–7032.
24. Kickham. J.E.: Loeb, S.J.; Murphy, S.L. Molecular receptors for adenine and guanine employing metal coordination, hydrogen-bonding and π-stacking interactions. Chem. Eur. J. 1997, 3. 1203–1213.
25. Cameron, B.R.; Loeb, S.J. Calixarene metalloreceptors. Upper-rim functionalized calix[4]arenes containing an organopalladium binding site. Chem. Commun. 1996, 2003–2005.
26. Cameron, B.R.; Loeb, S.J.; Yap, G.P.A. Calixarene metalloreceptors. Synthesis and molecular recognition properties of upper-rim functionalized calix[4]arenes containing an organopalladium binding site. Inorg. Chem. **1997**, *36*, 5498–5504.
27. Cameron, B.R.; Loeb, S.J. Calixarene metalloreceptors. Demonstration of size and shape selectivity inside a calixarene cavity. Calixarene for separations. ACS Symp. Ser. 2000, 757, 283–295. Chapter 21.
28. Dalrymple, S.A.; Parvez, M.; Shimizu. G.H.K. Supramolecular encapsulation of hexaaquo metal ions by second-sphere coordination. Chem. Commun. 2001, 2672–2673.

Secondary Bonding

Ionel Haiduc
Universitatea "Babeş-Bolyai," Cluj-Napoca, Romania

S

INTRODUCTION

The "secondary bond" concept was introduced by N.W. Alcock[1] *and describes interactions characterized by interatomic distances longer than single covalent bonds but shorter than van* der Waals *distances. These interactions are weaker than covalent or dative bonds but are strong enough to play a structure-determining role in the solid state. perhaps even in solution. The secondary bonds can be* intra- *or intermolecular. In the context of* supramolecular *chemistry, intermolecular secondary bonds leading to self-assembly and self-organization are of primary* importance, *both in* inorganic[1] *and in* organometallic compounds,[2,3] *in which discrete* supermolecules *or* supramolecular *polymeric arrays can be* formed *by connecting individual molecules (tectons). Intramolecular secondary bonds will not be discussed here, although interesting structural effects are produced by this type of* interactions.[4,5]

Some formal analogy between secondary bonding and hydrogen bonding can be noted. In both cases, there is a trinuclear. basically linear (but not always) and unsymmetrical $X–A\cdots X'$ *system, in which* $A–X$ *is a normal covalent bond.* and $A\cdots X'$ *is a weaker interaction. called an hydrogen bond (when* $A=H$*) and secondary bond (when* $A\neq H$*)*(Scheme 1). *In rare cases, the hydrogen bonds are symmetrical, and this happens more often with secondary bonds.* Symmetrical $X\cdots A\cdots X$ *systems are* formed *by an electron density redistribution by which the covalent bond is elongated. and the secondary bond is shortened, until the interatomic distances are equalized. In this case, the* $A\cdots X$ *bond order is* 0.5, *sensibly more than in common secondary bonds.*

There are: however. some significant differences between hydrogen bonds and secondary bonds; in the former, *the centrai atom hydrogen is monovalent: whereas. in the secondary bonds,* the *central atom A can be* plurivalent, i.e., *can form several covalent bonds. Thus. the number and variety of synthons able to participate* in *secondary bond formation. and therefore in* supramolecular self-assembly, *is considerably greater. In Scheme 2. some secondary bond synthons are illustrated.*

In some *cases.* the *hydrogen bonds can be bifurcated, but rarely* trifurcated. *In the case of secondary bonds. this is a* frequent *occurrence. As an example, the* diorganoditellurium(IV) *halides can be* cited,[6,7]; *these compounds* display *several coordination patterns and* numerous modes *of supramolecular self-assembly.*

THEORY

The structure-determining role of the secondary bonds even in simple inorganic molecules and ions cannot be underestimated. Their formation results in increased coordination numbers and distortions of the coordination geometries. This matter was discussed in terms of valence bond and VSEPR theories, [8,9] *and* a *remarkable analysis of the coordination geometries of* Sb(III) *halides influenced by secondary bonds could serve as a* model *for similar discussion of other main group elements.*

The secondary bond is *now explained as a result of donation from the lone pair of* X' *into a* σ^* orbital *of the* $A–X$ *bond or (alternatively and equivalently) as an asymmetric four-electron three-center system, with three* σ-symmetric atomic *orbitals on A and* X, X' *combined to form three molecular orbitals: one filled bonding* MO *located between A and* X, *one filled nonbonding or weakly bonding* MO *located between A and* X' *and one* empty *antibonding orbital (Fig. 1). It seems that the secondary bonding is associated with a high electron density at the acceptor binding site (usually having one or* more *lone pairs of electrons). The bonding in such systems was studied in detail on simple* triatomic *models, and the conclusions can be extended to similar synthons incorporated in more complex* structures.[10–13]

Secondary bonds are common *in compounds of heavier* main *group elements and can be regarded as a particular case of donor–acceptor bonds. Strong acceptors, such as metals of upper rows of the Periodic Table, associated with strong donors such as fluorine. oxygen, or nitrogen (generally described as hard acids and bases) tend to form two-electron dative bonds (classical coordinative bonds). Seldom. if ever, secondary bonds of the type discussed here are observed for hard donor–hard acceptor pairs* (e.g., *Be.* Zn, Al/F, O, *N). The metals and nonmetals in the bottom rows of the Periodic Table (soft acids and bases) tend to form weaker donor–acceptor bonds and "secondary bonds." Unfortunately, there is* still some *ambiguity about these interactions, and there is not even an*

Encyclopedia of Supramolecular Chemistry
DOI: 10.1081/E-ESMC *120012970*

X—A···X'	X—H···X'
normal covalent bond / secondary bonding	normal covalent bond / hydrogen bonding
A Hg, Tl, Sn, Pb, Sb, Bi, Se, Te, etc.	X = or ≠ X'

Scheme I Analogies between hydrogen bonds and secondary bonds.

unanimously accepted mode of naming them; in addition to using the term "secondary bonds," they are referred to in the literature as soft–soft interactions. closed-shell interactions, nonbonding interactions, or semibonding interactions, with the tendency to cover a broad range of interactions under this umbrella. The complexity of the matter was analyzed in a comprehensive review.[14]

Self-assembly through secondary bonds results in the formation of discrete supermolecules (dimers, trimers, tetramers) or supramolecular polymeric arrays, both in purely inorganic systems[1] and in organometallic compounds.[2,15–18] They are frequently found in derivatives of mercury,[19,20] thallium,[20] tin,[21] lead,[22–24] antimony,[25,26] bismuth,[27–29] selenium,[30,31] tellurium,[6,7] iodine[32,33] paired with sulfur, selenium. or heavy halogens. and sometimes even with oxygen and nitrogen ligands. Some are well illustrated by the main group derivatives of phosphor-1,1-dithiolato and related ligands.[15–18]

The most common are the heteroatomic secondary bonds, but homoatomic systems containing Sb–Sb···Sb–Sb···[34,35] Bi–Bi···Bi–Bi···[36] or Te–Te···Te–Te···[37] assays are known. Also, Se···Se interactions (3.07 Å) dimerize the five-membered Se_2SN_2 rings in Se_2SN_2Cl, but $Se_2S_2N_4$ eight-membered ring molecules are associated through Se···N secondary bonds.[38] Such interactions are common between sulfur- and selenium-containing inorganic rings and lead to interesting physical properties for the design of new materials (e.g., molecular conductors).[39] Iodine...iodine interactions are important in polyiodides and produce a broad variety of supramolecular structures.[40]

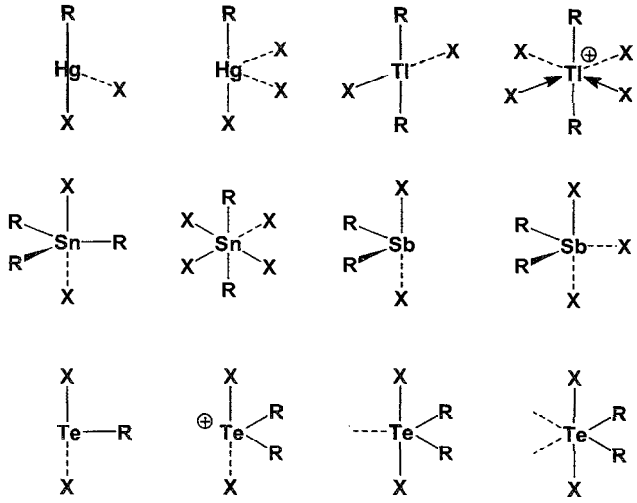

Scheme 2 Some secondary bond synthons

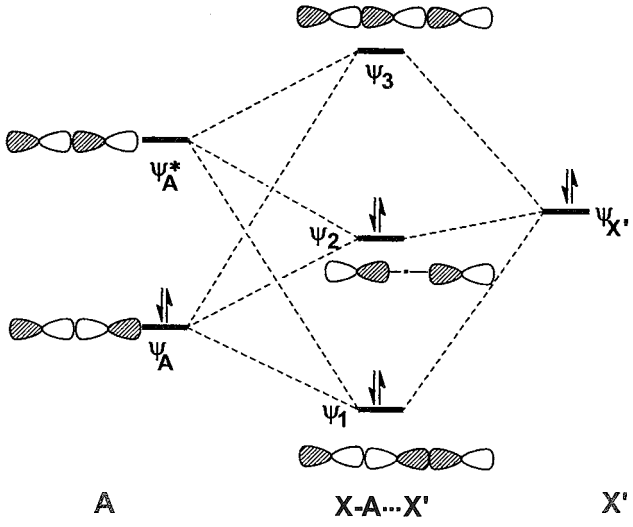

Fig. 1 Molecular orbital diagram of secondary bonding.

DINUCLEAR SUPERMOLECULES

There is a large number of dimers formed through secondary bonds. A few selected illustrative examples include organomercury halides, e.g., $[PhN{=}NC_6H_4HgCl]_2$,[41] and phosphor-1,1-dithiolates, e.g., $[MeHgS_2PPh_2]_2$,[42] and lead phosphor-1,1-dithiolates.[43] Some organoantimony phosphor-1,1-dithiolates and dithioarsinates, $[R_2SbS_2ER'_2]_2$ (E = P,As) are also dimers,[44,45] but others form polymeric arrays.[46–48] In dimeric $[Ph_2SbS_2EPh_2]_2$, the eight-membered rings are formed through Sb···S secondary interactions. The bismuth(III) analogues, $Bi(S_2ER_2)_3$ (E = P or As). are also dimers.[49–51] In $[Me_2TlSPh]_2$ supermolecules, the four-membered Tl_2S_2 rings are nearly symmetrical (TI-S 2.748 and 2.991 Å), but the difference between the two interatomic distances is significant.[52] The eight-membered cyclic adduct $[PhSeSePh.I_2]_2$[31] can be cited to illustrate a unique type of quasicyclic structure.[30] Phenyltellurium tetraphenyldithioimidodiphosphinate. $[PhTeSPh_2PNPPh_2S]_2$, is but one of many dimeric supermolecules based upon Te···S interaction~.'~Some of the cited species are shown in Scheme 3.

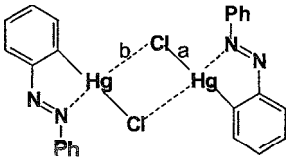

a = 2.309;b = 3.362 Å

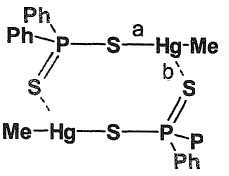

a = 2.370;b = 3.152 Å

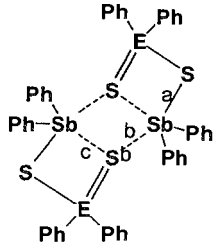

E = P: a = 2.490;b = 3.474;c = 3.440 Å
E = As: a = 2.486;b = 3.369;c = 3.500 Å

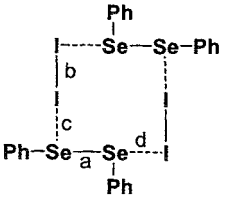

a = 2.347; b =2.775;
c = 2.992; d = 3.588 Å

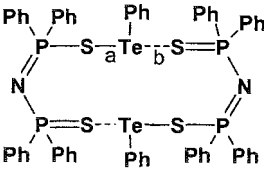

a = 2.557;b = 2.843 Å

Scheme **3** Dinuclear superrnolecules

TRINUCLEAR SUPERMOLECULES

Trimers formed through secondary bonds are rare, probably because of inadequate bond angles, which are far from linearity. An example includes the bismuth chloro derivative, $[\{(C_5H_4Me)Fe(CO)_2\}_2BiCl]_3$, containing bent Cl–Bi···Cl units.[55] In $[(Me_3Si)_3C–PbCl]_3$, the lead–chlorine bonds are symmetrized (Pb–Cl, 2.71 and 2.74 Å), whereas in a related dimer $[(PhMe_2Si)_3C–PbCl]_2$ the difference in the bond lengths is more significant (Pb–Cl, 2.729 Å; Pb···Cl 2.962 Å).[56] Probably the nonlinearity of the Cl–Pb···Cl and the tendency of symmetriza-

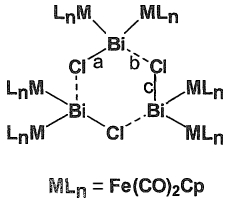

$ML_n = Fe(CO)_2Cp$

a = 2.914; b = 2.852; c = 2.955 Å

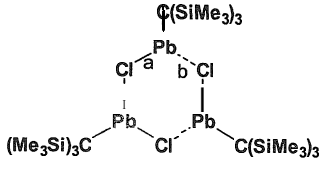

a = 2.71; b = 2.4 Å

Scheme 4 Trinuclear supermolecules.

tion are related to formation of the four- and six-membered rings (Scheme 4).

TETRANUCLEAR SUPERMOLECULES

Some tetrameric supermolecules based upon secondary bond self-assembly are illustrated in Scheme 5. Bulky organomercury chlorides, i.e., $[\sigma\text{-}(Me_2BuSi)C_5H_4HgCl]_4$ and (2-pyridylphenyl)mercury(II) chloride,[57] the heterocyclic antimony chloride $[C_4H_8SbMeCl_2]_4$,[58] and the organotellurium iodo derivative $[o\text{-}C_6H_4(CH_2TeMe_2I)_2]_2$ containing a Te_4I_4 cube,[59] demonstrate a great diversity of such structures. Another tetranuclear species $[Sb_4Cl_{16}]^{4-}$ [investigated as a *bis*(diphenylphosphino)ferrocenium salt][60] is a tetramer formed through secondary bond association of four $SbCl_3$ molecules (Sb–Cl in the

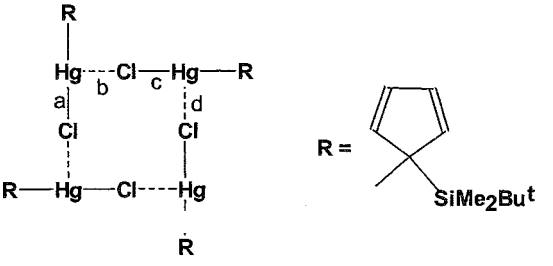

a = 2.333; b = 3.117; c = 2.336; d = 3.105 Å

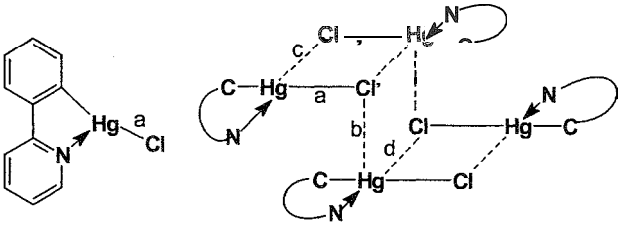

a = 2.314; b = 3.184; c = 3.442; d = 3.410 Å

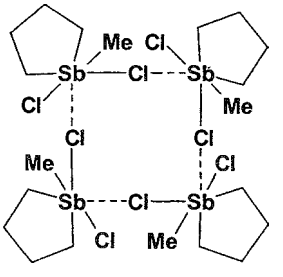

Sb-Cl 2.485; 2.519 Å; Sb···Cl 3.613 Å

Scheme 5 Tetranuclear superrnolecules

range 2.397–2.547 Å), with four Cl^- anions through S b . Cl^- secondary bonds ($Sb\cdots Cl^-$ in the range 2.743–3.329 Å). Each antimony atom is six-coordinate (distorted octahedral) and participates in three orthogonal Cl–$Sb\cdots Cl$ systems.

SUPRAMOLECULAR POLYMERIC ARRAYS

This is the most comprehensive family of supramolecular architectures involving self-assembly and self-organization promoted by secondary bonds. Selected examples are collected in Schemes 6 and Scheme 7. Scheme 6 comprises organometallic halides.

Among organometallic halides, organomercury(II) compounds. such as 1,2-$C_6F_4(HgCl)_2$ and 1,3,5-$C_6H_3(HgCl)_3$,[61,62] several triorganotin halides, R_3SnCl[63,64] and triorganolead(IV) halides, R_3PbX,[22–24] can be cited. Triorganotin chlorides are chain-like polymeric arrays. Thus, in Me_2Bu^tSnCl[65] and Me_3SnCl,[66] the secondary bond system is unsymmetrical and linear. Diorganotin dichlorides are also associated, e.g., Me_2SnCl_2.[67] In triorganolead halides, there is some tendency for bond equalization in the colinear bond system, as found in $Ph_2(PhCH_2)PbBr$,[22] but in the iodide Me_3PbI, the lead–iodine distances are significantly different.[23]

Organoantimony(III) and organobismuth(III) halides, R_2EX and REX_2 (E = Sb, Bi: *R* = Me, Ph, *X* = Cl,

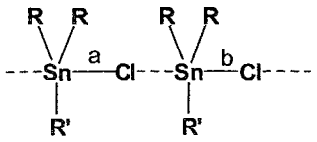

R = R' = Me: a = 2.430; b = 3.269 Å

R = Me, R' = Bu^t: a = 2.405; b = 3.662 Å

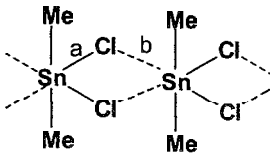

Sn-Cl = 2.389; Sn···Cl = 3.433 Å

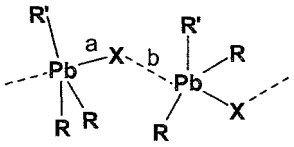

X = I; R = R' = Me: a = 3.038; b = 3.360 Å

X = Br; R = Ph, R' = CH_2Ph: a = 2.885; b = 2.985 Å

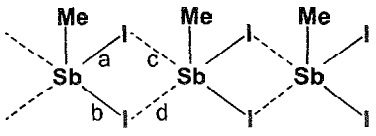

a = 2.799; b = 2.761; c = 3.467; d = 3.398 Å

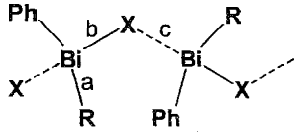

X = Cl, R = Ph: b = 2.746; c = 2.763 Å

X = R = Br: a = 2.684; b = 2.825; c = 3.038 Å

X = R = I: a = 2.882; b = 3.056; c = 3.227 Å

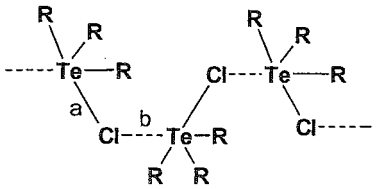

R = C_6F_5; Te-Cl 2.670; Te ···Cl 3.47 Å

Scheme 6 Chain-like supramolecular organometallic halides

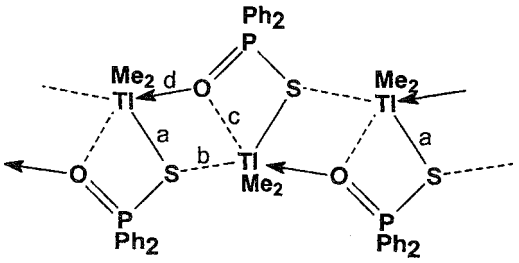

a = 2.919; b = 3.402; c = 3.143; d = 2.509 Å

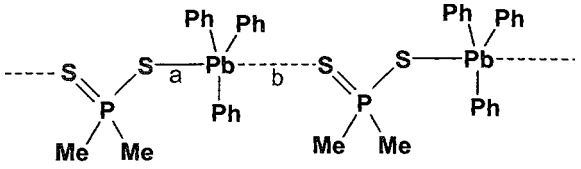

a = 2.708; b = 3.028 Å

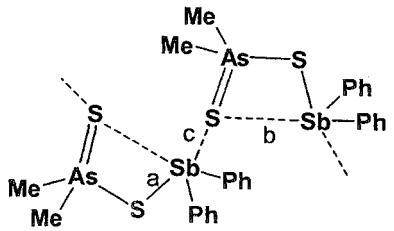

a = 2.655; b = 3.652; c = 2.830 Å

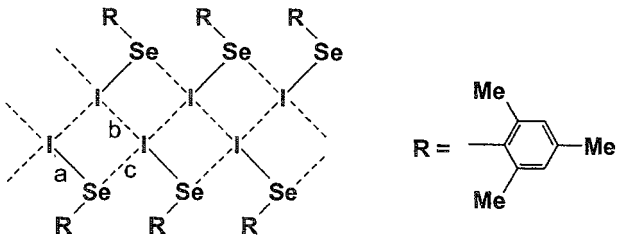

a = 2.535; b = 3.841; c = 3.839 Å

Scheme 3 Other supramolecular chain-like arrays.

Br, I),[25–29,68,69] are almost without exception. polymeric arrays formed through secondary bond self-assembly. As an example. Me_2SbI is cited; which is a chain-like polymeric array with basically linear fragments.[25] In Ph_2BiCl, the linear secondary bond system is again symmetrized,[23] but in the dibromide $PhBiBr_2$, and diiodide $PhBiI_2$, the interatomic distances are significantly different, although the difference is small.[28] Alkylbismuth diodides, $RBiI_2$, form a family of linear-chain supramolecular arrays with symmetrized triatomic systems, resulted from electron redistribution in the I–Bi···I tricenter moieties.[27,28] Organotellurium halides also form supramolecular polymeric arrays.[6,7] The most recent examples are $MeTeCl_3$,[70] $(C_6F_5)_3TeCl$,[71] and $(C_6F_5)_3$-TeBr.[72]

Suprainolecular coinpounds other than halides are numerous. Among these; methylmercury xanthates, $MeHgS_2COR$,[73] and organothalium thiophosphinates[74] can be cited. Tin–oxygen (Sn···O 3.337 A) and lead–oxygen (Pb···O 3.180 Å) secondary bonds. much longer than usually observed between these elements. connect 2-nitrobenzenethiolato triphenylmetal molecules. Ph_3-$MSC_6H_4NO_2$-2 (M= Sn. Pb) into supramolecular chains; the oxygen atoms belong to the nitro groups. and the S–M···O systems are linear.[75] Lead and organolead phosphor-1,1-dithiolates. e.g., $Pb(S_2PR_2')_2$ and Ph_3PbS_2-PMe_2;[76,77] and organoantirnony oxides and amides. e.g., $(Me_2Sb)_2O$ and $(Ph_2Sb)_3N$[78,79] provide other examples. Diphenylantimony dimethyldithioarsinate, Ph_2SbS_2-$AsMe_2$, is the first supramolecular polymer associated through dithioarsinate bridges.[77] Mesitylselenenyl iodide. 2,4,6-$Me_3C_6H_3SeI$,[80] organotellurium azides, $ArTe(N_3)_3$,[81] and numerous others can be cited. Iodo–nitro interactions (I···O=N secondary bonds) are also important and can lead to formation of supramolecular polymeric arrays.[82] In (arylsulfonylimino)iodoarenes, $ArI–NSO_2Ar'$, supramolecular one-dimensional (ID) chains. ladders. two-dimensional (2D) layers. and three-dimensional (3D) stepladders are formed through I···O and I···N secondary bond interactions.[83] Some of the above are illustrated in Scheme 7.

SECONDARY BONDS ENHANCED BY ELECTROSTATIC INTERACTIONS

Like in the hydrogen-bond systems. when secondary bonding interactions occur between charged species, the strength of the bond is increased. Numerous examples of anion–cation secondary bond interactions can be cited, but only a few will be mentioned here for illustration. Thus. secondary bonds are responsible for the formation of the dimeric diphenyliodonium halides. $[Ph_2IX]_2$ (X = Cl, Br. I). built through secondary interactions between Ph_2I^+ cations and X-anions: the X···I···X system is symmetrical. and the I···X interatomic distances are each 0.77 Å longer than covalent I–X(g) distances.[77] A tetramer $[R_2IBr]_4$, coexisting with the dimer $[R_2IBr]_2$ in the same crystal. both built from R_2I^+ cations (R = p-MeC_6H_4) and Br^- anions kept together by secondary bonds. was also reported.[85]

Some interesting organoiin examples can be cited (Scheme 8). In the solid-state structure of $[O(Sn$-$Me_3)_3]^+Cl^-$, trigonal planar cations interacting with Cl^- anions through both secondary bonds and electrostatic

interactions form graphite-like 2D layers.[86] In another tin–oxygen supramolecular array, trinuclear cations $[Me_3Sn(\mu\text{-}OH)SnMe_3(\mu\text{-}OH)SnMe_3]^+$, formed through dative-coordinate bonds between two Me_3SnOH molecules and a Me_3Sn^+cation, are interconnected through $Me_3Sn\cdots Br^-$ secondary bonds, and additionally through $O–H\cdots Br^-$ hydrogen bonds, into a complex 3D architecture. Cation–anion electrostatic interactions probably contribute significantly to the lattice energy.[87]

In the structure of triphenylselenonium chloride monohydrate, hydrogen bonds participate in addition to secondary bonds and electrostatic interactions between Ph_3Se^+ cations and Cl^- anions.[88]

SELF-ASSEMBLY THROUGH COOPERATION OF SECONDARY BOMBS WITH OTHER TYPES OF INTERMOLECULAR INTERACTIONS

Innumerable possibilities exist based upon the cooperative use of classical dative-coordinate and secondary bonds for supramolecular synthesis. This strategy is only in its infancy but can serve for the controlled design of materials with predictable structures. In a first alternative, discrete supermolecular species formed through dative bonds are further associated into polymeric arrays through secondary bonds. This case can be illustrated by the adduct of trimethyltin chloride with the dimeric tristannoxane $[ClMe_2SnOSnMe_2(OSnMe_3)]_2$. The dimer is formed through dative coordinate oxygen–tin bonds. In the crystal, $Sn\cdots Cl$ secondary bonds from the terminal $OSnMe_3$ moiety of the dimer to $ClSnMe_3$ molecules and from $ClSnMe_3$ molecules to the terminal Me_2SnCl moieties of the dimer. connect the two compounds in a supramolecular architecture.[89]

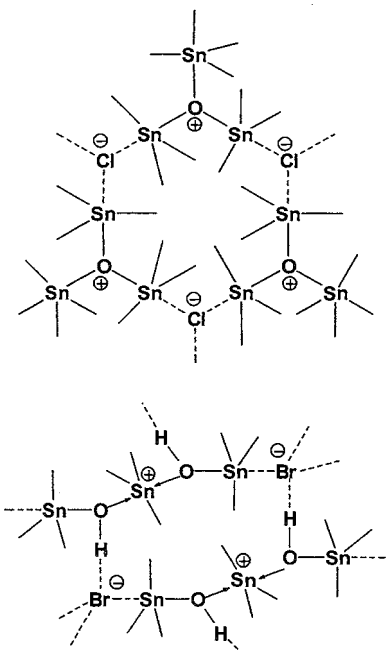

Scheme 8 Supramolecular structures formed through cooperativity of secondary bonds and electrostatic interactions.

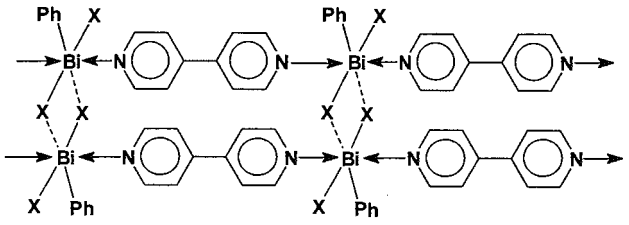

Scheme 9 Supramolecular structures formed through cooperativity of secondary bonds and dative-coordinate bonds.

A second alternative is illustrated by the supramolecular architectures built from 4,4′-bipyridyl and arylbismuth(III) halides, in which infinite chains of *trans*-$[BiX_2Ph(4,4'\text{-bipy})]_x$ (formed through coordination of the ditopic ligand 4,4′-bipy) are interconnected into intricate 3D structures through $Bi\cdots X$ secondary interaction ~ [(Scheme 9).

Complex supramolecular structures involving intermolecular $Sn\cdots S$, $S\cdots S$ secondary bonds and $N–H\cdots S$ hydrogen bonds were observed in organotin derivatives of substituted 5-mercapto-1,3,4-thiadiazoline-2-thione.[91] The simultaneous presence of $S–Sb\cdots Cl^-$ secondary bond synthons and $Cl^-\cdots H–N$ hydrogen bonds in the solid-state structure of dichlorobis(trimethylenethiourea)antimony(III) chloride also leads to an interesting supramolecular self-organization.[92] The cooperation of secondary bonds and $Te\cdots\pi$ aryl interactions also produces some spectacular supramolecular architectures.[93]

CONCLUSION

Secondary bonds, alone or in cooperation with other types of intermolecular interactions, can serve as a versatile bonding motif for the supramolecular self-assembly and self-organization, and therefore, may be exploited for the design of novel materials. A great diversity of compositions and structures, based mostly on heavier main group elements, can be expected. A new chapter of supramolecular chemistry, based upon intermolecular secondary

bonding, is emerging, and significant progress along these lines can be expected in the near future.

ARTICLES OF FURTHER INTEREST

Hydrogen Bonding, p. 658
Self-Assembly: Definition and Kinetic and Thermodynamic Considerations, p. 1248
Self-Assembly: Terminology, p. 1263

REFERENCES

1. Alcock, N.W. Secondary bonding to nonmetallic elements. Adv. Inorg. Chem. Radiochem. *1972. 15*. 1
2. Haiduc. I.: Edelmann. F.T. *Supramolecular Organometallic Chemistry*; Wiley-VCH: Weinheirn. 1999. Chapters 1 and 4.
3. Starbuck. J.; Norman. N.C.; Orpen, A.G. Secondary bonding as a potential design element for crystal engineering. New J. Chem. 1999, 23.969.
4. Vargas-Baca. I.; Chivers, T. Weakly bonding interactions in organochalcogen chemistry. Phosphorus Sulfur Silicon *2000.* 164, 207.
5. Cea-Olivares, R.: Garcia-Montalvo, V.: Munoz-Hernandez. M.-A.; Jimenez-Sandoval. O.: Garcia y Garcia. P.; Cardoso. M.L. The conformational relationships in group 14 and 15 oxadithia- and trithia-metallocanes. Main Group Chem. News *1996.* 4, 20.
6. Haiduc, I.: Zukerman-Schpector, J. Supramolecular self-assembly through secondary bonds in organotellurium chemistry. Phosphorus Sulfur Silicon *2001.* 171. 171.
7. Zukerman-Schpector, J.: Haiduc, I. Diorganotellurium(IV) dihalides and secondary bonding: revisiting the coordination polyhedra. Phosphorus Sulfur Silicon 2001. 171, 73.
8. Brown. I.D. Bond valence as an aid to understanding the stereochemistry of O and F complexes of Sn(II), Sb(III), Te(IV), I(V) and Xe(VI). J. Solid State Chem. *1974.* 11. 214.
9. Sauyer. J.F.: Gillespie, R.J. The stereochemistry of Sb(III) halides and some related compounds. Progr. Inorg. Chem. 1986. 34, 65.
10. Landrum, G.A.; Coldberg, N.; Hoffmann. R. Bonding in the trihalides (X_3^-), mixed trihalides (X_2Y^-) and hydrogen bihalides (X_2H^-). The connection between hypervalent. electron-rich three-center, donor–acceptor and strong hydrogen bonding. J. Chem. Soc., Dalton Trans. 1997, 3605.
11. Landrum. G.A.: Hoffmann. R. Secondary bonding between chalcogens or pnicogens and halogens. Angew. Chem. Int. Ed. 1998. 37. 1887.
12. Landrum. G.A.: Goldberg. W.: Hoffmann, R.: Minyaev, R.M. Intermolecular interactions between hypervalent molecules: Ph_2IX and XF_3 (X = Cl, Br, I) dimers. New J. Chem. 1998. *22.* 883.
13. Munzarova. M.L.; Hoffmann. R. Electron-rich three-center bonding: Role of s,p interactions across the p-block. J. Am. Chem. Soc. 2002. 124.1787.
14. Pyykko. P. Strong closed-shell interactions in inorganic chemistry. Chem. Rev. *1997.* 97. 597.
15. Haiduc. I. Supramolecular associations, secondary bonds. quasi-cyclic structures and heterogeometrism in metal derivatives of phosphorus- and arsenic-based thioacids and oxo analogs. Coord. Chem. Rev. *1994.* 158, 325.
16. Haiduc, I. Thiophosphorus and related ligands in coordination. organometallic and supramolecular chemistry. J. Organomet. Chem. *2001.* 623. 29.
17. Haiduc, I.: Sowerby, D.B.: Lu. S.F. Stereochemical aspects of phosphor-1,1-dithiolato metal complexes (dithiophosphates, dithiophosphinates): Coordination patterns. molecular structures and supramolecular associations. Polyhedron *1995,* 14. 3389.
18. Haiduc. I.; Sowerby, D.B. Stereochemical aspects of phosphor-1,1-dithiolato metal complexes: Coordination patterns. molecular structures and supramolecular associations in dithiophosphinates and related compounds. Polyhedron *1996, 15*, 2469.
19. Kuz'mina. L.G.; Struchkov, Yu.T. Structural chemistry of organomercury compounds. Role of secondary interactions. Croat. Chem. Acta *1984.* 57. 701.
20. Casas, J.S.; Garcia-Tasende. M.S.; Sordo, J. Structural aspects of the Coordination chemistry of organothallium(III) and organomercury(II) derivatives. Coord. Chem. Rev. 1999, *193/195*, 283.
21. Alcock, N.: Sawyer, J.F. Secondary bonding. Part 2. Crystal and molecular structures of diethyltin dichloride. dibromide and diiodide. J. Chem. Soc., Dalton Trans. 1977, 1090.
22. Fahrenkampf. U.; Schürmann, M.: Huber. F. Benzyl(bromo)diphenyllead. Acta Crpstallogr. *1994. C50*, 1252.
23. Hillwig, R.; Kunkel. F.; Harms. K.: Neumiiller, B.; Dehnicke. K. Die Kristallstrukturen von Trimethylbleiiodid und Diphenylbismutchlorid. Z. Naturforsch. 1997, *52b*, 149.
24. Edelmann. F.T.; Haiduc, O.; Schmidt. H.-G.; Noltemeyer, M.: Silvestru. C. Supramolecular self-assembly in triphenyllead(IV) dimethyldithiophosphinate, $_x^1[Ph_3PbS_2PMe_2]$, a chain polymer built through intermolecular Pb· S secondary bonds. Polyhedron *1998.* 17. 2043.
25. Breunig, H.: Althaus, H. Ring and chain systems in structures of organo antimony(III) and bismuth(III) halides. Phosphorus Sulfur *2001,* 168. 123.
26. Mundt. O.: Becker. G.; Stadelmann, H.: Thurn, H. Element-element-bindungen. VII. Intermolekulare Wechselwirkungen bei Dihalogen(phenyl)stibanen. Z. Anorg. Allg. Chem. *1992,* 617. 59.
27. Mitzi. D.B. Synthesis and crystal structure of the alkylbismuth diiodides: A family of extended one-dimensional organometallic compounds. Inorg. Chern. *1996.* 35, 7614.
28. Wang, S.; Mitzi. D.B.; Landrum, G.A.; Genin, H.: Roffmann. R. Synthesis and solid state chemistry of CH_3BiI_2: A structure with an extended one-dimensional organometallic framework. J. Am. Chem. Soc. *1997,* 119. 724.
29. Clegg, W.: Errington, R.J.: Fisher. G.A.: Hockless. D.C.R.: Norman, N.C.: Orpen, A.G.; Stratford. S.E. Structural studies on phenylbismuth halides and halogenoanions. J. Chem. Soc., Dalton Trans. 1992. 1967.

30. Du Mont, W.W.; Martens-von-Salzen, A.; Ruthe, F.; Seppala. E.: Mugesh, G.; Devillanova. F.A.; Lippolis, V.; Kuhn, N. Tuning selenium-iodine contacts: From secondary soft–soft interactions to covalent bonds. J. Organomet. Chem. 2001, 623. 14.
31. Du Mont, W.W. The fate of neutral selenium iodides. Main Group Chem. News 1994. 2. 18.
32. Alcock. N.W.; Countryman. R.M. Secondary bonding. Part 1. Crystal and molecular structures of diphenyliodonium chloride. bromide and iodide. J. Chem. Soc., Dalton Trans. 1977. 217.
33. Alcock, N.W.; Countryman. R.M. Secondary bonding. Part 14. Structural isomerism in diaryliodonium halides and the structure of di(*p*-tolyl)iodonium bromides. J. Chem. Soc., Dalton Trans. 1987. 193.
34. Mundt. O.; Riffel, H.; Becker. G.; Simon. A. Element–element Bindungen. III. Intermolekular Sb···Sb-Wechselwirkungen im kristallinen Tetramethyldistiban. Z. Naturforsch. 1984. *39b*. 317.
35. Ashe. A.J., III; Ludwig, E.G.; Oleksyszyn. J. The structure of tetramethyldistibine. Organometallics 1984. 3. 337.
36. Ashe. A.J.. III; Kampf. J.W.; Puranik. D.B.: Al-Taweel, S.M. Secondary bonding in organobismuth compounds. Comparison of the structures of 2,2′,5,5′-tetramethyl-1,1′-dibismaferrocene and 2,2′,5,5′-tetramethylbibismole. Organornetallics 1992. 11. 2743.
37. Newton, M.G.: King, R.B.: Haiduc, I.; Silvestru, A. Aunique supramolecular structure of *catena*-poly[bis(μ-diphenylphosphinodithioato) ditellurium(I)(*Te–Te*)], $[Te_2(S_2PPh_2)_2]_n$, containing Te–Te···Te–Te··· chains. Inorg. Chem. 1993. *32*. 3795.
38. Maaninen, A.: Ahlgren, M.; Ingman, P.; Laitinen. R.S. Phosphorus. sulfur and silicon. The pathway of the reaction between $[(Me_3Si)_2N]_2S$ and $SeCl_4$. Phosphorus Sulfur Silicon 2001. 169. 161.
39. Oakley. R.T. Chemical binding within and between inorganic rings: the design and synthesis of molecular conductors. Can. J. Chem. 1993. 71. 1775.
40. Stenzel. V.; Jeske, J.: du Mont. W.; Jones. P.G. Supramolecular soft–soft interactions of diiodo(*tert*-butyl)-(isopropyljphosphonium cations with μ_2 to μ_5—Bridging iodide anions. Formation of chains. helixes and columnar structures. Inorg. Chem. 1997. 36. 443.
41. Ali, M.; McWhinnie, W.R.; Hamor. T.A. The crystal structure of phenylazophenyl-C,N′)mercury(II) chloride: A dimeric transmetallation reagent. J. Organomet. Chem. 1989. 371. C37.
42. Zukerman-Schpector. J.; Vázquez-López, E.M.; Sánchez, A.: Casas. J.S.; Sordo, J. Synthesis and structural characterization of diphenyldithiophosphinates of methyl- and phenylmercury(II). Crystal structure of $MeHgS_2PPh_2$. J. Organomet. Chern. 1991. 405. 67.
43. Silvestru. C.: Haiduc. I.: Cea-Olivares. R.; Hernandez-Ortega. S. A new eight-membered $Pb_2S_4P_2$ inorganic ring. Crystal and molecular structure of dimeric $[Pb(S_2PMe_2)_2]_2$, associated into polymeric chains through intermolecular Pb···S interactions. Inorg. Chim. Acta 1995. 233. 151.
44. Gibbons, M.N.; Silvestru. C.; Haiduc. I.; Sowerby, D.B. Reduction of antimony(V) by dithiophosphinates and the crystal structure of dimeric diphenylantimony(III) dimethyldithiophosphinate, $[Ph_2SbS_2PMe_2]_2$. Polyhedron 1996. 15. 4573.
45. Silvestru, C.: Haiduc, I.; Kaller, R.; Ebert. K.H.; Breunig. H.J. Synthesis, spectroscopic characterization and molecular structure of dimeric (diethyldithiophosphinato) di(para-tolyl)antimony(III), $[(p\text{-}CH_3C_6H_4)_2SbS_2\text{-}P(C_2H_5)_2]_2$, containing a novel monocyclic $P_2S_4Sb_2$ inorganic ring system, formed through Sb···S semibonding interactions. Polyhedron 1993.12.2611.
46. Silvestru, C.; Curtui, M.; Haiduc. I.; Begley, M.J.; Sowerby, D.B. Phenylantimony(III) diorganophosphorodithioates: The crystal structure of diphenylantimony(III) diisopropylphosphorodithioate, $Ph_2SbS_2P(OPr^i)_2$; unusual polymerization through semibonding interactions. J. Organomet. Chem. 1992, 426, 49.
47. Sowerby, D.B.: Begley, M.J.: Silaghi-Dumitrescu, L.; Silaghi-Dumitrescu, I.; Haiduc. I. Antimony(III) and phenylantimony(III) dimethyldithioarsinates. Synthesis and mass spectral study. Crystal structure of $Ph_2SbS_2\text{-}AsMe_2$, the first coordination polymer associated via bridging dimethyldithioarsinate ligands, J. Organomet. Chem. 1994, *469*, 45.
48. Ebert. K.H.; Breunig, H.J.; Silvestru, C.; Haiduc, I. Crystal and molecular structure of (dimethyldithiophosphinato)dimethylantimony(III), $_x{}^1[Me_2SbS_2PMe_2]$, a chain polymer built through secondary, intermolecular Sb···S interactions. Polyhedron 1994, 13. 2531.
49. Begley, M.J.: Sowerby, D.B.: Haiduc. I. The crystal structures of the diphenyl–dithiophosphinates of antimony(III) and bismuth(III): $M(S_2PPh_2)_3$ (M=Sb or Bi). J. Chem. Soc., Dalton Trans. 1987. 145.
50. Edelmann, F.T.; Noltemeyer, M.; Haiduc. I.; Silvestru. C.: Cea-Olivares, R. Bismuth(III) dimethyldithiophosphinate, $Bi(S_2PMe_2)_3$: Another dimer formed through secondary bonding. The stereochemically active lone pair revisited. Polyhedron 1994. *13*, 547.
51. Cea-Olivares, R.; Ebert, K.H.; Silaghi-Dumitrescu. L.; Haiduc. I. Bismuth(III) dimethyldithioarsinate, $Bi(S_2\text{-}AsMe_2)_3$: A new dimer formed through Bi–S secondary bonding. Heteroat. Chem. 1997, *8*, 317.
52. Burke. P.J.: Gray. L.A.; Hayward, P.J.C.: Matthews, R.W.; McPartlin. M. X-Ray structures of the dimeric dimethylthallium(III) derivatives, $[(CH_3)_2TlX]_2$ ($X=OC_6H_5$-OC_6H_4Cl-*o*, SC_6H_5). J. Organomet. Chem. 1977. 136. C7.
53. Haiduc, I.: King, R.B.; Newton, M.C. Stereochemical aspects of tellurium complexes with sulfur ligands. Molecular compounds and suprarnolecular associations. Chern. Revs. 1994, 94. 301.
54. Husebye. S. Recent developments in the structural chemistry of tellurium with sulfur and selenium containing ligands. Phosphorus Sulfur Silicon 1998. *136/137*. 377.
55. Clegg, W.: Compton. N.A.; Errington, R.J.; Norman, N.C. Synthesis and X-ray crystal structure of $[\{(C_5H_4Me)\text{-}Fe(CO)_2\}_2BiCl]_3$: A compound containing a planar six-membered Bi_3Cl_3 ring. Polyhedron 1987, 6. 2031.

56. Eaborn. C.: Hitchcock, P.B.: Smith, J.D.; Sozerli, S.E. Synthesis and crystal structures of the compounds $[Sn\{C(SiMe_2Ph)_3\}Cl]_2$, $[Pb\{C(SiMe_3)_3\}Cl]_3$ and $[M\{C(SiMe_3)_2(SiMe_2OMe)\}Cl]_2$ (M = Sn or Pb). Organometallics *1997. 16.* 5653.
57. Constable, E.C.: Leese. T.A.: Tocher, D.A. Polynuclear intermediates in the synthesis of cyclometallated complexes and molecular structure of (2-pyridylphenyl)mercury(II) chloride tetramer. J. Chem. Soc., Dalton Trans. *1989.* 570.
58. Meinema, A.H.; Noltes, J.G.; Spek, A.L.; Duisenberg. A.J.M. The structure of 1,1-dichloro-1-methyl-1λ^5-stibacyclopentane. Recl. Trav. Chim. Pays–Bas *1988,* 107. 226.
59. Hill. N.J.; Lewason. W.: Reid. G.: Ward, A.J. Synthesis and molecular structures of dimeric assemblies of telluronium salts derived from *o*-$C_6H_4(CH_2TeMe)_2$ and PhMeTe. J. Organomet. Chein. *2002. 642,* 186.
60. Razak. I.A.: Usman, A.: Fun, H.K.; Yamin, B.M.; Kasim, N.A. Bis[1,1′-bis(diphenylphosphino)ferrocenium] hexadecachlorotetraantimony(III) ethanol solvate. Acta Crystallogr. *2002. C58.* m162.
61. Beckwith, J.D.; Tschinkl. M.; Picot, A.; Tsunoda. M.: Bachman, R.; Gabbaï, F.P. Interaction of the bifunctional Lewis acid 1,2-bis(chloromercurio)tetrafluorobenzene with aldehydes. nitriles and epoxides. Organometallics *2001. 20,* 3169.
62. Rot. *N.;* de Kanter, F.J.J.; Bickelhaupt. F.; Smeets. W.J.J.; Spek, A.L. Synthesis of 1,3,5-tri- and 1.2.4.5-tetrasubstituted tin and mercury derivatives of benzene. Crystal structure of 1,3,5-*tris*(chloromercurio)benzene. J. Organomet. Cheni. *2000. 593/594,* 369.
63. Harrison. P.G. Silicon, Germanium, Tin and Lead. In *Comprehensive Coordination Chemistry,* Volume *3,* Main *Group and Early Transition* Metals; Wilkinson. G.. Gillard. R.D.. McCleverty, J.A., Eds.; Pergamon Press: Oxford, 1987; 183.
64. Davies, A.G. *Organotin Chemistry*; VCH: Weinheim. 1997: 131.
65. Apodaca, P.: Cervantes-Lee. F.; Pannell, K.H. Mixed aryl–alkyl organotin compounds. Main Group Met. Chem. *2001. 24.* 597.
66. Lefferts. J.L.: Molloy, K.C.: Hossain. M.D.: Van der Helm, D.; Zukerman. J.J. The crystal and molecular structure of trimethyltin(IV) chloride. a chlorine-bridged, linear polymer. J. Organomet. Chem. **1982**. *240.* 349.
67. Reuter. *H.:* Pawlak, R. Zinnhalogenverbiiidungen.. III. Neuere daten zur Kristall- und Molekulstruktur von Dimethylzinndichlorid Me_2SnCl_2. Z. Kristallogr. **2001**. *216.* 56.
68. Althaus. H.: Breunig. H.J.: Lork, E. Synthesis and chemistry of methylantimony and methylbismuth dihalides. An extended two-dimensional framework in the crystal structure of CH_3BiCl_2 and molecular units in the structures of $[CH_3ECl_2(2,2'\text{-bipyridine})]$ (E = Sb. Bi). Organometallics **2001**. *20.* 586.
69. Clegg, *W.:* Elsegood. M.R.J.: Errington, R.J.; Fisher. G.A.; Norman. N.C. Structure of $BiBr_2Ph$: A solid-state architecture involving secondary bonding and π–π interactions. J. Mater. Chem. *1994. 4.* 891.
70. Pietikainen, J.: Laitinen, R.S.; Konu. J.; Valkonen. J. Formation and crystal structure of polymeric $(MeTeCl_3)_n$. Z. Naturforsch. *2001. 56b.* 1369.
71. Klapotke. T.M.; Krumm. B.: Mayer. P.; Polborn, K.: Ruscitti, O.P. The reactivity of perfluorophenyltellurium(IV) dihalides towards cyanide. Crystal structures of $(C_6F_5)_3$-TeCl and $C_6F_5TeTeC_6F_5$. J. Fluorine Cheni. **2001**, *112,* 207.
72. Naumann. D.: Tyrra, W.; Herrmann. R.; Pantenburg, I.; Wickleder, M.S. Syntheses and properties of tetrakis-(pentafluorophenyl)tellurium, $Te(C_6F_5)_4$, and related compounds. Single crystal structure of *tris*(pentafluorophenyl)-tellurium bromide, $Te(C_6F_5)_3Br$. Z. Anorg. Allg. Chem. *2002. 628.* 833.
73. Casas. J.S.; Castellano. E.E.: Ellena, J.; Haiduc. I.: Sanchez, A.; Semeniuc, R.F.; Sordo, J. Supramolecular self-assembly in the crystal structures of methylmercury xanthates. MeHgS(S)COR, R = Et. 'Pr, and CH_2Ph. Inorg. Chim. Acta *2002. 329,* 71.
74. Casas. J.S.: Castiiieiras, A.; Haiduc. I.: Sánchez. A.; Sordo. J.; Vázquez-López, E.M. Supramolecular self-organization in *catena*-poly[(dimethylphosphinothioato) thallium(III)], $[TlMe_2\{S(O)PPh_2\}]_n$, a polymer with secondary interactions between the chain segments. Polyhedron **1994**. *13.* 1805.
75. Aupers. J.H.; Cox. P.J.: Doidge-Harrison. S.M.S.V.; Howie. R.A.; Low, J.N.; Wardell, J.L. Non-bonded interactions involving oxygen in 2-nitrobenzenethiolato compounds: Structures of $Ph_3MSC_6H_4NO_2$-2 (M = Ge, Sn, Pb). Main Group Chem. *1999.* 3, 23.
76. Ebert, K.H.: Breunig. H.J.; Silvestru, C.: Stefan, I.; Haiduc. I. Crystal and molecular structure of *bis*(diphenyldithiophosphinato)lead(II) $_x{}^1[Pb(S_2PPh_2)_2]$, a new type of polymer associated through Pb···S secondary interactions. Inorg. Chem. *1994. 33,* 1695.
77. Silvestru, C.; Haiduc, I.: Cea-Olivares. R.; Hernandez-Ortega, S. A new eight-membered $Pb_2S_4P_2$ inorganic ring. Crystal and molecular structure of dirneric $[Pb(S_2PMe_2)_2]_2$, associated into polymeric chains through intermolecular Pb···S interactions. Inorg. Chim. Acta **1995**, *233.* 151.
78. Breunig. H.J.; Lork. E.; Rosler, R.; Becker. G.; Mundt. O.; Schwarz. W. Common features in the crystal structures of the compounds *bis*(dimethylstibanyl)oxane and -sulfane, and the minerals valentinite and stibnite. Z. Anorg. Allg. Chem. *2000. 626.* 1595.
79. Balazs. L.; Breunig, H.J.: Krüger, T.; Lork, E. Bildung und Struktur von Tris(diphenylstibino)amin. Z. Naturforsch. **2001**. *56b.* 1325.
80. Jeske. J.: Jones, P.J.: Martens-von-Salzen. A.; Du Mont. W.W. Mesitylselenenyl iodide. Acta Crystallogr *2002. E58.* o350.
81. Klapotke. T.M.: Krum. B.: Mayer, P.: Piotrowski. H.: Ruscitt. O.P.: Schiller. A. Novel organotellurium(IV) diazides and triazides. Inorg. Chern. *2002. 41.* 1184.
82. Allen, H.F.: Goud. B.S.: Hoy, V.J.: Howard. J.A.M.: Desiraju, G.R. Molecular recognition via iodo···nitro and

iodo···cyano interactions: Crystal structures of the 1:1 complexes of 1,4-diiodobenzene with 1,4-dinitrobenzene and 7,7,8,8-tetracyanoquinodimethane (TCNQ). J. Chem. Soc., Chem. Commun. 1994, 2729.

83. Boucher. M.; MacIkenas, D.: Ren. T.; Protasiewicz, J.D. Secondary bonding as a force dictating structure and solid-state aggregation of the primary nitrene sources (arylsulfonylimido)iodoarenes ($ArINSO_2Ar'$). J. Am. Chem. Soc. 1997. 119. 9366.
84. Alcock. N.W.; Countryman, R.M. Secondary bonding. Part 1. Crystal and molecular structures of diphenyliodonium chloride, bromide and iodide. J. Chem. Soc., Dalton Trans. 1974. 217.
85. Alcock. N.W.: Countryman, R.M. Secondary bonding. Part 14. Structural isomerism in diaryliodonium halides and the structure of di(*p*-tolyl)iodonium bromide. J. Chem. Soc., Dalton Trans. 1987. 193.
86. Rake, B.: Miiller. P.; Roesky, H.W.; Uson, I. Synthesis and structural characterization of graphite-like $[(Me_3Sn)_3O]Cl$. Angew. Chem., Int. Ed. 1999, *38*, 2050.
87. Pavel. I.; Cervantes-Lee. F.; Pannell, K.H.; Haiduc, I. Supramolecular self-assembly involving cooperative use of dative coordinate, secondary and hydrogen bonding in solid $[Me_3Sn(\mu\text{-}OH)SnMe_3(\mu\text{-}OH)SnMe_3]^+Br^-$. Inorg. Chem. Commun. 2001, 4, 530.
88. Mitcham. R.V.; Lee, B.: Mertes. K.B.: Ziolo. R.F. The nature of triphenylselenonium chloride. Crystal and molecular structure of the monohydrate: Triphenylselenoniurn chloride hydrate. Inorg. Chem. 1979. *18*. 3498.
89. Mitzel, N.W.; Lustig, C.: Scharfe, S. Cocrystallization of trimethylchlorostannane with a distannoxane. Z Naturforsch. 2001, *56b*. 440.
90. James, S.C.; Norman. N.C.; Orpen, A.G.; Starbuck, J. Crystal synthesis using secondary and dative coordinate bonding: 4,4′-Bipyridyl adducts of arylbismuth dihalides. CrystEngComm 2000, 10.
91. Bercean, V.; Crainine. C.: Haiduc. I.: Mahon, M.F.; Molloy. K.C.: Venter. M.M.; Wilson. P.J. The structural chemistry of organotin derivatives of 5-mercapto-3-phenyl-1,3,4-thiadiazoline-2-thione: Supramolecular structures involving intermolecular Sn···S, N–H···S or S···S interactions. J. Chem. Soc. Dalton Trans. 2082. 1036.
92. Razak, I.A.; Usman, A.; Fun, H.K.: Yamin, B.M.; Keat, G.W. Dichlorobis-(trimethylenethiourea)antimony(III) chloride. Acta Crystallogr 2002, *C58*, m122.
93. Zukerman-Schpector, J.; Haiduc, I. Tellurium···π-aryl interactions: A new bonding motif for supramolecular self-assembly and crystal engineering. CrystEngComm 2002. 4. 178.

Selectivity: Thermodynamic and Kinetic

Franz P. Schmidtchen
Munich Institute of Technology, Garching, Germany

INTRODUCTION

The introduction of selectivity into chemical systems and the understanding of its foundations are major motives for dealing with supramolecular chemistry. Examples from the living world clearly show that it is the capacity to distinguish compounds and their conversions with respect to a particular function that enables the concerted and balanced interplay of components in a complex system. Selectivity in the supramolecular context is. therefore, intimately connected to a purposefully integrated function. let it be a simple reversible adhesion phenomenon of two particles or highly sophisticated vectorial processes like catalysis. transport, or information transfer (signaling). This also includes the targetted blocking or annihilation of these functions. The basic platform defining the stage for observation of selectivity and ultimately providing a means for its deliberate alteration is the molecular complex formed reversibly from at least two, in many instances. however, many more. molecules. For the present discussion. I arbitrarily designate the species participating in this interaction as host and guest binding partners. Selectivity emerges from two stages tied to the occurrence of the noncovalently bound and truly supramolecular associate species (Scheme 1, Fig. 1).

At the level of complex formation, compounds can compete for binding at a molecular target and will thus be differentiated according to their chemical affinities. Selectivity here arises from the differential extent of binding reflected in unequal concentrations of the various host–guest complexes formed from identical guest concentrations in reversible binding equilibria. With a defined set of environmental limits given, selectivity will be time invariant and a sole function of the thermodynamic state of the system. Thus. it is termed thermodynamic selectivity. expressed as a ratio of binding constants of the competing guests.

Alternatively. selectivity may relate to a nonequilibrium process. to the differential transformation of two (or more) molecular complexes that may be formed even in similar concentrations from the various host–guest partners. In this case. the discrimination of one complex species over the others depends on differences in the respective rates of the forward reactions leading from the complex or the starting state (depending on the concentration domain) to the final function (Fig. 2). As a corollary, it is the rate of change of the system that determines the selectivity pattern under these irreversible conditions, justifying the designation as kinetic selectivity.

Both strategic versions of the origin of selectivity are widespread in nature as well as in technological applications. Typical examples for thermodynamic selectivity include molecular aggregations, like the formation of rnicelles from amphiphilic molecules (soaps), or gels from certain proteins (gelatine), or artificial gelators, respectively. Also the strand pairing of DNA. the assembly of molecular capsules from urea-appended calixarene derivatives, or the construction of virus coats from monomeric protein building blocks belong to this class. Thermodynamic selectivity principles lend themselves to the rational development of technical applications, as in the unperturbed detection of analytes with selective electrodes or the extraction and recycling of precious elements from sea water or nuclear waste.

Kinetic selectivity. on the other hand, is a constitutive part of all living systems, which necessarily operate far from chemical equilibrium. Material fluxes across membranes via dedicated carriers or molecular channels are governed by this type of selectivity, as are the generation of signals, e.g., the light emission of the firefly. Enzyme catalysis probably is the most prominent realization of kinetic selectivity. providing not only the balanced and just-in-time supply of all vital materials but also insuring high fidelity in the information transfer in DNA replication and protein synthesis. The technical exploitation of kinetic selectivity using supramolecular approaches in general is. as yet. less amenable to design than its thermodynamically based counterpart. Nevertheless. kinetic optical resolutions and asymmetric chemical inductions are shiny examples of the implementation of kinetic selectivity in high added-value industrial processes, and they demonstrate feasibility and utility.

THERMODYNAMIC SELECTIVITY

Differentiation between molecular species A. B. or C (deliberately designated heie as guests) that compete for a certain function can be established through their reversible fixation at another molecular target (named the host),

Encyclopedia of Supramolecular Chemistry
DOI: 10.1081/E-ESMC 120012656

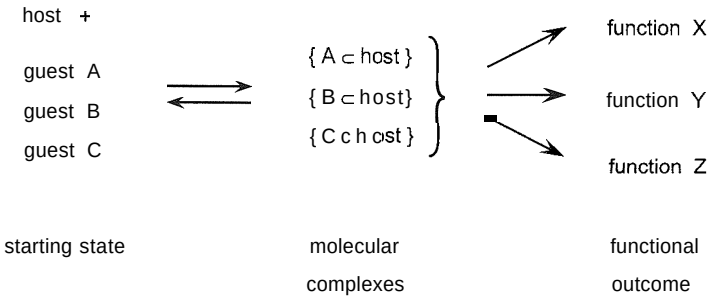

Scheme 1 Schematic division of the molecular events producing selectivity from the pairwise interaction of supramolecular binding partners (the host and the various guests). Thermodynamic selectivity (left-hand side) relates to the differential concentrations at equilibrium of the molecular complexes formed whilst kinetic selectivity (right-hand side) refers to their differential rates of breakdown to produce some function.

resulting in a host–guest complex (Scheme I). In principle; mutual adhesion of molecules is nothing but a universal property of matter. Selectivity comes into play only if the interaction between host and guest dramatically exceeds the usual level. As a consequence, a potential well is formed that characterizes the mutual distance and orientation of the binding partners and the energetic gap separating this peculiar configuration (the host–guest complex structure) from the multitude of random collision complexes. For expression of selectivity, this state needs to be more populated in thermal equilibrium than any alternative molecular arrangement. Because the abundance of energetic states for host–guest structures of higher energy is much greater than the unique "best" structure. the preferential population of the latter can be reached only if either the thermal energy (i.e., the temperature) is very low or the energy gap is substantial. This requirement also defines the frame for the observable selectivity between competing guests, because the respective differences in their interactions with the host can only be great if the absolute size of the interaction is even greater. The central criterion here is the affinity constant K_{ass}, which describes the thermodynamic equilibrium of associated and separated binding partners, including all solvation changes. The association constant K_{ass} is related to the Gibbs energy AG" of the associative event by $\Delta G^\circ = -RT \ln K_{ass}$ (R=universal gas constant; T=absolute temperature). Thus, the optimization of thermodynamic selectivity requires maximizing $\Delta\Delta G^\circ = \Delta G^\circ\{\text{Achost}\} - \Delta G^\circ\{B \subset \text{host}\}$, which is equivalent to the ratio of the corresponding association constants $K_{ass}\{A \subset \text{host}\}/K_{ass}\{B \subset \text{host}\}$. In this scenario, selectivity is independent of the presence of the variety of other guest species. However. arguments based on statistical thermodynamics led to the conclusion that, at least in the biological context involving many potential competitors, the observable selectivity will depend on the type and concentration of every competing species in the entire ensemble.'" So far, our understanding of thermodynamic selectivity is tied to the concept of a peculiar structure that host and guest will attain. The rather frequent observation of enthalpically neutral or even endothermic host–guest binding in polar hydrogen-bonding solvents and especially in water, point to the conclusion that a unique structure as implied by a potential well (i.e., a negative enthalpy of association) is not a mandatory requirement for selectivity. The negative Gibbs energy necessary for high-affinity binding results from a compensatory interplay of enthalpy and entropy, as shown by the fundamental Gibbs–Helmholtz equation ($\Delta G = \Delta H - T$ AS) and may originate exclusively from a large and positive entropy component that outmatches any unfavorable (positive) enthalpy contribution. However, highly positive association entropies imply less-structured modes in the associated versus the starting state that most

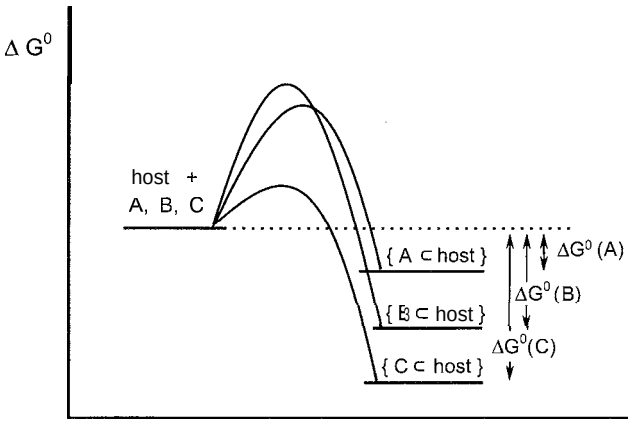

Fig. 1 Free-energy diagram relating the pertinent energy quantities to the thermodynamic selectivity of three competing guest species. The host–guest complexes are formed according to their respective host–guest affinities represented by free energies of association ΔG°. Preferential binding is expressed as AAC° [e.g., $\Delta\Delta G^\circ = \Delta G^\circ(A) - \Delta G^\circ(C)$].

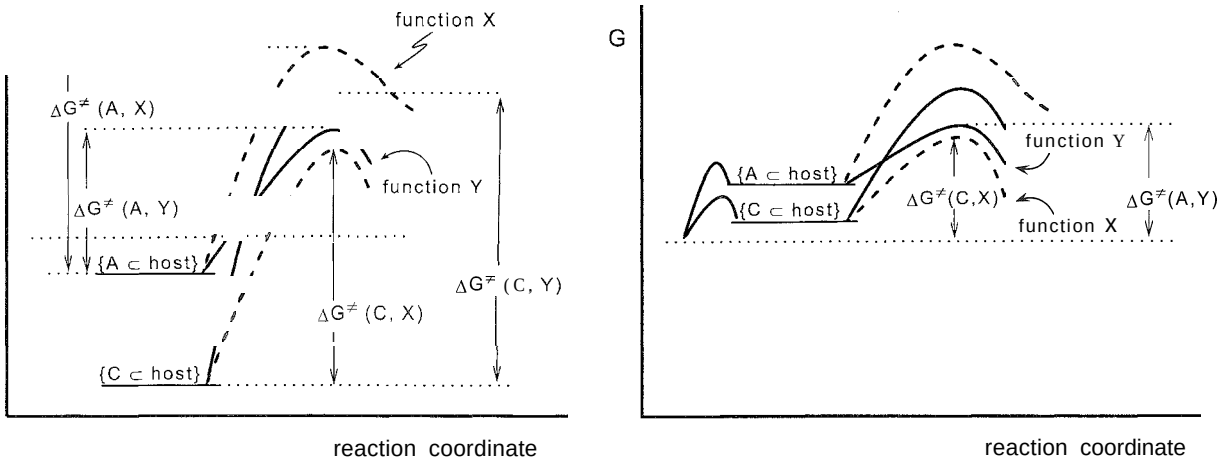

Fig. 2 Free-energy diagram relating the various barriers of activation for two competing guests (A and C) with respect to two different functions (e.g., two catalytic pathways leading to different products) to the kinetic selectivity. Two limiting situations need to be considered: The left panel shows the case when saturation of the molecular complexes occurred {[A], [C] $\gg 1/K_{ass}$ (A, C)}. In the scenario shown, Guest A would be kinetically selected to perform function *Y*, because this is the process with the lowest barrier. However, using low concentrations of the guests {[A], $[C] \ll 1/K_{ass}$ (A. C), panel on the right}, the free energies of the host–guest complexes are elevated. and the barriers relative to the starting conditions take over. This causes Guest C acting in function X to be kinetically selected.

likely do not only emerge from solvent reorganization. It is conceivable that on association of the binding partners, certain conformational restrictions present in the uncomplexed species are relieved. yielding an associated ensemble that has more degrees of freedom and thus less pairwise correspondence of atomic positions, including solvent molecules. than before the binding event. The relaxation of structural definition is compatible with the selectivity-based function but eludes ready comprehension using popular complementarity models like the lock-and-key picture of molecular recognition.[2]

Though maximizing affinity is a profitable way to boost thermodynamic selectivity, there is an upper limit to it due to practical limitations. Taking the well-studied avidin–biotin system as a prototypical example of a high-affinity supramolecular complex ($K_{ass} = 10^{15}$ M^{-1}) and assuming the fastest possible association of host and guest (diffusion controlled rate $\sim 10^9$ M^{-1} sec^{-1}), one arrives at a dissociation rate constant of $k_{off} = k_{on}/K_{ass} = 10^{-6}$ sec^{-1} corresponding to a half-life for dissociation of ca. 10 days or about 3 months for establishing equilibrium conditions. There are not many relevant processes known that rely on the exploitation of thermodynamic selectivity in this time regime.

Biological systems. which usually operate on a much shorter time span but are nevertheless in need of high affinity and seiectivity, bypass the problem of slow dissociation by polyvalent binding.[3] This binding mode refers to the simultaneous fixation of several moieties (anchor groups) of one binding partner capable of dedicated interaction with a set of corresponding substructures of the other. The participation of multiple interaction sites results in the accumulation of all free-energy contributions. compounding the total energy available for differentiating action. Contrary to single-site binding. the adhesion of host and guest can be destroyed in steps by cornpetition with monovalent guest analogues, leading to greatly improved dissociation kinetics.[3] In addition, polyvalent binding can be modulated by the mutual influence of the anchor groups on one another.[5] This influence can turn out to be opposing to binding, i.e., the following binding steps addressing the second. third. etc., anchor groups occur with smaller affinities (smaller microscopic K_{ass} values) than the preceeding ones. Though the interaction is progressively weakened in each step, the overall affinity increases with every supplementary site, contributing some free energy ΔG_i° ($\Delta G_{total}^\circ = \Sigma \Delta G_i^\circ$; ΔG_i° is more negative than ΔG_{i+1}°). Cooperativity between the various anchor groups is negative, and in general, this situation appears to be more common. However, the alternative scheme in which the affinities in subsequent binding steps are progressively strengthened, giving rise to positive cooperativity (ΔG_i° more positive than ΔG_{i+1}°), holds a peculiar virtue with respect to function: low-affinity binding of the first anchor group to a inolecular target can trigger the binding of all subsequent steps, thus providing an overall free energy of interaction that can exceed a certain threshold value defined for initiating some function. Synergistic action here approaches an all-or-nothing switch that is useful on

many occasions in supramolecular chemistry—from the clearance of antigens from the bloodstream by the immune system[3] to the formation of kinetically stable molecular capsules from calixarene building blocks.[6–8]

Tailored shaping of thermodynamic selectivity requires considerable insight into intimate molecular details. In comparison, the blocking of such delicately balanced functions by brute binding force interference should be easier to achieve. This lays the foundations for the best-established application in tailoring thermodynamic selectivity: the rational drug design. Guided by complementarity principles. artificial compounds are looked for that would interact best with a target site, for instance, in a protein that is essential for some biological function. Better binding of the artificial guest prevents binding of the natural substrate and interrupts its proper function. The need for selectivity is basically twofold, because drug binding has to override the natural host–guest process but also must avoid interfering at any other potential target site (here disregarding the equally important so-called ADME [Absorption, Distribution, Metabolism, Excretion] characteristics[9]). The approach chosen most frequently employs the computational maximization of the interaction enthalpy of drug and target. with or without taking solvent participation and the internal flexibility of the binding partners explicitly into account (docking). However. the tacit assumption that the enthalpies of interaction ΔH° derived in this way reflect or even parallel binding free energies ΔG° is not founded. Rather, it is common experience that owing to the phenomenon of enthalpy–entropy compensation,[10,11] dramatic trends in enthalpy variation do not materialize in equilibrium affinities. Nevertheless. in the absence of practicable methods to account for association entropies and with the proviso of conscience of their fundamental limitations; docking procedures can provide guidelines in thermodynamic selectivity optimization.

KINETIC SELECTIVITY

While the conversion of a supramolecular complex back into its constituent components is part of the equilibration process and, as such, is contained in thermodynamic selectivity. any alternative transformation leading to a function is characterized by a rate and a corresponding monomolecular rate constant. Principally, it can refer to just one elementary reaction yielding the function, but more likely, function generation will be composed of several successive steps. In any case, a pathway is defined that features a certain activation barrier that, in turn, determines the total flux on this route. Typical kinetically controlled vectorial processes include the transport of compounds across membranes, the photosynthetic electron translocation, or chemical transmutations of starting compounds into products using a molecular catalyst. Because a flux mandates nonequilibrium conditions, this defines a sine-qua-non restriction for establishing kinetic selectivity. In essence: the term refers to the different rates with which a single supramolecular complex decays along the various options for reaction (Scheme 1, Fig. 2). Alternatively, the differences in rates shown by the set of host–guest complexes of competing guests for eliciting the same function are addressed. The route requiring to pass the lowest activation barrier generates the highest flux and is thus preferred.

Optimizing kinetic selectivity does not necessarily require a barrier to be lowered and the speed of the corresponding process to be increased. Because it is the relative height of the barriers that counts, the uniform enhancement of the rate-determining barriers of all competing pathways excepting the desired one would be equally effective. This concept is realized in some natural catalytic systems, where it is termed "negative catalysis."[12] If the desired process cannot be accelerated sufficiently to insure preference over another fast side-reaction, inhibition of the latter may be the only means by which to foster kinetic selectivity. Another facet of the same principle is realized in the kinetic shielding (dynamic protection) of highly reactive species generated in the interior cavity of helnicarcerand hosts."'' For instance, photolytic decomposition of suitable precursor molecules trapped in the cavity of these encapsulation hosts can furnish exotic molecular species like cyclobutadiene,[14] which are too reactive to survive in free solution but can be observed and studied readily when

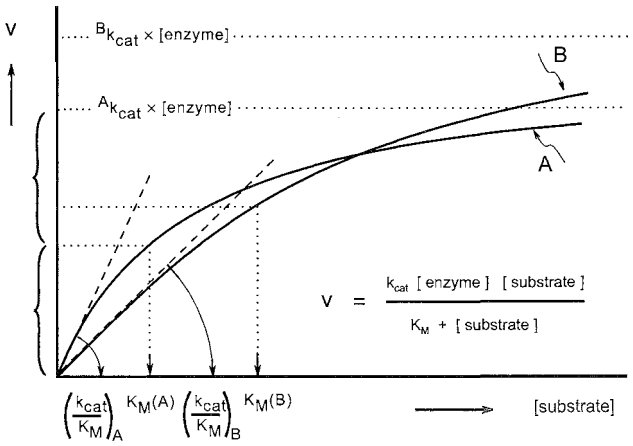

Fig. 3 Michaelis–Menten enzyme kinetics. Rate versus concentration profile for two competing substrates A and *B*. both showing simple saturation behavior. The kinetic domains are defined relative to the respective Michaelis constants K_M that represent the substrate concentrations at which just one half of the maximal rate is reached.

protected from attack from potential reaction partners behind the walls of the molecular cage. Control experiments that address the porosity of the cage can confirm that the elongated lifetime of the encapsulated species is a consequence of kinetically selective shielding rather than due to ground-state stabilization contributed by the host–guest interaction.

The most prominent example in observing kinetic selectivity is enzymatic catalysis. By definition, catalysis is a kinetic phenomenon, and though the origin of enzymic catalysis at present is not totally lucid and is still under vivid debate, it is undisputed that it mandatorily relies on the formation of a molecular complex (the so-called Michaelis complex) that determines the further fate and rate of conversion of the substrate. If it were for this fact only, it would be justified to describe enzymic catalysis as a process that provides an alternative mechanistic pathway from starting materials to products, however, with a lower activation barrier than in the uncatalyzed reaction. As a consequence of the formation of Michaelis complexes of the two competing substrates A and *B* and on the basis of fundamental Michaelis–Menten enzyme kinetics that describes the typical nonlinear rate versus concentration profile (saturation kinetics). by a hyperbolic function (Fig. 3), two kinetic regimes must be distinguished. The first can be described as follows: at high concentration of substrates A or *B*, respectively. the rates become independent of concentration. and the kinetic selectivity approaches the ratio of the unimolecular rate constants $k_{cat}(A)/k_{cat}(B)$, featuring the decomposition of the Michaelis complexes (cf. Fig. 21). Second. conversely, at low substrate concentration, the kinetic selectivity is set by the ratio of second-order rate constants $(k_{cat}/K_M)_A/(k_{cat}/K_M)_B$ representing the slopes of the tangents in the origin in the rate versus the concentration plot of the substrates. Formally, this ratio corresponds to the ratio of bimolecular productive encounter of the substrates with the enzyme molecule on the forward reaction pathway. On the basis of this scheme, it is conceivable that the kinetic selectivity will change with reaction progress (decreasing concentrations) and may even switch its preference. That is why nonlinear effects are commonplace and are regularly observed in applications that involve molecular complexes, e.g., in kinetic asymmetric inductions or dynamic racemate resolutions.[""] In spite of these complications, the kinetic selectivity can reach exorbitant values. In the enzymatic interconversion of lactate and pyruvate using lactate dehydrogenase and the coenzyme NAD, the enantiodifferentiation of the prochiral faces of the nicotinamide ring of the coenzyme is stereospecifically reliable to an error of 1 in 5×10^7 turnovers,[16] corresponding to an enantiomeric excess of L-lactate formation of about 99.999994.

Kinetic selectivity is profitably engaged in instances where high fidelity in the selective outcome must be guaranteed at reasonable speed. In the biological context. the transmission of genetic information from one generation to the next, i.e., replication of the genome,[17] or in another example, the translation of the base sequence of messenger RNA into the primary sequence of amino acids of a growing peptide strand,[18,19] provide well-studied cases. In either case, it is the kinetic distribution of a high-energy intermediate between hydrolysis and incorporation into the growing biopolymer chain that allows, e.g., in replication, the intrinsic thermodynamic selectivity of base pairing (A-T versus A-C $\sim 1{:}10^4$) to elevate to the required $1{:}10^8$ fidelity ratio mandated by prokaryotic survival. Nature set up a kinetic editing mechanism in DNA polymerase that double-checks the incorporation of the correct base that is complementary to the one in the parent strand of the duplex. Editing involves the kinetic interplay of an initial ligating step that attaches the incoming nucleotide according to the Watson–Crick rules of base complementarity and a subsequent step of its hydrolytic expulsion. If a less well-fitting nucleotide is adventitiously incorporated, an exonuclease activity inherent in DNA polymerase cleaves the misincorporated nucleotide off again, opening another chance for correct elongation of the duplex. The hydrolytic exonuclease action is not specific, and in order to avoid any erroneous incorporation. part of the correctly ligated nucleotides is also cleaved. Proofreading of the copied message as described is costly for the organism, because phosphate ester linkages are destroyed that were introduced at the expense of high-energy triphosphates and because part of the correctly formed sequence is eradicated. The formal analysis reveals that selectivity increases only if a substantial cost in erroneously excised bases is tolerated. In the concrete case of *Escherichia coli*, an enhancement of the fidelity of correct base pairing by a factor of 10^3–10^4 requires about 10% of all correctly incorporated nucleotides to be excised again in the editing step.[20]

In biological systems, kinetic schemes for selectivity augmentation are widespread but are usually built upon highly sophisticated interwoven reaction networks. Naturally, this finding obviates easy adaptation and implementation into abiotic mimicks. though the principles seem clear. and attractive applications to artificial chemical flux systems are readily envisaged.

CONCLUSION

The diversity around us, including the biological world (life), emerges from and depends on the ability to distinguish and exploit alternatives (selectivity). This discriminative process can rest on the energetic differences in thermodynamically definable and thus time-invariant states representing. however, in many cases, a

crude abstraction of the real situation in which the selectivity is expressed. Owing to the projection of reality onto the panel of concepts offered by current thermodynamic theory and to the. at times, unscrupulous introduction of framing conditions as well as to the simple omission of as yet untreatable factors (e.g., entropy), rudimentary understanding and even prediction of selective behavior is possible. The results of thermodynamic selectivity are especially helpful for the purposive destruction of selective function as demonstrated by the undisputable success of tailored drug–receptor bonding.

Even more demanding is the comprehension of kinetic selectivity, because here the appreciation of energetic differences at multiple stages along competing functional pathways is required. Additional obstacles arise from the fuzzy and experimentally hard-to-define nature of transition-state structures in chemical conversions or other functional processes that need to be correlated with the energetic profiles. Minute misassignments there can easily ruin all attempts aimed at informed design. It is not clear at present whether just one model structure chosen to picture a particular position of the profile can be taken as a reliable representation of the ensemble of actually populated states.

Beyond doubt, we are making progress in unfolding the subtleties of selectivity generation, yet we have not reached the position at which to decide whether a deeper understanding of selectivity of either type expressed in condensed phases is open to encompassing reductionistic analysis.

ACKNOWLEDGMENT

The long-lasting and continuing support of our supramolecular research activities by Hans–Fischer–Gesellschaft, Muenchen. is gratefully acknowledged.

ARTICLES OF FURTHER INTEREST

Artificial Enzymes, p. *76*
Enzyme Mimics: p. *546*
Induced Fit, p. *717*
The Lock and Key Principle, p. *809*
Preorganization and Complementarity, p. *1158*

REFERENCES

1. Janin. J. Quantifying biological specificity: The statistical mechanics of molecular recognition. Proteins 1996. *25*, 438–445.
2. Lichtenthaler. F.W. 100 Years ''Schlüssel–Schloss–Prinzip'': What made Emil Fischer use this analogy? Angew. Chem., Int. Ed. Engl. 1994. 33. 2363–2374.
3. Mammen, M.: Chio. S.-K.: Whitesides. G.M. Polyvalent interactions in biological systems: Implications for design and use of multivalent ligands and inhibitors. Angew. Chem.. Int. Ed. Engl. 1998. 37, 2755–2793.
4. Rao. J.: Lahiri, J.; Isaacs, L.; Weis, R.M.: Whitesides. G.M. A trivalent system from vancomycin-D-Ala-D-Ala with higher affinity than avidin–biotin. Science 1998, *280*. 708–711.
5. Di Cera, E. Site-specific thermodynamics: Understanding cooperativity in molecular recognition. Chem. Rev. 1998, *98*. 1563–1591.
6. Vysotsky. M.O.; Thondorf, I.; Boehmer, V. Hydrogen bonded calixarene capsules kinetically stable in DMSO. Chem. Cornmun. 2001. 1890–1891.
7. Boehmer. V.; Shivanyuk, A. Calixarenes in self-assembly phenomena. Calixarenes in Action 2000, 203–240.
8. Shivanyuk, A.; Rebek, J., Jr. Hydrogen-bonded capsules in polar. protic solvents. Chem. Commun. 2001, 2374–2375.
9. Thompson, T.N. Early ADME in support of drug discovery: The role of metabolic stability studies. Current Drug Metabolism 2000. 1. 215–241.
10. Dunitz, J.D. Win some. lose some: Enthalpy–entropy compensation in weak intermolecular interactions. Chern. Biol. 1995. 2. 709–712.
11. Calderone, C.T.: Williams, D.H. An enthalpic component in cooperativity: The relationship between enthalpy, entropy and noncovalent structure in weak associations. J. Am. Chem. Soc. 2001. *123*. 6262–6267.
12. Retey, J. Reaction selectivity of enzymes through negative catalysis or how enzymes work with highly reactive intermediates. Angew. Chem. 1990. *102*. 373–379.
13. Warmuth, R.: Yoon, J. Recent highlights in hernicarcerand chemistry. Acc. Chem. Res. 2001. 34, 95–105.
14. Cram, D.J.: Tanner. M.E.; Thomas, R. The taming of cyclobutadiene. Angew. Chem.. Int. Ed. Engl. 1991, *30*. 1024–1027.
15. Kagan. H.B. Nonlinear effects in asymmetric catalysis: A personal account. Synlett 2001, 888–899. Spec. Issue.
16. Anderson, V.E.; LaReau, R.D. Hydride transfer catalyzed by lactate dehydrogenase displays absolute stereospecificity at C4 of the nicotinamide ring. J. Am. Chem. Soc. 1988. *110*, 3695–3697.
17. Fersht. A.R. *Structure and Mechanism in Protein Science;* Freeman: New York, 1999; 377.
18. Cramer. F.: Freist. W. Molecular recognition by energy dissipation, a new enzymatic principle: The example isoleucine–valine. Acc. Chem. Res. 1987. *20*. 79–84.
19. Freist, W.; Sternbach, H.: Pardowitz. I.; Cramer. F. Accuracy of protein biosynthesis: Quasi-species nature of proteins and possibility of error catastrophes. J. Theor. Biol. 1998. *193*. 19–38.
20. Fersht. A.R.: Knill-Jones, J.W.: Tsui. W.-C. Kinetic basis of spontaneous mutation. Misinsertion frequencies, proofreading specificities and cost of proofreading by DNA polymerases of *Escherichin coli*. J. Mol. Biol. 1982. *156*, 37–51.

Self-Assembling Capsules

Dmitry M. Rudkevich
The University of Texas at Arlington, Arlington, Texas, U.S.A.

INTRODUCTION

Self-assembly is the spontaneous. noncovalent association of two or more molecules under equilibrium conditions into stable. well-defined aggregates.[1,2] In nature. self-assembly is a ubiquitous strategy responsible for the formation of cell membranes, double-stranded nucleic acids. and viruses. In chemistry, self-assembly offers a rapid way to construct receptors. catalysts, and materials.''' With appropriate curvature and careful positioning of self-complementary bonding sites. self-assembling systems generate capsules.

That noncovalent dimerization of self-complementary structures may lead to closed surfaces, capable of encapsulating smaller molecules. was initially recognized by Julius Rebek. Jr., a decade ago,[4] while describing the structure of synthetic self-replicator 1 (Fig. I). By definition, self-assembling capsules are receptors with enclosed cavities that are formed through the reversible noncovalent interactions between two or more subunits.[5] Typically. capsules assemble through hydrogen bonding and metal–ligand interactions.[6] Hydrogen bonding is directional and specific. On the other hand. metal–ligand forces are much stronger. and metal–induced assemblies are more robust. At the same time, their strength can be controlled by solvent polarity and pH. Another way to classify capsules is by their dimensions; which vary between 50–1500 A^3.

In this article. we do not intend to cover hundreds of publications on self-assembling capsules. Instead, we will overview the most recognized examples. These frequently appear in original publications. The analysis will be developed on the basis of the increasing complexity of the capsule's structures, which is determined by the capability to form stable and specific molecule-within-molecule aggregates. Subsequently. we will examine unique features of encapsulating complexes that make them so attractive and promising for chemists.

VARIETY OF CAPSULES

Early generations of self-assembling capsules include Rebek's sports balls (Fig 1) The ''tennis ball' 2 assembles via eight C═O H—N hydrogen bonds between the self-complementary glycoluril NH and C═O groups [7] The inner volume of 2 is -50 A', which allows for the encapsulation of small molecules such as CH_4, C_2H_6, and Noble gases. Larger bisglycoluril-containing balls possess extended spacers and are capable of encapsulating two benzene-sized molecules. For example, the enclosed cavity of the ''softball'' 3 is ~ 300 $Å^3$.[8]

Typical molecular complexes depend on stereoelectronic complementarity between receptor and substrate. They are held together by hydrogen bonding: metal–ligand attractions; ion–ion; ion–dipole. CH–π, and π–π interactions; and van der Waals and solvophobic forces. In contrast. self-assembling capsules rely on so-called constrictive binding: the stability of these complexes is mostly provided not through the intrinsic host–guest attraction but through mechanical inhibition of the decomplexation process. In other words, encapsulation is influenced by energetic barriers for the guest exchange. The guest's size and its shape reflect the binding ability of the hosts. In the absence of additional intermolecular forces, recognition-through-encapsulation is largely determined by host and guest volumes. An extensive analysis of occupancy factors, or packing coefficients, of molecule-within-molecule complexes in solution gave the optimal value of 55% occupancy.[9] This is believed to also be a feature of natural biological cavities such as of enzymes. Importantly. the encapsulation takes place under subtle control. because the capsule's formation-dissipation occurs under equilibrium conditions. Capsules form reversibly on time scales of 10^{-3}–10^3 s. in between diffusion complexes (-10^{-10} s) and carceplexes ($\sim 10^{10}$ s).[5,6]

Dimeric calix[4]arene tetraurea capsules **4**, which arrived shortly after the sports balls. are probably the most studied to date.[10] Noteworthy. calixarenes and their relatives had a great impact in the history of self-assembling capsules. Their rigid, concave surface, commercial availability. and rich synthetic chemistry have made them extremely popular platforms for elaboration. In this article. we will have more examples of calixarene-based capsules. In dimers 4. a seam of 16 intermolecular C═O···H—N hydrogen bonds at the upper rim is formed. Eight urea moieties. four from each hemisphere. assemble head-to-tail. as shown in Fig. 2. This results in a rigid cavity of -200 $Å^3$, which can accommodate a benzene-sized guest molecule. The encapsulated guest exchange is slow on the NMR time scale. Experimentally. capsules 4

Encyclopedia of Supramolecular Chemistry
DOI: 10.1081/E-ESMC 120012777

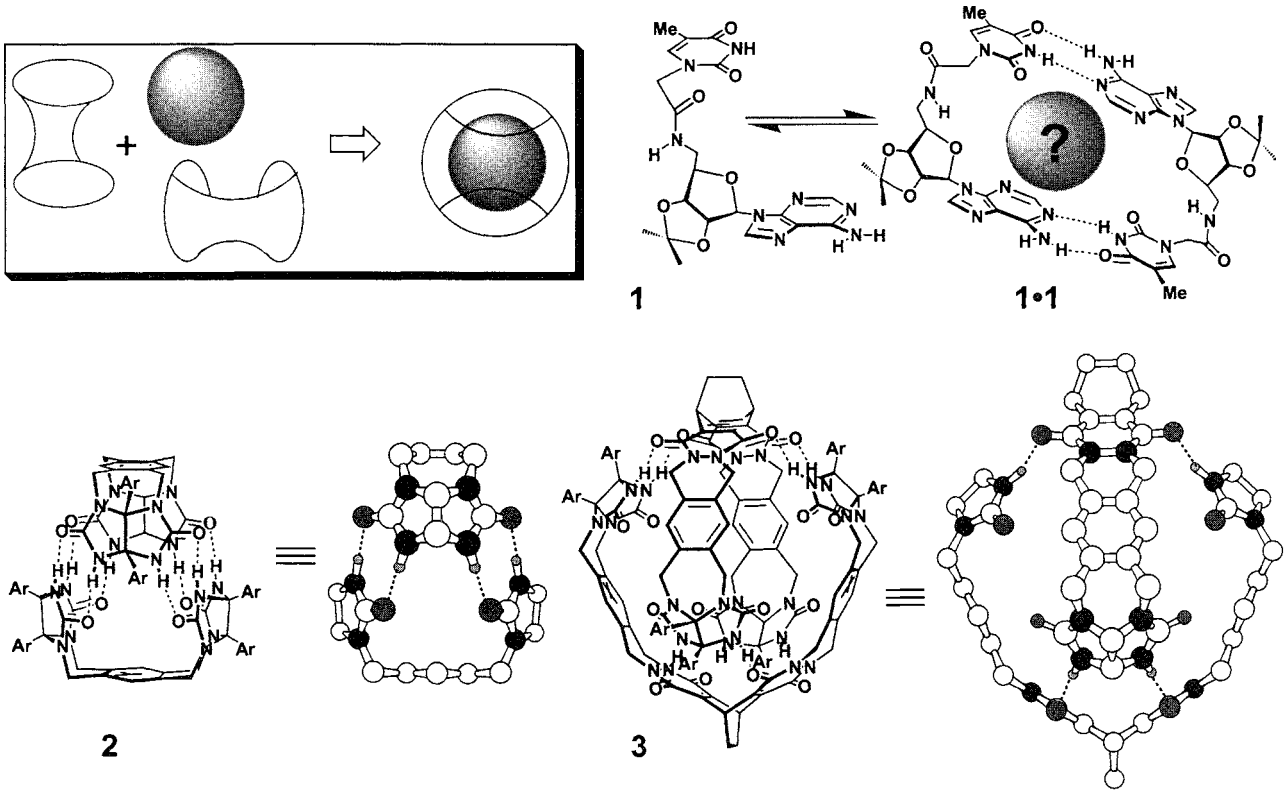

Fig. 1 Capsule formation and early examples of Rebek's self-assembling capsules: self-replicating dimer 1·1, the tennis ball 2. and the softball 3.

include benzene, toluene; halobenzenes, and polycyclic aliphatics (e.g., camphor derivatives, 3-methylcyclopentanone). The encapsulated benzene molecule. for example, is observed at -4 ppm in deuterated p-xylene. For the encapsulated fluorobenzene, the CH protons are seen between 5.5 and 3 ppm and the para- and ortho-hydrogens are separated by more than $\Delta\delta=2$ ppm. Encapsulated aliphatic guests are seen upfield of 0 ppm. From nuclear Overhauser effect spectroscopy (NOESY) experiments with the lower-symmetry capsule 4, a rate constant for the benzene exchange of $0.47\pm0.1\ s^{-1}$ was obtained.[11] The guest exchange time can, however, be significantly prolonged by introducing sterically bulky substituents (e.g., 2.6-diisopropylphenyl; 3,5-di-*t*-butylphenyl; trityl; p-tritylphenyl) to the urea moieties.[12] Some of these capsules are stable even in polar solvents.

When two different calixarene tetraureas are mixed together. heterodimers form along with the corresponding homodimers.[13] From a mixture of tetraurea and tetrasulfonyl urea. heterodimers form exclusively.[14] The increased acidity of the $-SO_2NH$ urea proton may be the reason for such selection. The preference of the aryl urea/sulfonyl urea could possibly be the basis of a binary molecular code.

Electrospray ionization mass spectrometry (ESI MS) was successfully used to characterize capsules **2**–**4** in solution and in the gas phase. Ion labeling in this case was achieved through the encapsulation of quaternary ammonium ions in $CHCl_3$.

Larger capsules entrap more than one guest. Self-complementary cyclic tetraimides built up on the resorcinarene platform and dimerize through hydrogen bonding into cylindrical capsule **5**.[15] Its estimated internal volume is 460 Å^3, and the internal dimensions are 6 x 15 Å (Fig. 2). In deuterated mesitylene, which is too bulky to fit inside, capsule 5 dissociates. but the addition of benzene or toluene immediately results in complex **5**·2Guest; two benzene or toluene molecules were quantitatively encapsulated inside 5 (^{1}H-NMR). The complexes are kinetically stable at ambient temperatures, and the encapsulation processes are slow on the NMR time scale. capsule 5 was used to entrap such useful chemical reagents as dicyclohexylcarbodiimide (DCC) and dibenzoyl peroxide (DBPO). Chemical stability of DCC and DBPO complexed inside capsule **5** was greatly improved. For example, inside the capsule, DBPO is stable for at least 3 days at 70°C in mesitylene-d_{12} solution, while in the absence of **5**, it decomposes within 3 h under those

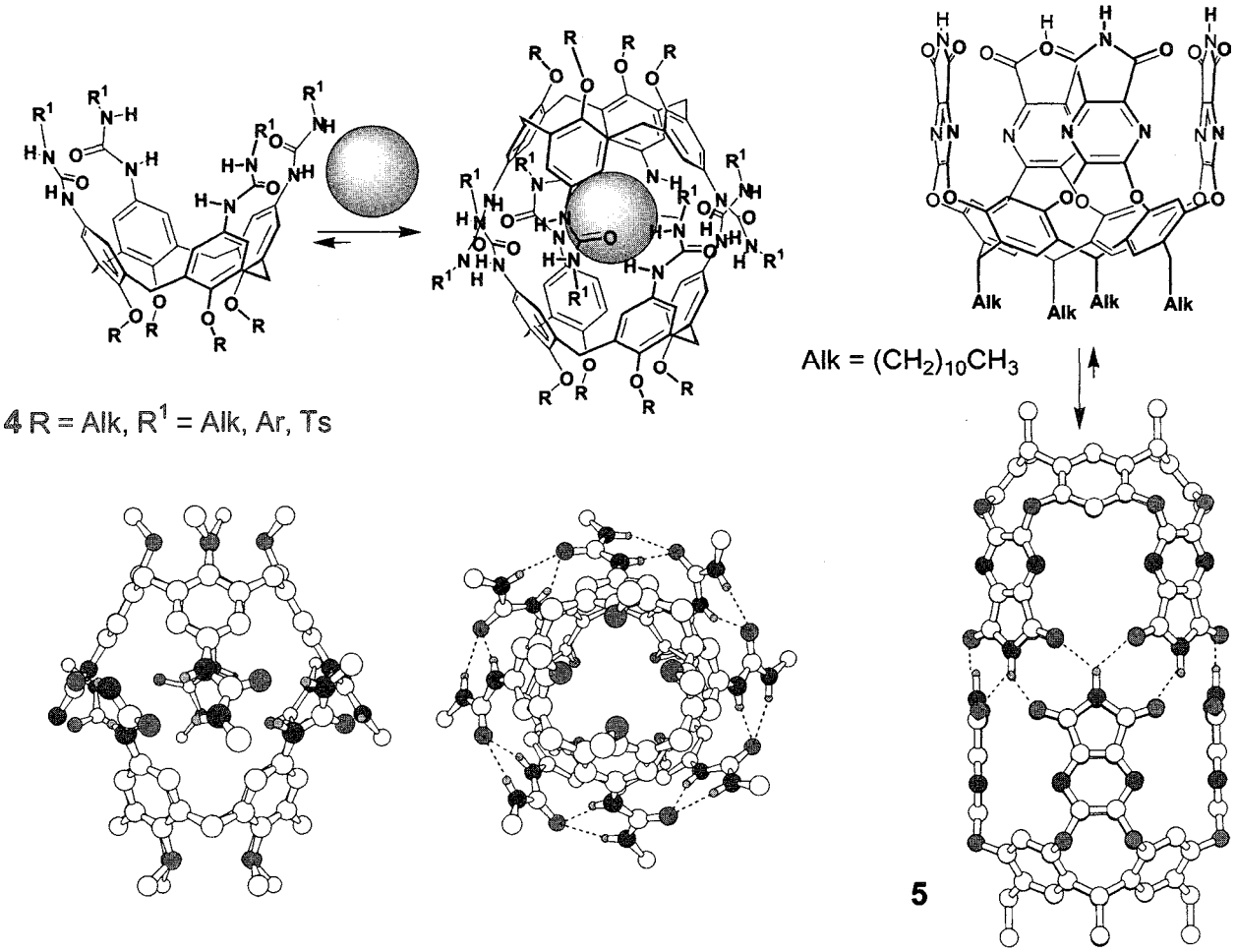

Fig. 2 Left: calix[4]arene tetraurea dimers 4. with the X-ray structure: Right: cylindrical capsule **5** and its computer-generated molecular model.

conditions. Due to the reversible nature of the hydrogen bonds stitching 5. competitive guest molecules or polar solvents can release the encapsulated DCC and DBPO.

Metal-induced capsular self-assembly **6** (Fig. 3) of two deep. resorcinarene-based cavitands was described by Dalcanale and coworkers.[16] Two tetracyanocavitands were connected through four square-planar Pd(II) or Pt(II) entities in CH_2Cl_2, $CHCl_3$, and acetone. Evidence of encapsulation of one triflate anion upon dimerization was obtained (^{19}F-NMR, x-ray analysis). For the Pt(II) case, the assembly process was shown to be reversible: Et_3N dissociated the capsule 6. while the addition of trifluoroacetic acid restored it.

Examples of Co(II) and Fe(II)[17] resorcinarene-based cages **7** came from the group of Harrison (Fig. 3). These are water-soluble and formed by combining $CoCl_2$ or $FeCl_2$ in aqueous solution at pH > 5 with the cavitand, functionalized with four iminodiacetic acid moieties. Upon synthesis, six water molecules initially occupy the inner cavity. When the appropriate guest molecule is present in the reaction mixture; it usually goes inside, replacing the water. Benzenes, halobenzenes. chlorinated hydrocarbons, (cyclo)alkanes, and alcohols were thus trapped in aqueous solution. Due to the paramagnetic nature, these complexes may act as NMR shift reagents, as they cause substantial upfield isotropic hydrogen shifts ($\Delta\delta = 25 - 40$) in the guest molecules with a signal separation of $\delta - 12$ ppm. At lower pH, the Iigand becomes protonated, the metal ion is no longer coordinated to the cavitand, and the assembly falls apart.

Fujita and coworkers elegantly combined triangular azaheterocyclic ligands with cis-protected square-planar Pd and Pt entities into highly symmetric capsules 8 and **9**.[18] The positively charged metal centers provided with water solubility on these capsules, and their hydrophobic interiors were able to accommodate a wide variety of organic guests. In capsule 8, Pd- or Pt-atoms occupy each corner of an octahedron. formed by four *tris*(4-pyridyl)

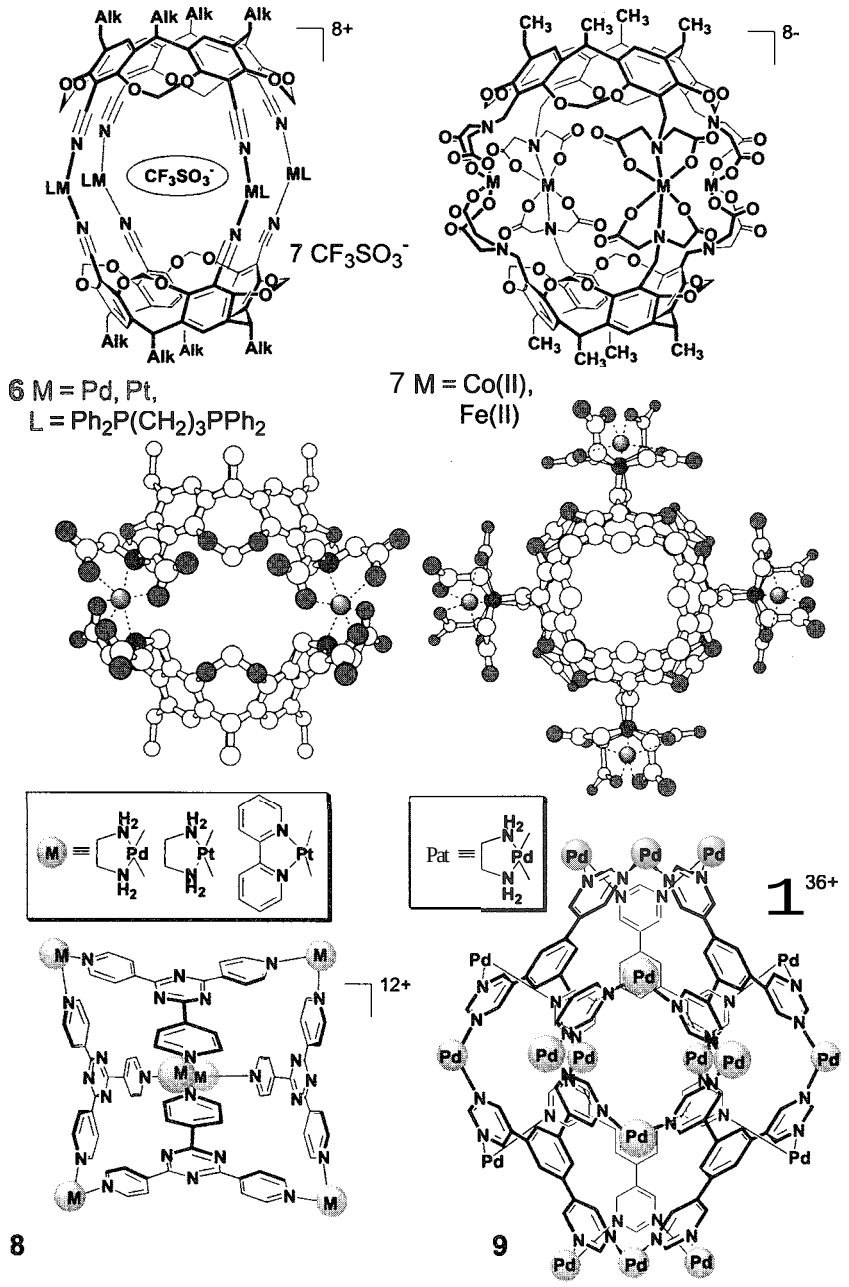

Fig. 3 Metallocapsules 6 and **7** and the x-ray structure of 7 [M=Co(II)]. Below: Fujita's self-assembling cages 8 and 9.

triazine molecules, with the longest metal–metal separation of 19 Å and the internal volume of ~500 $Å^3$ (Fig. *3*). The Pt-based assembly **8** is remarkably stable, even in HNO_3 and aqueous K_2CO_3. Cavities 8 are large enough to encapsulate four guests with the size of adamantane. two cis-azobenzenes, or two cis-stylbenes. Mixing six *tris*(pyrimidyl)benzenes with I8 Pd-complexes resulted in spectacular hexahedral capsule 9. Unlike 8. each face of the hexahedral capsule **9** is completely enclosed by the planar threefold-symmetric ligands (Fig. *3*). The volume of the inner cavity is considerably larger and ~900 Å. This means that guests like C_{60} can easily fit inside. However, only water or oxygen molecules may pass through the narrow pores (2×2 Å) in the structure.

By similar design, homooxacalix[3]arenes bearing 4-pyridyl groups at the upper rim form dimeric capsule **10** with $Pd(II)(Ph_2P(CH_2)_3PPh_2)(OTf)_2$ in a 2:3 ratio in dichloromethane[19] ((Fig. 4). A kinetically stable complex between capsule 10 and fullerene C_{60} was detected (^{1}H-

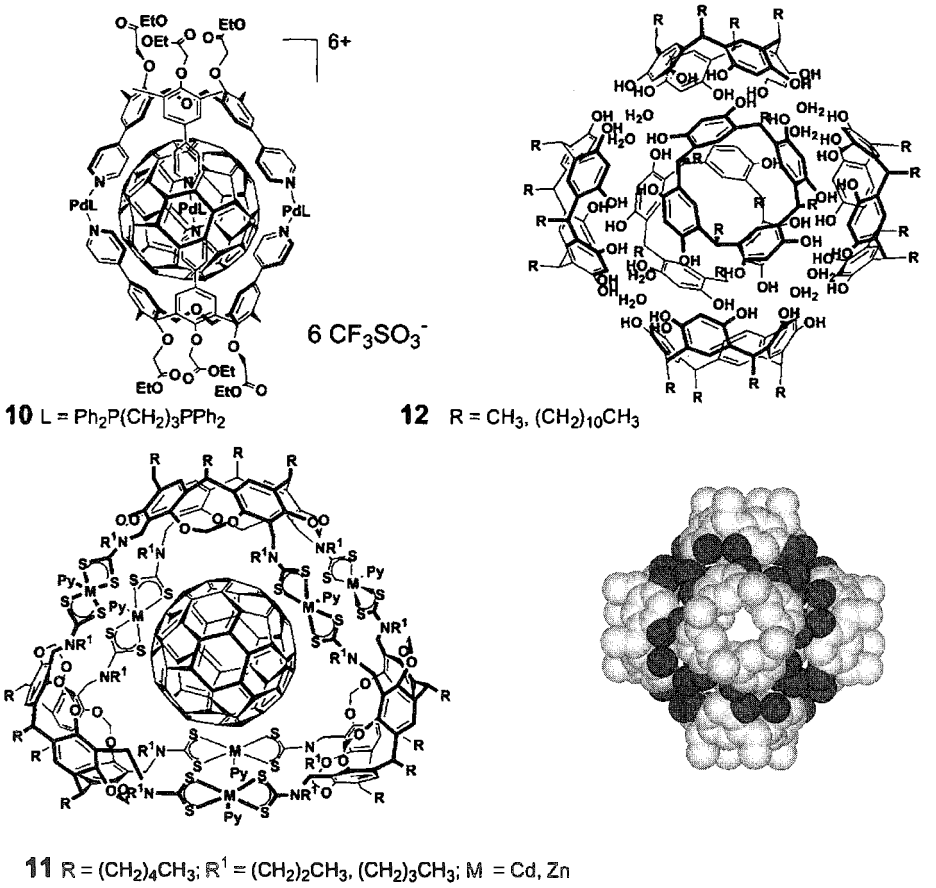

Fig. 4 Self-assembling capsules **10** and **BB** for fullerene entrapment. Atwood's hexamer 12 and its x-ray structure

and ^{13}C-NMR) in $Cl_2CDCDCl_2$; values for the association constant K_{ass} of 39 M^{-1} at 30°C and 54 M^{-1} at 60°C were obtained. Complexation of Li^+ cation at the calixarene lower rims induced their more flattened conformation, and this appeared to be even more suitable for the C_{60} inclusion: the K_{ass} value jumped to 2100 M^{-1} (30°C).

Spectacular trimeric assemblies **11** of cavitands functionalized with four dithiocarbamate units were obtained upon their mixing with Zn(II) and Cd(II) salts in EtOH/H_2O (Fig. 4).[20] In apolar solvents, the ^{1}H-NMR spectra were broad, but the complexes nicely crystallized from pyridine/H_2O; they were characterized by x-ray crystallography. Trimers **11** form stable 1:1 complexes with fullerene C_{60} in benzene and toluene solutions: the logK_{ass} values are within the range 3.5–6 (UV/Vis spectroscopy).

Six molecules of resorcinarene (R=Me or n-undecyl) and eight H_2O molecules self-assemble into a spectacular spherical nanocavity 12 with a diameter of 17.7 Å and an internal volume of ~1375 Å^3.[21] Sixty hydrogen bonds hold the nanocavity together (Fig. 4). In wet $CDCl_3$, hexamer 12 entraps bulky tetraalkylammonium and tetraalkylphosphonium cations.[22] Molecular modeling suggests that 12 is large enough to accommodate even fullerenes or porphyrins.

CAPSULES IN ACTION

The main feature of self-assembling capsules is, obviously: reversibly formed cavities, capable of encapsulating smaller molecules. Small capsules entrap single molecules, and nanosized capsules, for example **12**, may embrace up to a dozen molecules. By design, the motion of encapsulated guests may be restricted, and the guest release may be fast or slow. Chirality of capsules is also an important issue.[6] Even combinatorial libraries of capsules were invented. The level of molecular recognition, achieved within the capsule's interiors, is extremely high. Of particular importance are binary guest selection and the control of chemical reactivity.

The early case of pairwise guest selection through encapsulation was described for cylindrical capsule **5**. When benzene and *p*-xylene were added in a 1:1 ratio to a me-

sitylene-d_{12} solution of capsule 5. an unsymmetrically filled complex formed[23] (Fig. 5*)*. Such pairwise selection of the guests was also observed for benzene with *p*-trifluoromethyltoluene, p-chlorotoluene, 2.5-lutidine, and p-methylbenzyl alcohol to give new species with one of each guest inside. Moreover, capsule **5** exhibits complexation of smaller hydrogen-bonded pairs such as 2-pyridone/2-hydroxypyridine diiner. benzamide and benroic acid dimers, and *trans*-1,2-cyclohexanediol dimers.[15] When equal amounts of $\bar{\alpha}$, $\bar{\beta}$, and $\bar{\gamma}$picolines were added to a mesitylene-d_{12} solution of **5,** in addition to the corresponding homocapsules, nonsymmetrically filled heterocapsules were also formed (^{1}H-NMR).[24]

The idea of multiple guest encapsulation can also be expressed in polymeric self-assembling capsules. When two calix[4]arene tetraureas are covalently linked at their lower rims (see **13**; Fig. 5). hydrogen bonding results in a polymer chain of capsules, or polycaps.[25] The polycaps form only when a guest of proper size and shape is present; in competitive solvents such DMSO or MeOH. the polycaps dissociate. By analogy with parent capsules 4. the formation of heterodimeric systems was explored. Specifically, the polycap rapidly broke down to a dumbbell-shaped assembly when treated with an excess of the simple dimeric capsule (e.g., 4). The dumbbell featured a well-resolved NMR spectrum that showed all of the expected resonances. Combination of aryl- and sulfonylurea biscalixarenes effectively afforded heteromeric polycaps.[14] Monomers **13** were also functionalized with long alkyl groups capable of forming a liquid-like sheath

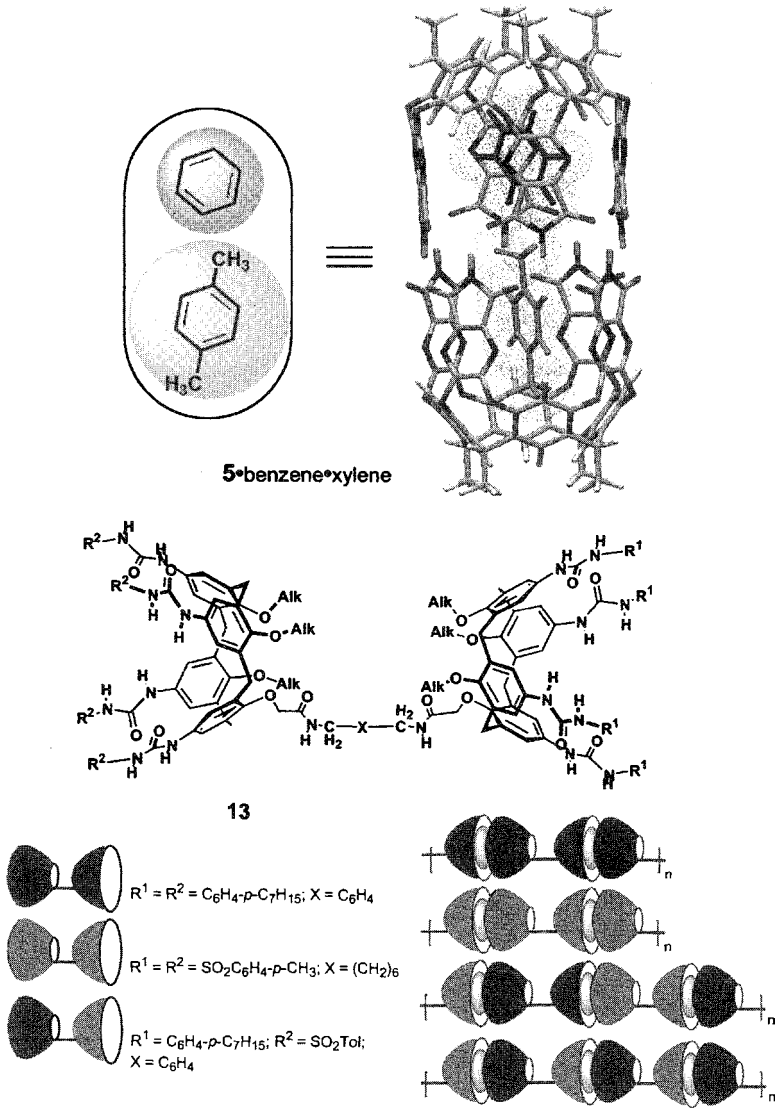

Fig. 5 Top: pairwise selection of guests aithin capsule 5: Bottom: reversibly formed polymeric capsules — Rebek's polycaps.

about them. At high concentrations. the resulting polycaps self-organize into polymeric liquid crystals.

Fujita used his capsules 8 for the stabilization of unfavored conformations. The treatment of an aqueous solution of capsule 8 with a solution of 4,4-dimethylazobenzene (*cis-trans*, 1:6) in hexane resulted in the formation of an unusual complex within the capsule walls:[26] the capsule selectively entrapped two equivalents of the cis-isomer (2D NMR). The cis-azobenzene molecules were stabilized within this encapsulation complex (Fig. 6): exposing the solution to visible light for several weeks did not result in the production of any of the thermodynamically favored *trans*-azobenzene. Most probably: the dimeric hydrophobic guest complex was formed inside the capsule: it is too large to penetrate as is. so it enters as a single species.

Another example of stabilization through encapsulation was demonstrated with capsule **5.** Upon encapsulation within 5. the tertiary anilide, *p*-[*N*-methyl-*N*-(*p*-tolyl)toluamide, is fixed in its *Z*-configuration[27] (Fig. 6). In bulk solution. these anilides exist as mixtures of E- and *Z*-isomers. with the E-configuration favored. The E-isomer, however, cannot fit inside capsule **5,** and its inherent stability is overcome by the CH–π, van der Waals, and dipolar interactions offered by the interior surface of the capsule.

Enclosed cavities in self-assembling capsules can even stabilize labile molecules formed in situ by the reaction of smaller molecular components. Thus, the condensation reaction of trimethoxysilanes in the cavity of 8 led exclusively to cyclic. trirneric silanol **14**, which was never isolated before.[28] In a typical reaction, phenyltrimethoxysilane was suspended in D_2O solution of **4** at 100°C (Fig. 6). After 1 h. the ^{1}H-NMR spectrum showed the exclusive presence of only one complex **8·14**. The formation **8·14** was also evidenced by ESI-MS and single-crystal x-ray crystallography. Not only the cyclic trimers **14** are formed in a "ship-in-a-bottle" fashion. but they were protected

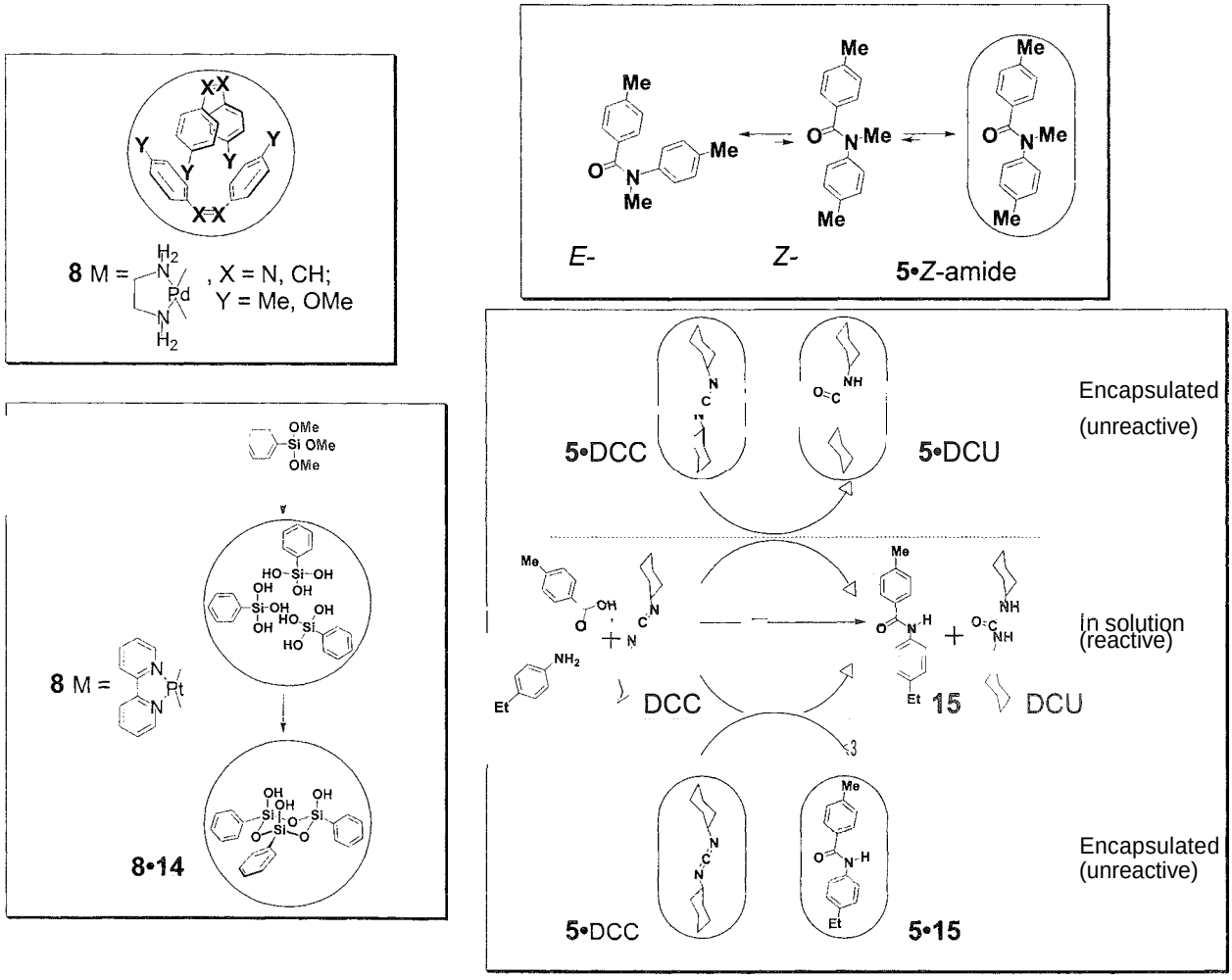

Fig. 6 Capsules in action: examples of stabilization unfavored isomers and controlling chemical reactivity through encapsulation.

by the cavity. They were stable even in acidic aqueous solutions and isolable as pure clatharate compounds.

A recent paper from the Rebek's laboratory offers a novel concept — autocatalysis with encapsulated reagent~.~''When DCC was trapped by capsule 5 (Fig. *6*), reaction between *p*-toluic acid and p-ethylaniline exhibited a complex kinetic behavior. Trace amounts of DCC free in solution proinoted the initial formation of an amide bond between the acid and the amine. The products of this reaction were anilide 15 and dicyclohexylurea *(DCU)*, and both are better guests for capsule 5 than *DCC*. Accordingly, increasing amounts of DCC are displaced from the capsule by emerging 15 and DCU, so the rate of the reaction increases as the reaction proceeds. The kinetics possesses a sigmoidal character. Such nonlinear kinetics can be viewed as an emergent property of the system as a whole. with the partnership of compartmentalization and molecular recognition giving rise to chemical amplification.

CONCLUSION

The impact of self-assembling capsules in chemistry is impressive and fully expected to grow. They already made an enormous inteliectual contribution to the field of molecular recognition, aggressively attacking the problems of intermolecular interactions and generating new supramolecular functions. The 'eversible formation of an enclosed cavity is a spectacular function. The notion of molecular cavities emerged alinost two decades ago, first with cyclodextrins and then with calixarenes and their analogs. The ambitious desire of chemists to have totally synthetic molecules permitting great structural variation; and to control the cavity's size and shape, led to the discovery of exclusive molecular containers — cavitands, carcerands and hemicarcerands, and subsequently, self-assembling capsules.[30] The functions came with cavities — sensing. separation. stabilization. and controlled release of active reagents. In some cases. significant NMR shifts of the entrapped molecules offer the possibility to deduce their structural features ''from inside,'' to determine the orientation of the guests and their interaction with each other and the receptor's interior walls. In principle. such host–guest complexes can be used for structural information/memory storage. Moreover, as two or even more guests are encapsulated. reaction/catalytic chambers can be envisioned. In biocheinistry and molecular biology. capsules are aiming at drug encapsulation, drug active transport through the cell membranes. and drug delivery. Approaches toward water-soluble assembling cavities and capsule-based polymeric materials were introduced. Construction of novel architectures will offer even wider perspectives.

ARTICLES OF FURTHER INTEREST

Anion-Directed Assembly, p. *51*
Calixarenes and Their Analogues: Molecular Complexation. p. *145*
Carcerands and Hemicarcerands, p. *189*
Cryptophanes, p. *340*
Glycoluril-Based Hosts. p. *597*
Hydrogen Bonding, p. *658*
Micelles and Vesicles. p. *861*
Molecular Squares, Boxes, and Cubes, p. *909*
Platonic and Archimedean Solids. p. 1100
Self-Assembly: Definition and Kinetic and Thermodynamic Considerations. p. *1248*
Self-Assembly: Terminology, p. *1263*
Soft and Smart Materials, p. *1302*

REFERENCES

1. Whitesides. G.M.; Grzybowski, B. Self-assembly at all scales. Science *2002.* 295 (5564). 2418–2421.
2. Philp. D.: Stoddart, J.F. Self-assembly in natural and unnatural systems. Angew. Chem., Int. Ed. Engl. 1996. *35* (11). 1155–1196.
3. Prins. L.J.; Reinhoudt, D.N.: Timmerman, P. Noncovalent synthesis using hydrogen bonding. Angew. Chem., Int. Ed. *2001. 40* (13). 2382 -2426.
4. Feng. Q.; Park. T.K.: Xebek, J.. Jr. Crossover reactions between synthetic replicators yield active and inactive recombinants. Science 1992. *256* (5060). 1179–1180.
5. Conn. M.M.; Rebek. J.. Jr. Self-assembling capsules. Chem. Rev. 1997. *97* (5). 1647–1668.
6. Hof. F.: Craig. S.L.; Nuckolls. C.: Rebek, J.. Jr. Molecular encapsulation. Angew. Chem., Int. Ed. *2002.41* (9). 1488–1508.
7. Branda. N.: Wyler. R.: Rebek. J.. Jr. Encapsulation of methane and other small molecules in a self-assembling superstructure. Science 1994. *263 (*5151). 1267–1268.
8. Meissner, R.S.; Rebek. J.. Jr.: de Mendoza. J. Autoencapsulation through intermolecular forces: A synthetic self-assembling spherical complex. Science 1995. *270* (5241). 1485–1488.
9. Mecozri. S.: Rebek. J.. Jr. The 55% solution: A formula for molecular recognition in the liquid state. Chem. Eur. J. 1998. 4 (6). 1016–1022.
10. Rebek. J.. Jr. Host–guest chemistry of calixarene capsules. Chem. Commun. 2000. (8). 637–643.
11. Mogck. 0.: Pons. M.; Bohmer. V.: Vogt, W. NMR studies of the reversible dimeriration and guest exchange processes of tetra urea calix[4]arenes using a derivative with lower symmetry. J. Am. Chem. Soc. 1997. *119* (24). 5706–5712.
12. Vysotsky. M.O.; Thondorf. I.: Böhmer. V. Self-assembled hydrogen-bonded dimeric capsules with high kinetic stability. Angew. Chern.. Int. Ed. *2008.39* (7). 1264–1267.
13. Mogck. O.; Bohmer, V.: Vogt. W. Hydrogen bonded homo-

and heterodimers of tetraurea derivatives of calix[4]arenes. Tetrahedron 1996. *52* (25). 8489–8496.

14. Castellano. R.K.: Rebek, J., Jr. Formation of discrete. functional assemblies and informational polymers through the hydrogen-bonding preferences of calixarene aryl and sulfonyl tetraureas. J. Am. Chem. Soc. 1998, *120* (15). 3657–3663.
15. Komer. S.K.; Tucci. F.C.; Rudkevich, D.M.; Heinz. T.: Rebek. J.. Jr. A self-assembled cylindrical capsule: New supramolecular phenomena through encapsulation. Chem. Eur. J. 2000, *6* (1), 187–195.
16. Fochi. F.: Jacopozzi, P.: Wegelius, E.: Rissanen. K.: Cozzini, P.; Marastoni, E.: Fisicaro, E.; Manini. P.; Fokkens, R.: Dalcanale. E. Self-assembly and anion encapsulation properties of cavitand-based coordination cages. J. Am. Chem. Soc. 2001, *123* (31). 7539–7552.
17. Fox. O.D.; Leung, J.F.-Y.; Hunter. J.M.: Dalley, N.K.: Harrison, R.G. Metal-assembled cobalt(II) resorc[4]arene-based cage molecules that reversibly capture organic molecules from water and act as NMR shift reagents. Inorg. Chem. 2000, *39* (4). 783–790.
18. Fujita, M.: Umemoto. K.; Yoshizawa, M.; Fujita, N.: Kusukawa, T.: Biradha. K. Molecular paneling via co-ordination. Chem. Commun. 2001. (6). 509–518.
19. Ikeda. A.; Yoshimura, M.; Udzu, H.: Fukuhara, C.: Shinkai. S. Inclusion of [60]fullerene in a homooxacalix[3]arene-based dimeric capsule cross-linked by a Pd(II)-pyridine interaction. J. Am. Chem. Soc. 1999. *121* (17). 4296–4297.
20. Fox. O.D.; Wilkinson. E.J.S.: Beer. P.D.; Drew, M.G.B. Cadmium- and zinc-directed assembly of nano-sized. resorcarene-based host architectures which strongly bind C_{60}. Chem. Commun. 2000. (5). 391–392.
21. MacGillivray, L.R.: Atwood. J.L. A chiral spherical molecular assembly held together by 60 hydrogen bonds. Nature (Lond.) 1997, *389* (6650), 469–472.
22. Shivanyuk, A.; Rebek, J., Jr. Reversible encapsulation by self-assembling resorcinarene subunits. Proc. Natl. Acad. Sci. U.S.A. 2001. *98* (14), 7662–7665.
23. Heinz, T.; Rudkevich, D.M.; Rebek. J.. Jr. Pairwise selection of guests in a cylindrical molecular capsule of nanometer dimensions. Nature (Lond.) 1998, *394* (6695). 764–766.
24. Tucci. F.C.; Rudkevich, D.M.: Rebek. J., Jr. Stereochemical relationships between encapsulated molecules. J. Am. Chem. Soc. 1999. *121* (20). 4928–4929.
25. Castellano, R.K.; Rudkevich, D.M.; Rebek, J.. Jr. Polycaps: Reversibly formed polymeric capsules. Proc. Natl. Acad. Sci. U.S.A. 1997, *94* (14), 7132–7137.
26. Kusukawa, T.; Fujita. M. "Ship-in-a-bottle" formation of stable hydrophobic dimers of cis-azobenzene and -stilbene derivatives in a self-assembled coordination nanocage. J. Am. Chem. Soc. 1999, *121* (6). 1397--1398.
27. Heinz, T.; Rudkevich, D.M.: Rebek, J., Jr. Molecular recognition within a self-assembled cylindrical host. Angew. Chem., Int. Ed. 1999. *38* (8), 1136–1139.
28. Yoshizawa, M.; Kusukawa, T.: Fujita, M.; Yamaguchi. K. Ship-ill-a-bottle synthesis of otherwise labile cyclic trimers of siloxanes in a self-assembled coordination cage. J. Am. Chem. Soc. 2000. *122* (26), 6311–6312.
29. Chen, J.; Komer. S.; Craig, S.L.; Rudkevich. D.M.; Rebek, J.. Jr. Amplification by compartmentalization. Nature 2002. *415* (6870), 385–386.
30. Rudkevich. D.M. Nanoscale molecular containers. Bull. Chem. Soc. Jpn. 2002, *75* (3). 393–413.

S

Self-Assembling Catenanes

Gerhard F. Swiegers
Junhua Huang
Commonwealth Scientific and Industrial Research Organization (CSIRO), Melbourne, Victoria, Australia

INTRODUCTION

Perhaps the most challenging class of molecules to synthesize using classical organic chemistry is the intertwined species known as catenanes. Catenanes involve two or more cyclic molecular strands that are mechanically interlocked with each other.[1] The resulting attachment is not chemical in nature, although it is created by the formation of chemical linkages. The cycles are instead considered to be "topologically" bound to each other.

The preparation of a catenane involves two processes, each of which is difficult to perform using classical preparative techniques: (i) the formation of cyclic species, and (ii) the interlocking of two or more such species.[2] Because traditional synthetic organic chemistry must rely on statistical chance in high dilution processes to obtain cyclic species, only low yields can generally be obtained. Interlocking steps are similarly unfavorable, so that achieving cyclization and interlocking simultaneously is a challenging exercise.

Self-assembly techniques can, however, be used to favorably skew the probability of these processes taking place and thereby greatly simplify the preparation of catenanes.[3] In such techniques, noncovalent interactions are exploited to favorably dispose the assembly constituents for cycle formation and interlocking, thereby ensuring high-yielding procedures. A wide range of catenanes were obtained using self-assembly processes mediated by complementary n-donor–acceptor-, coordinate-, and hydrogen-bonding interactions, among others.

In this article. a brief and general review of catenanes in terms of their nomenclature, self-assembly, and a few pertinent properties; will be presented. Examples of the concepts discussed were limited to representative transition metal-mediated processes.

NOMENCLATURE

The simplest class of catenane involves two interlocked rings, as depicted in Fig. 1a. Such singly-interlocked species are termed 2-crossing catenanes and are formally given the nomenclature 2-crossing-[*n*]catenane, where *n* indicates the number of interlocked rings.[4] Multiply-interlocked catenanes, such as the doubly-interlocked species shown in Fig. 1b, have also been prepared. Such species are formally named *m*-crossing-[*n*]catenanes, where *m* refers to the number of times one strand crosses the other in traversing its full length.[4] The term "catenane" may be replaced in these terminologies with the term "catenate" or ''metallocatenate''[1,5] to indicate the involvement and presence of metal–ion coordination. Demetallation of a catenate has also been said to produce a catenand.[1]

Various multiring catenanes are known. One class involves several rings interlocked with a single. central ring as depicted in Figs. 1c,d. Such species are termed "molecular necklaces" (MN) and described using the nomenclature [*n*]MN, where *n* refers to the total number of cycles present.[6] The structure in Fig. 1c depicts a [4]MN, while that in Fig. 1d is that of a [5]MN. Two classes of linear oligocatenanes are known. Illustrated in Fig. 1e is the general structure of an [*n*]polycatenane, where *n* refers to the number of cycles present, while depicted in Fig. 1f is a poly-[2]catenane.[7] Sanders and Hamilton describe the former as catenane polymers. that is, polymers created by a series of interlocked rings. The latter are polymers containing [2]catenane structures within their backbones.[7]

SELF-ASSEMBLY OF CATENANES

Two self-assembly techniques are predominantly employed in the preparation of catenanes: "thermodynamic" self-assembly and self-assembly with covalent "modification."

Thermodynamic self-assembly involves the establishment of a dynamic equilibrium between the reagents and products in which catenane structures are energetically highly favored.[3] If such systems are kinetically labile. the products obtained in greatest proportions will be those that are also the most thermodynamically stable: that is. catenane structures. In such processes, thermodynamic influences drive the cyclization and the interlocking steps required in the formation of catenanes. Different types of

Encyclopedia of Supramolecular Chemistry
DOI: 10.1081/E-ESMC 120012778

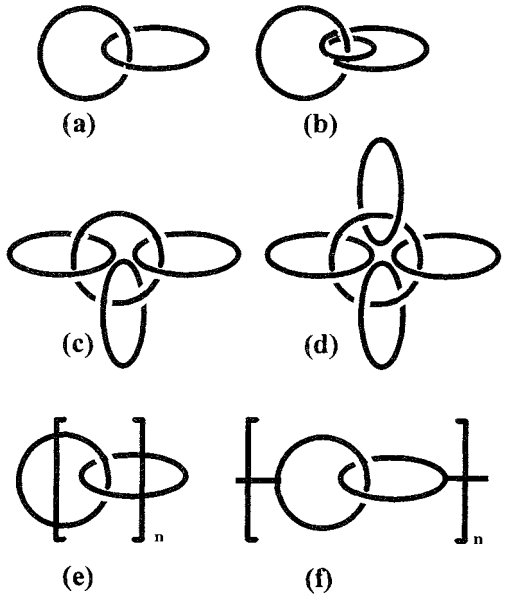

Fig. 1 Catenane structures: (a) a 2-crossing-[2]catenane, (b) a 4-crossing-[2]catenane, (c) a [4]MN, (d) a [5]MN, (e) an [*n*]polycatenane. and (f) a poly[*n*]catenane.

thermodynamic driving forces may: however, be employed for the different steps. For example, the formation of one type of noncovalent interaction may induce interlocking. while the formation of another creates cyclization. Entropy may also be employed to drive one of the steps.[3]

In self-assembly with covalent modification. conventional organic reactions are typically performed on self-assernbled structures in order to lock them into a kinetically stable state."'] For the preparation of catenanes, the self-assembly step is generally used to generate a precursor molecule with a disposition that allows for ready conversion to a kinetically stable catenane structure. The self-assembly step is most often employed to bring about interlocking. giving rotaxane or pseudorotaxane intermediates. These are subsequently converted to catenanes by simple cyclization reactions.

THERMODYNAMICALLY SELF-ASSEMBLED CATENANES

Illustrated in Fig. 2 is one of the most famous examples of a metal-mediated, thermodynamically self-assembled catenane. The reaction of 1 (M = Pd) with the angled bipyridyl ligand 2 was found by Fujita and coworkers to lead to the formation of cycle **3,** along with the interlocked catenane **4.**[5,8] The nature of the self-assembly process was elucidated by the fact that the relative proportions of 3 and 4 could be varied by altering the metal ion employed, the reaction solvent, the concentration of the reagents, and the substituents on the central phenyl moiety in the ligand. Thus. the use of Pt(II) led to the formation of the equivalent metallocycle 3 (M = Pt) but not the spontaneous formation of the catenane 4 (M = Pt). Concentration of an aqueous mixture of 1 and 2 (M = Pd) from 2–50 mM caused the equilibrium to shift strongly in favor of 4. Increased proportions of 4 were also obtained when using D_2O as solvent. Substitution of the central phenyl ring in 2 with fluorine atoms led to cycle 5 (M = Pd), however, no corresponding catenane structure was formed.[5]

While the lability of the Pd—N bonds clearly induced cyclization and allowed interlocking, the interlocking step itself must have been brought about by other influences. The fact that **5** would not interlock with itself, despite the lability of its Pd—N bonds, indicates that π-aromatic donor–acceptor interactions between the phenyl groups on the interlocking species played an important

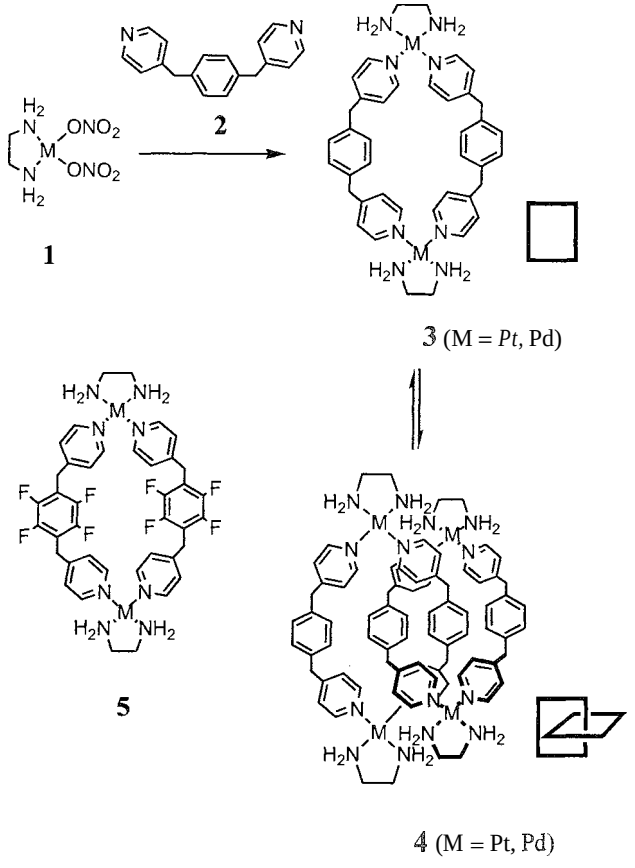

Fig. 2 Thermodynamic self-assembly: Formation of a [2]-catenane. mediated by coordinative and other noncovalent interactions.

role in the formation of catenane 4. The fact that changing the solvent from water to the more polar D_2O increased the proportion of catenane produced indicates that hydrophobic interactions between the central phenyl groups in each iigand also contributed to interlocking. Finally, entropy must also have played a role in the interlocking step, because concentration of the system led to more of the catenane, consistent with the expected response of the equilibrium, as predicted by Le Chatelier's principle.[3] The role of the noncoordinate interactions was to double the free-energy change of the process, allowing quantitative self-assembly of the catenane at high reagent concentrations.[5,8]

The formation of 4, therefore, involved several different noncovalent interactions. The cyclization step was brought about by the formation of Pd—N coordinate bonds; that is, by a metal-mediated process. The interlocking step involved n- and hydrophobic/hydrophilic-mediated processes, along with an entropic effect. Catenane 4 can. therefore, be considered an example of a "'multi-mediated," multiple-interaction self-assembly.[9] Fujita referred to such processes as "double-molecular recognition" procedures, in which the two interlocking molecules bind each other in their cavities.[5,8]

The equivalent reaction with M = Pt is also interesting and informative.[5,8] As noted earlier, the reaction of 2 with 1 (M = Pt) led exclusively to the kinetically inert metallocycle ***3*** (M = Pt). Because Pt—N bonds are inert under normal conditions, the cycle is "locked" in its cyclized state. However, at high temperatures in a concentrated, highly polar medium, the coordination bonds become labilized, allowing interlocking to occur. Thus, the cycle 3 (M = Pt) was spontaneously transformed into 4 (M = Pt) by the addition of $NaNO_3$ with accompanying concentration of the mixture at 100°C. The resulting catenane could then be trapped by dilution and cooling of the mixture. Fujita referred to this procedure as a ''molecular lock," which mimics. on a molecular scale, the interlocking rings trick used by conjurers and magicians.[5,8]

While the simultaneous use of several different classes of noncovalent interactions provides an elegant means of preparing a catenane. such systems are not always easily designed. Another method of thermodynamically self-assembling catenanes involves using two or more metal-mediated interactions to carry out the cyclization and interlocking steps. Illustrated in Figs. 3 and 4 are examples of thermodynamic self-assembly of this type.

In Fig. 3 is depicted the spontaneous self-assembly of the ligand strand 6 with Fe(II) and Ag(I) to give the metallocatenate **7**.[10] Each cycle in 7 may have either *P*- or *M*-helicity, so that 7 is formed as an equal mixture of *meso* (*P*,*M*)- and racemic (*P*,*P*)/(*M*,*M*)-diastereoisomers. In this assembly, the octahedral Fe(II) ion selectively

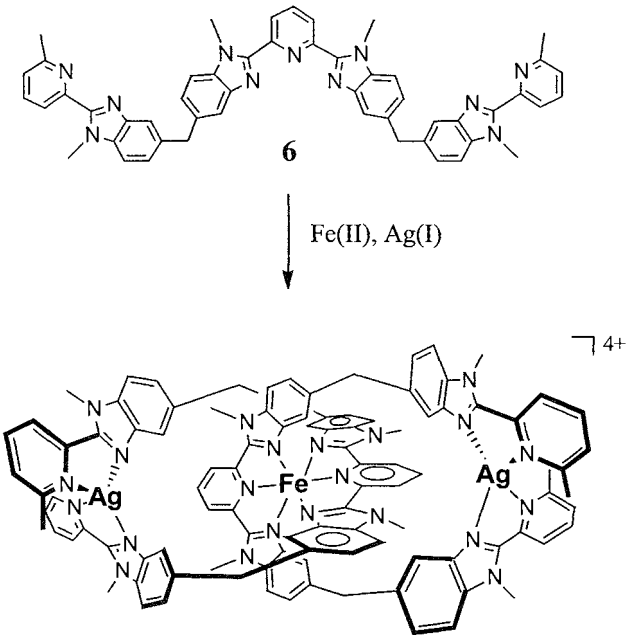

(*P*,*M*)-**7**

(One stereoisomer depicted only)

Fig. 3 Thermodynamic self-assembly: Formation of a [2]catenane, mediated by selective coordinative interactions only.

binds the central binding sites on the ligand, inducing interlocking. Tetrahedral Ag(I) binds the outer binding sites on the ligand, inducing ring closure.[9]

In Fig. 4 is illustrated a similar class of self-assembly. The [2]metallocatenate **11** could be prepared as a mixture of (*P*)- and (*M*)-stereoisomers either by the sequential addition of Cu(I) and Ru(II) to a 1:1 mixture of 8 and **9** (left route) or by the simultaneous addition of Cu(I) and Ru(II) to the mixture of ligands (right route).[11] Because both approaches give **11,** a thermodynamic equilibrium must be present with two self-assembly processes operating. In the one process, Cu(I), which strongly favors tetrahedral four-coordination. selectively interacts with the phenylene sites on the two ligands, generating the interlocked pseudorotaxane **10**. In the other process, Ru(II), which favors octahedral six-coordination. selectively binds the *tris*(pyridyl) sites on 8, causing the arms of this ligand to cyclize. The interlocking step is therefore mediated by Cu(I), and the cyclization step by Ru(II). Because the interlocking and cyclization steps are both metal-mediated, the formation of 7 and **11** are examples of "uni-mediated," multiple-interaction self-assembly.[9]

The system depicted in Fig. 4 illustrates another noteworthy feature of catenane self-assembly; the thermodynamically most stable moiety, which would arguably

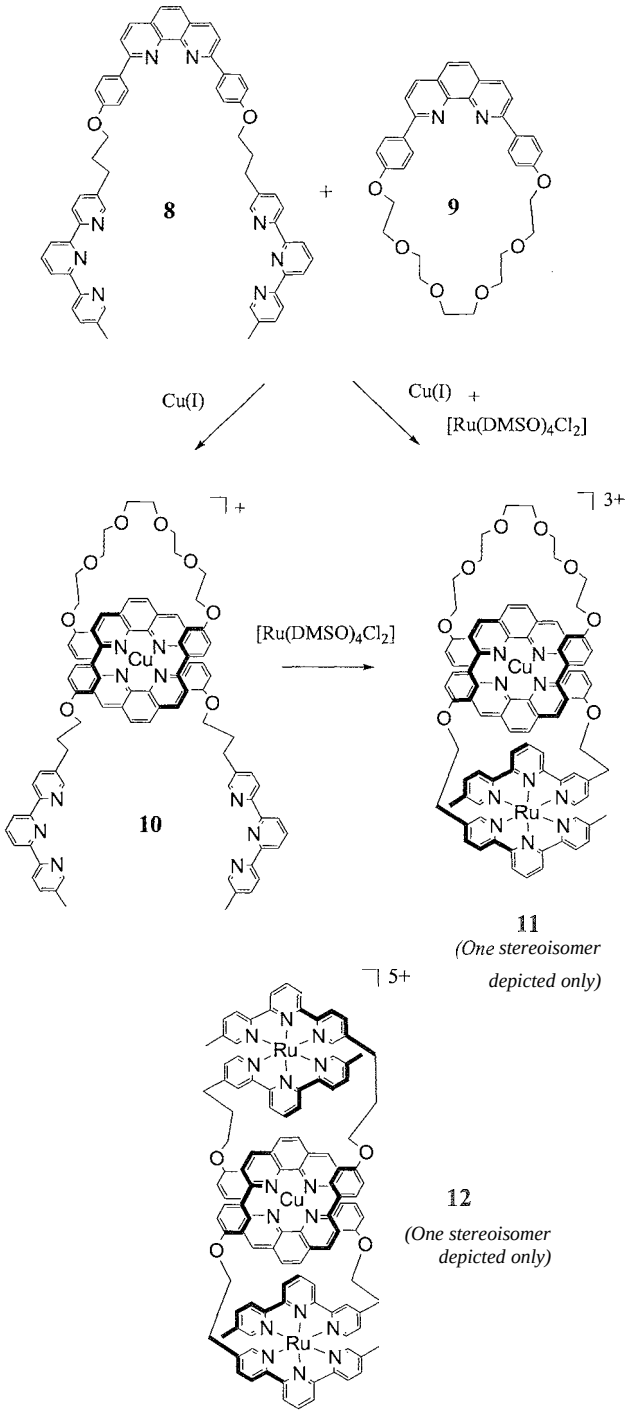

Fig. 4 Thermodynamic self-assembly: Formation of a [2]catenane, mediated by selective coordinative interactions only, in which the therniodynamically most stable moiety is not formed.

be the species 12 in Fig. 4, is not obtained.[77] This is because the stoichiometry of the reaction mixture, which involved a 1:1:1:1 ratio of 8:9:Cu(I):Ru(II), means that the formation of 12 would have to be accompanied by the formation of $[Cu(\mathbf{9})_2]^{2+}$, a species made unstable by the steric hindrance of the polyether linkages in 9 The system, therefore. transformed itself to achieve the greatest overall thermodynamic stability rather than the most stable product per se This result illustrates the usefulness of stoichiometry as a means of manipulating self-assembly processes and the dangers of attempting to predict the products of a thermodynamic self-assembly without considering the other species present

CATENANES PREPARED BY SELF-ASSEMBLY WITH POSTMODIFICATION

Catenanes have also been prepared by performing conventional organic reactions on self-assembled precursor molecules. In such cases. the interlocking step is typically carried out by a self-assembly process. with cyclization then achieved using an organic reaction.

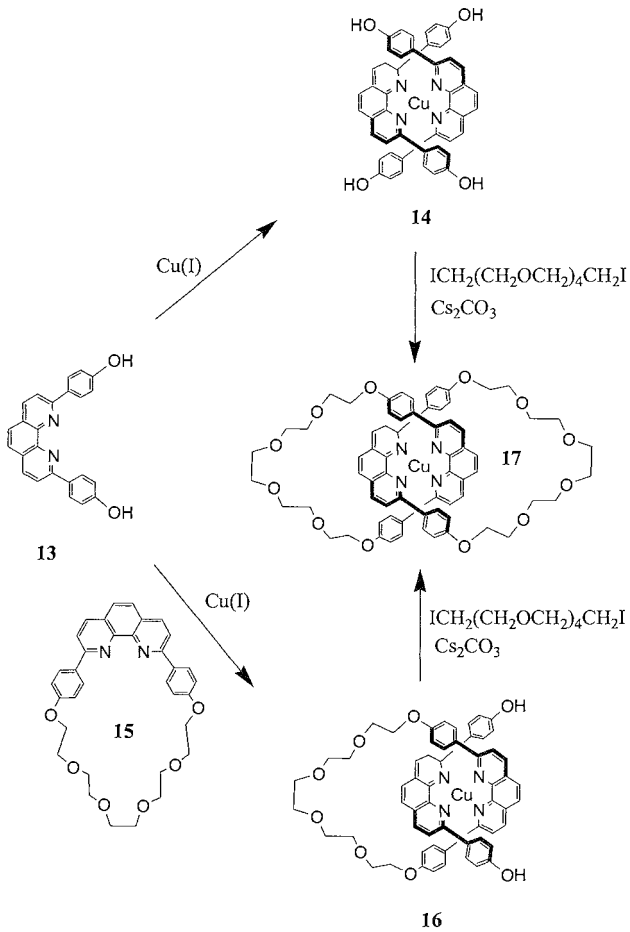

Fig. 5 Self-assembly with postmodification: Preparative routes to a [2]catenane.

Examples of such processes are depicted in Fig. 5 in which the precursor **14**. which is well-disposed for interlocking. and the pseudorotaxane **16** are self-assembled from 13 and Cu(I)/**15**.[13] When treated under high dilution conditions with a suitable polyether diiodide, **14**

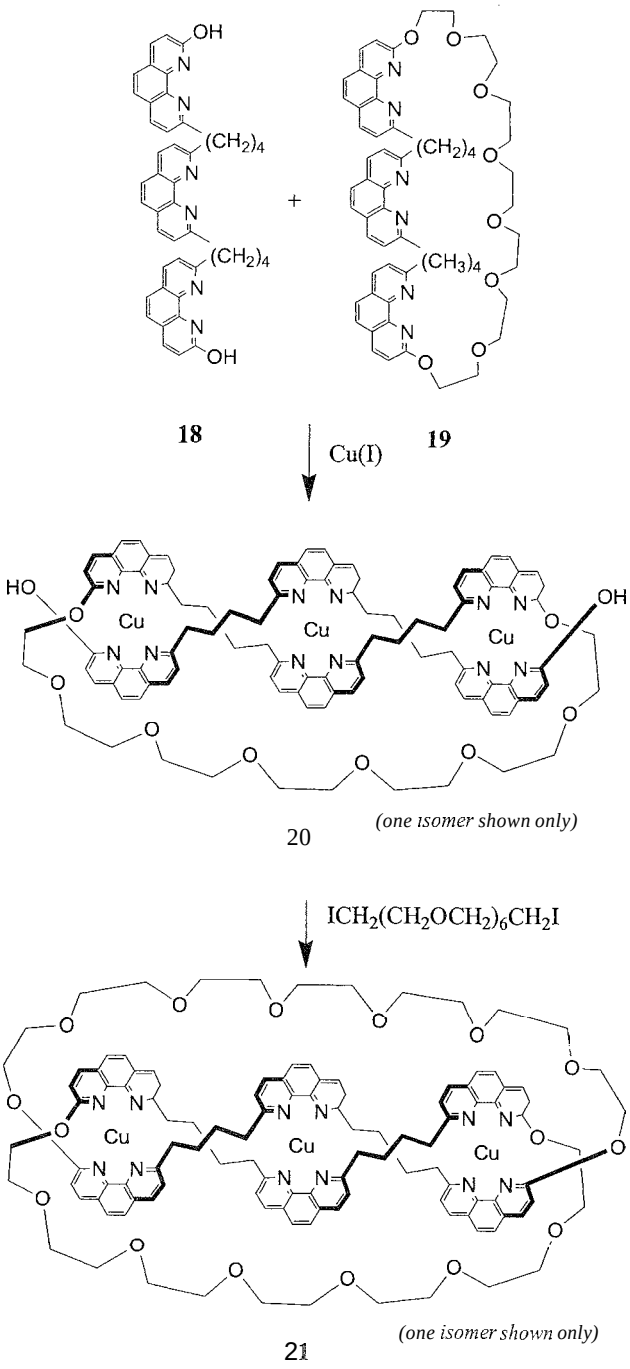

Fig. 6 Self-assembly with postmodification. Preparative routes to a 4-crossing-[2]catenane.

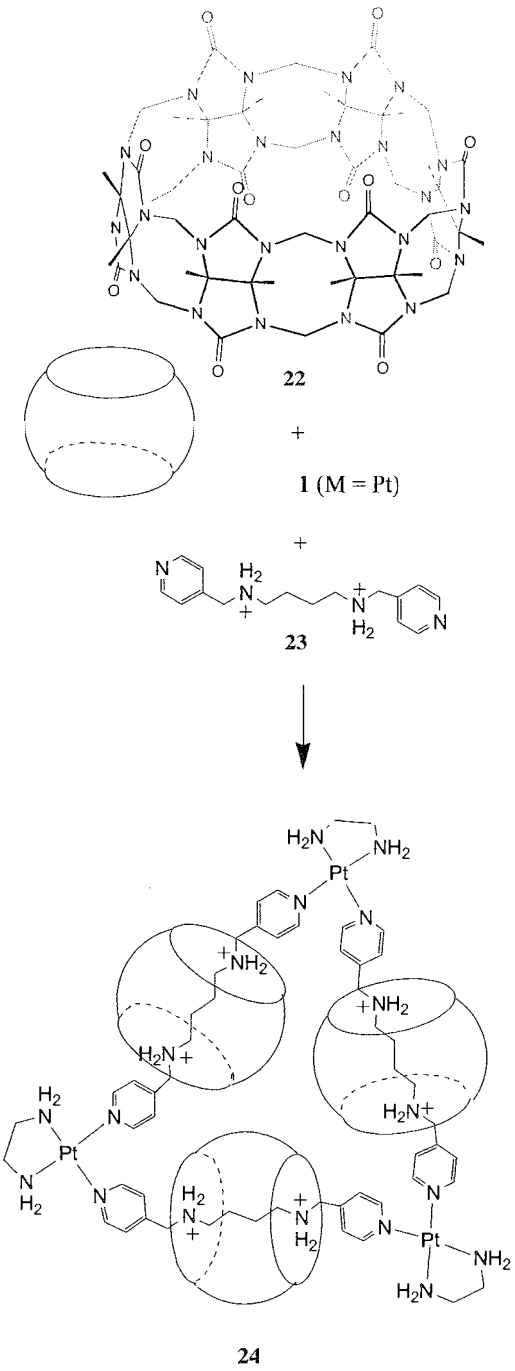

Fig. 7 Thermodynamic self-assembly of multiring catenanes—Molecular necklaces. Formation of a [4]MN, mediated by coordinative and other noncovalent interactions.

or 16 generate the interlocked catenane **17** in 27% yield (top route) or 42% yield (bottom route).[13]

This class of reaction proved particularly useful in the preparation of more complicated intertwined structures.

such as multiple crossing catenanes and molecular knots. Depicted in Fig. 6 is the formation of a 4-crossing-[2]catenane as described by Sauvage and coworkers.[14] The reaction of the tritopic ligands 18 and 19 with Cu(I) generates the double-helical complex 20, as well as its corresponding side-by-side complex (not shown in Fig. 6). When *20* is cyclized, by treatment with an equivalent polyether diiodide under high dilution conditions, it produces the 4-crossing-[2]catenane 21. Demetallization of 21 produces the equivalent, Cu-free catenand. Both 21 and its corresponding catenand are chiral thanks to the helicity of the precursor 20.

MULTIRINGED CATENANES

A range of multiringed catenanes have been prepared. One class of such molecules contain multicyclic cores.[15] Somewhat simpler species involve a single-ring core and are termed molecular necklaces (MN).[6] Depicted in

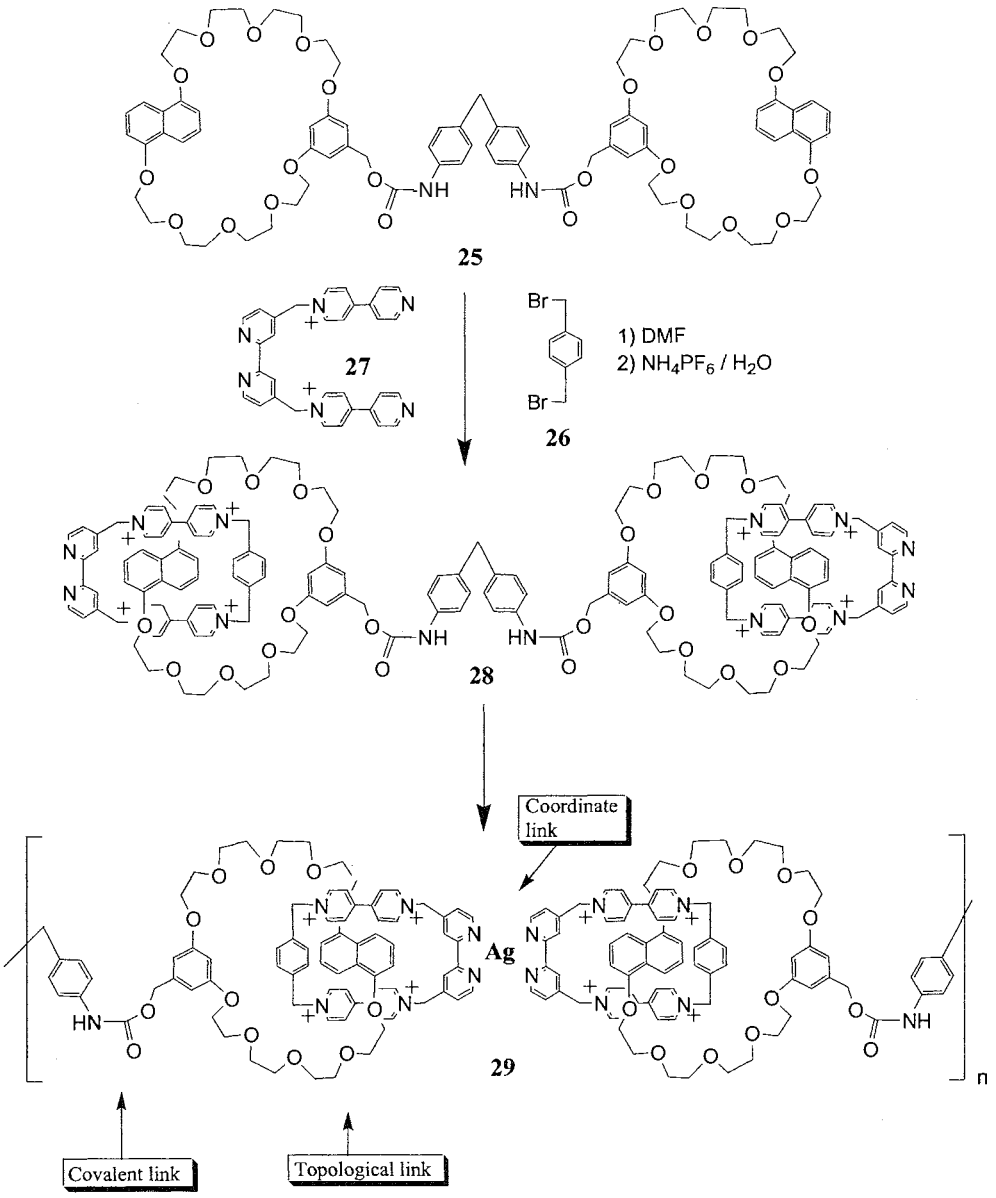

Fig. **8** Thermodynamic self-assembly of a polycatenane. Formation of a linear poly[2]catenane containing covalent, topological, and coordinative linkages.

Fig. 7 is the assembly of a [4]MN by the reaction of 1 equivalent of the cyclic molecule cucurbituril 22 with 1 equivalent of the angled metal complex 1 (M = Pt) and 1 equivalent of the dipyridyl molecule 23 after reaction for 1 day at 100°C in water.[6] Interactions between 22 and 23 result in cucurbituril spontaneously threading onto 23, completing the intertwining step. Cyclization is brought about by the formation of the Pt—*N*(pyridyl) bonds. As Pt—N bonds are labile at high temperature, either step may occur first. The structure of 24 was confirmed by an x-ray crystal structure determination. as well as by mass spectrometry and NMR. Several other [4]- and [5]MNs were prepared in a similar vein.[16]

The self-assembly of [*n*]polycatenanes having structures of the type depicted in Fig. 1e. offers perhaps a pinnacle of achievement in catenane synthesis. Unfortunately, it has thus far proved impossible to prepare such ensembles by a one-step thermodynamic self-assembly. Stoddart and Vogtle have, however. obtained [*n*]polycatenane structures by multistep, statistically based procedures.[17,18] The central problem with the thermodynamic self-assembly of oligomers of this type involves inducing an oligomerization process and then controlling it. This must be achieved in addition to the interlocking and cyclization processes required. While Sauvage suggested theoretical strategies in which the cyclization and the oligomerization steps are combined into one process. with a separate step for interlocking,[1] this approach has not yet been successfully demonstrated. Controlled oligomerization of a similar type has been achieved in only one case to the best of our knowledge — the self-assembly of a dendritic wedge."'' This technique is therefore far from being mastered in wider applications.

Poly[*n*]catenanes having the structure depicted in Fig. 1f are significantly more easily prepared than [*n*]polycatenanes: relatively few examples are nevertheless known. Illustrated in Fig. 8 is the formation of a poly-[2]catenane from a precursor 25 containing two covalently linked ringed polyethers.[20] When treated with the dibromide 26 and dication 27, the dicatenated structure 28 is obtained. Subsequently. treatment with Ag(I) produced the corresponding poly[2]catenane 29 that contained covalent-, topological-, and coordinate-linking units down its backbone.

HIGHER STRUCTURE IN CATENANES

As noted in a previous article in this *Encyclopedia*, self-assembly processes often generate compounds and materials displaying hierarchies of structure. also known as higher structures.[3] Self-assembled catenanes display similar structural hierarchies. although these are different to the hierarchies common in biology and chemistry. The interconnectivity of the individual components of a catenane must be considered the primary structure; that is. the lowest level of structural arrangement. Upon self-assembly, a secondary structure is created in the form of the closed cycles. The interlocked arrangement can also be considered a secondary structural element. However. as the term "interlocking" describes the way in which the closed cycles are organized relative to one another, it is perhaps more conveniently considered a feature of tertiary structure. Quaternary structure can be observed in oligocatenanes; Figs. 1e.f describe. for example, two different quaternary structural arrangements involving catenanes.

CONCLUSION

Several decades ago. catenanes were considered to be exotic and rare molecules. Today, thanks to self-assembly techniques. they are far more prevalent, acting even as convenient models for studies of ''molecular'' machines and motors.[21] In the future. we will see further simplifications in the preparation of catenanes, leading, perhaps, to oligomeric catenane structures with novel material and chemical properties. New types of noncovalent interactions will also be harnessed in the preparation of catenanes. Aurophilic. Au(I)–Au(I) attractions. having about the same bond strength as a hydrogen bond. have: for example, recently been plausibly employed in the synthesis of organometallic gold(I) acetylide catenanes.[22] Some practical applications of catenanes are already in the offing. Catenanes are, for example, being seriously examined as potential molecular switches, on the smallest possible scale, in information storage technologies.[23]

ARTICLES OF FURTHER INTEREST

Anion-Directed *Assembly*, p. 51
Catenanes and Other Intel-locked *Molecules*, p. 206
Chemical Topology, p. 229
Cucurbituril, Its *Homologues,* and *Derivatives*, p. 390
The Diphenylmethane Moiety, p. 452
Interpenetration, p. 735
Macrocycle Synthesis. p. 830
Rotaxanes and Pseudorotaxanes. p. 1194
Self-Assembly: Definition and Kinetic *and Thermodynamic Considerations*, p. 1248
Self-Assembly: Terminology, p. 1263
Strict Self-Assembly and *Self-Assembly with Covalent Modifications*, p. 1372
The Template Effect. p. 1493

REFERENCES

1. Sauvage, J.-P. Interlacing molecular threads on transition metals: Catenands. catenates, and knots. Acc. Chern. Res. 1990. *23*. 319–327 and references therein.
2. Kern. J.-M.: Sauvage, J.-P.; Weidemann. J.-L. Multiring interlocked systems via transition metal-templated strategy: The single-cyclization synthesis of [3]-catenates. Tetrahedron 8996, 52. 10921–10934.
3. Swiegers, G.F.: Malefetse. T.J. New self-assernbled structural motifs in coordination chemistry. Chem. Rev. 2008, 100. 3483–3537 and references therein.
4. Nierengarten, J.-F.; Dietrich-Buchecker, C.O.; Sauvage, J.-P. Copper(I) template synthesis of a 4-crossing [2]-catenane. New J. Chem. 1996, *20*. 685–693.
5. Fujita. M. Self-assembly of [2]catenanes containing metals in their backbones. Acc. Chem. Res. 1999. 32, 53–61 and references therein.
6. Whang, D.; Park. K.-M.; Heo. J.: Ashton. P.; Kim, K. Molecular necklace: Quantitative self-assembly of a cyclic oligorotaxane from nine molecules. J. Am. Chem. Soc. 1998, *120*, 4899–4900.
7. Raehm, L.: Hamilton, D.C.; Sanders. J.K.M. From kinetic to thermodynamic assembly of catenanes: Error checking, supramolecular protection, and oligocatenanes. Synlett 2002. 11, 1743–1761. and references therein.
8. Fujita. M.: Ibukuro, F.: Hagihara, H.; Ogura, K. Quantitative self-assembly of a [2]catenane from two preformed molecular rings. Nature 1994, 367. 720–722.
9. Swiegers. G.F.: Malefetse, T.J. Multiple-interaction self-assembly in coordination chemistry. J. Incl. Phenom. Macrocyc. Chern. 2001, 40. 253–264.
10. Piguet, C.: Bernardinelli, G.: Williams. A.F.; Bocquet. B. Formation of the first isomeric [2] catenates by self-assembly about two different metal ions. Angew. Chem., Int. Ed. Engl. 1995. 34. 582–584.
11. Cardenas, D.J.: Gaviña. P.: Sauvage. J.-P. Construction of interlocking and threaded rings using two different transition metals as templating and connecting centers: Catenanes and rotaxanes incorporating Ru(terpy)2-units in their framework. J. Am. Chem. Soc. 1997. *119*. 2656–2664.
12. Cardenas, D.J.: Sauvage. J.-P. Templating and clipping coordination reactions leading to heteronuclear trimetallic complexes containing interlocking rings. Inorg. Chem. 1997, *36*. 2777–2783.
13. Dietrich-Buchecker. C.: Sauvage, J. Effect template induit par le cuivre (I): Application à la synthèse de caténanes et de nœuds moléculaire. Bull. Soc. Chim. Fr. 1992; 129. 113–120.
14. Nierengarten. J.-F.; Dietrich-Buchecker. C.O.; Sauvage, J.-P. Synthesis of a doubly interlocked [2]-catenane. J. Am. Chem. Soc. 1994, 116, 375–376.
15. Dietrich-Buchecker, C.; Sauvage. J.-P.; Vogtle. F.; Frommberger, B.; Lüer, I. Multiring catenanes with a macrobicyclic core. Angew. Chem.. Int. Ed. Engl. 1993. *32*, 1434–1437.
16. Kim. K. Mechanically interlocked molecules incorporating cucurbituril and their supramolecular assemblies. Chem. Soc. Rev. 2002. *31*. 96–107 and references therein.
17. Amabilino, D.B.: Ashton, P.R.; Reder, A.; Spencer, N.; Stoddart, F.J. Olympiadane. Angew. Chem., Int. Ed. Engl. 1994. 33. 1286–1290.
18. Schwanke, F.: Safarowsky. O.; Heim, C.; Silva, G.: Vogtle, F. Amide-based oligocatenanes by an iterative template strategy. Helv. Chim. Acta 2000. 83. 3279–3290.
19. Huck, W.T.S.: van Veggel, F.C.J.M.; Kropman. B.L.; Blank, D.H.A.: Keim, E.G.; Smithers, M.M.A.; Reinhoudt. D.N. Large self-assembled organopalladium spheres. J. Am. Chem. Soc. 1995. 117, 8293–8294.
20. Hammers. C.; Kocian. O.; Raymo. F.M.: Stoddart. J.F. A poly(bis[2]catenane) containing a combination of covalent, mechanical, and coordinative bonds. Adv. Mater. 1998.10. 1366–1369.
21. Sauvage. J.-P. Transition-metal-containing rotaxanes and catenanes: Toward molecular machines and motors. Acc. Chem. Res. 1998. 31. 611–619 and references therein.
22. McArdle, C.P.: Irwin, M.J.; Jennings, M.C.: Vittal. J.J.: Puddephate. R.J. Self-assembly of gold(I) rings and reversible formation of organometallic [2]catenanes. Chem. Eur. J. 2002. 8. 723–734.
23. Collier, C.P.; Mattersteig. G.: Wong. E.W.; Luo. Y.; Beverly, K.; Sampaio, J.; Raymo, F.M.; Stoddart, J.F.: Heath. J.R. A [2]catenane-based solid state electronically reconfigurable switch. Science 2000. 289, 1172–1175.

Self-Assembly: Definition and Kinetic and Thermodynamic Considerations

Jim *A. Thomas*
University of Sheffield, Sheffield, United Kingdom

INTRODUCTION

Self-assembly is often called upon to explain a variety of molecular processes, from the spontaneous assembly of discrete biological structures, through complex organic syntheses. to the design of new materials. This review outlines how these processes are classified, delineates the enthalpic and entropic factors that drive such phenomena, and discusses models developed to interpret the limiting factors involved in self-assembly.

WHAT IS SELF-ASSEMBLY?

Self-assembly is one of the core concepts of supramolecular chemistry. It is often defined as the spontaneous formation of higher-ordered structures from molecular building blocks. This hypothesis first arose through research into biological systems. As the complex architectures found in living cells were delineated. the concept that such constructs were built by the convergent assembly of smaller subunits was increasingly invoked.[1] In particular, its relevance to one of the core principles of molecular biology soon became apparent.

The central dogma holds that genetic information is stored. read, and duplicated by the nucleic acids DIVA and RNA, and when required, this information is translated into the specific amino acid sequence of a protein, that then folds into its functional native form. As this model was developed. it became clear that it was underpinned by another assumption: that the final three-dimensional structure of a protein. or a nucleic acid, is inherent in the linear sequence of its building blocks. In groundbreaking work on ribonuclease, the Nobel Laureate Christian Afinison labeled this supposition the "Thermodynamic Hypothesis," suggesting that, in physiological conditions, the native structure of a protein is the one in which the Gibbs free energy of the system is at its lowest.[2] This concept of self-assembly was then extended, as subsequent discoveries revealed that. in many cases; protein folding is facilitated by other factors.[3]

CLASSIFYING SELF-ASSEMBLY

In an attempt to provide a general framework for discussion and research, Lindsey introduced a wide-ranging classification scheme. built upon the work of others, that encompasses self-assembly processes in biology and chemistry.[4] This definitive scheme is broken up into seven broad, overlapping, classes.

Class 1. Strict Self-Assembly

As will be discussed later, in many ways, strict self-assembly is a restatement of Afinison's Thermodynamic Hypothesis and encompasses all processes in which components assemble reversibly. The archetype of strict self-assembly is tobacco mosaic virus (TMV).[5,6] The TMV particles consist of a single helical strand of RNA embedded in a right-handed helix composed of identical coat protein subunits. The TMV particles will dissociate into their component parts by changes in pH, temperature. or even pressure. However. once the correct conditions are again attained. protein subunits and RNA spontaneously reassemble into virus particles that are indistinguishable from the original TMV.

Glass 2. Irreversible Self-Assembly

This class is the obverse of the previous case. As steps toward the final assembly are unalterable, usually full covalent interactions, building blocks must come together into the final correct structure with no margin of error. Under the guise of tandem or domino reactions. this class of process is currently attracting much attention in synthetic organic chemistry.[7,8]

Unlike most self-assembly processes (vide infra), irreversible self-assembly is under kinetic control. Consequently. in most irreversible multistep assembly processes, the initial architectures must be precisely located and aligned.[8] However. in some cases, highly complex architectures can result from apparently nontemplated, irreversible self-assembly.[9]

Encyclopedia of Supramolecular Chemistry
DOI: 10.1081/E-ESMC 120012779

Class 3. Precursor Modification Followed *by* Self-Assembly

These processes involve the synthesis of precursors that are subsequently structurally modified. A biological example is collagen synthesis. Collagens are fibrous proteins that form the major component of skin and bone. They are the most abundant mammalian protein and are found in long, extracellular polymeric structures called fibrils. In turn, these fibrils are often aggregated into larger cables, known as fibers, that are big enough to be viewed under light microscopes.[10]

The assembly of such structures within a cell would be fatal. To prevent such an occurrence, a precursor. known as procollagen, is synthesized. Procollagen consists of triple helical polypeptide strands capped at their terminal ends by amino acid chains, called propeptides, that prevent aggregation of procollagen molecules. Once synthesized, procollagen is secreted out of the cell, where proteolytic enzymes remove the propeptides. The resulting collagen molecules are several orders of magnitude less soluble than their precursors, and self-assembly of fibrils is rapidly initiated.''''

Class 4. *Self-Assembly with* Postmodification

In this case, the self-assembly process precedes the final modifications that lead to the targeted architecture. Using this powerful methodology, self-assembled structures can be irreversibly locked into position. Within supramolecular chemistry: this strategy is most commonly employed in the elegant syntheses of catananes, rotaxanes, knots. and other interlocked species.''''

Class 5. Assisted Self-Assembly

Here. external factors that are not part of the final assembly mediate the self-assembly process. This concept was developed as the function of molecular chaperones became apparent.'''' Chaperones help in folding nascent polypeptide chains by preventing aggregation of peptide sequences, and they modulate refolding of denatured proteins. Chaperones do not affect the thermodynamics of folding—the ratio of folded and unfolded polypeptides is left unchanged—but they influence the kinetics of the process. It is thought that this is accomplished by stabilizing intermediates along the folding pathway, thus decreasing activation-energy barriers.

Class 6. Directed Self-Assembly

In Lindsey's original definition, this class includes processes in which a template participates as a structural element in the self-assembly process but does not appear in the final assembled architecture. An example from biology is the scaffolding protein directed assembly of viral capsids. External and internal scaffolding protein frameworks direct the construction of the protein coat that houses the viral DNA. Packaging of DNA is then accompanied by withdrawal of the internal scaffolding, and the final virion is produced after removal of the external scaffold.[12]

An example from chemistry is the use of vesicles, liquids, and foams to direct biomimetic mineralization and polymerization. Such templates, that may only have a transitory existence: were used to template the assembly of structurally complex, three-dimensional architectures.[13]

Subsequently, within supramolecular chemistry, the term ''directed self-assembly'' has become more generally understood to include any templated process that brings together molecular components, even if the directing moiety is part of the final structure.[14]

Class *7. Self-Assembly with Intermittent* Processing

This final class incorporates elements from all the proceeding classes. It includes all processes where there are sequential phases of self-assembly and irreversible modification. Such complex processes are still the exclusive domain of biology.

WHAT DRIVES SELF-ASSEMBLY?

With the exception of the previously discussed irreversible processes. the key steps in self-assembly tend to involve the interplay of dynamic. relatively weak. interactions. In these conditions. thermodynamic products. where free energy is maximized. will be favored. Consequently. entropic and enthalpic state functions must be considered.

Solvophobic Effects

Superficially, the synthesis of discrete, ordered structures from a set of subunits would seem to be a solely enthalpically driven process—the formation of new favorable interactions is at the cost of losing translational, vibrational, and rotational degrees of freedom. However. it has long been established that the hydrophobic effect, which drives amphiphilic subunits to assemble into micelles and lipid bilayer structures such as liposomes, is largely an entropic phenomenon.[15]

Water molecules that sunound nonpolar regions of a solute form cage-like cavities. Although these arrays of

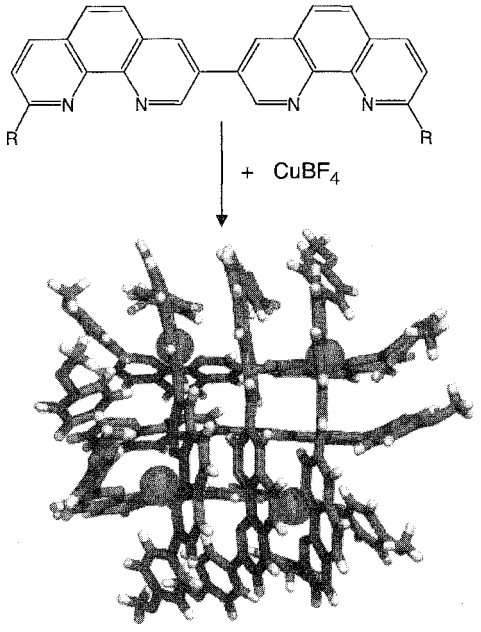

Fig. 1 Synthesis of a 3 x 3 molecular grid. Physical studies indicate that recognition processes in this assembly involve solvation effects analogous to the hydrophobic effect. (Adapted from Ref. [16].)

water molecules are fluxional, there is overall increase in local order. Creation of a bilayer means that while the polar part of the amphiphile is solvated, the nonpolar sections are not. allowing water molecules to be released into the bulk solvent. thus increasing the degrees of freedom in the system. Even in nonaqueous solvents, analogous effects drive recognition processes.

Investigating self-assembly processes involving acetonitrile solutions of ditopic 2,2′-diaryl-8,8′-*bis*-1,10-phenanthroline ligands and copper(I) metal centers, Siegal and co-workers observed the formation of a 3 x 3 molecular grid with four ligands coordinated to metal centers, forming a molecular square host, while two additional ligands filled interstitial spaces as guests (Fig. 1).[16]

Studies using the sterically demanding ligand 2,2′-dimesityl-8,8′-*bis*-1,10-phenanthroline indicated that the grid was not the product of a two-step process involving self-assembly of the square followed by a host–guest interaction, but it was, rather, a genuine cooperative process involving host and guest components. Furthermore, spin saturation transfer spectroscopy studies indicated that the host–guest interaction had a large entropic component. These observations hint that a solvation effect, analogous to the hydrophobic effect, partially drives the self-assembly process.

Further evidence of a generai solvophobic effect was revealed in an isothermal titration calorimetry study probing the recognition of carboxylates by guanidinium residues. a common motif in protein–substrate binding. When investigating this interaction in acetonitrile solution~.~Schmidtchen and colleagues obtained evidence that the entropic component to the free energy of binding—the release of solvent molecules and counterions engaged in the solvation of the free binding site—is not a marginal factor but may constitute the major part of ΔG°.

However. even if such solvent effects are disregarded, it may be argued that for strict self-assembly processes, discrete structures are still thermodynamically favored.

Enthalpy and Entropy Considerations

Consider a simple hypothetical system. where 12 components can reversibly associate. via a single, weak, enthalpically favored interaction, into a discrete four-membered cyclic structure; or alternatively, an open oligomeric structure (Fig. 2). Clearly. the formation of any oligomeric structure is enthalpically favored, as new interactions are created. but. as Lawrence et al. pointed out,[18] discrete structures are slightly favored.

The number of interactions per component created in the assembly of tetramers (one interaction per unit) is larger than that in the formation of the open oligomer (0.9167 interactions per unit). If there is more than one interaction between components, then assembly of the

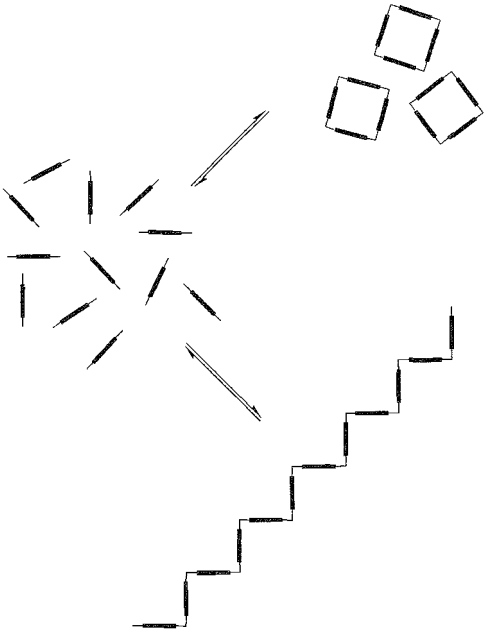

Fig. 2 Subunits that can assemble into two possible products: a discrete four-membered cyclic structure or an open oligomeric structure.

tetramer is even more advantageous. For example, if there are two interactions between individual components, then the tetramer has two interactions per unit, while the oligomer only has 1.834 interactions per unit. While it is clear from an extension of such arguments that the enthalpic advantage of assembling tetramers over open polymeric structure incorporating a large number of components will rapidly become extremely small; it is also true that a cyclic structure with N components will be enthalpically favored over an open structure with N components.

Conversely, due to losses of translational and conformational degrees of freedom, the formation of any oligomeric structure is entropically unfavorable. Nevertheless, compared to self-assembly of discrete structures, generation of open oligomers (and especially polymers) is particularly unfavorable. Again, consideration of the system shown in Fig. 2 illustrates this argument. Relative to the tetramer, it seems likely that self-assembly of the less rigid, open oligoiner results in a smaller change in conformational degrees of freedom. On the other hand, the formation of one oligomer particle, as opposed to three tetramer particles, will result in a much larger loss in translational degrees of freedom. If more components are incorporated within this polymer, the entropic disadvantage, relative to the tetramer, increases.

Seen in this light, preferential self-assembly of discrete architectures over open oligomeric structures is related to the widely studied phenomenon known as enthalpy–entropy compensation[19,20]—the enthalpic benefits of interactions are balanced by the entropic costs in losing degrees of freedom. In reports by Fujita and colleagues and Hong et al., the subtlety of this interplay is revealed.

FLUXIONAL SELF-ASSEMBLY AND DYNAMIC COMBINATORIAL LIBRARIES

In 1990, using the suitably hindered square-planer metal center [(en)Pd(NO_3)$_2$] (en=ethylene-1,2-diamine) and 4,4′-bipyridine, Fujita and coworkers reported the self-assembly of macrocyclic supramolecular squares.[21] Later work revealed that the replacement of 4,4′-bipyridine with more flexible dipyridyl ligands such as *trans*-1,2-*bis*(4-pyridyl)ethylene resulted in an equilibrating mixture of molecular squares and triangles (Fig. 3).

The ratio of products in this equilibrium was found to be concentration and temperature dependent. At low concentrations, the equilibrating reaction mixture contains significant amounts of the triangular product, while at higher concentrations, the square is the predominant product. At very high concentrations, the product mixture contains significant amounts of unidentified oligomeric structures.[22] A similar equilibrium shift toward the triangle is observed on heating the reaction mixture. These results suggest that this system is held in a fine thermodynamic balance: entropically, the triangle is favored. because it is assembled from fewer components, while enthalpically, the less-strained square assembly is favored.

In further studies on the same system, Hong and coworkers found that by exploiting host–guest interactions. it is possible to bias the equilibrium toward a specific product architecture.[23] The addition of p-dimethoxybenzene to the reaction mixture induced an equilibrium shift toward the triangle, while the addition of sodium 1.3-adamantanedicarboxylate resulted in the formation of the square as the only product (Fig. 3). The directing principal is supplied by hydrophobic interactions: in an example of the thennodynamic template effect, the free energy difference created by the appropriate guest is enough to make a specific host the favored product. These studies illustrate the protean nature of systems at the interface of self-assembly and receptor–substrate recognition. This interface was further exploited in the creation of dynamic combinatorial libraries (DCL).

A DCL consists of higher-order molecular architectures that reversibly self-assemble from a set of molecular building blocks.[24] Because the whole system is held in thermodynamic equilibrium. it is highly fluxional: a template that binds to one member of the library will drive the preferential assembly of this library member. Thus, through Le Chatlier's principle, the equilibrium shifts, evolving toward architectures that tightly bind the target template. Work by Sanders and colleagues delineates the power of this rapidly developing technique. Using hydrozone-based pseudopeptides that interconvert via transimination at the hydrozone bond, they utilized an equilibrating covalent DCL to identify and isolate a macrocyclic receptor that binds to N-methyl alkylammonium salts such as acetylcholine chloride.[25] This approach is not just limited to the design of new hosts: Lehn and coworkers showed that a DCL of folding isomers can be directed toward a specific folded form of a linear molecule.[26] While in work reported by Karan and Miller, a DCE consisting of various salicylamides ligands and Cu^{2+} ion was used to identify a compound that binds to an RNA hairpin with a high affinity, showing remarkable selectivity relative to DNA.[27]

SWITCHING FROM THERMODYNAMIC TO KINETIC REGIMES

While strict self-assembly is a particularly attractive strategy in the construction of complex molecular architectures, there are disadvantages. As the disaggregation of

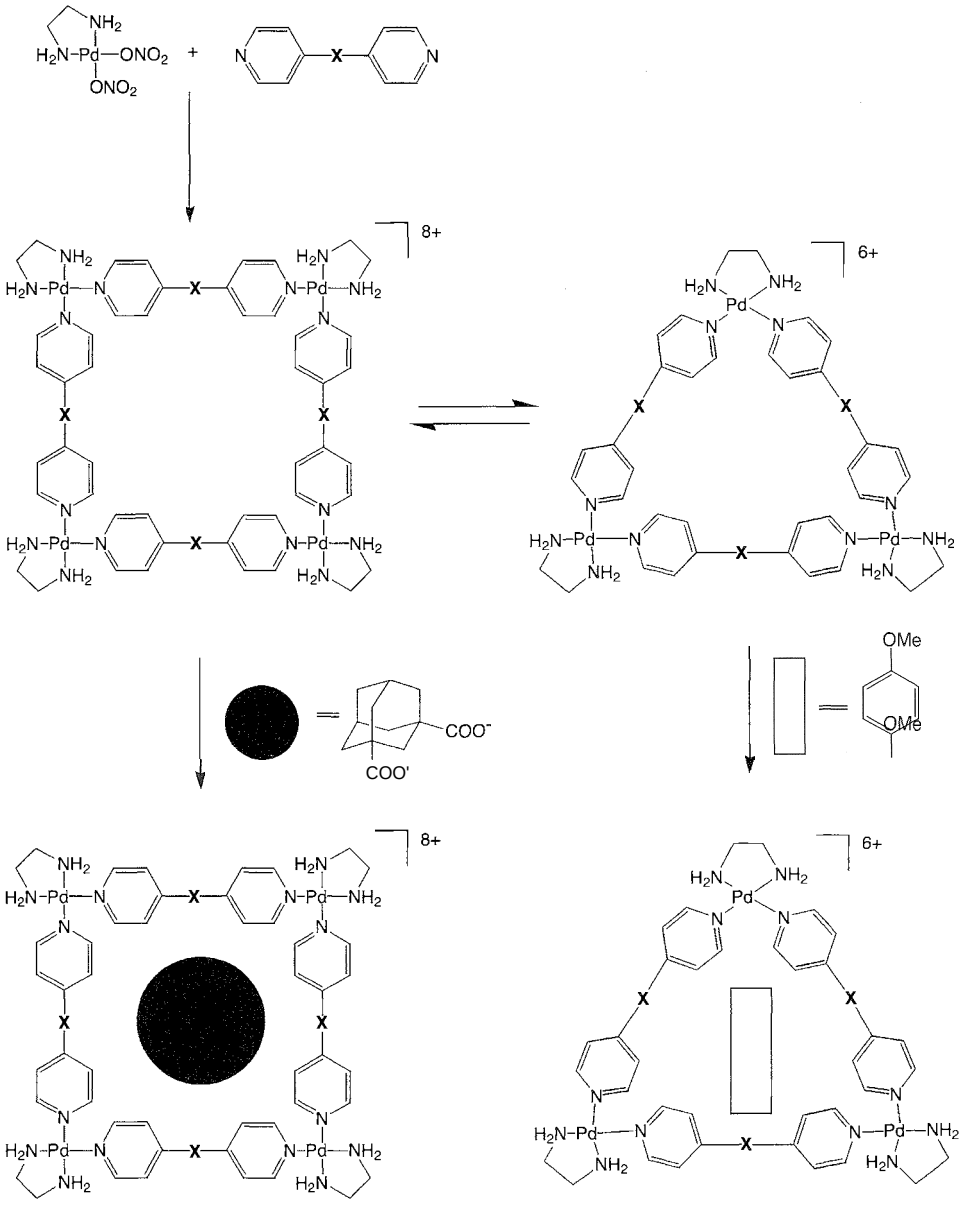

Fig. 3 Reaction of square planar inetal centers with flexible dipyridyl ligands leads to an equilibrating product mixture containing a square and triangle inacrocycle. Host–guest recognition processes bias this mixture toward specific products. (Adapted from Refs. [22,23].)

TMV particles illustrates. as the final product is thermodynamically selected, it is not necessarily kinetically robust. Consequently. synthetic chemists working to create functional architectures often adopted self-assembly with postmodification strategies.[11] However. another strategy was also pursued — one in which construction by strict self-assembly is then followed by whole-system switching into the kinetic regime. thereby locking complex architectures into structurally resilient entities.

That such an approach was possible became apparent with the work of Lehn and colleagues on Ni^{II} ternplated triple helicate complexes.[28] It was found that on crystallization. spontaneous partial resolution of A- and Δ-enantiomers rook place. Presumably due to cooperativitp inherent within such structures, these complexes racemized at much reduced rates, compared to related monomeric systems. The first true approach to kinetic locking, reported by Williams and colleagues, involved an

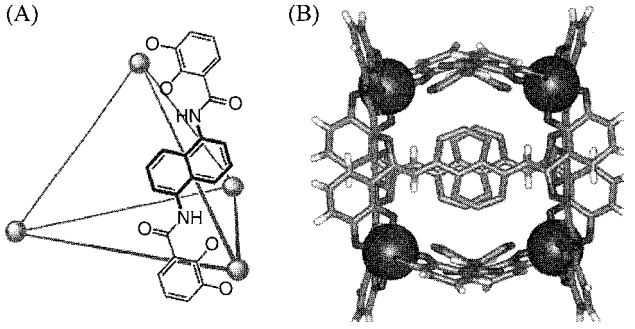

Fig. **4** Self-assembly using labile Ga^{III} results in the synthesis of kinetically stable tetrahedral cages. (A) Structure; (B) Crystal structure of AAAA-tetrahedral cage. NEt_4—guest was removed for clarity. (Adapted from Ref. [33].)

electrochemically active dinuclear triple helicate.[29] In this case, self-assembly was ternplated via Co^{II}, and then locking was achieved by oxidation of the labile Co^{II} metal centers to relatively kinetically inert Co^{III}. The racemic product mixture was then resolved into its component enantiomers via chromatography.

Fujita and coworkers developed a generalized strategy for the kinetic locking of self-assembled architecture~.['~. They exploited the dual character of platinum(II)-pyridine coordination, which in normal ambient conditions is kinetically inert. However, at elevated temperatures and in highly polar media. or in the presence of a suitable template, this interaction becomes relatively labile. Using this effect, they reacted $(en)Pt(NO_3)_2$ with appropriate ligands to isolate macrocyclic, catenated,'"] and nanosized cage'"'] architectures. Unlike their Pd(II)-based analogues, these structures are remarkably stable. For example, the isolated catananes do not dissociate at temperatures as high as 100°C. The addition of excess $(en)Pt(NO_3)_2$ to the square macrocycle constructed in this manner showed no sign of subsequent product redistribution.

Using a similar high-temperature approach to labilize Ru^{II}. Thomas and colleagues reported the self-assembly of a molecular cube incorporating eight $[Ru([9]aneS_3)]^{2+}$ ([9]aneS$_3$=1,4,7-trithiacyclononane) corners and 4,4′ bipyridine edges. The final structure enhanced the kinetic stability of the individual components. While the analogous monomeric complex, $[Ru([9]aneS_3)(bpy)3]^{2+}$, is relatively kinetically labile toward ligand substitution reactions, the final assembly was stable even at elevated temperatures.[32]

However, perhaps the most spectacular example of kinetic locking was reported by Raymond et al. Using highly labile gallium(III) metal ion (M) to template the self-assembly of inflexible C_2 symmetric bis-catecholate ligands (L), the researchers prepared chiral tetrahedral $[M_4L_6]$ assemblies[33] (Fig. 4). In the presence of a chiral anion, *N*-methylnicotinium, which is encapsulated within the cluster cavity. the homoconfigurational *ΛΛΛΛ* and *ΔΔΔA* clusters were completely resolved.

Usually. raceniization of *tris*(catecholate)gallium(III) complexes takes place quickly via a Bailar twist mechanism. Even in bimetallic helicates, where there is strong mechanical coupling between metal centers, racemization rater of 0.10 s^{-1} were determined by NMR studies. In contrast, the tetrahedral $[M_4L_6]$ assemblies are so inflexible that metal centers cannot independently racemize. Once formed. the guest *N*-methylnicotinium molecule can be replaced by Et_4N^+ with complete retention of chirality—the clusters retain enantiopurity even after remaining in aqueous solution for months. Racemization is still not observed after extended boiling of such solutions. The rigidity of the assembly results not from the individual components but the way they

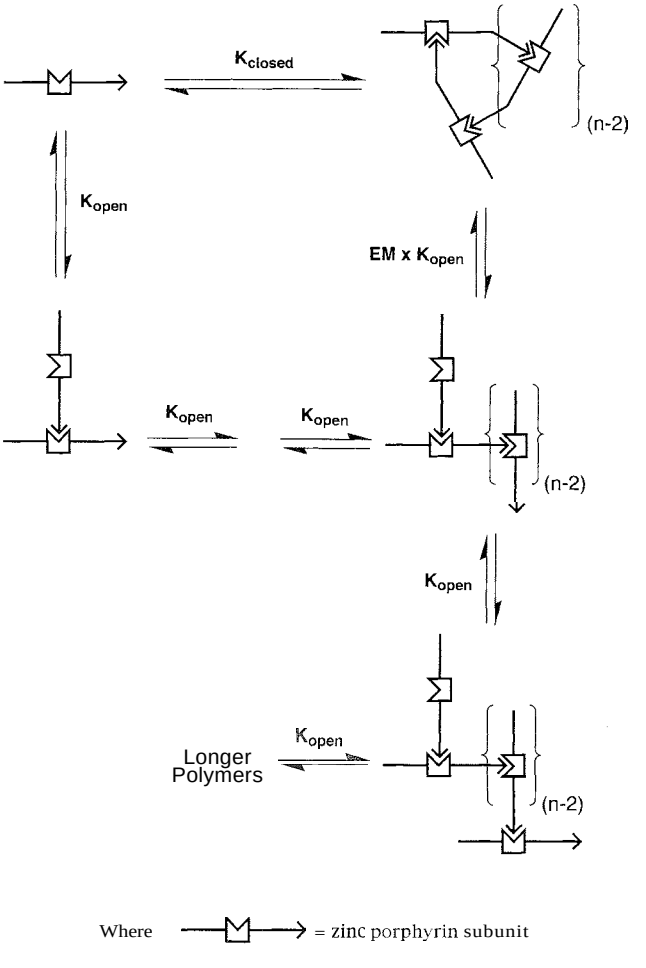

Fig. **5** Equilibria involved in the self-assembly of porphyrin macrocycles. (Adapted from Ref. [34].)

are assembled. This work demonstrates that. through judicious design. highly labile components can be made to self-assemble into architectures of extraordinary kinetic stability.

THEORETICAL MODELS OF SELF-ASSEMBLING SYSTEMS

While synthetic studies on self-assembly are rapidly developing in number and sophistication, thermodynamic models for such systems are relatively less common. One of the first studies to address this issue was presented by Hunter and colleagues.[''''] Exploiting the relatively weak coordination of pyridine to zinc porphyrins, they investigated the strict self-assembly of cyclic porphyrin oligomers. Using structural variants of porphyrin subunits, a variety of macrocycles we e targeted. Although the individual interactions used to drive these assemblies are almost identical. their behavior is quite different. A comparison of dimeric and tetrameric systems illustrates this point.

Defining critical self-assembly concentration (csac) as the concentration at which half the porphyrin inonomers are assembled into a macrocycle. the concentration dependence of the self-assembly process was investigated. It was found that csac for the dimer is 3×10^{-9} mol dm^{-3}, while the tetramer only assembles at much higher concentrations, csac $= 3 \times 10^{-5}$ mol dm '. These results were rationalized by considering the equilibria shown in Fig. 5 and the relationship between csac and the effective molarity, EM ($EM = K_{closed}/K_{open}$), leading to Eq. 1:

$$\text{csac} = \frac{1}{n^{1/(n-1)} \text{EM}^{1/(n-1)} K_{ref}^{n/(n-1)}} \quad (1)$$

Where n is the number of subunits within a structure, and K_{ref} is the equilibrium constant for the association of a zinc porphyrin subunit with a reference ligand structurally analogous to those used in the self-assembly process but incapable of assembling into a closed structure. This equation indicates that as n increases, csac rises. Furthermore, as $n \rightarrow \infty$, csac $= 1/K_{ref}$. In these conditions, significant self-assembly occurs only between $1/K_{ref}$ and EM. This analysis indicates that provided EM is kept high

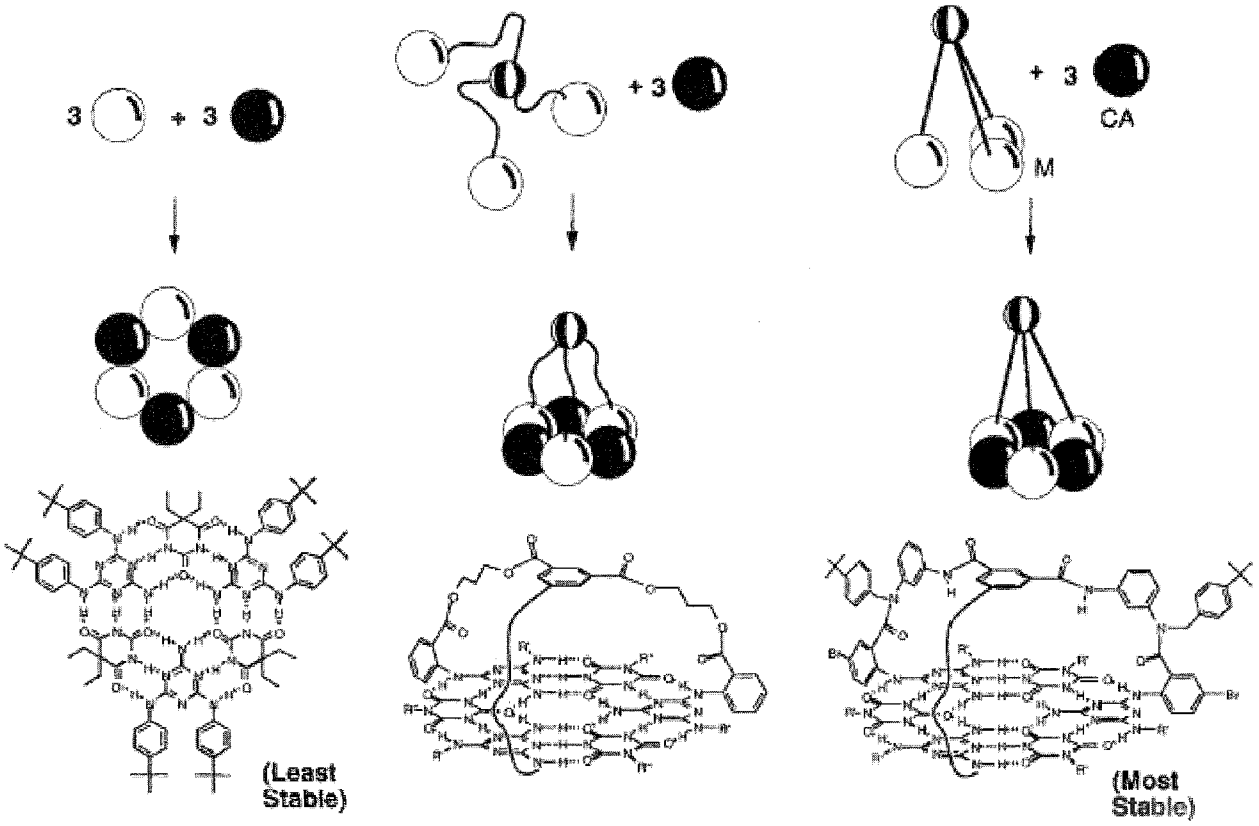

Fig. 6 Molecular structures of hydrogen-bonded cyanuric acid·melamine aggregates and corresponding schematics based on ball. rods. and string (BRS) models. (Reprinted with permission from Ref. [36].)

by using preorganized monomers, even very large multicomponent systems will self-assemble into stable. discrete structures.

In studies on derivatives of cyanuric acid and mel- amine (Fig. 6), Whiteside and coworkers developed a model to predict the relative stability of a series of hydrogen-bonded aggregates.[35] This model was developed after an analysis, analogous to that of Hunter and colleagues, revealed that the extent of aggregation is not directly reflected by the magnitude of ΔG° but depends strongly on N, the number of particles in the aggregate. Further consideration revealed that for self-assembly of a given aggregate, $\Delta S \propto (N-1)$ and the number of hydrogen bonds. HB $\propto$ AH. Using these relationships, indices that estimate the stability of cooperative and noncooperative assemblies in terms of N and HB were introduced. In particular, they showed that the index I_{TM} = HB/N 1, relates to ΔH/ΔS, and, for cooperative assemblies. correlates well with experimental stability measurements obtained from studies of deaggregation using polar solvents such as DMSO.

In a related study, Whiteside and colleagues went on to particularly focus on the entropic cost of assembling these aggregates.[36] After partitioning the entropy of self-assembly into translational. rotational, vibrational, and conformational components, they pointed out that, while there are adequate theoretical treatments for rotational and vibrational entropy, models for conformational and translational entropy changes are not accurate.

Translational entropy, S_{trans}, reflects the possible number of unique arrangements of a collection of molecules in a given space. Classically, this is described by the Sackur–Tetrode equation:

$$S_{\text{trans}} = RIn\left[\left(\frac{10^{-15/2}}{N_A^4[X]}\right)\left(\frac{2\pi MkTe^{5/3}}{h^2}\right)^{3/2}\right] \quad (2)$$

Where M and T, $[X]$ are the mass (g/mol), temperature (K), and concentration (mol/L) of the particle, respectively, and R, h, k, e, and N_A are constants with their usual meanings. This equation is a good predictor of the entropy of monoatomic gases. However, S_{trans} of molecules in liquid or solution phase is significantly lower than that predicted by the equation. By taking into account the volume occupied by the molecules in a solution. Whiteside and his colleagues used free volume theory to obtain an extended version of the Sackur–Tetrode equation that offers a significantly improved estimate of S_{trans}. This new model was used to predict the entropy of association of a six-particle aggregate compared to that of a four-particle aggregate, and agreement with experimentally obtained free energy differences was obtained.

Going on to consider conformational entropy changes on self-assembly. the researchers employed a model based on balls (hydrogen-bonding subunit) that may be free or connected by rods (rigid covalent linkers) or strings (flexible tethers) (Fig. 6). This model indicated that the conformational entropic cost of self-assembling an aggregate connected by flexible tethers would be approximately 23 kJ mol^{-1} more than that of an assembly with rigid tethers: figures that were, again, in agreement with experimental data on the free energy of aggregate assembly.

CONCLUSION

If complex and/or functional molecular assemblies are to be derived from supramolecular chemistry, a comprehensive exploration of the factors that govern self-assembly processer will be required. While theoretical models for these processes are sparse, progress in synthetic arpects of self-assembly has been relatively swift, leading to entirely new concepts such as DCLs. Concurrent to these developments, methodologies for irreversibly locking self-assembled stuctures are also beginning to emerge.

ARTICLES OF FURTHER INTEREST

Anion-directed Assembly, p. 51
Catenanes and Other Interlocked Molecules, p. 206
Hydrophobic Effect, p. 673
Molecular Squares, Boxes, and Cubes, p. 909
Rotaxanes and Pseudorotaxanes, p. 1194
Selectivity: Thermodynamic and Kinetic, p. 1225
Self-Assembling Capsules, p. 1231
Self-Assembling Catenanes. p. 1240
Self-Assembly in Biochemistry, p. 1257
Self-Assembly: Terminology, p. 1263
Strict Self-Assembly and Self-Assembly with Covalent Modifications, p. 1372
The Template Effect, p. 1493
Viruses as Host Assemblies, p. 1563

REFERENCES

1. Kushner. D.J. Self-assembly of biological structures. Bacteriol. Rev. **1969**, 33, 302–345.
2. Afinson, C.B. Principles that govern the folding of protein chains. Science **1973**, *181*, 223–228.
3. Ellis, R.J.; Hemmingsen, S.M. Molecular chaperones: Proteins essential for the biogenesis of some macromolecular structures. TIBS 1989. *14*, 339–342.
4. Lindsey, J.S. Self-assembly in synthetic routes to molecular devices. Biological principles and chemical perspectives: A review. New J. Chem. **1991**. 15, 153–179.
5. Klug, A. The tobacco mosaic virus particle: Structure and

assembly. Phil. Trans. R. Soc. Lond. B. 1999, *354*, 531–535.

Butler. P.J.G. Self-assembly of tobacco mosaic virus: The role of an intermediate aggregate in generating both specificity and speed. Phil. Trans. R. Soc. Lond. B. 1999. *354*. 537–550.

Bunce. R.A. Recent advances in the use of tandem reactions for organic synthesis. Tetrahedron 1995. 48, 13103–13159.

McCarroll. A.J.; Walton. J.C. Programming organic molecules: Design and management of organic syntheses through free-radical cascade processes. Angew. Chem. Int. Ed. 2001. 40, 2224–2248.

Gibb. C.L.D.: Stevens, E.D.; Gibb. B.C. The self-assembly of benzyl alcohol derived deep-cavity cavitands: A new. highly efficient moiety for irreversible assemblies? Chem. Commun. 2000. 363–364.

10. Kucharz. E.J. The *Collagens: Biochemistry* and *Pathophysiology*; Springer-Verlag: New York, 1992.
11. Ambalino, D.B.: Stoddart, J.F. Interlocked and intertwined structures and superstructures. Chem. Rev. 1995, *95*, 2725–2828.

Dokland. T.: McKenna, R.; Ilag, L.L.; Bowman, B.R.; Incardona. N.L.; Fane, B.A.: Rossmann, M.G. Structure of a viral procapsid with molecular scaffolding. Nature 1997, 389. 308–313.

Mann, S.J. Biomineralization: The form(id)able part of bioinorganic chemistry! Chem. Soc., Dalton Trans. 1997, 3953–3961.

Recognition-Mediated Self-Assembly of Organic Systems; Rotello, V.M., Ed.: Tetrahedron. Symposium in Print Special Edition. 2002: Vol. 48, 621–844.

15. Tanford. C. *The Hydrophobic* Effect: John Wiley and Sons: New York, 1973.
16. Toyota. S.; Woods. C.R.: Benaglia, M.: Haldimann. R.: Warnmark. K.: Hardcastle. K.; Siegel, J.S. Tetranuclear copper(i)-biphenanthroline gridwork: Violation of the principle of maximal donor coordination caused by intercalation and CH-to-N forces. Angew. Chem. Int. Ed. 2001. 40. 751–754.

Haj-Zaroubi, M.; Mitzel, N.W.: Schmidtchen. F.P. The rationale design of anion host compounds: An exercise in subtleenergetics. Angew. Chem. Int. Ed. 2002, *41*, 104–107.

18. Lawrence, D.S.: Jiang, T.: Levett. M. Self-assembling supramolecular complexes. Chem. Rev. 1995, *95*. 2229–2260.
19. Williams. D.H.: Westwell. M.S. Aspects of weak interactions. Chem. Soc. Rev. 1998, *27*. 57–63.
20. Liu, L.; Guo, Q.-X. Isokinetic relationship, isoequilibrium relationship. and enthalpy–entropy compensation. Chern. Rev. 2001. 101. 673–695.

Fujita, M.: Yazaki. J.; Ogura, K. Preparation of a macrocyclic polynuclear complex, $[(en)Pd(4,4\text{-}bpy)]_4(NO_3)_8$ which recognizes an organic molecule in aqueous media. J. Am. Chern. Soc. 1990, *112*. 5467–5645.

Fujita. M.: Sasaki, O.; Mitsuhashi, T.; Fujita. T.: Uazaki. J.: Yarnaguchi. K.: Ogura. K. On the structure of transition-metal-linked molecular squares. Chem. Commun. 1996, 1535.

23. Lee. S.B.: Hwang, S.: Chung, D.S.; Yun, H.; Hong. J.-I. Guest-induced reorganization of a self-assernbled Pd(II) complex. Tetrahedron Lett. 1998, *39*. 873–876.
24. Lehn. J.-M. Dynamic coinbinatorial chemistry and virtual combinatorial libraries. Chem. Eur. J. 1999. *5*. 2455–2463.
25. Cousins. G.R.L.: Furlan. R.L.E.; Kg. Y.-F.; Redman. J.E.; Sanders, J.K.M. Identification and isolation of a receptor for N-methyl alkylammonium salts: Molecular amplification in a pseudo-peptide dynamic combinatorial library. Angew. Chem. Int. Ed. 2001. *40*. 423–428.
26. Berl. V.; Krische, M.J.: Huc, I.: Lehn, J.-M.; Schmutz. M. Template-induced and molecular recognition directed hierarchical generation of supramolecular assemblies from molecular strands. Chem. Eur. J. 2000. 6. 1938–1946.
27. Karan. C.: Miller, B.L. RNA—selective coordination complexes indentified via dynamic combinatorial chemistry. J. Am. Chem. Soc. 2001. *123*. 7455–7456.
28. Krämer, R.; Lehn. J.-M.: De Cian. A.; Fischer, A. Self-assembly. structure. and spontaneous resolution of a trinuclear triple helix from an oligobipyridine ligand and Ni^{II} ions. Angew. Chem. Int. Ed. Engl. 1993, *32*. 703–706.
29. Charbonniere. L.J.: Bernardinelli. G.; Piquet, C.: Sargeson, A.M.: Williams. A.F. Synthesis, structure and resolution of a dinuclear Co^{III} triple helix. J. Chem. Soc., Chem. Commun. 1994. 1419–1420.
30. Fujita. M.: Ibukuro. F.: Yamaguchi, K.: Ogura. K. A molecular lock. J. Am. Chem. Soc. 1995. *117*. 4175.
31. Ibukuro, F.: Kusukawa. T.: Fujita, M.A. Thermally switchable molecular lock. Guest-templated synthesis of a kinetically stable nanosized cage. J. Am. Chem. Soc. 1998, *120*. 8561–8562.
32. Roche, S.; Haslam. C.; Adams. H.: Heath, S.L.: Thomas. J.A. Self-assembly of a supramolecular cube. Chem. Commun. 1998. 1681.
33. Terpin, A.J.; Ziegler. M.: Johnson. D.W.; Raymond. K.N. Resolution and kinetic stability of a chiral supramolecular assembly made of labile components. Angew. Chem. Int. Ed. 2001, 40. 157–160.
34. Chi. X.: Guerin. A.J.: Haycock. R.A.: Hunter. C.A.: Sarson. L.D. The thermodynamics of self-assembly. Cheni. Commun. 1995. 2563.
35. Mammen, M.: Simanek. E.E.; Whitesides, G.M. Predicting the relative stabilities of multiparticle hydrogen-bonded aggregates based on the number of hydrogen bonds and the number of particles and measuring these stabilities with titrations using dimethyl sulfoxide. J. Am. Chem. Soc. 1996. *118*. 12614–12623.
36. Mammen. M.; Shakhnovich, E.I.; Deutch. J.M.: Whitesides. G.M. Estimating the entropic cost of self-assembly of multiparticle hydrogen-bonded aggregates based on the cyanuric acid, melamine lattice. J. Org. Chem. 1998, *63*. 3821–3830.

Self-Assembly in Biochemistry

Tamara D. Hamilton
Leonard R. MacGillivray
University of Iowa, Iowa City, Iowa, U.S.A.

INTRODUCTION

The term "self-assembly" has been used to describe a wide range of processes, including the capiliary force-*driven association of micrometer-sized* plates[1] *and the* arrangement *of protein monolayers* on *gold surfaces.*

For the scope of this article, we will limit *our survey to those processes that occur naturally* (i.e., *within living systems). and we will define self-assembly as the spontaneous, reversible association of large molecular components to form larger. ordered structures by way of* noncovalent *forces. The process leads the components* from *a less-ordered state to one of higher order.'" The self-assembled product then carries out a task not achievable by the* individual *components.*

Though an exhaustive description of self-assembly processes in living systems could fill many books. our goal is to provide representative examples that illustrate the diversity of the process.

THE IMPORTANCE OF SELF-ASSEMBLY TO LIFE PROCESSES

Self-assembly is important to life processes. If self-*assembly did not occur, it is certain that life could not exist.'" Natural selection has long been a central tenet in theories of the origin of life on* earth, *but it alone is not likely to* have *given rise to the emergent order of* life. *This order* can *be explained by considering that nature is operating under the influence of inherent principles of self-assembly.*[3]

The conventional method *that a chemist employs to synthesize new compounds in the laboratory relies on the sequential formation of covalent bonds. This approach is, however.* limited. *when it comes to constructing large or complex entities* (e.g., a *cell). One can imagine the sorts of difficulties that would arise if the* components *of a cell. for example. were all covalently bonded and part of one giant inolecule. Synthetic chemists have met* tremendous *challenges* in making *natural products with procedures* that *can involve upwards of 30* steps.[4] If *nature approached synthesis of these molecules or even more complicated structures* in *the same manner. not only would the kinetics of life processes be inordinately slow, but each step would need to be carried out with absolute* fidelity.[5] *Mistakes could not easily be corrected because of the comparatively high energy required to break and reform a covalent bond. Nature circumvents these limitations by creating relatively simple building blocks that spontaneously assemble into* more complex structures.[5]

Nature uses self-assembly to build highly structured systems for specific functions. Examples include the transfer and storage of genetic information in nucleic acids,[6] *the organization of lipids into protective cell membranes that serve as molecular receptors for the cell, and the hierarchical structure of spider silk, still one of the strongest known fibrous* materials.[7] *yet flexible enough to absorb the* impact *energy of an unlucky fly.*

ASYMMETRICAL SELF-ASSEMBLY: PROTEIN FOLDING

The mechanism whereby complementary parts of a long peptide *chain. often located far apart in the amino acid sequence, find each other and form a unique, biologically active, three-dimensional structure predetermined by that sequence remains* puzzling. *Because proteins need to recognize a diverse array of molecules through complex three-dimensional interactions. their secondary structure varies widely. Within this panoply of secondary structures, however, there are recognizable regularities.*

Kendrew's x-ray crystal structure of myoglobin from 1958. the first of a globular protein. revealed that the amino acid side chains found on the interior of the protein were almost exclusively hydrophobic.[8] *Further structural studies of small proteins led to the idea that the main driving force behind folding of water-soluble globular proteins is to pack hydrophobic side chains into the core. leaving a hydrophilic surface. The problem* comes *when one considers that the hydrophilic main chain (with one NH hydrogen bond donor and one CO acceptor per residue) must assemble, or fold, into the interior along with any hydrophobic side chains. The main chain is neutralized by the formation of regular hydrogen bonds to create (usually) one of two common motifs within the protein interior: the* α-helix *or the* β-sheet *(Fig.* 1), *each*

Encyclopedia of Supramolecular Chemistry
DOI: 10.1081/E-ESMC 120012694

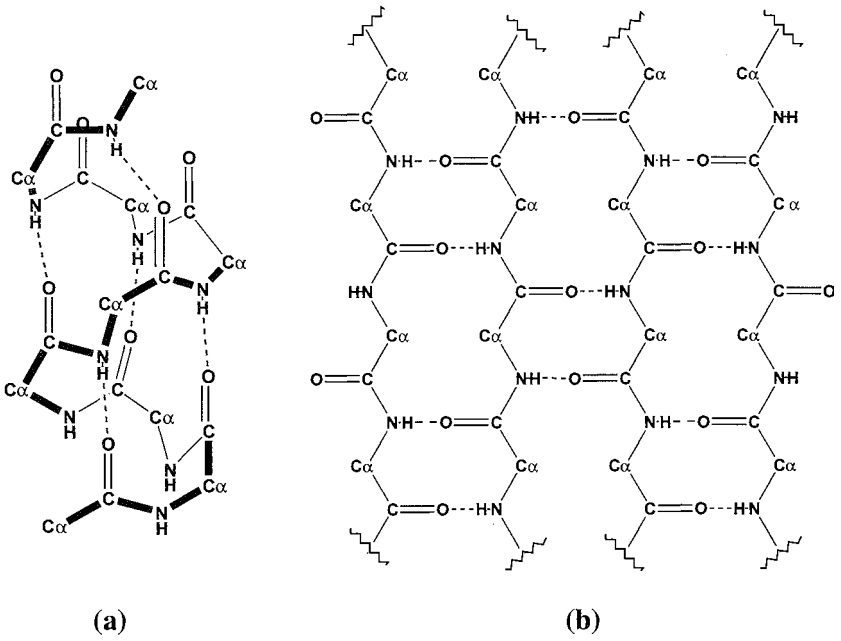

Fig. 1 Two common protein folding motifs: (a) the α-helix, (b) the β-sheet. Side chains are omitted for clarity

with a distinctive hydrogen-bonding pattern. These motifs are connected by short loop regions.[9]

THREE-DIMENSIONAL "SPHERICAL" STRUCTURES

Icosahedral Viruses

A virus consists of a strand of nucleic acid contained in a protective protein shell, the capsid, which serves to relay the genetic information of the core to a host cell, where it may arrest the cell machinery and replicate. Some viruses have an additional lipid bilayer membrane. an envelope, enclosing the capsid. There are two main structural types of simple virus:[10] icosahedral, discussed here, and helical, discussed later.

Crick and Watson were the first to suggest that small viruses were built up of small protein subunits packed together symmetrically to form a protective shell for the nucleic acid.[11] They reasoned that formation of small identical molecules was an efficient use of the limited information contained in the virus nucleic acid. They also realized that, of the types of symmetry possible for a three-dimensional structure enclosing space, only the cubic point groups could lead to an isometric particle, which was the known symmetry of many viruses at the time. Three types of cubic symmetry exist; namely, tetrahedral. octahedral, and icosahedral. For a virus particle, these imply, respectively, 12, 24, or 60 subunits, arranged identically on the surface of a sphere.

To account for large molecular weights of viruses, Caspar and Klug introduced the idea of ''quasi-equivalent'' structure units.[12] They showed that an icosahedron, with 20 equilateral triangular facets, has therefore 60 T structure units, where T is the triangulation number (Fig. 2), given by $T=Pf^2$ [P is any number of the series (1, 3, 7, 13. 19. 21. 31…). and f is any integer]. Subunits can therefore be arranged on the facets of an icosahedron to give icosahedral symmetry. The same types of noncovalent contacts are used between the structure units in the shell, even though they are not in equivalent environments.

The genetic material of a virus, then, contains the code for one of these structure units, which is read many times to make the number of proteins needed to assemble via

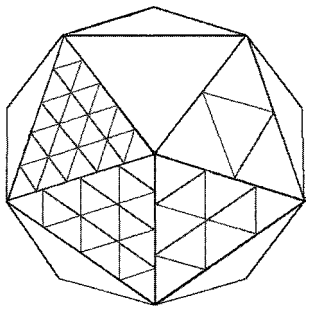

Fig. 2 An icosahedron with each face showing triangulation numbers of, clockwise from top, $T=1$, $T=4$, $T=9$, $T=16$, and $T=25$, respectively. (*View this art in color at www.dekker.com.*)

noncovalent forces into a convergent, icosahedral capsid. In addition to the capsid, enveloped viruses like Sindbis virus are enclosed on the outside by a self-assembled lipid bilayer. The *400* Å diameter capsid of Sindbis virus has $T=3$ icosahedral symmetry and is therefore composed of 180 subunits. It is surrounded by a polyhedral lipid membrane 40 Å thick. Finally, anchored in this membrane are 80 large spikes projecting from the surface, visible by electron microscopy. The spikes are arranged in a $T=4$ icosahedral lattice. The volume of each spike, as measured from electron density maps, corresponds to three copies of each of the two different spike polypeptide chains. The RNA in the core, therefore, codes for three separate protein subunits: one for the capsid and two for the spikes.[9]

Ferritin

Ferritin has two functions within the body: it protects cells from the potentially toxic effects of free iron by sequestering the metal in a mineralized form within a protein shell, and it stores iron for later use by the cell in the synthesis of heme. The shell is made of cylindrically shaped protein subunits. each composed of a bundle of four long helices, a short helix. and an extended loop. Twenty-four of these subunits self-assemble[13] to give a hollow shell with octahedral symmetry and a cavity (diameter −80 Å) capable of storing up to 4500 Fe(III) atoms (30% by weight)'''' as the mineral ferrihydrite ($5Fe_2O_3{\cdot}9H_2O$).[15] The shell is thermally stable and stable to treatment with urea or guanidinium chloride. This stability is largely due to intra- and intersubunit salt bridges and hydrogen bonds.[14]

Iron(II) atoms are oxidized at specific ferroxidase sites on the protein shell and can then enter the host through one of six hydrophobic channels about 4–5 Å wide, which lie along the fourfold symmetry axes. Once core nuclei are formed inside the structure, iron(II) oxidation can occur on the mineral surfaces.[16]

Lipid Membranes

Lipids are amphipathic inolecules composed of a polar, hydrophilic ''head'' connected to a nonpolar, hydrophobic hydrocarbon ''tail.''[17] When in an aqueous environment, lipids tend to associate noncovalently. There are two driving forces for this association: the hydrophobic effect due to the nonpolar tails. and the van der Waals interactions between the hydrocarbon portions of the molecules. This behavior in water can cause lipids to spontaneously form surface monolayers, bilayers, micelles, or vesicles, depending on the structures of the head and tail of the lipid molecule. We shall direct our attention here to the cell membrane bilayer, the most important of these biological assemblies.

The lipids of cell membranes fall into four groups: phospholipids, sphingolipids, glycolipids, and sterols (Fig. 3). The acyl chains generally have chain lengths from C_{10} to C_{28} and can be saturated or unsaturated. Notably, the dominant lipids in membrane formation have highly polar head groups and, usually, two hydrocarbon

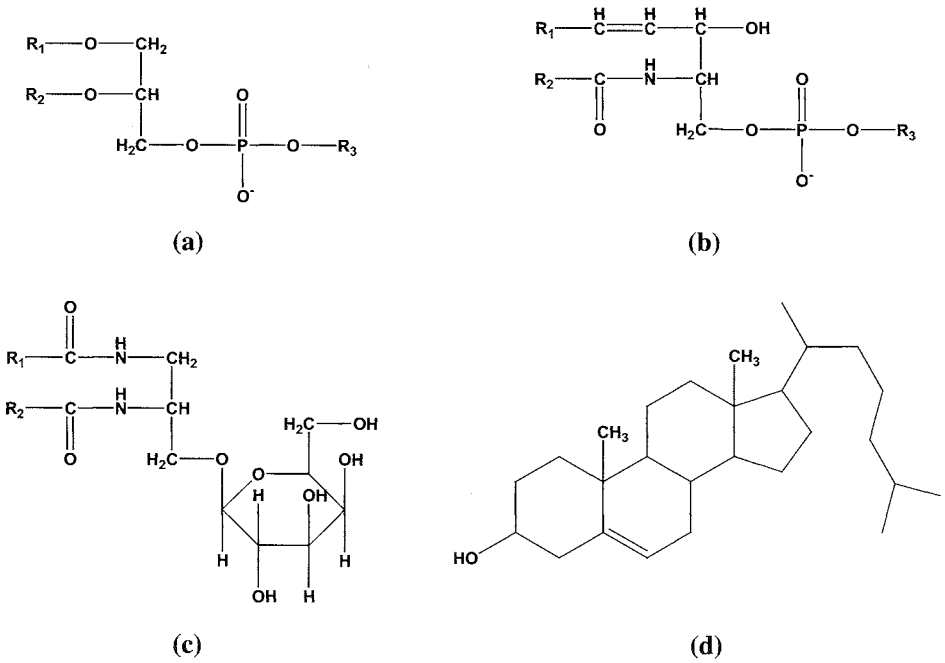

Fig. 3 The four principal groups of cell membrane lipids: (a) phospholipids, (b) sphingolipids. (c) glycolipids (cerebroside pictured), and (d) sterols (cholesterol pictured).

tails. If a large head group were attached to a single hydrocarbon chain, the resulting wedge-shaped molecules would tend to form spherical micelles upon self-association. A double tail results in molecules that can easily pack in parallel to form extended bilayer membrane sheets, with the hydrophilic head groups facing inside and outside toward the aqueous regions.

To say that a cell membrane is essentially a lipid bilayer would be an oversimplification. The basic structure of the lipid bilayer abounds with specific proteins contained within the membrane or attached to its surface. These serve as transport and recognition agents for the cell. Animal and some plant and fungal cells contain sugar residues on their surfaces. These have an important role in cell recognition processes, antigenic properties. and hormone reception.[17]

ROB-SHAPED, HELICAL, OR CYLINDRICAL STRUCTURES

Helical Viruses

Viruses with helical symmetry, or "linear" viral capsids, have their genetic material encased in a helix of identical protein subunits, the length of which is determined by the length of the encased nucleic acid. There are three main classes of simple helical viruses: the rigid rod viruses, the flexuous plant viruses, and the filamentous bacteriophage~.~The most studied of these viruses is the rigid rod Tobacco Mosaic Virus (TMV).

The TMV is composed of about 2100 identical protein subunits. each of molecular weight ~18,000. These self-assemble to form a right-handed helix with 16 $^1/_3$ subunits per turn. The final rod measures 3000 Å in length and 180 A in diameter. A single strand of RNA follows the basic turns of the helix from the inside, at a radial distance of 40 Å from the central axis, with three nucleotides binding to each protein subunit. Assembly is initiated by a preformed protein disk that serves as a sort of jig upon which the first few turns of the viral helix can assemble to reach sufficient size to be stable. It also provides a mechanism for the recognition by the protein of its RNA.[18]

Electron microscopy studies of the elongation process[19,20] showed that during elongation, the 5' and the 3' ends of the RNA extend from the same end of the growing nucleocapsid. As elongation proceeds, the 5' end of the RNA is pulled up and through the central channel of the growing rod. Assembly of the capsid around the 3' end is much slower and may not occur until the 5' end is entirely coated. It is possible that coat proteins are continually synthesized in vivo during the encapsulation of the remainder of the RNA.[10]

There are two charge clusters in the viral structure that provide stability for the capsid through electrostatic interactions. The largest is found near the inner surface of the virus, between 20 and 50 Å from the central axis. It is composed of a number of carboxyl groups in close proximity, which was described as a "carboxyl cage." Such intersubunit carboxyl clusters are a characteristic feature of many virus structures. A smaller charge cluster is found between 55 and 60 Å from the axis.[21]

Motion Machines

Biological systems have a number of ways of producing motility, where self-assembly plays a central role. The most familiar is muscle contraction that produces bodily movement, where the interaction of two proteins, actin and myosin, is critical.[6] For smaller organisms, including cells and the chromosomes and organelles of cells inside the bodies of larger organisms. motion is produced through interactions with microtubules, which are filamentous assemblies of the protein tubulin.[22]

Actin and myosin

Actin exists as a long, fibrous. helical polymer (*F*-actin) of a globular protein monomer (*G*-actin).[6] The polymerization is initiated by binding ATP to a 6-actin monomer. Myosin, on the other hand, is composed of six polypeptide chains: two identical heavy chains and two each of two different light chains. The two heavy chains have long α-helical tails. which intertwine to form a coil at the end of the myosin structure, and globular heads to which the light chains are bound. Between the head and tail domains of the heavy chain is a flexible stalk. The helical tails of myosin can join together to form a bipolar thick filament. Actin and myosin filaments interact to form long myofibers, or individual muscle cells. When a muscle moves from a relaxed to a contracted state, the headpieces of the thick (myosin) filaments pull the thin (actin) filaments together, shortening the myofibril by successively making and breaking cross-bridges in conjunction with binding and hydrolyzing ATP.[6]

Microtubule systems

Microtubules are noncovalent assemblies of the protein tubulin (Fig. 4). There are two closely related types of tubulin subunit, a and β, which alternate in the helical microtubule structure, with 13 subunits per turn. Each subunit weighs 55,000 Da. Assembly is initiated when an $\alpha\beta$ dimer binds to a molecule of GTP. The resulting microtubule is a hollow cylinder of 250 Å outside diameter and 15 Å internal diameter. The length is variable by assembly or disassembly of the subunits. a process that is sensitive to changes of cellular activity and conditions. In vivo. a continuous flow exists between assembled microtubules and the pool of free tubulin (which may represent up to 50% of the total tubulin). Because of the weak forces that hold them together, microtubules can be assembled

when and where they are requested and disassembled when they are of no more use.[22]

Microtubules are used in such diverse places as the mitotic spindle. protozoan and sperm flagella. and nerve axons.[22] They, along with actin filaments, provide the rod-like tracks upon which molecular engines (the proteins dynein and kinesin) transport packages around the cell; as well as provide scaffolding upon which a cell can alter its shape—an amoeba extending a pseudopod, for example. Cilia, used to propel microorganisms through solution and to push dirt-filtering mucus around the respiratory tract, and eukaryotic flagella, which propel the cell by an undulatory motion. both achieve movement with a highly organized bundle of microtubules called an axoneme.

BIOMINERALIZATION

The process of biomineralization involves the well-ordered construction of discrete or extended self-assembled arrangements of organic inolecules (the "organic matrix"), which subsequently associate with inorganic solids in vivo to give precisely controlled biomineral structures. The incorporation of iron into ferritin illustrates biomineralization within a discrete organic structure, the type predominant inside cells. Here we will discuss the case of biominei-alization arising from extended organic matrices, which happens mostly in the intercellular spaces of multicellular organisms to produce structures such as bones. shells. and teeth.[23]

The topology of the organic matrix involved in biomineralization (e.g., tubular, fibrous. pleated sheet) differs depending on the targeted structure. but there is a common theme underlying the process. Hydrophobic proteins first assemble into a structural framework. Then. acidic proteins like aspartic acid. often associated with sulfated polysaccharides. are built onto the insoluble framework and draw minerals, like $CaCO_3$ or SiO_2, out of the surrounding aqueous environment and into an ordered arrangement. It is thought that this molecular recognition process is controlled by electrostatic. structural. and stereochemical complementarity at the organic–inorganic interface.[23]

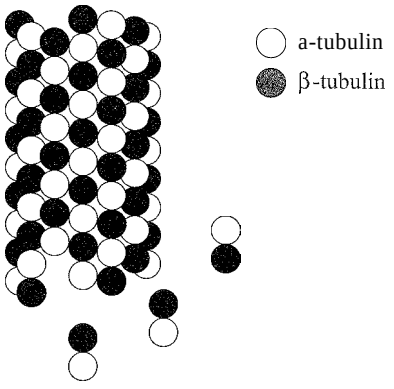

Fig. 4 Assembly of a microtubule from tubulin dimers. α-Tubulin is shown in white: β-tubulin is shown in black.

From a few simple inorganic salts, nature can construct a wide array of mineralized structures able to perform diverse functions. This shows the degree of control that can be exercised by the organic matrix, simply by controlling the crystal growth environment.[24]

For example, molluscan shells are organized composites of two different polymorphs of calcium carbonate (calcite and aragonite) arranged within a matrix of glycoproteins rich in acidic amino acid residues. The shell has a strength ~ 3000 times greater than that of its composite crystals. Different arrangements of crystals are formed, depending on the composition of the organic matrix, to give nacreous, prismatic: foliated. or crossed lamellar layers. It is thought that the chemical structure of the matrix surface complements a specific crystal face of the mineral so that nucleation is directed along a preferred crystallographic axis.[''] It is known that after a layer of calcite has grown on the nucleating protein sheet of a molluscan shell; there is an abrupt transition to production of aragonite to form nacre (mother of pearl). The production of each crystal type is accompanied by production of specific polyanionic proteins, allowing the organism to induce phase changes as needed by controlling the state of the organic–inorganic interface.[25] Though the matrix proteins typically make up less than 2 wt% of the shell. they determine its structural organization and properties.

WHY IS SELF-ASSEMBLY UBIQUITOUS IN NATURE?

Self-assembly is driven by many weak, reversible interactions to obtain a final structure that represents a thermodynamic minimum. In other words. it operates under equilibrium control. Consequently, incorrect structural units are easily rejected in the dynamic equilibrium assembly. giving the process high fidelity.[26]

Self-assembly is highly efficient. because it proceeds by organizing many small subunits that were made by sequential covalent processes to form the final, large structure. For example. if the protein coat of TMV were coded by a single, continuous gene. then the structure would require a section of RNA approximately 1×10^6 base pairs long. As 2130 identical subunits capable of self-assembling are utilized to form the protein coat. the complete structure may be coded for in a gene of around 500 base pairs in length.[26] This represents an economy of information. Additionally, only a few different molecules are normally involved in self-assembly. This means that a limited set of binding interactions is required to cause the final structure to form. allowing for further economy of information.

Finally, complementarity in molecular shape provides the foundation for association between components. This allows for molecular recognition between two specific components.

CONCLUSION

Nature has demonstrated an ability to outperform humans in efficiency of design and strength of materials. If materials scientists can learn to mimic the controlled synthetic processes employed to make durable materials such as bones, teeth, and shells, significant advances could be realized.

Thus. in a coming age of nanotechnology, it is likely that synthetic chemists will strive to make molecules of larger molecular weights, while lithography will make possible the reduction of engineered structures to roughly 1 ym. Indeed, the size gap between these two efforts is converging within a range of many self-assembled biological structures. It is therefore reasonable to assert that a better understanding of self-assembly processes in biological systems will lead to the engineering of functional molecular structures with nanometer-scale dimensions, and beyond.

ARTICLES OF FURTHER INTEREST

Anion-Directed Assembly, p. 51
DNA Nanotechnology, p. 475
Enzymes: Characteristics and Mechanisms, p. *554*
Micelles and Vesicles, p. *861*
Molecular-Level Machines, p. *931*
Self-Assembly: Definition and Kinetic and Thermodynamic Considerations, p. 1248
Strict Self-Assembly and Self-Assembly with Covalent Modifications, p. 1372
Viruses as Host Assemblies, p. *1563*

REFERENCES

1. Whitesides, G.M.; Grzybowski, B. Self-assembly at all scales. Science **2002.** *295.* 2418–2421.
2. Whitesides, G.M.; Boncheva, M. Beyond molecules: Self-assembly of mesoscopic and macroscopic components. Proc. Natl. Acad. Sci. **2002.** *99,* 4769–4774.
3. Kauffman, S. At Home in *the Universe*; Oxford University Press: New York, 1995.
4. Nicolaou, K.C.; Yang, Z.; Liu, J.J.; Ueno, H.; Nantermet. P.G.; Guy, R.K.: Claiborne, C.F.; Renaud, J.; Couladouros, E.A.: Paulvannan. K.: Sorenson, E.J. Total synthesis of taxol. Nature **1994,** *367,* 630–634.
5. Lawrence, D.S.; Jiang, T.; Levett, M. Self-assembling supramolecular complexes. Chem. Rev. **1995,** *95.* 2229–2260.
6. Mathews, C.K.; van Holde. K.E. Bioclzenzistn; Benjamin-Cummings: Menlo Park, 1996; 8. Ch. 4.
7. Smith, B.L.; Schaffer, T.E.; Viani. M.: Thompson, J.B.: Frederick, N.A.; Kindt. J.: Belcher, A.: Stucky, G.D.: Morse. D.E.; Hansma, P.K. Molecular mechanistic origin of the toughness of natural adhesives. fibres and composites. Nature **1999,** 399. 761–763.
8. Kendrew, J.C.; Bodo, G.; Dintzis, H.M.; Parrish, R.G.: Wyckoff, H.; Phillips, D.C. A three-dimensional model of the myoglobin molecule obtained by x-ray analysis. Nature **1958,** *181.* 662–666.
9. Branden, C.: Tooze, J. Introduction to Protein *Structure*: Garland: New York. 1991; Ch. 11.
10. Makowski, L. Structural studies of the assembly of simple viruses. Prog. Clin. Biol. Res. **1980,** *40,* 158–233.
11. Crick, F.H.C.; Watson, J.D. The structure of small viruses. Nature **1956,** *177.* 473–475.
12. Caspar. D.L.D.: Klug, A. Physical principles in the construction of regular viruses. Cold Spring Harbor Symp. Quant. Biol. **1962,** *27,* 1–24.
13. Caulder, D.L.; Raymond, K.N. The rational design of high symmetry coordination clusters. J. Chem. Soc. Dalton Trans. **1999.** *8,* 1185–1200.
14. Harrison, P.M.; Arosio, P. The ferritins: Molecular properties. iron storage function and cellular regulation. Biochim. Biophys. Acta **1996,** *1275,* 161–203.
15. Crichton. R.R.: Ward, R.J. Iron metabolism—New perspectives in view. Biochemistry **1992,** *31,* 11255–11264.
16. Proulx-Curry. P.M.: Chasteen, N.D. Molecular aspects of iron uptake and storage in ferritin. Coord. Chem. Rev. **1995.** *144.* 347–368.
17. Jones. M.N.; Chapman. D. Micelles, *Monolayers,* aizd *Biomembranes*; Wiley-Liss: New York, 1995.
18. Klug, A. From macromolecule to biological molecular assembly (Nobel lecture). Angew. Chem., Int. Ed. Engl. **1983.** *22,* 565–582.
19. Butler, P.J.G.; Finch, J.T.; Zimmern, D. Configuration of tobacco mosaic virus RNA during virus assembly. Nature **19'77,** *265,* 217.
20. Lebeurier, G.: Nicolaieff, A.; Richards, K.E. Inside-out model for self-assembly of tobacco mosaic virus. Proc. Natl. Acad. Sci. U. S. A. **1977.** *74,* 139.
21. Namba, *K.;* Stubbs, G. Structure of tobacco mosaic virus at 3.6 Å resolution: Implications for assembly. Science **1986,** *231.* 1401–1406.
22. Dustin; P. *Microtubules*; Springer-Verlag: New York, 1984.
23. Mann. S. Molecular tectonics in biomineralization and biomimetic materials chemistry. Nature **1993,** *365.* 499–505.
24. Aizenberg, J. Patterned crystallization of calcite in vivo and in vitro. J. Cryst. Growth **2000.** *211,* 143–148.
25. Belcher. A.M.; Wu. X.H.: Christensen, R.J.; Hansma. P.K.: Stucky, G.D.; Morse, D.E. Control of crystal phase switching and orientation by soluble mollusk-shell proteins. Nature **1996,** *381.* 56–58.
26. Philp, D.; Stoddart, J.F. Self-assembly in natural and unnatural systems. Angew. Chem., Int. Ed. Engl. **1996,** *35.* 1154–1196.

Self-Assembly: Terminology

Gerhard F. Swiegers
Commonwealth Scientific and Industrial Research Organisation (CSIRO), Melbourne, Victoria, Australia

INTRODUCTION

Self-assembly processes can today be found in a variety of fields ranging from biology to materials science and electronics. While self-assembly has proven to be a valuable tool in the formation of supramolecular assemblies, it remains less a discipline in its own right than a compilation of principles that have been applied to an apparently disparate collection of research fields. One outcome of this historical development is that the concepts of self-assembly were typically defined in discipline-specific and sometimes overlapping ways. This fragmentation obscures their underlying coherence and universality. It also hinders a widespread understanding of self-assembly.

In this article. the various terminologies used to describe important concepts in thermodynamic self-assembly will be reviewed. In so doing, an attempt is made to illustrate. wherever possible, the underlying unity of the concepts and eliminate confusion arising from the different terminologies used. Most of the terminologies derive from the fields of chemistry. biology, and biochemistry.

TERMINOLOGIES TO DESCRIBE HIERARCHICAL SELF-ASSEMBLED STRUCTURES

The dramatic development of biochemistry in the twentieth century can largely be attributed to breakthroughs in the understanding of the supramolecular structure of biomolecules. Pauling and Corey's work on the structure of proteins and the discovery of the DNA double helix[1,2] demonstrated the critical importance of supramolecular structure in biology and stimulated interest in its study as well as in the processes by which it is formed.

One of the most remarkable properties of self-assembly is its ability to generate exceedingly coinplicated supramolecular structures frorn fairly simple components. Perhaps the most elegant embodiment of this phenomenon is protein structure. Proteins exhibit at least four hierarchies of structure: primary, secondary, tertiary. and quaternary structures.[1,2] Primary structure describes the covalent connections making up the sequence of amino acids in each strand. Secondary structure involves local architectural elements created when portions of a strand twist or loop into regularly repeating arrangements, like α-helices or β-sheets. The overall folding of each polypeptide chain is considered to be tertiary structure: while the spatial arrangement of several strands relative to each other is known as quaternary structure. Some of the hierarchies may be further subdivided. For example. repetitions of a secondary structural feature within one particular fold of a protein are sometimes referred to as supersecondary structures.[1,2] The tertiary structures of large proteins may also consist of domains, each of which comprises a fold or series of folds having their own interior surface and connected to other domains by an interconnecting strand of the backbone.[1,2] The individual constituents of an extended quaternary structure are typically known as protomers.[1,2]

These levels of organization are hierarchical, because each level cannot exist without the preceding level. For example. a tertiary structure requires the presence of secondary structural elements. These cannot exist without a primary structure. When viewed in a widening perspective, from an atomic level to a more macroscopic level. each of the hierarchies of organization becomes progressively obvious.

Similar levels of structural hierarchy can be discerned in nonbiological self-assembled compounds such as coordination complexes.[3] Metal helicates display secondary structure in their overall helical architectures and primary structures in the covalent connections of the organic ligands.[4] Tertiary structure can be observed in the cyclized metal helicates known as circular helicates,[5] while quaternary structure is present in certain coordination polymers.[3] The only important difference, from a self-assembly point of view. between an r-helix in biology and a metal helicate in coordination chemistry is the type of noncovalent interactions that drive the self-assembly process, i.e., the formation of coordination bonds in the latter case and the formation of hydrogen bonds. ion-pairing interactions, and hydrophobic–hydrophilic interactions in the former. While coordinate interactions are more directional and stronger (bond energies ca. 10–30 kcal mol^{-1}) than the biological interactions (bond energies ca. 0.6–7 kcal mol^{-1}), all are nevertheless noncovalent in nature.

In the study of self-assembled supramolecular assemblies directed by π donor–acceptor interactions, Stoddart

DOI: 10.1081/E-ESMC 120012878

noted the existence of structural hierarchies. In his terminology,[6] assemblies exhibiting secondary structure are termed supermolecules, with individual components that are designated as primary molecules or tectons. Assemblies displaying tertiary structures are called supramolecular arrays. while quaternary structures are found in macroscopic conglomerates.

These descriptions and terminologies are conceptually analogous, differing only in their discipline-specific framing and the nature of the interactions involved.

TERMINOLOGIES FOR DYNAMIC SELF-ASSEMBLY PROCESSES

Self-assembly in biology — the so-called dance of life — is largely driven by the enthalpy of formation of the three fundamental noncovalent interactions mentioned earlier. Other classes of interaction employed in self-assembly include coordinate bond formation and π–π acceptor–donor interactions. Steric factors, conformational preferences, and entropic driving forces also play significant roles.[3] In a kinetically rapid, dynamic, thermodynamic self-assembly; all of these possible contributions are continuously at play. They act to ensure a never-ending association and dissociation of all possible products, with the lowest-energy products being present in the greatest proportion at any one time.[7] Thus. a combinatorial library of products, each with their own structural architecture. exists in self-assembling mixtures.[8] Because of their high energies, most of the members of such a library are present in infinitesimally small proportions; the assembly can therefore be considered to be a virtual combinatorial library.[8] Each member of the library, nevertheless, represents the whole library, because it can be disassembled and reassembled into every other member. The main constituents of the library can be changed by varying an external factor. like temperature or concentration. which affects the thermodynamic stabilities of the members. Thermodynamic self-assembly is therefore truly a dynamic combinatorial process.[8]

TERMINOLOGIES DESCRIBING REPRODUCIBILITY IN SELF-ASSEMBLY

The existence of life depends, crucially, on the reproducibility of self-assembly processes in biology. Without unqualified fidelity. protein-based ion-pumps and enzymes. among other biological devices, could not operate.[2] But what are the origins of this noteworthy characteristic?

The property of reproducibility generally arises from the thermodynamic equilibrium present. In strict self-assembly,[3] the system uniformly seeks and settles upon the lowest-energy arrangement.[7] Thermodynamics dictates that this state will always be the product of the self-assembly under a determined set of physical conditions. "Strict" or "thermodynamic" self-assembly refers to processes dominated by a kinetically rapid, reversible thermodynamic equilibrium. This equilibrium exists at all times during the assembly. The products are, therefore: obtained in proportions determined by their relative thermodynamic stabilities.

It has long been known that certain types of components can drive the self-assembly of particular structures. For example, the amino acid residues alanine and leucine promote α-helix formation when they are present within a polypeptide chain, while glycine and tyrosine are considered "helix breakers."[1]

These preferences usually originate in stereochemical and structural limitations that affect the thermodynamics of the system. As such, they can be considered instructions that direct the self-assembly process.[9] In some cases, the preferences are extreme, so that they dominate the system regardless of alternative influences. In others, they are less intense and must be weighed against other factors. In a complicated multicomponent system. for example, not all of the component preferences will be aligned, i.e., the instructions may be contradictory. In such a case; self-assembly becomes a process in which the preponderance of instructions and their intensities dominate. But how does this take place?

Lehn proposed considering self-assembly in coordination chemistry to be akin to a computer program driven by an ".interactional" algorithm.[9,10] The algorithm is established by the interplay between the structure of the ligands and the stereochemistry of the metal ions. i.e., by the preferences of the components. Algorithms, however, involve a linear hierarchy of commands that execute to completion and then stop. As mentioned earlier, thermodynamic self-assembly is, by contrast; entirely pathway independent. and it never stops. Where then is the linearity and hierarchy implied in the analogy? It is energetic in nature, and it applies to the system as a whole rather than to any one constituent molecule. Thus, thermodynamic self-assembling systems transform themselves. linearly. from a high-energy to a low-energy state.[7] While many individual pathways may be followed in this process, all are characterized by a process known as positive cooperativity. This effectively involves the stepwise optimization of structural elements from those producing the greatest thermodynamic stabilization to those producing the smallest.[7] The strongest and most intense preferences or instructions must be finalized first, followed by a hierarchy of instructions from most to least energetically important. For example, self-assembly of a metal helicate involves the initial formation of an increasing number of coordination bonds. However, the instruction for the characteristic helical twisting is, for all pathways, carried out only during the last step.[7] Self-assembly processes

involving the formation of coordination bonds (strong) and π–π acceptor–donor interactions (weak) must, therefore, first optimize elements involving the former interactions and then those involving the latter. In following this linear hierarchy of thermodynamic instructions, it is, of course, conceivable that the combined instructions at the lower end of the hierarchy may overturn those at the top. but this can only happen after the former are satisfied.

This concept has important implications. It explains, for example, how proteins fold as fast as they do. For example, a protein containing 100 amino acid residues should take at least 10^{27} years to reach its lowest energy state if it does so by exploring all of its possible conformations.[12] Instead. such proteins typically fold within minutes. This can only occur because energetically highly favored local folds are formed first, and these then serve as nuclei that attract and stabilize other elements of secondary structure.[2]

Instructed, reproducible self-assembly of this type can be seen in numerous disciplines. In polymer chemistry, certain oligo(phenylene ethylenes) undergo solvophobic folding into helical conformations in polar solvents.[11] In peptide science. synthetic polypeptides containing unnatural β-amino acids spontaneously adopt helical dispositions in solution, despite being unable to form the hydrogen bonds that drive self-assembly in normal biopolymers.[12]

TERMINOLOGIES DESCRIBING THE COMPLEXITY OF SELF-ASSEMBLY PROCESSES

The thermodynamic hierarchies discussed in the previous section offer important opportunities to manipulate self-assembly processes. In particular, they raise the possibility of innovatively assembling novel structures that display unusual physical properties or that can be switched between different physical states. The latter aspect is particularly important, because it prospectively provides a means of creating a molecular computational[13] or information storage system.[14] As many self-assembled structural motifs cannot be easily obtained by other means, this concept also opens the way to a wide variety of supramolecular compounds displaying novel properties, such as self-assembling catalysts.[15]

Several researchers recognized and sought to exploit this approach. Fujita and coworkers. for example, developed so-called multiple-molecular recognition processes, in which the self-assembly of coordination bonds is accompanied in situ by the formation of weaker interactions: such as π donor–acceptor and hydrophobic/hydrophilic interactions.[16] Illustrated in Fig. 1 is an example of such an assembly. in which a molecular switch is created by the interlocking or diassociation, upon command, of two cyclic molecules.[17]

Lehn and coworkers developed a similar approach. which they term double code or double subroutine self-assembly.[18] In this technique: different metal ions in a mixture are induced to selectively interact with different binding sites on a single. hybrid ligand, giving assemblies displaying novel structures. An example of such a process is shown in Fig. 2.[19]

In general, it is possible to distinguish two classes of self-assembly in this respect:[20] single-interaction self-assembly and multiple-interaction self-assembly. Single-interaction self-assembly, also referred to as single-code self-assembly, involves the formation of one specific interaction during the self-assembly process. In Fig. 3a, an example of a single-interaction process is depicted in which a metal ion interacts with a multitopic ligand strand by forming the same type of metal–ligand coordination bond at each binding site.

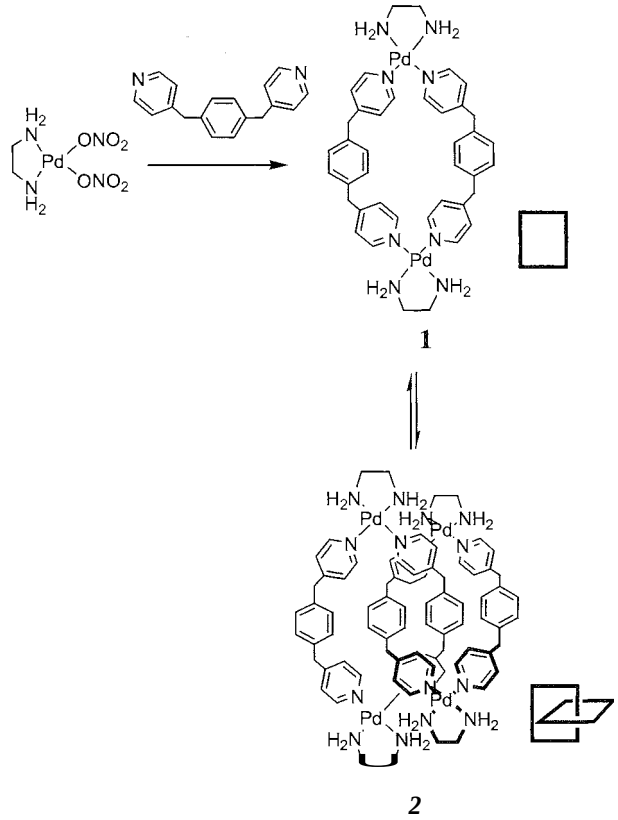

Fig. 1 Multiple molecular recognition: Free metallocycle **1** is formed in dilute solution because of the enthalpy of formation of the Pd—N coordination bonds. When the solution is concentrated from 2–50 mM, the lability of these bonds allows the in situ formation of the interlocked catenane **2**. This is driven by hydrophobic interactions to minimize the contact of the metallocycle cavities with the water solvent, the formation of π-stacking interactions between two such rings. and an entropic effect due to a decline in the number of species present in solution after interlocking.

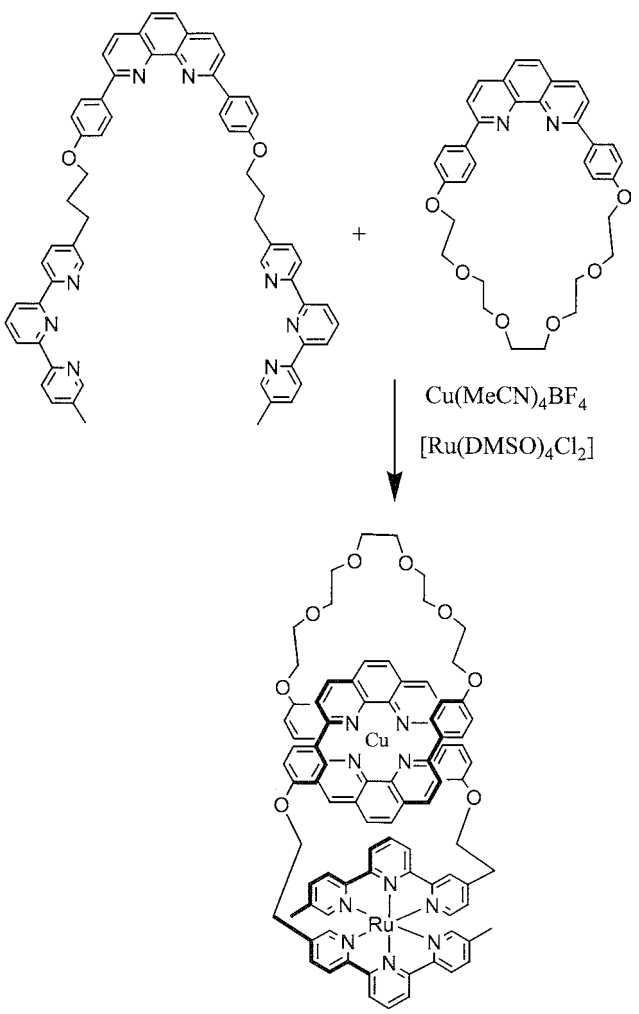

Fig. *2* Double subroutine self-assembly: The formation of a metallocatenane. (From Ref. [19].)

Multiple-interaction self-assembly involves the formation of more than one type of interaction. Illustrated in Fig. 3b is a multiple-interaction process in which two types of coordinate bonds are formed (i.e., double subroutine self-assembly). Depicted in Fig. 3c is a multiple-interaction process in which one type of coordinate bond and one type of hydrogen bond are formed (i.e., a multiple inolecular recognition process). Processes like that depicted in Fig. 3b involve mediation by one class of interaction only, and can therefore be referred to as unmediated.[20] Processes of the type depicted in Fig. 3c involve mediation by two different classes of interaction and are therefore referred to as multimediated.[20]

The three processes illustrated in Fig. 3 differ fundamentaliy in their self-assembly properties, because they exhibit different thermodynamic hierarchies.[20] Their potentials in regard to self-assembly are therefore also quite different. For example. in Fig. 3a, only one bond angle is possible: the range of architectural alternatives is therefore similarly limited. In Fig. 3b, two types of bond angles are possible, so that a greater range of possible architectures are available. The self-assembly in Fig. 3c prospectively allows for the most architectural variety. because the noncoordinate interactions are weak and poorly directed.

TERMINOLOGIES TO DESCRIBE 2-D AND 3-D CYCLIC ASSEMBLIES

Self-assembled two-dimensional (2-D) and three-dimensional (3-D) cyclic assemblies are known in fields including biology (e.g., spherical viruses) and chemistry (e.g., cryptands, polyoxometallates). While such capsules are exceedingly important entities. their architectures are highly diverse,[21] a fact which long hindered their systematic classification. MacGillivray and Atwood have. however, formalized the description of such species using an analogy based on the principles of solid geometry.[22] Their system employs the Platonic and Archimedean solids, along with prisms, antiprisms, duals. irregular polyhedra, and other pseudospherical arrangements as models of spheroidal design. The structure of a self-assembled capsule is classified according to its resemblance to these structures. The comparative nature of this approach is topologically correct, because most of the above solids

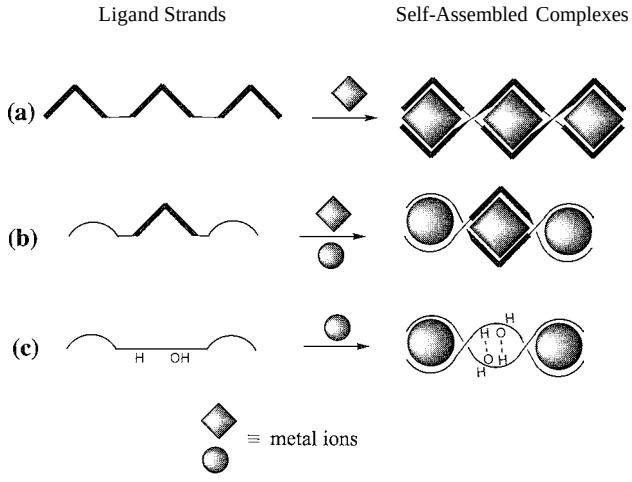

Fig. 3 Classes of self-assembly: The forination of metal helicates by: (a) single-interaction self-assembly. (b) unimediated multiple-interaction self-assembly. and (c) multimediated multiple-interaction self-assembly.[20] The circles and diamonds represent metal ions with preferences to bind the semicircular and half-diamond binding sites, respectively. on the hybrid ligand strands.

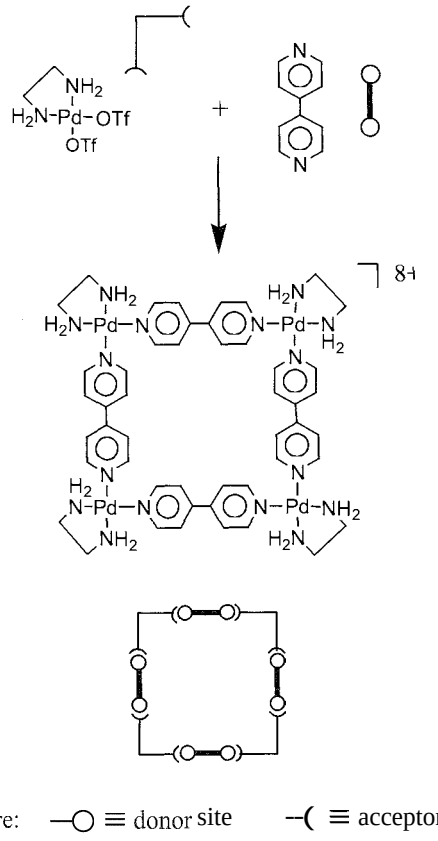

Fig. 4 Self-assembly of an edge-defined molecular square by the Molecular Library approach (From Ref. [25].)

can be continuously deformed into spheres. However. as noted elsewhere.[23] it can produce ambiguities due to the sometimes subjective nature of the comparisons; real supramolecular structures do not always clearly correspond to idealized polyhedral structures.

Various techniques were developed to aid in the rational design of self-assembling systems. The best known of these are the Molecular Library method and the Symmetry Interaction method.

The Molecular Library approach employs complementary components to generate geometrically shaped assemblies.[24] The highly directional formation of coordination bonds between suitably rigid, complementary donor (ligand-based) and acceptor (metal-based) components makes this approach most appropriate to coordination chemistry. In Fig. 4. the formation of a inolecular square by this approach is illustrated.[25] A wide variety of secondary structures displaying polygonal and polyhedral geometries have been self-assembled using this technique, including molecular triangles; hexagons, triangular prisms, octahedra, cubes. and adamantanoid and other boxes.[26] The Molecular Library approach is most suitable to the formation of edge-defined polyhedra, in which the components lie on the corners and edges of the structures.

The basis of the Symmetry Interaction approach lies in the recognition that many natural suprarnolecular assemblies are formed in symmetry-driven processes involving incoinmensurate lock-and-key interactions.[27] A polyhedral structure can therefore be designed by determining the symmetry interactions and the associated geometric relationships necessary to generate that structure from a combination of preorganized ligands and metal ions. The following terms describe these relationships in coordination chemistry.[27] The coordinate vector of a binding group bisects the chelate in the direction of the metal ion to which it is bound. The chelate plane of a metal ion is the plane that contains all of the coordinate vectors of the bound groups. The approach angle describes the arrangement of three bidentate chelators about a metal ion: it defines the angle between the plane holding the coordinating atoms of a bidentate chelating group and

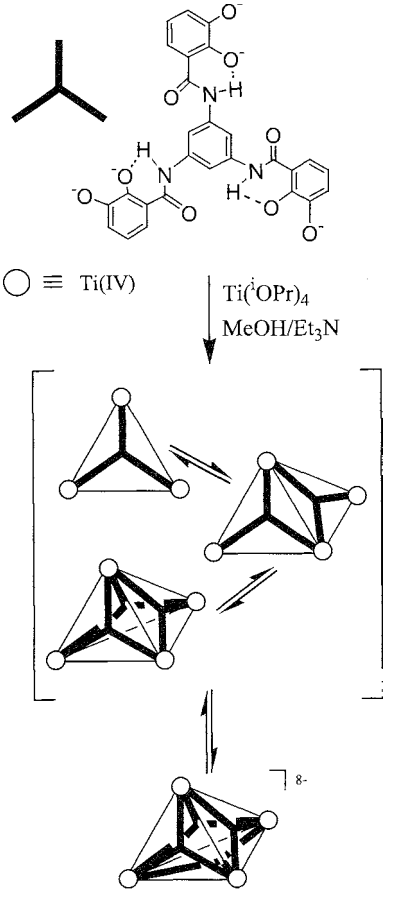

Fig. 5 Self-assembly of a face-occupied inolecular tetrahedron by the Symmetry Interaction approach (From Ref [28])

the major symmetry axis of the metal center. Each class of polyhedra involves different relationships between these variables. The Symmetry Interaction approach is particularly suited to the formation of face-defined polyhedra, in which the components lie on the corners and faces of the structure.[23] Illustrated in Fig. 5 is the formation of a face-occupied tetrahedron.[28]

Several terminologies were created to describe the composition of self-assembled structures and therefore also of the self-assembly process. Stang's assembly descriptor terminology involves treating the assembly components as linear (L), or angular (A), and then listing the numbers and types of each constituent with superscripts to describe their respective topicities.[26] An assembly, such as the square shown in Fig. 4 is therefore assigned the descriptor $A_4{}^2L_4{}^2$, because it consists of four ditopic angular units and four ditopic linear units. This approach offers a convenient abbreviation of the self-assembly process and also provides information about the number of linkages formed and the coordinative saturation of the resulting cycle.

Stang's assembly descriptor terminology was recently amended to include a designation of the nature of the linkage sites on the assembly components.[29] In this terminology, each component is further superscripted with d's or a's to indicate the types of binding sites present. The designation d signifies a donor site and a an acceptor site. A unique descriptor is thereby obtained that fully describes the self-assembly process. This approach has a number of advantages: it allows for a systematic analysis of all of the self-assembly pathways leading to a particular polygonal or polyhedral structure.[30] It also offers a simple means of identifying commonalities between different self-assembly processes, including identical processes.

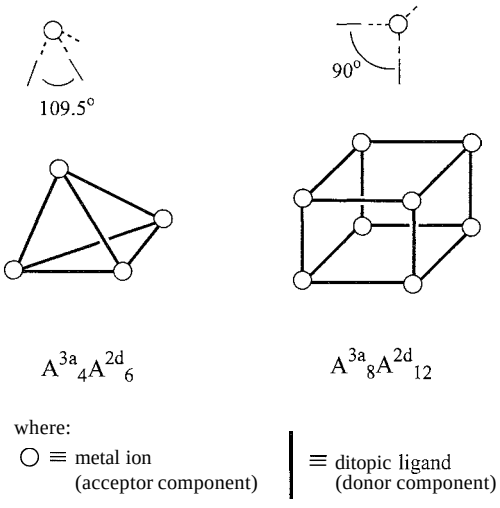

Fig. **6** Switchable molecular structures displaying the same stoichiornetries and component topicities.

near-identical processes, and processes involving common components.[29,30] Polygons and polyhedra that can be switched between structures are easily identified using this approach.[29] For example, illustrated in Fig. 6 are an $A_4{}^{3a}L_6{}^{2d}$ molecular tetrahedron and an $A_8{}^{3a}L_{12}{}^{2d}$ cube. Despite their different overall shapes, these structures have the same stoichiometry and component topicity and would therefore likely switch from one to the other if the directing angles of the angled component were toggled between 109.5" (tetrahedron) and 90° (cube).[29]

CONCLUSION

Self-assembly processes offer important opportunities to inexpensively fabricate novel, molecular-based structures and devices. Underlying all thermodynamic self-assembly processes is a set of common principles with a complexity that has not yet been fully exploited. Recent advances provided significant new insights into self-assembly. These are already generating new ways to manipulate self-assembly in the formation of coinplicated nonbiological entities. Developments such as these are mere precursors for what is still to come. Thanks to self-assembly, molecular engineering will undoubtedly take over from nanoscopic engineering as the dominant and topical theme of the day.

ARTICLES OF FURTHER INTEREST

Anion-Directed Assembly, p. 51
Enzymes: Characteristics and Mechanisms, p. 554
Hydrogen Bonding, p. 658
Molecular *Squares,* Boxes, *and* Cubes, p. 909
Molecular-Level Machines, p. 931
Protein *Supramolecular Chemistry*, p. 1161
Racks, Ladders, and Grids, p. 1186
Self-Assembling *Catenanes*, p. 1240
Self-Assembly: Definition and Kinetic and *Thermodynamic* Considerations, p. 1248
Self-Assembly in *Biochemistry*, p. 1257
The Template Effect. p. 1493

REFERENCES

1. Kuchel, P.W.: Ralston. G.B.: Bersten. A.M.: Easterbrook-Smith. S.B.: Jones, A.R.; Montague, M.D.: Slaytor, M.B.: Thomas, M.A.W.: Wake, R.G. *Chapters 3–5. Schaums Outline of Theory and Problems of Biochemistry*; McGraw Hill Inc.: New York, 1988; 50–140.
2. Stryer, L.B. Chap 2 4 . In *Biochemistry, Third Edition;*

W. H. Freeman and Company: New York. 1988; 15–90.
3. Swiegers, G.F.: Malefetse. T.J. New self-assembled structural motifs in coordination chemistry. Chem. Rev. 2000, 100. 3483–3537. and references therein.
4. Lehn, J.-M. Perspectives in supramolecular chemistry—From molecular recognition towards molecular information processing and self-organisation. Angew. Chem.. Int. Ed. Engl. 1990. 29. 1304–1319.
5. Hasenknopf, B.: Lehn, J.-M.: Boumediene. N.; Dupont-Gervais. A.; van Dorsselaer. A.; Kneisel. B.; Fenske. D. Self-assembly of tetra- and hexanuclear circular helicates. J. Am. Chem. Soc. 1997. 119, 10956–10962.
6. Fyfe. M.C.T.: Stoddart. J.F. Synthetic supramolecular chemistry. Acc. Chem. Res. 1997. 30. 393–401.
7. Pfeil, A.: Lehn. J.-M. Helicate self-organisation: Positive cooperativity in the self-assembly of double-helical metal complexes. J. Chem. Soc.. Chem. Commun. 1992. 838–840.
8. Lehn, J.M. Dynamic cornbinatorial chemistry and virtual combinatorial libraries. Chem. Eur. J. 1999. *5*, 2455–2463.
9. Lehn. J.-M. Supramolecular chemistry—Molecular information and the design of supramolecular materials. Makromol. Chem., Macromol. Symp. 1993, 69. 1–17.
10. Machado. V.G.; Baxter. P.N.; Lehn, J.M. Self-assembly in self-organized inorganic systems: A view of programmed rnetallosupraniolecular architectures. J. Braz. Chem. Soc. 2001, 12. 431–462. and references therein.
11. Nelson. J.C.; Saven. J.C.: Moore. J.S.; Wolynes. P.G. Solvophobically driven folding of nonbiological oligomers. Science 1997. *277*, 1793–1796.
12. Stigers, K.D.: Soth. M.J.; Nowick, J.S. Designed molecules that fold to mimic protein secondary structures. Curr. Opin. Chem. Biol. 1999. 3. 714–723.
13. Rothemund. P.W.K. Using lateral capillary forces to compute by self-assembly. Proc. Natl. Acad. Sci. U. S. A. 2000. *97*. 984–989.
14. Lehn. J.-M. Programmed chemical systems: Multiple subprograms and multiple processing/expression of molecular information. Chem. Eur. J. 2000. 6. 2097–2102.
15. Hill. C.L.: Zhang. X. A smart catalyst that self-assembles under turnover conditions. Nature 1995. *373*. 324–326.
16. Fujita, *M*. Self-assembly of [2]catenanes containing metals in their backbones. Acc. Chem. Res. 1999. 32. 53–61.
17. Fujita, M.; Ibukuro. F.: Hagihara, H.; Ogura. K. Quantitative self-assembly of a [2]catenane from two preformed molecular rings. Nature 1994. *367*. 720–722.
18. Funeriu. D.P.; Lehn. J.-M.; Baum, C.: Fenske, D. Double subroutine self-assembly, spontaneous generation of a nanocyclic dodecanuclear Cu^{I} inorganic architecture. Chem. Eur. J. 1997, *3*. 99–104.
19. Cárdenas, D.J.; Gaviiia, P.; Sauvage. J.-P. Construction of interlocking and threaded rings using two different transition metals as templating and connecting centers: Catenanes and rotaxanes incorporating $Ru(terpy)_2$-units in the framework. J. Am. Chem. Soc. 1997. 119, 2656–2664.
20. Swiegers. G.F.; Malefetse. T.J. Multiple-interaction self-assembly in coordination chemistry. J. Incl. Phenom. Macrocycl. Chem. 2001. 40, 253–264.
21. Conn. M.M.; Rebek. J. Self-assembling capsules. Chem. Rev. 1997. *97*, 1647–1668.
22. McGillivray, L.R.; Atwood. J.L. Structural classification and general principles for the design of spherical molecular hosts. Angew. Chem.. Int. Ed. Engl. 9999. *38*, 1018–1033.
23. Swiegers. G.F. Chapter 1.99. In Topologies *of Assemblies*; Lever. A.B.P., McCleverty, J., Meyer, T.J., Eds.: Comprehensive Coordination Chemistry II, Elsevier Scientific: Oxford, Vol. I. *in* press.
24. Stang. P.J.; Olenyuk, B. Self-assembly, symmetry, and molecular architecture: Coordination as the motif in the rational design of supramolecular metallacyclic polygons and polyhedra. Acc. Chein. Res. 199'7. *30*. 502–518. and references therein.
25. Fujita. M.: Yakazi, J.; Ogura. K. Preparation of a macrocyclic polynuclear complex, $[(en)Pd(4,4'\text{-bpy})]_4(NO_3)_8$, which recognises an organic molecule in aqueous solution. J. Am. Chem. Soc. 1990.112.5645–5647.
26. Leininger. S.: Olenyuk, B.; Stang. P.J. Self-assembly of discrete cyclic nanostructures mediated by transition metals. Chem. Rev. 2000. 100. 853–908. and references therein.
27. Caulder. D.L.: Raymond. K.N. Supermolecules by design. Acc. Chem. Res. 1999. *32*, 975–982, and references therein.
28. Briickner, C.: Powers. R.E.: Raymond, K.N. Symmetry driven rational design of a tetrahedral supramolecular Ti_4L_4 cluster. Angew. Chem., Int. Ed. Engl. 1998. *37*, 1837–1839.
29. Swiegers, G.F.: Malafetse. T.J. Classification of coordination polygons and polyhedra according to their mode of self-assembly. Chem. Eur. J. 2001, *7*. 3637–3643.
30. Swiegers, G.F.: Malefetse. T.J. Classification of coordination polygons and polyhedra according to their mode of self-assembly. 2. Review of the literature. Coord. Chem. Rev. 2002. *225*, 91–121.

Semiochemistry

Antony M. Hooper
John A. Pickett
Rothamsted Research, Harpenden, Hertfordshire, United Kingdom

INTRODUCTION

A semiochemical, derived from the Greek word *semeion* meaning sign. is a chemical signal mediating interactions between organisms, either of the same species (pheromones) or between different species (allelochemicals). Examples of sex pheromones employed by mating moths are well known. Male moths. with their large antennae, locate females using an odor plume of sex pheromone. The first chemically characterized example was bombykol **1**, the sex pheromone of the silkworm moth *Bombyx mori*,[1] an organism still used as a study model (see below). Identifying the sex pheromones of insect pest species, particularly lepidopterous pests, led to pest inanagement strategies in agricultural systems that disrupt mating by the release of competitively high concentrations of the sex pheromone. An alternative strategy is illustrated by use of the aphid sex pheromone[2,3] to lure pests away from crops to areas where biological control or localized pesticide spraying can be used, minimizing the environmental iinpact of conventional pesticides.[4] Pheromones can elicit behaviors other than the familiar mating response. Alarm pheromones elicit escape behavior in aphids or muster an attack in social hymenopterous insects, such as honeybees and some ant species. The aggregation pheromone of the ladybird. *Coccinella septempunctata*, is an example of an epideictic or dispersal pherornone. The mosquito, *Culex quinquefasciatus*, has an oviposition pheromone. All these are important aspects of insect behavior that may be regulated by semiochemistry.

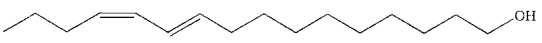

I - Bombykol

Allelochemicals are most notable in examples of host–plant and nonhost–plant selection, a process that is vital for phytophagous pest insects to locate food plants and avoid unsuitable or toxic hosts. Aphids have taxonomically unrelated summer and winter hosts. The bird-cherry-oat aphid, *Rhopalosiphum yadi*. is able to detect species-specific odors from each of its hosts, the bird-cherry tree. *Prunus padus*, in winter and summer cereal crops. One such allelochemical from the winter host is methyl salicylate 2, and the aphid's behavioral response changes from attraction in winter to repulsion, as it migrates to its summer host. Hematophagous insects such as mosquitoes or midges also use chemical odors from their animal hosts for location. These are examples of kairomones. which are defined as semiochemicals where only the receiver of the semiochemical benefits from the interaction. Insect antifeedants such as ajugarin are examples of allomones, compounds that benefit the emitter of the semiochemical. Ajugarin is not toxic at natural concentrations but prevents susceptible insects from feeding on the labiate plant, *Ajuga remota*. Synomones benefit emitter and receiver, for example, the attraction of pollinating insects to flowers; and apneumones are compounds emitted from nonliving material. It is common for semiochemical components to have multiple roles and exert effects on multiple trophic levels. Nepetalactone **3a** is the sex pheromone of the grain aphid, *Sitobion avenae*, but also attracts parasitic braconid wasps. e.g., *Praon* sp., that inject an egg into the aphid, which subsequently develops, consuming the host. Nepetalactone therefore acts as a sex pheromone and also as a kairomone. An even more sophisticated example is the release of isothiocyanates by cruciferous plants under attack from herbivores, such as the diamondback moth, *Plutella xylostella*. Herbivorous insect attack on the plant releases myrosinase enzymes (specific thioglucosidases) in the damaged plant tissue that catalyze the decomposition of glucosinolates to isothiocyanates. These compounds are repellent to many insects, but *P. xylostella* is adapted to feed on crucifers and is attracted by them. Furthermore, compounds such as allyl isothiocyanate 4 also attract parasitoids, such as *Cotesia xylostella*, that can destroy the herbivore, thereby acting as a synomone working in a tritrophic system.

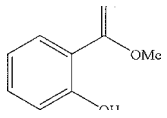

2

Semiochemical biogenesis employs biosynthetic pathways common to many organisms. and this, combined

Encyclopedia of Supramolecular Chemistry
DOI: 10.1081/E-ESMC 120012785

with the requirements for most semiochemicals to be lipophilic, of low molecular weight, and, therefore, volatile. limits their structural diversity. As a consequence, behavioral response often depends on the detection of more than one semiochemical component in a blend. These blends are often detected at the same site of the antenna by co-located olfactory organs, and so the semiochemicals must be in the same odor plume to be recognized, verifying to the insect that they originate from the same source. Many species of aphid use nepetalactone **3a** and nepetalactol **3b** as their sex pheromone but respond to species-specific ratios. Also, the aphid alarm pheromone, (*E*)-β-farnesene **5** is a ubiquitous plant semiochemical, but in plants, it is generated along with *β*-caryophyllene, which is inhibitory to the behavioral response. Pure **5**, however, elicits the full-alarm response. Despite the existence of thousands of moth species, structural diversity of their sex pheromones is also low, and only a few hundred compounds, derived from fatty-acid metabolism, are used. By utilizing species-specific blends, as well as temporal, geographic. or habitat parameters, mating signals are not confused.

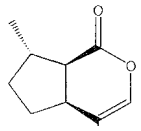

3 - Nepetalactone

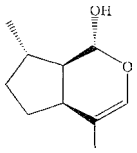

3b - Nepetalactol

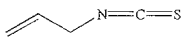

4

The use of single semiochemicals in the field is not usually sufficient for pest control, but by combining semiocheinicals, substantial protection can be achieved using an integrated approach called the push–pull system. The push is located in the crop and may comprise antifeedants, nonhost serniochemicals, attraction of predators or parasitoids, oviposition deterrents, or epideictic pheromones. The pull component comprises lures or trap areas away from the crop containing the sex pheromone, host odors, oviposition stimulants, or aggregation pheromones. The effectiveness of this approach can reduce broad-spectrum pesticide use by preventing, or even just delaying. the point at which pest populations reach economically damaging levels, so reducing the number of pesticide applications. Insect resistance to pesticides results from mutations that either allow enhanced detoxification of the chemical or that change the target site protein. These insects. which cannot be destroyed by the pesticide and so are at a significant selective advantage in treated areas, can subsequently multiply to produce a resistant population. Semiochemicals, however, affect insect behavior and prevent the damaging population explosions that occur in agricultural monocrops, so maintaining wild-type populations and avoiding a selection process comparable to pesticide use. Semiochemicals can, therefore, provide part of a successful, long-term pest-management strategy.

The primary difficulty in researching the field of semiochemicals is structure elucidation. Semiochemicals are produced in small quantities and are typically available in the range of subnanogram to microgram quantities and in complex mixtures. While modern NMR techniques of Microcell- or Microprobe-NMR using high-field instruments make the upper range amenable to elucidation, gas chromatography-mass spectrometry (GS-MS) is the usual analytical method. As structural data are limited and stereochemical data are severely limited from mass spectra, structure verification by chemical synthesis is almost always required. The structure of the sandfly *Lutzomyia longipalpis* sex pheromone was determined by GC-MS as methyl-α-himachalene **6**. however, syntheses of all four diastereoisomers and subsequent syntheses of both enantiomers of the correct diastereoisomer were required to determine the structure.[5] The synthesis of semiochemicals appears straightforward due to their low molecular weight. but it requires rigorous stereochemical control, as isomers (geometric, diastereomeric, or enantiomeric) can have different biological activities and interfere with the desired response. The field-scale of application also presents problems in the synthesis of the necessary quantities.

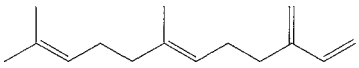

5

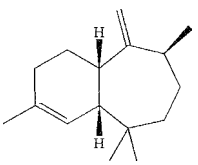

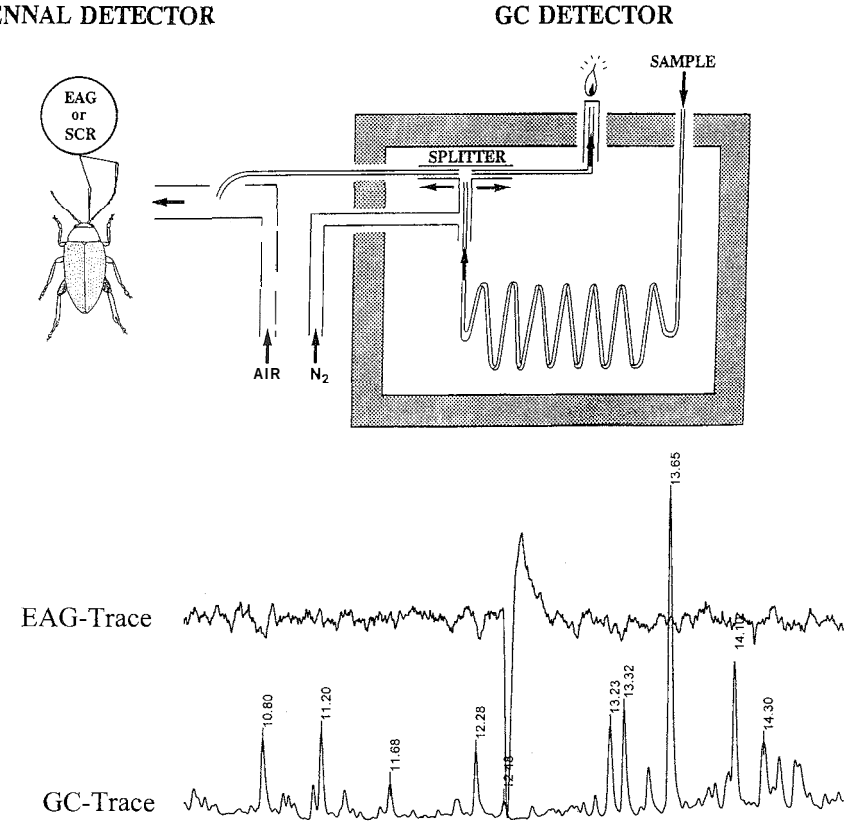

Fig. 1 GC-EAG response of the banana weevil, *Cosmopoiltes sordidus*. to host-plant volatiles

Biologically active isolates, especially plant volatiles. are extremely complex mixtures of compounds. By GC analysis, there may be 200–300 compounds. Insects, however, only detect and utilize a limited number of these, and as the compounds that insects need to detect are specific to a plant or insect, they are often not major peaks. presenting the problem as to which peaks should be analyzed. This problem has been tackled by a technique called gas chromatography coupled electro-antennography (GC-EAG), whereby the analytical GC effluent is split (Fig. I). One half is passed through the flame ionization detector as usual, while the other is simultaneously passed over an insect antenna that has electrodes attached to each end. Antennal response can be correlated to specific peaks. and these peaks are subsequently analyzed by mass spectrometry. This was developed further to a technique called single-cell recording (SCR). In this case, an electrode can be placed in an individual olfactory cell within the antenna. so locating the actual site of olfaction for particular semiochemicals.[6] These techniques show that the insect is capable of detecting a particular odor at the peripheral system and avoid the problems of demonstrating such detection through observing a behavioral response, which is only observed after the detection process is neurally processed and is less reproducible. Despite these techniques, electrophysiological responses are often observed to such vanishingly small quantities that peaks cannot be detected in the GC trace. The large number of compounds in the traces also means that although a compound in the active region may be identified, the activity actually comes from a much smaller co-eluting peak.

INSECT OLFACTION

Insect perception of volatile semiochemicals is mediated through olfactory sensilla, located mainly on the antennae. These sensilla have a porous cuticular surface through which semiochemicals can pass and make contact with the sensillum lymph. Semiochemicals are usually hydrophobic. organic chemicals. For land-living insects, these molecules must be transferred across the aqueous lymph to membrane-bound *G*-protein-coupled receptors (GPCRs) on the olfactory neurones, from which signal transduction occurs.[7] Transfer across the sensillum lymph is an evolutionary adaptation to terrestrial habitation and is mediated by odorant-binding proteins (OBPs). These are small (14–20 kDa), acidic,

water soluble. and highly concentrated (~10 mmol) in sensillum lymph. Initially it was thought that the function of OBPs was passive transport of any suitable hydrophobic, organic compounds across the aqueous sensillum lymph, and protection of the chemicals from degradative enzymes. However, it is now suggested that OBPs may bind a particular odorant specifically, or with at least some degree of specificity. and deliver it by dissociation at the receptor, or allow the receptor to recognize the entire odorant/OBP complex. Most current research is investigating the role OBPs play in molecular recognition of specific chemicals at the cuticular surface and at the interface with GPCRs, where molecular recognition must also reside.

ODORANT-BINDING PROTEINS

Insect OBPs were initially identified from lepidopteran species such as the tobacco hawkmoth. *Manduca sexta*, and silk moths, *Antheraea* sp.,[8] but they have now been found in examples from the orders Diptera (*Culex quinquefasciatus*—mosquito), Hymenoptera (*Apis melli*-,fern—honeybee). Coleoptera (*Exomala orientalis*—Oriental beetle), and Hemiptera (*Lygus lineolaris*—tarnished plant bug). The molecular techniques used to identify OBPs are numerous: as outlined in a recent review.[9]

OBPs are classed into three groups based primarily on sequence homology and tissue expression patterns:

Pheromone-binding proteins (PBP). These are expressed mainly in male antennae and are concentrated in sensilla responding to pheromones (sensilla trichoidea in lepidopterans). although smaller quantities are commonly found in female antennae. They show little amino acid sequence identity between species, although they have higher homology if the insect pheromones are structurally related.

General odorant-binding proteins (GOBPs). These are expressed in male and female antennae and are localized in sensilla responding to food or host semiochemicals (sensilla basiconica in lepidopterans). They exhibit higher sequence similarity between different species, suggesting that they may bind to a broad range of common semiochemicals, though it is still possible they selectively bind particular chemicals. There are two groups of these. GOBP1 and GOBP2. that differ from each other in their C-terminal amino acid sequences, and both differ considerably from PBPs.

The amino acid sequences of OBPs show little homology between orders and no homology to analogous proteins found in vertebrate olfaction systems. implying convergent evolutionary processes. However. there is conservation of six cysteine residues in all insect OBPs, and these form disulfide bridges important for the protein structure. The cysteine pattern in insect OBPs can be generalized as X_{18}-C-X_{30}-C-X_3-C-X_{42}-C-$X_{8\ 10}$-C-X_8-C-X_{24-26}. There are other classes of small, putative binding proteins related to insect olfaction, including the rapidly expanding group of chemosensory proteins (CSPs). These have only four cysteines, and, as many CSPs are not antennal specific and there are no ligands yet identified, they are not examined further in this review.

Pheromone-Binding Proteins

Experiments to probe the specificity of PBPs to insect pheromones were carried out by chemical synthesis of pheromone analogues and measurement of the electrophysiological response of the insect antennae by EAG. This technique, however, only reveals the result of PBP binding and receptor response and does not reveal where any discrimination resides. Analogues of the gypsy moth sex pheromone. (7*R*,8*S*)-*cis*-2-methyl-7,8-epoxyoctadecane. or (+)-disparlure **7**, have been synthesized in attempts to create behavioral agonists, antagonists, or pheromone synergists to use in mating disruption of this pest species. Analogues with different methyl group or epoxide positions proved unsuccessful, and a study where electronic properties were analyzed by replacing the epoxide of (+)-**7** with various cyclopropanes or aziridine, revealed the overall system of detection at the antennal level to be highly stringent.[10] Studies probing the structural requirements of the sex pheromone of the turnip moth, *Agrotis segetum*, were done by synthesizing conformationally restrained analogues of the pheromone component, (*Z*)-5-decenyl acetate. The enantiomers of cis- and *trans*-3-(4-propyl-cyclopent-2-enyl)-propyl acetate (Fig. 2) mimic both enantiomers of the cisoid and *transoid* conformations of the sex pheromone.[11] Electrophysiological recordings from single sensilla showed the cisoid (1*S*,4*R*)-conformation to be two orders of magnitude more active than its enantiomer and three orders more than the *transoid* isomers, providing evidence of a cisoid conformation of the pheromone in its bioactive state. A complementary study in the same moth, A. *segetum*, tested analogues of (*Z*)-5-decenyl acetate, in which the acetate group was replaced by different polar functional groups.[12] By comparing molecular electrostatic potentials determined by ab initio calculations with

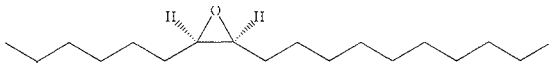

7 - (+)-disparlure

the results of electrophysiological single-cell recordings, the results indicated a probable H-bonding interaction of

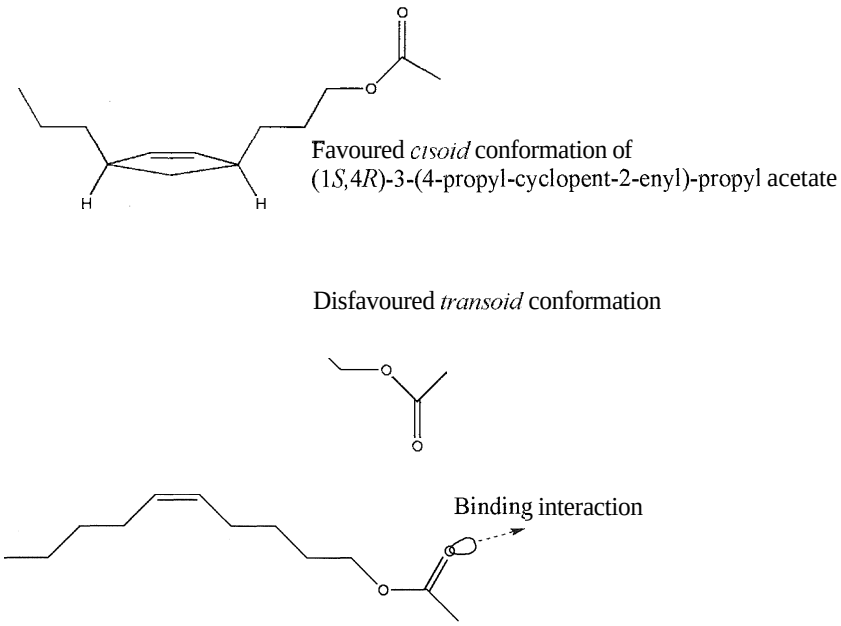

Fig. 2 (*Z*)-5-decenyl acetate and conformationally restrained analogues reveal structural requirements for peripheral detection by the turnip moth, *Agrotis segetum*.

the carbonyl group in a direction pointing away from the hydrocarbon moiety (Fig. 2).

The question as to what degree molecular recognition resides at the OBP binding level remains. The insect is able to identify particular chemicals in an environment containing structurally related compounds, isomers, or even enantiomers, so how much molecular recognition resides at the OBP level? Many lepidopterous species use two or three compounds in their pheromone blends, often the same chemicals as related species but in different ratios, so it is possible that each component is recognized by a specific PBP. Incubation of Bombyx mori pheromone-binding protein (BmPBP) with its pheromone, bombykol 1, produced a complex stable enough to undergo mass spectrometric analysis to reveal a noncovalently bound complex at neutral pH (see the following section describing pH dependence).[13] However, other structurally related molecules also bound to the protein, albeit with lower binding efficiencies. Of three PBPs from the cabbage armyworm, *Mamestra* brassicae, only two isoforms bound the pheromone component (*Z*)-11-hexadecenyl acetate.[''' This PBP was also found in the female antennae at low concentration, belying the concept that only males can detect the pheromone. As mentioned before, the gypsy moth, L. *dispar*, uses (+)-disparlure 7 as its sex pheromone, but the (−)-enantiomer acts as an antagonist. Two recombinant PBPs from gypsy moth antennae reversibly bound with each enantiomer, but one PBP had a higher affinity to the (−)-enantiomer, and the other bound preferentially to the (+)-enantiomer. Two sibling moth species, A. *polyphemus* and *A*, pemyi, use the same three compounds in their sex pheromone blends. (*E*,*Z*)-6,11-hexadecadienyl acetate, (*E*,*Z*)-4,9-tetradecadienyl acetate, and (*E*,*Z*)-6,11-hexadecadienal. Three PBPs were isolated from each moth species and displayed a range of >1000-fold binding affinites measured for structurally related chemicals.[15] These PBPs also showed different binding affinities to different components of the pheromone blends, with *K*d values ranging from 0.6–30 μM. These examples, and others of lepidopteran PBPs that also bind their respective pheromones with Kd values of 0.1–10 μM, imply that an insect PBP will selectively bind its pheromone. However, in contrast to the ligand selectivity described above, only one PBP gene encoding an identical protein was isolated from two strains of the European corn borer, *Ostrinia nubilalis*, and from the closely related Asian corn borer, *O. furnacalis*. These insects use different pheromone isomers, suggesting that the molecular recognition here does not reside on the PBP.[16] In addition, two species of scarab beetle, the Osaka beetle (Anomala osakaaa) and the Japanese beetle (Popillia japonica), use opposite enantiomers of (*Z*)-5-(1-decenyl)oxacyclopentan-2-one 8 as their sex pheromone. The pheromone enantiomer of one species is a behavioral antagonist to the other species, yet the PBP from both species' antennae had the same binding affinity to both enantiomers,[17] suggesting that molecular recognition lies at the membrane receptor in this case. However, the finding that there are at least 38 OBP genes annotated in the *Drosophila melanogaster* genome[18] suggests some specificity between OBPs and particular ligands. In addition, more than 50 genes en-

coding putative receptors were also identified, so it may well be that semiochemical olfaction involves combinatorial interactions between OBPs and GPCRs and molecular recognition at both proteins.

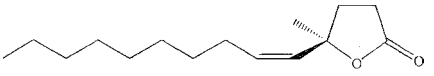

8 - (*R*)-japonilure

Early attempts to characterize the binding site structure of PBPs were performed by Prestwich, who was the first to purify high levels of recombinant PBP from the moth Anfhemca *polyphemus*, by gene expression in *E.* coli. The active site of the PBP was probed by photoaffinity labeling using analogues of two components of the natural sex pheromone (6*E*,11*Z*)-hexadecadienyl acetate and (4*E*,9*Z*)-tetradecadienyl acetate. The photoaffinity labels prepared were [^{3}H]-(6*E*,11*Z*)-hexadecadienyl diazoacetate **9** and [^{3}H]-(4*E*,9*Z*)-tetradecadienyl diazoacetate. On photoactivation, these compounds degrade into a highly reactive carbene that forms a covalent bond, presumed to be with the nearest amino acid, i.e., one in the binding pocket. Subsequent degradation of the protein can identify this amino acid and its position in the protein sequence.[19] The 16-carbon label covalently bonded to a major hydrophobic domain comprising a helix-sheet-helix motif that shows sequence variation among insect PBPs and could explain the hydrophobic binding site of the alkyl chain. The bound amino acid, however, was threonine-44. found in a hydrophilic subfragment. next to arginine-46. a highly conserved amino acid. that could be involved in binding the acetyl group. The 14-carbon photoaffinity label was found bound to two sites in the binding pocket, one in the same region as the 16-carbon unit and one at aspartate-32. This is explained as a result of different chain lengths. allowing a different fit into the binding pocket. Indeed, the PBP binds the pheromone component (4*E*,9*Z*)-tetradecadienyl acetate poorly compared to the 16-carbon component. which may explain why the labeled pheromone analogue fits into the binding site less specifically.

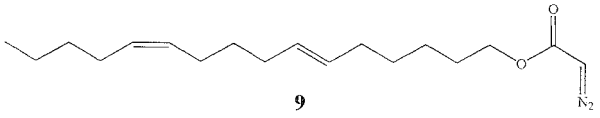

9

PBP/Pheromone-binding mechanism

Analysis of recombinant bombyko! pheromone-binding protein. BmPBP, has given information on the protein structure and suggested a mode of action that is pH dependent. BmPBP can exist as a dimeric structure at neutral or slightly acidic or basic pH but dissociates at low pH and undergoes conformational change.[20] Single-crystal x-ray diffraction studies were carried out on the protein with bound bombykol, and they revealed some interesting structural features.[21] The structure contains many α-helices and has a novel protein fold different from that found in vertebrate olfactory proteins. The surface is covered in charged residues, as expected for a highly water-soluble protein, and it contains residues that may interact to form an asymmetric dimer. The monomeric structure shows bombykol bound in a large flask-shaped cavity with a very small opening. The residues most conserved between lepidopteran PBPs, including some highly conserved aromatic residues, form the hydrophobic surface of the cavity around the bound bombykol. The opening to the bombykol-binding pocket is small, and it is unclear from the x-ray structure how bombykol enters or leaves the binding pocket, as the hydroxyl end of bombykol is covered by a loop, stabilized by hydrogen bonding. that acts as a rigid lid. This lid. however, can be destabilized by a drop in pH, causing protonation of conserved histidine residues allowing release of the bound pheromone. Structural NMR studies show that BmPBP undergoes reversible conformational change on acidification between pH 6 and pH 4.9: and as expected, the more basic form generates better-dispersed NMR data, i.e., it is more structurally rigid, than the data from the acidified protein.[22] The BmPBP binds the pheromone only at neutral and basic pH. A. *polyphemus* PBP also only binds its pheromone above pH 5.6. There is evidence that the structural rearrangement of PBPs under acidic conditions may be more fundamental. The NMR studies of the BmPBP at pH 4.5 show a G-terminal helix occupying the pheromone-binding site.[23] Complementary reports from a hymenopteran (*Apis mellifera*—honeybee) OBP called ASP2, expressed in the yeast *Pichia* pastoris, found that ASP2 had cysteine residues identical to BmPBP and was dimeric at neutral pH.[24] The ASP2 protein bound a number of floral odorants. but this was reversed at pH 3 when the protein also became monomeric. The proposed mechanism is that the PBP binds the pheromone at neutral surface lymph pH. transports it across the aqueous sensilla lymph to the membrane-bound receptor. where lower pH at the membrane surface. or other local ionic conditions. cause the PBP structure to alter with concomitant release of the molecule that then elicits signal transduction.

General Odorant-Binding Proteins

While many molecular genetic approaches to studying COBP proteins were reported, little has been achieved by chemistry-based studies. Current theories propose that these proteins bind either a wide range of semiochemicals

poorly or have a high affinity to one of a broad range of semiochemicals. This makes determination of ligands for study extremely problematic. So, work has generally focused on PBPs, where ligand identification (the sex pheromone) is simpler. A recombinant GOPB from the moth. *Manduca sexta*, could be photoaffinity labeled by the moth pheromone analogue [^{3}H]-(*E*,*Z*)-6,11-hexadecadienyl diazoacetate, but plant odors (3-3-hexen-1-01, geraniol, and limonene displaced it in competitive binding studies.[25] These same plant volatiles, however. were unable to displace the pheromone analogue when it was bound to its PBP. This suggests that the GOBP is tuned to a broad range of plant volatiles, although it is also possible that it binds highly selectively to a different semiochemical not used in the study. The GOBP also displayed similar properties to insect PBPs, as ligand binding was dependent on pH and salt concentration. and the protein structure was highly α-helical. In another study, a *D. melanogaster* mutant was created that lacked an antennal-specific gene containing six conserved cysteines named LUSH.[26] The nomenclature is derived from the mutant's attraction to abnormally high concentrations of ethanol. propanol. and butanol that repel wild-type flies. In low concentrations, these alcohols are attractive to both wild-type and mutant flies and are important semiochemicals in nature, as the flies feed on, and lay eggs in. fermenting plant material. where short-chain alcohols are present.

SEMIOCHEMICAL DEACTIVATION

After the olfactory receptor is activated, the semiochemical signal must be destroyed to prevent continued stimulation. Esterase, dehydrogenase. aldehyde oxidase, epoxidase, and glutathione-S-transferase activities have all been detected in the sensillum and could degrade the signal. A further example is found in the pale-brown chafer. *Phyllopertha diversa*, which uses 1,3-dimethyl-2,4-(1*H*,3*H*)-quinazolinedione **10** as its sex pheromone.

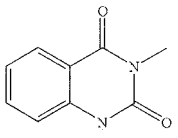

10

Degradative hydroxylation and dernethylation were observed. and a species-specific membrane-bound P450 system was found only in male antennae.[27] Signal degradation must be extremely fast, especially for insects locating odor plumes in flight. and it has been argued that enzymic methods are too slow to achieve this. An alternative model was suggested in A. *polyphemus*, where it is proposed that signal inactivation occurs by modification of the pheromone/PBP complex.[28] In this case, A. *polyphemus* PBP was found to exist in a reduced state with two disulfide bridges that bound the pheromone, [^{3}H]-(*E*,*Z*)-6,11-hexadecadienyl acetate, and oxidized in the presence of sensory hair material to a complex with three disulfide bonds. The concept is that oxidation of the pheromone/PBP coinplex occurs at the activated receptor, and the oxidized form traps the pheromone and prevents further stimulation. Subsequently, the complex is degraded enzymically.

CONCLUSION

The extraordinary ability of insect antennae to recognize particular odorants and blends of odorants in highly complex olfactory environments. through molecular recognition, has led to research into technologies to exploit this. Using live insects or excised antennae linked to electrodes, volatiles from a desired medium can be analyzed for specific signals. A mobile robot linked to a B. *mori* antenna was able to locate the organism's pheromone source.[29] Also. a company, Inscentine, is making efforts to detect food deterioration semiochemicals for quality control of supennarket foods.[30] In addition. fingerprint patterns using multiple antennae can be used to analyze anthropogenic signals, and American scientists are creating detectors for illegal drugs or explosives. This approach is vastly superior to other artificial nose technologies in that it relies on molecular recognition rather than simple physical properties. making it possible to analyze highly complex samples.

ACKNOWLEDGMENTS

Rothamsted Research receives grant-aided support from the Biotechnology and Biological Sciences Research Council of the U.K.

ARTICLES OF FURTHER INTEREST

Biological Ligands, p. 88
Enzymes: Characteristics and Mechanisms. p. *554*
Hydrogen Bonding, p. 658
The Lock and Key Principle, p. *809*
Nuclear Magnetic Resonance Spectroscopy, p. 981
X-Ray Crystallography, p. 1586

REFERENCES

1. Butenandt. A . Beckmann. R . Stamm. D . Hecker, E On the sex attiactant of the silkworm moth *Bombyx mori*

Isolation and structure. Z. Naturforsch.. B 1959, 14. 283–284.
2. Dawson, G.W.: Griffiths, D.C.: Janes. N.F.; Mudd. A.; Pickett. J.A.; Wadhams. L.J.; Woodcock. C.M. Identification of an aphid sex pheromone. Nature 1987, *325*, 614–616.
3. Boo. K.S.: Choi, M.Y.: Chung. I.B.; Eastop. V.F.; Pickett, J.A.; Wadhams. L.J.: Woodcock. C.M. Sex pheromone of the peach aphid. *Tuberocephalus momonis*. and optimal blends for trapping males and females in the field. J. Chem. Ecol. 2000. 26 (3), 601 - 609.
4. Agelopoulos. N.; Birkett, M.A.: Hick, A.J.; Hooper. A.M.; Pickett. J.A.: Pow, E.M.: Smart. L.E.; Smiley, D.W.M.: Wadhanis, L.J. Exploiting semiochemicals in insect control. Pestic. Sci. 1999. 55. 225--235.
5. Hamilton, J.G.C.; Hooper, A.M.; Mori. K.; Pickett, J.A.; Sano. S. 3-Methyl-α-himachalene is confirmed, and the relative stereochemistry defined. by synthesis as the sex pheromone of the sandfly *Lutzomyia longipalpis* from Jacobina. Brazil. Chem. Commun. 1999, 4. 355--356.
6. Wadhams. L.J. Coupled gas chromatography—Single cell recording: A new technique for use in the analysis of insect pheromones. Z. Naturforsch. 1982, *37c*. 947–952.
7. Krieger, J.; Breer. H. Olfactory reception in invertebrates. Science 1999. *286*, 720–723.
8. Vogt, R.G.: Riddiford. L.M. Pheromone binding and inactivation by moth antennae. Nature (Lond.) 1981, *293*. 161–163.
9. Field. L.M.; Pickett, J.A.: Wadhams. L.J. Molecular studies in insect olfaction. Insect Mol. Biol. 2000. *9* (6). 545–551.
10. Dickens, J.C.: Oliver. J.E.; Mastro, V.C. Response and adaptation to analogs of disparlure by specialist antennal receptor neurons of gypsy moth. *Lymantria dispar*. J. Chem. Ecol. 1997. 23 (9). 2197–2210.
11. Gustavsson. A.-L.; Larsson, M.C.: Hansson, B.S.: Liljefors. T. Enantiomers of *cis*- and trans-3-(4-propylcyclopent-2-enyl) propyl acetate. A study on the bioactive conformation and chiral recognition of a moth sex pheromone component. Bioorg. Med. Chem. 1997. *5* (12). 2173–2183.
12. Gustavsson, A.-L.; Tuvesson, M.; Larsson, M.C.; Wenqi. W.; Hansson. B.S.; Liljefors, T. Bioisosteric approach to elucidation of binding of the acetate group of a moth sex pheromone component to its receptor. J. Chem. Ecol. 1997, *23* (13). 2755–2776.
13. Oldham. N.J.: Krieger. J.; Breer. H.: Fischdick, A.; Hoskovec, M.: Svatos. A. Analysis of the silkworm moth pheromone binding protein-pheromone complex by electrospray-ionisation mass spectrometry. Angew. Chem., Int. Ed. 2000. *39* (23). 4341 –4343.
14. Maibeche-Coisne, M.; Sobrio. F.: DeLaunay, T.; Lettere. M.: Dubroca, J.; Jacquin-Joly, E.: Nagnan-Le Meillour, P. Pheromone binding proteins of the moth *Mamestra brassicae*: Specificity of ligand binding. Insect Biochem. Mol. Biol. 1997. 27 (3). 213–221.
15. Du, G.: Prestwich, G.D. Protein structure encodes the ligand binding specificity in pheromone binding proteins. Biochemistry 1995. *34*. 8726–8732.
16. Willet. C.S.: Harrison, R.G. Pheromone binding proteins in the European and Asian corn borers: No protein change associated with pheromone differences. Insect Biochem. Mol. Biol. 1999, *29*. 277–284.
17. Wojtasek, *W.:* Hansson. B.S.; Leal. W.S. Attracted or repelled?—A matter of two neurons. one pheromone binding protein. and a chiral center. Biochem. Biophys. Res. Commun. 1998. 250. 217–222.
18. Graham. L.A.; Davies. P.L. The odorant-binding proteins of *Drosophiln melanogaster*: Annotation and characterization of a divergent gene family. Gene 2002. *292*. 43–55.
19. Du, G.; Ng, C.-S.; Prestwich. G.D. Odorant binding by a pheromone binding protein: Active site mapping by photoaffinity labeling. Biochemistry 1994.33.4812--4819.
20. Leal, W.S. Duality monomer-dimer of the pherornone-binding protein from *Bombyx nzori*. Biochem. Biophys. Res. Commun. 2000. *268*. 521–529.
21. Sandler. B.H.: Nikonova. L.: Leal. W.S.: Clardy, J. Sexual attraction in the silkworm moth: Structure of the pheromone-binding-protein-bombykol complex. Chem. Biol. 2000. 7 (2), 143–151.
22. Damberger, F.: Nikonova. L.: Horst. R.: Peng, G.; Leal, W.S.; Wuthrich, K. NMR characterization of a pH-dependent equilibrium between two folded solution conformations of the pheromone-binding protein from *Bombyx nzori*. Protein Sci. 2000. *9* (5), 1038– 1041.
23. Horst. R.; Damberger. F.: Luginbuhl, P.; Guntert. P.; Peng. G.: Nikonova. L.: Leal. W.S. NMR structure reveals intamolecular regulation mechanism for pheromone binding and release. Proc. Natl. Acad. Sci. 2001, *98* (25). 14374–14379.
24. Briand. L.: Nespoulous, C.; Huet. J.-C.: Takahashi. M.; Pernollet, J.-C. Ligand binding and physico-chemical properties of ASP2. a recombinant odorant-binding protein from honeybee (*Apis mellifera* L.). Eur. J. Biochem. 2001. 268. 752–760.
25. Feng. L.; Prestwich. G.D. Expression and characterization of a lepidopteran general odorant binding protein. Insect Biochem. Mol. Biol. 1997. 27 (5). 405–412.
26. Kim, M.-S.: Repp. A.; Smith. D.P. LUSH odorant-binding protein mediates chemosensory responses to alcohols in *Drosophila melanogaster*. Genetics 1998. *150*. 711–721.
27. Wojtasek, H.: Leal. W.S. Degradation of an alkaloid pheromone from the pale-brown chafer. *Phyllopertha diversa* (Coleoptera: Scarabaeidae). by an insect olfactory cytochrome P450. FEBS Lett. 1999. *458*, 333–336.
28. Ziegelberger, G. Redox-shift of the pheromone-binding protein in the silkmoth *Antheraea polyphemus*. Eur. J. Biochern. 1995, *232*. 706–711.
29. Kuwana. Y.: Nagasawa. S.; Shimoyama, I.: Manzaki, R. Synthesis of the pheromone-oriented behaviour of silkworm moths by a mobile robot with moth antennae as pheromone sensors. Biosens. Bioelectron. 1999. *14*. 195–202.
30. Pickett. J.A. *Detection of Volatile Compounds Related to Food Deterioration*: Foodlink News. DEFRA Publications: London. December 2002: Vol. 41. 5 pp.

Siderophores

Robert C. Hider
Zu Dong Liu
King's College London, London, United Kingdom

INTRODUCTION

Siderophores are compounds produced by microorganisms for scavenging iron from the environment. They are low-molecular-weight compounds (500–1000 daltons) possessing a high affinity for iron(III) ($K_f > 10^{30}$), the biosynthesis of which is regulated by iron levels and the function of which is to supply iron to the cell. Because of these roles, siderophores are of interest to biomedical researchers who are working on treating anemia and helping recipients of blood transfusions. This article briefly describes the classification and chemical properties of siderophores, before outlining the research on siderophore transport and interactions with metals.

BACKGROUND

During the period 1949–1952. three different siderophores were isolated and identified as growth factors. namely. mycobactin 1, ferrichrome 2A and coprogen **3.** Snow, in a classic study, largely characterized mycobactin, correctly identifying its coordination groups and demonstrating that mycobactin possesses a high affinity for iron(III).[1,2] This seminal work was followed in 1960 by the discovery of the ferrioxamines 4.[3] A key observation concerning the mode of action of these growth factors was made by Garibaldi and Neilands in 1956,[4] when it was demonstrated that the production of ferrichrome A **2B** was enhanced by growing the organism *Ustilago sphaerogena* in a medium deficient in iron. This finding was subsequently confirmed for mycobactin and other hydroxamate siderophores. The first tricatechol siderophore. enterobactin ***5*** was independently isolated by Pollock and Neilands from *Salmonella typhimurium*[5] and O'Brien and Gibson from *Escherichia coli*.[6] The isolation and characterization of siderophores was greatly facilitated in recent years by the use of HPLC and mass spectrometry, thus, the number of well-characterized siderophores has risen to over 500. The majority of these molecules fall into ihe hydroxamate. catecholate. or hydroxycarboxylate classes and. despite considerable structural variation, chelate iron in a hexadentate fashion. In addition, there are some tetra-. tri-. and bidentate ligands that also function as siderophores.

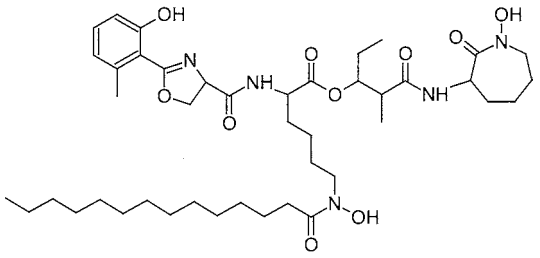

1

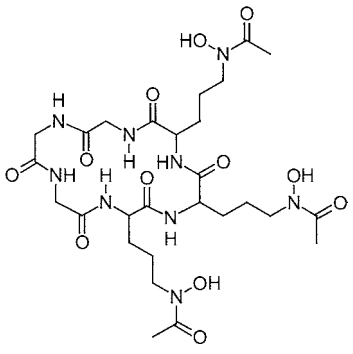

2A

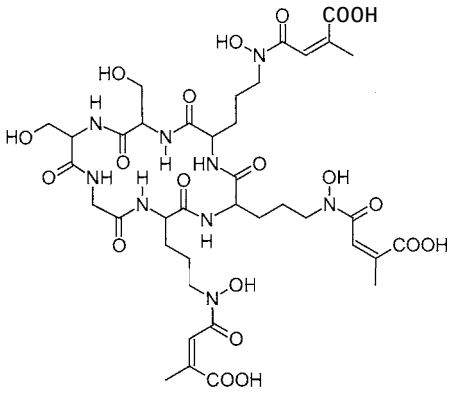

2B

Encyclopedia of Supramolecular Chemistry
DOI: 10.1081/E-ESMC 120012714

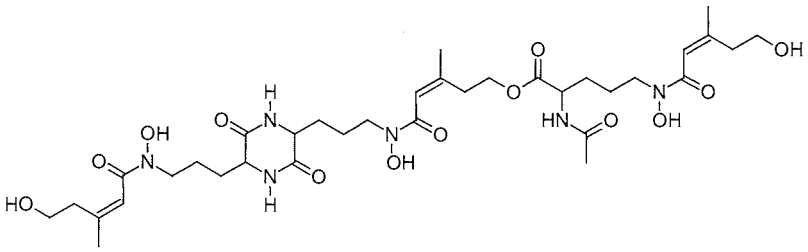

3

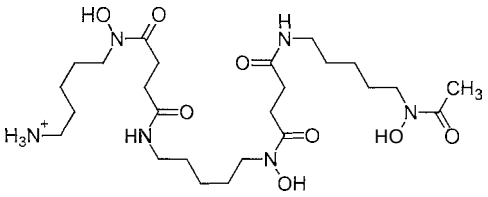

4

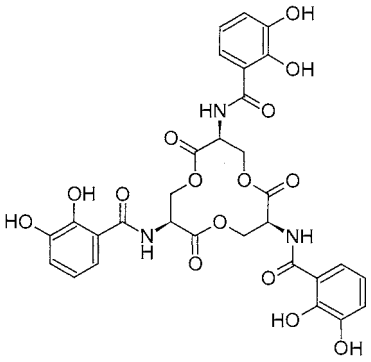

5

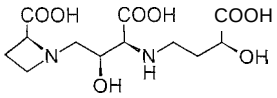

6

Iron is not a rare element, but its availability is limited by the inherently low solubility of iron(III); under aerobic conditions. the limiting concentration of ferric ions is close to 10^{-18} M at pH 7.0. For this reason. microorganisms evolved strategies for the solubilization and absorption of iron, iron being essentia! for all living processes. Siderophores are products of the vast majority of microorganisms, be they bacteria. or fungi. live in soil, fresh water. or the sea. For some microorganisms. a correlation was established between siderophore production and virulence.[7] The synthesis of all known siderophores is controlled by iron availability to the cell. Under conditions of high iron availability. the biosynthesis of siderophores and the corresponding transport proteins are repressed: however, as soon as the soluble iron levels drop below approximately 1 μM, siderophore synthesis and secretion are activated.

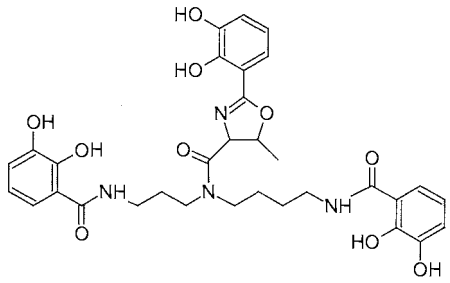

7

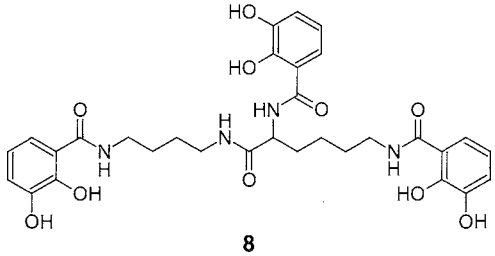

8

There is no evidence for siderophore-like molecules in multicellular animals, and with the exception of grasses and the related cereals, there is no evidence for the existence of siderophores in plants. Grasses secrete phytosiderophores,[8] for instance, mugeneic acid 6. into the soil under low iron conditions and. consequently. are able to thrive in alkaline soils.

Table 1 Hexadentate siderophores

Siderophore	*Organism*	*Structure*	Ligands
Enterobactin	*Escherichia coli*	**5**	Catechol
Agrobactin	*Agrobacterium tumefaciens*	7	Catechol and hydroxyphenyloxazoline
Protochelin	*Azotobacter*	8	Catechol
Desferrioxamine-B	*Nocardia*	**4**	Hydroxamate
Desferrioxamine-E	*Nocardia*	9	Hydroxamate
Ferrichrome	*Ustilago sphnerogena*	**2A. 2B**	Hydroxamate
Triacetylfusarine	*Fusarium roseum*	**10**	Hydroxamate
Coprogen	*Penicillium*	**3**	Hydroxamate
Exochelin	*Mycobacterium smegmatis*	**11**	Hydroxamate
Mycobactin	*Mycobacterium*	**1**	Hydroxamate and hydroxyphenyloxazoline
Pseudobactin	*Pseudomonas*	**12**	Catechol, hydroxamate, and a-hydroxycarboxylate
Aerobactin	*Klebsiella pneumonia*	**13**	Hydroxamate and a-hydroxycarboxylate
Rhizobactin	*Rhizobium meliloti*	**14**	α-Aminocarboxylate and a-hydroxycarboxylate
Mugineic acid	*Hordium vulgare*	6	α-Aminocarboxylate and α-hydroxycarboxylate
Rhizoferrin	*Rhizobus*	**15**	α-Hydroxycarboxylate

CLASSIFICATION OF SIDEROPHORES

The major chelating functions found in siderophores are catechol, hydroxyphenyloxazolone, hydroxamate, phenol, a-hydroxycarboxylic acid, α-aminocarboxylic acid, and thiazole (Tables 1 and 2).

Hexadentate Siderophores

The basic design of hexadentate siderophores is such that the bidentate functional units are placed at suitable distances in order to create a stable intermolecular complex. This spacing is achieved via cyclic and acyclic esters **(3, 5,** 10); by cyclic and acyclic α-amino acid amides (2. 12. 13) by cyclic and acyclic ω-amino acid amides (4. 9. 11), and by mixtures of ester and amide bonds (1). The structural framework can also be based on spermidine, related polyamines, and citrate. The advantage of a cyclic structure appears to be twofold. First, they are more resistant to attack by proteolytic enzymes. Second, due to a decreased entropy difference between the free ligand and the complex as compared with the acyclic analogue, they possess a higher affinity for iron(III) than their acyclic analogues. A wide range of siderophore–iron(III) complexes were subjected to x-ray diffraction studies.[9] As typified by ferrioxamine D 25, all possess a distorted octahedral coordination, the distortion being greater in complexes possessing non-equivalent ligands, for instance, mycobactin P. Although most hydroxamate siderophores possess three identical ligands. relatively few possess a threefold symmetry, examples being triacetylfusarine 10, desferrioxamine E 9, and enterobactin 5.

Table 2 Tetra-. tri-. and bidentate siderophores

Siderophore	*Organism*	*Structure*	Ligands
Rhodotorulic acid	*Rhodotorula*	**16**	Hydroxamate
Azotobactin	*Azotobacter vinelandii*	**17**	Catechol
Amonabactin	*Aeromonus hydrophilia*	**18**	Catechol
Uersiniophore	*Yersina enterocolitica*	**19**	Phenol. thiazole. and carboxylate
Desferrithiocin	*Streptomyces antibioticus*	**20**	Phenol, thiazole, and carboxylate
Chrysobactin	*Erwinia chrysanthemi*	**21**	Catechol
Aspergillic acid	*Aspergillus flavus*	**22**	Hydroxypyridinone
Pyridoxatin	*Acremonium*	**23A**	Hydroxypyridinone
Cepabactin	*Pseudomonas cepacia*	**23B**	Hydroxypyridinone
Aminochelin	*Azotobacter vinelandii*	**24**	Catechol

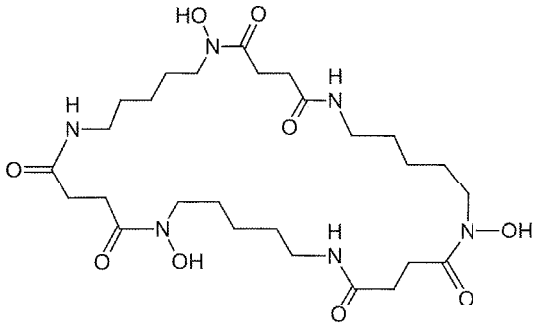

9

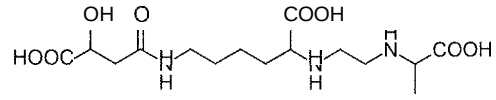

14

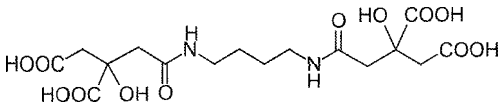

15

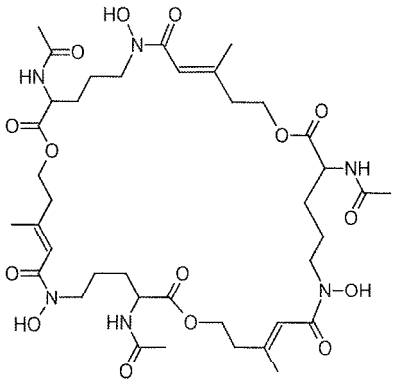

10

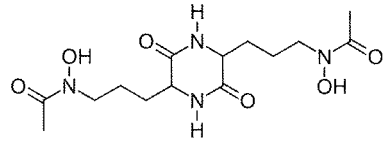

16

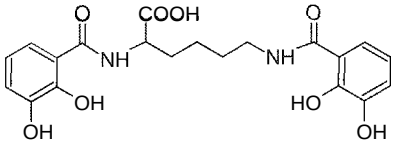

17

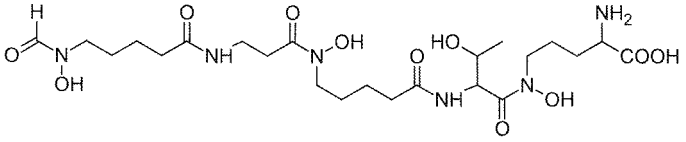

11

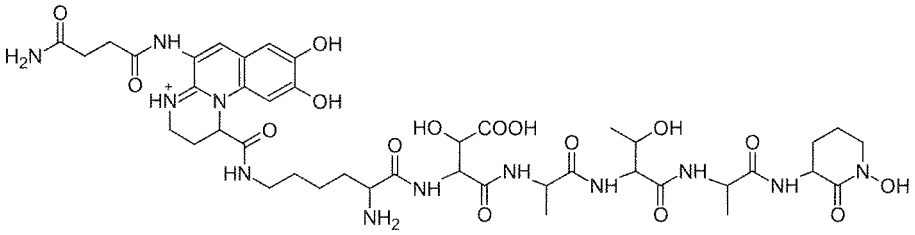

12

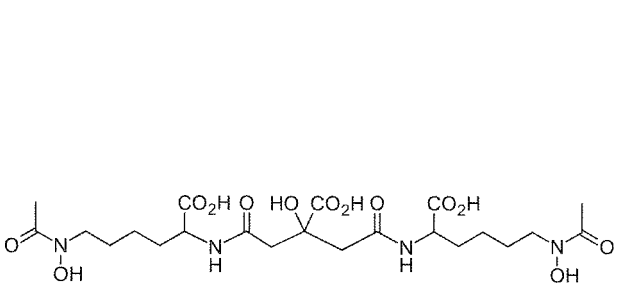

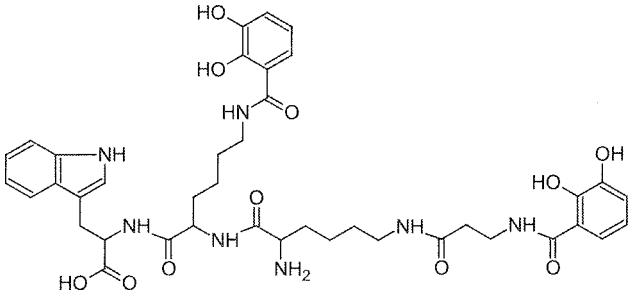

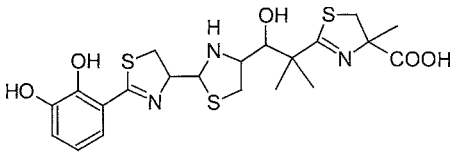

19

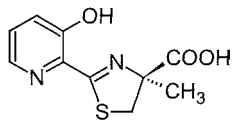

20

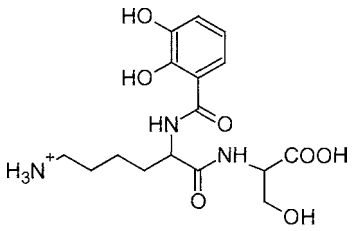

21

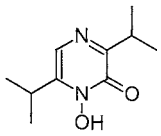

22

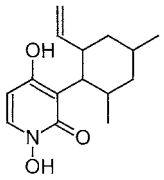

23A

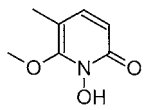

23B

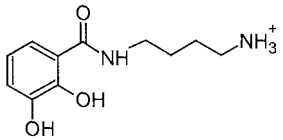

24

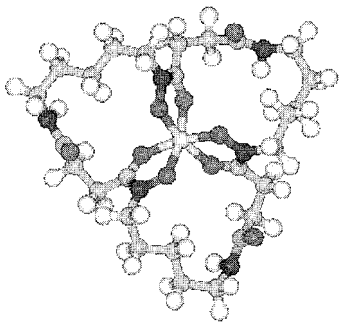

25

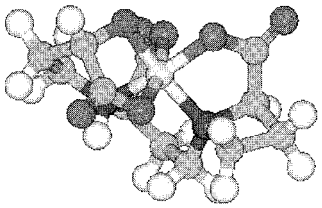

26

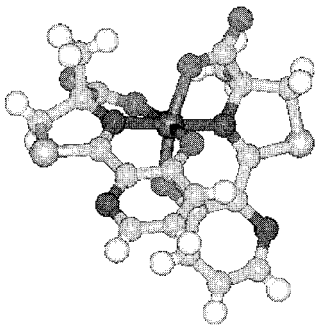

27

Most hexadenlate hydroxamate and catecholate siderophores are stereochernically restricted to the ***cis*** isomers. The stereochemistry of a range of siderophore iron complexes was determined by x-ray and CD methods (Table 3).[10] These isomers are stable in aqueous solution. Although iron(III) phytosiderophore complexes have not beer, crystallized. structures of the analogous cobalt(III) complexes were determined. Again. a distorted octahedral geometry is observed but with two of the ligands being nitrogen atoms **26**.

Table 3 Stereochemistry of siderophore metallate(III) complexes

Siderophore	Structure	Stereochemistry
Ferrichrome	**2**	A-cis
Rhodotorulic acid	**16**	A-cis
Aerobactin	**13**	A
Mycobactin P	**1**	A-cis
N,N,N-triacetylfusarinine	**10**	A-cis (solid state); predominately A-cis (solution)
Ferrioxamine E	**9**	Racemate-cis
Ferrioxaniine B	**4**	Racemate-cis and *-trans*
Enterobactin	**5**	A-cis
Enantioenterobactin		***A-cis***
Agrobactin	**7**	A-cis

Tetradentate Siderophores

Tetradentate siderophores interact with iron(III) in three different manners, forming a 1:1 complex or a 3:2 complex (Fig. 1). The vacant coordination sites on the 1:1 complex can be occupied by a bidentate ligand forming a ternary complex. and thus, the coordination chemistry is more complex for this type of ligand when compared to the corresponding hexadentate molecule. The 3:2 complexes are generally favored at high concentrations ($>10^{-4}$ M), whereas the 1:1 complex will predominate at lower concentrations ($<10^{-6}$ M). For some tetradentate ligands, e.g., rhodotorulic acid **16**, the 1:1 complex is sterically forbidden, and only the 3:2 complex was characterized. With simple alkyl links between two bidentate functions. a chiral trihelical conformation is formed in the 3:2 complex.[111]

Tridentate Siderophores

As with tetradentate ligands, more than a single complex species can exist in aqueous solution, namely, the 1:1 and the 2:1 complexes. The 2:1 complex, for instance, ferrithiocin 27. will be favored under nonacid conditions and at high concentrations.

Bidentate Siderophores

The only well-characterized bidentate siderophores are based on the catechol or hydroxypyridin-2-one function. Some are probably intermediates in the synthesis of hexadentate siderophores. Nevertheless, they can be present at high concentrations in the immediate vicinity of secreting organisms and undoubtedly mobilize iron from insoluble ores. Bidentate catechols favor the 2:1 complex over the pH range 4.0–8.0, whereas the hydroxypyridinones 22 and 23 favor the 3:1 complex, which carries a net zero charge.[''''] The structure of the iron(III) complex of the parent 1-hydroxypyridin-2-one is a cis-distorted octahedron 28. By virtue of their neutrality and hydrophobicity, these ligands and their iron(III) complexes are toxic to some microorganisms and, as such, are recognized as antibiotics, e.g., aspergillic acid, 22.

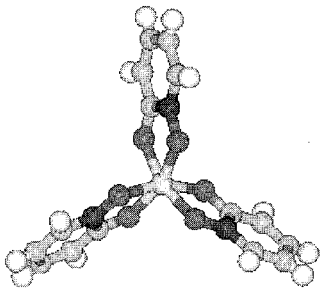

28

CHEMICAL PROPERTIES

Thermodynamic Stability

Mexadentate ligands are likely to possess higher iron(III) stability constants than the corresponding tri- and bidentate ligands. due to entropy factors. However, the effect is

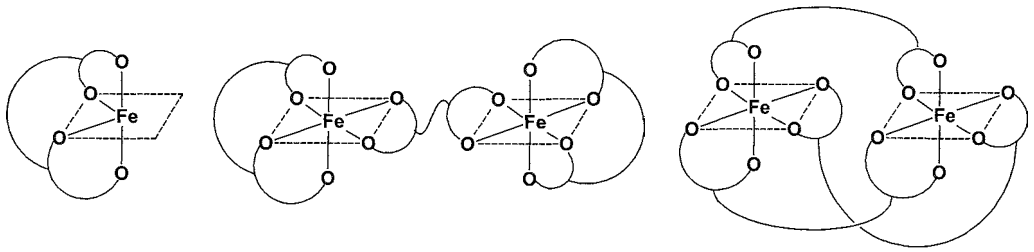

Fig. 1 Modes of iron(III) chelation by tetradentate ligands: A. 1:1 complex: B. 3:2 complex with ligands in nonequivalent positions; C. 3:2 complex with ligands in equivalent positions.

frequently suboptimal due to deviation from ideal stereochemistry and the associated influence on the enthalpy of the interaction. The smaller the conforinational space of the free ligand, the higher the stability of the complex: as the flexibility of the ligand and its corresponding iron complex decreases. so does the entropy difference. Thus, cyclic ligands typically possess a higher affinity than linear analogues and ligands with a good deal of preorganization in their structures, for instance, enterobactin 5, possesses particularly high affinities for iron(III). Irrespective of the framework. catechol and hydroxamate functions provide excellent iron(III) coordinating centers. as indicated in Table 4. The pM parameter provides a more reliable comparison of the affinity of the various ligands for iron(III) under physiological conditions.[''''] The pM is defined as pM = L o g $[Fe(H_2O)_6^{3+}]$, thus a large. positive value of pM corresponds to a low concentration of free Fe(III) and, hence, effective binding by the ligand. The most powerful ligands at pH 7.0 are the hexadentate triscatechols as exemplified by enterobactin (pM = 35); the hexadentate *tris*hydroxamates have appreciably lower pM values. typically 25–28. The substitution of a single hydroxamate function by a hydroxycarboxylate leads to a significant drop in the pM value, as indicated by aerobactin **13** (pM = 23). Due to the concentration dependence of the tri- and bidentate ligands, their pM values are lower than those of the hexadentate class (22–25). The amino carboxylate phytosiderophores also possess relatively low pM values. typically in the range of 17–18.

Kinetic Stability

As the affinity of hexadentate siderophores for iron(III) is so high, the dissociation rate of iron from the complex is extremely low at neutral pH values. Thus, the exchange of iron between two siderophores is also exceedingly slow. The halftime for exchange of ^{59}Fe between desferrioxamine-B 4 and ferrichrome-A **2B** (4 mM, pH 7.4) is over 200 h, although the rate can be increased by acidification of the medium. Tri- and bidentate siderophores are more kinetically labile. and this results from the relative ease of removing one of the ligands from the complex.[14] With bidentate ligands, even at pH 7.0. there will be a trace of the 2:1. ligand:iron complex, and thus, the reactions indicated in Eqs. 1 and 2 reach equilibrium rapidly. For this same reason, the iron complexes of bidentate hydroxamates, in contrast to those of hexadentate hydroxamates, undergo rapid racemization in aqueous solution.

$$L_3Fe \rightleftharpoons L + L_2Fe \quad (1)$$

$$L_2Fe + L' \rightleftharpoons L_2L'Fe \quad (2)$$

Thus, the role of bidentate siderophores may be to solubilize iron and, by virtue of their kinetic lability, then donate the iron to the more kinetically inert hexadentate siderophores. for specific delivery to the secreting organism.

Redox Activity of Catechol Ligands

In contrast to hydroxamates, catechols are susceptible oxidation. The oxidation products, semiquinone and quinone. are also able to coordinate cations. but generally with reduced affinity. Assignment of a formal oxidation state to the coordinated metal is not always unambiguous; as the orbitals involved are delocalized over the metal and at least one ring. The electronic structure of the iron chelate ring can be viewed in terms of three isoelectronic forms 29. These various complex types can be induced

Table 4

Siderophore	Ligands	Denticity	$K_{Fe^{3+}}$ (M^{-1})	pFe^{3+a}
Enterobactin **5**	Catechol	6	49	35
Protochelin **8**	Catechol	6	44.6	29
Desferrioxamine B 4	Hydroxamate	6	30.5	27
Ferrichrome 2A	Hydroxamate	6	29.1	25
Coprogen *3*	Hydroxamate	6	30.2	28
Aerobactin 13	Hydroxainate and α-hydroxycarboxylate	6	22.5	23
Mugineic acid 6	a-Aminocarboxylate	6	18	17
Rhizoferrin 14	a-Hydroxycarboxylate	6	25.3	20
Rhoclotrulic acid 16	Hydroxainate	4	31.2	22
Ainonabactin 18	Catechol	4	34	26
Desferrithiocin 20	Phenol. thiazole. and carboxylate	3	29.6	20
2,3-Dihydroxybenzoic acid	Caiechol	2	42	15
Aminochelin	Catechol	2	41.3	17.6
1-Hydroxy-4-methoxy-3-methyl-pyridin-2-one 23B	Hydroxypyridinone	2	28	16

[a]The pFe^{3+} is defined as log $[Fe^{3+}]$ when $[Fe^{(III)}]_{Total} = 1$ μM and $[Ligand]_{Total} = 10$ μM, pH 7.4.

electrochemically by the addition or removal of electrons via an electrode surface or a chemical agent. Thus, iron catechol complexes are capable of undergoing intramolecular electron transfer reactions. Such internal redox reactions are strongly influenced by pH, thus at pH 7.0. the iron(III) catechol complex is most stable, but under more acidic conditions: for instance, pH<5.0, the corresponding iron(II) semiquinone complex becomes the dominant species.[15]

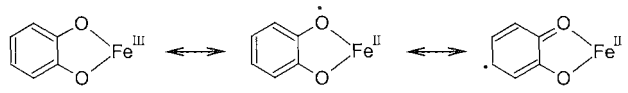

29

TRANSPORT OF IRON–SIDEROPHORE COMPLEXES

Bacteria

A large proportion of bacterial siderophore uptake studies were centered on enteric bacteria as typified by E. *coli* and S. *typhimurium*. These bacteria possess a cell wall consisting of an outer membrane layer and a peptidoglycan layer. The former acts as a molecular sieve-type barrier, and the latter confers mechanical stability. Thus, the metabolically active cytoplasmic membrane is protected against bile salts and hydrolytic enzymes found in the mammalian gastrointestinal tract. The outer membrane consists of a lipid bilayer, rich in lipopolysaccharide and porins, which renders the outer membrane freely permeable toward small hydrophilic molecules. The region between the outer and cytoplasmic membranes is termed the periplasmic space and contains approximately 20% of the total cell water. As iron(III) siderophores possess molecular weights in excess of 600, their ability to permeate porin structures is low, and specific carrier proteins are necessary. Studies with mutants provided evidence for independent carriers being associated with iron–enterobactin, iron–hydroxamates. and iron–citrate (Fig. 2).[16]

The outer membrane proteins, for instance FecA. FepA, and FhuA, were recently characterized by x-ray crystallography and shown to be homologous structures with molecular weights in the region of 80.000.[17,18] The basic structure consists of a transmembrane β-barrel consisting of 22 transmembrane β-strands. The barrel is "corked" by a globular domain constructed from a mixed α-helical/β-strand framework. There is also an extracellular domain that covers the surface of the barrel and is fully exposed to the extracellular environment. The different proteins are selective for particular iron complexes. for instance, FepA (ferric-enterobactin permease) is selective for iron–enterobactin. The affinity of the outer membrane receptors for the iron–siderophore complexes is high (0.5–50 nM), and thus, they are able to scavenge the complexes from the environment. The complexes bind to the top of the β-barrel, and as a result of a conformation change in the cork domain, which is transmitted by the TonB protein. are translocated to the periplasmic space."'' Here they are picked up by binding proteins

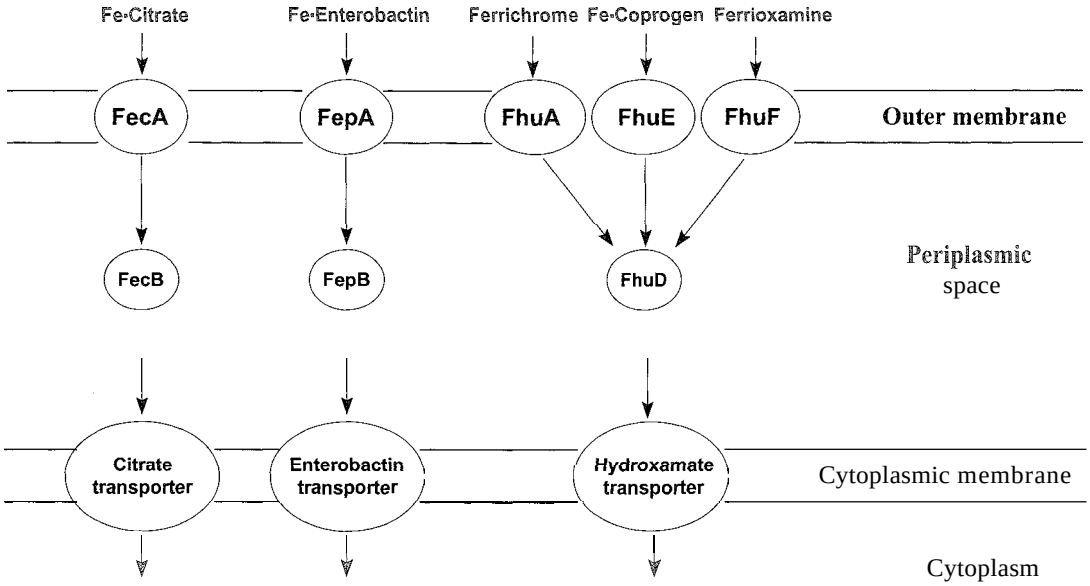

Fig. 2 Iron(III) transport system in E. coli and other enterobactriaceae. The donation of the iron–siderophore complex to the periplasrnic binding protein is facilitated by the cytoplasmic protein TonB. The cytoplasmic iron–siderophore transporters function via a typical ABC-type mechanism. which is driven by ATP hydrolysis.

with μM affinities. e.g., FepB, and translocated to the cytoplasmic membrane. where they are transported to the cytoplasin by ABC-type transporters.

Inevitably. the field is dominated by studies centered on the two organisms. E. coli and *S. typhimurium*, although with the discovery of the plasmid-mediated aerobactin system,[20] other bacterial families are monitored, for instance, *Shigella flexneri*. Virulent strains of *Vibrio anguillarum* contain a plasmid that influences the efficiency of iron uptake by the organism. When grown under low iron conditions, these strains induce the synthesis of outer membrane proteins, in the 80,000 molecular weight range. In similar fashion. Vibrio *cholerae*. *Aeromonas salmonicida* (a fish pathogen), and *Agrobacterium tumefaciens* (a plant pathogen), all induce similar siderophore transport systems when grown under conditions of low iron availability. Many enteric bacteria possess transport systems for exogenous siderophores, for instance, E. coli possesses the Fhu complex of transporters even though it does not normally produce hydroxamate siderophores. This property. together with the ability to harbor plasmids for the synthesis and transport of siderophores, for instance. aerobactin. demonstrates the considerable evolutionary pressure experienced by bacteria to obtain iron from the environment.

Mycobactin species produce a range of siderophores, the water-soluble exochelins (for instance, exochelin MS **11**), mycobactin P **1** (a hydrophobic siderophore, which is not secreted from the organism), and the carboxymycobactins (which are also secreted) (Table 5). The carboxymycobactins are similar to mycobactin P, the only difference being the introduction of a ω-carboxyl function on the central lipid substituent. It is proposed that the exochelins and carboxymycobactins scavenge iron from the environment and donate it to mycobactin P. which acts as an intracellular ion store.[21,22]

Iron(III) complexes of hexadentate siderophores are kinetically and thermodynamically stable, which although being ideal for their scavenging roles. presents problems to the organism with respect to iron release. Redox processes were implicated in this mechanism, as the resulting iron(II) siderophore complexes are kinetically and thermodynamically much less stable than the corresponding iron(III) complexes. Furthermore, such a mechanism renders it possible to reutilize the siderophore and renders it unlikely for an organism to assimilate aluminum. another common tribasic element in the environment. Aluminum is not susceptible to a reductive release mechanism. The enzyme ferrisiderophore reductase is widely distributed. It was suggested that such a mechanism involving catecholate siderophores is not possible due to their extremely low redox potential (−750 mV). This is much lower than a typical intracellular reductant, NADH (−320 mV). As a consequence, the involvement of a siderophore esterase was proposed. However, there is no firm evidence for the existence of such an esterase, and such a mechanism would fail to explain how iron is released from the iron(III) complex of MECAM, a synthetic analogue of enterobactin 5. MECAM 30 can donate iron to *E.* coli and related microorganisms.[23] If the reduction process is carried out in the presence of a powerful iron(II) sink, for instance. protoporphyrin, then such a reduction is readily achievable under physiological conditions. as demonstrated by Byers and coworkers.[24]

Table 5 Microorganisms possessing multiple siderophores

Organism	Siderophores
Mycobactin smegmatis	Mycobactin P **I**, carboxymycobactin. and exochelin MS **11**
Ustilago	Ferrichrome **2A** and ferrichrome-A **2B**
Neurospora	Coprogen **3** and ferricrocin
Fusarium	Fusarine-c and nialonichrome
Aspergillus	Triacetylfusarine **10** and ferricrocin
Azotobacter vinelandii	Protochelin 8. aminochelin 24. and azotochelin **17**

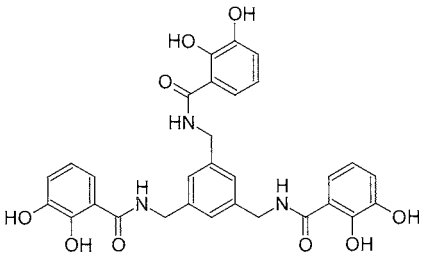

30

Fungi

Fungi are eukaryotic organisms and possess a single cytoplasmic membrane. usually surrounded by a hyphal wall. This hyphal wall does not contain an integral lipid membrane. and thus. unlike enteric bacteria. the iron only has to permeate a single bilayer structure. Siderophores were isolated from many fungi classes. including Basidiomycetes (*Ustilago*), Ascomycetes (*Neurospora* and *Rhodotorula*), Zygomycetes (*Rhizopus*), and Deuteromycetes (*Penicillum*, *Aspergillus*, and *Fusarium*).[25] In general. fungi secrete siderophores into the environment. some are able to donate iron to the external surface of the membrane. whereas others are transported into the cytoplasm as an intact iron(III) complex. This latter process involves active transport and is dependent on the presence of membrane potential and ion gradients. Many fungi

secrete more than one siderophore (Table 5). The function of multiple siderophores is not clear. but their syntheses appear to be under independent control. Under different environmental conditions. the secretion of one or another of the siderophores will predominate. With some pairs. one will be a more potent scavenger for polymeric inorganic iron and will exchange iron prior to cellular uptake. Sorne siderophores are used as storage molecules for iron and do not rapidly donate iron once gaining entry to the cell. Iron is released from siderophores via specific ferrisiderophore reductases. *Neurospora crassa* produces coprogens and ferrichromes (Table 5), and whereas the fersichrome-type siderophores release their bound iron rapidly,[26] iron(III) coprogen is not rapidly reduced and remains largely unchanged in the cytoplasm, possibly acting as a storage form of iron. With *Fusarium roseum*, two different siderophore classes are produced: the fusarines and malonichrone. It is likely that the negatively charged malonichrome is a more efficient scavenger than the fusarines and, thus, is only induced under conditions of extreme iron scarcity. A similar phenomenon probably occurs with *Ustiligo*, which produces ferrichrome **2A** and the superior scavenger ferrichrome A **2B**.

Structure activity studies with the cyclic hexapeptide siderophores demonstrate that modification of the amino acid sequence in the cyclic peptide does not appreciably influence the ability of the resulting siderophore to transport iron. However, the nature of the hydroxamate acyl substituent has a major influence. the presence of one or more *trans* anhydromevalonic acid residues severely inhibits the process. Furthermore. the chiral nature of the iron complex has a dominant influence, the cyclic hexapeptide siderophore receptor with a marked preference for the Λ complex.[27]

Graminaceous Plants

Grasses, cereals, and rice secrete phytosiderophores into the soil when grown under iron-deficient conditions, for instance. alkaline soils. The iron–phytosiderophore complex is then transported via the root cells to the phloem,[28] where the iron is transferred to nicotianamine **31.** a molecule closely related to mugineic acid 6 and translocated to the rest of the plant tissues. Many phytosiderophores are hydroxylated, and this results in a lowering of the pK_a values of the amino functions and, hence, reduces the ability of protons to compete with the binding of iron.

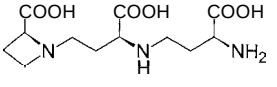

31

Such trends have relevance to the ability of different cereals to grow in acidic soils. It is probably significant that barley and rye. which are relatively resistant to iron-induced chlarosis, produce highly hydroxylated phytosiderophores.[29]

INTERACTION OF SIDEROPHORES WITH METALS OTHER THAN IRON

Aluminum and gallium form trivalent cations with similar radii to that of iron(III) and, therefore, possess high affinities for siderophores. Gallium is a scarce metal, and therefore. competition with iron in the biosphere in unlikely. In contrast, aluminum is plentiful, and although it binds less tightly to hydroxainate ligands than does iron(III), it possesses a similar affinity for catecholato ligands. The stability constants (β_3) of iron(III) and aluminum(III) for acetohydroxamic acid are 10^{28} and 10^{22} and for catechol are 10^{44} and 10^{46}, respectively. Thus, there is the possibility that aluminum could be absorbed by phenolate siderophores. However, its release from the siderophore, unlike iron, would not be facilitated by a reduction step. Thus, absorbed aluminum would tend to remain bound to the siderophore and not be available for protein coordination. For these reasons, it is unlikely that aluminum enters mammalian food chains via microorganisms. Some actinides, for instance, plutonium(IV), by virtue of possessing similar charge densities to that of iron(III), also possess high affinities for hydroxamate and catechol siderophores.

Three other metals. namely, copper. vanadium. and molybdenium, possess appreciable affinities for siderophores. It is possible that siderophores or siderophore-like molecules are involved in the microbial transport of these metals. Copper(II) forms stable complexes with hydroxamate siderophores (for instance, schizokinen, desferrioxamine B. and desferrithiocin) and catechol siderophores (for instance, enterobactin). However, copper(II), unlike iron(III), also possesses a high affinity for amino acids and small peptides, and this property renders it unlikely that copper uptake is dependent on siderophore-mediated transport.

Molybdenum VI

Molybdenum behaves differently than most metals that are essential for living processes, in that it exists predominantly in an anionic form in neutral aqueous solution. The reason for this difference is that the most stable valence state of molybdenum in aerobic aqueous solutions is six. Because the Mo(VI) cation possesses an extremely high charge density (radius = 0.73 A), it reacts with water,

forming the MoO_2^{2+} and MoO_4^{2-} species. The MoO_2^{2+} cation does not behave as a typical divalent cation insofar as it binds anions strongly and thus is more like a trivalent cation. The effective charge on the molybdenuin atom is 3.6^+, and therefore, the surface of the cation not occupied by oxygen atoms is similar to that of iron(III). Not surprisingly, therefore, molybdenum(VI) forms complexes with catechol 32, which possess a characteristic yellow color (λ_{max}=325 nm).

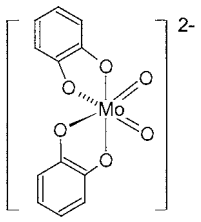

32

The nitrogen fixing organism *Azobacter vinelandii* was demonstrated to produce a range of molybdenum-binding catecholates, which also function as siderophores. for instance, azotochelin 17 and protochelin 8. The levels of molybdenum in culture medium have a dramatic influence on siderophore production (Fig. 3).[30] At high concentrations of molybdate, the production of the tetradentate siderophore **17** is reduced to zero and replaced by the hexadentate siderophore, protochelin 8. In the presence of high molybdate levels. the tetradentate molecule is an inefficient scavenger of iron(III) hydroxide due to the formation of a molybdenum complex. In contrast, the hexadentate siderophore is still able to scavenge iron, as one catechol function is free when the molecule binds molybdate. Thus, the frequently observed toxicity of high molybdate levels is likely to be a result of iron deficiency (Mo–Fe antagonism). However. this effect will be minimized in the presence of hexadentate catecholate siderophores. Other nitrogen fixing organisms, for instance, *Azospirillum lipoferum* and *Paracoccus denitrificans*, produce catechol siderophores and molybdenum accumulation was demonstrated to be dependent on the iron status of these organisms.

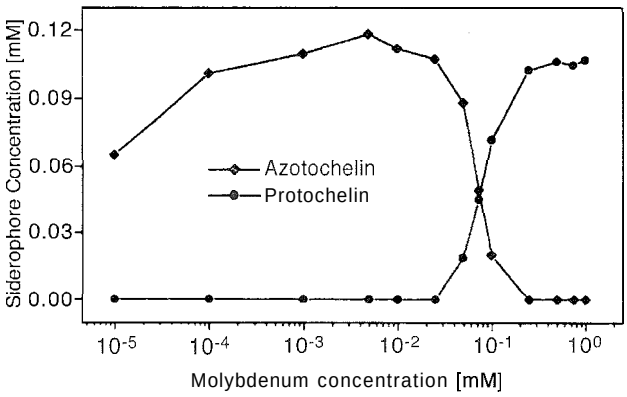

Fig. **3** Effect of rnolybdate on azotochelin 17 and protochelin 8 production by A *vinelandii* as determined by HPLC

Vanadium ascidians (sea squirts), possess the ability to sequester and reduce vanadium in specialized blood cells termed vanadocytes. Vanadium is present in these cells at high concentrations, most probably in the simple mononuclear form $[V^{(III)}SO_4(H_20)_5]^+$. Tunichromes 33, which are produced by ascidians, possess a rigid backbone and, as a result. are unable to form stable tetradentate or hexadentate monomeric vanadium complexes: unlike enterbactin **5.** which binds V^{IV} avidly. As a result. it is more likely that tunichrome acts as a transient ligand and reductant of vanadium(V), which is accumulated by the organisms as the vanadate anion,[31] leading to its ultimate storage as V^{III} in vanadophoric granules of low pH.

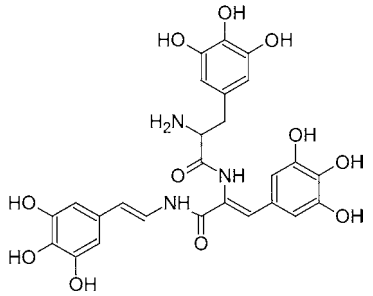

33

CLINICAL APPLICATION OF SIDEROPHORES AND ANALOGUES

Selective Iron Chelation

Currently, there is considerable demand for a highly specific chelator of iron. which is suitable for clinical administration to iron-overloaded patients. The most widely adopted method of treating β-thalassaemia, is regular blood transfusion. and this leads to iron overload. In 1962. Sephton Smith demonstrated that desferrioxamine **B** 4 given intramuscularly to iron-overloaded patients. increased the excretion of iron in the urine.[32] However, early experiences with this hydroxamate siderophore were disappointing, and it was not until regular bolus injections were introduced that any consistent success was obtained. Following this. administration of the drug by slow continuous infusion was introduced. and although unpleasant. the treatment is effective.[33] Desferrioxarnine is also used in the treatment of acute iron poisoning and for the removal of aluminum. Unfortunately, desferrioxamine is not orally active, and it has become increasingly important to identify a nontoxic orally active

iron chelator. A wide range of siderophores were investigated together with close synthetic analogues, for instance, **5,** 16, and **20**. In order to achieve good oral bioavailability, molecules with molecular weights <500 are required, and this excludes most of the hexadentate siderophores. However, the bidentate 3-hydroxypyridin-4-ones were demonstrated to be effective, and deferiprone **34** is now an approved medicine in Europe.[34]

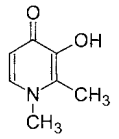

34

Iron-Transport-Mediated Drug Delivery

Some natural antibiotics contain a siderophore structure, for instance, δ_1-albomycin **35,** which is produced by *Streptomyces subtropicus*. The linear tripeptide portion chelates Fe(III) and, thereby, is able to utilize the iron-transport system of a range of microorganisms. Subsequent to uptake, peptidases localized in the cytoplasmic membrane hydrolytically release the toxic thioribosyl moiety. In principle, this property can be used for selective drug delivery. Preliminary studies indicated that substantial modification of the siderophore framework can be tolerated by microbial iron-transport systems.[35,36] Surprisingly, simple modifications can be made to cephalosporin molecules, which endow them with the ability to interact with microorganism iron-transport mechanisms. Thus, simple incorporation of a catechol moiety, as in 36, endows this molecule with enhanced activity against *Pseudomonas aeruginosa* when compared with other cephalosporins.[37]

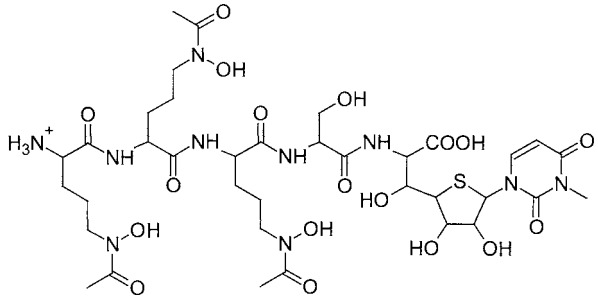

35

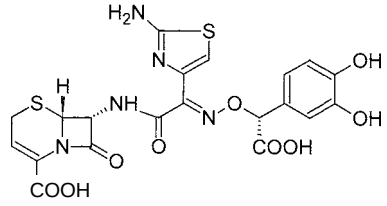

36

ARTICLES OF FURTHER INTEREST

Biological Ligands, p. *88*
Hemoglobins: O_2 Uptake and Transport, p. 636
Ionophores, p. 760
Podands, p. 1106
Stability Constants: Definition and Determination, p. 1360

REFERENCES

1. Snow, G.A. Mycobactin. A growth factor for Mycobacterium johnei. Part II. Degradation and identification of fragments. J. Chem. Soc. 1954. 2588–2596.
2. Snow, G.A. Mycobactin. A growth factor for Mycobacterium johnei. Part III. Degradation and tentative structure. J. Chem. Soc. **1954**, 4080–4093.
3. Bickel, H.; Bosshardt, R.; Gäumann, E.: Reusser. P.: Vischer. E.; Voser. W.; Wettstein. A.: Zahner, H. Über die isolierung und charakterisierung der femoxamine A–F; neuer wuchsstoffe der sideramin-gruppe. Helv. Chim. Acta 1960. 43. 2118–2123.
4. Garibaldi, J.A.; Neilands, J.B. Formation of iron-binding compounds by microorganisms. Nature 1956. 177. 526–527.
5. Pollack. J.R.: Neilands. J.B. Enterobactin. an iron transport compound from *Salmonella typhimurium*. Biochem. Biophys. Res. Commun. 1970. *38*. 989–992.
6. O'Brien, I.G.: Gibson, F. The structure of enterochelin and related 2.3-dihydroxy-N-benzoylserine conjugates from *Escherichia coli*. Biochem. Biophys. Acta 1970. *215*, 393–402.
7. Bullen, J.J.: Griffiths. E. *Iron and Infection.* 2nd Ed.: Wiley: New York, 1999.
8. Mori, S. The Role of Mugineic Acid in Iron Acquisition: Progress in Cloning the Genes for Transgenic Rice. In *Plant Nutrient Acquisition*; Ae. *N.*, Arihara. J.. Bkada, K.. Srinivason, A.. Eds.; Springer-Verlag: Tokyo, 2001: 120–139.
9. van der Helm. D.: Jalal. M.A.F.: Hossain. M.B. The Crystal Structures, Conformations and Configurations of Siderophores. In *Iron Transport* in *Microbes, Plants and Animals:* Winkelmann. *G.*, van der Helm. D.. Neilands, J.B.. Eds.; VCH: Cambridge. UK. 1987; 135–165.
10. Raymond. K.N.; Müller, G.: Matzanke, F. Complexation of iron by siderophores: A review of their solution and structural chemistry and biological function. Top. Curr. Chem. 1984. *123*. 49–102.
11. Meyer, M.: Kersting. B.; Powers, R.E.; Raymond. K.N. Rearrangement reactions in dinuclear triple helicates. Inorg. Chern. 1997. *36*. 5179–5191.
12. Liu, Z.D.: Hider, R.C. Design of iron chelators with therapeutic application. Coord. Chem. Rev. 200%*232*, 151–171.
13. Harris, W.R.: Raymond, K.N. Ferric ion sequestering

agents 3. The spectrophotometric and potentiometric evaluation of two new enterobactin analogues: 1,5,9-N,N^{I},N^{II}-Tris(2,3-dihydroxybenzoyl)triaminomethylbenzene. J. Am. Chem. Soc. 1979, *101*. 6534–6541.
14. Liu. Z.D.: Hider. R.C. Design of clinically useful iron(III)-selective chelators. Med. Res. Rev. 2002, *22*. 26–64.
15. Hider, R.C.: Liu. Z.D.: Khodr, H.H. Metal chelation of polyphenols. Methods Enzymol. 2001, *335*. 190–203.
16. Braun. V.; Hantke, K. Receptor-Mediated Bacterial Iron Transport. In *Transition Metals* in Microbial Metabolism: Winkelmann, G., Carrano. C.J., Eds.; Harwood Academic Publishers: London. 2000: 81–116.
17. Ferpuson. A.D.; Hofmann, E.: Coulton, J.W.: Diederichs, K.: Welte, W. Siderophore-mediated iron transport: Crystal structure of FhuA with bound lipopolysaccharide. Science 1998. 282. 2215–2220.
18. Buchanan. S.K.: Smith. B.S.: Vankatramani. L.; Esser. L.: Palnitkar, M.: Chakraborty, R.; van der Helm. D.; Deisenhofer. J. Crystal structure of the outer membrane active transporter FepA from *Escherichia* coli. Nat. Struct. Biol. 1999, *6*. 56–63.
19. Ferguson, A.D.: Chakraborty, R.; Smith. B.S.: Esser, L.: van der Helm. D.; Deisenhofer, J. Structural basis of gating by the outer membrane transporter FecA. Science 2002, 295. 1715–1719.
20. De Lorenzo, V.; Bindereif, A.; Paw. B.H.: Neilands, J.B. Aerobactin biosynthesis and transport genes of plasmid ColV-K30 in Escherichicr coli K-12. J. Bacteriol. 1986, *165*. 570–578.
21. Sharman. G.J.: Williams, D.H.: Ewing. D.F.: Ratledge, C. Isolation, purification and structure of exochelin MS. the extracellular siderophore from *Mycobacterium smegmatis*. Biochem. J. 1995. *305*. 187–196.
22. Gobin. J.: Horwitz. M.A. Exochelins of *Mycobacterium tuberculosis* remove iron from human iron-binding proteins and donate iron to mycobactins in the *M. tuberculosis* cell wall. J. Exp. Med. 1996. *183*. 1527–1532.
23. Heidinger. S.; Braun. V.; Pecoraro. V.L.; Raymond. K.N. Iron supply to *Escherichia* coli by synthetic analogues of enterochelin. J. Bacteriol. 1983. *153*, 109–115.
24. Lodge. J.S.; Gaines, C.G.; Arceneaux. J.E.L.: Byers. B.R. Non-hydrolytic release of iron from ferrienterobactin analogues by extracts of Bacillus *subtilis*. Biochem. Biophys. Res. Commun. 1980. *97*. 1291–1295.
25. Leung. S.A.: Winkelmann. G. Molecular Biology of Iron Transport in Fungi. In Metal *Ions* in Biological Systems: Sigel. A.. Sigel, H., Eds.; Dekker: New York, 1998: Vol. 35. 147–186.
26. Huschka, H.; Naegeli, H.U.; Leuenberger-Ryf, H.: Keller-Schierlein. W.; Winkelmann, G. Evidence for a common siderophore transport system but different siderophore receptors in *Neurospora* crassa. J. Bacteriol. 1985, *162*. 715–721.
27. Drechsel. H.: Winkelmann, G. Iron Chelation and Siderophores. In *Transition* Metals in Microbial Metabolism; Winkelmann, G., Carrano. C.J., Eds.: Harwood Academic Press: London, 2000: 1–49.
28. Mori. S. Iron Transport in Graminaceous Plants. In *Metal Ions in* Biological *Systems*; Sigel. A., Sigel. H., Eds.: Dekker: New York. 1998: Vol. 35. 215–238.
29. Von Wirén. N.; Khodr. H.; Hider, R.C. Hydroxylated phytosiderophore species possess an enhanced chelate stability and affinity for iron(III). Plant Physiol. 2000. *124*. 1149–1157.
30. Duhme, A.K.; Hider. R.C.: Naldrett. M.J.: Pau, R.N. The stability of the molybdenum–azotochelin complex and its effect on siderophore production in *Azotobacter vinelandii*. J. Biol. Inorg. Chem. 1998. *3*, 520–526.
31. Oltz. E.M.; Bruening, R.C.: Smith, M.J.; Kustin. K.: Nakanishi, K. The tunichromes. A class of reducing blood pigments from sea squirts: Isolation, structures and vanadium chemistry. J. Am. Chem. Soc. 1998, *110*. 6162–6172.
32. Hershko. C.: Konijn, A.M.; Link. G. Iron chelators for thalassaemia. Br. J. Haematol. 1998. *101*. 399–406.
33. Porter. J.B. Practical management of iron overload. Br. J. Haematol. 2001. *115*. 239–252.
34. Liu, D.Y.; Liu. Z.D.: Hider. R.C. Oral iron chelators—Development and application. Best Pract. Res. Clin. Haematol. 2002, *15*. 369–384.
35. Miller, M.J.; Malouin. F. Microbial iron chelators as drug delivery agents: The rational design and synthesis of siderophore—Drug conjugates. Acc. Chem. Res. 1993. *26*. 241–249.
36. Wittmann, S.: Schnabelrauch. M.: Scherlitz-Hofmann, I.: Mollmann. U.; Ankel-Fuchs. D.; Heinisch. L. New synthetic siderophores and their β-lactam conjugates based on diamino acids and dipeptides. Bioorg. Med. Chem. 2002, *10*. 1659–1670.
37. Silley. P.: Griffiths, J.W.: Monsey, D.: Harris. A.M. Mode of action of GR69153, a novel catechol-substituted cephalosporin and its interaction with the *ton*-B-dependent iron transport system. Antimicrob. Agents Chemother. 1990. 34. 1806–1808.

Simultaneous Binding of Cations and Anions

Bradley D. Smith
Joseph M. Mahoney
University of Notre Dame, Notre Dame, Indiana, U.S.A.

INTRODUCTION

Synthetic receptors for cations or anions have potential applications in many different chemical technologies, and a large number of receptor designs have been evaluated over the past three decades. Many of these synthetic receptors are uncharged molecules that operate in organic solvents. Under these conditions, the target salts may exist as associated ion pairs that can hinder the single-ion recognition process. Two strategies can be employed to simultaneously bind both ions of a target salt. The dual-receptor strategy uses a binary mixture of anion and cation receptors: alternatively, a single ditopic receptor can be designed with specific cation and anion binding sites. These salt-binding receptors can be organic or organometallic molecules. They are prototypes for more complicated self-assembly systems that may eventually be used as components in molecular machines.

IONS AND ION PAIRS

An important goal in supramolecular chemistry is to develop high-affinity synthetic receptors for specific target ions. Because the target ion is necessarily accompanied by a counterion. the recognition process can become complicated, because salts do not exist as free ions in most organic solvents, instead they are present as solvent-separated ion pairs, contact ion pairs. or aggregated contact ion pairs (Fig. 1).[1] Thus. for a receptor to associate with a target ion. it must compete with the counterion. Historically, this situation was avoided by using noncompeting counterions such as tetralkylammonium cations or tetrarylborate anions. However. in many real-life separation or sensing situations. the luxury of noncompeting counterions is not available, and ion pairing of the target ion with its counterion can lead to diminished receptor/ion association constants. For example, titration of the simple acetate receptor. *N*-octyl-*N*′-phenyl urea, in DMSO with tetrabutylammonium acetate leads to an association constant of $K_{acetate}$=310 M^{-1}. Repeating the titration experiment in the presence of one molar equivalent of sodium tetraphenylborate lowers $K_{acetate}$ to 90 M^{-1}.[2] In chis case. the sodium forms an ion pair with the acetate, which lowers the receptor1 acetate association constant. The associated sodium cation sterically hinders the receptor/acetate interaction. and it lowers the acetate's effective charge by a polarization effect or a shielding effect.

DUAL-RECEPTOR STRATEGY

One way to alleviate this counterion-induced inhibition of receptorlion binding is to use a dual-receptor strategy, that is. a binary mixture of anion and cation receptors.[3–6] Examples of dual-receptor strategies reported so far include mixtures of crown ether 1 and tripodal amide 2 to extract $CsNO_3$,[3] and a mixture of cation-binding calixarene **3** and anion-binding calixpyrrole 4 to bind butylammonium chloride (Chart 1).[4] A major advantage of the dual-receptor strategy is structural simplicity and the associated economic savings. Thus, dual-receptor systems should be useful for industrial solid/liquid extraction and membrane transport of salts.

DITOPIC RECEPTORS

An alternative to the dual-receptor strategy is to design a single ditopic salt receptor that simultaneously binds the cation and the anion.[7] A potential advantage gained by covalently linking the anion- and the cation-binding sites is the possibility of binding cooperativity. That is. the binding of the first ion to the receptor alters the receptor's affinity for the second ion. Positive cooperativity is when the presence of the first ion raises the receptor's affinity for the second ion, whereas negative cooperativity is the reverse. Many of the early ditopic salt receptors described in the literature have spatially separated cation and anion binding sites. so that the anion and the cation are not in contact with each other when they are bound to the receptor.[8–10] As a result; cooperative binding effects are expected to be small. One of the earliest ditopic salt receptors is Compound **5,** which has two crown ether rings to bind metal cations such as K^+ and a Lewis acidic UO_2^+ center to bind anions such as $H_2PO_4^-$.[8]

Encyclopedia of Supramolecular Chemistry
DOI: 10.1081/E-ESMC 120012715

$$M^+ + A^- \rightleftharpoons M^+A^- \rightleftharpoons [M^+A^-]_n$$

Fig. 1 Salts can exist as free ions. ion pairs, or aggregated ion pairs in organic solvents. (Reprinted with permission from Ref. [9]. Copyright 2000. American Chemical Society.)

Positive cooperativity is produced when the binding of an ion alters the ditopic receptor structurally (induced fit) or electronically (receptor polarization) in a way that improves binding of the counterion. The induced-fit concept is particularly intriguing. because it is a central feature in the allosteric effect used by many enzymes and biological receptors. An early example of a flexible receptor that uses an induced-fit strategy to simultaneously bind K^+ and Cl^- is Compound 6.[11] The central polyamine linker wraps around a Cl^- ion, which brings the two crown ether rings together to bind a K^+. A more recent example is the dibenzo-30-crown-10 derivative **7**, which acts in reverse; that is. the receptor wraps around a K^+ ion and forms a preorganized binding site for diphenylphosphate anion.[12] A receptor that probably uses both induced-fit and polarization effects. is the tripodal *tris*(amido benzo-15-crown-5) 8. which simultaneously binds Na^+ and ReO_4^-.[13] In this case, the presence of the Na^+ improves the receptor's affinity for ReO_4^- by a factor of 20.

A variation of the receptor polarization effect is the binding strategy shown by schematic Complex 9. In this case; the binding of an ion to one face of an appropriately designed receptor polarizes (and perhaps preorganizes) the receptor so that it can bind the counterion to the opposite face with increased affinity. Two examples that use this strategy are the macrocyclic phosphine oxide 10, which can simultaneously bind a monoalkylammonium cation and Cl^-,[14] and the cyclopeptide **11**, which simultaneously binds an alkyltrimethylammonium cation and tosylate anion[15] (Chart 2).

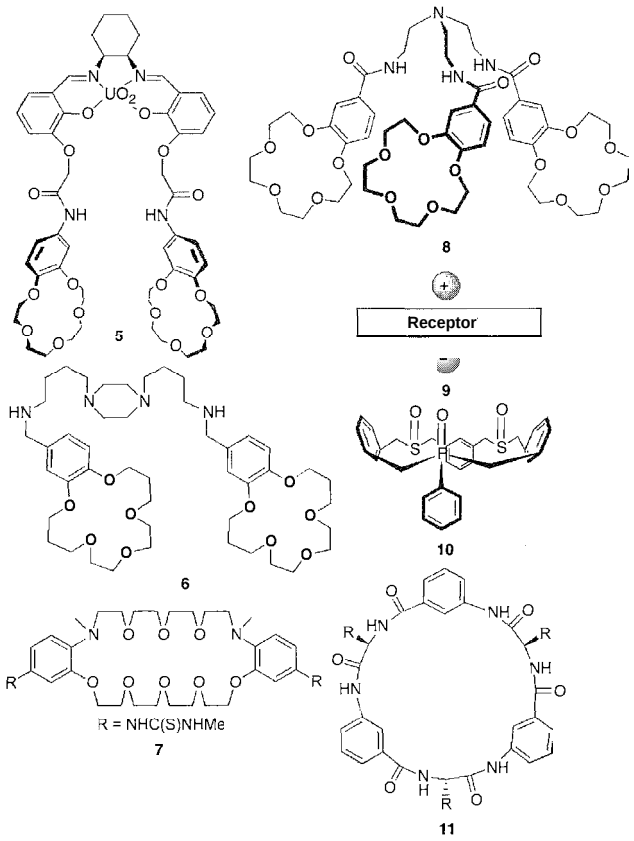

Chart 2 Ion-pair recognition using ditopic salt-binding hosts.

ORGANOMETALLIC DITOPIC RECEPTORS

A number of organometallic receptors were developed to take advantage of the anion coordination ability of inorganic atoms. A conceptually important early example is the crown boronate 12, which can simultaneoirsly bind cations such as K^+ and anions such as F^-. The F^- forms a strong coordinate bond with the boron, and the K^+ associates with the crown ether ring.[16] More recently. the simple monodentate ligand, 3-*t*-butylpyrazole, was found to act as a ditopic receptor for Zn(II) halide salts.[17] The system self-assembles to form Complex 13 with one halide anion coordinated to the zinc and the other hydrogen bonded to the pyrazole NH.

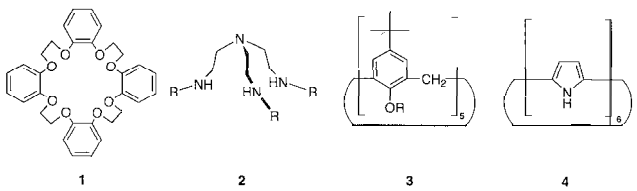

Chart 1 Compounds 1–4 used for dual-receptor recognition of cations and anions.

DITOPIC RECEPTORS THAT RECOGNIZE ASSOCIATED ION PAIRS

Another way to view salt binding is to accept the fact that salts prefer to form ion pairs and. thus. develop ditopic receptors that bind salts as associated ion pairs (Fig. 2). Two examples are the macrobicycles 14 and **15** with juxtaposed anion- and cation-binding sites. In the case of 14, the presence of Na' cation enhances Cl binding by about a factor of 10. An x-ray crystal structure of the **14**·NaCl complex shows that the salt is bound as a solvent-separated ion pair.[18] The Na^+ sits in the crown ring, and

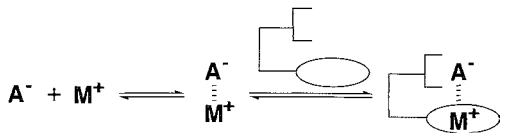

Fig. 2 Ion-pair recognition using ditopic salt-binding hosts. (Reprinted with pennission from Ref. [9] Copyright 2000, American Chemical Society.)

the C l is hydrogen bonded to the two receptor NH residues with a chloroform molecule sandwiched between the two ions. The positive binding cooperativity for this receptor is due to the anion interacting with the cation via the bridging chloroform. The binding cooperativity effect is greatly magnified in the case of the smaller macrobicycle **15**, because the NaCl salt is bound as a contact ion pair."'' This increases the Cl^- ion's electrostatic attraction to the receptor/Na^+ complex. In the case of **15**, the receptor/salt complexes are so stable that they can survive column chromatography using silica gel and weakly polar solvents (Chart 3).

CONCLUSION

In the future, salt-binding receptors are likely to be employed in various separation and sensing applications. It appears that both design strategies, dual-receptor mixtures, and single ditopic receptors, should be useful. Salt binding is a relatively new topic in supramolecular chemistry, and it is likely to be actively pursued in the near future. Hints of possible new research directions are provided by two examples from the recent literature. The first is the self-assembled pseudorotaxane **18**, which is prepared by simply mixing ion-pair **16** with macrocycle **17**[20] (Chart 3). This work and a related report[21] show how salts can be employed as "molecular glue" to assemble complex supramolecular structures. The second example. illustrated in schematic form in Fig. 3, is a permanently interlocked [2]rotaxane with salt-binding ability.[22] In polar DMSO solvent, the rotaxane is conformationally mobile, with the wheel rotating slowly around the axle. This motion is stopped by the presence

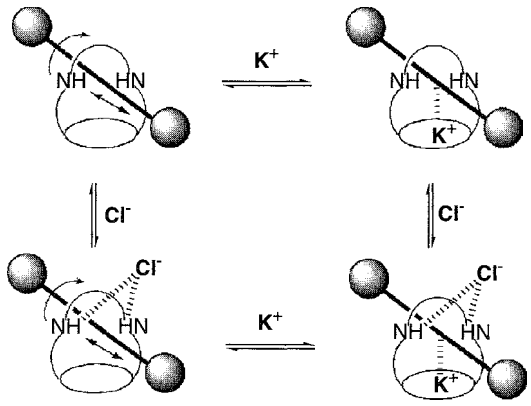

Fig. 3 In polar aprotic solvent, a salt-binding [2]rotaxane populates multiple axle/wheel orientations. Binding Cl^- does not measurably alter the rotaxane's dynamic properties, whereas binding K^+ freezes out a single coconformation (molecular brake). (Reprinted with permission from Ref. [22]. Copyright 2002, Elsevier Science.)

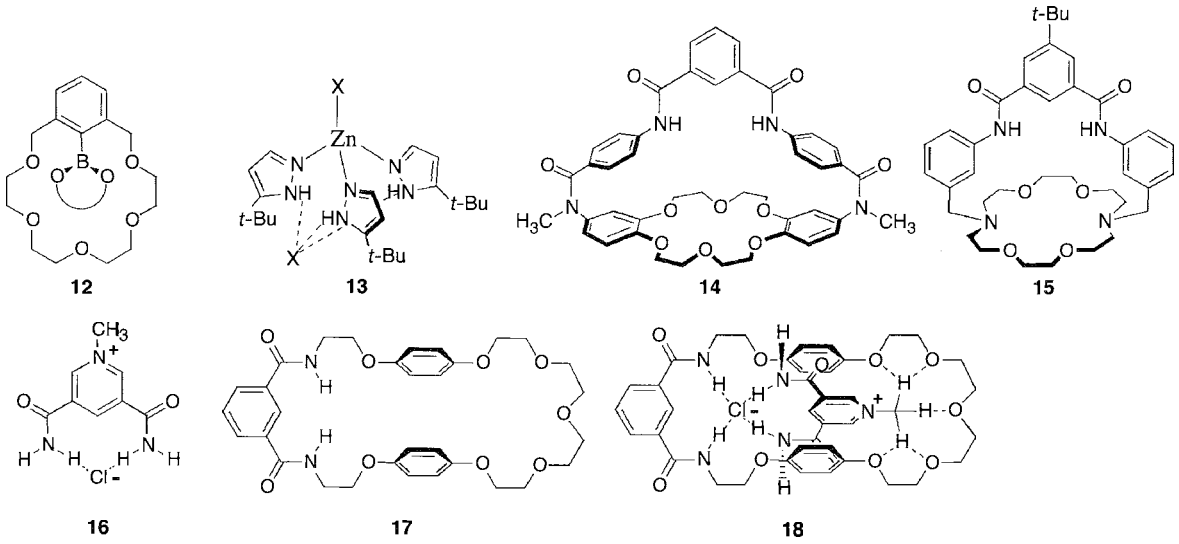

Chart 3 Compounds 12–15 are recent examples of salt receptors. Compounds 16–18 are examples of salt recognition as a method of supramolecular self-assembly.

of K^+ ions that bind to a crown ether unit in the wheel. Binding Cl^-, however, does not measurably alter the rotaxane's dynamic properties. This supramolecular system can be viewed as a potential molecular machine component. with dynamic properties that can be regulated by chemical effectors.

ACKNOWLEDGMENTS

We gratefully acknowledge support by the National Science Foundation and the University of Wotre Dame.

ARTICLES OF FURTHER INTEREST

The Allosteric Effect, p. 20
Calixarenes and Their Analogues: Cation Complexation, p. 137
Crown Ethers, p. 326
Cryptands, p. 334
Ionophores, p. 760
Lariat Etlzers. p. 782
Organometallic Anion Receptors. p. 1006
Pyrrole- and Polypyrrole-Based Anion Receptors, p. 1176
Rotaxanes and Pseudorotaxanes, p. 1194
Spherands, p. 1344

REFERENCES

1. Smid. J. Structure of ion-pair solvation complexes. Angew. Chem. Int. Ed. 1972, 11. 112–127.
2. Shukla, R.; Kida. T.; Smith, B.D. Effect of competing alkali metal cations on neutral host's anion binding ability. Org. Lett. 2000, 2. 3099–3102.
3. Kavallieratos. K.; Danby. A.; Van Berkel, G.J.; Kelly, M.A.; Sachleben, R.A.: Moyer. B.A.: Bowman-James, K. Enhancement of $CsNO_3$ extraction in 1,2-dichloroethane by *tris*(2-aminoethyl)amine triamide derivatives via a dual-host strategy. Anal. Chem. 2000, 72. 5258–5264.
4. Cafeo, G.; Gattuso, G.; Kohnk, F.H.; Notti, A.; Occhipinti, S.; Pappalardo, S.; Parisi. M.F. Remarkable boosting of the binding of ion-paired organic salts by binary host systems. Angew. Chem. Int. Ed. 2002. 41, 2122–2126.
5. Chrisstoffels, L.A.J.: De Jong, F.: Reinhoudt, D.N.: Sivelli. S.: Gazzola. L.; Casnati. A.; Ungaro, R. Facilitated transport of hydrophilic salts by mixtures of anions and cation carriers and by ditopic carriers. J. Am. Chem. Soc. 1999; 121, 10142–10151.
6. Rudkevich, D.M.: Shivanyuk, A.N.: Brzozka. Z.; Verboom, W.; Reinhoudt, D.N. A self-assembled bifunctional receptor. Angew. Chem.. Int. Ed. Engl. 1995. 34. 2124–2126.
7. Gale, P.A.: Beer, P.D. Anion recognition and sensing: The state of the art and future perspectives. Angew. Chem.. Int. Ed. Engl. 2001. 40. 486–516.
8. Rudkevich, D.M.; Brzozka, Z.: Palys, M.: Visser. H.C.; Verboom. W.: Reinhoudt. D.N. A difunctional receptor for the simultaneous complexation of anions and cations. recognition of KH_2PO_4. Angew. Chem., Int. Ed. Engl. 1994. 33. 467–468.
9. Scheerder, J.: van Duynhoven, J.P.; Engberson, J.F.; Reinhoudt, D.N. Solubilization of NaX salts in chloroform by bifunctional receptors. Angew. Chem.. Int. Ed. Engl. 11996, 35. 1090–1093.
10. Antonisse. M.M.G.; Reinhoudt, D.N. Neutral anion receptors: Design and application. J. Chem. Soc., Chern. Commun. 1998. 443–447.
11. Arafa, E.A.; Kinnear. K.I.: Lockhart. J.C. New pocket ionophores with potential for simultaneous chelation of anions and cations. Synthesis and scope of chelating properties. J. Chem. Soc., Chem. Commun. 1992. 61–64.
12. Tozawa. T.; Misawa. Y.; Tokita, S.: Kubo, Y. A regioselective *bis*(thiourea)-substituted dibenzo-diaza-30-crown-10: A new strategy for the development of multisite receptors. Tetrahedron Lett. 2808. 41. 5219–5223.
13. Beer. P.D.: Hopkins. P.K.: McKinney, J.D. Cooperative halide. perrhenate anion-sodium cation binding and pertechnetate extraction by a novel tripodal *tris*(amide benzo-15-crown-5) ligand. J. Chem. Soc., Chem. Commun. 1999. 1253–1254.
14. Savage, P.B.; Holmgren. S.K.; Gellman. S.H. Anion and ion pair complexation by a macrocyclic phosphine oxide dirulfoxide. J. Am. Chem. Soc. 1994. 116. 4069–4070.
15. Kubik. S. Large increase in cation binding affinity of artificial cyclopeptide receptors by an allosteric effect. J. Am. Chem. Soc. 1999, 121. 5846–5855.
16. Reetz. M.T.; Niemeyer. C.M.; Harms. K. Heteroditopic host molecules for binding two different guests. Angew. Chem., Int. Ed. Engl. 1991. 30. 1474–1476.
17. Liu. X.: Kilner. C.A.: Halcrow. M.A. 3{5}-*tert*-butylpyrazole is a ditopic receptor for zinc(II) halides. J. Chem. Soc., Chem. Commun. 2002. 704–705.
18. Deetz. M.J.: Shang, M.; Smith, B.D. A macrobicyclic receptor with versatile recognition properties: Simultaneous binding of an ion pair and selective complexation of dimethylsulfoxide. J. Am, Chem. Soc. 2000. 122, 6201–6207.
19. Mahoney, J.M.; Beatty, A.M.; Smith. B.D. Selective recognition of an alkali halide contact ion-pair. J. Am. Chem. Soc. 2001, 123. 5847–5848.
20. Wisner. J.A.: Beer. P.D.: Berry. N.G.; Tornapatanaget, B. Supramolecular chemistry and self-assembly special feature: Anion recognition as a method for templating pseudorotaxane formation. Proc. Natl. Acad. Sci. U. S. A. 2002. 99 (8). 4983–4986.
21. Shi, X.; Fettinger. J.C.: Davis. J.T. Ion-pair recognition by nucleoside self-assembly: Guanosine hexadecamers bind cations and anions. Angew. Chem.. Int. Ed. Engl. 2001.40. 2827–2830.
22. Shukla. R.; Deetz, M.J.; Smith, B.D. Recognition-directed assembly of salt-binding [2]rotaxanes. Tetrahedron 2002. *58* (4). 799–805.

Simultaneous Binding of Cations and Neutral Molecules

Michaele J. Hardie
University of Leeds, Leeds, United Kingdom

INTRODUCTION

The simultaneous binding of cations and neutral molecules within a single host–guest system usually involves a metal as the cationic species, although there are a handful of examples involving an organic cation. Molecules that include metal cations but also bind neutral molecules may do so through a number of mechanisms, including coordinating the neutral guest with a metal cation that is bound within a host; binding the cation and neutral guest in different host receptor sites; and making the metal cation an intrinsic part of the molecular architecture of the host molecule (a metallohost). which includes the metal-templated self-assembly of a receptor molecule that subsequently binds a neutral molecule. Simple macrocyclic coordination complexes, such as metallated crown ethers, porphyrins, and phthalocyanines, where neutral ligands bind to the metal in axial positions, may also be regarded as simultaneous binding of cations and neutral molecules. These will not be considered here. Also, pseudomacrocyles, which are metal-assembled macrocycles analogous to traditional organic macrocycles. will not be presented. Metallohosts were extensively reviewed in recent years,[1–3] hence only a few representative recent examples will be highlighted herein. The main focus of this article will be host molecules that simultaneously bind cations and neutral molecules in different receptor sites.

TRADITIONAL HOST MOLECULES

Crown Ethers

The earliest reported examples of a system binding cations and neutral molecules simultaneously employed traditional inacrocyclic host molecules, such as calixarenes 1, which are described more fully below, and cyclic polyethers. Incorporating pyridyl or Schiff base groups into crown ethers leads to macrocycles with two possible binding modes.'" in the complex 2,6-pyrido[27]crown-9.$LiClO_4$.urea, both the Li^+ cation and urea are encapsulated within the crown ether cavity with interactions between them. In contrast, the Ni^{2+} complex of a Schiff-base-derived crown ether 2 has the Ni^{2+} immobilized at the Schiff-base binding sites in a square-planar geometry, with a water guest molecule bound in the macrocyclic cavity and showing no association with the metal. Uranyl cations UO_2^{2+} may likewise be bound within the Schiff-base cavity of Schiff-base-derived crown ether macrocycles, and the uranyl complex may be used as a metallohost that binds neutral molecules in the macrocyclic cavity through interactions with the uranyl cation and polyether oxygens. Guests include urea, formamide, dimethyl sulfoxide (DMSO) and (2-pyridylmethyl)urea.[4]

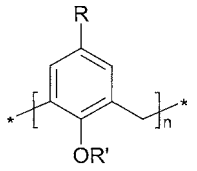

1

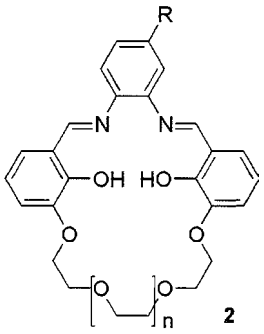

2

The crown ether tetrabenzo-24-crown-8 shows selective binding of large alkali metals Cs^+ and Rb^+ in preference to the smaller Na^+.[5] On complexation of Cs^+ or Rb^+, the tetrabenzo-24-crown-8 organizes into a cage-like structure about the cation, with the crown ether backbone resembling the seam of a tennis ball. The alternating benzo groups are thereby arranged to face one another, creating two molecular clefts. Neutral molecules may be bound within the clefts.[5,6] When crystallized from aqueous dioxane, host–guest species $[M(\text{tetrabenzo-24-crown-8})(\text{dioxane})_2(H_2O)_n]^+$, where $M=Cs^+$ or Rb^+, were isolated.[5] A dioxane molecule occupies one cleft of the assembly, while the other cleft contains dioxane and water guest molecules. Remarkably. a similar complex can be found with a traditionally "noncoordinating" sol-

DOI: 10.1081/E-ESMC 120012716

vent as the neutral guest molecule.[6] The complex [Cs(tetrabenzo-24-crown-8)(1,2-dichloroethane)$_2$](NO$_3$).(H$_2$O) forms a cage-like structure about the cation, with two molecular clefts. A molecule of 1,2-dichloroethane occupies each cleft, with weak bidentate coordination to the Cs^+ cation via the chlorine atoms, Fig. 1. Notably, the 1,2-dichloroethane molecules bind in preference to the nitrate anions, despite there being no obvious steric reason for this. It is postulated that this is more electronically favored, as some slightly electropositive hydrogen atoms of the 1,2-dichloroethane are within 3 A of an arene ring. Furthermore, the authors propose that the structure of the complex in the solid state persists in solution on the basis of liquid–liquid extraction studies. A distinguishing feature of these molecular clefts is that the cation is easily dissociated or replaced from the crown ether and may not be an intrinsic part of the host assembly, noting that the unmetallated acetonitrile complex of tetrabenzo-24-crown-8 has a similar conformation to acetonitrile molecules bound within the molecular clefts.'''

Calixarenes and Related Host Molecules

Traditional host molecules, the calix[*n*]arenes **1**, are cyclic phenols bridged by –CH_2- groups [$RC_6H_4(OR')CH_2]_n$ (*R'*=H in unsubstituted calixarene) that may adopt different conformations according to the value of *n* and the substituents *R* and R'. The most common calixarenes are *n*=4, and they have several important conformations, including the cone conformation or 1,3- alternate. In the cone conformation. calix[4]arenes possess a molecular cavity capable of binding cationic or neutral guest molecules, and additional host functionality can be imparted by the judicious use of functional groups at the lower rim of the calixarene. the R' position, allowing neutral and cationic guests to be bound simultaneously.

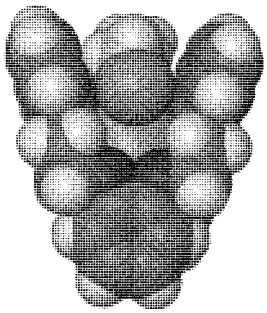

Fig. 1 Space-filling diagram showing the binding of 1,2-dichloroethane to Cs^+ within a molecular cleft from the crystal structure of [Cs(tetrabenzo-24-crown-8)(1,2-dichloroethane)$_2$](NO$_3$)·(H$_2$O). Minor disorder of the 1,2-dichloroethane was omitted. This diagram was adapted from Ref. [6].

An early example of this is found in *p-tert*-butylmethoxycalix[4]arene *R*=C(CH$_3$)$_3$, *R'*=CH$_3$, where in the solid state, a Na^+ cation is bound by the methoxy groups at the lower rim of the calixarene, and a molecule of toluene is contained within the molecular cavity.[7] The neutral calixarene *p-tert*-butyl-ethylacetatecalix[4]arene may likewise bind Wa or K^+ as a 1:1 complex. and this facilitates the transfer of these ions across a water-1,2-dichloroethane interface.[8] The crystal structure of the Na^+ complex reveals that the Na^+ is bound within the tetraethyl acetate cage of the calixarene lower rim in a distorted cube coordination geometry. Despite the presence of a tetraphenylborate anion. which is known to cooperatively occupy the upper-rim molecular cavity of alkali metal calixarene complexes, a molecule of ethanol is included as a loosely bound guest molecule. The smaller alkali metal ion Li^+ is bound by the lower-rim ether oxygens of the unsymmetrically substituted calixarene, 5,7-*bis*(9-fluorenyl)-25,26,27,28-tetrapropoxy calix[4]arene.[9] Although in a cone form, the metal-free calixarene has a pinched conformation that does not allow for the inclusion of guest molecules within the molecular cavity. Binding of the Li^+ cation opens the calixarene to a pseudo-C_{4v} cone conformation, however. simple complexation of a neutral guest molecule is not observed. Instead. the metallocalixarene dimerizes to give a capsule assembly that complexes a molecule of toluene (Fig. 2). The capsule is stabilized by interactions with the toluene and π–π interaction between fluorenyl groups of the different calixarenes.

Molecular capsules may likewise be formed by related host molecules such as calixresorcinarenes. Tetraethylresorcin[4]arene, for instance, forms a capsule-like assembly when cocrystallized with tetraethylammonium cations.[10] The capsule is composed of a neutral resorcin[4]arene and an anionic monodeprotonated resorcin[4]arene molecule hydrogen bonded in a head-to-head fashion via eight water molecules. In contrast to the capsule described above, the cationic guest molecule. tetraethylammonium, is bound within the capsule, and the neutral ethanol molecules form an interdigitating association with the lower rim of each tetraethylresorcin[4]arene molecule.

An entirely different mode of alkali metal cation inclusion is found in the complex {Cs(*p-tert*-butylcalix[4]-arene-H)(CH$_3$CN)}.[11] Notably, there is no lower-rim substitution, and the calixarene is monodeprotonated to form a phenoxide. The Cs^+ cation is not bound by the phenolic/phenoxide oxygen atoms but rather is contained within the molecular cavity of the calixarene. The Cs–C distances are sufficiently short to suggest a polyhapto coordination of the Cs^+ to the four aromatic rings of the calixarene, which is consistent with delocalization of the phenolate charge over the rings. The neutral CH$_3$CN guest molecule coordinates with the included Cs^+ cation.

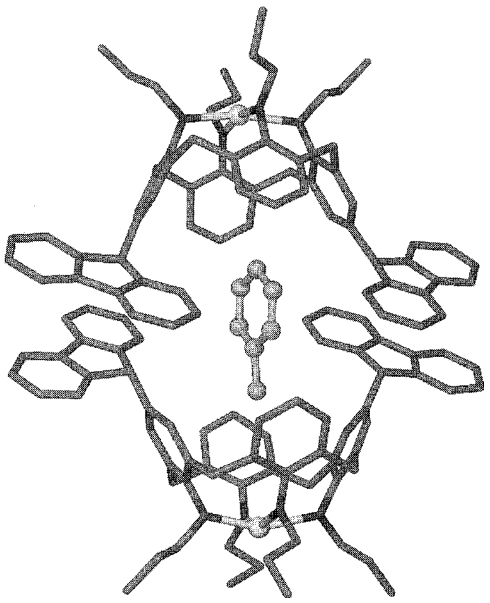

Fig. 2 X-ray structure of the molecular capsule formed by two Li[5,7-*bis*(9-fluorenyl)-25,26,27,28-tetrapropoxy calix[4]arene]$^+$ cations dimerizing around a toluene guest molecule. Diagram adapted from Ref. [9].

Transition or post-transition metals may be bound at the lower rim of a calixarene to form a metallocalixarene that may act as a metallohost. Calixarenes have a tendency to bind UO_2^{2+} cations, for example. A well-characterized recent example is the uranyl complex of (*p-tert*-butyltetrathiacalix[4]arene-H)$^{4-}$, where the $-CH_2-$ bridges of the calixarene are replaced by –S–. The UO_2^{2+} cation is bound by the four phenoxide O in a square plane. Further complexation of guest molecules is not precluded by one of the uranyl O atoms being directed into the molecular cavity from the lower rim of the calixarene, and a molecule of *N,N'*-dimethylformamide is found in the upper-rim cavity.[12] The zinc complex of the functionalized calix[6]arene hexa-*tert*-butyl-trimethoxy-tris{(1-methyl-2-imidazolyl)methoxylcalix[6]arene} has a cone conformation, with the Zn^{2+} cation coordinated by the tris(imidazolyl) groups on the lower rim and an aquo ligand.[13] The labile aquo ligand is constrained inside the molecular cavity of the calixarene and can be substituted for other neutral ligands. The hydrophobic calixarene cavity acts as a selective molecular funnel, allowing only guest molecules with complementary steric factors to be bound. Other examples of metallocalixarenes include a series of anionic {(*p-tert*-butylcalix[4]arene-4H)W≡CR}$^-$ hosts that host neutral solvent molecules."'' These may be linked into *bis*(calixarene) ditopic receptors by the binding of other metal cations such as Ag^+ and Mg^{2+}, which act as bridges.[14]

There are a number of other examples of similar ditopic metallocalixarenes binding neutral molecules. such as the crystalline complex $[NH_2(CH_3)_2][Mo_2(\eta^4\text{-}p\text{-}tert\text{-butylcalix[4]arene-}4H^+)_2]\cdot 4NC_5H_5$, where the anionic calixarenes are bridged by a $[Mo{\equiv}Mo]^{6+}$ moiety. and a molecule of pyridine is bound within each calix[4]arene molecular cavity.[15] An unusual example of a ditopic metallocalixarene that binds an organic cation and a neutral molecule is the anionic receptor {di-*p-tert*-butylcalix-[4]areneditungstate(III)}$^{2-}$, where a $[W{\equiv}W]^{6+}$ core is bridged by two fourfold deprotonated *p-tert*-butylcalix[4]-arene molecules.[16] The x-ray structure reveals that one calix[4]arene moiety binds a dimethylammonium countercation, while the other binds a molecule of acetonitrile. Interestingly. in the Mo analogue, both calix[4]arene molecular cavities are occupied by dimethplammoniurn cations. and acetonitrile molecules occupy holes within the molecular packing of the crystal structure.[16]

The water-soluble *p*-sulfonatocalix[*n*]arenes also form calixarene-based metallohosts that may bind transition or alkali metal cations at their upper-rim sulfonate groups. Representative examples of such chemistry are discussed below. The crystalline complex $Na_8\{Co(H_2O)_4(p\text{-sulfonatocalix[5]arene})_2\}.2CH_3C(O)N(CH_3)_2\cdot 37H_2O$[17] features two calix[5]arenes in cone conformations coordinating to a single $Co(H_2O)_4^{2+}$ moiety through sulfonate groups in a cis fashion. The calix[5]arenes are oriented in a face-to-face manner that results in the formation of a "supercavity." One *N,N'*-dimethylacetamide guest molecule is bound within each calix[5]arene host molecule. ^{1}H-NMR studies indicate that the coordination complex breaks up in solution. and there was no evidence of complexation of the *N,N'*-dimethylacetamide guest by the calix[5]arene. This is in direct contrast to the related Ni(II) complex $Na_8\{Ni(H_2O)_4(p\text{-sulfonatocalix[5]arene})_2\}.2NC_5H_5\cdot 38H_2O$, which in solution exists as a fluxional coordination complex with intracavity complexation of the pyridine guest molecules.[17] The complex $\{[Sc_2(OH)_2(H_2O)_8][Sc(H_2O)_4]_2[p\text{-sulfonatocalix[4]arene-H}]_2\text{-}([18]\text{crown-6})\}.16H_2O$ features a two-dimensional (2-D) coordination polymer formed through bridging coordinate interactions between $[Sc(H_2O)_4]^{3+}$ and lower-rim phenolate calix[4]arene oxygen atoms, and $[Sc_2(OH)_2(H_2O)_8]^{4+}$ and upper-rim sulfonate groups.[18] The neutral host molecule 18-crown-6 acts as a guest molecule in this structure. being bound within calix[4]arene capsule-like dimers in a similar manner to the binding of toluene by 5.7-*bis*(9-fluorenyl)-25,26,27,28-tetrapropoxy calix[4]arene that was discussed above.

Calixarenes may also be linked through covalent interactions to form ditopic receptors, such as in the symmetric linking of two *p-tert*-butylcalix[4]arene molecules via ethylene linkages to form a calix[4]tube. The calix[4]tube shows remarkable selectivity toward K^+ cations.[19] with K^+ bound within the central ethylether cage of the calix[4]tube. Molecular mechanics calculations suggest that the uptake of K^+ cations requires an

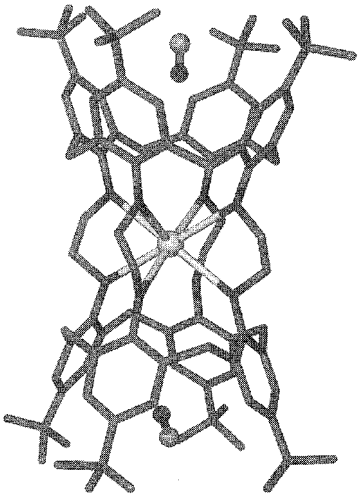

Fig. 3 X-ray structure of a calix[4]tube, with K^+ bound in the ethylether cage and ethanol guest molecules within the calixarene molecular cavities. Diagram adapted from Ref. [19].

initial complexation of the K^+ within the calix[4]arene cavity, with subsequent channel transportation to the ethyleiher cage. A crystalline species $\{K(calix[4]tube)\}^+ \cdot I^- \cdot 3CHCl_3 \cdot 4CH_3OH \cdot H_2O$ was isolated and structurally characterized with the host–guest species shown in Fig. 3. The K^+ cation is 8-coordinate with a flattened cube geometry, and each calix[4]arene receptor binds one molecule of ethanol.

Another family of calixarene-based ditopic receptors are the 1,3-calix[4]arene-*bis*(crown ethers). where the calixarene is locked into the 1,3-alternate conformation, and substrate binding normally occurs at the crown ether loops. These may form mononuclear or dinuclear complexes with alkali inetal cations, or may bind neutral guest molecules. The unsymmetrical 1.3-alternate calix[4]arene-1,3-crown-6;2,4-(1,2-phenylene)-crown-6 forms a 1:1 complex with Cs^+. The crystal structure shows that the cation is bound only within the adapted phenylene-crown-6 loop, and a molecule of acetonitrile is bound within the unmodified crown-ether loop.[20]

OTHER METALLOHOSTS

As described above. metallocalixarenes and metal-crown-ether complexes may act as host systems for neutral guest molecules. Many other types of coordination complexes may also act as host molecules, either through the formation of molecular cavities within the complex that may bind neutral molecules, or molecular clefts, where vacant coordination sites on the metal cation may be employed to bind neutral molecules. the latter termed metalloclefts. Recent examples of such chemistry are discussed below.

The structured binding sites of metalloclefts mean that they are often highly selective hosts. An example is the salophen-uranyl-based metallocleft **3,** which complexes neutral molecules. provided that the two phenyl groups of the host are parallel to one another. The salophen-uranyl unit may be employed as a catalyst for Michael additions, and the high steric requirements of the metallocleft of **3** result in it acting as a highly selective supramolecular catalyst.[21] Metalloclefts of Type 4 selectively bind SO_2 molecules and may be incorporated into dendritic materials that show catalytic activity.[22]

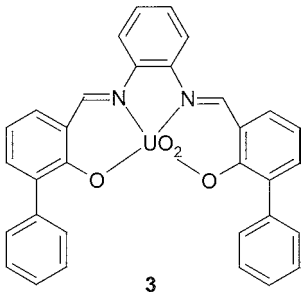

3

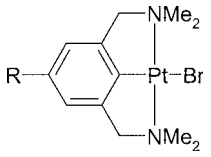

4

Self-assembly processes are employed to link molecules together to create molecular hosts. Metal-templated self-assembly was used to create supramolecular systems, where neutral molecules are bound by the metal complex that acts as a metallohost, however, without direct interactions between the metal cation and guest molecule. unlike in the metalloclefts discussed above. The molecular recognition or receptor sites can be intrinsic parts of the molecular building biock, or the receptor site can be created within the supermolecule.[2,3] An example of the former situation is seen with a 2.2'-bipyridine-substituted calix[5]arene.[23] Two calix[5]arenes self-assemble around an Ag^+-cation to bring the two molecular cavities into close proximity. The Ag^+-*bis*(calix[5]arene) is capable of binding large neutral guest molecules. and an intracavity 1:1 complex with fullerene-C_{60} was characterized by nuclear magnetic resonance (NMR) and electrospray ionization mass spectrometry (ESIMS). Binding of the larger fullerene-C_{70} was likewise demonstrated by ESIMS.[23]

Complexes that are capable of binding neutral molecules but where the molecular building blocks have no intrinsic binding properties may be constructed through similar self-assembly processes.[3] An example is the ligand 5. where binding of transition metal cations via the

alcohol and deprotonated carboxylic acid groups results in a water-soluble host with a pre-organized cavity, which binds hydrophobic guest molecules such as naphthalene.[24] The spiro-bridged bis-phenanthroline ligand **6** forms a self-assembled cyclic tetranuclear complex $[Cu_4\mathbf{6}_4]^{4+}$ with Cu(I).[25] The bis-phenanthroline ligands are arranged in a face-to-face arsangement in solution and in the solid state. effectively forming a molecular cavity. In ^{1}H-NMR experiments, anthracene guest molecules were demonstrated to be bound within the tetranuclear complex, and a 1:1 host–guest complex was formed in solution. Similarly, self-assembly processes result in the formation of a hexahedral coordination cage $[(NH_2CH_2CH_2NH_2)Pd]_{15}\mathbf{7}_6^{30+}$, a molecular capsule. The hexahedron has two open sites where guest molecules may enter or exit: encapsulating two molecules of CBr_4.[26] Related coordination cages may be employed as nanoscale reaction vessels, leading, for instance. to stereoselective reactions. An example is the quantitative formation of the *syn* dimer of acenaphthylene in a [2+2] photodimerization of guest acenaphthylene bound within the octahedral coordination cage $[(NH_2CH_2CH_2NH_2)Pd]_6\mathbf{8}_4^{12+}$.[27] In many cases, the manner of metal-cation-directed self-assembly of a metallohost is dependent on neutral guest molecules present during the self-assembly processes. Such templating effects are particularly predominant in coordination polymers. Discrete metallohelicates also provide some recent examples of this effect. For instance, triple helicates of stoichiometry M_2L_3 formed by bridging *bis*-bidentate ligands and octahedral metals may form helical or *meso* structures. When H_2L is the *bis*-hydroxypyridinone ligand 9, $[M_2L_3]$ complexes (M=Al, Ga) may form as either a *meso* or a helicate structure, where the helicate structure is stabilized by the incorporation of a guest water or DMSO. Furthermore, on addition of guest molecules in solution, a *meso*-helicate equilibrium is established, indicating that the structures are interconvertible.[28]

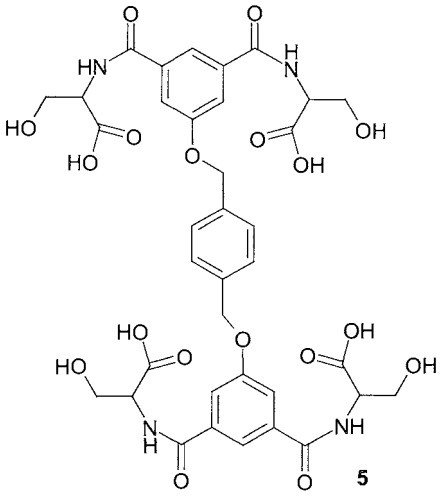

5

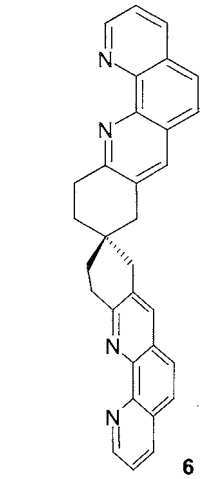

6

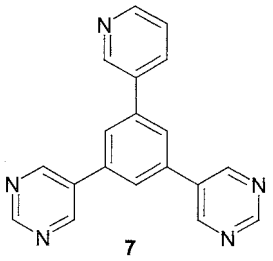

7

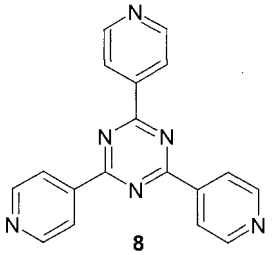

8

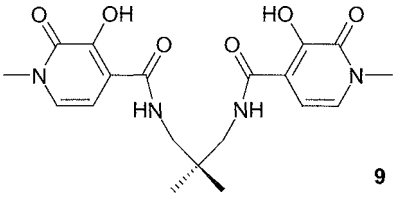

9

FRAMEWORK MATERIALS

Negatively charged solid-state framework materials may show inclusion behavior where both countercations and neutral molecules are included. The most obvious example is the zeolites and related materials, however, a discussion of the inclusion characteristics of these materials is beyond the scope of this article. A relatively new field where such inclusion behavior may be observed is based on coordination polymers. Most coordination polymers are cationic or neutral, however one exception is

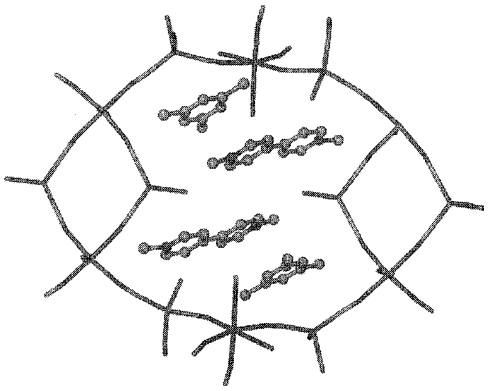

Fig. 4 Neutral mesitylene and cationic 1,1′-dimethyl-4,4′-bipyridicium $[MV]^{2+}$ guest molecules contained within a $[Cd_3(CN)_6Cl_2]^{2-}$ framework—from the x-ray structure of $[MV]^{2+}[Cd_3(CN)_6Cl_2]^{2-}.C_6H_3(CH_3)_3$. Diagram adapted from Ref. [29].

the series of mineralomimetic structures formed by cadmium cyanide derivatives, where the framework is anionic. In these cases, clathrate complexes with the simultaneous inclusion of cationic and neutral molecules may result. An interesting recent example is the clathrate complex $[MV]^{2+}[Cd_3(CN)_6Cl_2]^{2-}.C_6H_3(CH_3)_3$, where MV^{2+} is methylviolopen (1,1′-dimethyl-4,4′-bipyridinium).[29] The $[Cd_3(CN)_6Cl_2]^{2-}$ host framework has bridging cyanide ligands and terminal chlorides with an overall infinite three-dimensional structure. Cavities within the framework structure are occupied by methylviologen dications and mesitylene molecules that form a MV^{2+}-mesitylene charge-transfer complex. The crystal structure of $[MV]^{2+}[Cd_3(CN)_6Cl_2]^{2-}.C_6H_3(CH_3)_3$ reveals that the MV^{2+} acceptor and mesitylene donor molecules stack in a near coplanar manner and are very close, with an interspacing of 3.30(1) Å, (Fig. 4). Similar MV^{2+}-aromatic donor charge-transfer complexes are found in related polycyano–polycadmate clathrate complexes, with ethylbenzene, anisole, phenol: cresol, aniline or pyrrole in place of mesitylene.[29]

CONCLUSION

The simultaneous binding of cations and neutral molecules can be achieved by different types of molecular hosts or assemblies. Traditional host molecules such as crown ethers and calixarenes can complex both a cation and neutral molecule within different receptor sites. Metallohosts, where a metal cation is an intrinsic part of the host assembly, can complex neutral molecules within molecular clefts or capsule arrangements. Negatively charged framework materials such as mineralomimetic metal cyanide polymers may feature cavities that simultaneously contain both cations and neutral molecules.

ARTICLES OF **FURTHER** INTEREST

Calixarenes and Tlzeir Analogues: Cation Complexation, p. 137
Calixarenes and Their Analogues: Molecular Complexatiorz, p. 145
Crown Ethers, p. 326
Mineralomimetic Structures, p. 868
Self-Assembling Capsules, p. 1231
Zeolites: Structures and Inclusion Properties: p. 1623

REFERENCES

1. Verboom. W.: Reinhoudt, D.N. Simultaneous Binding of Cations and Neutral Molecules. In *Comprehensive Supramolecular Chemistry*; Atwood. J.L.. Davies. J.E.D.. MacNichol. D.D.. Vögtle, F.. Eds.; Pergamon: Oxford, 1996: Vol. 2. 495–517.
2. Canary. J.W.: Gibb, B.C. Selective Recognition of Organic Molecules by Metallohosts. In Progress in *Inorganic Chemistry*; Karlin. K.D., Ed.; John Wiley & Sons, Inc.: New York, 1997: Vol. 45, 1–81.
3. Linton. B.; Hamilton, A.D. Formation of artificial receptors by metal-templated self-assembly. Chem. Rev. 1997. 97. 1669–1680.
4. van Staveren. C.J.: van Eerden. J.: van Veggel. F.C.J.M.: Harkema, S.: Reinhoudt. D.N. Cocomplexation of neutral guests and electrophilic metal cation in synthetic macrocyclic hosts. J. Am. Chem. Soc. 1988, *110*. 4994–5008.
5. Bryan, J.C.: Sachleben, R.A.: Hay. B.P. Structural aspects of cesium ion selectivity by tetrabenzo-24-crown-8. Inorg. Chim. Acta 1999. *290*. 86–94.
6. Levitskaia. T.G.: Bryan. J.C.: Sachleben. R.A.: Lamb. J.D.: Moyer, B.A. A surprising host–guest relationship between 1.2-dichloroethane and the cesium complex of tetrabenzo-24-crown-8. J. Am. Chem. Soc. 2000, *122*. 554–562.
7. Bott, S.G.; Coleman, A.W.: Atwood, J.L. Inclusion of both cation and neutral molecule by a calixarene. Structure of [*p-tert*-butylmethoxycalix[4]arene-sodium-toluene]$^+$ cation. J. Am. Chem. Soc. 1986. *108*. 1709–1710.
8. Wickens. J.: Dryfe, R.A.W.: Mair, F.S.; Pritchard. R.G.: Hayes. R.; Arrigan, D.W.M. Calixarene facilitated transfer of alkali metal ions across the polarized liquid–liquid interface. New J. Chem. 2000. 24. 149–154.
9. Faldt. A.; Krebs. F.C.; Jørgensen, M. Lithium-ion induced conformational change of 5,17-bis(9-fluorenyl)-25,26,27,28-tetrapropoxy calix[4]arene resulting in an egg-shaped

dimeric clathrate. Tetrahedron Lett. 2000, *41*. 1241–1244.
10. Murayama, K.: Aoki, K. Resorcin[4]arene dimer linked by eight water molecules and incorporating a tetraethylammonium ion: Guest-driven capsule formation via cation-n interactions. Chem. Commun. 1998, 607–608.
11. Harrowfield. J.M.: Ogden, M.I.: Richmond, W.R.; White. A.H. Calixarene-cupped caesium: A coordination conundrum? J. Chem. Soc., Chem. Commun. 1991, 1159–1161.
12. Asfari. Z.: Bilyk. A.: Dunlop, J.W.C.; Hall. A.K.; Harrowfield, J.M.; Hosseini, M.W.; Skelton, B.W.: White, A.H. Subtleties with sulfur: Calixarenes as uranophiles. Angew. Chern., Int. Ed. 2001. *40*. 721–723.
13. Sénèque, O.: Rager. M.-N.; Giorgi, M.; Reinaud, O. Calix[6]arenes and zinc: Biomimetic receptors for neutral molecules. J. Am. Chem. Soc. 2000. *122*, 6183–6189.
14. Giannini, L.: Solari, E.; Dovesi, S.: Floriani. C.; Re. N.: Chiesi-Villa. A.; Rizzoli, C. Genesis, redox, acid–base relationships among W–C, W=C, and W≡C functionalities over an oxo surface modeled by calix[4]arene. J. Am. Chem. Soc. 1999, *121*, 2784–2796.
15. Chisholm, M.H.; Folting. K.; Streib. W.E.; Wu, D.-D. Preparation and characterization of the kinetic and thermodynamic isomers of dinuclear molybdenum and tungsten complexes with metal–metal triple bonds supported by *p-tert*-butylcalix[4]arene anions. Chem. Commun. 1998, 379–380.
16. Radius, U.; Attner. J. Dinuclear molybdenum(III) and tungsten(III) calix[4]arene complexes—Metal–metal triple bonds supported by bridging calix[4]arene ligands. Eur. J. Inorg. Chern. 1998. 299–303.
17. Johnson, C.P.; Atwood. J.L.; Steed, J.W.; Bauer, C.B.: Rogers, R.D. Transition metal complexes of *p*-sulfonatocalix[5]arene. Inorg. Chem. 1996. *35*. 2602–2610.
18. Webb. H.R.: Hardie. M.J.: Raston. C.L. Scandium(III) coordination polymers containing capsules based on two *p*-sulfonatocalix[4]arenes. Chem. Eur. J. 2001. 7, 3616–3620.
19. Schmitt, P.; Beer. P.D.: Drew. M.G.B.: Sheen. P.D. Calix[4]tube: A tubular receptor with remarkable potassium ion selectivity. Angew. Chem., Int. Ed. Engl. 1997, 36, 1840–1842.
20. Asfari, Z.; Thuéry, P.: Nierlich, M.; Vicens. J. Unsymmetrical calix[4]-*bis*-crowns-6 with unequivalent crown loops. Tetrahedron Lett. 1999. *40*. 499–502.
21. van Axel Castelli. V.: Cort, A.D.; Mandoliai. L.: Reinhoudt, D.N.: Schiaffino. L. Catalysis of the addition of benzenethiol to 2-cyclohexen-I-ones by uranyl-salophen complexes: A catalytic metallocleft with high substrate specificity. Chem. Eur. J. 2000, 6. 1193–1198.
22. Albrecht, M.; Hovestad, N.J.: Boersma, J.; van Koten. G. Multiple use of soluble rnetallodendritic materials as catalysts and dyes. Chem. Eur. J. 2001, 7. 1289–1294.
23. Haino. T.; Araki. H.; Yamanaka. Y.; Fukazawa, Y. Fullerene receptor based on calix[5]arene through metal-assisted self-assembly. Tetrahedron Lett. 2001. *42*, 3203–3206.
24. Lee, S.B.: Hong, J.-I. A new water-soluble bowl-shaped host by metal-induced self-assembly. Tetrahedron Lett. 1998. *39*, 4317–4320.
25. Ziessel, R.: Charbonnière, L.: Cesario. M.; Prangé, T.; Nierengarten, H. Assembly of a face-to-face tetranuclear copper(I) complex as a host for an anthracene guest. Angew. Chem.. Int. Ed. 2002, *41*. 975–979.
26. Umemoto, K.; Tsukui, H.; Kusukawa, T.: Biradha, K.; Fujita, M. Molecular paneling by coordination: An $M_{15}L_6$ hexahedral molecular capsule having clefts for reversible guest inclusion. Angew. Chern., Int. Ed. 2001. *40*. 2620–2622.
27. Yoshizawa. M.: Takeyama. Y.; Kusukawa. T.; Fujita, M. Cavity-directed. highly stereoselective [2+2] photodimerization of olefins within self-assembled coordination cages. Angew. Chem.. Int. Ed. 2002, *41*. 1347–1349.
28. Xu. J.; Parac. T.N.: Raymond, K.N. *Meso* Myths: What drives assembly of helical versus *meso*-$[M_2L_3]$ clusters? Angew. Chem.. Int. Ed. 1999. *38*, 2878–2882.
29. Yoshikawa. H.: Nishikiori, S.; Suwinska, K.; Luboradzki, R.: Lipkowski. J. Crystal structure of a polycyanopolycadmate host clathrate including a charge-transfer complex of methylviologen dication and mesitylene as a guest. Chem. Commun. 2001, 1398–1399.

Soft and Smart Materials

Dmitriy V. Soldatov
National Research Council Canada, Ottawa, Ontario, Canada

INTRODUCTION

The term "soft materials" refers to a large group of bulk materials where the inorganic, organic. or composite components link weakly through van der Waals forces, hydrogen bonding, additional coordination, or other secondary interactions. The term "smart materials" is attributed to materials that possess at least two functions: to sense an external signal ("sensor function") and to respond to that signal with a useful response ("actuator function"). An intrinsic feature of soft and smart materials is their resemblance to living systems, such that the former models supramolecular organization inherent in biological material, whereas the latter can mimic important functions in living organisms. Soft supramolecular materials form the basis for the rational design of a new generation of smart materials.

SOFT SUPRAMOLECULAR MATERIALS

The range of soft supramolecular materials embraces a variety of crystalline supramolecular compounds;[1] organic–inorganic nanocomposites;[2] partially crystalline or glassy low-dimensional organic polymers;[3] materials formed by nanoparticles and self-assembled supramolecular layers;[*] and liquid-like systems such as liquid clathrates, liquid crystals, and gels.[*] All of these materials exhibit supramolecular organization of varying complexities, with a prominent hierarchy of covalent, specific, and weak nonspecific interactions among their components. An example of soft supramolecular materials of practical interest are the naturally occurring clathrate hydrates. a huge reservoir of hydrocarbon fuel deposited in the world's permafrost regions and offshore on the continental margins. The water molecule, a species containing two covalent bonds, forms a host hydrate framework linking water molecules to each other by hydrogen bonds. while guest hydrocarbon molecules are retained in the cavities of the framework due to van der Waals forces.

Since the structures of the first materials having supramolecular organization were identified by Powell half a century ago,[6] extensive efforts produced entire generations of inclusion compounds. micro- and mesoporous sorbents, coordination polymers, and other supramolecular materials.[7–9] Clathrate chemistry provided a historical breakthrough in the intentional production of thousands of soft supramolecular materials and in a comprehensive understanding of their natures, structures, and properties.[10] The best-known classes of such materials include Hofmann-type clathrates; Werner clathrates; clathrate hydrates; inclusion compounds of urea, thiourea, and selenourea; cyclodextrins; calixarenes; gossypol; hexahosts: hydroquinone; phenol and Dianin's compounds; graphite intercalates; natural and pillared clays; and others. Such studies contributed to the birth of supramolecular chemistry, with relevance to a new understanding of the world of materials that was emphasized with a Nobel Prize.[11]

The general principle for building all soft materials is the bulk supramolecular assembly or aggregation of building units into a regular structure, with strong bonding within building units and weaker bonding between them. The nature of the building units may vary from simple molecules to nanoparticles, and the forces linking the units may vary from coordinative to van der Waals. On the one hand, weaker bonding among the building units allows for the variation of the units within the same type of material and, on the other hand, makes soft supramolecular materials sensitive to external conditions and leads them to have a propensity for structural or conformational changes, a property characteristic of biologically active materials. Therefore, the most attractive features of soft supramolecular materials, from a practical point of view, are their wide variability, easy conversion from one structure to another, and active response to external stimuli."

The variability of soft supramolecular materials makes it possible to modify each into a family of analogs, where a sought property will change by small steps over a wide range. An illustration of this is given by Werner complexes—the first metal complexes utilized for creating supramolecular materials in the 1950s and 1960s.[12,13] About 10 different metals (M), 15 anionic groups (X), and >100 organic ligands (A) were incorporated successfully

[*] Note that a number of supramolecular materials of practical importance today, such as zeolite inclusion compounds. microporous silicas. and most 3D coordination polymers. do not satisfy one or more of the listed conditions.

Encyclopedia of Supramolecular Chemistry
DOI: 10.1081/E-ESMC 120012877

Table 1 Selected data on inclusion of various isomers by $[Ni(Y\text{-}C_6H_4\text{-}CHR\text{-}NH_2)_4(NCS)_2]$

Guest isomers	Host Y	Host R	Percentage of isomers (*o*, *m*, *p*) Feed			Extract			Selectivity
Xylenes	y-Br	i-C_4H_9	34	32	34	86	11	3	*o*
	p-F	C_6H_{13}	34	33	33	6	84	10	m
	m-Cl	CH_3	32	34	34	10	7	83	P
Ethyltoluenes	*p*-Cl	i-C_4H_9	34	33	33	97	3	0	*o*
	H	C_6H_{13}	34	32	34	8	84	8	m
	m-Br	C_2H_5	34	33	33	5	10	85	*p*
Bromotoluenes	H	C_4H_9	33	32	35	87	13	0	*o*
	H	C_5H_{11}	45	40	15	7	88	5	*m*
	m-Br	CH_3	33	32	35	2	6	92	P

(Data from Ref [13])

into this host of general formula $[MA_4X_2]$ to give hundreds of new host receptors, each able to include a variety of guest components. Detailed studies made it evident that for every guest. a characteristic host receptor specifically selective toward the particular guest, could be found. Shown in Table 1 experimental data. a few entries of many such available, strongly support the above statement.''']

The variability of soft supramolecular materials also provides a basis for their rational design. Although crystal structure prediction is a difficult problem, some crystal engineering approaches, such as Etter's rules[14] and the concept of the supramolecular synthon,[15] were successfully applied. A fascinating example of intentional design by the systematic variation of a component is given by the guanidinium disulfonates.[16] The sulfonates in the pillars (Fig. la) form a two-dimensional hydrogen-bonded network with guanidinium cations (Fig. lb), the pillared interlayer space being available for the hydrophobic inclusion of guest aromatics (Fig. lc). A library of pillars controlling the interlayer space from 3–17 Å with ~1 Å increments provides a diverse set of soft organic frameworks with systematically adjustable pore characteristics.

The existence of several energetically similar forms for the same compound is another typical feature of soft supramolecular materials. This property is a result of the weak linkage between building units and the variety of ways the units can assemble into a structure. A small change in external conditions can lead to another thermodynamically stable form, or. a little change in preparative conditions can lead to another kinetically stable product. The problem may show as polymorphism for forms having the same (polymorphs) overall composition, or pseudopolymorphism. where the components are present in different proportions. or as so-called supramolecular isomerism[18] for forms having the same composition of the host framework. Water exemplifies such a structural diversity. giving rise to dozens of ice and hydrate frameworks, each appearing under specific conditions of temperature and pressure with different guest types and transforming into each other as conditions change.[19,20]

The ability of soft supramolecular materials to respond to changing external conditions with dramatic structural reorganization reveals tremendous potential for their applications. Liquid crystals were utilized extensively in liquid-crystal displays and thermometers, optical imaging, and recording. Evidence for a growing practical interest in soft supramolecular materials is provided by the rapid evolution in design of microporous metal–organic frameworks. Three generations of frameworks were distinguished:''' 1) ''unstable to the loss of included guest'': 2) ''stable frameworks, reversibly losing and readsorbing guest species without undergoing a change in phase or morphology''; and 3) ''dynamic structures that change their frameworks responding to external stimuli.'' This last type of ''third generation,'' or ''dynamic.'' frameworks is also referred to. by other authors, as ''soft''[17] or ''flexible''[22] frameworks. In the context of a general tendency for materials science to move toward innovation and design,''' the growing interest in soft supramolecular materials can be seen in the concepts of functional materials and smart materials.

FUNCTIONAL AND SMART MATERIALS

Functional materials are major output targets of contemporary supramolecular design. Functional materials possess a certain designed functionality, making possible their implementation as elements in specific processes. Molecular magnets,[24] catalysts,[25] molecular sieves and chemical sensors,[26] materials displaying useful optical and conductivity effects.'''' ion-exchange materials,~''' materials switchable on molecular level through

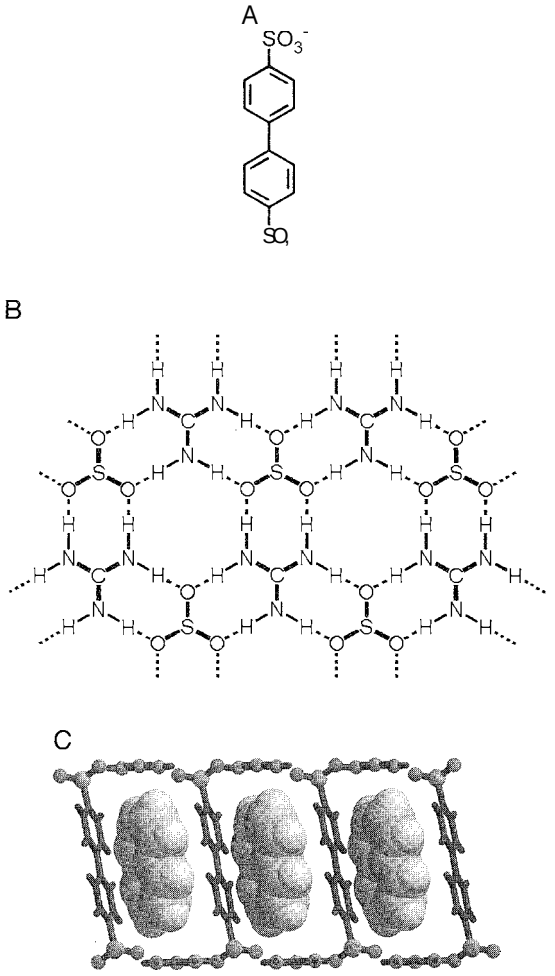

Fig. 1 Inclusion compound $[C(NH_2)_3]_2(SO_3C_6H_4C_6H_4SO_3)\cdot(C_{10}H_8)$.[17] *(A)* Disulfonate dianion pillar. (B) Hydrogen-bonded layer of guanidinium cations and sulfonate groups. (C) Guest naphthalene (van der Waals dimensions) included in the interlayer space of the guanidinium disulfonate host framework. (Using data from CSD.)

coordination.'''' isomerization,[30] and other reversible in situ changes[22] are only a few examples of supramolecular materials that may be qualified as being functional.

Smart materials are functional materials that, according to essential definition,'''' function as both sensors and actuators. In other words, smart materials must possess at least two important functions inherent to living organisms: to sense an external signal (sensor function) and to respond to that signal with a useful response (actuator function). The first generation of smart materials comprises mainly covalently bonded materials exhibiting useful physical properties: ferroelectrics, piezoelectrics. electrostrictors. relaxor ferroelectrics. magnetostrictive actuators. shape-memory metals. and others.[31]

An example of a smart material is one developed by Toyota.[32] The multilayer piezoelectric ceramic inside an automobile shock absorber has about five layers for sensing road vibrations. The multilayer stacks positioned near each wheel of the auto also have about 100 layers that act as the actuator, all part of the same ceramic. After analyzing the vibrational signals, a voltage is fed back to the actuator stack, and a response occurs by pushing on the hydraulic system of the auto to cancel the vibration.

Soft supramolecular materials. with their high sensitivities to environmental conditions and easy responses to environmental changes. thus possess the qualities that make their implication as smart materials a rnatter of an appropriate engineering solution. An essentially endless variability of soft supramolecular materials, arising from the vast variability of their organic and inorganic components and multitude of ways that these components can be assembled to form a 3D structure, allows that it should be possible to create a proper material for any particular task and provides an area where the rational design of such materials can be foreseen. The above reasons provide convincing evidence that progress in the chemistry of soft supramolecular materials predestines the appearance of a new generation of smart materials.

Examples of soft supramolecular materials that are ''smart'' as they interact physicaily with the environment are available.[27,33] More complicated are systems in which the interaciion involves a chemical process.[28,29] A further advantage of soft materials, though, is that they allow even more complex process schemes to be organized. as exemplified by one-way cycles.[34,35]

A one-way cycle involving dense (α-form) and microporous (0-form) polymorphs of a host compound, and an inclusion form, is shown in Fig. 2: Step 1—The α-form converts into the inciusion form in an atmosphere of a suitable guest template; Step 2—The inclusion form converts into the empty β-form by means of guest template removal: this process is driven thermodynamically and is reversible; Step 3—The β form. which exists for kinetic reasons, collapses into the more stable α-form upon applying certain conditions. an irreversible step. Mainly because of the last stage. the complete cycle α form $\rightarrow$ inclusion form $\rightarrow \beta$ form $\rightarrow \alpha$ form may be run only in one direction.

Smart sorbents are a vivid application of one-way cycles; such a sorbent was recently developed on a basis of a copper complex.[22,36] It is the microporosity of the material that arises or disappears as a response to external stimuli. The a-form of the complex is not active as a sorbent with respect to many guest sorbates (e.g., xenon, methane. propane). Consecutive application of a helium flow containing a guest template and then a flow without the guest template (Steps I and 2 in Fig. 2. respectively) transforms the α-form into an empty β-form that acts as a

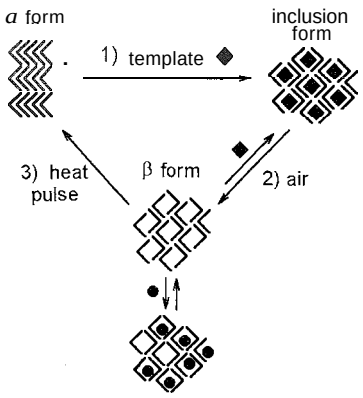

Fig. 2 One-way cycle: the phase interconversion scheme: 1) Guest template (diamonds) converts α-form into inclusion form: 2) ternplate removal gives the empty β-form that can work as a sorbent by including other guests (circles): and *3)* a heat pulse induces collapse of the empty β-form back to the u-form.

versatile sorbent with a pore diameter of —6 A. The application of a short-term heat pulse or appropriate catalyst returns the system to the "inactive" α-form. All of the processes proceed in situ, quantitatively, do not include any solvents, and may be controlled according to the degree of switching by an operator. The system is ‘‘smart,'' not only instantly responding to certain conditions but also recognizing the sequence under which the conditions change.

CONCLUSION

Soft supraniolecular materials are an extensive class combining organic, inorganic, and composite materials, where nonvalent interactions constitute at least one of several levels of bonding among the components. Recently, these materials attracted a great deal of attention because of their variability and mimicry of living matter. These properties predestine the appearance of soft supramolecular material libraries in the near future that exhibit useful functions, including those of living organisms. The ultimate targets in the engineering of new soft supramolecular materials start with functional materials for sensors, conductors, magnets. and catalysts. Smart materials are at the next level of complexity. as these materials combine the abilities of sensing external signals and responding to the signals with useful responses. Further levels may include materials with a learning or tuning function, that is. materials that become smarter with age. and materials able to choose and make correct decisions where multiple choices exist.

ACKNOWLEDGMENT

The author is thankful to John Ripmeester for his kind suggestions.

ARTICLES OF FURTHER INTEREST

Calixarenes: Synthesis and Historical Perspectives. p. 153
Clathrate Hydrates, p. 274
Crystal Structure Prediction, p. 371
Cyclodrxtrins, p. 398
Gossypol, p. 606
Hofmann-Type Clathrates, p. 645
Hydrogen Bonding, p. 658
Hydroquinone, p. 679
Liquid Clathrates, p. 804
Polymorphism, p. 1129
Supramolecular Chemistry: Definition, p. 1401
Swelling Clays (Smectites) and Nanofilms, p. 1478
van der Waals Forces, p. 1550

REFERENCES

1. Solid-State Supramolecular Chemistry: Crystal Engineering. *Comprehensive Supramolecular Chemistry*; Atwood, J.L., Davies, J.E.D., MacNicol. D.D.. Eds.; Pergamon Press: Oxford. *1996;* Vol. *6*.
2. *Special Issue on Organic–Inorganic Nanocomposite Materials:* Eckert. H., Ward, M.. Eds.: Chem. Mater. 200%.13 (10).
3. *Polyphenylene Oxide and Modified Polyphenylene Oxide Membranes. Gas, Vapour and Liquid Separation*; Chowdhury. G., Kruczek, B., Matsuura, T., Eds.: Kluwer: Boston. *200*1.
4. Shimomura. M.: Sawadaishi, T. Bottom-up strategy of materials fabrication: A new trend in nanotechnology of soft materials. Curr Opin. Colloid Interface Sci. 2001. 6 (1), *11–16.*
5. Esch. J.H.; Feringa. B.L. New functional materials based on self-assembling organogels: From serendipity towards design. Angew. Chem.. Int. Ed. 2000. 39 (13), 2263–2266.
6. Powell, H.M. The structure of molecular compounds. Part IV. Clathrate compounds. J. Chem. Soc. 1948, (I), *61–73.*
7. *Inclusion Compounds*; Atwood. J.L.. Davies. J.E.D., MacNicol, D.D.. Eds.: Academic Press: London, 1984.
8. *Comprehensive Supramolecular Chemistry*; Atwood. J.L.. Davies, J.E.D.. MacNicol, D.D., Vogtle, F., Eds.: Pergamon: Oxford, *1996.*
9. Nanoporous Materials II. *Studies in Surface Science and Catalysis*; Sayari. A., Jaroniec, M., Pinnavaia, T.J.. Eds.; Elsevier: Amsterdam, *2000;* Vol. *129.*
10. Dyadin, Yu.A.: Terekhova, I.S.: Rodionova, T.V.; Soldatov. D.V. Half-century history of clathrate chemistry. J. Struct. Chem. 1999. 40 *(5).* 645–653.

11. Pedersen, C.J.: Lehn, J.M.; Cram, D.J. Nobel Lectures. 1987: The discovery of crown ethers. Supramolecular chemistry—Scope and perspectives: Molecules—Supermolecules—Molecular devices. The design of molecular hosts. guests. and their complexes. J. Incl. Phenom. 1988, 6 (4). 337–413.
12. Lipkowski. J. Inclusion Compounds Formed by Werner MX_2A_4 Coordination Complexes. *Inclusion Compounds*; Atwood, J.L., Davies, J.E.D., MacNicol, D.D., Eds.: Academic Press: London, 1984: Vol. 1; 59–103.
13. Hanotier. J.: Radzitzky, P. Inclusion Compounds of Diisothiocyanatotetrakis(α-Arylalkylamine) Nickel(II) Complexes. *Inclusion Compounds*; Atwood, J.L., Davies, J.E.D., MacNicol. D.D.. Eds.; Academic Press: London. 1984; Vol. 1; 104–134.
14. Etter. M.C. Encoding and decoding hydrogen bond patterns of organic compounds. Acc. Chem. Res. 1990.23 (4), 120–126.
15. Desiraju, G.R. Supramolecular synthons in crystal engineering—A new organic synthesis. Angew. Chem., Int. Ed. 1995. 34 (21), 2311–2327.
16. Holman, K.T.: Pivovar. A.M.: Swift, J.A.; Ward. M.D. Metric engineering of soft molecular host frameworks. Acc. Chem. Res. 2001. 34 (2), 107–118.
17. Swift. J.A.: Pivovar, A.M.: Reynolds, A.M.; Ward, M.D. Template-directed architectural isomerism of open molecular frameworks: Engineering of crystalline clathrates. J. Am. Chem. Soc. 1998. *120* (24), 5887–5894.
18. Moulton, B.: Zaworotko, M.J. From molecules to crystal engineering: Supramolecular isomerism and polymorphism in network solids. Chem. Rev. 2001. 101 (6), 1629–1658.
19. Franks, F. The Properties of Ice. Water. A *Comprehensive* Treatise: Franks, F.. Ed.; Plenum Press: New York, 1972; Vol. 1; 115–149. Chapter 4.
20. Davidson. D.W. Clathrate Hydrates. Water. A Comprehensive Treatise; Plenum Press: New York. 1973; Vol. 2; 115–234. Chapter 3.
21. Kitagawa, S.: Kondo. M. Functional micropore chemistry of crystalline metal complex-assembled compounds. Bull. Chem. Soc. Jpn. 1998. *71* (8), 1739–1753.
22. Soldatov, D.V.; Ripmeester, J.A. Flexible Metal-Organic Frameworks with Isomerizing Building Units. Studies in *Surface Science and Catalysis*; Elsevier: Amsterdam, 2002; Vol. 141; 353–361.
23. Olson, G.V. Designing a new material world. Science 2000. 288, 993–998.
24. Miller, J.S.; Epstein, A.J. Organic and organometallic molecular magnetic materials—designer magnets. Angew. Chem., Int. Ed. 1994, 33 (4). 385–415.
25. Aoyama, Y. Functional organic zeolite analogues. Top. Curr. Chem. 1998. 198. 131–161.
26. Dinolfo, P.H.; Hupp, J.T. Supramolecular coordination chemistry and functional microporous molecular materials. Chem. Mater. 2001. 13 (10). 3113–3125.
27. Langley, P.J.; Hulliger, J. Nanoporous and mesoporous organic structures: New openings for materials research. Chem. Soc. Rev. 1999. *28* (5). 279–291.
28. Min. K.S.; Suh, M.P. Silver(I)-polynitrile network solids for anion exchange: Anion-induced transformation of supramolecular structure in the crystalline state. J. Am. Chem. Soc. 2000. 122 (29), 6834–6840.
29. Albrecht. M.; Lutz, M.; Spek, A.L.; Koten, G. Organoplatinum crystals for gas-triggered switches. Nature 2000. 406, 970–974.
30. Soldatov. D.V.; Ripmeester. J.A.; Shergina. S.I.; Sokolov. I.E.: Zanina, A.S.; Gromilov, S.A.; Dyadin, Yu.A. a- and β-Bis(1,1,1-trifluoro-5,5-dimethyl-5-methoxyacetylacetonato)copper(II): Transforming the dense polymorph into a versatile new microporous framework. J. Am. Chem. Soc. 1999, 121 (17). 4179–4188.
31. Newnham, R.E. Molecular mechanisms in smart materials. Mater. Res. Soc. Bull. 1997, 22 (5), 20–34.
32. Uchino, K. Piezoelectric *Actuators* and Ultrasonic Motors; Kluwer Academic Publishers: Boston, 1997.
33. Kim, S.J.: Reneker. D.H. A mechanochromic smart material. Polim. Bull. 1993, 31 (3), 367–374.
34. Soldatov, D.V.; Ripmeester. J.A. Novel 4-vinylpyridine-extended metal-dibenzoylmethanate host frameworks: Structure. polymorphism, and inclusion properties. Chem. Eur. J. 2001, 7 (14), 2979–2994.
35. Soldatov. D.V.; Ripmeester. J.A. Inclusion in microporous β-bis(1,1,1-trifluoro-5,5-dimethyl-5-methoxyacetylacetonato)copper(II), an organic zeolite mimic. Chem. Mater. 2000, *12* (7). 1827–1839.
36. Nossov, A.V.: Soldatov. D.V.; Ripmeester, J.A. In situ switching of sorbent functionality as monitored with hyperpolarized ^{129}Xe NMR spectroscopy. J. Am. Chem. Soc. 2001. 123 (15), 3563–3568.

Solid-State Nuclear Magnetic Resonance Spectroscopy

John A. Ripmeester
Christopher I. Ratcliffe
National Research Council Canada, Ottawa, Ontario, Canada

INTRODUCTION

Nuclear magnetic resonance (NMR) spectroscopy evolved into a major technique for the characterization of materials in just about all areas of chemistry. Most researchers and students will be familiar with solution applications, where chemical shifts and J couplings of spin $^1/_2$ nuclei can be used for simple spectral analysis of reaction products as well as the complex multidimensional techniques used to determine the structure and conformation of molecules as complex as proteins. A fundamental strength of NMR spectroscopy is that there is one-to-one correspondence between a chemically distinct nucleus and a chemically shifted line in the resonance spectrum: thus, spectra are quantitative fingerprints of the material under investigation.

DIFFERENCES BETWEEN SOLIDS AND LIQUIDS

In the solid state, WMR spectroscopy differs from solution spectroscopy in a number of ways. The main one is that in solution spectroscopy, all anisotropic interactions are averaged by rapid molecular motion, so that usually only the two aforementioned interactions, chemical shifts and J couplings. survive at their isotropic averages. However, because in the solid state molecular motion is seldom isotropic, all spin interactions behave as second-rank tensors. This means that interactions such as the chemical shift depend on the orientation of a molecular fragment with respect to the magnetic field, and on the details of the motion of the fragment. In single crystals, this then gives rise to an orientation-dependent chemical shift spectrum, and for powdered samples, where all orientations are allowed. a powder pattern results. Overlapping powder patterns cause obvious problems in resolving contributions from inequivalent nuclei, so much effort is spent on developing methods that give better-resolved spectra.

Another factor in solid-state spectroscopy is that some interactions not encountered in the spectral analysis of liquids contribute to the solid-state spectrum. These include the through-space coupling of magnetic spins, known as the nuclear dipolar interaction, and the quadrupolar interaction between the nuclear electric quadrupole moment and the electric field gradient. Although both complicate the spectra, each contributes unique information and different possibilities for probing the solid state.

NMR SPECTRA IN SOLIDS

Below, we present a brief account of solid-state NMR spectroscopy that will point the interested researcher to more detailed accounts. General references are given[1–8] that will give the interested reader a detailed account of a variety of solid-state NMR topics. Refs. [1,2] give an encyclopedic overview of NMR spectroscopy that is updated regularly.

Spin—1/2 Nuclei

Carbon and hydrogen are of particular importance in supramolecular chemistry. as both organic and metal–organic components are in prominent use. A closer examination of these two nuclei provides a good starting point for discussion of all spin $^1/_2$ nuclei.

The proton (^{1}H) is an abundant nucleus (99.8%), it has a large magnetic moment, and hence, a high NMR frequency. The dipolar coupling between protons is the main broadening interaction and varies as $\gamma^2(3\cos^2\theta - 1)/r^3$ (where γ = magnetogyric ratio of the proton, r = internuclear distance, and θ = angle between the internuclear vector and the magnetic field direction), so that the ^{1}H spectrum of most organic compounds is a line. usually featureless. as broad as 10–50 kHz. Because the chemical shift range is small (−20 ppm), if fine structure is seen, it almost always arises from dipolar couplings. For certain geometries, this allows for the analysis of internuclear distances. Sufficiently rapid molecular motion averages the dipolar couplings, thus narrowing the resonance line. Only center-of-mass diffusion reduces the dipolar coupling to zero. Molecular motions also affect the rate at which nuclear magnetization is lost, and from studies of the relaxation time as a function of temperature, the activation energy E_a for a motion can be obtained. Chemical shift information for ^{1}H. therefore, is difficult to

Encyclopedia of Supramolecular Chemistry
DOI: 10.1081/E-ESMC *120012821*

obtain directly, and recourse must be taken to specialized techniques. The ^{1}H spins can be manipulated by multiple pulse cycles that remove homonuclear dipolar couplings. The chemical shift tensors that result can then be averaged to their isotropic values (plus a set of spinning side bands that are separated from the main resonance by the spinning frequency) by application of magic angle spinning (MAS). This involves rotating the sample rapidly about an axis that is inclined to the magnetic field at 57.3°, known as the "magic angle," the angle where $(3\cos^2\theta - 1)$ vanishes. The CRAMPS experiment (Combined Rotation and Multiple Pulse Sequence) combines the two approaches to produce high-resolution ^{1}H spectra in solids.

If the dipolar couplings are not too large, or if they were partially averaged by molecular motion, fast MAS (−35 kHz) used by itself can be employed to obtain a high-resolution spectrum. In such cases, many of the complex experiments designed for liquids can be applied to these "soft" solids.[2]

The ^{13}C nucleus, on the other hand. at 1% natural abundance, is considered to be a "rare" nucleus. The main line-broadening mechanisms are the anisotropic chemical shift and dipolar couplings to protons. In order to observe a high-resolution spectrum. it is necessary to apply high-power ^{1}H decoupling (50–100 kHz, values that are considerably larger than the dipolar coupling) and to apply MAS to average the chemical shift tensors to their isotropic values. The usual way of recording ^{13}C-NMR spectra is to transfer polarization from an abundant nucleus, usually ^{1}H to the rare ^{13}C nucleus. This double-resonance experiment is referred to as CP/MAS (cross-polarization with magic angle spinning). Although it is usually easier to generate a spectrum this way rather than by generating ^{13}C magnetization directly by applying a single pulse at the "63 frequency and decoupling the ^{1}H, quantitation is more difficult, as the spectral line intensities depend on the strength of dipolar coupling, the length of the cross-polarization sequence applied. and the ^{1}H spin-lattice relaxation time in the rotating frame, which all must be taken into account when performing a CP/MAS experiment.

Other "rare" nuclei for which spectra can be recorded in the same way as for ^{13}C include "Si. ^{15}N, ^{31}P, ^{77}Se, ^{125}Te, ^{113}Cd, and ^{129}Xe.

Quadrupolar Nuclei (Spin > 1/2)

By far. the majority of nuclides with spin are quadrupolar nuclei ($I > 112$). It should be remembered that for a spin I, there are $21 + 1$ energy levels and $2I$ allowed transitions. Of those with spin $\mathbf{I} = 1$. ^{2}H is by far the most popular. The magnetic moment of ^{2}H is a factor of 7 smaller than that of ^{1}H, resuliing in a lower resonance frequency and much smaller homonuclear dipolar couplings. The quadrupolar interaction. usually 300 KHz or less, is then a small perturbation on the Zeeman energy levels. giving rise to a quadrupolar fine structure. In a single crystal, each inequivalent ^{2}H nucleus gives rise to a doublet with a separation chat depends on the orientation of the quadrupolar coupling tensor in the magnetic field.

In a powder, because all orientations are allowed. the spectrum is broadened into a characteristic powder pattern that can be analyzed in terms of a quadrupole coupling constant (C_Q) and an asymmetry parameter (η). One attractive feature is that at low-to-medium magnetic fields, the quadrupolar coupling is the only interaction required to interpret the spectra; at higher fields, the chemical shift anisotropy must be taken into account as evident from asymmetry in the spectrum. The main use of ^{2}H-NMR is to study dynamics of molecules or molecular fragments, usually as a function of temperature. Dynamics cause narrowing of the line shapes as the quadrupolar coupling tensor reorients in the magnetic field. and details of the motion can be worked out from the shapes of the narrowed lines. The rate of motion and. thus, the line shape depend on temperature, and by fitting line shapes to dynamic models at specific rates, activation energies (E,) can be obtained from Arrhenius plots of rate versus $1/T$. Another property of ^{2}H-NMR. which can be of use in supramolecular chemistry. is that C_Q is a sensitive indicator of the strength of hydrogen bonds: the stronger (and hence, shorter) the bond, the smaller C_Q is for the ^{2}H atom in the bond.

Most quadrupolar nuclei are half-integral spins. and these have a central transition, affected by the second-order quadrupolar coupling. plus a set of satellite transitions with splittings related to the first-order quadrupolar coupling. A full discussion of the spectroscopy of half-integral quadrupolar nuclei is beyond the scope of this article, but the key features of the second-order central line shape are its inverse dependence on the magnetic field strength. a second-order shift (from the isotropic shift). and the fact that MAS alone will not coinpletely remove the anisotropy.

SOLID-STATE NMR SPECTROSCOPY AND SUPRAMOLECULAR CHEMISTRY

Structure, Disorder, and Dynamics

Why should a supramolecular researcher be interested in solid-state NMR spectroscopy?[7,9] After all, with advances in diffraction methods, it would appear that many if not most problems can be solved by crystallographic methods. A chief distinction between NMR and diffraction is that the former is a local-order technique. whereas the latter is a long-range-order technique. One

piece of information related to long-range symmetry in crystalline materials obtainable from NMR is that not only chemical inequivalence but also crystallographic inequivalence give rise to splittings in the spectrum. In this way, it is often possible to get a snapshot of the unit cell contents. and this has, on occasion, been used to guide the choice of space group.

In many complex supramolecular systems, usually still considerably less complicated than biological systems, there may be problems of disorder that are often dynamic. It must be remembered that for diffraction models. all disorder is projected back into the unit cell, whereas NMR spectroscopy will be sensitive to the local symmetry in all parts of the crystal. Thus. it is possible that the lattice symmetry for a diffraction-derived structural model can be higher than that indicated by NMR, as the former is affected by space averaging. For example. in Dianin's compound with *p*-xylene[10] (Fig. 1), with the x-ray structural solution. a spatially averaged sixfold symmetry of the host and disordered guest can be seen. If this were the true local symmetry, then each chemically (and crystallographically) distinct C should have only one resonance in the ^{13}C-NMR. whereas at room temperature, these resonances show splittings. indicating a static p-xylene disorder. The splitting pattern shows that each cavity lost its threefold axis and the center of symmetry: the high x-ray symmetry coupled with the observed disorder indicates that the distortions are not correlated through the lattice. The splittings disappear at higher temperatures as the disorder becomes dynamic. and on

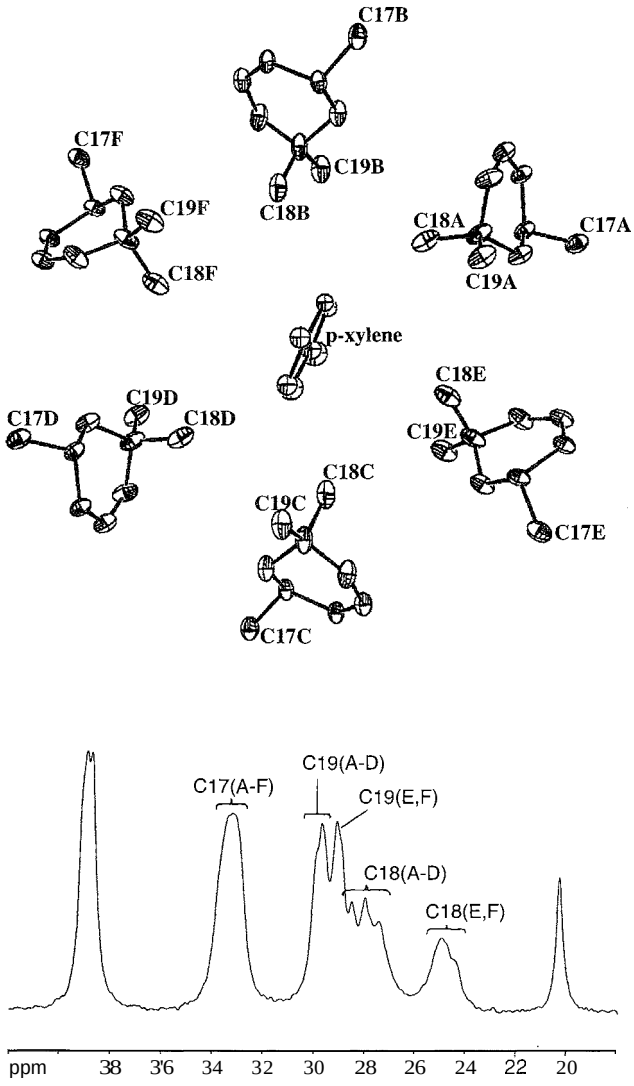

Fig. 1 Dianin's compound with p-xylene guest. (From Ref. [10].) (Top) Packing of six Dianin's host molecules around a p-xylene molecule. looking down the sixfold axis of the x-ray diffraction model (only part of each Dianin's inolecule is shown). (Bottom) Room-temperature ^{13}C-CP/MAS spectrum showing the multiple splittings for the methyl groups (18 and 19. pointing into the cavity) that arise because the p-xylene molecule is static. and the sixfold symmetry is lost.

time average each set of carbons becomes a sixfold equivalent. On the other hand, it is possible for the symmetry indicated by NMR to be greater than that derived from crystallography. This is often the case if there is sufficiently rapid molecular motion, and the NMR spectrum is affected by time averaging. For example, the ^{13}C-NMR of n-pentane in *t*-butyl-calix[4]arene shows only a single methyl resonance, rather than the two lines expected for the two distinct methyls seen in the crystal structure, one inside the calix cavity and the other outside.[11,12] The NMR, therefore, indicates dynamic exchange of the two ends of the pentane.

A great deal can be gained through the combined use of NMR and crystallography in a synergistic approach to refining structures. With NMR, we can determine if the disorder is static or dynamic and often define the exact nature and activation energies of the motions of both guest molecules and components of the host. Another contribution of NMR is in the detection of phase transitions and the possible involvement of dynamics and disorder in the transition process. Another example of where the combined use of NMR and x-ray diffraction led to a better understanding of the material and to an improved refinement of the structure is the toluene calix-[4]-arene inclusion compound.[13,14] At room temperature, the structure refines as P4/*n* in which the calix has a fourfold axis, and the toluene is disordered. Below a phase transition at 248 K (initially detected by NMR), the ^{13}C-NMR

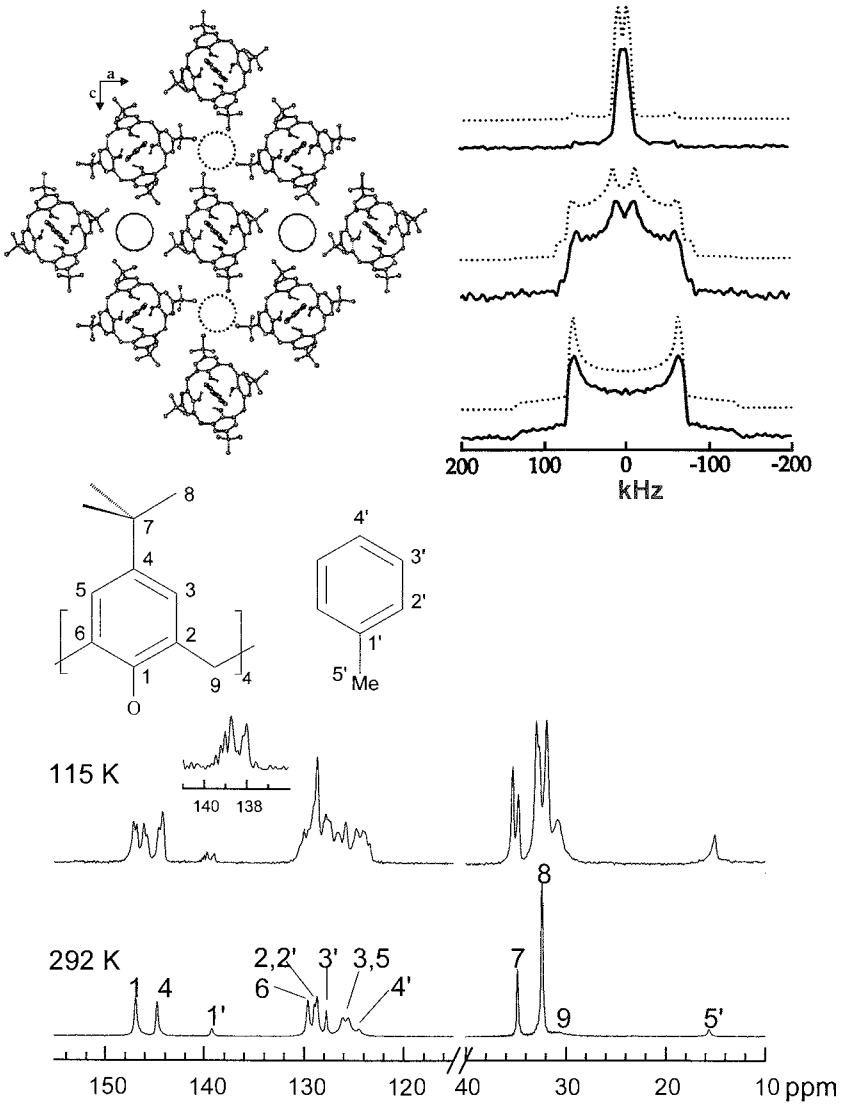

Fig. 2 (Top left) The 173 K P2/*c* structure of toluene-t-butyl-calix-[4]-arene, showing guest-induced twofold distortion of the host molecules. (From Ref. [14].) (Top right) ^{2}H-NMR line shapes, showing, from the bottom up, static (129 K), twofold flip (179 K), and fourfold rotation (337 K). (From Ref. [13].) (Bottom) The increased multiplicity of lines in the ^{13}C-CP/MAS spectra between 292 K and 115 K. (From Ref. [13].)

lines show splittings indicating a Iowering of symmetry. Shown by ^{2}H-NMR is that the toluene is static at 129 K, undergoes rapid twofold reorientation at 179 K and only goes into fourfold reorientation above the phase transition. An initial x-ray structure determination of this low-temperature phase appeared to show no difference from the room temperature phase (P4/*n*), but clearly this was not compatible with the NMR results. Further investigation of fine details in the diffraction data, including a set of superlattice lines, revealed a more complex structure in which the calix has twofold symmetry. P2/*c* (Fig. 2). Also of interest in this system and shown by x-ray and ^{13}C-NMR is the observation that 90–95% of the toluenes have their methyl groups inserted into the cavity, versus 5–10% out. For the external methyl, a weak line is observed close to the resonance seen for liquid toluene, whereas a stronger line is observed for the methyls in the cavity shifted by ~6 ppm to lower frequency, due to ring current effects from the aromatic rings of the calix.

To demonstrate static disorder in numerous cadmium cyanide host structures,[15,16] ^{113}Cd-NMR was used, because the number of resonances observed depends on whether the CN groups are ordered. statically disordered, or dynamically disordered (Fig. 3). The ^{13}C- and ^{15}N-NMR helped to establish or confirm connectivities in other mixed-metal cyanide frameworks, where it is more difficult to probe the metal nuclei directly. by making use of dipolar and J-couplings.[7,17] Likewise, ^{27}Al, ^{29}Si, and ^{31}P were used to establish connectivities in zeolite and aluminophosphate frameworks.[5,18,19]

Static line shapes arising from chemical shift anisotropy (CSA) and quadrupolar coupling also reflect the local symmetry of the nucleus. Isotropic lines occm for high-symmetry sites, such as tetrahedral, cubic, or octahedral, where these interactions are zero [e.g., in the ^{63}Cu-NMR of tetrahedral copper centers in $N(CH_3)_4$-$CuZn(CN)_4$ and $N(CH_3)_4CuCd(CN)_4 \cdot$guest framework~],'~whereas the lines have characteristic shapes for sites with axial symmetry or for lower-symmetry sites. In the case of ^{129}Xe. the sign of an axial CSA line shape also indicates whether the cavity is oblate or prolate.[20,21]

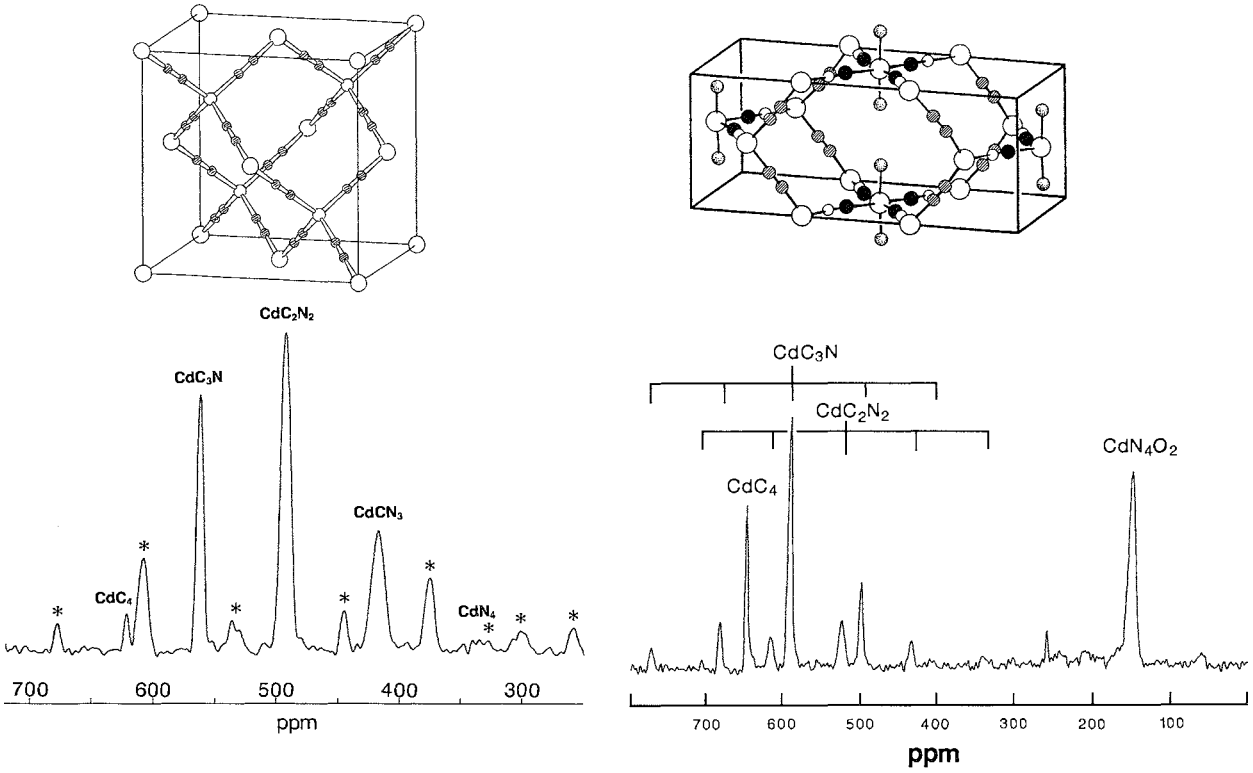

Fig. 3 (Left) The ^{113}Cd-NMR MAS spectrum of $Cd(CN)_2 \cdot C_6H_{12}$. The five lines arise from tetrahedral Cd attached to C_4, C_3N, C_2N_2, CN_3, and N_4, and indicate static disorder of the CN in the Cd–C–N–Cd linkages (* indicates spinning side bands). (From Ref. [15].) (Right) The ^{113}Cd-NMR CP/MAS spectrum of $Cd(CN)_2 \cdot 2/3\ H_2O \cdot$t-BuOH is shown. indicating ordering of the CN connecting the Oh Cd site to Td Cd sites (all N on the Oh Cd), with static disorder of the CN between Td Cd sites (the combs indicate the spinning side bands for CdC_3N and CdC_2N_2). (From Ref. [16].) X-ray structural studies previously established that this material could fall into one of five space groups. and a choice was made on the basis of the lowest *R*-factor. The NMR showed that this choice was not tenable and narrowed the choice to three of the five space groups. The structures of the frameworks are shown above the spectra: large open circles are Cd atoms; hatched circles are disordered C/N; and black circles are N atoms.

^{2}H-NMR is used extensively in studies of dynamics and disorder of guests and hosts in numerous supramolecular systems. These include clathrate hydrates, *t*-butylcalixarenes, cyclodextrins, metal cyanide clathrates, *tri-ortho*-thymotide, crown ethers, Dianin's compound, urea. thiourea, and numerous others. The benzene and pyridine t-butylcalixarenes provide an example where there is agreement between the orientations of the guest molecules with respect to the calix axis determined by NMR and diffraction, and where two guest molecules of similar shape have distinct differences in their dynamics.[22] It often comes as a surprise to the uninitiated that there can be large-scale motions in solids, yet solid-state NMR spectroscopy provided ample evidence of this over the years; a fine example being 18-crown-6, a large host macrocycle consisting of a ring of 18 atoms, which reorients rapidly in many of its solid complexes at room temperature.[23,24] In the malononitrile complex, the ring is

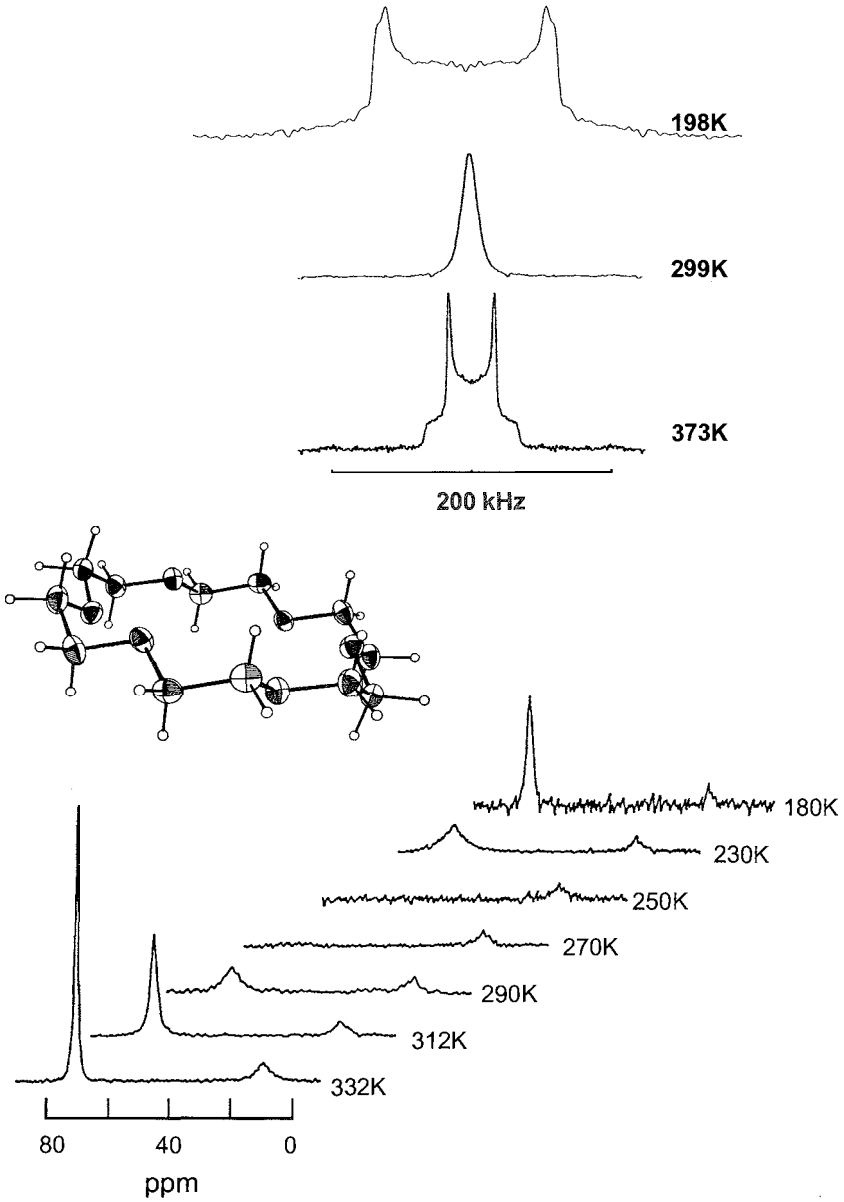

Fig. 4 The molecular merry-go-round in the solid complex 18-crown-6·$2CH_2(CN)_2$. (Middle) The ring adopts an almost D_{3d} symmetry. (Bottom) The ^{13}C-CP/MAS spectra as a function of temperature, showing fade-out of the resonance of the macrocycle carbons at 69.5 ppm near 250 K due to interference of incoherent reorientational motion with the coherent ^{1}H decoupling. (From Ref. [23].) (Top) The ^{2}H-NMR line shapes of the deuterated macrocycle as a function of temperature. indicating reorientation around the ring with a concomitant flip in orientation of each C–D bond between equatorial and axial. (From Ref. [24].)

in a D_{3d} conformation, and each $O—CH_2—CH_2$ unit rotates among adjacent sites around the ring. In the process, the CH_2 groups flip up and down. performing a motion resembling that of a merry-go-round (Fig. 4).

Similarly. effects of dynamics on line width and line shape can be observed for static NMR spectra of the following:

1. The chemical shift anisotropy, e.g., ^{13}C in CO_2 clathrate hydrate (which rhows a line considerably narrowed from that of a static CO_2 molecule,[25]), likewise for ^{77}Se in H_2Se clathrate hydrate[26] and ^{15}N in pyridine in *t*-butyl-calixarene.[22]
2. Noninteger quadrupolar nuclei. e.g., the central transition line shapes

   a. Of ^{17}O in water in THF clathrate hydrate, which narrows from a broad static quadrupolar line shape at 140 K to a line shape indicating rapid pseudoisotropic reorientation just below the melting point.

   b. Of alkali metals, such as ^{23}Na and ^{87}Rb in zeolites, which show isotropic lines that retain a field-dependent second-order shift, which indicates that these lines arise from dynamic averaging over sites with significant quadrupolar coupling.

The changes in line shape can often be used to derive details of the motions.

Evidence of dynamics can also be found in ^{13}C-CP/MAS spectra, where modulation of the $^{13}C—^{1}H$ dipolar coupling due to reorientation can interfere with the ^{1}H decoupling, causing broadening and a fade out of the signal over a specific temperature range (i.e., at specific rates of reorientation) (Fig. 4),[23,27] or prevent complete elimination of the resonances of carbons with attached ^{1}H in interrupted decoupling (also known as dipolar dephased or nonquaternary suppression) experiments.

Many supramolecular systems have pore spaces, usually, but not always. occupied by guest species. The ^{129}Xe-NMR can be applied to study the pore spaces or the exchange or competitive adsorption of guest species.

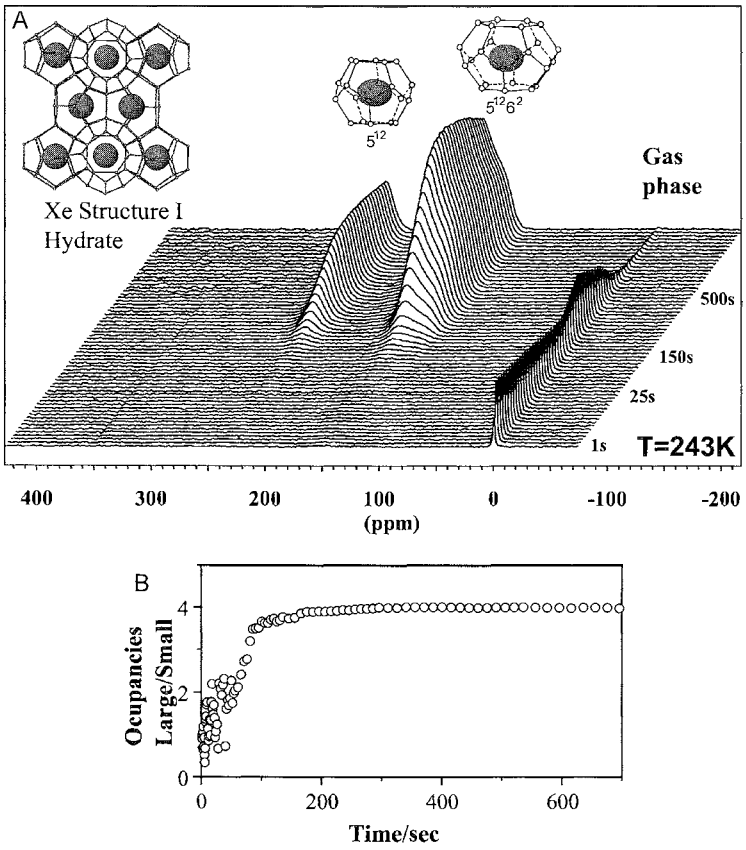

Fig. **5** Hyperpolarized ^{129}Xe-NMR spectroscopy of the formation of xenon hydrate on ice. (From Ref. [28].) (A) Single-scan spectra taken as a function of time, showing the development of Xe clathrate hydrate when HP Xe is admitted to powdered ice at 243 K. There is an initial induction period where only the gas line is observed. followed by a rapid rise of the lines due to Xe in the small and large cages of the clathrate hydrate. (B) The Xe-NMR intensity ratio of large:small cages shows an initial relative excess of Xe in small-cage environments. before eventually approaching the ratio in equilibrium Xe hydrate.

Although ^{129}Xe ($I = 1/2$) is a low-boiling gas under normal conditions, most of its NMR applications are in porous solids. The Xe atom is inert but highly polarizable. and as such. its chemical shift is sensitive to changes in its local environment: smaller cavities give larger chemical shifts. and the chemical shift anisotropy is sensitive to cavity shape. Thus. its signal, with the isotropic and anisotropic chemical shifts; is often diagnostic of whether the Xe atom behaves more like a trapped solid or adsorbed gas inside the pore system. The ^{129}Xe can also be hyperpolarized using optical pumping techniques such that its spin polarization is several orders of magnitude larger than the normal thermal spin polarization. This results in a greater NMR sensitivity. allowing for time-resolved studies of formation and decomposition processes. diffusion processes, and competitive adsorption between Xe and other guest molecules in supramolecular systems.[28,29] An example is shown in Fig. 5.

Of course, there are numerous other more sophisticated and hence less routine NMR experiments (refer to more specialized reviews[1,2,5,8] that can be applied to give information about supramolecular systems, such as the following:

1. The ^{1}H spin-counting technique can be used to determine the number of ^{1}H in a local cluster, and thus count the number of molecules in a cavity.[30,31]
2. Solid-echo double resonance (SEDOR) and rotational-echo double resonance (REDOR) techniques can be used to determine the proximity of the two types of nuclei, e.g., to determine which Na ions are closest to Al atoms in the framework of a zeolite, or to determine internuclear distances, or to help locate the position of a guest molecule relative to the host framework.[2,8]
3. MQMAS (Multiple Quantum MAS) is used to resolve resonances of noninteger quadruplar nuclei: complete narrowing of the second-order quadrupolar line shape cannot be achieved by MAS alone, but this is feasible when MAS is combined with multiple quantum pulse sequences.[2,5,8] This was used extensively in studies of zeolites.
4. Magnetic resonance imaging (MRI) can be used for diffusion measurements in porous systems, by monitoring the distribution of such nuclei as ^{1}H and ^{129}Xe as a function of time.[1,32]

CONCLUSION

It is clear that solid-state NMR has developed into a powerful tool for the supramolecular chemist who is interested in developing a true understanding of systems that are complicated and that, in fact, need to be flexible, responsive, or have dynamic components in order to be functional. On examining the development of NMR spectroscopy, it is remarkable that periodically there were major developments in hardware, software. or some fundamental aspects of spectroscopy. All of these led to increased prospects for spectroscopy as a research tool for the sciences. This is also the case for solid-state spectroscopy as it is applied to supramolecular chemistry, where the technique has now diffused from a few specialized labs into the mainstream. There is no reason to suppose that such developments will stop. Soon the impact of the general availability of higher fields to solid-state spectroscopists will give unprecedented sensitivity. thus giving access to smaller samples as well as nuclei that have lower sensitivity or low gamma. The wide range of fields will also allow for the development of complex spectroscopy of half-integral quadrupolar nuclei, thus giving the researcher a whole new range of probes for material studies as well as dynamic processes.

ARTICLES OF FURTHER INTEREST

Alkalides and Electrides, p. 12
Calixarenes and Their Analogues: Molecular Complexation, p. 145
Channel Inclusion Compounds, p. 223
Chiral Guest Recognition, p. 236
Clathrate Hydrates, p. 274
Crown Ethers, p. 326
Crystalline Microporous Silicas, p. 380
Cyclodextrins, p. 398
Hofmann-Type Clathrates, p. 645
Hydrogen Bonding, p. 658
Hydroquinone, p. 679
Inclusion Compounds: Selectivity, Thermal Stability, and Kinetics, p. 696
Mesoporous Materials, p. 845
Mesoporous Silica and Silica–Organic Hybrids, p. 852
Mineralomimetic Structures, p. 868
Nuclear Magnetic Resonance Spectroscopy, p. 981
Organic Zeolites, p. 996
X-Ray Crystallography, p. 1586
X-Ray and Neutron Powder Diffraction, p. 1592
Zeolites: Structures and Inclusion Properties, p. 1623

REFERENCES

1. *NMR Basic Principles and Progress;* Springer-Verlag: Berlin. 1976: Vol. 11, 1993: Vol. 29. 1994: Vols. 30–33.
2. *Encyclopedia of NMR;* Grant.. *D.M.*. Harris, R.K.. Eds.; John Wiley: New York. 1996. Periodic supplements.
3. Fyfe, C.A. *Solid State NMR for Chemists*: CFC Press: Guelph, 1983.

4. Bryce. D.L.: Beniard, G.M.: Gee. M.: Lumsden. M.D.; Eichele. K.; Wasylishen. R.E. Practical aspects of modern routine solid-state multinuclear magnetic resonance spectroscopy: One-dimensional experiments. Can. J. Anal. Sci. Spectrosc. 2001. *46*. 46–82.
5. Solid-State *NMR Spectroscopy:* Principles *and* Applications; Duer, M.J.. Ed.: Blackwell Science: Oxford. 2002.
6. Schmidt-Rohr. K.: Spiess, H.W. *Multidimensional Solid*-State NMR *and Polymers*; Academic Press: London. 1994.
7. Ripmeester. J.A.: Ratcliffe. C.I. Solid-State NMR Spectroscopy: Applications to Supramolecular Chemistry. In *Comprehensive Supramolecular Chemistry*; Atwood, J.L.. Davies. J.E.D., MacNicol, D.D., Vogtle. F., Lehn. J.-M., Eds.; Pergamon: New York. 1996; Vol. 8, 323–380.
8. Laws. D.D.; Bitter, H.-M.L.; Jerschow, A. Solid-state NMR spectroscopic methods in chemistry. Angew. Chem. Int. Ed. 2002. *41*. 3096–3129.
9. Brouwer. *E.B.;* Enright, G.D.; Ratcliffe. C.I.; Ripmeester. J.A.: Udachin. K.A. Dynamic Structures of Host–Guest Systems. In *Calixarenes 2001;* Asfari, Z., Bohmer. V.. Harrowfield, Vicens. J.. Eds.; Kluwer Academic: Dordreclit. 2001: 296–311. Chap. 16.
10. Enright, G.D.: Ratcliffe. C.I.: Ripmeester, J.A. Crystal structure and ^{13}C CP/MAS NMR of the p-xylene clathrate of Dianin's compound. Mol. Phys. 1999, 97. 1193–1196.
11. Brouwer, E.B.: Udachin. K.A.: Enright, G.D.; Ratcliffe. C.I.: Ripmeester. J.A. A chlorophobic pocket in the cavity of tert-butylcalix[4]arene: A test site for molecular recognition investigated by ^{13}C CP MAS NMR and x-ray crystallography. J. Chem. Soc., Chern. Commun. 1998. 587–588.
12. Brouwer. E.B.: Enright, G.D.; Ripmeester. J.A. n-Methyl interactions and p-tert-butylcalix[4]arene-guest stability: WMR and crystallographic studies of cyclohexane and n-pentane inclusion compounds. Supramol.Chem. 8996, 7. 143–145.
13. Brouwer, E.B.: Enright, G.D.: Ratcliffe, C.I.; Ripmeester. J.A. Dynamic molecular recognition in solids: A synoptic approach to structure determination in t-butylcalix[4]-arene-toluene. Supramol. Chem. 1996. 7. 79–83.
14. Enright, G.D.; Brouwer. E.B.: Udachin, K.A.: Ratcliffe. C.I.: Ripmeester. J.A. A re-examination of the low temperature crystal structure of the p-*tert*-butylcalix[4]-arene toluene inclusion compound: Differences in spatial averaging with Cu and Mo K radiation. Acta Crystallogr., B 2002, *58*, 1032–1035.
15. Nishikiori. S.: Ratcliffe, C.I.; Ripmeester, J.A. ^{113}Cd NMR studies of Hofmann type clathrates and related compounds: Evidence for two room temperature orientational glasses. Can. J. Chem. 1990, *68*. 2270–2273.
16. Nishikiori. S.: Ratcliffe. C.I.; Ripmeester, J.A. Framework ordering in solid cadmium cyanides from ^{113}Cd NMR spectroscopy. J. Cliem. Soc.. Chem. Commun. 1991. 735–736.
17. Curtis. R.D.: Ratcliffe, C.I.: Ripmeester. J.A. Structure and ordering in metal cyanide lattices: The use of doubly labelled cyanide (^{13}C–^{15}N) to simplify the ^{13}C MAS NMR spectrum. J. Chem. Soc.. Chem. Commun. 1992. 1800–1802.
18. Engelhardt, G.; Michel, D. High *Resolution* Solid-State NMR of Silicates *and* Zeolites: John Wiley and Sons: New York. 1987.
19. Fyfe. C.A.; Mueller. K.T.: Grondey, H.; Wong-Moon, K.C. Dipolar dephasing between quadrupolar and spin—112 nuclei. REDOR and TEDOR NMR experiments on VPI-5. Chem. Phys. Lett. 1992. *199*. 198–204.
20. Ripmeester. J.A.: Ratcliffe, C.I.; Tse, J.S. The NMR of ^{129}Xe trapped in clathrates and some other solids. J. Chem. Soc., Faraday Trans. 1 1988. *84*, 3731–3745.
21. Jameson, C.J.: de Dios. A.C. Xe nuclear magnetic resonance line shapes in nanochannels. J. Chem. Phys. 2002. 116. 3805–3821.
22. Brouwer. E.B.: Enright, G.D.; Facey, G.A.: Ratcliffe. C.I.: Ripmeester, J.A. Weak intermolecular interactions: Structure and dynamics of the benzene and pyridine p-tert-butylcalix[4]arene inclusions. J. Phys. Chem., B 1999, *103*, 10604–10616.
23. Buchanan. G.W.; Morat. C.; Ratcliffe, C.I.; Ripmeester, J.A. Macrocyle reorientation in solid 18-crown-6 complexes detected by 'H and ^{13}C NMR. J. Chem. Soc., Chem. Commun. 1989, 1306–1308.
24. Ratcliffe. C.I.: Ripmeester. J.A.: Buchanan. G.W.; Denike. J.K. A molecular merry-go-round: Motion of the large macrocyclic molecule 18-crown-6 in its solid complexes studied by ^{2}H NMR. J. Am. Chem. Soc. 1992. *114*. 3294–3299.
25. Udachin. K.A.: Ratcliffe. C.I.; Ripmeester, J.A. Structure, composition and thermal expansion of CO_2 hydrate from single crystal x-ray diffraction measurements. J. Phys. Chem.. B 2001. *105*. 4200–4204.
26. Collins, M.J.; Ratcliffe. C.I.: Ripmeester, J.A. NMR studies of guest species in clathrate hydrates: Lineshape anisotropies. chemical shifts and the determination of cage occupancy ratios and hydration numbers. J. Phys. Chem. 1990. *94*. 157–162.
27. Buchanan. G.W.: Morat, C.: Charland. J.P.: Ratcliffe. C.I.: Ripmeester. J.A. A novel 1:1 benzenesulfonamide: 18-crown-6 complex as uncovered via ^{13}C solid phase NMR spectroscopy and x-ray crystallography. Can. J. Chem. 1989. 67. 1212–1218.
28. Moudrakovski. I.L.: Sanchez. A.A.: Ratcliffe. C.I.: Ripmeester, J.A. Nucleation and growth of hydrates on ice surfaces: New insights from ^{129}Xe NMR experiments with hyperpolarized xenon. J. Phys. Chem.. B 2001. *105*. 12338–12347.
29. Nossov, A.V.; Soldatov, D.V.; Ripmeester, J.A. In situ switching of sorbent functionality as monitored with hyperpolarized ^{129}Xe NMR spectroscopy. J. Am. Chem. Soc. 2001. *123*. 3563–3568.
30. Baum. J.: Pines, A. NMR Studies of clustering in solids. J. Am. Chem. Soc. 1986, *108*, 7447–7454.
31. He, J.; Ba, Y.; Ratcliffe. C.I.: Ripmeester. J.A.; Klug. D.D.; Tse, J.S.: Preston, K.F. Encapsulated silicon nanoclusters in zeolite Y. J. Am. Chem. Soc. 1998. *120*. 10697–10705.
32. Moudrakovski. I.L.: Sanchez. A.; Ratcliffe. C.I.: Ripmeester, J.A. Applications of hyper-polarized xenon to diffusion in vycor porous glass. J. Phys. Chem.. B 2000. *104*. 7306–7310.

Solid-State Reactivity/Topochemistry

Leonard R. MacGillivray
Giannis S. Papaefstathiou
University of Iowa, Iowa City, Iowa, U.S.A.

INTRODUCTION

Topochemical solid-state reactions take place in a crystal lattice[1,2] and are typically initiated by irradiation [e.g., ultraviolet (UV) energy] or thermal annealing. Generally, for such reactions to occur, the reactive groups must be separated by <4.2 Å, consistent with the topochemical postulate.[1] Because the organization of the reactants usually dictates the stereochemistry of the products, topochemical solid-state reactions typically take place more selectively than in the liquid phase and, as a result, can give rise to molecules, and polymers, less obtainable, or completely inaccessible. in solution.[3] In recent years, the application of supramolecular chemistry[4] to control topochemical solid-state reactions was shown to provide control over the organization of reactants such that it is possible to conduct topochemical solid-state reactions, in a similar way to a classical approach to organic synthesis, by design. The primary focus of this article will be on two well-established topochemical solid-state reactions, namely, the UV-induced [2 + 2] cycloaddition reaction'"] and the thermal polymerization of diacetylenes,[2] to demonstrate how supramolecular chemistry may be utilized to control such processes.

THE TOPOCHEMICAL POSTULATE

Extensive crystallographic and photochemical studies by Schmidt involving polymorphs of cinammic acid led to topochemical postulates that may be used to predict whether a photoinduced [2 + 2] cycloaddition reaction will occur in the solid state (Fig. 1).[1] According to Schmidt, the nature of a crystal determines whether or not reaction will take place and determines the molecular structure of the product. Moreover, if a solid displays such reactivity, then the reaction will involve nearest-neighbor molecules and will occur with minimum atomic and molecular movement.'"] Thus. for the [2 + 2] photoreaction, the double bonds of the reactants should, as determined by Schmidt, be separated by <4.2 Å and aligned in parallel. Such separation and parallel alignment ensures that the p(z) orbitals of the double bonds are nearly colinear and overlap sufficiently to react. Notably, there are exceptions to these empirical rules, involving photoactive and photostable compounds.[5] Nevertheless, these postulates provided useful geometry criteria to predict whether a [2 + 2] photoreaction will take place in a crystalline solid.

FROM THE TOPOCHEMICAL POSTULATE TO CRYSTAL ENGINEERING

Following the emergence of the topochelnical postulate, a variety of studies were developed to identify molecules that crystallize in a necessary arrangement for [2 + 2] photoreaction.[6] In addition to the [2 + 2] photocycloaddition, such studies led to molecules that undergo other transformations. such as [4 + 4] photocycloadditions,[7] decarbonylations,[8] and Diels–Alder reactions,[9] giving molecular and polymeric products. In effect, such studies illustrated that it is possible for chemists to modify structure at the molecular level to affect a bulk physical property of a solid (i.e., reactivity). This strategy of identifying molecules so as to engineer structures and properties of organic crystalline solids has, in recent years, led to the emergence of the general field of crystal engineering, which has been systematized by Desiraju.[10]

ENGINEERING THE [2 + 2] PHOTOREACTION

Following the initial work of Schmidt, two general strategies for engineering solids that undergo the [2 + 2] photoreaction were developed. These strategies involved intramolecular substitution or auxiliary components to organize reactants for photoreaction.

Intramolecular Substitution

In the first approach, substitutents are covalently attached to reactants to steer molecules, upon crystallization, into a necessary arrangement for reaction.[11–15]

Schmidt, for example, revealed that chlorine groups, attached to an aromatic ring, tend to steer a molecule, by way of Cl···Cl interactions, such that it adopts a P-structure, wherein neighboring olefins are photoactive.[11]

Encyclopedia of Supramolecular Chemistry
DOI: 10.1081/E-ESMC 120012761

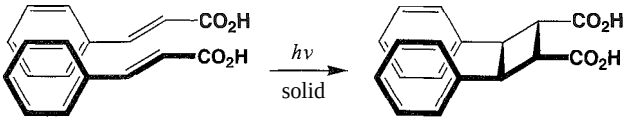

Fig. 1 Solid-state photodimerization of β-cinnamic acid.

Electrostatic[12] as well as donor–acceptor[13,14] interactions were also employed for steering the synthesis of molecules and polymers (Fig. 2a).

In a notable success, a J-shaped dicarboxylic acid was shown by Feldman to form a hydrogen-bonded molecular assembly held together by four O–H···O hydrogen bonds, wherein two olefins conform to the topochemical principle and are photoactive[15] (Fig. 2b). UV irradiation produced the expected photoproduct in quantitative yield. The covalently bound naphthalene unit served to preorganize the two double bonds within the discrete complex for reaction.

Auxiliary Components

In the second approach, an auxiliary component is employed to organize two olefins for [2 + 2] photoreaction. The auxiliary component is typically in the form of a molecule or cavity.[16–20]

Cavities based on cyclodextrins[16] and saponite,[17] for example. were used to organize olefins by way of van der Waals and electrostatic forces; respectively. In the former, the host accommodated the guests within a rigid tubular framework. while in the latter. the clay-like silicate accommodated the guests by swelling. In each case, the guest photodiinerized upon UV irradiation.

An auxiliary component that interacts with reactants by way of hydrogen bonds was also described (Fig. 3). Specifically, tetraaryl diols were shown by Toda to accommodate guests within cavities wherein the host interacted with two guests by way of two O–H···O hydrogen bonds.[18] The guests packed within the cavities such that two olefins of two guests conformed to the topochemical principle and, upon UV irradiation, photodimerized.

An approach that utilizes hydrogen bonds and electrostatic forces, in the absence of cavities, was also reported.[19,20] Specifically, Ito revealed the ability of flexible diamines (e.g., ethylenediamine) to undergo acid–base reactions with cinnamic acids, wherein each ammonium group forms an N^+–H···O^- hydrogen bond with a cinnamate. Combinations of acid and base were found to be photoactive, which was accounted for by the formation of three-component assemblies wherein each base, in a syn conformation. organizes two anions for reaction.

SOLID-STATE REACTIVITY AND CHEMICAL SYNTHESIS BY DESIGN

Although substituents and auxiliary components were successfully employed to achieve [2 + 2] photoreaction in the solid state. the ability to organize two double bonds in a solid for reaction has been a difficult challenge. This difficulty is largely due to insufficient knowledge of weak interactions that govern crystal packing (e.g., van der Waals forces). Reactions of homologous compounds $R'(CH_2)_nR''$ (n=1,2,3...), for example, were not found to be identical, in contrast to the liquid phase, for all values of n in the solid state owing to the sensitivity of molecular packing to unique electronic and steric demands of reactants.[1] Moreover; such sensitivity made

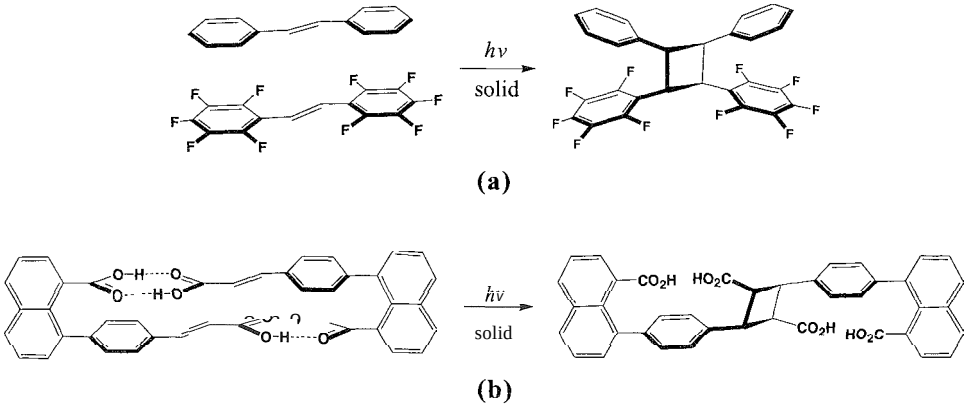

Fig. 2 The application of intramolecular substitution to control the [2 + 2] photodimerization in the solid state: (a) phenyl–perfluorophenyl interactions between two stilbenes and (b) a J-shaped dicarboxylic acid that self-assembles to form a hydrogen-bonded assembly.

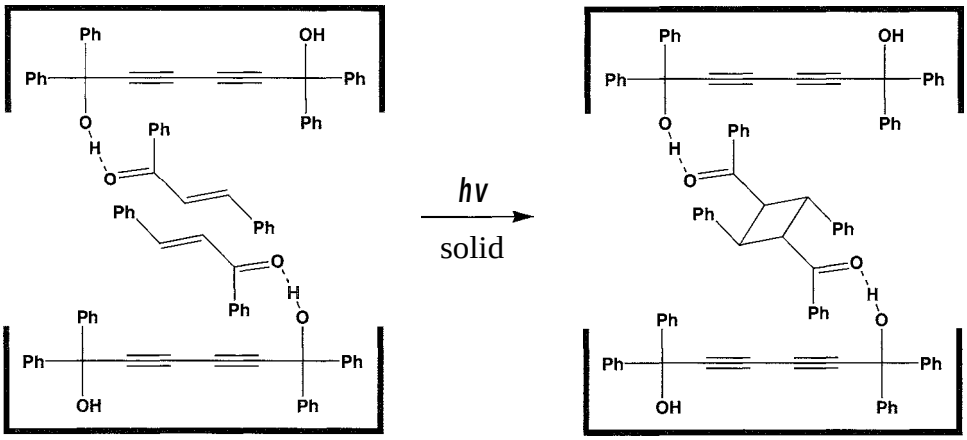

Fig. 3 The application of auxiliary components to control the [2 + 2] photodimerization in the solid state. A tetraaryl diol assembles to form a cavity and Interacts with olefins by way of hydrogen bonds.

it difficult to synthesize molecules in the solid state with degrees of freedom common to solution (e.g., reliability, functional group tolerance). In effect, products of solid-state [2 + 2] photoreactions were limited to specific topochemical strategies, a fact that has thwarted efforts toward an ability to conduct molecular solid-state synthesis by design.

SUPRAMOLECULAR CONTROL OF THE [2 + 2] PHOTOREACTION

To control the [2 + 2] photoreaction such that it is possible to conduct molecular solid-state synthecir by design, recent efforts were directed toward the application of supramolecular chemistry.[4] Specifically, the field of

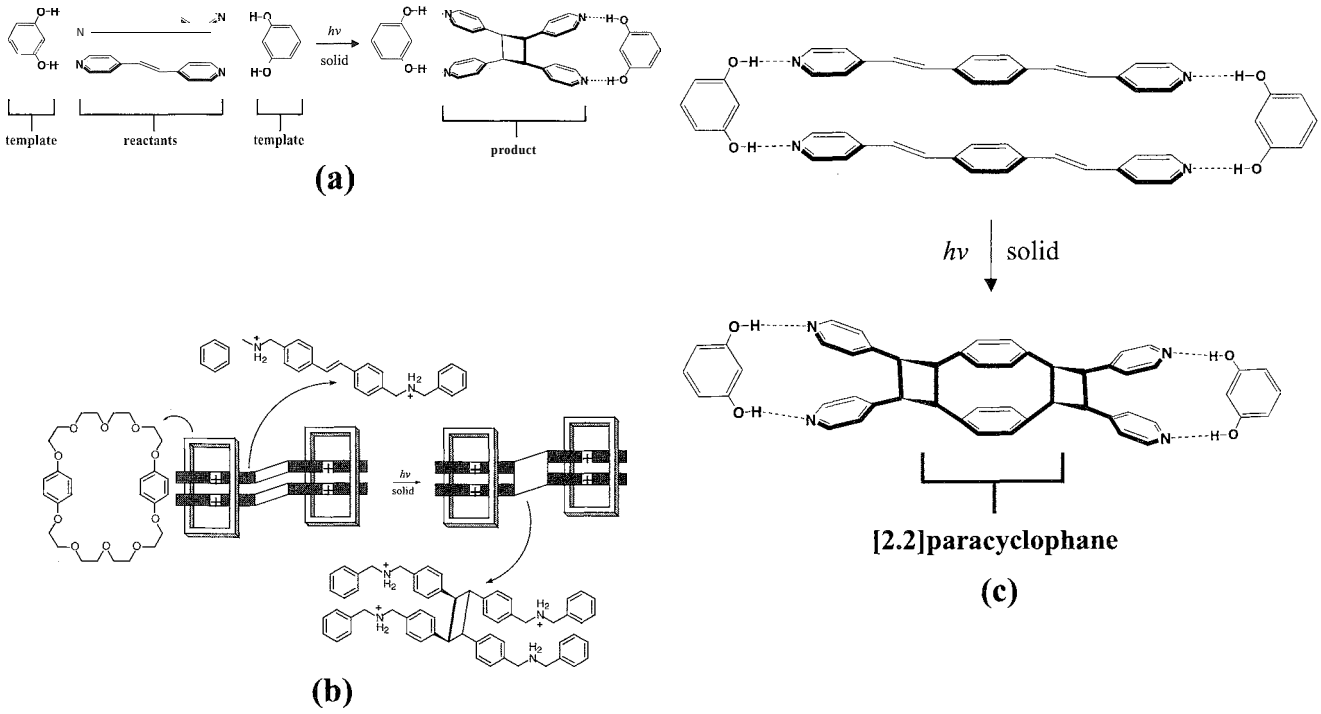

Fig. 4 The application of molecular receptors to achieve supramolecular control of the [2 + 2] photodimerization in the solid state. Control of reactivity using (a) resorcinol and (b) a crown ether, and (c) the targeted solid-state synthesis of a [2.2]paracyclophane using a resorcinol.

host–guest chemistry[21] was shown to provide access to molecules. termed molecular receptors, which recognize and preorganize molecules in the solid state for photoreaction. The receptors were shown to largely eliminate problems of intermolecular forces that made such topochemical reactions difficult to control by preorganizing the reactants. via noncovalent forces (e.g., hydrogen bonds), within discrete molecular assemblies for reaction.

MacGillivray, for example, demonstrated the ability of 1,3-dihydroxybenzene (resorcinol) and 1.8-naphthalenedicarboxylic acid (1,s-nap) to function as molecular receptors able to direct the [2 + 2] photoreaction by serving as bifunctional hydrogen bond donors in the solid state.[22,23] Specifically, cocrystallization of resorcinol or 1,8-nap with *trans*-1,2-*bis*(4-pyridyl)ethylene (4,4′-bpe) was shown to give discrete four-component molecular assemblies. 2(resorcinol)·2(4,4′-bpe) and 2(1,8-nap)·2(4,4′-bpe), respectively, held together by four O–H···N hydrogen bonds, wherein two double bonds of 4,4′-bpe are separated by <4.2 Å and are aligned in parallel (Fig. 4a). UV irradiation of each solid produced the expected photoproduct, *rctt-tetrakis*(4-pyridyl)cyclobutane (4,4′-tpcb), stereospecifically (yield: 100%). Owing to the ability of the receptors to organize the olefins linearly, the receptors were regarded as linear templates.[24]

A method that utilizes a crown ether to control a [2 + 2] photoreaction in the solid state has also been reported.[25] In particular, cocrystallization of *bis*paraphenylene[34]-crown-10 with a *bis*(dialkylammonium ion)-substituted stilbene was demonstrated by Garcia-Garibay and

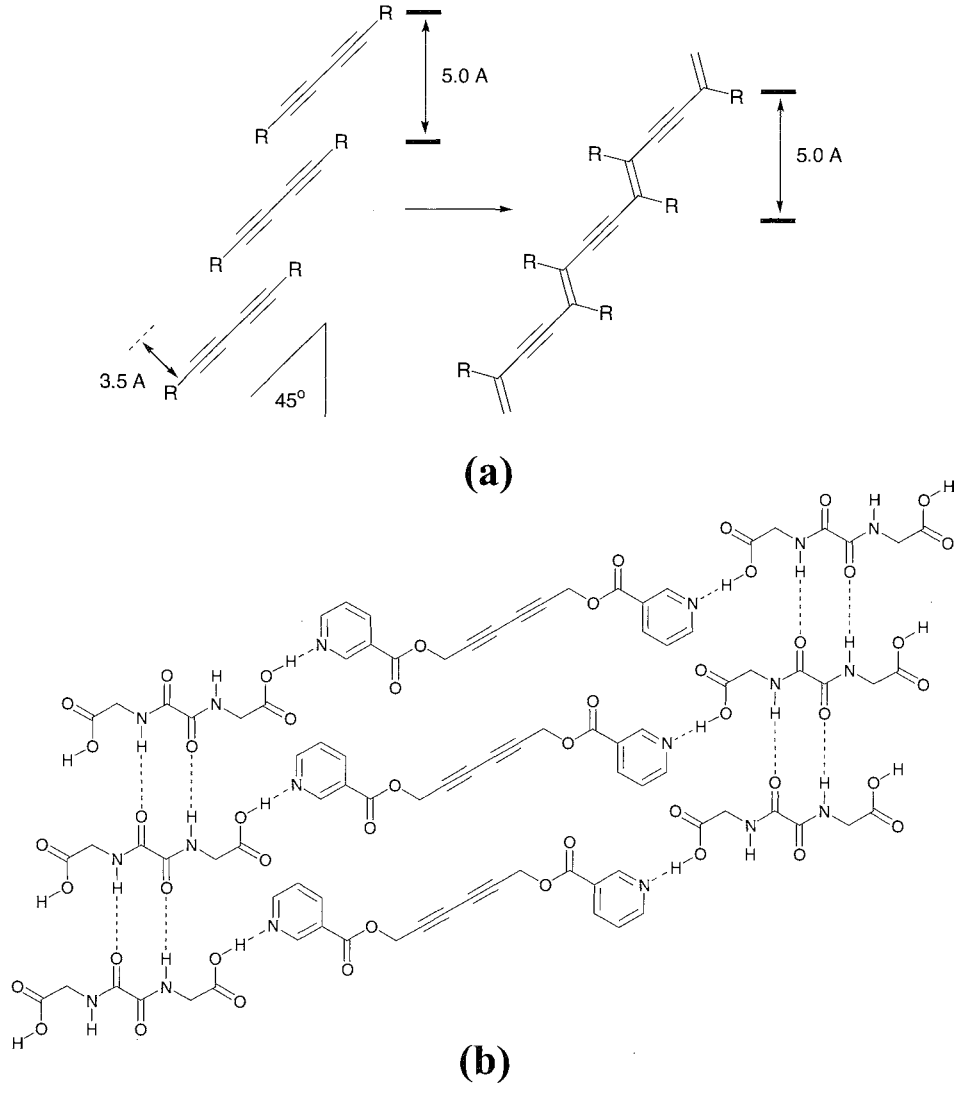

Fig. 5 Topochemical polymerization of diacetylenes in the solid state: (a) topochemical requirements and (b) a host–guest strategy for controlling polymerization of diacetylenes using an oxalamide of glycine as a supramolecular host.

Stoddart to give a 2:2 host–guest complex, wherein two olefinic bonds of two stilbenes are organized in a stacked geometry for photoreaction (Fig. 4b). UV irradiation of the solid resulted in a stereospecific solid-state photochemical dimerization that produced a single diastereoisomer. The stereochemistry of the photoproduct was determined by way of x-ray crystallography.

The ability of resorcinol to function as a linear template to organize reactants in the solid state for [2 + 2] photoreaction also led to a molecular solid-state synthesis by design.[22] Specifically. cocrystallization of 1,4-*bis*[2-(4-pyridyl)ethenyl]benzene (1.4-bpeb) with 5-methoxyresorcinol (5-OMe-res) yielded a four-component assembly. 2(5-OMe-res)·2(1,4-bpeb), wherein four olefins, as two reaction centers, conformed to the topochemical principle. UV irradiation of the solid produced. regio- and stereoselectively. a targeted [2.2]paracyclophane (yield: 60%) (Fig. 4c).

SUPRAMOLECULAR CONTROL OF DIACETYLENE POLYMERIZATION

The thermal polymerization of diacetylenes to form polydiacetylenes is also known to proceed under topochemical control in the solid state.[1] To achieve polymerization. reactant inonomers must be organized such that the carbons atoms of the reactive sites are generally separated by <3.8 Å. Thus. for a 1,4-topochemical polymerization to give a polydiacetylene, linear alignment of monomers with an intermolecular repeat spacing of approximately 5.0 Å and tilt angle of 45" with respect to the translation axis must be achieved[2] (Fig. 5a). Most diacetylenes, however. do not crystallize in accordance with structural requirements for solid-state polymerization.[1] Moreover, the application of host–guest chemistry to preorganize diacetylenes in molecular solids, similar to the [2 + 2] photoreaceion, for solid-state polymerization offered a solution to this problem.[26,27]

A host–guest strategy for controlling the polymerization of diacetylenes in the solid state was described by Fowler and Lauher.[26] Specifically. the method is based on the utilization of molecules that self-assemble into one-diiiiensional hydrogen-bonded β-networks. The networks serve as hosts by imposing a characteristic intermolecular repeat distance and tile angle upon the diacetylene guests such that the guests conform to topochemical requirements for solid-state polymerization. In particular, cocrystallization of the oxalamide of glycine with a *bis*-pyridyl substituted diacetylene was shown to impose a repeat distance and tilt angle of 4.97 Å and 43°, respectively, upon the diacetylene (Fig. 5b), an orientation suitable for solid-state polymerization.[26] The resulting oxalamide crystalline solids were observed to slowly polymerize crystal-to-crystal at room temperature to give the targeted diacetylene polymer. Notably, thermal annealing at a slightly elevated temperature increased the rate of conversion.[26] In addition to a diacetylene polymerization, the method was recently applied to an unprecedented solid-state topochernical polymerization involving a triacetylene.[27]

CONCLUSION

Topochemical solid-state reactions are, in general, more selective than liquid-phase reactions and can yield molecular and polymeric products which, in many cases, may be difficult, or impossible, to obtain in solution.[1,2] Owing to the ability of such reactions to occur under strict geometric requirements in an organized environment, topochemical solid-state reactions provided useful targets for applying principles of supramolecular[4] and host–guest[21] chemistry to direct such transformations. It is expected that as principles for controlling topochemical reactions using such host–guest design strategies continue to develop. it should be possible to routinely access molecules and polymers, as well as solid-state materials, less available by a more classical approach to covalent synthesis.[22–27]

ARTICLES OF FURTHER INTEREST

Artificial Enzymes, p. 76
Chemical Topology, p. 229
Concepts in Crystal Engineering, p. 319
Crystal Engineering with Hydrogen Bonds, p. 357
Enzyme Mimics, p. 546
Hydrogen Bonding, p. 658
π–π Stacking as a Crystal Engineering Tool, p. 1093
Preorganization and Complementarity, p. 1158
Solid-State Reactivity/Topochemistry, p. 1316
Space Groups and Crystal Packing Modes, p. 1337
Supramolecular Photochemistry, p. 1434
The Template Effect. p. 1493

REFERENCES

1. Schmidt, G.M.J. Photodimerization in the solid state. Pure Appl. Chem. 1971, 27, 647–678.
2. Enkelmann. V. Structural aspects of the topochemical polymerization of diacetylenes. Adv. Polym. Sci. 1984. *63*. 91–136.
3. Tanaka. K.: Toda. F. Solvent-free organic synthesis. Chem. Rev. 2000. 100. 1025–1074.

4. Lehn, J.-M. *Supramolecular Chemistry*; Wiley-VCH: Weinheim. 1995.
5. Kearsley. S.K.The Prediction of Chemical Reactivity within Organic Crystals Using Geometric Criteria. In *Organic Solid* State *Chemistry*; Desiraju. G.R.. Ed.; Elsevier: New York. 1987: 69–115.
6. Ramamurthy, V.: Venkatesan. K. Photochemical reactions of organic crystals. Chem. Rev. 1987. *87.* 433–481.
7. Kohmoto, S.: Ono. Y.: Masu. H.: Yamaguchi. K.: Kishikawa. K.; Yamamoto, M. Enantioselective intramolecular aromatic [4+4] photocycloaddition in crystalline state: Parameters for reactivity. Org. Lett. 2001. *3*, 4153–4155.
8. Yang. Z.; Ng, D.; Garcia-Garibay, M. Engineering reactions in crystalline solids: Photochemical generation of secondary and tertiary enol radical pairs from crystalline ketodiesters. J. Org. Chem. 2001. *66*, 4468–4475.
9. Kishan. K.V.R.: Desiraju. G.R Crystal engineering a solid-state Diels–Alder reaction. J. Org. Chem. 1987, *52*, 4640–4641.
10. Desiraju, G.R. Supramolecular synthons in crystal engineering—A new organic synthesis. Angew. Chem.. Int. Ed. Engl. 1995. *34.* 2311–2327.
11. Sarma, J.A.R.P.: Desiraju. G.R. The role of Cl···Cl and C–H···O interactions in the crystal engineering of 4-A short-axis structures. Acc. Chem. Res. 1986, 19. 222–228.
12. Coates. G.W.: Dunn. A.R.; Henling, L.M.: Ziller. J.W.: Lobkovsky, E.B.: Grubbs. R.H. Phenyl-perfluorophenyl stacking interactions: Topochemical [2+2] photodimerization and photopolymerization of olefinic compounds. J. Am. Chem. Soc. 1998, 120. 3641–3649.
13. Sharma. C.V.K.; Panneerselvam, K.; Shimoni. L.: Katz. H.: Carrell, H.L.: Desiraju. G.R. 3-(3′,5′-dinotrophenyl)-4-(2′,5′-dimethoxyphenyl)cyclobutane-1,2-dicarboxylic acid: Engineered topochemical synthesis and molecular and supramolecular properties. Chem. Mater. 1994. *6.* 1282–1292.
14. Maekawa, Y.; Kato. S.; Hasegawa. M. Quantitative formation of a highly strained tricyclic [2.2]paracyclophane derivative from a mixed crystal of ethyl and propyl α-cyano-4-[2-(4-pyridyl)ethenyl]cinnamates through a topochemical reaction. J. Am. Chem. Soc. 1991. *113.* 3867–3872.
15. Feldman. K.S.: Campbell, R.F. Efficient stereo- and regiocontrolled alkene photodimerization through hydrogen bond enforced preorganization in the solid state. J. Org. Chem. 1995. 60. 1924–1925.
16. Brett. T.J.; Alexander. J.M.: Clark, J.L.: Ross. C.R., II; Harbison. G.S.; Stezowski. J.J. Chemical insight from crystallographic disorder: Structural studies of a supramolecular β-cyclodextrin/coumarin photochemical system. Chem. Commun. 1999. 1275–1276.
17. Takagi, K.: Usami, H.: Fukaya. H.: Sawaki. Y. Spatially controlled photocycloaddition of a clay-intercalated stilbazolium cation. J. Chem. Soc., Chem. Commun. 1989. 1174–1175.
18. Tanaka. K.; Tocla, F.: Mochizuki. E.: Yasui. N.: Kai. Y.: Miyahara, I.: Hirotsu. K. Enantioselective single-crystal-to-single-crystal photodimerization of coumarin and thiocoumarin in inclusion compounds with chiral host compounds. Angew. Chem.. Int. Ed. Engl. 1999. *38,* 3523–3525.
19. Ito. Y.: Borecka. B.: Trotter. J.: Scheffer. J.R. Control of solid-state photodimerization of trans-cinnamic acid by double salt formation with diamines. Tetrahedron Lett. 1995. *36,* 6083–6086.
20. Ito, Y.: Borecka. B.: Olovsson, G.; Trotter, J.: Scheffer. J.R. Control of the solid-state photodirnerization of some derivatives and analogs of *trans*-cinnamic acid by ethylenediamine. Tetrahedron Lett. 1995. *36*, 6087–6090.
21. Cram, D.J. The design of molecular hosts, guests, and their complexes. Science 1988. *240.* 760–767.
22. MacGillivray, L.R.: Reid. J.L.; Ripmeester. J.A. Supramolecular control of reactivity in the solid state using linear molecular templates. J. Am. Chem. Soc. 2000. 122, 7817–7818.
23. Papaefstathiou. G.S.: Kipp, A.J.: MacGillivray, L.R. Exploiting modularity in template-directed synthesis: A new linear template to control reactivity within discrete hydrogen-bonded molecular assemblies in the solid state. Chern. Commun. 2001, 2462–2463.
24. Anderson. S.; Anderson. S.L. *Templated* Organic *Synthesis*; Diederich, F.. Stang, P.J.. Eds.: Wiley-VCH: New York, 2000: 1–38.
25. Armisakis. D.G.: Garcia-Garibay. M.A.: Rowan. S.J.: Stoddart. J.F.: White. A.J.P.: Williams. D.J. Host–guest chemistry aids and abets a stereospecific photodimerization in the solid state. Angew. Chem., Int. Ed. 2001. *40.* 4256–4261.
26. Kane, J.J.: Liao, R.-F.: Lauher. J.W.: Fowler, F.W. Preparation of layered diacetylenes as a demonstration of strategies for supramolecular synthesis. J. Am. Chem. Soc. 1995. *117.* 12003–12004.
27. Xiao. J.; Yang. M.: Lauher. J.W.: Fowler. F.W. A supramolecular solution to a long-standing problem: The 1,6-polymerization of a triacetylene. Angew. Chem., Int. Ed. Engl. 2000. *39*, 2132–2135.

Solvation Effects in Guest Binding

Mikhail Rekharsky
Entropy Control Project, International Cooperative Research Project (ICORP), Osaka, Japan
Yoshihisa Inoue
Entropy Control Project, International Cooperative Research Project (ICORP), Toyonaka, Japan

INTRODUCTION

A large variety of noncovalent weak interactions can take place in the solution of a guest. The guest–solvent interactions, or guest solvation, involve electrostatic (ion–ion, ion–dipole, dipole–dipole, dipole–induced dipole), van der Waals, hydrogen bonding, n – staking, and other weak forces that strongly depend on the physicochemical properties of the particular guest–solvent combination under consideration. As a consequence of the diversity of guest–solvent interactions, the association process of a guest with a supramolecular host can be dramatically altered or totally changed depending on the solvation properties.

WHAT IS GUEST SOLVATION?

The solvation of a neutral or ionic guest in any solvent, including hydration in aqueous solution, is represented by the process of guest transfer from the ideal gas to the solution. both in the standard state:

$$\text{Guest(gas)} \rightarrow \text{Guest(solution)} \quad (1)$$

The standard states correspond to a hypothetical ideal gas at atmospheric pressure (101,325 Pa) and a hypothetical ideal 1 M aqueous solution. The standard molar Gibbs free energy, enthalpy. and entropy changes for the above reaction are donated by symbols ΔG°, ΔH°, and ΔS°, respectively.

Certainly, it should be emphasized that the solvation of a supramolecular host is also altered upon switching from one solvent to another. Taking into account the generally more complicated structure and functionality of supramolecular hosts in comparison to guests, it should be stated that in many cases, the alteration of host solvation can lead to a more profound impact in its binding behavior.

The host–guest association process, incorporating solvent molecules, may be illustrated by a rather simple scheme shown in Fig. 1. The extent of the solvation, i.e., the amount and location/position of the solvent molecules as well as the strength of the host–solvent and guest–solvent interactions, critically varies depending on the nature of the solvent employed. However, in principle, the combined surface area of host and guest, which is accessible to solvent, is significantly reduced upon host–guest complexation, limiting the number of solvent molecules able to associate with the complex. Concurrently, a number of solvent molecules are released into the bulk solvent upon host–guest complexation, and therefore. the interaction of solvent molecules in the bulk solution also plays a crucial role in guest binding. More detailed discussion on this issue may be found in the literature.[1,2]

DESOLVATION UPON GUEST–CYCLODEXTRIN ASSOCIATION

One group of representative examples of host–guest desolvation upon association are the complexation reactions of cyclodextrin in water. Cyclodextrins (CDs), cyclic oligosaccharides composed of 6, 7, or 8 glycopyranose units, are truncated cone-shaped macrocyclic molecules with hollow, tapered cavities (Fig. 2) (see *Cyclodextrins* article for more details). In aqueous solution, the cavity is occupied by several water molecules that are excluded from the cavity upon inclusion of a proper guest. As a result of the α-1,4-linkage of each glucopyranose unit, all of the hydrophilic 2-. 3-, and 6-hydroxyl groups are located on the exterior of the hydrophobic cavity (Fig. 2), as is amply exemplified in the literature.[2,3] The most common binding mode of native and modified CDs with various guests involves penetration of the less hydrophilic (nonpolar) part of a guest molecule into the CD cavity, while the more hydrophilic. often charged. part of the guest stays just outside the primary or secondary rim of the cavity.

The diameters of simple aliphatic hydrocarbon chains match well with the size of α-cyclodextrin's (a-CD) hydrophobic cavity, which in aqueous solution contains in its interior several water molecules (Fig. 3). Sequential insertion of methylene groups of the hydrocarbon chain into the a-CD cavity is accompanied by expulsion of water molecules into the bulk solvent. In addition. several water

Encyclopedia of Supramolecular Chemistry
DOI: 10.1081/E-ESMC 120012739

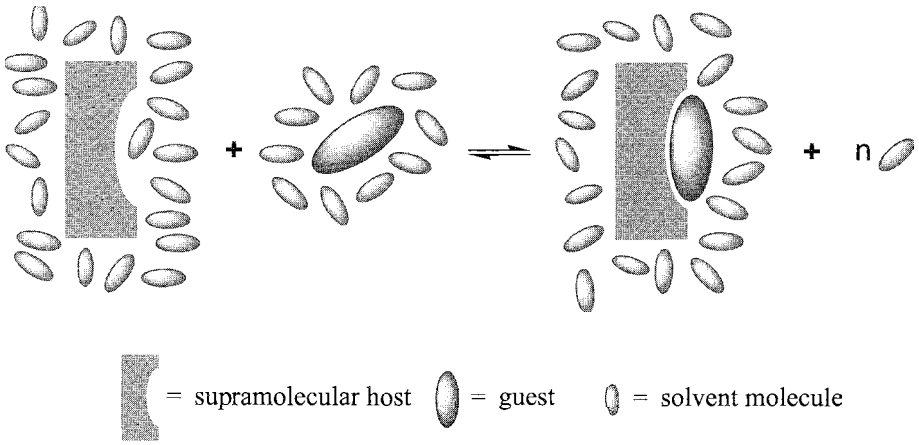

Fig. 1 Schematic drawing of host-guest deiolvation upon complex formation. (*View this art in color at www.dekker.com.*)

molecules that were located around the inserted methylene group in solution are also returned to the bulk solvent upon complexation. The longer the chain. the stronger the complexation.[3] Furthermore, the incremental change of the ΔG° value (as well as other thermodynamic parameters) for the complexation reaction is constant with the stepwise increase of the aliphatic chain length.'''

One of the intriguing issues observed in guest inclusion by native CDs is that only the specific part of the guest penetrating into the cavity contributes to the overall complexation thermodynamics. The introduction of a methyl group to the less-polar penetrating part of a guest consistently enhances the binding constant by a factor of 2–4, while the methylation of a charged group. such as an ammonium which stays outside the cavity upon complexation (Fig. 3), does not at all affect the complexation thermodynamics.[3] Furthermore, the chemical nature, structure, and even sign of the charged group do not play any significant thermodynamic roles upon cornplexation with native CDs as far as the same hydrophobic past of the guest is included in the cavity.''' This is obviously nonclassical. or unusual. thermodynamic behavior from the viewpoint of ordinary solute–solvent interactions or for the conventional solute transfer from water to nonpolar solvent.

Another major difference between conventional solute transfer and supramolecular association is the crucial influence of the shape of the guest molecule in the latter case. This is clearly demonstrated upon complexation of β-CD with 2- and 3-phenylbutyric acids. The apparently trivial variation in the methyl position results in a profound difference in complexation thermodynamics. Despite virtually the same hydrophobicity (i.e., the distribution ratio between water and nonpolar organic solvent). the affinity of 3-phenylbutyric acid toward β-CD (K=402–430 M^{-1}) is more than four times larger than that of 2-phenylbutyric acid (K=94–95 M^{-1}).[4,5] This difference arises from the significantly greater degree of steric hindrance occurring in the 2-phenylbutyric acid case. The crucial steric effect on guest binding is also found in the cornplexation of ortho-substituted phenyl guests. which always exhibit much lower complexation affinities toward β-CD than their *para* counterparts, due to the steric hindrance caused by the ortho-methyl group.[4,5] This is a good example of the critical role that steric factors play in CD complexation and in supramolecular association in general, highlighting the intrinsic difference between inclusion complexation by CD and classical hydrophobic processes (e.g., transfer from water to nonpolar organic media) (see Hydrophobic Effects article for more details).

EFFECT OF SOLVENT MOLECULE SIZE ON GUEST BINDING

As discussed above, improper molecular size and shape of a guest often prevent it from fully enjoying the most comfortable association with hosts such as cyclodextrins. In this light, it would be intriguing to investigate the effect

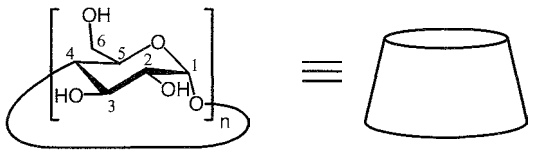

α-, β-, γ-Cyclodextrin (n = 6-8)

Fig. 2 Chemical structures of α-, β-, and γ-cyclodextrin (CD).

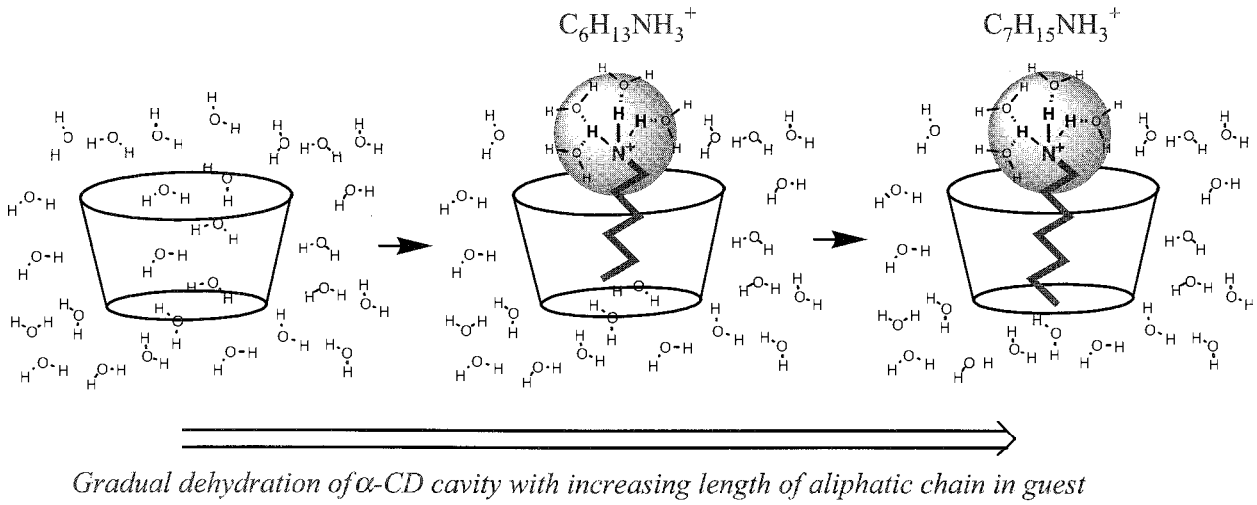

Fig. 3 Dehydration of r-CD cavity upon guest complexation. (*View this art in color at www.dekker.com.*)

of the size and shape of the solvent molecule on supramolecular association. For instance, the cyclophane host (see *Cyclophanes* article for more details) with functionalized tethers, illustrated in Fig. 4, can bind a small guest such as imidazole in ethers and chlorinated hydrocarbons.[6] However. the binding constant for imidazole varies dramatically by two to three orders of magnitude from 29 M^{-1} in THF to 1067 M^{-1} in Me_4-THF and from 240 M^{-1} in CH_2Cl_2 to 128,000 M^{-1} in $CHCl_2CHCl_2$, critically depending on the size of the solvent used. Some of the solvent molecules are larger in size than the guest, and the relatively small binding site of the host is hardly accessible for the large solvent molecules, which facilitates the guest's access to the interacting site. Consequently, the association constant increases gradually with increasing size of the solvent molecule in both series of solvents, i.e., ethers and chlorinated hydrocarbons. Probably, the size/shape of the largest $CHCl_2CHCl_2$ molecule prevents it from entering the inner sphere of the host, thus giving the largest affinity of 128,000 M^{-1} in the absence of competitors for the binding site.

When the guest and host interact with the solvent, the guest binding is expected to become weaker. In the above case, both imidazole and the host (Fig. 4) can more strongly interact with ether solvents, in comparison to

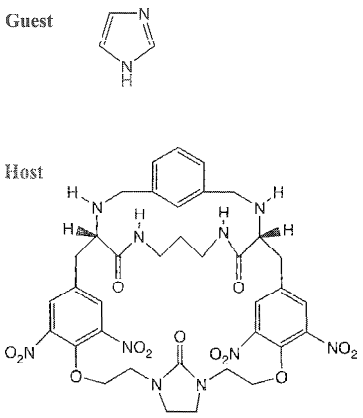

Solvent	$K_a(M^{-1})$
CH_2Cl_2	240
$CHCl_3$	490
CH_3CCl_3	8161
$CHCl_2CHCl_2$	128000
Tetrahydrofurane(THF)	29
2-Me-THF	77
1,4-dioxane	87
Tetrahydopyran	104
2,2-Me_2-THF	156
2.5-Me,-THF	185
2,2,5,5-Me_4-THF	1067

Fig. 4 Effect of solvent molecule size on complex stability between imidazole and cyclophane host. (*View this art in color at www.dekker.com.*)

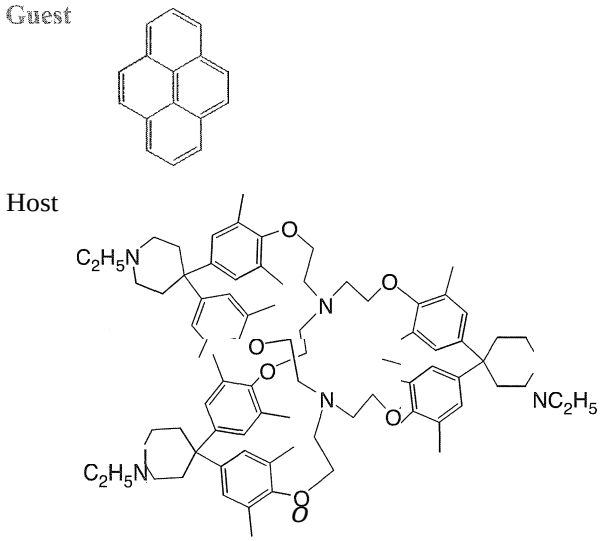

solvent	log K	$E_T(30)$ kJ/mol
water	6 8	264
methanol	4.6	232
ethanol	4 4	217
acetone	3 1	177
[illegible]	2.8	188
[illegible]	1 9	164
carbon disulfide	1 0	136

Fig. 5 Effect of solvent polarity on complex stability between pyrene and cyclophane host. (*View this* art *in color at www.dekker.com.*)

chlorinated hydrocarbons, through hydrogen-bond formation (see *Hydrogen Bonding* article for more details). Hence, the host–guest association is always much stronger in chlorinated hydrocarbons than in ethers of similar size.

EFFECT OF SOLVENT POLARITY ON NONPOLAR ASSOCIATION

I? is also interesting to examine the solvent effect on the binding behavior of neutral nonpolar pyrene with the three-dimensional (3D) cyclophane host, as shown in Fig. 5, in a wide variety of solvents. Using this host–guest system. we can make a valuable comparison, because it was shown that in all solvents (Fig. 5) the coinplex has the same structure and geometry. and that the large cyclophane cavity is freely accessible to all solvents, assuring complete solvation.[7] The highest affinity for pyrene was observed in water and the lowest in nonpolar solvents such as benzene and carbon disulfide. A somewhat linear relationship was found between log K and the solvent polarity parameter $E_T(30)$, which was applied successfully to the interpretation of solvent effects observed for a variety of reactions and equilibria.[8]

Analogous correlations between solvent polarity and the strength of nonpolar interactions were found for other systems, such as for aromatic interactions in metal *tris*-bipyridine complexes.[9] These observations are consistent with the solvophobic nature of aromatic interactions. which is strengthened in polar solvents, lacking the ability to properly solvate to the nonpolar surfaces of the aromatic ring.

BINDING OF NEUTRAL AROMATIC GUEST VERSUS ION

Complexation of neutral hydrophobic organic guests and hydrophilic metal cations is usually characterized by different solvent dependencies. In this context. it is of interest to examine the binding behavior of the cyclophano-crown-ether host (shown in Fig. 6) in solvents of varying

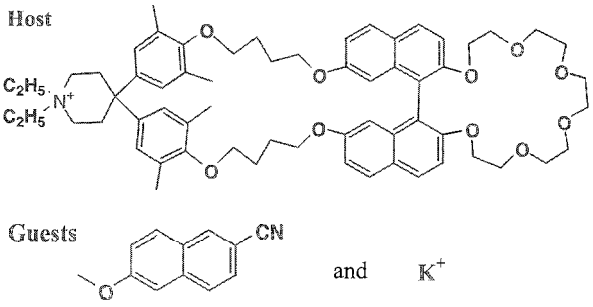

Methanol content (% vol) in water	log K	
	K^+	6-Methoxy-2-naphthonitrile
40	1.1	3.6
60	1.9	2.6
80	2.0	2.1
100	3.2	1.4

Fig. **6** Interaction of potassium ion and 6-methoxy-2-naphthonitrile with cyclophane-crown ether host various water-methanol mixtures. (*View this art in color at www.dekker.com.*)

polarity.[10] Possessing crown ether and cyclophane moieties in a single molecule, the cyclophano-crown-ether host can simultaneously bind a potassium cation and 6-methoxy-2-naphthonitrile in a water–methanol mixture. Similar to the binding of pyrene by the 3D-cyclophane shown in Fig. 5, 6-methoxy-2-naphthonitrile forms a 160 times more stable complex with the cyclophane moiety in the more hydrophilic 60:40 water–methanol mixture than in pure methanol. In contrast, the affinity toward the potassium ion is enhanced 120 times in pure methanol compared to the 60:40 water–methanol mixture.

This opposite solvent polarity dependence is generally observed for solvophobically versus electrostatically driven complexation processes; see, for instance. the recent study by Mizutani et al.[11] This general phenomena is used to create a wide variety of supramolecular devices. such as molecular shuttles based on rotaxanes as well as other so-called .'molecular machines.''[12]

SOLVOPHOBIC THEORY AND SURFACE TENSION

Obviously, the simple unmodified 18-crown-6 (Fig. 7) (see *Crown Ethers* article for more details) is a better binder for potassium cation in water and methanol compared to the cyclophano-crown ether (Fig. 4). Nevertheless, the tendency of affinity is the same in both cases. Indeed, both hosts interact strongly with the potassium cation in methanol, while the affinity in water is relatively weak. The logarithm of the association constant of the potassium cation with the crown ether (Fig. 7)[13] correlates with the solvent surface tension (y), whereas the correlations with other solvent parameters such as relative permeability and dipole moment'''' are not as good. This is not the only case in which a direct correlation is observed between solvent γ and host–guest affinity. A linear correlation of ΔG° against γ was observed experimentally for several complexation reactions of cyclodextrin, e.g., indole + β-CD (1:1 complex)[15] and adainantanecarboxylate + β-CD (1:1 complex).[16]

According to the ''solvophobic theory.' originally proposed in Sinanoglu's pioneering papers.[17] the free-energy change of complex formation is regarded as a linear function of the solvent's surface tension (γ). To visualize this idea applied to the inclusion complexation of hydrophobic organic guests in CDs, one could imagine a sort of ''cavity'' or ''solvent cage'' that exists around the hydrophobic part of a guest in bulk water but disappears upon insertion of the hydrophobic part into a CD cavity. However, as is the case with the other hypotheses; the ''''slvophobic theory'' has limitations as to what it can explain, for instance, the higher complex stabilities in D_2O in comparison to H_2O are simply because the surface tension of D_2O is slightly smaller than that of H_2O.[18]

Host Guest K^+

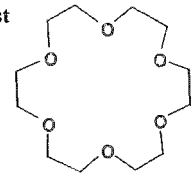

Solvent	Physical properties			log *K*
	Surface tension IN m^{-1}	Relative permeability	Dipole moment /D	
Water	0.072	78.4	1.8	2.0
Dimethylsulfoxide	0.043	46.7	3.9	3.7
Benzyl alcohol	0.040	13.1	1.7	4.1
N,N-Dimethylformamide	0.035	36.7	3.9	4.3
Acetonitrile	0.028	37.5	3.4	5.7
Acetone	0.023	20.7	2.7	6.0
Methanol	0.022	32.7	2.9	6.2
Ethanol	0.022	24.6	1.7	6.1

Fig. 7 Correlation of stability of crown ether-potassium ion complex with physical properties of various solvents. (*View this art in color at www.dekker.com.*)

THERMODYNAMIC VIEW FOR GLOBAL UNDERSTANDING OF MOLECULAR RECOGNITION

In quantitatively discussing molecular recognition phenomena in various solvents from the viewpoint of supramolecular chemistry. it is indispensable to determine the thermodynamic parameters for the relevant (supra)-molecular system of interest. For a wide variety of chemical and biological molecular recognition systems, the thermodynamic quantities were already compiled: analyzed, and discussed in order to extract insights into the mechanistic profile of molecular recognition. However, most of the foregoing discussion and conclusions. though certainly self-consistent within the particular and closely related systems. unfortunately seem ad hoc in many cases and are not always applicable to other molecular recognition systems composed of different categories of host–guest combinations. Probably the most general thermodynamic approach to global understanding of molecular recognition is the comprehensive analysis of the compensatory enthalpy–entropy relationship observed in many supramolecular systems.

The enthalpy–entropy compensation in general has long been a hot topic in the chemical literature, because in principle. no explicit relationship between the enthalpy change and the entropy change can be derived from

Table 1 Slope (Y) and Intercept *(TASo)*of AH–TAS plots for suprarnolecular Interactions of natural and synthetic hosts with a variety of ionic. molecular. and biomolecular guests in homogeneous and heteiogeneouc solutions

Host	Guest	Solvent	α	$T\Delta S_0^\circ$
Glyme	Ion	Aqueous	0.89	2.0
Crown ether	Ion	Aqueous	0.77	2.9
Crown ether (solvent extraction)	Ion	Binary	0.73	2.6
Crown ethei (sanduich complex)	Ion	Aqueous	0.93	3.2
Long glyme	Ion	Aqueous	1.03	4.2
Cryptand	Ion	Aqueous	0.42	4.0
Ionophore antibiotic	Ion	Aqueous	0.93	5.4
Lariat ether	Ion	Aqueous	0.89	4.3
Bis(crown ether)	Ion	Aqueous	1.03	4.6
Cyclodextrin	Organic molecule	Aqueous	0.93	3.3
Quinone-receptor porphyrin	Quinone	Organic	0.60	0.0
Metalloporphyrin	Pyridine	Organic	0.61	1.6
Cyclophane/calixarene	Organic molecule	Aqueous	0.78	3.4
Enzyme	Coenzyme/substrate/inhibitor	Aqueous	1.11	7.0
Antibody	Antigen	Aqueous	0.88	8.7
DNA/RNA	DNA/RNA/intercalator	Aqueous	1.03	8.5

fundamental thermodynamics. Nevertheless. the compensatory enthalpy–entropy relationship is often observed in activation and therinodynamic quantities determined for a wide variety of reactions and equilibria.

The linear AH–AS relationship observed experimentally leads to Eq. 2, where the proportional coefficient β has the dimension of temperature. From Eq. 2 and the differential form of the Gibbs–Helmholtz Eq. 3, we obtain Eq. 4.

$$\Delta H^\circ = \beta\Delta\Delta S^\circ \tag{2}$$

$$\Delta G^\circ = \Delta\Delta H^\circ - T\Delta\Delta S^\circ \tag{3}$$

$$\Delta G^\circ = (1 - T/\beta)\Delta\Delta H^\circ \tag{4}$$

Eq. 4 clearly indicates that, at the critical point. or so-called isokinetic or isoequilibrium temperature (β), the rate or equilibrium constant is independent of the enthalpic change caused by any alterations in substituent, solvent, and so on. It is interesting that such phenomena have been abundantly observed for a wide variety of reactions and equilibria.

ENTHALPY–ENTROPY COMPENSATION AS A PRACTICAL TOOL FOR UNDERSTANDING AND ANALYZING GUEST SOLVATION AND MOLECULAR RECOGNITION

From the compensatory enthalpy–entropy relationship, the $T\Delta S^\circ$ value can be linearly correlated with the AN^o value to give Eq. 5. When integrated. this gives Eq. 6. Subsequent combination with Eq. 3 affords Eq. 7.

$$T\Delta\Delta S^\circ = \alpha\Delta\Delta H^\circ \tag{5}$$

$$T\Delta S^\circ = \alpha\Delta H^\circ + T\Delta S^\circ_0 \tag{6}$$

$$\Delta\Delta G^\circ = (1 - \alpha)\Delta\Delta H^\circ \tag{7}$$

Thus. the slope (α) of the $T\Delta S^\circ$-versus-ΔH° plot (Eq. 6) indicates to what extent the enthalpic gain ($\Delta\Delta H^\circ$), which is induced by any alterations in host, guest, or solvent, is canceled by the accompanying entropic loss (AAS^o). In other words, only a fraction ($1r$) of the enthalpic gain can contribute to the enhancement of complex stability. On the other hand. the intercept ($T\Delta S^\circ_0$) represents the inherent complex stability (AC^o) obtained at AN^o=O, which means that the complex is stabilized even in the absence of enthalpic gain, as long as the $T\Delta S^\circ_0$ term is positive. From comparative analyses of the thermodynamic data for cation binding by three types of ionophores with different topologies and rigidities (i.e., glyme, crown ether, and cryptand),[19] the slope (α) and the intercept ($T\Delta S^\circ_0$) of the regression line were related to the degree of conformational change and to the extent of desolvation upon complexation. respectively. Using α and $T\Delta S^\circ_0$ as quantitative measures for changes in conformation and desolvation of both host and guest, diverse chemical and biological supramolecular systems can be analyzed consistently, despite the different weak interactions involved in each supramolecular system.[''']

The slopes (α) and the intercepts (TAS^o_0) obtained for a variety of supramolecular systems are presented in Table 1. It is obvious that conformational changes and desolvation

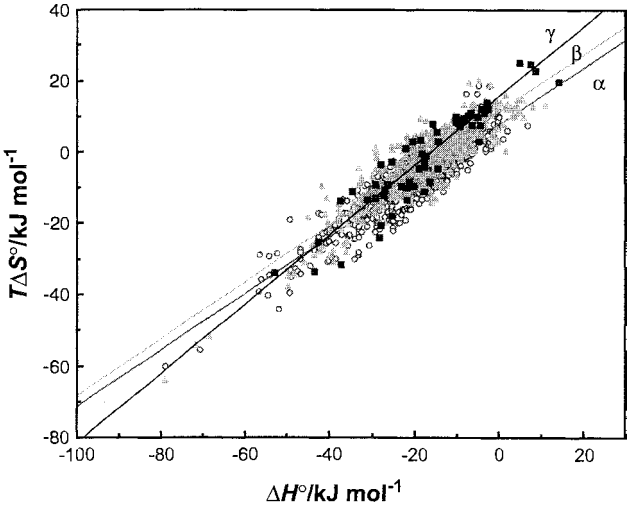

Fig. 8 Individual entropy compensation plots for natural a-, β-, and γ-cyclodextrins. (*View this art in color at www.dekker.com.*)

are much larger for the association reactions involving enzymes, antibodies, and DNA/RNA than for simple crown ethers. In accordance with that, the slope α and intercept $T\Delta S^\circ_0$ are larger for the former biological systems than for the latter synthetic systems. It should be emphasized that even closely related systems, such as cyclodextrins of different sizes (Fig. 8), can be consistently analyzed in terms of the slope α and intercept $T\Delta S^\circ_0$ as measures of the conformational changes and desolvation, respectively. The slope α and the intercept $T\Delta S^\circ_0$ increase from α-CD to P-CD and then to γ-CD in accordance with the increased conformational changes and extent of desolvation upon guest inclusion.

GRUNWALD THEORY OF ENTHALPY–ENTROPY COMPENSATION

The general concept and methodology developed by Grunwald et al.[20] provides us with a reliable tool for analyzing the complexation thermodynamic parameters and, particularly, for predicting the existence or nonexistence of meaningful enthalpy–entropy compensation in a particular set of limited thermodynamic data. The idea is based on the separation of overall complexation thermodynamic parameters into two terms: *nominal* and *environmental*. The nominal part (ΔG_{nom}, ΔH_{nom}, and AS_{nom}) is associated with the complexation of the solvated host with solvated guest to form a solvated host–guest complex. while the environmental part (ΔG_{env}, AH_{env}, and ΔS_{env}) is associated with water molecules involved in solvation/desolvation processes upon complexation. It was shown that ΔG_{env} is equal to zero in dilute solution, and thus, only AH_{env} and AS_{env} terms are subject to distinct enthalpy–entropy compensation.[21]

Recently, experimental confirmation of the Grunwald theory was achieved by comparing the qualities of differential enthalpy–entropy compensation plots for the exchange equilibrium between (*R*)- and (*S*)-enantiomers of chiral guests in β-CD's cavity (Eq. 8),[4] and the exchange equilibrium between native P-CD and 6-ammonio-6-dexoy-β-CD (am-β-CD) for chiral and achiral guests (Eq. 9):[5]

$$[\beta\text{-CD} \cdot \text{R}] + S = [\text{P-CD} \cdot \text{S}] + \text{R} \quad (8)$$

$$[\beta\text{-CD} \cdot \text{G}] + \text{am-}\beta\text{-CD} = [\text{am-}\beta\text{-CD} \cdot G] + \text{P-CD} \quad (9)$$

Differential thermodynamic parameters calculated for the hypothetical exchange equilibria (Eqs. 8 and 9) are used to build the compensation plot shown in Fig. 9a and 9b, respectively. Interestingly, despite the same accuracy level

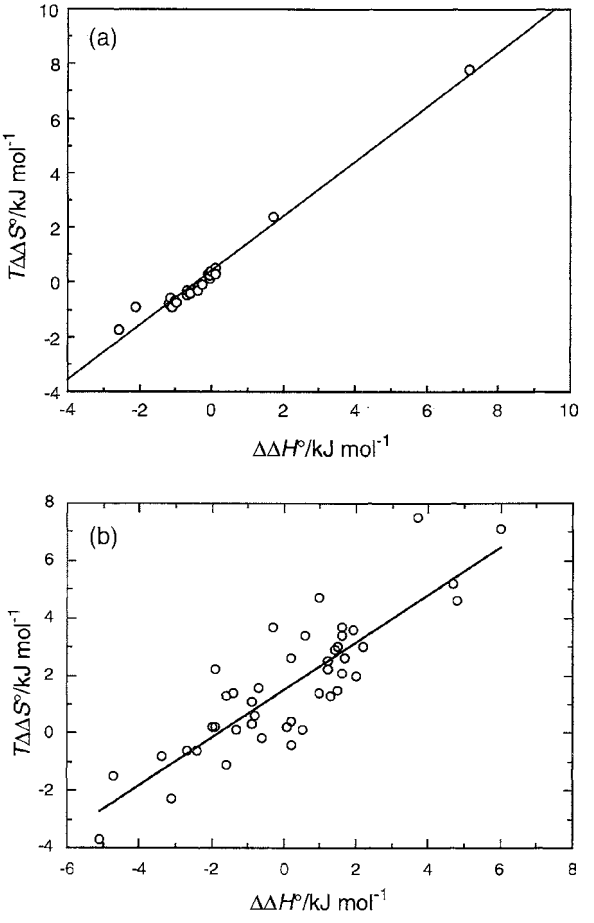

Fig. **9** (a) Compensation plot for differential entropy change ($T\Delta S^\circ_{D/L}$ or $T\Delta S^\circ_{R/S}$) against the differential enthalpy ($\Delta H^\circ_{D/L}$ or $\Delta H^\circ_{R/S}$) upon complexation of various D/L and *R/S*-enantiomeric pairs with β-cyclodextrin in aqueous buffer solution. (b) Compensation plot for differential entropy change ($T\Delta S^\circ_{am}$) against the differential enthalpy (ΔH°_{am}) upon transfer of various guests from β-cyclodextrin to 6-amino-6-deoxy-β-cyclodextrin in aqueous buffer solution.

and encompassing range of original data, the two compensation plots show strikingly different scattering levels. These compensatory enthalpy–entropy relationships are a direct experimental confirmation of the Crunwald's prediction that ΔG_{env} is equal to zero in dilute solution, and thus. only AH_{env} and AS_{env} are subject to the enthalpy–entropy compensation. It is obvious that a larger contribution from the nominal part (ΔG_{nom}, $A H_{nom}$, and $A S_{nom}$), associated with the particular complex structure, is expected for the host exchange from β-CD to am-β-CD than for the enantiomeric guest exchange in the same β-CD cavity.

CONCLUSION

It is demonstrated that, irrespective of the type of host. guest, and solvent systems employed, the solvation of the guest, host, and resulting complex plays a crucial role in supramolecular chemistry, where several weak interactions work together. However. the seemingly complicated solvation/desolvation behavior as well as the conformational changes upon suprainolecular interactions can be rationaliy understood, first by determining the thermodynamic parameters for a wide variety of chemical and biological supramolecular systems, and then by analyzing the compensatory enthalpy–entropy relationship that is frequently observed in weakly interacting supramolecular systems by applying the Grunwald theory.

ACKNOWLEDGMENT

We would like to thank Dr. Guy A. Hembury for assistance in the preparation of this manuscript.

ARTICLES OF FURTHER INTEREST

Crown Ethers, p. 326
Cyclodextrins, p. 398
Cyclophanes: Endoacidic, Endobasic, and Endolipophilic Cavities, p. 424
Hydrogen Bonding, p. 658
Hydrophobic Effects. p. 673

REFERENCES

1. Diederich. F. *Cyclophanes*; Royal Society of Chemistry: Cambridge, 1991.
2. *Comprehensive Supramolecular Chemistry (Cyclodextrins)*; Szejtli, J.. Osa, T., Eds.: Pergamon: Oxford, 1996: Vol. 3.
3. Rekharsky, M.V.: Inoue, Y. Complexation thermodynamics of cyclodextrins. Chem. Rev. 1998. *98*, 1875–1917.
4. Rekharsky. M.V.; Inoue, Y. Chiral recognition thermodynamics of β-cyclodextrin: The thermodynamic origin of enantioselectivity and the enthalpy–entropy compensation effect. J. Am. Chem. Soc. 2000, *122*. 4418–4435.
5. Rekharsky, M.V.; Inoue. Y. Complexation and chiral recognition thermodynamics of 6-amino-6-deoxy-0-cyclodextrin with anionic, cationic, and neutral chiral guests: Counterbalance between van der Waals and coulombic interactions. J. Am. Chem. Soc. 2002. *124*. 813–826.
6. Chapman, K.T.; Still, W.C. A remarkable effect of solvent size on the stability of a molecular complex. J. Am. Chem. Soc. 1989. *111*, 3075.
7. Smithrud, D.B.: Diederich. F. Strength of molecular complexation of apolar solutes in water and in organic solvents is predictable by linear free energy relationships: A general model for solvation effects on apolar binding. J. Am. Chem. Soc. 1990. *112*. 339–343.
8. Reichardt. C. *Solvents and* Solvent *Effects* in Organic *Chemistry*, 2nd Ed.: VCH: Weinheim. 1998.
9. Breault. G.A.: Hunter. C.A.: Mayers, P.C. Influence of solvent on aromatic interactions in metal tris-bipyridine complexes. J. Am. Chem. Soc. 1998. *120*. 3402–3410.
10. Diederich, *F.;* Hester. M.R.: Uyeki. M.A. 2,2′,7,7′-Tetrahydroxy-1-1'-binaphthyl based novel chiral mono- and ditopic cyclophanyl host compounds with nonpolar bonding positions. Angew. Chem. 1988, *100*, 1775–1777.
11. Mizutani. T.; Wada. K.; Kitagawa. S. Molecular recognition of amines and amino esters by zinc porphyrin receptors: Binding mechanisms and solvent effects. J. Org. Chem. 2000. *65*. 6097–6106.
12. Balzani. V.: Credi. A.: Raymo. F.M.; Stoddart, J.F. Artificial molecular machines. Angew. Chem.. Int. Ed. 2000. *39*, 3348–3391.
13. Izatt, R.M.; Pawlak. K.: Bradshaw, J.S.: Bruening, R.L. Thermodynamic and kinetic data for macrocycle interaction with cations. anions. and neutral molecules. Chem. Rev. 1995. 95. 2529–2586. and references cited therein.
14. Marcus. Y. *Ion Solvation*; John Wiley: Chichester, 1985.
15. Orstan. A.; Ross. J.B.A. Investigation of the β-cyclodextrin-indole inclusion complex by absorption and fluorescence spectroscopies. J. Phys. Chem. 1987. *91*. 2739–2745.
16. Harrison, J.C.: Eftink. M.R. Cyclodextrin-adamantanecarboxylate inclusion complexes: A model system for the hydrophobic effect. Biopolymers 1982. 21. 1153–1166.
17. Sinanoglu. O. *Molecular Associations* in Biology; Pullman. B., Ed.: Academic: New York. 1968; 427.
18. Rekharsky. M.V.; Inoue. Y. Solvent and guest isotope effects on complexation thermodynamics of α-, β-, and 6-amino-6-deoxy-β-cyclodextrins. J. Am. Chem. Soc. 2002. *124*. 12361–12371.
19. Inoue, Y.; Wada, T. Molecular Recognition in Chemistry and Biology as Viewed from Enthalpy–Entropy Compensation Effect. In *Advances in Supramolecular Chemistry*; Gokel. G.W.. Ed.: JAI Press: Greenwich, CT, 1997: Vol. 4. 55–96.
20. Grunwald. E.: Steel. C. Solvent reorganization and thermodynamic enthalpy–entropy compensation. J. Am. Chem. Soc. 1995. 117. 5687–5692.
21. Grunwald. E. *Thermodynamics* of *Molecular* Species: Wiley-Interscience: Sen· York, 1996.

Solvatochromism

Marcos Caroli Rezende
Universidad de Santiago de Chile, Santiago, Chile

INTRODUCTION

The term "solvatochrornism" describes a significant change in position or intensity of an absorption or emission band of a compound in solution, when the polarity of the medium is changed. A bathochromic (or red) shift of the absorption band with increasing solvent polarity is known as positive solvatochromism The corresponding hypsochromic (or blue) shift is termed negative solvatochromism.

Solvatochromic compounds exhibit large differences between the dipole moments of their ground and excited states. This behavior is commonly found in two families of compounds. Organic molecules where an electron-donating group is linked by a conjugated system to an electron-accepting fragment constitute the first group. Organometallic complexes composed of central metal and organic ligands with a π-electron system comprise the second important family.

Significant solvent-dependent spectral variations may also arise from self-aggregation of dyes in solution. The monomer rnay be solvatochromic. and it may not be easy to distinguish the contribution of self-aggregation to the observed solvatochrornism, especially in media where the dye is poorly soluble.

Because of their sensitivities to environmental changes. wide applications for solvatochromic compounds were found in the study of solute–solvent interactions, mainly in the characterization of bulk or microenvironments. Various polarity scales employing solvatochromic dyes as solvent probes were proposed. Because these empirical scales may be used to characterize any solvent or solvent mixture, solvatochromism played an important role in the study of a wide variety of solvent-dependent processes.

GENERAL PRINCIPLES

Spectra of a solvatochromic compound show significant shifts of absorption or emission bands in solvents of different polarities. Solvatochromism is thus a measure of the sensitivity of a compound to environmental changes, expressed by changes of its spectra in solution.[1,2] It is related with other environment-dependent spectral changes, such as thermochromisin and halochromism. In the former, spectral changes occur as a result of variations of the solvent temperature.[3,4] In the latter. spectral changes are observed by the addition of a salt to the solution. Depending on the nature of the ionic species capable of inducing absorption shifts, one may further distinguish a cationic and an anionic halochromism.[5,6]

These spectral changes may be ascribed to variations of solute–solvent interactions, when a given factor (solvent, temperature, or added salt) is changed. Because these are related processes. it is not uncommon for a solvatochromic compound to also show a thermochromic or halochromic behavior.

Solvent-dependent spectral changes are common in chemistry. However, only compounds that exhibit pronounced spectral changes are properly considered solvatochromic. A general requirement for this to occur is that large differences between the dipole moments of their ground and excited states must exist. The resulting solvatochromism may be explained in terms of the simplified scheme shown in Fig. 1.

According to the Franck–Condon principle. electronic excitation is much faster ($\sim 10^{-15}$ s) than solvent reorganization around the molecule ($\sim 10^{-12}$–10^{-10} s).

Therefore, the excited species has the same solvation pattern of its ground state. When large differences exist between the dipole moments of ground and excited states, the relative stabilities of the two solvated species change considerably with the solvent. Two possibilities exist: in case (a), the excited state of the solvatochromic compound is more polar than its ground state. Transfer to a more polar solvent has the result of stabilizing its excited state relative to its ground state. The new transition energy $\Delta E'$ is smaller than ΔE, and the cot-responding absorption band is shifted bathochromically (red-shifted) by a more polar solvent (positive solvatochromism).

Case (b) depicts the opposite situation, with a ground state more polar than the excited state of the molecule. In this case. increasing the polarity of the solvent has the effect of increasing the transition energy $\Delta E'$, and the corresponding absorption band is shifted hipsochromically (blue-shifted) in more polar media (negative solvatochromism).

This simplified scheme may be illustrated with two specific examples.[1,2,7]

Encyclopedia of Supramolecular Chemistry
DOI: 10.1081/E-ESMC 120019192

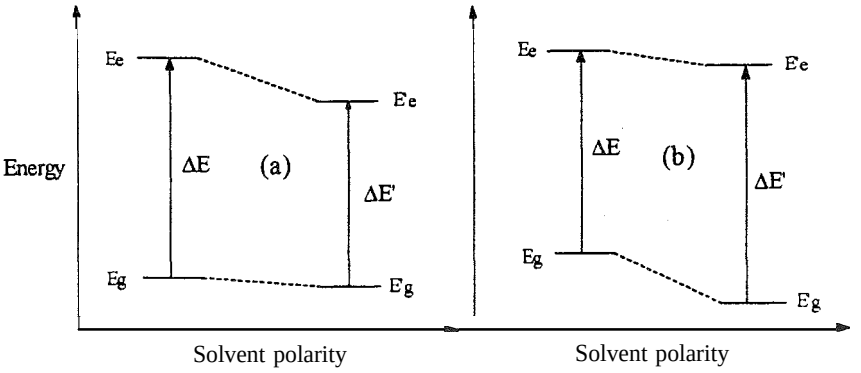

Fig. 1 The origins of positive (a) and negative (b) solvatochromism

Stilbene **1**, a hybrid of canonical structures (I) and (II), exhibits positive solvatochromism (Fig. 2). Its ground state resembles a neutral structure (I), with a calculated dipole moment of 9.85 D. Its more polar excited state, with the total electron density heavily concentrated on the acceptor fragment, has a calculated dipole moment of 23.5 D.

Compound 2 ($R_1 = R_2 = H$) shows an opposite behavior. Its zwitterionic ground state has a calculated dipole moment of 22.6 D, which is reduced in its quinoid, excited state to a value of 13.7 D. An increase in solvent polarity destabilizes the charge-transfer transition of this compound. shifting the λ_{max} value of its longest wavelength band hypsochromically, from 620 nm in nonpolar $CHCl_3$ to 442 nm in water (negative solvatochromism) (Fig. 3).

Similar considerations apply to the interpretation of solvatochromism in emission spectra. Here, however, the excited species may live long enough to allow for solvent rearrangement in its solvation shell. If. for example, the resulting solvated excited state has a larger dipole moment than it has in its ground state, it will be further stabilized, relative to its ground state, in a more polar environment. The emitted photon will have less energy with increasing solvent polarity, and a red shift of the fluorescence band will be observed.

Many emitting molecules may have two solvent-dependent excited states, arising from an intramolecular charge-transfer (ICT) and a twisted intramolecular charge-transfer (TICT) process. For these molecules, the existence of these two interconvertible excited states may give rise to two solvatochromic fluorescence bands.

Significant solvent-dependent spectral variations may also arise from self-aggregation of dyes in solution. Monomer association gives rise to different dipolar species. according to their aggregation patterns in solution. Cyanines constitute a particularly well-studied example of such behavior.[8] The observed spectral shifts are ascribed to different aggregation patterns of the dye. *J*-aggregates generate red-shifted bands, while H-aggregates give rise to blue-shifted bands. A J-dimes results from an end-to-end stacking. in a head-to-tail arrangement. An *H*-dimer forms a sandwich-type arrangement. with a parallel plane-to-plane stacking. Several dyes form *J*- and H-aggregates in solution.

The solvatochromism of fullerene solutions was studied by several authors and constitutes an example of a difficult distinction between contributions from solute–solvent interactions of monomeric species and contributions arising from aggregation. The C-60 solutions are

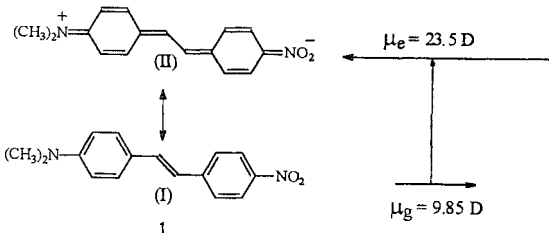

1

Fig. 2 Transition to a more polar excited state—positive solvatochromism.

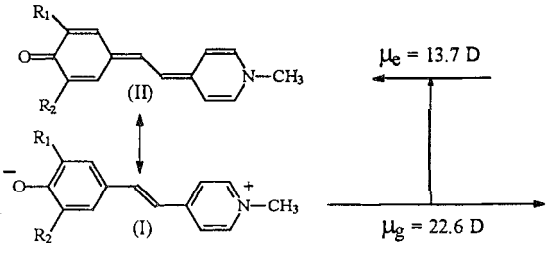

2

Fig. 3 Transition to a less polar excited state—negative solvatochromism.

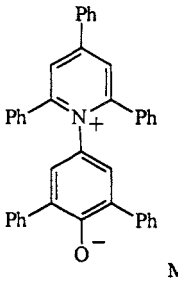

3

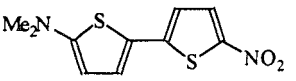

4

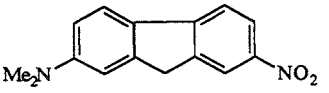

5

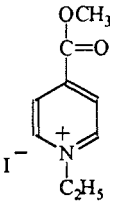

6

magenta in toluene, pink in fluorobenzene, and bluish-violet in anisol. In spite of changing color with concentration, solutions of C-60 in dimethoxybenzene follow the Lambert–Beer law, pointing to the absence of aggregates in solution.[9] Because transitions to the lowest excited states are forbidden by the highly symmetrical structure of the C-60 molecule, its spectral behavior must be ascribed to symmetry-breaking environmental interactions. The observed solvatochromism is then ascribed partly to complexation of the electrophilic C-60 molecule with π-electron-donating aromatic solvents and to the formation of aggregates.[10,11]

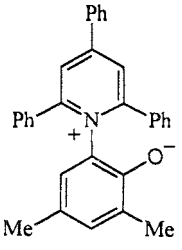

7

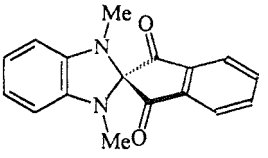

8

The requirements for a solvatochromic behavior are generally fulfilled by molecules exhibiting ICT excitations. Two families of compounds commonly behave in this way. The first comprises organic molecules with a donor and an acceptor fragment linked directly or through a conjugated π-system. Besides compounds **1** and 2, dyes **3–5** illustrate this general structural feature.[1,2] The ICT may also originate from the interaction of a donor–acceptor ion pair. Compound **6** is a classical example of this behavior.

Although coplanarity of the donor and acceptor fragments might be expected to be necessary for full conjugation and ICT. there are examples of solvatochromic compounds where these fragments are practically orthogonal. X-ray diffraction analysis of the strongly solvatochromic betaine **7** yielded a dihedral angle of 90° between the donor phenoxide and the acceptor pyridinium moieties of the molecule.[12] The CT band of the spiro dye 8, where donor and acceptor groups are mutually perpendicular, showed pronounced solvatochromism.[13]

A second important family of solvatochromic compounds comprises organometal complexes with ligands possessing a π-electron system.[1,2] The spectra of these cornpounds may exhibit more than one solvatochromic band. Two distinct processes may give rise to solvatochromism: a metal-to-ligand charge transfer (MLCT), where charge is transferred on excitation from the metal donor to an acceptor ligand, and a ligand-to-metal charge transfer (LMCT), where the opposite situation occurs. Compound **9** is an example of the former, and compound **10** is an example of the latter. The solvato- and halochromism of **11** arises from a transition from a square-planar to an

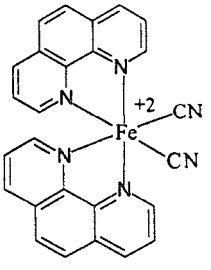

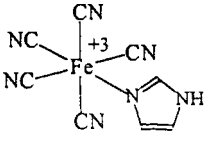

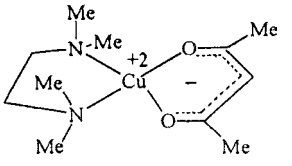

10

octahedral geometry. by interaction with an axial donor solvent or anion.[14]

THEORETICAL TREATMENTS

When developing theoretical models with which to interpret and predict the solvatochromic behavior of molecules. a distinction must be made between specific and nonspecific effects. The former are caused by specific interactions, such as complexation or hydrogen bonding with the solvent. The latter is a sum of different solute–solvent dielectric interactions.[15]

When only nonspecific effects are responsible for the solvatochromic behavior, the change of the molecule dipole moment upon excitation may be estimated from a continuum model.

For fluorescent molecules in nonpolar solvents of the same refractive index, solvatochromic shifts are governed by the change of the molecule dipole moment $\Delta\mu_{ge}$ and by a solvent polarity function $f(D)$, which depends on the static dielectric constant D of the medium.

$$f(D) = 2(D-1)/(2D+1) \tag{1}$$

For solvatochromic shifts between solvents 1 and 2, Eq. 2 applies, where $\Delta(E_{\text{flu}-\text{abs}})_{1-2}$ is the energy difference between the fluorescence and the first absorption bands, a_o is the radius of the solute molecule, and $\Delta f(D)_{1-2}$ is the difference between the polarity functions of the two solvents. This relationship. originally derived by Lippert,[16] allows for the calculation of $\Delta\mu_{ge}$:

$$\Delta(E_{\text{flu}-\text{abs}})_{1-2} = -(\Delta\mu_{ge})^2 a_o^{-3} \Delta f(D)_{1-2} \tag{2}$$

According to the McRae formalism,[17] the solvatochromic shifts in absorption frequencies of a molecule may be expressed as follows:

$$\nu_{\text{solv}} - \nu_{\text{vac}} = A[(n^2-1)/(2n^2+1)] + B[(\varepsilon-1)/(\varepsilon+2) - (n^2-1)/(n^2+2)] \tag{3}$$

where ν_{solv} and ν_{vac} are the frequencies of transition (s^{-1}) in a solvent and in the vacuum, respectively; n is the refractive index: ε is the dielectric constant of the solvent; and A and B are constants. The slope B may be obtained from a plot of transition frequencies in a series of solvents, and the excited-state dipole moment μ_e is estimated with the aid of the following relationship:[7]

$$B = 2[\mu_g(\mu_g - \mu_e \cos\phi)]/4\pi\varepsilon_o h a_o^3 \tag{4}$$

where ε_o is the permeability of the vacuum. h is Planck's constant. a, is the radiur of a spherical cavity occupied by the solute. μ_g is the ground-state dipole moment of the molecule, and ϕ is the angle formed by vectors μ_g and μ_e. The value of ϕ is often assumed equal to 180°.

Quantum chemical methods were employed with variable success in theoretical studies of solvatochromism.[18,19] Electronic transition energies of molecules in the gas phase may be calculated by ab-initio and semiempirical methods. The latter are more frequently used because of their much smaller computational cost and also because of the existence of programs. like CNDO/S and INDO/S, that were parametrized for spectral studies. Calculation of solvent effects poses a major problem in the prediction of solvatochromic shifts. Several methods exist that are based on a continuum model, where changes in the electronic levels of the molecule are treated as perturbations by the solvent dielectric constant. This model was extended to include the effect of an added salt.[20] Alternatively, the bulk solvent may be replaced by point charges.[21,22]

None of these treatments is capable of reproducing specific solute–solvent interactions, which become increasingly important in more polar, or in protic solvents. In this case. one has to resort to calculations involving supramolecules. formed by solute–solvent complexes.[23]

SOLVATOCHROMISM AND SOLVENT POLARITY

The use of solvatochromic compounds as polarity sensors in a variety of environments constitutes one of the most important applications of these molecules. Solvent polarity scales were designed that rely on the solvatochromic behavior of one or a set of compounds.[1,2]

In order to be a useful polarity indicator. a solvatochromic dye should meet a number of requirements. It should be easily available, stable on storage and in solution, soluble in extremely polar and nonpolar solvents. with a range of solvatochromic shifts as large as possible. High absorptivities should allow for the use of dilute solutions, so as to discard the possibility of aggregation. This last requirement is considered fulfilled if all solutions follow the Lambert–Beer law.

One of the first examples of a polarity scale based on a solvatochromic probe was Kosower's Z values.[24] defined as the transition energy of the longest wavelength absorption band of dye 6.

Transition energies of betaine 3 were used as the bases of the widely employed E_T (30) scale.[1,2] Its negatively solvatochromic charge-transfer absorption band is shifted by ca. 360 nm on going from diphenyl ether ($\lambda_{\max} = 810$ nm) to water ($\lambda_{\max} = 453$ nm). This high sensitivity prompted its use as a polarity indicator for over 350 pure solvents. besides a variety of solvent mixtures; micellar systems; and electrolyte solutions.

The large number of empirical polarity scales derived from solvatochromic sensors raises the question of the degree of correlation among them. In principle. there is no reason to expect a correlation between any pair of these einpirical scales. The solvatochromic behavior of a given compound reflects a sum of specific and nonspecific solute–solvent interactions that vary from probe to probe. Good correlations are to be expected only between scales based on solvatochromic compounds that present a similar response to a range of solvents. As a result of this, the concept of solvent polarity is elusive and the claims of a universal polarity scale based on solvatochromic probes cannot be maintained. Different solvents may assume different polarity values, according to the nature of the scale employed to define them.

One approach aimed at overcoming this relativity is the definition of polarity as a weighted sum of contributions from more specific effects. This approach, originally introduced by Kamlet, Abboud, and Taft,[25] distinguishes a hydrogen-bond donor, or acidity contribution (α values): a hydrogen-bond acceptor. or basicity contribution (β values); and a dipolarity-polarizability contribution (π^* values) of the solvent. Various probes were proposed for the measurement of these values. according to their nature as sensors for a given contribution. In order to isolate a particular effect. sets or pairs of homomorphic compounds are sometimes employed. Homomorphs are molecules that have the same, or closely similar geometries. and similar spectral responses. The spectral differences between a pair of hoinomorphs are due to the fact that one is capable of interactions with the solvent that should be absent. or nearly absent with the other. A cornparison of their spectra allows a distinction to be made between solute–solvent interactions that are shared by both probes, from those interactions characteristic of only one compound. An exainple of such a pair, employed to build a scale for acidity values, is the *o-tert*-butylstilbazolium betaine DBSB (2. $R_1 = R_2$ = t-butyl) and its homomorph TBSB (2. R_1 = t-butyl, R_2 = H), which were used in the classification of 121 organic solvents.[26] A comparison of the spectra of TBSB, a basic probe capable of interactions with hydrogen-bond-donor solvents. with DBSB, a homomorph where these interactions are absent because of the steric hindrance of the two t-butyl groups, allows for the quantification of the specific contribution of solvent acidity to the observed solvatochromism of the two probes.

The iron complex **9** is another example of a probe for solvent acidity. whereas the planar copper complex **11** was proposed as a basicity or β sensor.[27]

Compound 4, which displays large positive solvatochromic shifts and good solubility in a wide range of solvents. was proposed as a π^* probe.[28] Another example involves the homomorphic pair 2-(dimethylamino)-7-nitrofluorene (**5**)/2-fluoro-7-nitrofluorene that were suggested to be the basis of a solvent dipolarity-polarizability (SPP) scale.[29]

The use of solvatochromic compounds as polarity indicators may be extended to solvent mixtures and micellar systems. In this case, an additional difficulty is introduced in the assessment of systems that are not homogeneous from a microscopic point of view. The microenvironment actaally "seen" by the sensor does not correspond to the bulk characteristics of the medium. In a binary solvent mixture, a solvatochromic probe may be more solvated by one of the components, thus reflecting through its spectrum a solvent composition that may be different from that of the bulk mixture. In micellar systems. the solvatochromic response of a probe reflects the nature of its microenvironment and is dependent on the relative solubility of the sensor in the aqueous or the organic pseudophases, or in the micellar interphase.

APPLICATIONS **AND** FUTURE PROSPECTS

The use of solvatochromic compounds for characterizing common laboratory solvents was extended to other media. such as liquid organic salts[30] and supercritical solvent systems.[31] Solvatochromic probes were widely employed in the characterization of microenvironments. such as the interphase of micellar systems.[1,2]

By adsorbing or chemically binding a solvatochromic compound to a solid matrix. its surface polarity may be estimated, thus extending the applications of these compounds to the solid phase. A few examples include the evaluation of the surface polarity of various silicas[13] and polysaccharides.[33]

In the design of new materials for optical devices. crystal soivatochromism plays an important role in understanding intermolecular interactions in the solid phase.[34]

The field of nonlinear optical (NLO) materials constitutes another area of research related to the synthesis of solvatochromic compounds. Asymmetric molecules possessing donor and acceptor substituents linked by a π-backbone exhibit large hyperpolarizabilities, being potential candidates far NLO materials with interesting properties.[7] It is, therefore, not surprising that many solvatochromic dyes also exhibit NLO properties. Solvatochromism is an important property in the design of NLO-functionalized macromolecules.[7,11]

The development of chiro-solvatochromic compounds should lead to interesting applications. These probes should be capable of distinguishing pairs of enantiomers, as a result of stereoselective interactions. giving rise lo significant spectra! differences between solutions of the diastereomeric complexes. One may envisage simple and fast methods for the determination of the enantiomeric

purity of chiral compounds. based on the visual inspection of chiro-solvatochromic dyes. Such compounds might also present interesting chiroptical properties. So far, attempts to prepare such probes yielded solvatochromic compounds with little sensitivity to the chiral environment.[1,2,36,37]

CONCLUSION

The phenomenon of solvatochromism has caused a wide range of applications to be directed in chemistry, in the study of solute–solvent interactions. The design of new molecules with increased solubility and sensitivity to environmental changes will probably remain a subject of interest in the future, especially as probes in less-developed areas, such as, for example, the solvatochromic discrimination of a chiral environment. Theoretical approaches to the problem of describing the influence of the medium on the spectral behavior of these compounds will benefit from the availability of faster programs and computers. Finally, research on the solvatochromism of organic and organometallic compounds will remain an area of active interest, because of its connections with the development of new nonlinear optical materials.

ARTICLES OF FURTHER INTEREST

Chiral Guest Recognition, p. 236
Dye Inclusion Crystals, p. 497
Energy and Electron Transfer in Supramolecular Systems, p. 535
Fluorescent Sensors, p. 572
Hydrogen Bonding, p. 658
Ionophores, p. 760
Luminescent Probes, p. *821*
Nonlinear Optical Materials, p. 973
Solvation Effects in Guest Binding, p. 1322
Supramolecular Photochemistry, p. 1434

REFERENCES

1. Reichardt. C. Solvatochromic dyes as solvent polarity indicators. Chem. Rev. 1994. 94, 2319–2358.
2. Reichardt, C. Solvatochromic Compounds. In *Solvents and Solvent Effects in Organic Chemistry*, 3rd Ed.: VCH-Wiley: Weinheim. 2002.
3. Zhao. X.H.: Burt. J.A.: Knorr, F.J.; McHale. J.L. Thermosolvatochromism of betaine-30 in CH_3CN. J. Phys. Chern.. A 2001, *105*. 11110–11117.
4. El-Ayaan, U.; Murata, F.: Fukuda. Y. Thermochromism and solvatochromism in solution. Monatsh. Chem./Chem. Mon. 2001. *132*. 1279–1294.
5. Reichardt, C.: Asharin-Fard. S.; Schafer, G. The halochromism of pyridinium *N*-phenoxide betaine dyes in acetonitrile solution. Chem. Ber. 1993, *126*, 143–147.
6. Lavallee, R.J.; Zimmt, M.B. Interaction between electrolyte and charge-transfer status: Evidence for complex formation. J. Phys. Chem. 1994. 98, 4254–4260.
7. Kanis. D.R.; Ratner, M.A.: Marks, T.J. Design and construction of molecular assemblies with large second-order optical nonlinearities. Quantum chemical aspects. Chem. Rev. 1994. *94*, 195–242.
8. Mishra. A.; Behera. R.K.: Behera, P.K.; Mishra. B.K.; Behera. G.B. Cyanines during the 1990s: A review. Chem. Rev. 2000, *100*, 1973–2011.
9. Catalán. J.; Saiz, J.L.: Lainez, J.L.; Jagerovic, N.; Elguero, J. The colors of C60 solutions. Angew. Chem.. Int. Ed. Engl. 1995. 34, 105–107.
10. Rudalevige, T.; Francis, A.H.; Zand, R. Spectroscopic studies of fullerene aggregates. J. Phys. Chem.. A 1998. *102*. 9797–9802.
11. Nath, S.; Pal. H.; Palit, D.K.; Sapre. A.V.; Mittal. J.P. Aggregation of fullerene, C-60, in benzonitrile. J. Phys. Chem.. B 1998, *102*. 10158–10164.
12. Paley, M.S.; Meehan, E.J.: Smith. C.D.; Rosenberger. F.E.: Howard, S.C.: Harris, J.M. Synthesis and characterization of a novel betaine dye: 2,4-Dimethyl-6-(2,4,6-triphenyl-*N*-pyridinio)phenolate. J. Org. Chern. 1989, *54*. 3432–3436.
13. Maslak, P.; Chopra. A.: Moylan. C.R.: Wortmann, R.: Lebus. S.; Rheingold. A.L.; Yap, G.P.A. Optical properties of spiroconjugated charge-transfer dyes. J. Am. Chem. Soc. 1996. *118*, 1471–1481.
14. Zanotto. S.: Scremin, M.C.; Machado. C.: Rezende. M.C. Cationic and anionic halochromism. J. Phys. Org. Chern. 1993, *6*. 637–641.
15. Suppan, P. Solvatochromic shifts: The influence of the medium on the energy of electronic states. J. Photochem. Photobiol.. A Chem. 1990. *50*. 293–330.
16. Lippert, E. Spectroscopic determination of the dipole moment of aromatic compounds in the first excited singlet state. Z. Elektrochem. 1957, *61*. 962–975.
17. McRae. E.G. Theory of solvent effects on molecular electronic spectra. Frequency shifts. J. Phys. Chem. 1957. *61*. 562–572.
18. Ishida. *T.;* Rossky. P.J. Solvent effects on solute electronic structure and properties: Theoretical study of a betaine dye molecule in polar solvents. J. Phys. Chem.. A 2001. *105*, 558–565.
19. Morley. J.O.; Padfield. J. Experimental and computational studies on the solvatochromism and thermochromism of 4-pyridiniophenolates. J. Chem. Soc., Perkin Trans. 2 2002. 1698–1707.
20. Mulder, W.H.: Parkanyi. C. Theory of the salt effect on solvatochromic shifts and its potential application to the determination of ground-state and excited-state dipole moments. J. Phys. Chem., A 2002. *106*. 11932–11937.
21. Da Silva, L.; Machado, C.; Rezende, M.C. On the solvatochromic reversal of merocyanine dyes. Part 1. The

UV–Vis spectroscopic behaviour of vinylogous γ-pyridones. J. Chem. Soc., Perkin Trans. 2 1995. 483–488.

22. Baraldi, I.: Momicchioli, F.; Ponterini. G.; Vanossi. D. Solvent effects within the CS INDO method. Geometrical distortion and solvatochromism of merocyanine dyes. Chern. Phys. 1998, *238*, 353–364.
23. Alencastro, R.B.: Motta Neto. J.D.; Zerner. M.C. Solvent effects on the electronic spectrum of Reichardt's dye. Int. J. Quantum Chem.. Quantum Chem. Symp. 1994. *28*. 361–377.
24. Kosower, E.M. The effect of solvent on spectra. I–A new empirical measure of solvent polarity: Z-values. J. Am. Chern. Soc. 1958. *80*. 3253–3260.
25. Kamlet. M.J.: Abboud. J.-L.M.: Abraham, M.H.; Taft, R.W. Linear solvation energy relationships. 23. A comprehensive collection of the solvatochrornic parameters π*, α, and β and some methods for simplifying the generalized solvatochromic equation. J. Org. Chem. 1983. *48*, 2877–2887.
26. Catalán, J.; Diaz. C. A generalized solvent acidity scale: The solvatochrornism of *o-tert*-butylstilbazolium betaine dye and its homomorph *o,o′*-di-*tert*-butylstilbazolium betaine dye. Liebigs Ann./Recueil 1997. 1941–1949.
27. Migron, Y.: Marcus, Y. Two reintroduced solvatochromic indicators for hydrogen-bond-donation and acceptance. J. Phys. Org. Chem. 1991. *4*. 310–314.
28. Effenberger. *F.;* Wiirthner, F. 5-Dimethylamino-5'-nitro-2,2′-bithiophene—A new dye with pronounced positive solvatochromism. Angew. Chem.. Int. Ed. Engl. 1993. *32*. 719–721.
29. Catalan, J.: López, V.; Perez. P.: Martin-Villamil, M.: Rodriguez, J.-G. Progress towards a generalized solvent polarity scale: The solvatochromism of 2-(dimethylamino)-7-nitrofluorene and its homomorph 2-fluoro-7-nitrofluorene. Liebigs Ann. 1995. 241–252.
30. Bart. E.; Meltsin. A.; Huppert. D. Solvation dynamics of Coumarin 153 in molten salts. J. Phys. Chem. 1994. *98*, 3295–3299.
31. Eberhardt. R.; Lobbecke, S.; Neidhart. B.: Reichardt. C. Determination of $E_T(30)$ values of supercritical carbon dioxide at various pressures and temperatures. Liebigs Ann./Recueil 1997, 1195–1199.
32. Zimmermann, Y.: El-Sayed, M.; Prause. S.: Spange. S. The solvent-like nature of silica particles in organic solvents. Monatsh. Chem. 2001, *132*. 1347–1361.
33. Fischer. K.; Spange, S. Empirical surface polarity parameters for native polysaccharides. Macroinol. Chem. Phys. 2000. *201*. 1922–1929.
34. El-Sayed. M.: Müller. H.: Rheinwald, G.: Lang, H.; Spange, S. Solvatochromism, crystallochromism, and solid state structures of hydrophilically functionalized aromatic amino ketones containing furan and thiophene rings. Chem. Mater. 2003, *15*, 746–754.
35. Dobrev, I.D.: Karamancheva. I.R. Solvatochromic determination of second-order polarizabilities of chromophore-functionalized dextran and amylose derivatives. Supramol. Chem. 2002, *14*. 491–495.
36. Reichardt. C. Solvatochromism, thermochromism, piezochromism, halochromism and chiro-solvatochrornism of pyridinium *N*-phenoxide betaine dyes. Chem. Soc. Rev. 1992. *21*. 147–153.
37. Reichardt. C.: Blum, A.; Harms, K.: Schafer, G. Synthesis and UV–Vis spectroscopic properties of solvatochromic, halochromic. and chiro-solvatocliromic pyridinium *N*-phenolate betaine dyes with four stereogenic centers. Liebigs Ann./Recueil 1997, 707–720.

Space Groups and Crystal Packing Modes

Chick C. Wilson
University of Glasgow, Glasgow, United Kingdom;
Central Laboratory of the Research Councils (CLRC) Rutherford Appleton Laboratory, Oxon, United Kingdom

INTRODUCTION

The internal symmetry of a crystal structure is described. The concepts of the unit cell and lattice are developed, leading naturally to a definition of symmetry elements and, hence. to the crystallographic space groups. The relevance of space groups and symmetry elements to the formation of the extended networks found in supramolecular chemistry is summarized. A discussion of common crystal packing modes follows, and the relevance of space group symmetry is discussed in this context.

THE CRYSTAL AND ITS INTERNAL SYMMETRY

The regularity of a macroscopic crystal gives a clear indication of the underlying construction. which describes the crystal structure as a convolution between the lattice. a conceptual array of points in space. and the motif (or basis). the structural unit repeated regularly at the lattice points. That is, the motif is placed at each lattice point in turn, the resulting function (the crystal structure) being the cumulative result of this folding together of the two components.

The geometry of the lattice is governed by crystallographic unit cell, a parallelepiped uniquely defined by six parameters: the lengths of the cell edges (a, b, c) and the angles between these (α, β, γ) (Fig. 1). The parallelepiped chosen is generally the smallest (or occasionally some more convenient) volume containing the unique structural component in the crystal. Repetition of this unit by translation through space forms the crystal. The unit cell contains the structural motif. The origin of each unit cell sits at one of the conceptual lattice points.

The Lattice

Replicating the unit cell through space along the directions of the three axes of the paralellepiped forms the complete crystal. containing all structural components. This is shown in Fig. 2, where one unit cell is shown to sit at each of the conceptual arrays of lattice points.

With the unit cell and lattice constructed, the remainder of the geometry of crystallography follows. For example, we can define sets of lattice planes according to the intercept of a plane within the unit cell with the three axes of the parallelepiped (Fig. 3). The lattice planes are defined by the Miller indices (hkl), where *hkl* are defined in terms of their intercept with the a, b, and c axes, respectively. The plane intercepts the *a*-axis at the position alh. the 0-axis at the position blk, and the c-axis at the position *c/l*. There are equivalent parallel lattice planes passing through all translationally related points in the lattice, and the set of lattice planes of this type is denoted (hkl). The related lattice direction [*hkl*] is the direction parallel to the line through the origin and the point (*ha*, kb, *lc*). For a cubic crystal, the [hkl] direction is perpendicular to the (hkl) planes. A considerably fuller description of geometrical crystallography is available in many other places.[1–7] It is worth mentioning at this point that the unit cell is bounded by the planes (100). (010), and (001), obvious from a brief study of Fig. 3.

The lattice is defined not only by the unit cell, principally by its external dimensions (defining the crystal system), but also by aspects of its internal constitution (defining the lattice type) and symmetry within the unit cell. There are seven crystal systems: triclinic. monoclinic. orthorhombic. tetragonal, cubic. trigonal, and hexagonal. These are defined on the basis of the external geometry of the unit cell. The constraints defining the crystal system can easily be summarized:

Crystal system	*Constraints on cell dimensions*
Triclinic	$a \neq b \neq c$; $\alpha \neq \beta \neq \gamma \neq 90°$
Monoclinic	$a \neq b \neq c$; $\alpha = \gamma = 90°$, $\beta > 90°$
Orthorhombic	$a \neq b \neq c$; $\alpha = \beta = \gamma = 90°$
Tetragonal	$a = b \neq c$; $\alpha = \beta = \gamma = 90°$
Cubic	$a = b = c$; $\alpha = \beta = \gamma = 90°$
Trigonal	$a = b \neq c$; $\alpha = \beta = 90°$, $\gamma = 120°$ or $a = b = c$; $\alpha = \beta = \gamma < 120°$
Hexagonal	$a = b \neq c$; $\alpha = \beta = 90°$, $\gamma = 120°$

The internal structure of the unit cell also plays a role in the definition of the lattice type. Unit cells containing a

Encyclopedia of Supramolecular Chemistry
DOI: 10.1081/E-ESMC 120012762

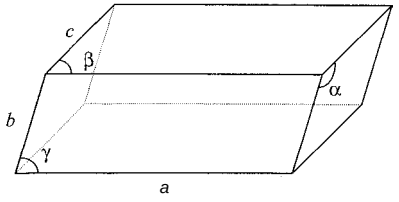

Fig. 1 The parallelepiped model used for a unit cell. The example shown is for a skew (triclinic) unit cell. with all lengths different and all interaxial angles non-90". The majority of unit cells found in nature are more regular than this example.

single lattice point are termed primitive. denoted **P.** Under certain circumstances: it is convenient to introduce unit cells that contain more than one lattice point. Such unit cells are called nonprimitive, and in general, the practical advantages to be gained from using nonprimitive unit cells can far outweigh the disadvantage of the larger unit cell volume.

Such nonprimitive or centered cells can occur in all crystal systems higher than triclinic and introduce an extra seven lattice types to those already defined by the crystal system. The conventional types of nonprimitive lattice are C-centered (C), with an extra lattice point in the center of the (001) face at unit cell position ($^1/_2,^1/_2$,0); body-centered **(I),** with an extra lattice point at the unit cell center at ($^1/_2,^1/_2,^1/_2$,); face-centered **(F),** with extra lattice points in the center of the unit cell faces at positions ($^1/_2{}^1/_2$0), ($^1/_2$0$^1/_2$), (0$^1/_2{}^1/_2$); and the rhombohedrai *R* setting of the trigonal lattice. There are also nonstandard settings of these, such as A-centered monoclinic cells, but these do not represent distinct lattice types.

There are thus 14 possible lattice types, termed the Bravais lattices:

Crystal system	*Lattice type*	*Number of lattice points*
Triclinic (one Bravais lattice)	P	1
Monoclinic (two Bravais lattices)	P	1
	C (or A)	2
Orthorhombic (four Bravais lattices)	P	I
	C (or A or B)	2
	I	2
	F	4
Tetragonal (two Bravais lattices)	P	1
	I	2
Cubic (three Bravais lattices)	P	1
	I	*2*
	F	4
Trigonal (one Bravais lattice)	R	3 or 1
Hexagonal (one Bravais lattice)	P	1

Symmetry Elements and Space Groups

Further symmetry occurs within the unit cell. This internal symmetry introduces relationships among the unit cell contents and can be due to rotation, reflection, and combinations of these with fractional translations. The internal symmetry of the unit cell allows the complete description of the entire contents on the basis of a unique structural unit, the asymmetric unit. Applying the internal unit cell symmetry to the asymmetric unit, followed by imposition of the lattice structure, leads to a complete description of the crystal.

The internal symmetry elements of the unit cell are of two types (Fig. 4): those involving purely reflections and rotations (symmorphic elements — mirror planes and rotation axes), and those additionally involving translational components (nonsymmorphic elements — glide planes and screw axes).

When the symmetry elements are introduced into the possible lattices, the symmorphic elements combine to yield a total of 32 so-called point groups, while inclusion of symmorphic and nonsymmorphic elements leads to the 230 crystallographic space groups. Space groups. symmetry elements, and other aspects of crystal symmetry are tabulated in great detail in the International Tables for Crystallography.[8]

CRYSTAL PACKING MODES

The periodicity conferred by the crystallographic symmetry described above also, of course, plays a major role in governing the intermolecular interactions that are so important in supramolecular chemistry. We now consider the implications for crystal packing modes. Crystal packing modes is a term used to describe the packing of molecular units inside a crystal structure. Specifically, the aim of their study is to find common patterns, with the aim of understanding, classifying. and potentially predicting the way in which these molecular units will pack to form crystal structures.

Crystal packing is governed by the interinolecular interactions between molecules, whether ionic, hydrogen bonds or other weaker nonbonded contacts. These intermolecular interactions are, in turn, governed by the relative disposition of molecules in the crystal, more often than not a consequence of the space group symmetry. An exception to this is when there are intermolecular interactions between distinct molecular units in the unit cell, usually in crystal structures with more than one formula unit in the unique part of the unit cell ($Z' > 1$).

There have been many attempts to categorize crystal packing modes and their implications for understanding and potentially predicting patterns of intermolecular

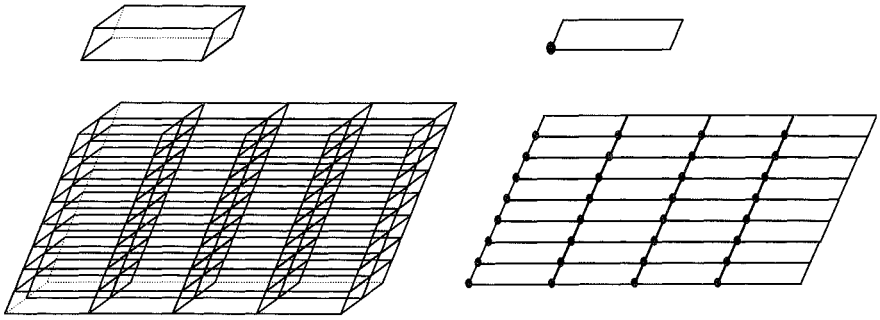

Fig. 2 The construction of a crystal from its unit cell (left) in three dimensions and (right) a two-dimensional projection, also showing the lattice points.

interactions, supramolecular assembly, and hence. crystal structures; from the earliest days of molecular crystallography.[1] The work of Kitaigorodskii[10,11] represented some of the earliest attempts at gaining insight into crystal packing via systematic studies of organic crystal structures. This included an enunciation of the principles of close packing and also set the initial framework for systematic analyses of crystal packing, using. for example, the Cambridge Structural Database,[12,13] which now contains over 250,000 organic crystal structures.

Several methods were adopted in attempting to describe and understand crystal packing and its implications for supramolecular chemistry. These include studies of commonly occurring intermolecular motifs, surveys of crystallographic databases. examinations of space group frequencies. analytical and predictive studies of simple molecular compounds and classes of molecules, and lattice dynamical and other computational/theoretical methods. The area was surveyed recently in the context of crystal packing[14] and its relation to supramolecular chemistry and crystal engineering discussed in many review articles. The latter subject is covered elsewhere in this volume, but is intimately related to the subject of this article. This is evident from the fact that the field of crystal engineering depends upon understanding the nature of intermolecular forces and their role in assembling molecular building blocks into extended structures and architectures.[15] A definition of crystal engineering by Desiraju brings home clearly this link between the topics. This definition of crystal engineering is "the understanding of intermolecular interactions in the context of crystal packing and in the utilisation of such understanding in the design of new solids with desirable physical and chemical properties."[16]

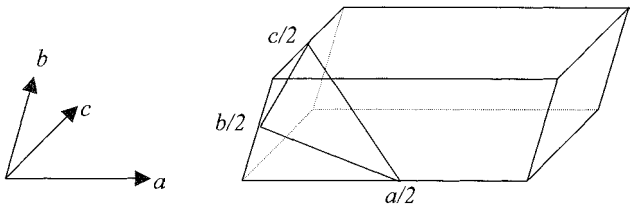

Fig. 3 A lattice plane and definition of its Miller indices. The plane shown intercepts halfway along each axis. It is described by the Miller indices according to $(a/2, b/2, c/2) = (a/h, b/k, c/l)$. This is. therefore, the (222) plane.

Commonly Occurring Intermolecular Motifs

Because the aim of supramolecular chemistry is to predict and control the arrangement of neighboring molecules or motifs by intermolecular forces, an understanding of how specific commonly occurring functional groups or motifs are likely to interact in the crystalline environment is important. Some of the earliest but still highly relevant studies in this area were carried out on carboxylic acids[17] and on primary[18] and substituted[19] ainides.

For carboxylic acid structures,[17] it is clear that for monocarboxylic acids, cyclic hydrogen-bonded pairs are the motif of choice (for achiral or racemic compounds: these are often generated by a syminetry center), while chains linked by O—H···O linear hydrogen bonds are also common. For chiral monocarboxylic acids, a chain motif is often formed along a twofold screw axis. Dicarboxylic acids tend to form chains in which the cyclic dimeric pair acts as the linking motif along the chains. In the other dimension. these carboxy-group-containing molecules tend to stack with neighboring units offset along either the C=O or C—OH bond direction. There also tend to be interplanar contacts via antiparallel arrangements of C—O bonds.

For amides R-$CONH_2$, the molecules generally form hydrogen-bonded rings linked by a pair of C=O···H—N hydrogen bonds that are then linked in several ways—by translation via NH···O bonds. by glide planes. or by a twofold screw axis. In cases where the dimer is not formed. helical motifs can be formed about a 2_1 screw

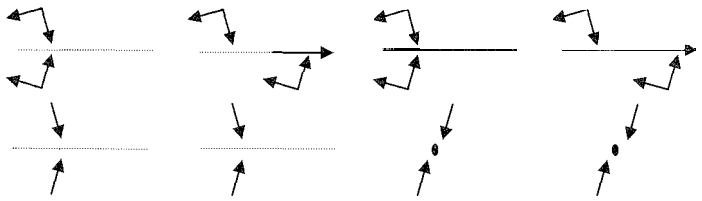

Fig. 4 The effect of four types of symmetry elements in elevation (upper) and projection (lower). From left to right are a mirror plane. a glide plane. a twofold rotation axis. and a twofold screw axis.

axis. and the molecules can also pack via a combined 2_1 axis and a translation axis (of length -5 Å) and by a hexameric, rhombohedra1 crown arrangement. For the diineric groups, parallel and antiparallel ribbon planes can be formed in the crystal packing. as can nonparallel ribbon planes. The detailed description of the formation of such motifs is given in the work by Leiserowitz and Hagler,[19] which also emphasizes the general principles of construction of crystal packing modes via various space group symmetry elements.

These two representative examples illustrate the type of general principle one seeks in trying to quantify crystal packing modes. They also illustrate the need for simple, general ways of classifying the ways in which molecules link together. Of several schemes advanced for such classification, perhaps the most widely applied currently is the graph set description of hydrogen-bonding motifs,[20] of particular relevance in supramolecular chemistry. as hydrogen bonds are frequently the sources of intermolecular interactions. In trying to look for similarities in patterns of crystal packing. it is also useful to have a means of classifying identical or similar organic molecules. This problem was tackled by Malman et al.[21] with their definition of isostructural systems (identical packing motifs of isometric. necessarily closely similar. molecules) and homeosrructural systems (similar packing motifs of nonisomeiric molecules). In a similar vein is the extensive body of work of Zorky et al.[22] This worli involved the concept of structural class as a descriptor of molecular packing arrangements in crystals. going beyond the normal definition of the space group in reflecting the topology of the molecular crystal.

Database Surveys and Space Group Frequencies

The Cambridge Structural Database (CSD)[12,13] contains deposited information from over 250,000 organic and organometallic crystal structures, and this can be extracted (mined) using powerful search tools, including fragment [one-dimensional(]-D), two-dimensional(2-D). and three-dimensional(3D)], unit cell and space group searches. These allow trends within motifs to be identified and followed, along with frequencies of occurrence of space groups. etc.,[22–24] and the implications of these for the formation of intermolecular interactions and supramolecular structures. Among the general conclusions of such surveys[1,2] are that space groups containing mirror planes occur if ail the mirror planes are occupied,[23,24] and that among rotation axes, only twofold axes are common in molecular systems.[23,25] The presence of inversion centers also tends to be favorable for crystal packing.

Among the 230 possible space groups. it is found that few are occupied with any great frequency among molecular crystal structures. For example, over 80% of structures in the CSD occur in the seven most common space groups: $P2_1/c$, $P1$, $P2_12_12_1$, $P2_1$, $C2/c$, Pbca. and Pnma.[26] However, space group frequencies depend on the type of compound in the crystal. as the intermolecular interactions will vary, governing the packing. For example, more ionic compounds, salts. and solvates are most likely to crystallize in high-symmetry space groups. Wilson found that normally. the relative frequency of occurrence of molecular compounds in particular space groups is governed by the ease of packing.[24] The presence of internal molecular symmetry and of symmorphism (lack of screw axes and glide planes) is an additional factor to take into consideration in such studies.

A further conclusion is that the occurrence of structures with $Z' > 1$ tends to be low. and the percentage of structures with this property tends to increase as the symmetry of the space group decreases, being most common in space group Pi. When there is more than one crysiallographically independent molecule in a unit cell. these molecules tend on the whole to have similar conformations.[27,28]

It is possible that as the number of structures in the CSD increases. general einpirical rules may become apparent that help predict particular packing patterns for certain types of molecules. Clearly, the principle of close packing (cosresponding to an energy minimum in the crystal) will always be important in governing the pacliing adopted. The principles of closest packing in molecular crystal structures are well illustrated by studies of the

distribution of molecular centers in crystallographic unit cells.[26] In these, there is a tendency for the preferred locations of these centers to cluster around positions between centers of symmetry or screw axes. Such studies also indicate the wide occurrence of layers of molecules and confirm the importance of close packing.

Studies of Simple Molecular Compounds

The study of crystal packing modes in simple molecular systems has long been seen as a tractable approach to quantifying the interactions underlying the adoption of packing patterns. Given their relatively simple shapes. fused ring planar aromatic hydrocarbons are an obvious case to choose, and these were studied on several occasions. The early work in this area[9,29,30] was extended in a series of studies by Gavezotti and Desiraju.[31,32] These studies examined the energetic and geometric factors controlling the packing of such condensed aromatics, using atom–atom and molecular–molecular packing energy calculations. It is found that the structures can be characterized in four structural types, called Herringbone, Sandwich-Herringbone, γ (a flattened Herringbone), and β (graphitic-like planes), which is determined by the relative orientation of molecular planes in the crystal. The major motifs present are built from stacks and glides of molecules.

The adoption of a particular structure type is found to depend on the relative importance of different intermolecular interactions — part of the molecule being likely to result in stack formation (C···C interactions) and part in the formation of glides (C···H interactions). In these simple molecules, some degree of prediction was found to be possible based on the assignment of a ''stacking'' ability or ''glide-forming'' ability to each atom in the molecule: equivalently, an overall molecular size/shape descriptor can be defined.

This work was extended to a study of the general crystal packing of hydrocarbons,[33] in which the correlation of packing energy with various parameters defining the molecular size/shape is exploited. These parameters include the total number of atoms. the number of carbon and hydrogen atoms. the van der Waals envelope volume and surface, the molecular mass, and the number of valence electrons. The best correlation is found to be between the packing potential energy and the number of carbon atoms in the molecule. A self-packing coefficient can be defined that describes the ''smoothness'' of the molecular envelope. high values of which tend to improve packing energy. More complex structures subjected to such packing analysis include those containing hexafluorobenzene or fluoranil,[34] nitrobenzene derivatives,[35,36] and the carboxylic acids and amides discussed

Computational/Theoretical Approaches

In addition to the packing energy calculations discussed above, there are many other examples of computational methods being used to quantify or interpret crystal packing modes. These included studies on the discrimination of the energies and stabilities of racemic crystals from equivalent chiral structures[37] and on the influence of directional molecular dipole interactions on crystal packing (in fact, this is found not to be as significant as was commonly supposed[38]). Recent systematic work on predicting the packing of paracetamol molecules showed the sensitivity of lattice energy minimization calculations to variations in the observed molecular structure.[39] Calculations were also used in studies of the important phenomenon of polymorphism — in particular, in this context: on the differing crystal packing modes that may be adopted by polymorphic forms of the same molecules.[40] It is found that many plausible structures have energies within a few $kJ.mol^{-1}$ of the global minimum, emphasizing the difficulty of reliable crystal structure prediction. The possibility of reducing the number of plausible predicted structures using calculations of other, macroscopic, properties was investigated.[41]

A related topic is the use of observed molecular conformation and crystal packing patterns for the deduction of possible mean molecular geometries, reaction pathways, and transition states. This so-called structure-correlation method[42] makes the assumption that observed molecular structures tend to adopt conformations and packing motifs that are close to low-energy regions in the solid state. These are, however, by no means fully quantitative[39] and, in particular, quantitative deductions from molecular conformations in different structural environments are not established. This point is emphasized in a study of the systematics of crystal packing in biphenyl structures.[44] in this case, close-to-planar conformations are found in crystal structures more often than would be expected — the effects of crystal packing would tend to favor this ''distortion'' to an apparently higher energy molecular conformation in a range of environments. However, there is a notable increase in dynamic and static disorder in these ''planar-distorted'' structures.

CONCLUSION

The study of crystal structure remains a vital underpinning component of much research in supramolecular chemistry in the solid state. The implications of crystallographic

symmetry for the solid-state packing of molecular systems are complex, with competing intramolecular, intermolecular, and lattice effects. The systematic study of crystal-packing modes yields vital clues about the relative influence of each of these on molecular association. and thus, toward a fuller understanding of crystal packing and crystal structure and the eventual goal of their prediction.

ARTICLES OF FURTHER INTEREST

Tlze Cambridge Structural Database, p. 161
Concepts in Crystal Engineeving, p. 319
Crystal Engineering with Hydrogen Bonds. p. *357*
Hydrogen Bonding, p. *658*
Hydrogen Bonds to Metals and Metal Hydrides, p. 666
Isostructurality of Inclusion Compounds, p. 767
Modulated Structures, p. 873
Polarity Formation: Markov Chain Model, p. 1120
Polymorphism, p. 1129
Racks, Ladders, and Grids. p. 1186
X-Ray Crystallography, p. 1586

REFERENCES

1. Hammond. C. *The Basics of Crystallography and Diffraction*: IUCr Texts on Crystallography 3; Oxford University Press: Oxford, 1997.
2. Sherwood. D. *Crystals, X-rays and Proteins:* Longman: London, 1976.
3. McKie, D.: McKie. C. *Essentials of Crystallography*; Blackwell: Oxford, 1986.
4. Glusker, J.P.; Lewis, M.: Rossi, M. *Crystal Structure Analysis for Chemists and Biologists:* VCH: New York, 1994.
5. Stout, G.H.: Jensen. L.H. *X-ray Structure Determination: A Practical Guide,* 2nd Ed.: Wiley: New York, 1989.
6. Woolfson, M.M. *An Introduction to X-ray Crystallography*; Cambridge University Press: Cambridge, 1997.
7. Sands, D.E. *Vectors and Tensors in Crystallography*; Dover: New York, 1995.
8. *International Tables for Crystallography: Volume A—Space Group Symmetry*; Hahn. Th.. Ed.: International Union of Crystallography; Kluwer: Dordrecht, 1996.
9. Pauling, L. *Tlze Nature of the Chemical Bond:* Cornell University Press: Ithaca, 1960.
10. Kitaigorodskii, A.I. *Organic Chemical Crystallography*; Consultants Bureau: New York. 1961.
11. Kitaigorodskii. A.I. *Molecular Crystals and Molecules*: Academic Press: New York. 1973.
12. Allen, F.H.; Kennard, O.; Taylor, R. Systematic analysis of structural data as a research technique in organic chemistry. Acc. Chern. Res. **1983.** 16, 146–153.
13. Allen. F.H.: Kennard. O. 3D search and research using the Cambridge Structural Database. Chem. Des. Autom. News **1993**, *8*, 31–37.
14. Brock, C.P. Systematic Study of Crystal Packing. In *Implications of Molecular and Materials Structure for New Technologies*; Howard. J.A.K., Allen. F.H., Shields. G.P., Eds.: NATO Science Series E. Kluwer: Dordrecht, 1999: Vol. 360. 251–262.
15. Aakeroy, C.B. Crystal engineering: Strategies and architectures. Acta Crystallogr., Sect. B **1997**, *53*. 569–586.
16. Desiraju. G.R. *Crystal Engineering: Tlze Design of Molecular Solids:* Elsevier: Amsterdam. 1989.
17. Leiserowitz, L. Molecular packing modes. Carboxylic acids. Acta Crystallogr.. Sect. B **1976,** *32*. 775–802.
18. Leiserowitz. L.; Tuval, M. Molecular-packing modes. *N*-methylarnides. Acta Crystallogr.. Sect. B **1978,** 34, 1230–1247.
19. Leiserowitz. L.: Hagler. A.T. The generation of possible crystal structures of primary amindes. Proc. R. Soc. Lond., A **1983.** *388*. 133–175.
20. Etter. M.C. Encoding and decoding hydrogen-bond patterns of organic compounds. Acc. Chem. Res. **1990.** *23*. 120–126.
21. Kalman. A.; Parkanyi. L.: Argay. G. Classification of the isostructurality of organic molecules in the crystalline state. Acta Crystallogr.. Sect. B **1993.** *49*, 1039–1049.
22. Belsky. V.K.: Zorkaya, O.N.; Zorky. P.M. Structural classes and space groups of organic homomolecular crystals: New statistical data. Acta Crystallogr., Sect. A **1995. 51.** 473–481.
23. Brock. C.P.; Dunitz. J.D. Towards a grammar of crystal packing. Chem. Mater. **1994.** 6. 1118–1127.
24. Wilson, A.J.C. Space groups rare for organic structures. III. Symmorphism and inherent molecular symmetry. Acta Crystallogr.. Sect. A **1993,** *49*. 795–806.
25. Cole. J.C. Systematic Computational Analyses and Novel Search Procedures for Crystallographic Information. Ph. D. Thesis: University of Durham, UK, 1995.
26. Motherwell. W.D.S. Distribution of molecular centres in crystallographic unit cells. Acta Crystallogr., Sect. B **1994. 53.** 726–736.
27. Gautham. N. A conformational comparison of crystallographically independent molecules in organic crystals with achiral space groups. Acta Crystallogr., Sect. B **1992.** *48*, 337–338.
28. Zorky, P.M. A new view on the structure of organic crystals. Russ. J. Phys. Chem. **1993.** *68*, 870–876.
29. Robertson, *J.M.* The measurement of bond lengths in conjugated molecules of carbon centres. Proc. R. Soc. Lond., A **1951,** *207*, 101–110.
30. Kitaigorodskii, A.I. The principle of close packing and the condition of thermodynamic stability of organic crystals. Acta Crystallogr. **1965. 18.** 585–590.
31. Gavezzotti, A.; Desiraju, G.R. A systematic analysis of packing energies and other packing parameters for fused-ring aromatic hydrocarbons. Acta Crystallogr.. Sect. B **1988**, *44*. 427–434.

33. Desiraju, G.R.: Gavezzotti. A. Crystal structures of polynuclear aromatic hydrocarbons. Classification, rationalization and prediction from molecular structure. Acta Crystallogr.. Sect. B 1989, *45*. 473–482.
33. Gavezzotti, A. Crystal packing of hydrocarbons. Effects of molecular size, shape and stoichiometry. Acta Crystallogr., Sect. B 1990, *46*, 275–283.
34. Dahl. T. Molecular packing analysis of molecular complexes containing hexafluorobenzene or fluoranil. Acta Crystallogr.. Sect. B 1990, *46*. 283–288.
35. Andre. I.; Foces-Foces, C.; Cano, F.H.: Martinez-Ripoll, M. Packing modes in nitrobenzene derivatives. I. The single stacks. Acta Crystallogr., Sect. B 1997, 53, 984–995.
36. Andre. I.: Foces-Foces, C.: Cano, F.H.; Martinez-Ripoll. M. Packing modes in nitrobenzene derivatives. II. The "pseudo-herringbone" mode. Acta Crystallogr., Sect. B 1997. *53*. 996–1005.
37. Brock. C.P.; Schweizer. W.B.: Dunitz, J.D. On the validity of Wallach's rule. On the density and stability of racemic crystals compared with their chiral counterparts. J. Am. Chem. Soc. 1991, 113, 9811–9820.
38. Whitesell, J.K.; Davis. R.E.; Saunders, L.L.: Wilson, R.J.; Feagins, J.P. Influence of molecular dipole interactions on solid state organisation. J. Am. Chem. Soc. 1991. 113, 3267–3270.
39. Beyer, T.; Price, S.L. The errors in lattice energy minimisation studies: Sensitivity to experimental variations in the molecular structure of paracetamol. CrystEngComm 2000. 2, 183–190.
40. Gavezzotti, A.: Filippini, G. Polymorphic forms of organic crystals at room conditions: Thermodynamic and structural implications. J. Am. Chem. Soc. 1995, 117, 12299–12305.
41. Beyer. T.; Day, G.M.: Price. S.L. The prediction, morphology. and mechanical properties of the polymorphs of paracetamol. J. Am. Chem. Soc. 2001. *123*, 5086–5094.
42. Burgi. H.B.: Dunitz, J.D. From crystal statics to chemical dynamics. Acc. Chem. Res. 1983. 16. 153–161.
43. Burgi. H.B.; Dunitz. J.D. Can statistical analysis of structural parameters from different crystal environments lead to quantitative energy relationships? Acta Crystallogr.. Sect. B 1988. *44*, 445–448.
44. Brock, C.P.; Minton. R.P. Systematic effects of crystal packing forces: Biphenyl fragments with H atoms in all four ortho positions. J. Am. Chem. Soc. 1989. 111. 4586–4593.

Spherands

john C. Sherman
University of British Columbia, Vancouver, British Columbia, Canada

INTRODUCTION

Soon after crown ethers came on the scene as the first synthetic host molecules capable of binding guests, cryptands followed, and soon thereafter, the spherands. The preorganization of these three classes of molecules follows the order of their invention, as does overall binding affinity, i.e., crowns<cryptands<spherands. Spherand **7** (Chart 1) is the prototypical spherand, but there are a number of subfamilies that will be discussed. Donald J. Cram, 1987 Nobel Laureate, was the creator of the family of hosts that he named spherands. The spherand story began shortly after the genesis of supramolecular chemistry, and it demonstrates how quickly the field matured. as complex syntheses and methods of characterization enhanced the rapid sophistication of host–guest chemistry.

PREORGANIZATION

The topic of preorganization is discussed in a separate article, and spherands were used there as an example of this principle. A further example is given here. Shown in Chart 1 are the structures of hosts, starting from a simple crown ether (**1**) and progressing to Spherand **7** via successive replacement of an aliphatic ether group with rigid anisole units (**2**–**7**). In Table 1, the binding free energies for selected cations are given.[1] Although guest selectivity changes (the anisole units are larger and create a smaller cavity), the general trend is still marked: increased preorganization increases overall binding affinity for the most strongly bound guest. Note that this is despite the sacrifice in ligand strength. That is, aryl ethers are poorer electron donors than aliphatic ethers due to delocalization of the lone pairs into the aromatic rings. The enhanced

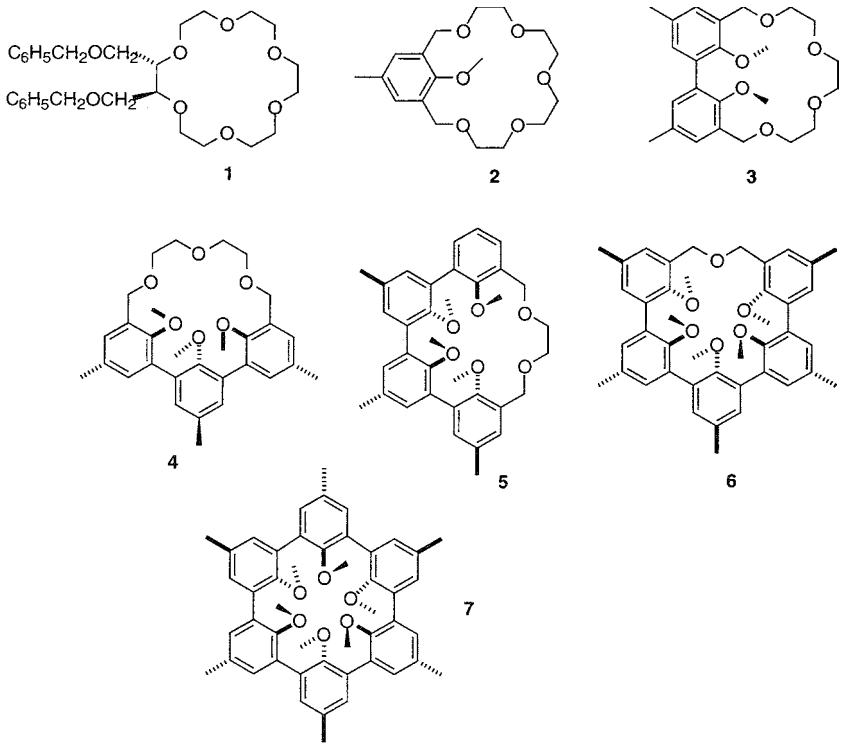

Chart 1 Compounds 1–7.

Encyclopedia of Supramolecular Chemistry
DOI: 10.1081/E-ESMC *120012717*

Table 1 Binding affinities ($\Delta G°$, kcallmol) for guests by hosts in $CDCl_3$ saturated with D_2O at 25°C

Host	Li^+	Na^+	K^+
1	6.3	8.4	11.4
2	5.5	6.4	8.5
3	6.5	8.7	7.5
4	7.2	12.2	11.7
5	7.2	13.5	10.7
6	12.8	14.4	10.4
7	>23	19.2	

preorganization of the anisole groups more than compensates for this electronic loss, once the effect of preorganization kicks in at three anisole units.

SYNTHESIS

The highly strained spherands took great synthetic effort to bring to fruition. Cram had to invent a reaction to couple arenes in an efficient manner. The key development was the use of $Fe(acac)_3$ as the coupling agent. Thus, for example, spherand **1**·Li^+ could be prepared starting from arene **8**, *bis*-arene **9**, or *tris*-arene **10** (Chart 2), in 3, 7.5, and 28% yields, respectively, as follows: 1) BuLi; 2) $Fe(acac)_3$; 3) EDTA; and 4) HCl. Decomplexation to give free spherand **1** was achieved by heating the Li^+ complex in H_2O/MeOH at 125°C.[2]

CHARACTERIZATION

Spherands and their relatives are characterized like any organic molecule, largely by NMR and mass spectrometry, as well as by elemental analysis. The key binding experiment used to determine the free energy of complexation of cations is typically done via a picrate extraction procedure developed by Cram.[''] Picrate salts of the cation in question were partitioned along with the host between $CDCl_3$ and D_2O. The partition of the picrate, and thus the cation, was determined by UV/Vis spectroscopy. Thus. equilibrium constants and free energies of complexation were generated. This method is effective for binding energies in the range of 6–16 kcallmol. Beyond that. competition experiments are needed between the host in question with a host with known binding properties. In addition, rates of complexation and decomplexation were used to yield free energies of binding.[''''']

Another key tool for characterization of spherands and related species is x-ray crystallography. This is the definitive method for deriving structural information. Numerous structures of free and complexed hosts were obtained for this family of compounds. Such structures make it clear just how preorganized a host is and how significantly it is solvated. They also clearly depict the size and shape of the cavity.

Another crucial element in host–guest characterization is modeling. This is, of course, critical in the design stages, but there is an iterative process of design and characterization. Cram's key here was the use of CPK molecular models. Nothing can replace the visual effect of holding a physical model in your hands. Cram spent considerable time studying models and calibrating himself using the binding data and crystal structures he had at hand. With experience, binding energies could be predicted within a few kcallmol using CPK models. Even strain energy could be appreciated, as some models needed to be shaved to be built. Strain was also evident from analysis of crystal structures, as adjacent oxygens were often closer than the sum of their van der Waals radii (and had to be shaved in CPK models). In addition, the arene carbons and their substituents deviated up to 10° and 0.5 Å from the plane of the ring.[6] Such strain was largely relieved upon complexation of cationic guests, as **O—O** repulsion was eliminated.[6] The glut of data and the highly preorganized nature of spherands made them an attractive system for computational chemists to hone their force fields for supramolecular applications.[7]

CLASSES OF SPHERANDS

The closest member of the spherand family to the prototype (i.e., **7**) are the bridged spherands such as **11** (Chart 3).[2] Bridges of different lengths could be incorporated, even those containing an extra oxygen. The bridges could be *syn* or *anti*. as could the two methyl groups on the remaining anisoles. These bridges change the size and shape of the cavity. making some oxygen ligands closer to the guest, some farther. The effective diameter of Li^+ could be measured from crystal structures of its complex with various such spherands. and it ranged

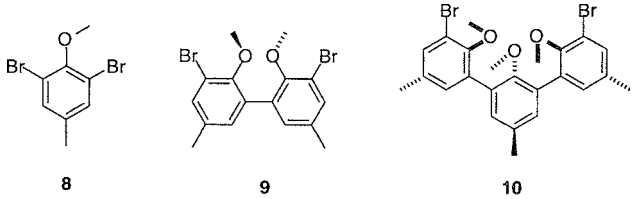

8 9 10

Chart 2 Starting units to produce spherand 1.

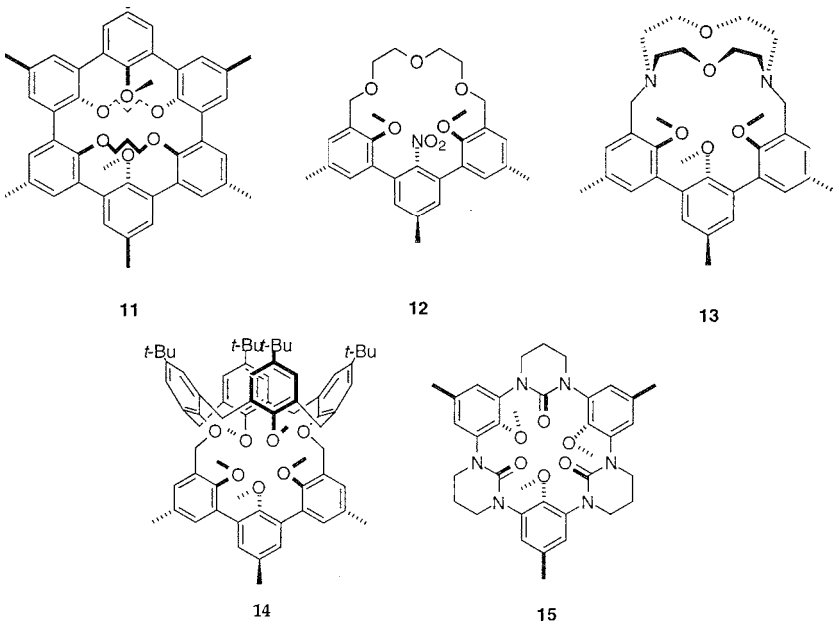

Chart **3** Compounds 11–15

as follows: 1.28 Å with five coordinating oxygens, 1.48 Å with six coordinating oxygens, and 1.72 Å with seven coordinating oxygens. These distances agreed with complexes found in the literature. though no other seven-coordinate lithium was known. The spherands, being the most preorganized ionophores, manifest the strongest binding and the highest selectivity of all alkali cation-binding hosts.[8] They also have the slowest decomplexation rates. For **7**·Li^+, heating to 400 K in MeOH/water is required for decompiexation. For **11**·Li^+, even such rigorous treatment is not sufficient for decomplexation. Thus, **11**·Li^+ can be considered a carceplex.[9]

The next class in the spherand family is the hemispherands. These consist of at least half preorganized ligands. Typically. the remainder of the host is a corand. that is. part of a crown ether. Compounds **4**–**6** fit in this category. The length of the corand could be varied. and functional groups were incorporated into the central aromatic rings of compounds such as **4**, in place of the methoxy group. This way. the ligating ability of a variety of functional groups could be explored. Functional groups such as nitro (e.g., **12**), N-oxide. amides, and esters were incorporated.[10] The hemispherands typically bind strongest to Na^+ and K^+, with binding energies typically 9–12 kcal/mol.[8]

Similar to the hemispherands are the cryptahemispherands. Instead of a corand part. there is a cryptand part; the rest of the host again is a highly preorganized spherand unit. Cryptahemispherand **13** binds Na^+ as a seven-coordinate ligand. The size and number of ligating sites can be varied considerably within this family, and complexes fi-om Na^+ to Cs^+ were studied.[8] Binding affinities for these guests are in the range of 19–21 kcal/mol for the best guests.[8]

Loosely related to crytaheinispherands are the calix-spherands. e.g., **14**. in which as the name suggests, half a spherand is capped with a calixarene. Binding energies for K^+ of 14 kcal/mol were reported.[12]

Other classes of spherands were reported. Some will be discussed in other articles. such as those used for chiral recognition of amino acids and those used as rate enhancers for polymerization and acylation reactions.[8] The serine protease enzyme mimic developed by Cram made use of a unit that is worthy of mention here. Cyclic urea units were incorporated into spherands to give another subfamily of spherands, which manifest some unique features. In addition to alkali metal cations, spherands bind to ainmoniums. In these cases: instead of the guest being encapsulated in the cavity of the host. the guest perches like a tripod onto three of the potential ligating oxygens. Typically, binding of ammonium guests is lower than for the alkali cations (typically 3–4 kcal/mol), largely because of the differential binding geometries.[8] That is. the alkali cations can access six ligating oxygens. while the ammoniums can access only three. Thus, Cram developed the cyclic urea unit as a particularly strong ligand for ammoniums. as it is a strong hydrogen-bond acceptor. For example, *tris*-urea spherand **15** binds

ammonium and methyl ammonium with 14.4 kcal/mol, and the best guest, K^+, with similar affinity at 15.6 kcal/mol. Measurement of bond angles from crystal structures of relatives of tris-urea **15** led Cram to conclude that the oxygens of the ureas can adjust their hybridization as needed to the task at hand. i.e., to the needs of the guest in question.[13] This makes these spherands useful. In addition, they are highly soluble in organic solvents, and their complexation/decomplexation rates are high compared to hosts that bind guests with comparable affinity.[14]

A CHROMOGENIC IONOPHORE

Applications are always a strong selling point for a field. and nothing is more satisfying than when fundamental studies lead to a useful application, especially if the development of that application actually leads to more fundamental work. Creation of a sensor for a particular guest has and continues to be a common goal in applications of supramolecular assemblies. A particularly challenging problem is the detection of K^+ in blood serum. The problem is that there is $\sim$100-fold greater concentration of Na^+ over K^+ in blood serum. As K^+ is only slightly larger than Na^+, one cannot simply design a host with a cavity that is too small for Na^+. One cannot simply use the concept that two things cannot occupy the same space, at least without paying a large price. In this case, what one needs is a highly preorganized host that is complementary to K^+, and thus shows a high selectivity over Na^+; if it can conform (i.e., collapse) to a cavity complementary to Na^+, there will be little or no selectivity. Such a tall order in binding properties was available from the huge databank of spherands and related hosts that Cram and others (Jean-Marie Lehn in particular) developed over a period of 20 years. What remained was a way to turn such hosts into sensors. For a simple application, the hosts should change color upon binding K^+, and the assay should be fast. One does not want to have to wait days for equilibrium to take place to get a meaningful result. Thus; cryptahemispherand **16** (Chart 4) was developed and commercialized.[15] Cryptahemispherand **16** binds K^+ over Na^+ by a factor of 1500, the equilibrium is reached rapidly, and a chromophore was incorporated that gets activated upon binding of a metal cation (the host deprotonates). Cryptahemispherand **16** has a pK_a value of 7.05 in the presence of KBr, and a value of 7.75 in the presence of NaBr. Such a differential allows complexation of K^+ to be observed colorimetrically in the presence of 100-fold excess Na^+.[15]

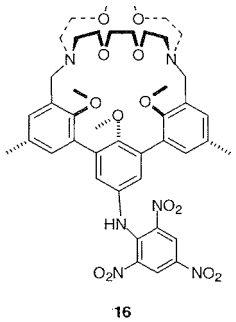

16

Chart 4 Chomogenic ionophore 16.

CONCLUSION

Presented here is a brief summary of several decades of work. In addition to the original literature, the reader is directed to more comprehensive reviews.[2,16,17] The spherands and their immediate family begot many other supramolecular families, each of which is covered in subsequent articles in this encyclopedia. Thus, the spherands represent a daunting example of design and effort, synthetically, and in terms of characterization. This immense body of work is exemplary of how we can and should conduct our business in supramolecular chemistry.

ARTICLES OF FURTHER INTEREST

Alkali Metal Cations in Biochemistry, p. 1
Anticrowns, p. 68
Artificial Enzymes, p. 76
Biological Ligands, p. 88
Calixarenes and Their Analogues: Cation Complexation, p. 137
Chiral Guest Recognition, p. 236
Crown Ethers, p. 326
Cryptands, p. 334
Enzyme Mimics, p. 546
Ion-Selective Electrodes, p. 747
Ionophores, p. 760
Kinetics of Complexation, p. 776
Lariat Ethers, p. 782
Macrocycle Synthesis, p. 830
Podands, p. 1106
Preorganization and Complementarity, p. 1158
Siderophores, p. 1278
Solvation Effects in Guest Binding, p. 1322
Stability Constants: Definition and Determination, p. 1360

REFERENCES

1. Helgeson. R.C.: Selle, B.J.; Coldberg. I.: Knobler. C.B.: Cram, D.J. J. Am. Chem. Soc. 1993, *115*, 11506.
2. Cram, D.J.; Kaneda, T.: Helgeson. R.C.; Brown. S.B.; Knobler, C.B.: Maverick. E.: Trueblood, K.N. J. Am. Chem. Soc. 1985. 107, 3645.
3. Helgeson. R.C.; Weisman, G.R.; Toner, J.L.; Tarnowski, T.L.: Chao, Y.: Mayer, J.M.: Cram, D.J. J. Am. Chem. Soc. 1979. 101, 4928.
4. Cram. D.J.: Lein. G.M. J. Am. Chem. Soc. 1985. 107. 3657.
5. Artz. S.P.: Cram. D.J. J. Am. Chem. Soc. 1984. 106, 2998.
6. Cram, D.J.: Lein. G.M.; Kaneda, T.; Helgeson, R.C.: Knobler. C.B.: Maverick. E.: Trueblood, K.N. J. Am. Chem. Soc. 1981. 103. 6228.
7. Vacek, J.; Kollman, P.A. J. Phys. Chem. A 1999, 103. 10015.
8. Cram. D.J.: Cram. J.M. Container Molecules and Their Guests. In *Monographs in Supramolecular Chemistry*; Stoddart, J.F.. Ed.; Royal Society of Chemistry: Cambridge, 1994.
9. Helgeson. R.C.; Knobler, C.B.; Maverick, E.F.; Trueblood, K.N. Acta. Cryst. 2000. *C56*. 795.
10. Bryant, J.A.; Helgeson, R.C.: Knobler, C.B.: de Grandpre. M.P.; Cram, D.J. J. Org. Chem. 1990, *55*. 4622.
11. Cram. D.J.; Ho. S.P.; Knobler. C.B.; Maverick. E.F.: Trueblood. K.N. J. Am. Chem. Soc. 1986, *108*, 2989.
12. Groenen. L.C.; Brunink. J.A.J.: Bakker, W.I.I.: Harkema, S.: Wijmenga, S.S.; Reinhoudt. D.N. J. Chem. Soc., Perkin Trans. 1992. 2. 1899.
13. Doxsee. K.M.; Feigel, M.: Stewart, K.D.: Canary, J.W.; Knobler, C.B.; Cram, D.J. J. Am. Chem. Soc. 1987. 109. 3098.
14. Anthonsen. T.; Cram, D.J. J. Chem. Soc., Chem. Cornmun. 1983, 1414.
15. Helgeson, R.C.: Czech. B.P.: Chapoteau. C.R.; Kumar. A.: Cram, D.J. J. Am. Chern. Soc. 1989. *111*, 6339.
16. Cram, D.J. Angew. Chem., Int. Ed. Engl. 1986. 25, 1039.
17. Maverick, E.F.; Cram. D.J. *Comprehensive Supramolecular Chemistry*; Lehn. J.-M., Atwood, J.L.. Davies. J.E.D.. MacNicol. D.D.. Vogtle. F., Eds.; Pergamon: New York, 1996; Vol. 1, 213–244.

Spontaneous Formation of Homochiral Supramolecular Architectures

S

Yasuhiro Ishida
The University of Tokyo, Tokyo, Japan

INTRODUCTION

The first observation of homochiral supramolecular architecture dates to Pasteur's historical experiment in 1848 on the resolution of sodium ammonium tartrate."' Since then, spontaneous formation of homochiral architectures attracted scientists' attention as an important phenomenon relevant to the emergence of biochemical homochirality. The origin of chirality in nature is of long-standing interest in physics, chemistry, biology, and geology.[2] However, answers to the following questions have not yet been provided: what is the first step of symmetry breaking, and how can an amplification of an apparently small initial enantiomeric excess be achieved? Although several hypotheses were proposed, homochiral segregation of a racemate and subsequent homochiral polymerization have been considered critical steps in biochemical evolution.[3]

Spontaneous separation of enantiomers also attracts practical attention because the phenomenon has a potential to provide attractive optical resolution methods, in view of simplicity and no requirement of chiral auxiliary. In fact, optical resolution by direct crystallization of racemates was operated on a large scale to prepare several economically important compounds, such as monosodium L-glutamate.[4] The key of the process is homochiral crystallization, where a racemic liquid or solution yields a mixture of crystals composed of only D or L isomers, so-called "conglornerate." In such a system, one can often sort the enantiomers by hand. or one can induce preferential crystallization of one enantiomer. This method cannot be applied for the resolution of racemates that undergo heterochiral crystallization, giving rise to crystals containing both enantiomers. However. the prediction of racemate types, the homochiral versus heterochiral packing, has been one of the most challenging subjects in this field, although more than 150 years have past since the discovery of Pasteur.[5]

Recent studies in supramolecular chemistry revealed that spontaneous separation of enantiomers is a phenomenon coinmonly observed in many phases, from the crystalline state to a dilute solution. Starting with early studies of the morphology of chiral crystals by optical microscopy, the scale for the observation of chiral supramolecular assemblies approaches that of the molecules themselves (Fig. 1). In the following sections. the achievements in this area, which would shed some lights on the unsolved problems as described above, will be summarized and compared. The examples of homochiral assemblies in heterogeneous systems. investigated by direct morphology observation are described in the second section. Then, described are the recent examples of homochiral architectures formed in homogeneous systems. which were characterized by various spectroscopic techniques. In the last section, the question of how to manipulate homochiral supramolecular architectures, in order to apply the attractive entities for practical use, is addressed.

HOMOCHIRAL AGGREGATES IN HETEROGENEOUS SYSTEMS

Homochiral Domain in Two-Dimensional Crystal

Pasteur's observation not only uncovered the existence of enantiomers but stimulated scientists' desire for direct observation of supramolecular chirality without resorting to diffraction techniques. Recent progresses in scanning prove that microscopy, such as atomic force microscopy (AFM) and scanning tunneling microscopy (STM), enable us to observe two-dimensional (2-D) chiral crystals at molecular resolution. Eckhardt and coworkers reported the first example of spontaneous separation of chiral phases in monolayer crystals. Langmuir–Blodgett films of a racemic tetracyclic alcohol (1), formed on the water surface, were transferred onto mica.[6] The AFM of the ordered films revealed the domains of mirror-image structures, indicating separation into domains of pure enantiomers. Such chiral symmetry breaking was also observed from achiral molecules. Zasadzinski and coworkers presented AFM images of monolayer crystals of calcium arachidate (2). where these achiral molecules separated spontaneously into lattices with'chiral packing of opposite handedness."'

DOI: 10.1081/E-ESMC 120019193

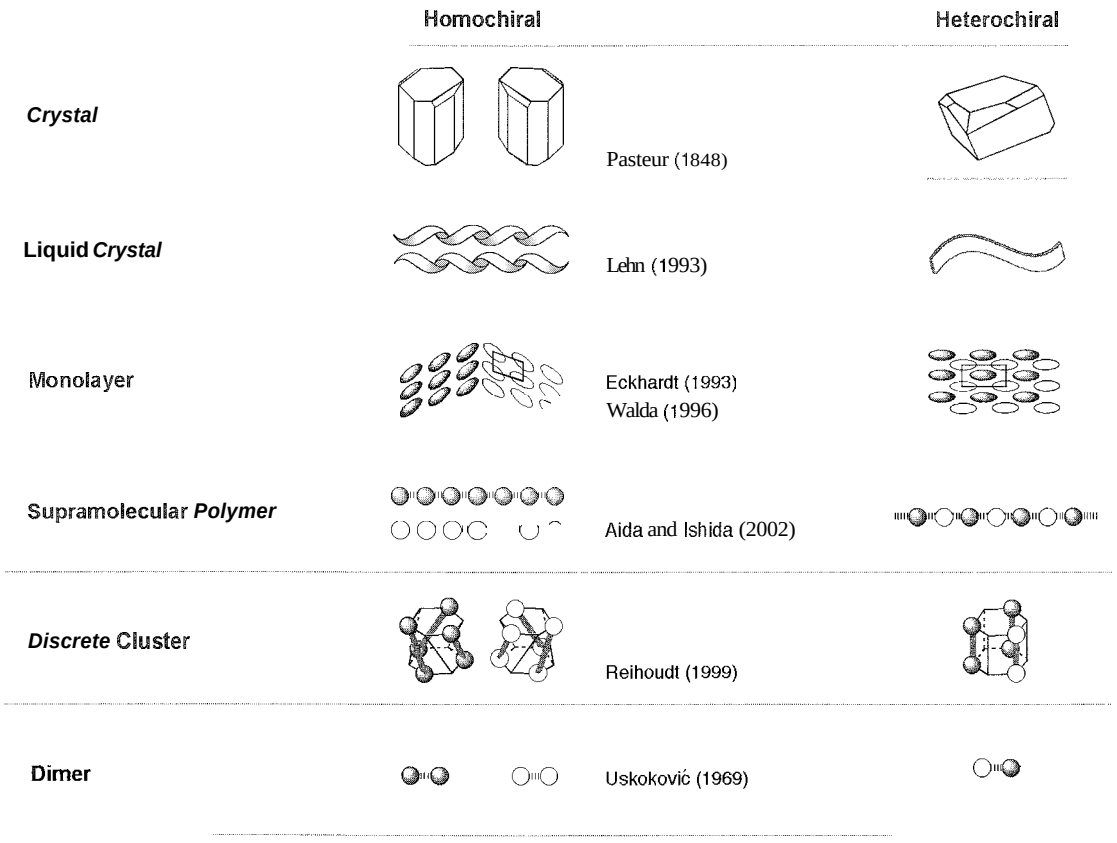

Fig. 1 Homochiral and heterochiral supramolecular architectures.

More recently, Walda et al. reported that a racemic mixture of mesogen *3* produced images of coexisting enantiomorphous domains, which were indistinguishable from the domains obtained from the enantiomerically pure materials (Fig. 2).[8] Observation of enantiomorphous domains in 2-D crystals can result from two different mechanisms:

1. The racemic material spontaneously resolves into monolayer crystals of pure *R* and *S* material forming a 2D conglomerate.
2. Both enantiomorphous domains are composed of racemate packed in chiral orientation.

The crystals formed through these two mechanisms must be diastereomeric, but it is not possible to distinguish between these two possibilities by measuring physical properties such as optical activity. If resolution occurs, and the monolayer crystal domains are enantiomerically pure, the chiral images observed from the racemic material must be identical to those obtained from one or the other of the pure enantiomers. Over 100 images were analyzed for each material [enantiomerically pure (*R*)- and (*S*)-**3**, and racemic **3**], and the unit cells from the pure enantiomers and from the racemate were found to be the same within experimental error. These results provide strong evidence for chiral symmetry breaking to give a 2-D conglomerate.

Mesoscopic Superhelix in Liquid Crystal

Molecular chirality is sometimes amplified to chirality at the mesoscopic level, through the self-assembling process of a monomeric building block with low molecular mass.[9] Especially, helices with nanometric or micrometric pitches are fascinating entities for scientists, as they are often observed in crystalline fibers, liquid crystals, and physical gels. Chirality of such mesoscopic helices can be easily detennined by direct morphology observation using microscopy. Recent studies revealed that symmetry breaking can occur through superhelix-formation processes of racemic or achiral components.

Lehn and coworkers reported that a racemic mixture of monomeric components spontaneously formed long superhelices of opposite handedness that coexist in the same

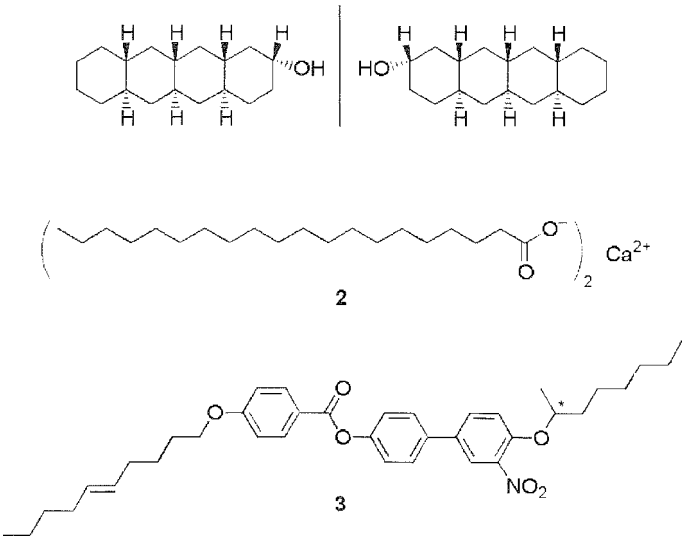

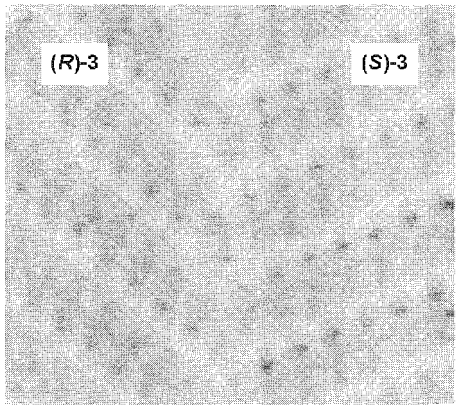

Fig. 2 A scanning tunneling microscopy (STM) image obtained from racemic **3** (nght) (Reproduced by permission of the American Chemical Society from Acc Chem Res. 1996, 29. 591–597.)

sample.[10] They designed mesogens consisting of two recognition units connected with D- and L-tartaric acid: Structures 4 and **5** derived from 2,6-diaminopyridine and uracile derivatives, respectively. Because 2,6-diaminopyridine and uracile moieties form a stable dimer via triple hydrogen-bonding interactions, equimolar mixtures of 4 and 5 lead to the progressive assembly of supramolecular–polymolecular entities (see the next section for more information on supramolecular polymers). Though the individual species L-4, L-**5**, D-**4**, and D-**5** were solids, the mixtures (L-**4**+L-**5**) and (D-**4**+D-**5**) showed liquid crystalline phases at room temperature. Electron microscopic observations of these mixtures revealed that (L-**4**+L-**5**) and (D-**4**+D-**5**) formed very long superhelical strings with right- and left-handed helicity, respectively [Fig. 3a (left) and (middle)]. Interestingly, in the case of a racemic mixture of L-**4**, L-5, D-**4**, and **D-5,** long superhelices of opposite handcdncss were formed [Fig. 3a (right)], which suggests the occurrence of spontaneous optical resolution in the supramolecular liquid crystalline polymers.

Since the discovery of the first liquid crystalline material in 1888, helicity has proven to be one of the most fascinating topics in this field.[9,11] Several liquid crystalline phases with helical structurc were reported, such as chlolesteric phase, blue phase, ferroclectric and antiferroelectric smectic phases, and helical smectic A phase. In most of these helical phases, at least a fraction of the constituent molecules have an asymmetric carbon, and it was long believed that chirality at a molecular level is a prerequisite to construct chiral architectures at the mesoscopic level. However, Watanabe et al. reported the first example of spontaneous helix formation in liquid crystalline systems comprised of achiral molecules.[12] They employed banana-shaped mesogene **6,** which showed thermotropic smectic phases. Interestingly, the achiral mesogen **6** formed a helical structure in the smectic phases. Although right- and left-handed helices were observed with equal probability in this system, they spontaneously segregated to form the domains of opposite handedness, which was confirmed by cross-polarized microscopy and circular dichroism spectroscopy (Fig. 3b). Moreover, millimeter-ordered homochiral domains could be grown, upon cooling the sample from isotropic melt to the smectic phase. It should be emphasized that such intriguing phenomena were specifically observed in the liquid crystalline state of such banana-shaped mesogens. Despite not yet knowing the precise mechanism, these phenomena are presumably attributed to the unique bent structurc of 6.

HOMOCHIRAL ASSEMBLIES IN HOMOGENEOUS SYSTEMS

Homochiral Dimer

In a solution of a chiral compound, the enantiomers should display identical physical properties, if any foreign optically active substance does not exist in the system. However, this notion holds truc only in on ideal dilute solution. To the extent that there is some degree of solute aggregation, chiral differentiation of enantiomers may be possible without the aid of any foreign optically active substance. As Uskoković and coworkers discovered in

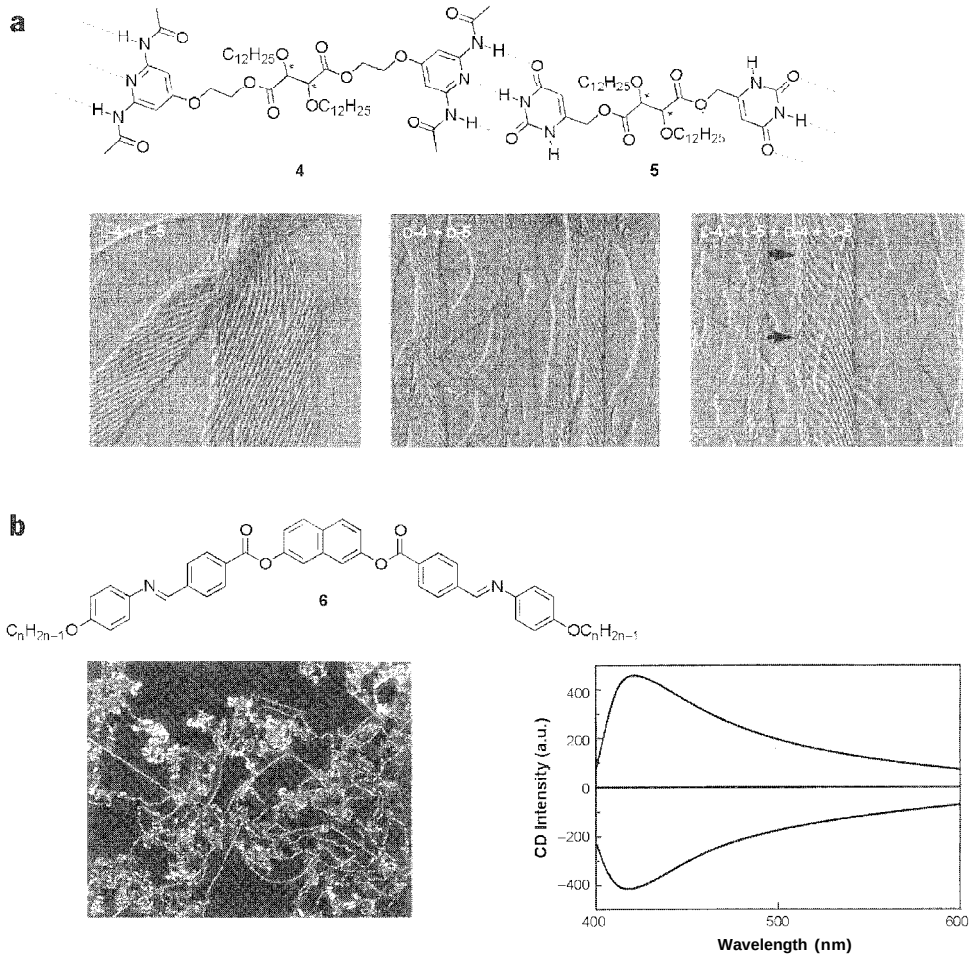

Fig. 3 (a) Electron micrographs of thin layers of (L-**4**+L-**5**) (left), (D-**4**+D-**5**) (middle). and (L-**4**+L-**5**+D-**4**+D-**5**) (right). (Reproduced by permission of the National Academy of Sciences from Proc. Natl. Acad. Sci. USA 1993, 90. 163–167.) (b) Cross-polarized optical micrograph of the smectic phasc of 6 (left) and circular dichroism spectra of two domains in the amectic blue phasc of 6 (right). (Courtesy of Prof. J. Watanabe.)

1969 for the case of dihydroquinine,[13] diastcreoisomeric solute–solute interactions can cause nonraccmic mixtures of cnantiomcrs to give distinct NMR spectra. To date, several reports of this phenomenon appeared, most of which can be elucidated as the results of the dimerization of solutes via noncovalent interactions (Fig. 4a).[13-17] Enantiodiffcrcntiation through dimcr formation is of paramount importance, because this process should be involved in the formation of all homochiral aggregates.

Harger ct al. reported the discrimination by NMR spectroscopy of both enantiomers of alkylphenylphospinic amides **7**.[14] Thc observed spectra can be rationalizcd in tcrms of dimerization through hydrogen bonds [Fig. 4a (top)]. In this system; there was no marked preference for homochiral or heterochiral dirncrization, and the partner-exchanging was fast on the NMR time scale. In an cnantiomcrically unbalanced sample, thc major enantiomer was, on average, associated mainly with partners with thc same chirality, whereas the minor one was for the most part paired with partners of opposite handedness. Therefore; the major and minor cnantiomcrs were related differently to their time-averaged local environments and exhibited distinct NMR spectra. Hara et al. described the self-induced nonequivalence in the association of amino acid derivatives **8**.[15] In this case, thc homochiral dimer and the hctcrochiral dimcr gavc different signals in NMK due to thc same reason as the example of Hargcr, where dimcrization via hydrogen-bonding interactions again played an important role [Fig. 4a (middlc)]. At room temperature, stabilities of thc homochiral and the heterochiral dimers were cssentially thc same. I-Iowever, upon lowering the temperature, the homochiral dimer bccame relatively more stable compared with the heterochiral dimer, which was supported by NMR and IR spectroscopy.

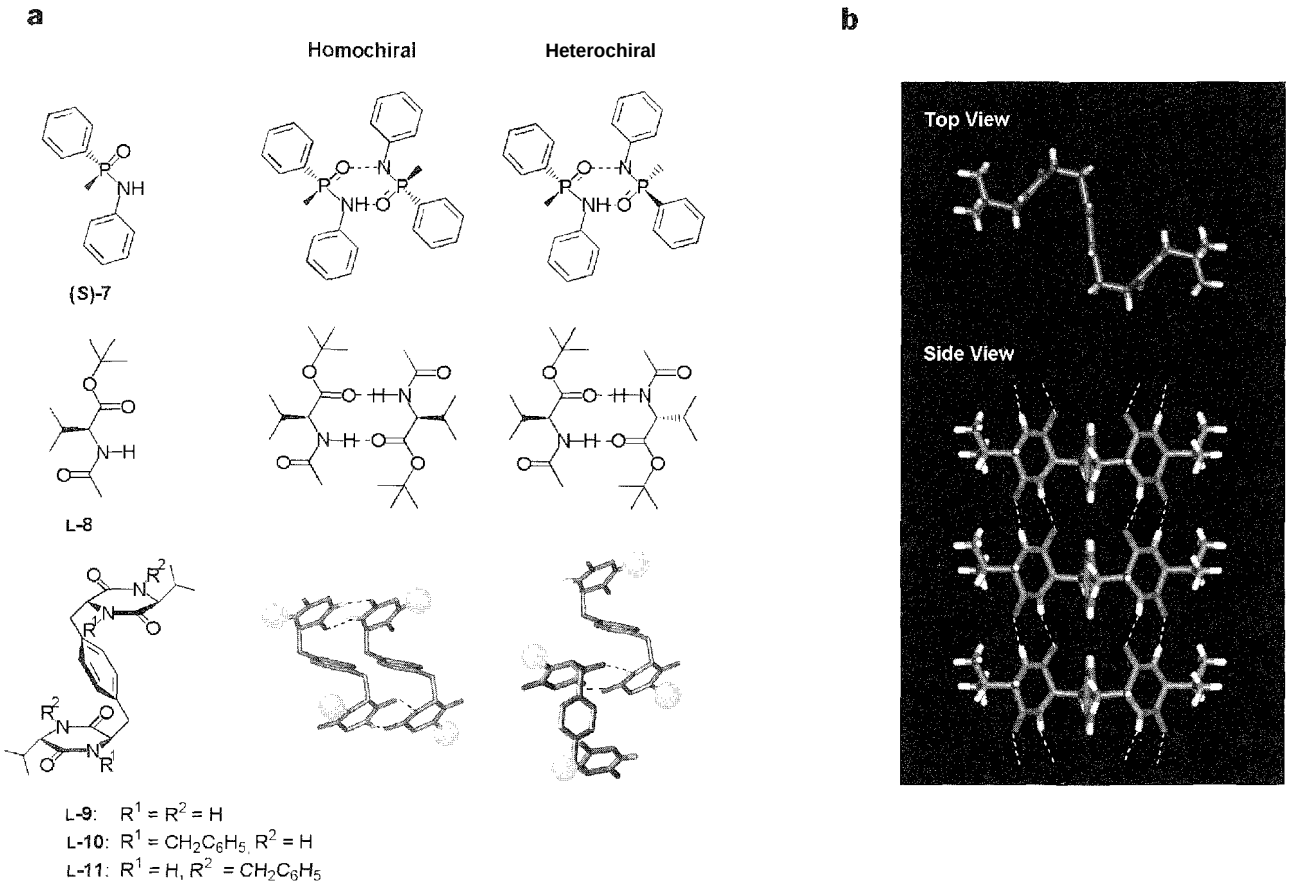

Fig. 4 (a) Homochiral and heterochiral dimerization. (b) Crystal structure of L-9 viewed along the *c*-axis (top) and u-axis (bottom). The dotted lines represent hydrogen bonds. Solvent molecules are omitted for clarity. (Reproduced by permission of the American Chemical Society from J. Am. Chem. Soc. **2002,** 124, 14017–14019.) ***(View*** this *art* ***in*** color *at www.dekker.com.*)

Recently, Aida and Ishida demonstrated the example of exclusive homochiral-dimer formation, where the enantioselection mechanism was clearly elucidated by the number of hydrogen bonds [Fig. 4a (bottom)].[18] The hydrogen-bonded dimer motifs **10** and **11** were designed based on a xylyiene-bridged *bis*(cyclic dipeptide) 9. Conformational studies on cyclic dipeptides with benzylic side chains indicated that the aromatic groups "hover over" the diketopiperadine unit due to a dipole–dipole interaction. Hence, 9 having a p-xylylene bridge adopts an "*S*" -shaped conformation with the aromatic ring stacked by the two diketopiperadine units, which was confirmed by x-ray crystallography of L-**9** [Fig. 4b (top)]. Furthermore, crystallographic studies showed that 9 possesses arrays of two-amide functionalities, (NH⇒CO)⇒(CO⇒NH) and (CO→NH)⇒(NH⇒CO), on each edge of the "*S*"-shape. When the sequences and the shapes of the arrays are complementary, the two arrays can efficiently interact with each other through multiple hydrogen bonds. In fact, L-9 formed a columnar assembly in the crystalline state, via complementary hydrogen bonds at both edges of the molecule [Fig. 4b (bottom)]. Contrary to this, the association of **L-9** with D-**9** is expected to be unfavorable, because the steric requirement allows only one of the two diketopiperadine units to take part in the association event. By protecting either of the two edges of L-**9**, **L-10** and L-**11** were derived, which are expected to posses "S" -shaped (NH⇒CO)⇒(CO⇒NH) and "anti-*S*"-shaped (CO⇒NH)⇒(NH⇒CO) arrays, respectively. Because of the steric and sequential requisites for the association as described above, **10** and **11** should form a stable hetero dimer 10.11 only when they are homochiral [Fig. 4a (bottom)]. In fact, the amide–NH signal of L-**11**, upon mixing with L-**10**, showed a 1 ppm downfield shift due to the hydrogen-bonding interactions, whereas the signal was totally intact due to the addition of D-**10**. The association constant for the homochiral dimer L-**10**·L-**11** was estimated to be $5 \times 10^3\ M^{-1}$ by ^{1}H-NMR dilution technique. Such high stability is most likely due to the simultaneous participation of the two diketopiperadine units, because a

model compound possessing only a single diketopiperadine ring did not show any sign of hydrogen-bonding interactions under the same condition

Homochiral Discrete Cluster

Supramolecular approaches to self-assembly often rely upon reversible noncovalent interactions. These strategies inherently involve an error–correction process, and as a consequence, the thermodynamically favored structures are preferentially constructed.[19] Particularly in the self-association of racemic components, the error–correction process often leads to the selective formation of the homochiral clusters, although the diastereomeric clusters with similar stability are potentially formed as the final products.[20]

Enantiomeric self-recognition of biomolecules such as amino acids attracted exceptional attention, because symmetry breaking of these materials might play a significant role in a prebiotic process, which was proposed to explain the transformation from a racemic chemistry to a chiral biology.[3] Recently, Cooks et al. reported chiroselective self-directed oligomerization of serine (**12**).[21] An unusually strong magic number cluster of L-12, observed as the protonated, sodiated, or potassiated octamer, was identified by electospray ionization mass spectrometer (ESIMS). Tandem mass spectrometry results and ab initio calculations suggested that the serine octamer $(L\text{-}\mathbf{12})_8$ is composed of four dimeric units: the individual dimers are bound through carboxylic acid groups, while additional hydrogen bonding involving the hydroxyl and amino groups generates the final drum-shaped structure (Fig. 5a). Furthermore, preliminary results showed the formation of "clusters of clusters," which is predicted to arise as a result of oligomerization of $(L\text{-}\mathbf{12})_8$, held together by the "sticky ends" present on the top and bottom faces via hydrogen bonds between the amino and hydroxy groups. The most intriguing discovery about the octamer was its chiral dependence. Under ESIMS conditions, the relative abundance of the protonated $\mathbf{12}_8$ significantly depended on the enantiomeric composition of the sample. For example, the mass spectra recorded for solutions of enantiomerically pure L- and D-**12** were essentially identical, while the absolute intensity attributed to the octamer was reduced by a factor of five when using a racemic mixture. Furthermore, ESIMS spectrometry results of isotopically labeled samples (mixtures of L-[$^{13}C_1$]-**12** and D-**12**) confirmed the homochirality of the octameric cluster. These results may have implications for the evolution of homochirality of amino acids in living organisms.[3]

Such chiroselective oligomerization was also achieved in the self-organization of nucleoside derivatives. Davis

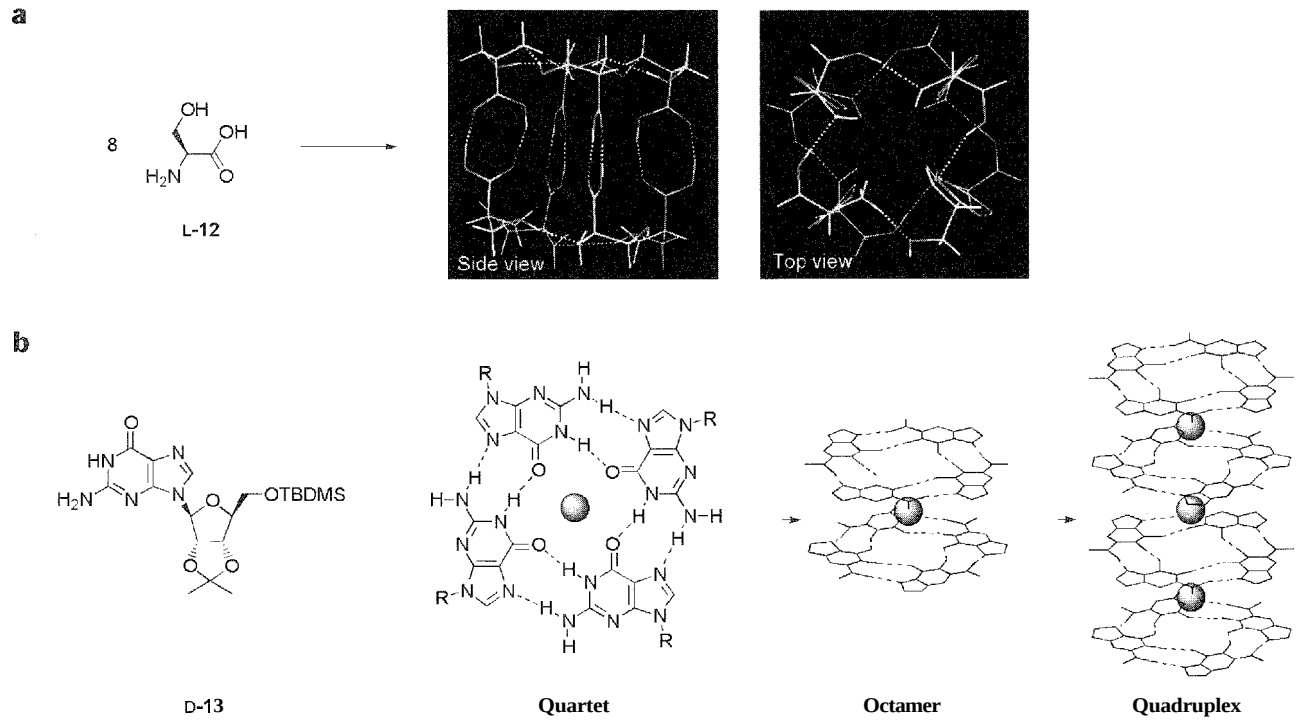

Fig. 5 (a) Calculated HF/6-31G structure of the protonated octamer of **12**. (Reproduced by permission of the American Chemical Society from Anal. Chem. **2001,** *73*, 3646–3655.) (b) The formation of the quartet, the octamer, and the quadruplex of **13.** (*View this art in color at www.dekker.com.)*

et al. employed a guanosine derivative 13 for cation-templated formation of homochiral clusters.[22] It is known that guanosine derivatives (G) self-associate to form quartets G_4 in the presence of cations M^{n+} (n= 1 or 2). Individual G_4-quartets, stabilized by hydrogen bonds between the base moieties: stack to give G_8-M^{n+} sandwiches and higher-ordered C-quadruplexes (Fig. 5b). For example. Ba^{2+} picrate ternplates the formation of a complex with eight equivalents of D-**13** bound to each Ba^{2+} picrate. X-ray crystallographic study indicated that the formation of a huge discrete cluster consisting of 16 units of D-13 associates around two Ba^{2+} cations to give a complex with four 6-quartet layers. This hexadecamer $(D\text{-}\mathbf{13})_{16}\cdot 2Ba^{2+}$ was composed of two coaxially stacked C_4-symmetric octamers, $(D\text{-}\mathbf{13})_8\cdot Ba^{2+}$, and the octamers are linked by four picrate anions that hydrogen bond to the "inner" *G*-quartets. The NMR studies indicated that the hexadecamer structure was retained in solution. While studying the structure and dynamics of *G*-quadruplexes, they discovered that Ba_2^{+} picrate directs enantiomeric self-recognition of 13. The homochiral hexadecainers with opposite handedness. $(D\text{-}\mathbf{13})_{16}\cdot 2Ba^{2+}$, and $(L\text{-}13)_{16}\cdot 2Ba^{2+}$, were predominantly generated by the treatment of a CD_2Cl_2 solution of racemic 13 with Ba^{2+} picrate. The ^{1}H-NMR spectrum of the mixture showed that the homochiral pair accounted for at least 90% of all of the diastereomers observed at equilibrium. In contrast, such enantiomeric recognition did not occur when the templating cation was the monovalent K^+, where NMR signals attributed to heterochiral diastereomers were observed. Taking advantage of the reversible nature of these nucleoside assemblies, the homochiral assemblies can be reconstructed: upon treatment of the diastereomeric $(D,L\text{-}\mathbf{13})_{16}\cdot 4K^+$ with Ba^{2+}, an equilibrium favoring the homochiral $\mathbf{13}_{16}\cdot 2Ba^{2+}$ was attained. Because Ba^{2+} and K^+ are similar in size, the cation's charge density is considered to be the major factor in controlling the enantioineric self-association at the supramolecular level.

Homochiral Supramolecular Polymer

Supramolecular polymers, 1-D aggregates of monomers formed via noncovalent interactions, attracted increasing attention as a new class of environment-responsive polymeric materials because of their reversible polymerization and depolyrnerization characteristics.[23] In general, monomers possess two interactive moieties at which they can be connected to each other via noncovalent interactions. in supramolecular polymerization, every chain-elongation process could be regarded as equivalent events, because the associations, monomer with monomer, monomer with polymer, and polymer with polymer. involve the same chemical process. In sharp contrast, through the formation of discrete clusters in a supramolecular manner. several types of association events should be involved, which are often complicatedly related to each other (see the previous section).

In the case of a chiral monomer, sequences of the resultant polymer should be directly influenced by the stereoselectivity of these interactive moieties."'' if the interactive moiety prefers homochiral association, two enantiomeric polymers of individual optical antipodes should be afforded. Contrary to this, when the interactive moiety possesses a strong tendency to adhere another monomer with opposite handedness, an alternative copolymer of each enantiomer is expected to arise. On the other hand, the monomer with no stereoselectivity will give a random copolymer. Studies on the supramolecular polymerization of racemic monomers are of significant importance, because these three extreme cases are regarded as the simplest models of the molecular arrangements in crystalline states. conglomerates, racemic compounds, and racemic mixtures. respectively.

In supramolecular polymerization of chiral monomers, molecular weights of polymers and distribution (MWD) are generally affected by the stereoselectivity of the association event as well as optical purity of the monomer.[16] Shown in Fig. 6b are three extreme cases of supramolecular polymerization of an enantiomerically unbalanced monomer (e.g., [D]>[L]). For nonstereoselective supramolecular polymerization, size-exclusion chromatography (SEC) profiles [monitored by absorption (UV) and circular dichroism (CD) detectors], shown in Fig. 6b (top). are expected, where MWD is unimodal, as in the case of polymerization of optically pure monomers, and should not change with [L]/[D], whereas the CD intensity response should reflect the enantiolneric purity of the monomer. Shown in Fig. 6b (middle) are SEC profiles, as expected for perfect homochiral supramolecular polymerization, where a bimodal MWD should result due to the formation of poly(L) and poly(D) with different molecular weights, depending on chiral monomer concentrations [L] and [D], respectively. According to a theoretical prediction, the CD response should initially be positive (or negative) but display a sudden drop to the baseline level at the beginning of the second peak, due to partial cancellation in ellipticity of poly(D) by Iower molecular-weight poly(L) ([D]>[L]). On the other hand, Fig. 6b (bottom) shows SEC characteristics as expected for perfect heterochiral supramolecular polymerization, in which a CD-silent copolymer with an alternating sequence of L- and D-monomers should be formed. In the SEC profile. D-monomer, which exists in excess with respect to L-monomer, should be observed as a CD-active, sharp peak at the end of the chromatogram.

Recently, Aida and Ishida demonstrated the first example of ''homochiral supramolecular polymerization,"

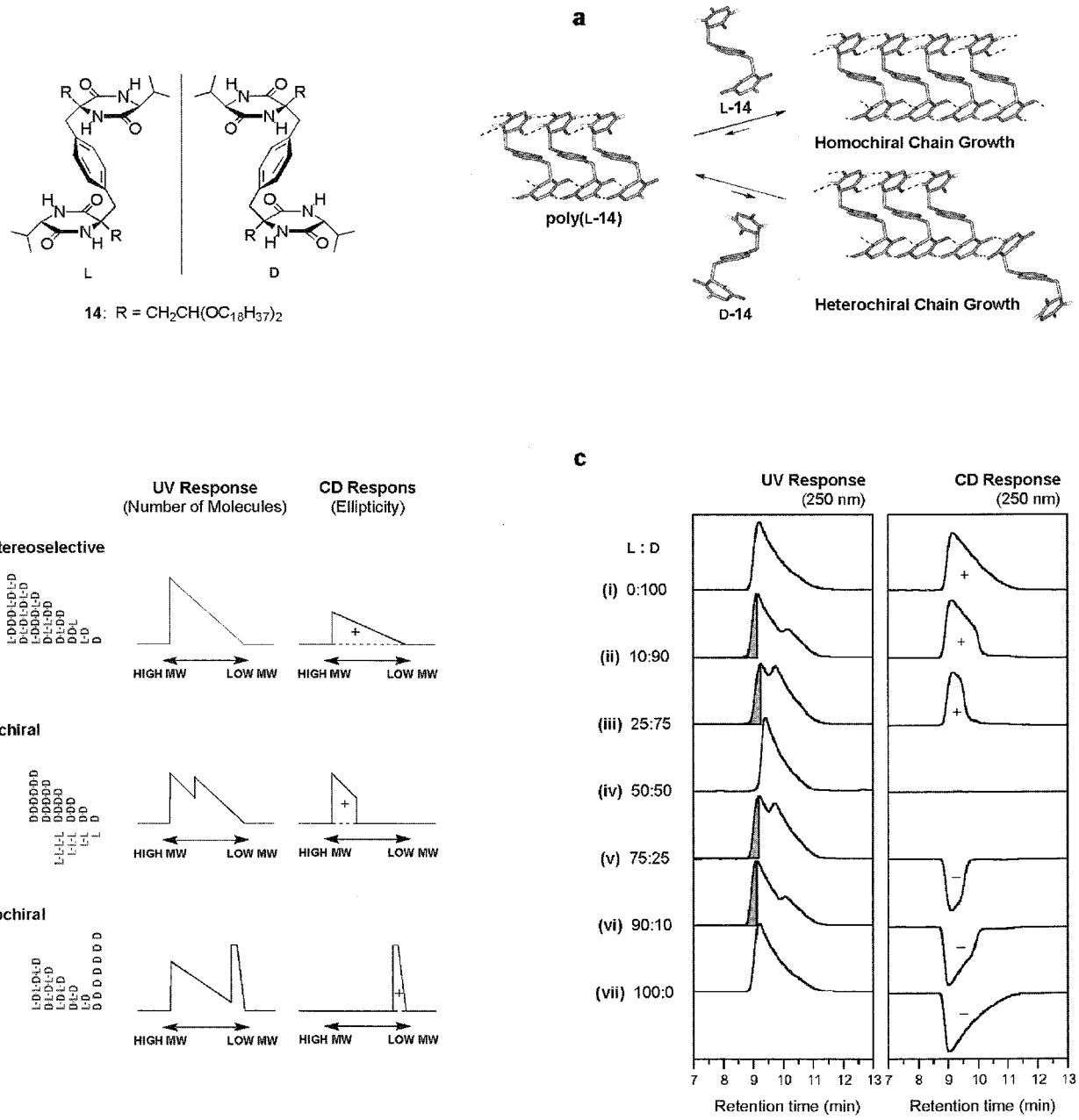

Fig. 6 (a) The homochiral supramolecular polymerization of **14**. (b) Size-exclusion chromatographic (SEC) profiles of an enantiomerically unbalanced (D-enriched) monomer, as expected for nonselective (top), homochiral (middle), and heterochiral (bottom) polymerization. (c) UV (left) and circular dichroism (CD) (right) responses in SEC traces of mixtures of L-**14** and D-**14**. (Reproduced by permission of the American Chemical Society from J. Am. Chem. Soc. **2002**, *124*, 14017–14019.) (*View this art in color at www.dekker.com.*)

which can be regarded as the formation of a discrete 1D conglomerate (Fig. 6a).[16] The chiral monomer **14** was designed based on **9**, by introducing long alkyl chains to improve solubility. In aprotic solvents, **14** formed a supramolecular polymer via hydrogen-bonding interaction, which was confirmed by ^{1}H-NMR, FT-IR, SEC, and vapor pressure osmometry. As an inherent property of supramolecular polymer, significant dependence of the average molecular weight on monomer concentration was observed for poly-**14**. Noteworthy, the homochiral association of **14** interactions preferentially proceeds compared with the heterochiral one, and as a consequence,

racemic 14 in solution forms two enantiomeric supramolecular polymers of individual optical antipodes, poly(L-14) and poly(D-14). Such homochiral association is undoubtedly due to the same reason as the homochiral dimerization of 10 and 11 (see previous section entitled "Homochiral Dimer"). The SEC profile of the supramolecular polymerization of 14 was consistent with the expectation as described above (Fig. 6b,c). When the mole ratio [L]:[D] was gradually changed from 100:0 to 0:100 at a constant concentration of 14 (Fig. 6c), the two peak tops once merged at [L]:[D]=50:50 (Fig. 6c, iv), and then they were separated once again. The CD profiles of the chromatograms thus observed, were also consistent with what was expected for the homochiral supramolecular polymerization. When the SEC trace of an optically unbalanced mixture of L-14 and D-14 was monitored by CD detector. the chromatogram, initially with a positive sign, displayed a steep drop to the baseline level at the beginning of the second peak and remained almost unchanged thereafter (Fig. 6c. vi). By virtue of this homochiral supramolecular polymerization; enantiomerically pure L-14 and D-14 could be isolated from the fractions corresponding to the shaded parts of the chromatograms in Fig. 6c, ii, iii. v, and vi.

CONCLUSION

By means of various analytical techniques. we can observe homochiral supramolecular architectures in a wide range of phases, from the crystalline state to a dilute solution, as described above. If we want to apply these systems for practical use. such as in optical resolution of racemates, the next crucial subject is how to manipulate the homochiral assemblies. In the case of separation of conglomerates. one can often sort the enantiomers by hand, as was performed by Pasteur.[1] Although this method can be applied only when crystals have sufficient size to allow determination of their sign of rotation, an alternative technique named "preferential crystallization" was developed, which has its origin in 1866 in the work of Gernez.[4] He observed that a supersaturated solution of racemic dextrorotatory salt yielded only

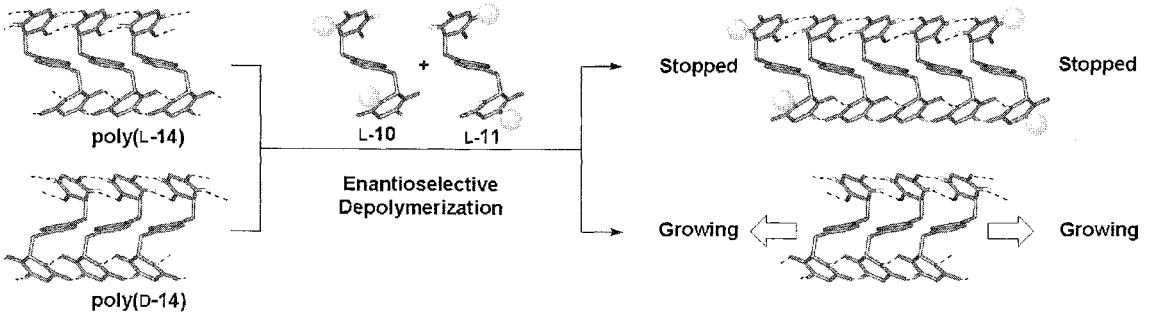

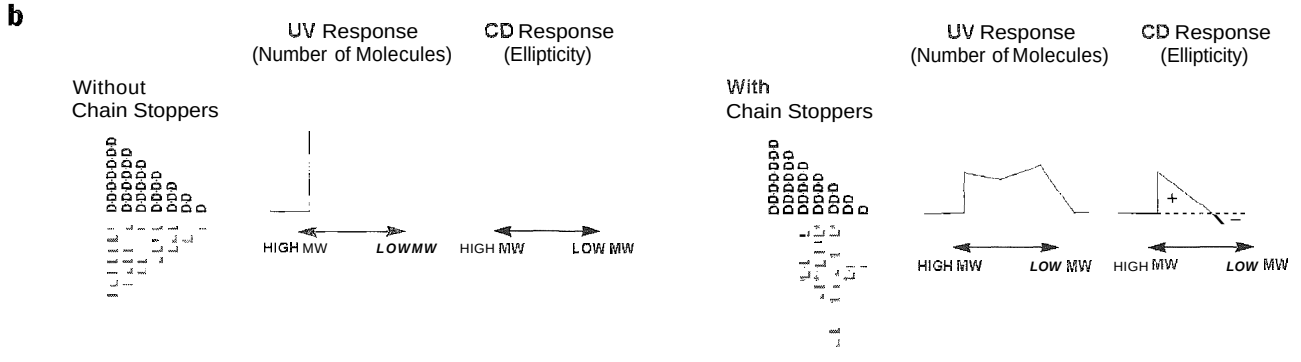

Fig. 7 (a) The optical resolution of poly-14 by enantioselective depolymerization with L-10 and L-11. (b) The SEC profiles of a racemic monomer for homochiral polymerization in the absence (left) and the presence (right) of chain stoppers. (View *this art in color at www.dekker.com.*)

L-isomer crystals, when a particle of L-dextrorotatory salt was seeded. However, in other phases than the crystalline states, attempts to manipulate homochiral assemblies were surprisingly limited.

As a preliminary result, Aida and Ishida demonstrated the optical resolution of a homochiral supramolecular polymer by controlling its MWD via the enantioselective depolymerization. As described above, 10, **11,** and 14 are expected to possess similar structures, because they are all derived from 9 (see the previous sections entitled "Homochiral Dimer" and "Homochiral Discrete Cluster"). Therefore, hydrogen-bonded homochiral complexes **10**·**14** and **11**·**14** are likely to be formed. Taking advantage of the reversible nature of hydrogen-bonded complexes, enantioselective depolymerization of the supramolecular polymer of racemic 14 was attained by using a mixture of L-**18** and L-**11** as chain stoppers (Fig. 7a). In this case, L-**10** and L-**11** could enantioselectively bind the two respective termini of poly(L-**14**), to reduce its molecular weight (Fig. 7a,b). For example, *SEC* traces of racemic 14 displayed a monodisperse chromatogram with a broad tail [Fig. 7b (left)], typical of noncovalent polymeric aggregates. In contrast, when an equimolar mixture of L-**10** and L-11 was added to a $CHCl_3$ solution of racemic 14, the *SEC* trace of the supramolecular polymer was considerably broadened due to two overlapped fractions [Fig. 7b (right)]: a fast-eluting (higher molecular-weight) fraction with a positive CD sign and a slow-eluting (lower molecular-weight) fraction with a negative CD sign. Because the CD signs of the L-forms of 14, poly-14, **10**, and **11** are all negative, and those of their D-forms are positive, the above observations strongly indicate that poly(L-**14**) in poly(*rac*-**14**) is enantioselectively depolymerized by the action of L-**10** and L-**11** to provide poly(L-**14**) with a lower molecular weight than that of poly(D-**14**).

ACKNOWLEDGMENTS

The works in homochiral supramolecular polymerization were carried out when I was a postgraduate student under the guidance of Prof. Takuzo Aida, to whom I am greatly indebted. I am also grateful to the JSPS Young Scientist Fellowship.

ARTICLES OF FURTHER INTEREST

Amino Acids: Applications, p. 42
Anion-Directed *Assembly*, p. 51
Chiral Guest Recognition, p. 236
Chiral *Induction*, p. 245
Crystal Growth Mechanisms, p. 364
DNA Nanotechnology, p. 475
Emergence of Life, p. 528
Gels, p. 586
Protein *Supramolecular* Chemistry, p. 1161
Scanning Tunneling Microscopy, p. 1202
Self-Assembly *in* Biochemistry, p. 1257
Supermicroscopy: AFM, *SNOM,* and *SXM*, p. 1394

REFERENCES

1. Pasteur, L. Mémorie sur la relation qui peut exister entre la form cristalline et la composition chimique, et sur la cause de le polarisation rotatorie. Acad. Sci. Paris 1848, *26*, 535–538.
2. Feringa, B.L.; van Delden, R.A. Absolute asymmetric synthesis: The origin, control and amplification of chirality. Angew. Chem.. Int. Ed. Engl. 1999, *38.* 3418–3438.
3. Hazen, R.M.; Filley, T.R.: Goodfriend. G.A. Selective adsorption of L- and D-amino acids on calcite: Implications for biochemical homochirality. Proc. Natl. Acad. Sci. U. S. A. 2001. *98*, 5487–5490.
4. Jacques, J.; Collet, A.; Wilen, S.H. *Enantiomers, Racemates and* Resolutions; Keieger Publishing: Florida, 1994.
5. Jacques, J.; Lelercq, M.; Brienne, M.-J. La formation de sels auqmente-t-elle la fréquence des dédoublements spontanés. Tetrahedron 1981. 37. 1727–1733.
6. Eckhardt, C.J.; Peachey, N.M.; Swanson, D.R.; Takecs. J.M.; Khan, M.A.; Gong, X.; Kim, J.-H.; Wang. J.; Uphaus, R.A. Nature 1993. *362.* 614–616.
7. Viswanathan. R.; Zasasdzinski, J.A.: Schwartz, D.K. Spontaneous chiral symmetry breaking by achiral molecules in a Langmuir–Blodgett film. Nature 1994. *368.* 440–443.
8. Stevens: *F.;* Dyer. D.J.; Walba, D.M. Direct observation of enantiomorphous monolayer crystals from enantiomers by scanning tunneling microscopy. Angew. Chem., Int. Ed. Engl. 1996, *35*, 900–901.
9. Fuhrhop, J.-H.; Koning, J. *Membranes and* Molecular Assemblies: The *Synkinetic* Approach; The Royal Society of Chemistry: Cambridge, 1994.
10. Gulik-Krzywicki, T.; Fouquey, C.: Lehn, J.-M. Electron microscopic study of supramolecular liquid crystalline polymers fonned by molecular-recognition-directed self-assembly from complementary chiral components. Proc. Natl. Acad. Sci. U. S. A. 1993, *90.* 163–167.
11. Goodby, J.W. Chirality in liquid crystals. J. Mater. Chem. **1991**, **1,** 307–318.
12. Thisaykta, J.; Kanee, H.; Kawauchi. S.; Watanabe. J. Spontaneous formation of a chiral structure in an achiral banana-shaped molecular system. Mol. Cryst. Liq. Cryst. 2000, *346*, 63–75.
13. Williams, T.; Pitcher, R.C.; Bommer. P.; Cutzwiller. J.; Uskokovid, M. Diastereomeric solute–solute interactions

of enantiomers in achiral solvents. Nonequivalence of the nuclear magnetic resonance spectra of racemic and optically active dihydroquinine. J. Am. Chem. Soc. 8969. *91*. 1871–1874.
14. Harger, M.J.P. Proton magnetic resonance no-equivalence of the enantiomers of alkylphenylphosphinic amides. J. Chem. Soc., Perkin Trans., II 1977. 1882–1887.
15. Dobashi, A.; Saito, N.: Motoyama. Y.; Hara, S. Self-induced nonequivalence in the association of D- and L-amino acid derivatives. J. Am. Chem. Soc. 1986. 108, 307–308.
16. Ciordano, C.: Restelli. A.; Villa, M. A case of self-induced anisochrony in the proton nuclear magnetic resonance spectra of 1.5-benzothiazepines. J. Org. Chem. **1991**, *56*. 2270–2272.
17. Kitamura. M.; Okada, S.: Suga, S.: Noyori, R. Enantioselective addition of dialkylzinks to aldehydes promoted by chiral amino alcohols. Mechanism and nonlinear effect. J. Am. Chem. Soc. 1989, *111*. 4028–4036.
18. Ishida. Y.; Aida. T. Homochiral supramolecular polymerization of an ''*S*''-shaped chiral monomer: Translation of optical purity into molecular weight distribution. J. Am. Chem. Soc. **2002**, *124*, 14017–14019.
19. Lehn, J.-M. Dynamic combinatorial chemistry and virtual combinatorial libraries. Chem. Eur. J. 8999. *5*, 2455–2463.
20. Prins. L.J.; Huskens. J.; de Jong. F.: Timmerman. P.: Reinnhoudt. D.N. Complete asymmetric induction of supramolecular chirality in a hydrogen-bonded assembly. Nature 1999. 398. 498–502.
21. Cooks, R.G.; Zhang, D.: Koch, K.J. Chiroselective self-directed octamerization of serine: Implications for homochirogenesis. Anal. Chem. **2001**, 73. 3646–3655.
22. Shi, X.; Fettinger, J.C.: Davis. J.T. Homochiral G-quadruplexes with Ba^{2+} but not with K^{+}: The cation programs enantiomeric self-recognition. J. Am. Chem. Soc. 2001. 123. 6738–6739.
23. Brunsveld, L.; Folmer, B.J.B.; Meijer, E.W.: Sijbesma. R.P. Supramolecular polymers. Chem. Rev. 2001. *101*, 4071–4098.

Stability Constants: Definition and Determination

Peter Cans
The University of Leeds, Leeds, United Kingdom

Alberto Vacca
Università degli Studi di Firenze, Sesto Fiorentino, Italy

INTRODUCTION AND DEFINITIONS OF STABILITY CONSTANTS

The following entry defines the commonly used stability constants (stepwise, overall. conditional, association, dissociation, and pK) and relates the values to a rigorous thermodynamic definition of equilibrium constants. In addition. the article briefly outlines experimental techniques (potentiometric titration, spectroscopic methods involving ultraviolet/visible, infrared, Raman, fluorescence. and nuclear magnetic resonance spectroscopy), together with the numerical methods and computer programs that can be used to derive stability constants from such experimental data.

THERMODYNAMIC DEFINITION

For a reaction of the type $pA+qB+.. \rightleftharpoons A_pB_{q..}$ a thermodynamic equilibrium constant, β^0_{pq} . is defined by the equality Eq. 1.

$$\{A_pB_{q..}\} = \beta^0_{pq..}\{A\}^p\{B\}^q.. \quad (1)$$

where {A) signifies the activity of a reagent, denoted by A, etc., and the species $A_pB_{q..}$ is said to be an adduct, or complex. A stability constant (or formation constant) is a particular kind of equilibrium constant that relates to the stability of a complex species.

Activities are, by definition, unit-less quantities. In practice it is more convenient to use concentrations. The activity. {A}. of a species A is related to its concentration, [A], by {A)=[A]γ_A, where γ_A is the activity coefficient that has units which are the inverse of the concentration unit. It follows that the thermodynamic stability constant can be defined by Eq. 2:

$$[A_pB_{q..}]\gamma_{pq..} = \beta^0_{pq..}[A]^p[B]^q..\gamma_A^p\gamma_B^q.. \quad (2)$$

The stability constant can be expressed as a product of two terms. a concentration quotient and an activity quotient, Eq. 3:

$$\beta^0_{pq..} = \frac{[A_pB_{q..}]}{[A]^p[B]^q..} \times \frac{\gamma_{pq..}}{\gamma_A^p\gamma_B^q..} \quad (3)$$

Stability Constants Based on Concentrations

If the activity quotient can be regarded as a constant, a stability constant can be defined as a concentration quotient, Eq. 4:

$$\beta_{pq..} = \frac{[A_pB_{q..}]}{[A]^p[B]^q..}$$

The activity quotient can be made effectively constant by performing the measurements in a medium of high ionic strength relative to the concentrations of the species involved in the equilibria. The stability constants obtained from measurements at relatively high ionic strength have the thermodynamic significance of setting that medium as the standard state: in terms of this definition of thermodynamic standard state, the activity quotient has a value of unity. This can clearly be seen in the relation between the stability constant and the standard free-energy change for the equilibrium: $\Delta G^0 = -RT\log_e\beta_{pq}..$. Thus, any stability constant has meaning only in terms of the standard state conditions.

Other forms of stability constant can be derived from the fundamental definition given in Eq. 2. For example, if one of the reagents is H^+, the hydrogen ion activity can be measured with a suitable electrode, and this will give rise to a mixed stability constant when the other species are represented by concentrations.

Conditional constants

A conditional constant is obtained when the measurements are made in the presence of a substance that affects the equilibria in a fixed way, but these effects are ignored. In fact, stability constants derived from measurements in an ionic medium are conditional in the sense that they are valid only under those experimental conditions. Each concentration term in Eq. 4 should be considered as the sum of the concentrations of all species that have the same stoichiometry in regard to the explicit reagents A,B.. but containing different quantities of the implicit reagents, such as the solvent or ions present in the ionic medium. The concentrations of the implicit reagents

Encyclopedia of Supramolecular Chemistry
DOI: 10.1081/E-ESMC 120012822

usually remain constant as long as the solvent or ionic medium is not changed.

The term "conditional" (or alternatively, apparent or effective) constant is sometimes used in analytical chemistry and frequently used in biological chemistry. A conditional constant is a concentration quotient that applies only when the concentration of one or more reactants or products is fixed at a particular constant value. For example, when the equilibrium $M+H_nL \rightleftharpoons ML+nH$ is studied at fixed pH, an effective constant can be defined by Eq. 5:

$$[ML] = K_{eff}[M][H_nL] \quad (5)$$

where n may be nonintegral, and H_nL may represent an equilibrium mixture of species with $n=0$, 1, etc.[1]

Overall and stepwise constants

The equilibrium constant defined in Eq. 4 is an overall constant. A stepwise constant refers to an equilibrium in which a single reagent molecule or ion is added to a complex species or another reagent. For example, the equilibrium constant for $A_pB_{q-1}..+B \rightleftharpoons A_pB_q..$ is given by Eq. 6:

$$K^{B}_{pq..} = \frac{[A_pB_q..]}{[A_pB_{q-1}..][B]} \quad (6)$$

An overall constant is simply the product of the stepwise constants leading to the complex of given stoichiometry. For example, $\beta_{12}=K_1K_2$, where $K_1=[AB]/[A][B]$, and $K_2=[AB_2]/[AB][B]$. The logarithm of the overall constant is the sum of the logarithms of the stepwise constants: $\mathrm{Log}\beta_{12}=\mathrm{Log}K_1+\mathrm{Log}K_2$.

Association and dissociation constants

The stability constant given in Eq. 4 is an association constant. A dissociation constant is numerically equal to the reciprocal of the corresponding association constant. It is common practice to quote dissociation constants for acids (particularly organic acids), while association constants are used for complexes. For a monobasic acid, HL. there are no further complications. But for polybasic acids, the numerical order of the two sets is reversed. For example, for a dibasic acid, the first stepwise dissociation constant is equal to the reciprocal of the second stepwise association constant and vice versa.

Variation of stability constants with temperature

Equilibrium constants vary with temperature according to the following well-known expression (Eq. 7):

$$\mathrm{Log}K = \frac{-\Delta H^0}{2.303RT} + \frac{\Delta S^0}{2.303R}$$

If ΔH^0 is measured by means of calorimetry, the value of the equilibrium constant at a temperature other than that of the standard state can be calculated. It has to be assumed that ΔH does not vary with temperature, which is only approximately true. The same assumption is made when deriving AH' from stability constant values obtained at different temperatures—the so-called Van't Hoff method, in which Log$K$ is plotted against $1/T$ to give a straight line with slope $-\Delta H^0/2.303$ R. Use of this method requires stability constants of high precision, because the error on ΔH^0 is considerably magnified with respect to the error on Log$K$.

Variation of stability constants with ionic medium

When a stability constant is derived from measurements in an ionic medium. the value will vary when the medium is changed. This is a subject of considerable importance, because often the medium of interest is different from the medium of measurement; for example, in biomedical applications, the medium of interest is a biological medium such as blood, but that medium is unsuitable for stability constant measurements. Corrections for variation of ionic strength can be made by using the Davies equation (Eq. 8) to estimate activity coefficients:

$$\mathrm{Log}\ \gamma = -Az^2\{[I^{1/2}/(1+I^{1/2})] - 0.31I\} \quad (8)$$

where I is the ionic strength; A is the Debye–Hückel limiting slope; and z is the electrical charge on the species under consideration. A better approximation can be made by application of the theory of specific interactions between ions.[2]

TYPES OF MEASUREMENT

In order to derive a stability constant. it is necessary to measure one (or more) concentration (or activity). When that quantity is measured over a range of experimental conditions, the method of least squares may be applied to the data to yield one (or more) stability constant.

Potentiometric Measurements

The most common quantity measured is the hydrogen ion concentration. This is measured by means of a glass electrode. The response of the glass electrode is assumed to follow a near-Nernstian law (Eq. 9):

$$E = E^0 + s\ \mathrm{Log}[H^+] \quad (9)$$

E^0 and s (ideal value $2.303\ RT/F$) are calibration parameters. The recommended calibration procedure involves the titration of a known quantity of a strong acid with a

base of known concentration; this procedure ensures that the electrode is calibrated in terms of hydrogen ion concentration. The data can be analyzed using the program GLEE.[3] which employs Gran's method.[4]

The term pH in this context must be understood to mean $-\mathrm{Log}[H^+]$: from Eq. 9, $pH=(E^0-E)/s$. Another point to note is that in Eq. 9, the measured potential; E, is expected to depend linearly on the logarithm of the concentration, for the glass electrode deviations occur at low and high pH values. At low pH, the effect can be partly corrected by adding a term proportional to $[H^+]$ to Eq. 9. At high pH, an additional term, proportional to [OH]. may be added. These additional terms are loosely described as correction for variation in junction potentials, and the proportionality constant(s) may be determined empirically. At high pH. the glass electrode is susceptible to interference from Na^+ ions (it also becomes a Na^+ ion-selective electrode). For this reason. the use of KOH as alkali is preferable to the use of NaOH when using a glass electrode.

In a typical stability constant determination, an acidified mixture is titrated with alkali; after each addition, the pH is measured to produce a so-called potentiometric titration curve.

Absorbance Measurements

The second most common quantity measured is UV/Visible absorbance. obtained by means of a spectrophotometer. Optical density (OD), is assumed to follow the Beer–Lambert law Eq. 10:

$$OD = LC_{pq..}[A_pB_{q..}] \tag{10}$$

where L is the path length of the cuvette. and $\varepsilon_{pq..}$ is the molar absorbance of the complex $A_pB_q...$ For pure substances, ε can be determined directly from a set of experimental measurements, but for species that only exist in equilibrium, the molar absorbance must be regarded as an unknown quantity. Measurements may be performed at a single wavelength or at multiple wavelengths. If a reagent is added in a stepwise manner, a spectrophotometric titration curve will result.

NMR Measurements

In recent years, NMR spectroscopy has been used more for stability constant determination. It can be used in two different ways. In systems where exchange is slow, each species gives a separate NMR spectrum; the (integrated) intensity of the signal from any one set of chemically equivalent nuclei is related to the concentration of the species containing that set of nuclei. Where exchange is rapid, the separate resonances merge to a single resonance with a chemical shift, δ, that is the average of the individual shifts, weighted according to the fractional population of a single nucleus (Eq. 11):

$$\delta = \sum_j \frac{x_j C_j}{T_x} d_j$$

where T_x is the total concentration of the reagent containing the nucleus under consideration; x_j is the stoichiometric coefficient (p, q, etc., in the chemical formula) of reagent X in the jth chemical species; and d_j is its chemical shift in that species.

Other Measurements

Other indicators of a species' concentration include fluorescent intensity, infrared intensity, Raman scattering intensity, and electron spin resonance. These will not be discussed in detail.

METHODS OF CALCULATION

A Simple System

A simple system involves the protonation of a base. L, in the equilibrium $L+H \rightleftharpoons LH$. Working with concentrations and omitting electrical charges, the system is defined by Eqs. 12–14:

$$[LH] = K[L][H] \tag{12}$$

$$T_L = [L] + K[L][H]$$

$$T_H = [L] + K[L][H] \tag{14}$$

where T_L and T_H are the total (analytical) concentrations of the base L and mineral acid. Both T_L and T_H must be known experimental quantities. The [L] and [H] are called the free concentrations of the reagents L and H, respectively. The term LH is conveniently called a complex species. If [H] is measured by means of a glass electrode (Eq. 10), the three equations can be solved for the three unknown quantities [L], [LH], and K. However, rather than obtain a K value at each point in a titration curve, it is preferable to treat the whole data set by the method of least squares.

A General Procedure

The most general method is as follows. Each stability constant is defined by an expression of the type given in Eq. 4, and for each reagent there is an equation of mass balance. of the general form as follows in Eq. 15:

$$T_A = [A] + \Sigma p\beta_{pq..}[A]^p[B]^q.. \tag{15}$$

Then. if values of the stability constants are "known." there are as many mass-balance equations as unknown free concentrations of the reagents [A], [B], ... The solution of these nonlinear simultaneous equations provides the values of the free concentrations and thence, from the definitions such as Eq. 4, the concentrations of all the complex species. Armed with these concentrations, it is then possible to calculate quantities that correspond to the quantities observed and to minimize a sum of squared residuals (differences between observed and calculated values) with respect to the stability constants, that is, to use the least-squares method to find the values and standard deviations on the stability constants. A large number of computer programs for stability constant determination were published.[5] The discussion below concentrates on the programs most familiar to the authors and that are of a completely general nature, having no restrictions regarding the number of reagents, the stoichiometry of the complexes formed (p, q .. values), or the number of measurements collected.

The least-squares problem is also nonlinear and so must be solved by an iterative procedure. This means that initial values of the stability constants must be estimated before the iterations can begin. One way to obtain the estimates is by finding values for analogous compounds in one of two extensive stability constant databases.[6,7]

Potentiometric data

This form of data typically consists of one or more titration curves, each curve containing a number of data points of the form titre volume. electrode reading. The electrode is an ion-selective electrode (ISE). The most common electrode used is the glass-electrode, which is sensitive to the hydrogen ion, H^+, but other ISEs may be used just as well. The electrode potential is supposed to follow a modified Nernst equation. such as Eq. 9.

The computer program Hyperquad[5] may be used to determine stability constants from potentiometric data. This program employs the general procedure outlined above with the following specifics for implementation.

Solution of the mass-balance equations at any titration point provides the concentration of free hydrogen ions $[H^+]$ so that a potential can be calculated for Eq. 10. The objective function to minimize can be written (in simplified form) as $\Sigma w(E^{obs} - E^{calc})^2$. It is immediately obvious that the objective function contains no explicit reference to the stability constants. Therefore, in order to use the powerful Gauss–Newton method of minimization, it is necessary to perform an implicit differentiation. details of which can be found in the literature."]

Absorbance data

Hyperquad can also handle absorbance data. Indeed, Hyperquad can handle potentiometric and absorbance data obtained on the same solutions. With absorbance data the Beer–Lambert law (Eq. 10) applies at each wavelength where measurements were made. Nowadays. it is common practice to record complete spectra at fixed wavelength intervals, though in principle, measurements need only be made at a single wavelength. Once the free concentrations are found by solving the equations of mass balance, the molar absorbances can be obtained by solving the set of equations (Eq. 10) with measured absorbances in place of OD. This is a linear least-squares system, so no iteration or initial estimates are required. There is a linear least-squares system at each wavelength measured. Once the molar absorbances are deduced, the optical density may be calculated, and the (simplified) objective function $\Sigma w(OD^{obs} - OD^{calc})^2$ may be minimized. Once again, the stability constants are implicit parameters of the objective function.

Another computer program that can be applied to absorbance data is pHab.[8] The main difference is that pHab assumes that pH was set for each solution. This means that there is one less free concentration to calculate, but otherwise. the program functions in a similar manner.

These programs can also be used with fluorescence data on the assumption that the fluorescent intensity due to any species is a linear function of the concentration of that species. This assumption is usually valid for dilute solutions. but as the concentration rises, self-absorption, or quenching, causes deviations from linearity to occur.

NMR data

The data from slow-exchange systems can be treated as though it were absorbance data. When exchange is fast on the NMR timescale. the chemical shift of any given nucleus is given by Eq. 11. The computational procedure used in the computer program HypNMR[9] is similar to that used for absorbance data. Free concentrations are obtained by solving the equations of mass balance, and the individual chemical shifts are derived by means of a linear least-squares calculation. The objective function $\Sigma w(\delta^{obs} - \delta^{calc})^2$ is, once again, an implicit function of the stability constants.

Common Features

The three programs Hyperquad. pHab, and HypNMR use an objective function that contains weights. represented by the symbol w. Ideally: the weight associated with any measured quantity should be equal to the reciprocal of the variance on the measurement. When this is so, the objective function divided by the number of degrees of freedom (reduced objective function) has an expectation value of unity. This means that there can be an objective criterion of the goodness of fit. However. estimation of experimental errors is tedious and difficult. so the ideal weighting scheme is hard to realize in practice. When a

single type of measurement is made (e.g., NMR chemical shift), the weighting scheme has little bearing on the values to be calculated for the stability constants.

The programs provide a means for finding good initial values for the stability constants by manual fitting, with a display of observed and calculated values; the stability constants are adjusted by hand so as to reduce the systematic differences between observed and calculated values. This phase of the computation is important, because it serves to validate the choice of species taken to be present in the equilibria. In particular, in cases other than the simple one where only a 1:1 host:guest complex is formed, manual fitting will be useful to establish the stoichiornetry of the complexes formed.

CONCLUSION

The fundamental question to answer is as follows: Are the calculated values equal to the experimental values within experimental error? Implicit in this question is the need to have estimates of experimental error. With programs in the Myperquad suite, these estimates are entered as data such that the expectation value of the reduced objective function is unity. In practice, any value near unity (perhaps less than three) indicates an acceptable fit. However, other criteria should also be satisfied. In particular, the residuals (observed minus calculated values) should not show any systematic trend along a titration curve. The existence of a systematic trend implies the presence of a systematic error, most probably that the wrong set of chemical species was chosen to represent the equilibria.

Another indication of the quality of the results is given by the estimates of standard deviation on the stability constants. It should be remembered that these estimates depend only on random experimental errors. The 95% confidence limits are usually taken as ± 2 standard deviations. It should also be remembered that standard deviation refers only to precision. The accuracy of a derived stability constant is lower because of the inevitable presence of systematic errors in the measurements.

ARTICLES OF FURTHER INTEREST

Nuclear Magnetic Resonance Spectroscopy, p. 981
Selectivity: *Thermodynamic* and Kinetic, p. 1225

REFERENCES

1. Flashka, H.A. EDTA Titvations; Pergamon Press: Oxford, 1964.
2. Ciavatta. L. The specific interaction theory in equilibrium analysis. Some empirical rules for estimating interaction coefficients of metal ion complexes. Ann. Chim. (Rome) **1980.** *80,* 255–263.
3. Gans, P.; O'Sullivan, B. GLEE, a new computer program for glass electrode calibration. Talanta **2000.** *43,* 1739–1753.
4. Gran, G. Determination of the equivalence point in potentiometric titrations. Part II. Analyst **1952,** 77. 661–671.
5. Gans, P.; Sabatini, A.: Vacca, A. Investigation of equilibria in solution. Determination of equilibrium constants with the HYPERQUAD suite of programs. Talanta **1996,** *43.* 1739–1753.
6. Pettit, L.D.: Powell. K.J. IUPAC *Stability Constants Database—SC-Database*: Academic Software: Otley, UK, 1999. http://www.acadsoft.co.uk.
7. Smith, R.M.; Martell, A.E. NIST *Critically* Selected Stabilit); Constants of Metal *Complexes* Database, *Version 4.0;* U.S. Department of Commerce. National Institute of Standards and Technology: Gaithersburg, MD 20899 USA. 1997.
8. Gans, P.; Sabatini, A.; Vacca, A. Determination of equilibrium constants from spectrophotometric data obtained from solutions of known pH: The program pHab. Ann. Chim. (Rome) **1999**, *89,* 45–49.
9. Frassineti, C.; Ghelli, S.; Gans. P.; Sabatini, A.: Moruzzi, M.S.; Vacca, A. Nuclear magnetic resonance as a tool for determining protonation constants of natural polyprotic bases in solution. Anal. Biochem. **1995,** 231. 374–382.

Steroid-Based Anion Complexation Agents

Anthony P. *Davis*
University of Bristol, Bristol, United Kingdom

INTRODUCTION

Supramolecular chemistry depends critically on preorganization, the correct and reliable positioning of functional groups and surfaces to achieve specific binding, etc. In principle, this may be achieved with flexible but conformationally biased architectures. However, in practice, it is difficult to operate without rigid spacers and scaffolds. While these roles are often filled by aromatic rings, fused aliphatic systems can be equally rigid and have certain advantages. For example, they are usually chiral and possess two valencies (and thus two orientations) at each nonbridging center. Also, they are readily available in the form of inexpensive natural steroids such as cholesterol **1** and cholic acid **2**.[1–4] In the field of anion recognition. the steroid nucleus has made notable contributions by providing a scaffold on which to mount polar functional groups. and lipophilic surfaces that can be used to maintain solubility in nonpolar media. This brief account of the area is divided into two parts, covering electroneutral anion receptors derived from cholic acid and positively charged steroid-based anion complexers.

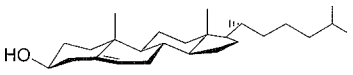

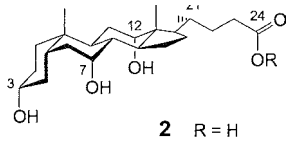

2 R = H
3 R = Me

ELECTRONEUTRAL ANION RECEPTORS BASED ON CHOLIC ACID

The history of anion complexation in supramolecular chemistry is almost as long as that of cation binding.[5,6] However, it developed differently. Whereas the first cation-binding agents (crown ethers, cryptands, etc.) were electroneutral and compatible with organic solvents, the early anion complexers were cationic and highly hydrophilic.[7] It is only recently, perhaps since the early 1990s. that much attention has been paid to the design of electroneutral, lipophilic anion-binding molecules.

One obvious approach to electroneutral anionophores is the deployment of neutral H-bond donor functionality around a central binding site. However, the execution of this strategy is nontrivial. Anions are generally larger than cations, while convergent H-bond donor centers must be spaced more widely than, for example. electron pair donors (compare O—H· ·X^-· ·H—O versus O· ·M^+· ·O). Both factors imply that large, elaborate frameworks may be required. Moreover, most neutral H-bond donor groups are also H-bond acceptors, raising the pcssibility of intramolecular H-bonding within the receptor.

The steroid nucleus provides an attractive solution to these problems. It is extended, and thus able to support well-separated functional groups, and rigid, such that these groups cannot easily interact with each other. Of the readily available steroids. cholic acid 2 is especially useful.[1,2] It possesses a curved profile, with three codirected hydroxyl groups emerging from the concave α-face. This structure naturally lends itself to the creation of macrocyclic or cleft-type architectures with polar interiors and apolar exteriors. The hydroxyl groups may be differentiated and converted to a range of other functional groups, while the side-chain carboxyl affords further possibilities.

Cholic acid has been converted into a series of electroneutral anionophores targeted at inorganic anions. These may be divided into two categories: acyclic and macrocyclic receptors that exploit the H-bonding properties of (at least some of) the secondary hydroxyls, and acyclic podands in which all the hydroxyl groups were modifed to give alternative binding functionality. These two classes are considered separately below.

Hydroxysteroid Anion Receptors Derived from Cholic Acid

The hydroxyl groups already present in 2 are, of course, H-bond donors, so that simple esters such as 3 might be expected to have anion-binding properties. Indeed, 3 was found to associate with tetrabutylammoniurn (TBA) bromide, tosylate, mesylate. and hydrogen phenylphosphonate in benzene and benzene–hexane mixtures.[8,9]

Encyclopedia of Supramolecular Chemistry
DOI: 10.1081/E-ESMC 120012780

However, there was no detectable complexation in $CDCl_3$ or more polar solvents. Some improvement resulted from the incorporation of a single -NH-CO group. Thus. the acetamido derivative 4 showed modest affinities for TBA chloride and bromide in $CDCl_3$ (K_a=53 and 36 M^{-1}, respectively).[9,10] Further, significant increases could be obtained using a more elaborate, cyclodimeric architecture. The cryptand ***5*** was specifically designed to encapsulate a small, spherical anion such as fluoride or possibly chloride. It was synthesized from 2 via degradation of the C21–C24 side chain, introduction of a short spacer plus an externally directed solubilizing group. and cyclodimerization. NMR titrations reveaied binding constants of 3320, 990, and 250 M^{-1} to TBA fluoride, chloride, and bromide, respectively.[10]

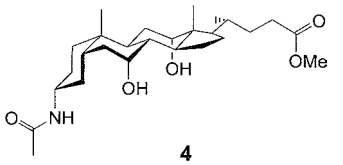

4

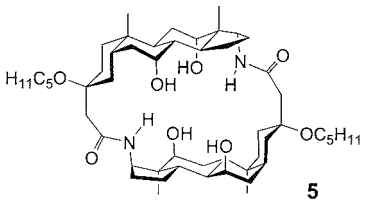

5

Steroidal Podands with Multiple NH Groups

As H-bond donors in supramolecular chemistry, NH units are far more versatile than OH groups. The third valence on the nitrogen can be exploited structurally and can also be used to tune the H-bond donor power. Accordingly, steroidal podands with three or more NH groups proved more effective than 4 or ***5***. Early studies involved the sulfonamide *bis*-carbamate 6 and the iris-sulfonamide **7**.[11] Both systems provide well-defined binding sites for anions. In 6, free rotation is possible about the C3–N bond. but the carbamate NH groups are preorganized to some extent through restricted rotation about the axial C7/C12-O bonds and the preference for *Z,Z*-conformations across the carbarnate units." In 7, restricted rotation about the C7/C12-N bonds (Eq. 1) holds the NH groups firmly in place for anion recognition. NMR titrations revealed the binding constants shown in Table 1, significantly higher than those for 5.

Table 1 Association constants (K_a, M^{-1}) of 6 and **7** with TBA Salts in $CDCl_3$ (NMR titrations)

Anion	*Complex* **with** 6	*Complex* **with** 7
F^-	15.400	Not determined
Cl^-	7200	92,000
Br^-	7200	9200
I^-	930	525
TsO^-	865	950

Data from Ref. [11]

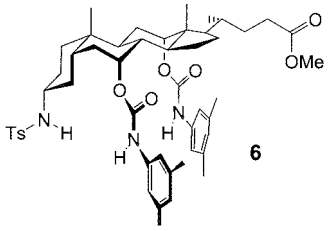

6

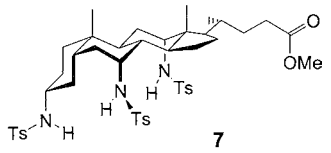

7

The steroidal podand architecture clearly had potential for further development. Electron-withdrawing substituents could be used to increase H-bond donor potency, and further NH groups could be added. Progress was hindered by problems of measurement: at $K_a \sim 10^5$ M^{-1}, receptor **7** had already attained the upper limit compatible with NMR titrations. However, a solution was found in Cram's extraction-based methodology, whereby binding constants are determined from the ability of the receptor to extract a hydrophilic substrate from water into an organic medium.[12]b Once this method was calibrated for use with tetraethylammonium (TEA) chloride and bromide, it was possible to investigate a second generation of podands.[13,14] Receptors 8–13 feature a lipophilic side chain (to minimize loss during extraction experiments) and acidifying, nitrophenyl substituents. As shown in Table 2. the binding constants to TEA chloride and bromide increase through the series as the number of H-bond donors increases. The sequence also illustrates the

[a] *Ab initio* calculations on *O,N*-dimethylcarbamate (6–31G* basis set) indicate that the *Z,Z*-conformation lies 5.58 kJ mol^{-1} below the next lowest energy minimum.

[b] Alternatively, NMR titrations could have been continued in more competitive solvents, such as DMSO. However, it was thought preferable to retain the nonpolar medium, as being more relevant to (for example) biological membranes.

Table 2 Association constants (K_a, M^{-1}) of **8–13** with TEA chloride and bromide in water-saturated $CHCl_3$ (extraction measurements)

Receptor	Complex with TEACl	Complex with TEABr
8	3.2×10^6	1.1×10^6
9	3.4×10^7	2.9×10^7
10	4.77×10^8	2.26×10^8
11	1.05×10^9	3.24×10^8
12	6.60×10^{10}	1.68×10^{10}
13	1.03×10^{11}	2.59×10^{10}

Data from Refs. [13,14]

slight advantage of thiourea over urea groups in anion recognition. The affinities of the stronger receptors are exceptional; at the time of writing, the binding constant of 10^{11} M^{-1} for **13**+TEACl is the highest published value for an electroneutral, purely organic anionophore.

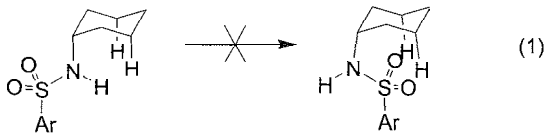

(1)

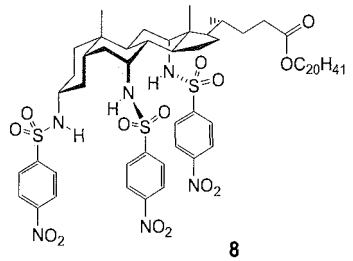

8

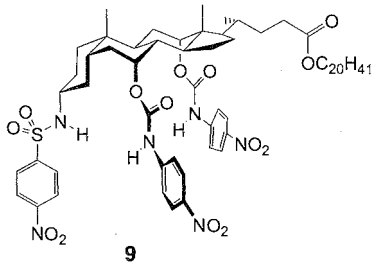

9

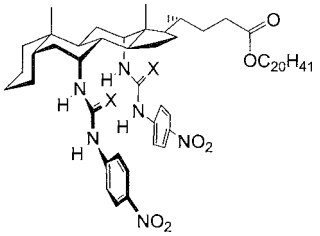

10 X = O
11 X = S

The advent of these powerful and highly lipophilic anionophores raises the possibility of new applications, for example, in the area of membrane chemistry. An early result is the discovery that **14** and **15** can serve as translocases for phospholipids. promoting the *trans*-membrane shuttling of polar, phosphate-containing head groups.[15]

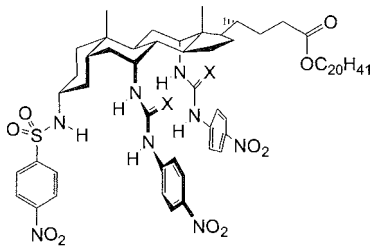

12 X = O
13 X = S

STEROID-BASED ANION RECEPTORS WITH NET POSITIVE CHARGE

The steroid nucleus has also been exploited in a variety of positively charged anion complexers. These fall naturally into two categories: those employing guanidinium units as the major binding centers and those bearing protonated amino groups.

Steroidal Guanidinium Cations as Anion Receptors

The guanidinium cation is well-established as a center for carboxylate recognition, through formation of electroneutral, H-bonded complexes **16**. High affinities are observed, even in polar solvents.[16] Placed on a steroidal scaffold. a guanidinium group can therefore position a carboxylate within a well-defined (and chiral) environment created by other substituents. Cholic acid. once again. is an attractive starting material for such systems. Elaboration of the secondary hydroxyl groups can lead to a variety of receptors in which three independent contacts are made with a substrate. For example. a series of cations **17** was prepared with a view to enantioselective carboxylate recognition.[17,18] The receptors could be tested by straightforward extraction experiments, in which **17** served as both extractant and chiral NMR shift reagent. As shown in Table 3. good selectivities were observed with *N*-acetyl amino acids as substrates. Perhaps surprisingly. the asymmetrically derivatized receptors **17c–e** did not generally perform better than their symmetrically substituted relatives; indeed. symmetrically substituted **17b** gave (marginally)

Table 3 Enantioselectivities (L:D) shown by receptors **17a–e** in extraction experiments

Receptor	*N*-Ac-DL-alanine	*N*-Ac-DL-valine	*N*-Ac-DL-tryptophan
17a	7:1	7:1	7:1
17b	10:1	9:1	9:1
17c		2:1	1:1
17d	3:1	4:1	4:1
17e	6:1	9:1	6:1

Data from Refs. [17,18]

the best overall results. Receptor 18, a lipophilic variant of this system; proved capable of transporting *N*-acetylphenylalanine enantioselectively, with turnover. through nonpolar solvents. As well as the traditional "U-tube" apparatus. a "hollow-fiber membrane" separator was used in this work, raising the possibility of industrial-scale separations.[19]

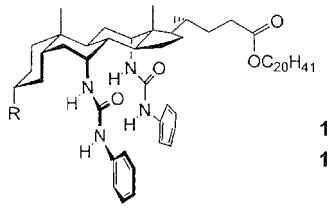

14 R = H
15 R = OAc

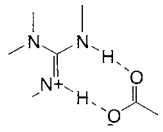

16

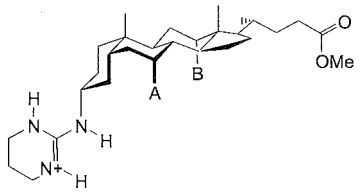

17a A = B = OCONHPh
17b A = B = $OCONHC_6H_4(p\text{-}CF_3)$
17c A = OH, B = OCONHPh
17d $A = OCONHBu^t$, B = OCONHPh
17e $A = OCONHC_6H_3(o,o\text{-}Cl_2)$, B = OCONHPh

Two units of cholic acid were linked through a guanidinium moiety to create receptor **19**.[20] The targets in this case were glucuronic acid salts such as **20**. The steroidal units caused a small but significant increase in binding to *20* (K_a=7000 M^{-1} versus 2800 M^{-1} for a nonsteroidal control). A framework derived from corticosterone was used to position *bis*-guanidinium units relative to an imidazole, as in **21**. The imidazole was

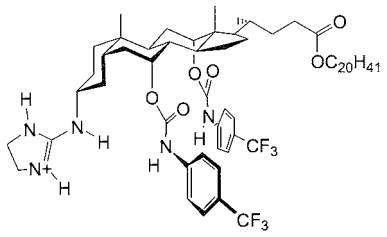

18

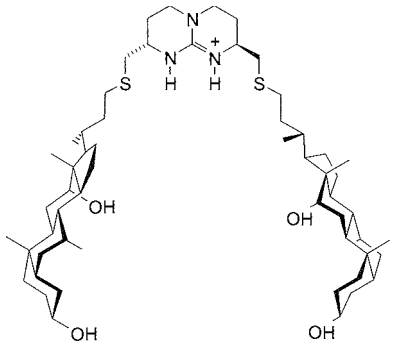

19

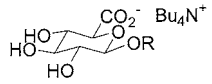

20

expected to act as a general base, promoting cleavage of bound RNA. Dication **21** was capable of cleaving RNA models, although accelerations over background were only moderate.[21]

Protonated Aminosteroids

Finally, a range of steroidal polyamines were found to promote transport across cell/liposome membranes or bind to nucleic acids and promote gene transfection. Although these compounds have not in general been studied as receptors. their interactions with anionic centers are presumably central to their activities. For example, **22**[22] and **23**[23] were incorporated in vesicle membranes and shown to discharge pH gradients across the membranes. Their mechanisms of action are

uncertain. but symport transfer of H^+X^- is a likely option.

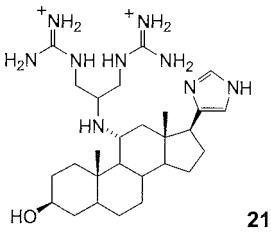

21

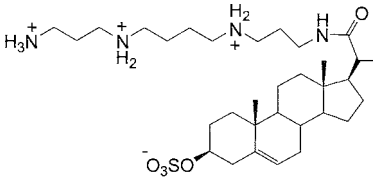

22

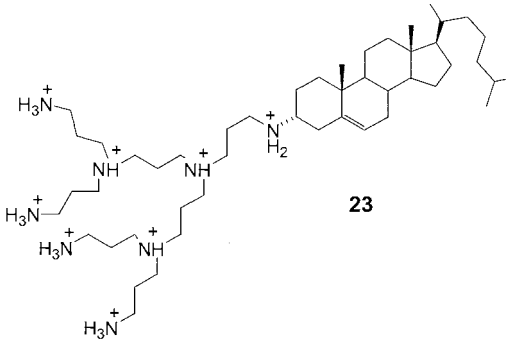

23

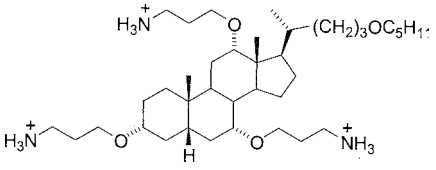

24

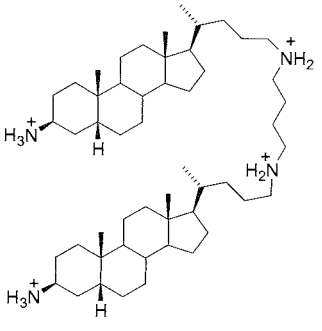

Triamine 24 and relatives permeabilize the membranes of gram-negative bacteria and possess antibiotic activity.[24] A series of polyamines derived from deoxycholic acid, lithocholic acid. or cholesterol were shown to strongly bind DNA.[25,26] Especially effective was 25, showing higher affinities than the natural DNA-complexer spermine.[25] Other steroidal amines were shown to act as cytofectins, promoting the delivery of DNA from liposomes to cell nuclei.[27] Examples are CTAP **26**[28] and the facial amphiphiles **27**[29] and **28**.[30]

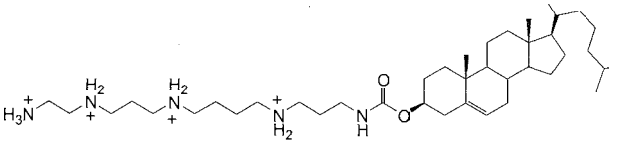

26

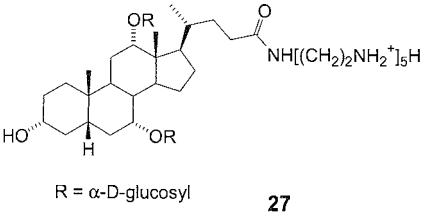

R = α-D-glucosyl

27

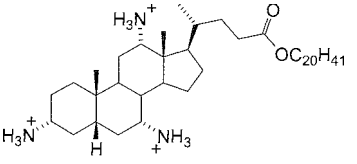

28

CONCLUSION

Steroid-based anion receptors show exceptional binding constants, encouraging enantioselectivities and a range of membrane-related activities. Much structural space remains unexplored. especially in the series derived from cholic acid 2. and further advances can be expected. In particular, the podand architecture of 6–15, 17. and 18 is amenable to variation through combinatorial chemist ~ ~ . and this technique may expand the scope and effectiveness of steroid-based anion recognition in years to come.

ACKNOWLEDGMENTS

The author thanks his coworkers, whose names appear in the references, for their contributions to the research described in this article. Funding for our program on steroidal anion receptors was provided by the EPSRC, the European Commission, the University of Bristol, and Enterprise Ireland.

ARTICLES OF FURTHER INTEREST

Amide- and Urea-Based Anion Receptors, p. 31
Amino Acids: Applications, p. *42*
Chiral Guest Recognition, p. 236
Deoxycholic, Cholic, and Apocholic Acids, p. *441*
Fluorescence Sensing of Anions, p. 566
Guanidinium-Based Anion Receptors, p. 615
Hydrogen Bonding, p. 658
Ionophores, p. 760
Organometallic Anion Receptors, p. 1006
Protonated Aza-Macrocycles for Anion Complexation, p. 1170
Pyrrole- and Polypyrrole-Based Anion Receptors, p. *1176*
Simultaneous Binding of *Cations and Anions,* p. 1291

REFERENCES

1. Davis, A.P. Cholaphanes et al.; steroids as structural components in molecular engineering. Chem. Soc. Rev. 1993. 22 (4). 243–253.
2. Davis. A.P.; Bonar-Law. R.P.; Sanders, J.K.M. Receptors Based on Cholic Acid. In Comprehensive *Supramolecular Chemistry*; Murakami, Y., Ed.: Suprainolecular Reactivity and Transport: Bioorganic Systems, Pergamon: Oxford, 1996: Vol. 4, 257–286.
3. Li. Y.X.; Dias, J.R. Dimeric and oligomeric steroids. Chem. Rev. 1997. *97* (1), 283–304.
4. Wallimann. P.; Marti, T.: Furer, A.; Diederich, F. Steroids in molecular recognition. Chem. Rev. 1997. 97 (5), 1567–1608.
5. Beer, P.D.; Gale, P.A. Anion recognition and sensing: The state of the art and future perspectives. Angew. Chem., Int. Ed. 2001, *40* (3), 487–516.
6. Bianchi, A.; Bowman-James, K.; Garcia-Espafia, E. *Supramolecular Chemistry* of Anions; Wiley-VCH: New York. 1997.
7. Park. C.H.; Simmons, H.E. Macrobicyclic amines. III. Encapsulation of halide ions by in,in-1,(k+2)-diazabicyclo[k.l.m]alkane-ammonium ions. J. Am. Chem. Soc. 1968; *90* (9), 2431–2432.
8. Davis, A.P.; Perry. J.J.: Wareham, R.S. Anion recognition by alkyl cholates: Neutral anionophores closely related to a natural product. Tetrahedron Lett. 1998, *39* (25), 4569–4572.
9. Perry. J.J. Steroid-Based Receptors for Anions and Polar Molecules. Ph.D. Thesis; University of Dublin, 1995.
10. Davis. A.P.; Gilmer. J.F.; Perry. J.J. A steroid-based cryptand for halide anions. Angew. Chem., Int. Ed. Engl. 1996. *35* (12). 1312–1315.
11. Davis, A.P.; Perry, J.J.; Williams. R.P. Anion recognition by tripodal receptors derived from cholic acid. J. Am. Chem. Soc. 1997, *119* (7), 1793–1794.
12. Kyba, E.P.; Helgeson. R.C.; Madan, K.: Gokel, G.W.; Tarnowski, T.L.; Moore, S.S.; Cram, D.J. Host–guest complexation. 1. Concept and illustration. J. Am. Chem. Soc. 1977, *99* (8), 2564–2571.
13. Ayling, A.J.; Pérez-Payán, M.N.; Davis, A.P. New "cholapod" anionophores; High-affinity halide receptors derived from cholic acid. J. Am. Chem. Soc. 200%.*123* (50). 12716–12717.
14. Ayling, A.J.; Broderick, S.; Clare, J.P.; Davis, A.P.; Pérez-Payán, M.N.; Lahtinen, M.; Nissinen, N.J.; Rissanen, K. An extraction-based assay for neutral anionophores: The measurement of high binding constants to steroidal receptors in a non-polar solvent. Chem. Eur. J. 2002. *8* (9). 2197–2203.
15. Lambert, T.N.; Boon, J.M.; Smith, B.D.; Pérez-Payán, M.N.: Davis, A.P. Facilitated phospholipid flip-flop using synthetic steroid-derived translocases. J. Am. Chem. Soc. 2002. *124.* 5276–5277.
16. Fan, E.; Arman, S.A.V.; Kincaid. S.; Hamilton, A.D. Molecular recognition: Hydrogen-bonding receptors that function in highly competitive solvents. J. Am. Chern. Soc. 1993. *115* (1), 369–370.
17. Davis. A.P.; Lawless, L.J. Steroidal guanidinium receptors for the enantioselective recognition of N-acyl a-amino acids. Chem. Commun. 1999, (1). 9–10.
18. Lawless. L.J.; Blackburn. A.G.; Ayling, A.J.; Pérez-Payán, M.N.; Davis, A.P. Steroidal guanidines as enantioselective receptors for N-acyl α-amino acids. Part 1. 3α-guanylated carbamates derived from cholic acid. J. Chem. Soc., Perkin Trans. 1 2001, (11), 1329–1341.
19. Baragafia. B.; Blackburn, A.G.: Breccia, P.; Davis, A.P.; de Mendoza. J.: Padrón-Carrillo, J.M.: Prados, P.; Riedner. J.; de Vries, J.G. Enantioselective transport by a steroidal guanidiniurn receptor. Chem. Eur. J. 2002. *8.* 2931–2936.
20. Segura, M.; Alcazar. V.; Prados, P.; de Mendoza, J. Synthetic receptors for uronic acid salts based on bicyclic guanidinium and deoxycholic acid subunits. Tetrahedron 1997, *53* (38). 13119–13128.
21. Oost, T.; Kalesse, M. Synthesis of RNAse active site model systems using a steroid template. Tetrahedron 1997, *53* (25). 8421–8438.
22. Merritt. M.; Lanier, M.: Deng. G.; Regen, S.L. Sterol-polyamine conjugates as synthetic ionophores. J. Am. Chem. Soc. 1998, *120* (33), 8494–8501.
23. Sakai. N.; Matile. S. Transrnembrane ion transport mediated by amphiphilic polyamine dendrimers. Tetrahedron Lett. 1997, *38* (15), 2613–2616.

24. Li, C.H.: Budge. L.P.: Driscoll, C.D.; Willardson, B.M.: Allman. G.W.: Savage, P.B. Incremental conversion of outer-membrane permeabilizers into potent antibiotics for Gram-negative bacteria. J. Am. Chem. Soc. 1999, *121* (5). 931–940.
25. Hsieh. H.-P.: Muller, J.G.; Burrows, C.J. Structural effects in novel steroidal polyamine-DNA binding. J. Am. Chem. Soc. 1994. *116* (26). 12077.
26. Geall. A.J.: Taylor, R.J.: Earll, M.E.: Eaton. M.A.W.; Blagbrough. I.S. Synthesis of cholesterol-polyamine carbarnates: pK_a studies and condensation of calf thymus DNA. Chem. Commun. 1998. (13), 1403–1404.
27. Miller, A.D. Cationic liposomes for gene therapy. Angew. Chem., Int. Ed. 1998, 37 (13–14), 1768–1785.
28. Cooper, R.C.: Etheridge, C.J.; Stewart, L.; Marshall. J.; Rudginsky, S.; Cheng, S.H.: Miller, A.D. Polyamine analogues of 3 β-[*N*-(*N*′,*N*′-dimethylaminoethane)carbamoyl]cholesterol (DC-Chol) as agents for gene delivery. Chem. Eur. J. 1998, 4 (1), 137–151.
29. Walker, S.; Sofia. M.J.: Kakarla. R.: Kogan, N.A.: Wierichs. L.: Longley, C.B.; Bruker. K.; Axelrod. H.R.: Midha, S.; Babu, S.; Kahne, D. Cationic facial amphiphiles: A promising class of transfection agents. Proc. Natl. Acad. Sci. U.S.A. 1996. 93 (4). 1585–1590.
30. Vandenburg. Y.R.: Smith. B.D.; Pérez-Payán, M.N.; Davis, A.P. Non-leaky vesicle fusion and enhanced cell transfection using a cationic facial amphiphile. J. Am. Chem. Soc. 2000. *122* (13). 3252–3253.
31. Boyce. R.; Li. G.: Nestler, H.P.; Suenaga, T.; Still. W.C. Peptidosteroidal receptors for opioid peptides. Sequence-selective binding using a synthetic receptor library. J. Am. Chem. Soc. 1994. *116* (17), 7955.
32. De Muynck, H.: Madder. A.; Farcy. N.; De Clercq, P.J.; Pérez-Payán, M.N.: Öhberg, L.M.: Davis. A.P. Application of cornbinatorial procedures in the search for serine-protease-like activity with focus on the acyl transfer step. Angew. Chem., Int. Ed. 2000. 39 (1). 145–148.

Strict Self-Assembly and Self-Assembly with Covalent Modifications

Bruce C. Gibb
University of New Orleans, New Orleans, Louisiana, U.S.A.

INTRODUCTION

At the most general level, the words "self-assembly" are used to identify the phenomenon whereby some kind of higher-level pattern emerges from the interactions of multiple simple components (Fig. 1). We are concerned here with the phenomenon of molecules coming together in a specific fashion so as to engender the formation of a higher species that is precisely defined at the molecular level. An example from the Fujita group is shown in Scheme 1.[1] To sets this particular type of self-assembly in its proper context. we should note that in the field of chemistry. ihe term "self-assembly" is used to describe two distinct types of processes. On the one hand, there are assemblies that lead to the formation of essentially infinite arrays, while on the other hand; there are assemblies such as that shown in Scheme 1 that lead to distinct, bounded species. Furthermore. within each of these categories, it is possible to make a further distinction that reflects the scale of organization. For example, for infinite arrays. we can consider processes such as crystallization,[2] where the molecules are ordered at the molecular level (ca. 10^{-9} m), or the formation of self-assembled monolayers[3] and bilayers,[4] where there is little order between individual molecules, but a larger scale of organization is evident across say the 10^{-6}m level. Likewise. the scale of organization for assemblies leading to distinct species can be broken down into similar categories. Briefly stepping out with the bounds of molecular assemblies. we can note the self-assembly of macroscale objects (10^{-3} m) is currently being investigated.[5] However, as far as the interaction of molecules to form distinct species goes, we can consider the formation of micelles[3] and vesicles[4] that constitutes assembly at the 10^{-6}m level, while the formation of the discrete molecular assemblies of interest here represents system ordered at the 10^{-9}m level.

The essential features of chemical assembly processes is that they share a common self-correcting mechanism.[6–8] In other words, strict self-assemblies are fully reversible, dynamic. systems that lead to a product that represents the global thermodynamic minimum for the system. Sometimes an additive or template"-"' is needed to boost the efficiency of the assembly. but this is the only true variable if we are speaking of strict self-assembly. *At* their *cores, strict molecular assemblies consist of subunits, product, and an equilibrium that relates the two.*

One addition to the assembly lexicon added a layer of complexity to the above definition. Thus, one of the seven different classes of self-assembly originally proposed by Lindsey.[11]—which are strict self-assembly processes (with or without a template) positioned in different chemical settings—is commonly known as "irreversible self-assembly." This term is used to describe two-step processes, whereby a strict self-assembly processes is followed by irreversible reactions that covalently knit together the array of subunits. As Whitesides noted, strictly speaking this term is a misnomer.[7] Hence, along with other types of post-assembly modified self-assemblies, we categorize these processes as "self-assembly with covalent modification." Postmodification generally comes in the form of a series of covalent bond formation steps and is of less interest to us here. The crux of any self-assembly process is the self-assembly.

Even within the strict confines given above. self-assembly processes come in all shapes and sizes. One of the results of this complexity is that defining self-assembly is difficult. Thus, although definitions from Hamilton,[6] Whitesides,[7] and Lehn[8] were highly influential in clarifying the *quality* of self-assembly, signs of confusion still appear in the literature. Perhaps part of the problem lies in Kelvin's dictum: if we cannot put a number to it, we do not understand it. Put another way, without a unifying quantitative description of self-assembly. our appreciation of self-assembly is limited. With the idea of a unifying quantitative description of self-assemblies, Lehn pointed out[12] that our approach must require a kind of molecular information science, of "molecular informatics." Hence, chemists have, over the last 15 years or so. been busy contributing to this information data bank. As this collection of data increases. it becomes possible to begin to quantify assemblies. This process is. in effect, writing the rule book that will ultimately allow inolecular subunits to be readily designed and synthesized for a required self-assembly. The purpose of this article is not to review the stream of data that was collected: there are many good reviews for this purpose.[8,11,13–17] Rather, it is to define self-assembly by bringing together the less well-appreciated examples of quantitative descriptions of

Encyclopedia of Supramolecular Chemistry
DOI: 10.1081/E-ESMC 120012781

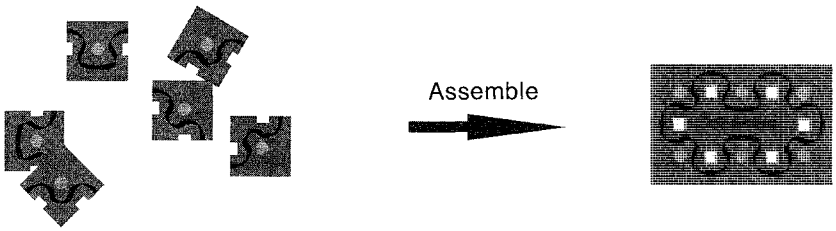

Fig. 1 Cartoon of a self-assembly process.

self-assembly, so that these can be tied into the well-established qualitative descriptions given above.

SELF-ASSEMBLY: THE CURRENT STATE OF AFFAIRS

To describe self-assembly, we need to consider the three components of any process: the subunits: the products, and the (complex) equilibrium that relates the two. As yet, there is no unification of these different aspects. Consequently. we will review the work from each category separateiy. In general. progress toward a quantitative description can be approached from two different fronts. The first of these is based on first principles. and produces detailed models that fully describe specific assembly processes. There are literally only a handful of systems described in this manner. For some recent examples, the reader is directed toward the literature.[18–20] The basis of the second approach is philosophically different. Here. the developing classifications are not derived from first principles but are symmetry based. In this way, they are applicable to more than one specific type of self-assembly. In this entry we focus on this latter methodology.

The Molecular Subunits

Molecules that constitute assembly subunits are generally described qualitatively. For example, the term, "possessing information'' is routinely used. What is this ''information''? A considerable amount of effort has gone into describing and classifying the assembly information contained within molecular subunits. Perhaps not surprising, the bulk of these descriptions has been applied to the most successful type of self-assembly to dace; self-assembly utilizing metal ions (acceptors) and coordinating ligands (donors). The assembly shown in Scheme 1 from the Fujita group is an admirable example.[21]

Assembly subunits can be broadly categorized as rigid or flexible. This absolute, and imperfect. distinction is made because, as we will see. the inherent flexibility in a subunit has a major impact in the way assembly (and assembly information) is viewed. Peter Stang and co-workers were some of the early pioneers in regard to the categorization of rigid subunits. Thus, they described[22] how rigid subunits coinprised of donor ligands and acceptor metal ions can be broken down into two kinds: those that are linear and those that are angular. Linear units can only be comprised of two donor–acceptor sites, but the angular subunits can have any number of sites

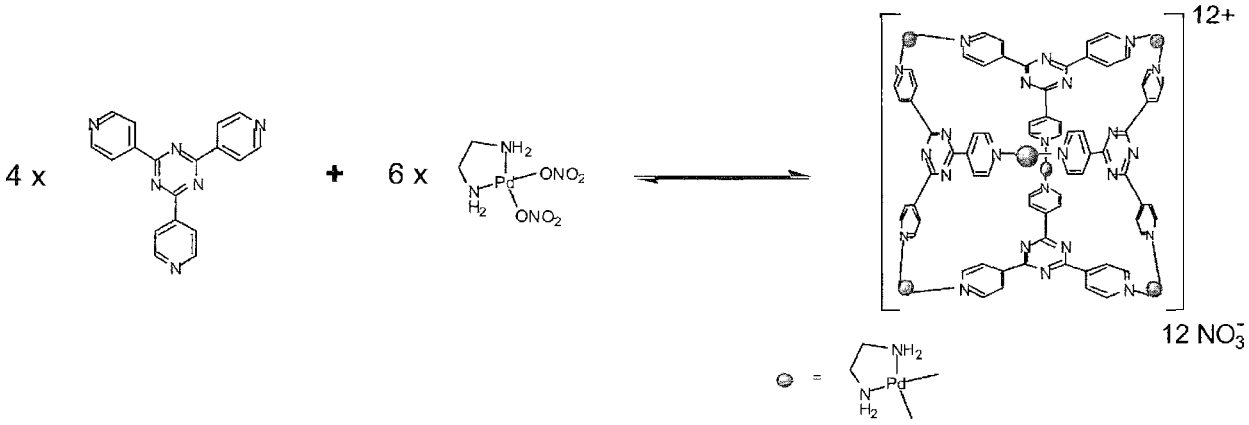

Scheme 1 A typical strict self-assembly from the Fujita group. (From Ref. [1].) (*View this art in color at www.dekker.com.*)

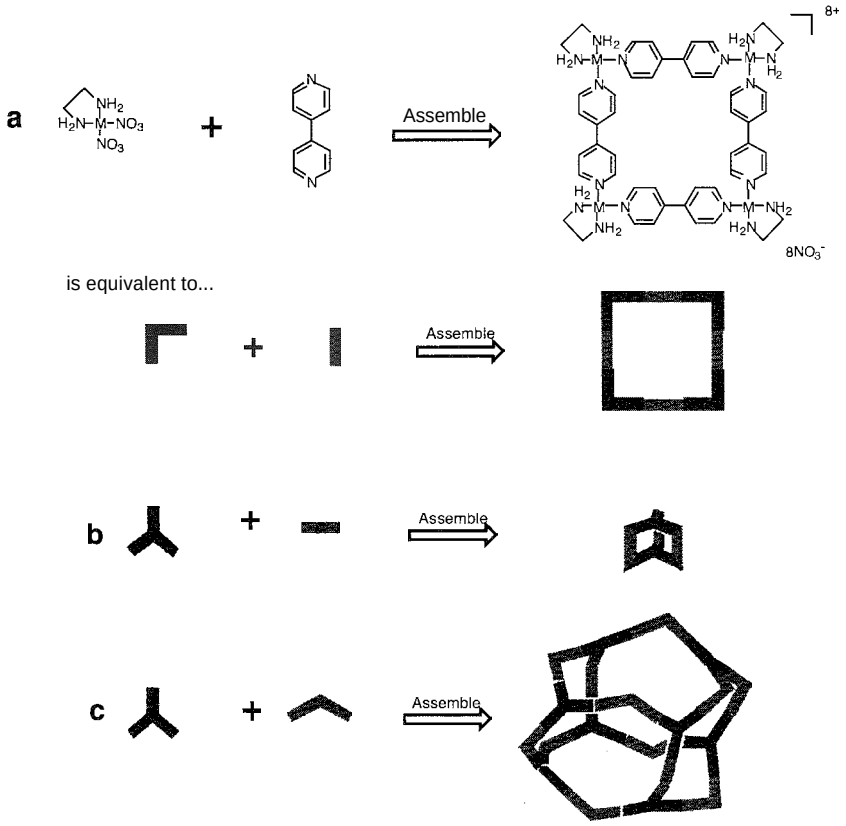

Fig. 2 Three successful assembly predictions from the combination of (a) four 90° angular units and four linear units: (b) two trigonal planar units and three linear units; and (c) Eight trigonal planar units and 12 109° angular units. **(View *this* art *in* color at *www.dekker.com.*)**

(>1), and possess any set angle between them. From this simple premise. it became possible to consider many assemblies arising from rigid subunits (Fig. 2).

Swiegers and Malefetse recently proposed[23] an extension to the Stang assembly analysis technique to precisely define the chemistry and geometry of each subunit. Consider the assemblies shown in Fig. 2. We can define each subunit as linear (*L*) and angular (A) and the blue and red subunits as acceptors *(u)*and donors (d), respectively. Having done this and taking the convention that the order of listing of subunits is acceptors, then mixed (acceptor–donor) subunits, then donors, we can classify these types of assemblies. Hence, the assembly in Scheme 1 is an $A_6^{2a}A_4^{3d}$ process, because it involves the coming together of six angular ditopic acceptors and four tritopic angular donors. Similarly, the assemblies in Fig. 2 are $A_4^{2a}L_4^{2d}$, $A_2^{3a}L_3^{2d}$, and $A_8^{3a}A_{12}^{2d}$, respectively. This approach to categorizing is useful, because it can be tied in with the categorizing of assembly products (vide infra) to reveal which type of assembly subunits are required for a target polyhedron with corners, edges. or faces that are formed from donors or acceptors. However, it must be noted that this approach was designed specifically for assemblies such as those shown in Scheme 1 or Fig. 2. Outside the bounds of these types of processes, the approach runs into problems. For example, the assembly shown in Fig. 3 cannot be described in this manner. Likewise. it will require modification if it is to be able to describe assemblies involving subunits such as proteins that interact via a multitude of moieties.

The above approach to describing subunits is difficult if the subunit possesses several degrees of rotational freedom or some other form of disorganization. How does one define, say, the ligation directionality of di-3-pyridyl ketone? Recently, Raymond and coworkers proposed rules that describe the assembly of their more flexible subunits.[24] In these cases, the organic subunits are relatively flexible and possess inultiple chelator groups. Hence, the principle focus of attention has not been on the directional relationships of the donor groups. but rather on describing the mode of ligation of the subunits to the metal ion subunits using coordinate vectors. chelate planes, and approach vectors (Fig. 3). Hence, the information contained within each subunit is not considered with the molecule or fragment in isolation, but in the context of the assembled species. Approaches to describe the assembly products (vide infra) have, therefore. much in common in this regard.

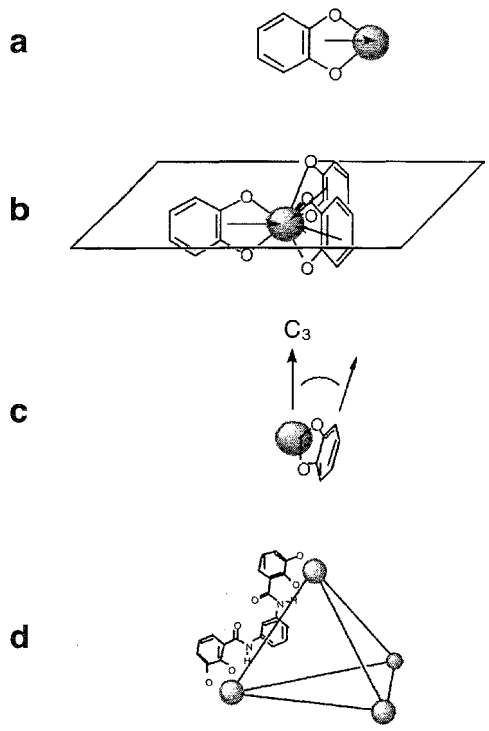

Fig. **3** *(a)The coordinate vector* for *catechol coordination to* a *metal center.* (b) *The chelate plane defined by a metal* ion *and the coordinate vectors in a tris-catechol complex. (c). The approach angle* for *each chelate of the tris-catechol complex.* (d) *A* M_4L_6 *tetrahedral cluster (adapted from Ref.* [24]). (*View this art in color at www.dekker.com.*)

Mirkin et al. recently worked on a slightly different metal-ion-directed self-assembly in which thermodynamically controlled covalent modification is applied to the product.[''''] In this approach. the assembly part of this, ''self-assembly with covalent modification,'' involves chelate donors and is perhaps best described with the Raymond analysis. However, in contrast, the postmodified products are probably best described using the method proposed by Stang. This double-barreled approach is not ideal and indicates that there is still a large amount of work to be done before a more uniformly applicable description of self-assembly is reached.

The Assembly Product

There are an infinite number of shapes that can be formed by self-assembly. How do we classify all of them? It may be possible to broadly classify assembly products as, e.g., star-shaped, but it is hard—at least from a chemist's point of view—to justify at the moment why snowflake-shaped assemblies need to be divided into different subclasses ad infinitum. There is, however, at least one exception to this ''classify assembly product or not'' quandary; spherical or quasi-spherical assembly products. As MacGillivary and Atwood pointed out,[25] in a chemical system, there are only so many ways in which subunits can be brought together to form these types of assemblies. This is fortunate, because with potential applications including catalysis, drug delivery, or molecular devices. hollow sphericallquasi-spherical assembly products are probably one of the most important classes of assembly product. Within this subgroup there are two general categories of products: arising from either two (curved) subunits, or those formed from more than three regular polyhedral subunits. The latter of these lead to assembly products based on the five Platonic solids, the 13 Archimedean solids, or one of the two (infinite) families of prisms and antiprisms. Classifying the assembly product in such a manner complements the categorization of the assembly subunits. In combination, they allow the visualization of which assembly subunits can potentially lead to which assembly products.

The Assembly Process

In a chemical sense. what relates molecular subunits with their assembly product? To answer this question precisely is to define self-assembly. From a qualitative standpoint, we can state that the two sets of molecules are related by a complex series of intertwining equilibria; some of them dead-ends. some of them leading as directly to the assembly product as possible.[26] As a step toward analyzing this type of complex system, we recently described a general, semiquantitative analysis of self-assemblies.[27] This probabilistic approach'' focuses on the options available to each molecular subunit as the assembly occurs and engenders a common frame of reference by which the efficiency of all assemblies leading to discrete species can be compared.

Because different assemblies involve the coming together of different numbers of subunits, quoting a yield for an assembly system tells us nothing about the efficiency of the assembly process. Yields tell us what went right during the assembly but not what potentially could have gone wrong with the process, and it is the difference between these that dictates assembly efficiency. To gauge the efficiency of a process, we need to measure the probability that an assembly will occur

''To the author's knowledge. the first consideration of probability of assembly in a self-assembling system (the folding of bovine pancreatic ribonuclease via the pairing of the eight sulfhydryl groups) was made by Anfinsen: Ref. [28].

successfully, and compare this to the actual yield of the process to see if it is better or worse than probability suggests. To determine the probability of assembly, two approximations must be made. First, the examination of possible assembly options must be constrained to the possibilities that can arise between the number of subunits that appear in the product. Put another way, to prevent an analysis into infinity, the possibility that molecules or random polymers larger than the product are formed must be assumed to be zero. This limits the analyses to a practical level. The other approximation also restrains the analyses and, perhaps more importantly, levels the playing field for all analyses. Thus, we assume that assembly occurs between subunits for which bond rotation is the only allowed motion, and that barring impossible molecular motions (such as moieties passing through moieties). all intermolecular and intramolecular processes occur on a flat potential energy surface. Thus, there is no bias because of conformational sampling of the subunit or supramolecular array, or bias because activation energies arising from the building processes are taken into account. These natural biases are, in actuality, what makes an assembly successful, and they are part of the actual yield of the assembly. The probability value calculated is therefore representative of a worst-case scenario, where the subunit is devoid of information. The approach centers around the construction of a standard probability tree that details the successful and the nonsuccessful pathways of assembly. This "assembly tree" leads to the calculation of a probability (p) for forming the product and, hence, a theoretical yield. An example best illustrates the approach. Consider the $A_6^{2a}A_4^{3d}$ assembly shown in Scheme 1 and its corresponding assembly tree (Fig. 4). Assembly is initiated by joining two triangular subunits by one metal ion (not shown) to form the first, bow-tie, intermediate. The probability of this occurring correctly is one in one. Note that although the assembly is reversible, for convenience, we assume that each step is irreversible. There is no going back: either we form an intermediate that can go on to form product, or we form an intermediate that cannot. Next, the bow-tie can undergo eight possible reactions: four intrainolecular and four intermolecular. All the intramolecular reactions lead to an intermediate that cannot go on to form product. These pathways are therefore terminated. All four intermolecular reactions give the same linear, trimer intermediate. Thus, the probability of this compound forming is 1/1 x 4/8, i.e., $\rho = 0.5$. Likewise, the probability of forming each of the three, next-generation, possible tetramers is 1/1 x 4/8 x 1/13 or one in 26 for the three-pointed star derivative, and two in 1/1 x 4/8 x 4/13 or two

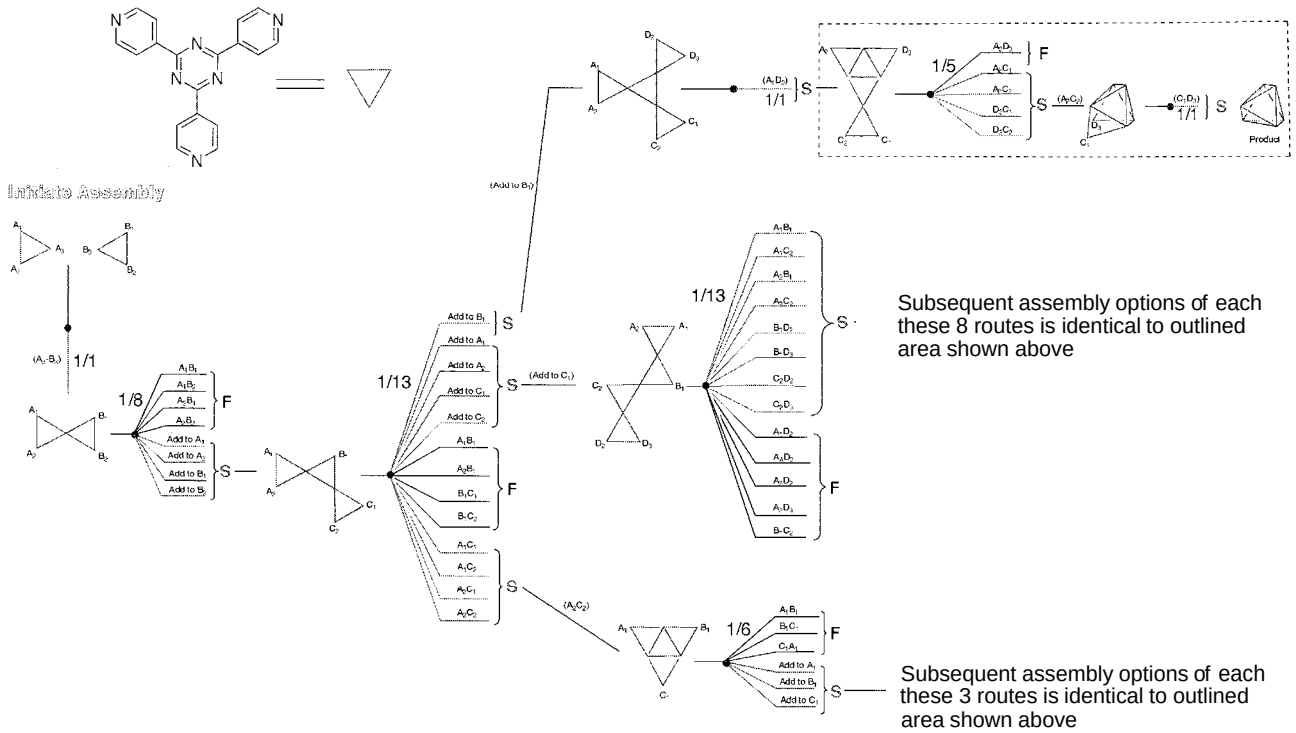

Fig. 4 The assembly tree of the shown in Scheme 1 (adapted from Ref. [27]). (*View* this *art in color at www.dekker.com.*)

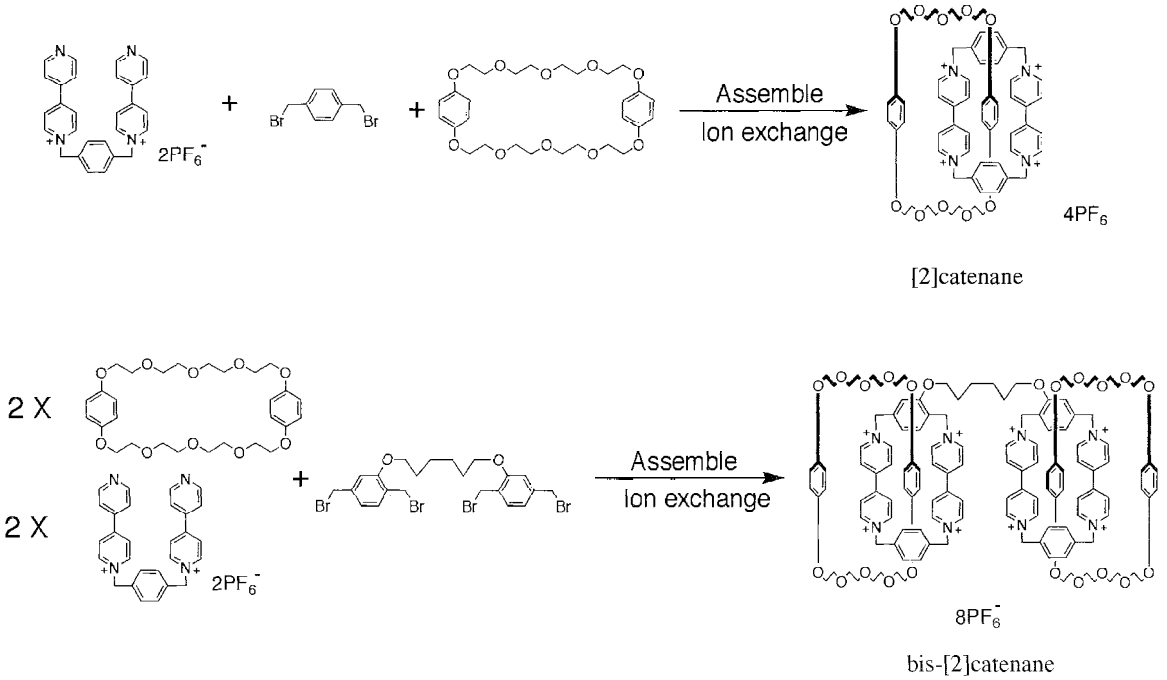

Scheme *2* The formation of a [2]catenane and a *bis*-[2]catenane. (From Refs. [29,30])

in 13 for the linear and equilateral triangle species. Repeating this process until the product is formed, we can determine that the probability of successful assembly is $\rho=0.1301$ or 13%. In actuality, the product is formed quantitatively, and thus the ratio of these two values is 7.68. The actual yield is 7.68 times better than probability suggests. We call this ratio the assembly number (AN). The higher the assembly number the better.

By considering the probability of assembly, it is possible to evalute the effifiency of different assemblies. Consider the formation of the [2]catenane[29] and the *bis*-[2]catenane[30] shown in Scheme 2. The first is isolated in a yield of 70% and the second in a yield of 31%. However, by forming the corresponding assembly trees. it is possible to determine their respective AN values as 1.4 and 3.72. It is the formation of the *bis*-[2]catenane that is more efficient.[27]

Whether or not an assembly follows a theoretical assembly tree can only be determined by garnering information about intermediates in the process—a difficult task for complex assemblies.[26] Nevertheless, as a starting point to assembly analysis, assembly trees offer information regarding the statistically prevalent species in an assembly mixture. They suggest where we should start looking when wishing to determine the mechanism of an assembly. Moreover, in addition to the information they provide regarding the efficiency of a process, assembly trees represent unique fingerprints for specific types of assembly. Hence, they represent a powerful means by which assemblies can be analyzed and categorized.

CONCLUSION

It is apparent that although chemical self-assembly is defined in qualitative terms, there is still a considerable amount of work to be done to quantify self-assembly. However, advances are being made in the categorizing of assembly subunits, assembly products, and the chemical relationships between the two. On another front, specific systems are beginning to be described from first principles. These advances amount to an increasingly more accurate definition of self-assembly in chemical systems. They also constitute a developing rulebook with which we will ultimately be able to manipulate the increasing pool of knowledge of "molecular informatics."

ACKNOWLEDGMENTS

This work was supported by the National Science Foundation (CHE-0111033) and the Donors of the Petroleum Research Fund, administering by the American Chemical Society.

ARTICLES OF FURTHER INTEREST

Self-Assembling Capsules, p. 1231
Self-Assembling Catenanes, p. 1240
Self-Assembly in Biochemistry, p. 1257
Self-Assembly: Definition and Kinetic and Thermodynamic Considerations, p. 1248
Self-Assembly: Terminology. p. 1263
The Template Effect, p. *1493*

REFERENCES

1. Fujita, M.: Oguro. D.; Mlyazawa, M.: Oka. H.; Yarnaguchi, M.: Ogura, K. Nature 1995. 378. 469–471.
2. Desiraju. G.R. Nature 2001. 412. 397–400.
3. *Micelles, Membranes, Microemulsions, and Monolayers*; Gelbart. W.M., Ben-Shaul. A., Roux, D.. Eds.: Springer-Verlag: New York, 1994.
4. Fendler, J.H. *Membrane Mimetic Chemistry*; John Wiley and Sons: New York. 1982.
5. Bowden. N.B.: Weck. M.: Choi. I.S.: Whitesides. C.M. Acc. Chem. Res. 2001. 34. 231–238.
6. Tecilla. P.: Dixon. R.P.; Slobodkin. G.; Alavi. D.S.; Waldeck. D.H.: Hamilton. A.D. J. Am. Chem. Soc. 1990. 112. 9408–9410.
7. Whitesides. G.M.: Mathias. J.P.: Seto. C.T. Science 1991. 254. 1312–1319.
8. Lehn. J.-M. *Supramolecular* Chemistn: VCH: Weinheim. 1995.
9. *Templated Organic Synthesis*; Diederich. F.. Stang. P.J., Eds.: Wiley-VCH: Weinheim. 2000.
10. Busch. D.H. J. Incl. Phenom. Mol. Recognit. Chem. 1992. 12. 389–395.
11. Lindsey, J.S. New J. Chem. 1992. 12, 153–180.
12. Lehn, J.-M. Angew. Chem.. Int. Ed. Engl. 1990. 29. 1304–1319.
13. Chapman. R.G.: Sheman, J.C. Tetrahedron 1997. 53. 15911–15945.
14. Fyfe, M.C.T.: Stoddart. J.F. Acc. Chem. Res. 1997. 30. 393–401.
15. Conn, M.M.: Rebek, J. Jr. Chem. Rev. 1997. 97. 1647–1668.
16. Fujita. M. Chem. Soc. Rev. 1998. *17*, 417–425.
17. Leininger, S.: Olenyuk, B.; Stang, P.J. Chem. Rev. 2000. 100. 853–908.
18. Bielejewska, A.G.: Marjo, C.E.; Prins, L.J.; Timmerman, P.; de Jong, F.: Reinhoudt. D.N. J. Am. Chem. Soc. 2001, 123. 7518–7533.
19. Ercolani, G. J. Phys. Chem.. B 2001, 102. 5699–5703.
20. Cort, A.D.: Ercolani. G.: Iamiceli, A.L.; Mandolini. L.: Mencarcelli. P. J. Am. Chem. Soc. 1994. 116. 7081–7087.
21. Holliday. B.J.: Mirkin, C.A. Angew. Chem.. Int. Ed. Engl. 2001, 40. 2022–2043.
22. Olenyuk. B.: Fechtenkdtter. A.; Stang. P.J. J. Chem. Soc., Dalton Trans. 1998, 1707. 1701–1728.
23. Swiegers, G.F.: Malefetse. T.J. Chem. Eur. J. 2001, 7. 3637–3643.
24. Caulder, D.L.: Raymond, K.N. Acc. Chem. Res. 4999. 32. 975–982.
25. MacGillivray, L.R.: Atwood, J.L. Angew. Chem., Int. Ed. Engl. 1999. 38. 1018–1033.
26. Levin, M.D.: Stang. P.J. J. Am. Chem. Soc. 2000, 122. 7428–7329.
27. Gibb. C.L.D.:Gibb. B.C. J. Supramol. Chem. 2001. *1*, 39–52.
28. Sela, M.: White, F.H.; Anfinsen. C.B. Science 1957. 125. 691.
29. Ashton, P.R.: Goodnow, T.T.: Kaifer. A.E.: Reddington. M.V.: Slawin. A.M.Z.: Spencer. N.; Stoddart. J.F.: Vincent. C.: Williams, D.J. Angew. Chem.. Int. Ed. Engl. 1989. 28. 1396–1399.
30. Ashton. P.R.: Preece, J.A.; Stoddart, J.F.; Tolley, M.S. Synlett 1994. 789–792.

Strong Hydrogen Bonds

Christer B. Aakeröy
Kansas State University, Manhattan, Kansas, U.S.A.

INTRODUCTION

Hnterrnolecular forces are ultimately responsible for the way in which discrete molecular building blocks are assembled into infinite architectures and crystalline materials, and for providing the necessary specificity and selectivity in host–guest chemistry. Although it is important to acknowledge that every crystal structure and host–guest interaction is the result of a subtle balance between a multitude of noncovalent forces; the hydrogen bond remains a crucial element in supramolecular chemistry. In this article, some of the parameters that are commonly used when characterizing and examining strong hydrogen bonds, particularly in the context of supramolecular solid-state chemistry. will be outlined.

BACKGROUND

Strong Hydrogen Bonds—What Are They?

The strength and directionality of the hydrogen bond,[1–5] as compared to other intermolecular forces, account for its significance and has made it the most important interaction in molecular recognition and crystal engineering. Despite the fact that hydrogen bonds are employed regularly and successfully as structure-directing forces in natural and synthetic supramolecular systems,[6] there is still considerable debate about how to define a hydrogen bond and how to distinguish between "weak," "moderate." and "strong" hydrogen-bond interactions.[7–11] in many ways, such classifications will suffer from a considerable degree of arbitrariness, as it is impossible to find boundaries with experimental or theoretical methods that correspond to real physical distinctions. Hydrogen bonds. in general. as well as weak hydrogen bonds are covered elsewhere (see articles on hydrogen bonding and weak hydrogen bonds). The main focus of this section will be on "strong" hydrogen bonds. Defined in Scheme I are the geometric parameters that will be used throughout this section. Despite the lack of fully satisfactory definitions, hydrogen bonds that are frequently referred to as being strong display many common traits in terms of their properties and behaviors. Strong hydrogen bonds tend to display significant infrared (IR) shifts (over 25%) for the D—H bond. large downfield 'H-WMR shifts (14–22 ppm). and bond energies over 50 kJ/mol. In the solid state, common features include a lengthening of the D—H bond (0.08–0.25 Å), short H···A distances (1.2–1.5 Å), and 0 in the range of 170–180° (these numbers should be taken as guiding values only).[12] Strong hydrogen bonds are often referred to as low-barrier hydrogen bonds. because they involve a single-minimurn potential energy well or a double-well with a small barrier. Such interactions: which usually involve charged species. have a significant covalent component. They tend to form when a proton is shared by two strong bases. as demonstrated by the charge-assisted hydrogen bonds between bifluoride ions. $[FHF]^-$, which have bond energies greater than those displayed by some covalent interactions.[13] For the purpose of this section, a strictly operational "definition" of strong hydrogen bonds will be employed: only hydrogen bonds that involve O. N, or X heavy atoms (where X=F, Cl, or Br) and display some of the structural or spectroscopic features listed above will be considered as strong (and no distinction between hydrogen bonds involving neutral and charged species will be made).

Relevance of Strong Hydrogen Bonds

Strong hydrogen bonds are important stabilizing factors in enzymes and are relevant to proton-transfer reactions in biological systems.[7–9] For example. a key step in many enzyme-catalyzed processes is the formation of a thermodynamically unfavorable enolate in the presence of an acid catalyst. The required stabilization energy may be provided when a weak enzyme···substrate hydrogen bond is replaced with a strong enzyme···intermediate hydrogen-bond interaction.[14] Strong O—H···O and N—H···O hydrogen bonds are also responsible for the formation of α-helices and β-sheets in proteins, base pairing in nucleic acids. and many protein–nucleic acid interactions.[10] It was suggested that the formation of strong hydrogen bonds is instrumental in ester hydrolysis catalyzed by cholinesterases.[15] Strong hydrogen bonds were also implicated as possible conduits for magnetic exchange interactions,[16,17] and near-symmetric $N—H^+\cdots N$ hydrogen bonds are observed in proton sponges.[18] Strong hydrogen bonds are important in some

Encyclopedia of Supramolecular Chemistry
DOI: 10.1081/E-ESMC 120012763

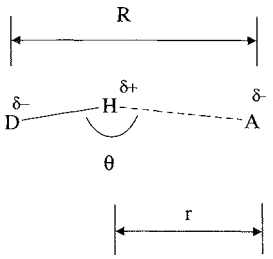

Scheme 1 A generic hydrogen bond (r=H···A distance: R=D···A distance: θ=D—H A angle).

ferroelectric materials,[19] which is indicated by changes in transition temperatures that occur upon deuterium substitution. They are also known to play key roles in several structures that display pyrelectricity (polarity induced by heating). piezoelectricity (polarity induced by pressure). and ferroelasticity (polarity induced by mechanical stress).[19]

DETECTING HYDROGEN BONDS

In a generic hydrogen bond, D—H···A, the overall thermodynamic effect is a lowering of the potential energy as compared to the sum of the energies of the two isolated monomers. In addition. as the distance between the two species decreases and the D—H···A interaction approaches its maximum stability, there is a corresponding weakening of the covalent D—H bond. Consequently. it is possible to employ a variety of spectroscopic. crystallographic, and thermodynamic tools (in addition to the use of high-level ab initio or density functional theory)[20] in the study and detection of strong hydrogen bonds.

Infrared Spectroscopy

Changes in molecular geometries that take place when hydrogen bonds are formed can be studied using vibrational spectroscopy, but the relative strength of a hydrogen bond can also be determined due to its behavior in the IR region.[7,9] For weak hydrogen bonds. the bands are not far removed from those in a discrete D—H system, however, a strong hydrogen bond gives a broad band in the 1600–3000 cm^{-1} region, with three discernible maxima. Particularly strong hydrogen bonds give a broad band below 1600 cm^{-1}, which is indicative of a highly polarizable system. Even with this information, it is sometimes difficult to analyze and interpret IR spectra that involve strong hydrogen-bond interactions, as the region below 1400 cm ' tends to be overlaid with a large number of other absorption maxima. By selectively replacing hydrogen atoms with deuterium. it is often easier to accurately assign correct hydrogen-bond modes; the isotope frequency ratio ν_{AH}/ν_{AD} varies as a function of internuclear separation.[22]

Possible correlations between the chemical nature of the donor and the acceptor, and the resulting hydrogen-bond behavior were examined extensively.[1–5] For example,[23] a systematic study of the mid-and far-IR regions for a series of carboxylic acid···pyridine complexes (in chloroform) showed that even the weakest acid in this sequence, acetic acid, forms a 1:1 complex with pyridine held together by a short O—H···N hydrogen bond. The potential energy of this hydrogen bond is described by a highly asymmetrical double-minimum curve. With increasing acidity (or decreasing temperature), the O—H···N hydrogen bond becomes stronger. the O···N distance shortens, and the potential energy curve has a more symmetric appearance. The height of the barrier between the two minima in the potential-energy curve decreases with increasing acid strength. In the trifluoroacetic-acid–pyridine complex. the equilibrium is shifted toward the right-hand side of the equilibrium, O—H···N⇌O^-···$^+$H—N. The partial proton transfer is most efficient when the acceptor and the donor have similar proton affinities (PA), and the dissociation energy of D—H···A decreases as ΔPA increases. The gradual physical changes that take place (as a function of variations in the donor strength of D—H). can be monitored effectively using IR spectroscopy. However, this study also shows that there is a continuum between the relatively weak acetic acid···pyridine hydrogen bond and the charge-assisted O^-···$^+$H—N hydrogen bond.

NMR Spectroscopy

The findings from the use of nuclear magnetic resonance (NMR) spectroscopy for interrogating systems with strong hydrogen bonds can be divided into four categories: changes in chemical shifts, hydrogen-bond dissociation and exchange times, relaxation processes, and location of hydrogen atoms in crystalline materials. When a hydrogen-bond donor, D—H. is in close proximity of a suitable hydrogen-bond acceptor. the corresponding ^{1}H-NMR signal is shifted to higher frequencies, consistent with deshieiding of the proton. Observed shifts are significantly larger for species capable of forming strong hydrogen bonds, cf. HF and H_2O.[7–9]

By correlating hydrogen-bond distances (obtained from neutron-diffraction data) with chemical shift tensors obtained from solid-state ^{1}H-NMR spectroscopy, it was shown that there is a linear relationship between the O···H distance and the anisotropic chemical shift. The observed shifts translate to −20 ppm per 1.0 Å change in O···H distance.[24] The change in chemical shift for

strong hydrogen bonds can also distinguish single-minimum systems from the double-minimum, low-barrier type.[25] For example, the following data were found for the hydrogenphthalate ion: $\delta(H)=21.00$; $\Delta\delta(H,D)=-0.15$; and $\Delta\delta(H,T)=-0.25$ ppm (the negative change indicates a single-minimum hydrogen bond). Whereas for acetylacetone, the following was determined: $\delta(H)=16.1$: $\Delta\delta(H,D)=0.61$; and $\Delta\delta(H,T)=0.83$ ppm, which is typical of a hydrogen bond with a double-well energy profile.

Crystallography

The presence or absence of hydrogen bonds in a crystalline material is often inferred by applying one or several geometric criteria such as D···A and H···A distances shorter than their combined van der Waals radii [e.g., R(O···O) <3.10 A. r(H···O) <2.75 Å, R(N···O) <3.25 Å, θ (D—H···A) greater than 90–120°, etc.]. Unfortunately, there is still debate about which values to use for van der Waals radii. and it has become clear that rigid applications of geometric criteria as a way of identifying hydrogen bonds is inadequate, especially when examining weaker interactions.

A way around these difficulties can be provided by systematic statistical studies of extant structural data obtained from the steadily growing Cambridge Structural Database.[26] Such efforts provide a crucial base from which our understanding of hydrogen-bond interactions can be further developed. By correlating geometric parameters of hydrogen-bond interactions with the nature of the participating donor and acceptor moieties, several important trends were identified.[27] An increase in H···A distance is likely to be accompanied by large deviation from linearity of θ. And, O—H···O interactions are more often close to linear geometries than are N—H···O hydrogen bonds.

There is also an inverse relationship between the covalent O—H and the intermolecular H···O distance in an O—H···O hydrogen bond. In the case of strong D—H···A hydrogen bonds, the D···A distances are typically significantly less (>0.3 A) than the sum of the combined van der Waals radii of D and A. Furthermore, the proton is normally located near the center of D···A. Of course, any reliable examination of geometric parameters involving the hydrogen atom requires access to neutron-diffraction data: the large neutron-scattering power of hydrogen-atom nuclei means that they can be located with the same accuracy as many heavier atoms.

Electron-density maps (obtained through a combination of neutron-diffraction, x-ray diffraction, and high-level theory) can offer unique insights into the subtle, but significant, electron rearrangements that accompany the formation of hydrogen bonds.[28,29] In hydrogen bonds of weak and intermediate strengths, it is common to approximate the electron distribution in the bond to a simple superpositioning of the electron densities of the individual. unperturbed, donor and acceptor moieties. In essence, these interactions can be adequately represented by an electrostatic model, because attractive charge transfer and repulsive exchange interaction are small and tend to cancel each other. In strong hydrogen bonds, the charge distribution is more symmetrically arranged. as there is less charge buildup on either side of the proton, as well as in the D—H bond and in the H···A region.

Theory and Physical interpretations

Because electrons are responsible for all chemical bonding, it is desirable to discuss hydrogen-bond interactions in terms of quantities that directly describe electron densities rather than concepts like σ-and π-bonding, electronegativity, etc.[20]

The total interaction energy of a hydrogen bond can be partitioned into four (sometimes five) constituents. The sum of these terms should represent the total energy difference, ΔE_{HB}, between the hydrogen-bonded system at equilibrium and the total energy of the isolated, unperturbed, components. The electrostatic contribution represents the energy change that would take place if two isolated components. D—H and A. were positioned in such a way that the geometry represents the hydrogen-bonded complex, D—H···A, but without perturbing their respective charge distributions and without any electron exchanges taking place. The polarization energy represents the energy gain that would arise if the charge distributions of the isolated components were deformed to resemble the charge distribution of the hydrogen-bonded complex (still without allowing for any charge transfer between D—H and A). The charge transfer contribution represents the energy change that would result from electron transfer between D—H and A. The notion of "covalency" in a hydrogen bond is related to the latter term; charge transfer results in a buildup of charge in the overlap region, where it is shared between the original components D—H and A. The dispersion energy (another stabilizing component) is the energy change resulting from the correlated motion of electrons on D—H and A. The only destabilizing term. the exchange energy between D—H and A. essentially corresponds to the repulsion that arises when too many electrons are located within the same region of space (a violation of the Pauli exclusion principle)—this exchange energy also prevents the system from collapsing. The way the energy is partitioned in a positively charged hydrogen bond is similar to the situation in a neutral system, with the main difference being that there is a decrease in exchange contribution. This is due to the fact that wave functions in positive ions

are more compact, resulting in less overlap between donor and acceptor moieties.

Through high-level calculations. it was shown[30] that there is a linear relationship between the strength of O—H···O hydrogen bonds and the difference in proton affinity. ΔPA, of the donor and the acceptor (there is also a correlation between O···O distance and strength). Single-well or low-barrier double-well hydrogen bonds tend to arise when $\Delta PA \approx 0$ (this is corroborated by IR studies).

STRENGTH OF THE HYDROGEN BOND

As so many different donor and acceptor moieties can participate in a strong hydrogen bond. it is not surprising that the strengths vary considerably. The hydrogen-bond energy (increased stabilization) is typically defined with respect to the lower-energy coinponents [D—H] + [A] or [D] + [H—A]. Strong hydrogen bonds involving neutral species tend to be in the range of 10–65 kJ mol^{-1}, but for charge-assisted interactions. the range of bond strengths rises to 40–90 kJ mol^{-1}.[13] The strongest known hydrogen bonds typically involve $[FHF]^-$ anions with commonly reported values of 155–252 kJ mol^{-1},[31–34] which is comparable to the strength of covalent single bonds.

Interionic Hydrogen-Bond interactions

Despite conflicting reports,[35] interion O—H···O^- interactions of the type often observed in monoanions of dicarboxylic acids. dihydrogenphosphates, and hydrogensulfates. behave similarly to strong hydrogen bonds between molecular species.[36] The IR absorption spectrum of potassium hydrogenoxalate displays the expected features of a strong (and stabilizing) hydrogen bond. There is also a significant lengthening of the covalent 8 — H bond distance (as determined by single-crystal neutron diffraction).''' Finally, the C—O bond distance of the acceptor moiety of the anion is significantly longer than the C—O bond distance of the moiety that does not participate in the near-linear O—H···O^- interaction. In addition, solution WMW studies of hydrogenoxalate anions demonstrate that interactions between anions display characteristics that one would conventionally associate with strong hydrogen bonds, e.g., significant shortening of the O···O distances.[38] These results have important ramifications for supramolecular synthesis, because they show that charge-assisted hydrogen bonds between anions can be employed as active structure-directing tools. The commonly observed short intermolecular distances are not the result of a ''least-destabilizing'' arrangement.

SPECIFIC EXAMPLES OF STRONG HYDROGEN BONDS AND THEIR BEHAVIORS

Strong O—H^+···O hydrogen bonds are typically associated with oxonium ions, H_3O^+. Other ''hydrated protons.'' like the diaqua oxonium ion. $H_5O_2^+$, often appear in structures of strong mineral acids.[39]

Strong O—H···O hydrogen bonds between neutral species are well known from crystal structures of β-diketo enols and certain dicarboxylic acids. The shortest O···O distances are associated with intramolecular interactions (exemplified by pyridine 2.3-dicarboxylic acid). The increased strengths of such interactions are the result of a resonance contribution. This n-bond cooperativity or resonance-assisted hydrogen bonding[40] involves multiple bonds. whereas the cooperative effects between hydroxyl groups in carbohydrates and cyclodextrins are usually described as σ-bond cooperativity.[41] Resonance-assisted hydrogen bonds also contribute to the stability of heteromeric interactions. e.g., 2-pyridone ··2-aminopyrimidine, and are therefore particularly important in inolecular recognition processes involving purines and pyrimidines.

Strong N—H^+···N hydrogen bonds are characteristic of proton sponges, fused-ring diamines with extraordinarily high basicities.[''' These molecules readily accept a proton, which interacts simultaneously with two nitrogen-based lone pairs that face each other. These hydrogen bonds range from very short (possibly centrosymmetric) to conventional hydrogen bonds without significant lengthening of the covalent N—H bonds.

The N—H···N^- hydrogen bonds were studied crystallographically, as exemplified by intramolecular N—H···N interactions between adjacent acetamido

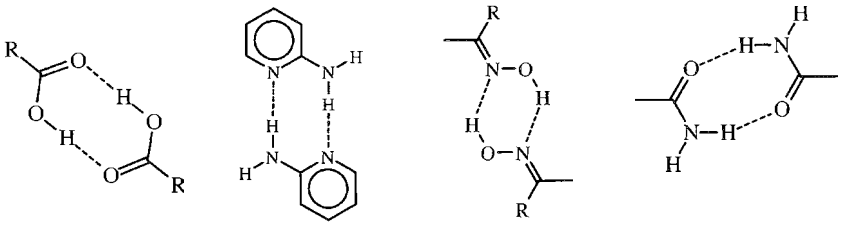

Scheme 2 Some examples of self-complementary hydrogen-bond interactions

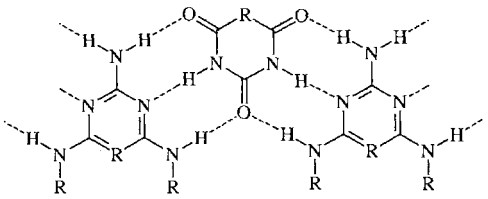

Scheme 3 A typical hydrogen-bonded tape generated by hydrogen bonds between complementary aminotriazine-··barbituric acid building blocks.

moieties (where one of the acidic protons was removed). In addition, ab initio calculations estimate that the $[H_3N\cdots H\cdots NH_3]^-$ complex has a hydrogen-bond energy of 56 kJ/mol, which is 48 kJ/mol less than the calculated value for the corresponding positive complex ion.[42]

STRONG **HYDROGEN BONDS** AND **SUPRAMOLECULAR ASSEMBLY**

One of the most well-known hydrogen-bond motifs is the carboxylic acid dimer. This particular intermolecular interaction is not only present among simple organic acids (there are few examples of chain-like, catemeric interactions between carboxylic acids), but self-complementary head-to-head carboxylic acid dimers are also often observed in coordination compounds as well as in organometallic species.[43] The availability of these robust and transferable intermolecular interactions (Scheme 2) allows for the assembly of discrete building blocks into extended networks of well-defined and predictable connectivities.

The improved understanding of interinolecular interactions. hydrogen bonds in particular. is invaluable to the development of crystal engineering — an interdisciplinary area concerned with the rational design, synthesis, and assembly of functional materials through noncovalent interactions.[44] Several aspects of this field are covered extensively elsewhere (see articles on hydrogen bonds,

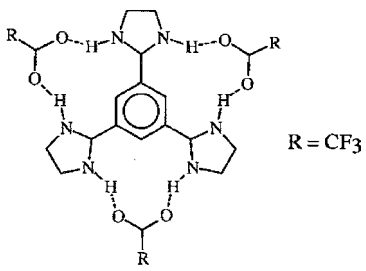

Scheme 4 Six charge-assisted N—H···O hydrogen bonds give rise to a tetrameric structure.

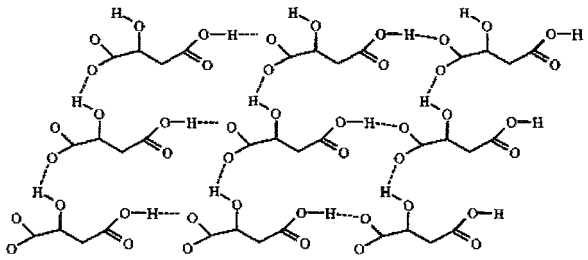

Scheme 5 Charge-assisted O—H···O hydrogen bonds between hydrogenmalate anions lead to an infinite sheet.

weak hydrogen bonds, crystal engineering with hydrogen bonds) and a few examples of hydrogen-bond-directed crystal, engineering are given below.

Construction of Extended Organic Architectures

The complementarity of some triaminotriazines (and related heterocycles) and barbituric acid was employed extensively in the assembly of a variety of discrete multicomponent structures as well as of extended ribbons, tapes, and rosettes (Scheme 3).[45–48] A collection of strong hydrogen bonds can impart sufficient stability to allow these structures to stay intact in solution as well as in the gas phase.

It was shown[49] that anions of trimesic acid generate hydrogen-bonded lamellar structures with alkyl- or aryl-substituted ammonium moieties.[50] The complementarities

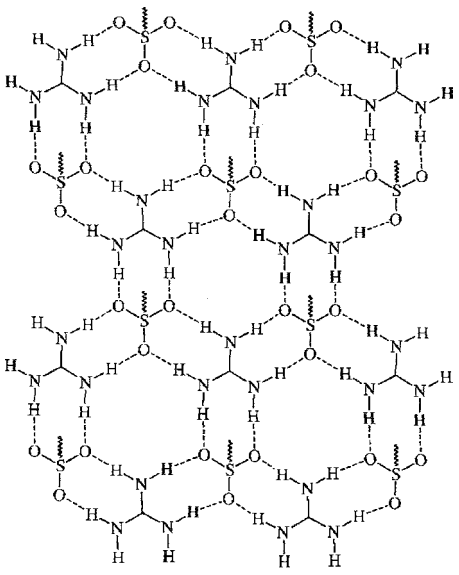

Scheme 6 Charge-assisted N—H···O interactions in a guanidinium/sulfonate system produce highly reliable layers (shown face on).

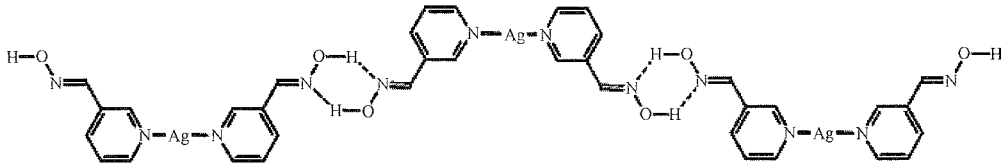

Scheme 7 Infinite chain of Ag(I)(3-aldoximepyridine)$_2$ cations held together by oxime···oxime dimeric hydrogen bonds.

of pyrimidine-2.4.6-triamines and 1,3,5-triazine-2,4,6-triones were used to create infinite ribbons that were subsequently connected into sheets via ammonium ··carboxylate hydrogen-bond interactions.[''] A combination of directional hydrogen bonds and electrostatic interactions between complementary units (dicarboxylic acids and cyclic bisamidine) were also employed in the design of discrete and infinite assemblies.[52,53] Charge-assisted N—H···O hydrogen bonds were utilized in the construction of tetrameric structures from a *tris*(imidazoline) base and four carboxylate anions (Scheme 4).[54] Charge-assisted interactions were also instrumental in building two-dimensional ionic networks using chiral hydrogen-*L*-malate ions (Scheme 5).[55]

The most thoroughly studied supramolecular organic host framework capable of reversible incorporation of guests is arguably the guanidinium/organic sulfonate-two-component system.[56–58] The host structure is built with the aid of complementary hydrogen-bond sites on guanidinium cations and substituted sulfonaie anions, leading to robust infinite hydrogen-bonded sheets (Scheme 6).

Strong Hydrogen Bonds and Extended Inorganic Assemblies

Hydrogen bonds also enabled the directed assembly of coordination complexes into extended architectures.[59–63]

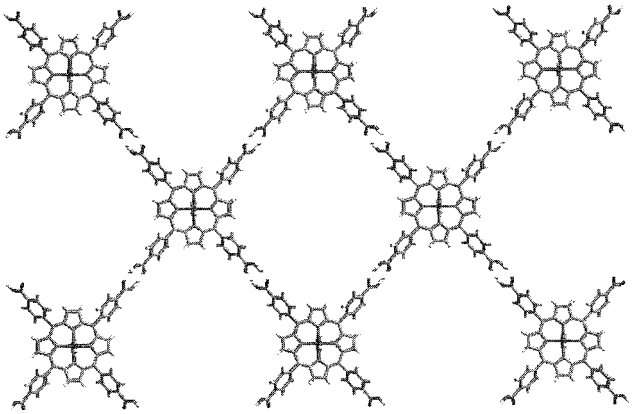

Fig. 1 Metal porphyrins assembled into infinite square grids through O—H···O hydrogen bonds between adjacent carboxylic acids.

For example, self-complementary oxime···oxime and amide···amide interactions[64–66] were used to propagate the inherent linear geometry of some Ag(I) complexes into infinite chains (Scheme 7).

Ligand-based, charge-assisted carboxylic acid···carcarboxylate hydrogen bonds in combination with Pt(II) ions. produced square grids that extend infinitely in two dimensions.[67] Even porphyrin complexes were connected into flat, grid-like networks through amide··amide and acid··acid hydrogen-bond interactions (Fig. 1).[68–70]

CONCLUSION

The concept of molecular recognition has a profound impact upon our understanding of a wide range of fundamental events, e.g., biomolecular activity. crystallization processes, and physicochemical signaling mechanisms. The relevance of strong hydrogen bonds to such phenomena remains unchallenged, and it is likely that further studies of the nature of such interactions will have important ramifications for supramolecular chemistry as a whole.

ARTICLES OF FURTHER INTEREST

Crystal Engineering with Hydrogen Bonds, p 357
Hydrogen Bonding, p 658
Self-Assembling Capsules, p 1231
Self-Assembly in Biochemistry, p 1257
Weak *Hydrogen Bonds*, p 1576

REFERENCES

1. *Hydrogen Bonding:* Hadži, D., Thompson. W.H., Eds.; Pergarnon Press: Oxford. 1959.
2. Pimentell. G.C.: McClellan, A.L. *The Hydrogen Bond:* W.H. Freeman: San Francisco, 1960.
3. *The Hydrogen Bond. Recent Developments in Theory and Experiment, Vols 1–3:* Schuster, P.. Zundel, G., Sandorfy, C.. Eds.; North Holland: Amsterdam. 1976.
4. Pauling, L. *The Nature of the Chemical Bond:* Cornell University Press: Ithaca. 1963.

5. Hamilton, W.C.: Ibers, J.A. *Hydrogen Bonding in Solids;* Benjamin: New York, 1968.
6. Lehn, J.-M. *Supramolecular Chemistry*; VCH: Weinheim. 1995.
7. Emsley, J.E. Very strong hydrogen bonds. Chem. Soc. Rev. 1980. 9. 91.
8. Tuck. D.G. Structural properties of HX_2^- and HXY^- anions. Prog. Inorg. Chem. 1968. 9. 161.
9. Speakman. J.C. Acid salts of carboxylic acids. crystals with some "very short" hydrogen bonds. Struct. Bond. 1972, *16.* 141.
10. Jeffrey. G.A.; Saenger, W. *Hydrogen Bonding in Biological Structures*; Springer-Verlag: Berlin, 1991.
11. Steiner, T. The hydrogen bond in the solid state. Angew. Chem., Int. Ed. 2002. *41.* 48.
12. Jeffrey. G.A. *An Introduction to Hydrogen Bonding:* Oxford University Press: New York. 1997.
13. Aakeroy. C.B.: Seddon, K.R. The hydrogen bond and crystal engineering. Chem. Soc. Rev. 1993. 2. 397.
14. Cerlt. J.A.: Gassman. P.C. Understanding enzyme-catalyzed proton abstraction from carbon acids: Details of stepwise mechanisms for β-elimination reactions. J. Am. Chem. Soc. 1992. *114,* 5928.
15. Viragh. C.; Harris, T.K.: Reddy, P.M.; Massiah. M.A.: Mildvan. A.S.; Kovach. I.M. NMR evidence for a short. strong hydrogen bond at the active site of a cholinesterase. Biochemistry 2000. *39,* 16200.
16. Hernandez. E.; Mas, M.; Molins. E.; Rovira, C.: Veciana. J. Hydrogen bonds as a crystal design element for organic molecular solids with intermolecular ferromagnetic interactions. Angew. Chem.. Int. Ed. Engl. 1993, 32. 882.
17. Akita. T.: Mazaki. Y.; Kobayashi, K. Ferromagnetic spin interaction in a crystalline molecular complex. J. Chem. Soc.. Chem. Commun. 1995. 1861.
18. Staub, H.A.; Saupe. T.: Kruger, C. 4,5-Bis(dimethylamino) fluorene. a new "proton sponge.''Angew. Chem., Int. Ed. Engl. 1983. 22. 731.
19. Abrahams. S.C. Structure relationship to dielectric. elastic and chiral properties. Acta Crystallogr. 1994. *50.* 658.
20. Scheiner. S. *Hydrogen Bonding.* A *Theoretical Perspective;* Oxford University Press: Oxford, 1987.
21. Hadži. D. IR spectra of strongly hydrogen bonded systems. Pure Appl. Cheni. 1965. *11.* 435.
22. Novak. A. Hydrogen bonding in solids. Con-elation of spectroscopic and crystallographic data. Struct. Bond. 1974. 18. 177.
23. Langner. R.: Zundel, C. FTIR investigation of polarizable hydrogen bonds in carboxylic acid-pyridine complexes in the mid- and far IR region. J. Chem. Soc.. Faraday Trans. 1995. *91.* 3831.
24. Jeffrey. G.A.: Yeon. Y. The correlation between hydrogen-bond lengths and proton chemical shifts in crystals. Acta Crystallogr. 1986. *B42,* 410.
25. Altman. L.A.; Laungani. D.: Gunnarsson. G.; Wennerstrom, H.; Forsen, S. Proton. deuterium, and tritium nuclear magnetic resonance of intramolecular hydrogen bonds. Isotope effects and the shape of the potential energy function. J. Am. Chem. Soc. 1978, *100.* 8264.
26. Allen. F.A. The Cambridge structural database: A quarter of a million crystal structures and rising. Acta Crystallogr.. Sect. B. 2002, *58.* 380.
27. Taylor, R.: Kennard. O. Hydrogen-bond geometry in organic crystals. Acc. Chem. Res. 1984. *17.* 320.
28. Becker, P. *Electron and Magnetization Densities in Molecules and Crystals*; Plenum: New York, 1980.
29. Stevens. E.D.; Coppens, P. Experimental electron density distributions of hydrogen bonds. High-resolution study of [alpha]-oxalic acid dihydrate at 100 K. Acta Crystallogr. 1980. *B36.* 1864.
30. Chen. J.: McAllister. M.A.: Lee. J.K.: Houk. K.N. Short. strong hydrogen bonds in the gas phase and in solution: Theoreticai exploration of pka matching and environmental effects on the strengths of hydrogen bonds and their potential roles in enzymatic catalysis. J. Org. Chem. 1998, *63,* 4611.
31. Waddington, T.C. The lattice energies of potassium, rubidium. and caesium bifluorides and the strength of the bonds in the bifluoride HF_2^- ion. Trans. Faraday Soc. 1958. *54.* 25.
32. Almlöf. J. Hydrogen bond studies. 71. Ab initio calculations of the vibrational structure and equilibrium geometry in HF_2^- and DF_2^-. Chem. Phys. Lett. 1972. *17.* 49.
33. Harrell. S.H.: McDaniel. D.H. Strong hydrogen bonds. II. The hydrogen difluoride ion. J. Am. Chem. Soc. 1964. *86.* 4497.
34. Wenthold, P.; Squires, R. Bond dissociation energies of F_2^- and HF_2^-. A gas-phase experimental and G2 theoretical study. J. Phys. Chem. 1995, *99.* 2002.
35. Braga, D.: Grepioni, F.; Novoa. J.J. Inter-anion O—H$^-$···O$^-$ hydrogen bond like interactions: The breakdown of the strength–length analogy. Chem. Commun. 1998. 1959.
36. Steiner, T. Inter-anion O—H···O interactions are classical hydrogen bonds. Chern. Commun. 1999. 2299.
37. Moore, F.H.: Power, L.F. The crystal structure of potassium hydrogen oxalate by neutron diffraction. Inorg. Nucl. Chem. Lett. 1971. *7.* 873.
38. Mascal. M.: Marjo, C.E.: Blake, A.J. Breakdown of the hydrogen bond strength–length analogy: A revision. Chem. Commun. 2000. 1591.
39. Rathcliffe. E.I.: Irish. D.E. *Water Science Reviews Vol. 2;* Franks. F.. Ed.: Cambridge University Press. 1985: 149–214.
40. Gilli. G.; Belluci. F.; Ferretti. V.: Bertolasi. V. Evidence for resonance-assisted hydrogen bonding from crystal–structure correlations on the enol form of the β-diketone fragment. J. Am. Chem. Soc. 1989. *111.* 1023.
41. Tse, Y.C.: Newton. M.D. Theoretical observations on the structural consequences of cooperativity in H···O hydrogen bonding. J. Am. Chem. Soc. 1977. 99. 611.
42. Del Bene. J.E. An ab initio molecular orbital study of the structures and energies of neutral and charged bimolecular complexes of nh_3 with the hydrides AH_n (A = N. O. F, P, S, and Cl). J. Comput. Chem. 1989. *10,* 603.
43. Braga, D.: Crepioni. F. Intermolecular interactions in nonorganic crystal engineering. Acc. Chem. Res. 2000. *33,* 601.
44. Aakeroy. C.B.: Beatty, A.M. Crystal engineering of

hydrogen-bonded assemblies—A progress report. Aust. J. Chem. 2001, *54*, 409.
45. Whitesides, C.M.: Mathias, J.-P.; Seto, C.-T. Molecular self-assembly and nanochemistry. Science 1991,254, 1312.
46. Mathias, J.-P.; Seto, C.T.; Simanek, E.E.; Whitesides. G.M. Self-assembly through hydrogen bonding: Preparation and characterization of three new types of supramolecular aggregates based on parallel cyclic ca3···m3 "rosettes". J. Am. Chem. Soc. 1994. *116*, 1725.
47. Lehn. J.-M.; Mascal, M.; DeCian, A.; Fischer. J. Molecular recognition directed self-assembly of ordered supramolecular strands by cocrystallization of complementary molecular compounds. Chem. Commun 1990, 479.
48. Marsh, A.: Silvestri, M.; Lehn. J.-M. Self-complementary hydrogen bonding heterocycles designed for the enforced assembly into supramolecular macrocycles. Chem. Commun. 1996. 1527.
49. Melendez, R.E.; Sharma, C.V.K.; Zaworotko, M.J.; Bauer. C.; Rogers. R.D. Toward design of organic porous solids: Modular honeycomb grids sustained by anions of trimesic acid. Angew. Chem.. Int. Ed. Engl. 1996, 35, 2213.
50. Sharma. C.V.K.; Bauer, C.B.; Rogers, R.D.: Zaworotko, M.J. Interdigitated supramolecular laminate. Chem. Commun. 1997, 1559.
51. Mascal, M.: Hansen, J.: Fallon, P.S.; Blake, A.J.: Heywood, B.E.; Moore. M.H.; Turkenburg, J.P. From molecular ribbons to a molecular fabric. Chem. Eur. J. 1999, 5, 381.
52. Felix, O.: Hosseini, M.W.: DeCian, A.; Fischer. J. The simultaneous use of H-bonding and Coulomb interactions for the self-assembly of fumaric acid and cyclic bisamidine into one- and two-dimensional molecular networks. Angew. Chem.. Int. Ed. Engl. 1997. 36. 102.
53. Felix, O.; Hosseini, M.W.; De Cian, A.: Fischer. J. Crystal engineering of 2-D hydrogen bonded molecular networks based on the self-assembly of anionic and cationic modules. Chem. Commun. 2000, 281.
54. Kraft. A.; Frohlich, R. Star-branched non-covalent complexes between carboxylic acids and a tris(imidazoline) base. Chem. Commun. 8998. 1085.
55. Aakeroy, C.A.: Nieuwenhuyzen, M. Hydrogen-bonded layers of hydrogenmalate anions: A framework for crystal engineering. J. Am. Chem. Soc. 1994, 116. 10983.
56. Russell. V.A.: Etter. M.C.: Ward, M.D. Layered materials by molecular design: Structural enforcement by hydrogen bonding in guanidinium alkane- and arenesulfonates. J. Am. Chem. Soc. 1994. *116*. 1941.
57. Russell. V.A.; Ward. M.D. Molecular crystals with dimensionally controlled hydrogen-bonded nanostructures. Chem. Mater. 1996. *8*. 1654.
58. Russell, V.A.; Evans, C.C.; Li, W.; Ward, M.D. Nanoporous molecular sandwiches. Science 1997, *276*. 575.
59. Beatty, A.M. Hydrogen bonded networks of coordination complexes. Cryst. Eng. Comm. 2001, *51*, 1–13.
60. Burrows, A.D.; Chan, C.-W.; Chowdry, M.M.; McGrady, J.E.; Mingos, D.M.P. Multidimensional crystal engineering of bifunctional metal complexes containing complementary triple hydrogen bonds. Chem. Soc. Rev. 1995, 24, 329.
61. Chowdhry. M.M.; Burrows, A.D.; Mingos. D.M.P.; White. A.J.P; Williams. D.J. Synthesis and crystal structure of 5-(2-pyridylmethylene)hydrotoin and complexes of pyhy with nickel(II) and copper(II). Chem. Commun. 1995, 1521.
62. Houlton, A.; Mingos, D.M.P.; Williams, D.J. Multidimensional crystal engineering of metal complexes based on complementary hydrogen bonding. Transit. Met. Chem. 1994, 19, 653.
63. Houlton, A.; Mingos. D.M.P.; Williams, D.J. Molecular recognition of nucleotide bases by a metal complex. A novel bifunctionality with implications for metallo-drug design. Chem. Commun. 1994. 503.
64. Aakeroy. C.B.; Beatty, A.M. Low-dimensional architectures of silver(I) coordination compounds assembled via amide–amide hydrogen bonds. Cryst. Eng. 1998, I, 39.
65. Aakeroy, C.B.; Beatty, A.M. Supramolecular assembly of low-dimensional silver(I) architectures via amide–amide hydrogen bonds. Chem. Commun. 1998. 1067.
66. Aakeroy, C.B.; Beatty, A.M.; Leinen. D.S. The oxime functionality: A versatile synthon for supramolecular assembly of metal-containing hydrogen-bonded architectures. J. Am. Chem. Soc. 1998. *120*, 7383.
67. Aakeroy. C.B.: Beatty. A.M.; Leinen. D.S. A versatile route to porous solids: Organic–inorganic hybrid materials assembled through hydrogen bonds. Angew. Chem., Int. Ed. 1999. 38. 1815.
68. Dastidar, P.: Stein. Z.; Goldberg, I.; Strouse. C.E. Supramolecular assembly of functionalized metalloporphyrins. Porous crystalline networks of zinc tetra(4-carboxyphenyl)porphyrin. Supramol. Chem. 1996. 7. 257.
69. Krishna Kumar, R.: Balasubramanian. S.; Goldberg. 1. Crystal engineering with tetraarylporphyrins, an exceptionally versatile building block for the design of multidimensional supramolecular structures. Chem. Commun. 1998. 1435.
70. Diskin-Posner. Y.; Goldberg. I. From porphyrin sponges to porphyrin sieves: A unique crystalline lattice of aquazinc tetra(4-carboxyphenyl)porphyrin with nanosized channels. Chem. Commun. 1999. 1961.

Structural Engineering in Organic–Inorganic Perovskites

S

Karen R. Maxcy
IBM T.J. Watson Research Center, Yorktown Heights, New York, U.S.A.

Roger D. Willett
Washington State University, Pullman, Washington, U.S.A.

INTRODUCTION

Layer perovskite materials of the type $(RNH_3)_2MX_4$ and $(NH_3RNH_3)MX_4$ (M = divalent metal ion; X = Cl^-, Br^-, or I^-) form an extensive family of organic–inorganic hybrid materials. These contain layers of corner-sharing metal-halide octahedra separated by layers of organic cations. The metal ions employed have typically been from the first transition series or the heavier members of group 12 and group 14 elements, although a number of other divalent ions as well as trivalent ions have also been incorporated. With the appropriate choice of M and X ions, it is possible to incorporate a large variety of organic R groups into these materials. Often, the R groups play a passive role in the behavior of these materials, but much of the current research focuses on systems where there may be synergistic interactions between the organic and inorganic subsystems.

The compounds containing magnetic transition metal ions were extensively studied as model low-dimensional ferro- or antiferromagnetic systems. Variations in the size and shape of the organic groups are used to modify the strength of intra-and interlayer exchange coupling. When the metal is Sn^{2+} or Pb^{2+}, the systems are semiconductors that can be of use in device applications. The labile, ionic nature of these compounds allows for many of the hybrid materials to be processed using solution techniques.

A common feature of these hybrid materials is structural phase transitions involving the onset of disorder of the organic *R* groups. For compounds containing long-chain aliphatic *R* groups, this led to organic layers being studied as crystallographic models for lipid bilayers. Another interesting application is to use the inorganic layers as templates to hold unsaturated organic groups in favorable juxtaposition for photopolymerization.

STRUCTURAL CHARACTERISTICS OF LAYER PEROVSKITE MATERIALS

The parent perovskite rtructure has the formula AMX_3, where A and *M* are metal ions, and X is a monatomic anion.''' The structure consists of a three-dimensional (3D) network of corner-sharing MX_6 octahedra, while the A cations fill the 12-fold coordination holes within the 313 framework, as shown in Fig. 1a. The oxide perovskites can incorporate a broad range of A and *M* metal ions and have been extensively studied because of their interesting and useful physical properties. With the halide perovskites, it is possible to incorporate small organic cations in the A sites when the M cation has a large ionic radius.[2] However, the dimensionality of the framework must be reduced in order to extend this framework to incorporate larger organic cations. This is typically accomplished by slicing out a $(MX_4^{2-})_\infty$ (100) sheet, as seen in the left-hand diagram in Fig. 1b. The 12-fold holes in the parent AMX_3 structure now become eightfold square cavities that decorate each face of the inorganic framework. These have appropriate size to accommodate the $-NH_3^+$ moieties of the organoammonium cations. In this manner, $(RNH_3)_2MX_4$ layers are formed in which the inorganic frameworks are sheathed by the organic R groups. The crystalline materials thus formed are fragile, because only van der Waals interactions occur between these sheathed layers. If 3D stability is desired. diammonium cations (right-hand diagram in Fig. 1b) may be used to provide a covalent linkage between the inorganic frameworks.[3] In a few cases, a zigzag inorganic framework is observed, where the slices of the AMX_3 parent structure are cut out parallel to the (110) direction.''' Another variation. observed when a small A' ion such as $CH_3NH_3^+$ is present, has a multilayered inorganic framework of stoichiometry $(A)_2(A')_{n-1}M_nX_{3n+1}$.[5]

The inorganic framework is able to accommodate most divalent metal ions that can assume octahedral coordination geometry. From the first transition series, structures with Cr^{2+},[6] Mn^{2+},[7] Fe^{2+},[8] and Cu^{2+}[3] are known (Fig. 2a). However, the perovskite structure is not found with metal ions that have a strong preference for tetrahedral geometry or have a small radius. For metal ions like $Mn^{2+}$and Fe^{2+}, the bridging M–X distances are relatively invariant. so the sizes of the eightfold cavities vary little from compound to compound. In contrast. the

Encyclopedia of Supramolecular Chemistry
DOI: 10.1081/E-ESMC 120012554

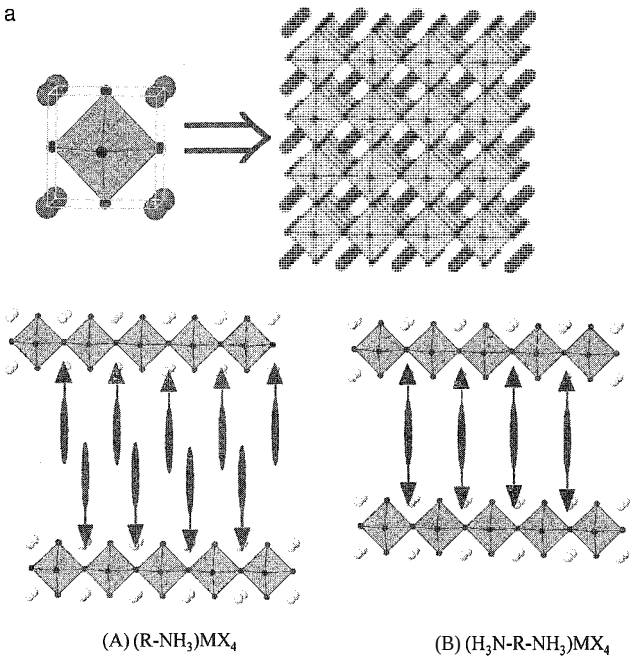

Fig. 1 (a) The cubic AMX_3 perovskite structure. (b) Single-layer perovskites with (A) monoammonium (RNH_3^+) of (B) diammonium ($^+NH_3RNH_3^+$) organic cations. (*View this art in color at www.dekker.com.*)

Cu^{2+} and Cr^{2+} ions are subject to a tetragonal elongation of their octahedral coordination due to the Jahn–Teller effect. This leads to an asymmetrical *M–X···M* linkage, with one normal *M*–X bond and one longer semi-coordinate *M···X* bond. The length of the semicoordinate bond is variable over a range $\geq$0.8 A. Thus, these lattices can adapt to accommodate more complex organic cations. For the main group metals. Cd^{2+},[9] Sn^{2+},[10] and Pb^{2+} [10] salts were prepared. Other more unusual metal ions that were incorporated include Eu^{2+}[11] and Pd^{2+}.[12]

The $-NH_3^+$ hydrogen-bonding linkage into the eightfold square cavity provides the interesting topological challenge of inserting an objeci with threefold symmetry into a cavity with fourfold symmetry. As a result. the C–N bond tips so that the $-NH_3^+$ is able to hydrogen bond to both the bridging and terminal halide ions. Two limiting cases exist: hydrogen bonds to two terminal and one bridging halides (the 2b,1t scheme) or to one terminal and two bridging halides (the 1b,2t scheme). The former is illustrated in Fig. 2b. These two schemes result in different conformations for the hydrocarbon backbone attached to the ammonium ion. These interactions have two effects on the inorganic framework. A $\sqrt{2} \times \sqrt{2}$ superlattice (or more complex) is produced that involves a 45° rotation of the in-plane crystallographic axes. The second effect is to cause the *M–X–M* bonding interactions to be nonlinear. This leads to a washboard effect for frameworlis based on transition metals. as seen in Fig. 2a. With Group 14 metal ions. an in-plane bending occurs. Both distortions adapt the eightfold cavities to the shape of the organic *R* groups.

The inorganic framework provides a template to which the organic *R* groups must accommodate. For *M* = first row transition metal and X = Cl or Br, the edges of the cavity typically range from 5.1–5.5 A. Thus. primarily straight-chain hydrocarbon groups can be accommodated. However, for the Jahn–Teller active ions. the variable length of the semicoordinate *M···X* allows for greater flexibility in the length of the sides of the cavity. Thus, these salts can accommodate *R* groups with simple ring systems. For cornpounds based on the larger metal or halide ions, the cavity edges now range from 6.0–6.4 A. This allows the incorporation of more complex *R* groups. In order to give sufficient flexibility to accominodate these more complex organics. it is conventional to tether them to the $-NH_3^+$ moiety via methylene or ethylene linkages.

PHYSICAL PROPERTIES AND APPLICATIONS OF HYBRID LAYER PEROVSKITES

Magnetic Properties

Because of their interesting magnetic properties. hybrid layered perovskites containing transition metal ions were

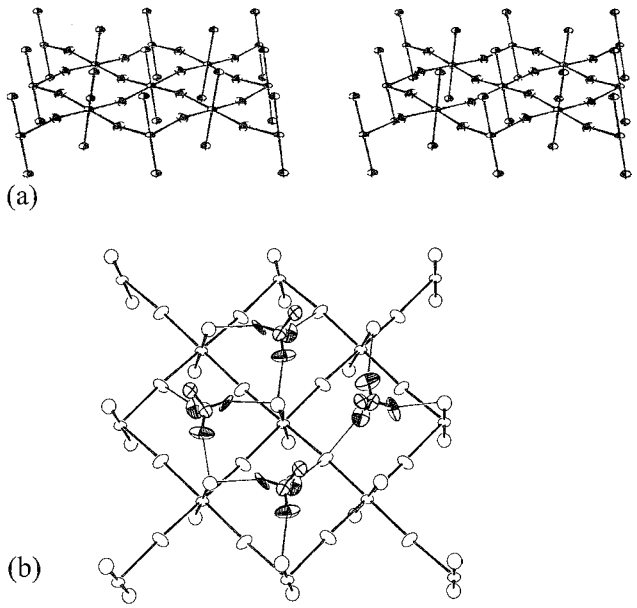

Fig. 2 The structure of $(NH_3C_3H_6NH_3)MnCl_4$ showing (a) the inorganic framework and (h) the 2t.1b hydrogen-bonding scheme (Adapted from Ref [8])

the most intensely studied. The corner sharing of the octahedra within the inorganic framework gives direct *M–X–M* superexchange pathways between the metal ions. while the organic sheathing of the layers generally restricts the interactions between the layers to those of dipolar nature. Thus, they are excellent realizations of two-dimensional (2D) magnetic systems. The ability to change spin quantum number and magnetic anisotropy through variation of the metal and halide ions has made these extremely interesting systems to study. In the Mn^{2+} salts, the symmetric Mn–X–Mn pathways lead to antiferromagnetic exchange coupling.[13] With the $S = 5/2$ ground states, the Mn^{2+} salts provide excellent model systems for classical 2D antiferromagnetic coupling. Short-range antiferromagnetic correlations lead to a maximum in the magnetic susceptibility in the 80–90 K range (Fig. 3a), with the onset of long-range magnetic order occurring at 40–50 K. Because of the nonlinear nature of the Mn–X–Mn exchange pathways, adjacent spins are not precisely antiparallel, so these actually show canted antiferromagnetic behavior. The creation of domain wall movements in these canted antiferromagnetic systems at the 3D ordering temperature leads to the spike seen in Fig. 3a. For the $S = 2$ Fe^{2+} systems, the presence of zero field-splitting leads lo further complications in describing the details of the antifersomagnetic-coupled 2D layer.[14]

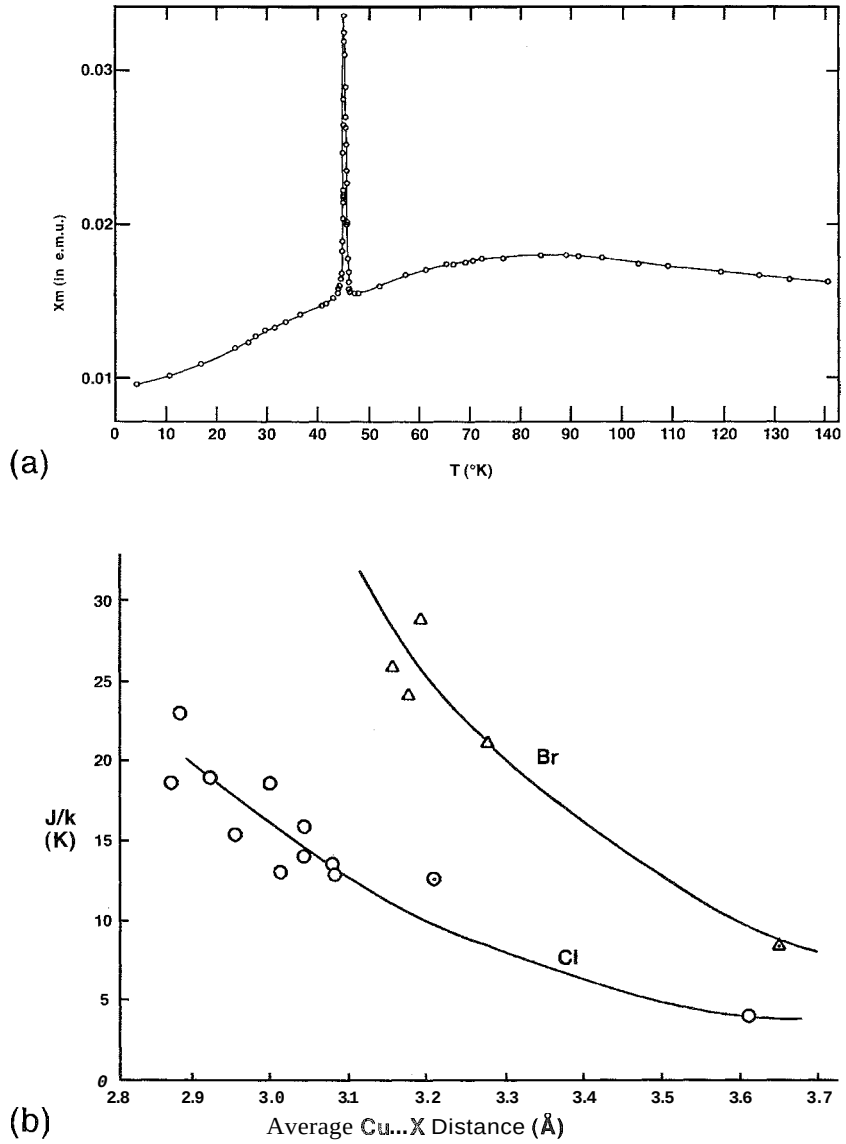

Fig, 3 (a) Magnetic susceptibility of $(CH_3NH_3)_2MnCl_4$ (Gerstein, B.C.; Chang, K.; Willet, R.D. *J. Chem. Phys.* 1974, *60,* 3454). (b) Correlation of interlayer exchange coupling with the Cu···X distance in $(RNH_3)_2CuX_4$ salts. (From Ref. [4].)

Ferromagnetic interlayer coupling is found in salts of the Jahn–Teller active d^4 Cr^{2+} and the d^9 Cu^{2+} ions. The antiferrodistortive nature of the tetragonal elongation of the octahedra within the layers leads to orbital arrangements that favor ferromagnetic interlayer coupling within the layers in these systems. The type of 3D ordering will depend upon the nature of the coupling between the layers. Dipolar and superexchange interactions between layers usually lead to antiferromagnetic coupling. However, examples with ferromagnetic 3D ordering are known. The Cr^{2+} salts typically undergo 3D ferromagnetic interlayer ordering around 40–45 K. pointing the way to the possibility of high T_c molecular magnets.[6] $(MeNH_3)_2CuCl_4$ (among other Cu^{2+} salts) orders at 8.9 K.[15] The Cu systems were extensively studied as realizations of the quantum (S = 1/2) 2D ferromagnetic interlayer. The strength of the FM intralayer exchange coupling (and thus the ordering temperature) was shown to decrease monotonically (Fig. 3b) as the length of the semicoordinate Cu···X distance increases.[3] Magnetization and, electron paramagnetic resonance (EPR) studies showed that the spins align normal to the layers in the Cl salts and in the plane in the Br salts. This is due to the role of the ligand spin-orbit in determining the anisotropy of the magnetic interactions.[14] lor the diammonium $(NH_3RNH_3)CuCl_4$ series. it is found that as n decreases, strong interlayer antiferromagnetic superexchange coupling occurs via so-called "two-halide" Cu–X···X–Cu interaction~.~'~'

PHASE TRANSITIONS

The combination of different hydrogen-bonding schemes and the possibility of thermal reorientation of the part or all of the organic R groups leads to the potential for multiple phase transitions in these materials. The R = n-propyl series (M = Mn, Cu, Cd) exhibits interesting behavior. with multiple transitions and the presence of modulated phases. The phase transitions in the Cu^{2+} salt involve not only disorder of the cations but also perturbation of the inorganic framework.[17,18] In the low-temperature phase. the n-propyl groups form an ordered arrangement that leads to a pseudohexagonal arrangement for the terminal methyl groups. However. the disorder in the high-temperature phases causes packing of the methyl groups to mimic the square arrangement of the underlying ammonium groups. The high-temperature phase differs from the lower-temperatme phase in three significant ways: the average orientation for the N–C bonds is parallel to the normal to the plane; the bridging Cl atoms are not displaced from the planes; and the cations are disordered. An incommensurate phase, found at intermediate ternperatures, is characterized by the superposition of a wave-like sinusoidal displacement of each layer.[17,18] The displacements in adjacent layers are out of phase, so the distance between layers is also sinusoidally modulated.

The diammonium salts can also undergo phase transitions. The high- and low-temperature phases of $(NH_3C_3H_6NH_3)MnCl_4$ have the usual $\sqrt{2} \times \sqrt{2}$ superlattice of the inorganic framework and 2t,1b hydrogen-bonding scheme.[19] In the high-temperature phase, the cations are disordered across a mirror plane. with a rotation angle of 40° between the two orientations. However, the intermediate phase has a 2 x 2 superlattice. The cations are again disordered across a mirror plane. The hydrogen bonding is intermediate between the 2t,1b and 1t,2b schemes, so the angle between the two orientations is only 20°.

The phase transitions in compounds with long-chain R groups—C_{10} or longer—were touted as analogues of the phase transitions in lipid bilayers.[20] However, a major difference exists between the two systems. Although the R groups in the perovskites can undergo various types of motion. the-NH_3^+ head groups are anchored to an inorganic framework. Nonetheless. some similarities exist. The perovskite materials typically show two primary thermal anomalies. one with $\Delta S_{tr} \sim$ 5–10 cal/mol-K and the second with $\Delta S_{tr} \sim$ 30–40 callmol-K. The sequence in which these anomalies occurs depends on the length of the hydrocarbon chain and the size of the

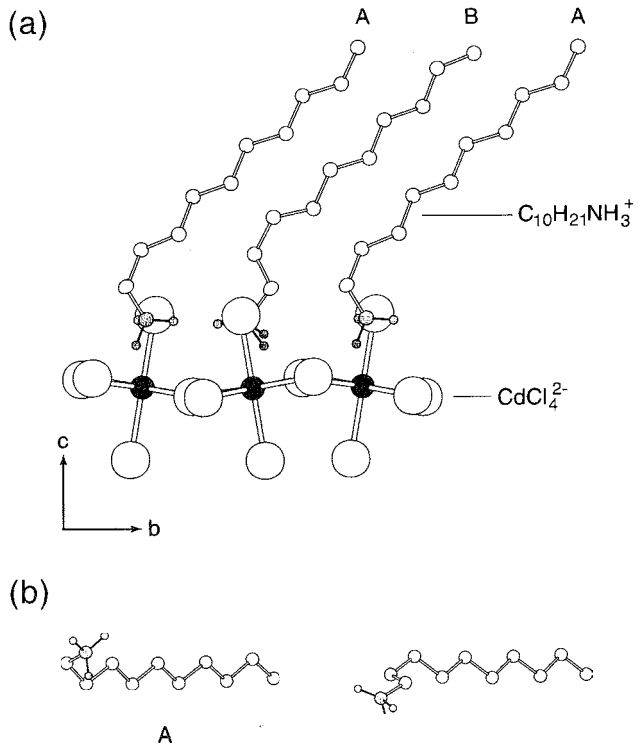

Fig. 4 The room-temperature structure of $(C_{14}H_{29}NH_3)_2CdCl_4$. (From Ref. [27].)

inorganic framework. In the low-temperature phase, the majority of hydrocarbon chains are in extended *trans* conformations that are tilted 30–40° from the normal to the plane, although some *gauche* bonds exist near the head group to accommodate the packing of the chains (Fig. 4). The major thermal anomaly corresponds to "chain melting"—the introduction of *gauche-trans-gauche* kinks into the chain and a realignment of the chains perpendicular to the layers.[21] When the smaller anomaly occurs first, this corresponds to a twofold flipping motion of the *trans* portions of the chains. When it occurs after the chain melting, it corresponds to a twofold disorder of the melted chains due to disorder of a gauche bond by the head group. Thus, these studies helped to shed light on the possible behavior in lipid layers.

Electrical Properties

Hybrid layer perovskites designed with metals from Group 14 possess a variety of favorable properties for the fabrication of electronic devices. These metal halides have excitonic transitions related to their band gap, which result in spectral transitions dependent on the metal cations and halides contained within the inorganic sheet of the perovskite. The 2D A_2MX_4 perovskite structure as well as the dielectric modulation between the organic and inorganic layers allows for strong exciton binding energy and observation of the electroluminescence at room temperature. The exciton binding energy and the oscillator strength also lead to strong photoluminescence,[10,22,23] nonlinear optical effects,[24,25] and tunable polarization absorption.[26] The Pb^{2+} perovskites demonstrated thermal and mechanical stability as well as room-temperature photoluminescence in the visible range,[27] while the Sn^{2+} perovskites possess high carrier mobility.

Incorporation of AEQT, the cation of the oligothiophene derivative 5,5‴-*bis*(aminoethyl)-2,2′:5′,2″:5″,2‴:5‴,2‴-quaterthiophene into the lead halide perovskite framework results in a characteristic absorption/emission of the given material. The organic-inorganic framework is tethered between the layers of PbX_6 octahedra by the ethylammonium groups of the dication. The AEQT is held between the metal-halide sheets in a herringbone arrangement with respect to the other AETQ cations in the lattice (Fig. 5). Organic-inorganic light-emitting diodes (OILED) were fabricated using thin films of the (AEQT)$PbCl_4$ perovskite.[28–30] The OILED devices based on (AEQT)$PbCl_4$ emit bright green-yellow light (λ_{max} = 530 nm) in a well-lit room when the devices are forward biased under ambient conditions.

Organic-inorganic TFTs (thin-film field effect transistors) were formulated as low-cost alternatives for the development of display and storage technologies.[31] The semiconducting organic-inorganic perovskite, $(C_6H_5C_2H_4NH_3)_2SnI_4$ [$(PEA)_2SnI_4$], was used in the fabrication of TFTs using solution-processed thin films (Fig. 6).[31] Devices fabricated from the $(PEA)_2SnI_4$ perovskite are *p*-channel transistors with field effect mobilities of 0.61 $cm^2/V\text{-}s$ and I_{on}/I_{off} ratio of $\sim 10^6$.[32] Flexibility in the choice of the inorganic anion and the organic cation

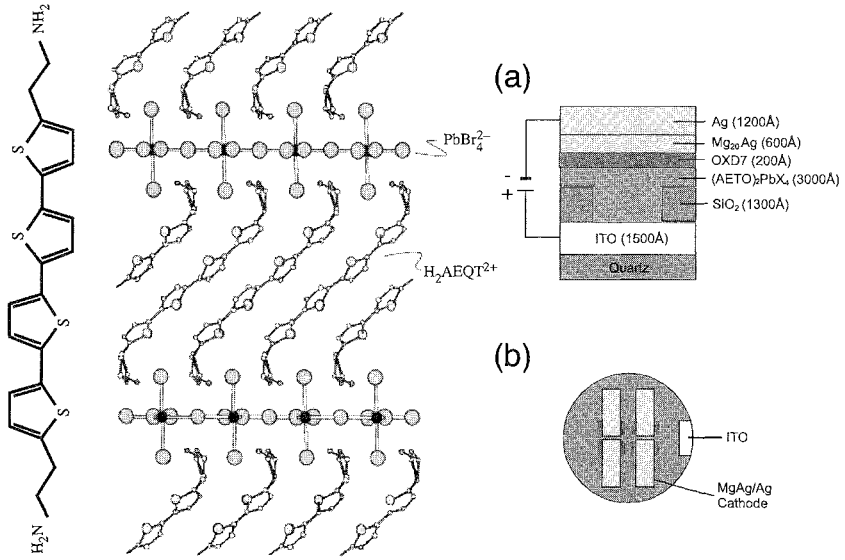

Fig. 5 (Left) The 5,5‴-*bis*(aminoethyl)-2,2′:5′,2″:5″,2‴:5‴,2‴-quaterthiophene molecule. (Center) perovskite structure of the (AEQT) $PbBr_4$. (Right) (a) Cross section of the OILED device structure (not to scale): (b) view of the circular substrate containing four devices. For clarity, the OXD7 layer (on the top of the patterned hybrid perovskite layer) is not shown. (Adapted from Ref. [32].) (*View this art in* color *at www.dekker.com.*)

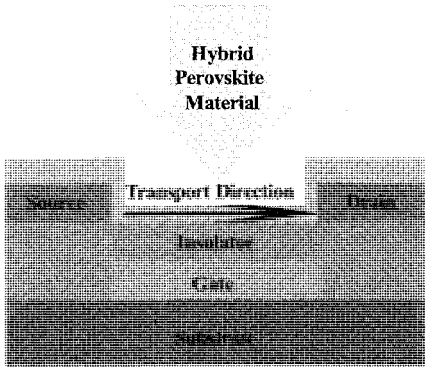

Fig. 6 A TFT device. The organic/inorganic perovskite material is deposited as an upper onto prefabricated source and drain electrodes. (Adapted from Ref. [31].) (View, *this* art in color at *www.dekker.com.*)

allowed for the development of processable TFTs. The $(PEA)_2SnI_4$ perovskite contains alternating layers of corner-sharing SnI_6 octahedra and PEA cations. The $-NH_3^+$ group present on PEA cation hydrogen bonds to the SnI_6 octahedra, and weak van der Waals interactions between the PEA groups hold the layers together. The weak interactions between the layers allow the material to be solution processed.

Enhanced physical properties of materials where the thickness of the inorganic layer sheathed between the organic cation layers is of interest in the fabrication of devices with conductive properties. A semiconductor ⟷ metal transition is observed for tin(II) compounds $(C_4H_9NH_3)_2(CH_3NH_3)_{n-1}Sn_nI_{3n+1}$ as a function of increasing n value. The n = 1 compound $(C_4H_9NH_3)_2SnI_4$ is a large band-gap semiconductor with a room-temperature resistivity of approximately 10^5 Ωcm.[5] Increasing the value of n results in reduced resistivity of the material, with metallic behavior seen for materials $n \geq 3$. The 3d perovskite $(CH_3NH_3)SnI_3$ (n = ∞) is a low-carrier-density p-type metal with a room-temperature Hall mobility of approximately 50 $cm^2V^{-1}s^{-1}$ and a carrier density of approximately $10^{19}cm^{-3}$.[32] As the number of inorganic layers increases, the conductivity also increases.

CONCLUSION

The family of layered perovskites designed with divalent cations grew from systems, which use organic cations as placeholders in the lattice, to materials that can be tailored to possess unique properties. Systems were developed with specific properties inherent to the organic and inorganic components. Crystal engineering was used with the layers structure to design materials with potential commercially useful properties, such as magnetic and electronic characteristics. The recent developments in magnetic materials and device fabrication of TFTs and OILEDs highlighted the practical applications that can be explored with the ability to consistently work in the same structural framework.

REFERENCES

1. Wyckoff, R.W.G. Crystal Structures, (Inorganic *Compounds RX_m, R_nMX_2, R_nMX_3)*; John Wiley & Sons: New York, 1964, Vol. 2, 394.
2. Mitzi, D.B.; Liang. K.J. Synthesis, resistivity, and thermal properties of the cubic perovskite $NH_2CH{=}NH_2SnI_3$ and related systems. Solid State Chem. 1997, *134*, 376.
3. Willett, R.D.; Place, H.; Middleton, M. Crystal structures of three new copper(II) halide layered perovskites: Structural, crystallographic. and magnetic correlations. J. Am. Chem. Soc. 1988, *110*, 8639.
4. Mitzi, D.B.; Wang, S.; Feild, C.A.; Chess, C.A.; Guloy, A.M. Conducting layered organic–inorganic halides containing (110)-oriented perovskite sheets. Science 1995, *267*, 1473.
5. Mitzi, D.B.; Feild, C.A.; Harrison, W.T.A.; Guloy, A.M. Conducting tin halides with a layered organic-based perovskite structure. Nature 1994, *369*. 467.
6. Bellitto. C.; Day, P.: Wood, T.E. Magnetic susceptibilities and optical study of the organic-intercalated two-dimensional ionic ferromagnet bis(benzylammonium)tetrachorochromate(II). J. Chem. Soc. Dalton Trans. 1986, *847*.
7. Peterson, E.R.; Willett, R.D. The crystal structure of $(CH_3CH_2CH_2NH_3)_2MnCl_4$. J. Chem. Phys. 1972, *56*, 1879.
8. Willett. R.D.; Riedel, E.F. A neutron diffraction study of the crystal structures of $(NH_3CH_2CH_2CH_2NH_3)MnCl_4$ and $(NH_3CH_2CH_2CH_2NH_3)FeCl_4$: Layer structures with two-dimensional magnetic interactions. Chem. Phys. 1975, *8*, 112.
9. Willett, R.D. Propylenediammoniumtetrachlorocadmate(II). Acta Crystallogr. 1997, *B33*, 1641.
10. Mitzi, D.B. Synthesis, crystal structure. and optical and thermal properties of $(C_4H_9NH_3)_2MI_4$ (M = Ge, Sn, Pb). Chem. Mater. 1996, *8*, 791.
11. Mitzi, D.B.: Liang, K.N. Preparation and properties of $(C_4H_9NH_3)_2EuI_4$: A luminescent organic–inorganic perovskite with a divalent rare-earth metal halide framework. Chem. Mater. 1997, *9*, 2990.
12. Willett, J.J.; Willett, R.D. Bis(propylammonium)tetrachloropalladate(II). Acta Crystallogr. 1977, *B33*, 1639.
13. Achiwa, N.; Matsuyama, T.; Yoshinari, T. Weak ferromagnetism of the layered perovskite$(C_{10}H_{21}NH_3)_2MnCl_4$, $(C_{11}H_{23}NH_3)_2MnCl_4$ and $(C_{12}H_{25}NH_3)_2MnCl_4$. Phase Transit. 1990, 28, 79.
14. Patyal, B.R.; Willett, R.D. Theory of EPR linewidths in low-dimensional magnetic insulators and application to data on ferromagnetic Cu(II) layer systems. Magn. Reson. Rev. 1990, *15*, 47.

15. de Jongh, L.J. Observation of lattice- and spin-dimensionality crossovers in the susceptibility of quasi 2-dimensional Heisenberg ferromagnets. Physica 1976, *82B*, 247.
16. Snively, L.O.; Tuthill, G.F.; Drumheller, J.E. Measurement and calculation of the superexchange interaction through the two-halide bridge in the eclipsed layered compounds $[NH_3(CH_2)_nNH_3]CuX$ for n = 2-5 and X = Cl_4 and Cl_2Br_2. Phys. Rev., B 1981, *24*, 5349.
17. Doudin. *B.;* Chapuis, G. Structure analysis of the high-temperature phases of $[NH_3(C_3H_7)]_2CuCl_4$. I. The commensurate phase. Acta Cryst. 1998, *B46*, 175. Doudin, B.; Chapuis, G. Structure analysis of the high-temperature phases of $[NH_3(C_3H_7)]_2CuCl_4$. II. The modulated phase. Acta Cryst. 1990, *B46*, 180.
18. Crowley, J.C.; Dodgen, H.W.; Willett, R.D. The crystal structures of the three phases of $(NH_3C_3H_6NH_3)MnCl_4$ and a ^1H NMR investigation of its phase transitions. J. Phys. Chem. 1982. *86*, 4046.
19. Needham. G.F.; Willett. R.D.; Franzen, H.F. Phase transition in crystalline models of lipid bilayers, I. DSC and x-ray studies of $(C_{12}H_{25}NH_3)_2MCl_4$ and $(C_{14}H_{29}NH_3)_2MCl_4$ salts (M = Mn^{2+}, Cd^{2+}, Cu^{2+}). J. Phys. Chem. 1984. *88*, 674.
20. Vacatello. *M.;* de Girolamo, M.; Busico. V. Relationships between structure and properties in long chain bis(n-alkylammoniumtetrabromocuprates(II) and bis(n-alkylammonium)tetrabromomanganates(II). J. Chem. Soc., Faraday Trans. 1, 1981, *77*, 2367.
21. Papavassiliou. G.C.; Koutselas, I.B. Structural, optical and related properties of some natural 3-dimensional and lower-dimensional semiconductor systems. Synth. Met. 1995, *71*, 1713.
22. Ishihara, *T.;* Takahashi, J.; Goto, T. Exciton state in two-dimensional perovskite $(C_{10}H_{21}NH_3)_2PbI_4$ semiconductor. Solid State Commun. 1989, *69*, 933.
23. Xu, C.; Kondo, T.: Sakakura, H.; Kumata, K.; Takahashi, Y.; Ito. R. Optical third harmonic generation in layered perovskite-type material $(C_{10}H_{21}NH_3)_2PbI_4$. Solid State Cornmun. 1991, 79, 245.
24. Calabrese. J.; Jones, N.L.: Harlow, R.L.; Herron, W.; Thorn. D.L.; Wang. Y.J. Preparation and characterization of layered lead halide compounds. Am. Chem. Soc. 1991. 113.2328.
25. Fujita, T.; Sata, Y.; Kuitani, T.: Ishihara. T. Tunable polariton adsorption of distributed feedback microcavities at room temperature. Phys. Rev., B 1998, *57*, 12428.
26. Mitzi, D.B. Synthesis, structure and properties of organic–inorganic perovslutes and related materials. Prog. Inorg. Chern. 1999. *48.* 1.
27. Chondroudis. K.; Mitzi, D.B. Electroluminescence from an organic–inorganic perovskite incorporating a quaterthiophene dye within lead halide perovskite layers. Chem. Mater. 1999. *11*, 3028.
28. Mitzi. D.B.; Chondroudis. K.: Kagan, C.R. Design, structure, and optical properties of organic–inorganic perovskites containing an oligothiophene chromophore. Inorg. Chem. 1999. *38.* 6246.
29. Chondroudis, *K.:* Mitzi, D.B. The use of ionic salt dyes as amorphous, thermally stable emitting layers in organic light-emitting diodes. Appl. Phys. Lett. 2000, *76.* 58.
30. Kagan, C.R.: Mitzi, D.B.; Dimitrakopoulos, C.D. Organic–inorganic hybrid materials as semiconducting channels in thin-film field-effect transistors. Science. 1999. *286.* 945.
31. Mitzi, D.B.; Chondroudis, K.; Kagan, C.R. Organic–inorganic electronics. IBM J. Res. Dev. 2001. *45*, 29.
32. Mitzi, D.B.; Feild. C.A.: Schlesinger, Z.: Laibowitz, R.B. Transport, optical, and magnetic properties of the conducting halide perovskite $CH_3NH_3SnI_3$. J. Solid State Chern. 1995, *114*, 159

Supermicroscopy: AFM, SNOM, and SXM

Steven De Feyter
Frans C. De Schryver
Katholieke Universiteit Leuven (K.U.Leuven), Leuven, Belgium

INTRODUCTION

The development of scanning probe techniques is a blessing for the study of suprarnolecular structures. These supermic oscopy techniques open new ways not only to visualize the architecture of supramolecular structures but also to allow insight into chemical and physical processes related to their supramolecular identities with unprecedented spatial resolution.

The birth of scanning probe techniques revolutionized the way small objects or domains can be visualized. Common to all scanning-probe techniques is a tiny probe that scans a surface at a very small distance from it, and the interaction between probe and object is translated into a signal. The ultimate control in positioning is achieved by using piezoelectric elements. Since the invention of the scanning tunneling microscope (STM),[1] several experimental schemes were developed that allow detection of a great variety of interactions between probe and surface. Probably. atomic force microscopy (AFM) is the most popular.[2] Among those techniques. scanning near-field optical microscopy (SNOM)[3,4] takes a special place due to its optical resolution below the diffraction limit. All of these techniques have in cominon that they almost exclusively probe surface structures and properties. A major benefit of these techniques with respect to other surface characterization techniques is their noninvasiveness. Moreover, these techniques can be used under a large variety of experimental conditions, such as ultrahigh vacuum, under ambient conditions, in liquids. and at different temperatures.

In general. these supermicroscopy tools can be used for the investigation of two types of supramolecular structures> based upon the way they are "deposited" on the subst ate. On the one hand, these techniques can be exploited to investigate supramolecular assemblies that form in. e.g., solution, and that do not lose their structural integrity upon deposition on the surface. On the other hand, these techniques are also ideally suited to probe the supramolecular structures with forination is driven by the presence of the substrate. in any case, one has to take into consideration that upon deposition of supramolecular structures from solution. their nature can be affected substantially by the deposition process due to, for instance, adsorbate–substrate interactions and changes in concentration; and one should not neglect the role of the substrate.

SCANNING TUNNELING MICROSCOPY

STM for Structure Elucidation

In STM. a metallic tip is brought very close to a conductive substrate. and by applying a voltage between both conductive media. a tunneling current may result (Fig. 1). The exponential distance dependence of the tunneling current provides an excellent means with which to control the distance between the probe and the surface. High resolution (atomic) can be achieved, but the use of this probe technique is limited to conductive substrates. Of major importance is its ability to probe not only bare surfaces such as metals or semiconductors but also molecules, which are physisorbed or chemisorbed on these conductive surfaces. However, due to the specific nature of probing. only very thin molecular layers can be investigated.

Reducing the mobility of the molecules is a prerequisite for successful STM imaging. This can be achieved by working at low temperatures. Under these conditions. submonolayer assemblies can be investigated. Some examples include the formation of surface-supported supramolecular structures with size and aggregation patterns that are rationally controlled by tuning the noncovalent interactions between individual adsorbed molecules. Using low-temperature ultrahigh vacuum scanning tunneling microscopy. it was shown that porphyrin molecules adsorbed on a gold surface form monomers, trimers, tetramers. or extended wire-like structures. based upon dipole–dipole interactions."' Other examples include the formation of wire-like structures by hydrogen-bond formation[6] and the two-dimensional self-assembly of supramolecular clusters (containing precisely 10 molecules) and chains formed by 1-nitronaphthalene.[7] In the latter case. it was shown that these clusters could be manipulated (translated) while maintaining their structural and chiral integrities.[8]

Another way to reduce the mobility is by forming two-dimensional monolayers under ambient conditions. Adsorbate–substrate and adsorbate–adsorbate interactions lower the molecular mobility and are responsible for the two-dimensional ordering, ''Dry'' monolayers can be formed by drop casting and evaporation or by the horizontal lifting technique.[9] It is also possible to measure

Encyclopedia of Supramolecular Chemistry
DOI: 10.1081/E-ESMC 120012823

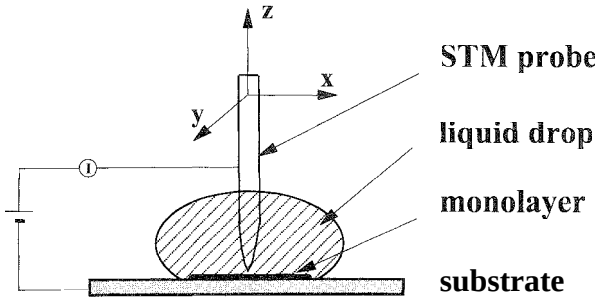

Fig. I An STM setup in liquids. (Reprinted with permission from the American Chemical Society.)

in liquids. With respect to sample preparation, the latter approach is attractive, as one needs only to apply a drop of a solution on the substrate, and by physisorption, a two-dimensional layer can be formed.[11] Examples include the study of supramolecular grids[11] and catenanes.[12] Within our research group, the "liquid" approach was extensively used to investigate and to control the formation of two-dimensional supramolecular structures by dicarboxylic acid type and urea-containing compounds.

Shown in Fig. 2a is a STM image of a monolayer of a 5-alkyloxy-isophthalic acid derivative physisorbed from 1-phenyloctane on the graphite surface. The larger bright spots in this functionalized hydrocarbon monolayer correspond to the aromatic moieties. The darker regions in the image correspond to the alkyl groups, which are interdigitated over their full length and aligned with their long axis parallel to the graphite substrate. The distance between adjacent isophthalic acid moieties allows for intermolecular hydrogen bonding within a lamella and between adjacent lamellae. In Fig. 2b, the ordering of an isophthalic acid derivative with a semifluorinated alkyl chain is shown (model: Fig. 2c). There is a clear change in contrast along the alkyl chain, illustrating the chemical sensitivity of STM. When isophthalic acid derivatives are

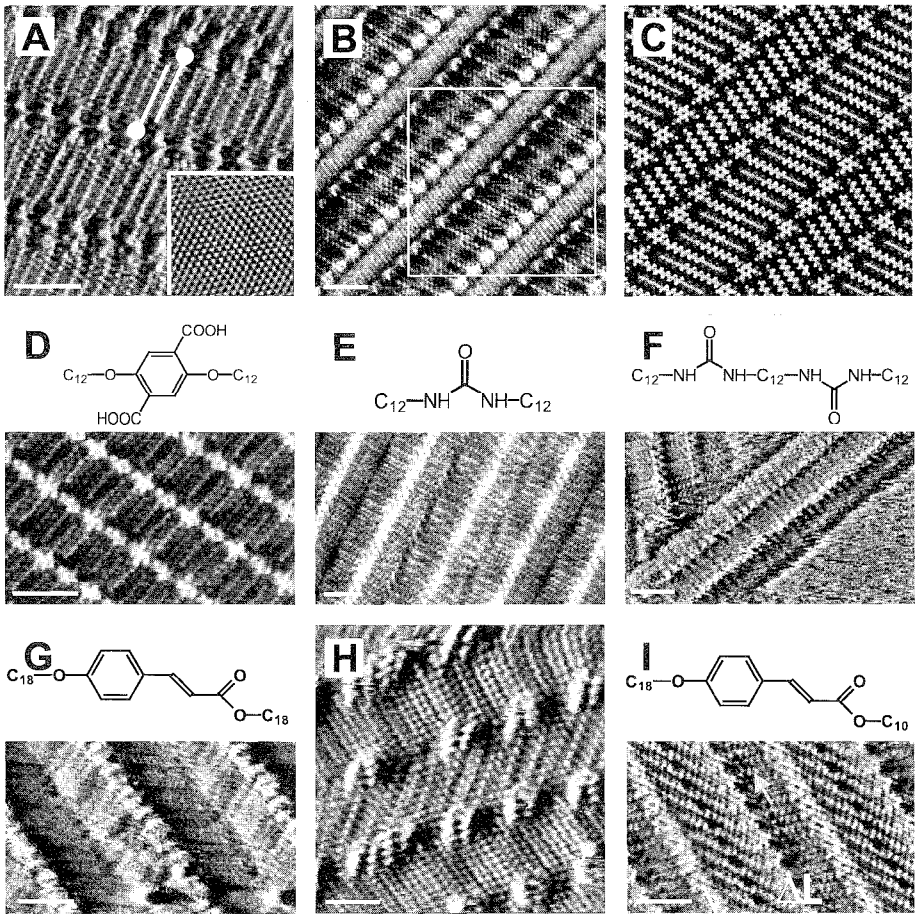

Fig. 2 STM images of (a) An isophthalic acid derivative. (h) A semifluorinated isophthalic acid derivative. (c) A model of the area in (b). (d) A terephthalic acid derivative. (e) A monourea compound. (f) A his-ureum compound. (g) A symmetric cinnamic acid derivative. (h) A photodimer monolayer of (g). (i) An asymmetric cinnamic acid derivative (not reactive). The scale bar is 2 nm. (Reprinted in part or adapted with permission from the American Chemical Society.) ***(View*** this art in color *at www.dekker.com.*)

dissolved in 1-octanol or 1-undecanol, solvent molecules are often incorporated in the monolayer (Figs. 2b–c). The 1-octanol molecules are codeposited and are stabilized by hydrogen bonding. Some functionalized hydrocarbons may display stabilizing hydrogen bonding along the lamella axis. For example, in monolayers of alkylated terephthalic acid derivatives (Fig. 2d), the terephthalic acid groups (bright) are linked by hydrogen bonds, and the alkyl chains, which are oriented perpendicular to the lamella axis, are interdigitated. This interdigitation allows for a two-dimensional stabilization.[17] For those systems lacking interacting groups at the termini of the alkyl chains, quasi-discrete supramolecular structures can be formed, even in liquid conditions. Urea groups are capable of forming up to four hydrogen bonds. Therefore, for the symmetrically substituted monourea compound. lamellae are formed, and the intermolecular distance (0.46 nm) is determined by hydrogen bonding (Fig. 2e). On the other hand, the interaction between adjacent lamellae is rather weak. For example, some *bis*-urea derivatives showed stable lamella formation.[14] In combination with relatively strong adsorbate–substrate interactions. the lamellae were stabilized enough to prevent or limit molecular diffusion on the graphite support. and isolated lamellae could be observed (Fig. 2f).

STM as Probe for Supramolecular Chirality, Dynamics and Reactivity

These simple examples illustrate how by carefully designing the molecules. one can control the supramolecular patterns in two dimensions. We took advantage of the control of the supramolecular patterns formed by these types of molecules to carry out reactions at the liquid–solid interface. In addition to investigations related to the structure of the two-dimensional assemblies, topics such as chirality, dynamics, and light-induced reactions can be studied. For instance, chirality is known to often have a major influence on the handedness of supramolecular structures formed in solution. and its effect also shows up in two-dimensional layers and in clusters. In general, it is found that enantiomers form enantiomorphous monolayers or clusters (the monolayers or clusters formed by enantiomers are related to each other by mirror symmetry). The same holds for achiral compounds, but now both mirror-image-related structures—monolayers or clusters—are formed. Of course, in these kinds of investigations, the study of the behavior of racemic mixtures is also of main interest.[8,15,16] Supramolecular structures, both in solution and on solid supports exposed to solution, are often "equilibrium structures" and show continuous exchange with the reservoir of building blocks. The STM is ideally suited to probe the dynamics in physisorbed supramolecular structures. For instance. assemblies formed at the liquid–solid interface are in dynamic equilibrium with the supernatant solution, and STM is the ideal tool to investigate desorption and adsorption dynamics in those supramolecular assemblies. To elucidate these dynamic processes, one can take advantage of the chemical sensitivity of STM by incorporating marker molecules in the supramolecular assembly.[17] Reactivity can be controlled by the structures of the supramolecular assemblies. For example, the photodimerization of two cinnamate derivatives was investigated at the graphite–liquid interface (Figs. 2g–i). The symmetrically substituted derivative was found to pack in two patterns, and photodimerization was observed upon in situ illumination. On the other hand. an asymmetrically substituted cinnamate derivative was found not to photodimerize, which could be related to a different supramolecular packing, inducing too great of an intermolecular distance between the reactive centers.[18]

ATOMIC FORCE MICROSCOPY

In contrast to STM. in AFM, forces exerted by the sample on the tip (or vice versa) are recorded, and several detection schemes are possible. The AFM scans a sample with a sharp tip, which is mounted on a cantilever spring (Fig. 3). The cantilever senses the interaction forces between tip and sample. A distance sensor monitors the reflection of the cantilever. Nowadays, beam deflection is nearly the only used detection scheme. The laser beam is reflected onto a segmented photodiode. As the deflection of the cantilever changes, the laser spot on the photodiode will shift accordingly. The detected deflection is then converted into an AFM image. Due to the flexibility of AFM with respect to the nature of the samples that can be studied and the measuring conditions (ambient conditions, liquids. etc.), AFM is intensively used. In most

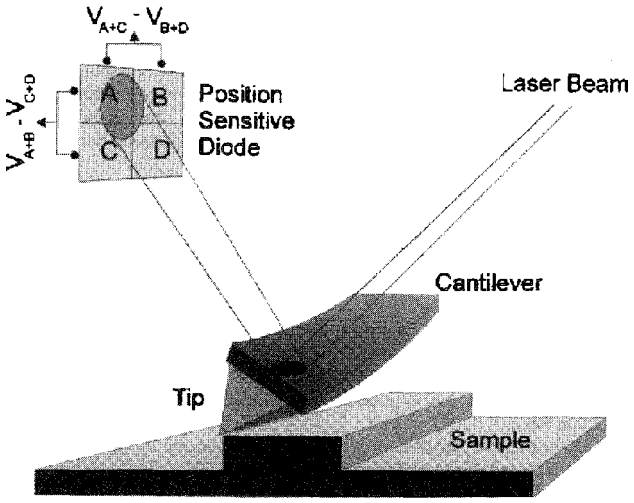

Fig. 3 An AFM setup.

applications, AFM is used as a topography sensing tool, but in certain measuring conditions, AFM is also sensitive to the mechanical properties of the sample, such as adhesion and stiffness.

The AFM was used to investigate various supramolecular structures. An example includes the study of the vertical profiles along the molecular long axes within a microtube made up of a boloamphiphile, which illustrates the usefulness of AFM for studying the molecular packing as well as the morphological dimensions of supramolecular assemblies.[19] Another recent study focused on the aggregation process of conjugated (sexithiophene)/nonconjugated [poly(ethylene glycol)] rod–coil copolymers[20] They all show regular arrangements of microfibrillar structures. This fibrillar morphology appears to be a typical signature of the organization of these conjugated copolymers in the solid state. If, on the other hand, this compound is deposited on the surface of a silicon wafer, thin fibrils are also formed, but they present a helical shape. The influence of substrates is a factor one has to be aware of. For instance, we investigated by means of noncontact AFM, individual polyphenylene dendrimers and their self-assembled nanostructures, prepared by spin coating and solvent casting on various substrates, such as mica: silanized mica, and graphite.[21] Besides globular clusters and monolayers, the polyphenylene dendrimer self-organizes into micrometer-long nanofibers on a graphite surface (Figs. 4a–c). Fibrillar nanostructures were also visualized on a silanized mica surface, while on a mica surface, the dendrimers only aggregate into globular structures. On the other hand, alkyl-substituted polyphenylene dendrimers do not form fibers but monolayers, including complex two-dimensional arrangements and suprarnolecular ordering.[22]

Of course, the use of AFM is not restricted to the investigation of supramolecular structures in the material sciences. 'Xrtificial" biomaterials were also recently probed by AFM. For instance, two-dimensional crystalline forms of DNA that self-assemble from synthetic DNA double-crossover molecules were assembled, and their patterned crystals were visualized by AFM. Intermolecular interactions between the structural units are programmed by the design of "sticky ends" that associate according to Watson–Crick complementarity.[23] Recently, biohybrids, formed by the association of two biotinylated polystyrene

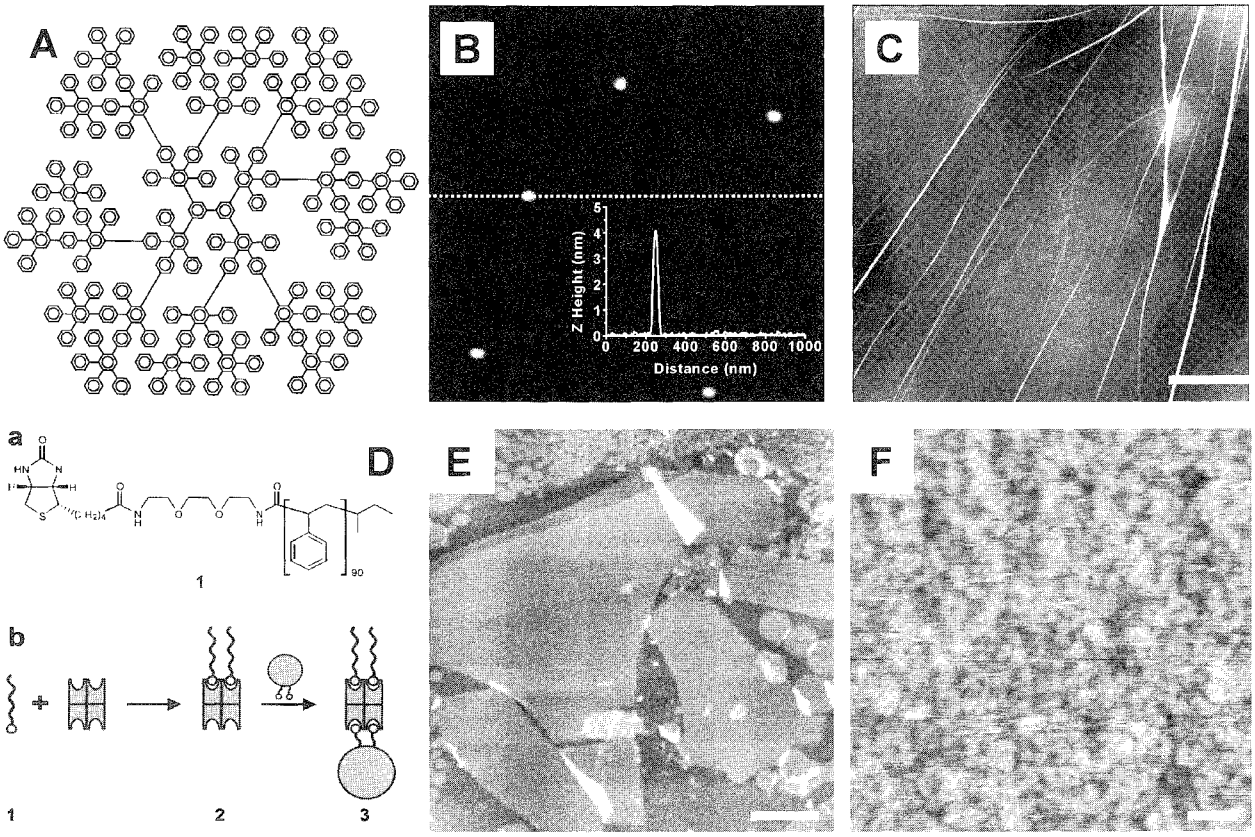

Fig. 4 (a) Dendrimer structure. (b) AFM image of isolated dendrimer molecules on mica. (c) Fibers imaged after solvent casting a dilute solution from chloroform. (Reprinted in part or adapted with permission from the American Chemical Society.) (d) Structure of biotinylated polystyrene 1; giant amphiphile 2. (e) AFM topographic image of pure polymer 1. (f) AFM topographic image of polymer with bound streptavidin 2. The scale bar is 10 μm. (From Ref. [24].)

molecules and streptavidin (leading to the formation of "giant amphiphiles"), were investigated.[24] In addition to AFM imaging (Figs. 4d–f). the nature of the monolayers was characterized by confocal fluorescence microscopy imaging of dye-labeled hybrids. The combination with optical techniques brings us to the last technique discussed in this entry (SNOM). The analysis of supramolecular structures becomes more powerful when topography data can be related to spectroscopy data.

SCANNING NEAR-FIELD OPTICAL MICROSCOPY

The SNOM combines the possibilities of AFM and optical microscopy. On the one hand, it allows for probing of the surface and obtaining information on the topography. On the other hand, in aperture SNOM, the probe contains an aperture, and the sample can be illuminated locally (Fig. 5). The diameter of the aperture at the end of the probe is typically of the order of 50–100 nanometer, and therefore. the illuminating spot is not diffraction limited. Both transmission and tluorescence in combination with polarization provide appropriate contrast mechanisms.

There are a number of excellent reviews on SNOM[25,26] and its applications in the study of organic materials.[27] The reader is referred to these reports for detailed information on the technique and some of its applications. We focus on some of our results on the use of SNOM for illustrating its usefulness in the study of supramolecular structures.

Porphyrin Wings

'The formation of ring-like structures was observed in the evaporation process of organic solutions containing porphyrin derivatives.[28] In particular, the deposition of these solutions on a substrate led to micron-scale ring-shaped arrangements of the solute/dispersed materials. Using SNOM, a deeper insight into the morphology and the local optical properties of solvent-evaporated porphyrin thin films was reached. Evaporation of a 10^{-6} M solution of PtP (Figs. 6a,b) in $CHCl_3$ on glass yielded symmetric rings for which the topography and fluorescence images are highly correlated. The ring diameter ranges between 100 nm to 10 μm, while the height of the rims, determined from the SNOM topographic image, varies between 10–300 nm. The fluorescence intensity measured inside the rings equaled the background value, indicating the absence of porphyrin material at these positions. The use of a more dilute solution (10^{-7} M) resulted in the formation of incomplete ring-shaped assemblies that were made from individual isolated structures which were observed in the topography and in the fluorescence image (Fig. 6c). A further characterization of the films in terms of the local optical properties and molecular organization was perfoimed using fluorescence polarization imaging. Similar experiments were performed using samples prepared by evaporation of another porphyrin derivative (BP_6)/$CHCl_3$ (Fig. 6a) solution. For the samples studied before annealing, the images corresponding to the different polarization configuration were identical (images are not presented). On the other hand, the annealed sainples exhibit strong polarization contrast. When the fluorescence intensity distributions in the rings are compared to what was found for PtP, a much smoother profile is observed. For the BP_6 samples, the intensity distribution depends, over a longer range, on the excitation polarization with parallel emission polarization. When the excitation polarization is oriented horizontally in the image (Fig. 6e), the upper and lower parts of the rings have a relative higher intensity than the left and the right parts of the rings. Turning the excitation polarization 90° (Fig. 6f) results in

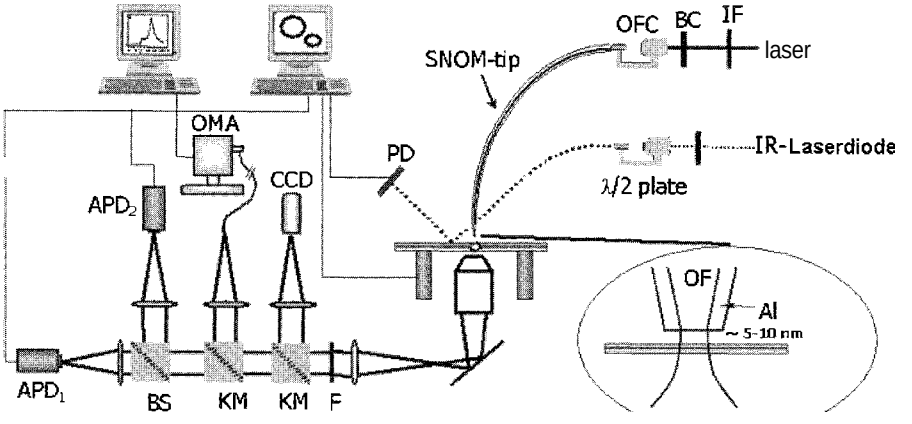

Fig. 5 Experimental setup of SNOM: The inset is a zoom of the optical fiber end. (Chem. Com. 2001. 7, 585—Reproduced by permission of the The Royal Society of Chemistry.)

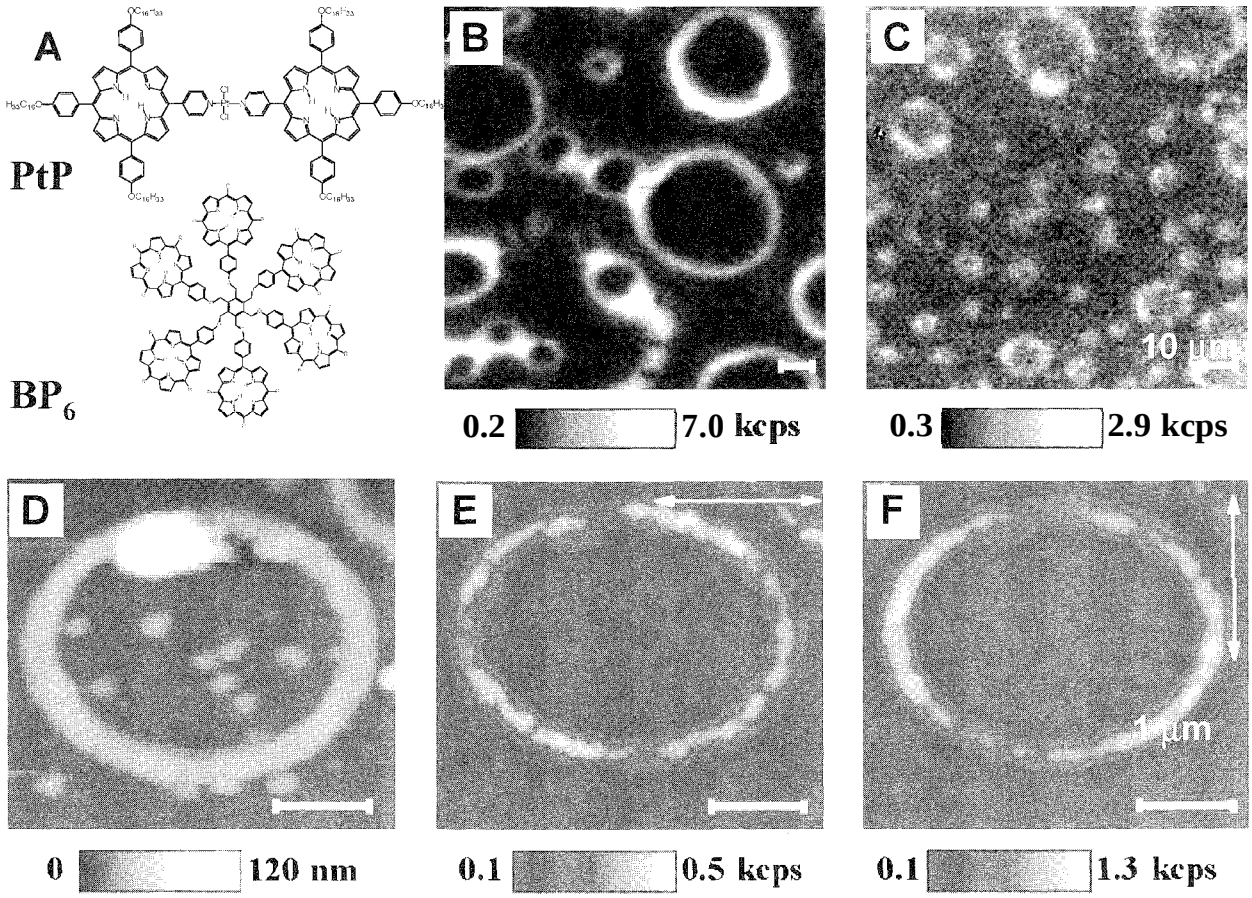

Fig. 6 (a) Porphyrinc derivatives. (b,c) SNOM fluorescence images of evaporated films of PtP/$CHCl_3$ solutions on glass by solvent casting at different concentrations. Scale bar is 10 μm. (d,e,f) A set of SNOM topographic and fluorescence polarization images acquired from a BP_6/$CHCl_3$ solution on glass. The orientation of the excitation polarization is indicated with the white arrows on the images. All tluorcscence images arc acquired with a parallel polarization configuration. Scale bar is 1 μm. (Chein. Com. 2001, 7, 585—Reproduced by permission of the The Royal Society of Chemistry.)

higher fluorescence intensity for the left and right parts of the ring. The observed fluorescence pattern can only be explained if there is a preferential orientation of the molecules in the rings. Using polarized excitation results in a preferential absorption of the excitation light at the positions where the polarization and the absorption dipole of the chromophore are parallel. This results in higher fluorescence intensity at the respective positions. If the molecules are schematically presented as disks, the orientation should be preferentially perpendicular to the sample plane. A possible arrangement of the disks in the rings could be one with the planes parallel or perpendicular to the radial of the ring.

CONCLUSION

In summary, the invention and development of scanning-probe microscopy techniques opened new ways to study supramolecular systems on solid supports The strength of these techniques is the local natures of the probing modes and their general applicability, even under ambient conditions, combined with the high resolution

ARTICLES OF FURTHER INTEREST

Chiral Induction, p. 245
Dendrimers, p. 432
Hydrogen Bonding, p. 658
Imaging and Targeting, p. 687
Inclusion Reactions und Polymerization, p. 705
Luminescent Materials, p. 816
Luminescent Probes, p. *821*
Scanning Tunneling Microscopy, p. 1202
Supramolecular Photochemistry, p. 1434

REFERENCES

1. Binnig, G.; Rohrer. H. Scanning tunneling microscopy. Helv. Phys. Acta 1982. *55* (6). 726–735.
2. Binnig, G.: Quate, C.F.: Gerber. C. Atomic force microscopy. Phys. Rev. Lett. 1986. *56* (9). 930–933.
3. Dürig, U.: Pohl, D.W. Near-field optical-scanning microscopy. J. Appl. Phys. 1986. 59 (10), 3318–3327.
4. Betzig. E.: Lewis, A.; Harootunian. A.; Isaacson, M.: Kratschmer, E. Near-field scanning optical microscopy (NSOM)—Development and biophysical applications. Biophys. J. 1986. *49* (1). 269–279.
5. Yokoyama, T.: Yokoyama, S.; Kamikado. T.: Okuno, Y.: Mashiko, S. Selective assembly on a surface of supramolecular aggregates with controlled size and shape. Nature 2001. *413*. 619–621.
6. Barth, J.V.: Weckesser. J.: Cai, C.: Günter, P.; Bürgi, L.: Jeandupeux, O.; Kern. K. Building supramolecular nanostructures at surfaces by hydrogen bonding. Angew. Chem., Int. Edn. Engl. 2000. *39*, 1230–1234.
7. Bohringer, M.; Morgenstern, K.: Schneider, W.-D.; Berndt. R.: Mauri, F.; De Vita. A.; Car. R. Two-dimensional self-assembly of supramolecular clusters and chains. Phys. Rev. Lett. 1999; *83* (2). 324–327.
8. Bohringer, M.: Morgenstern. K.: Schneider. W.-D.: Berndt, R. Separation of a racemic mixture of two-dimensional molecular clusters by scanning tunneling microscopy. Angew. Chem.. Int. Ed. 1999. *38* (6). 821–823.
9. Zhang. G.; Kuwahara, Y.; Wu. J.; Akai-Kasaya, M.: Saito, A.: Aono. M. Scanning tunneling microscopy observation of binary monolayers of 10.12-tricosadiynoic acid and stearic acid deposited by horizontal lifting method. Surf. Sci. 2001. *476*, L254–L258.
10. Rabe. J.P.; Buchholz. S. Commensurability and mobility and two-dimensional molecular patterns on graphite. Science 1991. *253* (5018), 424–427.
11. Semenov. A.; Spatz, J.P.: Möller, M.: Lehn, J.-M.: Sell. B.: Scliubert. D.: Weidl, C.H.: Schubert, U.S. Controlled arrangement of supramolecular metal coordination arrays on surfaces. Angew. Chein.. Int. Ed. 1999. *38* (17). 2547–2550.
12. Samori. P.: Jäckel, F.: Unsal, O.: Godt, A.; Rabe. J.P. Ordered nanostructures of a [2]catenane through self-assembly at surfaces—An STM study with sub-molecular resolution. ChemPhysChem 2001. *2* (7), 461–464.
13. De Feyter, S.: Gesquière, A.; Abdel-Mottaleb. M.M.; Grim. P.C.M.: De Schryver, F.C.: Meiners. C.: Sieffert. M.: Valiyaveettil, S.: Müllen. K. Scanning tunneling microscopy: A unique tool in the study of chirality. dynamics, and reactivity in physisorbed organic monolayers. Acc. Chem. Res. 2000. *33*. 520–531.
14. De Feyter, S.: Grim. K.: van Esch. J.: Kellogg. R.M.; Feringa. B.L.: De Schryver, F.C. Non-trivial differentiation between two identical functionalities within the same molecule studied by STM. J. Phys. Chem., B 1998. *102*. 8981–8987.
15. De Feyter. S.; Gesquière, A.; Wurst. K.; Amabilino. D.B.; Veciana. J.: De Schryver. F.C. Homo- and hetero-chiral supramolecular tapes from achiral. enantiopure and racemic promesogenic formamides: Expression of molecular chirality in 2- and 3-dimensions. Angew. Chern.. Int. Ed. 2001. 40 (17), 3217–3320.
16. De Feyter. S.: Grim, P.C.. M.: Rücker, M.; Vanoppen. P.: Meiners. C.; Sieffert. M.; Valiyaveetiil. S.: Müllen. K.: De Schryver. F.C. Expression of chirality by achiral coadsorbed molecules in chiral monolayers observed by STM. Angew. Chem.. Int. Ed. Engl. 1998. *37*. 1223.
17. Gesquière, A.: Abdel-Mottaleb. M.; De Feyter. S.: De Schryver. F.C.: Sieffert. M.: Müllen. K.: Calderone, A.; Lazzaroni. R.; Brédas. J.L. Dynamics in physisorbed monolayers of 5-alkoxy-isophthalic derivatives at the liquid/solid interface investigated by scanning tunneling microscopy. Chem. Eur. J. 2000, 6 (20). 3739–3746.
18. Abdel-Mottaleb. M.M.S.: De Feyter. S.: Gesquière, A.: Sieffert. M.; Müllen, K.: De Schryver, F.C. Photodimerization of cinnamate derivatives studied by STM. Nano Lett. 2001, *1* (7). 353–359.
19. Shimizu, T.: Ohnishi. S.: Kogiso. M. Cross-section molecular imaging of supramolecular nticrotubes with contact atomic force microscopy. Angew. Chem.. Int. Ed. 1998. *37* (23). 3260–5262.
20. Schenning. A.P.H.J.: Kilbinger, A.F.M.: Biscarini, F.: Cavallini, M.: Cooper. H.J.: Derrick. P.J.: Feast. W.J.: Lazzaroni, R.: Leclère, P.; McDonell, L.A.: Meijer, E.W.: Meskers. S.C.J. Supramolecular organisation of α,α'-disubstituted sexithiophenes. J. Am. Chem. Soc. 2002. *124* (7), 1269–1275.
21. Liu, D.; Zhang, H.: Grim. P.C.M.: De Feyter. S.; Wiesler. U.-M.: Berresheim, X.J.: Müllen. K.: De Schryver. F.C. Self-assembly of polyphenylene dendrimers into micrometer long nanofibers: An atomic force microscopy study. Langmuir 2002. *18*. 2385–2391.
22. Loi, S.: Wiesler. U.-M.: Butt. H.-J.; Müllen, K. Self-assembly of alkyl-substituted polyphenylene dendrimers on graphite. Macromolecules 2001. *34*. 3661–3671.
23. Winfree. E.: Liu. F.: Wenzler. L.A.: Seeman. N.C. Design and self-assembly of two-dimensional DNA crystals. Nature 1998, *394* (6693). 539–544.
24. Hannink. J.M.: Cornelissen. J.J.L.M.: Farrera, J.A.: Foubert. P.: De Schryver, F.C.: Sommerdijk, N.A.J.M.: Nolte. R.J.M. Protein–polymer hybrid amphiphiles. Angew. Chem., Int. Ed. 2001. *40* (24), 4732–4734.
25. Betzig. E.: Trautman, J.K. Wear-Field optics—Microscopy, spectroscopy. and surface modification beyond the diffraction limit. Science 1992. *257* (5067). 189–195.
26. Hecht. B.: Sick. B.: Wild. U.P.: Deckert. V.: Zenohi. R.: Martin. O.J.F.: Pohl. D.W. Scanning near-field optical microscopy with aperture probes: Fundamentals and applications. J. Chem. Phys. 2000, *112* (18), 7761–7774.
27. Barbara. P.F.; Adams, D.M.: O'Connor. D.B. Characterization of organic thin film materials with near-field scanning optical microscopy (NSOM). Annu. Rev. Mater. Sci. 1999; *29*. 433.
28. Hofkens, J.: Latterini, L.: Faes. H.; Vanoppen. P.: Jeuris, K.: De Feyter. S.: Kerimo, J.: Barbara. P.F.: De Schryver. F.C.: Rowan. A.E.: Nolte. R.J.M. Mesostructure of evaporated porphyrin thin films: Porphyrin wheel formation. J. Phys. Chem. 1997. *101* (49). 10588–10598.

Supramolecular Chemistry: Definition

Jonathan W. Steed
University of Durham, Durham, United Kingdom

INTRODUCTION

It is an almost impossible task to write a useful definition of supramolecular chemistry. The field is ever changing as it advances, and researchers will have their own understanding and sets of terminology. Rather than trying to limit the field or "claim" certain areas, what follows will attempt to be a simple introduction for the newcomer into the sorts of areas in which the concepts of supramolecular chemistry, broadly defined, may be of some use. In short, here are some things to think about to get you started.

In this article, for a practical exploration of the definition and scope of supramolecular chemistry, we will consider the viewpoint within the following interrelated subfields, all of which lend something to our understanding of supramolecules:

- Molecular host–guest chemistry.
- Solid-state host–guest chemistry (also known as inclusion or clathrate chemistry).
- Crystal engineering.
- Supramolecular devices.
- Self-assemblylself-organization.
- Soft/smart materials.
- Nanochemistry/nanotechnology.
- Biological chemistry.

BACKGROUND

In 1978, Jean-Marie Eehn introduced the modern concept of supramolecular chemistry, which he defined as the "...chemistry of molecular assemblies and of the intermolecular bond,"[1] although the term itself made a much earlier appearance (in *Webster's Dictionary* in 1903). Traditionally, phrases such as "chemistry beyond the molecule." "the chemistry of the non-covalent bond," and "non-molecular chemistry" or even "Lego chemistry" were also used to describe the field. In the beginning, supramolecules mainly comprised two components. a host and a guest, which interact with one another in a noncovalent fashion (Fig. 1). The area rapidly evolved to encompass molecular devices and molecular assemblies. More recently (2002), Lehn added a further functional definition: "Supramolecular Chemistry aims at developing highly complex chemical systems from components interacting by non-covalent intermolecular forces."[2] The current emphasis is thus on increasing complexity and, hence, increasingly sophisticated functionality, and on the information stored in molecular coinponents that allows this complexity to be achieved.

Fundamentally, supramolecular chemistry concerns the mutual interaction of molecules or molecular entities with discrete properties. This interaction is usually of a noncovalent type (an "intermolecular bond," such as a hydrogen bond, dipolar interaction or x-stacking). Key to many definitions of supramolecular chemistry is a sense of modularity. Supramolecules, in the broad sense: are aggregates in which a number of components (of one or more type) come together, either spontaneously or by design, to form a larger entity with properties derived from its components. These aggregates can be of the host–guest type in which one molecule encapsulates the other, or they can involve mutually complementary, or self-complementary, components of similar size, in which there is no host or guest (Fig. 2).

The broad general field of interactions between molecules is, in fact, of relevance to a number of loosely related disciplines, both within chemistry and at the interface of chemistry with biology, condensed matter physics, and materials science. Some of these disciplines—particularly solid-state clathrate chemistry and biological chemistry (see articles of further interest)—predate the rise of modern supramolecular chemistry. as shown by the rough timeline of some supramolecular milestones given in Table 1. It would be inappropriate to describe workers in this diverse group of disciplines as supramolecular chemists. However. the evolving language and framework provided by supramolecular chemistry facilitates cross-fertilization and communication between disciplines concerned with the interactions between molecules (of whatever size and chemical composition). Moreover. a great deal can be learned by the comparative study of such loosely related areas, and the juxtaposition may inspire important new areas of activity.

Encyclopedia of Supramolecular Chemistry
DOI: 10.1081/E-ESMC 120012662

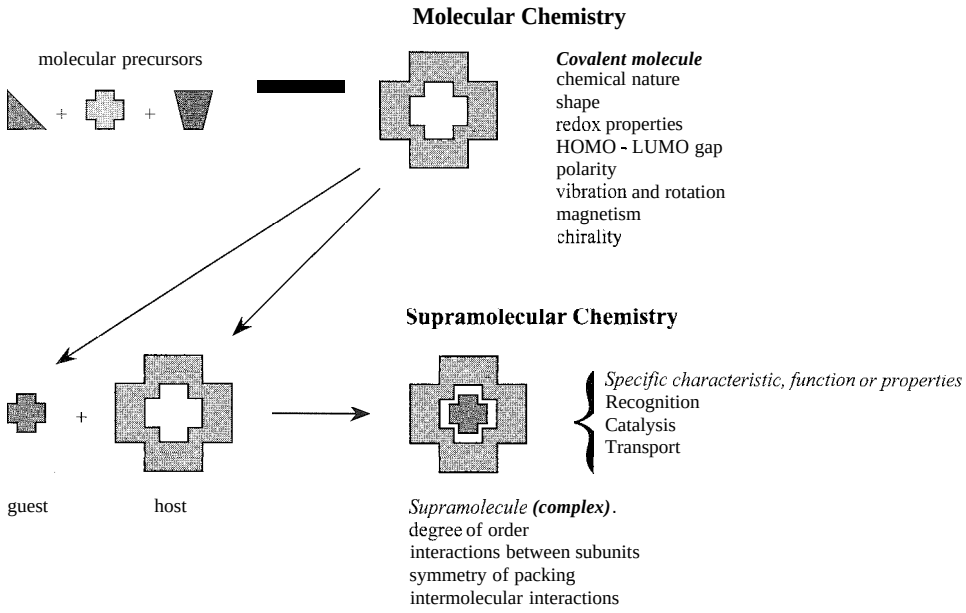

Fig. 1 Coinparison between the scope of molecular and supramolecular chemistry according to Lehn. (From Ref. [1].) (View *this art* in color *at www.dekker.com.*)

MOLECULAR HOST–GUEST CHEMISTRY

A host–guest complex was defined by Donald Cram,[3] who shared the 1987 Nobel Prize in Supramolecular Chemistry, in the following way:

> Complexes are composed of two or more molecules or ions held together in unique structural relationships by electrostatic forces other than those of full covalent bonds. . .molecular complexes are usually held together by hydrogen bonding. by ion pairing, by π-acid to π-base interactions, by metal-to-ligand binding, by van der Waals attractive forces, by solvent reorganizing. and by partially made and broken covalent bonds (transition states). . .High structural organisation is usually produced only through multiple binding sites. . .A highly structured molecular complex is composed of at least one

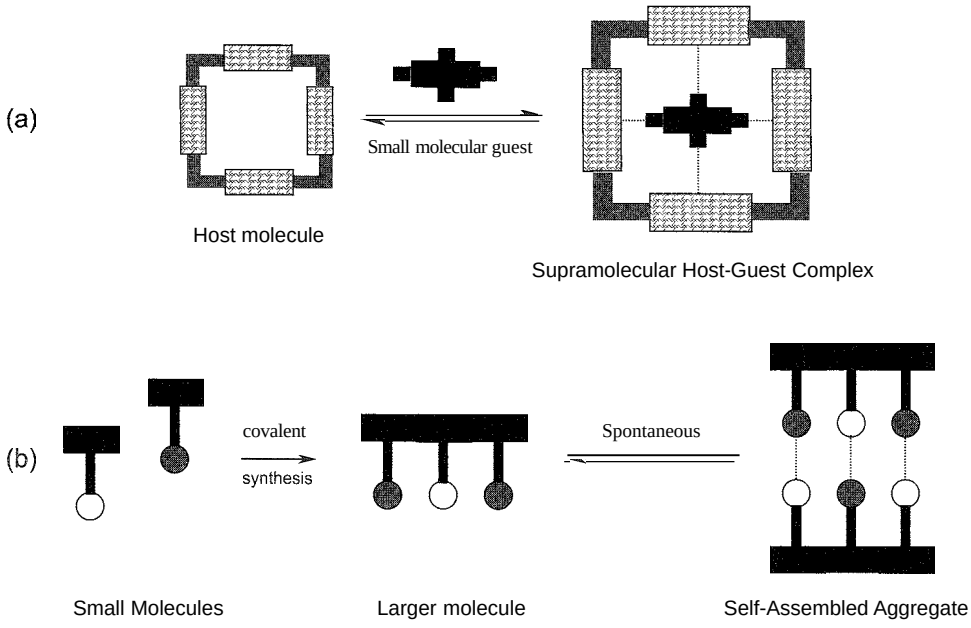

Fig. 2 The development of a supramolecular system from molecular building blocks. (a) Host–guest complexation and (b) self-assembly between complementary species (circles represent binding sites). (*View* this *art in* color *at www.dekker.com.*)

Table 1 Timeline showing some milestones of interest in supramolecular chemistry

1810—Sir Humphrey Davy: Discovery of chlorine hydrate
1823—Michael Faraday: Formula of chlorine hydrate
1841—C. Schafhäutl: Study of graphite intercalates
1849—F. Wohler: β-Quinol H_2S clathrate
1891—Villiers and Hebd: Cyclodextrin inclusion compounds.
1893—Alfred Werner: Coordination chemistry
1894—Emil Fischer: Lock and key concept
1906—Paul Ehrlich: Introduction of the concept of a receptor
1937—K.L. Wolf: The term *Ubermolekül* is coined to describe organized entities arising from the association of coordinatively saturated species (e.g., the acetic acid dimer)
1939—Linus Pauling: Hydrogen bonds are included in the groundbreaking book *The Nature* of *the Chemical Bond*
1940—M.F. Bengen: Urea channel inclusion compounds
1948—R.M. Powell: X-ray crystal structures of β-quinol inclusion compounds; the term "clathrate" is introduced to describe compounds where one component is enclosed within the framework of another
1949—Brown and Farthing: Synthesis of [2.2]paracyclophane
1953—Watson and Crick; Franklin and Wilkins: Structure of DNA
1953—Max F. Perutz: Structure of hemoglobin
1956—Dorothy Crowfoot Hodgkin: X-ray crystal structure of vitamin B_{12}
1959—Donald Cram: Attempted synthesis of cyclophane charge-transfer complexes with $(NC)_2C{=}C(CN)_2$
1961—N.F. Curtis: First Schiff's base macrocycle from acetone and ethylene diamine
1964—Busch and Jäger: Schiff's base macrocycles
1967—Charles Pedersen: Crown ethers
1968—Park and Simmonds: *Katapinand* anion hosts
1969—Jean-Marie Lehn: Synthesis of the first cryptands
1969—Jerry Atwood: Liquid clathrates from alkyl aluminium salts
1973—Donald Cram: Spherand hosts produced to test the importance of preorganization
1978—Jean-Marie Lehn: Introduction of the term "Supramolecular Chemistry" defined as the "...chemistry of molecular assemblies and of the intermolecular bond"
1979—Gokel and Okahara: Development of the lariat ethers as a subclass of host
1981—Vogtle and Weber: Podand hosts and development of nomenclature
1987—Award of the Nobel Prize for Chemistry to Donald J. Cram, Jean-Made Lehn. and Charles J. Pedersen for their work in Supramolecular Chemistry
1996—Atwood, Davies. MacNicol. and Vogtle: Publication of *Comprehensive Supramolecular Chemistry* containing contributions from many key groups and summarizing the development and state of the art
1996—Award of the Nobel Prize for Chemistry to Kroto, Smalley. and Curl for their work on the chemistry of the fullerenes
2003—Award of the Nobel Prize for Chemistry to Agre and MacKinnon for their work on channels in cell membranes

> host and one guest component...A host–guest relationship involves a complementary stereoelectronic arrangement of binding sites in host and guest...The host component is defined as an organic molecule or ion whose binding sites converge in the complex...The guest component as any molecule or ion whose binding sites diverge in the complex...

The key point here is the convergent arrangement of binding sites on a host molecule. This disposition is deliberately introduced during the host synthesis and is an intrinsic property of the host. A preorganized host such as the spherand 1 (which binds a Li' guest) will maintain a convergent arrangement of binding sites at all times, irrespective of the presence of guest species. More flexible hosts such as [18]crown-6 (2) display some flexibility and may undergo a conformational change to a more convergent geometry upon guest complexation (metals such as K^+ in the case of 2) (Fig. 3).

Hosts such as 1 and 2 use their molecular cavity (whether preorganized or binding induced) to bind effectively to metal cations and were among the first modern host systems, The range of guest species is not limited to cations, however, and can include hosts for anions (e.g., **3,** which binds effectively to Cl^-[4]) or neutral molecules as in cavitands such as 4 that complexes CS_2.[5]

SOLID-STATE HOST–GUEST CHEMISTRY

Solid-state host–guest chemistry dates to the discovery of chlorine clathrate hydrate by Davey in 1810 and represents cocrystallization of two or more chemically

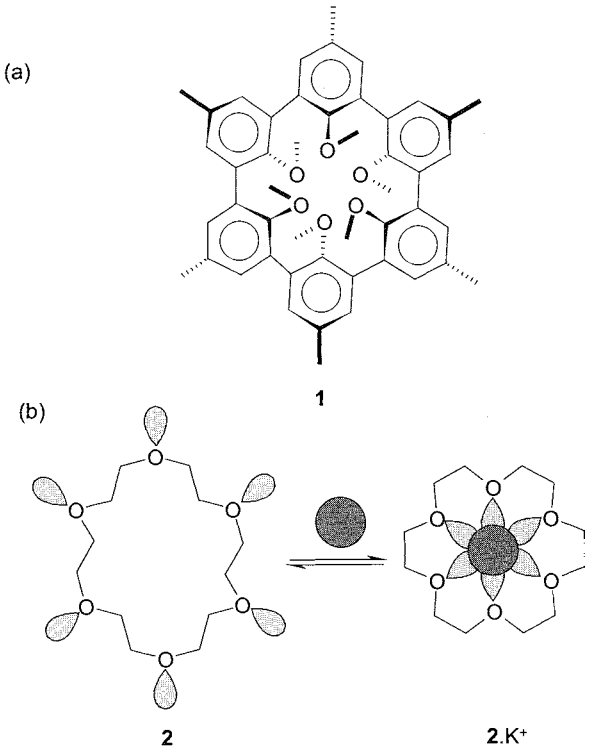

Fig. 3 Molecular hosts (a) preorganiaed spherand. (b) flexible crown ether—in polar solvents. the oxygen lone pairs point outwards to interact with solvent but converge upon guest binding. (*View this art in color at www.dekker.com.*)

distinct species. The nature of solid-state host–guest complexes was first elucidated by Powell in the 1940s using x-ray crystallography. He introduced the term "clathrate" to indicate a guest molecule trapped in a cavity formed by the host, formally a kind of inclusion compound "in which two or more components are associated without ordinary chemical union, but through complete enclosure of one set of molecules in a suitable structure formed by another." More recently. Vogtle and Weber[6] proposed the division of host–guest complexes into two general categories according to the relative topological relationship between guest and host. Cavitands may be described as hosts possessing intramolecular cavities. This means that the cavity available for guest binding is an intrinsic molecular property of the host and exists both in solution and in the solid state. Compounds 1–4 fall into this category. Conversely, clathrands are hosts with extramolecular cavities (the cavity essentially represents a gap between two or more host molecules) and is only of relevance in the crystalline or solid state. The host–guest aggregate formed by a cavitand is termed a cavitate, while clathrands form clathrates.

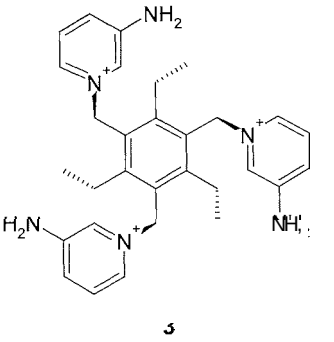

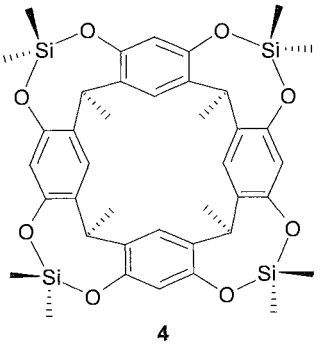

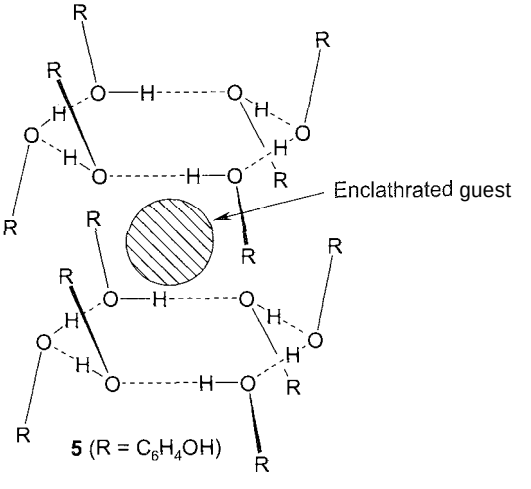

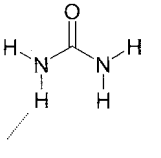

In principle, any cocrystal may be regarded as a clathrate: however. there are certain well-known classes of host molecules that regularly and reliably form solid host–guest clathrate-type compounds. and in many cases, these materials were extensively studied for a number of decades. Typical examples include hydoquinone (5), urea (6), tri-o-thymoiide (7). cyclotriveratrylene (8), gossypol (9), perhydrotriphenylene (10), etc. Urea clathrates are perhaps the most well-known with the urea molecules forming double-helical hexagonal channels via N H . ·O═C hydrogen bonds. The channels are able to include long, linear guest species such as *n*-alkanes (Fig. 4). Guests do not usually interact with the channel walls, and packing is often incommensurate. However, Hollingsworth et al. reported a number of complexes of ketone guests in which host–guest interactions result in interesting stress-induced orientational changes.[7]

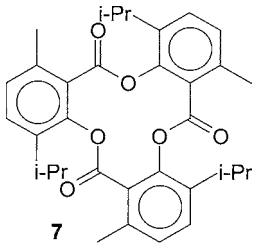

7

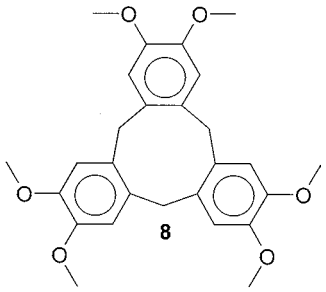

8

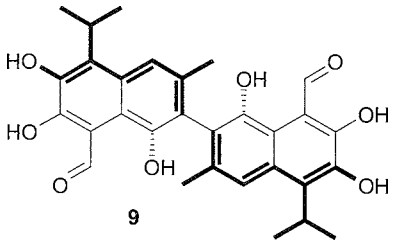

9

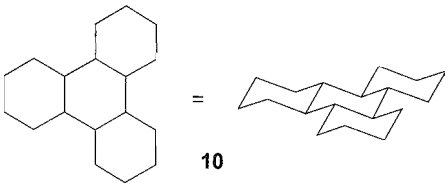

10

An interesting example of the interplay between solid-state clathrands and solution-phase cavitands is provided by cyclotriveratrylene (CTV, 8). In the solid state, the "saucer-shaped" CTV molecules stack one on top of another in the two most common phases (x and β),[8] and hence, while the molecules possess shallow molecular cavities, they do not include guests such as solvent molecules, which instead are located in voids between host stacks. However. larger guests such as buckminsterfullerene C_{60},[9] organometallic sandwich compounds,[10] or carboranes[11] form intracavity inclusion compounds, and the association persists in the solid state, with potential applications, for example, in the selective purification of fullerenes.[12] Thus, CTV is both a cavitand and a clathrand. The cavitand behavior of CTV is highlighted by the chemistry of the double-CTV cryptophanes that form very stable solution complexes with a variety of halocarbon guests.[13,14]

CRYSTAL ENGINEERING

In a recent article."'' Dario Braga summed the impact of supramolecular concepts in the following way:

> The supramolecular perception of chemistry generated a true paradigm shift: from the one focused on atoms and bonds between atoms to the one focused on molecules and bonds between molecules. In its burgeoning expansion the supramolecular idea abated, logically, all traditional barriers between chemical subdivisions (organic, inorganic, organometallic, biological) calling attention to the collective properties generated by the assembly of molecules and to the relationship between such collective properties and those of the individual component.

In the context of crystal engineering. he goes on to say the following:

> When applied to crystalline solids, the paradigm shift leads directly from supramolecular chemistry to crystal engineering. What is a (molecular) crystal if not an organized entity of higher complexity held together by intermolecular forces (J.M. Lehn)? Who can deny that the collective properties of such a giant supermolecule are the result of the convolution of intermolecular non-covalent bonding between molecular/ionic components with the periodicity of the crystal.

So, while traditionally crystal engineering had its birth in the "topochemistry" of Schmidt,[16] or even the earlier ideas on control of crystal packing presented by Pepinsky in 1955,[17] the modern discipline is simply supramolecular chemistry applied to periodic molecular solids. The aim is the rational design of interesting or

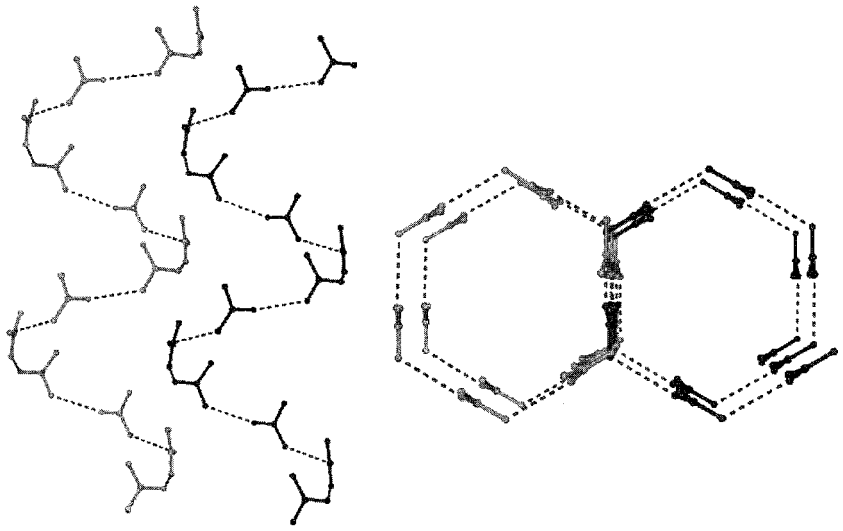

Fig. 4 The hexagonal urea host channel. Two urea helices viewed from the side of the channel and along the channel axis

functional crystalline materials. For example, a recent report by Hosseini et al. of the University of Strasbourg, France, demonstrated the designed synthesis of a double helical chain in the solid state via the assembly of ligands such as **11** and Ag^+ (Fig. 5).[18] Hosseini advocates the use of the term "molecular tectonics" instead of crystal engineering to emphasize the building block nature of the discipline (see article on *Tectons: Definition and Scope* in this *Encyclopedia).*

There is also continued interest in the systematic placement of reactive groups in the solid such that their chemical reactivities are determined by the reactants' spatial relationships.[19] This was the original premise of Schmidt's topochemistry and has important implications in modern solventless ("green") synthesis[20,21] and even mechanochemistry.[22] For example, work by MacGillivray resulted in the solid-phase photochemical synthesis of paracyclophane **12** by a strategy termed "template switching" (Fig. 6).[23]

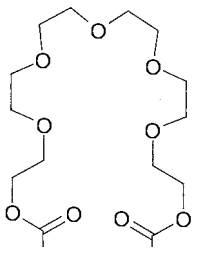

The crystal engineering community is also at the forefront of work into new kinds of intermolecular interactions. Recent single-crystal neutron diffraction studies revealed detailed information on OH···π interactions[24] and on unconventional hydrogen bonds to metal centers as well as MH···HX-type interactions, where MH is a hydridic metal hydrogen moiety, and HX contains protic hydrogen.[26,27]

Supramolecular Devices

A supramolecular device is a molecular-level system that acts or carries out a function of some kind in the same way as a larger-scale device, such as an electronic component (switch, rectifier) or mechanical object (motor, spring). The basis for the device's operation can be supramolecular in the sense that two or more components interact in a noncovalent manner. This is the case with rotaxane **13** (Fig. 7), in which the paraquat-derived macrocycle switches back and forth between the two biaryl "stations" in response to changes in pH. The interaction between the paraquat "train" and the two stations on the polyethyleneglycol "track" is entirely supramolecular and involves n-stacking. charge transfer, and CH···O hydrogen bonds.

In the construction of molecular devices, however, the focus is on the functional interactions between the components rather than the chemical nature of their connectivity. This means that a supramolecular device can be an entirely covalent molecule if it possesses characteristics of a supramolecular nature. Thus, a supramolecular device may be defined as a complex system made up of molecular components with definite individual properties.

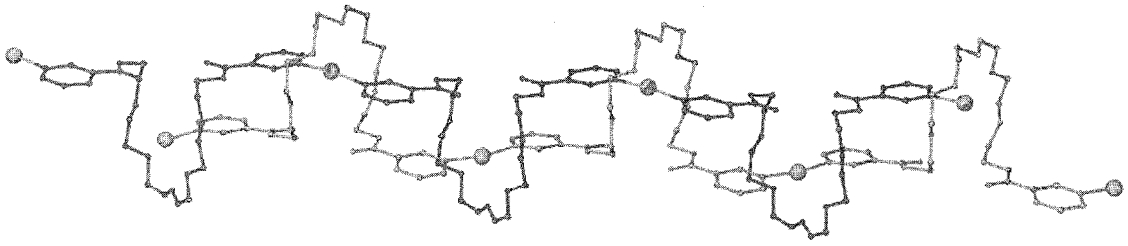

Fig. 5 Double-helical polymer chain formed from an interaction of Ag^+ with **11**. (From Ref. [18].) ***(View** this art **in** color at www.dekker.com.)*

These properties are intrinsic to the molecular component. whether they are part of the device or not. Another way of saying this is that the interaction energy between the components of the supramolecular device must be small compared with other energy parameters relevant to the system. It does not matter, therefore, how the components are connected in the device (covalently, hydrogen bonded, coordination interaction, etc.); all that matters is that each component should contribute something unique and identifiable with that component alone. within the system. If this does not hold true, and the functionality of the system is identifiable with the molecule as a whole, as opposed to the individual parts, then the complex is best thought of as a "large molecule" and is not supramolecular.

The relative unimportance of the nature of the bonding is illustrated by compounds 14 and **15**, both of which are devices designed to transport a photoexcited electron from the zinc porphyrins to the Fe(III) center, reducing it to Fe(II).[28] In the case of 14, the link between the two compounds is noncovalent, whereas in **15**, it is covalent. Remarkably. not only are both systems effective at carrying out this process, but the photoelectron transfer rate constants of 8.1×10^9 and 4.3×10^9 s^{-1} for 14 and 15, respectively, suggest that the carboxylic acid double hydrogen bond is more effective at transmitting the excited electron than the σ-framework in **15**. despite the fact that some dissociation might occur in solution.

Self-Assembly and Self-Organization

Strict supramolecular self-assembly involves the spontaneous formation of a multicomponent aggregate under thermodynamically controlled conditions based on information encoded within the individual building blocks (tectons). The aggregate might comprise only one kind of molecule (as in the multiple copies of the same protein that comprise the coat of many viruses, such as the tobacco mosaic virus) or more than one type of component. In the latter case, the different components are usually mutually complementary. Strict self-assembly implicitly

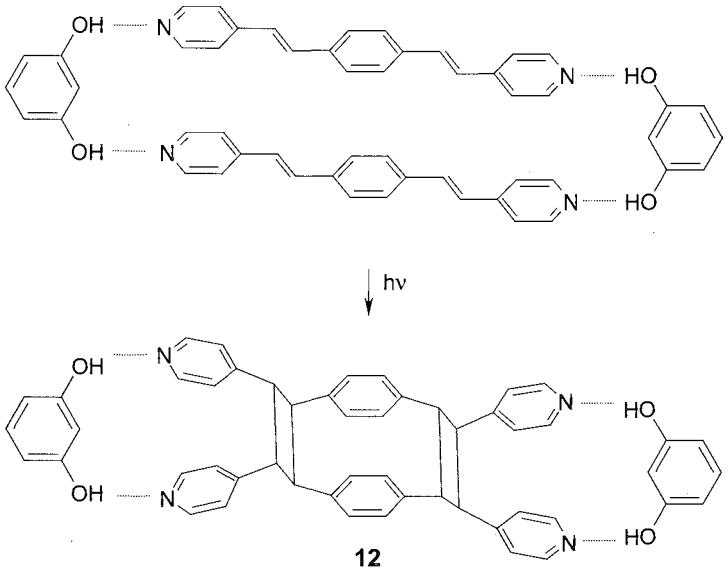

Fig. 6 "Template switch" synthesis of tetrapyridylparacyclophane 12. (From Ref. [23].)

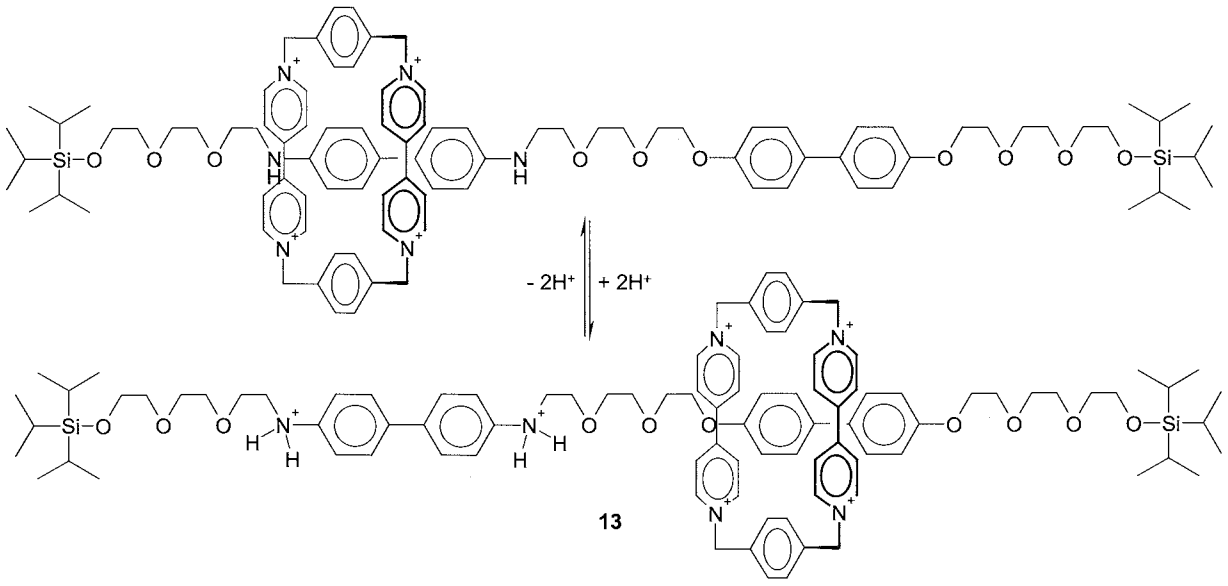

Fig. 7 The pH switched molecular switch based on a two-component rotaxane.

carries with it the notion of reversibility of intercomponent bond formation in that the final aggregate is the most thermodynamically stable structure under the prevailing conditions. This means that there is an in-built error-checking mechanism—malformed aggregates are less stable than the true minimum energy structure and decompose and are reassembled correctly if sufficient time is allowed to pass. Self-assembly processes may be regarded as the result of a series of supramolecular templated steps that build the aggregate. In turn, the interactions and synergy of self-assembled components, leading to collective behavior and, ultimately, intelligent "soft" functional systems, may be regarded as self-organization. The hierarchical sequence of templation leading to self-assembly leading to self-organization represents the ideal manifestation of the supramolecular information concept outlined in the introduction.

One simple and elegant example of supramolecular self-assembly is the synthesis of a molecular cube by Jim Thomas from the University of Sheffield, U.K.[29] Starting from the simple geometric observation that a cube comprises eight corners and 12 edges (a ratio of

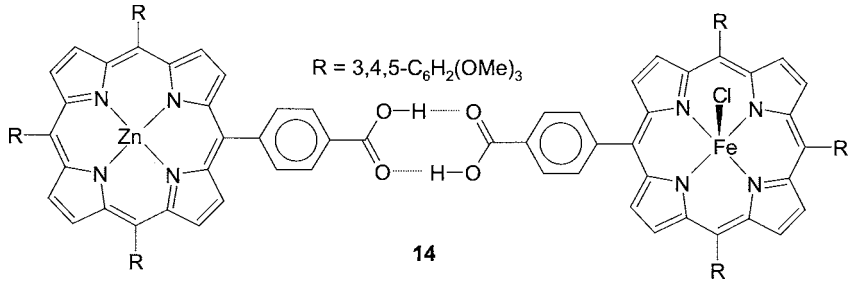

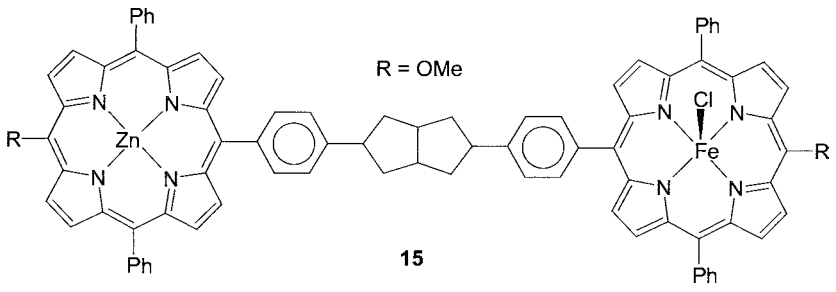

2:3), Thomas et al. reacted $\{Ru([9]aneS_3)Cl_2(OSMe_2)\}$ as a "corner" with 4,4′-bipyridyl as an "edge" in a *2:3* ratio. The result was the displacement of the chloride and $OSMe_2$ ligands to give the predicted molecular cube $[\{Ru([9]aneS_3)\}_8(\mu\text{-}4,4'\text{-bipyridyl})_{12}]^{16+}$ **16**. Thomas' faith in the tenets of self-assembly were demonstrated by the fact that the reaction had to be allowed to reflux for a month before reaching the thermodynamically most stable cube structure. In this particular case, the ''supramolecular'' interactions are relatively covalent ruthenium(II)-pyridyl interactions, and the cube structure **16** is formally a molecule, or a coordination complex (albeit a fancy one) rather than a supramolecule in the strict sense. However, the slow but inevitable thermodynamically reversible formation of the Ru-N interactions obeys all of the same supramolecular rules that the hydrogen-bond-driven self-assembly of the DNA double helix does. The concepts are transferable even if the chemistry is hugely different.

Soft/Smart Materials

The term "materials" carries with it images of durable solids; organic materials like plastics and polymers, or inorganic materials like semiconductors and coatings. More generally, however, the term "material" can be applied constructively to any (usually solid) chemical compound with interesting or useful physical properties. We can readily distinguish between hard materials (often inorganic) and soft materials (often organic). Soft materials are held together by supramolecular interactions, such as hydrogen bonds, van der Waals forces, or other weaker intermolecular bonds. Hard materials involve much less easily deformed ionic or covalent interactions. A great deal of supramolecular chemistry, particularly the types of activities we termed crystal engineering above, represents de facto the design and synthesis of soft materials.

A smart material is a material that can, in effect, make a decision based on external stimuli. In other words, it is able to sense an external event such as an electrical signal, change in pH, or irradiation, and respond with an action of some kind (change in binding behavior, cooler, conformation, etc.). The ability of supramolecular chemists to use intermolecular interactions to design and construct soft materials (perhaps via self-assembly) may pave the way to the tailored design of smart materials. The concept has been articulated by Dima Soldatov of the Steacie Institute, Canada, and a wealth of detail is contained in his article in this *Encyclopedia* (see *Soft and Smart Materials).*

Nanochemistry/Nanotechnology

The prefix nano-refers to objects with dimensions approximately of the order of a nanometer (10^{-9} m). Broadly speaking, there are two approaches to the nanoscale dimension — "synthesizing-up" and "engineering-down." The engineering-down approach includes the latest in modern techniques for producing electronic components and originates in a bulk sense. Engineering-down to the nanoscale involves doing the same sorts of things that an engineer or artisan does on a macroscopic scale but using specialized techniques in order to miniaturize. In contrast, the synthesizing-up approach is modeled on biology, particular biological self-assembly, and aims to produce nanoscale functional components (perhaps with molecular device or molecular-scale computing applications in mind) by chemical synthesis. The first reports of functional molecular computing using supramolecular species have already begun to appear.[30] Somewhere in between these two complementary approaches to the preparation of new systems come a variety of scanning-probe-microscopy-based techniques such as STM and AFM (see articles on *Supermicroscopy: AFM, SNOM, and SXM* and *Scanning Tunnelling Microscopy).* Because they operate on the nanometer scale, these techniques give unique insight into molecular behavior. Microscopists are not necessarily innocent observers, however, and microscope tips may be used to carry out molecular manipulations and redox chemistry. Tips may even be modified by attaching a probe molecule and using molecular recognition to examine a surface. Chemical reactions may even be carried out by physically pushing individual molecules into close mutual proximity using an STM tip.[31] Chemical assembly, thus, represents one facet of the preparation and study of nanoscale materials, and it is particularly through the concepts of self-assembly and self-organization that the nanoscale world can be addressed by chemists in a well-defined and molecularly precise way.

Biological Chemistry

The world of biological molecules is governed almost entirely by supramolecular chemistry: hydrogen bonding, van der Waals, π-stacking, and hydrophobic interactions responsible for protein secondary and tertiary structure; enzyme–substrate binding and transition-state stabilization; viral and oligonucleotide self-assembly; intracellular sensing and signaling; semiochemistry — supramolecular concepts are everywhere. Of course, biochemistry is a vast, well-established and distinct field that dwarfs abiotic supramolecular chemistry. To date, much of the inspiration in the latter discipline has come from biology, however, and supramolecular chemistry is beginning to contribute to the understanding and mimicry of biochemical systems. While the language of biochemistry is often distinct from the parallels in supramolecular chemistry, no supramolecular chemist can function without a rudimentary knowledge of biological principles. Indeed, in his article in this *Encyclopedia* on *Terminology in*

Self-Assembly, Gerry Sweigers goes a long way toward bridging the gap.

CONCLUSION

In this article. a brief survey is provided of some critical areas in which the concepts that underlie supramolecular chemistry have found utility and application. It is a moot point whether all such chemical systems should be described using the adjective "supramolecular." Indeed, Ian Dance of the University of New South Wales made a spirited argument in favor of strictly limiting the use of the term ''supramolecular'' to systems that involve the "philosophies and strategies of grand assembly." The term "grand assembly" is taken to mean "a strategy of controlled organization of multiple separate components." This definition is particularly designed to exclude "intermolecular" chemistry (well-known weak and long interactions between molecules) and more or less elaborate metal coordination compounds that may be described by the language of coordination chemistry.[32] The crucial point is that in any discussion of science. nomenclature and language should be precise and unambiguous. On the other hand, concepts should be flexible and widely applicable.

ACKNOWLEDGMENT

I thank the Royal Society of Chemistry for a travel award and for their unceasing efforts on behalf of the chemical sciences.

ARTICLES OF FURTHER INTEREST

Classical Descriptions of Inclusion Compounds, p. 253
Clathrate Hydrates, p. 274
Concepts in *Crystal Engineering*, p. 319
Crown Ethers, p. 326
Cryptands, p. 334
DNA Nanotechnology, p. 475
Enzyme Mimics, p. 546
The Lock and Key Principle, p. *809*
Molecular-level Machines, p. 931
Selectivity: Thermodynamic and Kinetic, p. 1225
Self-Assembly: Definition and Kinetic and Thermodynamic Considerations, p. 1248
Self-Assembly: Terminology, p. 1263
Soft and Smart Materials, p. 1302
Spherands, p. 1344

REFERENCES

1. Lehn. J.-M. Supramolecular chemistry—Scope and perspectives. molecules. supermolecules and molecular devices. Angew. Chem.. Int. Ed. Engl. **1988.** *27.* 89–112.
2. Lehn, J.-M. Supramolecular chemistry and self-assembly special feature: Toward complex matter: Supramolecular chemistry and self-organization. Proc. Natl. Acad. Sci. U. S. A. 2002. 99, 4763–4768.
3. Cram. D.J. Preorganisation—From solvents to spherands. Angew. Chem.. Int. Ed. Engl. **1986.** *25.* 1039–1134.
4. Abouderbala. L.O.; Belcher, W.J.: Boutelle, M.G.: Cragg. P.J.; Fabre, M.: Dhaliwal, J.: Steed, J.W.; Turner, D.R.: Wallace. K.J. Anion sensing 'Venus flytrap' hosts: A modular approach. Chem. Commun. 2002, 358–359.
5. Cram. D.J.; Karbach. S.: Kim, H.E.: Knobler. C.B.; Maverick, E.F.: Ericson, J.L.: Helgeson, R.C. Host guest complexation. 46. Cavitands as open molecular vessels form solvates. J. Am. Chem. Soc. **1988,** *110*, 2229–2237.
6. Weber, *E*. Clathrate chemistry today—Some problems and reflections. Top. Curr. Chem. 1987, 140. 2–20.
7. Hollingsworth, M.D.; Brown. M.E.; Hillier, A.C.: Santarsiero, B.D.; Chaney. J.D. Superstructure control in the crystal growth and ordering of urea inclusion compounds. Science **1996.** *273.* 1355–1358.
8. Steed. J.W.: Zhang. H.M.; Atwood. J.L. Inclusion chemistry of cyclotriveratrylene and cyclotricatechylene. Supramol. Chem. 1996, *7.* 37–45.
9. Steed, J.W.; Junk. P.C.: Atwood, J.L.; Barnes, M.J.: Raston. C.L.: Burkhalter, R.S. Ball-and-socket nanostructures—New supramolecular chemistry based on cyclotriveratrylene. J. Am. Chem. Soc. 1994. *116*, 10346–10347.
10. Holman, K.T.; Atwood, J.L.; Steed. J.W. Intra cavity inclusion of $[CpFe^{II}(arene)]^+$ guests by cyclotriveratrylene. Angew. Chern., Int. Ed. Engl. **1997.** *36.* 1736–1738.
11. Hardie. M.J.: Raston. C.L.: Wells, B. Altering the inclusion properties of CTV through crystal engineering: CTV. carborane, and DMF supramolecular assemblies. Chem. Eur. J. 2000, *6*, 3293–3298.
12. Atwood, J.L.: Koutsantonis, G.A.: Raston, C.L. Purification of C_{60} and C_{70} by selective complexation with calixarenes. Nature **1994.** *368.* 229–231.
13. Canceill, J.; Cesario, M.; Collet, A.; Guilhem, J.: Riche, C.: Pascard, C. Selective recognition of neutral molecules — study of the complexation of CH_2Cl_2 and CH_2Br_2 by cryptopliane-D in solution and crystal-structure of its CH_2Cl_2 cavitate. J. Chem. Soc., Chem. Commun. **1986.** 339–341.
14. Crassous. J.; Collet. A. The bromochlorofluoromethane saga. Enantiomer 2000, *5*, 429–438.
15. Braga, D. Crystal engineering, Where from? Where to? Chem. Commun. 2003, *22*, 2751–2754.
16. Schmidt, C.M.J. Molecular Engineering. Pure Appl. Chem. 1971. *27.* 647–678.
17. Pepinsky. R. Crystal engineering: A new concept in crystallography. Phys. Rev. 1955, *100.* 952.
18. Jouaiti, A.; Hosseini. M.W.; Kyritsakas, N. Molecular tectonics: Infinite cationic double stranded helical coordination networks. Chem. Commun. 2003. 472–473.

19. MacGillivray, L.R. From engineering crystals to engineering molecules: Emergent consequences of controlling reactivity in the solid state using linear templates. Cryst. Eng. Commun. **2002.** 37–41.
20. Raston. C.L.; Scott. J.L. Chemoselective, solvent-free aldol condensation reaction. Green Chem. **2000. 2.** 49–52.
21. Raston. C.L. Green chemistry down under. Green Chem. **2000. 2.** G74.
22. Kaupp. G. Solid-state molecular syntheses: Complete reactions without auxiliaries based on the new solid-state mechanism. Cryst. Eng. Commun. **2003.** 5. 117–133.
23. Friscic. T.; Macgillivray, L.R. 'Template-switching': A supramolecular strategy for the quantitative, gram-scale construction of a molecular target in the solid state. Chem. Commun. 2003, 1306–1307.
24. Allen, F.H.; Howard, J.A.K.; Hoy, V.J.; Desiraju, G.R.; Reddy. D.S.: Wilson. C.C. Neutron study of adamantane alkyne-ol. J. Am. Chem. Soc. **1996. 118.** 4081.
25. Brammer, L.; McCann, M.C.; Bullock, R.M.; McMullan, R.K.: Sherwood, P. $Et_3NH^+Co(CO)_4^-$—Hydrogen-bonded adduct or simple ion-pair—Single-crystal neutron-diffraction study at 15 K. Organometallics **1992,** *11*, 2339–2341.
26. Crabtree. R.H.: Siegbhan. P.E.M.; Eisenstein, O.; Rheingold, A.L.: Koetzle, T.F. Unconventional hydrogen bonding review. Acc. Chem. Res. **1996.** 29. 348.
27. Patel, B.P.; Wessel, J.; Yao. W.B.; Lee, J.C.: Peris, E.: Koetzle. T.F.; Yap. G.P.A.; Fortin. J.B.; Ricci. J.S.: Sini. G.; Albinati, A.; Eisenstein. **O.;** Rheingold, A.L.: Crabtree. R.H. Intermolecular N–H···H–Re interactions involving rhenium polyhydrides. New J. Chem. **1997.** 21, 413–421.
28. Derege, P.J.F.: Williams. S.A.: Therien, M.J. Direct evaluation of electronic coupling mediated by hydrogen-bonds—Implications for biological electron-transfer. Science **1995.** 269. 1409–1413.
29. Roche, S.: Haslam, C.; Adams. H.; Heath, S.L.: Thomas. J.A. Self-assembly of a suprarnolecular cube. Chem. Commun. **1998.** 1681–1682.
30. Collier. C.P.; Wong, E.W.; Belohradsky, M.; Raymo, F.M.: Stoddart. J.F.: Kuekes, P.J.; Williams, R.S.: Heath. J.R. Electronically configurable molecular-based logic gates. Science **1999. 285,** 391–394.
31. Hla, S.W.; Bartels, L.: Meyer. G.: Rieder, K.H. Inducing all steps of a chemical reaction with the scanning tunneling microscope tip: Towards single molecule engineering. Phys. Rev. Lett. **2000, 85,** 2777–2780.
32. Dance. I. What is supramolecular? New J. Chern. 2003, *27*, 1–2.

Supramolecular Electrochemistry

Angel E. Kaifer
University of Miami, Coral Gables, Florida, U.S.A.

INTRODUCTION

The field of supramolecular chemistry is concerned with a large number of systems ranging from simple host–guest complexes to more complicated solution assemblies, as well as two-dimensional (organized monolayers) and three-dimensional assemblies (crystalline solids). Noncovalent interactions play an important role in the kinetic assembly and thermodynamic stabilization of all these systems and constitute their most distinctive feature. Electron-transfer reactions can obviously be affected by supramolecular structures, but the reverse is also true. It is possible to alter the structure and the thennodynamic stability of supramolecular assemblies using electrochemical (redox) conversions. In other words, electron-transfer reactions can be utilized to exert some degree of control on supramolecular aggregates. Provided in this article is an overview of the interplay between supramolecular structure and electron-transfer reactions.

REDOX CONTROL ON HOST–GUEST COMPLEXES

Consider a host–guest complexation equilibrium and assume that the guest (G) is redox active, while the host (H) is not. Obviously, redox or electrochemical reactions on the guest introduce pronounced changes in electric charge and hydrophobic character. These changes usually translate into considerable changes in the stability of the corresponding host–guest complex (HG). In other words, changes in the oxidation state of the guest will affect the equilibrium constant (K) for the formation of the complex. The best way to represent the coupling between the electron-transfer and binding processes is through a square scheme. such as that shown in Scheme 1.

In Scheme 1, K and K' represent the binding constants corresponding to the association of each of the oxidation states of the guest with the host, and E^o_f and E^o_c represent the formal potentials for the electron-transfer reactions (taken arbitrarily as oxidations in the scheme) of the free and complexed guest. These thermodynamic values are related by the following equation:

$$K/K' = \exp[nF(E^o_c - E^o_f)/RT] \quad (1)$$

where n is the number of electrons transferred, F is Faraday's constant, R is the ideal gas constant, and T is the Kelvin temperature. Clearly revealed by this equation is that the molecular recognition of the guest by the host may affect its formal potential (E^o versus $E^{o\prime}$). In fact, other electrochemical parameters may also be affected by the complexation reactions. For instance, voltammetric peak currents, which depend on the effective diffusion coefficients of the electroactive species, are usually depressed by molecular association phenomena, as the diffusion coefficient of the complex is lower than that of the free components. In general terms, this means that electrochemical techniques are useful experimental tools for the study of host–guest binding interactions, provided that there is a redox-active center (electrophore) in the guest, the host or both.[1]

The chemical literature already contains numerous examples of redox control on host–guest binding interactions, and the topic was the subject of several reviews.[2–6] In this article, selected examples that illustrate particularly well the possibilities of the research field will be presented. As a first example. let us consider the cobaltocenium ion (Cob^+), an 18-electron organometallic complex that can be reversibly reduced to its neutral form, cobaltocene **(Cob).** The reduced form is hydrophobic and is an excellent guest for the water-soluble host β-cyclodextrin (β-CD), which has a cavity that also has an inner surface with pronounced hydrophobic character. In contrast to this, the positively charged cobaltocenium is not bound by the β-CD host in aqueous solution.[7] This system illustrates the idea of electrochemically enhanced binding, as the initial and more stable form of the electroactive guest is not significantly bound by the host, but its one-electron reduction triggers the formation of an inclusion complex (see Scheme 2), with stability that is derived from the hydrophobic character of the guest in its reduced form.

The positive charge on the cobaltocenium ion makes it an excellent guest for water-soluble, anionic calix[6]arene hosts. Specifically, the hexasulfonatocalix[6]arene (1^{8-}), with its structure given in Scheme 3, was shown to bind two Cob^+ ions on the equivalent binding sites indicated by the arrows.[8,9] Therefore, one can think of an aqueous solution containing cobaltocenium, and the two hosts, β-CD and calixarene 1^{8-}, as a redox-switchable system in which, initially, two Cob^+ ions form a 2:1 complex with

Encyclopedia of Supramolecular Chemistry
DOI: 10.1081/E-ESMC 120012664

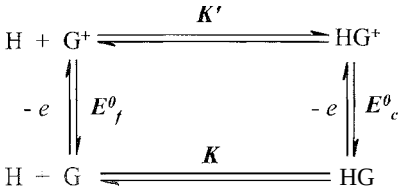

Scheme 1 Square scheme showing the redox and complexation equilibria that describe the interactions between a redox active guest (G) and an electroinactive host (H).

the anionic host $\mathbf{1}^{8-}$. Upon a one-electron reduction of the guest to the neutral Cob form. the predominant bimolecular species in the solution is the 1:1 inclusion complex β-CD.Cob. This example clearly illustrates a case in which the oxidation state of the guest determines host selection for complex formation. as well as the stoichioinetry of the resulting complex.

The Cob^+/β-CD host–guest system can also be adapted to the preparation of much larger supramolecular aggregates in the solution phase. For instance, multiple cobaltocenium groups can be covalently attached to the periphery of dendrimers. In these macromolecules. the reduction of the peripheral cobaltocenium units takes place in just one voltammetric wave. regardless of their number (dendrimers with 4, 8, 16, and 32 cobaltocenium units were prepared).[9] This finding reveals that all the reducible cobaltoceniurn units are equivalent and show no degree of electronic communication with one another on the dendrimer surface. When the reduction takes place in the presence of excess β-CD host. the reduced cobaltocene units are complexed by the freely diffusing hosts. Thus, the dendrimer can be considered as a molecular scaffold for the organized assembly of the CDs upon cobaltocenium reduction (see Scheme 4), and this provides another interesting example of electrochemically driven self-assembly.

A completely different example illustrates the flexibility of this general approach. For instance. the tetracationic

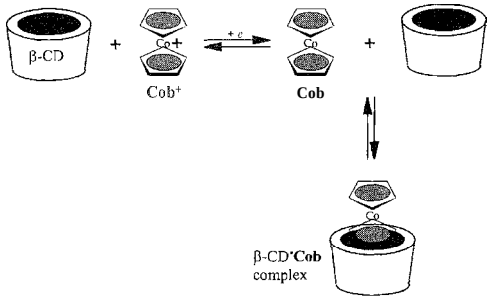

Scheme 2 Interplay between electron transfer and complexation equilibria in the cobaltocenium/β-CD system. **(View *this art in color at www.dekker.com.*)**

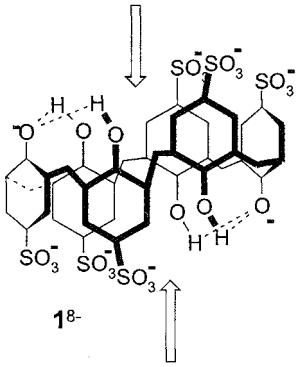

Scheme **3** Molecular structure of the anionic host hexasulfonatocalix[6]arene at neutral pH. The arrows point to the two pockets for the binding of cationic species.

cyclophane host [$\mathbf{2}^{4+}$, *bis*(paraquat-*p*-phenylene)], forms a stable inclusion complex with the guest tetrathiafulvalene (TTF). in which the stability of the complex is rationalized by a combination of solvophobic forces and charge-transfer interactions between the π-donor guest and the

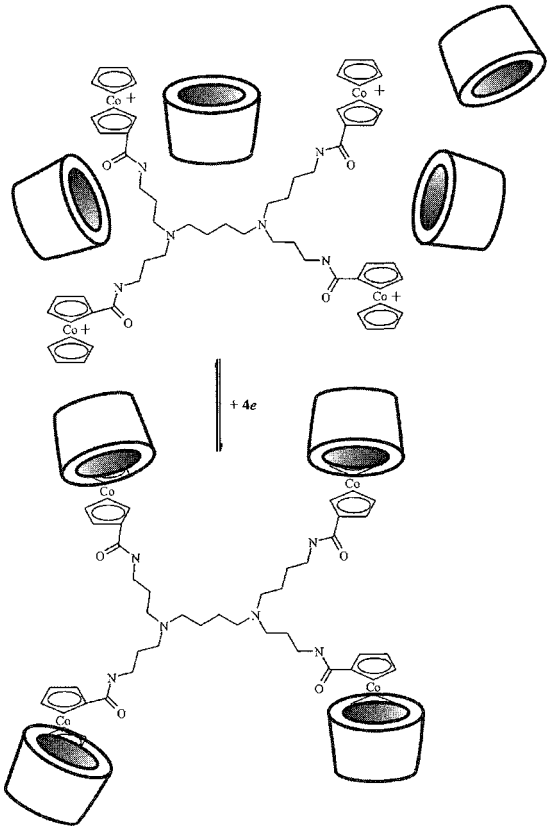

Scheme 4 Electrochemically triggered self-assembly of β-CD hosts around a dendrimer with four peripheral cobaltocenium units.

π-acceptor (4,4′-bipyridinium) residues of the host.[10] In this case, oxidation of the guest to its cation radical leads to complex dissociation due to the loss of π-donor character by the guest, and, perhaps more importantly, the coulombic repulsion between the tetracationic host and the cationic guest. The binding affinity can be restored, because the one-electron oxidation of the TTF guest is fully reversible (Scheme 5). Furthermore, the stability of the TTF–cyclophane complex can also be decreased by the one-electron reduction of the two 4,4′-bipyridinium residues on the cyclophane host. This system exhibits additional features due to the possibility of further oxidizing the cation radical TTF^{+} to yield a dication TTF^{2+}, which constitutes an excellent guest for the crown ether **3**.[10] Therefore, the three accessible oxidation states of TTF have different selectivities for these two hosts, and conditions can be found to form either complex or none.

Hydrogen-bonding interactions are extremely important in living systems, and their redox control has been the subject of a good number of interesting reports. For instance, Rotello and coworkers extensively investigated

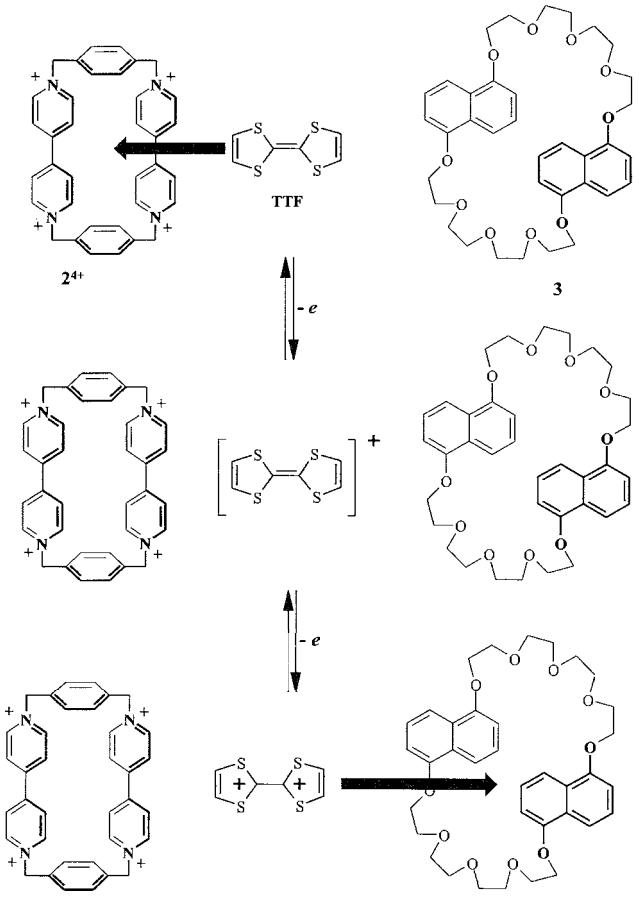

Scheme 5 Redox control on the guest properties of TTF in the presence of two possible hosts (2^{4+} and **3**).

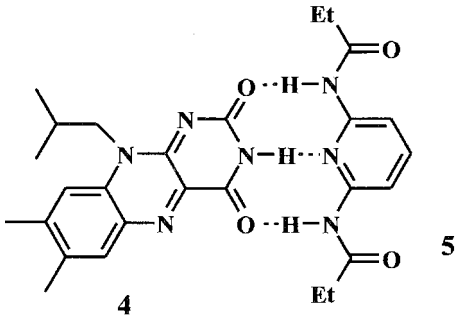

Scheme 6 Hydrogen bonding between flavin 4 and diamidopyridine derivative **5**.

the binding interactions between the flavin 4 and the 2,6-diamidopyridine derivative **5** (Scheme 6).[11] In CH_2Cl_2 solution, the three-point hydrogen bonding between these two compounds leads to a shift of +155 mV in the one-electron reduction of the flavin to its anion radical. This reflects the enhanced binding constant between $4^{-}\cdot 5$ as compared to that observed for $4\cdot 5$. The binding pair between flavoprotein models, such as 4, and a number of diaminopyridine and diamidopyridine derivatives was extensively investigated, as it has considerable importance to understanding the wide range of redox potentials observed in flavoproteins.[12]

Tucker and coworkers prepared and investigated the ferrocene-containing host 6, which was specifically designed to recognize and bind urea and barbiturate derivatives (Scheme 7).[13] This host binds barbital in organic solvents forming a 1:1 complex, with a crystal structure that was reported. However, the ferrocene residue in 6 does not act as an effective voltammetric reporter for the binding, because the formal potential for ferrocene oxidation shifts only by ~20 mV in the presence of excess barbital guest. Drawing from this example, we can conclude that the design of redox-active hosts as

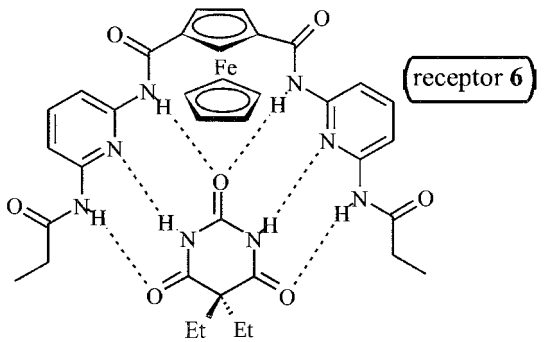

Scheme 7 Hydrogen bonding between receptor 6 and barbital.

voltammetric sensors poses special requirements, because it is highly desirable that the sought-after binding event will shift the formal potential of the reporter electrophore *as much as possible. To* accomplish *this goal, the molecular design must focus on two fundamental points: 1) the binding site and the* redox *center must be spatially very close; and* 2) *the binding event must alter the microenvironment around the* redox *center or cause a considerable change in the electronic density of the electrophore.*

Typically, redox *conversions in the host or the guest give rise to pronounced changes in the stability of the corresponding complex. The* β-CD/Cob^+ *host–guest system and any complexes between n-donor compounds and host* 2^{4+} *constitute excellent* examples *of electrochemically induced complex formation or dissociation. Furthermore, in cases where the guest's electron-transfer reaction is associated with substantial changes in the host–guest affinity, the actual electron-transfer step takes place on the free guest. not on the inclusion complex, as both species undergo dynamic equilibrium in the solution. This somewhat surprising fact was first demonstrated by Evans and coworkers in a* seminal *study of the electrochemistry of ferrocenecarboxylic acid in the presence of the host* β-CD.[14] *The author's groups reached similar conclusions on electrochemical investigations of the host–guest systems between several* ferrocene *derivatives and* β-CD[15] as *well as the* cobaltocene/β-CD system.[7] *However, recent work on the complexation of methylviologen* (MV^{2+}) *by the host* cucurbit[7]uril (CB7) *shows different behavior (see Scheme* 8).[16] *The* CB7 *inclusion complex of* MV^{2+} *exhibits a high binding constant* ($\sim 1 \times 10^5$ L/mol) *in aqueous media. However, a one-electron reduction of the guest to its cation radical* MV^+ *decreases the binding constant by* a *modest factor of only two. As a result of the high stability of both complexes, the electrochemical behavior of the* MV^{2+}/MV^+ redox *couple in the presence of one equivalent of* CB7 *does not show any signs of coupling with* association/dissociation *chemical steps, which reveals that the electron-tranfer process actually takes place on the inclusion complexes.*

REDOX CONTROL OF ROTAXANES AND CATENANES

Rotaxanes are molecules that consist of one or more macrocyclic rings (wheels) threaded by a linear component (axle) with bulky stopper groups at both ends. The sliding, back-and-forth motion of the macrocyclic *rings is spatially limited by the stopper groups, which prevent axle–wheel dissociation. A catenane is composed of two or more interlocked macrocycles. The relative positions of the interlocked components in these fascinating molecules can be determined to some extent by noncovalent interactions, and thus, the possibility to exert interactive control by* redox *conversions quickly became a goal in the development of molecular machines. A review of the extensive work in this area* is available.[17] *Here, we will discuss* some *key examples.*

In collaboration with Stoddart, the authors' group reported in 1994 *a rotaxane in which the relative position of the wheel could be controlled by chemical and electrochemical* methods.[18] *This rotaxane contains two n-donor stations in the axle: benzidine and biphenol. The* macrocyclic *wheel fcyclophane* 2^{4+}) *interacts preferentially with the benzidine station. Thus, at* 299 *K in* CH_3CN *solution, 84% of the rotaxanes have the wheel located around the benzidine station, and* 16% *have it around the biphenol group (Scheme 9). At higher temperatures, the exchange between these two translational conformers is too fast in the NMR timescale, and the lines broaden extensively. Electrochemical experiments demonstrated that the one-electron oxidation of the benzidine station to form its cation radical results in the effective translation of the wheel over to the biphenol station.''''* The *wheel sliding motion is mostly due to the coulombic repulsions that the oxidized, positively charged benzidine station exerts on the tetracationic wheel. Switching back to the original situation is possible, as the* electrochemical *oxidation of benzidine is reversible under these conditions. A nice aspect of this rotaxane is that similar control on the wheel position can be attained by proton-transfer reactions, as the protonation of the benzidine station leads*

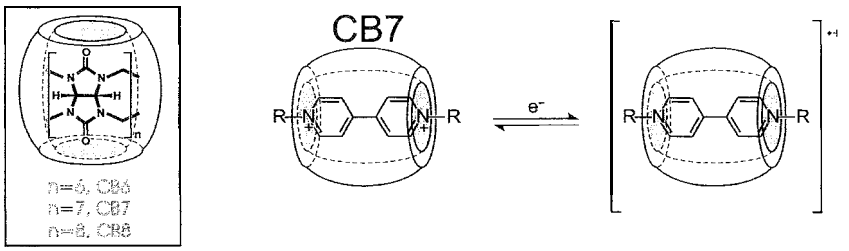

Scheme 8 *Electron transfer between the* CB7 *inclusion complexes of* MV^{2+} and MV^+. *The structure of three* cucurbituril *hosts* (CB6, CB7, *and* CB8) *is* shown *in the* insert *at the right.*

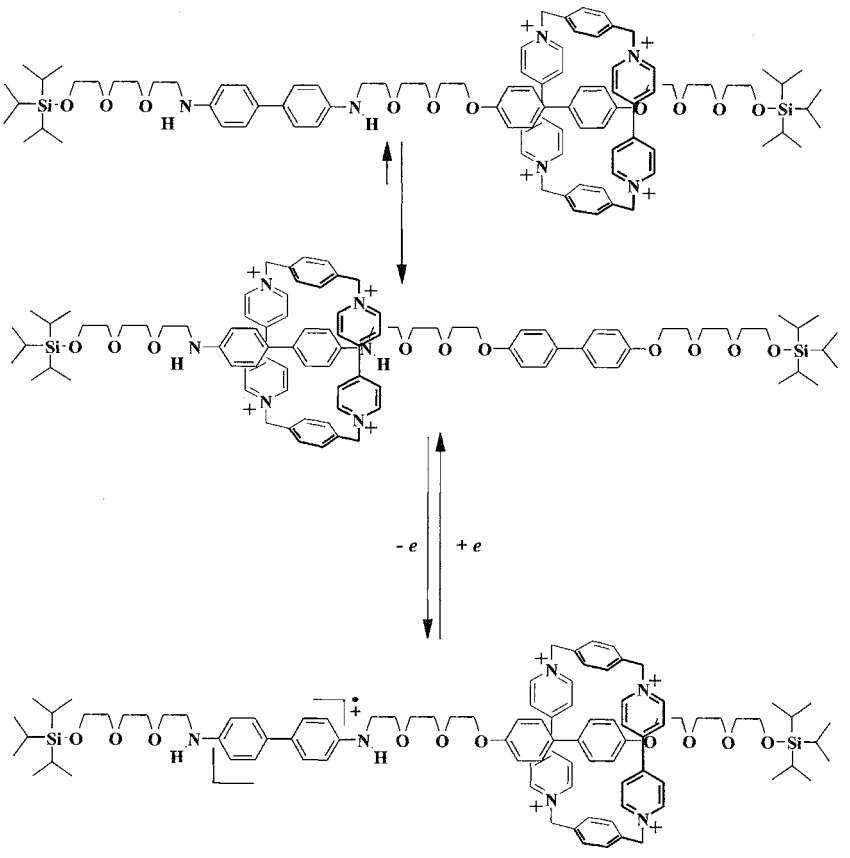

Scheme 9 Electrochemical switching of the average location of the wheel component (cyclophane 2^{4+}) in the rotaxane. taking advantage of the reversible oxidation of the benzidine station in the axle.

to wheel binding on the biphenol's region of the axle. Therefore, this rotaxane clearly exhibits properties corresponding to a molecular machine that can be switched by electrochemical and chemical means.

Similar electrochernical and chemical control on the conformation of catenanes was reported by the groups of Stoddart and Balzani. A prominent example is given in Scheme 10. The catenane in question is composed of two macrocyclic rings; the first is the already familiar electron-acceptor cyclophane $\mathbf{2^{4+}}$, while the second contains TTF and binaphthol aromatic donor units.[19] Given that TTF is the strongest π-donor, the most stable conformation of the catenane has the TTF unit sandwiched between the two bipyridinium units of the electron-acceptor ring. However, electrochemical (or chemical) oxidation of the TTF unit gives rise to a conformational change, as the catenane structure minimizes the coulombic repulsions between the oxidized TTF^+ and the tetracationic cyclophane ring by inserting the binaphthol unit between the bipyridinium groups and leaving the TTF^+ unit "alongside." This process is completely reversible, and the reduction of TTF^+ back to TTF returns this unit to the "inside" position.

These examples show how redox conversions can be utilized to control internal motions and the relative positions of functional groups in interlocked structures, such as catenanes and rotaxanes. Recently, the groups of Stoddart and Heath demonstrated that these compounds can be used to build monolayers, anchored with phospholipid counterions, which exhibit properties like those of solid-state. electronically addressable, switching devices.[20]

ELECTROCHEMISTRY **OF ENCAPSULATED** WEDOXCENTERS

Most redox proteins contain a redox-active group that is partially or completely buried inside their polypeptide backbones. Clearly, this design is meant to discriminate between possible electron-transfer partners, in such a way that only those approaching the protein at the right locations will be allowed to exchange electrons with the redox functional group. Therefore. the electron-transfer reactions of encapsulated redox centers are the subject of considerable current interest.[21–23] Most groups

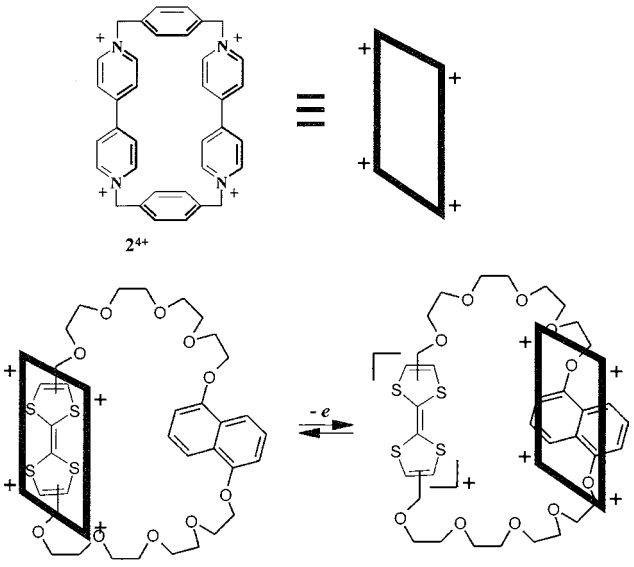

Scheme 10 Electrochemical switching of the average location of the 2^{4+} macrocycle in the catenane, taking advantage of the reversible oxidation of the TTF unit on the other macrocycle.

approached this problem by preparing large macromolecules containing redox-active groups covalently attached to their cores. In particular, this approach was popular in dendrimer chemistry, and a number of dendrimers with electroactive cores were synthesized and their electrochemical properties investigated.[23] Generally; dendrimer growth around a redox-active center results in the quick attenuation of the corresponding electron-transfer rates: although dendrimers with viologen cores appear to be exceptions to this trend.[24] This research topic is still open, and much work must be done to fully understand the effects of dendrimer encapsulation on the electrochemical properties of the redox cores.

An alternative way to attack this problem would rely on noncovalent encapsulation. In other words, use host–guest interactions to trap a redox active guest inside an electroinactive host. However, full encapsulation is not so easy to accomplish. and. as mentioned before, many complexes dissociate once the redox-active guest undergoes electron transfer. As a result of these complications, the literature contains few examples of truly encapsulated redox guests by noncovalent means. A few years ago; the author's group reported the electrochemistry of ferrocene fully encapsulated inside Cram's hemicarcerands.[25] This is a case of constrictive binding in which the complex is formed at high temperatures, at which the collisions between the fersocene (Fc) and the host molecules may lead to ferrocene encapsulation in the central cavity of the host, by sliding through one of the equatorial portals in the hemicarcerand. Cooling of this solution to room temperature effectively traps the Fc guest inside the host. We prepared hosts 7 and 8 (Scheme 11) and their respective ferrocene inclusion complexes, as previously described by Quan and Cram.[26] While $Fc\cdot 7$ was only soluble in tetrachloroethane. $Fc\cdot 8$ was soluble in dichloromethane and tetrachloroethane. Guest release from $Fc\cdot 8$ in CD_2Cl_2 was monitored at 25°C by ^{1}H-NMR spectroscopy. The half-life for the dissociation process was found to be slow enough ($t_{1/2}$ > 300 h) and to provide a long time in which to perform the electrochemical experiments with the encapsulated guest.[27]

Voltammetric experiments with $Fc\cdot 7$ in $C_2H_2Cl_4$ and $Fc\cdot 8$ in $C_2H_2Cl_4$ and CH_2Cl_2 were performed, and the results were compared with those obtained with free ferrocene in the same media. The data showed that encapsulation shifts the half-wave potential for fessocene oxidation to more positive values. Also, fersocene encapsulation by either host leads to a decrease in the diffusion coefficient and the standard rate constant for the heterogeneous electron transfer.[27] The observed effect on the potential values can be rationalized by the poor solvation provided by the inside walls of the host to the oxidized. ferrocenium ion. On the other hand, the observed decrease of the diffusion coefficient is easily explained by the increase in the molecular weight (and size) experienced by fersocene upon encapsulation inside the massive host. Finally, the decreased rate of electron transfer is probably the result of the increased average distance between the electrode surface and the ferrocene center upon its encapsulation. These results are similar to those obtained with dendrimer systems containing a redox center covalently attached to their cores,[21–23] which reveals general agreement between two different types of experiments. In any instance, additional work is necessary to fully understand

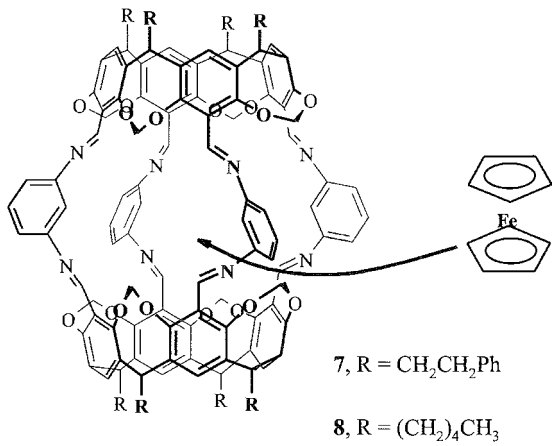

Scheme 11 Structures of Cram's hemicarcerands 7 and 8 for the constrictive encapsulation of ferrocene.

the ways in which encapsulation and site isolation affect electron-transfer reactions in synthetic systems and, by extension. in natural ones.

SUPRAMOLECULAR CHEMISTRY *AT THE ELECTRODE–SOLUTION INTERFACE*

Another area of work that received considerable attention in the last few years focuses on the design of the molecular architecture at the electrode–solution interface and the utilization of supramolecular interactions and effects to increase the selectivity of the electrode response. For instance, several years ago, the author's group prepared self-assembled monolayers on gold containing β-CD units.[28] The electrode-immobilized CD cavities were shown to bind ferrocene at low concentrations, increasing the sensitivity of the electrode and making possible the electrochemical detection of ferrocene under those conditions. Reinhoudt and coworkers extensively worked on the design and preparation of supported monolayers containing preformed binding sites.[29] The recent efforts of Nupp and coworkers also deserve mention in this area. This group developed electrode coatings based on cavity-containing coordination compounds. These film coatings are then capable of molecular sieving,[30] that is, they can size-select the electroactive materials for access to the underlying electrode surface, where they can undergo electron transfer.

CONCLUSION

The work summarized in this article relates to some of the most exciting areas of supramolecular chemistry. The interdependence of electron-transfer reactions with supramolecular interactions is at the core of the development of switchable molecular devices. Furthermore, research in areas of supramolecular electrochemistry may open the way for technological applications such as responsive (intelligent) materials. A possible impact in the field of electrochemical sensors is also readily visualized from the work described here.

ACKNOWLEDGMENTS

The author is grateful to the National Science Foundation for continued support of the research work described here.

ARTICLES OF FURTHER INTEREST

Carcerands and Hemicarcerands, p. *189*
Electrochemical Sensors, p. *505*
Ion-Selective Electrodes, p. *747*

REFERENCES

1. Kaifer, A.E.; Gbmez-Kaifer, M. *Supramolecular Electrochemistry*; Wiley: New York, 1999. Chapter 9.
2. Boulas. P.; Gbmez-Kaifer, M.; Echegoyen. L. Electrochemistry of supramolecular systems. Angew. Chem. Int. Ed. **1998.** *37*, 216.
3. Kaifer. A.E. Interplay between molecular recognition and redox chemistry. Acc. Chem. Res. **1999,** *32*. 62.
4. Amendola, V.; Fabbrizzi. L.; Pallavicini, P. Controlling the assembling/disassembling process of metal-containing superstructures. Coord. Chem. Rev. 2001. *216*. 435.
5. Beer. P.D.; Gale, P.A. Anion recognition and sensing: The state of the art and future perspectives. Angew. Chem. Int. Ed. **2001.** 40. 487.
6. Tucker, J.H.R.; Collinson, S.R. Recent developments in the redox-switched binding of organic compounds. Chem. Soc. Rev. **2002,** *31*, 147.
7. Wang. Y.; Mendoza, S.: Kaifer, A.E. Electrochemical reduction of cobaltoceniurn in the presence of β-cyclodextrin. Inorg. Chem. **1998**, *37*, 317.
8. Wang, Y.; Alvarez, J.; Kaifer, A.E. Redox control of host-guest recognition: A case of host selection determined by the oxidation state of the guest. Chem. Commun. **1998.** 1457.
9. González, B.; Casado, C.M.; Alonso, B.: Cuadrado. I.; Morán, M.; Wang, Y.; Kaifer, A.E. Synthesis, electrochemistry and cyclodextrin binding of novel cobaltocenium-functionalized dendrimers. Chem. Commun. **1998;** 2569.
10. Ashton. P.R.; Balzani. V.: Becher, J.; Credi. A.; Fyfe, M.C.T.; Matterstig, G.; Menzer. S.; Nielsen, M.B.; Raymo, F.M.; Stoddart, J.F.; Venturi, M.; Williams. D.J. A three-pole supramolecular switch. J. Am. Chem. Soc. **1999,** *121*. 3951.
11. Breilinger, E.: Niemz. A.; Rotello. V.M. Model systems for flavoenzyme activity. Stabilization of the flavin radical anion through specific hydrogen bond interactions. J. Am. Chem. Soc. **1995**, *117*, 5379.
12. Neimz, A.: Rotello, V.M. From enzyme to molecular device. Exploring the Interdependence of redox and molecular recognition. Acc. Chem. Res. **1999.** *32*. 44.
13. Collinson, S.R.; Gelbrich, T.; Hursthouse. M.B.; Tucker, J.H.R. Novel ferrocene receptors for barbiturates and ureas. Chem. Cornmun. **2001,** 555.
14. Matsue. T.; Evans. D.H.; Osa, T.: Kobayashi, N. Electron-transfer reactions associated with host-guest complexation. Oxidation of ferrocenecarboxylic acid in the presence of β-cyclodextrin. J. Am. Chem. Soc. **1985,** *107*. 3411.

15. Isnin, R.: Salam. C.; Kaifer, A.E. Bimodal cyclodextrin complexation of ferrocene derivatives containing n-Alkyl chains of varying length. J. Org. Chem. 1991, 56. 35.
16. Ong, W.: Gómez-Kaifer. M.; Kaifer. A.E. Cucubit[7]uril: A very effective host for viologens and their cation radicals. Org. Lett. 2002. 4, 1791.
17. Balzani, V.; Credi. A.: Raymo. F.M.; Stoddart, J.F. Artificial molecular machines. Angew. Chern. Int. Ed. 2000. *39*, 3348.
18. Bissell. R.A.; Córdova. E.: Kaifer, A.E.; Stoddart, J.F. A chemically and electrochemically switchable molecular shuttle. Nature 1994. 369. 133.
19. Asakawa, M.: Ashton, P.R.: Balzani. V.; Credi, A.; Hamers. C.; Mattersteig, C.; Montalti. M.: Shipway, A.N.; Spencer. N.: Stoddart, J.F.; Tolley. M.S.; Venturi, M.: White, A.J.P.: Williams, D.J. A chemically and electrochemically switchable [2]catenane incorporating a tetrathiafulvalene unit. Angew. Chem. Int. Ed. 1998, *37*. 333.
20. Collier. C.P.: Mettersteig. G.; Wong, E.W.: Berverly. K.: Sampaio, J.: Raymo. F.M.; Stoddart, J.F.; Heath, J.R. A [2]catenane-based solid state electronically reconfigurable switch. Science 2000. 289. 1172.
21. Cardona, C.M.: Mendoza. S.: Kaifer, A.E. Electrochemistry of encapsulated redox centers. Chem. Soc. Rev. 2000, 29. 37.
22. Gorman, C.B.: Smith. J.C. Structure-property relationship in dendritic encapsulation. Acc. Chem. Res. 2001. 34, 60.
23. Cameron, C.S.; Gorman, C.B. Effects of Site Encapsulation on electrochemical behavior of redox-active core Dendrimers. Adv. Funct. Mater. 2002. *12*, 17.
24. Toba. R.: Quintela. J.M.; Peinador, C.; Román, E.; Kaifer, A.E. A new series of dendrimers with 4,4′ -birpyridinium cores capable of fast electron transfer reactions. Chem. Commun. 2001. 857.
25. Cram. D.J.: Cram. J.M. Container Molecules and Their Guests. In Monographs in *Supramolecular Chemistry*; Stoddart, J.F., Ed.; Royal Society of Chemistry: Cambridge, 1994; Vol. 4. Chapter 8.
26. Quan, M.L.C.; Cram. D.J. Constrictive binding of large guests by a hemicarcerand containing four portals. J. Am. Chem. Soc. 1991. *113*, 2754.
27. Mendoza. S.: Davidov, P.D.: Kaifer. A.E. Electrochemistry of encapsulated guests: Ferrocene inside cram's hemicarcerands. Chern. Eur. J. 1998, 4, 864.
28. Rojas, M.T.: Koniger, R.: Stoddart, J.F.; Kaifer, A.E. Supported monolayers containing preformed binding sites. Synthesis and interfacial binding properties of a thiolated β-cyclodextrin derivative. J. Am. Chem. Soc. 1995, *117*. 336.
29. Flink. S.; van Veggel. F.C.J.M.; Reinhoudt, D.N. Sensor functionalities in self-assembled monolayers. Adv. Mater. 2000, 12, 1313.
30. Bélanger, S.: Hupp, J.T. Porphyrin-based thin-film molecular materials with highly adjustable nanoscale porosity and permeability characteristics. Angew. Chem. Int. Ed. 1999, 38, 2222.

Supramolecular Isomerism

Martin Schröder
Neil R. Champness
The University of Nottingham, Nottingharn, United Kingdom

INTRODUCTION

Described in this article is the phenomenon of supramolecular isomerism, using examples derived from coordination framework materials. The terminology, as applied to this complex area, is discussed via the description of ''isomerism'' within one-, two-, or three-dimensional arrays.

DEVELOPMENTS

The construction of crystal-engineered frameworks using either coordinative bonding or hydrogen-bonding interactions is an extremely topical area of inorganic and materials chemistry. In the case of coordination frameworks, notable advances have been made in understanding the factors that influence network topology using the building-block methodology as originally advanced by Robson et al.[1] This straightforward concept of using transition metal geometries to develop extended arrays is highly adaptable, but framework structures can be readily influenced by weaker supramolecular forces and by the coordinating ability of the anion.[2] Thus, it is possible for different forms of the extended array to be formed in which the same molecular components are used to construct the array, but different connectivities or orientations are observed. The realization that different forms, or '.isomers,'' of highly related compounds can be formed led to a dilemma of how such compounds can be described most usefully. Confusion, and conflicting opinions. have resulted in a variety of terminologies being used in the literature, which we seek to clarify in this article.

TERMINOLOGY

A large number of terms have been used to describe forms of isomerism in extended supramolecular arrays observed in the solid state. These include architectural isomerism,[3] topological isomerism,[4] and older terms that have specific and often well-defined meanings, including polymorphism, pseudopolymorphism, and structural isomerism.[5]

The term ''supramolecular isomerism'' was first used by Zaworotko[6] to describe distinct forms of highly related coordination polymer materials. This is complicated by the observation that supramolecular isomerism for a given network system is commonly combined with a variation in guest solvent molecules within the extended structure. Variation of guest molecules within a framework does not, of course, define new supramolecular isomers of the framework if the latter is unchanged. In a recent review, Zaworotko et al.[7] stated that supramolecular isomerism is closely related to the ''well-documented subject of polymorphism in crystalline solids.'' Zaworotko defined supramolecular isomerism in this context as ''the existence of more than one type of network superstructure for the same molecular building blocks'' and related the phenomenon ''to structural isomerism at the molecular level.''

Supramolecular isomerism represents a broad term for which the following subdivisions need to be considered:

Class I. Frameworks built from the same molecular components using the same interactions, i.e., supramolecular synthons (M-L, H-bonding, etc.), giving rise to the same localized connectivities but different framework topologies.

Class II. Frameworks built from the same molecular components using different interactions, i.e., supramolecular synthons (M-L, H-bonding, etc.), giving rise to different framework topologies.

Class III. Frameworks built from the same molecular components but with different noninteracting guest molecules giving rise to different framework topologies.

All of these subdivisions of supramolecular isomerism can be related to previously used terminology; thus, Class I can be considered as polymorphism; Class II as structural isomerism, and Class III as pseudo-polymorphism.

Other subsets of these classes also exist that can be considered as further forms of supramolecular isomerism but that are perhaps more usually associated with molecular species. Therefore, the term supramolecular isomerism offers little additional information. In particular, conformational changes of one, or more; of the molecular

Encyclopedia of Supramolecular Chemistry
DOI: 10.1081/E-ESMC 120012924

constituents of the extended array can lead to isomerism of the supramolecular array. Similarly, it is possible to prepare chiral frameworks for which two enantiomers can be envisaged and often isolated. Another form of isomerism. classified as a subset of supramolecular isomerism, is catenane isomerism, which distinguishes between catenatedlinterpenetrated and noncatenated/interpenetrated forms.

We will now discuss the classes of supramolecular isomerism using illustrative examples to show the complexity of the issues that arise in this area.

Class I—Polymorphic Supramolecular Isomers

We define polymorphic supramolecular isomers as supramolecular frameworks built from the same molecular components using the same interactions, i.e., supramolecular synthons (M-L, H-bonding, etc.). in all isomers giving rise to the same localized geometries but different framework topologies. To illustrate this terminology, we outline three examples of this class of isomerism.

Two distinct polymorphic supramolecular isomers of $\{[Ag(4\text{-}CNpy)_2]BF_4\}_\infty$ (4-CNpy = 4-cyanopyridine) have been reported.[8] In both isomers, each Ag(I) cation is coordinated by two pyridyl and two nitrile donors. In the first isomer, the Ag(I) cation adopts a flattened tetrahedral environment in which both pyridyl and nitrile donors adopt conventional Ag—W bond lengths, [Ag—$N_{(pyr)}$, 2.270(6) A: Ag—$N_{(CN)}$, 2.350(10) Å]. Propagation of the polymer via the 4-cyanopyridine ligands from these tetrahedral nodes results in the formation of a three-dimensional diamondoid assay (Fig. la), which exhibits fourfold interpenetration.

The second isomer of $\{[Ag(4\text{-}CNpy)_2]BF_4\}_\infty$ shows a distorted square-planar geometry at Ag(I) with different bond lengths for Ag—$N_{(pyr)}$ and Ag—$N_{(CN)}$, [Ag—$N_{(pyr)}$, 2.175 Å; Ag—$N_{(CN)}$, 2.71(1), 3.06(1) Å]. Thus, the two Ag—$N_{(CN)}$ contacts can only be considered as weak interactions. Polymeric propagation via the bridging ligands in this isomer results in a two-dimensional sheet structure of (4,4) topology (Fig. lb), in contrast to the three-dimensional diamondoid assay observed in the first isomer. The difference in polymeric dimensionality of the two compounds, i.e., two- versus three-dimensional, is therefore a direct result of the different geometries adopted at the Ag(I) cation, square-planar versus tetrahedral.

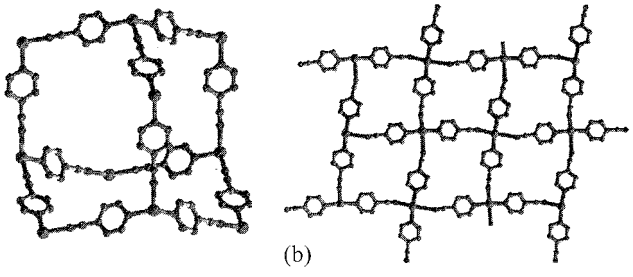

Fig. 1 Class I supramolecular isomers of $\{[Ag(4\text{-}CNpy)_2]BF_4\}_\infty$, in which the flexible Ag(I) coordination geometry leads to three-dimensional diamondoid (a) or two-dimensional (4.4) grid structures.

Cu(TCNQ) (TCNQ = 7,7,8,8-tetracyanoquinodimethane) exists as two polymorphic supramolecular isomers; which have been described as polymorphs by the original authors.[9] The two isomers exhibit distinct morphologies, needle (A) and platelet (B), and different magnetic and charge-transport properties. Interestingly. Isomer A can be converted to Isomer B by simply suspending Isomer A in MeCN solution for several days. Structural characterization of the two isomers shows that they exist as doubly interpenetrated three-dimensional coordination polymers in which the Cu(I) center is bound by four nitrile donors from four separate TCNQ ligands. The isomers exhibit subtly different four-coordinate geometries that lead to significantly different three-dimensional topological arrangements. Whereas, in Isomer A, neighboring TCNQ ligands around the Cu(I) center are rotated through an angle of 90° with respect to each other, in Isomer **B**, infinite assays of coplanar TCNQ molecules are arranged in the same orientation but in two perpendicular planes.

The series of compounds $[M(dca)_2(pyz)]_\infty$ (M = Mn,[10,11] Co [10] Ni,[10] Cu [12] Zn;[10] dca = dicyanamide, pyz = pyrazine) forms two distinct isomers termed the α and β forms. In both cases. the M(II) cation is coordinated by four dca nitrile donors and by two pyrazine donors that adopt a *trans* assangement. Thus, essentially the same coordination sphere is adopted at the M(II) cationic network node. In the case of the Cu(II) salt, Jahn–Teller distortion is observed via elongation of two of the dca nitrile–copper Cu—N bonds.[12]

In α-$[Cu(dca)_2(pyz)]_\infty$, the dca ligands bridge each Cu(II) cation to four nearest-neighbor metal nodes forming a square-grid framework derived from $[M(dca)_2]_\infty$ units. The pyrazine ligands link these $[M(dca)_2]_\infty$ square-grids into a three-dimensional α-Po network (Fig. 2a) which exhibits two-fold interpenetration. In contrast, in β-$[Cu(dca)_2(pyz)]_\infty$, the dca ligands bridge metal centers via double bridges such that each M(II) is only linked to two other metal nodes leading to $[M(dca)_2]_\infty$ chains. These chains are then linked through bridging pyrazine ligands to give two-dimensional sheets with a square-grid topology, if one considers the double-bridges as a single link (Fig. 2b). Interestingly. in the case of $[Cu(dca)_2(pyz)]_\infty$, the α form can be converted. over a period of hours. to the β isomer by suspension of the α

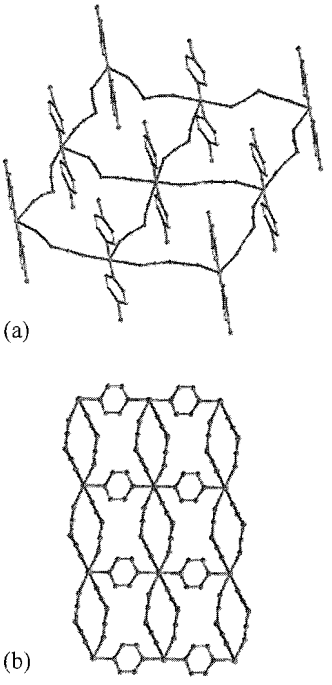

Fig. 2 Class I supramolecular isomers (a) α-$[M(dca)_2(pyz)]_\infty$, a three-dimensional coordination framework with ʏ-Po topology and (b) β-$[M(dca)_2(pyz)]_\infty$. a two-dimensional framework (M = Mn, Co. Ni, Cu, Zn) (*View this art in* color *at www dekker com*)

form in aqueous solution: this interconversion of phases is not observed for other metal cations.

Class II Structural Supramolecular Isomers

We define structural supramolecular isomers as supramolecular frameworks built from the same molecular components using different supramolecular interactions. Examples of structural supramolecular isomerism in coordination polymers are relatively rare, which probably reflects the requirement of inultiple interactive modes being present in a single building-block, ligand, or hydrogen-bonding moiety.

The complex [Cu(SCN)(dpt)] [dpt = 2,4-*bis*(4-pyridyl)-1,3,5-triazine] exhibits structural supramolecular isomerism. with the two isomers adopting either a three-dimensional lattice A or a one-dimensional ribbon polymer B.[13] Isomer A exhibits N_3S binding via two dpt ligands and two S C N anions. The chains of (CuSCN), are single stranded and are linked via bridging bidentate dpt ligands (Fig. 3a); therefore, SCN^- anions and dpt ligands lead to polymer propagation. The (CuSCN), chains on opposing ends of any given dpt ligand are orthogonally disposed. leading to the three-dimensional framework structure with a $6^5.8$ topology [$Cd(SO_4)$-type structure]. Such frameworks have been previously observed for coordination polymers with bridging bipyridyl ligands, but this structural type is more commonly associated with square-planar metal centers.[14 15]

Isomer **B** of $[Cu(SCN)(dpt)]_\infty$ exhibits a one-dimensional ribbon polyiner structure constructed from dpt-decorated (CuSCN), stair-polymers (Fig. 3b). Each Cu(I) center adopts a N_2S_2 coordination sphere formed by three SCN^- anions and a single dpt ligand. In contrast to Isomer A, each dpt ligand is only monocoordinated and, therefore, is not involved in polymer propagation.

Class III Pseudopolymorphic Supramolecular Isomers

We define pseudopolymorphic supramolecular isomers as supramolecular frameworks built from the same molecular components but with different noninteracting guest molecules giving rise to different framework topologies.

The complex $[(CuI)_2(bpds)]_\infty$ [bpds = *bis*(4-pyridyl)-disulfide] adopts two different structural motifs depending upon the solvent of crystallization. In both cases, the $[(CuI)_2(bpds)]_\infty$ consists of Cu_4I_4 cubane tetramers linked by two bpds ligands to form a square-shaped cavity.[''] When crystals of $[(CuI)_2(bpds)]_\infty$ are grown from $EtCN/CH_2Cl_2$, the tetrahedral Cu_4I_4 cubane junctions are linked by bpds ligands to give a necklace structure, $\{[(CuI)_2(bpds)] \cdot 0.5\ EtCN\}_\infty$ (Fig. 4a). The tetrahedral geometry of the Cu_4I_4 cubane results in alternating square-shaped units being orientated perpendicular to each other in adjacent links of the necklace, with the square-shaped cavities packed to give channels that accommodate EtCN molecules.

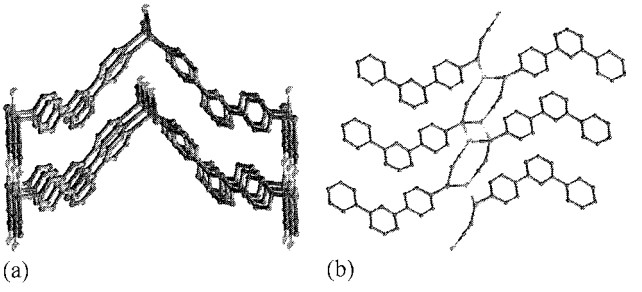

Fig. *3* Class II supramolecular isomers of $[Cu(SCN)(dpt)]_\infty$. in which the different $(CuSCN)_\infty$ motifs lead to the formation of three-dimensional (a) or one-dimensional (b) coordination polymers. (*View this art in* color *at www.dekker.com.*)

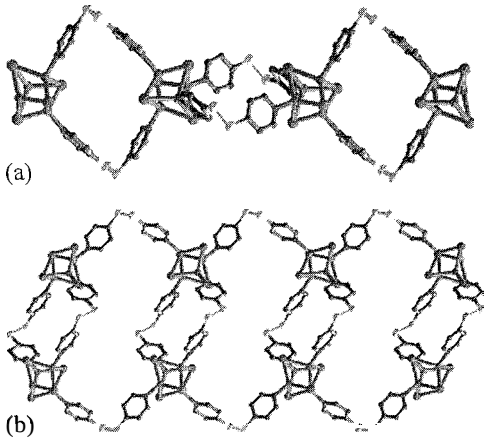

Fig. 4 (a,b) Two Class III supramolecular isomers of $[(CuI)_2(bpds)]_\infty$ [bpds = *bis*(4-pyridyl)disulfide] in which Cu_4I_4 cubane tetramers are linked via bridging bipyridyl ligands. (*View this art* in color *at www.dekker.com.*)

Use of $MeCN/CH_2Cl_2$ as the crystallization solvents results in a different isomer; $\{[(CuI)_2(bpds)] \cdot 0.5\ MeCN\}_\infty$. As in the first isomer discussed. Cu_4I_4 cubane tetramers are linked by two bpds ligands to form a square-shaped cavity. However. the tetrahedral junctions of these cubane units now allow these squares to interlink via two further bpds ligands. forming a tubular polymer (Fig. 4b). Despite interdigitation between adjacent tubular polymers, the packing arrangement allows the formation of two criss-crossed channels occupied by MeCN solvent molecules. Powder X-ray diffraction studies confirm that the formation of each isomer is exclusively dependent on solvent of crystallization. As both isomers of $[(CuI)_2(bpds)]_\infty$ are formed under similar reaction conditions, but with a change in the nitrile solvent. it is reasonable to conclude thatr there are oniy relatively minor, but significant. energy differences in the formation of the two polymers.

A wide family of network architectures can be formed when $M(NO_3)_2$ (M = Co, Ni, Cd) salts are reacted with bridging bipyridyl ligands.[6,16–23] Many of these compounds adopt a seven-coordinate geometry in which the metal center is coordinated by two chelating nitrate anions, leaving th ee sites for pyridyl ligation, arranged in a *mer* configuration in the equatorial plane of a pentagonal bipyramid. These compounds have a T-shaped asrangement of pyridyl sites and have been shown to adopt a range of coordination polymer architectures, including ladder,[16,23] bilayer,[17,18,20,21] three-dimensional architectures,[19] herringbone,[22,23] and brick-wall[23] motifs. Systems that exhibit architectural flexibility are particularly likely to exhibit supramolecular isomerism, and this is the case for the family of compounds, $[Co_2(NO_3)_4(4,4'\text{-bipy})_3]_\infty$. The supramolecular isomerism exhibited by this particular system was extensively studied, and it was shown that the architecture adopted by $[Co_2(NO_3)_4(4,4'\text{-bipy})_3]_\infty$ is highly dependent on the nature of guest species included in the host. Thus. $Co(NO_3)_2$ reacts with 4,4′-bipy in either MeOH/$CHCl_3$ or MeOH/MeCN to afford the complex $\{[Co_2(NO_3)_4(4,4'\text{-bipy})_3] \cdot solv\}$, (solv = MeCN or $CHCl_3$), which exhibits a ladder motif, Isomer A (Fig. 5a).[16] Despite the cavity between the rungs of the $[Co_2(NO_3)_4(4,4'\text{-bipy})_3]_\infty$ ladder being large enough to allow interpenetration of further ladders. the structure exhibits no such interpenetration but rather includes guest solvent molecules, $CHCl_3$ or MeCN in the two reported instances.

In contrast, reaction of $Co(NO_3)_2$ with 4,4′-bipy in the presence of CS_2[17] or H_2O[18] affords a molecular bilayer motif. Isomer **B**, in which each Co(II) center still acts as a T-shaped connecting junction. The guest molecule, CS_2 or H_2O, is clathrated within the framework and presumably acts as a template for the formation of the bilayer motif.

Reaction of $Co(NO_3)_2$ with 4,4′-bipy in the presence of pyridine and benzene templates leads to the formation of a further structural motif.[19] In this case, a three-dimensional lattice (Fig. 5c) is observed which again is a supramolecular Isomer C of the ladder structure. In this structure, the T-shaped connections are arranged such that pairs are oriented at 180° with respect to each other and then at 90° to the adjacent pair of connections. This affords a complicated three-dimensional lattice that is triply interpenetrated, leaving channels that are occupied by guest benzene solvent molecules.

These three distinct architectures of the $[Co_2(NO_3)_4(4,4'\text{-bipy})_3]_\infty$ family all contain guest solvent molecules,

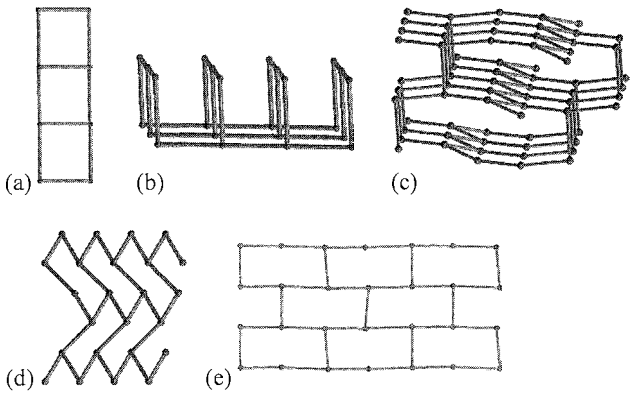

Fig. 5 Coordination frameworks constructed using a T-shaped connecting unit: (a) ladder: (b) bilayer: (c) three-dimensional framework; (d) herringbone; and (e) brick-wall motifs. (View *this* art *in* color *at* 1tww.dekker.com.)

MeCN, $CHCl_3$ (ladder),[16] CS_2, H_2O (bilayer),[17,18] benzene (three-dimensional framework)[19] and, thus, can be considered pseudopolymorphic supramolecular isomers. Of course, it is a debatable point as to whether the guest molecules are "noninteracting." At the least, the molecules will act as shape templates encouraging the formation of one supramolecular isomer over another or will act as kinetic templates. However, one method of assessing the extent of host–guest interaction is to investigate the ease of guest removal and the stability of the guest-free framework. In this respect, it is notable that the bilayer motif of $[M_2(NO_3)_4(4,4'\text{-bipy})_3]_\infty$ (M = Co, Ni, Zn) shows that not only is this structure robust to guest removal, but it also adsorbs N_2, CH_4, O_2,[18] CO_2, N_2O, MeOH,[20] and EtOH.[20,21] This indicates that host–guest interactions are not sufficiently important in the final product such that upon guest removal the host framework is structurally robust.

The reactions of $Co(NO_3)_2$ with the elongated analog of 4,4′-bipyridine, 1,2-*bis*(pyrid-4-yl)ethyne, have also been studied, and supramolecular isomers have been prepared.[22,23] Two isomers have been structurally characterized, the familiar ladder motif (Fig. 5a) and a herringbone structure (Fig. 5d), both using a $Co(NO_3)_2(py)_3$ as a T-shaped junction. The two isomers can be produced from the same reaction mixture (MeOH/MeCN),[22] but samples of pure ladder material can be isolated from an acetone–EtOH mixture.[23] The ladder structure is analogous to those observed previously. except that the ladders interpenetrate in a perpendicular fashion to afford a polycatenated three-dimensional structure. Each square-space between the rungs of the ladder is filled by two other square units from two further perpendicular ladders. In the case of the second, "herringbone" isomer triple parallel interpenetration gives rise to a polycatenated two-dimensional sheet.[22] Powder x-ray diffraction studies of the products from simple precipitation reactions of 1,2-*bis*(pyrid-4-yl)ethyne and $Co(NO_3)_2$ yield intriguing results.[23] If an acetone solution of $Co(NO_3)_2$ is added to a solution of the ligand in EtOH, then pure samples of the interpenetrating ladder compound are isolated, but if the addition process is reversed, then powder x-ray studies reveal that the product is ca. 20% ladder and 80% of a further structural motif, the brick-wall (Fig. 5e). The brick-wall structure is highly related to the herringbone motif but with a different orientation of the rectangular cavities within the structure. These results further reinforce the subtle differences between the different supramolecular isomers based on the $Co(NO_3)_2$ unit.

Reaction of $Co(NO_3)_2$ with 1,2-*bis*(pyrid-4-yl)ethane in a 1:3 ratio affords three different pseudopolymorphic supramolecular isomers of formula $\{[Co_2(NO_3)_4(1,2\text{-}bis(\text{pyrid-4-yl})\text{ethane})_3] \cdot x(\text{guest})\}_\infty$, depending upon the ternplating conditions used.[6] In all three cases the

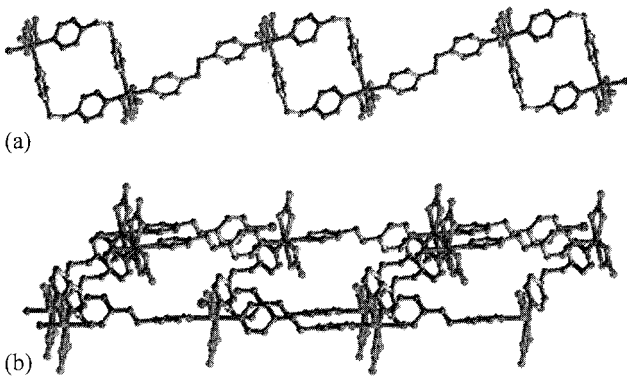

Fig. 6 Class III supramolecular isomers of $\{[Co_2(NO_3)_4(1,2\text{-bis(pyrid-4-yl)ethane})_3] \cdot x(\text{guest})\}_\infty$, (a) isomer exhibiting ligands with both *gauche* and *anti* ligand conformations to afford a one-dimensional polymer; (b) isomer again containing both *gauche* and *anti* ligand conformations. but in this case. forming a two-dimensional bilayer structure. *(View this art in color at www.dekker.com.)*

Co(II) cation is coordinated by two nitrate anions in a bidentate fashion to form a T-shaped $Co(NO_3)_2(py)_3$ junction, but the 1,2-*bis*(pyrid-4-yl)ethane ligand is flexible and can adopt either *gauche* or *anti* isomers. When crystallized from MeOH/MeCN, the complex illustrated in Fig. 6a is isolated, in which two ligands adopt a *gauche* arrangement and link two $Co(NO_3)_2$ units in a square-shaped unit which are then linked by ligands in the *anti* arrangement into a one-dimensional polymer. In complete contrast, if the crystallization process is performed in MeOH/MeCN but in the presence of a ferrocene-templating agent, then a molecular bilayer structure is formed. For every ligand in a *gauche* conformation, two ligands in an *anti* conformation are observed in the structure. The ligands in the *anti* configuration bridge T-shaped $Co(NO_3)_2$ junctions in a linear arrangement, and these chains are then linked through the *gauche* ligand to form the bilayer structure (Fig. 6b). By varying the solvent combination to MeOH/$CHCl_3$, a more familiar molecular ladder motif (Fig. 5a) is formed in which the ligands adopt *anti* conformations. As with the 4,4′-bipy analog of this complex, the spaces between the rungs of the ladder are filled with guest $CHCl_3$ solvent molecules that inhibit interpenetration of adjacent ladders. The supramolecular isomerism observed in these cases arises by variation of the conformation of the 1,2-*bis*(pyrid-4-yl)ethane ligand building block. Zaworotko described this type of supramolecular isomerism as ''conformational supramolecular isomerism.''[7] With the aim of simplifying the terminology in this area, we suggest that the example of supramolecular isomerism described in this family of compounds be classified as pseudopolymorphic supramolecular isomerism (i.e., Class III), as many instances

of supramolecular isomerism will also exhibit minor differences in the arrangements of the ligand or other building blocks within the overall network structure.

CONCLUSION

It is clear from the examples discussed that supramolecular isomerism can be encountered in a range of systems. Such isomerism is particularly important when there are only subtle energy differences between highly related structures. This is clearly the case when the metal coordination environment remains the same in the different isomers (Class I and III), and so the differences in structure arise purely through different orientations of metal nodes within the coordination polymer. For Class II, structural supramolecular isomerism. it is rare to observe such a subtle balance between different metal coordination spheres, and this is reflected in the small number of examples of this type of isomerism.

In conclusion. we seek in this article to clarify the terminology used to describe supramolecular isomerism observed in coordination polymer frameworks. The terminology used has wider implications and can readily be applied to hydrogen-bonded arrays and also to non-polymeric architectures.

ARTICLES OF FURTHER INTEREST

Chemical Topology. *p. 229*
Classification and Nomenclature of Supramolecular Compounds, *p.* 261
Concepts in Crystal Engineering, p. *319*
Crystal Engineering with Hydrogen Bonds, p. 357
Nomenclature in Crystal Engineering, p. *967*
Polymorphism, p. 1129
Supramolecular Isomerism, p. 1420

REFERENCES

1. Robson. R.; Abrahams. B.F.; Batten, S.R.; Gable. R.W.: Hoskins. B.F.: Liu. J.P. Crystal engineering of novel materials composed of infinite 2-dimensional and 3-dimensional frameworks. ACS Symp. Ser. 1992, 499. 256–273.
2. Blake. A.J.: Champness. N.R.; Hubberstey, P.; Li. W.S.: Withersby. M.A.; Schröder, M. Inorganic crystal engineering using self-assembly of tailored building-blocks, Coord. Chern. Rev. 1999.183. 117–138.
3. Swift, J.A.: Pivovar, A.M.: Reynolds, A.M.: Ward, M.D. Template-directed architectural isomerism of open molecular frameworks: Engineering of crystalline clathrates. J. Am. Chem. Soc. 1998.120 124). 5887–5894.
4. Blake. A.J.: Brooks, N.R.; Champnesr. N.R.: Crew. M.; Deveson, A.; Fenske, D.: Gregory. D.H.: Hanton. L.R.: Hubberstey. P.; Schroder. M. Topological isomerism in coordination polymers. Chem. Commun. 2001, (16), 1432–1433.
5. Wells, A.F. *Structural Inorganic Chemistry*, 5th Ed.; Clarendon Press: Oxford, 1984.
6. Hennigar. T.L.; MacQuarrie, D.C.: Losier, P.: Rogers. R.D.: Zaworotko. M.J. Supramolecular isoinerism in co-ordination polymers: Conformational freedom of ligands in $[Co(NO_3)_2(1,2\text{-bis(pyrid-4-yl)ethane})_{1.5}]_n$. Angew. Chern., Int. Ed. Engl. 1997, 36 (9). 972–973.
7. Moulton. B.; Zaworotko. M.J. From molecules to crystal engineering: Supramolecular isomerism and polymorphism in network solids. Chem. Rev. 2001. *101* (6). 1629–1658.
8. Carlucci, L.; Ciani. G.: Prosperio, D.M.: Sironi. A. Interpenetrating diamondoid frameworks of silver(I) cations linked by N,N′-bidentate molecular rods. J. Cheni. Soc., Chem. Commun. 1994. (24). 2755–2756.
9. Heintz. R.A.: Zhao. H.; Ouyang, X.: Grandinetti. G.: Cowen, J.: Dunbar, K.R. New insight into the nature of Cu(TCNQ): Solution routes to two distinct polymorphs and their relationship to crystalline films that display bistable switching behaviour. Inorg. Chem. 1999. 38 (1), 144–156.
10. Jensen, P.: Batten. S.R.: Moubaraki. B.: Murray. K.S. Synthesis. structural isomerism. and magnetism of co-ordination polymers $[M(dca)_2(pyz)]_n$, M = Mn, Fe. Co, Ni and Zn. dca = Dicyanamide ($N(CN)_2^-$), and pyz = Pyrazine. J. Solid State Chem. 2001. 159 (2). 352–361.
11. Manson, J.L.: Incarvito, C.D.: Rheingold, A.L.: Miller. J.S. Structure and magnetic properties of $Mn^{II}[N(CN)_2]_2$(pyrazine). An antiferromagnet with an interpenetrating 3-D network structure. J. Chem. Soc., Dalton Trans. 1998, (22), 3705–3706.
12. Jensen. P.; Batten. S.R.; Fallon. G.D.; Hockless. D.C.R.; Moubaraki, B.: Murray. K.S.: Robson. R. Synthesis. structural isomerism, and magnetism of extended framework cornpounds of type $[Cu(dca)_2(pyz)]_n$, where dca = Dicyanamide ($N(CN)_2^-$) and pyz = Pyrazine. J. Solid State Chem. 1999, 145 (2), 387–393.
13. Barnett, S.A.; Blake. A.J.; Champness, N.R.; Wilson, C. Structural isomerism in CuSCN Co-ordination polymers. Chem. Commun. 2002. (15). 1640–1641.
14. Carlucci, L.; Ciani. G.: Macchi, P.; Proserpio, D.M. An unprecedented triply interpenetrated chiral network of 'square-planar' metal centres from the self-assembly of copper(II) nitrate and 1,2-bis(4-pyridyl)ethyne. Chem. Commun. 1998. (17). 1837–1838.
15. Power, K.N.: Hennigar. T.L.: Zaworotko, M.J. X-ray crystal structure of $\{Cu[1,2\text{-Bis(4-pyridyl)ethane}]_2(NO_3)_2\}n$: The first example of a co-ordination polymer that exhibits the NbO 3-D network architecture. Chem. Commun. 1998. (5). 595–596.
16. Losier. P.: Zaworotko, M.J. A noninterpenetrated molecular ladder with hydrophobic cavities. Angew. Chem., Int. Ed. Engl. 1996.35 (23 24), 2779–2782.
17. Power. K.N.: Hennigar. T.L.; Zaworotko, M.J. Crystal

structure of the co-ordination polymer $[Co(bipy)_{1.5}(NO_3)_2] \cdot CS_2$ (bpy = 4.4'-bipyridine). a new motif for a network sustained by 'T-shape' building blocks. New J. Chem. 1998, *22* (2). 177–181.

18. Kondo. M.: Uoshitomi, T.; Seki. K.: Matsuzaka, H.: Kitagawa, S. Three-dimensional framework with channeling cavities for small molecules: $\{[M_2(4,4'\text{-bpy})_3(NO_3)_4] \cdot xH_2O\}_n$ (M = Co, Ni. Zn). Angew. Chem.. Int. Ed. Engl. 199'7.36 (16), 1725–1727.
19. Gudbjartson. H.: Biradha. K.: Poirier, K.M.; Zaworotko. M.J. Novel nanoporous co-ordination polymer sustained by self-assembly of T-shaped moieties. J. Am. Chem. Soc. 1999, *121* (11), 2599–2600.
20. Fletcher, A.J.: Cussen, E.J.; Prior, T.J.; Rosseinsky. M.J.: Kepert, C.J.: Thomas, K.M. Adsorption dynamics of gases and vapors on the nanoporous metal organic framework material $Ni_2(4,4'\text{bipyridine})_3(NO_3)_4$: Guest modification of host sorption behaviour. J. Am. Chem. Soc. 2001, 123 (41). 10001–10011.
21. Kepert. C.J.; Rosseinsky. M.J. Zeolite-like crystal structure of an empty microporous molecular framework. Chem. Commun. 1999. (4), 375–376.
22. Dong. Y.B.; Layland, R.C.: Pschirer, N.G.: Smith. M.D.; Bunz. U.H.F.: zur Loye, H.C. New crystalline frameworks formed from 1,2-bis(4-pyridyl)ethyne and $Co(NO_3)_2$: Interpenetrating molecular ladders and an unexpected molecular parquet pattern from T-shaped building blocks. Chem. Mater. 1999. 11 (6). 1413–1415.
23. Carlucci, L.: Ciani, G.: Proserpio, D.M. Self-assembly of novel co-ordination polymers containing polycatenated molecular ladders and intertwined two-dimensional tilings. J. Chem. Soc.. Dalton Trans. 1999. (11). 1799–1804.

Supramolecular Libraries

Sijbren Otto
Jeremy K. M. Sanders
University of Cambridge, Cambridge, United Kingdom

INTRODUCTION

Over the two last decades, the pharmaceutical industry has gone to great lengths in the development of combinatorial methods for drug discovery. Although combinatorial chemistry has perhaps not been able to live up to the overstretched expectations, it claimed its rightful place as another tool among the diverse approaches toward drug development. Combinatorial methods are now starting to penetrate other fields of science, where they can be efficient tools for exploring structural space just beyond the boundaries of what we know; understand, and can predict. in this article, we summarize the progress made using combinatorial libraries of noncovalent assemblies. These libraries were mainly developed for the discovery of supramolecular receptors for small guest molecules, although some work was also carried out on the complementary approach, where libraries of noncovalent assemblies were screened for affinity for biological targets.

COMBINATORIAL LIBRARIES OF NONCOVALENT ASSEMBLIES

Supramolecular assemblies held together by noncovalent forces have some unique characteristics. Even the strongest of the noncovalent forces (metal–ligand coordination and hydrogen bonding) tend to be weak enough to allow, under relatively mild conditions, for the exchange of the building blocks that make up the assemblies. This reversibilitp ensures that, upon mixing different supramolecular building blocks together. the composition of the resulting library is typically controlled by thermodynamics rather than by kinetics. Hence, most libraries in which building blocks are held together by noncovalent interactions are dynamic combinatorial libraries (DCLs).[1–3] Because of the possibility of interchange of building blocks. DCLs are able to respond to external influences. For instance, other noncovalent interactions can be used to shift the equilibria (and. hence, the library distribution). Thus, after introduction of a guest into a DCL of hosts. binding of the guest to the best available host will lead to stabilization of this host, which induces a shift in the equilibrium. The best host will be amplified at the expense of the inferior receptors (Fig. 1). Screening the libraries for the best receptors is then simply a matter of comparing product distributions before and after addition of the guest.

RECEPTORS FROM LIBRARIES OF NONCOVALENT ASSEMBLIES

In early work in 1995, just before the concept of dynamic combinatorial chemistry was first explicitly recognized,[4] Hamilton et al. screened a combinatorial library of ruthenium *bis*(terpyridyl) complexes.[5] From five differently substituted terpyridine ligands, a series of 15 different coordination complexes was synthesized and isolated. The library was screened for affinity for dicarboxylate or diammonium guests using microcalorimetry or picrate extraction. and several receptors were identified (Fig. 2).

More recently. Morrow and coworkers developed a dynamic combinatorial approach to identify complexes that extract metal ions [Zn(II) and Cd(II)] from an aqueous phase into organic solution.[6] Diversity was achieved on a covalent level and on a noncovalent level: metal ions were extracted into the organic phase by coordination to two Schiff base ligands, each of which was assembled from an aldehyde or ketone and an amine through reversible covalent bond formation. In a more recent study, the authors used a set of 25 acylhydrazones as ligands.[7] Although. in theory. diversity in these systems can be achieved through hydrazone exchange as well as metal–ligand exchange, the former process was found to be too slow for practical use. Under thermodynamic control, the product distribution of the libraries will be biased toward the most stable complexes. This might be beneficial, as extraction efficiency is likely to be correlated with complex stability. However, other factors not directly correlated to stability, such as the solubility of the complex in the organic phase, will influence the efficiency of extraction.

Huc, Lehn. and coworkers used the coordination of bipyridine ligands to Cu(I) or Pd(II) metal centers to form four-coordinate tetrahedral or square-planar complexes, respectively.[8] Mixing two bipyridine ligands. one with and one without hydrogen-bonding capabilities, resulted in the formation of a small dynamic library of three

DOI: 10.1081/E-ESMC 120013880

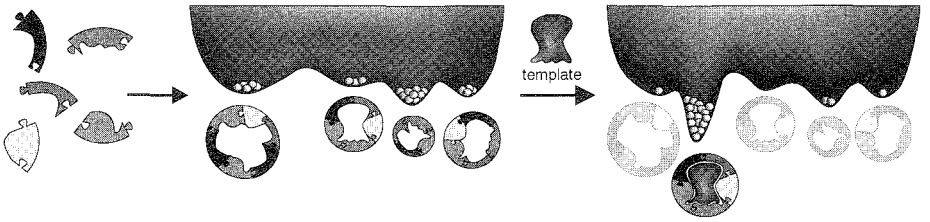

Fig. 1 Free-energy landscape of a small dynamic combinatorial library of potential receptors. Addition of a guest that is selectively bound by one of the receptors leads to the formation of an additional free-energy well and shifts the equilibrium in the direction of the fittest host. (View *this art* in color at www.dekker.com.)

possible ternary complexes. Introduction of guest molecules presenting complementary hydrogen-bond recognition motifs resulted in modest shifts in the equilibrium in favor of complexes that maximize host–guest hydrogen bonding.

Work on combinatorial supramolecular libraries nearly exclusively uses metal–ligand interactions to hold the assemblies together. Crego Calama, Timmcrman, Reinhoudt, and coworkers, however, used well-known complementary hydrogen-bond motifs to build up supramolccular structures of impressive complexity. Three calix[4]arene units (1a) each functionalized with two melamine groups and six complementary barbiturate building blocks (2) self-assemble cooperatively into a $\mathbf{1}_3\mathbf{2}_6$ superstructure that is held together by 36 hydrogen bonds (Fig. 3). By starting from two different calixarene building blocks (not shown) the researchers were able to build a small DCL.[9] NMR studies indicated rapid exchange of building blocks at room temperature. In a separate study, the authors prepared a calixarene functionalizcd with two melamine and two Zn-porphyrin units (**1b**).[10] The Zn-porphyrins have an affinity for nitrogen ligands, giving the resulting structures potential receptor properties. Mixing the barbiturate 2 with the parent calixarene 1a and the porphyrin-functionalized calixarene **1b** generated a small DCL of four superstructures with different numbers of Zn-porphyrin recognition sites. Addition of a tripyridine guest (3) resulted in a shift of the equilibrium in favor of the host–guest complex $(\mathbf{1b})_3\mathbf{2}_6\mathbf{3}_2$, forcing the remaining 1a to form $(\mathbf{1a})_3\mathbf{2}_6$. After addition of the guest, no mixed **1a1b** structures could be detected.

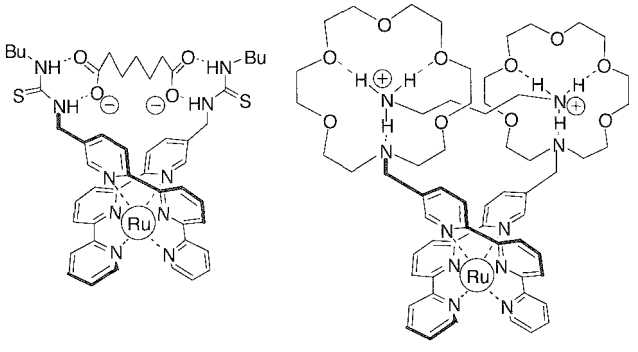

Fig. 2 Some of the first receptors identified using a combinatorial approach. (Adapted from Ref. [5].)

In recent work in our laboratories, we used the efficient coordination of phosphine ligands to Rh(III) porphyrins to construct DCLs of mixed-metal arrays of Zn(II)- and Rh(III)-porphyrins (Fig. 4).[11] The porphyrin building blocks 4 and **5** are bifunctionalized, thus allowing access to a theoretically unlimited range of linear and macrocyclic oligomeric structures. Using the interaction of Zn-porphyrins with the nitrogen ligand 4,4′-bipyridine led to the selection and quantitative amplification of host–guest complex 6.

The last two examples demonstrate convincingly how host–guest interactions can quantitatively transform a complex mixture into the optimal host, illustrating the power of dynamic combinatorial chemistry for selection and amplification of the fittest receptors.

DYNAMIC LIBRARIES OF NONCOVALENT CAGE COMPOUNDS

Cage-like compounds are among the more complex supramolecular structures and are formed through the connection of tripodal or even more complex building blocks in a specific manner. It is perhaps one of the areas in supramolecular chemistry that has benefited most from noncovalent thermodynamically controlled synthetic methods.

Rebck and coworkers extended their studies on the hydrogen-bond-bascd self-assembly of tetrameric capsules around guest molecules using a combinatorial approach.[12] Starting from two different monomers, a small dynamic library of guest-filled capsules was produced. The distribution of capsule compositions was analyzed by MS and found to depend on the nature of the guest, with methylquinuclidinium cation as the most

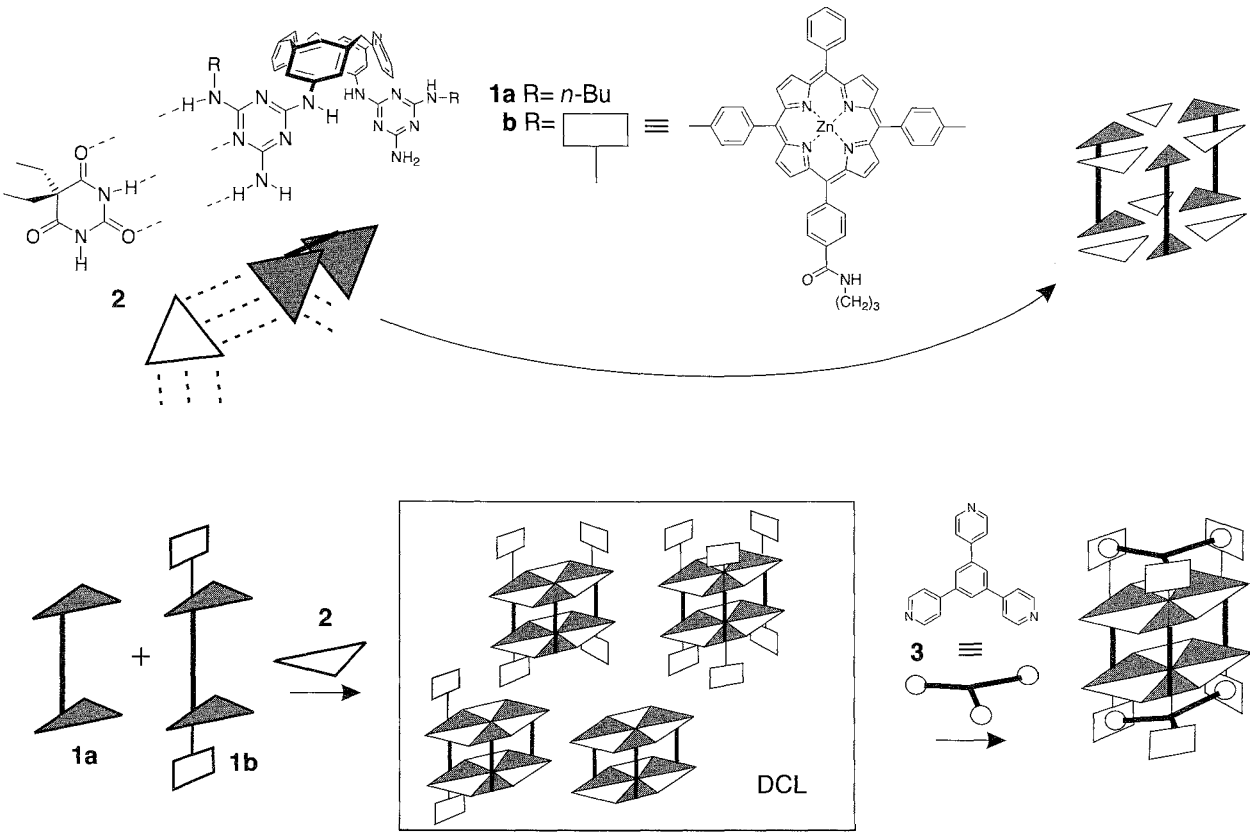

Fig. 3 Self-assembly of three calix[4]arenes (1a) functionalired with two melamine groups and six complementary barbiturate building blocks (2) into a $(\mathbf{1a})_3\mathbf{2}_6$ superstructure. Mixing in of another calixarene building block functionalized with Zn-porphyrin units (1b) generates a small DCL of four superstructures. Addition of a tripyridine guest (3) shifts the equilibrium in favor of the host–guest coinplex $(\mathbf{1b})_3\mathbf{2}_6{\cdot}\mathbf{3}_2$. (Adapted from Refs. [9] and [10].)

selective guest amplifying the formation of the largest capsule. Similar, but less clear-cut, changes in product distribution were observed in a more diverse library made from five (or seven, when counting enantiomers separately) building blocks.

Raymond and coworkers published a thorough study of a series of dynamic libraries made from dipodal biscatecholate ligands linked together by Ga(III) metal centers.[11] The ligands are predisposed to assemble into tetrahedral Ga_4-ligand$_6$ complexes. The kinetics of equilibration and equilibrium distribution of a 12-component dynamic library made from two different ligands were analyzed in detail. Analysis by ESI-FTICR-MS of larger libraries made by mixing three different ligands confirmed the

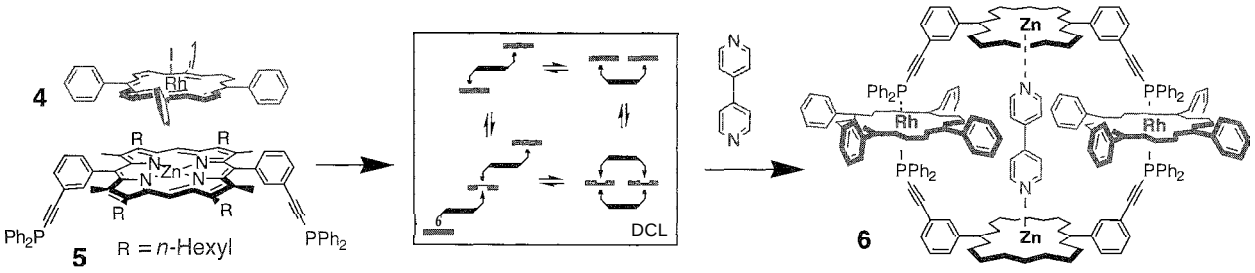

Fig. 4 A dynamic combinatorial library of cyclic and linear arrays of mixed metalloporphyrins which. upon addition of a 4.4′-dipyridine guest. transforms quantitatively into a macrocyclic porphyrin tetramer. (Adapted from Ref. [1 I].) (*View* this *art in color at www.dekker.com.*)

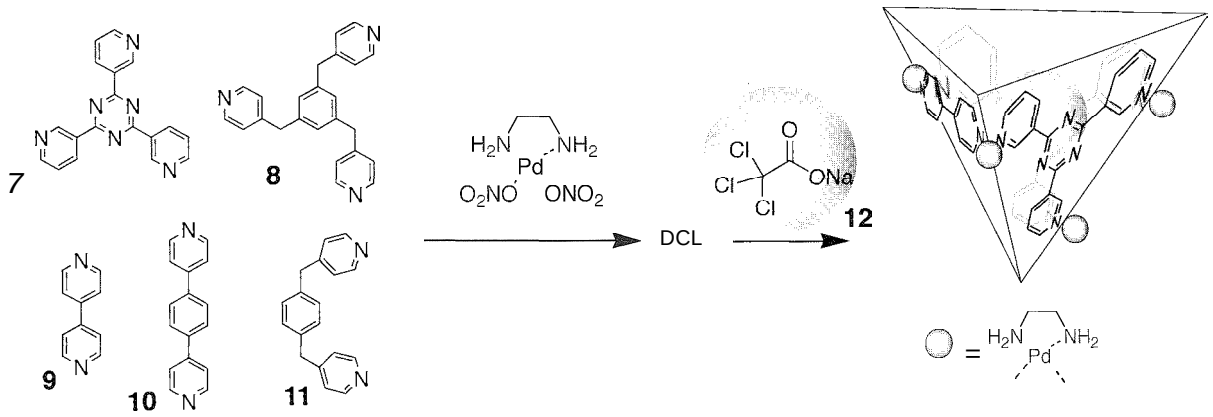

Fig. 5 Mixing di- and tripyridyl ligands (7–11) with Pd(en) produces a diverse dynamic combinatorial library of cyclic and cage coordination compounds. Exposure of this library to sodium trichloroacetate (12) results in the amplification of a new receptor. (Adapted from Ref. [17].)

presence of most of the statistically most probable products. Although the capsules are known to bind Et_4N^+ ions indiscriminately, screening of these libraries for more specific host–guest systems has yet to be performed.

Albrecht and coworkers used Ga(III) and Zn(II) centers to link ligands containing two bidentate hydroxyquinoline units.[14] In the absence of any guests, dynamic libraries of metal–ligand complexes were formed that were not further characterized. However, upon addition of Na^+, K^+, Rb^+, or NH_4^+ ions to the Ga(III)–ligand solutions. well-defined structures were formed containing three ligands held together by two Ca centers surrounding a central cation guest. Similar structures were observed upon addition of Li^+, Na^+, or $K^+$to the Zn(II)–ligand solutions. Receptor amplification is driven by the interaction of the six oxygen atoms of the three ligands with the central cation.

In elegant work, Fujita and coworkers extensively explored Pd-pyridyl interactions to build capsule-like structures. In one of the first dynamic combinatorial approaches toward encapsulation. an asymmetric tripodal pyridine ligand was used to construct an equilibrium mixture of two isomeric complexes containing two ligands held together by three bridging Pd centers.[15] Exposure of this equilibrium mixture to globular guest molecules such as $CBrCl_3$ and CBr_4 induced a shift toward one of the isomers, whereas flatter guests (xylene and 1.3.5-benzenetricarboxylic acid) amplified the other capsule isomer. This selectivity was rationalized on the basis of differences in the shapes of the two isomeric capsules. In a separate study. another slightly larger tripodal ligand was added to the prototypical library, increasing the number of two-ligand capsules to four.[16] Significant shifts in the capsules distributions were observed upon adding suitable guests. For instance. $CBrCl_3$ was now found to selectively amplify the formation of the heteroligand capsule. Recently. Fujita and coworkers increased capsule diversity further by mixing two tripodal pyridine ligands (**7** and 8) with three dipodal ones (**9**–**11**) (Fig. 5*)*, once again using Pd centers to link the ligands together.[17] The authors were able to identify a new receptor for sodium trichloroacetate (12) from this full-grown DCL. Analysis of a difference NMR spectrum obtained by subtracting the spectrum of the library in the absence of guest from that in the presence of guest led to the identification of the selected building blocks. A second round of similar NMR experiments was necessary to obtain the building block stoichiometry. The newly discovered receptor was found to consist of two units of **7** bridged by one unit of **9** (Fig. 5).

NONCOVALENT LIBRARIES AND BIOLOGICAL SYSTEMS

The discussion of noncovalent libraries has so far been limited to cases where a guest selects its optimal receptor from a library of hosts. When targeting biological systems, the reverse approach of screening a library of guests against a macromolecular host becomes relevant.[18] Several cases were reported where a macromolecule amplifies the formation of its best binder.

Sasaki and coworkers used coordination of *N*-acetyl galactose (GalNAc) functionalized bipyridine ligands to a central Fe(II) ion to generate a small dynamic library of four $(ligand)_3Fe$ complexes differing in the spatial arrangement of the three GalNAc units[19] (Fig. 6). The

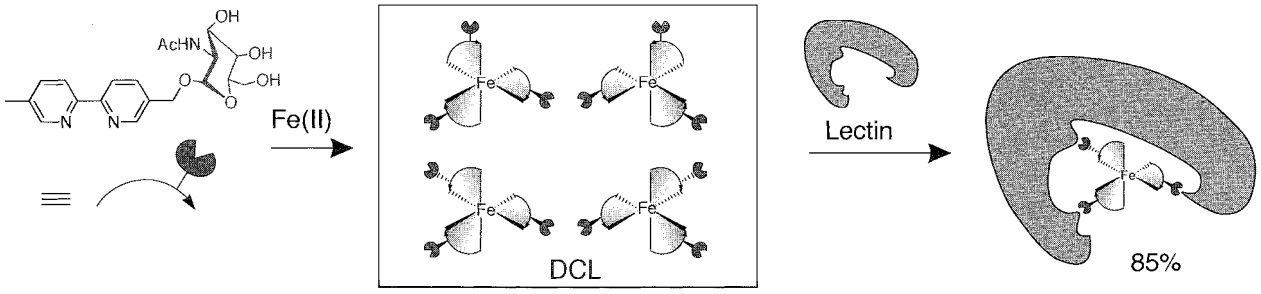

Fig. 6 Mixing Fe(II) with a bipyridine ligand functionalized with a N-acetylgalactose residue produces a small dynamic library of coordination compounds. Exposure of the library to a lectin leads to selection and amplification of the strongest binding complex. (Adapted from Ref. [19].) (*View this urt* in color *at www.dekker.com.*)

authors screened this library against two different lectins (proteins with carbohydrate-binding sites; the two lectins used were known to have affinity for GalNAc). They found that exposure of the library to one of the lectins led to the amplification of the Fe complex with the highest affinity for the protein, whereas the second lectin selected and amplified a different complex.

Miller and coworkers targeted DNA using libraries of metal–ligand complexes.[21,22] A DCL was made through coordination of different salicylaldimine ligands to a central Zn(II). Exchange between library building blocks can take place through metal–ligand exchange as well as through breaking and forming the covalent C=N bond in the ligands. The library was screened against double-stranded DNA immobilized on a cellulose resin. The optimal DNA binders were identified by monitoring depletion of the selected building blocks from solution as a result of binding to the immobilized DNA. In more recent work,[23] the same group also targeted RNA using libraries made from square planar Cu(II) complexes containing one or two salicylamide ligands. A dynamic library was prepared using six such ligands carrying different amino-acid sidegroups. The library was exposed to an RNA hairpin sequence contained within a dialysis tube. The selected ligands were identified by monitoring their depletion from the library solutions. As the total concentration of library members was much higher than the RNA concentration, several rounds of exposure to RNA were required to observe significant effects. The authors found that the Cu(II) complex of the salicylamide derived from histidine bound the RNA hairpin with nanomolar affinity and with remarkable 300-fold selectivity over the homologous DNA sequence. Unfortunately, the experimental setup does not allow for quantification of the level of amplification of the selected complex.

Dynamic libraries of noncovalenl assemblies can also be used to address issues related to protein folding. In this case, no additional guest or host is added to the system, but molecular recognition occurs internally, leading to the amplification of the most stable folded arrangement. In one of the first studies in this area, McLendon and coworkers grafted short α-helical peptides onto bipyridine ligands.[24] Three such ligands differing in hydrophobicity were allowed to compete for the binding sites on an octahedral Fe(II) center, producing a small dynamic library of three-helix bundles. The authors found that the most hydrophobic helix was preferentially incorporated in the bundles, leaving the remaining two less hydrophobic helices behind in solution. Denaturation studies on the analogous but more robust Ru(II) complexes, that were synthesised independently, confirmed that the amplified three-helix bundle is the most stable. These results demonstrate that dynamic combinatorial chemistry is a useful tool to identify the global minima in free-energy landscapes.

FIXATION OF NONCOVALENT STRUCTURES

The use of noncovalent interactions for the assembly of libraries of supramolecular assemblies has one serious disadvantage: the resulting structures are inherently labile, because they are held together by relatively weak bonds. This will limit their practical utility as receptors or selective binders to macromolecules. Hence. there is a need for methods of fixation of the noncovalent structures after selection and amplification have taken place. One approach is to equip the building blocks with functional groups that can be used to covalently link them together after selection has taken place. This strategy was used successfully by Reinhoudt and coworkers to stabilize their hydrogen-bond-based assemblies.[25] The calixarene building blocks (1 in Fig. 3) were equipped with terminal alkenes that can undergo ring-closing metathesis to form stable assemblies that are held together by alkene bonds.

Another approach was reported by the groups of Eliseev[26] and Constable[27] who made elegant use of the difference in kinetic stability between Co(II) and Co(III) complexes. The former are kinetically labile and can be used to generate dynamic libraries of different metal–ligand complexes. However, upon oxidation to Co(III), ligand exchange becomes very slow, and the resulting complexes are kinetically inert. An admirable feature of this system is that the change in oxidation state does not affect the coordination geometry around the Co center.

CONCLUSION

The key concept of dynamic combinatorial chemistry—molecular recognition-induced amplification of the fittest—has laid dormant in the literature for decades. For instance, there are many examples where a complex of interest crystallized from a mixture of "hopeless" and unintentional diversity. Nevertheless. researchers have. in the past, largely steered away from making use of complex mixtures and. instead, focused on more "well-behaved" systems that were easier to study. It was not until the concepts of dynamic combinatorial chemistry were first articulated that interests shifted, and efforts are now made to actively generate diverse and complex mixtures and screen them for components that are good at recognition. As illustrated by some of the examples in this review, the first successes have appeared, illustrating that handing control back to the (right) molecules can be a fruitful approach.

ACKNOWLEDGMENTS

We are grateful to the Royal Society (SO) and EPSRC (JKMS) for financial support.

ARTICLES OF FURTHER INTEREST

Anioiz-Directed Assembly, p. 51
Nanocasting Strategies and Porous Materials. p. 950
Preorganization and Complementarity, p. 1158
Racks, Ladders, and Grids, p. *1186*
Self-Assembling Capsules, p. *1231*
Self-Assembly: Definition and Kinetic and Thermodynanzic Considerations, p. *1248*
Soft and Smart Materials, p. 1302
The Template Effect, p. *1493*

REFERENCES

1. Otto, S.: Furlan, R.L.E.: Sanders, J.K.M. Recent developments in dynamic combinatorial chemistry. Curr. Opin. Chem. Biol. 2002. *6.* 321–327.
2. Lehn, J.-M.: Eliseev, A.V. Dynamic combinatorial chemistry. Science 2001. *291*, 2331–2332.
3. Karan, C.: Miller. B.L. Dynamic diversity in drug discovery: Putting small-molecule evolution to work. Drug Discov. Today 2000. *5.* 67–75.
4. Brady. P.A.; Bonar-Law. R.P.; Rowan. S.J.; Suckling, C.J.: Sanders, J.K.M. 'Living' macrolactonisation: Thermodynamically-controlled cyclisation and interconversion of oligocholates. Chem. Commun. 1996. 319–320.
5. Goodman. M.S.: Jubian. V.; Linton, B.: Hamilton. A.D. A combinatorial approach to artificial receptor design. J. Am. Chem. Soc. 1995, 117. 11610–11611.
6. Epstein. D.M.: Choudhary. S.: Churchill, M.R.: Keil, K.M.; Eliseev, A.V.: Morrow. J.R. Chloroforn-soluble Schiff-base Zn(II) or Cd(II) complexes from a dynamic combinatorial library. Inorg. Chem. 2001. 40. 1591–1596.
7. Choudhary, S.: Morrow. J.R. Dynamic acylhydrazone metal ion complex libraries: A mixed-ligand approach to increased selectivity in extraction. Angew. Chem., Int. Ed. 2002. 41. 4096–4098.
8. Huc. I.; Krische. M.J.; Funeriu. D.P.: Lehn. J.–M. Dynamic combinatorial chemistry: Substrate H-bonding directed assembly of receptors based on bipyridine–metal complexes. Eur. J. Inorg. Chem. 1999. 1415–1420.
9. Crego Calama, M.; Hulst. R.; Fokkens, R.; Nibbering, N.M.M.: Timmerman, P.: Reinhoudt. D.N. Libraries of non-covalent hydrogen-bonded assemblies, cornbinatorial synthesis of supramolecular systems. Chem. Commun. 1998. 1021–1022.
10. Crego Calama. M.; Timmerman. P.; Reinhoudt, D.N. Guest-templated selection and amplification of a receptor by noncovalent combinatorial synthesis. Angew. Chem.. Int. Ed. 2000. 39. 755–758.
11. Stultz. E.; Ng. Y.-F.; Scott, S.M.: Sanders. J.K.M. Amplification of a cyclic mixed-metalloporphyrin tetranier from a dynamic combinatorial library through orthogonal metal coordination. Chem. Commun. 2002. 524–525.
12. Hof. F.: Nuckolls. C.: Rebek, J., Jr. Diversity and selection in self-assembled tetrameric capsules. J. Am. Chem. Soc. 2000. 122. 4251–4252.
13. Ziegler. M.: Miranda. J.J.: Andersen, U.N.; Johnson, D.W.: Leary. J.A.: Raymond. K.N. Combinatorial libraries of metal-ligand assemblies with an encapsulated guest molecule. Angew. Chem.. Int. Ed. 2001. 40. 733–736.
14. Albrecht, M.; Blau, O.; Frohlich. R. An expansible metallacryptand as a component of a supramolecular cornbinatorial library formed from di(8-hydroxyquinoline) ligands and gallium(III) or Zn(II) ions. Chem. Eur. J. 1999, 5. 48–56.
15. Hiraoka. S.: Fujita. M. Guest-selected formation of Pd(II)-linked cages from a prototypical dynamic library. J. Am. Chem. Soc. 1999. *121*, 10239–10240.
16. Hiraoka. S.; Kubota. Y.; Fujita, M. Self- and heterorecognition in the guest-controlled assembly of Pd(II)-

linked cages from different ligands. Chem. Commun. 2000, 1509–1510.
17. Kubota. Y.: Sakamoto. S.: Yamaguchi. K.; Fujita, M. Guest-induced organization of an optimal receptor from a dynamic receptor library: Spectroscopic screening. Proc. Natl. Acad. Sci. U. S. A. 2002. 99. 4854–4856.
18. Ramstrom, O.: Bunyapaiboonsri. T.; Lohmann. S.: Lehn. J.–M. Chemical biology of dynamic combinatorial libraries. Biophys. Biochim. Acta 2010%.*1572*. 178–181.
19. Sakai, S.; Shigemasa, Y.: Sasaki, T. A self-adjusting carbohydrate ligand for GalNAc specific lectins. Tetrahedron Lett. 1997. *38*. 8145–8148.
20. Sakai, S.; Shigemasa. Y.: Sasaki, T. Iron(II)-assisted assembly of trivalent GalNAc clusters and their interactions with GalNAc-specific lectins. Bull. Chern. Soc. Jpn. 1999, 72, 1313–1319.
21. Klekota. B.: Hammond. M.H.; Miller. B.L. Generation of novel DNA-binding compounds by selection and amplification from self-assembled combinatorial libraries. Tetrahedron Lett. 1997. *38*. 8639–8642.
22. Klekota. B.; Miller. B.L. Selection of DNA-binding compounds via multistage molecular evolution. Tetrahedron 1999. *55*. 11687–11697.
23. Karan, B.; Miller, B.L. RNA-selective coordination complexes identified via dynamic combinatorial chemistry. J. Am. Chem. Soc. 2001. *123*. 7455–7456.
24. Case, M.A.: McLendon, G.L. A virtual library approach to investigate protein folding and internal packing. J. Am. Chem. Soc. 2000. *122*. 8089–8090.
25. Cardullo. F.; Crego Calama, M.; Snellink-Ruel, B.H.M.; Weidmann, J.–L.: Bielejewska, A.; Fokkens. R.: Nibbering. N.M.M.; Timmerman. P.: Reinhoudt, D.N. Covalent capture of dynamic hydrogen-bonded assemblies. Chem. Commun. 21000. 367–368.
26. Goral, V.; Nelen. M.I.: Eliseev. A.V.: Lehn. J.–M. Double-level "orthogonal" dynamic combinatorial libraries on transition metal template. Proc. Natl. Acad. Sci. U. S. A. 2001, *98*. 1347–1352.
27. Constable. E.C.; Housecroft. C.E.; Kulke, T.: Lazzarini. C.; Schofield, E.R.: Zimmermann, Y. Redistribution of terpy ligands — Approaches to new dynamic combinatorial libraries. J. Chem. Soc.. Dalton Trans. 2001. 2864–2871.

Supramolecular Photochemistry

Sandra Monti
Francesco Barigelletti
Istituto per la Sintesi Organica e la Fotoreattività CNR-ISOF, Bologna, Italy

INTRODUCTION

Following a classical view, supermolecules assemble because of recognition properties that are expressions of molecularly stored information in the interacting partners.[1,2] Noncovalent, weak interactions (e.g., hydrogen-bonding, van der Waals. and electron donor–acceptor) are generally recognized to assist the structural organization of a supermolecule. Metal-coordination may represent a type of stronger interaction, frequently responsible for the building up of multicomponent arrays that can still be regarded as supermolecules.[3] According to a largely shared understanding, in an assembly of weakly interacting molecular components, the local properties are preserved, and the overall behavior cannot be reduced to the simple sum of the intrinsic properties of each component. In other words, a supermolecule shows a richer spectrum of properties with respect to the components; this happens because the additional properties basically rest on the intercomponent interactions. This outcome has nothing to do with holistic effects; instead it is traceable to molecularly stored information at the component level that went unexpressed until formation of the multicomponent assembly.[4]

ARE THERE SEVERAL CLASSES OF SUPERMOLECULES?

Discrete local and overall properties may also be identified in multicomponent systems. where electronically isolated molecular moieties, recognized as the active components, are connected by covalent bonds.[1,2] In this sense, this type of molecule can be regarded as a second class of supramolecular systems. Mere. the bridges are bound to play a structural role while providing only a small degree of electronic communication between the active components. When such electronic mediation is sufficiently weak, the bridged multicomponent system becomes similar to a self-assembled supermolecule. The extension of the concept of supramolecular system to include covalently connected assemblies proved to offer the remarkable advantage that a spatial assangement of the various components can be designed and subsequently made through suitable synthetic procedures. In this way, it is frequently possible to deal with components at fixed geometry, a key requisite in view of successful studies of the intercomponent processes originated after placing light energy at one of the components.

Molecular assemblies made of interlocked components like catenanes, knots, and rotaxanes[6–8] crucially rely on weak forces and covalent bonds and can be considered a further step forward along a higher degree of complexity of the organized matter (i.e., a hierarchically superior step). With such systems, provided some of the interlocked components can store energy (supplied by chemical, electrochemical, or photochemical methods), it is possible to spark off cycles of intercomponent displacements (see below).

Supramolecular photochemistry is the science of the interaction between light and supermolecules. It has to do with the consequences on the structural and electronic organization of the supramolecular system of the extra energy placed by light within it[9] and with the signaling properties of light.[10] Below, we introduce a distinction between photoactive and innocent units of a supermolecule. Then, we briefly describe a few selected cases from the literature. These, in our opinion, illustrate the type of approach followed in supramolecular photochemistry and. at the same time, show how fertile the supramolecular approach is in combination with the use of light. The examples are from solution chemistry; for the experimental details (e.g., type of solvent, concentrations employed, and so on), the reader should consult the original work. Of course, behind and next to the few examples we deal with in the following. there currently stand broad, diversified, and extremely important areas of study that we have not mentioned.

PHOTOACTIVE AND INNOCENT COMPONENTS

The understanding of the light effect relies on the clear-cut attribution of individual component-based properties and on properties regulated by the intercomponent interactions taking place within the assembly. Having in mind an extended view of supramolecular systems. we

Encyclopedia of Supramolecular Chemistry
DOI: 10.1081/E-ESMC 120012792

recall notions that are of help to understand their behavior under illumination. The primary event that triggers any subsequent process is obviously light absorption. This may occur selectively, i.e., depending on the frequency of the radiation, some of the components may be excited and others may not. Thus, to a first approximation, the light-absorbing subunits may be regarded as photoactive; for the others, an innocent behavior seems foreseeable (the bridging units, when present, are always expected to exhibit an innocent behavior, otherwise one is not dealing with a supermolecule but with a big molecule).[9]

This is, however, an oversimplified approach, at least from four different viewpoints that we illustrate with reference to Fig. 1 (here. cases for two-component systems are examined; extension to a higher number of components is given for granted). First, a molecular subunit undergoing no direct light absorption and apparently regarded as innocent, may play some role from an electronic viewpoint (for instance, a perturbation effect over the electronic properties of other subunits) (Fig. 1a). Second. use of radiation of sufficiently high frequency can lead to population of excited levels spatially centered on all subunits (i.e., in this case, all subunits are photoactive against absorption). Cascade steps, both of intra- or cross-component nature, can then take place and finally lead to population of the lowest-lying excited level. The cascade paths take place with various degrees of efficiency as governed by the electronic properties of the involved subunits, including those presumed to be innocent (Fig. 1b). Third (a clear-cut case), because of intercomponent interactions, one may observe the appearance of electronically excited levels not present in the separate components; of course, this corresponds to the manifestation of an additional property according to the basic supramolecular approach. For instance, donor–acceptor interactions frequently result in low-lying excited levels of intercomponent nature, which may be involved in light absorption and light emission events (Fig. 1c). Four, and most important, a light-absorbing subunit temporarily stores an excess of energy. Provided some energetic requirements are met, this may result in a transfer of energy (Fig. 1d) or electron (Fig. 1e. f) to and from, respectively, the other unit, which being not photoactive with regard to light absorption turns out to be not innocent.

In conclusion, the definition of a subunit as innocent with respect to the interaction with light should be employed after careful inspection of the spectroscopic properties of the supermolecule and of the separated components. and after monitoring the occurrence of light-induced processes. As a practical short-cut, use of light at a selected frequency (for instance, a low-frequency radiation to selectively excite the lowest-available electronic levels of a supermolecule, both of localized or

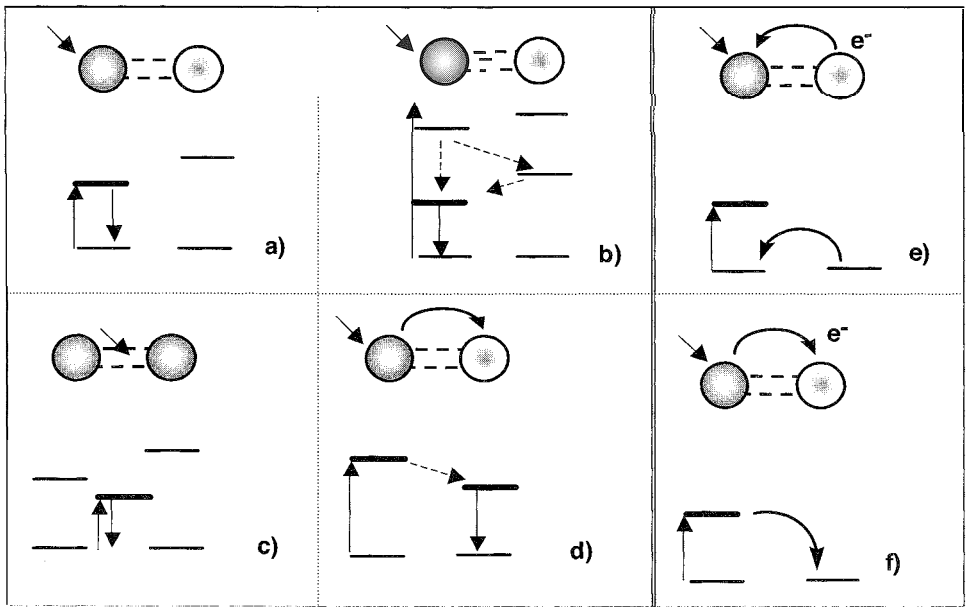

Fig. 1 Photoactive (dark sphere) and innocent (empty sphere) units and possible intercomponent effect? in self-assembled or covalently-linked two-component systems undergoing illumination: for the cases in which (a) one unit absorbs and emits light: (b) both units process the absorbed light; (c) photoactivity is of intercomponent origin: and (d) the unit that absorbs light transfers excitation energy to the other unit. which becomes emissive: and an orbital description for the case in which (e) the photoactive unit undergoes reduction: and (f) the photoactive unit undergoes oxidation.

intercomponent origin) and observation of luminescence properties (a localized emission is identified upon comparison with the luminescence properties of a suitable reference molecular unit) may lead to the understanding of which subunits precisely display a photoactive behavior and which can be regarded as innocent.

SYSTEMS POWERED BY LIGHT: LOOKING FOR THE STOWAGE OF CHEMICAL ENERGY

Extension of the dyad schemes of Fig. 1 to triads and multicomponent systems with carefully balanced electrochemical and spectroscopic properties has led to remarkable achievements along the mimicking of the fundamental processes of light energy collection and storage (via charge separation. CS) taking place in natural systems.[11,12] Dealt with in Fig. 2 is a representative example that conveniently illustrates the approach followed by studying light-induced processes in covalently-linked multicomponent systems.[13] In the figure, the behavior of a porphyrin-fullerene dyad-type reaction center ($P\text{-}C_{60}$) is compared with that of a carotenoporphyrin-fullerene triad ($C\text{-}P\text{-}C_{60}$). For the latter, the presence of the third component results in a two-step sequential transfer of electron; with an overall final quantum yield of charge separated state, Φ_{cs}, not far from unit. The chemical energy stored within the final CS state of the triad is less than that of the dyad, 1.1 versus 1.39 eV, respectively. However. the storage time. τ_{cs}, is three orders of magnitude longer. 340 ns versus 480 ps. respectively. which suggests an easier utilization of its energy content. In line with a supramolecular view. the energy schemes of Fig. 2 are drawn by combining the spectroscopic and electrochemical properties of the single components.

A related area in supramolecular photochemistry has to do with the transduction and collection of excitation energy in the presence of a convenient energy gradient. This type of process is frequently a multistep one and was

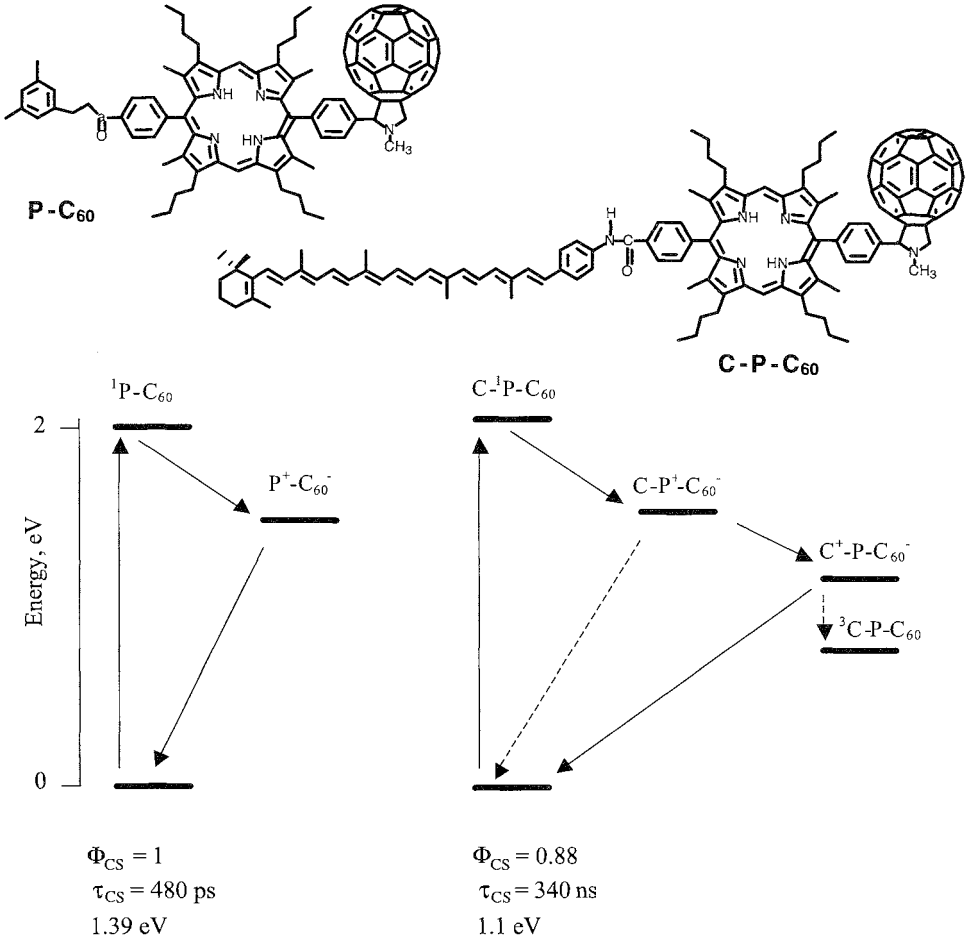

Fig. *2* Artificial photosynthesis: photoinduced storage of chemical energy inspired by the behavior of natural systems;[11,12] comparison of the performance of a dyad and related triad.[13]

extensively studied in linear and dendritic-type assemblies. In the former case, it can be initiated by light absorption at one terminal of the linear system (usually termed molecular wire). and after vectorial transfer of the excitation, it can lead to final population of excited states localized at the opposite terminal.[14] Cases are also known where a vectorial energy migration takes place along chromophores linked to a polymer backbone.[15] In dendritic-type systems, light absorption may take place at one peripheral/central unit and result in the subsequent energy conveyance at a central/peripheral unit.[16] The final localization of the excitation at the periphery or at the center of the assembly can be driven by carefully organizing and integrating the active components.[17,18] As an example, the behavior of a polyphenylene-framed, rigid-shape system performing a periphery-to-center excitation collection is depicted in Fig. 3.[18] The active components are naphthalene dicarboxmonoiimide (N), perylene dicarboxmonoimide (P), and terrylene tetracarboxdiimide (*T*). These components exhibit conveniently

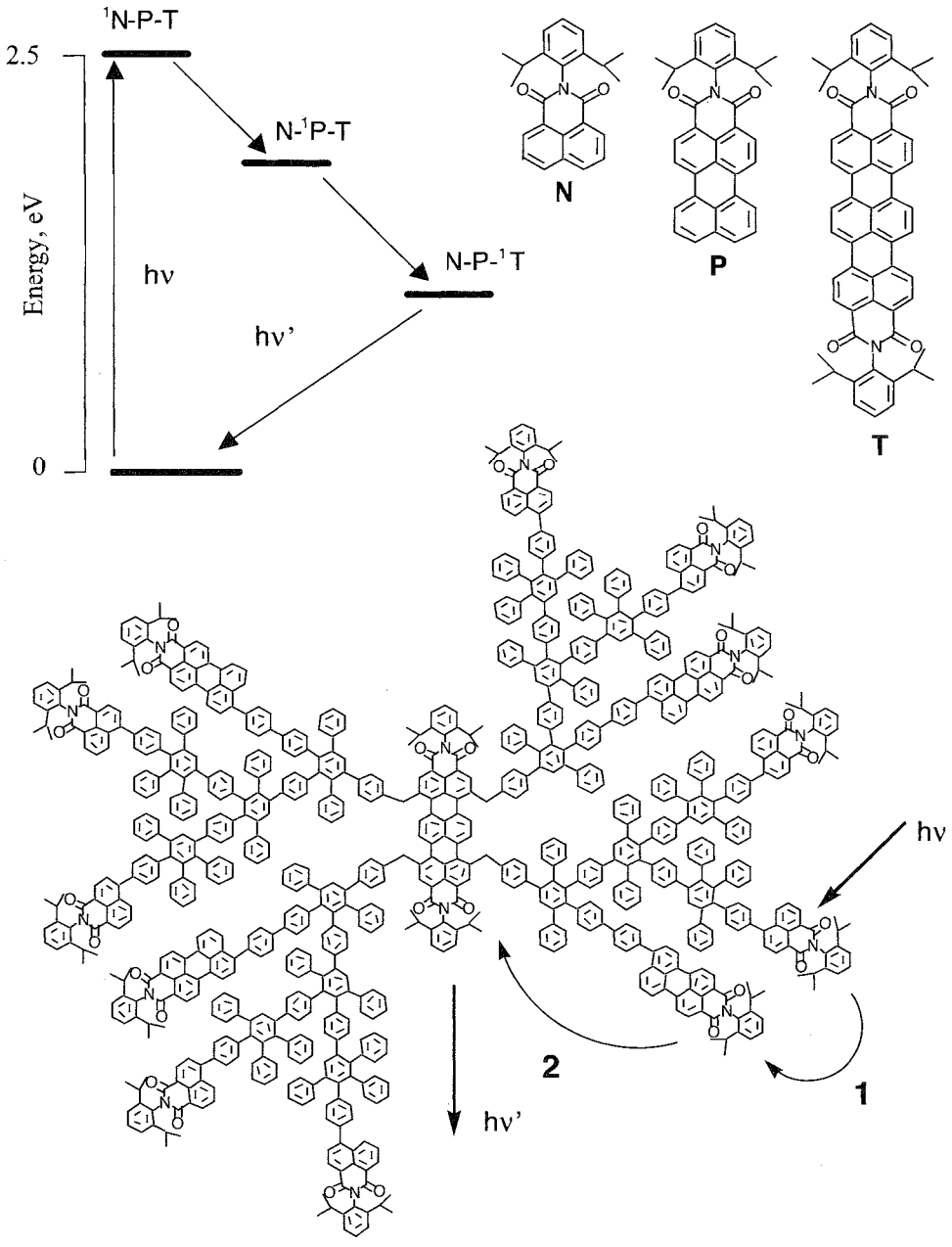

Fig. 3 A two-step periphery-to-center excitation energy collection driven by the energy gradients between the excited levels of the three luminactive components.[18]

scaled luminescent levels, and from the luminescence properties of the dendrimer, it is inferred that upon excitation of a peripheral *N* chromophore, a two-step, nearly quantitative final collection at the single central T unit is taking place. Clearly, assemblies may be envisaged that combine the funnelling of excitation energy at one component of a dendritic array with its subsequent utilization for performing CS steps. a scheme that is reminiscent of the behavior of natural systems.[11 12]

SYSTEMS POWERED BY LIGHT: MACHINES AT THE MOLECULAR LEVEL

Numerous interlocked assemblies were designed in connection with attempts to gain control of rotational and translational motions at the molecular level. a stepping stone toward possible outstanding development. As regards light-operated cases, a representative shuttling scheme for a rotaxane-based "molecular abacus" is depicted in Fig. 4.[21] As active components, the rotaxane axle contains a $[Ru(bpy)_3]^{2+}$ photosensitizer (which also plays the role as a stopper) and two MV-type electron-accepting stations exhibiting a slightly different accepting aptitude [bpy is 2.2'-bipyridine. MV is 4.4′-bipyridinium (methylviologen)]. An electron-donor ring, a macrocycle containing two dioxybenzene units, is wired around the axle that is terminated by a tetraarylmethane group as a second stopper. The streamed arrangement of the two accepting stations sets up the stage for molecular displacements based on donor–acceptor interactions through the following steps: a) positioning of the macrocyclic ring according to the more favorable donor–acceptor interactions; b) the better acceptor turns into the worse acceptor by the photoinduced event, electron transfer; and c) displacement of the ring. This half-cycle is expected to be followed by restoration of the starting a) position after some time. Actually, the timing of the various steps represents the most critical factor within the scheme of Fig. 4. This is basically due to the fact that the ring displacement is usually exceedingly slow compared to the light-triggered events. Despite these difficulties, successful systems were reported

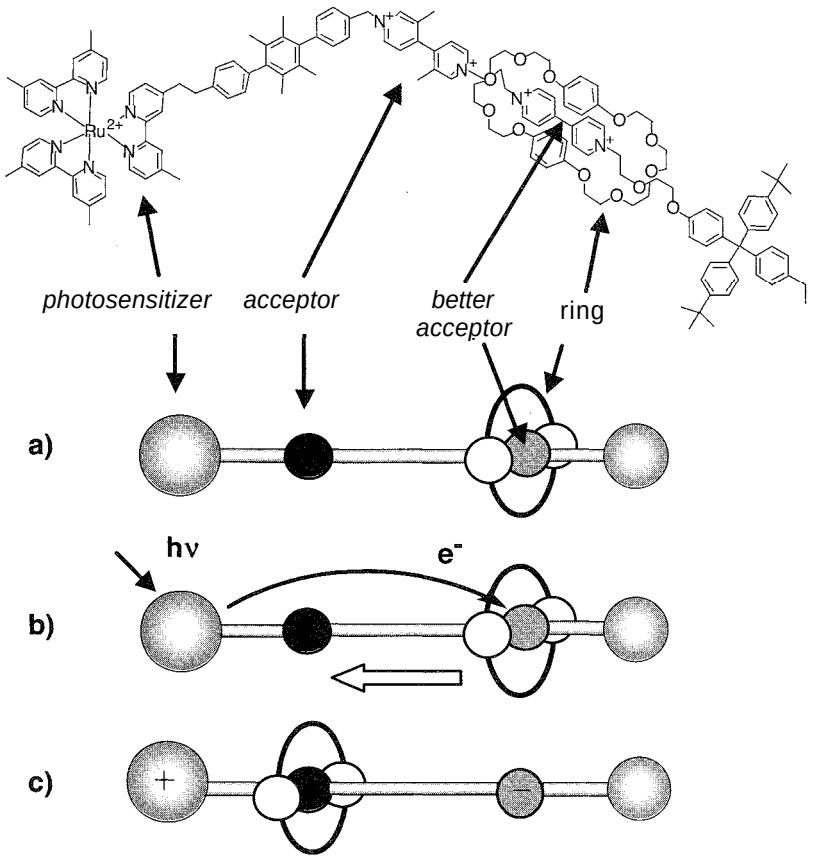

Fig. 4 A light-driven "molecular abacus" with movements that are mediated by the covalent bonds and are stationed by the establishment of weak (donor–acceptor) interactions.[21]

where the light-induced intercomponent displacements are fast in comparison to the competing deactivation processes.[22,23]

SENSING AND SIGNALING BY LIGHT UPON MOLECULAR RECOGNITION

Biomedical applications as well as environmental and food quality control fostered the development of systems for easily sensing and fast reporting the presence of a chemical species, the analyte. With this purpose, a variety of supramolecular sensors were designed in the last decade, able to signal binding of a substrate via large changes in the overall optical properties. These structures generally possess a receptor for associating the analyte, a spacer, and a signaling unit that converts the recognition event into changes of the light absorption or emission features of the system. Receptors such as crown ethers, functionalized calixarenes, cryptands, podands, chelators, and coronands are expressly designed for recognition of cations: polyammonium derivatives and functionalized metal ions are suitable for anions, whereas aromatic moieties of calixarenes and cyclodextrins easily bind neutral species. Various intercomponent interactions may work, such as H-bonding, hydrophobic forces, electronic effects, donor–acceptor interactions, metal coordination, and covalent bond formation.

Because of their intrinsic higher sensitivities and selectivities, the luminescent sensors are considered to be convenient. The signaling events rely on emission quenching or enhancement related to photoinduced electron transfer (PET sensors), on new emissions originating by excimer or exciplex formation, on changes in λ_{max}, quantum yield, and lifetime of the luminescence by intramolecular charge transfer (PCT sensors).[24,25]

Compared to systems based on a single interaction, cooperative sensors based on multiple, concerted, intermolecular interactions between the components exhibit higher discrimination capabilities and enhanced functions.[26,27] As examples for this class of sensors, two systems, both based on the absorption/luminescence properties of the porphyrin nucleus: are illustrated in Fig. 5. Structure (a) represents a ditopic receptor where cooperative binding of a cation by the amide-appended calixarene and of an anion by the Zn-porphyrin allows recognition of complete binary metal salts.[27] Structure (b) incorporates two cyclodextrin cavities and relies on the modification of the Fe(III) complex spectroscopic properties by inclusion of guests in these hydrophobic sites.[28] This species is able to sense the presence of benzylmercaptane and 1-adamantanecarboxylate in four

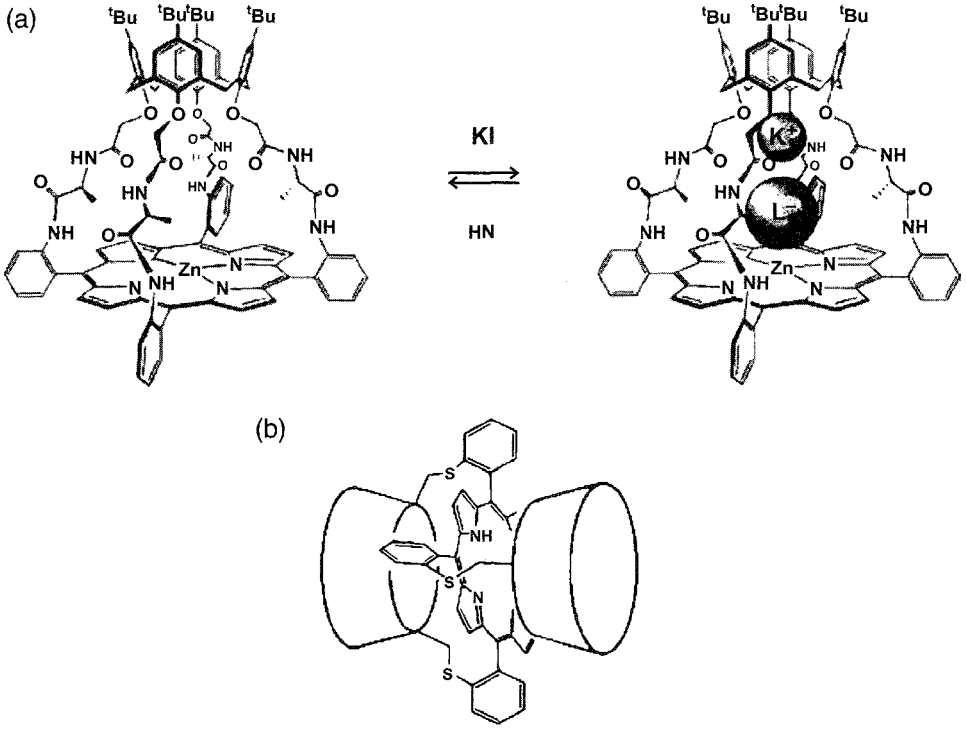

Fig. 5 Two examples of porphyrin-based cooperative optical sensors. (a) A ditopic receptor for binary metal salts.[27] (b) A cyclodextrin-capped porphyrin system able to sense and report in four distinguishable association modes.[29]

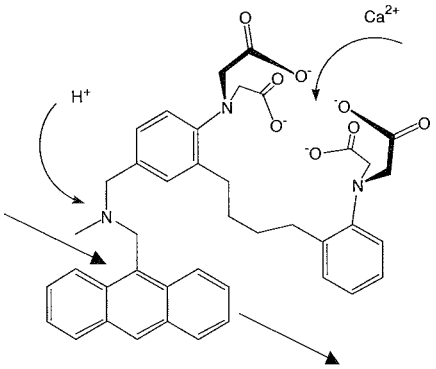

AND logic gate		
Input1 H^+	Input2 Ca^{2+}	Output
0	0	0
0	1	0
1	0	0
1	1	1

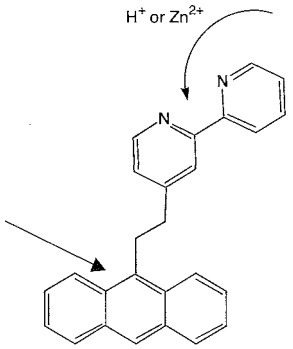

NOR logic gate		
Input1 H^+	Input2 Zn^{2+}	Output
0	0	1
0	1	0
1	0	0
1	1	0

Fig. 6 Molecular-scale implementation of logical gates based on the fluorescence signals of the anthracene unit. Inputs: $H^+ = 0$ means $[H^+] = 10^{-7}$; $M^{2+} = 0$ means $[M^{2+}] \leq 10^{-9}$; and H^+, Zn^{2+}, $Ca^{2+} = 1$ are for concentrations $\geq 10^{-3}$ M. Output: 1 = strong fluorescence, 0 = no or weak fluorescence.[33,34] The light input/output is indicated by straight arrows.

different binding conditions. Empty cavities, singly-occupied cavity, doubly-occupied cavities in homo- or heterocomplexes are easily distinguished by UV/Vis spectra. The system coupled sensing properties with catalytic action, by trapping an oxidizable substrate near an activated iron center or carrying out biomirnetic electron transfer reactions with quinones as guests.[29,30]

Cooperative binding in supramolecular sensors is a main requirement for obtaining other sophisticated, environmentally effective, functions like the selective transport of molecules.[26]

FROM OPTICAL SIGNALS TO LOGIC FUNCTIONS FOR MOLECULAR ELECTRONICS

As seen above, thanks to a suitable structural organization and functional integration of the components, the energy addition via light input can start useful energy conversion processes within a supermolecule. These may be exploited to achieve various types of luminescent sensors[24,25] and switches[31,32] and may lead, along with increasing complexity of components and their integration; to the development of nanoscale devices for information processing and molecular computing. In principle, these devices may be based on logic gates that combine the effect of chemical inputs on the optical output (luminescent signals) of a suitable chromophore. Nowadays, optical functions of two inputs are amenable to AND, OR, XOR, WAND, NOR, and XWOR behaviors via exploitation/inhibition of electron- or energy-transfer processes involving the excited luminescent level of the selected chromophore. Two simple model examples are illustrated in Fig. 6.[33,34] For the upper case, amine protonation or reception of Ca^{2+} by the carboxylate groups prevents the occurrence of photoinduced electron transfer from these fragments to the excited anthracene unit; for the bottom case, protonation of the bpy unit or its coordination with Zn^{2+} results in the quenching of the anthracene-based fluorescence. This probably happens because H^+ and Zn^{2+} cause a stabilization of the lowest-lying levels of bpy so that an anthracene-to-bpy energy-transfer step becomes energetically allowed. Notably, the implementation of elaborate electronic functions at the

molecular level is further made possible by the combination in series or in parallel of the two-inputlone-output gates of the type shown in Fig. 6.[33,34]

CONCLUSION

In supramolecular chemistry, concepts like recognition and self-organization based on the expression of molecularly stored infosmation appear to be strictly derived from a biomimetic approach, the one taught at the school of nature.[2,4,35] Supramolecular photochemistry, with the emphasis placed on the use of energy consequent to its spatial localization at some selected and active component of a molecular array, appears to enforce prospects along the design of artificial systems, where preorganization of the stereochemical features holds the spotlight. For the supramolecular science, it is reasonable and tempting to envisage developments toward systems of higher degrees of complexity that incorporate more infosmation. This means that they can display improved self-organizing abilities (which are stored in the components) and that novel molecular architectures are at once made available because of the designing abilities of molecule makers, the chemists. These developments are sometimes claimed to possibly include molecular adaptive and evolutive schemes,[35,36] until now an exclusive power of nature, exerted over time scales of hundreds of millions of years.[37] We shall soon see what the future brings.

ARTICLES OF FURTHER INTEREST

Classification and Nomenclature of Supramolecular Compounds, p. 261
Crown Ethers, p. 326
Cryptands, p. 334
Cyclodextrins, p. 398
Cyclodextrins, Applications, p. 405
Dendrimers, p. 432
Fluorescence Sensing of Anions. p. *566*
Fluorescent Sensor-s, p. 572
Molecular Logic Gates, p. 893
Molecular Squares, Boxes. and Cubes, p. 909
Molecular Switches. p. 917
Molecular Wires, p. 925
Molecular-Level Machines, p. 931
Photochemical Sensors, p. 1053
Rotaxanes and Pseudorotaxanes, p. 1194
Self-Assembling Catenanes, p. *1240*
Self-Assembly: Definition and Kinetic arid Thermodynamic Considerations. p. 1248
Supramolecular Chemistry, Definition, p. 1401
Supramolecular Electrochemistry, p. 1412

S

REFERENCES

1. Lehn. J.-M. *Supramolecular Chemistry. Concepts and* Perspectives; VCH: Weinheim. 1995.
2. Lehn, J.-M. Programmed chemical systems: Multiple subprograms and multiple processing/expression of molecular information. Chem. Eur. J. 2000. 6. 2097–2102.
3. Swiegers, G.F.; Malefetse. T.J. New self-assembled structural motifs in coordination chemistry. Chem. Rev. 2000. *100,* 3483–3537.
4. Monod, J. *Chance* and Necessity; Penguin Books: London, 1971: 79–80.
5. *Supramolecular Photochemistry*; Balzani, V., Ed.; Reidel Publishing Company: Dordrecht, Holland, 1987.
6. Dietrich-Buchecker, C.O.; Sauvage, J.-P. Interlocking of molecular threads: From the statistical approach to the template synthesis of catenands. Chem. Rev. 1987. 87, 795–810.
7. Amabilino, D.B.: Stoddart, J.F. Interlocked and intertwined structures and superstructures. Chem. Rev. 1995, *95,* 2725–2828.
8. Vögtle, F.: Diinnwald. T.; Schmidt, T. Catenanes and rotaxanes of the amide type. Acc. Chem. Res. 1996. 29, 451–460.
9. Balzani, V.; Scandola, F. Supramolecular *Photochemistry*; Ellis Horwood: New York. 1991.
10. deSilva, A.P.; Gunaratne, H.Q.N.; Gunnlaugsson. T.; Huxley, A.J.M.: McCoy. C.P.; Rademaclier, J.T.; Rice, T.E. Signaling recognition events with fluorescent sensors and switches. Chem. Rev. 1997. 97. 1515–1566.
11. Wasielewslti. M.R. Photoinduced electron transfer in supramolecular systems for artificial photosynthesis. Chem. Rev. 1992, 92, 435–461.
12. Gust. D.: Moore. T.A.; Moore, A.L. Mimicking photosynthetic solar energy transduction. Acc. Chem. Res. 2001, *34.* 40–48.
13. Kaciauskas, D.; Liddel, P.A.; Lin. S.: Stone. S.; Moore, A.L.: Moore, T.A.: Gust, D. Photoinduced electron transfer in carotenoporphyrin-fullerene tryads: Temperature and solvent effects. J. Phys. Chem.. B 2000. *104.* 4307–4321.
14. Barigeiletti, F.: Flamigni. L. Photoactive molecular wires based on metal complexes. Chetn. Soc. Rev. 2000.29.1–12.
15. Fleming, C.N.: Maxwell. K.A.; DeSimone. J.M.; Meyer. T.J.: Papaniltolas. J.M. Ultrafast energy migration dynamics in an efficient light-harvesting antenna polymer based on Ru(II) and Os(II) polypyridyl complexes. J. Am. Chem. Soc. 2001, *123,* 10336–10347.
16. Adronov, A.; Frechet, J.M.J. Light-harvesting dendrimers. Chem. Commun. 2000, 1701–1710.
17. Balzani. V.: Juris. A.; Venturi. M.; Campagna. S.: Serroni. S. Designing dendrimers based on transition metal complexes. Light harvesting properties and predetermined redox patterns. Acc. Chem. Res. 1998. *31.* 26–34.

18. Weil. T.: Reuther. E.; Müllen, K. Shape-persistent. fluorescent polyphenylene dyads and triads for efficient vectorial transduction of excitation energy. Angew. Chem.. Int. Ed. 2002. *dl*. 1900–1904.
19. Pease. A.R.: Jeppesen, J.O.;Stoddart. J.F.; Luo, Y.; Collier, C.P.: Heath. J.R. Switching devices based on interlocked molecules. Acc. Chem. Res. 2001. 34, 433–444.
20. Collier. C.P.: Jeppesen, J.O.; Yi, L.; Perkins, J.; Wong, E.W.; Heath, J.R.: Stoddart, J.F. Molecular-based electronically switchable tunnel junction devices. J. Am. Chem. Soc. 2001. *123*, 12632–12641.
21. Ashton, P.R.: Ballardini. R.; Balzani. V.; Credi. A.; Dress. K.R.; Ishow, E.: Kleverlaan. C.J.: Kocian. O.; Preece, J.A.; Spencer. N.: Stoddart. J.F.; Venturi, M.; Wenger, S. A photochemically driven molecular-level abacus. Chem. Eur. J. 2000. *6*, 3558–3574.
22. Brouwer, A.M.: Frochot. C.: Gatti, F.G.; Leigh. D.A.; Mottier, L.: Paolucci, F.: Roffia, S.: Wurpel, G.W.H. Photoinduction of fast, reversible translational motion in a hydrogen-bonded molecular shuttle. Science 2001. *291*, 2124–2128.
23. Balzani. V.; Credi, A.; Marchioni, F.; Stoddart. J.F. Artificial molecular-level machines. Dethreading-rethreading of a pseudorotaxane powered exclusively by light energy. Chem. Commun. 2001, 1860–1861.
24. Lunzinescenr Sensors; Fabbrizzi, L., Ed.: Coord. Chem. Rev.. Elsevier: Amsterdam. 2000; 1–228.
25. Valeur, B.: Brochon. J.-C. *New* Ti-ends *in Fluorescence Spectroscopy—Applications* to Chenzical and Life Sciences: Springer-Verlag: Berlin, 2001.
26. Robertson. A.; Shinkai. S. Cooperative binding in selective sensors. catalysts and actuators. Coord. Chem. Rev. 2000, *205*. 157–199.
27. Nagasaki, T.: Fujishima, H.: Takeuchi. M.: Shinkai, S. Design and synthesis of a C4-symmetrical hard-soft ditopic metal receptor by calixarene-porphyrin coupling. J. Chem. Soc., Perkin Trans. I 1995, 1883–1995.
28. Bortolus. P.: Monti. S. Photochemistry in cyclodextrin cavities. Adv. Photochem. 1996, *21*. 1–133.
29. Kuroda. *Y.*: Hiroshige. T.: Sera. T.: Shiroiwa. Y.; Tanaka. H.: Ogoshi. H. Cyclodextrin-sandwiched porphyrin. J. Am. Chem. Soc. 1989, *111*. 1912–1913.
30. Kuroda. Y.; Ito, M.: Sera. T.; Ogoshi. H. Controlled electron transfer between cyclodextrin-sandwiched porphyrin and quinones. J. Am. Chem. Soc. 1993. *115*, 7003–7004.
31. Rurack. K.: Resch-Genger. U. Rigidization. preorientation and electronic decoupling-the 'magic triangle' for the design of highly efficient fluorescent sensors and switches. Chem. Soc. Rev. 2002. 31, 116–127.
32. Feringa, B.L. *Molecular* Switches: Wiley–VCH: Weinheim, 2001.
33. de Silva. A.P.: Dixon, I.M.: Gunaratne, H.Q.N.; Gunnlaugsson, T.: Maxwell. P.R.S.: Rice, T.E. Integration of logic functions and sequential operation of gates at the molecular-scale. J. Am. Chem. Soc. 1999, *121*. 1393–1394.
34. de Silva, A.P.: McClenaghan, N.D. Proof-of-principle of molecular-scale arithmetic. J. Am. Chem. Soc. 2000. *122*, 3965–3966.
35. Brakmann. S. On the generation of information as motive power for molecular evolution. Biophys. Chem. 1997. 66. 133–143.
36. Lehn. J.M. Toward complex matter: Supramolecular chemistry and self-organization. Proc. Natl. Acad. Sci. U.S.A. 2002. *99*. 4763–4768.
37. De Duve, C. *Vital Dust*; Basic Books: New York. 1995.

Supramolecular Polymers

Alberto Ciferri
University of Genoa, Genova, Italy

INTRODUCTION

Conventional linear polymers are characterized by main-chain covalent bonds and by nonbonded interactions among groups localized at specific sites of repeating units. Supramolecular polymers (SPs) recently investigated display purely nonbonded interactions or unconventional combinations of covalent chains and supramolecular interactions. Novel structures, properties, and applications are displayed by SPs with respect to conventional polymers. The study of this exciting class of new inaterials is of interest for the formation of nanostructures with prescribed molecular order assembling hierarchically to mesoscopic dimensions, for the understanding of self-assembling processes in complex biological systems, and for the use of concepts cutting across traditional boundaries between colloid, polymer, and solid-state science.

DEFINITION, CLASSIFICATION

A classification of several systems described as SPs was recently presented.[1,2] For the fully supramolecular polymers (Class A) the interactions holding the unimers along the main-chain are of a supramolecular nature. These polymers are open, self-assembled, equilibrium sequences of bifunctional unimers polymerizing to a high degree of reversible supramolecular polymerization (DP) according to mechanisms significantly different from those of conventional polymers. Unimers can be of several forms and sizes: from small molecules to covalent polymers terminated by supramolecular bonding units. In the latter case, a SP should be regarded as a "polymer of polymers." Assembly of multifunctional unimers results in multidimensional structures. Class B includes self-assembled, closed structures such as aggregates of a small number of molecules (supermolecules), helical, globular, and side-chain associations of monofunctional sites. Class C includes self-assembled systems based on supramolecular structures irreversibly associated to covalent polymers, as in the case of dendrimeric chains or single-stranded globular proteins. Finally. engineered (as distinct from self-assembled) supramolecular structures. ofien involving covalent polymers, are included in Class D.

GENERAL ASSEMBLY PRINCIPLES

Localized Interactions

For all types of SPs, the stabilization of well-defined structures is due to combinations of interactions that may be localized at specific atomic groups of the unimers, or more uniformly distributed over the assembly surface. In all cases, shape complementarity is an integral part of the process of molecular recognition. Detailed quantitative assessment of the role of classical localized interactions (Coulombic. van der Waals, hydrogen. and solvophobic bonds) is described in the literature of low-molecular-weight host–guest complexes.[3] In the case of SPs, most important types of localized interactions are based on H-bonds, charged groups, π–π stacking, or metal-ion coordination.[2–6] Several combinations of these interactions may addiively contribute to the overall contact energy. H-bonds are a primary source of stabilization due to their strong directionalities allowing positional control. For multiple H-bonds, the product of single-binding constants may be increased or decreased by parallel (e.g., AAA–DDD) or antiparallel placements.[4–6]

Solvents may compete or enhance the formation of localized bonds. For instance, H-bonds are stronger in apolar solvents, ionizable groups are sensitive to pH. and π–π interactions are not largely affected. Solvents also display nonlocalized effects on the formation of supramolecular bonds, as described below.

Site Distribution, Unimer Functionality, Assembly Dimensionality

The number of sites per unimer *(S)* and their distributions control the functionalitjj (F) of the unirners and the dimensionality of the assembly. Complementarity of shapes and interaction. localized at the north and south contacting surfaces of bifunctional unimers, results in the formation of unidimensional (linear) assemblies (Fig. 1a: $F = 2$, $S = 2$). Functionalities greater than 2 result in the formation of more complex geometries (Fig. 1b).[1] Helical supramolecular chains are expected when two additional sites are located on the same side (i.e., NE and SE) of the unimer.[7] Planar assemblies are expected when four sites are distributed along the circumference of a disk,

Encyclopedia of Supramolecular Chemistry
DOI: 10.1081/E-ESMC 120012808

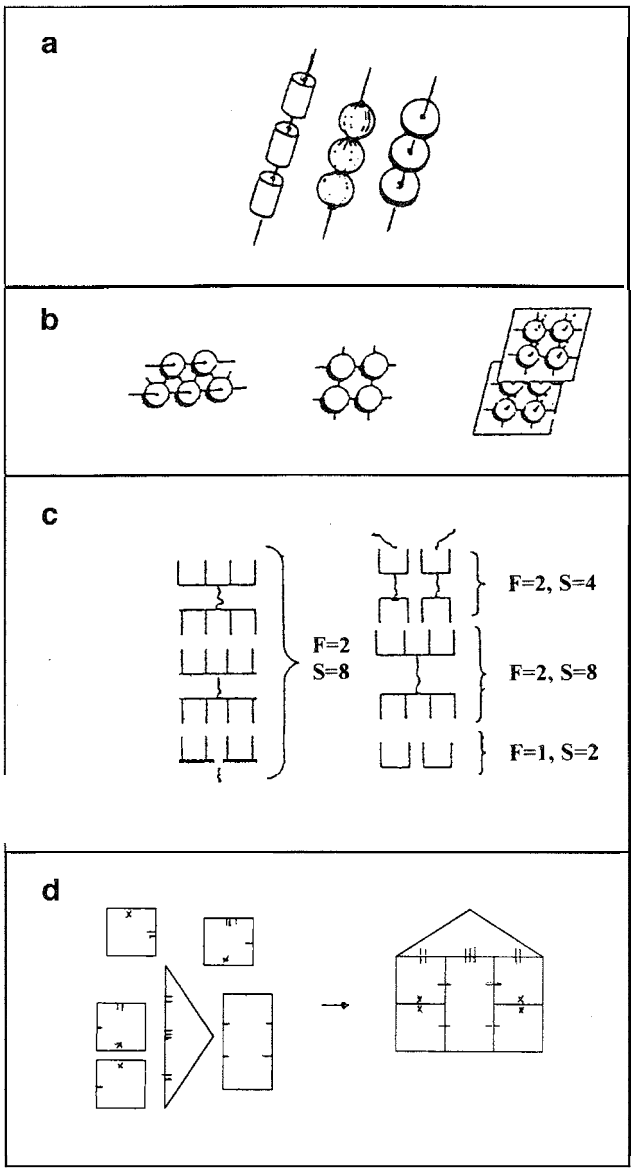

Fig. 1 Shapes and functionality. (a) linear assemblies of bifunctional rod-like, spherical. disk-like unimers (F= 2. S = 2); (b) helical. planar. three-dimensional assemblies (F> 2. S > 2): (c) linear polymers, branching. and termination for various F and S; and (d) assembly of unimers with different shapes and functionalities.

or the equatorial plane of a quasi-spherical unimer.[8] Three-dimensionally ordered arrays are expected if N and S interacting sites increase (longitudinally) the functionalities of the planar systems.

Supramolecular unimers can be of large size, and often more than one binding site occurs over each complementary surface (cf. Fig. lc). If full compensation occurs. there will be no alteration of the functionality of the unimer or the dimensionality of the assembly. Multiple sites on properly designed complementary surfaces have a high probability of being mutually compensated. Should a mismatch occur, or unimers with different functionalities or numbers of sites be mixed. alterations in the above assembling patterns are expected, i.e., termination or random network formation. as shown schematically in Fig. lc. More complex patterns are expected upon mixing unimers differing in shape, functionality, and bond type (Fig. 1d). These situations are not yet under active investigation: computational and simulation methods (algorithmic assembling) might be used for describing assemblies of increasing complexities.[9]

Smoothed-Out interactions

Wonlocalized interactions play a unique role in the assembly of SPs. particularly in their hierarchical evolution from nano to mesoscopic dimensions. One type of smoothed-out interaction is described by thermodynamic parameters of compatibility between solute and solvent species (i.e., the χ parameter). and another type is related to thermodynamic parameters describing excluded volume effects for unimers and growing SPs.[6,10]

Incompatibility

The *solvophobic bond*[11] describes the poor affinity of a nonpolar solute (i.e., a hydrocarbon) for a polar solvent (i.e., water). The ensuing phase separation amounts to a recognition of compatible components and hence is a driving force for self-assembly.[6] If the solute is a ditopic, amphiphiiic molecule (i.e., a surfactant[11] or a block copolymer[12]) dissolved in a selective solvent, the combined incompatibility of the components leads to micellization.[6,11,12] For ditopic molecules in the absence of a solvent. the inacroscopic phase separation expected for the unconnected components is replaced by a microsegregation in domains separated by the surface comprising the intersegmental bonds. A detailed mean-field theory satisfactorily explains the self-assembly of amorphous diblock copolymers into hexagonal, lamellar, and other phases by a balance of the thermodynamic incompatibility of components and their relative sizes and flexibilities.[13]

Excluded volume

The tendency to reduce excluded volume leads to a driving force for the orientation of rods having length/diameter ratio $X = L/D > \sim 6$.[14] and for the stacking of thin disks ($0 < L/D < 0.1$[15]). This hard interaction effect is detectable even in diluted isotropic solution and leads, above a critical concentration, to an orientational transition to

nematic and higher-order phases. Excluded volume is therefore an important driving force for self-assembly. It is important to stress the predicted differences between rod- and disk-like particles.[10] The relatively large axial ratios indicated above for rod-like mesogens suggest that only rigid assemblies or covalent polymers with large DP will attain the nematic phase. On the other hand, a strong tendency to form nematic phases is exhibited even by low MW disk-like unimers, provided their thicknesses are sufficiently small.

Assembling Mechanisms

The general thermodynamic formalism regarding growth of supramolecular aggregates was highlighted by Israelachvili.[16] The growth of two- and three-dimensional systems can be described as a true phase transition (crystallization): the aggregation number tends to infinity above a critical aggregate concentration (CAC). Unidimensional assemblies (linear. helical, columnar. including spherical micelles), may instead display large cooperativity above the CAC but not a true transition: size distributions will occur. In line with the above considerations, three distinct mechanisms were identified for unidimensional growth.[6]

Multistage Open Association (MSOA) is the basic step-by-step process (not involving critical nucleus or cooperativity) similar to the molecular polycondensation of bifunctional monomers.[17] Each step is described by a single binding constant K that includes all possible contributions to the contact energy and determines (Fig. 2a) the rate of increase of DP with unimer concentration. Detailed calculations[1,4,6] reveal that values of $K > 10^6$ M^{-1} are needed to produce SPs exhibiting DP in the range of interest (>100) in diluted (<1%) solutions. For H-bonded polymers, the above condition requires a minimum of three bonds (S=6, $F=2$, assuming a value of $K \sim 500$ M^{-1} for a single H-bond[18]).

Helical growth (HG) occurs when a sequence of linear steps according to MSOA leads to a critical concentration C^* at which cooperative helical growth begins (Fig. 2b). Because more bonds per unimer are expected in the helical than in the linear chain, the sudden increase of DP at $C > C^*$ is described by a constant $K_h > K$ and by the familiar Zimm–Bragg cooperativity parameter.[11,12] The original theory was developed by Oosawa for the nucleus schematized in Fig. 1b and applied to the $G \rightleftharpoons F$ transformation of actin.[7] A recent extension by van der Schoot and coworkers,[13] applied to helical assemblies of discotic molecules, does not require the specification of the critical nucleus.

Growth-coupled-to-orientation(SLC), also described as the open supramolecular liquid crystal,[20] is an inter-

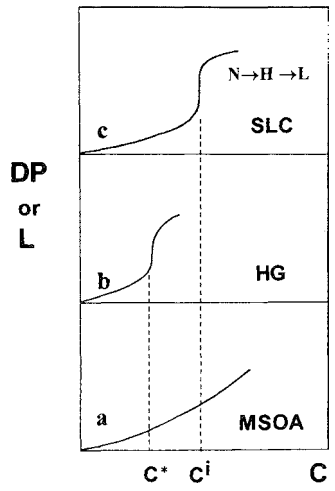

Fig. 2 Growth mechanisms. Schematic theoretical variation of DP (or length) with unimer concentration for linear supramolecular polymerization according to (a) multistage open association; (b) helical growth: (c) growth-coupled-to-orientation. C^* and C^i are critical concentrations corresponding to (b) and (c). Occurrence of liquid-crystalline phases (N. H, L) is indicated. From Ref. [1]. Copyright 2002 Wiley-VCH.

assembly cooperative process occurring at a critical concentration C^i at which growth of bifunctional unimers occurs siinultaneously with the formation of a nematic phase (Fig. 2c). The sudden increase of DP at C^i is controlled by suitable combinations of contact energy and rigidity (persistence length) of the formed assembly.[20–23] The original theory,[21] developed for linear assemblies of cylindrical micelles in nematic solutions, was later extended to discotic molecules displaying hard interactions and showing nematic. hexagonal, and higher-order phases.[22,23] Theory predicts that the nematic phase may be skipped for particular combinations of contact energy and rigidity.[23]

CLASS A SPs

Representative examples of linear, helical. and columnar assemblies are summarized in Fig. 3.[1,4] The growth mechanism. the magnitude of the solution DP, and the nature of the main contact forces are evidenced. The figure highlights essential features of supramolecular polymerization. Note, for instance, how the geometry of the assembly is not necessarily related to the growth mechanism or the nature of contact forces. In particular. Polymers **1** and **3** assemble through the MSOA mechanism, but one is a linear chain. and the other is a columnar stack of disks. Polymers 4 and 6 assemble through the HG mechanism, but one is a double helical chain, and

	Unimer and/or Polymer	Mech.	DP	Bond
1	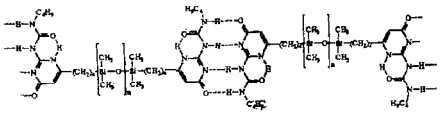	MSOA	→1000	H-bonds
2	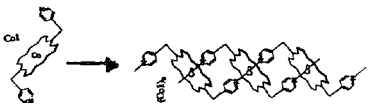	MSOA	→100	Metal ion
3	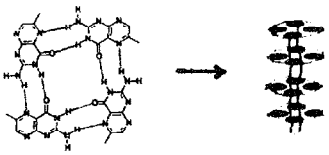	MSOA	→10	Salt inter.
4		HG	→4000	H-bonds
5	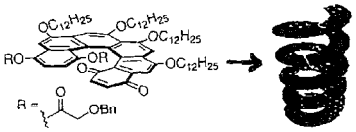	HG	---	π-π
6	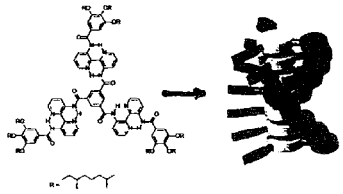	HG	→1000	π-π H-bonds
7	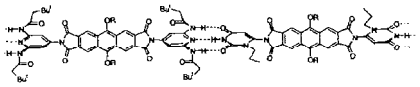	SCL	---	H-bonds
8	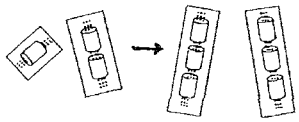	SCL	→22000	Solvophobic
9	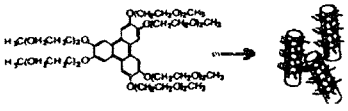	SCL	---	π-π Solvophobic

Fig. *3* Class A SPs. 1: Ureidopyrimidone-based linear chains;[4,24] 2: porphyria-based linear chains;[25] **1:** folic acid tetramers columnar stacks;[1,26] 4: actin double-helical chains;[6,27,28] 5: helicene helical chains;[29,30] 6: C_3-symmetrical molecules forming helical columnar stacks;[7] 7: uracyl or pyridine-terminated anthracene forming linear chains;[5] 8: surfactant micelles linear polymers;[6,21] 9: 2,3,6,7,10,11-hexa(1,4,7-trioxoacetyltriphenylene) columnar stacks.[8]

the other is a columnar helix. Polymers **7,** 8, 9 assemble through the SLC mechanism, but 7 is a linear chain, 8 is a linear micelle, and 9 is a columnar stack of disks. Also to be noticed is the difference in the structure of the disk-like unimer in Polymer **3:** a superrnolecular tetramer,[26] and in Polymer 9: an amphiphilic molecule. The cooperative growth of Polymer 6 is attributed to a conformational transition from a flat to propeller shape in each disk, allowing maximization of interaction.''' The chirality of the unimer is usually expressed and reinforced in helical SPs.[4,26,30,31] Not included are "tubular" polymers containing a large central cavity and based on MSOA stacking of peptide rings,[32] or on a spiralization (HC) of globular proteins, as in the case of microtubules,[6] and helical assemblies of oligomeric foldamers such as m-phenylene ethylene.[33,34]

The extent of polymerization (DP) appears to be directly related to the strength of contact forces and cooperativity effects. In particular, Polymer 1 attains DP well above the value reported for other MSOA polymers due to the large dimerization constant ($K = 6 \times 10^7\ M^{-1}$ in $CDCl_3$)[4] of ureidopyrimidone forming four (self-cornplementary) Id-bonds. The still larger DPs reported for Polymers 4 and 8 reflect the occurrence of cooperative growth mechanisms, HG and SLC, respectively (reported DPs refer to dilute isotropic solutions for MSOA or HG and to relatively concentrated anisotropic phases for SLC). It is theoretically predicted that DP will increase with unimer concentration, the largest DPs being expected in the undiluted state. If the assembly becomes oriented in a nematic phase, a sequence of transitions to hexagonal columnar and lamellar phases upon increasing concentration represents a hierarchical ordering to mesoscopic

Planar systems resulting from a crystallization process are exemplified by self-assembling S-layers (Fig. 4a), the protective monolayers for the external surface of bacterial cells.[8] The constituent proteins have a quasi-spherical shape with an equatorial distribution of H-bonding sites (Fig. 1b) and an additional site on the south pole, allowing weaker electrostatic anchoring to the cell membrane. Proteins were isolated and reassembled in vitro as single free-standing monolayers over inert surfaces. revealing a tendency for this system to form open planar assemblies. More complex is the behavior of the in vivo assembly when features of a dynamic closed-surface crystal are exhibited. The curvature and finite size effects are controlled by the curvature of the bilayer cell membrane to which the protective layer is anchored. The assembly $\longleftrightarrow$ disassembly process of the crystalline layer responds to cell growth and division by incosporating fresh protein at dislocation sites (intussusceptive growth). Nanotechnology applications of S-layers were described.[8]

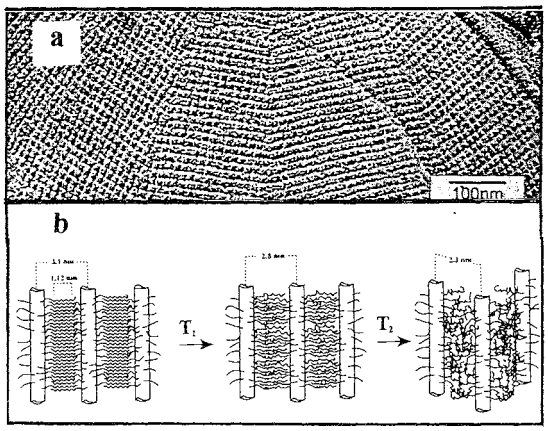

Fig. 4 (a) A planar assembly of S-layers showing square symmetries and edge dislocations (sites for intussusceptive growth). From Ref. [8]. Copyright 2000 Marcel Dekker. (b) Thermal transition for a three-dimensional assembly of comb-like PαAA-18. Loosely interdigitating clusters occur in the LC phase between T_1 and T_2. From Ref. [35]. Copyright 1995 ACS.

Three-dimensional assemblies of spheres with a symmetrical distribution of equivalent sites (cf. Fig. 1b) form regular crystalline arrays. More interesting are situations in which a geometrical anisotropy of the unimer or differences in the recognition pattern of different components exists allowing consideration of modes of growth along longitudinal and transverse directions. An interesting example is a comb-like polymer poly(α-*n*-alkyl-β,L-aspartate) (Fig. 4b) based on a helical backbone and aliphatic side chains.[35] At the highest temperature investigated, the flexible segments were completely molten within a nematic phase, due to orientation of the helical backbones. At lower temperature; another LC phase was observed in which rigid helices were correlated by interdigitation with partly molten side chains. At still lower temperatures, the latter crystallized in a separate hexagonal lattice. Thus, it appears that a supramolecular unimer based on an elementary cluster of helices correlated by interdigitating side chains was a precursor of the solid-state structure.'''' This led to the suggestion of describing systems showing complex and mesoscopic structuralization in terms of supramolecular polymerization of specifically designed building blocks.[1,10] A similar concept was used to describe the solid-state organization of interpenetrating nets.[36] The future evolution of this concept for building patterns of increasing complexity could be handled by methods of molecular computing[''' ((Fig. 2c) and cellular automation.[37]

The SPs in Class A exhibit strong growth (DP may exceed that of conventional polycondensation[1,17]) and labile bonds. DPs may reversibly change by altering concentration. temperature, and other external variables.

The linear systems conforming to the MSOA mechanism exhibit relatively minor changes of DP in response to the above variables. Rheological data offer compelling evidence for the persistence of polymer-like behavior in spite of reversible polymerization.[24,38] Therefore, applications in areas expanding the uses of conventional polymers were suggested.[1,4,5,24,39] In particular, the following applications were suggested: easier processing despite a large DP: topology control in networks; tunable, smart, self-repairing materials; increase of DP for covalent polymers: recycling; supramolecular block copolymers; and chiral and sequential control promoted by the high selectivity of molecular recognition.

In the case of helical SPs, when major length changes occur in response to the above variables. microengines mimicking the mechanical behavior of biological systems and engineered for new practical applications were suggested. Particularly important is the coupling of an external stimulus, or a chemical reaction, to the assembly–disassembly process, thus extending the use of SPs materials to complex, coupled systems.[6,27,28] For instance, ATP hydrolysis causes an alteration of polymerization–depolymerization rates at the two ends of a growing actin filament. As a result, the polymer translates.[27,28]

Interesting nonlinear optical properties were shown by chiral helicenes (5) forming LB films with larger second-order susceptibility than corresponding racemic structures.[29] Nanotubes based on cyclic peptides[32] were reported to form membranes with ion-selective channels.

CLASS B SPs

Scheme 10a in Fig. 5 represents the formation of low-MW closed assemblies such as host–guest complexes, supermolecules, and cyclic oligomers. Examples include the supermolecules 11 and 12 and the cyclic folic acid tetramer (**3** in Fig. 3). These compounds aroused interest due to their pronounced thermotropic behaviors compared to the unbound components. The enhancement of liquid crystallinity for Complex **11** is explainable by general consideration of soft interactions in low-MW mesogens.[41] More complex is the case of Complexes 12 and **3** that. due to discotic shape, can form columnar stacks. A close relationship between liquid crystallinity and columnar growth was anticipated.[4,5,26] However. recent analysis[11] showed that columnar growth of the folate tetramer receives only a minor contribution from contact forces. The large excluded volume effect of thin disks is the main driving force for liquid crystallinity and self-assembly.

Scheme 10b in Fig. 5 represents the formation of closed side-chains SPs. Electrostatic binding of salts and

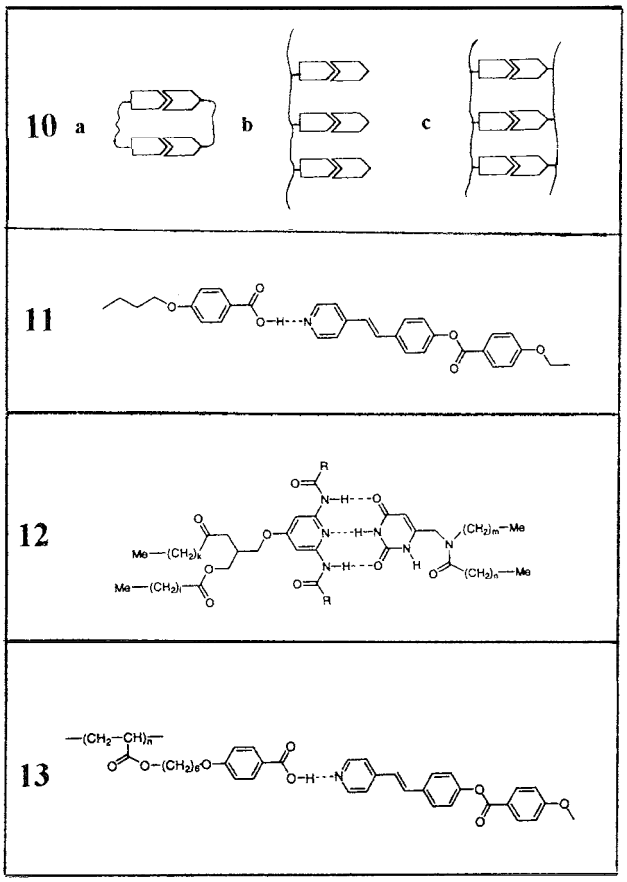

Fig. 5 Class B SPs. 10: Schemes for (a) closed low-MW assemblies; (b) side-chain polymers: and (c) multichain assemblies; 11: supermolecule of 4-butoxybenzoic acid and stilbazole;[40,42] 12: supermolecule of derivatives of 2.6-diaminopyridine and uracil;[5] 13: polyacrylate with hexyloxy benzoic acid side chains H-bonded to stilbazole.[42]

amphiphilic molecules to polyelectrolytes or polar polymers is an important topic of supramolecular interaction but is not usually described in the context of supramolecular polymers. Side-chain binding of small mesogens through H-bonding was pioneered by Kato and Fréchet.[42] Example **13** in Fig. 5 illustrates how the interaction of the supermolecule 11 can be transferred to a covalent polymer. In this case, a broad nematic phase occurred over a wider temperature range (140–252°C) than that for the individual components.

Scheme 10c in Fig. 5 represents the forination of closed supramolecular assemblies involving two (or a small number) covalent chains. There may be direct recognition of complementary groups attached to complementary chains. or ditopic units may be used to link (by electrostatic charge or H-bonds) identical chains. Conspicuous examples of this type of assembly are described in the literature of multistrand proteins and nucleic acids

but. again. are not usually described in the context of supramolecular polymers. It is to be noted that complete internal compensation of all sites carried by the polymers must occur for a closed structure to develop. Residual uncompensated sites still allow growth to occur, causing a mixed behavior of closed and open systems. For instance, the stoichiometry of the tropocollagen triple-helix is strictly defined. but occurrence of uncompensated chain-ends and reduction of electrostatic repulsion cause side-by-side and head-to-tail aggregation of triple-helices at neutral pH. Ultimately, network structures may be formed.

Formation of H-bonding between synthetic polymers is used as a way to improve compatibility in blends.'''' Interesting examples of switching from closed to open assemblies are the reversible transformation of the structure of folic acid **3** into linear ribbon-like aggregates (by salt concentration changes),[44] and of cyclic octapeptides into linear chains (by UV radiation).[32]

CLASS C SPs

Polyrotaxanes and poly[2]catenanes, exemplified by 14 and **15** in Fig. 6, are a class of mechanically interlocked macromolecules[45–47] deriving from the extensively studied low-MW compounds **16**.[48,49] Polyrotaxane **14**. prepared from the condensation of tetraarylmethane-based diols and acid chlorides in the presence of a crown ether, attained $M_n \sim 25.000$ with rings mechanically trapped between two large tetraarylmethane groups. The poly[2]catenane **15**, prepared from a bisfunctionalized [2]catenane, attained $M_n \sim 800.000$ including numerous mechanical linkages. Interest in this unconventional type of polymers is due to the possibility of inducing relative movements of their noncovalently bound components under the action of external stimuli. In Scheme **16**, rings of dibenzol[24]crown-8 can flip around interactions localized at the NH_2^+ centers. Relative motion can be triggered by electrochemically or photocheinically induced reduction/oxidation reactions.[49] Molecular microengines and abacuses may thus be conceived.

The components of the "shish-kebab" composite (17) based on α-cyclodextrin rings over poly(ethylene oxide)[50] are not irreversibly interlocked as for true Class C SPs. The assembly belongs to the class of clathrates (inclusion compounds) that have interest for separation processes. Single chains are confined in small channels (diameter -6 Å) for a wide variety of crystalline adducts. These systems suggests that smoothed-out effects assist rhe formation of host–guest polymeric assemblies in addition to localized interactions. The nonlocalized effects may arise from the suppression of undulation modes of the polymer due to the presence of rings. and from excluded volume effects favoring elongated assemblies."]

A covalent polymer (18) was synthesized starting from dendritic 7-oxanorbornene macromonomers. The solid-state structure of the polymer revealed helical columnar stacks of disks. Each disk included four tapered monodendrons (spanning two repeating units), with the main chain running in the central cavity and complying with the supramolecular organization of side chains.'''''''' The formation of columnar stacks of disks was documented for other monodendritic, tapered units having a crown ether at the focal point. When the latter was replaced with an oligoxyethylenic segment connected as a side chain to a polymethylacrylate chain, the columnar stack was transformed into a helical column.

The organization of tapered monodendrons, connected or not to a covalent chain, can be regarded as a model roi. the assembly of the tobacco mosaic virus, 19. included for comparison in Fig. 6. Here, the guest is a RNA molecule: and the host is a hollow column composed of 2130 identical tapered protein molecules following a helix with 16.3 units per turn.'''' The whole structure can be disassembled by pH change and reassembled with and without RNA. In the latter case. however, the spiralization is lost, and the host is simply a stack of disks, each including 17 protein units. It appears. therefore, that a polymer hosted in the cavity of a columnar stack induces spiralization, irrespective of the nature (covalent or supramolecular) of the bond with the host. The model of internal crank-shaft coupling features of Class A and Class C systems is suggested.[20] Additional features of biological assemblies were reproduced by polymers with dendritic side chains.[51,52] In particular, spherical assemblies. modeling icosahedral virus. were obtained with low-DP dendritic polymers.

The self-assembled monolayers 20 (SAMs) are two-dimensional assemblies of short hydrocarbon chains [i.e., decanethiol HS(CH2)10X] grafted to a planar surface [i.e., AU(111)].[54] A covalent bond actually occurs between the head-group HS and gold. The organization of alkyl segments involves. with increasing coverage, a phase with molecular axes parallel to the surface and a final phase with all *trans* segments tilting $\sim 30°$ from the normal axis. Properties and applications of SAMs are influenced by the nature of the terminal functional group and by subsequent chemical transformations, including the attachment of polymers. Patterning of SAMs is most conveniently done by microcontact printing, confinement in areas of nanometric dimension was verified by AFM. Applications are in areas of nanotechnology: molecular electronics. optical devices, biological and chemical sensors, and tissue engineering.

CLASS D SPs

Engineered assemblies may be produced by controlled addition of components, chemical reactions or additives, external forces such as flow fields, and dissipative processes.[6] Supramolecular interaction still assists the final organization, but the assembly mechanisms are outside the theoretical framework discussed above. Thus, only a few examples will be outlined.

The complexation of complementary polyelectrolytes can allow the formation of assemblies attaining macroscopic dimensions. Spherical skins may, for instance, be

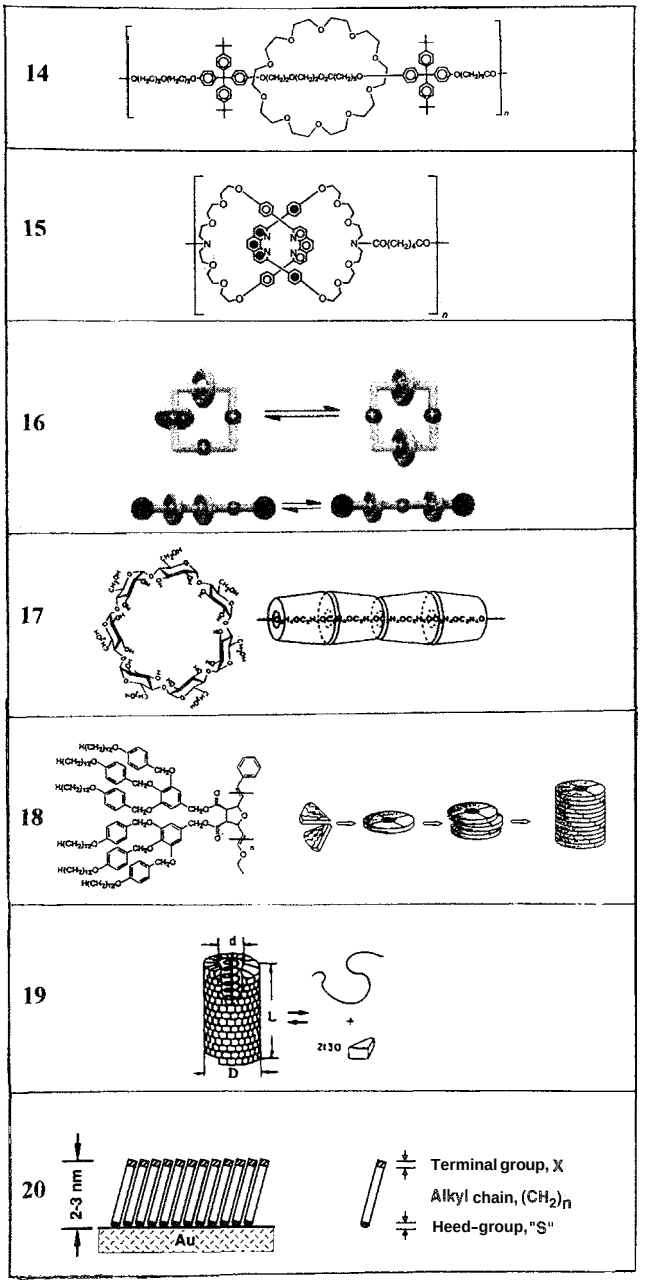

Fig. 6 Class C SPs. 14: Polyrotaxane;[45,46] 15: poly[2]catenane;[45,47] 18: linear dendritic hybrid chain from 7-oxanorbornene monomers substituted with two tapered monodentrons;[52] and 20: SAMs of n-alkanethiolates on gold.[54] Structures 16: [3]catenane and [3] rotaxane with two dibenzol[24]crown-8 rings;[48] 17: α-cyclodextrin+poly(ethylene oxide);[50] and 19: tobacco mosaic virus[**] are included for comparison.

produced by letting drops of a polycation solution free fall into a solution of a polyanion.[55] The theoretical basis for the forination of micellar-like aggregates within a gel of complementary polyelectrolytes was discussed.[55] Stratified deposition of complementary polyelectrolytes, colloids.~bola-type amphiphiles may be achieved by alternating deposition of components anchored to a suitable surface; for instance, a substrate compatible with poly-(styrene sulfonate) alternatively dipped in poly(allylamine hydrochloride). and PSS solutions.[56,57] Uncompensated sites and intermediate rinsing steps prevent uncontrolled coprecipitation. The method has several advantages over the classical LB deposition and was applied to a wide variety of systems. It allows micropatterning and tailored performance in applications such as biocompatibility, biocatalysis, and integrated optics and electronics.[56,57]

DNA nanotechnology allows the fabrication of nanostructured composites based on gold particles regularly distributed within a DNA matrix.[▾▾▾] Complex functionalities leading to branched and two-dimensional matrices lead to programmable nanodevices extending the assembling modes from periodic to algorithmic ones.[9]

ARTICLES OF **FURTHER INTEREST**

Biological Models and Their Characteristics, p. 101
Catenanes and Other Interlocked Molecules, p. 206
Classification and Nomenclature of Supramolecular Compounds, p. 261
Clathrate Inclusion Compounds, Phase Transitions in, p. 289
Crystal Growth Mechanisms. p. 364
Dendrimers, p. 432
The Diphenylmethane Moiety, p. 452
Hydrophobic Effects, p. 673
Ion Channels and Their Models, p. 742
Micelles and Vesicles, p. 861
Molecular Switches, p. 917
Molecular-level Machines, p. 931
Nonlinear Optical Materials, p. 973
Peptide Nanotubes, p. 1035
π–π Interactions: Theory and Scope, p. 1076
Rotaxanes and Pseudorotaxanes, p. 1194
Self-Assembly: Definition and Kinetic and Thermodynamic Considerations, p. 1248
Strict Self-Assembly and Self-Assembly with Covalent Modifications, p. 1372
Strong Hydrogen Bonds, p. 1379
Supramolecular Polymers, p. 1443
Surfactants, Part I: Fundamentals, p. 1458
Surfactants, Part II: Applications, p. 1470
van der Waals Forces. p. 1550

REFERENCES

1. Ciferri, A. Supramolecular polymerizations. Macromol. Rapid Commun. **2082,** *23,* 511.
2. *Supramolecular* Polymers; Ciferri. A., Ed.: Marcel Dekker. Inc.: New York, 2000.
3. Schneider. H.-J. Mechanisms of molecular recognition—Investigations of organic host guest complexes. Angew. Chern.. Int. Ed. **1991,** *30,* 1417.
4. Brunsveld. L.: Folmer. B.J.B.; Meijer, E.W.: Sijbesma, R.P. Chem. Rev. **2001.** *101.* 4071.
5. Lehn, J.-M. *Supramolecular Polymers*; Ciferri, A., Ed.; Marcel Dekker, Inc.: New York, 2000; 615.
6. Ciferri, A. Mechanism of supramolecular polymerizations. J. Macromol. Sci-Pol R. **2003,** *C43.* 271.
7. Oosawa, *F.;* Asakura, S. *Thermodynamics of* the Polymerization of Protein; Academic Press: London, 1975.
8. Sleytr, U.B.; Sara, M.; Pum. D. *Supramolecular Polymers*; Ciferri, A., Ed.; Marcel Dekker. Inc.: New York, 2000; 177.
9. Seeman, N.C. In the nick of space: Generalized nucleic acid complementarity and DNA nanotechnology. Synlett **2000,** *11*, 1536.
10. Ciferri. *A.* Fundamental aspects of supramolecular polymerization. Recent Res. Devel. Macromol. Res. 2002. 6. 129.
11. Tanford, C. Formation of *Micelles and* Biological Membranes; Wiley: New York. 1980.
12. Halperin. A. *Supramolecular* Polymers; Ciferri. A., Ed.; Marcel Dekker, Inc.: New York, 2000; 93.
13. Matsen, M.W.: Bates. F.S. Unifying weak- and strong-segregation block copolymer theories. Macromolecules **1996.29.** 1091.
14. Ciferri. **A.** *Liquid Crystallinity* in *Polymers*; Ciferri. A., Ed.: VCH: New York. 1991: 209.
15. Bates, M.A.: Frenkel. D. Infinitely thin disks exhibit a first order nematic-columnar phase transition. Phys. Rev.. E **1998, 57,** 4824.
16. Israelachvili, J.N. *Intermolecular* and *Surface* Forces: Academic Press: London. 1992.
17. Odian, G. Principles of *Polymerization*; McGraw-Hill: New York. 1991.
18. Lee. J.Y.; Painter, P.C.: Coleman, M.M. Hydrogen-bonding in polymer blends. 4. Blends involving polymers containing methacrylic-acid and vinylpyridine groups. Macromolecules 1988, 21. 954.
19. van Gestel. J.: van der Schoot. P.: Michels, M.A.J. Helical transition of polymer-like assemblies in solution. J. Phys. Chem., B **2001.** *105*, 10691.
20. Ciferri; *A.* Supramolecular liquid crystallinity as a mechanism of supramolecular polymerization. Liq. Cryst. 1999, 26. 489.
21. Odijk. T. Effect of micellar flexibility on the isotropic-nematic phase transition in solutions of linear aggregates. J. Phys. **1987,** *48.* 125.
22. Hentschke. *R.:* Edwards. R.: Boden. P.J.B.; Bushby, R.J. A model for isotropic. nematic. and columnar ordering in a self-assembling system—comparison with the phase-

behavior of 2,3,6,7,10,11-hexa-(1,4,7-trioxaoctyl)-triphenylene in water. Macromol. Symp. 1994. *81.* 361.
23. van der Schoot, P. Phase ordering of marginally flexible linear micelles. J. Phys., II 1995. *5.* 243.
24. Tessa ten Cate, A.; Sijbesma, R.P. Macromol. Rapid Commun. in *press.*
25. Michelsen. U.; Hunter. C.A. Self-assembled porphyrin polymers. Angew. Chem., Int. Ed. 2000. *39,* 764.
26. Gottarelli. G.: Masiero. S.: Spada, G.P. Self-assembly in organic solvents of a deoxyguanosine derivative induced by alkaly metal picrates. J. Chem. Soc., Chern. Commun. 1995, 2555.
27. Oosawa. F. *Supramolecular Polymers*; Ciferri. A., Ed.; Marcel Dekker, Inc.: New York, 2000: 643.
28. Oosawa, F. Physical-chemistry of actin—Past. present and future. Biophys. Chemist. 1993. 47. 101.
29. Nuckolls. C.; Katz, T. Synthesis. structure, and properties of a helical columnar liquid crystal. J. Am. Chem. Soc. 4998. *120.* 9541.
30. Verbiest. T.; van Elshocht. S.; Karuanen. M.; Heliemans. L.; Snauwaert, J.: Nuckolls. C.: Katz, T.J.; Persoons. A. Strong enhancement of nonlinear optical properties through supramolecular chirality. Science 1998, *282,* 913.
31. Palmans. A.R.A.; Vekemans. J.A.J.M.; Fischer, H.: Hikmet. R.A.M.; Meijer, E.W. Extended-core discotic liquid crystals based on the intramolecular H-bonding in N-acylated 2.2'-bipyridine-3.3'-diamine moieties. Chem. Eur. J. 1997. *3.* 300.
32. Vollmer, M.S.: Clark. T.D.; Steinem, C.: Ghadiri. M.R. Photoswitchable hydrogen-bonding in self-organized cylindrical peptide systems. Angew. Chem.. Int. Ed. 1998. *38.* 1598.
33. Hill. D.J.: Mio. M.J.: Prince, R.B.: Hughes. T.S.; Moore, J.S. A field guide to foldamers. Chem. Rev. 2001. *101,* 3893.
34. ten Cate. A.T.: Sijbesma. R.P. Coils. rods and rings in hydrogen-bonded supramolecular polymers. Macromol. Rapid. Commun. 2002. *23,* 1094.
35. Lopez-Carrasquero. F.: Monserrat. S.: Martinez de Harduya. A.; Muñoz-Guerra, S. Structure and thermal properties of new comblike polyamides. Macromolecules 1995. *28.* 5535.
36. Batten. S.R.: Robson. R. Interpenetrating nets: Ordered. periodic entanglement, Angew. Cheni.. Int. Ed. 1998. *37,* 1460.
37. Wolfram. S. A *New Kind of* Science: Wolfram Media. 2002.
38. Castellano. R.K.: Clark. R.: Craig. S.L.: Nuckolls. C.: Rebek. J.. Jr. Emergent mechanical properties of self-assembled polymeric capsules. Proc. Natl. Acad. Sci. U. S. A. 2000. *97.* 12418.
39. Gohy, J.F.; Lohmeijer. B.G.G.: Schubert, U.S. Reversible metallo-supramolecular block copolymer micelles containing a soft core. Macromol. Rapid Commun. 2002, *23.* 555.
40. Paleos. C.M.: Tsiourvas. D. Supramolecular hydrogen-bonded liquid crystals. Liq. Cryst. 2001, *28.* 1127.
41. Flory, P.J.: Ronca, G. Theory of systems of rodlike particles. 2. Thermotropic systems with orientation-dependent interactions. Mol. Cryst. Liq. Cryst. 1979, 54. 311.
42. Kato, T.: Fréchet, J.M.J. Stabilization of a liquid crystalline phase through non covalent interaction with a polymer side chain. Macromolecules 1989. 22. 3818.
43. Demeftahi. M.V.: Fréchet. J.M.J. Study of the compatibility of blends of polymers and copolymers containing styrene, 4-hydroxystyrene and 4-vinylpyridine. Polymer 1988. *29.* 477.
44. Kato. T.; Mizoshita. N.: Kanie, K. Hydrogen-bonded liquid crystalline materials: Supramolecular polymeric assembly and the induction of dynamic function. Macromol. Rapid Commun. 2001. *22,* 797.
45. Raymo. F.M.; Stoddart, J.F. *Supramolecular* Polymers: Ciferri, A., Ed.: Marcel Deltker. Inc.: New York, 2000; 323.
46. Gong, C.; Ji. Q.: Glass. T.E.; Gibson, H.W. A strategy to eliminate dethreading during the preparation of poly(ester/crown ether rotaxane)s: Use of difunctional blocking groups. Macromolecules 9997. *30.* 4807.
47. Shimada. S.: Ishiwara, K.: Tamaoki, N. Synthesis and switchable condensation reaction of bifunctional [2]catenane. Acta Chem. Scand. 1998, *52.* 374.
48. Sheng-Hsien. C.: Elizarov. A.M.: Glink. P.T.; Stoddart. J.F. Org. Lett. 2902. 4, 3561.
49. Balzani. V.: Credi, A.: Raymo, F.M.: Stoddart, J.F. Artificial molecular machines. Angew. Chem., Int. Ed. 2000. *39.* 3348.
50. Huang. L.: Tonelli. A.E. J.M.S. Polymer inclusion compounds. Rev. Macromol Chem. Phys. 1998. *C38.* 781.
51. Tomalia. D.A.; Majoros. I. *Supramolecular Polymers*; Ciferri. A.. Ed.; Marcel Dekker. Inc.: New York. 2000: 359.
52. Percec, V.; Schlueter. D. Mechanistic investigations on the formation of supramolecular cylindrical shaped oligomers and polymers by living ring opening metathesis polymerization of a 7-oxanorbornene monomer substituted with two tapered monodendrons. Macromolecules 4997. *30.* 5783.
53. Klug. A. From macromolecules to biological assemblies. Angew. Chern., Int. Ed. 1983, *22,* 565.
54. Yan, L.; Huck. W.T.S.; Whitesides, G.M. *Supramolecular Polymers*; Ciferri. A., Ed.; Marcel Dekker, Inc.: New York. 2000: 435.
55. Larez. C.: Crescenzi. V.; Dentini, M.; Ciferri, A. Assemblies of amphiphilic compounds on rigid polymers. II. Interaction of sodium dodecylbenzenesulfonate with chitosan-scleraldehyde gels. Supramol. Sci. 1995. *2.* 141.
56. Arys, X.: Jonas, A.M.; Laschewsky, A.; Legras. R. *Supramolecular Polymers*; Ciferri. A.. Ed.: Marcel Dekker, Inc.: New York. 2000; 505.
57. Decher. G.; Schelenoff, J.B. *Multilayer Thin Films: Sequential Assembly*; Wiley: Europe. 2002.
58. Mirkin, C.A. Programming the assembly of two- and three-dimensional architectures with DNA and nanoscale inorganic building blocks. Inorg. Chem. 2000. *39.* 2258.

Supramolecular Stabilization

Dmitriy V. Soldatov
John A. Ripmeester
National Research Council Canada, Ottawa, Ontario, Canada

INTRODUCTION

Supramolecular stabilization means stabilization of certain chemical species. their different forms, and assemblies in a particular supramolecular environment. Supramolecular stabilization is responsible for the existence of "energetically unfavorable" conformations. different spatial isomers, unexpected oligomers, "unstable" molecules. highly reactive radicals, elements in unusual oxidation states. certain ionic species, and so on, in supramolecular phases. Such species decompose. change, or equilibrate with alternative forms once they are brought out of their "stabilizing" environment. The best-known chemical reaction based strictly on supramolecular stabilization is the so-called "blue reaction." where iodine reversibly polymerizes in the presence of starch.

Supramolecular stabilization provides an excellent opportunity to store highly reactive species or to obtain species not available by traditional methods in high concentration. The phenomenon plays an important role in stabilizing drugs and may be useful in the creation of new methods of separation and purification. the design of new functional and smart materials. and the development of new approaches to chemical and biological research.

KINETIC VERSUS THERMODYNAMIC STABILIZATION

Kinetic and therinodynamic stabilization are intrinsically distinct and. therefore. should be treated separately. Kinetic stabilization occurs because of the restrictions that a supramolecular environment superimposes on highly reactive species. These restrictions increase the activation barrier for decomposition routes. thus increasing the lifetime of the species. Typical restrictions include the isolation of reactive species from each other or from other possible issues relating to their instability: oxygen, water, light, radiation, and so on. Thermodynamic stabilization occurs because of a change in the energy balance created by the supramolecular environment. thus favoring formation of stabilized species. This can be attributed to a specific set of noncovalent interactions, such as van der Waals forces, hydrogen bonding, additional coordination, or other secondary interactions. Although each individual interaction is weak. the cumulative contribution of multiple intermolecular contacts may have an impact significant enough to stabilize supramolecular complexes or solids with "unusual" chemical species.

Kinetic stabilization is iinportant for increasing the useful lifetime of drugs. The active drug content of various pharmaceutical formulations decreases with time upon heating, oxidation, hydrolysis. and self-degradation. The guarantee of chemical and mechanical stability for a pharmaceutical product for periods of at least 2 years is a key factor for marketing the product. Stabilization of photosensitive drugs by inclusion in cyclodextrins was reported."' The stabilization of prostaglandins and other pharmaceuticals using cyclodextrins is successful, and inclusion products are marketed in Japan and other countries.[2] Kinetic stabilization plays an important role in the chemistry of radicals. For example, stabilization or destabilization of nitroxides in redox processes and hydrolysis in the presence of cyclodextrins is well documented."'

Thermodynamic stabilization reflects a drive to the lowest overall energy of the final phase. This tendency may cause flexible chemical species to change in order to accept the most favorable geometry in context of the resulting supramolecular environment. Thermodynamic stabilization falls into several types. depending on the kinds of species that are stabilized. The most common types are dealt with below.

SPECIES THAT CAM BE STABILIZED

Conformational Isomers

Three experimental observations provide good estimates of how strongly molecular geometry is influenced by surroundings in molecular crystals. The first observation is "contact conformational isomerism.." where different conformations are encountered for the same molecule in a single phase.[4] The statistical analysis of crystals having two or more symmetrically independent molecules in the same structure reveals that about 20% contain molecules with different conformations.[4] A second observation is

DOI: 10.1081/E-ESMC 120013466

conformational polymorphism, the existence of different conformations of the same molecule frequently observed in polymorphs.[5] A third observation is conformational isomerism induced by a guest template. the appearance of different conformations of the same molecule in a range of inclusion compounds.[6–8]

Monomers, Oligomers, Polymers

First described in the literature in 1814,[9] the "blue reaction" of iodine with starch is the best-known example of a polymerization process induced by supramolecular stabilization. Structural studies indicate that amylose (the linear fraction of starch) forms a helix with six glucose residues per turn to include guest iodine molecules.[10] Inside this helix, iodine molecules form a polymeric chain with a periodicity of 3.1 Å, which is much shorter than the nonbonded distance between iodine atoms (4.3 Å) but greater than the single I–I bond distance (2.7 A).[11] The amylose–iodine reaction is widely used in analytical chemistry and was utilized for the solubilization and purification of carbon nanotubes.[12]

Oligomerization of metal complexes induced by a template drastically changes properties of materials. Exposure of a polymeric copper(I) complex to toluene vapor leads to the disappearance of its blue emission and the appearance of yellow emission because of the formation of a new tetrameric complex which forms an inclusion compound with guest toluene.[13] Nickel(II) dibenzoylmethanate monomer, a brown diamagnetic material. rearranges into a trimer, green paramagnetic material. in the presence of benzene, as the trimeric form accommodates guest benzene in its void space.[14] The material transformations described above are reversible and selectively sensitive to a specific transforming template and, therefore. may be used in the design of functional and smart materials.

Spatial Isomers

Several types of isomers can be stabilized in supramolecular solids,[11] and the temperature. or the presence of various templates, may factor in switching molecules from one isomer to another. These may be inorganic ions,[16] polar molecules like water,[17] or typical organic molecules like *o*-xylene.[18] Guest-induced stabilization of stereo- (*cis–trans*) isomers has the most potential: stereoisomers are usually similar in energy (because they have the same set of chemical bonds), but they can form different inaterials (due to dramatic differences in molecular geometry).

The utility of the stabilization of spacial isomers is vividly illustrated by a system of two conjugated polymorphs of a copper β-diketonate complex.[15,19] The *r*-form of the complex contains cis and *trans* units that assemble into a dense structure, whereas the β-form contains only *trans* units that assemble into a microporous framework (Fig. I). Therefore, the α-to-β (or reverse) transition involves cis-to-trans (or reverse) isomerization on a molecular level and switches on (or off) the microporosity, an integral property of the material. The identification of appropriate conditions that control the isomerization made it possible to utilize the system as a first smart sorbent, that is. a sorbent with microporosity that may be switched off and on in situ by an operator.[20]

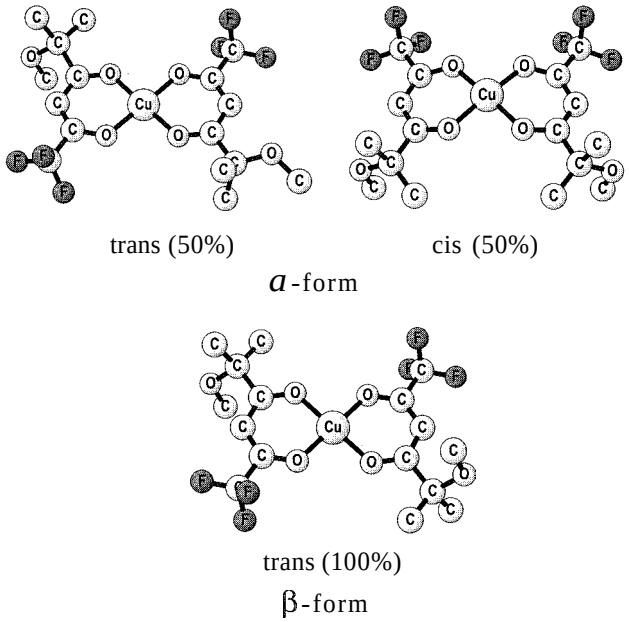

Fig. 1 Isomer distribution in the two polymorphs of (1,1,1-trifluoro-5,5-dimethyl-5-methoxyacetylacetonato)copper(II). The n-form has *trans* and cis isomer units, whereas in the P-form, they are all *trans*. For clarity, fluorine atoms are dark.

Host *Molecules*

The stabilization of host molecules in van der Waals clathrate matrices is referred to as "contact stabilization,"[21–23] This type of stabilization is most striking, as the molecule can exist only in a "stabilizing" supramolecular environment and cannot form a stable solid phase without a template. In other words, a favorable set of noncovalent interactions prevents the molecule from decomposition.

Contact stabilization is observed in the binary system pyridine (Py)–cadmium nitrate. The phase diagram of the system[24] indicates formation of an inclusion coinpound $[CdPy_4(NO_3)_2]$*2Py (Fig. 2). The compound comprises molecules of the $[CdPy_4(NO_3)_2]$ host complex[25] (Fig. 3)

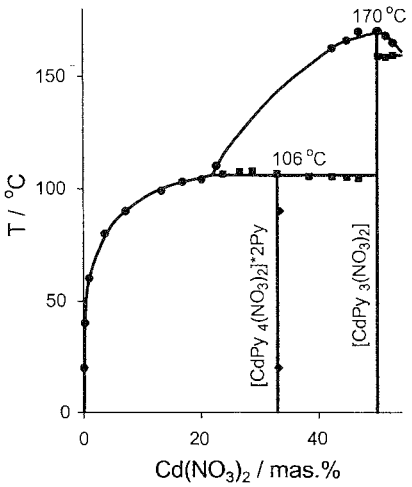

Fig. 2 The phase diagram of the pyridine (Py)–cadmium nitrate system (fragment). The host complex $[CdPy_4(NO_3)_2]$ does not exist in the system as a solvent-free compound.

that build a crystal with guest pyridine included in cavities. As follows from the phase diagram, the host complex does not form an individual phase; the molecules of the $[CdPy_4(NO_3)_2]$ complex exist only in the inclusion compound and instantly decompose upon removal of the guest component:

$$[CdPy_4(NO_3)_2]*2Py = [CdPy_3(NO;),] + 3Py$$

In quantitative terms,[26] the contact stabilization phenomenon appears when the stability of a molecule is comparable with the stability of its decomposition products, and noncovalent interactions in a particular solid phase play a decisive role favoring or disfavoring formation of the molecule.

Guest Species

The stabilization of highly reactive or easily dissociating guest species included in host molecules or in a host framework is related to the contact stabilization phenomenon. Various fluoride complexes of boron, silicon. and germanium are stabilized through creation of favorable hydrogen bonds with crown ethers.[27] Oxonium and other ions of biological significance are stabilized in calixarenes or coordination polymers, such as H_3O^+,[28] $H_5O_2^+$,[29] $H_7O_3^+$,[30] and $N_2H_7^+$.[31]

MOLECULAR VERSUS SUPRAMOLECULAR STRUCTURE

In the past. chemists underestimated the importance of noncovalent interactions, resulting in much confusion. The development of supramolecular concepts in chemistry made it possible to understand and rationalize a number of experimental observations. One such example is the so-called "hexapyridine metal complexes," representing dozens of compounds with the general formula MX_2*6Py (M is a metal(II), X is (–1) anion, *Py* is pyridine or its derivatives). A priori, these compounds were described as complexes where six pyridine ligands coordinate to the central atom M with ionic packing comprising $[MPy_6]^{2+}$ cations and A^- anions. Recent studies revealed that this is not the case.[32] The compounds should be described by the formula $[MPy_4X_2]$*2Py, as the *X* anions and only four pyridines are coordinated to the central atom, whereas the remaining two pyridines are included as guest species. Therefore. the compounds contain only neutral species in their van der Waals lattices. Exclusively using the language of chemical bonds, it would be difficult to explain why such poor ligands as nitrate or perchlorate compete with pyridine for the coordination sites around the metal center.[26] It is the noncovalent interactions that are responsible for the fact that hexapyridine metal species are rarely observed in the solid state. while the chemical analogue hexaammine complexes are common.[33]

STABILIZATION OF MOLECULAR ENSEMBLES

In a broader sense, supramolecular stabilization is responsible for the regular arrangement of species in supramolecular structures. The following examples show some of the applications of the phenomenon.

Inclusion compounds of urea[34] display linear arrays of guest species inside cylindrical channels. This property makes it possible to conduct stereoregular poiymerization

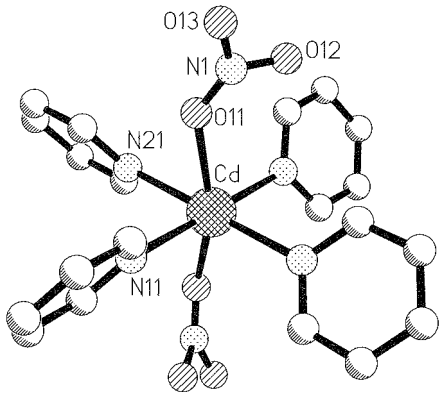

Fig. *3* Structure of the $[CdPy_4(NO_3)_2]$ coinplex molecule in the clathrate phase.

reactions of included species inside the channels. Another application is to constrain polymers in the ordered environment of the urea tunnel structure to simplify the spectroscopic and diffraction properties of the polymers. Orienting unsaturated molecules in certain supramolecular environments with appropriate hydrogen bonding makes it possible to conduct stereoregular condensation reactions in the solid phase in quantitative yield.[35] In more detail, the subject is reflected in other topics, see for example the following topics in this *Encyclopedia*: inclusion reactions and polymerization; hydrogen bonding; inclusion compounds; polarity in crystals; preorganization and complementarity; soft and smart materials; solid-state reactivity and topochemistry; and strong hydrogen bonds.

CONCLUSION

Supramolecular stabilization is an important concept that needs to be introduced when considering the influence of the supramolecular environment on the structures and stabilities of chemical species. The kinetic component of the phenomenon is responsible for increasing or decreasing the lifetime of chemical species included in host structures. The thermodynamic component of the phenomenon explains the existence of unusual, or one of many possible, chemical entities in supramolecular solids. Our current understanding of these phenomena allows a number of experimental facts to be explained and makes qualitative predictions possible in some cases. Further development of these concepts to more quantitative levels will allow improved predictions and the purposeful design of desired species stabilized in supramolecular environments.

ARTICLES OF FURTHER INTEREST

Anion-Directed Assembly, p. 51
Bond-Stretch Isomerism, p. 120
Calixarenes: Synthesis and Historical Perspectives, p. 153
Crown Ethers, p. 326
Crystal Structure Prediction, p. 371
Cyclodextrins, p. 398
Hydrogen Bonding, p. 658
Hydrophobic Effects, p. 673
Inclusion Compounds: Selectivity, Thermal Stability, and Kinetics, p. 696
Inclusion Reactions and Polymerization, p. 705
Preorganization and Complementarity, p. 1158
Secondary Bonding, p. 1215
Soft and Smart Materials, p. 1302
Solid-State Reactivity/Topochemistry, p. 1316
Strong Hydrogen Bonds, p. 1379
The Template Effect, p. 1493
van der Waals Forces, p. 1550

REFERENCES

1. Tomono, K.; Hiroko, G.; Okamura, M.; Ueda, H.; Saitoh, T.; Nagai, T. Effect of β-cyclodextrin and its derivatives on the photostability of photosensitive drugs. Yakuzaigaku 1988, 48 (4). 322–325.
2. Nagai, T.: Ueda, H. Aspects of Drug Formulation with Cyclodextrins. In *Comprehensive Supramolecular Chemistry;* Atwood, J.L., Davies. J.E.D., MacNicol, D.D., Vogtle, F.. Eds.: Pergamon: Oxford. 1996; Vol. 3, 441–450.
3. Fenyvesi. E.: Szente, L.; Russell, N.R.; McNamara, M. Specific Guest Types. In Comprehensive *Supramolecular* Chemistn: Atwood, J.L., Davies, J.E.D., MacNicol, D.D., Vogtle, F., Eds.; Pergamon: Oxford, 1996; Vol. 3,305–366.
4. Zorkii. P.M.: Razumaeva. A.E. The coexistence of molecules having different structures in organic crystals. J. Struct. Chem. 1979. 20 (3). 390–393.
5. Bernstein, J. Conformational Polymorphism. In Organic Solid State *Chemistry*; Desiraju, G.R., Ed.; Studies in Organic Chemistry. Elsevier: Amsterdam. 1987; Vol. 32. 471–518.
6. Soldatov, D.V.; Grachev. E.V.; Lipkowski, J. Crystal structure of a 1:2:1 packing complex formed by bis(isothiocyanato)tetrakis(pyridine)nickel(II), triphenylmethane, and methanol. J. Struct. Chem. 1996, 37 (4). 658–665.
7. Soldatov, D.V.; Ripmeester, J.A. Novel 4-vinylpyridine-extended metal-dibenzoylmethanate host frameworks: Structure. polymorphism, and inclusion properties. Chem. Eur. J. 2001, 7 (14), 2979–2994.
8. Barbour, L.J.: Atwood, J.L. Non-covalent interactions exert extraordinary influence over conformation and properties of a well-known supramolecular building block. Chem. Commun. 2001, (19), 2020–2021.
9. Colin, M.M.; Gaultier de Claubry, H. Sur les combinaisons de l'iode avec les substances végétales et animales. (On the reactions of iodine with vegetable and animal materials.) Ann. Chim. 1814, 90. 87–100.
10. Rundle, R.E.; French, D. The configuration of starch in the starch–iodine complex. III. X-ray diffraction studies of the starch–iodine complex. J. Am. Chem. Soc. 1943, *65* (9), 1707–1710.
11. West. C.D. Structure-optical studies. I. X-ray diffraction by addition compounds of halogens with hydrophilic organic polymers. J. Chem. Phys. 1947, *15* (9), 689.
12. Star, A.; Steuerman, D.W.; Heath, J.R.; Stoddart, J.F. Starched carbon nanotubes. Angew. Chem. Int. Ed. 2002. 41 (14), 2508–2512.
13. Cariati, E.: Bu, X.; Ford, P.C. Solvent- and vapor-induced isomerization between the luminescent solids $[CuI(4\text{-pic})]_4$ and $[CuI(4\text{-pic})]_\infty$ (pic = methylpyridine). The structural basis for the observed luminescence vapochromism. Chem. Mater. 2000, 12 (11), 3385–3391.
14. Soldatov, D.V.; Henegouwen, A.T.; Enright, G.D.: Ratcliffe, C.I.: Ripmeester, J.A. Nickel(II) and zinc(II)

dibenzoylmethanates: Molecular and crystal structure, polymorphism, and guest- or temperature-induced oligomerization. Inorg. Chem. **2001**, *40* (7). 1626–1636.
15. Soldatov, D.V.; Ripmeester, J.A. Flexible Metal–Organic Frameworlts with Isomerizing Building Units. In *Studies* in *Surface Science and Catalysis*; Delmon, B., Yates, J.T.. Eds.; Elsevier: Amsterdam, 2002; Vol. 141, 353–362.
16. Guilard, R.: Siri, O.; Tabard, A.: Broeker, G.; Richard, P.; Nurco, D.J.: Smith. K.M. One-pot synthesis, physicochemical characterization and crystal structures of cis- and *trans*-(1,4,8,11-tetraazacyclotetradecane)dichloroiron(III) complexes. J. Chem. Soc., Dalton Trans. **1997**. (19), 3459–3463.
17. Adams, R.P.: Allen. H.C.; Rychlewska, U.; Hodgson, D.J. The EPR spectrum of Mn(II) doped into cis-diaquobis (1,1,1,5,5,5,-hexafluoroacetylacetonato)zinc(II) and *trans*-diaquobis(1,1,1,5,5,5-hexafluoroacetylacetonato)-zinc(II) and the crystal structure of the host crystals. Inorg. Chim. Acta *1986. 119* (1). 67–74.
18. Nassimbeni. L.R.: Niven, M.L.: Zemke, K.J. Synthesis of diisothiocyanatoterakis(1-phenyl-1-ethylamine)nickel(II): Enclathration of organic guests with host isomerization. Acta Crystallogr. *1986, B42* (5). 453–461.
19. Soldatov. D.V.; Ripmeester, J.A.; Shergina, S.I.; Sokolov, I.E.; Zanina, A.S.; Gromilov, S.A.; Dyadin, Yu.A. *α*- and β-Bis(1,1,1-trifluoro-5,5-dimethyl-5-methoxyacetylacetonato)copper(II): Transforming the dense polymorph into a versatile new microporous framework. J. Am. Chem. Soc. *1999, 121* (17), 4179–4188.
20. Nossov, A.V.; Soldatov, D.V.; Ripmeester, J.A. In situ switching of sorbent functionality as monitored with hyperpolarized ^{129}Xe NMR spectroscopy. J. Am. Chem. Soc. 2001. *123* (15), 3563–3568.
21. Dyadin, Yu.A.; Kislykh, N.V. The contact stabilization of the frameworks and molecules of the host in guest–host systems. Russ. J. Phys. Chem. *1992,* 66 (1), 60–65.
22. Dyadin, Yu.A.; Soldatov, D.V.; Logvinenko. V.A.; Lipkowski. J. Contact stabilization of host complex molecules during clathrate formation: The pyridine–zinc nitrate and the pyridine–cadmium nitrate systems. J. Coord. Chem. *1996, 37* (1–4), 63–75.
23. Dyadin, Yu.A. At the interface between coordination and supramolecular chemistry: Contact stabilization of molecular complexes. Russ. J. Coord. Chem. *1996, 22* (5), 402–404.
24. Soldatov, D.V.; Dyadin, Yu.A; Ukraintseva, E.A.; Kolesov, BA.; Logvinenko, V.A. Clathrate formation and phase equilibria in the pyridine–cadmium nitrate system. J. Incl. Phenom. *1996. 26* (4). 269–280.
25. Soldatov, D.V.: Kolesov, B.A.: Lipkowski, J.: Dyadin, Yu.A. Polymorphous transformation of a clathrate in the pyridine–cadmium nitrate system. J. Struct. Chem. *1997. 38* (5), 819–828.
26. Soldatov, D.V.; Ukraintseva, E.A.: Logvinenko, V.A.; Dyadin, Yu.A.: Grachev, E.V.; Manakov, A.Yu. Thermodynamic dissociation constants for $[MPy_4(NO_3)_2]$*2Py clathrates (M = Mn, Co, Ni. Cu). Supramol. Chem. *2000. 12* (2), 237–246.
27. Simonov, Yu.A.: Fonari, M.S.; Lipkowski. J.: Gelmboldt. V.O.: Ganin, E.V. Inclusion compounds: The products of the interaction of silicon. germanium and boron fluorides with crown ethers. J. Incl. Phenom. **1996**, *24* (2), 149–161.
28. Atwood, J.L.; Bott, S.G.; Coleman, A.W.: Robinson. K.D.; Whetstone, S.B.; Means, C.M. The H_3O^+ cation in aromatic solvents. Synthesis, structure, and solution behavior of $[H_3O^+$*18-crown-6] [Cl–H–Cl]. J. Am. Chern. Soc. **1987**, *109* (26), 8100–8101.
29. Junk, P.C.; Atwood, J.L. Synthesis and x-ray crystal structure of $[H_5O_2^+$*21-crown-7] $[WOCl_5^-]$, a complex in which the 21-crown-7 molecule adopts a rigid, bowl-like conformation. J. Chem. Soc., Dalton Trans. *1995.* (15). 1551–1552.
30. Shirnizu, C.K.H.; Enright, G.D.; Rego, G.S.: Ripmeester, J.A. One-dimensional ribbons of solvated Ag sulfonates. Can. J. Chem. *1999, 77* (3), 313–318.
31. Atwood, J.L.; Barbour, L.J.; Jerga, A. Supramolecular stabilization of $N_2H_7^+$. J. Am. Chem. Soc. *2002, 124* (10). 2122–2123.
32. Soldatov, D.V.; Lipltowski, J. Structural reinterpretation and determination of the clathrate nature of the compounds of the general formula MX_2*6Py. J. Struct. Chem. *1995, 36* (6), 979–982.
33. Cotton, F.A.: Wilkinson, G.; Murillo, C.A.: Bochmann. M. Advanced Inorganic *Chemistry*, 6th Ed.; Wiley: New York, 1999.
34. Hollingsworth, M.D.; Harris, K.D.M. Urea, Thiourea, and Selenourea. In *Comprehensive Supramolecular* Chemistry: Atwood. J.L., Davies, J.E.D.. MacNicol. D.D.. Vogtle, F.. Eds.: Pergamon: Oxford, 1996; Vol. 6, 177–237.
35. MacGillivray, L.R.; Reid. J.L.; Ripmeester, J.A. Supramolecular control of reactivity in the solid state using linear molecular templates. J. Am. Chem. Soc. 2000, *122* (32), 7817–7818.

Surfactants, Part I: Fundamentals

John F. Scamehorn
David A. Sabatini
Jeffrey H. Harwell
University of Oklahoma, Norman, Oklahoma, U.S.A.

INTRODUCTION

Surfactants are important, or even crucial, in a wide variety of phenomena, including wetting, surface tension reduction, micelle formation, solubilization of organic solutes in micelles, emulsification: dispersion formation. adjusting solution rheology, and foaming. The two articles on ''Surfactants'' in this encyclopedia are split into "'Fundamentals.' and "Applications," with fundamental aspects of surfactant behavior being discussed in this article. The article in which a certain topic appears is arbitrary, because fundamental and applied aspects of surfactant behavior are involved in certain topics (e.g., wetting. emulsification, adsorption on solids). The purpose of this article is to outline the important physical behavior of surfactants, primarily in aqueous solution, because this is where most studies have been done.

OVERVIEW

The term "surfactant" is a contraction of "surface active agent." because a characteristic of surfactants is their tendency to adsorb or concentrate at interfaces between bulk phases. such as at the water–air surface or at the solid–liquid surface.

A surfactant molecule is composed of two basic parts: a water-soluble (hydrophilic) head group and an oil-soluble (hydrophobic) tail group, as shown in Fig. 1. While the tail group is often a hydrocarbon chain. the head group can be charged or uncharged. The basic surfactant structure is illustrated by sodium dodecyl sulfate in Fig. 1. The anionic sulfate is the head group. the linear dodecyl chain is the tail group. and sodium is the counterion (ion of opposite charge to the head group). Based on the hydrophilic and hydrophobic regions of surfactant molecules. they are sometimes referred to as amphiphiles or amphipaths.

In aqueous solution: the driving force for a surfactant's tendency to adsorb at interfaces and to form aggregates is the incompatibility of the tail group with water. Because of their hydrophobic nature, tail groups tend to insert themselves into a hydrophobic phase, or tend to self-assemble by forming aggregates in which the tails intertwine to form a hydrophobic environment from which water is largely excluded. If the tails cannot distribute into an oil-like phase. they essentially form their own oil phase, a process known as hydrophobic bonding. This term should not be misconstrued to imply that chemical bonds are formed between tail groups; rather, aggregation permits the hydrophobic tails to escape from water, eliminating this unfavorable tail–water interaction.

Shown in Fig. 2 are several of the many aggregates formed by surfactants. For these systems, unaggregated surfactant (monomer) is in equilibrium with the aggregate. If an aqueous solution of surfactant is in contact with air. the surfactant molecules adsorb at the air–water interface as a monolayer, with the head groups immersed in the water and the tails sticking in the air phase. If the aqueous solution forms an interface with a hydrophilic solid (e.g., cotton fabric or a clay). under select conditions, bilayered aggregates. known as an admicelles, will form on the surface. In this case. the head groups of the first layer of surfactant can have attractive interactions with the solid surface (e.g., electrostatic attraction or hydrogen bonding), and the second surfactant layer has head groups exposed to the water. In admicelles, the tail groups interact to form a hydrophobic interior.

The surfactant can also form aggregates in solution, such as micelles and vesicles. The spherical or cylindrical micelles shown in Fig. 2 have a core of interacting tail groups, coated by the head groups exposed to water, a configuration in which both dichotomous regions of the surfactant molecules can be in favorable environments. In contrast. if the surfactant is dissolved in an organic solvent. reverse or inverse micelles can form. where the tail group is at the micelle surface exposed to the solvent, and the head groups are exposed to a droplet of water at the reverse micelle core. Vesicles have structures similar to cell membranes, and in solution, the phospholipids of the cell membrane spontaneously fo m vesicles. Surfactants can form many other aggregated structures, only a few of which are shown in Fig. 2. In each case, the basic driving force for self-assembly is for each of the surfactant molecule's dissimilar parts to be in a favorable

Encyclopedia of Supramolecular Chemistry
DOT: 10.1081/E-ESMC 120012809

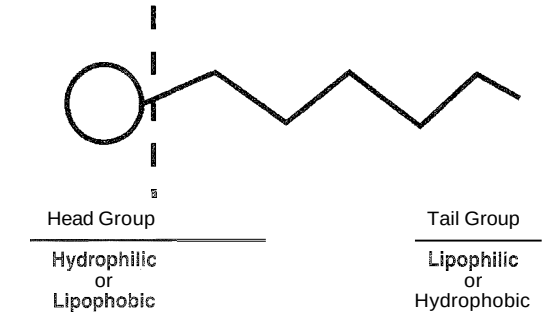

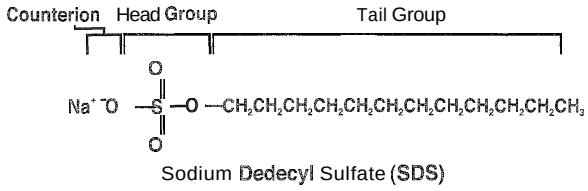

Fig. 1 Surfactant architecture—general representation of a surfactant molecule.

environment: for aqueous solutions, this means that the tail group should avoid contact with water.

While the tail group of commercial surfactants can be fluorocarbon or silicon based. the vast majority of surfactants have a hydrocarbon group as the tail. This hydrocarbon tail Is generally derived from natural sources like animal fat or vegetable oil, or from synthetic sources like petroleum derivatives. The head groups can vary dramatically between surfactants. Based on their head groups, surfactants are normally classified into five major classes. as illustrated in Fig. 3. Anionic surfactants are the largest volume of surfactants produced, with the linear alkylbenzene sulfonate (EAS). shown in Fig. 3, being the largest volume anionic surfactant produced commercially. For LAS. the head group is the negatively charged sulfonate group. while the linear alkyl chain (approximately 12 carbons in length) with the benzene ring is the tail group. The counterion (sodium) completely disassociates from the surfactant when the surfactant dissolves in water. As with many commercial surfactants. LAS is a coinplex mixture of hornologues with varying alkyl chain lengths, and isomers with varying points of benzene ring attachment to the alkyl chain. This natural heterogeneity produces performance advantages compared to a single surfactant molecule, including improved water solubility. In contrast to anionic surfactants. cationic surfactants, like ihose based on quaternary ammonium, have a positively charged head group. Nonionic surfactants typically have a polymeric group or an uncharged hydrophilic group like poly(ethylene oxide) as the head group (see Fig. 3). Zwitterionic surfactants have positive and negative charges on the head group. Amphoteric surfactants have a head group with a pH-dependent charge. The amine oxide shown in Fig. 3 is zwitterionic at high pH, but becomes cationic as protonation occurs at low pH. Because amphoteric surfactants are generally zwitterionic at some pH. and zwitterionic surfactants are often amphoteric. in practice, the terms zwitterionic and amphoteric are used as synonyms, and the term ampholytic is used to describe both surfactant types.

MICELLES

As illustrated in Fig. 4. a number of surfactant properties experience discontinuity in slope at a specific concentration called the critical micelie concentration (CMC). Below the CMC, an insignificant concentration of micelles is present. and essentially all the surfactant is present as monomer. Above the CMC. incremental surfactant forms micelles, and the monomer concentration remains nearly constant. Surfactant molecules contribute differently to a given property when present as monomer versus in a micelle. accounting for the discontinuity in slope in Fig. 4. The monomer concentration is often nearly proportional to the thermodynamic activity of the surfactant, and it is this activity that determines such properties as adsorption at interfaces. surface tension reduction, and precipitation. Monomer concentrations become nearly constant above the CMC (for single-component surfactants), resulting in many physical properties plateauing above the CMC. For example. as shown in Fig. 4, surface tension at the air–water interface levels off above the CMC—this is the dominant method of measuring the CMC. Even practical properties. such as

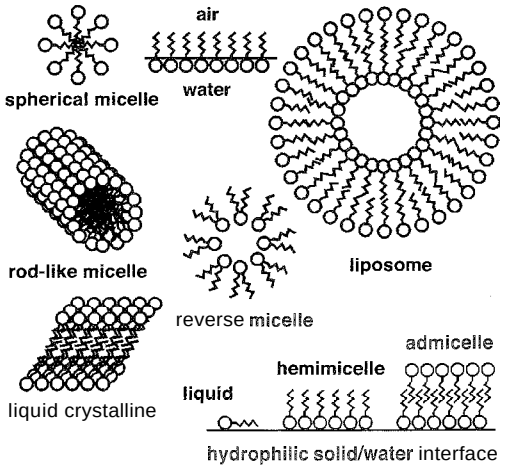

Fig. 2 Examples of surfactant aggregates.

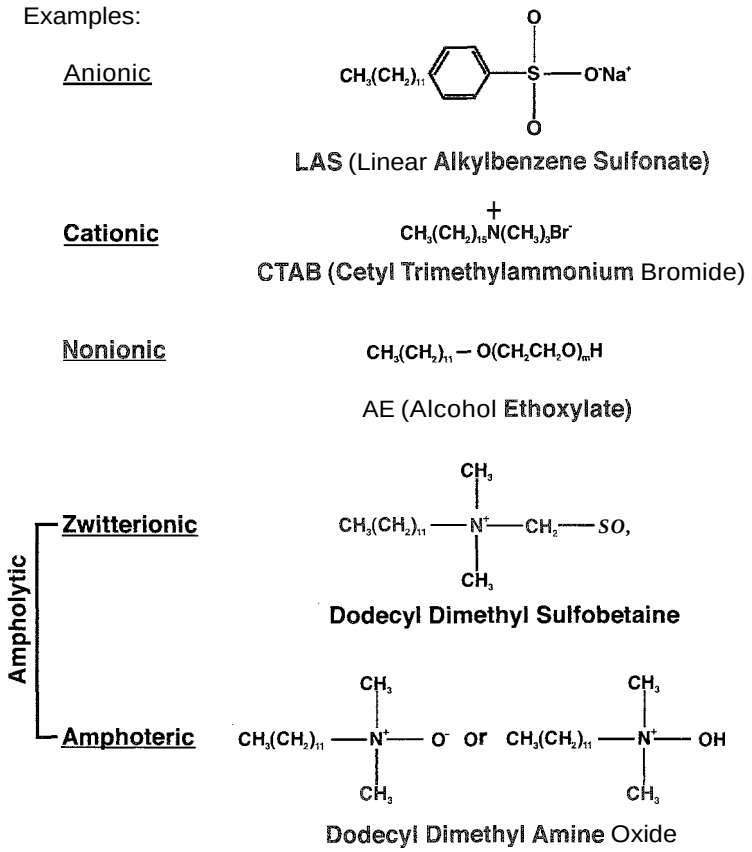

Fig. 3 Major surfactant groups.

particulate soil detergency, can plateau above the CMC. Charged or ionic surfactants contribute less to equivalent conductance in micellar form than as a monomer, resulting in the change in slope for this variable illustrated in Fig. 4; conductance is used to measure CMC of ionic surfactants at low ionic strength. Because the organic solutes dissolve (partition) into micelles (a phenomena called solubilization), the aqueous solubility of organic solutes increases with surfactant concentration above the CMC; conversely, surfactants do not significantly affect the aqueous solubility of organic solutes below the CMC, as illustrated in Fig. 4.

As illustrated in Fig. 2, micelies can be classified as normal (tail groups forming the core and head groups coating this oil-like interior) in aqueous solution; or reverse (inverse) where the tail groups are on the micelle exterior exposed to an organic solvent. There are fewer studies of reverse micelles compared to those on normal micelles, because the vast majority of surfactant applications are in aqueous solution, and normal lnicelles are much easier to form than reverse micelles. The focus in this article will be on surfactants in aqueous solution, due to this emphasis and space limitations.

A typical spherical micelle in aqueous solution has an average number of surfactant molecules, or aggregation number, of 40–100. The diameter of a spherical or cylindrical micelle is around 4–6 nm for typical surfactants. The shape of the micelle depends on surfactant molecular structure, solution ionic strength, temperature, and presence of organic solutes in solution, among other factors.

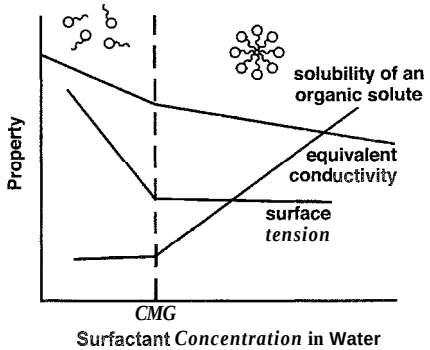

Fig. 4 Some properties of aqueous surfactant solutions related to CMC.

For example, micellar structures commonly transition from spherical to cylindrical to planar to reverse micelles as the tail group length decreases, branching of the tail group increases, diameter of the head group decreases, ionic strength of solution increases (for ionic surfactants), or surfactant concentration increases. This can be understood in terms of how the surfactant molecules best fit together to form the aggregate. For a large head group and small diameter tail group. each surfactant can be approximated as a cone, which best fits together as a sphere in water. As the tail group becomes more branched, each surfactant molecule becomes more like a cylinder in shape, which aggregates best as a planar structure. As the tail group becomes even more branched. the molecules can invert to form reverse micelles. with the head group surrounding a droplet of water in the reverse micelle interior. This transition in aggregate type is shown in Fig. 5. The shape of the micelle can influence important physical properties. For example. cylindrical micelles (particularly when they become long or thread-like) can substantially increase solution viscosity, even at a fairly low surfactant concentration, a phenomenon sometimes used in shampoos.

It is easy to think of micelles as stable species when viewing depictions such as that in Fig. 2. However, micelles are dynamic structures. The average lifetime of a surfactant molecule going into and out of the micelle is normally on the order of 1–10 μsec, and the average lifetime of an individual micelle is commonly around 1–10 msec. Thus, at a given condition, the fraction of surfactant present as monoiner versus micelles is that at equilibrium. because equilibration times are so fast. This rapid kinetics can affect such processes as foaming or wetting, where the micelles act as reservoirs for surfactant monomer and replenish this monomer readily. as it is used by adsorbing at an interface.

While rnicelles are the most studied surfactant aggregate. the driving force for forming other surfactant aggregates often mirrors those for micelle formation. Thus, knowledge of how variables affect the CMC can provide guidance on the anticipated effect of variables on. e.g., the surfactant aggregate adsorbed on solids or at the air–water interface as monolayers. The analogous behaviors between aggregates composed of surfactants give substantial importance to knowledge of micelle formation tendencies. Thus. as a broad generalization, the CMC is the single most important physical property of water-soluble surfactants in aqueous solution.

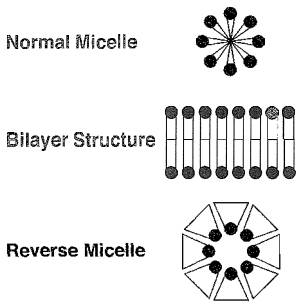

Fig. 5 How tail group share can influence micelle shape

The thermodynamics of micelle formation is unusual compared to formation of condensed or structured phases in systems not involving contact between water and hydrophobic groups. For example, when a vapor condenses to form a liquid, the entropy decrease is compensated for by a large endothermic effect. so a condensed phase can be in equilibrium with a vapor phase. The heat of micelle formation is not large; while it can be endothermic or exothermic. it is always small. In micelle formation, the entropy decrease for surfactants in the aggregate is offset by an entropy increase in another part of the system, the water. Water forms highly structured layers. known as iceberg structures. adjacent to the hydrophobic groups of surfactant monomer. When the ice-like sheath is disrupted as the monomer moves into a micelle, the increase in disorder as these structured water molecules become ordinary bulk water. approximately offsets the increase in order of the surfactant molecules as they form the structured micelles. The overall result is that the entropy change for the system is small when micelles form, consistent with small heat changes and resultant lack of free energy change when micelles form at the CMC. with the monomer in equilibrium with micelles. Sometimes. micelle formation is referred to as entropy-driven in the surfactant literature. This is a misleading term and results from the lack of the large entropy decrease normally associated with formation of a condensed phase, rather than a large entropy increase upon micelle formation. which the term implies.

There are two basic approaches to modeling the thermodynamics of micelle formation. The mass action model views the micelles as reversible complexes of the monomer that are aggregating and predicts the sharp change in tendency of incremental surfactant to form micelles instead of monomer at the CMC: this sharp transition is a consequence of the relatively large number of molecules forming the aggregate. The mass action model predicts that micelles are present below the CMC but at very low concentrations. The ocher major model used to describe micelle formation is the pseudophase separation model, which views micelles as a separate thermodynamic phase in equilibrium with monomer. Because micelle formation is a second-order phase transition. micelles are not a true thermodynamic phase. and this model is an approximation. However. the assumption that there are no micelies present below the CMC, and that the surfactant activity becomes constant above the CMC. is close to reality. and the mathematical simplicity of the pseudophase

separation model is attractive. In fact, some version of the pseudophase separation model is predominantly used in modeling mixed surfactant systems (almost all practical applications involve surfactant mixtures). The distribution of the different surfactant components between monomer and micelle can be calculated using solution-mixing models to describe surfactant mixing in mixed micelles; regular solution theory is frequently used and results in simple mathematical relationships with a single parameter describing nonideality of mixing.

Micelle fornmtion is enhanced (the CMC is lowered) by increasing the length of the hydrophobic gioup due to the increased tendency for hydrophobic bonding. For ionic surfactants, the repulsion between the like-charged head groups at the micelle surface must be overcome by hydrophobic bonding for the micelle to form. So, for a given tail group, the CMC of nonionic surfactants can be an order of magnitude or more below an ionic surfactant, because no electrostatic repulsion must be overcome for nonionic surfactants to form micelles. For ionic surfactants, the CMC decreases as this repulsion force decreases; this can be induced by increasing solution ionic strength or by inserting nonionic hydrophilic groups between the charged head groups by using a mixture of nonionic and ionic surfactants. This type of synergism from the use of surfactant mixtures is observed in many properties of the surfactant system, and use of surfactant mixtures is one of the most common ways to adjust properties and performance.

LIQUID CRYSTALS/SURFACTANT PRECIPITATION

As the surfactant concentration increases above the CMC, many surfactants form solutions in which the micelles are no longer randomly distributed but are organized into structures called liquid crystals. Surfactants form four main types of liquid crystals, as shown in Fig. 6. Hexagonal liquid crystals involve cylindrical micelles packed hexagonally, where six micelles surround a central micelle. Lamellar liquid crystals are composed of bilayers of surfactants separating layers of water. Cubic liquid crystals are also known as the viscous isotropic phase. These are called cubic because they were originally thought to be composed of spherical micelles packed in a cubic structure. The current view is that there are two types of liquid crystals called cubic, although neither exhibits cubic packing. One of these is the discontinuous cubic liquid crystal, where oblong micelles are arranged in a highly structured fashion. Bicontinuous cubic liquid crystals have a continuous bilayer of surfactant extending through solution as a "plumbing-type" of structure separating the water, which is also a continuous phase; hence, the term bicontinuous.

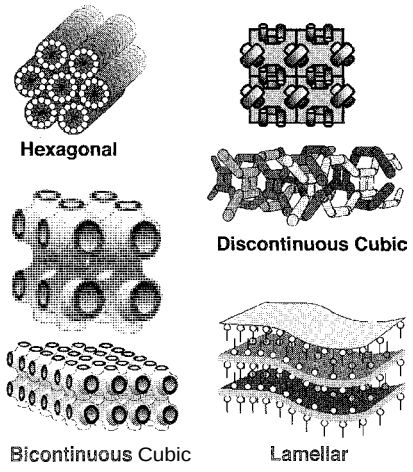

Fig. 6 Classes of surfactant liquid crystals

As the surfactant concentration increases, surfactant structures commonly transition as follows: spherical micelles, cylindrical micelles, discontinuous cubic liquid crystals, hexagonal liquid crystals; bicontinuous cubic liquid crystals, and lamellar liquid crystals. However, viscosity increases in the order as follows: lamellar liquid crystal, hexagonal liquid crystal, and cubic liquid crystals, with both types of cubic liquid crystals being the most viscous (cubic liquid crystals are commonly deduced to be present from high viscosity). Lamellar liquid crystals can exhibit relatively low viscosity despite high surfactant concentrations due to the existence of shear planes, along which the aggregated surfactant layers can move easily. The cylindrical micelles in hexagonal liquid crystals can shear past each other, but there are no shear planes in discontinuous cubic liquid crystals and bicontinuous surfactant structures, which must be broken for flow to occur, so both types of cubic liquid crystals exhibit high viscosity. Liquid crystal formation or transition of one type of liquid crystal to another can be induced by other variables, such as ionic strength and temperature. Liquid crystals have substantially longer lifetimes than micelles; transitions between different liquid crystal types often occur in a few seconds. Optical microscopy under polarized light is often used to detect liquid crystals, because hexagonal and lamellar liquid crystals are birefringent.

As the temperature of an aqueous solution of nonionic surfactants is increased, at some temperature, called the cloud point, the solution transitions from a one-phase to a two-phase system. If the solution is allowed to equilibrate, a coacervate phase (highly concentrated in surfactant, as much as 70 wt %) and a dilute phase separate. The solution appears cloudy at the cloud point, because an emulsion of coacervate phase exists in the dilute

phase. The cloud point is an important temperature for nonionic surfactant solutions; for example, nonionic surfactants are used above their cloud points in automatic dishwashing formulations to promote low foaming. In addition, optimum laundry detergency is observed around the cloud point.

If the solubility product of a charged surfactant monomer with an ion of opposite charge is exceeded, precipitation will occur. Hydrophobic bonding in the surfactant precipitate causes precipitation to occur at low counterion concentrations, particularly if the counterion is multivalent. Hard water cleaning has always been challenging, because hardness ions (calcium or magnesium) readily form a precipitate with many anionic surfactants. Surfactant precipitation is generally undesirable, because when the surfactant is present as a crystal, it is unavailable for adsorption at interfaces and interfacial tension adjustment, or for forming other aggregates. such as micelles and vesicles. When the surfactant is a fatty acid or soap, the precipitate formed is called soap scum. The use of anionic and cationic surfactant mixtures is limited by their tendency to precipitate over a wide concentration range. Precipitation can be avoided by manipulation of the surfactant structure so that the molecule will not fit well into a crystal lattice. for example, by making the tail group more highly branched and increasing the solubility product. As shown in Fig. 7, another strategy is to synergize micelle formation, thereby reducing the CMC and monomer concentration. Because the surfactant activity is reduced, a higher counterion concentration (called hardness tolerance in this case) is required to exceed the solubility product. Micelle formation can be made more favorable by adding nonionic or amphoteric surfactants to ionic surfactants, by increasing ionic strength of nonprecipitating counterions for ionic surfactants, etc. Manipulation of conditions to favor one type of aggregate over another is a common technique used by surfactant technologists to improve system performance. Recently introduced industrial surfactants are designed to preferentially fonn micelles rather than precipitate, for example, by judiciously introducing branching in the hydrophobe; this is an example of molecular engineering to manipulate surfactant physical properties and system performance.

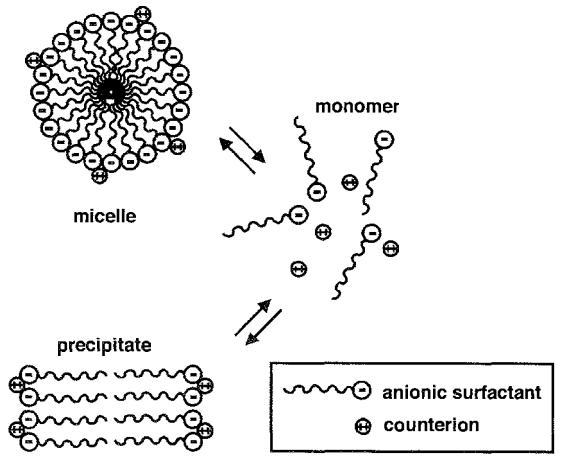

Fig. 7 Equilibria between anionic surfactant precipitating with a hardness cation and surfactant monomer and micelles.

SURFACE TENSION REDUCTION/FOAMS/WETTING

One of the most important properties of surfactants is their ability to reduce surface or interfacial tensions between bulk phases: which results from their surface activity or adsorption at the interface. Surface tension is the energy per unit area required to create new surface area and is the consequence of dissimilarity between phases. When a vapor and liquid are in equilibrium for a single-component system, as the critical point is approached. the vapor–liquid surface tension approaches zero as the two phases become identical. Surface tensions result from the reduction in intermolecular interactions when a molecule is moved from bulk phase to a surface and a reduction in interaction with nearest neighbors of the same structure. Surfactants reduce surface tensions due to their tendencies to adsorb at the surface. and they act as linkers to make these phases more compatible with each other. This is illustrated in Fig. 8 for an air–water interface. At room temperature, air–surfactant-free water surface tension is about 72 mN/m (same as mJ/m^2), while a typical air–alkane interfacial tension is 30 mN/m. When a surfactant monolayer adsorbs at the air–water surface, the head groups are immersed in or adjacent to the water, while the tail groups stick in the air. The 72 mN/m air–water interface was replaced by a head group–water interface and a tail group (oil-like layer)–air interface. The sum of the surface tensions of these two new interfaces is that of an oil–air surface (about 30 mN/m) and a head group–water surface (very low surface tension). As a result of the surfactant linking the air and water phases, the surface tension is reduced from 72 mN/m to about 30 mN/m. Surfactant-induced surface tension modification is used in a wide range of applications. For example, air–water surface tension reduction is important to processes such as wetting of an aqueous solution on a hydrophobic surface or production of foam; interfacial tension reduction at an oil–water interface is important in the removal of oily soil from fabric in laundry detergency.

The air–water surface tension decreases with increasing surfactant concentration below the CMC and

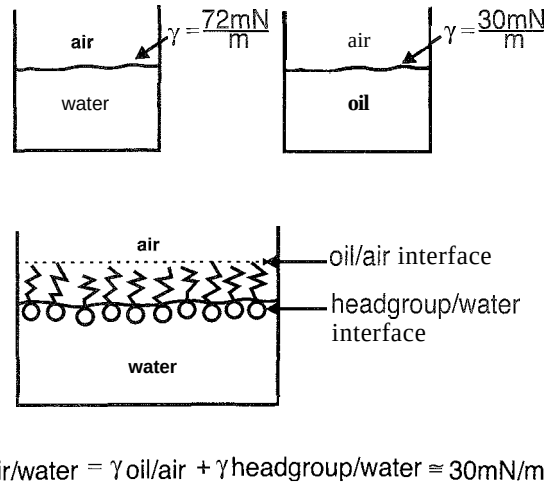

Fig. 8 Using adsorption to lower surface tension of water: surfactant acts as linker between phases.

plateaus above the CMC for single-component surfactants. Because the tendency of the surfactant to adsorb at the air–water interface and its tendency to form micelles is affected similarly by changes in many conditions, the plateau surface tension does not vary greatly within a homologous series of surfactants. For example, as the number of carbons within a linear hydrocarbon tail group increases. to attain a specified surface tension, a lower surfactant concentration is needed, but the concentration at which no further surface tension reduction occurs (the CMC) is also lowered. As a result. the plateau surface tensions between meinbers of a homologous series vary little with alkyl chain length of the surfactant. Similar trends are true for other variables that synergize micelle formation. such as increasing ionic strength for ionic surfactants or adding a nonionic surfactant to the ionic surfactant. This is illustrated for the addition of NaCl to an aqueous solution of the cationic surfactant cetylpyridinium chloride in Fig. 9. It is difficult to attain a plateau air–water surface tension of less than about 25 mN/m with hydrocarbon-based tail groups in surfactants. Silicon-based hydrophobic groups allow surface tensions as low as 20 mN/m, and fluorocarbon-based hydrophobic groups exhibited surface tensions as low as 13 mN/m.

When a droplet of liquid is on a solid surface, the contact angle describes whether the droplet wets the surface (spreads) or beads up, as shown in Fig. 10. A contact angle through the droplet of 0° would correspond to wetting and 180° to dewetting. As a liquid spreads over a solid surface and the contact angle decreases. a liquid–vapor surface and a solid–liquid surface are created. and a solid–vapor interface is destroyed. This process is made thermodynamically favorable when surfactant adsorbs at the two newly created interfaces. reducing their surface tensions; total system energy decreases upon wetting in this case. as illustrated in Fig. 10. In part because it is easily measured, liquid–vapor surface tension is often considered the dominant force that affects wetting of an aqueous solution on a hydrophobic solid, and surfactants cause an increased tendency to wet due to surface tension reduction. The most effective wetting agents in water are fluorinated surfactants, followed by silicon surfactants. Wetting is important in many applications, including spreading of an aqueous solution of herbicide sprayed on crops in agriculture, spreading of inks on a plastic film upon printing. and spreading of a detergent solution over dishware in automatic dishwashing. to name a few.

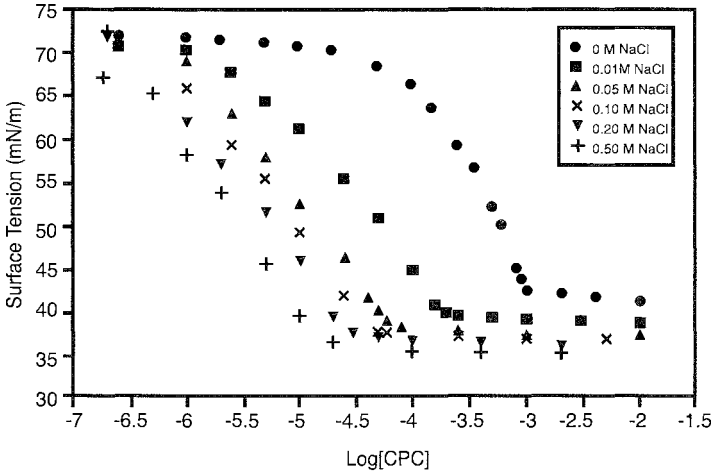

Fig. 9 Surface tension of cetylpyridinium chloride (CPC) solutions at different salinities.

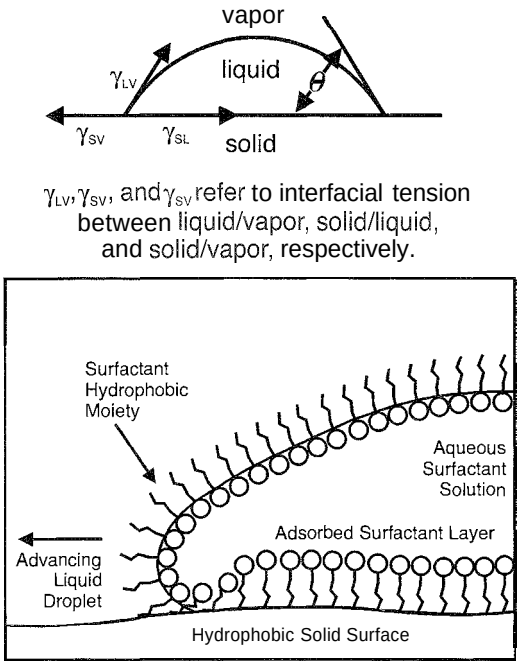

Fig. 10 Contact angle (0) for liquid wetting a solid and role of surfactant adsorption in aiding spreading (0 decreases).

Foams are dispersions of gas in a liquid. The thin-liquid film (film lamellae) separating the discrete gas bubbles is continuous. Surfactants are critical to effective foam formation and stability for two basic reasons: 1) the reduction in liquid–vapor surface tension reduces the energy required to creaie the large surface areas in a foarn; and 2) the adsorbed surfactant monolayers on each side of the film lamellae repel each other. thereby opposing thinning and the ultimate rupture of the film, as shown in Fig. 11. If the head groups are ionic, there is electrostatic repulsion between the charged monolayers: if the head groups are large polyethoxylate nonionic groups, steric (space-filling) repulsion exists between layers. These electrostatic and steric repulsive forces, generically referred to as a disjoining pressure, are crucial to stabilization of the foam. Because electrostatic forces are often stronger than steric forces. ionic surfactants are generally the best foaming agents. Foam stability is particularly good when using mixtures of ionic and zwitterionic surfactants, because they form stable monolayers. Fortnation of cylindrical micelles or liquid crystals in the foarn lamellae can increase viscosity in the film and increase foam stability. As a foam ages and the liquid drains from the liquid film. the foam becomes dryer, and the gas bubbles transition from spheres to polyhedrons. The minimum free energy of a foaming system occurs when the foam breaks. demonstrating the instability of these systems. Foams can be formulated. however. to be stable for months or even years. One foam of academic interest has ultrathin liquid films separated by gas bubbles. so thin that no light reflects from them. and they appear to be black. These black films were first observed by Newton and can be stable. because repulsive and attractive forces between the two surfaces of the liquid film can be in balance. This is a quasiequilibrium state. however; at equilibrium. these black film-based foams will break due to the large energy gained by the system when the film surface area is destroyed.

Surfactants improve foam formation by inducing film elasticity. which is helpful when the film is stretched as a gas bubble emerges from a liquid solution to become part of the foam matrix. As the film stretches, differentia! surfactant adsorption at the interface leads to surface tension gradients and healing of the film (so it thins with approximately uniform thickness). The optimum surfactant concentration for foam formation (although not foam stability) is around the CMC.

Water-insoluble surfactants (particularly silicoa-based) can act as antifoams (prevent foarn formation) or defoamers (break existing foams) due to displacement of water-soluble surfactants from the air–water interface. resulting in inelastic adsorbed monolayers. poor foam formation, and poor resistance of an existing foam to rupture upon stretching (due. for example, to mechanical vibrations). So, surfactants can help make or help break foams, depending on the desired effect.

EMULSIONS/MICROEMULSIONS

Emulsions and microemulsions are widely used in a range of products. including pharmaceuticals, cosmetics, food products. and cleaning. to name but a few. as well as in industrial operations. such as in the production of

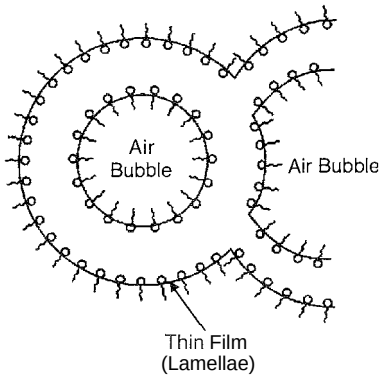

Fig. 11 Formation of surfactant monolayers at the air–water interface that stabilizes foam.

emulsion polymers. An emulsion, or macroemulsion, is a thermodynamically unstable mixture of oil and water. Surfactants can help to stabilize these emulsions for months, or even years, depending on the desired shelf life for a given product. By contrast, a microemulsion is a thermodynamically stable system. The surfactant selection approach to stabilize a macroemulsion and to form a microemulsion are similar in some ways but different in others. The discovery that microemulsion formation and macroemulsion stability are linked is rapidly changing the designs of macroemulsion surfactant systems.

Macroemulsions are opaque dispersions of an oil and water phase, taking on a milky-white appearance when the oil is colorless (as in the case of milk). The milky-white appearance results from the emulsion droplet size, typically on the order of 0.5–1.0 microns, which is large enough to scatter visible light. Stable macroemulsions cannot have droplets much larger than this, as the buoyant forces that result from the oil–water density difference will cause the droplets to "cream out," rising to the top of the continuous phase. By contrast, microemulsions are generally transparent, a result of their much smaller droplet size—larger than a micelle, 4–6 nm, but much less than 100 nm. As microemulsion systems approach or exceed this upper limit. they evidence a blue-white or hazy appearance; this region is sometimes known as a miniemulsion, or swollen micelles.

Droplet size plays an important role in macroemulsion stability. Forming a macroemulsion requires energy input because of the increased interfacial area between the oil and water phases (Fig. 12). Conversely, as the emulsion breaks and the system returns to the original state, energy is released. In the example in Fig. 12, 31 J of work is required to form one micron droplet of 100 mLs of heptane in 1 L of water. If smaller droplets were desired, more energy input would be required because of the increased interfacial area. At the same time, smaller emulsion droplets experience less buoyancy effect and creaming (coalescence as the droplets rise to the surface). Surfactants help the emulsion process in two important ways: 1) by reducing the interfacial tension, surfactants decrease the energy input required to form a certain droplet size (or, for the same energy input, smaller droplets are formed); and 2) as surfactants accumulate at the oil–water interface, they provide electrostatic or steric hindrances to droplet coalescence. It is by producing smaller emulsion droplets and hindering the coalescence process that surfactants help to form stable macroemulsions. Once a macroemulsion breaks, energy must again be added to reform the macroemulsion.

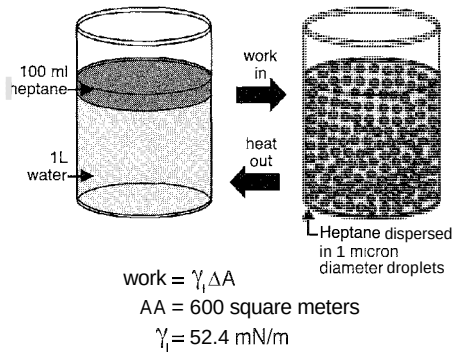

Fig. **12** An example of energy required to form a macroemulsion.

As a general description, a microemulsion is a homogeneous phase that contains a substantial fraction of both oil and water, their mixing being induced by the dissolved surfactant. In contrast with macroemulsions, microemulsion systems form spontaneously in solution. As with micelles, microemulsions are thermodynamically stable. As a result, in contrast to macroemulsions, microemulsion formation is reversible. For example, if changes in a system parameter (e.g., temperature) alter the microemulsion system, when the system parameter returns to its original state, so does the microemulsion system. In contrast to macroemulsions, a microemulsion forms virtually independent of the volume of the oil phase, but once formed, the microemulsion enhances the aqueous solubility of the oil phase. Most often, an excess oil phase persists in the presence of a microemulsion phase—the oil and water phases do not completely mix.

Macroemulsions can occur in two basic forms: oil in water (O/W) or water in oil (W/O). In an O/W emulsion, the system has bulk properties of a water phase, and thus behaves like oil droplets dispersed in a water continuous phase. Conversely, for a W/O emulsion, the system has properties of water dispersed in a continuous oil phase. An obvious questions is: how does one design a surfactant system to form or stabilize an O/W or a W/O emulsion'? A traditional rule-of-thumb, Bancroft's Rule, indicates that an O/W emulsion will result when the emulsifying agents (surfactants) are more soluble in the water phase, while W/O emulsions result when the emulsifying agents are more soluble in the oil phase. The more quantitative hydrophilic–lipophilic balance (HLB) is an indicator of a surfactant's water or oil solubility. Surfactants with relatively high HLB values (e.g., 16 or greater) are highly water soluble. while relatively low HLB values (e.g., six or less) indicate surfactants that are oil soluble. As expected, increasing the surfactant tail length decreases the HLB, while increasing the number

of ethylene oxide groups or going from a carboxylate to sulfate or sulfonate head group increases the HLB. As the HLB of a surfactant, or surfactant mixture. decreases between these extreme values, it transitions from being water soluble (micelles) to oil soluble (reverse micelles). This transition occurs at intermediate HLB values (approximately eight to 12, depending on the oil). An emulsion has its highest stability when the HLB of the surfactant is tailored to the HLB of the oil. In this case. the surfactant concentrates at the oil–water interface, lowering the interfacial tension and providing electrostatic and steric hindrances to emulsion coalescence. If the surfactant is too oil or too water soluble (the HLB is too low or too high). the surfactant will preferentially be in the oil or water phase rather than at the interface stabilizing the emulsion. Surfactant mixtures help optimize the MLB. increase the surfactant packing density at the oil–water interface, lower the interfacial tension, and enhance the electrostatic/steric hindrances to coalescence. all of which improve emulsion stability. The HLB method is widely used. because it provides a single value that characterizes the water solubility of a surfactant or mixtures thereof. Within a class of surfactants. the lower the HLB. the greater the tendency to form aggregates from aqueous solution [such as micelles (reduced CMC), precipitate (for ionic surfactants. higher Krafft temperature)]. form monolayers at the air–water interface, etc. However, at the same HLB, surfactants from different classes (e.g., anionic versus nonionic) can behave differently.

One limitation of the HLB concept is its failure to account for variations in system conditions from that at which the HLB is measured (e.g., temperature. electrolyte concentration). For example. increasing temperature decreases the water solubility of a nonionic surfactant. ultimately causing phase separation above the cloud point. an effect not captured in a temperature-independent HLB value. When both water and oil are present. the temperature at which a surfactant transitions from being water soluble to oil soluble is known as the phase inversion temperature (PIT). Below the PIT, nonionic surfactants are water soluble, while above the PIT. they are oil soluble. Thus, from Bancroft's rule. a nonionic surfactant will form an O/W emulsion below its PIT and a W/O emulsion above its PIT. Likewise, increasing salt concentrations reduces the water solubility of ionic surfactant systems. At elevated salt concentrations, ionic surfactants will eventually partition into the oil phase. This is illustrated in Fig. 13. which shows aqueous micelles at lower salt concentrations and oil-phase inverse micelles at higher salt concentrations. Increasing the system temperature will likewise cause this same transition for nonionic surfactant systems.

Interesting things happen in the region where a surfactant transitions from being water soluble to oil soluble. At the incipient point of transition. the surfactant dislikes the water and the oil phases and prefers to be at the interface, but there is not sufficient room at the interface to accommodate all of the surfactant. In this case, a new phase forms, which we call a middle-phase microemulsion. The middle-phase microemulsion combines virtually all of the surfactant with portions of the oil and water phases, giving it an intermediate density. and exists in equilibrium with virtually surfactant-free oil and water phases. Middle-phase microemulsions appear at the intermediate salt concentrations shown in Fig. 13. Unlike oil–water emulsions. which break given sufficient time, a middle-phase microemulsion system is thennodynamically stable and does not break with time (given that system conditions remain constant). Winsor referred to this middle phase as a Type III microemulsion. as opposed to Type I (micelles) and Type II (inverse micelles) microemulsions. Middle-phase microemulsions have several highly desirable properties; including ultralow interfacial tensions with the water or the oil phases, potentially less than 10^{-4} mN/m, and ultrahigh solubilization potentials for oil or water, potentially two to three orders of magnitude higher than in simple micellar systems. as illustrated in Fig. 13. To illustrate the remarkable ability for oil and water to coexist in a middle-phase microemulsion. a few weight % surfactant can cause equal amounts of oil and water to be contained in the microeinulsion.

While the middle-phase microemulsion appears at a discrete point in the temperature or salinity scan, system properties change continuously through the scan. As illustrated in Fig. 13. the interfacial tension decreases

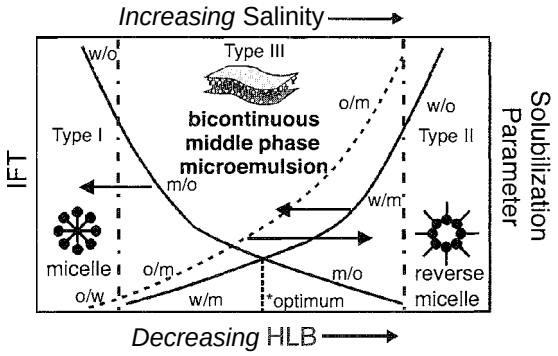

Fig. 13 Effect of electrolyte concentration on Winsor microemulsion type (salinity scan). w: water: o: oil: m: microemulsion: solubilization parameter: volume of oil solubilized per mass of surfactant.

continuously as the system transitions through the Type I region toward the Type III boundary, and it will decrease by orders of magnitude prior to the appearance of a middle-phase microemulsion. Likewise, the solubilization potential will increase by an order of magnitude or more prior to the appearance of a middle phase. We refer to the Type I microemulsion region just before a Type III microemulsion forms as the supersolubilization region.

As the surfactant concentration increases. there is more surfactant in the middle-phase region. Because the surfactant is accumulating at the oil–water layers within the middle phase, as the surfactant concentration increases, the volume of the middle phase must increase to accommodate the additional surfactant. Eventually, at elevated surfactant concentrations. the volume of the middle phase grows sufficiently to consume all of the oil and water phases, and we are left with a single-phase microemulsion. In this Winsor Type IV microemulsion, the oil and water become miscible, the system interfacial tension reaches a global minimum. and the solubilization potential reaches a global maximum. In order to form a single phase, a Type IV microemulsion requires elevated surfactant concentrations, but the improved performance may warrant additional costs for certain applications. As a microemulsion transitions from a Type I toward a Type III system, micelles become swollen. and eventually, a bicontinuous structure forms with a monomolecular surfactant film separating regions of oil from regions of water. (See Fig. 13.) Hence. water and oil are continuous; this bicontinuous structure is present, not only in middle-phase microemulsions containing approximately equal volumes of oil and water. bur also as we approach the Type I or II microemulsion boundaries within the middle-phase region.

Emulsion stability is also a function of surfactant concentration. As discussed above. if the surfactant HLB is not tailored to the HLB of the oil, the surfactant will be in the oil or water phase rather than accumulating at the interface. But in addition to having the right surfactant system (HLB matched to the oil phase), there must be sufficient surfactant present to cover the interfacial area of the optimally sized emulsion droplets. In addition to saturating the oil–water interface: enough surfactant must be added to maintain the aqueous CMC, as this equilibrates with the desired level of surfactant at the interface. If the surfactant concentration is less than this optimal concentration. then larger emulsion droplets will occur, and increased buoyancy forces will result in a shorter shelf life than desired. Thus, optimal emulsion stability requires selecting the right surfactant system. as guided by the HLB concept, and the right amount of this surfactant system, as estimated from the oil–water interfacial area and the area per head group of the surfactant present as an adsorbed monolayer.

CONCLUSION

The tendency of surfactants to adsorb at interfaces and self-assemble results in unique physical properties and behavior. Formation of micelles, liquid crystals. macroemulsions, microemulsions. and foams, as well as surface tension reduction and improving wettability of aqueous solutions, are just a few phenomena exhibited by surfactants. This behavior is of both fundamental interest as a unique subset of physical chemistry as well as leading to many practical applications.

ARTICLES OF FURTHER INTEREST

Hydrophobic *Effects*, p. 673
Micelles and Vesicles, p. 861

SUGGESTED READING

General

Adamson, A.W. *Physical Chemistry of Surfaces*, 6th Ed.: Wiley-Interscience: New York. *1997.*

Analysis of Surfactants, 2nd Ed.: Schmidt. T.M.. Ed.; Marcel Dekker: New York. *200*1.

Ash, M.; Ash. I. *Industrial Surfactants Electronic Handbook.* Gower: Brookfield, VT. 2000.

Clint. J.H. *Surfactant Aggregation:* Chapman and Hall: New York. *1992.*

Handbook of Detergents, Part A: Properties: Broze, *G.*, Ed.; Marcel Dekker: New York, *1999.*

Handbook of Surfactants, 2nd Ed.: Porter. M.R.. Ed.: Blacltie: London, *1994.*

McCutcheon's Emulsifiers and Detergents, International Edition: McCutcheon Division. Manufacturing Confectioner Publishing Co.: Glen Rock, NJ. published annually.

Myers. D. *Surfactant Science and Technology;* VCH: New York. *1988.*

O'Lenick. A.J.. Jr. *Surfactants: Chemistry and Properties*; Allured Publishing Corp.: Carol Steam. IL. *1999.*

Rieger. M.M. *Surfactant Encyclopedia:* Allured Publishing: Carol Steam. IL, *1996.*

Rosen. M.J. *Surfactants and Interfacial Phenomena*, 2nd Ed.: Wiley-Interscience: New York, *1989.*

Surfactants: A *Practical Handbook*; Lange. K.R.. Ed.: Hanser Gardner: Cincinnati, OH. *1999.*

Micelles

Micellization, Solubilization, and Microemulsions; Mittal. K.L., Ed.; Plenum: New York. *1977:* Vols. *1* and 2.

Mixed Surfactant Systems; Ogino, *K.*, Abe, M., Eds.; Marcel Dekker: New York, 1993.
Phenomena in Mixed Surfactant Systems; Scamehorn. J.F.. Ed.; ACS Symp. Ser. 311. American Chemical Society: Washington, DC. 1986.
Solubilization in Surfactant Aggregates; Christian, S.D.. Scamehorn. J.F.. Eds.: Marcel Dekker: New York. 1995.
Solution Behavior of Surfactants; Mittal, K.L.; Fendler, E.J.; Plenum: New York. 1982: Vols. 1 and 2.

Liquid Crystals/Surfactant Precipitation

Laughlin, R.C. *The Aqueous Phase Behavior of Surfactants*; Academic Press London. 1994

Surface Pension Reduction/Foams/Wetting

Defoamiag: Theory and Industrial Applications; Garrett, *P.R.*, Ed.; Marcel Dekker: New York, 1992.
Fluorinated Surfactants and Repellents, 2nd Ed.; Kissa, E., Ed.; Marcel Dekker: New York, 2001.
Foams: Physics, Chemistry and Structure: Wilson. A.J.. Ed.; Springer-Verlag: London. 1989.
Foams: Theory, Measurements, and Applications; Prud'homme, *R.B.*, Ed.: Marcel Dekker: New Uork, Basel. Hongkong, 1996.
Sebba, F. *Foams and Biliquid Foams - Aphrons*; Wiley: New York, 1987.
Silicone Surfactants; Hill. R.M., Ed.: Marcel Dekker: New Uork. 1999.
Wettability; Berg. J.C.. Ed.; Marcel Dekker: New York. 1993.

Emulsions/Microemulsions

Becher, P. *Encyclopedia* of *Emulsion Technology*; Marcel Dekker: New York. 1983: Vol. 1.
Bourrel. M.: Schechter, R.S. *Microemulsions and Related Systems*; Marcel Dekker: New York, 1988.
Food Emulsions and Foams; Dickinson. *E.*, Stainsby. F.. Eds.; Elsevier: London. 1988.
Handbook of Microemulsion Science and Technology; Kumar. *P.*. Mittal. K.L., Eds.: Marcel Dekker: New York, 1999.
Modern Aspects of Emulsion Science: Binks, B.P.. Ed.; Royal Society of Chemistry: London. 1999.

Surfactants, Part II: Applications

john F. Scamehorn
David A. Sabatini
Jeffrey H. Harwell
University of Oklahoma, Norman, Oklahoma, U.S.A.

INTRODUCTION

Surfactants are used in many applications, including consumer products. industrial products and processes, and environmental remediation. The total annual value of surfactants is on the order of $\$6 \times 10^9$. As an example of the commercial importance of applications in which surfactants are crucial, the worldwide annual market for detergent or cleaning products. in which surfactants are an important component, is approximately $\$60 \times 10^9$. The two articles on ''Surfactants'' in this encyclopedia are split into "Fundamentals" and "Applications," with this article discussing applied aspects of surfactant behavior. The article in which a certain topic is included is arbitrary. because fundamental and applied aspects of surfactant behavior are involved (e.g., wetting, emulsifying. adsorbing on solids). The purpose of this article is to extend the discussion of fundamental surfactant behavior from Part I, to discuss some applications, like detergency and surfactant-based separations. and to describe environmental aspects of surfactants that influence their use in applications.

SURFACTANT ADSORPTION ON SOLIDS/DISPERSIONS

Surfactants tend to accumulate at the solid/liquid interface just as they accumulate at the vapor/liquid and liquid/liquid interfaces. Surfactants also tend to form aggregates at the solid/solution interface, just as they tend to form inicelles in solution. Bilayered aggregates of adsorbed surfactants are called admicelles.

Shown in Fig. I is a typical adsorption isotherm for a single-component surfactant adsorbing from an aqueous solution surface for which the head group of the monomer has an attractive interaction, such as an anionic surfactant adsorbed on a positively charged surface. The *x*-axis is the equilibrium concentration of surfactant in solution, and the y-axis is the amount of adsorbed surfactant. in moles or molecules or mass per area or adsorbent weight.

The surfactant adsorption isotherm is usefully divided into four regions. Region I is called the Henry's Law Region, where adsorption is proportional to concentration. In Region I. monomers adsorb independently on the solid surface, without cooperation or competition for adsorption sites, because the number of available adsorption sites greatly exceeds the number of adsorbed molecules. Region II is characterized by the formation of admicelles (adsorbed bilayers) in patches on the surface. The Region I/Region II transition is marked by a sharp increase in the slope of the adsorption isotherm. as the surfactant molecules begin to cooperate, and hydrophobic bonding causes formation of admicelles. The Region II/Region III transition is characterized by a competition between admicelles for available formation sites, as the number of adrnicelles can approach the number of sites available for admicelles. Thus, while Region II is dominated by cooperative interactions between surfactant monomers to form admicelles, Region III is dominated by competition between the admicelles for the available surface area of the solid. Region III may not exist in some systems where surface coverage of admicelles is sparce. Region IV begins as the monomer concentration in solution reaches the critical micelle coacentration (CIVIC). Because the last admicelle forms at the same chemical potential as the first micelle to form. surfactant added above the CMC goes into forming more inicelles with little change in the chemical potential of the surfactant molecules. resulting in a nearly constant adsorption above the CMC in Region IV. The level of adsorption above the CMC is often called the plateau adsorption. In cases where the head group has a neutral or even repulsive interaction with the surface. as might occur with a hydrophobic surface or with a surface having the same charge as the head group, the admicelles will tend to be local monolayers called hemimicelles. with a tail-down, head-out configuration. In this case. the driving force for self-assembly is less than that for the systems shown in Fig. 1. so a gradual increase in surfactant adsorption with concentration instead of an abrupt transition upon surface aggregate formation is observed. However, adsorption still plateaus above the CMC in these cases.

It is hard to overstate the observation that the admicelle has properties similar to a micelle. Counterion binding on the adrnicelle is nearly identical to that on the micelle:

Encyclopedia of Supramolecular Chemistry
DOI: 10.1081/E-ESMC 120016053

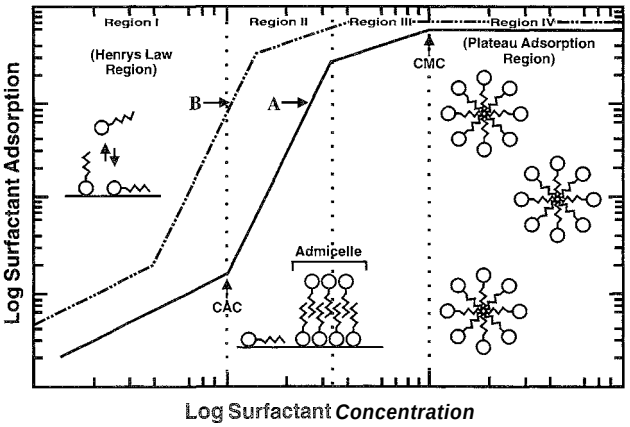

B -- *Longer* alkyl *chain length or higher electrolyte concentration (for ionic* surfactants) than A

CAC -- Critical Admicelle *Concentration*

Fig. 1 A typical surfactant adsorption isotherm on a hydrophilic surface from water.

admicelles will soiubilize organic solutes, a phenomenon called adsolubilization. to about the same extent as the same solute is taken up by a micelie. A consequence of this is that the transition from Region I to Region II—often called the CAC, or critical admicelle concentration in analogy to the CMC—will decrease with added electrolyte in nearly the same manner as the CMC decreases for ionic surfactants. In Fig. 1, Isotherm B can represent the same surfactant as in Isotherm A. adsorbing on the same surface; Isotherm B is shifted to the left. because added electrolyte reduced the CAC along with the CMC. Isotherm B could also represent a surfactant with a larger hydrophobic g oup than Isotherm A. As with added electrolyte for ionic surfactants, increased hydrophobicity lowers the CAC and the CMC and shifts the Isotherm to the left. For all concentrations of surfactant between the CMC and the CAC, the adsorption for Isotherm B is higher than the adsorption in Isotherm A: however. because the electrolyte or increased hydrophobe size lowered the CMC, the CMC occurs at a lower surfactant concentration. and the level of adsorption above the CMC is practically unchanged. Above the CMC, the plateau adsorption level may be at or near complete biiayer coverage but may be significantly less if there is not a strong interaction between the surface and the hydrophilic group of the surfactant.

While ionic surfactants will always adsorb strongly on surfaces oppositely charged to the head group. nonionic surfactants adsorb strongly on some substrates, like silica (due to hydrogen bonding), but have low adsorption on substrates like alumina. A nonionic surfactant may adsorb to form a complete bilayer on silica but may not even begin to form admicelles on alumina. Anionic and. nonionic surfactants can form monolayers (hemirnicelles) on hydrophobic surfaces and can form admicelles on hydrophilic surfaces.

All hydrocarbon mixed surfactant systems with dissimilar head groups. such as ionic/nonionic, ionic/amphoteric, and anionic/cationic, tend to have increased adsorption relative to the pure component adsorption at the same surfactant concentration. This synergisin is analogous to the effect of mixed surfactant systems in forming low CMC surfactant mixtures. It is easier to form a mixed admicelle rather than a pure component admicelle, just as it is easier to form a mixed micelle.

Adsorption of surfactant at the solid/solution interface is important in technologies such as ore flotation (a separation process). stabilization of dispersions. wetting. and surface cleaning. Surfactants are important components in paints. drilling muds; printing inks, and ceramic green bodies. There are many similarities in the phenomenologies of dispersions and emulsions. In both phenomena, adsorption of surfactants at the solvent interface lowers the interfacial energy and also imparts steric and electrostatic repulsion between particles; this inhibits aggregation of the particles, thus preventing the buoyant force on the aggregate from becoming significant enough to reduce the stability of the dispersion. The role of the adsorbed surfactant layer in stabilizing a dispersion of hydrophobic particles (e.g., carbon black) is illustrated in Fig. 2. In emulsions, in contrast to dispersions. optimization of the surfactant systems results in smaller liquid droplets. so that the buoyant force becomes negligible. For solids, the particle size does not adjust when surfactants are added (although surfactants can cause small particles to agglomerate into assemblies or flocs—this is not the same as adjusting the primary particle size). This means that for solid particles too large to be suspended by Brownian motion, the negative buoyant force will cause the particles to settle. no matter

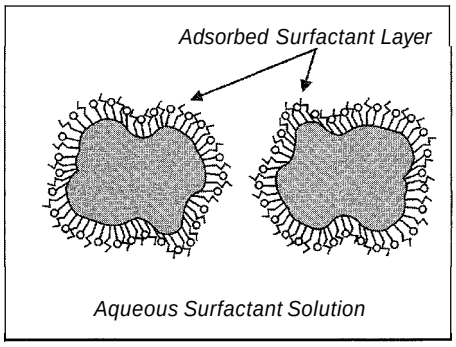

Fig. 2 The role of adsorption in solid/liquid dispersions

how effectively the surfactant adsorbs at the particle/solution interface.

Despite the central role of surfactants in stabilizing solid/liquid dispersions. the most important variables affecting dispersion stability are the particle size and the volume fraction of the solid. These variables essentially determine the strategy to be used to form a stable dispersion of the particles in liquid. Only in the case of a low volume fraction of submicron particles will surfactant adsorption on the surface, and the resulting electrostatic and steric repulsion between the particles, be sufficient to form a stable suspension of dispersed particles. When the solid particles are too large to be suspended by Brownian motion, as is generally the case for particles of micron size or larger, if the particles are completely, uniformly dispersed, then the dispersion stability remains low. To form stable suspensions in such systems, it is important that the particles have a small amount of "stickiness" between one another. Sticky particles form high volume fraction aggregates that, even though too large to be suspended by Brownian motion, form a large volume fraction clay or floc that is readily redispersed by shear forces and does not form a dilatant (shear thickening or nonredispersable) clay. Formation of high volume fraction aggregates that keep one another suspended is easier as the volume fraction of the solid increases.

There is a strong correlation between surfactant concentration and cossesponding adsorption, and the type of dispersion obtained. Consider, for example, an aqueous suspension of silica particles to be stabilized by adsorption of a nonionic surfactant. The silica particles have a negatively charged surface above pH 2; consequently, submicron silica particles at neutral pH tend to remain suspended even in the absence of added surfactant, because the charged surfaces repel one another. When the particles are greater than a micron in size; however, the density of silica (specific gravity of two) causes rapid settling of the particles, despite their electrostatic repulsion. Addition of surfactant to a level where the surfactant equilibrates in Region I of the adsorption isotherm has little effect on the suspension because of the low level of adsorbed surfactant. When the surfactant equilibrates in Region II, however, the silica particles begin to aggregate. The aggregation is caused by the simultaneous coadsorption of individual admicelles on two silica particles. resulting in the formation of an admicelle bridge linking the particles together. So, when the surfactant adsorption density is such that surfactant-covered patches on one particle interact substantially with bare patches on other particles, the surfactant can decrease dispersion stability or cause aggregation. The extent of aggregation and the size of the aggregates will vary throughout Region II, and there will generally be an optimum level of surfactant for stabilizing the dispersion. Once the surfactant adsorption level reaches Region III, however, a high fraction of adsorption sites can become filled. and there can be a decrease in aggregation. By the time the plateau or Region IV adsorption is reached, the adsorbed nonionic surfactant admicelles cause steric repulsion of the particles, and a stable dispersion can result.

In selecting a surfactant for use in modifying dispersions, the most important consideration is whether or not the surfactant adsorbs on the solid. Ionic smfactants adsorb best on oppositely charged surfaces of oxides like silica, alumina, or titanium dioxide. The opposite charge is determined by the pH of the solution. For example. silica gels generally have what is called a point-of-zero charge (PZC) between pH 2 and pH 3. Below pH 2 the silica surface is positively charged, and anionic surfactants will adsorb best; above pH 3 the silica surface will be negatively charged, and cationics will adsorb best. In contrast, zinc oxides generally have a PZC around pH 9. Below pH 9 the zinc oxide has a positively charged surface, and anionic surfactants adsorb best and are better able to affect the stability of zinc oxide dispersions. Above pH 9 the zinc oxide will have a negatively charged surface, and cationic surfactants will adsorb best and be more effective.

As in the earlier example. where nonionic surfactant decreases then increases dispersion stability of silica as surfactant concentration increases from Region I on the adsorption isotherm to the CMC. ionic surfactants can exhibit the same qualitative behavior with hydrophilic solids. If the surfactant has an opposite charge to that of the particle (e.g., anionic surfactant with alumina at pH below its PZC of 9), adsorption of surfactant can reduce the absolute value of electrical potential of the particle, reducing electrostatic repulsion between particles and reducing dispersion stability. As surfactant concentration and adsorption are increased further, the surfactant adsorption density can cause the net charge on the particle to change from positive to negative (or vice versa), a phenomena known as charge reversal. Further increases in surfactant concentration, up to the CMC, can increase charge density on the particles. increase electrostatic repulsion, and increase dispersion stability. Charge reversal is possible, because hydrophobic bonding in admicelles can overcome electrostatic repulsion between charged surfactant head groups. So charge reversal can be yet another factor causing surfactant to act as an agglomeration agent or as a dispersant, depending on concentration. Dispersion stability approximately plateaus above the CMC, because surfactant adsorption also plateaus (Region IV in Fig. 1). Unlike hydrophilic particles, where dispersion stability can exhibit a minimum with surfactant concentration, the higher the adsorption (higher concentration up to the CMC), the greater the dispersion stability of hydrophobic

particles in water (see Fig. 2), because electrostatic and steric stabilization improve with increasing surfactant adsorption. In designing dispersed systems. relating equilibrium surfactant concentration to the CMC is crucial. rather than using empirical rules related to a wt% of dispersant recommended for a given system.

DETERGENCY

Detergency can be defined as removal of unwanted materials from a solid surface. Most detergent applications occur in aqueous solution. although in laundry dry cleaning. organic solvents are used. We will restrict discussions here to water-based systems. Detergent products include laundry detergents (mostly powders, liquids. tablets), hand dishwashing detergents, automatic dishwashing detergents, hard surface cleaners, shampoos, bar soaps and body washes for cleansing of the skin, carpet cleaners, glass cleaners, car washes, and many other products. While a universal formulation could do a reasonable job of cleaning most surfaces, the consumer demands high performance. so products are designed for specific applications with differing compositions. Surfactants are a key component in the detergency process. In some applications (e.g., inexpensive bar soaps, most hand dishwashing detergents). surfactants are the only additive responsible for cleaning.

Unwanted materials (or soils as they are referred to in detergency) to be removed from the substrate are normally classified as oily, particulate, or solid non-

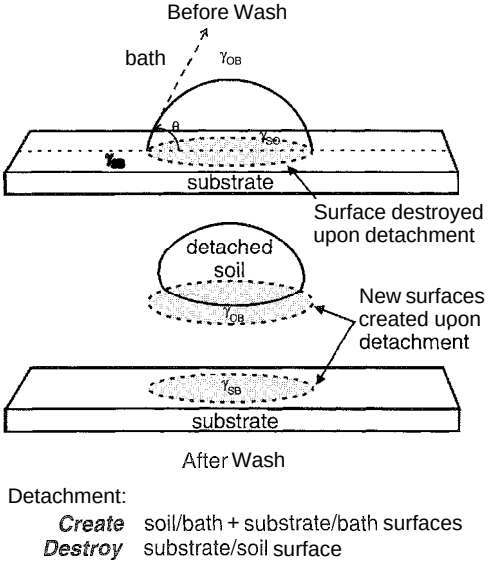

Fig. 3 Destruction and creation of surfaces upon oily soil detachment.

Time

Fig. 4 Removal of oily soil by the roll-up mechanism.

particulate. Oily soils are any liquid substances that can spread out or bead up (contact angle change) on the substrate; motor oil or vegetable oils are typical model oily soils used in detergency studies. Particulate soils are hard particles such as carbon black (model hydrophobic soil) or clay (model hydrophilic soil). Solid nonparticulate soils are sebum from human skin. which can contain enough crystallinity (due to fatty acids) so they do not flow, yet they do not remain intact as discrete particles like particulate soils. Soils are different from stains; stains involve a chemical bond between the contaminant and substrate (e.g., blood, coffee, blueberries), whereas soils are attracted to the substrate by physical forces like van der Waals, electrostatic, and hydrophobic forces. Enzymes and bleaches are generally used to treat stains, whereas surfactants are critical to removal of soils. Substrates to be cleaned are generally classified into textiles or hard surfaces (e.g., dishes, kitchen counters), although there are a number of surfaces that do not fall into either of these categories. Another way of classifying substrates is as hydrophobic (e.g., synthetic clothing, polyethylene food storage containers) or hydrophilic (e.g., cotton fabric, ceramic dishes). This latter classification is mechanistically more convenient, as illustrated by the example that the toughest detergency challenge is oily soil on a hydrophobic surface.

The general principle of surfactant action to remove soils from a surface is illustrated for oily soil in Fig. 3. When the soil is detached from the substrate, the surface between soil and substrate is destroyed. but two new surfaces are created—that between soil and bath and between substrate and bath. Detachment will be thermodynamically favorable when the sum of the interfacial tensions of the two new surfaces is less than that of the destroyed surface. A primary function of surfactants is to adsorb at the soil/bath and substrate/bath interfaces and reduce these interfacial tensions to make detachment more thermodynamically favorable. As surfactants adsorb and modify interfacial tensions, the contact angle (8 in Fig. 3) increases. and the contact area between soil and substrate decreases. As shown in Fig. 4, this results in the

"roll up" mechanism of detergency as the oily droplet rolls up and detaches. However, as shown in Fig. 4, when the substrate/bath interfacial tension is not sufficiently reduced, a phenomena called snap-off can occur where the oil droplet becomes elongated. forms a neck. and only part of the drop is removed. For particulate soil detergency. surfactants act to adsorb onto the newly created soil/bath and substrate/bath interfaces, reducing these interfacial tensions to make detachment more thermodynamically favorable. However, because removal is all or nothing in this case, there are no contact angles or roll-up mechanisms. As shown in Fig. 5. for solid nonparticulate soil, the surfactant diffuses into the soil and loosens pieces of the soil. thereby promoting detachment of these dispersed particles. Thus, the surfactant acts as a dispersing agent as well.

Whatever the type of soil removed, once this soil is detached from the substrate, barriers must be set up to inhibit reattachment or redeposition. The chemicals used to achieve this are known as antiredeposition agents. Surfactants can achieve this by adsorbing onto the detached soil and setting up electrostatic and steric barriers to redeposition. For example, anionic surfactant can adsorb onto a particle to induce a negative charge. and the resultant repulsion of these particles from negatively charged cotton. Nonionic surfactants can adsorb onto the surface of oily soil droplets, form a macroemulsion, and set up steric barriers to redeposition. In practice. water-soluble polymers (e.g., sodium carboxymethylcellulose) are used for antiredeposition. but the mechanisms are electrostatic and steric stabilization.

Anionic surfactants are generally most effective in removing particulate soils, while nonionic surfactants are most effective at removing oily soils. Cationic surfactants adsorb strongly onto negatively charged fabrics like cotton and act as fabric softeners. as they set up an adsorbed monolayer with hydrophobic groups sticking out to give a smooth feel to the fabric.

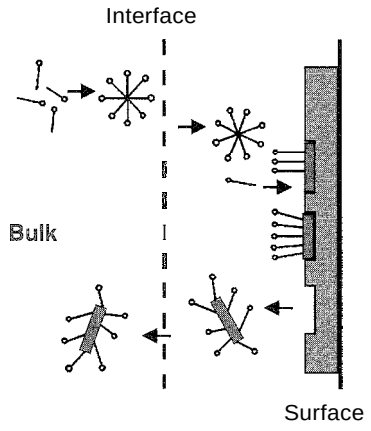

Fig. 5 Detergency of solid nonparticulate soil

INDUSTRIAL APPLICATIONS OF SURFACTANT-BASED SEPARATIONS

Separation techniques using surfactants are valuable in industrial operations and in analytical chemistry. We will briefly discuss several industrial applications of surfactant-based separations to illustrate how surfactants are used in such important operations as wastewater clean-up and recovery and purification of valuable materials.

Detergency aside, ore flotation is the largest industrial use of surfactants. Ore is mined. crushed into small particles, mixed with water, and placed into a flotation cell. In the froth flotation process, as illustrated in Fig. 6. surfactant is added to the slurry, and air is bubbled into the solution through a sparger at the bottom of the vessel. Surfactant adsorbs at the air/water interface as a monolayer and (under the right condition) adsorbs as a bilayered structure onto the valuable ore (colligend) that is to be collected. When the air bubble collides with the ore particle, the minimum free energy corresponds to the configuration shown in Fig. 6, where the surfactant acts as a bridge between the air and ore surfaces. Surfactant is chosen that does not adsorb well onto the mineral to be rejected (gangue), which then does not stick to the air bubbles and stays suspended in the water. The colligend is carried up to the foam (called a froth in this case). where it is suspended in the froth and carried overhead as the froth flows over a weir or is skimmed off. Depending on the ore type, anionic surfactant or cationic surfactant is chosen; pH is a crucial parameter for maximizing adsorption of surfactant onto the colligend. Calcium is sometimes added as an activator with anionic surfactant. coadsorbing or acting as a bridge between the ore surface and the surfactant. Foam stabilizers are sometimes added to make the froth strong enough and stable enough to hold the ore particles.

During paper deinking, ink removal permits recycling of the paper as secondary fiber. Paper is pulped (blended into small pieces), and the ink is detached from the paper by immersing in a surfactant solution, which is basically a detergency process. In flotation deinking, the slurry of paper fiber and ink is placed in a flotation cell (same type of equipment as used in ore flotation), and air is sparged through the solution. As with ore flotation. under the correct conditions. certain materials (in this case, ink) attach to the air bubbles as they rise through solution. leaving the paper fibers behind for reuse. Nonionic surfactants are often used in the detachment step. while fatty acids. with calcium as an activator. are often used in the flotation operation. The calcium synergizes the anionic surfactant adsorption onto ink.

As illustrated in Fig. 7. in micellar-enhanced ultrafiltration, surfactant is added to water at concentrations well above the CMC. Dissolved organic solutes (e.g., chlorinated organic pollutants) and multivalent ionic solutes

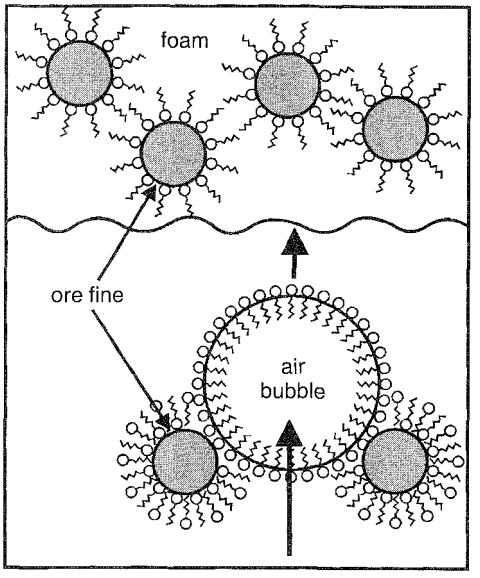

Fig. 6 Froth flotation for ore separation.

(e.g., cadmium, copper, chromate, arsenate) are incorporated into the micellcs via solubilization and counterion binding, respectively. When solubilizing nonionic organic solutes, any type of surfactant can be used, but surfactants of opposite charge to the target multivalent ions arc used for their removal. The solution is then treated by ultrafiltration, with membrane pore sizes sufficient to block or reject micelles. The solution passing through the membrane contains only unsolubilized solute, unbound counterions, and monomeric surfactant. If insufficient concentration reduction is attained, the process can be staged. One intriguing application is the use of optically active surfactants or solubilized ligands to selectively remove biologically active enantiomers in a bioseparation.

In surfactant-enhanced subsurface remediation, surfactant solutions are pumped through a subsurface contaminated with organic pollutants, such as a chlorinated solvent (e.g., trichloroethylene) or components from a fuel spill (e.g., gasoline). The pollutant is trapped between soil grains due to capillary forces. As illustrated in Fig. 8, a concentrated surfactant solution is pumped between the injection and recovery wells. The flush solution is treated above-ground and reinjected. There are two mechanisms by which the surfactant solution enhances pollutant removal: solubilixation into micelles; and sufficient reduction of interfacial tension between the organic phase and the aqueous phase so the organic droplets are mobilized or removed intact from the pores. Which mechanism is desirable depends on the pollutant and aquifer characteristics. For organics less dense than water (LNAPLs, or light-nonaqueous-phase liquids), the more efficient mobilization process is generally desired, but for organics heavier than water (DNAPLs, or dense-non-aqueous-phase liquids), solubilization may be favored, because if mobilized, the organics might sink into previously uncontaminated aquifer regions and get retrapped. So, solubilization capacity and the ability to attain ultralow interfacial tensions are crucial properties of the surfactants, in addition to high hardness tolerance and low adsorption onto the soil. In addition, the residual surfactant left behind must be biodegradable, often under anaerobic conditions. Cationic and nonionic surfactants tend to have unacceptably high soil adsorption. Ethoxylated anionic surfactants, gemini surfactants, and branched-tail surfactants are three types of popular surfactants for this application. For economical operation for multiple pore volume flushes (greater than four), the surfactant has to be reused. In above-ground operations, the flush solution is treated to remove the organic pollutant (for volatile organics, pervaporation or air stripping can be used; for nonvolatile organics, liquid–liquid extraction can be used) and to concentrate the surfactant that was diluted during

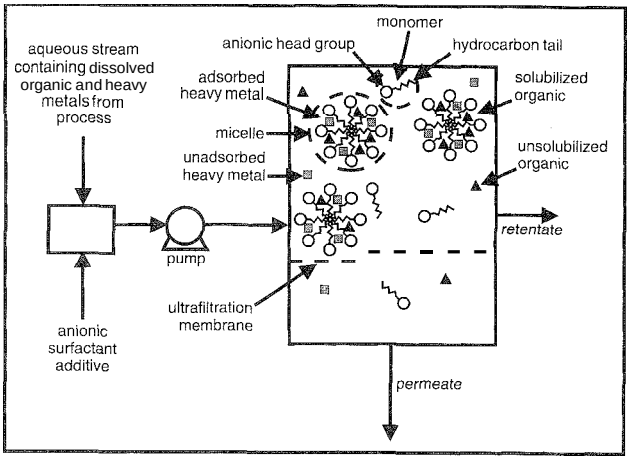

Fig. 7 Micellar-enhanced ultrafiltration

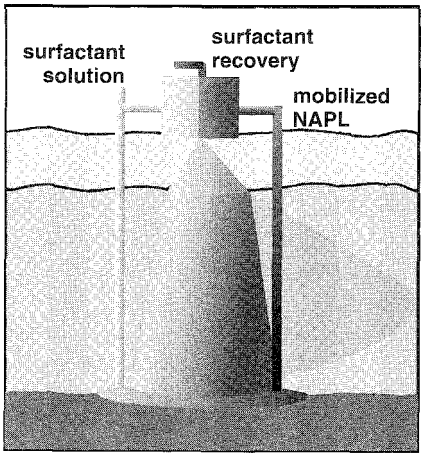

Fig. 8 Recovery of organic contaminant by surfactant-enhanced subsurface remediation.

the subsurface operation by the use of micellar-enhanced ultrafiltration. These operations further constrain surfactant selection, because excessive foaming makes stripping difficult, and micelles must be big enough to be ultrafiltered. Following the flushing operation, bioremediation is often used to remove the small residual pollutant concentration in a polishing step.

ENVIRONMENTAL AND HEALTH ISSUES

Over the past several decades, chemical impacts on the environmental and human health have been an increasing concern. Fortunately, the human toxicity of surfactants is relatively low compared to many other environmental contaminants. However, surfactants can be toxic to aquatic life at relatively low concentrations (1–10 mg/L) and can cause foaming in rivers at even lower concentrations. It was through these effects that the deleterious effects of surfactants were first observed in the environment. Introduction of the highly branched (tetrapropyl) alkylbenzene sulfonate (ABS), which is highly resistant to biodegradation in wastewater treatment plants, resulted in the widespread occurrence of surfactants in the environment. This had not been a problem before, because soaps are readily biodegradable. To help combat this situation. ABS was replaced by linear alkylbenzene sulfonate (LAS), which readily biodegrades in wastewater treatment plants. Once again, surfactant being discharged into the environment reached acceptable levels. This shift from tetrapropyl to linear ABS started a trend to eliminate ali branching in surfactant molecules. Recently. it was found that a mild degree of branching in the tail group can lead to performance advantages without sacrificing biodegradability. The majority of surfactant biodegradation work focused on aerobic environments. However, recently, the fate of surfactants in anaerobic environments is receiving increased scrutiny.

Nonionic surfactants have the lowest oral toxicity. while cationic surfactants have the highest toxicity, and anionic surfactants have an intermediate toxicity. One measure of toxicity is the lethal dose for 50% fatality (LD_{50}). The LD_{50} of nonionic surfactants with rats (1000–25,000 mg/kg) is slightly higher than that of anionic surfactants (700–15,000 mg/kg), which is higher than that for cationic surfactants (300–600 mg/kg). By contrast to surfactants, the LD_{50} of dioxin, a highly toxic compound, is 0.02 mg/kg. The high LD_{50} values for hydrocarbon-based surfactants indicate how safe they are to consumers or industrial workers. Fluorinated surfactants are recalcitrant to biodegradation and can bioaccumulate in the liver, leading to toxicity.

Surfactants can also cause irritation to skin. mucous membranes, etc. This irritation tends to be greatest for cationic surfactants, with decreasing irritation from anionic to nonionic and amphoteric surfactants. The irritation also tends to be greatest for 12-carbon alkyl groups and decreases with increasing ethoxylation of nonionic surfactants. This same trend is observed for a wide range of surfactant impacts on the environment and human health. In addition, for certain systems, the irritant results from an impurity or by-product of the surfactant manufacturing process rather than the surfactant.

Likewise, in some surfactant systems, the environmental or toxicity concern results from an additive or impurity in the formulation rather than the surfactant. Sultone or chlorosultone impurities in some anionic surfactants can lead to irritation. As another example, polyphosphates used to be commonly added to detergents as builders (i.e., to bind calcium and magnesium and prevent hardness precipitation of the surfactant). In some surface water bodies, phosphorous scarcity limits the growth of algae: discharging additional phosphorous into such water bodies can cause algal blooms and eutrophication. For this reason, phosphate builders were removed from many detergent systems, in some cases being replaced with zeolites for hardness sequestration. But there is some uncertainty as to how much impact phosphate builders have on the environment as compared to other phosphorous sources, and many areas of the world still use phosphates in formulations.

CONCLUSION

Surfactants are used in a wide range of industrial and consumer applications from washing fabric to remediating polluted water. Understanding and applying the fundamental properties of surfactants is resulting in a continuing expansion of practical uses of surfactants.

ARTICLES OF FURTHER INTEREST

Hydrophobic Effects, p. 673
Micelles and Vesicles. p. 861

SUGGESTED READINGS

Adsorption from Solution at the Solid/Liquid Interface; Parfitt, G.D., *Rochester*. C.H., Eds.; *Academic Press: London. 1983:* 105–152.

Adsorptive Bubble Separation Techniques: Lemlich, R., *Ed.; Academic Press: New York. 1972.*

Biodegradability of Surfactants; *Marsa, D.R.. Porter. M.R.. Eds.; Blackie: London. 1995.*

Detergency; *Cutler*, W.G., *Davis. R.C.*, Eds.; *Marcel Dekker*, Inc.: *New York*, 1973–1981. *Parts* I–III.

Detergency of Specialty Surfactants; *Friedli. F.E., Ed.; Marcel Dekker*. Inc.: New *York. 2001.*

Detergents and Cleaners: A Handbook for Formulators; *Lange, K.R.. Ed.: Hanser: Munich. 1994.*

Detergents and Textile Washing: Jakobi, G., *Lohr. A.. Eds.: VCH: Weinheim. Germany. 1987.*

Handbook of Separation Process Technology; Rousseau. R.W., Ed.; Wiley: New York, 1987. Chaps. 16, 17, and 19.

Handbook of Separation Techniques for Chemical Engineers, 2nd Ed.: Schweitzer, P.A., Ed.; McGraw-Hill: *New York*, 1988. *Chaps. 2.5 and 5.2.*

Leja. J. *Surface Chemistry of Froth Flotation:* Plenum *Press:* New *York. 1982. Chap. 9.*

Liquid Detergents; *Lai, K-Y.. Ed.: Marcel* Dekker. *Inc.: New York. 1997.*

Napper, *D.H. Polymeric Stabilization of Colloidal Dispersions*; *Academic Press: London. 1983.*

Powdered Detergents: Showell, *M.S., Ed.: Marcel Dekker, Inc.:* New York. *1998.*

Scamehorn. J.F.; *Christian,* S.D.; *Harwell, J.H.: Sabatini, D.A. Surfactants in the Environment. In New Horizons: An AOCS/CSMA Detergent Industry Conference;* Coffey, *R.T.. Ed.: AOCS Press: Champaign, IL, 1996: 79–96.*

Soap Technology for the 1990's; Spitz. L., *Ed.; American Oil Chemists' Society: Champaign, IL. 1990.*

Solid/Liquid Dispersions: Tadros, T.F.. Ed.; Academic Press: London, 1987.

Surfactant-Based Separation Processes: Scamehorn, J.F.. Harwell, J.H., Eds.: Marcel Dekker. Inc.: New York, 1989.

Surfactant-Based Separations, Science and Technology; *Scamehorn. J.F.. Harwell. J.H.. Eds.:* Symposium *Series, American Chemical Society: Washington. DC. 2000; Vol. 240.*

Surfactarit-Enhanced Subsurface Remediation: Emerging Technologies; *Sabatini. D.A.. Knox, R.C., Harwell. J.H.,* Eds.: *Symposium Series, American Chemical Society: Washington, DC, 1995: Vol. 594.*

Surfactants in Consumer Products, Theory, Technology and Application: Falbe, J.. Ed.: Springer-Verlag: Berlin, 1987. Chaps. 5 and 11.

Swisher, R.D. Surfactant Biodegradation, 2nd Ed.: *Schick, M.J.. Fowkes,* F.M., *Eds.; Surfactant Science Series. Marcel Dekker,* Inc.: *New York. 1987.*

Tai, L.H.T. Formulating Detergents and Personal Care Products: A Guide to Product Development; AOCS Press: Champaign. IL, 1999.

The Effect of Polymers on Dispersion Properties; Tadros, T.F.. Ed.: Academic Press: London. 1982.

Thomas. H. Surfactants and the Environment—An *Overview. In Industrial Applications of Surfactants IV: Karsa, D.R., Ed.: Royal Society of Chemistry: Cambridge. UK, 1999; 23–39.*

Use of Ordered Media in Separatiorzs; Hinze, W.L., Armstrong, D.W.. Eds.; Symposium Series. American Chemical Society: Washington, DC, 1987: Vol. 342.

Swelling Clays (Smectites) and Nanofilms

Robert A. Schoonheydt
Katholieke University Leuven, Leuven, Belgium

INTRODUCTION

Smectites or swelling clays are almost ideally suited for fabrication of functional nanofilms. Self-assembling, also called fuzzy assembling or layer-by-layer assembly, and the Langmuir–Blodgett technique were explored. The functionality is introduced in the nanofilrns by ion exchange of amphiphilic molecules. In that way, films with nonlinear optical properties were prepared. Highly dispersed organoclays are also used in nanocomposites of polymers and in coatings to increase the mechanical strength, the photostability, and the heat resistance. and to prevent leakage.

SMECTITES

Clay is a general term for inorganic inaterials in the nano- and micrometer-size range that show plasticity.[1] Clay minerals form the crystalline fraction of clays. They belong to the class of the phyllosilicates. This class is subdivided into 1:1 and 2:1 clay minerals. The elementary sheet of the 1:1 clay minerals consists of a layer of SiO_4 tetrahedra and one layer of Al- or Mg-octahedra, which share a layer of oxygen atoms. In 2:1 clay minerals, the Al- or Mg-octahedral layer is sandwiched between two SiO_4 tetrahedral layers. Isomorphous substitution of Si^{4+} with trivalent cations. mainly Al^{3+}, or Al^{3+} in the octahedral layer by Mg^{2+} or Mg^{2+} in the octahedral layer with Li^{+} leads to negative layer charges compensated by exchangeable cations. When the isomorphous substitution amounts to 0.2–0.6 e per unit cell formula of 2:1 clay minerals. we have smectites or swelling clays. They are the subject of this article. Typical unit cell formulae are given in Table 1.

The superscripts IV and VI stand for the tetrahedral and octahedral layers. respectively. Smectites with Mg in the octahedral layer are called trioctahedral: those with an Al-octahedral layer are called dioctahedral.

SWELLING

The elementary sheets form aggregates. and the exchangeable cations are located at the surfaces of the sheets in the interlamellar spaces.[2] Depending on the size and charge of the cations. one or two layers of water molecules are associated with the exchangeable cations in the interlamellar space. In liquid water. additional water molecules are taken up, leading to the swelling of the aggregates. The limiting case is that of complete swelling into elementary clay sheets or platelets. which diffuse independently of each other in the aqueous suspension. Whether such a state can ever be achieved is a matter of debate. Two opposing forces determine the extent of swelling: on the one hand, the cations, which attract water molecules through ion–dipole interactions; on the other hand. the interaction exchangeable cation-negative layer charge. The former promotes swelling; the latter prohibits swelling. As a consequence. most extensive swelling is observed for the smallest monovalent cations, Li^{+} and Na^{+}. but swelling decreases significantly with increasing cationic radius (Cs^{+}). Di- and trivalent cations have strong interactions with the negative lattice charge, which limits the degree of swelling: the ion–dipole interaction is too weak to overcome the ion-negative lattice charge attraction.

Swelling is an extremely important property of the smectites. because it makes the interlamellar surface available. e.g., ion exchange with almost any type of cation. be it organic or inorganic. Cationic surfactants such as long-chain alkylammonium cations are selectively ion exchanged and form well-defined supramolecular assemblies at the surface. depending on the negative charge density of the clay mineral and the length of the alkyl chain. These so-called organoclays[3] are hydrophobic, swell in suitable organic solvents, e.g., methanol or ethanol. and form stable suspensions in these organic solvents. In principle. it is possible to prepare smectites with well-defined hydrophobicity or hydrophilicity. This property together with the nano/micrometer size of the elementary clay sheets is at the basis for the development of functional nanomaterials. starting from natural or synthetic smectites.

CATIONIC DYES

Cationic dyes such as methylene blue. rhodamine B or 6G, and many others are extremely selectively adsorbed by ion exchange.[4] The reaction is instantaneous. The dyes form aggregates around the smectite particles in aqueous

Encyclopedia of Supramolecular Chemistry
DOI: 10.1081/E-ESMC 120012831

Table 1 Typical unit cell compositions of smectites

$(Si_8)^{IV}(Al_{3.34}(Mg_{0.66})^{VI}O_{20}(OH)_4\ M^+_{0.66}\ mH_2O$: montmorillonite
$(Si_{7.34}Al_{0.66})^{IV}(Mg_6)^{VI}O_{20}(OH)_4M^+_{0.66}\ mH_2O$: saponite
$(Si_8)^{IV}(Mg_{5.34}Li_{0.66})^{VI}O_{20}(OH)_4\ M^+_{0.66}\ mH_2O$: hectorite

suspension, from which the dye molecules slowly redistribute over the surface of the smectite particles.[5] The extent of redistribution and the time scale of the event depend on the type of clay. This means that aggregation and desaggregation phenomena of the elementary clay sheets and the layer charge (position and amount) come into play. The result is that a mixture of monomers, dimers. and aggregates of dye molecules are usually present on the clay surface. The relative proportion of each of these species depends on the loading, the particle size of the smectite, and the location of the isomorphous substitution (octahedral layer versus tetrahedral layer). Two additional interesting observations were made in the study of smectite–dye systems in aqueous suspensions:

1. When water is removed, the dye aggregates redistribute into monomers.[6] This means that in excess water, dye–dye interactions dominate, while in the absence of water, dye–clay particle interactions dominate.
2. The hyperpolarizability of adsorbed methylene blue in a methylene blue–smectite suspension is 11 times higher than that of methylene blue in a methanolic solution.[7] This effect disappears with increasing loading. Thus, two effects play a role: weak electronic interaction of the methylene blue molecule with the clay surface and organization of the dye molecules at the surface.

FILMS

The nanosize of the elementary sheets (1 nm thickness). ion exchange, swelling. and hydrophobic and hydrophilic balance are the basic properties of smectites for layer-by-layer construction of nanofilms and the development of nanodevices. Films can be prepared by casting and spin coating. However. the two most important techniques. which allow a layer-by-layer construction of the nanofilms, are self-assembling (SA) or fuzzy assembling (FA) and the Eangmuir–Blodgett (LB) technique.

Self-Assembling (SA), Fuzzy Assembling (FA), or Layer-by-Layer Assembling (LBL)

Self-assembling is based on the Coulombic attraction between negative and positive charges. In that way. nanocomposite films of oppositely charged polyelectrolytes can be constructed, but the technique can also be applied with smectite particles, because the elementary sheets are negatively charged. Multilayered nanofilms can be constructed by alternate deposition of a layer of a cationic polyelectrolyte and of a layer of smectite particles on a suitable substrate such as glass, quartz, Si, or mica. The latter is preferable, because it is also a 2:1 phyllosilicate with a very high negative charge density and therefore not swellable in water. The cationic polyelectrolyte is strongly adsorbed from a dilute aqueous solution on the surface of the mica sheet. After washing and drying of the polyelectrolyte film, a dilute suspension of a smectite is deposited. The smectite particles are retained by electrostatic attraction with the cationic polyelectrolyte. Excess smectite is washed away, and the film is dried in air. This procedure can be repeated several times to produce multilayer films of the type $(PE/clay)_n$, where PE stands for polyelectrolyte and n is the number of layers.[8] A linear increase of the film thickness with the number of deposited layers is obtained. The average layer thickness is proportional with the concentration of the polyelectrolyte in the solution used for deposition. The clay particles are essentially single sheets (no aggregates) that are randomly oriented in the layer and are partially overlapping. They also form a submonolayer, which means that they do not completely cover the surface. As a consequence, the films have a significant roughness, which is proportional to the amount of polyelectrolyte. This observation gives a hint for the mechanism of film formation. In a thick layer of polyelectrolyte, there is a high density of positive charges, giving a medium with high ionic strength. When a dilute clay suspension is deposited, the high local ionic strength causes clay particle aggregation, thus increasing the roughness. This is schematically shown in Fig. 1. In a thin layer of polylectrolyte molecules, the positive charge density is low, as is the ionic strength; and the polyelectrolyte molecules are stretched. Clay particles will mainly deposit as individual sheets, aggregation is minimal, and the roughness of the film is minimal. The main advantages of such a layer-by-layer assembly are simplicity, control of thickness on the nanometer scale, universal applicability, and easy incorporation of a functionality.[9] This functionality is necessary if the nanofilms are going to be implemented into a device. Two strategies were described in the literature.

In the first. developed by us,[10] a layer of clay mineral particles is covered with the cationic polyelectrolyte poly(diallyldimethylammoniumchloride) (PDDA) and subsequently with the anionic, noncentrosymmetric dye 4-{4[*N*-allyl,*N*-methylamino]phenylazo} benzene sulphonic acid (NAMC). Thus, the monolayer consists of clay/PDDA/NAMO. It is supported on a glass substrate. derivatized with 3-aminopropyl-trimethoxysilane (APTS)

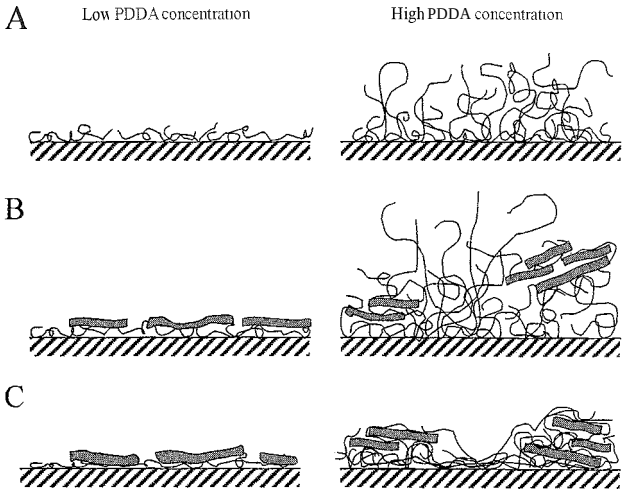

Fig. 1 Model of self-assembling of clay mineral particles (represented as gray slabs) and PDDA (represented as thin curled lines) on a substrate. (A) PDDA only: (B) PDDA + clay mineral particles in the presence of water: and (C) dried film of PDDA + clay mineral particles.

or *N*-trimethoxysilylpropyl-*N*,*N*,*N*-trimethylammonium chloride (TMSPA) and exhibits nonlinear optical properties (Fig. 2). The amount of PDDA is the most important parameter, determining the intensity of the second harmonic signal. $I_{2\omega}$. The type of clay and the type of derivatization of the glass substrate seem to have a less pronounced influence on the $I_{2\omega}$ signal. The NAMO molecules are probably adsorbed with their SO_3^- groups toward the positive charges of the PDDA. If the latter molecules are more or less stretched on the surface of the clay, a noncentrosymmetric organization of the NAMOs can be realized. At high PDDA loadings. a stretched configuration of the PDDA molecules is impossible at the clay surface. Chains of PDDA stick out of the clay surface in different directions and adsorb NAMO molecules. The positive charges on PDDA are randomly distributed, as are the NAMO molecules, and the noncentrosymmetric organization fades away, leading to a decrease of the $I_{2\omega}$ signal.

LBL assembling is not restricted to two-dimensional particles such as smectites. Spherical particles, which carry some negative charge, can also be organized in nanofilms. Such particles include Fe_3O_4, CdTe, PbS, and TiO_2.[9] Thus, the assembly can be $(PDDA/Fe_3O_4)_n$ with $n=1-30$. Smectite layers can also be included, thus giving, e.g., $(PDDA/clay/PDDA/Fe_3O_4)_{30}$ or $(PDDA/clay/PDDA/CdTe)_{20}$. The smectite particles have at least two positive effects: avoidance of interpenetration of the Fe_3O_4 or CdTe layers or isolation of the magnetite layers and the CdTe layers from each other, thus strongly influencing the magnetic properties (Fe_3O_4) and the luminescence properties (CdTe) of the nanofilms.[11]

A special case is that of the free-standing nanofilms.[12] In this case, the glass substrate is covered with a layer of cellulose acetate (CA). This layer is partially hydrolyzed, thus generating negative charges, on which PDDA and Fe_3O_4 or PDDA. smectite. PDDA and Fe_3O_4 can be deposited, thus giving films of composition glass/CA/PDDA/Fe_3O_4 or glass/CA/PDDA/clay/PDDA/Fe_3O_4. The film is peeled off, and cellulose acetate is dissolved in acetone without damage to the nanofilm. The latter is freely suspended in acetone and maintains its magnetic properties.

Langmuir–Blodgett Technique (LB)

In the LB technique, a monolayer of amphiphilic molecules, prepared at the air–water interface, is transferred to a substrate, thus giving a monomolecular film. The molecules must be solvable in a volatile, water-insoluble (organic) solvent. but not, or to a very limited extent. in water. Thus. when the solution of the molecules in the organic solvent is spread over the surface of water, the solvent evaporates, leaving a monolayer of molecules at the air–water interface. This monolayer can be compressed and transferred to a substrate. When the molecules are replaced by colloidal. nanosized particles. monolayers of these particles on a substrate are obtained. Smectites are especially well suited for the LB technique. The elementary clay sheets are about 1 nm thick and a few tens to hundreds nm wide and long. In the alkali- or alkaline earth form. they are hydrophilic, but by ion exchange with suitable amphiphilic cations. they become hydrophobic. There are then two ways to prepare monolayers of smectite clay particles by the LB technique.

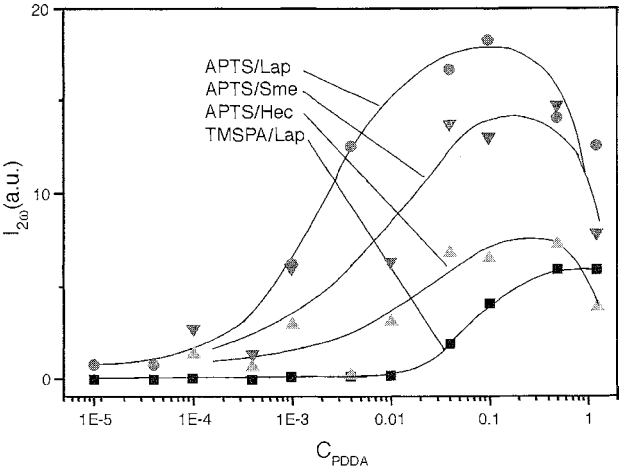

Fig. 2 Intensity of the second harmonic signal versus the amount of PDDA offered in solution (C_{PDDA} in moles/L) for the film: glass/clay/PDDA/NAMO. Lap= laponite; Hec= hectorite; Sme= synthetic saponite: APTS=3-aminopropyltrimethoxysilane: and TMSPA=trimethoxysilylpropyltrimethymammonium.

The first starts with the preparation of a hydrophobic smectite, which forms a colloidal suspension in chloroform. This suspension is spread over the water surface in the EB trough, chloroform evaporates almost instantaneously, and the remaining monolayer of clay particles is transferred to a hydrophobic glass plate.[13] The procedure is laborious because of the preparation of the organophilic smectite. In addition, it is not at all evident that the aggregates of organophilic smectite particles swell in chloroform to such an extent that they break up into individual elementary sheets necessary for the monolayer film formation. An alternative and, in principle, easier approach is schematically shown in Fig. 3. The LB trough is filled with a dilute aqueous suspension of smectite particles. The amphiphilic cations are spread at the air–water interface. The organic solvent evaporates, and the amphiphilic cations undergo an ion exchange reaction with the elementary clay sheets at the air–water interface. Thus, a monolayer smectite sheet–amphiphilic cations is formed at the air–water interface, which is compressed and transferred on a substrate (e.g., glass) by vertical or horizontal dipping. The advantage of this procedure is that the preparation of the organoclay is avoided. A dilute aqueous suspension of a Na^+-smectite guarantees that the smectite suspension contains a large fraction of individual eleinentary clay sheets. This is proven by visualization of the smectite particles in the monolayer film with AFM.

The technique was developed with octadecylammonium cations as amphiphiles. However, short-chain, water-soluble alkylammonium cations can also be used.[14,15] In that case, some of the alkylammonium cations are picked up by the eleinentary clay sheets and stabilized at the air–water interface and some dissolve in the aqueous subphase. In any case, the alkylammonium-smectite sheet can be compressed at the air–water interface and transferred to the substrate. This proves that the ion exchange reaction between the smectite particles and the alkylammonium cations at the air–water interface is an extremely fast and selective reaction. Multilayers can be prepared, and their formations can be followed by measuring the intensities of the C–H stretching vibrations of the ion-exchanged alkylammonium cations. The linear increase of the intensities with the number of deposited layers indicates that, on average, the same amount of eleinentary clay sheets and alkylammonium cations are deposited in each layer.

If functional films are to be made. the alkylammonium cations have to be replaced, at least partially, with functional molecules. Thus, if the optical isomers or the racemic mixture of $[Ru(phen)_2(dcC_{12}bpy)](ClO_4)_2$ (phen=1.10-phenanthroline; $dcC_{12}bpy$=4,4′-carboxyl-2.2'-bipyridyl didodecylester). is used as an amphiphile. monolayer and multilayer films are obtained that have nonlinear optical properties.[16] That means that they generate a second harmonic signal upon illumination with a Nd-YAG laser. When the Ru complex is diluted in octadecylammonium cations. the signal intensity increases quadratically with the number of layers deposited. indicating that films with noncentrosymmetric organization of the Ru complexes are realized. This is not the case in the absence of octadecylamrnonium cations. The latter observation suggests that in the absence of octadecylammonium cations, the Ru complexes form aggregates at the clay surface. In principle then, one can control the organization of amphiphilic cations at the smectite surfaces and tune it into the desired direction. Amphiphilic dyes can also be used. If the right couple of dyes is used, energy transfer can be realized in the films. This has been shown for 3.3'-dioctadecyloxacarbocyanine and octadecyl-rhodamine B.[17] The former is the donor. Upon excitation around 460 nm, the fluorescence of rhodamine B in the region 500–580 nm is monitored. The advantage of the clay films is that they stabilize the dye molecules against degradation by light and that the organization of the molecules can be monitored in the presence of octadecylamrnonium cations.

With a single layer of elementary clay sheets and a single layer of adsorbed molecules, one can now start studies of the clay sheets with x-ray techniques,[18] vibra-

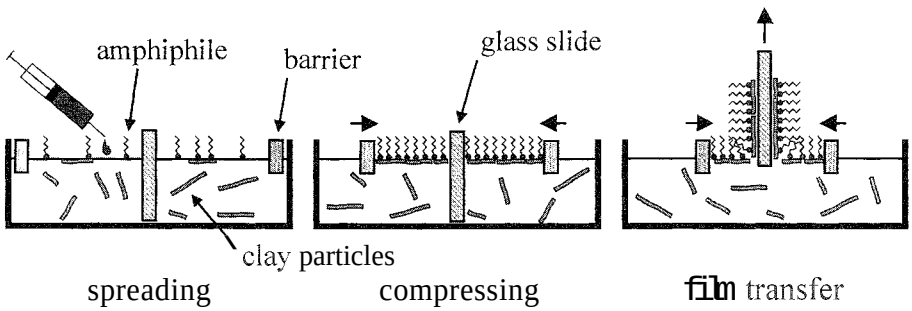

Fig. 3 The preparation of clay mineral-amphiphilic cation films by the Langmuir–Blodgett method.

tional and electronic spectroscopies. The same holds for the adsorbed molecules.

Highly Dispersed Organoclays

One of the essential conditions for formation of smectite nanofilms is the presence of elementary clay sheets in the system. This is not only the case for LB and SA films, discussed above, but also for a number of modern developments in fabrication of devices and formulations of polymeric materials. Thus, Ecke and Decher[19] fabricated organic light-emitting devices (OLEDs) with an isolating barrier of single sheets of montmorillonite in the active medium between the two electrodes. This isolating montmorillonite layer plays a key role in the electrooptical properties of the device, increasing the light output. But the exact mechanism of action of the isolating montmorillonite layer is not yet known.

Single clay layers or 100% dispersion of the clay in polymer matrices is also the ideal situation in which to obtain nanocomposite materials with enhanced mechanical properties. This was achieved by researchers at the Pennsylvania State University[20] with a semifluorinated organic surfactant to modify the montmorillonite, which is subsequently compounded with polypropylene (functionalized with, e.g., maleic anhydride). In The Netherlands,[21,22] the clay is intercalated with polyethyleneoxide block copolymer. This material is swollen in the monomer (methylmethacrylate). which polymerizes to poly(methylmethacrylate) by radical polymerization. The swelling ensures complete dispersion of the clay.

Organophilic clays can also be homogeneously dispersed in coatings, giving them improved corrosion resistance, thermal stability. and barrier properties (decreased permeability toward water and oxygen). If the organic modifier of the clay is a dye, improved color stability against. e.g., UV irradiation, is obtained.[23,24]

Organoclays in an adequate solvent provide microenvironments for formation of quantum-sized semiconductor particles, such as CdS and ZnS.[25] Finally, they are excellent adsorbents of pesticides, which leads to improved stability of the pesticides: higher resistance against photodegradation and reduced leaching into water.[26]

CONCLUSION

It has been convincingly shown that functional nanofilms on the basis of smectites can be prepared. Properties that must be under control are complete swelling of the clay minerals into individual elementary sheets, selective and fast ion exchange of functional molecules, and organization of the molecules at the clay surface.

These nanofilms open two directions of research. First and for the first time they allow the fundamental study of single elementary clay mineral sheets and of their adsorbed molecules. Second. there is still a long way to go from nanofilms to devices. These hurdles can only be solved by research. Thus, there is a bright future for more research on clay minerals.

ACKNOWLEDGMENT

The author acknowledges financial support of the FWO-Vlaanderen of the bilateral agreement Flanders–Hungary and of the K.U.Leuven.

ARTICLES OF FURTHER INTEREST

Biosensorr, p. 115
Electrochemical Sensors, p. 505
Fluorescent Sensors, p. 572
Layered Supramolecular Solids and Their Intercalates, p. 791
Mesoporous Materials, p. *845*
Mesoporous Silica and Silica–Organic Hybrids. p. *852*
Nonlinear Optical Materials, p. 973
Photochemical Sensors, p. 1053

REFERENCES

1. Nemecz, E. Clay Minerals; Akademiai Kiado: Budapest, 1981.
2. Güven, N.; Pollastro. R.M. Clay–Water Interface *and* Its *Rheological Implications*; The Clay Minerals Society, 1992: Vol. 4.
3. Yariv. S.; Cross, H. *Organo-Clay* Compleses *and Interactions*; M. Dekker Inc.: New York. 2001.
4. Schoonheydt. R.A. Organization and Spectroscopy of Dyes on Submicron-Sized Crystalline Solids. In *Microchemistry. Spectroscopy and Chemistry* in *Small Domains*; Masuhara. H., Ed.: Elsevier Science B.V.: Amsterdam, 1994; 469–482.
5. Jacobs, K.Y.; Schoonheydt, R.A. Time dependence of the spectra of methylene-blue–clay mineral suspensions. Langmuir **2001**, 17. 5150–5155.
6. van Duffel. B.: Jacobs. K.Y.; Schoonheydt. R.A. Methylene Blue–Hectorite Complexes: From Suspensions to Films. In *Proceedings* of *the 11th International Clay Conference*; Kodama. H., Ed.; Marcel Dekker, Inc.: New York. 1999: 475–481.
7. Boutton, C.: Kauranen. M.: Persoons, A.; Keung, M.P.: Jacobs, K.Y.: Schoonheydt, R.A. Enhanced second-order optical nonlinearity of dye molecules adsorbed into laponite particles. Clays and Clay Min. **1997**, *45*, 483–485.
8. van Duffel, B.; Schoonheydt, R.A.: Grim. C.P.M.: De

Schryver, F.C. Multilayered clay films: Atomic force microscopy study and modeling. Langmuir 1999, *15*, 7520–7529.
9. Kotov, N.A. Ordered layered assemblies of nanoparticles. MRS Bulletin **2001**, 992–997.
10. van Duffel. B.; Verbiest, T.: Van Elshocht. S.; Persoons, A.: De Schryver, F.C.; Schoonheydt, R.A. Fuzzy assembly and second harmonic generation of clay-polymer-dye monolayer films. Langmuir 2001. 17. 1243–1249.
11. Mamedov, A.; Ostrander, J.: Aliev, F.; Kotov, N.A. Stratified assemblies of magnetite nanoparticles and montmorillonite prepared by the layer-by-layer assembly. Langmuir 2000, 16, 3941–3949.
12. Mamedov. A.A.; Kotov. N.A. Free-standing layer-by-layer assembled films of magnetite nanoparticles. Langmuir **2000**. 16. 5530–5533.
13. Inukai. K.; Hotta, Y.: Taniguchi, M.; Tomuro, S.: Yamagishi, A. Formation of a clay monolayer at an air–water interface. Chem. Comm. 1994, Vol. 959.
14. Umernura, Y.; Yamagishi, A.: Schoonheydt, R.; Persoons. A.: De Schryver. F.C. Fabrication of hybrid films of alkylammonium cations ($C_nH_{2n+1}NH_3^+$; n = 4–18) and a smectite clay by the Langmuir–Blodgett method. Langmuir **2001**, 17. 449–455.
15. Umemura, Y.; Yamagishi, A.; Schoonheydt. R.A.; Persoons. A.; De Schryver. F. Formation of hybrid monolayers of alkylammoniurn cations and a clay mineral at an air–water interface: Clay as an inorganic stabilizer for water-soluble amphiphiles. Thin Solid Films 2001, *388*, 5–8.
16. Umemura, Y.: Yamagishi, A.: Schoonheydt. R.A.: Persoons. A.; De Schryver. F.C. Langmuir–Blodgett films of a clay mineral and ruthenium(II) complexes with a noncentrosymmetric structure. J. Am. Chem. Soc. 2002. *124*. 992–997.
17. Ras. R.H.A.: van Duffel, B.: Van der Auweraer. M.; De Schryver, F.C.; Schoonheydt. R.A. Molecular and Particulate Organization in Dye–Clay Films Prepared by the Langmuir–Blodgett Method. In Proceedings 12th *International* Clay Conference; Cravero, F., Mas. G., Dominguez, E.. Eds.; Elsevier: Amsterdam. in ***press.***
18. Takahishi, S.; Taniguchi. M.; Omote, K.; Wakabayashi, N.; Tanaka. R.; Yamagishi. A. First observation of in-plane x-ray diffraction arising from a single inorganic compound film by a grazing incidence x-ray diffraction system with a conventional laboratory x-ray source. Chem. Phys. Lett. 2002. *352*, 213–219.
19. Eckle, M.; Decher, G. Tuning the performance of layer-by-layer assembled organic light emitting diodes by controlling the position of isolating clay barrier sheets. Nanoletters 2001, **1,** 45–49.
20. Manias, E. A direct blending approach for polypropylene1 clay nanocomposites enhances properties. MRS bulletin 2001, 862–863.
21. Dortmans, L.J.M.G.; Batenburg. L.F.; Fischer, H.; Nelissen, R.G.W.J.; Koster. T.P.M. Nanocomposite materials: From postdoc's work to prototypes. Klei, Glas, Keramiek 2002, *23*. 5–9.
22. Eckle, *M.;* Decher, G. Tuning the performance of layer-by-layer assembled organic light emitting diodes by controlling the position of isolating clay barrier sheets. Nanoletters 2001. *1*, 45–49.
23. Fischer, H.R.; Batenburg, L.F.; Meinema. H.A.: Hogerheide, M.P.; Rentrop, C.H. Nanocomposite Coatings. WO Patent 01104050, January 18. 2001.
24. Fischer. H.R.: Batenburg, L.F. Coloring Pigment. WO 01/04216, January 18, 2001.
25. Dékany, I.: Turi, L.; Tombacz, E.: Fendler. J.H. Preparation of size-quantized CdS and ZnS particles in nanophase reactors provided by binary liquids adsorbed at layered silicates. Langmuir **1995. 11,** 2285–2292.
26. El-Nahlal, Y.: Undabeytia. T.; Polubesova, T.; Mishael. Y.G.; Nir. S.; Rubin, B. Organo-clay formulations of pesticides: Reduced leaching and photodegradation. Appl. Clay Sci. 2001, *18*. 309–326.

Tectons: Definition and Scope

Pierangelo Metrangolo
Giuseppe Resnati
Polytechnic of Milan, Milan, Italy

INTRODUCTION

Many molecules tend to be involved in a pattern of several intermolecular interactions of comparable relative strength. the structure of the resulting aggregated system being determined by the balanced cooperation of these interactions. The relative relevance of these interactions often depends on the properties of the partners with which the molecules are connected. This is the case of molecules that can give rise to weak interactions only. In contrast. there are molecules with interactions that are dominated by particular associative forces that induce the self-assembly of an organized network with specific architectural or functional features. In 1991. James D. Wuest proposed naming these molecules tectons. from the Greek, τεκτων. which means "builder" and is the root of such words as architect."] Water is among the simplest tectons.[2]

Tectons interact with their neighbors in strong and well-defined ways, as they inherently possess the molecular structure and intermolecular recognition features to predictably self-assemble into crystalline networks. The interactions pattern of a tecton is robust enough to be exchanged from one network structure to another, thus securing generality and predictability in self-assembly processes. Within their structure. tectons contain the recognition sites and a specific assembling algorithm that will operate when complementary sites are available. Tectons can be considered to consist of peripheral "sticky sites" that direct molecular association, as well as of scaffolds that hold the sticky sites in pa ticular orientations. Together, these features help tectons control how their neighbors are positioned, despite the competing effects of other intermolecular interactions that are weaker and less specific."] Tectons must fulfil energy and structural criteria (interaction robustness and scaffold geometry. respectively). An effective method for making tectons is to attach selected functional groups that are known to participate reliably in specific intermolecular interactions to geometrically suitable molecules."" Various interactions are used to direct association. thanks to their strength, directionality, and specificity. e.g., metal coordination. hydrogen bond. and halogen bond.

The concept of tecton can be better understood if contrasted with the concept of supramolecular synthon. Paraphrasing Corey's historic definition of synthon,[5] Desiraju defined that a supramolecular synthon is a structural unit within a supermolecule that can be formed or assembled by known or conceivable synthetic operations involving intermolecular interactions.[6] The supramolecular synthon concept is backwardly oriented (i.e., is useful in supramolecular retrosynthesis) and focuses on the part of a supermolecule that is formed or can be formed through an intermolecular interaction. The tecton concept is forwardly oriented (i.e., is useful in supramolecular synthesis) and focuses on a molecule that predictably gives supermolecules, thanks to its tailored structure and robust binding sites.

Various derived terms were also introduced. Molecular tectonics is the art and science of supramolecular construction using tectonic subunits[7] and describes the chemical construction of systems with an order higher than the molecular scale."" The term "metallatecton" is used to indicate tectons having a metal ion coordinated in their core,[9,10] but its employment could be extended to indicate all the tectons where a metal is present [see the discussion of metal coordination presented later in this article[11,12]]. The term tecton is also used to address synthetic polymers [13] and DNA strands.[14] When structures of inorganic frameworks are considered. the word tecton is used to address oligomeric groups of polyhedra that enable a desired topology to be formed.[15]

TECTONS

Metal-ligand dative bonds are always highly directional. While their strength spans over a wide range. depending on the nature of the species involved, in most cases. metal coordination overpowers a number of weaker interactions. Being a dominant supramolecular interaction. it is perfectly tailored for the design and synthesis of tectons. The studies of Peter J. Stang on the self-assernbly-driven formation of high-symmetry coordination cages are simultaneously elegant in their simplicity and in their complexity and are particularly well-suited for a case

Encyclopedia of Supramolecular Chemistry
DOI: 10.1081/E-ESMC 120019167

Ditopic 180°

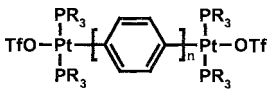

	R	n
1a	Et	1
b	Ph	2

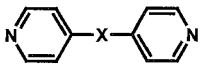

	R
6 a	/
b	(*E*)–≡–
c	–(≡)$_2$–

Ditopic 120 - 108°

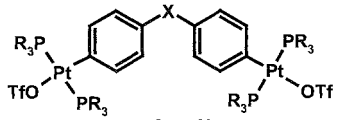

	R	X
2 a	Ph	CO
b	Et	CMe_2

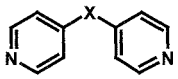

	R
7 a	CO
b	$C(OCH_2)_2$
c	$SiMe_2$

Di, tri-. tetratopic 90°

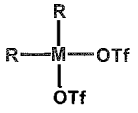

	M	R
3 a	Pt	PEt_3
b	Pd	PEt_3

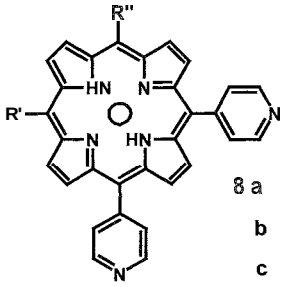

	R'	R''	○
8 a	Ph	Ph	–
b	4-Me-Ph	4-Me-Ph	$2Zn^{++}$
c	4-Py	4-Me-Ph	$2Zn^{++}$
d	4-Py	4-Py	$2Zn^{++}$

Ditopic 0°

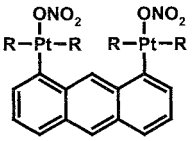

	R
4	PEt_3

Tritopic 120°

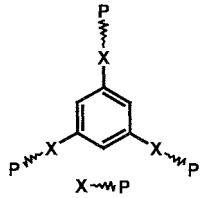

	X~P
5 a	–≡–$Pt(PPh_3)_2OTf$
b	–≡–$Pt(PEt_3)_2OTf$

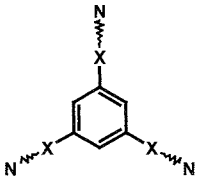

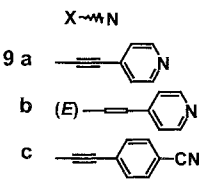

	X~N
9 a	–≡–
b	(*E*)–≡–
c	–≡–CN

Tritopic 108°

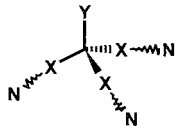

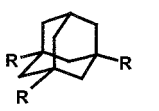

	Y	X~N
10 a	OH	–≡–
b	OH	–≡–CN
c	OCOCHPhEt	–≡–

	R
10 d	–≡–

history on tectons exploiting inetal coordination."[1,12] Stang's paradigm is the recognition between two complementary tectons. one bearing the metal sites and the other bearing the ligands. Two libraries of tectons were prepared (Scheme 1). Platinum atoms are typically used as metal sites, and the nitrogen atoms of pyridine moieties are used as ligand sites. Less frequently. palladium atoms and cyano groups are also employed with comparable success.[16] Metal tectons (1–5) and ligand tectons (**6–10**) can be classified as functions of the recognition sites number; namely. they can be differentiated into ditopic tectons (**1–4**, 6–8a.b). tritopic tectons (5, 8c, 9, P0), and tetratopic tectons (8d). A further differentiation can be made in relation to the angle between the recognition sites. Ditopic 180° tectons are typically obtained by the 1,4-difunctionalization of a benzene ring (1a) or by the 4-functionalization of a pyridine (6a). If metric engineering requires the distance between the recognition sites to be tuned, ethylene. acetylene. and benzene spacers are used (Pb, **6b**,**c**).[17] Ditopic 120° tectons are obtained by interposing an sp^2 atom between two para-substituted benzenes (2a) or pyridines (7a). Siinilarly, ditopic 108" tectons are obtained by intei-posing an sp^3 atom (2b, 7b,c). Ditopic 90° ligand tectons are formed by appending two 4-pyridyl residues in positions 5,10 of a porphyrin system (8a,b). When a third and fourth 4-pyridyl substituent are added in positions 15 and 20 of the porphyrin scaffold, the tritopic and tetratopic 90" tectons **8c** and **8d** are obtained. respectively.[18] The 90° ditopic metal tectons (3a,b) are obtained by resorting to dicoordinating platinum or palladium ions. Metal tectons with different topicity and geometry are obtained by using other metals with different numbers or geometries of coordination. For instance, Ag(I) is frequently used as a ditopic 180° metal tecton in the coordination of pyridyl ligands[19] and Cu(I) as a tetratopic tetrahedral tecton for oligo(2,2′-bipyridine) ligands.[20] Tritopic tectons with either a planar (5 and 9) or a tetrahedral (10) arrangement of the "sticky sites" were also developed. The 1,3,5-trisubstitution of a benzene core is the standard approach to tritopic planar tectons, while the trisubstitution of a methane (10a–c) or adamantane (10d) moiety affords tetrahedral tectons. Once again, their metrics are controlled by using rigid acetylene and phenyl spacers.

By combining tectons 1–10 as the bricks of a molecular Lego, Stang obtains several cage molecules, and among them, some of the Platonic and Archimedean solids (Scheme 2). On self-assembly. the pyridyl or nitrile nitrogen atoms replace the triflate, or nitrate, residues at the metal. Dodecahedranes **11** are formed by self-assembly of 30. 180° ditopic tectons **1** and 20, 108° tritopic tectons 10, yields being nearly quantitaiive independent from the metric of the employed ditopic tecton. The same three-dimensional geometries can be obtained

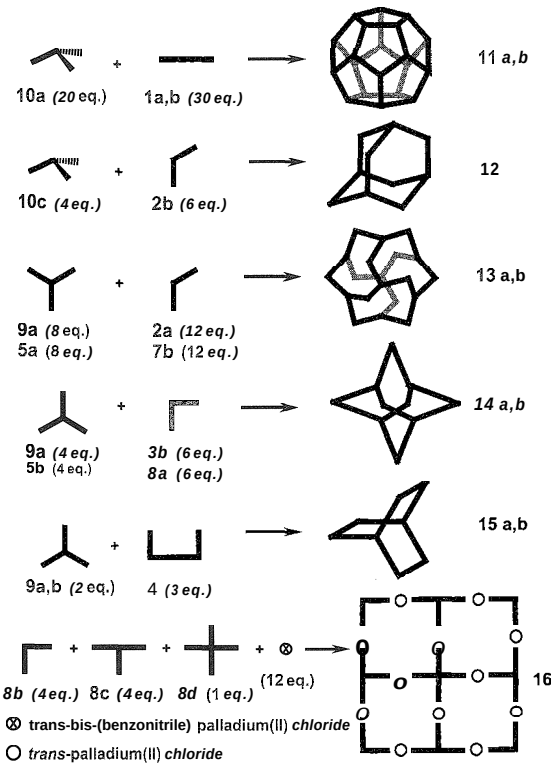

Scheme 2

by switching the donor and acceptor sites between ditopic and tritopic tectons. For instance. cuboctathedrons 13 and truncated tetrahedrons 14 can be obtained by self-assembly of metal tritopic tectons ***5*** with ligand ditopic tectons **7** and 8 or of ligand tritopic tectons 9 with metal ditopic tectons 2 and **3.** Selective self-assembly of different tectons can also occur. When 12 equivalents of *trans*-bis(benzonitrile)palladium(II) chloride are mixed with four equivalents of '1-shaped" tectons 8b. four equivalentss of ''T-shaped'' tecton 8c, and one equivalent of "X-shaped'' tecton 8d, a 21-membrered discrete square array is obtained, where the "L-shaped" tectons form the corners of the array, the ''T-shaped'' tectons the sides, and the ''X-shaped'' tecton the central core.[18]

Hydrogen bonding is the most frequently occurring interaction in self-assembled systems of living organisms. forcefully indicating the outstanding power and effectiveness of the interaction. It is not surprising that several tectons were developed by exploiting hydrogen bonding. As described above, tectons based on metal coordination bear donor or acceptor sites. On the other hand. tectons exploiting hydrogen bonding bear both donor and acceptor sites, and it is important that an equal number of complementary sites be present so that robustness and predictability during the self-assembly process are maximized. In most cases, tectons exploiting hydrogen

bonding were built by endowing them with the ability to participate in multiple intermolecular hydrogen bondings. Simple. well-known hydrogen-bonding motifs, which were carefully studied and shown to be particularly strong and reliable, were selected and repeatedly inserted on a core to construct the tectons via a modular approach.

In the solid state and in solution, 2(1*H*)-pyridinone (**17a**) shows a well-established tendency to self-associate and to form cyclic hydrogen-bonded dimers (**17b**, Scheme 3). This preference is used effectively to control the association of more complex derivatives that incorporate multiple 2-pyridiaone groups[1] and have some of the desirable properties of zeolites, including high structural integrity, potential large void volumes, and adjustable microporosity. Compound **18a** is a tetratopic and tetrahedral tecton that have four 2-pyridone groups appended to a methane core through phenylacetylene spacers. The intermolecular hydrogen bondings of these tetrahedrally oriented pyridones direct the self-assembly of a diamandoid network. The enormous voids in this structure are filled by a combination of interpenetrating, independent, diamondoid networks and enclathrated molecules of carboxylic acids (acetic, propionic, butyric, or valeric acids). The hydrogen-bonded networlts are porous enough to permit the exchange of the acid (e.g., valeric by acetic acid) and robust enough to remain intact. Compound **18b**. where the tetrahedral core is a silicon atom, also crystallizes in diamondoid interpenetrated networks. The Si—C covalent bond is approximately 0.33 Å longer than the C—C bond, and the intertectonic separation in the crystal of **18b** is approximately 0.7 Å larger than that in the crystal of **18a**. The structural similarity between **18a** and 18b extends also to functional properties, as **18b** also enclathrates carboxylic acid molecules in the void channels of the crystal.[7] To have contracted diamandoid networks, the tecton **18c** was constructed. Its smaller size results in a decreased intertectonic separation (11.7 Å) and reduced interpenetration (twofold in **18c**. sevenfold in **18a**. eightfold in **18b**) but leaves unchanged the ability to selectively enclose carboxylic acid guest molecules in the void channels. When the silicon core of **18c** is replaced by a more flexible tin core (**18d**), the direct hydrogen bonding of pyridone rings still links each tecton to four neighbors, but because the core is more susceptible to angular deformation. cyclic quartets are present instead of diamondoid networks. Nevertheless, functional properties are retained. and carboxylic acid molecules are once again enclosed in the channels.[21]

Also, simple aryl boronic acids form cyclic hydrogen-bonded dimers in the solid state. Tetraboronic acids **18e,f**, bearing four $-B(OH)_2$ groups oriented tetrahedrally by cores derived from tetraphenylmethane and tetraphenylsilane, afford isostructural. fivefold interpenetrated, and diamandoid networks held together by hydrogen bondings of the $-B(OH)_2$ groups. Both networks present void channels available for the inclusion of disordered guests, and their crystallization affords inclusion compounds of approximate composition $18 \cdot 5CH_3COOC_2H_5 \cdot xH_2O$.[22]

The 2,4-diamino- and the 2.4.6-triaminotriazine (melamine) motifs proved particularly effective in tecton construction. The pentaerythritol derivative **18g**, having four 2,4-dimethylaminotriazine residues appended to the tetrahedral core through flexible spacers. affords crystals where, despite the eightfold interpenetration, 60% of the volume is available for including guests. which can be exchanged quantitatively without loss of crystallinity.[3] A similar inclusion behavior is shown by other tectons bearing four tetrahedrally oriented 2,4-diaminotriazine residues, e.g., **18h**.

In synthetic chemistry; the reactivity profile of a functional group is inherently invariant, as only some of its marginal aspects are affected by the overall structure of the molecule in which the functional group is inserted. Similarly. the interactions pattern of a tecton is strong enough to be exchanged from one network structure to another. but some slight changes may occur as a function of the properties of the partner with which it is interacting.

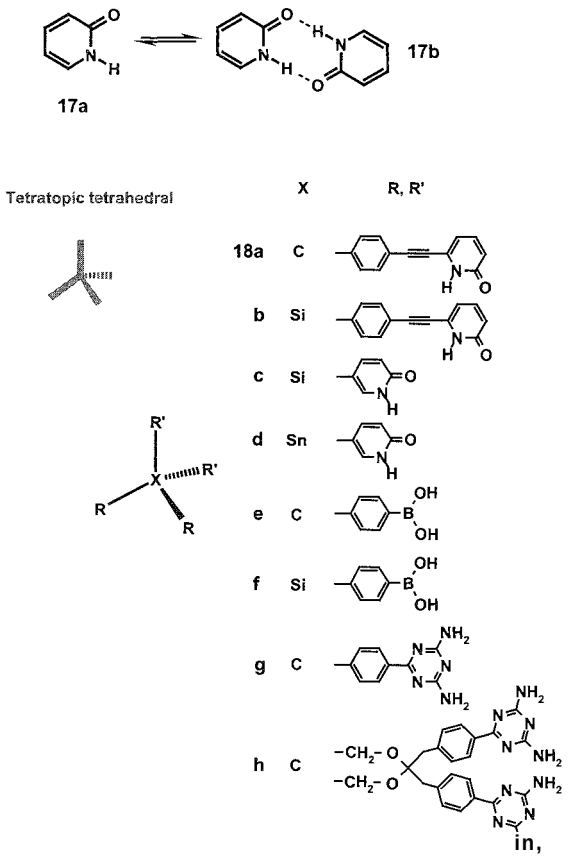

Scheme **3**

The pairing of melamines and barbituric acids, two tritopic 120° tectons, gives a telling example.[23] 5,5-Diethylbarbituric acid (**19**) cocrystallizes with *N*,*N*′-bis (4-methylphenyl)melamine (**20a**) to form the linear, polymeric, tape-like array **21a** (Scheme 4). On replacement of the methyl group of the melamine subunit with the sterically bulkier carbomethoxy substituent, as in **20b**, the crinkled tape **21b** is generated in the solid to relieve unfavorable lateral nonbonding interactions that would be present in a hypothetical linear tape. Placing highly encumbering *tert*-butyl substituent on the melamine subunit, as in **20c**, effects the production, in the solid state, of the rosette-like supermolecule **21c**.

All tectons described above give rise to nonionic hydrogen bonds. Other tectons form intermolecular recognition patterns dominated by directional hydrogen bonds and strong but less directional ionic interactions. This is the case, for instance, of cyclic *bis*-amidinium dications interacting with dihydrogenophosphate anions, iso- or terephthalate dianions, fumarate, pyromellitate, or acetylenedicarboxylate dianions.[24]

Halogen bonding[25] is another directional, strong, and selective interaction that allowed several iodo-substituted compounds. and to a lesser extent their bromo analogues, to work as reliable tectons. The "sticky sites" here are the halogen atoms. Chlorine atoms give rise to

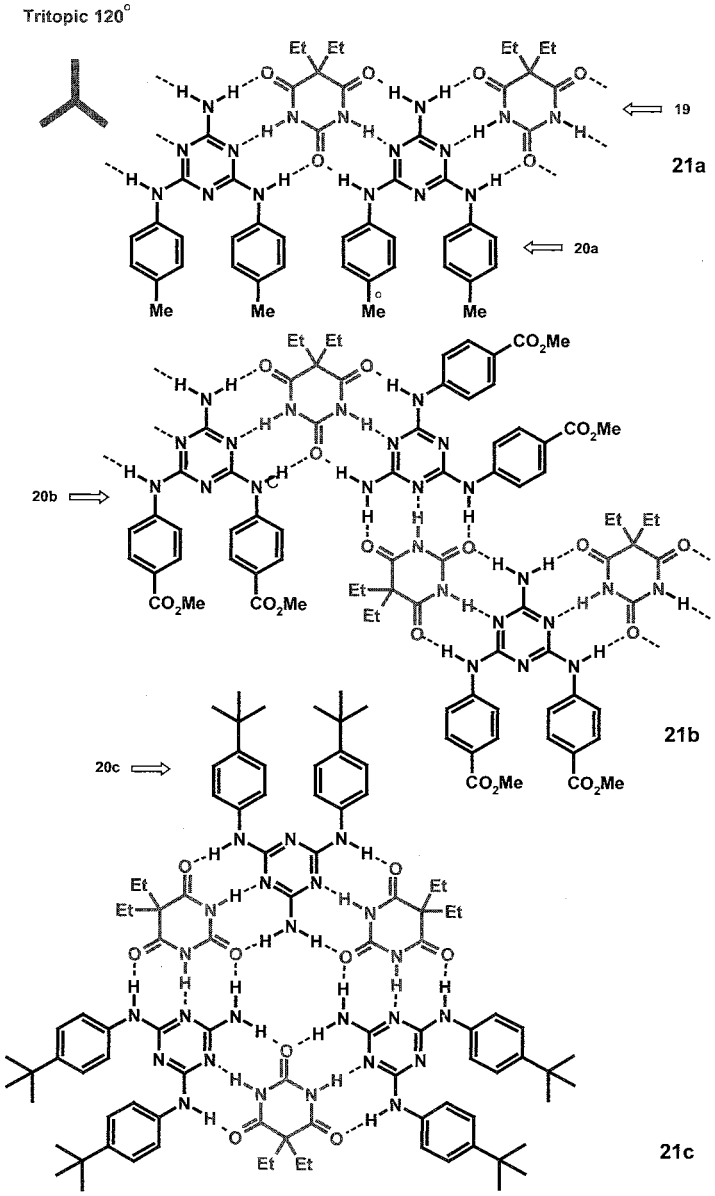

weak halogen bondings that do not dominate the associative forces driving self-assembly processes. Bromine atoms give stronger halogen bonds, but in the reported tectons, the bromines are usually appended to electron-withdrawing scaffolds in order to strengthen the interaction.[26] Iodine atoms give strong halogen bonds, and a wide diversity of tectons was described where the iodines were bound to cores, which are quite different from the structural point of view.

Strategies employed to prepare halogen-bonding based tectons strictly parallel those described above for metal-coordination-based tectons. 1,4-Difunctionalization of a benzene ring affords ditopic 180° tectons (**22a–c**, Scheme 5). Perfluoroalky chains, due to limited conformational flexibility, behave as rigid bars, and α,ω-diiodoperfluoroalkanes **23a–d** are ditopic 180° tectons for which the metric can be controlled by simply varying the difluoromethylene units number. Ditopic 108° tectons are obtained by interposing an sp^3 atom between two pam-substituted benzenes (**24a,b**), and 1,2-difunctionalization of a benzene ring affords ditopic 60° tectons **25a,b**. Tetrabromomethane 26 is a tetratopic and tetrahedral tecton.

Several one-dimensional and infinite chains are formed when ditopic halogen tectons 22–25 interact with ditopic electron donor tectons (Scheme 6). Noncovalent copolymers **27a–h** are formed when **22a–c** interact with dipyridyl 6a and its analogues **6b** and **6d**, where an (*E*)-ethylene and ethane spacer separate the two pyridine rings. X-ray analysis of these one-dimensional chains shows a remarkable crystal packings arrangement consistent with the self-assembly being dominated by the algorithm of the starting tectons.[27,28] Infinite chains are also obtained on the interaction of **6a** with the ditopic halogen tectons **24b** and **25a,b**. Because the geometry of the supramolecular chains is controlled by the geometry of the "sticky sites" on starting tectons, the noncovalent copolymers given by **24b** and **25a,b** show a wave-like or screwed arrangement rather than the linear arrangement of **27a–h**. 1,4-Diiodobenzenes **22a,c** also afford one-dimensional infinite chains when interacting with ditopic tectons, where the electron donor sites are oxygen atoms (e.g., 4,4′-dipyridyl *N*,*N*′-dioxide and 1,4-dinitrobenzene, **27i,j**)[27,29] or sulfur atoms (e.g., 2-mercapto-1-methylimidazole, **27k**).[30] Similarly, α,ω-diiodoperfluoroalkanes **23a–d** give infinite chains **28a–g** upon interaction with a wide variety of ditopic tectons, where the electron donor sites are either neutral (e.g., primary, secondary, and tertiary amines, anilines, pyridines, ethers) or anionic (e.g., fluoride or iodide anions).[31] In all reported structures, the perfluoroalkyl chains adopt a twisted *trans* conformation and behave as rigid, linear spacers of the two terminal "sticky sites."

When the tetratopic and tetrahedral halogen tecton 26 interacts with an electron donor with a similar topicity and geometry, for instance, hexamethylenetetramine, diamondoid networks are obtained.[6] The tecton **24a** bears two iodine atoms (halogen-bonding donor sites) and two nitro groups (halogen-bonding acceptor sites) that are oriented after a tetrahedral geometry. On crystallization, the system behaves as a tetratopic and tetrahedral tecton and affords a fivefold interpenetrated diamondoid network.[32]

Finally, tectons based on two other interactions types were reported.

The van der Waals interactions-driven recognition processes between diconcave and diconvex tectons afforded one- and two-dimensional inclusion networks.[33] Calix[4]arene units in the cone conformation offer preorganized and tuneable hydrophobic pockets that include a wide variety of neutral molecules. Fusion of two calix[4]arene units in the cone conformation and in a face-to-face arrangement (by bridging their eight OH groups with two silicon atoms), gives diconcave tectons, the "sticky sites" of which are the two cavities arranged in a divergent fashion. Mexadiyne and p-xylene are used as diconvex tectons. Being included in the calixarenes cavities thanks to van der Waals interactions, these hydrocarbons work as connectors and form one-dimensional networks.

With metals, tetracyanoethylene can work as a polydentate ligand via several different bonding modes. In addition, with a number of organic π systems, it sustains π–π stacking interactions as a result of a combination of electrostatic and charge-transfer interactions. In this last context, it was considered a tecton prone to give, in the

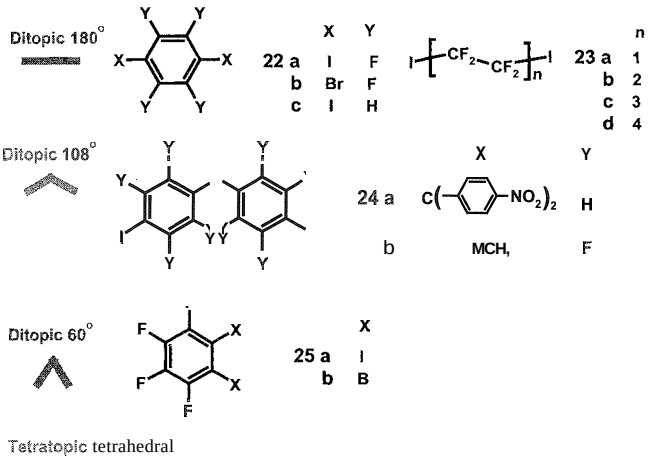

Scheme 5

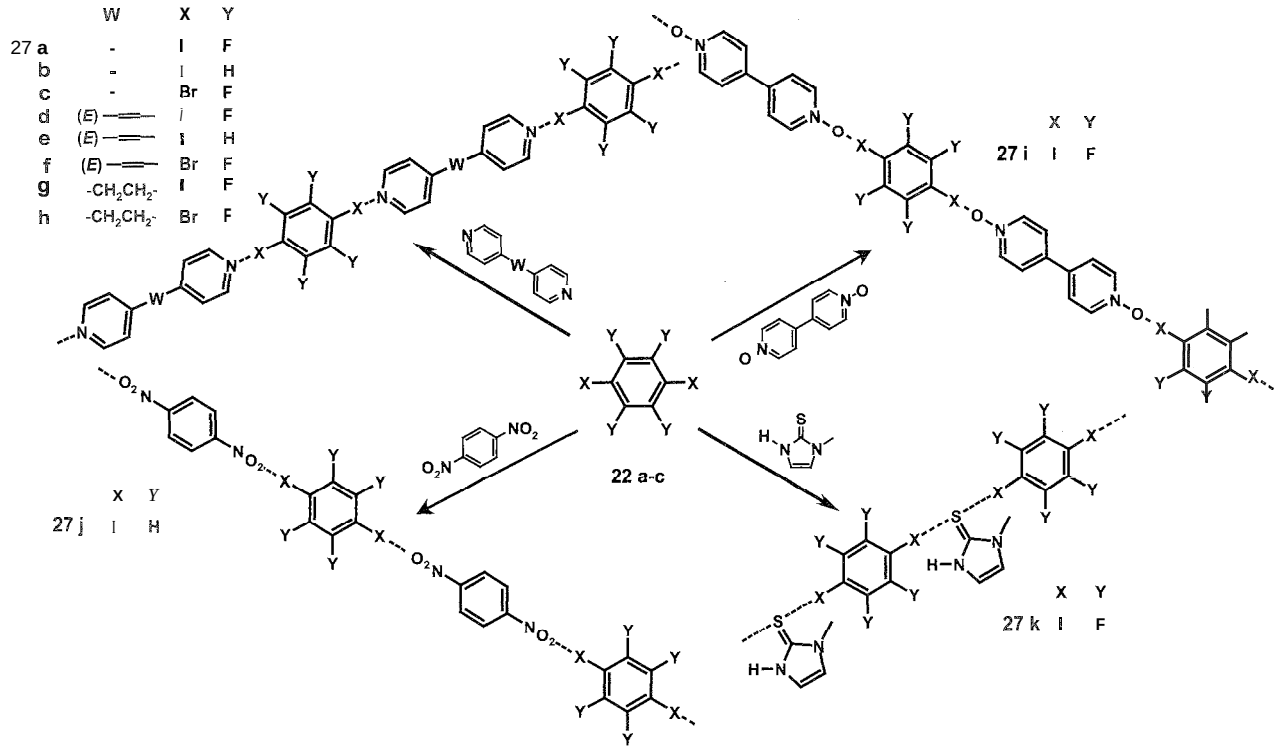
W X Y
27 a - I F
b - I H
c - Br F
d (E)—═— I F
e (E)—═— I H
f (E)—═— Br F
g -CH2CH2- I F
h -CH2CH2- Br F
X Y
27 i I F
X Y
27 j I H
22 a-c
X Y
27 k I F

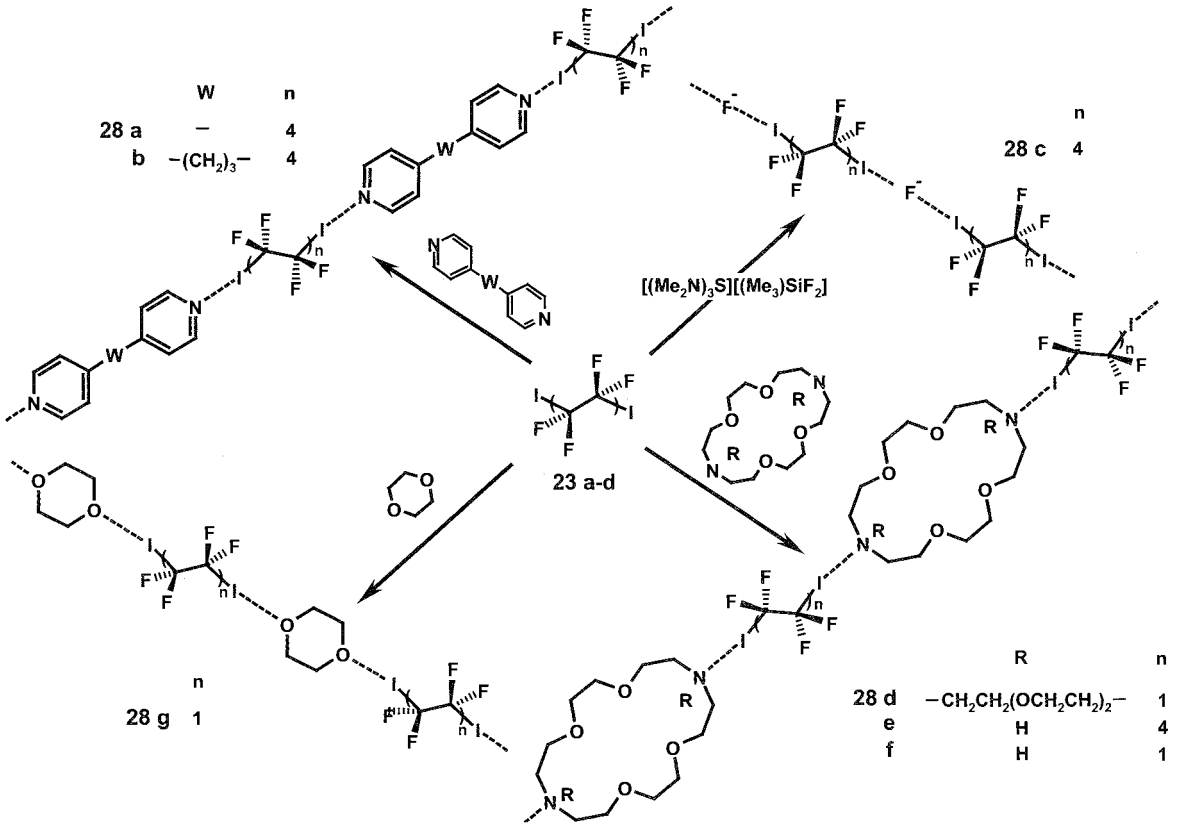
W n
28 a — 4
b —(CH2)3— 4
n
28 c 4
[(Me2N)3S][(Me3)SiF2]
23 a-d
n
28 g 1
R n
28 d —CH2CH2(OCH2CH2)2— 1
e H 4
f H 1

Scheme 6

solid state, infinite and one-dimensional stacks with 1,4-dialltoxybenzene partners.[34]

CONCLUSION

The term tecton does not address a "yes-or-no phenomenon." It is applied to molecules with interactions that thanks to energetic and structural characteristics, are dominated by particular associative forces that induce the self-assembly of organized networks with specific architectural or functional features. The term pinpoints aspects of the suprainolecular behavior of molecules. As is always the case in behavioral matters and in dominance affairs, the use of the term is somewhat subjective. This becomes more true when the extremity of weak interaction patterns is approached, and the possibility of exchanging the pattern from one network structure to another becomes more remote. For this reason and with the aim to avoid a biased selection, the tectons described in this article were. in most cases, drawn from the compounds already named in this way in the primary scientific literature.

Nevertheless, the term can be applied and should be applied to many other molecules and whenever the pertinent aspects of the supramolecular behavior of molecules have to be stressed. For instance. purine and pyrimidine bases are reliable tectons. as their intermolecular recognition patterns are predictably defined by the well-known hydrogen bonds to which they give rise. However, to the best of our knowledge, they were never named in this way. The introduction of the term tecton declared the need for molecules with predictable and invariant self-assembly features. Identifying new tectons can be equated to devising molecules to be discussed in a graduate textbook of supramolecular chemistry or to be included in a hypothetical "Aldrich catalogue for supramolecular chemistry..

ARTICLES **OF** FURTHER INTEREST

Calixarenes and Their Analogues: Molecular Complexation, p. *145*
Crystal Structure Prediction, p. 371
Halogen Bonding, p. 628
Hydrogen Bonding, p. *658*
Interpenetration, p. 735
Organometallic Oligomers and Polymers, p. *1014*
π–π Stacking as a Crystal Engineering Tool, p. 1093
Preorganization and Complementarity, p. *1*158
Self-Assembly: Definition and Kinetic und Thermodynamic Considerations, p. 1248
Self-Assembly in *Biochemistry*, p. 1257

REFERENCES

1. Simard, M.; Su. D.: Wuest. J.D. Use of hydrogen bonds to control molecular aggregation. Self-assembly of three-dimensional networks with large chambers. J. Am. Chem Soc. 1991. *113* (12), 4696–4698.
2. Schmidtchen. F.P. The anatomy of the energetics of molecular recognition of calorimetry: Chiral discrimination of camphor by α-cyclodextrin. Chem. Eur. J. 2002. 8 (15), 3522–3529.
3. Sauriat-Dorizon, H.: Maris, T.; Wuest. J.D. Molecular tectonics. Construction of porous hydrogen-bonded networks from bisketals of pentaerythritol. J. Org. Chem. 2003. *68* (2). 240–246.
4. Vaillancourt, L.; Simard. N.; Wuest. J.D. Synthesis and self-association of 2-pyrimidinones. J. Org. Chem. 1998. *63* (26), 9746–9752.
5. Corey, E.J. General methods for the construction of complex molecules. Pure Appl. Chem. 1967. *14* (1), 19–37.
6. Desiraju, G.R. Supramolecular synthons in crystal engineering—A new organic synthesis. Angew. Chem., Int. Ed. 1995, *34* (21). 2311–2327.
7. Su, D.; Wang. X.: Simard. M.: Wuest, J.D. Molecular tectonics. Supramol. Chem. 1995. 6 (2), 171–178.
8. Mann. S. Molecular tectonics in biornineralization and biomimetic material chemistry. Nature 1993. *365* (6446). 499–505.
9. Akdas, H.; Graf, E.: Hosseini, M.W.; De Cian. A.; Harrowfield, J.McB. Design, synthesis and structural investigation of 2-D coordination network based on the self-assembly of the tetracarboxylate derivative of tetrathiacalix[4]arene and silver cation. Chem. Commun. 2000. (22). 2219–2220.
10. Jouaiti. A.; Jullien. V.: Hosseini, M.W.; Planeix, J.-M.; De Cian. A. Controlling the formation of discrete complexes or a 1-D directional coordination network by the binding ability of anions. Chem. Commun. 2001. (13), 1114–1115.
11. Stang, P.J.; Olenyuk, B. Self-assembly, symmetry, and molecular architecture: Coordination as the motif in the rational design of supramolecular metallacyclic polygons and polyhedra. Acc. Chem. Res. 1997. 30 (12), 502–518.
12. Seidel. S.R.: Stang, P.J. High-symmetry coordination cages via self-assembly. Acc. Chem. Res. 2002. *35* (11), 972–983.
13. Polarz, S.: Antonietti. M. Porous materials via nanocasting procedures: Innovative materials and learning about soft-matter organisation. Chem. Commun. 2002, (22), 2593–2604.
14. Sha. R.: Liu. F.: Millar. D.P.: Seeman, W.C. Atomic force microscopy and parallel DNA branched junction arrays. Chem. Biol. 2000. 7 (9), 743–751.
15. Férey, G. Microporous solids: From organically templated inorganic skeletons to hybrid frameworks. Ecumenism in Chemistry. Chem. Mater. 2001. 13 (10), 3084–3098.
16. Ferlay. S.; Koenig, S.; Hosseini, M.W.: Pansanel, J.: De Cian, A.; Kyritsakas. N. Design of 3-D coordination

networlts: Topology and metrics. Chem. Commun. 2002. (3). 218–219.
17. Kryschenko. Y.K.; Seidel. R.S.: Arif. A.M.; Stang. P.J. Coordination-driven self-assembly of predesigned supramolecular triangles. J. Am. Chem. Soc. 2003. *125* (17), 5193–5198.
18. Drain. C.M.: Nifiatis. F.: Vasenko, A.; Batteas. J.D. Porphyrin tessellation by design: Metal-mediated self-assembly of large arrays and tapes. Angew. Chem.. Int. Ed. 1998, 37 (17). 2344–2347.
19. Khlobystov, A.N.: Blake, A.N.: Champness. N.R.; Lemenovskii. D.A.; Majouga. A.G.; Zyk, N.V.: Schroder, M. Supramolecular design of one-dimensional coordination polymers based on silver(I) complexes of aromatic nitrogen-donor ligands. Coord. Chem. Rev. 2001. 222. 155–192.
20. Lehn, J.-M.; Rigault. A.M.: Siegel. J.: Harrowfield. J.: Chevrier. B. Spontaneous assembly of double-stranded helicates from oligobipyridine ligands and copper(I) cations: Structure of an inorganic double helix. Proc. Natl. Acad. Sci. U.S.A. 1987. 84 (9). 2565–2569.
21. Wang, X.: Simard. M.; Wuest. J.D. Molecular tectonics. Three-dimensional organic networks with zeolitic properties. J. Am. Chem. Soc. 1994, *116* (26). 12119–12120.
22. Fournier. J.-H.; Maris, T.: Wuest, J.D.; Guo, W.; Galoppini. E. Molecular tectonics. Use of the hydrogen bonding of boric acids to direct supramolecular construction. J. Am. Chem. Soc. 2003. *125* (4). 1002–1006.
23. Zerkowski, J.A.; Seto. C.T.; Whitesides, G.M. Solid-state structures of rosette and crinkled tape motifs derived from the cyanuric acid melamine lattice. J. Am. Chem. Soc. 1992. *114* (13), 5473–5475.
24. Vincent, B.; Planeix, J.-M.; Félix. O.; Hemmerlé. J.: Schaaf, P.; Hosseini. M.W.; Voegel. J.C. Molecular tectonics: Abiotic control of hydroxyapatite crystals morphology. Cryst. Growth Des. 2002. 2 (6). 489–492.
25. Metrangolo, P.; Resnati. G. Halogen bonding: A paradigm in supramolecular chemistry. Chem. Eur. J. 2001. 7 (12), 2511–2519.
26. De Santis, A.; Forni, A.; Liantonio. R.: Metrangolo, P.: Pilati. T.; Resnati, G. N···Br Halogen bonding: 1D infinite chains through the self-assembly of dibromotetrafluorobenzenes with dipyridyl derivatives. Chem. Eur. J. 2083, 9 (16). 3974–3983.
27. Corradi. E.; Meille, S.V.: Messina, M.T.: Metrangolo, P.: Resnati, G. Halogen bonding versus hydrogen bonding in driving self-assembly processes. Angew. Chem.. Int. Ed. 2000. 39 (10). 1782–1786.
28. Walsh, R.B.: Padgett, C.W.: Metrangolo. P.: Resnati, G.: Hanks. T.W.: Pennington. W.T. Crystal engineering through halogen bonding: Complexes of nitrogen heterocycles with organic iodides. Cryst. Growth Des. 2001. *1* (2). 165–175.
29. Allen. F.H.; Goud. B.S.; Hoy. V.J.: Howard. J.A.K.: Desiraju. G.R. Molecular recognition via iodo···nitro and iodo···cyano interactions: Crystalò structure of the 1:1 complexes of 1.4-diiodobenzene with 1,4-dinitrobenzene and 7,7,8,8-tetracyanoquinodimethane (TCNQ). Chem. Commun. 1994. (23). 2729–2730.
30. Jay, J.I.; Padgett. C.W.: Walsh. R.D.B.: Hanks, T.W.: Pennington, W.T. Noncovalent interactions in 2-mercapto-1-methylimidazole complexes with organic iodides. Cryst. Growth Des. 2001. *1* (6). 501–507.
31. Farnham. W.B.; Dixon, D.A.: Calabrese, J.C. Novel fluorine-bridged polyfluorinated iodine structures. Presence of fluorine as the central atom in a five-center. six-electron bond. J. Am. Chem. Soc. 1988. *110* (25). 8453–8461.
32. Thaimattam. R.: Sharma. C.V.K.: Clearfield, A.; Desiraju. G.R. Diamondoid and square grid networks in the same structure. Crystal engineering with the iodocnitro supramolecular synthon. Cryst. Growth Des. 2001. *1* (2). 103–106.
33. Martz. J.: Graf. E.: Hosseini. M.W.: De Cian, A.; Gruber, N.K. Molecular tectonics: Design and structural analysis of 1-D and 2-D self-inclusion molecular networks in the crystalline state. C. R. Chimie 2082, *5*, 481–486.
34. Colonna. B.; Menzer, S.: Raymo, F.M.; Stoddart, J.F.; Williams, D.J. Noncovalent synthesis of donor/acceptor stacks. Tetrahedron Lett. 1998, *39*. 5155–5158.

The Template Effect

Daryle H. Busch
University of Kansas, Lawrence, Kansas, U.S.A

INTRODUCTION

Template reactions have been used to produce new molecules with remarkable chemical architectures." The field of macrocyclic ligand chemistry and the closely related field of cage-like ligand chemistry had their beginnings in their template synthesis as the new concept ligands of their era. As the sophistication of templates grew, interlocked molecular structures emerged, including catenanes (interlocked rings), rotaxanes (axle inolecules locked in cyclic molecules by large end groups), oligocatenanes and oligo-rotaxanes of various kinds, and molecular knots (see Fig. 1).

DEFINITION AND ILLUSTRATION OF THE TEMPLATE EFFECT

By definition,[2] "a molecular template organizes an assembly of atoms, with respect to one or more geometric loci. in order to achieve a particular linking of atoms." Such a template plays an active role in the construction of a new molecular entity, and this involves two essential features: 1) the template organizes some specified assembly of atoms, thereby influencing their chemical reactions; and 2) the results of this organization are found in some spatial, geometric. and topological relationships built into the structure of the new molecule.[2,3]

The basic concept of the template effect is illustrated by the first example of such a reaction (Fig. 2). In this seminal case, the template effect results from the binding to the nickel(II) ion of the ligand that is precursor to the macrocyclic product. The ideal behavior results from the fact that the tetradentate ligand is just the right size to wrap around the metal ion (complementarity); the sulfur nucleophiles of the ligand are still active while bound to the metal ion, while the nitrogen donors are not; and the length of the xylylene unit in the α,α-dibromo-*o*-xylene reagent is right for spanning between the two sulfur nucleophiles (again, complementarity). Finally. the coordination sphere of the metal ion has an appropriate geometry, square planar, bringing the sulfur nucleophiles into adjacent locations. Here is what happens. The metal ion wraps the long ligand molecule about itself, binding to all four donor atoms, S and *N*. and bringing the two, still reactive, terminal donors (sulfur atoms) into adjacent positions. This new metal complex encounters one of the α,α-dibromo-*o*-xylene molecules, and a bound sulfur nucleophile displaces Br from one end of that reagent. This produces an intermediate in which the second active functional group, the second sulfur atom. is ideally located to displace the second bromide, closing a ring that now encircles the metal ion. Thus, a neighboring group effect favors ring closure and formation of only a single product in a system that ordinarily would have given a useless mixture of products, including linear oligomers and polymers, rings of various sizes, and mixed oligomer/ring structures.

This first example not only illustrates the template effect, but it also shows certain elements of a molecular template. The metal ion serves as an anchor that holds certain groups of atoms in place, and it also bends a long linear molecule into what is usefully termed a molecular turn. These are basic elements of a molecular template. Anchoring the ligand to the metal ion in the form of a molecular turn facilitates tying the ends of the turn together with a complementary reagent; and that results in the formation of a large ring that encircles the metal ion. It follows that the essential elements for the formation of a macrocycle by a template reaction are an anchor, a molecular turn, and its complement.

A less obvious part of the template concept is that. once formed, the products of these template reactions are not dependent on the template that guided in their generation. Thus, the macrocyclic ligands formed by template reactions of the kind shown in Fig. 2 can be removed from their metal ions and moved to other chemical applications. The great promise of the template effect rests on that fact. Templates facilitate the synthesis of complicated molecular architectures composed solely of the light atoms typical of organic molecules.

KINETIC AND THERMODYNAMIC TEMPLATE EFFECTS

Two different kinds of template effects have long been known. One of these is an equilibrium phenomenon and is

"For a brief history of the field see Ref. [1]

Encyclopedia of Supramolecular Chemistry
DOI: 10.1081/E-ESMC 120012668

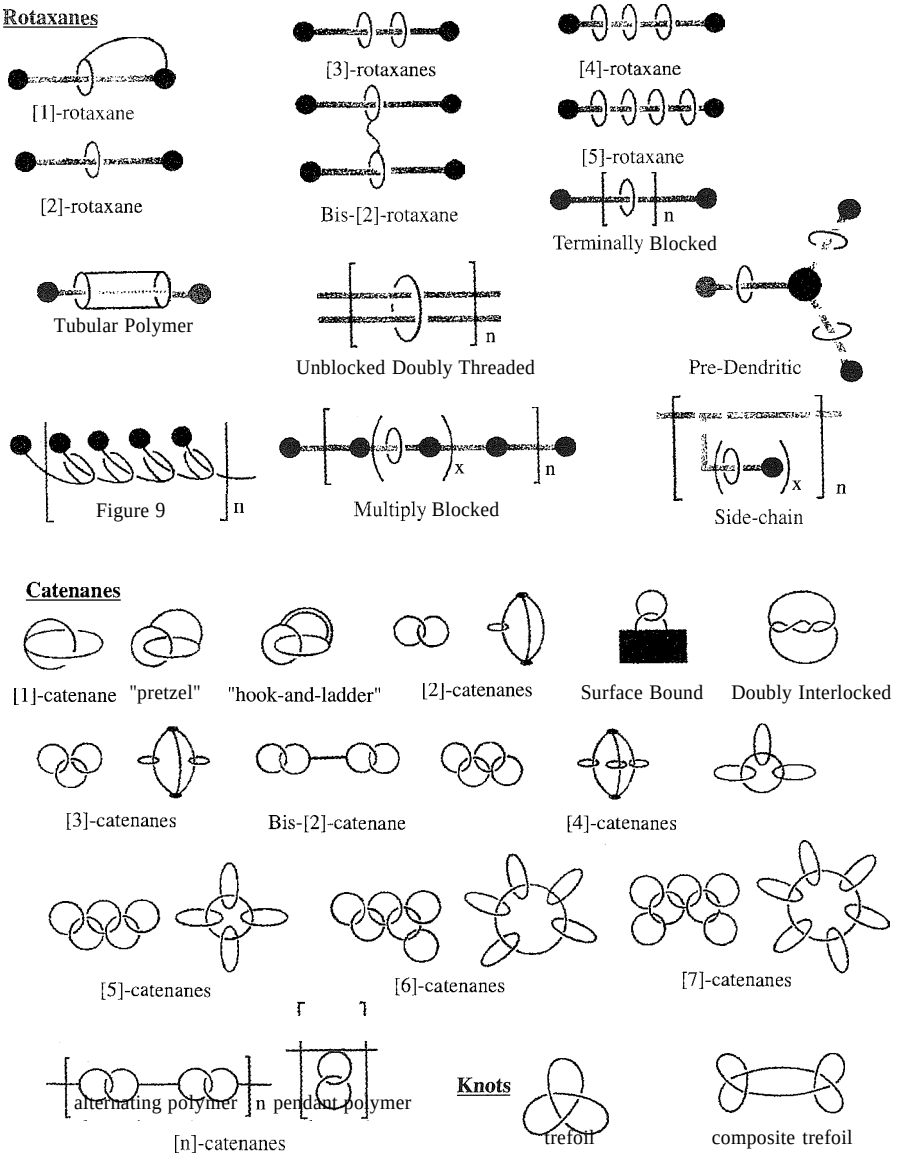

Fig. 1 Rotaxanes, catenanes, and knots formed by template reactions.

therefore of thermodynamic origin, while the other is mechanistic: or kinetic, in its fundamental nature. The example in Fig. 2 exemplifies the kinetic template effect. As described, the template controls a sequence of reaction steps by constraining reactant molecules. Examples of the thermodynamic template effect were first invoked when, as a result of a chemical reaction, a metal complex of a new ligand was discovered, and that new ligand was known to be unstable in the absence of the metal ion.[4] The organic components chat form the new ligand are capable of equilibrating to form a variety of products, but one of them binds to the metal ion much more strongly than do the others. Consequently, the metal ion sequesters that product and shifts the equilibrium in the direction of its for-mation.

COMPONENTS OF **TEMPLATES**

Maximum value of templates will be achieved only through an intimate understanding of how they function. As pointed out in the discussion of Fig. 2, a template for macrocycle formation need only consist of a molecular turn, an anchor, and a complementary reagent to link the two ends of the turn. Anchors and turns recur repeatedly in template reactions and are among the most important

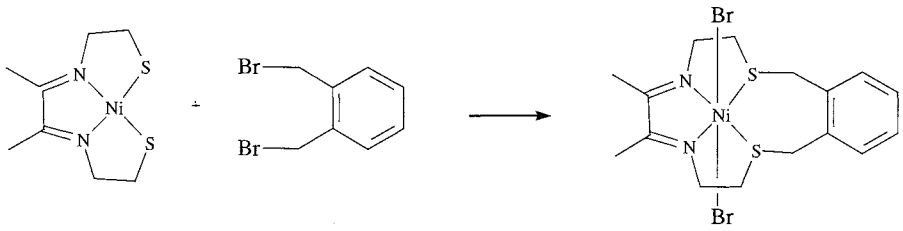

Fig. 2 The seminal example of a template reaction; the product is a coordinated macrocycle.

basic elements of a template.[5] Shown in Fig. 3 are a number of important examples. In Fig. 3a, two turns are united by an anchor to create another basic element of templates. a crossover. Crossovers template the formation of catenanes (interlocking rings) and rotaxanes (axles threaded through rings. with the ends of the axles blocked). If a linking group makes a ring from one of the turns, a rotaxane is formed. If two linking groups convert both turns to rings, a catenane if formed. Shown in Fig. 3b is how closing a fused pair of turns, using a fused linker, produces a bicycle, or cage-like molecule. Linearly connected pairs of turns that are mutually inverted can be used in pairs, with pairs of anchors, as a template for tying a trefoil knot (Fig. 3c). Further doubling of the number of turns and anchors to eight and four: respectively. led to the formation of molecules having the configurations of square knots and granny knots. In addition to anchors, turns, and crossovers, threading are elements of general applicability in templates. Threading of an axle molecule through a cyclic molecule obviously produces a rotaxane. Almost as simply; if a turn is threaded through a ring, and the two ends of the threaded turn are then linked, a catenane is formed. Further. a second way to generate a trefoil knot is by threading through a loop created by a crossover using a single linear molecule. The product is a mathematically acceptable knot if the ends of the molecule are then joined. Multiple crossovers anchored onto a single ring lead to oligocatenanes.

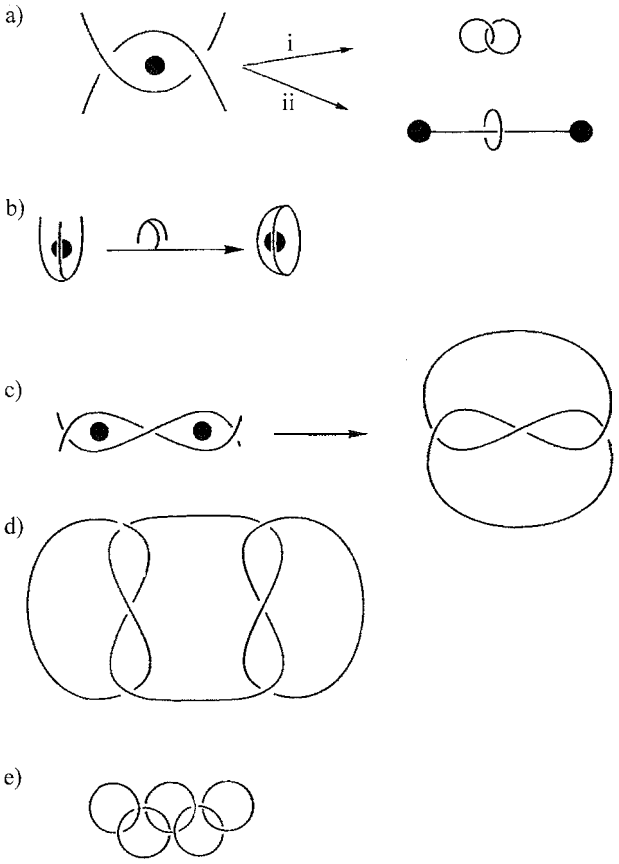

Fig. **3** Elements of molecular templates: (a) a crossover reacts with a linker to give (i) a catenane and (ii) a rotaxane; (b) a fused turn closed with a fused linker gives a macrobicycle; (c) two anchors and two pairs of inverted ditopic turns template a trefoil knot: (d) composite knots require two two-anchor templates; and (e) oligocatenanes can be formed with multicrossover templates on a single anchor.

VARIOUS USES OF THE TERM ""TEMPLATE"

The word "template" occurs in the vocabularies of biochemists, materials scientists, synthetic chemists, and elsewhere. reflecting broad usage in the chemical literature. Here, template refers to controlling the outcome of a chemical reaction, commonly in chemical synthesis, by organizing components that are being united or rearranged in the templating process—all on the molecular scale. Thus. the formation of very small, but macroscopic, fibrils and tubules within molds provided by the pores of a membrane does not qualify as the product of a molecular template reaction—the scale is not molecular. On the other hand. the astounding control over pore size in aluminosilicate molecular sieves[6] and the molecularly imprinted macroporous polymers[7] represent limits of the realm of molecular templates. In biology, the word has been applied to the biosynthesis of DNA and other natural

products. However. the obvious extension into the realm of continuous hydrogen-bonded supramolecular arrays is supramolecular chemistry, but not template chemistry. Beautiful and complicated architectures in which metal ions participate in their backbones, including polymers. cages, catenanes of metallocycles, inetallo-macrocycles. and dendrimers make use of the metal ion coordination spheres in determining supramolecular structures. but they do not involve template reactions. Fisher's "lock and key" concept (e.g., enzyme/substrate selectivity) is sometimes suggested as the equivalent of the molecular template. That is incorrect; the key is the complement of the lock, and this is an excellent example of complementarity,[8] not a template. Also, foundational components upon which other moieties may be appended are sometimes referred to as templates. Such components might better be called platforms; one is adding superstructure, not conducting a template reaction. The critical aspects of a template reaction are the creation of a structure that is otherwise difficult to produce, often for reasons of entropy. and that would still exist if the anchoring component were removed.

PRIMARY EXAMPLES

Metal Ion Templates

The seminal example (Fig. 2) produced a family of macrocyclic complexes in high yield with no apparent byproducts, in accord with the expectations of a well-designed template.[b] This was followed by the use of inetal ion anchors for the template syntheses of hundreds of macrocycles varying from nine-membered tridentate rings, through a plethora of tetradentate rings. to 24-membered and greater rings with as many as eight donors, that is best known for binding two inetal ions simultaneous ~Macrobicycles were first produced using metal ion templates[10] to make the cage complexes. Many hexadentate cage ligands having only saturated amine donors were produced by template reactions.[b] Cyclidenes, bicyclic ligands of a different kind, were produced using inetal ion templates.[12] They are bicycles, but they contain two distinctive cavities, one having four donor atoms that binds a metal ion. while the second is essentially hydrophobic and provides a cave-like site for binding a second species, either a ligand for the metal ion or an organic molecule that might be a substrate.

The first template synthesis of catenanes[13] made use of ligands that were turns and a copper(I) ion as anchor (Fig. 4). Terminal phenolic functions provided the reactive sites to combine with linking groups and produce two interlocked inacrocycles, a catenane. The same copper(I) anchor and the same molecular turns were used in the tying of knots[b] using multicentered templates (Fig. 5).

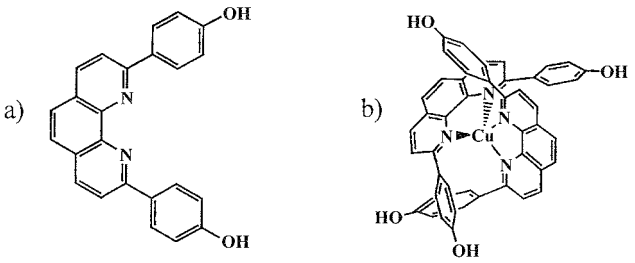

Fig. 4 Sauvage's template composed of two molecular turns bound to a copper(I) anchor: phenolic functions were reaction sites for ring closures and catenane or rotaxane formation.

Hydrogen-Bonded Templates

Although elegant results were obtained with metal ion templates, the ultimate applications of rotaxanes. catenanes, knots. and the production of the as yet unavailable polymers. molecular braids, or woven molecular materials will depend oil simpler materials, such as those presently found in synthetic fibers. Arguably the most likely candidate for an anchor in such long-term developments will be a proton. or multiple protons, anchoring axles, or turns through hydrogen bonding. The early demonstration that the ammonium ion forms a complex with a crown ether was harbinger to these systems.[15] The difficulty of the threading process was emphasized by low yields in the early work, for example. a system that yielded 30% for a [2]rotaxane gave only 10% for the corresponding [3]-rotaxane.[16] For high-yield syntheses. the threading and the blocking reactions must be efficient. Such a successful synthesis was reported in 1998, with the yield of a [3]-rotaxane at 84%.[17]

A high dilution reaction that might have been expected to produce a macrocycle, serendipitously yielded an entirely new kind of catenane (Fig. 6) and led to the characterization of a different family of hydrogen-bonded templates.[18] Structural and isomer studies led to the conclusion that the threaded macrocycle is the critical intermediate in the catenane formation. making this a classic template process.[19]

Templates with More Complex Anchors

Short tube-shaped cyclodextrins, consisting of six (α), seven (β), or eight (γ) x-1.4-linked D-glucose units. act as

[b] An earl) review of macrocyclic ligand chemistry. (Ref. [9].)

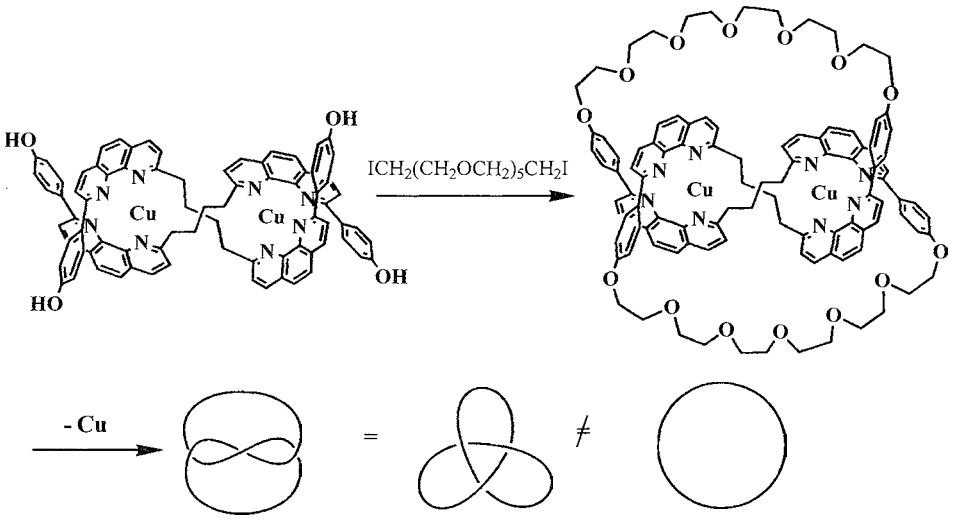

Fig. 5 Template synthesis of a trefoil knot

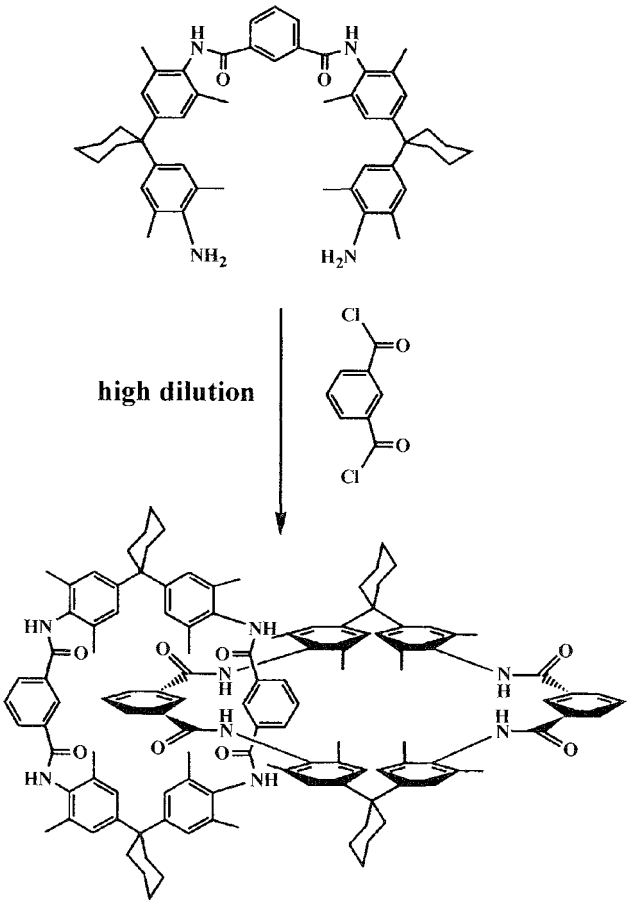

Fig. 6 The hydrogen-bonded amide template and its first catenane product.

anchors in a broad range of template reactions. The cyclodextrins bind an axle molecule within their cylindrical cavities through a combination of weak intermolecular interactions such as hydrophobic effects, van der Waals interactions, and hydrogen bonds, the latter at the periphery of the cavity. Although their guest–host complexes have been studied for many years,[20] its use as the anchor in template formation of catenanes and simple rotaxanes is relatively recent. Remarkably, linear polymers heavily laden with threaded β-cyclodextrins were prepared as early as 1976 and have been studied extensively. In a particularly striking example of a template reaction, cyclodextrin rings strung along a linear polymer were bound together by reaction of their peripheral OH groups with epichlorohydrin. Removal of the polymer anchor then liberated the first synthetic tubular polymer.[21]

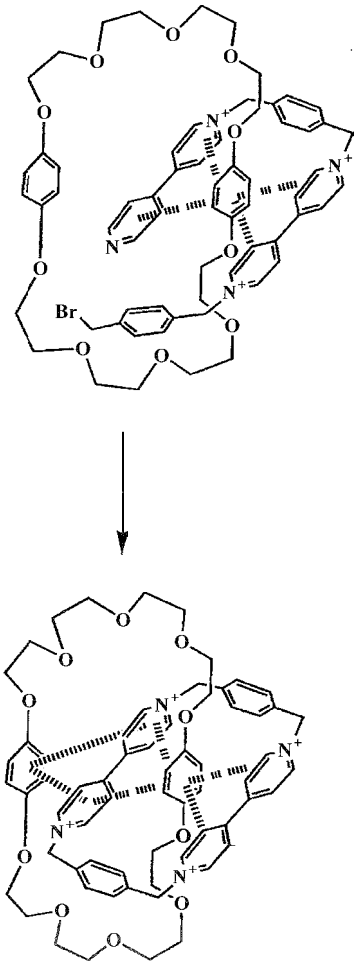

Fig. 7 The $\pi-\pi$ template in use to form a catenane.

As the above example illustrates, the discovery of a new template can lead to voluminous chemistry with exciting new results. Such has been the case with the development of templates based on guest–host complexes between derivatives of the electron-deficient herbicide paraquat and π-donor molecules like *bis-p*-phenylene-34-crown-10.[22] Powerful noncovalent forces lead to appreciable yields of predictable products. The strong interactions between the π-systems may be viewed as playing the role of the anchor. In some cases, more complicated interactions create tums from the mutually attracted molecules, but a phenylene-linked bis-paraquat wraps about an electron-rich aromatic ring forming a prototypical molecular turn. The latter stages of [2]-catenane formation in such a system are shown in Fig. 7. These systems have been used to produce oligo-catenanes up to a [7]-catenane,[23] Olympiadane, the [5]-catenane, being best known.'''' An enormous assembly of interlocked molecular structures has been designed and synthesized using this template, including functional species not previously described here, like molecular switches.

CONCLUSION

It is remarkable how much new chemistry emerges when a new molecular template is discovered. This is especially true of the discovery and development of a new molecular turn. Sauvage's turn and Stoddart's turn have been exceptionally productive in leading to new molecular architectures. New turns will continue to create new opportunities. For example, there is no turn specific for cyclodextrins. although it is reasonably clear how to proceed in attempts to design such a potent addition to the toolbox of parts for interlocked molecules.

Other new kinds of fundamental elements for template chemistry await development. A relatively new arrival[25] is what has been called the divergent turn.[3] This requires re-labeling the previously known turns as convergent. Convergent turns extend across the anchor with which they associate in a molecular template, whereas divergent turns extend away from their anchor. Illustrated in Fig. 8a is a divergent turn. Shown in Fig. 8b is how a divergent and convergent turn might be combined to produce noninterlocked rings of different sizes. Shown in Fig. 8c is how using a half-blocked divergent turn along with a convergent turn could result in a blocked trefoil knot. The latter concept, knots stabilized by blocking groups after the fashion of rotaxanes, appears not to have been tested in the laboratory as yet. Envisioned in Fig. 8d and 8e is the use of a combination of divergent/convergent turns to produce new interloclied figure eights. A possible new template element. the templated loop. may be used to

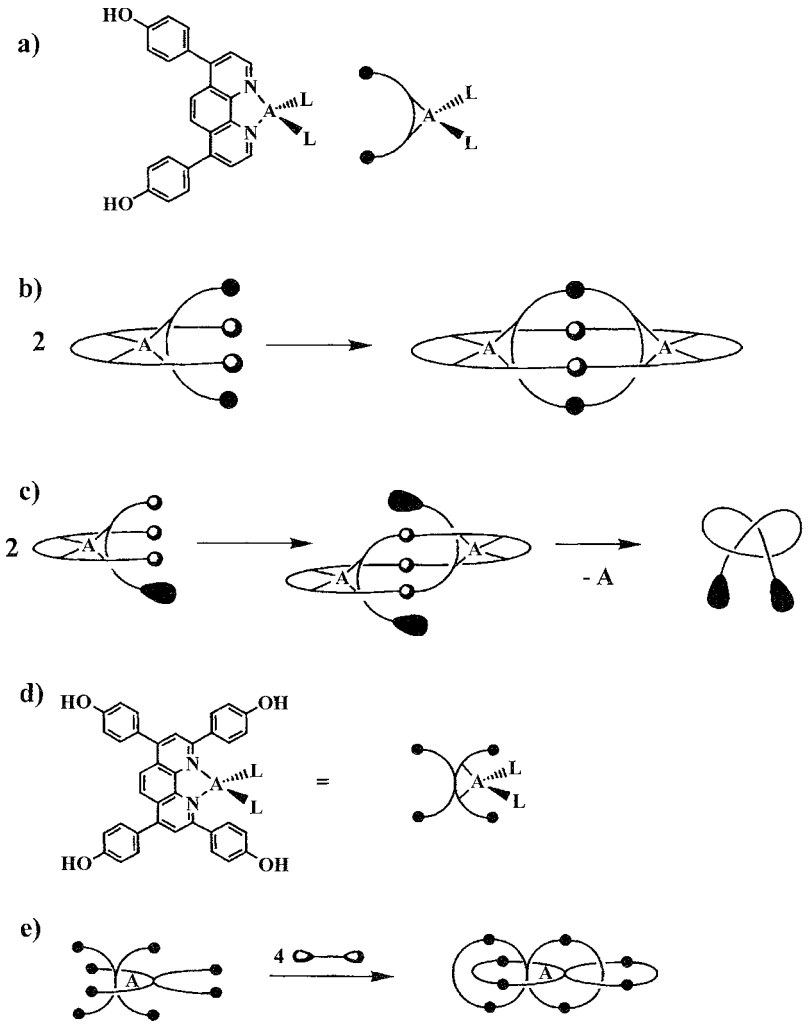

Fig. 8 (a) A hypothetical divergent turn; (b) combining convergent and divergent turns in a template produces a complex with a ring in a ring; (c) a knot designed after a rotaxane. using divergent and convergent turns: (d) and (e) a hypothetical combined convergent and divergent knot gives an interlocked set of figure eights.

form temporary rings for threading, and this might be helpful in the formation of still more complicated architectures as the field advances.

The development of rack complexes[26] and the overlaps of strands observed in a star-shaped circular double helicate[27] give promise of the eventual success of attempts at molecular weaving, an ultimate goal of interlocked molecular structures. Through molecular weaving and molecular braids, the development of materials may be possible that multiply the strengths of covalent bonds. The three-dimensional equivalent of a woven material is easily envisioned on the molecular scale and may present microscopic structures with no macroscopic counterparts. Molecular switches, traditional and Boolean, and molecular-scale inactive information storage remain viable goals of chemistry controlled at the inolecular level by templates.

ARTICLES OF FURTHER INTEREST

Anion-Directed Assembly, p. 51
Catenanes and Other Interlocked Molecules, p. 206
Cation–π Interactions, p. 214
Chemical Topology, p. 229
Cryptands, p. 334
Cryptophanes, p. 340
Cyclodextrins, p. 398
Cyclodextrins: Applications, p. 405
Macrocycle Synthesis, p. 830

Molecular Logic Gates, p. 893
Molecular Switches, p. 917
π–π Interactions: Theory and Scope, p. 1076
Rotaxanes and Pseudorotaxanes, p. 1194
Self-Assembling Capsules, p. 1231
Self-Assembling Catenanes, p. 1240
Self Assembly: Definition and Kinetic and Thermodynamic Considerations, p. 1248
Supramolecular Polymers, p. 1443

REFERENCES

1. Busch. D.H.: Vance, A.L.; Kolchinski, A.G. Molecular Template Effect: Historical View. Principles and Perspectives. In *Comprehensive Supramolecular Chemistry*; Lehn, J.-M.. Ed.; Elsevier Science: New York, 1996: Vol. 9. 1–42.
2. Busch. D.H. Structural definition of chemical templates and the prediction of new and unusual materials. J. Inclus. Phen. Molec. Recog. Chem. 1992, 12. 389–395.
3. Hubin. T.J.: Busch. D.H. Template routes to interlocked molecular structures and orderly molecular entanglement. Coord. Chem. Rev. 2000. *200–202*, 5–52.
4. Thompson. M.C.: Busch, D.H. Reactions of coordinated ligands. IX. Utilization of the template hypothesis to synthesize macrocyclic ligands in situ. J. Am. Chem. Soc. 1964. 86. 3651–3656.
5. Hubin. T.J.: Kolchinski. A.G.; Vance, A.L.: Busch. D.H. Template control of supramolecular architecture. Advan. Supramol. Chem. 1999. *5*. 237–357.
6. Beck. J.S.; Vartuli. J.C.: Roth. W.J.: Leonowicz. M.E.; Kresge. C.T.: Schmitt. K.D.; Chu, C.T.W.: Olson, D.H.; Sheppard, E.W.: McCullen. S.B.: Higgins, J.B.; Schlenker, J.L. A new family of mesoporous molecular sieves prepared with liquid crystal templates. J. Am. Chern. Soc. 1992. *114* (27). 10834–10843.
7. Wulff, G.: Dederichs, W.: Grotstollen, R.; Jupe. C. On the chemistry of binding sites. Part II. Specific binding of substances to polymers by fast and reversible covalent interactions. Anal. Chem. Symp. Ser. 1982. 9, 207–216. (Affinity Chromatogr. Relat. Tech.).
8. Busch. D.H. Ligand design for enhanced molecular organization-selectivity and specific sequencing in multiple receptor ligands, and orderly molecular entanglements. NATO ASI Ser.. Ser. C 1994, 448, 55–80.
9. Busch. D.H. Transition metal complexes of the new synthetic macrocyclic ligands. Helv. Chim. Acta 1963. 174. fasc. Extraord. Alfred Werner.
10. Boston. D.R.: Rose. J.J. Encapsulation reaction. Synthesis of the clatliro chelate 1,8-*bis*(fluoroboro)-2,7,9,14,15,20-hexaoxa-3,6,10,13,16,19-hexaaza-4,5,11,12,17,18-hexamethylbicyclo[6.6.6]eicosa-3,5,10,12.16,18-hexaenecobalt-(III) ion. J. Am. Chem. Soc. 1968, 90. 6859.
11. Sargeson, A.M. Developments in the synthesis and reactivity of encapsulated metal ions. Pure Appl. Chem. 1986, 58 (11). 1511–1522.
12. Busch. D.H.; Alcock. N.W. Iron, cobalt and nickel 'lacunar' complexes as dioxygen carriers. Chem. Rev. 1994. 94, 585.
13. Sauvage. J.-P. Interlacing molecular threads on transition metals: Catenands, catenates, and knots. Acc. Chem. Res. 1990, 23 (10). 319–327.
14. Dietrich-Buchecker, C.O.: Sauvage. J.-P.; De Cian. A.: Fischer, J. High-yield synthesis of a dicopper(I) trefoil knot containing 1,3-phenylene groups as bridges between the chelate units. J. Chern. Soc., Chern. Commun. 1994, (19). 2231–2232.
15. Pedersen. C.J.; Frensdorff, H.K. Macrocyclic polyethers and their complexes. Angew. Chern.. Int. Ed. Engl. 1972, *11* (1), 16–25.
16. Ashton. P.R.: Fyfe. M.C.T.: Glink. P.T.; Menzer, S.: Stoddart. J.F.; White. A.J.P.: Williams, D.J. Multiply stranded and multiply encircled pseudorotaxanes. J. Am. Chem. Soc. 1997. 119 (51). 12514–12524.
17. Kolchinski, A.G.; Busch, D.H. Molecular riveting: High yield preparation of a [3]-rotaxane. J. Chem. Soc., Chem. Commun. 1998. 1437.
18. Adams. H.; Carver. F.J.: Hunter. C.A. [2]Catenane or not [2]catenane? J. Chem. Soc., Chem. Commun. 1995. (8), 809–810.
19. Ottens-Hildebrandt, S.; Meier. S.: Schmidt. W.: Voegtle. F. Isomeric catenanes of lactam type and their formation mechanism. Angew. Chem.. Int. Ed. Engl. 1994. 33 (17), 1767–1770.
20. Fenyvesi, E.: Szente. L.: Russell. N.R.: McNamara, M. Specific guest types. Compr. Supramol. Chem. 1996. 3. 305–366.
21. Harada. A.; Okada, M.: Kamachi, M. Complex formation between poly(oxytrimethylene) and cyclodextrins. Acta Polym. 1995. 46 (6). 453–457.
22. Allwood, B.L.; Spencer, N.; Shahriari-Zavareh. H.: Stoddart. J.F.; Williams, D.J. Complexation of paraquat by a bisparaphenylene-34-crown-10 derivative. J. Chem. Soc., Chem. Commun. 1987. (14), 1064–1066.
23. Amabilino. D.B.; Ashton, P.R.; Boyd, S.E.; Lee, J.Y.: Menzer. S.: Stoddart, J.F.: Williams. D.J. The five-stage self-assembly of a branched heptacatenane. Angew. Chem., Int. Ed. Engl. 1997, 36 (19). 2070–2072.
24. Amabilino. D.B.; Ashton, P.R.; Reder. A.S.: Spencer, N.; Stoddart. J.F. Olympiadane. Angew. Chem.. Int. Ed. Engl. 1994. 33 (12), 1286–1290.
25. Benniston. A.C.: Mackie, P.R.; Harriman, A. Artificial photosynthesis: Mimicking redox asymmetry. Angew. Chem.. Int. Ed. 1998. 37 (3). 354–356.
26. Baxter, P.N.W.: Lehn. J.-M.: Fischer. J.: Youinou. M.-T. Self-organization and structure of an inorganic 3 x 3 lattice from nine silver ions and six ligands. Angew. Chem., Int. Ed. Engl. 1994. 33 (22). 2284–2287.
27. Hasenknopf. B.; Lehn. J.-M.; Kneisel. B.O.: Baum. G.; Fenske. D. Self-assembly of a circular double helicate. Angew. Chem., Int. Ed. Engl. 1996. *35* (16). 1838–1840.

Thiourea inclusion Compounds

Kenneth *D. M. Harris*
Cardiff University, Cardiff; Wales

INTRODUCTION

It has been known since 1947[1] that thiourea forms crystalline inclusion compounds in the presence of appropriate guest molecules. These thiourea inclusion compounds have a tunnel host structure (Fig. 1) that is similar in some respects to the urea tunnel structure but has a larger cross-sectional area. As a consequence, the urea and thiourea host structures typically accommodate different types of guest molecules. with the thiourea host structure able to incorporate larger guest molecules that cover a more diverse range of chemical types. For example, the thiourea tunnel structure can include guest inolecules such as cyclohexane and its derivatives, ferrocene and other organometallics, and compounds containing aromatic rings. Such guest molecules do not generally form inclusion compounds with urea. Empirical generalizations on the characteristic features of guest molecules that form inclusion compounds with thiourea have been discussed elsewhere.[2–4]

The host structure in thiourea inclusion compounds is generally rhombohedral or monoclinic. For guest molecules that have fairly isotropic shapes (such as cyclohexane, chlorocyclohexane, and ferrocene). the host structure at ambient temperature is usually rhombohedral. and the guest molecules generally exhibit reorientational dynamics. In many cases, this rhombohedral structure transforms (via one or more solid-state phase transitions) to a monoclinic structure at sufficiently low temperature. On the other hand, guest molecules with a more planar shape (such as 2.6-diethylnaphthalene: 2,3-dimethylbutadiene; and 1,5-cyclooctadiene) tend to favor the monoclinic host structure at ambient temperatme, with the guest molecules constrained to adopt an ordered arrangement. Lowering the symmetry from rhombohedral to monoclinic is associated with a deformation of the tunnel, leading to greater orientational ordering of the guest molecules.

While the tunnel in conventional urea inclusion compounds is fairly cylindrical (with fairly constant cross-sectional diameter), the thiourea tunnel structure contains bulges and constrictions at different positions along the tunnel. As a consequence, it is often more appropriate to regard the thiourea host structure as ''cage''-type rather than ''tunnel''-type, and many properties of thiourea inclusion compounds can be understood more directly on this basis. Thus, the guest molecules in thiourea inclusion compounds usually occupy specific preferred sites along the tunnel, cossesponding to one guest molecule per cage and a stoichiometric guest/thiourea molar ratio of 1/3. Thus, most thiourea inclusion compounds have a commensurate relationship between the host and guest substructures.

In this article, an overview of structural aspects of thiourea inclusion compounds is provided and some of the interesting properties of these materials are elaborated upon, such as the dynamic and conformational properties of the guest molecules, chemical reactions, and applied aspects. Also highlighted are the types of techniques and approaches that have been used in order to acquire an understanding of these properties. Several review articles[5–7] have been published on thiourea inclusion compounds, and contain comprehensive lists of references to the original literature in this field.

STRUCTURAL PROPERTIES

Structural Aspects of ''Conventional'' (Rhombohedral) Thiourea Inclusion Compounds

The host structure[8–10] in ''conventional'' thiourea inclusion compounds is rhombohedral [usual space group $R\bar{3}c$; $a \approx 15.5$–16.2 Å, $c = 12.5$ Å (hexagonal setting)] and exhibits a significant variation in tunnel diameter on moving along the tunnel, with constrictions (minimum diameter ca. 5.8 Å) and bulges (minimum diameter ca. 7.1 Å). In most thiourea inclusion compounds, the guest molecules occupy specific sites along the host tunnel, corresponding to one guest molecule within each ''cage'' in the host structure and corresponding to the commensurate relationship $c_h = 2c_g$ (where c_h is the periodic repeat distance of the host structure along the tunnel, and c_g is the periodic repeat distance of the guest molecules along the tunnel). Thus, there are two guest molecules within the periodic repeat distance of the thiourea host structure along the tunnel, leading to a guest/thiourea molar ratio of 1/3. The well-defined positioning of the guest molecules at specific locations within each tunnel gives rise directly

Encyclopedia of Supramolecular Chemistry
DOI: 10.1081/E-ESMC 120012521

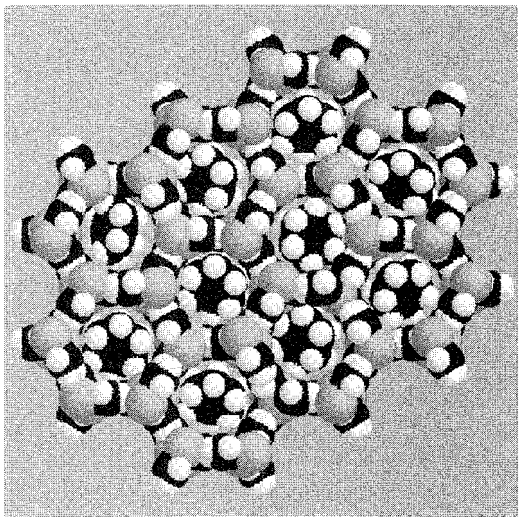

Fig. I Structure of the cyclohexane/thiourea inclusion compound at ambient temperature, showing 10 complete tunnels (with van der Waals radii) viewed along the tunnel axis. Guest molecules have been inserted into the tunnels, illustrating orientational disorder. The positions of the guest molecules are not actually determined from x-ray diffraction data at ambient temperature. (View this art *in color at www.dekker.com.*)

to three-dimensional (3-D) positional ordering of the guest molecules controlled by the 3-D periodicity of the host structure. However, in many cases, as discussed below, there is orientational disorder of the guest molecules.

Much progress has also been made in understanding the structural properties of conventional thiourea inclusion compounds below their phase transition temperatures. The rhombohedral structure of the high-temperature phase usually transforms to a monoclinic structure in the low-temperature phase[7] and is associated with changes in the dynamic properties and the degree of ordering of the guest molecules. Powder x-ray diffraction studies of the chlorocyclohexane/thiourea[12] and cyclohexane/thiourea[13] inclusion compounds have highlighted the advantages of using powder diffraction techniques when transformation to the low-temperature phase is associated with crystal twinning.

Structural Aspects of Some Thiourea Inclusion Compounds with Monoclinic Host Structures

As discussed above, a number of thiourea inclusion compounds have monoclinic structures that can be considered as distorted forms of the conventional (rhombohedral) thiourea tunnel structure. Two examples of inclusion compounds in this category are discussed here.

In the monoclinic structure of the 2,3-dimethylbutadiene/thiourca inclusion compound,[14] the planar guest molecules are arranged longitudinally (rather than stacked) within the tunnels and occupy 6.3 A per guest molecule along the tunncl. The cross-sectional dimensions of the guest molecules perpendicular to the tunnel are ca. 4.0 Å $\times$ 7.0 Å, and the tunnel is considerably deformed from the regular hexagonal cross section found in the conventional (rhombohedral) thiourea inclusion compounds, but with the same N — H. ·S hydrogen-bonding scheme. The guest molecules do not exhibit orientational disorder with respect to the tunnel axis. In the monoclinic structurc of the 2,6-diethylnaphthalene/thiourea inclusion compound,[15] the cross section of the tunnel is a deformed hexagon, and the asymmetric unit comprises three thiourca molecules and half the 2,6-diethylnaphthalene molecule. Thus, in contrast to the conventional thiourea inclusion compounds, there is one guest molecule per unit repeat distance of the host structure along the tunnel, and the molar guest/thiourea ratio is 1/6.

CASE STUDIES: STRUCTURAL AND DYNAMIC PROPERTIES OF SOME SPECIFIC THIOUREA INCLUSION COMPOUNDS

Cyclohexane/Thiourea

In many respects, the cyclohexanetthiourea inclusion compound is regarded as the prototypical example of conventional thiourea inclusion compounds, and its properties have been investigated widely. At ambient temperature, cyclohexanetthiourea has the conventional rhombohedral thiourea host structure,[8] and the cyclohexane guest molecules are located at the sites of 32 symmetry along the tunnel. Three distinct phases have been identified:[7,9,10] Phase I (above 149 K) is rhombohedral (space group $R\bar{3}c$); Phase II (149–129 K) is monoclinic (space group $P2_1/a$, with twice the volume of the rhombohedral unit cell); and Phase III (below 129 K) is also monoclinic (space group $P2_1/a$), with a discontinuity in the lattice parameters between Phases II and III at 129 K. The phase transition between Phases I and II is second order, and the phasc transition between Phases 11 and III is first order. A comprehensive investigation of the structural and symmetry properties associated with these phase transitions has been reported,[13] including the application of Landau theory to establish a detailed understanding of the mechanisms of the phasc transitions.

Early studies of the dynamic properties using wide-line solid-state ^{1}H-NMR of cyclohexane/thiourea-d_4[11,16] concluded that molecular motion of the guest molecules occurs in all three phases I–III. More details of the dynamic processes have been elucidated subsequently

from ^{2}H-NMR studies of cyclohexane-d_{12}/thiourea,[17,18] although confiicting interpretations of the dynamic properties have emerged from these studies. The most comprehensive study of the dynamics of cyclohexane/thiourea to date[13] has involved the application of single-crystal ^{2}H-NMR techniques. In Phase I, the dynamic properties of the cyclohexane guest molecules are described by a model of jumps of the C_3 symmetry axis of the molecule among six equiprobable orientations (corresponding to the D_6 point group symmetry of the site occupied by the guest molecules within the host structure), together with rapid reorientation of the guest molecule about its C_3 axis. The dynamics in Phase II involve reorientation of the C_3 axis of the guest molecule among six inequivalent orientations, although with specific relationships between these orientations. Order parameters driving the transition from Phase I to Phase II have been identified. and the orientational ordering process in Phase II has been elucidated. In Phase III, an abrupt ordering of the C_3 axis of the guest molecule takes place, due to freezing the motions of this axis relative to the host structure, although rapid reorientation of the guest molecule about its C_3 axis still occurs at the temperatures investigated within this phase. The information obtained on the dynamic properties together with the structural information obtained from powder x-ray diffraction studies were both important in developing a detailed description of the phase-transition mechanisms in this material. Molecular dynamics simulation studies[19] have also been exploited to understand the dynamic properties of cyclohexane/thiourea.

Ferrocene/Thiourea

At ambient temperature. ferrocene/thiourea has the conventional rhoinbohedral thiourea host structure.[10] The Fe atoms of the fessocene guest molecules occupy the sites of 32 symmetry within the host tunnel, and the cyclopentadienyl rings are disordered. Heat capacity measurements[20] have suggested that there are five phase transitions (at ca. 147, 160, 171, 186, and 220 K) between 13–280 K, which led to the proposal that the transitions at 147 K and 160 K are associated with reorientational order–disorder processes involving the molecular axis of ferrocene.

Early studies of the dynamic properties focused on ^{1}H-NMR of ferrocene/thiourea-d_4,[21] from which it was concluded that the fivefold axes of the ferrocene molecules are frozen in a number of nonequivalent orientations at low temperature. and that the phase transition at 160 K is associated with the onset of reorientational motion of these axes. Anisotropic ^{13}C-NMR chemical shielding spectra,[22] ^{57}Fe Mossbauer spectroscopy,[23] and solid-state ^{2}H-NMR[24] studies have also shed significant light on the orientational and dynamic properties of the guest molecules. The most recent ^{2}H-NMR study of fessocene-d_{10}/thiourea[25] proposed that there are four distinct orientations of the ferrocene guest molecules in the thiourea tunnel. In three of the orientations; the principal axis of the fessocene molecule is perpendicular to the tunnel axis, whereas in the fourth orientation, it is parallel to the tunnel axis. Below the phase transition at 160 K. the only motion effective on the ^{2}H-NMR timescale is rapid reorientation of each cyclopentadienyl ring about its C_5 axis. In this temperature regime, each fessocene molecule is confined (at least within the ^{2}H-NMR timescale) to one of the four molecular orientations defined above. The phase transition at ca. 160 K is associated with the onset of reorientational motion of the C_5 axes of the ferrocene molecules; between 165 and 220 K. the ^{2}H-NMR spectra are interpreted in terms of interchange of molecules between the three orientations perpendicular to the tunnel axis (with activation energy 6.4 kJ mol^{-1}) together with interchange between the perpendicular and parallel orientations (with activation energy 10.1 kJ mol^{-1}). The populations of these orientational states were determined as a function of temperature. At ambient temperature, the motion of the fessocene molecules is rapid on the ^{2}H-NMR timescale (i.e., frequency >10^7 Hz) and is still anisotropic, but by 340 K, the guest motion is effectively isotropic.

Carbon Tetrachloride/Thiourea

The CCl_4/thiourea inclusion compound has a rhombohedral host structure[26] (space group $R\bar{3}$; a = 15.54 A, c = 12.53 A) at 170 K. The crystal structure determination developed a model for the disordered CCl_4 guest molecules, with the carbon atoms of these molecules coplanar with the three sulfur atoms of thiourea molecules that point toward the center of the tunnel. Heat capacity measurements[27] between 15–300 K give evidence of a first-order phase transition at 41 K and a second-order phase transition at 67 K. Possible types of molecular disorder in the high-temperature phase have been related to the transition entropy and the molecular and site symmetries of the guest molecules. The heat capacity of the lowest temperature phase is unusually large, perhaps indicating very low-frequency vibrational modes or labile configurational excitation of the guest molecules. ^{35}Cl-NQR studies[28] have elucidated details of the dynamic properties of the guest molecules in CCl_4/thiourea.

Adamantane/Thiourea

Adamantane/thiourea has the conventional rhombohedra1 thiourea host structure.[29] In the crystal structure determination. the adamantane molecules were considered as

rigid bodies, and a model of twofold disorder of these molecules was invoked. Dynamic properties of the adamantane guest molecules have been studied by solid-state ^{2}H-NMR spectroscopy.[30] Motionally narrowed isotropic ^{2}H-NMR line shapes are observed throughout the temperature range studied (119–333 K), and ^{2}H-NMR T_1 measurements indicate that the guest molecules reorient on the picosecond timescale at 300 K. There is only one solid phace over the temperature range studied, and the effective barrier to overall reorientation of the adamantane guest molecules is estimated to be about 11 kJ mol^{-1}.

CONFORMATIONAL PROPERTIES OF THE GUEST MOLECULES

Guest molecules in solid host structures are often constrained to exhibit uncharacteristic conformational properties, which can be exploited inter alia as a means of carrying out spectroscopic characterization of such conformations. A classic illustration of such unconventional conformational behavior is provided by monohalogenocyclohexane ($C_6H_{11}X$; X=Cl, Br, I) guest molecules within the thiourea tunnel structure. For monohalogenocyclohexanes in liquid and vapor phases, the dynamic equilibrium between equatorial and axial conformations favors the equatorial conformation, and in the solid state (at sufficiently low temperature or high pressure), only the equatorial conformation is found. In contrast, however, when included as guests in the thiourea tunnel structure, $C_6H_{11}Cl$, $C_6H_{11}Br$, and $C_6H_{11}I$ exist predominantly in the axial conformation. These results have been established from infrared,[31] Raman,[32] and high-resolution solid-state ^{13}C-NMR[33,34] techniques. From the ^{13}C-NMR studies,[34] the mole fraction of the equatorial conformation is in the range 0.05–0.15, in contrast to the corresponding range (0.75–0.81) for the same molecules in $CFCl_3/CDCl_3$ (3:1) solution (all values quoted are for temperatures in the range 159–220 K). There is also a marked contrast between the conformational properties of these guests in the thiourea tunnel structure and in various zeolitic hosts, within which the equatorial conformation predominates. Bromine K-edge extended x-ray absorption fine structure (EXAFS) spectroscopy[35] has also confirmed that the axial conformation of bromocyclohexane predominates within the thiourea tunnel structure. This technique provides a direct measurement of the intramolecular Br···C(3) distance (3.27 Å), and on this basis, the axial and equatorial conformations may be distinguished directly. The ^{13}C-NMR results also demonstrate that for monohalogenocyclohexane guests in the thiourea tunnel at sufficiently high temperature, there is dynamic interconversion between the axial and equatorial conformations.

For guest molecules $C_6H_{11}X$, with X=CH_3, NH_2, and OH, the equatorial conformation is preferred (mole fraction 0.82–0.97) inside the thiourea tunnel structure.[34] Thus, for these guests, the conformational properties resemble those of the same molecules in solution, in contrast to the behavior of the monohalogenocyclohexane guests discussed above.

Further diversity of behavior is observed for fluorocyclohexane ($C_6H_{11}F$) guest molecules in the thiourea tunnel structure, for which there are approximately equal amounts of guest molecules in the axial and equatorial conformations. The conformational properties of this system and the ring inversion dynamics have been probed in detail[36] using a variety of different high-resolution ^{19}F-NMR techniques (with high-power ^{1}H decoupling) and triple-resonance ^{13}C-NMR experiments (with ^{1}H and ^{19}F decoupling).

A number of experimental techniques have also been used to show that certain disubstituted cyclohexanes can adopt uncharacteristic conformations inside the thiourea tunnel structure. For *trans*-1-bromo-2-chlorocyclohexane, intramolecular Br···Cl and Br···C(3) distances of 4.5 Å and 3.27 Å determined from bromine K-edge EXAFS spectra[35] demonstrate that the diaxial conformation is preferred. In contrast, the diequatorial conformation is preferred in dispersed phases.

CHEMICAL REACTIONS OF GUEST MOLECULES IN THIOUREA INCLUSION COMPOUNDS

Although the thiourea tunnel structure can accommodate guest molecules containing a diverse array of functional group types, reported studies of reactions in thiourea inclusion compounds have primarily concerned polymerization reactions. Classical work in this field[13] reported polymerization reactions of 2,3-dimethylbutadiene; 2,3-dichlorobutadiene; 1,3-cyclohexadiene; cyclohexadiene monoxide; iso-butylene; and vinylidene chloride. In all but the latter two cases, high-melting, crystalline polymers were obtained. There have been many subsequent reports of polymerization reactions carried out within the thiourea host structure. A computational study investigating the size requirements of polymers within the thiourea tunnel structure has also been reported.[37]

Another example of a chemical reaction within the thiourea tunnel structure concerns the Diels–Alder reaction between maleic anhydride and cyclopentadiene, which is reported to occur with high conversion and high stereoselectivity.[38] The two guest components were

cocondensed with the vapor of thiourea at 77 K. On subsequent heating, the Diels–Alder reaction occurs with 90% conversion, and more than 95% of the product comprises the *endo* isomer of the Diels–Alder adduct.

APPLIED ASPECTS OF THIOUREA INCLUSION COMPOUNDS

Nonlinear Optical Properties of *Thiourea* Inclusion Compounds *Containing* Organometallic *Guests*

It has been shown by Tam and coworkers[39,40] that thiourea inclusion compounds containing appropriate organornetallic guests can exhibit second-harmonic generation (SHG), i.e., doubling of the frequency of light as it passes through a material. Materials exhibiting SHG are important in a range of applications in optoelectronics and other fields. In order for a crystalline solid to exhibit SHG. the crystal structure must be noncentrosymmetric. If the crystal structure is centrosymmetric, the SHG will be zero, even if the constituent molecules have high second-order hyperpolarizabilities (β). The organometallics [e.g., (η^6-C_6H_6)$Cr(CO)_3$] studied have large values of β, but the structures of their "pure" crystalline phases are centrosymmetric and therefore do not exhibit SHG. Under the proposal that dipole organization may be favored inside the thiourea host structure, a large number of thiourea inclusion compounds containing organometallic guest molecules were prepared, and several of these materials were found to exhibit significant SHG. Structure determination of the SHG-active crystals confirmed the expected dipole organization of the guest molecules. For example, the crystal structures of (η^6-benzene)$Cr(CO)_3$/thiourea, (η^4-trimethylenemethane)$Fe(CO)_3$/thiourea, and (η^5-cyclohexadienyl)$Mn(CO)_3$/thiourea are isomorphous (space group R3c), and contain head-to-tail arrangements of the guest molecules along the tunnel. This work suggests, inter alia, that inclusion compound formation may be a widely applicable strategy for the formation of SHG-active materials. It was also shown that the SHG activity of these materials arises predominantly from the organometallic guest molecules, rather than the thiourea molecules (which also have significant β).

Application *of a Thiourea* Inclusion Compound *as* **an** Analyzer for **X-ray** Polarization Analysis

In the case of visible light, studies of polarization are dominated by the use of dichroic filters (e.g., the Polaroid sheet), for which photons with polarization parallel to a certain axis in the material are preferentially attenuated over those with polarization perpendicular to this axis. In principle, materials analogous to the Polaroid sheet may be developed for applications as dichroic filters in other regions of the electromagnetic spectrum, and there is interest in the development of materials for analysis of polarized x-ray radiation (which may be produced, for example, from a synchrotron radiation source). A suitable dichroic filter would be a crystal for which the absorption of polarized x-rays depends significantly on the orientation of the crystal, and such materials are of interest in a range of applications, such as in studies of magnetic x-ray scattering. Recently, it has been shown[41] that the 1-bromoadamantane/thiourea inclusion compound exhibits essentially optimal properties as a dichroic filter for polarized x-ray radiation (with x-ray energy close to the bromine K-edge). In this inclusion compound. the thiourea molecules form a tunnel host structure that differs to some extent from the conventional thiourea host structure. Within the repeat distance (24.75 Å) along the tunnel, there are three crystallographically independent 1-bromoadamantane guest molecule sites, corresponding to a guest:thiourea molar ratio of 1/4. At each site, there is disorder between two orientations (with essentially equal occupancies) of the guest molecule, but importantly, the C—Br bond of each guest molecule lies parallel to the thiourea host tunnel. It has been shown theoretically that this structural feature promotes optimal perforinance of such materials as dichroic filters for polarized x-rays.

CONCLUSION

As discussed above, the fact that thiourea inclusion compounds display a wide range of interesting structural and dynamic properties is well established. As with many solid inclusion compounds: structural constraints imposed upon the guest molecules by means of confinement within the host structure can confer properties upon the guest molecules chat differ significantly from those of the same molecules in dispersed phases. In view of the fact that the thiourea host structure can incorporate a diverse range of guest species, in terms of size, shape, and chemical functionality, there appears to be considerable potential for the design of thiourea inclusion compounds for applications in a range of scientific fields, and significant future developments in this regard may be anticipated.

ARTICLES OF FURTHER INTEREST

Incommensurate and Commensurate Structures. p. 712
Urea Inclusion Compounds, p. 1538

REFERENCES

1. Angla. B. Molecular complexes of thiourea. Compt. Rend. 1944. *224*, 1166.
2. Fetterly, L.C. In *Non-Stoichiometric Compounds*; Mandelcorn, L., Ed.; Academic Press: New York, 1964: 491.
3. Brown, J.F.; White. D.M. Stereospecific polymerization in thiourea canal complexes. J. Am. Chem. Soc. 1960. *82*. 5671.
4. Takemoto, *K.*: Sonoda. N. In *Inclusion Compounds*; Attwood. J.L.. Davies. J.E.D.,MacNicol, D.D., Eds.: Academic Press: London. 1984: Vol. 2. 47.
5. Hollingsworth. M.D.: Harris. K.D.M. *Comprehensive Supramolecular Chemistry*; MacNicol, D.D., Toda, F., Bishop, R.. Eds.; Pergamon Press 1996; Vol. 6. 177.
6. Harris, K.D.M. Understanding the properties of urea and thiourea inclusion compounds. Chem. Soc. Rev. 1997, *26*, 279.
7. Harris, K.D.M. Towards a fundamental understanding of urea and thiourea inclusion compounds. J. Chin. Chem. Soc. 1999, *46*. 5.
8. Lenné, H.-U. Rontgenographische Strukturuntersuchungen hexagonaler Einschlussverbindungen des Thioharnstoffs. Acta Crystallogr. 1954, *7*. 1.
9. Harris, K.D.M.: Thomas. J.M. Structural aspects of the chlorocyclohexane/thiourea inclusion system. J. Chem. Soc., Faraday Trans. 1990, *86*. 1095.
10. Hough, *E.:* Nicholson. D.G. X-ray crystallographic studies on ferrocene included in a thiourea host lattice. J. Chem. Soc., Dalton Trans. 1948. 15.
11. Clément, R.: Mazières, C.; Gourdji, M.; Guibè. L. Phase changes and molecular motion in the thiourea-cyclohexane inclusion compound. J. Chem. Phys. 1977. *67*, 5381.
12. Jones. M.J.: Shannon. I.J.; Harris, M.D.M. Temperature-dependent structural propel-ties of the chlorocyclohexane/thiourea inclusion compound investigated by synchrotron X-ray powder diffraction. J. Chem. Soc., Faraday Trans. 1996. *92*. 273.
13. Desinedt. *A.:* Kitchin, S.J.: Guillaume. F.: Couzi. M.; Harris. K.D.M.; Bocanegra. E.H. Phase transitions and molecular dynamics in the cyclohexane/thiourea inclusion compound. Phys. Rev.. B 2001. *64*. 054106.
14. Chatani. Y.: Nakatani. S. Crystal structure of the monoclinic adduct of thiourea with 2,3-dimethylbutadiene. Z. Kristallogr. 1977. *144*. 175.
15. Shindo, *T.:* Shindo, M.: Ohnuma. H.; Kabuto. C. Crystal structure of the adduct of thiourea with 2,6-diethylnaphthalene. Bull. Chem. Soc. Jpn. 1993, *66*, 1914.
16. Clément. *R.;* Gourdji. M.; Guibè. L. Nitrogen pure quadrupole resonance and proton magnetic resonance in the thiourea–cyclohexane inclusion compound. Evidence for phase transitions. Mol. Phys. 1978. *21*, 247.
17. Meirovitch. E.: Krant, T.: Vega. S. A deuterium nuclear magnetic resonance study of conformational and dynamic characteristics of cyclohexane while trapped within thiourea inclusion-compound channels. J. Phys. Chem. 1984. *87*, 1390.
18. Poupko, *R.;* Furman. E.; Müller, K.: Luz. Z. Reinvestigation of the thiourea-cyclohexane inclusion compound by deuterium NMR spectroscopy. J. Phys. Chem. 1991, *95*. 407.
19. Soetens. J.-C.; Desmedt. A.: Guillaume. F.; Harris. K.D.M. Molecular dynamics simulation study of cyclohexane guest molecules in the cyclohexane/thiourea inclusion compound. Chem. Phys. 2000. *261*, 125.
20. Sorai. M.; Ogasahara, K.: Suga, H. Thermodynamic properties of ferrocene crystal. Mol. Cryst. Liq. Cryst. 1981. 73. 231.
21. Clément. R.: Gourdji. M.; Guibè, L. Molecular motions in the thiourea-d_4-ferrocene inclusion compound. Chem. Phys. Lett. 1980. *72*. 466.
22. Nakai, T.: Terao. T.: Imashiro, F.; Saika. A. A ^{13}C WMR study of the dynamic structure of the thiourea-ferrocene inclusion compound. Chem. Phys. Lett. 1986, *132*. 554.
23. Gibb, T.C. Anisotropic relaxation of the electric field gradient tensor in the ^{57}Fe Mossbauer spectra of a thiourea-ferrocene clathrate. J. Phys., C 1976. *9*, 2627.
24. Lowery. D.M.; Wittebort, R.J.; Sorai, M.: Hendrickson. D.N. Dynamics of ferrocene in a thiourea inclusion matrix. J. Am. Chem. Soc. 1990, *112*. 4214.
25. Heyes, S.J.; Clayden, N.J.; Dobson, C.M. Ferrocene molecular reorientation in the (thiourea)$_3$·ferrocene inclusion compound as studied by deuteron NMR spectroscopy. J. Phys. Chem. 1991; *95*. 1547.
26. Fait, J.F.; Fitzgerald. A.: Caughlan, C.N.; McCandless. F.P. Carbon tetrachloride-thiourea (113) adduct at 170 K. Acta Crystallogr. 1991. *C47*. 332.
27. Sekii. M.: Matsuo. T.; Suga. H. Calorimetric study of phase transitions in the thiourea carbon tetrachloride inclusion compound. J. Incl. Phenom. Mol. Recognit. Chem. 1990. 9. 243.
28. Adolphi. N.; Conradi. M.S.; Matsuo, T. ^{35}Cl NQR study of thiourea-CCl_4 and thiourea-CCl_3Br inclusion compounds. J. Phys. Chem. 1994, *98*. 1968.
29. Gopal, R.: Robertson. B.E.: Rutherford, J.S. Adamantane inclusion complexes with thiourea and selenourea. Acta Crystallogr. 1989. *C45*. 257.
30. MacIntosh. M.R.: Fraser, B.; Gruwel, M.L.H.: Wasylishen, R.E.; Cameron, T.S. Deuterium NMR study of the adamantane-thiourea and bicyclo[2.2.2]octane-thiourea inclusion compounds. J. Phys. Chem. 899%.*96*. 8572.
31. Fukushima, K. Far-infrared spectra and structure of monochlorocyclohexane in a thiourea adduct. J. Mol. Struct. 1976. *34*. 67.
32. Allen. A.; Fawcett. V.: Long. D.A. A Raman spectroscopic investigation of the conformation of the cyclohexyl halides $C_6H_{11}X$ (X= chlorine, bromine. and iodine) in thiourea clathrates. J. Raman Spectrosc. 1976, 4. 285.
33. McKinnon, M.S.; Wasylishen, R.E. A carbon-13 cp/mas NMR investigation of the conforniation of substituted cyclohexanes in thiourea inclusion compounds. Chem. Phys. Lett. 1986. *130*. 565.
34. Aliev, *A.E.:* Harris. K.D.M. Conformational properties of monosubstituted cyclohexanes in their thiourea inclusion compounds and in solution: Variable-temperature

one-dimensional and two-dimensional carbon-13 NMR investigations. J. Am. Chem. Soc. **1993,** *115*, 6369.
35. Shannon, I.J.: Jones, M.J.; Harris, K.D.M.: Siddiqui. M.R.H.; Joyner. R.W. Probing the conformational properties of guest molecules in solid inclusion compounds *via* EXAFS spectroscopy: Bromine K-edge EXAFS studies of the bromocyclohexane/thiourea and *trans*-1-bromo-2-chlorocyclohexane/thiourea inclusion compounds. J. Chem. Soc., Faraday Trans. **1995**, 91. 1497.
36. Harris. R.K.; Nordon. A.; Harris. K.D.M. Ring inversion of fluorocyclohexane in its solid thiourea inclusion compound. Magn. Reson. Chem. **1999,** *37*, 15.
37. Tonelli. A.E. Can polymers containing rings in their backbones form inclusion cornpounds with small-molecule, host clathrates? Comput. Polym. Sci. **1992.** *2*. 80.
38. Sergeev, G.B.; Komarov. V.S.: Zvonov. A.V. Reaction of cyclopentadiene with maleic anhydride in an inclusion compound with thiourea prepared in the solid phase at low temperatures. Dokl. Akad. Nauk. SSSR **1983,** *270*. 139.
39. Anderson, A.G.; Calabrese, J.C.; Tam. W.: Williams, I.D. Thiourea inclusion complexes of organometallics: Optically non-linear materials. Chem. Phys. Lett. **1987,** *134*. 392.
40. Tam, W.; Eaton, D.F.: Calabrese, J.C.; Williams, I.D.; Wang, Y.; Anderson, A.G. Channel inclusion complexation of organometallics: Dipolar alignment for second harmonic generation. Chem. Mater. **1989. 1.** 128.
41. Chao. M.-H.; Kariuki, B.M.; Harris, K.D.M.; Collins. S.P. Design of a solid inclusion compound with optimal properties as a linear dichroic filter for X-ray polarization analysis. Angew. Chem., Int. Ed. 2003. *42*, 2982.

Torands

Thomas **W. Bell**
University of Nevada, Reno, Nevada, U.S.A.

INTRODUCTION

The term "torand," derived by combination of "toms" and "ligand," denotes a macrocyclic ligand in which the perimeter of the large ring is completely formed by fusion of smaller rings. Three kinds of torands are currently known, dodecahydrohexaazakekulene (**1**, $R^1 = R^2 = H$)[1,2] and its substituted derivatives,[3–7] "expanded" torand 2 (R = butyl) containing 1,8-naphthyridine units,[5,6,8,9] and mixed pyridine/pyrrole macrocycle **3** (R = butyl), an expanded porphyrin.[5,6] The structures of these torands are shown in Fig. 1, along with those of related molecules. The latter include kekulene (**4**),[10] cyclosexipyridine (**5**),[11] Shiff-base pyridomacrocycles **6** and **7**,[4,5,12] and a heterohelicene molecular coil (**8**).[7,13,14] These systems are included in the following discussion of the background for torands. Current methods for synthesis of torands **1** and 2 are presented, followed by a summary of their binding properties. Torand **1** forms complexes with a wide variety of metal cations, including alkali metals, and expanded torand 2 binds guanidinium cation via hydrogen bonds. These relatively rigid hosts form stronger complexes than less highly preorganized analogues.

RELATED MOLECULES

Kekulene (4)

The ^{1}H-NMR spectrum[10,15] and crystal structure[16] of kekulene (4) disproved the concentric [18]annulene/[30]annulene character implied by the resonance form shown in Fig. 1. Instead, kekulene is better represented by a D_{6h}-symmetric structure including six benzenoid sextets.[16,17] Computational studies confirmed the semilocalization of π electrons in six benzene rings[17] and also produced current-density maps contradicting the annulene model."[17] Torands of Type **1**, formally dodecahydrohexaazakekulenes, have six pyridine rings in the same positions as the six benzenes of the D_{6h} kekulene structure. Fully unsaturated torands were not reported, but a D_{3h}-symmetric hexaazakekulene with three inner and three outer nitrogen atoms is known.[19] Lacking solubilizing substituents, this macrocycle only has appreciable solubility in strong acids. An insoluble dodecahydrodiazakekulene may have been prepared from the corresponding dodecahydrodioxoniakekulene.[20] Kekulene (4) represents only one of a hypothetical family of "cycloarenes" derived by fusion of benzene rings to form macrocyclic hydrocarbons.[15] To date, **1** and "expanded" torand 2 are the only known torands formally derived from cycloarenes.

Cyclosexipyridine (5)

The ultimate bridged-pyridine macrocycle,[21] cyclosexipyridine (**5**), was a synthetic target for numerous research groups for decades prior to the 1983 reports by Newkome and Lee[11] and Toner[22] on the parent and diaryl-substituted systems, respectively. These two communications did not give full details pertaining to synthesis and characterization and implied contrasting solubilities and sodium-scavenging properties. A thorough investigation of the synthesis of threefold symmetric triarylcyclosexipyridines was reported recently by Masciello and Potvin.[23] The *tris*(*p*-tolyl), *tris*(4-chlorophenyl), and *tris*(4-*tert*-butylphenyl) derivatives of **5** were obtained as mixed Na^+ and K^+ complexes and were insoluble amorphous solids. On the other hand, the *tris*(4-neopentoxyphenyl) analogue is soluble in nonaromatic solvents and was characterized (NMR, UV/Vis, and matrix-assisted laser desorption ionization mass spectrometry (MALDI-MS)) as a 5:2 mixture of Na^+ and K^+ complexes. Thus, the tendencies of cyclosexipyridines toward problematic aggregation and alkali metal sequestration are well established.

Schiff-Base Pyridomacrocycles (6 and 7)

Metal complexes of Schiff-base macrocycle **6**[4,5] can be prepared by cyclocondensation of pyridine-2,6-dicarboxaldehyde with benzene-1.2-diamine in the presence of Sr^{2+}[24,25] Pb^{2+}, or Cd^{2+}.[26] The metal-free macrocycle is prepared by replacement of Sr^{2+} with K^+,[24] followed by decomplexation with excess 18-crown-6.[12] While 6 adopts the circular conformation shown in Fig. I in complexes with Sr^{2+}[25] and other metals, the cavity collapses in the absence of a guest.[5,12] Despite this conformational flexibility, 6 binds both Na^+ and K^+ better than 18-crown-6 in dimethyl sulfoxide (DMSO), and it is

Encyclopedia of Supramolecular Chemistry
DOI: 10.1081/E-ESMC 120019187

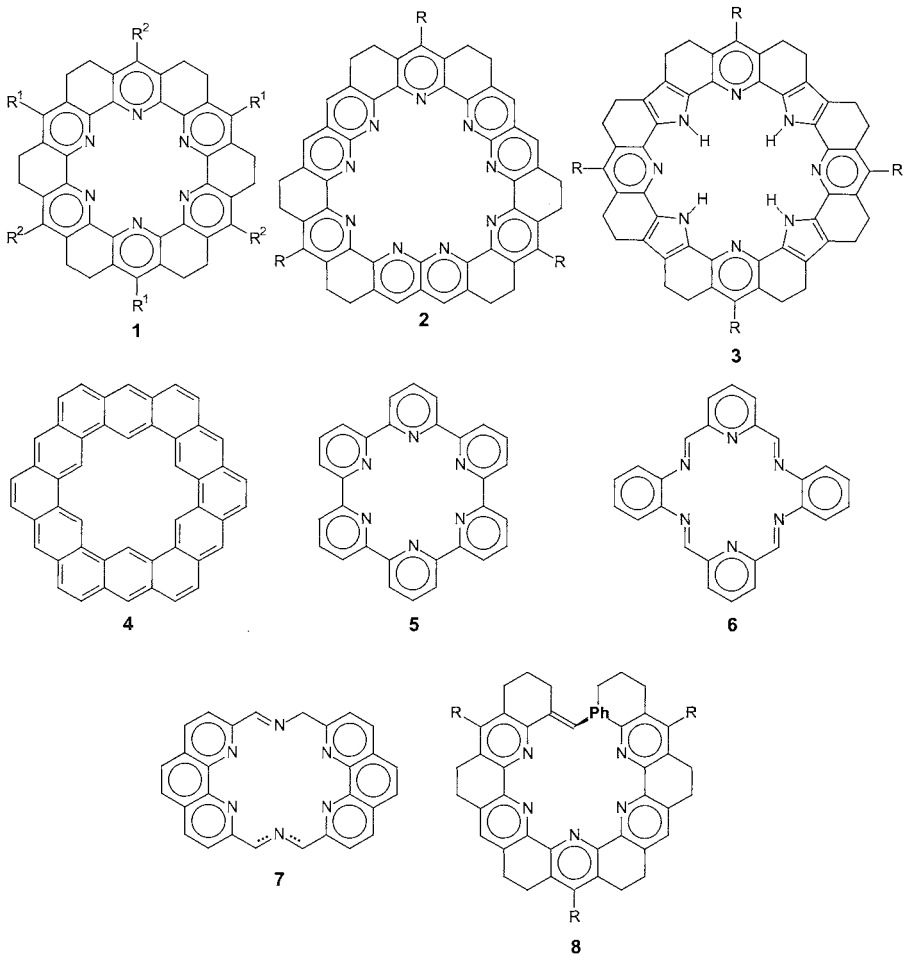

Fig. 1 Known torands (1–3) and related molecules: kekulene (4), cyclosexipyridine (5). Schiff-base pyridomacrocycles (6 and 7), and a molecular coil (8).

slightly selective for K^+ over Na^+.[25] Condensation of 1,10-phenanthroline-2,9-dicarboxaldehyde with 2,9-*bis* (aminomethyl)-1,10-phenanthroline in the presence of strontium triflate gave a *2:*1 mixture of diimine macrocycles (7) as very stable Sr^{2+} complexes.[4,5] These complexes of 6 and **7** are among the first complexes of "hard" alkaline earth ions with hosts containing only "soft" nitrogen donors.[21] This apparent contradiction is, however. consistent with the large dipole moments associated with pyridine and imine ligand sites[24,25] and the importance of ion–dipole interactions in the stabilization of alkaline earth (as well as alkali metal) complexes.

Molecular Coils (8)

Torand 1 consists of alternating, angularly fused pyridine and six-membered carbocyclic rings. When this molecular architecture is applied to open-ended systems, the ends overlap when a total of *12* rings is reached, or when a benzylidene group is introduced as a steric barrier in an 11-ring system, as in **8**.[7,13,14] This expanded heterohelicene. or "molecular coil." and a 13-ring analogue lacking the benrylidene group were synthesized.[7,13] While the metal-free ligands were isolated, they were found to sequester Na^+ or Ca^{2+} from chromatographic sorbents (silica or alumina). Careful examination of sodium binding by **8** revealed that a double-helical 2:2 complex was formed.[14] These results underscore the affinities of preorganized polypyridines toward alkali metal and alkaline earth cations.

TORAND SYNTHESIS

Dodecahydrohexaazakekulenes (1)

A lengthy synthesis of the parent dodecahydrohexaazakekulene (1, $R^1 = R^2 = H$) was reported by Ransohoff and Staab.[1] The final, macrocyclization step apparently gave the torand in 3% yield as a sparingly soluble solid,

which was characterized only by mass spectrometry and ^{1}H-NMR spectroscopy. Anticipating solubility problems with the parent torand, Bell and Firestone developed a method for synthesis of butylated heptacyclic terpyridines[27] and applied it to tributyldodecahydrohexaazakekulene (1, R^1 = H. R^2 = butyl).[3] The rnacrocyclization step in both approaches involved the reaction of two components to form a *bis*(pyrylium) dicationic intermediate. In the Ransohoff/Staab case, a single compound representing about half of the torand ring was dimerized. In the case of the Bell/Firestone synthesis, two different octahydroacridines each comprising one-third of the torand were combined, then the final third was incorporated during macrocyclization. The strategy is illustrated in Fig. *2,* which shows current approaches to both the parent and tributyl torands.

Two routes were originally developed for the synthesis of intermediate diketone 18 (*R*= butyl).[3,28] One involved introduction of the two carbonyl groups by oxidation of the corresponding dibutyl heptacyclic terpyridine.[27] The other route is similar to that shown in Fig. 2, except that 14 was prepared by pyrolysis of the trimethylhydrazonium derivative of 12. An improved method for this ''1/3+1/3'' coupling reaction involves condensing the HCl salt of Mannich derivative 13 with ketone 12 and ammonium acetate, giving heptacyclic terpyridyl 14 in 70% yield. The synthesis of 9-butyloctahydroacridine (9) and its conversion to N-oxide 10 are part of an Organic *Syntheses* procedure,[29] and various routes to diketone 18 are documented in an article describing its complexation properties.[28] The overall yield of the tributyl torand is 3% for the 11-step synthesis shown in Fig. 2.[6] The route was also applied to the unsubstituted torand (1, $R^1 = R^2$ = H), in which case the overall yield is *2%*. The synthesis of torand I is tedious, but the route shown in Fig. 2 can be used to prepare gram-quantities of the trifluoroinethanesulfonate (triflate) salt. The triflate salt of the tributyl torand can be converted to the free-base form by reaction with tetrabutylammonium hydroxide in butanol/acetonitrile.[30]

Similar pyridine annelation reactions were used to produce cleft-shaped molecules and torands bearing substituents capable of modifying their solubilities and aggregation properties. For example, 9-(4-t-butoxybutyl) octahydroacridine was prepared and used to synthesize corresponding disubstituted heptacyclic terpyridines and an undecacyclic quinquepyridine similar to 8.[31] Several β-arylenones resulting from condensation of ketone 12 (*R*= butyl) with aromatic aldehydes were condensed again with 12 and ammonium acetate to give. after oxidation, analogues of 14, in which the central pyridine ring bears a phenyl, 4-methoxyphenyl, 4-chlorophenyl. or 4-nitrophenyl substituent.[32] By an approach analogous to that shown in Fig. 2, this method was applied to the synthesis of triaryltrialkyltorands (1, R^1 = butyl, R^2 = aryl), which were obtained in 15–30% macrocyclization

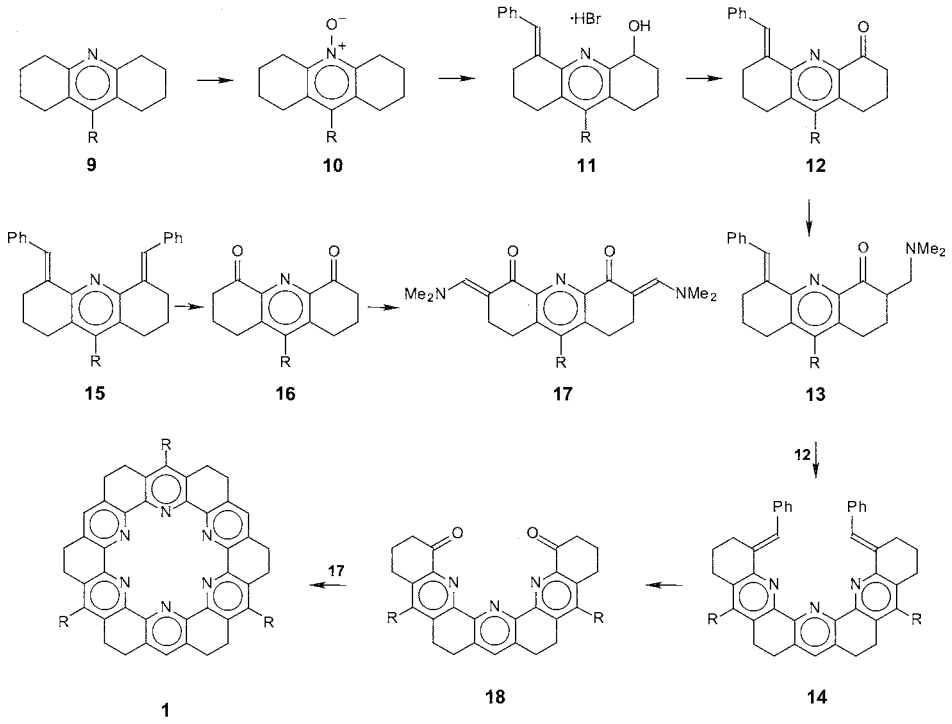

Fig. 2 Synthesis of dodecahydrohexaazakekulene torands (*R*=H or butyl)

yield.[6,7] Substituents in the four-positions of the three aryl groups may potentially be used to introduce ionic groups or steric barriers.

Expanded Torand 2

Angular fusion of six-membered rings produces torand 1 with an 18-membered central ring; incorporation of three linearly fused pairs of pyridines produces three 1,8-naphthyridine units and a larger cavity defined by a 24-membered ring in torand 2. Annelated 1.8-naphthyridines are conveniently prepared by Friedlander condensation of 4-aminopyrimidine-5-carboxaldehyde (19, Fig. 3), with a cyclic ketone, hydrolysis of the pyrimidine ring, and Friedlander condensation of the resulting *o*-aminoaldehyde with a second ketone.[''''] This method was applied to benzylideneketone 12 (R = butyl) to synthesize expanded torand 2, as shown in Fig. 3. as well as a nonmacrocyclic (or U-shaped) analog.[5,6,8,9] The macrocyclization step involves trimerization of ketoaminoaldehyde 22, which is obtained by ozonolysis of 21, the hydrolysis product of Friedlander derivative 20. The cyclotrimerization yield (50% max.) is sensitive to the amount of cesium hydroxide used to promote the reaction. Torand 2 precipitates as a complex with cesium and is obtained as the free ligand after removal of the metal by boiling in water.

TORAND COMPLEXATION

Metal Cations

Torand 1 (R = butyl) forms remarkably strong complexes with alkali metal salts. Lithium, sodium. potassium, and cesium picrate are completely extracted from water into chloroform, indicating that the stability constants of their 1:1 complexes exceed $10^{''}$ M^{-1}.[5,30] Competition experiments were performed by adding [2.2.1]- or [2.2.2] cryptand to solutions of the 1:1 complexes of 1 with alkali metal picrates, following the binding equilibrium by ^{1}H-NMR spectroscopy under slow exchange conditions. The resulting logK_s values were calculated: Li^+, 13.4; Na^+, 14.7; and K^+, 14.3. [5,30] As shown in Fig. 4, under these conditions, torand 1 binds Na^+ and K' with higher affinity than does cryptahernispherand 23, spherand 24, [2.2.2] cryptand (25). or naphtho-18-crown-6 (26). The cavity of 1 is more open than those of the other hosts, so these findings refute the notion that encapsulation is required for strong binding. Moreover. the low size-selectivity of 1 contradicts the usual preference for the metal that best fits the cavity. The torand cavity radius is nearly fixed at a previously estimated value of 1.3 Å, and the hexacoordinate radii of potassium, sodium, and lithium are 1.38, 1.02, and 0.76 Å, respectively.[5]

The stability constants of the 1:1 alkali metal picrate complexes of diketone 18. heptacyclic terpyridyl 27 and flexible terpyridine 28 were estimated by liquid–liquid extraction,[28] and the resulting logK_s values for Na^+ and K^+ are also given in Fig. 4. The affinities of 18 and 27 for these alkali metals are remarkably high for hosts containing only five or three ligand atoms, respectively. In water-saturated chloroform, pentadentate host 18 binds Na^+ and K^+ more strongly than do most crown ethers. Compared to naphtho-18-crown-6 (26), 18 binds Na^+ 4000 times better, and K^+ 40 times better. Even tridentate host 27 extracts alkali metal picrates into chloroform, whereas flexible model system 28 is ineffective under the same experimental conditions. The potent complexation

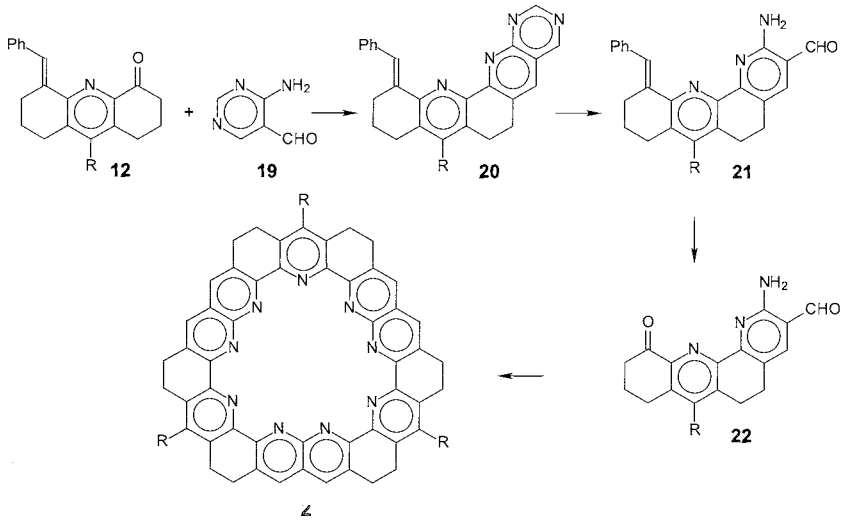

Fig. 3 Synthesis of expanded torand 2 (R = butyl) by Friedlander trimerization

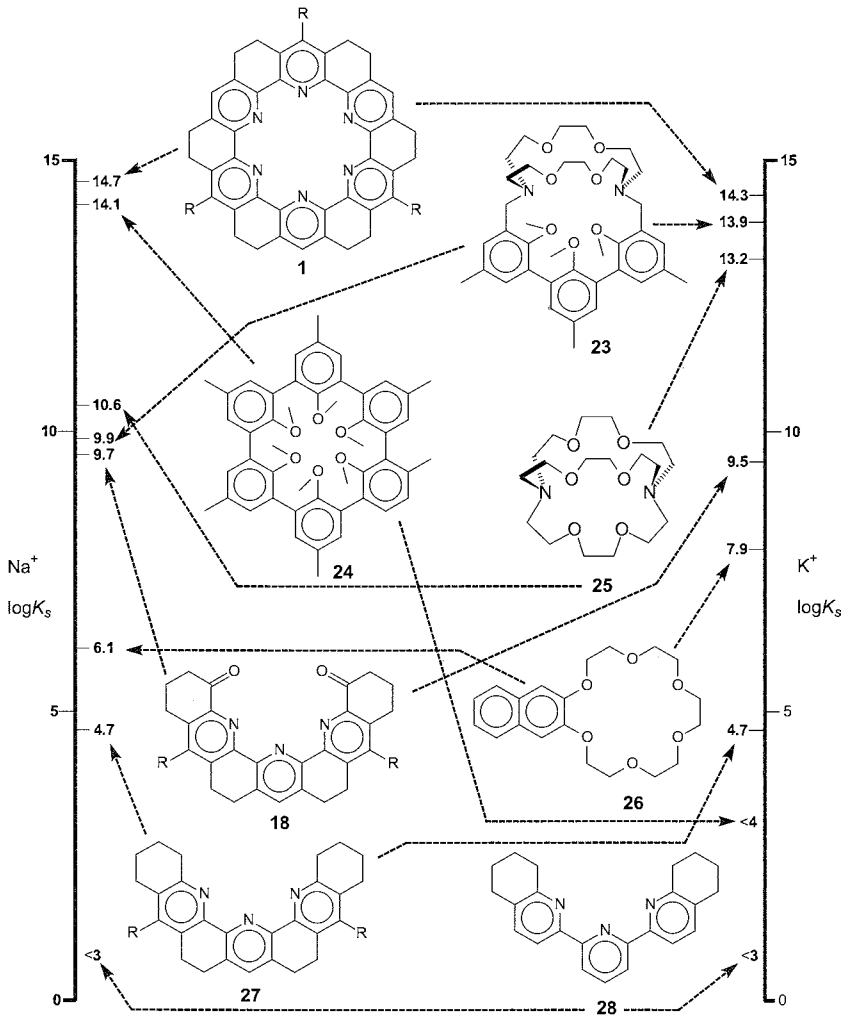

Fig. 4 Stability constants ($\log K_s$) of sodium and potassium picrate complexes in H_2O-saturated $CHCl_3$ (or D_2O-saturated $CDCl_3$) for torand 1. cryptahemispherand 23, spherand 24. cryptand ***25.*** terpyridyldiketone 18. crown ether 26, preorganized terpyridyl 27. and flexible terpyridyl 28 (R = butyl in **1. 18**, and 27).

abilities of heptacyclic terpyridyl hosts 18 and 27 can be attributed to enforced orientation of relatively large ligand functional group dipoles toward the center of the molecular cleft. As observed for torand **1**. selectivity is modest. Diketone 18 binds sodium and potassium slightly better than lithium, rubidium, and cesium, whereas 27 shows a slight preference for lithium among all the alkali metals.[28]

The x-ray crystal structures of the lithium, potassium. and rubidium picrate complexes of torand 1 (R = butyl) were determined.[5,34–37] and the structures of the potassium and rubidium complexes are shown in Fig. 5. In ihese two complexes. the metal atoms rest in the center of the cavity of 1, which adopts the staggered pseudo-D_{3d} conformation predicted by molecular modeling.[34,35] Potassium is clearly an excellent fit to the torand cavity, because it lies only 0.23 Å out of the best plane of the six nitrogen atoms. with K–N distances ranging from 2.73–2.85 Å. Potassium has a seventh contact to picrate, suggesting that the cavity radius of 1 should be revised to nearly 1.46 A, the ionic radius of seven-coordinate potassium.[5] The torand adopts the same conformation in $1 \cdot Rb^+$, but rubidium lies 1.06 Å out of the best nitrogen plane. and picrate is bidentate.

In contrast to K^+ and Rb^+, lithium picrate crystallizes with torand 1 as a 2:2 complex containing three water molecules.[36,37] The two torands are coaxially stacked and threaded by a hydrated dilithium chain: H_2O–Li^+–H_2O–Li^+–H_2O. Each lithium cation binds unsyinmetrically to two of the six nitrogens in each torand, and two water molecules complete the tetrahedral Li^+ coordination sphere. No anion coordination is observed, and hydrogen

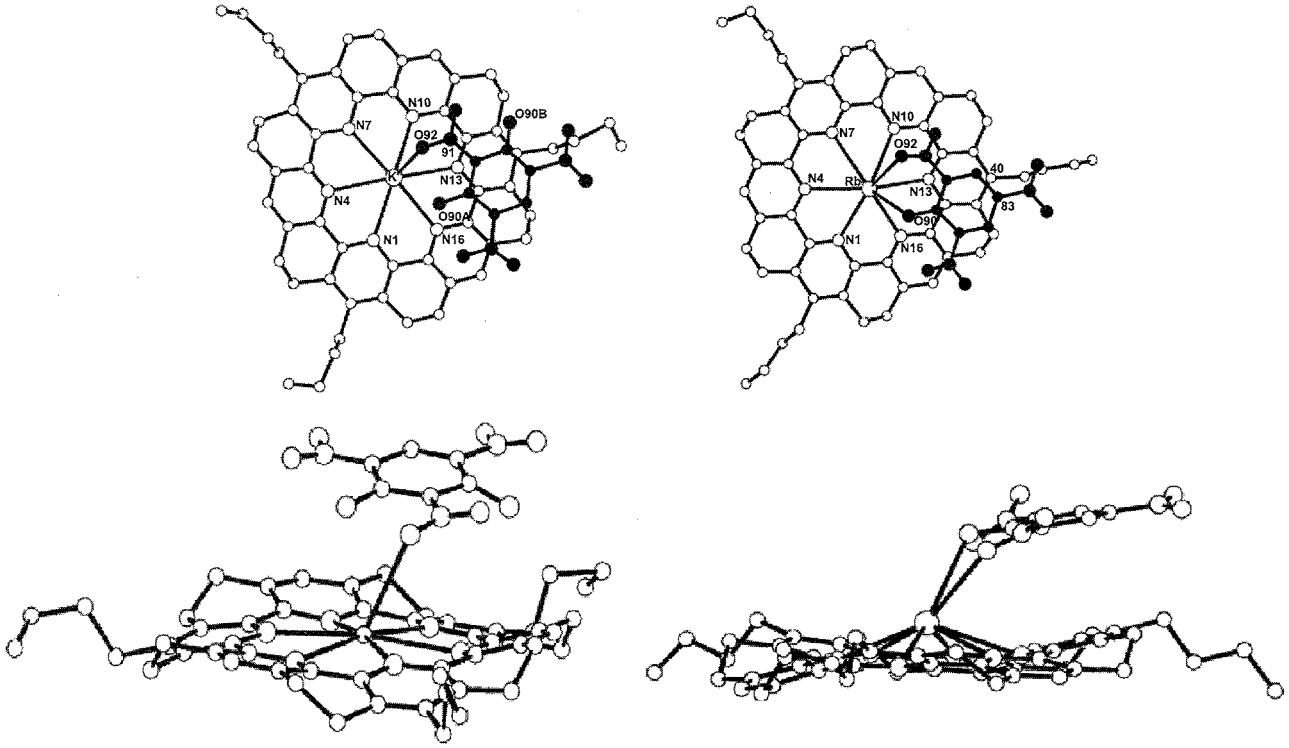

Fig. 5 Crystal conformations of cationic complexes of torand **1** (R' = H, R^2 = butyl) with potassium (top left, bottom left) and rubidium (top right, bottom right). (*View this* art *in* color *at www.dekker.com.*)

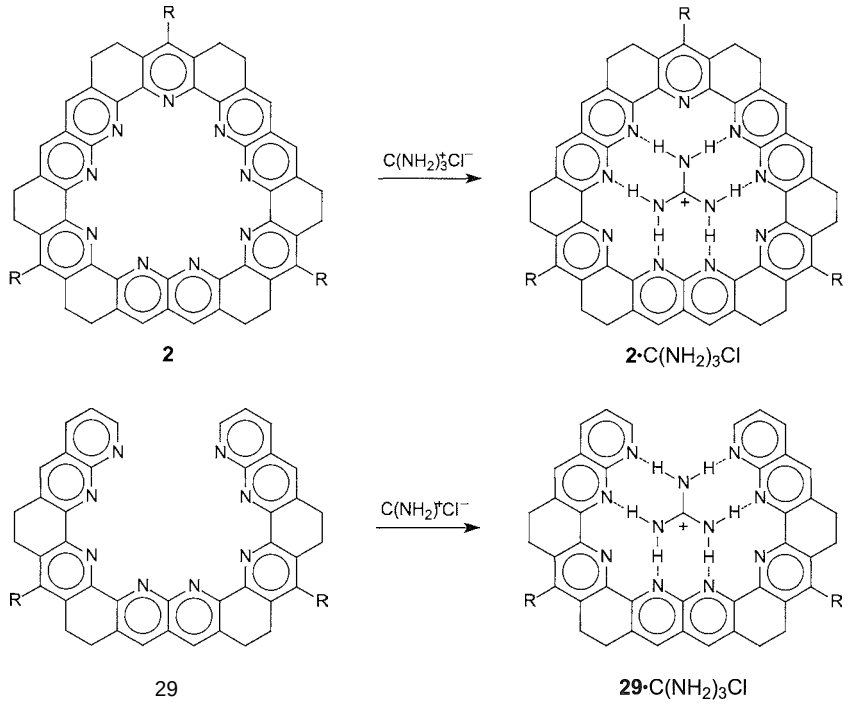

Fig. 6 Complexation of guanidinium by expanded torand 2 and flexible analogue 29

bonding between Li^+-coordinated water molecules and vacant N binding sites apparently enhances the stability of the supramolecular assembly. Torand stacking interactions are also implied by the cation response of thin films of torand **1** at the air–water interface.[38] Even though **1** is substituted only with three butyl chains, it is sufficiently hydrophobic to form compressible thin films on water. Surface pressure/molecular area isotherms are dramatically affected by metal cations in the aqueous subphase. Transitions at 100–120 $Å^2$/molecule suggest the formation of stacked-torand dimers in the presence of Li^+, Cs^+, and Pb^{2+}.[7,38] Despite the relatively large cavity size of **1**, and unusual hexagonal planar ligand geometry, complexes are formed with metal cations throughout the periodic table.[5] Fluorescence of protonated **1** is quenched upon binding certain metals (e.g., Pb^{2+}), so it might be useful as a sensor for detection of metals in solution.[39]

Organic Guests

Torand **2** (*R*= butyl) presents a nearly ideal array of hydrogen-bond-accepting pyridines for complexation of the guanidinium cation, as shown in Fig. 6. This nearly perfect registry of host and guest geometries led conceptually to the family of "hexagonal lattice receptors" for organic guests.[39] Flexible U-shaped host **29** has nearly the same array of pyridine rings as **2**. but its minimum energy geometry is expected to be nonplanar, placing the terminal nitrogen nuclei nearly 7.3 Å apart.[8,9] Thus, **2** should bind guanidinium with little change in host conformation, while **29** must adjust to a more planar conformation in the complex. Accordingly, the UV/Vis spectrum of **2** shows no significant response to complexation, while **29** binds guanidinium with bathochromic shifts of the longer wavelength absorption maxima.[8,9,39] Both *2* and **29** quantitatively extract guanidinium chloride into anhydrous CH_2Cl_2. Titration studies led to calculation of a stability constant of 2×10^6 M^{-1} for **29**·$C(NH_2)_3Cl$ in 95:5 ethanol/CH_2Cl_2,[39] and the stability constant of **2**·$C(NH_2)_3Cl$ is apparently even higher.

CONCLUSION

Torands and closely related molecules, such as cycloarenes, sexipyridines, and expanded heterohelicenes (molecular coils). still constitute a relatively small group of known compounds. The main reason for this is purely synthetic: fusion of multiple rings requires many synthetic steps; and low-yield macrocyclization reactions compound the problem. Clearly, better methods are needed for the synthesis of torands to enable more complete exploration of their complexation properties and other potential uses. Easier synthetic access would pave the way for application of these rigid molecules as, for example, scaffolds, dendrimer cores, mesogens, and nanoscale molecular devices. The binding properties of partial structures of torands also demonstrate the value of preorganization in supramolecular chemistry. Fused-ring hexagonal lattice receptors can form strong complexes, and macrocyclic structures may not be necessary or desired for many applications.

ARTICLES OF FURTHER INTEREST

Annulenes, p. 59
Anficrowns, p. 68
Calixarenes and Their Analogues: Cation Complexation, p. 137
Cavitands, p. 219
Guanidinium-Based Anion Receptors, p. 615
Hydrogen Bonding, p. 658
Induced Fit, p. 717
Ionophores, p. 760
Macrocycle Synthesis, p. 830
π–π Interactions: Theory and Scope. p. 1076
Preorganization and Complementarity, p. 1158
Pyrrole- and Polypyrrole-Based Anion Receptors, p. 1176
Spherands, p. 1344
Stability Constants: Definition and Determination, p. 1360

REFERENCES

1. Ransohoff. J.E.B.: Staab, H.A. En route to hexaaza–kekulene. Tetrahedron Lett. 1985. 26, 6179–6182.
2. Bell, T.W.: Tidswell, J. Torands. In *Macrocycle Synthesis:* A Practical Approach; Parker. D., Ed.: Oxford University Press: Oxford, 1996: 119–143.
3. Be?:. T.W.: Firestone. A. Torands: Rigid toroidal macrocycles. Calcium sequestration by a member of this new ligand class. J. Am. Chem. Soc. 1986, 108. 8109–8111.
4. Bell, T.W.: Firestone, A.; Guzzo. F.; Hu, L.-Y. Torands: Planar polyazamacrocyclic ligands for metal ions. J. Incl. Phenom. 198'7, *5*. 149–152.
5. Bell, T.W. From Crowns to Torands and Beyond. In *Crown Compounds: Toward* Future *Applications*; Cooper. S.R.. Ed.: VCH Publishers: New York, 1992; 303–316.
6. Bell, T.W.: Cragg. P.J.; Drew, M.G.B.; Firestone. A.; Kwok. A.D.-I.; Liu. J.; Ludwig. R.T.: Papoulis, A.T. Synthesis of new torands and new uses for old torands. Pure Appl. Chem. 1993. *65*. 361–366.
7. Bell. T.W.; Heiss. A.M.: Jousselin. H.; Ludwig, R.T. Toward Columns and Channels from Torands and Molecular Coils. In *Supramolecular Stereochemistry*;

Siegel, J.S.. Ed.: Kluwer: Dordrecht. The Netherlands. 1995: 161–168.
8. Bell. T.W.: Liu. J. Torand synthesis by trimerization— New receptors for guanidinium. Angew. Chem. 1990. *102.* 931–933.
9. Bell, T.W.: Liu. J. Torand synthesis by trimerization— New receptors for guanidinium. Angew. Chem.. Int. Ed. Engl. 1990, 29. 923–925.
10. Diederich. F.; Staab, H.A. Benzenoid versus annulenoid aromaticity: Synthesis and properties of kekulene. Angew. Chem., Int. Ed. Engl. 1978. *17,* 372–374.
11. Newkome, G.R.: Lee, H.-W. 18[(2,6)Pyridino$_6$coronand-6]: "Sexipyridine". J. Am. Chem. Soc. 1983, *105.* 5956.
12. Bell. T.W.; Guzzo. F. Isolation and conformation of a fully unsaturated nitrogen analogue of 18-crown-6. J. Chem. Soc., Chem. Commun. 1986. 769–771.
13. Bell. T.W.: Jousselin. H. Expanded heterohelicenes: Molecular coils that form chiral complexes. J. Am. Chem. Soc. 1991. *113,* 6283–6284.
14. Bell, T.W.; Jousselin. H. Self-assembly of a double-helical complex of sodium. Nature 1994. *367,* 441–444.
15. Staab. H.A.; Diederich. F. Synthesis of kekulene. Chem. Ber. 1983. *116.* 3487–3503.
16. Staab. H.A.; Diederich, F.: Krieger, C.; Schweitzer, D. Molecular structure and spectroscopic properties of kekulene. Chem Ber. 1983, *116.* 3504–3512.
17. Jiao. *H.*: Schleyer, P.v.R. Is kekulene really superaromatic? Angew. Chem.. Int. Ed. Engl. 1996. *35.* 2383–2386.
18. Steiner. E.; Fowler. P.W.: Jenneskens. L.W.; Acocella, A. Visualization of counter-rotating ring currents in kekulene. J. Chem. Soc., Chem. Commun. 2001. 659–660.
19. Tatibouet. A.: Hancock. R.; Demeunynck, M.; Lhomme, J. Synthesis of 3,9,15,19,21,23-hexaazakekulene. Angew. Chem.. Int. Ed. Engl. 1997. *36.* 1190–1191.
20. Katritzky, A.R.; Marson, C.M. Synthesis of a dodecahydro-18.21-dioxoniakekulene. J. Am. Chem. Soc. 1983. *105.* 3279–3283.
21. Bell, T.W.: Sahni, S.K. Bridged Pyridine Hosts. In *Inclusion Compounds*; Atwood. J.E.. Davies, E.. MacNicol. D.. Eds.: Key Organic Host Systems. Oxford University Press: Oxford. 1991: Vol. 4. 325–390.
22. Toner, J.L. Cyclosexipyridines. Tetrahedron Lett. 1983, *24.* 2707–2710.
23. Masciello, L.; Potvin, P.G. One-pot synthesis of terpyridines and macrocyclization to C_3-symmetric cyclosexipyridines. Can. J. Chem. 2003. *81.* 209–218.
24. Bell. T.W.: Guzzo. F. Stable potassium complex of a pyridine-fused hexaaza[18]annulene. A new rival for 18-crown-6. J. Am. Chem. Soc. 1984. *106.* 6111–6112.
25. Bell. T.W.: Guzzo. F.: Drew. M.G.B. Molecular architecture 1. Sodium. potassium and strontium complexes of a hexaazamacrocycle; an 18-crown-6/torand analogue. J. Am. Chem. Soc. 1991. *113.* 3115–3122.
26. Marchetti. P.S.: Bank. S.; Bell. T.W.: Kennedy. M.A.; Ellis. P.D. Cadmium-113 NMR spectroscopy. Long bond interactions and chemical shielding in the cadmium complex of an unsaturated nitrogen analogue of 18-crown-6. J. Am. Chem. Soc. 1989. *111.* 2063–2066.
27. Bell, T.W.: Firestone. A. Construction of a soluble heptacyclic terpyridine. J. Org. Chem. 1986. *51.* 764–765.
28. Bell. T.W.; Cragg. P.J.: Firestone. A.; Kwok, A.D.-I.; Liu. J.; Ludwig, R.; Sodoma. A. Molecular architecture 2. Synthesis and ion-binding properties of heptacyclic terpyridyl molecular clefts. J. Org. Chem. 1998, *63,* 2232–2243.
29. Bell, T.W.: Cho, Y.-M.; Firestone. A.: Healy. K.: Liu. J.; Ludwig. R.: Rothenberger, S.D. 9-*n*-Butyl-1,2,3,4,5,6,7,8-octahydroacridin-4-01, In *Organic Syntheses,* Collective Volume *VIII*: Freeman. J.P., Ed.: Wiley Books: New York. 1993: 87–93.
30. Bell; T.W.: Firestone, A.: Ludwig, R. Exceptionally stable alkali metal complexes of a torand. J. Chem. Soc., Chem. Commun. 1989. 1902–1904.
31. Ait-Haddou, H.: Fontenas. C.: Bejan, E.; Daran. J.-C.; Balavoine, G.G.A. Synthesis of new soluble annelated polypyridines. Eur. J. Org. Chem. 2000, 987–994.
32. Bell. T.W.: Heiss. A.M.; Ludwig, R.T.: Xiang, C. An effective route to highly substituted pyridines. Synlett 1996. 79–81.
33. Bell, T.W.: Beckles, D.L.; Debetta. M.; Glover. B.R.; Hou. Z.: Hung, K.-Y.: Khasanov, A.B. An improved preparation of 4-aminopyrimidine-5-carboxaldehyde. Org. Prep. Proced. Int. 2002, *34.* 321–331.
34. Bell, T.W.: Cragg. P.J.; Drew. M.G.B.: Firestone, A.: Kwok, D.-I.A. Conformational preference of the torand ligand in its complexes with potassium and rubidium picrate. Angew. Chem. 1992. *104.* 319.
35. Bell, T.W.: Cragg. P.J.; Drew, M.G.B.: Firestone. A.: Kwok, D.-I.A. Conformational preference of the torand ligand in its complexes with potassium and rubidium picrate. Angew. Chem.. Int. Ed. Engl. 1992, *31.* 345–347.
36. Bell, T.W.: Cragg. P.J.; Drew. M.G.B.; Firestone. A.: Kwok, D.-I.A. A supramolecular assembly of two torands, two lithium ions and three water molecules. Angew. Chem. 1992, *104.* 321.
37. Bell. T.W.: Cragg. P.J.: Drew. M.G.B.: Firestone. A.; Kwok, D.-I.A. A supramolecular assembly of two torands, two lithium ions and three water molecules. Angew. Chem., Int. Ed. Engl. 199%.31. 348–350.
38. Boguslavsky, L.: Bell. T.W. Cation response of torand thin films at the air–water interface. Langmuir 1994. *10.* 991–993.
39. Bell, T.W.; Beckles, D.L.: Cragg. P.J.; Liu, J.: Maioriello. J.: Papoulis, A.T.: Santora. V.J. Intrinsic Chromophores and Fluorophores in Synthetic Molecular Receptors. In *Fluorescent Chemosensors* ,for *Ion and Molecule* Recognition: Czarnik, A., Ed.: ACS Books: Washington. DC. 1993: 85–103.

Tröger's Base Derivatives

Gerd Kaupp
University Oldenburg, Oldenburg, Germany

INTRODUCTION

Troger's base derivatives (5,6,11,12-tetrahydro-5,11-methanodibenzo[b,f][1,5]diazocines) are V-shaped or roof-shaped chiral bases. They are potential concave receptors. The angles between the two aryl rings vary from 92" to 104° in the crystal. Calculated ab initio DFT (density functional theory) values for isolated molecules are larger (112° for Troger's base). These compounds are frequently synthesized from primary aromatic amines and formaldehyde or in related synthetic procedures. Numerous derivatives (the Chemical Abstracts Service (CAS) Registry file contains 532 entries at present) are known, and 24 of them are well characterized by x-ray crystallography. The racemates can be optically resolved to give pure enantiomers that racemize slowly in acidic inedia via reclosure of iminium intermediates. Troger's bases can be used for optical inductions.

They were complexed with heavy-metal salts and quaternized with alkylating agents. The quaternary salts are better hosts for formation of inclusion complexes with various guests. The receptor qualities and molecular as well as chiral recognition capabilities rely on the armature function for larger clefts and for larger pockets in trögerophanes via embedding in large ring systems when they exert their armature function. This leads to biological and pharmaceutical actions that are promising for medical treatments.

Various related ring systems of the *nor*, *iso*, and *homo* types are available. and most of them show promise for applications in supramolecular chemistry. The V-shape in all of these systems is the common structural motif.

SYNTHETIC ASPECTS

Tröger's base [**I** (Fig. 1). R=CH_3, X=H] (5,6,11,12-tetrahydro-2,8-dimethyl-5,11-methanodibenzo [b,f][1,5]diazocine) was first obtained from *p*-toluidine, formaldehyde, and acid in 1887.[1] The yields are not very high in that procedure but may reach 70% under carefully selected conditions.[2] Numerous derivatives, including double Troger's bases. were prepared by this one-pot approach. however, only p-substituted aniline derivatives were successful.[3] The unsubstituted system nor-Troger's base **3** (Fig. 1) (**1**, R=X=H) required a bromine-lithium exchange of **I** (R=Br, X=H) followed by hydrolysis[4] or a four-step synthesis from anthranilic acid methylester. The last step is the reaction of the tetrahydrodibenzodiazocine 4 (Fig. 1) with formaldehyde.[5] An elegant synthesis starts with commercial 1,3,5-triphenylhexahydrotriazine (2. Fig. 1) (easily synthesized from aniline and paraformaldehyde in boiling xylene), which is dissolved in trifluoroacetic acid to provide a 90% yield of **3** in a one-pot cascade reaction.[6] Further derivatives of Tröger's base were synthesized in a corresponding manner, using triaryl-2 with free *o*-position.[6]

The intermediate labile iminium salt was isolated as its chloride in a gas–solid reaction between 2 and HCl. Water vapor produced 3 and aniline after final neutralization.[6] Racemic Troger's base derivatives can be optically resolved by chromatography at chiral stationary phases.[7] Absolute configurations of Troger's bases **1** were determined and recently corrected: (−)-(*R,R*)-**1**; (+)-(*S,S*)-**1**.[8] The configurational stability decreases upon monoalkylation.[9,10] Alkylations provide monoquaternized salts, complexations of (+) or (±)-Tröger's base with heavy metal salts (e.g., $HgBr_2$) yield 2:1 complexes that were characterized by x-ray crystal structure determination (e.g., 5. Fig. 1).[10] An enantiopure 1:1 complex **6** (Fig. 1) of Troger's base was formed with methyl rheniumtrioxide and was equally characterized by x-ray crystal structure analysis.[11] X-ray structures were reported for Troger's bases with condensed aromatics, such as **7** (Fig. 1)[12] and for the bis-Troger's base 8 (Fig. 1).[13] Highly functionalized (*R,R*)-Tröger's bases, such as 9, (Fig. I), and also their (*S,S*)-enantiomers were prepared.[14] A polycyclic Troger's base **10** (Fig. 1) is easily obtained by acid-catalyzed self-condensation of *o*-aminobenzaldehyde.[15] Several derivatives are known.

INCLUSION **REACTIONS**

Troger's bare **11** (Fig 2) includes 1.4-dioxane (1 0 33 ratio) [16] Mole versatile are inclusions of the quaternary salt 12 (Fig 2) (X=*I*) which includes toluene *p*- and *m*-xylene. p- and *m*-chlorotoluene, diethyl ketone, cyclohexanol. dioxane. and THF The characteristic ratios vary

Encyclopedia of Supramolecular Chemistry
DOI: 10.1081/E-ESMC 120019139

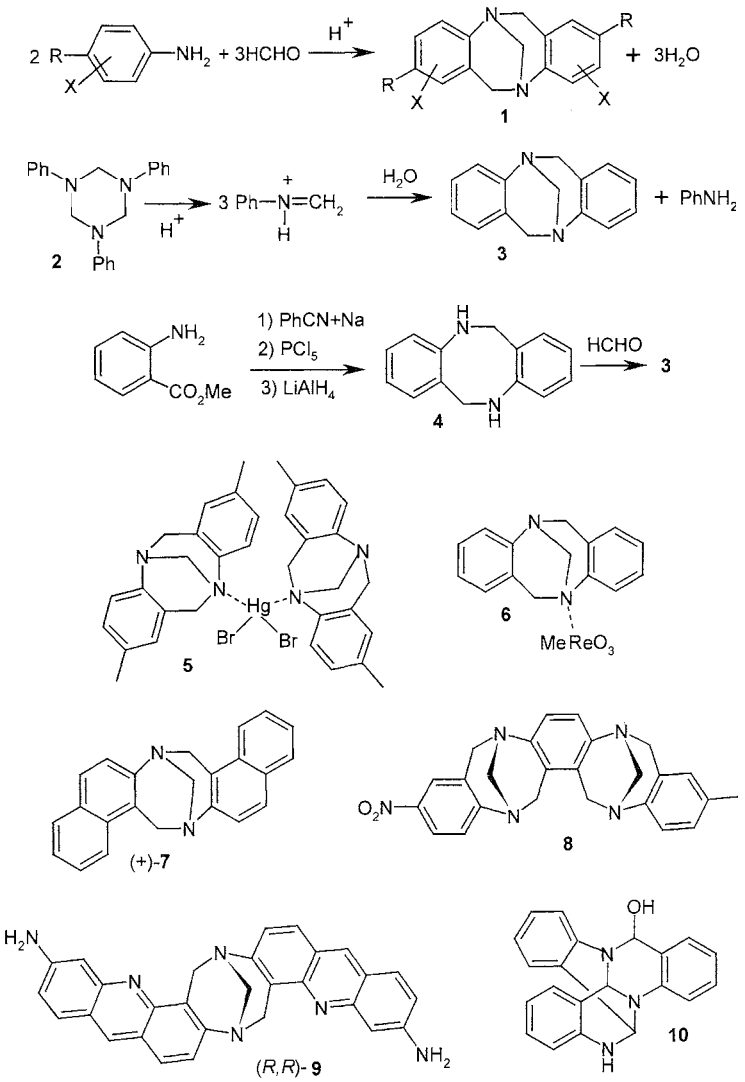

Fig. 1 Syntheses schemes for Troger's bases and some varied structures.

from 1:0.5 to 1:1.25. In all cases, water is also included and is capable of being the sole guest (1:2.25).[16]

Open-chain alcohols, cyclohexane, and p-cymene are not included. The inclusion capacity of **12** is slightly higher than that of **13a** (Fig. 2). The 1:1-competition experiments showed that p-xylene is selectively included by 12 from mixtures with benzene or toluene. whereas **13a** (*X*=*I*) selectively included benzene from these mixtures. Furthennore, 1,4-dioxane is selectively included by **13a** from mixtures with benzene or toluene.[17] The chain length of the alkyl group in the salts **13a–d** influences the stoichiometry of the inclusion, for example, with p-xylene (1:0.5, 1:1. 1:1.25, 1:0.75 host–guest ratio, respectively).[16] The quaternary salts **13a–e**, 14, and **15** (Fig. 2) exhibit a remarkable preference for aromatic guest solvents. Compound **13f** prefers less voluminous guests, including acetone, *n*-BuOH, and EtOH (not MeOH) for 1:1 incorporation into the crystal lattice.[17] Host 15 compares closely with 13f in its inclusion selectivity. Furthermore, compound **14a** corresponds to **13a** (*X*=CH_3OSO_3): phenylmethanol, 1-phenylethanol, acetophenone, mesitylene, cyclohexanone. benzaldehyde, *o*-xylene, chlorobenzene, ethylbenzene are additionally included. Structure 14b resembles **13f** in its inclusion behavior.[17] The reason for the increased enclosure capabilities of the alkylated Tröger's base cations was not investigated further. According to DFT ab initio calculations at the B3LYP/6-31G* level, the dihedral angle between the planes of the benzene rings of the cation **13a** is predicted to be 109°, smaller than for **I**

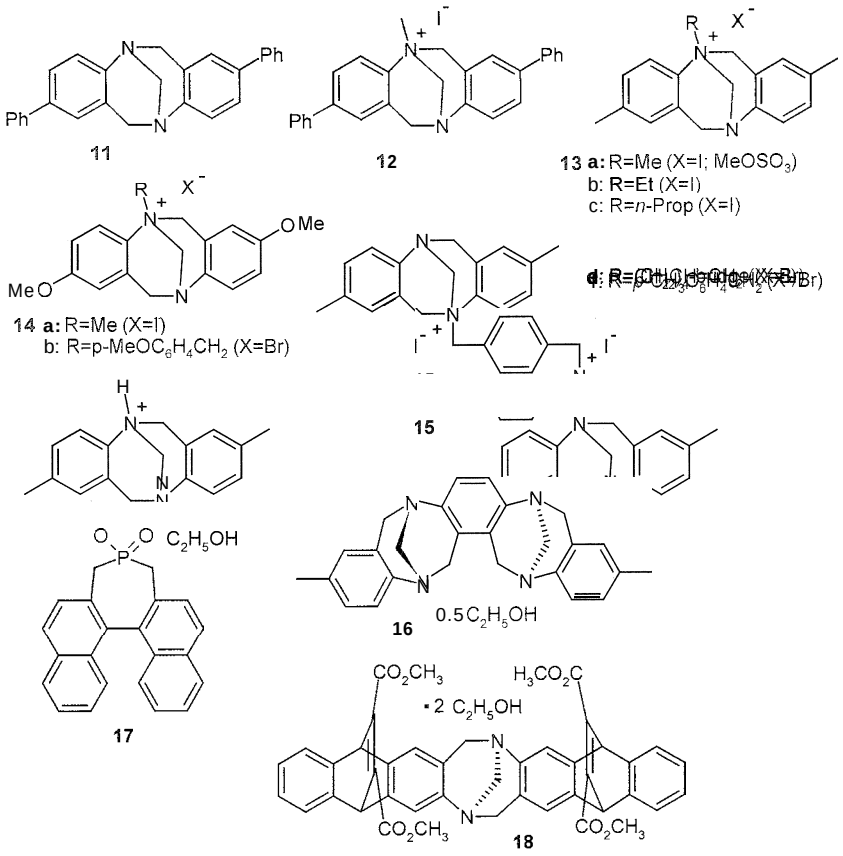

Fig. 2 Troger's base inclusion compounds

(R=CH_3, X=H), with 112°. The angles at the methano bridges are found to be 110" and 111.5°, respectively. Obviously, the inclusion lattices are further improved by alkylation. X-ray crystal analysis of **13a** (X=I)·0.5 1,4-dioxane established an enclathration-type inclusion.[17] An investigation of the molecular packing of the published structure reveals that the dioxane does not immerse into the cleft of the V-shaped host molecules **13a**. It is surrounded by two of them with their cleft open to it and two of them facing the outside of their cleft. Apparently, the V-shape may provide inclusion lattices that accommodate the guest, but the cleft is not the site where the guest resides. This important question was addressed further. The resolved *exo-endo*-bis-Tröger's base inclusion compound 16 (Fig. 2) packs in such a way that both of the U-shaped clefts go in the clefts of the next molecules: every two molecules are intercalated with each other.[15] The ethanol molecules are situated between the rows according to the published crystal structure. The salt 17 (Fig. 2) (inclusion of EtOH) has the counteranion out of ihe cleft, a peripheral aryl ring of the bisnaphthyl moiety covers the cleft of the protonated Troger's base, and ethanol is hydrogen-bonded to the anion at the backside of the cleft, according to the reported crystal structure.[18] A much larger U-shaped cleft (8–9 Å wide. 5–7 Å deep) is formed in the inclusion compound 18 (Fig. 2).[19] Two ethanol molecules are located within the cleft defined by the esters, with the Troger's base moiety at the bottom. The guest molecules are relatively disordered. They are held by hydrogen bonds to the ester groups and are clathrated in a molecular chamber, the fourth side of which is defined by the next molecule in the stack.

The V-motif is certainly used in the herringbone stacking of the crystalline Troger's base (1, R=CH_3, X=H) at a distance of ca. 5.5 Å.[20] Further Tröger's base derivatives use the same stacking motif (for example, **11**).[16] An U-inside-inverted-U-packing requires the much larger U-shaped cleft in the *endo-endo*-bis-Tröger's base **8**.

It could not be shown that the Troger's base cleft is used by included guest molecules. Rather, the clefted molecules are able to create lattices that can accomodate guest molecules, in particular. when they are protonated or alkylated.

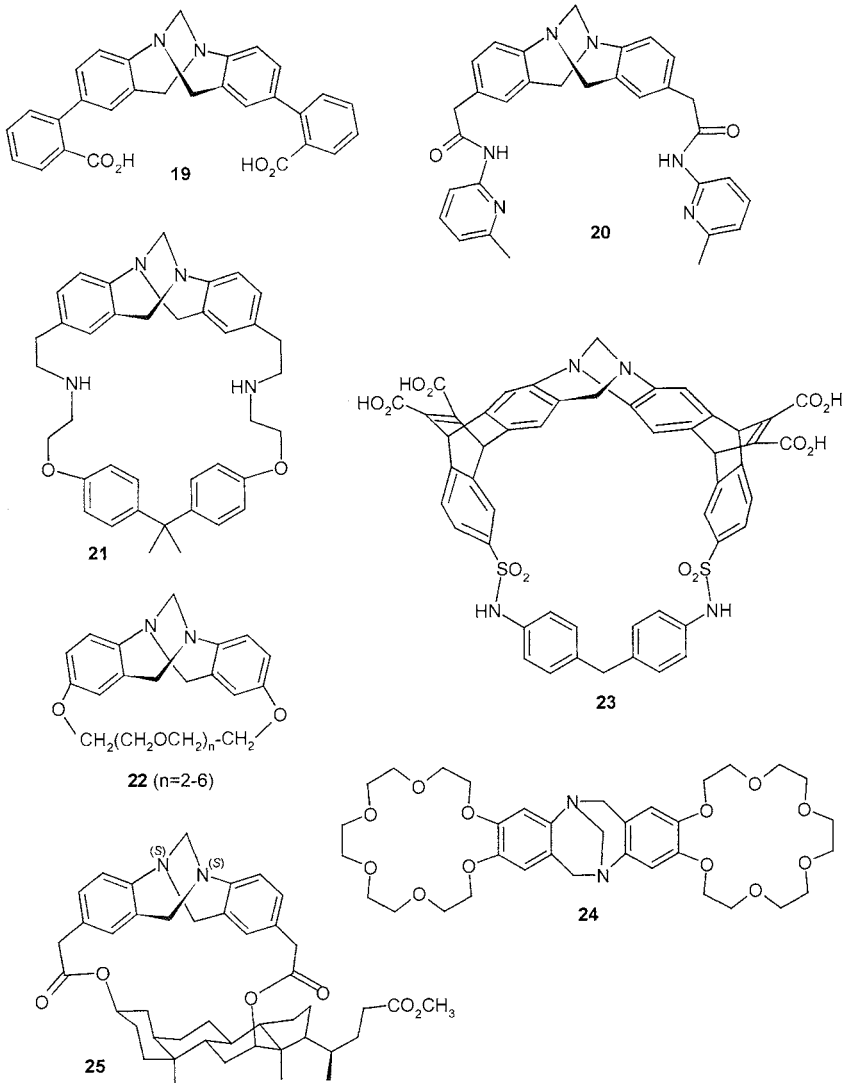

Fig. 3 Troger's base as an armature for systems with molecular recognition.

MOLECULAR RECOGNITION IN SELF-ASSEMBLING SYSTEMS

The cleft of Troger's bases provides only limited success in supramolecular applications, however, their well-defined structures were used as armatures for aligning further functionality in order to provide receptors for molecular and chiral recognition. That goal was achieved with scaffold-type derivatives 19, 20, 24 (cf. 18) and by embedding Troger's bases in macrocycles that were called trogerophanes (21–23, 25) (Fig. 3).

Scaffold 19 with two carboxyl groups intersecting at an angle of 120" forms hydrogen-bonded complexes by host–guest interaction with weak bases and exhibits large association constants (K).[21,22] Thus. 2-aminopyrimidine (K=2600 M^{-1}), dimethyleneurea (K=44,000 M^{-1}), trimethyleneurea (K=33,000 M^{-1}), 2-imidazolidone (K= 21.000 M^{-1}), biotin methyl ester (K=17,000 M^{-1}), and 9-ethyladenine (K=45,000 M^{-1}) are all bound in $CDCl_3$, as determined by ^{1}H-NMR titration. Scaffold 20 is an artificial receptor for dicarboxylic acids by virtue of selective binding.[23]

The trogerophane **21** forms association complexes with various phenols and p-toluenesulfonic acid.[3] It forms complexes with benzenoid substrates in acidic aqueous solutions. The crown ether trogerophanes 22 do not include solvent molecules for n=1–3. The complexation of LiSCN (not NaSCN, KSCN) with 22 (n=3) is weak. However, the larger rings in 22 (n=4–6) exhibit supramolecular cation-binding properties, as was shown for

NH_4^+, K^+, Na^+, Cs^+, Li^+ using Cram's picrate extraction method.[24]

The large trogerophane 23 is particularly versatile for molecular recognition.[21,22] It complexes *trans-tert*-butylcyclohexanol (K=8600 M^{-1}) and much more efficiently *cis-tert*-butylcyclohexanol (K=41,000 M^{-1}) from aqueous (D_2O) phosphate buffer. The enantiopure receptor 23 (tetraammonium salt in D_2O) binds cyclohexanoid and alicyclic alkanes, stereoisomeric menthols, diastereomeric cyclohexane derivatives, and steroids. Furthermore. it is a chiral shift reagent. The differentiation of (−)-menthol (K=2500 M^{-1}) and (+)-menthol (K=2000 M^{-1}) is not pronounced. but (+)-isomenthol (K=1000 M^{-1}) is disfavored. The axial substituent is less welcome in the pocket.[25] Two crown-6 moieties in 24 recognize primary bisammoniuin salts, and the enantiopure Troger's base 24 discriminates *D*- and *L*-lysine.[26] Even larger and more rigid clefts were constructed with Troger's base by [*a*,*b*]- and [*e*,*b*]-condensation to two pyrazino[*b*,*a*]porphyrins. Thus, a templated assembly by superstructure encapsulation is known.[27] The dendrimer *N*,*N*,*N*′,*N*′-tetra-(3-aminopropyl)-1,4-diaminobutane coordinates with all four of its primary amino groups to two clefted Troger's base molecular receptors with two pyrazino[*b*,*a*]-tetra-(3,5-di-*tert*-butylphenyl)-zincporphyrin moieties each condensed to them. The binding sites are at the zinc atoms of the four assembled porphyrins. and a spherical supramolecular capsule results.

The trogerophane based on the deoxycholic acid chiral template in 25 [and in its (*R*,*R*)-epimer] was used for an asymmetric synthesis of the enantiopure Tröger's base analogues after hydrolysis.[28,29] As the two hydroxyl groups of deoxycholic acid have different reactivities for esterification, unsymmetric Troger's bases could be asymmetrically synthesized as well.

OPTICAL INDUCTION BY TRÖGER'S BASES

Resolved Troger's base (**1**) interacts with chiral alcohols as a chiral NMR shift reagent.[21,22] It is also possible to use enantiopure Troger's bases for chiral resolution and chiral induction. When **1** (*R*=CH_3, *X*=H) was imprinted in methacrylic acid–ethylene glycol dimethylacrylate copolymers; enantioselectivity of the synthetic receptors was observed in high-performance liquid chromatography (HPEC) experiments with the polymer as stationary phase.[30] A (+)-Tröger's base. when used as preadsorbed chiral modifier of a Pt/alumina catalyst; provided enantioselective hydrogenation of ethyl pyruvate (65% ee in AcOH).[31] The application of (+)-(*S*,*S*)-Tröger's base (**1**) as ligand in 1,4-additions of lithium aryls to α,β-unsaturated tert-butyl esters provided ee-values up to 57% that compare to those obtained with (−)-sparteine (**37**, below).[32] The (+)-(*S*,*S*)-Tröger's base (**1**) (*R*=CH_3, *X*=H) is a relatively poor chiral ligand in the asymmetric addition of diethylzinc to benzaldehydes.[33] However, the enantiomeric excesses were as high as 86% if 5% of 5*S*.11*S*-6-exomethylene-**1** was applied.

BIOLOGICAL AND PHARMACEUTICAL APPLICATIONS OF TRÖGER'S BASE DERIVATIVES

Troger's base moieties are attractive pharmacological groups. The interaction of drugs with living materials is of a supramolecular nature, and interactions with DNA are particularly important. Thus; compound (−)-**9**, which contains two proflavine units, binds in enantio- and sequence-specific fashions to DNase I. Conversely, (+)-**9** interacts poorly with DNA in a nonsequence-selective fashion.[14] The (−)-enantiomer preferentially recognizes certain DNA sequences containing both A·T and G·C base pairs, such as the motifs 5′-GTT·AAC and 5′-ATGA·TCAT. Similarly, the asymmetrical compound 26 (Fig. 4) containing a proflavine unit and a phenanthroline unit intercalates DNA topoisomerase I, as indicated by linear and circular dichroism experiments and biochemical assay.[34] The data are compatible with a model in which the proflavine moiety intercalates between DNA base pairs, and the phenanthroline moiety occupies the DNA groove. Cleavage experiments revealed the sequence preference of the hybrid ligand, and a well-resolved footprint was detected at a site encoinpassing two adjacent 5'-GTC.5-GAC triplets. The chiral *bis*-(1,10-phenanthroline) Troger's base copper(I) complex **27** (Fig. 4) interacts with DNA and causes strand scission as determined by the almost complete conversion of the covalently closed circular pVC18 plasmid to open circular DNA.[35]

Compound 28 (Fig. 4) is an effective inhibitor of the enzyme thromboxane A_2 (T x A_2) synthase, with an ED_{50} of 30 ng ml^{-1} in a specified in vitro assay.[36]

The trogerophane 29 (Fig. 4) was synthesized for treatment of malignant tumors. It restores c-fos expression disorder in neuroblastoma cells.[37]

The known data indicate that further applications of Troger's bases in pharmacology and medicine are to be expected. However. this prediction is also valid for related clefted systems.

RELATED SYSTEMS WITH CLEFT STRUCTURE

The 5,6,11,12-tetrahydrodibenzo[*b*,*f*][1,5]diazocines such as 4 become Troger's-base-like if they are complexed

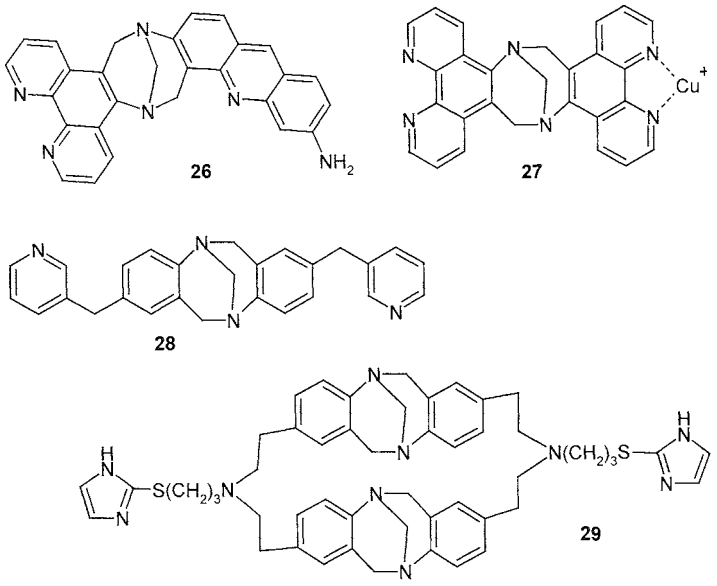

Fig. 4 Tröger's bases with biological and pharmacological action (see also 9).

with heavy-metal salts. The inclusion compound 30 (Fig. 5) is a well-studied example.[38] The methano bridge is formally replaced by the metal salt.

In the *pseudo*-Tröger's bases **31**[39] and ***32*** (Fig. 5),[40] the methano or imino bridge connects the carbons instead of the niirogens of the dibenzo[*b*,*f*][1,5]diazocine. According to DFT B3LYP/6-31G* calculations, the molecular skeleton of 31 (totally unsubstituted) is more stable than compound **3** by 13.6 kcal mol^{-1}. Seven derivatives of 31 were prepared from p-methylamino-benzaldehyde, $POCl_3$, and diethylmalonate or other reagents with two α-H atoms next to an activating heterocycle. The cleft

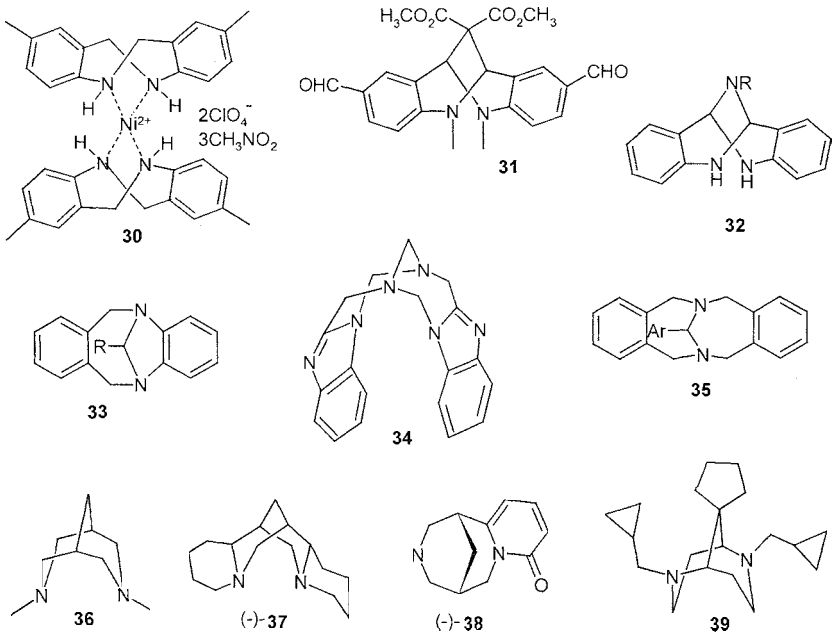

Fig. 5 Clefted molecular systems related to Tröger's base

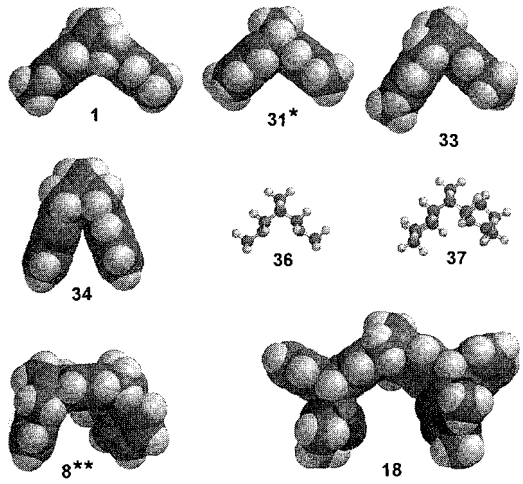

Fig. 6 Visualization of clefts in Troger's base and related systems. (* CH_3 instead of *CHO*, CH_3, and CO_2CH_3 replaced by H; ** NO_2 and CH_3 replaced by *H*.)

shapes (calculated angle between the aryl rings: 109°) do not considerably change with respect to Troger's base. and inclusion of water or acetonitrile occurs.

Compound 32 has an imino bridge instead of the methano bridge and is synthesized by reacting a primary aromatic or benzylic amine with o-(triphenylphosphoranylidene) aminobenzaldehyde. Isomers 33 (Fig. 5) of Troger's bases have long been known.[''] They are prepared from 5,6,11,12-tetrahydrodibenzo[*b*,*f*][1,4] diazocine and formaldehyde. Compound 33 (*R*=H) is 10.1 kcal mol^{-1} less stable than *nor*-Tröger's base (3), according to ab initio DFT calculations at the B3LYP/6-31G* level. The reactions of compounds 33 proved "comparable" to those of 3. even though the calculated cleft angle between the aromatic rings is considerably smaller (81° versus 112°), which leads to a considerably sharper cleft (see Fig. 6).

The homologous Troger's base analogue 34 (Fig. 5) is selectively available in a one-pot synthesis from 2-chloromethylbenzimidazole and hexamethylenetetramine with a 56% yield.[42] The isomeric products of the multimethenylation in the absence of template catalysts are not formed under these conditions.[42] The clefted conformer of the bridged tetrazecine 34 is the most stable (endo-endo-34 is 5.4 or 14.2 kcal mol^{-1} better than exo-rndo- or *exo-exo*-34. respectively) according to ab initio DFT calculations at the B3LYP/6-31G* level. The cleft is very narrow in this case (40°), and more detailed investigations of the supramolecular properties of 34 are clearly indicated. Two related benzo derivatives 35 (Fig. 5) were reported.[43] They were synthesized from 5,6,7,12,13,14-hexahydrodibenzo[*c*,*h*][1,6]diazecine and aromatic aldehydes.

Finally. the saturated bispidines 36 and (−)-sparteine 34 (Fig. 5) exhibit interesting clefts for supramolecular use. Bispidines form metal salt complexes. The *N,N'*-dimethylbispidine (36) has as its most stable conformer the twin-chair V-shape, according to ab initio DFT calculations at the B3LYP/6-31G* level (5.7 or 8.4 kcal mol^{-1} better than boat-chair or twin-boat conformers, respectively).

This preference is not overridden by slight differences in the aqueous solvation energy. The bispidine moiety was combined with crown-ether functionality to form a molecular cavity (19 ring members, including the cleft of bispidine, two *N* and four *O*).[44] Sparteine (37) is less stable than its 11β-diastereomer genisteine (by 9.3 kcal mol^{-1} according to B3LYP/6-31G* calculations). The (−)-sparteine is V-shaped (Fig. 6) and forms versatile chiral bases with lithium alkyls for enantioselective syntheses.[45] These reactions are usually formulated via double coordination of the Li in the cleft of the (−)-sparteine conformer 37. Similarly, bidentate metal salt complexes of (−)-sparteine form readily. The complexing nitrogens in the clefts of the pharmaceuticals (−)-cytisine (38) and tedisamil **(39)** (Fig. 5) (with an isomeric ring system) are certainly involved in the blocking and release of calcium and potassium cations. The (−)-cytisin (38) is a neuronal nicotinic acetylcholine receptor. It activates $\alpha 3\beta 4$ receptors and blocks $\alpha 3\beta 2$ receptors.[46] Tedisamil (39) is a new bradycardic agent that exerts antiischemic and antiarrythmic effects by blockading the different cardiac and vascular K^+ currents.['']

CONCLUSION

The unifying structural motif in this article is the molecular cleft. Clefts may be wide or sharp. If they are formed by (nearly) planar groups in molecules of C2 symmetry, they are most easily characterized by the dihedral angle between the planes. Space-filling models indicate the amount of free space. Space-filling models of ab initio DFT B3LYP/6-31G* calculations are contained in Fig. 6, as experimental values are only available for some of them. Both cleft arms are exactly vertical on the image plane in Tröger's base **(I,** *R*=CH_3, *X*=**H)**, pseudo-Troger's base (31. but CH_3 instead of CHO: CH_3 and CO_2CH_3 replaced by H). iso-Trogers base (33, *R*=H), and the 10-ring compound 34. The alicyclic clefts of dimethylbispidine (36) and (−)-sparteine (34) are better depicted in ball-and-spoke representation. In the *bis*-Troger's base 8 (NO_2 and CH_3 replaced by H). two of the aromatic rings are vertical on the image plane, and the five-clefts compound 18 (semiempirical PM3 calculation)

has the aryl rings for one dibenzo[2.2.2]cyclooctatriene moiety and both olefinic bridges vertical.

A wide cleft (112°; isolated molecule) is present in **I**. It is not much different from the upper dibenzobicyclo[2.2.2]octatriene clefts in **18** (DFT angle for the main cleft of dibenzobicyclo[2.2.2]octatriene: 118°). The cleft shape does not change much in **31** (109°). However. 33 has a considerably sharper cleft (81°), and 34 is very sharp (40°). The clefts of 36 and **37** are of different character, because their nitrogens (distances 2.958 and 3.054 Å, respectively) are not inaccessibly shielded. The nitrogen shielding in Troger-type clefts leads to outside protonation. alkylation. and heavy-metal salt complexation (5, 6, 17). The cleft angles determine the size, but included organic guest molecules profit only from the crystal lattices. Inclusions in 8 profit from a large double cleft. The huge cleft of 18 is created by substitution, and the Tröger's base moiety serves primarily as armature. as in the trogerophanes (21–23 and **25**), with their large rings and pockets. Only these or similar elaborate systems are suitable for molecular and chiral recognition. The supramolecular properties of bispidine and sparteine are of different character. The field is far from being exhausted.

ARTICLES OF FURTHER INTEREST

Cavitands, p. 219
Chiral Guest Recognition, p. 236
Chiral Induction, p. *245*
Concave Reagents, p. 311
Crown Ethers, p. 326
Cyclophanes: Endoacidic, Endobasic, and Endolipophilic Cavities, p. 424
Inclusion Compounds: Selectivity, Thermal Stability, and Kinetics, p. 696
Molecular- Clefts and Tweezers, p. *887*
Podands, p. 1*106*
Protonated Aza-Macrocycles for Anion Complexation, p. *1170*
Self-Assembling Capsules, p. 1231

REFERENCES

1. Triiger. J. Ueber einige mittelst nascirenden Formaldehydes entstehende Basen. J. Prakt. Chem. N.F. **1887**, 36. 225–235.
2. Baring, M. Preparation of 5.11-endomethylenetetrahydrophenhomazines and 5-alkyltetrahydrophenhomazines. Helv. Chim. Acta **1963**. 46. 2970–2982.
3. Sucholeiki, I.; Lynch, V.: Phan, L.: Wilcox. C.S. Chemistry of synthetic receptors and functional group arrays. 7. Molecular armatures. Synthesis and structure of Troger's base analogs derived from 4-, 2.4-, 3,4-, and 2.4,5-substituted aniline derivatives. J. Org. Chem. 1998. *53*, 98–104.
4. Jensen. J.; Tejler. J.: Wärnmark, K. General protocols for the synthesis of C2-symmetric and asymmetric 2.8-disubstituted analogues of Troeger's base via efficient bromine-lithium exchanges of 2.8-dibromo-6H.12H-5.11-methanodibenzo[b,f][1,5]diazocine. J. Org. Chem. **2002**, *67*, 6008–6014.
5. Cooper. F.C.; Partridge. M.W. Cyclic amidines. IV. 5,6,11,12-Tetrahydro-5,11-endomethylenephenhomazine and Tröger's base. J. Chem. Soc. **1955**. 991–994.
6. Kaupp, G.; Schmeyers, J.: Boy, J. Iminium salts in solid-state syntheses giving 100% yield. J. Prakt. Chem. 2000, 342, 269–280.
7. Prelog, V.: Wieland. P. The resolution of Troger's base into its optical antipodes. a note on the stereochemistry of trivalent nitrogen. Helv. Chim. Acta 1944.27. 1127–1133.
8. Aaniouche, A.: Devlin, F.J.: Stephens. P.J. Structure, vibrational absorption and circular dichroism spectra. and absolute configuration of Troger's base. J. Am. Chem. Soc. 2000, *122*, 2346–2354.
9. Trapp, O.: Trapp. G.: Kong. J.: Hahn, U.: Vogtle, F.; Schurig. V. Probing the stereointegrity of Tröger's base—A dynamic electrokinetic chromatographic study. Chem. Eur. J. 2002. *8*. 3629–3634.
10. Lenev, D.A.; Lyssenko, K.A.; Kostyanovsky, R.G. Asymmetric nitrogen 82. Tröger base: Study of its complex with $HgBr_2$ and its methiodide. Russ. Chem. Bull. (Transl. from Izvestija Akad. Nauk. SSSR, Ser. Khim.) 2000; 49. 1241–1249.
11. Herrmann. W.A.: Kuehn. F.E.; Mattner. M.R.: Artus. G.R.J.: Geisberger. M.R.: Con-eia. J.D.G. Multiple bonds between transition metals and main-group elements. 163. Nitrogen-donor adducts of organorhenium(VII) oxides: Structural and catalytic aspects. J. Organomet. Chem. **1997**. 538. 203–209.
12. Talas, E.: Margitfalvi, J.: Machytka. D.: Czugler. M. Synthesis and resolution of naphthyl-Tröger's base. Tetrahedron: Asymmetry **1998**. 9, 4151–4156.
13. Pardo, C.: Sesmilo. E.; Gutierrez-Puebla. E.: Monge, A.; Elguero, J.: Frucliier. A. New chiral molecular tweezers with a bis-Troger's base skeleton. J. Org. Chem. **2001**. 66. 1607–1611.
14. Tatibouet, A.: Demeunynck. M.: Andraud, C.; Collet. A.; Lhomme. J. Synthesis and study of an acridine substituted Tröger's base: Preferential binding of the (−)-isomerto B-DNA. J. Chem. Soc. Commun. 1999. 161–162.
15. McGeachin. S.G. The structures of two self-condensation products from o-aminobenzaldehyde. Can. J. Chem. 1966. 44. 2323–2328.
16. Bond. D.R.; Scott. J.L. Clathrate formation with Troger base analogs. J. Chem. Soc.. Perkin Trans., II 1991. 47–51.
17. Weber. E.; Müller. U.: Worsch, D.; Vögtle, F.: Will, 6.: Kirfel. A. Quaternary Tröger bases as new inclusion hosts: The first x-ray structures of a Triiger base and of a dioxane clathrate. J. Chem. Soc.. Chem. Commun. **1985**. 1578–1580.

18. Wilen. S.H.: Qi, J.Z.: Williard, P.G. Resolution, asymmetric transformation. and configuration of Troger's base. Application of Troger's base as a chiral solvating agent. J. Org. Chem. 1991, *56*, 485–487.
19. Wilcox, C.S.; Greer, L.M.: Lynch. V. Synthesis of chiral molecular clefts. New armatures for biornimetic systems. J. Am. Chem. Soc. 1984. 109. 1865–1867.
20. Larson. S.B.: Wilcox. C.S. Structure of 5,11-methano-2,8-dimethyl-5,6,11,12-tetrahydrodibenzo[b,f][1,5]diazocine (Troger's base) at 163 K. Acta Crystallogr.. Sect. C 1986. 42. 224–227.
21. Wilcox. C.S.; Adrian. J.C.; Webb. T.H.; Zawacki. F.J. Chemistry of synthetic receptors and functional group arrays. 18. Approaches to quantitative supramolecular chemistry. Hydrogen-bond-based niolecular recognition phenomena and sigmoidal behavior in multicomponent mixtures. J. Am. Chem. Soc. 1992. 114. 10189–10197.
22. Adrian. J.C.: Wilcox, C.S. Orderly functional group dyads. Recognition of biotin and adenine derivatives by a new synthetic host. J. Am. Chem. Soc. 1989. **111,** 8055–8057.
23. Goswami, S.; Chosh. K.: Dasgupta. S. Troger's base molecular scaffolds in dicarboxylic acid recognition. J. Org. Chern. 2000, 65. 1907–1914.
24. Manjula. A.: Nagarajan, M. New supramolecular hosts: Synthesis and cation binding studies of novel Troger's base-crown ether composites. Tetrahedron 1997. *53*. 11859–11868.
25. Wilcox. C.S.: Webb. T.H.: Zawacki, F.J.; Glagovich. N. Chemistry of synthetic receptors and functional group arrays. 21. Selectivity in molecular recognition of steroids, alkanes and alicyclic substrates in aqueous media. Supramol. Chem. 1993. 1. 129–137.
26. Hansson, A.P.: Norrby, P.O.: Warnmark. K. A bis(crown-ether) analog of Troger's base: Recognition of achiral and chiral primary bisammonium salts. Tetrahedron Lett. 1998, 39. 4565–4568.
27. Reek, J.N.H.: Schenning, A.P.H.J.: Bosman. A.W.: Meijer. E.W.: Crossley. M.J. Templated assembly of a molecular capsule. J. Chem. Soc. Commun. 1998, 11–12.
28. Maitra. U.: Bag. B.G.: Rao. P.: Powell. D. Bile acids in asymmetric synthesis. 5. Asymmetric synthesis of steroidal Tröger's base analogs. X-ray molecular structure of methyl 3α,12α-{6H,12H-5.11-methanodibenzo[b,f][1,5]diazocine-2,8-bisacetoxy}-5β-cholan-24-oate. J. Chem. Soc., Perkin Trans. 1 1995, 2049–2507.
29. Maitra, U.: Bag. B.G.; Rao. P.: Powell. D. First asymmetric synthesis of the Troger's base unit on a chiral template. J. Org. Chem. 1992, *57*. 6979–6981.
30. Adbo. *K.:* Andersson. H.S.; Ankarloo. J.; Karlsson. J.G.: Norell, M.C.: Olofsson, L.; Svenson. J.: Ortegren. U.: Nicholls, I.A. Enantioselective Troger's base synthetic receptors. Bioorganic Chem. 1999. 27. 363–371.
31. Minder. B.: Schuerch, M.: Mallat, T.; Baiker, A. Chiral nitrogen compounds as new modifiers for the enantioselective hydrogenation of ethyl pyruvate. Catal. Letters 1995. *31*, 143–151.
32. Xu, F.; Tillyer, R.D.: Tschaen, D.M.: Crabowski, E.J.J.; Reider. P.J. Enantioselective 1.4-addition of aryllithium reagents to α,β-unsaturated tert-butyl esters in the presence of chiral additives. Tetrahedron: Asymmetry 1998. 9. 1651–1655.
33. Harmata, M.; Kahraman. M. Congeners of Troger's base chiral ligands. Tetrahedron: Asymmetry 2000, 11. 2875–2879.
34. Baldeyrou, B.; Tardy. C.: Bailly. C.: Colson, P.: Houssier, C.: Charmantray, F.; Demeunynck, M. Synthesis and DNA interaction of a mixed proflavine-phenanthroline Troger base. Eur. J. Med. Chem. 2002. *37*. 315–322.
35. Yashima. E.: Akashi, M.: Miyauchi, N. Chiral bis(1,10-phenanthroline) with Troger's base skeleton. Synthesis and interaction with DNA. Chem. Lett. 1991. 1017–1020.
36. Johnson. R.A.; Gorman. R.R.: Wnuk. R.J.: Crittenden. N.J.; Aiken. J.W. Troger's base. An alternate synthesis and a structural analog with thromboxane A2 synthetase inhibitory activity. J. Med. Chem. 1993. *36*, 3202–3206.
37. Suzuki. T.: Miyake, M. Preparation of Cyclophane Derivative for Treatment of Malignant Tumor. JP Patent 2003073379. Chem. Abstr. 2003, *38*. 221609.
38. Hussain, M.S. Structure of bis(5,6,11,12-tetrahydro-2,8-dimethylphenhomazine)nickel(II) perchlorate. J. Cheni. Soc., Dalton Trans. 1982. 2545–2547.
39. Brack. A. Bicyclic Tetrahydroquinolinecarboxaldehydes and Their Use. Ger. Offen. DE 82-3218202. Cheni. Abstr. 1984. 101. 7135 (to Bayer, A.G.).
40. Molina, P.; Arques. A.; Tarraga, A.; Del Rosario Obon, M.: Foces-Foces, C.: Jagerovic. N.: Elguero. J. Synthesis and x-ray crystallographic study of 6,12-epiiminodibenzo[b,f][1,5]diazocines. Tetrahedron 1998. 54. 997–1004.
41. Yale, H.L.: Spitzmiller. E.R. 5,12-Diacylated-5,6,11,12-tetrahydrodibenzo[b,f][1,4]diazocines and related compounds. J. Heterocycl. Chern. 1976, 13. 443–448.
42. Kaupp, G.: Sailer. K. Hexaazapolycycles by selective multimethylenations with dichloromethane and base or with hexamethylenetetramine. J. Prakt. Chem. 1996, *338*, 47–50.
43. Maki, E.: Pihlaja. M.: Kleinpeter, E.: Hartmann. J.; Schroth, W. Electron impact ionization mass spectra of some 4,9-dihetero-(X,X)-cyclodeca-1,6-dienes: Mono- and di-benzo analogs. Acta Chem. Scand. 1994. *48*. 319–323.
44. Carcanague, D.R.; Knobler, C.B.; Diedrich. F. Water-soluble cyclophane receptors with convergent functional groups. J. Am. Chem. Soc. 1992. 114. 1515–1517.
45. Hoppe, D.: Hense. T. Enantioselective synthesis with lithium/(−)-sparteine carbanion pairs. Angew. Chern.. Int. Ed. Engl. 1997, 36. 2282–2316.
46. Colquhoun, L.M.: Patrick. J.W. α3, P2. and β4 form heterotrimeric neuronal nicotinic acetylcholine receptors in Xenopus oocytes. J. Neurochem. 1997. 69, 2355–2362.
47. Mitrovic. V.; Oehm, E.: Thormann. J.; Pitschner. H.: Haberbosch. W. Comparison of the potassium channel blocker tedisamil with the β-adrenoceptor blocker esmolol and the calcium antagonist gallopamil in patients with coronary artery disease. Clin. Cardiol. 1998. *21*. 492–502.

Unimolecular Electronics and Unimolecular Rectifiers

Robert M. Metzger
The University of Alabama, Tuscaloosa, Alabama, U.S.A.

INTRODUCTION

"Molecular electronics" (ME) (*sensu stricto*), or "molecular-scale electronics" or "unimolecular electronics" (UE) is the study of electrical and electronic processes measured or controlled on a molecular scale or on the nanometer scale.[1,2] A wider definition of molecular electronics (*sensu lato*), or "molecule-based electronics" encompasses electronic p ocesses by molecular assemblies of any scale, including macroscopic crystals and conducting polymers.[1,3] This article deals with UE and focuses on electrical conduction (asymmetric or not), through single molecules or through a monolayer of molecules measured in parallel.

In the 1950s, ME was discussed in the U.S. Defense Department and was presaged by Richard P. Feynman's visionary comment "there is plenty of room at the bottom."[4]

THE AVIRAM–RATNER ANSATZ, THE FIRST UE PROPOSAL

The first concrete proposal for UE was the 1974 Ansatz by Ari Aviram and Mark A. Ratner that a rectifier of electrical current could be achieved with a single molecule.[5] A rectifier is an electronic device through which electrical current is conducted asymmetrically, i.e., preferentially from left to right. rather than vice versa: the IV curve is asymmetrical with voltage.

Since the late 1940s, the solid-state inorganic rectifier has consisted of a pn junction, where the p region is a semiconducting Si or Ge crystal "doped" with a small excess of substitutional impurities (electron-poor group-3 elements such as Al, Ga, In) that create a small excess of mobile "holes" (lack of electrons). The n region is a Si or Ge crystal doped with a small percentage of electron-rich group-5 atoms (N. P. As, etc.), creating a small excess of mobile electrons. Such *pn* rectifiers. where electrons flow preferentially from the *n* region to the p region, are used in electrical circuits and in integrated circuits.

Aviram and Ratner proposed that a unimolecular rectifier be a single D-σ-A molecule, where D is a good one-electron donor with relatively first low ionization potential, σ is some saturated covalent "sigma" bridge, and A is a good one-electron acceptor with relatively high electron affinity. when this molecule is placed between two appropriate metal contacts M_1 and M_2.[5] The bridge σ decouples the donor moiety D from the acceptor moiety A. If the decoupling between D and A is complete, then intramolecular electron transfer becomes impossible. The molecular ground state of D-o-A has a low dipole moment and can be written as D^0-σ-A^0, while the first excited state is much more polar, and is the zwitterionic state D^+-σ-A^-.

The Aviram–Ratner mechanism consists of two resonant electron transfers across metal–organic interfaces:

$$M_1 + D^0\text{-}\sigma\text{-}A^0 + M_2 \rightarrow M_1^- + D^+\text{-}\sigma\text{-}A^0 + M_2 \quad (1)$$

$$M_1^- + D^+\text{-}\sigma\text{-}A^0 + M_2 \rightarrow M_1^- + D^+\text{-}\sigma\text{-}A^- + M_2^+ \quad (2)$$

followed by an inelastic downhill intramolecular electron transfer:

$$M_1^- + D^+\text{-}\sigma\text{-}A^- + M_2^+ \rightarrow M_1^- + D^0\text{-}\sigma\text{-}A^0 + M_2^+ \quad (3)$$

which moves one electron from M_2 to M_1.[5] This electron transfer is possible if the molecule has reasonable oscillator strength in an intramolecular optical intervalence transfer (IVT) band.

The Aviram–Ratner proposal involves an electronic transition.[5] which is inherently fast (*ps* to ns), compared with translations, conformational transitions, or molecular rearrangements.

PHYSISORPTION (LANGMUIR–BLODGETT, LB) VERSUS CHEMISORPTION (""SELF-ASSEMBLY")

Aviram and Ratner did not specify how such a device could be interrogated electrically. There are two choices. The Langmuir–Blodgett (LB) technique allows for the assembly of one-molecule-thick ("monolayer") films or of several-molecule-thick films (multilayers):[6,7] the assembly onto surfaces by physisorption has the advantage that the transfer of ainphiphilic molecules from the

Encyclopedia of Supramolecular Chemistry
DOI 10.1081/E.ESMC.120012788

air–water interface to suitable solid substrate could be quantitative: the disadvantage is the weakness of the binding of these layers to the substrate. (The transfer ratio is the area covered by the LB monolayer on the solid substrate, divided by the area lost from the monolayer at the air–water interface.)

A competing technique is the formation of chemisorptive monolayers that are covalently bonded to the substrate:"' this is now called "self-assembly."[9] Self-assembly has the advantage of strong binding, but its disadvantage is that the surface coverage by a self-assembled rnonolayer (SAM) is rarely quantitative and is difficult to measure.

EARLY INTEREST IN ME AND UE

ME was launched with some fanfare,[10–12] then languished for several years. Recently. UE registered significant results, thanks to advances in how to place electrodes above LB monolayers of organic molecules without "frying them." and to studies of SAMs (thiols covalently bonded to gold) by either a scanning tunneling microscopy (STM) tip. by conducting-tip atomic force microscopy (AFM), or by gold "brealc junctions."[13] The interest in UE is due to projections that the technological progress in ultraminiaturization of Si-based integrated circuits. which makes computers faster as the distance ("design rule") between individual components shrinks (Gordon E. Moore's law[14]). may not reach nanoscopic dimensions. At design rules of 3 nm, one-molecule electronic devices (resistors. capacitors. rectifiers, and amplifiers) may present a significant technological alternative.

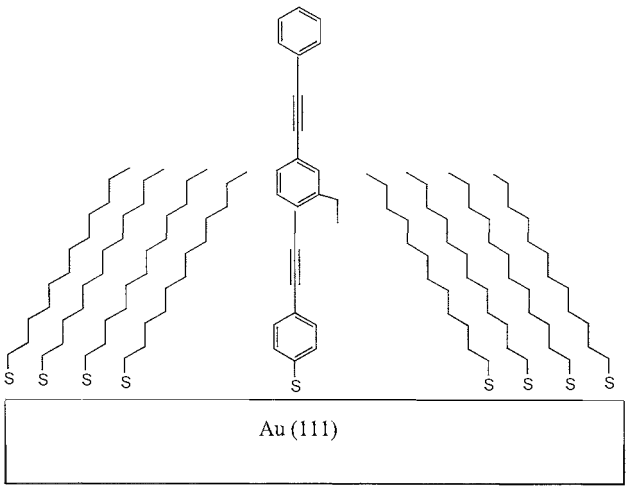

Fig. 1 Insertion of 4,4-di(phenylene-ethynylene)-benzenethiolate into a SAM of *n*-dodecylthiolate on Au{111}. (From Ref. [Ih].)

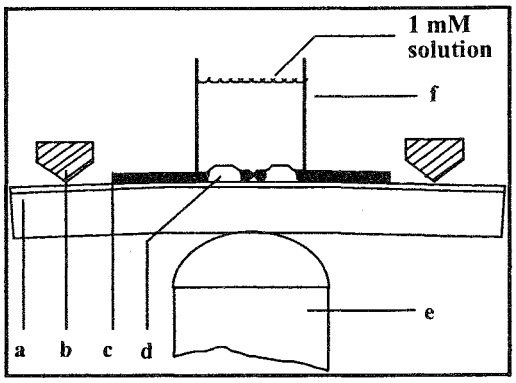

Fig. 2 Lever (b). piston (e). and beaker (f) with 1.4-benzenedithiol solution (From Ref [13])

THE EIGHT MILESTONES OF UE

Here is a subjective list of eight milestones. i.e., recent significant advances in UE:

1. Henry Taube showed that electron transfer between two different metal ions bridged by a shared ligand in solution was faster if the ligand was conjugated than if it was saturated, i.e., nonconjugated.[15] In *Milestone*

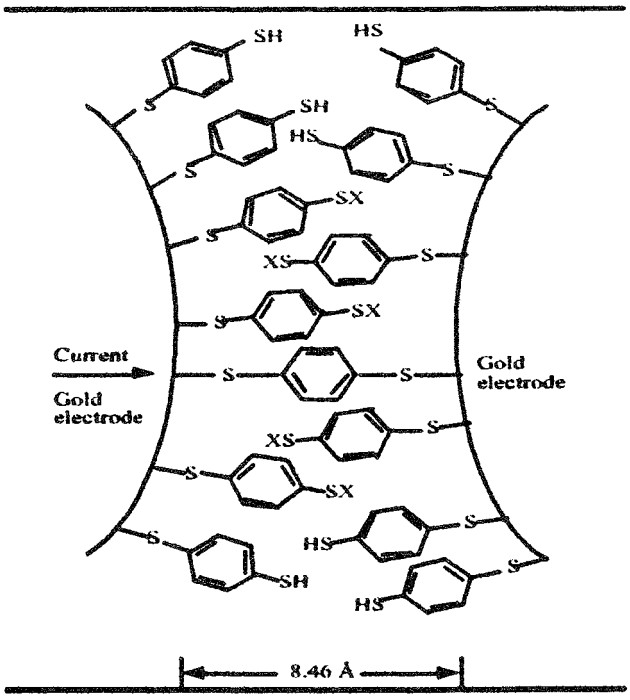

Fig. 3 Depiction of Au shards. and of 14-benzenedithiol molecules attaching themselves to one electrode. the other. or both electrodes. (From Ref. [13].)

One, a STM was used by Paul S. Weiss, David L. Allara, James M. Tour, and coworkers and confirmed Taube's result directly. by measuring the electrical current through individual ''molecular wires.''[16] The current through an aromatic 4,4-di(phenylene-ethynylene)-benzenethiolate bonded to an Au(111) surface is larger than that through an aliphatic *n*-dodecanethiolate bonded to the same substrate[ii6, (Fig. 1).

2. Rolf Landauer proved that the minimum resistance of any single-channel wire (composed of atoms or molecules or polymers), measured between any two macroscopic electrodes. is the quantum of resistance $R = (h/2e^2) = 12.91$ kΩ, where h is Planck's constant, and e is the electronic charge.[17] In *Milestone Two*, this Landauer quantum of resistance was measured by Walt de Heer and coworkers at room temperature between a multiple-walled carbon nanotube (MWCNT), glued to a conducting AFM tip, and a pool of liquid Hg.[18]
3. *Milestone Three* occurred when a break junction was fabricated by Mark A. Reed and coworkers, by evaporating a thin Au wire onto a Si wafer, then compressing this wafer between two static levers and a movable piezoelectric piston. When the Si wafer cracked, the Au wire sepa ated, creating two Au shards. with a mutual separation that could be controlled to ±0.01 nm by the voltage on the piston (Fig. 2).[13] When a benzene solution of 1,4-benzene-dithiol was put into the gap (Fig. 2), some 1.4-benzenedithiol molecules bonded covalently, either to one electrode or to the other or to both (Fig. *3)*. When the latter happened. a one-molecule bridge was created, with a resistance of 22 MΩ (Fig. 4a),[13] which was three orders of magnitude larger than the Landauer resistance quantum, because the lowest unoccupied molecular orbital (LUMO) of the benzene-dithiolate was not in resonance with the work function of Au. The resistances were reproducible (Fig. 4b). If two molecules bonded to both Au shards (two one-molecule bridges). 13 MΩ was measured (Fig. 4c).[13]
4. *Milestone Four* took place when Mark A. Weed developed a "nanopore" technique. Into a thinned-out region of a Si wafer, Au was evaporated to form a 50-nm-wide, few-nm-deep "bowl" of Au{*11*1}, onto which thiols were self-assembled (Fig. 5). The nanopore was then covered with Ti (and its oxide), then Au. Thus. sandwiches ''Au |thiolate|Ti/TiO_2| Au'' could be studied, with maybe a thousand SAM molecules of area 2 nm^2 each. in parallel. A SAM of 4-ethynyl-phenyl-4′-ethynylphenyl-benzene-1-thiolate was a Schottky barrier rectifier."'' In contrast, a SAM of 2'-amino-4-ethynylphenyl-4'-ethy nylphenyl-5′-nitro-benzene-1-thiolate gave a surprise. a negative differential resistance (NDR) peak, useful if this molecule could replace a tunnel diode in a device (Fig. 6).[20] STM suggests that the molecule changes its orientation on Au{111} and thus its conductivity.[21]
5. *Milestone Five* is as follows. When a single-walled carbon nanotube (SWCWT) was deposited by Louis Pasteur's method onto a Si substrate with a 70-nm-wide Au source and drain electrodes, and was studied by STM (Fig. 7), with the STM tip acting as a gate electrode. the nanotube acted as a semiconductor,

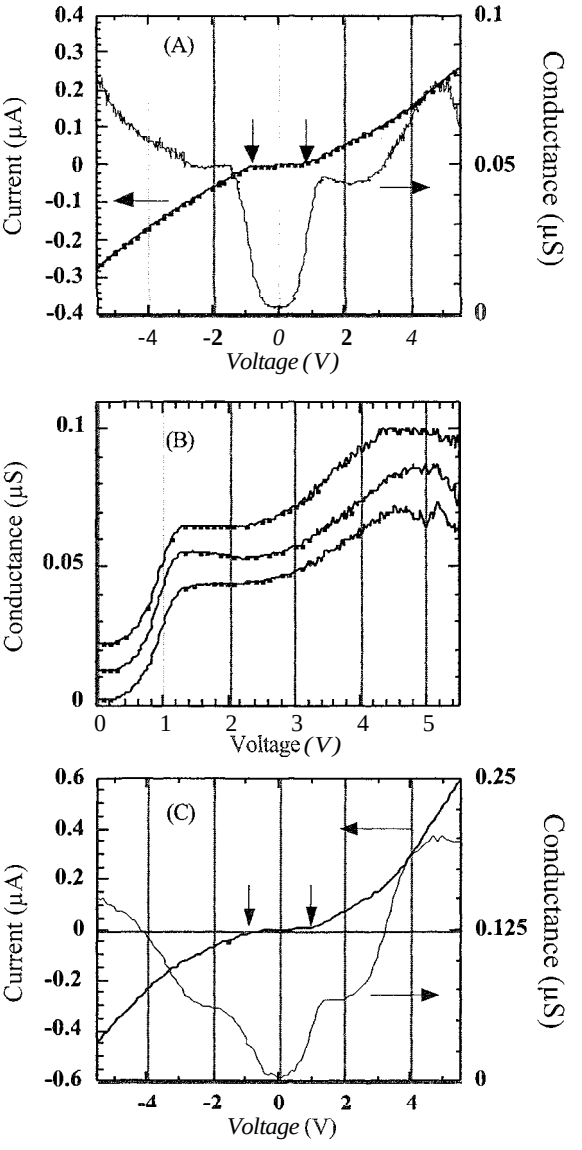

Fig. 4 IV curves (left) and dI/dV (right) for (A) one-molecule bridge, with Coulomb blockade: (B) three separate one-molecule junctions; and (C) a junction with two one-molecule bridges in parallel (From Ref [13])

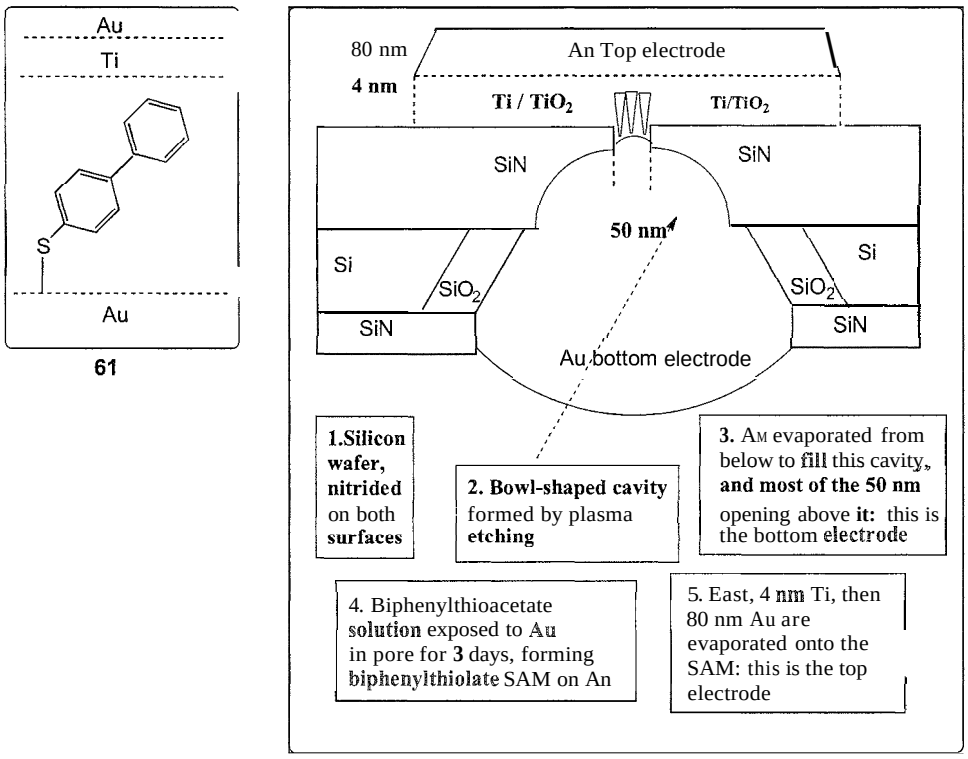

Fig. 5 Construction of nanopore. (Redrawn from Ref. [19].)

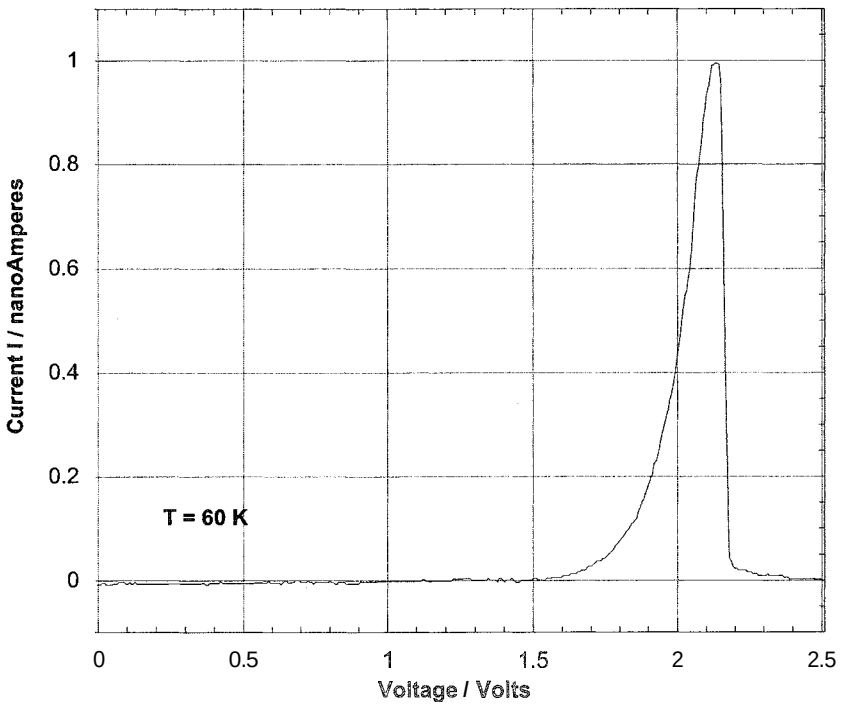

Fig. 6 Current-voltage (IV) curve for Au ¦ 2′-amino-4-ethynylphenyl-4′-ethynylphenyl-5′-nitro-1-benzenethiolate ¦ Au at 60 K, exhibiting NDR. to wit, $(dI/dV) = R < 0$ for $V > 2.1$ Volts. (Redrawn from Ref. [20].)

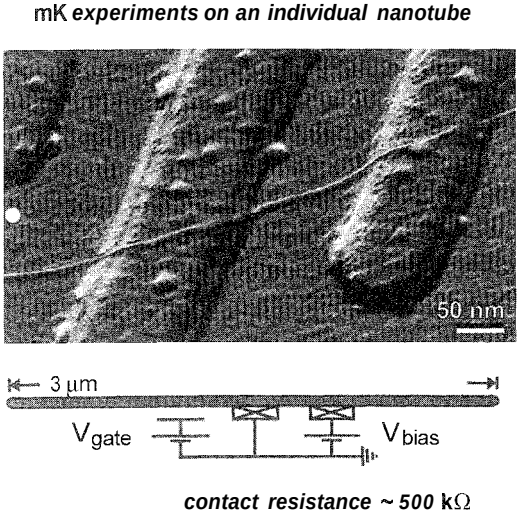

Fig. 7 A SWCNT acting as the semiconductor in a FET measured by STM. (From Ref. [22].)

and field-effect transistor (FET) behavior was observed.[22] FETs are a major source of power amplification in Si-based integrated circuits. They are three-electrode devices, where the current from the source electrode to the drain electrode traverses an electrical semiconductor region, with an effective width (and therefore electrical conductivity) controlled by the electric field between the gate electrode and source and drain electrodes. Thus, a FET requires only that a semiconductor of any dimension be placed between the three electrodes. Its efficiency is due to the sizes and placements of the three electrodes. The gain in the SWCNT FET was only 0.33,[22] but later improvements showed much higher gain.[23,24]

FET behavior in LB physisorbed multilayers of conducting polymers were seen,[25] as was FET behavior in thin-film organic semiconductors, e.g., sexithiophene.[26,27] The assembly of SWCNT in the FET[22-24] is limited to "Pasteur's method" of studying the one SWCNT that fortuitously landed across the "right" Au electrodes. This is a major shortcoming of all carbon nanotube-based devices.

6. In *Milestone Six*, a change in electrical conductivity, presumably tied to a molecular translation, was reported. A cyclic bistable [2]catenane, with two different electron donor moieties (the closed "track") and a cyclic acceptor traveling on the catenane (the "train" on the closed track) (Fig. 8) was measured as a LB monolayer between polysilicon and Ti electrodes. The two donor moieties are naphthalene, a weak donor, and tetrathiafulvalene, a much stronger donor (in the sense that it is more easily oxidized. The electron acceptor is a paraquat salt. The current–voltage plot was asymmetric (Fig. 9), as the train moves from the lower-conductivity station to the higher-conductivity station, although it is not clear which signal is due to which station.[28] The device speed is low, because it depends on a fast electronic transition followed by a slow molecular translation.
7. *Milestone Seven* is as follows. The metal–organic equivalent of a single-electron transistor (SET), which is a Coulomb blockade device with no gain. was recently reported.[29] A Coulomb blockade occurs in a nanodevice (quantum dot, or small metal particle) if adding an extra charge to a finite set of charges on that nanodevice is hindered by Coulomb repulsion, and extra energy is required to add that charge in spite of the Coulomb repulsion. A hexacoordinate Co(II) complex, shown in Fig. 10, was attached at many points to a prefabricated Au wire with a narrow kink in it atop an oxide-covered n-type degenerate Si wafer.[29] The attachment to Au was through one or two thiols.[29] When current was passed through the Au wire at 4.2 K, at some point, the device melted at the kink, and the bithiol then bonded between the two

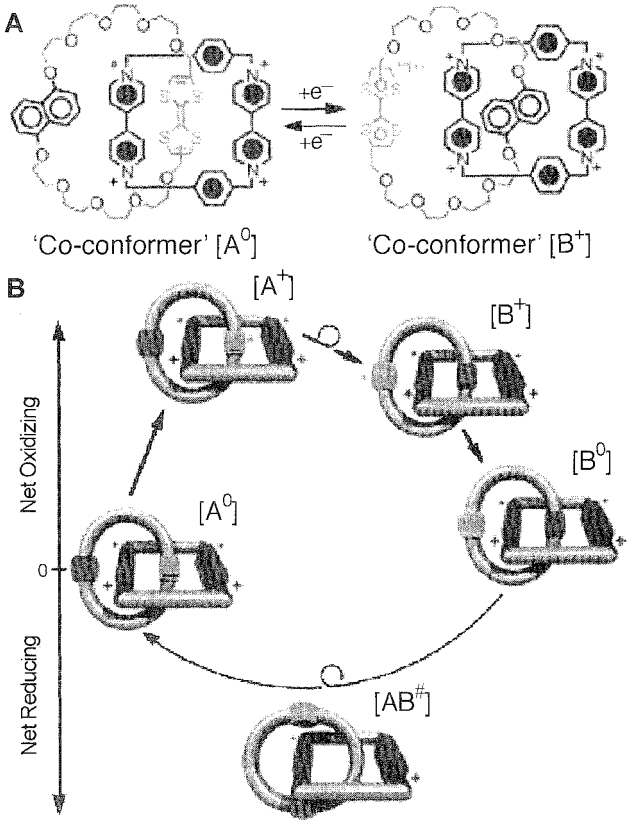

Fig. 8 Train+track. (From Ref. [28].)

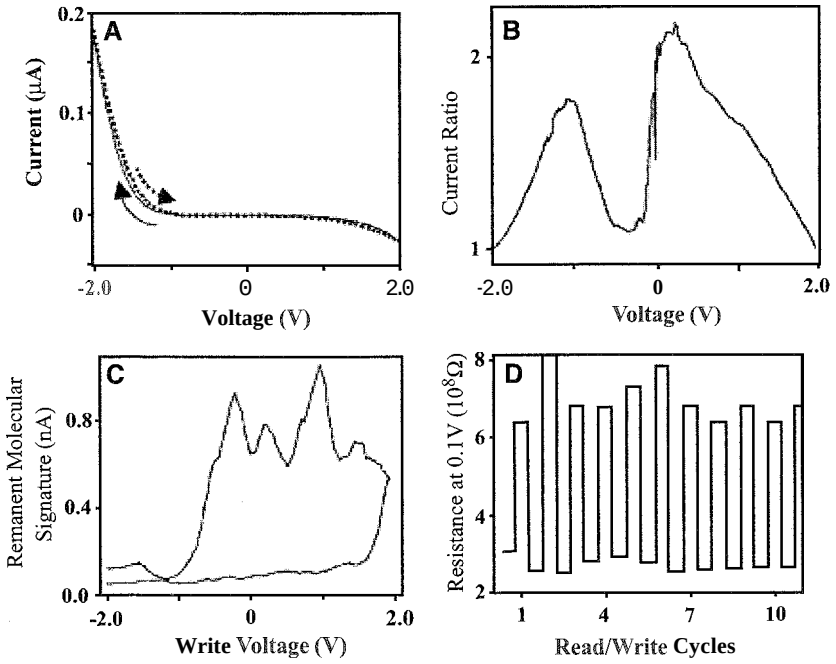

Fig. 9 Current-voltage plots and read–write cycles. (From Ref. [28].)

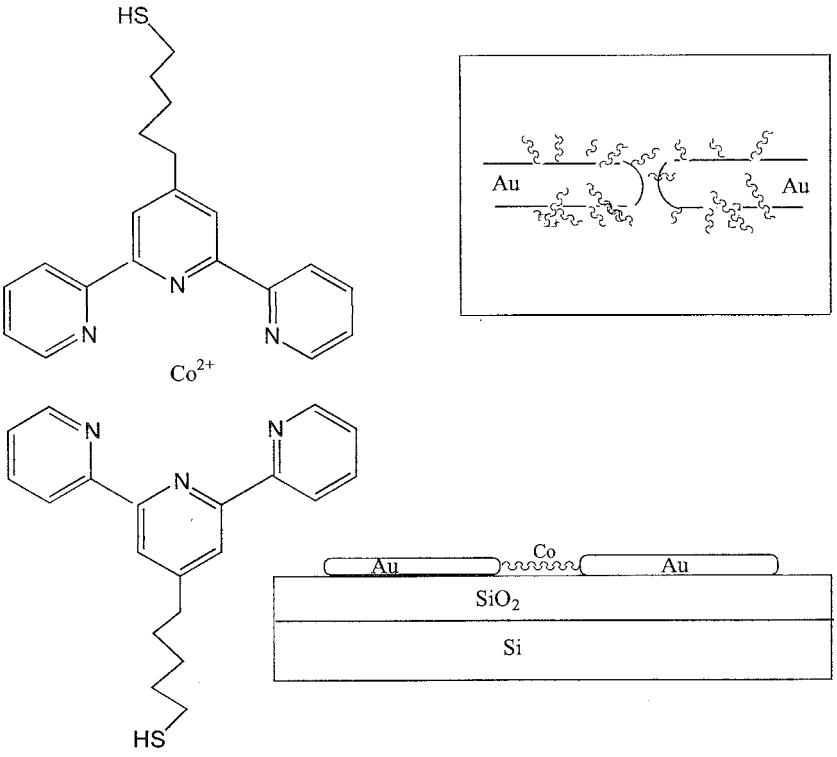

Fig. 10 Electromigration to create an "Au | Co (II) coordination complex | Au" sandwich at 4 K. (From Ref [29])

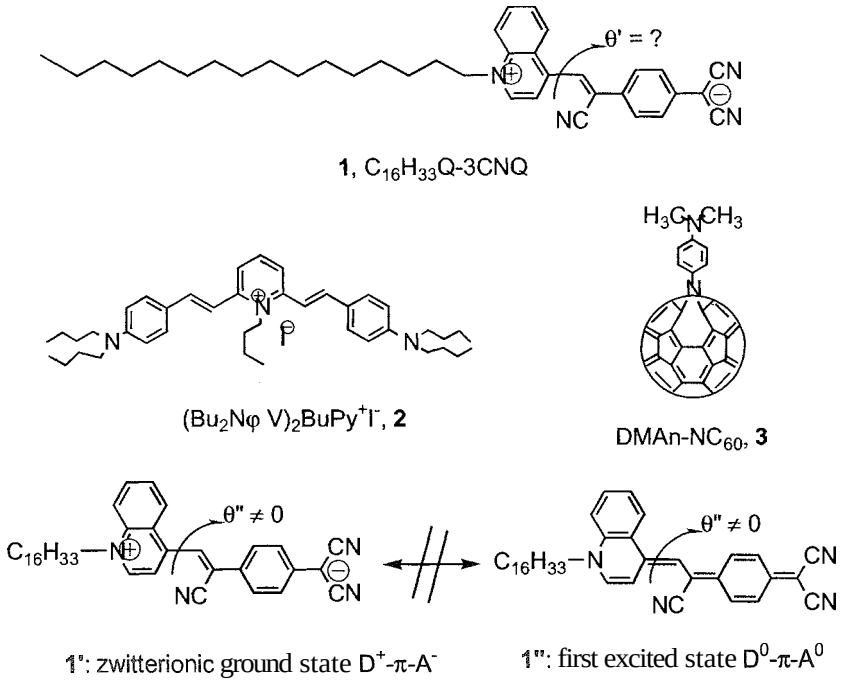

Fig. 11 Three unimolecular rectifies (**1**, **2**. and **3)**

Au shards, with a success rate of a few percent.[29] When a potential was applied to the Si gate electrode. the conductivity through the complex at 0.1 K changed. This change was ascribed to oxidation from Co(II) to Co(III).[29]

8. In *Milestone* Eight, unimolecular rectification was confirmed by Robert M. Metzger and coworkers for an LB monolayer of hexadecylquinolinium tricyanoquinodimethanide. C_{16} H_{33} Q-3CNQ, **1** (Fig. 11) sandwiched at first between oxide-bearing Al electrodes (Fig. 12),[30–32] and later across oxide-free Au electrodes (Fig. 13).[33,34]

The next two rectifiers were dimethylanilinoazafullerene, DMAn-NC_{60} (**2**), a D-σ-A molecule,[35] and 2,6-di[dibutylamino-phenylvinyl]-1-butylpyridinium iodide, $(Bu_2N\varphi V)_2BuPy^+$ I^- (**3**), a charge-transfer salt or interionic rectifier.[36] Details and recent reviews are given elsewhere.[37–40]

RECTIFICATION BY A SINGLE MOLECULE

The electrical conduction through macroscopic matter follows Ohm's law, $\mathbf{I} = V/R$, where **I** is the current, V is the applied potential or bias or voltage, and R is the resistance. Ohm's law is obeyed if the conduction is limited by scattering from impurities or lattice defects.

On the nanoscopic level, the current **I** is limited by quantum-mechanical tunneling in some form and depends exponentially on some power c of V: $\mathbf{I} = A \exp(b V^c)$ (the prefactor A also depends on some power of V). For $V < 0$, **I** is also negative: $\mathbf{I} = -A \exp(b|V|^c)$, so the current–voltage is sigmoidal, or symmetrical with V: $\mathbf{I}(-V) = -I(V)$.

In contrast, electrical rectification, or asymmetrical conduction implies the following:

$$I(V) \neq -I(-V) \tag{4}$$

This asymmetrical conduction, or rectification. for a single molecule or for a monolayer of molecules measured in parallel, can have three causes:

1. A Schottky barrier (dipole layer) at the metal–molecule interface: due to differences in Gibbs free energies of the metal and the molecule or the formation of a dipolar layer of charges on the two sides of the interface. This is ''S'' (for Schottky) rectification.[41]
2. The asymmetric placement between two electrodes of the "chromophore," or electron-rich region of the molecule. This is ''A'' (for asymmetric) rectification.[42]
3. The asymmetric placement between the electrodes of the significant molecular orbital coefficients of the energy levels relevant for electron transfer. This is ''U'' (for unimolecular) rectification.

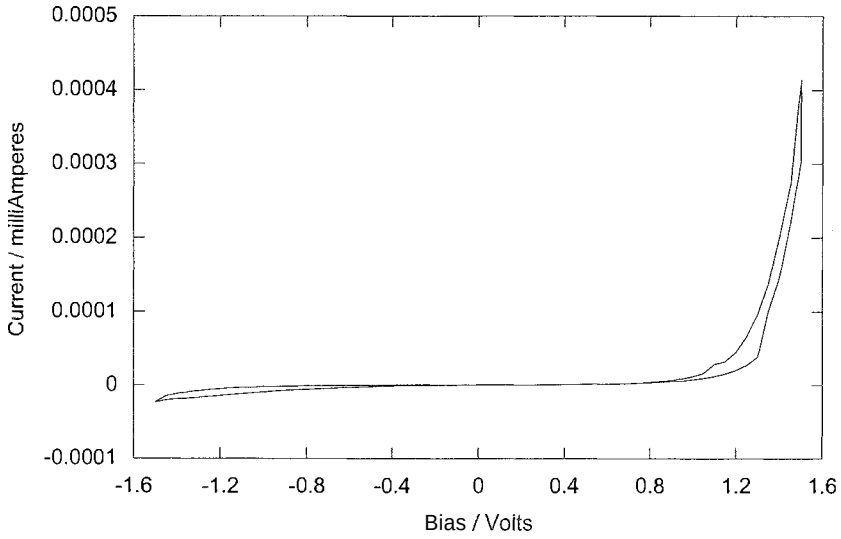

Fig. 12 I–V plot for a monolayer of 1 sandwiched between Al electrodes. (From Ref [30])

For example. molecule 1 is an "A" rectifier (because of the long hexadecyl ''tail'' needed for LB assembly) and. most importantly. a ''U'' rectifier.

Rectification by Molecule 1

The rectification for 1 was first detected by J. Roy Sambles and coworkers between Mg and Pt electrodes.[43,44] A monolayer of 1 was placed by Metzger and coworkers between two electrodes of the same metal [at first Al,[30–32] then Au[33,34] (Fig. 14)]. Also, Molecule 1 was thoroughly characterized.[45,46] The ground-state static electric dipole moment of 1 is $\mu_{GS} = 43 \pm 8$ Debyes.[30] There is a strong and narrow absorption band peaked between 600 and 900 nm. which is strongly hypsochromic; this IVT[30,45] fluoresces in the near-IR region.[45] The excited-state dipole moment is estimated to be $\mu_{ES} = 3$–9 Debyes:[45] 1 is zwitterionic in the ground state

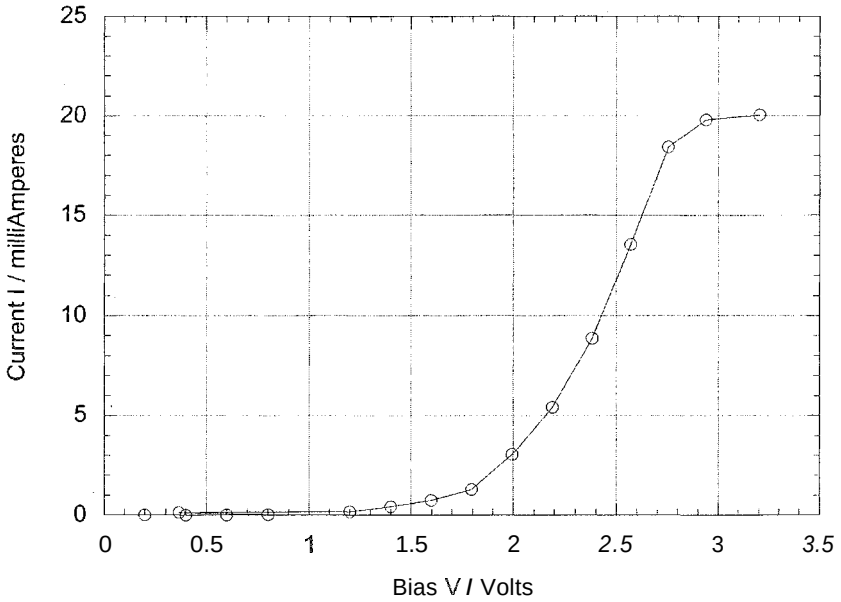

Fig, 13 I–V plot for a monolayer of 1 sandwiched between Au electrodes. with saturation in the forward current. (From Ref. [34].)

$(D^+\text{-}\pi\text{-}A^-, \mathbf{1}')$, and less dissociated $(D^0\text{-}\pi\text{-}A^0, \mathbf{1}'')$ in the first excited state. Molecule 1 forms amphiphilic Pockels–Langmuir monolayers at the air–water interface, with a collapse pressure of 34 mN m^{-1} and a collapse area of 50 $Å^2$ at 20°C.[30] It transfers well on the upstroke, with transfer ratios around 100% onto hydrophilic glass, quartz, or aluminum,[30] or fresh hydrophilic Au.[33,34] The LB monolayer thickness of **1** was determined as 2.3 nm[30] or 2.9 nm[34] (x-ray diffraction), 2.3 nm (spectroscopic ellipsometry),[34] 2.2 nm (surface plasmon resonance),[30,46] and 2.5 nm (x-ray photoelectron spectrometry, XPS).[46] The molecule in the monolayer is estimated to lie at 46° from the surface normal.[30] To perform rectification measurements, LB monolayers and multilayers of **I** were sandwiched between macroscopic Al electrodes[30] and then between Au electrodes.[33,34] For Au deposition, the sample holder is cryo-cooled to 77 K, and 10^{-3} torr of Ar gas is added to the evaporation chamber. Also. the substrate is shielded from direct thermal radiance from the heated Au source.[34]

When a monolayer of **1** is placed between Al electrodes (with their patchy and defect-ridden Al_2O_3 coating), then a dramatically asymmetric current is seen (Fig. 12).

The rectification ratio (RR) at potential V is the current at a positive bias V divided by the absolute value of the current at the corresponding negative bias −V:

$$RR(V) = |I(V)|/I(-V) \tag{5}$$

For **1**, RR = 26 at 1.5 Volts; this corresponds to a current of 0.33 electrons molecule $^{-1}s^{-1}$.[30] This same asymmetry is seen also for multilayers of **1**, for a sample covered

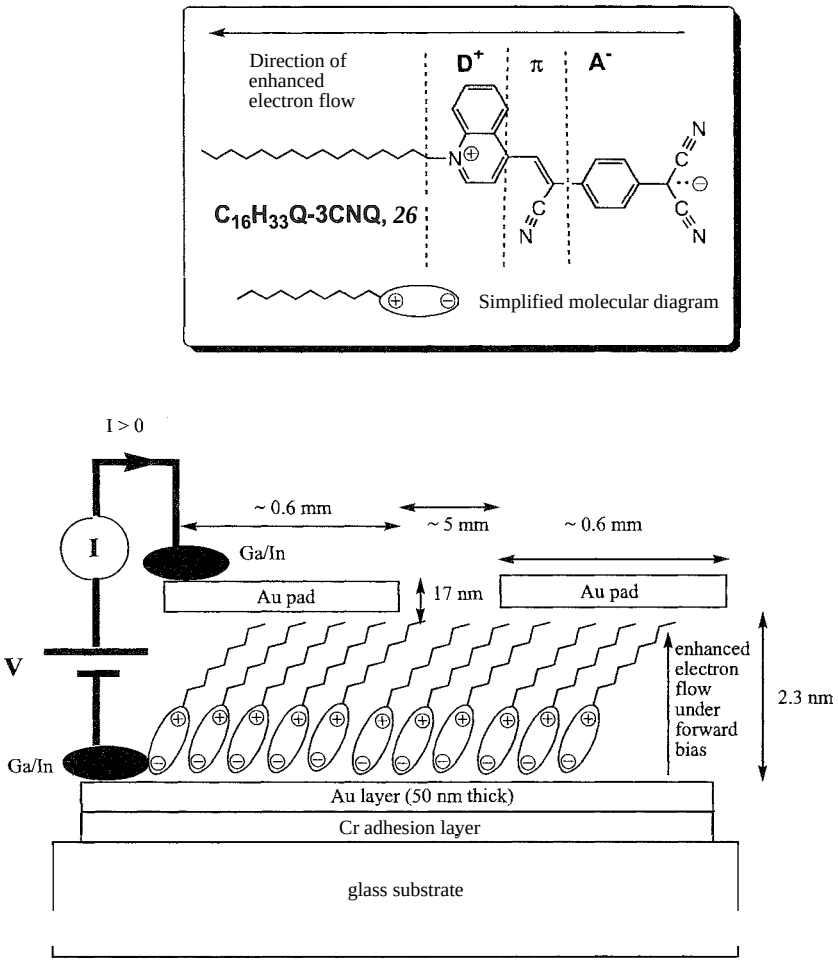

Fig. 14 Molecular structure and geometry of LB monolayer of **1** sandwiched between Au electrodes with direction of enhanced electron flow. The substrate was glass. 50 mm x 50 mm *x* 0.4mm, covered either by a Cr adhesion layer or by a hydrophobic xylene covering, followed by an evaporated Au film 50 mm x *50* mm *x 50* nm. then the LB monolayer or multilayer, then by 48 cylindrical Au pads. 17 nm thick and with an area of *0.283* mm^2. (From Ref. [34].)

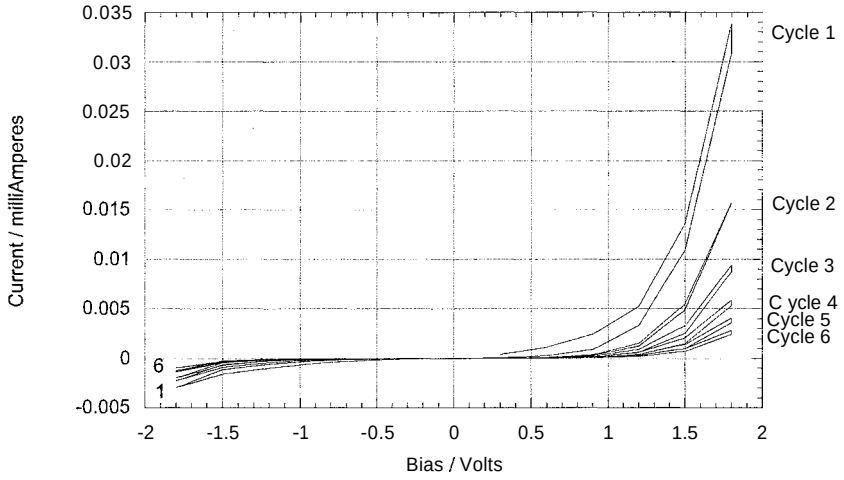

Fig. 15 I–V plots for 2 measured in an ''Au | LB monolayer of 2 | Au'' cell. for six successive cycles of measurement. RR = 12.7. 5.4. 3. 3. for cycles 1 through 6, respectively. (From Ref. [35].)

by Mg pads topped by Al pads,[30,43,44] for monolayers and multilayers of 1 on graphite studied by scanning tunneling spectroscopy,[30] and even for a solution of 1 in dimethylsulfoxide placed in the STM.[30] The RR varies from pad to pad because it is obtained in two-probe measurements. It was suggested that any molecule with RR<2 at maximum V should not be considered a rectifier.'''] As high potentials are scanned, RR decreases gradually, presumably because in an electric field of (1.5 Volts/2.3 nm) = 0.65 GV m^{-1}, molecules in the monolayer may turn around, end over end. to minimize the total energy.[30] Measurements in the temperature range 105 K < T < 390 K established that the asymmetry is not temperature dependent.[32]

When the ''cold gold'' evaporation technique[42] was used, the current through the Au pads increased dramatically.[33,34] The best rectification ratio was 27.5 at 2.2 Volts.[34] The maximum current was 90,400 electrons $molecule^{1}s^{-1}$.[34] Some cells exhibited. as in Fig. 13, the saturation in the forward current[34] predicted by the Aviram–Ratner model.[5]

These results confirm experimentally the Aviram–Ratner Ansatz.[5] but the low-polarity and high-polarity states are interchanged.[45]

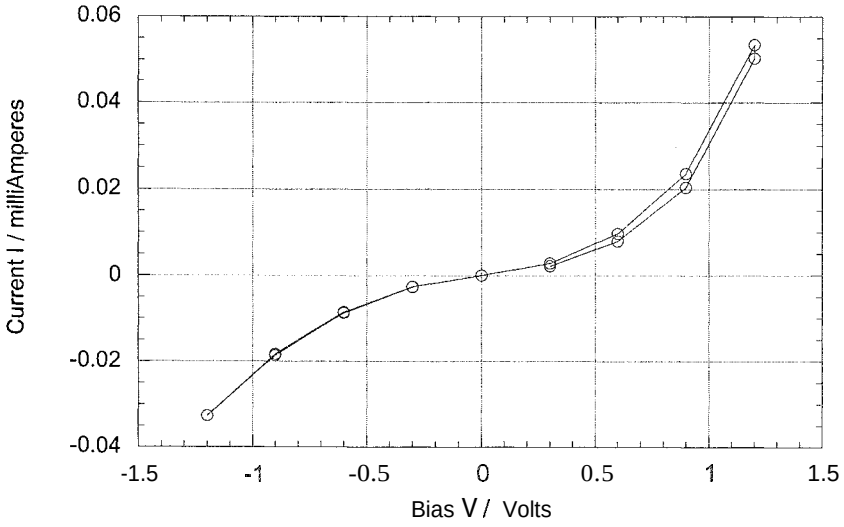

Fig. 16 Current–voltage plots for **3** measured in an ''Au LB monolayer of **3** | Au'' cell. (From Ref. [36].)

Rectification by Molecule 2

The $(Bu_2N\varphi V)_2$ $BuPy^+I^-$, *Molecule 2 forms a* Pockels–Langmuir *film at the air–water interface and transfers to hydrophilic substrates as a Z type* LB multilayer[35] (*"Z-type" means that all dipoles are in the* same *direction). The* monolayer *thickness values were* 0.7 *nm* (ellipsometry) *and 1.15 nm (surface* plasmon *resonance) and 1.3* nm *(x-ray* diffraction).[35] *The films exhibit an absorption* maximum *at* 490 *nm (slightly hypsochromic in solution, attributable to iodide-to-pyridiniuln back-charge transfer). and a second-harmonic signal* $\chi^{(2)}=50$ *pm* V^{-1}.[35] The *rectification in Fig.* 15 *shows a decrease of rectification upon successive cycles. Some cells have* initial RRs *as high as 60. The favored direction of electron* flow *is from the gegenion to the* pyridinium *ion.* i.e., *in the direction of "back-charge transfer," and the rectification in* $(Bu_2N\varphi V)_2$ $BuPy^+I^-$, *2* is *attributed to an interionic process rather than to an intramolecular* process.[36]

Rectification by Molecule 3

The azafullerene DMAn-NC_{60}, **3** *is a weak electron donor* (dimethylaniline) *bonded to a moderate electron acceptor (N-capped* C_{60}), *with a significant* IVT *peak at* 720 nm.[36] *The molecular areas in the monolayer at the air–water interface are only* 70 $Å^2$ at *extrapolated zero pressure.* and 50 $Å^2$ *at 22* mN m^{-1}, *whereas the molecular area of* C_{60} is *close to* 100 $Å^2$. *The* molecules **3** *are probably transferred in a slightly staggered* mode.[36] *The* XPS *film* thickness *is* 2.2 nm.[36] The *monolayer* is *covered, as* previously,[34,45] *by Au* pads.[36] *The current–voltage plot in Fig.* 16 *shows* a *"marginally" rectifying current"'] in the forward direction, with RR of about* 2.[36]

CONCLUSION

Although unimolecular *rectification has been confirmed. there are* still *questions:*

1. *How fast* is *the rectification process?*
2. Can *inelastic electron tunneling spectroscopy* confirm *that the electron really goes through the molecule (instead of tunneling through space)?*
3. Can *the device be made* more *sturdy.* e.g., *by anchoring the molecules covalently to both* metal *electrodes?*
4. Can *one investigate optically what occurs during the electrical* measurements?
5. Can *rectifiers and strands of conducting polymers be grafted together to form a molecular amplifier with power gain?*

ACKNOWLEDGMENTS

This work was generously supported by the United *States National Science Foundation (grants* NSF-DMR-FRG-00-95215 *and* DMR-00-99674) *and was made possible by the help, the ideas, the patience, and the friendship of many colleagues. students, and post-doctoral fellows.*

ARTICLES OF FURTHER INTEREST

Energy and Electron Transfer in Supramolecular Systems, *p.* 535
Ionic, Dipolar, and Interfacial Processes. p 753
Molecular Logic Gates, p. 893
Molecular Switches, p. 917
Molecular Wires. p. 925
Soft and Smart Materials. p 1302
Supramolecular Electrochemistry, p. 1412

REFERENCES

1. Metzger. R.M. Prospects for Truly Unimolecular Devices. In *Lower-Dimensional Systems and Molecular Electronics*; Metzger, R.M.. Day, P., Papavassiliou. C.C.. Eds.; NATO ASI Ser. B248. Plenum Press: New Uork, NY. 1991: 659–666.
2. Rawlett. A.M.: Mickelson, E.T.; Reinerth. W.A.: Jones. L.. II: Kozaki. M.: Burgin, T.P.: Tour, J.M.; Chen, J.; Zhou. C.-W.: Muller. C.J.: Deshpande. M.R.: Reed, M.A.: Bumm, L.A.; Cygan. M.T.: Dunbar, T.D.; Weiss. P.S.: Allara, D.L. Molecular scale electronics. Mater. Res. Soc. Proc. **2001**, *582.* H9.2.1–H9.2.8.
3. Kittlesen. C.P.: White. H.S.; Wrighton. M.S. Chemical derivation of microelectrode arrays by oxidation of pyrrole and N-methylpyrrole: Fabrication of molecule-based electronic devices. J. Am. Chem. Soc. 1984, *106.* 7389–7396.
4. Feynman. R.P. *There is Plenty of Room at the Bottom. [Reprinted Version of Talk Given at the American Physical Society Meeting. California Institute of Technology, Pasadena, CA 29 December 1959 First Transcript Printed in Engineering and Science. California Institute of Technology, February 1960]. Reprinted in Miniaturization*; Gilbert. *H.D.*, Ed.; Reinhold: New Uork, 1961; 282–296.

5. Aviram, A.: Ratner. M.A. Molecular rectifiers. Chem. Phys. Lett. 1974, *29*, 277–283.
6. Rlodgett, K.B. Films built by depositing successive unimolecular layers on a solid surface. J. Am. Chem. Soc. 1935, *57*. 1007–1022.
7. Blodgett, K.B.; Langmuir, I. Built-up films of barium stearate and their optical properties. Phys. Rev. 1937, *51*. 964–982.
8. Bigelow, W.C.; Pickett, D.L.; Zisman, W.A. Oleophobic monolayers. I. Films adsorbed from solution in nonpolar liquids. J. Coll. Sci. 1946, *1*, 513–538.
9. Laibinis, P.E.; Hickman, J.J.; Wrighton. M.S.: Whitesides. G.M. Orthogonal self-assembled monolayers: Alkanethiols on gold and alkane carboxylic acids on alumina. Science 1989. *245*. 845–847.
10. *Molecular Electronic Devices;* Carter, F.L., Ed.; Dekker: New York. 1982.
11. *Molecular Electronic Devices 11;* Carter. F.L., Ed.; Dekker: New York. 1987.
12. *Molecular Electronic Devices, Proc. 3rd Intl. Symp.*; Carter, F.L., Siatkowski, R.E., Wohltjen, H., Eds.: North-Holland: Amsterdam, 1988.
13. Reed. M.A.: Zhou, C.; Muller, C.J.; Burgin, T.P.; Tour, J.M. Conductance of a molecular junction. Science 1997. *278*. 252–254.
14. Moore. G.E. Cramming more components onto integrated circuits. Electronics 19 April 1965. 114–117.
15. Taube, H. Angew. Chem., Int. Ed. Engl. 1984, *23*. 329.
16. Bumm, L.A.; Arnold. J.J.: Cygan, M.T.; Dunbar, T.D.: Burgin, T.P.; Jones, L., II; Allara, D.L.; Tour, J.M.; Weiss, P.S. Are single molecular wires conducting? Science 1996. *271*. 1705–1707.
17. Landauer. R. Spatial variation of currents and fields due to localized scatterers in metallic conduction. IBM J. Res. Develop. 1957. *1*. 223–231.
18. Frank, S.; Poncharal. P.; Wang, Z.L.; de Heer, W.A. Carbon nanotube quantum resistors. Science 8999, *280*. 1744–1746.
19. Zhou. C.; Deshpande. M.R.; Reed, M.A.; Jones, L.. II; Tour, J.M. Nanoscale ruetallself-assembled monolayer/ metal heterostructures. Appl. Phys. Lett. 1997. *71*, 611–613.
20. Chen, J.; Reed. M.A.; Rawlett, A.M.; Tour, J.M. Large on-off ratios and negative differential resistance in a molecular electronic device. Science 1999, *286*, 1550–1552.
21. Donhauser, Z.J.: Mantooth, B.A.; Kelly, K.F.; Bumm. L.A.; Monnell. J.D.; Stapleton, J.J.; Price, D.W., Jr.; Rawlett, A.M.; Allara, D.L.; Tour, J.M.; Weiss, P.S. Conductance switching in single molecules through conformational changes. Science 2001. *292*, 2303–2307.
22. Tans. S.J.; Devoret, M.H.: Dai, H.; Thess, A.; Smalley, R.E.; Ceerligs, L.J.: Dekker, C. Individual single-wall carbon nanotubes as quantum wires. Nature 1997. *386*. 474–477.
23. Derycke, *V.:* Martel, R.: Appenzeller. J.; Avouris. Ph. Carbon nanotube inter-and intramolecular logic gates. Nano Lett. 2001, **I**, 453–456.
24. Bachtold, A.; Hadley, P.; Nakanishi, T.; Dekker, C. Logic circuits with carbon nanotube transistors. Science 2001, *294*. 1317–1320.
25. Paloheimo. J.: Kuivalainen, P.; Stubb, H.; Vuorimaa. E.: Yli-Lahti, P. Molecular field-effect transistors using conducting polymer langmuir-blodgett films. Phys. Lett. 1990, *56*. 1157–1159.
26. Gamier, F.; Horowitz. G.; Peng, X.; Fichou, D. An all-organic 'soft' thin film transistor with very high carrier mobility. Adv. Mater. 1990, *2*. 592–594.
27. Turner-Jones, E.T.; Chyan, O.M.; Wrighton, M.S. Preparation and characterization of molecule-based transistors with a 50-nm source-drain separation with use of shadow deposition techniques: Toward faster, more sensitive molecule-based devices. J. Am. Chem. Soc. 1987, *109*. 5526–5528.
28. Collier, C.P.; Mattersteig. G.; Wong, E.W.; Beverly. K.: Sampaio, J.; Raymo, F.M.; Stoddart. J.F.; Heath, J.R. A [2]catenane based solid-state electronically reconfigurable switch. Science 2000, *289*, 1172.
29. Park, J.; Pasupathy, A.N.; Goldsmith. J.I.; Chang, C.; Yaish, Y.; Petta, J.R.; Rinkoski. M.; Sethna, J.P.; Abruña, H.D.: McEuen, P.L.; Ralph. D.C. Coulomb blockade and the kondo effect in single atom transistors. Nature 2002, *417*. 722–725.
30. Metzger. R.M.; Chen, B.; Höpfner, U.; Lakshmikantham, M.V.; Vuillaume. D.; Kawai, T.; Wu. X.: Tachibana. H.; Hughes. T.V.: Sakurai, H.; Baldwin, J.W.; Hosch. C.; Cava, M.P.; Brehmer, L.: Ashwell, C.J. Unimolecular electrical rectification in hexadecylquinoliniurn tricyanoquinodimethanide. J. Am. Chem. Soc. 1997, *119*, 10455–10466.
31. Vuillaume, D.; Chen, B.; Metzger, R.M. Electron transfer through a monolayer of hexadecylquinoliniurn tricyanoquinodimethanide. Langmuir 1999, *15*, 4011–4017.
32. Chen. B.; Metzger, R.M. Rectification between 370 K and 105 K in hexadecylquinolinium tricyanoquinodimethanide J. Phys. Chem. 1999, *B103*, 4447–4451.
33. Xu, T.; Peterson, I.R.; Lakshmikantham, M.V.: Metzger, R.M. Rectification by a monolayer of hexadecylquinolinium tricyanoquinodimethanide between gold electrodes. Angew. Chem., Int. Ed. 2001, *40*. 1749–1752.
34. Metzger, R.M.; Xu, T.; Peterson. I.R. Electrical rectification by a rnonolayer of hexadecylquinolinium tricyanoquinodimethanide measured between macroscopic gold electrodes. J. Phys. Chem. 2801. *B105*, 7280–7290.
35. Baldwin, J.W.: Amaresh, R.R.; Peterson. I.R.: Shumate, W.J.; Cava, M.P.; Amiri, M.A.; Hamilton, R.; Ashwell, C.J.; Metzger, R.M. Rectification and nonlinear optical properties of a Langmuir-Blodgett monolayer of a pyridinium dye. J. Phys. Chem. 2002, *B106*, 12158–12164.
36. Metzger. R.M.; Baldwin, J.W.; Shumate, W.J.; Peterson, I.R.; Mani, P.; Mankey, G.J.; Morris, T.; Szulczewski, G.: Bosi, S.; Prato. M.; Comito, A.; Rubin, Y. Large current asymmetries and potential device properties of a Langmuir-Blodgett monolayer of dimethyanilinoazafullerene

sandwiched between gold electrodes. J. Phys. Chem. 2003, *B107*, *1021* – 1027.

37. Metzger, R.M. The unimolecular rectifier: Unimolecular electronic devices are coming. J. Mater. Chem. 1999. 9. 2027–2036.
38. Metzger, R.M. All about y-hexadecylquinolinium tricyanoquinodimethanide, a unimolecular rectifier of electrical current. J. Mater. Chem. 2000, *10*, 55–62.
39. Metzger, R.M. Electrical rectification by a molecule: The advent of unimolecular electronic devices. Acc. Chem. Res. 1999, 32. 950–957.
40. Metzger. R.M. Unimolecular electrical rectifiers. Chem. Rev.. accepted and *in* press.
41. Schottky, W. Simplified and extended theory of barrier-layer rectifiers. Z. Phys. **1942**, *118*, 539–592.
42. Krzeminski, C.: Delerue, C.; Allan, G.; Vuillaume, D.; Metzger, R.M. Theory of rectification in a molecular monolayer. Phys. Rev. **2001**, *B64*, #085405.
43. Ashwell. G.J.; Sambles, J.R.: Martin, A.S.: Parker, W.G.: Szablewski, M. Rectifying characteristics of Mg | ($C_{16}H_{33}$-Q3CNQ LB Film) | Pt structures. J. Chem. Soc., Chem. Commun. 1990. 1374–1376.
44. Martin, A.S.; Sambles, J.R.: Ashwell, G.J. Molecular rectifier. Phys. Rev. Lett. 1993, *70*. 218–221.
45. Baldwin, J.W.; Chen. B.; Street, S.C.: Konovalov. V.V.; Sakurai. H.; Hughes, T.V.; Simpson, C.S.; Lakshmikantham, M.V.: Cava, M.P.: Kispert, L.D.: Metzger. R.M. Spectroscopic studies of hexadecylquinolinium tricyanoquinodimethanide. J. Phys. Chem. 1999. *B103*, 4269–4277.
46. Xu. T.; Szulczewski, G.J.: Morris, T.A.; Amaresh. R.R.; Gao, Y.; Street, S.C.; Kispert. L.D.; Metzger. R.M.; Terenziani, F. A spectroscopic study of hexadecylquinolinium tricyanoquinodimethanide as a monolayer and in bulk. J. Phys. Chem. **2002**, *B106*, 10374–10381.

Urea Inclusion Compounds

Kenneth D. M. Harris
Cardiff University, Cardiff, Wales

INTRODUCTION

Urea inclusion coinpounds were first discovered in the 1940s with the serendipitous preparation by Bengen[1] of an adduct between I-octanol and urea. Many different families of guest molecules based on long alkane chains are now known to form inclusion compounds with urea, and x-ray diffraction studies[2,3] have been that the host structure in these crystalline solids contains linear. parallel tunnels that are constructed from an extensively hydrogen-bonded arrangement of urea molecules. The guest molecules are densely packed along these tunnels. A remarkable fact is that the vast majority of different urea inclusion compounds (containing different types of guest molecules) have essentially the same urea host structure at ambient temperature, and we refer to such cases as "conventional" urea inclusion compounds (guest molecules that represent exceptions are discussed later in this article). The conventional urea inclusion compounds are characterized at ambient temperature by: a hexagonal host tunnel structure (Fig. 1: space group $P6_122$ or $P6_522$; $a = b \approx 8.2$ Å; $c \approx 11.0$ Å; effective tunnel "diameter" ranging between 5.5 Å and 5.8 Å on moving along the tunnel): an incommensurate relationship (see below) between the periodicities of the host and guest substructures along the tunnel axis; and substantial dynamic disorder (reorientation about the tunnel axis) of the guest inolecules (see below). In the conventional urea inclusion compounds, the urea inolecules form hydrogen bonds only to other urea molecules. and there is no hydrogen bonding between urea molecules and guest molecules. The host structure comprises a spiral arrangement of urea molecules, and a given single crystal contains only right-handed spirals ($P6_122$) or only left-handed spirals ($P6_522$). Thus. the host tunnel is a chiral structure.

Structural compatibility between host and guest components is fundamental to most inclusion phenomena. and the conventional urea tunnel structure is formed only with guest molecules that are based on a sufficiently long alkane chain and with only a limited degree of substitution of this chain allowed. Examples of appropriate guest molecules are *n*-alkanes and derivatives such as α,ω-dihalogenoalkanes, diacyl peroxides, carboxylic acids, alkanones, carboxylic acid anhydrides, and α,ω-alkane dicarboxylic acids. In general. rnolecules containing benzene or cyclohexane rings do not form inclusion compounds with urea. presumably because these structural components are too wide to fit comfortably inside the tunnel. Several empirical generalizations have been made[4,5] concerning the geometric and steric features of guest molecules that form inclusion compounds with urea. The requirement for size and shape compatibility between host and guest components leads to the possibility of using urea inclusion compounds in applications based on molecular separation. such as the separation of mixtures of linear and branched alkanes. Such applications provided the motivation for much early research (particularly within the petrochemicals industry) on urea inclusion compounds. before it was found that zeolites and related materials offer several advantages in such applications. Nevertheless, the formation of urea inclusion compoiinds is still used on the laboratory scale as a method for isolating linear molecules.

The empty urea tunnel structure is unstable, and it has been shown by experiment and computer simulation that the tunnel collapses if the guest molecules are removed from the inclusion compound. leading to the ''pure'' crystalline phase of urea, which does not contain empty tunnels. The instability of the "empty" urea tunnel structure clearly limits the potential for developing certain applications of urea inclusion compounds.

In addition to forming tunnel inclusion compounds, urea can also form specific complexes with a variety of organic and inorganic nlolecules and ions. Discussion of these complexes is beyond the scope of this article. which is focused on tunnel inclusion compounds of urea.

In this article, an overview of structural aspects of urea inclusion compounds is provided, and some of the interesting properties of these materials. such as the dynamic and conformational properties of the guest molecules. chemical reactions, and applied aspects, are elaborated upon. Also highlighted are the types of techniques used to investigate these properties. Several review articles have been published on urea inclusion compounds,[5–10] and they contain comprehensive lists of references to the original literature in this field. The reader is encouraged to consult these review articles. and the original papers cited therein, in order to obtain more information.

Encyclopedia of Supramolecular Chemistry
DOI: 10.1081/E-ESMC 110012728

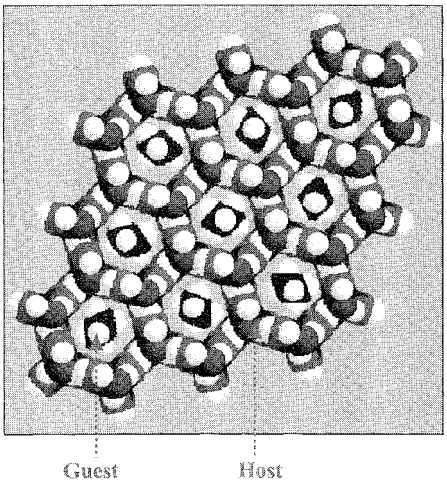

Fig. 1 Structure of the hexadecane/urea inclusion compound at ambient temperature, showing 9 complete tunnels (with van der Waals radii) viewed along the tunnel axis. Guest molecules have been inserted into the tunnels. illustrating orientational disorder. The positions of the guest molecules are not actually determined from X-ray diffraction data at ambient temperature. (View *this art* in color *at www.dekker.com.*)

STRUCTURAL PROPERTIES

Periodic Structural Properties

As discussed above, the conventional urea inclusion compounds are characterized by the hexagonal urea tunnel structure shown in Fig. I at ambient tempcrature, and by an incommensurate relationship between the host and guest substructures along the tunnel axis (Fig. 2). The periodic repeat distance of the guest molecules along the tunnel (c,) depends directly on the length of the guest molecule in the linear type of conformation required to fit inside the tunnel, and the periodic repeat distance of the urea molecules along the tunnel (c_h) is fixed by the host structure (c_h is essentially invariant at ca. 11 A for urea inclusion compounds containing different guest molecules). The incommensurate relationship between c_g and c_h in conventional urea inclusion compounds is readily evident from x-ray diffraction photographs (see Fig. 2 of article on "Incommensurate and Cornmcnsurate Structures").

Although the focus in this article is on the conventional urea inclusion compounds, we note that the inclusion compounds formed between urea and certain specific gucst molecules arc commensurate tunnel structures. For such commensurate systems, the host structure is usually distorted from the hexagonal tunnel structure shown in Fig. 1. Examples are the inclusion compounds formed between urea and the guest molecules 1,6-dibromohexane,[11] sebaconitrile[12] and (a + 1),(ω - 1)-alkanediones.[13] The inclusion compounds of urea and (a + 1),(ω - 1)-alkanediones exhibit an interesting diversity of commensurate superstructures in which there is direct hydrogen bonding between urea molecules and the guest molecules. Furthermore, a number of tunnel inclusion compounds of urea containing polymeric guests have been found to exhibit host structures that differ from the conventional urea tunnel structure.[14-16]

Many conventional urea inclusion compounds exhibit three-dimensional (3-D) ordering of the guest molecules, and thus there are well-defined structural relationships between guest molecules both within each tunnel and between adjacent tunnels. The mode of intertunnel ordering (characterized by the intertunnel offset A_n, defined in Fig. 2) is found to depend on the functional groups present on the guest molecule, and different homologous families of guest molecules exhibit characteristic modes of intertunnel ordering. Results for selected families at ambient temperature are: alkanelurea, $A_n = 0$ A; diacyl peroxide/urea, $A_n = 4.6$ Å;[17] α,ω-dibromoalkane/urea, A_g and c_g are related by the exact relationship $\Delta_g = c_g/3$;[18] and carboxylic acid anhydride/urea, $A_n = 0$ Å, with the exception of heptanoic anhydride/urea, for which $A_n = 2.3$ Å.[19] The complete 3-D arrangement of guest molecules is understood by extending the Δ_g concept into three dimensions, leading to monoclinic, rhombohedral, and hexagonal guest structures for diacyl peroxide/urea, α,ω-dibromoalkane/urea, and alkane/urea inclusion compounds, respectively. For the alkanelurea and α,ω-dibromoalkane/urea inclusion compounds, these average symmetries require disorder of the guest molecules with respect to reorientation about the tunnel axis. In many cases, a given single crystal contains

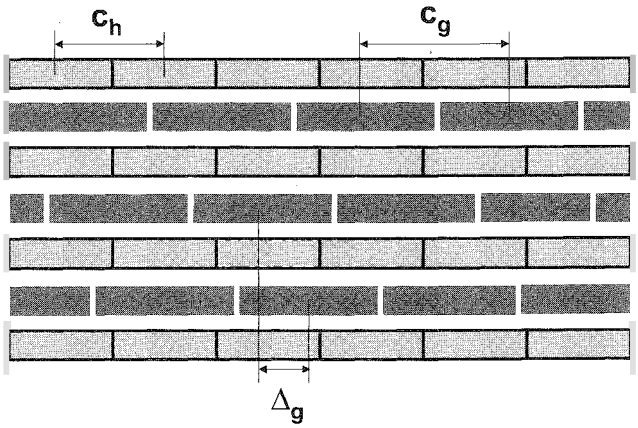

Fig. 2 Schematic two-dimensional representation of a urea inclusion compound viewed perpendicular to the tunnel axis and indicating the definitions of c_g, c_h and A_n. (View *this art in color at* www.deklcer.com.)

different domains of the guest substructure: each domain has an identical packing of guest molecules but has a different (although equivalent) orientation relative to the host structure. Although, as discussed above, diffraction data allow the average periodicity and symmetry of the basic guest structure to be determined, dynamic disorder of the guest molecules in conventional urea inclusion compounds can limit the ability to obtain detailed information on the guest structure. One consequence of the dynamic disorder of the guest molecules is the appearance of different forms of diffuse scattering in diffraction patterns of urea inclusion compounds.

As a consequence of the incommensurate nature of urea inclusion compounds, the symmetry of the composite inclusion compound (i.e., considering host and guest components implicitly together) cannot be described by a 3-D space group, and instead. a four-dimensional (4-D) superspace group is required. Descriptions of the symmetry properties of urea inclusion compounds in superspace groups have been developed,[20] and attempts to determine the incommensurate modulations in the host and guest substructures by solving the structure of the composite inclusion compound in a superspace group have been reported.[21,22] Much research[3,23–27] has been devoted to the study of all aspects of the diffraction patterns from incommensurate urea inclusion compounds (particularly alkanelurea inclusion compounds), including measurement of incommensurate satellite reflections and detailed characterization of different forms of diffuse scattering. The diffraction patterns of incommensurate urea inclusion compounds contain a rich variety of features: which promise to yield important fundamental inforination on the disorder properties and the incommensurate structural nature of these solids. A related aspect concerns the vibrational properties of the inclusion compound, and much attention has focused on the existence and observation of an extra acoustic vibrational mode (the "sliding mode") that may be expected to be observed for incommensurate systems.

Phase Transitions and Structural Properties at Low Temperature

At sufficiently low temperatu es, most conventional urea inclusion compounds undergo phase transitions associated with changes in the symmetry of the host structure and changes in the dynamic properties of the guest molecules. For alkanelurea and α,ω-dibromoalkane/urea inclusion compounds, structural[28–32] and dynamic[33–41] aspects of these phase transitions have been investigated extensively using a variety of techniques. Qualitatively, the alkane/urea and α,ω-dibromoalkane/urea inclusion compounds behave in a siinilar way with respect to these transitions. In both cases. the host structure in the low-temperature phase is orthorhombic and is based on a small distortion from the orthohexagonal description of the high-temperature structure. The structural relationship between the host and guest substructures along the tunnel remains incommensurate. Other urea inclusion compounds, such as 1,10-decanedicarboxylic acid/urea[42] exhibit more complicated structural behavior in the low-temperature phase, with the formation of large superstructures in directions perpendicular to the tunnel axis. Thus. the exact nature of the distortion of the host structure in the low-temperature phase depends critically on the type of guest molecule.

There have been various attempts to rationalize the phase transitions observed in urea inclusion compounds. One of these approaches[43] draws an analogy between the phase transition in alkane/urea inclusion compounds and the order–disorder phase transitions in alkali cyanide crystals and proposes that coupling between transverse acoustic phonons of the host structure and the orientational order of the guest molecules provides an indirect mechanism for orientational ordering of the guest molecules in the low-temperature phase.

The phase transitions for alkane/urea and α,ω-dibromoalkane/urea inclusion compounds are not associated with changes in the mode of 3-D ordering of the guest molecules. However, the behavior of other urea inclusion compounds is different in this regard. For example. heptanoic anhydride/urea exhibits two phase transitions below ambient temperature.[44] The first transition (at 179 K on cooling) is associated only with a change in the mode of 3-D ordering of the guest molecules (A, = 2.3 A above 179 K: A, = 1.5 Å below 179 K), whereas the second transition (at 122 K on cooling) is associated with a distortion of the host structure as well as a further change in the mode of 3-D ordering of the guest molecules (A, = 0 A below 122 K).

Conformational Properties and Local Interactions of Guest Molecules

The structure of a crystalline solid determined from diffraction studies represents a space-averaged and time-averaged representation of the true structure. and in cases for which there is disorder (static or dynamic), structure determination from diffraction data cannot readily provide a complete description of the distribution of local (spatial or temporal) structural features about this averaged representation. As discussed below. there is substantial dynamic disorder of the guest inolecules in conventional\urea inclusion compounds, and although information on the average periodicity of the guest molecules can be established from diffraction data (as discussed above), eiucidating a detailed description of the structural

properties of the guest molecules from such data is far from straightforward. Nevertheless, other experimental and computational techniques can be used to obtain direct information on local structural properties, such as the conformational properties of the guest molecules, the interactions between guest molecules within the tunnel, and the orientational distributions of the guest molecules. Illustrative examples from such studies are now highlighted.

Raman spectroscopy has been used[45] to probe conformational properties of α,ω-dihalogenoalkane guest molecules [$X(CH_2)_nX$; $n = 8$ for $X = Cl$; $n = 7$–11 for $X = Br$: $n = 8$ for X = I] in urea inclusion compounds. In particular. the C–X stretching vibrations were used to assess the relative amounts of *trans* and *gauche* end groups as a function of the length (n) of the guest molecule. the identity of the terminal substituent X, temperature, and pressure. These investigations suggest that there is no well-defined relationship between the proportion of end groups in the *gauche* conformation and the length of the $Br(CH_2)_nBr$ guest molecules. The proportion of *gauche* end groups decreases significantly as the size of the terminal substituent is increased—at ambient temperature, the proportion of *gauche* end groups is 51% for $Cl(CH_2)_8Cl$, 7% for $Br(CH_2)_8Br$, and 1% for $I(CH_2)_8I$. For $Br(CH_2)_nBr$/urea inclusion compounds. the proportion of *gauche* end groups increases slightly as temperature is increased and increases markedly [for $Br(CH_2)_{11}Br$/urea] as the applied pressure is increased.

To directly probe the interaction between adjacent guest molecules in a urea inclusion compound, high-resolution solid-state ^{19}F-NMR spectroscopy (with high-power ^1H decoupling) was employed.[46] For the urea inclusion compound containing 1,10-difluorodecane [$F(CH_2)_{10}F$] guest molecules, the close proximity of the fluorine end groups of neighboring guest molecules gives rise to essentially isolated $^{19}F\cdots{}^{19}F$ spin pairs. Measurement of the $^{19}F\cdots{}^{19}F$ dipole–dipole interaction provides an opportunity to estimate the $^{19}F\cdots{}^{19}F$ distance. although such analysis is complicated by conformational disorder (the ^{19}F nucleus may be in *gauche* or *trans* positions with respect to the alkane chain. leading to the possibility of *trans–trans*, *tmrzs–gauche,* and *gauche–gauche* end group situations between adjacent end groups) and by reorientation of the guest molecules about the tunnel axis. Different ^{19}F-NMR techniques are in agreement that the average $^{19}F\cdots{}^{19}F$ dipole–dipole interaction is about 1 kHz at ambient temperature. This value is consistent with a random distribution over all mutual orientations for the *trans–gauche* and *gauche–guuche* situations. with little or no population of the *trans–trans* situation.

Bromine M-edge extended x-ray absorption fine structure (EXAFS) experiments were carried out[47] to investigate a variety of local structural properties of urea inclusion cornpounds containing α,ω-dibromoalkane guest molecules [$Br(CH_2)_nBr$; $n = 7$–11], and has led to unambiguous information on the intramolecular geometry around the bromine atom based on the Br C distances for the three intramolecular carbon atoms closest to the bromine atom. The value of the $Br\cdots C(3)$ distance indicates that the bromine end groups exist predominantly in the *trans* conformation, in agreement with results from Raman spectroscopy.

Recently,[27] information on the guest–guest interactions in urea inclusion compounds containing α,ω-diiodoalkane [$I(CH_2)_nI$] guest molecules has been established directly from analysis of the intensity distribution of diffuse sheets in their x-ray diffraction patterns. These diffuse sheets are often observed in x-ray diffraction patterns of urea inclusion compounds and correspond to 1-D ordering of the guest molecules along the tunnel axis. Thus, analysis of the intensities of the diffuse sheets provides information on the structural properties of the periodic linear array of guest molecules along an individual tunnel. Experimental measurements were made of the intensity distribution $I(l_g)$ obtained from 1-D scans of reciprocal space perpendicular to the diffuse sheets (where each diffuse sheet is specified by integer l_g). The 1-D Patterson maps constructed from the $I(l_g)$ data have a dominant peak at ca. 3.94 Å. which is interpreted as the projection: onto the tunnel axis, of the intermolecular $I\cdots I$ distance. This value is consistent with a model in which the iodine end groups are in van der Waals contact. with the $I\rightarrow I$ vector lying essentially parallel to the tunnel axis.

Guest molecules in solid host structures are often constrained to exhibit uncharacteristic conformational properties, which can be exploited as a means of carrying out spectroscopic characterization of such conformations. For example. guest molecules in the 1,6-dibromohexane/urea inclusion compound (a commensurate system) exist exclusively with both bromine end groups in the *gauche* conformation: allowing a definitive characterization of the vibrational properties of this conformation.[48]

Studies of End-Group Interactions for Unsymmetric Guest Molecules

For unsymmetric guest molecules of the type $X(CH_2)_nY$ in urea inclusion compounds, three different types of end-group interactions are possible within the tunnel (Fig. 3): $X\cdots X$ (head–head). $X\cdots Y$ (head–tail), and $Y\cdots Y$ (tail–tail). Thus. as proposed by Hollingsworth,[49] experimental measurements of the relative numbers of the different types of end-group interaction may yield fundamental information on the relative preferences for interactions between different types of functional groups. An advantage of this strategy for deriving fundamental information on functional group interactions is that, in a host tunnel

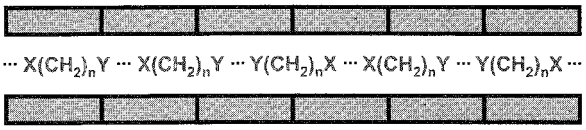

Fig. *3* Schematic illustration of the $X\cdots X$, $X\cdots Y$ and $Y\cdots Y$ intermolecular interactions for unsymmetric guest molecules of the type $X(CH_2)_nY$ inside the urea tunnel structure. (*View this art in color at www.dekker.com.*)

structure. the functional groups are constrained to approach each other in a well-defined and controlled geometry, allowing interactions between different types of fiinctional groups to be compared on a consistent geometric basis. Here we use $N_{X\cdots X}$, $N_{X\cdots Y}$, and $N_{Y\cdots Y}$ to represent the numbers of each type of end-group interaction in a given inclusion compound. For a random distribution of guest orientations, $N_{X\cdots X} + N_{Y\cdots Y} - 2N_{X\cdots Y}$, and any deviations from this relationship indicate the preferential formation of certain end-group interactions.

For many different types of unsymmetric guest molecules $X(CH_2)_nY$ in the urea tunnel structure, the ratio $N_{X\cdots X}/N_{X\cdots Y}$ and the ratio $N_{Y\cdots Y}/N_{X\cdots Y}$ can be determined from high-resolution solid-state ^{13}C-NMR spectroscopy, as many types of end groups show significant chemical shift differences in the presence of different neighboring end groups.[7,49] Examples include the ^{13}C resonances of methyl. aldehyde, nitrile, formate ester. formamide, methyl ester, alkene, alkyne. $-CH_2Cl$, $-CH_2I$, and thiocyanate end groups, the ^{29}Si resonances of SiH_3 end groups, the ^{19}F resonances of $-CH_2F$ and trifluoroacetyl end groups, and the ^{15}N resonances of nitrile end groups. Triple-resonance solid-state NMR techniques may also be exploited in the characterization of different types of end-group interactions.[50]

For a 1-D inclusion compound containing only $X(CH_2)_nY$ guest molecules. $N_{X\cdots X}$ and $N_{Y\cdots Y}$ are equal, and the ratios $N_{X\cdots X}/N_{X\cdots Y}$ and $N_{Y\cdots Y}/N_{X\cdots Y}$ are, therefore, also equal. Knowledge of this ratio from experimental measurements allows assessment of the preference for two $X\cdots Y$ interactions in comparison with one $X\cdots X$ interaction plus one $Y\cdots Y$ interaction, but it provides no information on the relative preferences of $X\cdots X$ interactions versus $Y\cdots Y$ interactions. It has been shown[51] that this limitation can be overcome by considering 1-D inclusion compounds containing two (or more) different types of guest molecules containing the end groups X and Y [for example, $X(CH_2)_nX$ and $X(CH_2)_nY$], and by studying a set of these inclusion compounds for which each member of the set has a different (known) molar ratio of the two types of guest molecules. Provided the molar ratio of the two types of guests in each member of the set is known from independent measurements (such as chemical analysis, elemental analysis, or spectroscopic measurements), the intrinsic relative preferences for all the $X\cdots X$, $X\cdots Y$, and $Y\cdots Y$ interactions can be extracted from the experimentally measured ratios $N_{X\cdots X}/N_{X\cdots Y}$ and $N_{Y\cdots Y}/N_{X\cdots Y}$.

DYNAMIC PROPERTIES

Several techniques have been used to investigate dynamic properties of urea inclusion compounds. including solid-state NMR, incoherent quasielastic neutron scattering; ESR, molecular dynamics simulation, Raman, infrared, dielectric loss, and x-ray diffraction. In addition to investigations of the dynamics of the guest molecules, the dynamic properties of the urea molecules have also been studied.

Early studies of guest motion in urea inclusion compounds focused on solid-state ^{1}H-NMR,[52] with measurements of line widths. second moments, and spin lattice relaxation times. Subsequent NMR work has mainly involved ^{2}H-NMR of urea inclusion compounds containing fully deuterated or selectively deuterated guest molecules.[33–35,38,39,53] These experiments probe the ^{2}H quadrupole interaction parameters, and line shape analysis of the ^{2}H-NMR spectra can provide detailed inechanistic information for motions with characteristic timescales between about 10^{-3} s and 10^{-8} s. ^{2}H-NMR provides information on reorientational motions of the guest molecules but does not yield direct information on translational motions. Progress in understanding translational motions (in addition to reorientational motions) has been made using incoherent quasielastic neutron scattering (IQNS),[36,37] which probes motions on characteristic timescales between about 10^{-10} s and 10^{-12} s. The ^{1}H isotope has a large incoherent neutron scattering cross-section and generally dominates the incoherent neutron scattering from organic solids. For urea inclusion compounds containing urea-d_4 and guest inolecules containing natural isotopic abundances, the incoherent neutron scattering arises predominantly from the guest molecules. BQNS studies of such materials selectively probe the dynamics of the guest molecules. By studying semioriented polycrystalline samples in which the tunnel axes of all crystals are aligned parallel to each other, and measuring the IQNS spectra either with the neutron momentum transfer vector parallel ($Q_\parallel$ spectra) or perpendicular ($Q_\perp$ spectra) to the tunnel axes. the translational motions of the guest molecules along the tunnel ($Q_\parallel$ spectra) can be investigated separately from the reorientational motions of the guest molecules about the tunnel ($Q_\perp$ spectra).

For alkane/urea and α,ω-dibromoalkane/urea inclusion compounds, ^{2}H-NMR studies have provided valuable

insights into the reorientational motions of the guest molecules about the tunnel axis in the high-temperature phase, although the timescale of the dynamics in the high-temperature phase is generally short in comparison with the timescale of the ^{2}H-NMR technique. IQNS spectroscopy has provided a more complete description of the translational as well as the reorientational dynamics of the guest molecules. and detailed studies of alkane/urea[36] and α,ω-dibromoalkane/urea[37] inclusion compounds have been carried out. In both cases, there is quasielastic broadening in the $Q_\perp$ spectra in the high-temperature phase, implying rapid reorientation of the guest molecules about the tunnel axis. This motion is diffusive (rather than discrete jumps) and can be modeled as uniaxial rotational diffusion in a onefold cosine potential. Rotational diffusion coefficients (0.3×10^{-12} s^{-1} for nonadecane/urea-d_4 at 306 K) and other parameters relating to this dynamic process have been determined as a function of temperature. The Q spectra indicate that there is also rapid translation of the guest molecules along the tunnel. This motion can be modeled as translational diffusion between impermeable boundaries, and the diffusion coefficient and translation length have been determined as a function of temperature. For nonadecane/urea-d_4, the translation length is 2.7 Å at 306 K and 1.1 Å at 160 K (just above the phase transition), and the translational diffusion coefficient at ambient temperature is 1.5×10^{-5} cm^{2}s^{-1}. Given the extent of motion of the guest molecules, it is remarkable that x-ray diffraction patterns at ambient temperature indicate both long-range intratunnel and intertunnel ordering of the guest molecules, and there is presumably a high degree of correlation between the translations of neighboring guest molecules both within a given tunnel and between adjacent tunnels.

The dynamics of the guest molecules in nonadecane/urea have also been probed in detail by molecular dynamics simulations.[54] The results indicate, inter alia, that the interaction between adjacent guest molecules in the tunnel exerts an important influence on their translational and reorientational motions and demonstrates that the reorientation of the guest molecules about the tunnel axis is coupled with movements of the host structure. Importantly, this work established links between the results from the molecular dynamics simulations and experimental results from IQNS spectroscopy.

Although the alkanelurea and α,ω-dibromoalkane/urea inclusion compounds exhibit similar dynamic behavior, the dynamic properties of other urea inclusion compounds can differ substantially. The dynamic properties of dioctanoyl peroxide guest molecules have been investigated[53] by a combined approach employing IQNS and ^{2}H-NMR. Both techniques indicate that the reorientation of the guest molecules about the tunnel axis can be described by a model of uniaxial rotational diffusion in a twofold potential, with two preferred orientations separated by 116". The orientational distribution of the dioctanoyl peroxide guest molecules is substantially more restricted than that for the guest molecules in alkanelurea and α,ω-dibromoalkane/urea inclusion compounds, and a mechanism involving conformational interconversion of the dioctanoyl peroxide molecules is consistent with the observed dynamic model. The translation of the guest molecules along the tunnel can be interpreted by a model involving jumps between sites with unequal probabilities of occupation, in contrast with the more continuous description of translational diffusion for alkanelurea and α,ω-dibromoalkane/urea inclusion compounds. There is agreement between the IQNS and ^{2}H-NMR techniques in describing the reorientational dynamics of the guest molecules in this system, and the combination of these techniques represents a powerful strategy for probing motions across a range of different timescales.

The dynamic properties of the urea molecules have also received attention. Thus, ^{2}H-NMR studies of the alkane/urea-d_4[55] and α,ω-dibromoalkane/urea-d_4[56] inclusion compounds have shown that, at sufficiently high temperatures, the urea molecules undergo 180° jumps about their C=O axes. For 1,10-dibromodecane/urea-d_4 at 293 K, the jump frequency is 5×10^6 s^{-1}, and there is no evidence for reorientation of the NH_2 groups about the C–N bond (on the ^{2}H-NMR timescale). The timescale of the 180" jumps of the urea molecules is substantially longer (at a given temperature) than the timescale of the guest motions described above, suggesting that the 180° jumps of the urea molecules are not correlated with the translational and reorientational motions of the guest molecules.

FUNDAMENTAL AND APPLIED ASPECTS

Practical Applications in Industrial, Commercial, and Laboratory Contexts

Many studies of urea inclusion compounds have focused on practical applications, such as inclusion polymerization. stabilization of liquids or unstable solids in an isolated form, and molecular separation and chromatography. Chemists studying fatty acids, for example. routinely use urea inclusion compounds to carry out molecular separations. Among industrial examples, urea inclusion compound formation has been used by the petroleum industry in the dewaxing of certain oil fractions. although zeolites are now routinely used in such applications. Other applications include stabilization of diacyl peroxides and peroxy acids in laundry products, and the use of urea inclusion compounds as solid supports in gas–liquid chromatography.

Chemical Reactions of Guest Molecules

Much early work relating to chemical reactions in urea inclusion compounds focused on studies,[57] primarily using ESR spectroscopy, of radicals generated from the guest molecules by x-ray irradiation. and provided fundamental information about the spin density and its anisotropy in a variety of radical species. Subsequently, a number of other workers have used ESR spectroscopy to identify radicals formed by x-ray or γ-ray irradiation and to study the dynamic, chemical. and electronic properties of these radicals.[''' Details of these studies were reviewed elsewhere.[7]

Detailed studies of the photodecomposition of diacyl peroxide guest molecules within the urea tunnel structure have been carried out. [7] and have provided interesting contrasts to the photodecomposition behavior of the same molecules in their ''pure.' crystalline phases, which have been investigated in considerable depth by McBride, Hollingsworth, and coworkers.

The photolysis processes of alkanone guest molecules in urea inclusion compounds have also been studied[59] and have been shown to involve Norrish Type II reactions. For 5-nonanonelurea and 6-undecanone/urea. the reactions show an almost complete diastereoselective preference for the *Z*-cyclobutanol product.

Papers concerning the physical properties of polymers as the guest components in urea inclusion compounds and polymerization reactions of guest monomer molecules within the urea tunnel structure have been reviewed elsewhere.[7,60] The polymers studied included poly(ethylene), poly(acrylonitrile), poly(1,3-butadiene), poly(ethylene oxide), poly(tetrahydrofuran), poly(acrolein), poly(vinyl chloride), poly(ethyl acrylate), poly(lactide), poly(lactic acid), poly(ethylene adipate). poly(ethylene succinate). acrylonitrile-ethyl acrylate copolymer. and poly(hexanediol diacrylate).

Host–Guest Chiral Recognition

The host structure in the conventional urea inclusion compounds is a spiral hydrogen-bonded arrangement of urea molecules. A given single crystal contains only right-handed spirals (space group $P6_122$) or only left-handed spirals (space group $P6_522$), and the host structure in a given single crystal is therefore chiral. This chirality is generated spontaneously during crystal growth of the inclusion compound. Clearly. the chiral nature of the host structure has the potential to influence the structural and chemical properties of chiral guest molecules. As the *R*-guest/($P6_122$)–host and *S*-guest/($P6_122$)–host systems have a diastereoisomeric relationship, a given crystal of the inclusion compound should have a preference to incorporate one particular enantiorner of a chiral guest species. and extensive experimental investigations by Schlenk[61,62] independently showed that the formation of urea inclusion compounds containing chiral guest molecules can be associated with significant chiral recognition. Recent computational investigations[63] have provided insights into the characteristics of host–guest interaction that underlie the chiral recognition. focusing on urea inclusion compounds containing chiral 2-bromoalkane [CH_3.C(Br)H.-$(CH_2)_nCH_3$] guest molecules. These studies have shown, inter alia, that there is a clear energetic preference for the R-enantiomer of the 2-brornoalkane guest molecules within the $P6_122$ urea tunnel. In assessing enantiomeric excesses for incommensurate systems. such as 2-bromoalkanelurea inclusion compounds, it is necessary to explore the host–guest interaction as a function of the position of the guest molecule along the tunnel. For example, for the lowest-energy conformation (Br *trans*/CH_3 *gauche*) of the 2-bromotridecane guest within the tunnel, the same enantiomer (*R*) is preferred at all positions along the $P6_122$ tunnel (for other conformations, such as Br *gauche*/CH_3 *trans*. the R enantiomer is preferred at some positions, and the S enantiomer is preferred at other positions). The assignment of the lowest-energy conformation (Br *trans*/CH_3 *gauche*) from these computational studies is in agreement with a direct experimental measurement of this property using bromine K-edge x-ray absorption spectroscopy.[64]

Orientation of Molecules for Spectroscopic Research

In general, confinement of guest molecules within the urea tunnel structure can be exploited as a means of isolating and orienting these molecules, or selecting a specific conformational state. in order that detailed spectroscopic studies can be carried out. One example concerns characterization of the spectroscopic properties of linear conjugated polyenes. An important property relating to the use of conjugated poiyenes in nonlinear optoelectronics and other applications is the orientation of the electronic transition dipole moment relative to the long-axis of the molecule. Experimental investigations are rendered difficult by the requirement to prepare perfectly oriented samples of the polyenes. This problem has been addressed[i6''' by constraining such molecules within the urea tunnel structure. ensuring that the molecular axes of all guest molecules are parallel and orientationally well-defined with respect to the crystal morphology. In these studies, octadeca-9,11,13,15-tetraenoic acid was considered as a dilute guest within the hexadecane/urea inclusion compound. and polarized fluorescence excitation spectra showed that the transition dipole lies at an angle of ca. 20 ± 1" with respect to the molecular axis of the guest. On

taking into account the effects of the surrounding medium, this value becomes modified to ca. 15 ± 1° for the isolated molecule. This result has important implications with regard to applications of these materials. There are clearly important prospects for exploiting the urea tunnel structure in such studies that require unidirectional alignment of molecules (guests) for measurement of electronic or other properties.

Control of Crystal Morphology

To explore several properties of crystalline solids and to exploit some of their applications, it is often crucial to obtain single crystals with a specific desired shape (morphology). However, the crystal morphology produced spontaneously by normal crystal growth procedures is often not the required morphology, and in such cases. experimental strategies must be devised to bias the crystal growth toward the desired morphology. Crystal growth is generally governed by kinetic factors, and to alter the crystal morphology requires control of the relative rates of crystal growth in different directions. A general strategy for controlling the crystal morphology of tunnel inclusion compounds (ranging from long-needle crystals to flat-plate crystals) has been developed and demonstrated for alkane/urea inclusion compounds. Spontaneous crystal growth of alkane/urea inclusion cornpounds produces a long hexagonal needle morphology as the rate of growth parallel to the tunnel ($k_{\|}$) is substantially greater than the rate of growth perpendicular to the tunnel ($k_{\perp}$). It has been shown that crystals of alkane/urea inclusion compounds can be induced to grow instead as hexagonal flat plates by using a selective crystal growth inhibitor (5-octadecyloxyisophthalic acid; 5-ODOIPA) that reduces the rate of crystal growth along the tunnel direction, such that $k \ll k_{\perp}$. Furthermore, by altering the concentration (c_{inh}) of inhibitor in the crystaflization solution. crystals with any desired morphology between the two extreme situations [long-needle crystals ($c_{inh} = 0$: $k_{\|} \gg k_{\perp}$) and flat-plate crystals (c_{inh} sufficiently large; $k_{\|} \ll k_{\perp}$)] can be grown, including (for intermediate values of c_{inh}) the growth of crystals that have comparable dimensions parallel and perpendicular to the tunnel axis (arising from $k_{\|} \approx k_{\perp}$).

Guest Exchange Processes

The ability to separate different types of molecules based on their structural characteristics is an important objective in many aspects of chemistry. Solid host structures can play an important role in such applications. as the host structure can display selectivity with regard to incorporation of guest molecules of differing size, shape. and in some cases also chirality. Many families of solid inclusion compounds (forexample. zeolites) are widely used in such applications. However, the fact that the "empty" urea tunnel structure is unstable limits much of the scope for using urea inclusion compounds in this regard. Thus, applications involving diffusion of guest molecules into, within, and out of the "empty" host structure are not feasible. However. it is, nevertheless, feasible to carry out exchange of guest molecules within urea inclusion compounds, provided that full occupation of the tunnel by guest molecules is maintained at all stages during the exchange process (with the actual identity of the guest molecules changing with time due to the exchange process). A general design strategy for achieving such exchange processes in urea inclusion compounds has been demonstrated.[68] Net transport of guest molecules in one direction along the tunnel can be achieved by inserting new (thermodynamically more favorable) guest molecules at one end of the crystal (e.g., by dipping it into the liquid phase of the new guest). with the original guest molecules expelled from the other end of the crystal. Such phenomena have considerable potential as the basis of highly selective microscale separation techniques. based on discrimination of molecular size, shape, and chirality.

Experimental Assessment of Host–Guest Interaction Energies

In order to derive a fundamental rationalization of the structural properties of molecular solids. it is essential to understand the intermolecular interactions that govern the observed molecular packing arrangement. However, while chemists have considerable intuitive understanding of preferred intermolecular interaction motifs, derived from observing common motifs in known crystal structures and from conducting computational studies of intermolecular interaction strengths, there is a paucity of direct quantitative experimental information on intermolecular interaction energies in molecular solids. A method has been developed[69] for estimating interaction energies in tunnel inclusion compounds directly from experimental investigations. The method focuses on the competitive coinclusion of two different types of guest molecules $X(S)_{ni}X$ and $X(S)_{nj}X$ within the same host tunnel structure. For each pair of guest molecule types [i, j), the inclusion compound is prepared for several different values of the proportion of $X(S)_{ni}X$ molecules in the crystallization solution (denoted by γ_i), and in each case. the proportion of $X(S)_{ni}X$ guest molecules in the inclusion cornpound (denoted by m_i) is measured. Thus. the experimental data comprise several values of (γ_i, m_i) for each pair of guest molecule types [i. j). The values of (γ_i, m_i) indicate the

relative extent of uptake of the two different types of guest molecules within the host tunnel structure, which in turn. depends on the interaction energies within the inclusion compound. A mathematical method has been developed for determining interaction energy terms for the tunnel inclusion compound directly from experimental measurements of (γ_i, m_i), and this method has been applied[70] to real experimental data for urea inclusion compounds containing binary mixtures of α.ω-dibromoalkane [$Br(CH_2)_nBr$] guest molecules. The interaction energy terms derived from the experiinental data are found to be in agreement with the corresponding interaction energy terms computed using a standard potential energy parameterization.

Analyzer Crystals for X-Ray Polarization Analysis

Studies of polarization of visible light are dominated by the use of dichroic filters (e.g., the Polaroid sheet), for which radiation with polarization parallel to a certain axis in the material is preferentially attenuated over radiation with polarization perpendicular to this axis. In principle, materials analogous to the Polaroid sheet may be developed as dichroic filters for polarized x-ray radiation and would have considerable potential in a range of applications (for example, in the field of magnetic x-ray scattering), although the development of a dichroic filter material for x-ray polarization analysis was demonstrated for the first time only recently.[71] The material studied was the 1.10-dibromodecanelurea inclusion compound, and the successful application of this material as a dichroic filter was demonstrated in a study of magnetic diffraction from antiferromagnetic holmium. In spite of this success, however. the efficiency of 1.10-dibromodecane/urea as a dichroic filter is limited by the fact that the C–Br bonds undergo reorientation around the tunnel axis at ambient temperature and are oriented at about 35° to this axis. Theoretical considerations suggest that a tunnel inclusion compound in which all C–Br bonds are aligned parallel to the tunnel would be a more effective material, and this situation has been realized subsequently for the 1-bromoadamantane/thiourea inclusion compound.

Properties of Commensurate Systems

While the focus of the majority of this article has been on the conventional (incommensurate) urea inclusion compounds. studies by Hollingsworth and coworkers have revealed a wide range of interesting physical properties of commensurate tunnel inclusion compounds of urea containing alkanone and $(\alpha + 1),(\omega - 1)$-alkanedione guest molecules. These studies have led to a profound level of understanding of the interactions within these materials and the ways in which these interactions control properties such as ferroelastic behavior (i.e., domain reorientation under the application of external anisotropic stresses)[72] and crystal growth mechanisms.[''' As an illustration, we highlight a study of stress-induced domain reorientation in the 2,10-undecanedione/urea inclusion compound, which is a commensurate system ($2\,c_g = 3\,c_h$) with a well-defined stoichiometric guestlurea ratio (1/9) and a well-defined positioning of the guest molecules with respect to the host structure. One out of every three urea molecules is oriented such that its two *syn* N–H groups form N–H···O hydrogen bonds with C=O groups of guest molecules in different tunnels. All C=O groups of the guest molecules are involved in host–guest hydrogen bonding in this way. producing an extended hydrogen-bonded network connecting the host and guest components throughout the structure and providing a direct mechanism for guest molecules in different tunnels to communicate with each other. Not surprisingly, the structure is distorted from the hexagonal structure of the conventional urea inclusion compounds and is orthorhombic. Crystals of this inclusion compound consist of domains; within a given domain, the planes of all guest molecules are oriented in the same direction, with different domains related to each other by rotation of the guest molecules by a multiple of ca. 60° about the tunnel axis. These domains are birefringent, allowing the different domain orientations to be observed directly by optical microscopy (striking optical micrographs illustrating the well-defined sectoring of crystals of this inclusion compound have been published[72]). A remarkable property of these inclusion compounds is that compressive stresses applied to the crystal can bring about reorientation of the domains. Reorientation of the guest molecules associated with this domain reorientation requires breakage and formation of hydrogen bonds (guest–host and host–host), and the requirement to reconstruct the guest–host hydrogen-bonding network underlies the large-scale cooperativity of this process. Interestingly, by incorporating 2-undecanone guest impurities (ca. 20%), the domain reorientation is spontaneously reversible, with the daughter phase reverting to the mother phase when the applied stress is removed. The 2-undecanone impurities disrupt the guest–host hydrogen-bonding scheme. influencing the energetic properties of the mother and daughter phases and the interface between them.

Among studies of other commensurate inclusion compounds of urea. it has been shown[''' that structural changes in the 1,6-dibromohexane/urea inclusion compound as a function of temperature (the metric symmetry

moves progressively toward hexagonal as temperature is increased) can be rationalized on the basis of motions of the guest molecules that occur as a mechanism for relaxation of strain within the inclusion compound.

CONCLUSION

As highlighted above, it is clear that urea inclusion compounds exhibit a diverse range of interesting and important physicochemical phenomena, including incommensurate structural properties, order–disorder phase transitions, molecular motion, properties relating to 1-D confinement, chemical reactivity, and ferroelastic properties. In spite of the apparent simplicity of the 1-D tunnel system in urea inclusion compounds, the quest to develop a fundamental understanding of the intricate details of the structural and dynamic properties of these materials, and the interrelationships between these properties, present many challenges that will continue to captivate the attention of chemists and physicists for many years to come. Furthermore, with continued progress in deepening the level of fundamental understanding of the properties of urea inclusion compounds, it may be expected that future advances in the design and development of applications based upon these materials will be forthcoming.

ARTICLES OF FURTHER INTEREST

Brillouin Scattering, p. 129
Channel Inclusion Compounds, p. 223
Disorder and Diffuse Scattering, p. 457
Halogen Bonding, p. 628
Hydrogen Bonding, p. 658
Inclusion Reactions and Polymerization, p. 705
Incommensurate and Commensurate Structures, p. 712
Modulated Structures, p. 873
Polarity Formation: Markov Chain Model, p. 1120
Soft and Smart Materials, p. 1302
Space Groups and Crystal Packing Modes, p. 1337
Thiourea Inclusion Compounds, p. 1501
X-Ray Crystallography, p. 1586

REFERENCES

1. Bengen, M.F. (I.G. Farbenindustrie). Ger. Pat. Appl., OZ 123438. **1940**.
2. Smith, A.E. The crystal structure of the urea-hydrocarbon complexes. Acta Crystallogr. **1952**, *5*, 224.
3. Harris, K.D.M.; Thomas, J.M. Structural aspects of urea inclusion compounds and their investigation by X-ray diffraction: A general discussion. J. Chem. Soc., Faraday Trans. **1990**, *86*, 2985.
4. Schiessler, R.W.; Flitter, D. Urea and thiourea adduction of C5–C42 hydrocarbons. J. Am. Chem. Soc. **1950**, *74*, 1720.
5. Fetterly, L.C. *Non-Stoichiometric Compounds*; Mandelcorn, L., Ed.; Academic Press: New York, 1964; 491.
6. Takemoto, K.; Sonoda, N. *Inclusion Compounds*; Atwood, J.L., Davies, J.E.D., MacNicol, D.D., Eds.; Academic Press: New York, 1984; Vol. 2, 47.
7. Hollingsworth, M.D.; Harris, K.D.M. *Comprehensive Supramolecular Chemistry*; MacNicol, D.D., Toda, F., Bishop, R., Eds.; Pergamon Press, 1996; Vol. 6, 177.
8. Harris, K.D.M. Understanding the properties of urea and thiourea compounds. Chem. Soc. Rev. **1997**, *26*, 279.
9. Harris, K.D.M. Towards a fundamental understanding of urea and thiourea inclusion compounds. J. Chin. Chem. Soc. **1999**, *46*, 5.
10. Guillaume, F. Des cristaux organiques d'intercroissance incommensurables 1-D: les composés d'inclusion de l'urée. J. Chim. Phys. (Paris) **1999**, *96*, 1295.
11. Hollingsworth, M.D.; Werner-Zwanziger, U.; Brown, M.E.; Chaney, J.D.; Huffman, J.C.; Harris, K.D.M.; Smart, S.P. Spring-loading at the molecular level: Relaxation of guest-induced strain in channel inclusion compounds. J. Am. Chem. Soc. **1999**, *121*, 9732.
12. Hollingsworth, M.D.; Santarsiero, B.D.; Harris, K.D.M. Zig-zag channels in the structure of sebaconitrile/urea. Angew. Chem. Int. Ed. Engl. **1994**, *33*, 649.
13. Brown, M.E.; Chaney, J.D.; Santarsiero, B.D.; Hollingsworth, M.D. Superstructure topologies and host-guest interactions in commensurate inclusion compounds of urea with bis(methyl ketone)s. Chem. Mater. **1996**, *8*, 1588.
14. Chenite, A.; Brisse, F. Structure and conformation of poly(ethylene oxide), PEO, in the trigonal form of the PEO-urea complex at 173 K. Macromolecules **1991**, *24*, 2221.
15. Chenite, A.; Brisse, F. Poly(tetrahydrofuran)-urea adduct: A structural investigation. Macromolecules **1992**, *25*, 776.
16. Eaton, P.; Vasanthan, N.; Shin, I.D.; Tonelli, A.E. Formation and characterization of polypropylene-urea inclusion compounds. Macromolecules **1996**, *29*, 2531.
17. Harris, K.D.M.; Hollingsworth, M.D. Structural properties of the guest species in diacyl peroxide/urea inclusion compounds: An x-ray diffraction investigation. Proc. R. Soc., A **1990**, *431*, 245.
18. Harris, K.D.M.; Smart, S.P.; Hollingsworth, M.D. Hollingsworth, Structural properties of α,ω-dibromoalkane/urea inclusion compounds: A new type of interchannel guest molecule ordering. J. Chem. Soc., Faraday Trans. **1991**, *87*, 3423.
19. Shannon, I.J.; Stainton, N.M.; Harris, K.D.M. Structural properties of urea inclusion compounds containing carboxylic acid anhydride guest molecules: Anomalous modes of guest-molecule ordering. J. Mater. Chem. **1993**, *3*, 1085.
20. van Smaalen, S.; Harris, K.D.M. Superspace group

descriptions of the symmetries of incommensurate urea inclusion compounds. Proc. R. Soc., A 1996. *452*. 677.
21. Weber, T.: Boysen, H.: Frey, F.; Neder, R.B. Modulated structure of the composite crystal urea/*n*-heptadecane. Acta Crystallogr. 1997. *B53*, 544.
22. Beral. I.: Madariaga, G.: Petricek, V.: Breczeivski, T. Superspace description of the structure of the composite crqstal urea/*n*-octane at room temperature. Acta Crystallogr. 2001, *B57*, pp. 378. 386.
23. Lefort. R.: Etrillard. J.: Toudic. B.: Guillaume, F.: Breczewski, T.: Bourges, P. Incommensurate intermodulation of an organic intergrowth compound observed by neutron scattering. Phys. Rev. Lett. 1996. 77.4027.
24. Welberry, T.R.: Mayo, S.C. Diffuse x-ray scattering and Monte Carlo study of guest-host interactions in urea inclusion compounds. J. Appl. Cryst. 1996. *29*, 353.
25. Mayo, S.C.; Welberry, T.R.: Brown. M.: Tarr. A. Order and disorder in *p*-dialkylbenzene-urea inclusion compounds. J. Solid State Chem. 1998. *141*. 437.
26. Le Lann, H.; Toudic. B.; Lefort. R.: Etrillard, J.; Guillaume, F.: Ruffle. B.; Ollivier. J.: Lechner. R.E.: Breczewski. T. Coherent neutron analysis of diffuse scattering in an alkane-urea composite. Physica, B 2000, 276. 298.
27. Chao, M.-H.; Harris, K.D.M.: Kariuki, B.M.; Bauer. C.L.: Foxman, B.M. Characterization of intermolecular interactions in a disordered solid via a one-dimensional Patterson synthesis. J. Phys. Chem. B. 2002, *106*. 4032.
28. Chatani, Y.; Taki. Y.; Tadokoro. H. Low-temperature form of urea adducts with *n*-paraffins. Acta Crystallogr. 1977, *B33*. 309.
29. Harris. M.D.M.: Carneson. I.: Thomas, J.M. Powder x-ray diffraction studies of a loiv-temperature phase transition in the n-hexadecane/urea inclusion compound. 3. Chem. Soc., Faraday Trans. 1990, *86*. 3135.
30. Yeo, L.; Harris. K.D.M. Definitive structural characterization of the conventional low-temperature host structure in urea inclusion compounds. Acta Crystallogr. 1997. *B53*, 822.
31. Ueo. k.: Kariuki, B.M.; Serrano-González, H.: Harris, K.D.M. Structural properties of the low-temperature phase of the hexadecane/urea inclusion compound. investigated by synchrotron x-ray powder diffraction. J. Phys. Chem., B 1997. *101*, 9926.
32. Le Lann, H.: Odin, C.: Toudic. B.; Ameline. J.C.; Callier. J.: Guillaume, F.: Breczewski, T. Single-crystal deuterium NMR study of the symmetry breaking in an incommensurate organic inclusion compound. Phys. Rev.. B 2000, *62*. 5442.
33. Casal, H.L.; Cameron, D.G.; Kelusky, E.C. A ^{2}H NMR study of inolecular motions of nonadecane-d_{40} in a urea inclusion adduct. J. Chern. Phys. 1984. *80*. 1407.
34. Greenfield. M.S.: Vold. R.L.; Vold. R.K. Deuterium relaxation and vibrationally averaged quadrupole coupling in an alkane/urea clathratc. J. Chem. Phys. 1985. *83*. 1440.
35. Harris. M.D.M.: Jonsen, P. ^{2}H NMR investigation of the dynamic behaviour of *n*-hexadecane in its urea inclusion compound. Chem. Phys. Lett. 1989, *154*. 593.
36. Guillaume. *F.*: Sourisseau. C.: Dianoux. A.-J. Rotational and translational motions of n-nonadecane in the urea inclusion compound as evidenced by incoherent quasi-elastic neutron scattering. J. Chim. Phys. (Paris) 1991, *88*. 1721.
37. Smart. S.P.: Guillaume. F.: Harris. K.D.M.: Dianoux. A.-J. Neutron scattering investigations of guest molecular dynamics in α,ω-dibromoalkane-urea inclusion compounds. J. Phys.. Condens. Matter 1994. 6. 2169.
38. Aliev. A.E.: Smart, S.P.: Shannon. I.J.: Harris. K.D.M. Structural and dynamic properties of the 1.10-dibromodecane/urea inclusion compound. investigated by variable-temperature powder x-ray diffraction, solid-state ^{2}H NMR lineshape analysis and ^{2}H NMR spin-lattice relaxation time measurements. J. Chem. Soc., Faraday Trails 1996. *92*. 2179.
39. El Baghdadi, A.; Dufourc, E.J.: Cuillaume. F. Chain end dynamical and conformational properties of *n*-nonadecane molecules in urea inclusion compounds: A study by deuterium NMR spectroscopy. J. Phys. Chem. 1996. *100*. 1746.
40. Etrillard. J.: Lasjaunias, J.C.: Toudic. B.: Guillaume. F.: Breczewski. T. Low-frequency dynamics in molecular incommensurate composite: Specific heat of nonadecane/urea inclusion compound. Europhys. Lett. 2000. *49*. 610.
41. Lefort. R.: Toudic. B.; Etrillard, J.; Bourges, P.: Currat. R.: Breczewski, T. Dynamical molecular disorder and diffuse scattering in an alkane/urea incommensurate inclusion compound. Eur. Phys. J., B 2001, 24. 51.
42. Yeo. L.: Harris. K.D.M.: Guillaume. F. Temperature-dependent structural properties of the 1,10-decanedicarboxylic acid/urea inclusion compound. J. Solid State Chem. 1997. *128*. 273.
43. kynden-Bell. R.M. The orientational order-disorder phase-transition of urea paraffin inclusion compounds. Mol. Phys. 199%. 79. 313.
44. Shannon, I.J.: Harris. K.D.M.: Guillaume. F.: Bocanegra. E.H.: MacLean. E.J. Phase transitions involving reordering of the guest molecules in a solid organic inclusion compound: Heptanoic anhydride/urea. J. Chem. Soc., Chem. Commun. 1995, *2341*.
45. Smart. S.P.: El Baghdadi, A.: Guillaume. F.: Harris. K.D.M. Conformational and vibrational properties of α,ω-dihalogenoalkane/urea inclusion compounds: Raman scattering investigation. J. Chem. Soc.. Faraday Trans. 1994, *90*. 1313.
46. Nordon, A.; Hughes. E.: Harris. R.K.: Yeo. L.; Harris. K.D.M. Direct measurement of the distance between adjacent guest molecules in a disordered solid inclusion compound using solid-state ^{19}F-^{1}H NMR spectroscopy. Chem. Phys. Lett. 1998. *289*, 25.
47. Shannon. I.J.: Harris. K.D.M.: Mahdyarfar. 4.: Johnston. P.; Joyner, R.W. EXAFS spectroscopic studies of the bromine environment in the crystalline inclusion compounds formed between urea and α,ω-dibromoalkanes. J. Chem. Soc., Faraday Trans. 1993. *89*. 3099.
48. Elizabe. L.: Smart. S.P.: El Baghdadi, A.: Guillaume, F.: Harris. K.D.M. Characterization of gauche end-groups in α,ω-dibromoalkanes: Vibrational properties of the 1.6-

dibromohexanelurea inclusion compound. J. Chem. Soc., Faraday Trans. 1996. *92.* 267.
49. Hollingsworth. M.D.: Cyr. N. Solid-state NMR studies of functional group recognition in channel inclusion compound formation. Mol. Cryst. Liq. Cryst. 1990. *187,* 135.
50. Nordon, A.: Harris. R.K.: Yeo. L.; Harris. K.D.M. Application of triple-channel ^{13}C-{^{1}H,^{19}F} NMR techniques to probe structural properties of disordered solids. Chern. Commun. 1997. 2045.
51. Harris, K.D.M.: Jupp. P.E. Stochastic models for guest-guest interactions in one-dimensional inclusion compounds. Proc. R. Soc. A 1997. *453.* 333.
52. Bell. J.D.: Richards. R.E. Nuclear spin relaxation studies on urea + hydrocarbon clathrates. Trans. Faraday Soc. 1969. *65,* 2529.
53. Girard, P.: Aliev. A.E.: Guillaume, F.: Harris. K.D.M.: Hollingsworth. M.D.; Dianoux. A.-J.: Jonsen. P. Dynamic properties of dioctanopl peroxide guest molecules constrained within the urea tunnel structure: A combined incoherent quasielastic neutron scattering and solid state ^{2}H nuclear magnetic resonance investigation. J. Chem. Phys. 1998. *109.* 4078.
54. Souaille. M.: Guillaume. F.: Smith. J.C. Molecular dynamics simulation of n-nonadecane in urea inclusion compound. II. Rotational distribution and elastic incoherent structure factor. J. Chem. Phys. 1996. *105.* pp. 1516. 1529.
55. Heaton, N.J.: Vold. R.L.: Vold. R.R. Deuterium quadrupole echo study of urea motion in urea/n-alkane inclusion compounds. J. Amer. Chem. Soc. 1989. *111,* 3211.
56. Aliev, A.E.: Smart. S.P.; Harris. K.D.M. Dynamic properties of the urea molecules in α,ω-dibromoalkane/urea inclusion compounds investigated by ^{2}H NMR spectroscopy. J. Mater. Chern. 1994, *4.* 35.
57. Griffiths, O.H. Electron spin resonance of RCHCOR' radicals in X-irradiated ketone-urea inclusion compounds. J. Chem. Phys. 1965. *42.* 2644.
58. Segre. *U.;* Brustolon, M.: Maniero. A.L.: Bonon. F. ESR and ENDOR relaxation study of molecular motions of a ketone/urea inclusion compound. J. Phys. Chem. 1993. *97,* 2904.
59. Casal. H.L.: de Mayo, P.: Miranda. J.F.: Scaiano, J.C. Photodecomposition of alkanones in urea inclusion compounds. J. Am. Chem. Soc. 1983. *105,* 5155.
60. Farina. M. *Inclusion* Compounds: Atwood, J.L., Davies, J.E.D.,MacNicol. D.D.. Eds.; Academic Press: New York, 1984: Vol. 3. 297.
61. Schlenk. W. Asymmetric urea inclusion lattice. Justus Liebigs Ann. Chem. 1973. *7.* 1145 (I. Separation of racements), 1156 (II. Stable configurational lattice coordination of the guest molecules), 1179 (III. Unstable configuration lattice coordination of the guest molecules), 1195 (IV. Absolute configuration of the lattice).
62. Arad-Yellin, R.: Green. B.S.: Knossow, M.: Tsoucaris, G. *Inclusion Compounds*; Atwood. J.L., Davies, J.E.D., MacNicol, D.D.. Eds.; Academic Press: New York. 1984: Vol. 3. 263.
63. Yeo, L.: Harris, K.D.M. A computational investigation of host-guest chiral recognition in incommensurate 2-bromoalkane/urea inclusion compounds. J. Chem. Soc., Faraday Trans. 1998. *94,* 1633.
64. Elizabé, L.: Yeo. L.: Harris. K.D.M.: Sankar. G.: Thomas. J.M. Conformational properties of guest molecules in constrained solid-state environments: Bromine K-edge x-ray absorption spectroscopy of 2-bromoalkane/urea inclusion compounds. Chem. Mater. 1998, *10.* 1220.
65. Shang, *Q.Y.;*Dou, X.: Hudson, B.S. Off-axis orientation of the electronic transition moment for a linear conjugated polyene. Nature 1991, *352.* 703.
66. Lee, S.-O.; Harris. K.D.M. Controlling the crystal morphology of one-dimensional tunnel structures: Induced crystallization of alkanelurea inclusion compounds as hexagonal flat plates. Chem. Phys. Lett. 1999. *307,* 327.
67. Kelly. N.E.: Lee. S.-O.; Harris. K.D.M. Fine-tuning the crystal morphology of tunnel inclusion compounds: A general strategy. J. Am. Chem. Soc. 2001, *123.* 12682.
68. Khan, A.A.; Bramwell. S.T.; Harris. K.D.M.; Kariuki, B.M.; Truter, M.R. The design of a molecularly selective capillary based on an incommensurate intergrowth structure. Chem. Phys. Lett. 1999, *307.* 320.
69. Harris, K.D.M.; Jupp. P.E.: Lee. S.-O. A theoretical framework for the experimental determination of host-guest interaction energies in solid inclusion compounds. J. Chem. Phys. 1999. *111,* 9784.
70. Lee, S.-O.; Harris, K.D.M.: Jupp, P.E.: Yeo. L. Experimental determination of interaction energies in a porous molecular solid. J. Am. Chem. Soc. 2001, *123.* 12913.
71. Collins, S.P.: Laundy. D.; Harris. K.D.M.: Kariuki. B.M.: Bauer. C.L.: Brown. S.D.: Thompson, P. X-ray linear dichroism in an α,ω-dibromoalkane/urea inclusion compound and its application to polarization analysis of magnetic diffraction. J. Phys.. Condens. Matter. 2002. *14.* 123.
72. Brown. M.E.; Hollingsworth. M.D. Stress-induced domain reorientation in urea inclusion compounds. Nature 1995. *376.* 323.
73. Hollingsworth. M.D.: Brown. M.E.; Hillier. A.C.: Santarsiero. B.D.; Chaney, J.D. Superstructure control in the crystal growth and ordering of urea inclusion compounds. Science 1996. *273.* 1335.

van der Waals Forces

Hans-Jörg Schneider
Universitat des Saarlandes, Saarbrucken, Germany

INTRODUCTION

Van der Waals forces play a decisive role in many supramolecular complexes, and in many other fields, such as in structure and function of proteins,[1] nucleic acids,[2,3] in adhesion phenomena including cell recognition, in membrane formation and transport, in self-assembly: in new materials from aromatic systems. in dendrimers, etc. A major problem is to distinguish van der Waals effects from hydrophobic interactions, also in supramolecular complexes: such as with cyclodextrins.[4] Van der Waals interactions belong to the most often invoked binding mechanisms in supramolecular systems, but they are the most difficult to quantitatively predict, and even pose serious problems in definition. These high-order interactions are treated in classical textbooks,[5–7] mostly in the context of intermolecular forces between simple "inert" molecules. such as noble gases.

Traditionally, one summarizes under van der Waals interactions high-order noncovalent binding mechanisms that do not rely solely on permanent charges but on polarization of electron clouds. Hydrogen bonds are not generally viewed this way, although one often uses here in force field description a Buckingham or Lennard-Jones potential (see below) in addition to the Coulombic interactions that prevail in hydrogen bonds of weaker or medium strength. The van der Waals attraction, e.g., between a permanent dipole and another dipole generated by polarization of the second is, finally. also based on interactions between permanent charges. Even the classical description of dispersive interactions in the form of the London–Eisenschitz forces involves a Coulomb-type attraction. only that in this case, it is considered to exist between fluctuating dipoles, some of which at a given time will have opposing, and hence attractive charge distributions.

COMPUTATIONAL DESCRIPTIONS

The only gradual distinction between low- and high-order effects in noncovalent binding is reflected by the classical potentials, as they are used in force fields. Noticeably, Coulombic attractions with, e.g., the benzene quadrupole (see below) already fall off with the power of three with the distance r, in contrast to the "soft" long-range potentials for interactions between point charges, which depend on r^{-1}. High-order effects. based on polarization of electron clouds, show increasingly steep dependencies on the distance r between the host and the guest site, and are usually described by simplified Lennard–Jones or Buckingham potentials:

$$\mathrm{EV} = a \cdot \mathrm{r}^{-12} - b \cdot \mathrm{r}^{-6} \quad (\textit{Lennard} - \textit{Jones} - \textit{potential}) \tag{1}$$

$$\mathrm{EV} = \underset{\textit{repulsive}}{10^4 \cdot \mathrm{e}^{-4\,6\mathrm{r}}} - \underset{\textit{attractive term}}{50 \cdot \mathrm{r}^{-6}} \quad (\textit{Buckirzgham} - \textit{potential})$$

The dependence of dispersive attractions on the polarizibilities α of the two interacting atom, or groups i and j is described by the Slates–Kirkwood Eq. 3. e.g., quantifying the factor b in Eq. 1. In Eq. 3, e and m refer to the electron charge and mass, n to the number of electrons in the valence shell, and $\hbar$ to the Planck–Dirac constant. The polarizibility increases with the size of the electron shell of atoms: typical values for α can be found in the literature and in parameters of force fields.[8]

$$b = [1.5\ \mathrm{e}\ (\hbar/m^{1/2})\ \alpha_i\alpha_j]/[(\alpha_i/n_i)^{1/2} + (\alpha_j/n_j)^{1/2}] \tag{3}$$

Force field calculations of such interactions in principle require explicit consideration of polarizibility even of lone pairs, with an appropriate treatment of electron correlation.[9] Several approaches were taken to describe polarizibilities and induced dipole moments within force fields, e.g., on the basis of the MM3 field.[10] Mutual polarizations can be included in the term for electrostatic interactions by describing Coulomb interactions with fluctuating atomic charges.[11–13] Multipole molecular mechanical models using a restrained electrostatic potential approach were shown to accurately reproduce aqueous solution-free energies of methanol and N-methyl acetamide. nucleic acid base, amide hydrogen bonding, and several chloroform and water partition coefficients.[14]

In quantum chemical descriptions,[9] *van der Waals* interactions correspond largely to electron correlation and

Encyclopedia of Supramolecular Chemistry
DOI: 10.1081/E-ESMC 120012665

necessarily need to include polarization. For this reason. density functional (DFT) calculations, which describe Coulomb. exchange, and correlation energy altogether as functional of electron densities in three dimensions, need at least the use of the MP2 (second order Mϕller–Plesset) method.[16–18] Still. the problem is that even for gas-phase modeling and with the fast DFT approach, the computational time is long. and it increases, e.g., with the MP2 method by a power of five with the molecular size of a given complex.

STACKING INTERACTIONS

Many well-known supramolecular complexes with aromatic components'[19–21] rely on coulombic-type attractions between electron-poor and electron-rich parts. and are for this reason often called donor–acceptor (D–A) interactions. An important clue to the dominating mechanism. also of practical significance. is that donor–acceptor and electrostatic interactions can be strong in organic solvents of lower polarity, whereas van der Waals forces relying on polarization effects reach their maximum in water due the extremely low polarizibility of this medium. The problem then is to distinguish the corresponding dispersive from hydrophobic interactions.

BENZENE–BENZENE INTERACTIONS: STACKING AND C—H—π BONDS

The classical example for stacking interactions seems to be the benzene dimer.[22] However, MD and ab initio MO calculations indicate a predominance of edge-to-face complexes over the stacked sandwich awangement by 3 kJ/mol in the gas phase and by 6 kJ/mol in water.[23–25] In contrast, the calculations predict for toluene in the gas phase, but not in water, a preference for stacking. Obviously. the permanent negative charges of π-electron clouds must lead to repulsion in parallel face-to-face complexes. In displaced stacks (Scheme 1). the repulsion between the π-moieties can be counteracted by electrostatic attraction between the positively charged aryl protons and the next π system. Such considerations lead to semiquantitative structure and energy predictions of stacked aromatic systems.[26,27] This treatment was criiicized also because ab initio molecular orbital calculations describe stacking between aromatic systems to a large degree by electron correlation.'''' which stands for dispersive interactions of fluctuating dipoles. The high polarizibility of the n-cloud enhances such forces also in less-displaced orientations. In the solid state. one

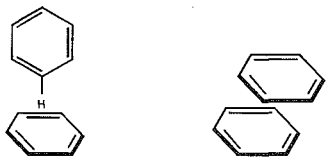

edge-to-face face-to-face

Scheme 1 Stacking and edge-to-face structures of benzene dimers

observes for larger. fused aromatic hydrocarbons a packing based most often on displaced stacking and on edge-to-face interactions. with typical herringbone structures'[29–31]

Experimental data on benzene association constants[iz1] show only values around 1 M^{-1} in water but they vary considerably. Magnetic field alignment NMR studies with benzene in water speak for an edge-to-face preference of up to 3 kJ/mol.[32] Significant pattern changes are observed with different substituents at phenyl rings.[33] In 1.8-diarylnaphthalenes. an increase of rotational barriers with the number of fluorine groups in one of phenyl rings was observed: the decreased electron density by the substituents leads to less unfavorable orientation in the enforced parallel stacks in the ground state. The quadrupoles of benzene rings with fluorine or hydrogen atoms have similar magnitudes but opposite signs with an inversion of the C—X bond polarity, which favors parallel stacks.[33,34]

Edge-to-face orientations are frequent motifs also in proteins,[35] and they can be viewed as hydrogen bonds between weakly acidic aromatic C—H bonds and π-moieties,[36] and will therefore noi be discussed in detail here. Due to small polarity. the strengths of such bonds are so small that they are mostly observable only in solid-state structures or with intramolecular balances set up to reflect particular interactions by changes in conformational equilibria.[37] However. it was concluded on the basis of force field calculations, including a solvation model, that van der Waals and solvation forces play a decisive role in the conformational equilibrium involving C—H—π bonds.[38]

INTERACTION OF CATIONS WITH π-MOIETIES AND WITH ELECTRON LONE PAIRS

Cation-π effects.[39,40] result largely from coulombic attraction. as long as metal cations interact with n-moieties: these effects are discussed in other chapters of this *Encyclopedia* and will therefore only be mentioned here

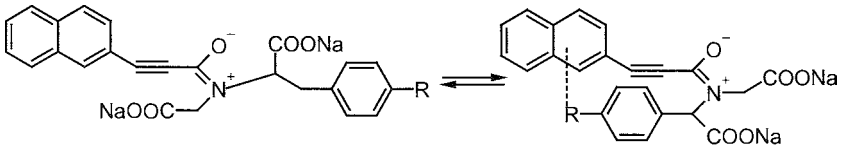

E **Z**

Scheme 2 Aryl–aryl interactions in an intramolecular balance, (see the text for further discussion)

with respect to van der Waals binding contributions. The MO calculations at the MP2 level speak for significant contributions of electron correlation effects in complexes between ammonium cations and aromatic systems.[41,42] Complexation of anions by aromatic clefts also indicates polarization as a dominant factor.[''] Even crown-ether complexes with metal ions are stabilized significantly by polarization effects on the oxygen electron lone pairs.[44]

STACKING DOMINATED BY DISPERSIVE INTERACTIONS

The dispersive interactions in stacking aggregations is expected to increase with the size of the interacting π-moieties. A similar increase would be predicted if hydrophobic forces dominate (see *Hydrophobic* Effects in this *Encyclopedia*). That dispersive interactions play a major role is, however, obvious by the fact that such a size-dependence is also seen in solvents such as chloroform: in a classical study with ethyladenine as guest and a series of hosts offering hydrogen bonds as the primary binding force and methyl, phenyl, naphthyl, and anthryl residues for stacking. the association free energies AG show a systematic increase of $\Delta\Delta G = 1.85 \pm 0.15$ kJ/mol for each additional benzene moiety interacting with the nucleobase.[45,46] Measurements of the EIZ equilibrium around the amide bond in the "balance" molecules in Scheme 2 show a preference for the *E* conformer, which for $R = H$ has the same small $\Delta G_{E/Z}$ difference to the *cis*-conformer in water (D_2O) as in chloroform. Only substituents *R* in the pam-position of the phenyl can in the *E* conformer reach the naphthyl moiety, and in water leads to an increase of $\Delta G_{E/Z}$, which is larger for R = phenyl than for R = cyclohexyl. This is in contrasi to expectations on the ground of the much higher hydrophobicity of cylohexane compared to benzene, and clearly speaks for dominant dispersive interactions. Noticeably, in chloroform. the ΔG_{EZ} values remain constant for the different substituents *R*.[47] The same evidence for dispersive instead of hydrophobic interactions between aromatic systems is seen if the aryl groups in the balance bear nitrogen atoms. Thus, with R = pyridyl, pyrimidyl, or quinolyl residues. one observes larger $\Delta G_{E/Z}$ differences, with a stronger preference for stacking with heterocycles than with arenes in spite of their smaller hydrophobicities.[48] The results emphasize the propensity of heteroaromatic systems for stacking, e.g., in nucleic acids, although the observed variations are small, with, e.g., $-\Delta G_{E/Z} = 0.43$ versus 0.79 kJ/mol for R = phenyl or R = pyrimidyl, respectively.

Stacking interactions can become so strong that other possible binding contributions cannot materialize, because optimal geometric disposition for all intermolecular forces is no longer possible. Thus, the observation of the same association energy between positively charged host compounds and either nucleotides or electroneutral nucleosides provides evidence for dispersive interaction mechanisms. *Bis*(phenanthridinium) receptors like **1** (Scheme 3) form equally strong complexes in aqueous media (lg K = 5–6) with both nucleotides and nucleosides. In spite of the positively charged nitrogen centers in the flat aromatic receptors, there is also no dependence on the ligand charges.[49]

PORPHYRIN COMPLEXES: DERIVING A SCALE FOR DISPERSIVE INTERACTIONS

Porphyrins are ideally suited for dispersive interactions due to their extended π-moiety, coupled with a relatively high flexibility that imposes small steric constraints on complexation with a variety of substrates. A porphyrin host has a surface often several times larger than the guest compound, and then it acts as receptor, with, e.g., twice as many binding sites, with a concomitant increase in binding strength. This effect can be further increased by doubling those interactions with a suitable porphyrin dimer **2** (Scheme 3, Fig. 1).[50] Measurements of porphyrin complexes with many ligands in water allowed the discrimination of hydrophobic from other binding mechanisms and the inference of free-energy increments of van der Waals interactions for many substituents.[51,52] The affinities of. e.g., benzoic acids to positively charged porphyrin derivatives, does not change significantly by alkyl substituents; in line with this, the binding constant

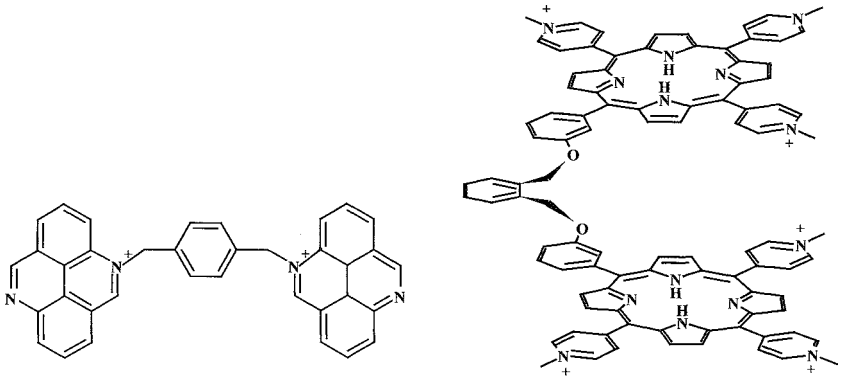

1 2

Scheme 3 *Bis*(phenanthridinium) 1 and porphyrin 2 as stacking units.

of cyclohexane carboxylic acid shows only the value expected for ion pairing. In contrast, the phenyl ring in benzoic acid has a similar surface as a cyclohexane ring, which leads to a value higher by about 8 kJ/mol.[53] Affinities of other aromatic compounds exhibit an increase of up to 18.5 kJ/mol for, e.g., acridine; a plot of the complexation free energies against the number of n-electrons is linear and gives an increment of about 2 kJ/mol per electron pair. That saturated systems show smaller interactions in spite of their larger lipophilicity is in line with the above-mentioned conclusions reached with the "balance" in Scheme 2. This emphasizes that dispersive and not hydrophobic mechanisms are the major driving force for intermolecular interactions of unsaturated systems in water, noticeably including cyclopropane (see Table 1).

Measurements of over 50 complexes with positively or negatively charged porphyrins showed additive substituent increments $\Delta\Delta G$ (Table 2), which describe the observed free energies accurately. Because electron-withdrawing and electron-pushing substituents on benzene rings increase the affinity the same way with all porphyrins, and there is a general increase of ΔG with the polarizibility of the groups, other mechanisms except for dispersive interactions can be excluded. The $\Delta\Delta G$ values in Table 2 have to be taken as relative numbers, much like substituent constants in, e.g., the Hammett equation. Their absolute magnitude will depend on the size of the acceptor molecule, which in the case of porphyrins is several times larger than, e.g., a single benzene unit, and also change with the reaction medium.

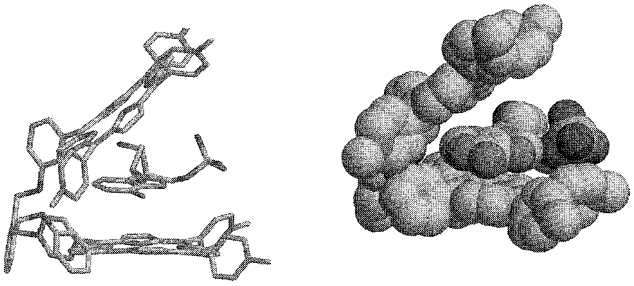

Fig. 1 Dispersive interactions between adenine in AMP and a porphyrin dimer. (For an interactive model, see http://www.uni-sb.de/matfak/fbll/schneider.) *(View this art in color at www.dekker.com.)*

Table 1 Calorimetric results for selected cyclodextrin complexes

	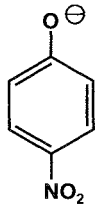	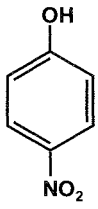	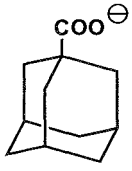
α—CD			
—ΔG	18.7	11.5	11.6
—ΔH	43	23	14
TΔS	−24	−11	−3
β—CD			
—ΔG	15.0	14.2	24.5
—ΔH	16	10	*22*
TΔS	−1	4	*3*

Table 2 Substituent increments—$\Delta\Delta G$ for van der Waals interactions. (Ref. [52.])

Substitutent R =	$\Delta\Delta G$ (kJ/mol)	n
—CH_3	<0.5	4
—$CH(CH_3)_2$	0.6	1
—$CH{=}CH_2$	2.4	6
—$C{\equiv}C$—	2.6	1
—cyclopropyl	1.65	2
—phenyl	8.3	6
—pyridyl	6.4	5
—F	0.3	3
—Cl	1.65	5
—Br	2.4	4
—I	2.95	3
—NH_2	0.9	1
—OCH_3	1.75	3
—$COOCH_3$	3.1	1
—$COCH_3$	3.15	1
—SCH_3	2.8	1
—CN	2.6	2
—NO_2	4.95	5
—$CONH_2$	2.85	5

Note: $\Delta\Delta G$ is derived from averaged association constants aith porphyrin derivatives (in water. 298 K. pH 7.00. phosphate buffer I=0.05 M); n: number of underlying systems for $\Delta\Delta G$ calculation: deviations of $\Delta\Delta G$ from different comnplexes: +/−0.25 kJ/mol; (+/−0.35 kJ/mol, R=I, $COCH_3$).

CYCLODEXTRIN COMPLEXES

Inclusion of guests in the cavity of cycloamyloses can have its origin in solvophobic effects as well as in a number of direct host–guest interactions. An empirical equation based on a iarge number cyclodextrin complexation constant K in water describes lgK as a function of solvent–solute and host–guest interaction energies resulting from hydrogen bond or electrostatic interactions. plus an additional term containing the change in accessible nonpolar surface area of the host upon complexation.[4] Calorimetric measurements can show if complex formation is dominated by a favorable entropy AS against an enthalpic disadvantage, as expected with the hydrophobic Frank–Evans effect as the major driving force. Unfortunately, the results are usually not as clear-cut, and often one observes entropy–enthalpy compensation.[54] Calorimetric studies of cyclodextrin complexes with guests of either low or higher polarizibility show systematically more favorable ΔH values for those with larger polarizibility, as long as the cavity size allows the tight fit necessary for dispersive interactions. If the polarizibility is smaller. like in nitrophenol instead of nitrophenolate, or in adamantanes, the ΔH contribution decreases, with more favorable entropy if the complex is not too tight (Table 2).

CHARGE-TRANSFER COMPLEXES

Associations between electron-rich and electron-poor molecules can be accompanied by an electron transfer from high-energy occupied molecular orbitals of the donor D to unoccupied acceptor A orbitals of lower energy: they can be described with linear cornbinations of wave functions corresponding to structures like A–D and A^+D^-.[55–57] Such orbital mixing leads to characteristic CT bands in the low-frequency part of UV/Vis spectra. which, however, do not correlate with the strength of the binding. The interaction free energy ΔG between the soft Lewis acid iodine I_2 as acceptor and a range of hydroxy-, thio-, and aminocompounds correlates linearly with the basicity of these donors, in line with significant polar contribution from the A^+D^- state.[58] The CT complexes are not to be confused with those between hard Lewis acids and bases, which usually are termed donor–acceptor complexes and were mentioned above. The CT complexes in solution are usually weak, with, e.g., ΔG = 4.6 kJ/mol in CCl_4 for the strong acceptor trinitrobenzene with the donor hexamethylbenzene. With toluene. the association constant is already lower than I. Nevertheless. CT complexes can. in contrast to those due to hydrophobic or dispersive interactions, also form in organic solvents and are. therefore. important for applications where solubility problems prohibit the use of aqueous media. Interesting complexations were observed with calixarenes and eiectron-deficient fullerene derivatives;[59] iodine substituents at the calixarene rim increase association constants with C_{60} from K = 460 M^{-1} for the unsubstituted host in benzene as solvent to K = 1840 M^{-1}.[60]

CONCLUSION

The few examples given in this article should illustrate the significance of van der Waals interactions in supramolecular systems. Space does not allow a detailed discussion of the results and views on stacking forces in and with nucleic acids. Only recently has it become clear that the major factor for the formation of the double helix is base stacking.[61] Investigations with a iarge number of heterocycles implemented instead of a natural nucleobase show only a rough correlation of duplex stability with the surface size of the base: a similar dependence holds for intercalators.[2,3,62] Based. i.e., on solvent effects, it was suggested that hydrophobic forces rule the duplex stability.[61,63] However, dispersive interactions would lead to similar solvent effects. and are. e.g., on the basis of calculations,[15] believed to be the major stacking factor. Obviously. much needs to be done to further clarify the

mechanisms of these chemically and biologically significant interactions.

ARTICLES OF FURTHER INTEREST

Biological Ligands, p. 88
Calixarenes and Their Analogues: Molecular Complexation, p. 145
Carbonic Anhydrase Models, p. 178
Carcerands and Hemicarcerands, p. 189
Cation–π Interactions, p. 214
Cavitands, p. 219
Classical Descriptions of Inclusion Compounds, p. 253
Classification and Nomenclature of Supramolecular Compounds, p. 261
Clathrate Hydrates, p. 274
Concepts in Crystal Engineering, p. 319
Crystal Structure Prediction, p. 371
Cyclodextrins, p. 398
Cyclophanes: Definition and Scope, p. 414
Cyclophanes: Endoacidic, Endohasic, and Endolipophilic Cavities, p. 424
Halogen Bonding, p. 628
Hydrogen Bonding, p. 658
Hydrophobic Effects, p. 673
Inclusion Compounds: Selectivity, Thermal Stability, and Kinetics, p. 696
Micelles and Vesicles, p. 861
Molecular Modeling and Related Computational Techniques, p. 901
π–π Interactions: Theory and Scope, p. 1076
Self-Assembly in Biochemistry, p. 1257
Soft and Smart Materials, p. 1302
Solvation Effects in Guest Binding, p. 1322
Stability Constants: Definition and Determination, p. 1360
Supramolecular Chemistry: Definition, p. 1401
Surfactants, Part II: Applications, p. 1470
Weak Hydrogen Bonds, p. 1576

REFERENCES

1. Feraht. A.R. *Structure and Mechanism in Protein* Science: A *Guide* to *Enzyme* Catalysis nnd Protein Folding: W.H. Freeman & Co: New York, 1999.
2. *Nucleic Acids* in *Chemistry* and Biology. 2nd Ed.: Blackburn. G.M., Gait. M.J.. Eds.: Oxford University Press: New York. 1996.
3. Mool. E. Chem. Rev. 1999. *97*. 1473–1487.
4. Connors, K.A. Chem. Rev. 1999, *97*. 1325–1357.
5. Israelachvili. J.N. *Intermolecular* and *Surface* Forces. 2nd Ed.: Academic Press: San Diego, 1991.
6. Rigby, M.: Smith, E.B.: Wakeham, W.A.: Maitland, G.C. The Foi-ces *between* Molecules: Clarendon: Oxford. 1986.
7. Huyskens. P.C.; Luck. W.A.: Zeegers-Huyskens. T *Intermolecular* Forces: Springer: Berlin, 1991.
8. Cornell, W.D.; Cieplak, P.: Bayly, C.I.; Gould, I.R.: Merz, K.M.; Ferguson, D.M.: Spellmeyer. D.C.; Fox. T.: Caldwell, J.W.; Kollman, P.A. J. Am. Chem. Soc. 1995, *117*, 5179.
9. Ferenczy. G.G.; Reynolds. C.A. J. Phys. Chern. 2001. *105* (51). 11470–11479.
10. Ma. B.U.: Lii. J.H.; Allinger. N.L. J. Comput. Chem. 2000. *21* (10), 813–825.
11. Mollhoff. M.; Sternberg. U. J. Mol. Model. 2001, *7* (4). 90–102.
12. Bret, C.; Field. M.J.: Hemmingsen, L. Mol. Phys. 2000. 98 (11), 751–763.
13. Mannfors, B.: Palnio, K.; Krimm, S. J. Mol. Struct. 2000. *556* (1–3). 1–21.
14. Cieplak. P.; Caldwell. J.: Kollman. P. J. Comput. Chern. 2001. *22* (10). 1048–1057.
15. Müller-Dethlefs, K.: Hobza, P. Chem. Rev. 2000. *100* (1), 143–168.
16. Feller. D.; Davidson. E.R. Basis Sets for Ab Initio Molecular Orbital Calculations and Intermolecular Interactions. In Computational *Chemistry*; Lipkowitz, K.B.. Boyd. D.B., Eds.: VCH Publishers: New York. 2001: Vol. 17. 1–43.
17. Lein. M.: Dobson. J.F.: Gross. E.K.U. J. Comput. Chem. 1999. 20. 12–22.
18. Furche, F. Phys. Rev., B 2001, *64* (19), 5120.
19. Balzani. V.; Credi. A.; Raymo. F.M.: Stoddart. J.F. Angew. Chem., Int. Ed. Engl. 2000, 39 (19). 3349–3391.
20. Nielsen. M.B.: Lomholt, C.; Becher. J. Chem. Soc. Rev. 2000, *29* (3). 153–164.
21. Klarner, F.-G.; Panitzky, J.: Blaser. D.; Boese. R. Tetrahedron 2001, *57*. 3673–3687.
22. Neusser, H.J.: Krause, H. Chem. Rev. 1994. 94. 1829.
23. Linse. P. J. Am. Chem. Soc. 1993, *115*. 8793.
24. Jorgensen, *W.L.*: Severance. D.L. J. Am. Chem. Soc. 1990. *112*. 4768.
25. Chipot, C.: Jaffe, R.: Maigret, B.; Pearlman. D.A.; Kollman. P.A. J. Am. Chem. Soc. 1996, *118*. 11217–12224.
26. Hunter. C.A. Chem. Rev. 1994. *94*. 101–109.
27. Hunter, C.A.; Lawson, K.R.: Perkins, J.; Urch, C.J. J. Chem. Soc., Perkin Trans. 2001, *2*. 651–669.
28. Hobza, P.; Spirko. V.: Selzle, H.L.; Schlag. E.W. J. Phys. Chem.. A 1998. *102*. 2501.
29. Desiraju, G.R.; Gavezzotti. A. Chem. Commun. 1989. 621.
30. *The Crystal* As *a Supramolecular Entity (Perspectives* in *Supramolecular Chemistry)*; Desiraju, G.R., Ed.: 1996: Vol. 2.
31. Desiraju, G.R. Crystal *Engineering*; Elsevevier: Amsterdam. 1989.
32. Laatiliainen. R.: Ratilainen, J.: Sebastian, R.: Santa. H. J. Am. Chem. Soc. 1995. *117*. 11006.
33. Cozzi. F.: Ponzini, F.: Annunziata. R.; Cinquini, M.: Siegel, J.S. Angew. Chem.. Int. Ed. Engl. 1995. *34*. 1019.

34. Adams, H.: Blanco, J.L.J.; Chessari, G.; Hunter, C.A.; Low, C.M.R.; Sanderson. J.M.; Vinter, J.G. Chem. Eur. J. 2001. 7, 3494–3503.
35. Burley, S.M.; Petsko, G.A. Adv. Protein Chem. 1988. 39. 125.
36. Nishio, M.; Hirota, M.; Umezawa, Y. *The CH-π Interaction*; Wiley: New York, 1998; etc.
37. Paliwal, S.; Geib, S.; Wilcox, C.S. J. Am. Chem. Soc. 1994, *116*. 4497.
38. Nakamura, K.; Houk, K.N. Org. Lett. 1999. 1, 2049–2051.
39. Ma, J.C.; Dougherty, D.A. Chem. Rev. 1997, 97, 1303.
40. Arnecke, R.; Bohmer, V.; Cacciapaglia, R.; DallaCort. A.; Mandolini, L. Tetrahedron 1997, *53*. 4901.
41. Kim, K.K.; Lee, J.Y.; Lee, S.J.; Ha, T.-K. J. Am. Chem. Soc. 1994. 116, 7399.
42. Minoux, H.; Chipot, C. J. Am. Chem. Soc. 1999,121 (44). 10366–10372.
43. Schneider, H.-J.; Werner, F.; Blatter, T. J. Phys. Org. Chem. 1993, 6, 590–594. Attractive interactions between negative charges and polarizable aryl parts of Host–Guest systems.
44. Golebiowski, J.; Lamare, V.; Martins-Costa. M.T.C.; Millot. C.; Ruiz-Lopez, M.F. Chem. Phys. **2001**, 272 (1), 47–59.
45. Rotello, V.M.; Viani, E.A.; Deslongchamps. G.; Murray, B.A.; Rebek, J.. Jr. J. Am. Chem. Soc. **1993**, 115 (2), 797.
46. Rebek, J., Jr. Angew. Chem. **1990**. 102, 261.
47. Gardner, R.R.; Christianson, L.S.; Gellman, S.H. J. Am. Chem. Soc. 1997, 119, 5041–5042.
48. McKay, S.L.; Haptonstall, B.: Gellman, S.H. J. Am. Chem. Soc. 2001, 123 (6), 1244–1245.
49. Žinić, M.; Vigneron, J.-P.; Lehn, J.-M. Chem. Commun. 1995. 1073.
50. Sirish, M.; Schneider, H.-J. J. Am. Chem. Soc. 2000. *112* (24), 5881–5882.
51. Schneider, H.-J.; Liu, T.; Sirish, M.; Malinovski, V. Tetrahedron 2002, *58*. 779–786.
52. Schneider. H.-J.; Liu, T. Angew. Chem. Int. Ed. Engl. 2002, 41. 1368–1370.
53. Schneider, H.-J.; Wang, M.J. Org. Chem. 1994, 59, 7464–7472.
54. Rekharsky, M.V.; Inoue, Y. Chem. Rev. **1998**, 98, 1875–1917.
55. Foster, R. Organic Charge-Transfer Complexes; Academic: New York, 1969.
56. Bender, C.J. Chem. Soc. Rev. 1986, 15, 475.
57. Mulliken, R.S.: Person, W.B. Molecular *Complexes—A* Lecture and Reprint *Volume*; Wiley Interscience: New York, 1969.
58. Bouab, W.; Esseffar, M.; Abboud, J.-L.M. J. Phys. Org. Chem. 1997, 10, 343.
59. Williams. R.M.; Zwier, J.M.; Verhoeven, J.W. J. Am. Chem. Soc. 1994, 116. 6965.
60. Haino. T.; Yanase, M.; Fukazawa, Y. Angew. Chem., Int. Ed. Engl. 1997, 36, 259.
61. Guckian. K.M.; Schweitzer, B.A.; Ren, R.X.F.; Sheils. C.J.; Tahmassebi, D.C.; Kool, E.T. J. Am. Chem. Soc. 2000, 122 (10), 2213–2222.
62. Schneider, H.-J.; Sartorius. J. J. Chem. Soc., Perkin Trans. 1997, 2, 2319–2327.
63. Pang, Y.-P.; Miller, J.L.; Kollman, P.A. J. Am. Chem. Soc. 1999, 121, 1717–1725.

Vibrational Spectroscopy

Carolyn A. Koh
King's College London, London, United Kingdom

INTRODUCTION

Vibrational spectroscopy is an important complementary tool to x-ray diffraction for structural characterization of materials. including supramolecular compounds. Unlike x-ray diffraction. where all the data must be collected to give the structure of the molecule. vibrational spectroscopy can be used to zero-in on part of the structure of interest. Furthermore, information on guest–host interactions of inclusion compounds can be readily determined from infrared (IR) and Raman spectra. whereas this information is not readily accessible from x-ray diffraction. Therefore, IR spectroscopy and more recently Raman spectroscopy are used to study the structure and dynamics of inclusion compounds. IR spectroscopy is also widely and routinely used to characterize supramolecular compounds containing macrocyclic molecules. The structures and dynamics of these compounds can also be studied using resonance Raman spectroscopy.

This article provides a brief overview of the theory of IR spectroscopy and Raman spectroscopy (for more in-depth descriptions of these methods see Refs. [1–3]). This is followed by a review of vibrational spectroscopic studies performed on clathrate hydrates (a class of inclusion compound) and macrocyclic suprainolecular compounds. Clathrate hydrates were highlighted in this article because of all the clathrate compounds. they are particularly amenable to vibrational spectroscopy and are of great industrial significance. Similar IR/Raman methods can be applied to other well-known clathrate compounds. including quinol[4] and urea[in] clathrates. Finally, future directions on the use of vibrational spectroscopy in supramolecular compounds will be given.

THEORETICAL BACKGROUND OF VIBRATIONAL SPECTROSCOPY

Atoms in a molecule vibrate within the wave number range $\sim 10-\sim 10^5$ cm^{-1}. with IR and Raman spectroscopic measurements of supramolecular compounds usually being performed within the region 10–3000 cm^{-1} The vibrational spectrum of a molecule reflects the properties of the molecule as a whole and characteristic features of separate chemical bonds. The compression and extension of a real bond of a diatomic molecule can be represented by an anharmonic oscillator model. The selection rules for an anharmonic oscillator are that the allowed vibrational energy transitions $\Delta v = \pm 1, a2, \pm 3$ (lines beyond this have very low intensities and therefore are not easily observed). Vibrational modes involving transitions of $\Delta v = \pm 1$ are the fundamental (or normal) modes. while those of $\Delta v \geq a2$ are the overtone modes.

Because a polyatomic molecule has more than one vibrational degree of freedom, a linear molecule containing N atoms will have *3M–5* normal modes of vibration (*3N*–6 for a nonlinear molecule). Each vibrational motion of a molecule is considered as a superposition of these normal modes of vibration. Therefore, a particular compound will have several characteristic frequencies that can be assigned to specific vibrational motions. Although a normal vibration in general involves all the atoms in a molecule, some vibrational modes such as O—H bond stretching, C—C—C bond angle bending. or C—N bond stretching always appear at approximately the same wave number region in spectra of different compounds. These characteristic vibrational modes are therefore used to identify specific functional groups present in a molecule. as well as to determine any changes in the bonding or environment of these groups. The symmetry of a molecule changes upon transition from the gas phase to condensed phases and can be detected from the vibrational spectrum. In solids, the situation is complicated by the occurrence of lattice vibrations, however. these are only observed if equivalent atoms in each unit cell vibrate in-phase.

Theoretical calculations and computer simulations can be used to predict the IR/Raman spectra of various molecules and can aid in the interpretation of vibrational spectral data. For example. calculating Raman spectra using molecular dynamics (MD) simulations[iii] involves expressing the energy of a vibrating molecule in a solvent as the sum of the inter- and intramolecular interactions (both contributions are expandable in terms of the normal coordinates). Intramolecular interactions consist of a harmonic part and an anharmonic part. Transitions between perturbed energy levels can be calculated by taking the intramolecular (anharmonic pari) and intermolecular interactions as perturbations to the energy levels of the anharmonic oscillator. Therefore. one can

Encyclopedia of Supramolecular Chemistry
DOI: 10.1081/E-ESMC 120012810

calculate the Raman shift that occurs due to intermolecular interactions.

Infrared Spectroscopy

The selection rule for a vibration to be infrared active is that the molecule must undergo a vibrational motion that changes the dipole moment of that vibrational mode. Hence. IR light of a frequency matching that of an IR-active vibrational motion will be directly absorbed by the molecule. This quantum of light will then promote the molecule to a higher vibrational energy state.

The development of Fourier Transform IR (FTIR) spectrometers led to the ability to measure vibrational spectra of supramolecular coinpounds with increased speed and sensitivity. The main feature of an FTIR instrument is the interferometer, which modulates the IR input waves by a moving mirror, M_M, moving back and forth toward and away from the beam splitter. Depending on the position of M_M, recombination of waves from M_M and the stationary mirror, M_S, at the beam splitter creates constructive or destructive interference that results in an output wave of varying intensity, i.e. the interferograin (see Fig. I).

Therefore. the interferograin is the sum of all the frequencies (plotted as intensity versus time). By performing a Fast Fourier Transform algorithm using a computer, the infrared spectrum is obtained in which intensity is now plotted versus frequency (usually given in cm^{-1}). Therefore, by means of the interferometer, an FTIR instrument can analyze all frequencies simultaneously. unlike a dispersive instrument that examines the frequencies one at a time.

Sampling methods used for IR analysis of clathrate hydrate compounds, which are largely composed of highly absorbing water molecules, were limited to mulls, thin films prepared by vapor co-deposition methods (the resulting amorphous deposit is warmed in a vacuum to the crystallization temperature[7]), or adamantane pellets (for samples to be analyzed below 125 cm^{-1}). These mulls, thin films, and pellets need to be prepared at cryogenic temperatures to maintain stability of the clathrate hydrate at atmospheric pressure. Conversely, macrocyclic supramolecular compounds are generally stable at ambient temperatures and pressures. Therefore, IR analysis of these compounds does not require cryogenic temperatures, and sampling methods include KBr disks and pellets and mulls.

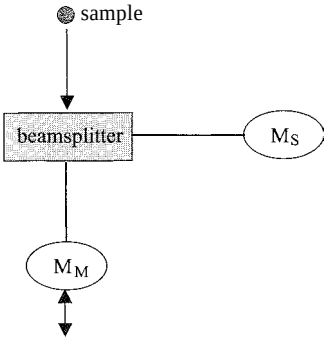

Fig. 1 *The Michaelson interferometer.*

Raman Spectroscopy

The selection rule for a vibration to be Raman active is that the molecule must undergo a vibrational motion that changes the polarizability of that vibrational mode. When a sample is irradiated with light (of visible, ultraviolet; or near-IR frequency), the molecule is excited to a virtual state of higher energy. Relaxation of the molecule to the original or a different vibrational energy state results in Rayleigh scatter or Raman scatter, respectively (see Fig. 2).

The Raman effect can be explained as follows. When a molecule is placed in a static electric field, it experiences some distortion that causes an induced dipole moment, μ, to be set up in the molecule. The molecule is then said to be polarized. The size of the induced dipole depends on the magnitude of the applied electric field, E, and the ease with which the molecule can be distorted, i.e.. its polarizability. α. If the field is supplied by electromagnetic radiation of frequency, ν_o, and the vibrational frequency, ν_{vib}, changes periodically, Eq. 1 is obtained:

$$\mu = \alpha_o E_o \cos(2\pi\nu_o t) + \frac{1}{2}(\delta\alpha/\delta q)_o \times E_o\, q_o \cos 2\pi t[(\nu_o + \nu_{vib}) + (\nu_o - \nu_{vib})] \quad (1)$$

where a, is the equilibrium polarizability, E_o is the maximum field strength, $(\delta\alpha/\delta q)_o$ is the rate of change of polarizability with distortion around the equilibrium position. and q, is the maximum distortion. Therefore. scattered radiation at frequencies ν_o, $(\nu_o+\nu_{vib})$, and $(\nu_o-\nu_{vib})$, are Rayleigh. anti-Stokes Raman. and Stokes Raman scatter, respectively.

Similar to the infrared instruments, there are two general types of Raman instruments: the dispersive and FT Raman spectrometers. The FT Raman instrument incorporates an interferometer that provides similar advantages to those given by the interferometer of an FTIR spectrometer (for further details. see Ref. [3]), although modern dispersive instruments with CCD detectors can measure a range of frequencies simultaneously.

Raman spectroscopy was recently used to study the structures of gas hydrates. It offers the advantage over IR analysis in that the sampling methods are significantly

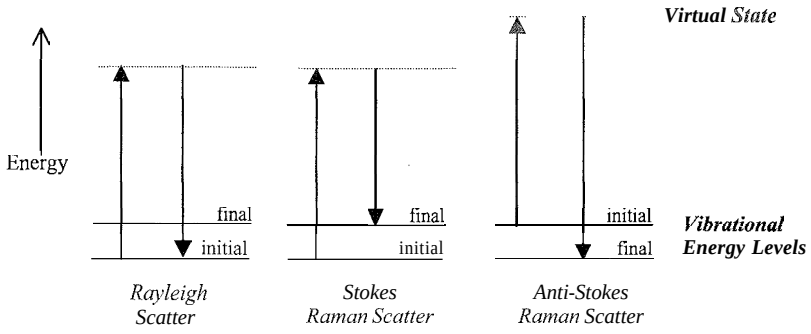

Fig. 2 Energy transitions of Rayleigh and Raman scatter.

simpler, i.e., glass cells and high-pressure cells can be used. Therefore, in situ measurements can be performed on clathrate hydrates at real conditions, which was not possible with previous IR studies.

Resonance Raman spectroscopy is a particularly powerful probe for studying the structures and dynamics of macrocyclic supramolecular compounds, e.g., metalloporphyrins. These compounds have strongly allowed electronic transitions in the visible or UV regions that can enhance the intensity of some Raman-active vibrations by a factor of 10^2–10^4, i.e., resonance enhancement or resonance Raman effect.

CLATHRATE HYDRATES

Clathrate hydrates are crystalline inclusion compounds composed of host water cages that trap guest molecule~.[~.The three most common types of clathrate hydrates are known as structure I, II, and H, which differ in the type of water cage they contain. The type of clathrate hydrate structure formed depends mainly on the size of the guest molecules present (for further details, see the article *Clathrate Hydrates* and Refs. [8,9]). The structures of these compounds were first determined from x-ray diffraction studies,[8] however, as mentioned previously, vibrational spectroscopy can provide important complementary information on the structures and dynamics of these compounds and can also detect the presence of any guest molecule–host lattice interactions.

Evidence of Guest–Host interactions

Far-IR transmission spectra were recorded of Structure I [ethylene oxide (EtO) hydrate][10] and Structure II [cyclopropane, trimethylene oxide (TMO), 1,3-dioxolane, tetrahydrofuran (THF), and cyclobutanone hydrates][11] hydrates. The slight water lattice stretching due to the large size of cyclobutanone was indicated by the most intense peak within the 120–200 cm ' region shifting by 2.5 cm ' lower than the corresponding peak for cyclopropane or 1,3-dioxolane deuterate guests. Guest vibrations were not found to significantly affect the water vibrational spectrum at 4.3 K at frequencies the guest does not absorb. This suggested that the interaction between guest–host vibrations is weak. particularly for THF. Further mid-IR spectral studies on EtO hydrate[1''' showed that only the water-network torsional modes couple with those of EtO molecules (the ring deformation modes of EtO at around 870 cm^{-1}). A later study by Fleyfel and Devlin[13] suggested that the large guest–host interaction of TMO hydrate caused disproportionate lengthening of the weaker H-bonds of the hose lattice.

IR studies on acetylene hydrate also suggested that guest rotation is significantly hindered in the water lattice.[''] This was concluded from the fact that the librational spectra of the hydrate showed no evidence of *P-R* band contours at any temperature, although the bandwidths showed pronounced temperature dependence. Free rotation of guest molecules in the cages would have led to its inertial constant providing a rotational band contour for ν_3 with P and *R* wings. The temperature dependence of the bandwidth was attributed to librational movement of the guest around some fixed orientation in the cage.

The above examples clearly demonstrate the importance of host–guest interactions in clathrate hydrate compounds. These interactions, together with the hydrogen-bonded water network, are important in stabilizing the hydrate system.

Differentiating Between Structure I and II Hydrates and Ice

From IR studies. absorptions by water molecules in EtO hydrate were found to be similar to those in ice.[12] This was expected. because the water lattice of the hydrate is similar to that of ice. with water molecules in EtO hydrate at 100 K being orientationally disordered and reorienting

extremeiy slowly (in contrast to the reorientation rate of EtO of about 10^{10} s^{-1}). However, preparing EtO hydrate from H_2O/D_2O dilutions, the O-H and 0-D stretching modes of isolated HOD rnolecules [ν_{OH}(HDO) and ν_{OD}(HDO), respectively] were found to be different for hydrate and ice materials. The frequency and half-width of ν_{OH}(HDO) and ν_{OD}(HDO) in Structure I hydrate are 2427 ± 3 cm^{-1} and 80 ± 10 cm^{-1}, respectively, compared to 2413 cm^{-1} and about 65 cm^{-1} for the corresponding values for hydrate containing ice. These differences in half-widths were explained in terms of the narrower range of O—O bond distances in ice compared to the hydrate. This was also confirmed later by FTIR studies on Structure I and Structure 11 hydrates.[15] The half-width of the ν_{OD} band of isolated HOD molecules was found to be sensitive to the distribution of O—O distances of the water lattice in ice, Structure I, and Structure II hydrates. Therefore, the ν_{OD} half-width is a useful test for confirming the structure of the hydrate and for detecting any ice impurities in hydrate samples.

Guest Occupancy

The guest IR spectra of EtO and H_2S hydrates indicated that EtO and H_2S occupy small and large water cages.[15] The spectra of Structure II mixed hydrates were used to identify the frequencies of these bands for guest molecules in small and large cages. H_2S molecules in the small cages of Structure I were found to absorb near 2610 cm^{-1}, while in the larger cages. they absorb near 2550 cm^{-1}. This finding'''' suggested that H_2S molecules are not more gas-like in larger cages, as one would intuitively expect. but rather the lower stretching frequency of the large cage reflects the theoretical prediction that small molecules occupy energy minima offset from the large cage centers.'''' This clearly demonstrates that vibrational spectroscopy offers an advancement on information obtained from x-ray diffraction, which only gives a vague picture of the position of a guest molecule in a hydrate cage.

Similarly, splitting of the ν_7 mode of ethane (a single peak in the gas phase) into components at 2982 and 2972 cm^{-1} on enclathration was interpreted as being due to the preferred molecular orientation of ethane in the large hydrate cage. resulting in a nonsymmetric interaction with the cage wall.[15] This will then eliminate the threefold molecular symmetry axis and split the degenerate vibrational states. A later study on EtO, H_2S, TMO, MeCl. and CO_2 hydrates also showed that the frequency of the stretching-mode bands for guest molecules in a small cage is usually greater than that in a large cage.[13] Similarly. FTIR studies of acetylene hydrates showed that the C-D stretching frequency of C_2D_2 guest molecules in large and small cages is at 2319 and 2431 cm^{-1}, respectively.[14] The integrated intensities ratio of these bands was found to be the same as the ratio of the number of large to small cages in Structure I hydrate (3:1).

In agreement with the above IR studies, Raman studies (performed at high pressure) show that the generai trend in vibrational frequencies of guest molecules in hydrate cages is that a guest in a larger cavity gives a lower vibrational frequency.[17] This was attributed to the qualitative ''loose cage–tight cage'' model of Pimentel and Charles. By monitoring the ratio of the vibrations of guest molecules in large and small cages, Raman spectroscopy[18] can be used to determine the relative occupancies of the large and small cavities and the hydration number for single and double gas hydrates (containing one and two types of guest molecules, respectively).

Recent Raman studies[17] also show that contrary to previous reports. ethane can be trapped in the small cage of Structure II hydrate at higher pressures ($\sim$70 MPa). Similarly. Raman microprobe studies of ethylene hydrate at 95 MPa and 303.9 K show that despite ethylene's large van der Waals radius; it can occupy the small cage of Structure I hydrate.[19]

It is assumed that only one guest molecule can be accommodated within each clathrate hydrate cage. However, recent measured[20] and calculated (using MD computer calculations[''']) Raman spectra showed that nitrogen can doubly occupy the large cage of Structure II nitrogen hydrate at higher pressures. The frequency of N_2 doubly occupying large cages (around 2332.5 cm^{-1}) is lower than that in singly occupied small cages (around 2335 cm^{-1}) but higher than that in singly occupied large cages (around 2330 cm^{-1}).

In Situ Studies of Hydrates

Raman spectroscopy provides a rapid and convenient tool for structure analysis without having to use diffraction techniques. Subsequently. Raman spectroscopy was used to study the structures. phase equilibria, and kinetics of gas hydrates at high pressure and close to ambient temperatures.[9] By monitoring the Rarnan spectra of guest molecules. the phase transition from Structure I to II hydrate for an ethane–methane gas mixture was identified for the first time. This was an unexpected result. because both methane and ethane form Structure I hydrate.[21]

Because in situ Raman spectra can be recorded, this provides a particularly convenient and useful tool for following the kinetics of gas hydrate formation and decomposition. For example, such studies we e performed during methane hydrate formation.[9,22–24] The evolution of two peaks at 2905 and 2915 cm^{-1} on hydrate formation from a single peak (at 2911 cm^{-1} for methane dissolved in water) can be monitored as a function of time/temperature/pressure. The effect of adding various chemicals that retard the hydrate formation process was also studied (Refs. [22–24]; see Fig. 3).

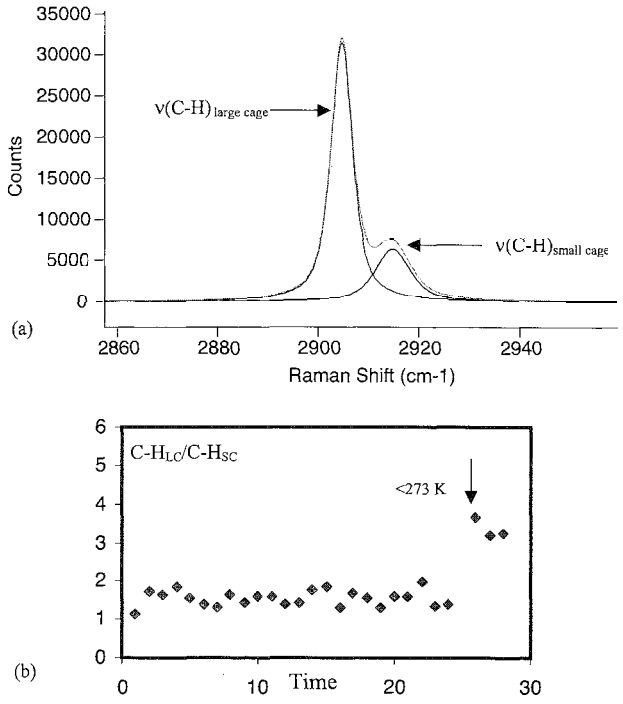

Fig. 3 (a) In situ Raman spectrum of the ν(C-H) symmetric mode of methane in methane hydrate:[23,24] and (b) intensity ratio of $\nu(C\text{-}H)_{large\ cage}/\nu(C\text{-}H)_{small\ cage}$ plotted as a function of time (in arbitrary units) for methane hydrate formation in the presence of a chemical inhibitor. Until the temperature is reduced, the intensity ratio is less than the usual 3:1 ratio. (From Refs. [23,24].) (View *this art in color at www.dekker.com.*)

SUPRAMOLECULAR COMPOUNDS CONTAINING MACROCYCLIC MOLECULES

IR and Raman spectroscopies were used to study the structures of a wide range of supramolecular compounds containing macrocyclic molecules. Some examples of the use of vibrational spectroscopy in structural studies of these compounds will now be given.[25–28]

Iron (IV, V) porphyrins were studied by resonance Raman spectroscopy.[25] These compounds have biological significance. because oxoferryl posphyrins {O=Fe (IV)(por)} are involved in enzymatic reactions of cytochrome P450, horseradish peroxidase (HRP). and related heme proteins. The mechanism of formation of the oxoferryl porphyrin π-cation radical was determined from resonance Raman measurements. The former radical is considered to be a model compound of HRP-I.

Resonance Raman spectroscopy was also used as a probe for detecting aggregation in porphyrin–DNA complexes.[26] For example. *t-bis*(*N*-methylpyridinium-4-yl)diphenylporphine (t_2-H_2-P_{agg})-DNA aggregation is indicated by intensity enhancements of bands due to bending motions of the pyridinium or phenyl groups. Microstructural changes occurring upon aggregation can also be detected from the resonance Raman spectrum.[26]

The study of time-dependent changes in protein structure is important in connecting their structures and functions. A recent Raman study of the heme macrocycle, myoglobin, revealed that a small absorption band, known as Band III. at 762 nm is allowed by means of vibronic coupling rather than the previously proposed Frank–Condon mechanism.[27] Band 111 was found to show an enhancement of non-totally-symmetric vibrational modes. Vibronic coupling involves the non-totally-symmetric modes that promote or enhance an electronic transition by lowering the symmetry of the molecule. Conversely, Frank–Condon active modes involve totally symmetric modes showing displacements of equilibrium positions upon excitation. It was suggested that these results change the interpretation of a large number of studies on myoglobin and will impact models connecting structure and dynamics in myoglobin.[27]

Structural trends in sandwich-type compounds [A-(*crown*)]$_2$[UO_2X_4] (where A=Li, Na, K; X=Cl, Br; crown=18-crown-6, 15-crown-5, 12-crown-4) were studied using IR and Raman spectroscopy in combination with x-ray diffraction and elemental analysis.[28] Understanding uranium coordination chemistry is crucial to the reprocessing and separation of uranium from nuclear energy and weapons industry waste streams. Separation and extraction of actinides in the waste stream by complexation with crown ethers to form coordination compounds is particularly attractive. This is because of the high chelating ability of the crown ethers and the tendency of actinides to adopt high coordination numbers. IR and Raman spectroscopy were used to characterize the structure of these compounds via the asymmetric ν(U-O) and symmetric ν_1(U-O) bands, respectively. In addition. Raman studies show that the coordination trends within this series of compounds are consistent with the principles of hard-soft-acid-base theory and Pearson's principle. i.e., "hard acids prefer to bind to hard bases and soft acids prefer to bind to soft bases." This is likely to be important for predicting binding. e.g., to remove actinide halides in a waste stream by coordination to form these sandwich-type compounds.

CONCLUSION

Vibrational spectroscopy is clearly a valuable tool for studying the structures and dynamics of supramolecular compounds, including inclusion compounds and macrocyclic compounds. In addition, resonance Raman mearurements were shown to be useful in studying the structure and function of biological molecules (containing macrocyclic moieties).

In terms of future directions, Raman spectroscopy will be important in further phase equilibria and kinetic rtudies

of clathate hydrates. These results coupled with macroscopic and x-ray and neutron diffraction measurements will aid in understanding how to control hydrate formation/dissociation in subsea pipelines and during energy exploitation. Finally, further advances are needed in theoretical calculations for interpreting measured vibrational spectra.

ACKNOWLEDGMENTS

Funding from the EPSRC, Chevron-Texaco, the Gas Research Institute, and NATO (PST.977638) are gratefully acknowledged.

ARTICLES OF FURTHER INTEREST

Clathrate Hydrates: Occurrence, Uses, and Problems, p. 281
X-Ray Crystallography, p. *1586*

REFERENCES

1. Banwell, C.N.; McCash, E. *Fundamentals* of Molecular Spectroscopy, 3rd Ed.: McGraw Hill: New York, 1994.
2. Smith, B.C. *Fundamentals* of *Fourier Transform* Infrared Spectroscopy; CRC Press Inc.: Boca Raton. 1996.
3. Hendra, P.J.; Jones, C.; Wames, G. *Fourier Transform Raman Spectroscopy—Instrumentation and Chemical Applications*; Ellis Horwood: U.K., 1991.
4. Davies. J.E.D. Clathrate and inclusion compounds. Part 8. An investigation of the usefulness of the spectral subtraction technique in analyzing the infrared spectra of clathrates. J. Incl. Phenom. **1985**, *3*, 269–279.
5. Elizabe, L.: ElBaghdadi, A.; Smart, S.P.: Cuillaume, F.: Harris, K.D.M. Characterization of gauche end-groups in α. ω-dibromoalkanes: Vibrational properties of the 1,6-dibromohexane/urea inclusion compound. J. Chem. Soc., Faraday Trans. 1996. *92* (2), 267–272.
6. van Klaveren. E.P.; Michels, J.P.J.; Schouten. J.A.: Klug, D.D.; Tse, J.S. Molecular dynamics simulation study of the properties of doubly occupied N_2 clathrate hydrates. J. Chem. Phys. 2001. 115 (22), 10500–10508.
7. Bertie, J.E.: Devlin. J.P. Infrared spectroscopic proof of the formation of the structure I hydrate of oxirane from annealed low-temperature condensate. J. Chem. Phys. 1983. 78 (10). 6340–6341.
8. Sloan, E.D. Clathrate Hydrates of *Natural Gas*, 2nd Ed.: Marcel Dekker: New York, 1998.
9. Koh. C.A. Towards a fundamental understanding of natural gas hydrates. Chem. Soc. Rev. 2002, 31. 157–167.
10. Bertie. J.E.: Othen, D.A. The infrared spectrum of ethylene oxide clathrate hydrate between 360 and 20 cm^{-1}, at 100 K. Can. J. Chem. 1972, *50*. 3443–3449.
11. Bertie, J.E.; Jacobs, S.M. Infrared spectra from 300 to 10 cm^{-1} of structure II clathrate hydrates at 4.3 K. J. Chem. Phys. 1978. *69* (9), 4105–4113.
12. Bertie. J.E.; Othen. D.A. The infrared spectrum of ethylene oxide clathrate hydrate at 100 K between 4000 and 360 cm^{-1}. Can. J. Chem. **1973**, *51*. 1159–1168.
13. Fleyfel, F.; Devlin. J.P. FTIR spectra of 90 K films of simple, mixed, and double clathrate hydrates of trimethylene oxide, methyl chloride, carbon dioxide, tetrahydrofuran, and ethylene oxide containing decoupled D_2O. J. Phys. Chem. 1988, *92* (3). 631–635.
14. Consani, K.; Pimentel, G.C. Infrared spectra of the clathrate hydrates of acetylene and of acetylene/acetone. J. Phys. Chem. 1987. *91* (2). 289–293.
15. Richardson, H.H.; Wooldridge, P.J.; Devlin, J.P. FT-IR spectra of vacuum deposited clathrate hydrates of oxirane, H_2S, THF. and ethane. J. Chem. Phys. **1985**, *83* (9), 4387–4394.
16. Barrer, R.M.; Edge. A.V. Vibrational spectroscopy. J. Proc. R. Soc. Lond., Ser. A. 1967. *300*, 1.
17. Subramanian, S.; Sloan. E.D. Trends in vibrational frequencies of guests trapped in clathrate hydrate cages. J. Phys. Chem., B 2002, *106* (17). 4348–4355.
18. Sum, A.K.: Burruss, R.C.; Sloan, E.D. Measurement of clathrate hydrates via Raman spectroscopy. J. Phys. Chem.. B 1997, *101* (38), 7371–7377.
19. Sugahara, T.; Morita. K.; Ohgaki, K. Stability boundaries and small hydrate-cage occupancy of ethylene hydrate system. Chem. Eng. Sci. 2000, *55*, 6015–6020.
20. Chazallon, *B.:* Kuhs, W.F. In situ structural properties of N_2, O_2, and air-clathrates by neutron diffraction. J. Chem. Phys. 2002. *117* (1). 308–320.
21. Subramanian, S.; Ballard. A.L.: Kini, R.A.: Dec, S.F.: Sloan, E.D. Structural transitions in methane+ethane gas hydrates—Part I: Upper transition point and applications. Chem. Eng. Sci. 2000. *55*. 5763–5771.
22. Sloan. E.D.; Subramanian, S.; Matthews, P.N.; Lederhos. J.P.; Khokhar, A.A. Quantifying hydrate formation and kinetic inhibition. Ind. Eng. Chem. Res. 1998, 37 (8), 3124–3132.
23. Carstensen. A.; Zugik, M.; Creek. J.; Koh. C.A. Clathrate hydrate formation and inhibition. Int. J. Vibr. Spec. 2002. *6*. 1–5. [www.ijvs.com].
24. Zugik, M. PhD thesis: King's College London, 2001.
25. Nakamoto. K. Resonance Raman spectra and biological significance of high-valent iron(IV,V) porphyrins. Coord. Chem. Rev. 2002. *226*. 153–165.
26. Pasternack, R.F.; Ewen, S.: Rao, A.; Meyer, A.S.; Freedman, M.A.; Collings, P.J.; Frey. S.L.: Ranen, M.C.; de Paula. J.C. Interactions of copper(II) porphyrins with DNA. Inorg. Chim. Acta 2001. 317. 59–71.
27. Franzen. S.; Wallace-Williams. S.E.; Shreve. A.P. Heme charge-transfer band III is vibronically coupled to the Soret Band. J. Am. Chem. Soc. 2002. *124* (24), 7146–7155.
28. Danis, J.A.; Lin. M.R.; Scott. B.L.; Eichhorn, B.W.: Runde, W.H. Coordination trends in alkali metal crown ether uranyl halide complexes: The series $[A(Crown)_2][UO_2X_4]$ where A=Li, Na, K and X=Cl, Br. Inorg. Chem. **2001**. *40* (14), 3389–3394.

Viruses as Host Assemblies

Michelle Flenniken
Mark Allen
Mark Young
Trevor Douglas
Montana State University, Bozeman, Montana, U.S.A.

INTRODUCTION

Viruses have long been recognized as being remarkable for their abilities to package. transport. and deliver their genornes using small well–defined containers: viral capsids. These viral containers span a wide range of size and shape, yet they are all essentially molecular assemblies with homogeneous properties.[1] These aspects of their biological functions have been recognized by chemists and materials scientists and are currently being exploited as a platform for the synthesis of inorganic nanomaterials, the attachment of biologically active ligands, the discovery of novel peptides, and the assembly of functionalized viral particles into well-ordered two- and three-dimensional arrays.

VIRUSES AS PROTEIN CAGES

The protein shell of a virus is assembled from multiple copies of virally encoded protein subunits.[2] The interaction among subunits is designed to provide maximum contact through non-covalent bonding.[3,4] Not surprisingly, the repetition of such interactions among a limited number of subunits results in regular structures with symmetry that describes the spatial interaction between protein building blocks. The protein shells of almost all virions are based on icosahedral or helical symmetry. Icosahedral symmetry is the largest closed structure that can be built from a repeating subunit in which the interactions between all subunits are chemically identical.[3] The T number (triangulation number) is a measure of the allowed arrangement of subunits to maintain icosahedral symmetry of the virus particle.

An icosahedron is defined by 20 triangular faces and 12 vertices related by two-, three-, and fivefold axes of rotational symmetry (Fig. 1). *A* spherical virion based on true icosahedral symmetry can be built from 60 copies of an identical coat protein subunit. However. a virion based on true icosahedral symmetry severely restricts the size of the genome that can be packaged. In nature. most spherical viruses are based on quasi-icosahedral symmetry that allows assembly of larger shells necessary to accommodate typical viral genomes (3–500 Kb). The basis for quasi-icosahedral symmetry is that the bonding properties of subunits in different structural environments are similar but not identical.[5] For example. a particle comprised of 180 copies of a single subunit (T = 3) arranges its subunits so that it retains the 12 vertices, but additional subunits arranged with sixfold symmetry are interposed between the fivefold symmetric clusters. In this type of arrangement, each subunit will be present in one of three slightly different chemical environments (designated A. B. and C). Even larger particles can be formed following the quasi-equivalent positions that allow the assembly of protein shells with diameters that typically range from 18–500 nm.

ICOSAHEDRAL VIRUS PARTICLES

Three icosahedral viruses emerged as useful templates with cage-like architectures for nanotechnology: cowpea chlorotic mottle virus (CCMV) and cowpea mosaic virus (CPMV) and Norwalk virus (NV) (Fig. *2)*. CCMV and *CPMV* are both plant viruses. while NV is an animal virus.

The CCMV is an RNA-containing plant virus. These 28 nm diameter virions contain 180 identical coat protein subunits (19.8 kDa each) arranged on an icosahedral lattice (T=3), which self-assemble to form a protein cage 2–4 nm thick and define a central cavity in which the viral *RWA* is packaged. The *N*-terminal 25 amino acid residues are basic, and negatively charged RNA is thought to interact electrostatically with this region of positive charge. In vivo. removal of this region of the protein prevents encapsulation of RNA but does not disrupt formation of empty virus particles in vitro.

The CPMV is also an RNA-containing plane virus. The icosahedral virus particle is formed from 60 copies of two different types of protein subunits (large *37* kDa and small *23* kDa). These proteins assemble into a pseudo (T = I) particle approximately 30 nm in diameter.[6] Very high

Encyclopedia of Supramolecular Chemistry
DOI: 10.1081/E-ESMC *120012697*

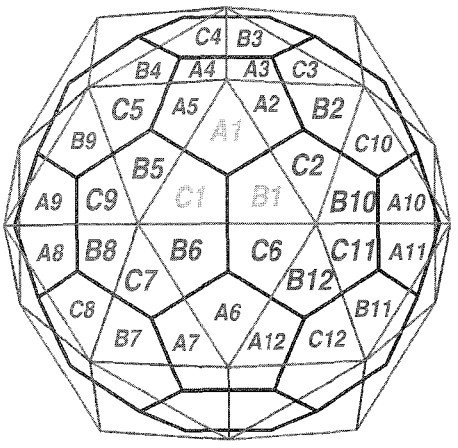

Fig. 1 Assembly of T = 3 icosahedral virus particle showing the three subunits of the asymmetric unit A1, BI, C1.[1] (Used with permission from http://mmtsb.scripps.edu/viper/viper.htm)

yields of virus can be obtained through a straightforward virus purification of infected plants. A kilogram of infected plant tissue can yield 1–2 g of virus. Unlike CCMV, this virus is not easily reconstituted into an empty protcin cage, but these particles are thermostable (up to 60°C) and noninfectious to animal cells.

The NV is a human calicivirus and contains a single-stranded RNA genome.[7] Particles of NV have T = 3 icosahedral symmetry with an approximate outer diameter of 38 nm and an average inner diameter of the central cavity that ranges from 20–29 nm. These virions contain 180 molecules of identical capsid protcin (56.6 kDa each), which has two principle domains, *S* and **P**. linked by a flexible hinge.[7] These viruses arc difficult to cultivate in tissue culture systems or animals,[8] making them difficult to study, and this factor limits their use as nanosynthctic reaction vessels.

Structural Transitions

The CCMV undergoes a reversible pH and metal-ion-dcpcndcnt swelling that results in a 10% increase in virus dimension."" This transition is the result of an expansion at the pseudo threefold axis of the virus particle,[10] which causes the formation of 60 separate 2 nm diameter openings in the protein shell (Fig. 2D). Under swollen conditions (pH>6.5), these openings allow free molecular exchange between the virus cavity and the bulk medium. In contrast, in the non-swollen form (pH < 6.5), there is no apparent exchange of large molecules between the cavity and the bulk medium. This transition can be viewed as analogous to reversible gating in molecular host–guest chemistry,[11,12] with the potential for selective entrapment and release of large molecules from the central cavity of the virion.

MINERALIZATION OF VIRAL CAPSIDS

Molecules can be packaged within the virion of CCMV and NV as crystalline solids that have a very high packing density. For example, it was shown that crystals of an ammonium salt of $H_2W_{12}O_{42}^{10-}$ can be packaged as a nanosizc crystalline solid within the CCMV protein cage,[13,14] and that modified viral cages will accommodate $Fe_2O_3{\cdot}nH_2O$.[15] The size and shape of the encapsulated nanomaterial is determined by the size and shape of the cavity created by the CCMV (or NV) protein cage. Therefore, the viral protein cage acts as a constrained reaction vessel to limit nanoparticle growth and morphology.

The crystallization of guest molecules can be achieved and controlled because the virion provides a charged protein interface (on the interior) that facilitates the aggregation and crystallization of ions. The plant virus CCMV has been a good model system for nanophase crystal growth, and a range of polyoxometalate species (vanadate, molybdatc, tungstate) can be crystallized within the CCMV protein cage. The same type of mineralization reaction (with tungstatc) is possible using NV. Thcse mineralization reactions are accomplished by providing an interface for molecular aggregation, based on complementary electrostatic interactions between the protcin and

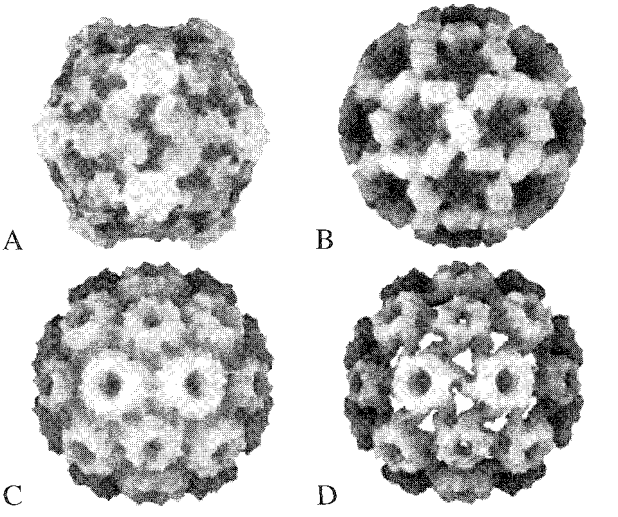

Fig. 2 Cryo electron microscopy and image reconstructions of (A) Cowpea Mosaic Virus (CPMV); (B) Norwalk Virus (NV); (C) Cowpea Chlorotic Mottle Virus (CCMV) unswollen; and (D) CCMV swollen.[1] (Used with permission from http://mmtsb.scripps.edu/viper/viper.htm) (*View this art in color at www.dekker.com.*)

the metal species, which creates a locally high concentration at the protein interface. Briefly outlined, the empty virions were incubated with the precursor ions (WO_4^{2-}, VO_3 , MoO_4^{2-}) at approximately neutral pH. Under these conditions, the virus exists in its open (swollen) form and allows all ions access to the cavity. The pH of the virus solution was then lowered to approximately pH 5.0. This induced two important complementary effects. The inorganic species underwent a pH-dependent oligomerization to form large polyoxometalate species such as $H_2W_{12}O_{42}^{10-}$, which were readily crystallized as ammonium salts. In addition, the viral capsid particle underwent a structural transition in which the pores in the protein shell closed, trapping crystallized mineral or mineral nuclei within the virus. Crystal growth of the polyoxometalate salt continued until the virion container was filled. Thus, the material synthesized was constrained by the size and shape of the interior of the viral protein cage. The resulting product could be easily purified (by centrifugation on sucrose gradients or size exclusion chromatography) and was visualized by transmission electron microscopy (TEM).

To test the dominance of electrostatic effects in the mineralization model, a mutant of CCMV was constructed (subE) in which all the basic residues on the N-terminus of the coat protein were substituted for glutamic acid (E), thus dramatically altering the electrostatic character of the interior of the assembled protein cage.[11] This mutant was able to catalyze the oxidative hydrolysis of Fe(II) to form an iron oxide nanoparticle encapsulated within the protein cage of the modified virus. High-resolution spectral imaging allowed the elemental composition of a protein–mineral composite material to be resolved (1 nm spatial resolution, Fig. 3). This clearly showed that the mineral nanoparticle was completely encapsulated within the protein cage structure. This mutant is able to bind Fe(II), facilitate its autoxidation to Fe(III), and engage in subsequent hydrolysis to form a ferric oxide mineral within the virion. The nanomaterial within the cage is size and shape constrained by the internal dimensions of the particle. Wild-type CCMV showed none of this spatially defined catalytic activity, and when incubated in the presence of Fe(II), bulk autoxidation and hydrolysis was observed, and no virion-encapsulated mineral was detected. Thus, selective engineering of the virion is possible, illustrating the synthetic plasticity of these architectures as biotemplates.

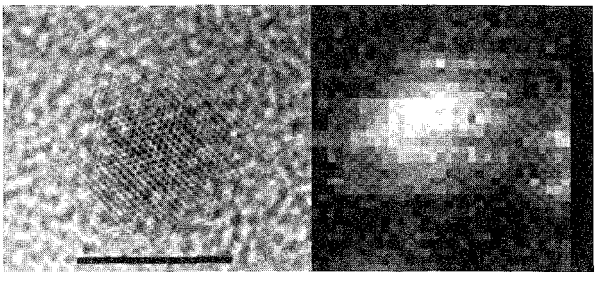

Fig. 3 Iron oxide nanoparticle cores synthesized within the mutant form of CCMV (subE). High-resolution TEM (left) of a single core (scale bar 30 nm) and (right) energy loss spectral imaging of a single particle showing N (dark pixels) and Fe (light pixels). (*View this art in* color *at www.dekker.com.*)

Encapsulation Based on Structural Transitions

Reversible virus gating (swelling) appears to play a role in the selective entrapment and release of materials from the protein cage.[13,14] The selective entrapment of the large anionic organic polymer poly(anetholsulfonic acid) (average molecular weight of 10,000 kDa) was used as a test of the role of gating. Empty virions were incubated under swollen conditions (pH 7.0) in a low concentration of poly(anetholsulfonic acid). When the virion is swollen, the polymer has free access to the interior through the 2 nm holes opened at the quasi-threefold axes and binds strongly to the highly cationic protein inner surface. When the pH of the solution was lowered, closing the holes, the polymer remained trapped inside and could be isolated as an organic composite, as demonstrated by TEM analysis and sedimentation on sucrose gradients. The poly (anetholsulfonic acid) loaded particles isolated from the gradients were subsequently dialyzed at pH 7 in buffer lacking the polymer, whereupon the poly(anetholsulfonic acid) was released from the particles. The release of the polymer was indicated by reanalysis of the particles on sucrose gradients that showed the sedimentation velocity of an empty particle (50S) and the loss of the unique poly(anetholsulfonic acid) absorbance at 315 nm. When the virion was incubated with polymer under nonswollen conditions, no uptake was observed. The same result was achieved with other polyanions such as poly(dextran sulfate). These results suggest that gating can be manipulated to play a central role in the selective entrapment and release of large molecules.

SURFACE MODIFICATION OF VIRUS PROTEIN CAGES

A recent series of articles illustrated the potential of using viruses as addressable nanoblocks having a variety of chemical and physical properties. These icosahedral virus particles can be derivatized using fluorescent organic labels[16,17] or particles of nanogold.[18] This is an illustration of the use of chemical functionality in a

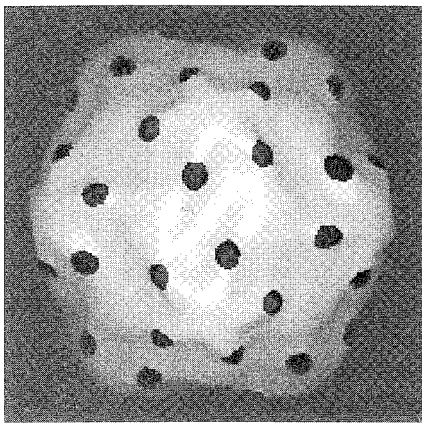

Fig. 4 Cryro electron micrograph and image reconstruction of Au-labeled CPMV. This illustrates the spatial selective labeling of engineered Cys residucs on the outer surface of CPMV. Adapted from Ref. [18] with permission. (*View this art in color at www.dekker.com.*)

biotemplate. Spatial selectivity of the derivatization process could be achieved using specific functionality enginecred into the virion structure.

The native CPMV virion could be reacted with the thiol reactive 5-maleimidofluoroscein, and it was found that 60 cysteine residues on the inside of each icosahedral particle could be derivatized.[16] A mutant form of CPMV was constructed with an exposed sulfhydryl on the exterior surface of the large subunit,[17] and the resulting two cysteine residucs could be differentially labeled, the exterior thiols reacting more rapidly than those on the interior. Qerivatization of thiol groups on the virus with a stilbene derivative for which antibodies wcre available showed the spatial differences between the location of thiols in the wild type and the mutant forms of the virus. The mutant, with thiols on the exterior of the virion, when derivatized with the stilbene, showed conjugate formation when reacted with the antibody. In contrast, attachment of the stilbene to the wild-type thiol on the interior of the virion showed no rcactivity with the antibody.

The surface-exposed thiols on the mutant virus wcre additionally reacted with monomalcimido-nanogold, and a three-dimensional image reconstruction was computed from cryo-electron microscopy.[18] As shown in Fig. 4, the gold particles are clearly visible at the positions of the inserted cysteine residues.

Derivatization of exposed lysine groups ($-NH_2$) on CPMV using rcactivity with *N*-hydroxysuccinimide esters or isothiocyanates provides additional flexibility for the use of viruses as biotemplates. Attachment of biotin to CPMV by this route, followed by reaction with avidin, resulted in c oss-linking of the virus particles to form a gel.[16] This is an initial step toward the programmed assembly of virus nanoblocks to form hierarchical structures with many levels of order.

Similarly, the wild type of CCMV could be chemically derivatized using amine-reactive fluorescent anhydrides or via activation of surface-exposed carboxylates and subsequent reaction with fluorophores bearing nucleophilic amine groups. In addition, genetically engineered CCMV with surface-exposed cysteine residues could be used for additional thiol selective attachment of fluorophores and peptides.

PHAGE DISPLAY

Phage display libraries arc "living" libraries of infectious *Escherichia coli* bacteriophage that were genetically engineered to express a library of small peptides on their exterior surface. A simplified overview of the phage display technique is illustrated in Fig. 5. The M13 filamentous phage (a virus) naturally infects and multiplies in the bacterium E. *coli,* and the genome of this phagc was completely sequenced. By inserting a library of peptide sequences into a "tail-like" protein of the phagc (three to five copies of which are located at one terminus of the assembled virion),[''] the living library is generated. The engineered phage present the corresponding novel peptides on their exterior surfaces and can then be used to test interactions with various targets, including inorganic and organic substrates. The first round of phage display involves introduction of the phagc library to the target and subsequently washing away those phage that do not interact with the target. The bound phage can then be eluted off the target by adding various compounds that

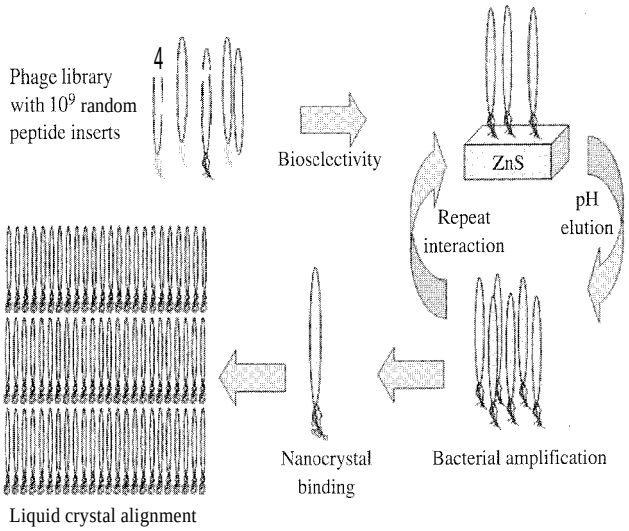

Fig. 5 The process used to generate nanocrystal alignment by the phage display method. (From Ref. [27].)

disturb the peptide–target interaction, without denaturing the remarkably resilient phage.[20] The eluted phage are amplified by re-infection of bacteria and then isolated and re-exposed to the same target (stringencies can be varied, if desired: in order to isolate peptides that interact with the target under certain experimentally relevant conditions). Typically. three to five rounds of phage–target exposure, unbound phage removal, elution (collectively referred to as "biopanning"), and amplification are performed. After the final amplification step, phage are isolated from infected bacteria, and their genetic inserts, corresponding to the novel peptides they each expressed, are sequenced. and the corresponding amino acid sequence of each peptide insert can be deduced. The biopanning results in the identification of several peptide sequences corresponding to those that interact strongly with their targets.

The use of phage display for the identification of proteins that specifically interacted with iron oxide targets was initiated[21,22] using slightly more complex systems than those depicted in Fig. 5. Similar peptide sequences were identified containing an RSK sequence domain. which correlates previous work that employed a bacterial display system.[21] Another sequence, identified by phage display, contained an RRSRHH sequence domain, again consistent with sequences identified in earlier work.[22]

The use of phage display was applied to the identification of a number of different peptides showing affinity for such materials as GaAs,[23] InP,[23] Si,[23] Ag,[24] SiO_2,[25] $CaCO_3$,[26] and ZnS.[27] In addition, the binding to different crystallographic faces of GaAs was probed. and peptide sequences were isolated that bound selectively to GaAS{100} faces but not GaAs{111} faces.[23] Interestingly. those peptides identified as having strong interactions with SiO_2 surfaces showed high sequence similarity to proteins isolated from the diatom *Cylindrotheca fusiformis*, which biomineralizes SiO_2.[28] The peptides identified by phage display were effective in inducing the mineralization of SiO_2 in synthetic reactions using silicic acid.

Recently. the isolation of a phage expressing a seven amino acid long peptide sequence that specifically bound to the surface of ZnS (Asn-Asn-Pro-Met-His-Gln-Asn) was reported.[27] When whole phage expressing this peptide were placed in precursor solutions of Zn^{2+} and S^{2-}, they induced the nucleation of nanoparticles of ZnS that remained bound to the phage. This concentrated solution of phage led to self-assembly of smectic. cholesteric. and nematic liquid crystal-like arrays comprising the filamentous phage bound to five ZnS crystals (2.66 ± 0.22 nm; Fig. 5*)*. The resulting ordered arrays of ZnS with phage showed periodicity of 895 nm corresponding to a separation of the nanocrystal domains (2.66 nm crystals in about a 20 nm cluster) by the dimensions of the phage (880 nm in length, 6.6 nm in diameter) stacking end to end giving a continuous lamellar morphology. This structure extended beyond the nanometer size regime to 72 μm domains that eventually form a film of cm dimensions (Fig. 5*)* but still have quantum dot properties. The value in this quantum dot function lies in an approach to computing based on a binary code that uses the semiconductor properties of ZnS nanocrystals.

In a similar set of experiments, phage display was used to identify peptides with high affinity for Ag.[24] These peptides were active toward the formation of Ag nanoparticles. and when the phage displaying these peptides were placed into a solution of silver ions (0.1 mM $AgNO_3$) for 16–48 h, they formed silver nanoparticles 60–150 nm in diameter. As in the case of the ZnS phage, it was possible to assemble these Ag nucleated phage into liquid crystal-like arrays in which layers of silver particles were separated by 680 nm, the dimensions of the phage.

The phage display technique was shown to have two important implications. For the first time, peptide sequences with high affinity for specific crystallographic mineral interfaces can be identified and were shown in some cases to influence the nucleation of specific minerals from solution. In addition, the ability to use self-assembly of the highly anisotropic and mineralized phage particles opened a new realm of supramolecular host–guest chemistry that combines high selectivity and long-range order.

CONCLUSION

The use of viruses and viral proteins for materials synthesis, encapsulation. and patterning, provides a number of unique advantages. The protein cages are biological in origin and, as such, are amenable to large-scale production (fermentation. farming, etc.) and are also inherently biodegradable. The icosahedral structures can be routinely modified using a genetic approach to impart specific chemical or structural functionality. The presentation of functionalizable reactive groups also allows a chemical approach to be taken to the attachment and presentation of organic and inorganic ligands. This structural and functional plasticity allows many of the protein cage systems described here to be engineered and redesigned for specific applications in materials science, homogeneous and heterogeneous catalysis. and biomedicine. The phage display technique provides a unique coinbinatorial approach to determining specific protein–mineral interactions, which can then be used to selectively synthesize mineral nanoparticles. In addition, the ability of the isotropic and anisotropic viral particles to make self-assembled superlattices and arrays in two and three

dimensions has the potential to make a significant impact in nanoelectronics. This chemistry is fundamentally biomimetic, and the lessons learned from how biological systems deal with issues of spatial control and assembly can now be applied to purely or partially synthetic systems.

ARTICLES OF FURTHER INTEREST

Biomaterials, p. 110
Carcerands and Hemicarcerands, p. 189
Crystal Growth Mechanisms, p. 364
DNA Nanotechnology, p. 475
Inclusion Reactions and Polymerization. p. 705
Micelles and Vesicles, p. 861
Nanocasting Strategies and Porous Materials, p. 950
Protein Supramolecular Chemistry, p. *1161*
Self-Assembling Catenanes, p. 1240
Self-Assembly in Biochemistry, p. 1257

REFERENCES

1. Reddy. V.; Natarajan. P.; Okerberg, B.: Li, K.; Damodaran. K.: Morton, R.; Brooks. I.C.: Johnson. J.E. Virus particle explorer (viper), a website for virus capsid structures and their computational analysis. J. Virol. 2001. *75.* 11943–11947.
2. Harrison. S.C.: Skehel. J.J.; Wiley. D.C. Virus Structure. In *Fundamental* Virology; Fields. B.N.. Knipe, D.M.. Howley. P.K., Eds.; Lippincott-Raven: New York. NY. 1996; 59–99.
3. Baker, T.S.; Johnson. J.E. Principles of Virus Structure. In *Structural* Biology of *Viruses*; Chiu. W.. Burnett, R.M.. Garcea. R.L., G.. Eds.: Oxford University Press: New York, NY, 1997: 38–79.
4. Rux. J.J.: Burnett, R.M. Spherical viruses. Curr. Opin. Struct. Biol. 1998, **1.** 142–149.
5. Johnson, J.E.; Speir. J. Quasi-equivalent: A paradigm for protein assemblies. J. Mol. Biol. **1997**, *269.* 665–675.
6. Lin. T.: Chen, Z.: Usha, R.; Stauffacher. C.V.; Dai. J.B.; Schmidt, T.; Johnson. J.E. The refined crystal structure of cowpea mosaic virus at 2.8 a resolution. Virology 1999, *265*, 20–34.
7. Prasad, B.V.; Dokland, T.: Bella, J.; Rossmann, M.G.; Hardy. M.E.; Estes. M.K. X-ray crystallographic structure of the norwalk virus capsid. Science 1999, *286*, 287–290.
8. Bertolotti-Ciarlet. A.; White. L.J.; Chen, R.; Prasad, B.V.; Estes, M.K. Structural requirements for the assembly of norwalk virus-like particles. J. Virol. 2002, *76*, 4044–4055.
9. Jacrot. B. Studies on the assembly of a spherical plant virus ii. The mechanism of protein aggregation and virus swelling. J. Mol. Biol. **1975**, *95*, 433–446.
10. Speir. J.A.; Munshi, S.; Wang, G.; Baker. T.S.: Johnson, J.E. Structures of the native and swollen forms of cowpea chlorotic mottle virus determined by x-ray crystallography and cryo-electron microscopy. Structure 1995. *3*, 63–78.
11. Houk. K.N.: Nakamura. K.: Sheu, C.; Keating, A.E. Gating as a control element in constrictive binding and guest release by hemicarcerands. Science 1996. *273*, 627–629.
12. Hof, F.; Craig, S.L.; Nuckolls, C.: Rebek. J. Molecular encapsulation. Angew. Chem.. Int. Ed. 2002. *41.* 1488–1508.
13. Douglas. T.; Young, M.J. Host–guest encapsulation of materials by assembled virus protein cages. Nature 1998. *393*, 152–155.
14. Douglas. T.; Young. M. Virus particles as templates for materials synthesis. Adv. Mater. 1999, *11*, 679–681.
15. Douglas. T.; Strable. E.; Willits, D.; Aitouchen. A.; Libera. M.: Young, M. Protein engineering of a viral cage for constrained nano-materials synthesis. Adv. Mater. 2002, *14.* 415–418.
16. Wang, Q.: Kaltgrad. E.; Lin. T.W.; Johnson. J.E.; Finn. M.G. Natural supramolecular building blocks: Wild-type cowpea mosaic virus. Chem. Biol. 2002. *9.* 805–811.
17. Wang, Q.: Lin, T.W.; Johnson, J.E.; Finn. M.G. Natural supramolecular building blocks: Cysteine-added mutants of cowpea mosaic virus. Chem. Biol. 2002. *9.* 813–819.
18. Wang, *Q.;* Lin, T.W.; Tang, L.; Johnson. J.E.; Finn. M.G. Icosahedral virus particles as addressable nanoscale building blocks. Angew. Chem., Int. Ed. 2002. *41.* 459–462.
19. Smith, G.P.; Scott. J.K. Searching for peptide ligands with an epitope library. Science 1990. *249*, 386–390.
20. Smith. G.P.; Petrenko. V.A. Phage display. Chem. Rev. **1997**, *97.* 391–410.
21. Brown. S. Engineered iron oxide-adhesion mutants of the *Escherichia coli* phage λ receptor. Proc. Natl. Acad. Sci. U. S. A. **1992**. *89*, 8651–8655.
22. Barbas, C.F., III: Rosenblum. J.S.: Lerner, R.A. Direct selection of antibodies that coordinate metals from semisynthetic combinatorial libraries. Proc. Natl. Acad. Sci. U. S. A. **1993**, *90*, 6385–6389.
23. Whaley. S.R.; English. D.S.: Hu, E.L.: Barbara, P.F.: Belcher. A.M. Selection of peptides with semiconductor binding specificity for directed nanocrystal assembly. Nature 2000. *405*. 665–668.
24. Naik, R.R.; Stringer. S.J.; Agarwal, G.: Jones, S.E.: Stone. M.O. Biomimetic synthesis and patterning of silver nanoparticles. Nat. Mater. 2002. *1*. 169–172.
25. Naik, R.R.: Brott. L.L.; Clarson, S.J.; Stone. M.O. Silica-precipitating peptides isolated from a combinatorial phage display peptide library. J. Nanosci. Nanotechnol. 2002, 2, 95–100.
26. Gaskin, D.J.H.; Starck. K.: Vulfson, E.N. Identification of inorganic crystal-specific sequences using phage display combinatorial library of short peptides: A feasibility study. Biotechnol. Lett. 2000. *22.* 1211–1216.
27. Lee, S.-W.; Mao, C.: Flynn, C.E.: Belcher. A.M. Ordering of quantum dots using genetically engineered viruses. Science 2002, *296.* 892–895.
28. Kroeger. N.: Deutzmann, R.; Sumper, M. Polycationic peptides from diatom biosilica that direct silica nanosphere formation. Science 1999. *286,* 1129–1132.

Vitamin B_{12} and Heme Models

V

Sabine Van Doorslaer
University of Antwerp, Wilrijk, Belgium

INTRODUCTION

Heme proteins, like the globins *and the cytochromes, fulfill important functions. They share the common structural feature of having a* heme *group,* i.e., *an iron posphyrin complex, embedded in the protein (Fig.* 1A). *Four types of* globin, *differing in structure, tissue distribution, and likely function, were discovered in man and in other vertebrates: hemoglobin (Hb), myoglobin (Mb), neuroglobin (Ngb), and cytoglobin* (Cgb).[1] Tetrameric *Hb, located in the red blood cells, serves to transport* O_2 *in the circulatory system. The* monomeric *Mb, present mainly in the cardiac and striated muscle, acts as an* O_2 *buffer, facilitates* O_2 *diffusion, and plays a role in NO removal. Ngb, predominantly expressed in nerve cells, and Cgb, expressed in* many *tissues, are two recently discovered members of the vertebrate* globin *family exhibiting a hexacoordinated heme. They are of ancient evolutionary origin, and their physiological roles are still not fully* understood.[1] *Besides the* globins, *the cytochromes. which are electron-transfer proteins, form an important class of heme proteins. Several cytochromes have* a *hexacoordinated heme. The most intriguing characteristics of the* cytochrome *family of electron-transfer proteins is the broad range of* redox *potentials featured by the* Fe^{III}/Fe^{II} *couple at the* electro-*active* heme *core.'''* *Cytochrome* P450 *proteins form a separate class of heme proteins, where a cysteine residue coordinates to the proximal site of the heme group. This membrane protein is ubiquitous, occurring in life forms ranging* from *bacteria to man. All cytochrome* P450 *proteins catalyze the oxidation of organic substrates by oxygen, performing essential roles in biosynthesis,* metab-*olism, and the detoxification of* harmful substances.[3]

The versatile functions of the heme proteins challenge chemists in various ways. In the past decades, a lot of effort was put into the synthesis of heme models. The goal of these syntheses is twofold. On the one hand, the models *can help to unravel* stepwise *the chemical process connected to biological* function. *On the other hand, the chemical knowledge attained in this way can be exploited to design new products aimed at* fulfilling *tasks like reversible* O_2 *binding or catalyzing specific electron-transfer reactions or atom-transfer reactions.* In *this article, we will give a brief overview of models put forward to mimic the biological functions of heme proteins and illustrate how modern spectroscopy is used to unravel and* understand *the active site mechanisms.*

The B_{12} *coenzyme (Fig.* 1B) *is highly intriguing. The* B_{12}-cofactors *play a role in enzymatic methyl group transfer. in enzymatic ribonucleotide reduction, and in the enzymatic* 1,2-rearrangements *of a hydrogen atom with heavy atom centers.''' The specific structure of the cofactor gives rise to several interesting questions. First, why did nature chose cobalt, a transition metal that is not very abundant on earth? Second, what is the origin of the corrin ligand? What can this ligand offer that a posphyrin ligand cannot? What is the nature of metal–ligand interactions, and how does the protein use these interactions in its enzymatic role? In order to unravel these points and to try to mimic the biological functions of the* B_{12}-dependent *proteins, several synthetic models were put forward. A brief overview will be given.*

In Fig. 1, *it is shown that the porphyrin and con-in ligand are related. They share a similar biosynthesis path as the one that leads from 6-Ala to uroposphyrinogen* III.[4] *The organic synthesis of vitamin* B_{12} *turned out to be a gigantic effort that took Eschenmoser and coworkers over 11 years and could only be obtained in a more than 90-step* synthesis.[5] *This also shows that nature must have had a clear reason to synthesize this extraordinary* corrinoid. *Therefore,* Co(II) *porphyrin complexes are often studied in* B_{12}-*related analyses, in order to pin down the specific advantage of the corrin ligand. Thus, some of the models mimicking heme proteins are also addressed in the* B_{12} *research domain.*

HEME MODELS

A wide variety of approaches was derived to synthesize model systems for heme proteins. In the following, we will summarize some of these designs. Although I *distinguish here three subsections, depending on the specific heme function that is aimed at, it should be noted that most synthetic strategies presented are of a general nature and are applicable to other subsections.*

Heme Models for Oxygen Transport

In order to mimic the biological functions *of heme proteins, one of* the *challenging targets is to realize*

Encyclopedia of Supramolecular Chemistry
DOI: 10.1081/E-ESMC 120012698

reversible O_2 binding. In globins, the heme is held in place by a coordination to the "proximal histidine" at the F8 site and by several noncovalent interactions with the surrounding protein residues. Heme hexacoordination, where the distal HisE7 residue directly coordinates to the heme iron atom is uncommon in Hb of vertebrates. In mammalian Mb and Hb, the protein superstructure shields the iron(II) heme cofactor against irreversible oxidation and μ-oxo dirner formation.[6] The peptide shell is also thought to play a determinant role in the affinity of the heme iron(II) for different diatomic molecules.[7] In the oxy forms of Hb and Mb, the distal histidine is thought to interact with the terminal O-atom of the dioxygen via H-bonding. Although the strength of the H-bond is still disputed; the interaction seems to play an important role in the discrimination of the heme proteins between O_2 and CO binding. The relative binding affinity of CO versus O_2, referred to as the M value, is a useful measure of a complex's susceptibility to poisoning by CO [$M = P_{1/2}(O_2)/P_{1/2}(CO)$, whereby $P_{1/2}$ is the partial pressure of O_2 or CO at half-saturation].

The basic requirements for synthetic heme models are, therefore, a five-coordinate iron(II) porphyrin in a high-spin state, with a proximal nitrogen base and a vacant site for dioxygen. Futhermore, the formation of chemochromes by axial coordinaton of two N-bases to the iron(II) prophyrin should be prevented.[8] Several approaches were put forward. It is found that a sterically hindered axial base, such as 1,2-dimethylimidazole, favors formation of a five-coordinate high-spin complex. Furthermore, covalent attachment of the axial ligand or steric hindrance of one of the two faces of the heme can also be used to prevent axial ligation of two bases. Finally, rapid decomposition of the O_2 adducts via μ-oxo-dimer formation has to be prevented. This can be achieved by attaching bulky substituents onto the iron(II) posphyrin or by bridging the macrocycle.[8]

The above requirements form a sort of blueprint for the synthesis of heme models for reversible oxygenation. The earliest structurally and functionally sound iron porphyrin model of the Hb and Mb active sites was the "picket fence" porphyrin[9] ((Fig. 2A). The CO affinity of the picket fence porphyrin turned out to be more than 30 times that of human Hb. If mammalian Hb or Mb would have the same M value as the picket fence porphyrins, mammals would suffocate in their own heme catabolism.[10] On the basis of this. Collman et al. proposed that the distal histidine plays a dual role of providing an H-bond to facilitate O_2 coordination and of decreasing CO affinity by steric hindrance of the CO binding in a linear manner.[8] In order to investigate this hypothesis further. Collman and coworkers synthesized "pocket" porphyrins, "hybrid" porphyrins. and "capped" posphyrins (for a review, see Ref. [8]). All of these models try to mimic the presence of the protein heme pocket in the natural proteins [see Fig. 2B as an example of a "pocket" porphyrin].[11] Collrnan and coworkers reported a versatile general method, the congruent multiple Michael addition, for attaching macrocycles over a posphyrin ring in a single high-yielding step, which opened interesting synthetic possibilities.[12] Finally, Collman and coworkers developed picnic basket porphyrins (Fig. 2C), a family of porphyrins consisting of a distal binding cavity with variable dimensions and an external bulky axial ligand on

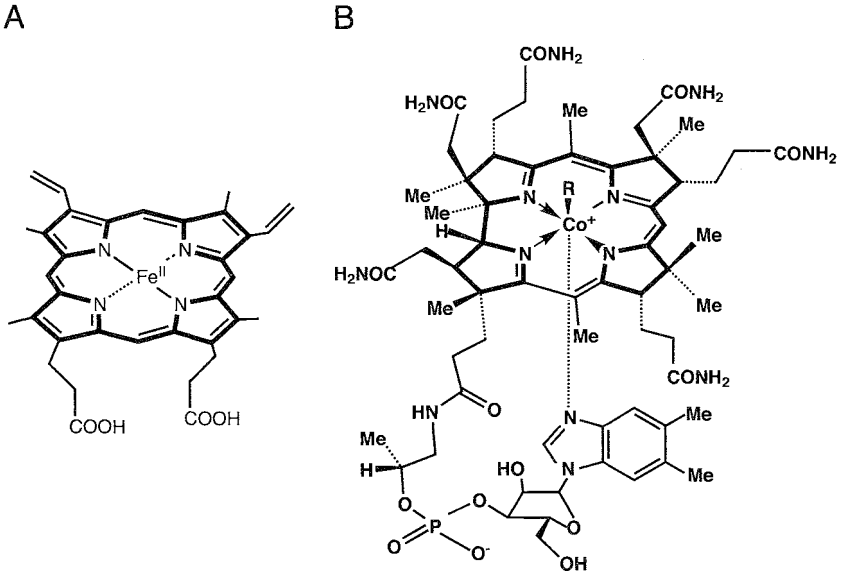

Fig. 1 (A) Heme group [iron(II) protoporphyrin IX]. (B) Vitamin B_{12} (R=CN) or coenzyme B_{12} (R=5′-deoxy-5′-adenosyl).

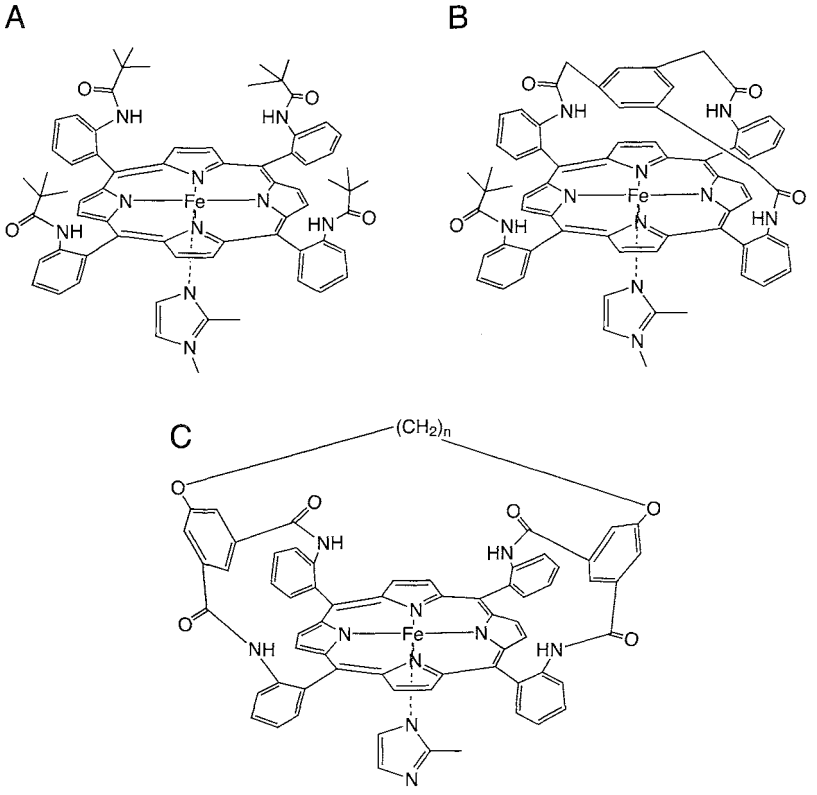

Fig. *2* Dioxygen-binding myoglobin analogues as synthesized by Collman and coworkers.[''] (A) Picket-fence porphyrin. (B) Pocket porphyrin. (C) Picnic-basket porphyrin.

the proximal side.[13] The ^{1}H-NMR and O_2 affinity measurements show that the iron(II) and cobalt(II) picnic basket porphyrins both bind O_2 reversibly at room temperature with high affinities. The O_2 affinity decreases when the size of the basket increases. This was attributed to a dipole–dipole interaction between the terminally bound O_2 and the amide protons. The O_2 affinities of the cobalt picnic basket porphyrins are more sensitive to changes in basket sizes than those of the corresponding iron posphyrin, consistent with the proposal that $Co—O_2$ adducts have more electron density on the oxygen ligand than do the $Fe—O_2$ adducts. Substitution of iron(II) by cobalt(II) in the porphyrin is, therefore, often used to get additional information on the influence of the surroundings of the dioxygen.

Over the past 5 years, the combination of metalloporphyrin with dendrirner chemistry led to a fascinating new class of Hb and Mb models,''''.''' with the dendritic superstructure mimicking the encapsulation of the heme in the natural protein environment. Modification of the dendritic shell around the iron(II) porphyrin core modulates the shape, density, and polarity of these model systems. thereby profoundly affecting the thermodynamics and kinetics of the complexes formed with O_2 and CO. Diederich and coworkers developed two classes of water-soluble dendritic iron(II) porphyrins with amide dendrons capable of H-bond donation and with ester dendrons lacking H-bond donor centers in the dendritic shell[15] (Fig. 3). Through UV/Vis titrations. it was revealed that the dendritic iron(II) porphyrins containing secondary amide groups in the dendritic branching undergo stable: reversible O_2 and CO complexation in dry toluene, whereby the O_2 affinity largely surpasses that of T-state Hb or Mb. The oxygenated complexes are stable for several hours due to the protection against μ-oxo dimer formation provided by the dendritic shell. The oxygenated Fe(II) complexes were found to be less stable in the presence of water. This suggested that in dry toluene, the dendritic cage is closely packed, and an H-bond is formed between the amide NH group and dioxygen. In water: the cage opens. and the H-bond is weakened, hence the reduced stability of the oxygenated complex. This seemed to be corroborated by the studies of the posphyrin with ester dendrons lacking H-bond donor centers. The UV/Vis analyses revealed that this receptor undergoes reversible stable CO binding in dry toluene, but that the oxygenated complexes are unstable and undergo facile oxidative decomposition. However, our recent pulse EPR (electron

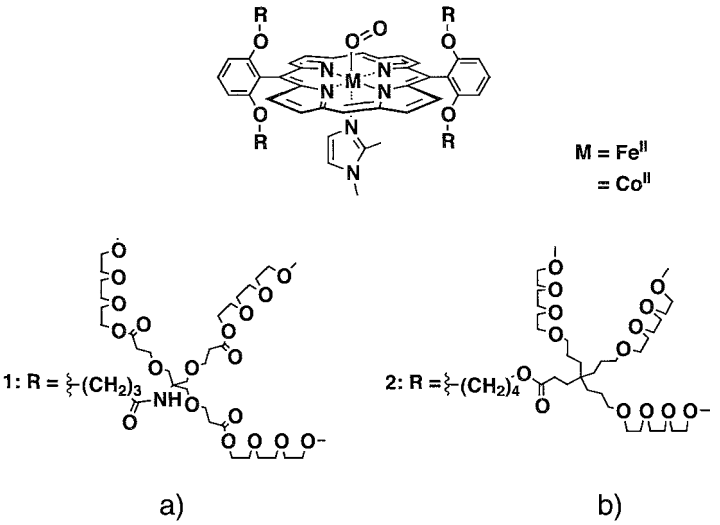

Fig. *3* Example of dendritic porphyrin complexes mimicking hemoglobin as proposed by Diederich and coworkers:[15] (a) amide dendrons; (b) ester dendrons.

paramagnetic resonance) studies of the corresponding Co(II) dendritic porphyrins shed a slightly different light on the subject.[16] Although the low hydrodynamic volume of the dendrimers in dry toluene could be experimentally confirmed, it was found that the difference in O_2 affinities between the amide-dendritic and ester-dendritic metalloporphyrins lies in the different packing and polarity of the dendritic branches. Our results clearly showed that observation of high O_2 affinity and the presence of functional groups capable of H-bond donation are no guarantee of the stabilization of dioxygen by an H-bond.

Heme Models Mimicking Cytochromes

The electron-transfer capacity of the cytochrome family of electron-transfer proteins is interesting, because the Fe^{III}/Fe^{II} couple of the heme core features a broad range of redox potentials.[2] In order to understand and mimic this behavior, several model systems were developed. The fact that the axial ligands of the heme groups in the different cytochrornes varies (the heme iron in Eukaryotic cytochrome c ligates to a histidine and a methionine, whereas cytochrome b_5 contains heme coordinated to two histidines): already shows that axial ligation to the iron center must be an important factor.[2] A variety of model studies indicated that the redox potential also depends on the nature of substituents in the porphyrin ring, H-binding to the axial ligands, and ruffling of the porphyrin macrocycle (see references within Ref. [17]). In the following, three recent models will be discussed that were developed to mimic the properties of cytochrornes.

One strategy to mimic the heme proteins is to embed the iron(II) porphyrins in a polymer. Bell et al. incorporated iron-5,10,15,20-tetraphenylporphyrin into films of a hydrogel polymer support medium, poly(γ-ethyl-L-glutamate) functionalized with imidazole pendent arms (PEG-Im) and studied the model in situ on silver electrodes using resonance Raman spectroscopy.[17] They found striking similarities between the properties of this model system, which contains multiple randomly oriented iron porphyrins bis-axially coordinated by imidazoles, and those of cytochrome c_3, which is a tetracheme protein of low molecular weight. In cytochrome c_3, the Fe^{III} hemes, which are *bis*-coordinated by histidine residues. lie close to each other (heme–heme distances ca. 1–1.5 pm), and they show efficient interheme electron transfer. The structure of the heme environment in the synthetic porphyrin-doped PEG-Im film model appears to be surprisingly close in structure and behavior to the

Another way of mimicking the electron-transfer properties of cytochromes is to use nature's own building blocks, e.g., by designing de novo polypeptides, where the porphyrin can be noncovalently introduced or covalently incorporated into a side chain of an amino acid residue in the peptide.[19]

Because observed environmental effects on the redox potential, such as heme solvation, polarity of the heme microenvironment, and nature of the surrounding protein shell are not well understood, it is important to design model systems with a unique local microenvironment around the electroactive core. Recently, dendritic iron porphyrins with tethered axial ligands were designed in which the dendritic branches guarantee a controlled microenvironment around the heme core.[17] The complexes are soluble in solvents of widely differing polarities, and the redox potential of the complexes was found to be solvent-independent.

Heme Models Mimicking Cytochrome P450 Activity

Cytochrome P450 is one of nature's oxidative workhorses. and it is involved in a wide variety of biological reactions, one of the most important being the detoxification of foreign bodies within the liver. A wide variety of approaches was developed to design and construct synthetic model systems of the cytochrome P450 family.[3] They vary from the earlier mentioned "capped" and "picnic basket" porphyrins, over supramolecular cytochrome P450 models, to dendritic porphyrins.[3]

B_{12} MODELS

Adenosylcobalamin or coenzyme B_{12} attracted great attention because of its interesting activity for selectively transforming organic substrates via homolytic (enzymatic ribonucleotide reduction and enzymatic 1,2-rearrangements) or heterolytic (methyl-group transfer) dissociation of carbon–metal bonds.[4] Structural aspects of the natural holoenzymes suggest a possible contribution of the protein matrix around the active site to the high selectivity of the transformation. In order to unravel the details of B12 functions, several Co^{III}, Co^{II}, and Co^{I} complexes have been synthesized. They can be divided in three groups depending on the equatorial ligand used: corrin, porphyrin, and other ligands.

Cobalt Corrins as B_{12} Models

Intuitively, one would think that one of the prerequisites of a good B_{12} model is a cobalt corrin complex. Cobalamin, however, is only soluble in polar solvents and oxidizes immediately to its Co^{III} form in the presence of O_2. This forms a drawback when one thinks in terms of a wide synthetic applicability, but it can also hamper mechanistic analyses. A change of the ligand substituents can solve this problem. Heptamethyl cobyrinate perchlorate (Fig. 4A), also named cobester, is soluble in polar and apolar solvents.[20] Our recent EPR studies showed that the Co(II) complex is stable at room temperature under air for months.[21] The temperature dependence of the oxygenation reaction of cobester could be monitored, and the complex was found to be in the deoxy form at room temperature. The addition of a nitrogen base was found to shift the oxygenation equilibrium in the direction of the oxygenated complex. Based on the cobester complex, several systems were synthesized that can model the methylmalonyl-succinyl rearrangement.[22,23]

In order to monitor the role of the nucleotide moiety in controlling radical reactions, different analogues of adenosylcobalamin were synthesized with modified α-D-ribose moiety and modified base moiety.[24] In diol dehydrase, it was found that the bulky base of the nucleotide moiety plays a pivotal role in stabilizing the highly reactive radical intermediates, and that it is, therefore. obligatory for catalytic turnovers. The upward distortion of the corrin ring induced by a bulky base to the

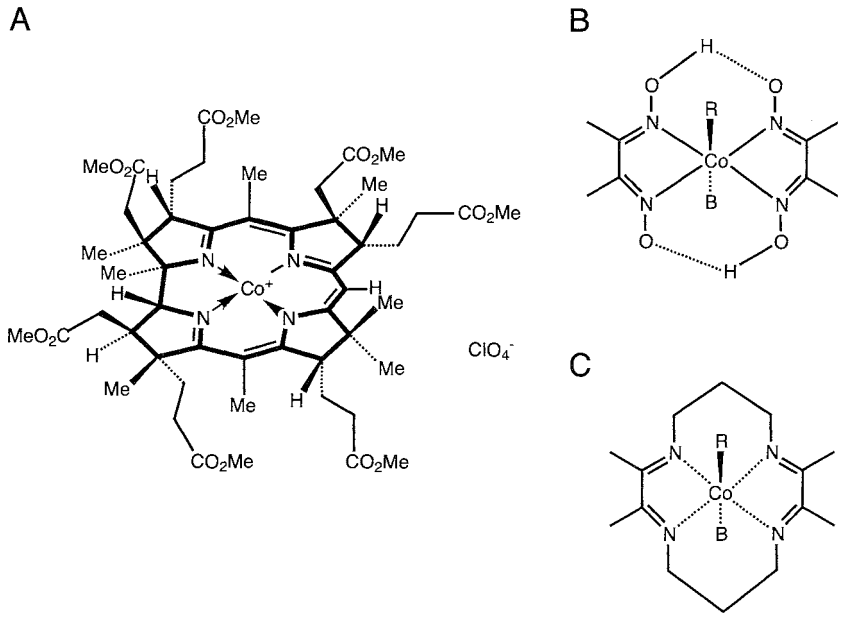

Fig. 4 B_{12} analogues. (A) Heptamethyl cobyrinate perchlorate.[20] (B) Cobaloxime as proposed by Schrauzer.[27] (C) The Costa complex as proposed by Costa et al.[29] (*B*=nitrogen base; *R*=alkyl group).

cobalt seems to be essential to prevent reactive radical intermediates from undesirable side reactions or from escaping out of the active sites during catalysis.[24]

Cobalt Porphyrins as B_{12} Models

One of the central questions in B_{12} research is why complex corrinoids are needed in B_{12} proteins. Cobalt porphyrins occur in nature, and an associated enzymatic reaction was discovered,[''] so why did nature not make use of these cobalt complexes? Can cobalt porphyrins nevertheless mimic some properties of B_{12}? Because porphyrin complexes are more easily synthetized than corrin complexes, this would broaden commercial applicability. In order to seek answers for these questions. cobalt porphyrins were studied in detail. Some of the heme models we discussed in the first section were also considered B_{12} models by replacing the central iron atom with cobalt.[8] Besides this, a lot of effort was put into fine-tuning cobalt porphyrins to perform specific chemical tasks. Recently, Uyemura and Aida successfully designed a novel model of coenzyme B_{12}, having a cobalt(II) porphyrin functionality encapsulated within a radical-tolerant, large poly(aryl ester) dendrimer cage. It was found to have a high potential for the steric control of 2,2′-azo*bis*(isobutyronitrile)-initiated transformation of alkynes.[26]

Other B_{12} Models

The synthetic importance of B_{12}-catalyzed reactions on the one hand and the reduced solubility and large autooxidation rate of cobalamin on the other hand, prompted chemists to design synthetic model systems that can overcome the drawbacks of cobalamin. In the 1970s. Schrauzer[27] recognized that cobaloxime (Fig. 4B) forms a good model for B_{12} systems. In cobaloxime, the two ligands are twofold H-bonded to form a quasi-macrocyclic chelate ring. Based on this early model, several bridged intramolecularly alkylated cobaloximes were synthesized to model the diol dehydratase reaction.[28] The Costa complex (Fig. 4C) is found to be an even better B_{12} mimic. because it exhibits a redox potential closer to the one of cobalamin.[29] An additional advantage of the relative simplicity of the model complexes is that they are of a size that is manageable in modern-day theoretical computations.[30] However, all of these synthetic model systems (and also the cobalt porphyrin systems) have a major disadvantage in that the supranucleophilic Co(I)-form is under physiological circumstances far less stable as in cobalt-corrin systems. Therefore, cobalt-corrin compounds are favored when methyl-transfer reactions are the goal.

CONCLUSION

In this overview, it is shown that the development of heme and B_{12} models has two goals: to gain a deeper understanding of the proteins' inner workings and the mimicking of specific enzymatic or transport functions of the heme and B_{12} proteins. Heme models have an iron porphyrin complex as base. The protein environment around the iron center can be modeled by means of targeted substituents of the porphyrin ring, like in picket-fence porphyrin, by dendritic branches. by a polymer, or by designing de novo polypeptides.

In order to model the extraordinary functions of B_{12} proteins: cobalt complexes with varying equatorial ligands were proposed. Besides cobalt-corrin complexes, cobalt porphyrin models and other cobalt complexes were suggested. The comparison between cobalt-corrin and porphyrin complexes is essential to unraveling nature's choice of the complex corronoid in coenzyme B_{12}.

ACKNOWLEDGMENT

I would like to thank Prof. Dr. B. Kraütler (University of Innsbruck, Austria), who introduced me to the wonders of B_{12} chemistry. I also would like to acknowledge Prof. Dr. L. Moens (University of Antwerp, Belgium). who, in the course of fruitful collaborations; taught me about heme proteins.

ARTICLES OF FURTHER INTEREST

Artificial Enzymes, p. 76
Biological Ligands, p. *88*
Biological Models and Their Characteristics, p. 101
Carbonic Anhydrase Models, p. 178
Enzyme Mimics, p. 546
Enzymes: Characteristics and Mechanisms, p. 554
Hemoglobins: O_2 Uptake and Transport, p. 636
Hydrogen Bonding, p. 658
Phthnlocyanines, p. 1069
Porphyrin Derivatives, Functional, p. *1*139

REFERENCES

1. Pesce, A.; Bolognesi. M.; Bocedi. A.; Ascenzi. P.; Dewilde. D.; Moens. L.; Hankeln. T.; Burmester. T. Neuroglobin and cytoglobin. Fresh blood for the vertebrate globin family. EMBO Rep. 2002. *3* (12). 1146–1151.
2. Mathews, F.S. The structure. function and evolution of cytochromes. Prog. Biopliys. Mol. Biol. 1985, *45* (1). 1–56.

3. Feiters, M.C.: Rowan, A.E.: Nolte. R.J.M. From simple to supramolecular cytochrome P450 mimics. Chem. Soc. Rev. 2000, *29* (6). 375–384.
4. Krautler. B. B_{12}-Coenzymes, The Central Theme. In *Vitamin B_{12} and B_{12}-Proteins*; Krautler, B., Arigoni. D.. Golding. B.T.. Eds.; Wiley-VCH. Verlag GmbH: Weinheim, 1998; 3–43.
5. Eschenmoser. A.; Wintner. C.E. Natural product synthesis and vitamin B_{12}. Science 1977. *196* (4297). 1410–1426.
6. Shikama, K. The molecular mechanism of autoxidation for myoglobin and hemoglobin: A venerable puzzle. Chem. Rev. 1998. *98* (4), 1357–1373.
7. Springer, B.A.; Sligar, S.G.: Olson. J.S.; Phillips. G.N., Jr. Mechanisms of ligand recognition in myoglobin. Chern. Rev. 1994. *94* (3). 699–714.
8. Collman. J.P.; Fu, L. Synthetic models for hemoglobin and myoglobin. Acc. Chem. Res. 1999, *32* (6), 455–463.
9. Collman. J.P.: Gagne. R.R.; Halbert, T.R.; Marchon, J.C.; Reed. C.A. Reversible oxygen adduct formation in ferrous complexes derived from a 'picket fence. porphyrin: A model for oxymyoglobin. J. Am. Chem. Soc. 1973, *95* (23). 7868–7870.
10. Collman. J.P.: Brauman. J.I.: Iverson, B.L.; Sessler, J.L.; Morris, R.M.; Gibson. Q.H. O_2 and CO binding to iron(II) porphyrins: A comparison of the 'picket fence' and 'pocket' porphyrins. J. Am. Chem. Soc. 1983, *105* (10). 3052–3064.
11. Collman, J.P.; Brauman. J.I.: Collins, T.J.; Iverson, B.: Sessler. J.L. The pocket porphyrin: A hemo-protein model with lowered CO affinity. J. Am. Chern. Soc. 1981, *103* (9). 2450–2453.
12. Collman, J.P.: Zhang, X.; Herrman, P.C.: Uffelman. E.S.: Boitrel, B.; Straumanis, A.; Brauman. J.I. Congruent multiple Michael addition for the synthesis of biomimetic heme analogues. J. Am. Chem. Soc. 1994. *116* (6), 2681–2682.
13. Collman. J.P.; Zhang, X.: Wong, K.: Brauman, J.I. Dioxygen binding in iron and cobalt picnic basket porphyrins. J. Am. Chem. Soc. 1994, *116* (14). 6245–6251.
14. Jiang. D.-L.: Aida. T. Dendrimer-encapsulated iron porphyrin as a novel hemoprotein mimic for dioxygen binding. J. Macromol. Sci., Pure Appl. Chem. 1997, *A34* (10). 2047–2055.
15. Zingg. A.; Felber, B.; Gramlich. V.; Fu. L.; Collman. J.P.: Diederich. F. Dendritic iron(II) porphyrins as models for hemoglobin and myoglobin: Specific stabilization of O_2 complexes in dendrimers with H-bond-donor centers. Hell. Chim. Acta 2002. *85* (1). 333–351.
16. Van Doorslaer. S.; Zingg. A.: Schweiger. A.; Diederich. F. Effects of the dendrimer cage on O_2 binding of dendritic cobalt(II) porphyrins. Chem. Phys. Chern. 2002. 3 (8). 659–667.
17. Weyermann. P.: Diederich. F.: Gisselbrecht. J.-P.; Boudon. C.: Gross. M. Dendritic iron porphyrins with tethered axial ligands: Neu model compounds for cytochromes. Helv. Chim. Acta 2002. *85* (2). 571–598.
18. Bell. S.E.J.; Devenney, M.D.: Grimshaw. J.: Hara, S.; Rice. J.H.: Trocha-Grimshaw. J. Resonance Raman and surface-enhanced resonance Raman studies of polymer-modified electrodes which mimic heme enzymes. J. Chem. Soc.. Faraday Trans. 1998. *94* (19). 2955–2960.
19. Tomizaki, K.: Murata, T.: Kaneko. K.: Miike. A.; Nishino. N. Chiral assembly of a pair of free base porphyrins and peroxidase-like activity of iron(III) porphyrins in four-α-helix bundle structures with dimerized two-%-helix polypeptides. J. Chem. Soc., Perkin Trans. 2000, 2 (5). 1067–1074.
20. Murakami, Y.: Hisaeda, Y.; Kajihara. A.: Ohno, T. Hydrophobic vitamin B_{12}. Coordination geometry and redox behavior of heptamethyl cobyrinate in non-aqueous media. Bull. Chem. Soc. Jpn. 1984. *57* (2). 405–411.
21. Van Doorslaer. S.; Schweiger, A.; Kräutler, B. A continuous wave and pulse EPR and ENDOR investigation of oxygenated Co(II) corin complexes. J. Phys. Chem. 2001. *105* (31). 7554–7563.
22. Keese. R.; Darbre. T.; Arx, U.; Müller, S.: Wolleb-Gygi. A.; Hirschi. D.; Sijegovic, V.: Pfammatter, M.; Amolins. A.; Otten. T. Model Studies for the Methylmalonyl-Succinyl Rearrangement. In Vitamin *B_{12} and B_{12}-Proteins*; Krautler. B., Arigoni. D., Golding, B.T.,Eds.: Wiley-VCH. Verlag GmbH: Weinheim. 1998: 289–301.
23. Sun, F.-P.; Darbre, R. Synthesis and irradiation of vitamin-B_{12}-derived complexes incorporating peripheral G.C base pairs. Helv. Chim. Acta 2002. *85* (9). 3002–3018.
24. Toraya, T. Recent Structure-Function Studies of B_{12} Coenzymes in Diol Dehydrase. In *Vitamin B_{12} and B_{12}-Proteins*; Krautler, B.. Arigoni. D.. Golding. B.T., Eds.: Wiley-VCH. Verlag GmbH: Weinheim. 1998; 303–320.
25. Dennis, M.; Kolattukudy, P.E. A cobalt-porphyrin enzyme converts a fatty aldehyde to a hydrocarbon and CO. Proc. Natl. Acad. Sci. U. S. A. 1992. *89* (12). 5306–5310.
26. Uyemura, M.: Aida, T. Steric control of organic transformation by a dendrimer cage: Organocobalt dendrimer porphyrins as novel coenzyme B_{12} mimics. J. Am. Chem. Soc. 2002. *124* (38). 11392–11103.
27. Schrauzer, G.N. New developments in field of vitamin B_{12}. Enzymatic reactions dependent upon corrins and coenzyme B_{12}. Angew. Chem.. Int. Ed. Engl. 1977. *16* (4). 233–244.
28. Rétey, J. Coenzymes B_{12}-Dependent Enzymes and Their Models. In *Vitamin B_{12} and B_{12}-Proteins*; Krautler, B.. Arigoni. D., Golding, B.T.. Eds.: Wiley-VCH. Verlag GmbH: Weinheim, 1998; 273–288.
29. Costa, G.: Mestroni. G.: Stefani. L. Organometallic derivatives of cobalt(III) chelates of *bis*(salicylaldehyde)-ethylenediimine. J. Organomet. Chem. 1967. 7 (3), 493–501.
30. Calligaris. M.; Ranaccio, L. Stereochemical analysis of cobal(II) complexes with tridendate imino- and amino-oxime ligands. Eur. J. Inorg. Chem. 2002. (11), 2920–2927.

Weak Hydrogen Bonds

Motorhiro Nishio
The CHPI Institute, Tokyo, Japan

INTRODUCTION

Properties of organic compounds are described as the consequence of various kinds of chemical forces. Strong covalent bonds bind the atoms together into an organic molecule or group. Weak interactions are important in deciding the three-dimensional (3D) shape of the molecule and play vital roles in supramolecular chemistry and in regulating biochemical processes. Among weak molecular forces, the hydrogen bond is one of the most abundant. The enthalpy of the ordinary hydrogen bond between OH or NH and electronegative atoms such as O or N is within the range of 3—7 kcal mol^{-1}. Pauling termed the above attractive force the hydrogen bond. In the conventional hydrogen bond, contribution from the Coulomb energy is the most important, because this is an interaction between a hard acid and a hard base in the context of the Pearson hard and soft acids and bases (HSAB) principle.

In the second half of the last century, evidence accumulated to show that weaker hydrogen bonds (2∼4 kcal mol^{-1}) are ubiquitous,[1] including XH/π and CH/*n* interactions (*n:* lone pair electrons, as contrasted to n). The former is hydrogen bonds between hard acids (HA) and soft bases (SB), while the latter is hydrogen bonds between soft acids (SA) and hard bases (FIB). More recently. a still weaker attractive force, the CH/π interaction (0.5∼2 kcal mol^{-1}), was shown to play a substantial role in a variety of chemical and biological phenomena. This is the hydrogen bond occurring between SA and SB. Stabilization of this bond, accordingly. comes essentially from the dispersion force and charge-transfer interaction. while contribution from the electrostatic energy is relatively unimportant. The HA/SB and SA/HB interactions fall between these two extremes. That the above interactions are all true hydrogen bonds was demonstrated by a number of spectral, crystallographic, and theoretical studies. Compared in Table 1 are characteristics of the four hydrogen bonds.

The characteristic of a hydrogen bond resides in its attractive nature and orientation dependence. This is shown in Fig. 1 for CH/π interactions as a typical example.[2] Notice that the directionality and H/π-plane distance correlate and depend on the strength of the proton donor. Analogous plots are also reported for other hydrogen bonds.

Shown in Fig. 2 are interaction energies as a function of intermolecular separation. An interesting point is that the stabilization by the weak CH/O hydrogen bond decreases more slowly than the ordinary hydrogen bond.[3]

Readers are referred to the following two monographs aimed at these nonconventional weak hydrogen bonds: *The Weak Hydrogen Bond in Structural Chemistry and Biology* by Desiraju and Steiner[4] and *The CH/π Interaction. Evidence, Nature, and Consequences* by Nishio. Hirota, and Umezawa.[5] The former is a thorough and in-depth treatise on the weak hydrogen bond, dealing largely with crystallographic evidence and consequences. The latter is aimed to a particular interaction, the CH/π hydrogen bond. dealing with various methods and aspects of this molecular force in chemistry and structural biology. Recently, Steiner wrote a review to give a survey of the hydrogen bonds, with a focus on the structure in the solid, on the ground of the modern theory and technology.[6]

Another source of information is a list of literature at the author's Web site (http://www.hi-ho.ne.jp/dionisio). The list is focused on the CH/π hydrogen bond and is updated regularly. The topics are categorized into several parts. such as crystal packing: clathrates, database analyses, structural biology, theoretical calculations, etc. The list also includes literature regarding XH/π and CH/*n* hydrogen bonds, though they are not intended to be complete. In this article, for space reasons, historically important papers are mentioned but not cited in the references. Citations are limited to the most relevant and informative. The interested reader is referred to information appearing in these books, articles, or web sites.

DETECTION OF WEAK HYDROGEN BONDS

The weak hydrogen bonds are studied by various methods. Experimentally. spectroscopy and crystallography are most often used. Formation constants or thermal properties of an interacting system also provide useful information. Conformational analyses of appropriate molecules may provide information, though indirect. for the weak

Encyclopedia of Supramolecular Chemistry
DOI *10* 1081/E-ESMC 120012761

Table 1 Four types of hydrogen bonds

Hydrogen bond	**Example**	ES	ER	CT	CORR
HA/HB (ordinary hydrogen bond)	H_2O/H_2O	Important	Important	Unimportant	Unimportant
HA/SB (OH/π, NH/π, OH/S, etc.)	H_2O/C_6H_6	Important	Moderate	Moderate	Unimportant
SA/HB (CH/O, CHIN, CH/X, etc.)	CH_4/H_2O	Important	Moderate	Moderate	Unimportant
SA/SB (CH/π, CHIS. CH/Se, etc.)	CH_4/C_6H_6	Unimportant	Unimportant	Moderate[a]	Important

ES: electrostatic; ER: exchange-repulsion: CT: charge-transfer: and CORR: London dispersion (correlation) term.
[a]A matter of current controversy.

hydrogen bonds operating between the interacting group.[5] Theoretically, ab initio calculations at high levels of approximation are used.

Spectroscopy

The IR spectroscopy, among others, is the most useful. The frequency shift of the X—H stretching band on complex formation ($\Delta\nu$) is known as the hydrogen-bond shift. The lower-frequency shift Av of ordinary hydrogen bonds varies from ca. 100–500 cm^{-1}, but the shifts are considerably smaller for weak hydrogen bonds. The NMR spectroscopy also provides information, especially if the electronic substituent effect is analyzed.

Crystallography

The x-ray diffraction method is most often employed.[4,6] Neutron diffraction provides information about the location of hydrogen atoms. Distance and angle parameters of the putative hydrogen-bonded atoms are used in evaluating the nature and strength of the interaction.

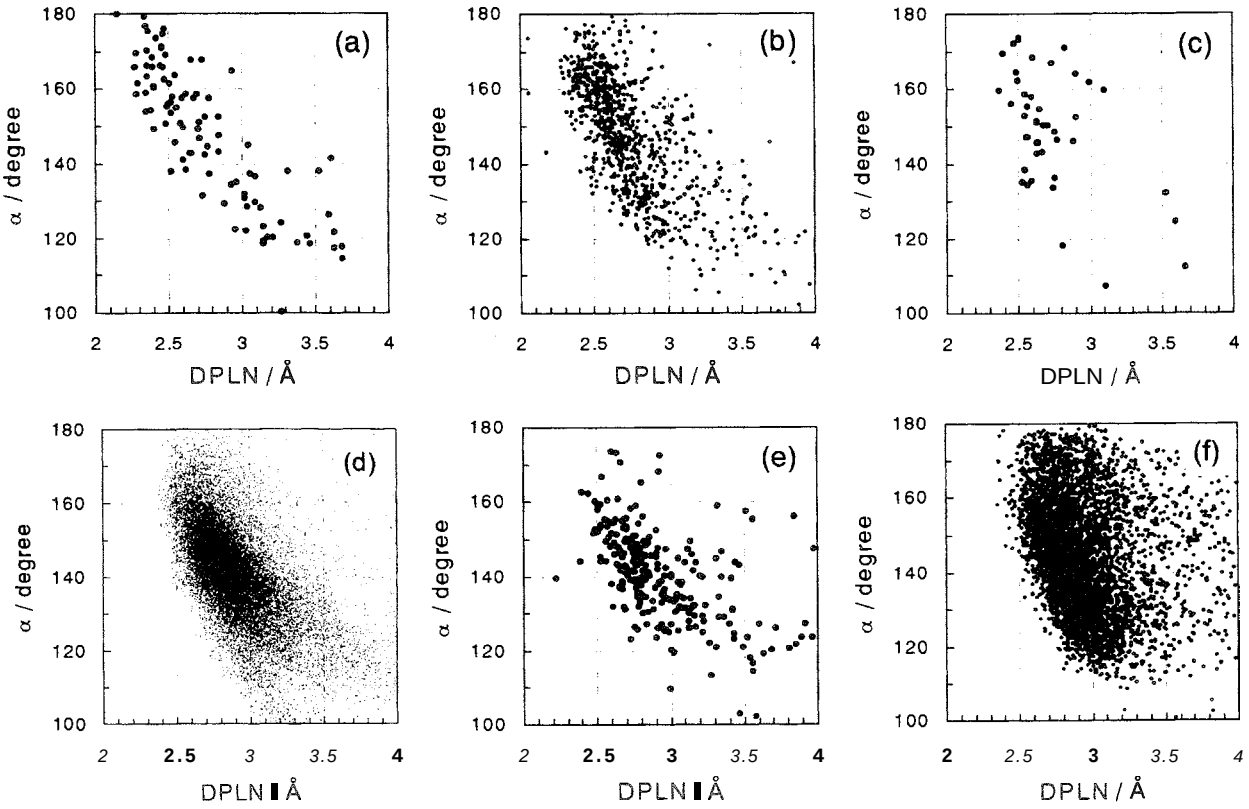

Fig. 1 Scatter plots showing the dependence of the CH/π access angle α on the Hln-plane distance DPLN. (a) $CHCl_3$, (b) CH_2Cl_2, (c) sp-CH, (d) sp2-CH (x-ray data), (e) sp2-CH (neutron data), and (f) sp3-CH (CCH_3). (From Ref. [2], Fig. 7.)

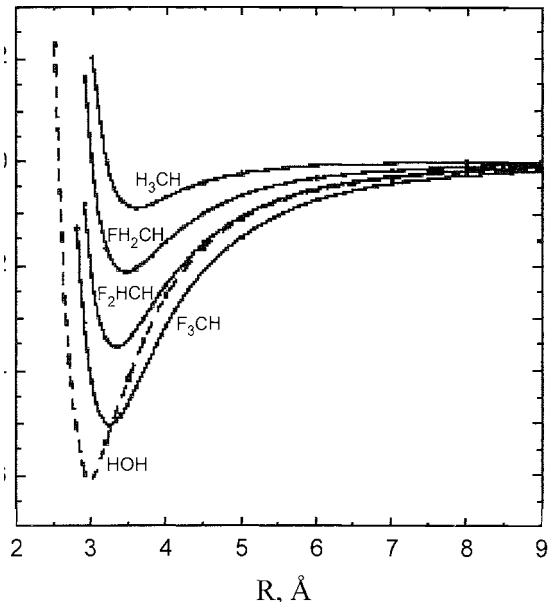

Fig. 2 Interaction energies as a function of intermolecular separation C···O in the *CWO* hydrogen bond. (From Ref. [3], Fig. 3.)

Database Analyses

The Cambridge Structural Database (CSD), Protein Data Bank (PDB). and Nucleic Acid Database (NDB) are used.[4,6] The CSD (http://www.ccdc.cam.ac.uk/) is equipped with programs QUEST3D for data retrieval and VISTA for statistical analyses. The January 2003 release includes more than 270,000 crystal structures of organic. organometallic, and coordination compounds. The PDB (http://www.rcsb.org.pdb/) and NDB (http://ndbserver.rutgers.edu/) are free for use through the Internet and contain more than 7000 protein and 2000 nucieic acid coordinates, respectively, from crystallographic and NMR determinations.

Theoretical Calculation

Ab initio MO calculations are used.[7,8] Correction to BSSE (basis set superposition error) is necessary for supramolecules. An MP2 or higher level of approximations should be employed. This is especially true for softer hydrogen bonds such as CH/π or CH/N. because contribution from the correlation energy is important. The density functional theory (DFT) method is used in calculating relatively large complexes. To analyze the contribution of energetic components. Morokuma partitioning or alternatives such as intermolecular perturbation theory method is used. The Bader's AIM (atoms in molecules) method is used to investigate the nature of the interaction.

HYDROGEN BONDS BETWEEN HARD ACIDS AND SOFT BASES

These bonds between hard acids and soft bases include the OH/π, NH/π. and XH/π (*X*=halogen) hydrogen bonds."."" These kinds of interactions were actively studied from the mid-1950s to the 1960s, by IR spectroscopy. For typical OH/π and NH/π interactions, the hydrogen-bond shift Δν falls between 20 and 100 cm^{-1}. The importance of the OH/π and NH/π hydrogen bonds in organic[9,10] and organometallic[11] crystals was reported.

Perutz suggested,[12] on the ground of vapor phase and crystallographic evidence, the role of aromatic rings as hydrogen-bond acceptors in molecular recognition. Recent MO calculations support this.[13–15] Novoa and Mota compared, by the AIM analysis. characteristics of the OH/π, CH/O, and CH/π interactions and concluded that they are all true hydrogen bonds.[16] Tsuzuki and coworkers examined the strength and directionality of the OH/π and NH/π interactions[17] and compared the results with the CH/π bond (Table 2). Notice that the electrostatic contribution decreases abruptly from an ordinary hydrogen bond to OH/π, NH/π, and then to CH/π hydrogen

Table *2* Interaction energies of XH/π hydrogen bonds

Type of H-bond	**Example**	**Total**	ES	ER	CORR	Ratio	Distance
OH/π[a]	H_2O/C_6H_6	−3.02[c]	−1.86	1.07	−2.23	0.62	3.4
NH/π[a]	NH_3/C_6H_6	−2.22[c]	−1.01	1.14	−2.36	0.45	3.6
CH/π[a]	CH_4/C_6H_6	−1.45[c]	−0.25	1.10	−2.30	0.17	3.8
Ordinary H-bond[b]	H_2O/H_2O	−5.23	−6.16	5.09	−2.20	1.18	

Energies in kcal mol^{-1}; distance: X···ring-centroid separation in Å; ES: electrostatic: ER: exchange-repulsion: CORR: London dispersion term: and ratio: *E*(ES)/*E*(total).

"(From Ref. [17].): MP2/cc-pVQZ.

[b](From Ref. [7].): MP4/6−31+G(2d,2p).

[c]Estimated CCSD(T) level interaction energy at the basis set limit.

Table 3 Mean *H*...O separation (Å) for *CHIX* hydrogen bonds from solvent molecules to various acceptor types (CSD analysis)

Donor	O-Acceptors	N-Acceptors	Cl^--Acceptors
$CHCl_3$	2.31	2.37	2.38
CH_2Cl_2	2.40	2.40	2.56
Sp-CH	2.49	2.53	2.59
MeCN	2.57	2.59	2.72
Me_2SO	2.56	2.65	2.94
Me_2CO	2.60	2.64	2.98

Source: Adapted from Ref. [33]

bond. The correlation energy, on the other hand, does not change appreciably.

Steiner and Koellner discussed the role of NH/π and OH/π hydrogen bonds in 592 high-resolution protein structures.[18] A brief review emphasizing the importance of NH/π, CH/O, and CH/π hydrogen bonds appeared.[19] The NH/π interactions are more frequently found than OH/π interactions,[20,21] presumably because NH is softer as an acid than OH. The OH/π bond is stronger than the NH/π and CH/π interactions, however, it is not common in proteins. It is likely that OH is harder as an acid and seeks a hard base as the partner in the physiological environment. More information on XH/π interactions in biology is available in Ref. [18] and in Chapter 5 of Ref. [4].

HYDROGEN BONDS BETWEEN SOFT ACIDS AND HARD BASES

Hydrogen bonds between soft acids and hard bases include the CH/*n* interaction. Thermochemical studies and measurements of CH stretching bands of the CH/O and CH/N complexed species suggested the capability of CH groups as hydrogen donors. The lower-frequency shifts Δν are of the order $10 \sim 100\ cm^{-1}$ depending on the system examined. The C—H absorption bands often shift to higher frequencies in CH/O and CH/π hydrogen bonds.[3,5]

In 1962, Sutor proposed the hydrogen-bond nature of the CH/O interaction on the ground of her crystallographic data. In 1982, Taylor and Kennard presented a monumental work in this field by surveying crystal structures in the CSD.[22] Thus, retrieval of neutron diffraction data and statistical analyses of the distance and angle parameters established, unequivocally, the hydrogen-bond nature of the CH/O, CH/N, and CH/halogen interactions. Desiraju, Steiner, and coworkers extensively studied CH/O interactions in crystals, and the results appear in several review articles.[23–27] In Table 3, the H···C distance in CH/X hydrogen bonds, examined by a CSD study is compared. Notice that the distance depends on the strength of the CH donor and the acceptor in the interacting system.

Stoddart and coworkers reported the role of CH/O interactions as a control element in supramolecular complexes.[28] Database studies demonstrated the importance of CH/O hydrogen bonds in the protein structure.[29–31] This topic is dealt with in great detail in Ref. [4].

Compared in Table 4 are the strengths of the CH/O hydrogen bonds calculated for methane and its fluorinated derivatives in complex with water or formaldehyde.[3] It is noted that the proportion of the electrostatic term is comparable to the ordinary hydrogen bond, whereas contribution from the correlation energy is unimportant. Acetylene, ethylene, and ethane were shown to interact favorably with H_2O and NH_3.[32] The interaction of CHs

Table 4 Interaction energies[a] of *CWO* hydrogen bonds (Morokuma energy decomposition analysis)

	Total	ES	EW	POL	CT	CORR
CH_4/H_2O	−0.29	−0.42	0.38	−0.13	−0.11	−0.08
CH_3F/H_2O	−1.34	−1.96	1.16	−0.24	−0.32	−0.20
CH_2F_2/H_2O	−2.53	−3.83	2.06	−0.36	−0.53	−0.25
CHF_3/H_2O	−3.70	−7.06	4.14	−0.69	−0.97	−0.25
CH_4/H_2CO	−0.37	−0.23	0.18	−0.08	−0.08	−0.21
CH_3F/H_2CO	−1.21	−1.40	0.62	−0.16	−0.21	−0.18
CH_2F_2/H_2CO	−2.11	−2.74	1.15	−0.28	−0.35	−0.10
CHF_3/H_2CO	−3.0[b]	−5.15	2.40	−0.61	−0.63	0.05
H_2O/H_2O	−4.51	−7.58	4.24	−0.71	−0.93	−0.30

ES: electrostatic: ER: exchange-repulsion: POL: polarization energy: CT: charge transfer; and CORR: London dispersion term
[a]Energies in kcal mol^{-1}. BSSE corrections were made for total energies but are not for components.
[b]Estimated.
Source: Adapted from Ref. [3]: MP2/6-31+G**.

Table 5 Comparison of CH/π bonds

Example	Total[d]	ES	ER	CORR	Ratio
CH_4/C_6H_6[a]	−1.45	−0.25	1.10	−2.30	0.17
C_2H_4/C_6H_6[a]	−2.06	−0.65	1.82	−3.22	0.32
C_2H_2/C_6H_6[a]	−2.83	−2.01	1.44	−2.26	0.71
C_6H_6/C_6H_6[b]	−2.46	−0.55	1.57	−3.48	0.16
CH_3Cl/C_6H_6[c]	−3.0	−1.1	1.4	−3.4	0.37
CH_2Cl_2/C_6H_6[c]	−4.5	−1.8	2.4	−5.1	0.40
$CHCl_3/C_6H_6$[c]	−5.6	−2.4	4.6	−7.9	0.43

ES: electrostatic; EK: exchange-repulsion; and CORR: London dispersion term.
Energies are in kcal mol^{-1}; ratio: *E*(ES)/*E*(total).
[a](From Ref. [44]): MP2/cc-pVQZ.
[b]Tsuzuki et al., *J. Am. Chem. Soc.* **2002,** *124,* 104–112: CCSD(T)/cc-pVQZ.
[c]Tsuzuki et al., *J. Phys.Chem.* **2002,** *109,* 4423–4428: MP2/cc-pVQZ.
[d]Estimated CCSD(T) level interaction energy at the basis set limit.

with N or halogen is important[4,33] but is less common than the CH/O hydrogen bond.

HYDROGEN BONDS BETWEEN SOFT ACIDS AND SOFT BASES

Interactions such as SH/π,[4] CH/S,[34] or CH/Se[35] may belong to this category but are not dealt with here. The most important is the CH/π hydrogen bond.[5]

In 1952, Tamres showed that benzene and analogues dissolve in chloroform exothermically. Huggins and Pimentel found, by measurement of IR spectra, that the interaction of chloroform with benzene showed behavior consistent with the criteria for hydrogen-bond systems. Many workers since demonstrated that the interaction of CH with π-bases was attractive. Argon matrix IR experiments provide good evidence.[6–9] Nuclear Overhauser effects of a series of simple organic compounds provided evidence for the hydrogen-bond nature of the CH/π interaction.[37] Crystallographic database analyses of organic[38,39] and transition metal compounds[40] support the conclusion. A number of theoretical studies supporting the concept appeared.[2,14,16,36,38,41–44]

Compared in Table 5 are the energies of CH/π bonds estimated by high-level ab initio calculations.[41] Notice that the electrostatic contribution is less than 20% when a nonpolar CH group is involved. A proportion of the electrostatic energy increases when going from sp3-CH to sp2-CH and then to sp-CH. A similar trend is obtained by substituting the hydrogens with an halogen atom. Interactions involving aromatic CHs are stronger than the aliphatic ones. The former is termed the aromatic CH/π interaction, but this is often referred to as the T-shape or edge-to-face π/π interaction.[45,46] A considerable part of the interactions between aromatic side chains in protein[47] may trace its origin in the aromatic CH/π interaction.

A unique feature of the CH/π bond is that a number of CH groups may simultaneously participate in the interaction with a π-base. This type of interaction is favorable, in view of entropy, because an assorted arrangement of CH groups is common in organic molecules. Every π-group has at least a plane of symmetry. The total Gibbs energy of the interaction thus increases; this point is

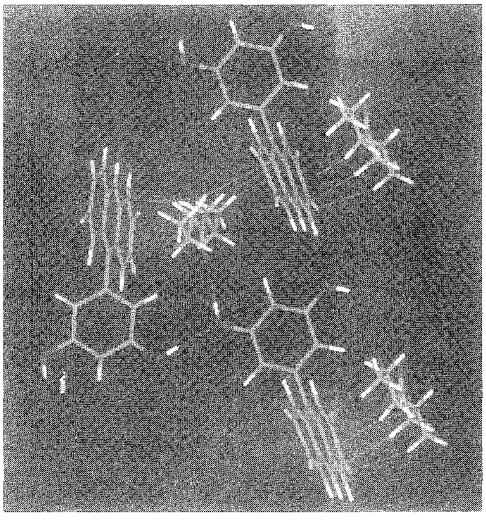

Fig. 3 Crystal structure of 9-(3,5-dihydroxyphenyl)anthracene heptane-4-one clathrate (CSD refcode REKMAV). Dotted lines and Dashed lines indicate CH/π and hydrogens bonds, respectively. (From Ref. [67], Fig. 2.)

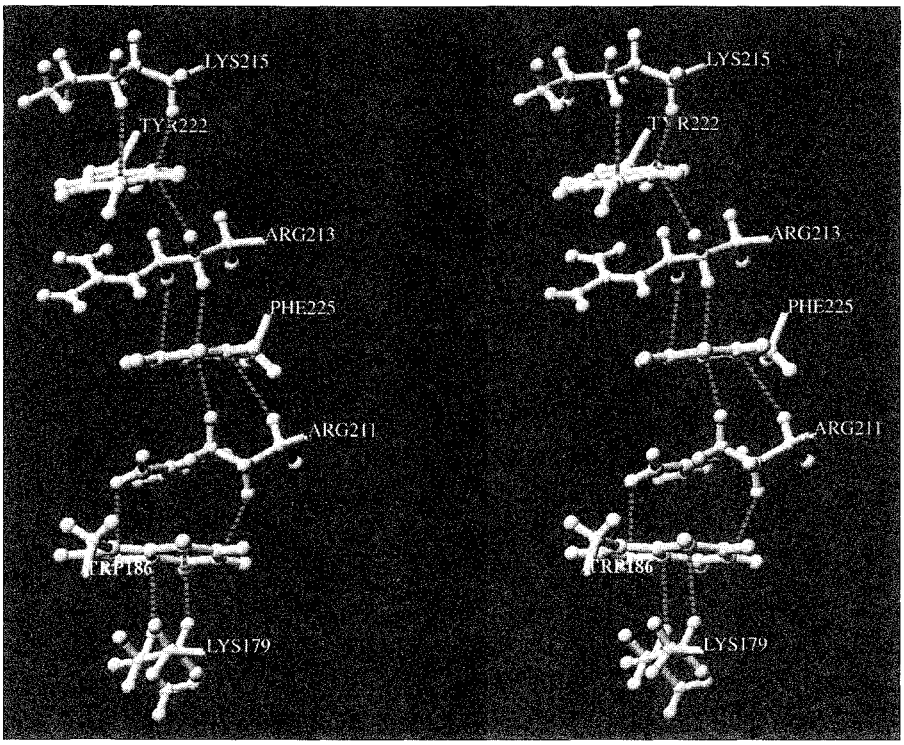

Fig. 4 CH/π interactions observed in human growth hormone-binding protein (PDB code 3HHR) Lys215/Tyr222/Arg213/Phe225/Arg211/Trp186/Lys179 (From Ref [68], Fig 10.)

crucial in understanding the role of CH/π interaction. Another characteristic, which is of supreme importance when considering biochemical processes, is that the CH/π interaction plays its role in protic media, such as water, as well as in nonpolar solvents. This is because most of its energy originates from the dispersion interaction. The specificity in supramolecules comes from weak forces of enthalpic origin, including van der Waals force and weak hydrogen bonds. The so-called "hydrophobic effect" is not the cause[48] of the specific interactions in molecular recognitions, including those of proteins.

The number of papers reporting the role of CH/π interaction is rapidly increasing. Only recent key papers are cited here. Chloroform interacts favorably with an arene π-cloud of fullerene complexes of calixarenes[49] and cyclotriveratrylene.[50] Evidence for the role of CH/π interaction in self-assembly was presented.[51,52] The significance in molecular capsules[53,54] and lattice-[55,56] and cavity-inclusion type clathrates[57,58] is well documented. Possibilities in designing useful drug[59] and liquid crystal[60] or agents for enantiomer separation[61] and enantioselective catalysts[62] were suggested. Houk and coworkers attributed the origin of a remarkable *endo*-stereoselectivity in Diels–Alder reactions to the CH/π and π/π interactions.[63] Importance in the efficiency and stereoselectivity in the photocycloaddition[64,65] and topochemical polymerization reactions[66] was demonstrated.

Illustrated in Fig. 3 is an example.[67] Notice that the nonpolar CH/π interactions dominate over the ordinary hydrogen bonds.

Significance in the structure of proteins, such as GTP-binding proteins, SH2 motif,[68] MHC antigens, and TATA-box binding protein/DNA complex[69] was reported. A stacked arrangement of carbohydrates with aromatic residues was interpreted as being a consequence of the CH/π interaction.[70] An inhibitor with a polyethylene glycol moiety was shown to effectively bind the substrate-binding cleft, lined with many aromatic residues, of acetylcholine esterase. The result was attributed to the CH/π interaction.[71]

An example is given in Fig. 4 for a sequence of CH/π bonds observed in human growth hormone-binding protein. Notice that the methylene hydrogens in Lys and Arg are involved in a stacked manner with aromatic residues, Phe, Tyr, and Trp.

By analyzing 19 adenine-cofactor specific enzymes, Chakrabarti and Samanta found CH/π interactions to play

an essential role in the binding of substrates.[72] Weiss and coworkers analyzed 1154 PDB entries and found that CH/π interactions are ubiquitously present in the protein structure.[73] Further information is available in several reviews[18,19,70,74] and in Chapter 11 of Ref. [5] CH/π interactions in DNA structure were also reported.[75]

CONCLUSION

The characteristics of the weak hydrogen bonds may be summarized as follows. The stronger the protoll-donating ability of XH, the stronger the attractive nature of the hydrogen bond. Thus, the following order obtains OH>NH>CH. Among carbon acids, sp-CH≫sp2-CH>sp3-CH. The H/acceptor distance decreases in the above order. As for the proton acceptor, O is stronger than N, S. and κ-bases. Among the κ-bases, the electron density of the acceptor (π-donor) is important. Directionality is a requisite for the hydrogen bonding, distinguishing it from the van der Waals force. This also follows the above order of strength: the stronger the hydrogen bond. the stronger the trend for linearity.

The implication of weak hydrogen bonds in supramolecular chemistry is immense, as shown in this and other articles in the *Encyclopedia.* A century has just begun where the interaction between molecules is becoming the most fascinating target in chemistry and biology; the weak hydrogen bonds undoubtedly play the central part.

ARTICLES OF FURTHER INTEREST

Biological Ligands, p. 88
Calixarenes and Their Analogues: Molecular Complexation, p. 145
Carbohydrates, Recognition of, p. 169
Carcerands and Hemicarcerands, p. 189
Catenanes and Other Interlocked Molecules. p. 206
Cavitands, p. 219
Chiral Guest Recognition, p. 236
Classical Descriptions of Inclusion Compounds, p. 253
Classification and Nomenclature of Supramolecular Compounds, p. 261
Complexation of Fullerenes, p. 302
Concepts in Crystal Engineering, p. 319
Crown Ethers. p. 326
Cryptands, p. 334
Cryptophanes, p. 340
Crystal Engineering with Hydrogen Bonds, p. 357
Crystal Structure Prediction. p. *371*
Cyclodextrins, p. 398
Cyclophanes: Endoacidic, Endobasic, and Endolipophilic Cavities, p. 424
Enzymes: Clzaracteristics and Mechanisms, p. 554
Glycoluril-Based Hosts, p. 597
Homocalixarenes, p. 649
Hydrogen Bonding, p. 658
Hydrophobic Effects, p. 673
Inclusion Compounds: Selectivity, Thermal Stability, and Kinetics, p. 696
Inclusion Reactions and Polymerization, p. 705
Interpenetration, p. 735
Layered Supramolecular Solids and Their Intercalates, p. 791
Liquid Clathrates, p. 804
The Lock and Key Principle, p. 809
Molecular Clefts and Tweezers, p. 887
Molecular Modeling and Related Computational Techniques, p. 901
Molecular Squares, Boxes, and Cubes. p. 909
Molecular Switches, p. 917
Molecular Wires, p. 925
Molecular-Level Machines, p. 931
Neutron Diffraction, p. 959
Nuclear Magnetic Resonance Spectroscopy, p. 981
π–π Interactions: Theory and Scope. p. 1076
Rotaxanes and Pseudorotaxanes, p. 1194
Secondary Bonding, p. 1215
Second-Sphere Coordination, p. 1209
Self-Assembling Capsules, p. 1231
Self-Assembling Catenanes, p. 1240
Self-Assembly: Definition and Kinetic and Thermodynamic Considerations, p. 1248
Self-Assembly in Biochemistry, p. 1257
Solid-Sfate Reactivity/Topochemistry, p. 1316
Spherands, p. 1344
Strong Hydrogen Bonds. p. 1379
Supramolecular Chemistry: Definition, p. 1401
Supramolecular Isomerism, p. 1420
Supramolecular Polymers, p. 1443
Supramolecular Stabilization. p. 1453
van rler Waals Forces. p. 1550
Vibrational Spectroscopy, p. 1557
X-Ray Crystallography, p. 1586

REFERENCES

1. Pimentel, G.C.; McClellan, A.L. *The Hydrogen Bond;* W. H. Freeman: San Francisco, 1960.
2. Takahashi, O.: Kohno, Y.; Iwasaki. S.; Saito, K.: Iwaoka, M.: Tomoda. S.: Umezawa. Y.; Tsuboyama. S.; Nishio, M. Hydrogen-bond-like nature of the CH/π interaction as

evidenced by crystallographic database analyses and ab initio molecular orbital calculations. Bull. Chem. Soc. Jpn. 2001, *74*, 2321-2430.
3. Gu, Y.; Kar, T.; Scheiner, S. Funciamental properties of the CH-O interaction: Is it a true hydrogen bond? J. Am. Chem. Soc. 1999. *121*, 9411-9122.
4. Desiraju, G.R.; Steiner, T. *The Weak Hydrogen Bond in Structural Chemistry and Biology;* Oxford Univ. Press: Oxford. 1999.
5. Nishio, M.; Hirota, M.; Umezawa, U. *The CH/π Interaction. Evidence, Nature, and Consequences*; Wiley-VCH: New Uork. 1998.
6. Steiner, T. The hydrogen bond in the solid state. Angew. Chem., Int. Ed. 2002. *41*, 48-76.
7. Stone, A.J. *The Theory* of *Intermolecular Forces;* Clarendon Press: Oxford, 1996.
8. Scheiner, S. *Hydrogen Bonding,* A *Theoretical Perspective:* Oxford Univ. Press: Oxford. 1997.
9. Bakshi, P.K.; Linden, A.; Vincent, B.R.; Roe, S.P.; Adhikesavalu, D.; Cameron, T.S.; Knop, O. Crystal chemistry of tetraradial species. Part 4. Hydrogen bonding to aromatic n-systems: Crystal structures of fifteen tetraphenylborates with organic ammonium cations. Can. J. Chem. 1994, *72*, 1273-1293.
10. Malone, J.F.; Murray, C.M.; Charlton, *M.H.;* Docherty, R.; Lavery, A.J. X-H/π (phenyl) interactions. Theoretical and crystallographic observations. J. Chem. Soc., Faraday Trans. 1997, 93, 3429–3436.
11. Braga, D.; Grepioni, F.; Tedesco, E. X-H/π (X=O, N, C) hydrogen bonds in organometallic crystals. Organometallics 1998. *17*, 2669–2672.
12. Peruiz, *M.F.* The role of aromatic rings as hydrogen bond acceptors in molecular recopnition. Phil. Trans. R. Soc., A 1993. *345*, 105-112.
13. Rozas, I.; Alkorta, I.; Elguero, J. Unusual hydrogen bonds: H/π interactions. J. Phys. Chem., A 1997, *101*, 9457–9463.
14. Sanianta, U.; Chakrabarti, P.; Chandrasekhar. J. Ab initio study of energetics of X-H/π (X=N, 0, and C) interactions involving a heteroaromatic ring. J. Phys. Chern., A 1998, *102*, 8964–8969.
15. Tarakeshwar, P.; Kim, K.S. Comparison of the nature of π and conventional H-bonds: A theoretical investigation. J. Mol. Struct. 2002. *615*, 227–238.
16. Novoa, J.J.; Mota, F. The CH-π bonds: Strength, identification, and hydrogen-bonded nature: A theoretical study. Chem. Phys. Lett. 2000, *318*, 345–354.
17. Tsuzuki, S.; Honda, M.; Uchimaru, T.; Mikaini, M.; Tanabe, K. The origin of the attraction and directionality of the NH/π interaction: Comparison with OH/π and CH/π interactions. J. Am. Chem. Soc. 2000. *122*, 11450–11358.
18. Steiner, T.; Koellner, G. Hydrogen bonds with π-acceptors in proteins: Frequencies and role in stabilizing local 3D structures. J. Mol. Biol. 2001. *305*, 535–557.
19. Weiss, M.S.; Brandi, M.; Sühnel, J.; Pal, D.; Hilgenfeld, R. More hydrogen bonds for the (structural) biologist. Trends Biochem. Sci. 2001, *26*, 521-523.
20. Flocco, M.M.; Mowbray, S.L. Planar stacking interactions of arginine and aromatic side-chains in proteins. J. Mol. Biol. 1994. *235*, 709–717.
21. Mitchell, J.B.O.; Nandi, C.L.; McDonald, I.K.; Thornton, J.M.; Price, S.L. Amino/aromatic interactions in proteins: Is the evidence stacked against hydrogen bonding? J. Mol. Biol. 1994. *239*, 315–331.
22. Taylor, R.; Kennard, O. Crystallographic evidence for the existence of CH-0, CH-N, and CH-Cl hydrogen bonds. J. Am. Chem. Soc. 1982, *104*, 5063–5070.
23. Desiraju, G.R. The CH-0 hydrogen bond in crystals: What is it? Acc. Chem. Res. 1991. *24*, 290–296.
24. Steiner, T. CH-O hydrogen bonding in crystals. Crystallogr. Rev. 1996. 6, 1-57.
25. Steiner, T. Unrolling the hydrogen bond properties of CH-O interactions. Chem. Commun. 1997, 727–734.
26. Nangia, A.; Desiraju, G.R. Supramolecular structures—Reason and imagination. Acta Crystallogr., A 1998, *54*, 934–944.
27. Nangia, A. Database research in crystal engineering. CrystEngComm 2002. *17*, 1–9.
28. Houk, K.N.; Menzer, S.; Newton, S.P.; Raymo, F.M.; Stoddart, J.F.; Williams, D.J. CH-O interactions as a control element in supramolecular complexes: Experimental and theoretical evaluation of receptor affinities for the binding of bipyridinium-based guests by catenated hosts. J. Am. Chem. Soc. 1999. *121*, 1479–1487.
29. Derewenda, Z.S.; Lee, L.; Derewenda, U. The occurrence of CH/O hydrogen bonds in proteins. J. Mol. Biol. 1995. *252*, 248–262.
30. Chakrabarti, P.; Chakrabarti, S. CH-0 hydrogen bond involving proline residues in α-helices. J. Mol. Biol. 1998, *284*, 867–873.
31. Fabiola, G.F.; Krishnaswamy, S.; Nagarajan, V.; Pattabhi, V. CH-O hydrogen bond in β-sheets. Acta Crystallogr., A 1997. *53*, 316–320.
32. Hartmann, M.; Wetmore, S.D.; Radom, L. C-HIX hydrogen bonds of acetylene, ethylene, and ethane with first- and second-row hydrides. J. Phys. Chem., A 2001, *105*, 4470–4479.
33. Steiner, T. Donor and acceptor strengths in CH-0 hydrogen bonds quantified from crystallographic data of small solvent molecules. New J. Chern. 1998. *22*, 1099–1103.
34. Cini, R.; Corsini, *M.;* Cavaglioni, A. Supramolecular aggregates of complex cations via unusual purine-purine base pairing in new organorhodium(III) compounds containing the antileukemic drug purine-6-thione. Inorg. Chem. 2080. 39, 5874–5878.
35. Iwaoka, M.; Komatsu, H.; Tomoda, S. Deuterium-induced isotope effects of a C-H···Se "hydrogen bond" on the IR and NMR spectra of 6*H*,12*H*-dibenzo[*b*,*f*][1,5]diselenocin. Bull. Chem. Soc. Jpn. 1996. 69, 1825-1828.
36. Sundararajan, K.; Sankaran, K.S.; Viswanathan, K.S.; Kulkarni, A.D.; Garde, S.R. H–π complexes of acetylene-ethylene: A matrix isolation and computational study. J. Phys. Chem., A 2002. *106*, 1504–1510.

37. Suezawa. H.: Hashimoto, T.; Tsuchinaga. K.: Yoshida. T.; Yuzuri, T.: Sakakibara, K.; Hirota, M.; Nishio, M. Electronic substituent effect on intramolecular CH/π interaction as evidenced by NOE experiments. J. Chem. Soc., Perkin Trans. 2 2000. 1243–1249.
38. Philp, D.: Robinson. J.M.A. A computation investigation of cooperativity in weakly hydrogen-bonded assemblies. J. Chern. Soc., Perkin Trans. 2 1998, 1643–1650.
39. Umezawa. Y.; Tsuboyama. S.: Honda. K.: Urawa, J.: Nishio, M. CH/π interaction in the crystal structure of organic compounds. A database study. Bull. Chem. Soc. Jpn. 1998. *71.* 1207–1213.
40. Suezawa. H.: Uoshida. T.: Umezawa. Y.: Tsuboyama. S.; Nishio, M. CH/π interactions implicated in the crystal structure of transition metal compounds. A database study. Eur. J. Inorg. Chem. 2002, 3148–3155.
41. Tsuzuki, S.; Honda. K.: Uchimaru, T.; Mikami, M.; Tanabe. K. The magnitude of the CH/π interaction between benzene and some model hydrocarbons. J. Am. Chem. Soc. 2000. *122.* 3746–3753.
42. Scheiner. S.: Grabowski. S.J. Acetylene as potential hydrogen-bond proton acceptor. J. Mol. Struct. 2002, *615.* 209–218.
43. Bagno, A.; Saielli, G.: Scorrano, G. Through-space spin-spin coupling in van der Waals dirners and CH/π interacting systems. An ab initio and DFT study. Chem. Eur. J. 2002, 8. 2047–2056.
44. Ugozzoli. F.; Arduini. A.; Massera. C.: Pochini. A.; Secchi. A. CH/π interaction between benzene and model neutral organic molecules bearing acid CH groups. New J. Chem. 2002. *26.* 1718–1723.
45. Hunter. C.A. The role of aromatic interactions in molecular recognition. Chem. Soc. Rev. 1994. 101–109.
46. Carver, F.J.: Hunter, C.A.: Seward. E.M. Structure-activity relationship for quantifying aromatic interactions. Chem. Commun. 1998. 775–776.
47. Burley, S.K.; Petsko. G.A. Weakly polar interactions in proteins. Adv. Protein Chem. 1988. 125–189.
48. Hildebrand. J.H. Is there a ''hydrophobic effect''? Proc. Natl. Acad. Sci. U. S. A. 1979, *76,* 194.
49. Atwood. J.L.: Koutsantonis, G.A.; Raston. C.E. Purification of C_{60} and C_{70} by selective complexation with calixarenes. Nature 1994. *368.* 229–231.
50. Steed, J.W.; Junk. P.C.; Atwood. J.L.: Barnes, M.J.: Raston. C.L.: Burkhalter. R.S. Ball and socket nanostructures: New supramolecular chemistry based on cyclotriveratrylene. J. Am. Chem. Soc. 1994. *116.* 10346–10347.
51. Lindenian, S.V.: Kosynkin, D.: Kochi. J.K. Unusually short (CH-n) hydrogen bonds for effective supramolecular (aromatic/aromatic) organization in edge-to-face motifs. J. Am. Chem. Soc. 1998. *120.* 13268–13269.
52. Cantrill, S.J.: Preece. J.A.: Stoddart. J.F.: Wang, Z.-H.: White. A.J.P.: Williams, D.J. The idiosyncracies of tetrabenzo[24]crown-8 in the solid state. Tetrahedron 2000. *56.* 6675–6681.
53. O'Leary, B.M.; Grotzfeld, R.M.; Rebek. J.. Jr. Ring inversion dynamics of encapsulated cyclohexane. J. Am. Chem. Soc. 1997. *119.* 11701–11702.
54. Chapman, R.G.Olovsson, G.: Trotter. J.; Sherman, J.C. Crystal structure and thermodynamics of reversible molecular capsules. J. Am. Chem. Soc. 1998. *120.* 6252–6260.
55. Madhavi, N.N.L.; Katz. A.M.; Carrell. H.L.: Nangia. A.; Desiraju, G.R. Evidence for the characterization of the CH/π interaction as a weak hydrogen bond: Toluene and chlorobenzene solvates of 2,3,7,8-tetraphenyl-1,9,10-anthridine. Chem. Commun. 1997, 1953–1954.
56. Biradha. K.: Dennis. D.; MacKinnonn. V.A.: Sharma. C.V.K.: Zaworotko, M.J. Supramolecular synthesis of organic laminates with affinity for aromatic guests: A new class of clay mimics. J. Am. Chem. Soc. 1998, *120,* 11894–11903.
57. Arduini. A.; Nachtigall, F.: Pochini, A.; Secchi, A.; Ugozzoli, F. Calix[4]arene cavitands: A solid state study on the interactions of their aromatic cavity with neutral organic guests characterized by acid CH_3 or CH_2 groups. Supramol. Chem. 2000, *12.* 273–291.
58. Takahashi, *H.:* Tsuboyama. S.: Umezawa. Y.: Honda, K.: Nishio, M. CH/π interactions as evidenced in the crystal structure of host-guest complexes. A database study. Tetrahedron 2000, *56.* 6185–6191.
59. Umezawa, K.: Kawakami, M.: Watanabe, T. Molecular design and biological activities of protein-tyrosine phosphatase inhibitors. Pharmacol. Ther. 2003. 99. 15–24.
60. Mori, A.: Hirayama, K.: Kato, N.: Takeshita. H.: Ujiie, S. New troponoid liquid crystalline compounds, 5-alkoxy-2-(4-alkoxybenzoylamino)troponons. Chem. Lett. 1997. 509–510.
61. Kinbara, K.: Oishi. K.; Harada. Y.: Saigo. K. Effect of a substituent on an aromatic group in diastereomeric resolution. Tetrahedron 2000. *56,* 6651–6655.
62. Yamakawa, *M.:* Yamada, I.; Noyori, R. CH/π attraction: The origín of enantioselectivity in transfer hydrogenation of aromatic carbonyl compounds catalyzed by chiral η6-arene-ruthenium(II) complexes. Angew. Chem.. Int. Ed. 2001, 40. 2818–2821.
63. Ujaque, G.; Lee. P.S.; Houk, K.N.: Henteniann. M.F.: Danishefsky. S.J. The origin of endo stereoselectivity in the hetero-Diels–Alder reactions of aldehydes with *ortho*-xylylenes: CH-π, π–π, and steric effects on stereoselectivity. Chern. Eur. J. 2002. *8,* 3423–3430.
64. Hasegawa, T.; Ikeda, K.; Yamazaki, Y. [2+2]photocycloaddition of 2-(dibenzylamino)ethyl 3-benzoylacrylate in a crystalline state: Weak intermolecular. J. Chem. Soc., Perkin Trans. 1 2001. 3025–3028.
65. Obata. T.: Shimo, T.; Yasutake, M.; Shinmyozu, T.: Kawaminami, M.: Yoshida, R.: Somekawa, K. Remarkable interaction effects of molecular packing on site- and stereoselectivity in photocycloaddition of 2-pyrones with maleimide in the solid state. Tetrahedron 2001, *57.* 1531–1541.
66. Nagahama, S.; Inoue. K.; Sada, K.: Miyata, M.; Matsumoto. A. Two-dimensional hydrogen bond networks

supported by CH/π interaction leading to a molecular packing appropriate for topochemical polymerization of 1,3-diene monomers. Cryst. Growth Des. 2003. 3. 247–256.

67. Suezawa, H.; Yoshida. T.; Hirota, M.: Takahashi. H.; Umezawa. Y.; Honda, K.: Tsuboyama. S.; Nishio. M. The CH/π interaction as an important factor in the crystal packing and in determining the structure of clathrates. J. Chern. Soc., Perkin Trans. 2 2001, 2053–2058.
68. Umezawa. Y.: Nishio. M. CH/π interactions in the crystal structure of guanine-nucleotide binding proteins, *src* homology-2 domains and human growth hormone in complex with their specific ligands. Bioorg. Med. Chem. **1998,** 6. 493–504.
69. Umezawa. Y.; Nishio, M. CH/π interactions in the crystal structure of TATA-box binding protein/DNA complexes. Bioorg. Med. Chem. 2000. *8*, 2643–2650.
70. Muraki, M. The importance of CH/π interactions to the function of carbohydrate binding proteins. Prot. Peptide Letters 2002, 9. 195–209.
71. Koellner, G.; Steiner. T.; Millard. C.B.: Silman, I.: Sussman, J.L. A neutral molecule in a cation-binding site: Specific binding of a PEG-SH to acetylcholineesterase from *Torpedo california*. J. Mol. Biol. 2002,320,721–725.
72. Chakrabarti, P.; Samanta, U. CH/π interaction in the packing of the adenine ring in protein structures. J. Mol. Biol. **1995.** 251, 9–14.
73. Brandi, M.; Weiss, M.S.; Jabs, A.; Sühnel, J.; Hilgenfeld, R. CH-π interactions in proteins. J. Mol. Biol. 2001. 307, 357–377.
74. Nishio, M.; Umezawa, Y.; Hirota. M.; Takeuchi, Y. The CH/π interaction: Significance in molecular recognition. Tetrahedron **1995.** *51*, 8665–8701.
75. Umezawa, Y.; Nishio. M. Thymine-methyl/π interaction implicated in the sequence-dependent deformability of DNA. Nucleic Acids Res. 2002, *30*, 2183–2192.

X-Ray Crystallography

Kari Rissanen
University of Jyväskylä, Jyväskylä, Finland

INTRODUCTION

X-ray crystallography is the most powerful tool in the structural analysis of crystalline solids. The extremely fast development of computers had a direct impact on the speed of x-ray diffraction analysis. Modern area detector-based diffractometers allow fast and accurate data collection and processing, giving the possibility of collecting and processing several. even very large, data sets in a day. Fast computers also speed structure solution and refinement. so that even complicated problems can be tackled within reasonable time frames. Supramolecular systems impose a demanding task on x-ray crystallography. The size of the structures to be solved are comparable to small proteins (up to MW 10000), yet protein crystallographic techniques cannot be applied to supramolecular systems. The methods developed for small molecule crystallography have to be adapted to large supramolecular systems, thus inaking the analysis of such structures demanding and, when successful, rewarding.

APPLICATION AREAS

This article is written for nonspecialists to give practical hints and advice to those supramolecular chemists designing and synthesizing systems they would like to study by x-ray crystallography with the help of an x-ray diffraction service or a collaborator. To learn the theoretical basis of x-ray crystallography, the reader is encouraged to read some of the recent x-ray crystallography textbooks to become acquainted with the principles [at introductory,"' intermediate[L2]' or advanced"'] levels]. Modem single-crystal x-ray crystallography has two major application areas. Small-molecule crystallography focuses on target structures with weights of the asymmetric unit, W_{au},[a] between 100–700, resulting in precise and accurate bond distances and angles with low crystallographic R-value (normally <0.07) due to good-quality crystals with no disorder and a high (usually >10) ratio of the number of observed reflections to the number of refined parameters. The R-value is a measure of the level of disagreement between the properly scaled observed structure factors (F_{obs}) and calculated structure factors (F_{calc}). It is usually given as %, i.e., an R-value of 0.07 is reported as 7%.

The other, technically quite different application area, is protein crystallography, which deals with very large structures, even virus structures, up to W_{au} of 10^6. However, these structures cannot be considered to be crystallographically accurate. Often, the resolution is not high enough to determine individual atom positions, and instead. amino acid residues are located. Protein R-values are seldom less than 0.15. and the ratio of the number of observed reflections and number of refined parameters is low (<5). However, protein x-ray structures are considered reliable structural information about the conformation and overall structure of the protein in the crystalline state.

Determination of the accurate structures of molecular inclusion complexes and molecular assemblies gained a lot of importance in supramolecular chemistry.

Since its birth, supramolecular chemistry was defined as "chemistry beyond-the molecule, bearing on the organized entities of higher complexity that result from the association of two or more chemical species held together by intermolecular forces.''[4] Detailed information about the nature of these weak intermolecular interactions is crucial in order to understand and further develop supramolecular systems. Particularly accurate structural inforination can be gained in the solid state by single-crystal x-ray crystallography.

THE CRYSTAL

By far the most important piece of the puzzle in structure determination by x-ray crystallography is the crystal. Without a good enough single crystal, nothing can be done. The first step in x-ray diffraction structural analysis is to produce crystalline material that contains at least one single crystal with certain properties. The most important property is good periodicity of the crystal lattice, viz..

[a] W_{au} is defined as the sum of the molecular weight of all atoms in the asymmetric unit. W_{au} of the system studied can be much higher than the MW of the (supra)molecule. For example, three molecules of MW 250 + four solvent molecules of MW 78 in the asymmetric unit will give W_{au} as high as 1062 (3 x 250 + 4 x 78 = 1062).

Encyclopedia of Supramolecular Chemistry
DOI: 10.1081/E-ESMC 120012825

packing of the molecules and solvent molecules (if present), to gain enough diffraction power. The periodicity is induced by crystal growth, a subtle and more or less spontaneous orderingldesolvation process of molecules, ions, and solvent molecules. No matter what technique is used to obtain the crystal. the only goal is to induce the best possible periodicity of the entities to be studied. The reader is encouraged to read some key articles on crystal growing[5,6] or search the World Wide Web for information, using the search term "crystal growth." With modern area detector diffractometers. the size of the crystal is not as important as it was earlier (well-diffracting crystals as small as 0.05 x 0.05 x 0.05 mm can give good data sets).

The periodicity of the crystal lattice is not the only item affecting the diffraction quality of the crystal. In addition, the types of the ordered atoms have a significant influence on the diffraction power of the crystal. Heavier and well-ordered atoms in the crystal lattice will produce the best diffraction power. In supramolecular systems, the crystal lattice consists mainly of light elements like carbon, hydrogen, oxygen, and nitrogen. and only when metallo-supramolecular systems are studied can heavier elements. such as transition metals, bromide. and iodine, be present. A rough but practical estimate for the intrinsic diffraction power of the compound can be simply calculated by dividing its molecular weight by the number of atoms in the molecule/assembly (N). viz. $dp = MW/N^b$, e.g., benzene $dp = 6.5$, hexaiodobenzene $dp = 49.5$. Therefore: the quality of the crystal. viz. perfect periodicity of the crystal lattice, is crucial for light-atom structures with high W_{au} (>1000) values. as frequently encountered in supramolecular systems.

The third important point about the crystal is its stability. The first two points related to diffraction quality of the crystal may be fine. but the crystal might be unstable under normal laboratory conditions. Large supramolecular assemblies are held together with weak intermolecular interactions. and crystals consisting of such entities are often fragile and sensitive to the environment. Solvent often plays a crucial role in the crystal growth of supramolecular systems and is needed in the construction of the crystal lattice. Due to this fact, many supramoleculer crystals are only stable in the solvent from which they were crystallized. It is not usually practical to change laboratory conditions to eehance crystal stability, and crystals can be easily handled inside the mother solvent and protected against decomposition. When no information about the stablity of the crystals exists, all crystals must be treated as extremely unstable. This starts immediately at the crystal growing phase. When and if crystals form in solution. the crystallization vessel must be closed to ensure that the mother solvent does not evaporate and that the crystals remain in solution. Also, mailing or transporting crystals must be done accordingly, in well-packed, sealed tubes, flasks, or ampoules.

For mounting sensitive and unstable crystals, two practical methods exist. The selected crystal is ''fished'' under a microscopy from the mother solvent by a "loop" crystal holder (see Fig. 1), dipped into perfluorinated polyether (so-called "Magic Oil"). This "oil" is viscous, oxygen free, and unreactive. and it forms a film around the crystal. protecting it from the hostile environment. During data collection. the crystal must not move inside the loop. This is best achieved when the crystal is cooled (with cooling devices available from x-ray diffractometer manufacturers) below 193 K (−80°C). This procedure has an additional advantage in that the low temperature maintained during data collection reduces the thermal movement of the atoms in the crystal. thus improving the quality of the data set.

If the crystal does not survive cooling (cracks appear or intensity of the reflections is lost) or it cannot be iransferred intact into the loop (or seems to react or decompose inside the oil, as happens occasionally). the crystal can be sealed into a capillary crystal holder (see Fig. 1). The advantages of this procedure are that the crystal is in contact only with the mother solvent (actually surrounded by it all the time) and that the data collection can be performed at room temperature. Disadvantages are the extreme care needed to seal and manipulate the fragile capillary crystal holder, which is unique for each crystal, and the possible movement of the crystal inside the capillary tube during data collection.

If the periodicity of the molecules. ions, and solvent molecules in the crystal lattice is good (no disorder, see below) and the structure contains some heavier atoms (sulfur or heavier) and data collection can be performed without decomposition of the crystal. all should be fine for the next phase of the x-ray analysis: data collection and structu e solution.

DATA COLLECTION AND STRUCTURE SOLUTION

Modern diffactometers have automated data collection routines after the crystal is placed into the center of the x-ray beam. With area-detector (e.g., CCD or image plate systems) diffractometers. it is advisable to take one image to check the diffraction quality of the

[b] More precisely dp should be calculated as $dp = W_{au}/N$, where N = number of atoms in the asymmetric unit. This. however, can be done only after the completed x-ray analysis, when the total contents of the asymmetric unit are known.

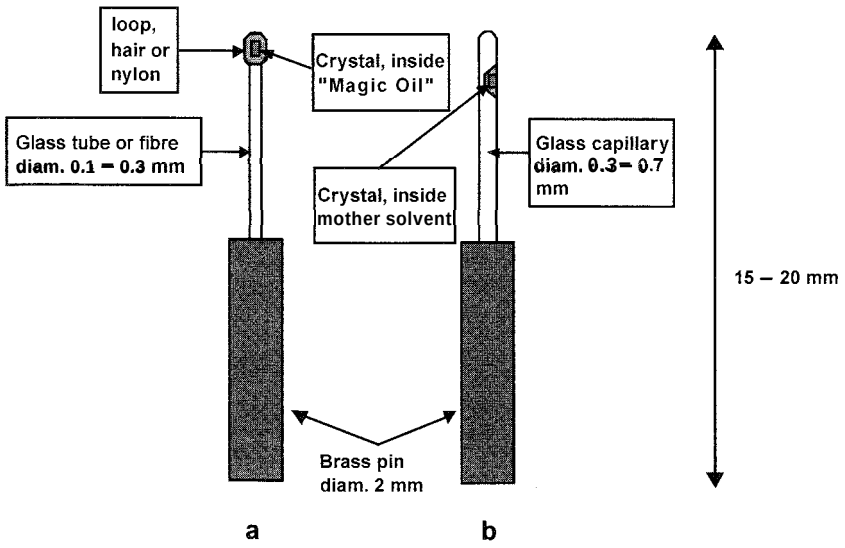

Fig. 1 "Loop" *(a)* and *capillary crystal holder (b)*

crystal. Single-reflection-detector diffractometers proceed directly to the unit-cell determination by randomly collecting reflections that are then used for unit-cell calculations. Before the actual data collection, the diffraction pattern image obtained should be carefully evaluated for two factors: Does the diffraction pattern indicate twinning of the crystal ("twin peaks" or two reflections systematically too close to each other)? Mow high a resolution does the crystal diffract to (visible reflections near the edge of the image. Fig. 2).

If either of these two factors is not acceptable, viz. crystal is clearly twinned or does not diffract well enough or not at all. select a new crystal. Only with persistent selection of a best possible crystal can success be reached. Do not give up with the first five crystals, test at least 15–20 crystals until you find a well-diffracting single crystal. Remember that even bad-looking (under the microscope) crystals can diffract well and give excellent results and, vice versa, good-looking samples might not diffract at all. If the batch of crystals you have does not have any good crystals, then recrystallize the whole batch. Working with a bad or defected data set obtained from poor-quality crystals will result in frustration and loss of time. It is advisable to start from the beginning and focus on getting good crystals rather than forcing data collection on a bad crystal. If you collected or obtained a bad data set (with a structure that cannot be solved), then return to the crystals and redo the crystallization or select a new crystal. The authors' laboratory has many examples of where only a persistent crystal selection procedure produced acceptable results. With a bad data set, you might be able to solve the skeleton of the structure. but you will not be able to refine or publish it.

Even though modern area detector diffractometers are able to collect a data set without first determining the unit cell, it is advisable to determine the unit cell first. The unit cell will tell you something about the constitution of the crystal. When starting the data collection, you do not know the W_{au} of your crystal. However, knowing W_{au} gives you an estimate of possible difficulties you may encounter when obtaining the structure solution. The unit-cell determination will give unit-cell volume (V), which is needed while evaluating W,. A simple equation holds:

$$d = \frac{Z \cdot W_{au}}{0.6023 \cdot V}$$

where d=density of the crystal (Mg m^{-3}), V=unit cell volume (A'), and Z=number of equivalent positions in a given space group. Reorganizing, we get:

$$W_{au} = \frac{(0.6023 \cdot d \cdot V)}{Z}$$

Because Z must be an integer [symmetry fixed. see Refs. [1–3]], we can only have values of 1, 2, 3, 4, 6, 8, 9, 12, 16, 24, 32, 48, 96. The density of the crystal can be measured using a flotation technique. but a plain intelligent guess (''light'' organic d=1.0 – 1.25, metal complex d=1.3 – 1.6) is enough. In the following imaginary example, crystallizing G-ethylresorcarene from pyridine produces nicely diffracting crystals. and the unit-cell determination gives a monoclinic crystal system (see Refs. [1–3]) with V=4952 Å^3. The MW of C-ethylresorcarene is 600.72 and that of pyridine 79.10. Z must

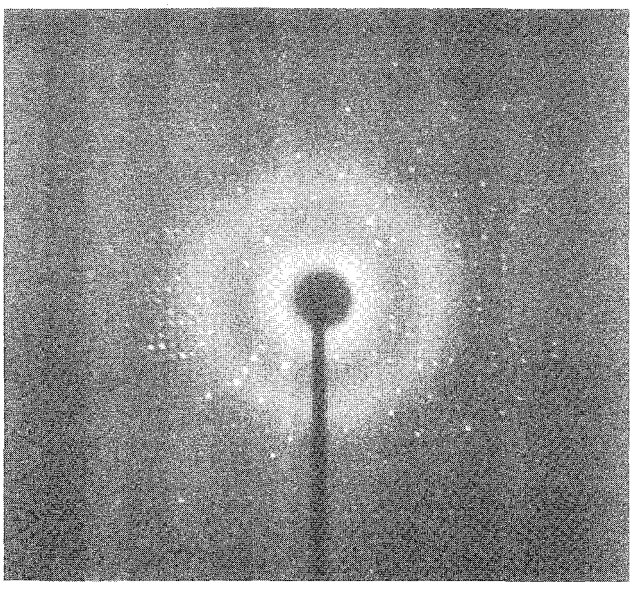

Fig. 2 *CCD* image *from* a *well-diffractingsingle crystal with large* W_{au} *(= 3293).*

have a value of 1, *2, 4, or 8 (in a monoclinic system). So, with d=1.2 (intelligent guess), Z=*1, *we get* W_{au}= *(0.6023 x 1.2 x* 4952)/1=3579.11. *In a* monoclinic *crystal system, Z=*1 *is rare, so calculate the same with Z=2 and Z=*4. *We get Z=2=>*W_{au}= *1789.55 or Z=*4*=>*W_{au}= 894.78. *The* W_{au} *of 1789.55 fits with asymmetric unit* contents *of two rcsorcarenes and seven pyridines* (W_{au}=1755.14) *and* W_{au} *of 894.78 fits with the sum of one resorcarene and four pyridines* (W_{au}=*917.12). So,* here, W_{au} *tells us that we have two resorcarenes and* seven *pyridines or one resorcarene and four pyridines in the asymmetric unit. This is not crucial at this moment, because after data* collection, *the space group (see* Refs. *11–31) will be determined, and Z will be fixed. In this example,* the *space group would be* $P2_1/c$ *and Z=*4, *and the* real *calculated d=1.23, and in the structure, the rcsorcarene would* be *solvated with four pyridines.*

The structure solution (see Refs. [1–3]) *is done using sophisticated* (semi)automatic *computer programs that* convert *the measured intensities (the data set) into* so-*called-structure factors and then use different techniques to solve "the phase problem" (again, see Refs.* [1–3]). *Modern structure solution programs [themost used* being SHELXS/SHELXD[7] *and* SIR97/SIR2000,[8] *others exist* too] need as *input only the* W_{au}, *in a form of reasonable chemical composition, and the collected data set. The success of the structurc solution depends mainly on two factors: the quality of the data collected (which, in turn, depends on the quality of the crystal) and how much of the data is observed over a certain threshold value (normally used criteria* for *an* observed *reflection is intensity, I* >2σ*I). Generally speaking, it can be said (fornontwinned structures) that the higher the percentage of the observed reflections, the better* the *data (severe* systematic *errors in the data can* overrule *this), and it is more* likely *that the structurc solution programs can produce a feasible model for the experimental electron density, viz. the program prints out three-dimentional coordinates for the best structure solution. Frequently, with smaller and* well-diffracting *structures* (W_{au} <700 *and dp* >10), all *atoms of the structure are output as the initial model by the program, and they just have to be named correctly and refined (see Refs. [I–31).* The *refinement process uses incremental movement of the atom coordinates and atomic displacement parameters (commonly called "thermal parametcrs") of the structure solution model, fits this model (the calculated structurc factors) against the data collected (the observcd structure factors), and calculates the R-value. However, with large supramolecular structures, all the atoms are* rarely *obtained directly from the structurc solution program, this is particularly true for the included guests and solvent molecules. The missing atoms (some of which will occur as atoms only at this stage of structural analysis) are located when the partial model and observcd data arc subjected* to *difference Fourier analysis (see Refs.* [1–3]), *which subtracts the electron density of the partial model from the observed electron density, revealing the missing atoms contributing to the observed electron* density. *The cycle,* refinement→diffrence *Fourier* analysis→refinement, *is repeated until the residual* elec-*tron density does* not *show any more peaks* (non-H *atom cut-offlevel is ca. 1.0* $e\text{Å}^{-3}$) *and the atomic parameters no longer shift during the refinement.*

The above applies to structures with good quality and well-behaved data. Unfortunately, this is not true in most cases for supramolecular structures due to the poor-quality crystals often used. Large supramolccules do not form *well-ordered crystal lattices (periodicity), the dps are low* (<10), *the* W_{au} *are* large (>1000), *and the crystal lattice can contain substantial amounts of (different) solvent molecules, which quite* often *are severely disordcrcd, further decreasing* the *periodicity.*

When you have ensured that you have the *best possible data set from your* supramolecular *crystal, proceed to the structure solution* phase. *Remember that the higher* W_{au} *you* have, the *greater difficulties the structure* solution *programs will havc in producing a good model for your structure.* Here, *the* same *principle applies as with crystals, do not* give *up* if *the first try with rhe default parameters of the structure solution program does not produce results.* The *programs have many other sets of parametcrs that will affect the structure solution procedure. A rule of thumb as to what set of values will actually produce success with your crystal cannot* be *given. Each crystal structure determination is unique,*

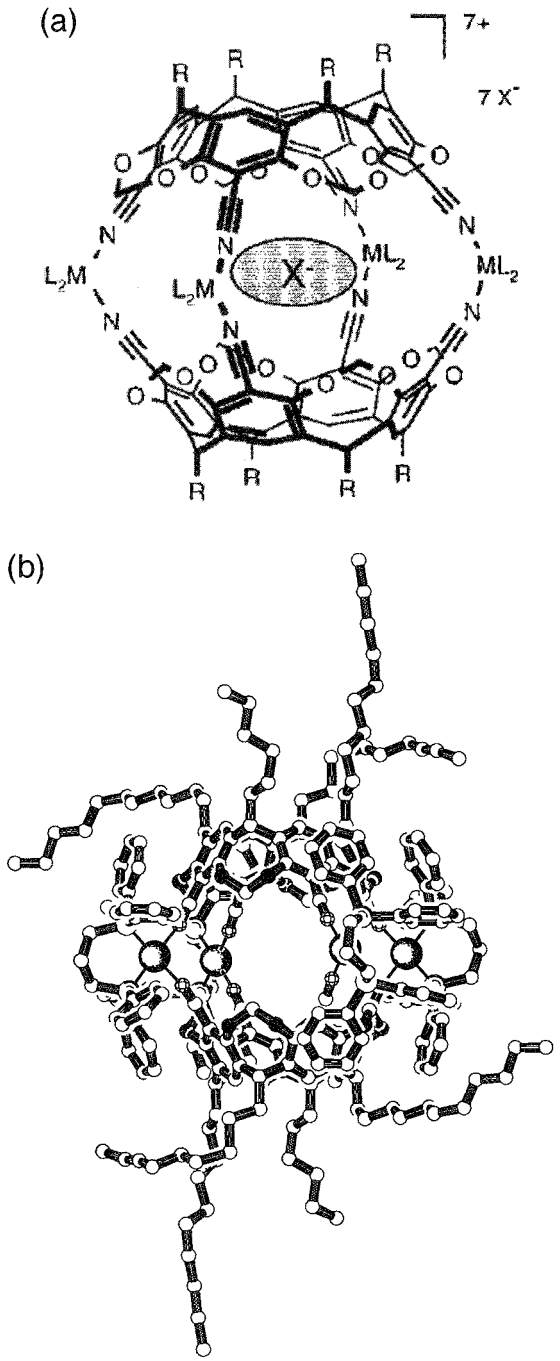

Fig. **3** Schematic (a) and x-ray (b) structure of a cavitand cage.[9] The H-atoms and the included disordered triflate anion are excluded for clarity

and it might be that you have to try various settings and even different structure solution programs in order to get a proper solution. If you tried your best with varying the set of parameters and still do not get a solution, you have to consider that your space group or crystal system may be incorrect (carefully check the data for systematic extinctions, and redetermine the crystal system). Sometimes a change to lower symmetry might help to solve the structure (e.g., going from monoclinic to triclinic). This, however, will double. triple: or quadruple. your W_{au}, thus making structure solution more difficult (if W_{au} grows large, this simplification will make structure solution impossible).

If the space group and the crystal system are correct, and you cannot find an alternative, then you must accept the fact that the quality of your data is not good enough for the structure solution and return to recrystallization of your compound.

DISORDER

Even if structure solution was successful. the task of completing the structure is not yet over. Supramolecular structures. almost by definition, contain included guest or solvent molecules inside the host coinpound or in the crystal lattice. This is, as such. not a problem. but quite often, these molecules are crystallographically disordered. This means that the electron density resulting from the guest or the solvent molecule cannot be clearly determined, and in severe cases, the guest or solvent cannot be located. This unwanted disorder is most prominent when the guest or solvent molecule has weak or nonexistent interactions with the host, e.g., inside molecular capsules and carcerands. Also. if the host compound contains long aliphatic chains, these are often seriously disordered, and it can be particularly difficult to solve and refine the structure to an acceptable level. However, careful control of the crystal growing process or change of the recrystallization solvent can reduce the disorder and thus improve the quality of the crystal. One example of such is a work from the authors' laboratory, where a large cavitand cage compound, $[(C_{268}H_{320}N_8O_{16}P_8Pt_4) @ CF_3SO_3]^{7+} \times 7\ CF_3SO_3^- \times 12.5\ C_6H_6$ was studied.[9] The first data collections produced a result where the core of the cage was clearly determined. but all together, 88 carbon atoms from the eight $C_{11}H_{23}$ alkyl chains could not be located. After 6 months of repeated recrystallizations and after 20 data coilections from 20 different crystals. an acceptable data set was obtained from which the structure with all atoms was obtained (Fig. 3).

CONCLUSION

The x-ray crystallography of supramolecular systems is a difficult but rewarding task. The success of an x-ray study of a supramolecular system requires a well-diffracting single crystal. Obtaining it is often the most difficult and

time-consuming part of the work. Being persistent with the diffraction quality of the crystals, viz. best possible periodicity of the crystal lattice with no twinning, is the key to success. Do not collect data on a bad crystal, test several different crystals and do data collection only for the best possible crystal. Repeat the crystal growing process and change the solvent system if needed. Do not worry which solvent you use, aim for a well-ordered and nicely diffracting single crystal. Only good data can bring you a structure solution. Even though the modern structure solution programs are powerful, do not underestimate the role of the crystal. Even good data does not necessarily produce instant structure solution. Be as persistent with the structure solution programs as you should be with the crystal quality. The larger the W_{au} of your system under study, the more difficulties you will face, but successful x-ray analysis of an interesting supramolecular system is always worth the time you put into it.

ARTICLES OF FURTHER INTEREST

The Cambridge Structural Database, p. 161
Carcerands and Hemicarcerands, p. 189
Concepts in *Crystal Engineering,* p. 319
Crystal Deconstruction, p. 349
Crystal Structure Prediction, p. 371
Neutron Diffraction, p. 959
Solid-State Nuclear Magnetic Resonance Spectroscopy, p. 1307
X-Ray and Neutron Powder Diffraction, p. 1592

REFERENCES

1. *Clegg. W. Crystal Structure Determination*; *Oxford University Press: Oxford,* 1998.
2. *Massa.* W. *Crystal Structure Determination: Springer: Berlin,* 2000.
3. *Fundamentals of Crystallography; Giacovazzo. C.,* Ed.; *IUCR, Oxford University Press: Oxford,* 1992.
4. *Lehn. J.-M. Supramolecular Chemistry*; *VCH: Weinheim,* 1995.
5. *Jones, P.G. Crystal growing. Chem. Br.* 1981. *17,* 222–225.
6. http://laue.chem.ncsu.edu/web/GrowXtal.html.
7. *SHELX Programs for Crystal Structure Analysis (Release 97-2); Sheldrick, G.M., Ed.; Institiit* für *Anorganische Chemie der* Universität: *Tammanstrasse 4,* D-3400 Göttingen, *Germany,* 1998. http://shelx.uni-ac.gwdg.de/SHELX/.
8. *Altomare,* A.; Burla, *M.C.; Camalli, M.: Cascarano, G.L.; Giacovazzo, C.; Guagliardi,* A.; *Moliterni, A.G.G.; Polidori,* G.; *Spagna, J.R. SIR; Appl.* Cryst. 1999. *32,* 115–119. http://www.irmec.ba.cnr.itJ.
9. *Fochi, F.: Jacopozzi, P.:Wegelius, E.; Rissanen, K.; Cozzini. P.; Marastoni, E.; Fisicaro, E.; Manini, P.; Fokkens, R.: Dalcanale, E. Self-assembly and anion encapsulation properties of cavitand-based coordination cages. J. Am. Chem.* Soc. **2001**, *123.* 7539–7552.

X-Ray and Neutron **Powder** Diffraction

John S. O. Evans
University of Durham, Durham, United Kingdom

INTRODUCTION

Powder x-ray and neutron diffraction are extremely powerful tools for probing the structural chemistry of materials in the solid state. Both techniques can be used to gain information about the composition of a bulk material, the degree of crystallinity of its components, information about its unit cell size and symmetry, and, in favorable cases, full three-dimensional (3-D) structural information comparable to that obtained from single-crystal methods. Powder diffraction experiments can be readily performed under the influence of external factors such as temperature, pressure, or applied magnetic field; under laser illumination of a sample; and even as a function of time or chemical environment during the synthesis of materials, giving valuable kinetic and mechanistic insight into their formation. In this article, an overview of the technique will be given along with guidelines on the collection of high-quality diffraction data and an indication of some of the information that can be derived from powder diffraction studies.

BACKGROUND

The techniques and information yielded by single crystal x-ray diffraction and single crystal neutron diffraction methods (see entries by Rissanen and Wilson) are well known and widely utilized by supramolecular chemists. The interaction of x-rays or neutron beams with wavelengths comparable to interatomic distances with an oriented crystal leads to interference effects that give rise to diffracted beams in certain specific directions and with characteristic intensities.[1] From their directions, information about the size and shape of the unit cell can be determined: from their intensities, information on the atomic positions within the unit cell can be determined. Thanks to improvements in single-crystal diffractometer design and the huge software advances of recent years, at the time of writing, there are some 281,000 crystal structure entries in the Cambridge Structural Database,[2] with approximately 30,000 being added annually. The majority of these were determined by single-crystal methods.

While single-crystal techniques will probably remain the primary tool for structural analyses of supramolecular materials in the solid state: the opportunities offered by powder diffraction methods should not be overlooked. In many cases, single crystals of interesting materials of sufficient size and quality for single-crystal methods simply cannot be prepared (though increasingly small microcrystals can now be studied at a synchrotron source). For such materials, structural information comparable to that from single-crystal studies may still be obtained using powder techniques. In other cases, powder diffraction may provide complementary information (such as bulk sample composition) to single-crystal techniques. Non-ambient studies (under extremes of temperature, pressure, magnetic field, or optical irradiation) are often simpler to perform on powdered samples than on single crystals, allowing for the potential to study functional materials under "real" operating conditions; powder studies become essential when phenomena such as phase transitions cause single crystals to shatter under working conditions. Recent advances in the speeds of powder diffraction studies (whole patterns being collected in a matter of minutes, seconds: or less) using advanced sources and detectors mean that phenomena such as host–guest inclusion reactions, chemical transformations in the solid state, and crystallization can now be followed in real time, allowing valuable kinetic and mechanistic insight into the process of chemical transformations. Despite powder diffraction being seen as a "poor cousin" to single-crystal techniques by many, it is a key member of the family of analytical methods that can be brought to bear on understanding structural problems. This article highlights areas of potential interest to supramolecular chemists. For more in-depth and mathematical descriptions of powder diffraction, the reader is referred elsewhere.[3–6]

POWDER DIFFRACTION

In a conventional single-crystal experiment, a beam of monochromatic x-rays/neutrons is incident on a suitably mounted and oriented single crystal. The phenomenon of diffraction leads to diffracted beams being produced in

Encyclopedia of Supramolecular Chemistry
DOI 10.1081/E-ESMC 120012724

certain directions in space.'" In a single-crystal diffraction experiment. the positions and intensities of these beams are recorded by film. point detector, or (most commonly nowadays) area detector methods.

In a powder experiment (Fig. I), instead of a single crystal. one has a collection of randomly oriented polycrystallites exposed to the beam. Each of these polycrystallites can be thought of as giving rise to its own diffraction pattern, and individual "spots" on a film become spread into rings of diffracted intensity (these rings are the intersections of cones of diffracted intensity with the film). The intensities of these rings can be recorded using film and area detector methods, but they are most commonly measured by scanning a point or one-dimensional (1-D) area detector across a narrow strip of the rings. In either case. one can represent the diffraction data as a plot of total diffracted intensity against the diffracted angle 28.

To understand at which values of 28 one may see peaks in a diffraction pattern, it is often convenient to treat the phenomenon of diffraction from a polycrystalline sample in terms of the interference of x-rays reflected from different planes within the unit cell of a crystal. In this way, Bragg's law, which reiates the 2θ angle at which diffraction peaks occur to distances between planes in the unit cell (d_{hkl}), can be readily understood (see Fig. 2). Planes are described by Miller indices, *hkl*. which are related reciprocally to the point at which the plane intercepts the cell edges, *a*. *b*, and c.

The information contained in Figs. 1 and 2 immediately shows one of the inherent problems of powder diffi-action. The 3-D intensity distribution of a single-crystal experiment is compressed onto the I-D of 28 space leading to a vast loss of information due to peak overlap. In a metrically cubic crystal, for example, the 221 and 300

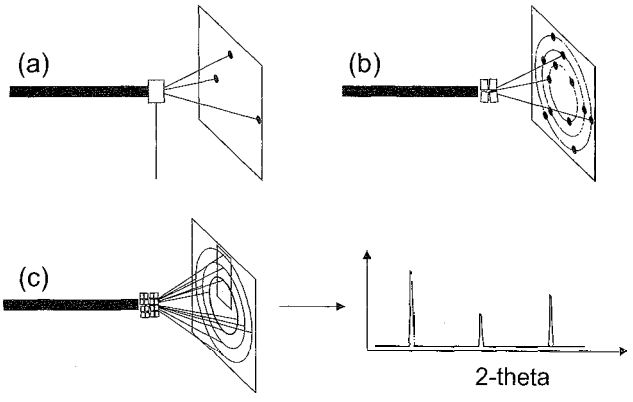

Fig. I (a) Diffraction from an oriented single crystal. (b) from a collection of four crystals at different orientations with respect to the incident beam. and (c) from a polycrystalline material. 2θ increases from the film center to the edge.

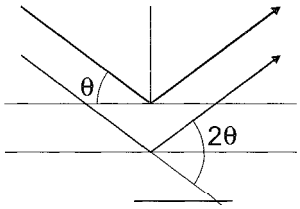

$$n\lambda = 2d_{hkl}\sin\theta$$

Fig. 2 Bragg's law. Constructive interference occurs when the path length difference, $2d_{hkl}\sin\theta$ between two beams is an integral multiple of ?. For cubic systems ($a=b=c$, $\alpha=\beta=\gamma=90°$), interplanar spacings are given by $d_{hkl}=a/(h^2+k^2+l^2)^{1/2}$, and the more complex relationships for noncubic systems are given elsewhere (see Ref. [1].).

reflections (which will generally be of different intensities) will occur at identical values of 28, and only information on their summed intensities is available from a powder diffraction experiment. For a triclinic cell of the complexity that would be routine for modern single-crystal methods (3400 Å^3) using a typical laboratory powder diffractoixeter, there would be —5500 reflections predicted between 0 and 90° 28 (d_{min}=1.09 A). Even for a highly crystalline material, this will lead to a considerable degree of peak overlap.[7,8] There are a number of methods that attempt to alleviate overlap problems. In one approach (see below), some separate information regarding overlapping peaks can be retrieved from intensity variations around the Debye–Scherrer rings of deliberately textured samples;[9] in another. one can make use of anisotropic thermal expansion to try and resolve different families of reflections at different temperatures. In the absence of such methods, overlap can only be reduced by recording the highest resolution data attainable for a given sample.

EXPERIMENTAL METHODS

There are a host of experimental methods available for recording powder diffraction data. each with inherent advantages and disadvantages. Those most commonly encountered in chemistry laboratories, and therefore most likely to be available to supramolecular chemists, are outlined here.

The two most commonly used geometries for obtaining x-ray diffraction data in home laboratories are shown in Fig. 3. In the simplest "reflection" or Bragg–Brentano setup (Fig. 3a), one has an x-ray line source at 3. A flat plate sample is mounted at 4 and a point detector at 6. The sample is scanned through θ degrees as the detector is moved through 20. The most common laboratory x-ray source is a sealed Cu tube. To produce monochromatic

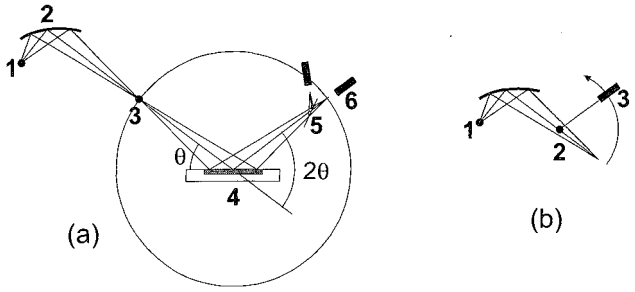

Fig. *3* Typical laboratory powder diffraction setups (see text for details). Diagrams are not to scale, typical distances 1–3. 3 4 . and 4–6 would be ~200 mm; a sample area of ~100 mm^2 would be illuminated.

radiation (Cu $K\alpha_1$ (λ=1.540596 Å), one can place the line source of the tube at Position 1 and a curved Johannsen monochromator (e.g., Ge 111) at Position 2 to produce an effective line source at Position 3. Either a scintillation counter or linear position-sensitive detector is commonly placed at Position 6. This arrangement gives high resolution but can suffer from high backgrounds for samples that fluoresce under Cu irradiation. Fluorescence effects can be reduced by placing a monochromator between the sample and detector. Perhaps the most common laboratory setup is a post-sample pyrolytic graphite monochromator placed at 5 giving an approximate 2:1 mixture of Cu $K\alpha_1$ (*h*=1.540596) and $K\alpha_2$ (h=1.544493) radiation.

Flat-plate samples can be prepared in a number of ways: as bulk powders pressed into a recessed holder or sprinkled onto an amorphous surface, such as glass. or (preferably) a "zero background" sample holder. such as a 511 cut Si wafer. Flat-plate methods are. however. prone to problems due to preferred orientation, whereby a non-random arrangement of crystallites is presented to the beam. This can severely skew diffraction intensities—in extreme cases. making experimental patterns appear completely different to calculated data or database standards. Several methods for reducing preferred orientation are described in the literature[3,10] The positions and intensities of reflections are also influenced by factors such as the sample surface roughness and sample absorption properties. For organic samples, low absorption can lead to a significant portion of diffracted intensity occurring from below the ideal sample surface, leading to peak shifts and broadening. This method of data collection is, therefore. perhaps best suited to relatively absorbing samples or "quick'' qualitative measurements.

The transmission setup of Fig. 3b is particularly well suited for studies on low-absorbing organic/molecular materials. Here, the sample is placed at Position 2. usually mounted in a thin-walled glass capillary of 0.2–1.0 mm internal diameter and spun in the plane of the page, though samples can also be mounted on thin mylar sheets. The use of capillaries significantly reduces preferred orientation effects, though sample mounting is slightly more time consuming.

As with any piece of scientific equipment. the performance of a powder diffractometer should be regularly checked. Various standard materials are available[11] to check the alignment and intensities of the system. There are several commercial suppliers of powder diffractometers. with many of the modern designs allowing for a number of different experimental configurations on the same basic instrument. The introduction of new optical devices such as x-ray mirrors to replace monochromators gives further flexibility in experimental design. A typical "quick" scan from 5–90° 28 on a conventional laboratory instrument might take 30 min, a higher-quality scan for Rietveld refinement may take 12 h or more. depending on instrument configuration.

Significantly higher fluxes and higher resolution are available at a synchrotron source. These also offer the possibility to select a precise wavelength for a specific experiment (allowing absorption edge studies. etc.) or to perform white beam diffraction. Synchrotron-based diffractometers such as ID31 at the ESRF receive a useful flux several orders of magnitude greater than a typical laboratory source and can give very high resolution data.

Powder neutron diffraction offers significant potential advantages over x-ray methods in some situations. In particular. because scattering occurs from the nucleus rather than electrons, one can detect light atoms in the presence of heavy atoms (e.g., O/H in the presence of metals). The penetrating nature of neutrons also gives more confidence that one is studying the bulk of a sample rather than a thin surface layer and allows the use of relatively complex sample environment equipment. Neutrons are also scattered by magnetic moments in a material. giving the possibility of magnetic structure determination. Neutron diffraction can be performed at a reactor (usually using constant λ neutrons) or at a spallation source (usually by the time-of-flight method). Perhaps the major drawback of this technique for the supramolecular chemist is the fact that H scatters neutrons incoherently. To avoid unreasonably high backgrounds. it is. therefore. nearly always necessary to deuterate samples.

INFORMATION IN A POWDER DIFFRACTION PATTERN

Any experimental powder diffraction pattern contains a wealth of information of potential use to the supramolecular chemist. The most important of these (arranged approximately in order of increasing complexity of analysis) are described below.

Phase Identification

Each (crystalline) phase present in a bulk sample will give rise to a characteristic set of peaks in a powder diffraction pattern. These can be compared to a database of known diffraction patterns or compared against patterns calculated from single-crystal diffraction data. Many powder diffractoineter manufacturers supply automatic search and match software to compare experimental data sets against the powder diffraction file (PDF), a collection of around 157.000 data sets maintained by the International Centre for Diffraction Data.[12] Many single-crystal refinement packages provide a facility for simulating a diffraction pattern from a refined structural model or directly from experimental single-crystal data. Recently, a large percentage of the Cambridge Structural Database (approximately 200.000 entries by November 2003) were made commercially available as calculated powder patterns in a format suitable for automated search and match algorithms. Many other resources for calculating powder patterns are available via the Web.

Perhaps the most important application of phase identification to the supramolecular chemist is in confirming whether the powder pattern of a bulk sample corresponds to a structure determined from a single crystal obtained during the same synthesis — there are innumerable examples where the few single crystals produced in a synthesis are due to minor products from side reactions or impurities. The presence of crystalline coproducts (e.g., KCl from a salt elimination reaction) can also be readily identified. A relatively quick powder diffraction experiment can often shed considerable light on otherwise conflicting pieces of analytical data.

Quantitative Analysis

it is also possible to obtain quantitative information about the composition of a multiphase sample from powder diffraction data. Various techniques have been developed based on the analyses of intensities of individual peaks due to different phases contributing to the pattern. on whole pattern intensity analysis. or multiphase Rietveld refinement (see below). Specific details are beyond the scope of this article. and the reader is referred elsewhere.[13] It is worth noting that extreme care should be taken when determining and interpreting quantitative composition. Results can be severely influenced by methods of sample preparation (see above), data collection. and analysis. Careful calibration experiments on the system of interest are recommended. It is also worth noting that it is possible to estimate the quantity of ainorphous material in a sample by powder diffraction measurements (amorphous materials generally give rise to a gradualiy oscillating contribution to the background of the diffraction pattern), by careful quantitative dilution of a powdered sample with an additional crystalline phase.

Peak Shape Information

While the position and intensity of peaks in a powder pattern are determined by the unit cell size and contents. their shapes and widths are determined by instrumental effects (which can be corrected for or modeled) and sample properties. such as the sizes and strains of crystallites and stacking faults.[3] The simplest expression for peak broadening due to sample size (the Scherrer formula) predicts that peak width and particle size are related by $fwhm = K*\lambda/size*\cos\theta$, where K is a shape factor (often 0.9), *fwhm* the peak full width at half maximum. and λ the wavelength: absolute numbers from this expression should be treated with caution. A sample strain leads to a peak width dependence on $\tan\theta$. In more sophisticated treatments. hkl-dependent peak widths can be used to obtain information on the anisotropies of size and strain in a sample. More details on the interpretation of peak shapes are given elsewhere.[14,15]

Rietveld Refinement

One of the main factors that has driven the explosion of powder diffraction methods in recent years is the popularization of the Rietveld method.[16–18] In this method, a powder pattern is expressed in terms of y_{obs}, the intensity observed at a given value of 20. One can use a structural model (equivalent to that used in a single-crystal refinement) and a mathematical model to describe how experimental peak widths vary as a function of 2θ to deterinine the calculated intensity. y_{calc}, at each experimental value of 2θ. The most commonly used function for describing powder peaks is a psuedo-Voigt (a mixture of Gaussian and Lorentzian contributions). though more sophisticated approaches can model peak shape contributions from the experimental setup and sample size and strain directly. One then typically uses a least-squares method to adjust structural parameters. such as unit cell size, fractional atomic coordinates, and temperature factors. to minimize the difference between y_{obs} and y_{calc} over the whole experimental pattern. The quality of a refinement can be monitored in terms of agreement factors R_{wp} or R_{Bragg} ($R_{wp} = [(\Sigma w_i[y_i(obs) - y_i(calc)]^2)/(\Sigma w_i[y_i(obs)]^2)]^{1/2}$; $R_{Bragg} = [(\Sigma|I_{hkl}(calc) - I_{hkl}(obs)|)/(\Sigma|I_{hkl}(obs)|)]$), though the best indication of the quality of a structural refinement is often a visual inspection of the agreement of observed and calculated patterns. An example of a Rietveld refinement of an inclusion compound is given in Fig. 4.[19] A number of commercial and academic software packages are available for Rietveld refinement. The most widely used are GSAS. Fullprof.

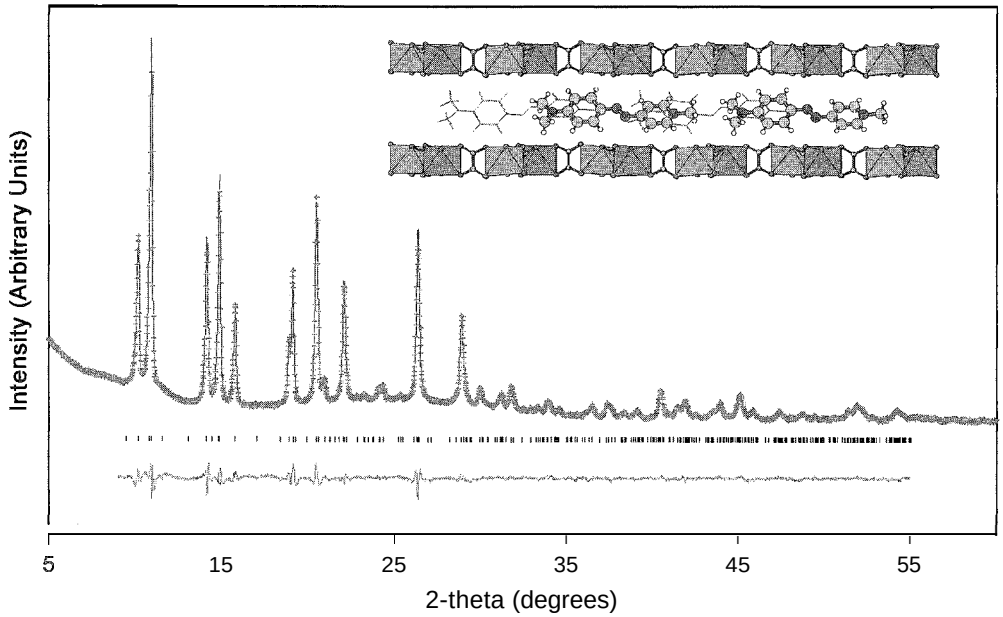

Fig. 4 A Rietveld refinement of an NLO-active-layered inclusion compound DAZOP[MnCr(ox)$_3$]0.6CH$_3$CN [DAZOP = 4-(4-dimethylamino-phenylazo)-1-methyl-pyridinium]. Observed data are shown as red crosses, the calculated pattern as a solid line, and the difference as the lower solid line. Small vertical tick marks show *20* values where retlections are predicted. (*View* this *art in color at www.dekker.com.*)

descendants of the DBWS code and Topas.[20–23] Many of these packages offer the opportunity to simultaneously refine a model against x-ray and neutron data. allowing one to utilize the often complementary information from the two techniques.

Structure Solution from Powder Diffraction Data

It should be emphasized that the Rietveld technique is a refinement method—one needs an approximate set of coordinates from which to refine a model. Until the late 1990s. this meant that Rietveld refinement was largely confined to extended metal oxides and chalcogenides. where starting models could be inferred from other known materials. In recent years, there have. however, been dramatic breakthroughs in solving structures ab initio from powder data; these will have considerable impact on the supramolecular community.[24.25]

The process of structure solution of an unknown material from powder data can be divided into several steps. First; one must record the highest-quality data possible on a (ideally) pure sample. One must then determine the unit cell parameters from observed peak positions (several software packages exist to tackle this nontrivial step). The space group symmetry must then be determined from systematic absences. At this stage. one of a number of different routes can be followed. One possibility is to extract integrated peak intensities from the pattern and use techniques similar to those employed in single-crystal studies, such as direct methods or Patterson synthesis, to solve the structure. Various software packages exist for this. some dedicated to overcoming the inherent uncertainties in intensities due to peak overlap and the inherent data shortage from a powder pattern. Structure completion can then be performed via a series of Fourier difference maps and Rietveld refinement.

Alternatively (and perhaps more powerfully for supramolecular chemistry). one can utilize information about the cell contents in the form of known molecular fragments and their geometric degrees of freedom and attempt direct space structure solution. From the molecular cell contents. one generates a trial structural model and compares its calculated diffraction pattern to the experimental data. Using a Monte Carlo or simulated annealing approach, the structural model can then be adjusted in a random fashion, and the agreement between the observed and calculated patterns can be examined again. The move is then accepted or rejected based on user-definable criteria, and the process is repeated until the best agreeinent between model and experiment is obtained. With efficient algorithms. many hundreds of thousands of trial structures can be generated and tested relatively rapidly, even on desktop computers, to produce a structural model that can be improved by Rietveld methods. Many variations on this general methodology

and alternative genetic and differential evolution algorithms have been developed. Materials of remarkable complexity have been solved by this method. The structure of the NLO-active-inclusion compound of Fig. 4. for which single crystals could not be grown. was solved by a related technique.[19]

It should, however, be noted that each stage of the structure solution pathway from indexing to refinement is complex and potentially insoluble. The range of techniques for overcoming each barrier is. however, expanding rapidly in what is a fast-moving area of research.

NONAMBIENT STUDIES

Experiments beyond a simple room-temperature diffraction pattern can yield considerable insight into the properties of materials. One of the most readily accessible thermodynamic variables experimentally is temperature. Commercial attachments are available for most diffractometers to cool and heat samples from liquid He temperatures to ~1600°C. Of particular relevance to supramolecular chemistry are cryofurnaces. which operate over the ''chemically interesting'' temperature range of 100–600 K, and gas-flow systems that typically operate from 77–373 K. Shown in Fig. 5. for example, is how a low-spin to high-spin phase transition in $[FeL_2](BF_4)_2$ [L = 2,6-di(pyrazol-1-yl)pyridine] is revealed by a marked discontinuity in unit cell parameter as a function of temperature at 260 M: structural information above and below T_C can be obtained directly from the experimental data.[26] Many single crystals of framework inaterials produced by crystal engineering studies are prepared in a solvated form. Structural changes on desolvation can be readily followed by powder methods, alleviating problems due to crystal degradation in single-crystal studies. Polymorphic phase transitions and the evolution of solvate and hydrate pseudopolymorphs, of particular relevance to the pharmaceutical industry, car! also be followed readily in simple sample stages.

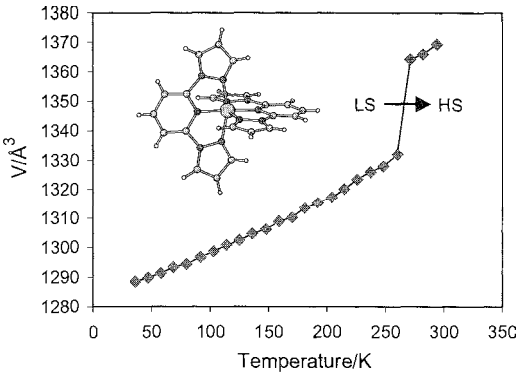

Fig. 5 The unit cell parameter of a powdered sample of $[FeL_2](BF_4)_2$ [L=2,6-di(pyrazol-1-yl)pyridine] determined from laboratory powder diffraction data. Structural changes at the low- to high-spin phase transition are readily visible. (*View this art in color at www.dekker.com.*)

The behaviors of materials under applied pressure are also readily studied by powder methods. Using small-volume diamond anvil cells most suitable for x-ray work, pressures of several hundred GPa at temperatures up to several thousand K can be achieved.[27] Larger volumes of samples can be studied by neutron techniques using gas-pressure cells (up to ~1 GPa on several cm^3 of sample) or more sophisticated designs such as the Paris–Edinburgh design cell (up to ~30 GPa/370 K on 30 mm^3). Such studies have revealed a wealth of important structural chemistry in a variety of molecular systems.

Finally, the possibility of perforining a powder diffraction experiment during a chemical reaction should not be overlooked. Various workers have shown that by using high-energy (and therefore highly penetrating) x-ray beams at synchrotrons, one can literally monitor reactions occurring in test tubes (or more sophisticated reactors) in real time by powder diffraction methods.[28,29] By way of an example. O'Hare and coworkers showed that diffraction patterns of ~100 mg of a suspension of solid SnS_2 in toluene can be recorded in as little as 5 sec. One can then introduce a molecule such as cobaltocene and monitor in real time the structural changes and kinetics of the host–guest intercalation reaction. The opportunities afforded by such a methodology to other areas of supramolecular chemistry must be considerable.

CONCLUSION

Powder diffraction studies can provide a wealth of structural and nonstructural information. Powder diffraction studies can provide quantitative information on multiphasic samples, atoinic coordinates similar to those from single-crystal studies. and give microstructural information on the properties of individual crystallites. The ease with which nonambient experiments can be performed makes powder diffraction one of the more powerful characterization tools available to the supramolecular chemist.

ARTICLES OF FURTHER INTEREST

The Cambridge Structural Database, p. 161
Concepts in Crystal Engineering, p. 319
Crystal Structure Prediction, p. 371
Disorder and Diffuse Scattering, p. 457
Inelastic Neutron Scattering, p. 727

Neutron Diffraction, p. 959
Nonlinear Optical Materials, p. *973*
Scanning Tunneling Microscopy. p. 1202
Solid-State Nuclear Magnetic Resonance Spectroscopy, p. 1307
Supermicroscopy: AFM, SNOM, and SXM, p. *1394*
Vibrational Spectroscopy. p. 1557
X-Ray Crystallography, p. 1586

REFERENCES

1. Giacovazro, C.; Artioli. G.; Viterbo. D.; Ferraris, G.; Monaco. H.L. *Fundamentals* of *Crystallography*; Oxford University Press. 2002.
2. http://www.ccdc.cam.ac.uk.
3. Klug, H.P.; Alexander. L.E. X-Ray *Diffraction* Procedures: For *Polycrystalline and Amorphous Materials*; Wiley-Interscience. 1974.
4. Jenkins. R.: Snyder, R.L. *Introduction* to X-Ray *Powder* Diffractornetn: Wile)?-Interscience, 1996.
5. Cullity, B.D.: Stock. S. *Elements* of X-Ray *Diffraction*: Prentice Hall College Div.. 2001.
6. Pecharsky. V.K.: Zavalij, P.Y. *Fundamentals* of *Powder Diffraction* and Structural Characterization of *Materials*: Kluwer Academic Publishers. 2003.
7. Sivia. D.S. The number of good reflections in a powder pattern. J. Appl. Crystallogr. 2000; *33,* 1295–1301.
8. David, W.I.F. On the number of independent reflections in a powder diffraction pattern. J. Appl. Crystallogr. 1999, *32.* 654–663.
9. Wessels. T.: Baerlocher. C.: McCusker. L.B. Single-crystal-like diffraction data from polycrystalline materials. Science 1999. *284.* 477–479.
10. http://www.mluri.sari.ac.uk/commercialservices/spraydrykit.html.
11. http://www.nist.gov.
12. http://www.icdd.com/.
13. Langford. J.I.; Louer, D. Powder diffraction. Rep. Prog. Phys. 1996. *59,* 131–234.
14. Scardi. P.: Leoni. M. Whole powder pattern modelling. Acta Crystallogr., A 2002. *58,* 190–200.
15. Warren; B.E. X-Ray Diffraction: Dover: New York. 1969.
16. McCusker. L.B.: Von Dreele, R.B.; Cox, D.E.: Louer, D.: Scardi. P. Rietveld refinement guidelines. J. Appl. Crystallogr. 1999. 32. 36–50.
17. Young. R.A. *The Rietveld Method*; Oxford University Press. 1995.
18. Rietveld. H.M. A profile refinement method for nuclear and magnetic srtuctures. J. Appl. Crystallogr. 1969, *2.* 65.
19. Evans, J.S.O.: Benard, S.; Yu, P.: Clement, R. Ferroelectric alignment of NLO chromophores in layered inorganic lattices: Structure of a stilbazolium metal-oxalate from powder diffraction data. Chem. Mater. 2001, *13,* 3813–3816.
20. Bruker AXS Ltd. Topas Bruker AXS: Karlsruhe, 2000.
21. Larson, A.C.: Dreele, R.B.V. GSAS. In Los *Alamos Internal* Report No. *86-748*; 1994.
22. Wiles. D.B.; Young, R.A. J. Appl. Crystallogr. 1981. *14,* 149.
23. Rodriguez-Carvajal, J. In FULLPROF: A *Program* for *Rietveld Refinement and* Pattern *Matching Analysis*, Abstracts of the Satellite Meeting on Powder Diffraction of the XV Congress of the IUCr, Toulouse. France. 1990: 127.
24. Harris. K.D.M.: Johnston, R.L.: Cheung, E.Y.; Turner. G.W.; Habershon, S.; Albesa-Jove. D.; Tedesco. E.: Kariuki. B.M. Recent advances in opportunities for solving molecular crystal structures directly from powder diffraction data: New insights in crystal engineering contexts. CrystEngComm 2002. 356–367.
25. Harris. K.D.M.: Tremayne. M.: Kariuki. B.M. Contemporary advances in the use of powder x-ray diffraction for structure determination. Angew. Chern.. Int. Ed. 2001. *40.* 1626–1651.
26. Money. V.A.: Evans. I.R.; Halcrow. M.A.: Goeta. A.E.; Howard, J.A.K. Light induced excited high spin-state trapping in [FeL2](BF4)(2) (L=2,6-di(pyrazol-1-yl)pyridine). Chem. Commun. 2003. 158–159.
27. Paszkowicz. W. High-pressure powder x-ray diffraction at the turn of the century. Nucl. Instrum. Methods Phys. Res.. B Beam Interact. Mater. Atoms 2002, 198. 142–182.
28. Evans. J.S.O.; Price. S.J.: Wong. H.V.; O'Hare. D. Kinetic study of the intercalation of cobaltocene by layered metal dichalcogenides with time-resolved in situ x-ray powder diffraction. J. Am. Chern. Soc. 1998. *120,* 10837–10846.
29. Francis, R.J.: O'Hare. D. The kinetics and mechanisms of the crystallisation of microporous materials. J. Chem. Soc. Dalton Trans. 1998. 3133–3148.

Zeolites in the Petroleum Industry

Christian Marcilly *(Retired)*
French Institute of Petroleum (IFP), Rueil Malmaison, France

INTRODUCTION

Since the first synthesis of a zeolite. the A zeolite, developed by Milton[1,2] in 1949. there has been constant development in the work on these special microporous solids and their applications. During the second half of the twentieth century, zeolite properties were chiefly exploited by the oil refining industry. but from the 1970s onwards. they gradually came to be used by the major intermediate petrocheinical industry and also by the end of the 1980s[3] by the promising field of fine chemicals. This article on the principal applications of zeolites will deal only with the refining and petrochemical industries. Nowadays, these applications concern two major categories of petroleum cut processing: the physical types of processing that belong to the field of adsorption and chemical types of processing by catalysis. These forms of processing produce petroleum cuts with characteristics that comply with the specifications laid down by government authorities. Shown in Table 1 are the chief characteristics that allow us to judge the qualities of four major petroleum fractions: liquefied petroleum gases (LPG), gasoline, gas oil, and lube oils. It also shows how the different types of hydrocarbon contribute to these characteristics and indicates the quality of the fractions produced by three typical refining processes.

The considerable success of zeolites is partly due to their shape selectivity, which has led to decisive progress in numerous applications in which they are involved: intensive drying and purification, fine separation. and improved catalytic activity. selectivity. and stability. Their shape selectivity is due to the very fine and regular pores present in their structure. Access to the pores is controlled by apertures with size that varies according to the zeolite considered. Zeolite success is also due to the confinement of molecules in the restricted pore space, which results in high molecule concentrations in the pores. This property is involved in adsorption and catalysis. promoting bimolecular reactions as opposed to monomolecular reactions in the latter. Shown in Table 2 are the structural types and pore aperture sizes of the zeolites used in the different processes of the refining and petrochemical industries. It also indicates the nature of the principal molecules capable of penetrating the pores and of some molecules that are too large to diffuse throughout the microporous structure.

APPLICATIONS IN ADSORPTION

Almost all the zeolites used in the field of adsorption are silicoaluminates.[4–8] Their adsorption properties depend on the concentration of intrazeolitic cations, which is governed by the concentration of aluminium in the zeolite framework, by the nature of the cations (valence and size), and by their crystallographic positions. The high degree of confinement of the molecules in the fine pores of the zeolites results in intensive adsorption of the molecules at low partial pressure, and it is significantly more intensive than with the traditional silica. alumina, or activated charcoal adsorbants. The intensive electrostatic field in the immediate vicinity of the zeolitic cations promotes the adsorption of the polar molecules (e.g., water, alcohols, H_2S) or the polarizable molecules (e.g., olefins). The adsorption properties differ greatly from zeolites rich in aluminium (hydrophilic zeolites). which have a strong affinity for polar molecules: and zeolites that contain little aluminium (and, consequently, zeolitic cations) (hydrophobic zeolites), which tend to adsorb preferably nonpolar molecules, such as saturated hydrocarbons. The transition from hydrophilic zeolites to hydrophobic zeolites corresponds to a silicon-to-aluminiin (Si/Al) atomic ratio of around 8–10.

Industrial adsorption applications in the refining and petrochemical industries fall into two main categories: the purification of various fluids, including intensive drying. and the fine separation of molecules within a mixture. These applications mainly involve two zeolite structures: LTA (zeolite A) and FAU (faujasite) (Table 2). Other zeolites are also of interest but to a lesser degree: for example. mordenite (MOR structure) is more resistant and was used in some catalytic reforming installations for drying recycle gas rich in HCl. and silicalite (silica-rich zeolite with the MFI structure) is potentially useful for removing some organic compounds present in refinery wastewater.

The choice of the zeolite structure to be used as adsorbent is based on three criteria: its adsorption capacity, its shape selectivity, and its varying affinity for removing or recovering the molecules. After adsorption. the zeolite has to be regenerated before it is used again. Three main regeneration techniques are used: thermal swing processes (TS). pressure swing adsorption

Encyclopedia of Supramolecular Chemistry
DOI: 10.1081/E-ESMC 120012811

Table 1 Some characteristics of the principal petroleum fractions. Contribution of the various hydrocarbon families to these characteristics. Qualities of the fractions produced by three typical catalytic refining processes (cracking, hydrocracking, hydroisomerization)

		Hydrocarbons to be promoted								Principal reactions		
Fractions	**Characteristics**	***n*-P**	***i*-P**	***n*-O**	***i*-O**	**Alkylnapht.**	**Polynapht.**	**Alkylaro.**	**Polyaro.**	**Crack.**	**HyCrack.**	**HyIsom.**
LPG	Olefinicity	0	0	xxx	xx	—	—	—	—	X××	0	0
	Branching	0	xx	0	xx	—	—	-	—	X×X	XX	XX
Gasoline	Octane number	0	xx	x	xx	x to xx	—	×xx	—	X×	X	XX
Gas oil	Cetane number	xxx	x to xx	xxx	x	x	0	× to ×x	0	0	XXX	XX
	Pour point	0	xx	0	xx	xx	xx	×x	—	0	0 to X	XX
Lubes	Viscosity index	xxx	x to xx	—	—	x to ××	0	× to ×x	0	0	XXX	XX
	Pour point	0	xx	—	—	x to xx	x to x:	× to ×x	0 to	0	0 to X	XX

Key: not relevant; 0: bad; x or X: poor to medium; xx or XX: good; xxx or XXX: excellent; 0 to x (X) and x to xx: according to the length of the alkyl chains; Alkylnapht: alkylnaphthenes; Polynapht: polynaphthenes; Alkylaro: alkylaromatics; Polyaro: polyaromatics; HyCrack.: hydrocracking; HyIsom.: hydroisomerization.

Table 2 Zeolites used in the refining and petrochemical industries Principal structural characteristics and applications

Zeolite structures	Zeolites	Pore apertures (Angström)	Principal accepted molecules	Principal unaccepted or barely accepted molecules	Applications
FAU	X, Y	7.4	P. N. Monoaro	Polyalkylnaphthenoaro Polyalkylpolyaro	Drying, purification, separation of C_8 aromatics Cracking (FCC) and hydrocracking of VGO, alkylation of aromatics
BEA	Beta	7.6 × 6.4	P. N. Monoaro	Polyalkylnaphthenoaro Polyalkylpolyaro	Cumene synthesis
LTL	K-L	7.1	P. N. Monoaro	Polyalkylnaphthenoaro Polyalkylpolyaro	Aromatization
MOR	Mordenite	7.0 × 6.5	P, N. xylenes. TMB	Trialkylrnonoaro	Hydroisornerization of n-P Xylene isomerization, transalkylation of aromatics, cumene synthesis
MFI	ZSM-5 Silicalite	5.3 × 5.6 5.1 × 5.5	*n*-P. MBP. Xylenes	2,2,4-TMC_5, TMB	FCC, dewaxing, aromatization. xylene isomerization. toluene disproportionation, ethylene-benzene alkylation Methanol—fuels or light olefins
AEL	SAPO-11	3.9 × 6.3	*n*-P, Slightly BP (MBP)	2,2,4-TMC_5	Isodewaxing
TON	ZSM-22	4.4 × 5.5	n-P, Slightly BP (MBP)	2,2,4-TMC_5	Isodewaxing
MWW	MCM-22	5.5 × 4	Cumene	?	*EB* and cumene synthesis
FER	Ferrierite	4.2 × 5.4 3.5 × 4.8	MBP	Gem-DMP	Butene isonierization
LTA	3A	2.9	H_2O, NH_3	n-P. *n*-O	Drying of alcohols and olefiins
	4A	3.8	H_2O, CO_2, C_2H_6	n-P and *n*-O>C_2	Drying, purification
	5A	4.4	*n*-P	*i*-P	*n*-P/*i*-P separation
CHA	SAPO-34	3.8 × 3.8	n-P and *n*-O	i-P, *i*-O. inonoaro	Methanol—light olefins
Undisclosed (IFP, UOP)		—	Xylenes	*TMB*	Xylene isomerization

Key: P: paraffins: **O:** olefins: N: naphthenes; aro: aromatic?: n: normal or linear: i: iso; BP: branched paraffins: MBP: monobranched paraffins: DMP: dimethylparaffins; TMC_5: trimethylpentanes: EB: ethylbenzene: TMB: trimethylbenzenes; DIPB: diisopropylbenzenes.

(PSA), or displacement by a fluid that may be inert or, on the contrary. may compete with the adsorbate.

Raising the temperature is the desorption method most commonly used in cyclic processes. It can be used in the liquid or gas phase and is much more effective when the adsorbate has a strong affinity for the zeoiite (as in the case of polar molecules like water). Reducing the pressure is a faster desorption method but is used preferably in the gas phase with gases that are only weakly adsorbed. Desorption by displacement may be used in liquid or gas phase and is the only method that can be used continuously (with countercurrent processes).

Drying and Purification sf Fluids

The choice of the adsorbent to be used for drying a fluid depends chiefly on the nature of the fluid. which in most cases, is a gas. For drying natural gas that contains only saturated hydrocarbons, the 4A zeolite (Si/Al=1, cation= Na. pore aperture ~0.4 nm) is generally used (Table 2). For drying olefin-rich gases [e.g., cracked gases from the fluid catalytic cracking(FCC) stream], the 3A zeolite (Si/Al=1, cation =M, pore aperture ~0.3 nm) is preferably used, because its pore size excludes hydrocarbons. The various impurities contained in the fluids are generally removed simultaneously with drying. as in the case of the purification of saturated acid hydrocarbon cuts (sour gases) containing sulfur compounds such as H_2S and mercaptans, CO_2, and water. The zeolite used is generally 13X ($1.2<Si/Al\leq 1.5$, cation=Na, pore aperture—0.74 nm), which has an adsorption capacity greater than that of the A zeolite. The affinities of the various impurities for the adsorption sites are in the following decreasing order: $H_2O>H_2S>CO_2$. Apart from drying. which is generally

carried out simultaneously, the sweetening of sour gases only requires the removal of the sulfur compounds (H_2S and mercaptans). so that regeneration of the molecular sieve is only necessary once these molecules, particularly H_2S, have broken through. However, a factor that often has to be taken into account is the forination of COS due to the reaction between CO_2 and H_2S. The formation of COS should be minimized. because only a small amount of the gas is adsorbed on the sieve, and H_2S may then be reformed by hydrolysis in the presence of traces of water. The use of a 10X zeolite (cation=Ca) instead of a 13X zeolite reduces this risk.

Drying and purification operations are almost all carried out in processes using at least two reactors and operating in a cyclic manner. Desorption by temperature switch (TS) is the technique most frequently used.

Separation Applications

The main applications in the field of hydrocarbon separation concern the recovery of *n*-paraffins contained in the light cuts from C_4 to C_6, or in heavier cuts such as kerosene from C_{10} to C_{15} approximately, and that of some isomers contained in the aromatic cuts (e.g., the recovery of paraxylene from C_8 aromatic cuts) (Table 2).

The separation of branched paraffins from a mixture of *n*- and isoparaffins with 4. 5, or 6 carbon atoms is almost always associated with an isomerization operation to maximize the production of isoparaffins for the gasoline pool (Table 1). It is performed on a 5A zeolite with pore apertures in the region of 0.45 nm that allow the passage of n-paraffins but not of other isomers (Table 2). A wide range of techniques for the use of this zeolite were adopted in the various existing industrial processes. Most operate in the gas phase according to a cyclical technique involving vacuum desorption or displacement by a gas. Two of them operate in liquid phase using a desorption technique invoiving chromatographic-type displacement.

Long straight paraffins from C_{10} to C_{15} contained in kerosene find applications in the detergent industry. Although these paraffins are strongly adsorbed on the 5A zeolite, a temperature-switch cyclic desorption process cannot be used, because it would require temperatures of over 350°C, at which coking inevitably occurs. The only possibilities. therefore, are vacuum desorption or displacement with a desorbent. The possible desorbents include hydrogen. *n*-pentane, or ammonia.

It is impossible to remove paraxylene from a mixture of xylenes and ethylbenzene by distillation, because the boiling points of para- and metaxylene are too close to each other. It is difficult and costly to do so by crystallization, mainly because of the existence of an eutectic between these two isomers that restricts the rate of paraxylene recovery to around 65%. The modern separation technique simulates a countercurrent flow between the isomer mixture and the adsorbent bed composed of the cationic form of an FAU structure zeolite (Table 2) and allows a rate of recovery of at least 92% of paraxylene of over 39.7% purity. This technique uses liquid-phase chromatography. and the recovery of paraxylene is realized by means of a desorbent. In order to make the operation continuous, the column in which the fixed adsorbent bed is located is equipped with multiple inlet/outlet connections, allowing liquid to be injected or drawn off. Countercurrent flow is simulated by the passage from one connection to the next in order to displace the level of injection of the mixture of liquid isomers and desorbent and that of the withdrawal of the extract (the paraxylene) and the raffinate, at the same speed as the displacement of the liquid in the fixed zeolite bed. The adsorbent used is an X or Y zeolite containing alkaline-earth ions. mainly Ba^{2+}, and possibly potassium ions, the role of which is to optimize the affinity of the zeolite for paraxylene.

The technique of desorption by simulated countercurrent flow displacement is also applied to other separation operations: the separation of ethylbenzene from a mixture of aromatics and that of olefins from a mixture of olefins and paraffins. The composition of the zeolite adsorbent is adjusted in each case to optimize the effectiveness of the separation: Na-Y or KSr-X zeolites for ethylbenzene and Ca-X or Sr-X for olefins. The nature of the liquid desorbent also depends on the molecule to be separated.

APPLICATIONS IN THE FIELD OF CATALYSIS

Refining

Cracking of heavy feedstocks

Cracking of vacuum gas oil (VCO) is the first catalytic application of zeolites.[9–14] From 1962–1963 onwards, the replacement of the former amorphous silica–alumina-based low-acid catalysts by catalysts containing the Y zeolite (FAU structure) with higher acidity resulted in considerably improved catalytic activity and gasoline yield. Today, cracking catalysts. except in rare cases. contain from 10–40% of Y zeolite dispersed in a more or less active solid matrix and are used in fluidized bed units (FCC or fluid catalytic cracking units). The role of the matrix is to ensure the precracking of the larger molecules in the feed. principally the alkylnaphthenoaromatics and the alkylpolyaromatics that cannot penetrate the micropores of the zeolite. which are limited by a circular

aperture with a diameter of around 0.74 nm (Table 2). The acidity of the zeolite is thus protected from these large coke precursor molecules and from large highly basic nitrogenous molecules, enabling it to effectively convert the smaller, less coking-prone molecules into gasoline with a satisfactory octane number (Table 1).

In an FCC unit, the fluidized catalyst constantly circulates between a reaction section where the temperature is about 500°C and where it is rapidly deactivated by the coke formed, and a regeneration section where the coke is burned in air at around 700–750°C. In the severe conditions prevailing in the regenerator, the framework of the Y zeolite is impaired, and fairly quickly it irrevocably loses its acid sites. The speed of the loss of acidity can be moderated by introducing varying amounts of rare earth (RE) ions into the zeolite. A strong concentration of RE ions maintains a high density of acid sites in the zeolite over a long period of time, which promotes the bimolecular hydrogen transfer (HT) reaction. In the absence of these ions, the density of the acid sites decreases rapidly, and the capacity of the Y zeolite to promote hydrogen transfer (HT) is considerably diminished. These ions are important with respect to the quality of the gasoline produced, because the HT reaction converts a large proportion of the olefins in this cut into paraffins and, at the same time, reduces its octane number.

Even when it does not contain any RE ions, the Y zeolite is always responsible for a drop in octane number compared to the old amorphous silica–alumina-based catalysts. In order to gain a few points in the octane number, many refiners add to the principal catalyst a small percentage of a ZSM-5-based additive that has pores 0.55 nm in diameter that can only be penetrated by linear aliphatic structures and, to a lesser degree, by monobranched aliphatic structures (Tables 1 and 2). These hydrocarbons, which are those with the lowest octane number, are mainly cracked to olefin-rich LPG, obviously at the expense of a few percentage points in gasoline yield.

Since the mid-1990s, the ZSM-5 zeolite has also been increasingly used to maximize light olefin production in fluid catalytic cracking.

Hydrocracking of heavy feedstocks

Cracking heavy feedstocks, such as VGO, at around 370–420°C, under high hydrogen pressure, is a more costly process than the previous one, but it is also more flexible, because it can be oriented toward the production of light products (LPG and gasoline), middle distillates (jet fuel, gas oil), and lube oil base stocks.[15–21] The gasoline produced has a poor octane number, but its high naphthene concentration makes it an excellent feedstock for catalytic reforming. The middle distillates possess good combustion characteristics (Table 1), because they are rich in hydrogen. The lube oil base stocks have excellent lubrication properties, in particular, a high viscosity index (Table 1). A high viscosity index indicates that the viscosity of the lube oil does not change much when the temperature increases. The hydrocracking catalysts are all of the bifunctional type and associate an acid function with a hydrodehydrogenation function (either a combination of nickel and molybdenum or tungsten sulfides, or noble metals such as palladium or platinum). Most of these catalysts contain a small proportion (approximately 5–30%) of Y zeolite, depending on the desired product (Table 2). The first zeolite catalyst, a Mg-Y catalyst containing Pd, was developed by Union Carbide and used industrially by Unocal in the early 1960s.[1] Modern catalysts generally contain a H-USY zeolite. (USY means ultrastable Y and refers to a Y zeolite treated at high temperature in the presence of steam to adjust its acidity and the stability of its structure.)

The first advantage of the Y zeolite compared to amorphous silica–alumina-based catalysts is its higher activity that allows it to operate at lower temperatures (ΔT of around 20–40°C), resulting in better hydrogenation and improved quality of middle distillates and lube oil base stocks. A further advantage is its greater stability over a period of time. Both advantages are mainly due to its higher acidity, which offers better resistance to nitrogen poisons, particularly ammonia, and also partly to its shape selectivity, which does not allow access of the larger and more coking-prone molecules to the acid sites. On the other hand, the limited pore size of the zeolite promotes the consecutive cracking of the larger molecules that are able to penetrate the pores because their diffusion is slower, which leads to a deterioration in both middle distillate selectivity and yield in relation to amorphous catalysts.

Zeolite catalysts are used in two main types of process:

1. Processes involving two reactors without any intermediate separation (one-stage process): the feed is hydrotreated in the first reactor with a conventional catalyst, and almost all the organic sulfur and nitrogen compounds are converted into H_2S and NH_3 gas, which are relatively well tolerated by the zeolite catalyst in the second reactor. The hydrodehydrogenation function added to the zeolite is usually of the metal-sulfide type.
2. Processes involving two reactors with an intermediate separation (two-stage process). The effluent from the reactors of the first stage is fractionated, and only the heaviest fraction, the nonconverted residue, from which all the sulfur and nitrogen compounds have

been removed, is treated by the zeolite catalyst in the second-stage reactor. The hydrodehydrogenation function is usually based on a noble metal.

Dewaxing of gas oils and lube oil base stocks

Some gas oils and lube oil base stocks. particularly those produced by hydrocracking, have cold flow properties that do not comply with specifications. The molecules responsible for these problems are mainly the long straight-chain alkyls, including those linked to a naphthene or aromatic ring (Table I). There are two ways to remove these chains—by selective hydrocracking or by selective hydroisomerization.

Dewaxing of Jet Fuels, Gas Oils, and Lube Oil Base Stocks by Selective Hydrocracking. In 1977, Mobil announced that it developed a selective acid ZSM-5-based catalyst for dewaxing jet fuels and gas oils (Table 2).[20,22] The pores of this zeolite (diameter around 0.55 nm) readily allow the penetration of straight-chain paraffins and long straight-chain alkyls juxtaposed to a ring, and to a lesser degree. alkyl chains that include a branched methyl group. These chains are cracked by the ZSM-5 zeolite at a temperature of between 300–400°C into smaller fragments that are distributed between the LPG and gasoline fractions. At the beginning of the 1980s, this application was extended to lube oil base stocks using the same zeolite.

Cracking all or part of the straight-chain paraffins improves cold-flow characteristics of the hydrocarbon cut processed. but on the other hand, it has the disadvantage of reducing its yield and of slightly deteriorating some important properties of the cut—the jet fuel smoke point, gas oil cetane number. and lube oil viscosity index. The dewaxing operation should therefore offer the best possible compromise between the desired cold-flow characteristics. the yield requirements, and the combustion or viscosity characteristics.

The feed does not require previous hydrotreating before dewaxing, because the organic base nitrogen molecules that it contains are too large to penetrate the pores of the ZSM-5 zeolite and inhibit its acidity. Hydrotreating would lead to the conversion of these bulky nitrogeneous organic molecules into ammonia that would penetrate the pores of the zeolite and inhibit its acidity. In such a case, this would impose the separation of ammonia upstream of the dewaxing reactor.

A large amount of the cracked products is present in the gasoline cut. In the absence of any strong hydrogenation function. the acid ZSM-5 zeolite produces olefinic gasoline with a high octane number as a by-product.

Isodewaxing. The second way of catalytically improving the cold-flow characteristics of a petroleum cut is to isomerize the paraffins while minimizing cracking so as to obtain a very high distillate or lube oil base stock yield.[20,23,24] This is an attractive solution in the case of lube oil base stocks. Their added value is much higher than that of distillates and so provides an incentive to minimize cracking into light by-products of lower value.

With the acid ZSM-5 zeolite used in dewaxing by selective hydrocracking, the cracking of n-paraffins is preceded by their isomerization into branched paraffins. The most branched of them are retained in the pores and are cracked into smaller fragments that may break free. There are two ways of avoiding or restricting the cracking: by using a more open zeolite such as the Beta zeolite (BEA structure), for example, which allows multibranched isomers to escape from the pores before they are cracked, or by finding a zeolite with a pore size and shape that do not allow the formation of multibranched isomers that are easily cracked. The first solution cannot prevent significant cracking, whereas the second solution appears more promising, provided the appropriate zeolite(s) can be found. The first results of removing linear paraffins by selective hydroisoinerization were published around 1987 and concern the treatment of lube oil base stocks by the SAPO-11 zeolite (Table 2). This zeolite has intermediate pore apertures (with a diameter of around 0.5 nm) and the required shape selectivity to inhibit the formation of easily cracked multibranched isomers and to allow the formation. even at a very high rate of conversion, of only slightly branched isomers that are difficult to crack. The catalyst used is bifunctional and possesses a strong hydrogenation function based on a noble metal (Pt or Pd) that requires operating with feeds that have low concentrations of organic sulfur and nitrogen compounds. Other zeolites possess properties comparable to those of the SAPO-11 zeolite: ZSM-22 and 23, and ferrierite, for example.

The first process for dewaxing by hydroisomerization was commercialized in 1993 for lube oil base stock treatment.

Isomerization of C_5–C_6 light paraffins

The most effective zeolite for this industrial application is an acid-modified mordenite (Table 2) associated with a small amount of Pt and has been used since 1970.[25–28] It does not involve the pollution and corrosion problems of conventional superacid catalysts with Pt on highly chlorinated alumina. It has much lower acidity. and therefore requires a high reaction temperature (220–250°C) that is thermodynamically not favorable to isomerization. It could rapidly be superseded by new

solid catalysts that are much more acidic. nonpolluting. and noncorrosive. such as sulfated zirconia.

Aliphatic alkylation

During the 1990s, considerable work was carried out on aliphatic alkylation for the purpose of replacing liquid acid HF and H_2SO_4 catalysts that were considered to be too dangerous for human beings and the environment.[29–33] The potential catalysts identified, including the USY and BEA, have selectivities similar to those of liquid acids, in spite of lower activity. but they are rapidly deactivated, and so a simple and economical procedure for regenerating their activity has to be designed. Several interesting processes were imagined. including suitable hydrogen treatments at low or medium temperature, but none has yet reached the industrial stage, because they do not provide sufficient gains in perforinance or investment and operating costs. At present, these new catalysts inay not make any headway unless substantial incentives are imposed by the authorities.

Aromatization of aliphatic hydrocarbons

Zeolites were used in various processes that convert paraffins or olefins into alkyl monoaromatics containing chiefly from six to nine carbon atoms.[34–37] There are various catalysts, and they involve a base or an acid zeolite. according to the type of process. The first catalyst, identified at the end of the 1970s. is composed of Pt deposited on the L zeolite (Table 2) exchanged with large alkaline ions such as potassium or alkaline earths. such as Ba. which gives it an alkaline nature. This cataiyst is monofunctional and is conceptually different from the conventional bifunctional acid catalysts based on Pt on chlorinated alumina. It selectively dehydrocyclizes the paraffins into aromatics, particularly hexane. which is the least reactive of them. The reaction takes place on the metal, which develops a special selectivity in contact with the alkaline zeolite. This aromatization process has not been successful so far. partly because of the extreme sensitivity of the catalyst to the slightest trace of sulfur compounds.

The other processes developed in the 1980s involve an acid catalyst. The purely acid H-ZSM-5 zeolite, for example. is used at around 500°C for cracking the olefins and paraffins in light FCC gasoline into smaller olefins. some of which are subsequently oligomerized and cyclized into monoaromatics.[22,36,37]

The bifunctional catalyst composed of gallium or zinc or. to a lesser degree, of Pt which are introduced into the ZSM-5 zeolite. is capable of aromaiizing saturated or unsaturated C_2 to C_4 hydrocarbons. particularly LPG, and hydrocarbons with five and six carbon atoms, at around 500°C[36 37] (Table 2)

The environmental constraints prevailing at the beginning of the twenty-first century are not likely to promote the commercial success of these processes. The scheduled reduction in the aromatics content of gasoline is likely to result in a surplus of these hydrocarbons on the market in the coming years.

Skeletal isomerization of linear olefins with four and five carbon atoms

This reaction produces the isobutene and isopentenes necessary for the synthesis of the principal ethers MTBE, ETBE, and TAME used as high-octane-number gasoline blending components.[38–41] On most of the nonzeolite acid solids, the isomei-ization of *n*-butenes takes place via two different mechanisms: the monomolecular one selectively produces isobutene, and the bimolecular one is not selective. Some zeolites of intermediate pore size, especially ferrierite (Table 2), with acidity and shape selectivity that strongly favor the monomolecular mechanism, have a selectivity for isobutene far greater than that of other solids. The situation is somewhat different in the case of pentenes. In this case. the selective monomolecular mechanism is dominant on all the solids and is not particularly favored by any acid zeolite. The superiority of ferrierite for the synthesis of isobutene was proven in a demonstration unit, but very few processes have yet been commercialized, due mainly to the threat that bangs over MTBE. The addition of this ether to gasoline might be permanently prohibited in a number of countries following the contamination of groundwater in California at the end of the 1990s due to leakage from MTBE storage tanks.

Oligomerization of olefins

The dimers and trimers of the light olefins ($C_3^=$ to $C_5^=$) produced with acid catalysts are generally branched and make good gasoline-blending components.[22,42] However. the open zeolites like the Y zeolite are less effective catalysts for this application. because they have a lower stability than amorphous silica-alumina catalysts. On the other hand, the shape selectivity of zeolites with small pore apertures. like the ZSM-5 zeolite (Table 2), only allows the formation of slightly branched oligomers. Around 200°C and a pressure of 2 MPa, the major parts of the hydrocarbons formed are aliphatic, of which the C_{12}–C_{25} fraction can be used, after hydrogenation, as jet fuel and diesel oil.[22] At higher temperatures, the oligomerization is followed by cracking. MT, and aromatization. all reactions that lead to a good-quality aromatic-rich

gasoline as the major product.[42] This type of process, commercialized in the early 1980s, is still far from being widespread, as the product qualities are just at the limit of the specifications imposed. For instance, the motor octane number of gasoline is below 85, and the cetane number of diesel oil is at the best only just above 50.

In another type of process. mordenite ion-exchanged with nickel is used to convert olefins from C_2 to C_5 into gasoline, jet fuel, and gas oil, under pressure and at a temperature between 200–280°C.[42]

Conversion of the aromatics of some petroleum cuts

The acid ZSM-5 zeolite is used to lower the benzene content of reformates to below 1%.[42] For this, the benzene of the light fraction of the reformate is alkylated by the light olefins, ethylene and propylene, present in the FCC fuel gas, into higher monoaromatics. This operation, which is performed in a fluidized fixed-bed reactor with a continuous catalyst regeneration, decreases the total gasoline yield of the reformate due to the cracking of part of the paraffins but slightly increases the octane number.

Conversion of methanol into gasoline

The first industrial unit for gasoline production by conversion of methanol on an acid ZSM-5 zeolite fixed bed (Table 2) came onstream in New Zealand in 1985.[22,43,44] The gasoline produced is rich in isoparaffins and aromatics and has a high octane number (NOR—93). A moving-bed process producing a slightly better gasoline was also developed but never went further than the demonstration stage. The main advantage of the ZSM-5 zeolite is its shape seiectivity that does not allow the formation of heavy aromatic products with over 10 carbon atoms and, hence, prevents the formation of coke. At present, this application is only viable in specific local political and economic situations and only limited success can be expected in the near future.

Petrochemicals

Applications of zeolites in the petrocheinical industry first concern the transformation of aromatics and second. light olefins—on one hand, their production from methanol and, on the other hand, their interconversion.

Isomerization of C_8 aromatics with transformation of ethylbenzene

The catalysts used differ considerably according to the nature of the desired transformation of the ethylbenzene present in the aromatics.[22 45–50]

Mordenite has been used since the second half of the 1970s in industrial xylene and ethylbenzene isomerization processes, chiefly for the production of paraxylene. the isomer for which there is the highest demand (Table 2). First, the isomerization of ethylbenzene into xylenes implies a bifunctional acid catalyst. Second. it requires a temperature of around 400°C and hydrogen pressure in the region of 1–1.5 MPa. The catalyst is. therefore. composed of acid mordenite associated with a strong hydrogenation function, supplied by Pt.

Although mordenite is much more active than the former amorphous silica–alumina-based catalysts. it is not fully selective for this application and should progressively be replaced by other high-performance acid zeolites such as that with a 10-membered ring aperture, which was recently developed[50] (Table 2).

The isomerization of xylenes and the dealkylation of ethylbenzene into benzene are other possibilities that have been industrially exploited on a large scale since the mid 1980s. This requires a catalyst that is more effective than mordenite; which is not very active in dealkylation. The best-suited catalyst is undeniably ZSM-5 (Table 2). If this zeolite is used in its purely acid form. the ethylene produced by dealkylation of ethylbenzene at around 350°C is alkylated on another ethylbenzene molecule mainly to form paradiethylbenzene. some of which is produced industrially by this method. In order to avoid the alkylation reaction in the dealkylation of ethylbenzene, it is necessary to operate under hydrogen pressure (~1.5 MPa) and to associate a small amount of Pi to the ZSM-5 zeolite, which hydrogenates the ethylene into ethane as it is produced.

Disproportionation and transalkylation of aromatics

The industrial disproportionation of toluene into benzene and xylenes on an acid zeolite has been performed since the 1970s.[22,45–47,51] At present. it is generally performed on the ZSM-5 zeolite (Table 2), but the practice is not widespread for economic reasons: the price of xylenes is not high enough above that of toluene. Moreover, the conversion of toluene is restricted to less than 50% by thermodynamics. which entails considerable recycling of the nonconverted reactant.

The acid ZSM-5 zeolite can be modified to selectively convert toluene into benzene and paraxylene. which is the least bulky of the xylenes. This modification requires the following: 1) reducing access to the channels by the two other xylenes through a suitable chemical or coking treatment; 2) passivating the external surface of the zeolite: and 3) limiting conversion to around 30%. When xylenes are produced by transalkylation of toluene and C_{9+} polymethylbenzenes, the ZSM-5 zeolite is unsuitable,

because its pores are too narrow for the latter. The acid zeolite most widely used for this application is mordenite (Table 2). associated with a mild hydrogenating function. sulfided Ni for example, which does not hydrogenate the monoaromatics but considerably improves the stability of the catalyst. especially when the feed to be processed contains a large amount of C_{9+}.

Alkylation of aromatics by olefins

The two most important applications in this field are the synthesis of ethylbenzene and cumene, in which zeolites replaced the former liquid HF and $AlCl_3$ catalysts.[22,52,53] These two applications reached the industrial stage in 1976 and the mid 1990s, respectively.

Shape selectivity is not a decisive parameter in achieving good performance, and consequently, acid zeolites with different apertures are used in the various rival industrial processes. For example, the synthesis of ethylbenzene is performed with ZSM-5 zeolites (pore diameter -0.55 nm) (Table 2), MCM-42, Beta (pore diameter $\sim 0.76 \times 0.64$ nm), and USY (pore diameter ~ 0.74 nm) zeolites (Table 2). Moreover. the small size of the pores is a handicap for the ZSM-5 zeolite with an operating temperature that is much higher than that of the other two zeolites, because the molecules diffuse less easily inside the pores. The most important parameter is zeolite acidity, which should be high enough to allow operation in the liquid phase ($T < 300°C$ approximately), which avoids the rapid deactivation associated with operation in the vapor phase.

For cumene synthesis through alkylation of benzene by propylene, four different zeolites are used industrially (Table 2): MCM-22, mordenite, Beta. and Y zeolites. The ZSM-5 zeolite cannot be used because of its restrictive pore size.

Other alkylaromatics synthesis processes are also of interest. The H–ZSM-5 zeolite is used industrially to selectively alkylate ethylene on toluene into paraethyltoluene, which is an intermediate for production of the monomer paramethylstyrene. The selective synthesis of paracymene was considered by selective alkylation of propylene on toluene with the H–ZSM-5 zeolite. Open zeolites (e.g., Y) are catalysts of potential interest for the alkylation of benzene by C_{10}–C_{15} linear olefins, which produce linear alkylbenzenes (LABs) used in manufacturing detergents. Good selectivities for 2.6-dialkylnaphthalene (alkyl = methyl or isopropyl) can be obtained by alkylation of naphthalene by methanol. propylene. or isopropanol on H-mordenite.

Conversion of methanol into C_2–C_4 olefins

This application was discovered in the mid-1980s but was little exploited until the beginning of the twenty-first century.[22,43,44,54] It could prove highly successful in the future due to the increasing demand for light C_2–C_4 olefins. particularly for ethylene and propylene, by the chemical industry. These two olefins, which are kinetically the first two formed from methanol. are rapidly converted into heavier products. particularly aromatics then coke precursors. if their desorption from the zeolite is too slow. Two properties can help to avoid this problem: 1) small pore size to inhibit the forination of heavy products; and 2) low acidity to enable operation at a sufficiently high temperature and hence rapid desorption of the olefins formed. The two most effective zeolites, silica-rich ZSM-5 and especially SAPO-34. at least partly fulfil these conditions (Table 2).

bight olefins interconversion

Some olefinic petroleum cuts produced in steam-cracking or FCC processes can be upgraded by converting their olefins into lighter ones, especially ethylene and propylene, that are sought by the chemical industry. through a complex set of oligomerization–cracking reactions.[▼▼] Olefin selectivity in the process is slightly deteriorated by a secondary reaction of aromatization. But. this latter reaction is limited, through the use of the acid ZSM-5 zeolite as a catalyst, to the production of a C_{5+} cut that principally contains monoaromatics and few polyaromatics.

CONCLUSION

Since zeolites were first used, in the 1950s for adsorption and in 1960 in catalytic applications in refining, they have made a considerable contribution to economic, technical, and scientific progress.[1,55] Their remarkable properties, due to their acidity confined within a restricted space and the small. regular size of their pores, have been largely instrumental in achieving this progress and will continue to be so in the future. The synthetic zeolite market has developed considerably and stood at 1.3 M tons in 1998, with over I M tons for the A zeolite alone: which has an enormous field of application in the detergent industry. In the field of refining, the largest market is for the Y zeolite, with over 150,000 tons produced in 1998. mainly in FCC. Although the tonnages of the other zeolites used are smaller. they are nevertheless important from the economic point of view. In the space of 50 years, the number of known zeolite structures increased significantly, from less than 30 structures identified at the end of the 1950s to over 125 in 2001.[1,55] Many new materials will probably be discovered in the years to come. with the hope of new industrial applications. However. at present, only a dozen

zeolite structures are used in industrial applications or applications with high industrial potential. This low success rate indicates the great difficulties that have to be overcome for an exciting laboratory discovery to become a genuine industrial success. Any application must satisfy a fundamental economic condition — it must be cost-effective and competitive in order to be viable.

ARTICLES OF FURTHER INTEREST

Inclusion Reactions and Polymerization, p. 705
Mesoporous Silica and Silica-Organic Hybrids, p. 852
Mesoporous Materials. p. 845
Organic Zeolites. p. 996
Zeolites: Catalysis, p. 1610
Zeolites: Separation Science, p. 1617
Zeolites: Structures and Inclusion Properties, p. 1623

REFERENCES

1. Rabo. J.A.; Schoonover. M.W. Early discoveries in zeolite chemistry and catalysis at union carbide. and follow-up in industrial catalysis. Appl. Catal.. A: Gen. 2001, *222 (1–2)*. 261–275.
2. Breck, D.W. *Zeolite Molecular Sieves, Structure, Chemistry and Use:* J. Wiley: New York, *1974: 771* pp.
3. *Handbook of Heterogeneous Catalysis;* Ertl. G., Knözinger. H.. Weitkamp. J.. Eds.: Wiley-VCH: Weinheim. FRG. *1997.*
4. Ruthvcn. D.M. *Principles of Adsorption and Adsorption Processes*; Wiley-Intersci. Publ.: New York, *1984.*
5. Basmadjian, D. *Adsorption Drying of Gases and Liquids, Advances in Drying*; Hemisphere Publishing Co.. *1984:* Vol. *3:* 305–357.
6. Carter. J.W. The Adsorption Separation Process. In *Properties and Applications of Zeolites;* Townsend. R.P., Ed.: Special Publication. Chemical Society: London, *1979;* Vol. *33; 79–91*.
7. Tondeur. D. Dual-Step Countercurrent Processes. In *Percolation Processes: Theory and Applications*; Rodrigues, A.E.. Tondeur, D.. Eds.; NATO ASI. Ser. *E.* Sijthoff and Noordhoff, Alphen van Rijn: Holland. *1981:* Vol. *33.* 517–538.
8. De Rosset. A.J.: Neuzil. R.W.; Broughton, D.B. Industrial Applications of Preparative Chromatography. In *Percolation Processes: Theory and Applications;* Rodrigues. A.E.. Tondeur. D.. Eds.; NATO ASI, Ser. E. Sijthoff and Noordhoff. Alphen van Rijn: Holland. *1981:* Vol. *33.* 249–281.
9. Magee, J.S.; Blazek. J.J. Preparation and Performance of Zeolite Cracking Catalysts. In *Zeolite Chemistry cmd Catalysis*; Rabo, J.A.. Ed.: ACS Monograph. American Chemical Society. *1976:* Vol. *171.* 615–679. Chap. 11.
10. Scherzer. J. Correlation Between Catalyst Formulation and Catalytic Properties. In *FCC: Science and Technology:* Magee, J.. Mitchell, M.M., Jr.. Eds.; Stud. Surf. Sci. Catal.. Elsevier, *1993:* Vol. 76. *145–182.* Chap. *5*.
11. Scherzer. J. Octane-enhancing zeolite FCC catalysts: Scientific and technical aspects. Catal. Rev.. Sci. Eng. 1989, *31 (3)*. 215–354.
12. Avidan, A.A. Origin, Development and Scope of FCC Catalysts. In *FCC. Science and Technology:* Magee, J., Mitchell, M.M., Jr., Eds.; Stud. Surf. Sci. Catal., Elsevier, *1993;* Vol. *76: 1–39*. Chap. *1*.
13. Bonifay. R.; Marcilly, C. Catalytic Cracking. In *Petroleum Refining, Vol. 3: Conversion Processes;* Leprince, P., Ed.: Technip Editions, *2001: 169–227*. Chap. *5*.
14. Venuto. P.B.; Habib, E.T. *Fluid Catalytic Cracking with Zeolite Catalysts, Chemical Industries*: Marcel Dekker. Inc.. *1979;* Vol. *1*.
15. Billon. A.; Bigeard. P.H. Hydrocracking. In *Petroleum Refining, Vol. 3: Conversion Processes*: Leprince. P., Ed.: Technip Editions. *2001:* 333–364. Chap. *10.*
16. Scherrer, J.; Gruia. A.J. *Hydrocracking Science and Technology:* Marcel Dekker. Inc., *1996.*
17. Ward, J.W. Upgrading Vacuum Gas Oil by Hydrocracking. In *Catalysts in Petroleum Refining*; Trimm, D.L., et al., Eds.: Stud. Surf. Sci. Catal.. Elsevier Sci. Publ. Co.. *1989;* Vol. *53.* 417–438.
18. Ward. J.W. *Design and Preparation of Hydrocracking Catalysts 111:* Stud. Surf. Sci. Catal.. Elsevier Sci. Publ. Co.. *1983:* Vol. *16,* 587–616.
19. Maxwell. I.E. Zeolite catalysis in hydroprocessing technology. Catal. Today Aug. 1987. *1 (4)*. 385–413.
20. Maxwell. I.E.: Minderhoud. J.K.: Stork. W.H.J.; van Veen, J.A.R. Hydrocracking and Catalytic Dewaxing. In *Handbook of Heterogeneous Catalysis:* Ertl. G., Knozinger. H., Weitkamp. J.. Eds.: Wiley-VCH: Weinheim. FRG, *1997;* Vol. *4.* 2017–2038. Chap. *3*.
21. Law, D.V. Hydrocracking: Past, present and future. Pet. Technol. Q. Winter 200012001. *55–63.*
22. Chen. N.Y.: Garwood, *W.E.:* Dwyer, F.G. *Shape Selective Catalysis in Industrial Applications, Chemical Industries;* Marcel Dekker. Inc., *1979;* Vol. *36.*
23. Miller. S.J. Studies on Wax Isomerization for Lubes and Fuels. In *Zeolites and Related Microporous Materials, State of the Art;* Weitkamp, J.. Karge, H.G.. Pfeifer, H., Holderich, W.. Eds.: Stud. Surf. Sci. Catal.. Elsevier: Amsterdam. *1994:* Vol. *84.* 2319–2326.
24. Angevine, P.J.: Buyan, F.M.; Pappal. D.A.: Partridge, R.D. In *MIDW—A New Dewaxing Process,* AIChE *1996* Spring Natl. Meet.. New Orleans, LA. USA, Feb. *25–29-1996.* paper 57d. *20* pp.
25. Sie, S.T. Isomerization Reactions. In *Handbook of Heterogeneous Catalysis*; Ertl, G., Knozinger. H., Weitkamp, J., Eds.: Wiley-VCH: Weinheim, FRG. *1997;* Vol. *4,* 1998–2017. Chap. *3*.
26. Gosling. C.; Shimizu, T.: Imai, T.: Rosin, R.: Bullen, P. Re\amp opportunities for isomerisation units. Pet. Technol. Q. Winker 1997198. *2 (4).55–59.*
27. Duchet. J.C.; Guillaume, D.; Monnier. A.: van Gestel. J.: Szabo, G.: Nascimento. P.; Decker. S. In *Isomerization of n-Hexane over Sulfated Zirconiu: Influence of Hydrogen*

and Platinum. Symp. on Paraffin and Olefin Isomer.. 218th A.C.S. Natl. Meet., Div. Pets. Chein.. New Orleans. LA. Aug. 22–26: ACS Publ. 1999: 425–429.
28. Duchet, J.C.: Guillaume. D.: Monnier, A.; van Gestel. J.; Szabo. C.: Nascimento. P.: Decker, S. Mechanism for isomerization of *n*-hexane over sulfated zirconia: Role of hydrogen. Chem. Commun. 1999. 1819–1820.
29. Corma. A.; Martinez. A. Chemistry, catalysts, and processes for isoparaffin olefin alkylation: Actual situation and future trends. Catal. Rev.. Sci. Eng. 1993. *35* (4). 483–570.
30. Weitkamp, J.; Traa. Y. Alkylation of Isobutane with Alkenes on Solid Catalysts. In *Handbook* of *Heterogeneous* Catalysis: Ertl. G., Knozinger, H.. Weitkamp. J.. Eds.; Wiley-VCH: Weinheim. FRG. 1997; Vol. 4. 2039–2069. Chap. 3.
31. Hommeltoft. S.I. Isobutane alkylation, recent developments and future perspectives. Appl. Cata.. A: Cen. 30 Nov. 2001, 221 (1–2), 421–428.
32. Peferoen. D.G.R.: Gilson. J.P.: Sie. S.T.: De Jong. K.P.: Stork (Shell). W.H.J. Process for Upgrading a Paraffinic Feedstock. EP 565197 A1. 1993.
33. Van Broekhoven, E.H.: Mas Cabre. F.R.: Bogaard, P.: Klaver. G.; Vonhof (Akzo Nobel), M. Process for Alkylating Hydrocarbons. US Patent No. 5.986.158 A1. 1999.
34. Bezukhanova. C.; Cuidot. J.: Barthomeuf. D.: Breysse. M.; Bernard. J.R. Platinurn–zeolite interactions in alkaline L zeolites (correlations between catalytic activity and platinum state). J. Chem. Soc., Faradaq· Trans., 1 1981. 77. 1595–1604.
35. Tamn. P.W.; Mohr. D.H.: Wilson. C.R. Octane Enhancement by Selective Reforming of Light Paraffins. In *Catalysis*; Ward. J.W.. Ed.: Stud. Surf. Sci. Catal., Elsevier. 1988; Vol. 38. 335–353.
36. Sivasanker. S.: Ratnasamy. P. Reforming for Gasoline and Aromatics. Recent Developments. In *Catalytic Naphta Reforming*. Science and Technology: Antos. G.J.. Aitani. A.M.. Parera. J.M.. Eds.: Marcel Dekker, Inc.: New York. 1995: 483–507. Chap. 15.
37. O'Connor. C.T. Aromatization of Light Alkanes. In *Handbook of Heterogeneous* Catalysis: Ertl. G., Knözinger. H.. Weitkamp. J.. Eds.: Wiley-VCH: Weinheim, FRG. 1997: Vol. 4. 2069–2074. Chap. 3.
38. Butler. A.C.: Nicolaides. C.P. Catalytic skeletal isomerization of linear butenes to isobutenes. Catal. Today 1993. 18. 443–471.
39. Houzvicka. J.: Ponec. V. Skeletal isomerization of *n*-butene. Catal. Rev., Sci. Eng. 1997. 39 (4). 319–344.
40. Mooiweer, H.H.: de Jong. K.P.: Kraushaar-Czarnetzki. B.: Storck. W.H.J.: Krutzen. B.C.H. Skeletal Isomerization of Olefins with the Zeolite Ferrierite as Catalyst. In Zeolites *and Related Microporous* Materials: State *of the Art* 1994; Weitkamp. J.. Karge. H.G.. Pfeifer. H., Hölderich. W.. Eds.: Stud. Surf. Sci. Catal.. Elsevier, 1994: Vol. 84. 2327–2334.
41. Grandvallet. P.; de Jong, K.P.; Krijn, P.: Mooiweer (Shell), H.H. Process for the Conversion of Feedstock Comprising Linear Olefins. Eur. Pat. Appl. EP 501.577. Feb. 1991.
42. Degnan. T.F. Applications of zeolites in petroleurn refining. Top. Catal. 2000. 13. 349–356.
43. Chang. C.D. Methanol to Hydrocarbons. In *Handbook of Heterogeneous* Catalysis; Ertl. G., Knozinger, H., Weitkamp. J., Eds.; Wiley-VCH: Weinheim, FRG. 1997: Vol. 4. 1894–1908. Chap. 3.
44. Chang. C.D. The Methanol-to-Hydrocarbons Reaction: A Mechanical Perspective. In *Shape* Selective *Catalysis, Chemicals Synthesis and* Hydrocarbon *Processing*; Song. C., Garcés, J.M., Sugi, Y.. Eds.; ACS Symp. Series. American Chemical Society, 1999; Vol. 738. 96–114. Chap. 7.
45. Beck. J.S.; Haag. W.O. Isomerization and Transalkylation of Alkylaromatics. In *Handbook* of *Heterogeneous Catalysis*; Ertl. G., Knozinger. H.. Weitkamp. J.. Eds.: Wiley-VCH: Weinheim, FRG. 1997: Vol. 5, 2136–2139. Chap. 4.
46. Guisnet, M. Procédés sélectifs et propres de production d'alkylaromatiques sur zéolithes. Actual. Chim.. Avril 1998. 4. 9–15.
47. Alario. F.: Barraqué, M.; Marcilly. C. Traitement des essences aromatiques pour la pétrochimie. Tech. Ing. 1997. *J 5* 920. 1–12.
48. Ransley. D.L. Xylenes and Ethylbenzene. In *Kirk–Othmer—Encyclopedia* of Chemical *Technology*, 3rd Ed.: Wiley-Interscience: New York. 1984: Vol. 24. 709–744.
49. John, H.H.: Neubauer, H.D.; Birke. P. Zeolite-containing-catalysts for the conversion of C_8 aromatics fractions. Catal. Today 1999. 49. 211–220.
50. Marcilly. C. Where and how shape selectivity of molecular sieves operates in refining and petrochemicals catalytic processes. Top. Catal. 2000. 13. 357–366.
51. Tsai, T.C.; Liu. S.B.: Wang, I. Disproportionation and transalkylation of alkylbenzenes over zeolite catalysts. Appl. Catal., A: Gen. 1999. *181*, 355–398.
52. Beck. J.S.: Haag. W.O. Alkylation of Aromatics. In *Handbook of Heterogeneous Catalysis*; Ertl. G.. Knözinger, H., Weitkamp. J.. Eds.; Wiley-VCH: Weinheim, FRG. 1997: Vol. 5. 2123–2136. Chap. 4.
53. Degnan, T.F.: Morris Smith. C.: Venkat. C.R. Alkylation of aromatics with ethylene and propylene: Recent developments in cominercial processes. Appl. Catal.. A: Gen. 30 Nov. 2001, 221 (1–2). 283–294.
54. Inui. T. Highly Selective Synthesis of Light Olefins from Methanol Using Metal-Incorporated Silicoaluminophosphate Catalysts. In *Shape Selective Catalysis, Chemicals Synthesis* and Hydrocarbon Processing; Song, C.. Garcés. J.M., Sugi, Y., Eds.: ACS Symp. Series. 1999: Vol. 738. 115–127. Chap. 8.
55. Marcilly. C. Evolution of Refining and Petrochemicals. What is the Place of Zeolites. In Zeolites *and Mesoporous Materials* at the *Dawn of* the *21st Century*; Stud. Surf. Sci. Catal.. Elsevier, 2001: Vol. 135. 37–60.

Zeolites: Catalysis

Takashi Tatsumi
Yokohama National University, Yokohama, Japan

INTRODUCTION

Zeolites and related microporous materials offer abundant chemical diversity. Over the past three decades. many new synthetic zeolites have been discovered. The Structure Commission of The International Zeolite Association have approved 145 framework types (November 2003). In addition. there are numerous other zeolites with structures that are not yet known or are only hypothetical. The goals of this article are to briefly mention the main categories and principal industrial uses of zeolites, before providing more detailed discussions of molecular sieving and redox reactions.

CLASSIFICATION

Zeolites are crystalline aluminosilicates with the structural formula $M_{x/n}(AlO_2)_x(SiO_2)_y$, where n is the valence of cation M, $x+y$ is the total number of tetrahedra per unit cell. and y/x is the Si/Al atomic ratio varying from a minimum value of 1 to infinite. Catalytic processes involve diffusion of molecules into the zeolite pores, only pores with a minimum of eight-membered oxygen ring (8-MR) apertures (eight tetrahedral and eight O atoms) are generally considered. Zeolites are usually classified into three categories: smail-pore zeolites with 8-MR apertures having free diameters of 0.30–0.45 nm; medium-pore zeolites with 10-MR apertures, 0.45–0.60 nm in free diameter: and large pore with 12-MR with free diameter 0.60–0.75 nm. The catalytic properties of zeolites can vary considerably by modifying them during or after the actual synthesis. The types of catalysis of zeolites can be roughly classified into four groups:

- Acid catalysis.
- Hydrogenation/acid bifunctional catalysis.
- Base catalysis.
- Redox catalysis.

INDUSTRIAL APPLICATIONS

Although there are I45 confirmed zeolite framework types, only a dozen zeolites and their modifications are used for industrial catalytic processes. Listed in Table 1 are the important industrial processes using zeolites as catalysts.

CATALYSIS

Among the primary tasks of catalysis of zeolites, the most important is shape-selective catalysis, which is the molecular-sieving function in action during a catalytic reaction that distinguishes between the reactants, the products, or the transition state species in terms of the relative sizes of the molecules and the pore space in which the reaction occurs. Over 40 years ago, Weisz and Frilette (1960) of Mobil Research Laboratories coined the term "shape-selective catalysis" to describe the then unexpected catalytic behavior of synthetic crystalline molecular-sieve zeolites. They found that the calcium ion exchanged zeolite A, having pore sizes of 4–5 Å selectively cracked straight-chain *n*-paraffins exclusively to straight-chain products. This is accounted for by the molecular sieving effect; branched-chain paraffins are too large to enter the pores of zeolite A. whereas straight-chain paraffins fit.

Shape Selective Catalysis

Since then, great strides have been made in the understanding and the use of shape-selective catalysis in commercial catalytic processes. Their applications have expanded well beyond the boundaries of traditional petroleum refining to petrochemical and fine chemicals manufacturing. Meanwhile. many new synthetic zeolites have been discovered; of particular importance was the discovery of the synthetic medium-pore zeolites (Table 1), having pore sizes of 5–6 Å (0.5–0.6 nm), which meet the industrial need for selective catalysts. Mobil produced ZSM-5, commercialized new petroleum refining and petrochemical processes. based on this zeolite, and the ZSM-5 catalyzed methanol-to-gasoline (MTG) processes attracted worldwide attention. Since the 1980s shape-selective catalysis has extended from the medium-pore zeolites to several large-pore zeolites, including zeolite L and zeolite β. A titanium-containing zeolite, TS-I. a novel derivative of ZSM-5, was first synthesized by the

Encyclopedia of Supramolecular Chemistry
DOI: 10.1081/E-ESMC 120012861

Table 1 Industrial processes using zeolite catalysts

Zeolite catalyst (framework code name)	*Process*
Large-pore zeolites (12-membered oxygen ring)	
Ultrastable H–Y and Rare-earth-Y (FAU)	Cracking of vacuum distillates and residues
Pt–Pd–H–Y (FAU)	Hydrocracking of vacuum gas oils
H-mordenite (MOR)	Transalkylation of aromatics: dimethylamine synthesis
Pt–H-mordenite (MOR)	Hydroisomerization of light gasoline: xylene isomerization
H–β (BEA)	Benzene alkylation (C_2, C_3); aromatics acylation
Pt–K–L (LTL)	Hexane aromatization
Medium-pore zeolites (10-membered oxygen ring)	
H-ZSM-5 (MFI)	Methanol to gasoline: toluene disproportionation: dewaxing: xylene isomerization: cyclohexene hydration
Silicalite-1 (MFI)	Beckmann rearrangement
GaMFI (MFI)	LPG to BTX
Pb-ZSM-5 (MFI)	Synthesis of pyridines from aldehydes and NH_3
TS-I (MFI)	Phenol oxidation; oxime synthesis; epoxidation
Fe-ZSM-5 (MFI)	Synthesis of phenol from benzene and N_2O
H-MCM-22 (MWW)	Benzene alkylation (ethylene. propylene)
H-ferrierite (FER)	Light olefins (C_4, C_5) isomerization
Small-pore zeolites (eight-membered oxygen ring)	
Ni-erionite (ERI)	Enhancement of light gasoline Octane No
SAPO-34 (CHA)	Methanol to olefin
H-rho (RHO)	Dimethylamine synthesis

researchers at ENI of Italy through the isomorphous substitution of titanium for silicon in ZSM-5 (Taramasso et al., 1983). A remarkable class of reactions having industrial importance was developed utilizing H_2O_2 as the oxidant.

The phenomenon of shape-selective catalysis is almost limited to the heterogeneously catalyzed reactions over zeolites and zeolite-related microporous solids. In a simplified manner, shape-selective catalysis can be described as the combination of catalysis with the molecular sieve effect. Shape selectivity effects can be produced if the sizes and shape of reactants, of products, of transition states. or of reaction intermediates are similar to the dimensions of pores and cavities of the zeolite. The zeolites contain intracrystalline pores and apertures having dimensions approximately equal to those of many of the molecules converted in catalytic processes, and they are classified according to the sizes of their apertures (Table 1). The number of oxygen atoms in the aperture of each molecular sieve[8,10,12] is shown in the table. There are also ultralarge-pore zeolites with apertures consisting of more than 12 oxygens. The aperture dimension ranges from about 0.4 nm to nearly 1 nm. The size of the aperture is also dependent on the size and number of the nearby cations. which may partially block it. The shape selectivity is also affected by the structure inside apertures: many zeolites have cavities (supercages) with internal dimensions that are larger than those of the apertures. Transition-state shape-selectivity is often governed by the sizes of these cavities. Recently, a variety of mesoporous molecular sieves such as MCM-41 and SBA-15 with apertures in the range of 2–20 nm have been synthesized and thus expected to be useful in converting large molecules such as those contained in heavy fractions of petroleum and fine chemicals intermediates.

Shape-selective catalysis is not limited to the use of the molecular sieve. There are many applications that involve transition metal species that are supported inside or synthesized inside the cages or pores channels of molecular sieves ("ship-in-a-bottle") that can be used for catalyzing many selective reactions, such as hydrogenation and oxidation.

Acid Catalysis

Zeolite catalysts are mainly used for a number of important acid-catalyzed reactions. Synthetic zeolites were developed for fluid catalytic cracking (FCC) in the early 1960s. This reaction occurs via carbonium ion intermediates and is. therefore. catalyzed by Brønsted acids. These sites normally consist of protons attached to bridging framework oxygen atoms and are introduced into the zeolite via ion exchange.

In general: zeolite synthesis yields the form neutralized by sodium ions. Usually, this is also the case if template molecules (structure-directing agents) are used; the

template removal step is followed by removal of Na^+ by ion-exchange techniques. However, many of the crystalline zeolites decompose when treated with strong acids. Therefore. the most effective and gentle methods for converting the sodium forms into the hydrogen forms involve exchange of the cation by ammonium from an aqueous solution of ammonium salt. Subsequent thermal treatment of the ammonium-exchanged zeolites results in the liberation of NH_3 and the formation of the proton (acidic) form of the zeolites (Eq. 1):

$$NH_4^+\{\text{zeolite}\} \rightarrow NH_3(g) + H^+\{\text{zeolite}\} \quad (1)$$

Thus. ideally. the total number of acid sites is equal to the total number of Al atoms on framework tetrahedral (T) sites. Because the acidity of zeolites is adversely affected by a small amount of residual Na^+, Na^+ must be exhaustively removed in order to obtain a highly active solid acid catalyst. Removal of Na^+ from zeolites usually requires repeated ion-exchange steps combined with calcination. in the temperature range of 823–1050 K. Only about 70% of the Na^+ ions are replaced by NH_4 ions during the first exchange. It is assumed that as a result of calcination Na^+ atoms. which were not accessible for ion exchange, are redistributed over the zeolite surface and made accessible. Simultaneously, solid-state reactions occur in the zeolite, and framework aluminum is removed. This phenomenon results in stabilization of the zeolite structure: the acid forms of low-silica zeolites are inherently unstable.

Although the enormous potential of zeolite Y as a cracking catalyst was recognized early. its low stability was a serious drawback to practical use. Therefore, efforts were made to develop techniques to enhance the thermal and hydrothermal stabilities of zeolite Y by increasing the Si/Al of the framework. During the dealumination treatment, pores with a diameter of ca. 20 nm are formed in the zeolite grains. The mesopores emerge when parts of the structure collapse, which is associated with removal of framework Al, leaving extra-framework Si as well as extra-framework Al. The mesoporous structure of the Y zeolites should be advantageous for use as an FCC catalyst; because the diffusivity of the feedstocks in the catalyst will be increased.

Hydrogen forms can be prepared in different ways. In general, zeolites with a Si/Al ratio of 5 or higher are resistant to acids. Direct treatment of high-silica zeolites with strong acids results in the progressive replacement of the cation by the hydronium ion. For mordenite, for example, this reaction is illustrated by the following reaction:

$$Na_8[(AlO_2)_8(SiO_2)_{40}].24H_2O + n\ H_3O^+ \rightarrow Na_{8-n}(H_3O)_n[(AlO_2)_8(SiO_2)_{40}].m\ H_2O + n\ Na^+ + (24 - m)H_2O \quad (2)$$

Replacement of all the original cations by the hydronium ions is possible. However. dealumination, removal of aluminum from the lattice, occurs to a certain extent. which is an unavoidable side effect.

Heating at high temperatures removes water from the Brønsted acid site, exposing a threefold coordinated Al ion, which has Lewis acid character. A reaction scheme for the formation of these sites is shown in Fig. 1,

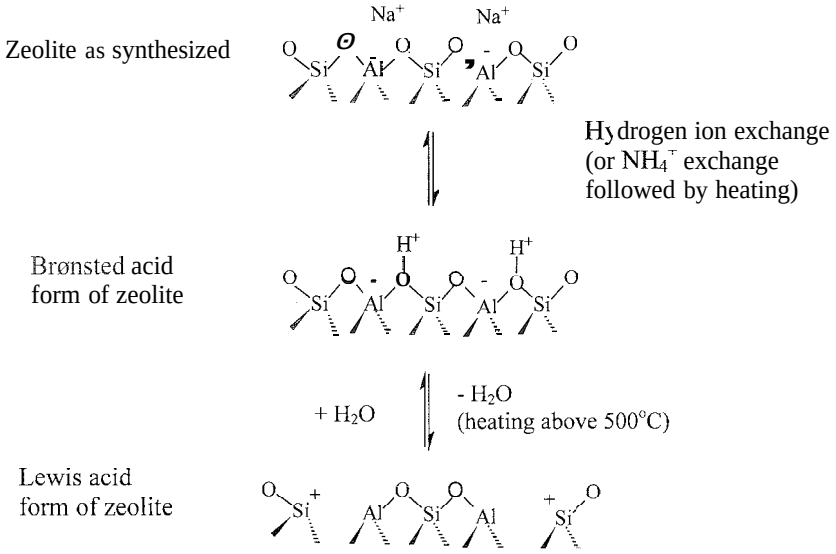

Fig. 1 Generation of Lewis and Brønsted acid sites in zeolites.

Table 2 Acid-form zeolites classified by their Si/Al ratios

Si/Al atomic ratio	*Zeolites*	*Properties*
Low (1–1.5)	*A*, X	Relatively low stability of framework: low stability in acid: high stability in base; and high concentration of acid groups with moderate acid strength
Intermediate (2–5)	Erionite, chabazite, clinoptilolite, mordenite, Y	
High (−10− x)	ZSM-5, erionite," β, MCM-22, mordenite,[a] Y[a]	Relatively high stability of framework: high stability in acid; low stability in base: low concentration of acid groups with high acid strength

"Formed by chemical framework modification (dealurnination): the Al is partially removed by treatment with steam or $SiCl_4$ at high temperatures.

although the structure of the Lewis acid is still a controversial issue.

The surfaces of zeolites can thus display Brønsted or Lewis acid sites or a combination of the two, depending on how the zeolite is prepared. Brønsted acid sites are converted into Lewis acid sites as the temperature is increased above approximately 500°C and water is driven off. The overall catalytic activity of zeolites as solid acids depends on the number and the properties of the acid site. The strength of the acid sites is directly related to the framework composition of the zeolite. Zeolites with low Si/Al ratios can have higher concentrations of catalytic sites. and zeolites with high Si/Al ratios show strong acidity. Their classifications are shown in Table 2. An H-Y or H-ZSM-5 zeolite with a low density of acid groups is like an ideal solution of dispersed noninteracting protons in a solid matrix.

Elements other than hydrogen are introduced into the zeolites by means of ion exchange in order to enhance catalytic activity. By polyvalent ion exchange followed by calcination. the zeolite is changed into the protic form:

$$M(H_2O)^{n+}Z \xrightarrow[(M = Ca\ \text{Rare earth elements, etc})]{} M(OH)^{(n-1)+}Z + H^+Z \quad (3)$$

The first generation of zeolite FCC catalyst involved the use of zeolite Y exchanged with trivalent rare earth ions and was activated by calcination according to Eq. 3.

There are other transitions in properties exemplified by the acid-form zeolites (those incorporating H^+ as the exchangeable ion). The zeolites with high concentrations of H^+ are hydrophilic, having strong affinities for polar molecules small enough to enter the pores. The zeolites with low H^+ concentrations (in the limit, silicalite-I (MFI), for example) are hydrophobic. taking up organic compounds from water–organic mixtures; the transition occurs at a Si/Al ratio near 10. The stability of the crystal framework also increases with increasing Si/Al ratios: decomposition temperatures of the different zeolites range from roughly 700–1300°C. Zeolites with high Si/Al ratios are stable in the presence of concentrated acids, but those with low Si/Al ratios are not; the trend is reversed for basic solutions.

Because of the need to develop new environmentally benign catalytic reaction processes. zeolites will continue to be applied. and their use will further diversify into various branches of chemicals synthesis and hydrocarbon processing. As catalysts, they offer less or no corrosion, little waste, are ready adaptation to continuous processes, exhibit high thermal stability, etc. These properties make zeolites the environmentally friendly catalysts, which could contribute to sustainability of the world. For example, acid zeolite catalysts could be substituted for highly corrosive and polluting acids such as $AlCl_3$, H_2SO_4, H_3PO_4, and HF. There are many reactions that utilize zeoites as a catalyst in clean synthesis processes. such as alkylation, catalytic cracking, aromatization, alcohol dehydration, rearrangements, base-catalyzed reactions, and oxidation, including ammoximation and epoxidation. There are only a few examples of industrial applications of zeolites to the syntheses of fine chemicals. such as pharmaceuticals, fragrances, liquid crystals, etc.: fine chemicals synthesis is mostly carried out in noncatalytic conventional ways through processes with poor atom economy or low E-factor, so often inefficient in reducing wastes. The application of zeolites catalysts to the fine chemicals synthesis is being developed.

Bifunctional Catalysis

Bifunctional (metallic and acidic functions) catalysts are applied to a variety of oil-refining and petrochemical processes. For example, paraffin hydroisomerization involves *n*-paraffins dehydrogenation to a-olefins over metal, skeletal isomerization of *n*-olefins to isoolefins over acidic sites. followed by hydrogenation of isoolefins to isoparaffins over metal. Zeolite-supposted noble metal catalysts are often used for these types of reactions, which

are conveniently prepared by ion exchange using an aqueous solution of a cationic metal complex. For platinum and palladium. $[Pt(NH_3)_4]^{2+}$ and $[Pd(NH_3)_4]^{2+}$ are used, respectively. The ion-exchanged product is then reduced in a stream of hydrogen to produce small metal particles inside the zeolite pores, ideally. This reduction is accompanied by formation of the Brønsted acid sites:

$$[M(NH_3)_4]^{2+}Z + H_2 \rightarrow M + 4NH_3 + (H^+)_2Z(M = Pt \text{ or } Pd) \quad (4)$$

If acidic activity is undesirable, the acid sites thus formed must be neutralized before catalytic use.

Because of the cost of noble metal. the inetal loading should be low. and the inetal must be well dispersed to make the exposed metal surface as high as possible. Each type of metal complex, the conditions for ion exchange, the calcination procedure. and the reduction conditions have profound effects on the dispersion of the metal.

Coordination Chemistry in Zeolites

Research on coordination chemistry in zeolites started in the 1970s. A metal complex of the appropriate dimensions can be encapsulated in a zeolite. being viewed as a bridge between homogeneous and heterogeneous systems. Complexes that are smaller than the free diameters of the channels and windows have access to the cavities. On the other band, complexes that are larger than the diameters of the windows must be synthesized in situ, namely, by adsorption of the ligands into the zeolites containing transition metal ions or by synthesis of the ligands in those zeolites. Herron et al. first referred to such zeolite guest molecules as "ship-in-a-bottle" complexes. Since the first report on the synthesis of a metal phthalocyanine inside zeolite Na^+-Y in 1977. numerous examples of encapsulation of metal phthalocyanine complexes have been discovered. Related porphyrin and N,N′-*bis*-(salicylidene)ethylenediimine (SALEN) complexes have been trapped in a zeolite cavity with restricted apertures. These are typical examples of ship-in-a-bottle complexes and are given names such as zeozymes and inorganic proteins in regard to their biomimetic chemistry, e.g., as a model for dioxygen binding and oxygenase.

Bass Catalysis

In zeolite catalysis. emphasis has been placed on the reactions catalyzed by acids. However. complete ion exchange with alkali metal cations such as K^+, Rb^+, and Cs^+ would allow for the preparation of weakly basic zeolites. Oxide ligands as counteranions of these alkali metal cations act as basic sites. Their basicity depends on the fractional negative charge they bear and, therefore, the composition of the zeolite, which can be quantified by the intermediate Sanderson electronegativity, S_{int}. It is also dependent on structural parameters such as bond length, bond angles, and Al distribution.

Redox Catalysis

For catalyzing redox reactions: one can introduce transition-metal active sites into the framework of zeolites. In current epoxidation processes: chlorine. hydroperoxides, and peracids are most commonly used as oxidants. Organic and inorganic compounds are coproduced in the reaction, which need to be recycled or disposed of. In the chlorohydrin route, generally preferred in the epoxidation of C_3 and higher olefins, stoichiometric amounts of sodium or calcium chlorides are produced by the dehydrohalogenation of intermediate chlorohydrins. Chlorinated organic by-products. such as halogen ethers and dichlorides. are formed as well in the process, further increasing the quantity of waste. A major breakthrough was the discovery that titanium silicate could be used as an efficient epoxidation catalyst with hydrogen peroxide as an oxidant. The reaction with TS-1 may be performed under mild conditions; for example, at room temperature in dilute aqueous or methanolic solution. Direct use of hydrogen peroxide is a more attractive epoxidation route based on ease and cleanliness of the process. The active oxygen content H_2O_2, 47 wt % (16/34), is much higher than that of organic peracids and hydroperoxides: water is the only co-product. Ti-silicalite catalyzes, besides epoxidation reactions, a broad range of oxidation reactions. with hydrogen peroxide as the oxidant, as shown in Table 3.

The most widely accepted mechanism for TS-1 catalyzed epoxidation is the peracid-like mechanism, which

Table 3 Catalytic chemistry with Ti-silicates

Substrate	Product
Olefins	Epoxides
Olefins and methanol	Glycol monomethyl ethers
Diolefins	Monoepoxides
Phenol	Hydroquinone and catechol
Benzene	Phenol
Paraffins	Alcohols and ketones
Primary alcohols	Aldehydes
Secondary alcohols	Ketones
Ammoximation of cyclohexanone	Oximes
N,*N*-Dialkylamines	*N*,*N*-Dialkylhydroxylamines
Thioethers	Sulfoxides

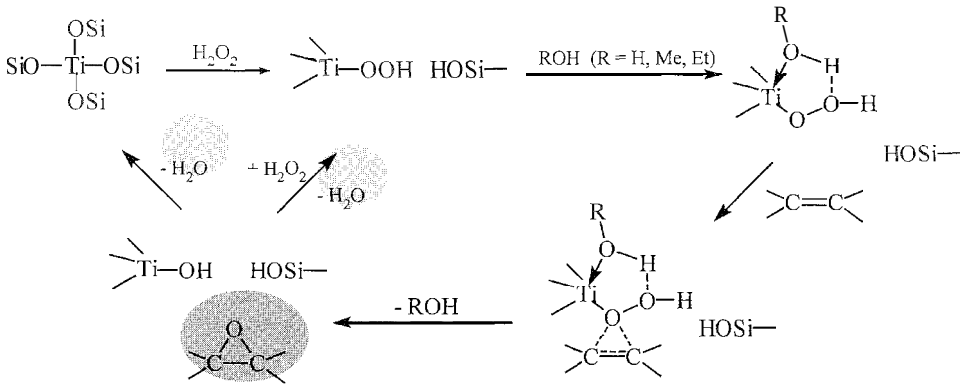

Scheme 1. Mechanisms of epoxidation on titanosilicates. (*View this art in color at www.dekker.com.*)

involves a hydroperoxo rather than a peroxo species, and coordination of an alcohol or water molecule to the site (Scheme 1). Ti seems to be isomorphously substituted for Si in the zeolite framework in tetrahedral coordination. This site is much more resistant to hydrolysis compared to titanium species on amorphous silica. A key characteristic of these materials is their relatively high hydrophobicity, resulting in the favorable adsorption of alkanes and other hydrocarbons. Thus. the low concentration of hydrogen peroxide present at all times in the catalyst results in its efficient use. The strong hydrophobicity also enables fast desorption of the product. Therefore. oxidations can occur up to high conversions with high H_2O_2 selectivities and high efficiencies.

The structure of TS-1 prevents all compounds with cross sections larger than ca. 0.55 nm from diffusing inside TS-1 channels and, therefore. from reacting or interfering with reactions occurring at Ti-sites. Although the discovery of TS-1 is a milestone in zeolite catalysis. the smaller pore size of the zeolite-type framework restricts its use, even for small molecules such as simple cyclic alkenes. Thus, new materials with various pore sizes are always sought. Ti-β and Ti-MWW (MCM-22) proved to be promising catalysts for similar oxidation reactions of larger substrates.

It was recently discovered that Sn-β catalyzes the Baeyer–Villiger oxidation of cyclic ketones to lactones without using peracids but using H_2O_2.

Pollution Abatement

The application of zeolite catalysts to pollution abatement is also promising. The main pollutants in gaseous emissions that can be potentially treated by zeolites are volatile organic compounds (VOCs) and NOx.

The treatments of VOCs by zeolite materials consist of adsorption/separation and catalytic oxidation. Although the VOCs adsorbed by zeolite are often recovered, at low VOCs concentrations, adsorption is followed by catalytic oxidation or incineration. Catalytic combustion is an efficient way to remove of VOCs. Zeolite-supported catalysts are favorable for VOC abatement, because they offer high selectivity to deep oxidation to CO_2 resulting from the highly developed microporosity. Both noble metals and base metals supported on zeolite catalysts can be used. Noble metals are preferable to base metals when VOCs do not contain chlorine or bromine atoms. Pd-zeolite such as Y(FAU) is most active for the combustion of hydrocarbons. One of the least combustible hydrocarbons is methane, which is widely used as a fuel, and emission of methane as a greenhouse gas must be controlled.

Zeolite catalysts constitute the best available technologies for reducing NOx and N_2O emissions from industrial activities. Emission levels of N_2O must be regulated. There are two types of N_2O emissions. Zeolites are not suitable for the simple abatement of highly concentrated N_2O (20–40%) gas discharged from adipic acid plants. However. direct oxidation of benzene to phenol was industrialized by using N_2O as an oxidant and Fe-MFI zeolites (AlphOx process). The treatments with N_2O of a low concentration remain challenging. Fe-exchanged zeolites show high activities in the catalytic decomposition of N_2O to N_2 and O_2, and the catalytic reduction of N_2O with reductants such as NH_3, CO, and H_2. Despite intensive work in the catalytic decomposition of NO. even the most promising system. Cu-MFI, is subject to poisoning by O_2, water, and SO_2, is efficient only at low space velocities. and has unsatisfactory catalyst activity. The selective catalytic reduction of NOx with hydrocarbons over zeolite-based catalysts has been widely investigated. This could be the best technology with which to achieve efficient NOx removal from off-gas emitted from power plants, stationary diesel engines, marine vessels; etc.

CONCLUSION

Zeolites are crystalline aluminosilicates and metallosilicates with distinct structures. The relationships between active site properties and chemical composition are more established than for analogous amorphous materials. Moreover. the structural diversity of zeolites is wide and still expanding. Zeolites can be industrially used not only for acid-catalyzed and bifunctional (metal–acid) processes but also for oxidation processes. Zeolite catalysts were mainly developed in the petroleum-refining and petrochemical industries; however. application of zeolite catalysts to fine chemicals synthesis is being developed, leading to the replacement of conventional noncatalytic processes or highly polluting processes with more environmentally friendly systems. To achieve these objectives. rational design of zeolite-based catalysts and methods for tailoring and fine-tuning zeolite catalysts, including control of active site arrangement, crystallite size. provision of mesoporosity. etc., as well as elaborate reaction engineering will be vitally important.

ARTICLES OF FURTHER INTEREST

Channel Inclusion Compounds, p. 223
Crystalline Microporous Silicas. p. 380
Inclusion Compounds: Selectivity, Thermal Stability, and Kinetics, p. 696
Inclusion Reactions and Polymerization, p. 705
Mesoporous Materials. p. 845
Mesoporous Silica and Silica–Organic Hybrids, p. 852
Mineralomimetic Structures, p. 868
Organic Zeolites. p. 996
Swelling Clays (Smectites) and Nanofilms, p. 1478
Zeolites in the Petroleum Industrv. p. 1599
Zeolites: Separation Scierzce, p. 1617
Zeolites: Structures and Inclusion Propel-ties, p. 1623

REFERENCES

1. *Introduction to Zeolite Science and Practice:\an* Bekkum, *H., Flanigen. E.M.. Jacobs, P.A., Jansen, J.C.. Eds.; Elsevier: Amsterdam.* 2001.
2. *Gates. B.C. Catalytic Chemistry*; *Wiley:* New *York. 1992.*
3. *Catalysis and Zeolites: Weitkarnp, J.*. Puppe, *L.. Eds.; Springer: Berlin, 1999.*
4. *Handbook of Porous Solids*: *Schueth. F., Sing. K.S.W.. Weitkamp. J.. Eds.: VCH: Weinheim,* 2002: *Vol. 4.*
5. *Zeolites for Cleaner Technologies: Guisnet, M.. Gilson. J.–P., Eds.:* Imperial *College Press: London.* 2002.
6. Corma. *A. Chern. Rev*. 1995. *95.* 559.
7. *Chen, N.Y.;* Garwood. *W.E.; Dwyer. F.G. Shape Selective Catalysis in Industrial Applications, 2nd Ed.; Marcel Dekker: New York, 1996.*
8. *Martens, J.A.;* Souveijns, *W.; van Rhyn, W.; Jacobs, P.A. Handbook of Heterogeneous Catalysis; Boudart,* M., *Ertl, G., Knozinger, H., Weitkamp, J.. Eds.: VCH:* Weinheim. *1997: Vol. 1.* 324.
9. *Shape-Selective Catalysis Chemicals Synthesis and Hydrocarbon Processing: Song,* C., Garcés, J.M., *Sugi. Y.. Eds.: American Chemical Society: Washington. DC.* 2000.
10. *Notari. B. Adv. Catal.* 1996, *41,* 253.
11. *Bellussi,* G.; *Peregp. C. Handbook of Heterogeneous Catalysis: Boudart.* M., *Ertl, G., Knozinger, H.*. Weitkamp, J., *Eds.; VCH: Weinheim. 1997: Vol.* 4, 2334.

Zeolites: Separation Science

Toshinori Tsuru
Yuko Takata
Hiroshima University, Higashi-Hiroshima, Japan

INTRODUCTION

Zeolites are used as detergent builders, adsorbents, and catalysts. In the past decade, we saw the development of a variety of zeoiite membranes, and a number of investigators reported on the preparation of such membranes and their applications to a variety of separation systems. These research activities are motivated by features common to inorganic membranes. such as thermal resistance and resistance to organic solvents, and features unique to zeolite materials. such as molecular sieving, selective adsorption, and catalytic activity.[1] In this article, the discussion will be restricted to zeolite membranes for use in separation and catalysis. First, an overview is presented on recent progress in zeolite membranes. followed by a discussion of our research activities.

ZEOLITE MEMBRANES—PREPARATION AND APPLICATION FOR SEPARATION AND REACTION

Zeolite membranes, which have been successfully prepared and applied to separations and reactions, are largely MFI, LTA (NaA), and FAU (NaY) membranes, as summarized in Table I. In terms of membrane preparation. a wide variety of preparation methods can be categorized into hydrothermal synthesis with or without seeds[2,3] and the dry-gei conversion method.[4] Sano et al.[2] reported on the successful preparation of MFI zeolite membranes (silicalite) on porous stainless steel supports by in situ hydrothermal synthesis without seeds; zeolite crystals nucleate and grow on the surface of supports. Kita et al.[3] developed NaA zeolite membranes by hydrothermal synthesis using micometer-size seed crystals. On the other hand. Lovallo and Tsapatsis[5] reported on the secondary growth of colloidal silicalite seeds, the size of which was approximately 100 nm, under hydrothermal conditions. and provided an evaluation of their gas permeation properties. The secondary growth of crystalline colloidal zeolites. in which the growth of seed crystals on the order of the seed crystal size would be expected to be sufficient to close the interzeolite pores, represents a potential method for the preparation of thin zeolite membranes rather than the use of microineter-size seed crystals. The secondary growth of seed crystals has an advantage in that nucleation and crystal growth can be independently controlled for the preparation of zeolite membranes. Another advantage in utilizing seed crystals is, the potential for preparing MFII membranes without organic structure-directing agents, that is. templates. such as tetrapropylammonium. Templates: which are required for the formation of MFI structures in hydrothermal synthesis but need to be burned out in order to open the pore structures, often cause microcracks as the result of thermal stress. It was reported that high-quality MFH zeolite membranes can be successfully prepared without a template by utilizing MFI crystal seeds.[6] Finally. in the dry-gel conversion method, a dry aluminosilicate gel is deposited on the support and then transformed to the zeolite layer in the presence of steam and template vapor.

Excellent separation was reported for various types of zeolite membranes. The focus of most articles has been on inorganic and organic gaseous permeation, including CO_2/N_2 separations,[7] C4 (*n*-/*i*-butane),[8] and C6[8] and C8 isomers (*o*-/*m*-/*p*-xylene).[9–12] Moreover, zeolite membranes were used to separate liquid mixtures by pervaporation.[2,3,13] Silicalite membranes, the surface property of which is hydrophobic. permit the preferential permeation of organic components rather than water, which has a smaller molecular size. Separation factors larger than 100 were achieved for ethanol over water by silicalite membranes. On the other hand. NaA zeolite membranes permit the selective permeation of water with the separation factor larger than 1000.[3] The NaY membranes showed high selectivities for the separation of organic liquid mixtures such as benzene/cyclohexane.[13] This excellent separation is based on molecular sieving effects (molecular size and pore size) and selective adsorption.[1] The mechanism by which gas permeates through porous membranes is classified into Knudsen diffusion, surface diffusion. and molecular sieving. Several permeation models were proposed in terms of amorphous silica membranes[14] and zeolite membranes.[15,16] Bakker et al.[15] proposed a permeation model for MFI membranes that combined surface diffusion (transport by adsorbed gaseous molecules) and configurational diffusion (activated diffusion based on molecular sieving). At present.

Encyclopedia of Supramolecular Chemistry
DOI: 10.1081/E-ESMC 120012862

Table I Zeolite membranes and applications for separation and reaction

Zeolite		Pore size [Å]	Si/Al	Preparation*	Separation/ permeation	Reaction**
LTA	A	3	2	HTS/WS	H_2O/EtOH[3]	Esterification[19]
MFY	Silicalite	5.5	∞	HTS/WS, HTS/WOS DGC	EtOH/H_2O[2] C4,[8,9] C6,[8] C8[10–12]	ODHP; butane dehydrogenation[20], MeOH to Olefin (CMR[21]); toluene methylation (CMR[24–26]); ODHP (CMR[23])
	ZSM-5	5.5	>20			
FER	Ferierite	5.5 x 3.8	10–20	DGC	Benzene, C8[4]	None
FAU	Y	7.3	3–6	HTS/WS	CO_2/N_2,[7] benzene/cyclohexane, MeOH/MTBE[13]	CO oxidation (CMR[22])
ERI + *OFF*	*T*	*3.8, 5.8*	*4*, 8	HTS/WS	H_2O/EtOH(PV)[27]	Esterification[27]

*TS/WS: hydrothermal synthesis nith seed: HTS/WOS: hydrothermal synthesis without seed: DGC: dry gel conversion.
**CMR: catalytic membrane reactor: no symbolic marks indicate membrane reactors without using inherent catalytic activity. ODHP: oxidative dehydration of propane.

the mechanism of permeation through microporous membranes (pore size: <1 nm) appears to remain a controversial subject, and for a complete understanding of this process. more experimental data will be required.

On the other hand. little attention was given to the use of zeolite membranes as membrane reactors, in comparison with separation applications. Several types of membrane reactor configurations were proposed. including the packed-bed meinbrane reactor (PBMR), the fluidized-bed membrane reactor (FBMR), and the catalytic membrane reactor (CMR).[17] Catalytic membranes can be categorized into two types. Catalytic membranes. the materials of which are inherently catalytic, represent the first class, while for the other class: catalysts are tightly bound to the separation membranes, that is, catalysts are attached to the membrane surface or on the pore surface.[17,18] As mentioned above, the features of zeolites not only involve separation but also catalytic activity for various types of reactions. and therefore, zeolite membranes have great potential for use as catalytic membranes. Zeolite A membranes were evaluated for use in the esterification of oleic acid with ethanol, resulting in an 100% conversion by the selective removal of water vapor.[19] Silicate membranes were examined for use in dehydration reactions of hydrocarbons.[20] In these cases, zeolite membranes were used as separation membranes and not as catalytic membranes. Catalytic activity would be expected for most zeolite membranes. such as Zeolite Y and ZSM-5. Masuda et al.[21] applied ZSM-5 membranes to the conversion of methanol to olefins (the MTO reaction), which is a consecutive reaction starting from methanol and then progressing through dimethylether and olefin finally to paraffin. They reported that the product composition of olefins could be controlled by appropriate adjustment of the pressure difference across the MFI membrane. Hasegawa et al.[22] applied Pt-impregnated Y-type zeolite membranes for the selective oxidation of CO, which was present at concentrations of several hundred ppm in a stream of hydrogen. The MFI membranes incorporated with vanadium (V-MFI) were found to be effective for the selective oxidation of propane to propene via dehydrogenation reactions.[23] Selectivity of p-xylene by the methylation of toluene with methanol was also reported to be enhanced using ZSM-5 catalytic membrane reactors.[24–26]

EXPERIMENTAL

Silicalite colloidal solutions with approximate diameters of 100 nm were prepared using distilled water, tetrapropylammonium hydroxide (TPAOM), and sodium hydroxide. Cylindrical α-alumina microfiltration membranes (average pore diameter 1 μm, outer diameter 10 mm, inner diameter 8 mmj were used as substrates for the zeolite membranes. A hydrothermal synthesis was carried out in a solution of distilled water, tetrapropylammonium bromide (TPABr), and sodium hydroxide in a molar composition of $TPABr/SiO_2/H_2O/NaOH = 0.1/1/80/0.1$.[2,26] For the case of ZSM-5 membranes, sodium aluminate was added at Si/Al molar ratios of 20 and 50. Seeded substrates were immersed in the solution contained in Teflon test tubes and hydrothermally treated in a stainless-steel vessel for 12 hr at 180°C. After controlled secondary growth, the membranes were rinsed with hot water several times. followed by drying at 75°C. They were then calcined in a muffle furnace at

500°C for 5 hr (heating rate 1°C/min) in an air atmosphere.

Gas permeation experiments were performed in the temperature range of 35–300°C. The feed stream was pressurized, while downstream pressure was maintained at atmospheric pressure; no sweep gas was used. The permeate flow rate was determined by a soap-film meter.

After the ion-exchange of MFI zeolite membranes from Na-type to H-type, the alkylation of toluene with methanol was carried out at temperatures of 450 and 500°C. The reactants, in a molar composition of 2 toluene: 1 methanol, were fed with a syringe pump. The carrier gas used from the outer to the inner side of the cylindrical membranes was He. The composition was analyzed by gas chromatography using a xylene-isomer separation column (Bentone 34, Supelco). The pressure difference across the membrane was controlled at approximately 10 kPa.

RESULTS AND DISCUSSION

Membrane Preparation

Shown in Figs. 1a and b are SEM photos of the synthesized MFI membranes with Si/Al ratios of ∞ and 20, which were prepared under the same conditions (180°C, 12 hr), respectively. The MFI membrane of Si/Al = ∞ showed a continuous and well-intergrown layer, and the zeolite layer, the thickness of which was approximately 15 pm, appeared to have grown from the inside of the α-alumina support to the outer surface. Moreover, the surface was oriented in the (101) plane, which was also confirmed by x-ray diffraction analysis.[26] On the other hand, an MFI zeolite membrane of Si/Al = 20 has a relatively thin thickness of approximately 5 μm and an agglomerate structure of smaller crystals (primary crystal size of 1 pm). The addition of aluminum ion to the synthesis solution appears to retard the secondary growth rate.

Gas Permeation Properly

Shown in Fig. 2a is the temperature dependency for the permeances of inorganic and organic gases through M-1 (Si/Al = ∞). The permeances for H_2 show a temperature dependency similar to Knudsen diffusion; the permeance decreases slightly with an increase in temperature, as shown by the dotted line in the iigure. This is probably because the pore sizes for H_2 permeation are sufficiently large, in comparison with the molecular size. On the other hand, CO_2 shows a decreasing tendency in pcrmeance in a steeper slope than was the case for H_2. The permeation mechanism can be simply described as surface diffusion, because these gases arc thought to be adsorbed to the MFI

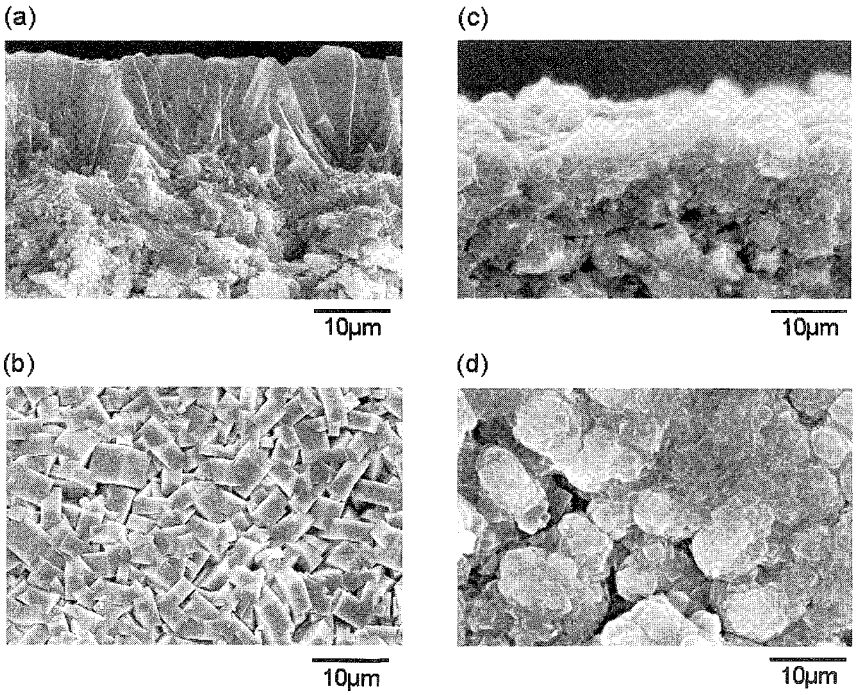

Fig. 1 MFI zeolite membranes: (a) cross-section (Si/Al = ∞); (b) surface (Si/Al = ∞); (c) cross-section (Si/Al = *20);* and (d) surface (Si/Al = *20).*

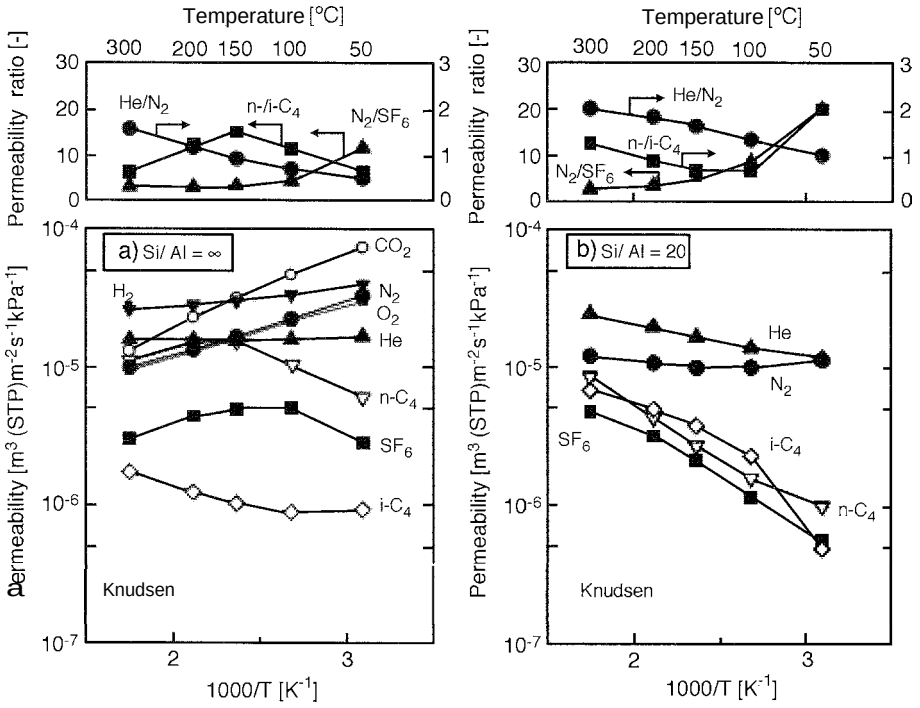

Fig. 2 Permeance and permeability ratio as a function of reciprocal temperature of M-1 (Si/Al = ∞) and M-2 (Si/Al = 20). (*View this art in color at www.dekker.com.*)

zeolite [15] N_2 and O_2, which are assumed to be non-adsorptive gases, also show a decreasing tendency, the slope tor which is intermediate between H_2 (Knudsen diffusion) and CO_2 (surface diffusion) Permeances of n-C_4H_{10} and SF_6 leached a maximum at 150°C and 100°C. respectively The maximal permeance can be explained as follows the number of adsorbed molecules decreases at temperatures higher than the maximum, while adsorption. which is enhanced at lower temperatures, causes a decrease in mobility (liquid-like diffusion of pore-filling molecules). On the other hand, the permeance of *i*-C_4H_{10} increased with temperature. and no peak was evident, which is similar to an activated diffusion mechanism.[14] The permeability ratio of *n*-C_4H_{10} over *i*-C_4H_{10}, based on pure gas permeances, shows a maximum of 15 at a temperature of 150°C, while the permeance of *n*-C_4H_{10} was 1.5 x 10^{-5} $m^3(STP)m^{-2}s^{-1}kPa^{-1}$. The M-1 membrane showed a large permeance and moderate selectivity,

Table 2 Summary of the methylation of toluene with methanol using MFI powders and membranes

Configuration	Si/Al	WHSV [$g_{feed}/(g_{catal}.h)$]	Temperature [°C]	Conversion [%]	Xylene composition [%]			Ref.
					o-	*m*-	*p*-	
Powder		33	400	23.5	21	47	32	[28]
Disc	50	34	450	26.7	3	18	79	[24]
Disc	50	17	450	37.8	3	20	76	[24]
Membrane	∞	9.7	500	4.3	22	22	*56*	[26]
Membrane	50	44	*500*	7 3	*6*	17	77	This work
Membrane	20	37	500	11.9 (initial conversion)	10	22	*68*	This work
Thermodynamic equilibrium			427	—	26	51	23	[24]

which might be caused by the formation of a thin zeolite layer by the secondary growth method, the existence of intercrystalline *pores, or the orientation of the* crystalline.[26] *On the other Band, as shown in Fig.* 2b, *M-2* (Si/Al *= 20) shows an increasing ten-iperature dependency for He.* SF_6, *n*-C_4H_{10}, *and i*-C_4H_{10}. *The effect of the* Si/Al *ratio on gaseous permeances is not yet clear. but the existence of* intercrystalline *pores for M-2* (Si/Al = *20) is strongly suggested. because since the permeability ratio of n*-C_4H_{10} *over i*-C_4H_{10} *was approximately 1.*

Methylation of Toluene

The reaction performances are summarized in Table 2, in terms *of* toluene *conversion and composition of o-/m-/p-xylene. Because toluene reacted with* methanol *in the case of an MFI membrane of* Si/Al = ∞, *it is clear that* aluminum *ions must have been incorporated into the MFI zeolite membranes. (The origin of the aluminum ions was probably* the α-alumina *support that was dissolved in strong alkali solutions during the hydrothermal synthesis.) The selectivity* for *p*-xylene *was as high as* 80%, *while the thermodynamic* equilibrium *was reported to have* a *composition of o-/m-/p-*xylene *of 26/51/23 at* 427°C.[24] *The alkylation reaction cakes place inside the ZSM-5 zeolite pores (intracrystalline pores) in the para-position, and the diffusioninside* ZSM-5 *also favors para*-selectivity *based on size selectivity. On the other hand. no para-selectivity would he expected on the external surface of the ZSM-5 crystals. including the intercrystalline pores. Furthermore. the* isomerization of *p-xylene. which is a primary product in the intracrystalline pores, to o- and m-xylene, occurs on the outer surface of the* H-MFI *zeolite. Therefore.* ZSM-5 *membranes, which have limited external surface area in comparison with powders, increased para*-selectivity.[24–26] *The present investigation confirms the possible* application *of MKP zeolite membranes to the alkylation* of *toluene with methanol.*

CONCLUSION

The MFI zeolite membranes containing different Si/Al *ratios were prepared by* the *secondary growth of colloidal* silicalite *on* α-alumina *microfiltration membranes. An* MFI membrane (Si/Al = ×), *the zeolite* layer *of which was oriented* in *the* (101) *plane. showed a n*-C_4H_{10} *permeance of* 1.5 *x* 10^{-} $m^3(STP)m^{-2}s^{-1}kPa^{-}$ *and a n-/i-*C_4H_{10} selectivity *of 15 at 150°C. After ion exchange of the* MFI *zeolite membranes* from *the Na-type to the* H-*type, the alkylation of toluene with methanol was carried out.* A *p*-xylene *selectivity of 80% was attained* using H-MFI *zeolite membranes at 450 ~ 500°C. confirming the possible application of an MFI zeolite* membrane *for use in a catalytic membrane reactor.*

ARTICLES OF FURTHER INTEREST

Mesoporous Materials, p. 845
Zeolites in the Petroleum Industry, p. 1599
Zeolites: Catalysis, p. *1610*
Zeolites: Structures and Inclusion Properties. p. 1623

REFERENCES

1. Coronas, J.: Santamaria. J. Separations using zeolite membranes. Sep. Purif. Methods **1999**, 28. 127–177.
2. Sano. T.: Yanagishita, H.: Kiyozumi, U.: Mizukami. F. Separation of ethanol/water mixture by silicalite membrane on pervaporation. J. Mernbr. Sci. **1994**, *95*. 221–228.
3. Kita. H.; Horii, K.; Ohtoshi. Y.; Tanaka. K.: Okamoto, K. Synthesis of a zeolite NaA membrane for pervaporation of water/organic liquid mixtures. J. Mater. Sci. Lett. **1995**. *14*. 206–208.
4. Nishiyarna. N.: Ueyama, K.; Matsukata. M. Synthesis of defect-free zeolite–alumina composite membranes by a vapor—Phase transport method. Microporous Mat. 1996. *7*, 299–308.
5. Lovallo. M.C.; Tsapatsis. M. Preferentially oriented submicron silicalite membranes. AIChE J. **1996**. *42*. 3020–3029.
6. Pan. M.: Lin. U.S. Template-free secondary growth synthesis of MFI type zeolite membranes. Microporous Mesoporous Mater. 2008. 43, 319–327.
7. Kusakabe, K.: Kuroda, T.; Uchino. K.; Hasegawa, Y.: Morooka. S. Gas permeation properties of ion-exchanged Faujasite-type zeolite membranes. AIChE J. 1999. *45*. 1220–1226.
8. Coronas. J.; Noble. R.; Falconer, J. Separations of C_4 and C_6 isomers in ZSM-5 tubular membranes. Ind. Eng. Chem. Res. 1998. 37. 166–176.
9. Gump, C.J.: Lin, X.: Falconer, J.L.; Noble. R.D. Experimental configuration and adsorption effects on the permeation of C_4 isorners through ZSM-5 zeolite membranes. J. Membr. Sci. **2000**. *173*. 35–52.
10. Nair, S.; Lai, Z.; Nikolakis. V.: Xomeritaks. C.: Bonila. G.; Tsapatsis. M. Separation of close-boiling hydrocarbon mixtures by MFI and FAU membranes made by secondary growth. Microporous Mesoporous Mater. **2001**. *48*. 219–228.
11. Burggraaf. A.J.; Vroon. Z.A.E.P.: Keizer, K.: Verweij, H. Permeation of single gases in thin zeolite MFI membranes. J. Membr. Sci. 1998. 144. 77–86.
12. Wegner. K.; Dong. J.: Lin. Y.S. Polycrystalline MFI

zeolite membranes: Xylene pervaporation its implication on membrane microstructure. J. Membrane Sci. 1999. *158*. 17–27.
13. Mita, H.; Fuchia. K.; Horita. T.: Asamura, H.: Okamoto. K. Preparation of Faujasite membranes and their permeation properties. Sep. Sci. Technol. 2001. *25*. 261–268.
14. Yoshioka. T.: Nakanishi. E.: Tsuru. T.: Asaeda. M. Experimental studies of gas permeation through microporous silica membranes. AIChE J. 2001, *47*. 2052–2063.
15. Bakker. W.J.W.: Broeke, L.J.P.; Kapteijn. F.; Moulijn, J. Temperature dependence of one-component permeation through a silicalite-1 membrane. AIChE J. 1997. *43*. 2203–2214.
16. Burggraaf, A.J. Single gas permeation of thin zeolite (MFI) membranes: Theory and analysis of experimental observations. J. Membrane Sci. 1999. *155*. 45–65.
17. Hsieh. H.P. *Inorganic Membranes* for *Separation* and *Reaction*; Elsevier: Amsterdam. 1996; 529.
18. Tsuru, T.: Tsuge, T.; Kubota, S.; Yoshida, K.; Yoshioka, T.: Asaeda. M. Catalytic membrane reaction for methane steam reforming using porous silica membranes. Sep. Sci. Technol. 2001. 36. 3721–3736.
19. Yamamoto. M.: Munehisa, N.: Kaibara. M.: Horii, K.; Tanaka. M.: Kita. H.: Okamoto. K. Vapor-permeation-aided esterification of oleic acid. Membrane 1995, 20. 143–148.
20. Cia\-arella, P.: Casanave, D.; Moueddeb, H.: Miachon. S.; Fiaty. K.; Dalmon, J.A. Isobutane dehydrogenation in a membrane reactor Influence of the operating conditions on the performance. Catal. Today 2001. 67. 177–184.
21. Masuda. T.: Asamura. T.: Kitamura, M.; Hashimoto. K.; Kobayashi. Y.: Koyama, T. Pervaporation of concentrated acetic acid solution and reaction of membrane of inethanol to olefin using cylindrical MFI-type zeolite membranes without any pin holes. Catal. Catal. 1998. *40*. 348.
22. Hasegawa. Y.: Kusakabe, K.: Moroolta. S. Selective oxidation of carbon monoxide in hydrogen-rich mixtures by permeation through a platinum-loaded Y-type zeolite membrane. J. Membrane Sci. 2001. *190*. 1–8.
23. Julbe, A.; Farrusseng. D.; Jalibert. J.C.; Mirodatos, C.: Guizard, C. Characteristics and performance in the oxidative dehydrogenation of propane of MFI and V-MFI zeolite membranes. Catal. Today 2000, *56*. 199–209.
24. Kiricsi, I.: Shimizu. S.: Kiyozuini, Y.; Toba. M.; Niwa, S.: Mizukami. F. Alkylation of toluene with methanol over zeolite-disc catalyst synthesized via solid-state reactions. Appl. Catal.. A 1997, *156*. 335–345.
25. Kiricsi, I.: Shimizu. S.: Kiyozumi, Y.: Toba, M.: Niwa, S.; Mizukami, F. Catalytic activity of a zeolite disc synthesized through solid-state reactions. Microporous Mesoporous Mater. 1998. *21*. 453–459.
26. Takata. Y.: Tsuru, T.: Yoshioka, T.; Asaeda. M. Gas permeation properties of MFI zeolite membranes prepared by the secondary growth of colloidal silicalite and application to the methylation of toluene. Microporous Mesoporous Mater. 2002, *54*, 257–268.
27. Tanaka, K.; Yoshikawa, R.: Ying, C.; Kita. H.; Okamoto. K. Application of zeolite membranes to esterification reactions. Catal. Today 2001, *67*, 121–125.
28. Yashima. T.: Sakaguchi, Y.: Namba, S. Selective formation of p-xylene by alkylation of toluene with methanol on ZSM-5 zeolites. Stud. Surf. Sci. Catal. 1981. 7. 739.

Zeolites: Structures and Inclusion Properties

Jiří Čejka
Academy of Sciences of the Czech Republic, Prague, Czech Republic

INTRODUCTION

Zeolite-based molecular sieves represent one of the most important groups of crystalline inorganic materials, with a great potential for application as adsorbents. ion-exchangers, and heterogeneous catalysts. The first natural zeolite, stilbite. was discovered about 250 years ago by Swedish mineralogist Crønsted, who showed that this mineral released water upon heating. Thus, this mineral was named *zeolite* after Greek *zeo* (to boil) and *lithos* (stone). Since that time, about 50 natural zeolites have been found in different parts of the world.[1]

Several hundreds of synthetic zeolites (crystalline microporous aluminosilicates) and zeotypes (crystalline microporous ferrisilicates, gallosilicates, titanosilicates, isomorphously substituted aluminophosphates, etc.) have been successfully synthesized in recent decades.[2] All these microporous materials have tetrahedral coordination of their central atoms (Si, Al, P, Fe, etc.), which are interconnected with four oxygen bridges to form a three-dimensional crystal structure. These structures exhibit regular micropores with dimensions up to 1.0 nm and cavities. high surface areas, and adsorption capacities, and shape selectivity toward reactants, products, and transition states.''''

In the last decade of the twentieth century, new types of zeolitic materials were synthesized, namely. mesoporous molecular sieves with pore sizes larger than 10 nm,[5] and delaminated or pillared zeolites, which preserve the zeolite structure but allow access of significantly larger molecules.[6,7] These materials attracted remarkable attention, as they enabled scientists to escape from the so-called ''1-nm prison'' imposed by the structures of classical zeolites.

At present, zeolites have found a wide array of applications ranging from ion exchangers, detergents, drying and separation agents. to catalysts. The estimated production of zeolites is to exceed 1,100.000 tons per year. In particular; the application of zeolites. as highly active. selective, and stable catalysts in large-scale technologies steadily increases and includes oil refineries, petrochemistry, and synthesis of fine chemicals and environmental catalysis.[4,8]

STRUCTURES OF ZEOLITES AND ZEOTYPES

Zeolites are crystalline microporous alurninosilicates with a three-dimensional framework consisting of tetrahedral SiO_4 and AlO_4, (Si, Al=T atoms) connected by oxygen bridges. Two neighboring tetrahedra are connected by one oxygen bridge. and no edge connection has yet been described. Tetrahedra SiO_4 and AlO_4 (or PO_4, FeO_4, GaO_4, etc., for various zeotypes) are the primary building units, which in turn. form the so-called secondary building units like 4-, 5-, and 6- membered rings, double 4-, 5-, and 6-membered rings. etc. By combining these secondary building units, a three-dimensional channel structure is formed. Depending on the connections among individual tetrahedra, channels of different shapes and dimensions in the microporous range and cavities can arise. The number of tetrahedra forming these windows controls their diameter. For microporous aluminosilicate and related aluminophosphate molecular sieves, the windows usually consist of 6. 8, 10. 12. 14, 18, and 20 tetrahedra.[2] Only one zeolite with an odd number of tetrahedra forming the windows has been described so far.''' The inne volume of zeolites contains cations (protons) that compensate the negative charge of the zeolite framework due to the presence of AlO_4 tetrahedra and water molecules. Clearly, a straiglztforward relationship exists between the sizes and shapes of zeolite entrance windows to the channel system imposing the molecular sieve effect and their application in catalysis and adsorption. Zeolites and zeotypes with even-membered rings are usually divided into the following four categories (some examples with channel dimensions and dimensionalities are given in Table 1):

1 Small-pore zeolites (eight-membered rings with pore dimensions up to 0 40 nm)—e g . chabazite. Linde type A. $AlPO_4$-34, $AlPO_4$-22
2 Medium-pore zeolites (10-membered rings with pore sizes up to 0 55 nm)—e g . ZSM-5. ZSM-11, ZSM-22, ZSM-23, $AlPO_4$-11. $AlPO_4$-31, and MCM-22 (in addition. they have large cavities defined by 12-membered rings)

DOI: 10.1081/E-ESMC 120012363

Table 1 Zeolites. zeotypes, and mesoporous molecular sieves, selected examples, and their characteristic features

Molecular sieve	IZA code	Main window	Channel dimensionality	Size (nm)
Zeolite				
CIT-5	CFI	14	1D	072x075
UTD 1	DON	14	ID	081x082
Zeolite Y	FAU	12	3D	0 74
Moıdenite	MOR	12	3D	065x070
Zeolite L	LTL	12	1D	0 71
ZSM-12	MTW	12	ID	056x060
Beta	BEA	12	3D	076x064
SSZ-42 ITQ-4	IFR	12	1D	0.62×0.72
ZSM-5	MFI	10	3D	054x056
Fenıeıite	FER	10	2D	042x054
ZSM-22	TON	10	1D	046x057
ZSM-23	MTT	10	1D	045x052
MCM-22	MWW	10	3D	0.40×0.55
Zeolite A	LTA	8	3D	041×0.41
Erionite	ERI	8	3D	036x051
Chabazite	CHA	8	3D	0 38
Zeotype				
Cloveıite	CLO	20	2D	040x1 32
$AlPO_4$ 8	AET	14	1D	079x087
$AlPO_4$-5	AFI	12	1D	0 73
$AlPO_4$-31	ATO	12	1D	054x054
$AlPO_4$-11	AEL	10	1D	0.40×0.65
$AlPO_4$ 41	AFO	10	1D	043x070
$AlPO_4$ 18	AEI	8	3D	038x038
$AlPO_4$-52	AFT	8	3D	0.32×0.38
$CoAlPO_4$ 34	CHA	8	3D	0 38
Mesoporous molecular sieves				
MCM 41			ID	3–10
MCM-48			3D	3–5
SBA 15			ID	5–20
Mesoporous alumina			ID	1–10

3. Large-pore zeolites (12-membered rings up to 0.75 nm)—e.g., zeolites Y and L, EMT, mordenite. Beta, and $AlPO_4$-5.
4. Extra-large-pore zeolites (at least 14-membered rings with pore sizes around 1.0 nm)—e.g., aluminosilicates CIT-5, UTD-1. aluminophosphates (VPI-5, JDF-20, gallophosphate. cloverite).

Typical examples of the individual structures. showing the type of secondary building units and entrance windows to the channel systems of zeolites ZSM-5 (10-membered rings), β (12-membered rings), CIT-5 (14-membered rings), and zeotype aluminophosphate $AlPO_4$-11 (10-membered rings) are shown in Fig 1 Summarized ın Table 1 are the structural characterıstıcs of the most Important zeolites. zeotypes, and mesoporous molecuiar sieves, including a three-letter code for different structure topologiei, based on the assignment of approved zeolite structures by the Structure Commission of the International Zeolite Association.[10]

The type of the individual zeolite structure is related to the chemical composition of the zeolite. The molar ratio of SiO_4 and AlO_4 tetrahedra can reach unity 1:1, which represents the regular periodicity of the $(Si–O–Al–O–Si–O–Al–O)_x$ structural motif. According to Lowenstein's rule, two neighboring Al atoms cannot be connected via one oxygen bridge. This finding implies that zeolites crystallizing with low Si/Al molar ratios are exclusively formed by secondary building units having an even number of T atoms. This is, e.g., the case of zeolites A and X (Si/Al=I) or zeolite Y (Si/Al=2.8). With decreasing concentration of Al in the zeolite framework, secondary building units with an odd number of T atoms are also utilized (ferrierite, Si/Al>8, ZSM-5, Si/Al>10, etc.). A similar rule is also valid in

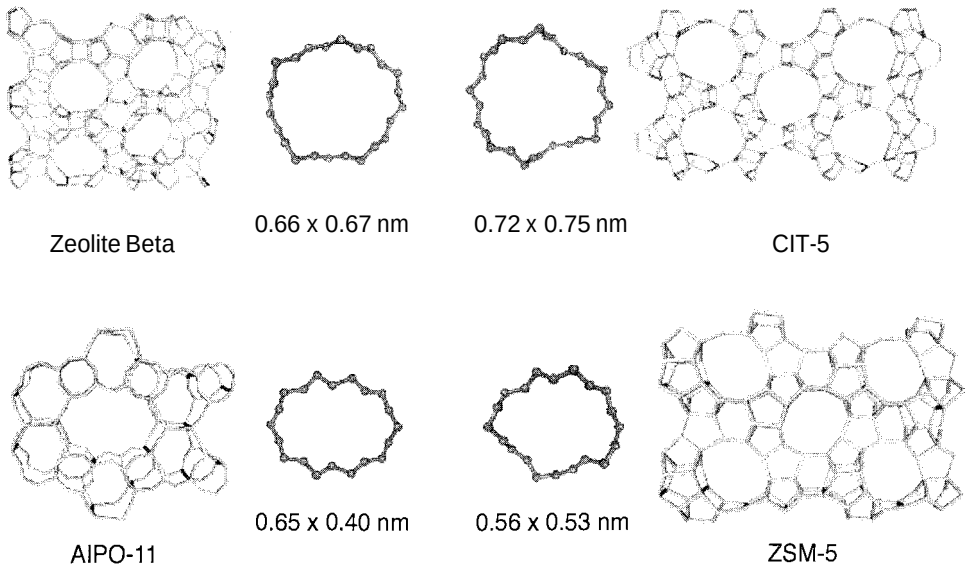

Fig. 1 Structure and entrance windows of zeolites β, CIT-5. ZSM-5. and zeotype $AlPO_4$-11. (*View this art in color at www.dekker.corn.)*

the case of aluminophosphate-based zeotypes, in which all the aluminum atoms are connected via oxygen bridges exclusively to four different phosphorus atoms. Thus, the secondary building units in aluminophosphates are limited to those with an even number of T atoms. Isomorphous substitution of aluminum by divalent metal cations like Co, Ni. Mn, Zn, Mg. or replacement of phosphorus by silicon can take place, resulting in the formation of negatively charged framework zeotypes.[2]

With the increasing concentration of aluminum in the framework (with the Si/Al ratio decreasing to 1), the hydrophilic character of zeolites rises. The same relation exists between the number of exchangeable cations and the affinity for polar molecules. On the other hand. thermal stability, stability in acidic solutions, hydrophobic character of zeolites, and their affinity for nonpolar molecules increases with the decreasing aluminum concentration (increasing Si/Al ratio).

The above-mentioned structural features of zeolite molecular sieves results in the following characteristic properties, which represent important advantages compared to other solid materials:

1. Well-defined inorganic crystalline structures yielding a large variety of structural types differing in the channel diameters, geometry, and dimensionality.
2. Precisely defined inner void volume providing high-surface areas up to 600 m^2/g.
3. Fine tuning of chemical properties through isomorphous substitution or various postsynthesis treatments.
4. Shape-selective properties related to the ratio between kinetic diameters of organic molecules and dimensions of the zeolite channels or cavities.
5. Environmental tolerance.

Based on the IUPAC nomenclature. microporous molecular sieves have pores with dimensions up to 2.0 nm in dimension. The mesopore dimension is between 2.0 and 50 nm, while macropores exhibit pores larger than 50 nm. Shown in Fig. 2 are the pore size and schematic structure of several zeolites. zeotypes, and mesoporous molecular sieves. Evidently, a large number of different zeolite or zeotype structures and mesoporous materials are available from which the optimum one for the given application can be selected.

EXTENSIONS OF ZEOLITE STRUCTURES

Although zeolites and zeotypes attracted attention in many areas of chemistry and its applications, much effort has been devoted in the last decade in particular to the enlargement of the size of their channels in order to allow larger molecules to reach the zeolite active sites. This work could have particular importance in fine chemical and pharmaceutical manufacturing and in petroleum refining. Access of larger organic molecules to the active sites of zeolites will significantly increase the number of reactions catalyzed by zeolites. The maximum size of zeolite channels is about 1.0 nm for

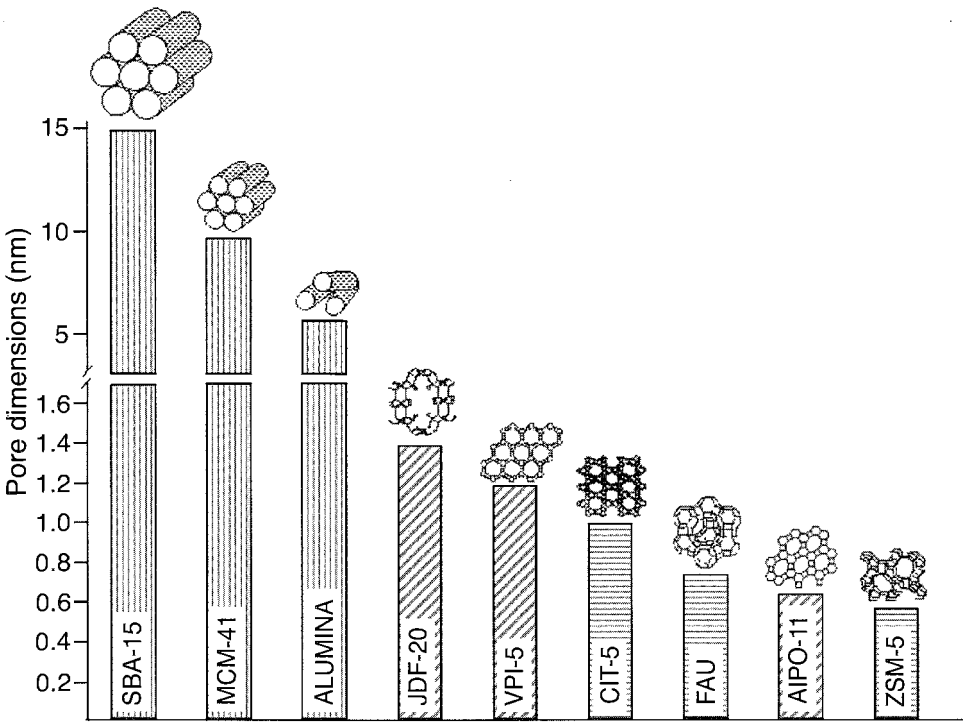

Fig. 2 Several zeolites. zeotypes, and mesoporous molecular sieves with dimensions of their channels

14-membered ring zeolites CIT-5 and UTD-1: while in zeotypes, channel sizes up to 1.4 nm in JDF-20 and cloverite have been achieved. However. further attempts to increase this pore size and at the same time to preserve the zeolite crystal structure unfortunately failed. Therefore, new synthetic approaches have been developed, namely, as follows:

1. Preparation of delaminated zeolites from zeolite precursors.
2. Preparation of pillared layered materials based on zeolite layers.
3. Synthesis of mesoporous molecular sieves with amorphous channel walls of various chemical compositions. different pore sizes, and dimensionalities.
4. Synthesis of mesoporous molecular sieves with crystalline zeolite phases embedded into the channel walls.

Several zeolites (e.g., MCM-22 and ferrierite) can be synthesized in the form of a layered precursor, which can be transformed into the three-dimensional crystalline structure by thermal treatment. These layered solids arouse interest due to their potential to intercalate guest molecules between the individual layers. Using a proper treatment. layered zeolite precursors can be delaminated, but their layered structure with surface areas exceeding 700 m^2/g is preserved. Such delaminated zeolites exhibit strong acidity and stability, which is characteristic for zeolite materials. In addition, they are better accessible for larger organic molecules.[6] Moreover, the layered nature of these materials enables zeolite-based pillared molecular sieves to be synthesized by inserting different inorganic materials (e.g., silica, alumina, heteropoly acids) into the interlayered space, yielding large-pore pillared materials with zeolitic properties.[11]

The invention of mesoporous molecular sieves at Mobil Research and Development Corporation, started a new era in the investigation of molecular sieves.[5] Mesoporous molecular sieves exhibit uniform pores with dimensions ranging from 2.0 to about 30 nm, surface areas often larger than 1000 m^2/g, and long-range ordering. These materials are obtained using supramolecular assemblies of surfactants, which template the inorganic components during the synthesis. Anionic: cationic. and neutral synthetic routes have been reported, defining the type of interaction among the head groups of inorganic and surfactant species in the initial steps of the synthesis of different mesoporous inaterials (MCM-41, MCM-48, SBA-15, mesoporous alumina).[12,13]

In order to overcome the limitations of individual micro- or inesoporous materials and to combine the advantages of these two types of molecular sieves, the synthesis of new molecular sieves incorporating porosity of both types presents a challenge. Several approaches and methods of synthesis of micro/mesoporous materials

have been described. One possible method of obtaining micro/mesoporous composite materials is by secondary teinplated crystallization of zeolites, starling from amorphous mesoporous materials containing structure-directing agents for the synthesis of the required zeolite phase. This approach consists of two steps: preparation of the amorphous mesoporous precursor and transformation of the amorphous mesopore walls into crystalline walls by additional hydrothermal treatment in the presence of a suitable organic template."'' Another approach is to impregnate mesoporous materials such as MCM-41 with tetrapropylarnmonium hydroxide followed by recrystallization at elevated temperatures to obtain a ZSM-5-like phase.[15] The dual-templating method through two-step crystallization represents another way of synthesizing micro/mesoporous molecular sieves.[16] Last but not least, direct assembly of nanoclustered alumosilicate precursors (zeolite seeds) with crystalline zeolite structure can be used under defined drying conditions.[17] Using this method, steam-stable aluminosilicate mesostructures assembled from zeolite Y, zeolite ZSM-5, and zeolite p seeds have been prepared.

A great deal of research effort aimed at enlargement of the zeolite and zeotype structures resulted in numerous papers on the synthesis, properties, and characterization of delaminated and pillared zeolitic materials and mesoporous molecular sieves with amorphous or partially crystalline channel walls. Also, evidence of their potentials for catalytic applications was reported. The individual synthetic approaches are summarized in Fig. 3. Depending on the reaction conditions and on the structure of organic template (structure-directing agent), various molecular sieve materials can be synthesized (zeolites—route A, delaminated zeolites—B. pillared layered zeolites—C, mesoporous molecular sieves—D, and mesoporous molecular sieves with zeolitic walls—E).

INCLUSION PROPERTIES OF ZEOLITES AND MESOPOROUS MATERIALS

The inclusion properties of zeolites and related molecular sieves are strongly controlled by the unique structures of their channel systems and the presence or absence of cavities. Introduction of various inorganic, organic. or organometallic species into the zeolite channels profoundly changes their properties. In addition, properties of guest molecules located in zeolite matrices can significantly differ from their bulk properties due to their nanoscale dimensions and locations in a constrained system. Crystalline structure of zeolites imposes important shape-selective properties, characterized by a negative framework charge and low

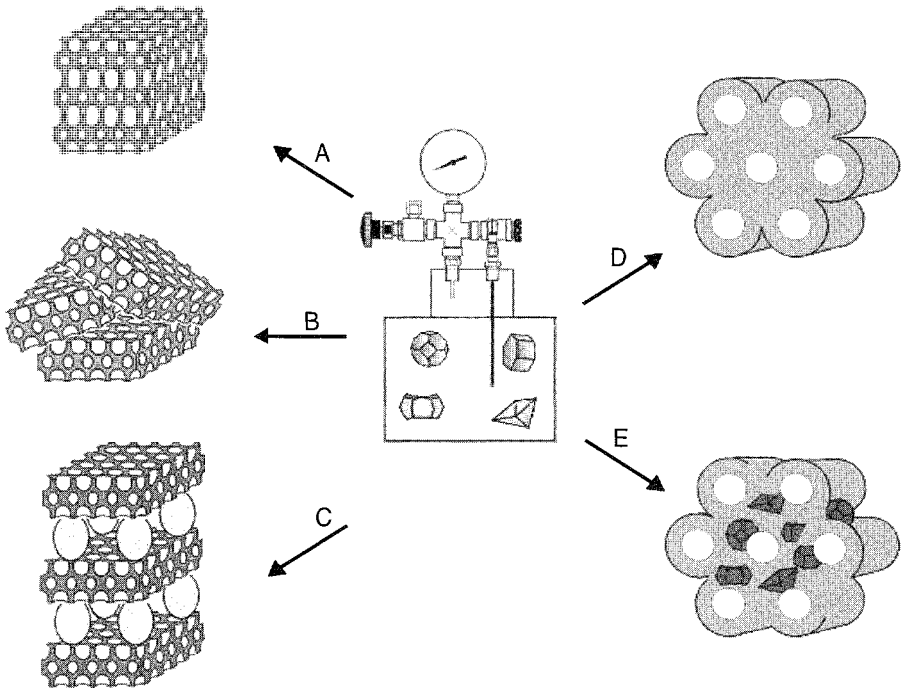

Fig. *3* Routes to zeolites (A), delaminated zeolites (B), pillared layered zeolites (C), mesoporous molecular sieves (D), and mesoporous molecular sieves with zeolitic walls (E).

flexibility of the zeolite structure. Excellent reviews covering this topic were recently published by Bein[18] and de Vos and Jacobs.[19]

Different synthetic approaches have been described for the formation of zeolite inclusion compounds, including direct adsorption. impregnation. ion-exchange from solutions or solid-state ion-exchange. ship-in-the-bottle synthesis. formation of large molecules (e.g., by polymerization reactions). and zeolite synthesis around the metal complex. Some examples of these approaches are given in the next sections.

METAL AND METAL-OXIDE **CLUSTERS**

Incorporation of metals or metal oxides into zeolite cavities leads to the formation of nanosized clusters exhibiting different catalytic properties from the bulk materials. These metal particles are usually introduced into zeolite channels through ion-exchange followed by reduction or oxidation/reduction to get their final dispersions.[20] Metal clusters can also be formed via zeolite impregnation by corresponding azides from methanolic solutions followed by thermal decomposition.[21] Catalytic activities of the bifunctional or basic catalysts prepared using these methods can be successfully combined with shape-selective properties of parent zeolites.

SHIP-IN-THE-BOTTLE SYNTHESIS

The ship-ill-the-bottle synthetic approach represents an elegant method of forming entrapped molecules within the zeolite channel system that are larger than dimensions of the channels of the zeolite. These entrapped molecules cannot be easily removed from the zeolite due to steric reasons. A typical example is the synthesis of Fe-phthalocyanine in the cavities of zeolite Y. Iron is introduced into the zeolite by ion exchange from its water solution followed by complexation with 1,2-dicyanobenzene. A schematic picture of the location of Fe-phthalocyanine in zeolite Y is provided in Fig. 4. This mechanism was examined in order to synthesize active catalysts for, e.g., oxidation and hydrogenation reactions and to mimic natural enzymes. It is expected that the mechanism of oxygen transfer of Fe-phthalocyanine in zeolite Y is analogous to the natural cytochrome P-450.[22] Complexes of other transition metals have been synthesized in zeolites using, e.g., bipyridine and salen ligands with application for epoxidation reactions. The ship-in-the-bottle synthesis was used by Meinershagen and Bein[23] for incorporation of the solvatochromic dye nile red in zeolite Y to test its sensing properties. This dye, located inside the zeolite. was shown to act as an optical sensor with extremely high sensitivity toward different organic compounds.

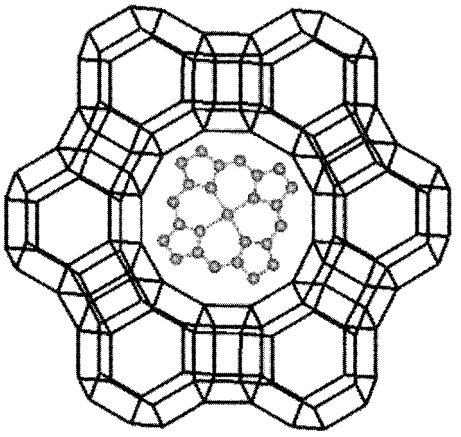

Fig. 4 Location of Fe-phthalocyanine in the cavity of zeolite Y. (*View this art in color at www.dekker.com.*)

FORMATION OF LARGE MOLECULES

The constrained geometry of the inner void volume of zeolites, and particularly of mesoporous materials, provides an important space of nanodimensions for accommodation of large molecules. It is expected that flexible polymers synthesized in the conditions of constrained geometry could exhibit different properties compared to nonconstrained systems. Considerable effort has been exerted to synthesize conducting polymers by polymerization of the respective monomers in the presence of zeolites ion-exchanged with some transition metals.

It has been shown that N-vinylcarbazole and vinyl ethers can be used for the cationic host–guest polymerization in MCM-41 and MCM-48 mesoporous molecular sieves. leading to new polymer/MCM-41 and polymer/MCM-48 host–guest hybrid materials.[24] It seems that the molecular weight and the degree of the loading of the enclosed polymers can be adjusted to a certain degree by modification of the polymerization conditions.

On the other hand. Balcar et al.[25] showed that the immobilization of $[Rh(cod)OCH_3]_2$ on mesoporous MCM-41 provides an inorganic hybrid catalyst, which is effective for polymerization of various substituted phenylacetylenes into substituted polyvinylenes (investigated for their interesting photoelectrical and optical properties) with molecular weight between 50.000 and 180,000 and high *cis-trans*oid structure.

ZEOLITE SYNTHESIS AROUND ORGANIC AND INORGANIC MOLECULES

A completely different approach involves organometallic complexes with a relatively rigid structure that can be used as templates for the synthesis of zeolites. Balkus et al.[26] showed that perrnethylated cobalticinium ion ($CoCp_2^+$) can be employed to synthesize a new zeolite UTD-1, which was the first zeolite with 14-membered ring channels. The ($CoCp_2^+$) complex was also used to synthesize ZSM-51 and AlPO-16. This zeolite and zeotype, respectively, exhibit cages into which this template nicely fits. Another example is the employment of 1-aminoadamantane for the synthesis of chabazite.

CONCLUSION

The continuous effort of numerous laboratories around the world resulted in the last decades in the synthesis of a number of new zeolites, zeotypes, and mesoporous molecular sieves of different chemical compositions. Hand in hand with the success of basic research in this area, zeolites found new industrial applications.

In the case of zeolites and related materials, unfortunately no breakthrough has been achieved in the synthesis of extra-large pore zeolites. UTD-1 and CIT-5 remain the only examples of 14-membered ring zeolites, while cloverite and JDF-20 represent the largest zeotypes with 20-membered rings. Therefore. much effort is exerted to enhance the accessibility of catalytically active sites by delamination and pillaring of zeolite precursors. while preserving the structure and properties of zeolitic layers. Several successful examples of these new types of materials are described in this article. Evidently, synthesis of other types of molecular sieves possessing chemical composition and properties can be expected. These synthetic activities are connected with the effort to increase the number of zeolitic materials applicable in industrial catalysis. Recently. synthesis of polymorph C of zeolite β and ITQ-21 has been reported, confirming the extremely high amount of research activity in this area.[27,28]

As for mesoporous molecular sieves. their synthesis opened a new subfield of molecular sieve chemistry. which has grown rapidly over the last 10 years. New synthetic approaches. different from those known for zeolites, have been applied. The variety of the synthetic procedures described and the differences in the textural properties due to different synthetic procedures, as well as to the high-temperature treatment, give evidence that mesoporous molecular sieves of different chemical compositions are interesting materials, not only for materials science but also for application as heterogeneous catalysts. support for immobilization of homogeneous catalysts, adsorbents, materials for synthesis of new types of inclusion compounds, etc. There is no doubt that research in this field will rapidly grow. and new types of mesoporous molecular sieves will be synthesized. Tailoring of the textural properties and industrial application of these materials in the near future are likely.

The first successful preparation of micro/mesoporous molecular sieves started an intensive search to optimize procedures of their synthesis, to increase their thermal stability, and to tailor their acid, base, and redox properties for possible application in heterogeneous catalysis. Although only a few syntheses of composite molecular sieves have been reported, it is clear that mastering this synthesis represents an important challenge in the area of porous materials. There is no doubt that molecular sieves represent a flourishing and expanding field of chemistry, and further interesting achievements and applications can be expected.

ACKNOWLEDGMENT

The long-term support of my projects focused on the synthesis, characterizations, and applications of zeolites and molecular sieves by the Grant Agency of the Academy of Sciences of the Czech Republic (A4040001) and the Grant Agency of the Czech Republic (104/02/0571 and 203/03/804) is gratefully acknowledged.

ARTICLES OF FURTHER INTEREST

Channel Inclusion Compounds, p. 223
Classical Descriptions of Inclusion Compounds, p. 253
Inclusion Compounds: Selectivity, Thermal Stability, and Kinetics, p. 696
Inclusion Reactions and Polymerization, p. 705
Organic Zeolites, p. 996
Zeolites in the Petroleum Industry, p. 1599
Zeolites: Catalysis, p. 1610
Zeolites: Separation Science, p. *1617*

REFERENCES

1. Armbruster, T.: Gunter. M.E. Crystal Structures of Natural Zeolites. In *Reviews in Mineralogy and Geology:* Bish, *D.L.*. Ming, D.W., Eds.; Mineralogical Society of America: Washington, 2001; Vol. 45. 1–67.
2. Szostak. R. *Molecular Sieves, Principles of Synthesis and Identification*; Blackie Acad. & Prof.: London. 1998.
3. Corma. A. From microporous to mesoporous molecular sieve materials and their use in catalysis. Chem. Rev. 1997. 97. 2373–2419.
4. Čejka, J.: Wichterlová, B. Acid-catalyzed synthesis mono-

and dialkyl benzenes over zeolites: Active sites, zeolite topology. and reaction mechanisms. Catal. Rev. 2802, 44 (3). 375–421.
5. Kresge, C.T.: Leonowicz. M.E.: Roth, W.J.: Beck. J.S. Ordered mesoporous molecular sieves synthesized by liquid-crystal template mechanisms. Nature 1992. 359, 710–712.
6. Corma, A.: Fornés. V.: Pergher. S.B.: Maesen. Th.L.M.: Buglass, J.G. Delaminated zeolite precursors as selective acidic catalysts. Nature 1998. 396. 353–356.
7. Corma, A.: Fornés. V.: Martinez-Triguero. J.; Pergher. S.B. Delaminated zeolites: Combining the benefits of zeolites and mesoporous materials for catalytic uses. J. Catal. 1999. 186. 57–63.
8. Sheldon. R.A.; Downing. R.S. Heterogeneous catalytic transformations for environmentally friendly production. Appl. Catal. A 1999, 189. 163–183.
9. Caniblor. M.A.; Diaz-Cabanas, M.J.: Pérez-Pariente. J.: Teat. S.J.; Clegg. W.: Shannon, I.J.: Lighfoot. P.; Wright, P.A.: Morris. R.E. SSZ-23: An odd zeolite with pore openings of seven and nine tetrahedral atoms. Angew. Chem., Int. Ed. Engl. 1998. 37. 2122–2126.
10. Baerlocher. Ch.: Meier. W.W.; Olson. D.H. *Atlas of Zeolite Framework Types*, 5th Ed.: Elsevier. 2001.
11. Roth. W.J.; Vartuli, J.C.; Kresge. C.T. Characterization of Mesoporous Molecular Sieves: Differences Between M41S and Pillared Layered Zeolites. In *Nunoporous Materials II*; Sayari. A., Jaroniec. M., Pinnavaia, T.J., Eds.; Studies in Surface Science and Catalysis, Elsevier, 2000: Vol. 129. 501–508.
12. Ying, J.Y.: Mehnert, Ch.P.: Wong, M.S. Synthesis and applications of supramolecular-templated mesoporous materials. Angew. Chem.. Int. Ed. 1999, 38. 56–77.
13. Schiith. F. Non-siliceous mesostructured and mesoporous materials. Chem. Mater. 2001. 13. 3184–3195.
14. On. D.T.; Lutic, D.: Kaliaguine, S. An example of mesostructured zeolitic material: UL-TS-1. Microporous Mesoporous Mater. 2001. 44–45. 435–444.
15. Verhoef. M.J.: Kooyman. P.J.; van der Waal, J.C.: Rigutto. M.S.; Peters. J.A.: van Bekkum. H. Partial transformation of MCM-41 inaterial into zeolites: Formation of nanosized MFI type crystallites. Chem. Mater. 2001. *13*, 683–687.
16. Huang. L.: Guo. W.: Deng, P.: Xue. Z.; Li. Q. Investigation of synthesizing MCM-41/ZSM-5 composites. J. Phys. Chem., B 2000, 104. 2817--2823.
17. Liu. Y.: Zhang, W.: Pinnavaia. T.J. Steam-stable MSU-S aluminosilicate rnesostructures assembled from zeolite ZSM-5 and zeolite β seeds. Angew. Chem.. Int. Ed. 2001. 40. 1255–1258.
18. Bein. T. Inclusion Chemistry of Organometallics on Zeolites. In *Comprehensive Supramolecular Chemistry*; Atwood, J.L.. Davies. J.E.D., MacNicol, D.D.. Vogtle, F.. Eds.: Pergamon. 1995; Vol. 7, 579–619.
19. de Vos, D.E.; Jacobs. P.A. Zeolite-Based Supramolecular Assemblies. In *Introduction in Zeolite Science and Practice*; van Bekkum. *H.*, Flanigen, E.M.. Jacobs, P.A., Jansen. J.C., Eds.: Elsevier, 2001: Vol. 137, 957–985.
20. van der Waal, J.C.; van Bekkum, H. Molecular sieves, multifunctional microporous materials in organic synthesis. J. Porous Mater. 1998. 5. 289–303.
21. Barthomeuf, D. Basic zeolites: Characterization and uses in adsorption and catalysis. Catal. Rev. 1996. 38. 521–612.
22. Parton, R.F.: Vankelecorn, I.F.J.; Bezoukhanova, C.P.; Casselman. M.; Uytterhoeven. J.: Jacobs. P.A. An efficient mimic of cytochrorne P-450 from a zeolite encaged iron complex in a polymer membrane. Nature 1994. 370. 541–544.
23. Meinershagen. J.L.; Bein. T. Optical sensing in nanopores. Encapsulation of the solvatochromic dye nile red in zeolites. J. Am. Chem. Soc. 1999. 121. 448–449.
24. Spange, S.: Graser, A.; Huwe, A.; Kremer. F.: Tintemann, C.: Behrens, P. Cationic host–guest polymerization of N-vinylcarbazole and vinyl ethers in MCM-41, MCM-48. and nanoporous glasses. Chern. Eur. J. 2001, 7. 3722–3728.
25. Balcar. H.: Sedláček. J.; Čejka, J.: Vohlidal. J. MCM-41-immobilized [Rh(cod)OCH3]2 complex—A hybrid catalyst for the polymerization of phenylacetylene and its ring-substituted derivatives. Macromol. Rapid Commun. 2002, 23. 32–37.
26. Freyhardt. C.C.: Tsapatsis. M.; Lobo. R.F.: Balkus, K.J.; Davis, M.E. A high-silica zeolite with a 14-tetrahedral-atom pore opening. Nature 1996, 381, 295–298.
27. Corma, A.; Navarro. M.T.: Rey. F.; Rius. J.: Valencia. S. Pure polymorph C of zeolite β synthesized by using framework isomorphous substitution as a structure-directing mechanism. Angew. Chem.. Int. Ed. 2001. 40, 2277–2280.
28. Corma. A.; Diaz-Cabanas. M.: Martinez-Triguero, J.; Rey. F.; Rius. J. A large-cavity zeolite with wide pore windows and potential as an oil refining catalyst. Nature 2002. 418. 514–517.

Zinc-Containing Enzymes and Their Models

Takashi Hayashi
Kyushu University, Fukuoka, Japan

INTRODUCTION

Zinc is one of the essential and widely used transition metals (Group 12) in biology, because it is the second most abundant transition metal in our body. Recently. the structures of over 300 zinc-containing proteins were determined, where the zinc atom acts as a strong catalyst as well as regulates the physiological process or fixation of the unique structural conformation of bioactive species. Zinc usually exists only in the dication state, Zn^{2+} with a closed d^{10} electronic configuration, indicating that no reduction-oxidation process occurs in physiological systems, whereas it is well known that zinc is the most common Lewis acidic metal cation in bioinorganic chemistry. A zinc-bound water molecule rapidly exchanges, because the ligand–zinc bond is kinetically labile. These features provide an effective hydrolysis function of the zinc complex through the activation of coordinated water. Therefore, it is of particular interest to study the metabolic conversion or degradation of biomolecules catalyzed by zinc enzymes. However, the mechanistic details of the enzyme function in the protein matrix are sometimes complicated, even though the structures of many zinc enzymes can be characterized by several different spectroscopies. On the other hand, a synthetic zinc complex related to the active site sphere will be a good tool with which to understand the role of the zinc ion and the complicated mechanism of catalytic reactions.[5,6] A great deal of interest focused on the design of excellent functional or structural models on zinc enzymes. In this article. several representative zinc enzymes and related functional models with supramolecular components will be discussed.

GENERAL MECHANISM OF HYDROLYSIS CATALYZED BY ZINC ENZYMES

It is known that the hydrolysis of peptides, proteins, or esters is accelerated by zinc-containing enzymes such as peptidases. lactamases, or dehydratases, even at neutral pH (Eq. 1), because a solvent water molecule readily binds to the strong Lewis acidic zinc ion to form $[Zn—OH_2]^{2+}$ (Eq. 2), and then the deprotonation of the coordinated water molecule occurs even at neutral pH (Eq. 3). In fact, a series of model studies demonstrated that the pK_a value of the coordinated water molecule decreases to as low as 7–8. The obtained metal-bound hydroxide species, $[Zn—OH]^+$ can then act as a nucleophile toward a hydrolyzable substrate. It is found that in some zinc-containing enzymes, the coordinated water molecule is not completely deprotonated. In such cases, a proton acceptor such as glutamate assists in the generation of the hydroxide complex (Eq. 4). In the enzymatic systems, the pK_a value of the coordinated water is controlled by the coordination number, ligand property, and amino acid residues near the zinc complex. Another catalytic pathway of the zinc enzyme is the displacement of a coordinated water molecule with a substrate (Eq. 5). For example, an alcohol is a substrate for a zinc complex in alcohol dehydrogenase, where a coordinated water molecule is replaced with an alcohol, and then deprotonation occurs to yield a zinc–alkoxide complex, $[Zn—OR]^+$, in the same manner as depicted by Eq. 3.

$$R—NH—CO—R + H_2O \rightarrow R—NH_2 + HO—CO—R \quad (1)$$

$$Zn^{2+}(\text{in protein}) + H_2O \rightarrow [Zn—OH_2]^{2+} \quad (2)$$

$$[Zn—OH_2]^{2+} \rightarrow [Zn—OH]^{+} + H^{+} \quad (3)$$

$$[Zn—OH_2]^{2+} + B^{-} \rightarrow [Zn—OH\cdots H\cdots B]^{+} \quad (4)$$

$$[Zn—OH_2]^{2+} + \text{Substrate} \rightarrow [Zn—\text{Substrate}]^{2+} + H_2O \quad (5)$$

INTRODUCTION TO REPRESENTATIVE ZINC ENZYMES

Shown in Fig. 1 is the three-dimensional active-site structures of four representative zinc-containing enzymes: carboxypeptidase[7] and β-lactamase[8] belong to the hydrolase family, while carbonic anhydrase[9] is one of

Encyclopedia of Supramolecular Chemistry
DOI: 10.1081/E-ESMC 120012699

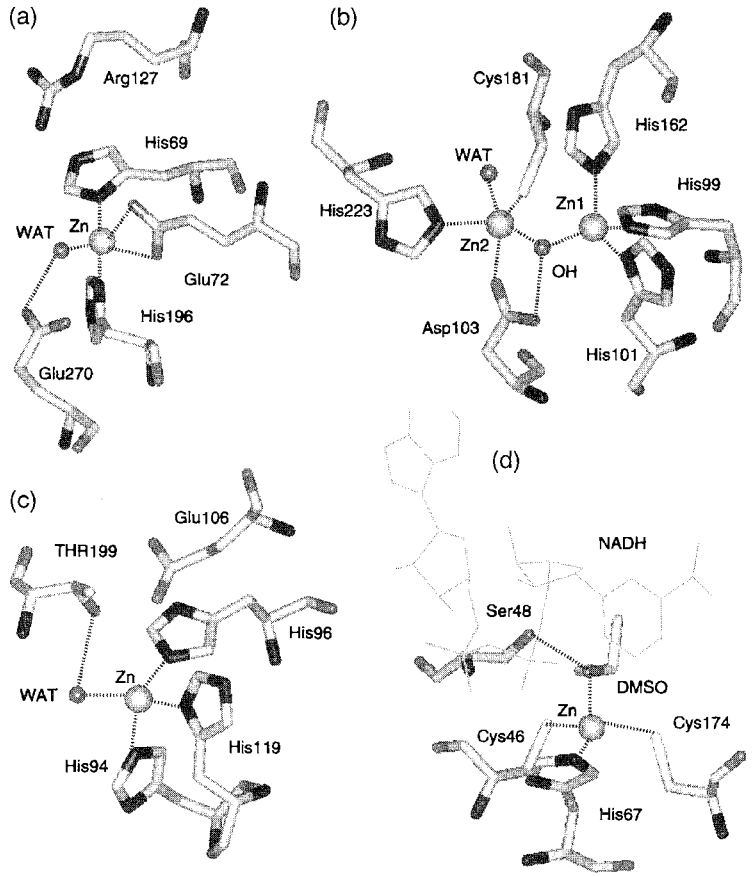

Fig. 1 Active site structures of four zinc-containing enzymes: (a) carboxypeptidase A from bovine pancreas. (b) β-lactamase from *Bacteroides fragilis*, (c) human carbonic anhydrase. and (d) horse liver alcohol dehydrogenase.

the famous lyases, and alcohol dehydrogenase[10] is classified as an oxidoreductase. All of these enzymes except for β-lactamase have four-coordinate zinc complexes with a normal or distorted tetrahedral geometry including a water molecule as the fourth ligand. In the case of some β-lactamases, there are two zinc sites, although the role of the second zinc atom is still not clear.

Carboxypeptidase A

The carboxypeptidase A, mainly isolated from bovine pancreas, is a metalloprotease that hydrolyzes peptide linkages. Particularly, the catalytic cleavage of the peptide in the presence of the enzyme preferably occurs at the C-terminal amide bond with a large hydrophobic amino acid side chain. such as phenylalanine, because the enzyme has a steady binding pocket for an aromatic ring. A proposed mechanism of initial step is shown in Fig. 2.[11] The zinc ion is coordinated by two histidines, one chelating (η^2-)glutamate and one water molecule, as shown in Fig. 1. The coordinated water is converted to the metal-bound hydroxide that is assisted by Glu270 as a general acid catalyst. The hydroxide then acts as the nucleophile to attack the peptide carbonyl carbon that is polarized with the assistance of Arg127. The tetrahedral obtained intermediate is stabilized by several interaction networks. It decomposes by proton donation from Glu270 and affords the final products via C—N bond cleavage.

β-Lactamase

The metallo-β-lactamases hydrolyze a series of β-lactam antibiotics, such as penicillin and cephalosporin derivatives. making them harmless to pathogenetic bacteria.[12] Thus. it is important to study the hydrolysis mechanism and prepare a clinically useful inhibitor. According to the three-dimensional structure of a zinc β-lactamase from *Bacteroides fraglis*, there are two zinc binding sites. where the two zinc ions, Zn1 and Zn2, are 3.5 Å apart and bridged by one hydroxide group; and Zn1 and

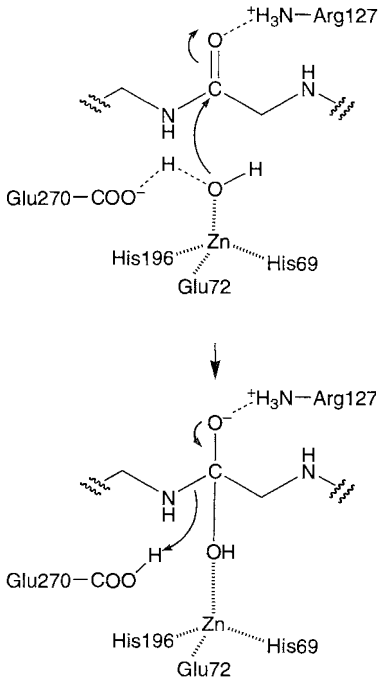

Fig. *2* A proposed mechanism of the nucleophilic attack of zinc-hydroxide to a carobonyl carbon of a peptide linkage.

Zn2 have a tetrahedral and trigonal-bipyramidal coordination geometry. respectively, as shown in Fig. 1. Although the mechanism of the N—C(=O) bond cleavage in the β-lactam is not completely clear, functional model studies suggested that the β-lactam antibiotics could be fixed at the active site by the interaction between a carboxylate of the β-lactam and one of the zinc ions (Zn2), and then the zinc-bound hydroxide acts as a nucleophile to attack the β-lactam. The intermediate species after the cleavage of the four-membered ring of the β-lactam is stabilized by two zinc ions. One zinc ion (Zn1) interacts with the carboxylate anion generated, and the other (Zn2) acts as a receptor of anionic nitrogen. Subsequent protonation of the intermediate species gives the hydrolytic opening product, which is antibiotic inactive.

Carbonic Anhydrase

The role of carbonic anhydrase is to reversibly convert carbon dioxide into bicarbonate. The structure of the active site containing one zinc ion is relatively simple compared to the carboxypeplidase A; however, it is one of the typical examples that demonstrates the nucleophilic attack at carbon by activated zinc-coordinated water.[''''] The catalytic zinc ion of carbonic anhydrase II is bound to three histidines and one water molecule to form a distorted tetrahedral geometry, as shown in Fig. 1. It is known that the pK_a value of the coordinated water molecule is approximately 7, indicating that the metal-bound hydroxide group is easily produced under physiological conditions, because deprotonation of the coordinated water is assisted by the Thr199 and Glu106 hydrogen-bonding network and a proton relay system including several histidines. The generated metal-bound hydroxide acts as a strong nucleophile to attack the carbon dioxide, and then the metal-bound carbonate is produced as an intermediate. The proposed reaction mechanism is summarized in Fig. 3. It is well-known that the hydrolysis equilibrium for CO_2 is fast. by diffusional control with a turnover number of 10^6 s^{-1}, indicating that the reaction is accelerated by a factor of 10^7 compared to that observed for the uncatalyzed reaction under physiological conditions, and hence, carbonic anhydrase represents a highly sophisticated catalyst.

Alcohol Dehydrogenase

Primary alcohols are metabolized to the corresponding aldehyde by mammalian liver alcohol dehydrogenase containing a catalytic site and a structural zinc site.[3,4] This enzyme requires a binding site for the dehydrogenase coenzyme NAD^+/NADH that directly catalyzes the oxidation of an alcohol or reduction of an aldehyde, because the zinc does not have any oxidation or reduction activity. The zinc ion located at the active site is tetrahedral coordinated by two cysteines, one histidine, and one water molecule. The coordinated water molecule must be replaced with the alcohol during the first step of the reaction. After the deprotonation of the alcohol to an alkoxide on the zinc ion, the subsequent proton transfer from the alkoxide to NAD^+ is accelerated to yield the corresponding aldehyde and NADH. For the reverse reaction from the aldehyde, the zinc ion interacts with the carbonyl oxygen of the substrate to polarize the C=O bond and accelerate the hydrogen transfer from NADH. According to the three-dimensional structure of the alcohol dehydrogenase, there is another zinc ion coordinated by four cysteines, and the role of the zinc might be fixation of the enzyme structure.

SEVERAL FUNCTIONAL **MODELS WITH SUPRAMOLECULAR** STRUCTURES FOR ZINC ENZYMES

The development of synthetic models for metalloenzymes is one of the most advanced fields in bioinorganic chemistry, because a well-defined model often gives us

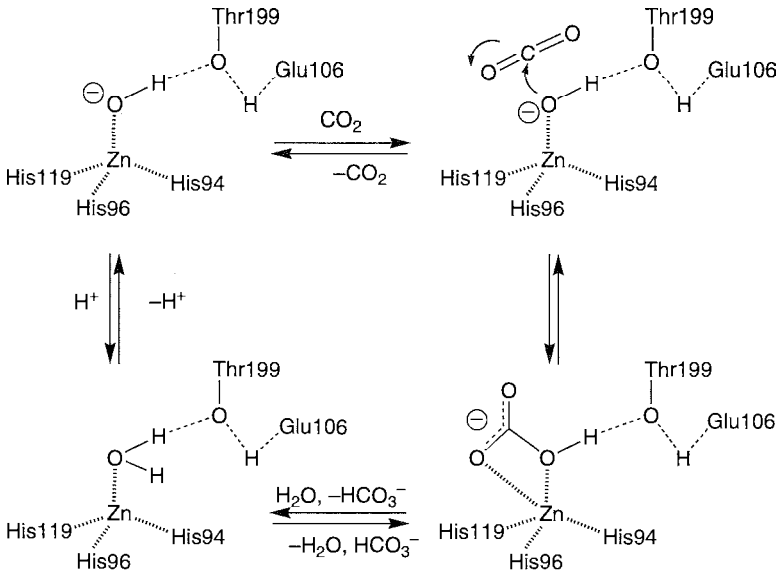

Fig. 3 A proposed catalytic mechanism of carbonic anhydrase.

a good suggestion about structure and function relationship\ and the complicated reaction mechanism of metalloproteins. Much effort on zinc enzyme modeling was devoted to demonstrating the catalytic importance of the Lewis acidity of the zinc atom by mimicking the active site. Reported herein are several representative models *focusing on the reactivity of zinc enzymes.*

Carboxypeptidase A Models

Model studies of carboxypeptidase A are limited. It is found that some zinc complexes can hydrolyze the carboxylic ester, however, there is no suitable functional model that demonstrates *the hydrolysis of normal* carboxamide *by* [Zn—OH]$^+$species.

β-Lactamase Models

It *is* important *to understand the mechanism of the cleavage of the (3-lactam ring catalyzed by* β-lactamase *involving a zinc atom as an active site, because the* zinc-containing *enzyme is a factor in bacterial resistance to the 0-lactam antibiotics such as penicillin, cephalosporin, and so on. The first functional model for* β-lactamase *was reported by* Kimura *and* coworkers.[14] They *demonstrated that the zinc complex involving* 1,4,7,10-tetraazacyclododecane ([12]aneN$_4$) forms *the* [Zn—OH]$^+$ *species under neutral conditions, and it accelerated the hydrolysis of benzylpenicillin in aqueous solution. In contrast, the native* β-lactamase *has two zinc atoms in the active site. From the three-dimensional structure information,* Lippard *and his coworkers recently prepared the unique functional models formed by dinuclear* Zn^{2+} *complexes as shown in Fig.* 4.[15,16] *For example, the observed rate constant for the hydrolysis of nitrocefin catalyzed by* [Zn_2 (BPAN)(μ-OH)(μ-O_2PPh_2)](ClO_4)$_2$, *where BPAN is* 2,7-*bis*[2-(2-pyridylethyl)aminomethyl]-*1.8-naphthyridine, is 2800–fold greater than that observed in the absence of a zinc complex at pH 7, whereas this value is comparable with that obtained by mononuclear zinc complexes. This finding indicates that the second* Zn^{2+} *does not activate the hydroxide as a nucleophile to nitrocefin. Moreover. the intermediate 2 in the (3-lactam hydrolysis based on the dinuclear zinc models* 1. *the* adduct *between dinuclear zinc complex and the opened nitrocefin, was characterized by* UV/Vis, *IR. and NMR spectroscopy, as shown in Fig.* 4.[17] *The structural data of the intermediate species suggest that two zinc* atoms *in the enzyme might play a role in the substrate binding sites, and the bridging hydroxide* intramolecularly *attacks the* β-lactam *antibiotics.*

Carbonic Anhydrase Models

Over the last two decades, a thousand structural and functional models for carbonic anhydrase were reported to address the features of the active site and the mechanism of the catalytic reaction. One of the earliest functional models is *the supramolecular composite of the* *bis*(histamino)cyclodextrin-Zn-imidazole *complex 3 that accelerates* CO_2 *hydration at* pH *7.0. although the catalytic activity is not good compared with the native*

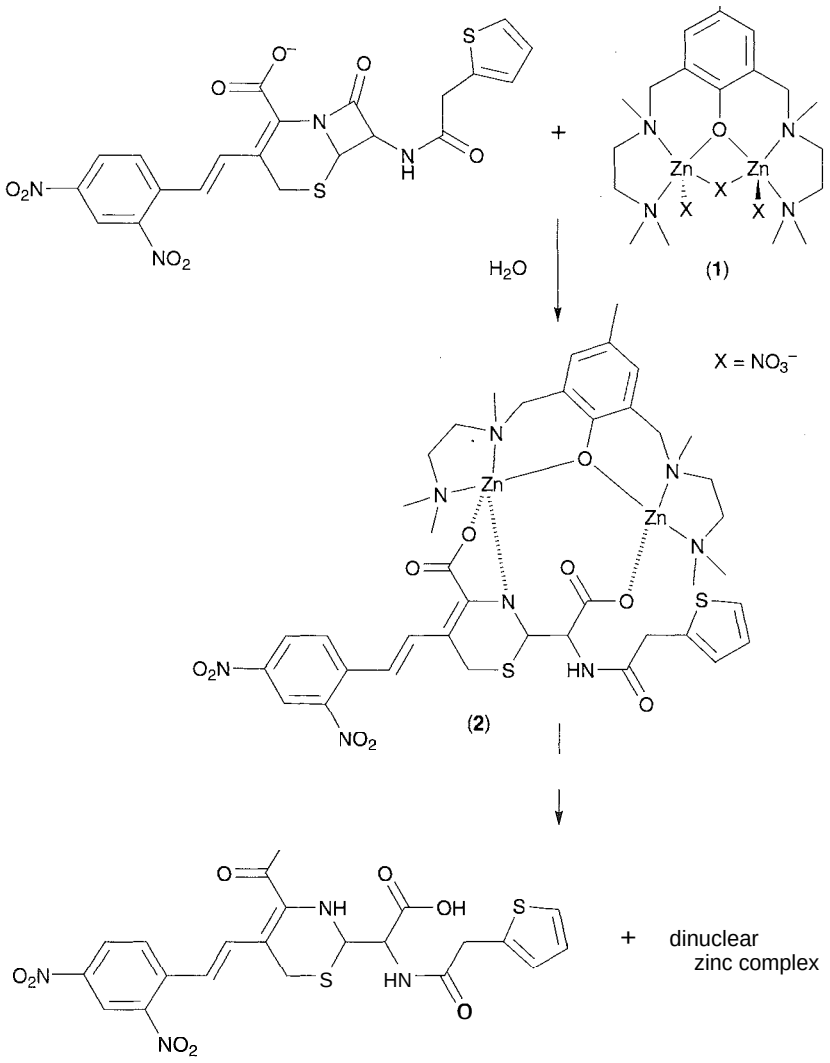

Fig. 4 Nitrocefin hydrolysis catalyzed by a dinuclear zinc(II) complex and its intermediate.

enzyme.[18,19] Kimura and coworkers demonstrated that the zinc(II) complex 4 with 1,5,9-triazacyclododecane, [12]aneN$_3$, as a ligand catalyzes the pH-dependent hydration of CO_2. Based on a titrimetric experiment, the pK_a value of Zn([12]aneN$_3$)·H$_2$O was determined to be 7.4. which is almost the same as that observed in the native carbonic anhydrase. The acceleration of CO_2 hydration was clearly observed in the region higher than pH 7.4. indicating that the zinc hydroxo species smoothly reacts with CO_2 under mild conditions.[20] The rate of the catalytic hydration of CO_2 also increased by 1,4,7,10-tetraazacyclododecane ([12]aneN$_4$) as a ligand. Eldik and coworker detcribed that an inflection point at pH 8.1 obtained in this reaction from the hydration rate by Zn([12]aneN$_4$)·H$_2$O 5 is almost comparable with the pK_a value of the deprotonation of the coordinated water.[21] Furthermore, Zn([12]aneN$_4$)·H$_2$O shows one of the highest catalytic activities of all reported zinc model complexes for the dehydration of HCO_3^- and hydration of CO_2, respectively. In contrast, Brown and coworkers prepared the *tris*(4,5-dialkyl-2-imidazolyl)phosphine-zinc complex 6, which mimics an active-site model for the carbonic anhydrase.[22] Although their models did not dramatically enhance the rate of interconversion between CO_2 and HCO_3^-, it is of interest to evaluate the catalytic mechanism using this system, because the coordination environment of the model zinc complex is an analog to that of the native enzyme, having a tetrahedra1 zinc center composed of three imidazoles and one water. Furthermore, Parkin, Vahrenkamp, and coworkers discussed the

intermediate of the catalytic reaction using *tris*(3,5-dialkylpyrazolyl)hydroboratozinc complex **7**.[23] Particularly. the hydroxide complex can smoothly react with CO_2 to yield a bicarbonate complex characterized by spectroscopy and then form the dimeric zinc complexes via a carbonate ligand bridge. The zinc complex obtained shows a unidentate or chelated bidentate coordination mode (8 or 9. respectively), which depends on the bulkiness of the substituted alkyl groups at the 3-position of the pyrazolyl ring, as shown in Fig. 5. From the ^{17}O-NMR study on the exchange of oxygen between CO_2 and $^{17}0$-labeled water, which is a critical process for the catalytic reaction of the carbonic anhydrase, it is concluded that the formation of a bidentate carbonate intermediate inhibits the displacement of the bicarbonate by water.[26,27] These results also rationalize the fact that the catalytic activity of $Zn[12]aneN_3$ is lower than that of $Zn([12]aneN_4)$, because the former complex may form the bidentate bicarbonate intermediate that decreases the displacement of the bound bicarbonate ligand by H_2O. In addition. Parkin and coworker recently reported the fact that protonation of the zinc hydroxide complex also inhibits the reactivity toward CO_2, indicating that the CO_2 hydration requires deprotonation of the coordinated water.[25] A series of model studies suggests that the catalytic activity of CO_2 hydration requires the deprotonation of the coordinated water and the prevention of the bidentate interaction of the carbonate with the zinc atom at the intermediate state.

Alcohol Dehydrogenase Models

To mimic the zinc-containing alcohol dehydrogenase enzyme, several groups focused on the complexation between an alcohol and the zinc complex and the subsequent hydrogen transfer from the obtained alkoxide complex to NAD^+ to yield the corresponding aldehyde derivatives (Fig. 6). Vahrenkamp and coworkers isolated the zinc alkoxide complex **10** with a *tris*(thioimidazolyl)hydroborate ligand from the reaction between the zinc hydroxide complex and phenols or trifluoroethanols.[26] Furthermore, the hydroxide and ethoxide interconversion in the zinc complex **7** with a *tris*(pyrazolyl)hydroborate as a ligand was also observed by Parkin and coworker.[27] In addition, Berreau and coworkers recently demonstrated that the zinc methoxide **11** with the *N*-2-(ethylthio)ethyl-*N*,*N*-*bis*(6-neopentylamino-2-pyridylmethyl)amine shows a significant hydrolytic stability due to the hydrogen bonding interaction between the methoxide and the N—H proton of the ligand, so the equilibrium is shifted to the zinc alkoxide from the zinc hydroxide, which mimics the native enzyme, where the alkoxide is stabilized by Ser48.[28] In contrast, Kimura and coworker demonstrated a hydride transfer reaction from 2-propanol to hydrogen acceptors such as a NAD^+ model or p-nitrobenzaldehyde by $Zn([12]aneN_3)$ **4**.[29] It is the first functional model for the alcohol dehydrogenase to demonstrate hydride transfer around the zinc coordination sphere.

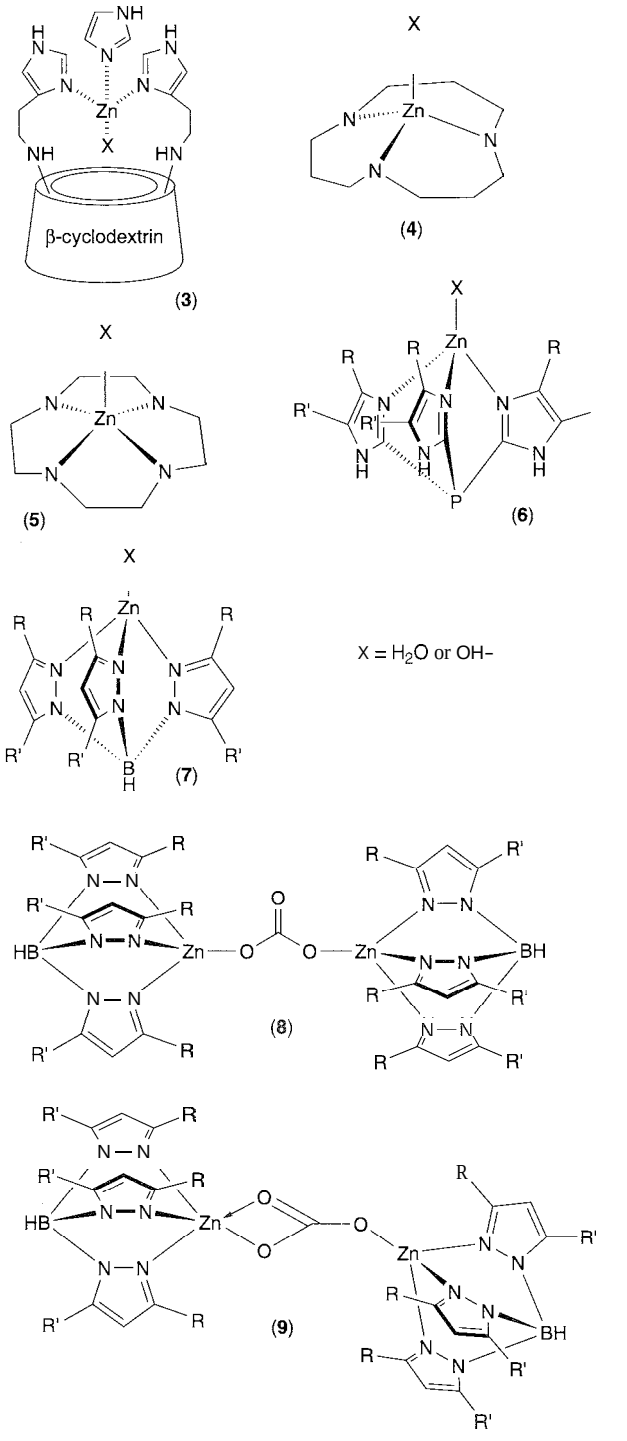

Fig. *5* Molecular structures of several functional models for carbonic anhydrase.

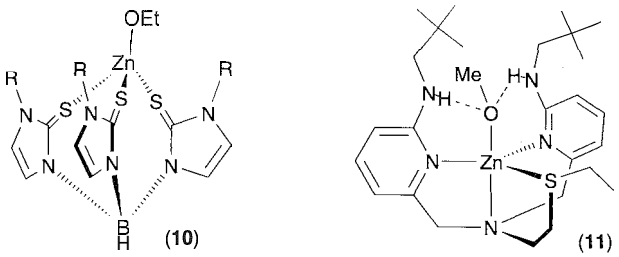

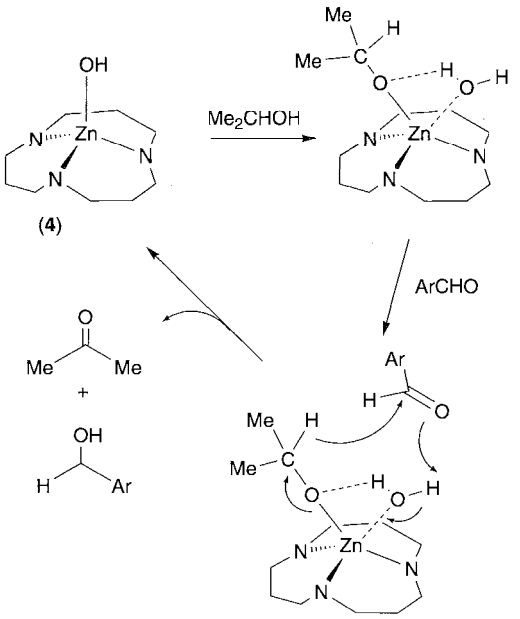

Fig. 6 Structure and function models for alcohol dehydrogenase.

CONCLUSION

Described in this article are four zinc enzymes and their representative functional models. Although the three-dimensional structures of many zinc enzymes were determined in the last decade, the dynamics and mechanisms of the catalytic process of the zinc enzyme are complicated and still not fully understood. Therefore, to resolve the nature of the active site in enzymes; it is necessary to prepare an appropriate model complex. From a series of studies by functional models, it is found that the pK_a of the coordinated water controlled by the ligand properties and the coordination mode of the substrate are essential to obtain catalytic activity for zinc enzymes. However, no functional models exhibit the activity observed by the native enzyme under physiological conditions. Thus, the goal that remains is to elucidate the significant difference in catalytic activity between the zinc enzymes and these models and then create a supramolecular composite of an artificial zinc enzyme that demonstrates the excellent catalytic function.

ARTICLES OF FURTHER INTEREST

Artificial Enzymes, p. *76*
Carbonic Anhydrase Models, p. *178*
Carboxypeptidase A, p. *183*
Enzyme Mimics, p. *546*
Enzymes: Characteristics and Mechanisms, p. *554*

REFERENCES

1. Auld, D.S. Zinc Sites in Metalloenzymes and Related Proteins. In Handbook on Metalloproteins; Bertini. I.. Sigel. A., Sigel, H.. Eds.: Marcel Dekker, Inc.: New York, 2001: 881–959.
2. Folkers, G.E.: Hanzawa, H.; Boelens, R. Zinc Finger Proteins. In Handbook on *Metalloproteins*; Bertini. I.. Sigel, A.. Sigel, H.. Eds.; Marcel Dekker, Inc.: New York, 2001; 961–1000.
3. Lipscomb. W.N.: Strater, N. Recent advances in zinc enzymology. Chem. Rev. **1996.** 96 (7). 2375–2433.
4. Holm, R.H.; Kennepohl, P.; Solomon, E.I. Structural and functional aspects of metal sites in biology. Chem. Rev. 1996, 96 (7), 2239–2314.
5. Kimura, E. Model studies for molecular recognition of carbonic anhydrase and carboxypeptidase. Acc. Chem. Res. 2001, 34 (2), 171–179.
6. Parkin. G. Synthetic Analogs of Zinc Enzymes. In Metal *Ions in* Biological Systems; Sigel, A., Sigel, H., Eds.: Marcel Dekker, Inc.: New York, 2001; Vol. 38, 411–460.
7. Teplyakov. A.; Wilson, K.S.; Orioli, P.: Mangani, S. *The* High *Resolution Crystal* Structure *of the Complex Between Carboxypeptidase* A and *L-Phenyl* Lactate: Acta. Crystallogr. D.. 1993. 49 (6). 534–540. Generated from PDB file 2CTB.
8. Concha, N.O.: Rasmussen, B.A.: Bush, K.: Herzberg. O. *Crystal Structure* of the Wide Spectrum *Binuclear Zinc* β-Lncfamase *from Bacteroides Fragilis*; Structure **1996.** 4 (7), 823–836. Generated from PDB file 1ZNB.
9. Alexander. R.S.; Nair. S.K.; Christianson. D.W. Engineering the hydrophobic pocket of carbonic anhydrase II. Biochemistry 199%. 30 (46), 11064–11080. Generated from PDB file 4CA2.
10. Al-Karadaghi, S.; Cedergren-Zeppezauer, E.S.; Petratos, K.: Hovmoeller, S.: Terry. H.; Dauter. Z.: Wilson, K.S. Refined *Crystal Structure* of *Liver* Alcohol *Dehydrogenase-NADH* Complex at *1.8 Å* Resolution; to be published. Generated from PDB file 2OHX.
11. Christianson. D.W.; Lipscomb, W.N. Carboxypeptidase A. Acc. Chem. Res. 8989. 22 (2), 62–69.
12. Massova. I.; Mobashery. S. Molecular bases for interactions between β-lactam antibiotics and β-lactamases. Acc. Chem. Res. 1997, 30 (4), 162–168.
13. Christianson, D.W.: Fierke, C.A. Carbonic anhydrase: Evolution of the zinc binding site by nature and by design. Acc. Chem. Res. 1996, 29 (7), 331–339.
14. Koike, T.: Takamura, M.: Kimura, E. Role of zinc(II) in β-lactamase II: A model study with a zinc(II)-macrocyclic

tetraamine (1,4,7,10-tetraazacyclododecane, cyclen) complex. J. Am. Chem. Soc. **1994.** *116* (19). 8443–8449.
15. Kaminskaia, N.V.: Spingler. B.: Lippard, S.J. Hydrolysis of β-lactam antibiotics catalyzed by dinuclear zinc(II) complexes: Functional mimics of metallo-β-lactamases. J. Am. Chem. Soc. **2000,** *122* (27). 6411–6422.
16. Karninskaia, N.V.; He, C.; Lippard, S.J. Reactivity of μ-hydroxodizinc(II) centers in enzymatic catalysis through model studies. Inorg. Chem. **2000.** *39* (15). 3365–3373.
17. Karninskaia. N.V.; Spingler, B.: Lippard, S.J. Intermediate in β-lactam hydrolysis catalyzed by a dinuclear zinc(II) complex: Relevance to the mechanism of metallo-β-lactamase. J. Am. Chem. Soc. **2001,** *123* (27). 6555–6563.
18. Tabushi, I.: Kuroda. Y. Bis(histamino)cyclodextrin-Zn-imidazole complex as an artificial carbonic anhydrase. J. Am. Chem. Soc. **1984,** *106* (16). 4580–4584.
19. Bertini. I.; Hayashi, T.; Kuroda, Y.; Luchinat, C.: Tabushi, I. ^{1}H NMR Characterization of the system cobalt(II)-*bis*(histamino)-β-cyclodextrin-imidazole. Gazz. Chim. Ital. **1988,** *118* (11). 777–781.
20. Kimura, E.; Shiota. T.; Koike. T.: Shiro, M.: Kodama, M. A zinc(II) complex of 1,5,9-triazacyclododecane ([12]aneN$_3$) as a model for carbonic anhydrase. J. Am. Chem. Soc. **1990,** *112* (15). 5805–5811.
21. Zhang, X.; van Eldik, R.A. Functional model for carbonic anhydrase: Thermodynamic and kinetic study of a tetraazacyclododecane complex of zinc (II). Inorg. Chem. **1995.** *34* (22); 5606–5614.
22. Brown. R.S.: Curtis, N.J.; Huguet, J. Tris(4,5-diisopropyl-imidazol-2-yl)phosphine:zinc(2+). A catalytically active model for carbonic anhydrase. J. Am. Chem. Soc. **1981.** *103* (23), 6953–6959.
23. Looney, A.: Parkin, G.; Alsfasse. R.: Ruf. M.; Vahrenkamp. H. Zinc pyrazolylborate complexes relevant to the biological function of carbonic anhydrase. Angew. Chem.. Int. Ed. Engl. **1992.** *32* (1), 92–93.
24. Looney. A.; Han, R.; McNeill, K.; Parkin, G. Tris(pyrazolyl)hydroboratozinc hydroxide complexes as functional models for carbonic anhydrase: On the nature of the bicarbonate intermediate. J. Am. Chem. Soc. **1993,** *115* (11). 4690–4697.
25. Bergquist. C.; Parkin. G. Protonation of the hydroxide ligand in a synthetic analogue of carbonic anhydrase. [Tp^{But,Me}]ZnOH: Inhibition of reativity towards CO_2. J. Am. Chein. Soc. **1999,** *121* (26), 6322–6323.
26. Tesmer. M.; Shu. M.: Vahrenkamp. H. Sulfur-rich zinc chemistry: New tris(thioimidazolyl)hydroborate ligands and their zinc complex chemistry related to the structure and function of alcohol dehydrogenase. Inorg. Chem. **2001.** *40.* 4022–4029.
27. Bergquist. C.; Perkin. G. Modeling the catalytic cycle of liver alcohol dehdrogenase: Synthesis and structural characterixation of a four-coordinate zinc ethoxide complex and determination of relative Zn—OR versus Zn—OH bond enegiees. Inorg. Chem. Acta **1999,** *38* (3). 423–442.
28. Garner. D.K.; Fitch, S.B.: McAlexander. L.H.; Bezold. L.M.: Arif. A.M.; Berreau, L.M. Mononulear nitrogen1 sulfur-ligated zinc methoxide and hydroxide complexes: Investigating ligand effects on the hydrolytic stability of zinc alkoxice species. J. Am. Chem. Soc. **2002.** *124* (34). 9970–9971.
29. Kimura. E.: Shionoya, M.: Hoshino. A.; Ikeda, T.: Yamada. Y. A model for catalytically active zinc(II) ion in liver alcohol dehydrogenase: A novel "hydride transfei" reaction catalyzed by zinc(II)-macrocyclic polyamine complexes. J. Am. Chem Soc **1992.** *114* (26). 10134–10137

Zwitterion Receptors

Stefano Di Stefano
Luigi Mandolini
Università degli Studi di Roma La Sapienza, Roma, Italy

Perla Breccia
Javier de Mendoza
Universidad Autónoma de Madrid, Madrid, Spain

INTRODUCTION

In a zwitterion, either of the charged functions is a likely site of recognition. Thus. a receptor specifically designed for the efficient recognition of a zwitterion should consist of at least two subunits, strategically arranged in a precise geometrical relationship. each of which is capable per se of binding one functional substructure of the substrate. The simultaneous recognition of additional part-structures of the guest should be performed in order to achieve selectivity and increased stability of the host–guest complex.

Since Pedersen's seminal article[1] published 35 years ago, the amount of research done in the field of molecular recognition of cations is overwhelming.[2] However. for a number of reasons, much less interest was focused for a long time on the molecular recognition of anions, and significant progress in the field has been achieved only recently.[3] Consequently, the entire field of molecular recognition of zwitterions was still in its infancy in the mid-1980s.

For the purpose of classification, this short article is divided into three sections, in accordance with the strategy used to achieve recognition of the ionic subunits of the zwitterion's guest. The strategy used in the design of receptors belonging to the first category is simply based on charge complementarity, which means that a major driving force for recognition is provided by a pair of antiparallel salt bridges. A second group is formed by receptors in which a neutral multidentate ligand is deputed to provide a recognition site for the cationic end of the zwitterion. Finally, in the third section, the only available example of a betaine receptor is discussed.

Becauce of their biological relevance, most of the work published in this field refers to the recognition, and the closely related problem of transport across liquid membranes. of the zwitterionic form of amino acids, which is the most abundant form in solution at pH values around neutrality (see Eq. I below).

ZWITTERIONIC RECEPTORS

a-Amino acids are mostly in zwitterionic form around neutral conditions. These are highly solvated species that represent a significant challenge for molecular recognition, because the electron densities of the carboxylate and the ammonium functions are greatly affected by their mutual vicinity, causing the binding forces of complementary groups of the receptor to be less effective for complexation. Although receptors based also on positively and negatively charged binding sites (zwitterionic receptors) would in principle be the molecules of choice for recognition, these designs are often of limited interest, because they tend to collapse internally or to aggregate into dimers or oligomers.

The first successful example of amino acid transport under neutral conditions, using a receptor designed in such a way as to provide charge complementarity to the zwitterionic form of the ainino acid (Eq. 2). was reported by Sunamoto and coworkers in 1982.[5] Upon UV irradiation, the photospiran 1 is converted to the purple form 2 bearing a merocyanine dye skeleton. When an aqueous suspension of single-walled liposomes containing the amino acid in the interior and I in the bilayer was

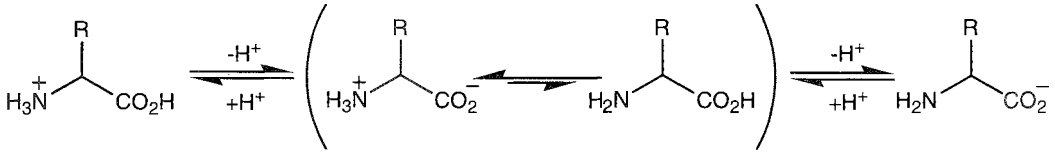

(1)

DOI: 10.1081/E-ESMC 120012722

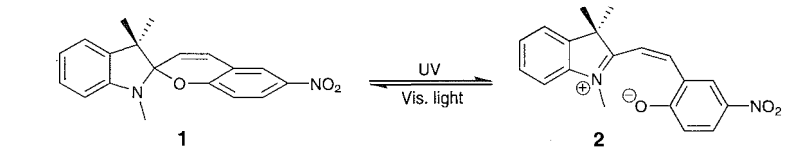

1 2

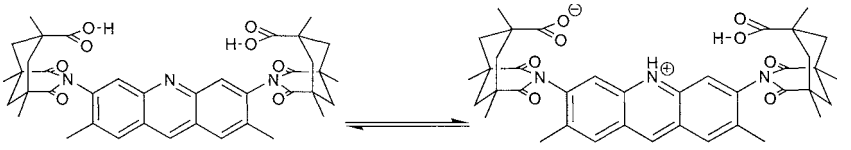

3 4

UV irradiated for 20 min. followed by being visible light irradiated for 5 min, a significant transfer of phenylalanine from the liposome to the outer solvent took place. No transport of amino acid was observed in the dark or in the absence of 1. The system suffers from several drawbacks, including the question of the integrity of the membrane under the conditions of the experiment and the photochemical instability of the photospiran **1.** However, in spite of such limitations. Sunamoto's work established for the first time the simple concept of charge complementarity for recognition and transport of the zwitterionic form of amino acids, as schematically depicted in Eq. 2 (see below).

This concept was adopted shortly afterwards by Rebek and coworkers.[6,7] Their acridine-based derivative ***3*** features a molecular cleft endowed with receptor properties toward guests of complementary size, shape, and hydrogen-bonding capacity. The zwiiterionic form 4 indicated by ^{1}H-NMR spectra to be the dominant species was held responsible for the successful extraction of phenylalanine, tryptophan, and tyrosine methyl ether from their aqueous solutions into chloroform with efficiencies of ca. 50%, accounted for by a 2:1 ternary complex. The same system was employed as an artificial carrier for amino acids across bulk liquid membrane. The aryl/aryl stacking interaction clearly revealed by NMR spectra, from which the structure of the intermolecular ternary complex 5 was established, provides a rationale for the finding that amino acids bearing a lipophilic side chain. such as leucine and isoleucine, were not extracted into chloroform.

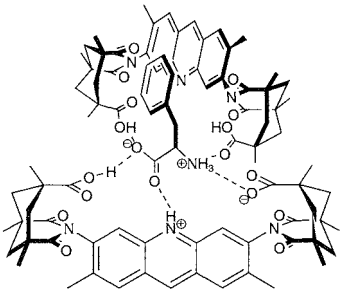

5

The schematic representation of the proposed structure of the complex between tryptophan and β-cyclodextrin modified with pyrrolidinyl and carboxyl subsiituents at neighboring AB (or BA) rings (6. only one regioisomer is shown) effectively illustrates Tabushi's design[s1] of receptors for amino acids based on triple recognition, namely, a combination of hydrophobic interaction between indolylmethyl and a cyclodextrin cavity, and a pair of complementary electrostatic interactions between ionic groups. Stability constants for complexation of D- and L-tryptophan in aqueous solution were in the range of 36–54 M^{-1} with little preference, if any, for the D-enantiomer. Comparison with a binding constant of 13 M^{-1} obtained with unsubstituited β-cyclodextrin shows that the hydrophobic effect is a major driving force for complexation.

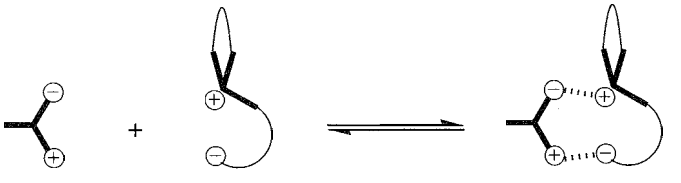

(2)

amino acid 2

The high stability of the amidinium-carboxylate salt bridge (K = *350* M^{-1} in Me_2SO at 35°C, based on simple model compounds) provides the basis for the simple self-replicating system described by von Kiedrowsky.[9] Anils of type **7** are not only capable of self-recognition via a pair of identical antiparallel salt bridges with four hydrogen bonds (as shown in duplex **10**), but also of acting as a template for Shiff-base bond formation between formylphenoxyacetate **8** and aminobenzamidinium **9** precursors. In this sense, anils **7** act as receptors of the zwitterionic transition states in the autocatalytic processes leading to self-replication.

The water-soluble macrobicyclic host **11** synthesized by Askew[10] features three quaternized nitrogens in the molecular backbone and an equal number of convergent

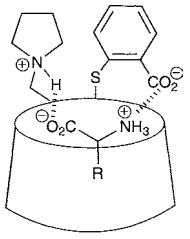

6

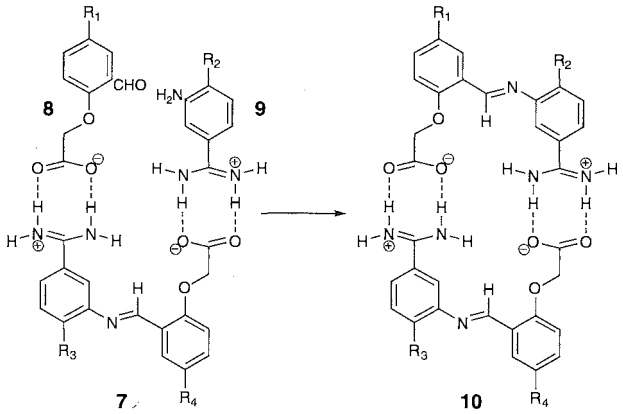

7 **10**

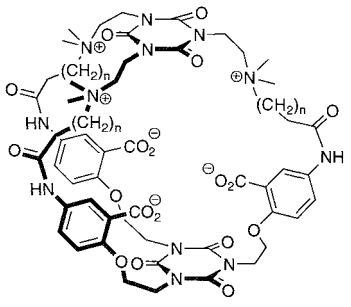

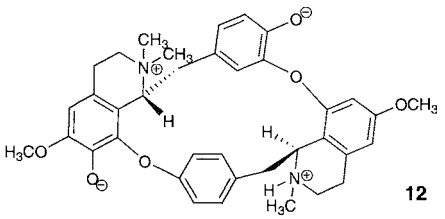

12

carboxylates. NMR evidence indicates that zwitterionic γ-aminobutyric acid (**GABA**), with size that matches that of the host cavity, is strongly complexed with a K value of about *3* x 10^3 M^{-1}. Much lower binding affinities are observed with glycine and 6-aminohexanoic acid, which are too short and too large, respectively, to match the host cavity size. The complexation properties of the zwitterionic form of the macrocyclic alkaloid (+)-tubocurarine **12** were investigated by Uatsimirsky et al.[11] The (+)-tubocurarine shows a moderate affinity toward phenylalanine at pH = 9.0, with a preference for the D-form (K = *30* ± 9 M^{-1}) over the L-form (K = 12 ± 2 M^{-1}).

RECEPTORS BASED ON CROWN ETHERS AND RELATED IONOPHORES

The discovery that crown ethers. besides metal ions. complex ammonium ions via hydrogen bonding to the oxygen donors dates to 1967.[1] Thus, the use of crown ethers and related ionophores as docking sites for the $-NH_3^+$ function of amino acids is an obvious choice. It must be borne in mind. however, that the nearby carboxylate considerably diminishes the likelihood that an ammonium will form hydrogen bonds with lone pair donors. This explains why a large number of receptors for amino acids were designed for single-charge substrates and not for zwitterions. Nevertheless, a sizable number of examples are available, where binding of zwitterionic amino acids was obtained by combining a crown ether or related ionophore moiety with a subunit suitable for carboxylate recognition. In addition, the rich variety of side chains of amino acids offers the potential for selective recognition.

The first attempts at receptors for carboxylate concentrated on protonated polyazamacrocycles.[12,13] These compounds bind their guests via a combination of electrostatic interactions and hydrogen bonds. An early example of a ditopic receptor composed of a macrocyclic polyamine and crown ether subunit was reported by Kimura.[14] The triprotonated form of **13** forms 1:1 complexes with zwitterionic compounds, such as glycine,

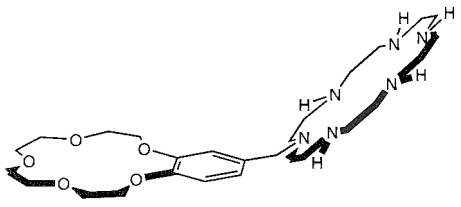

13

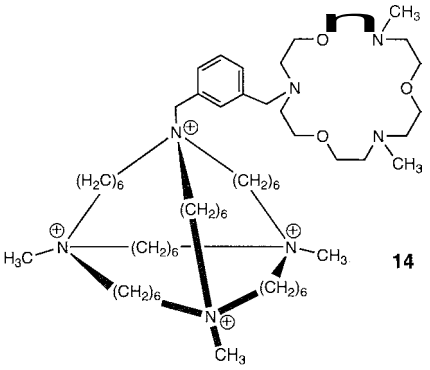

14

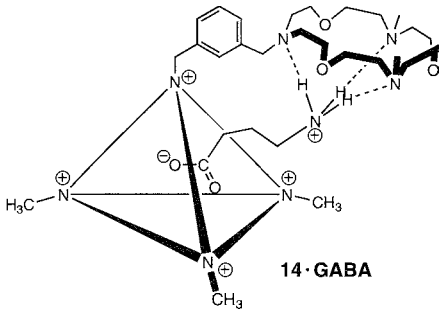

14·GABA

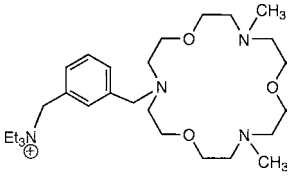

15

β-alanine, $H_2N(CH_2)_3CO_2H$, $H_2N(CH_2)_5CO_2H$, and diglycine in aqueous solution at pH values close to neutrality, with conditional binding constants of the order of $10^2\ M^{-1}$. Because the monotopic model compounds do not interact with the given amino acids under the same conditions, it was argued that the strong binding to **13** is a concerted action resulting from interaction of the carboxylate with the protonated azacrown moiety and from the primary ammonium function with the benzo-crown counterpart.

In place of a protonated macrocycle polyamine. Schmidtchen's ditopic receptor **14**[15,16] features a macrotricyclic quaternary ammonium unit for complexing carboxylate, and an azacrown macrocycle serving as an anchor group for the $-NH_3^+$ end, as schematically shown in the **14·GABA** complex. However, 14 showed no discrimination between GABA and its higher homologue $H_2N(CH)_6CO_2H$ in MeOH/H_2O 9:1, and the model compound 15 turned out to be a stronger binder than 14. Barboiu and coworkers[17] isolated in the solid state a series of complexes between a large number of L-amino acids and a macrocyclic receptor composed of a dibenzo-18-crown-6 unit endowed with two protonated 10-aminodecylcarbonyl side arms. Elemental analysis and spectroscopic data pointed to the formation of 1:1 complexes 16 in which the ammonium end group of the amino acid is bound to the crown ether, while the carboxylate forms a salt bridge with one of the ammonium end groups of the host.

An efficient combination of monotopic receptor subunits characterizes de Mendoza's tritopic receptor **17** [(S,S)-isomer shown] for the enantioselective recognition of α-amino acids.[18] Binding sites for carboxylate and ammonium are provided by nonself-complementary counterparts, such as a guanidinium and crown ether. respectively. Additional structural features are the aromatic surface of naphthalene for a stacking interaction of the side chain of aromatic amino acids and a chiral structure for enantioselective recognition. Thus, in a single extraction experiment, **17** removed about 40% of L-triptophan and L-phenylalanine from saturated aqueous solutions into dichloromethane, whereas the D-forms were extracted to a negligible extent. The high degree of chiral

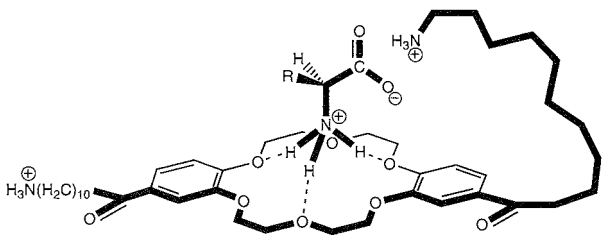

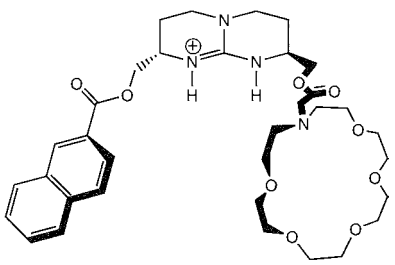

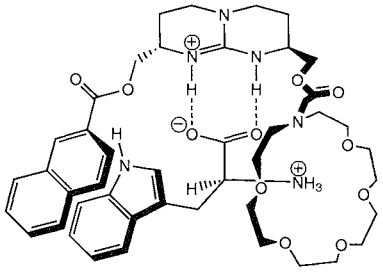

18

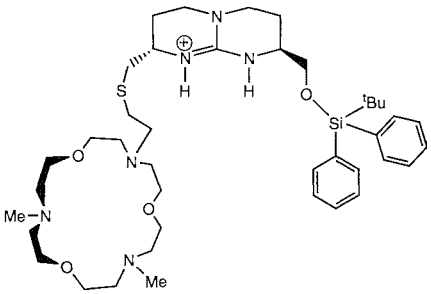

19

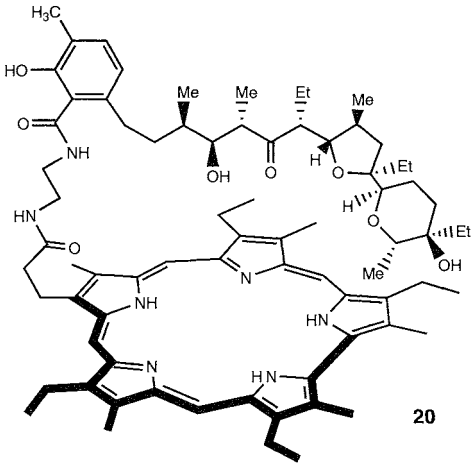

20

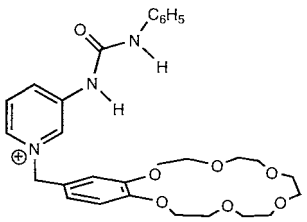

21

recognition is understood on the basis of three simultaneous interactions of the guest with the binding units of the host, as depicted in the proposed structure 18 of the complex with L-triptophan. Detailed molecular mechanics and dynamic calculations[19] showed that the salt bridge contributes about one half of the total binding, whereas the remaining attractive interactions are provided by the aza-crown ether and, to a minor extent. by the naphthalene moiety. The closely related receptor 19 was synthesized by Schmitdchen et al.[20] Thanks to the strongly hydrophobic silyl ether moiety, receptor 19 turned out to be much more effective than 17 in the extraction of a number of amino acid zwitterions from water to dichloromethane, but only a modest enantioselectivity was observed (40% ee for D,L-phenylalanine).

Although the underlying strategy is analogous to that of Kimura's receptor **13,** there are two elements of novelty in Sessier's design[21] of ditopic receptor 28 that features a sapphyrin unit for binding in its protonated form to carboxylate, and the naturally occurring ionophore lasalocid as the ammonium binding group. Receptor 20 acts as an efficient and selective carrier for aromatic n-amino acids, with a preference for phenylalanine > triptophan > tyrosine, and for L-amino acids over the corresponding D-enantiomers.

Instead of positively charged groups, neutral moieties can serve the purpose of providing docking units for carboxylate via hydrogen bonding. Receptor 21, synthesized by Joeng and Park,[22] combines benzo-18-crown-6 and urea functionalities for binding the ammonium and carboxylate groups, respectively, of zwitterionic amino acids. Receptor 21 extracted with high efficiency amino acids with nonpolar side chains. such as phenylalanine, isoleucine, leucine, and triptophan, from their aqueous solution into $CHCl_3$. Unlike 21, none of the model compounds 22 through 24 dissolved phenylalanine and isoleucine in $CHCl_3$. Clearly, the two binding subunits in 21 are cooperatively involved in the hydrogen-bonding

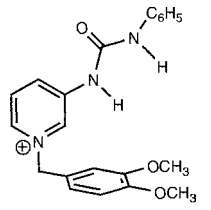

22

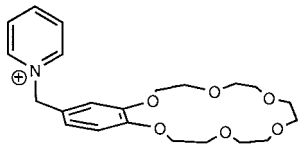

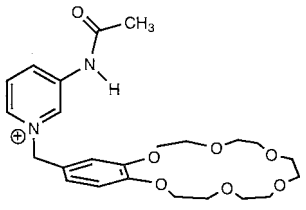

24

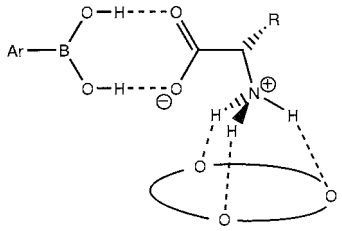

25

interactions with the ammonium and carboxylate end groups of the amino acids. Reetz's strategy[23] to bind and lipophilize zwitterionic amino acids involves the novel hydrogen-bonding interaction between arylboronic acids and the carboxylate group. in combination with the usual interaction between crown ethers and the ammonium function, as schematically depicted in 25. The transport rate of L-phenylalanine through $CHCl_3$ in the presence of crown-ether-modified arylboronic acids 26. **27a**, **27b** was very low for 26 and increased in the order 26 < 27a < **27b**. However, the transport rate in the presence of **27b** was lower than that observed in the presence of a mixture of phenylboronic acid and 18-crown-6, strongly suggesting that the geometry in **27b** is far from ideal for optimal cooperative binding of the two subunits.

Interaction with a metal ion may provide a suitable docking site for the carboxylate of a zwitterionic amino acid, on condition that the receptor molecule is endowed with a multidentate ligand substructure, in which the metal ion is implanted by a complexation process that leaves the cation coordinatively unsaturated. The above strategy is well illustrated by the ternary complex 28, isolated in the solid state (picrate or BF_4^- counterion) by Barboiu and coworkers.[24] Their bis-macrocyclic ligand is capable of multiple recognition of zwitterionic phenylalanine by combining various noncovalent interactions. The Na^+ cation, preferentially complexed by the benzo-15-crown-5, is anion paired to carboxylate, whereas the benzo-18-crown-6 moiety is hydrogen bonded to the $-NH_3^+$ function, and additional stabilization comes from a $\pi-\pi$ stacking interaction. Besides a benzo-18-crown ether moiety, ligand 29 contains the elements of the tetradentate nitrogen ligand *tris*(2-pyridyl-methyl)amine that forms stable complexes with metal ions such as Zn(II) and Cu(II). Canary et al.[25] measured the equilibrium constants for complexation of $29{\cdot}Cu^{2+}$ with a series of amino acids $^+H_3N(CH_2)_nCO_2^-$ in 50% aqueous acetonitrile at pH = 5.8. The measured K values (M^{-1}) were <40 for n = 2, 100 for n = 3. 91 for n = 4, 131 for n = 5, 57 for n = 6. and 22 for n = 7, to be compared with a K value of 40 for AcONa. Optimal complexation with 6-aminohexanoic acid was taken as an indication of a cleft-like arrangement of binding sites approximately 6.5 Å apart, with coordination of $-CO_2$ to the metal ion and concomitant hydrogen bonding of $-NH_3^+$ to the crown-ether oxygens. In addition to alkali and transition metal ions, lanthanides are used as carboxylate recognition sites in ditopic receptors for zwitterionic amino acids. Liquid–liquid extraction experiments of several amino acids from their aqueous solutions at pH = 5.9–6.2 into dichloromethane using ditopic receptor **30**,[26] showed that only with M = Er was the extraction ability of **30** higher than that obtained with a mixture of monotopic model receptors. This was taken as evidence that zwitterionic amino acids are cooperatively bound to the erbium center and to the crown-ether ring.

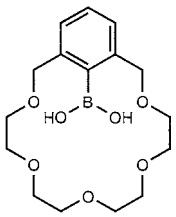

26

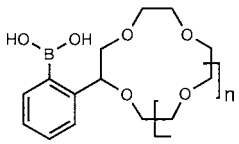

27 a: n=2
b: n=3

BETAINE RECEPTORS

Designing ditopic receptors for a betaine such as dioctanoyl-L-α-phosphatidylcholine **31** poses a difficult problem, because recognition of the trimethylammonium end group cannot take advantage of hydrogen-bonding interactions with negatively charged or electrically neutral

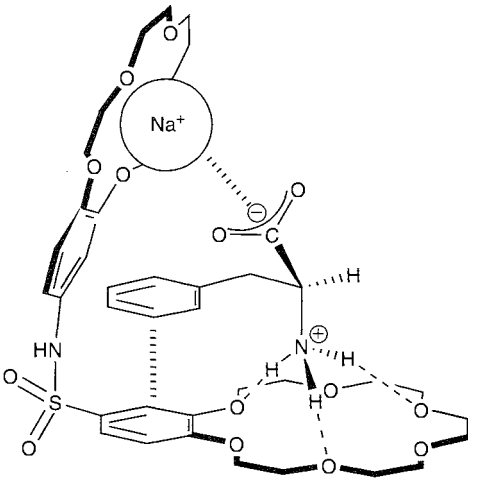

28

donors that have proved to be effective in the recognition of the primary ammonium function. Inspiration for the design of a suitable receptor for **31** came from the key interactions found in the crystal structure of the Fab domain of the McPC 603 antibody complexed with phosphorylcholine,[27,28] in which the phosphate group is engaged in a salt bridge with Arg 52H, and the quaternary ammonium head establishes a cation–π interaction with the aromatic residues of a number of amino acids. Thus, receptor **32**, designed by de Mendoza et al.,[29] contains a bicyclic guanidinium for the recognition of phosphate monoanion, and a calix[6]arene subunit for the complexation of the trimethylammonium head through cation–π interactions. NMR evidence was reported that upon mixing equimolar amounts of **31** and **32** in CD_2Cl_2 and $CDCl_3$, a stable complex is formed, in which the amide proton and one of the guanidinium protons are strongly hydrogen bonded to the phosphate, and the choline trimethylammonium head is included in the cavity of the

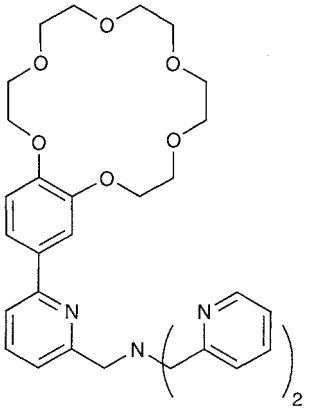

29

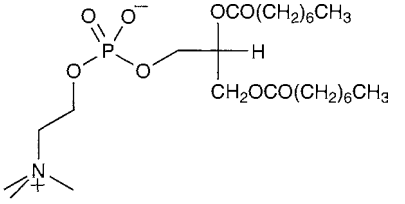

31

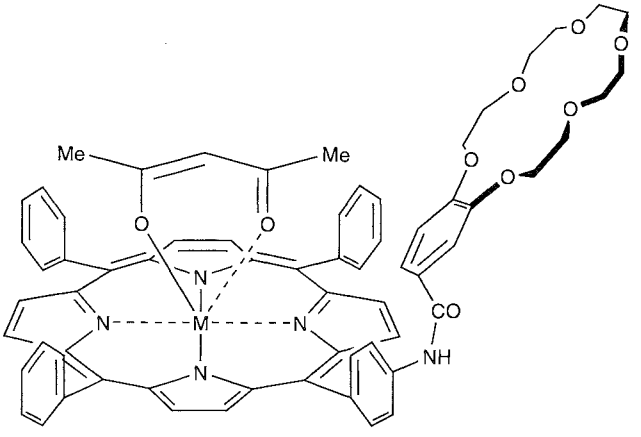

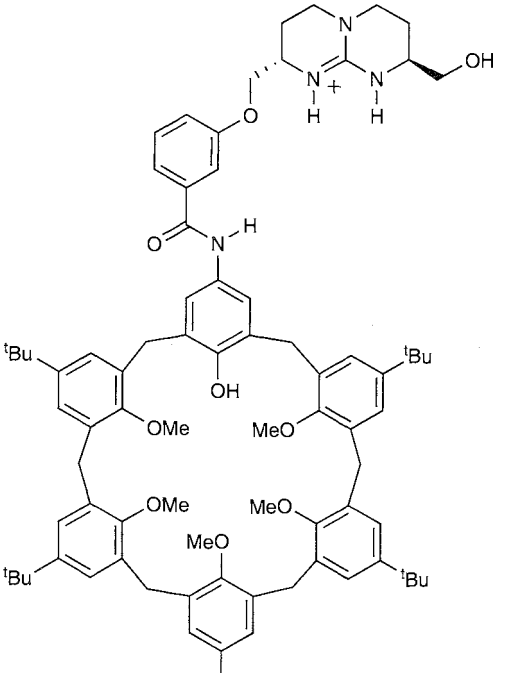

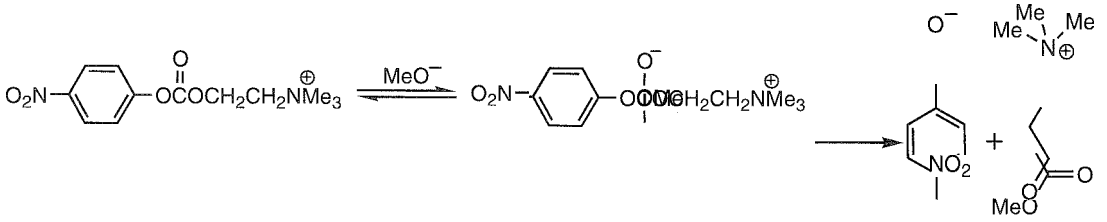

(3)

calix[6]arene in its cone conformation, as shown in the energy minimized structure 33, resulting from a detailed molecular dynamics study in a box of chloroform. Although binding of 31 by receptor 32 in chloroform ($\Delta G^\circ = -6.7$ kcal/mol) was as strong as binding of phosphorylcholine by McPC 603 in water ($\Delta G^\circ = -6.6$ kcal/mol), the former is enthalpically driven by the electrostatic contribution in the apolar solvent, while the latter has an entropic origin (desolvation of the charged ligand in water).

In view of the strong structural similarities of phosphate diesters with the tetrahedral intermediates involved in the $B_{Ac}2$ hydrolysis of esters, the former are good transition state analogues for the given reaction. This notion suggested that 32 would catalyze the cleavage of choline esters under basic conditions. In fact, it was found[13] that the methanolysis of choline p-nitrophenylcarbonate in $CH_3OH/CHCl_3$ 1:99 (v/v) in the presence of Hünig base buffer (Eq. 3) was catalyzed with high turnover efficiency by receptor 32 ($k_{cat}/k_{uncat} = 600$). Much lower rate enhancements were brought about by equimolar mixtures of monotopic model receptors, showing that the two subunits in 32 bind to the zwitterionic transition state with a high degree of synergism.

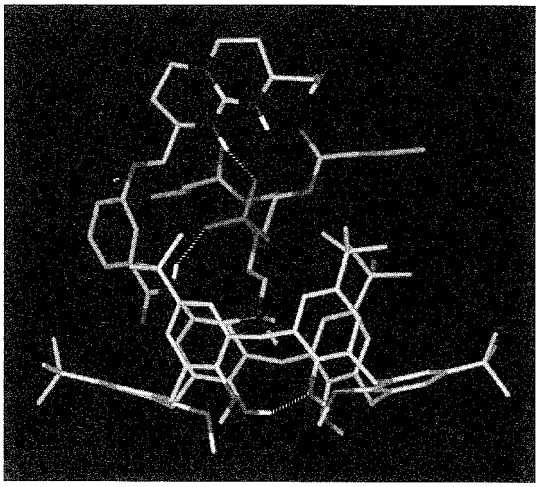

33

(View this art in color at www.dekker.com.)

CONCLUSION

Despite the above examples, the design of molecular receptors or membrane carriers for zwitterions such as natural amino acids is still a challenging task for the supramolecular community. Strong solvation and nearby opposite charges conspire against complexation or transport by complementary binding sites in synthetic candidates. Zwitterionic receptors are prone to collapse by self-assembly, so the designs have to be carefully drawn so as to use binding sites that are noncomplementary to each other. To achieve selectivity among the various members of the amino acids family is by no means free of difficulties, unless structural differences in the side chains (i.e., aromatic versus aliphatic side chains, presence of functional groups) smooth the way for efficient discrimination. This is closely related to the problem of chiral recognition, as the highest differences in binding constants among the enantiomers are to be expected for similarly weighted three-point contributions of the binding subunits.

ARTICLES OF FURTHER INTEREST

Amide- and Urea-Based Anion Receptors, p. 31
Cation–π Interactions, p. *214*
Chiral Guest Recognition, p. 236
Crown Ethers, p. 326
Cyclodextrins, p. 398
Lariat Ethers, p. 782
Podands, p. 1106
Simultaneous Binding of Cations and Anions, p. *1291*

REFERENCES

1. Pedersen. C.J. Cyclic polyethers and their complexes with metal salts. J. Am. Chem. Soc. 1967, *89*, 7017–7036.
2. Molecular Recognition: Receptors for Cationic Guests. In *Comprehensive Supramolecular Chemistry*, 1st Ed.; Atwood, J.L., Davies, J.E.D., MacNicol, D.D., Vögtle, F., Eds.; Pergamon: Exeter, UK, 1996; Vol. 1.

3. Beer, P.D.: Gale, P.A. Anion recognition and sensing: The state of art and perspectives. Angew. Chem., Int. Ed. Engl. 2001. *40*. 486–516.
4. *Supramolecular Chemistry* of Anions; Bianchi. A., Bowman-James. K.. Garcia-Espafia, E., Eds.; Wiley-VHC: New York. 1997.
5. Sunamoto, J.; Iwamoto, K.; Morhi, Y.; Kominato, T. Eiposomal bilayers. 13. Transport of an amino acid across liposomal bilayers as mediated by a photoresponsive carrier. J. Am. Chem. Soc. 1982. *104*, 5502–5504.
6. Nemeth. D.; Rebek, J., Jr. Molecular recognition: Three-point binding leads to a selective receptor for aromatic amino acids. J. Am. Chem. Soc. 1985, *107*, 6738–6739.
7. Rebek, J., Jr.; Askew, B.: Nemeth, D.; Parris, K. Convergent functional groups. 4. Recognition and transport of amino acids across a liquid membrane. J. Am. Chem. Soc. 1987, *109*, 2432–2434.
8. Tabushi, I.; Kuroda, Y.; Mizutani. T. Artificial receptors for amino acids in water. Local enviromental effect on polar recognition by 6A-amino-6B-carboxy- and 6B-amino-6A-carboxy-cyclodextrins. J. Am. Chem. Soc. 1986. *108*. 4514–4518.
9. Terfort, A.; von Kiedrowsky. G. Self-replication by condensation of 3-amino-benzamidines and 2-formylphenoxyacetic acids. Angew. Chem.. Int. Ed. Engl. 1992. *31*, 654–656.
10. Askew. B.C. The design and synthesis of macrobicyclic hosts featuring convergent functional groups. Tetrahedron Lett. 1990, *31* (30), 4245–4248.
11. Codoy-Alcántar, C.; Nelen, M.I.; Eliseev, A.V.; Yatsimirsky, A.K. Molecular recognition by natural macrocycles. Part II. Esterolytic activity and chiral discrimination of amino acid derivatives by the zwitterionic form of (+)-tubocurarine. J. Chem. Soc.. Perkin Trans. 2 1999, 353–361.
12. Kimura, E.; Sakawa, A.; Yatsunami, T.: Kadama, M. Macromonocyclic polyamines as specific receptors for tricarboxylate-cycle anions. J. Am. Chem. Soc. 1981. *103*, 3041–3045.
13. Dietrich, B.; Hosseini, M.W.: Lehn, J.M.; Sessions, R.B. Anion receptor molecules: Synthesis and anion-binding properties of polyammonium macrocycles. J. Am. Chem. Soc. 1981, *103*. 1282–1283.
14. Kimura, E.; Fujioka, H.; Kodama, M. A new ditopic receptor for ionic guest molecules. J. Chem. Soc., Chem. Commun. 1986. 1158–1159.
15. Schmidtchen. F.P. Synthesis of an abiotic ditopic receptor molecule. Tetrahedron Lett. 1984, 25 (39), 4361–4364.
16. Schimdtchen, F.P. Tetazac: A novel artificial receptor for binding w-amino carboxylates. J. Org. Chem. 1986. *51*. 5161–5168.
17. Barboiu. M.; Supuran, C.T.; Scozzafava, A.; Briganti, F.: Luca. C.: Popescu, G.: Cat, L.; Hovnanian, N. Supramolecular complexes of L-amino acids as efficient activators of the zinc enzyme carbonic anhydrase. Liebigs Ann./Recueil 1997. 1853–1859.
18. Galán, A.; Andreu. D.: Echavarren, A.M.; Prados, P.: de Mendoza. J. A receptor for enantioselective recognition of phenylalanine and triptophan under neutral conditions. J. Am. Chem. Soc. 1992. *115*. 7037–7038.
19. de Mendoza, J.; Gago, F. Molecular Recognition of Dinucleotides and Amino Acids by Artificial Receptors Containing a Byciclic Guanidinium Subunit. In *Computational Approches in Supramolecular Chemistry*; Wipff, G., Ed.; Kluwer: Dordrecht, 1994: 79–99.
20. Metzger, A.; Gloe, K.: Holger. S.: Schmidtchen. F.P. Molecular recognition and phase transfer of underivatized amino acids by foldable artificial host. J. Org. Chem. 1996. 61, 2051–2055.
21. Sessler. J.L.: Andrievsky, A. Efficient transport of aromatic amino acids by sapphyrin-lasalocid conjugates. Chem. Eur. J. 1998, *4* (1), 159–167.
22. Jeong, K.S.: Park, T.Y. Complexation and transport of zwitterionic amino acids by artificial receptor. Bull. Korean Chem. Soc. 1999, *20* (2), 129–131.
23. Reetz. M.T.; Huff, J.; Rudolph. J.; Tolner, K.; Deege. A.; Goddard, K. Highly efficient transport of amino acids through liquid membranes via three-component supramolecules. J. Am. Chem. Soc. 1994, *116*, 11588–11589.
24. Barboiu. M.D.; Hovanian. N.D.; Luca, C.: Cot, L. Functionalized derivatives of benzocrown-ethers, V multiple molecular recognition of zwitterionic phenylalanine. Tetrahedron 1999, *55*, 9221–9232.
25. dos Santos, O.; Lajmi, A.R.; Canary. J.W. Synthesis of a dinucleating with addressed ion binding sites. Tetrahedron Lett. 1997, *38* (25), 4383–4386.
26. Tsukube. H.; Wada. M.; Shinoda, S.: Tarniaki, H. Porphyrinatoerbium-crown ether conjugate for synergistic binding and chirality sensing of zwitterionic amino acids. J. Chem. Soc., Chem. Commun. 1999, 1007–1008.
27. Segal. D.M.; Padlan. E.A.; Cohen, G.H.; Rudikoff, S.: Potter. M.: Davies, R.D. Three dimensional structure of antigen binding site of McPC603 protein. Proc. Natl. Acad, Sci. U.S.A. 1974. 71. 4298.
28. Satow, Y.: Choen, G.H.; Padlan, E.A.; Davies. J.R. Phosphocholine binding immunoglobulin fab McPC603. An x-ray diffraction study at 2.7 Å. J. Mol. Biol. 1986. *190*. 593.
29. Magrans. J.O.; Ortiz, A.R.; Molins, M.A.; Lebouille, P.H.P.; Sánchez-Quesada, J.; Prados; P.; Pons. M.: Gago. F.; de Mendoza, J. A designed non-peptidic receptor that mimics the phosphocholine binding site of the McPC603 antibody. Angew. Chem.. Int. Ed. Engl. 1996.35. 1712–1715.
30. Cuevas, F.; Di Stefano, S.; Magrans, O.J.: Prados. P.; Mandolini. L.; de Mendoza, J. Toward an artificial acetylcholinesterase. Chem. Eur. J. 2000. *6*. 3228–3234.

Index

ENCYCLOPEDIA OF SUPRAMOLECULAR CHEMISTRY

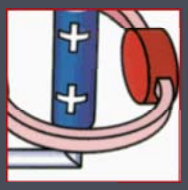

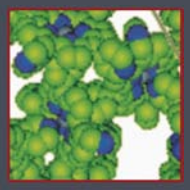

EDITED BY

JERRY L. ATWOOD
JONATHAN W. STEED

Pre-publication praise. . .

"...the time is ripe for an Encyclopedia of Supramolecular Chemistry...It will be of great value."—Jean-Marie Lehn, Supramolecular Chemistry Laboratory, Universite Louis *Pasteur, Strasbourg,* France, and Winner, 1987 Nobel Prize in Chemistry

"...the most ambitious undertaking in the field of supramolecular chemistry... well done!"—Jerald *S.* Bradshaw, *Brigham* Young University, Provo, Utah, U.S.A.

"...this Encyclopedia will be of immense use to both experts and those with growing interest in supramolecular science...[a] masterpiece."—Antonio Bianchi, University of Florence, Italy, and International Scientific Committee, International Symposium on Macrocyclic Chemistry

about the encyclopedia . . .

Crystallizing a rapidly expanding interdisciplinary field, this two-volume Encyclopedia of Supramolecular Chemistry offers authoritative, centralized information on the topic. Designed for specialists and students alike, the Encyclopedia simultaneously covers the fundamentals of supramolecular chemistry and sets the standard for relevant future research.

Commencing with a foreword by Jean-Marie Lehn, user-friendly and high-quality articles *parse* the latest supramolecular advancements in the areas of chemistry, biochemistry, biology, environmental and materials science and engineering, physics, computer science, and applied ma*thema*tics.

Guided by editors at the fore of supramolecular research and an elite international editorial advisory board, Atwood and Steed's Encyclopedia encompasses concepts in crystal engineering...DNA as a supramolecular scaffold...energy and electron transfer in supramolecular systems...imprinted polymers...macrocyclic synthesis—templates, high dilution, and high pressure...molecular-level machines...natural strategies for the molecular engineer...self-assembly...soft/smart materials...supramolecular chirality...and much more in the rich expanse of its more than 200 entries.

about the editors. . .

JERRY L. ATWOOD is Curators' Professor and Chair of the Department of Chemistry at the University of Missouri-Columbia. The founder or cofounder of three journals, current editor of The Journal of Supramolecular Chemistry, and an associate editor of Chemical Communications, he has over 550 refereed papers, 20 book chapters, and ten patents to his name. Along with Dr. Steed, he is coauthor of the influential textbook Supramolecular Chemistry (John Wiley & Sons, Inc.). Awarded the Izatt-Christensen International Macrocyclic Chemistry Award (2000) and the University of Missouri President's Award for Research and Creative Activity (2000), Dr. Atwood received the B.S. degree (1964) from Southwest Missouri State University, Springfield, and the Ph.D. degree (1968) from the University of Illinois at Urbana-Champaign.

JONATHAN W. STEED is a Reader in Inorganic Chemistry at the University of Durham, United Kingdom. An associate editor of the New Journal of Chemistry, Dr. Steed is the author of more than 170 research papers and numerous reviews, book chapters, and popular articles. Past collaborations with Dr. Atwood culminated in the development of a new class of supramolecular hosts for anions, as well as the publication of Supramolecular Chemistry (John Wiley & Sons, Inc.). The recipient of the Royal Society of Chemistry Meldola Medal (1998), Dr. Steed received the B.Sc. (1990) and Ph.D. (1993) degrees from University College London, United Kingdom.

Printed in the United States of America

DK056X

ISBN 0-8247-5056-X

CRC & Francis
Taylor & Francis Group
an informa business
A CRC PRESS BOOK
www.taylorandfrancisgroup.com

6000 Broken Sound Parkway, NW
Suite 300, Boca Raton, FL 33487

270 Madison Avenue
New York, NY 10016

2 Park Square, Milton Park
Abingdon, Oxon OX14 4RN, UK